THE 10th INDONESIA INTERNATIONAL GEOTHERMAL CONVENTION & EXHIBITION 2024

Supported by:
MINISTRY OF ENERGY AND MINERAL RESOURCES REPUBLIC OF INDONESIA

Hosted by:
ASOSIASI PANASBUMI INDONESIA (API)
INDONESIAN GEOTHERMAL ASSOCIATION (INAGA)

Endorsed by:
IGA
INTERNATIONAL GEOTHERMAL ASSOCIATION

ISSN 2986-1268
Volume 8, 2025

WORLD'S LARGEST GEOTHERMAL CONVENTION & EXHIBITION

POWERING TOGETHER: STAKEHOLDER UNITY IN GEOTHERMAL INNOVATION AND ACCELERATION

PROCEEDING BOOK

18-20 SEPTEMBER 2024
JAKARTA CONVENTION CENTER

Organized by:
ONUS ASIA

Proceeding Book 10th IIGCE 2024
Powering Together: Stakeholder Unity
in Geothermal innovation and Acceleration

ISSN 2986-1268
Volume 8, 2025

The 10th Indonesia International Geothermal Convention & Exhibition (IIGCE) 2024

September 18-20, 2024

Powering Together: Stakeholder Unity in Geothermal innovation and Acceleration

Editors:

Abadi Poernomo
Doddy Astra
Suryantini
Ali Ashat

Reviewers:

Ali Ashat (ITB)
Aquardi Suminar (SEGSD)
Christovik S (Baker Hughes)
Doddy Astra (INAGA)
Fernando Pasaribu (PGE)
Hari Widianto (Mannvit)
Hill Gendoet (ITNY)
Khasani (UGM)
Marino C. Baroek (INAGA)
Mulyanto (PGE)
Rizal Abiyudo (MCG)
Suryantini (ITB)
Yudi Indra Kusumah (SEGS)
Yunus Daud (UI)

Indonesian Geothermal Association

2025

ISSN 2986-1268
Volume 8, 2025

Published by:

Asosiasi Panasbumi Indonesia (API)

ISSN 2986-1268
Volume 8, 2025

Sanksi Pelanggaran Pasal 72 Undang-Undang Nomor 19 Tahun 2002 Tentang HAK CIPTA

1. Barangsiapa dengan sengaja dan tanpa hak melakukan perbuatan sebagaimana dimaksud dalam Pasal 2 ayat (1) atau Pasal 49 ayat (1) dan ayat (2) dipidana dengan pidana penjara masing-masing paling singkat 1 (satu) bulan dan/atau denda paling sedikit Rp. 1.000.000,00 (satu juta rupiah), atau pidana penjara paling lama 7 (tujuh) tahun dan/atau denda paling banyak Rp. 5.000.000.000,00 (lima miliar rupiah).
2. Barangsiapa dengan sengaja menyiarkan, memamerkan, mengedarkan, atau menjual kepada umum suatu Ciptaan atau barang hasil pelanggaran Hak Cipta atau Hak Terkait sebagaimana dimaksud pada ayat (1) dipidana dengan pidana penjara paling lama 5 (lima) tahun dan/atau denda paling banyak Rp. 500.000.000,00 (lima ratus juta rupiah).

ISSN 2986-1268
Volume 8, 2025

The 10th Indonesia International Geothermal Convention & Exhibition (IIGCE) 2024

September 18-20, 2024

COMMITTEE

ADVISOR
Director General of New, Renewable Energy and Energy Conservation (MEMR)

STEERING COMMITTEE
Director of Geothermal (MEMR)
Julfi Hadi (INAGA)
Riza Pasikki (INAGA)
Supriadinata Marza (INAGA)
Prijandaru Effendi (INAGA)
Abadi Poernomo (INAGA)
Rangga Wirapasa (INAGA)
Ahmad Yani (PGE)
Imron Gazali (MPI)
Rangga Wirapasa (SOL)
Agus Sandy (SEG)
Ali Sahid (KSO)
Dion Murdiono (Ormat)
Tommy Suryatama (Ecolab)
Pandu (Tiger Energy)
Dian Sari (SLB)

CHAIRMAN IIGCE 2024
Boyke Bratakusuma (SEG)

SECRETARIAT
Andry Susanto (INAGA)
Reva Sasistya (SEG)
Aldi (INAGA)

FIELD TRIP
Irwan Januar K Hasbullah (SEG)
Henri Kurniawan (SEG)
Indah Wardhani (SEG)

TECHNICAL PAPER
Alfiady (KSO)
Zerrynto (Supreme)
Ali Ashat (ITB)
Amsal Sihombing (SEG)
Angga (Ormat)
Aquardi Suminar (SEG)
Arias Sugandhi (SEG)
Budi Kristianto (GDE)
Chandra Salim (SOL)
Christovik S (Baker Hughes)
Deny Kurniawan (SEG)
Dhani Sanjaya (Chevron)
Doddy Astra (INAGA)
Doddy Darmawan (SEG)
Evans Satya (Supreme)
Fernando P (Pertamina)
Fitri Oktaviani
Hari Widianto (Mannvit)
Ichwan Elfajrie
Khasani (UGM)
Lutfhie (SEG)
Mahesa P. Saputra
Marina Sari
Mulyanto (PGE)
Prihatmaka
Redha Bhawika (KSO)
Remi Harimanda (Ormat)
Rex Soeparjadi (SEG)
Riki Irfan (ITS)
Riostantieka MS (ITB)
Rizal Abiyudo (MCG)
Suryantini (ITB)
Tommy S (Ormat)
Wintry Dimwan (SEG)
Yamin Wibisono (SEG)
Yudi Indra Kusumah (SEG)
Yunus Daud (UI)
Zerry Antro (SEG)

ISSN 2986-1268
Volume 8, 2025

This page is intentionally left blank

ISSN 2986-1268
Volume 8, 2025

SPEAKERS

H.E. Ir. H. Joko Widodo, President of the Republic of Indonesia

Hon. Bahlil Lahadalia, Minister of Energy and Mineral Resources of the Republic of Indonesia

Hon. Rosan Roeslani, Minister of Investment of the Republic of Indonesia (Represented by **Dedi Latip**, Deputy for Investment Planning, Ministry of Investment/Investment Coordinating Board)

Jisman P. Hutajulu, Director General of Electricity, Ministry of Energy and Mineral Resources of the Republic of Indonesia (Represented by **Wanhar**, Director of Electricity Program Development, the Ministry of Energy and Mineral Resources (ESDM)

Julfi Hadi, President Director of PT Pertamina Geothermal Energy Tbk

Hanif Osman, Director of Finance, Risk Management & General Affairs of PT Geo Dipa Energi (Persero)

Ahmad Yani, Director Operation of PT Pertamina Geothermal Energy Tbk

Peter Scrivener, Regional Director of Solenis

Vinesh Krishnan, Vice President, Energy Solution, Hub Asia of ABB Energy Industries

Novianto, VP Geothermal and General Manager of Medco Power Indonesia

Shuichiro Ikeda, Chief Operating Officer of Supreme Energy

H.E. Kevin Burnett, ONZM, New Zealand Ambassador to Indonesia

Eddy Soeparno, Deputy Chairman of Commission VII DPR RI

Eniya Listiani Dewi, Director General of New, Renewable Energy and Energy Conservation, Ministry of Energy and Mineral Resources of the Republic of Indonesia

Satyawan Pudyatmoko, Director General of the Conservation of Natural Resources and Ecosystem, Ministry of Environment and Forestry of the Republic of Indonesia

Hendra Soetjipto Tan, Group Chief Executive Officer of Star Energy Geothermal

Dr. Yan Tang, President Director of KS Orka Renewables Pte Ltd

Ann Robertson-Tait, President of SLB's GeothermEx Consulting Services

Ajit Menon, Vice President of Geothermal Baker Hughes

Ran Reshef, Vice President International Sales of Ormat Technologies

Ardyanto Fitrady, Center for Energy Studies, Gadjah Mada University (PSE UGM)

Marit Brommer, Executive Director the International Geothermal Association

Paul Ngugi, Managing Director & CEO of Geothermal Development Company - Kenya

ISSN 2986-1268
Volume 8, 2025

This page is intentionally left blank

ISSN 2986-1268
Volume 8, 2025

FOREWORD PRESIDENT OF INAGA

Global climate change remains one of today's most pressing challenges. Energy security is another critical issue exacerbated by the complex geopolitics unfolding globally. The transition toward renewable energy, particularly geothermal energy, has emerged as a vital solution to address these issues. Indonesia, with its vast geothermal resources lying untapped beneath chains of volcanoes, holds immense potential to accelerate the transition toward a sustainable energy future. This resource is key to Indonesia's renewable energy future, showcasing innovation and adaptability.

The 10th Indonesia International Geothermal Convention & Exhibition (IIGCE) 2024, held on **September 18 - 20, 2024**, at Assembly Hall, Jakarta Convention Center, was officially opened by **President of the Republic of Indonesia, His Excellency Joko Widodo**. Marking a decade of commitment to advancing geothermal development, this event continued to serve as a platform for dialogue and collaboration among geothermal stakeholders. With the theme **"Powering Together: Stakeholder Unity in Geothermal Innovation and Acceleration"**, IIGCE 2024 explored breakthroughs and solutions to support the global energy transition. Discussions emphasized overcoming commercial bottlenecks, fostering collaboration to refine business models for managing exploration risks, reducing development costs, optimizing production through technology, and working with the government to establish workable incentives.

As part of the 10th IIGCE, the **24th Annual Scientific Meeting (PIT)** achieved remarkable milestones, reflecting the growing enthusiasm for advancing geothermal research and development. A total of 278 abstracts were submitted, with contributions from professionals and academia, showcasing diverse perspectives.

These contributions spanned topics including Earth Science, Engineering, Resource Management, Beyond kWh, and other special focus areas. The Technical Papers Session served as an invaluable opportunity to share knowledge, insights, and best practices for the geothermal community.

I would like to take this opportunity to express my gratitude and appreciation to the Technical Paper Committee, Chairpersons, Authors, Presenters, and all contributors who made the 2024 Technical Papers Session a success. Your dedication and expertise ensured the continued impact of this platform, reflecting the innovation and collaboration that drive geothermal energy development forward.

On behalf of INAGA, I am pleased to present this year's Technical Papers Session, a valuable resource for our geothermal community. Let us collaborate to unlock geothermal's full potential for a sustainable future.

Yours Truly,

Julfi Hadi
President of INAGA

ISSN 2986-1268
Volume 8, 2025

This page is intentionally left blank

ISSN 2986-1268
Volume 8, 2025

Proceeding Book

The 10th Indonesia International Geothermal Convention & Exhibition (IIGCE) 2024

September 18-20, 2024

Published by

Asosiasi Panasbumi Indonesia
Apartemen Menteng Square, BR-9 Tower B
Jl. Matraman No. 30E, Jakarta Pusat – 10320, Indonesia

Topics

Earth Sciences (42 articles)
Engineering (56 articles)
Resource and Management (23 articles)
Social, Politics, Economics, and Community (21 articles)
General (33 articles)
TOTAL = 175 articles, 1748 pages

CONTENTS

Committee ..... **i**
Speakers ..... **iii**
Foreword President of INAGA ..... **v**

Paper Categories	Page
Part 1: Earth Sciences	1
Part 2: Engineering	405
Part 3: Resource Management	931
Part 4: Social, Politics, Economics, and Community	1125
Part 5: General	1393

ISSN 2986-1268
Volume 8, 2025

EARTH SCIENCES

Novel Accelerator of Geothermal Field Development: Transient Electromagnetic Method Utilizing Superconducting Quantum Magnetic Sensor (SQUID-TEM) **2**
Tsunehiro Hato, Hironori Wakana, Akira Tsukamoto, Keiichi Tanabe, Michael S. Zhdanov, Alex Gribenko, Indra A. Nugroho, and Herwin Azis

Stress Distribution Analysis to Characterize the Fault Permeability in Nage Field, Indonesia **11**
Muhammad Ikhwan

Identification of Geothermal Manifestation Using Remote Sensing Method in Slamet Mountain Area, Central Java **19**
Sisdeo Hutagaol, Fabyan Mark Alfons, Rowena Astika Rahamis, and Maulidiya Fathien Hamidah

A 3D Geological Model and Natural State Simulation of the Massepe Geothermal Field in South Sulawesi, Indonesia **30**
Fikri Rahmansyah, Michael Gravatt, and John O'Sullivan

Re-Evaluate The Sibayak Field Using 3D Inversion Model Based on Updated MT Data **43**
Inusa P Fauzi, Aditya A Juanda, Sotarduga S Nainggolan, and Mulyanto

Analog Study of Geothermal System of Telomoyo Mountain With Ungaran Mountain Using 3G Analysis Method (Geology, Geophysics and Geochemistry) **52**
M.D.A. Wulandari, A. S. Pintrandhita, and K. L. Fatihah

Imaging The Mass Distribution of The Semolon Geothermal Prospect, North Borneo, Using Satellite Gravity Data **57**
Sintia W. Niasari, Camelia Umar, and Mochamad Nukman

Interpolation Methods in Python for Geothermal Field Analysis: A Comparison of Cubic, Linear, and Nearest Neighbor Approaches **62**
Fanzly Togap Zisochi Lase, Prihadi Sumintadiredja, Tony Rahadinata, and Ahmad Zarkasyi

Preliminary Study of Mount Pandan Geothermal System at Bojonegoro Based on Surface Manifestation, Altered Minerals and Geochemical Fluids **71**
Juan Adhipermana, Bimo Putra Panggabean, Claudio Ronaldo Mendome, and Petrus Aditya Ekananda

The updates of 2021-2023 Patuha Drilling Campaign: Challenges and Successes in Expanding the Resource Areas **79**
Ezidin Reski, Khatis Jati Pamungkas, Dito Budi Sukarno, Randy Wijaya Atmaja, Eka Daya Samudra, and Yuris Ramadhan

Resistivity Model Using 3D Inversion MT at XX Geothermal Field **91**
Baskoro D and Zaky M

Kotamobagu Geothermal Field, Indonesia: Overview on the Geological Aspect **98**
Syayidu Guntur Maarif, Graniko Reza Pratama, Sigit Suryanto, Ben Ikhsan, David Paskareinold Timisela, and Dimas B E Rindingpadang

Unveiling Geothermal Potential by Leveraging SAR-assisted Fault Identification in Kotamobagu, North Sulawesi, using modified Segment Tracing Algorithm (mSTA) Method **112**
Ben Ikhsan, Israyudi, David P. Timisela, and Asep Saepuloh

Magnetotelluric Parameters with Variation in Synthetic Data in 3D Forward Modeling **126**
Serina Andiani Pongtuluran, Sari Widyanti, Lendriadi Agung, Imam B. Raharjo, Nicolas Silaen, Vicky Rai Chandra, Muhammad Ghassan Jazmi Shalihin, Astri Indra Mustika, Triwening Larasati, Galih Bayu Permadi, and Ferdino R. Fadhillah

ISSN 2986-1268
Volume 8, 2025

Radon Thoron in Fault-Controlled Geothermal Prospect: A Study Case in Sumatra **152**
Fraga Luzmi Fahmi, Jodhi Pramuji Giriarso, Fuad Nur Hussein, and Mulyanto

The Implications of Mineral Geothermometer, Geochemistry, and Pressure Temperature on Scaling in the Two-Phase Fluid Well, Dieng Geothermal System **161**
Iqbal Maratama, Rizkhy Ridoh A, Siti Olivinia Yusra, Rudy Martikno, Randy Wijaya Atmaja, and Denis Daya Pamungkas

Insights Into Permeability Heterogeneity: Seismic Monitoring and Focal Mechanism Studies at Wayang Windu Geothermal Field **171**
Wahyuddin Diningrat, Meiyanto Purnomo, and Wintry Dimwani

Towards a New Framework for the Systematic Assessment of Indonesia's Undeveloped Geothermal Resources **176**
John O'Sullivan, Winnie Alia, Armando Aloanis, Ken Dekkers, Ari Fuad, Michael Gravatt, Bei Nagoro, Rony Nugraha, Joris Popineau, Aulia Pratama, Fikri Rahmansyah, Theo Renaud, Jeremy Riffault, Alfia Syahrul, Iqbal Takodama, Ryan Tonkin, and Mike O'Sullivan

Untapped Geothermal Potential of Lahendong Concession, North Sulawesi **188**
Ristio Efendi, Antonius.R. Untoro, Sigit Suryanto, David. P. Timisela, and Dimas. B.E. Rindingpadang

Inter-tidal Hot Springs' Geochemistry in Atauro **196**
James C. Chang, Ardhya N.K. Nugroho, Joseph E. Ardine, and Nazario Gomes

Preliminary Survey of Tempuran Green Field Geothermal System Using Gravity Satellite Data and Fault Analysis **205**
Muhammad Faizal Zakaria, Ardhan Farisan, Y. Yatini, Nanda Ajeng Nurwantari, and Ismail Mutoriz

Identification of Hot Spring Aquifers Based on Vertical Electrical Sounding (VES) Method Using Schlumberger Configuration in Tempuran Area, Magelang Regency **213**
Latief D.U., Yatini, Indira A., Levana N., Faza N.A., and M. Faizal Z.

The Subsurface and Drilling Aspects of The Successful 2020-2021 Make-up Well Drilling in Wayang Windu Geothermal Field, Indonesia **222**
Shanti R. A. Sugiono, Ridha B. Nugraha, Rio Nugroho, and Wintry Dimwani

Utilizing Static Modeling to Analyze Paleosol Distribution to Reduce Its Impact on Stuck Well Drilling in Wayang Windu **228**
Meiyanto J. Purnomo, Ananyamatya B. Talita, Nevio M. Kamel, Dwiyogarani Malik, and Wintry Dimwani

Geology and Control for The Appearance of Hot Springs in The Northern Area of Mount Pandan Complex, East Java **236**
Solomon M. Timothi, Suryantini, and Alfend Rudyawan

Reservoir Fluid Movement Identification using 3-D Inversion Time-lapse Microgravity Monitoring (2015-2023) in the Lahendong Geothermal Field **250**
Lendriadi Agung, Mohammad Syamsu Rosid, Mochamad Tofan Sastranegara, Baiq Lola Riandari, Anita Fitria Sekar Arumsari, and David Paskareinold Timisela

Finding the Correlation Between Electrical Resistivity and Thermal Gradients in Geothermal Fields: A Case Study of Sumani, Way Selabung, and Kadidia **263**
Azralina Maysa Rahayu, Satriya Putra Baskara, Musa Zakariya, Sintia Windhi Niasari, Asep Sugianto, and Tony Rahadinata

Continuous Development of In-house Laboratory Capabilities of Wayang Windu Geothermal Field **270**
Dwiyogarani Malik, Indra Yudhistira, Nevio M. Kamel, Dodoh Abdullah, and Galang A. Purnama

ISSN 2986-1268
Volume 8, 2025

The Assessment of The Boundary Reservoir Expansion Based on Magnetotelluric and Wells Data of the Sorik Marapi Geothermal Field in North Sumatra, Indonesia **279**
Keshan Apriliyanthy, Alfiady, Tio Fernando,Wishnu Triananda, and Zammy Sarmiento

Unstable Formation Identification and Potential Drilling Hazard in Geothermal Borehole: Lesson from Sorik Marapi **287**
Tio Ferdinan, Alfiady, Keshan Apriliyanthy, Stephen Simamora, and Zammy Sarmiento

Time-Lapse Gravity Monitoring of the Tompaso Geothermal Field in Indonesia from 2016 to 2023 **295**
Astha Dandari Kusuma Wardhani, R. M. Tofan Sastranegara, Gylfi Pall Hersir, Egill Arni Gudnason, Lendriadi Agung, and Fadhilaz Digdaya Haq

Optimalize Geothermal Exploration Potential with Comprehensive Gravity and Landsat Method at Tanggeung Area, West Java, Indonesia **309**
Rahman F, Mawalid A, Fadrian D F, Herlambang K A, Kurniasih, and Pangestu F B

Reservoir Rock of the Lumut Balai Geothermal System Indonesia **321**
Vivi Dewi Mardiana Nusantara, Imam Muhamad Prasetya, Sapto Trianggo Nurseto, and Mulyanto

The Voyage of PGELabs Towards Geothermal Excellence **326**
Losendra Primamas Yonando, Henny Firdaus, Ragil Farhandimas Rizki, Helmi Sopari, M. Iqbal Al Kindi, Teza Permana, Hendra Hadriansyah, Nanda Najih H. A., and Ricsen Halomoan

Preliminary Assessment of Critically Stressed Fracture in Lumut Balai and its Effect on Permeability of the Field **334**
Muhammad Tajul Arifin, Sapto Trianggo Nurseto, and Mulyanto

Fracture Characterization Inside and Outside Salak Geothermal Reservoir **343**
Fanji J. Putra and Yudi Indra Kusumah

Characterization of Fluid Geochemistry from the New Pad in the Westernmost Section of Northern Wayang Windu **357**
Nevio Kamel, Dwiyogarani Malik, Stefano Pentury, and Wintry Dimwani

MT Conductors Below Volcanic Hosted Geothermal Prospects **364**
Friedemann Samrock[1], Wolfgang Soyer[1], Stefano Garanzini[1], Alice Pavesi[1], Randall Mackie[1], Chevy Iskandar[2], Elfina[2], Inusa Pamusyawara Fauzi[3], Aditya A Juanda[3], and Stephen Halinan[1]

Application of Long Offset Resistivity Tomography for Reservoir Characterization Improvement at The Darajat Geothermal Field, Indonesia **372**
Reka Tanuwidjaja[1], Chris Nelson[1], Bagus Endar B. Nurhandoko[2], and Amalia Nurani[3]

Constructing the Fault from Borehole Image and Drilling Fluid Movement in the Dieng Geothermal Field, Eastern Part of North Serayu Gea-Anticline **380**
Iqbal Maratama, Rizkhy Ridoh Alamsyah, Andhika Putera Utama, Aditya Yudha Kencana, Zakki Sabiq Purwaka, and Andy Wijaya Atmaja

Power Density Assessment of Geothermal Fields in Indonesia **391**
Eko Hari Purwanto and Andi Susmanto

Application of NDVI and VARI in Vegetation Monitoring Using GIS and Remote Sensing on Patuha Geothermal Area **396**
Muhammad Gantang Nugraha, Laurentia Mutiara Sani Widyawati, Agung Maulana, and R. Yulianto K.

ISSN 2986-1268
Volume 8, 2025

ENGINEERING

Integrated Strategy for Increasing Attractiveness and Competitiveness of Geothermal Drilling and Workover Market in Indonesia **406**
M. Rizqi Al Asy'ari, Daniel W. Adityatama, Nadya Erichatama, Vincentius Adven Brilian, Ferdino R Fadhillah, Desak Nyoman Inten Apriani, Dorman Purba, Astri Indra Mustika, and Triwening Larasati

Advances in High Temperature Directional Drilling **444**
John Clegg, Peter Harvey, Steve Krase, Gorka Plata, Shraddha Singh, and Matthew White

Estimating Pressure Drop in Two-Phase Geothermal Fluid Flow **452**
Sanjay Banerjee and Patrick Robinson

Monoblock Geothermal Power Plant Study in Dieng Geothermal Working Area **459**
Wahyu Festiawan Nurrochim, Rifki Yogiantara, Herdian Ardi Febrianto, and Andhika Yudiaji

Drilling Strategies in Red Clay Zone to Manage Iron Oxide Minerals Experience from P-Field, Indonesia **468**
Pradana Vian Prasetyo, Didin Chaeruddin Irwansyah, Vicki Agustino, Dicky Alamsyah, Eka Daya Samudera, Ingria Yunandra M Arrasy, and Budi Setiawan

Production Operations Optimization in Patuha Production Well **474**
Adiasa Dewa Pradipta, Ananda Riris Kurnia Pratama, Andrian Putra Wardana, Budi Santoso, and Hary Darmawan

Unlocking Geothermal Potential: The CaSil Technology **484**
Michael Schweig, James H. Johnston, Thomas Borrmann, and H. Putri Fraser

Case Study of the CaSil Technology at Dieng, Indonesia – Successfully Eliminating Silica Scale **492**
Thomas Borrmann, H Putri Fraser, James Johnston, Michael Schweig, Ilen Kardani, Delvirah Singkuang, Ayu Gracia Ade Sumartha, Andhika Putera Utama, and Aditya Yuda Kencana

Comparative Analysis of Steam Flowmeters for Enhanced Geothermal Power Plant Performance **500**
U. Anang Ischak

Condition Based Lubrication Drives Down Maintenance Costs and Downtime Cost in Patuha Geothermal **515**
Raka Anugrah Pratama, Andisyah Purdanto, and Yanuar Ramdhani

Geothermal Champaign a Success Story of GRE Pipe for Downhole Casing in Geothermal Well **525**
Nico Riyanto

Avoiding Stuck Pipe Incident Through Effective Management of Metasedimentary Rocks in Geothermal Drilling **533**
Gatra Kusuma, Umar Sidiq, Rully Putradi, Komang Wisnu, Wahyu Sutresno, Tesha, Timora, and Hargi

A Value to Reduce Overall Geothermal Cost – Unified Well Construction **540**
Gatra Kusuma, Ridha Budi, Doddy Darmawan, Komang Wisnu, Aufy, Hargi, and Timora

Geo-LOK Casing Hanger: A Superior Alternative to Conventional Cementing in Deep Geothermal Wells **549**
Kevin Gray, Daria Ivakhnenko, Ben Adams, Zander McDougall, and Garry Stephen

Reliability Analysis of Pressure Transmitter Integration with Flow Switch for Enhanced Seal Water System Performance in LRVP Systems at Geothermal Power Plants Kamojang **558**
Muhammad Indjra Dije, Ales Daniel, Fikrul Jihad, and Luhung Pravubinantaka

Upgrading Bently Navada 3300 to 3500: A Case Study of Wayang Windu Unit 1 Geothermal Power Plant **564**
Khansa Ambar Purbaranti, Teja Prasetya, Muhammad Ichsan, and U. Anang Ischak

ISSN 2986-1268
Volume 8, 2025

Inconsistent Quality of Class G Cements **575**
Ramil Joseph L. Bunac[1] and Lawrence Diehm Weber[2]

Debottlenecking Ulubelu: Optimizing Steam Supply **586**
A.H. Fauzi, A. Kuswantoro, I. Solikhin, A.T. Putra, M. Rofii, H.B. Setyawan, and M.W. Kusumah

Lesson Learned from a Forced Outage on April 14, 2024: Improving System Reliability in Power Generation Plants by eliminating nuisance trip due to improper setting of motor protection – A Case Study of Geothermal Power Plant Lumut Balai Unit 1 **591**
Surya H Silitonga, Muhammad Habib, Indrayanto, Erwandi Yanto, Edward Prananta Barus, Aris Kurniawan, and Catur Hendro Utomo Sukristiono

Energy Efficiency Potential at Steam Ejector 60% of Patuha Geothermal Power Plant Unit 1 **605**
Audi Ardika Paundratama, Ananda Riris Kurnia Pratama, and Muhammad Abdurrahman Saleh

DRJ-31 Scrubbing Facility to Sustain Darajat Unit-1 Steam Supply **611**
Surya Eko, Kalih Sholli, Wibisono, Sigit Winarno, Irfan Ismail, and Asiawan Hanindito

The Study of Safety Integrity Level (SIL) using A Layer of Protection Analysis (LOPA) Method in Geothermal Steam Field PT XYZ **615**
Putri Shavira, Efrata Pratenta Meliala, Adi Suparyanto, dan Wahyu Agung Pramudito

The First Bullhead Acidizing in Silangkitang Production Well **625**
Irfan Hamzah, Ayu A. Utami, Daniel Wilson, Grandy Danakusumah, Arsyan H. Sasoni, Zaky Mubarok, Albertus Ivan, Aditya Hernawan, Riza Pasikki, and Nur Choiri Amin

Dieng 2 Drilling Campaign Success Story **632**
Marzuki Nyakmat, Zakki Sabiq Purwaka, Budi Setiawan, Ingria Yunandra M. Arrasy, Jarot Pambudi, Adiwibowo Sitompul, and Didin Chaerudin Irwansyah

Acid Jetting Treatment for Scaled Up Production Well **638**
Gamal Hastriansyah, Benedict Amandus Hananto, Dhanie Marstiga Yuniar, and Fernando Pasaribu

Production Optimization Priorities Using the Analytical Hierarchy Process to Enhance Well Capacity in the Geothermal "X" Field **643**
Muhammad Thasril, Efrata Pratenta Meliala, and Aditya Tirta Pratama

Optimizing Performance of LP-Separator and Brine ORC Using Brine Reinjection System (BRS) Pumps in the 15 MW Combined Double Flash and Binary System at PT. Sorik Marapi Geothermal Power **650**
Hary Sumantry Aka, Guntur G. Lintang, Ezi Haili Ananta, Dedy Setiawan, and Ali Sahid

Slim–Core Hole Drilling Best Practices, Lessons Learned and Improvement Plan to Increase The Probability of Success in Reaching Exploration Objectives **668**
Tommy Souvanir, Hadi Permana, Sahat Nainggolan, Subur Arianto, Jefri Marthias, Andri Burnama, and Seto Tanimo

The Approach of Rock Muffler Design for a Typical 55 MW Net of Geothermal Power Plant in Indonesia **678**
Nursanty E. Banjarnahor, Agung W. Mukti, Agus Hendrayana, Fadil A. Lubis, Muhammad Tito Setiawan, Denis D. Pamungkas, Aqmal N. Kusuma, and Rezky Maulana Yusuf

A Drilling Learning Curve Continuous Improvement and Immediate Corrective Action **684**
Muhammad I, Tommy S, and Seto T

The Influence of Quicklime (CaO) Addition on pH and Silica Recovery in Brine of Dieng Geothermal Plant Indonesia **688**
Desy Hikmatul Siami and Jilda Sofiana Dewi

Improving Geothermal ORC Capacity by Using Chemical Method to Remove Silica Deposit **695**
Radhitya E Pradipta, Ryan Hidayat, Mona Natalia Siahaan, and Gabriel Mendoza

ISSN 2986-1268
Volume 8, 2025

UBL-M.3 Sidetrack to Recover Geological Prognosis **703**
Rivaldi Azhar Ramadhani and Fariz Grahadiningrat

Achievement of Drilling Incident Free Operation by Implementing of Safety Behavior Method **712**
Fachrul Subarkah, Budi Santoso, and Mangojak Siagian

Darajat H_2S Abatement System for Well Production Test **719**
Sigit Winarno, Wibisono, Thomas Agus Bayu Prasetyo, Windu Hasta Bayu, Irfan Ismail, Endik Sudarman, and Diah Ayu Pramesti

Total Loss Plugging Optimization in 26 Hole Section Using High-Vis + Cement **734**
Ade Dwi Prasetyo and Rivaldi Azhar Ramadhani

Steam Turbine Casing Leak Issue and On-site Repair Process **740**
Rasyid, Andrianto, and Hepy

Optimizing Open Cooling Tower Water Treatment in Star Energy Geothermal Darajat (SEGD) Unit-2 and Unit-3 Power Plants: A Five-Year Performance Review **747**
Tania Retno Kinasih, Wibisono Yamin, Ghina Thifal Ramadhani Eka Putri, Oscar Satria Ganda, Indra Kurniawan, Hasan Arief Supriatman, Dedi Kusnadi, and Bobby Nugroho Wicaksono

Towards Sustainable Power Generation: Optimizing Chemical Dosing System for Stable pH and Reduced Corrosion Rate at PLTP Darajat II Through the Use of Metering Pump and Non-Contact Transmitter **764**
Laila Sifha Urrohma, Toto Juniandri, Komar Wardana, Feriza Lukman, Muhammad Ichsan, Oscar Satria Ganda, and Tania Retno Kinasih

100% Coring Recovery in a High-Angle Well of Dieng Plateau's Geothermal Formation with a Combined Anti-Jamming System and Full-Closure System in One Assembly **778**
Benny Richard Wales, Triadi Herwasto Aribowo, Kurnia D. Huway, Arif Hudiman, Budi Setiawan, Yudi Hartono, and Zakki

Evaluating the Opportunity of Using General Motor Condition Monitoring in Early Failure Detection to Reduce the Frequency of Vibration Analysis by Applying Matthew Correlation Coefficient Method **789**
Muhammad Dhafier Mu'afa, Laila Sifha Urrohma, Firas Irfansyah Kurniawan, Toto Juniandri, Sekti Setiono, Fauzan, and Andry Hudarojat

Power Redundancy Strategy for Darajat Geothermal S1 and S4 Wellpads Using Photovoltaic-Battery System to Increase Plant Reliability **799**
Firas Irfansyah Kurniawan, Toto Juniandri, Agustiawan, Febrian Tommy, Asiawan Hanindito, Nixon Manik1, and Asep Cahyana Suarsa

Darajat Unit II Generator Lifetime Assessment **812**
Agustiawan, Agus Riyadi, and Febrian Tommy

Design of Steam Wash System as Deposition Prevention Method on Geothermal Turbine **819**
Bakhtiar Zaid Ariadji, Tubagus Ahmad Fauzi Soelaiman, Firman Bagja Juangsa, Yusniar Ully Andrianingtyas, Hanifah Bagus Sulistyardi, and Rahmad Harahap

Application of Rock Muffler Concept in Addressing Well Testing Challenges in Patuha-2 Geothermal Expansion Project, West Java, Indonesia **832**
Nurlianto Sadji, Asum Sumama, Randy Wijaya Atmaja, Dito Sukarno, Siti Olivinia Yusra, Rudy Martikno, and Ramonchito Cedric M. Malate

Analysis Of NCG, TDS, Wetness, Cl, $Si0_2$, And Na Parameters to Maintain The Quality Of 2 Phase Steam Gathering Line **838**
Ahmad A. and Bayan I

ISSN 2986-1268
Volume 8, 2025

Successful Drilling Campaign at Karaha Bodas Geothermal Field: Overcoming Challenges and Optimizing Performance **846**
Edyson, Priozky Purba, Gatra Kusuma, and Fery Malau

Rigorous Calculation for PSV Liquid Thermal Expansion in Cooling Water Service of Inter Condenser in Geothermal Operation **858**
Wijaya Jatmiko Putro and Wibisono Yamin

Implementing Deep Learning for Self-Diagnostic of Cooling Tower Fan Motor Vibration at Wayang Windu Geothermal Power Plant **867**
Syahrizal Faried Roosydi, Burhan Syahputra, Iman Kustaman, Toto Juniandri, and Mochamad Bhakti Prasastia

Bhakti Twist Phenomenon on an Old and or Refurbished Turbine Rotor **881**
Mochamad Bhakti Prasastia Utama and Indra Wening Maharsi

How to Avoid Derating by Installing Tune Mass Dynamic Absorber **889**
Mochamad Bhakti Prasastia Utama and Indra Wening Maharsi

Utilization of Refurbished PDC Bit in Geothermal Drilling in Sumatera: Performance Review and Lessons Learned **897**
Triadi Herwasto Aribowo, Mada Amatori Sutan, Arif Hudiman, Juliana Phan, Rahmad Febdiansyah Bas, and Kurnia Darmawan Huway

The Use of PE100 Polyethylene to Minimise Condensate Pipeline Corrosion at The Star Energy Wayang Windu Geothermal Power Plant **905**
Amos Tay and Alex Kartono

Evaluating the Effectiveness of Cooling Tower Fillpack Replacement for Improved Condenser Performance and Power Generation in Wayang Windu Unit-2 Geothermal Plant **914**
Wahyu Danumulyo, Anton Purwakusumah, and Indra Wening Maharsi

From Lab to Field: A Review of The Scaling Phenomenon in Geothermal **920**
Hande Sile, Duygu Disci, Argyro Spinthaki, and Ugur Kaymakci

Current Practices to Manage Silica-based Scaling in Geothermal Operations **926**
Duygu Disci, Argyro Spinthaki, Ugur Kaymakci, and Hande Sile

RESOURCE AND MANAGEMENT

Brine Management & Reinjection System for Dieng Two-Phase Fluid Geothermal Field **932**
Akbar Putra, Hendra Ardi Kurniawan, Bhaskara Aji Pawitra, Sarbeni Rangkuti, and Herdian Ardi Febrianto

Application of Geochemistry Monitoring for reservoir surveillance at Sorik Marapi Geothermal Field **947**
Radhitya E Pradipta, Ryan Hidayat, M Yamin Nasution, Zosimo Sarmiento, Jill Haizlip, and Zachary Brown

Modelling Non-Condensable Gas Reinjection Geochemical Dynamics in Geothermal Fields: A Case Study of Ngā Tamariki, New Zealand **955**
Yeftamikha Siahaan, Eylem Kaya, Dale E. Altar, John Mering, Denni Subekti, Ayu Utami, Roxanne Atayde, Kelly Melia, and Fabian Sepulveda

Transient Heat Conduction Modelling for Slim and Large Diameter Geothermal Well: A Case Study from Okuaizu Field, Tohoku, Japan **967**
Ken Prabowo

ISSN 2986-1268
Volume 8, 2025

The Advantages of Simple 3D Numerical Modeling in Characterizing a Localized Reservoir Boundary for New Wellpad Development in Wayang Windu **972**
Stefano Pentury, Mulyadi, Deoky Pandu Dewanto, and Meiyanto Joko Purnomo

Utilizing Numerical Pressure Transient Analysis across Diverse Well Challenges in the Wayang Windu Field **981**
Stefano Pentury and Mulyadi

A Conceptual Model of Maritaing Geothermal Green Field Prospect Area in East Nusa Tenggara, Indonesia Using Numerical Modelling **990**
Armando Ariakta Aloanis, John O'Sullivan, and Michael Gravatt

2023 Microearthquake Monitoring Result as Part of Reservoir Monitoring in Namora-I-Langit Geothermal Field **1001**
Yuris Ramadhan, Grandy B Danakusumah, Irfan Hamzah, David Sahara, and Aditya Hernawan

Analysis of Thermal Breakthrough Using Tracer Test in Geothermal Well W Field **1006**
Wily Rustam, Armando Ariakta Aloanis, Rivaldo Maurizio Tambahani, and Ricardo Kandoli

Quantification of Feedzone Contribution Based on PTS Flowing Survey on Wells JTG-3 and GMB-2 Karaha Geothermal Field **1012**
Ryandra S. Dharmawan, Welayaturromadhona, and Riska L. Sari

Positive Impact of Reinjection Infill on Geothermal Field Pressure Support **1021**
Fabiola Pardede, Wishnu Triananda, Rivan Yuono, Ryan Hidayat, and Radhitya Pradipta

Navigating Geothermal Challenges: A Decision Framework for Successful Well and Reservoir Interventions **1025**
Kennard Maturgo, John Gilliland, Martin Pujol, Neale Young, and Nadia Domanski

Targeting Two-Phase Steam Dominated Reservoir in Hot Water Geothermal System in Ulubelu Geothermal Field, Lampung, Indonesia **1032**
Imam M. Prasetyo, M. Ikhwan, Anita Fithriah S. A., Anjani Puspadianti, M. Permadi Sugiarto, M, R. M. Tofan S., and Teguh Prabowo

Production Improvement as Result of Injection Breakthrough Recovery: Case Study Sorik Marapi Geothermal Field, Indonesia **1038**
Wishnu Triananda, Fabiola Pardede, Rivan Tri Yuono, Keshan Apriliyanthy, Radhitya Pradipta, and Ryan Hidayat

The Analysis of Sokoria MTB A-03 Well Performance Post-Shallow Wellbore Perforation **1043**
Rivan Tri Yuono, Fabiola Pardede, and Wishnu Triananda

Analysis of Most Common Problems in Brine Injection Pump: Lesson Learned from Geothermal Dieng Site **1050**
Rizky Himawan, Hendra Ardi Kurniawan, and Ramdani Alfan Subekti

Application Transient Analysis at Later Stages of Production **1061**
Ahmad Fahmi Fanani, M Afif Habiburrahman, Dennis Grey, Dhanie Marstiga Yuniar, and Fernando Pasaribu

Formulation and Technical Implementation of Gazsol (Gas Abatement System with Zeolite and Sodium Hydroxide Liquid) for Geothermal Well Production Test in Kamojang Field **1068**
Nanda Najih Habibil Afif, Muhammad Iqbal Alkindi, Efrizal, Yanuaris Dwi Cahyono, Hendrik Kurniawan Sinaga, Hanifah Bagus Sulistyardi, and Teza Permana

Evaluating Reinjection Efficiency in The Kamojang Geothermal Field Using Gas and Isotope Chemistry Data **1079**
Baiq Lolla Riandari, Ristio Effendi, and R. Mochamad Tofan S

ISSN 2986-1268
Volume 8, 2025

3D Density Change Model to Support Well Targeting in Steam Cap Area: A Case Study on the Salak Geothermal Field, Indonesia **1089**
Azizatun Azimmah, Muhamad Wildan Perdana, and Yudi Indra Kusumah

Resource Assessment of Papandayan Geothermal Field, West Java, Indonesia **1097**
Winnie Tandri Alia, John O'Sullivan, and Michael Gravatt

Sizing and Optimizing Resources: A Decision Support System Applied to Lithium Extraction for Indonesia Geothermal Brine **1111**
Esty Mustika Suud, Suryantini, and Herbert Lubis

Geochemistry Monitoring During Drilling to Prevent Well Damage and Generation Loss in Darajat Geothermal Field **1116**
Yunia Syaffitri, Ngadi, Windu Hasta Bayu, and Hanna Melati Paramitasari

SOCIAL, POLITICS, ECONOMICS, AND COMMUNITY

Preliminary Study of Geothermal Separated Brine Utilization for District Heating at Dieng Plateau, Indonesia **1126**
Hendra Ardi Kurniawan, María Sigríður Guðjónsdóttir, Málfríður Ómarsdóttir, Sarbeni Rangkut, and Herdian Ardi Febrianto

Subsurface Stochastic Integrated Workflows with Downhole Measurements for Preferred Field Development Strategy: Utah FORGE Case Study **1138**
Mulyani, S., Khan, A.M., Wisnubroto, B., Widiatmoko, W., McLennan, J., Trikukuh, J.S., and Puspa, M.A

Using T2well for Simulating Tightly Coupled Wellbore-Reservoir Simulation in a Fully 3D Reservoir Model **1159**
Rony P. Nugraha, Ryan Tonkin, Theo Renaud, John O'Sullivan, and Michael J. O'Sullivan

The Design of COI (Cloud Control of Instrumentation) for Manpower Productivity and Carbon Credit Reduction Behavior at 55MW Geothermal Power Plant **1167**
Faris Abdillah, Nova Gandika and Mochammad Fa'iq Khasmadin

Increasing the Attractiveness of Low-Medium Temperature Geothermal Resources Development in Indonesia: A Discussion from the Techno-Economic Perspective **1175**
Vincentius Adven Brilian, Daniel W. Adityatama, Triwening Larasati, M. Rizqi Al Asy'ari, Nadya Erichatama, Dorman P. Purba, and Khasani

Empowering Coffee Farmers: A Strategic CSR Approach for Climate Resilience and Market Positioning at Supreme Energy Rantau Dedap **1238**
Andri Muhamad Affandi and M. Pradikta F. R

Preliminary Design of Waste Heat Recovery System Using Spiral Heat Exchanger from Geothermal Brine for Direct Use Utilization **1244**
Khasani, Shata Pramudya Ananda, Kevin Stephen Setiawan, and Andhika Putera Utama

Studithermal: An Integrated Geothermal Learning **1254**
Vera Aprianti, Muhammad Sidqi, Victor Gomgom P.S, Budiman Dwi Putra, M. Alzaid Ponka, Theresia Yolanda Sagala, Muchamad Harry, Hendryansyah William, Bagus M. Iqbal, Welly Prabata, and Jantiur Situmorang

Overview of Future Geothermal Development Plan in Indonesia: Resource Characteristics and Challenges for Future Development **1260**
M. Ghassan J. Shalihin, Triwening Larasati, Dewi Gentana, Daniel Adityatama, Ferdino R. Fadhillah, Astri I. Mustika, Vicky Ray Chandra, Galih B. Permadi, and Serina A. Pongtuluran

ISSN 2986-1268
Volume 8, 2025

Preliminary Assessment on the Hot Sedimentary Aquifer Geothermal System in the Midyan Basin in the Kingdom of Saudi Arabia **1277**
Vicky Rai Chandra, Triwening Larasati, M. Ghassan Jazmi Shalihin, Astri Indra Mustika, Ferdino R Fadhillah, Galih Bayu Permadi, and Serina Andiani Pongtuluran

Numerical Study on The Effects of Nanofluids on Heat Transfer Enhancement of a Closed Loop Geothermal Co-Axial System in an Unproductive-Idle Geothermal Well **1289**
Marcellinus Davinci, Khasani, Vincentius Adven Brilian, Budi Santoso Wibowo, and Fefria Tanbar

Lean Project Exploration Drilling Organization **1296**
Seto Tanimo, Tommy Souvanir, and Rifqi Alfaizi

Enhancing the Added Value of Organic Waste and Brine as a Secondary Geothermal Product Through COMBINE (Compost Brine) Innovation at PGE Karaha Area **1300**
Muhammad Sabdian Harwanda, Yanuaris Dwi Cahyono, Awaludin, and Muhamad Taufik

Upstream Digitalization and Software in Research Department of Pertamina Part I : PertaGAMANT **1311**
Taufiq[1], Irnaka, T.M., Suryanto, W., Koestono, H., and Mujihardi, B.

Enhancing Geothermal Resource Development in Indonesia: The Role of Personnel Certification and Capacity Building **1318**
Daniel Adityatama, M. Rizqi Al Asyari, Ferdino R. Fadhillah, Nadya Erichatama, Dorman Purba, and Desak Nyoman Inten Apriani

A Framework for Geothermal Drilling Data Integration for Preparing the Development of Geothermal Drilling Database in Indonesia **1328**
Dorman Purba, Desak Nyoman Inten Apriani, M. Rizqi Al Asyari, Nadya Erichatama, Daniel W. Adityatama, Ferdino R. Fadhillah, and Astri Indra Mustika

Thermoelectric Generator Application for Low-Temperature Geothermal Resources in Steam Field **1344**
Mochammad Ibrahim Agam, Alfian Rangga, Dyah Intan, and Hafid Agil

The Impact of Geothermal Coffee Process (GCP) As an Empowered Community of PT. Pertamina Geothermal Energy Tbk. AG Kamojang On the Development of Renewable Energy Discourse Among the Society **1349**
Ovinda Hariyesa, Muhammad N. Fauzan, Andre Mathew, and Dyah H. Kinanthi

Harnessing Low Enthalpy Energy: Innovatave Solutions for Sustainable Development **1358**
Fariz Alfarizi, Haris Mubarok, and Muhammad Farras Zahran Al-baihaqi

Digitalization of Geothermal Plant Facilities **1371**
Wasis Hartono

The Canaya Geothermal Coffee Process Revolutionizing Signature of Arabica Coffee Production with Geothermal Dryhouse in Kamojang, West Java, Indonesia **1380**
Muhammad N. Fauzan, Cecep U. Farouq, Adi Rahmadi, Aan Taryana, Syalva T.M. Yusuf, Ovinda Hariyesa, and Dyah H. Kinanthi

GENERAL

Optimizing Geothermal Investment in Indonesia: Adopting US Tax Credit Mechanisms **1394**
Nadya Erichatama, Vincentius Adven Brillian, Ferdino R. Fadhillah, M. Rizqi Al Asy'ari, Daniel Adityatama, Desak Inten Nyoman Apriani, and Dorman Purba

Geothermal Drilling Cost Landscape in Indonesia: Cost Trend, Outlier Cost, and Drilling Cost Component **1404**
Nadya Erichatama, Dorman Purba, Daniel Adityatama, and M. Rizqi Al Asy'ari

ISSN 2986-1268
Volume 8, 2025

Proposing Corporate Work Plan and Budget (WP&B) Based on Risk Management to Ensure the Sustainability of Business Operations in the Kamojang Geothermal Area **1412**
Darussalam, Harahap. R., and Iman. A.S.

Challenges in Meeting International Standards for Impact Assessments in Indonesia Geothermal Projects **1416**
Ni Putu Wulan Romianingsih, Suyud Warno Utomo, and Udi Syahnoedi Hamzah

Coexistence Study Between Wildlife Keystone Species and Darajat Geothermal Power Plant in West Java, Indonesia **1424**
Muhammad Riyadhi, Iqbal Abi Yaghsyah, and Toni Ahmad Slamet

Marketing Innovation and Utilization of Geothermal Coffee Products through Commercial Coffeeshop Schemes **1432**
Erwandi Yanto, Dian Pratomo, Mahmud Khairi, Teresia Maririsky, Ahmad Indra Sakti Harahap, Adi Rahmadi, Dewi Sri Utami, and Fajriyah Usman

Lifecycle Environmental Evaluation of Fossil and Renewable Energy Sources: Insights from Coal-fired and Geothermal Power Plant **1443**
Irhan Febijanto, Yudistian Yunis, Nadirah Nadirah, Ahmad Ismed Yanuar, Hismiaty Bahua, A. L. S. M. Sihombing, I. M.A.D. Susila, and Kris Pudyastuti

PROPER Implementation in Star Energy Geothermal Darajat II, Limited **1448**
Muhammad Riyadhi and Micia Zaputi Rohimah

Gender Action Plan: An Approach to Mitigate Risks and Impacts of Geothermal Projects **1456**
Maya Ryandita, Desak Nyoman Inten Apriani, Afandi, Eviyanti, Astri Indra Mustika, Dorman Purba, and Ferdino R Fadhillah

Indonesia Country Update 2024: Historical and Future Geothermal Development **1465**
Muchsin Chasani Abdul Qadir, Desak Nyoman Inten Apriani, Dorman Purba, Ferdino R Fadhillah, Andreas Suseno, and Astri Indra Mustika

Navigating Indonesia's Energy Transition: Comparative Advantages of Geothermal, Solar, and Wind Resources **1481**
Chandra Hasudungan, Desak Nyoman Inten Apriani, Dorman Purba, Andreas Suseno, Ferdino R Fadhillah, and Astri Indra Mustika

INSAN SMART - APIForestry and Natural Forest Succession Approach to Achieve Sustainable Community-Based Forest Restoration **1494**
Muhammad Riyadhi, M. Panji Pranadikusumah, and Iqbal Abi Yaghsyah

Analysis of CO_2 Emission Intensity of Geothermal Power Plant: Case Study Star Energy Geothermal Darajat II, Limited **1500**
Muhammad Riyadhi and Micia Zaputi Rohimah

Assessing Cost-Effective Exploration Methods: A Comparative Study for the Financial Viability of Indonesia's Geothermal Future **1505**
Dorman Purba, Ferdino R. Fadhillah, Desak Nyoman Inten Apriani, Daniel W. Adityatama, M. Rizqi Al Asyari, Nadya Erichatama, V. Adven Brilian, and Astri Indra Mustika

Insights for Developer Compliance to Lender Procurement Guidelines in Geothermal Exploration Financing **1533**
Aryani Amir, Desak Nyoman Inten Apriani, Ery Surandaru, Muchsin Qadir Jailani, Dorman Purba, and Astri Indra Mustika

Impact of Tax Facility Incentives to Geothermal Project Bankability: Comparison between National and Worldwide Practice **1540**
Andreas Adi Suseno, Desak Nyoman Inten Apriani, Muchsin Qadir Jailani, Aulia Pratama Bogy Ariyanto, Dorman Purba, and Ferdino R Fadhillah

ISSN 2986-1268
Volume 8, 2025

Pertamina Geothermal Energy Kamojang Restoration Management and Potential Carbon Sequestration from the Biomass Value **1549**
Syalva Taskia, Fauzi Ariq, and Hendrik K. Sinaga

Comparative Analysis of Geothermal PPPs: International Insights and Indonesia's Cases **1558**
Candra Sri Sutama, Ali Ashat, Suardi Nur, and Desti Alkano

Safeguard Requirements for Indonesia Geothermal Exploration Financing and De-Risking Facility **1578**
Eviyanti, Desak Nyoman Inten Apriani, Afandi, Dorman Purba, Maya Ryandita, Ferdino R Fadhillah, and Astri Indra Mustika

Implementing FPIC Stakeholder Engagement in Geothermal Projects **1592**
Satoshi Ishihara, Greg Guldin, Adi Prasetijo, Muchsin Qadir, and Annye Simbolon

Unlocking the Socioeconomic Opportunities of Geothermal Project Development and Operation **1602**
Stephanie A. Pinnington, Kavita Rai, Elin Hallgrimsdottir, and Muchsin Abdul Qadir

Role of Exploration Financing Program to De-risk Indonesia Geothermal **1612**
Ferdino R Fadhillah, Desak Nyoman Inten Apriani, Andreas Suseno, Muchsin Qadir Jailani, Dorman Purba, and Astri Indra Mustika

A Multi-Actor Analysis and Policy Analysis for Geothermal Development in Indonesia **1626**
Andi Susmanto and Akhmad Hidayatno

A 20 Year Retrospective: Analysis the Impact of Star Energy's Scholarship Program to Pangalengan Community Using MSC Technique **1642**
Mila Puspita, Firman Hidayat, Rahmat Hidayat, and Ismail Hidayat

Geothermal Beyond Electricity: A Study on Leveraging Various Geothermal Value Chain as Innovative Additional Revenue Option for Implementation in Indonesia **1648**
M. Rizqi Al Asy'ari, Daniel W. Adityatama, Nadya Erichatama, Vincentius Adven Brilian, Ferdino R Fadhillah, Desak Nyoman Inten Apriani, Dorman Purba, Astri Indra Mustika, and Triwening Larasati

Utilizing Geothermal Resources for Green Ammonia Production: A Techno-Economic Analysis for Decarbonizing Coal Power Plants in Indonesia **1662**
Annisa N Hidayah, Danny Kusuma, Yudithia Prastika, and Koichi Yamashita

Application Hydrogeochemical Studies in The Development of Geomedicine: A Lesson Learned of Mount Tampomas Geothermal Area as Geothermal Energy and Balneology Resource **1671**
Galih Bayu Permadi, Triwening Larasati, Zefanya Mesakh Dwi Cahya Wirya Putra, Andri E.A. Wibowo, Vicky Rai Chandra, and M. Ghasan Jazmi Shalihin

Enhancing Indonesia Geothermal Project Bankability Through Off-Grid Utilization **1684**
Desak Nyoman Inten Apriani, Muchsin Qadir Jailani, Dorman Purba, Andreas Suseno, Ferdino R Fadhillah, and Astri Indra Mustika

Geothermal Beyond Energy: Total Extraction and Circular Economy of Valuable Elements from Geothermal Brine **1692**
Himawan Tri Bayu Murti Petrus, Vincent Sutresno Hadi Sujoto, Chandra Edward Suryanaga, Dewa Putu Agus Sudarmaja, Sutijan, Agus Prasetya, Ferian Anggara, Siti Nurul Aisyiyah Jenie, Widi Astuti, Andhika Putera Utama, Syamsumin, Supremlehaq Taqwim, Delvirah Elisa Sabatini Singkuang, and Ayu Gracia Ade Sumartha

ISSN 2986-1268
Volume 8, 2025

Utilizing Geothermal Fluid By-products from Lahendong Geothermal Area for Liquid Nanosilica Geothermal Booster to Support Sustainable Farming in Tompaso, Minahasa Regency, North Sulawesi **1706**

Muhammad Gilang Madiantara, Muhamad Didih, Abdi Rayhan Garniwan, Navilia Hanin Pradipta, Pri Utami, Ronny Martien, and Ngadisih

The Utilization Scheme of Geothermal Brine for Balneotherapy Facilities in Dieng, Central Java **1712**

Danu Ari Wibowo, Muhammad Syakhis Qomaruddin, Azaria Dian Khoirunnisa, Dwi Ayu Kurniasih, Aafiansyah Su'daa, and Arief Putra Pratama

The Sustainable Impact of Patuha Geothermal Power Plant Project: A Carbon Trading Mechanism Case Study **1725**

Delvirah Elisa Sabatini Singkuang, Rosana Pribadi, Gina Lisdiani, Wien Pratama Abi Wicaksono, Agung Soni, Saltsa Prehtina Muryani, and Saktiyo Tri Nugroho

SMART Heating System: IoT-Enhanced Geothermal Brine Utilization for Efficient Space and Water Heating in Dieng Tourism Areas **1737**

Yoga Sanjaya, Bintang Putra Megantara, Farhan Izzat, M. Ihsan Fadhlurahman, and Sevilla Maharani

Part 1:
Earth Sciences

This page is intentionally left blank

Novel Accelerator of Geothermal Field Development: Transient Electromagnetic Method Utilizing Superconducting Quantum Magnetic Sensor (SQUID-TEM)

Tsunehiro Hato[1], Hironori Wakana[1], Akira Tsukamoto[1], Keiichi Tanabe[1], Michael S. Zhdanov[2], Alex Gribenko[2], Indra A. Nugroho[3], and Herwin Azis[3]

[1]SUSTEC, 2-11-19, Minowa-cho Kohoku-ku, Yokohama, Japan, 223-0051
[2]TechnoImaging,LLC and University of Utah, 4001 S. 700 E., Suite 500, Salt Lake City, UT 84107, USA
[3]PT Supreme Energy, Jl. Iskandarsyah Raya No. 1A, Kebayoran Baru, 12160, Indonesia

hato@sustec.jp

Keywords: Superconducting Quantum Interference Device (SQUID), Transient Electromagnetic (TEM), 3D inversion, grounded wire

ABSTRACT

We have developed a novel exploration system for the transient electromagnetic method (TEM) utilizing a superconducting quantum magnetic sensor (SQUID) with ultra-high sensitivity. Our SQUID-TEM enables the user to obtain a high-resolution three-dimensional (3D) geoelectrical imaging for any depth of interest (a few tens meters up to 3000-4000 m) in a quite user-friendly manner (e.g., a small amount of liquid nitrogen, less complicated pre-job preparation and simple field operation, etc.). Based on our field-deployment history in Indonesia, Japan, and some Middle East countries, it should be noted that SQUID-TEM, with 3D inversion data analysis, is able to contribute to the acceleration of the geothermal field-development process. The SQUID-TEM method can be a powerful tool not only for green-field geothermal development in the future but also to maintain or increase the generation capacity of geothermal power plants currently in operation, which largely contributes to the promotion of geothermal power generation.

1. INTRODUCTION

In 2009, we began developing a transient electromagnetic (TEM) exploration device using a superconducting quantum magnetic sensor SQUID that can be used at a liquid nitrogen temperature, and since 2012, it has been used by JOGMEC for mineral resource exploration (Hato et al., 2013). Subsequently, in order to realize equipment with the exploration depth of over 3000m required for geothermal exploration and carbon dioxide capture and storage (CCS) monitoring, we developed a SQUID sensor that operates more stably even in strong magnetic fields and a system that enables long- period TEM measurements as well as sufficiently long operation duration. We have also developed reliable cooling technology, signal processing technology that can efficiently remove noises, and 3D inversion technology.

There are four advantages to using the SQUID-TEM method in geothermal exploration.

- Among various electromagnetic exploration methods, the TEM method measures signals proportional to the cube of stratum conductance (Kaufman and Keller, 1983), while the magnetotelluric (MT) method and controlled source electromagnetic (CSEM: frequency domain) method observe signals only proportional to the first power. Thus, the TEM method is expected to provide a physically higher resolution.
- Since the TEM method uses an artificial magnetic field, repeated measurements are possible, and noise can be suppressed even in noisy environments. In addition, since the magnetic field signals from underground are measured after the artificial magnetic field is shut off, the artificial magnetic field does not influence the measured signals.
- SQUID measures the magnetic field itself, not the derivative of the magnetic field, as in the case of the induction coil sensor. Since the magnetic field attenuates more slowly than its derivative, the use of a highly sensitive SQUID sensor is advantageous for the measurement of late-time transients required for deeper exploration.
- SQUID magnetic sensor has advantageous characteristics for the TEM method - The sensitivity of sub-pico tesla, as well as the wide dynamic range and wide frequency bandwidth from DC to MHz range, make deep TEM exploration over 3000m possible. The conventional TEM method using an induction coil as a magnetic sensor does not have sufficient sensor sensitivity at low frequencies and thus has been used for exploration of relatively shallow underground below 1,000 meters depth, such as the case for mineral resource exploration.

As specific usage methods of SQUID-TEM in geothermal fields, we are considering two cases, as shown in Figure 1. One is the reduction of geothermal development risks through the hybrid use of MT and TEM methods. The exploration area of the TEM method is limited by the arrangement of the grounded wire source for the application of magnetic fields, which is a disadvantage compared with the MT method. As a result of a wide-area resource survey using the MT method, detailed exploration will be carried out using the TEM method at potential development sites. MT method using an electric field is sometimes affected by the relief of the ground, and MT data analysis without considering the relief of the ground produces distorted results. The SQUID-TEM method uses only a magnetic field, unaffected by the ground relief. The results obtained are useful for verifying the MT data analysis. We believe this hybrid approach effectively reduces risks in the early stages of geothermal exploration.

Another use of the method is for the exploration in the vicinity of geothermal power plants that are already in operation. Although it requires operation in a noisy environment, it is possible to explore using the SQUID TEM method, which can suppress noises. It is expected that the need to maintain and increase the output of geothermal power plants will increase in the near future.

The TEM method helps to determine the location of drilling for additional production wells and reinjection wells. We believe that such utilization will accelerate geothermal development.

In this paper, we describe the characteristics of the SQUID-TEM method and report on the interesting results of exploration case studies.

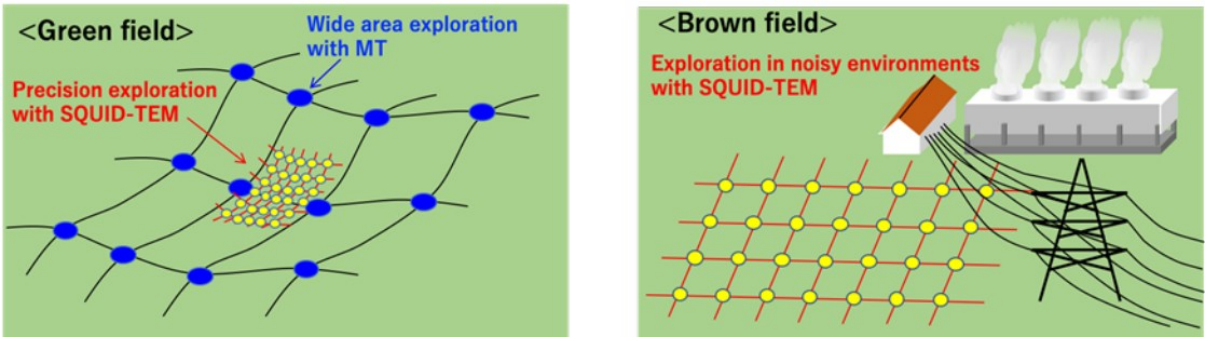

Figure 1: Image diagram of reducing geothermal development risks and accelerating development by utilizing SQUID TEM in green fields and brown fields around operating geothermal power plants.

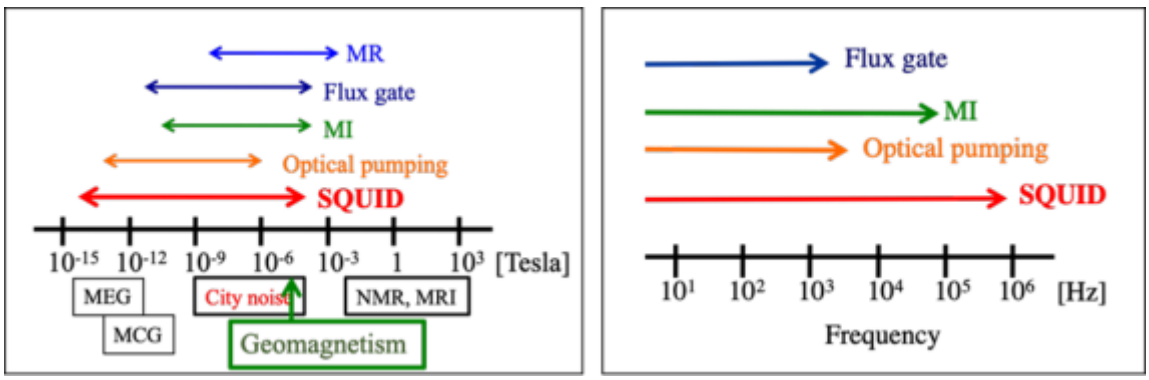

Figure 2: Dynamic range and frequency band of various magnetometers.

2. FEATURES OF SQUID-TEM

The significance of using a magnetometer such as a SQUID in the TEM method is that it allows direct observation of the magnetic field rather than the time derivative of the magnetic field, as is the case for induction coils. In geothermal exploration, cap layers and reservoirs have low resistivity, which slows down the decay of the magnetic field. In the TEM method, the attenuation of the magnetic field is measured after the primary magnetic field is shut off, but in order to conduct deep exploration, it is necessary to measure at late times. Direct measurement of the magnetic field reaches a noise level substantially later than time-derivative measurement, which is advantageous for deeper exploration. Figure 2 shows the dynamic range and frequency band for several types of magnetometers, including SQUID. SQUID magnetometer has (1) a sufficiently large dynamic range and (2) a wide frequency bandwidth from several hundred kHz to DC, which is suitable for the TEM method.

On the other hand, the issues that need to be overcome with SQUIDs are (1) the ability to follow changes in the magnetic field (slew rate), which is sufficient for stable operation when used outdoors, and (2) ease of cooling. Since we are able to design and manufacture SQUID magnetic sensors by ourselves, we have developed a specially designed SQUID for TEM measurements, which has a good balance between stability and high sensitivity for outdoor use. Figure 3 shows a photo of the developed TEM system named SUSTEM with three SQUIDs to measure x, y, and z field components. The total weight is approximately 20 kg. The SQUID is fabricated using high-temperature superconducting materials and can be operated at a liquid nitrogen temperature. By improving cooling and mounting technology, it is possible to operate the system continuously for up to 17 hours with 0.7 liters of liquid nitrogen. As a result, even if we carry it on expeditions in mountainous areas, once we fill it with liquid nitrogen, it can be used all day without having to refill it.

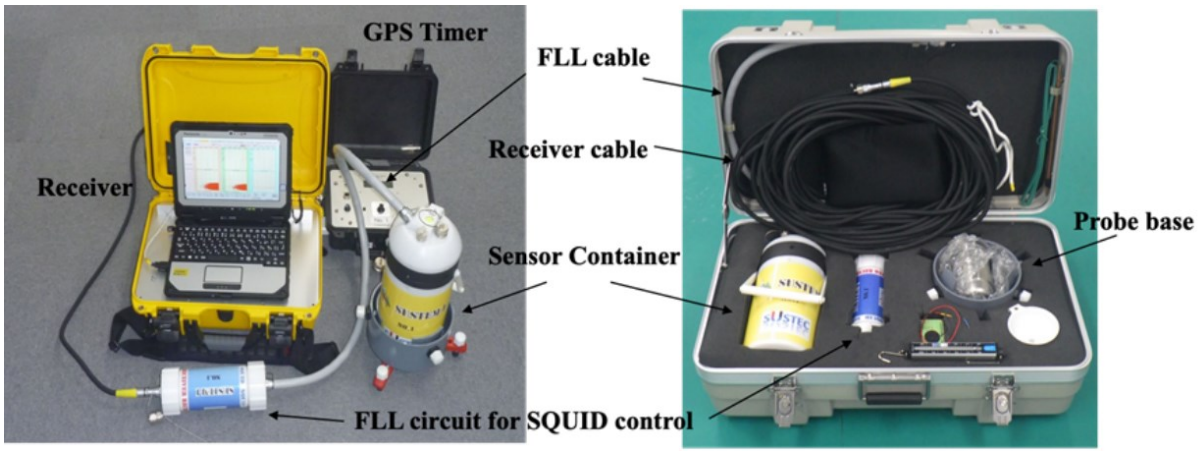

Figure 3: SQUID-TEM exploration system (SUSTEM®).

Figure 4 shows photos the system's transportation to a measurement site and its on-site operation. One set of measurement system can be transported by one person on flat ground, and two people can transport it even in mountainous areas, as shown in the photo. Both the sensor part and the receiver are installed on the ground surface to perform measurements without digging holes, making the measurement highly efficient and environmentally friendly. The area required to install the sensor section is approximately 50 cm square, and the receiver is installed approximately 30 m away from the sensor to avoid magnetic noises due to vibrations, for example, induced by the movement of people.

Figure 4: On-site operation of the SQUID-TEM system.

In the TEM method, we measure temporal changes in the secondary magnetic field created by the underground current induced and diffused after the primary DC magnetic field is shut off. Environmental noise is suppressed by performing averaging processing, such as stacking of the transients in response to a repetitive rectangular wave, as shown in Figure 5. This makes it possible to explore deep underground by measuring attenuated secondary magnetic field at late enough times. For the case of exploration depth of over 3000 m, a measurement time of 2 seconds is often required after the primary magnetic field is shut off. In that case, the measurement is usually repeated 1000 times with one cycle of 2 seconds plus ON, 2 seconds OFF, 2 seconds minus ON, and 2 seconds OFF, and each measurement at one point takes about 2.5 hours. By using two or three systems at the same time, it is possible to measure six points a day and 60 points in 10 days. The example shown in the measurement screen in Figure 5 shows a case of measurements with different time ratios, with ON for 1 second and OFF for 2 seconds. In this case, 1000 repeated measurements can be carried out in about 1.5 hours. It is possible to increase the efficiency of measurement further. For example, nine points can be measured per day, and 60 points can be measured in seven days when it is easy to approach the measuring points. The measured data undergo filtering,

trending, and stacking to remove noises such as those from power lines and geomagnetic fluctuations before resampling and inversion analysis.

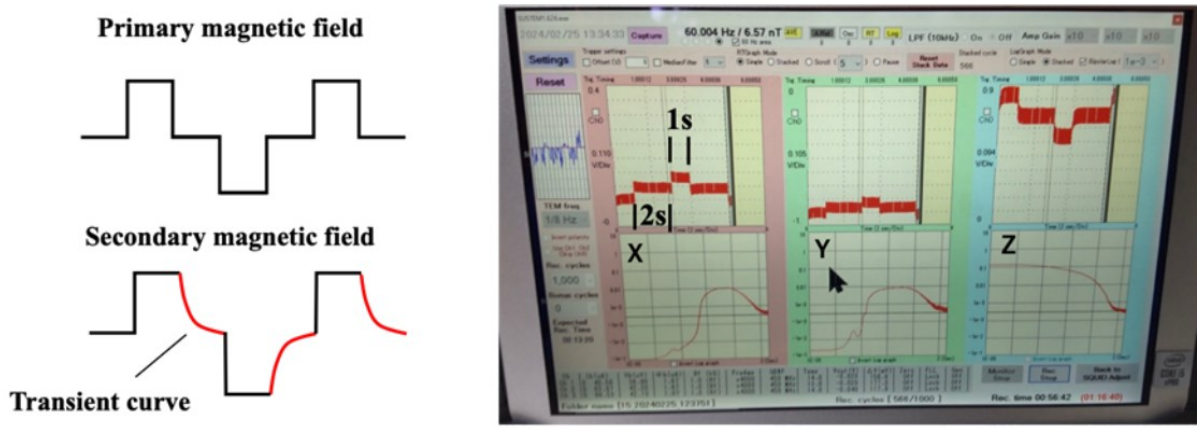

Figure 5: Transmission and reception signals in TEM method and real-time measurement screen of SUSTEM. (On the real-time measurement screen, the upper row shows the real-time received waveform of X, Y, and Z axis for each period, and the lower row shows the stacked waveform (decay curves) after the primary magnetic field is shut off).

3. EXAMPLE OF EXPLORATION IN GREEN FIELD

In Sumatra, Indonesia, an exploration was conducted using a grounded-wire source and the measurement point arrangement shown in Figure 6. The total length of the grounded-wire source was 5.1 km, and the measurement area was approximately 5 km east-west and 4 km north-south. In the figure, the points marked with crosses were not used in the analysis because they are close to the grounded-wire source and are greatly influenced by the shape of the grounded-wire source. In the 3D inversion, the shape of the grounded-wire source was assumed to be a straight line, indicated by the blue line. The analytical model shown in Figure 7 is 7 km east-west, 8 km north-south, 3500 m deep, and has a mesh size of 25 m x 25 m x 25 m.

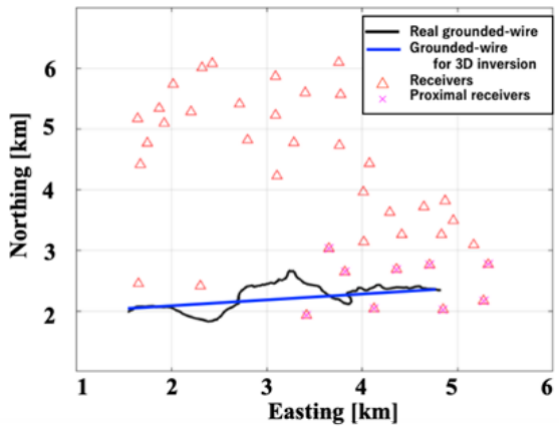

Figure 6: Arrangement of grounded-wire source and measurement points.

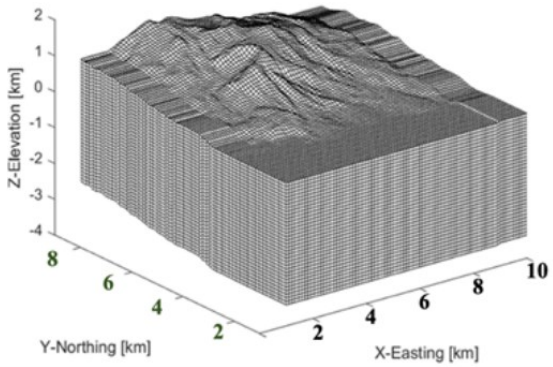

Figure 7: Mesh structure used for analysis.

In order to obtain unique and stable data, regularization is necessary, and a method that minimizes the Tikhonov objective function $P\alpha(\mathrm{m})$ was used (Tikhonov and Arsenin, 1977).

$$P\alpha(\mathrm{m}) = \phi(\mathrm{m}) + \alpha s(\mathrm{m}) = \min \tag{1}$$

Here, ϕ (m) is a misfit functional between the predicted and the observed SQUID TEM data, s(m) is the stabilization functional, and α is the regularization parameter that balances the misfit and stabilizing functional. The minimization problem formulated by (1) was solved via the re-weighted regularized conjugate gradient (RRCG) method (Zhdanov, 2002).

We used a data weighting scheme based on the known standard deviation to reduce the input of noisy data into the inversion result. Data weights were determined by using observed error Err_o (standard deviation of measurements) and theoretical errors Err_t as,

$$W_d = max\ (Err_o,\ Err_t)^{-1} \tag{2}$$

Theoretical errors Err_t were calculated assuming that the measurements are accurate to 1 pT or 3% of the observed fields B_{obs}.

$$Err_t = 1\ \text{pT} + 0.03 \cdot B_{obs} \tag{3}$$

The inversion converged to a global misfit χ^2 which is given by

$$\chi^2 = \frac{1}{N}\sum (W_d(d_i^p - d_i^o))^2 \tag{4}$$

where d^p are the predicted data and d^o are the observed data, respectively.

Figure 8 shows examples of decay curves of the observed with predicted data and the distribution of the local RMS misfit to illustrate the SQUID TEM data fit. The inversion converged to a global RMS misfit χ^2 of 3.61, which is a very statistically reasonable value indicating a relatively low misfit level between the observed and predicted data.

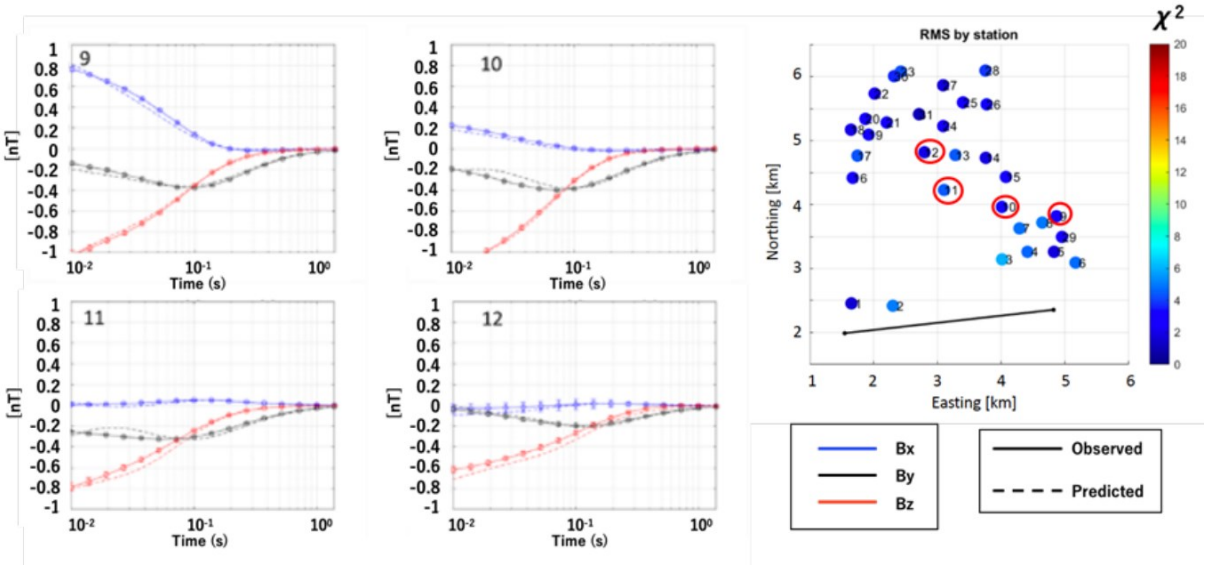

Figure 8: Observed and predicted decay curves for the measurement point 9-12, and the distribution of the local RMS misfit.

EMVision® software, developed by TechnoImaging, was used for the inverse analysis, with a starting homogeneous half-space background model of 25 Ωm, an upper limit of 10 kΩm, and a lower limit of 0.1 Ωm of the inverse resistivity. The iterative inversion of the RRCG method was terminated when the changes due to iterations became less than 0.1%. The contraction integral equation method was used for 3D numerical forward simulations (Zhdanov, 2018).

The isosurfaces of resistivities of 1, 10, and 100 Ωm are used. Red color corresponds to 1Ω m, yellow represents 10Ω m, and green corresponds to 100Ω m. Figure 10 presents a combination of several vertical sections (on the left) and a horizontal section at a depth of 500 m (on the right) to show the low resistivity anomaly. There are two zones of a few Ωm resistivity located at a depth of 500 m to 1000 m divided into two areas, and these are considered to be the clay cap layer of the geothermal reservoir.

This geothermal area has been explored using the MT method in the past. Therefore, we compared the results of the MT method and the SQUID-TEM method. Figure 11 shows a vertical cross section of resistivity at the same location. The intervals between the measurement points are almost the same, and the measurements were not made with increased measurement density, as shown in Figure 1. Analysis using the MT method shows that a low resistivity layer of several Ωm is spread over a wide area of more than 6 km, while analysis using SQUID-TEM shows almost the same depth but in a limited area of about 1.5 km. This suggests the existence of a low resistivity region in the area and points to a connection with a low resistivity region near the surface, indicating fumaroles

confirmed on the ground surface. In the future, it will be necessary to carry out a detailed investigation through drilling, but we believe that we have obtained relatively clear exploration results.

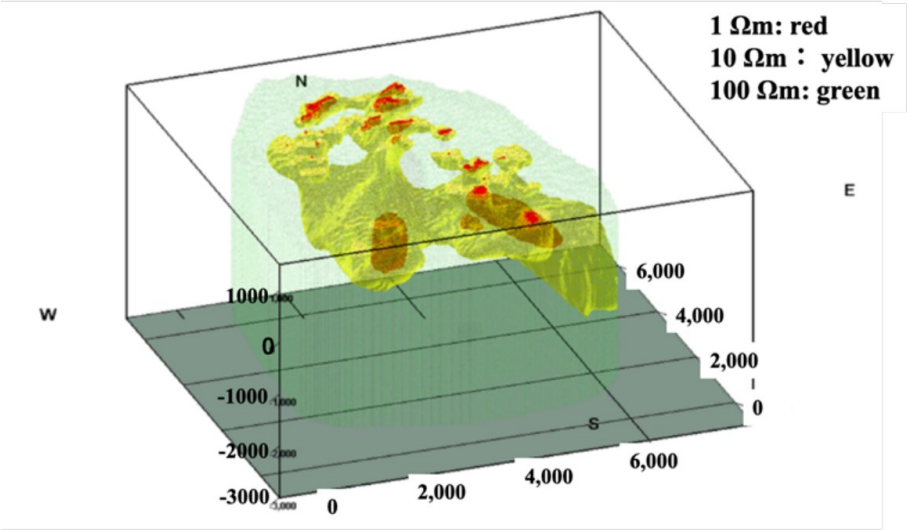

Figure 9: 3D view of the inverse model represented by isosurfaces at 1, 10, and 100 Ωm shown by red, yellow, and green color, respectively.

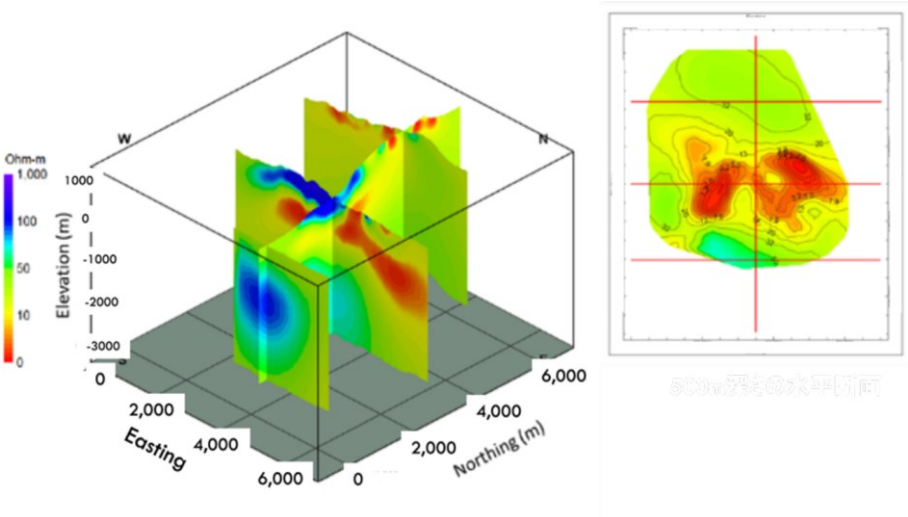

Figure 10: 3D image of resistivity distribution obtained by 3D inversion and horizontal section at 500 m depth.

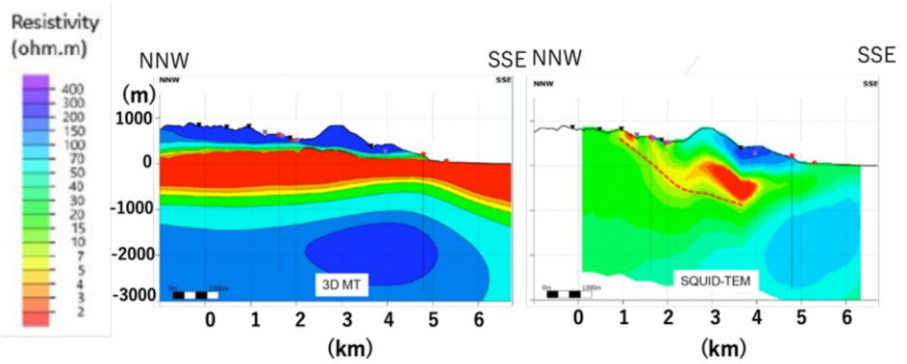

Figure 11: Comparison of the distributions of resistivity obtained by MT method (left panel) and SQUID-TEM method (right panel).

4. EXAMINATION OF EXPLORATION IN BROWN FIELD

We believe that the demand for exploration in so-called brownfield areas, which are areas around geothermal power plants that are already in operation, will continue to increase in the future.

There are following significant challenges in brownfield exploration:

- Electromagnetic noise from power plants and power lines.
- Influence on measurement of induced current generated in buried steel pipes of production wells and reinjection wells.

First, an example of measurement data taken in a field near a geothermal power plant and power lines is shown in Figure 12.

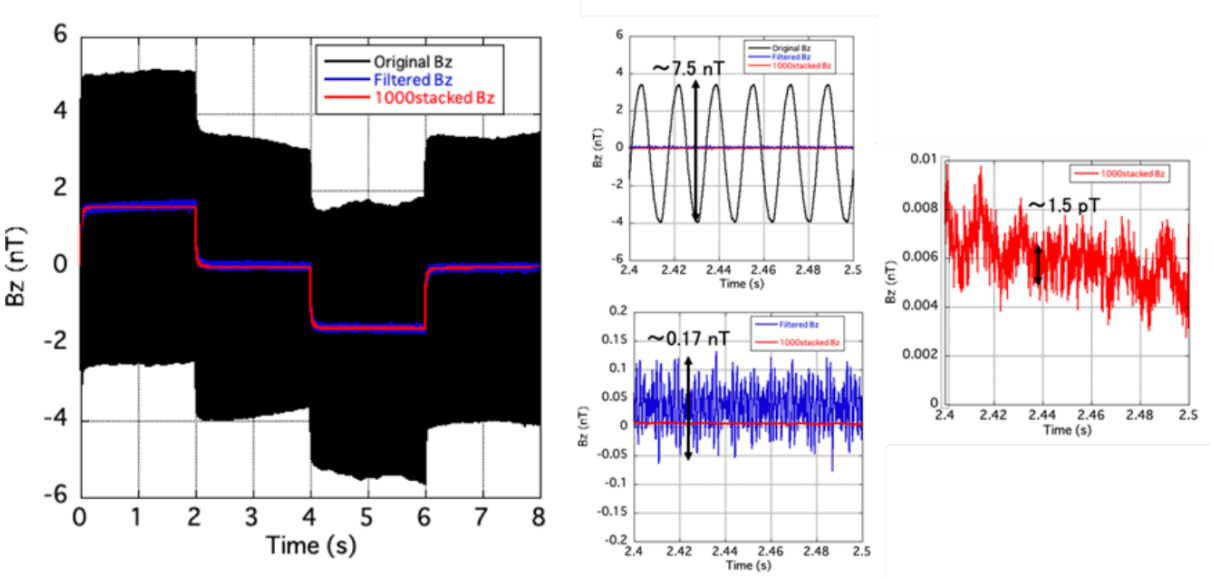

Figure 12: Effect of noise reduction by TEM method from measurement data taken in a brown field.

The figure on the far left shows an observed Bz waveform for one cycle. The amplitude of the noise with a sinusoidal waveform, mainly due to the power line in original Bz, reached 7.5 nT, as plotted in black. By using a filtering technique, the noise amplitude was reduced to 0.17 nT, as shown in blue. We took 1000 cycles of data and stacked them after the filtering process. Then the noise was reduced to pico tesla level. The theoretical noise level is given by

$$4 \times N_w \times \sqrt{\frac{f_s}{2}} \div \sqrt{N_s} \tag{5}$$

where N_w is the white noise level of the magnetometer, f_s is the sampling frequency, and N_s is the number of stackings, respectively (Hato et al., 2013). We used a SQUID sensor with a noise level of 50 fT/ √ Hz, sampling frequency of 50 kHz, and 1000 times stacking. The theoretical noise level is calculated to be 1.5 pT. We confirmed that the noise level of measured data is reduced to the theoretical noise level limited by the ultra-sensitive magnetometer, even in a brown field.

To examine the influence of steel pipes on production well, we carried out a forward simulation for models with and without steel pipes, assuming steel pipes and transmission sources in an actual brown field. Figure 13 shows the arrangement for the forward simulation. The borehole with a steel pipe is located at a distance of 1 km from the grounded wire source. Measurement points of No.35 and No.36 are placed just near the well entrance and almost directly above the steel pipe path. In this simulation, the transmission current was assumed to be 28.1A. The characteristics of the steel pipe were assumed to be 10 cm in diameter, 3 mm in thickness, and 10-7 Ohm-m in electrical resistivity.

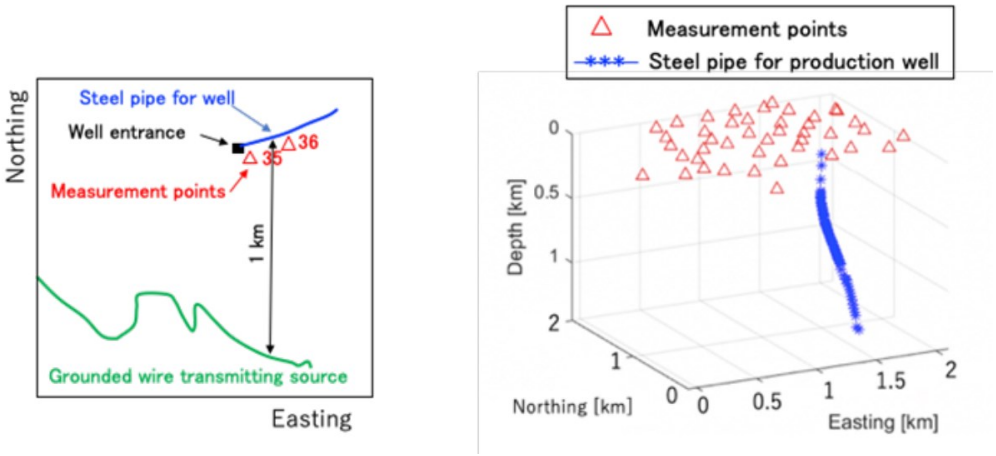

Figure 13: Arrangement for consideration of steel pipe influence on measurement.

The influence of the steel pipe on the magnetic field transients generated by underground induced currents was found to be less than 0.04%, even at these measurement points near the well. This is considered to be due to the small volume of the steel pipe and the structure that makes it difficult for a circulating current to occur. This result suggests that steel pipes in wells do not need to be considered in measurement point selection or analysis.

It is thus confirmed that the influence of power line noise can be effectively removed by signal processing utilizing repeated measurements in the TEM method, and the influence of the well steel pipe is limited. These results indicate that the SQUID-TEM method is an effective technique for geothermal development in brown fields.

5. SUMMARY

In order to accelerate the development of geothermal power generation, we have developed a TEM system with superconducting quantum magnetic sensors suitable for outdoor use, which enables exploration at over 3000 m depth. We applied 3D inversion analysis to SQUID-TEM exploration data collected at a geothermal site for the first time. This SQUID-TEM technology has already begun to be used at various sites, and it has been demonstrated that it is possible to clearly identify zones of conductivity anomaly.

It has been demonstrated that the noise level of measurement data, even in brown fields, can be reduced to near the theoretical limit calculated from the sensor's sensitivity by using this technology.

Noise-resistant electromagnetic exploration using artificial transmission sources enables deep exploration and is used not only for new geothermal development but also for exploration to maintain and increase the output of geothermal power plants already in operation. We believe that this will contribute to the acceleration of power generation.

ACKNOWLEDGEMENT

We received grants from NEDO for technology development, the Mitsubishi UFJ Technology Development Foundation, and Toshiaki Ogasawara Memorial Foundation for system mass production, and the Agency for Natural Resources and Energy for support to exploration in Indonesia.

REFERENCES

Hato, T., Tsukamoto, A., Adachi, S., Oshikubo, Y., Watanabe, H., Ishikawa, H., Sugisaki, M., Arai, E., and Tanabe, K. (2013): Development of HTS-SQUID magnetometer system with high slew rate for exploration of mineral resources, Supercond. Sci. Technol. 26, 115003.

Kaufman, A. A., and Keller, G. V. (1983): Frequency and Transient Soundings, Elsevierp.341.

Hato, T., and Tanabe, K. (2018): Long period of time cooling technique using liquid nitrogen for HTS-SQUID system, IEEE Trans. Appl. Super. 28, 1601404.

Tikhonov, A. N., and Arsenin, Y. V. (1977): Solution of ill-posed problems, V. H. Winston and sons, 258pp

Zhdanov, M. S. (2002): Geophysical inverse theory and regularization problems, Elsevier, ISBN: 978- 0-444-510891

Zhdanov, M. S. (2018): Foundations of Geophysical Electromagnetic Theory and Methods, Elsevier, ISBN: 978-0-444-638903

Stress Distribution Analysis to Characterize the Fault Permeability in Nage Field, Indonesia

Muhammad Ikhwan

The University of Auckland, New Zealand

ikhwan8823@gmail.com

Keywords: Nage, in-situ stress, geomechanics, structural geology, reservoir modelling

ABSTRACT

The fault zone is one of the critical aspect that controls permeability in the Nage geothermal field. It is composed of conjugate strike-slip faults that likely framework the hydrology in the field. Each fault has its own discontinuities and geometry, the most favorable part to host localized permeability. The boundary element method characterizes the stress distribution along these faults and maps the stress localization caused by fault intersections, orientation changes, or fault termination. The results show that these fault attributes generate local stress, indicated by the coulomb shear traction, dilation and normal traction changes. The highest stress perturbation is induced by the fault orientation changes, followed by termination and intersection. These local stress permeability-induced features are consistent with the occurrence of surface thermal manifestations in Nage, indicating that hydrothermal flow is most likely local and focused, and is strongly controlled by a discontinuity in the geological structures. These localized permeable zones accommodate the reservoir fluid's upwelling flow while also hosting the geothermal system. This study can support the geothermal conceptual model and well-targeting strategy for the next phase of Nage field exploration.

1. INTRODUCTION

Many geothermal fields are secondary permeability dependent where fault and fractures dominantly control the hydrology of geothermal fluid. They can act as the conduit or the horizontal barriers that dictate a geothermal reservoir continuum. As a result, many geothermal wells targeting these features expect the well will encounter a good permeability zone that can enhance the well's output. Therefore, it is critical to detail the fault and fracture zone mechanism and characterization to better understand these features.

The movement of faults, involving both kinematic and dynamic processes, has been suggested as an explanation for the positioning of hydrothermal upwelling relative to structural settings (Curewitz and Karson 1997; Siler et al. 2018). When a fault undergoes movement, stress is released along the faulted segments and transferred to the surrounding crust, resulting in strain, including shortening and dilation, in the adjacent areas. Studies have demonstrated that areas experiencing the highest stress and dilation are often associated with extensive geothermal features such as fumaroles, mud pools or hot springs. While any immediate increase in permeability from fault activity is expected to diminish rapidly due to secondary mineralization, repeated fault slips continue to generate and sustain permeability in specific stressed and strained areas. With successive earthquake cycles, these areas are continually subjected to stress and relief from minor slips, leading to the development of denser fracture networks or more open fractures compared to the surrounding crust. This makes these areas particularly conducive to hosting hydrothermal circulation.

Nage geothermal field considerably undergoes a complex tectonic and volcanic mechanism. This results in noticeable structural features and also the occurrence of surface thermal manifestation that seems to interconnect with each other. To assess the impact of fault slip on the development of permeability and fluid flow at structural discontinuities in Nage, and to understand the permeability development and surface thermal manifestation occurrence, I conducted stress distribution modelling focused on detected faults in Nage which play a key role in the geothermal systems, respectively. The research method and format in this paper were initiated by Siller (2023) and it is fairly applicable to understanding the relationship between structural framework with the hydrothermal fluid pathway in Nage. The data used in this work refer to a published previous geological study by Pradipta et al. (2021). This analysis provided with assumed geomechanics parameter for the slip and distribution modeling. Furthermore, applying these concepts to geothermal fields allows for a delineation of the favorable zones to drill the well in further development.

2. GEOLOGY AND STRUCTURAL SETTING IN NAGE

The island of Flores is situated within the Sundaland Block and lies at the boundary between the Eurasian and Indo-Australian Plates. The interaction between these two plates is characterized by the subduction of the Sunda

Arc to the west and the Banda Arc to the east, where the Indo-Australian oceanic crust subducts beneath the Eurasian Plate. The Indo-Australian Block is moving relatively north-northeast towards the Eurasian Plate, causing a counterclockwise rotation of Flores Island. This rotation has led to the formation of en-echelon volcanic chains on Flores Island, such as in the Nage area (Mccaffrey, 1988).

Research conducted by Koesoemadinata et al. (1994) and Muraoka et al. (2002) indicates that the Nage area consists of volcanic rocks ranging from the Tertiary to the Quaternary. These volcanic rocks in the research area are believed to originate from the eruptions of several volcanic cones, including Wolo Kenowe, Wolo Deru, Wolo Batulaba, Wolo Piu, Bena, Sinder Cone, and Mount Inirie. Generally, the volcanic rocks in the Nage area comprise lava, pyroclastic flows, pyroclastic falls, and alluvial deposits (Figure 1a). The lava has an andesitic composition, ranging from porphyritic to aphanitic texture, with occurrences of clay mineral alterations and columnar and sheet joints. Besides volcanic rocks, hydrothermal alteration with moderate to strong intensity has been observed in the research area, characterized by clay minerals found around fumarole manifestations in Wolo Puti, Keli hot springs, Nage hot springs, and the northern and eastern walls of the caldera.

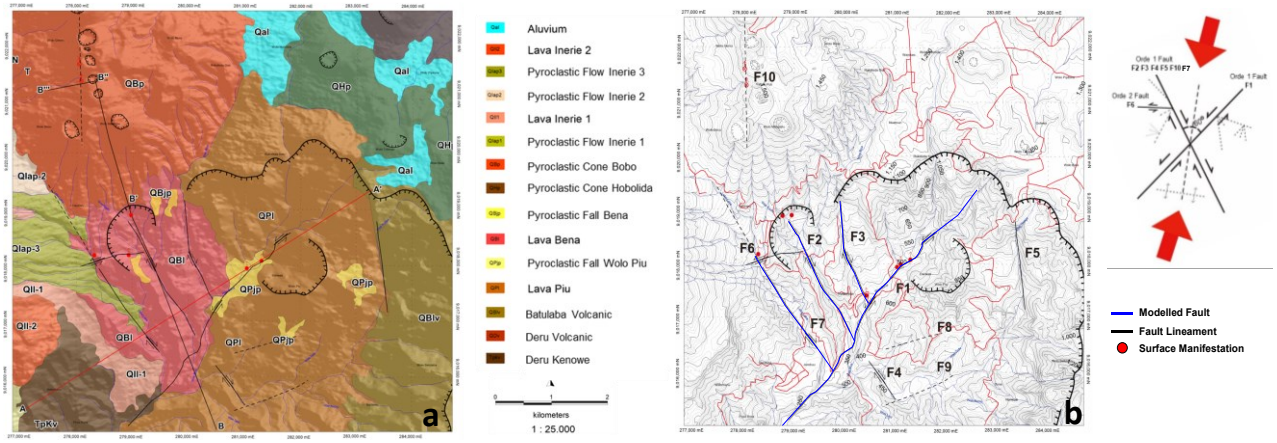

Figure 1: The geological information adapted from Pradipta et al. (2021): a) The geological map of the Nage field. b) The structural map of the Nage field. The blue line is the fault lineaments used for the stress transfer modelling

The geological structures in Nage were delineated by Pradipta et al. (2021) in Figure 1 by using the DEMNAS (Indonesia National Topographic) imagery and direct structural measurement on the surface. From the imagery, the noticeable structure also includes circular features indicating calderas and craters, as well as linear alignments of cinder cones oriented north-south. Field observations also reveal associated fault structures and zones of crushed rocks indicating strike-slip faulting oriented northeast-southwest and northwest-southeast. These structures are believed to influence the appearance of geothermal manifestations in the Nage area. They consist of secondary structures including oblique slip faults with a normal component in Nage noted as F1, oblique slip faults with a normal component noted as F2, oblique slip faults with a reverse component in noted as F3, oblique slip faults with a normal component noted as F4, oblique slip faults with a normal component in noted as F5, left-lateral slip faults in noted as F6, and oblique slip faults with a normal component noted as F7. DEMNAS imagery observations reveal several discontinuity surface lineations (faults noted as F8 and F9) and alignments of cinder cones believed to be structures representing faults noted as F10. In this study, I only use the prominent fault used has a clear appearance both on the surface and imagery, interpretatively. These faults are also been measured by the geological survey on Pradipta et al. (2021). They are F1, F2, F3 and F7. The maximum horizontal stress in the Nage field is interpreted relatively NNE-SSW or around N25^{o}E which is aligned with the regional horizontal stress in the southern cross of the Flores island as the result of subduction.

3. METHOD

Several factors that influence a fault mechanism and properties such as stress magnitude, lithology, rheology, and mineralization can result in a highly localised permeable zone that acts as the conduit for the fluid flow (Rowland & Sibson, 2004). This permeable zone can develop on the main fault segment and in the surrounding part of the fault including the structure near the slipping fault. The later condition is prone to better maintain the permeability due to its sensitivity to the stress changes during and afterslip, preventing rapid mineralization that can reduce the permeability magnitude. Therefore, the location of this well-maintained permeable zone will highly depend on the fault plane geometry, stress magnitude, and the fault and stress orientation.

The detail of the stress distribution analysis method was explained by Siller (2023). He used the boundary element method to calculate the three-dimensional displacement on triangular elements called Cut and Displace. The faults geometry was assigned to the 3D model and justified with the input stress. Two main aspects will be calculated on these inputs including the slip tendency of faults and the stress and strain changes on the fault planes and surrounding crust, resulting in four geomechanics parameters that can point out the local stress distribution impact including; 1) coloumb shear traction or coloumb friction, 2) dilation, 3) normal stress, and 4) shear stress.

Coulomb shear traction or coloumb friction refers to the force required to overcome the friction between two surfaces as they slide or move relative to each other. This force depends on factors such as the materials involved, the roughness of the surfaces, and the normal force pressing the surfaces together. The Coulomb friction model is often used in mechanics and engineering to calculate the forces and stresses in systems where sliding or relative motion between surfaces occurs. If the Coulomb friction is high, it means that there is a strong resistance to sliding or relative motion between the two surfaces in contact. In practical terms, this could mean that it requires a significant force to move or slide one surface against the other. High Coulomb shear traction can lead to difficulties in movement, increased wear and tear on materials, and potentially reduced efficiency in mechanical systems. On the other hand, if the Coulomb shear traction or friction is low, it indicates that there is less resistance to sliding or relative motion between the surfaces. This can make it easier to move one surface against the other with less force.

In geomechanics, dilation refers to the expansion or increase in volume that occurs within a rock mass when it is subjected to external forces. This concept is particularly relevant in the study of the mechanical behaviour of rocks under stress. When a rock is subjected to stress, such as compression or shearing forces, it can undergo deformation. Dilation specifically refers to the tendency of the material to increase in volume or expand perpendicular to the direction of the applied stress. This expansion occurs due to the rearrangement of particles or grains within the material as it experiences stress. The normal traction, also known as normal stress or normal force, refers to the force per unit area acting perpendicular (normal) to a surface, while shear traction, also known as shear stress, represents the force per unit area acting parallel to a surface or along a plane within a material.

The F1, F2, F3 and F7 faults are derived from the previous study. Due to subduction in the Flores, the Nage field is controlled by a compressional regime and by considering the topography of the field, the sense of movement of those faults is dominantly strike-slip faults. For the strike-slip faulting stress regime, the maximum horizontal stress (SHmax) is larger than the vertical stress (Sv), which is larger than the minimum horizontal stress (Shmin). For these structural settings which contain left and right-lateral strike-slip faults, SHmax is oriented to azimuth N25°E for the fault geometries. In the need stress modelling process, I assumed that strike-slip faults dip will be vertical as proposed by Anderson (1905).

The stress transferring model needs the input principal stress magnitude. For the input stress, I use the coefficient of friction of 0.6 and the crustal density of 2600 kg $^{m-3}$. The top of the reservoir in Nage is assumed distributed at 0 mASL which is typical of the top of the reservoir of the geothermal field on Flores Island (Muraoka et al., 2002). The mean surface level in the Nage field is assumed at 500 mASL, so the vertical overburden distance from the surface to the top of the reservoir will be 500 m in depth. An assumption was also made that the surface's stress and pore pressure values are zero and the overburden stress gradient is linear to depth.

Table 1: Input parameter for modelling

Young's modulus	75 Gpa
Poisson's ration	0.25
Coefficient of friction	0.6
Cohesive strength	0 Mpa
S_{Hmax} magnitude (at -0 mASL)	16.77 Mpa
S_{Hmax} direction	northeast – southwest
S_v magnitude (at -0 mASL)	12.74 Mpa
S_v direction	vertical
S_{Hmin} magnitude (at -0 mASL)	8.71 Mpa
S_{Hmin} direction	northwest-southeast
Pore pressure	9.79 Mpa

Stress variations and deformation arising from the simulated slip are computed across a grid of 256 points spaced evenly at 200-meter intervals within a 3-kilometre by 3-kilometre area, situated 500 meters below the surface. The input faults, extending beyond the grid by 1 kilometer, are assumed to have no stress or strain effects at the grid's edges. The stress changes are quantified in terms of Coulomb shear and normal tractions, specifically focusing on fractures with the greatest increase in Coulomb shear traction and a decrease in normal traction within a deviation of ± 1 standard deviation from the strike, dip, and rake of the input faults. These stress-induced

dilatation and shear tractions could potentially create permeable zones conducive to the upward flow of hydrothermal fluids to the surface.

The stress alterations are expressed as Coulomb shear and normal tractions. These are computed for fractures exhibiting the highest increase in Coulomb shear traction and the greatest decrease in normal traction for all fracture orientations within ± 1 standard deviation of the strike, dip, and rake of the input faults. Essentially, the stress changes discussed pertain to fractures that are optimally oriented similarly to the input faults. Assuming all strain is elastic, dilatation is calculated as the percentage of volume increase. The stress effects are illustrated as the percentage change in Coulomb shear traction and the percentage change in normal traction relative to the original (pre-slip and static) stress state (Siller 2023).

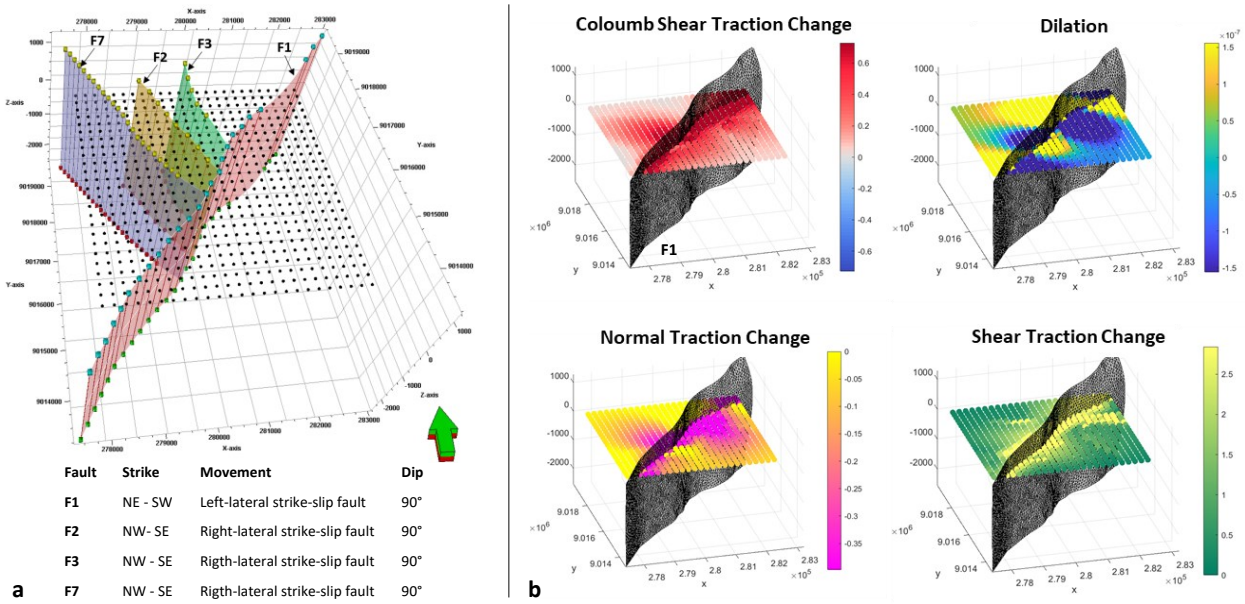

Figure 2: The modelling process to map the stress distribution on faults. A) The 3D view of the four modelled faults included in the study with the observation points at reservoir depth. B) The example of stress distribution analysis on Fault 1. Four stress components are measured on each observation point.

4. RESULT

4.1 Stress Distribution

In general, the fault orientation changes are the favorable area to undergo the stress changes impacted by the input stress parameter in the model. The stress changes could be both positive or negative, depending on the fault's geometry and orientation to the principle stress. Fault tip and fault intersections also experienced stress changes, that also correlate with the occurrence of surface manifestations.

For the percentage of coloumb shear traction change, the positive change (blue) indicates the resistance of the area around the fault plane that is hard to move while the negative change (red) indicates the opposite. Fault intersection between F1 and F2, F3 and the fault bend of F1 and F3 are the areas that have remarkable stress changes. The highest coloumb shear traction percentage decreasing (up to < 0.5% MPa) is concentrated at the most northern part of the F1, where the F1 strike significantly bends to far northeast about ~8°. This means that this area is prone to move when stress is applied due to the fault movement. The increase of the coloumb shear traction percentage occurs right on the intersection of F1 and F2, F3, remarks the most resistance area in the fault surrounding a movement. This also occurs on the fault bend area in the southern part of F2, whereas the relatively north-south fault bends ~15° to the southeast toward the F1. The resistance block around the fault will likely occur in the tips of the fault, such as the northern tips of F2 and F3 which indicates coloumb shear traction change increasing up to 3.25% MPa.

The dilation changes calculated from the input stress parameter follows the change of coloumb shear traction changes in the opposite way, if the coloumb shear traction changes are low in an area, the dilation changes should be positive. This is represented in the area of fault intersections, fault bends and fault tips. The most positive dilation change is located in the area between F1 and F2, right on the west side of the F1 strike bending, where the changes are up to 3.9×10^{-3}%. The dilation changes area could also controlled by the fault tips as shown by the northern tips of F2 and F3 with changes of 2.1×10^{-3}%. These areas with positive changes indicate the volume

increasing due to the applied stress. The negative dilation changes areas are controlled by the fault intersection as shown by the intersection of F1 with F2, F3 and F7, which remarks that instead of creating open space or permeability, the fault intersection zones are prone to compact under the applied stress parameters. Extensive negative dilation changes also appear on the east side of F3's northern tip. Most of these areas have < -1.2×10^{-3}% which indicates decreasing in area volume.

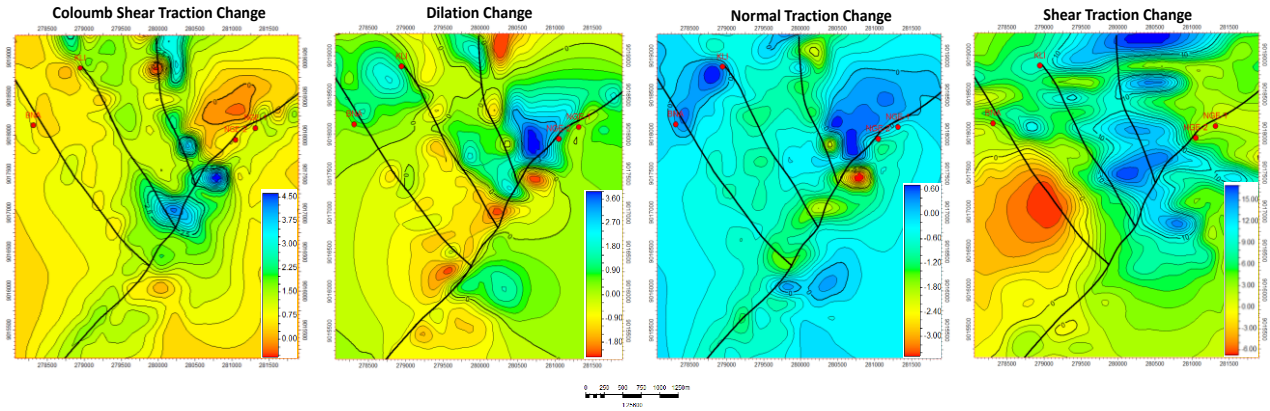

Figure 3: Contour maps show measured geomechanics parameters in the study area. The parameters anomaly mostly address the structural discontinuities zone, including fault bend, fault intersections and fault tips, and associates with the surface thermal manifestations.

The shear traction changes pattern also follows the coloumb shear and dilation, where the areas that undergo significant changes are controlled by the fault discontinuities. There are two areas that show the increasing shear stress, F1 northern fault bend and the northern tips of F2 and F3. The only area that indicates a significant shear stress decrease is the eastern side of the F1 and F3 intersection. This might also influenced by the bending of the F1. Meanwhile, the normal traction changes percentage in the Nage field is more distributed instead of focusing on the narrow area of the fault discontinuities. However, some thermal manifestations including KLI and BNA located on the location where the normal traction change increases. The increase of shear or normal traction should influence the fault slip susceptibility regarding the applied stress, which means that these areas are more prone to move.

4.2 Fault Slip Potential

Fault slip potential (FSP) analysis is a geomechanical assessment used to evaluate the likelihood of faults slipping or reactivating under certain stress and pore pressure conditions. If the stress distribution analysis investigates the stress on the rock around the fault, the fault slip potential analysis measures the stress along the fault sections. The application of fault slip potential is available in Walsh et al. (2023). Some assumption of stress parameters was made to predict the likelihood of the fault slip potential on structures in the Nage field, which required the stress gradients. I estimated the gradient of the maximum horizontal stress (SHmax) at 1.22 psi/ft, vertical stress (Sv) at 1.1 psi/ft, and minimum horizontal stress (Shmin) at 0.7 psi/ft, considering the possible formation composed of the Nage field. The assumption was also made for the initial reservoir pressure at 0.43 psi/ft. The fault slip potential analysis for the Nage field, as illustrated by the provided images and delta pore pressure (ΔP) colour bar, reveals significant insights into the stability and slip likelihood of key faults under varying pore pressure conditions. Some fault sections in F1, especially in the fault bend section, are shown in deep red on the fault map which requires the most minimal ΔP to slip, indicating it is critically stressed and highly sensitive to changes in pore pressure. Even minor increases in pore pressure could trigger slip along this fault section which means have a high favourability to create permeability. This also agrees with the occurrence of NGE-1 and NGE-2 thermal manifestations and the coloumb shear and dilation stress changes. The other sections of F1 also indicate slightly critically stressed sections. The north tip of F3 also indicates a similar fault section condition while the rest of the fault sections on F3 still need slightly moderate ΔP to slip. However, most of the F2 and F7 sections, depicted in yellow and orange, require moderate ΔP to slip, suggesting they are less sensitive than F1 and F3 but still pose a potential of reactivation under sufficient pore pressure changes. The Mohr circle diagram further supports this, showing red data points near the failure envelope for F1 and F3, while orange and yellow points for F2 and F7 are further from the envelope, indicating higher ΔP requirements for slip. The stereonet plot, which aligns maximum horizontal stress (SHmax) with fault planes, reveals that faults oriented in critical directions (red and orange) are highly susceptible to pore pressure changes. These results highlight that friction coefficient, SHmax azimuth, dip angle, fault strike orientation and also the relative location between faults are the most sensitive factors that control the fault slip potential measurement.

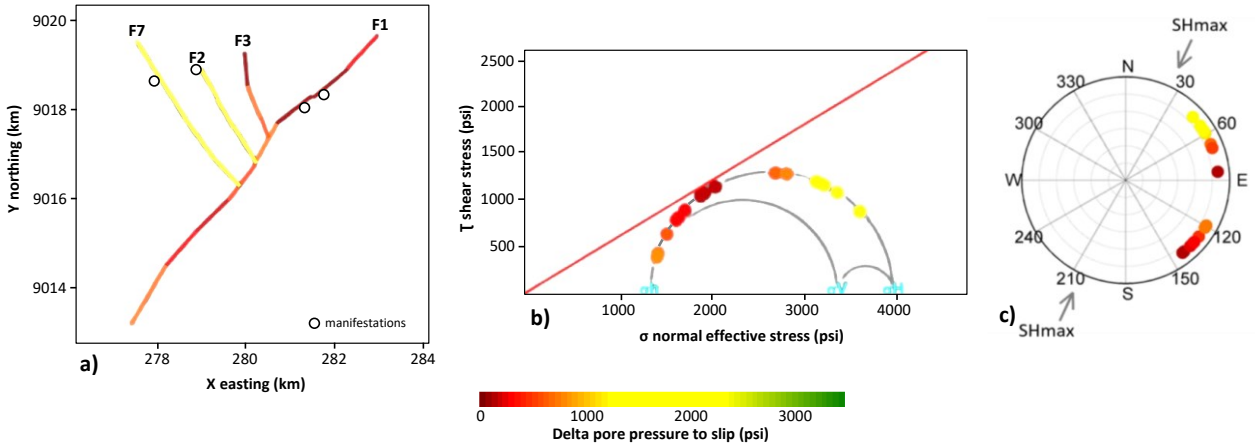

Figure 4: A) The fault map of the Nage field, identifying three major faults: F1, F2, F3, and F7 along with the fault sections on each of the faults. These fault sections are depicted in different colors indicating their slip potential. The colour scale at the bottom ranges from red (high slip potential) to green (low slip potential). B) Mohr circle diagram plotting the shear stress (τ) against the effective normal stress (σ effective) for the identified faults sections. C) Fault sections on the stereonet.

4.3 Hydrological Model

The occurrence of surface manifestation often relates to the permeability that provides the pathway to the hydrothermal fluid flow to reach the surface from the reservoir. These manifestations in the Nage field are interpreted as strongly controlled by the geological structure as they are all located in the vicinity of the prominent fault lineaments. The stress distribution analysis anomaly shows a good agreement between the changed stress area with the location of the surface manifestations. The NGE-1 and NGE-2 hotsprings exposed on the F1 fault bend or orientation changes, which conceptually will experience the stress changes. Accordingly, this area also indicates a favorable area to be fractured as it has negative coloumb shear traction change that indicates a weak zone, positive high dilation changes percentage as it indicates the volume increasing within the rock mass in this zone, and also the increasing of the shear stress that could trigger a slip of pre-existing fractures reactivation. This also happened for the BNA and KLI manifestations, where the stress distribution anomaly also supports the interpretation of surface manifestation pathways. These manifestations are concentrated at the north tips of F2 and F3. However, the magnitude of stress distribution anomaly intensity is not as high as the surrounding area of NGE-1 and NGE-2. This analysis supports the interpretation of structural-controlled permeability that accommodates the occurrence of surface thermal manifestation. The mechanism of structural discontinuities in the Nage field most likely forms a narrow secondary permeability (~500 m wide) that accommodates a vertically focused permeability. In addition, the interpretation of narrow and focused-vertical permeability in Flores is also strengthened by how the volcanic craters sporadically occur on the surface, forming the moon-liked surface topography.

Akasako et al. (2002) have concluded the geothermal conceptual model for the Nage field. There are two hydrology concepts proposed based on the occurrence of thermal manifestations in Nage and the surrounding area. First, the upway hydrology along the NE-SW fault, which also controls the occurrence of the Wae Bana River inside the Nage caldera, controls the NGE-1 and NGE-2 manifestations. Hot springs along the Wae Bana River, including NGE-1 and NGE-2, ranging from 7°C to 80°C, show significantly altered surfaces indicating strong hydrothermal activity, although the boundaries are unclear due to plant cover. This also indicates the localized permeability along this river and could be favorable in well targeting focusing on the fault bends section. Second, the lateral flow from the Wolo Bobo field on the northeast part of the Nage caldera. The volcanic activity along a north-trending fault across the Wolo Bobo to Nage caldera created numerous volcanic cones, indicating a good lateral permeability for a series of magma to arise. This relatively north-northwest flow is interpreted to control the occurrence of KLI and BNA surface manifestations. It could be a subsurface structure that is already covered by younger volcanic cone products and still permeable under the current stress condition. However, this interpreted fault is not included in this study as it is not discussed as a prominent fault in Pradipta et al. (2021). Therefore, a further study to detail the existence of this interpreted fault could be a benefit in interpreting the hydrology from Wolo Bobo toward the Nage caldera.

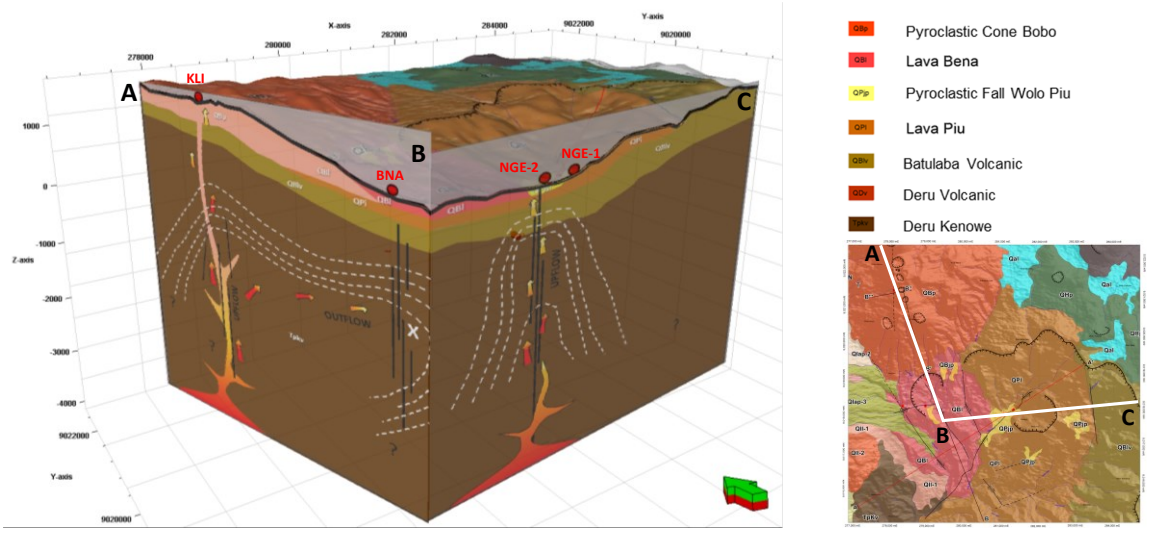

Figure 5: Proposed hydrology model of Nage geothermal field, which is strongly controlled by structure and fault damage zone. Vertical hydrology (upflow) controls the NGE-1 and NGE-2 manifestations while the BNA manifestation is interpreted as the outflow manifestation from the north-northwest upflow, indicated by the KLI manifestation.

5. DISCUSSION

The analysis of the stress distribution around fault planes in the Nage geothermal field reveals that certain fault discontinuities, such as fault bends or orientation changes, significantly enhance permeability. These discontinuities create vertical conduits for fluid flow, evidenced by substantial coulomb shear traction reduction and notable dilation increases. Areas around fault tips also contribute to permeability, particularly in regions where larger fault tips form positive or negative flower structures, facilitating fluid flow. Conversely, fault intersections are less favorable for permeability due to low coulomb shear traction changes and negative dilation, suggesting a higher rock strength resistance. The orientation of fault intersections relative to the maximum horizontal stress orientation plays a crucial role in this phenomenon.

The primary uncertainties in this study focusing to the assumptions about stress and mechanical properties, as well as fault geometry and propagation. The volcanic activity in the Nage area leads to varied volcano-stratigraphy, impacting overburden and sideburden stresses, potentially resulting in a non-homogeneous stress regime. Despite these uncertainties, the assumed stress parameters in this study seem to represent the current stress state in Nage fairly, as indicated by the alignment of results with expectations. Further detailed investigations into fault geometry, including lateral extensions and changes in strike and dip, are necessary due to their significant impact on stress distribution and anomalies across the study area.

6. CONCLUSION

This study emphasizes the critical role of fault discontinuities, such as fault bends or orientation changes, and fault tips, in enhancing permeability within the Nage geothermal field. The findings indicate that these features serve as effective vertical conduits for fluid flow, driven by stress-induced dilation and reduced coulomb shear traction. In contrast, fault intersections exhibit lower permeability potential due to their orientation relative to the maximum horizontal stress and inherent rock strength resistance. The primary challenges in this study include uncertainties in stress parameters assumptions and fault geometry, exacerbated by the varied volcanic stratigraphy in the Nage region. Nonetheless, the stress parameters used in this study provide a reasonable representation of the current stress state, supported by the agreement of the results with known conditions. Future research should focus on refining the understanding of fault geometry and propagation, considering their significant influence on stress distribution and permeability. Addressing these uncertainties will enhance the accuracy of permeability predictions and inform the development of more efficient geothermal resource exploitation strategies in volcanic regions. This comprehensive analysis contributes valuable insights into the permeability dynamics within geothermal fields, particularly those influenced by complex fault structures, and underscores the importance of integrating geological and geomechanical data for effective reservoir management.

REFERENCES

Akasako H., Matsuda K., Tagomori., Koseki., Takahashi H., and Dwipa S.: Conceptual Models for Geothermal Systems in the Wolo Bobo, Nage and Mataloko fields, Bajawa area, Central Flores, Indonesia, Bulletin of the Geological Survery of Japan, vol. 53 (2/3), p. 375-387, (2002).

Anderson, E.M.: The dynamics of faulting. Transactions of the Edinburgh Geological Society, 83, 387–402, https://doi.org/10.1144/transed.8.3.387 (1905).

Curewitz, D., and Karson, J.A.: Structural settings of hydrothermal outflow: Fracture permeability maintained by fault propagation and interaction: Journal of Volcanology and Geothermal Research, v. 79, p. 149– 168, https:// doi .org /10 .1016 /S0377 -0273 (97)00027 -9 (1997).

Siler, D.L., Hinz, N.H. and Faulds, J.E.: Stress concentrations at structural discontinuities in active fault zones in the western United States: implications for permeability and fluid flow in geothermal fields. Geological Society of America Bulletin, 130, 1273–1288, https://doi.org/10.1130/B31729.1 (2018).

Siler, D.L: Structural discontinuities and their control on hydrothermal systems in the Great Basin, USA. The Geological Society of London for GSL and EAGE, https://doi.org/10.1144/geoenergy2023-009, (2023).

Koesoemadinata, S., Noya, Y., and Kadarisman, D.: Peta Geologi Lembar Ruteng, Nusa Tenggara , Skala 1: 250,000, Pusat Penelitian dan Pengembangan Geologi, Bandung. (1994).

Mccaffrey R.: Active tectonics of the Eastern Sunda and Banda Arcs, Article in Journal of Geophysical Research Atmospheres, (1988)

Muraoka H., Nasution A., Ura M., Takahashi M., Takashima I., Simanjuntak J., Sundhor H., Aswin D., Nanlohy F., Sitorus K., Takahashi H., and Koseki T: Tectonic, volcanic and stratigraphic geology of the Bajawa geothermal field, central Flores, Indonesia, Bulletin of the Geological Survey of Japan, vol. 53 (2/3), p. 109-138, (2002).

Pradipta D., Permana L. A., and Ramdhan D. M.: Structural Geology Characteristics And Its Roles To The Nage Geothermal System, Ngada District, East Nusa Tenggara Province, Buletin Sumber Daya Geologi, Volume 16, No. 3 (2021).

Rowland, J.V. and Sibson, R.H.: Structural controls on hydrothermal flow in a segmented rift system, Taupo Volcanic Zone, New Zealand. Geofluids, 4, 259–283, https://doi.org/10.1111/j.1468-8123.2004.00091.x (2004).

Walsh, F.R.; Zoback, M.D.; Pais, D.; Weingarten, M.; Tyrell, T. FSP 1.0: A Program for Probabilistic Estimation of Fault Slip Potential Resulting from Fluid Injection. Available online: https://scits.stanford.edu/fault-slip-potential-fsp (accessed on 1 June (2023).

Identification of Geothermal Manifestation Using Remote Sensing Method in Slamet Mountain Area, Central Java

Sisdeo Hutagaol, Fabyan Mark Alfons,
Rowena Astika Rahamis, and Maulidiya Fathien Hamidah

Department Geological Engineering, Faculty of Mineral Technology, UPN "Veteran" Yogyakarta

sisdeohutagaol121@gmail.com

Keywords: Geothermal, GIS, Lineament, Remote sensing, Mount Slamet

ABSTRACT

These days, the globalization of energy transition efforts towards new renewable energy sources is intensively underway. In support of this, Indonesia is committed to achieving a target of 23% new and renewable energy (EBT) in the energy mix by 2025. As much as 40% of the world's geothermal reserves are located in Indonesia. However, in reality, geothermal exploration efforts in Indonesia still face several challenges, including many prospect areas that are difficult to reach, cost efficiency, and funding issues. This research was conducted to identify geothermal manifestations in the Mount Slamet area using remote sensing methods to minimize the existing exploration challenges. ASTER (Advanced Spaceborne Thermal Emission and Reflection) data with NDVI (Normalized Difference Vegetation Index) analysis is used to determine vegetation density, and LST (Land Surface Temperature) analysis is used to determine earth surface temperature anomalies. DEM (Digital Elevation Model) is used to conduct FFD (Fault Fracture Density) analysis, and Landsat-8 imagery to determine the distribution of hydrothermal alteration minerals as supporting parameters. The results of the LST (Land Surface Temperature) analysis found that the lowest temperature reached 9.1oC and the highest temperature reached 30.4oC. FFD (Fault Fracture Density) analysis shows the highest alignment density value of 3.3-4.4 km/km2. The results of data integration show that there are 8 new geothermal manifestation points in the study area. This research can be used as a reference in determining geothermal manifestation points, especially in this study the identified geothermal manifestation points are by the location of the manifestations that have been found previously.

1. INTRODUCTION

Geothermal is one of the energies currently being popularly looked for because it is a renewable energy that supports the energy transition process. The world is turning to new renewable energy, one of which is geothermal energy. Indonesia has over 40% of the world's geothermal reserves. Indonesia is committed to achieving a target of 23% new and renewable energy (EBT) in the energy mix in 2025 (ESDM, 2021). However, in reality, geothermal exploration efforts in Indonesia still face several challenges, namely the large number of prospect areas that are difficult to reach, to cost efficiency and funding issues. Therefore, there needs to be another alternative to identify manifestations of geothermal potential, one of which is the remote sensing method. This method can ease exploration challenges in terms of time efficiency, cost, and accessibility to exploration sites.

The Gunung Slamet area is an area with a geothermal potential of 110 MW which has a potential prospect area of about 60% of the Central Java region. From the results of research by Widagdo (2013), there are 5 geothermal manifestation points in the Gunung Slamet area (Table 1). Therefore, this research is expected to prove and identify potential points in the Gunung Slamet area using a more effective method.

2. METHODS

The method used is remote sensing. This research utilizes three data types, namely ASTER, Landsat-8 OLI/TIRS, and DEM, to identify geothermal potential based on geological and geomorphological data, nighttime surface temperature anomalies, lineament density, and land cover evaluation. Geological and geomorphological data serve as the basis for determining the presence of geothermal systems. Fault Fracture Density (FFD) and night time LST are used to locate geothermal manifestations such as hot springs and fumaroles. Meanwhile, the land cover map is used to evaluate areas that may become geothermal manifestations, such as disturbances in land cover. We used the analysis method of (Ghaly et al, 2023) modified with the addition of hydrothermal alteration map and only used ASTER Night Time data.

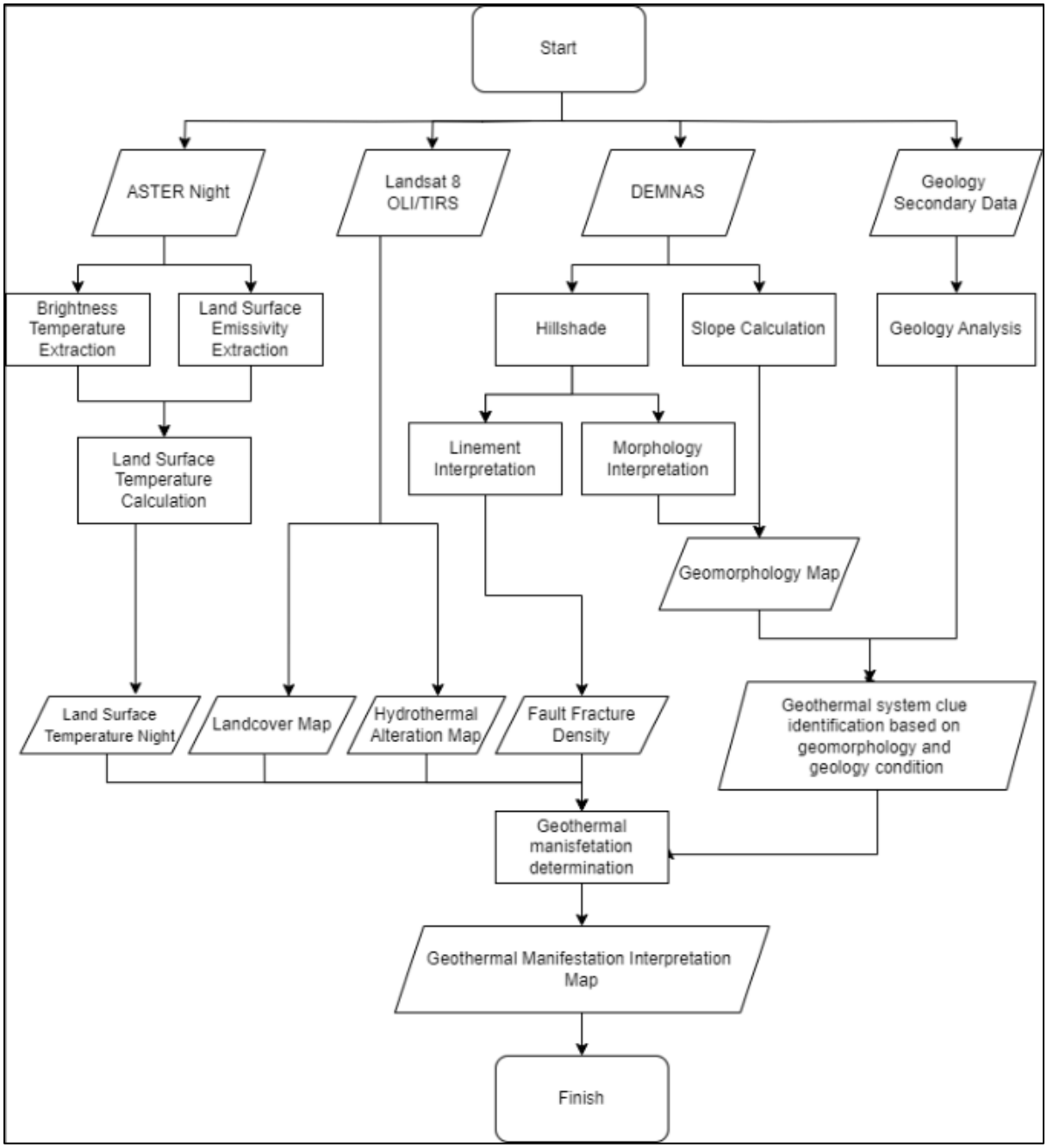

Figure 1: Research Flowchart.

Table 1: Location of Geothermal Manifestation Points (Widagdo, 2013).

No	Name	Location
1	Pancuran 5	Guci, Kec Bumijawa, Tegal
2	Pancuran 13	Guci, Kec Bumijawa, Tegal
3	Pancuran 7	Ketenger, Baturaden, Banyumas
4	Sigedong	Batusari, Kec Sirampok, Brebes
5	Pancuran 3	Karangmangu, Baturaden, Banyumas

Table 2: Image Data Use.

Image Name	Band	Resolution	Acquisition time
ASTER Night Time	TIR (10-14)	90 m	October 9th, 2023
Landsat-8 OLI/TIRS	Band 1- 6	30 m	September 8th, 2020
	Band 8	15 m	
DEMNAS		0.27 Arc second	Accessed on April 21th, 2024

2.1 Surface Temperature Calculation

This analysis uses ENVI software with nighttime ASTER data. The analysis begins with radiometric calibration correction and atmospheric correction to eliminate radiation errors. This is followed by temperature extraction using the emissivity normalization tool applied to the nighttime ASTER data.

2.1.1 Land Surface Emissivity (LSE) Calculation

Land Surface Temperature values require LSE values. Land Surface Temperature is obtained from NDVI processing, vegetation proportion, and emissivity calculations on ASTER images (Ndossi & Avdan, 2016). Normalized Difference Vegetation Index (NDVI) is a comparison of the reflectance value of the red band (Red Band) with the near infrared (NIR Band) which is normalized due to the reflection of land cover such as vegetation. This data can be used to estimate the density of vegetation on the earth's surface (Weirer, 2000 in Laksono, 2020).

To determine the NDVI value of the study area, we used band 4 (Red) and band 5 (NIR) data from the Landsat 8 OLI/TIRS image. With the following formula (Ndossi & Avdan, 2016):

a. NDVI (Ndossi & Avdan, 2016)

$$\text{NDVI} = (NIR - RED)/(NIR + RED) \quad (1)$$

NIR refers to reflected light in the near-infrared band, while RED refers to reflected light in the red channel on the ASTER instrument.

b. Proportion of Vegetation (Ndossi and Avdan, 2016)

$$Pv = (NDVI - NDVIs)/(NDVIv - NDVIs) \quad (2)$$

NDVIv refers to NDVI values for vegetated surfaces, while NDVIs refer to NDVI values for non-vegetated surfaces, which are obtained from sampling values at NDVI raster pixels.

c. Land Surface Emissivity

$$\varepsilon = \varepsilon v \times Pv + \varepsilon s(1 - Pv) \quad (3)$$

εv is the emissivity of the vegetated surface, while ε_s is the emissivity of the bare ground surface. These two values were obtained through sampling of PV values and then calculated using the following formula:

$$\varepsilon = 0.941 + 0.004\text{Pv} \quad (4)$$

2.1.2 Land Surface Temperature (LST) Calculation

The LST calculation was performed using the Plank Function inversion method formulated as follows (Ndossi and Avdan, 2016):

$$LST = \left(\frac{BT}{1 + \left[\frac{\lambda \times BT}{\rho} \right] \times ln\ \varepsilon} \right) \quad (5)$$

2.2 Fault Fracture Density (FFD) Map Construction

DEM data were processed with ArcGIS using the Hillshade tool qualitatively and quantitatively. Qualitatively, straightness was analyzed on each hillside with the direction of irradiation N 050° E, N 100° E, N 200° E, and N 315° E. Quantitative results in the form of Line Density values were obtained by combining the qualitative analysis of the straightness of each irradiation direction.

2.3 Hydrothermal Alteration Analysis

Hydrothermal Alteration was analyzed by creating an Alteration Map of the Study Area using Landsat 8 OLI/TIRS data, using Sabins's Band ratio Method. Using RGB Bands of 4/2, 6/7 and 6/5, to detect areas with hydrothermal alteration zones.

2.4 Manifestation Point Determination

Geothermal manifestation points are obtained from areas of high surface temperature anomalies at night. Then, the land cover was adjusted by removing the value of each pixel indicating settlements. Furthermore, the points that are outside the area with medium-high (FFD) are removed. Thus, the distribution points of geothermal manifestations can be identified.

3. REGIONAL GEOLOGY

3.1 Geological Condition

Mount Slamet is located in Central Java and is part of the Quaternary Sunda volcanic arc as a result of the subduction of the Indo-Australian Plate under the Eurasian Plate (Hamilton, 1979). This volcano arose at the boundary between two Miocene sedimentary basins in the North Serayu Mountains and the Bogor Zone. Both sedimentary basins were uplifted to form an east-west trending fold. This trend is more or less parallel to the which lies in the southern part of Java. The Bogor Zone extends from Slamet Volcano to the west, while the North Serayu spreads eastward from Slamet Volcano.

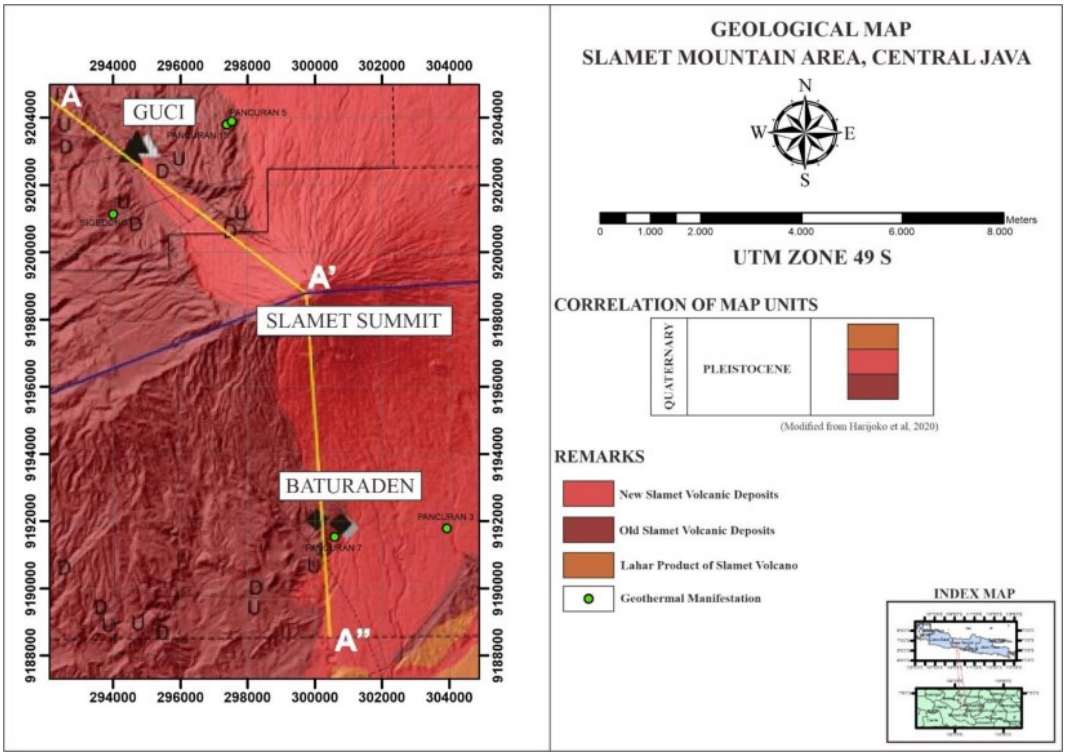

Figure 2: Geological Map (Modified from Harijoko, 2020; Kastowo, 1975; Sutawijaya et al., 1985; and Djuri et al., 1996).

Djuri et al. (1996) proposed that the substrate-tum rocks of the Slamet Volcano were sedimentary rocks of Rambatan, and the Halang Formation was part of North Serayu Mountain. Those sedimentary rock formations outcrop around the Slamet Volcano. Rambatan Formation was formed in an unstable back-arc basin flank (Husein et al., 2013), producing calcareous sandstone and conglomerate interbedded with shale, marl, and tuff (Djuri et al., 1996: Kastowo, 1975). During the sedimentation of the Halang Formation, the North Serayu region received a supply sediment of volcanic products indicated by the volcanic composition of the Halang Formation such as andesitic sandstone, tuffaceous conglomerate, and marl with intercalations of sandstone (Djuri et al., 1996).

3.2 Geological Structure

The regional geological structure assists in the interpretation of the faults. It is interpreted that there are two local faults right lateral fault. However, there is no evidence of a slicken side in the field except for the evidence on the ground except for fractures. There is a main fault structure that formed in the northeast of Mount Slamet, according to the Geological Map of Purwokerto-Tegal Sheet (Djuri, M. et al, 1996) are left and right horizontal faults with a southwest-northeast oriented. On the east, a horizontal fault structure develops on the left and northwest-southeast trending folds and west-east trending folds. This fold consists of two synclines (Mendelem and Majakerta) and two anticlines (Gombong and Karangmanggu). Most of the folds are relatively elongated from west to east except for the Majakerta syncline which runs northwest-southeast. Faults in the study area can only be observed from maps or satellite images.

Fractures are located in sandstone and no fractures are found in shale and igneous rocks. Field observations show fracture directions azimuths in two different dominant orientations, namely northeast-southwest and northwest-southeast. The fault direction from stereographic projections is interpreted as being dominated by the principle of transitional stress.

3.3 Alteration Condition

In the Gunung Slamet area, there are several types of alteration that develop due to fluid influence characterized by secondary minerals in the form of chlorite, quartz, pyrite, and calcite veins. Whereas in the area near the igneous intrusion, secondary minerals such as sericite, quartz, and pyrite are found, which are interpreted as subpropylitic alteration based on the alteration mineral graph (Prawiranegara et al, 2015).

There are polymictic breccia rocks with fragments consisting of tuff, basalt, metamorphic rock, and sandstone. The matrix has undergone oxidation and alteration to argillic (montmorillonite and halloysite) and silica in the Baturaden area (Indarto, 2017)

3.4 Geothermal

Geothermal manifestations around Mount Slamet appear as hot springs at several points in the study area. In the Baturaden area on the southern slope of Mount Slamet, there are Pancuran 3 and Pancuran 7 hot springs. In the Guci area on the northern slope of Mount Slamet, there are Pancuran 5 and Pancuran 7 hot springs, and on the northwestern slope, a hot spring manifestation also appears, known as Sigedong.

In general, geothermal manifestation points in the Gunung Slamet area are present in the breccia-lava-tuf unit (Qvs) which is a product rock of the Old Slamet volcano. Geothermal manifestations in the Mount Slamet area follow a northwest-southeast trending fault pattern.

According to research by Iswahyudi, et al (2020), hot water manifestations located at the five manifestation points in the research area are in immature water conditions. This condition indicates that there has been a process that causes the geothermal fluid to be unbalanced. This condition causes hot springs to be difficult to use in determining reservoir temperature with the geothermometer method. Based on the results of geoindicator analysis, there are three geothermal systems working in the study area, namely the Baturaden, Guci, and Sigedong systems or reservoirs. The recalculation of geothermal reservoir temperatures in the study area for Batudaren, Guci, and Sigedong using the silica-enthalpy method is 204°C - 220°C, 187°C - 196°C, and 181°C.

Table 3: Water Sample Types Used in this Study and the Types of Wall Rock Where the Springs Discharge (Modified from Harijoko et al., 2020).

Type	Location	UTM Coordinate		Elevation (m)	Sample Code	Temperature (°C)	pH	Estimated distance from Slamet summit (km)	Wall rock at the discharge point
		mE	mN						
Hot Spring	Baturaden, Pancuran Telu	304534	9191298	698	HP3	50	7	7.53	Basaltic lava
	Baturaden, Pancuran Pitu	303810	9191933	762	HP7	46	6	7.66	Basaltic lava
	Guci, Pengasihan	297197	9203712	1236	HPN	40.5	8	7.39	Volcanic breccia

4. RESULT AND DISCUSSION

4.1 Geomorphological Condition

In geothermal system modeling, geomorphology is important to determine the characteristics of the geothermal system, recharge areas, and source components. Geomorphological analysis of the Mount Slamet area using DEMNAS data, then hillshade analysis and slope calculation for landform interpretation.

The landform of the study area is a volcanic landform in the form of a crater, Old Volcanic Cone, Young Volcanic Cone, Foot Slope, and Lava Plain. The manifestation of the research area is associated with morphology in the rocks of the old Slamet volcano, especially in the morphology of the lava plain and Foot Slope. Areas with geothermal potential are usually associated with structures, and the volcanic regions are associated with foot slopes.

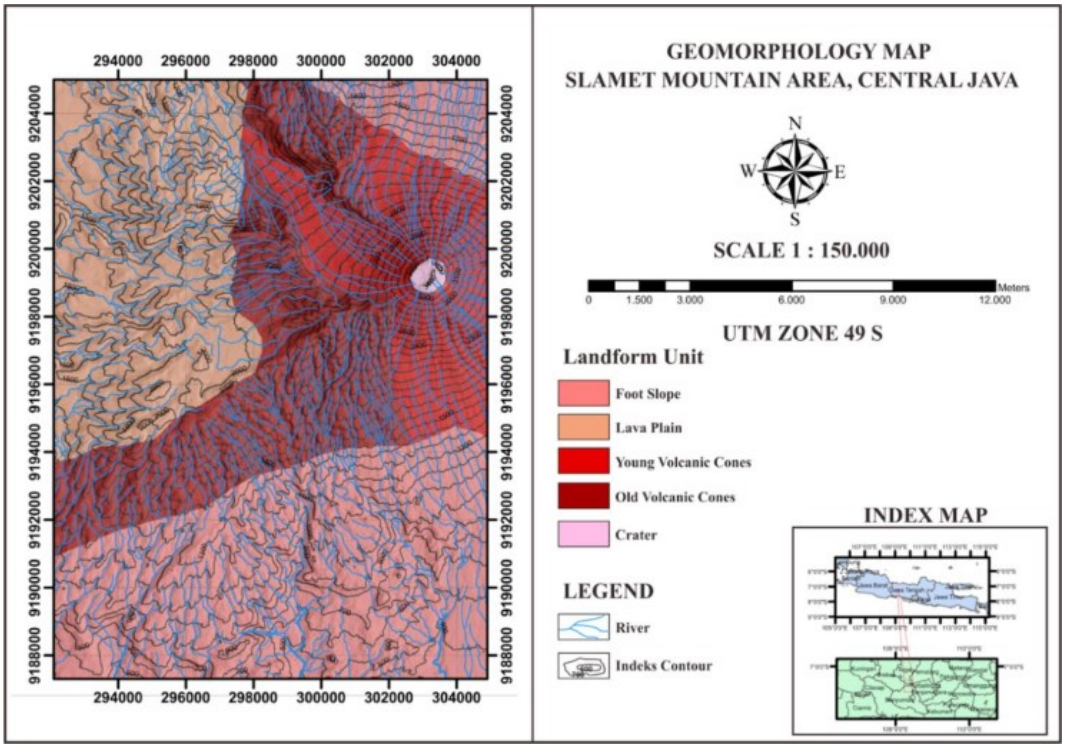

Figure 3: Geomorphological Map.

4.2 Land Cover Map

Land cover in the study area is classified into several objects, namely primary forest (dark green), secondary forest (light green), plantation (light orange), shrubs (dark orange), residential (red), agriculture land (yellow), paddy field (mint green). The results of the land cover map interpretation are used to make corrections to the results of data analysis from the land surface temperature (LST) map because it is likely to produce surface temperature anomalies influenced by residential areas.

4.3 Fault Fracture Density Map

In the Research Area, the previous manifestation point was associated with a high fracture density value, so the determination of a new manifestation point must also be associated with a high fracture density value. The manifestation point can also be associated with low fracture density values, so the point closes the possibility of a new manifestation point but additional data is still needed in the form of direct field checks in the field (Khoirunnisa et al., 2024).

4.4 Normalized Difference Vegetation Index

In the Research Area, the Vegetation Density Value is classified into 5 classes (Hakim et al., 2017). The NDVI value that dominates the research area is class 4 with a dominant distribution in the west, center and northeast of the lot. class 1 is associated with volcanic cone. Class 2 is dominantly distributed in the Southeast of the map due to clouds and west of the map due to settlements. Classes 3 and 5 do not dominate.

The purpose of this NDVI classification is to delineate geothermal hotspots by class. Areas with high vegetation density will have lower surface temperatures and low vegetation density will have higher surface temperature values (Hakim et al., 2017). In addition, it is also to help the calculation of land surface temperature values and regional corrections for hydrothermal alteration maps, because high vegetation density values will also produce inappropriate alteration maps.

The difficulty of using this NDVI map is the data used, if the image data used is a lot of clouds, the results will not be suitable. In addition, to help determine geothermal prospects, there has not been much research for areas with high vegetation density values, because they are prone to errors. However, it can be used because the previous manifestation point is associated with high NDVI values, so researchers concluded that NDVI is one of the determination parameters but the percentage is small. Table 3. NDVI Value Classification for Vegetation Density (Youhao, 2007)

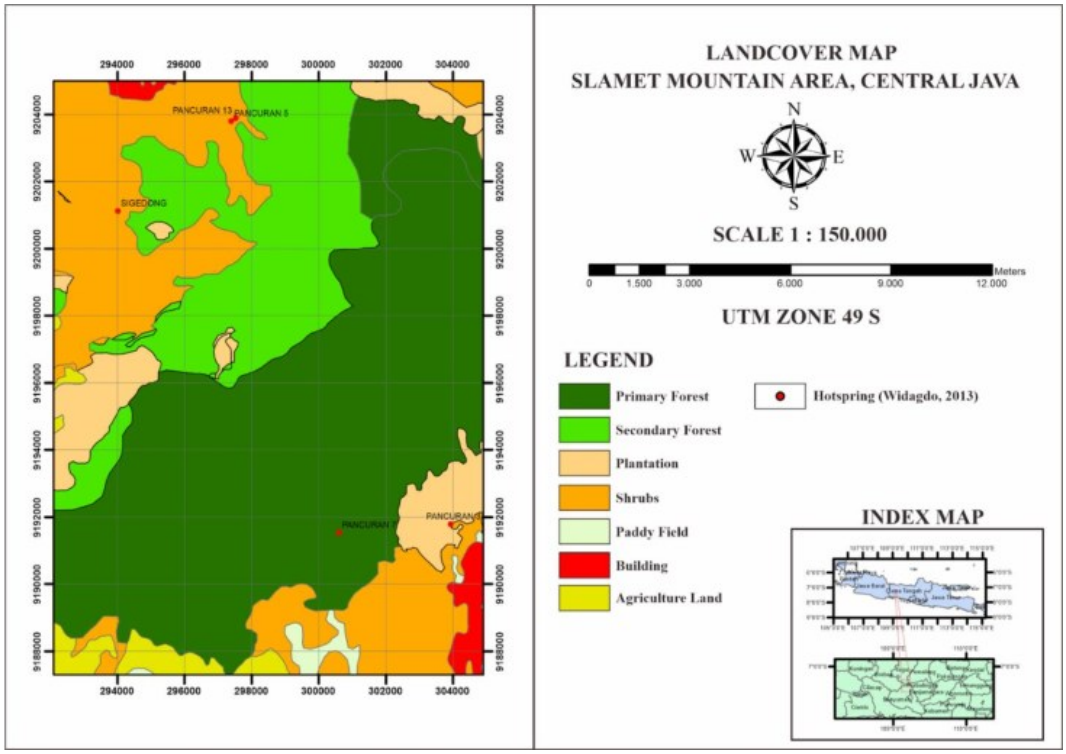

Figure 4: Land Cover Map.

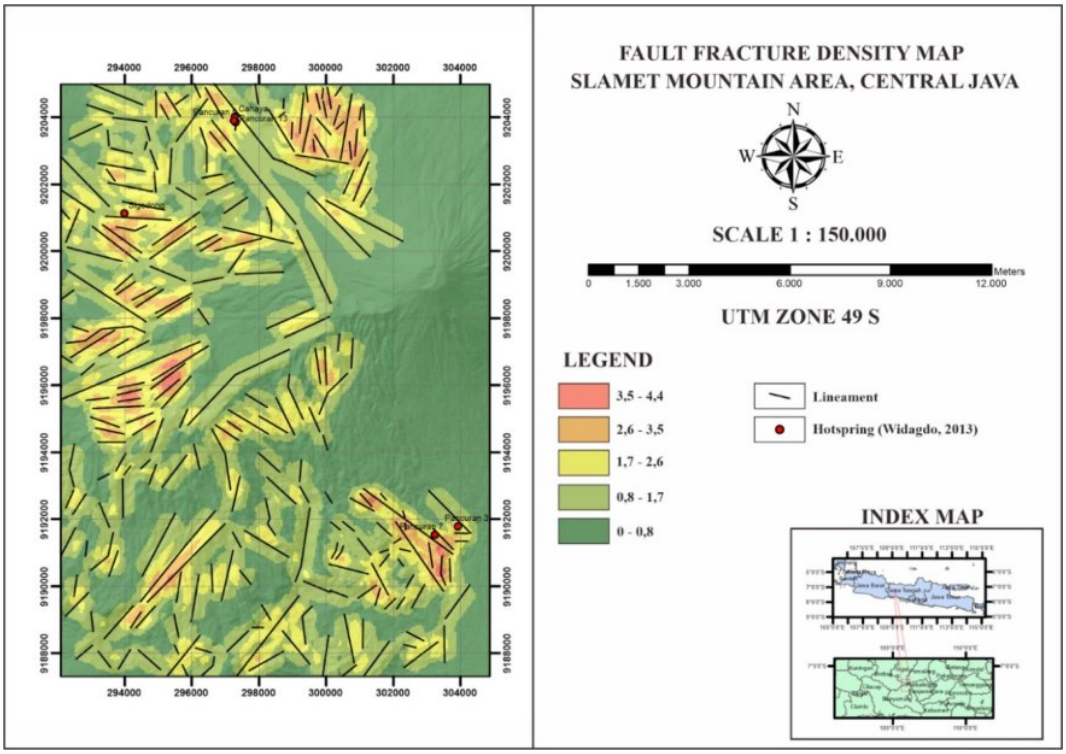

Figure 5: FFD Map.

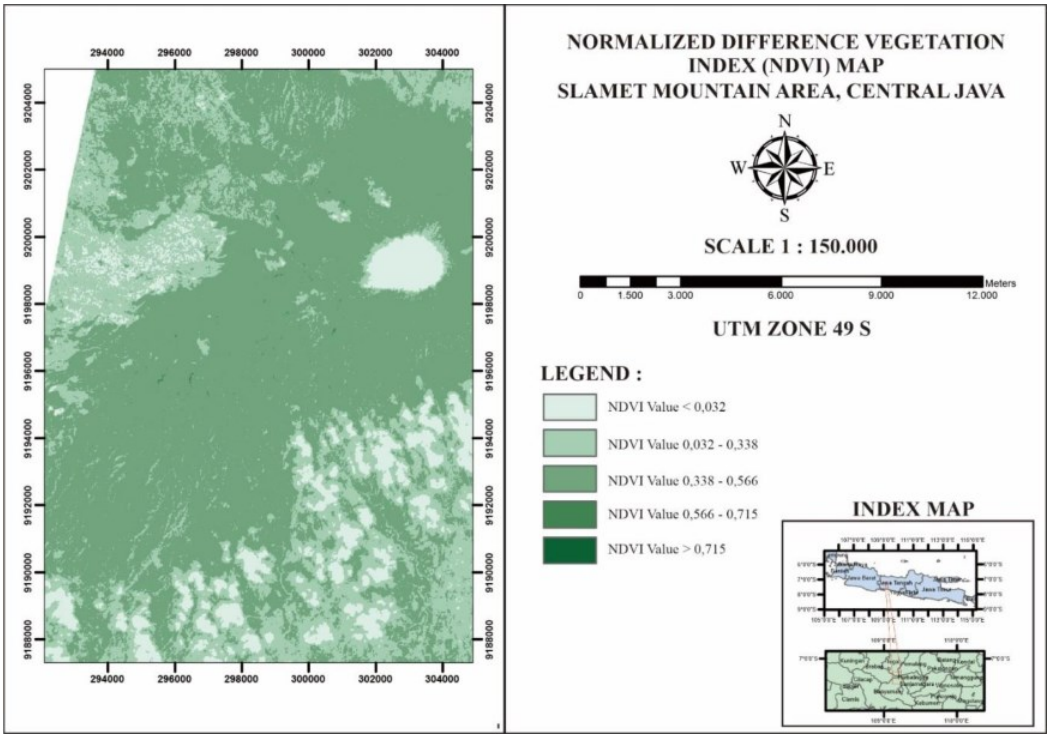

Figure 6: NDVI Map.

Table 4: NDVI Classification (Hakim et al., 2017).

No	NDVI Value	Classification
1	< -0,032	Aquatic, No Vegetation
2	-0,032 – 0,338	Clouds, Settlements
3	0,338 – 0,566	Rarely
4	0,566 – 0,715	Medium
5	> 0,715	Thick

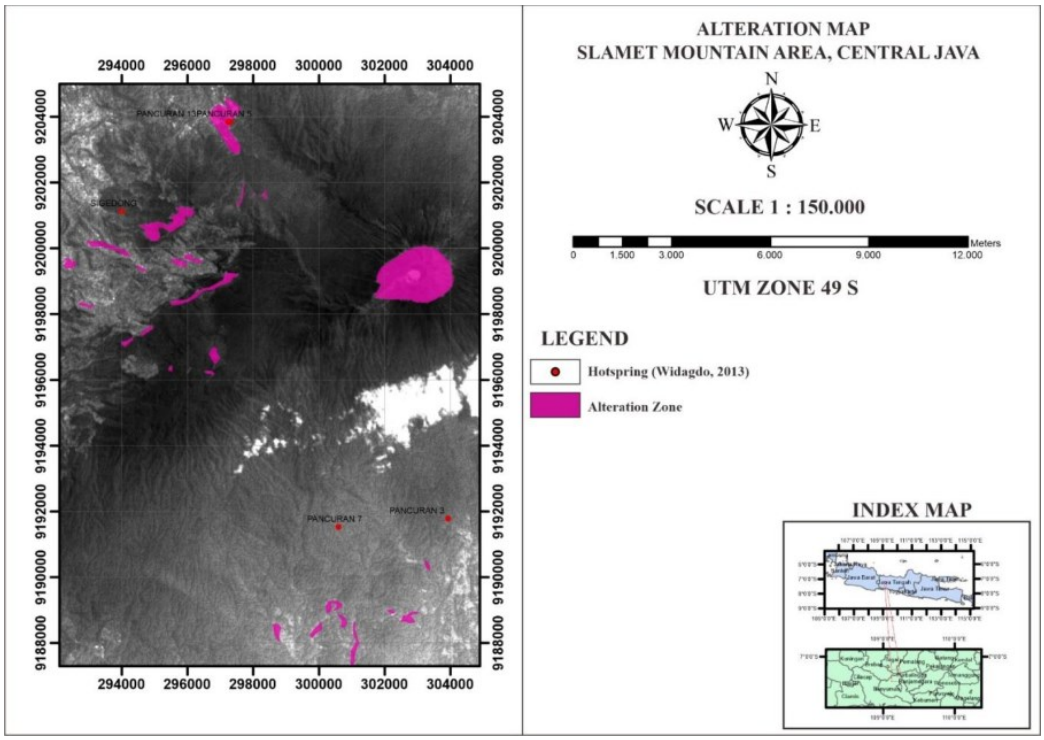

Figure 7: Alteration Map.

4.5 Hydrothermal Alteration Map

Hydrothermal alteration is an important component of a geothermal system. Because areas with geothermal potential usually have hydrothermal alteration zones. In this study, remote sensing analysis was carried out to determine the alteration zone, but it was not used as the main parameter in determining potential because of the high level of vegetation density that made it difficult to detect in remote sensing.

The Alteration Map of the Study Area was created using Landsat 8 OLI/TIRS data, using the Sabins's band ratio method. Using RGB bands of 4/2, 6/7, and 6/5, to detect areas with hydrothermal alteration zones. Band 4/2 - iron oxide, Band 6/7 - clay mineral, Band 6/5 - ferrous mineral. The distribution of alteration was also eliminated by NDVI map, high NDVI values cannot be used for zone determination due to the high failure rate.

4.6 Land Surface Temperature

LST Calculation Processing results from ASTER Night images, with a minimum temperature of 9.2°C and a maximum temperature of 30.4°C and an average temperature of 23.07°C. the temperature distribution in the volcanic cone area is relatively low because it is still influenced by higher elevations. The distribution of hot temperatures spreads around the foot slope to the north, south and west of the map.

Temperature anomalies are seen based on the characteristics of the area; the crater has the highest temperature because there is still active volcanism. Vegetation also affects temperature distribution, areas with high vegetation density tend to have lower temperatures, while low vegetation density tends to have higher temperatures, elevation also affects temperature distribution, the higher the elevation the lower the surface temperature.

The use of land surface temperature analysis results is very influential in determining geothermal prospect points, but it must be compared with other parameters to determine the location of new geothermal manifestations.

4.7 Temperature Determination

Based on the results of FFD Analysis, Geomorphology, NDVI, Land Cover, Geology, and LST Night and Hydrothermal Alteration as supporting data, Determination results are carried out qualitatively, with 5 data point locations of manifestations that have been previously identified as initial corrections marked with red dots in Figure 9.

Determination results obtained 8 new manifestation points marked with yellow dots in Figure 9, the manifestation point is included in the old Slamet volcanic deposit (Qvs) formation, and its geomorphology is included in the foot slope landform, old volcanic cone and lava plain. Determination results have 100% accuracy from previous manifestation data because 5 out of 5 initial manifestation points matches.

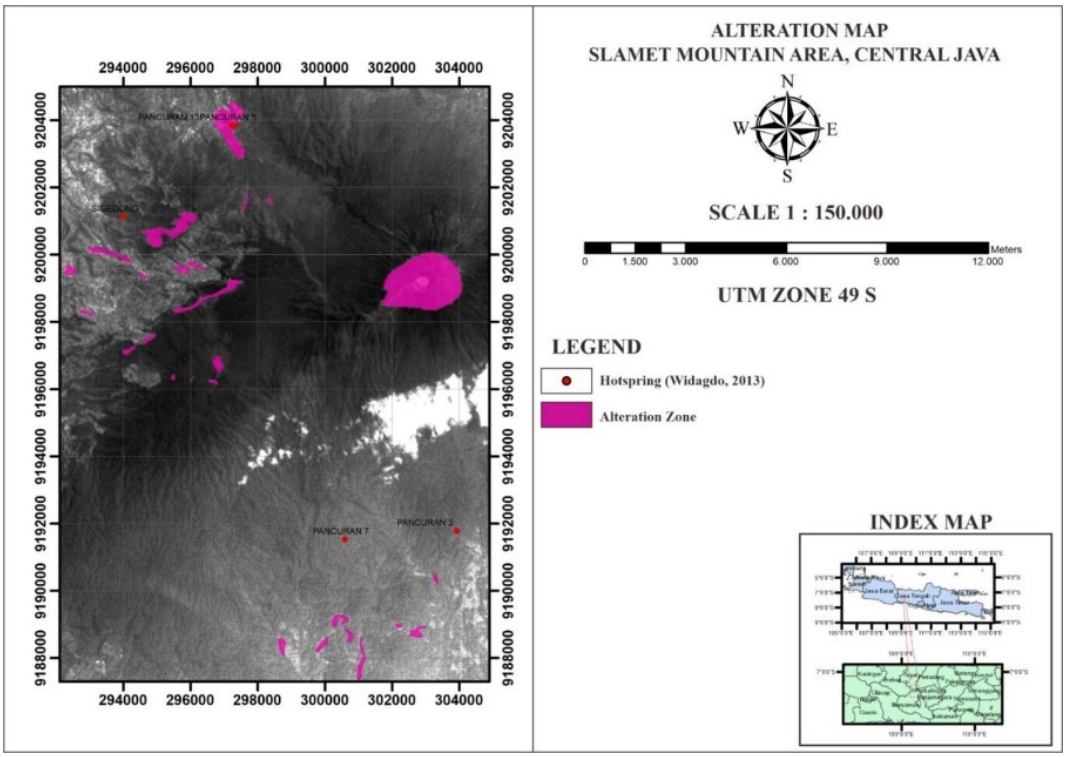

Figure 7: Alteration Map.

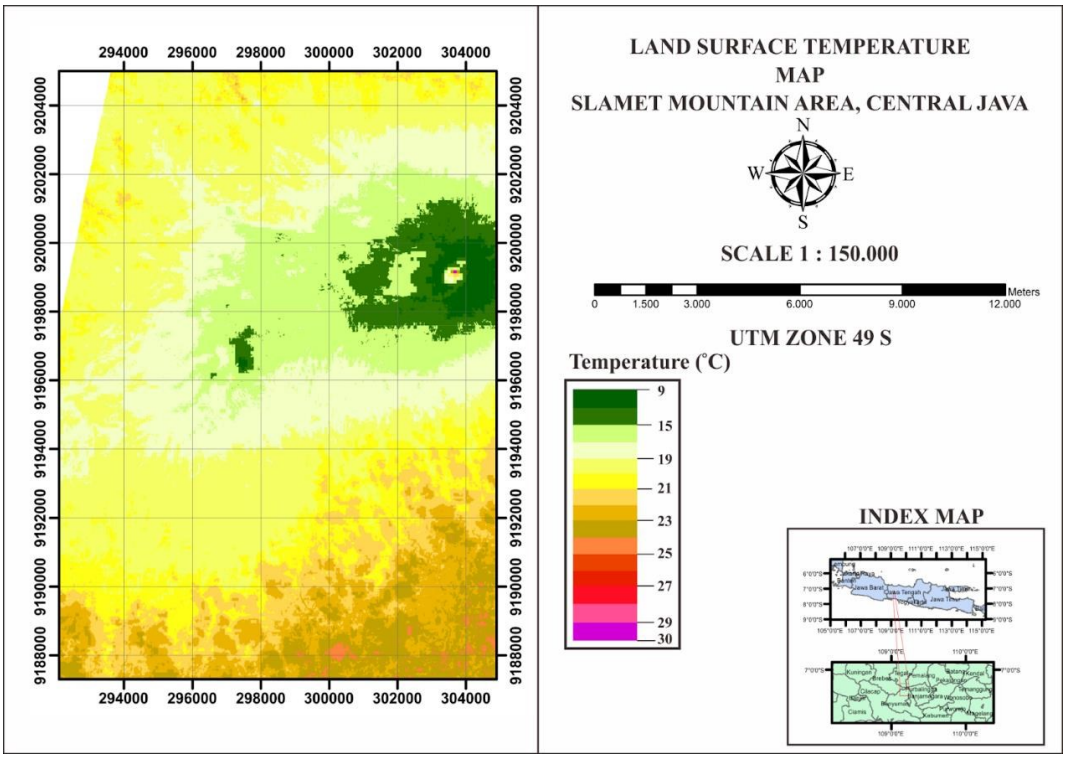

Figure 8: LST Map.

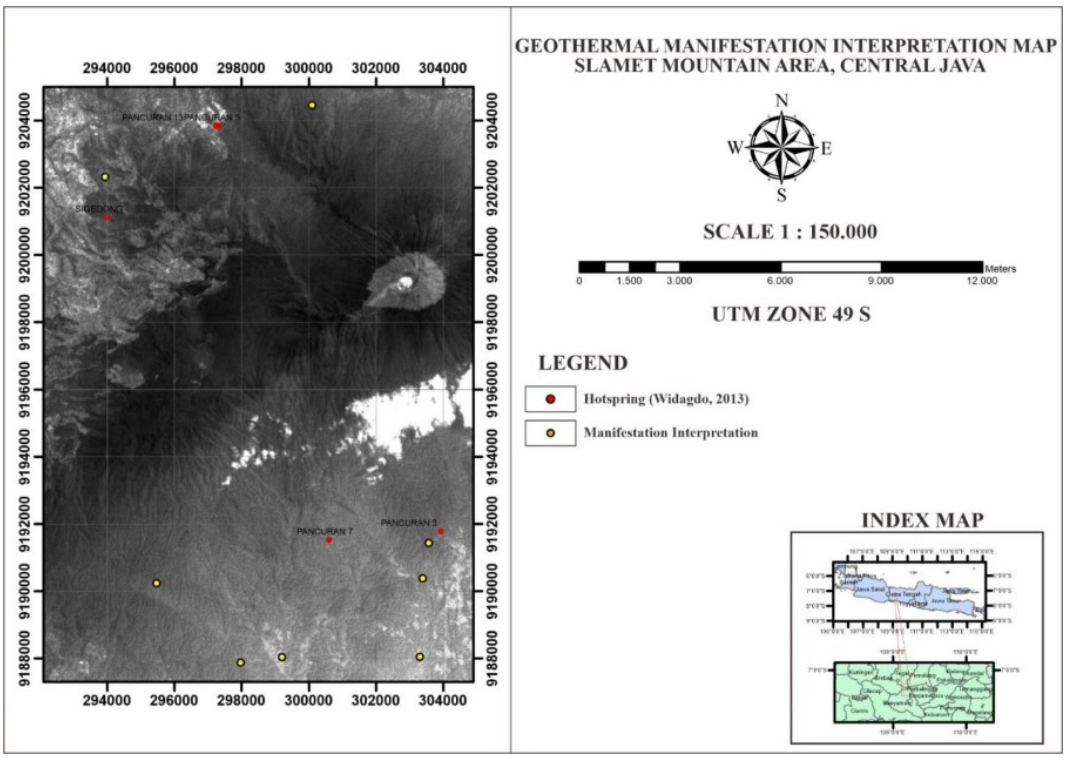

Figure 9: Geothermal manifestation interpretation map.

5. CONCLUSION

Identifying potential geothermal manifestation points in the Slamet Mountain area and its surroundings using remote sensing methods has proven to have a very good level of accuracy. This research can be used as a reference in determining geothermal manifestation points, especially in this study the identified geothermal manifestation points are in accordance with the location of the manifestations that have been found previously. From this

research, 8 new geothermal manifestation points were identified in the research area obtained from the analysis of Fault Fracture Density, Landcover map, Land Surface Temperature Night, and Hydrothermal Alteration map with 100% accuracy based on previous data. However, field mapping, subsurface analysis, and geochemical data are still needed to validate the research results and create a geothermal system.

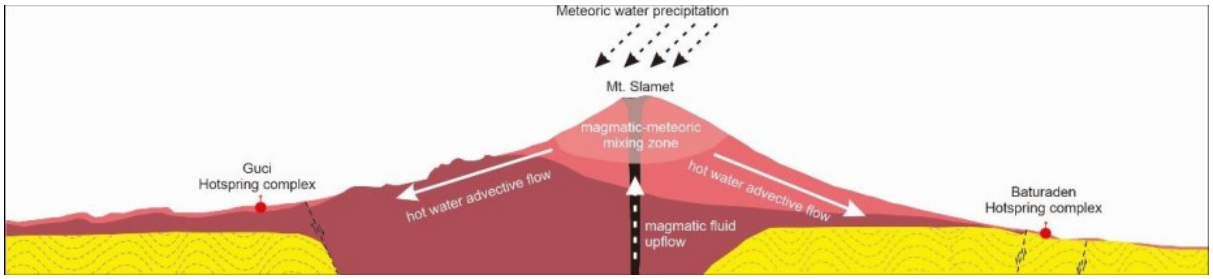

Figure 10: Geothermal Model (Modified from Harijoko, 2020).

REFERENCES

Candra, A., & Widagdo, A., 2011, Tinjauan Kondisi Geologi Gunung Slamet Dalam Mendukung Pemanfaatan Potensi Panas Bumi Bagi Kesejahteraan Masyarakat

Djuri, M., Samodra, H., Amin, T.C., and Gafoer, S. (1996). Peta Geologi Lembar Purwokerto dan Tegal, Jawa. Skala 1:100.000. Pusat Survei Geologi. Bandung.

Hakim, Lukmanul., Nazli Ismail., and Faisal. Kajian Awal Penentuan Daerah Prospek Panas Bumi di Gunung Bur Ni Telong Berdasarkan Analisis Data DEM SRTM dan Citra Landsat 8. Jurnal Rekayasa Elektrika, 13 (3), p.125-132. DOI: 10.17529/jre.v13i3.8332

Harijoko, A., Juhri, S., Taguchi, S., Yonezu, K., and Watanabe, K., 2020. Geochemical Indication of Formation Water Influx to The Volcanic Hosted Hot Springs of Slamet Volcano, Indonesia. Indonesian Journal on Geoscience, 7 (1), p.1-14. DOI: 10.17014/ijog.7.1.1-14

Indarto, Sri & Permana, H. & Gaffar, Eddy & Bakti, Hendra & Al Kausar, Andrie & Nurohman, Heri & Sudarsono, Sudarsono & Sudrajat, Yayat. (2017). STRUKTUR GEOLOGI DAN LITOLOGI SEBAGAI KONTROL MUNCULNYA MATA AIR PANAS DI GUCI DAN BATURADEN, JAWA TENGAH. RISET Geologi dan Pertambangan. 27. 97. 10.14203/risetgeotam2017.v27.287.

Isaya, Milton & Avdan, Ugur. (2016). Inversion of Land Surface Temperature (LST) Using Terra ASTER Data: A Comparison of Three Algorithms. Remote Sensing, 8(12). 10.3390/rs8120993.

Kementerian Energi dan Sumber Daya Mineral. (2021, 27 Juli). Pemerintah Optimistis EBT 23% Tahun 2025 Tercapai. Diakses pada 10 Juni 2024, dari https://www.esdm.go.id/id/berita-unit/direktorat-jenderal-ketenagalistrikan/pemerintah-optimistis-ebt-23-tahun-2025-tercapai

Prawiranegara, Dimas Aji Ramadhan. (2015). Integrated Data of Alteration, Geology, Geochemistry of Bantarkawung Area : Implication to Geothermal System." 4th ITB International Geothermal Workshop, 2015.

S. Khoirunnisa, N. B. Wibowo, H. Rosyida, I. Khaerunnisa, D. M. Jannah, F. Elsha C, and I. Mery S. A "Analisis keberadaan manifestasi panas bumi menggunakan fault fracture density (FFD) di Kecamatan Tempuran, Kabupaten Magelang," Kurvatek, vol. 9, no.1, pp. 63-72, 2024. doi: 10.33579/krvtk.v9i1.4701

Syahputra, Reza., Felix, Sihombing., Octaria, Prasojo. (2019). Correlation Between Fracture Azimuth, Surface Lineaments and Regional Tectonics: A case study from Belik District, Central Java, Indonesia. Journal of Geoscience, Engineering, Environment, and Technology, 4(1). DOI : 10.25299/jgeet.2019.4.1.2294

Widagdo, A., Adi, C., Sachrul, I., and Chalid, I.A. (2013). Pengaruh Struktur Geologi Gunung Slamet Muda dan Tua Terhadap Pola Sebaran Panas Bumi . Industrial Research Workshop and National Seminar

Yana Putra, Ghaly et al. (2023). Identification of New Geothermal Manifestation Using Remote Sensing Method at Solok, West Sumatera. Proceedings of 9th Indonesia International Geothermal Convention & Exhibition (IIGCE) 2023. Jakarta : 20-22 September 2023.

A 3D Geological Model and Natural State Simulation of the Massepe Geothermal Field in South Sulawesi, Indonesia

Fikri Rahmansyah, Michael Gravatt, and John O'Sullivan

Department of Engineering Science, University of Auckland,
70 Symonds Street, Grafton, Auckland 1010, New Zealand

fikri.rahmansyah@gmail.com, frah650@aucklanduni.ac.nz

Keywords: Geothermal Energy, Massepe Geothermal Field, Numerical Reservoir Modelling, Uncertainty Quantification

ABSTRACT

The Massepe Geothermal Field in South Sulawesi, Indonesia, presents promising geothermal energy potential. This study outlines a three-dimensional (3D) digital conceptual model and a numerical reservoir model of the Massepe field. A 3D digital conceptual model was developed utilizing geological, geophysical, and geochemical data. The model incorporates key formations, fault lines, and structural features, with a particular focus on the North-South Massepe fault. The integration of magnetotelluric data helped delineate the alteration zone, while surface manifestation data defined the model's temperature distribution.

A numerical reservoir model compatible with AUTOUGH2 and Waiwera geothermal simulators was subsequently developed. This model represents the temperature distribution, fluid flow, and heat transfer processes within the reservoir. The grid setup and boundary conditions were carefully designed to simulate the natural state of the geothermal system. Rock properties were assigned based on lithology, faults, and alteration zones. The natural state simulation was calibrated using estimated temperatures and the locations of surface manifestations.

The results indicate a geothermal upflow through the North-South Massepe fault, with lateral migration effectively restricted by adjacent geological structures. This study provides a robust understanding of the geothermal system's natural state, enhancing the knowledge necessary for strategic geothermal resource development in Indonesia.

1. INTRODUCTION

The Massepe Geothermal Field, located in South Sulawesi, Indonesia, is a promising site for geothermal energy development. Geographically, the field is situated between 119°44'15.5" - 119°51'17.25" E and 3°56'41" – 4°4'30.6" S in the Sidenreng Rappang (Sidrap) Regency, approximately 194 km from the provincial capital, Makassar City (Figure 1). The region, characterized by non-volcanic geothermal systems, offers significant opportunities for renewable energy exploration. Indonesia has substantial geothermal resources, with Sulawesi having the third-largest geothermal potential after Java and Sumatra, boasting approximately 3229 MWe identified across 76 locations, primarily in non-volcanic environments (Risdianto et al., 2015). Developing geothermal resources, particularly in greenfield sites like Massepe, is essential for diversifying energy sources and enhancing energy security.

This research aims to conduct a comprehensive assessment of the Massepe Geothermal Field using numerical reservoir modeling techniques. The study focuses on constructing a 3D digital conceptual model that integrates geological, geophysical, and geochemical data to reliably identify key formations, fault lines, and structural features. Additionally, a numerical reservoir model compatible with the AUTOUGH2 and Waiwera software platforms was developed to represent the temperature distribution, fluid flow, and heat transfer processes within the field. The natural state simulation was calibrated using estimated temperatures and the locations of surface manifestations to achieve a reliable model of the geothermal system.

The outcomes of this research will contribute significantly to the strategic development of geothermal resources, supporting Indonesia's goals of sustainable energy production and reduced reliance on fossil fuels.

2. GEOLOGICAL SETTING

Based on the Geological Map of the Majene and the Western Palopo Sheets, South Sulawesi (Sudjatmiko et al., 1998) and the Geological Map of the Pangkajene and the Western Watampone Sheets, South Sulawesi (Sukamto, 2012), the regional geology includes volcanic, intrusive, and sedimentary rocks dating from the Tertiary to the Quaternary periods. Risdianto et al. (2008) describe that the local geological formations consist of 13 rock units,

including one sedimentary rock unit, ten volcanic rock units, and two surface deposit units comprising lake and alluvial deposits (Figure 2).

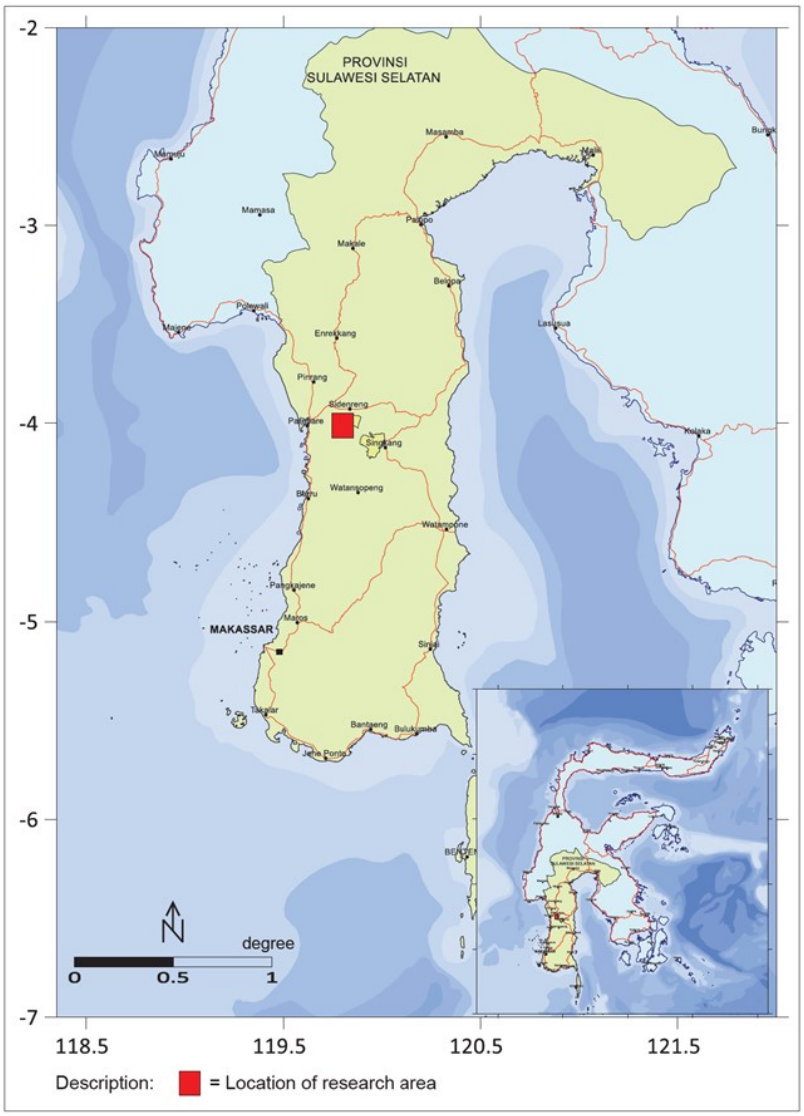

Figure 1: Map of the location of the Massepe Geothermal Field (Modified from Joni & Wahyuningsih, 2019, p. 144).

According to Risdianto et al. (2008), the oldest rocks exposed in the Massepe geothermal area are the Middle Miocene Soppeng volcanic rocks located south of the geothermal area. The Camba Formation volcanic rocks, ranging from the Middle to Late Miocene, extend from the south to the northwest. Late Miocene trachyte intrusive rocks are present in the central part of the geothermal area. The Late Miocene to Pliocene Walanae Formation, consisting of sandstone, siltstone, tuff, marl, claystone, conglomerate, and limestone, spreads from the central to the southeast of the area. The Pliocene Parepare volcanic rocks, including tuff, breccia, and volcanic conglomerate, are distributed in the northwest. Holocene-aged alluvial lake and coastal deposits, composed of clay, silt, mud, sand, and gravel, spread from the east to the north of the Massepe geothermal area.

The geological structure of the Massepe Geothermal Field is dominated by a series of faults and fractures that play a crucial role in controlling the geothermal system. The primary structural feature is the Walanae Fault, a major normal fault trending northwest-southeast, which has significantly influenced the regional geology by creating a graben (depression) that accommodates sedimentary deposits from the Tertiary Walanae Formation. Other significant faults include the Kalampee Fault, a dextral (right-lateral) strike-slip fault, and the Bulubaka Fault, a sinistral (left-lateral) strike-slip fault. The Massepe Fault, oriented north-south, controls the emergence of the Pajalele and Alakuang hot springs and is a key conduit for geothermal fluid flow (Risdianto et al., 2008).

The hydrogeology of the Massepe Geothermal Field is influenced by the area's geomorphology and the composition of its underlying rock formations. The recharge zones, where meteoric water infiltrates the ground,

are primarily in the hilly regions. The area experiences relatively high annual rainfall, significantly contributing to groundwater recharge, which interacts with the geothermal system, influencing the formation and characteristics of geothermal manifestations such as hot springs (Risdianto et al., 2008).

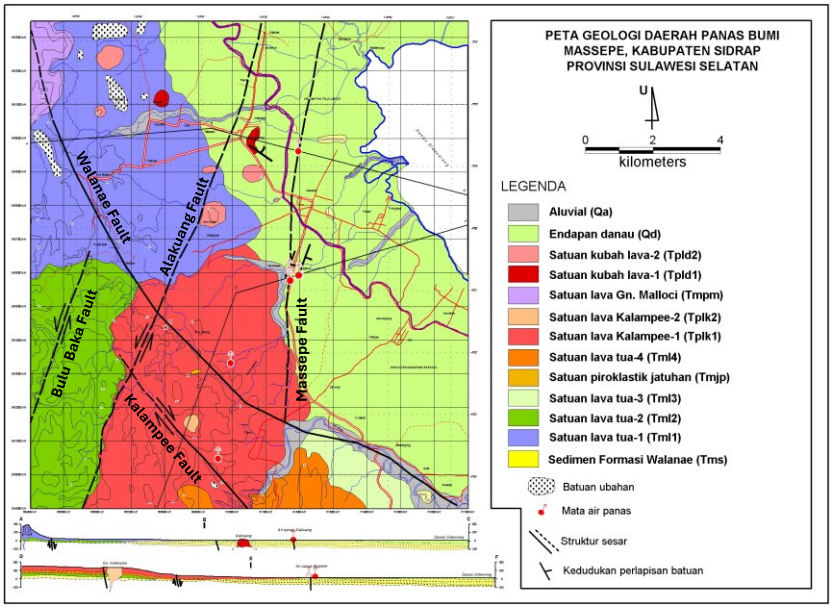

Figure 2: Local geological map of the Massepe Geothermal Field (Modified from Risdianto et al., 2008).

3. GEOCHEMICAL STUDIES

The geochemical survey of the Massepe Geothermal Field focused on analyzing the chemical composition of hot springs, geothermal fluids, and subsurface temperatures. The survey covered an area of approximately 13 x 15 km², featuring several hot spring manifestations with temperatures ranging from 29 to 68 °C, flow rates between 0.5 to 2.0 liters per second, and pH levels between 6.70 to 7.40 (Sulaeman et al., 2008).

The hot springs at Pajalele (Pajalele-1, Pajalele-2, and Pajalele-3) exhibit high concentrations of chloride (Cl), bicarbonate (HCO_3), and sulfate (SO_4), classifying them as bicarbonate-sulfate type waters and "immature waters" based on Cl-SO_4-HCO_3 triangular plots. The Alakuang hot spring, with a temperature of 45.3 °C, showed high concentrations of chloride and bicarbonate, indicating it as chloride-bicarbonate type water and "mature water" (Sulaeman et al., 2008).

Detailed ternary plots of Cl-SO_4-HCO_3 and Na-K-Mg (Figure 3) suggest that the Pajalele and Alakuang hot springs are on the borderline between immature water and partial equilibrium, indicating slight meteoric water dilution (Sulaeman et al., 2008).

High concentrations of bicarbonate and sulfate in the Pajalele hot springs indicate significant interaction between geothermal fluids and the surrounding rock formations. The elevated silica content supports a deep origin, as silica enrichment typically occurs through prolonged interaction with hot rocks at depth. The isotopic composition of the water confirms this deep origin, showing deviation from the meteoric water line and indicating geothermal fluid mixing with magmatic gases. (Sulaeman et al., 2008).

The estimated subsurface temperature for the Pajalele area using Na/K Giggenbach geochemical thermometers was around 193 °C, indicating a medium-temperature geothermal system. Soil and gas analysis showed Hg concentrations ranging from 7 to 259 ppb and CO_2 levels in the soil air from 0.03% to 6.34%, aligning with the north-south trending Massepe Fault and supporting the presence of underlying geothermal activity (Sulaeman et al., 2008). However, the reservoir temperature estimate is less accurate, considering that fluids from the Pajalele and Alakuang hot springs have been slightly diluted with meteoric water.

In conclusion, the geochemical survey highlights the potential for geothermal energy exploitation in the Massepe Geothermal Field, supported by significant ion concentrations, high subsurface temperatures, and distinct soil gas anomalies.

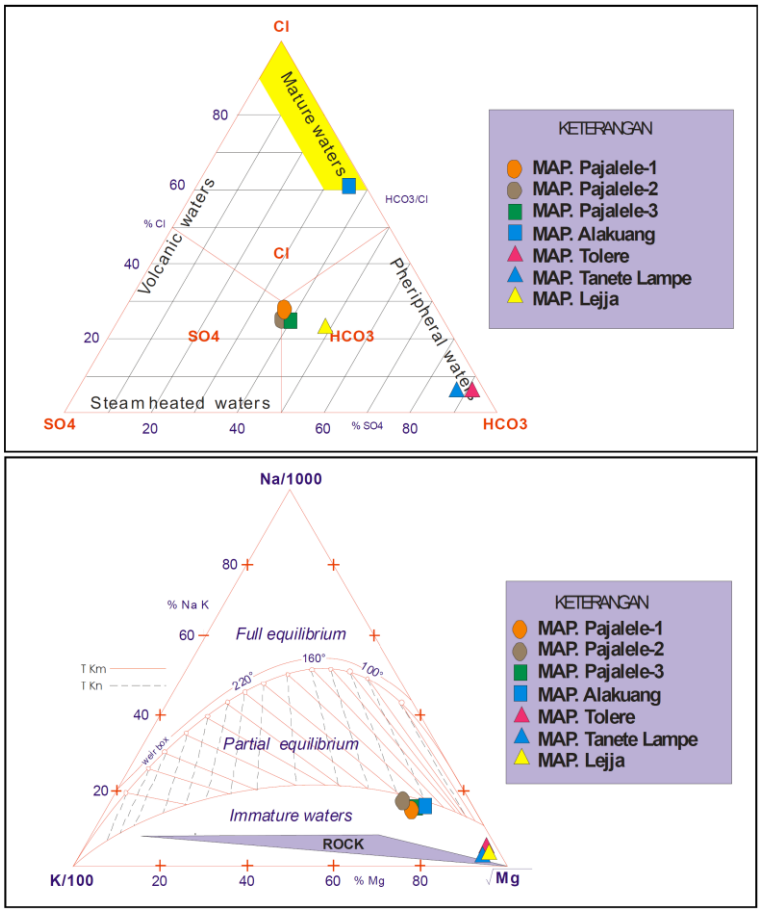

Figure 3: Ternary plots of the Massepe water sample: Cl-SO4-HCO3 (Top) and Na-K-Mg (Bottom) (Source: Sulaeman et al., 2008, p. 6,7).

4. GEOPHYSICAL SURVEYS

Advanced geophysical techniques were employed to investigate the subsurface conditions of the Massepe Geothermal Field. These techniques included geoelectrical resistivity, gravity, geomagnetic, and magnetotelluric (MT) surveys, each providing critical insights into the geothermal system.

4.1 Geoelectrical Resistivity

The geoelectrical resistivity surveys identified several low-resistivity zones indicative of hydrothermal alterations. These zones are primarily located around the Pajalele hot springs, suggesting the presence of conductive geothermal fluids. The resistivity profiles reveal a distinct contrast between the low-resistivity alteration cap and the underlying higher-resistivity zones, which are interpreted as unaltered rocks hosting geothermal reservoirs (Risdianto & Soetoyo, 2008).

4.2 Magnetotelluric (MT)

The MT surveys provided detailed resistivity structures down to several kilometers depth. The MT data delineated a prominent low-resistivity zone, interpreted as the clay alteration cap, which acts as an impermeable barrier above the geothermal reservoir. This alteration zone is primarily associated with the North-South Massepe fault. The MT resistivity cross-section (Figure 4) highlights areas of low resistivity extending from the surface to greater depths, indicating zones of intense hydrothermal alteration and potential geothermal upflow (Joni & Wahyuningsih, 2019).

4.3 Gravity

Gravity surveys revealed significant Bouguer gravity anomalies, indicating variations in subsurface density. A prominent low-gravity anomaly was detected in the central part of the field, corresponding to a graben structure filled with less dense sedimentary deposits of the Walanae Formation. Additionally, a high-density anomaly was identified beneath the Pajalele manifestation, suggesting the presence of an intrusive rock body (Figure 5). This intrusive body is likely contributing to the heat source for the geothermal system and is critical for understanding fluid flow and heat transfer within the reservoir (Risdianto & Soetoyo, 2008).

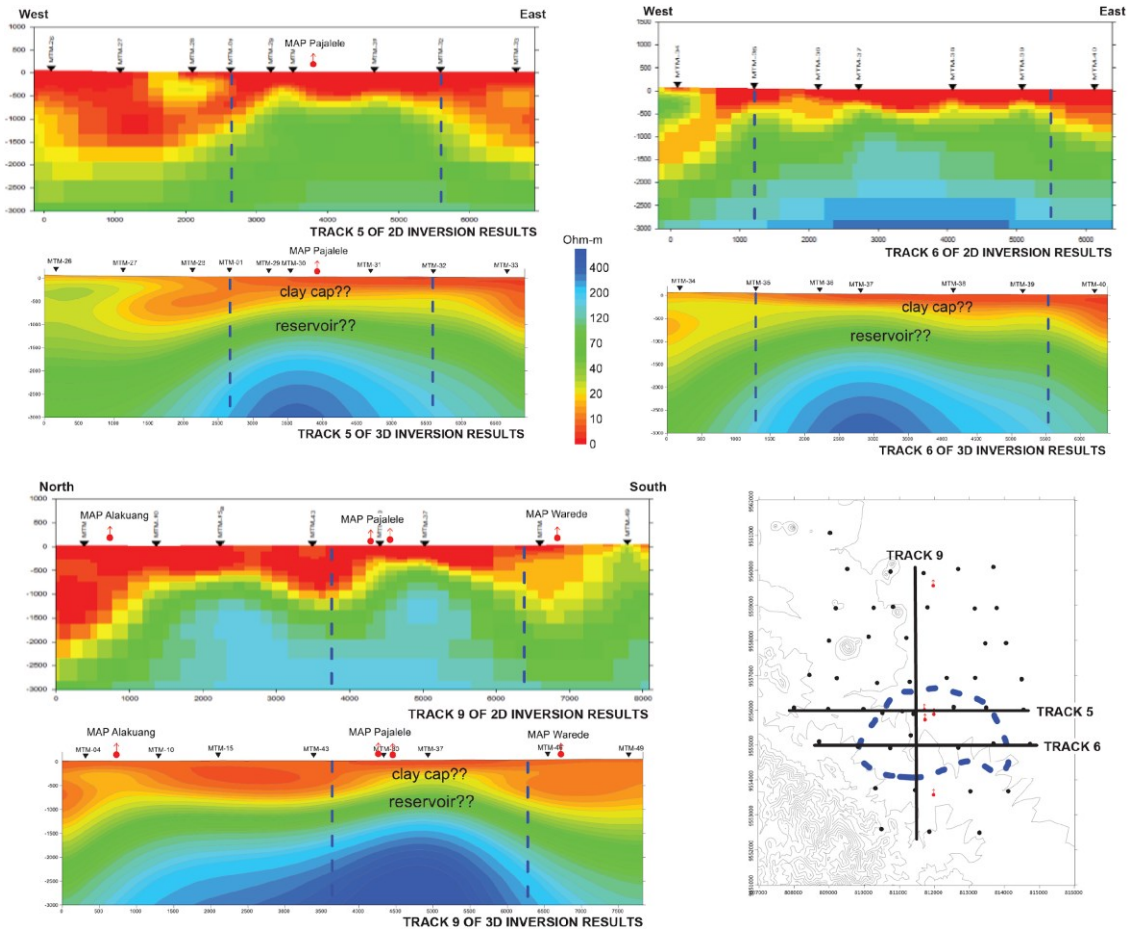

Figure 4: Cross-section resistivity results from 2-D and 3-D modeling along tracks 5, 6, and 9 (Modified from Joni & Wahyuningsih, 2019, p. 152).

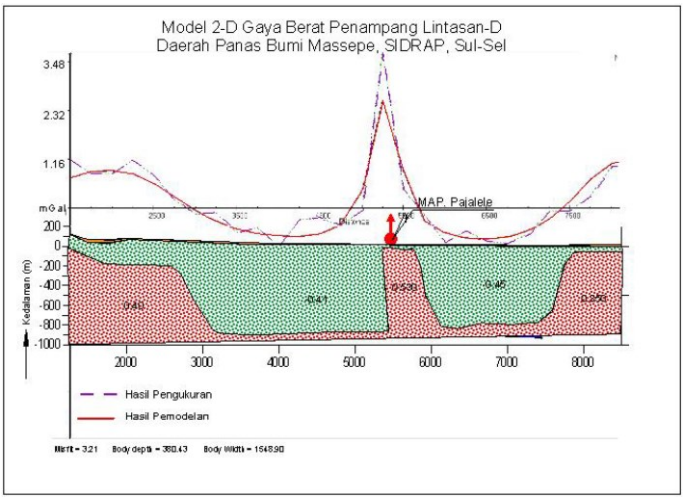

Figure 5: 2-D modeling of the gravity of the Massepe field (Source: Risdianto & Soetoyo, 2008).

4.4 Geomagnetic

The geomagnetic surveys detected notable magnetic anomalies associated with the volcanic rocks of the area. A strong magnetic anomaly correlates with the trachyte intrusive rocks in the central geothermal area. These anomalies suggest the presence of magnetically susceptible minerals, which could indicate heat sources contributing to the geothermal system. The magnetic data further delineates the structural trends and fault zones that control fluid flow and heat transfer (Munandar & Hermawan, 2008).

5. CONCEPTUAL MODEL OF THE MASSEPE GEOTHERMAL FIELD

The conceptual model of the Massepe Geothermal Field integrates geological, geophysical, and geochemical data, providing a comprehensive understanding of the subsurface conditions and geothermal system dynamics. The key geological formations include the Middle Miocene Soppeng volcanic rocks, the Middle to Late Miocene Camba Formation, the Late Miocene Walanae Formation, the Pliocene Parepare volcanic rocks, and the Holocene Alluvium deposits. The primary structural feature is the North-South trending Massepe Fault, which controls geothermal fluid flow and is associated with the Pajalele and Alakuang hot springs.

Hydrothermal alteration is evidenced by low-resistivity zones identified in MT surveys, with a prominent clay alteration cap acting as an impermeable barrier above the geothermal reservoir. Geothermal fluids ascend through the North-South Massepe Fault, driven by heat sources from intrusive rock bodies identified in gravity surveys. Geochemical analysis of hot springs shows high concentrations of chloride, bicarbonate, and sulfate, indicating significant interaction between geothermal fluids and surrounding rocks. Isotopic compositions confirm the deep origin of these fluids.

Figure 6 shows a top plan view of the conceptual model, highlighting the spatial distribution of key geological formations and structural features. Figure 7 provides cross-sections of the conceptual model, detailing the subsurface geology, hydrothermal alteration zones, and fluid flow pathways.

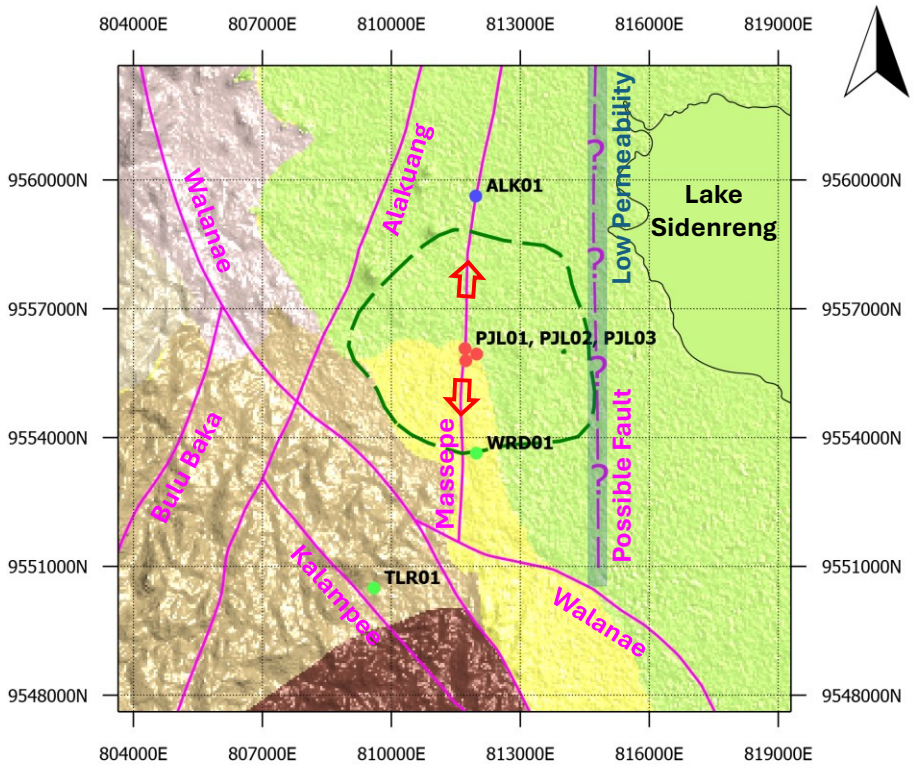

Figure 6: Top plan view of the conceptual model of the Massepe Geothermal Field. This includes faults (magenta line), bicarbonate-sulfate springs (red dots), bicarbonate springs (green dots), an alkali chloride spring (blue dots), and the boundary of the clay cap (green dashed line).

6. 3D MODELS CONSTRUCTION

The construction of 3D models for the Massepe Geothermal Field was essential to visualize and analyze the subsurface geological formations, structural features, and hydrothermal systems. The 3D geological and alteration models were developed using Leapfrog Energy software, which integrates various data sources to create a comprehensive representation of the geothermal field.

6.1 Geological Model

6.1.1 Topography Setup

The topography setup incorporated digital elevation model (DEM) data to represent the surface contours and elevation variations of the Massepe Geothermal Field. The model covered an area of approximately 44 km x 44 km around the Pajalele hot springs (Figure 8), highlighting significant elevation differences crucial for

understanding surface manifestations and recharge areas. The highest elevations are in the central and western parts of the field, influencing the direction of meteoric water recharge and surface runoff patterns.

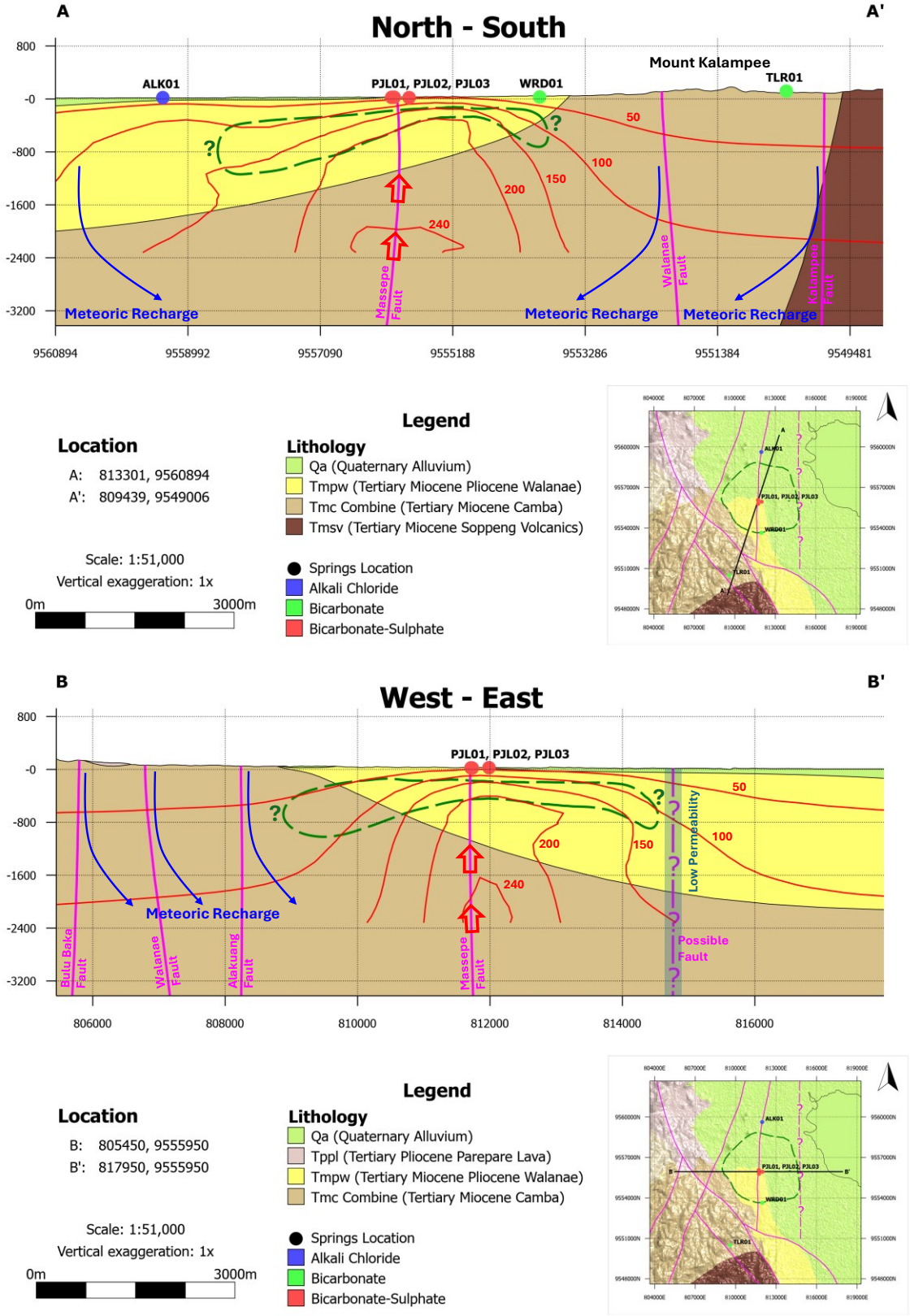

Figure 7: Cross sections of the conceptual model of the Massepe Geothermal Field. This includes the boundary of the clay cap (green dashed line) and the isotherm lines (red line).

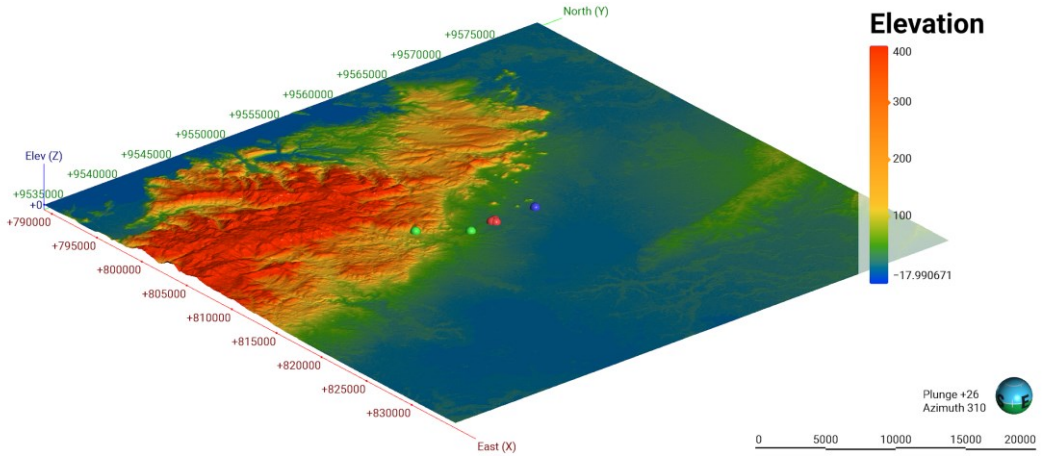

Figure 8: Topographic surface illustrated with an elevation color scale in Leapfrog. The Pajalele hot springs (Red dots) are situated at the centre of the map.

6.1.2 Lithology Setup

The lithology setup defined the spatial distribution of key rock types within the field using regional geological maps. Key formations modeled include the Middle Miocene Soppeng volcanic rocks, Middle to Late Miocene Camba Formation, Late Miocene Walanae Formation, Pliocene Parepare volcanic rocks, and Holocene Alluvium deposits. The lithology setup indicated that the Camba Formation and Soppeng volcanic rocks are predominant in the subsurface, with the Walanae Formation forming significant sedimentary layers that serve as both reservoirs and seals for the geothermal system.

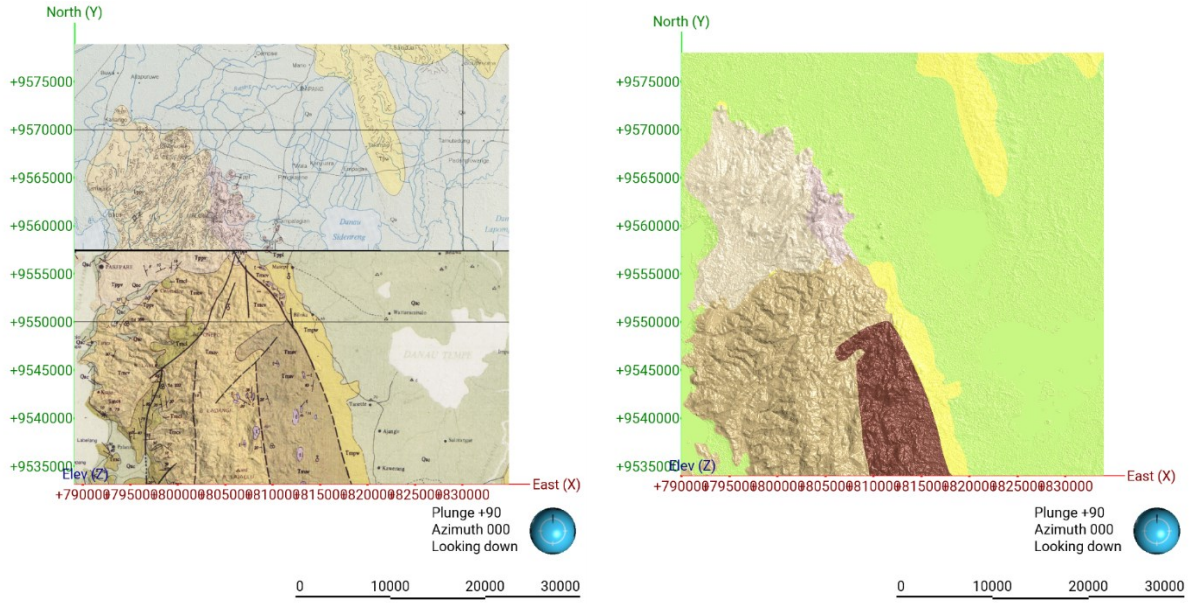

Figure 9: Lithological configuration of the Massepe geothermal system. The formation units from the newly developed digital conceptual model (left) are compared with the combined regional geological maps (right) (Modified from Sudjatmiko et al., 1998 and Sukamto, 2012).

6.1.3 Stratigraphy Setup

Stratigraphy was established using regional geological maps and cross-sectional profiles. This setup provided a detailed vertical sequence of geological formations, helping to understand the layering and thickness of each unit, which influences the geothermal reservoir's capacity and behavior. The stratigraphic sequence was developed according to the chronological age of the formations and their correlation with regional geological structures (Table 1). Figure 9 presents a comparison of the formation units from the newly developed digital conceptual model with those from the combined regional geological maps.

Table 1: Overview of the stratigraphic units within the Massepe geothermal system.

Formation Name	Abbreviation	Geologic Age	
		Period	Epoch
Alluvium	Qa	Quaternary	Holocene
Parepare Lava	Tppl	Tertiary	Pliocene
Parepare Volcanics	Tppv	Tertiary	Pliocene
Walanea	Tmpw	Tertiary	Late Miocene to Pliocene
Camba	Tmc	Tertiary	Middle to Late Miocene
Soppeng	Tmsv	Tertiary	Middle Miocene

6.1.4 Structural Interpretation

The structural interpretation involved digitizing major fault structures and fractures within the field. A total of seven active faults were identified and modeled (Figure 10). The North-South trending Massepe Fault is the primary conduit for geothermal fluid flow, controlling the emergence of the Pajalele and Alakuang hot springs. Another significant fault is the Walanae Fault, creating graben structures filled with sedimentary deposits, influencing fluid storage and migration. These faults were modeled to penetrate all geological formations with a vertical dip angle of 90°, providing possible pathways for fluid flow.

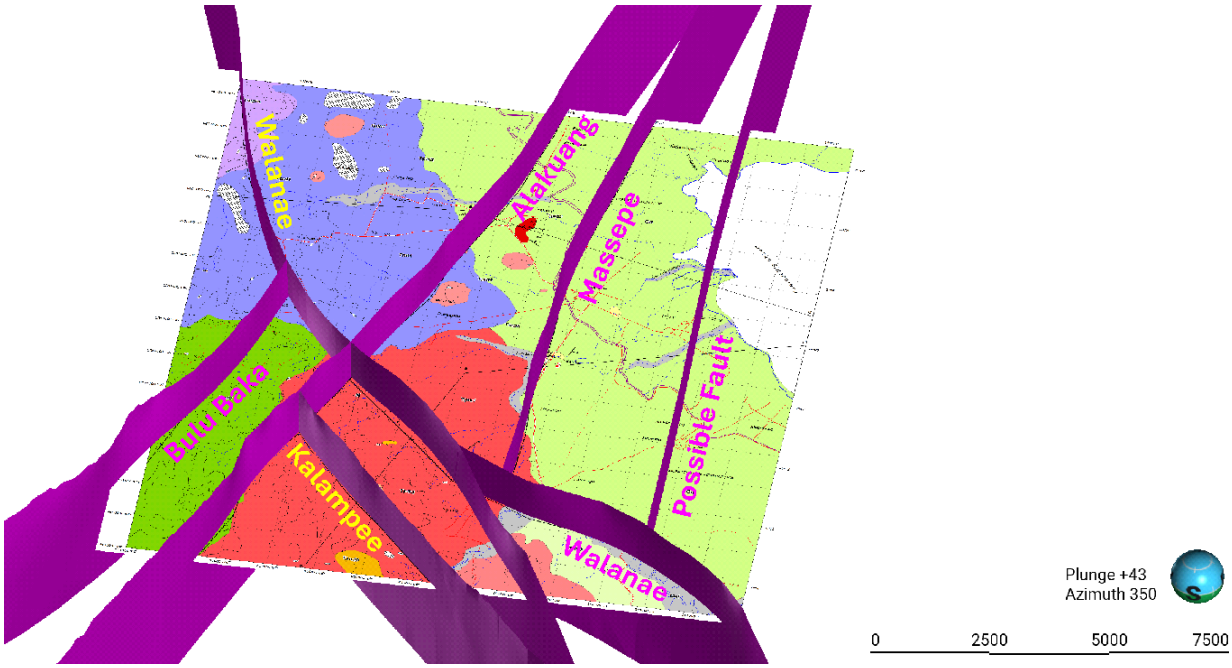

Figure 10: Fault structures in the Massepe Geothermal Field are highlighted in purple overlays on the modified local geological map (Source: Risdianto et al., 2008).

6.2 Alteration Model

The alteration model focuses on the clay cap zone, which acts as a barrier for fluid flow at the top of the reservoir. This zone was delineated using resistivity profiles from MT survey data, defining the boundaries and shape of the clay cap. The model indicates a widespread low-resistivity alteration cap, primarily associated with hydrothermal alteration processes driven by the underlying geothermal activity. The clay cap zone is delineated with a pronounced up-dome structure beneath the Pajalele hot springs, causing the clay cap to be significantly thinner in this region and thicker towards the edge of the reservoir (Figure 11).

7. NUMERICAL RESERVOIR MODEL

A numerical reservoir model is crucial for understanding the natural state of a geothermal system and forecasting its response to production and development activities. This model was constructed and executed using a geothermal simulator to represent the equilibrium conditions that existed before any exploration, production, or development took place. The reliability and accuracy of the simulation results depend on the detailed incorporation of rock parameters such as specific heat, permeability, porosity, and thermal conductivity, along with the thermophysical properties of the fluid and the fracture pattern (Franco & Vaccaro, 2014).

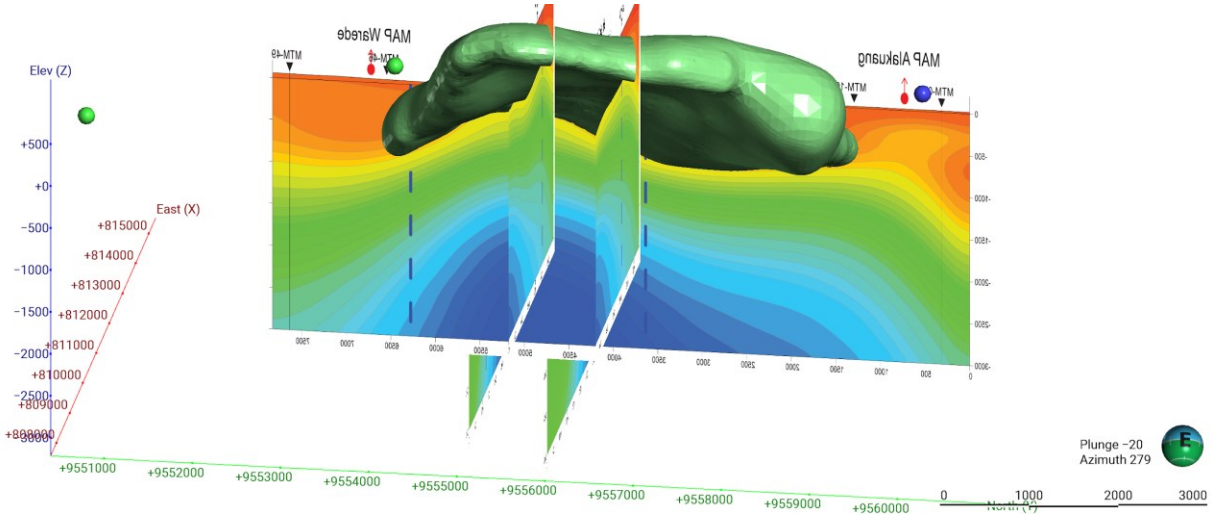

Figure 11: Clay cap zone (green volume) delineated from magnetotelluric data (Source: Joni & Wahyuningsih, 2019) and the distribution of surface manifestations. This includes bicarbonate-sulfate springs (red dots), bicarbonate springs (green dots), and an alkali chloride spring (blue dots).

7.1 Grid Setup

The grid for the model was constructed using data from the Leapfrog model. It was oriented at 0° azimuth to align with the main strike of the Massepe fault. The grid extends over an area of 16 km by 15.2 km, comprising 34,850 blocks, with the largest blocks measuring 800 m by 800 m. The vertical thickness of these blocks ranges from 500 m at the base to 20 m near the surface. To achieve higher accuracy in the zone of interest, the block size was reduced to 200 m by 200 m, providing a higher resolution in areas with significant fluid movement. Refinement in the shallow regions was also implemented to facilitate smooth numerical reservoir simulations in response to fluctuations in the water table.

7.2 TOUGH2 Model Generation

Once the grid was developed, it was imported into Leapfrog Energy to generate the TOUGH2 model input file. Leapfrog enables users to choose the geological model that will be the basis for creating the TOUGH2 model. This integration ensures that the methods available in Leapfrog for incorporating faults and alteration zones into the geological model can also be applied to the TOUGH2 model. Since the geological model in Leapfrog is dynamically updated with new data, it will be easy to implement these changes in later TOUGH2 model input files.

Figure 12 shows the TOUGH2 model that has been generated with the geological model mapped onto the grid. In Figure 13, the faults within the system are overlaid on the TOUGH2 model, with the bottom right half removed to reveal the fault blocks, which are highlighted in magenta. Similarly, Figure 14 presents the alteration model as a representation of the clay cap within the TOUGH2 model.

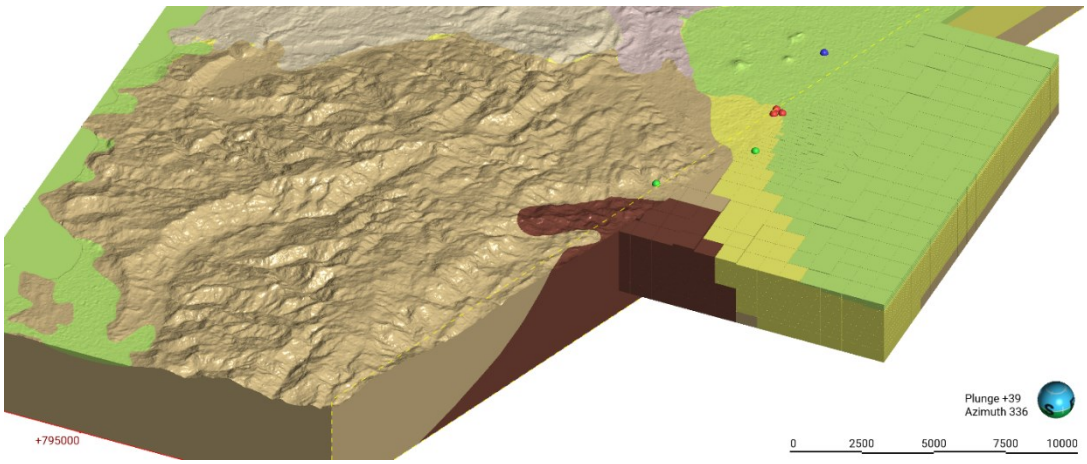

Figure 12: The Leapfrog model (top left) and the corresponding generated TOUGH2 model (bottom right), with hot springs marked.

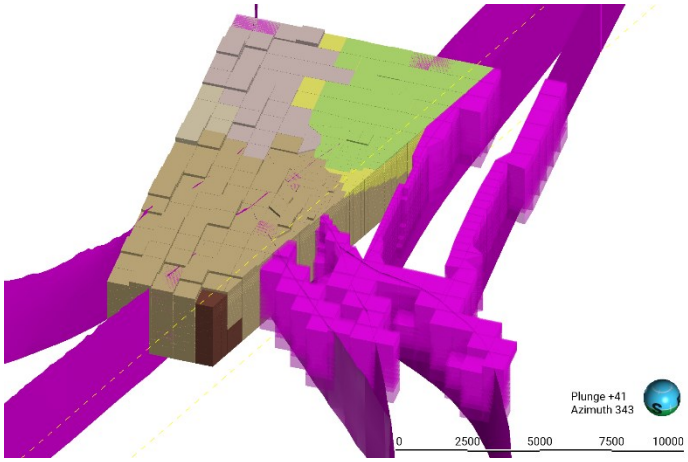

Figure 13: Visualisation of faults in the TOUGH2 model. The faults from the Leapfrog model are displayed in magenta, with the corresponding faulted TOUGH2 blocks visible in the cutaway section of the model.

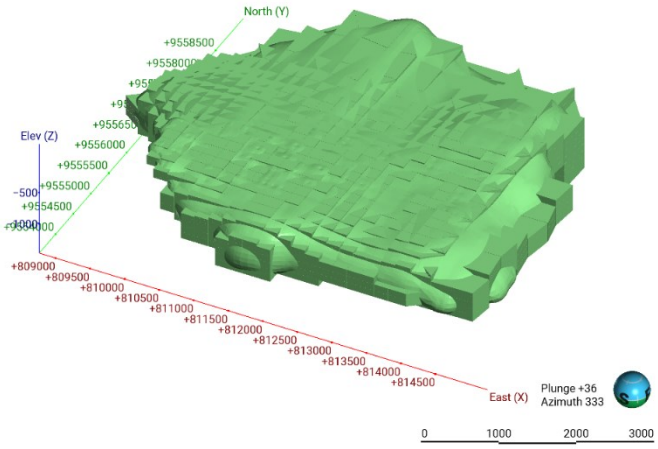

Figure 14: Visualisation of the clay cap in the Leapfrog model and the TOUGH2 model.

7.3 Boundary Conditions

Boundary conditions are essential in geothermal modeling as they define the limits and interactions of the model with its surrounding environment. They ensure that the model reasonably represents the natural physical conditions and processes in the geothermal system.

The top surface of the model simulates dry atmospheric conditions with a pressure of 1 bar and an average temperature of 26.8°C. The EOS3 module was employed to define the thermophysical properties of water and air, essential for solving mass and energy balance equations (Pruess et al., 1999). High permeability was attributed to the top surface blocks to facilitate rainwater infiltration consistent with the local topography. An annual rainfall of 1880 mm with a 10% infiltration rate was included to simulate realistic hydrological conditions.

A no-flow boundary condition was implemented on the sides of the model to encompass the entire convective geothermal system, eliminating the need for side flows. This setup ensures that the model reflects natural and induced flows within the reservoir without external influences.

The base boundary was assigned a uniform background heat flux of 80 mW/m². Additionally, as a result of the calibration process, a constant hot mass was assigned to 16 blocks with a total upflow rate of 28 kg/s and an enthalpy of 1050 kJ/kg. These blocks are strategically located along the Massepe fault to represent the upflow zone beneath the Massepe field, aligning with the conceptual model.

7.4 Rock Properties

Rock properties were directly assigned from the discretized zones of the combined model using PyTOUGH, categorized by lithology, fault zones, fault intersections, alteration, and heterogeneity. This approach resulted in up to 79 rock types with different permeabilities based on lithology, faults, and alteration, representing the geological complexities. The rock properties for the blocks were automatically assigned to align with those identified in the Leapfrog model and were set up using PyTOUGH (Popineau et al., 2018).

8. NATURAL STATE SIMULATION AND CALIBRATION

Model calibration is an iterative process used to align model outputs with measured data. Key parameters adjusted in this model include the mass of hot fluid introduced at the base and the permeabilities of various rock types affecting fluid flow. Permeabilities were modified based on lithology and fault structures, with the altered clay cap acting as a fluid barrier. The low permeability of the clay cap restricts fluid movement, directing the upflow through designated permeable zones. The natural state model was run for 5 x 10^{13} seconds to reach steady-state conditions.

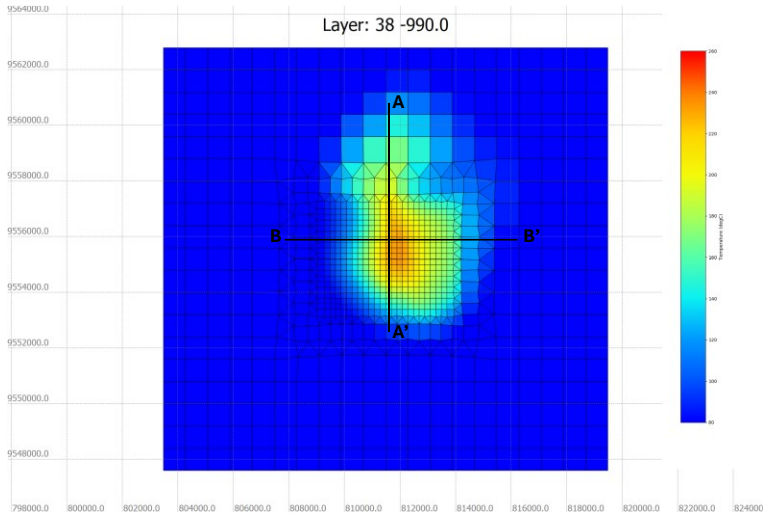

Figure 15: Temperature distribution in the natural state model at layer 38 (990 metres below sea level).

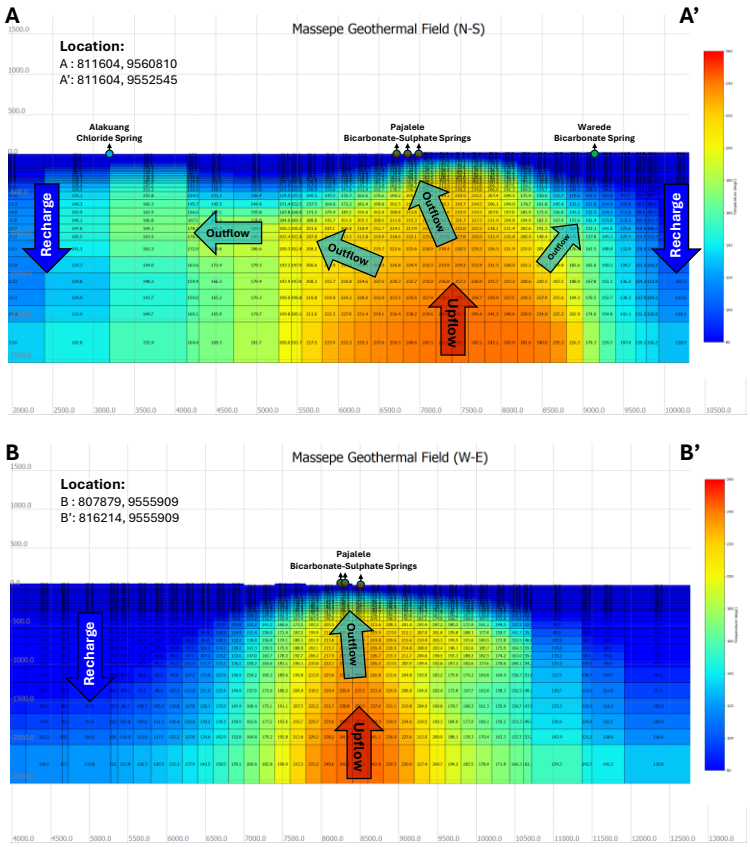

Figure 16: Temperature distribution and mass flow characteristics in the natural state model of the Massepe Geothermal Field. (A-A': North-South trajectory across the Massepe fault, B-B': West-East trajectory crosses Pajalele hot springs).

The natural state model was effectively calibrated using the estimated temperature at which the clay cap forms. The locations of surface manifestations helped in identifying upflows and outflows which can be mapped from simulation results. The presence of Pajalele springs indicates that upflow from the heat source seeps directly from the bottom, resulting in bicarbonate-sulfate manifestations. The outflow is evidenced by the Alakuang chloride spring to the north and the Warede bicarbonate spring to the south, both aligned with the Massepe fault. Figure 15 and Figure 16 show the temperature distribution resulting from the natural state calibration.

9. CONCLUSION

This study provides a detailed assessment of the natural state of the Massepe Geothermal Field using advanced numerical reservoir modeling techniques. The results indicate substantial geothermal potential, with a robust understanding of the temperature distribution, fluid flow, and heat transfer processes within the reservoir. The natural state simulation reveals a geothermal upflow through the North-South Massepe fault, with lateral migration restricted by adjacent geological structures. Continued exploration and model refinement, supported by field data and additional drilling, are essential for optimizing resource development and contributing to Indonesia's renewable energy goals.

ACKNOWLEDGMENTS

The authors would like to acknowledge the Directorate General of New, Renewable Energy and Energy Conservation (EBTKE) and the Geological Agency of the Ministry of Energy and Mineral Resources of Indonesia for providing the data related to the Massepe Geothermal Field. The authors also thank Seequent for providing a license for the Leapfrog Energy software, which was essential to this research.

REFERENCES

Franco, A., & Vaccaro, M. (2014). Numerical simulation of geothermal reservoirs for the sustainable design of energy plants: A review. Renewable and Sustainable Energy Reviews, 30, 987–1002. https://doi.org/10.1016/j.rser.2013.11.041

Joni, W., & Wahyuningsih, R. (2019). Pemodelan inversi 2-D dan 3-D menggunakan data magnetotelurik daerah panas bumi Massepe, kabupaten Sidenreng Rappang, provinsi Sulawesi Selatan. Buletin Sumber Daya Geologi, 14(2), 143–155. https://doi.org/10.47599/bsdg.v14i2.248

Munandar, A., & Hermawan, D. (2008). Penyelidikan geomagnet daerah panas bumi Massepe, kabupaten Sindenreng Rappang (Sidrap), provinsi Sulawesi Selatan. Pusat Sumber Daya Mineral, Batubara, dan Panas Bumi.

Popineau, J., O'Sullivan, J., O'Sullivan, M., & Archer, R. (2018). An integrated Leapfrog/TOUGH2 workflow for a geothermal production modelling. 7th African Rift Geothermal Conference.

Pruess, K., Oldenburg, C., & Moridis, G. (1999). TOUGH2 user's guide version 2. Lawrence Berkeley National Laboratory. https://tough.lbl.gov/assets/docs/TOUGH2_V2_Users_Guide.pdf

Risdianto, D., Adhitya Permana, L., Eko Ari, Wibowo, A., Sugianto, A., & Hermawan, D. (2015). Sistem panas Bumi non-vulkanik di Sulawesi. Pusat Sumber Daya Geologi - Badan Geologi Kementerian Energi dan Sumber Daya Mineral.

Risdianto, D., & Soetoyo. (2008). Survei terpadu geologi, geokimia, dan geofisika daerah panas bumi Massepe, kabupaten Sidenreng Rappang, Sulawesi Selatan. Pusat Sumber Daya Mineral, Batubara, dan Panas Bumi.

Risdianto, D., Soetoyo, & N, F. (2008). Penyelidikan geologi daerah panas bumi Massepe, kabupaten Sidenreng Rappang, Sulawesi Selatan. Pusat Sumber Daya Mineral Batubara dan Panas Bumi.

Sudjatmiko, D., Bachri, S., & Sukido. (1998). Geological map of the Majene and the Western part of Palopo Sheets, Sulawesi (Second) [Map]. Geological Survey Centre, Indonesia. https://geologi.esdm.go.id/geomap/pages/preview/peta-geologi-lembar-bungku-sulawesi

Sukamto. (2012). Geological map of the Pangkajene and Western part of Watampone Sheets, Sulawesi [Map]. Geological Survey Centre, Indonesia. https://geologi.esdm.go.id/geomap/pages/preview/peta-geologi-lembar-buru-maluku

Sulaeman, B., Ari, W. A., & Supeno. (2008). Penyelidikan geokimia daerah panas bumi Massepe, kabupaten Sindenreng Rappang, provinsi Sulawesi Selatan. Pusat Sumber Daya Mineral, Batubara, dan Panas Bumi.

Re-Evaluate The Sibayak Field Using 3D Inversion Model Based on Updated MT Data

Inusa P Fauzi, Aditya A Juanda, Sotarduga S Nainggolan, and Mulyanto

PT. Pertamina Geothermal Energy Tbk

fikri.rahmansyah@gmail.com, frah650@aucklanduni.ac.nz

Keywords: Magnetotelluric, Inversion Model, Sibayak, Bottom of Clay Cap

ABSTRACT

In 2023, PGE conducted Magnetotelluric (MT) and Gravity surveys to update the resistivity and density models of the Sibayak geothermal field. A 3D joint inversion was performed, leading to a refined understanding of the Sibayak reservoir. This study presents the updated models and reveals a significant finding: a highly conductive body (0.1-1 Ω.m) extending from deep outside the Singkut Caldera diagonally towards Mt. Pratektekan. This feature, not clearly identified in previous 2D models, underscores the enhanced image of the new 3D approach. Additionally, recent MT survey data, analyzed through 1D and 2D inversion, confirm the presence of this deep subsurface conductive anomaly. The delineation of the base of the clay cap interface with the underlying highly conductive body presents a challenge due to the absence of a distinct boundary between the two in our 3D resistivity model. Meanwhile, 1D could separate the bottom of clay cap and highly conductive body. This study emphasizes the value of updated geophysical data in understanding geothermal reservoirs and paves the way for further exploration and development in the Sibayak field.

1. INTRODUCTION

The Sibayak geothermal field, situated in North Sumatra, has been a contributing factor to Indonesia's geothermal energy production since 1996. Initially generating 2 MW, the field's capacity expanded to 12 MW in 2008 with the addition of two 5 MW units. However, an inactive steam sales contract with an Independent Power Producer (IPP) since 2012 prompted Pertamina Geothermal Energy (PGE) to re-evaluate Sibayak's potential to contribute to its ambitious 1 GW geothermal target.

Pertamina had conducted several geophysical data acquisitions. Initially, DC resistivity (Schlumberger) surveys were conducted to explore geothermal prospects with depth of investigation around 1000 meters, continued by MT survey in 1992 and Time Domain Electro-magnetic (TDEM) for static shift correction in 1997 (Mulyadi, 2000). A gravity survey was also conducted by PT. Gondwana in 1989 – 1990 using Lacoste Romberg gravity-meter (Daud, et al., 2001). In addition to the geophysical surveys, PGE undertook an update of the Sibayak reservoir model. The original model, developed in 2001, incorporated data from 10 wells drilled in the field (Atmojo, et al., 2001). Recognizing the potential impact of production history on reservoir characteristics, PGE created a new model in 2024 utilizing the available data since 2008 from the same 10 wells and incorporating a reflections of post-production conditions. (Firanda, et al., 2024).

A team of geoscientists and reservoir engineers from Pertamina Geothermal Energy (PGE) re-evaluated the Sibayak geothermal field's potential. This re-evaluation employed updated magnetotelluric (MT) data acquisition and resistivity inversion techniques to analyze the depth of the clay cap. Well cutting data from 10 wells have provided information on clay content, which will be useful in evaluating the clay cap. The updated resistivity model revealed a previously unidentified, highly conductive anomaly (less than 5 ohm.m) extending from the surface to a depth of approximately 4,000 meters below sea level (masl) with a lateral extent of about 4,000 meters. This anomaly exhibits an oval shape and trends southwest-to-northeast beneath Mount Sibayak. Notably, this anomaly was absent in previous resistivity models, However, PGE's recent MT data acquisition and resistivity model was thoroughly evaluated, resulting minor data masking for all decades above 160s (0.01 Hz) which PGE considered as satisfactory. It is also challenging to delineate the bottom of clay cap on our 3D resistivity model due to this high conductive body positions near the clay cap, resulting in a more smoothed and lower resolution view of the bottom of the clay cap (Cumming & Mackie, 2010).

Field Overview

Sibayak field is a volcanic geothermal system inside singkut caldera which formed at ~44 ka (Forni, et al., 2024) with two small conduit strato-volcano (Hochstein & Sudarman, 2015). Figure 1 visualizing two schematic conceptual model describing volcanic hosted system model and isotherm with alteration zone background derived from temperature log of the wells. The conceptual model was also used to update numerical simulation of Sibayak

Field (Firanda, et al., 2024) which consist of geothermal upflow beneath Mt. Sibayak outflowing towards Southeast and Northeast. Sibayak complex manifestations were founded in the crater of Sibayak Mountain and flank of Sibayak inside the Singkut caldera (Fahmi, et al., 2021). Figure 2 are the geological map of Sibayak with structure orientation NW-SE. Although Sibayak is a volcanic hosted system, tertiary sediments play major roles for the permeability in Sibayak reservoir.

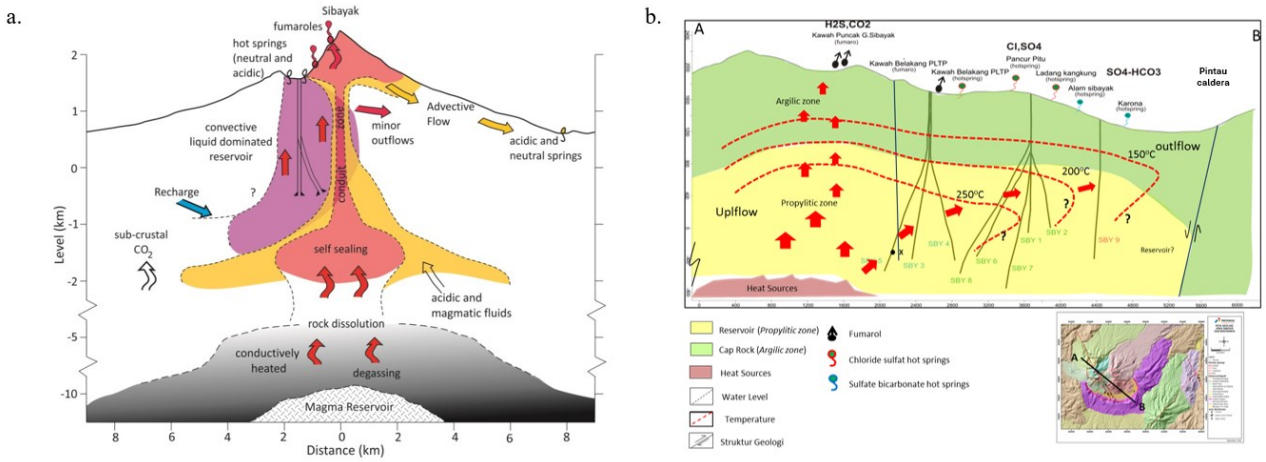

Figure 1: a. Sketch of Sibayak volcanic hosted conceptual model (Hochstein & Sudarman, 2015) and b. Isotherm conceptual model with hydrological setting of Sibayak along the alteration zone background developed from well temperature log (PT. Pertamina Geothermal Energy Tbk, 2022).

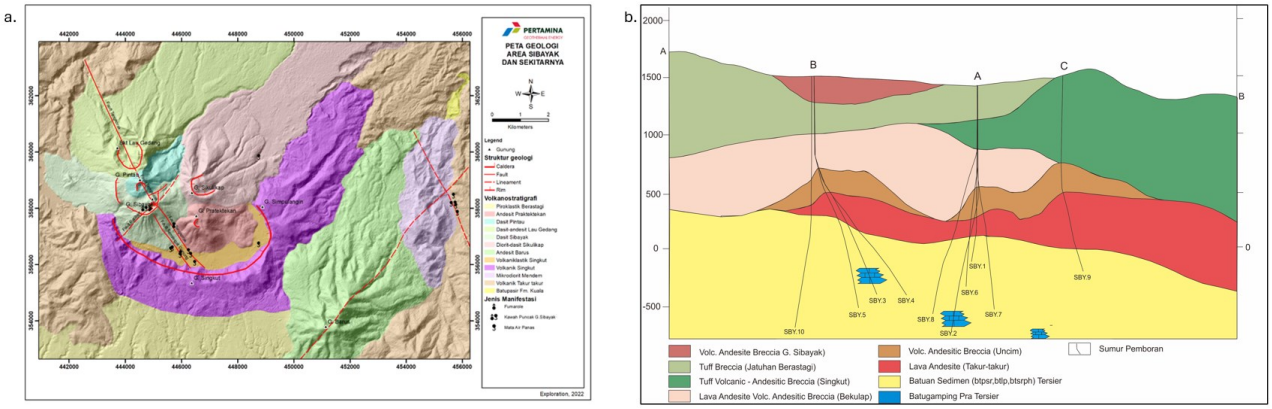

Figure 2: a. Updated geological map with stratigraphy of Sibayak field (PT. Pertamina Geothermal Energy Tbk, 2022) and b. Geological cross section interpreted from well cuttings data (PT. Pertamina Geothermal Energy Tbk, 2016).

2. SIBAYAK MT SURVEYS

Sibayak's old MT data, acquired in 1991 by PT Alico and in 1997 by PT Qodharwan Wirasta Konsultan, with total 51 MT stations, were utilized for 2D inversion techniques to verify the reservoir structure and its extent (Daud, et al., 2002). To achieve a more comprehensive understanding of the Sibayak geothermal field using modern software and technology, a 3D inversion approach was carried out. This re-modeling process aimed to enhance the three-dimensional visualization of the Sibayak Field, improving the accuracy of the geothermal resource assessment. However, limitations were encountered due to the incomplete recovery of historical MT data. To address this challenge and refine the remodeling efforts, a new MT data acquisition campaign was conducted. PGE's in-house geophysics department acquired 54 MT stations using proprietary tools and standardized acquisition procedures.

A three-receiver magnetotelluric (MT) system, including two operational units and one backup, facilitated simultaneous data acquisition at two stations per day in Sibayak. Each station utilized three MTC-80H coils with a frequency range of 1 kHz to 10,000 seconds and 4 electrode pots. Time series data processing is also run in-house using SSMT software resulting 4 excellent datasets, 48 good datasets and 2 fair datasets.

Figure 3 shows MT stations designed for capturing Sibayak reservoir. The station distributions were expected to be grid spaced or spread evenly with a target of 500 to 1000 m spacing in the inner core and 1500 m to 2000 m for the outer core with area of surveys around 100 m^2. Overall, the data acquisition was meeting the target although some part of the map such as in the North-East of Sibayak Mountain and South of Singkut Caldera cannot be acquired due to dense forest with minimum access and crowd residence with high voltage power line.

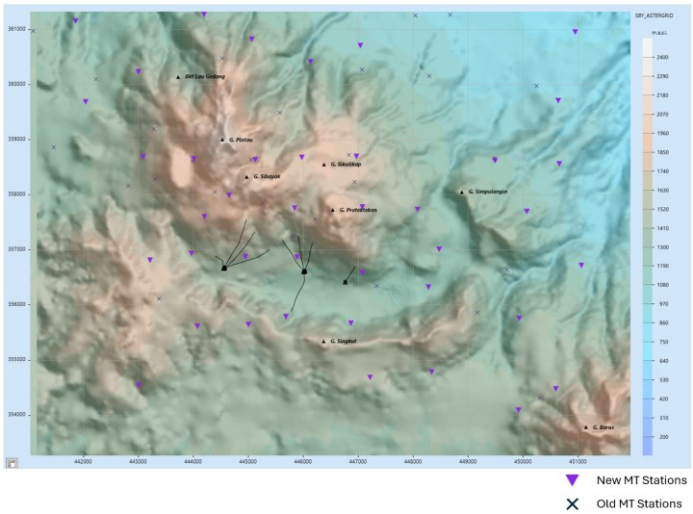

Figure 3: Distribution of MT stations from data acquisition in 2023 (purple triangle) and 1991 & 1997 (cross).

3. SIBAYAK MT INVERSIONS

Prior to this study, previous MT datasets from the Sibayak geothermal field had undergone several analyses. The first study showed that 1D inversion were used to delineate clay cap, reservoir and subsurface structure (Mulyadi, 2000). Understanding the limitation of 1D inversion, 2D inversion had been done to improve the interpretation of reservoir and basement from 1D inversion due to strong indication of 2D or 3D effects (Daud, et al., 2002). Advancements in technology have facilitated the routine application of 3D inversion techniques in recent years. Using a well-prepared MT dataset with recent technology, PGE conducted 3D inversion to create a better understanding of Sibayak reservoir.

To complement the re-evaluation, two complementary inversion approaches were incorporated alongside the contracted 3D MT inversion model. In-house 1D and 2D inversions were performed on newly acquired datasets using Geotools software. MT datasets were prepared to carry out 3D inversion. Datasets were rotated to 0-degree North, MT impedances and magnetic transfer function (tipper) were inverted. Notably, minimal data masking was only necessary for frequencies below 0.006 Hz due to anomalous behavior in the YX component at lower frequencies (Figure 4**)**. The resulting 3D resistivity model revealed a previously unidentified, highly conductive anomaly extending from the outer Singkut Caldera towards Sibayak Mountain. The validity of this anomaly was investigated through further analyses such as comparing it to the previous model, conducting 1D and 2D inversions and lastly conducting a sensitivity analysis.

3.1 Comparison of MT Inversions model

To verify the existence of the newly identified high conductive anomaly, several attempts were made to reconcile it with previous findings. As the original MT datasets used to generate the old 2D resistivity model were unavailable, the datasets of the old MT stations were plotted on the new 3D model, and the published image of the old 2D model was visually compared (Figure 5). Stations SBK-205, SBK-216, SBK-211, and SIB-128 are located within the footprint of the anomaly on the new 3D model. However, the old 2D model did not depict a conductive body at these locations. These restrictions could happen due to several reasons. First, the high conductive anomaly might exhibit a 3D effect that could not be adequately captured by the older 2D inversion algorithms. Second, due to the deep 3D nature, input data for the 2D model were restricted from 0.003 down to 30 seconds period (Daud, et al., 2002).

An additional effort to reconcile the anomaly with previous findings involved comparing published old MT curves to new MT curve nearby. Around 200 meters from SBK-211 is SBY-20 station with the same MT curve response (Figure 6). The most notable difference observed was a significantly higher initial resistivity (around 750 ohm.m) in the old SBK-211 curve (Mulyadi, 2000) compared to the new SBY-20 curve (around 40 ohm.m). This discrepancy could be attributed to the application of static shift correction using TDEM data in the processing of

the old MT data, which was not employed for the new dataset. Both curves exhibited a deflection in the Rho-YX component at a period of 1 second, while the Rho-XY component deflection occurred before 1 second in both datasets.

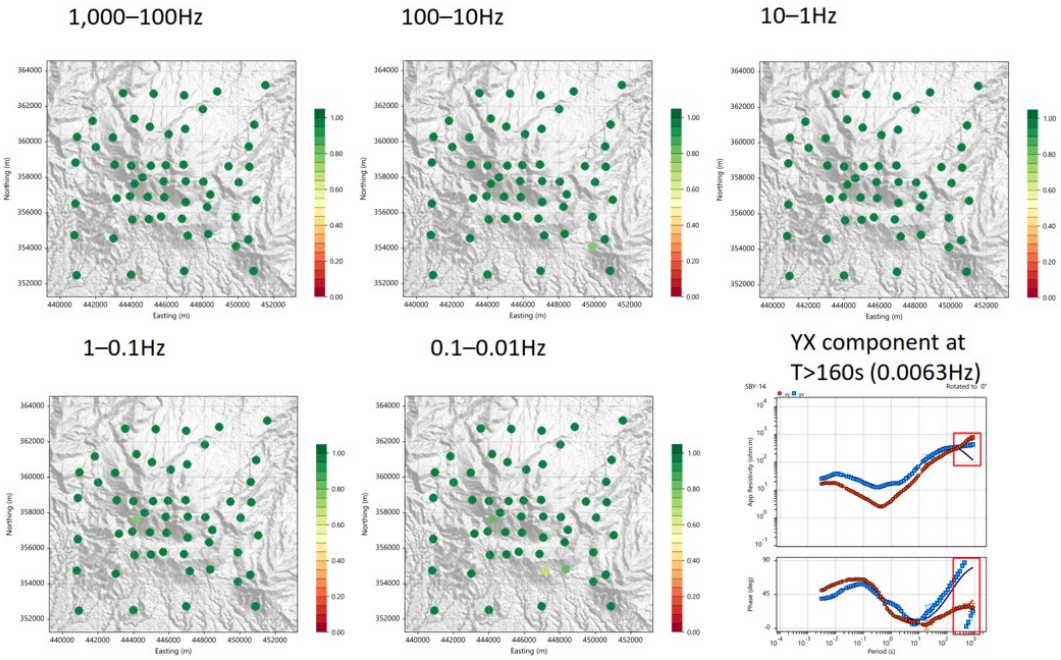

Figure 4: Data masking of MT datasets in every frequency start from 1000 – 0.01 Hz. Color bar green-red describing the percentage of data masked, value 1 or green means no data masking performed.

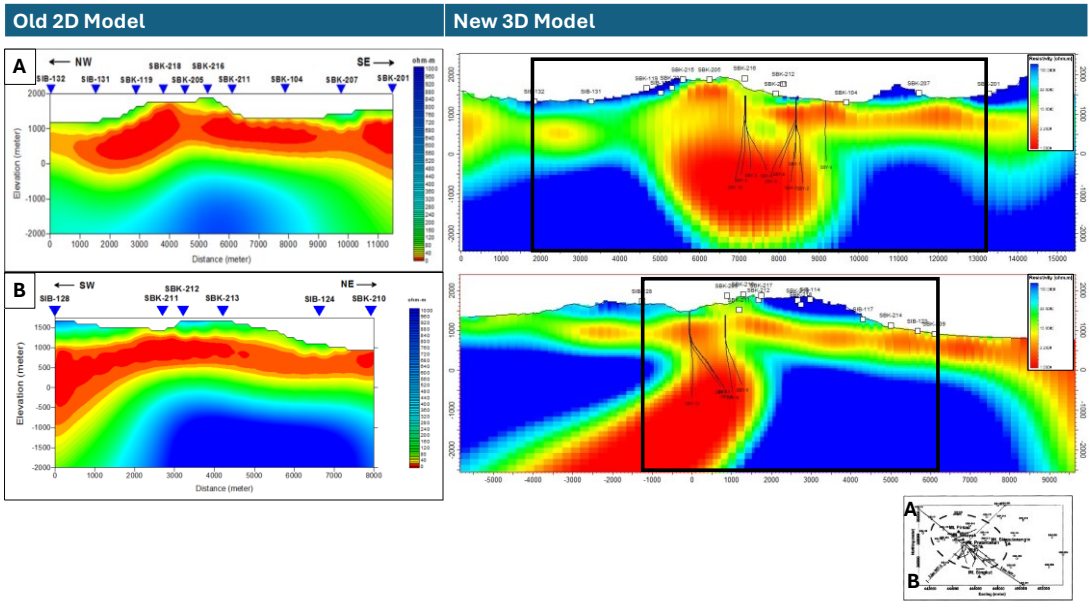

Figure 5: Cross-section comparation between old 2D model (left) and new 3D model (right). The boundary of old 2D model is visualized in a black box.

3.2 New MT Inversions of 1D, 2D and 3D Models

While 1D and 2D MT inversions using Geotools software offered a complementary approach, they presented limitations compared to 3D inversion. Unlike 3D models, 1D and 2D inversions relied on static shift correction obtained from TDEM surveys to process the MT data. This dependence on static shift correction can potentially introduce distortions in the dimensions of the geothermal clay cap as interpreted from the 1D and 2D models. However, the information derived from 1D and 2D models, when combined with alteration mineral data from wells, could still contribute to a comprehensive interpretation of the geothermal system.

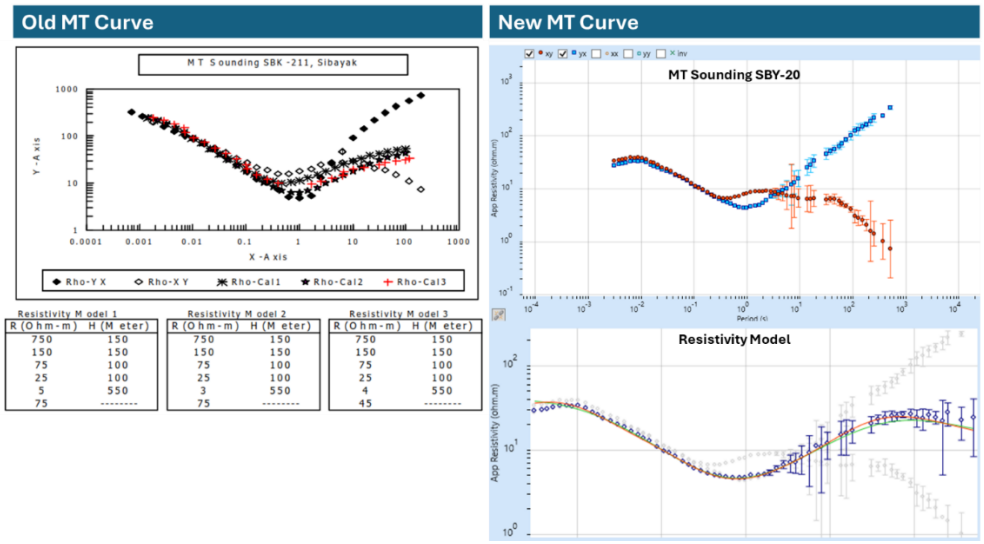

Figure 6: Comparison of nearby station between SBK-211 (old MT dataset) and SBY-20 (new MT dataset) including each 1D inversion.

To generate 1D model, smooth inversion (Occam) method were performed as it was good enough to delineate resistivity of geothermal clay cap (Cumming & Mackie, 2010). These 1D models were generated using TE and TM mode curves for all data within a frequency range of 1000 Hz to 0.001 Hz, incorporating a 5% apparent resistivity noise floor. Subsequently, the 1D Occam models were horizontally interpolated to create a cross-sectional image (Figure 7**)**. The resulting 1D model provides a clear representation of the resistivity down to a depth of approximately 1000 meters, with increased scatter at greater depths. This scattering might be attributed to the influence of 2D and 3D effect.

A 2D inversion was conducted utilizing TE and TM mode curves within the frequency range of 1000 to 0.01 Hz, as determined by data masking. Typically, 2D inversions serve as a preliminary step to refine inversion parameters before progressing to 3D modeling. However, in this study, the 2D inversion was employed to verify the presence of the high conductive body identified in the 3D model, particularly its position relative to the production wells. The 2D inversion confirmed the existence of the conductive body, although its depth was estimated to be greater than that observed in the 3D model Figure 7. This discrepancy underscores the importance of accurate static shift correction in both 1D and 2D inversions.

The 3D inversion was initiated with a uniform 50 ohm.m initial model and a 5% error floor, converging after 80 iterations to a root mean square (RMS) value of 1.08. By incorporating data from 0.006 to 251 Hz, reliable depth resolution was achieved to a depth exceeding 5000 meters. This depth coverage adequately captured the high conductive anomaly extending from outside the Singkut Caldera towards Sibayak Mountain. Notably, nine of the ten wells are located within the outer core of this conductive anomaly. However, a cautious interpretation is warranted due to the age of the well reports, which precludes further detailed analyses such as X-ray diffraction (XRD).

3.3 Sensitivity Test

To assess whether the deep conductive anomaly was an artifact of the inversion process or parameters, a sensitivity analysis was conducted (CGG Geoscience, Multiphysics, 2023). A modified 3D resistivity model (Figure 8a) was created by replacing the highly conductive anomaly with a less conductive body (50 ohm.m). The impact of this modification on the forward response was evaluated by comparing the TE-TM mode curves of the original and modified models at stations within the southwestern study area (Figure 8b). The apparent resistivity and phase curves from the original model (points) displayed significant deviations from those of the modified model (solid lines). This substantial difference in the forward responses demonstrates that the MT data possess sensitivity to the highly conductive body, suggesting its presence is required to accurately fit the observed data.

4. THE BOTTOM OF CLAY CAP FROM 1D AND 3D MT

Although the resolution of 3D model was lowered and smoothed, delineating the bottom of the clay cap using 3D resistivity models is often straightforward and typical for geothermal field evaluations. However, in the Sibayak field, the presence of a highly conductive body positioned near the clay cap in the 3D model presented a significant challenge. This proximity resulted in a blurred interface between the conductive clay cap and the anomaly, hindering clear separation. To address this limitation, 1D MT inversions were employed to provide a higher-

resolution characterization of the clay cap (Figure 7). Figure 7 illustrates a clear separation between the bottom of the clay cap (interpreted at 10 ohm.m) and the highly conductive body in the 1D model, in contrast to the ambiguity observed in the 3D model.

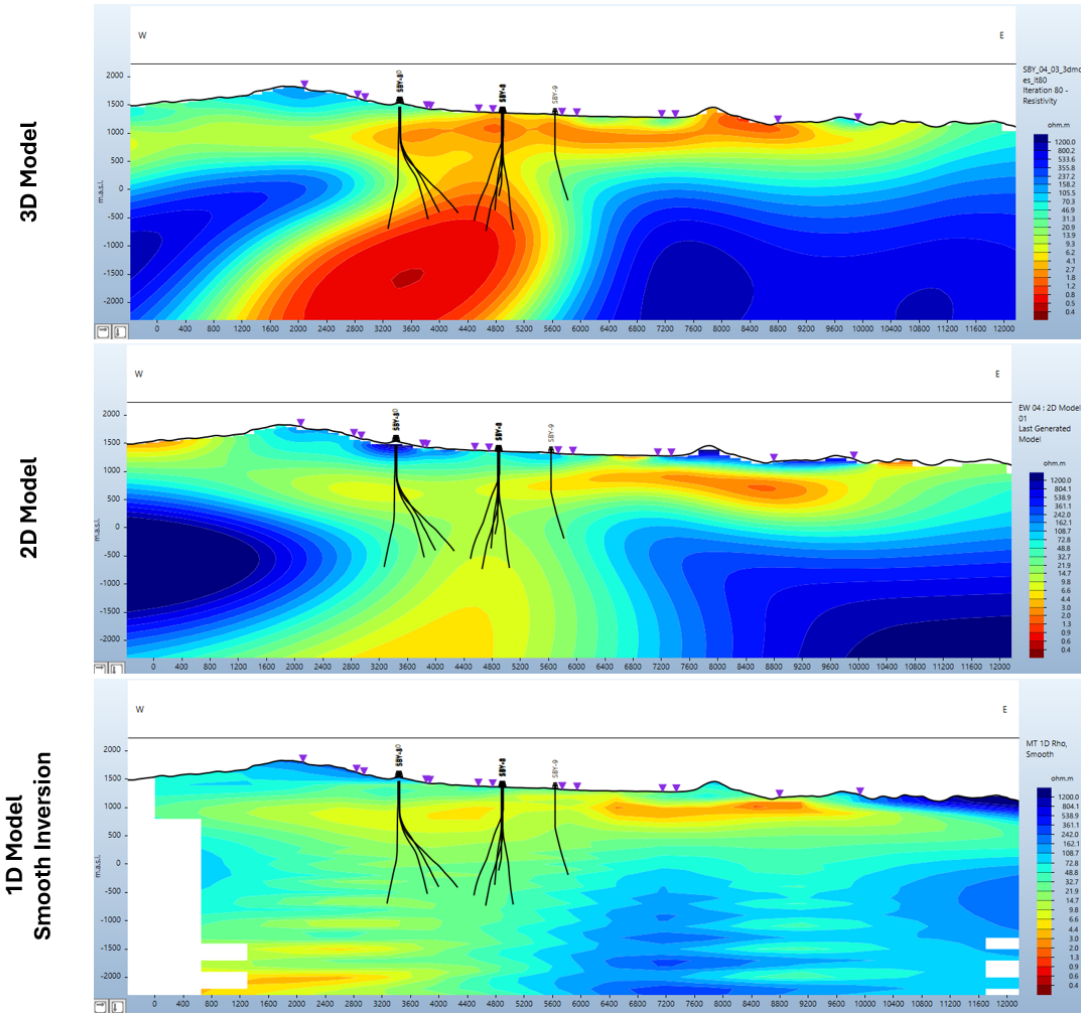

Figure 7: Three West-East Cross Section, crossing wells trajectory from 3D, 2D and 1D model sequentially.

The absence of static shift correction in the 1D model presented a significant challenge. While the integration of well data, including alteration zones, enhanced the interpretation of the geothermal system, the direct correlation between the 1D and 3D model-derived clay cap depths and well data proved to be inconsistent (Figure 9). The lack of Methylene Blue tests (MBT) in the legacy well reports, an uncommon practice at the time, hindered a more precise correlation between the clay cap and the argillic alteration zone.

To address these limitations, a combined approach was adopted. The bottom of the argillic alteration zone was used as a primary constraint, and the general trend of the bottom of clay cap from the 1D model was incorporated into the 3D model. This strategy aimed to mitigate the negative impacts of the low resolution associated with blurred resistivity value of the high conductive body and the clay cap on the 3D model at Figure 10.

5. DISCUSSIONS FOR FURTHER STUDY

While the integration of well data and 1D modeling provided valuable insights, challenges persisted in precisely defining the clay cap bottom. Moreover, the nature of the high conductive anomaly remains an open question. Potential causes for enhanced conductivity include graphite, ore minerals, saline fluids, and partial melting (Schilling, et al., 1997). However, given the likely presence of an impermeable barrier confining fluids, saline fluids are considered the most plausible explanations (Jones, 1992). Laboratory studies have established a correlation between high electrical conductivity and the presence of ore minerals, particularly sulfides. However, while this association is commonly observed, it is not universally applicable. Numerous case studies demonstrate that high conductivity can occur both with and without the presence of detectable sulfides (Lin, et al., 2023).

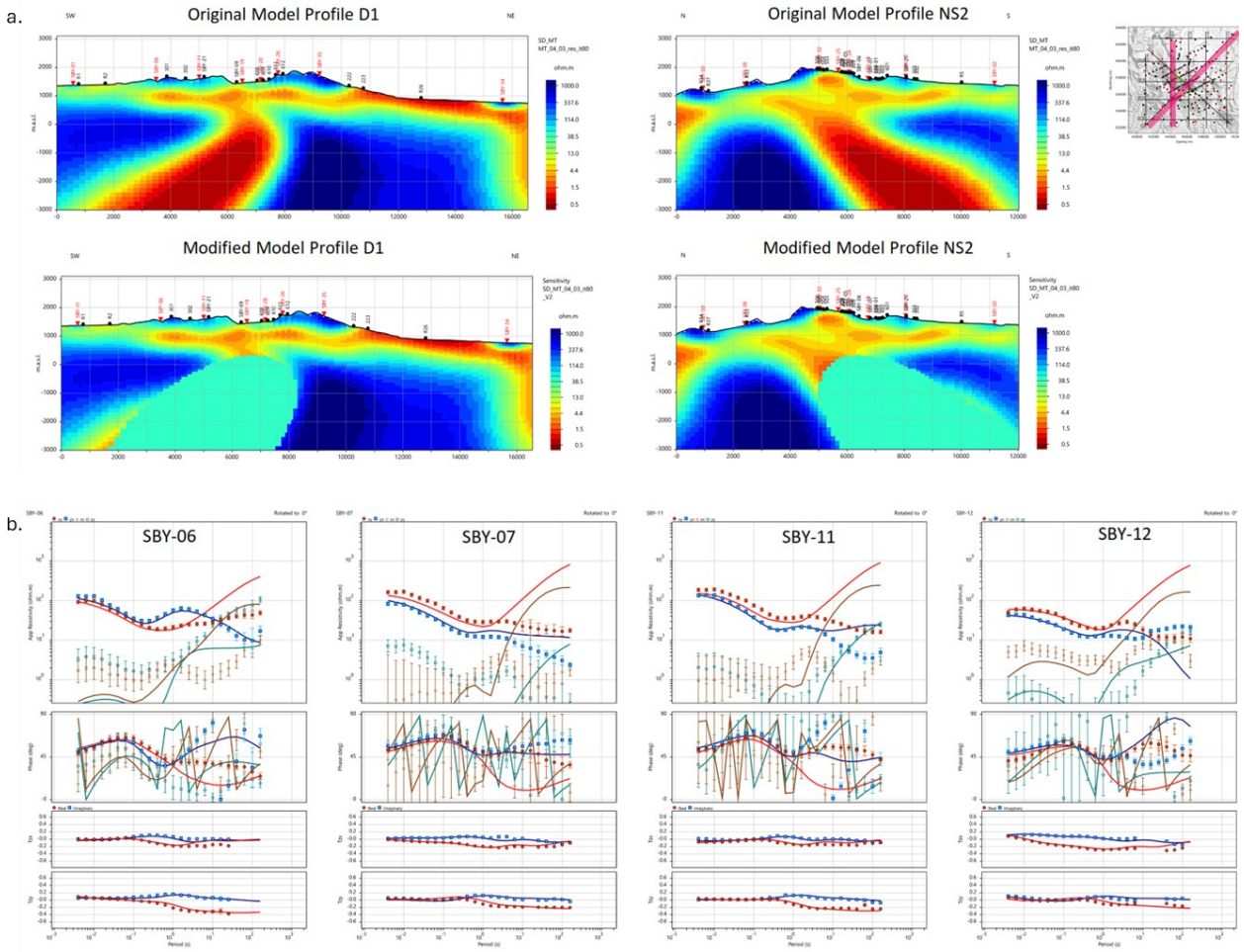

Figure 8: **a. Cross-section of two profiles comparing between modified 3D model from high conductivity into 50 ohm.m body. b. MT-curve sampled from MT stations above the high conductive body with MT curve from forward modelling of the modified body (solid lines) and original data (dots).**

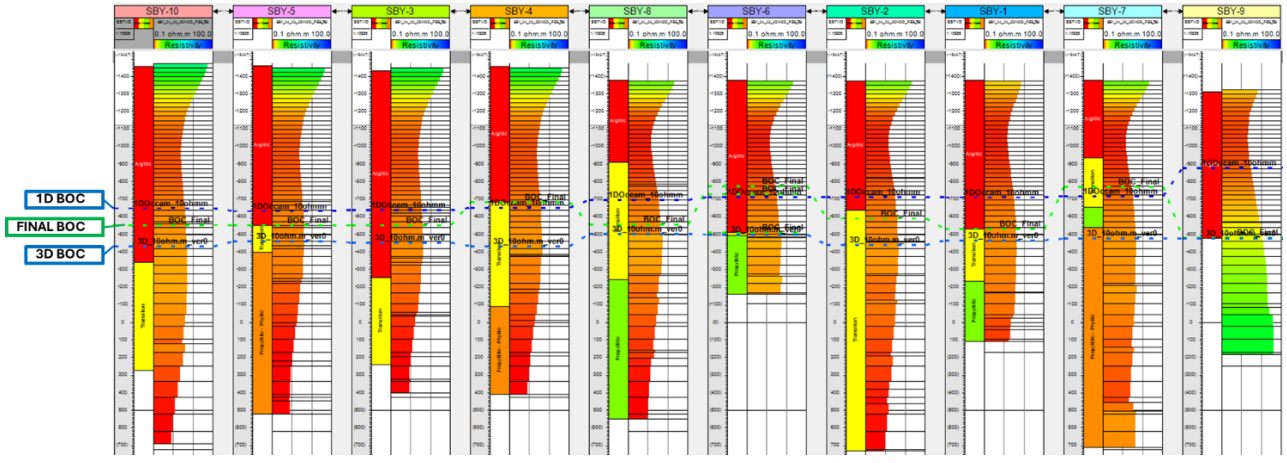

Figure 9: 1D and 3D interpreted bottom of clay cap with alteration data from Sibayak wells.

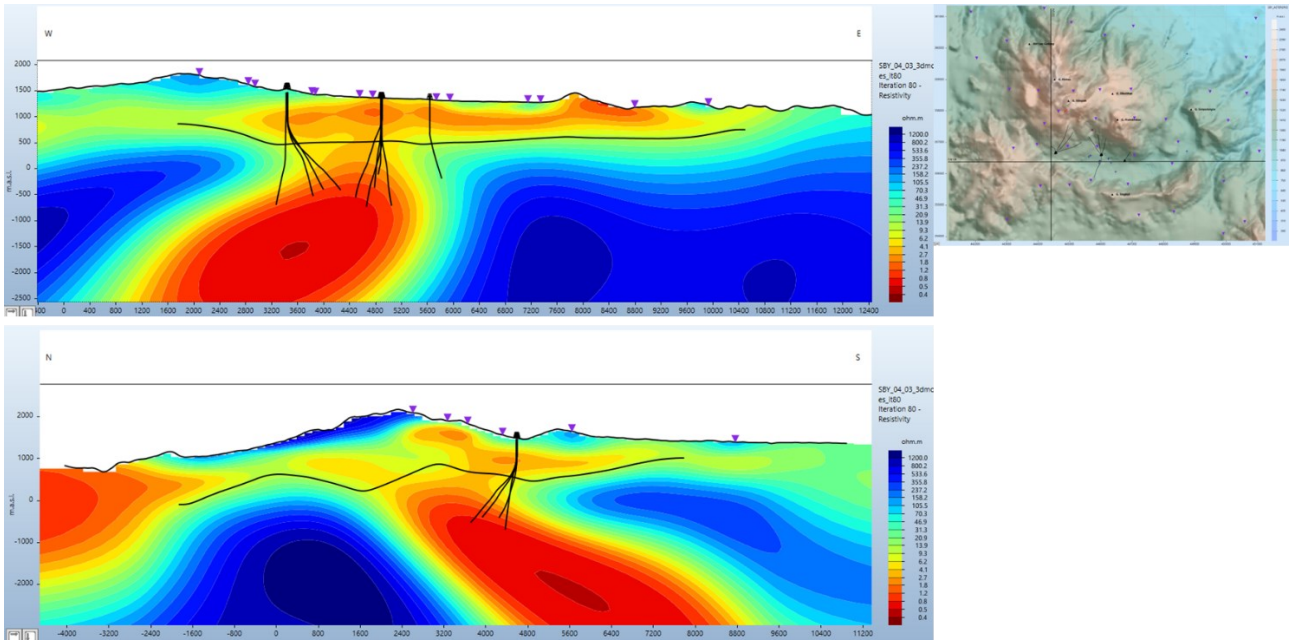

Figure 10: Cross-sections of 3D model with the interpolated bottom of clay cap from 3D interpretation BOC bound with well data and 1D BOC trends.

To discriminate between these possibilities, a comprehensive analysis of well data, including mineralogical studies and geochemical evaluations, are necessary. The characteristics of the fluids produced from the wells, combined with the spatial relationship between the wells and the conductive anomaly, will provide crucial information for determining the anomaly's origin. If the high conductivity is attributed to saline fluids, targeting this zone for future well development would be a logical strategy. Conversely, the presence of ore minerals within the anomaly might necessitate a more complex economic evaluation to assess the potential for mineral exploitation.

6. CONCLUSION

To enhance the definition of the geothermal clay cap, a combined approach utilizing 1D and 3D inversion models is recommended. While 1D inversion offers improved resolution, accurate static shift correction is essential for precise location determination. Conversely, 3D inversion captures the potential 3D and anisotropic nature of the subsurface but may suffer from reduced resolution due to smoothing effects. The resulting 3D clay cap interpretation was significantly refined, particularly in delineating the clay cap within the vicinity of the high conductive anomaly, guided by well data and 1D model interpretation.

7. ACKNOWLEDGEMENT

This study was supported by PT. Pertamina Geothermal Energy Tbk, Geoscience Exploration & Development Region 1 Division, Geoscience Department. Thank you for the support and permission to publish this paper.

REFERENCES

Atmojo, J. et al., 2001. Numerical Modelling Study of Sibayak Geothermal Reservoir, North Sumatra, Indonesia. Stanford, California, Twenty-Sixth Workshop on Geothermal Reservoir Engineering.

CGG Geoscience, Multiphysics, 2023. Pertamina Geothermal Energy Internal Report of 3D MT Inversion Modeling - Sibayak, CGG Geoscience, Multiphysics.

Cumming, W. & Mackie, R., 2010. Resistivity Imaging of Geothermal Resources Using 1D, 2D and 3D MT Inversion and TDEM Static Shift Correction Illustrated by a Glass Mountain Case History. Bali, Indonesia, World Geothermal Congress.

Daud, Y., Sudarman, S. & Ushijima, K., 2001. Sibayak Geothermal Field (Indonesia): Structure Assessed From Gravity and Hydrogeological Considerations.

Daud, Y., Sudarman, S. & Ushijima, K., 2002. Imaging Reservoir Structure of the Sibayak Geothermal Field (Indonesia) Based on Magnetotelluric Observations.

Fahmi, F. L. et al., 2021. Geochemistry Monitoring of Surface Thermal Manifestation in Sibayak, North Sumatra, Indonesia. Reykjavik, Iceland, World Geothermal Congress.

Firanda, E. et al., 2024. Updating Numerical Simulation Model of Sibayak Field, Indonesia. Standford, California, Forty-Ninth Workshop on Geothermal Reservoir Engineering.

Forni, F. et al., 2024. Remobilization and eruption of an upper crustal cumulate mush at the Singkut Caldera (North Sumatra, Indonesia). Journal of Volcanology and Geothermal Research, Volume 445.

Hochstein, M. P. & Sudarman, S., 2015. Indonesian Volcanic Geothermal Systems. Melbourne, Australia, World Geothermal Congress.

Jones, A. G., 1992. Electrical conductivity of the continental lower crust. In: D. M. Fountain, R. J. Arculus & R. W. Kay, eds. Continental Lower Crust. s.l.:Elsevier, pp. 81-143.

Lin, W., Yang, B., Han, B. & Hu, X., 2023. A Review of Subsurface Electrical Conductivity Anomalies in Magnetotelluric Imaging. Sensors, 23(1803).

Mulyadi, 2000. Magnetic Telluric Method Applied For Geothermal Exploration in Sibayak, North Sumatra. Kyushu - Tohoku.

PT. Pertamina Geothermal Energy Tbk, 2016. Internal Report : Geological, Geochemistry, Geophysical and Reservoir Evaluation of Sibayak Geothermal Field, North Sumatra, Jakarta, Indonesia: Resource Management Division of Planning and Development Directorate.

PT. Pertamina Geothermal Energy Tbk, 2022. Internal Report : Geological Mapping Report of Sibayak Area, Jakarta, Indonesia: Geoscience Region I Exploration Division of Exploration and Development Directorate.

Schilling, F. R., Partzsch, G. M., Brasse, H. & Schwarz, G., 1997. Partial melting below the magmatic arc in the Central Andes deduced from geoelectromagnetic field experiments and laboratory data. Physics of the Earth and Planetary Interiors, Volume 103, pp. 17-31.

Analog Study of Geothermal System of Telomoyo Mountain With Ungaran Mountain Using 3G Analysis Method (Geology, Geophysics and Geochemistry)

M.D.A. Wulandari, A. S. Pintrandhita, and K. L. Fatihah

Geophysical Engineering, Faculty of Mineral Technology,
University of Pembangunan Nasional "Veteran" Yogyakarta, 55283

115210020@student.upnyk.ac.id, 115210006@student.upnyk.ac.id, 115210051@student.upnyk.ac.id

Keywords: Geothermal System, GGMPlus, Telomoyo, Ungaran

ABSTRACT

The considerable geothermal energy potential in Indonesia is very possible to be developed and utilized, for example as a power plant and agricultural industry, because most of it has a fairly high enthalpy of the total potential of around 29 GWe. Java Island, especially in Central Java, has many geothermal potential points that can be utilized. There are geothermal potential points in Central Java that have been utilized for production, but there are also those that have not been utilized. Some geothermal potential points that have not been utilized well have some geological similarities or characteristics of the geothermal system with some points that have been utilized better. To be able to optimize other potential points, an analog study or comparison can be carried out on two or more geothermal systems to find out the similarity of the geothermal system conditions, so that later it can be maximally utilized. In this research, an analog study was conducted between the potential points of Telomoyo and Ungaran. The data used is based on the results of GGMPlus gravity satellite image processing and geological conditions in the potential point area. Based on GGMPlus data, in the Telomoyo potential point area the CBA values obtained range from low to high anomaly, where the low anomaly is located on Mount Andong and Mount Telomoyo. This is also shown in the processing results of the Ungaran potential point, where Mount Ungaran also shows a low anomaly. Furthermore, geological studies are carried out to determine the characteristics of geological conditions and validation of GGMPlus data, so that it can be used for potential development.

1. INTRODUCTION

The solo zone is formed by a complex of volcanoes that extends in a northwest-southeast direction, namely the series of Mount Ungaran - Mount Telomoyo - Mount Merbabu - Mount Merapi which is in the Quaternary volcanic geological environment. The Mount Telomoyo complex is one of the geothermal prospect areas indicated by the appearance of geothermal manifestations to the surface in the form of warm springs and rock alteration. Geothermal manifestations on Mount Telomoyo are found in the Candi Dukuh, Candi Umbul, Sepakung and Kendal Duwur areas. In addition, Mount Ungaran has geothermal prospect areas indicated by geothermal manifestations that appear on the surface in the form of fumaroles, hot spring pools and alteration rocks. Both mountains are located in the same zone, which is the solo zone, so there are indications of similarities in geothermal system conditions, geological and geochemical conditions.

Mount Telomoyo consists of several rock units, namely andesite lava unit, tuff breccia unit, pyroclastic breccia unit and alluvial unit. Manifestations that develop in this area are hot springs that have a Chloride - Bicarbonate water type and are a lateral outflow zone of the system. Furthermore, there is rock alteration that has an argillic - advanced argillic type which is an upflow zone that is above the boiling zone of a reservoir. Mount Ungaran is a quaternary volcano located in the north of the North Serayu Mountains, and is located on top of rocks and incorporated in Tertiary rock formations (Setiaji, et al, 2020). geothermal manifestations that develop in the form of warm to hot springs, including hot springs with characteristic deposits that develop in the form of sulfur and travertine. The geothermal manifestations appear to appear in the Kaligetas Formation, Gajahmungkur Volcanic Rocks, and Mount Sumbing Lava with rock distribution in the east - southeast - south of the foot of Mount Ungaran. Based on geochemical analysis, it has hydrothermal fluid types, which are Bicarbonate Water type and Chloride Water type (Trisnaning, 2021).

Geophysical methods are used in this study to find out the geothermal system under the surface of Mount Telomoyo and Ungaran. The method used is GGMPlus (Global Gravity Model Plus) satellite gravity data, which has advantages in terms of resolution of about 200 meters compared to other gravity satellites. Therefore, it can determine the geothermal system and subsurface conditions of the research area in detail.

There are several previous studies that explain the geothermal prospects of Telomoyo that can be developed and the exploration stage has been carried out. But in the Ungaran area no further utilization has been carried out, even though the two locations are still in the same zone. Hence, this research will discuss an analog study using geophysical, geological and geochemical data to determine the similarity of geological conditions and existing geothermal systems. This will help optimize the potential points on Mount Ungaran.

2. METHODS

The research used GGMPlus high-resolution gravity Landsat data, which was obtained from processing using Matlab software to obtain gravity acceleration values. To obtain the complete Bouguer anomaly value, terrain correction was carried out with Global Mapper software, then a complete Bouguer anomaly map and 2.5D modeling were made using Oasis Montaj software. The research locations are in two places, namely the Mount Telomoyo geothermal area and the Mount Ungaran area to see the potential in both geothermal development locations by looking at the similarity of geological, geochemical and geophysical conditions. Geochemical and geological data were obtained based on previous literature that has conducted previous research in the research area.

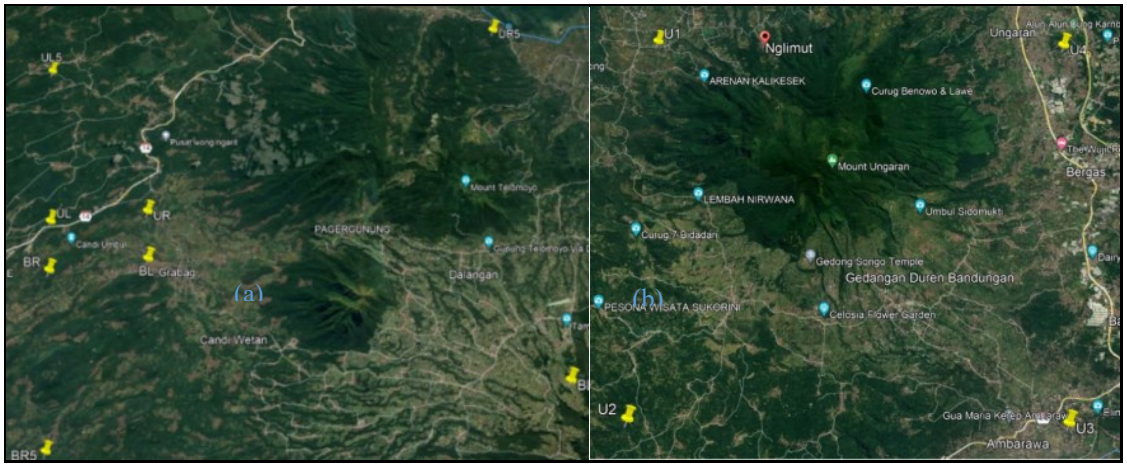

Figure 1: Location Research (a) Telomoyo Area; (b) Ungaran Area.

3. DATA AND RESULT

The Telomoyo area is a well-known geothermal area with the manifestation of hot springs from Candi Umbul and Pakis Dadu. Based on the gravity acceleration value of the Telomoyo area itself, the variation of acceleration values from high to low values is influenced by the geological conditions of the Telomoyo area. The map in Figure 4 shows that the gravity values range from 4 to 27.1 mGal, which can be classified into three zones, namely low, medium and high zones. The low zone in the Telomoyo area is in the area of Mount Telomoyo and Mount Kendil.

To ease the research, an overlay map was added between the Magelang-Semarang Geological Map Sheet and the Telomoyo Area CBA Map. Through the overlay, it is known that the lithology of the Telomoyo area comes from the Kaligetas Formation, Andong & Kendil Volcanic Rock Formation, and Gilipetung Volcanic Rock Formation, which are dominated by volcanic rocks, andesite and lava flows. The geologic map also shows the structures that control the geothermal system in the Telomoyo area.

In the previous research by Hutami, dkk in 2014 geochemical in Mt.Telomoyo geothermal Based on the analysis of the Cl - SO4 - HCO3 ternary diagram, the warm springs in the study area belong to the Chloride - Bicarbonate water type, where this water is formed due to the dilution of the chloride element by meteoric water while flowing to the surface. The presence of bicarbonate elements in the water is the result of vapor condensation below the groundwater level, which will move along the gradient of the groundwater level, the further away the influence of groundwater will be Based on the 18O and 2H isotopes of the warm spring fluid of Candi Dukuh and Candi Umbul, it shows that the fluid has experienced mixing with meteoric water. the zone of this manifestation is lateral outflow.

The Ungaran area is a geothermal area where there is a manifestation of hot springs from Gedongsongo Temple, where this area is surrounded by the Telomoyo and Guci Geothermal Areas. Based on the gravity acceleration values of the Ungaran area, the variation of acceleration values from high to low values is influenced by the geological conditions of the Ungaran area. The map in Figure 6 shows that the gravity values range from -6.8 to

19.9 mGal, which can be classified into three zones, namely low, medium and high zones. The low zone in the Ungaran area is in the area of Mount Sebangkong, which is an ancient volcano in the Ungaran area.

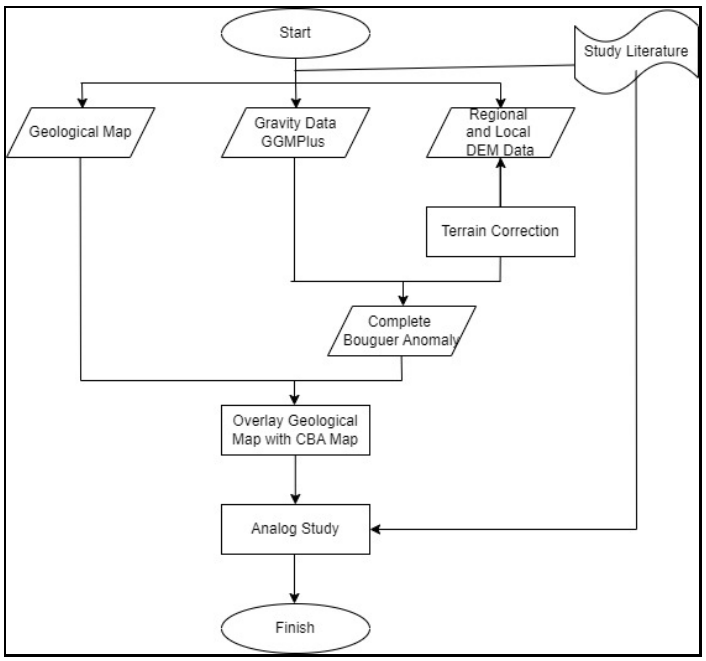

Figure 2: Research Flowchart.

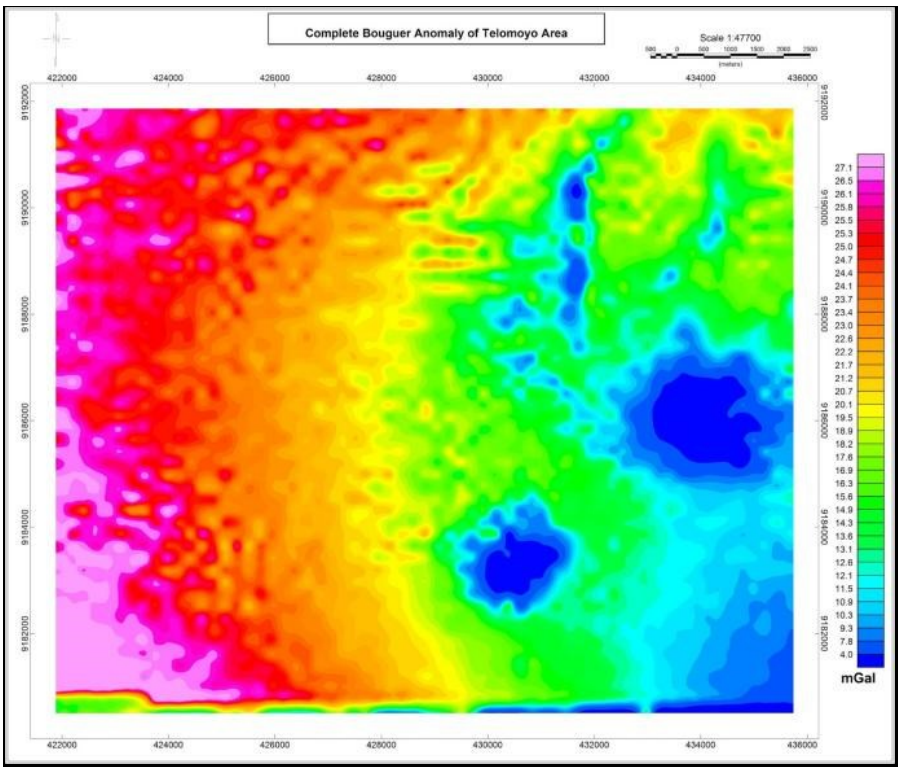

Figure 3: Complete Bouguer Anomaly of Telomoyo Area.

To ease the research, an overlay map was added between the Magelang-Semarang Geological Map Sheet and the Ungaran Area CBA Map. Through the overlay, it is known that the lithology of the Telomoyo area comes from the Jongkong Formation, Gajahmungkur Volcanic Rock Formation, and Kaligesik Volcanic Rock Formation, which are dominated by Andesite rocks with hornblende minerals and also basalt lava from the Jongkong Formation. In addition, the geological map also shows the structures that control the geothermal system in the Ungaran area.

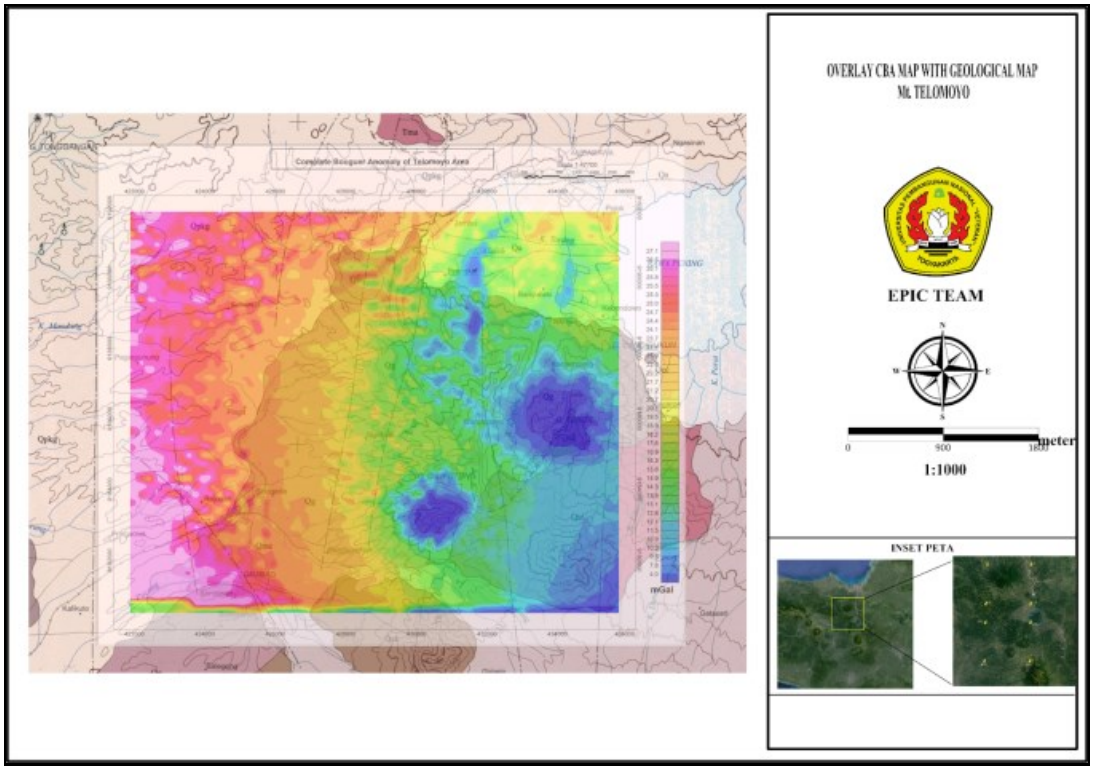

Figure 4: Overlay Complete Bouguer Anomaly of Telomoyo Area With Geological Map.

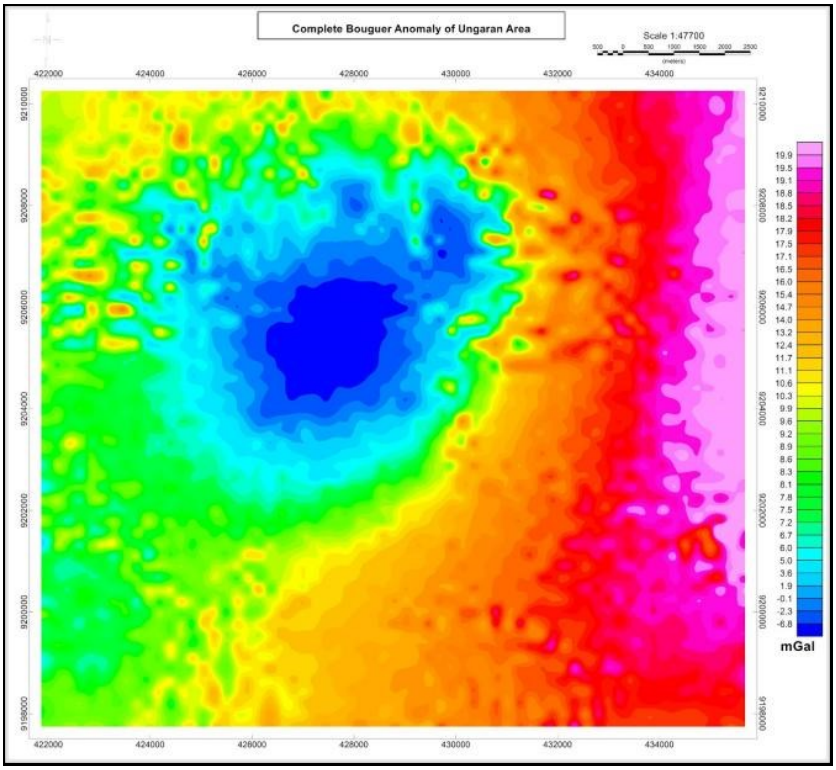

Figure 5: Complete Bouguer Anomaly of Ungaran Area.

Based on previous research by Emiyanto and Aribowo in 2011. geochemical data in Mt. Ungaran geothermal manifestation, hot water has type bicarbonate water fluid because from the results of chemical analysis, it is known that the element HCO3 (bicarbonate) is the most dominant element. This area is categorized as a steam heated water/steam condensates zone. The process that occurs in this zone is the heating of meteoric water by the underlying heat source, the water evaporates and condenses then comes to the surface with the dominant HCO3 element. Based on the plotting of the ternary diagram of the Cl-Li-B element content in hot water in Nglimut and

its surroundings. in the research area generally occurs in the edge zone (outflow). due to the less dominant Cl concentration, it indicates that the research location is quite far from the main flow of the geothermal system.

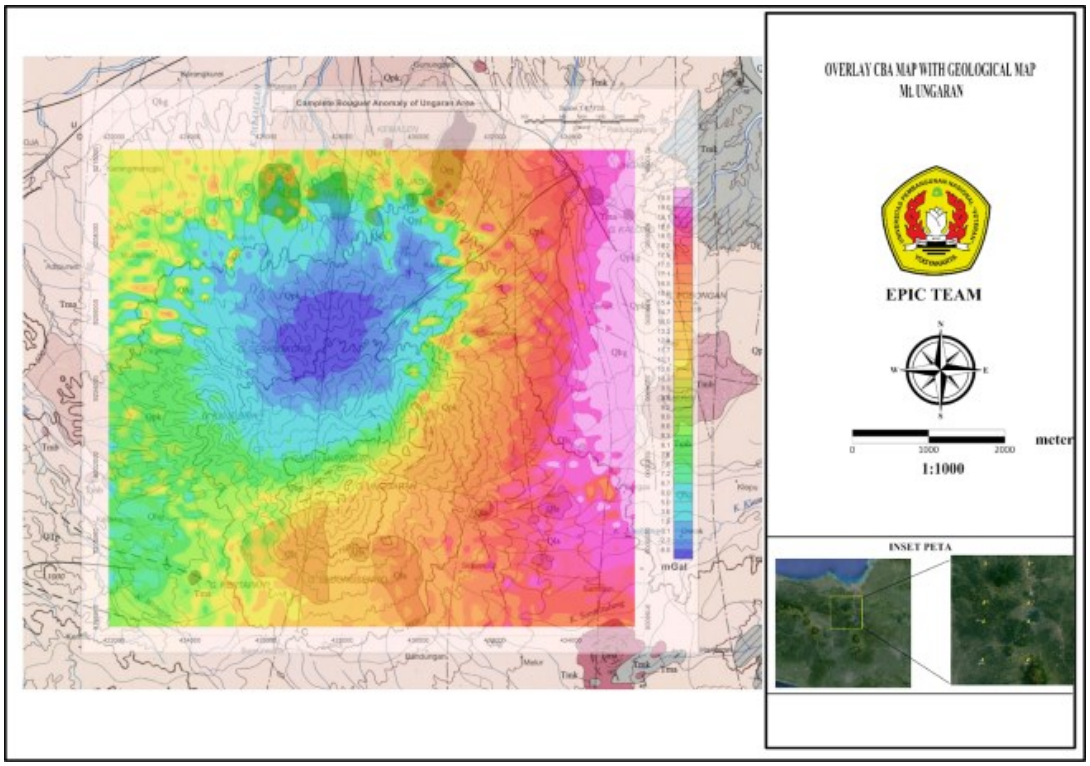

Figure 6: Overlay Complete Bouguer Anomaly of Ungaran Area With Geological Map.

3. CONCLUSION

From result and discussion above, we can know that:

1) Based on geological data Mt. Telomoyo and Mt. Ungaran have similar constituent lithology in the form of volcanic rocks. which consists of rocks as for the types of rocks that are pyroclastic rocks, alluvial, andesite.
2) Based on geophysical data It can be seen that the geothermal system in Mt. Ungaran and Mt. Telomoyo. have in common that there is a heatsource, reservoir faults and manifestations in the form of hot springs and alteration rocks on mt. telomoyo.
3) Based on geochemical data the hot water manifestation of geothermal between Mt. Telomoyo and Mt. Ungaran have a similar type of bicarbonate water. there is included as a outflow zone. but in Mt. Telomoyo Chlorine have a high domination and have higher temperature than Mt. Ungaran.
4) Based on the analog study that has been carried out, it can be concluded that Mt. Ungaran can be explored as in Mt. Telomoyo but the reservoir conditions are not mature enough and have a lower capacity compared to mt.telomoyo. so, it takes several geological years to explore and develop the uUngaran geothermal prospect.

REFERENCES

Emianto, Y. B., & Aribowo, Y. (2011). Studi Geokimia Fluida Panasbumi Daerah Prospek Panasbumi Nglimut, G. Ungaran Kecamatan Limbangan, Kabupaten Kendal Jawa Tengah. Teknik, 32(3), 230-233.

Hutami, R. T., Aribowo, Y., & Widiarso, D. A. (2014). Studi Pendahuluan Daerah Prospek Panasbumi Berdasarkan Data Manifestasi Panasbumi, Geokimia Dan Isotop Fluida Panasbumi Komplek Gunung Telomoyo, Kabupaten Semarang, Jawa Tengah. Geological Engineering E-Journal, 6(1), 233-245.

Setiaji, T. W., Khumayroh, R., & Muhammad, A. (2020). Analisa Struktur Geologi Pengontrol Reservoir Sistem Panas Bumi Ungaran Berdasarkan Data Gravitasi Dan Geomagnetik. Jurnal Geosains Terapan, 3(1), 72-72.

Trisnaning, P. T., & Fatimah, F. (2021). Tipe fluida hidrotermal sepanjang manifestasi panas bumi di daerah Ungaran dan sekitarnya. Angkasa: Jurnal Ilmiah Bidang Teknologi, 13(2). https://doi.org/10.28989/angkasa.v13i2.944

Imaging The Mass Distribution of The Semolon Geothermal Prospect, North Borneo, Using Satellite Gravity Data

Sintia W. Niasari, Camelia Umar, and Mochamad Nukman

Universitas Gajah Mada (UGM)

sintia_windhi@ugm.ac.id
cameliaumar1998@mail.ugm.ac.id
moch_nukman@ugm.ac.id

Keywords: Semolon Geothermal Prospect, North Borneo, Gravity Method

ABSTRACT

Indonesia has non-volcanic geothermal potential that can be found in Kalimantan, one of which is located in Semolon, Malinau Regency, North Kalimantan, indicated by the presence of geothermal manifestations such as hot spring. These manifestations can surface due to the presence of geological structures such as faults. The method that can be used to identify geological structures is the gravity method. This research aims to determine the distribution map of gravity anomalies, including complete Bouguer anomalies, regional anomalies, residual anomalies, and also to identify subsurface geological structures using First Horizontal Derivative (FHD) and Second Vertical Derivative (SVD) analyses. The research was conducted using secondary data from satellite gravity measurements, specifically GGMplus and SRTM data. Secondary gravity data is useful for preliminary surveys of geological targets that are difficult to access in the field. The research results show that the complete Bouguer Anomaly in the research area is in the range of 47.7 mGal to 193 mGal. Regional anomalies in the research area are in the range of 52.6 mGal to 190.9 mGal. Residual anomalies in the research area are in the range of -18.9 mGal to 13.1 mGal. Data analyses of residual Bouguer map resulted in indication of some faults in the study area. These faults should correlate with the fluid pathways. Additional study in this geothermal prospect is needed to understand more about the conceptual model of this system.

1. INTRODUCTION

Indonesia is located at the intersection of three active world plates, namely the Eurasian, Indo-Australian, and Pacific plates, which results in Indonesia having a complex tectonic structure. Sukendar et al (2016). This strategic position makes Indonesia one of the countries with the largest geothermal potential in the world, amounting to 29 GWe. Indonesia's geothermal potential is mostly distributed along the volcanic arc, from Sumatra, Java, Bali, Nusa Tenggara, Sulawesi to Maluku (Ahluriza and Udi, 2021).

Geothermal heat sources are often associated with volcanoes. Research discussing about non-volcanic geothermal system is still limited. Non-volcanic geothermal sources can be found in the Kalimantan region of Indonesia (Yushantarti, 2020; Zarkasyi and Dikdik, 2015). Medium to low enthalpy geothermal system can be considered for geothermal prospects in Kalimantan (Ahluriza and Udi, 2021). There are 14 geothermal prospects, including Semolon, located in Malinau Regency, North Kalimantan.

Indications of geothermal system in the Semolon area is the manifestation of warm spring with temperatures ranging from 51.4° to 60.2°C (Yushantarti, 2020). According to Dahlan et al. (2011), one of the geological structures in this study area is a normal fault with a relatively northwest-southeast direction.

Geophysical method can be used to determine the geological structure of the Semolon geothermal system. The gravity method is one of the geophysical methods that can be used to identify subsurface geological structures based on variations in the gravity field caused by differences in rock density (Asniar et al., 2020; Hoerunisa and Sismanto, 2020).

In this study, gravity satellite data were used. Satellite gravity data can be used for mapping subsurface geological structures. The GGMplus data is a global gravity model with very high resolution, having data point spacing of approximately ~200 m in the north-south direction (Hirt et al., 2013, 2019). GGMplus can provide a detailed description of the gravitational field conditions in an area such as density, depth, geometric shape of structures or objects that cause anomalies below the surface (Sudrajad, 2018).

The difference in anomaly value is due to the density contrast in the subsurface. The difference in density in the subsurface can be used as a starting point to predict the presence of fault structures in the research area.

2. METHOD

This study used Global Gravity Model Plus (GGMplus) and the Global Shuttle Radar Topography Mission (SRTM). GGMplus data and SRTM data can be obtained through official online database; from this link (http://ddfe.curtin.edu.au/gravitymodels/GGMplus/). These data sources provide access to high-resolution global gravity models. Data from http://ddfe.curtin.edu.au/gravitymodels/ERTM2160/ are also used.

The SRTM data is topographic data used for gravity field correction (Hirt et al., 2019). SRTM data is in the form of full-scale gravity with spacing between data points of ~220 m. SRTM data is used to correct GGMplus data to obtain the complete Bouguer anomaly for the research area, by subtracting GGMplus data from SRTM data. The complete Bouguer anomaly value is then processed to obtain regional and residual anomalies, then further analysis is carried out using First Horizontal Derivative Second Vertical Derivative to determine the presence or absence of faults and fault types (Trimulyati and Ardian, 2022).

3. RESULTS AND DISCUSSION

The complete Bouguer anomaly value is a gravity anomaly that represents the distribution of subsurface density in shallow and deep areas. Effects originating from shallow areas are called residual anomalies, while effects originating from deep areas are called regional anomalies (e.g. on Charisma et al., 2022). Based on the results of gravity data processing, the value distribution and complete Bouguer anomaly map are shown in Figure 1. The complete Bouguer anomaly in the research area is in the range of 47.7 mGal to 193 mGal.

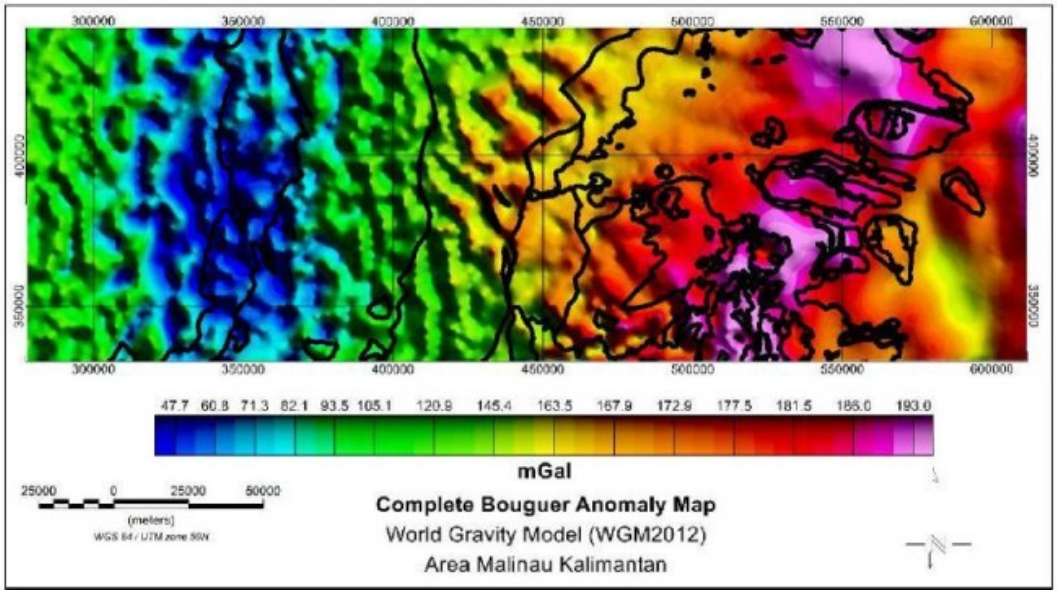

Figure 1: Complete Bouguer Anomaly Map of Semolon Geothermal Prospect Area. Red colour indicates high Bouguer anomaly.

The distribution of high anomalies in the research area ranges from 163.5 mGal to 193 mGal, depicted with color contrasts ranging from yellow to pink. The distribution of low anomalies in the research area ranges from 47.7 mGal to 145.4 mGal, depicted with color contrasts ranging from dark blue to green. The map shows that the distribution of high anomalies is on the east side of the research area and low anomalies are on the west side of the research area.

The regional anomaly in the research area is in the range of 52.6 mGal to 190.9 mGal (Figure 2). The regional anomaly pattern has a high tendency in the East with anomaly values of 164.9 mGal to 190.9 mGal and low in the West with anomaly values of 52.6 mGal to 145.0 mGal. The high value in the East indicates that the rocks in the area have a fairly high density compared to rocks in the West.

The formation of the Tarakan Basin and its deposition process cannot be separated from the existing tectonic phenomena. To the west of the Tarakan Basin lies the Kuching High, consists of metamorphic rock complexes from the Cretaceous age and a melange rock complex from Kalimantan Central Ranges of Early Eocene age (Achmad and Samuel, 1984). To the north of the study area is Sampurna Peninsula High. It consists of igneous and metamorphic rock complexes that have undergone uplift. In the southern part of the Tarakan Basin, there is the Mangkalihat-Peninsula High which is a thin sedimentary rock of Tertiary age deposited on top of uplifted bedrock. In the east, the Tarakan Basin is bordered by the Sulawesi Sea which continues to deepen and becomes the Makasar Trench.

The regional stratigraphy of the Tarakan Basin is divided into pre-Tertiary, Tertiary, and Quaternary. The oldest Tertiary rocks belong to the Danau Formation, which is composed of strongly tectonized rocks and metamorphic rocks with significant thickness. The age is still debated between Permian-Carboniferous or Jurassic-Cretaceous (Achmad and Samuel, 1984). The Sembakung Formation unconformably overlies the Danau Formation, consisting of red sandstones and conglomerates from the Middle Eocene (Achmad and Samuel, 1984).

The low regional anomalies in the western part of the research area are suspected to be caused by rocks with low density, this is in accordance with the geological data of the research area, indicating sedimentary rock deposits and geological structures such as faults or faults in the rock layers (Baharrudin , 2011; Dahlan et al (2011). In addition, there are geothermal manifestations such as hot spring, which can cause rock density to decrease due to alteration minerals produced by the circulation of hot water (Huenges, 2010).

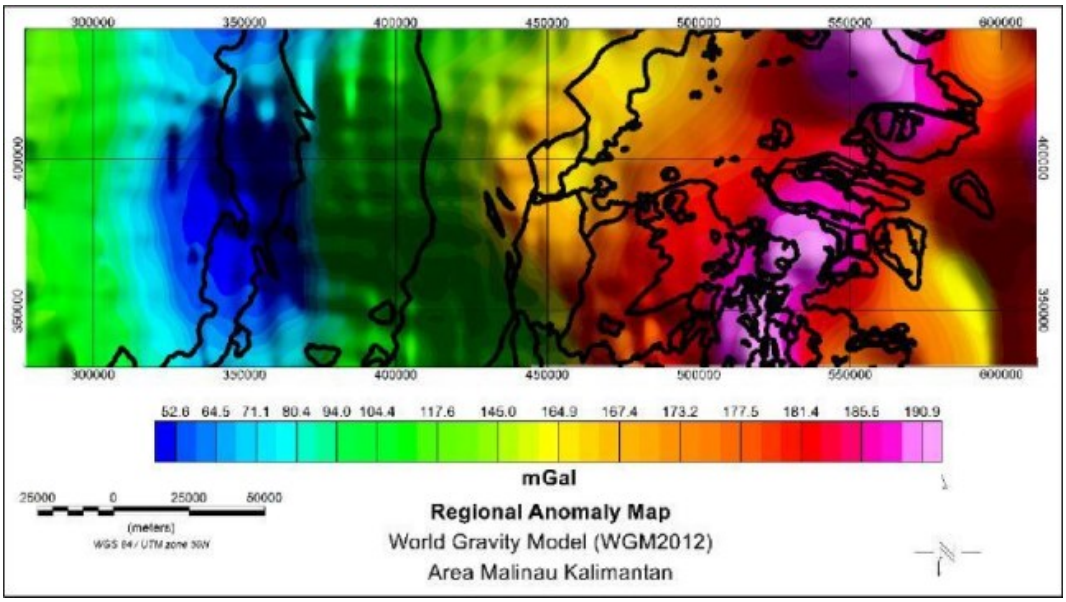

Figure 2: Regional Anomaly Map of Semolon Geothermal Prospect Area.

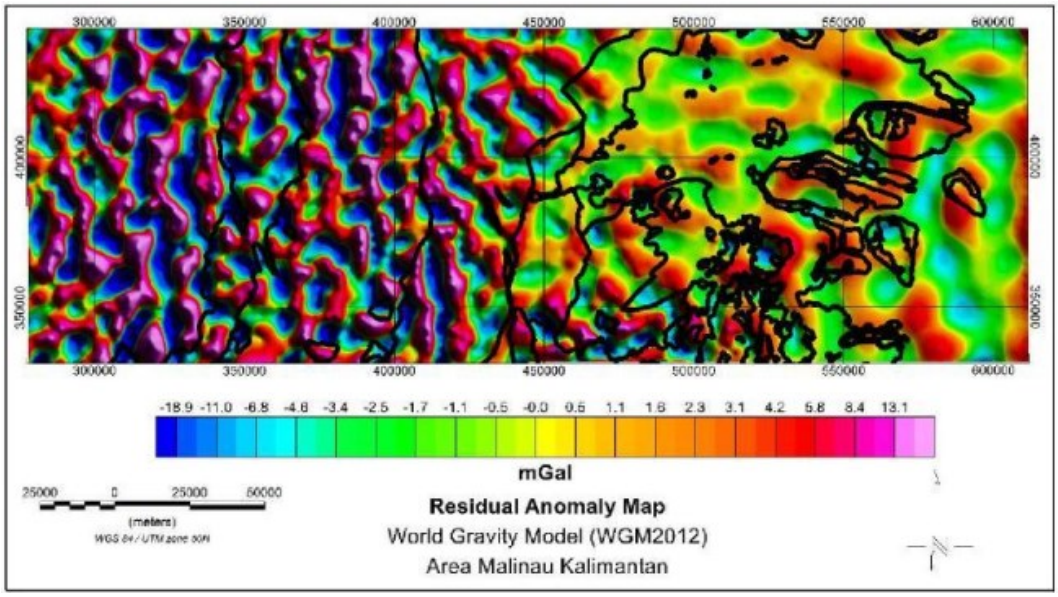

Figure 3: Residual Anomaly Map of Semolon Geothermal Prospect Area.

The results of the distribution of values and the residual anomaly map are shown in Figure 3. The residual anomaly in the research area is in the range of -18.9 mGal to 13.1 mGal. The negative anomaly value indicates that there is a much lower density value compared to the surrounding area. Low residual anomalies are in the range of -18.9 mGal to -0.5 mGal, depicted with dark blue to green color contrast. High residual anomalies are in the range -0.5 mGal to 13.1 mGal, depicted with orange to pink color contrast.

Based on the derivative analysis results, some faults were identified. These faults were identified due to maximum or minimum FHD (First Horizontal Derivative) that intersect with zero value of SHD (Second Horizontal Derivative).

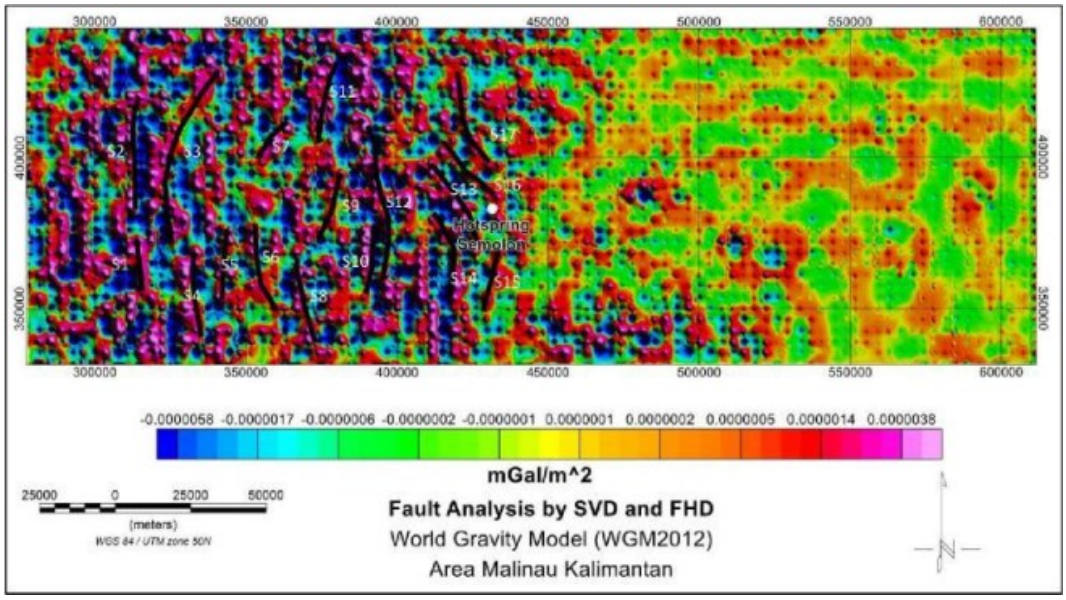

Figure 4: First Horizontal Derivative and Second Horizontal Derivative Map of Semolon Geothermal Prospect Area.

4. CONCLUSION

Gravity satellite data is very helpful to understand a geothermal prospect area in regional scale. Sedimentary layer and basement can be mapped as low and high Bouguer anomaly, respectively. Regional anomaly also displays similar result with Bouguer anomaly map. Derivative analyses shows that there are some faults indication with direction SE-NW, similar to Sampoerna Fault direction, close to Semolon warm spring.

REFERENCES

Achmad, Z. and Samuel, L.: Stratigraphy and Depositional Cycle in the NE. Kalimantan Basin, Proceedings, Ind. Petr. Assoc, 13th Ann. Convention, Jakarta (1984).

Ahluriza, P. and Udi, H.: Analysis of Indirect Utilization of Geothermal Energy Potential in Indonesia, Journal of Energy and Renewables, 2, (2020), 53-59.

Asniar, Jamhir, S. and Suryawan, A.: Estimation of Subsurface Structure in the North Buton Region, Southeast Sulawesi Province Based on Local Gravity Anomaly Data from GGMplus Satellite Imagery, Journal of Indonesian Geophysical Engineering, 2, (2020), 20-27.

Baharudin.: Petrology and Geochemistry of Jelai Tertiary Volcanic Rocks in the Malinau Region, East Kalimantan: Tectonic Implications, Jurnal Geologi dan Sumberdaya Mineral, 21, (2011), 203-211.

Charisma, P. A. W., Ahmad, Z., Suharno and Nandi, H.: Separation Using Polynomial Fittings and Second Vertical Derivative (SVD) Analysis to Identify Faults in The Geothermal Field of Pantar Island, Alor District, Journal of Geology and Mineral Resources, 23, (2022), 91-96.

Dahlan, Didik, R. and Edi M.: Preliminary Geothermal Investigation of Nunukan Regency, Bulungan Regency, and Malinau Regency, East Kalimantan Province, Proceedings, Activities of the Geological Resources Center (2011).

Hirt, C., Claessens, S., Fecher, T., Kuhn, M., Pail, R. and Rexer. M.,: New Ultrahigh-resolution Picture of Earth's Gravity Field, Geophysical Research Letters, 40, (2013), 4279-4283.

Hirt, C., Yang, M., Kuhn, M., Bucha, B., Kurzmann, A., and Pail, R.: SRTM2gravity: An Ultrahigh Resolution Global Model of Gravimetric Terrain Corrections, Geophysical Research Letters, 46, (2019), 4618–4627.

Hoerunisa, A. and Sismanto.: Interpretation of K51S Geothermal Area Gravity Data Anomalies Based on 3D Modeling, Journal of Physics Indonesia, 24, (2020), 136-140.

Huenges, E.: Geothermal Energy Systems: Exploration, Development, and Utilization. Weinheim: Wiley-VCH (2010).

Sudrajad, B.: Modeling of the Subsurface Structure of the Nabire Regency Area in the Northern Part of Bird's Neck on Papua Island Using Three-Dimensional (3D) Inversion Modeling and Derivative Horizontal Analysis Based on GGMplus Gravity Anomaly Data, Thesis, Gadjah Mada University (2018).

Sukendar, P. M., Bandi, S. and Arwan, P. W.: Analysis of the Distribution of Geothermal Potential Areas of Mount Salak with Surface Temperature, Vegetation Index and Geomorphology, Journal of Undip Geodesy, 5, (2016), 66-75.

Trimulyati, W. and Ardian, P.: Identification of the Subsurface Structure of Mount Tandikat Using Gravity Methods Based on Satellite Data. Journal of Unand Physics Journal. 1, (2022), 366-372.

Yushantarti, A.: Thermal Fluids Characteristics of Low Temperature Geothermal Systems at Kalimantan Island, Indonesia, Proceedings, 45th Workshop on Geothermal Reservoir Engineering Stanford University, Stanford, California, CA (2020).

Zarkasyi, A. and Dikdik, R.: Gravity Force and Audio Magnetotelluric (AMT) Survey in the Sajau Geothermal Area, Bulungan Regency, North Kalimantan Province, Proceedings, Activities of the Geological Resources Center (2015).

Interpolation Methods in Python for Geothermal Field Analysis: A Comparison of Cubic, Linear, and Nearest Neighbor Approaches

Fanzly Togap Zisochi Lase[1,2], Prihadi Sumintadiredja[1],
Tony Rahadinata[3], and Ahmad Zarkasyi[3]

[1]Faculty of Earth Science and Technology, Institut Teknologi Bandung
[2]IT-HC and Business Support Division, PT. Pertamina Geothermal Energy
[3]Pusat Sumber Daya Mineral Batubara dan Panasbumi

togaplase8668@gmail.com

Keywords: Cubic Interpolation, Geothermal, Interpolation, Linear interpolation, Nearest neighbor Interpolation

ABSTRACT

Interpolation in the world of geophysics has currently attracted a lot of attention because it can estimate unknown values at a certain time or location. Many interpolation methods have been developed in geophysical software such as Oasis Montaj, Surfer, Arc-GIS, and many other programs. In this research, we try to make Python programming using the Python Geophysics library and perform interpolation techniques with a focus on cubic interpolation techniques, linear interpolation, and nearest neighbor interpolation, and at the end, analyze the results of interpolation in the Cisolok-Cisukarame geothermal field. The data used is in the form of gravity data that has been measured in the field at 75 points and has undergone data processing to achieve a complete bouguer anomaly (CBA). Cubic interpolation analysis produces smooth estimates, can capture more complex variations in data and provides high accuracy but is computationally very intensive and requires a lot of memory and processing power. Linear interpolation is simple, easy to implement and suitable for linearly varying data but may not be accurate for non-linear and produces less accurate estimates. The nearest neighbor is like linear interpolation in its advantages but does not provide smooth estimates and produces a ladder-like appearance to the interpolated data. The Cubic technique produces excellent results over linear and nearest and maintains good value positivity.

1. INTRODUCTION

Geophysical data is often interpolated to generate a spatial data representation that can be described in the form of contour maps. Interpolation plays a crucial role in geophysical data analysis, especially when data points are unevenly scattered across the study area. In geophysical surveys, data are often collected at irregular intervals due to practical limitations or varying survey conditions. However, many analytical techniques in geophysics, such as fast Fourier transform for signal processing or equivalent layer methods for inversion, require regularly arranged data to allow efficient computation and interpretation (Gunn, 1975; Oldenburg, 1975). In geophysical interpolation, a lot of research has been conducted. Crain and Bhattacharyya (1967) introduced qualitative criteria to evaluate the balance between accuracy and computational time. The least-squares method with orthogonal polynomials generated through the Gram-Schmidt process showed the highest quantitative accuracy. Later, Bhattacharyya (1969) developed an interpolation method using cubic surfaces, which he stated was more accurate than using orthogonal polynomials. Several other studies followed this approach and proposed variations of the algorithm (Thomson, 1970; Heissing et al., 1972; Rasmussen and Sharma, 1979). Crain (1970) classified interpolation methods into two categories: (1) mathematical surface methods, and (2) numerical surface methods. The first method produces an analytical surface that passes through the observation points, while the second method develops interpolation points based on the distribution of neighboring observation points. Casanova P., and Alvarez R., (1985) presented a classification of Splines that featured the use of fast cubic spline algorithms operating on dense grids in an irregular area bounded by a rectangle.

Li W., et al. (2010) proposed a linear interpolation method by transforming rectangular coordinates into polar coordinates. owever, the algorithm error was high, and the operations were complex. W. Y., et al. (2012) proposed an improved method with a comparative point interpolation algorithm based on 8 directions, through maximum interpolation error analysis, analytical solutions, numerical comparisons, and computer computations, an error calculation method was obtained. This method demonstrated advantages in high interpolation precision, stable computation, and high computation speed. Zeng Min et al., 2016, found linear interpolation to be very promising for industrial applications due to its fast and promising calculations. Guilin (2020) presented missing data, and when experimental tests were conducted, linear interpolation showed good computational performance and efficiency. Dunlop, G. R. (1980) presented nearest neighbor interpolation, which had limited accuracy and was time-consuming. The presented interpolation methods are also used in many software applications such as Oasis Montaj, Surfer, Arc-GIS, and many other interpolation programs. In this study, we attempt to create Python

programming using modules that can perform interpolation techniques, focusing on cubic, linear, and nearest neighbor interpolation techniques.

2. METHODOLOGY

In this section, we will explain a little understanding of cubic, linear and nearest neighbor interpolation theory.

2.1 Cubic Interpolation

Bicubic interpolation is the simplest two-dimensional interpolation method that preserves the continuity of the function and its first derivatives (both normal and tangential) across cell boundaries (Russels W., S., (1995). It is a mathematical technique frequently used to generate new points within the range of a set of existing points. These new points represent function values of an interpolation function, known as a spline, which is composed of several cubic piecewise polynomials. This article describes the mathematical process behind this computation.

In the process of constructing the spline $\boldsymbol{f}$: $[x_1, x_{n+1}] \rightarrow$ R, where n consists of polynomials of degree 3 referred to as $\boldsymbol{f_1}$ to $\boldsymbol{f_n}$. The resulting function has the following structure:

$$f(x) = \begin{cases} a_1x^3 + b_1x^2 + c_1x + d_1 & \text{if } x \in [x_1, x_2] \\ a_2x^3 + b_2x^2 + c_2x + d_2 & \text{if } x \in [x_1, x_2] \\ \dots & \\ a_nx^3 + b_nx^2 + c_nx + d_n & \text{if } x \in [x_n, x_{n+1}] \end{cases} \quad (1)$$

Note that each polynomial is valid only within a specific interval; together, they form the interpolation function. While extrapolation predicts values beyond the range of the data, interpolation operates solely within the data boundaries $[x_n, x_{n+1}]$. With appropriately selected coefficients for the polynomials a_i, b_i, c_i, d_i, the resulting function passes smoothly through the points. To determine these coefficients, several equations are established, forming a system of equations that can be uniquely solved.

To solve the system of equations, two more pieces of information are needed. Arbitrary constraints, like setting the third derivative at a chosen point (for instance, the fourth point), to zero can be used. However, a commonly used method involves selecting boundary conditions, which consist of a pair of equations. Detailed explanations of four conditions—natural spline, not-a-Knot spline, periodic spline, and quadratic spline—are elaborated below.

2.1.1 Natural Spline

A natural spline is characterized by setting the second derivative of the initial and final polynomials to zero at the boundaries of the interpolation function.

$$\begin{aligned} 6a_1x_1 + 2b_1 &= 0 \\ 6a_nx_{n+1} + 2b_n &= 0 \end{aligned} \quad (2)$$

Visually, this means that the rate of change of the function approaches zero at both the beginning and end points.

2.1.2 Not-a-Knot Spline

For the not-a-knot boundary condition, the third derivatives of the first two polynomials are equal at the point where they meet (x_2). Similarly, the last two polynomials meet (x_n) at another point, with their third derivatives also being equal, resulting in

$$\begin{aligned} \frac{d^3}{dx^3}f1(x) &= \frac{d^3}{dx^3}f2(x) \quad |x = x_2 \\ \frac{d^3}{dx^3}f_{n-1}(x) &= \frac{d^3}{dx^3}fn(x) \quad |x = x_n \end{aligned} \quad (3)$$

After calculating these derivatives, this can be resolved by

$$\begin{aligned} a_1 &= a_2 \\ a_{n\text{-}1} &= a_n \end{aligned} \quad (4)$$

that is making the a -coefficients equal.

2.1.3 Periodic Spline

In periodic interpolation, the first polynomial's first and second derivatives are set equal to the last polynomial's corresponding derivatives. Visually, this ensures that the function can seamlessly repeat or tile. This helps if $\boldsymbol{f}$ $(x_1) = \boldsymbol{f}$ (x_{n+1}) but should work equally well with functions y where the first and last point values are different.

$$3a_1x_1^2 + 2b_1x_1 + c_1 = 3a_nx_{n+1}^2 + 2b_nx_{n+1} + c_n$$
$$6a_1x_1 + 2b_1 = 6a_nx_{n+1} + 2b_n \quad (5)$$

2.1.4 Quadratic Spline

The quadratic boundary condition specifies that both the first and last polynomials are quadratic, making this method the most straightforward. Mathematically, this means that the first coefficient of both polynomials is equal to zero:

$$a_1 = a_n = 0 \quad (6)$$

2.2 Linear Interpolation

In python programming, linear interpolation is constructed using triangulating inputs where each performed triangle uses barycentric linear interpolation (Gommers, R., (2022)). Given a sample sequence $f_n = f(nT)$ which is derived from a sample of uniform functions $f(x)$ taken in steps of T, the standard method of linear interpolation constructs a function $f_T(x)$ with the following process: for $x \in [(n-1)T, nT]$, $f_T(x) = a_nx + b_n$, where a_n and b_n are chosen such that $f_T((n-1)T) = f_{n-1}$ and $f_T(nT) = f_n$. This can be shown to be equivalent to (Blu, T., et al., 2024):

$$f_T(x) = \sum_{n\in\mathbb{Z}} f_n \, \mathrm{A}\left(\frac{x}{T} - n\right) \quad (7)$$

Where A is the 'hat' function, or linear B-Spline: A $(x) = |x|$ for $|x| \leqslant 1$ and A $(x) = 0$ for $|x| > 1$ (M. Unser, 1999).

2.3 Nearest Neighbor Interpolation

Xi, Yi are expressed as training samples for $i = 1, \ldots, n$. Given a data point x for testing, determine $R_{k+1}(x)$ to be the distance between x and its (k+1) nearest neighbor. Without loss of generality, let $X^1(x), \ldots, X^k(x)$ denote the unsorted k-nearest neighbor of x, and write as $X^1, \ldots, X^k$ for simplicity. Denote $\{R_i(x)\}_{i=1}^k$ and $\{Y^i(x)\}_{i=1}^k$ ($\{R_i\}_{i=1}^k$ and $\{Y^i\}_{i=1}^k$ in short) as distance between X^i and x and the corresponding responses. For regression models, the goal is to estimate $\Rightarrow(Y|X = x)$. Denote $\eta(x)$ as target the function, where $\eta(x) = \Rightarrow(Y|X = x)$, and $\sigma^2(x) = Var(Y|X = x)$. A Nearest Neighbor regression estimator at x, based on nearest k neighbors, is defined as

$$\eta k, n(x) = \sum_{i=1}^{k} W_i(x)\, Y^i, \quad (8)$$

Where $W_i(x)$ indicate the weight for each neighboring data point. For weight scheme $W_i \geqslant 0$ and $\sum k\, W_i = 1$, and traditional $W_i = 1/k$ for all $i = 1, \ldots, k$.

Figure 1 shows how interpolation processing is conducted in Python for gravity data in the Cisolok-Cisukarame geothermal field. The input used includes Python modules or libraries such as pandas, numpy, matplotlib, and scipy. The data is separated into two parts in CSV format: gravity data containing complete Bouguer anomaly data, and elevation data containing coordinate points and elevation. These are then displayed on a map to visualize data distribution and the values of each point. This process enables us to perform gridding interpolation using three different methods: cubic, linear, and nearest neighbor interpolation maps.

3. BACKGROUND GEOTHERMAL AREA

The Cisolok-Cisukarame geothermal field is situated in the western region of Java Island, within Cisolok village, Cisolok sub-district, Sukabumi district, West Java province, Indonesia (Figure 2). Evidence of subsurface hydrothermal activity in the field is demonstrated by surface manifestations such as hot springs and geysers with high temperatures and a relatively neutral pH, and flow rates of approximately 10 L/m. Additionally, the area features deposits of travertine and silica sinter in alteration zones (Herdianita & Mandradewi, 2010). These observations led to a pre-feasibility study in 1970, which involved a detailed 3G (geological, geochemical, and geophysical) survey. In Figure 3 the Cisolok-Cisukarame geothermal field is primarily composed of Quaternary rocks, including andesitic, basaltic, and pyroclastic lavas from Mount Halimun. Additionally, there are sedimentary rocks such as limestone (Sujatmiko & Santosa, 1992).

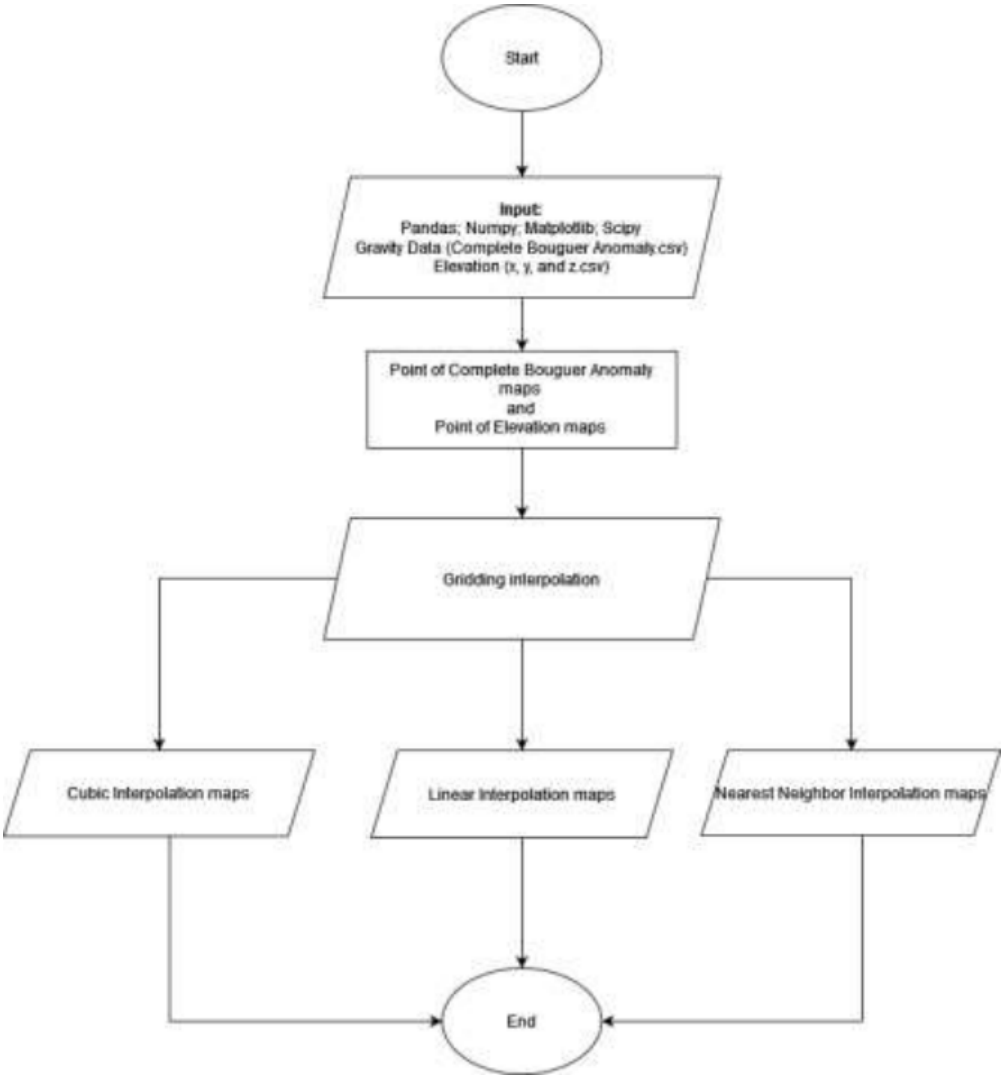

Figure 1: Flowchart of interpolation processing using python gravity data at Cisolok-Cisukarame geothermal field.

The geological structures in the study area, which trend north-south and northeast-southwest, formed during the Plio-Pleistocene period and are now covered by Quaternary volcanic deposits (Sujatmiko & Santosa, 1992; Herdianita & Mandradewi, 2010). The geothermal manifestations in the Cisolok-Cisukarame area are divided into two distinct regions: Cisolok and Cisukarame. In the Cisolok region, there are hot springs and geysers with temperatures ranging from 90 to 100°C and a relatively neutral pH of about 8 (Suryantini, 2009; Herdianita & Wulandari, 2010; Haty & Nugroho, 2013; Abdidallah et al., 2017).

The manifestations in Cisolok feature high sulfate and bicarbonate fluid types, likely influenced by limestone, as indicated by the presence of travertine deposits in the area (Sintawati, 2014; Kurniawan et al., 2018). Meanwhile, the Cisukarame region has hot springs with temperatures between 54 and 99°C and a relatively neutral pH of around 6.8 to 8.2 (Haty & Nugroho, 2013). The manifestations in Cisukarame contain sodium chloride fluid, reflecting the reservoir fluid (Sintawati, 2014). Consequently, it is believed that Cisolok and Cisukarame are characterized by different geothermal systems, as evidenced by the manifestation temperatures reaching the boiling point in both areas. The reservoir temperature in the Cisolok-Cisukarame area, estimated using a Na-K geothermometer and empirical equations from Fournier (1979) and Giggenbach (1988), ranges from 185 to 212°C (Kurniawan et al., 2018).

The geophysical survey utilized DC Resistivity, Magnetotelluric (MT), and Gravity methods, leading to the drilling of the first well (CSL-01) to a depth of 1477 meters. However, the CSL-01 well was used solely for publication purposes. DC Resistivity surveys, both 1-D and 2-D, were carried out in 1976 and 1982 by West Japan Engineering Consultants and Pertamina, encompassing 150 measurement points, with only 69 of these points deemed suitable for analysis due to data quality issues (Alhamid, 1982; Hochstein, 1988). These studies revealed a low resistivity anomaly (<10 ohm.m) in the Cisukarame area, open to the south, indicating it as the center of the

geothermal system and an upflow zone, whereas the Cisolok area is identified as an outflow zone. Kurniawan et al. (2018) concluded that MT results indicate a low resistivity anomaly zone beneath the Cisolok-Cisukarame area, forming a northeast-southwest pattern in the eastern part, associated with the clay cap zone and potential heat sources in the northeast.

Research by Lase & Soebakir (2022) identified a controlling structure through the low residual anomaly, evidenced by hot spring and spouting spring manifestations oriented NE-SW, N-S, and NW-SE. From the research of Lase et al., (2024) applying the gravity inversion model in the Cisolok-Cisukarame geothermal system, West Java, Indonesia. where there are 2 different heatsources where Cisukarame originates from the magmatic Halimun mountain and Cisolok is a cooling pluton that has a deeper depth than Cisukarame. Structures in the form of faults are identified and have directions that match the regional tectonic faults.

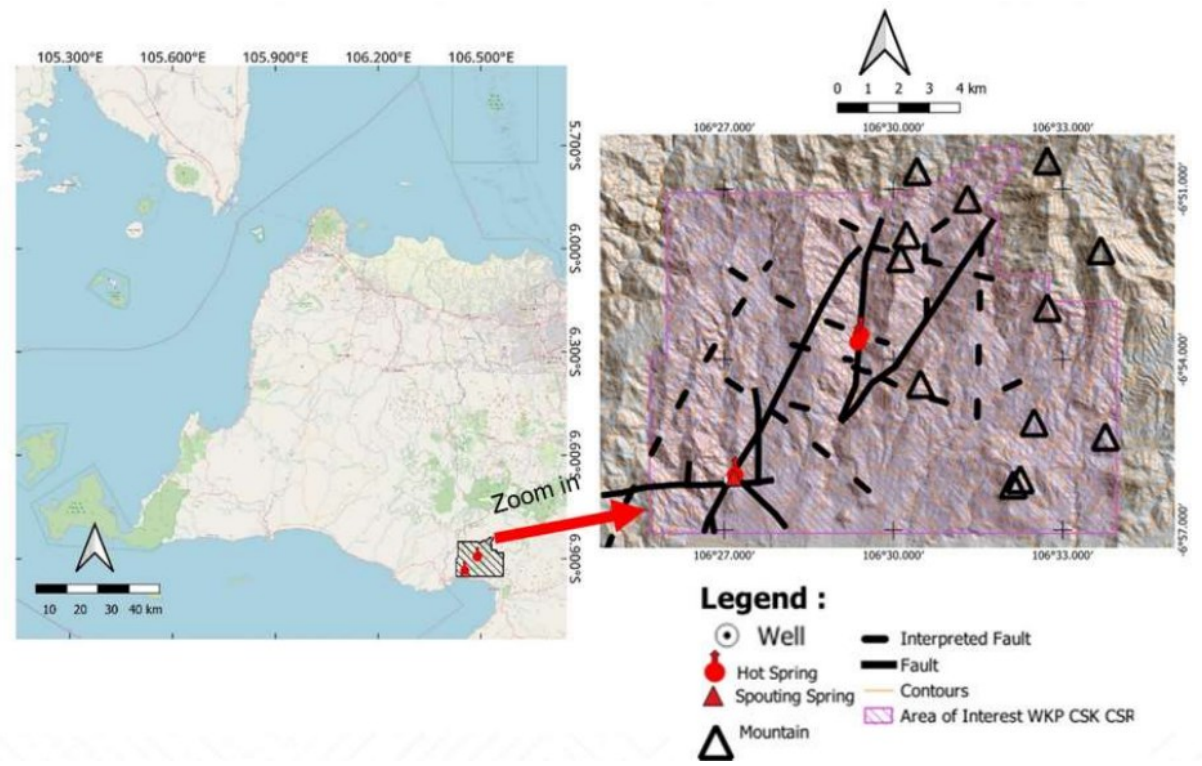

Figure 2: Location of the study area Cisolok-Cisukarame Geothermal Field in West Java, Indonesia. (modified Lase et al., 2024).

4. GEOLOGY SETTING

The Csk - Csr geothermal field is located to the southeast of Baya Mountain and consists of a large dome, Baya Dome, and several Upper Pleistocene mountains. This area is dominated by volcanic eruptions. Quaternary period with relatively steep topography ranging from 150 to 900 m above sea level. (Abdilla et al., 2017). In general, the lithology of the Csk - Csr region consists of three main types of rocks: sedimentary rocks (early sedimentary rocks); Miocene-Pliocene), acidic intrusive rocks (Miocene), and andesites (Pleistocene). Pleistocene andesite is the youngest volcanic product in the region.

Based on Figure 3, the Cikotok Formation, which consists of 12 rock units, is the oldest formation consisting of volcanic breccia, tuff, and lava. The Citarete Formation is composed of limestone and tuff, whereas the Cimapag Formation is dominated by breccia and conglomerate (Sujatmiko, 1992). Dacite occurs in the south, and in the west, granite is covered by lava and pyroclastic flow deposits (Sujatmiko, 1992). The Citorek Formation is composed of marine sediments and volcanic products deposited in the Cikotok, Citarete, and Cimapag Formations. Quaternary volcanic products are andesite and basalt, products of Mount Harimun (Sujatmiko, 1992). The alluvium is the youngest product in the region and is distributed around Cimaja and Pelabuhan Ratu in the south (KESDM, 2017).

In regional geology, the structural patterns that develop in the western part of Java Island are the Meratus pattern, the Java pattern, and the Sunda pattern. The southern part of the Leuwidamar geological map has a complex geological structure, which is caused by tectonic disturbances, resulting from the meeting between the geanthropic Java and the geanthropic Bukit Barisan in Sumatra. This area has a fault pattern with a general North-South

direction and there is also a northeast-southwest direction. There is a fold axis with a West-East to Northwest-Southeast direction. This geological structure is interpreted as a migration path for the emergence of geothermal discharges such as hot springs, spouting springs and the others in the Csk - Csr geothermal field.

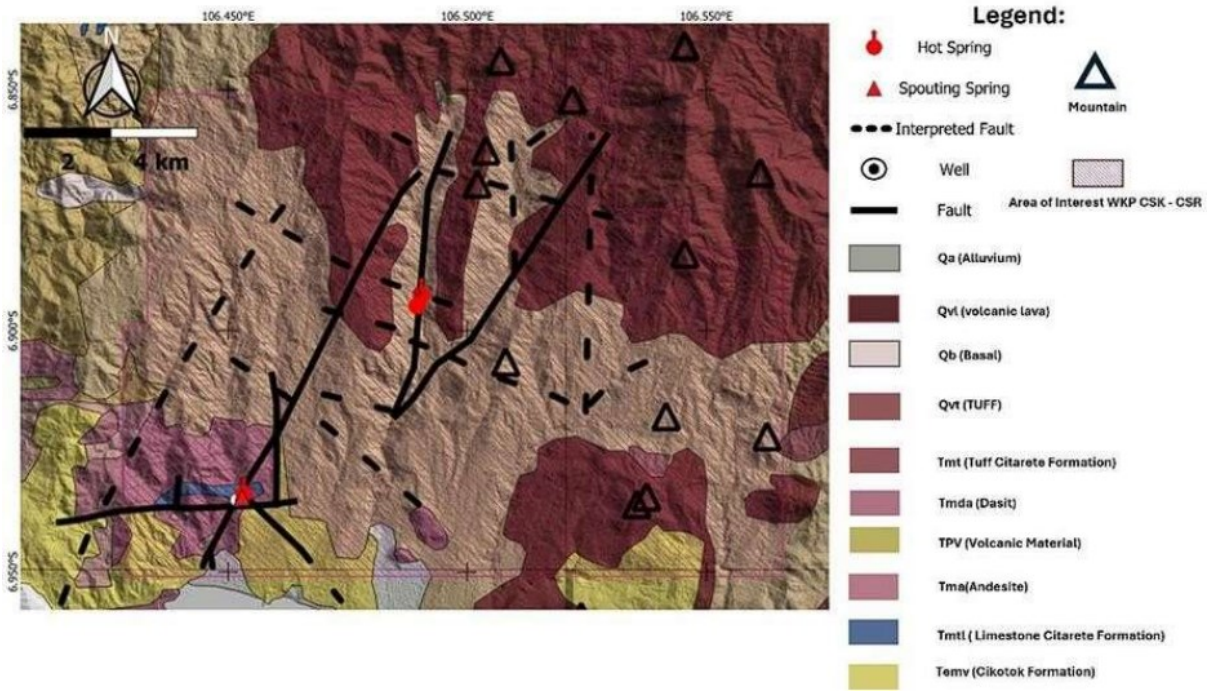

Figure 3: Regional Geology Cisolok-Cisukarame Geothermal (modified from Suryantini and Hendrasto F, 2009; Lase et al., 2023).

5. APPLICATION

5.1 Cisolok-Cisukarame Gravity Survey

The gravity acquisition in the Cisolok-Cisukarame geothermal field had 75 measurement points, with a spacing of 1 km between data points, covering an area of 100 km², and was conducted by PVMBG in 2011. Lase and Soebakir (2023) presented the GGMPLUS satellite gravity data of Cisolok-Cisukarame using minimum curvature to display CBA maps. Lase et al. (2024) presented gravity data acquisition in the Cisolok-Cisukarame geothermal field using minimum curvature to display CBA maps. In this study, we attempt to present all the data using the Python programming language, following the flowchart (Figure 1). Figure 4 shows the elevation points from the measured gravity points, where the darker purple color indicates lower elevations, and the brighter yellow color indicates higher elevations. Figure 5 shows the gravity data points, where the purple color indicates lower CBA values, and the redder color indicates higher CBA values.

5.2 Application in interpolating: Cubic, Linear and Nearest Neighbor Cisolok-Cisukarame Geothermal Field

Complete Bouguer Anomaly Maps were created using three different interpolation applications. Figure 6 shows the results of Linear interpolation, Figure 7 uses Cubic interpolation, and finally, Figure 8 shows the results of interpolation using Nearest Neighbor.

6. RESULT AND DISCUSSION

Linear interpolation (Fig. 6) offers simplicity, computational efficiency, and ease of implementation and understanding, making it well-suited for data that varies linearly. However, its drawback is its inability to accurately capture non-linear variations, resulting in piecewise linear estimates that may not represent the underlying data accurately. On the other hand, cubic interpolation (Fig. 7) provides smoother estimates and can capture more complex data variations, delivering higher accuracy, especially for data with non-linear patterns. Nevertheless, it is more computationally intensive and requires more memory and processing power, particularly for large datasets. Meanwhile, nearest neighbor (Fig 8.) interpolation excels in simplicity, computational efficiency, and preserving the original data points, making it suitable for discrete datasets or those with irregularly spaced points. However, it may not provide smooth estimates for continuously varying data and often results in a staircase-like appearance in the interpolated data.

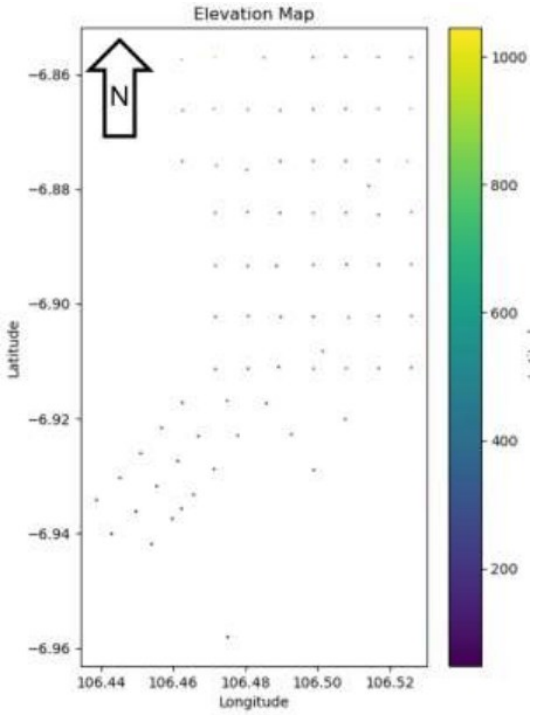

Figure 4: Elevation map from gravity station using python at cisolok-cisukarame geothermal field.

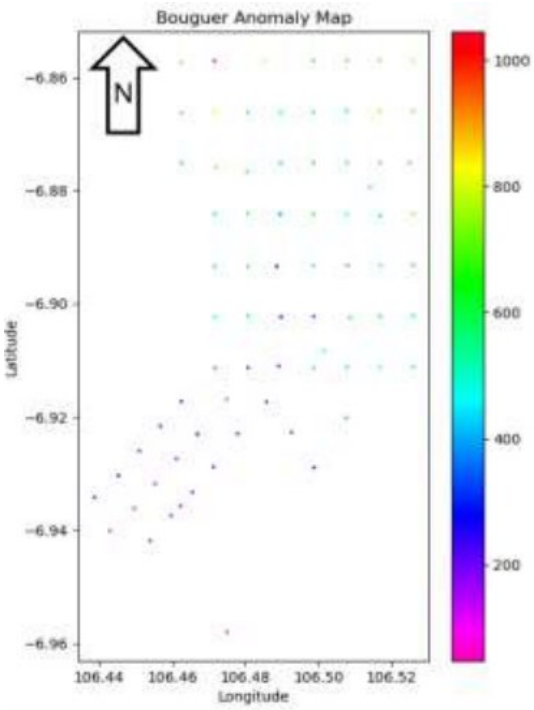

Figure 5: Complete Bouguer Anomaly map from gravity station using python at cisolok-cisukarame geothermal field.

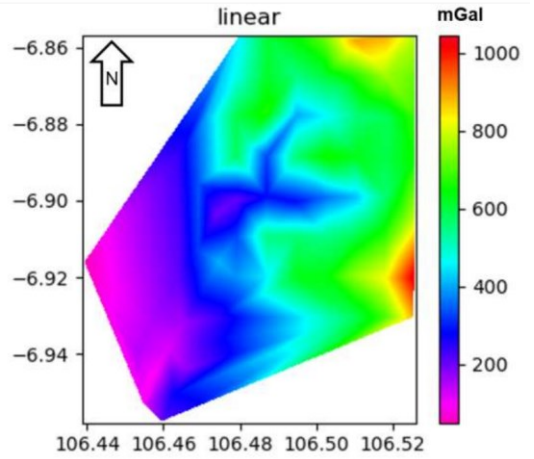

Figure 6: Elevation map from gravity station using python at cisolok-cisukarame geothermal field.

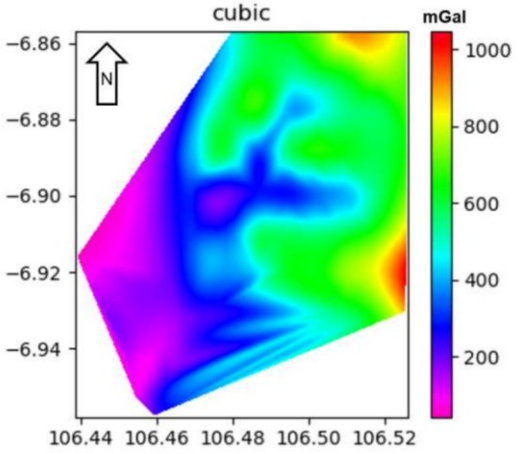

Figure 7: Complete Bouguer Anomaly map from gravity station using python at cisolok-cisukarame geothermal field.

7. CONCLUSION

We have presented a comparison of interpolation methods to test and generate interpolation performance using Python programming. The research demonstrates that there are advantages and disadvantages to each interpolation method, whether in terms of complex computations, linear or non-linear data, comprehensible learning, or using programming languages without software. Cubic interpolation yields interesting and good estimates, and it significantly has good accuracy despite the intensive and numerous computations involved. In summary, the cubic interpolation method performs better compared to Linear and Nearest-Neighbor methods.

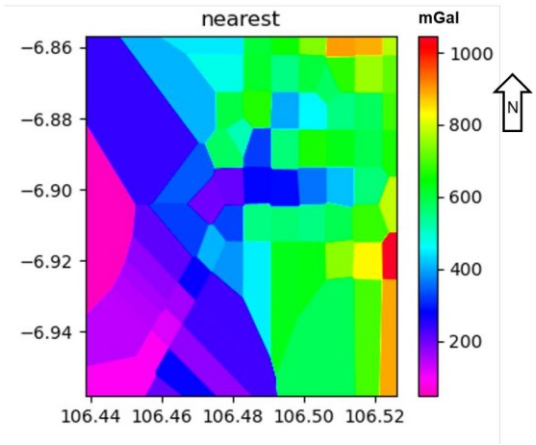

Figure 8: Elevation map from gravity station using python at cisolok-cisukarame geothermal field.

REFERENCES

Abdillah, M. R., Aditio, M., Alamsyah, M. S., Haryanto, A. D., and Rosana, M. F., Hidrogeokimia air manifestasi panas bumi di daerah Cisolok – Cisukarame, Kabupaten Sukabumi, Provinsi Jawa Barat.(2017), Padjadjaran Geoscience Journal, 1(3).

Alhamid, I., Resistivity Survey of the Cisolok-Cisukarame Geothermal Area, West Java, Indonesia. UNU Geothermal Training Programme National Energy Authority. (1982).

Bhattacharyya, B. K., : Bicubic spline interpolation as a method for treatment of potential field data: Geophysics, 34, (1969), 402-423.

Blu, T., Thévenaz, P., and Unser, M. : Linear interpolation revitalized. IEEE Transactions on Image Processing, 13(5), (2004), 710-719.

Crain, I. K., and Bhattacharyya, B. K., :Treatment of non equispaced two-dimensional data with a digital computer: Geo explor., 5, (1967), 173-194.

Crain, I. K., :Computer interpolation and contouring of two dimensional data: A review: Geoexplor., 8, (1970), 71-86.

Dunlop, G. R : A rapid computational method for improvements to nearest neighbour interpolation. Computers & Mathematics with Applications, 6(3), (1980), 349-353.

Fournier, R.O.: A revised equation for the Na/K geothermometer. Geothermal Resources Council Transactions, 3, (1979).

Giggenbach, W.F.: Geothermal solute equilibria. Derivation of Na-Mg-Ca geoindicator, Geochimica et Cosmochimica Acta, 52, (1988)

Gommers, R., Virtanen, P., Burovski, E., Weckesser, W., Oliphant, T. E., Haberland, M., ... & Moore, E. (2022). scipy/scipy: SciPy 1.9. 0rc2. Zenodo.

Guilin H: Missing data filling method based on linear interpolation and lightgbm. In Journal of Physics: Conference Series (Vol. 1754, No. 1, p. 012187). (2021, February). IOP Publishing.

Gunn, P. J., : Linear transformations of gravity and magnetic fields: Geophys. Prosp., 23, 1975, 300-312

Haty, I. P. and Nugroho, A. N. "Geothermometer dan Heat Loss Dalam Eksplorasi Geokimia Lapangan Panasbumi Daerah Cisukarame, Kabupaten Sukabumi, Propinsi Jawa Barat". (2013).

Heissing, R. C., Lee, H. K., Price, A., and Powers, E. N :Automatic contouring using bicubic functions: Geophysics, 37, (1972) 669-674.

Herdianita, N. R., and Mandradewi, W., Evolution of Cisolok–Cisukarame Geothermal System, West Java–Indonesia, Based on Its Surface Manifestation. (2010). In Proceedings World Geothermal Congress.

Hochstein, M.P., Assessment and Modelling of Geothermal Reservoirs (Small Utilization Schemes). (1988).Geothermics.

Sumartha, A. G. A., Kurniawan, I., Wiradinata, R., Nandaliarasyad, N., Pratama, H. B., and Prabata, T. W., Updating the Conceptual Model of Cisolok-Cisukarame Geothermal field, West Java, Indonesia. In IOP Conference Series: Earth and Environmental Science (Vol. 417, No. 1, p. 012025). (2020). IOP Publishing.

Lase, F. T. Z., and Soebakir, D. B. INVESTIGATION OF PERMEABLE ZONE USING MAGNETIC AND GGMPLUS GRAVITY DATA IN CISOLOK-CISUKARAME GEOTHERMAL FIELD, (2022, September).

Lase, F. T. Z., Soebakir, D. B., Rahadinata, T., and Zarkasyi, A., EVALUATION OF CISOLOK-CISUKARAME GEOTHERMAL SYSTEM USING GRAVITY INVERSION, (2023, September)

Lase, F. T. Z., Zarkasyi, A., Rahadinata, T., and Sumintadiredja, P., Interpretation of Gravity Data using Horizontal Gradient, Analytic Signal, Tilt Angle, and Total Horizontal Derivative of the Tilt Angle on Cisolok Cisukarame Geothermal Field, (2024, September)

Li W, Fan N, Yang C, : "The Study for Algorithm of Linear Interpolation Based on Bipolar Coordinates" [J]. Intelligent Computation Technology & Automation International Conference on, 3, (2010) , 977-979.

M. Unser, "Splines: A perfect fit for signal and image processing," IEEE Signal Process. Mag., (Nov. 1999), vol. 16, pp. 22–38.

Oldenburg, D. W :The inversion and interpretation of gravity anomalies, Geophysics, 39, (1975), 526-536. Rasmussen, K. L. and Sharrna, P. V: Bicubic spline interpolation: A quantitative test of accuracy and efficiency: Geophys. Prosp., 27, (1979), 394--408.

Russell, W., S,: "Polynomial interpolation schemes for internal derivative distributions on structured grids," Appl. Numer. Math. 17(2), 129–171 (1995).

Sintawati, F., Analisis Prospek Panasbumi Cisolok Cisukarame Menggunakan Data Magnetotellurik dan Gravitasi. Skripsi. Universitas Indonesia. (2014).

Sujatmiko and Santosa, S., Geologi lembar Leuwidamar, Jawa (lembar : 1109-3), skala 1:100.000, (1992).

Suryantini and Hendrasto F., Geothermal excursion Geothermal Magister Program Institut Teknlogi Bandung. (2009).

Thomson, R. F: Spline interpolation on a digital computer: Preprint X-692-70-261, Goddard Space Flight Center, Greenbelt, Maryland (1970)

Wei Y, Baosheng Y, Xinqiao Q., "Optimization of point-by-point comparison linear interpolation algorithm" [J]. Journal of Wuhan University of Science and Technology, (2012) 3:017

Preliminary Study of Mount Pandan Geothermal System at Bojonegoro Based on Surface Manifestation, Altered Minerals and Geochemical Fluids

Juan Adhipermana, Bimo Putra Panggabean,
Claudio Ronaldo Mendome, and Petrus Aditya Ekananda

University of Diponegoro

juanadhipermana@gmail.com

Keywords: Geothermal, Geochemical, Altered Minerals, Mount Pandan, Bojonegoro

ABSTRACT

Geothermal comes from the words Geo which means earth and Thermal which means heat, so it can be define as an energy source that comes from natural heat in the earth. Indonesia has high geothermal potential. Indonesia stores 40% of the world's geothermal reserves. Based on the Geological Agency of the Ministry of Energy and Mineral Resources (December 2020), Indonesia has total geothermal energy potential estimated to reach 23.7 GW. The research located on Jari, Samongrejo, and Sengaten village at Gondang District, Bojonegoro Regency, East Java. This area became a research location because there were indications of the potential for geothermal resources originating from Mount Pandan. Mount Pandan is a volcano in Bojonegoro Regency, East Java with geothermal manifestations in the form of mud pools and hot springs. The emergence of this manifestation can be used as data to measure the potential and existing geothermal systems. Besides that, It was discovered some alteration minerals in this area, such as travertine and pyrite. The research method used in this research was geological mapping, petrographic analysis of thin section, XRD analysis and fluid analysis. Based on the results of the geological mapping, it was found that there are several types of lithology, including mudstone interbedded with sandstone which has a gray color and this rock has carbonate cement. Then it was also found that there was andesite breccia lithology which had a brownish color, matrix supported and travertine minerals were found at some location, and also there was porphyry andesite lithology which had a grayish color dominated by plagioclase minerals and several other minerals such as quartz and biotite. Based on the results of petrographic observations, it is known that the presence of altered minerals is still very minimal, so it can be interpreted that our research area is an area with low-medium alteration intensity. Then, from the XRD results of rock samples that taken near the mud pool, it is dominated by the minerals smectite, and illite, so it can be interpreted that this location is located in the argillic zone. From the three fluid samples, located in the Keramat, Selogajah and Jari areas, it can be seen that this area has chloride fluid and it can be interpreted that this sample is included in the Mature Waters category. Based on the results found in the field, it can be interpreted that this research area is included in the upflow zone, as evidenced by the presence of chloride fluid, several travertine deposits, and clay minerals in the form of illite and smectite.

1. INTRODUCTION

Indonesia is one of the countries that has great potential for geothermal energy, because tectonically Indonesia is located at the three large plates which form a subduction zone and produce magmatism activity in the form of a row of active volcanoes (Ring of fire). The Ministry of Energy and Mineral Resources (ESDM) has estimated the total size of Indonesia's geothermal resources at 27,000 MW. However, only about 800 MW has been developed in seven locations with five of them located in Java (Setijadji, 2010).

Mount Pandan is one of the products of early Pleistocene-aged Quaternary magmatism located in the Wilis-Lasem arc segment in Bojonegoro Regency, East Java Province (Lunt et al., 1998; Smyth et al., 2005). The mountain was formed in the anticlinorium of the Kendeng Zone and is near back-arc volcanism. Mount Pandan is a quaternary mountain composed of andesite breccia and intrusions. This area has the potential for geothermal energy as indicated by several Geothermal manifestations that appear on the northern slope of Mount Pandan such as hot spring pools, mud pools and alteration rocks.

The potential for geothermal energy in Mount Pandan is associated with the volcanic environment. This research was conducted in the Gondang area, Bojonegoro Regency. The research was conducted using primary data with a geological approach such as geological mapping, petrological and mineralogical analysis of the constituent rocks of the study area, XRD analysis of altered rocks, spatial analysis, especially structures that are expected to control the appearance of manifestations on the surface. In addition, this research also using secondary data in the form of water geochemical data from the manifestation of hot springs which will later be used to determine the reservoir fluid temperature of the Mount Pandan geothermal system.

This research aims to collect detailed surface data such as the rock stratigraphy of the study area, alteration zones, and also the presence of manifestations which will later be used for zoning the geothermal system area of Mount Pandan. In addition, it is also to update existing alteration map in the research area.

2. REGIONAL GEOLOGY

The research site is located in Jari, Samongrejo, and Sengaten villages in Gondang District, Bojonegoro Regency, East Java. This area became the research location because of indications of the potential for geothermal resources originating from Mount Pandang. Bojonegoro itself is located in the Kendeng Zone or called the Kendeng Mountains, an anticlinorium with a west-east direction. The Kendeng Zone is a continuation of the North Serayu Mountains Zone that developed in Central Java. In the north, it is bordered by the Randublatung Depression, and the south is bordered by part of the mountain range (Solo Zone). The kendeng zone is composed of several formations, including:

- Kerek Formation, which is characterized by a mixture of clay, clayey marl, marl, silty tuffaceous sandstone, and tuffaceous sandstone. Also found is a typical graded bedding sedimentary structure that characterizes flysch.
- Kalibeng Formation, a formation that lies harmoniously above the Kerek Formation, is divided into two formation members namely Lower Kalibeng Formation and Upper Kalibeng Formation.
- Pucangan Formation, which develops as volcanic facies and black clay facies.
- Kabuh Formation, composed of sandstone lithology with non-volcanic materials such as Quartz, cross-bedded structure with conglomerate and tuff inserts, containing Mollusc fossils
- Notopuro Formation, composed of lava breccia lithology interspersed with tuffaceous sandstone and volcanic conglomerate.
- Undah Bengawan Solo Formation, consisting of polymict conglomerate with fragments of limestone, marl, and andesite, along with sandstones containing vertebrate fossils.

3. METHODS

This research was prepared using several types of methods, including field data collection in the form of water samples, as well as rock samples. Then further analysis is carried out on the existing data so that the results are obtained from several stages of analysis, including:

- Geochemical analysis, an analysis of the chemical composition of water to identify and determine the concentration of elements and chemical compounds contained in water, which is carried out by taking water samples in the field which are then tested in the laboratory.
- Petrographic analysis, an analysis that requires a thin section the sample rock that has been taken in the research area, this analysis requires the help of a polarizing microscope to observe the incision of a rock which is useful for knowing the minerals that make up the rock as well as the structure and texture of the rock and helps in knowing the geological history and formation.
- XRD analysis, an analytical method carried out by taking rock samples in the field then these samples are observed with an X-ray machine so that the results can be used to identify and determine the crystal structure of an alteration rock.

4. RESULTS

4.1 Surface Manifestation

4.1.1 Hot Springs

This manifestation is located in Jari Village, Bojonegoro. Where the water samples at this location have a clear color with the appearance of iron colour around the manifestation (Figure 1). Based on Ramadhani, 2018 water samples in this manifestation had a temperature of around 43^{o}C.

4.1.2 Mud Pools

This manifestation is located in Jari Village, Bojonegoro. Where the mud samples at this location have a grey color with strong scent of suplhur (Figure 2). Based on Ramadhani, 2018 water samples in this manifestation had a temperature of around 48^{o}C.

4.2 Petrology & Petrography

4.2.1 Porphyry Andesite

This rock has brownish-gray color, holocrystalline texture, where the condition of the entire rock composition consists of crystals. These rocks are usually formed where magma cools slowly. Based on the grain size, it is classified as medium to coarse. The relationship between the grains can be classified as euhedral, where the

crystals grow with a perfect shape, where the crystal boundaries correspond to the original crystal plane, growing with an ideal shape. The grain shape is classified as prismatic and granular. Prismatic is usually found in rocks that experience slow cooling, and granular where minerals have the same size. A special texture in these rocks is porphyritic (inequigranular), where minerals have grain sizes that are not the same as the texture of the rock where large crystals (phenocrysts) are embedded in a finer base.

Figure 2 : Mudpools manifestation & alteration minerals at Jari village.

If based on the petrology, there are several minerals identified. The first mineral identified is plagioclase, where plagioclase usually has a white color, with bright white, light luster, perfect cleavage, with a hardness of 6 - 6.5 Mohs. Hornblende was also found which has a greenish-black color, white spout, glassy luster, with a translucent tendency.

The mineral content found in this sample is quite diverse. By interpreting it using three different viewpoints (Figure 3) known from cutting the rock into thin sections, the following was obtained. On the phenocrysts, if based on the three identified viewpoints, this sample is composed of 37% plagioclase, with a colorless-gray-white appearance, euhedral, partly having a zoning texture. Hornblende was found at 13% with yellow-brown appearance, high relief, euhedral. In phenocrysts, sanidine is present with a percent found only in the third field of view, characterized by colorless-gray-white, euhedral. The rock mass is composed of plagioclase, hornblende, quartz and another unidentified minerals/glass.

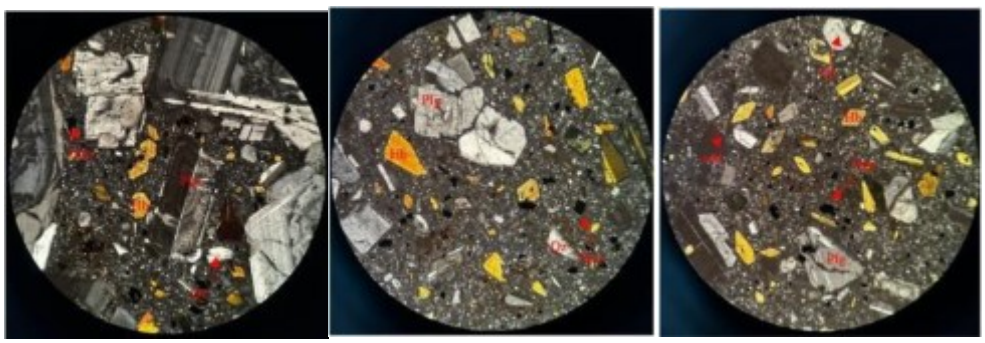

Figure 3: Petrography analysis for Porphyry Andesite (Plg : Plagioclase, Hb : Hornblend, Qz : Quartz, Opq : Opaq. Minerals, Md : Rock Mass)

From the three viewpoints and the interpretation carried out, it is known that the rock is an Porphyry Andesite (Russel B Travis, 1955). This rock has a porphyritic texture containing phenocrysts that are fused with the base mass, namely the matrix. The magma that forms porphyry andesite is an intermediate magma type. Apart from that, things that can explain that the rock is porphyry andesite, where the composition is a lot of plagioclase, pyroxene, and hornblende.

This porphyry andesite itself is interpreted to be formed from magma containing moderate amounts of silica. These magmas usually originate from subduction processes, where oceanic plates press down on continental plates, causing rock melting. When the magma reaches the Earth's surface or shallower depths, it undergoes rapid

cooling. This cooling causes crystallization of minerals present in the magma, such as plagioclase, quartz, and other minerals.

4.2.2 Volcanic Breccia

This rock has a greenish-gray color with fresh conditions. It has a grain size of gravel to sand. The mineral composition includes pyroxene, plagioclase, and hornblende with igneous rock fragments. In terms of physical properties of minerals, breccias have coarse grains, where grain size is usually > 2mm. The rock color tends to be dark blackish.

The mineral identification is known from several identification results. Pyroxene itself, has a color that tends to be dark green to black, which has a white spout, glass gloss, hardness of 5 - 6.5 Mohs, paramagnetic magnetism, with brittle properties. Plagioclase has a white color, with a glass gloss, hardness of 6 - 6.5 Mohs, with a prismatic structure, with a translucent classification. For the latter, it is hornblende with the appearance of black color, glass gloss, hardness 5 - 6 Mohs, two-way cleavage, classified as non-magnetic.

Petrographically, using three different viewpoints, the following minerals was obtained. There are porphyry andesite fragments which has some mineral such as plagioclase, hornblend and quartz. Besides that there are some minerals, such as pyroxene is subhedral in shape, the colors tends to be greenish brown. It has high relief with almost 90° cleavage and biaxial optical properties. Then there are plagioclase that has a sheet shape, with colors tending to be gray-white. Its relief is low, with a less pronounced texture when compared to other minerals. The cleavage is not clear. Hornblende has an euhedral or subhedral shape with colors that tend to be brownish green. The relief is high which means the mineral has a clearer texture and is easier to recognize.

This volcanic breccia is formed from volcanic eruptions that produce pyroclastic material and lava, which are also assisted by flow mechanisms, which then undergo a reworked process and are deposited in a marine environment.

4.2.3 Carbonate Claystone

This rock has clay grain size. It also has rounded grain shape, which causes the incision to be classified as a closed pack. The grain contact of this rock is classified as matrix Supported, where the majority of sedimentary rocks are fine-grained matrix, not clasts (in the case of conglomerates) or allochtonous (in the case of limestone). Rock porosity is classified as primary interparticle porosity, where interparticle porosity is a pore that exists between grains in the rock. Interparticle porosity is a type of porosity found in sedimentary or igneous rocks, where the spaces between larger grains are filled by smaller particles. This porosity is formed during the process of rock deposition and formation, and can affect the physical and chemical properties of the rock.

From petrography analysis (Figure 4), this rock is composed mostly of matrix at 80.6%, which is composed of microcrystalline calcite and a little quartz. The dominant matrix content has a rounded texture, good sorting and closed packing. Grains amounted to 14.3%, consisting of foraminifer fossils, one of which is Nodosaria sp. which is a benthonic foraminifera, is a type of foraminifera that lives on the seabed, which is contained between the rock matrix, and cement by 5% in the form of carbonate cement resulting from the dissolution of carbonate minerals such as calcite.

Using Embry Klovan's (1971) classification, the rock is a mudstone, which was formed through the process of weathering and erosion of other rocks. The foraminifera microfossils contained in the rock were deposited along with clay particles. These clay particles and microfossils were carried by water and deposited on the seabed then experienced deposition and formed a clay layer. This claystone underwent compaction, mineral replacement.

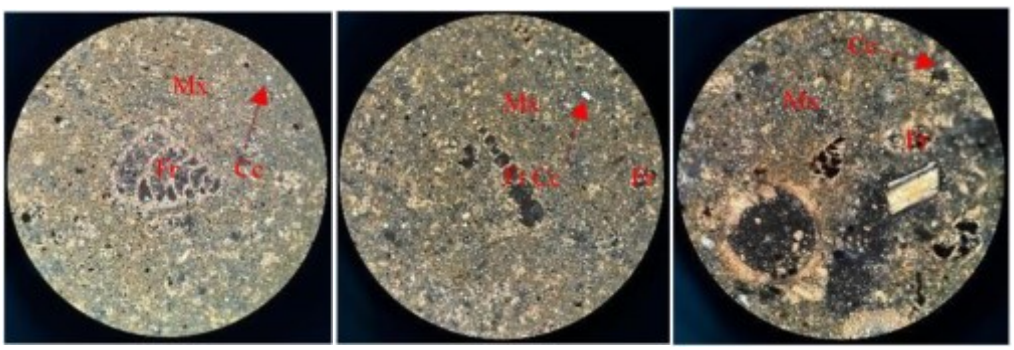

Figure 4: Petrography analysis for Carbonate Claystone (Fr : Foramnifira, Cc : Calcite, Mx : Matrix, Md : Rock Mass).

4.3 Fluid Geochemistry & Alteration

To be able to know the composition of geothermal fluids, the anion components in the form of Cl, SO4, and HCO3 are needed, which in these three anion components can help to interpret the conditions and processes that occur in the geothermal fluid source area.

In this study, there is 4 samples that we used from Hanindya's research, 2018. These included the Jari, Banyukuning, Sokogajah, and Keramat samples (Figure 1). The high Cl content of spring water can indicate that the hot water comes from a direct reservoir (minimal mixing or cooling by conduction), but water with low Cl content or that does not indicate the presence of hot spring steam is characteristic of groundwater dilution (Concentration ± <10 - >100,000mg/kg). The results obtained based on the existing fluid samples have been input into the diagram below (Figure 5):

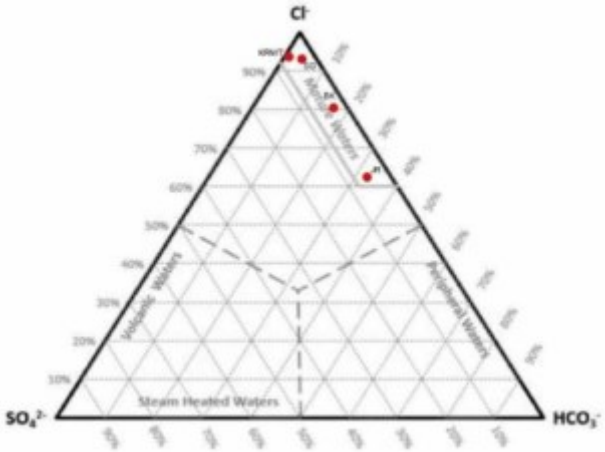

Figure 5: The results of the fluid type plot on the Cl-SO4-HCO3 diagram.

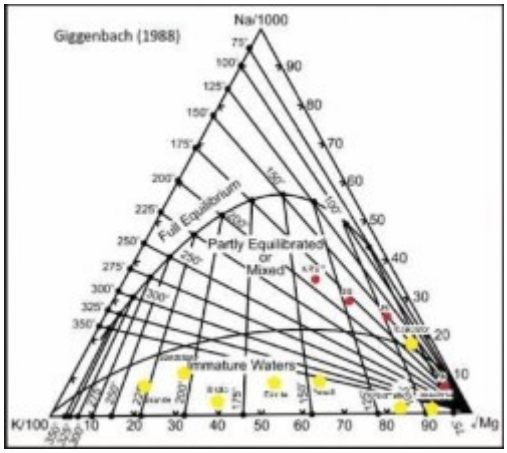

Figure 6: Geothermometer Na-K-Mg diagram.

Based on the results of data processing, it can be seen that the type of geothermal fluid in this research area is Mature Water.

In this geothermometer calculation method based on the Na/1000-K/1000- Mg diagram (Figure 6) due to the high Ca content with knowledge or theory that is classified as empirical and carried out with several literature studies. It is interpreted that the equilibrium between Na and K-Feldspar and the conversion of calcium alumino silicate minerals can become calcite. As well as the results of geothermometer calculations as follows (Table 1).

Table 1: Geothermometer Calculation Results.

Location Sample	Geothermometer Na/K/Mg (Giggenbach, 1988)
Jari	153
Banyukuning	222
Sokogajah	176
Keramat (Mud)	187

Calculations from this geothermometer have been adjusted based on the ion balance of the anions and cations, so that the data can be used is Jari's geochemical data that has a reservoir heat of 153°C (ion balance <5%).

Some alteration minerals that can be found in fields are : pyrite, travertine and clay minerals. From XRD analysis, clay minerals that can be identified is smectite. We can interpreted this area as an outflow zone, because the mineral association that can be found and also the fluid geochemistry analysis.

5. CONCLUSION

Mount Pandan has some manifestasion, such as : hot springs & mud pools. Some lithologies that can be found in this area are porphyry andesite, volcanic breccia, and carbonate claystone. From andesite & volcanic breccia thin section, there are some minerals that can be found such as : plagioclase, pyroxene, hornblend and rock mass. And from carbonate claystone thin section, there are some materials that can be found such as : foraminifera fossils, calcite and mud matrix. From water geochemical analysis at surrounding areas, it can be classified as mature water with interpretation of reservoir heat is 153°C based on geothermometer Na-K-Mg. Some altered mineral that can be found are : smectite, pyrite and travertine. So it can be interpreted this area as an outflow zone, because the mineral association that can be found and also the fluid geochemistry analysis

REFERENCES

Verma, A., and Pruess, K.: Enhancement of Steam Phase Relative Permeability Due to Phase Transformation Effects in Porous Media, Proceedings, 11th Workshop on Geothermal Reservoir Engineering, Stanford University, Stanford, CA (1986).

Wang, C.T., and Horne, R.N.: Boiling Flow in a Horizontal Fracture, Geothermics, 29, (1999), 759-772.

a) Geological Map

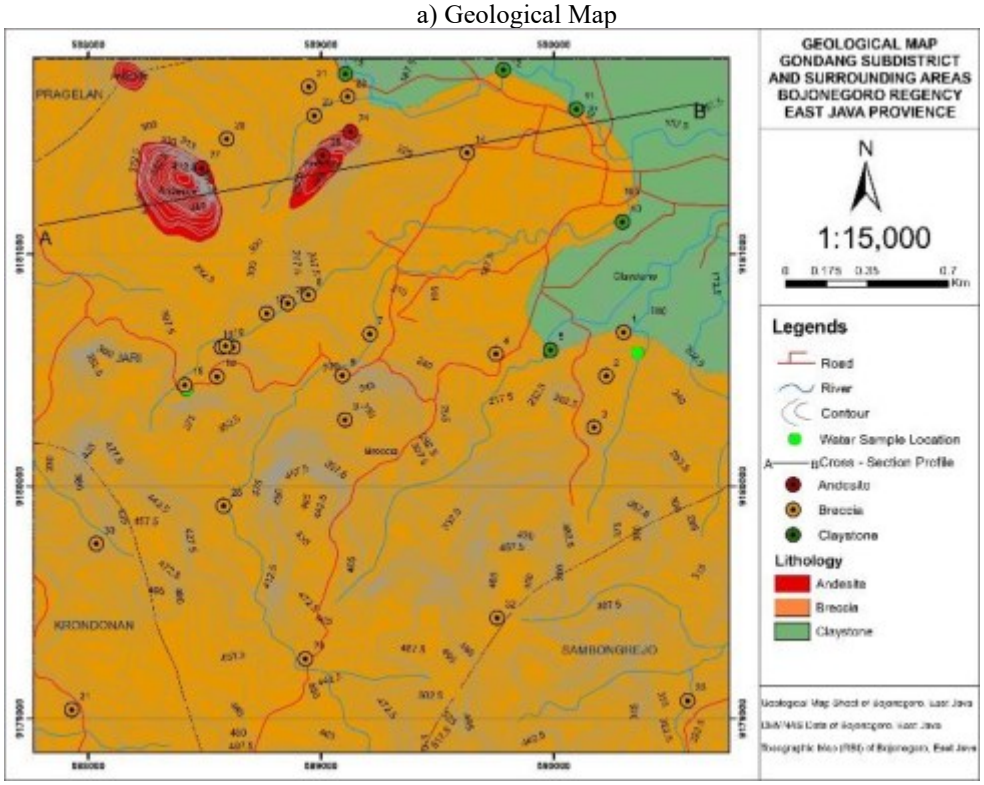

b) Geological Profile

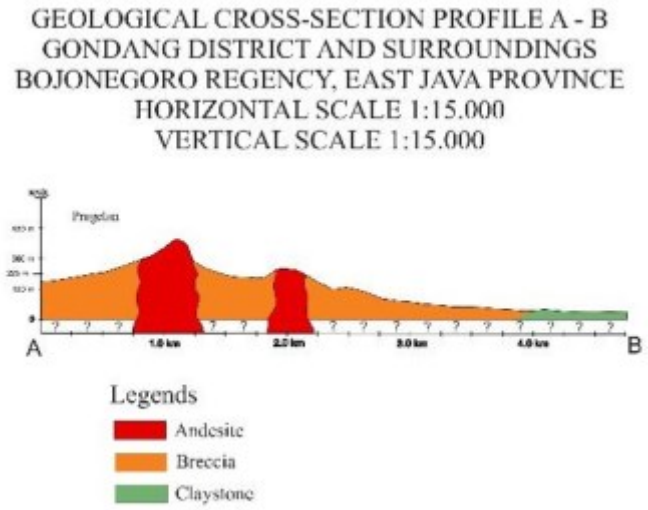

Figure 7: Geological Map & Geological Profile of Research Area.

a) Geomorphology Map

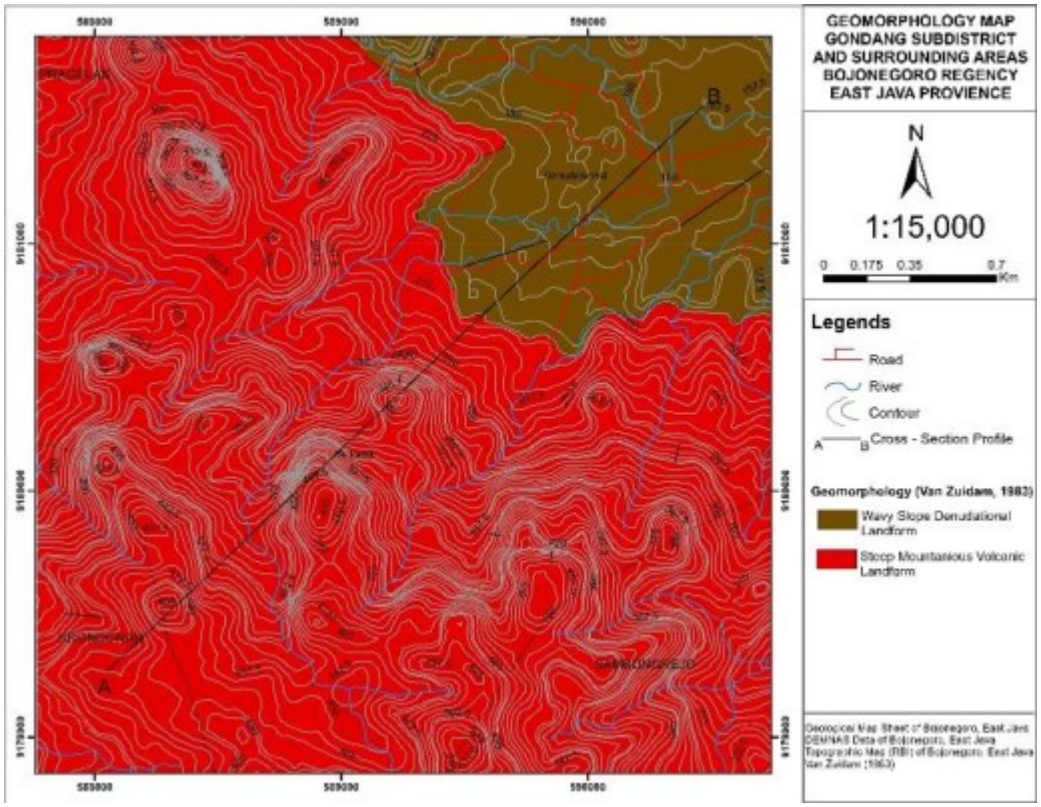

b) Geomorphology Profile

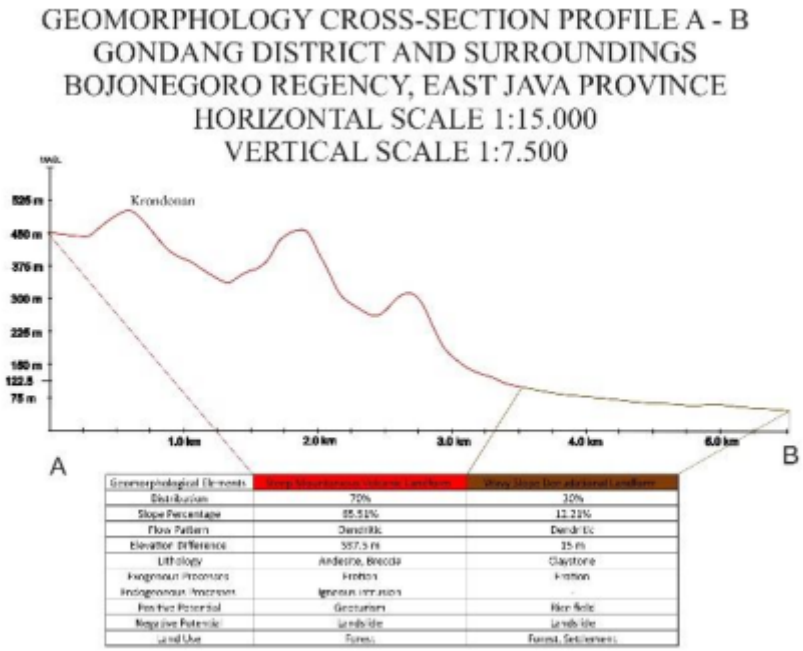

Figure 8: Geomorphology Map & Geomorph Profile of Research Area.

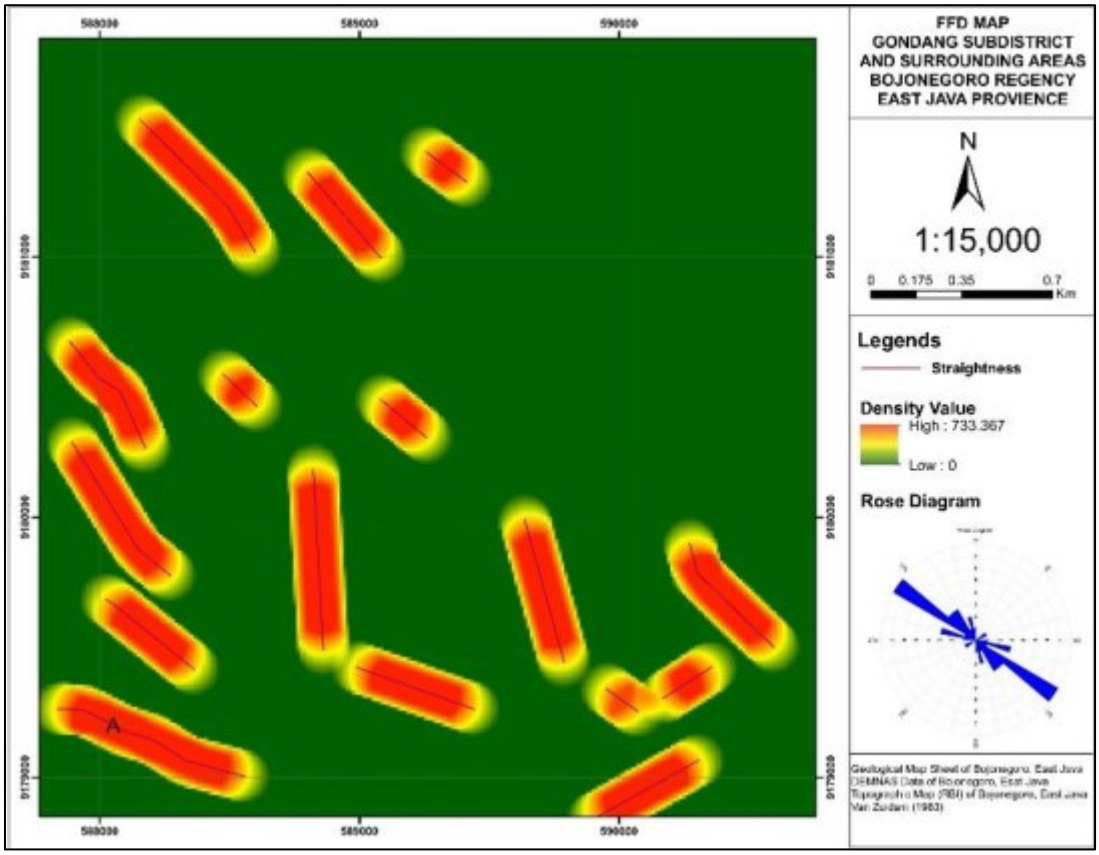

Figure 9: Fault Fracture Density Map of Research Area.

The updates of 2021-2023 Patuha Drilling Campaign: Challenges and Successes in Expanding the Resource Areas

Ezidin Reski, Khatis Jati Pamungkas, Dito Budi Sukarno,
Randy Wijaya Atmaja, Eka Daya Samudra, and Yuris Ramadhan

PT Geo Dipa Energi, Akses Tol Soroja street, Blok Sumakamanah Parungserab, No.22, Soreang, Bandung

ezidin.reski@gmail.com

Keywords: Patuha, Resource Area, Drilling Campaign, Red bed

ABSTRACT

PT. Geo Dipa Energy successfully completed a drilling campaign (2021-2023) to expand the Patuha geothermal field in West Java, Indonesia. This project aimed to utilize the area's geothermal potential for a new 55 MW power plant (Patuha Unit-2). Despite challenges like complex fractures and unstable formations, the drilling reached northwest towards the Patuha Mountains, significantly expanding the proven geothermal area.

This expansion was confirmed by a separate study that analyzed geological and drilling data. The study revealed a significant increase in the usable geothermal zone, extending both north and west from previous estimates. This finding highlights the importance of a comprehensive data approach in exploring geothermal potential. By incorporating diverse datasets – including recent drilling data, geological data (lithology and structural geology), and reservoir data (pressure and temperature measurements) – we were able to create a more holistic understanding of the geothermal field. This approach not only confirmed the expansion of the resource area, but also provided valuable insights into the geothermal system itself.

The successful drilling campaign and the confirmation of an expanded resource area pave the way for further development of the Patuha field. In the next phase, understanding the behavior of the unstable formations encountered during drilling will be studied more deeply. This knowledge will be instrumental in developing more effective drilling practices, ensuring the continued success of future geothermal projects in Patuha. Additionally, these insights can be transferable, informing advancements in geothermal drilling technologies that can be applied in other geothermal fields around the world.

1. INTRODUCTION

Located in the volcanic heartland of West Java, Indonesia, lies the Patuha geothermal area. This site harnesses the Earth's internal heat to generate clean and renewable energy. Located roughly 50 kilometers southwest of Bandung, Patuha's geothermal potential stems from its unique geological setting. The area sits within a chain of volcanic mountains, including North and South Patuha, where hot molten rock heats underground water. This interaction creates steam and hot water reservoirs, a valuable resource for geothermal energy production. Surface features like fumaroles and hot springs offer a glimpse into the geothermal activity below.

Patuha plays a significant role in Indonesia's renewable energy goals. Geothermal plants convert geothermal steam into electricity, providing a clean and reliable alternative to fossil fuels. This contributes to reducing greenhouse gas emissions and fostering a sustainable future. The Patuha geothermal system is a captivating subject for scientific study. Understanding its geological structure, fluid flow patterns, and overall energy potential is crucial for optimizing its development and ensuring its long-term sustainability.

Managed by PT Geo Dipa Energi, Patuha harnesses a vapor-dominated geothermal system and has been a reliable source of clean energy since 2014, with a current capacity of 55 MW (Unit-1). In response to growing regional energy demands, PT Geo Dipa Energi commenced a project in 2021 to expand Patuha's capacity. The expansion project, designated Unit-2, involves drilling new wells to achieve a targeted increase in steam output of 55 MW.

2. SURFACE ANALYSIS RESULT

To enhance the interpretation of geological features and optimize resource development for Patuha Unit-2, a comprehensive suite of surveys and studies were undertaken:

- LiDAR Survey (2020, with MI): This high-resolution topographic survey provided detailed digital elevation data, crucial for infrastructure planning and well-site selection.
- Structure and Stratigraphy Study (2020, UGM): Geologists from Universitas Gadjah Mada conducted this study to refine the understanding of the subsurface geological structure and stratigraphy within the

Patuha field. This information is critical for identifying potential geothermal reservoirs and predicting fluid flow patterns.

- Microseismic (MeQ) Monitoring (November 2019 - October 2020, ITB): The Institut Teknologi Bandung deployed a microseismic monitoring system to detect and locate micro-earthquakes associated with geothermal activity. This data provides valuable insights into subsurface fluid movement and reservoir dynamics.
- Magnetotelluric (MT) and Gravity Survey (2020, Elnusa): Elnusa conducted geophysical surveys utilizing MT and gravity techniques. These surveys provide information about subsurface electrical conductivity and density variations, aiding in delineating the extent and characteristics of the geothermal reservoir.
- Well Surveillance (2019-2020): Continuous monitoring of existing wells during drilling and production operations allows for real-time data collection and analysis of wellbore pressure, temperature, and fluid flow. This data is vital for reservoir management and well optimization.
- Structural Model and Permeability Evaluation (during drilling): Geologists and engineers conducted ongoing evaluations of the subsurface structure and permeability characteristics encountered during drilling operations. This real-time analysis allows for informed decisions about well trajectory adjustments and optimization of geothermal resource extraction.

By integrating data from these diverse surveys and studies, a comprehensive understanding of the Patuha geothermal field was established. This information serves as a crucial foundation for the successful development of Patuha Unit-2 and the sustainable utilization of its geothermal potential.

2.1 Regional Tectonic Setting

The Patuha geothermal field, situated on the Indonesian island of Java, lies at the heart of a dynamic tectonic zone. This region is significantly influenced by subduction, a geological process where one tectonic plate dives beneath another. In the case of Patuha, the oceanic crust of the Indo-Australian Plate is subducting underneath the continental crust of the Eurasian Plate. This subduction occurs at a remarkable pace of 6-7 centimeters per year, with a N20°E subduction angle (Tregoning et al., 1994). This ongoing process plays a crucial role in shaping the regional stress patterns and geological structures that define the Patuha geothermal field.

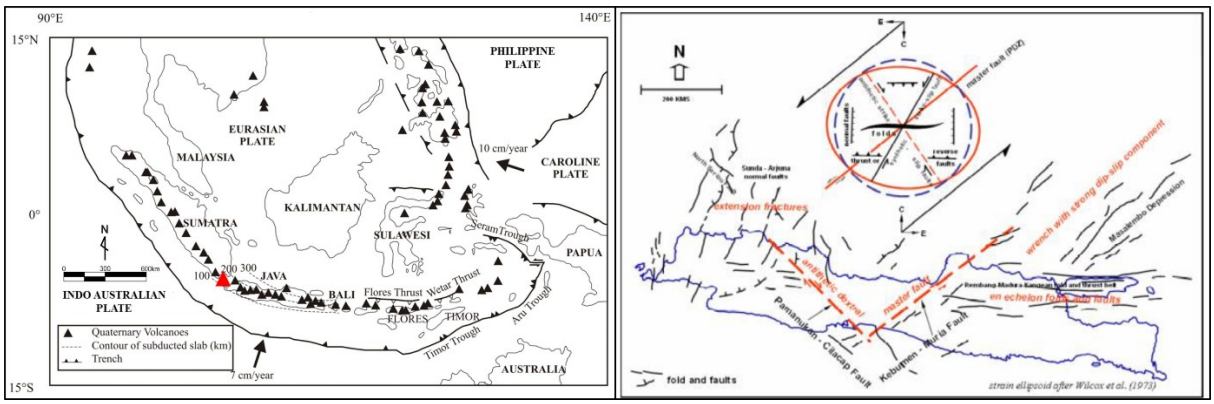

Figure 1: Java regional tectonic framework.

The island of Java, particularly its western region, is a fascinating tapestry woven by powerful tectonic forces. Three major structural trends dominate the region's geological makeup:

- N-S Trending Sunda Trend: This prominent trend reflects the influence of a large tectonic element called the Sunda Plate.
- NE-SW Trending Meratus Trend: This trend originates from another tectonic plate, the Meratus Microplate, interacting with the region.
- E-W Trending Java Trend: This trend reflects the overall east-west directionality of the vast Eurasian Plate.

Focusing specifically on West Java, Satyana (2007) have identified NE-SW, NW-SE, and E-W as the dominant structural trends (Figure 1). These trends are believed to be a consequence of a series of events related to the ongoing subduction process occurring beneath the region.

Subduction, a process where one tectonic plate dives beneath another, plays a significant role in shaping the geological landscape. Understanding the regional stress field, major plate boundaries, and faults (as depicted in Figure 1, modified from Hall and Morley, 2004 in Stingay et al., 2010) is crucial for deciphering the complex interplay of forces that have shaped West Java's unique tectonic setting.

2.2 Structural Geology Framework Update

An integrated evaluation of various data sources has shed light on the structural framework governing the Patuha geothermal field. This study incorporated field measurements, LiDAR lineament data, geophysical data, and drilling data to construct a comprehensive model (Figure 2). The analysis reveals that the Patuha field is dominated by three key structural trends:

- NE-SW Trend: This prominent trend appears to be the principal controlling factor within the field.
- N-S Trend: A secondary trend also plays a significant role in shaping the structural framework.
- Circular Patterns (Northern Gunung Patuha): Notably, the northern region of Gunung Patuha exhibits a distinct pattern of circular structures.

This structural model bears a strong resemblance to strike-slip systems as described by Woodcock and Fisher (1986). The main controlling influence appears to be a major NE-SW trending fault, with a network of en-echelon faults trending roughly NNE-SSW acting as secondary structures (Reski et al., 2023).

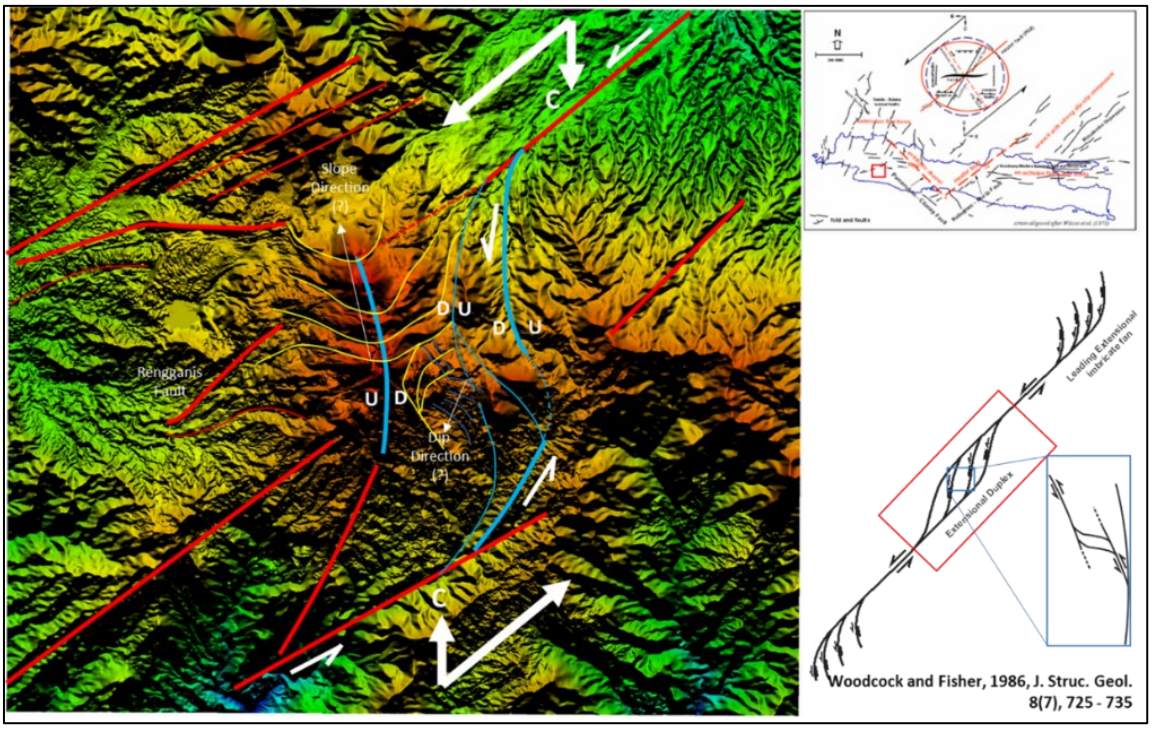

Figure 2: Patuha structural geology framework after Reski, et.al. (2023).

High-resolution image logs from wells 4X, 2Z, and 7Z, combined with permeability indicators observed during drilling and production testing, provide strong evidence for the presence of a mature fault zone within the Patuha geothermal field.

The analysis of these data sets reveals a fascinating interplay of geological features:

- Scattered Fault Network: The identified faults exhibit a scattered distribution, suggesting a complex fracture system within a relatively confined area.
- Strike-Slip and Compartmental Faults: The presence of both strike-slip and compartmental faults points towards a multi-directional stress regime that has shaped the subsurface structure.

These findings, obtained through an integrated analysis of borehole image logs and well testing results, support the established structural model for the Patuha field (Figure 3). This model depicts the field as a sinistral strike-slip system dominated by a major NE-SW trending fault. Secondary en-echelon faults trending NNE-SSW define an extensional duplex – a structural feature favorable for geothermal reservoir development.

Intriguingly, the observed presence of circular fracture patterns within this zone might not be directly related to the regional tectonic forces. As suggested by Reski et al. (2023), these patterns could be attributed to localized deformation or non-tectonic events. Further investigation into these unique features is warranted.

Well monitoring during the Patuha Unit-2 drilling campaign played a crucial role in confirming the presence and characteristics of faults within the geothermal field (Pamungkas, 2024). This monitoring focused on gas breakthroughs, specifically analyzing trends in residual gas and CO2 content.

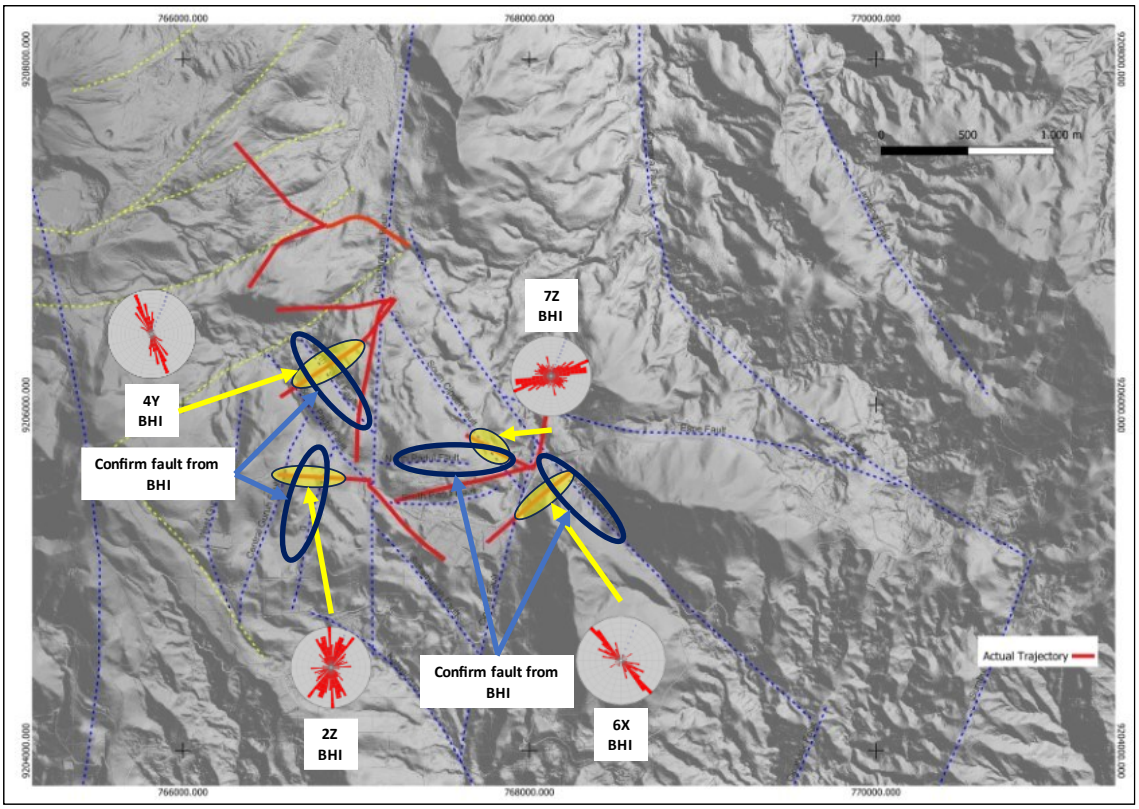

Figure 3: Patuha Bore Hole Image After Reski, et.al., 2024.

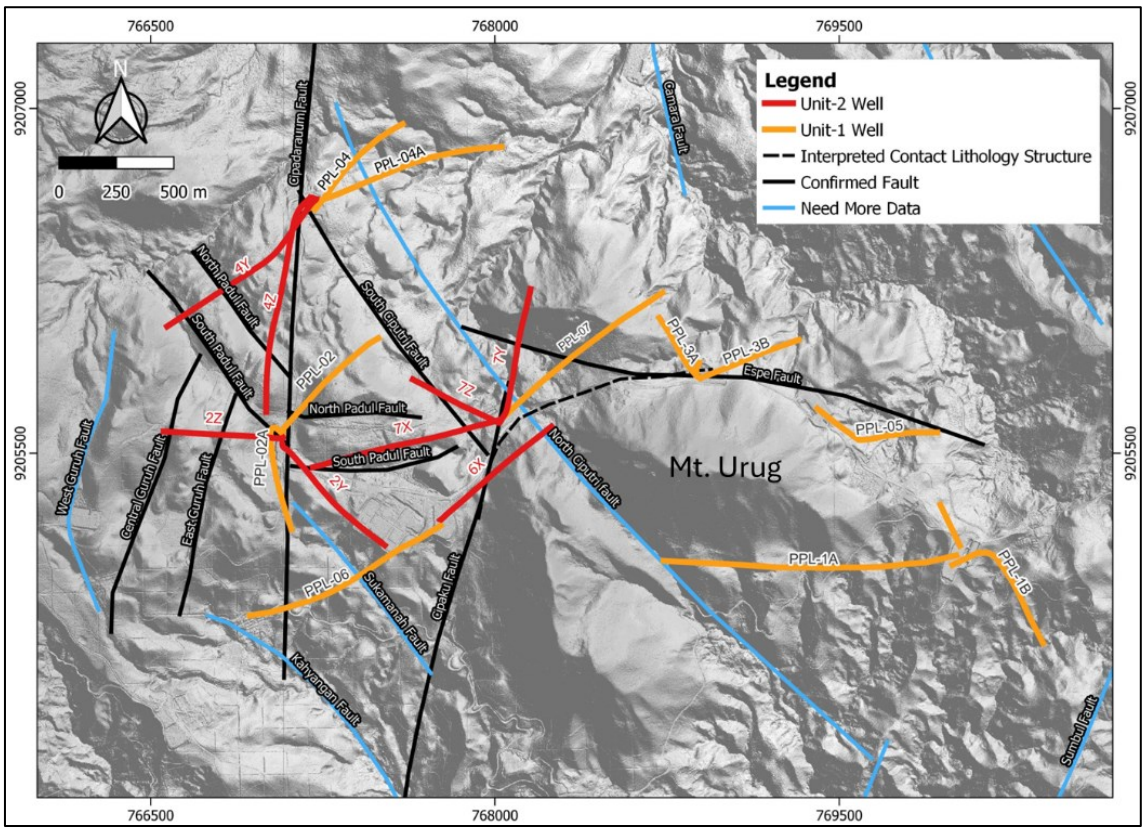

Figure 4: Map of confirmed fault by well monitoring during Patuha Unit-2 drilling campaign after Pamungkas, et.al. (2023).

When a well intersects a productive zone and utilizes an aerated drilling method, an increase in residual gas and a decrease in CO2 content are typically observed. The Patuha Unit-2 drilling campaign identified anomalies in these gas breakthrough trends, particularly in wells targeting the same fault or intersecting faults. This behavior indicates that faults act as pathways for geothermal fluids and can be used to confirm their existence within the reservoir.

The well monitoring results, along with existing geological knowledge, shed light on the interplay between regional tectonics and the Patuha geothermal field (Figure 4).

- Alignment with Regional Stress Field: The identified fault orientations, primarily NE-SW and N-S, align well with the dominant horizontal maximum compressional stress field of Java, which trends roughly N-S (Koesmono et al., 1996). This suggests a potential link between regional tectonic forces and the development of the strike-slip system governing the Patuha field.
- Local Amplification: The observed NE-SW and N-S trends in the fracture networks could be further amplified by local deformation processes associated with strike-slip faulting (Harding, 1973).

2.3 Geophysical Result

3D magnetotelluric (MT) modeling has been utilized to map the electrical conductivity distribution beneath the Patuha geothermal field. This information plays a vital role in pinpointing the boundaries of the valuable geothermal reservoir.

3D MT model show a detailed map of the geothermal reservoir within the Patuha field. This map relies on two key electrical conductivity boundaries:

- Conductive Layer Base (BOC): This boundary, identified by a significant shift from conductive layers (potentially indicating hot, saline fluids) to resistive layers (potentially drier, less conductive rocks), is interpreted as the interface between the geothermal reservoir and the underlying impermeable rock formations. Estimates suggest the BOC depth in Patuha ranges from 8-10 ohm-meters.
- Outer Reservoir Boundary: This boundary marks the transition from the highly permeable reservoir zone to the less permeable surrounding rocks. It is identified by a shift in the electrical conductivity gradient, moving from a positive value (updoming or thinning) to a flattening or thickening trend.

To account for inherent uncertainties in geophysical data and well information, two key interpretations have been employed:

- P50 Interpretation: This method merges 3D MT model data with existing well data (Top of Reservoir or TOR). It utilizes a conservative approach to define the gradient change, aiming for a balanced representation of the reservoir's extent.
- P90 Interpretation: This method relies solely on the 3D MT model and employs a more optimistic interpretation of the gradient change (focusing on a flattening trend). As a result, it potentially identifies a larger reservoir extent.

By combining these two interpretations, we can account for potential variations in data and present a range of feasible reservoir boundaries within the Patuha field (Figure 5). This information is critical for optimizing well placement and maximizing the utilization of this geothermal resource.

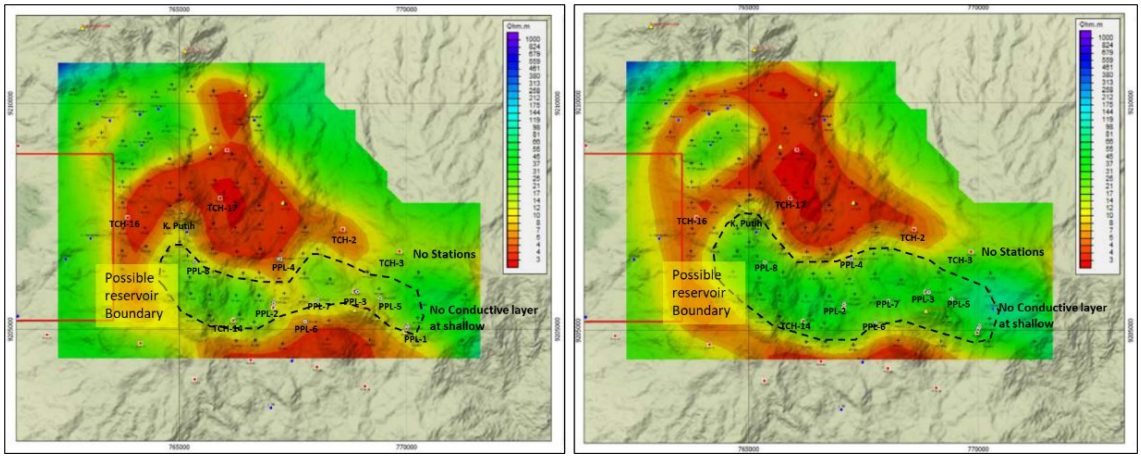

Figure 5: Outer reservoir boundary from resistivity map at 1250 mASL (Left) and 1000 mASL (Right).

2.4 Geochemical Result Update

Several wells drilled as part of the Patuha-2 campaign have been subjected to testing and sampling. Interestingly, the majority of the wells exhibited a dry steam condition with similar geochemical properties to Unit-1 wells, except for wells 4Y and 4Z which produced water condensate after the LECM.

The available gas chemistry data includes components like CO_2, H2S, NH_3, Ar, N_2, CH_4, and H_2. A ternary diagram utilizing CO_2-N_2-Ar can be used to analyze the origin of the geothermal fluids. Here, a lower CO_2/H_2S ratio suggests proximity to the upflow zone, while an increasing ratio indicates more extensive migration (Nicholson, 1993).

Wells 2Y, 7X, 7Y, and 7Z displayed low non-condensable gas (NCG) content (less than 1%wt) and a low CO_2/H_2S ratio (Table 1). This might indicate their location close to the upflow zone. In contrast, wells drilled towards the west encountered higher NCG content (1-3%wt) and a higher CO_2/H_2S ratio. This is interpreted as being caused by condensation processes occurring at shallower depths.

The majority of gas chemistry data points plotted on the CO_2-N_2-Ar diagram (Figure 6) cluster around the air zone. This suggests that the wellbore chemistry might still be significantly influenced by drilling fluids. However, well test results indicate a relatively neutral fluid with no signs of acidity, even in well 9X, which is closest to the Kawah Putih crater. Despite this initial assessment, continuous geochemical sampling during stable production conditions is crucial for ongoing reservoir monitoring.

Table 1: NCG value and the CO_2/H_2S ratio in Patuha Unit-2 wells.

Well Name	NCG (%wt)	CO_2/H_2S
2Y	0.36	19.37
2Z	0.62	31.76
4Y	1.00	56.77
4Z	2.11	49.61
7X	0.48	21.20
7Y	0.74	29.83
7Z	0.33	18.21
9X	3.00	62.83

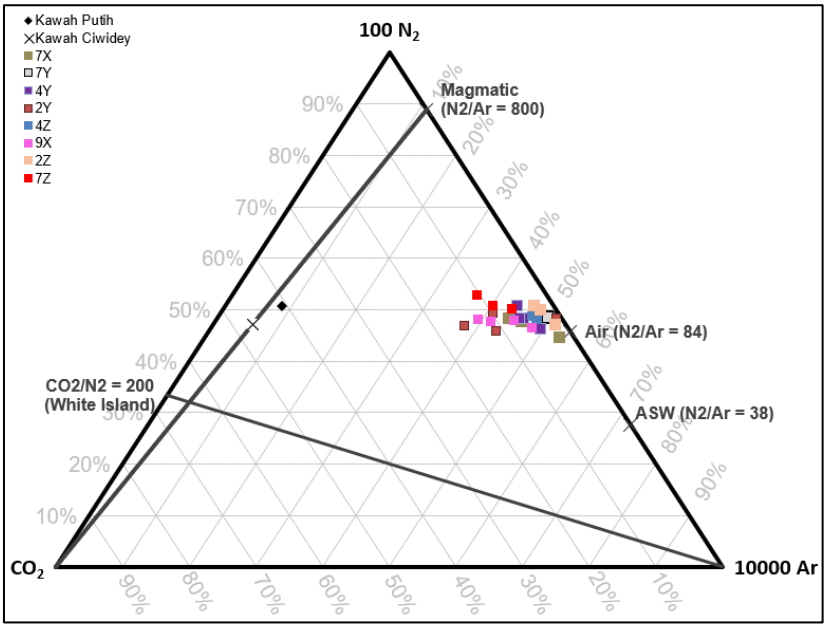

Figure 6: CO_2-N_2-Ar Ternary Diagram of Patuha Unit-2 wells, indicating air contamination from drilling fluid.

3. DRILLING RESULT

The Patuha Unit-2 drilling campaign, a key milestone in expanding geothermal energy production at the Patuha field, commenced in November 2021 and completed in March 2024 with the successful completion of 12 wells. To efficiently execute this drilling program, a strategic approach utilizing five well pads was implemented. Four of these pads were existing infrastructure within the field, while a new pad was strategically positioned near the Kawah Putih area to target promising geothermal resources in that sector.

3.1 Drilling Performance

The Patuha Unit-2 drilling campaign encountered various obstacles during its execution. These challenges, arising from both equipment limitations and complex geological formations, resulted in extended drilling times compared to the initial program. The initial plan anticipated an average well depth of 1800-2000 meters and a completion time of 45 days per well, unexpected difficulties necessitated adjustments.

Drilling on well pads 4 and 9 proved particularly demanding, requiring sidetracking maneuvers in each well to bypass formation-related problems. The primary obstacle in the Production Zone was red bed formations, which presented significant drilling challenges. Figure 7 shown that the most of Non-Productive Time (NPT) in Patuha area caused by stuck pipe.

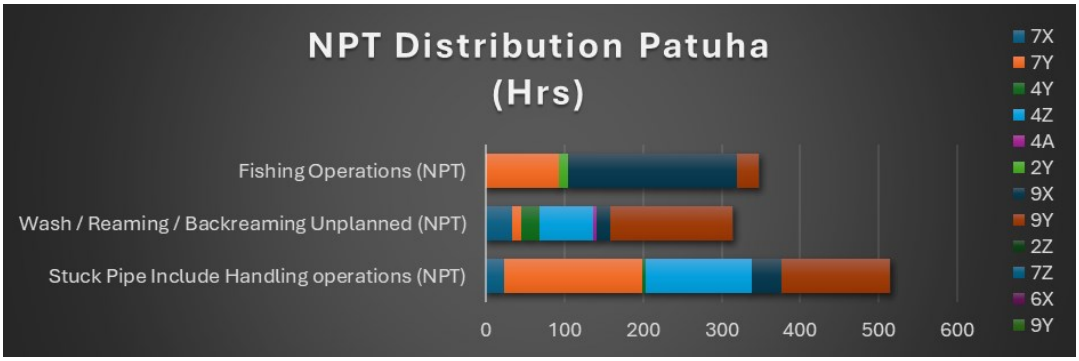

Figure 7: NPT Distribution during Patuha-2 drilling campaign.

The Patuha Unit-2 drilling campaign encountered initial challenges, but the drilling team's adaptability and collaborative approach led to significant performance improvements. Through continuous learning and close collaboration with the subsurface team to refine drilling strategies, they were able to tackle unforeseen challenges.

This resulted in a notable reduction in drilling times for later wells. These wells were completed within a timeframe of 26-30 days, with an average depth ranging from 1600 to 1700 meters. Furthermore, the team successfully eliminated formation-related issues that could have caused stuck pipe incidents. This achievement culminated in drilling a well with zero Non-Productive Time (NPT).

3.2 Permeability Update

Evaluating permeability, the ease with which fluids can flow through rock formations, is critical for optimizing geothermal well productivity. Patuha geothermal field rely on a multifaceted approach that integrates data from various sources:

- Drilling Parameters: During drilling, encountering zones where drilling fluid disappears underground (Loss Zones) or experiencing sudden changes in drilling parameters (Drilling Breaks) can indicate encountering formations with potentially high permeability. These parameters provide valuable clues about subsurface conditions. Total loss zones are particularly significant, as they directly indicate enhanced fluid movement within the rock. Drilling breaks, on the other hand, can be caused by encountering softer formations or changes in rock strength, which can be indirectly linked to increased permeability. By analyzing the depth, duration, and severity of these events, a comprehensive picture of subsurface permeability variations builds.
- Geological Hazard Indicators: The release of gases and the occurrence of kicks (sudden wellbore pressure increased) during drilling can also be associated with permeable formations. These events can occur when the drill bit encounters a zone with high pore pressure or fractures that allow pressurized fluids to flow rapidly into the wellbore. While these events can pose safety challenges during drilling, they also provide valuable information about the presence and characteristics of permeable zones.

An analysis of permeability indicators within the Patuha geothermal field has revealed a critical finding that geological structures, especially faults and fractures, exert the most significant influence on permeability. This

aligns perfectly with the established concept of Patuha being a "structurally controlled" geothermal system, where geological formations play a major role in directing the flow of geothermal fluids.

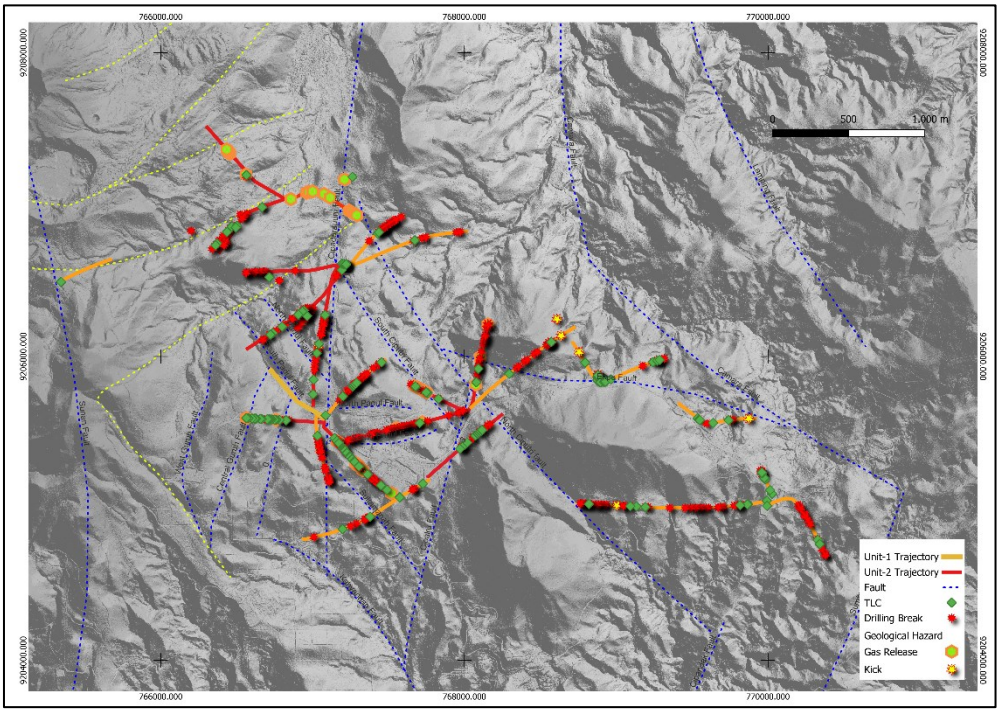

Figure 8: Patuha Permeability Indication During Drilling.

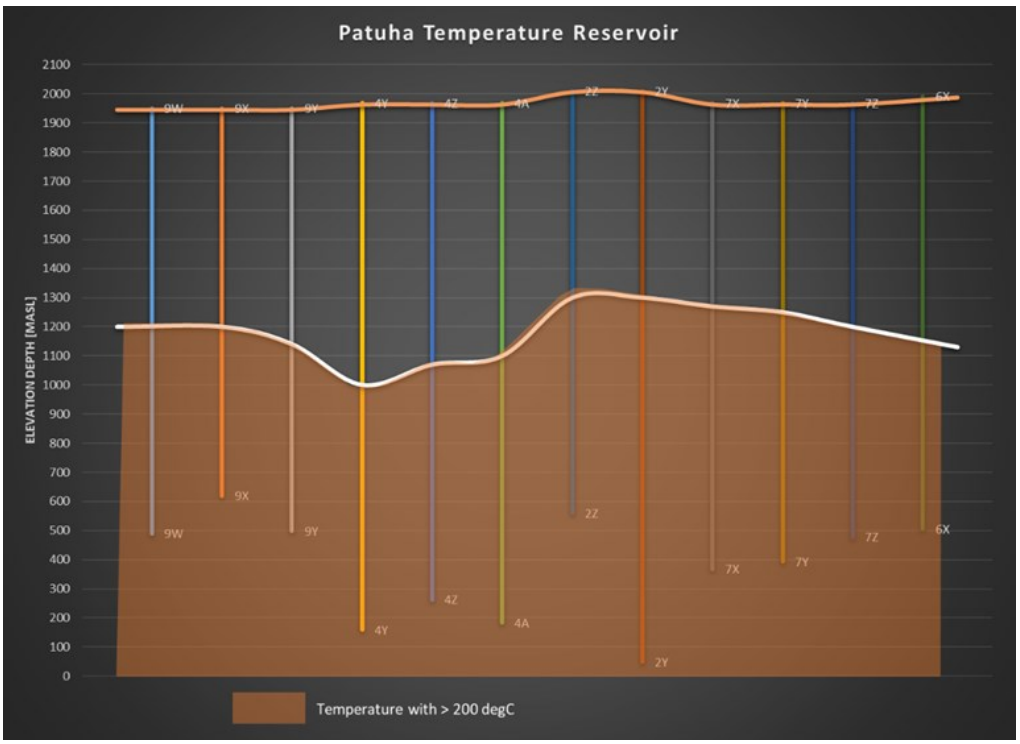

Figure 9: Patuha Temperature Distribution.

3.3 Pressure and Temperature Distribution

Following the completion of drilling for each well in Patuha Unit-2, a Pressure and Temperature (PT) survey was conducted to assess the geothermal potential of the field. This survey provides valuable insights into the presence and characteristics of geothermal reservoirs. A PT survey typically involves measuring pressure and temperature along the entire depth of a well while maintaining a consistent well condition throughout the process. These

measurements can be taken under various well conditions, including shut-in (closed wellbore), injection, or flowing conditions. In Patuha Unit-2, the PT data was acquired with the wells in a shut-in state.

For optimal results, a recommended PT survey schedule involves measurements at specific time intervals, often including 1, 3, 7, 14, 28, and 60 days after well completion. The acquired PT data can then be plotted versus measured depth, vertical depth, or elevation depth. Once the wells have reached a stable condition, plotting the PT data versus elevation depth allows for the estimation of the proven geothermal area. In this analysis, a temperature of 200°C is often used as a threshold to define the reservoir section within the wellbore.

Analysis of temperature data from the Patuha geothermal field reveals a compelling possibility for resource expansion. The central and northern regions exhibit temperatures exceeding 200°C at 1100 mASL (Figure 10), a strong indicator of the presence of viable geothermal reservoirs. This promising finding suggests that extending geothermal exploration activities towards the western and northern areas of Patuha holds significant potential. Further investigation in these regions can lead to the discovery of additional geothermal resources.

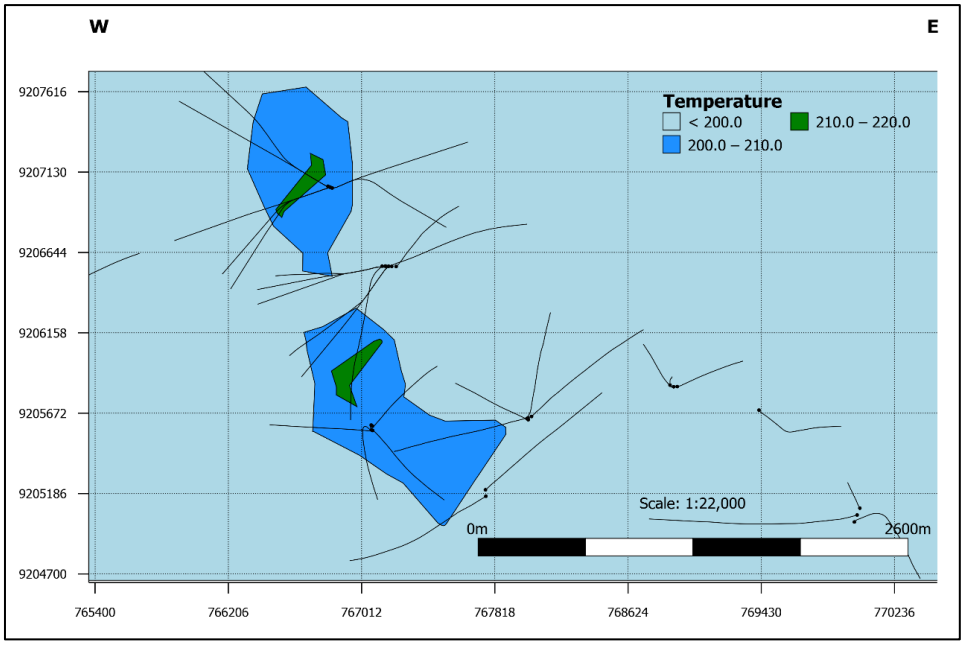

Figure 10: Temperature Distribution at 1100 mASL.

4. SUBSURFACE CHALLENGE

The Patuha Unit-2 drilling campaign encountered a multitude of challenges that demanded innovative solutions from the drilling and subsurface teams. These challenges stemmed from complex geological conditions and the need to optimize drilling efficiency while ensuring wellbore stability and safety.

4.1 Geological Hazard

Drilling operations in the Patuha geothermal field have consistently encountered a specific geological obstacle – a reddish-brown rock layer informally known as the "red bed" due to its characteristic color and oxidation evidence. This layer, in some sections, also contains elevated concentrations of clay minerals.

The red bed presents a significant challenge during geothermal well drilling due to its problematic interaction with water-based drilling fluids, particularly within the target reservoir zone. Contact with water can trigger the red bed to swell and disintegrate, leading to critical issues like stuck drill pipes. Analyses of past drilling data from Patuha reveal a concerning trend – nearly 45% of wellbore issues, including tight holes and stuck pipes, can be traced back to the red bed.

The red bed encountered in the Patuha geothermal field exhibits some internal variations, particularly in its location within the wellbore. Here's a breakdown of the key observations:

- Red Bed Above Reservoir: Commonly found above the target geothermal zone, this variant features a high visual clay content. In simpler terms, this high clay content translates to a soft, crumbly texture, and when these clays come into contact with water-based drilling fluids, they tend to become sticky. This stickiness can contribute to wellbore issues.

- Red Bed Within Reservoir: Encountered within the reservoir zone, this variant possesses a lower visual clay content but often displays a spike in the Methylene Blue (MeB) value. Despite the lower clay content, it maintains a soft and crumbly consistency. However, it visually differs from the first variant by exhibiting a shale or platy shattered appearance.

Figure 11: Type of Red Bed Occur above reservoir zone (left) and in reservoir zone (right).

Analysis of wellbore data, incorporating elevation and well correlation techniques, has revealed the presence of at least 16 distinct red bed layers within the Patuha Unit-2 geothermal field (Figure 12). These red bed layers occur at varying elevations, and interestingly, nearly every well drilled in Patuha area encountered this red bed layer. A noteworthy observation is the higher concentration of red beds encountered in wells located within the central Patuha area. This finding could be attributed to two potential factors. Firstly, the well paths in this region may have traversed a zone with a more concentrated presence of red beds. Alternatively, the central Patuha area itself might be situated within a section where the red bed formation is inherently thicker.

Research on the red bed's characteristics and impact on drilling is an ongoing process. Future studies will incorporate data from various laboratory analyses, including petrography, XRD, and Linear Swelling Tests. Integrating this data with other relevant information will contribute to the development of more robust models for understanding and mitigating the challenges posed by the red bed during Patuha geothermal well drilling.

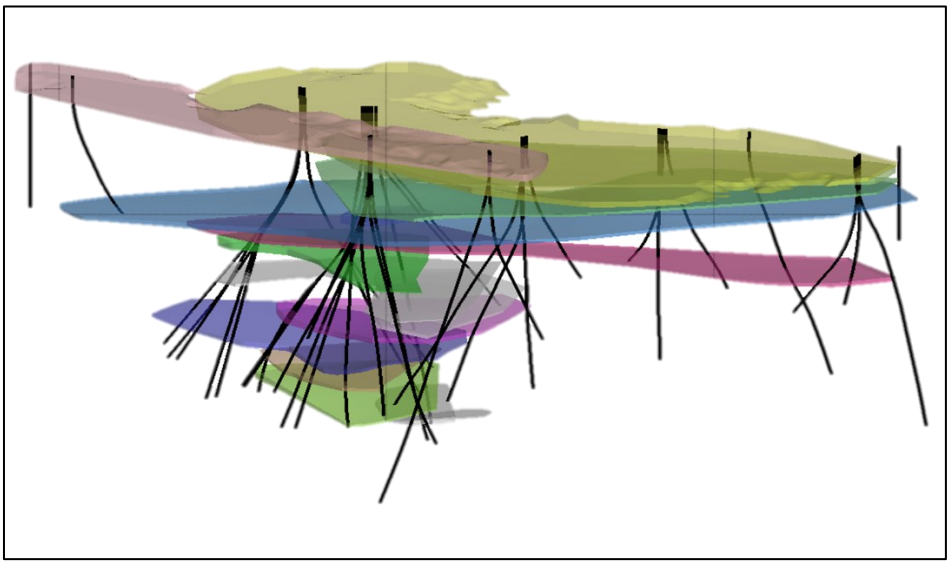

Figure 12: 16 Red Bed Layers Based on Elevation.

4.2 Drilling Challenge

The Patuha Unit-2 drilling campaign encountered a significant challenge in the production zone: unstable formations. These formations are particularly fragile when exposed to water, making them susceptible to collapse during drilling.

- Combating Formation Collapse: This presented a dilemma. Traditional drilling methods rely on water-based drilling fluids. However, with unconsolidated formations, these fluids could exacerbate the problem by further weakening the formation. The solution: a technique known as Slightly Underbalance

Drilling (SUBD). SUBD minimizes water contact with the formation by maintaining a slightly lower pressure in the wellbore compared to the surrounding rock.

- Balancing Challenges: While SUBD addressed the formation collapse issue, it introduced another challenge: high temperatures. Due to limitations with directional drilling tools that cannot withstand high temperatures, the team had to switch to a rotary drilling assembly. This compromised directional control, making it more difficult to maintain a precise well path.
- Adaptability and Innovation: The drilling team displayed remarkable adaptability. They implemented modifications to surface equipment to handle the high temperatures and extend its lifespan. This ensured continued drilling operations.
- Collision Averted: Drilling in close proximity to existing wells carries the risk of collision. However, meticulous wellbore monitoring and meticulous planning ensured no such incidents occurred during the Patuha Unit-2 drilling campaign.

Despite encountering unforeseen geological challenges, the Patuha Unit-2 drilling campaign emerged successful. The team's adaptability, collaborative problem-solving, and meticulous planning ensured efficient well construction and avoided potential wellbore issues.

5. CONCLUSION

Our exploration of the Patuha Unit-2 geothermal field, utilizing a combination of techniques, has yielded significant insights into its geological makeup, permeability characteristics, and overall geothermal potential. Geological analysis revealed a mature fault zone within the field, which may play a role in directing geothermal fluid flow. Real-time data analysis during drilling allows for adjustments to well trajectories, maximizing the extraction of geothermal resources. A specific rock layer, known as the red bed, presents a challenge due to its interaction with drilling fluids. Ongoing research is focused on developing mitigation strategies. Pressure and temperature (PT) surveys provided valuable information about the presence and characteristics of geothermal reservoirs. The encouraging discovery of temperatures exceeding 200°C in the central and northern regions suggests the potential for significant resource expansion in these areas. Continuous monitoring and data collection are essential for optimizing the development of Patuha Unit-2 and ensuring its long-term sustainability. Furthermore, spurred by the promising temperature data, further exploration of the western and northern regions holds the key to unlocking additional geothermal resources, contributing to Indonesia's clean energy goals.

ACKNOWLEDGEMENTS

The authors would like to express acknowledgment to PT. Geo Dipa Energi (Persero) for their important assistance in completing this study. We want to express our gratitude to Subsurface and Drilling Division PMU for their essential help throughout the research process. We would also like to thank the Management of PT. Geo Dipa Energi (Persero) for obtaining permission to publish this work. Their effort and teamwork were essential to the successful completion of this research.

REFERENCES

Al Amin, T., Reski, E., Ramadhan, Y., Atmaja, R. W., & Mackenzie, K. (2023). Permeability evaluation while drilling: A case study of slightly overbalanced drilling in Patuha Field, West Java, Indonesia. *Proceedings*, 12th ITB International Geothermal Workshop 2024, Institut Teknologi Bandung, Indonesia.

Ashat, A., Pratama, H. B., & Itoi, R. (2019). Updating conceptual model of Ciwidey-Patuha geothermal using dynamic numerical model. IOP Conference Series: Earth and Environmental Science (Vol. 254, No. 1, p. 012002). IOP Publishing.

Chandra, V. R., Iskandar, Ramadhan, Y., Akmala, I., & Atmaja, R. W. (2022). Fault and structure study for field development strategy in Patuha Geothermal Project. *Proceedings*, 47th Workshop on Geothermal Reservoir Engineering, Stanford University, Stanford, CA.

Elfina, N. S. (2017). Subsurface geology and hydrothermal alteration of the Patuha geothermal field, West Java: A progress report. ResearchGate, 6(1), 1-7.

Harding, T. P. (1973). Newport-Inglewood trend, California—An example of wrenching style of deformation. AAPG Bulletin, 57(1), 97-116.

Kusdji, A. F. (2013). Geothermal exploration in Indonesia: Challenges and opportunities.

Koesmono, M., Kusnama, & Suwarna. (1996). Peta Geology Lembar Sindangbarang dan Bandarwaru, Jawa [Geological Map of Sindangbarang and Bandarwaru Sheets, Java]. Geology Research and Development Center.

Pamungkas, K. J., Reski, E., Ramadhan, Y., Atmaja, W. R., & Muryani, S. P. (2024). The determination of fluid flow movement from geochemical monitoring during drilling to prove the fault geometry existence in Patuha Geothermal Area. *Proceedings*, 13th ITB International Geothermal Workshop 2024, Institut Teknologi Bandung, Indonesia.

Pradipta, R. A., Saepuloh, A., & Suryantini. (2016). Geology structure identification based on Polarimetric SAR (PolSAR) Data and Field Based Observation at Ciwidey Geothermal Field. IOP Conference Series: Earth and Environmental Science.

Pulunggono, A., & Martodjoyo, W. (1994). Peta Geologi dan Stratigrafi Lembar Bandung (45-12) [Geological and Stratigraphic Map of Bandung Sheet (45-12)]. Pusat Penelitian dan Pengembangan Geologi.

Reski, E. (2024). Updating fault model with using borehole image data on Patuha Geothermal System, West Java, Indonesia. Proceedings, 49th Workshop on Geothermal Reservoir Engineering (SGP-TR-227), Stanford University, Stanford, California, February 12-14, 2024.

Reski, E., Al Amin, T., Ramadhan, Y., Atmaja, R. W., & Wilmarth, M. (2024). Structural model update on Patuha Geothermal System, West Java, Indonesia. IOP Conference Series: Earth and Environmental Science, 1293(1), 012005.

Satyana, A. K. (2007). Peta Struktur Geologi Bandung dan Sekitarnya, Jawa Barat [Geological Structure Map of Bandung and its Surroundings, West Java]. Jurnal Geologi Indonesia, 4(1), 1-12.

Stingay, H. R., et al. (2010). Model tektonik dan distribusi sumber daya panasbumi di Jawa Barat [Tectonic model and distribution of geothermal resources in West Java]. Jurnal Sains Teknik Sipil, 15(3), 85-94.

Woodcock, Nigel H., Fischer, and Mike.: Strike-slip duplexes. Journal of Structural Geology, 8 (7). 725-735 (1986).

Resistivity Model Using 3D Inversion MT at XX Geothermal Field

Baskoro D and Zaky M

Geothermal Exploration Magister Program, Graduate Program of Physical Sciences, Department of Physics, Faculty of Mathematics and Natural Sciences, Universitas Indonesia, Kampus Depok 16424, Indonesia

dibaskoros@gmail.com, javabinas@gmail.com

Keywords: updated resistivity model, 3D inversion

ABSTRACT

Like most geothermal fields producing for more than 5 (five) years, XX has had problems with wells performance. This is most likely due to the result of inappropriate of subsurface data. The problem has been approached with the proper application of MT technology such as selecting and reprocessing raw data to reproduce 3D inversion. However, the analysis is frequently conflicted with the others data, primarily due to incorrect interpretation of noise and low deep resistivity.

The appropriate modelling scheme of MT data and observation of anomalous resistivity feature are interpreted as thick-conductive zone, self-sealing fracture, steep gradient of BOC, reservoir barrier at weak altered zone which separate zone between production and reinjection wells. This anomaly is strongly correlated with the temperature changes in hydrothermal minerals. This variation shows the up-dome shape of temperature contour and low resistivity zone above upflow zone. The results are confirmed from hot water and fumarole characteristics (such as altered rock and acid spring) and resistivity model.

The aim of this paper is to rebuild the resistivity model, which can be expected to analyze and integrate the distribution of alteration minerals, top of reservoir (TOR), base of conductor (BOC), hence the outflow zone and fault barrier zone that corresponds to reservoir partition at field can be identified.

1. INTRODUCTION

XX area is a volcanic, high-enthalpy resources geothermal environment, reservoir is characterized by shallow intrusion, high permeability, hosting benign fluid chemistry. The lithology setting at XX area field are composed of Quaternary volcanic rocks, both lava and pyroclastic, lahar, breccia, and tuff that comprise several formations underlying the south-western boundary of reservoir occurs to form the youngest product and high elevation (andesite) at XX area. Subtle variations in fluid chemistry allow the field to be subdivided into four distinct sectors or “cells” that are likely bounded by faults. There is clear evidence that dikes and sills have intruded into some fault zones during recent episodes of volcanism and may have either sealed existing permeability or created new pathways near the boundaries of these cells. The four sectors have been termed the three different partition.

High permeability in SW - NE profile is controlled by high temperature, presence of shallow heat source and distribution of altered mineral, while most of TOR delineation are speculatively described in large reservoir and no-barrier fluids flow. Although the distribution of clay cap spreads all over XX area, the fault / lithologic contact barrier, dike and geochemical variation divided into 3 (three) main intrusion play the significant factor in overall understanding model and how much resistivity anomaly of upflow and outflow zone can build conceptual model from previous analysis. As a consequence of disagreement between interpretation of 1D MT inversion, conducted in 2002 and improved joint inversion in 2013, also analysis of TOR (top of reservoir) or BOC (base of conductor), production and injection well can be encountered deep conductive layer and fault barrier after well completion, which for data validation needs good agreement of thickening in conductive layer and well data as the primary purpose of this publication. Proper application, quality control of magnetotellurite data and re-processing can eliminate contradiction of large prospect area with drilling data as well as mismatch of TOR and thickening of conductive layer (Figure 1 and 2).

2. GEOLOGY AND STRUCTURE FEATURE

For the compilation of stratigraphy and structure of XX site, the formations can be determined as andesite tuff – rhyodacite and lava 180,000 – 280,000 years ago, which is composed of ruptured Caldera and floored further to the west, northwest and north area and filled by the older rhyolite dome, lava and the younger tuff. In terms of the fracture zones, a major lineament is expected to exist with post-caldera units show prominent 0°~50° N to NE direction and 330°~340° NW (Figure 3 (A) and (B)).

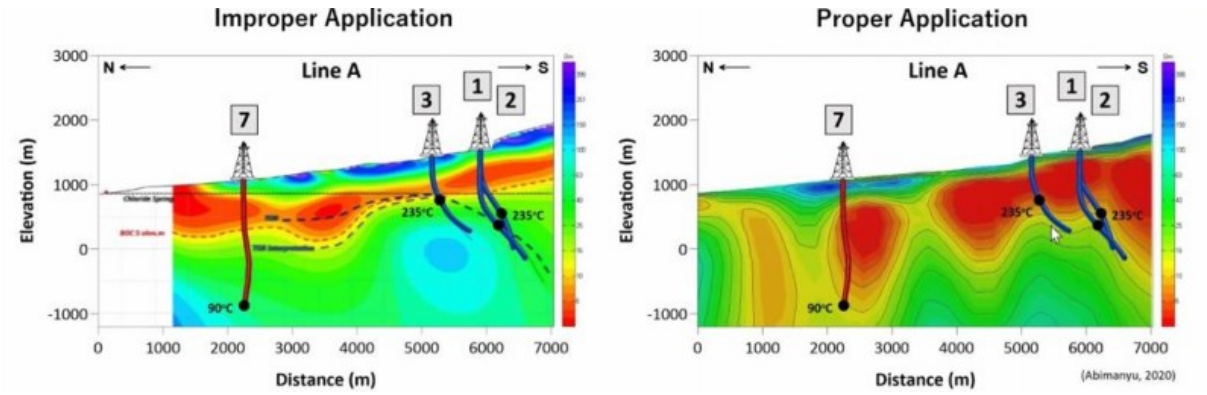

Figure 1: Application of quality control and re-processing MT data, (Daud Y. et al., 2015).

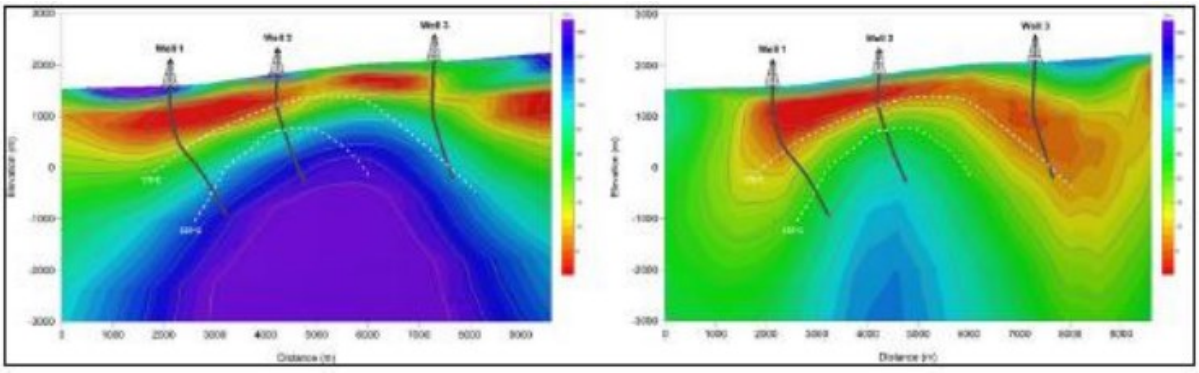

Figure 2: Correlation of MT and drilling data before (left) and after (right). Innovated application to define actual reservoir geometry and deep alteration zone (Daud Y. et al., 2017).

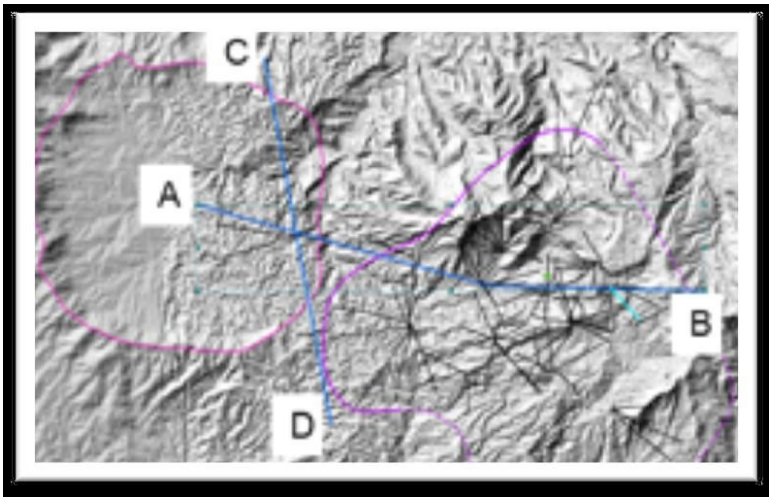

Figure 3: DEM Map shows fault lineament and surface manifestation.

The five regionally extensive basaltic–andesite to andesite volcanic centers described are the (1) the older andesite (670-1610 ka), that consists of andesitic cone that forms the rim of the caldera to the west; (2) Basaltic Andesite (420-860 ka); (3) Middle Basaltic Andesite (400-320 ka); (4) Young Andesite (180-280 ka); and (5) Rhyolite Lava (113-120 ka). Both the Middle and Upper Volcanic Formations consist of a series of dacitic (at their base) and andesitic rocks overlying each other. This new interpretation approach suggests that the separation of the volcanic rocks into ductile and brittle is impractical. Thus, the temperature and the permeability changes in volcanic altered rock interpreted as upflow and outflow zone. In addition, 3 (three) main intrusions are spread across at XX geothermal field.

NNE-trending normal faults are the dominated faults which correlated with recent volcanic vents, playing as a key indicator in forming the system, and allowing the descent of shallow fluids into the eastern, western and northern portion of the geothermal reservoir. Main fault forms an important cell boundary and it will be shown later that together with these structures bound of an fault intersection, anomalous-resistive zone, and recent

volcanism that host a thicker and highly permeable volcanic pile than the adjacent areas. Figure 3 represents the mapped faults and lineaments identified at XX area showing fault intersection, upflow, outflow and confidence on their surface feature. Thermal decrease is an evidence of boundary divided into several sectors or "cells" that are likely bounded by faults, permeability barrier or lithological contact, which are shown as an abrupt temperature change. The most common cause for such discontinuities in thermal regimes is a spatially change in permeability.

The main fault, at surface manifestations (fumarole) also main altered zone, intersect with E-W trending fault zones identified nearly parallel to the lithological contact. It serves as an outstanding example of a mapped fault zone in the area (Figures 3). The fault zone consists of a nearly vertically trending zone that is 5 m wide and that is filled with mixed of shear and broken formations. The surface formations are clay-altered tuffs that do not maintain permeable fractures. The oldest tuffs are bedded red-brown deposits that are collectively called the Lower Brown Tuff, whereas the youngest units are the Orange Tuff and a thin overlying brown ashy soil. Apparent offset on the Orange Tuff (age estimated at 8,400 to 40,000 years based on C-14 ages on overlying and underlying units) in Figure 3 (A), suggest the fault is down-to-the-north. A dip of about 75° is forming a normal fault. Slow changes in the bed dip at the fault margin may be interpreted as high permeability zone. However, no slickensides or hydrothermal alteration were observed in the fault zone or at its margins. This zone dips too steeply to represent a paleozoic channel. It is most likely to represent a young (<40,000 year old) fault with normal or oblique-normal slip.

3. 3-D INVERSION OF MT DATA

The 3-D inversion method was applied for the 123 MT soundings with a frequency range of 100 to 0.01 Hz. The overall quality of the MT data used varied from bad (20.2 %) to very good (17.5 %). The 3-D MT inversion was carried out using the MT3DInv-X software program (Daud et al., 2012). It is a user-friendly software program that utilizes the Occam's inversion data space algorithm developed by Siripunvaraporn (2011). With this software program, the 3-D inversion process was performed more effectively. The result of the 3-D inversion in this software program was integrated with the GeoSlicer-X software program (Daud and Saputra, 2010). The output of the MT3DInv-X was exported into the (x, y, z) value data format, which was used as data input in the GeoSlicer-X software to visualize the data in three dimensions.

3.1 Mesh Grid Parameter

The 3-D model consisted of blocks in the 3-D mesh-grid in the dummy coordinate system. The center of the dummy coordinate system was situated in the center of the station distribution. In the MT3DInv-X software, the x-axis was oriented from north to south (with north as positive), the y-axis was oriented from east to west (with east positive), and the z-axis was positive downwards. The 3-D MT inversion process used a 100 ohm-m homogeneous half-space as the initial model. The number of blocks was 72 from north to south and 80 from west to east, with 22 vertical layers (without air layers). Thus, the total number of model blocks was M = 72 x 80 x 22 = 126,720.

3.2 Data Input

The data input for the 3-D MT inversion process were the real and imaginary parts of the impedance tensor (Zxx.real, Zxx.imag, Zxy.real, Zxy.imag, Zyx.real, Zyx.imag, Zyy.real, Zyy.imag). To constrain the data from high errors, the error floor of the impedance tensor was set as 5% to ensure that the model response fitted well with the observed data. The total number of data (N) depended on the number of stations, frequencies, and impedance tensor elements. The total number (N) for the 3-D inversion of MT data was 110 stations, 9 periods with the frequency range of 320 to 0.01 Hz, and all eight impedance tensor elements. Thus, the total number of data (N) is 110 x 8 x 8 or 2,448.

3.3 3-D Inversion Process

The 3-D MT inversion process was run on a PC with specifications as follows: Intel Pentium core i7 with 16 GB of RAM. For one iteration, it took about 2 hours and the total time to reach the 4^{th} iteration was about 148 hours. The 3-D inversion process using MT3Dinv-X was stable and convergent before finally reaching the best fit. Thus, it produced a good subsurface resistivity structure representing the real condition. The final RMS misfit achieved was 7.3%.

4. VARIATION IN OBSERVED RESISTIVITY

In recent days, there are three (3) type of inversion as follow, inversion 1 D, inversion 2 D, and 3 D. 1D Inversion is conducted with assumption of homogenous in earth properties, thus subsurface resistivity value varies only with deep. Inversion 1D is used for simple interpretation describing complexity of subsurface condition, however 3D inversion is analyzed with time-consuming and processed using large memory database. In any special cases, which the assumption of 2D subsurface structure using valid data, 2D method could be an alternative to obtain

updated model (Baranwal V.C., 2010). Following are the stages of the research, the first step is to select 3D MT data and its interpretation of resistivity distribution, and the next step, build conceptual model by re-processing MT 3D data, others geophysical and data validation with data from previous drilling results. MT price has generally been inexpensive method compared to drilling, 123 MT stations is about 4 % of one drilling price, which can demonstrate clearly interpretation of target area than drilling data.

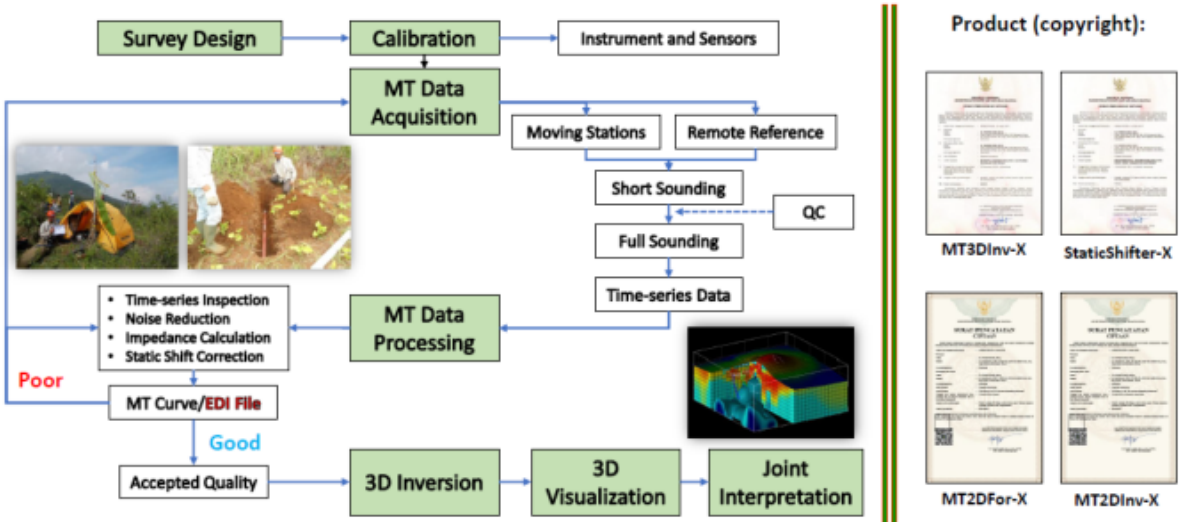

Figure 4: Workflow of MT Technology (Daud Y, 2020).

MT technology and processing program developed for various research projects are being evaluated and applied into the overall module. User documentation is being enhanced, including templates for typical application problems and improved user features. Additional time-series inspection, noise reduction, impedance calculation enhancements and applications of static-shift correction to difficult reservoir problems are ongoing. Accurate modelling criteria for MT data is essential to resemble the real 3D volcanic environment. 3D inversion method can be used in 3D complex structure area as usually correspond to volcanic formation. The MT sensitivity of conductive zone, such as clay cap, fracture zone and lithological contact, can also benefit from 3D modelling scheme based on resistivity distribution obtained from clean and genuine MT data. Proper MT technology can delineate geothermal system components such as altered rock layer (Clay cap) above the reservoir, vertical and lateral boundaries of reservoir, basement or possible heat source, well target zone (boundary of promising zone), high temperature and permeability zones.

Argillic Alteration is dominated by *smectite clay* that formed at temperatures less than about 180°C. The rocks within this alteration zone typically have resistivity below about 10 ohm-m and a conductive temperature profile indicating very low fracture permeability. The transitional argillic to propylitic zone can span up to 300 m in thickness, and is dominated by mixed layered smectite–illite clay. The propylitic alteration zone is corresponded to measured reservoir temperatures between about 220 and 270 °C.

4.1 Interpretation of Resistivity and Permeability Distribution

The update three-dimensional model shows resistivity distribution at all levels, with particularly at each elevation of 250 m. msl. At elevation – 3500 to – 1000 corresponds to the high resistivity zone as single extensive unit of resistive body and were related to the intrusion or heat source. Primary structural and stratigraphic controls on upflow system where the resistive (blue) zone extends into the sediments and lithological contact of youngest volcanic unit. Thick clay cap in the middle of prospect area is likely the barrier of two heat source and hypothesized as fault-controlled reservoir. Therefore, the upflow is interpreted to occur between the fault and deep BOC, beneath the area where the <5 ohm-m part of the clay cap (red) extends to about 2500 m depth.

Elevation – 1000 to - 500 m indicates narrowed reservoir geometry becomes 3 separated resistive zone (intrusion). Thick clay cap is found in the middle of prospect area, beneath of fumarole, and between hot spring. One important finding, believed to be interpreted for the first time: reservoir margin is described with contrast on surrounding conductive zone. This indicates that prospect area heterogeneity (and its structural details) may give a narrow and limited reservoir geometry and may explain much of the significant resistivity anomalies.

The average deep of BOC results from the resistivity mapping on a shallow deep is shown in Figure 5, elevation from – 500 to surface. It looks like a structure that hosts an upflow that extend almost 2000 m from surrounding the updome zone at about -500 m depth and dissipate near the reservoir boundary. The resulting of 3D inversion

are rich in information, illustrating a wide distribution of "anomalies" ranging from conductive or resistive class to sealed fractures and permeable fault. Importantly, the results illustrate that the three resistive zones separated by clay rich-barrier between these zones.

The three (3) main upflow zone are dominated by low permeability rocks. These intrusion may be related with heat source, fractured and high permeability zone, most likely along faults and intrusive margins (fault as conduit/vein), beneath main altered zone, barrier zone (clay rich tuff). The change of resistivity value with boiling depends on porosity and surface conduction, and was much larger for the high-permeability hydrothermal breccia and rhyolite lava from young phreatic eruption (8400 ka). Improved understanding, in three dimensions MT and correlation of well data may interpret high permeability fracture in volcanic rocks at the middle of main reservoir, such as andesite, dacite, rhyodacite, tuff, lava and breccia. Total changes in resistivity with boiling are appeared from andesite at well data and much larger for a hydrothermal breccia. Large resistivity changes associated with boiling for the highly permeable breccia (at southern kawah and thick clay barrier) suggest that a resistivity increase would correlate with high-permeability zones if steam is present.

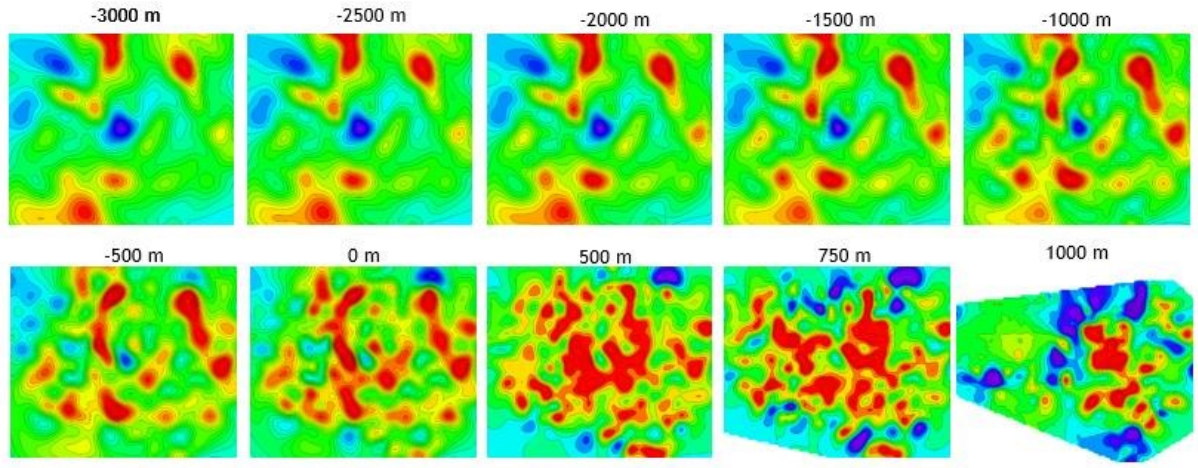

Figure 5: Distribution Map of Resistivity, shows spacious geometry of reservoir and thick clay cap in the centre (-1000 m), narrowed reservoir and three (3) main resistive zone (-500 m), clay rich tuff as barrier of the three resistive zone (0 m).

4.2 Inconsistencies of Resistivity Interpretation between 3D Inversion and 1D MT

This paper is focusing on revising the previous interpretation of 1D inversion that appear to be not exactly consistent with the real distribution of resistive zone interpretation at W - E which are speculatively described in a large reservoir from west – east . The decription of thick clay cap at W – E section and fumarole until elevation - 250 masl and no-barrier between large reservoir is not realistic to updated model. Thin conductive layer and shallow at Figure 8 is expected to represent main heat source or intrusion in 1D inversion, but in 3D model, low resistive layer is thick to nearly -750 masl. The most recent updome pattern is showed by upflow zone at updated 3D MT section and top of updome pattern (reservoir zone) at a depth of about -500 m until 500 m, which we infer to be the top of the reservoir after reviewing BOC and characteristic of upflow zone. The hotter part at conductive zone, has higher resistivity data, interpreted also as the alteration mineral product. This means a change of smectite zone into illite or chlorite with lower conductivity value. Porosity tends to decrease versus depth, so that reduce portion of fluids (Usher, Harvey & Johnstone, 2000).

Importantly, reservoir boundary is obviously determined by anomaly contrast which is analyzed using resistivity map at – 1000 until -500 m, the impermeable zone at west of the hottest production well, east of fumarole and southern hot spring. While thick, deep clay cap and sealed fractures have been known as permeability border, beneath southern hot water, 2 (two) major faults, and NW hot spring. Intrusion temperature above ~235 °C indicates a resistivity anomaly. Initial observations suggest that the resistive data could lead to reveal the occurrence of a geothermal system evidenced by discontinuous of resistivity value, at depth between - 4000 and - 3000 m. This is assumed to be the root of the igneous intrusion in the caldera area. This anomaly is present also outside the reservoir boundary but with minor presence of conductive layer.

The interpretation of revised 3D inversion is increasing the understanding of XX conceptual model. Authors suggested, based on the resistivity map layer by layer, that the reservoir margin corresponds to the sealed fault boundary; others suggested that this permeability transition occurs in areas where the conductive layer indicates greater deep than –1500 m, also explain the clay rich tuff or impermeable fracture as the barrier of reservoirs on the integrated interpretation of MT and geochemical data from production well.

Deep outflow to the northeast area (chloride spring), bicarbonate spring is supported by an extensive low-resistivity anomaly and the distribution of surface thermal features. Low permeability and temperature decline indicate outflow zone at reservoir boundary. 70 – 200^{o}C zone is represented by low resistivity (conductive, range between 1 – 10 ohm-m), characterized also by smectite mineral content (low permeability). Low resistivity at outflow zone or the presence of low resistive layer due to tertiary sediment strongly affects, compared with conductive zone identified as upflow zone. This paper suggests that the resistivity anomaly is the secondary fault filled with minerals that, in turn, intersects WE-trending fault as high permeability fractures (upflow).

The evidence for both the highest temperatures at main production well, thick clap cap as barrier, suggest that an exceptionally spacious geometry is not described in this research. This conclusion is consistent with 3D MT E-W section. The conductive layer at east area is unlikely to have been significantly thicker. In contrast, the updome pattern and temperature match and range up to 230 – 250 ºC. Previous 1D interpretation have not proven to be at shallow BOC elevation, however it is certainly thicker clay cap, at – 750 m and – 1500 m (Figure 8). The comparison here of all interpretation of MT_2004_1D-Occam does suggest that resistive and conductive layer is not similar with Top of Reservoir (TOR) from well data. 1D interpretation may not be providing appropriate elevation of high resistive value (Figure 8). Perhaps the key to intrusion feature is a lack of illustration of resistivity variation which show permeability boundaries. The images of the predictive indicator of reservoir boundary is limited because the thickening of conductive layer has no significant indication.

5. SUMMARY AND RECOMMENDATION

1. 3D MT inversion has a strong correspondence only with good criteria and interpolation/software correction of EDI file, realistic curve trend for determining resistivity distribution and deep clay cap feature instead of using fair and bad quality of EDI file.
2. Misinterpretation of geothermal conceptual model remains the potential and important issue at XX field. The result of 3D inversion improvement, lithology, surface manifestation and others data correlation can indicate reliability of the proven BOC, deep conductive zone, barrier of permeability, and upflow in reservoir as an expedient measure for revising the existing conceptual model.
3. XX is a volcanic altered zone that exhibits thick and low resistivity anomaly detected at centre of prospect area, west part of fumarole, beneath of centre barrier and feature of high resistive zone at separated region. In vicinity of clay cap or sealed fracture, heat source was mapped as well.
4. This paper outcome is improved understanding, in three dimensions MT, geological feature and surface manifestation (geochemical) in volcanic-geothermal settings. Disagreement between Base of Conductor and TOR geometry at main reservoir has been corrected with new resistivity model which produce good agreement with TOR from drilling data as well as thickening of conductive layer in unsuccessful well.
5. Comprehensive geophysical methods especially corrected timeseries/static shift of raw data can play an important role to connect and reconstruct several data.
6. This study must be able to take many lessons from the “MT vs Drilling” experiences by utilizing the valuable drilling data in order to be successful in the upcoming drilling campaign and disseminated through collaboration of university, government and operator company for further research, journal and papers or publication.

ACKNOWLEDGEMENTS

Author is very grateful and kindly thank the counselors from Geothermal Submajor, University of Indonesia for the support and guidance and PT NewQuest Geotechnology for facilitating the data processing.

REFERENCES

Daud Y. et al., Identification of Subsurface Geological Structure in a Geothermal System Using MT Imaging Technology Proceedings of World Geothermal Congress 2015, Melbourne, Australia, 19-25 April, 2015

Daud Y., Magnetotellurite (MT) Technology for Geothermal Exploration. Scientific Article. For GEOCAP, 2018. Daud Y., Nuqramadha WA., Resistivity characterization of the Arjuno-Welirang Volcanic Geothermal System (Indonesia) through 3-D Magnetotelluric Inverse Modeling, 2019.

Fahmi F, Ichwan WN, et al., Simulation of 3-D Effect in Magnetotelluric (MT) Data and Its Influence on Inversion Modeling, The 5th Indonesia International Geothermal Convention & Exhibition (IIGCE), 2017.

Kurniawan, I W, Evaluation of Reinjection Well and Analysis of Geothermal Reservoir Using 3D MT, MEQ, and Well Data at Salak Field, (2015)

Nordquist, G.A Microearthquake (MEQ) Monitoring., International Geothermal Association and Indonesian Geothermal Association Workshop Indonesia, Bali, (2008).

Stimac J A and Sugiaman F., The Awi 1-2 Core Research Program Part I: Geologic overview of the Geothermal Field, Indonesia Proc., World Geothermal Congress, Kyushu-Tohoku, Japan, (2000).

Supijo Marchel C, Wahyono Akbar D, Lesmana A., Updating Conceptual Model Using Numerical Modelling for Geothermal Green Field Prospect Area in Atadei, East Nusa Tenggara, Geothermal Master Program, Institute Technology of Bandung, Indonesia Jl. Ganesha No. 10 Bandung, (2018).

Younger P L,. Geothermal Energy: Delivering on the Global Potential, Journal Energies (ISSN 1996-1073), Basel, Switzerland, (2015).

Yoshioka K, Stimac J., Geologic and Geomechanical Reservoir Simulation Modeling of High Pressure Injection., Proceedings World Geothermal Congress, Bali, (2010)

Kotamobagu Geothermal Field, Indonesia: Overview on the Geological Aspect

Syayidu Guntur Maarif, Graniko Reza Pratama, Sigit Suryanto,
Ben Ikhsan, David Paskareinold Timisela, and Dimas B E Rindingpadang

PT Pertamina Geothermal Energy Tbk.

Syayidu.maarif@pertamina.com

Keywords: Kotamobagu Geothermal Field, Geology, Volcanology

ABSTRACT

The Kotamobagu geothermal field is located in North Sulawesi, Indonesia. Tectonically, the Kotamobagu geothermal field is on the southern side of the northern arm of Sulawesi Island, which is an active tectonic zone flanked by two NE-SW trending subductions on the northwest (Molucca Oceanic Plate) and southeast sides (Sangihe Double Subduction Zone). The tectonic processes resulted in volcanoes appearing in the Kotamobagu geothermal field.

Based on the results of geological mapping and satellite image analysis, the Kotamobagu geothermal field consists of lithology divided into four groups: tertiary rocks unit, tertiary-quaternary rocks unit, quaternary rocks unit, and the recent depositional unit. The formation of the Kotamobagu Geothermal Field is deeply intertwined with regional tectonic activities, particularly the subduction and extension phases in the northern arm of Sulawesi. These subduction processes influenced volcanic activity in Kotamobagu with the direction of the main tectonic forces acting, which are aligned with the straightness of the existing volcanic cone with the direction of northwest to southeast with the oldest volcano on the northwest, including Mt. Kolokot, Mt. Moyayat while the youngest volcano is on the southeast included Mt. Moaat and Mt. Ambang resulting in the diverse geological features observed in the field today. The extension phase, in particular, facilitated the formation of NE-SW trending structures, such as the Ambang-Makaaroyen structure, which is crucial for understanding the region's geothermal potential.

1. INTRODUCTION

The Kotamobagu geothermal field is one of the concession areas under PT Pertamina Geothermal Energy Tbk. Administratively, the Kotamobagu Geothermal Field is located in four districts in North Sulawesi Province (Figure 1). This field is tectonically located on the northern arm of Sulawesi, or approximately 200 km to the south of Manado City. In the middle of this field is the Mount Ambang complex, characteristic of volcanic activity. Geological surveys in the Kotamobagu field have been carried out since the 1980s. In 1993, three shallow wells were spread across the Kotamobagu field, and in 2010-2011, two large hole wells were drilled on the south flank of Mount Ambang.

2. REGIONAL GEOLOGY

2.1 Regional Tectonic

Based on regional tectonics, Sulawesi Island is a complex tectonic zone associated with magmatic arcs, metamorphic rocks of varying grades, ophiolites, and microcontinental fragments that formed during the Late Mesozoic and Cenozoic (Hall, 2002). This tectonic zone can be divided into five tectonic provinces (Figure 2): the western, northern, central, and eastern Sulawesi Arms and microcontinental fragments (Cottam et al., 2011). Each of these tectonic provinces is separated by major regional faults.

2.1.1 Western Arm of Sulawesi

The tectonic province of the western arm of Sulawesi extends from the north in Gorontalo Bay to the south in Makassar. This tectonic province characterizes the continental margin segment (Leeuwen et al., 2007). The western arm of Sulawesi began to form in the Late Mesozoic on the southeastern border of Sundaland (Elburg et al., 2003). The basement of the western arm of Sulawesi is composed of several metamorphic rock complexes exposed on the southern side of this tectonic province, such as the Bantimala Complex (Wakita et al., 1996 in Elburg et al., 2003). This basement was formed during the subduction process beneath Sundaland in the Late Cretaceous (van Leeuwen, 1981; Hasan, 1991; Sukamto and Simandjuntak, 1983; van Leeuwen and Muhardjo, 2005 in Leeuwen et al., 2007). The subduction process continued until the Early Tertiary when the western arm of Sulawesi rifted away from Borneo, resulting in the thinning of the lithosphere in the Makassar Strait (Calvert

and Hall, 2007). Volcanic arcs appeared continuously and intermittently until the Early Miocene and produced carbonate and siliciclastic deposits on the south and north sides of the western arm of Sulawesi.

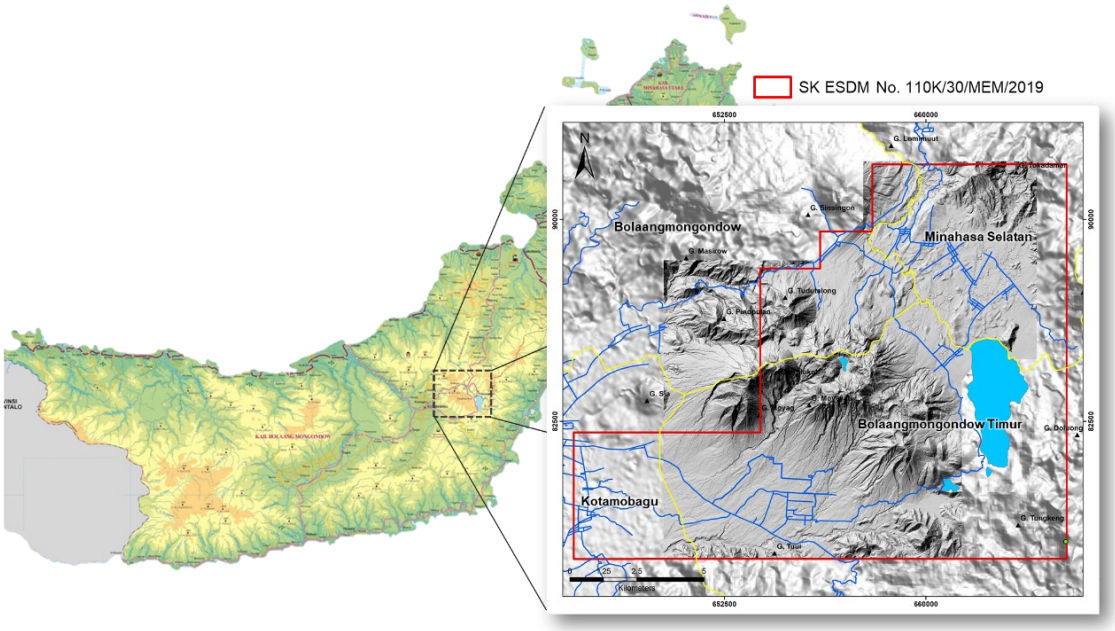

Figure 1: Location map of Kotamobagu Geothermal Field.

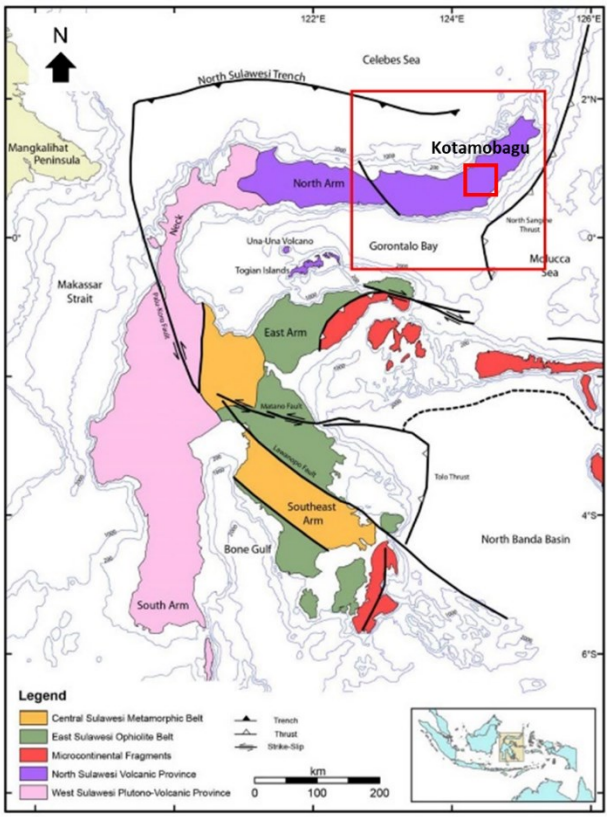

Figure 2: Tectonostratigraphic province of Sulawesi. Modified after Cottam et al. (2011).

2.1.2 Eastern Arm of Sulawesi

The tectonic province of the eastern arm of Sulawesi is located around the Tojo Una-una and Luwu areas. This tectonic province is composed of Ophiolites, which consist of sequences of dunites, lherzolites and harzburgites, ultramafic cumulates, layered gabbros, isotropic gabbros, sheeted dykes and basaltic pillows and lavas

(Simandjuntak 1986; Parkinson 1991,1998 in Cottam et al., 2011). Based on K-Ar dating, the ophiolites that make up this tectonic province are Cretaceous to Eocene in age (Simandjuntak, 1986 in Cottam et al., 2011).

2.1.3 Central Sulawesi

The central tectonic province of Sulawesi is divided into two parts: the northern part around Poso and the southern part around Kendari. This tectonic province is a metamorphic belt that separates the western and eastern arms of Sulawesi (Cottam et al., 2011). Lithologically, this location is composed of the Pomangeo schist complex, predominantly composed of interbanded phyllitic marble, calcareous phyllite, graphitic schist, and quartzite, rocks of terrigenous to shallow marine origin (Parkinson, 1998). This tectonic province was formed at the same time as the subduction process on the western arm of Sulawesi at the end of the Mesozoic (Parkinson, 1998).

2.1.4 Microcontinental Fragments

The microcontinental fragment tectonic province is in the Banggai-Sula complex on the eastern side of Sulawesi. This tectonic province comprises a basement of Palaeozoic or older metamorphic rocks intruded by Permo-Triassic granites associated with felsic volcanic rocks. These rocks are overlain by undated, probably Lower Jurassic, terrestrial sediments and by Jurassic and Cretaceous marine shales and limestones. There are Eocene to Neogene limestones in the western parts of the islands (Garrard et al., 1988; Supandjono & Haryono, 1993; Surono & Sukarna, 1993 in Cottam et al., 2011). Even though this tectonic province is relatively small, the collision processes that occur in this province are often interpreted as the cause of regional deformation in Sulawesi and Borneo. One of them is the Early Miocene collision of the Sula Spur with the North Arm volcanic arc and East Arm Ophiolite, and this continental area was then fragmented during extension caused by subduction rollback into the Banda embayment (Cottam et al., 2011).

2.1.5 Northern Arm of Sulawesi

The tectonic province of the northern arm of Sulawesi extends from Gorontalo to Manado and consists of a dominantly tholeiitic Tertiary volcanic arc built on the Eocene oceanic crust (Cottam et al., 2011). Kotamobagu Geothermal Field is located in this complex tectonic province of North Sulawesi. Its current position is at the meeting point of four plates: the Eurasian, Philippine/Celebes Sea, Molucca Sea, and Indo-Australian. The volcanism in this tectonic province was controlled by the northward subduction of the Indian Ocean lithosphere beneath the north arm of Sulawesi in the Eocene (Figure 3; Cottam et al., 2011; Hall 2002; 2012).

The volcanic products representing this subduction period are bimodal volcanic rocks (felsic and mafic in composition) categorized by Elburg et al. (2003) as Old Series volcanism on Sulawesi Island. The Old Series volcanism (51–17 Mya) in Sulawesi has a Chalk-Alkaline to Tholeiitic affinity spread throughout the West Sulawesi tectonostratigraphic province (Elburg et al., 2003). This indicates that the western and northern arms of Sulawesi were part of a volcanic arc in the Eocene (Elburg et al., 2003).

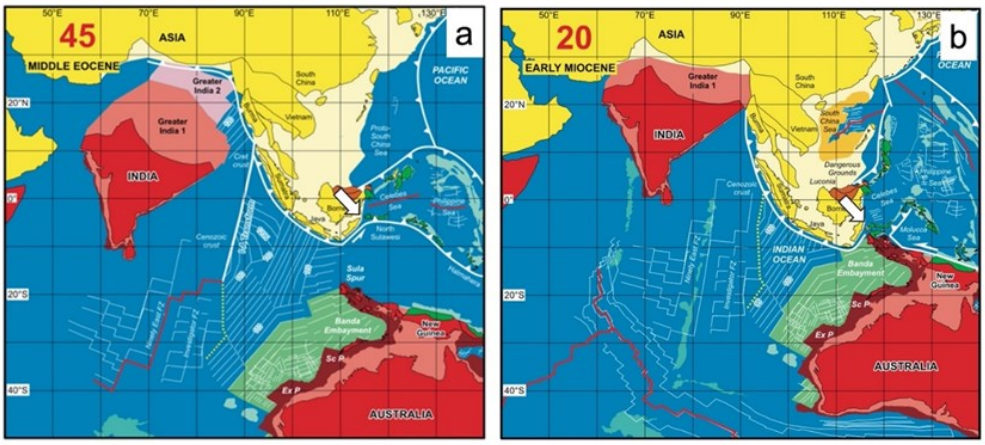

Figure 3: Tectonic reconstruction of the formation of the Northern Arm of Sulawesi volcanic arc through northward subduction of the Indian Ocean lithosphere beneath the north arm of Sulawesi during the Middle Eocene (a) and Early Miocene (b) (Hall 2002; 2012). The white arrow shows where the northern arm of Sulawesi is located.

The easternmost products of volcanism on the northern arm of Sulawesi from this subduction are represented by Ratatotok (12–14 Mya), Lake Tondano (3 Mya), Mount Lokon, and Manado Tua, which have a Calc-Alkaline affinity with potassium values varying from medium-K to shoshonitic (Elburg and Foden, 1998). Elburg and Foden (1998) assume that these volcanic rocks are part of the Sangihe Arc, which resulted from the subduction of the Molucca Sea plate to the west. This is confirmed by the results of seismic analysis of the subducting plate in

North Sulawesi (Cottam et al., 2011). Geochemical isotope trends show that the younger the age of volcanism, the melting of subducting sedimentary material increases (Elburg and Foden, 1998). This is possibly caused by the slowing speed of subduction of the Molucca Sea plate due to the collision process between the Sangihe Arc and the Halmahera Arc (Elburg and Foden, 1998).

The Celebes Sea, which formed in the Middle Eocene, was then subducted under the North Sulawesi arm in the Pliocene (Figure 3.2a; Hall, 2002; 2012). The tectonic process of this subduction also causes the northern arm of Sulawesi to experience a clockwise rotation process with the center of rotation at its western tip (Hall, 2019). The rotation and subduction process also causes the formation of right-hand strike-slip faults that limit segments of the upper crust, for example, Gorontalo, Buol, Malino, Tambarana, and Palu-Koro strike-slip faults (Hall, 2019).

2.2 Regional Stratigraphy

Based on the order of formation from old to young (Figure 4), the formations that make up the Kotamobagu Geothermal Prospect Area and its surroundings (Apandi & Bachri, 1997; Effendi & Bawono, 1997) are as follows:

2.2.1 Bilungala Volcanic Rock Formation (Tmbv)

This formation has a thickness of approximately 1000 meters and was deposited in a radius with the Bilungala Volcanic Limestone Member (Tmbl). Based on the fossil content in the limestone inserts, this unit is Early Miocene - Late Miocene. Bilungala Volcanic rocks are composed of breccia, tuff, and lavas, which are also composed of andesite, dacite, and rhyolite. In the rocks that make up breccia, zeolite, and calcite fragments are often found.

2.2.2 Bilungala Volcanic Rock and Limestone Member (Tmbl)

Members of this formation are composed of gray limestone, and their fossil content indicates that this unit is from the Early Miocene to the Late Miocene.

2.2.3 Tapadaka Formation (Tmts)

The Tapadaka Formation is composed of sandstone, greywacke, eroded sandstone, and shale. Based on the fossil content found, it is of Early Miocene—Late Miocene age.

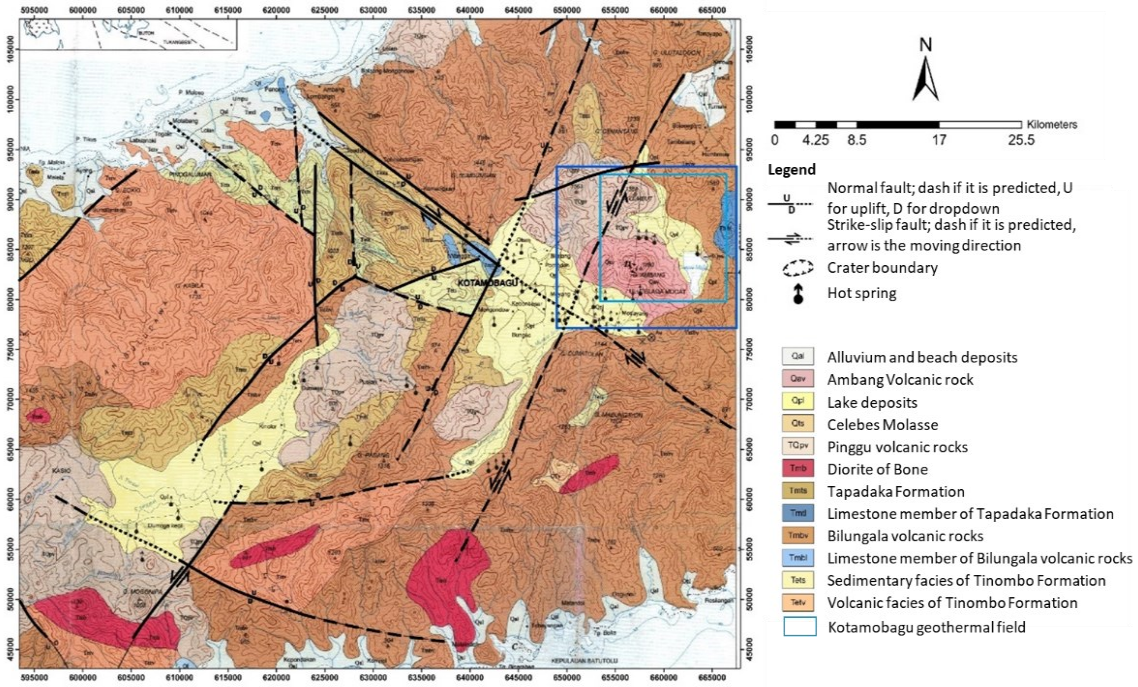

Figure 4: Regional geological map of Kotamobagu (Apandi & Bachri, 1997; Effendi & Bawono, 1997).

2.2.4 Pinogu Volcanic Rocks (TQpv)

This formation comprises tuff, lapilli tuff, volcanic breccia, and lava. Volcanic breccia is generally composed of andesite pyroxene and dacite. The tuff exposed on Mount Lemibut and Mount Lolombulan contains pumice fragments interspersed with lava. This rock unit is estimated to be Pliocene-Pleistocene in age.

2.2.5 Lake Deposits (Qpl)

Lake deposits consist of gray mudstone. In some places, it contains plant remains and lignite. Based on drill data, this unit has a thickness of 94 m.

2.2.6 Ambang Volcanic Rock (QAv)

This formation is composed of tuff, agglomerate, lahar deposits, lava, and sulfur deposits in the crater. Ambang Volcano is an active volcano with a strato cone shape and there are five fumarole fields.

3. DATA AND METHODOLOGY

The geological interpretation in Kotamobagu Geothermal Field is done by doing detailed geological mapping on the 20 x 20 km area. The steps of this research are collecting secondary data and lithology distribution mapping on the 137 observation points, including volcanostratigraphy and volcanic facies, distribution of alteration, and geological structure patterns in the Kotamobagu geothermal field and its surroundings. It also combines the subsurface data from the two existing wells on the southern flank of Mount Amban.

From the detailed mapping, hand specimens were taken and used for petrography and XRD analysis. These two analyses interpret the distribution of volcanostratigraphy and volcanic facies. The volcanostratigraphy and volcanic facies are then displayed on the 2D geological map and 2D cross-section.

4. KOTAMOBAGU GEOLOGICAL SETTING

4.1 Geomorphology

The Kotamobagu geothermal field has unique geomorphological conditions. The main location for this geothermal prospect is in the center, a row of young volcanoes surrounded by hillsides that look like caldera walls. Based on analysis of LiDAR data, topography, and aerial photography, the geomorphological units in the Kotamobagu geothermal field were divided into six units (Figure 5), namely:

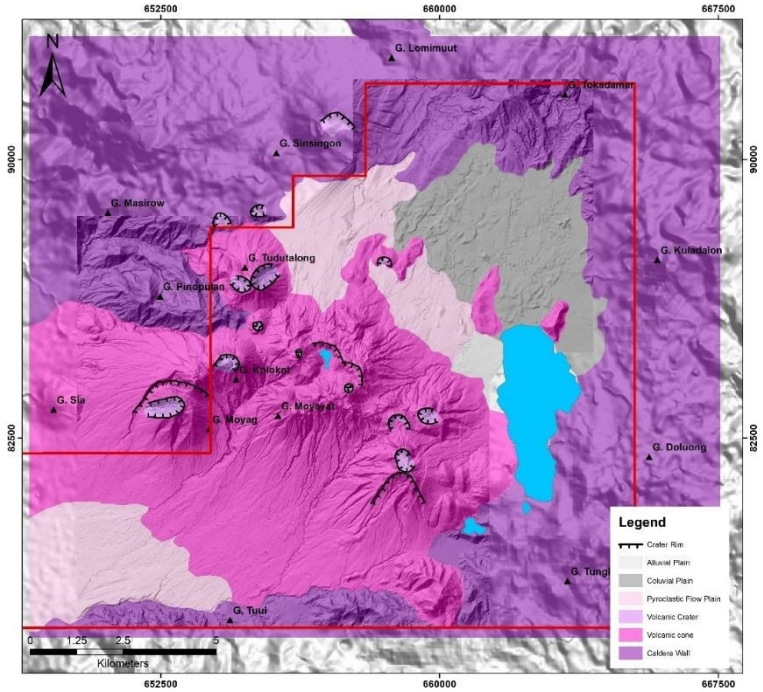

Figure 5: Geomorphological map of Kotamobagu geothermal field.

4.1.1 Alluvial Plain Unit

This unit is located in the middle of the Kotamobagu geothermal field on the northwest side of Lake Moaat. Its highest point is 1075 meters above sea level, and its lowest point is 1070 meters above sea level in the southwest, creating a height difference of 5 meters. The slope in measured units is approximately 1°. This unit is composed of loose deposits of fine material and soil.

4.1.2 Colluvial Plain Unit

This unit is located in the middle of the Kotamobagu geothermal field on the northside of Lake Moaat towards Makaaroyen. Its highest point is 1100 masl in the northeast, and its lowest point is 1079 masl in the southwest,

thus creating a slope that decreases towards the southwest. The slope in the measured unit starts at approximately 1°; however, the northwestern part of this unit has a wavy plain relief.

4.1.3 Pyroclastic Flow Plain Unit

This unit is located within the caldera wall and is a medial-distal slope on the southwest side of Mt. Ambang and north of Mt. Moyayat. This unit on the southwest side of Mt. Ambang has the highest point at 509 meters above sea level and the lowest point at 325 meters above sea level. On the north side of Mount Moyayat, the highest point is 1270 meters above sea level, and the lowest is 938 meters above sea level. The slopes on both parts of the measured unit start at approximately 3°. This unit is composed of lithology in the form of pyroclastic flow deposits and lahar.

4.1.4 Volcano Crater Unit

This unit is spread in the middle of the Kotamobagu geothermal field, especially along a row of mountains. It is the peak of these mountains, including Mt. Lemibut, Mt. Masiron, Mt. Tadutolong, Mt. Guaan 4, Mt. Kolokot, Mt. Kolokot Muda, Mt. Moyag, Mt. Ambang Muda 3, Mt. Ambang Muda 6, Mt. Ambang Muda 7, and Mt. Mooat. The geomorphological appearance of the volcanic crater unit is a volcanic depression at the top of the volcanic cone formed by pyroclastic flows and lava. This unit is included in the central facies, which is the center of the eruption.

4.1.5 Volcano Cone Unit

This unit extends to the center and surrounds the volcanic crater unit. This unit appears to be spread out in an NW-SE direction from Mount Moaat on the southeastern side to Mount Tudutalong and Mount Moyag on the northwest side. This type of unit has the highest point at 1701 meters above sea level and the lowest point at 347 meters above sea level, so it has a height difference of up to 1356 meters. The geomorphological appearance of the volcanic cone unit is a cone formed by pyroclastic flows and lava. This unit is included in the proximal-medial facies close to the eruption center.

4.1.6 Caldera Wall Unit

This unit is spread around the Kotamobagu geothermal field. This unit is interpreted as a horseshoe-shaped moat caldera wall with an opening to the southwest. This unit is the remains of Mount Tuui and Mount Tungkeng on the south and southeast sides, Mount Kuladalon and Mount Doluong on the east side, Mount Tokadamar and Mount Lomimuut on the northside, and Mount Masirow and Mount Pinopulan on the Northwest. This unit has the highest point at 1539 meters above sea level and the lowest point at 302 meters above sea level, so it has a height difference of up to 1237 meters. The geomorphological appearance of the caldera wall unit is a medium slope with wavy to steep relief composed of lava, breccia, and pyroclastic flows.

4.2 Stratigraphy

Based on observations at 137 points and after carrying out petrographic and XRD analysis on selected samples, the rock units in the Kotamobagu geothermal field can be separated into four units (Figure 6). This division is based on rock characteristics and interpretation of their associations. Then, comparisons are made with regional geological data to group these rock units based on the estimated age at which these units were formed because age dating has not been carried out on the existing samples. Based on this, the following rock units in the Kotamobagu geothermal field are sorted from oldest to youngest estimated units, namely:

4.2.1 Tertiary Volcanic Rock Unit

This rock unit is the oldest rock unit in the Kotamobagu geothermal field. This unit is spread around the Kotamobagu geothermal field. This unit is the remnant of an old Moaat volcanic cone. The lithology that makes up this unit includes andesite lava, which is the dominant constituent. Lithology is also found locally in the form of tuff breccia. Among the constituent lithologies, andesite lava is still exposed throughout the entire caldera wall, but the tuff breccia has experienced quite intense weathering, so no fresh samples were found (Figure 7).

Based on field analysis, andesite lava shows a yellowish gray to dark gray color, has a phenocryst size of 1-4 mm and a groundmass of <0.1 mm, is hypocrystalline, porphyro-aphanitic, with a phenocryst composition of plagioclase, pyroxene, hornblende, and fine-size groundmass. Photos of outcrops in the field can be seen in Figure 7a. Based on petrographic analysis (Figure 8), andesite lava has a porphyro-aphanitic texture and hypocrystalline crystallinity with phenocrysts in the form of plagioclase, biotite, and clinopyroxene as primary minerals. Phenocrysts measure 0.1-1.6 mm. Volcanic glass and plagioclase microliths are present as groundmass. Meanwhile, secondary minerals identified were sericite, opaque minerals, and fe-oxide. The name based on petrographic observations is pyroxene andesite (Streickesen, 1978 in Le Maitre, 2002).

Observation of the tuff breccia shows a grayish brown to brownish red color, some of the rock has experienced weathering and alteration, the material is fine ash - chunks. The rock fragments are brownish gray to reddish gray

andesite, have a porphyro-aphanitic texture, have a hypocrystalline rock structure with phenocrysts measuring 1-3 mm, and the groundmass is fine. The phenocryst composition consists of plagioclase, pyroxene, hornblende, biotite fine-sized groundmass, and secondary minerals. The matrix of the tuff breccia is grayish brown to yellowish brown, and the material is fine gray – coarse gray. The appearance of the outcrop in the field can be seen in Figure 7b.

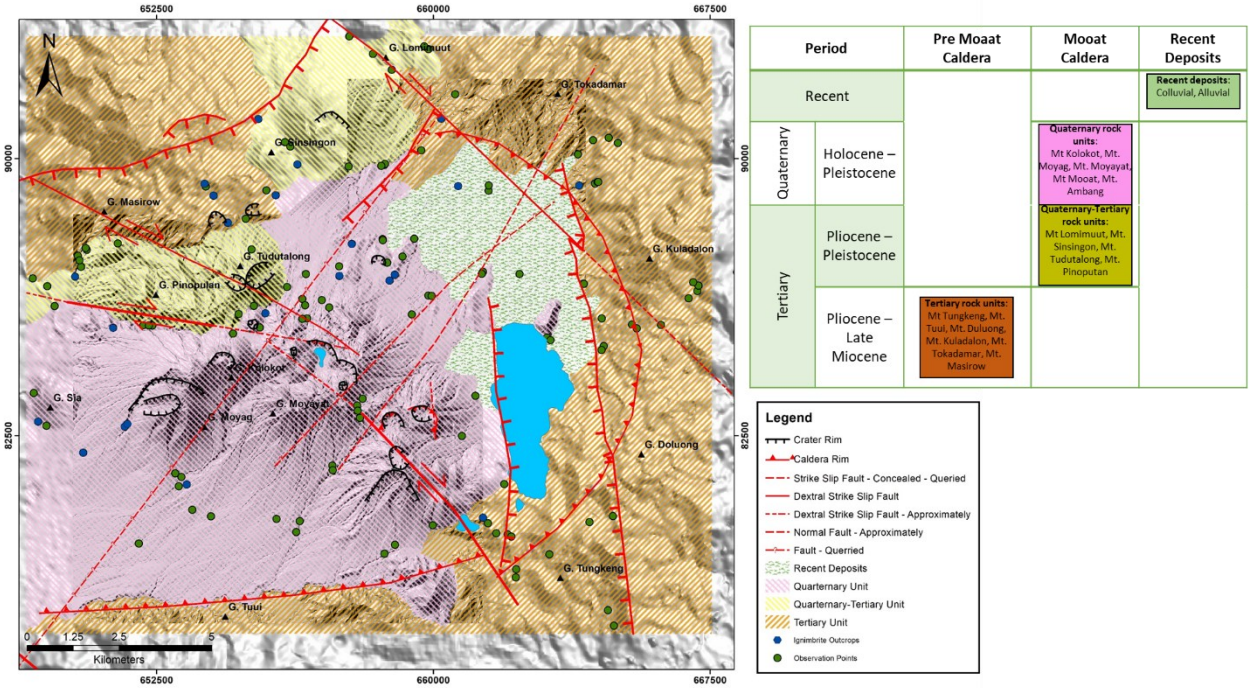

Figure 6: Geological map of Kotamobagu geothermal field. The lithological unit can be divided into four units based on the correlation with regional geology.

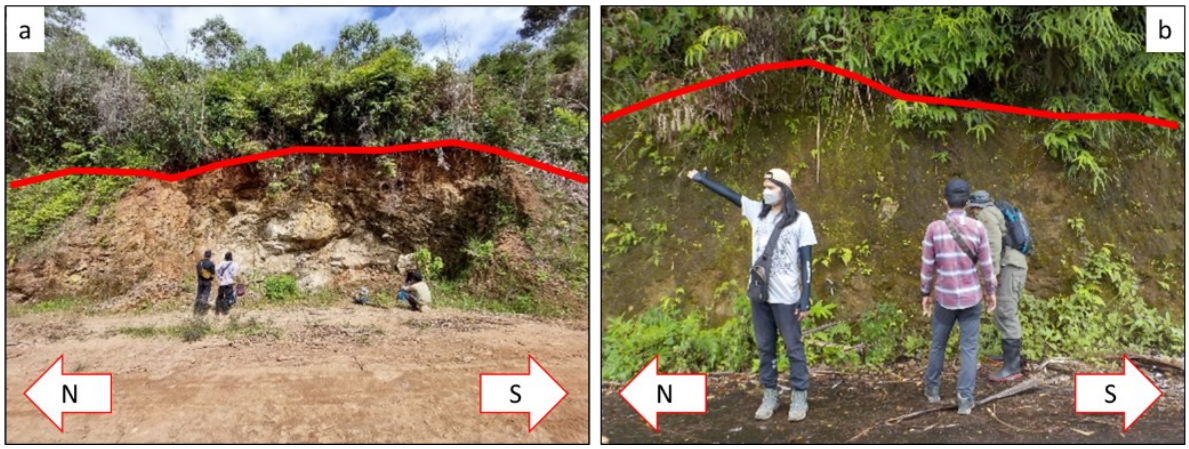

Figure 7: Outcrop of tertiary rock unit, a) Andesite lava outcrop near MT. Duluong, b) Tuff breccia outcrop near Mt. Kuladolon.

parallel and cross nicols respectively.

4.2.2 Quaternary-Tertiary Rock Unit

Quaternary-tertiary rock units are limited to the north and northwest sides of the Kotamobagu geothermal field. This unit appears in the northwesternmost part of the sill volcanic series and is deposited on top of tertiary rock units. Lithologically, the composition of this unit is not much different from that of tertiary rock units, namely composed of andesite lava and tuff breccia. However, what is different is that the tuff breccia lithology in this unit is only limited to around MT. Tudutalong and MT. Pinopulan and has fresher characteristics than the tuff breccia in the tertiary unit, although sampling cannot still be carried out.

The andesite lava that makes up the quaternary-tertiary rock unit shows a light to dark gray color, has a phenocryst size of 1-5 mm, and a fine groundmass, hypocrystalline, porphyro-aphanitic texture. The phenocryst composition

is plagioclase, pyroxene, hornblende, and fine groundmass. Photos of outcrops in the field can be seen in Figure 9a. Based on petrographic analysis (Figure 9c and Figure 9d), andesite lava has a porphyro-aphanitic texture and hypocrystalline crystallinity with phenocrysts in the form of plagioclase, clinopyroxene, biotite, and hornblende as primary minerals. Phenocrysts measure 0.1-1 mm. Volcanic glass and plagioclase microliths are present as groundmass. The rock experienced intensive alteration (IA = 0.6), which presented secondary minerals in the form of sericite, iron oxide, opaque minerals, quartz, and clay minerals. The name based on petrographic observations is biotite andesite (Streickesen, 1978 in Le Maitre, 2002).

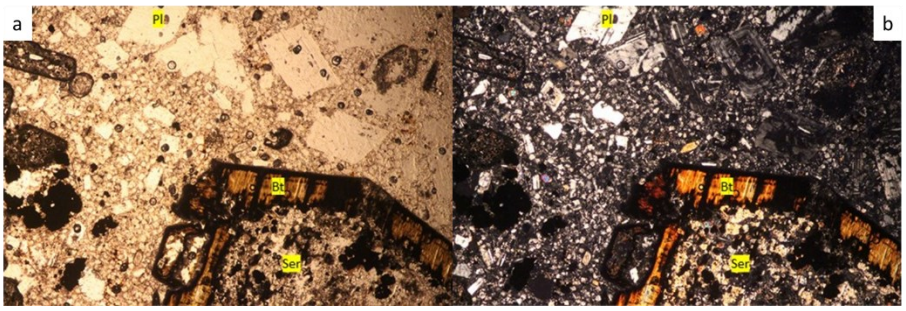

Figure 8: Andesite lava of tertiary rock unit under petrographic analysis. a) parallel nicols, b) cross nicols.

Figure 9: Outcrop of quarternary-tertiary rock unit, a) Andesite lava outcrop, b) Tuff breccia outcrop. Both of the outcrop located near Mt.Pinopulan, (c) and (d) are thin section of andesite lava in

The tuff breccia in Mount Pinopulan shows a characteristic brown color; some of it has experienced weathering (Figure 9b). The rock fragments are dark gray andesite, porphyro-aphanitic texture, hypocrystalline, and 1-3 mm phenocrysts. The groundmass is fine. The phenocryst composition consists of plagioclase, pyroxene, and fine groundmass minerals. The matrix of the brown tuff breccia is composed of fine ash - coarse ash-sized material.

4.2.3 Quaternary Rock Unit

This rock unit is in the central part of the Kotamobagu geothermal field and is the deposit of a row of young volcanoes that emerged in Kotamobagu. This rock unit is spread from Mt. Kolokot on the northwest side to Mt. Moaat on the southeastern side. The distribution of this rock unit is closely related to the geological structure in the form of the Ambang-Poopo dextral strike-slip fault with an NE-SW direction (Figure 13). The lithology exposed in this rock unit is closely related to the formation and eruption period of the existing volcano.

The dominant lithology that makes up this rock unit is andesite lava. These rocks are scattered throughout the volcanoes along the NE-SW Ambang-Poopo fault, including on Mt. Moyayat, Mt. Kolokot, Mt. Moyag, Mt. Moaat, Guaan, and Mt. Ambang, which are the youngest volcanoes in the Kotamobagu area. Andesitic lava has field characteristics showing a brownish gray, reddish color, has a phenocryst size of 1-3 mm, and a fine, hypocrystalline, and porphyro-aphanitic groundmass. The phenocryst composition consists of plagioclase minerals, hornblende, and fine groundmass (Figure 10a). Based on petrographic observations, a porphyritic

texture and hypocrystalline crystallinity were found, with the main phenocryst composition being plagioclase, biotite, hornblend, clinopyroxene, and opaque minerals (Figure 11a and Figure 11b). The phenocrysts in this rock measure between 0.1 to 4 mm and are euhedral-subhedral. The groundmass is composed of plagioclase microliths, biotite microliths, pyroxene microliths, and glass material. The secondary minerals that appear are alunite, chlorite, iron oxide, clay minerals, opaque minerals, and sericite.

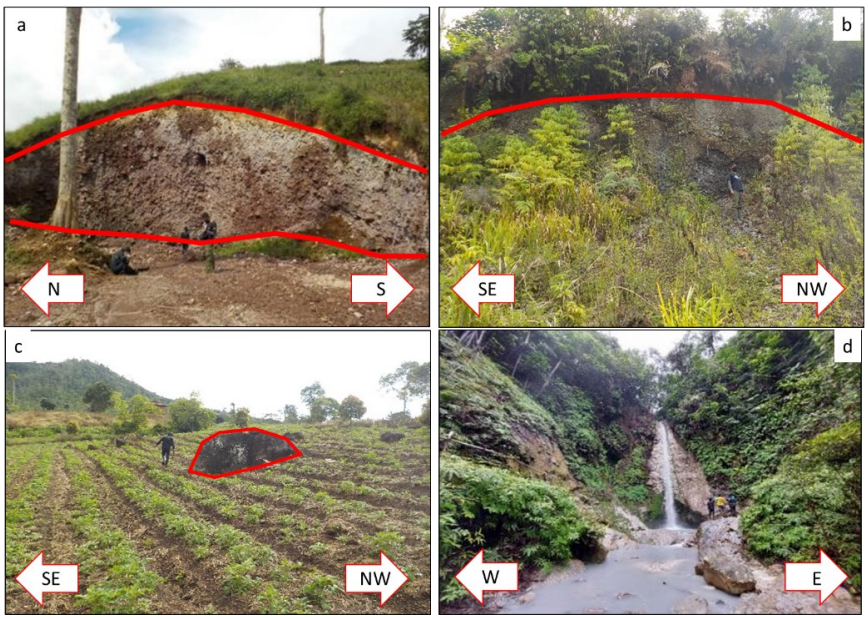

Figure 10: Outcrop of quarternary rock unit, a) Andesite lava near Guaan, b) Tuff breccia near Mt. Moyayat, c) Laharic breccia near Mt. Moyayat, d) Dacitic breccia near Mt. Ambang.

The other lithology that makes up Quaternary rock units is tuff breccia, which appears locally in Mt.Moaat, Mt.Moyag, Mt.Kolokot, and Mt.Moyayat (Figure 10b). Tuff breccia shows a yellowish-brown color that has undergone alteration and is composed of fine ash-lump-sized material. The rock fragments are gray andesite, porphyro-aphanitic, and hypocrystalline texture with phenocrysts measuring 1-4 mm; the groundmass is fine. The phenocryst composition consists of plagioclase, pyroxene, hornblende minerals, and a groundmass of fine-sized intermediate minerals. The matrix of the yellowish-brown tuff breccia is composed of fine ash - coarse ash-sized material.

Laharic breccia deposits were also found at several points in this Quaternary rock unit, especially in the Mt. Kolokot and Mt. Moyayat areas. This deposit was identified from chunk-sized andesite fragments in the middle of rice fields. These fragments were identified as a matrix of laharic breccia that had experienced intense weathering (Figure 10c).

The final lithology that makes up the Quaternary rock unit is dacite lava, which appears in the youngest volcanoes in the Kotamobagu area, including Mt. Moaat and Mt. Ambang (Figure 10d). This dacite lava often appears around the Mt. Ambang crater, especially on the southwest slopes. Observations of dacite in the field show a bright gray color, a phenocryst size of 1-5 mm, a fine hypocrystalline, and porphyro-aphanitic groundmass. The phenocryst composition consists of plagioclase, quartz, hornblende, pyroxene, biotite, and a groundmass of fine-sized intermediate minerals. Based on petrographic observations, a porphyritic texture and hypocrystalline crystallinity were found, with the main phenocryst composition being plagioclase, biotite, quartz, clinopyroxene, and hornblend (Figure 11c and Figure 11d). The phenocrysts in this rock measure between 0.1 to 4 mm and are euhedral-subhedral. The groundmass is composed of plagioclase microliths and glass material. The secondary minerals that appear are opaque minerals and sericite. The name of the rock is based on the petrographic description, namely biotite dacite (Streickesen, 1978 in Le Maitre, 2002).

4.2.4 Recent Depositional Units

Recent deposit units are spread on the north side of Lake Moaat towards Makaaroyen and reach the walls of the Moaat caldera. In terms of field appearance, there are two groups of rocks from recent sedimentary units. These, namely colluvial deposits, are the result of erosion of the caldera walls on the north and east sides (Figure 12a and Figure 12b). Colluvial deposits are composed of sand-gravel depositional lithology. Observations in the field showed a whitish-brown color and fine sand grain size, but they were not consolidated. The composition consists of sand-sized volcanic material and pebble-sized tuff - gravel. Based on petrographic analysis of this depositional fragment, a porphyritic texture, and hypocrystalline crystallinity were found, with the main phenocryst

composition being plagioclase, biotite, clinopyroxene, and hornblende. The phenocrysts in this rock measure between 0.1 to 3 mm and are euhedral-subhedral (Figure 12c and Figure 12d). The basic mass is composed of plagioclase microliths and glass material. The secondary minerals that appear are opaque minerals and sericite. There is also mineral filling in the form of alunite. The naming of the rock is based on the petrographic description, namely biotite andesite (Streickesen, 1978 in Le Maitre, 2002).

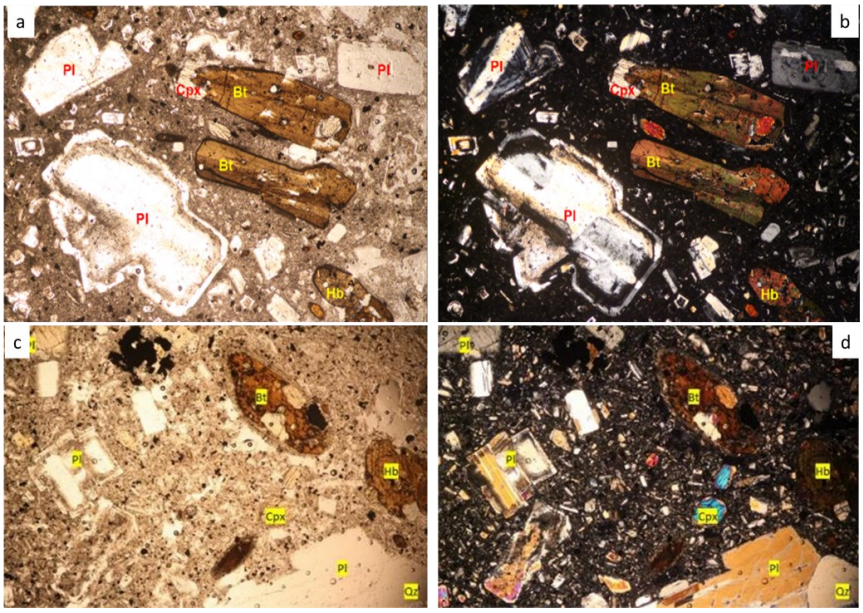

Figure 11: Thin section of quaternary rock units. (a) and (b) parallel and cross nicols of Andesite lava, (c) and (d) are parallel and cross nicols of Dacitic lava.

Figure 12: Outcrop of recent depositional units (a) and (b). Thin section of colluvial deposit in parallel and cross nicols (c) and (d).

In contrast to colluvial deposits, other recent depositional units are composed of alluvial deposits. This deposit is the result of the deposition of a moat lake, which has the characteristics of being composed of sand-gravel depositional lithology. Observations in the field showed a whitish-brown color, fine sand grain size, and gravel that was not consolidated. The composition consists of sand-sized volcanic material and pebble-sized tuff.

4.3 Geological Structure

Interpretation of geological structures in the Kotamobagu geothermal field is quite difficult. This is because most outcrops have experienced weathering, and alluvial and colluvial deposits cover the middle part of the location. Based on an analysis of satellite and LiDAR images, there is an NE-SW trend lineament (Ambang-Makaaroyen

Fault) that extends from Ambang Mountain to Makaaroyen. This lineaments interpreted to connect the manifestations in the Mt. Ambang crater and the Makaaroyen manifestations. The structure characterized by this lineament is not exposed on the surface because it is buried by colluvial sediment units deposited in the last sedimentation period.

The main geological structure that controls the evolution of volcanoes in the Kotamobagu geothermal field is the Ambang-Poopo fault, which is at the center of this field. This geological structure is exposed on the southeast side of the Kotamobagu geothermal field on the caldera wall (Figure 13). The outcrop is a cliff with dimensions of 2 x 4 x 4 meters (Figure 13a). Indications of the geological structure found at this location are stepping on the fault plane with an average orientation of N312°E/78° from 15 measurements. The stepping pattern on the fault plane at this location shows right-hand (dextral) shear dynamics.

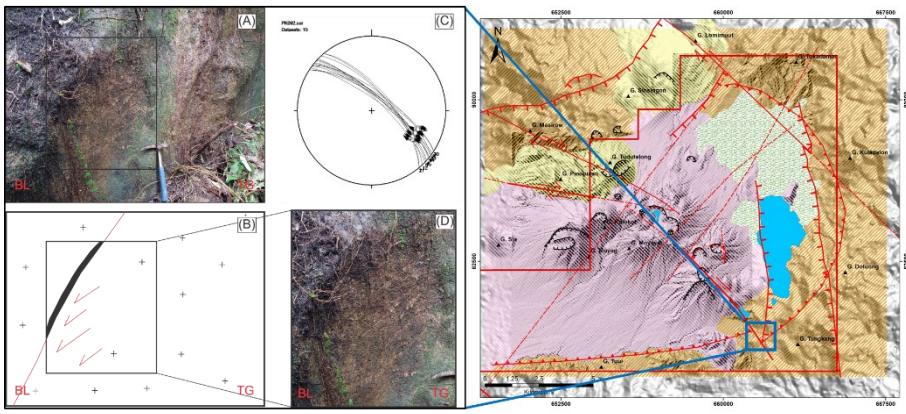

Figure 13: Field features and a sketch of the main geological structure trending NW-SE, a dextral strike-slip fault.

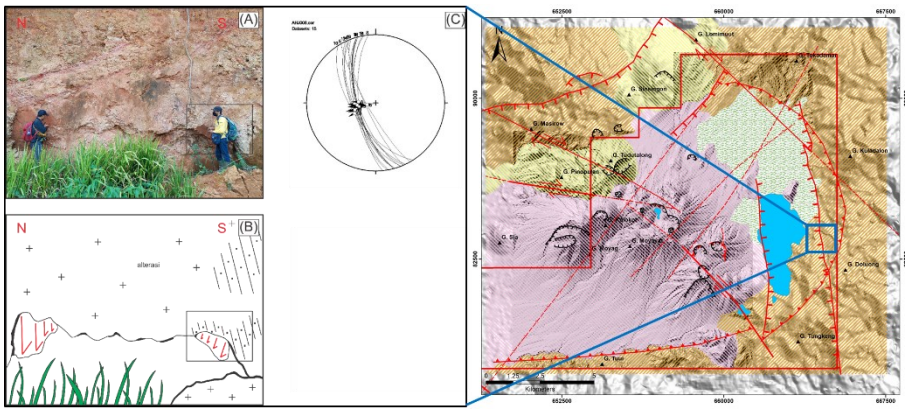

Figure 14: Field features and a sketch of the N-S normal fault near Mt. Duluong.

Another geological structure in the Kotamobagu geothermal field is found on the east wall of the Mooat caldera (Figure 14). This structure was found in the andesite lava lithological unit and is an outcrop in a field measuring 15 x 20 meters. Indications of the geological structure found at this location are structural mirror striations with a fault plane orientation with an average of N164°E/69° from 15 measurements (Figure 14). Observation and measurement of striations at this location indicate downward movement of the deformed block to the west.

4. DISCUSSION

The evolution of the formation of the Kotamobagu geothermal field is interpreted using existing data, including lithology, geological structure, and geomorphology data. Based on the interpretation of the existing topography and geomorphological units, the Kotamobagu geothermal field began to form during the Tertiary with the presence of the old Mooat Volcano, which then erupted and produced the Moaat Caldera. Evidence of this eruption is marked by the appearance of ignimbrite deposits around the Kotamobagu location and reaching the Tutuyan area (Figure 6). The ignimbrite was spread out when the big eruption of the old Mooat Volcano happened. It is characteristic of pumice that is vesicular and filled with quartz in the cavity (Figure 15).

In the Late Miocene to Pliocene, based on regional tectonics, the subduction process of two tectonic plates, namely the Celebes Sea and the Sula-Button, resulted in the formation of NW-SE trending dextral strike-slip faults along the northern arm of Sulawesi (Figure 16) (Hall & Wilson, 2000; Hall, 2012), one of the faults that appears is the

Ambang fault. The appearance of this Ambang fault started the process of volcanism in the Kotamobagu field, where this Ambang fault was interpreted as a way for magma to escape, forming a row of volcanoes in the Kotamobagu field (Figure 17).

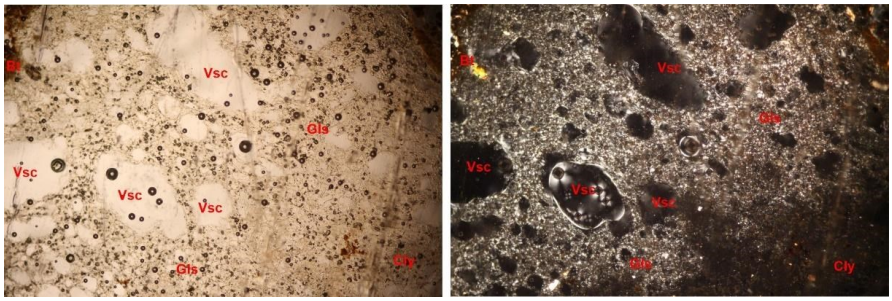

Figure 15: Thin section of the pumice with the vesicular is filled by quartz.

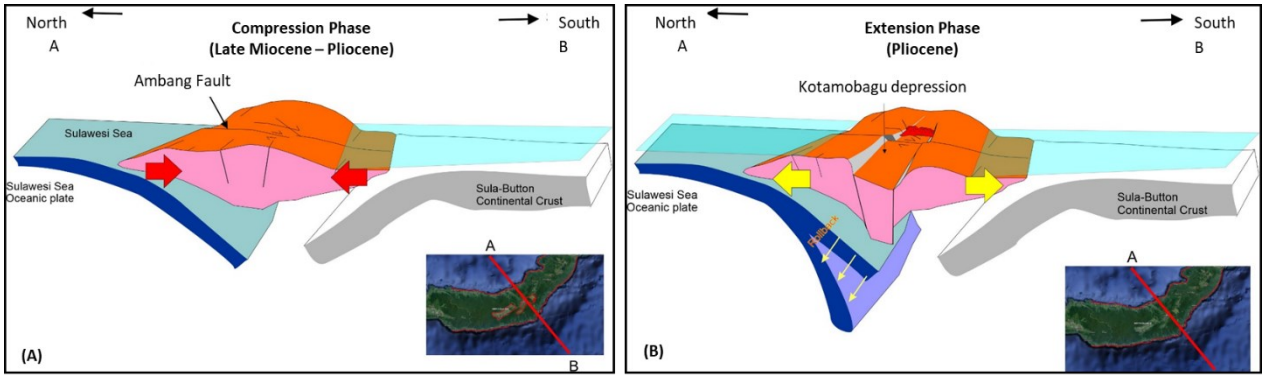

Figure 16: Tectonic process in North arm of Sulawesi at Late Miocene – Pliocene (A) compression phase, (B) extension phase (modified from Hall & Wilson, 2000; Hall, 2012).

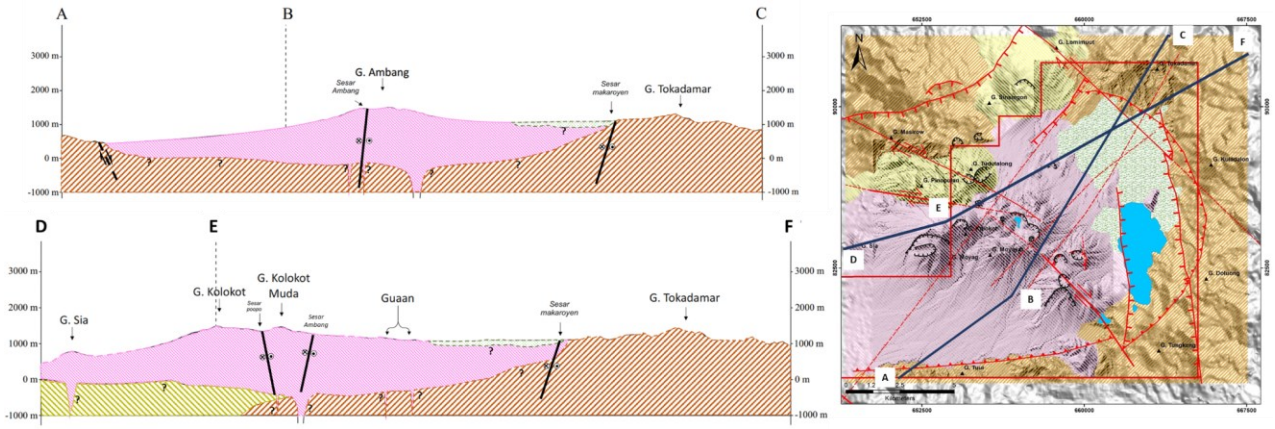

Figure 17: Cross section of the geological map. Showing the Quaternary rock units intruded the Tertiary rock units near the Ambang Fault.

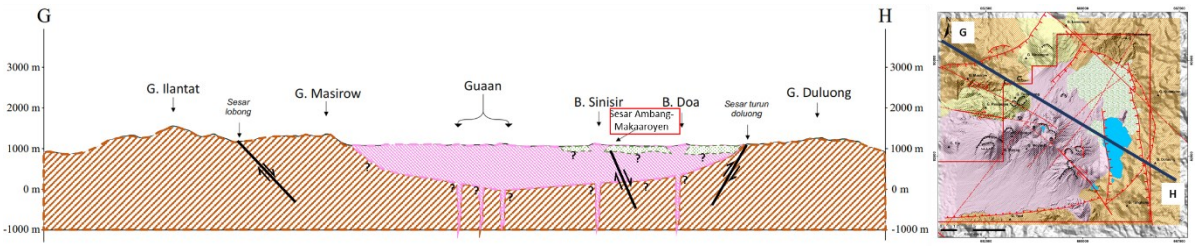

Figure 18: Geological cross section showing Ambang-Makaaroyen Fault (red square).

The process of magmatic evolution in the series of volcanoes in Kotamobagu starts from the northwest side, which is identified with the emergence of Mt. Tudutalong, Mt. Pinoputan, Mt. Kolokot, and Mt. Moyayat. Then, the magma evolution moved southeast towards Mt. Moaat and Mt. Ambang, which are the youngest volcanoes in the

Kotamobagu field. This magma evolution is categorized by a difference in the magmatic content of the lava in the northwest volcanoes, which are dominated by andesite-type lava. Meanwhile, on the mountains on the southeast area, there is dacitic-type lava, which has more acidic characteristics caused by the magma differentiation process.

During the process of volcanism during the Pliocene, it is interpreted that an extension phase occurred in the northern arm of Sulawesi (Hall & Wilson, 2000; Hall, 2012). This extension phase causes a rollback in the Celebes Sea tectonic plate, which provides an extension force and causes NE-SW trending structures to appear, one of which is the Ambang-Makaaroyen Structure, which is interpreted from drilling data on the southwest side of Mount Ambang and the alignment in satellite image data (Figure 18). Furthermore, due to the weathering process on the rocks on the moat caldera walls and rocks along the volcano, materials were deposited that filled the NE-SW structure (Ambang-Makaaroyen Fault), which was formed at a lower location.

5. CONCLUSION

The geological interpretation of the Kotamobagu Geothermal Field, conducted through detailed geological mapping, reveals a complex and dynamic geological history. The study covers a 20 x 20 km area, incorporating 137 observation points and integrating subsurface data from two wells on the southern flank of Mount Amban. The research methodology involves collecting secondary data, lithology distribution mapping, and analyzing volcanostratigraphy, volcanic facies, alteration distribution, and geological structure patterns. Hand specimens collected during the mapping were analyzed using petrography and X-ray diffraction (XRD) to interpret the distribution of volcanostratigraphy and volcanic facies, subsequently displayed on 2D geological maps and cross-sections.

The geomorphology of the Kotamobagu Geothermal Field is characterized by diverse units, including alluvial plains, colluvial plains, pyroclastic flow plains, volcano craters, volcano cones, and caldera walls. Each unit displays unique topographical features and geological compositions. For instance, the alluvial plain unit is composed of loose deposits of fine material and soil. In contrast, central to the geothermal field, the volcano crater unit consists of volcanic depressions formed by pyroclastic flows and lava. The stratigraphic analysis identifies four primary rock units, ranging from the oldest Tertiary rock units, predominantly andesite lava and tuff breccia, to the youngest Quaternary rock units, which include andesite and dacite lavas.

Despite the challenges posed by weathered outcrops and sediment cover, geological structure analysis highlights the significance of the NE-SW trending Ambang-Poopo fault. This fault plays a crucial role in the magmatic and volcanic evolution of the Kotamobagu field, facilitating magma escape and the formation of volcanoes. The magmatic evolution appears to progress from northwest to southeast, transitioning from andesite-dominated lavas to more acidic dacitic lavas due to magma differentiation.

The study concludes that the formation of the Kotamobagu Geothermal Field is deeply intertwined with regional tectonic activities, particularly the subduction and extension phases in the northern arm of Sulawesi. These tectonic processes influenced volcanic activity, resulting in the diverse geological features observed in the field today. The extension phase, in particular, facilitated the formation of NE-SW trending structures, such as the Ambang-Makaaroyen structure, crucial for understanding the region's geothermal potential.

REFERENCES

Apandi, T., & Bachri, S. (1997). *Peta Geologi Lembar Kotamobagu, Sulawesi*. Pusat Penelitian dan Pengembangan Geologi.

Calvert, S. & Hall, R. 2007. Cenozoic evolution of the Lariang and Karama regions, North Makassar Basin, western Sulawesi, Indonesia. Petroleum Geoscience, 13, 353–368

Cottam, M. A., Hall, R., Forster, M. A., & Boudagher-Fadel, M. K. (2011). Basement character and basin formation in Gorontalo Bay, Sulawesi, Indonesia: new observations from the Togian Islands. *Geological Society, London, Special Publications*, *355*(1), 177-202.

Effendi, A. C., & Bawono, S. S. (1997). *Peta Geologi Lembar Manado, Sulawesi Utara*. Pusat Penelitian dan Pengembangan Geologi.

Elburg, M., van Leeuwen, T., & Foden, J. (2003). Spatial and temporal isotopic domains of contrasting igneous suites in western and northern Sulawesi, Indonesia. *Chemical Geology*, *199*(3-4), 243-276.

Hall, R. & Wilson, M. E. J. 2000. Neogene sutures in eastern Indonesia. Journal of Asian Earth Sciences, 18, 787–814

Hall, R. (2002). Cenozoic geological and plate tectonic evolution of SE Asia and the SW Pacific: computer-based reconstructions, model and animations. *Journal of Asian Earth Sciences*, *20*(4), 353-431.

Hall, R. (2012). Late Jurassic–Cenozoic reconstructions of the Indonesian region and the Indian Ocean. *Tectonophysics*, *570*, 1-41.

Hall, R. (2019). The subduction initiation stage of the Wilson cycle. *Geological Society, London, Special Publications*, *470*(1), 415-437.

Parkinson, C. 1998. An outline of the petrology, structure and age of the Pompangeo Schist complex of central Sulawesi, Indonesia. Island Arc, 7, 231–245

van Leeuwen, T., Allen, C., Kadarusman, A., Elburg, E., Palin, J. M., Muhardjo, & Suwijanto 2007. Petrologic, isotopic, and radiometric age constraints on the origin and tectonic history of the Malino metamorphic complex, NW Sulawesi, Indonesia. Journal of Asian Earth Sciences, 29, 751–777

Unveiling Geothermal Potential by Leveraging SAR-assisted Fault Identification in Kotamobagu, North Sulawesi, using modified Segment Tracing Algorithm (mSTA) Method

Ben Ikhsan[1], Israyudi[1], David P. Timisela[1], and Asep Saepuloh[2]

[1]PT Pertamina Geothermal Energy Tbk.
[2]Institut Teknologi Bandung

ben.ikhsan@pertamina.com, saepuloh@itb.ac.id

Keywords: Geothermal, geological structures, fault identification, rock permeability, mSTA method, Synthetic Aperture Radar (SAR), SENTINEL-1 satellite, lineament detection, tectonic structures, volcanic structures, radial pattern, hot springs, environmental constraints, North Sulawesi, Kotamobagu

ABSTRACT

During the exploration phase, identification of geological structures, especially faults, has a very important role in determining geothermal potential based on rock permeability characteristics. However, in its implementation, there are a number of technical obstacles that hinder the accuracy of identifying these structures, including the complexity of field conditions which is often caused by the presence of cloud cover, dense vegetation, and subjectivity in the lineament delineation process. This study tackles the challenge of identifying geological structures, like faults, crucial for geothermal exploration in Kotamobagu, North Sulawesi.

This study introduces the application of the mSTA (modified Segment Tracing Algorithm) method as a solution for automatically detecting alignment from Synthetic Aperture Radar (SAR) images produced by the SENTINEL-1 satellite in the Kotamobagu geothermal area, North Sulawesi. Analysis of the results shows that the mSTA method is able to produce identification of 1657 lineaments in the ascending orbit and 2089 in the descending orbit. The identified lineament patterns depict strong associations with existing tectonic and volcanic structures.

By categorizing lineaments based on orientation and length, we discern a dominant radial pattern in the central study area. Furthermore, the high frequency density (Lf) anomaly observed on this lineament is significantly correlated with the local geological structure and the presence of hot springs. These findings underscore the promising utility of mSTA in overcoming environmental constraints for geothermal exploration.

1. INTRODUCTION

The use of remote sensing methods is remarkably effective in identifying geological structures to estimate subsurface geological features from the Earth's surface. In geothermal exploration, pinpointing geological structures, particularly faults, helps locate potential geothermal areas by assessing rock permeability. Visual analysis correlating lineaments with geological structures is commonly employed to gauge surface rock permeability. However, challenges such as cloud cover, vegetation, and the subjective nature of lineament delineation often hinder the accuracy of these assessments.

Remote sensing methods have been extensively and effectively utilized in geological tasks such as mapping alterations, distinguishing lithologies, and exploring minerals (Van der Meer et al., 2012). The advancement of satellite remote sensing systems has thus provided geologists with a potentially cost-effective substitute for conventional methods, which are known to be expensive, time-consuming, and labor-intensive. In utilizing these advantages, the lineament detection method is automated using the mSTA (modified Segment Tracing Algorithm) to estimate the presence of faults and fracture permeability in the Kotamobagu geothermal field, North Sulawesi (Figure 1).

The mSTA method is an automated lineament detection technique applied to Synthetic Aperture Radar (SAR) imagery, based on digital value contrast to detect lineament segments (Saepuloh et al., 2018). SAR imagery obtained from radar satellite sensors at microwave wavelengths can overcome cloud cover and vegetation canopy, thus enabling detected lineaments to closely approximate actual geological structure features (Saepuloh, 2021). The accuracy of lineament detection determines the precision of identifying geological structures (faults) and surface fracture permeability.The study utilizes automated detection of geological structure lineaments through the mSTA method, followed by statistical analysis to identify faults. Fracture permeability calculations are then derived from the identified mSTA lineaments. Verification of both structure and fracture permeability accuracy is conducted using full polarimetric SAR imagery.

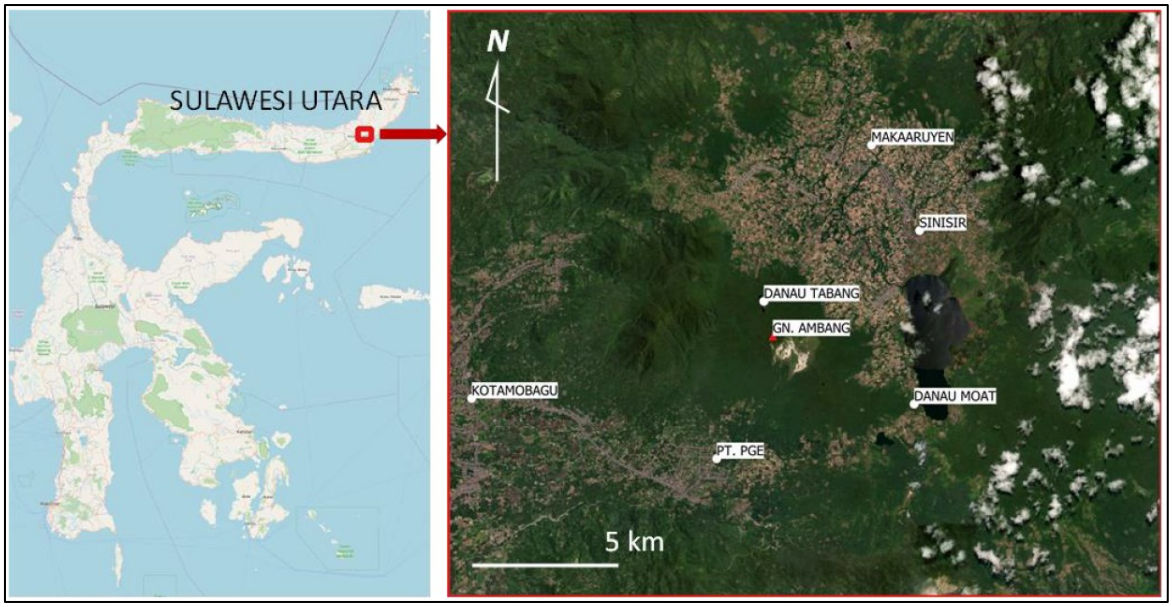

Figure 1: Location of Kotamobagu, North Sulawesi.

2. GEOLOGICAL SETTING

Sulawesi Island, shaped by complex tectonic since the Late Mesozoic and Cenozoic periods (Figure 2), exhibits a diverse geological landscape comprising magmatic arcs, metamorphic rocks, ophiolites, and microcontinental fragments. These features are organized into distinct tectonic provinces separated by major faults (Hall, 2002; Cottam et al., 2011).

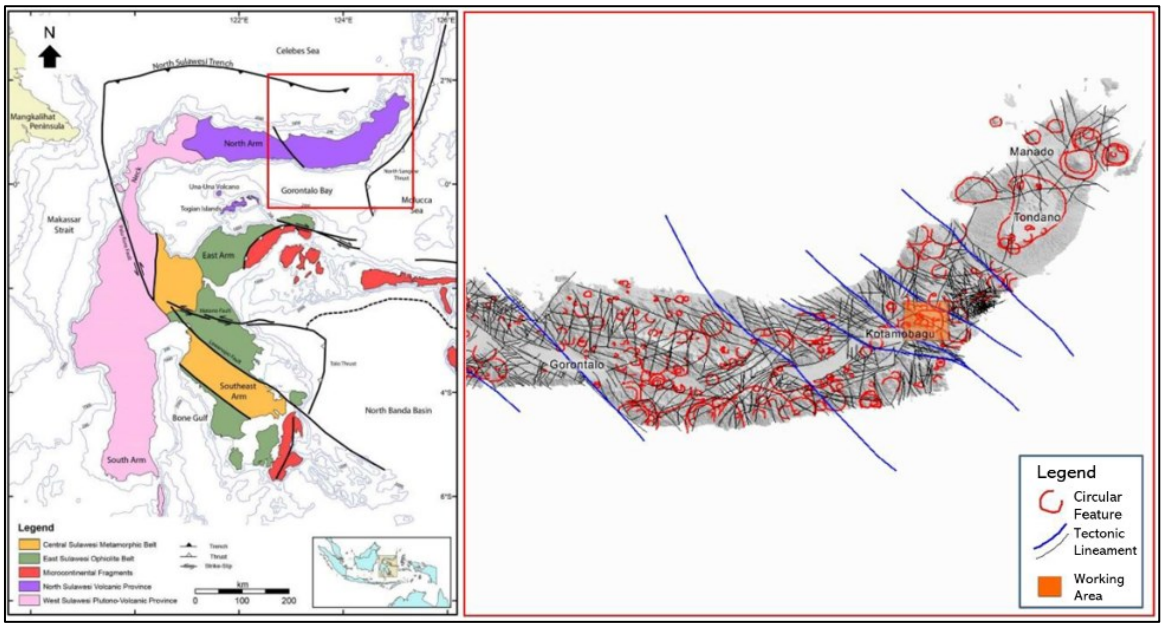

Figure 2: Tectonic Complex of Sulawesi (left) and North Sulawesi (right).

The western arm of Sulawesi spans from Gorontalo Bay to Makassar and developed as a continental margin in the Late Mesozoic on Sundaland's southeastern edge. Its basement includes metamorphic complexes like the Bantimala Complex, formed during Late Cretaceous subduction beneath Sundaland. Rift processes in the Early Tertiary thinned the lithosphere in the Makassar Strait, accompanied by intermittent volcanic activity until the Early Miocene, which deposited carbonate and siliciclastic deposits.

The eastern arm, encompassing areas such as Tojo Una-una and Luwu, is characterized by ophiolites dating from the Cretaceous to Eocene periods. Central Sulawesi, divided into northern Poso and southern Kendari regions, acts as a metamorphic belt separating the western and eastern arms. The Banggai-Sula complex hosts

microcontinental fragments with Palaeozoic metamorphic rocks intruded by Permo-Triassic granites and associated volcanic rocks, including Eocene to Neogene limestones.

The northern arm of Sulawesi, from Gorontalo to Manado, features a Tertiary volcanic arc on Eocene oceanic crust, influenced by northward subduction of the Indian Ocean lithosphere. This area, which includes the Kotamobagu Geothermal Field, illustrates complex interactions among tectonic plates such as the Eurasian, Philippine/Celebes Sea, Molucca Sea, and Indo-Australian plates. Volcanic formations range from Eocene bimodal rocks to recent Calc-Alkaline formations, shaped by ongoing tectonic processes and subduction activities (Elburg and Foden, 1998; Hall, 2012). These geological insights highlight Sulawesi's dynamic tectonic history, providing a framework for understanding its diverse geological formations and their implications for resource exploration and hazard assessment in the region.

The Kotamobagu Geothermal Field (Figure 3) is situated within four districts in North Sulawesi Province, positioned on the northern arm of Sulawesi, approximately 200 km south of Manado City. At its core lies within the Mount Ambang complex, indicative of the volcanic activity prevalent in this area.

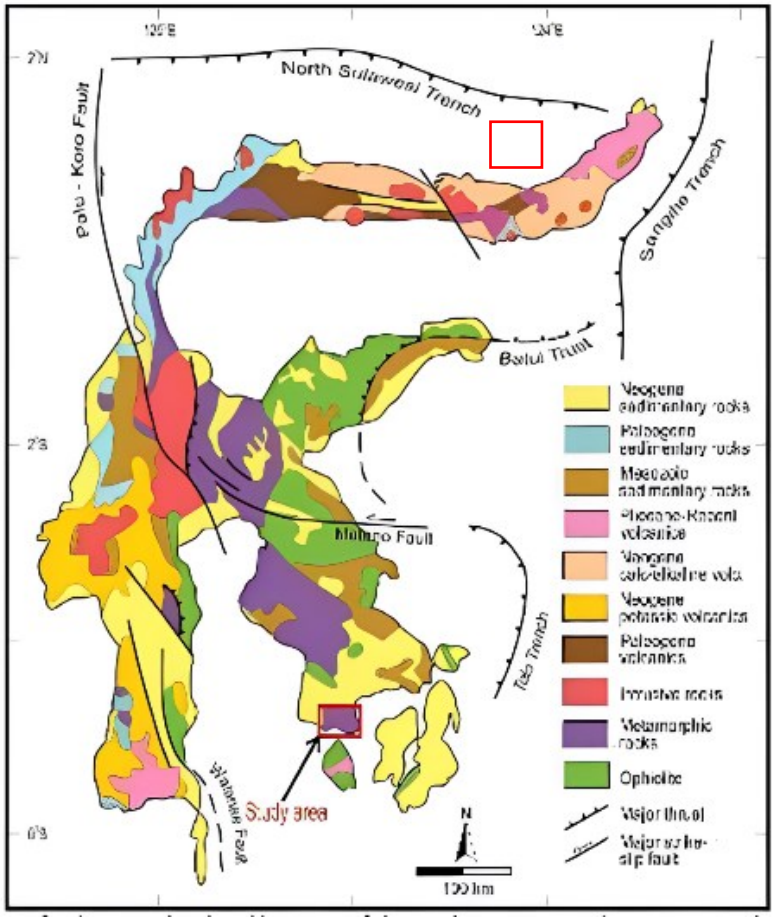

Figure 3: Sulawesi Regional Tectonic (left; Leeuwen and Pieters, 1992).

3. DATA AND METHOD

3.1. Data

3.1.1 Sentinel-1A/B

Sentinel-1 is the first satellite constellation of the Copernicus Program operated by the European Space Agency (ESA). The Sentinel-1 mission consists of two satellites, Sentinel-1A and Sentinel-1B, sharing the same orbit. They carry C-band Synthetic Aperture Radar (SAR) instruments capable of providing all-weather, day-and-night data with spatial resolution up to 5 meters and swath width up to 400 kilometers. The satellite constellation operates in a near-polar, sun-synchronous orbit (98.18°), completing 175 orbits per 12-day cycle. Two scenes of Sentinel-1 images, in ascending and descending orbits with dual polarization, are utilized for lineament detection, geological structure identification, and fracture permeability assessment.

3.1.2 ALOS PALSAR

The Phased Array type L-band Synthetic Aperture Radar (PALSAR) is an active microwave sensor utilizing L-band frequency for cloud-free land observation both day and night. Installed on the ALOS satellite, this sensor offers enhanced performance compared to previous generation SAR sensors like JERS-1. The development of PALSAR was a collaborative project between JAXA and the Japan Resources Observation System Organization (JAROS). Two scenes of ALOS PALSAR images in ascending orbit with full polarization are employed for visual verification of geological structures and fracture permeability.

3.2 Pre-Processing

The Sentinel-1 image footprint in both ascending and descending orbits has covered the study area adequately, requiring only one scene each (Figure 4). In contrast, the ALOS PALSAR image footprint in ascending orbit with full polarization requires two scenes due to the study area being located at the boundary edge of the scene.

NO	SENSOR	ID	TANGGAL	ORBIT	POLARISASI
1	SENTINEL-1B	S1B_IW_SLC__1SDV_ 20210716T100236	2021/07/16	ASCENDING	VV VH
2	SENTINEL-1A	S1A_IW_SLC__1SDV_ 20221115T212619	2022/11/15	DESCENDING	VV VH
3	ALOS PALSAR	ALPSRP064990000	2007/05/30	ASCENDING	HH HV VH VV
4	ALOS PALSAR	ALPSRP064990010	2007/05/30	ASCENDING	HH HV VH VV

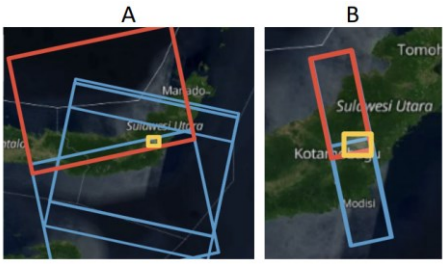

Figure 4: Dataset of Alos Palsar (left) and Sentinel-1A/B (right).

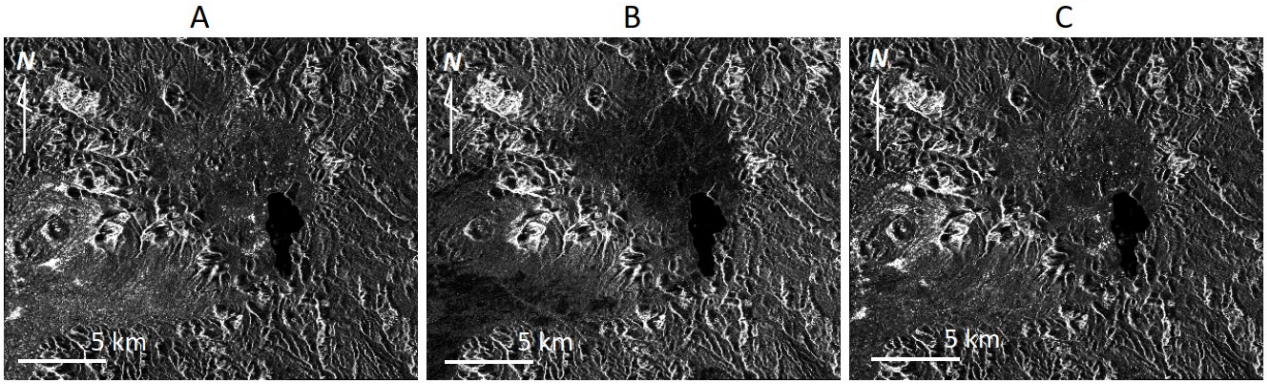

Figure 5: ALOS PALSAR HH, HV, and VV polarizations.

The study commences by obtaining data from ALOS PALSAR, followed by extracting images and performing polarimetric decomposition using the Yamaguchi method. Processing ALOS PALSAR data involves seven distinct steps, starting with: (1) data preprocessing, (2) multilooking, (3) ALOS deskewing, (4) geometric correction, (5) polarimetric matrix generation, (6) polarimetric speckle filtering, and (7) polarimetric decomposition. The geometrically corrected polarimetric image displays different tones and textures for HH, HV, and VV polarizations (Figure 5). The H and V polarizations represent the horizontal and vertical orientations of the wave propagation transmitted by the sensor and returned by objects on the surface.

Meanwhile, the processing of Sentinel-1 data involves seven distinct steps, starting with: (1) data preprocessing, (2) Multilooking, (3) Speckle filtering, (4) geometric correction, (5) automated lineament detection using mSTA. These processing stages are conducted using the SNAP software platform and subsequently continued with MATLAB scripts. Geometrically corrected Sentinel-1 images from both ascending and descending orbits exhibit clear morphological features from two different viewing perspectives (Figure 6).

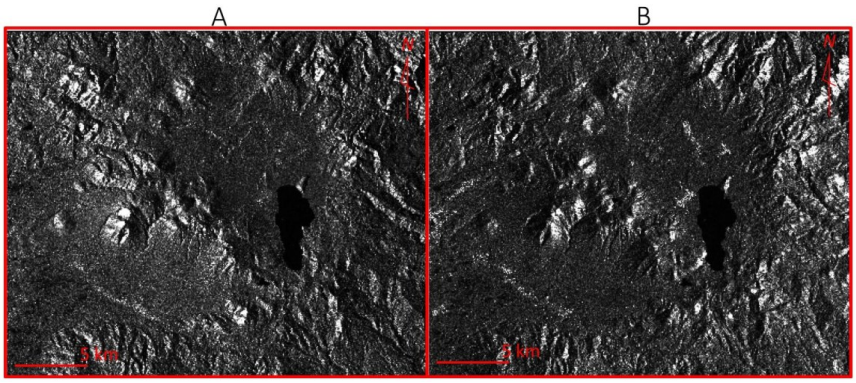

Figure 6: SENTINEL-1/B Pre-Processed Data.

4. PROCESSING

4.1 Lineament Detection

In detecting the geological structure lineaments, Synthetic Aperture Radar (SAR) images from dual-orbit observations of the same surface object are used. These observations include ascending orbits, which move from south to north, and descending orbits, which move from north to south. Illustration of ascending and descending orbits of SAR satellites.

The detection of geological lineaments utilizes SAR (Synthetic Aperture Radar) images from dual-orbit observations, crucial for reducing geometric distortions from off-nadir SAR image acquisitions and providing information from both viewing directions. Automated extraction of geological lineaments employs the modified Segment Tracing Algorithm (mSTA) on processed SAR images (Saepuloh et al., 2018). Initially, a window size of 11×11 pixels is set to assess whether the center of the window represents a line element.

16 directions at intervals of 11.25 degrees passing through the window center are defined to examine local variations in grayscale intensity. The orientation is determined by calculating deviations from the center pixel along the defined scan lines. The direction with the minimum value is assumed as the line direction and denoted as kmin. In the second step, along the perpendicular direction to kmin, denoted as kmax, analysis is conducted based on the equation:

$$\Lambda = \sum_{i=-(a-1)}^{a-1} \lambda_i = \sum_{i=-(a-1)}^{a-1} \left[\frac{(Z_{i+1} - 2Z_i + Z_{i-1})^2}{Z_i} \right]$$

where Zi is the grayscale intensity at pixel i. Λ is used to create a dynamic threshold (T), so line elements closer to the azimuth angle have lower threshold levels. The average (m) and standard deviation (σ) of Λ define the threshold (T) as $T = m + \mu\sigma$, with μ calculated using equation (3).

In the third step, evaluation determines whether the center pixel represents a ridge or a valley. Along the scan line from kmax, the sum of grayscale levels at i = -a to -1 and l to a are calculated and denoted as $\tau 1$ and $\tau 2$. If $\tau 1 \geq \tau 2$, the center pixel is assumed to be located in a valley (potential pixel). The fourth step involves connecting the line elements obtained from the previous steps. For a specific center pixel (p) in the direction kmin, it is linked to another center pixel within the direction range of kmin - 11.25 degrees to kmin + 11.25 degrees. The distance between p and the farthest potential pixel within the distance range (D) is calculated using equation (4).

Lastly, if multiple pixels align along the same valley, they may form multiple intersecting line elements with the same direction. Step five transforms complex line elements and curved valleys into straight lines using Principal Component Analysis.

4.2 Fracture Permeability Identification

After extracting lineaments successfully from dual-orbit SAR images, a grouping process is conducted to eliminate lineaments originating from backscatter or noise. Density calculations are then performed for each grid of a specified size to obtain three density parameters: length density (l), intersection density (i), and frequency density (f). Length density represents the total length of lineaments within each grid. Intersection density indicates the number of intersections of lineaments within each grid.

Frequency density denotes the total number of detected lineaments within each grid. A grid size of 1×1 km is considered optimal for extracting geological features, given the image size of approximately 800×800 pixels (Figure 7; Saepuloh et al., 2018).

4.3 Visual Analysis of Polarimetric SAR Images

The use of full-polarization SAR data channels is highly effective for identifying surface geological features in tropical regions. Polarimetric images can map the boundaries of volcanic products, which serve as the basis for determining volcanic stratigraphic units such as khuluk and gumuk, as well as visualizing geological structures for 1:30,000 scale mapping. Analysis of the distribution boundaries of volcanic products and geological structures is based on patterns of tone, texture, and brightness of SAR backscatter intensity pixels. The morphology and structure of volcanoes play a crucial role in geothermal exploration. Detected morphological and structural features include lava flow patterns filling valleys on volcanic slopes, structural fractures, and circular and radial patterns formed by eruption centers such as craters, domes, and lava flows (Figure 8). Bright tones indicate high backscatter from complex-geometry volcanic products and/or high rock reflectivity. Dark tones indicate volcanic products with simpler geometries like plains and water surfaces, or low reflectivity rocks like dry alluvial sands. Dark and bright contrasts can be analyzed to potentially identify geological structures such as faults visually.

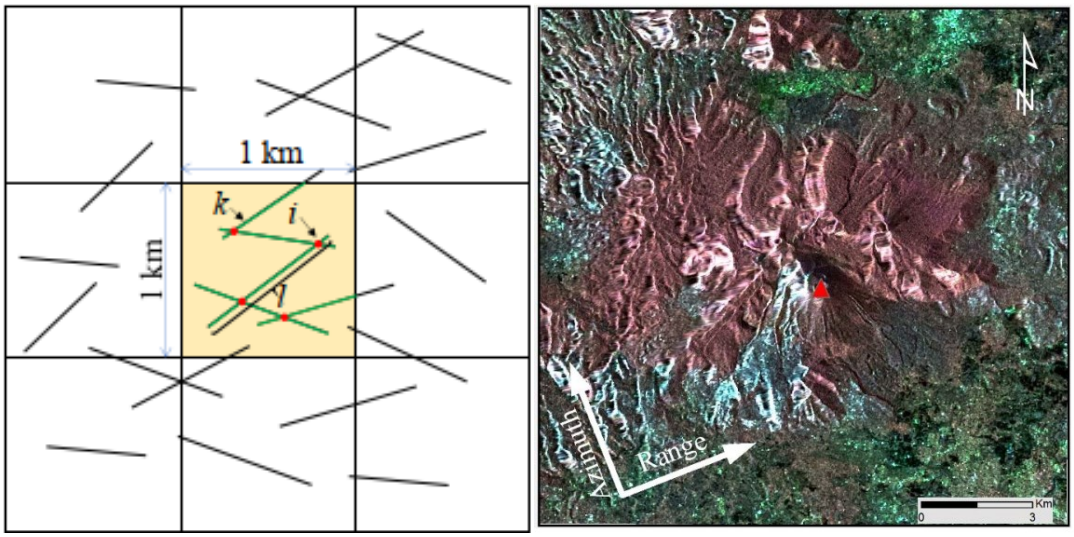

Figure 7: (Left): Illustration of lineament density for each 1×1 km grid; Figure 8 (Right): The composite polarimetric SAR backscatter intensity image from ALOS PALSAR with R,G,B = σHH, σHV, σVH highlights the morphology and structural features of volcanic products originating from eruption centers, marked by the red triangle (Bakker and Saepuloh, 2017).

4.4 Lineament Detection using modified Segment Tracing Algorithm (mSTA)

The modified Segment Tracing Algorithm (mSTA) detects linear features automatically. Essentially, mSTA utilizes differences in backscattering intensity (contrast and relief) from the image to identify linear patterns (Saepuloh et al., 2018). The mSTA method implemented here utilizes a MATLAB script developed by Saepuloh et al. (2018). There are several steps involved in the mSTA method for detecting linear features or lineaments in SAR images: (1) setting the observation area in pixels to detect linear elements, (2) determining secondary quadratic differentiation for grayscale levels, (3) evaluating each line representing ridge or valley features, (4) defining linear elements, and (5) performing principal component analysis to identify features with the same direction intersecting each other.

5. IMAGE PROCESSING

5.1 SAR Images Extraction

The satellite ALOS PALSAR level 1.1 images were classified using polarimetric methods, including matrix generation, speckle filtering with a refined Lee filter, and Yamaguchi decomposition. The refined Lee filter was applied to smooth out speckles in the intensity data, preserving image sharpness while reducing noise. The Yamaguchi decomposition yielded four scattering models: surface scattering, volume scattering, helix scattering, and double bounce (Figure 8). This decomposition aimed to separate scattering contributions for each type of information and generate distinct scattering types. Subsequently, the processed results were color-composited to facilitate easier classification and interpretation of the images.

Image compositing is a process where three channels are merged into a single image, showcasing the strengths of each individual channel. This composite image is utilized due to the limitations of human vision, which struggles to differentiate color gradients and finds it easier to comprehend with added color. Human vision can only

distinguish prominent objects in a single channel, making it difficult to identify other objects. Therefore, image compositing is conducted to facilitate the identification of objects in the image.

In this study, a color composite was created using the following parameters: the red channel represents the double bounce scattering parameter, the green channel represents the volume scattering parameter, and the blue channel represents the surface scattering parameter. This resulted in Figure 10, which aids in the classification of objects at the research site.

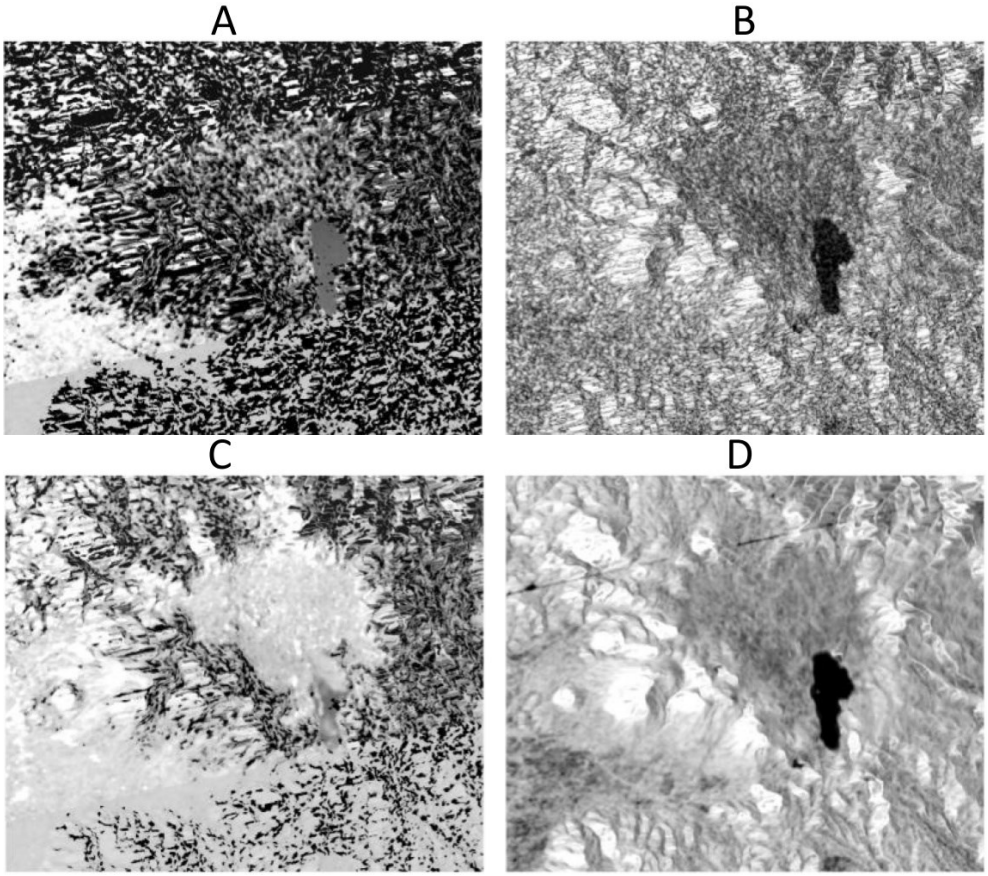

Figure 8: Yamaguchi decomposition of full polarization resulted in four scattering models from the ALOS PALSAR image at the observation site: double bounce (A), helix scattering (B), surface scattering (C), and volume scattering (D).

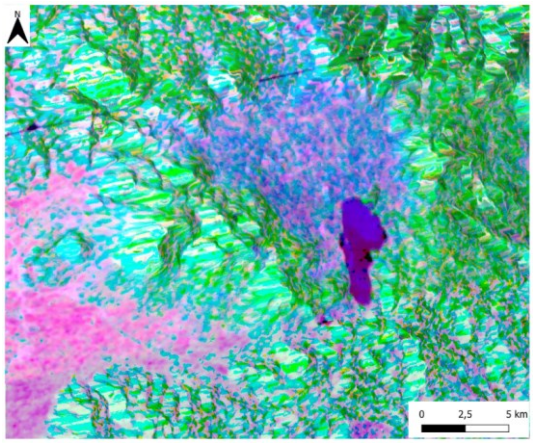

Figure 9: The RGB composite result from various Yamaguchi decomposition parameters for surface scattering, double bounce, and volume scattering types.

5.2. Lineament Extraction

The mSTA method produces linear features and interpretive structural analysis similar to the Yamaguchi method. This study applies the mSTA method to SAR data with a 25-meter resolution. Due to radar viewing geometry,

linear features with strike angles of 0 – 10° from the radar look direction (range) cannot be detected. Therefore, the dual-orbit mode of SENTINEL-1, with two different viewing directions, is used to detect linear features and interpret structures. The mSTA method automates linear feature detection using MATLAB scripts, resulting in significantly more detections compared to manual methods. Features are extracted based on surface roughness changes and slope steepness variations.

The mSTA method eliminates short linear features originating from noise with low backscatter intensity, primarily detecting features on both front and back slopes. It detects more linear features compared to the previous STA method. In the research location, mSTA identifies linear features interpreted as faults or fractures using SENTINEL-1 data in ascending and descending modes. A total of 1419 linear features are detected in the ascending direction and 1267 in the descending direction. More linear features are extracted from the ascending images, indicating directional influence on feature visibility.

In addition to extracting linear features, the study generates rose diagrams combining features from ascending and descending images. Based on linear features extracted from SENTINEL-1 images using the mSTA method, dominant strike directions are identified as northwest-southeast for both ascending and descending images (Figure 10).

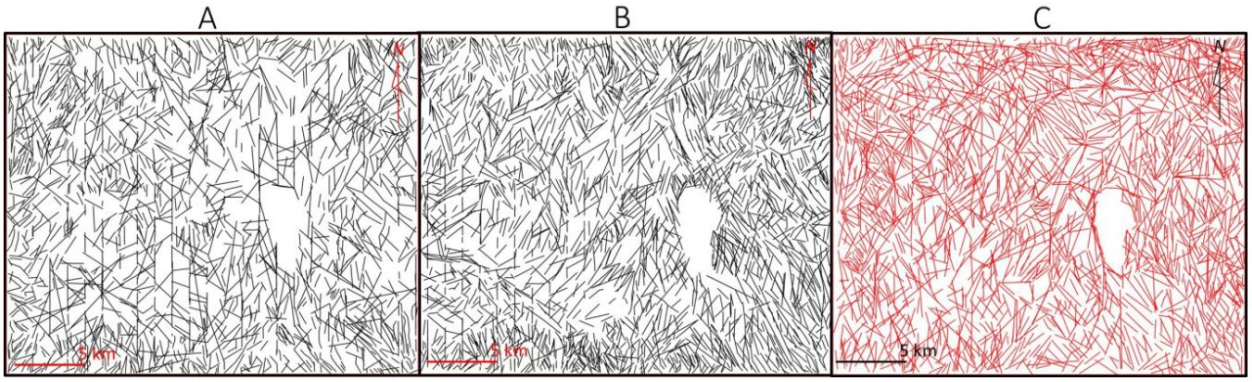

Figure 10: The map of detected lineaments using the mSTA method for Sentinel-1 images in ascending orbit (A), descending orbit (B), and their combination using grouping process (C).

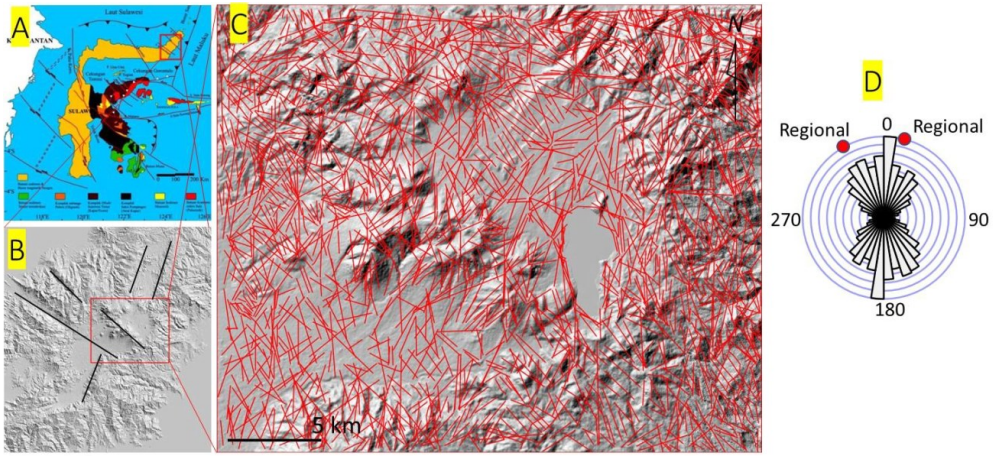

Figure 11: Regional Structure of Sulawesi Island (A), major alignments based on SRTM 30 m imagery (B), alignments derived from grouping Sentinel-1 images with ascending and descending orbits, and directional statistics presented in a rose diagram (D).

5.3 Lineament Structure Grouping and Verification

After extracting lineaments from both ascending and descending Sentinel-1 images, the next step involved grouping these lineaments. Enhanced mSTA data was obtained by merging lineaments from both orbits and subsequently grouping and eliminating short lineaments, resulting in the identification of the main directions of mSTA lineaments after merging. The processed lineaments totaled 160, predominantly oriented northwest-southeast, corresponding to the main structural trend at the study site (Figure 11).

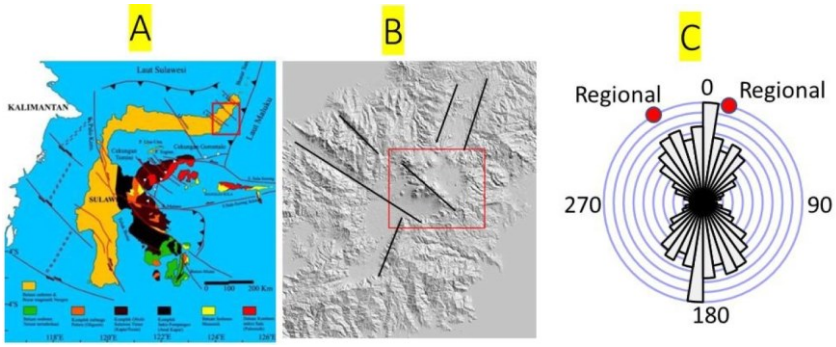

Figure 12: Regional geological structure map at the research site (A and B), and the frequency of alignments obtained from the mSTA method indicates similar directions (C).

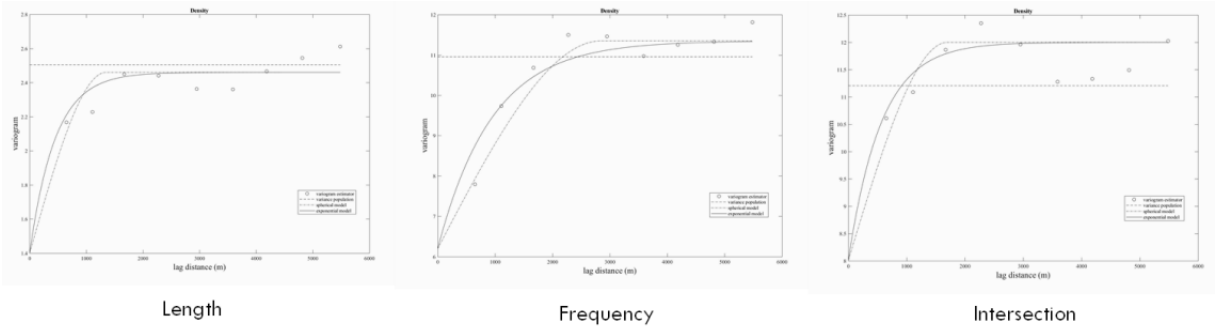

Figure 13: Experimental omnidirectional semivariogram of lineament density indices Li (left), Lf (middle), and Ll (right) for lineament distribution within 1×1 km² grid cells.

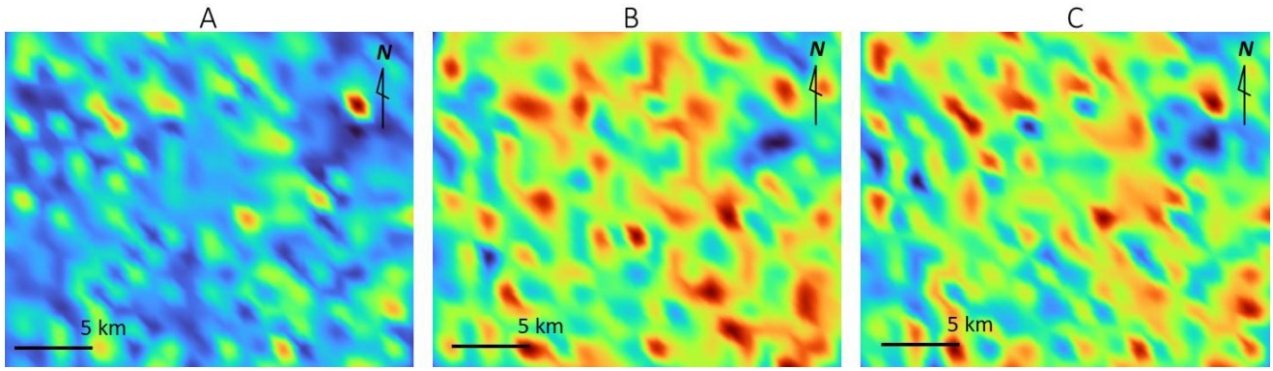

Figure 14: Ordinary kriging maps of three lineament indices: length Ll (A), intersection Li (B), and frequency Lf (C), depicting the spatial concentration of lineaments in Kotamobagu.

The mSTA method is employed to detect lineaments in the research area and identified a total of 1419 lineaments with a dominant northwest-southeast trend. This dominant trend aligns with the regional structure at the study site. This consistency demonstrates that the use of mSTA yields a representative detection of lineaments aligned with regional structures in the research area (Figure 12). This similarity validates that the mSTA method effectively identifies lineaments associated with geological structures in SAR images, defined as continuous and linear morphological features.

5.4 Calculation of Lineament Structure Density

From the grouping of these alignments, three lineament density indices are obtained: Li (Lineament intersection), Lf (Lineament frequency), and Ll (Lineament length), where their semivariograms are computed omnidirectionally and all data fit well to an exponential model (Figure 13).

These variograms are used to generate lineament maps using ordinary kriging in three index maps, where high and low index values are depicted in red and blue, respectively (Figure 14). The strong correlation observed between faults and lineament density across all three index maps validates the mSTA method's capability in detecting geological structure lineaments.

6. RESULTS AND DISCUSSIONS

To facilitate the analysis of lineaments in relation to tectonic and volcanic controls, lineament grouping was conducted based on two criteria: Lineament Direction Grouping and Length Grouping. (a) Lineament Direction Grouping: Lineaments were classified according to their directional alignments. The methodology involved utilizing the mSTA method to derive directional statistics, which are indicative of regional geological structures. Lineaments aligned with these regional structures were interpreted as products of tectonic activity, whereas lineaments exhibiting diverse directional orientations were associated with volcanic activity. A direction frequency threshold of 100 was determined based on histogram analysis, where predominant lineament directions aligned with regional geological structures (N 320° E and N 20° E) were observed at a frequency of 100 (Figure 14A). Lineaments exceeding this frequency threshold were classified as tectonically influenced, while those below were categorized as volcanically influenced. (b) Lineament Length Grouping: Lineaments were also categorized based on their lengths. Longer and continuous lineaments were considered characteristic of regional geological structures, while shorter lineaments converging to a point were deemed indicative of volcanic activity. A lineament length threshold of 1000 m was established from histogram data, showing a concentration of lineaments at approximately 1000 m in length (Figure 14B). Lineaments longer than 1000 m were identified as likely products of tectonic activity, whereas those shorter than 1000 m were associated with volcanic processes. Histograms of lineament direction and length were analyzed to establish threshold values for distinguishing between tectonically and volcanically influenced lineaments (Figure 15). These criteria and thresholds provide a systematic approach for delineating and interpreting lineaments in terms of their geological origins within the study area.

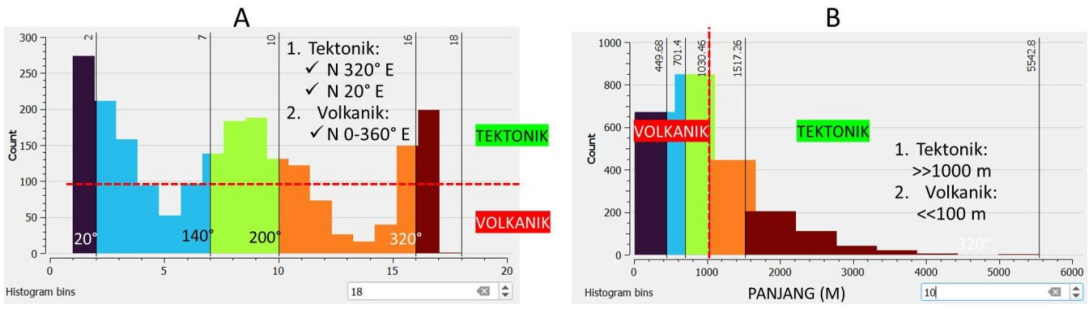

Figure 15: Histogram of lineament directions derived from mSTA analysis every 20° from the north (A), and histogram of lineament lengths resulting from mSTA analysis with 10 different length classes (B).

6.1 Lineament Direction Grouping

Lineament direction classification associated with tectonic and volcanic processes was performed using 20° class intervals (Figure 15A). The merging process of azimuth and back azimuth directions facilitated analysis, resulting in nine lineament classes (Figure 16). Tectonic lineament classification was based on directions aligned with regional geological structures, specifically N 320° E and N 20° E. Lineaments outside this range were assumed to be volcanic in origin, categorized into four tectonic-associated classes and five volcanic-associated classes.

Tectonically associated lineaments clustered in specific locations with nearly identical directions, while volcanic-associated lineaments exhibited a dispersed pattern ranging from N 0° E to N 180° E. When combined, volcanic lineaments displayed a radial pattern indicative of volcanic features such as flow structures, volcanic unit contacts, erosion surfaces, faults, fractures, and surface depressions. Typically, radial patterns converge towards a focal point where volcanic material is erupted, known as a volcanic vent. Locating older Tertiary or older volcanic vents in the field is challenging in Indonesia due to intense erosion and weathering processes. However, with lineaments detected using the mSTA method, identifying volcanic vents can be expedited. Field verification is essential to confirm that these lineaments are indeed associated with the intended target.

6.2 Lineament Length Grouping

Length classification of lineaments associated with tectonic and volcanic processes was conducted using a threshold value of 1000 m based on the histogram frequency of lineament lengths (Figure 15B). Lineaments longer than 1000 m, falling within quartiles 3 and 4, were assumed to be tectonically associated, whereas those shorter than 1000 m, falling within quartiles 1 and 2, were considered volcanic in origin. Tectonically associated lineaments exhibited a pattern predominantly oriented NW-SE and NE-SW (Figure 17A), with little significant presence around the lake area. Volcanically associated lineaments displayed a radial pattern emanating from several centers (Figure 17B). Radial patterns clustered in the central part of the study area, while circular patterns formed from continuous lineaments in the NE and terminal lineaments in the SW.

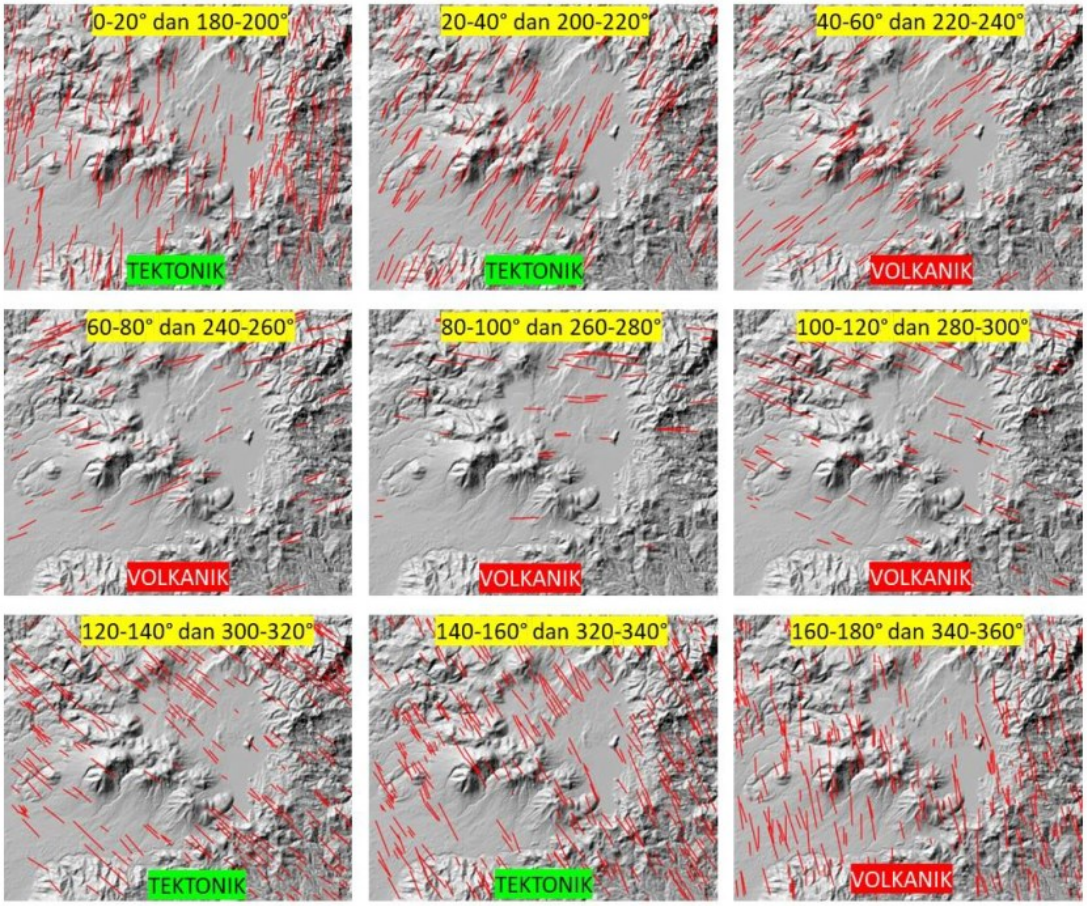

Figure 16: Classification of lineaments from mSTA analysis, grouped every 20° by combining azimuth and back-azimuth, to estimate lineaments associated with tectonic and volcanic processes.

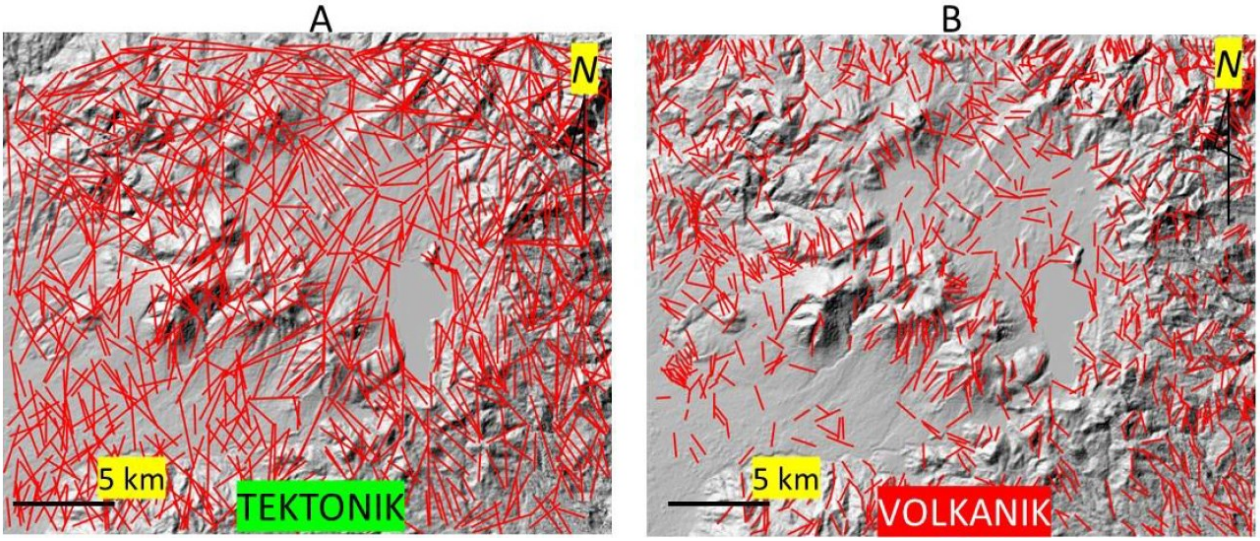

Figure 17: Classification of lineament lengths longer than 1000 m associated with tectonics (A) and less than 1000 m associated with volcanic activity (B).

6.3 Fault Identification

Based on two classification scenarios of detected lineaments using the mSTA method, the presence of faults is defined as lineaments that share similar orientation with regional structures and exhibit continuity or elongation. Fault presence is indicated by the continuity of several detected lineament segments.

In the direction classification scenario, the continuity of lineament segments largely corresponds to local geological structures (Figure 18). Some faults can be identified from continuous segments aligned with regional geological structures.

In the length classification scenario, the continuity of lineament segments follows the direction of local geological structures (Figure 19). Some faults can be identified from continuous segments aligned with regional geological structures (Figure 19A). Circular structures are detected from segments less than 1000 m in length, represented by short continuous segments (Figure 19B).

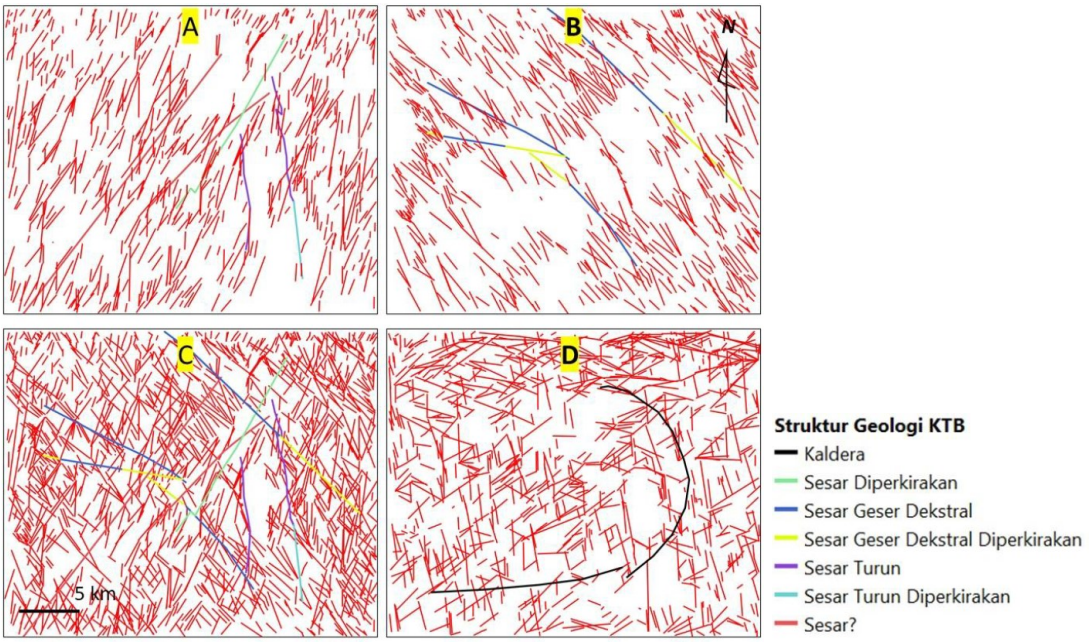

Figure 18: Classification of lineaments from mSTA results with tectonic orientations 0-40° (A), 120-160° (B), total (C), and volcanic lineament orientations (D), overlaid with local geological structures.

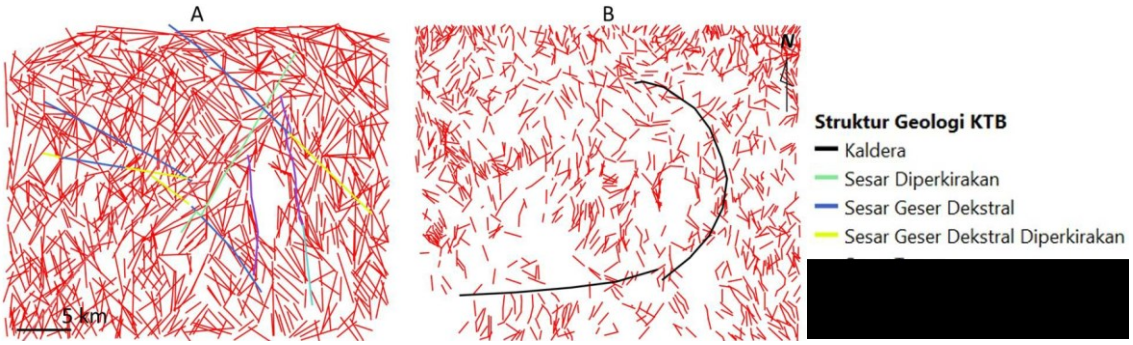

Figure 19: Classification of lineament lengths less than 1000 m (A) and greater than 1000 m (B) in relation to the presence of local geological structures.

6.4 Surface Permeability Identification

Surface permeability identification through fracture density calculation, as detailed in the previous section, was conducted. The concept revolves around the idea that a higher density of detected lineaments indicates potentially higher permeability compared to lower densities. Lineament density was computed using three parameters: length (Ll), intersection (Li), and frequency (Lf). High anomalies in these three density parameters were identified using the fourth quartile threshold of their respective histograms (Figure 20).

Among these density parameters, high anomalies in frequency density (Lf) showed the highest correlation with local geological structures, particularly at fault intersections. Another correlation was observed with the presence of hot springs, all of which coincided with high density values of lineament frequency (Lf) (Figure 21). Dark red shades in the central study area indicated high Lf anomalies on relatively flat terrain. Despite low topographic contrast, Sentinel-1 radar sensors detected lineaments suspected to originate from near-surface geological features. Surface roughness contrast and rock dielectric values are key factors recorded by radar sensors, aside from topographic factors. The high anomalies in the central area were within circular features indicating concentrations

of high permeability associated with volcanic processes. Verification with subsurface geophysical data is necessary to understand the manifestation of high permeability on the surface relative to subsurface geological features.

Figure 20: High anomalies of mSTA lineament density for Length Ll (A), intersection Li (B), and frequency Lf (C) overlaid with local geological structures.

Figure 21: High-frequency density anomalies overlaid on ALOS PALSAR polarimetric composite imagery and local geological structures such as faults. Backscattering mechanisms for the study area are illustrated by the three images on the left.

7. CONCLUSION

The processing of SENTINEL-1 images using mSTA for lineament extraction detected 1657 lineaments in ascending orbits, 2089 in descending orbits, and grouped 1971 with dominant trends at N 320° E and N 20° E. The sensitivity analysis of the mSTA method demonstrated representative results with dominant trends aligned parallel to regional structures at the study location.

Classification of lineament directions associated with tectonics and volcanics separated based on the regional geological trends of N 320° E and N 20° E. Tectonically associated lineaments clustered in specific locations with nearly identical directions, whereas volcanic lineaments exhibited a dispersed pattern ranging from N 0° E to N 180° E. Length classification of lineaments associated with tectonics and volcanics utilized a threshold of 1000 m based on histogram frequency. Tectonic lineaments displayed NW-SE and NE-SW directional trends, while

volcanic lineaments showed radial patterns and clustered in the central study area. Circular patterns formed from continuous lineaments in the NE and terminal segments in the SW.

Processing of ALOS PALSAR level 1.1 imagery involved several stages including data preparation, multilooking, terrain correction, matrix generation, and polarization decomposition. High-frequency density anomalies (Lf) corresponded well with local geological structures, as indicated by anomalies at fault intersections and the presence of hot springs associated with high Lf frequency lineament densities. Dark red shades in the central study area indicated high Lf anomalies despite low topographic contrast, demonstrating the Sentinel-1 radar sensor's ability to detect lineaments possibly originating from near-surface geological features.

These findings underscore the effectiveness of radar imaging and mSTA analysis in delineating geological structures and highlighting potential areas of high permeability associated with volcanic processes. Further validation through subsurface geophysical data is recommended to enhance understanding of these surface manifestations relative to subsurface geological features.

REFERENCES

Cottam, M.A., Hall, R., Forster, M., Boudagher-Fadel, M. (2011): Basement character and basin formation in Gorontalo Bay, Sulawesi, Indonesia: New observations from the Togian Islands. In: R. Hall, M.A. Cottam, M.E. Wilson (Eds.), *The SE Asian Gateway: History and Tectonics of the Australia-Asia collision*. Geological Society of London Special Publication 355, 177–202.

Elburg, Marlina, and J. Foden (1998): Temporal Changes in Arc Magma Geochemistry, Northern Sulawesi, Indonesia. *EARTH AND PLANETARY SCIENCE LETTERS*, 163 (1–4), 381–98.

Haeruddin, H., Saepuloh, A., Heriawan, M. N., and Kubo, T. (2016): Identification of linear features at geothermal field based on Segment Tracing Algorithm (STA) of the ALOS PALSAR data, *IOP Conference Series: Earth and Environmental Science*, 42, 012003.

Hall, R. (2002): Cenozoic geological and plate tectonic evolution of SE Asia and the SW Pacific: computer-based reconstructions, model and animations. *Journal of Asian Earth Sciences*, 20, 353–431.

Hall, R. (2012): Late Jurassic–Cenozoic reconstructions of the Indonesian region and the Indian Ocean. *Tectonophysics*, 570-571, 1–41.

Leeuwen, Theo (2011): Mineral deposits of Sulawesi. 10.13140/2.1.3843.2322.

Saepuloh, A., Haeruddin, H., Heriawan, M. N., Kubo, T., Koike, K., and Malik, D. (2018): Application of lineament density extracted from dual orbit of Synthetic Aperture Radar (SAR) images to detecting fluids paths in the Wayang Windu geothermal field (West Java, Indonesia), *Geothermics*, 72, 145–155. https://doi.org/10.1016/j.geothermics.2017.11.010

Saepuloh, Asep (2021): *Prinsip dan aplikasi pengindraan jauh geologi gunung api pendekatan fisis dan observasi geologi lapangan* (2nd ed.), ITB Press, Bandung, Indonesia, 197.

Van der Meer, F.D., Van der Werff, H.M.A., Van Ruitenbeek, F.J.A., Hecker, C.A., Bakker, W.H., Noomen, M.F., Van der Meijde, M., Carranza, E. John M., Boudewijn de Smeth, J., Woldai, T. (2012): Multi- and hyperspectral geologic remote sensing: a review. *Int. J. Appl. Earth Obs. Geoinf.*, 14, 112–128.

Magnetotelluric Parameters with Variation in Synthetic Data in 3D Forward Modeling

Serina Andiani Pongtuluran[1], Sari Widyanti[2], Lendriadi Agung[3], Imam B. Raharjo[2], Nicolas Silaen[3], Vicky Rai Chandra[1], Muhammad Ghassan Jazmi Shalihin[1], Astri Indra Mustika[4], Triwening Larasati[1], Galih Bayu Permadi[1], and Ferdino R. Fadhillah[4]

[1]PT Geoenergi Solusi Indonesia, Cibis Nine 11th Floor, Jakarta Selatan 12560, Indonesia
[2]Universitas Pertamina, Jl. Teuku Nyak Arief, RT.7/RW.8, Simprug, Jakarta Selatan 12220, Indonesia
[3]PT Pertamina Geothermal Energy, Jl. Medan Merdeka Tim. No.11-13 6, RT.6/RW.1, Gambir, Jakarta Pusat 101110, Indonesia
[4]PT Sarana Multi Infrastruktur, Sahid Sudirman Center, Lantai 47-48, Jakarta Pusat, 10220, Indonesia

Serina.pongtuluran@geoenergis.com, Serina.pongtuluran@gmail.com

Keywords: magnetotelluric, polar diagram, phase tensor, induction arrow, forward modeling

ABSTRACT

Magnetotelluric (MT) is a common geophysical method used in exploring a geothermal system, as it is one of the powerful tools for delineating subsurface conditions. A common challenge in this method is the complexity of the subsurface condition that influences the dimensionality of its inversion. Which produces a model that may not accurately represent the actual condition and lead to misinterpretation. This study aims to construct several synthetic models to understand its impact on MT parameters, such as polar diagram, phase tensor, and induction arrow/tipper.

The result shows that polar diagrams form a circular shape when the MT station is located at a model with the same resistivity value laterally and on conductive zones that are relatively far from resistive boundaries while forming elliptical or peanut shapes on transitioning to resistive boundaries. The phase tensor phi value ranges between 0 to 45 degrees for resistivity increasing with depth, for models with lateral resistivity differences ranging between 40 to 50 degrees. The induction arrow/tipper will always have the highest value when the station is located far from the conductive anomaly.

1. INTRODUCTION

The Magnetotelluric (MT) method is a passive geophysical technique that measures changes in electric and magnetic fields over time to determine the distribution of rock resistivity under the Earth's surface. The Magnetotelluric (MT) technique can penetrate to enormous depths. As a result, it can examine a wide range of deep and geological features on Earth. The form of geological features, such as two-dimensional arrangements in sedimentary rocks or three-dimensional configurations in more complicated geological settings, influences subsurface resistivity. The mapping of subsurface resistivity is based on MT data processing, which typically includes 1-D and 2-D analysis. 3D processing needs more powerful computing resources. The main objective of MT data processing is to get a transfer function represented by the impedance tensor (Z), which consists of four impedance components (Simpson & Bahr, 2005). The MT technique is frequently used as the default instrument for investigating particular natural resources, such as groundwater and geothermal (Abdelzaher et al. 2012; Kebede and Saibi 2016; Kerbadj et al. 2017; Saibi et al. 2018). Its cost-effectiveness improves geothermal resource exploitation by aging reduced resistivity anomalies in geothermal systems (Cumming and Mackie 2010). A geothermal system is identified by considerably lower resistivity anomalies than the surrounding rocks and the degree of mineralization, water quantity, and temperature, which correspond to resistivity fluctuation (Spichak et al., 2007).

It is essential to remember that increasing the complexity of data processing does not necessarily result in a more accurate depiction of the real subsurface conditions. Ledo's (2006) research shows that when a 3-D conductive anomaly exists under the surface, 2-D modeling fails to reflect the anomaly adequately. This study aims to examine Transverse Electric (TE) and Transverse Magnetic (TM) mode curves, assess the dimensionality of resistivity zones, calculate geoelectrical strike, and map the distribution of conductive anomalies using MT modeling.

2. MT DATA

This study's data is synthetic and consists of 25 MT measurement points. The collected data was in MT data in EDI file format, which included tensor impedance and phase tensor values relative to time. Five north-south lines and five west-east lines exist. Four synthetic models with varied resistivity values were created using the 25 MT station location.

2.1 Model 01

The resistivity values in model 01 vary with depth. The thickness of each layer is one kilometer. Surface layers have resistivity values of 10 Ω m, 100 Ω m, 500 Ω m, and 1000 Ω m, respectively.

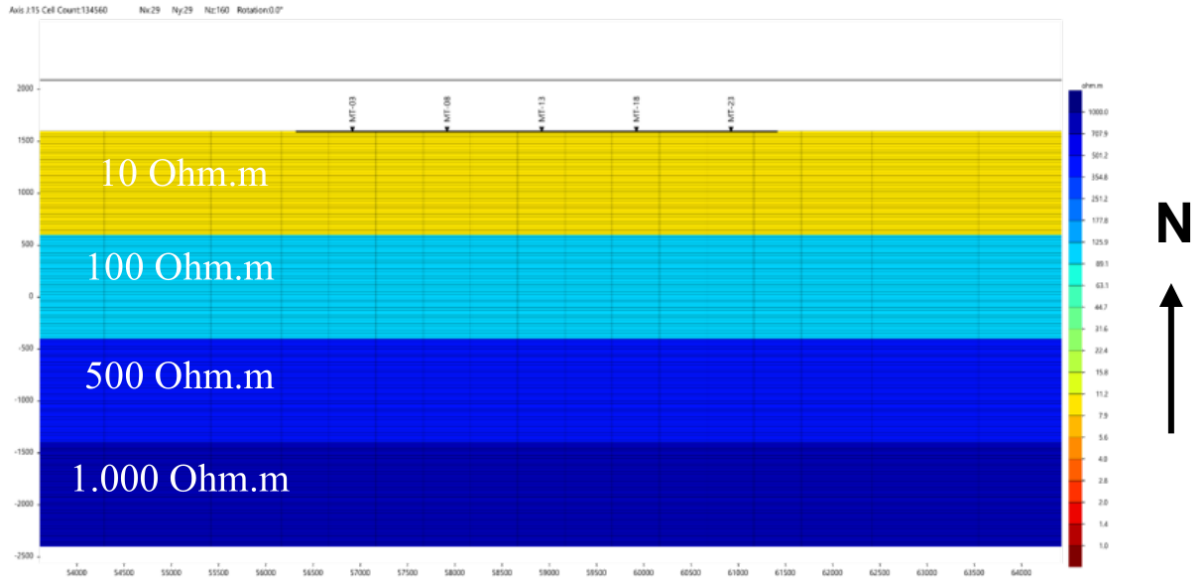

Figure 1: Model 01.

2.2 Model 02

Model 02 is a two-block model with contrasting resistivity values. The resistivity values for the right and left blocks are 1 Ωm and 1000 Ωm, respectively. The depth of each block is 4 kilometers.

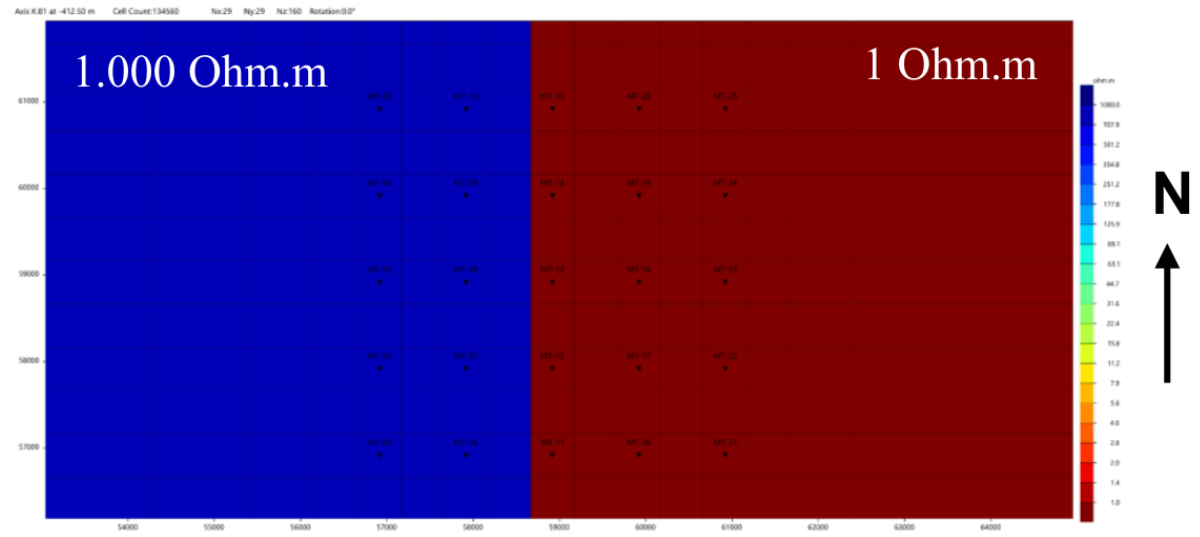

Figure 2: Model 02.

2.3 Model 03

Model 03 consisted of a diagonal conductivity anomaly model with a thickness of 2 km. Conductive anomalies have a resistivity value of 1 Ωm compared to an ambient value of 100 Ωm.

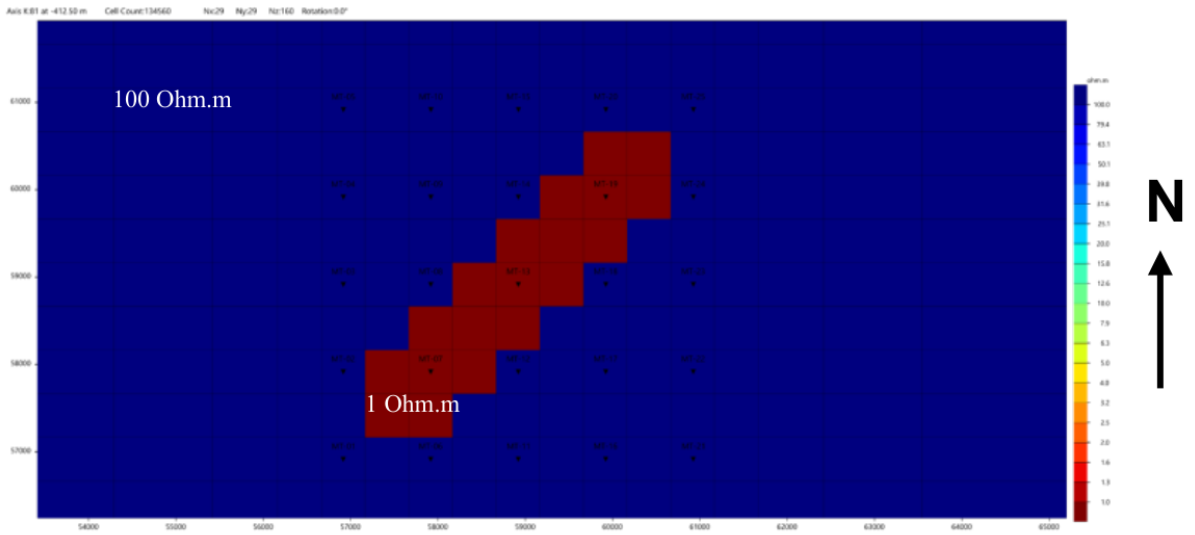

Figure 3: Model 03.

2.4 Model 04

Model 04 includes an anticline with a conductive anomaly value of 1 Ωm and a surrounding layer of 100 Ωm. The conductive anomaly is located 500 meters below the surface.

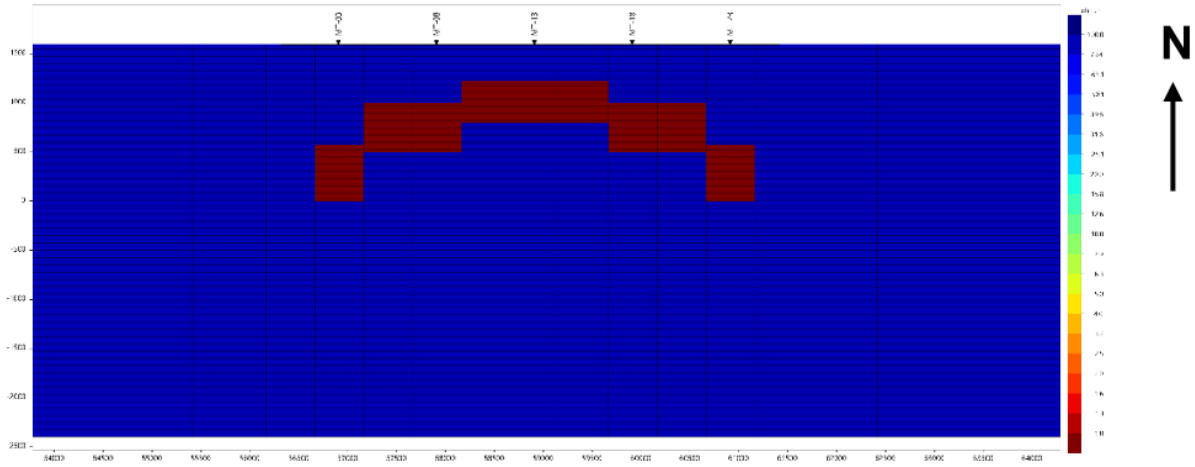

Figure 4: Model 04.

3. MAGNETOTELLURIC METHOD

The Magnetotelluric (MT) method is a geophysical method that utilizes natural electromagnetic waves from the source interaction of the solar wind and/or meteorological activity to take the distribution of resistivity values below the surface. The MT method measures the earth's magnetic field and the earth's electric field simultaneously with a function of time. Electromagnetic waves have a frequency range (0.00001 Hz - 10000 Hz). The lower the frequency value, the deeper the penetration, and vice versa; the higher the frequency value, the shallower the depth penetration will be (Vozzof, 1991). Electromagnetic signals are generated by the interaction of solar wind and lightning, which creates a magnetic field that penetrates Earth. The time-varying magnetic field penetrating the Earth interacts with rock strata, causing eddy currents and generating a primary electric field. The temporal fluctuation of the primary electric field produces a secondary magnetic field. The temporal change of the secondary magnetic field produces a secondary electric field. Magnetotelluric surveys in the field measure secondary electric and magnetic fields.

3.1 Forward Modeling

Forward modeling, a computational process, is employed to derive observational measurement outcomes based on specified physical parameters. This technique is pivotal in hypothesizing subsurface conditions (Turkoglu, 2009). Initially, the geometry is constructed using a synthetic model, which is then aligned with the target model to mitigate potential impacts on subsequent analysis. The horizontal cell value is defined in meters, and padding

is incorporated to ensure complete polarization of resistivity data at the MT station points. Additionally, the "enable outer core area" option should be selected to include the observation's external core area while configuring the cell size and extension.

In forward modeling, padding plays a critical role; insufficient padding can introduce edge effects at MT points during modeling, leading to data loss. It is advisable that the padding be ten times the size of the MT measurement layout to facilitate proper interpolation of resistivity data and prevent data loss. Subsequently, the appropriate depth limit is specified, followed by the width of the vertical axis cell, which is then expanded as necessary.

The next step involves generating a model by inputting the resistivity value and the population property of the total resistivity value. The desired synthetic data's resistivity values are then distributed along the i (length), j (width), and k (vertical/map view) axes within each segment relative to the distance. To refine the modeling, frequency range parameters and points per decade are introduced, indicating the interpolation of several points within a decade. Following the forward modeling of the generated 3-D synthetic data, the EDI data is exported with a complete tensor and subsequently utilized for MT curve parameter analysis.D synthetic data, the EDI data is exported with complete tensor and then loaded in for MT curve parameter analysis.

3.2 Impedance Tensor

MT measures orthogonal variations in electric fields (E) and magnets (H) on the earth's surface. Simpson and Bahr (2005) compare electric and magnetic field components coupled with an impedance tensor (Z). Z is a complex number made up of real and imaginary numbers. As a result, each impedance component (Zij) has its own magnitude and phase. The number Z must be transformed to pseudo-resistance and phase as a function of time. It is important to convert since Z is a complex number made up of real (Pseudo-Resistivity) and imaginary (Phase) values.

3.3 Phase Tensor

The Phase Tensor compares the real and imaginary parts of the complex impedance tensor. According to Caldwell et al. (2004), the phase tensor is defined by an angle α, which is not an invariant rotation. There are three invariant rotation parameters: the maximum axis (Φxy), the minimum axis (Φyx), and the skew angle (β). Phase Tensors help identify the distribution of conductive anomalies and determine the direction of the geoelectrical strike at the measurement site. In a 1-D medium, the phase tensor is diagonal with identical values for Φxy and Φyx, forming a perfect circle. In a 2-D medium, the phase tensor is also diagonal but with different values for Φxy and Φyx, resulting in an elliptical shape. The skew angle (β) in 2-D media is zero ($\beta = 0$). In a 3- medium, the phase tensor has distinct values for Φxy and Φyx, meaning the skew angle (β) is not zero ($\beta \neq 0$) and is often greater than 3.0. The phase tensor in 3-D is represented as an ellipse. Ellipses are created by mapping phase angle values in polar coordinates over a frequency range from 0° to 360° (Caldwell et al., 2004).

3.4 Induction Arrow (Tipper)

The Induction Arrow is a vector that represents the ratio of complex numbers, which include both real and imaginary parts. Induction arrows help us see if there are changes in conductivity across different areas. If the Earth is uniform, the induction arrow value is zero. However, if there is a conductive object underground, the induction arrow will point towards that object (Simpson and Bahr, 2005). There are two types of induction arrow representations: reversed and non-reversed. The reversed convention, introduced by Parkinson in 1959, shows the vector pointing towards the concentration of internal electric current anomalies. The non-reversed convention, introduced by Wiese in 1962, shows the vector pointing away from the concentration of internal electric current anomalies.

3.5 Polar Diagram

A Polar Diagram provides information about the characteristics of the subsurface medium based on changes in the impedance tensor (Z). The direction of the polar diagram's axis indicates the dimensional changes relative to the strike. In a 1-D medium, the polar diagram forms a perfect circle because $Zxx = Zyy = 0$. A 2-D medium is represented by an elliptical shape in the polar diagram, as variations in resistivity occur in one lateral direction and depth, indicated by the impedance amplitude where ($Zxy \neq Zyx$) with components $Zxx = Zyy = 0$. In contrast, a 3-D medium has measurement coordinate axes that are not aligned (Berdichevsky, 2008).

3.6 Inverse Modeling

Inverse Modelling is a mathematical process used to directly obtain a subsurface geophysical model based on geophysical measurement data. This differs from forward modeling, which relies on a trial-and-error approach to match measured data with calculated data. The type of inversion used in this study is Non-Linear Conjugate Gradients (NLCG). The inversion process using the NLCG algorithm aims to find a model solution that minimizes the objective function (ψ) based on data residuals and the second derivative of resistivity values (Rodi and Mackie, 2010). This study employs both 1-D and 2-D inversion modeling steps.

3.6.1 1-D Inversion

One-dimensional (1-D) inversion can be effectively conducted after performing 1-D modeling at each MT (Magnetotelluric) measurement point along the survey line. This process involves fitting the observed and calculated curves to determine the thickness of each subsurface layer accurately. Following the 1-D modeling at each measurement station, interpolation is applied between stations to derive the spatial distribution of resistivity values across the survey profile.

3.6.2 2-D Inversion

In 2-dimensional (2-D) inversion modeling, it is essential to first construct a grid that aligns with the initial geometry. The parameters to be defined include the width of the horizontal cells, the presence of top elevation, padding to avoid edge effects, and the boundaries of the left and right cells. Next, the vertical cells are arranged by setting the boundaries of each layer and the thickness of the cells, with an option for vertical cell enlargement if needed.

Once the grid dimensions are established, an initial model with a background value tailored to the specific model is created, as this initial model will influence the inversion results. The following step involves inputting the inversion parameters based on the analysis of the MT (Magnetotelluric) data. These parameters include the selection of the MT transfer mode that is parallel to the geoelectrical strike, frequency modeling boundaries, the number of interpolation points per decade, and smoothing.

Performing inversion requires a trial and error approach for each parameter to ensure that the resulting model accurately represents the subsurface conditions. This iterative process helps prevent errors in data interpretation due to incorrect modeling.

4. RESULT AND DISCUSSION

4.1 Variations in TE and TM Curves

The responses of the TE and TM curves from each model exhibit unique characteristics, which are influenced by the geometry and resistivity values of the conductive anomalies. The shapes of the TE and TM curves in each synthetic model can be utilized to identify the distinctive features of each modeling curve. When the resistivity values vary solely with depth, the TE and TM curves demonstrate consistent trends across all MT station points.

4.1.1 Model 1

The TE and TM curves will overlap when there are no lateral changes in resistivity. Consequently, the resistivity values indicated by both TE and TM are identical across the period from 0.01 to 1000 seconds. Therefore, a single curve is selected, as shown in Figure 4.1, where the apparent resistivity value increases with the period, consistent with the synthetic model. From the period of 0.08 to 0.9 seconds, the response from the first layer is obtained, the second layer response is acquired from 0.9 to 10 seconds, and the third layer response is observed from 1 to 10 to 100 seconds. The subsequent layer responses appear in the period of 100 to 1000 seconds. At the 100-second mark, the TE and TM curves begin to flatten, indicating proximity to the last layer, with an apparent resistivity value of 1000 Ωm and a total layer thickness of 4 km. The phase of the TE and TM curves shows a 45-degree angle from 0.08 to 0.1 seconds, then decreases to 10 degrees at 0.6 seconds. It returns to 45 degrees at 1000 seconds. The phase decreases with increasing depth due to higher resistivity in deeper layers, reducing the angle between the electric and magnetic fields. The phase increases again as the electric field propagation tends to shift towards the more conductive upper layers.

4.1.2 Model 2

Regarding the geometry of Model 02, which features a resistivity contrast between two blocks, the discussion will focus on a single transect perpendicular to the vertical contact, comprising five points, as illustrated in Figure 6. This transect spans 4 km. In the figure, the two graphs on the left are within the resistive medium, while the three graphs on the right are in the conductive medium. The x-axis represents the period, and the y-axis indicates apparent resistivity and phase.

First, the TE curve response is discussed. The TE curve, which is the Ex/Hy component, shows a decrease in apparent resistivity with increasing depth, influenced by the Ex component's direction towards the conductive zone. At stations located above the resistive block, a resistive response (1000 Ωm) is observed at low periods, which then transitions to a conductive response as the period increases. The phase flattens at 45 degrees around a period of 20 seconds.

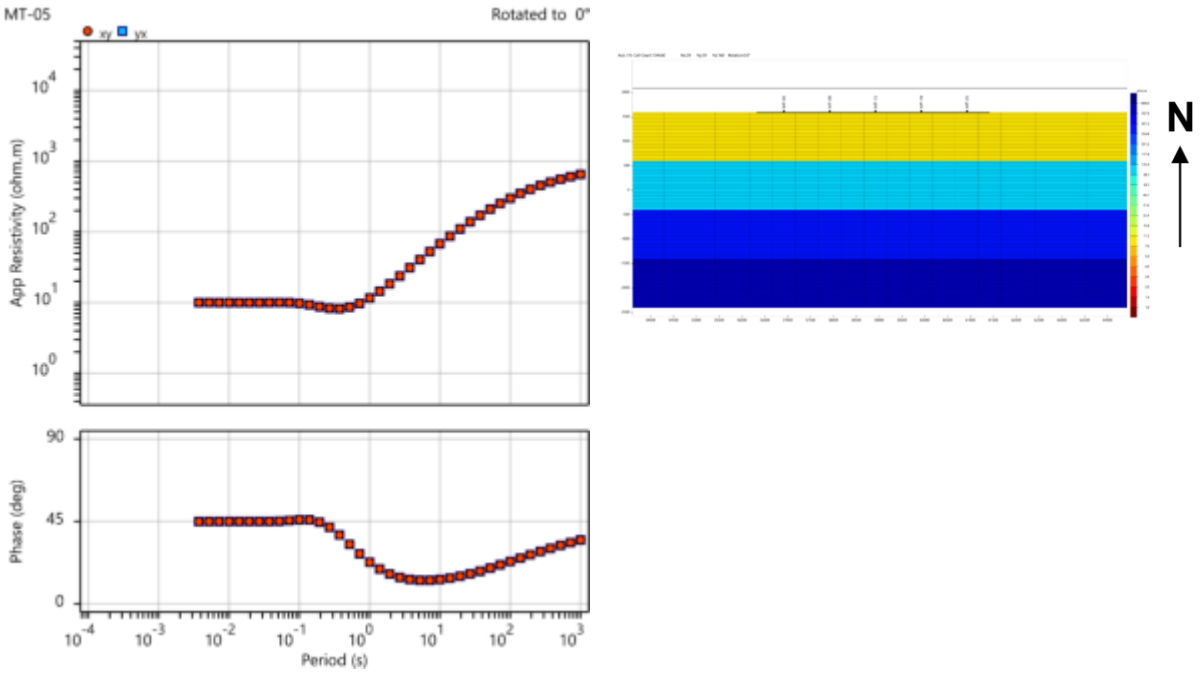

Figure 5: TE and TM Curves for Model 01.

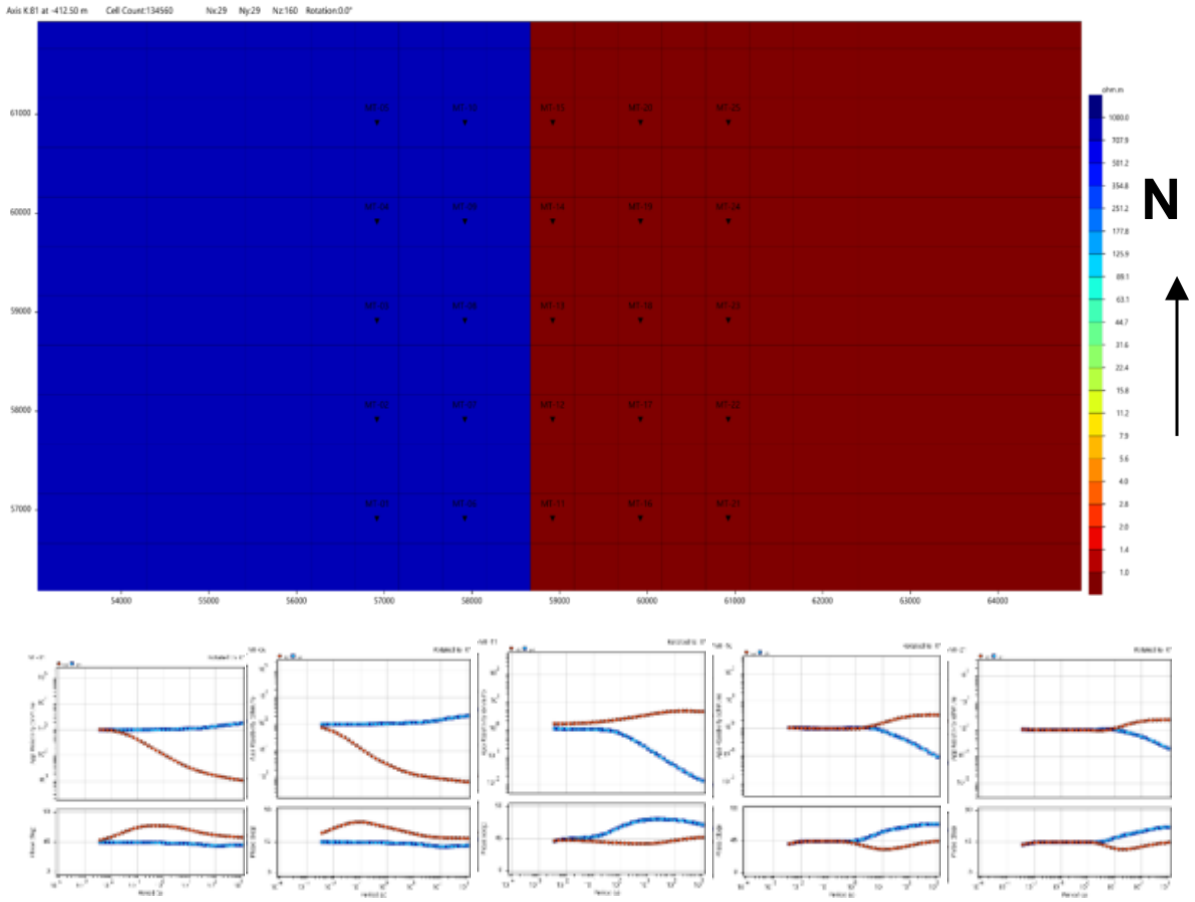

Figure 6: Characteristics of TE (red) and TM (blue) curves across resistivity contrast of two blocks.

Secondly, the TM response provides an intriguing observation. In the resistive block, from low to high periods, the TM response remains relatively constant at 1000 Ωm, then increases to approximately 1100 Ωm at higher periods. The phase remains flat at 45 degrees across all periods.

At MT stations situated above the conductive block and near the resistivity contrast, an inversion of the TE and TM curves is observed. At low periods, the TE curve's apparent resistivity exceeds 1 Ωm and rises to 8 Ωm at high periods. The TM curve, however, decreases from 1 Ωm at low periods to 0.01 Ωm at high periods. The TE phase starts at 45 degrees at low periods and drops to around 40 degrees, while the TM phase follows a similar trend as the TE phase until 0.6 seconds, then diverges at 0.4 seconds, with the TM phase increasing to about 70 degrees at 1 second. The maximum separation between the TE and TM phases is approximately 30 degrees.

The inversion of the TE and TM curves in terms of both apparent resistivity and phase at observation points near the resistivity contrast is attributed to boundary charges. The accumulation of electric charges at the vertical contact plane on the conductive side enhances the electric field reading during MT data acquisition. At points within the conductor and further from the resistivity contrast, the TE and TM curve separation occurs at higher periods. This is also influenced by the direction of the surrounding electric and magnetic fields. The TE and TM apparent resistivity values are identical from 0.08 seconds and begin to diverge at around 2 seconds. The TE phase flattens at 0.08 seconds, then slightly decreases to 35 degrees at 2 seconds. The TM phase remains flat at 45 degrees at 0.08 seconds, rises to 65 degrees at 10 seconds, and then decreases to 45 degrees at 100 seconds.

4.1.3 Model 3

Model 03 has a more complex resistivity structure compared to Models 01 and 02, featuring different resistivity values and geometries. Therefore, the discussion is divided into three sections: points above the anomaly, points near the anomaly, and points at the edge of the conductive anomaly.

a. Points at the Center of the Conductive Anomaly

As shown in Figure 7, the TE and TM curves overlap from low to high periods with a response of 1 Ohm.m, decreasing to 0.7 Ωm from 2 to 1000 seconds. The phase starts at 45 degrees, rises to 55 degrees, and then drops back to 45 degrees as the period approaches 1000 seconds. In this model, there are three station points exhibiting similar characteristics because the anomaly is on the surface and does not extend deeply, affecting the response at higher periods.

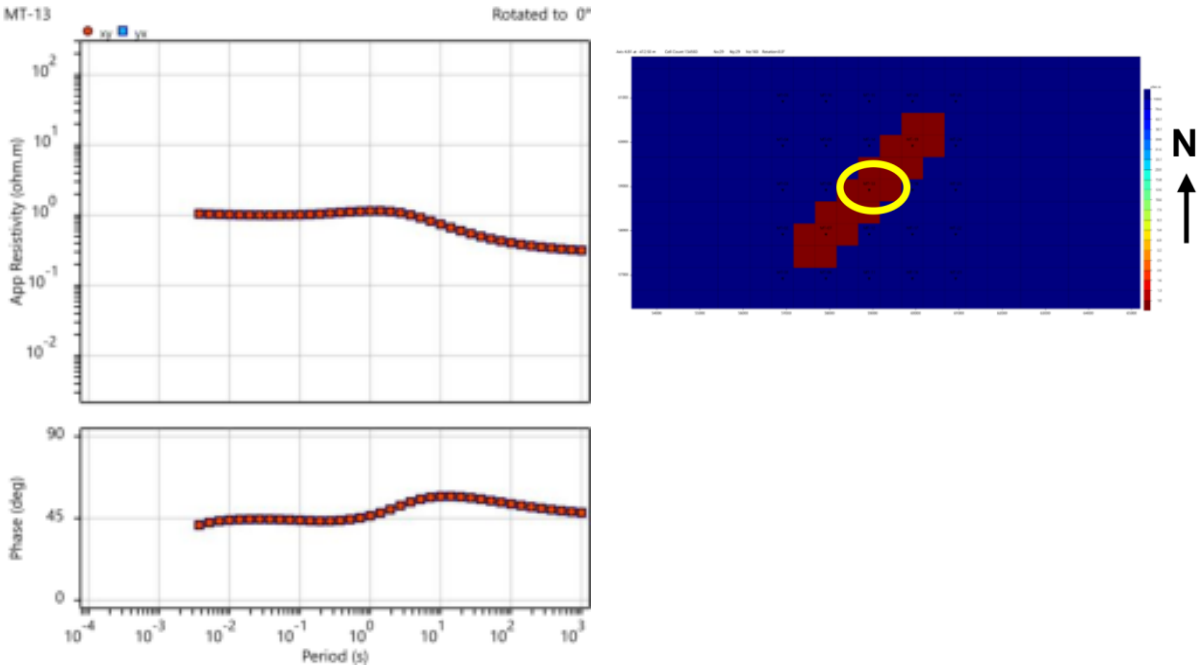

Figure 7: TE and TM curves of the diagonal conductive anomaly model at the center of the conductive anomaly.

At the stations located at the center of the conductive anomaly, the TE and TM curves overlap, with apparent resistivity values ranging from 0.01 to 0.1 seconds 100 Ωm. From 0.1 to 1000 seconds, there is a slight decrease in apparent resistivity to 90 Ωm. The phase values for TE and TM also overlap, forming a 45-degree angle. The overlapping of the TE and TM curves occurs because the measurements are taken precisely at the center of the conductive anomaly.

b. Points Near the Conductive Anomaly

The separation of the TE and TM curves as a function of the period can be observed at MT points near the anomaly, as shown in Figure 8, at a distance of 500 meters from the conductive anomaly. This study identified six stations with similar characteristics, detailed as follows. The apparent resistivity value from the TE response is 20 Ωm at a period of 0.08 seconds. This value decreases to 10 Ωm as the period increases and flattens at 10 Ωm from a period of 100 seconds. The phase angle is approximately 47 degrees at a period of 0.08 seconds, then drops to 45 degrees at a period of 0.1 seconds, rises to 50 degrees at a period of 20 seconds, and flattens at 45 degrees.

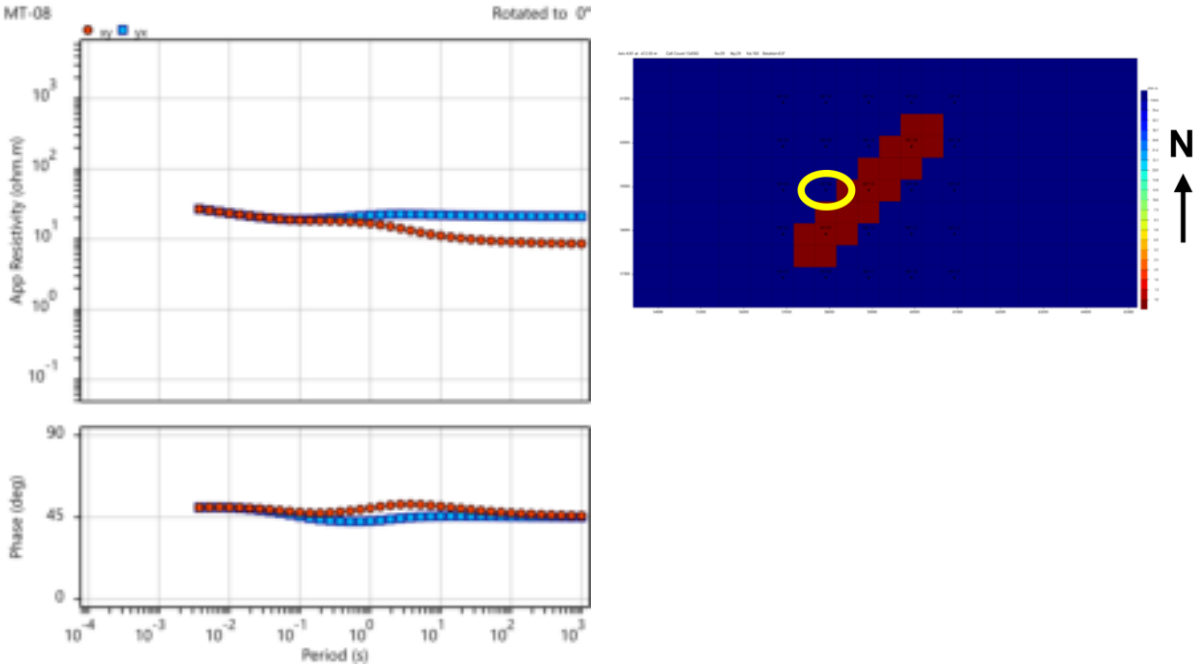

Figure 8: TE and TM curves of the diagonal conductive anomaly model at stations near the conductive anomaly.

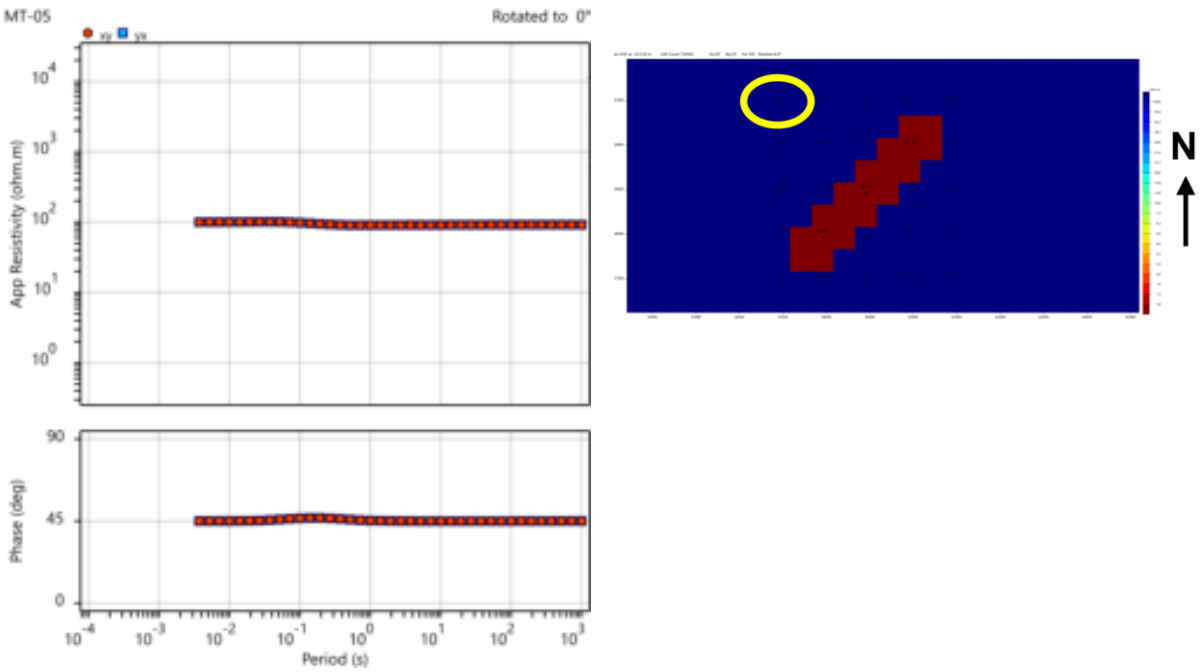

Figure 9: TE and TM curves of the diagonal conductive anomaly model at stations furthest from the conductive anomaly.

The TM response has an apparent resistivity of 30 Ωm at a period of 0.08 seconds, which then decreases to 20 Ωm at a period of 0.5 seconds and flattens towards 30 Ωm. The TM phase is around 47 degrees at a period of 0.08 seconds, then flattens at 45 degrees as the period increases. The characteristics of the TE and TM curves near the conductive anomaly exhibit separation. This separation is crucial for identifying the presence of an anomaly near the observation point. The separation occurs due to anisotropy, in this case, a diagonal-shaped conductive anomaly, where both the size and depth of the anisotropy influence the separation of the TE and TM curves. At higher periods, surface anisotropy does not affect lower periods. The degree of separation between the TE and TM phase curves is around 10 degrees.

c. Stations Furthest from the Conductive Anomaly

Measurements of the TE and TM points at the furthest measurement station from the 3-D anomaly are shown in Figure 9. At this distance, the conductive anomaly does not affect the shape of the TE and TM curves, and both have the same apparent resistivity value of 100 Ωm across all periods. Similarly, the phases of the TE and TM curves overlap at 45 degrees throughout the period. It is important to note that this condition may not hold if the size of the anomaly is increased while maintaining the same distance.

4.1.4 Model 4

Model 04 features a resistivity structure in the form of an anticline. The discussion is divided into three sections: points above the anomaly, points near the anomaly, and points at the edge of the conductive anomaly. The responses of the TE and TM curves from the anticline model are categorized as follows:

a. Points Above the Conductive Anomaly

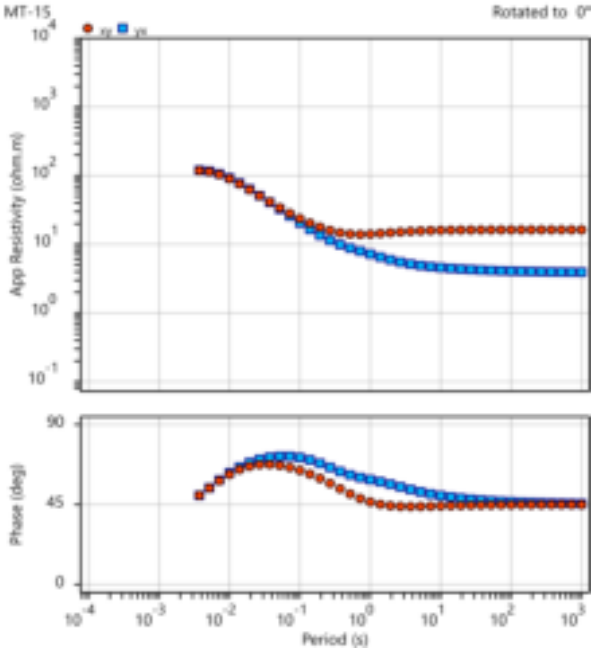

Figure 10: TE and TM curves of the anticline model at measurement points above the anticline.

The separation of the TE and TM curves at observation points above the anticline is shown in Figure 10. The characteristics of the TE and TM curves can be described as follows: The apparent resistivity value from the TE response is 100 Ωm at a period of 0.08 seconds and flattens at 20 Ωm from a period of 0.01 seconds. The phase angle starts at 45 degrees at a period of 0.08 seconds, rises to 60 degrees at a period of 0.8 seconds, then drops and flattens at 45 degrees. The TM response follows the TE response until a period of 0.9 seconds, then drops to 2 Ωm at a period of one second and flattens towards 2 Ωm up to a period of 1000 seconds. The initial TM phase matches the TE phase, but the TM curve begins to separate at a period of 0.01 seconds, with a slightly larger angle than the TE curve at a period of 0.1 seconds, then the phase decreases and flattens from a period of 20 seconds at an angle of 45 degrees.

In general, it can be concluded that the TE and TM curves above the conductive anomaly will overlap up to a certain period, then begin to separate. The apparent resistivity of the TE curve follows the resistivity of the anomaly, while the apparent resistivity of the TM curve follows the resistivity of the surrounding area. The phase curves initially and finally overlap, with slight separation in between. The phase separation between the TE and TM curves is approximately 20 degrees. The separation of the TE and TM curves is caused by the presence of the conductive anomaly at a period of 0.1 seconds.

b. Stations Adjacent to the Conductive Anomaly

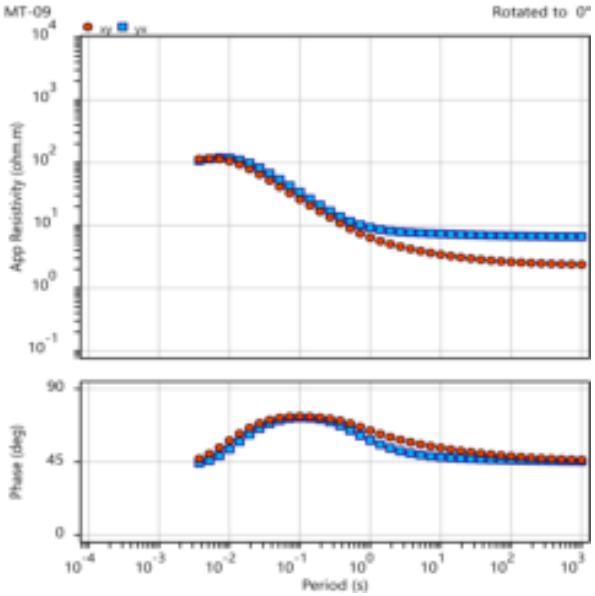

Figure 11: TE and TM curves of model 04 at stations adjacent to the conductive anomaly.

The characteristics of the TE and TM curves at stations adjacent to the conductive anomaly can be described as follows: The apparent resistivity value from the TE response is 100 Ωm at a period of 0.08 seconds, then it decreases from 0.01 to one second and flattens at an apparent resistivity value of 2 Ωm. The phase angle starts at 45 degrees at a period of 0.08 seconds, rises until a period of 0.1 seconds, then drops and flattens at 45 degrees. The TM response is similar to the TE response until a period of 0.01 seconds, then it decreases to 10 Ωm at a period of 0.9 seconds and flattens at 10 Ωm up to a period of 1000 seconds. The initial TM phase matches the TE phase, but the TM curve's angle decreases earlier at a period of 0.9 seconds, with a slightly smaller angle than the TE curve, and flattens from a period of 9 seconds at an angle of 45 degrees.

The characteristics of the TE and TM curves near the conductive anomaly begin to show separation at a period of 0.01 seconds, though the separation is not very pronounced. The separation becomes more distinct from a period of 0.9 seconds, where the conductive anomaly is located. In general, the TE and TM curves above the conductive anomaly will overlap up to a certain period and then begin to separate. The apparent resistivity of the TE curve follows the resistivity of the anomaly, while the apparent resistivity of the TM curve follows the resistivity of the surrounding area. The phase curves initially and finally overlap, with slight separation in between. The phase separation between the TE and TM curves is approximately 8 degrees. The separation of the TE and TM curves is caused by the presence of the conductive anomaly at a period of 1 second.

c. Stations Furthest from the Conductive Anomaly

The characteristics of the TE and TM curves at stations located at the edge of the anticline wing, as shown in Figure 12, can be described as follows: The apparent resistivity value from the TE response is 100 Ωm at a period of 0.08 seconds, then it decreases from 0.5 seconds and flattens at an apparent resistivity value of 10 Ωm. The phase angle starts at 45 degrees at a period of 0.08 seconds, rises until a period of 0.1 seconds, then drops and flattens at 45 degrees. The TM response is similar to the TE response until a period of 0.9 seconds, then it decreases to 70 Ωm at a period of 0.3 seconds, rises again, and flattens at 100 Ωm up to a period of 1000 seconds. The initial TM phase matches the TE phase, but the TM curve forms a smaller angle compared to the TE curve, despite experiencing a phase increase, and flattens from a period of one second at an angle of 45 degrees.

The characteristics of the TE and TM curves near the conductive anomaly start to show separation at a period of 0.1 seconds, where the conductive anomaly is located. In general, the TE and TM curves above the conductive anomaly will overlap up to a certain period, then begin to separate. The apparent resistivity of the TE curve follows the resistivity of the anomaly, while the apparent resistivity of the TM curve follows the resistivity of the surrounding area. The phase curves initially and finally overlap, with slight separation in between. The phase separation between the TE and TM curves is approximately 20 degrees. The separation of the TE and TM curves at the edge of the anticline wing occurs at a period of 0.1 seconds, due to the presence of the conductive anomaly at that period.

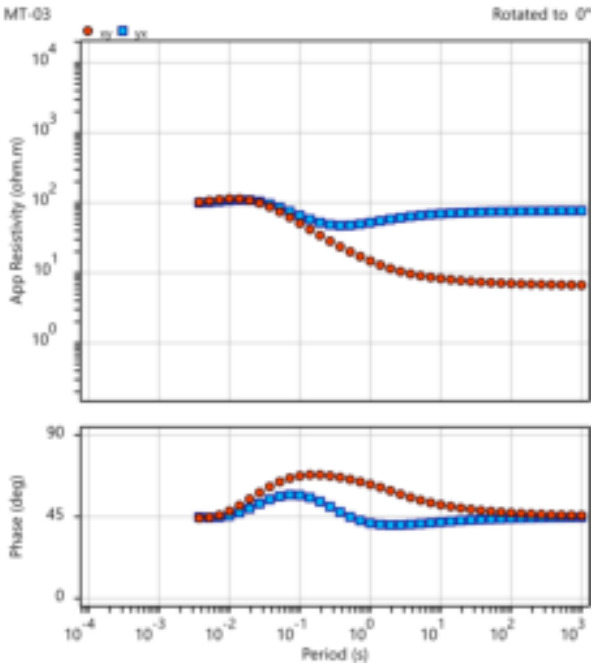

Figure 12: TE and TM curves of model 04 at stations located at the edge of the anticline wing.

4.2 Dimensionality of MT Data

4.2.1 Model 1

The changes in the polar diagram shape and the angles formed on the beta phase tensor can provide dimensionality information of MT data as a function of the period. The dimensionality derived from the polar diagram and the beta phase tensor can validate each other. The information obtained from these two parameters will serve as the basis for selecting the modeling method and determining the data constraints to be modeled.

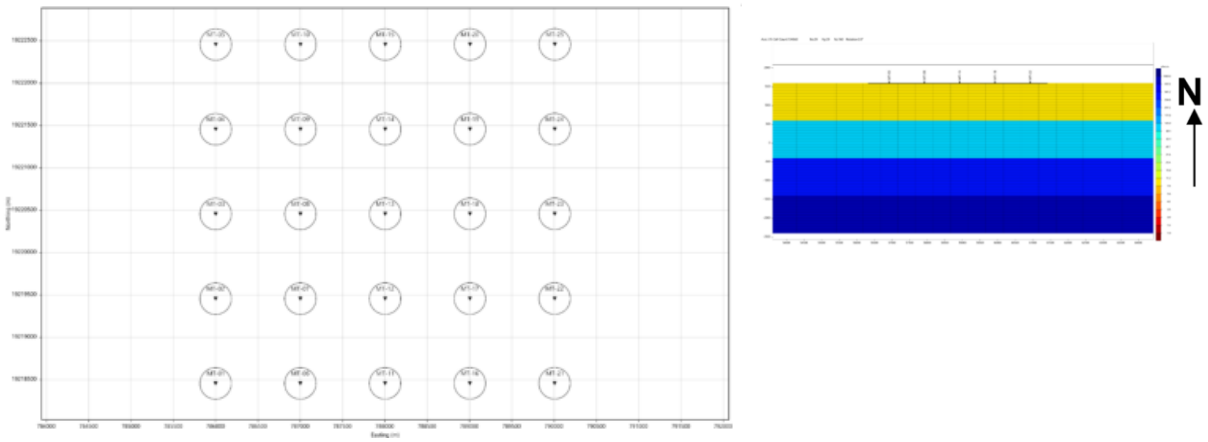

Figure 13: Polar diagram of model 01.

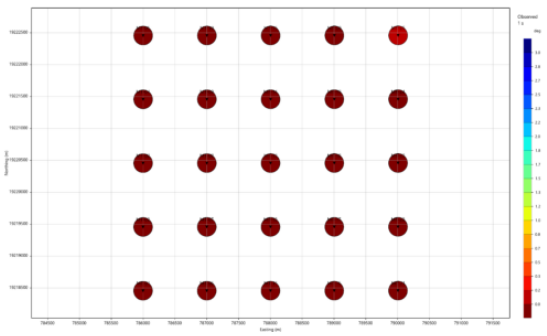

Figure 14: Beta phase tensor of model 01 at a period of 0.01 Seconds

In Model 01, the shape of the polar diagram at each period is a perfect circle, which means Zxy = -Zyx and Zxx = Zyy = 0. The dimensionality at each period is 1-D. An example of a polar diagram at a period of 0.01 seconds is shown in Figure 13. The circular polar diagram physically means that the resistivity measurement will give the same value in all directions.

Figure 14 provides information on the beta phase tensor where the angle formed is close to 0 degrees (indicated by the brown color). This beta angle remains the same at each period. The observation of the beta phase tensor has a consistent relationship with the polar diagram discussion above.

4.2.2 Model 2

The shape of the polar diagram for Model 02 varies as a function of the period, including circles, ellipses, and a peanut shape. At low periods, such as 0.01 seconds, the circular shape is observed at nearly all observation points, indicating that the vertical contact has not yet been detected. Points close to the vertical contact can capture the effect of resistivity contrast, shown by a weak north-south elongation. At this period, points near the resistivity contrast between two blocks exhibit a slightly elliptical polar diagram with a north-south orientation.

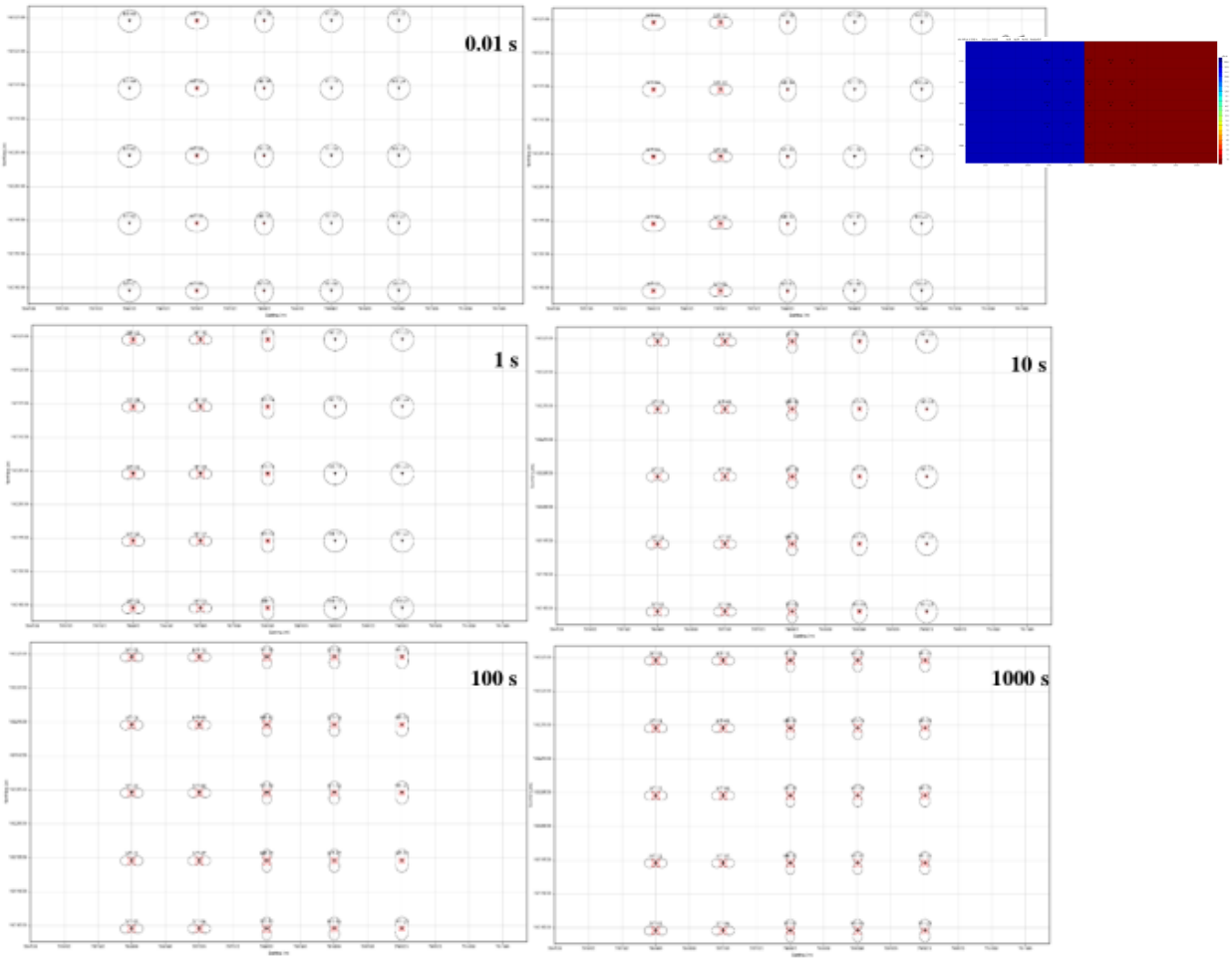

Figure 15: Polar Diagram of Model 02.

At a period of 0.1 seconds, the transition begins to detect the presence of resistivity contrast at all points, shown by the polar diagram in the resistive block. Points above the resistive block exhibit a west-east orientation, while the conductive block shows a north-south orientation. At a period of 1 second, the response from the resistivity contrast between the two blocks is recorded by all points. However, points above the resistive block already show a peanut-shaped polar diagram with a west-east orientation, while points above the conductive block still exhibit an elliptical shape. Notably, MT points near the resistivity contrast between the two blocks have a peanut-shaped polar diagram.

The characteristics of the polar diagram at a period of 10 seconds are similar to those at 1 second, with the following observations: the presence of a peanut shape in the conductive block at points near the resistivity contrast, and as the distance from the contrast increases, the shape in the conductive block becomes elliptical. At higher periods, represented by 100 seconds and 1000 seconds, the polar diagram response shows that as the period

increases, the peanut shape appears at all measurement points, both above the resistor and the conductor. The peanut shape becomes more pronounced above the conductor, where it becomes clearer. Measurement points above the conductor, whether near or far from the vertical contact, have a similar polar diagram shape.

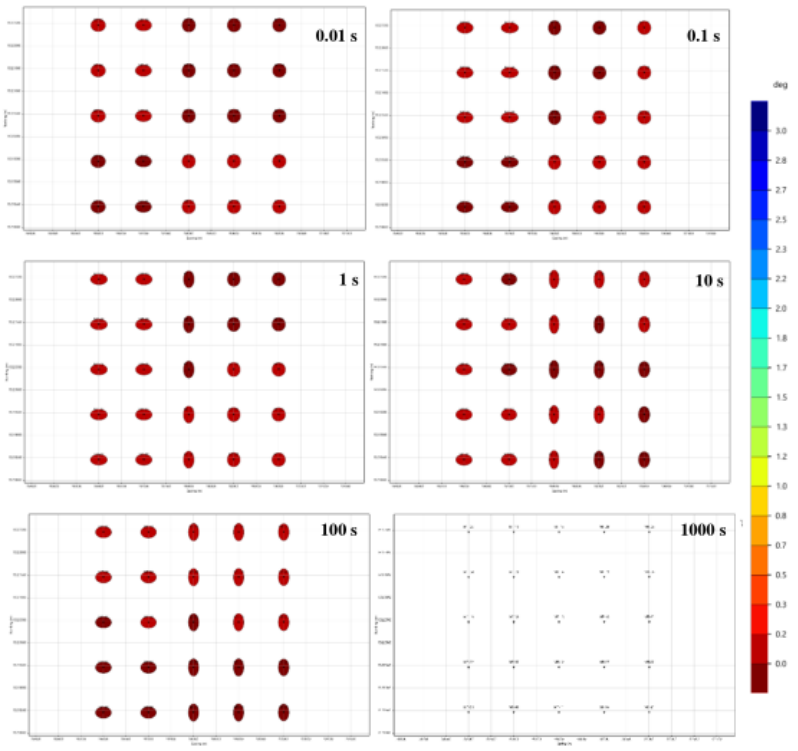

Figure 16: Beta phase tensor of model 02.

The dimensionality analysis of the beta phase tensor for Model 02 is shown in Figure 16, covering periods from low to high. At a glance, the beta phase tensor analysis indicates a 1-D dimensionality, where the angle formed is 0 degrees. This is understandable because the synthetic model is a simple 2-D model. However, upon closer examination, starting from a period of 0.01 seconds, the value of the beta phase tensor slightly increases to 0.2 degrees, indicating the presence of minor 2-D data.

4.2.3 Model 3

The shape of the polar diagram for Model 03 varies as a function of the period, including circles, ellipses, and a peanut shape. At low periods, such as 0.01 to 0.1 seconds, a circular shape is observed over the resistive part far from the conductive anomaly and at observation points above the conductive anomaly. However, measurement points near the conductive anomaly exhibit weak elliptical elongation perpendicular to the conductive anomaly.

At a period of 1 second, the presence of the conductive anomaly begins to be detected, with the polar diagram pattern changing to a radial shape relative to the anomaly's geometry. For example, at five points on the north side of the measurement area, the direction of elliptical elongation changes from southeast (MT-05) to south (MT-20), and then to southwest (MT-25). A similar pattern is observed at five points in the center of the measurement area, with the peanut shape elongation changing from southeast at MT-03 and MT-08 to northeast at MT-13 above the anomaly. However, at MT-18 and MT-23, the elongation is northeast. The radial pattern is also observed at periods of 10 to 100 seconds, with strong peanut shape elongation at measurement points above and near the conductive anomaly. Observation points far from the conductive anomaly still show weak elliptical elongation. Overall, anisotropy effects are detected at MT points as a function of the period and distance from the anomaly. These anisotropy effects will be further analyzed with the beta phase tensor.

The dimensionality analysis of the beta phase tensor for Model 03 is shown in Figure 18. Generally, at periods of 0.01 and 0.1 seconds, the beta phase tensor is 0 degrees, indicating that the response from the conductive anomaly is not clearly visible at these periods. Specifically, at MT measurement points near the conductive anomaly, the angle ranges from 0 to 1 degree. For points far from the conductive anomaly, the beta phase tensor remains at 0 degrees. This clarifies the previous analysis that the position of the conductive anomaly does not affect distant measurement points.

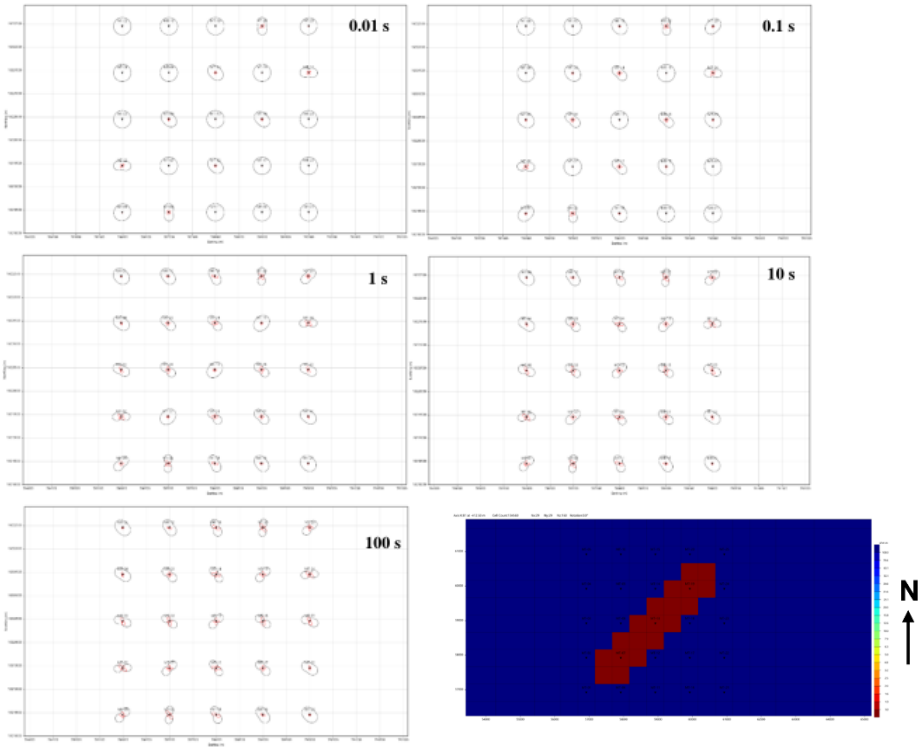

Figure 17: Polar diagram of model 03.

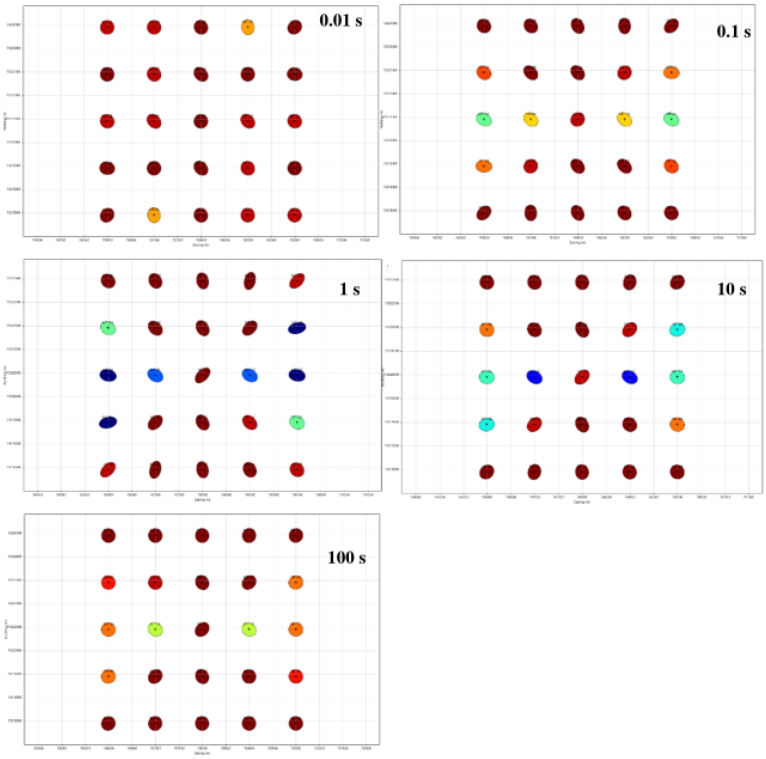

Figure 18: Beta phase tensor of model 03.

At a glance, the beta phase tensor analysis from 0.01 to 0.1 seconds indicates a 2-D dimensionality, with angles less than 3 degrees. The conductive anomaly's response starts to be recorded at all measurement points at a period of 1 second. Near the anomaly, the beta phase tensor shows a 3-degree angle. At this point, the angle between Φ\PhiΦ and the conductive anomaly is 3 degrees. For points near the center of the conductive anomaly, the beta phase tensor angle is 2.7 degrees, while other nearby points have a 0-degree angle. Above the conductive anomaly, the beta phase tensor angle is 0 degrees, and points far from the anomaly also have a 0-degree angle, indicating 3-D dimensionality.

At higher periods, such as 10 to 100 seconds, the beta phase tensor angle at MT stations decreases from 3 degrees to 1.7 degrees. However, near the conductive anomaly, particularly in the center, the angle remains at 2.7 degrees. Measurement points above the conductive anomaly show a slight increase to 0.2 degrees, while distant points remain at 0 degrees. In conclusion, the analysis of the polar diagram and beta phase tensor for Model 03 confirms that this model exhibits 3-D dimensionality.

4.2.4 Model 4

The shape of the polar diagram for Model 04, as shown in Figure 19, varies as a function of the period, including circles, ellipses, and a peanut shape. At low periods, such as 0.01 seconds, the polar diagram at all MT measurement points is circular, as it is not yet influenced by the deeper conductive anomaly. A similar pattern is observed at 0.1 seconds, where the response from the conductive anomaly is still not clearly visible.

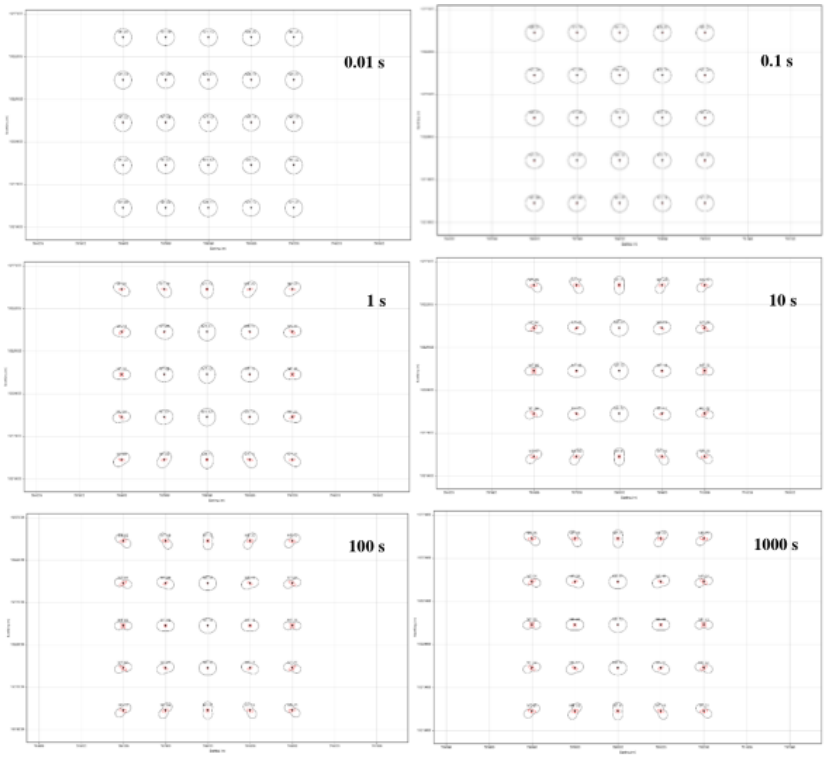

Figure 19: Polar diagram of model 04.

At a period of 1 second, the presence of the transition starts to be detected at measurement points above the edge of the anticline wing, marked by a change in the polar diagram shape at MT points near the conductive anomaly, shown by medium elliptical elongation. The direction of the polar diagram from the MT measurement points is perpendicular to the location of the conductive anomaly, which is in an east-west direction. MT measurement points above the conductive anomaly exhibit a circular polar diagram, while points above the anticline wing show very low elliptical elongation. This indicates that the conductive anomaly significantly influences the polar diagram shape at the edge of the anticline wing.

At higher periods, such as 10 to 1000 seconds, the polar diagram shows a similar pattern. MT measurement points at the edge of the anticline wing exhibit strong peanut shape elongation, points above the anticline wing show strong elliptical elongation, and points above the anticline show weak elliptical elongation. Based on this observation, the discussion will continue with the beta phase tensor analysis.

The dimensionality analysis of the beta phase tensor for Model 04 is shown in Figure 20. At low periods, particularly 0.01 seconds, the angle formed by the beta phase tensor is 0–0.3 degrees at each measurement point. This is influenced by the deeper location of the conductive anomaly, which does not significantly affect the measurement points at this period. The beta phase tensor angle begins to increase at MT points near the edge of the anticline wing, particularly in the northeast and southwest directions at a period of 0.1 seconds. The increase in the beta phase tensor angle at these points is due to the conductive anomaly starting to be recorded at this period. The beta phase tensor angle formed ranges from 0.2 to 1 degree.

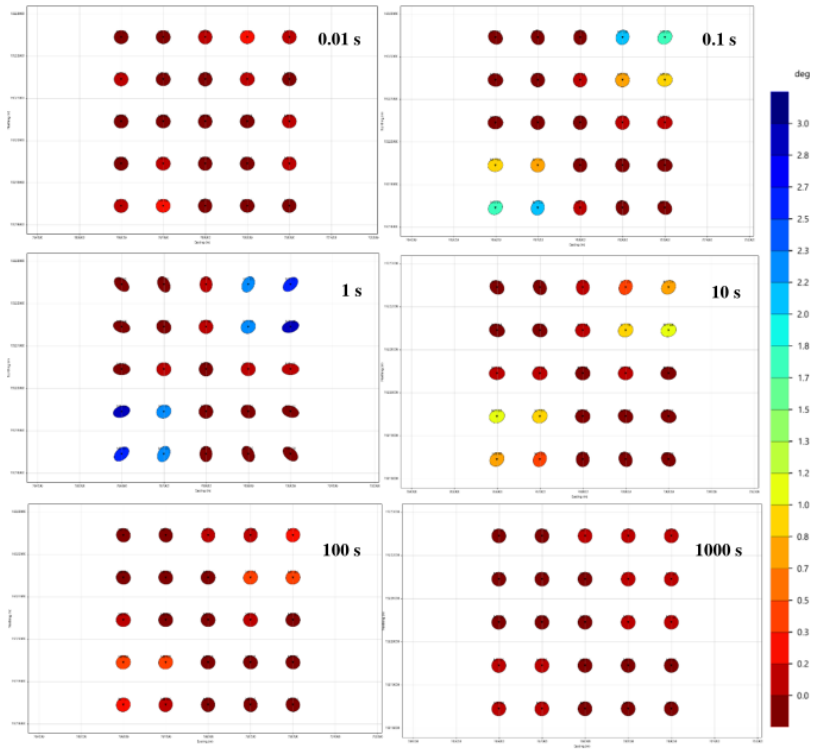

Figure 20: Beta phase tensor of model 04.

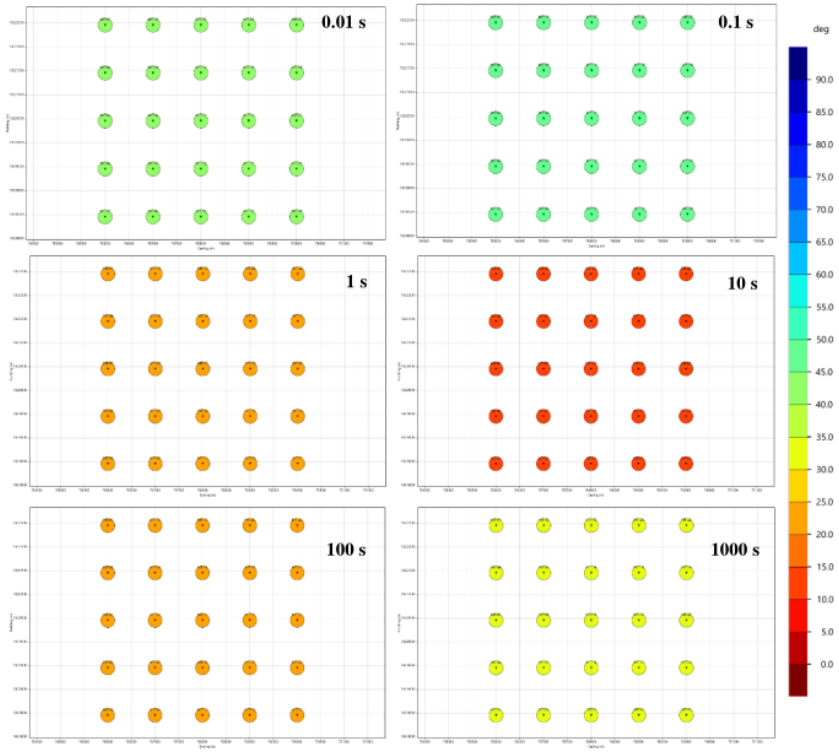

Figure 21: Phase Tensor Φ of Model 01.

The response of the conductive anomaly is recorded at all measurement points at a period of 1 second. At MT measurement points at the edge of the anticline wing, particularly in the northeast and southwest directions, the beta phase tensor response shows a beta angle of 3 degrees. At these points, the angle between Φ and the conductive anomaly is 3 degrees, indicating the presence of 3-D dimensionality at this period. At higher periods (10 to 1000 seconds), the beta phase tensor angle returns to 0 degrees, as the conductive anomaly is no longer detected at these periods.

4.3 Direction of Linearity

4.3.1 Model 1

The phase tensor Φ of Model 01 is shown in Figure 21. At a period of 0.01 seconds, the angle formed is 45 degrees, indicating that the electric and magnetic fields are perpendicular to each other. As the period increases, the Φ angle decreases to 10 degrees at a period of 10 seconds due to increasing resistivity with depth. However, the Φ angle at periods of 100 and 1000 seconds increases again because the electric field tends to move toward the surface where a conductive layer is present. Model 01 exhibits resistivity variation with depth, so there is no linear zone, as evidenced by the constant phase tensor Φ across all periods.

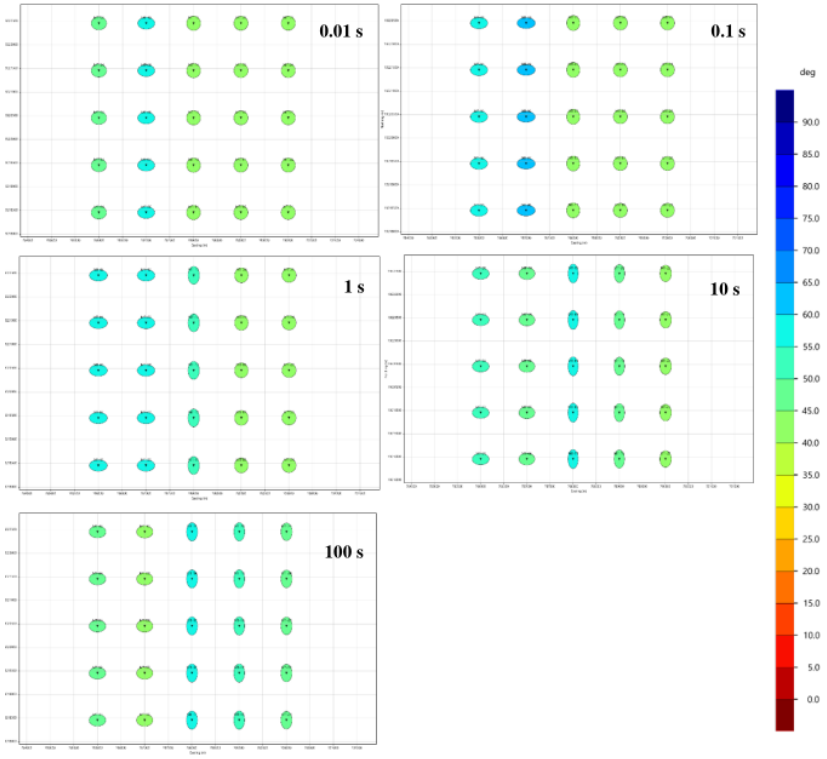

Figure 22: Phase tensor Φ of model 02.

4.3.2 Model 2

The Φ phase tensor of Model 02 is shown in Figure 22. In Model 02, the Φ phase tensor values range from 45 to 60 degrees. At a period of 0.01 seconds, a resistive layer is observed, with MT measurement points near the geoelectrical strike showing an angle of 60 degrees. The resistivity contrast between the two blocks at this period has little effect on the resistive block measurement points, while other points are not yet influenced. As the period increases, the impact of the resistivity contrast becomes more apparent, indicated by the increasing Φ angle from the resistive block to the conductive block. At a period of 1 second, the strong influence of the resistivity contrast is evident, with the resistive block having a Φ phase tensor direction perpendicular to the conductive block. The conductive block shows linearity in the Φ phase tensor direction, and as the period increases, the conductive block has a larger Φ phase tensor value compared to the resistive block. At this period, the resistive block has an electric and magnetic field angle of 45 degrees, indicating perpendicularity.

4.3.3 Model 3

The Phi phase tensor values for Model 03, ranging from 45 to 60 degrees, are shown in Figure 23. From 0.01 to 0.1 seconds, the influence of the conductive anomaly is not clearly recorded. As the period increases, the direction of the polar diagram containing the Phi phase tensor values for the resistive block becomes perpendicular to the conductive anomaly. MT points above the conductive anomaly show a diagonal linearity in the Phi phase tensor direction with a northeast-southwest orientation. At higher periods, such as 10 to 100 seconds, the Phi angle formed by the Phi phase tensor of the conductive block is larger than that of the resistive block. At these periods, the Phi phase tensor has electric and magnetic field angles of 45 degrees, indicating perpendicularity.

4.3.4 Model 4

In Model 04, the Phi phase tensor values range from 45 to 60 degrees. From 0.01 to 0.1 seconds, MT points above the conductive anomaly have larger angles compared to other MT points, with angles of 80 degrees at 0.01 seconds and 85 degrees at 0.1 seconds. This indicates that the influence of the conductive anomaly starts to be recorded at

these periods. The response from the conductive anomaly can still be recorded up to a period of 1 second, indicating proximity to the anomaly. The linear zone shown by Model 04 is in the middle of the MT measurement points with an east-west orientation. As the period increases, the Phi phase tensor angle approaches 45 degrees, indicating perpendicularity between the electric and magnetic fields, and no longer showing linearity.

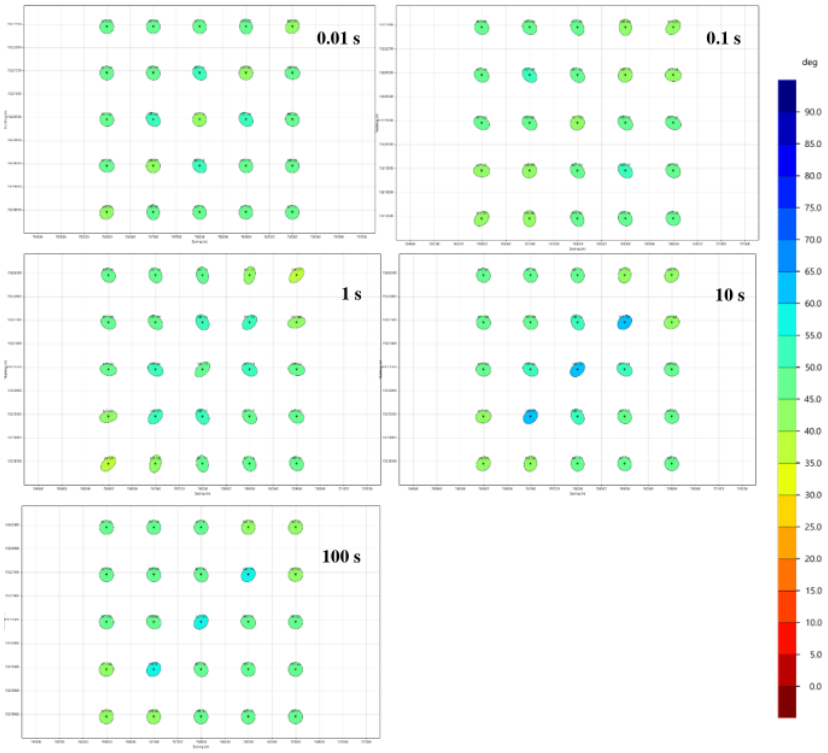

Figure 23: Phase tensor Φ of model 03.

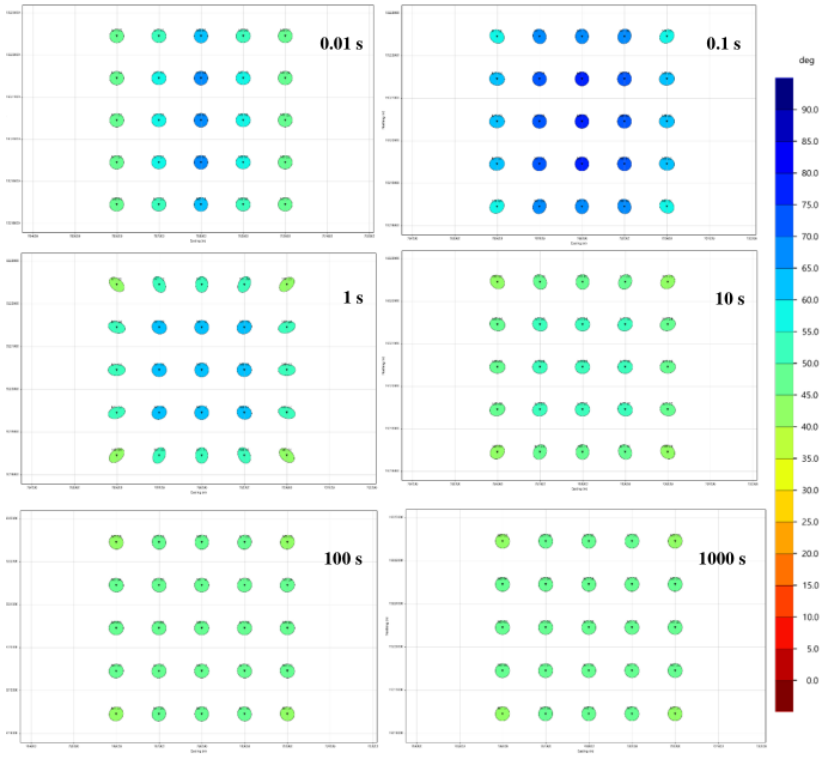

Figure 24: Phase Tensor Φ of Model 04.

4.4 Distribution of Conductive Anomalies

The distribution of conductive anomalies can be identified using phase tensors and induction arrows. Changes in the phase tensor values are displayed over several periods to observe angle variations with depth. Phase tensor maps with high and constant angles as depth increases can represent the presence of conductive anomalies. Induction arrow analysis is used to observe changes in subsurface resistivity structures. Using Parkinson's conversion, vectors approach conductive materials from the surrounding environment. The induction arrow discussion is focused on points above the resistor.

4.4.1 Model 1

Model 01 represents a layer with varying resistivity values with depth. The induction arrow for Model 01 points toward the surface at all MT point periods, indicating that the conductive layer is at the surface. The distribution of conductive anomalies in Model 01 can also be observed with the Phi phase tensor shown in Figure 21. At low periods, the angle formed is 45 degrees, decreasing with increasing period. At high periods, the Phi phase tensor increases because the electric field tends to flow to the more conductive surface layer.

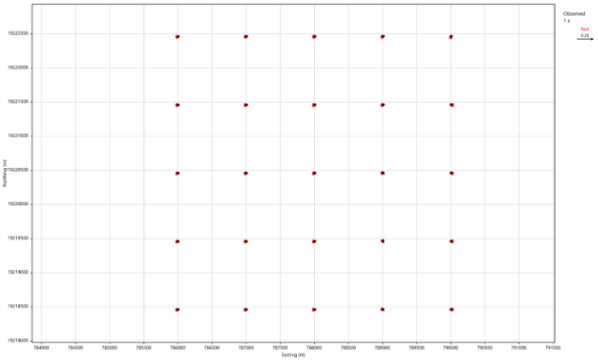

Figure 25: Induction Arrow of Model 01.

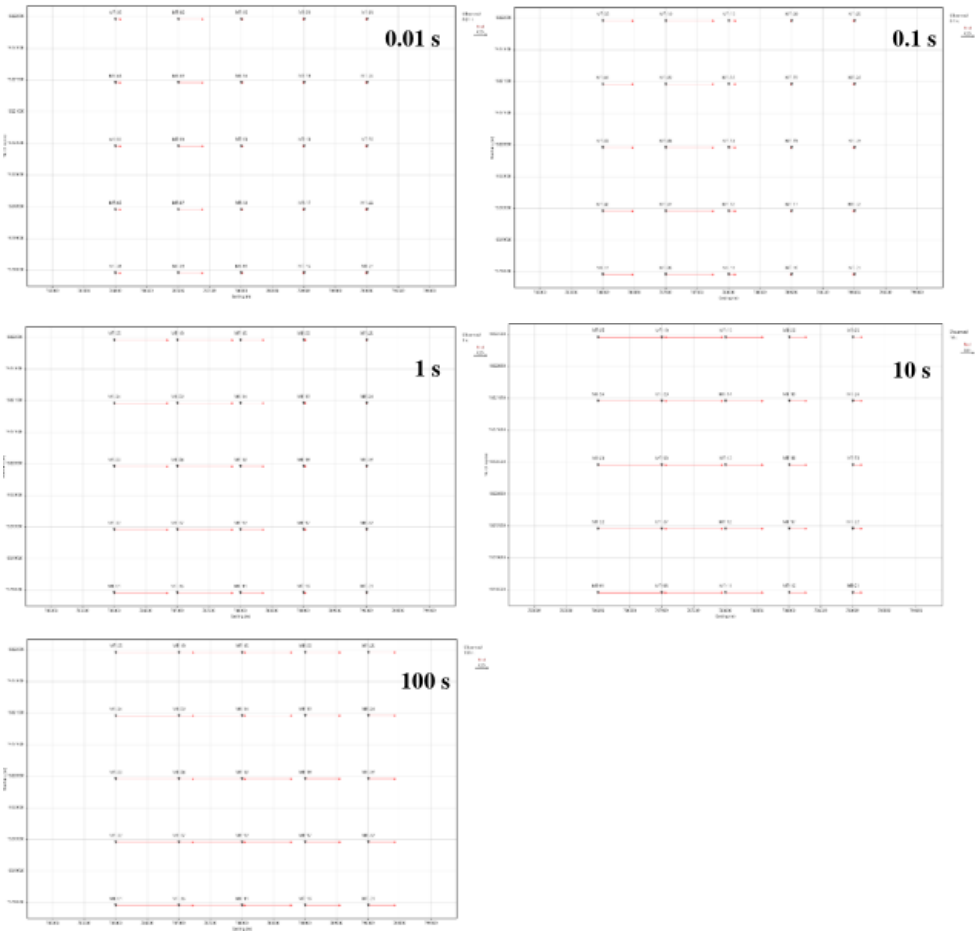

Figure 26: Induction arrow of model 02.

4.4.2 Model 2

The distribution of conductive anomalies in Model 02 is shown in Figure 26. At low periods (0.01 seconds), weak induction arrows are observed pointing east, indicating the location of the conductive medium. Across all periods, the magnitude of the induction arrow increases with the period. The conductive block shows arrows pointing east, influenced by the rectangular padding used. The distribution of conductive anomalies in Model 02 can also be analyzed using the Phi phase tensor shown in Figure 22. At high periods, the conductive block has a higher Phi phase tensor angle compared to measurement points above the resistor.

4.4.3 Model 3

The direction of the induction arrow for Model 03 is shown in Figure 27. From a period of 0.01 seconds, the response from the conductive anomaly is recorded, indicated by the induction arrow pointing toward the center. The magnitude of the induction arrow increases at 0.1 seconds, indicating the presence of the conductive anomaly. The magnitude decreases with depth, meaning the anomaly's influence lessens. Induction arrows at the center of the conductive anomaly point to the surface. MT points beside the conductive anomaly point toward the center with greater magnitude than points at the edge of the anomaly. The distribution of conductive anomalies in Model 03 can also be observed with the Phi phase tensor shown in Figure 23. The conductive anomaly has a larger Phi angle compared to the resistive block as depth increases.

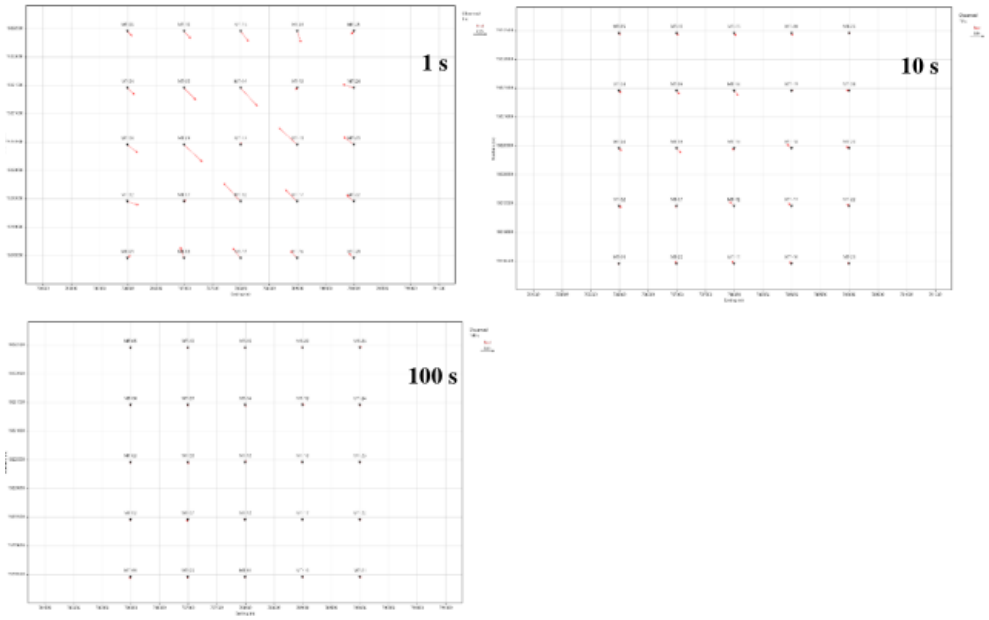

Figure 27: Induction arrow of model 03.

4.4.4 Model 4

The distribution of conductive anomalies in Model 04 using induction arrows is shown in Figure 28. At low periods (0.01 seconds), the response from the conductive anomaly is very weak, with induction arrows pointing below the surface. At 0.1 seconds, the conductive anomaly response begins to show a weak central direction. Clearer induction arrows start to appear at 1 second, pointing toward the center. With increasing periods, the induction arrow magnitude weakens as the distance from the conductive anomaly increases. This can also be analyzed with the Phi phase tensor shown in Figure 24. At low periods (0.01 to 1 second), the conductive anomaly response is recorded, indicated by a larger Phi angle in the conductive anomaly compared to the resistive part. At 0.01 seconds, the Phi phase tensor already shows a large angle due to the proximity to the conductive anomaly. At 0.1 and 1 second, the Phi phase tensor response indicates the presence of the conductive anomaly.

4.5 MT Data Modeling

4.5.1 1-D Interpretation

The 1-D model has resistivity values that vary with depth (Figure 29). The period range used for the 1-D model in Model 01 is from 0.01 to 1000 seconds, whereas for the other models, the 1-D model is only applicable at a period of 0.01 seconds. The 1-D modeling is performed by first conducting forward modeling, followed by inversion to produce a resistivity model that accurately depicts the subsurface resistivity values. The 1-D interpretation serves as an initial approach for modeling and interpretation in the preliminary stage. The inversion

results for Model 01 show that the 1-D modeling is consistent with the synthetic MT curve parameter analysis. The layer thickness from the 1-D inversion more accurately represents the synthetic model conditions compared to the 2-D inversion model. The layer thickness obtained is 1 km for each layer.

The analysis of Model 02 reveals the presence of both 1-D and 2-D dimensionalities. The 1-D inversion modeling results for Model 02 show a lateral distribution of resistivity values consistent with the synthetic model. However, the elevation does not match the synthetic model, with the 1-D model indicating elevations greater than -3000 masl, while the synthetic model reaches only up to - 2400 masl.

The 1-D inversion results for Model 03 show that the lateral distribution of resistivity values aligns with the synthetic model, but the elevation is not accurate. The conductive anomaly elevation produced by the 1-D model is greater than 5000 m, whereas the synthetic model indicates around -1400 m.

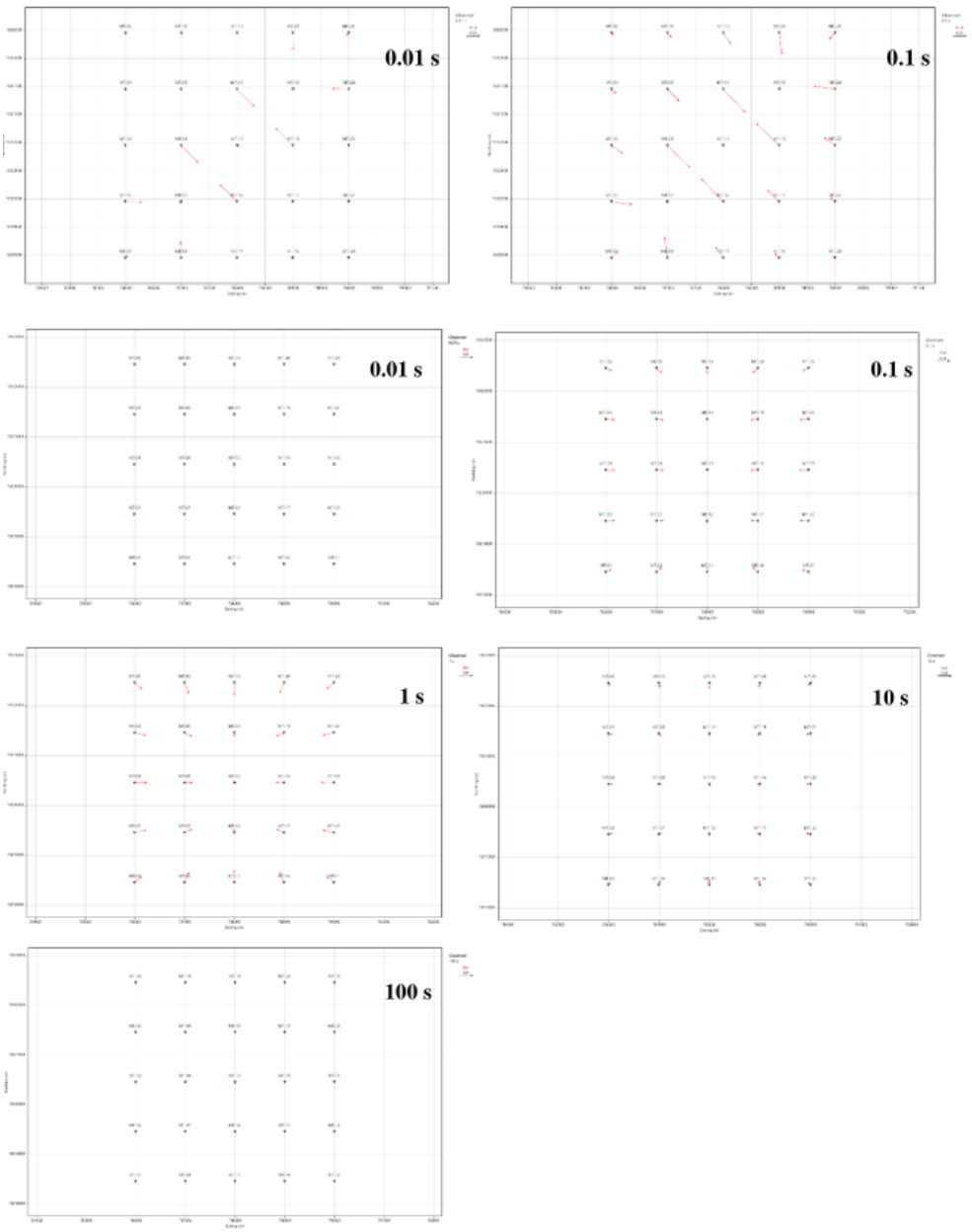

Figure 28: Induction Arrow of Model 04.

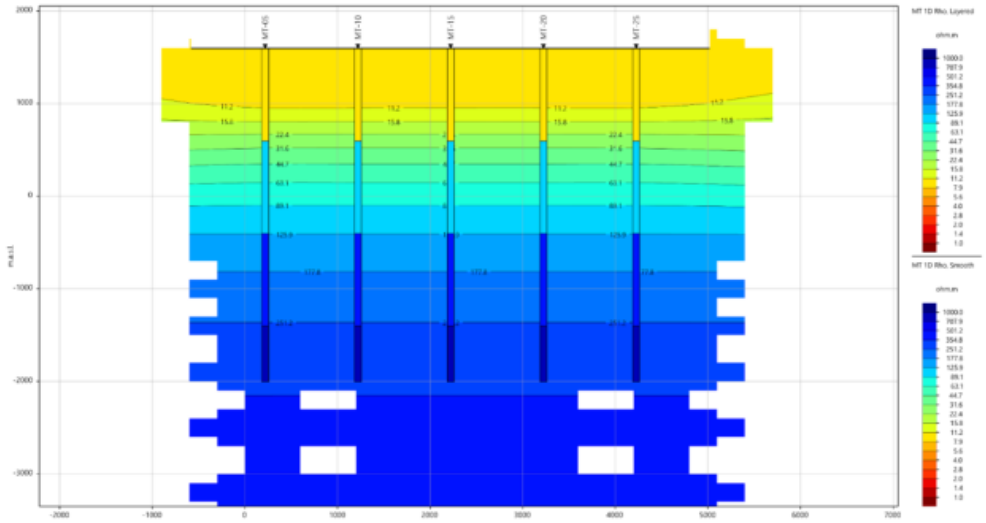

Figure 29: 1-D model for model 01.

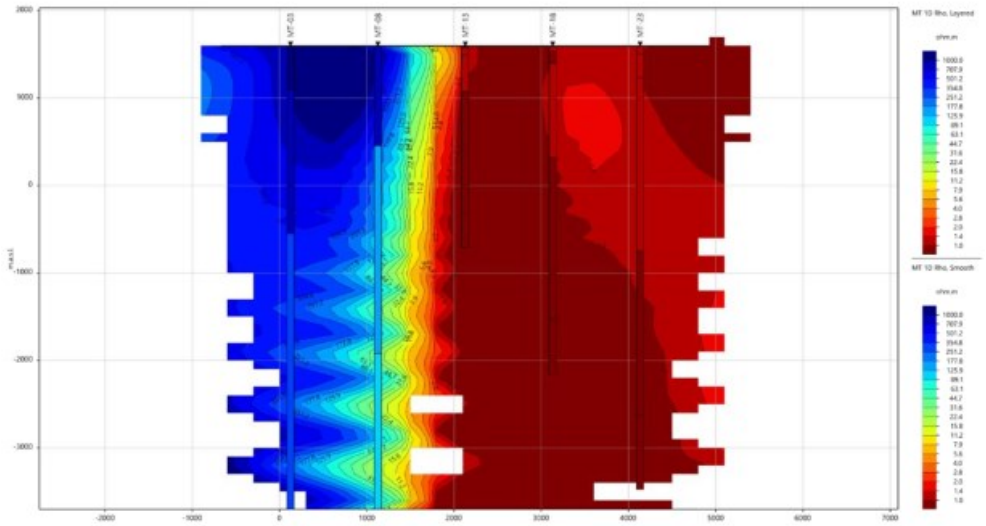

Figure 30: 1-D model for model 02.

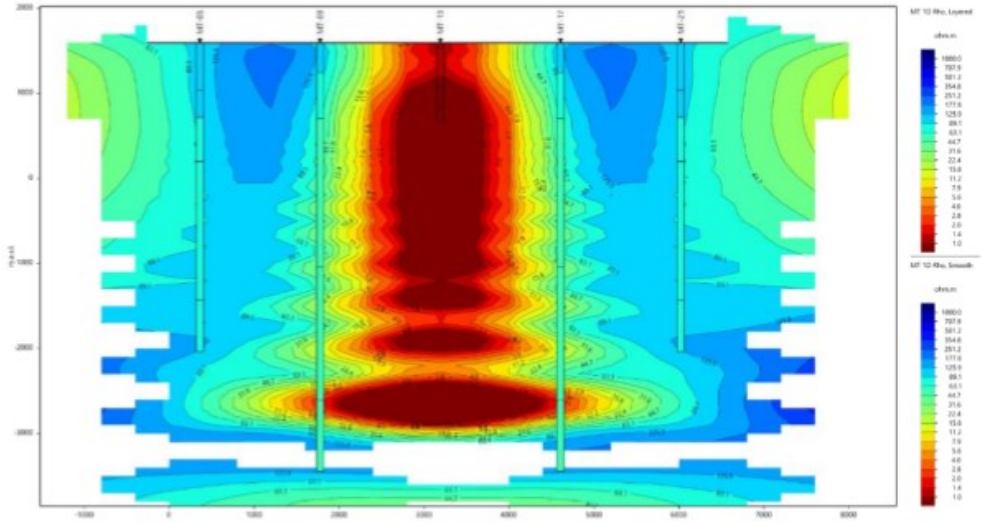

Figure 31: 1-D dodel for model 03.

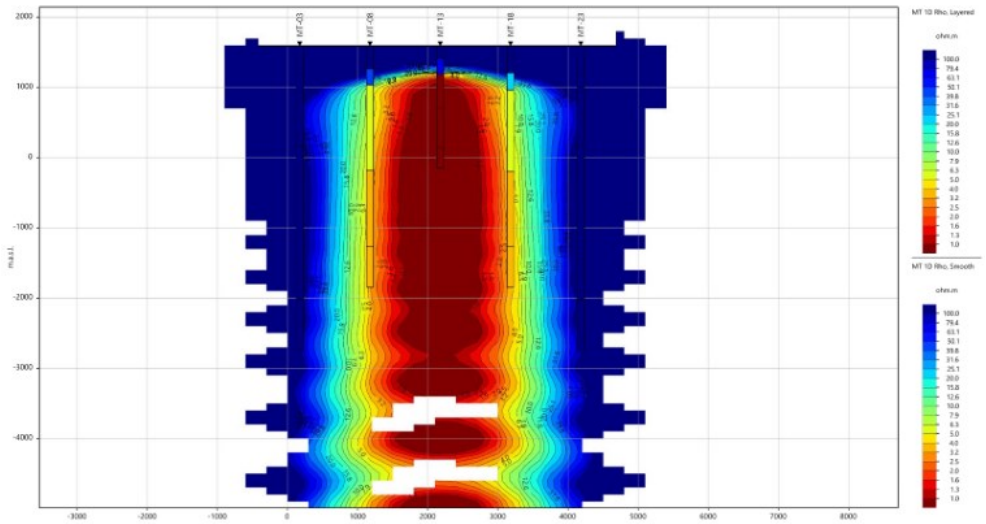

Figure 32: 1-D model for model 04.

In Model 04, the lateral distribution of the conductive anomaly matches the synthetic model, but the depth does not align with the synthetic data. The depth of the conductive anomaly from the 1-D modeling is more than -4000 masl.

4.5.2 2-D Interpretation

In 2-D modeling, trial and error are performed to find the appropriate inversion parameter size that matches the subsurface conditions. The geometry and inversion parameter size significantly affect the resistivity distribution results. 2-D MT modeling is carried out using the same transect to observe subsurface resistivity distribution with respect to distance and depth. In constructing the 2-D model, the geometry of each cell affects the resistivity distribution results, as do the background resistivity values and inversion input parameters.

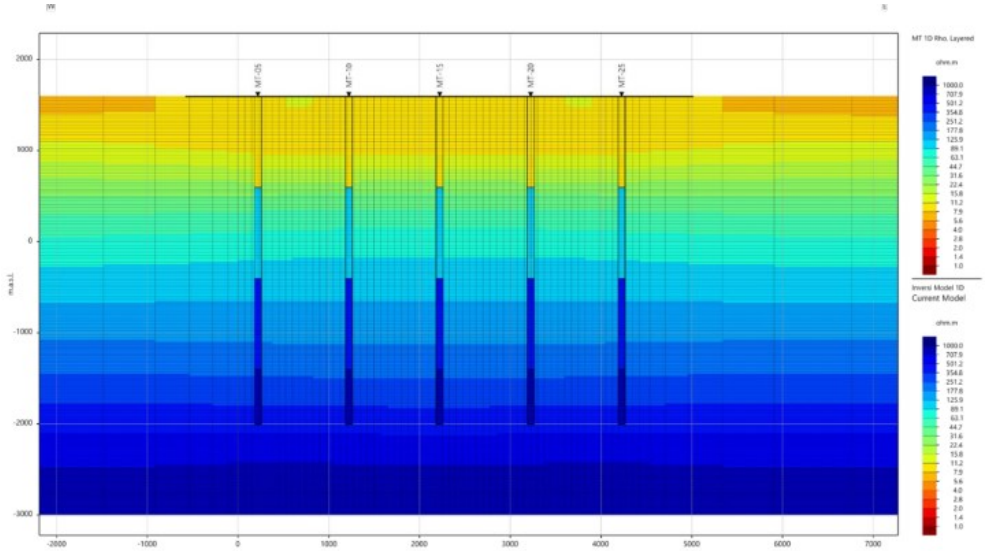

Figure 33: 2-D model for model 01.

Based on the MT curve parameter analysis, Model 01 has 1-D dimensionality. When 2-D inversion modeling is applied to Model 01, the layer elevation from the 2-D inversion does not match the synthetic model. For example, the first layer's thickness does not reach 1 km. The geometry used in the inversion includes horizontal cell widths of 500 m, an elevation range of 1600 to -2400 m, padding of 1000 m with a padding factor of 1.5, and vertical cell thickness of 25 m. The inversion parameters used include the entire period range (0.01 to 1000 seconds) and a background resistivity value of 100 Ωm.

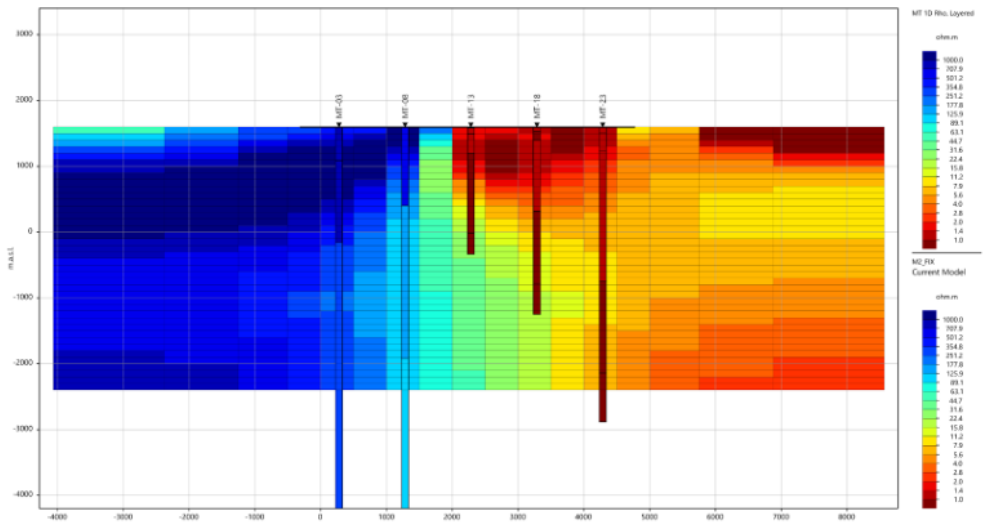

Figure 34: 2-D model for model 02.

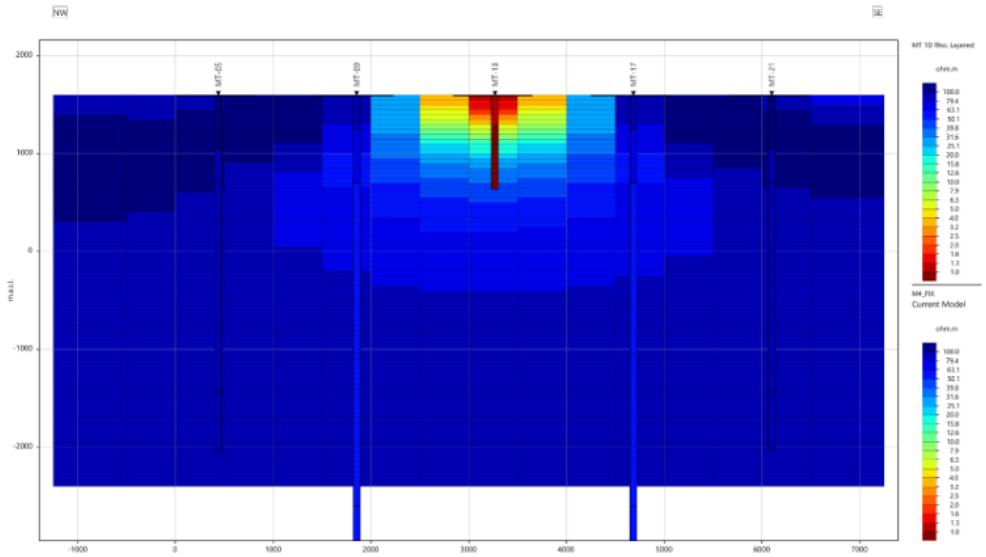

Figure 35: 2-D Model for Model 03.

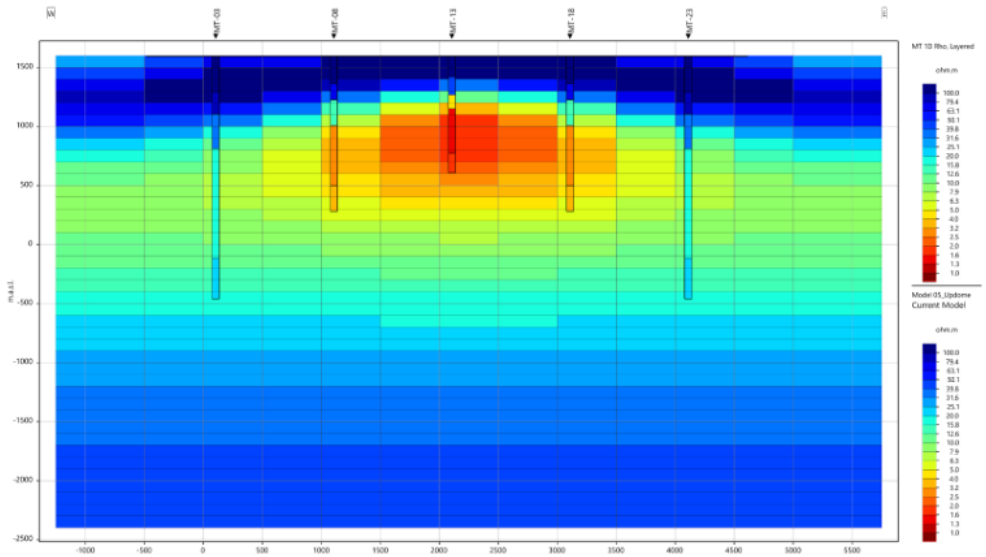

Figure 36: 2-D model for model 04.

The MT curve parameter analysis for Model 02 indicates 2-D dimensionality. The lateral resistivity distribution aligns with the synthetic model, and the 2-D inversion depth also represents the synthetic model depth. The geometry used in the inversion for Model 02 includes horizontal cell widths of 500 m, an elevation range of 1600 to -2400 masl, padding of 1000 m with a padding factor of 1.5, and vertical cell thickness of 100 m. The inversion parameters used include the entire period range (0.01 to 1000 seconds) and a background resistivity value of 100 Ωm. The MT transfer function used is TM mode, as the geoelectrical strike direction aligns with the magnetic field. Additionally, Model 02 has 2-D dimensionality due to the simple lateral resistivity distribution and geometry.

For Model 03, the 2-D inversion results with a transect perpendicular to the geoelectrical strike up to a period of 0.1 seconds do not accurately represent the conductive anomaly distribution in elevation. In the synthetic model, the conductive anomaly depth is around 2 km from the surface, but the 2-D inversion results are only reliable up to 0.1 seconds, as the 2-D modeling limit is at this period. Therefore, 3-D inversion modeling is needed for more representative results. The geometry used in the inversion for Model 03 includes horizontal cell widths of 500 m, an elevation range of 1600 to -2400 masl, padding of 1000 m with a padding factor of 1.5, and vertical cell thickness of 100 m. The inversion parameters used include the entire period range (0.01 to 0.1 seconds) and a background resistivity value of 100 Ωm. The complex geometry and resistivity distribution influence the dimensionality of the diagonal resistivity contrast.

In Model 04, the 2-D inversion results up to a period of 0.1 seconds show that the lateral resistivity distribution aligns, but the depth of the conductive layer does not match the synthetic model. The synthetic model indicates a depth of 2 km from the surface, but the 2-D inversion results only show a depth of 503 m. The geometry used in the inversion for Model 04 includes horizontal cell widths of 500 m, an elevation range of 1600 to -2400 m, padding of 500 m with a padding factor of 1.5, and vertical cell thickness of 100 m. The inversion parameters used include the entire period range (0.01 to 0.1 seconds) and a background resistivity value of 100 Ωm. The MT transfer function used is TE mode, as the geoelectrical strike direction aligns with the electric field. 3-D inversion modeling is needed for more accurate data modeling, similar to Model 03, where the complex geometry and resistivity distribution influence the dimensionality of the anticline resistivity contrast.

5. CONCLUSION

The research conducted to analyze the MT curve parameters from 3D synthetic MT data concluded that the TE and TM curves separate when crossing the geoelectrical strike, whereas they align when the resistivity values are the same. If the polar diagram is circular, further processing can be done up to 1-D; if elliptical, processing can extend to 2-D; and for a peanut shape, processing can be up to 3-D. If the beta phase tensor value is zero, the dimensionality is 1-D, and if it is more than three, the dimensionality is 3-D. The dimensionality of the polar diagram is closely related to the beta angle in the beta phase tensor. If there is no change in the polar diagram shape, the Phi phase tensor value is homogeneous at each period, and the induction arrow points to the surface, there is no linear zone. However, if the polar diagram shape changes, the Phi value varies at each period, and the induction arrow points towards the conductive layer, a linear zone can be identified. Conductive anomalies are indicated by the direction of the induction arrow pointing towards the conductive layer, and the phase tensor value will be higher than that of other stations with higher resistivity values.

REFERENCES

Abdelzaher M, Nishijima J, Saibi H, El-Qady G, Massoud O, Soliman M, Younis A, Ehara S .: A coastal aquifer study using magnetotelluric and gravity methods in abo Zenema, Egypt. Pure Appl Geophys 169(9), (2012), 1679–1692.

Berdichevsky, M. N.: Models and methods of magnetotellurics. Springer Science & Business Media (2008).

Caldwell, T. G.: The magnetotelluric phase tensor. Geophysical Journal International, 158(2), (2004), 457-469.

Kebede, Y. and Saibi H. : 2-D inversion of magnetotelluric data from Tendaho geothermal field (NE Ethiopia). Int Workshop on Earth Resources Technology, Kyushu University, Fukuoka, Japan, 8–9 December 2016 (2016).

Kerbadj N., Saibi H., A. Bouzid, M.O. Bounif, S. Bougchiche.: 2-D inversion of magnetotelluric data at Dar-Chioukh region (Djelfa, Arab J Geosci (2019) 12: 766 Page 17 of 18 766 Algeria). The 4th international conference on engineering geophysics (ICEG), Al-Ain, UAE, 9–12 October 2017 (2017).

Ledo, J: 2-D versus 3-D magnetotelluric data interpretation. Surveys in Geophysics, 26(5), (2005), 511- 543.

Rodi, W.L. and Mackie, R.L.: Nonlinear Conjugate Gradients Algorithm for 2-D Magnetotelluric Inversion. Geophysics, 66, (2001) ,174-187.

Saibi H, Khorsravi S, Smirnov M, Kebede Y, Gabr A.: 2D inversion of magnetotelluric data from Al-Mubazzarah geothermal area, Al-Ain, United Arab Emirates. European Geosciences Union General Assembly 2018, Vienna, Austria, 8–12 April 2018,(2018).

Simpson, F. & Bahr. K: Practical magnetotellurics. Cambridge University Press.(2005).

Vozoff, K.: The Magnetotelluric Method. In M. N. Nabighian (Ed.), Electromagnetic Methods in Applied Geophysics, 22, (1991), 1943-1961.

Radon Thoron in Fault-Controlled Geothermal Prospect: A Study Case in Sumatra

Fraga Luzmi Fahmi, Jodhi Pramuji Giriarso, Fuad Nur Hussein, and Mulyanto

Pertamina Geothermal Energy, Grha Pertamina, Pertamax Tower 5th floor,
Jl. Medan Merdeka Timur No.11-13 Jakarta, Indonesia

fraga.fahmi@pertamina.com

Keywords: radon, thoron, RAD8, fault-controlled geothermal system, Sumatra

ABSTRACT

Radon-thoron survey was measured using Durridge RAD 8 radon detector of 63 locations in Pertamina Geothermal Energy's geothermal green field site at central region of Sumatra, which is being explored for geothermal prospecting. The object was to determine the geothermal system's permeability based on radon surface anomaly. The study area was located in a major fault of the Sumatra Fault System (SFS), and this geological structure controlled the evidence of surface manifestation, suggesting a fault-controlled geothermal prospect. The sampling distance was 500 m. As a result, anomalies here were scattered along the fault and corresponded mainly with the surface thermal manifestation and granitic rocks at the surface. The results suggested the high anomaly of radon and thoron was related to the heat flow of the system, indicated by the surface manifestation distribution. Another cause isthe granitic rock that is exposed near the surface, may result higher radon emanation. A tectonic graben area covered by paddy soil usually had measured radon levels of near zero because of the slow diffusion of radon in stagnant water. Measurements along the fault zone show variations in radon measurement values that correlate with the appearance of manifestations.

1. INTRODUCTION

Geothermal energy has received much attention as a renewable and sustainable energy source, with the potential to play a critical role in meeting global energy demands and mitigating the consequences of climate change. The assessment of geothermal resources frequently relies on various geological, geophysical, and geochemical indicators, with the detection of naturally occurring noble gases, such as radon (^{222}Rn-222) and thoron, emerging as a valuable tool for evaluating geothermal potential. Radon soil gas investigations have had varying success rates in geothermal exploration (Dyck, 1968; Wollenberg, 1974; Nielson, 1978; Whitehead et al., 1983, Cox, 1980; Whitehead et al., 2007; and Prasetio et al., 2023). Previous study on Sumatra was conducted by Haerudin et al. (2016), located on Way Ratai, one of geothermal prospect in southern part of Sumatra.

2. LOCATION AND GEOLOGICAL SETTING

The study area is a geothermal prospect under exploration phase located along the Sumatra Fault System (Figure 1). According to Sieh and Natawidjaja (2000), this prospect is located on the edge of 1N segment and terminated with 1O segment, a part of 19 segments of Sumatra Fault System (SFS). This fault termination creates a pull-apart basin on the southeast area of the geothermal prospect. The surface manifestation appears along the fault, as hot springs and warm springs. No steam features or fumarole were identified on this prospect. The distribution of the faults follows the pattern of the Sumatra Fault System with NW-SE fault pattern. Previous study by PGE (2016) suggests this prospect as a geothermal fault-controlled system, where the deep-seated fault is controlled the heat flow from the heat source to the surface as a boiling hot spring. The study area is located on the Tertiary volcanic rocks, granite rocks, and sedimentary rocks in southeast area as Quaternary alluvium covering the area of pull-apart basin (PGE, 2016).

3. METHODOLOGY

3.1 Radon and Thoron Measurements for Geothermal Prospecting

Radon is a noble gas that is colorless, odorless, and not easily chemically compounded with other natural nuclides. There are three isotopes of radon in nature, namely ^{219}Rn (Actinon) with a half-life of 4 seconds derived from the Actinium decay series, ^{220}Rn (thoron) with a half-life of 55.6 seconds derived from the ^{232}Thorium decay series and ^{222}Rn with a half-life of 3.824 days. The ^{222}Rn isotope is the decay product of ^{226}Rn in the ^{238}U decay series, decaying by emitting alpha (α) particles. ^{222}Rn detection was widely used as a natural tracer for several applications such as groundwater dynamics studies, surface water and groundwater interaction studies, and fault zone investigation studies in earthquake and geothermal system studies.

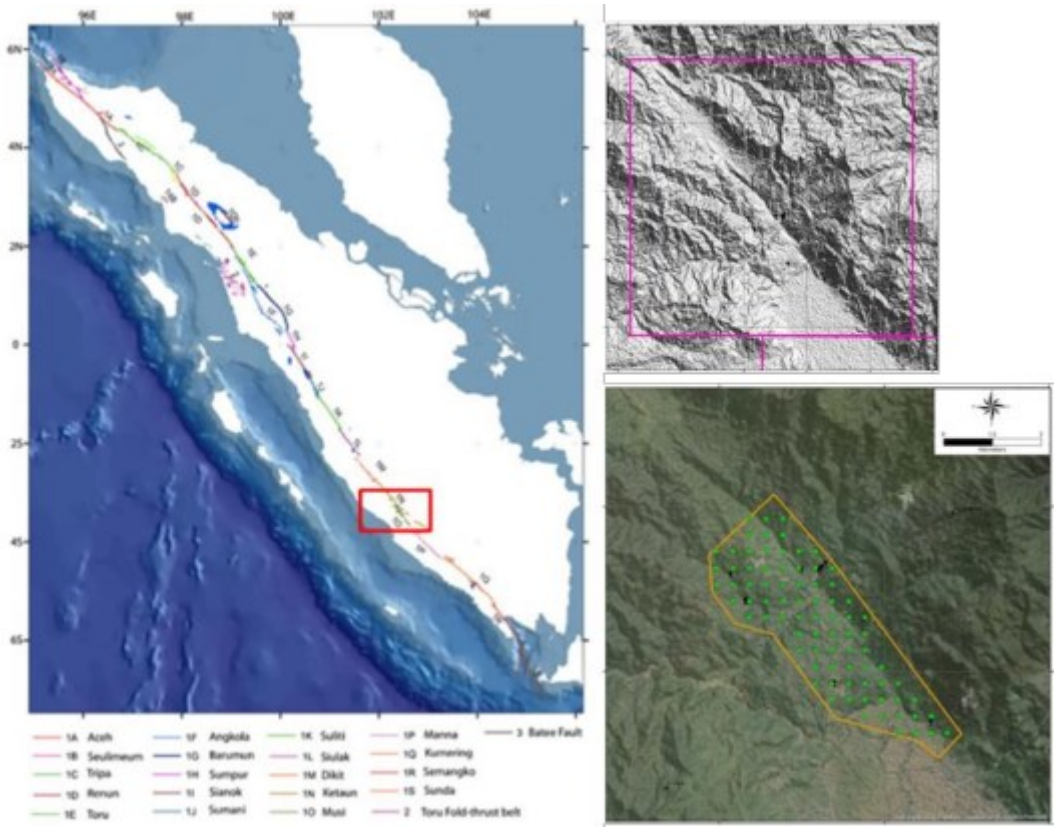

Figure 1: The location of this study related to the Sumatra Fault System (SFS), the picture shows the Sumatra Fault segment from Sieh and Natawidjaja (2000). The green dot lines indicate the distribution of data acquisition along the Sumatra Fault.

Radon can be a useful indicator in geothermal exploration because its presence can signal the indication of permeable zone due to its mobility tendency and its inert property of noble gas. Radon soil gas study allows geothermal geoscientists to locate and delineate fault-controlled geothermal systems. This data is critical for targeting geothermal wells and evaluating the viability of a geothermal resource (Figure 2).

3.2 Field Data Acquisition to Measure Radon and Thoron Soil Gas

The soil gas radon (^{222}Rn) and thoron (^{220}Rn) were measured in the field using Sniff method with a Durridge RAD8 radon detector and a soil gas probe located approximately 60-80 cm below the surface (Figure 3). To reduce air pollution, proper flushing was performed for 5 minutes before and following sampling. The radon (^{222}Rn) and thoron (^{220}Rn) measurements were performed with humidity levels below 10%. Previous study for radon soil gas from many researchers uses RAD7 as radon detector. Since early 2023, Durridge company has released a new version of the radon detector called RAD 8. In this study, Pertamina Geothermal Energy (PGE) was the first user of RAD 8 in Indonesia who apply RAD 8 as a soil gas detector in a geothermal geoscience study. A total of 63 point locations were chosen for radon soil gas measurements with consideration of geological setting and surface thermal manifestation distribution. The field data acquisition was conducted at October to November 2023. The challenges during data acquisition was heavy rainfall, extreme terrain, and heavy vegetation of forestry area.

4. RESULT AND DISCUSSION

4.1 Radon and Thoron Statistics

The soil gas radon (^{222}Rn) and thoron (^{220}Rn) findings were statistically analysed using a probability plot, a technique extensively used in exploratory geochemistry (Reimann et al., 2005; Sinclair, 1974; Ciotoli et al. 2016; and Prasetio et al., 2023). In principle, making a probability graph will determine the normality of the data, which refers to the trend line in the graph. A series of data that deviates from the normal line or has a different trend line is considered an anomaly. Thus, the threshold value can be determined, which is the value that limits the two trend lines in the probability graph. This study determined two thresholds to divide the data into low anomaly, background, and high anomaly.

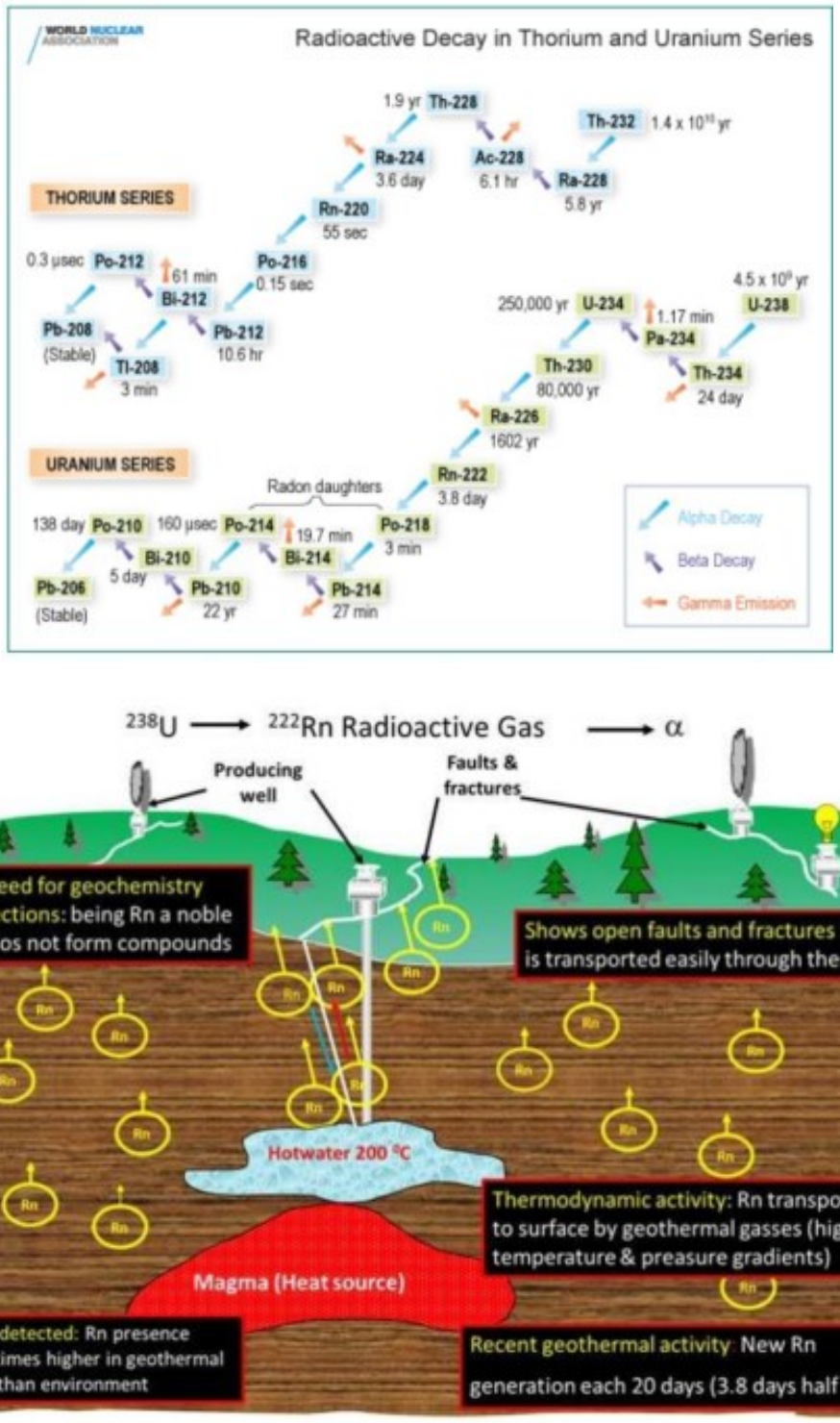

Figure 2: Top: Radioactive decay in Thorium and Uranium series as the source of radon in nature. Bottom: Radon for geothermal. exploration prospecting (Balcazar et al., 2014).

The normal probability plot tool in NCSS 2023 statistical software was used to examine the data. To explain the statistic of radon and thoron statistic, a series of normal probability plot from radon, thoron, and radon + thoron can be viewed from the graph on Figure 4. Radon (^{222}Rn) concentrations of soil gas in the research area range from 15,80 Bq/m3 to 4.132,00 Bq/m^3, with an average of 607,86 Bq/m^3. Thoron (^{220}Rn) concentrations of soil gas in the research area range from 20,00 Bq/m^3 to 16.180,00 Bq/m^3, with an average of 3.331,21 Bq/m^3. Radon + thoron values range from 122,00 Bq/m^3 to 18.480,00 Bq/m^3, with an average of 3.741,84 Bq/m^3 (Table 1). Geothermal and volcanic sites typically have values ranging from 1.500 to 250.000 Bq/m^3 (Inguaggiato et al., 2000; Bonforte et al., 2013; Mismanos and Vasquez, 2015).

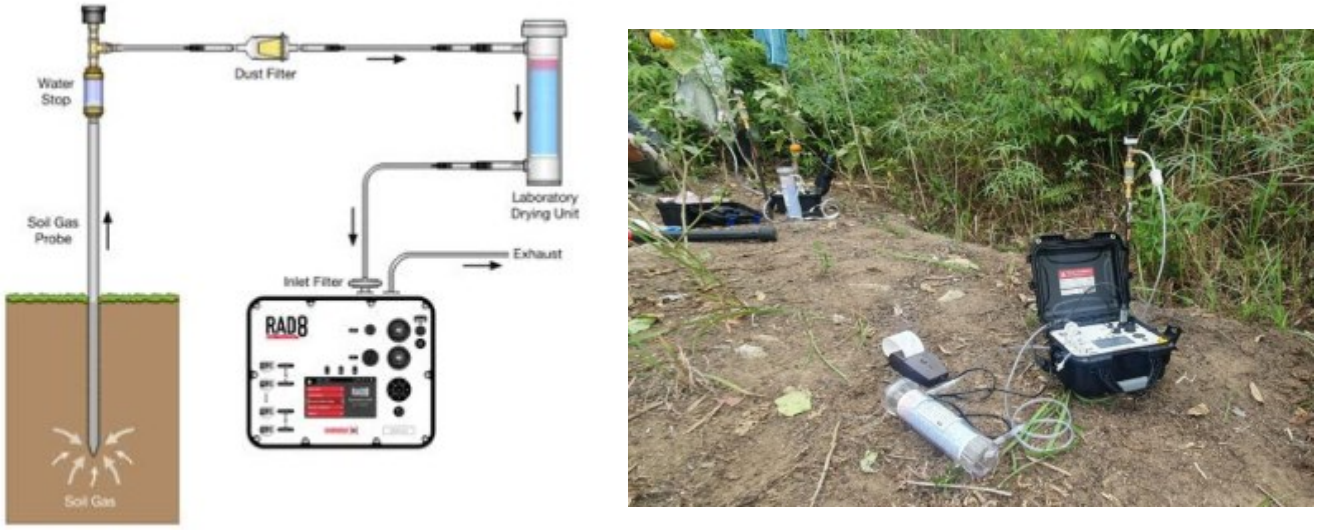

Figure 3: Soil gas probe and Rad8 radon detector configuration for field data acquisition (left), Rad8 during operation (right).

Table 1: The main statistics of soil gas data of radon, thoron, and radon + thoron (Bq/m^3).

Count of Data Samples	Soil Gas Data	Mean	Standard Deviation	Standard Error	Minimum	Maximum	Range
63	radon (Bq/m^3)	607,86	769,24	96,92	15,80	4.132,00	4.116,20
63	thoron (Bq/m^3)	3.331,21	3.226,59	406,51	20,00	16.180,00	16.160,00
63	radon + thoron (Bq/m^3)	3.939,07	3.741,84	471,43	122,00	18.480,00	18.358,00

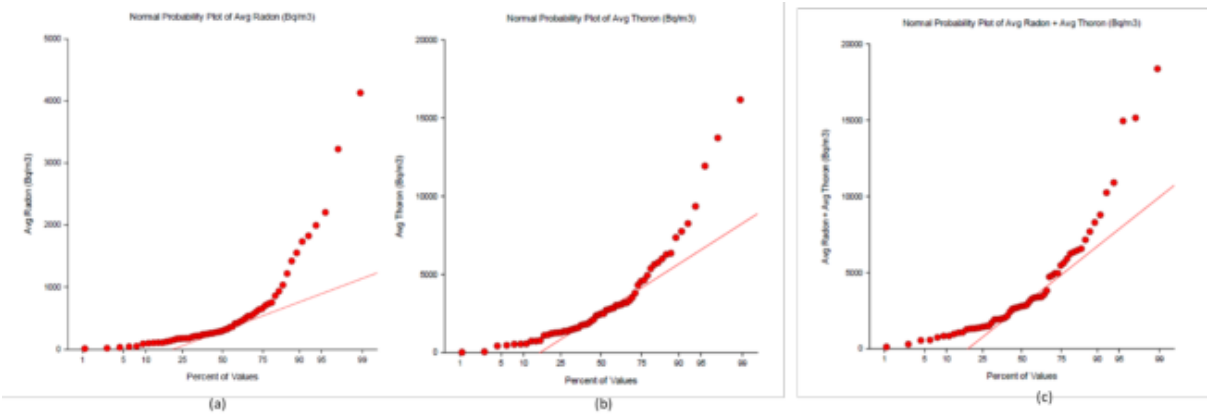

Figure 4: The graph of normal probability plot of radon (a), thoron (b), radon + thoron (c).

4.2 Distribution Maps of Radon and Thoron

The distribution map or contour of soil gas concentration was created to analyze the vicinity of high soil gas concentration to fault structures using Kriging interpolation to assess the lateral distribution of radon (^{222}Rn) and thoron (^{220}Rn) soil in the research region, which was then mapped over existing structures, which was done by Surfer and ArcGIS software (Figure 5, Figure 6, Figure 7). The structural geology data was derived from a previous study conducted by PGE (2016).

Site locations with radon (^{222}Rn) and thoron (^{220}Rn) background values were found in the central, south, and northwest area, despite the presence of major fault structures (Sumatra Fault System) along the northwest to southeast. High and anomalous values were primarily identified in the north-northeast and southeast of the research area, which is located around the AP and BR hot spring complex. Based on the lateral distribution of radon, thoron, and radon + thoron, all show generally similar patterns. The occurrence of a lateral distribution of high radon values is more widespread in the north-north-east area than the lateral distribution of thoron values, although in terms of measured values thoron is higher than radon. From the distribution of the anomaly map, it

can also be concluded that radon and thoron anomaly values do not show the same high values along the Sumatra Fault System, as seen from the low radon and thoron emanation values from measurements in the central area. High values of radon (> 2.000 Bq/m^3) and thoron (> 10.500 Bq/m^3) do not always correlate with the appearance of geothermal manifestations. From the maps in Figure 5, Figure 6, and Figure 7, it can be identified that radon values around the K2 & K3 hot spring and AK warm spring, as well as L warm spring show insignificant radon and thoron values. The surface geology data and geothermal conceptual model in Figure 8 may correlate with the radon and thoron distribution data, where high radon and thoron values are found in locations around hot springs and granitic rock outcrops at the surface. These granitic rock outcrops on the surface follow the pattern of high radon and thoron, it can also be correlated that radon and thoron may indicate heat flow from fault-controlled geothermal systems. High radon and thoron values appear around the upflow zone following with the appearance of boiling hot springs and neutral chloride water. The low radon and thoron values in the south-southeast area may correlate with the surface rock type of moist paddy soil. Many researchers have concluded that radon values are low if the measurement location is on a water-saturated soil surface because the presence of shallow water on the surface can block radon readings on surface radon detectors. The radon and thoron distribution pattern at the surface was modeled using Leapfrog software with the same cross-section direction as the geological model (NE-SW), which is perpendicular to the Sumatra Fault System (SFS) pattern (Figure 9).

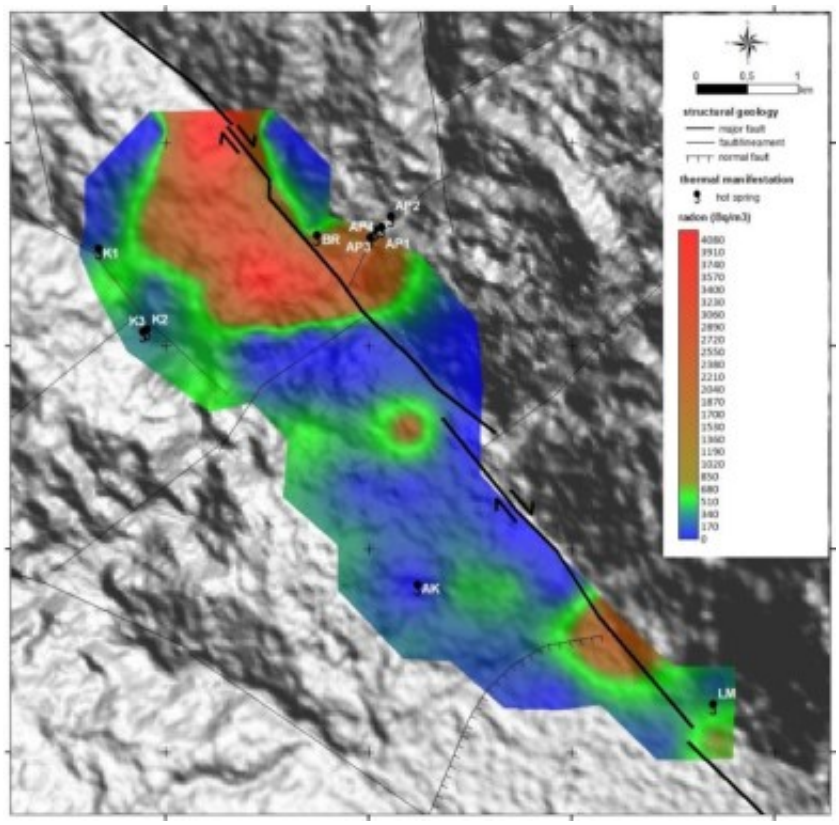

Figure 5: Anomaly map of radon.

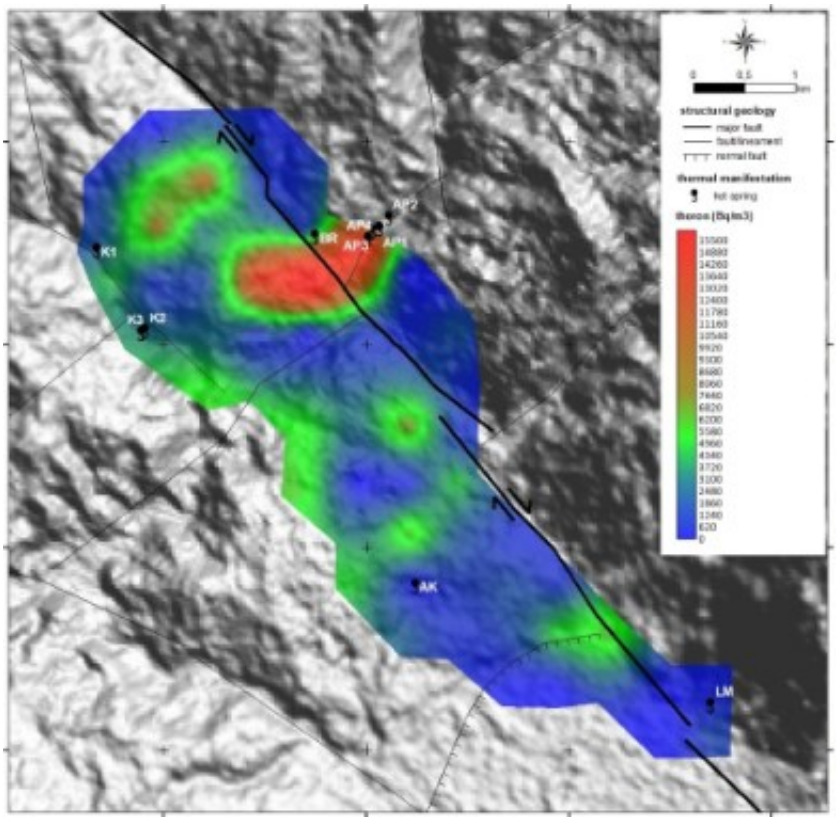

Figure 6: Anomaly map of thoron.

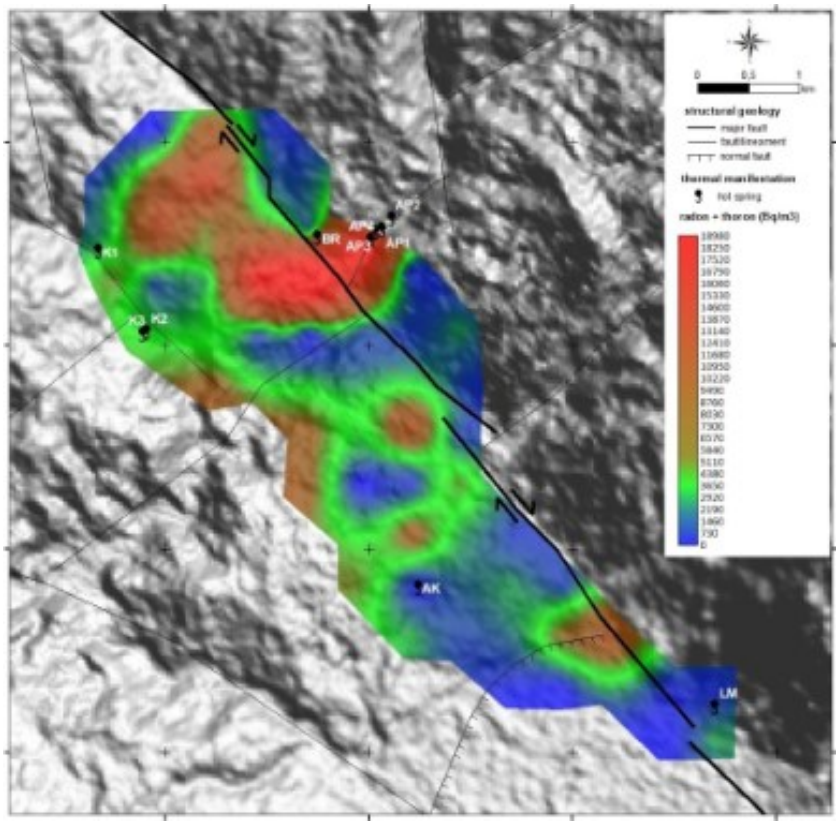

Figure 7: Anomaly map of radon+thoron.

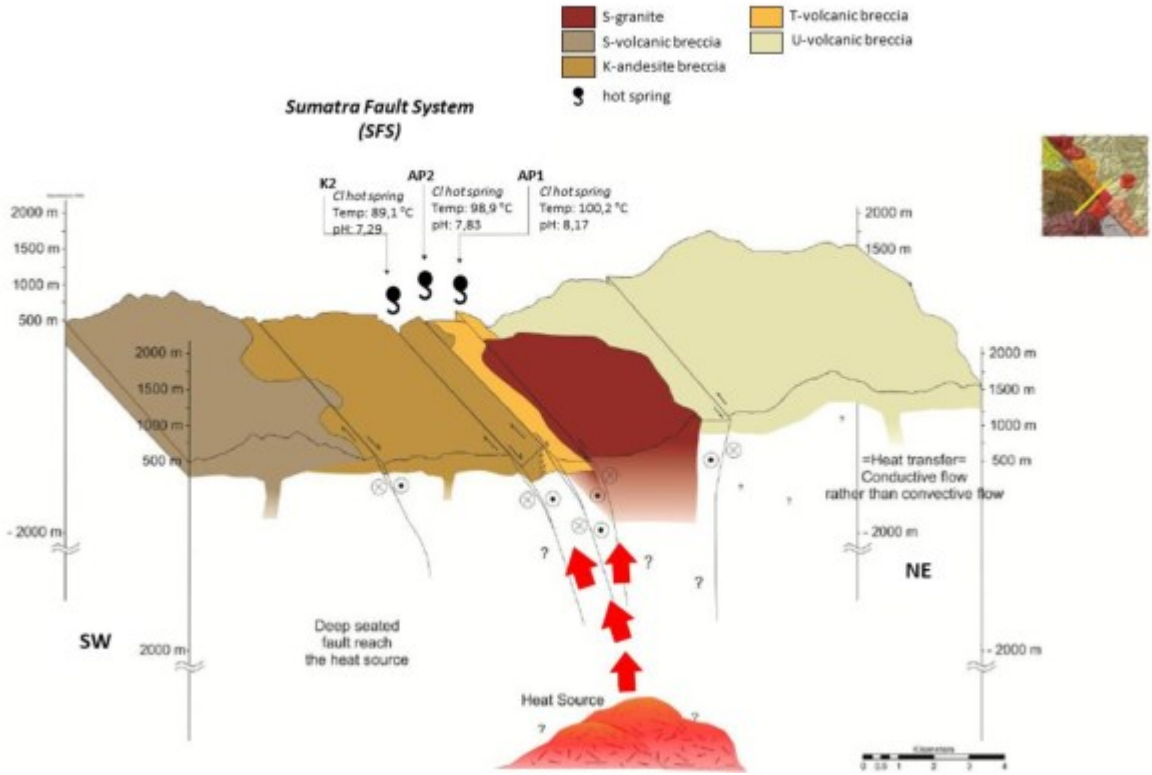

Figure 8: 3D-geological cross section and geothermal conceptual model of study area (modified from PGE, 2016).

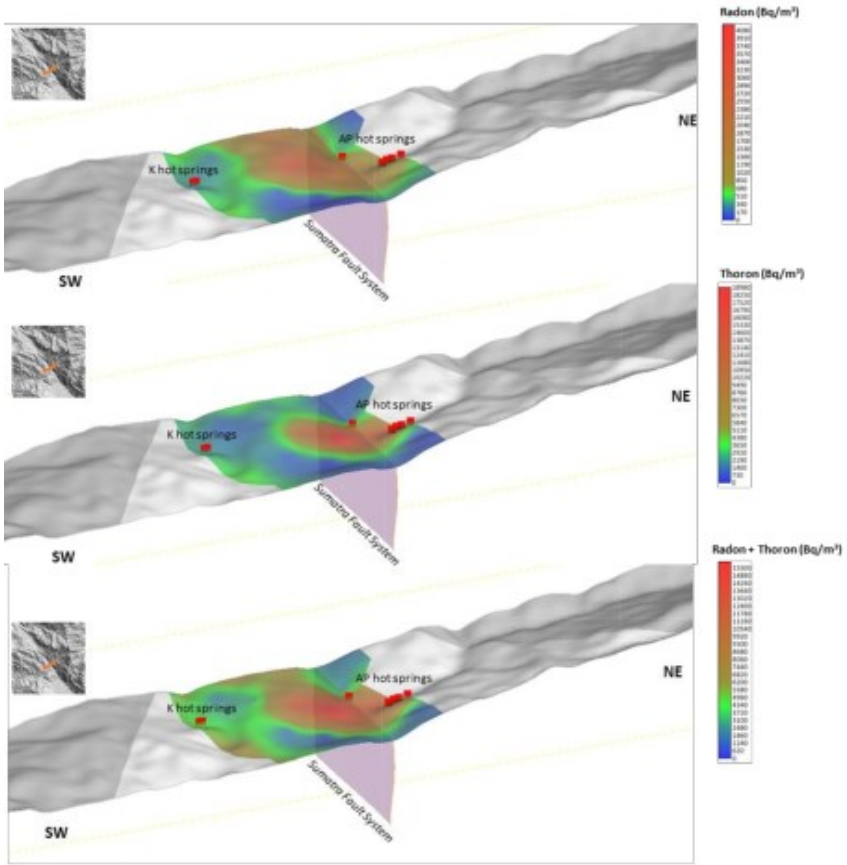

Figure 9: radon, thoron, and radon+thoron anomaly map cross section with terrain model. The cross sections (NE-SW) are perpendicular to Sumatra Fault orientation (NW-SE fault pattern).

5. CONCLUSION

The soil gas of radon (^{222}Rn) and thoron (^{220}Rn) and thoron distribution in this study area showed high concentration in the northern to northeastern of study area, which related to some fault segments of Sumatra Fault Sytem and appearance of natural boiling hot spring and chloride water, which represents as upflow zone of this geothermal system. The high values of radon also correlate with the lithological distribution of granitic rock in the surface, while the low radon and thoron values in the south-southeast area may correlate with the surface rock type of moist paddy soil.

ACKNOWLEDGEMENTS

The authors would like to express gratitude to our colleagues in Pertamina Geothermal Energy (PGE)'s exploration geoscience team who provided assistance during field and laboratory works. The authors want to thank to the management of PGE for supporting and allowing this study to be published.

REFERENCES

Balcazar, M., Lopez, A., Flores, M., and Marciano H., Natural Radiation Contribution to Renewable Energy Searching, Proceedings of the XIV International Symposium on Solid State Dosimetry, (2014), p. 1035-1063

Bonforte, A., Federico, C., Giammanco, S., Guglielmino, F., Liuzzo, M., Neri, M.: Soil gases and SAR measurements reveal hidden faults on the sliding flank of Mt. Etna (Italy). Journal of Volcanolology and Geothermal Research 251, (2013) 27–40

Ciotoli, G., Alessandra, S., Livio, R., Aldo, A., Sabina, B.: Soil gas geochemical behaviour across buried and exposed faults during the 24 August 2016 central Italy earthquake. Annals of Geophysics 59 (2016).

Cox, M.E.: Ground Radon Survey of a Geothermal area in Hawaii, Geophysical Research Letters, 7, (1980), 283-286.

Dyck, W; Radon-222 emanations from a Uranium deposit; Economic Geology, 63, (1968), No.3

Haerudin, N., Karyanto, dan Kuntoro, Y.: Radon and thoron mapping to delineate the local-fault tn the Way Ratai Geothermal Field, Lampung, Indonesia. ARPN Journal of Engineering and Applied Sciences, vol. 11 (7), (2016) pg. 4804-4809

Hernandez, P., Prerez, N., Salazar, J., Sato, M., Notsu, K., Wakita, H.: Soil gas CO2, CH4, and H2 distribution in and around Las Canadas caldera, Tenerife, Canary Islands, Spain. Journal of Volcanology and Geothermal Research. 103, (2000), 425–438.

Inguaggiato, S., Pecoraino, G., D'Amore, F.: Chemical and isotopical characterisation of fluid manifestations of Ischia Island (Italy). Journal of Volcanology and Geothermal Research. 99, (2000) 151–178

Lombardi, S., Voltattorni, N.: Rn, He and CO2 soil gas geochemistry for the study of active and inactive faults. Applied Geochemistry25, (2010) 1206–1220

Mismanos, J.W., Vasquez, A.A.: Scouting for permeable structures in geothermal systems using soil gas radon. Proceedings World Geothermal Congress, (2015).

Nielson, D.L; Radon emanometry as a geothermal exploration technique. Theory and an example from Roosevelt Hot Springs KGRA, Utah. University of Utah, Research Institute Report ESL-14, (1978) 31 p

Prasetio, R., Hutabarat, J., Daud Y., Hendarmawan: Distribution of 222Rn and CO2 across faults and its origin in Wayang Windu geothermal area, West Java – Indonesia, Geothermics 110, (2023), 102691

PGE: The Study of Structural Geology of "X" Prospect Area, internal report, not published, (2016)

Reimann, C., Filzmoser, P., Garrett, R. G.: Background and threshold: critical comparison of methods of determination. Sci. Total Environ. 346, (2005). 1–16.

Sieh, K. and Natawidjaja D.: Neotectonics of the Sumatran fault, Indonesia, Journal of Geophysical Research, 105, (2000) pp.28295-28326

Sinclair, A.J., Selection of Threshold Values in Geochemical Data Using Probability Graphs. Journal of Geochemical Exploration, 3, (1974), 129–149.

Voltattorni, N., Sciarra, A., Quattrocchi, F.: The application of soil gas technique to geothermal exploration: study of "hidden" potential geothermal systems. Proceedings World Geothermal Congress 2010, (2010) pp. 1–7.

Whitehead, N.E., Gingrich, J.E., and Fischer, J.L.: A New Zealand test of the Track-Etch Method of Prospecting for Geothermal Steam, Journal of Volcanology and Geothermal Research,15, (1983), p.339-354

Whitehead N.E., Barry, B.J., Ditchburn, R.G. Morris, C.J., Stewart, M.K.: Systematics of radon at the Wairakei geothermal region, New Zealand, Journal of Environmental Radioactivity 92, (2007), 16-29

Wollenberg, H.A.: Radon alpha-track survey of a potential geothermal resource area; Lawrence Berkley Laboratory Report, (1974) LBL- 3225 P14

The Implications of Mineral Geothermometer, Geochemistry, and Pressure Temperature on Scaling in the Two-Phase Fluid Well, Dieng Geothermal System

Iqbal Maratama, Rizkhy Ridoh A, Siti Olivinia Yusra, Rudy Martikno,
Randy Wijaya Atmaja, and Denis Daya Pamungkas

PT Geo Dipa Energi, Jl. Akses Tol Soroja,
Blok Sumakamanah Parungserab, No.22, Parungserab, Soreang, Bandung

iqbalmrtm@gmail.com

Keywords: scaling, geothermometer, geochemistry, Dieng

ABSTRACT

Scaling is a mineral or mineral combination that forms and precipitates in response to pH, pressure, and temperature changes. Scaling is one of the challenges in the geothermal industry, particularly in medium enthalpy geothermal systems with high silica content, such as Dieng. This situation becomes disruptive when minerals deposit in brine pipeline and injection wellbores, reducing the flow rate of the fluid. To prevent scaling, it is crucial to understand mineral geothermometers, geochemistry, and pressure temperature in well and surface facilities.

This case study goes over the appearance of scaling in well testing activities. This data from well testing activity is essential as a key to understanding the development of scaling before the well is generated and hooked in to the power plant. The data came up from Well Testing activity, PTS survey, TFT and XRD analysis of scaling samples. It's interesting to note that when WT is conducted, the stuffs formed in the borehole and well testing facilities. Based on Well Testing Activity, the well can generate a total mass flow of approximately 136 kg/s at an enthalpy of roughly 1470 kJ/kg at WHP 45 bara. The liquid level was measured during the PT shut-in survey, which somewhat is located at 500 mASL. Based on the geochemistry data, geothermometer, and SSI analysis were obtained to gain a more comprehensive result to analyze potential scaling issues, as there are scaling issues when the well is flowing. Scaling in the research area typically takes the form of silica, metal sulfides, and so on.

The objective of this research is to investigate the influence of the mineral geothermometer, fluid geochemistry, and PT on scaling deposition in geothermal fields with high enthalpy characterization in two-phase fluid well. It is hoped that the findings of this study will help to identify scaling depositional characteristics and locations related to solution solubility and saturation. Further research is required to overcome or reduce the formation of scaling by modifying the level of pressure and other changes to the well testing facility in the well.

1. INTRODUCTION

Located on the Dieng Plateau in Central Java, Indonesia, the Dieng geothermal field stands as a testament to the region's unique geological characteristics and renewable energy potential. Nestled amidst the volcanic complex of the Dieng Plateau, this field boasts a diverse array of geothermal features owing to its location within the volcanic arc of the Sunda-Banda magmatic arc. Sileri, one of the areas in Dieng, for instance, governs and hosts the two phase-liquid dominated reservoir with neutral fluid as it marked by presence of high chloride and silica concentration. Chloride content is ranging from 8000 to 24000 ppm and silica content from 600 to 1300 ppm, respectively. The first Commercial Operation Date (COD) for Dieng Unit-1 was in 2002 with 1x60 MW installed capacity. Right now, the power plant had produced less electricity than the initial capacity because one of the problems is scaling.

In 2020, GDE started to develop the second power plant unit for Dieng Field. The development program of Dieng Unit 2 aims to obtain capacity of approximately 55 MWe plus 10% steam buffer. After drilling, production well need to be tested. This paper will be focused in one of the well that tested in development program of Dieng Unit 2, Well 1. Well 1 is production well that already drilled in Sileri area. One of the issues in well testing activity in Dieng is about scaling related in wellbore or well testing equipment. This case study goes over the appearance of scaling in well testing activities. This data from well testing activity is essential as a key to understanding the development of scaling before the well is generated and hooked in to the power plant.

The research framework of this study begins with an overview of the Dieng geothermal area, highlighting its geological characteristics and the prevalent types of scaling, such as halite, sylvine, and amorphous silica. The next phase involves conducting detailed analyses, including geothermometer to assess subsurface temperatures, geochemical analysis to determine the composition of geothermal fluids, and pressure-temperature profiling to

understand the dynamic conditions within the wellbore. These analyses provide a comprehensive understanding of the scaling processes and the conditions that favor their formation. The final phase of the study focuses on evaluating and implementing anti-scaling and descaling methods, such as high-pressure separation and chemical injections of inhibitors or acids, to develop effective strategies for preventing scaling in the Dieng geothermal wells and surface facilities. This holistic approach aims to enhance the efficiency and longevity of geothermal operations in the Dieng area.

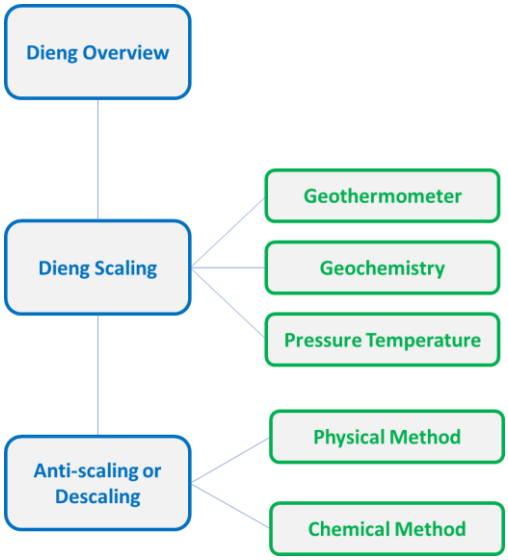

Figure 1: The research framework of this study.

2. DIENG SCALING TYPE

2.1 Overall Scaling Dieng

Scaling is a mineral or mineral combination that forms and precipitates in response to pH, pressure, and temperature changes. Scaling is one of the challenges in the geothermal industry, particularly in medium enthalpy geothermal systems with high silica content, such as Dieng. This situation becomes disruptive when minerals deposit in brine pipeline and injection wellbores, reducing the flow rate of the fluid. To prevent scaling, it is crucial to understand mineral geothermometers, geochemistry, and pressure temperature in well and surface facilities. In Dieng, scaling can form from wellbore until turbine. While well testing activity, scaling still found even the activity still in a short time. Some of mineral scaling already found in Dieng such as silica, metal sulfide, halite, calcite, and etc.

2.2 Scaling in the Well Testing Activity

The scaling process in geothermal wells can have significant implications for the effectiveness and efficiency of well testing activities. In a recent well testing conducted in a new geothermal well, scaling was found in various equipment used during well testing, such as in pipelines, mist pads in the LECM, and potential on the wellbore itself. The presence of scaling in the wellbore was identified by running a sample catcher in the hole to obtain scaling samples, which were then tested using X-ray diffraction (XRD) to determine the type of scaling present. This information is crucial for understanding the potential scaling issues that may arise in the future in the Dieng geothermal field, allowing for better mitigation strategies to be implemented to maintain the integrity and efficiency of geothermal well testing activities. By identifying and analyzing scaling in geothermal wells, GDE can proactively address scaling-related challenges and optimize the performance of geothermal wells in the long term.

3. GEOCHEMISTRY AND WELL TESTING RESULT

3.1 Geothermometer

From the Na-K-Mg geothermometer to determine the geothermal temperature in the Dieng Geothermal field, revealing a calculated temperature of approximately 340°C. However, it was noted that this temperature was higher than the actual temperature recorded in boreholes, which typically averaged around 304°C. This discrepancy raised questions about the accuracy of the geothermometer and the factors that could potentially influence the results.

One possible explanation for the higher temperature readings could be attributed to the presence of fluids with differing chemical compositions within the geothermal reservoir. These variations in fluid chemistry can affect the equilibrium between the geothermal minerals and the fluids, leading to deviations in temperature estimates. Additionally, the complexity of the geological structure and fluid flow dynamics in the Dieng Geothermal field could also play a role in influencing the temperature calculations.

Geothermometers estimate subsurface temperatures by analyzing the equilibrium state of minerals dissolved in geothermal fluids. Higher temperatures indicated by geothermometers suggest that the geothermal fluids have equilibrated at significant depths where temperatures are higher. As fluids ascend to the surface or shallower depths, they cool, leading to changes in mineral solubility. As the fluid cools, these minerals can precipitate out, forming scale in wellbores, pipelines, and surface equipment.

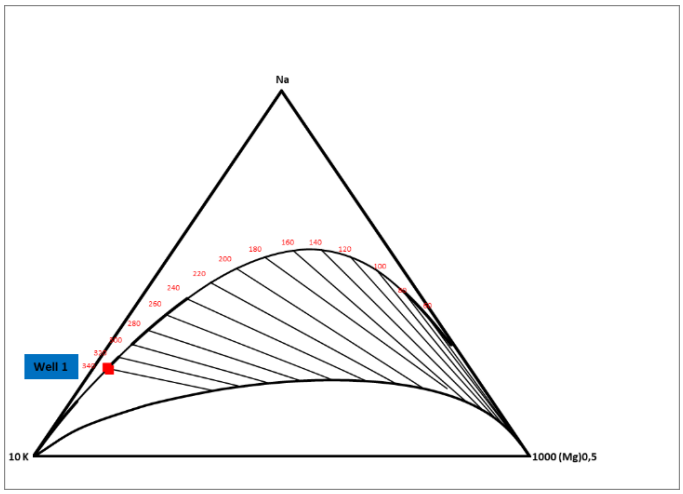

Figure 2: Na-K-Mg Ternary Diagram of the study area to estimate the temperature of reservoir fluids.

3.2 Geochemistry

Geochemistry analysis of reservoir fluid from Well 1 has revealed interesting findings. The first sampling showed that the fluid was still influenced by drilling fluids, with a high nitrogen/argon chemistry content. This is likely due to the use of aerated drilling fluid that incorporates air from the atmosphere during the drilling process. The presence of these gases indicates that the reservoir fluid may still be in contact with the drilling fluids, which could impact the overall geochemical composition of the fluid.

However, subsequent samplings at different times have yielded more promising results. The second and third sampling data show that the reservoir fluid has transitioned to a composition more characteristic of natural reservoir gases. The geochemical analysis suggests that the fluid is no longer heavily influenced by the drilling fluids, indicating that the reservoir gases are now the dominant component. This shift in composition is a positive sign, as it suggests that the reservoir fluid is evolving towards a more stable and natural equilibrium.

The analysis of the geochemical results from the reservoir fluid in the well 1 highlights the dynamic nature of fluid composition in a production well. The initial influence of drilling fluids has given way to a more natural reservoir gas composition over time. This evolution in composition is crucial for understanding the behavior of the reservoir and optimizing production strategies.

During the well testing activity at Well 1, geochemistry fluid sampling revealed a high Chloride content in the geothermal fluid. This elevated Chloride content poses a significant risk for scaling potential within the geothermal pipelines and injection wells. Chloride ions in high concentrations can react with minerals and metals present in the geothermal fluid, leading to the formation of scale deposits. These scale deposits can cause corrosion and blockages within the pipelines and injection wells, decreasing the efficiency of the geothermal system. In order to mitigate the scaling potential associated with high Chloride content in geothermal fluids, proper monitoring and treatment procedures must be implemented. Regular testing and analysis of the fluid chemistry, along with the use of scale inhibitors and corrosion inhibitors, can help prevent scaling issues and ensure the longevity and effectiveness of the geothermal infrastructure.

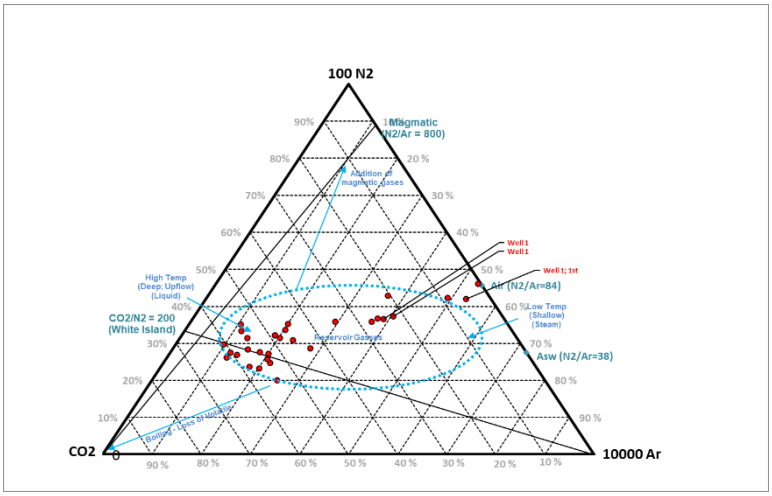

Figure 3: N2-CO2-Ar Ternary Diagram to explain gas chemistry.

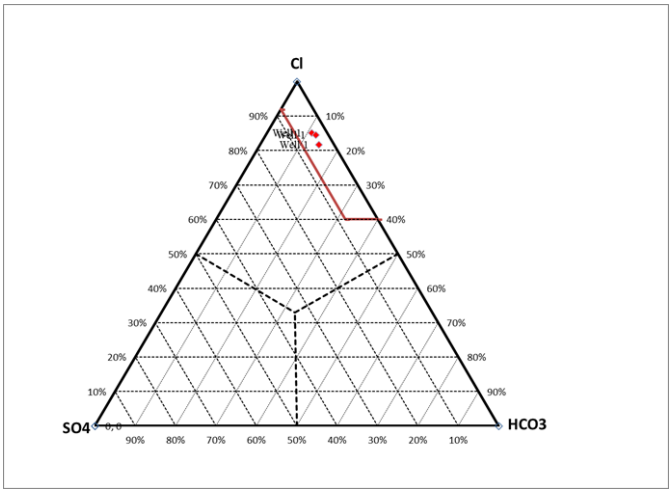

Figure 4: Cl-SO4-HCO3 Ternary Diagram about fluid chemistry.

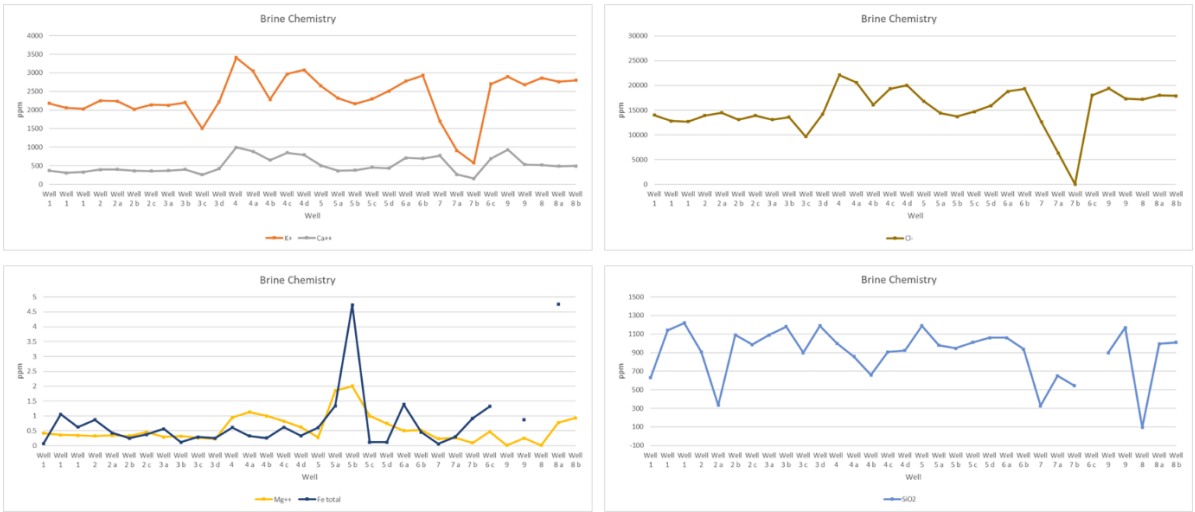

Figure 5: Brine chemistry of well 1 and existing wells.

The chemistry of geothermal brine plays a crucial role in determining the scaling potential within a geothermal well, with specific ions like potassium (K), calcium (Ca), chloride (Cl), magnesium (Mg), iron (Fe), and particularly silica (SiO2) being key indicators. In the case of the research well (Well 1), the SiO2 concentration is notably high, around 1200 ppm, while the concentrations of other ions such as K, Ca, Cl, Mg, and Fe remain consistent with those found in existing wells. This elevated silica concentration significantly increases the risk of silica scaling, which is one of the most common and problematic types of scaling in geothermal systems.

Silica tends to precipitate as the geothermal fluid cools during its ascent from the reservoir to the surface, especially when its concentration exceeds the solubility limit. In Well 1, the high SiO2 concentration suggests that silica scaling could occur in areas where there is a significant temperature drop, such as within the wellbore, in surface pipelines, or in heat exchangers. The scaling is likely to form as amorphous silica deposits, which can obstruct fluid flow and reduce the efficiency of geothermal operations. Although the other brine chemistry parameters are similar to those in existing wells, indicating a stable chemical environment for minerals like calcium carbonate or iron oxide, the unique challenge in Well 1 is the management of silica scaling.

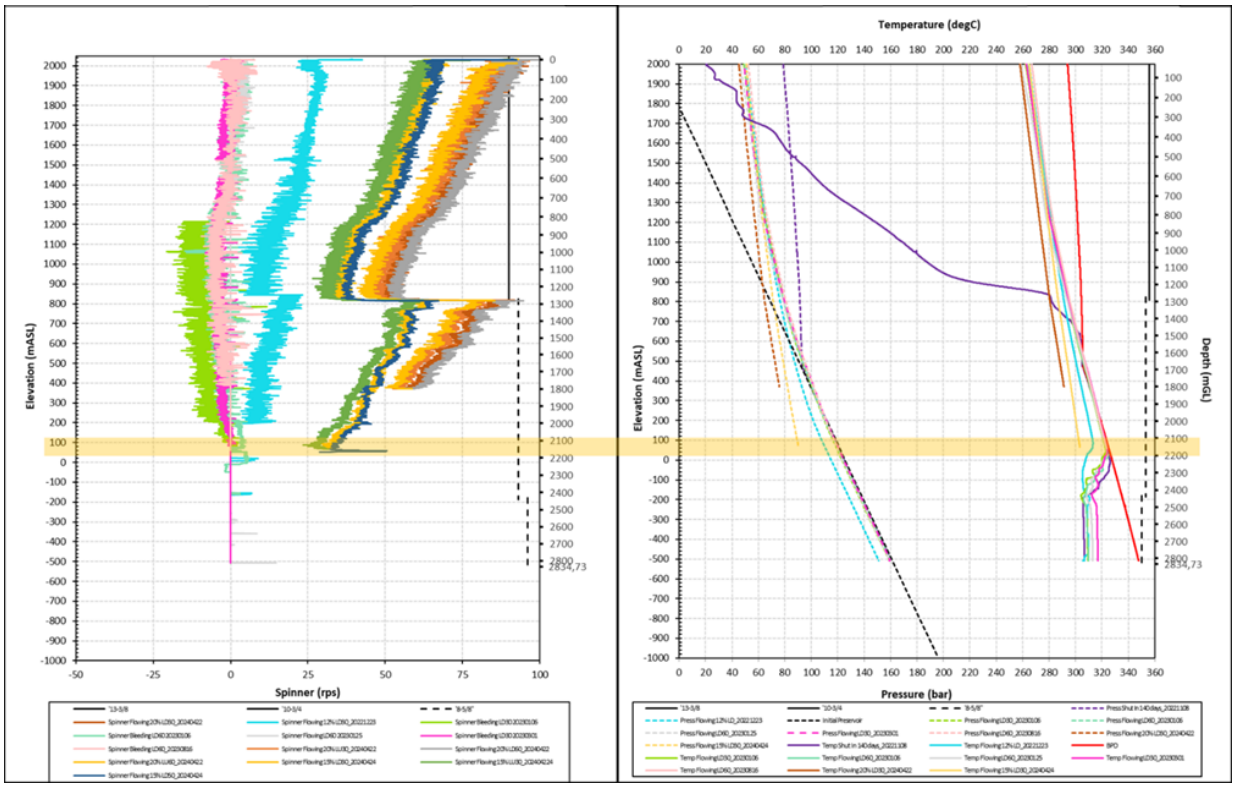

Figure 6: Pressure-Temperature-Spinner survey in the well 1.

3.3 Pressure-Temperature

A Pressure Temperature Spinner (PTS) survey conducted during bleeding and flowing in Well 1 revealed significant insights into the reservoir's behavior. The PTS surveys were performed at four different surveys to monitor the inflow and outflow feed zones within the reservoir section. The flashing point was identified at approximately 2157-2161 meters below ground level (mGL) or 65 meters above sea level (mASL), indicating a crucial zone where the pressure drops significantly enough for the liquid to vaporize. Temperature readings from the survey showed values higher than those recorded during the 140-day heating up period, suggesting increased thermal activity in the reservoir or well already in the stable condition.

Throughout the PTS surveys, a consistent issue was noted where the spinner readings were lost around 2000-2100 mGL. This anomaly occurred in every survey, indicating a potential obstruction or consistent interference at that depth. Additionally, scale samples were found on the spinner blades during each survey, which could be contributing to the spinner reading losses. These findings emphasize the need for further investigation into the cause of the obstructions and the thermal dynamics within the identified flashing point and feed zones. Based on Well Testing Activity, the well can generate a total mass flow of approximately 136 kg/s at an enthalpy of roughly 1470 kJ/kg at WHP 45 bara. The liquid level was measured during the PT shut-in survey, which somewhat is located at 500 mASL.

The flashing point in geothermal wells, where the geothermal fluid undergoes a phase change from liquid to vapor due to a drop in pressure, plays a crucial role in determining the scaling potential. As the pressure decreases and the temperature drops during the ascent of the fluid, especially near the flashing point, the solubility of dissolved minerals such as silica and calcium carbonate significantly decreases. This rapid change in conditions leads to the precipitation of these minerals, forming scale on the wellbore walls, pipelines, and surface equipment. The location and intensity of scaling are directly influenced by the pressure and temperature changes near the flashing point, making it a critical factor to monitor and manage in geothermal operations.

4. SCALING IN THE WELL TESTING EQUIPMENT

During well testing in Well 1, significant scaling was found in various pieces of equipment, which has implications for the operation and efficiency of the well. In the pipe flow line, scaling was discovered, indicating a buildup of mineral deposits that could potentially restrict fluid flow and reduce the efficiency of the well testing result. Amorphous silica scaling was also identified in the mist pad of the LECM. This is a critical issue because the mist pad is essential for preventing brine carryover, which can lead to operational inefficiencies and potential equipment damage. The presence of scaling on the mist pad compromises its ability to function correctly, reducing the overall efficiency of the LECM and posing a risk to the integrity of the entire system. Addressing this scaling is crucial to ensure the LECM operates effectively and prevents brine from contaminating other parts of the system.

Amorphous silica scaling occurs when dissolved silica in geothermal fluids precipitates out of solution, forming hard deposits. This process typically happens as the geothermal fluid cools and loses pressure, causing the solubility of silica to decrease. The chemical element involved in this scaling is silicon (Si), which combines with oxygen (O) to form silicon dioxide (SiO_2). Environments prone to amorphous silica scaling include well testing equipment where rapid temperature and pressure changes occur, such as LECM.

Additionally, scaling was found during Pressure Temperature Spinner (PTS) logging within the wellbore. The spinner was unable to spin properly due to scaling deposits, leading to inaccurate measurements and potential operational issues. A sample catcher was used to collect samples from the wellbore, confirming the presence of scaling. This scaling not only affects the accuracy of PTS surveys but also poses a risk to the longevity and functionality of the wellbore equipment. Regular descaling and monitoring are necessary to ensure accurate data collection and maintain the integrity of the well.

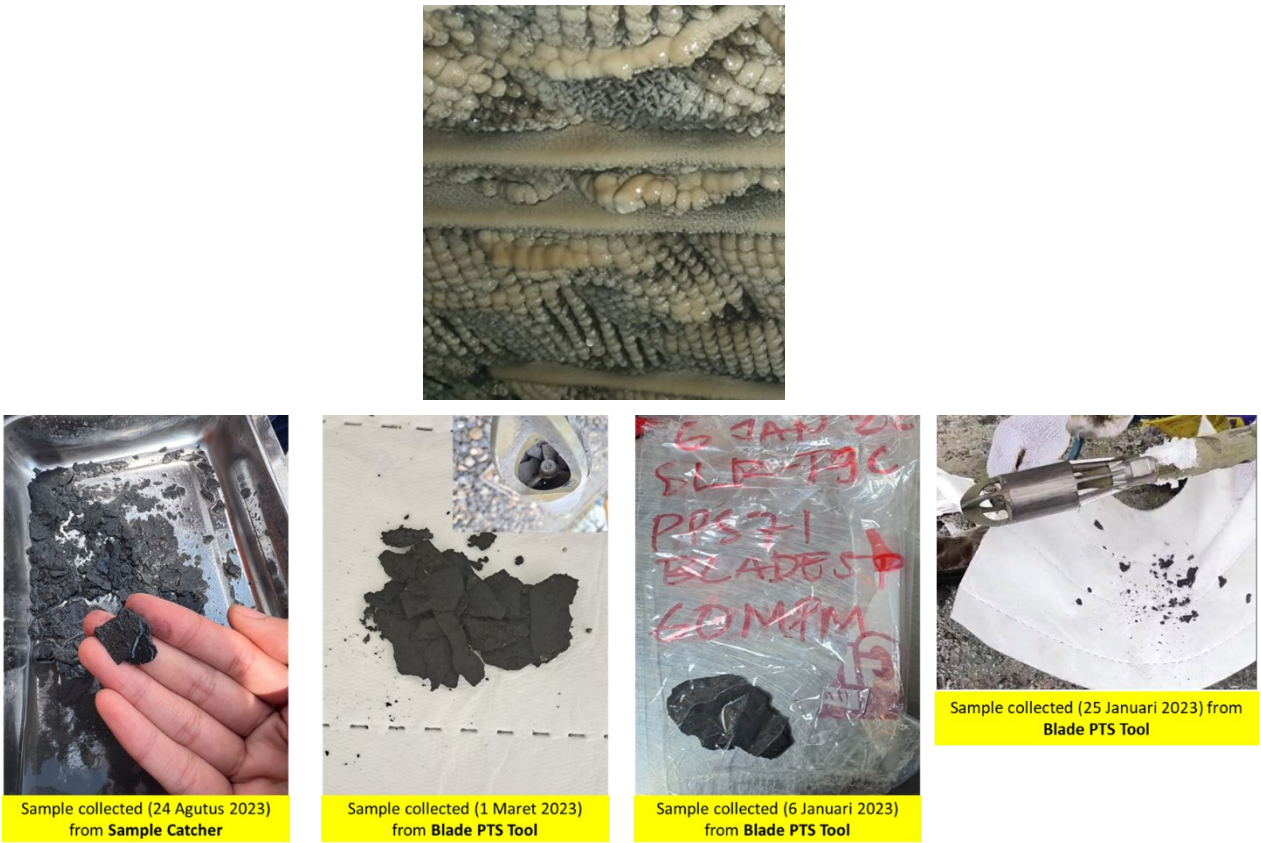

Figure 7: Scaling in the LECM (top pict), sample from sample catcher and blade PTS (bottom pict).

Data from Well 1 indicate that silica scaling index (SSI) issues occurred at temperatures below 200 degrees Celsius. Even with separation occurring at 21.2 bara, the conditions remain below the threshold for preventing silica scaling. This suggests that the thermal and pressure conditions within Well 1 are conducive to silica deposition, which can lead to significant operational challenges. The findings highlight the critical need to monitor and adjust these parameters to minimize the risk of scaling and ensure the well operates efficiently.

Furthermore, analysis of the LECM brine output and sampling conditions supports the presence of scaling. The brine, when plotted on a scaling potential graphic, consistently falls within the scaling zone. This indicates that despite separation efforts, the conditions within the LECM are still favorable for scale formation. The correlation between the low temperature and high-pressure environment and the observed scaling underscores the importance of implementing mitigation strategies.

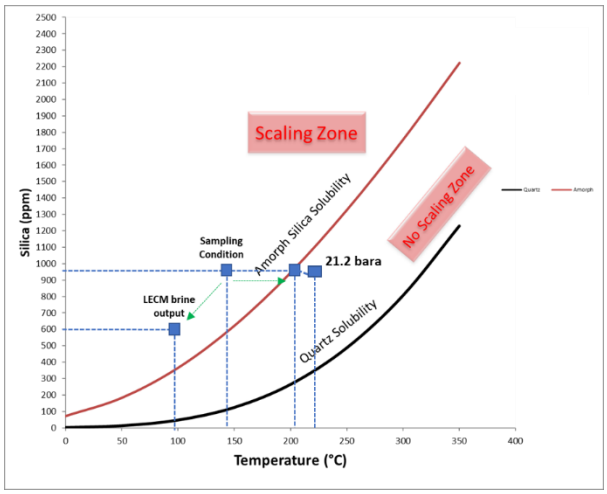

Figure 8: Silica-Temperature graphic related with scaling - no scaling zone.

XRD Analysis

XRD analysis of the scaling sample from the well 1 in the Dieng area revealed the presence of three primary minerals: halite, sylvine, and magnetite. Halite, or sodium chloride (NaCl), is commonly formed in geothermal wells due to the evaporation of saline water. As the geothermal fluid ascends and experiences pressure and temperature changes, the dissolved salts precipitate, leading to the formation of halite scales. These scales can obstruct fluid flow and reduce the efficiency of the well.

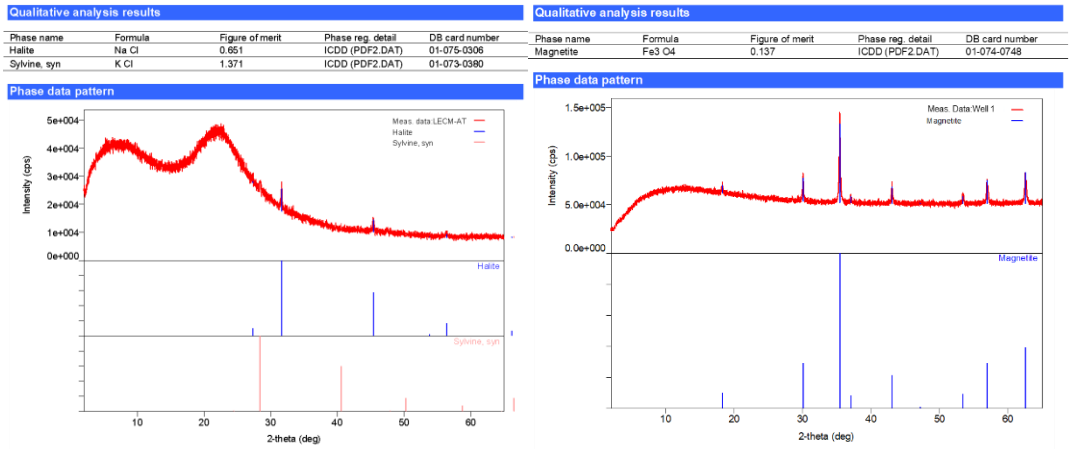

Figure 9: XRD qualitative analysis of scaling samples.

Sylvine, or potassium chloride (KCl), was also identified in the scaling sample. Similar to halite, sylvine forms as a result of the evaporation and concentration of geothermal fluids. The presence of sylvine indicates a high potassium content in the geothermal brine, which can further compound scaling issues by creating harder and more adherent deposits within the wellbore. These deposits can cause significant operational challenges, including increased maintenance requirements and potential well shutdowns.

Magnetite, or iron oxide (Fe3O4), found in the scaling sample, points to the corrosion of wellbore materials and the precipitation of iron from the geothermal fluid. The formation of magnetite scales can be particularly problematic as they are hard and dense, leading to severe blockages. The identification of these minerals through XRD analysis provides crucial baseline data for understanding the scaling processes in the Dieng geothermal wells. This information is invaluable for developing strategies to mitigate scaling and for predicting scaling patterns in newly drilled wells in the area.

5. ANTISCALING/ DESCALING

In geothermal wells, scaling can significantly impair the efficiency and functionality of the system. Mitigating silica scaling in geothermal systems involves two main approaches: physical methods and chemical methods. Each method targets the silica saturation index (SSI), a critical factor influencing silica precipitation. Increasing the pressure in the geothermal system can reduce the SSI.

According to the Fournier equation, maintaining higher pressures helps keep silica in a dissolved state, thereby preventing its deposition as scale. Modifying the pH of the geothermal fluid can shift the equilibrium of silica solubility. Lowering the pH tends to increase silica solubility, reducing the likelihood of scale formation. Chemical inhibitors can interfere with the nucleation and growth of silica particles, thus preventing scale formation.

5.1 Physical method

The value of SSI for mitigate silica scaling shall < 1. Increase pressure (to increase temperature) on the system to reduce value of SSI (silica saturation index) based on Fournier equation.

$$\log C = \left(\frac{-731}{10\,(T+273.15)}\right) + 4.52$$

$$SSI = \frac{A}{C} \quad (1)$$

Where:
T = Temperature system (Saturation pressure on the system)
C = Solubility of Amorphous silica (mg/kg)
A = Concentration of SiO_2 on the system from fluid chemistry analysis (mg/kg)

5.2 Chemical Method

1. pH Modification
   Injected acid either Sulfuric Acid or Acetic Acid on the system. It can delay polymerization of Silica occurs and thus rate of deposition of silica from the brine (Kingston Morrison, 1997). Sulfuric acid injection used on the many Geothermal Industries of the world because readily available, and relatively low cost. The key success on its method is depend on controlling or on the automation of injection due to sulfuric acid is a strong acid and the titration curve is steepest around pH 5, which is the normal target for pH modification. This means that if the acid is even slightly overdosed, the pH can go very low. Carbon steel piping tolerates acid conditions to about pH 4.6-4.8, but any lower pH can cause rapid corrosion of carbon steel (depending on the amount of silica scale already deposited in the pipe). Thus, even small fluctuations in brine flow can have a large change in pH, either leading to scaling, or corrosion. (Jacobs, 2020)
2. Inhibitor
   Many places on the world especially Indonesia is intensively developing chemical inhibitor to solving silica scaling mitigation without corrosion and health safety environment problem. Usually, they use water-based inhibitor. But it can't be said to be successful today, more research is needed to developing it chemical.

Even though we have done with value of SSI or delay of polymerization of silica, we should check on the pipeline physically view of deposition. We can install retractable coupon on the bypass pipeline to check periodically while the operation of production.

Commonly in Geothermal Industries on the surface facilities (from well head to power plant) we can separately handling Silica Scaling based on the location:

- 2-phase pipeline and production well
  Increase Well-head pressure (WHP) or throttle valve on the pipeline to reduce value of SSI on it place
- Brine pipeline
  Increase pressure separation on the separator to reduce value of SSI
- Injection well
  Reaming and Acidizing on workover activity can recover injection well from silica deposition either at the wellbore or the reservoir. But its activity is worst condition if we can't mitigate silica on the surface facility.
- Steam pipeline
  Silica deposition on the steam line is uncommonly because naturally silica is growing on the brine

phase. Silica deposition on the steam line is happen due to brine carry over to steam or silica is vaporized because normally geothermal steam is saturated steam change into superheated steam.

- Ensure efficiency of separator is >99.95%
- Ensure the quality steam outlet separator or demister/scrubber is <100%
- Loop seal installation on the separator to mitigate brine carry over to steam

5.3 Technology Selection

Based on pilot plant testing with JV Mannvit on 2021-2022 Higher pressure separation will be implemented on Dieng 2 steam field production to ensure value of SSC at 2-phase line and brine line is < 1 or minimum close than 1, so silica scaling on the injection facilities is still manageable without chemical injection. Dieng 2 power plant planned for 30 years operation, chemical injection either pH modification or inhibitor will add value of CAPEX and OPEX for 30 years operation. On other perspective pH modification with H_2SO^4 have a potential metal sulfide deposition due to H_2SO^4 reaction with metals content on the brine fluid.

- Average SiO_2 content D1 production wells = 1000-1100 ppm
- Projection of SSI for D2 operation = 0.95-1.05

From equation 1 previously, to get projection of SSI for D2

- Minimum pressure separation = 21.1 bar.a
- Temperature saturation = 215◦C

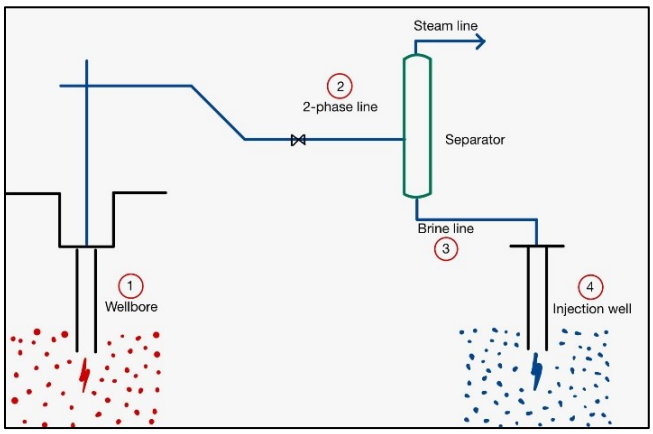

Figure 10: Common scaling location in Dieng (1,2,3,4) and higher-pressure separation will be implemented to ensure value of SSC at 2-phase line and brine line is < 1 or minimum close than 1.

6. CONCLUSION

Scaling in geothermal wells is intrinsically linked to the chemistry of the geothermal reservoir fluids. The types and concentrations of dissolved minerals such as silica, potassium, and iron play a critical role in the formation of scales. When geothermal fluids ascend and experience changes in temperature and pressure, their solubility characteristics alter, leading to the precipitation of minerals like halite, sylvine, and amorphous silica. These precipitates form hard deposits that can obstruct fluid flow, reduce efficiency, and cause significant operational challenges within the wellbore and surface facilities.

Additionally, the scaling process is heavily influenced by environmental changes within the wellbore and surface facilities. Variations in pressure and temperature, such as those occurring during fluid separation or rapid cooling, can trigger the formation of scales. The introduction of physical and chemical anti scaling method to control scaling demonstrates the dynamic nature of the wellbore environment and the necessity for continuous monitoring and adjustment of conditions. Understanding these relationships is essential for developing effective scaling prevention and mitigation strategies, ensuring the long-term efficiency and reliability of geothermal wells, particularly in areas like Dieng.

REFERENCES

Dieng Subsurface Team: Chemistry Update, *Internal Report* (2024).

Dieng Subsurface Team: Detail Well Targeting Dieng, SPDEP Phase 2, *Internal Report of Geodipa* (2021).

Dieng Subsurface Team.: Dieng Well Prognosis and Resources Risk & Uncertainty Mitigation Plan, SPDEP Phase 3, *Internal Report of Geodipa* (2021).

Dieng Subsurface Team: Well Condition History, *Internal Report* (2023).

Dieng Subsurface Team: Chemistry Update, *Internal Report* (2024).

Jacobs: Geodipa Dieng Unit-1 Optimization Study Report (2020).

Kingston Morrison: Geothermal Module (1997).

Layman, B Erik., Irzarwadi Agus., and Samsudin Warsa.: The Dieng Geothermal Resource, Central Java, Indonesia, Geothermal Resources Council Transactions, (2002).

Insights Into Permeability Heterogeneity: Seismic Monitoring and Focal Mechanism Studies at Wayang Windu Geothermal Field

Wahyuddin Diningrat, Meiyanto Purnomo, and Wintry Dimwani

Star Energy Geothermal (SEG), Wisma Barito Pacific II, 17th – 21st floor
Jl. Let. Jen. S. Parman Kav. 60. Jakarta 11410, Indonesia

wahyuddin.diningrat@starenergy.co.id

Keywords: Geothermal, fractures, permeability, fault, microearthquake, Wayang Windu, focal mechanism, double-difference

ABSTRACT

Deciding where to drill to improve the well success rate is one of the most important issues for geothermal field development. The biggest challenge in Wayang Windu as in many geothermal fields is understanding permeability heterogeneity which is commonly associated with structural irregularity. One geophysical approach to characterize the structural irregularity is monitoring seismic activity associated with fluid production and injection activities. Ten monitoring stations have been established to cover the most seismicity active areas of Wayang Windu field. Since 2021, more than 1400 absolute locations of high-quality micro-earthquake events have been recorded. High-quality microearthquake events must be identified by at least four stations, have at least eight phases, and have an azimuthal gap of less than 210 degrees. With the help of the double-difference (hypoDD) software, 662 events were successfully relocated and grouped into the north and south clusters with better location uncertainties. The north cluster, which is connected to the steam zone, is comparatively shallower and denser than the south cluster. Both clusters show the encapsulated fault-controlled event distributions, i.e., Kijang and Cibitung-1 faults at the north; Cibolang and Sukaratu faults at the south. Processing of the focal mechanism was applied to the chosen hypoDD events, requiring at least four stations with a signal-to-noise ratio of at least five. A Python program was used to process the focal mechanism. The outcome demonstrates a variation of the maximum stress orientation. Further analysis of the stress regime has revealed variation: in the north-west the stress regime having more reverse-faulting, while in the northern and southern production areas are both tend to have strike-slip and normal-faulting type.

1. INTRODUCTION

Located roughly about 40 kms south of Bandung, capital province of West Java, Indonesia, the Wayang Windu geothermal field has been commercially producing steam since 2000. The field now has 230.5MWe of installed capacity totaling 110 MWe from Unit-1 and 117 MWe from Unit-2, and 450 kg/s of steam is needed to maintain 230.5MWe of generation.

Figure 1: Location of geothermal fields in West Java, Indonesia.

There are several high terrain andesitic strato-volcanoes geothermal system in the area such as Darajat, Kamojang, Tampomas, Tangkuban Perahu, Salak, Karaha-Talaga Bodas, and Patuha. The strato-volcanoes are associated with the Sunda Volcanic Arc. It was resulted from the activity of subduction where Australian plate underneath Eurasian plate at the southern of Java.

Numerous seismicity monitoring projects have been carried out at Wayang Windu field. In 1998, the first microearthquake monitoring was carried out to track the induced seismicity of the field's southernmost wells, which located in the STW and STF pads. In 2005, three wells which located in the NTD, STS and NTQ pads were subjected to an additional round of induced monitoring to follow the seismicity in the central area. One well in the NTB pad was used in 2007 to track generated seismicity in the north. The massive reservoir monitoring was also carried out in 2012 as more than 30 continuous monitoring stations covering the field. The monitoring continued until the last equipment was dismantled in 2016.

Currently, there are 10 permanent seismic monitoring stations covering the field since 2020. Each of monitoring stations equipped with GEObit GEOthree data logger and force-balance C100 sensor that was put at 5 m depth. The sensors have a wide response of 10s – 98Hz, and 1500 V/m/s sensitivity. The sampling rate was set to 500 sps.

Data acquisition is conducted weekly, this include replacing the batteries of each station. SEISGRAM2K program (http://alomax.free.fr) is used for phases picking, this include P-phase polarity determination, while the absolute hypocenter location inversion was carried out using HYPOINVERSE program (https://www.usgs.gov). Relative location Double Difference was then carried out by utilizing HYPODD software (https://www.ldeo.columbia.edu/~felixw/hypoDD.html). The focal mechanism inversion was completed within python environment. The study will focus on the microearthquake focal mechanism result of 2021-2023 monitoring activity and its correlation with the updated geological structure, stress regime and geomechanics study.

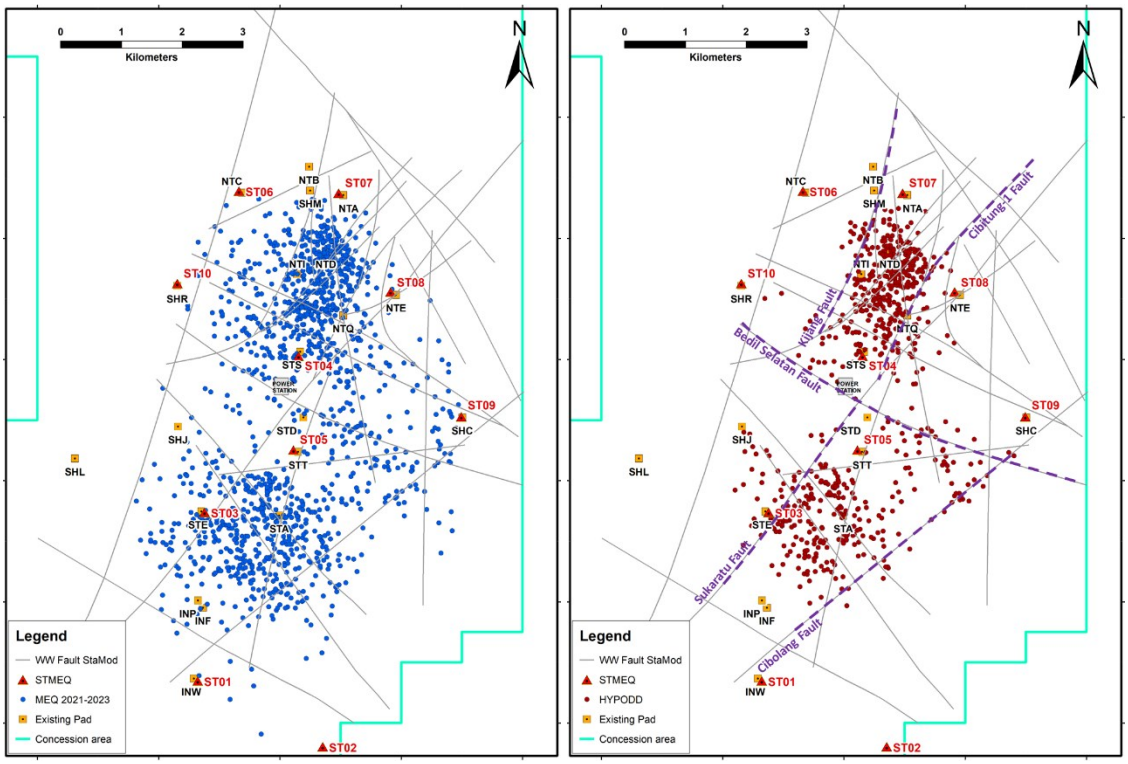

Figure 2: Hypocenter distribution during 2021-2023 monitoring period, [Left] Absolute; [Right] HypoDD.

2. SEISMICITY

Microearthquakes are small earthquake that has magnitude less than 3 (Lee and Stewart, 1981). Microearthquakes commonly occurs in reservoirs as a result of injection or exploitation activities that may be due to the change in the stress distribution. Microearthquake occurrences can also be caused by localized volcanic and tectonic activities.

2.1 Microearthquake Distribution

Wayang Windu geothermal field has been producing steam for more than 2 decades and thousands of microearthquake events have been recorded in the area since then. The distribution of seismic monitoring stations is designed to monitor the reservoir proven area. The deployment of 10 monitoring stations was distributed into two stages. The first five was deployed in 2020, and another five in 2021. Almost all stations are located in the

well pads except one that is placed further south at the edge of concession area (ST02). The well pads occupied are production pads i.e., STT (ST05), NTC (ST06), NTA (ST07), and NTE (ST08); injection pad, STW (ST01); SlimHole pads i.e., SHC (ST09), and SHR (ST10); and idle wells i.e., STS (ST04) and STE (ST03).

Figure 2 showing the distribution of microearthquake events overlaid with the interpreted fault in the area. The field's geological structure was better understood in 2019 thanks to an extensive LIDAR survey. New insights into geological structure were obtained by combining the high-resolution Digital Terrain Model (DTM) with earlier LANDSAT data, gravity processing, and modeling outcomes (Purnomo, et al., 2023).

There are more than 2000 microearthquake events recorded since the deployment of seismic monitoring stations, but only about 1400 events that are detected by minimum 4 stations (8 phases) and maximum azimuthal gap of 210º are accepted and kept for advance processing. The HypoDD processing was conducted to enhance the accuracy of hypocenter determinations. As a result, 662 hypocenter locations were refined, revealing the presence of two distinct clusters. This improved accuracy is crucial for detailed seismic analysis and understanding the underlying geological structures and fault mechanisms in the study area.

Two significant clusters have been identified: the northern and southern clusters (Figure 2). The northern cluster, which is the most productive area, is confined between the Kijang and Cibitung-1 faults, whereas the southern cluster is located between the Cibolang and Sukaratu faults. Both clusters are situated in regions dominated by production wells. In terms of seismicity, the Bedil Selatan fault separates the shallower northern cluster from the deeper southern cluster. Tritium tracer injection tests were performed in the central area in 2014 and 2016 and confirmed vertical connectivity between the deep liquid reservoir and the current main production area, the Northern steam cap (D. Malik, et al., 2020).

2.2 Signal to Noise Ratio

The advantages of placing the monitoring stations within the pads are easy access, more secure, and no additional budget needed for land leasing; while the disadvantage tends to have more noisy data, thus reducing signal to noise ratio (SNR). The SNR was calculated from the ratio of P-phase signal and the background noise about 0.5 second before the P-phase amplitude. SNR ≥ 5 was taken as the good SNR for focal mechanism processing. Figure 3 shows the statistic of events detection and SNR of each station since all ten stations are installed. It shows that station ST07 and ST08 are both have the lowest SNR and event detection, while ST06, ST09 and ST10 are three stations with the highest SNR and event detection. The ST02 is unique, because it was installed rather late, Nov 2021.

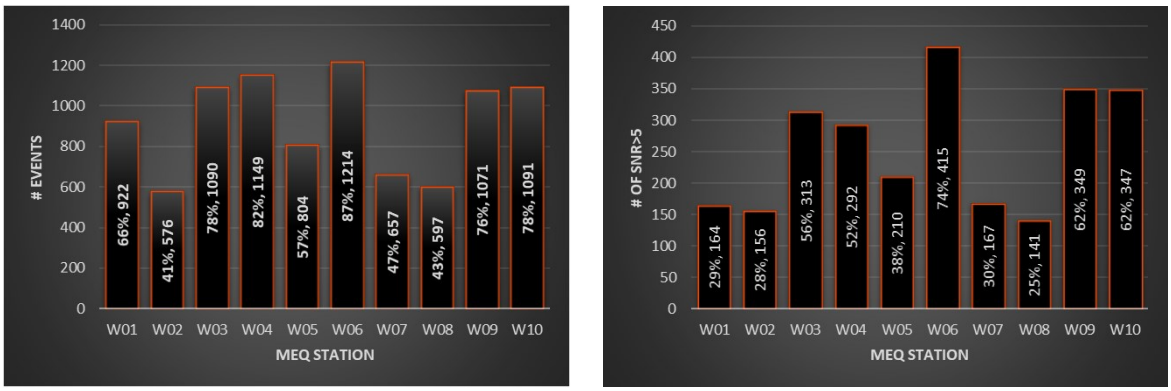

Figure 3: (Left) Number of events detected on each station during 2021-2023 monitoring period. (Right) Number of SNR ≥ 5 of events detected by each station.

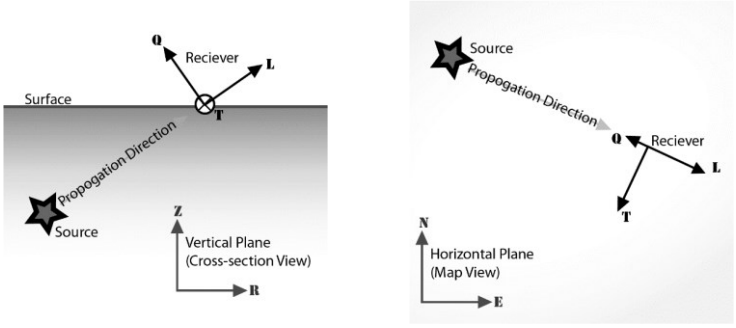

Figure 4: The illustration of LQT orientation system (https://service.iris.edu/).

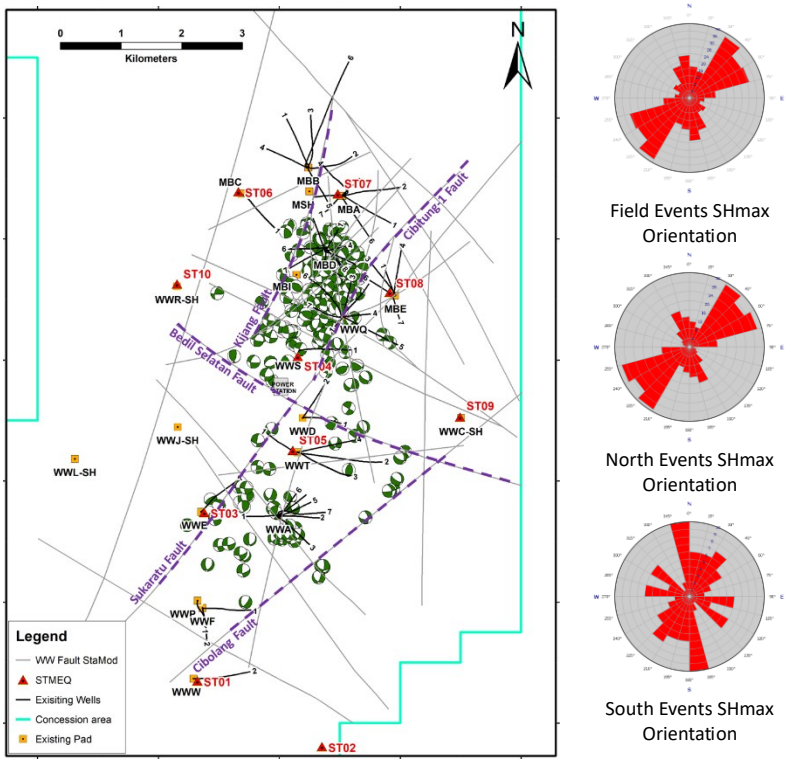

Figure 5: [Left] Distribution of focal mechanism, [Right] Rose diagram of SHmax orientation.

3. FOCAL MECHANISM

A total of 223 hypoDD microearthquake events were chosen for investigation of the focal mechanism. The selection of events is based on a minimum of eight phases and a signal-to-noise ratio of more than five, as observed by a minimum of four stations. During the computation of the hypoDD, azimuth and takeoff angle were calculated simultaneously. P, SV, and SH amplitudes were obtained by rotating the event waveforms into the LQT orientation system, where L aligned with the P wave propagation direction, Q with the SV phase movement, and T with the SH phase movement (Figure 4).

The microearthquake (MEQ) focal mechanism are distributed into two main clusters: north and south (Figure 5). The northern cluster, which is confined by Kijang and Cibitung-1 fault, is characterized by shallower events compared to the southern cluster. This difference in depth correlates with the distinct reservoir type in the area: the north is a vapor-dominated zone, while the south is a two-phase zone. Consequently, most of the steam production originates from the northern area, highlighting its significance in geothermal energy extraction. The focal mechanism analysis reveals that the SHmax orientation in the northern cluster is NE-SW, while in the southern cluster, it is NNW-SSE.

The SHmax orientation varies between the clusters (Figure 5), indicating distinct stress regimes essential for understanding fracture dynamics and optimizing geothermal extraction. The geological faults significantly influence the seismic activity and reservoir behavior, with the northern cluster being more productive.

The SHmax orientations are crucial for assessing regional stress fields and their impact on seismicity and reservoir behavior. This understanding helps predict potential fault slips, improving risk management in geothermal energy production. The stress orientation data guides drilling and stimulation activities to enhance resource recovery while minimizing seismic risks.

4. CONCLUSION

The investigation into the focal mechanisms of 223 hypoDD microearthquake events has provided valuable insights into the seismicity and subsurface characteristics of the study area. The selection of events was rigorous, based on a minimum of eight phases and a high signal-to-noise ratio, ensuring the reliability of the data. The computation of azimuth and takeoff angles, along with the rotation of event waveforms into the LQT orientation system, allowed for precise determination of P, SV, and SH amplitudes.

The findings emphasize the northern cluster's importance for geothermal energy extraction, suggesting focused exploration and production strategies of Wayang Windu. The different stress regimes in the clusters highlight the

need for region-specific analysis. Continuous monitoring and analysis are essential for optimizing geothermal production.

Future research should deepen the understanding of the relationship between seismicity, reservoir characteristics, and geothermal production. Advanced modeling techniques and higher-resolution data can offer more insights into subsurface processes and improve understanding of the geothermal field. Additionally, evaluating signal-to-noise ratios at monitoring stations can further enhance data quality and interpretation.

In summary, the focal mechanism analysis of hypoDD microearthquake events has revealed critical information about the Wayang Windu geothermal field's seismicity and subsurface structure. These findings enhance the understanding of regional geology and stress fields, providing useful information for geothermal energy extraction, reservoir management, and well targeting.

REFERENCES

Lee, W. H. K., and Stewart, S. W.: Principles and Application of Microearthquake Networks, Advance in Geophysics, Supplement 2, Academic Press, p. 4. (1981).

Malik, D., Abidin, Z., and Pramono, B.: Tritium tracer Injection test at Wayang Windu Geothermal Field, West Java, Indonesia, *Geothermics*, **83**, (2020) 101718.

Purnomo, M., Diningrat, W., Kamel, N., Talita, A., and Dimwani, W.: Updated Geological Structure and 3D Intrusion Model as Veritable Fracture Driver of Fracture Characterization in Wayang Windu Geothermal Field, Indonesia, *Handbook*, 45th New Zealand Geothermal Workshop, Auckland, NZ (2023).

HypoDD. (n.d.). https://www.ldeo.columbia.edu/~felixw/hypoDD.html

HYPOINVERSE Earthquake Location | U.S. Geological Survey. (n.d.). https://www.usgs.gov/software/hypoinverse-earthquake-location

NSF SAGE: IRISWS: Rotation: Docs: v. 1: Help. (n.d.). https://service.iris.edu/irisws/rotation/docs/1/help/

Towards a New Framework for the Systematic Assessment of Indonesia's Undeveloped Geothermal Resources

John O'Sullivan, Winnie Alia, Armando Aloanis, Ken Dekkers, Ari Fuad, Michael Gravatt, Bei Nagoro, Rony Nugraha, Joris Popineau, Aulia Pratama, Fikri Rahmansyah, Theo Renaud, Jeremy Riffault, Alfia Syahrul, Iqbal Takodama, Ryan Tonkin, and Mike O'Sullivan

Department of Engineering Science, University of Auckland,
70 Symonds Street, Grafton, Auckland 1010, New Zealand

jp.osullivan@auckland.ac.nz

Keywords: Geothermal resource assessment, Indonesia, Numerical reservoir models, Renewable energy, Geoscientific data

ABSTRACT

The National Energy General Plan (RUEN) of Indonesia targets the production of 10 GWe from geothermal by 2030 and further increases to 17.5 GWe by 2050. Robust assessments of Indonesia's undeveloped geothermal resources are required to help prioritize systems for development.

A new method for resource assessment has been developed by the Geothermal Institute at the University of Auckland, which leverages modern geothermal modelling tools and cloud computing. This approach provides more realistic estimates of the potential of a geothermal resource than the traditional stored heat method and has been applied to commercial and research projects.

This paper discusses the application of this method to six undeveloped geothermal systems in Indonesia. The study was understaken in collaboration with the Geological Agency (GA) of Indonesia and the Directorate-General of New Renewable Energy and Energy Conservation (EBTKE) as a step towards establishing a new framework for the systematic assessment of Indonesia's undeveloped geothermal resources. The resource assessment framework was applied to each of the six systems; Ciremai, Kepahiang, Kotamobagu, Maritaing, Massepe, and Papandayan. This included the development of new digital conceptual models and numerical reservoir models for each system using geoscientific data from The Geological Agency. The resource assessment results for each field are presented in a standard format, and it is envisioned that they could be made publicly available in a database of Indonesia's geothermal resources in the future.

1. INTRODUCTION

Indonesia is positioned along the boundaries of active plates and boasts an impressive geothermal potential estimated at 23.36 GW distributed across 356 locations. Recognizing this vast potential, the Indonesian government has set targets to increase geothermal energy production to 10 GWe by 2030, with further expansion to 17.5 GWe by 2050 (Rencana Umum Energi Nasional, 2017). However, despite these promising prospects, the current exploitation of geothermal resources in Indonesia remains limited. Currently, 16 geothermal fields are operational, collectively generating 2,342 MW, representing less than 15% of the targeted capacity for 2050 (Alhusni et al., 2023).

The exploration and development of new geothermal resources face many challenges. The early stage of exploration is particularly risky due to the limited availability of data and the substantial investment required. Consequently, stakeholders must ensure that the potential of a geothermal resource is sufficient to justify the investment. This is typically assessed by estimating the potential electrical power output of the geothermal field.

Traditional methodologies for estimating geothermal resource potential are plagued by high levels of uncertainty, primarily due to reliance on numerous assumptions and a lack of consideration for the physical processes within the reservoir and wellbore. A new framework has been developed that incorporates a more realistic energy extraction scenario using numerical modelling and cloud computing to address these limitations (Croucher et al., 2020; Dekkers et al., 2022; O'Sullivan & O'Sullivan, 2016). This innovative approach reduces the uncertainty in power output calculations and enhances investor confidence by providing a more reliable assessment of geothermal potential.

This paper presents the application of this novel approach to six undeveloped geothermal systems in Indonesia. Conducted in collaboration with the Geological Agency (GA) of Indonesia and the Directorate-General of New

Renewable Energy and Energy Conservation (EBTKE), this study marks a significant step toward establishing a systematic framework for assessing Indonesia's untapped geothermal resources.

2. METHODOLOGY

Numerical modelling for geothermal reservoirs has been carried out since the 1970s (Stanford Geothermal Program, 1980; O'Sullivan, 1985; O'Sullivan et al., 2001; O'Sullivan and O'Sullivan, 2016). In this paper, we propose a new method for assessing the potential of geothermal power output using numerical modelling, available data and innovative algorithms. This method requires simulations of a large number of different reservoir models, making it highly dependent on computational speed. Fortunately, highly parallelized geothermal simulators like Waiwera, developed by the University of Auckland and GNS Science (Croucher et al., 2020), can leverage high-performance computing resources to make this new method feasible.

The advantage of the resource assessment method presented in this work is that the geothermal power estimations are based on numerical reservoir simulations. These simulations include reservoir physics, wellbore physics and realistic energy extraction scenarios. The method of resource assessment also produces robust estimates of the uncertainty using well-established uncertainty quantification techniques (Dekkers et al., 2022).

2.1 Steady state models

The first step for our resource assessment is to use the 3D digital conceptual model to set up a numerical model where the geology, alteration zone, structural settings and potential deep upflow locations define a large set of model parameters. We then generate an ensemble of possible models by randomly sampling model parameters from statistical distributions based on realistic ranges. These sample models are simulated to a steady state before any production simulations are carried out. Over 2000 sample models were generated for each of the systems presented in this paper to estimate the power output of each geothermal system.

2.1.1 Uncertain parameters

Generally, when we develop a new numerical model, we start with an initial guess based on expert knowledge of rock permeabilities and upflow rates. These parameters are then manually calibrated using the available data. During the exploration stage of a geothermal field, the calibration process is rapid because few data is available. However, the lack of data means there is significant uncertainty in the model parameters. To represent this uncertainty, an ensemble of reservoir models is created by randomly sampling model parameters from realistic probability distributions. The distribution of each parameter is centred around the calibrated model parameters. Collaboration by geothermal stakeholders to specificy a standardised list of required exploration data could help reduce uncertainty in the future by providing more data to condition the sample models.

2.1.2 Conditioning on the clay cap

The second step of our approach is to filter the steady state models based on the location and temperature of the clay cap. This process is called "conditioning" and involves discarding sample models that do not fit the available reservoir engineering data. We do this using approximate Bayesian computation (ABC) (Beaumont, 2019; Marin et al., 2012) as described in Dekkers et al. (2022). Thus, to apply our methodology, some data giving the location of the clay cap is required, e.g., MT survey data, clay mineralogy from drilling cuttings or downhole temperatures. A clay cap is formed by alteration of the rock structure due to heating. Temperatures of approximately 200 °C are needed to form a clay cap. After the clay cap is formed, the hot fluids do not flow easily through the clay cap due to its low permeability. Thus, the location of the clay cap can be used as a proxy for the temperature distribution at the top of the geothermal system. The resistivity boundary and estimates of the location of the top of the reservoir are used in a similar way to traditional stored heat calculation. However, a stored heat calculation neglects the physics of subsurface fluid flow and does not make use of the full three-dimensional interpreted clay cap. Expert interpretation of resistivity is still required in both a traditional stored heat calculation and our new approach to account for phenomena such as relic alteration and clay sediments. The temperature threshold for conditioning can also be modified where mineralogy indicates it is appropriate.

2.2 Production models

After filtering the steady state models to an ensemble containing only those that match the geophysical data, we apply an innovative method to run production scenarios that maximize the power output of each sample model. We use the steady state model as an initial state for the production model and then simulate 25 years of future production extracting energy using a typical flash power plant configuration. This method can be easily modified to accommodate different power plant designs and operating conditions depending on the geothermal system that is being analyzed.

One of the challenges with using uncertainty quantification of geothermal models for resource assessment is that the optimal production strategy is different for each model sample. Typically, the design of future scenarios for a

geothermal model is done manually by geothermal reservoir modellers and then optimized to achieve maximum energy extraction. However, this manual approach is clearly not viable with thousands of sample models.

The innovative method we have developed is an iterative algorithm that can select the best targets for production and reinjection for any given sample model. The iterative algorithm continues selecting targets until the additional energy produced is less than 5% of the previous iterative step, indicating diminishing returns on adding new wells.

Wellbore modelling is used to represent the behaviour of each of the production wells. Before running the iterative algorithm, wellbore models are run for all possible target depths under all the likely range of thermodynamic conditions. This process can be completed on a standard desktop computer within 2-3 days. Vertical, single-feed wells with typical completion designs are assumed in this work to demonstrate the approach. However, the parameters of production wells, including the completion design and number of feeds, could easily modified. Additionally, areas where wells can (or cannot) be sited (e.g., due to factors such as topographical constraints or consent boundaries) can be easily specified.

It is important to remember that the objective of this method is to calculate the production potential for each sample model efficiently using a realistic extraction scenario. It does not aim to design the perfectly optimal extraction scenario for each sample model or the system in general. Designing an optimal extraction scenario for the system is expected to take place during the development of the production stage once exploration drilling and early production testing have taken place. The details of the iterative algorithm of our innovative method are provided in Dekkers et al. (2022).

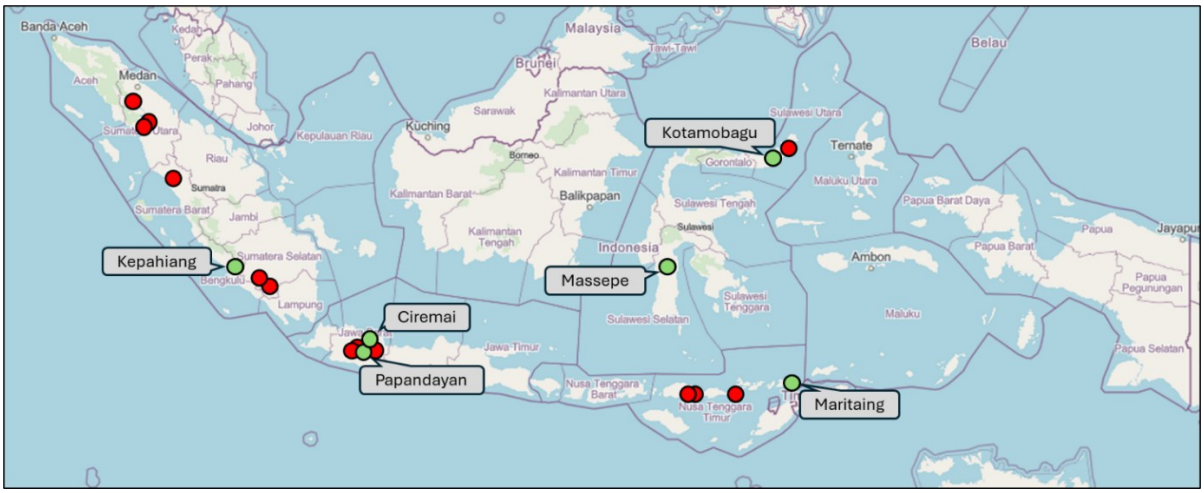

Figure 1: Exploitation stage geothermal fields (red) and six undeveloped geothermal fields (green).

3. UNDEVELOPED GEOTHERMAL FIELDS

Indonesia has an abundant amount of geothermal potential mainly due to its location at the junction of several tectonic plates. Its location produces volcanic arcs and tectonically active zones along many of the islands across the country. Sunda Arc, which is the subduction product between Indo-Australian plate and Eurasian plate, hosts from Sumatra to Java and then through to Nusa Tenggara (MacPherson & Hall, 2002; Varekamp et al., 1989). Modern volcanoes in the area were formed during the Quaternary period and have mainly generated basaltic andesite to andesite effusive and explosive products (Pacey et al., 2013). Different to the islands in Sunda Arc, the regional area of Sulawesi Island was formed by interactions of three different plates, namely Eurasian, Indo-Australian, and Pacific plates (Hall, 2002; Hamilton, 1979; Katili, 1975; Nugraha et al., 2022). A unique K-shape feature in Sulawesi is the evidence of robust tectonics and volcanics activity since Miocene to Late Pliocene (Katili, 1978).

This study applied the new resource assessment framework to six undeveloped geothermal fields namely Ciremai and Papandayan (Java); Maritaing (Nusa Tenggara); Kepahiang (Sumatra); and Massepe and Kotamobagu (Sulawesi) (Figure 1). The sections below discuss the newly developed numerical and 3D geological model for each geothermal field. Data from Geological Agency of Indonesia, the Directorate-General of New Renewable Energy and Energy Conservation (EBTKE) and previous publicly available research were used to support this paper.

3.1 Ciremai

The Ciremai geothermal field, located in West Java, Indonesia, is a volcanic-type geothermal system with promising potential for energy development. Situated around the prominent stratovolcano Mount Ciremai, the field covers an area of approximately 38,560 hectares, making it a possible target for Indonesia's geothermal development strategy. The geological setting of Ciremai is characterized by a complex stratigraphy that includes the Cinambo Formation, Halang Formation, Ciherang Formation, and various volcanic deposits dating from the Tertiary to Quaternary periods (Djuri, 2011; Silitonga et al., 1996). The area is dominated by the northwest-southeast trending fault system, which serves as the primary conduit for geothermal fluids (Sukaesih et al., 2021) (see Figure 2). Notable geothermal manifestations include the Cilengkrang, Sangkanhurip, and Ciniru hot springs, which provide surface evidence of the geothermal activity beneath the surface.

The hydrogeology of the Ciremai geothermal field reveals a complex interaction between volcanic aquifers, fracture zones, and recharge areas. The system is influenced by two primary flow mechanisms: a porous media system and a fracture-driven volcanic aquifer system resulting in a relatively low water table. Recharge occurs in the highlands, discharging at lower elevations (250-650 meters above sea level) through numerous springs (Irawan & Puradimaja, 2006). This hydrogeological framework is vital for understanding the geothermal system and is integral to developing accurate conceptual and numerical models (Irawan et al., 2009).

3.2 Kepahiang

The Kepahiang geothermal field is located within the volcanic complex of Mount Kaba in Bengkulu Province, Sumatra, Indonesia. The site covers the Kepahiang and Rejang Leboh regions at altitudes ranging from 250 to 1600 meters above sea level. Characterized by its volcanic nature, the area hosts various volcanic products and manifestations, such as fumaroles, solfataras, and hot springs, which indicate active geothermal activity (Kusnadi et al., 2011). The primary geological formations include the Kaba Tua and Kaba Muda eruption products, along with surrounding volcanic structures such as Bukit Lumut, Taba Penanjung, and Bukit Malintang (Sugianto & Hadi, 2011).

Based on the geophysical surveys, the dynamics of the system are controlled by key fault structures, including the Sempiang and Bogor faults, which facilitate the movement of geothermal fluids (Arsadipura et al., 2011; Nurdiyanto et al., 2022) and the reservoir is estimated to be under a thick clay cap layer (1500-2500m), which is in the Old Kaba Volcanic (Nurdiyanto et al., 2022). The complex hydrogeology of the area is further influenced by volcanic activity, with fluid recharge occurring from the slopes of Mt. Kaba and surrounding areas. These factors contribute to the rich geothermal manifestations observed in the region (Kusnadi et al., 2011).

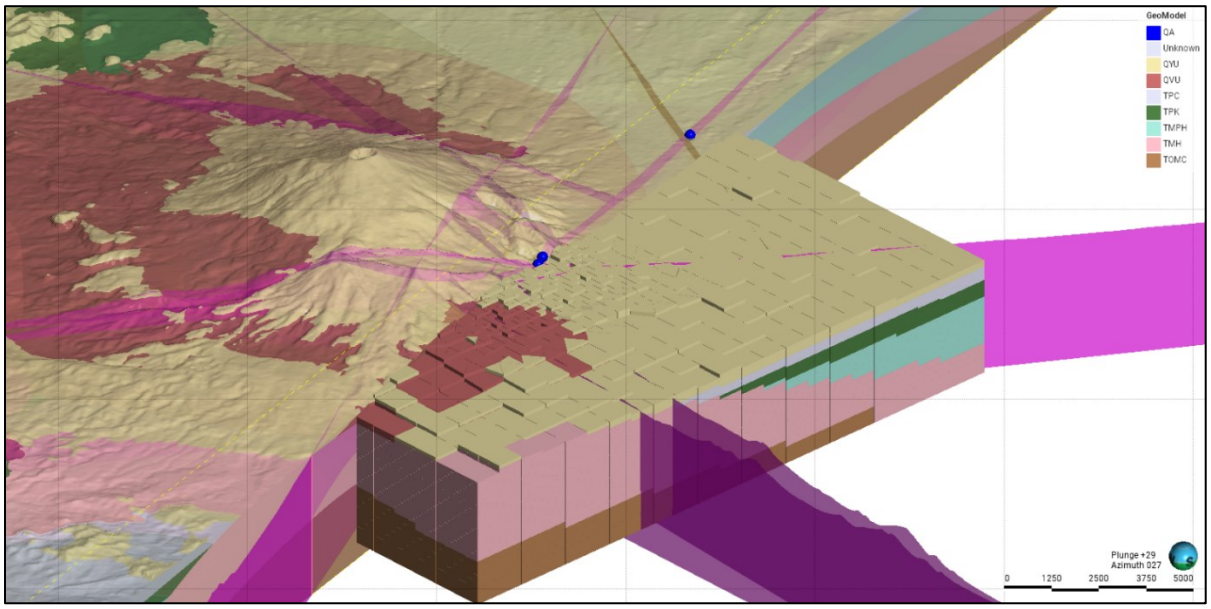

Figure 2: Ciremai geological model alongside the numerical model. Magenta planes represent NE-SW and NW-SE faults. Blue dots represent alkali chloride surface manifestations.

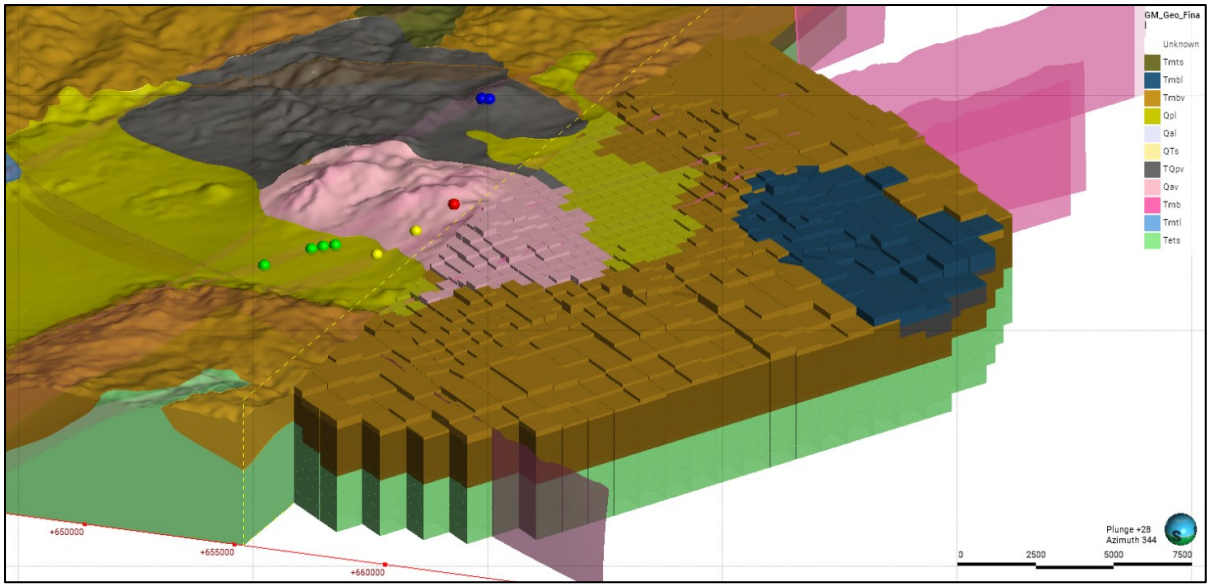

Figure 3: Kotamobagu geological model alongside the numerical model. Magenta planes represent NE-SW and NW-SE faults. Colored dots represent survey manifestations as acid sulphate (red), sulfate-chloride (yellow), and bicarbonate (green), and alkali chloride (blue).

3.3 Kotamobagu

The Kotamobagu geothermal field is located in North Sulawesi, Indonesia, approximately 200 km southwest of Manado City. This geothermal site, situated within the Minahasa region, is known for its significant potential as a geothermal energy resource. The field is characterized by a complex geological setting, with stratigraphy including sedimentary rocks of the Tinombo Formation, Bilungala Volcanics, Tapadaka Formation, and Pinogu Volcanic deposits. Recent volcanic deposits from the Ambang Volcanics also play a crucial role in the geothermal system (Apandi & Bachri, 1997) (see Figure 3). The field's geology features formations from the Eocene to the Holocene, reflecting a dynamic volcanic and tectonic history shaped by regional geological processes.

A previous conceptual model has been made and geochemical surveys have identified key features of the Kotamobagu geothermal system (Riogilang et al., 2011b, 2011a; Riogilang, Itoi, & Taguchi, 2012; Riogilang, Itoi, Tanaka, et al., 2012). The presence of fumaroles and hot springs around the Mt. Muayat area indicates an active, liquid-dominated reservoir with temperatures ranging from 230°C to 320°C (Riogilang et al., 2013). The system is influenced by NE-SW and NW-SE trending fault lines, which serve as pathways for geothermal fluids and control the distribution of manifestations across the field. These fault structures are critical for understanding the geothermal dynamics and potential resource area within the Kotamobagu site.

3.4 Maritaing

The Maritaing Geothermal Field, situated on Alor Island in East Nusa Tenggara province, Indonesia, holds a modest geothermal potential. The field is located approximately 800 km from the Ulumbu field and about 700 km from Maritaing. The area encompasses 3 km² and is characterized by a reservoir temperature estimated at 170-200°C as indicated by Na-K geothermometer analyses through a partial-equilibrium Kura hot spring (Setiawan et al., 2015). Preliminary studies have focused on its geological, geophysical, and geochemical properties. The geological composition mainly includes volcanic and sedimentary rocks such as andesite lava, pyroclastic flows, conglomerates, and limestone. These formations are part of the Alor formation, which consists of various lava and breccia layers interspersed with tuff.

The geological structure of the Maritaing field features prominent NW-SE and NE-SW trending faults, forming the Maritaing depression and acting as fluid controls for the Kura hot springs (Supriyadi et al., 2015). Faults in this region are crucial for the geothermal system's dynamics, as they facilitate the movement of fluids and recharge the reservoir. A recent gravity survey shows high amplitude values in the complete Bouguer anomaly signal, suggesting the presence of andesitic lava rocks (Boling et al., 2024). The magnetotelluric (AMT and TDEM) surveys have revealed low-resistance zones (<10 Ohm.m) indicative of altered rock formations acting as a caprock (Rahadinata et al., 2017).

A previous conceptual model (Setiawan et al., 2015) proposes that the geothermal system is linked to young magmatic activity, with meteoric water infiltrating the Maritaing Depression and heating up due to residual magmatic heat. This results in a convective hydrothermal system, with hot fluids emerging at the surface as hot

springs. A new 3D geological model was developed to give better understanding of the system (Aloanis, 2024) (see Figure 4).

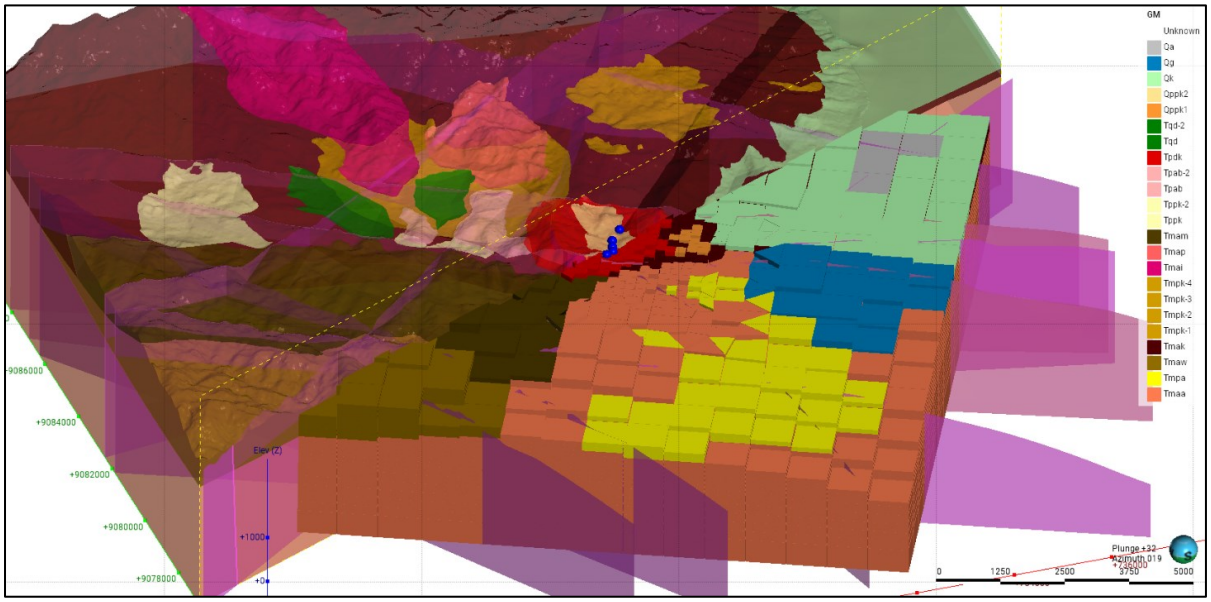

Figure 4: Maritaing geological model alongside the numerical model. Magenta planes represent NW-SE and NE-SW faults. Blue dots represent alkali chloride surface manifestations.

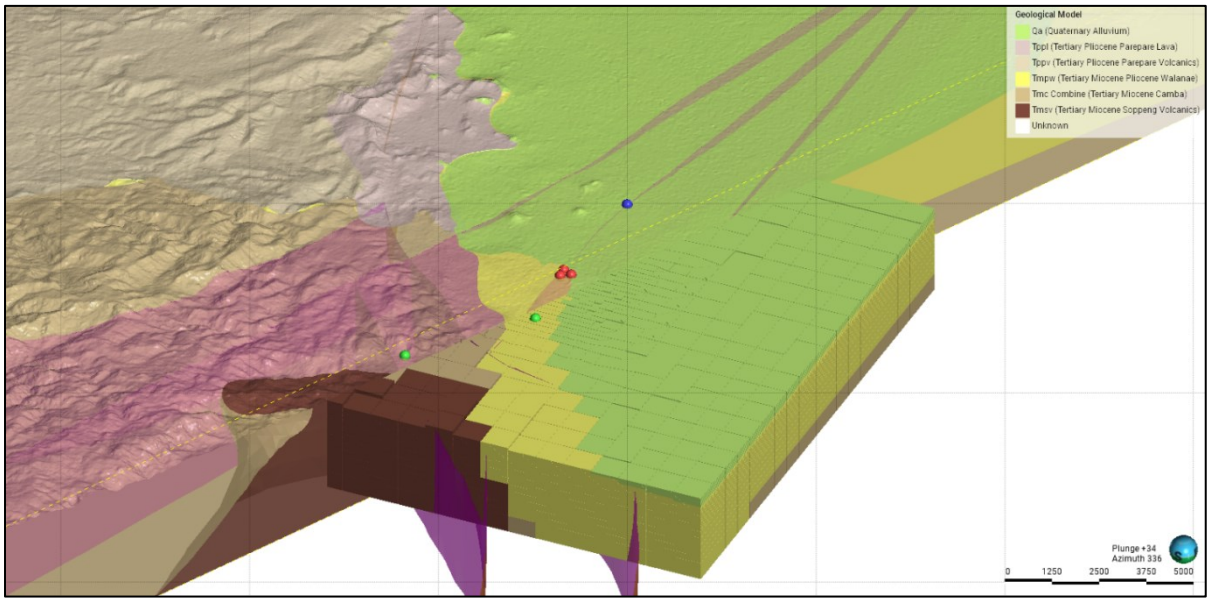

Figure 5: Massepe geological model alongside the numerical model. Magenta planes represent the N-S faults. Colored dots represent survey manifestations such as bicarbonate sulphate (red), bicarbonate (green), and alkali chloride (blue).

3.5 Massepe

The Massepe Geothermal Field, located in South Sulawesi, Indonesia, presents a promising opportunity for geothermal energy development due to its potential. Geographically situated within the Sidenreng Rappang Regency and approximately 194 km from Makassar City, the Massepe field is characterized by diverse geological formations and notable geothermal activity. The region consists of volcanic, intrusive, and sedimentary rocks dating from the Tertiary to Quaternary periods (Sukamto, 2012). Key stratigraphic units include the Soppeng, Camba, Walanae, Parepare formations, and more recent alluvial deposits (Risdianto et al., 2008). Notably, the geological structure is dominated by the north-south trending Massepe fault, which acts as the primary conduit for geothermal fluids and plays a crucial role in the hydrothermal system. The hydrogeology of the area includes recharge zones in the hilly regions where meteoric water infiltrates and interacts with deep-seated geothermal

fluids, leading to surface manifestations such as the Pajalele and Alakuang hot springs (Risdianto & Soetoyo, 2008) (see Figure 5).

The geophysical surveys provide detailed subsurface features. The Bouguer anomaly resulted from the gravity survey show low-mid-high values, which associated with altered and less dense volcanic rock, sedimentary rocks, and shallow andesitic intrusions rocks, respectively (Risdianto & Soetoyo, 2008). The resistivity anomalies confirm the geological structures, particularly in the north-south Massepe Fault, which contribute to the emergence of hot springs at Pajalele and Alakuang. The low resistivity anomaly (<20 Ωm) suggests to be the upflow zone of the system, while the values between 20-60 Ωm thought to be the reservoir zone which clustered around the Pajelele hot spring, extending towards the Alakuang and Warede hot springs (Joni et al., 2019).

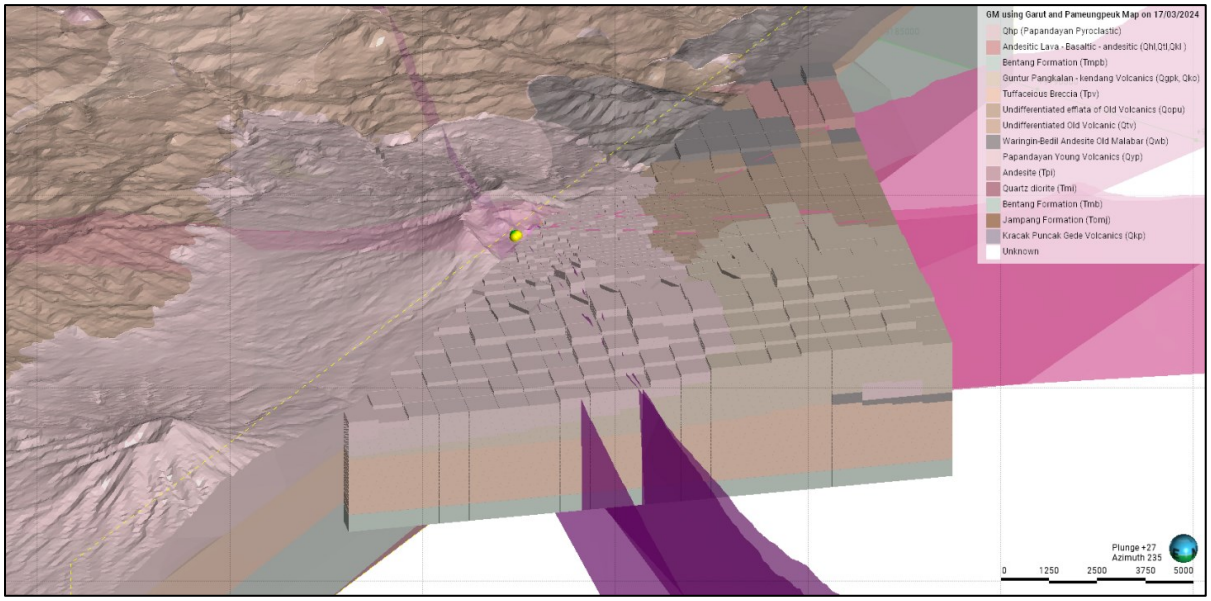

Figure 6: Papandayan geological model alongside the numerical model. Magenta planes represent NW-SE and NE-SW faults. Yellow dots represent acid sulphate manifestations.

3.6 Papandayan

The Papandayan geothermal field, located in West Java, Indonesia, offers potential for geothermal energy development. Mount Papandayan, a prominent stratovolcano, rises from 1,100 to 2,665 meters above sea level and is situated between Bandung and Garut District. The site has been studied since the early 2000s, with investigations focusing on lithology mapping, geologic structures, ground deformation, alteration, and fluid analysis from thermal features, which include solfataras, fumaroles, mud pools, and hot springs (Alzwar et al., 1992; Byrdina et al., 2018; Mazot et al., 2008; Nasution et al., 2008; Z. Abidin et al., 2003). The field's geological framework comprises several rock formations, ranging from Quaternary Holocene volcanic deposits to Tertiary Miocene formations such as the Bentang and Jampang formations. These formations are linked to ongoing volcanic activity, which provides a heat source that elevates the temperature of permeable rocks, creating geothermal reservoirs (see Figure 6).

A key feature of the Papandayan geothermal system is its complex fault structure, which significantly influences fluid flow and geothermal activity. The fault system in the area includes NE-SW and NW-SE trending faults that create pathways for geothermal fluids, impacting the distribution and intensity of thermal features (Sulastri et al., 2014). The presence of a clay cap dome below the area with many acidic thermal features, particularly in the Mas Crater, presents a challenge, as it is not feasible for drilling.

4. RESOURCE ASSESSMENT RESULTS

The resource estimates were made using the method outlined in Section 2 with the calibrated natural state model of each geothermal field as the initial input. Key parameters such as rock permeabilities, porosities and heat upflows were sampled from distributions to establish realistic parameter ranges for developing an ensemble of sample models. Note that these distributions could also be constrained by any available lab analysis data. Each sample model was then run to achieve a steady state before undergoing the filtering process. The models that successfully converged to a steady state were conditioned based on their temperature distribution at the base of the clay cap. These selection criteria required models to reach temperature between 180-200°C beneath the

alteration zone, indicating an accurate representation of the geothermal conditions during the formation of the clay cap.

The accepted models were subsequently used to estimate the maximum power output using the production scenario algorithm outlined in Section 2. By combining the predictions from the thousands of sample models, the uncertainty range of the power output can be quantified and expressed probabilistically using P10, P50, and P90 estimates.

A 25-year production scenario was applied to each of the six undeveloped geothermal fields in this study (Alia, 2024; Aloanis, 2024; Fuad, 2024; Nagoro & O'Sullivan, 2023; Rahmansyah, 2024; Syahrul, 2024). All scenarios had a separator pressure of 6.5 bar and a conversion rate of 2.5 kg/s of steam per MWe.

Stored heat calculation from published sources by EBTKE (Direktorat Panas Bumi, 2017), The Geological Agency (Badan Geologi, 2019), and Rahmansyah (2024) are also presented in this study as direct comparison with the result obtained from numerical methods. The stored heat calculation estimates the total thermal energy output and accounts for the recovery factor, conversion efficiency, and parasitic load (Zarrouk & Simiyu, 2013). Depending on the field, 10-20% can be used for the recovery factor and conversion efficiency. Monte Carlo simulation is typically used to quantify the uncertainty for parameters including reservoir size, average reservoir temperature, and porosity. This allows P10, P50, and P90 estimates to be made using the stored heat method. Table 1 presents the resource estimation results using both approaches for each of the geothermal fields studied.

Table 1: Result of the resource assessment using a traditional stored heat approach and the numerical modelling framework applied to six undeveloped geothermal fields. Stored heat calculations carried out by EBTKE (Direktorat Panas Bumi, 2017) [1], Rahmansyah (2024) [2], and The Geological Agency (Badan Geologi, 2019) [3].

Geothermal Field	Stored Heat Estimate (MWe)			Numerical Modelling Estimate (MWe)		
	P90	P50	P10	P90	P50	P10
Ciremai[1]		150		28.6	37.5	55.1
Kepahiang[1]		180		36.6	50.2	63.1
Kotamobagu[1]		225		70	160	270
Maritaing[1]		17		10.2	16.7	22.9
Massepe[2]	24.4	39.4	55.4	25.8	34.5	43.4
Papandayan[3]	16	21	26	12.3	18.5	28.4

The results in Table 1 show that the stored heat method yields higher resource estimates than the numerical model approach for the fields considered in this study. However, the stored heat estimates are subject to important limitations, primarily due to their high sensitivity to key input parameters and simplifying assumptions. The stored heat method neglects the importance of a heterogeneity typical of geothermal systems by using average temperature to represent the entire reservoir. Numerical reservoir models can capture reservoir heterogeneity. The stored heat method also assumes simplified reservoir geometries and ignores reservoir physics, which further bias thermal energy estimates. Importantly, the recovery factory parameter used in stored heat calculations is very uncertain and cannot reflect the complexities producing from different geothermal systems.

Our numerical modelling approach presented in this work provided robust estimates of the potential power output for each geothermal field, as the methodology accounts for reservoir and wellbore physics and fluid flow dynamics. The approach also allows additional insights into the nature of the geothermal resource. For example, it was found that accurately modelling the water table level was critical for the Ciremai system. The initial numerical resource assessment yielded a very low power estimate due to the system having a very deep water table. The deep water table strongly affects the reservoir pressure in the system and the ability of geothermal wells to flow without pumping. Our research indicated that it was unlikely for conventional wells to self-discharge at the Ciremai system. Thus, a scenario involving drilling highly-deviated wells from lower elevations was considered. Development scenarios such as this can only be considered using numerical reservoir modelling techniques. The stored heat calculation for Ciremai can only account for the low reservoir pressure crudely through the recovery factor and most likely overestimated the resource potential as a result.

Similarly the Kepahiang system has a very deep top of the reservoir due to a thick conductor. The effect of the deep reservoir can be accurately estimated using our approach which models the production wellbore physics. The result is a more conservative estimate then the stored heat calculation which likely overestimates the recovery factor once again.

For Kotamobagu the results are quite similar with our numerical modelling approach estimating a lower resource potential. For this system the MT data and their interpretation are quite uncertain and as a result our interpretation of the target reservoir was slightly smaller than the resistivity boundary used in the stored heat calculation. The target reservoir zone could be expanded once more geoscientific data or exploration drilling more clearly identify its extent.

5. CONCLUSION

This study presents six case studies demonstrating a new framework for assessing the resource potential of geothermal systems. This framework uses early-stage exploration data to constrain numerical reservoir models and estimate the potential power output of a geothermal system. This approach can provide a more realistic estimate of geothermal resource potential than traditional methods, such as stored heat calculations, as it can represent the complex reservoir dynamics that affect how much energy can be extracted.

For each system, a new 3D geological model was constructed using publicly available data and data from the Geological Agency (GA) and the Directorate-General of New Renewable Energy and Energy Conservation (EBTKE). These 3D models provide a better conceptual understanding of each system and allow critical geological structures and features to be visualized. Subsequently, numerical models compatible with AUTOUGH2 and Waiwera were developed representing key aspects of the geothermal system, such as temperature distribution, heat transfer, and fluid flow.

The methodology then uses the calibrated models to generate an ensemble of sample models from sets of reasonable parameters, thereby representing the uncertainties inherent at the exploration stage. Our method is also adaptable, enabling refinement of production strategies as additional data becomes available and allowing for seamless updates when geological models are revised. The production algorithm calculates realistic maximum energy extraction scenarios for each of the thousands of sample models and can also be adjusted to suit specific project criteria.

The case studies presented show that our novel approach can be used to estimate the early resource potential of geothermal systems with diverse geological settings and thermodynamic conditions. They have also highlighted some typical flaws in estimates made using the stored heat method. The method can be implemented using only publicly available data (see Kotambagu) though the availability of comprehensive exploration data, including geoscience and exploration well data, is preferable, as it enhances the accuracy of the conceptual model and provides more data to constrain the numerical reservoir models.

By working with the Geological Agency (GA) and the Directorate-General of New Renewable Energy and Energy Conservation (EBTKE) to combine high quality geoscientific surveys and exploration data with our robust numerical modelling approach we hope this framework can help to address some of the challenges in estimating the capacity of geothermal resources during early exploration, and contribute to the broader goals set by the Indonesian government for expanding geothermal energy production.

REFERENCES

Alhusni, H., Satria, T., Perdana, P., Purwanto, E. H., & Setyawan, H. (2023). Geothermal Business Outlook in Indonesia. 48th Workshop on Geothermal Reservoir Engineering.

Alia, W. T. (2024). Quantifying Geothermal Resource Potential and Uncertainty Analysis using a Natural State Model of Papandayan Geothermal Field in West Java Province, Indonesia. University of Auckland.

Aloanis, A. A. (2024). Resource Assesment of Maritaing Geothermal Green Field Area East Nusa Tenggara, Using Numerical Modelling and Uncertainty Quantification. University of Auckland.

Alzwar, M., Akbar, N., & Bachri, S. (1992). Geological Map of Garut and Pemeungpeuk Sheet, Java. [Map].

Apandi, T., & Bachri, S. (1997). Peta Geologi Lembar Kotamobagu, Sulawesi.

Arsadipura, S., Kholi, M., & Djukardi, , Dedi. (2011). Penyelidikan Geofisika Terpadu Gaya Berat, Geomagnet dan Geolistrik Daerah Panas Bumi Kepahiang, Kecamatan Kaba Wetan, Kabupaten Kepahiang, Provinsi Bengkulu.

Badan Geologi. (2019). Laporan Evaluasi Data Geosains Panas Bumi untuk Pengusulan WK Panas Bumi TA. 2019 - Papandayan.

Boling, R. A., Tanesib, J. L., Sutaji, H. I., Lapono, L. A. S., & Lewerissa, R. (2024). Re-evaluation of a geothermal system model based on high-resolution gravity field inversion: A case study of the Maritaing geothermal

field, Alor Regency, East Nusa Tenggara Province, Indonesia. Kuwait Journal of Science, 51(2), 100187. https://doi.org/https://doi.org/10.1016/j.kjs.2024.100187

Byrdina, S., Grandis, H., Sumintadireja, P., Caudron, C., Syahbana, D. K., Naffrechoux, E., Gunawan, H., Suantika, G., & Vandemeulebrouck, J. (2018). Structure of the acid hydrothermal system of Papandayan volcano, Indonesia, investigated by geophysical methods. Journal of Volcanology and Geothermal Research, 358, 77–86. https://doi.org/10.1016/j.jvolgeores.2018.06.008

Croucher, A., O'Sullivan, M., O'Sullivan, J., Yeh, A., Burnell, J., & Kissling, W. (2020). Waiwera: A parallel open-source geothermal flow simulator. Computers and Geosciences, 141. https://doi.org/10.1016/j.cageo.2020.104529

Dekkers, K., Gravatt, M., Maclaren, O. J., Nicholson, R., Nugraha, R., O'Sullivan, M., Popineau, J., Riffault, J., & O'Sullivan, J. (2022). Resource Assessment: Estimating the Potential of a Geothermal Reservoir. 47th Workshop on Geothermal Reservoir Engineering.

Direktorat Panas Bumi. (2017). Potensi Panas Bumi Indonesia Jilid 1-2 (Geothermal Potential of Indonesia 1st and 2nd Edition) (2nd ed.).

Djuri. (2011). Geological map of the Arjawinangun, Java. [Map].

Fuad, A. A. (2024). Resource Potential Assessment of Mount Ciremai Geothermal Field using Reservoir Modeling and Uncertainty Quantification Method. University of Auckland.

Hall, R. (2002). Cenozoic geological and plate tectonic evolution of SE Asia and the SW Paci®c: computer-based reconstructions, model and animations. In Journal of Asian Earth Sciences (Vol. 20). www.elsevier.com/locate/jseaes*

Hamilton, W. B. (1979). Tectonics of the Indonesian region. In Professional Paper. https://doi.org/10.3133/pp1078

Irawan, D. E., & Puradimaja, D. J. (2006). The hydrogeology of the volcanic spring belt, east slope of Gunung Ciremai, West Java, Indonesia. International Association for Engineering Geology.

Irawan, D. E., Puradimaja, D. J., Notosiswoyo, S., & Soemintadiredja, P. (2009). Hydrogeochemistry of volcanic hydrogeology based on cluster analysis of Mount Ciremai, West Java, Indonesia. Journal of Hydrology, 376(1), 221–234. https://doi.org/https://doi.org/10.1016/j.jhydrol.2009.07.033

Joni, W., Wahyuningsih, R., Sumber, P., Mineral, D., Dan, B., & Bumi, P. (2019). 2-D AND 3-D INVERSION MODELLING USING MAGNETOTELLURIC DATA AT MASSEPE GEOTHERMAL AREA, SIDENRENG RAPPANG REGENCY, SOUTH SULAWESI PROVINCE. In Buletin Sumber Daya Geologi (Vol. 14).

Katili, J. A. (1975). Volcanism and plate tectonics in the Indonesian island arcs. Tectonophysics, 26(3), 165–188. https://doi.org/https://doi.org/10.1016/0040-1951(75)90088-8

Katili, J. A. (1978). PAST ANR PRESENT GE~TECTONIC POSITION OF SULAWESI, INDONESIA (Vol. 45).

Kusnadi, D., Nurhadi, M., & Suparman. (2011). Penyelidikan Terpadu Geologi dan Geokimia Daerah Panas Bumi Kepahiang, Kabupaten Kepahiang, Bengkulu.

MacPherson, C. G., & Hall, R. (2002). Timing and tectonic controls in the evolving orogen of SE Asia and the western Pacific and some implications for ore generation. Geological Society Special Publication, 204, 49–67. https://doi.org/10.1144/GSL.SP.2002.204.01.04

Mazot, A., Bernard, A., Fischer, T., Inguaggiato, S., & Sutawidjaja, I. S. (2008). Chemical evolution of thermal waters and changes in the hydrothermal system of Papandayan volcano (West Java, Indonesia) after the November 2002 eruption. Journal of Volcanology and Geothermal Research, 178(2), 276–286. https://doi.org/10.1016/j.jvolgeores.2008.06.022

Nagoro, B. B. R., & O'sullivan, J. (2023). Quantifying Geothermal Resource Potential and Uncertainty Analysis using a Natural State Model of Kotamobagu Geothermal Field in North Sulawesi, Indonesia. 45th New Zealand Geothermal Workshop.

Nasution, A., Widarto, D. S., Hutasoit, L., Yuliani, D., & Hadisoemarto, S. (2008). Geothermal Geophysical Study of Mt. Papandayan, Garut District, West Java Indonesia. Proceedings of the 8th Asian Geothermal Symposium.

Nugraha, A. M. S., Hall, R., & BouDagher-Fadel, M. (2022). The Celebes Molasse: A revised Neogene stratigraphy for Sulawesi, Indonesia. Journal of Asian Earth Sciences, 228. https://doi.org/10.1016/j.jseaes.2022.105140

Nurdiyanto, B., Daud, Y., & Zarkasyi, A. (2022). Application of MT and Gravity Method to Potential Analysis of Kepahiang Geothermal, Bengkulu. Proceeding Confrenece on Applied Electromagnetic Technology (AEMT). https://doi.org/10.31219/osf.io/wc764

O'Sullivan, M. J., & O'Sullivan, J. P. (2016). Reservoir modeling and simulation for geothermal resource characterization and evaluation. In Geothermal Power Generation: Developments and Innovation (pp. 165–199). Elsevier Inc. https://doi.org/10.1016/B978-0-08-100337-4.00007-3

Pacey, A., Macpherson, C. G., & McCaffrey, K. J. W. (2013). Linear volcanic segments in the central Sunda Arc, Indonesia, identified using Hough Transform analysis: Implications for arc lithosphere control upon volcano distribution. Earth and Planetary Science Letters, 369–370, 24–33. https://doi.org/10.1016/j.epsl.2013.02.040

Rahadinata, T., Zarkasyi, A., & Dewi, R. (2017). Survei Magnetotelluric (MT) dan Time Domain Electromagnetics (TDEM) Daerah Panas Bumi Maritaing, Kabupaten Alor, Provinsi Nusa Tenggara Timur.

Rahmansyah, F. (2024). A Resource Assesment Using Numerical Reservoir Modelling of the Massepe Geothermal Field, North Sulawesi, Indonesia. University of Auckland.

Rencana Umum Energi Nasional, Pub. L. No. Presidential Decree No.22/2017 (2017).

Riogilang, H., Itoi, R., & Taguchi, S. (2012). Recharge Elevation of Hot Spring Study in The Mt. Muayat at The Kotamobagu Geothermal Field, North Sulawesi, Indonesia using The Stable Isotope O and H. 36th Workshop on Geothermal Reservoir Engineering.

Riogilang, H., Itoi, R., & Taguchi, S. (2013). Conceptual Model of Hydrothermal System at Kotamobagu Geothermal Field, North Sulawesi, Indonesia. Procedia Earth and Planetary Science, 6, 83–90. https://doi.org/10.1016/j.proeps.2013.01.012

Riogilang, H., Itoi, R., Taguchi, S., Yamashiro, R., Yamashita, S., & Masloman, H. 3. (2011a). Geochemical Study of Hot Spring Water Discharging on the Northern Slope Mt. Muayat in The Kotamobagu Geothermal Fields, North Sulawesi, Indonesia. Proceedings of the 9th Asian Geothermal Symposium.

Riogilang, H., Itoi, R., Taguchi, S., Yamashiro, R., Yamashita, S., & Masloman, H. 3. (2011b). Geochemical Study on Hot Spring Water in Kotamobagu geothermal Field, North Sulawesi, Indonesia. PROCEEDINGS, Thirty-Sixth Workshop on Geothermal Reservoir Engineering.

Riogilang, H., Itoi, R., Tanaka, T., & Jalilinasrabady, S. (2012, November). Natural State Model of the Kotamobagu Geothermal System, North Sulawesi, Indonesia.

Risdianto, D., & Soetoyo. (2008). Survei terpadu geologi, geokimia, dan geofisika daerah hpanas bumi Massepe, Kabupaten Sidenreng Rappang Sulawesi Selatan.

Risdianto, D., Soetoyo, & Freddy N. (2008). Penyelidikan Geologi Daerah Panas Bumi Massepe, Kabupaten Sidenreng Rappang Sulawesi Selatan.

Setiawan, D. I., Wibowo, A. E., & Hermawan, D. (2015). Geologi dan Geokimia Panas Bumi Daerah Maritaing Kabupaten Alor, Provinsi Nusa Tenggara Timur.

Silitonga, P. H., Masria, M., & Suwarna, N. (1996). Geological map of the Cirebon, Java. [Map].

Sugianto, A., & Hadi, M. N. (2011). Survei Terpadu Daerah Panas Bumi Kepahiang Kabupaten Kepahiang, Bengkulu.

Sukaesih, Permana, Lano. A., & Rezki, Y. (2021). Survei Rinci Geologi Daerah Panas Bumi Gunung Ciremai Kabupaten Kuningan, Provinsi Jawa Barat.

Sukamto. (2012). Geological map of the Pangkajene and Western part of Watampone Sheets, Sulawesi. [Map].

Sulastri, M., Menur Mandriati, D. S., & Andi Agus Nur, I. (2014). Geothermal Development Potential of Papandayan Volcano, Garut City, Wets Java Province Through Geochemical Analysis Study and Field Activity. Proceedings Indonesia International Geothermal Convention & Exhibition 2014, 4–6.

Supriyadi, Y., Taokdama, I., & Nurdin, N. M. (2015). Survei Terpadu Gaya Berat dan Audio Magnetotelluric (AMT) Daerah Panas Bumi Maritaing, Kabupaten Alor, Provinsi Nusat Tenggara Timur.

Syahrul, A. (2024). Resource Assessment: Estimating the Potential of Kepahiang Geothermal Field. University of Auckland.

Varekamp, J. C., Van Bergen, M. J., Vroon, P. Z., Poorter, R. P. E., Wirakusumah, A. D., Erfan, R., Suharyono, K., & Sriwana, T. (1989). Volcanism and tectonics in the Eastern Sunda Arc, Indonesia. Netherlands Journal of Sea Research, 24(2–3), 303–312. https://doi.org/10.1016/0077-7579(89)90156-7

Z. Abidin, H., Andreas, H., Gamal, M., K. Suganda, O., Meilano, I., & Hendrasto, M. (2003). Ground Deformation during Papandayan Volcano 2002 Eruption as Detected by GPS Surveys. ITB Journal of Engineering Science, 35(1), 45–60. https://doi.org/10.5614/itbj.eng.sci.2003.35.1.4

Zarrouk, S. J., & Simiyu, F. (2013). A REVIEW OF GEOTHERMAL RESOURCE ESTIMATION METHODOLOGY. In 35 th New Zealand Geothermal Workshop.

Untapped Geothermal Potential of Lahendong Concession, North Sulawesi

Ristio Efendi, Antonius.R. Untoro, Sigit Suryanto,
David. P. Timisela, and Dimas. B.E. Rindingpadang

PT Pertamina Geothermal Energy Tbk.
Grha Pertamina Building 5th Floor, Medan Merdeka Timur St. No. 11-13 Jakarta 10110

Ristio.efendi@pertamina.com

Keywords: Mahawu, Geothermal

ABSTRACT

An unexplored prospect within the Lahendong Concession or WKP is Mount Mahawu. Limited research publications and data constraints have prompted PGE to initiate geological and geochemical studies from 2019 to 2023. Mount Mahawu's geological structure is part of the Quaternary volcanic arc situated east of the Lokon Volcano complex, formed by tectonic subduction in North Sulawesi's northern arm, known as the Sangihe Arc. Classified as a Type-A volcano, Mount Mahawu features low activity fumarole within its central eruption crater and sits atop an older volcanic complex.

The geothermal system of Mount Mahawu is indicated by thermal manifestations extending from its central eruption area to the northern volcanic complex. These manifestations include hot water with temperatures of 88.7°C and neutral pH, Cl-SO4 hot water with a pH of 2 on the northeastern slope, and argillic alteration on the southern side. Weak fumarole emissions are observed in the central eruption crater.

The heat source is attributed to the Quaternary-aged volcanic activity of Mount Mahawu, associated with the active volcanic emergence of Mount Lokon. The cap rocks are the result of hydrothermal alteration of volcanic products such as basaltic andesite lava, pyroclastic breccia, and tuff, producing clay minerals dispersed around the geothermal hydrology system. The geothermal reservoir temperature, estimated using the cation geothermometer, is approximately 216°C.

This medium-enthalpy reservoir, as inferred from manifestation data, holds significant geothermal potential and presents an opportunity for further development.

1. INTRODUCTION

Lahendong Geothermal Concession (WKP) is a geothermal working area located in North Sulawesi, Indonesia. This area is managed by Pertamina Geothermal Energy (PGE) based on Minister of Energy and Mineral Resources Decree No. 2067K/MEM/2012 dated 18 June 2012. The Lahendong Concession covers an area of 106,800 hectares and has very promising geothermal prospects. In this area, there are two geothermal potentials that have been developed, namely Lahendong and Tompaso. Lahendong Unit I, which produces 20 MWe, began operating in 2001 and has operated consistently. Capacity development of 40 MWe was carried out in 2007-2009, and an additional 20 MWe began operating in 2011. Currently, Lahendong's total generating capacity reaches 80 MWe from 4 power plants, and Tompaso produces 2x20 MWe which is also included in this Concession. Apart from that, there is still other potential in this Concession that has not been explored, showing great opportunities for the development of geothermal energy in the future.

One of the other geothermal prospects in the WKP is located in the Mahawu Area. Based on a preliminary survey conducted by the Center for Geological Resources (PSDG) in 2013, two manifestations in the form of hot springs were found in the Kaleosan Area. These manifestations show great potential, and further and detailed research is needed to understand the geothermal system and evaluate the geothermal energy potential in this area. In 2023, PGE conducted geochemical and geological survey to assess preliminary evaluation of Mahawu prospect.

2. METHOD

Geological survey were conducted to find out the distribution of rock formations, identify tectonic features, and evaluate the physical characteristics of geothermal manifestations. Furthermore, geochemical survey were carried out to determine the fluid characteristics and conditions within geothermal reservoirs. This involves analyzing various parameters, including the type of manifestation and the concentration of solute to understand estimated temperature reservoir base on geothermometry.

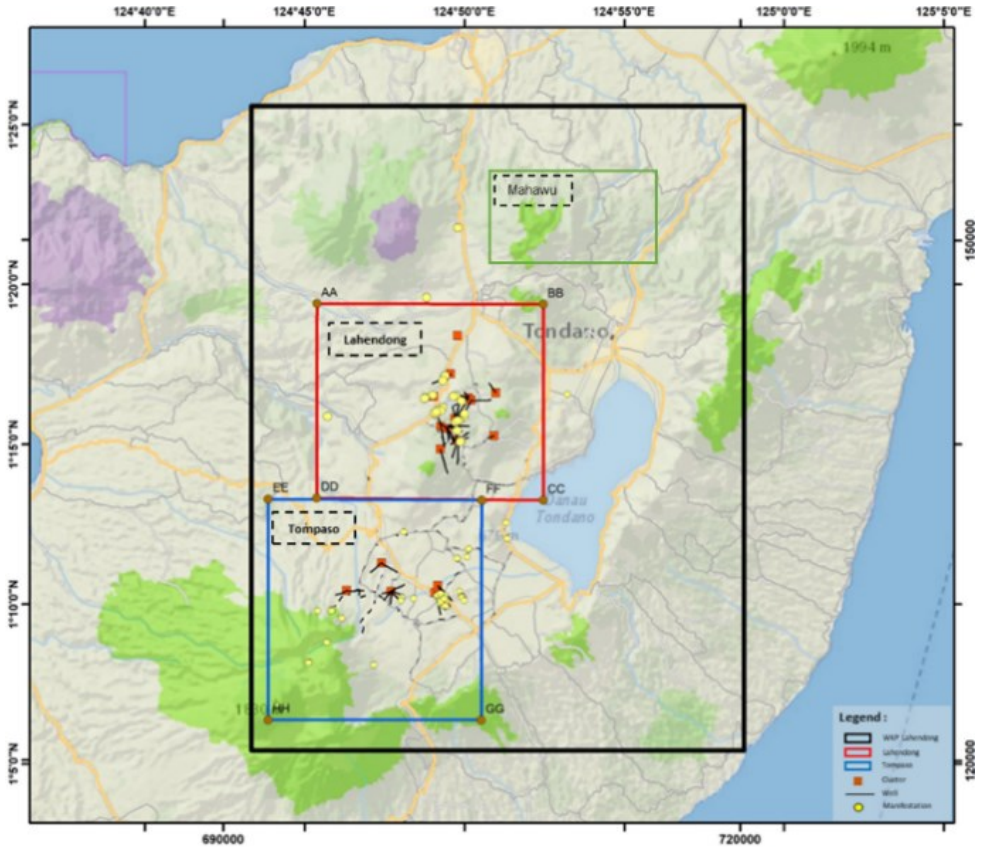

Figure 1: Geothermal prospect in the Lahendong Concession (Black square), Tompaso prospect at the South (Light blue square), Lahendong prospect (Red square), and Mahawu Prospect at the North (Green square).

3. REGIONAL GEOLOGY

The Mahawu Volcanic Complex is situated in the eastern part of the Northern Arm of Sulawesi Island, an area commonly referred to as the Minahasa Compartment (Siahaan et al., 2005). The Northern Arm of Sulawesi was formed by convergent tectonic processes, which include the subduction of the North Sulawesi Plate to the north and the East Sangihe Plate to the east, adjacent to Halmahera (Hall and Wilson, 2000). The subduction of North Sulawesi has been driven by the interaction between the Molucca Sea Oceanic Plate and the East Banda Arc since the Middle Miocene (Hamilton, 1979; Katili, 1975; Walpersdorf et al., 1998). The formation of geological structures in the Minahasa Compartment is primarily influenced by the tectonic evolution resulting from the interaction between the Sangihe Arc Subduction and the Halmahera Arc Subduction. This interaction has caused the Minahasa Compartment to move west to northwest (Walpersdorf et al., 1998) and rotate counterclockwise (Szentpeteri et al., 2015). On the surface, these tectonic processes have manifested in three major geological structures within the Minahasa Compartment: the Amurang-Malompar Fault, the Manado-Kema Fault, and the Tondano Volcanotectonic Depression Structure (Effendi and Bawono, 1997; Lecuyer et al., 1997). The Manado-Kema Fault borders the Minahasa Compartment to the north, while the Amurang-Malompar Fault borders it to the south.

The regional geological framework of the Mahawu and Klabat volcanic complexes in North Sulawesi is profoundly shaped by the tectonic dynamics within the Minahasa Compartment and result of significant volcanic activity during Quarternary period. The Mahawu Volcanic Complex, a stratovolcano located east of the Lokon-Empung volcano, exhibits complex geological features including pyroclastic cones and a crater lake formed from historical volcanic activity. Mount Klabat, the tallest volcano in Sulawesi, is distinguished by its summit crater lake, although it lacks recorded eruptions. These volcanoes are integral to the volcanic arc formed by the subduction of tectonic plates, underscoring their intricate geological and geothermal properties.

4. RESULT AND DISCUSSION

4.1 Local Geology

The delineation and relationship of volcanostratigraphic units were determined based on observations from a Digital Elevation Model (DEM), using references from previous publications and geological maps (Effendi et al., 1993; Effendi and Bawono, 1997; Wibowo et al., n.d.). There are 10 geological units in the study area, ranging from the oldest to the youngest: Tertiary Volcaniclastics, Tondano Tuff, Masarang Lava, Tombuluan Lava, Titingon Lava, Mahawu Lava, Klabat Lava, Klabat Pyroclastic, and Alluvium.

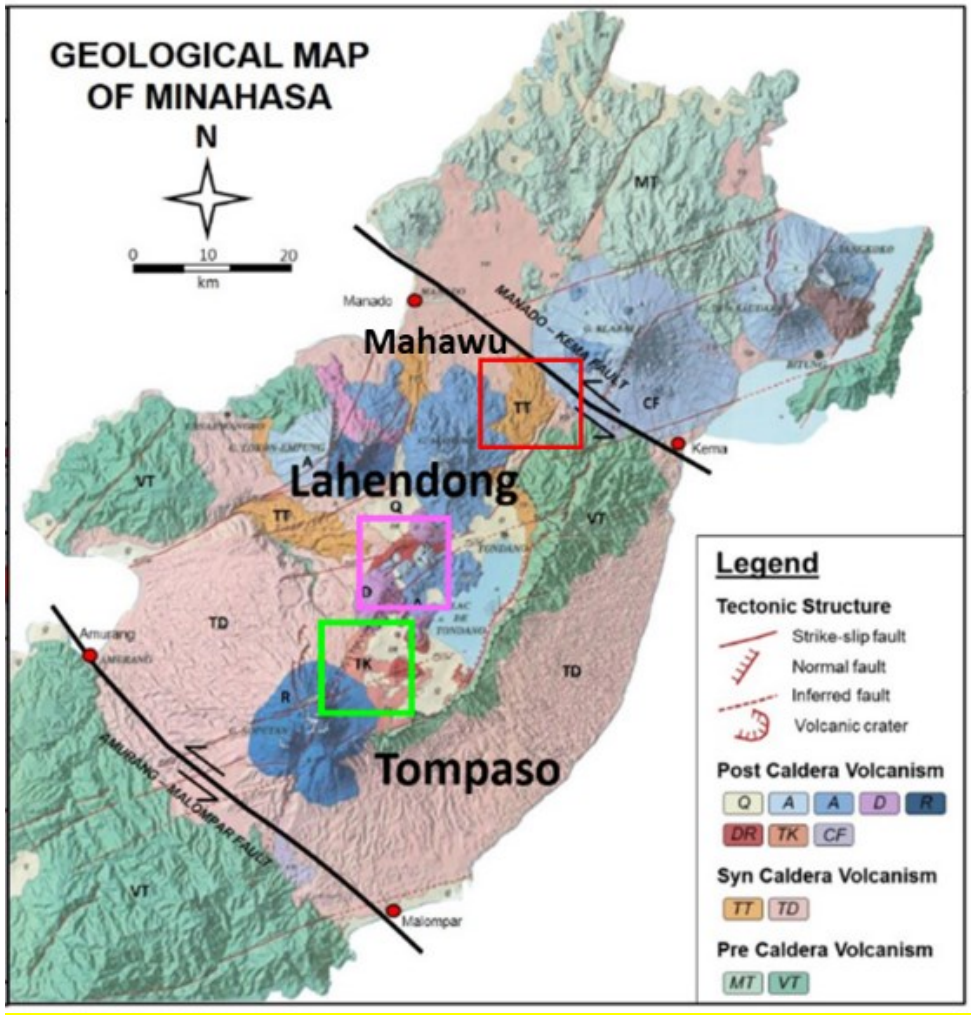

Figure 2: The geological map of the Minahasa Compartment (Lecuyer et al., 1988) shows the Tondano Volcanotectonic Depression, which is composed of pre-, syn-, and post-volcanic products of Tondano. The map also highlights two major strike-slip structures that bound the Minahasa Compartment to the north and south.

The oldest rocks found in the study area are products of the Tertiary volcanism, including breccia, andesite-basalt lava, and tuff (Effendi and Bawono, 1997). Additionally, mapping by Effendi et al. (1993) indicates that Quaternary volcanism began with the Tondano volcanic episode, which produced widespread tuff, pumice, and ignimbrite with flow structures. This massive Tondano volcanism also contributed to the formation of the Tondano Caldera. Volcanic activity continued with eruptions from Mount Wawo, Mount Masarang, Mount Tombuluan, Mount Titingon, and Mount Klabat, and Mount Mahawu, which remains active to this day, with the last recorded eruption occurring on November 16, 1977 (Global Volcanism Program, 2024). Futhermore, the volcanic products found in the Mahawu Volcanic Complex are generally lava with compositions ranging from basalt to dacite, as well as pyroclastic flow and lahar deposits (Siahaan et al., 2005; Yamin et al., 2015).

The determination of the geological structures in the Mahawu area was based on several previous publications (Effendi et al., 1993; Wibowo et al., n.d.) and interpretations using Digital Elevation Model (DEMNAS) data. The geological structures in the Mahawu area generally have a northwest-southeast orientation, aligning with the direction of subduction, as well as northeast-southwest and, to a lesser extent, north-south orientations. The major

faults in the study area are the Kuwil Fault and the Taedei Fault (Wibowo et al., n.d.), which are part of the sinistral strike-slip Manado-Kema Fault, one of the major northwest-trending faults that delineate the Minahasa Compartment to the northeast (Effendi and Bawono, 1997; Lecuyer et al., 1997). The presence of these faults is also believed to control the occurence manifestations observed in the study area.

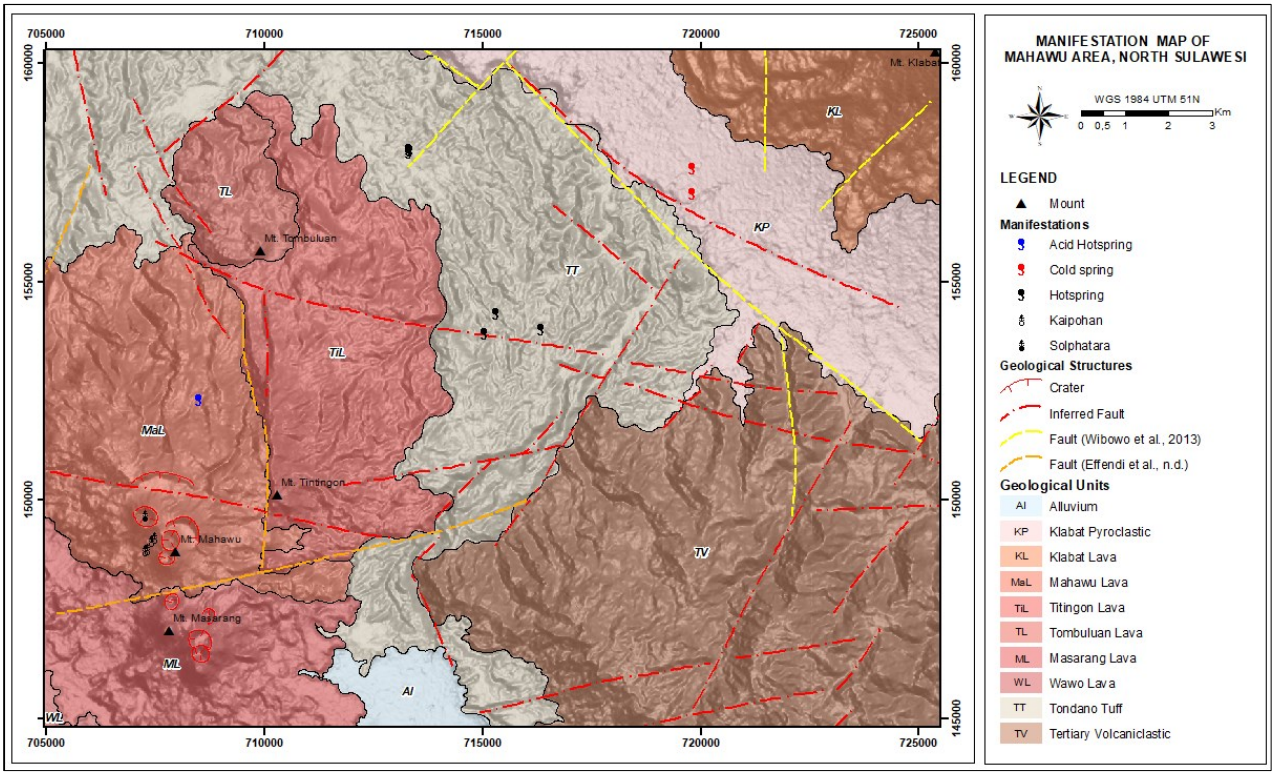

Figure 3: Geological map of the Mahawu-Klabat area with geological structures shown in yellow dash (Wibowo et al., 2013), orange dash (Effendi et al.), and red dash representing inferred faults.

Table 1: Physical parameter of surface manifestation.

No	Lokasi	Jenis_mani	Id/Code	Ambience Temp	Manifestation Temp	PH	Total Disolve Solid
1	Mahawu	Hotspring	MHW-1	30.2	57.3	2.92	1182
2	Kaleosan	Hotspring	KLS-1	32.9	74.1	7.96	1001
3	Mahawu (Kaipohan)	Kaipohan	MHC-1	22.5	28.8	N/A	N/A
4	Air Madidi Tumatenden	Cold spring	AMD-1	28.4	26.6	7.67	84.31
5	Air Madidi	Cold spring	AMD-2	28	26.7	6.58	118
6	Sampiri	Hotspring	SAM-2	31.8	42.3	6.92	263
7	Sampiri	Hotspring	SAM-1	32.4	28	7.01	98.7
8	Sawangan	Hotspring	SAW-1	26.4	40.4	6.66	115.8
9	Mahawu (Kaipohan)	Kaipohan	MHB	26.4	22.6	3.25	260.7
10	Kaleosan	Hotspring	KLS-2	36.5	53	7.98	490

4.2 Water Geochemistry

The prospect area is featured by manifestations around the crater of Mount Mahawu and hotsprings at northeast. Additionally, hotsprings located between Mount Mahawu and Mount Klabat were the key targets for this survey. Data collection for manifestations was conducted concurrently in 2023. The manifestations and cold springs in the Mahawu prospect can generally be categorized as follows:

- Mount Mahawu Group: Includes altered ground or kaipohan to the south of Mount Mahawu, Solfatar at the crater of Mount Mahawu, and acidic hot springs (MHW-1) on the northeastern flank.
- Sampiri-Kaleosan Group: Comprises hotspring manifestations in Sampiri (SAM1, SAM2, SAW1) and Kaleosan (KLS- 1, KLS-3). No thermal activity was found in Air Madidi.

The Mahawu Prospect is generally characterized by hotsprings and some acidic hot springs, with no active fumaroles (kaipohan and altered ground) and the crater of Mount Mahawu. Hotsprings are distributed across the northeast region of the Mount Mahawu complex. Field observations indicate that the spring water temperatures range from 28-57°C with pH values between 2.9 and 8. Anion, cation, and isotope sampling was conducted in the hotsprings based on these observations.

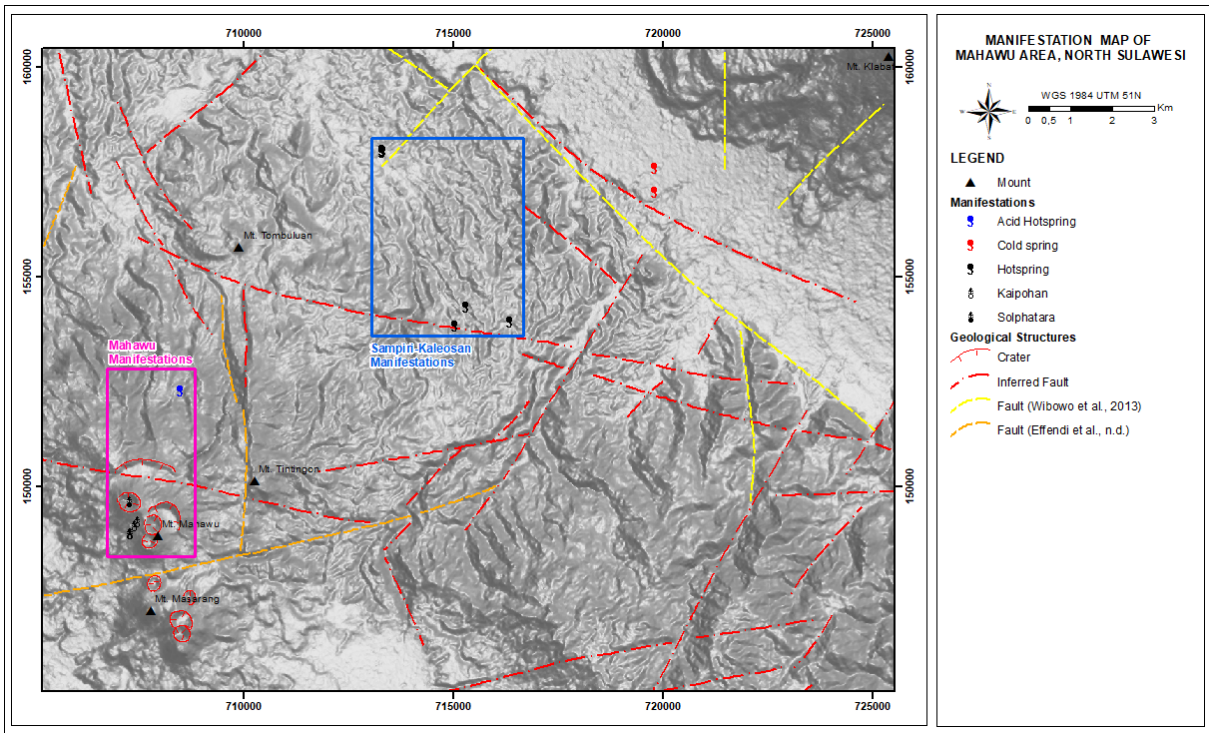

Figure 4: Map distribution of data and manifestations of the Mahawu prospect. The Mahawu complex is marked in pink, and the Sampiri and Kaleosan complex is marked in blue.

4.3 Geochemistry Evaluation

Based on the geochemical survey carried out in 2023, cold spring samples were taken from various locations and then analyzed by a third party laboratory. Table 1 presents the results of the water chemistry analysis. Initial quality control of the data was performed using ion balance calculations before further evaluation. Acid fluid manifestations with an ion balance value exceeding 5% (e.g. MHW-1, MHB-1, MHW-4) were included in the geochemical interpretation due to evidence of oxidation. Other manifestations with an ion balance value below 5% exhibited good data quality.

The ternary diagram of Cl-HCO_3-SO_4 indicates that manifestations around the Kaleosan area (KLS 1) exhibit water characteristics close to chloride/mature water. Acidic springs in Mahawu and the river from Mount Mahawu are classified as sulfate water types. In contrast, the cold springs in Air Madidi Village (AMD-1 & AMD-2) and the warm springs in Sampiri Village (SAM-1 & SAM-2) are classified as bicarbonate water types. Within the Mahawu geothermal system, chloride hot springs are found exclusively in Kaleosan village (KLS-1 to KLS-3), with a significant number of points around the Kaleosan River and some occurring directly in the river.

Data plotted on the Na-K-Mg diagram shows that all manifestations and springs in the Mahawu Geothermal system are classified as immature water. This suggests significant mixing with meteoric water during the transportation from the reservoir to the surface. Only the sample from the KLS-1 manifestation is positioned on the partial equilibrium line, indicating a stronger influence from the reservoir compared to other hot springs.

The Cl/B (Conservative element) diagram reveals two distinct groups of springs: the Kaleosan trend (KLS 1 and KLS 2) and the MHW acid manifestations. The Kaleosan group shares similar characteristics with the Sampiei and Sawangan manifestations, as well as several springs from Mount Mahawu. Conversely, the hot springs in Mahawu and those to the north of Mount Mahawu (MHW 1) exhibit an acidic pH, likely due to sulfate condensation in meteoric water, while maintaining high chloride levels indicative of a magmatic origin.

Isotope analysis provides insights into the fluid properties and processes of the manifestations and springs in this area. The Oxygen-18 ($\delta^{18}O$) vs. Deuterium (δD) plot shows that both cold and hot springs, including those from Sampiri and Kaleosan, display a slight shift to the right of the Local Meteoric Water Line (LMWL). This minor

shift suggests a limited influence, as the water type in these locations is predominantly chloride and remains mixed with surface water. The samples do not indicate a significant influx of magmatic fluid; rather, there is a subtle shift to the left in the plot.

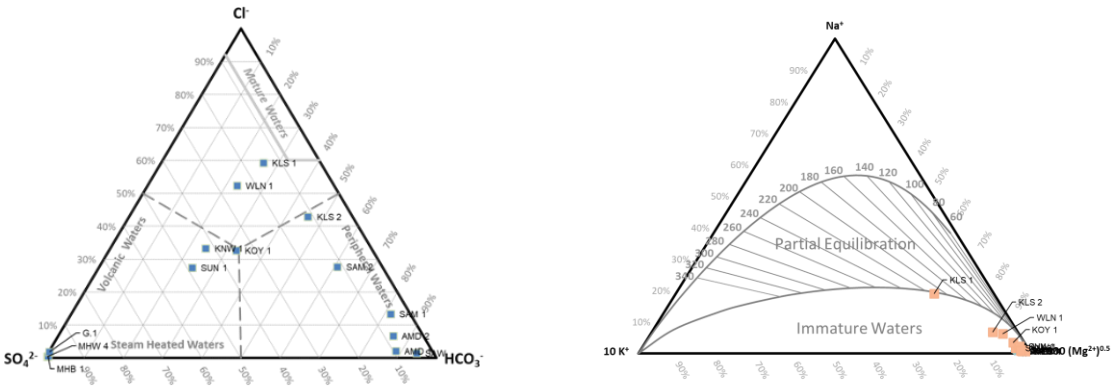

Figure 5: Ternary diagram of Mahawu water chemistry data.

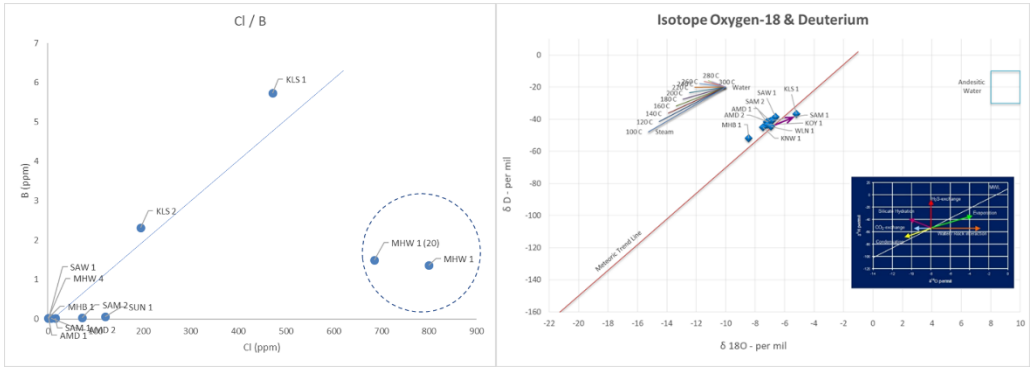

Figure 6: Diagram Cl/B of Mahawu water chemistry data (left) and Isotopes Oxygen-18 vs Deuterium data (right).

4.4 Geothermometry

Geothermometer is one of the methods in estimating reservoir temperature based on chemical composition from brine and gas samples. In this study, geothermometer approach is utilized to estimate the change in reservoir fluid temperature using solute geothermometer.

Silica geothermometer approach utilizes silica solubility as a function of temperature. While cation geothermometer is based on the equilibrium between minerals. Both geothermometer have different apporach. The fluid in the reservoir has reached equilibrium and when it rises to the surface, the Na/K ratio does not change much. The fluid migration to the surface might cause slight changes in temperature. Silica is very sensitve to temperature change, either because of pressure change or mixing with surface water. Therefore, the silica geothermometer method provides a lower temperature estimate compared to the cation geothermometer method which calculates temperature estimation at greater depth. When calculating geothermometry near the surface, the Na/K geothermometer should be corrected using calcium and magnesium conceentration for a more accurate temperature estimation.

Based on the results of water chemistry analysis, geothermometer calculations can be carried out to determine the temperature of the subsurface reservoir, while gas geothermometers cannot be used because there is no gas data that can be taken. All manifestations associated with the Mahawu system are not chloride water types that reflect fluid directly from the reservoir except for the Kaleosan Manifestation. Subsurface temperature can only be interpreted using 1 data which is still experiencing mixing based on the Cl-HCO3-SO4 and Na-K-Mg diagrams. The geothermometer results show a subsurface temperature range of 170 ºC – 216 ºC based on the Silica, Na/K, Na-K-Ca, and Na-K-Mg Correction geothermometer.

4.5 Tentative Conceptual Model

The hydrology of the Mahawu geothermal system remains a critical area of investigation. Based on the presence of chemical manifestations and existing data, the upflow is likely located beneath Mount Mahawu, where volcanic cones and craters exhibit minimal residual activity. In contrast, fumaroles to the south have undergone cooling and condensation. The northeast outflow direction is suggested by the presence of chloride manifestations in Kaleosan and chloride traces in the Sampiri area. Additionally, the presence of acidic hot spring manifestations on the northeastern flank of Mahawu is likely indicative of shallow fluid flow resulting from the oxidation of H2S gas within the groundwater aquifer. The prospect boundary towards Mount Klabat is defined by the Manado-Kema Fault, which is interpreted as a sealing fault. This is corroborated by the absence of other manifestations east of the fault, with only minor chloride traces observed in the cold springs of Air Madidi (AMD-1 & AMD-2). To develop a more robust conceptual model, further research into the distribution of clay caps and detailed geological structures is essential.

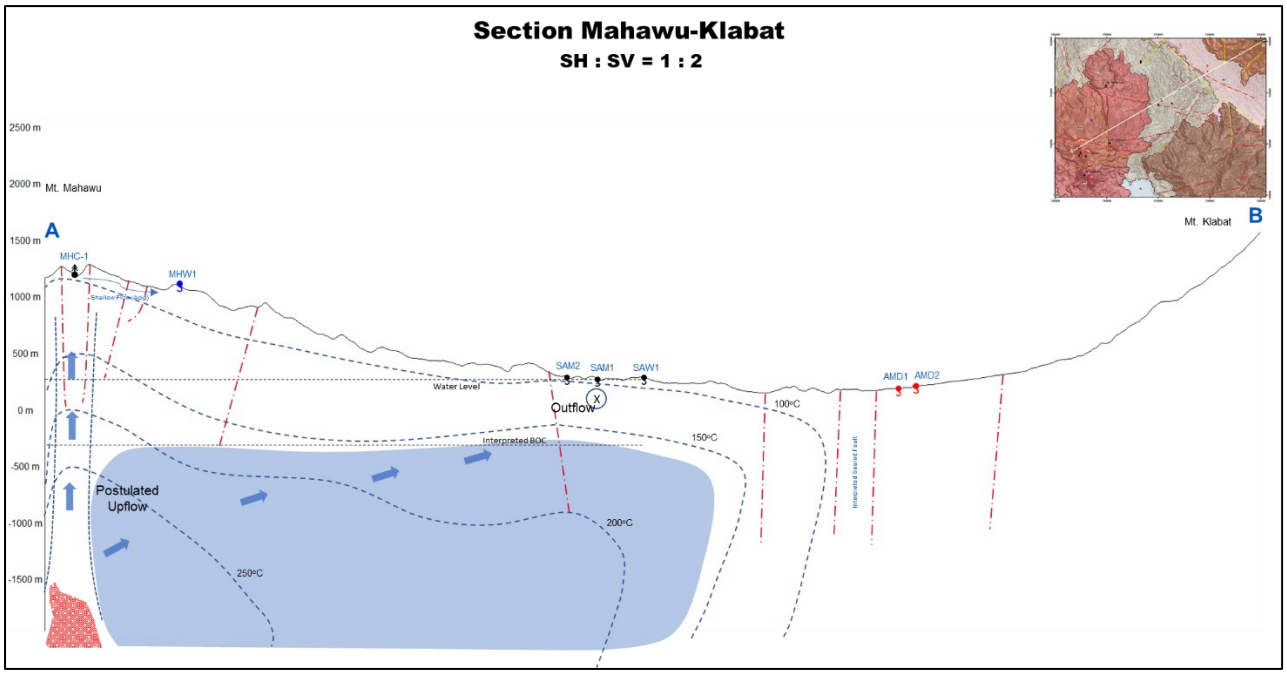

Figure 8: Tentative conceptual model which built from Geology and Geochemistry data of Mahawu Prospect.

5. CONCLUSION

The region's geological framework, shaped by the tectonic interactions of the Sangihe and Halmahera Arc Subductions, has resulted in a complex structural configuration within the Minahasa Compartment. These findings underscore the area's considerable geothermal prospects. The Lahendong Concession in North Sulawesi, particularly the Mahawu area, holds significant untapped geothermal potential, representing a promising frontier for future energy development. Comprehensive geological and geochemical surveys conducted from 2019 to 2023 by PGE have revealed substantial geothermal manifestations, including hot springs, acid hot spring, kaipohan, and low activity fumarole, indicative of a medium-enthalpy geothermal system with reservoir temperatures approximating 216°C. Continued exploration and in-depth studies are essential to harness the Mahawu area's full potential, which could play a pivotal role in augmenting Indonesia's geothermal energy resources.

REFERENCES

Effendi, A.C., and Bawono, S.S.: Geological Map of the Manado Sheet, North Sulawesi, Pusat Penelitian dan Pengembangan Geologi, Bandung, (1997).

Effendi, W., Kusnadi, I., Irawan, W., and Mulyadi, E.: Geologic Map of Mahawu Volcano, Minahasa, North Sulawesi, *Map*, Direktorat Vulkanologi, Bandung, (2013).

Global Volcanism Program: Mahawu (266110), *Database*, Volcanoes of the World, (2024).

Hall, R., and Wilson, M.: Neogene Sutures in Eastern Indonesia, *Journal of Earth Sciences*, **18**, (2000), 781-808.

Hamilton, W.: Tectonics of the Indonesian region, *Professional Paper*, **1078**, (1979), 345.

Katili, J.A.: Volcanism and Plate Tectonics in the Indonesian Island Arcs, *Tectonophysics*, **26**, (1975), 165-188.

Lécuyer, K., Bellier, O., Gourgaud, A., and Vincent, P.M.: Active tectonics of north-east Sulawesi (Indonesia) and structural control of the Tondano Caldera, *Comptes Rendus de l'Académie des Sciences - Series IIA - Earth and Planetary Science*, **325**, (1997), 607-613.

Siahaan, E.E., Soemarinda, S., Fauzi, A., Silitonga, T., Azimudin, T., and Raharjo, I.B.: Tectonism and Volcanism Study in the Minahasa Compartment of the North Arm of Sulawesi Related to Lahendong Geothermal Field, Indonesia, *Proceedings,* World Geothermal Congress, Antalya, Turkiye (2005).

Szentpeteri, K., Albert, G., and Ungvári, Z.: Plate tectonic and stress-field modelling of the North Arm of Sulawesi (NAoS), Indonesia, to better understand the distribution of mineral deposit styles, *Proceedings*, World-Class Ore Deposits: Discovery to Recovery, Tasmania, AU (2015).

Walpersdorf, A., Vigny, C., Manurung, P., Subarya, C., and Sutisna, S.: Determining the Sula Block Kinematics in the Triple Junction Area in Indonesia by GPS, *Geophysical Journal International*, (1998).

Wibowo, A.E.W., and Risdianto, D.: Survei Terpadu Geologi Daerah Panas Bumi Kalawat, Kabupaten Minahasa Utara, Provinsi Sulawesi Utara, *Map*, PSDG, Bandung, (n.d.).

Yamin, R.A., Patonah, A., Hardiyono, A., and Hadi, M. N.: Sistem Panas Bumi Kalawat , Kabupaten Minahasa Utara, Provinsi Sulawesi Utara, *Bulletin of Scientific Contribution,* **13**, (2015), 44-56.

Inter-tidal Hot Springs' Geochemistry in Atauro

James C. Chang[1], Ardhya N.K. Nugroho[1], Joseph E. Ardine[1], and Nazario Gomes[2]

[1]Department of Geological Engineering, Faculty of Mineral Technology, UPN "Veteran" Yogyakarta
[2]Department of Petroleum Engineering, Dili Institute Technology

Ristio.efendi@pertamina.com

Keywords: Atauro Island, inter-tidal hot springs, seawater intrusion, ternary diagram

ABSTRACT

Atauro is a volcanic island formed 3 Ma as a result of the magmatism from arc-continent subduction to collision between the Banda Arc and Australian Passive Margin, recognized from its 2 distinctive volcanic edifices in the southern part of the island with traces of northward-moving volcanism. The ancient volcanism leaves 4 hot springs as its traces, which is adjacent to the coastlines on the eastern part of the island. Therefore, it is strongly affected by the inter-tidal activity. Unfortunately, prior research on inter-tidal hot springs in this area are insufficient. Hence, it is necessary to understand the characteristics of these inter-tidal hot springs by using field observation and water geochemistry analysis, complemented by geothermometric studies with various ternary diagrams and calculations. There are four hot springs on the coastal plain of the eastern Atauro Island, namely, Makili, Pala, Biqueli 1, and Biqueli 2, which all are exposed only at low tide and submerged by seawater at high tide. The rocks around these hot springs are characterized by argillic alteration. The Pala hot spring's water emerged from joints in dacitic rock, while the water of the other three hot springs emerged from alluvial deposits on the coastal plain. The average water temperature of these hot springs is 73.88°C, with pH of 7.15, and the average of 19,525 mg/L for TDS and 39,837.5 µmhos/cm for EC. The Biqueli 2 hot spring has warm ground and a weak sulfuric odour, while the Biqueli 1 hot spring only has sulfuric odour but weaker than Biqueli 2 hot spring. Based on Giggenbach's Na-K-Mg ternary diagram shows that only the Biqueli 1 hot spring is in partial equilibrium with the estimated reservoir temperature 130-140°C, whereas the other three are immature waters. Based on the TCSH and TCLB diagram plots, all samples fall in the mature water zone with high Cl- content, with the average of 15,406.60 mg/L. Thus, considering the high Cl- concentration, along with TDS and EC parameters, indicates that all hot springs have been strongly intruded by seawater. Therefore, a correction using seawater fraction is required to normalize the water geochemistry data. Unfortunately, the seawater sample was not taken and currently there is no available geochemistry data of seawater around this island from previous studies, thus, the correction cannot be performed in this research.

1. INTRODUCTION

Atauro is a volcanic island located around 30 km north of Dili, East Timor. It is a part of the Inner Banda Arc and has 2 distinctive volcanic edifices on its southern part (Ely, et al., 2011). This elongated-shaped island indicates the northward changing volcanism due to the collision between Banda Arc and Australian Passive Margin (Ely, et al., 2011). Consequently, the volcanic activity ceased (Abbot and Chamalaun, 1981) and left several indications of hydrothermal activity and the existence of a geothermal system, such as altered rocks and hot springs. It is necessary to conduct assessments on these hot springs' potential, as it might be developed for a power plant or tourist attraction. Moreover, most of the inhabitants depend on electricity from a diesel-powered power plant, and the availability of which is based on a frequently limited fuel supply. Hence, geothermal energy might become an alternative to provide electricity in this island.

However, these manifestations are mostly located on the eastern shoreline of the island. Interestingly, the hot springs are situated in the intertidal zone and can only be seen when low tide. The absence of previous research on coastal hot springs in this region makes it difficult to understand the processes involved in the geothermal system, particularly the possibility of sea water intrusion, which might influence these manifestations. Therefore, it is necessary to conduct research on these hot springs to unravel their characteristics before determining their potential.

The aim of this paper is to understand the characteristic of inter-tidal hot springs in Atauro Island by utilizing geochemistry analyses of its surface hot spring water and field observation. There are 4 locations where the water samples were taken (Figure 1), namely, Makili (HSM), Pala (HSP), Biqueli 1 (HSB1), and Biqueli 2 (HSB2). Furthermore, water geochemistry data from these samples were plotted in Microsoft Excel using several diagrams, such as Schoeller (1965), Gibbs (1970), and Giggenbach's TCSH, TCLB, and Na-K-Mg (1991).

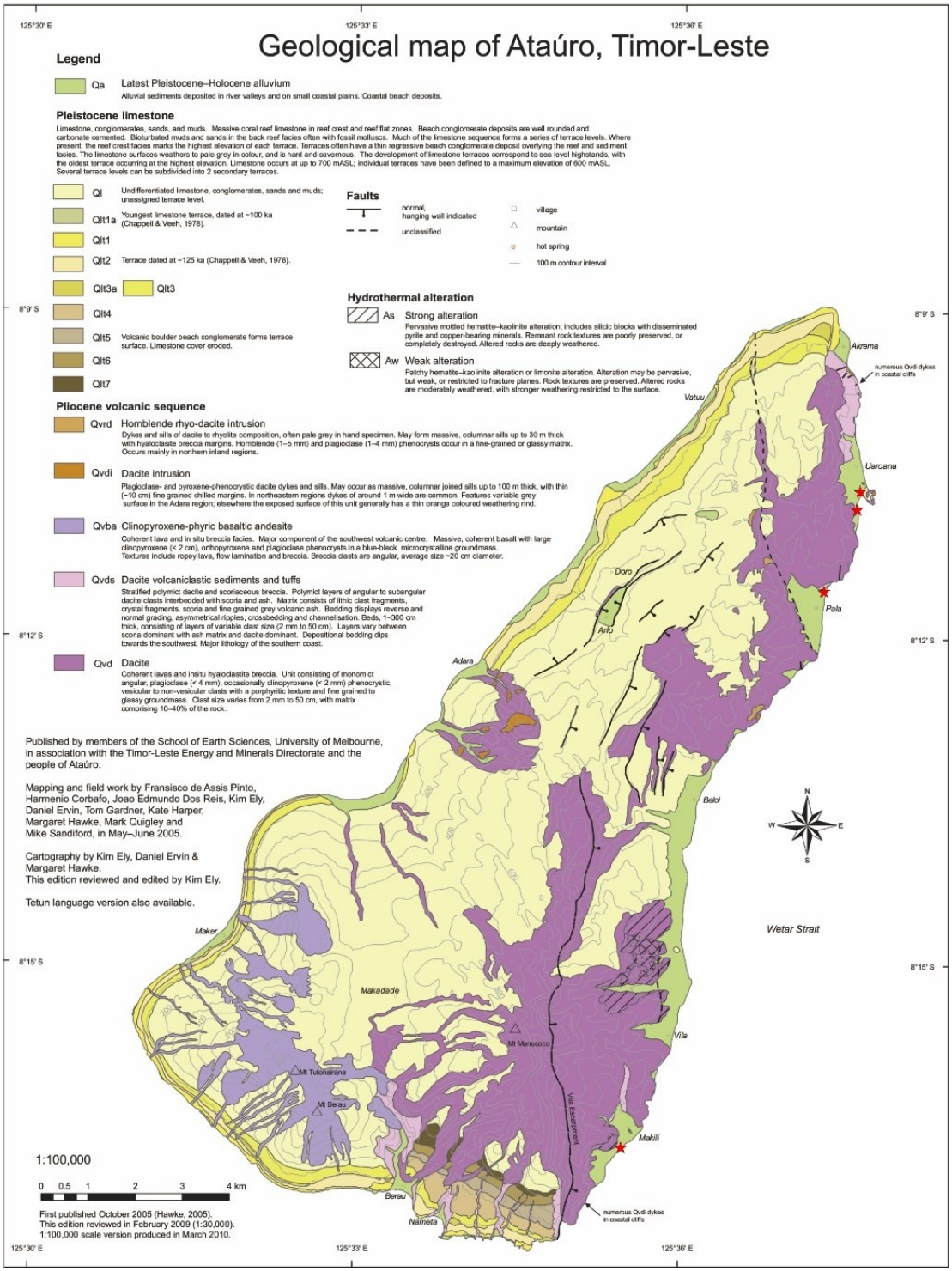

Figure 1: Geological Map of Atauro Island (Ely et al., 2011). Hot Springs are shown with red star symbol.

2. GEOLOGICAL SETTING

The research site is situated within the Southeast Asian tectonic framework, influenced by the convergent interactions of the Pacific, Eurasian, and Australian plates. Atauro Island, positioned in the neotectonic context (Figure 2), is located south of the Wetar Thrust and is impacted by the Timor Trough to its southeastern side (Harris, 2011). Geomorphologically, it is characterized by volcanic landforms and structural features (Chang, 2023).

The tectonic evolution of the study area commenced in the Late Miocene epoch, marked by the subduction-to-collision transition between the Banda Arc and the Australian continent. During the Late Miocene to Pliocene (4-6 Ma), this transition progressed gradually, leading to the uplift of Proto-Timor as a consequence of the shortening of the accretionary zone on the passive margin of the Australian continent due to active tectonic forces. In the Pleistocene epoch, compressional forces persisted, resulting in the shortening and uplift of Timor Island, accompanied by the development of back-arc thrusts and the Banda Volcanic Arc (Hall and Wilson, 2000; Spakman and Hall, 2010; Harris, 2011). The geological structures observed on Atauro Island include normal faults, strike-slip faults, and joints (Chang, 2023). In the context of tectonic evolution, the stratigraphic development in the research area is categorized into the Pliocene Volcanic Sequence, Pleistocene Limestone, and Pleistocene-Holocene Alluvial Deposits, with limestone overlaying volcanic highlands (Abbot and Chamalaun, 1981; Ely et al., 2011).

This tectonic setting has given rise to a volcanic arc that has been inactive since the Pleistocene epoch. However, hydrothermal alteration processes continue actively, facilitating the ongoing presence and potential development of geothermal resources (Abbot and Chamalaun, 1981).

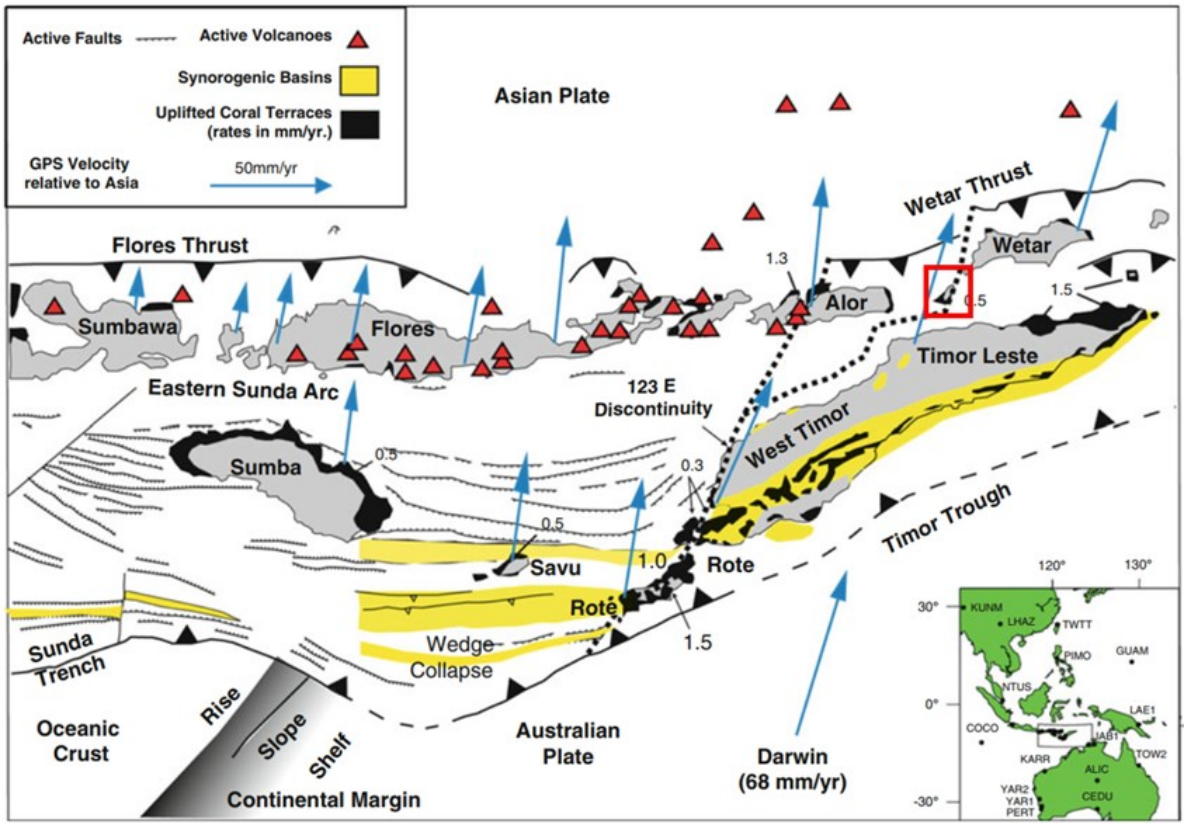

Figure 2: Neotectonic Map around the study area by Harris (2011). Research site is shown in red rectangle.

3. SAMPLING AND LABORATORY ANALYSIS

The sampling was conducted between 8:00 and 10:00 AM (UTC+9) during low tide in the wet season (February 2023). Water sample was collected directly from the water output (indicated by air bubbles) from each location and stored in a 900 mL polyethylene bottle that had been rinsed with groundwater and sample water. We ensured that the bottle was airtight an no water bubbles inside to prevent biological and chemical reaction. The temperature of the hot spring water was directly measured using Fann® Metal Stem Dial Thermometers (Part no. 206037), as well as pH value which was determined using Universal Test Paper. For temperature measurement, the thermometer's stem was dipped around 4 inches under water for 2 minutes, whereas the pH measurement was done by quickly dipping the test stripe (<1 second) and match it with the standard colour. Afterwards, the samples were sent to the Yogyakarta Centre for Environmental Health Engineering and Disease Control (BBTKLPP Yogyakarta) for water geochemistry analysis. The water samples were not filtered (using 0.45-micron membrane filter) except for Na, Li, K, and B parameter.

4. RESULTS AND DISCUSSION

4.1 Makili Hot Spring (HSM)

This hot spring was located at the coastal plain in Makili Village, at the southeastern part of the Island (UTM Zone 51S; 785907 m E, 9082818 m S). This location was accessible via 4-wheeled vehicle until Vila Village, followed by roughly 3,25 kilometres walk along the coastline. The Makili hot spring has a temperature of 187 – 192°F (86.1 – 88.89°C). Temperature measurements were taken at several points where the hot water emerged, characterized by the presence of water bubbles in several small puddles. In the area around the hot spring, there was a slight smell of sulphur and it felt warm with the presence of wet steam. The hot spring emerged from beneath alluvial ranging from fine sand to boulders (Figure 3). The boulders surrounding the hot spring had a reddish colour. It was an altered andesite rock from Mt. Manucoco, indicated by argillic alteration zone on the nearby hill (Chang, 2023).

Figure 3: Makili landscape around hot spring with altered hill in the background (left); small puddles where the hot water came out (middle); hot spring temperature (right).

Figure 4: Pala hot spring puddle (left); fracture where the hot water came out (middle); hot spring temperature (right).

4.2 Pala Hot Spring (HSP)

This hot spring was located in Pala Village at the northeastern side of the island (UTM Zone 51S; 790329 m E, 9094769 m S). This location was accessible by 4-wheeled vehicle and roughly 100 metres walk from the main road. The water came out from fractured rock (Figure 4), which was an altered dacitic rock (Ely, 2011) and had a trace of argillic alteration in the surrounding area. The temperature was measured on the fracture where the water flowed and it showed 149 – 151°F (65 – 66.1°C). This area had a slight smell of sulphur and little amount of steam observed.

4.3 Biqueli 1 Hot Spring (HSB1)

This hot spring was located in Biqueli Village (UTM Zone 51S; 790903 m E; 9096499 m S). This location was accessible by 4-wheeled vehicle and adjacent to the main road. The water came out under the bedding of an unconsolidated coastal deposit with sand-sized grains (Figure 5). This area had light steam and little smell of sulphur, and several brownish-orange alterations. The average of measured temperature was 145°F (62.8°C) on several water flow.

4.4 Biqueli 2 Hot Spring (HSB2)

This hot spring was accessible by 4-wheeled vehicle until the main road and roughly 150 metres walk (or by motorcycle ride) from the main road. The hot spring was located around 30 metres from the seawater, and the surrounding area was a peat land (UTM Zone 51S; 791101 m E, 9096855 m S). However, it become a pond when the high tide. The water flowed and formed a small river, with a quite strong smell of sulphur and steams that were observable (Figure 6). The measured temperature was 166°F (74.4°C) on a single spot that had bubbles, indicating a flow of fluid from beneath.

Figure 5: Biqueli 1small puddles where the hot water came out (left); Landscape around hot spring (middle); small puddles where the hot water came out with brownish-orange altered rocks (right).

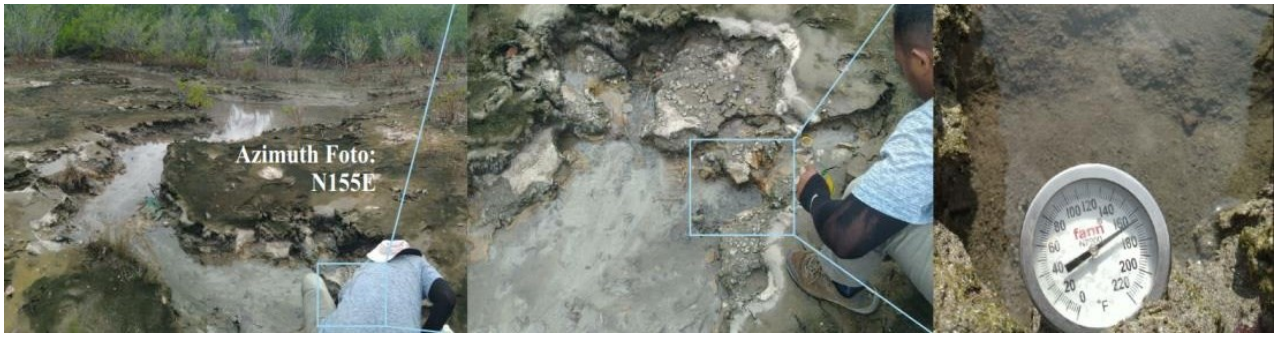

Figure 6: Biqueli 2 landscape around hot spring (left); small puddles where the hot water came out (middle); hot spring temperature (right).

4.5 Hot Spring Water Geochemistry

Chemistry of fluid is an important part in geothermal study and plays a crucial role as a tool to unravel the characteristic of a geothermal field. Four water samples were taken, one for each hot springs on the island, to analyse the chemical composition of geothermal system in Atauro Island. The result of chemical fluid composition of geothermal hot springs is given in Table 1.

Table 1: Major water geochemistry data from inter-tidal hot springs in Atauro Island.

Sample		HSM	HSP	HSB1	HSB2	Method
Na	mg/L	4434.05	5115	5659	5358.48	APHA 2017, Section 3120 B
K		248.3865	188.7212	213.1370	210.4250	APHA 2017, Section 3120 B
Ca		38.21	19.10	26.27	25.47	SNI 06-6989.12-2004
Mg		1197.83	1463.32	1023.74	1266.02	SNI 06-6989.12-2004
Li		1.9069	1.0600	1.0601	0.4549	APHA 2017, Section 3120 B
Cl		15881.6	11996.4	17866.8	15881.6	SNI 6989.19-2009
SO4		1099	844	1265	1814	SNI 6989.20.2019
SiO2		10.167	15.702	9.501	6.718	APHA 2017, Section 4500 C
CO3		18.6	19.5	33.7	30.1	APHA 2017, Section 2310 & 2320 B
B		18.6429	8.6581	8.8203	7.5534	APHA 2017, Section 3120 B
HCO3		138.2	113.1	125.7	125.7	APHA 2017, Section 2310 & 2320 B
TDS		20160	16350	20710	20880	In House Method
EC	umhos/cm	41170	33350	42250	42580	SNI 06.6989.1-2019
PH		7.2	7.2	6.9	7.3	SNI 06-6989.11-2019

4.5.1 Schoeller Diagram

Schoeller (1965) is one of the methods used for water chemistry analysis which based on cationic and anionic concentration comparative between groundwater samples. This diagram plots each ion concentration using six

ions such as Ca^{2+}, Mg^{2+}, $Na^{+} + K^{+}$, Cl^{-}, SO_4^{2-}, and HCO_3^{-} to represent groundwater type from its ionic dominations. Ionic concentrations are relatively similar on all four hot spring water samples, with the order of cationic concentration is $Na^{+} + K^{+} > Mg^{2+} > Ca^{2+}$ and for the anionic concentration is $Cl^{-} > SO_4^{2-} > HCO_3^{-}$ (Figure 7).

Schoeller diagram (Figure 7) shows there are spikes of Cl^{-} anion concentration values ranging from 338.4 Meq/L to 504 Meq/L for all four samples. These values, backed with DHL values of 33.350 µmhos/cm to 42.580 µmhos/cm from four samples (Table 1), represents saline water (saltwater). Classification standard of groundwater with electrical conductivity for fresh groundwater is less than 900 µmhos/cm (low EC), 900-2000 µmhos/cm for brackish water (medium EC), and higher than 2000µmhos/cm for saltwater (high EC) (Davis in Ruseffandi & Gusman, 2020). The presences of saline water indicated that there is sea water intrusion into the geothermal system, especially to the reservoir, which correlated to its location as all four hot springs are located in the inter-tidal of coastal zone and only exposed to the surface on low tide.

4.5.2 Gibbs Diagram

Gibbs (1970) constructed the diagram of TDS v/s $Na^{+}/(Na^{+}+Ca^{2+})$ and TDS v/s $Cl^{-}/(Cl^{-}+HCO_3^{-})$ as an instrument to study the water chemistry relationship due to the interaction with rainwater, aquifer material, rock weathering and evaporites crystallization as water flows in the subsurface. This diagram shows the origin and distribution of dissolved components from water-rock interactions and explained the variable that responsible for controlling groundwater chemistry (Rengarajan and Balasubramanian, 1990). Cation (a), anion (b), and TDS data from water samples plotted into the diagram (Figure 8) and it's shows that the chemistry of hot spring water in the study area are falls into the low precipitation or runoff zone and heavily influenced with seawater. This suggested that high concentrations of Cl^{-} anion from all four hot springs in Atauro Island most likely caused by sea water intrusion.

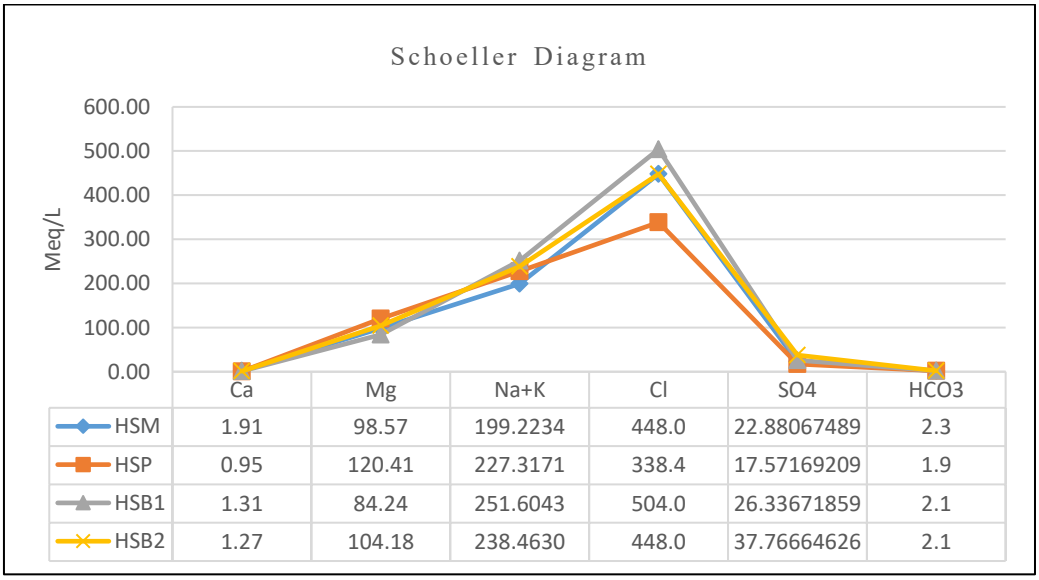

	Ca	Mg	Na+K	Cl	SO4	HCO3
HSM	1.91	98.57	199.2234	448.0	22.88067489	2.3
HSP	0.95	120.41	227.3171	338.4	17.57169209	1.9
HSB1	1.31	84.24	251.6043	504.0	26.33671859	2.1
HSB2	1.27	104.18	238.4630	448.0	37.76664626	2.1

Figure 7: Schoeller Diagram result for showing the domination of major anions and cations.

4.5.3 Water Type / TCSH / Cl-SO_4-HCO_3 Diagram

The ternary of Cl-SO_4-HCO_3 shows the proportions of the significant anion concentrations in the hot spring water samples. This diagram is used to tell or classify types of geothermal water present in the area, which distinguished into four types of thermal waters such as mature waters, peripheral waters, volcanic waters, and steam heated waters. (Giggenbach, 1991). Through this diagram based on the results of plotting the anions (Figure 9), shows that all hot springs water classified as mature water which is a type of water that high in Cl^{-} concentration and low content of sulphate and bicarbonate.

Ideally geothermal water with high value of Cl^{-} is an indication of water dominated by the geothermal reservoir system, but in this case the water came from the sea water intrusion as shown in Schoeller Diagram (Figure 9) and Gibbs Diagram (Figure 9). The Cl^{-} anion values from four hot springs are too high to be classified as a water from the geothermal reservoir. So, the anionic concentration from Maliki, Pala, Biqueli 1, and Biqueli 2 can't be used to determine the water type without further research and more comprehensive sampling procedures.

4.5.4 Water Source / TCLB / Cl-Li-B Diagram

This ternary diagram is used as an instrument to distinguish the geothermal water that influenced by absorption of high temperature steam from different sources (Powell and Cumming, 2010). The B concentration of fluids is

reflected to some degree the maturity of a geothermal system, in which because of its volatility it is expelled during the early heating up stages (Mnjokava, 2007). Result from plotting each element into the ternary diagram shows that all hot spring water samples fall at the top of the diagram (Figure 10). Low content of Boron and Lithium concentrations and high content of Cl^- concentrations is suspected influenced by sea water intrusion into the system. This result is consistent with Schoeller Diagram (Figure 10) and Cl-SO_4-HCO_3 ternary diagram (Figure 10) that also shown the indication of sea water intrusion.

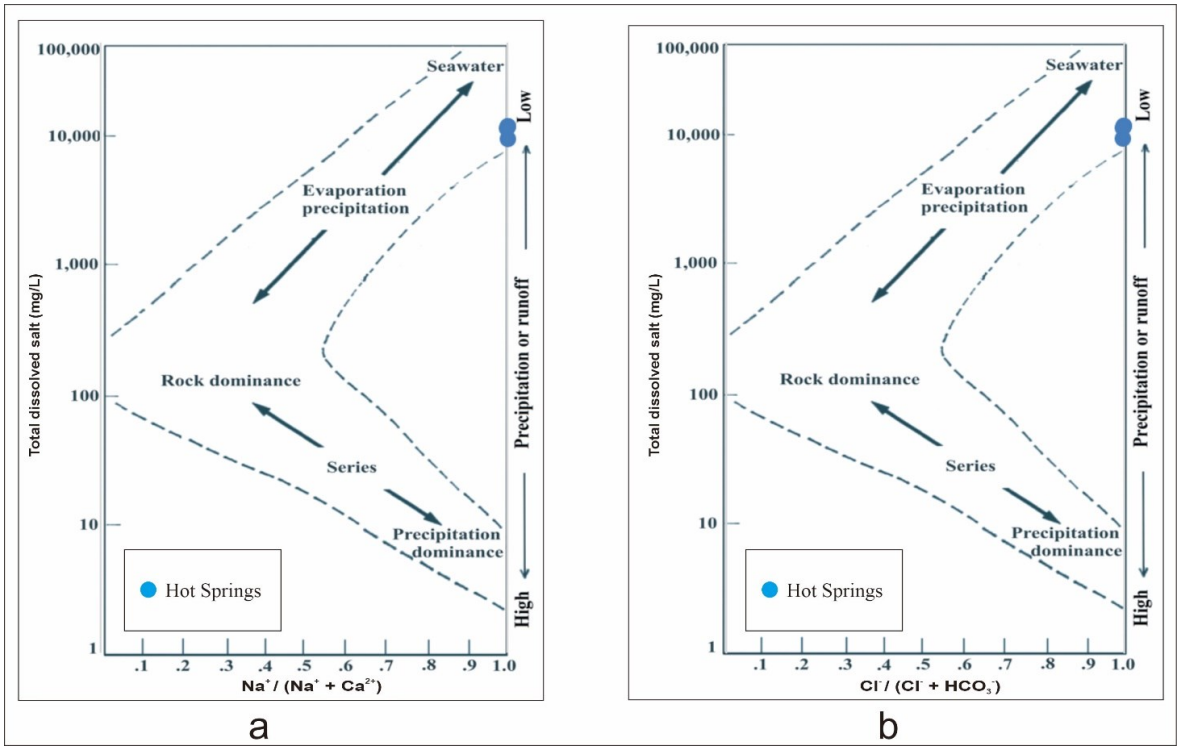

Figure 8: Gibbs Diagram shows the chemical relationship of water interaction.

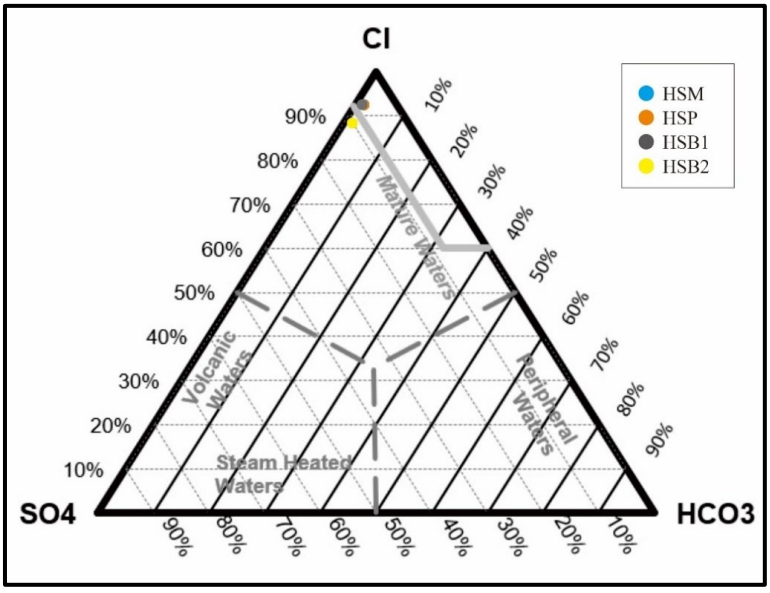

Figure 9: TCSH / Cl-SO4-HCO3 Diagram to determine the water type.

4.5.5 Equilibrium and Temperature

Na-K-Mg ternary is a diagram which used geoindicator ionic elements as a classification tool that divided water into three different classifications of water such as immature water, partially equilibrated water, and fully equilibrated water (Giggenbach, 1988). This diagram can be used to apply geothermometry only to partially equilibrated water and equilibrated water (Shah et al, 2021). The prediction of equilibrium temperature is based on the temperature dependency of full equilibrated assemblage of sodium and potassium minerals that formed

after isochemical recrystallization of average crustal rock under the geothermal interest condition (Giggenbach, 1988).

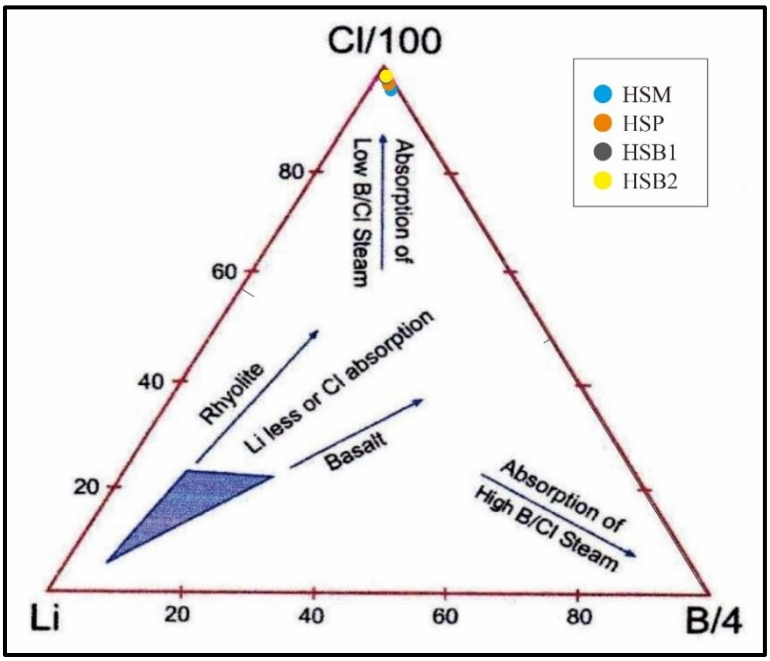

Figure 10: TCLB / Cl-Li-B Diagram to determine the water source.

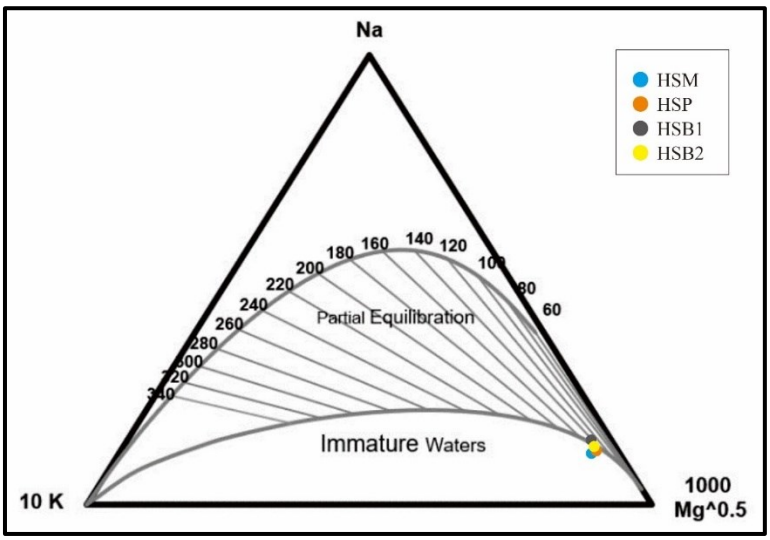

Figure 11: Na-K-Mg ternary diagram as a geoindicator to determine the equilibration.

According to Figure 11, the chemical data plotted from each hot springs shows that all hot springs have similar concentration that close to Mg concentration but only one sample falls just above the immature and partially equilibrated water boundary, which is HSB1 hot spring. The interpretation is that there is high concentration mixing of relatively cold meteoric water (groundwater) into the system, hence the high concentration of Mg ion. Hot springs that classified as immature water aren't suitable for temperature estimation (Giggenbach, 1988). However, the reservoir temperature from HSB1 hot spring that falls just above the boundary and classified as a partially equilibrated water is estimated to be 120 ^{0}C – 140 ^{0}C.

5. CONCLUSION

Field study on the Atauro Island revealed there are four hot springs as geothermal manifestations, namely, Makili (HSM), Pala (HSP), Biqueli 1 (HSB1), and Biqueli 2 (HSB2), which are located at the inter-tidal zone and only exposed on low tide. Furthermore, based on the ternary plots, HSM, HSP, and HSB2 hot springs are classified as immature water, whilst HSB1 is classified as partially equilibrated water with its estimated temperature of 120 ^{0}C – 140 ^{0}C. However, geochemistry data of the water samples from all hot springs shown that the hot springs are intensely mixed with cold groundwater and were suspected that there is a high amount of sea water intrusion into

the geothermal system. This occurrence was indicated by the high concentration of Cl^- anion, ranging from 338.4 - 504 Meq/L, with DHL values of 33.350 - 42.580 µmhos/cm. Therefore, obtaining the geochemistry of seawater around this island is necessary to normalize the hot spring water samples. Unfortunately, the seawater sample was not taken and currently there is no available geochemistry data of seawater around this island from previous studies. Thus, further research with the corrected hot spring water is required to remove the effect of sea water intrusion in order to conduct more accurate geothermometric analyses.

REFERENCES

Abbot, M., and Chamalaun, F.: Geochronology of some Banda Arc Volcanics, In S. Wirosuyono (Ed.), *The Geology and Tectonics of Eastern Indonesia*, **2**, (1981), 253-271.

Chang, J. C.: Geologi dan Evolusi Tektonik serta Implikasi Pola Struktur Geologi terhadap Keberadaan Manifestasi Panas Bumi di Daerah Makili dan Vila, Pulau Atauro, Timor Leste, *Bachelor Thesis*, UPN "Veteran" Yogyakarta, Yogyakarta, Special Province of Yogyakarta, Indonesia, Retrieved from http://eprints.upnyk.ac.id/38372/

Ely, K. S., Sandiford, M., Hawke, M. L., Phillips, D., Quigley, M., and Reis, J. E.: Evolution of Atauro Island: Temporal Constraints on Subduction Processes Beneath the Wetar Zone, Banda Arc, *Journal of Asian Earth Science*, (2011), 1 - 17. doi:10.1016/j.jseaes.2011.01.019

Gibbs, R.J.: Mechanism Controlling World Water Chemistry, *Science* **17**, (1970), 1088-1090.

Giggenbach, W.F.: Geothermal Solute Equilibria, Derivation of The Na-K- Mg-Ca Geoindicators, *Geochem, Cosmochim*, Acta **52**, (1988), 2749-2765.

Giggenbach, W.F.: Chemical Techniques in Geothermal Exploration. In: *UNITAR/UNDP Guidebook: Application of Geochemistry in Resources Development*, (1991a), 119-144.

Giggenbach, W.F.: The Composition of Gases in Geothermal and Volcanic Systems as a Function of Tectonic Setting. In: *Kharaka, Maest (Eds.)*, Water-Rock Interactions. Balkema Rotterdam, (1991b), 873-878.

Harris, R.: The Nature of the Banda Arc-Continent Collision in the Timor Region, In D. Brown, *Arc-Continent Collision*, (2011), 163-211.

Schoeller, H.: "Qualitative Evaluation of Groundwater Resources," In: H. Schoeller, Ed., Methods and Techniques of Groundwater Investigations and Development, The United Nations Educational, *Scientific and Cultural Organization*, Paris, (1965), 54-83.

Spakman, W., and Hall, R.: Surface Deformation and Slab-Mantle Interaction During Banda Arc Subduction Rollback. *Nature Geoscience*, **3**, (2010), 562-566.

Mnjokava, T.T.: Interpretation of Exploration Geochemical Data for Geothermal Fluids from The Geothermal Field of the Rungwe Vulcanic Area, SW-Tanzania, *Report of Geothermal Training Programme*, United Nation University, Iceland (2007).

Powell, T., and Cumming, W.: Spreadsheets for Geothermal Water and Gas Geochemistry, *Proceedings*, Thirty-Fifth Workshop on Geothermal Reservoir Engineering. Stanford University, California, (2010), 110.

Preliminary Survey of Tempuran Green Field Geothermal System Using Gravity Satellite Data and Fault Analysis

Muhammad Faizal Zakaria[1], Ardhan Farisan[2], Y. Yatini[1],
Nanda Ajeng Nurwantari[3], and Ismail Mutoriz[1]

[1]Geophysical Engineering, University of Pembangunan Nasional "Veteran" Yogyakarta
[2]The National Research and Innovation Agency
[3]Geology Engineering, University of Pembangunan Nasional "Veteran" Yogyakarta

mfaizal@upnyk.ac.id

Keywords: Tempuran, Geothermal, GGMPlus, Gravity, Fault

ABSTRACT

The emergence of hot springs in the Tempuran area, Magelang, Central Java is a natural phenomenon that has been utilized and manage as a public thermal bath by the locals. The appearance of these hot springs is a sign of the existence of a geothermal system in the area. The source of the geothermal system developing in this area is still unknown. This research aims to provide initial information specifically regarding the green field geothermal system present in the Tempuran area. This research uses high-resolution satellite gravity data from The Global Gravity Model Plus (GGMPlus) to analyze density of the sub-surface rocks. In addition, this research uses DEMNAS data as a basis for fault continuity analysis. This gravity data will be supported by field geological measurements and local geological structures measurement. The results of this research show that there is a low gravity anomaly around the hot springs (-0.31 mgal to -0.007 mgal) which indicates that the geothermal system aquifer is located in the Alluvium Quarter rocks. there is a high anomaly (0.1 mgal to 0.3 mgal) in the southern part of the study area which is the response of Oligo-Miocene volcanic rocks, and high anomaly (0.1 mgal to 0.3 mgal) in northern part of study area which is the response of Quarter Volcanic deposits. Using DEM data to obtain the general direction of the structure using morphotectonic methodology, the Tempuran area, Magelang has a general (major) direction of lineaments ranging from NW – SE with a minor direction N – S. This data shows that the geothermal system in the study area is most likely included in the geothermal system of Mount Sumbing.

1. INTRODUCTION

The Java arc is located along the southern edge of the Eurasian plate, where the Indo-Australian plate subducts it. This arc has been active in its current position since approximately 10 million years ago in the late Miocene (Smyth et al., 2005; Soeria-Atmadja et al., 1994). The volcanoes in this chain vary in height, with some exceeding 3000 meters, forming the island's backbone with the existence of geothermal manifestation. The dominant composition of today's volcanic products is basaltic andesite (Nicholls et al., 1980), and their eruptive and epiclastic materials cover a substantial portion of the island. Most active volcanoes are located about 100 km above the subducting slab(England et al., 2004) and roughly 300 km north of the subduction margin.

Geothermal manifestations in the study area are one of the products of active volcanoes on the island of Java. The study locations are Tempuran District, Magelang Regency, Central Java Province. This geothermal area called Tempuran Geothermal Field due to the district of the existing geothermal manifestation. The site is located between the active mountain ranges of Sindoro-Sumbing Active Volcano and Merapi Active Volcano. The north of Merapi Volcano lies the currently inactive Mount Merbabu (Figure 1). The study area includes geotourism sites with hot springs, specifically the Ngasinan Hot Springs and Umbul Banyu Roso. Geographically, the location is near the confluence of the Setro and Progo Rivers (Figure 2) and is located approximately 30 km southeast of Sumbing Volcano.

Identification of the Geothermal system of Tempuran Geothermal Field is needed to make a long-term develompment plan of the area. This paper will provide a preliminary information of the Tempuran Geothermal Field using Gravity GGMPlus data (Hirt et al., 2013) and DEM data from DEMNAS (https://tanahair.indonesia.go.id/demnas) for structure deliniation. Those data will be confirmed by mapping of local geology. The use of GGMPlus in Geothermal field exploration has been carried out in several previous studies. Lase used GGPPlus Gravity data to modelling the heat source of Amohola-Sumbersari geothermal, and has been successful to locate the heatsource (Lase et al., 2022). Bahtiar also associated the low Gravity anomaly with some geothermal manifestations in Mount Iyang-Argopuro Geothermal Field (Abi Bahtiar et al., 2021). The topographic data from DEM could also used to deliniate the surface geologic structure (Hooper et al., 2003; Jordán et al., 2005).

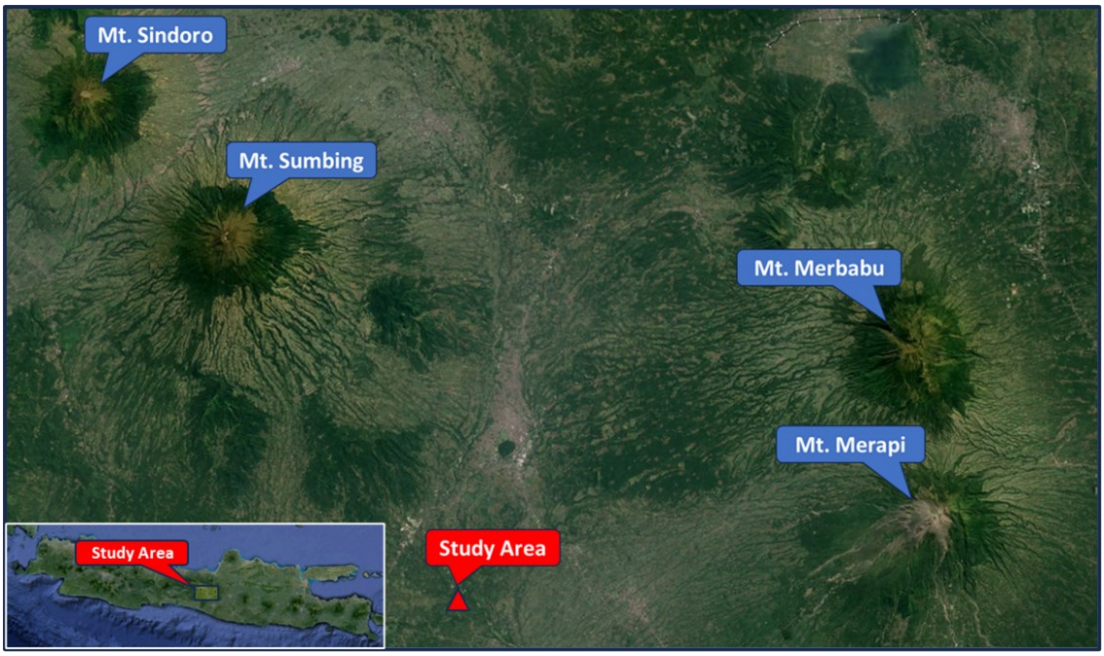

Figure 1: The study area is located between Sindoro-Sumbing Volcano and Merapi Volcano.

Local Geology

Geologically, based on the geological map of the Yogyakarta Sheet (Rahardjo et al., 1995) (shown in Figure 2, the study area is located in the Young Sumbing Deposits (Qsm), which consist of tuffaceous sand, sandy tuff, and andesite breccia. To the east and northeast are Volcanic Breccia deposits (Qb) comprising volcanic breccia, lava flows, tuff, tuffaceous sandstone, and lahar. To the west and northwest are Old Sumbing Deposits (Qsmo) consisting of andesite breccia, agglomerate, and tuff. The study area is located southeast of Mount Sumbing (Figure 1). Based on these geological conditions, it is suspected that the geothermal manifestations in the study area are products of geothermal activity from Sumbing Volcano. This preliminary study aims to uncover the geothermal sources of the Tempuran Geothermal Field based on morphotectonic analysis, aerial photography, and field surveys to validate the morphotectonic analysis results.

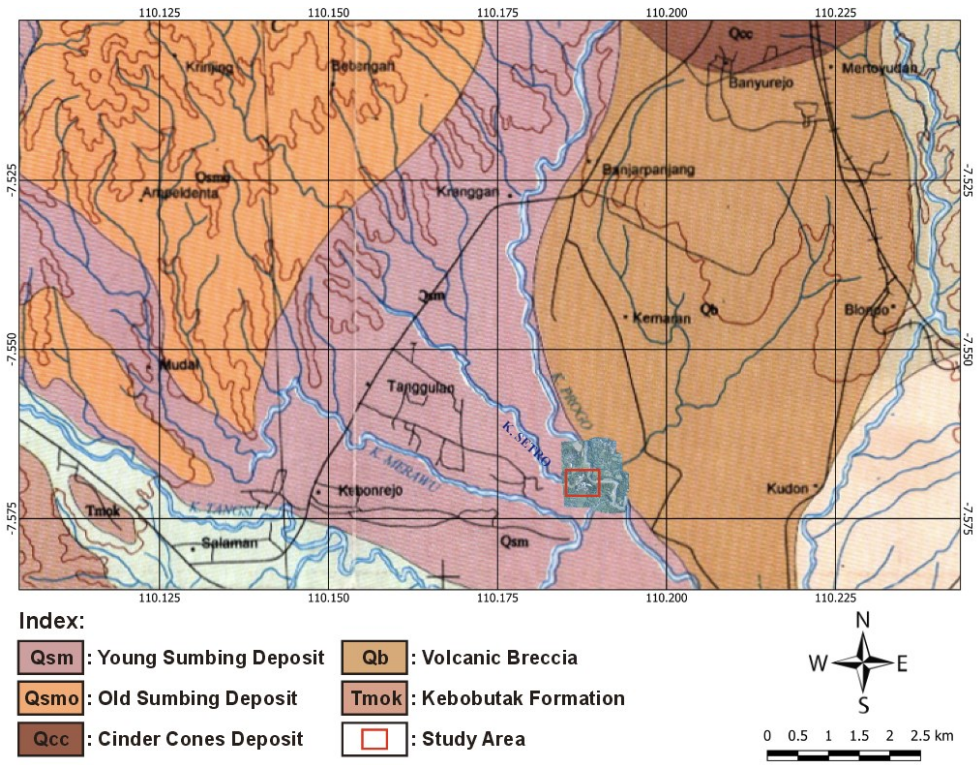

Figure 2: Geological Map of the Study Area (Rahardjo et al., 1995).

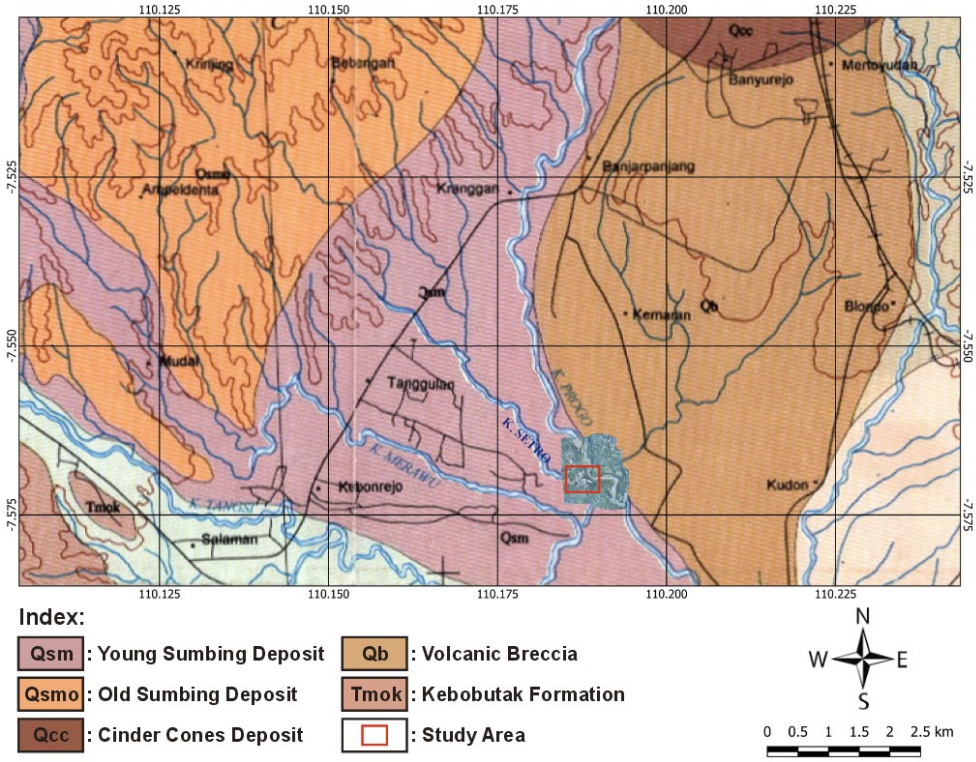

Figure 2: Geological Map of the Study Area (Rahardjo et al., 1995).

2. METHOD

This research is a long-term activity aimed at mapping and identifying geothermal systems in the Tempuran geothermal field in detail. Data yang digunakan adalah data GGMPlus Gravity Data. This data is released by theWestern Australian Centre for Geodesy and Curtin University Perth. This data consist of high resolution high resolution Earth's Gravity data over all continent, including Java and Indonesia. This data obtained through augmentation of satellite (GOCE/GRACE) data, EGM 2008 data, and terrestrial gravity with topography data and delivering detail at ~200 m spatial resolution (Hirt et al., 2013, 2019). The data is collected in research area and processed through standard processing of Gravity data(LaFehr & Nabighian, 2012; Zakaria, 2021). Result of the processing data is Bouguer anomaly and will be analysed. The workflow of gravity data processing can be seen in Figure 3.

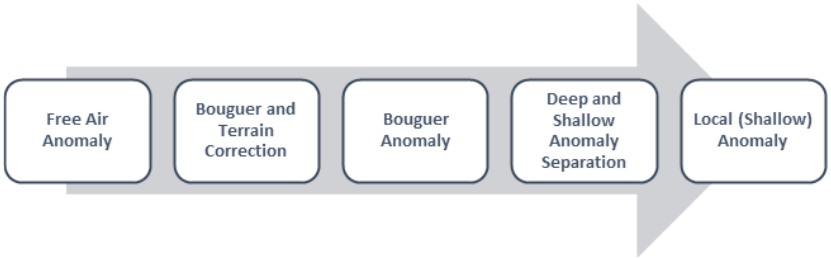

Figure 3: Workflow of GGMPlus Gravity data.

Detailed mapping of the morphotectonic in the study area utilizes Google Earth images, SRTM (Shuttle Radar Topographic Mission) from DEMNAS (Digital Elevation Model Nasional Indonesia), Shp data (https://tanahair.indonesia.go.id/demnas), drone aerial photography, and on-site field surveys. The mapping process identifies diverse lineations, focusing on slope, elevation, shape, and variations of these features. Terrain analyses utilized the DEM to investigate various aspects, including elevation, slope, aspect, topographic profiles, and longitudinal river profiles. Slope and aspect maps were generated from the DEM using Global Mapper and QGis. DEM analysis is crucial for studying elevation-related characteristics in fault zone areas (Duncan et al., 2003; Menges, 1990). The tonal variations in the elevation map provide insights into regional topography and structural features (e.g., Duncan et al., 2003; Hooper et al., 2003; Kassaras et al., 2020; Menges, 1990).

Morphotectonic mapping is divided into two parts, focusing on the Old Sumbing Deposits (Qsmo) and Young Sumbing Deposits (Qsm), due to suspicion that the study area represents a geothermal manifestation originating

from Sumbing Volcano. The morphotectonic mapping was validated using field data consisting of structural manifestations observed at the outcrop scale. Validation was conducted along several rivers near the geothermal manifestations because geological structures are often more visible along riverbanks. Field validation commenced at the first point near the Ngasinan Hot Springs and Umbul Banyu Roso, involving aerial photography, followed by two additional points northwest of Ngasinan Hot Springs and Umbul Banyu Roso based on interpreted lineaments from the morphotectonic map. Furthermore, thorough field observations have been crucial to the study, aiding in verifying, reinforcing, and interpreting the findings derived from the morphotectonic analysis. The workflow analysis can be seen in Figure 4.

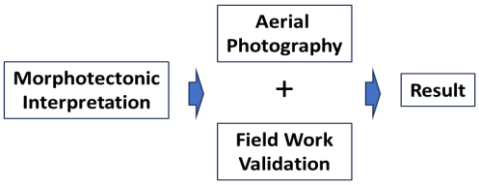

Figure 4: Workflow.

3. RESULT AND DISCUSSION

3.1 Geothermal Manifestation

Tempuran Geothermal Field located in Sumberarum Area, Tempuran District, Magelang Regency, Central Java. The main attraction of this area is the appearance of old hot spring in this area. Nowadays, there are several local residents to exploit this natural phenomenon by drilling around the main hot springs, and using it as public hot spring. This hot spring has been visited by many local residents and became a public bath recreational afterwards (magelangekspres, 2022). As seen in the picture, there are several hot springs appearing: 1. Original Hot Spring, 2. Ngasinan Public Bath, 3. Umbul Roso Public Bath, 4. Lintang Waterpark, 5. Tirta Madu Public Bath, 6. Tirta Sambara Public Bath, 7. Azirza Tirta Public Bath. Tourism development in this area of course requires careful planning so that the existance of hot water and also the temperature of the hot water is maintained. so detailed information about the Tempuran Geothermal System is needed

Figure 5: Location of local public bath appearing in Research area.

3.2 GGMPlus Gravity Data

Figure 6 shows the distribution of local (shallow) gravity anomaly values in research area. Manifestations are in the center of the map and are marked in red. The contour color shows the gravity anomaly value, with variations between -0.223 mgal to 0.148 mgal. Blue values are low anomalies and red are high anomalies.

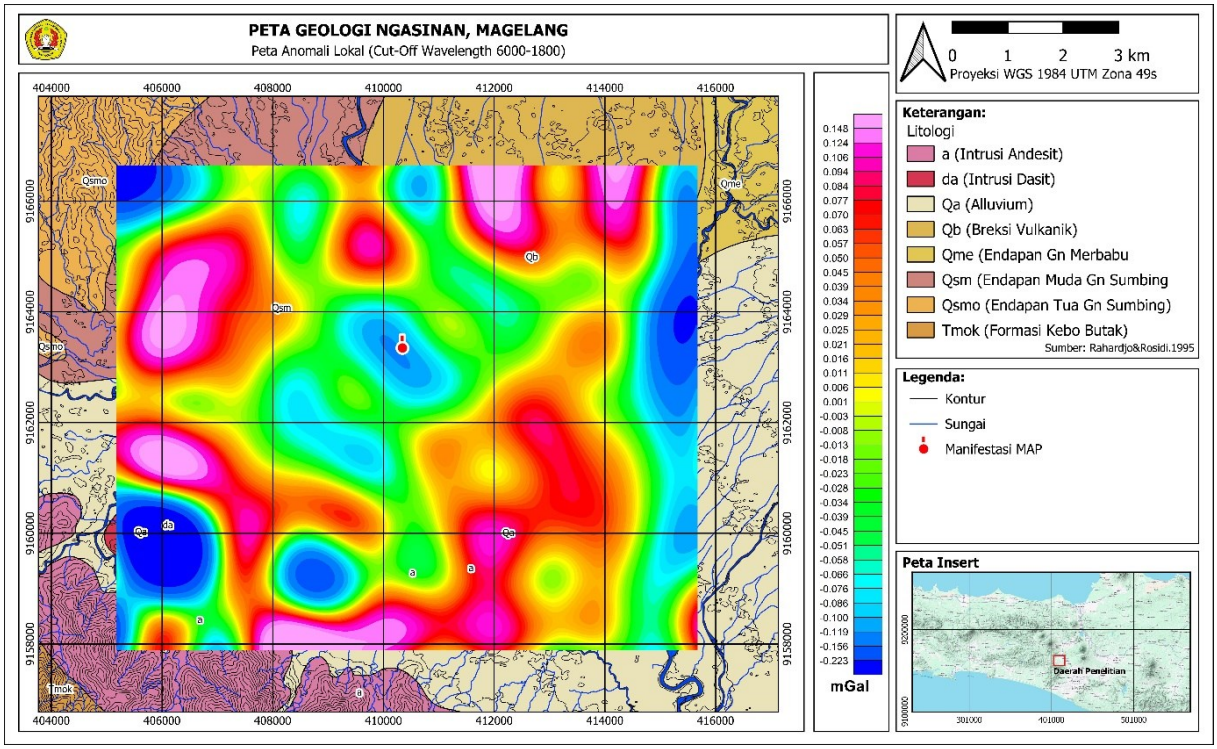

Figure 6: Map of Local Bouguer Anomaly data from GGMPlus Gravity Data on Tempuran Geothermal Field.

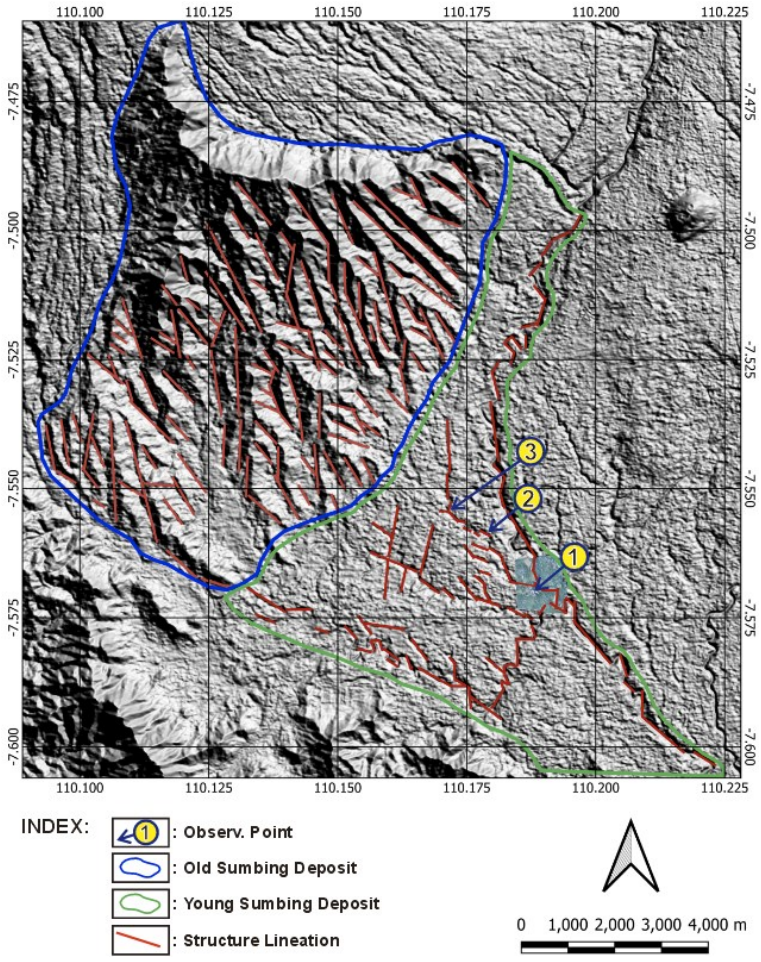

Figure 7: Morphotectonic Map and Observation Point of Study Area.

Rock formations in the research area are dominated by quarter volcanic rocks, products from Sumbing Volcano and Merbabu Volcano. These rocks tend to have a high density so they should provide a high response to gravity anomalies, in the red color. This high anomaly is spread over areas with low anomalies in the central part of the study area. The low anomaly in the middle is interpreted as a change zone or alteration zone caused by the emergence of hydrothermal fluid. Hydrothermal fluid comes out through structures that mix with meteorite water near the surface and change the volcanic rocks into clay rocks. This clay rock is thought to be the cover rock of the geothermal system in the research area.

3.3 Structure Identification and Delineation

Topography can provide valuable insights into the structure of the near-surface crust (Edward & Nicholas, 2002; Pérez-Peña et al., 2009) and deeper lithospheric processes, such as upper mantle dynamics). A relatively easy-to-observe topographic expression is the linearity found on slopes and rivers. In this paper, the author divides the study area into two sections for analysis of general orientation: the Old Sumbing Deposit (Qsmo) and the Young Sumbing Deposit (Qsm), as shown in Figure 7. The results, derived from morphotectonic interpretation data, indicate that the main structural direction of lineaments in both the Old Sumbing Deposit (Qsmo) and the Young Sumbing Deposit (Qsm) is predominantly NW-SE (Figure 8a and b). The author conducted this main direction analysis using rose diagrams.

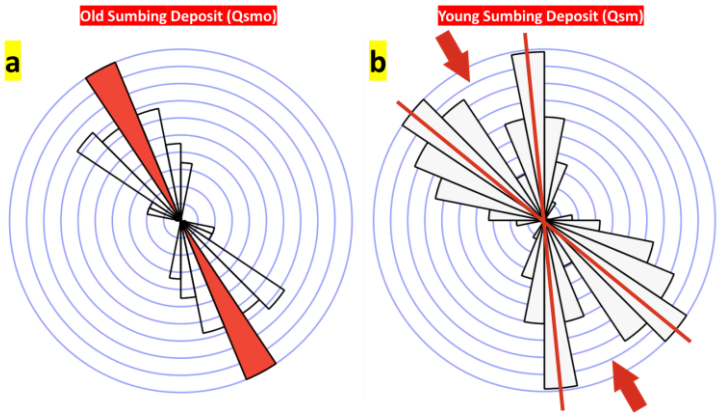

Figure 8: a) Rose Diagram of Old Sumbing Deposit (Qsmo); b) Rose Diagaram of Young Sumbing Deposit (Qsmo).

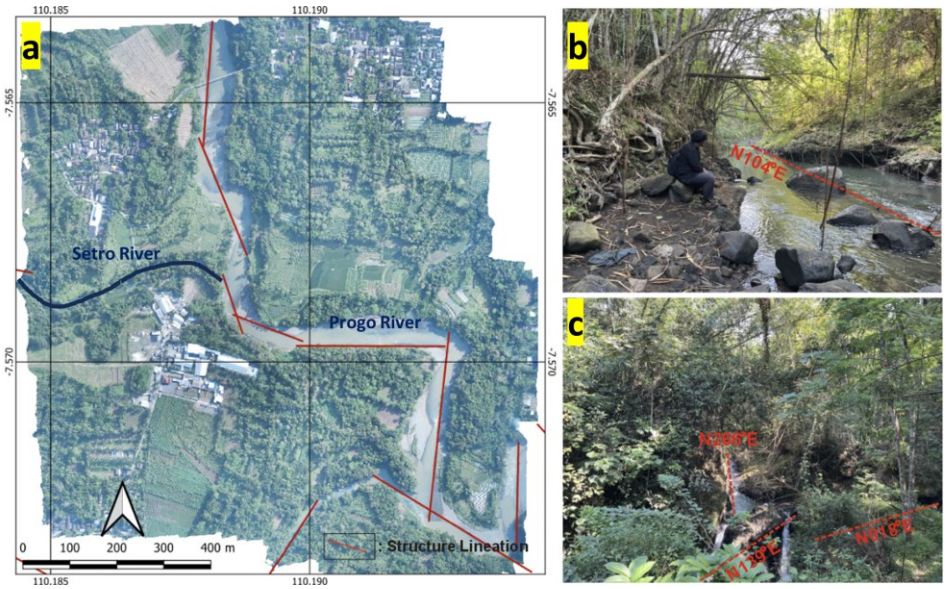

Figure 9: a) Aerial photography (orthophoto) of obvservation Point 1; b) The lineation of obvservation. Point 2; c) The confluence of these three rivers in obvservation point 3.

We analyze The Old Sumbing Deposit (Qsmo) using a rose diagram. The result of the rose diagram shows the main direction of the lineament structures is identified as NW-SE. In Qsmo, it is relatively easy to delineate the lineament structures due to the clear morphological expressions, as the rocks in Qsmo are relatively more resistant, resulting in steep and hilly terrain (Figure 8a).

In contrast, the Young Sumbing Deposit (Qsm) exhibits a flatter morphology due to the influence of younger volcanic deposits, which have not yet consolidated into hard rock. The delineation of lineament structures in Qsm is conducted in river areas, where the features are relatively fresh and easier to observe. The results show that in Qsm, there are two general orientations: approximately N-S and NW-SE. Based on the rose diagram in Figure 8b, the main stress direction is determined to be NNW-SSE.

The validation of lineament delineation was conducted using several methods (Figure 9). In addition to direct field cross-checking, the author also utilized aerial photography (orthophotos) to validate the lineament delineation. Figure 6a shows validation using aerial photography, confirming that the delineation based on the morphological map corresponds to the actual conditions around the Ngasinan Hot Springs and Umbul Banyu Roso. The structure around the Ngasinan Hot Springs and Umbul Banyu Roso is relatively complex, and this area marks the confluence of the Progo River and its tributary, the Setro River.

Field observations were carried out at observation points 2 (Figure 9b) and 3 (Figure 9c). At observation point 2, a river lineament oriented at N104°E was identified. This lineament confirms the validity of the morphotectonic interpretation conducted. At observation point 3, a confluence of three small rivers was found. The orientations of these small rivers are N286°E, N018°E, and N139°E, which are the downstream directions of these rivers. The confluence of these three rivers is likely due to geological structures, as evidenced by the irregular rock formations in this area.

4. CONCLUSION

Gravity data conclude that there are low anomaly around the hot spring geothermal manifestation. This area is corresponding to alteration zone of the Tempuran Geothermal Field System. Morphotectonic analysis indicates that the study area, which includes the Young Sumbing Deposit (Qsm) and the Old Sumbing Deposit (Qsmo) to the northwest, has a predominant lineament orientation of Northwest-Southeast. The author interprets the geothermal source in the study area as originating from Sumbing Volcano, located approximately 30 kilometres to the northwest.

REFERENCES

Abi Bahtiar, E., Suprianto, A., & Supriyadi, S. (2021). Identification of The Geothermal Heat at Mount Iyang-Argopuro Based on a Data Image of Landsat 8 Satellite and a Data Gravity of GGMPlus Satellite. Computational And Experimental Research In Materials And Renewable Energy, 4(1), 44–59.

Duncan, C., Masek, J., & Fielding, E. (2003). How steep are the Himalaya? Characteristics and implications of along-strike topographic variations. Geology, 31(1), 75–78.

Edward, K. A., & Nicholas, P. (2002). Active tectonics: earthquakes, uplift, and landscape. New Jersey: Prentice Hall.

England, P., Engdahl, R., & Thatcher, W. (2004). Systematic variation in the depths of slabs beneath arc volcanoes. Geophysical Journal International, 156(2), 377–408.

Hirt, C., Claessens, S., Fecher, T., Kuhn, M., Pail, R., & Rexer, M. (2013). New ultrahigh-resolution picture of Earth's gravity field. Geophysical Research Letters, 40(16), 4279–4283.

Hirt, C., Yang, M., Kuhn, M., Bucha, B., Kurzmann, A., & Pail, R. (2019). SRTM2gravity: an ultrahigh resolution global model of gravimetric terrain corrections. Geophysical Research Letters, 46(9), 4618–4627.

Hooper, D. M., Bursik, M. I., & Webb, F. H. (2003). Application of high-resolution, interferometric DEMs to geomorphic studies of fault scarps, Fish Lake Valley, Nevada–California, USA. Remote Sensing of Environment, 84(2), 255–267.

Jordán, G., Meijninger, B. M. L., Van Hinsbergen, D. J. J., Meulenkamp, J. E., & Van Dijk, P. M. (2005). Extraction of morphotectonic features from DEMs: Development and applications for study areas in Hungary and NW Greece. International Journal of Applied Earth Observation and Geoinformation, 7(3), 163–182.

Kassaras, I., Kapetanidis, V., Ganas, A., Tzanis, A., Kosma, C., Karakonstantis, A., Valkaniotis, S., Chailas, S., Kouskouna, V., & Papadimitriou, P. (2020). The new seismotectonic atlas of Greece (v1. 0) and its implementation. Geosciences, 10(11), 447.

LaFehr, T. R., & Nabighian, M. N. (2012). Fundamentals of Gravity Exploration. In Fundamentals of Gravity Exploration. Society of Exploration Geophysicists. https://doi.org/10.1190/1.9781560803058

Lase, F. T. Z., Aprina, P. U., Ferucha, I., & Alawiyah, S. (2022). Modelling of Heat Source in the Geothermal field based on Euler Deconvolution and Occam Inversion using GGMPlus Gravity data. The 47th Annual Scientific Meeting of Himpunan Ahli Geofisika Indonesia, 1–6.

magelangekspres. (2022). Viral Pemandian Air Hangat di Tempuran, Ternyata Sumber Airnya dari Sini. https://magelangekspres.disway.id/read/649102/viral-pemandian-air-hangat-di-tempuran-ternyata-sumber-airnya-dari-sini

Menges, C. M. (1990). Late Quaternary fault scarps, mountain-front landforms, and Pliocene-Quaternary segmentation on the range-bounding fault zone, Sangre de Cristo Mountains, New Mexico. Reviews in Engineering Geology, 8, 131–156.

Nicholls, I. A., Whitford, D. J., Harris, K. L., & Taylor, S. R. (1980). Variation in the geochemistry of mantle sources for tholeiitic and calc-alkaline mafic magmas, western Sunda volcanic arc, Indonesia. Chemical Geology, 30(3), 177–199.

Pérez-Peña, J. V., Azañón, J. M., Azor, A., Delgado, J., & González-Lodeiro, F. (2009). Spatial analysis of stream power using GIS: SLk anomaly maps. Earth Surface Processes and Landforms, 34(1), 16–25.

Rahardjo, W., Sukandarrumidi, & Rosidi, H. M. D. (1995). Peta geologi lembar Yogyakarta, Jawa [peta]. https://opac.perpusnas.go.id/DetailOpac.aspx?id=141772

Smyth, H., Hall, R., Hamilton, J., & Kinny, P. (2005). East Java: Cenozoic basins, volcanoes and ancient basement.

Soeria-Atmadja, R., Maury, R. C., Bellon, H., Pringgoprawiro, H., Polve, M., & Priadi, B. (1994). Tertiary magmatic belts in Java. Journal of Southeast Asian Earth Sciences, 9(1–2), 13–27.

Zakaria, M. F. (2021). Analisis Kedalaman Sumber Anomali Gravitasi menggunakan Spectral Statistical Technique di daerah Godean Yogyakarta. Jurnal Fisika Flux: Jurnal Ilmiah Fisika FMIPA Universitas Lambung Mangkurat, 18(1), 75–82.

Identification of Hot Spring Aquifers Based on Vertical Electrical Sounding (VES) Method Using Schlumberger Configuration in Tempuran Area, Magelang Regency

Latief D.U., Yatini, Indira A., Levana N., Faza N.A., and M. Faizal Z.

latiefdhiyya@gmail.com, jeng_tini@upnyk.ac.id, abadiindira@gmail.com, levana.noviyanti@gmail.com, fazanaa09@gmail.com, mfaizal@upnyk.ac.id

Keywords: Aquifer, Geothermal, Resistivity, Schlumberger

ABSTRACT

The Tempuran area, Magelang Regency is an area that has many hot springs that are close together. Hot springs are a manifestation that characterizes the existence of a geothermal system in a place. These geothermal manifestations are used by the local community to support the economy which has the potential to be further developed by knowing the orientation outflow of the hot fluids that exist below the surface. Based on geological studies, the research area is included in the young Mount Sumbing sedimentary formation which is composed of sedimentary rocks associated with volcanic material. This research uses Resistivity Vertical Electrical Sounding which is spread at several points around the research area to determine the groundwater aquifer that enters the Outflow Zone of the geothermal system in the research area. The acquisition process uses Syscal Jr with a Schlumberger configuration with 7 acquisition points and a stretch of 600 meters each. The results obtained based on the Vertical Electrical Sounding profile show that the top aquifer is at a depth of 100 meters with an average resistivity value ranging from 24 Ωm to 39 Ωm. Subsurface interpretation based on 1D profiles shows the distribution of the aquifer which has an average thickness of 44 meters.

1. INTRODUCTION

Indonesia is part of the Pacific Ring of Fire, which results in the emergence of numerous volcanoes, both active and inactive (Basith et al., 2012). A volcano that has been inactive for a long time is not entirely free from visible volcanic activity. Some long-dormant volcanoes can be utilized as sites for geothermal energy development. Geothermal energy can serve as an alternative to reduce the use of non-renewable energy sources such as fossil fuels.

An area with potential geothermal energy is characterized by surface manifestations. One such area with geothermal manifestations is Tempuran in Magelang Regency. This is indicated by the presence of many hot springs located close to each other. These manifestations appear on the surface due to fractures that allow hot fluids to escape. Geological studies indicate that the study area is part of the Young Sumbing volcanic deposit formation, composed of sedimentary rocks associated with volcanic materials (Rahardjo et al., 1995).

This study aims to identify groundwater aquifers that are part of the outflow zone of the geothermal system using the Vertical Electrical Sounding (VES) resistivity method with a Schlumberger configuration, spread across the study area. The survey involves injecting electrical current into the earth's subsurface to determine the electrical properties, either electrical conductivity or resistivity, of the subsurface medium (Todd, 1980). These electrical properties will reveal the subsurface conditions, including the mineral composition and the porosity of the medium. The distribution of resistivity values will provide information on the distribution of groundwater aquifers in the study area.

2. LITERATURE REVIEW

2.1 Geology of The Research Area

Regionally, the research area consists of 5 rock units, namely volcanic breccia units, Merbabu deposits, Young Sumbing deposits, Old Sumbing deposits, and alluvial deposits (Figure 1). Locally, the research area itself is in the Young Sumbing sedimentary unit (Qsm) which belongs to the medial volcanic facies consisting of tuff breccia, sandy tuff, sandstone and clay lithologies (Nuur, M.F., et, al., 2015). In the mid-Quaternary era, volcanic activity was still ongoing, but the type of eruption became more explosive in the form of large eruptions that ejected pyroclastic material ranging from fine sand to gravel. The pyroclastic material is then carried through the air and falls down under the influence of gravity to reach the area of study and forms the Young Sumbing pyroclastic breccia unit in harmony with the Old Sumbing volcanic breccia and not align with the Kaligesing monomict

breccia. Volcanic activity continued during the Pleistocene but did not continue until the Holocene (Nuur, M.F., et, al., 2015).

2.2 Vertical Electrical Sounding (VES)

The Vertical Electrical Sounding (VES) method is one type of electrical sounding geophysical method. According to Simpen (2015), the geoelectric method is a method that studies the electrical flow properties within the earth and how to detect them from the earth's surface. The physical quantity sought is the specific resistivity of rocks due to the presence of potential fields and currents injected beneath the earth's surface. The measurable depth beneath the surface depends on the electrode spacing. The greater the electrode spacing, the deeper the measured depth. The configuration used in the Vertical Electrical Sounding (VES) geoelectric method is the Schlumberger configuration. This configuration uses four electrodes arranged as Figure 2.

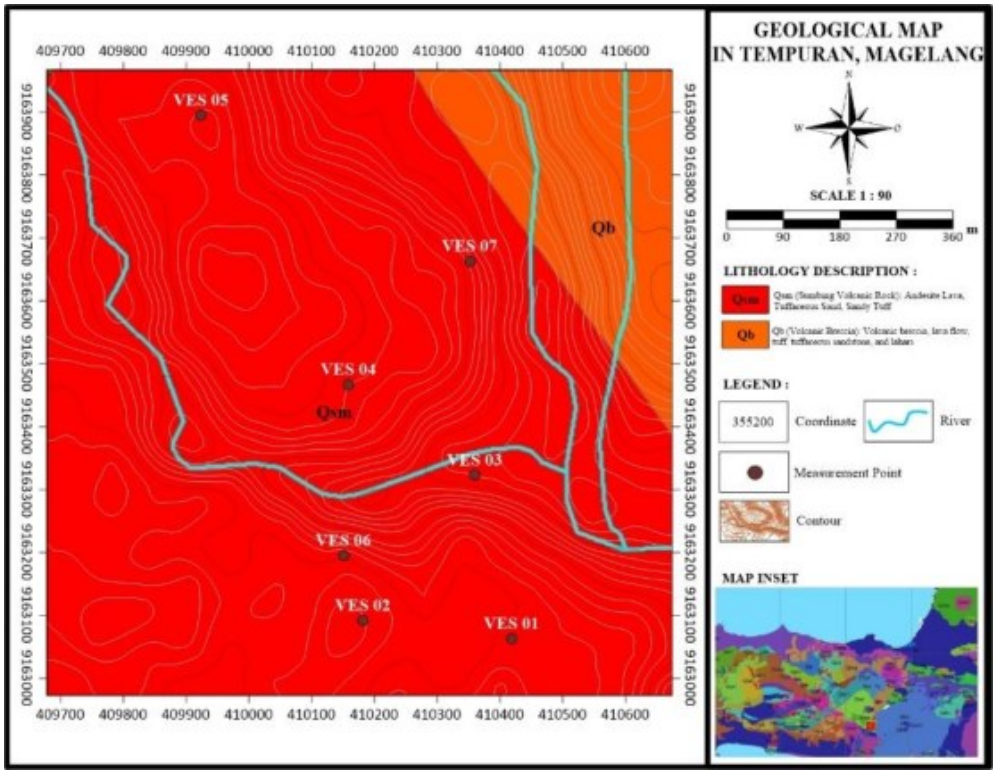

Figure 1: Geological Map of Magelang Regency (modified from Rahardjo, W. et al, 1995).

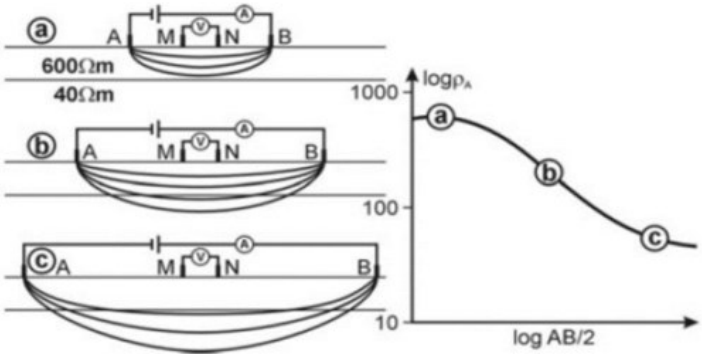

Figure 2: Schlumberger Configuration (Wardana, 2019).

2.3 Types of Aquifer

An aquifer is a subsurface layer capable of storing water due to its high porosity and permeability. Aquifers serve two important functions: as water storage and as water conduits. Each type of aquifer plays a distinct role in the hydrological cycle and water management. Based on lithology, aquifers can be classified into four types (Suharyadi, 1984) :

a. Unconfined aquifer, is an aquifer where the upper boundary is the water table and the lower boundary is confined. This type is also known as a shallow aquifer due to its maximum depth of about 15 meters.

b. Confined aquifer, is an aquifer located between impermeable layers, with pressure greater than atmospheric pressure.
c. Leakage aquifer, is an aquifer where the upper boundary is a semi-permeable layer and the lower boundary is impermeable.
d. Perched aquifer, is an aquifer where the groundwater mass is separated from the main groundwater mass by an impermeable layer and is located in a saturated zone. This type of aquifer is known for having limited water availability.

3. RESEARCH METHODOLOGY

In this hot spring aquifer identification research using the Vertical Electrical Sounding (VES) method, there are several steps in data acquisition and processing as shown in Figure 3a. The first step in conducting this research is to conduct data acquisition using a stretch in accordance with the target to be achieved. The data acquisition will produce primary data in the form of AB/2, MN/2, electric current value (A), and resistivity value (Ω). The data is then processed using Microsoft Excel and arranged in order and coherent so that the processing process is easier. Primary data that has been processed is then further processed by making resistivity profiles and lithology profiles to be given lithology symbols and lithology colors according to Agus Santoso (2013) rock resistivity table. After that, make a discussion of all the results of the lithology profile that has been produced.

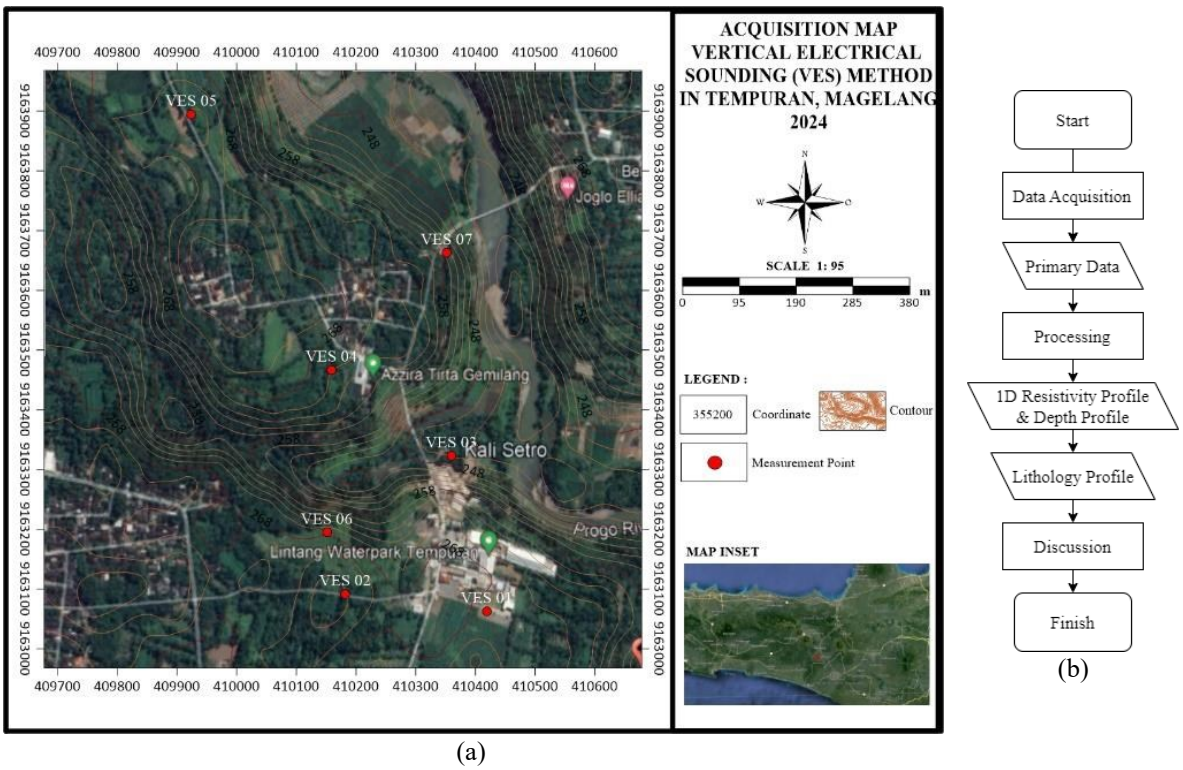

(a) (b)

Figure 3: Research Methodology, (a) Acquisition Map in The Research Area, (b) Flow Diagram.

4. RESULT AND DISCUSSION

4.1 Subsurface 1D Profiling

4.1.1 Subsurface Profile VES-01

In VES-01 sounding resistivity profile there are 5 layers with 3 kinds of lithology, namely soil with a resistivity range of 13.16 - 73.97 Ωm, sandstone with a resistivity range of 24.50 - 47.22 Ωm, and claystone with a resistivity range of 2.13 - 9.04 Ωm with a maximum depth of 240m. Processing of resistivity values based on inversion in Progress software has an error value of 9%. At this point, the presence of a hot water aquifer at a depth of 160 m can be identified because it can be seen in the lithology profile that the resistivity value of the lowest sandstone is at that depth. So it can be indicated that the VES-01 point is passed by the outflow of the geothermal system which originates from Mount Sumbing.

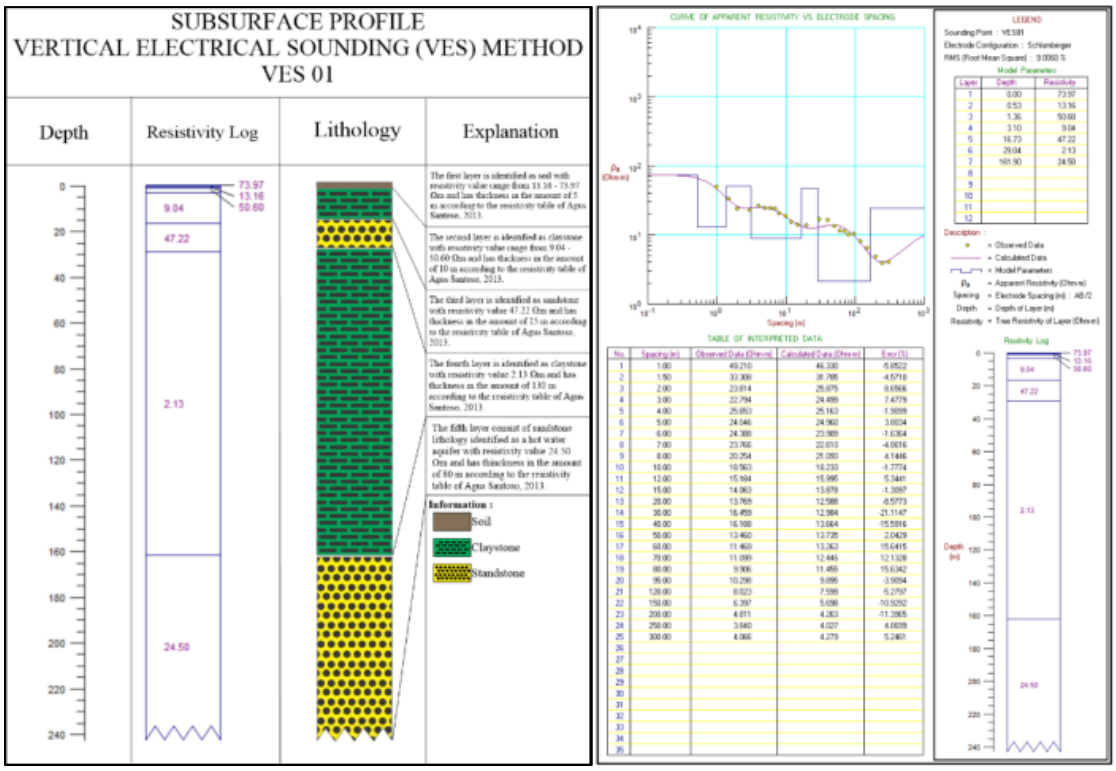

Figure 4: VES-01 Profile.

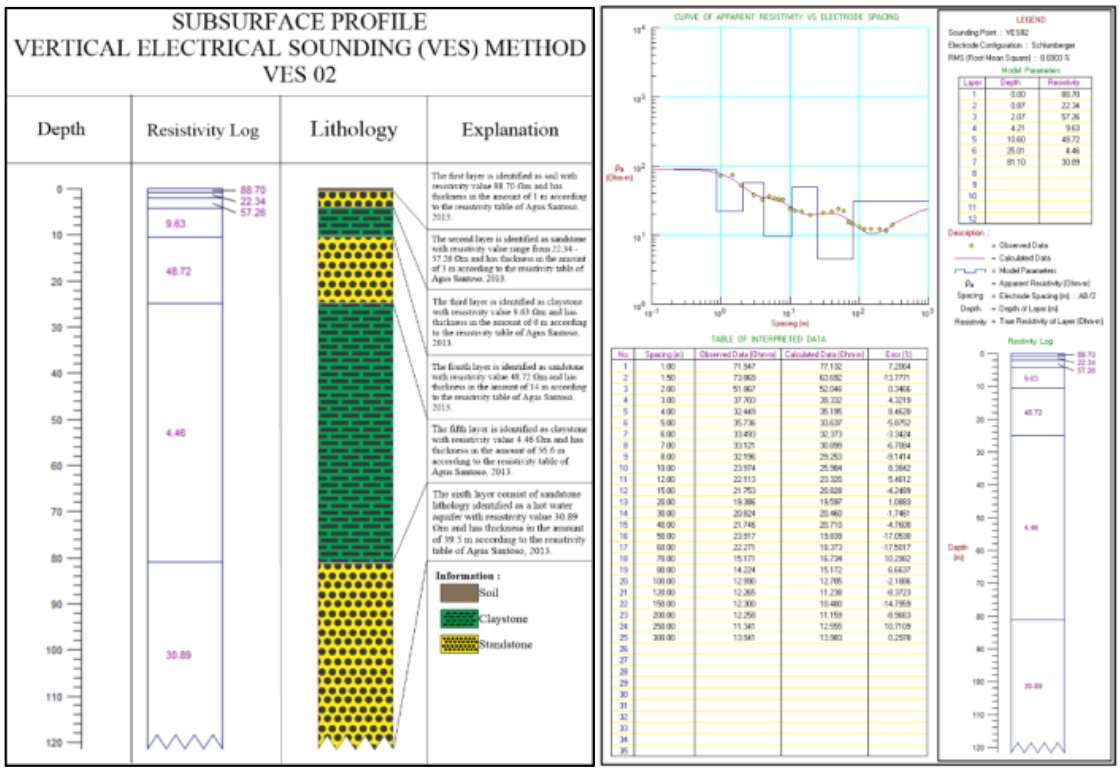

Figure 5: VES-02 Profile.

4.1.2 Subsurface Profile VES-02

In VES-02 sounding resistivity profile there are 6 layers with 3 kinds of lithology, namely soil with a resistivity of 88.70 Ωm, sandstone with a resistivity range of 22.34 - 48.72 Ωm, and claystone with a resistivity range of 4.46 - 9.63 Ωm with a maximum depth of 120m. Processing of resistivity values based on inversion in Progress software has an error value of 8.6903%. At this point, the presence of a hot water aquifer at a depth of 80 m can be identified because it can be seen in the lithology profile that the resistivity value of the lowest sandstone is at

that depth. So it can be indicated that the VES-02 point is passed by the outflow of the geothermal system originating from Mount Sumbing.

4.1.3 Subsurface Profile VES-03

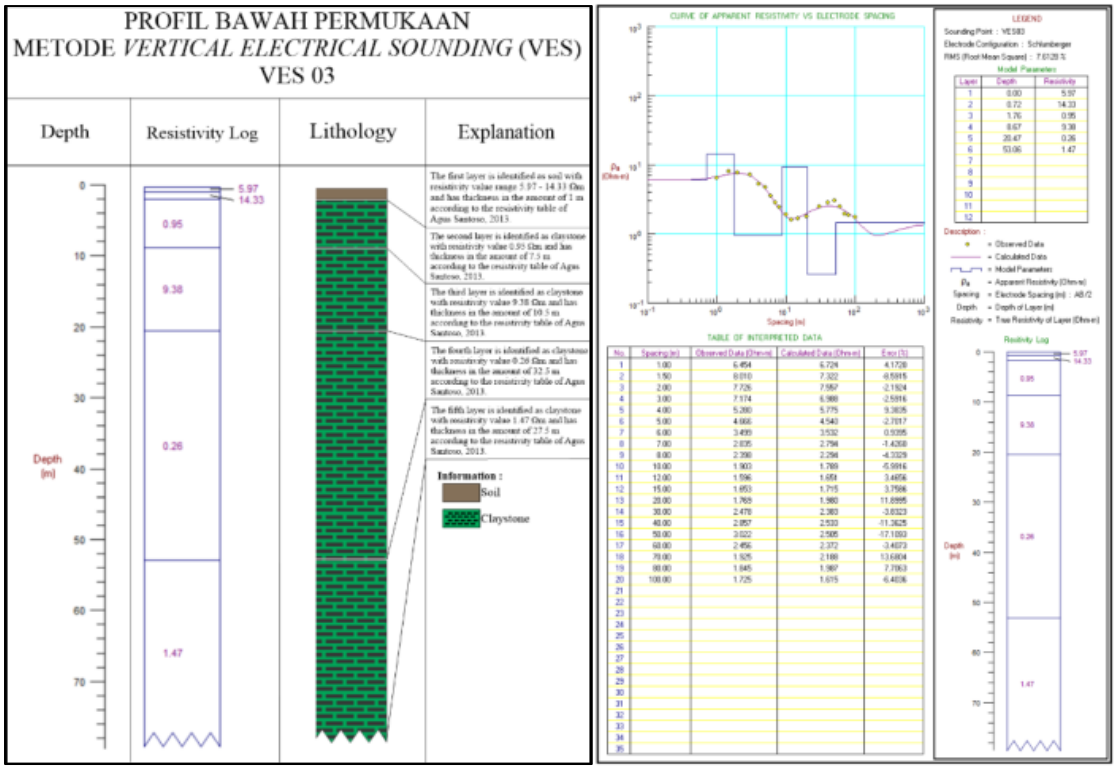

Figure 6: VES-03 Profile.

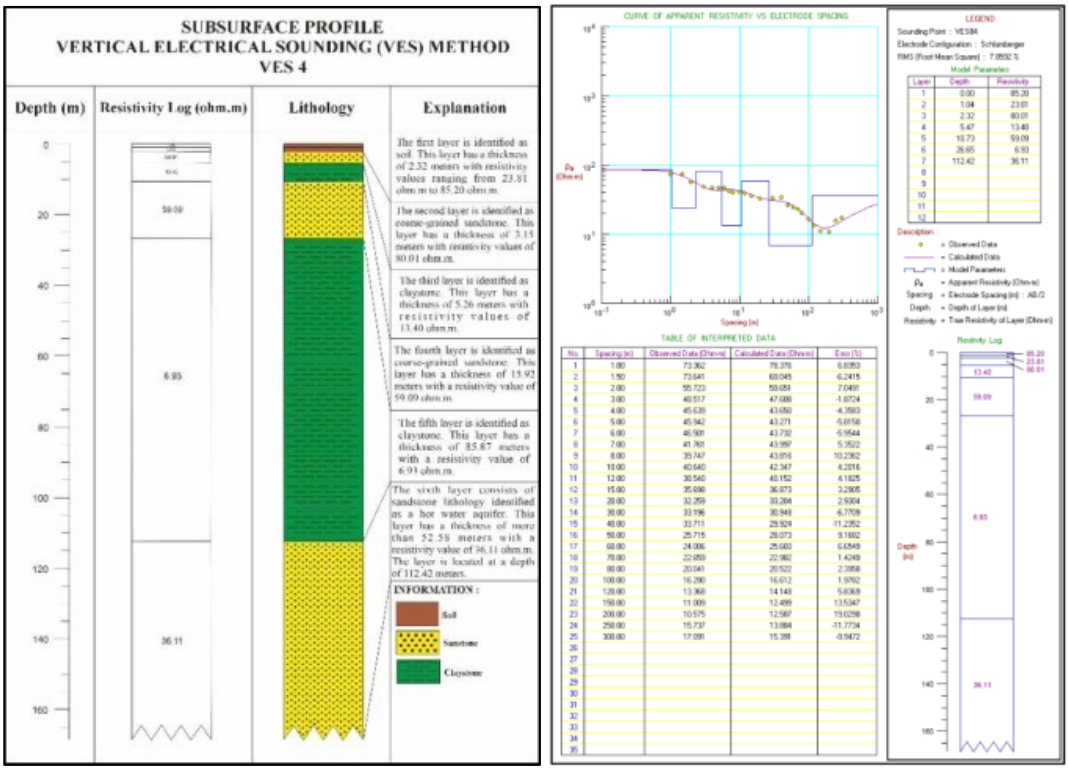

Figure 7: VES-04 Profile.

In VES-03 sounding resistivity profile there are 2 layers with 2 kinds of lithology, namely soil with a resistivity range of 5.97 - 14.33 Ωm, and mudstone with a resistivity range of 0.26 - 9.38 Ωm with a maximum depth of 80m. Processing of resistivity values based on inversion in Progress software has an error value of 7.6128%. At this point, the presence of a hot water aquifer cannot be identified because it can be seen in the lithological profile that the resistivity value of mudstone, which has very low permeability properties due to its very small pores and the cohesive nature of its particles, is usually not ideal as a flow medium for hot water aquifers. Therefore, it can be indicated that the VES-03 point is not passed by the outflow of the geothermal system originating from Mount Sumbing.

4.1.4 Subsurface Profile VES-04

In VES-04 sounding resistivity profile there are 6 layers with 3 types of lithology, namely soil with a resistivity range of 23.81 - 85.20 Ωm, sandstone with a resistivity range of 36.11 - 80.01 Ωm, and claystone with a resistivity range of 6.93 - 13.40 Ωm, with a maximum depth of up to 165 m . Processing resistivity values based on inversion in progress software has an error value of 7.85%. At this point it can be identified that there is a hot water aquifer at a depth of 112.42 m because it can be seen in the profile that the lowest resistivity value of the sandstone is at that depth. So it can be said that at the VES-04 point the Outflow from the Geothermal System which originates from Mount Sumbing passes through.

4.1.5 Subsurface Profile VES-05

In VES-05 sounding resistivity profile there are 6 layers with 3 types of lithology, namely soil with a resistivity range of 18.08 - 39.47 Ωm, sandstone with a resistivity range of 33.38 - 54.72 Ωm, and claystone with a resistivity range of 4.45 - 9.25 Ωm, with a maximum depth of up to 160 m. Processing resistivity values based on inversion in progress software has an error value of 12.94%. At this point it can be identified that there is a hot water aquifer at a depth of 107.41 m because it can be seen in the profile that the resistivity value of the sandstone is the lowest and is not shallow at that depth. So it can be said that at the VES-05 point the Outflow from the Geothermal System which originates from Mount Sumbing passes through.

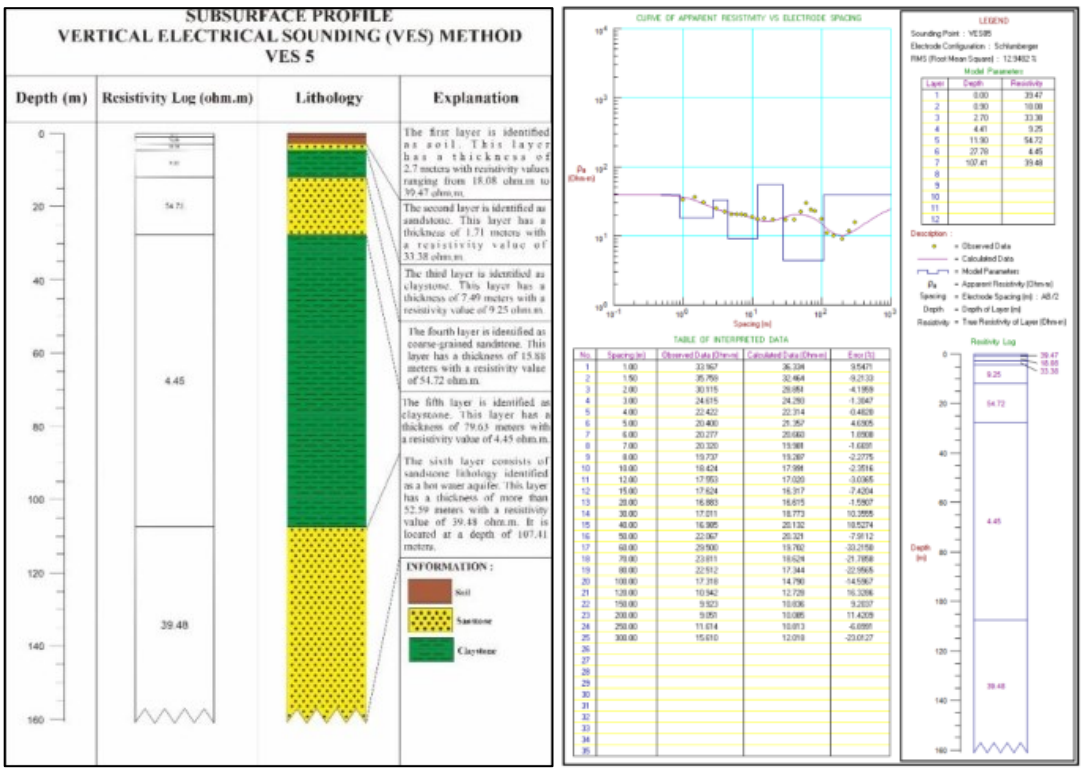

Figure 8: VES-05 Profile.

4.1.6 Subsurface Profile VES-06

In VES-06 sounding resistivity profile there are 6 layers with 3 types of lithology, namely soil with a resistivity range of 41.81 - 49.40 Ωm, sandstone with a resistivity range of 21.83 - 96.66 Ωm, and claystone with a resistivity range of 2.01 - 12.09 Ωm, with a maximum depth of up to 155 m. Processing resistivity values based on inversion in progress software has an error value of 7.59%. At this point it can not be identified that there is a hot water aquifer in this VES Point. So it can be said that at the VES-06 point it is not passed by the Outflow from the Geothermal System.

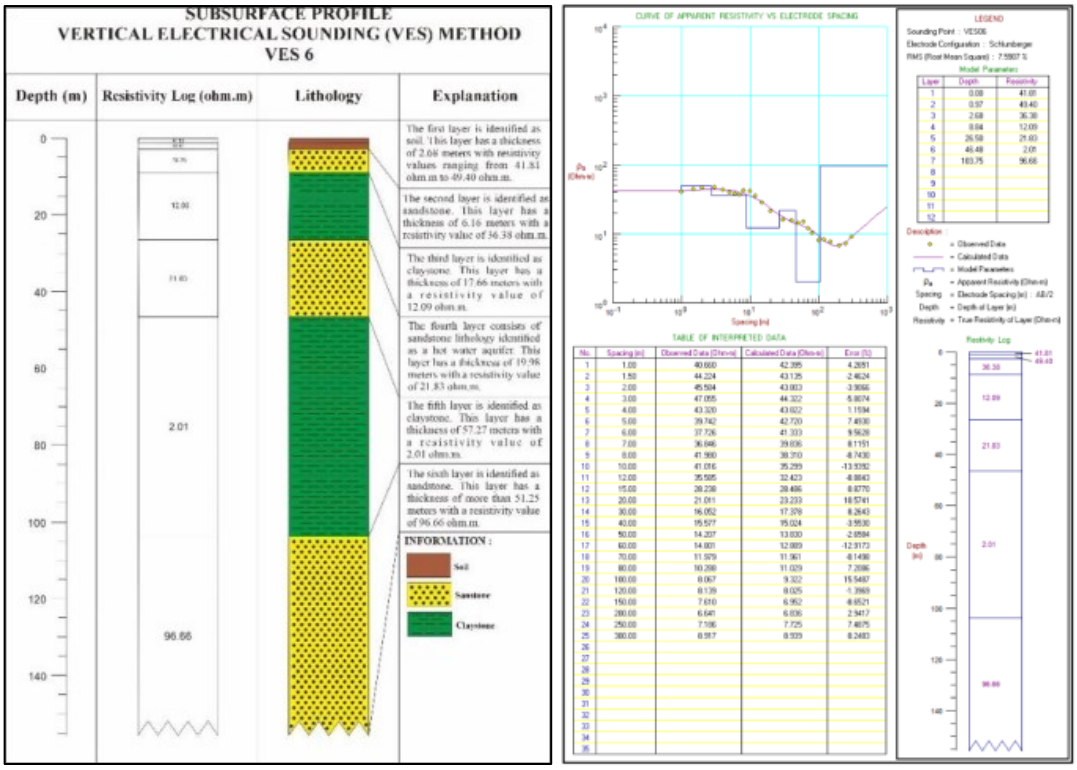

Figure 9: VES-06 Profile.

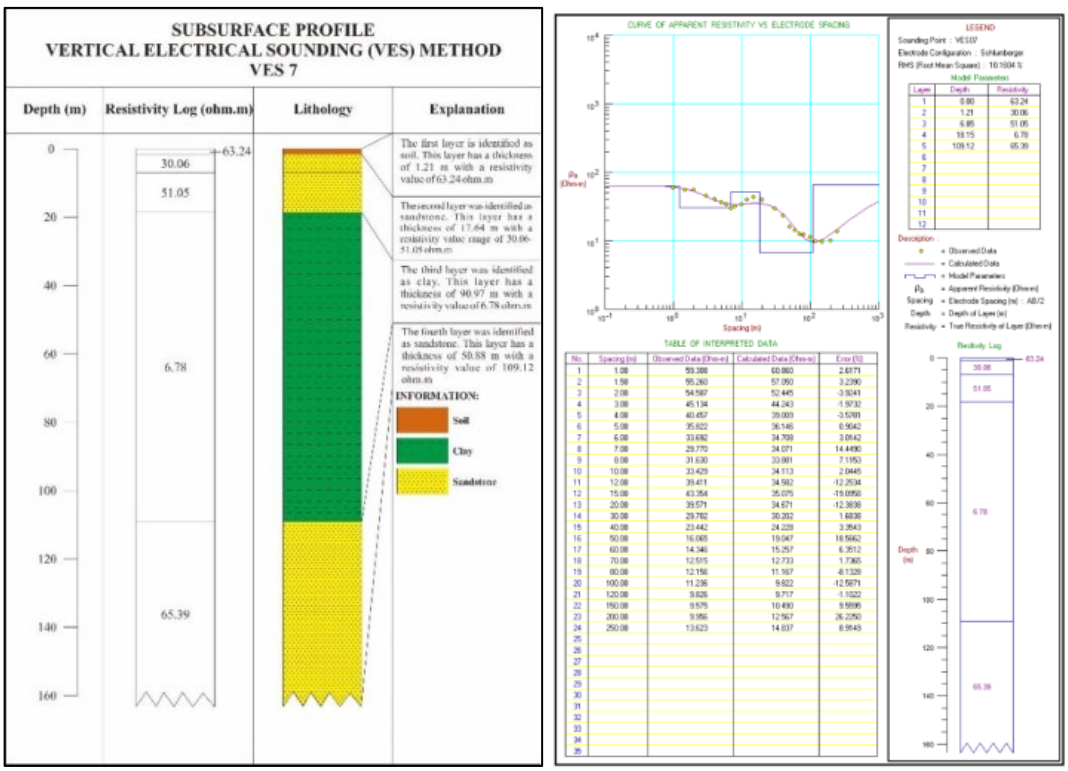

Figure 10: VES-07 Profile.

4.1.7 Subsurface Profile VES-07

In VES-07 resistivity sounding profile, there are 4 layers with 3 types of lithology, namely soil with a resistivity of 63.24 Ωm, sandstone with a resistivity range of 65.39-30.06 Ωm, and claystone with a resistivity of 6.78 Ωm, with a maximum depth of up to 160 m. The resistivity values were processed based on inversion using the Progress software, resulting in an error value of 10.16%. At this point, no hot water aquifer was identified at deeper depths because, as can be seen from the profile, the resistivity value of the sandstone appears high at a depth of 110 m,

indicating that there is no water contained in the pores of the sandstone. Therefore, it can be said that at the VES-07 point, the outflow from the geothermal system sourced from Mount Sumbing does not pass through.

4.2 VES Profile Correlation

Based on the correlation of line 1 and line 2, it can be said that the aquifer is at a depth of >110 meters with lithology in the form of sandstone. From the correlation above, it can be seen that the continuity of the outflow that fills the aquifer zone only passes through the measurement points of VES-01, VES-02, VES-04, and VES-05 with a range between acquisition points is ±500 meters. In line 1 all lithological layers are connected so that there are no missing layers, and in line 1 you can see the continuity of the aquifer zone in the last layer. In line 2 the lithology of the last layer based on data is still the same, namely sandstone, however in VES-07 and VES-06 there is no indication of water content because the resistivity value is quite high. It can be concluded that the outflow from Mount Sumbing is oriented from northwest to southeast.

4.3 Resistivity Map Each Elevation

Figure 12 shows the difference in resistivity values for each elevation difference. The resistivity value of the aquifer has a higher value range between 19 Ωm to 24.6 Ωm. It can be seen from Figure 12 that the elevations of 240 masl and 220 masl have high resistivity values in the western part, but the value gets smaller as the elevation decreases. However, at elevations of 200 masl and 180 masl, the northwest area shows higher resistivity values. The aquifer zone can be identified by its high resistivity value while still looking at its depth. Where this zone begins to appear at an elevation of 200 masl. While the elevation area above it is identified as a sandstone layer that does not contain aquifers.

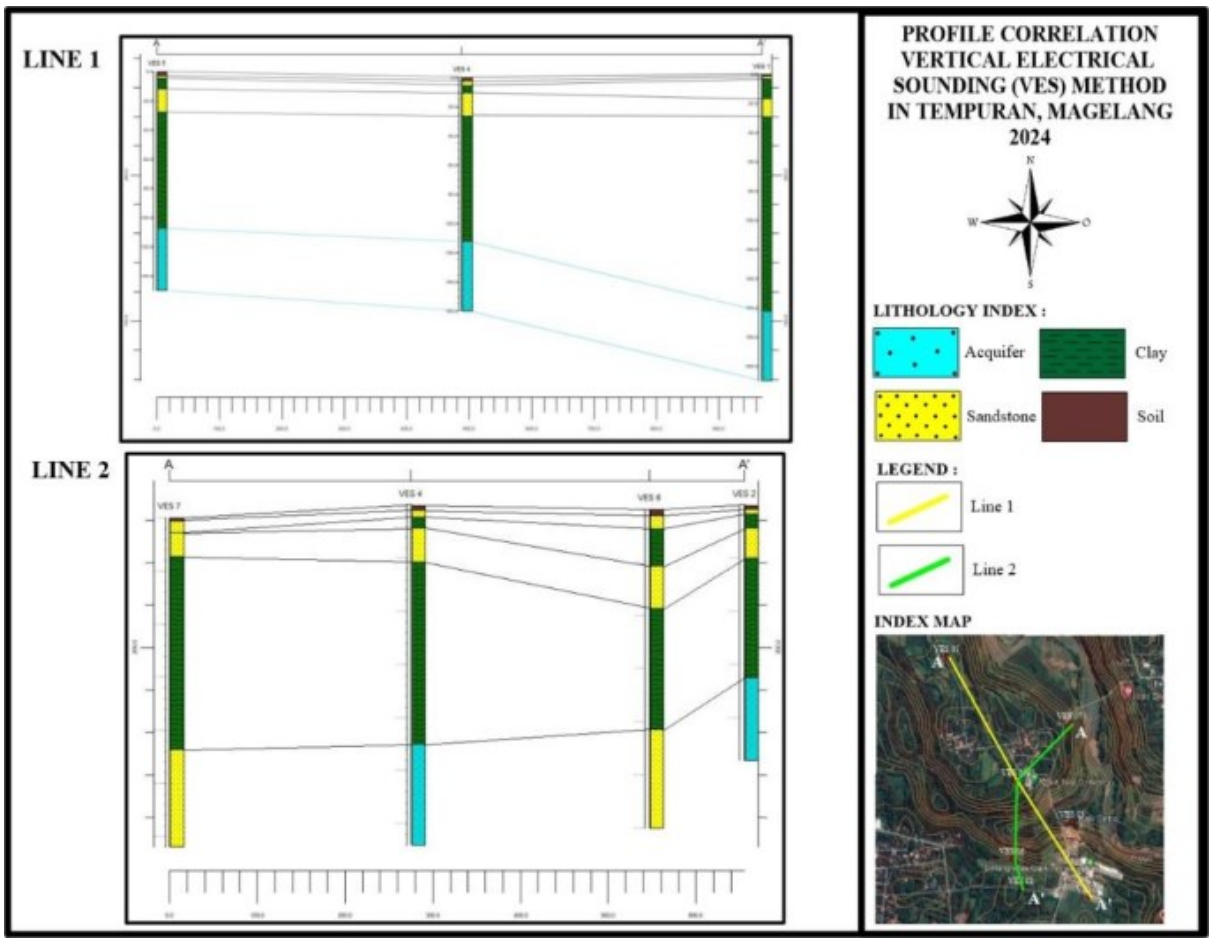

Figure 11: Profile Correlation Line 1 and Line 2.

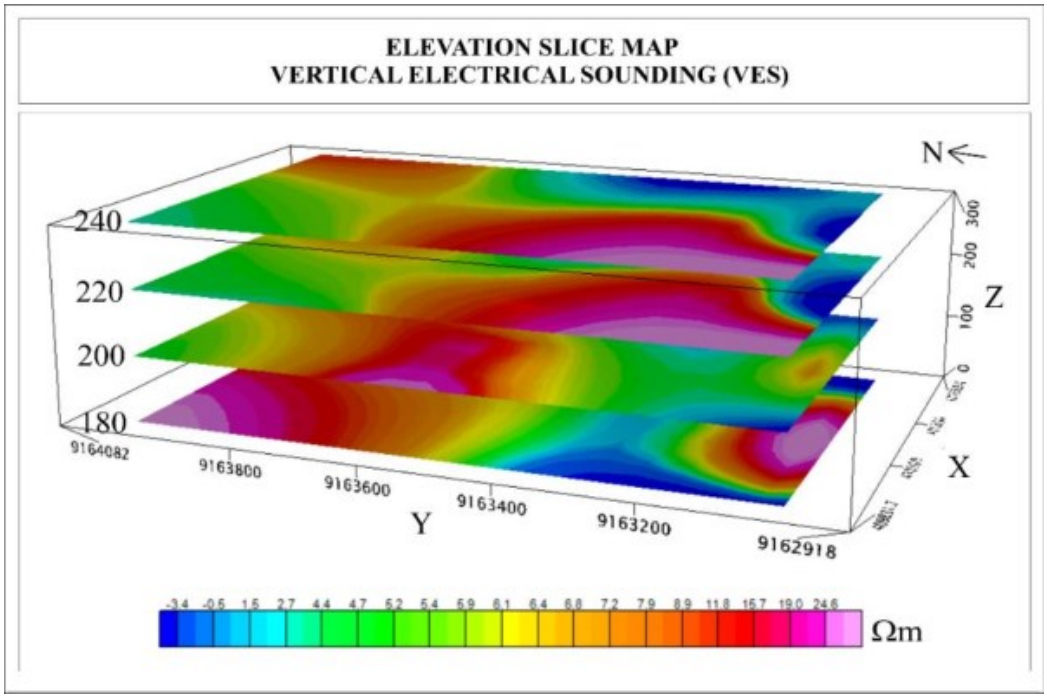

Figure 12: Resistivity Stack Map Elevation.

5. CONCLUSION

Based on the research that has been conducted, it shows that in the study area there is a layer of sandstone that is identified as an aquifer zone at a depth starting from 100 meters with average thickness of 44 meters. The existence of the aquifer zone is identified as arising from the outflow of the Geothermal System sourced from Mount Sumbing is oriented from northwest to southeast.

REFERENCES

Basith, A., Kongko, W., & Oktaviani, N.: Pemodelan Spasial Landaan Tsunami Menggunakan Variasi Lokasi Sumber dan Magnitude Gempa Studi Kasus Kota Padang. In Conference on Geospatial Science and Engineering. Yogyakarta. (2012).

Nuur, M.F., Purwanto, Raharjo, S.: Geologi Kendali Sifat Fisik - Mekanik Tanah Terhadap Potensi Bencana Gerakan Tanah Daerah Tanjunganom, Kecamatan Salaman, Kabupaten Magelang, Jawa Tengah. Jurnal Ilmiah Geologi Pangea. 2(2), (2015), 51-67.

Rahardjo, W., Sukandarrimidi dan Rosidi, H. M.: Peta Geologi Lembar Yogyakarta, Jawa, Skala 1:100.000. Bandung: Puslitbang Geologi. (1995).

Santoso, Agus.: Tabel Resistivitas Batuan Daerah Yogyakarta. Modul Geolistrik. (2014).

Simpen, I.N.: Solusi Permasalahan Sumur Bor versus Sumur Gali dengan Metoda Geolistrik dan Uji Pemompaan Sumur (Suatu Studi Kasus di Bugbug Karangasem Bali). Prosiding Seminar Nasional Sains dan Pembelajarannya. Malang : Jurusan Fisika Fakultas Matematika dan Ilmu Pengetahuan Alam Universitas Negeri Malang. (2015).

Suharyadi.: Geohidrologi. Yogyakarta : Fakultas Teknik Universitas Gajah Mada. (1984).

Todd, D.K.: Groundwater Hydrology. Second Edition: New York: John Wiley & Sons, Inc. (1980).

Wardana, G. G.: Identifikasi Zona Akuifer Air Tanah Menggunakan Metode Vertical Electrical Sounding (VES) Pada Daerah Banyumas Kabupaten Pringsewu. Universitas Lampung, Bandar Lampung. (2019).

The Subsurface and Drilling Aspects of The Successful 2020-2021 Make-up Well Drilling in Wayang Windu Geothermal Field, Indonesia

Shanti R. A. Sugiono, Ridha B. Nugraha, Rio Nugroho, and Wintry Dimwani

Star Energy Geothermal, Wisma Barito Pacific II, Jl. Letjen S. Parman Kav. 60, Jakarta 11410, Indonesia

shanti.sugiono@starenergy.co.id

Keywords: Star Energy Geothermal, Wayang Windu, Drilling, Make-up well, Subsurface

ABSTRACT

Star Energy Geothermal completed the make-up well drilling campaign in 2020-2021 to maintain steam supply for the existing power plants with a total installed capacity of 227 MWe at the Wayang Windu geothermal field. As a primary objective, based on the steam supply profile, 6 (six) production wells were required to be drilled in this campaign, three wells producing from the steam reservoir and three wells producing from the deep brine reservoir. This combination was necessary to maintain field pressure decline by balancing steam and liquid reservoirs production. Wells prepared in this campaign consist of one re-drill well, four new wells drilled from the existing pad, and one well from the new well pad. Based on historical data, drilling deep into the brine reservoir has been particularly challenging in Wayang Windu field. Several initiatives have been implemented to achieve the objective of this campaign, including lessons learned from previous drilling campaigns as part of continuous improvement. The initiatives in the subsurface area include refining well targeting assessment and detailing potential geological hazard identification, especially in the deep reservoir section. While in the drilling area, several initiatives were made, such as better well planning and improvement in drilling practice. As a result, the drilling campaign was completed with significant success: steam output above the target, successful drilling to the deep brine reservoir, and finishing the campaign with a faster and lower cost than the plan. Moreover, the success of this campaign in drilling deep brine wells has provided more information for the resource team to characterize better the deep brine reservoir for resource assessment to enable future field development and maximize Wayang Windu asset value.

1. INTRODUCTION

Wayang Windu geothermal field (Wayang Windu) is located at Pangalengan district, West Java Province, Indonesia. It lies within the high thermal flow region among other geothermal fields such as Kamojang, Darajat, and Patuha (Figure 1). Wayang Windu is operated by Star Energy Geothermal Wayang Windu Ltd. with a total installed capacity of 227 MW from two power plant units. The field has been running since the first power plant unit generation started in 2000 (110 MW), followed by the second unit in 2009 (117 MW). As part of the field management Star Energy has developed a continuous program to ensure sufficient steam supply to run the power plant at full capacity. The programs include well workovers/interventions and other initiatives such as make-up well drilling. The latter initiative is programmed and scheduled when the well capacity decreases towards minimum steam supply requirement.

From November 2020 to June 2021, Star Energy Geothermal conducted a make-up well drilling program in Wayang Windu. The main objective of this drilling campaign is to maintain the steam supply for the current generation by obtaining steam from both steam and brine reservoirs. The combination of steam and brine wells also aims to achieve optimum production between steam and brine reservoirs and prolong the steam cap reservoir performance.

One of the challenges in this drilling campaign is to drill the well down to the brine reservoir, which has a low historical success rate (less than 50% field-wide). Despite the challenges, this drilling campaign was successfully conducted with the total steam output above the target, completed with faster drilling days, and cheaper well costs. This paper discusses the subsurface and drilling aspect that plays an essential role in the success of this campaign.

2. WAYANG WINDU GEOTHERMAL RESERVOIR IN BRIEF

Wayang Windu is a two-phase liquid reservoir that is transitional from a vapor-dominated reservoir in the northern portion of the field to a more liquid-dominated reservoir in the southern part (Figure 2). Three upflows have been identified at Wayang Windu, lining up from the north to the south called Gambung, Wayang, and Windu upflows. These upflows represent different reservoir regions based on their temperature, pressure, and chemistry. However, the reservoir area is connected laterally and vertically between steam and brine, as confirmed by the tracer injection test across the field (Malik et al., 2020).

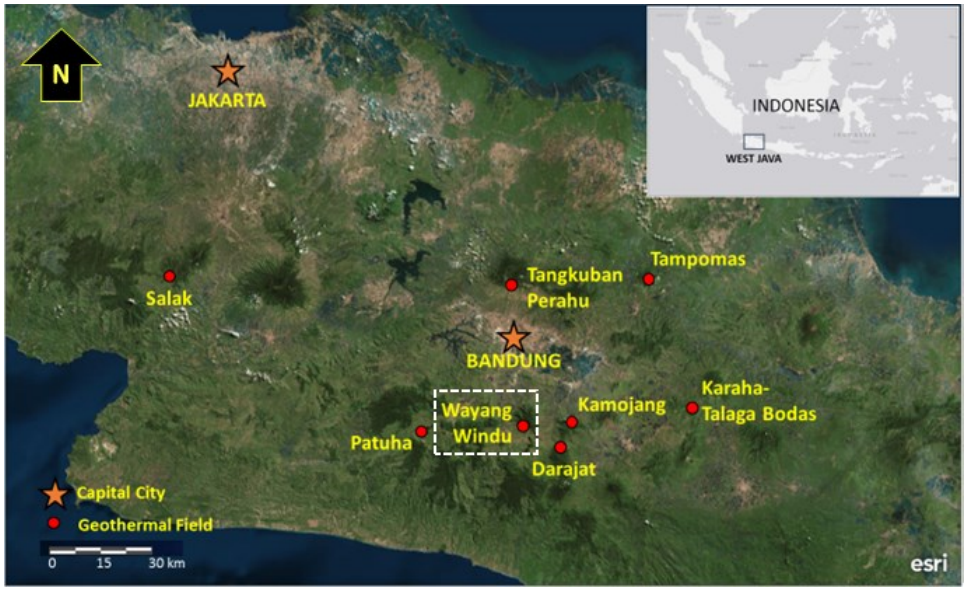

Figure 1: Location of Wayang Windu geothermal field (in the white rectangle) and other nearby high-temperature geothermal field in the West Java province, Indonesia.

The vapor reservoir/steam cap temperature is about 250-260 °C and about 280-290 °C in the liquid/brine reservoir. The steam cap in the northern area is relatively thicker compared to the central and southern parts of the field (Figure 3). The permeability of the steam reservoir in the northern area is also higher than in the other parts of the field, making commercial production in this area more favorable. Currently, about 90% of the steam production is coming from the steam cap in the northern area (MBA, MBB, MBD, MBE, and WWQ wells) and about 10% from the two-phase reservoir in the central area. The southernmost area of the field is currently the locations of the brine and condensate re-injection wells (WWF and WWW wells).

Most of the wells drilled in the northern area penetrated only the steam cap with no direct brine indication, and therefore no clear steam-brine contact can be observed. The steam-brine contact can be observed in the central area as most wells penetrate the brine reservoir. While in the southern part, because the wells are currently re-injection wells, no clear steam-brine contact can be observed (Figure 3, left). Due to the higher production rate of the northern steam cap, the pressure decline is higher in the steam reservoir, although it is still within a tolerable range (about 1 bar/year). On the other hand, the deep-seated liquid reservoir is relatively stable due to lower pressure drawdown (Mulyadi et al., 2023). To maintain pressure decline in the steam cap, one of the initiatives is to optimize the production between steam and brine reservoirs by producing more brine to create more steam from below.

3. WAYANG WINDU MAKE-UP WELL DRILLING 2020-2021

3.1. Well Selection and Targeting

Before the drilling campaign, well trajectory option/catalog that could be drilled in the existing production area (by new wells, sidetrack, re-drill, or deepening the existing wells) were listed and updated based on the latest drilling result. The well catalog was developed considering the subsurface target and surface facility condition (well pad). The list also considers multiple subsurface target options with various depth, azimuth, and inclination. For this campaign, the list is ranked based on the target area (i.e., reservoir temperature), permeability (i.e., potential steam production), potential subsurface risk (i.e., problematic formation issue, scaling, possible cooling/marginal recharge, and interference with the nearby well), potential drilling risk (i.e., well stuck), and surface facility consideration. In addition to the list, a new well pad (MBI) was also constructed for this campaign to extend the northern production area to avoid rapid production and interferences between the existing wells.

This campaign was programmed to provide steam for the full generation of Unit-1 and 2 power plants until 2023. With the current field decline rate and average well production, at least 5-6 wells would be required to meet the steam target of 122 kg/s. From the well catalog, several steam and brine wells at the top rank on the list were selected and assessed to get an optimum option with the highest total steam output while minimizing the drilling costs. Based on the evaluation, six wells (three targeted steam and three targeted brine) were selected for this campaign. The wells consist of one re-drill well from the MBD well pad, four new wells drilled from MBE and WWA well pads, and one from the new MBI well pad (Figure 2).

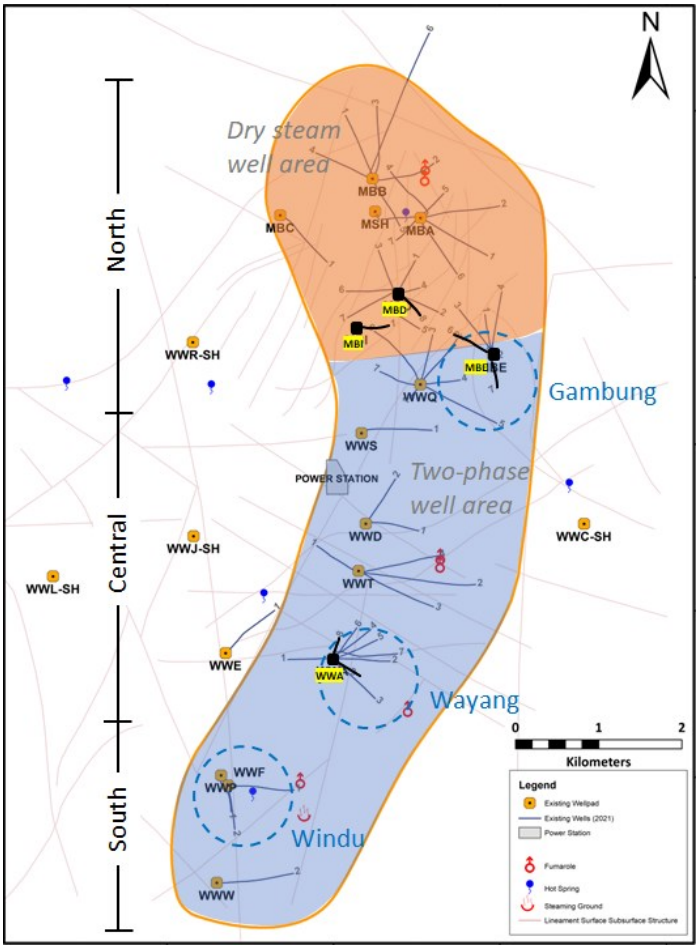

Figure 2: Map of Wayang Windu geothermal field with well courses, two-phase reservoir area, and upflows location (after Malik et al., 2020).

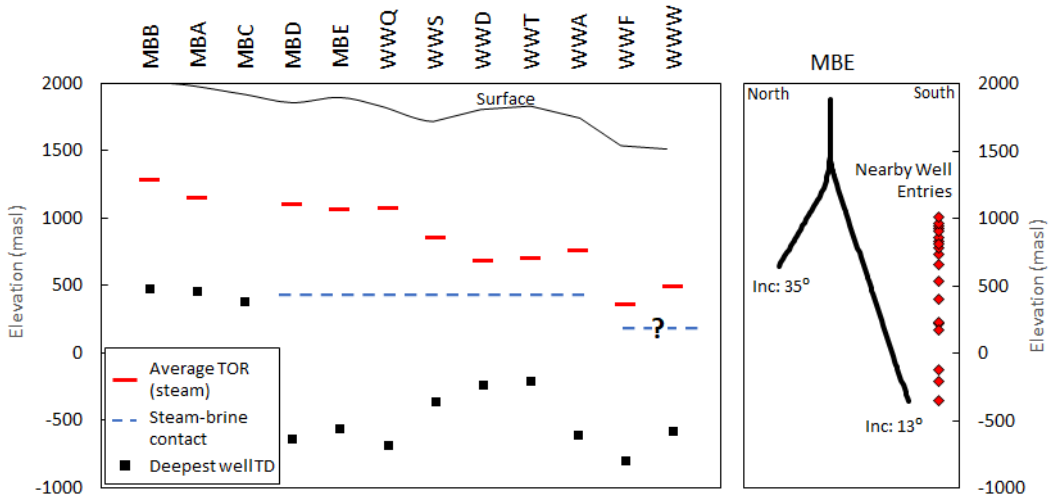

Figure 3: Left: a simplified N-S section of Wayang Windu geothermal field with average top of reservoir steam (TOR), steam-brine contact and deepest well TD at each well pad. Right: example of well trajectory in 2020-2021 drilling campaign for steam (left) and brine well target (right). See Figure 2 for well pad location.

Well trajectory of each well candidate was designed to penetrate either steam reservoir only or a steam and brine reservoir. The well targeting considers the optimum direction related to the strike of the open fractures and the depth of the productive zone based on the nearby wells. To minimize a potential higher risk of doing directional drilling in the reservoir section, a 2-D J-shaped well design was selected for all wells. The well design is

considered optimum as the target of productive zone can be achieved while maintaining the allowable distance with the nearby wells to avoid production interference. Figure 3 (right) shows the example of well trajectories prepared from the MBE well pad. One of the MBD well targets the steam reservoir with a 35º inclination to the northeast, while the other well targets the brine reservoir with a 13º inclination to the south. The average total depth for the steam well is 1,370 meters and for brine well is 2,100 meters measured depth (mMD).

The well targeting of the selected wells relied heavily on the nearby wells' information. It includes the location of the permeability target at both steam and brine reservoirs (well entries) and potential subsurface risk. In this campaign, a new and improved approach to calculate the steam output and the location of the well entries was applied carefully, especially for the well at the new well pad and the brine well, which have limited data.

In Wayang Windu, drilling the brine reservoir, especially in the central and northern areas, is challenging. In addition to the limited subsurface information in the deep brine reservoir, the drilling risk is historically high (less than 50% of the drilling success rate). One of the subsurface risks encountered when drilling the brine well is the limited information on the formation-related drilling difficulties like tuffaceous siltstone (TS). The TS is a reactive smectite-rich formation that could swell when exposed to the drilling fluid within ~48 hours and can lead to a stuck pipe (Putra et al., 2021). The TS is a common formation in volcanic regimes like in Wayang Windu that was originated from the volcanic ash which reacted with water to form clays and iron oxides. The thickness of this formation can vary, and its distribution can be identified based on the offset wells. Figure 4 shows the distribution of TS layers at WWA well pad based on the latest study conducted before this drilling campaign. At least nine layers of TS were observed in most wells at the WWA well pad. The TS occurs above and within the reservoir section and can lead to the stuck pipe under certain conditions.

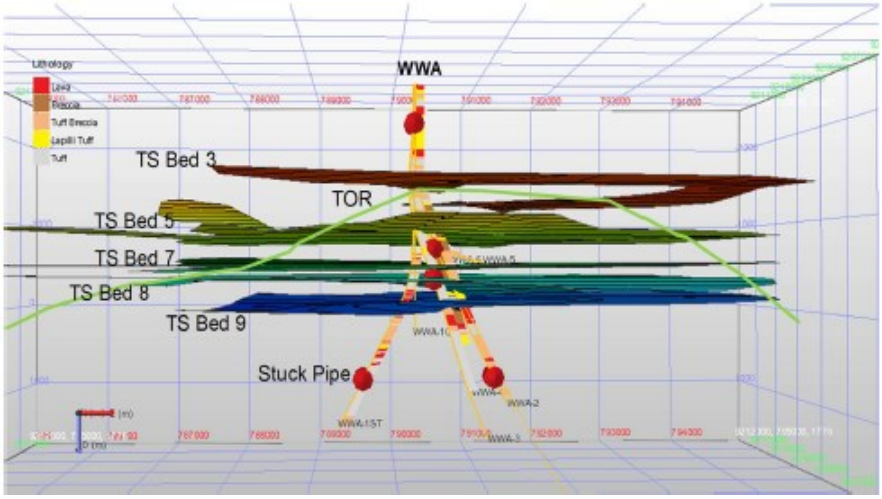

Figure 4: Distribution tuffaceous siltstone at WWA wellpad as part of the detail study (Star Energy, 2020).

3.2. Well Planning and Well Drilling

The drilling in Wayang Windu has improved over time, as reflected by the faster drilling, fewer stuck pipe events, and lower drilling cost (Putra et al., 2021). However, there is still some room for improvement that can be done to get better results, especially in the well planning and drilling practice.

An example of well planning is that an improved understanding of the behavior of the problematic formation, such as TS leads to a better selection of the drilling fluid. A better understanding of identifying clay mineral content using XRD analysis helps to design suitable drilling fluid based on formation needs. A behavior study of a similar formation in Salak (Ganefianto, 1994) shows that only a few drilling problems encountered above the reservoir are related to TS. In addition, using KCl as clay inhibitor below top of reservoir section was ineffective in inhibiting the swelling (Ganefianto, 1994). A thorough study was conducted to identify the stuck pipe mechanism that occurred in the reservoir section. The study concluded that drilling without clay inhibitors such as KCl is suitable to be used in Wayang Windu. It is because the presence of high Cl^- in drilling fluid coming from KCl is counter-effective since it can initiate the propagation of high illite-chlorite clay structure. In Wayang Windu, the drilling fluid without KCl has successfully mitigated the problematic formation in the reservoir section.

The predictive offset well monitoring and real-time drilling monitoring are implemented in this campaign as it effectively improves the drilling operation. The system's effectiveness has been identified since the previous drilling campaign (Putra et al., 2021); therefore, it is maintained as one of the best practices for this drilling campaign. Real-time drilling monitoring displays the data collected from the sensors at the rig site and then

transmitted lively and can be monitored by the field and office team 24 hours daily. One example of utilizing this system is predicting the well's entries/possible feed zones to enhance the rate of penetration (ROP) and cutting management to ensure well cleaning during the drilling (Figure 5). With this approach, in this drilling campaign, the ROP is improved from 120 m/day to 358 m/day in the reservoir section.

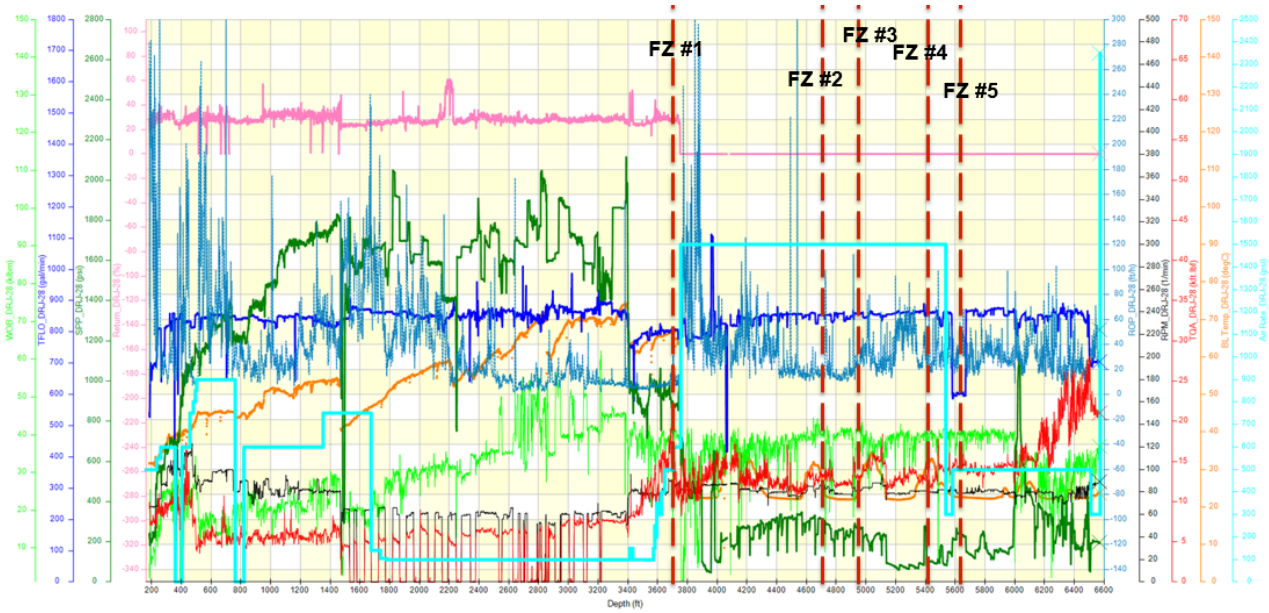

Figure 5: Example of the real-time drilling monitoring to predict entries/feedzone (FZ) to assist when to accelerate or when we have to hit the break.

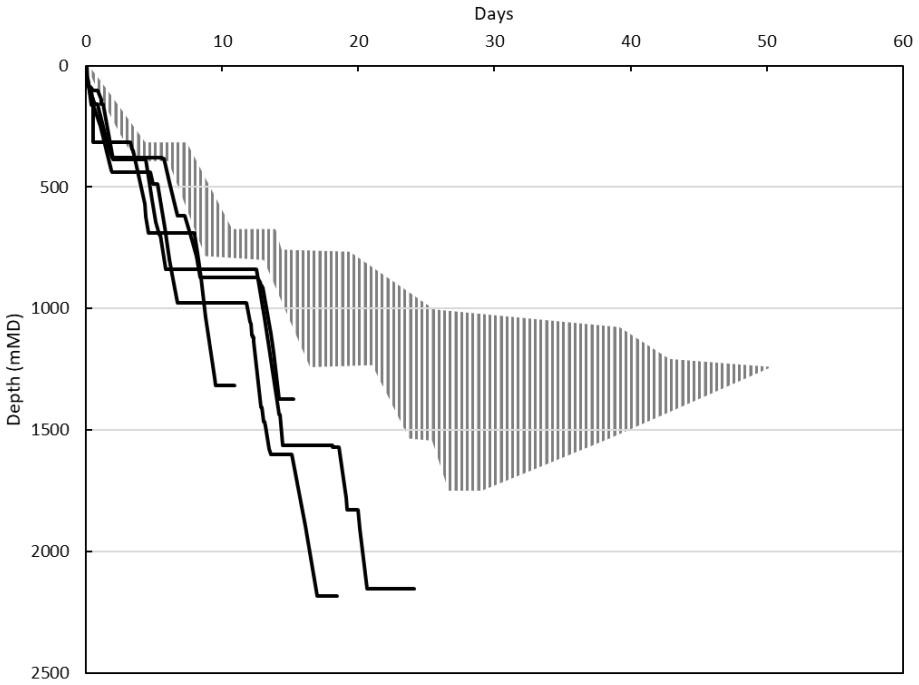

Figure 6: Time (days) vs. depth (meter measured depth) comparison of the MUW 2020-2021 (black lines) with the last drilling campaigns in Wayang Windu (shaded area).

3.3. Drilling Results

Six wells were drilled in this campaign, starting with the re-drill well in the MBD well pad, then two wells in the MBE well pad (one steam well and one brine well), two wells in the WWA well pad (two brine wells) and completed in the MBI new well pad (steam well). This sequence represents the drilling started from the well with the lowest drilling risk to the higher drilling risk, allowing the drilling to be improved over time. The total steam gained in this campaign is 131 kg/s (9 kg/s above the target), where four wells delivered the steam above the

expected target, and the other two were near and below the target. The actual location of the feed zones in the steam reservoir generally fits with the planned depth. In contrast, for the brine wells, the actual depth of the feed zones is offset for several targets, showing that the limited data in the brine well leads to high uncertainty. However, all the expected major feed zones from steam and brine reservoirs are obtained.

The total drilling days in this campaign is142 days (63 days faster than the plan), with most of the wells successfully drilled to the planned TD. Compared to the last drilling campaign, this campaign has improved significantly in terms of drilling days for each well and successfully drilled to the deep brine wells with an average well TD of 2,100 mMD (Figure 6). Moreover, the new well at MBI was successfully drilled to the planned TD at 1,308 mMD in 11 days, breaking the whole-time drilling record for the steam well in Wayang Windu. The average well cost in this campaign also decreased significantly to less than USD 3 million per well. The main contribution to the efficiency came from the faster drilling time and the elimination of the KCl in the drilling fluid.

The make-up well drilling in 2020-2021 is not only successfully providing steam supply for the current generation but also providing vital information for the future development of the Wayang Windu field. The successful drilling of the brine reservoir in MBE and WWA well pad has provided confidence in drilling in the brine wells, especially in the northern area. It is also found that commercial productivity appears in the brine reservoir and can sustain as indicated since the well started producing.

4. CONCLUSION

The 2020-2021 make-up well drilling in Wayang Windu was completed successfully, providing steam supply to the existing power generation. This success was the result of continuous improvement in the drilling campaign. The total steam production in this campaign is above the planned target, with faster drilling days. In addition, the success of this campaign in drilling deep brine wells has provided vital information for the resource team to characterize better the deep brine reservoir for resource assessment to enable future field development and maximize Wayang Windu asset value.

ACKNOWLEDGEMENT

The authors would like to thank the Asset Management team of PT Star Energy Geothermal and the management for their support and permission to publish this paper. Special acknowledgement to Rifqa A Wicaksono as the Project Manager of Wayang Windu 2020-2021 Make-up Well Drilling Campaign.

REFERENCES

Bogie, I., Kusumah, Y.I., Wisnandary, M.C.: Overview of the Wayang Windu Geothermal Field, West Java, Indonesia, Geothermics, 37, (2008), 347-365

Ganefianto, N.: Awibengkok Paleosoil Study, Unocal unpublished report (1994)

Malik, D., Abidin, Z., Pramono, B.: Tritum tracer Injection test at Wayang Windu Geothermal Field, West Java, Indonesia, Geothermics, 83, (2020), 101718

Mulyadi, Subekti, D., Pentury, S., Azwar, L.S.: Response of Wayang Windu Geothermal Reservoir to Over 20 Years of Production, Proceedings, World Geothermal Congress, Beijing, China (2023)

Putra, R.B., Souvanir, T., Purba, E., Irfan, M., Darmawan, D.: Significant Improvements in the 2018-2019 Wayang Windu Drilling Campaign, Proceedings, World Geothermal Congress, Reykjavik, Iceland (2021)

Star Energy: Brine reservoir drilling task force close out report, Star Energy unpublished report (2020)

Utilizing Static Modeling to Analyze Paleosol Distribution to Reduce Its Impact on Stuck Well Drilling in Wayang Windu

Meiyanto J. Purnomo, Ananyamatya B. Talita,
Nevio M. Kamel, Dwiyogarani Malik, and Wintry Dimwani

Star Energy Geothermal Wayang Windu Ltd., Wisma Barito Pacific II 17th Floor, Jakarta 11410, Indonesia

meiyanto.jokopurnomo@starenergy.co.id

Keywords: Static model, paleosol, Wayang Windu

ABSTRACT

Paleosol, or ancient soil formed in the past and buried under more recent deposits, is commonly observed in volcanic environments, which often host geothermal systems worldwide. The presence of paleosol has been reported in several geothermal fields in Indonesia, such as Salak, Wayang Windu, and Sarulla. Paleosols developed in volcanic environments mainly consist of weathered volcanic materials, such as volcanic ash, cinder, and pumice. Soils derived from volcanic products are classified as Andosols. In Wayang Windu area, paleosol is well-known as Tuffaceous Siltstone (TS) material, predominantly composed of weathered tuff with a silt grain size. Physically, paleosol at Wayang Windu appears reddish-brown-grey and primarily consists of fine-grained tuff. The mineralogy of the paleosol mainly comprises smectite and/or mixed layers with illite or chlorite. Generally, it can be classified as either sticky or non-sticky (brittle).

Paleosol at Wayang Windu has been a significant concern due to its suspected correlation with stuck pipe incidents during drilling. There is a strong conjecture that the characteristic of the paleosol, which tends to swell upon contact with drilling fluid and has poor mechanical strength, is responsible for many stuck pipe incidents. Therefore, modeling the distribution of paleosol at Wayang Windu has critical implications.

The updated static model of Wayang Windu in 2023 was constructed based on formation distribution, enabling the modeling of paleosol distribution at the formation scale. Single well paleosol distribution analysis has revealed that paleosol deposition at Wayang Windu occurs in three types: continuous thin layers, single thin layers, and single thick layers. The distribution of paleosol within and beyond individual wellpads has been synthesized by incorporating each single well analysis with data from other wells within the same formation using 2D and 3D correlation and modeling techniques. The 2D correlation method has successfully differentiated at least three paleosol layers within each formation at Wayang Windu. Combining the results of 2D correlation with the 3D structural and static models makes it possible to interpret paleosol distribution beyond the existing wells. This distribution provides valuable information for identifying potential subsurface hazards related to paleosol distribution (stuck pipe incidents) during well planning activities.

1. INTRODUCTION

The Wayang Windu Field is geographically located in the Pangalengan district, about 40 km South of Bandung, the capital city of West Java Province, and about 150 km southeast of Jakarta, the capital city of Indonesia. Wayang Windu is a two-phase geothermal field with an electricity generating capacity of 230.5 MW. This field is surrounded by several high-terrain geothermal systems such as the Darajat, Kamojang, Patuha, and Karaha-Talaga Bodas fields (Figure 1).

The volcanological setting shows that Wayang Windu lies on the southern slopes of a large andesitic stratovolcano called Mt. Malabar, along with a series of smaller volcanoes trending southward, including Mt. Wayang and Mt. Windu. This setting permits paleosol development across the Wayang Windu field. Paleosol in Wayang Windu, mostly known as the Tuffaceous Siltstone (TS) layer, consists of fine-grained tuff with a reddish-brown and grey color, high smectite content (either as smectite layer or mixed layer smectite) and is categorized into two types: sticky and non-sticky (brittle) material.

The impact of paleosol on drilling activity has been under special investigation since the beginning of Wayang Windu development. The initial exploration stage, undertaken by PERTAMINA, drilled the discovery well of the Wayang Windu field in 1991. The first paleosol study was conducted internally in 1997 with Kingston Morrison, which aimed to establish the cause of the instability of the paleosol, suspected to be a problematic formation causing drilling problems at Wayang Windu (Kingston Morrison, 1997). In 2019, an update on the paleosol (tuffaceous siltstone) study was conducted as part of drilling lookback to better understand the impact of the paleosol (TS) to the drilling problem in order to increase the probability of success (POS) to drill deep brine

reservoir in WW (Earth Science AM WW, 2019), The objective of the study was to update the paleosol characterization based on physical appearance, mineral composition, distribution, and its correlation with the drilling problems (i.e. stuck pipe incident). Paleosol distribution was initiated based on bed correlation referring to the 1997 paleosol study under pad basis. The assessment in Wayang Windu in 2019 concluded that 20% of the stuck pipe incidents in central Wayang Windu correlated with paleosol existence, while in the north Wayang Windu area, 30% of the stuck pipe incidents were related to paleosol. Hence, modeling the distribution of paleosol at Wayang Windu has critical implications for the success of the next make-up well drilling campaign.

Figure 1: The location map shows the geographical location of Wayang Windu and its relative position to the surrounding geothermal fields.

In 2023, Wayang Windu updated the static model by incorporating the petrophysical group and paleosol layer to define formation distribution. The use of the paleosol layer as a marker is based on the recommendation of the 1997 paleosol study, which concluded that at least five beds of paleosol have extensive occurrence and distribution in the north of Wayang Windu. Thus, it is useful to use the paleosol as a marker horizon. The update of the static model identified eleven formations spread across the Wayang Windu area (Purnomo et al., 2023). The established 2D and 3D distribution of the formations improved the understanding of their spatial distribution in Wayang Windu. Therefore, this paper discusses the utilization of formation distribution by incorporating detailed paleosol categorization to define the paleosol distribution in Wayang Windu. By having detailed distribution in 2D and 3D, a more accurate paleosol distribution model can be acquired, aiding in identifying the paleosol zone during drilling and defining mitigation strategies when encountering this zone.

2. PALEOSOL CHARACTERIZATION

Two major descriptions of paleosol are accepted today, related to two branches of geoscience: soil science and geology. In soil science, paleosol refers to a soil layer that formed a long time ago and has a different chemical and physical composition compared to the recent soil layer, which is controlled by present-day climate or vegetation. In geology, particularly paleontology, paleosol refers to ancient soil that is preserved due to being buried by other sediments or volcanic deposits. These sediments might consist of alluvium or loess, while volcanic deposits can include lava from lava flows or pyroclastic material such as volcanic ash deposits. Paleosol formed in volcanic environments is categorized as Andosols (or Andisols in some publications; this paper will use Andosols). The common concept of Andosols is that they are paleosols derived from loose volcanic ejecta such as volcanic ash, cinders, and pumice. Another source of the materials forming Andosols might be other explosively erupted, fragmental volcanic material (tephra) and volcaniclastic or reworked volcanic materials (McDaniel et al., 2012).

Paleosol in Wayang Windu, known as the Tuffaceous Siltstone (TS) layer, can be distinguished into four categories based on physical appearance (megascopic) identified at the drilling site as follows: a) Reddish brown sticky clay, b) Grey sticky clay, c) Reddish brown non-sticky/brittle, and d) Grey non-sticky/brittle as seen in the Figure 2 (Earth Science AM WW, 2019). To further understanding its composition, the TS is also defined based on laboratory analysis results of samples using petrography, XRD, and SEM-EDAX. In the case of blind drilling and no cutting return from the wellbore, potential TS presence can still be identified by involving borehole image (BHI) analysis. A combination of physical and laboratory characterization of TS shows characteristics of reddish-brown and grey, very fine-grained tuff with high smectite content (Ca-smectite with more than 80% smectite in the form of interlayered Illite-Smectite). The origin of TS in Wayang Windu is concluded to be derived from

volcanic ash (unconsolidated, easily reworked and filled the lake) that reacted with water to form clays and iron oxides. Relating to the geothermal system in Wayang Windu, the TS is not in equilibrium with the Wayang Windu hydrothermal system (mineralogy composition indicates a temperature of less than 170°C, while the measured temperature is almost 200°C).

The distribution of paleosol in Wayang Windu is mostly observed interlayered with other pyroclastic rocks, and minorly with volcanogenic sandstone or conglomerates. The paleosol study in 1997 suggested that paleosol is divided into 13 layers (from 17 wells), with the depths of the top and thicknesses of TS beds based on the continuous core data obtained from four slim holes. Five beds have extensive occurrences, with bed 8 (450-330 masl) being the most widespread, extending to the NE and the most useful as a marker horizon. The study also concluded that variation in elevation could be due to variation in paleo topography at the time of deposition combined with the subsequent structural modification. The study in 2019 examined Methylene Blue (MeB), XRD and physical appearance under microscope to analyze the characteristic of paleosols, where indicating that the majority of the sticky paleosol was encountered above the reservoir section, while in the reservoir, most paleosols are not sticky and brittle. The additional data from the 2019 study are more distributed to the north and infield, and generally, the number of TS encountered in the reservoir section is greater than above the reservoir, where it is absent toward MBB pads (Figure 3).

The relationship between paleosol existence and drilling problems in Wayang Windu is mostly due to the reaction of the paleosol with the drilling fluid. On a mineralogical scale, the Ca-smectite which abundant in paleosol, will swell when in contact with water, causing swelling in paleosol. This causes the rock to have very poor mechanical strength. A study in 1997 observed that swelling is also affected by temperature and salinity, being strongest at low temperatures (<100°C) and low salinity. When in contact with Na/Ca rich solution, Na will exchange with Ca to form Na-smectite and increase the volume. The initial grace period before paleosol collapses into the hole is around 48 hours. When sudden massive losses of circulation are encountered, severe collapse of paleosol can occur due to the reduction of confinement pressure. In such instances, extensive reaming and tripping have rarely improved the hole condition sufficiently. The study in 2019 also concluded that, in correlation to drilling problems, paleosol at Wayang Windu can easily swell when in contact with water/drilling fluid and has very poor mechanical strength (easily sloughing as a respond to the reduction of hydrostatic pressure due to total loss circulation). The study also observed that the majority of drilling problems associated with paleosol occurred in the reservoir hole section.

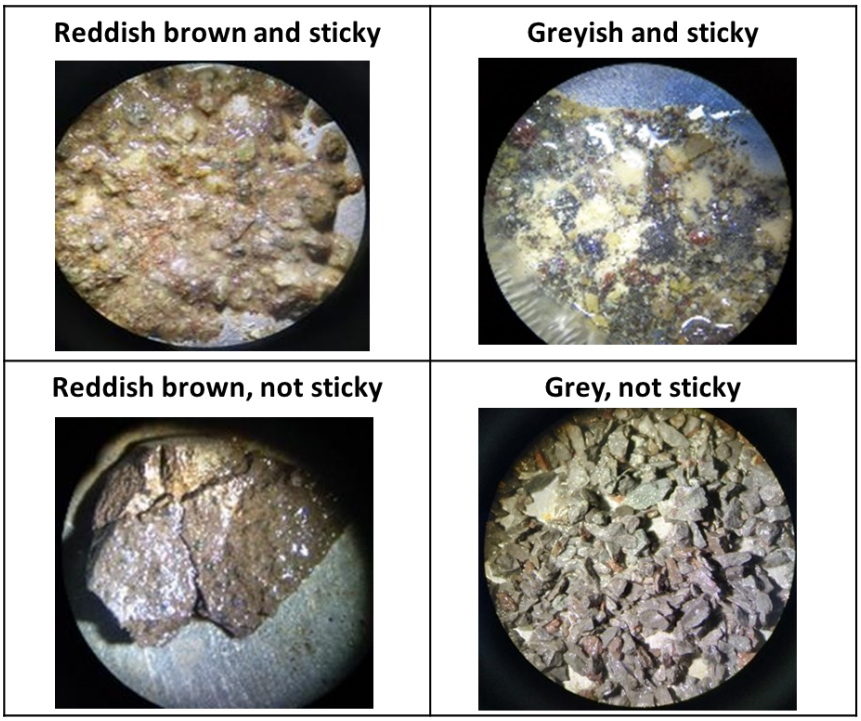

Figure 2: The megascopic view of paleosol in Wayang Windu based on early drilling observations. There are four groups based on the color and physical characteristics of the paleosol (sticky or not sticky).

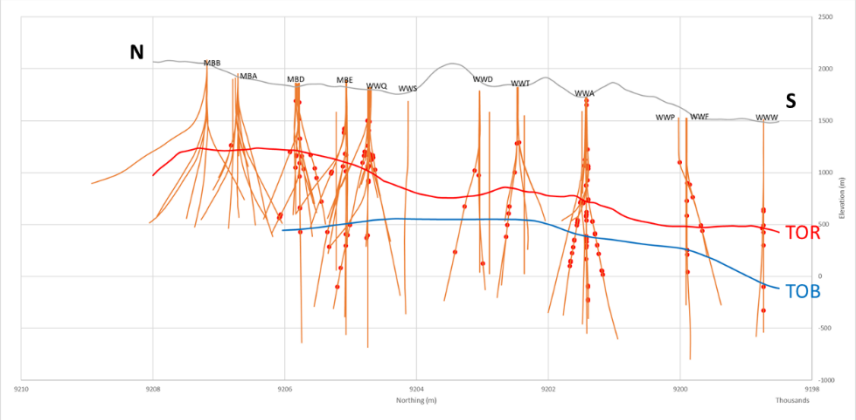

Figure 3: The location of paleosol in Wayang Windu's well (red dot in the well trajectory). It shows that the paleosol is mostly observed in the reservoir section (below TOR) and is getting absent toward the MBB pad in the north.

3. PALEOSOL DISTRIBUTION BASED ON STATIC MODEL

Several initiatives have been conducted at Wayang Windu as part of updating the static model. One major initiative correlated with paleosol distribution is formation profiling. Formation profiling in Wayang Windu is based on grouping PGs in the well by composition (in %), where the differences between each formation are based on distinct differences in PG composition (in %), compared to the above or below PG groups (Purnomo et al., 2023). Some formation profiles have markers that are easy to distinguish (e.g., conglomerate and basaltic andesite lava in Pangalengan formation, dacite lava in Gambung-B formation and Young Wayang formation); however, some formation profiles do not. Hence, formation profiling includes paleosol analysis to help define petrophysical group distribution (Boogie and McKenzie, 1986 and Purnomo et al., 2003).

The basis of the paleosol analysis in helping define the formation profiling is that the paleosol layer present between formation profiles acts as a formation depositional break marker (paleosol develops when the volcanic depositional process is stopped and taken over by the weathering-erosion process). According to the origin of the paleosol, two processes might produce paleosol represented by illitization types. The two major types of illitization in paleosol are pedogenic and diagenetic processes. Pedogenic illitization is associated with the formation of soil on the earth's surface, while diagenetic illitization is associated with compaction after deposition, involving factors such as water-rock reaction and microbial activity. Therefore, the paleosol containing illite from pedogenic illitization represents paleosol as a depositional break marker (soil formed during a volcanic depositional break on the earth's surface) (Purnomo et al., 2023).

Three TS samples have undergone special analysis to define the correlation of their illitization process with the type of depositional process they represent. The TS samples were collected from clear sections that represent boundaries of formation deposition. TS-1 was taken from the boundary between the Gambung-A and Puncak Besar formations, where there is no age deposition gap. TS-2 and TS-3 were collected from formation boundaries that have age deposition gaps, specifically between Young Wayang and Old Wayang formations, and Young Wayang and Pangalengan formations, respectively. According to the diagenetic and pedogenic characteristics explained by Purnomo et al. (2023), TS-1 does not exhibit pedogenic characteristics compared to TS-2 and TS-3. This conclusion aligns with the depositional relations of TS-1, TS-2, and TS-3, where TS-1 indicates diagenetic processes, while TS-2 and TS-3 show pedogenic characteristics. This analysis provides evidence that the formation profiling in Wayang Windu is valid, as demonstrated by the characteristics of the paleosol (TS) layers in Wayang Windu. Moreover, the paleosol layers in Wayang Windu show significant evidence of being markers that define formation depositional breaks.

The positive correlation between the type of paleosol layer and the distribution of formations in Wayang Windu allows for further analysis by combining paleosol and formation distribution data. To gain a good understanding of the paleosol layer deposition in the wells, single well analysis is conducted to categorize the type of paleosol in each well in Wayang Windu. This categorization is based on the location of the paleosol layer relative to the unique distribution of several petrophysical groups (PG). The single well analysis identified the pattern of paleosol distribution in each well, which can be divided into three groups: continuous thin paleosol layers, single thin paleosol layers, and single thick paleosol layers (Figure 4). The continuous thin paleosol layers are well observed when the paleosol exists within the thick PG distribution. The single thin and thick paleosol layers might exist within a single PG or between two different PGs.

To map the distribution of paleosol beyond individual wells, 2D and 3D correlations are conducted. The 2D correlation is developed prior to the 3D correlation to refine the category of each paleosol in each well by observing the consistency of the relationship between specific groups of paleosol deposition patterns and unique PG distributions across the wells. The correlation is conducted within the same formation, where the paleosol layers within the same formation are likely deposited during the same age and represent a continuous deposition regime. This effort helps detail the depositional sequence of several groups of paleosol layers, with the 2D correlation successfully defining up to three paleosol layers for each formation in Wayang Windu. Some discontinuities in deposition are observed, which, based on paleosol studies from 1997, might represent a combination of variations in paleo topography at the time of deposition and subsequent structural modifications. These discontinuities will be useful for the 3D correlation to determine whether they are controlled by paleo topography or structural geology. Additionally, the 2D correlation allows for the possibility of subdividing formations based on unique PG distributions and existing paleosol groups, enhancing the understanding of depositional sequences in Wayang Windu.

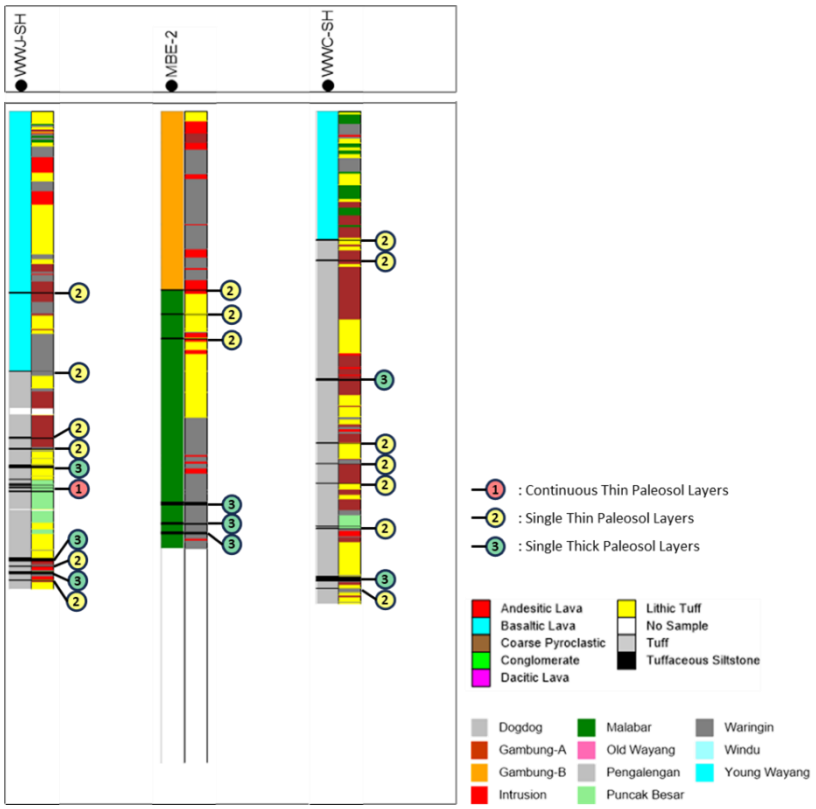

Figure 4: Example of the application of paleosol single well analysis to determine the group of paleosol layers within the well. The continuous thin paleosol layers group is usually clearly observed in the thick PG deposition, while the single thin and thick paleosol layers might be observed in a single PG or exist between different PGs.

An example of 2D correlation constructed in the North of Wayang Windu, from wellpad WWR to MBE (West to East), is applied in the Puncak Besar Formation (Figure 5). This correlation suggests that the Puncak Besar Formation might be divided into three sub-formations: Puncak Besar-1 (PB1), Puncak Besar-2 (PB2), and Puncak Besar-3 (PB3). The determination of the sub-formations refers to a combination of paleosol layers and unique PGs, as not all the complete sequences of paleosol layers are observed in the wells. This is due to geologic factors such as structure and depositional heterogeneity or data availability issues like lost zones.

In the Puncak Besar Formation, four groups of paleosol layers are observed, namely paleosol D, D.1, D.2, and D.3. The determination of the paleosol follows the single well analysis. For example, paleosol D is a single thick paleosol layer found in thick lithic tuff at the shallow elevation of the Puncak Besar Formation. Another example is paleosol D.1, observed in the middle of thick coarse pyroclastic with a lava layer in between. This paleosol layer is observed at the middle elevation of the Puncak Besar Formation. The relation of each paleosol layer is also concluded from the single well analysis, showing that paleosol D is the shallowest one, deposited above D.1 in WWQ-2 and D.3 in MBC-1ST2. Paleosol D.1 is found above D.2 in MBI-1, and D-3 is observed below D.2 in MBE-3. An additional paleosol layer, D.a, is observed above D as indicated in MBB-1 and MBE-3 (?).

By adding the unique PG, the sub-formation PB1 is deduced from the existence of thick lithic tuff upwards in the shallow part of the Puncak Besar Formation, which is associated with paleosol D. There is a possibility of paleosol D.a being observed above paleosol D. The distribution of PB1 is observed between MBC-1ST2 and MBB-1 (eastward) and is discontinued in the middle of the correlation line. PB1 is observed again in the eastern part from WWQ-2, thickening towards MBE-4. PB2 is in the middle of the Puncak Besar Formation, dominated by coarse pyroclastic-lava and related to paleosol D.1 and D.2. PB2 is observed continuously from West to East, with the western part (WWR-SH) exposed near the surface. PB2 has a unique relationship with paleosol layers, as the paleosol layer is not observed from the west (WWR-SH) to the center of the correlation line (MBD-6). However, PB2 in MBI-1, WWQ-2, and MBE-3 is clearly associated with paleosol D.1 and D.2. This discontinuity is interesting, as it occurs within the same sub-formation, creating an area of Puncak Besar Formation free of paleosol layers between MBB-1 and MBI-1. PB3 is observed at the deeper part of the Puncak Besar Formation, at the bottom of MBC-1ST2 and MBE-3 (?), associated with thick lithic tuff and paleosol D.3.

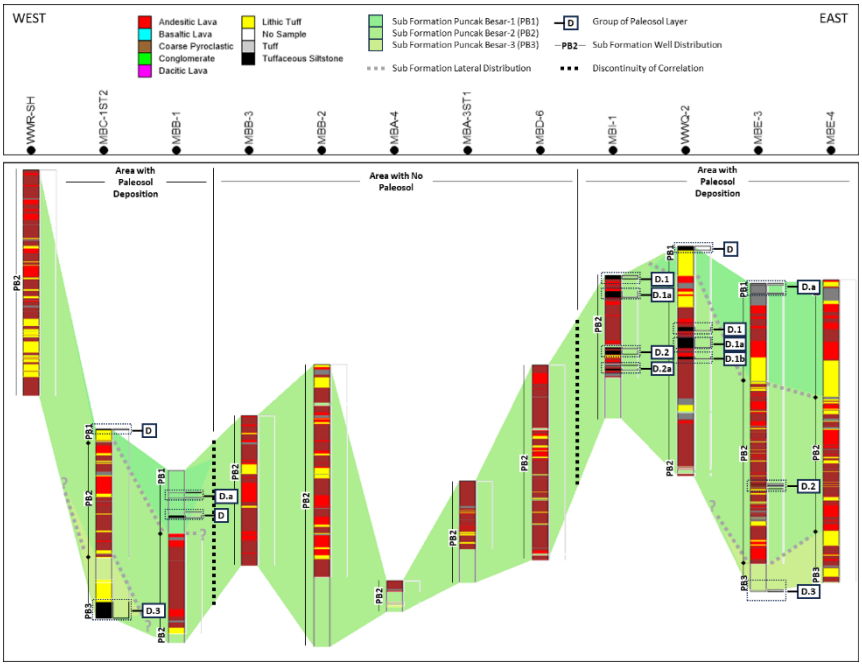

Figure 5: The application of 2D correlation of paleosol layers in the North of Wayang Windu. The correlation suggests two discontinuities: the first is the PB1 discontinuity in the west to the center of the correlation line. The second is the paleosol discontinuity in PB2, which creates an area with no paleosol in Puncak Besar Formation in wellpads MBB-MBA-MBD.

Following the construction of the 2D correlation, the 3D correlation is developed. The 3D correlation considers either paleo topography or structural impact on the paleosol deposition to explain the discontinuities observed in the 2D correlation. Additionally, the trajectory plot showing the actual direction of trajectory might add supplemental insight regarding the distribution of paleosol layers in a well and their relationship with paleo topography and structural setting. The information gathered in the 2D correlation has been plotted into the faulted 3D static model, which already incorporates a 3D structure model and shows its structural impact on the development of formations in Wayang Windu (Figure 6). By observing the correlation between the area of paleosol layer distribution from the 2D correlation and the structure, it can be concluded that area ① and ② is divided by the Kawah Burung fault, while area ② and ③ are divided by the Cibitung fault.

Focusing on area ①, it is concluded that paleosol layers D and D.a represent the boundary between the Puncak Besar Formation and the Gambung-A Formation. A gap between paleosol layers, from D to D.3, is observed in well MBC-1ST2. This well intersects the Kawah Burung fault at a deeper depth and has a relatively low inclination, with the fault showing upward movement at the bottom of the well. As a result, paleosol layer D.1 and D.2 are missing, and paleosol D.3 is found at nearly the same elevation. Following this logic, in area ②, paleosol layers D.2, D.1, and D might be present above paleosol D.3. This issue will be further discussed in the explanation of area ②.

Area ② is an interesting part for discussion due to the absence of paleosol in this area. Only paleosol D.3 is observed in area ②. Paleosol D.3 might be related to the boundary of the Puncak Besar Formation and the Malabar Formation underneath it. Relating to the nature of the Kawah Burung Fault, paleosol D.3 might have been uplifted to the recent depth. According to the same logic, another paleosol layer should be observed above paleosol D.3 in

wells drilled in area ②, but in fact, none are found. An interpretation to explain the absence of paleosol layers is related to the deposition of the Gambung-A Formation above the Puncak Besar Formation in this area. The paleosol layers D.2, D.1, and D might have existed in the shallowest part of this area, but as this area acts as the deposition basin of the Gambung-A Formation, those paleosol layers were destroyed when the paleo topography of the Gambung-A Formation was formed, leaving only paleosol layer D.3 undisturbed.

Area ③ is also a very interesting topic. In this area, a complete sequence of paleosol layers is observed (from paleosol D.a to D.3). Paleosol D and D.a are related to the boundary of the Puncak Besar Formation and the Gambung B formation. Paleosol D.1 is also observed as the boundary of the Puncak Besar Formation and the Gambung-A Formation, instead of D and D.a. This might be result of the same process that caused the absence of the paleosol layer in area ②. The striking fact is the incomparable depth of paleosol D and D.a in this area compared to area ①. According to the geometry of the Puncak Besar Formation deposition and assuming that the paleosol in the Puncak Besar Formation is continuously deposited, an uplifting process pushed up the Puncak Besar Formation in this area, creating a significant gap in paleosol depth between area ① and this area. The existence of the Malabar Horst Structure, a regional structural object, might explain this condition, as the development process of this structure corresponds to the observed paleosol distribution in this area.

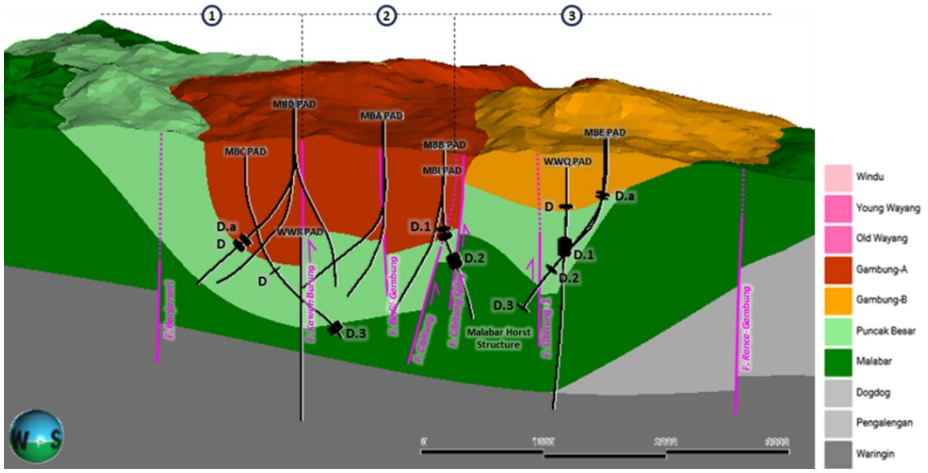

Figure 6: The application of 3D correlation of paleosol layers in the North of Wayang Windu extends the understanding of paleosol distribution from the 2D correlation. The 3D correlation might explain the first discontinuity of PB1 in area ①, where it is bounded by uplifted area ② driven by the Kawah Burung Fault. The paleosol discontinuity in PB2, which creates an area with no paleosol in area ②, can also be explained. It is related to the fact that area ② is the main part of the depositional basin of the Gambung-A Formation. Hence, the paleosol layer in the shallow part of this area is destroyed when the paleo geography of the basin is formed. Related to the distribution of paleosol layers in area ③, the Malabar Horst Structure might explain how this structure uplifted the Puncak Besar Formation in area ③. This structure creates a wide gap in depth between the same paleosol layers in area ③ and area ①.

Regarding the paleosol layer distribution for drilling purposes, the 3D correlation will be useful to expect potential paleosol distribution in the Puncak Besar Formation. It can be concluded that wells that will be drilled in area ① intersect the deep part with potentially two paleosol layers (D and D.a). Another paleosol layer might be observed below paleosol D, as this area is undisturbed, though no well data supports this assumption. Wells in area ② will not intersect paleosol layers in the Puncak Besar Formation but might intersect layer D.3 at depth, close to the Malabar Formation. Wells in area ③ might intersect a complex of paleosol layers (D.a to D.3) at shallow depths. Therefore, wells that will be drilled in this area should be aware of the abundant paleosol layers in the Puncak Besar Formation. As this interpretation is specific to the Puncak Besar Formation, it should be taken into account when considering the paleosol layers in the formations above and below the Puncak Besar Formation and incorporating the results to have a comprehensive well assessment of paleosol existence along the well.

5. CONCLUSION

Paleosol distribution in Wayang Windu has been characterized since 1997 and updated recently in 2019. Physically, paleosol can be categorized into sticky and non-sticky (brittle) types. It is concluded that the paleosol in Wayang Windu originates from volcanic ash, which is unconsolidated and easily reworked, then filled the lake and reacted with water to form clays and iron oxides. In relation to the geothermal system in Wayang Windu, the paleosol is not in equilibrium with the hydrothermal system, as the mineralogical composition indicates temperatures of less than 170°C, while the measured temperature is almost 200°C. The paleosol distribution is

mostly within the reservoir and is dominated by non-sticky (brittle) paleosol. Several paleosol layers have extensive occurrence and distribution, making them useful as marker horizons. However, variations in elevation for each paleosol layer are observed and interpreted as a result of paleo topography variations at the time of deposition and subsequent structural modifications. The relation between paleosol existence and drilling problems in Wayang Windu is primarily due to the reaction of paleosol with the fluids used in drilling activities. Paleosol in Wayang Windu can easily swell upon contact with water or drilling fluid and has very poor mechanical strength, making it prone to sloughing when hydrostatic pressure is reduced due to total loss circulation, leading to stuck pipe incidents.

Paleosol has been incorporated into the development of the static model in Wayang Windu to help define formations based on unique petrophysical group distributions. Following this concept, detailed analysis of paleosol layers aims to define sub-formations and map their distribution within specific formations. Single well analysis categorized the paleosol layers into three groups: continuous thin paleosol layers, single thin paleosol layers, and single thick paleosol layers. Continuous thin paleosol layers are well observed when paleosol exists within thick petrophysical group distributions. Single thin and thick paleosol layers might exist within a single petrophysical group or between two different petrophysical groups.

Following single well analysis, 2D correlation was conducted for each formation by incorporating the paleosol layer with unique petrophysical groups to define sub-formations. The 2D correlation generally identified up to three paleosol layers for each formation in Wayang Windu. Discontinuities in the paleosol layer observed in 2D correlation were then incorporated and further evaluated using faulted 3D formation distribution. In the example of paleosol layer correlation in the Puncak Besar Formation, single well analysis identified four groups of paleosol layers. The 2D correlation identified three sub-formations within the Puncak Besar Formation and observed two discontinuities. The 3D correlation explained the contributions of two faults (Kawah Burung and Cibitung) and the Malabar Horst Structure, which are responsible for these discontinuities. Paleo topography is also responsible for the discontinuity observed in the middle of the Puncak Besar Formation, creating a zone with no paleosol distribution. The formation of a depositional basin in this area might have destroyed the paleosol layers that would have been found there, based on the 2D-3D correlation.

ACKNOWLEDGEMENT

The authors gratefully acknowledge and thank Colleagues and Leaders of Asset Management SEG for reviewing the manuscript. We also thank the Management of SEG for the permission to publish this paper.

REFERENCES

Bogie, I., and McKenzie, K.M.: The Application of a Volcanic Facies Model to an Andesitic Stratovolcano Hosted Geothermal System at Wayang Windu, Java, Indonesia, *Proceedings,* 20th New Zealand Geothermal Workshop, Auckland, New Zealand. (1998).

Earth Science AM WW, 2020. Tuffaceous Siltstone Study Wayang Windu Geothermal Field. Unpublished Star Energy Geothermal Presentation, March 2020.

F.H. Beinroth, W. Luzio L., F. Maldonado P., and H. Eswaran., 1985. Proceedings of the Sixth International Soil Classification Workshop, Chile and Ecuador. Part 1: Papers. Sociedad Chilena de la Ciencia del Suelo, Santiago, Chile.

Kingston Morrison, 1997. Report on Tuffaceous Siltstone from Wayang Windu Geothermal Project, West Java, Indonesia for Mandala Nusantara, Ltd. Unpublished Star Energy Geothermal Report.

McDaniel, P.A., Lowe, D.J., Arnalds, O., Ping, C.-L., 2012. Andisols. In: Huang, P.M.; Li, Y; Sumner, M.E. (editors) "Handbook of Soil Sciences. 2nd edition. Vol. 1: Properties and Processes". CRC Press (Taylor & Francis), Boca Raton, FL, pp.33.29-33.48.

Purnomo, M., Diningrat, W., Sugiono, S., Kamel, N., Malik, D., Talita, A., Dimwani, W., 2023. Updated Geological Framework of Wayang Windu Geothermal Field, Indonesia. *Proceedings*, World Geothermal Congress 2023, Beijing, China (2023).

Ramadhan, Y., Sutrisno, L., Tasrif, A., Bogie, I.: Geological Evaluation of the Waringin formation as the host of a Vapor-Dominated Geothermal Reservoir at the Wayang Windu Geothermal Field, *Proceedings,* 2012 New Zealand Geothermal Workshop, Auckland, New Zealand. (2012).

Geology and Control for The Appearance of Hot Springs in The Northern Area of Mount Pandan Complex, East Java

Solomon M. Timothi[1], Suryantini[1,2], and Alfend Rudyawan[1]

[1]Geology ITB
[2]Geothermal ITB

solomonsimarangkir@gmail.com, suryantini@itb.ac.id, alfend@itb.ac.id

Keywords: Geology, springs, physical characteristics, fault

ABSTRACT

Mount Pandan is one of the geothermal prospecting areas in Indonesia. This is shown by the appearance of several warm springs, such as Banyu Kuning, Jari Hot Spring, and others in the north of Mount Pandan Area. However, there has been no study about control for the appearance of Mount Pandan Area, and there are still very few studies about detailed geology in Mount Pandan Area. The purpose of the study is to determine the geological conditions and understand the control for the appearance of springs in the north Mount Pandan Area. Understanding geological conditions is based on field mapping, which includes geological mapping, geological structure, and volcanostratigraphy analysis. Meanwhile, the control for the appearance of springs is based on the physical characteristics of the springs and geological condition.

The study area can be divided into 5 Crown of and 13 Hummock of based on the volcanostratigraphy analysis and 40 informal lithological units based on the geological mapping. The main geological structure is a left slip fault with a trending NNW-SSE (tear fault). This causes the formation of normal left slip faults trending NE-SW, reverse right slip faults trending NW-SE, and small folds trending ENE-WSW.

Spring mapping shows there is 7 hot springs. Springs can be divided into 3 groups, fault spring in Wackestone Unit aquifer with high TDS value and neutral pH, fault spring with dome unit aquifer with lower TDS value than Wackestone Unit aquifer and neutral pH, and depression spring in Wackestone Unit aquifer with low TDS value and acid pH. The water flow is controlled by faults and lithology orientation. The faults also control the secondary permeability to increase heat flow as heat source of the hot springs. Radiogenic heat production and gradient geothermal also make the springs have higher temperatures.

1. INTRODUCTION

Mount Pandan is a stratovolcano on Java Island, in the middle of Kendeng Basin and north of the Quaternary volcano on Java Island (Figure 1). Mount Pandan is one of the geothermal prospecting in Indonesia. The geothermal activity is shown by appearance of several hot spring such as Banyu Kuning, Jari Hot Spring, and others in the north of Mount Pandan Area. However, there has been no study about control for the appearance of hot spring in Mount Pandan Area, and there are still very few studies about detailed geology in Mount Pandan Area. To understand the control for the appearance of hot springs, understanding geological condition is necessary. Purpose of this study is determining the geological conditions and understand the control for the appearance of springs in the north Mount Pandan Area. Understanding geological conditions is based on field mapping, which includes geological mapping, geological structure, and volcanostratigraphy analysis. Meanwhile, the control for the appearance of springs is based on the physical characteristics of the springs and geological condition.

There are many classifications of springs based on the spring's temperatures. This paper will use hot springs classification based on Zhou et al. (2023). There are two types of hot springs: low to moderate temperature hot springs (equal to and greater than 25 ◦C to below the local boiling point), and high temperature hot springs (equal to and greater than the local boiling point). There are appearances of low to moderate temperature hot springs in the northern area of Mount Pandan. Hot springs are one of the important geothermal features on the Earth's surface. A hot spring results from special geological and tectonic factors, and specific geothermal and hydrogeological conditions. Hot springs occurring at different places with different tectonic backgrounds exhibit a wide variety of hydrothermal activities and geochemical constituents due to the differences in the circulation depth of groundwaters, the nature of the heat source, the size of tectonic structures, the distance and elevation difference between the recharge area and the spring orifice and the permeability of the geothermal reservoir (Huang, 1993 in Zhou et al.,2023). There are 5 questions raised when we study the origin of hot springs (Zhou et al., 2023): (1) what are the factors controlling the occurrence of a hot spring? (2) what causes the emergence of a hot spring at a certain location? (3) what determines the temperature, flow rate, and geochemical constituents? (4) why are hot springs frequently encountered in some places, but are sparse in other regions? (5) why do the

temperatures and flow rates of hot springs occurring in different places vary so widely? This paper is trying to answer that questions in the northern area of Mount Pandan area based on geological conditions and physical characteristics of the springs.

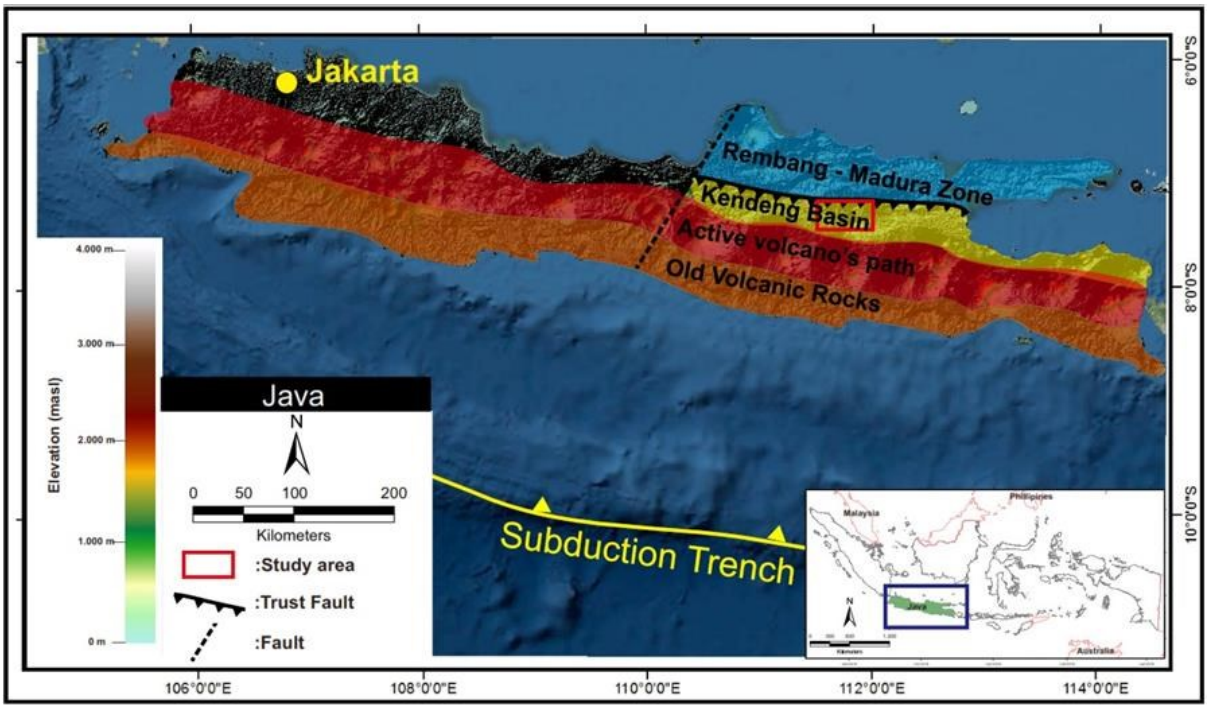

Figure 1: Location of the study area (Jati et al., 2021).

2. DATA AND METHODS

The data of this study consists of primary and secondary data. The primary data is based on geological mapping and laboratory analysis. Lithology, geological structure, and physical characteristics of springs are geological mapping data. Based on geological mapping, there are 160 observation stations, 120 shear fractures data, and 7 physical characteristics of springs data. Laboratory analysis is needed to make sure the megascopic description with petrography analysis. This study used 23 thin section data. The physical characteristics of springs consist of air temperature, spring temperature, Total Dissolved Solids (TDS), and pH. There are also secondary data, such as 100 shear fractures data from Jati et al. (2021) and Bojonegoro Geological Map from Pringgoprawiro and Sukido (1992).

The research began by conducting a literature study regarding the geology and hydrology of the study area. Continue with making the volcanostratigraphy interpretation based on contour and topography. The collecting data stage is carried out by conducting geological and spring mapping. Then the data analyzed to make a geological map of the study areas. The geological condition knowledge and physical characteristics of springs will help in understanding control for the appearance of hot springs. Conceptual models are carried out to understand control for the appearance of hot springs.

3. GEOLOGY OF THE STUDY AREA

3.1 Geology and Stratigraphy

Geological understanding and stratigraphy of the study area used the volcanostratigraphy concept based on Indonesian Stratigraphy Codes by Martodjojo and Djuhaeni (1996). Analysis and overview of geological conditions is based on Bojonegoro Geological Map by Pringgoprawiro and Sukindo (1992). Then, the volcanostratigraphic map is interpreted to indicate the cores in the form of conical and circular features, and to indicate the expulsion from the core. Volcanostratigraphic analysis is done on a scale of 1:100.000 and :50.000 to identify stratigraphy units. Naming the core with no specific name yet is based on geographical and cardinal directions if it is in the same geographical location.

Volcanostratigraphic map 1:100.000 (Figure 2) shows there are 5 Crown in the study area, such as Crown of Jari, Crown of Senganten, Crown of Pandan, Crown of Buntung, and Crown of Tritik. Crown of Jari and Crown of Senganten show an isolated hills. Crown of Pandan shows isolated hills and flowing texture from Mount Pandan in contour analysis. Crown of Tritik and Crown of Buntung show isolated hills. Volcanostratigraphic map

1:50.000 (Figure 3) shows there are 23 Hummock in the study area, consisting of 9 Hummock part of Crown of Pandan, 3 Hummock part of Crown of Senganten, and 11 Hummock part of Crown of Jari.

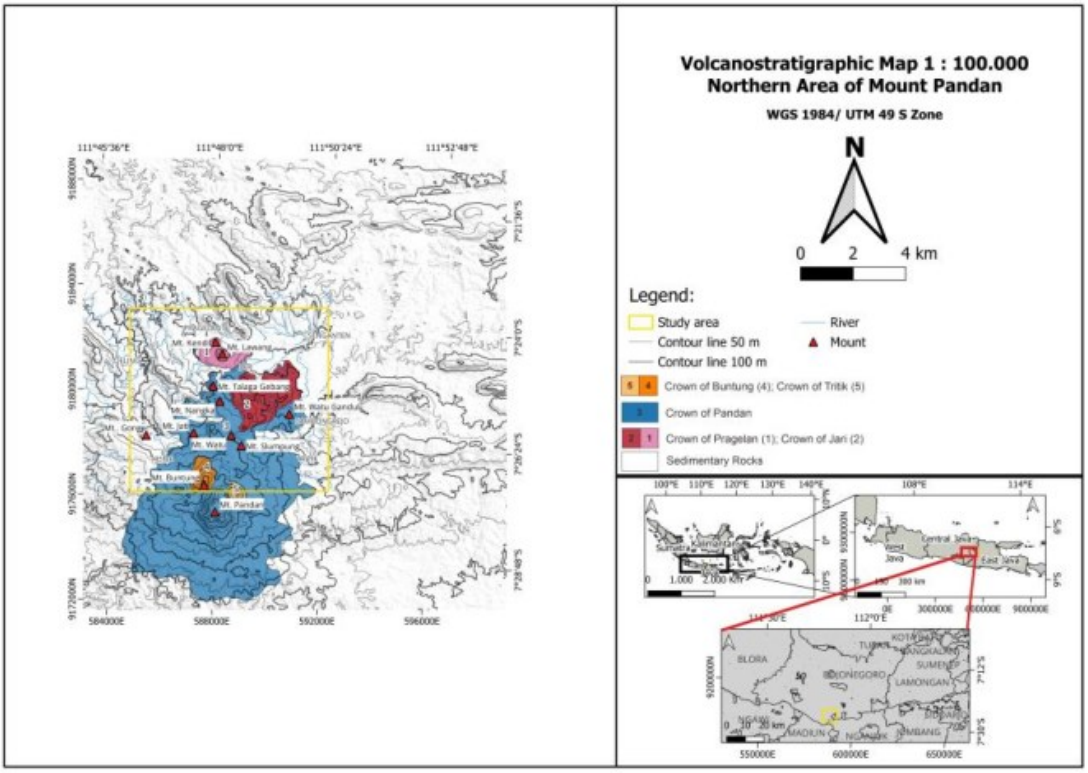

Figure 2: Volcanostratigraphic map 1:100.000.

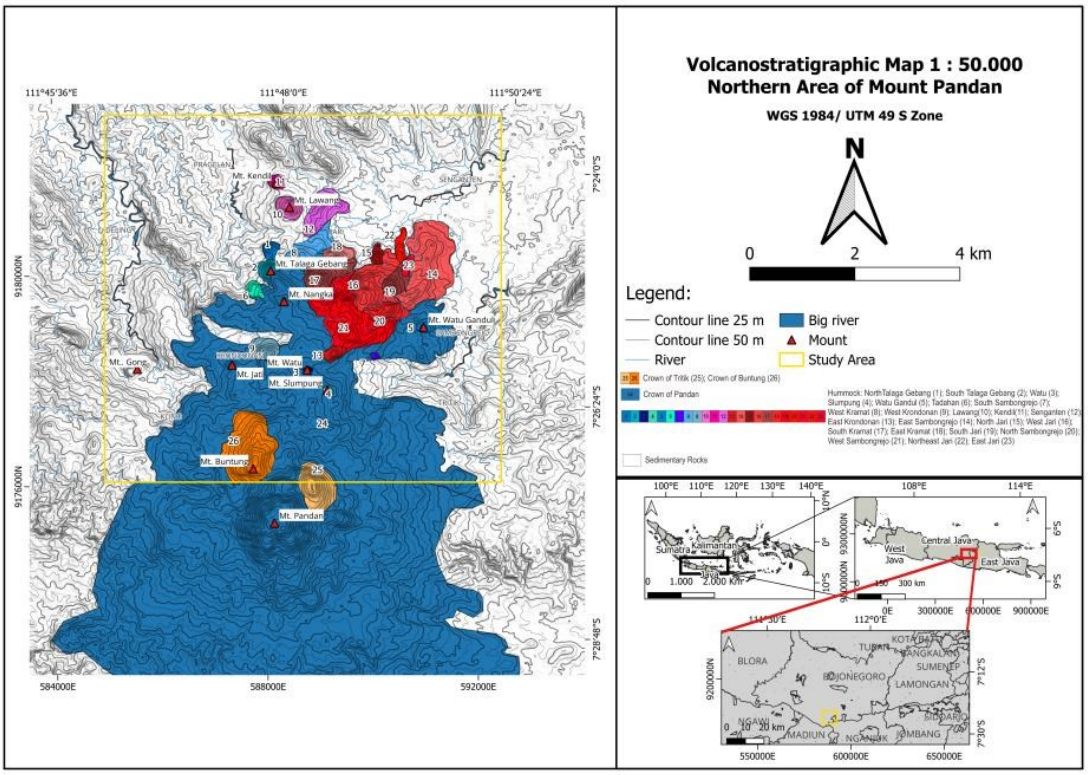

Figure 3: Volcanostratigraphic map 1:50.000.

Based on topographic analysis, shows that the topography of the Crown of Senganten and Crown of Jari is rougher than Crown of Pandan, Crown of Tritik, and Crown of Buntung. In Crown of Pandan, several hills show a deflection pattern texture from the flowing texture. This shows the hills are older than the Pandan deposits.

Meanwhile, the flow texture deposits from Crown of Pandan are relatively younger than Crown of Jari due to the deflection of the flow texture. The Crown of Buntung and Crown of Tritik were identified as younger Crown than Crown of Pandan based on the presence of lava flow texture buried by other flow in the west of Crown of Buntung deposits.

A geological map was made based on descriptive similarities of rocks and a volcanostratigraphic map (Figure 4). the stratigraphy of 39 informal lithological units in the study area is shown in Table 1. The core geometry was identified based on residual magnetic anomaly based on Maubana et al. (2019). There is a low magnetic anomaly in the Crown of Jari. This indicates the small size of the core geometry due to intrusion rock will have a high magnetic anomaly. There are many circular features in the study area with dome morphology. The dome units in the study area are defined as monogenetic volcano. Monogenetic volcano commonly consists of large numbers of volcanic clusters and/or alignments that include hundreds of structures (Condit and Connor, 1996; Connor, 1987, 1990; Con-nor et al., 1992, 2000; Connor and Conway, 2000; Conway et al.,1998; Valentine et al., 2006; in Németh, 2010).

3.1.1 Wackestone Unit

Wackestone Unit is the oldest unit in the study area. This unit consists of light grey calcareous claystone (Figure 5 (a)) with many fractures in the station. Based on petrography analysis, this unit consists of wackestone (Dunham, 1962) with many microfossils like Foraminifera Globigerina, other foraminifera, and coral. The Wackestone Unit is equal to the Kalibeng Formation in the Bojonegoro Geological Map by Pringgoprawiro and Sukindo (1992) in the Upper Miocene-Lower Pliocene.

3.1.2 Breccia-1 Unit

Breccia-1 (Figure 5 (b)) Unit is a younger unit than Wackestone Unit. Breccia-1 Unit consists of brown breccia lithology with andesite fragments with fine sand matrix. Breccia-1 Unit is equal to Atasangin member of Kalibeng Formation in Bojonegoro Geological Map by Pringgoprawiro and Sukindo (1992) in the Upper Miocene.

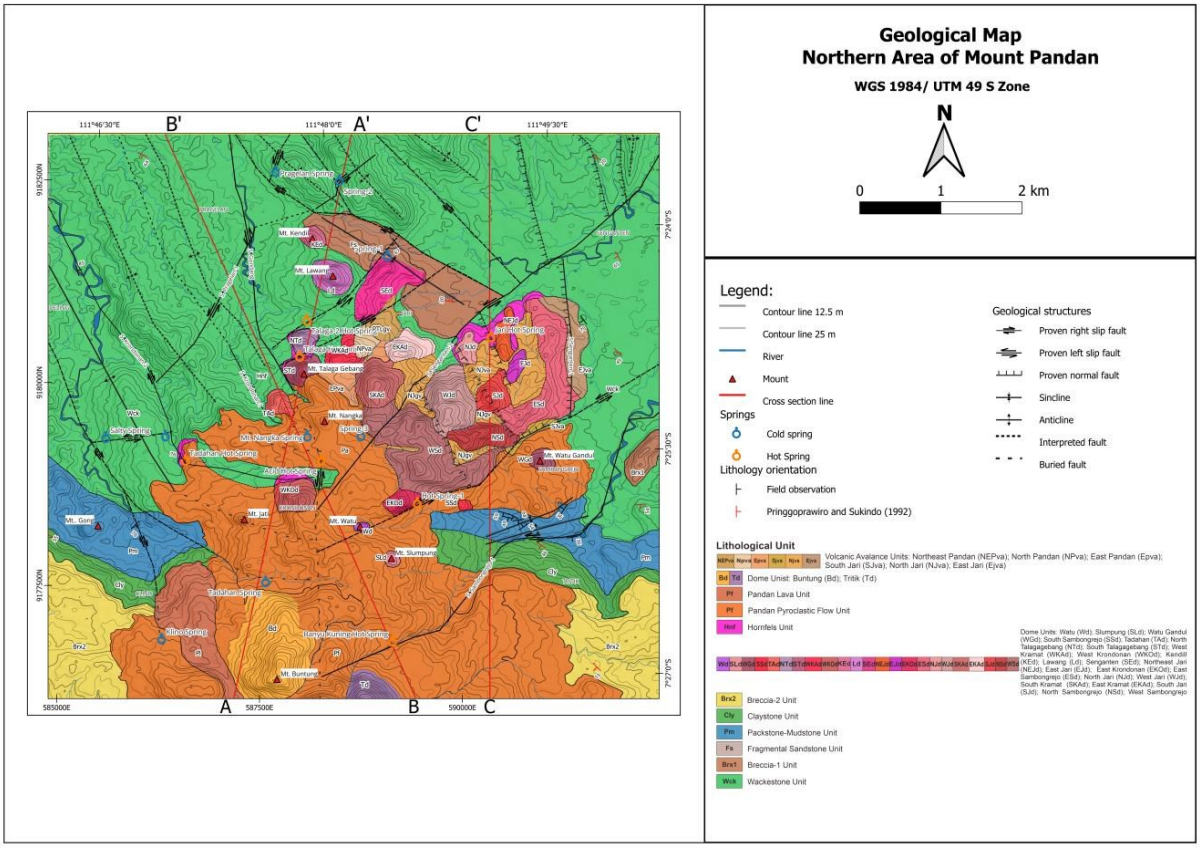

Figure 4: Geological Map of the study area.

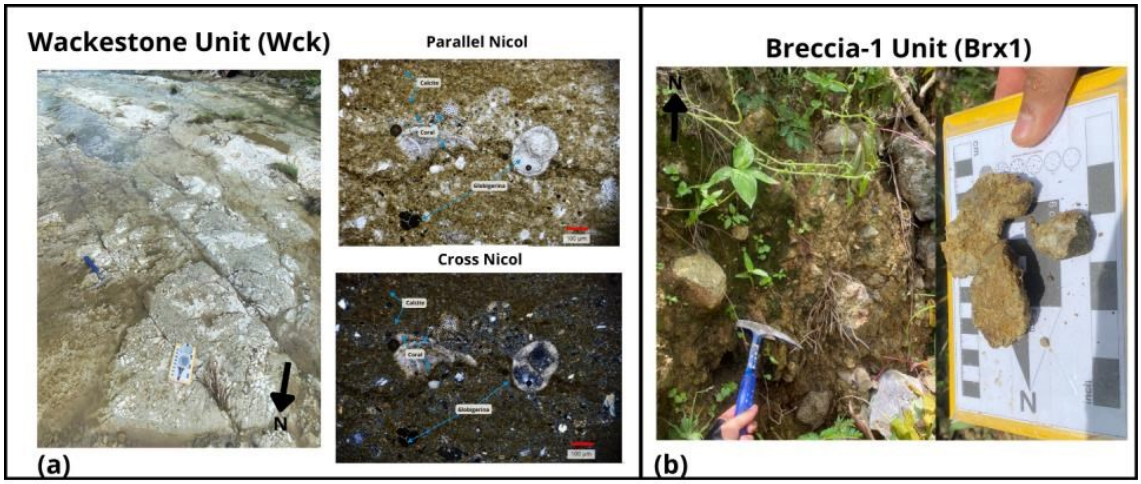

Figure 5: Wackestone (a) and Breccia-1 (b) Unit characteristic.

Table 1: Stratigraphy of the study area.

Relative Age			ACTIVITY PERIOD	Stratigraphical Unit		LITHOLOGY			
Period	Epoch	Equivalent Formation (Pringgoprawiro & Sukando, 1992)		Crown	Hummock	PRIMARY lava dome	lava	flow	SECONDARY volcanic avalanche
Quaternary	Pleistocene	Pandan Breccia	Pandan-Jari volcanic avalanche period	Jari; Pandan					SJva NJva EJva NEPva Npva Epva
			Tritik and Buntung lava dome period	Tritik; Buntung		Td Bd			
			Mount Pandan eruption period	Pandan			Pl		
		Intrussion Unit	Pandan, Senganten, and Jari lava dome period	Pandan: Senganten Jari	Watu; Slumpung; Watu Gandul; South Sambongrejo; Tadahan; North Talagagebang; South Talagagebang; West Kramat; West Krondonan; Kendil; Lawang; Senganten; East Jari ; Northeast Jari; East Krondonan; East Sambongrejo; North Jari; West Jari; South Kramat; East Kramat; South Jari; North Sambongrejo; West Sambongrejo	WdSLdWGdSSdTAdNTdSTdWKAdWKOdKed Ld SEdNEJdEJdEK0dESdNJdWJdSKAdEKAdSJdNSdWSd		Pf	
Tertiary	Pliocene	Pucangan Formation				Breccia-2 Unit (Brx2)			
		Sonde Formation				Claystone Unit (Cly)			
		Klitik Formation				Packstone-Mudstone Mudstone (Pm)			
	Late Miocene	Kalibeng Formation				Breccia-1 Unit (Brx1)			
						Wackestone Unit (Wck)			

3.1.3 Packstone-Mudstone Unit

Packstone-Mudstone Unit (Figure 6 (a)) is a younger unit than Breccia-1 Unit. This unit consists of interbedded light grey calcarenite with dark grey calcareous claystone. Based on petrography analysis, this unit consists of packstone (Dunham, 1962) and mudstone (Dunham, 1962). There are ENE-WSW syncline and anticline structures in this unit. Packstone-Mudstone Unit is equal to Klitik Formation in the Bojonegoro Geological Map by Pringgoprawiro and Sukindo (1992) in Lower Pliocene-Middle Pliocene.

3.1.4 Claystone Unit

Claystone Unit (Figure 6 (b)) is a younger unit than the Packstone-Mudstone Unit. This unit consists of black claystone with Brachiopoda, pelecyopoda macrofossil fragments, and Packstone-Mudstone Unit lithic fragments. This unit is equal to the Sonde Formation in the Bojonegoro Geological Map by Pringgoprawiro and Sukindo (1992) in the Middle Pliocene.

3.1.5 Breccia-2 Unit

Breccia-2 Unit (Figure 6 (c)) is a younger unit than Breccia-2 Unit. This unit breccia with andesite and basalt fragments and fine sand matrix. Based on petrography analysis shows clastic texture with lithic and minerals as fragments and mud as matrix in the unit. This unit is equal to the Pucangan Formation in the Bojonegoro Geological Map by Pringgoprawiro and Sukindo (1992) in the Upper Pliocene-Pleistocene.

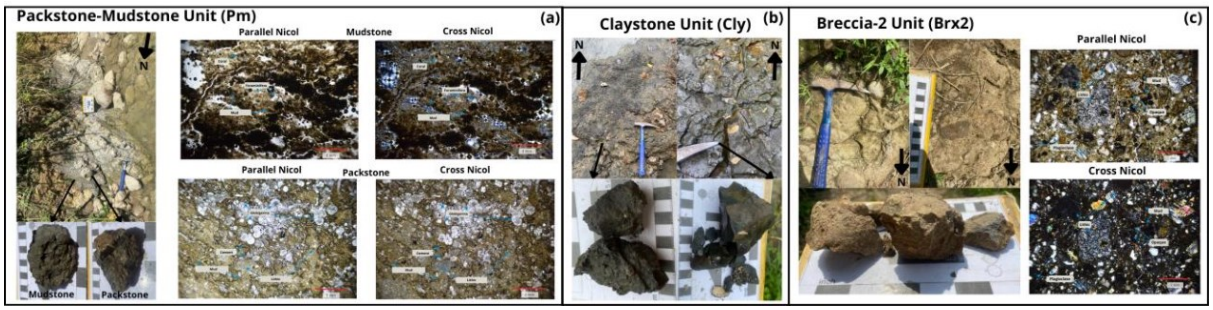

Figure 6: Packstone-Mudstone (a), Claystone b), and Breccia-2 Unit characteristic.

3.1.6 Crown of Senganten

Crown of Senganten (Figure 7) is in the north of the study area which was formed at the same age as the Crown of Jari. Crown of Senganten consists of three Hummock, such as Hummock of Lawang, Hummock of Kendil, and Hummock of Senganten. Crown of Senganten consists of 3 informal lithological units, such as Lawang Dome Unit (Ld), Kendil Dome Unit (KEd), and Senganten Dome Unit (SEd). The lithology of Ld, KEd, and SEd is hornblende andesite (Williams et al., 1998). Lithology identification of Lawang Lava Unit was based on Thoha et al., (2014). The dome Units in the study area are defined as monogenetic volcanoes. Crown of Senganten is equal to the Intrusion Rock Unit in the Bojonegoro Geological Map by Pringgoprawiro and Sukindo (1992) in the Pleistocene.

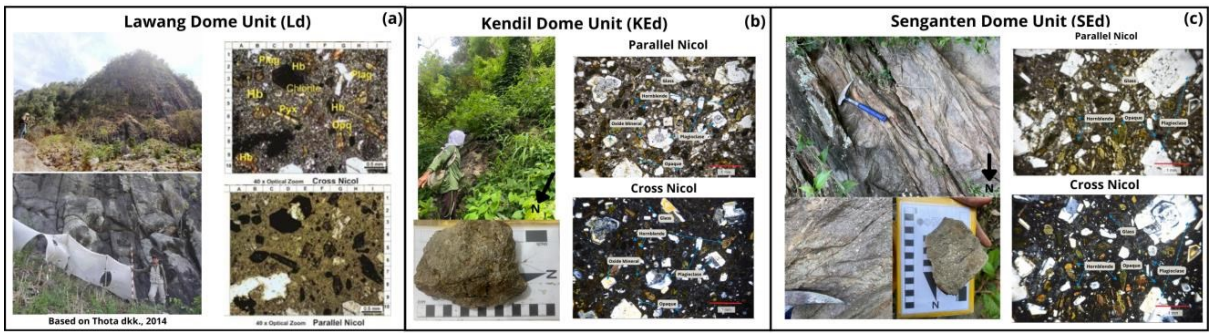

Figure 7: Crown of Senganten Unit characteristic.

3.1.7 Crown of Jari

The Crown of Jari (Figure 8) is in the east of the study area which was formed at the same age as the Crown of Senganten. Crown of Jari consists of eleven hummock with 13 informal lithological units, such as East Jari Dome Unit (EJd), Northeast Jari Dome Unit (NEJd), East Krondonan Dome Unit (EKOd), East Sambongrejo Dome Unit (ESd), North Jari Dome Unit (NJd), West Jari Dome Unit (WJd), South Jari Dome Unit (SJd), West Sambongrejo Dome Unit (WSd), South Kramat Dome Unit (SKAd), East Kramat Dome Unit (EKAd), South Jari Volcanic Avalanche (SJva), East Jari Volcanic Avalanche (EJva), North Jari Volcanic avalanche (NJva). The dome Units in the study area are defined as monogenetic volcanoes. The lithology of dome units is hornblende andesite (Williams et al., 1998). SJva and NJva were identified as volcanic avalanches from dome units in Crown of Jari. Besides that, Ejva was identified as volcanic avalanche from East Sambongrejo Dome Unit (ESd). Dome units are equal to Intrusion Rock Unit and volcanic avalanche units in Crown of Jari are equal to the Pandan Breccia Unit in the Bojonegoro Geological Map by Pringgoprawiro and Sukindo (1992) in the Pleistocene.

3.1.8 Crown of Pandan

The Crown of Pandan (Figure 9) is in the south-north of the study area and relatively younger than the Crown of Senganten and Crown of Jari. Crown of Pandan consists of nine Hummock with 14 informal lithological units, such as Watu Dome Unit (Wd), Slumpung Dome Unit (SLd), Watu Gandul Dome Unit (WGd), South Sambongrejo Dome Unit (SSd), Tadahan Dome Unit (TAd), North Talagagebang Dome Unit (UTd), South Talagagebang Dome Unit (SJd), West Kramat Dome Unit (WKAd), West Krondonan Dome Unit (WKOd), Pandan Flow Unit (Pf), Pandan Lava Unit (Pl), North Pandan Volcanic Avalanche (NPva), Northeast Pandan Volcanic Avalanche (NEPva), and East Pandan Volcanic Avalanche (EPva). The dome Units in the study area are defined as monogenetic volcanoes. The lithology of Dome and lava units is hornblende andesite (Williams et al., 1998), except the SLd Unit consists of pyroxene andesite (Williams et al., 1998). Pandan Flow Unit consists of pyroclastic breccia with andesite fragments. The size of the fragments shows finer to the north of the study area or further away from Mount Pandan Core. NPva and EPva were identified as volcanic avalanches from lava units and pyroclastic breccia units in Crown of Pandan. Besides that, NEPva was identified as a volcanic avalanche West Kramat Dome Unit (WKd). Dome units is equal to the Intrusion Rock Unit; besides that, volcanic avalanche units, Pandan Flow Unit, and Pandan Lava Unit in Crown of Pandan are equal to the Pandan Breccia Unit in the Bojonegoro Geological Map by Pringgoprawiro and Sukindo (1992) in the Pleistocene.

3.1.9 Crown of Buntung and Crown of Tritik

Crown of Buntung and Tritik is in the Southwest and Southeast of the study. The Crown of Buntung and Tritik was formed after Crown of Pandan. The interpretation of the age is based on the contour pattern changed in the East of Pandan Lava Unit. The Crown of Buntung consists of Buntung Dome Unit (Bd). The Crown of Tritik consists of Tritik Dome Unit (Td). Bd and Td are interpreted younger Pandan Breccia Unit in the Bojonegoro Geological Map by Pringgoprawiro and Sukindo (1992) in the Pleistocene.

3.1.10 Hornfels Unit

Hornfels Unit is in around of some lava units. The Hornfels unit was formed because of contact metamorphism which was changed by the Wackestone Unit.

3.2 Geological Structure

The Geological structure section consists of kinematic analysis based on field data and previous study data, and identification order of the fault and the fault implication to the geological condition of the study area.

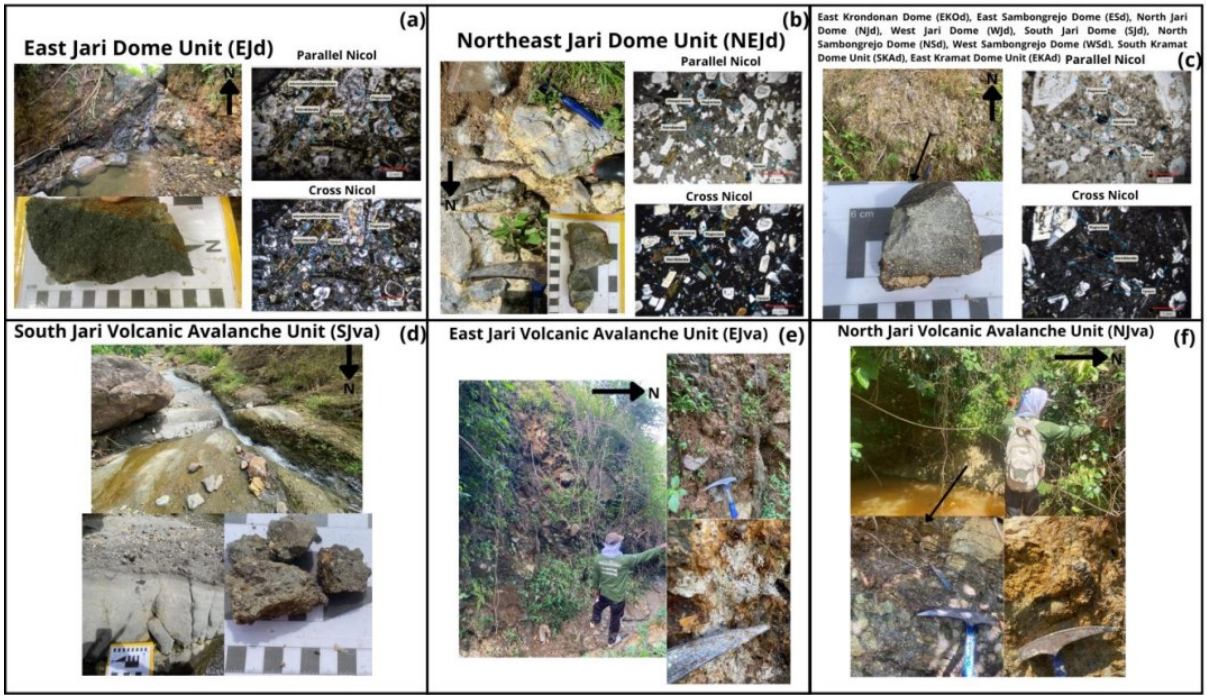

Figure 8: Crown of Jari Unit characteristic.

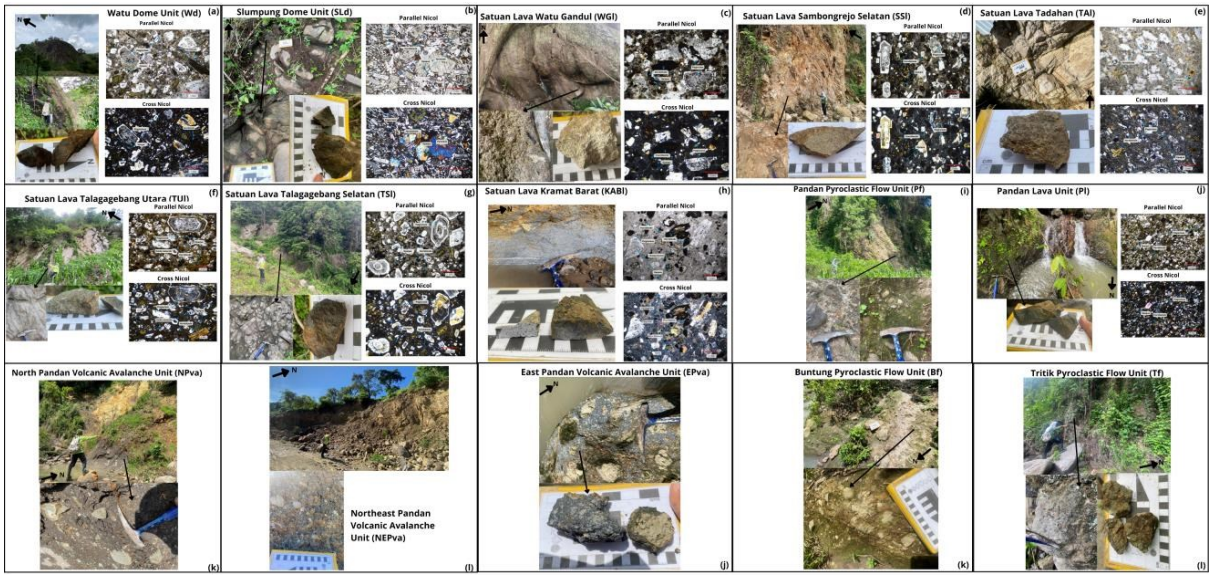

Figure 9: Crown of Pandan characteristic.

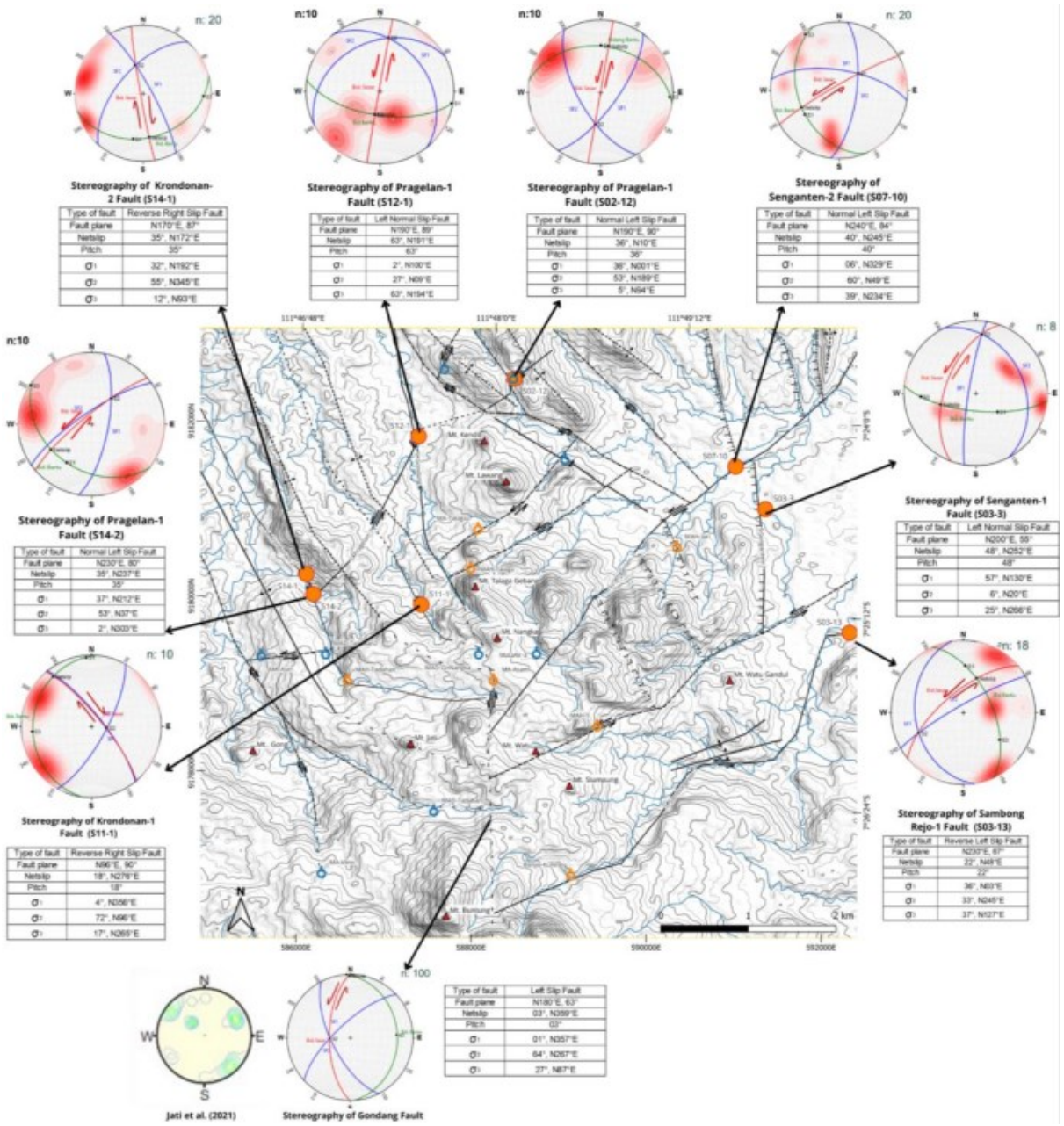

Figure 10: Mount Pandan fractures and locations.

3.3.1 kinematic Fault Analysis

Kinematic analysis is based on shear fracture data and lineament. The trend of lineament is interpreted as a strike of the fault plane. Identification of the stress and relative movement of the fault plane used stereonet software and classification from Rickard (1972). 6 faults were identified based on the field mapping data and 1 fault was identified based on the previous study from Jati et al. (2021). Reanalysis of the fault was done because there was a mistake in determining the movement of the fault. The spatial distribution of the fault analysis is shown in Figure 10.

- Pragelan-1 fault is a Normal Left Slip Fault, N190ºE/90ºNW (Rickard, 1972).
- Sambongrejo-1fault is a Reverse Left Slip Fault, N230ºE/90ºNW (Rickard, 1972).
- Senganten-1 fault is a Left Normal Slip Fault, N200ºE/55ºNW (Rickard, 1972).
- Senganten-2 fault is a Reverse Right Slip Fault, N96ºE/90ºSW (Rickard, 1972).
- Krondonan-1 fault is a Reverse Right Slip Fault, N96ºE/90º SW (Rickard, 1972).
- Krondonan-2 fault is a Reverse Right Slip Fault, N170ºE/87º SW (Rickard, 1972).
- Gondang fault is a Left Slip Fault, N180ºE/63º SW (Rickard, 1972).

3.3.2 Order of The Fault and The Implications

Based on the Cinematic analysis, there are several faults in the study area. In the geological map, Gondang fault has a trend NNW-SSE in the study area. There is a different position of Packstone-Mudstone Unit and Claystone Unit in the east and west of the study area. The east area is a relative left movement than the west area. The movement is caused by the Gondang Fault movement. If the fault is seen in the smaller scale map, the Gondang Fault has a continuity to the north from the study area. The Strike of the Gondang Fault is relatively perpendicular to the strike of Kendeng Anticlinorium (W-E trend). Based on previous pure shear or simple shear models, nothing has been explained yet about strike slip fault parallel to the dominant stress (Sigma1). Gondang Fault is identified as a tear fault that is formed when the folding process. A tear fault is a strike-slip fault that runs across the strike of a contractional or extensional belt and accommodates differential displacement between two segments of the belt. Like transfer faults, tear faults are usually confined to hanging walls of detached systems (Burg, 2020). Tear fault is normally found in the folding areas, such as the Andong Fault Area in Gyeongsang Basin, South Korea (Choi et al., 2002), the Zaghouan Thrust Belt, Tunisia (Aridhi et al., 2011), and others.

Gondang Fault was identified as a cause form other faults in the study area. This identification is validated with the model by Riedel (1929). North-South Left Slip Fault will make left slip fault with trend NE-SW (Pragelan-1 Fault, Sambongrejo-1 Fault, and Senganten-2 Fault) is identified as R Shear, right slip fault with trend NW-SE (Krondonan-1 Fault and Krondonan-2 Fault) is identified as R' Shear, and fold with trend ENE-WSW in the Southeast of the study area. NW-SE Right slip fault causes movement of the fold trend in the study area. Gondang fault is also identified as a permeable zone to form Mount Pandan, other cores, and the continuity trend of springs.

Senganten-1 Fault is a normal fault with trend N-S. The movement of the Senganten-2 Fault and the interpreted left slip fault in the south of the Senganten-2 Fault caused Senganten-1 Fault and other normal faults (identified as a normal fault zone). This normal fault zone is identified as a permeable zone that controls the form of cores in Crown of Jari with every Hummock having a relative trend N-S and Jari Warm Spring.

Table 2: Physical Characteristic of Springs.

Springs Name	X (m)	Y (m)	TDS (ppm)	pH	Water Temperature (°C)	Air Temperature (°C)	Elevation (mdpl)	Spring Classification		
								Temperature	TDS	pH
Talaga 2	588082.1	9180758	16200	6.52	31	32.8	283.65	Warm spring	Salt water	Neutral
Banyu Kuning	589139.9	9176800	2970	6.17	35.6	25.9	494.76	Warm spring	Brackish water	Neutral
Acid Spring	588257.7	9179029	350	3.95	31.2	32.5	455.63	Warm spring	Fresh water	Acid
Hot Spring-1	589443.3	9178504	2240	6.15	33.6	29.1	425.52	Warm spring	Brackish water	Neutral
Talaga	587995.7	9180311	756	6.32	32.6	30.3	323.87	Warm spring	Fresh water	Neutral
Jari	590353.6	9180551	7800	6.3	43.9	33.6	200.54	Warm spring	Brackish water	Neutral
Tadahan	586586.4	9179028	1070	6.81	31.1	30.7	327.29	Warm spring	Brackish water	Neutral

4. CONTROL FOR THE APPEARANCE OF HOT SPRINGS

4.1 Characteristic of Springs

Understanding the Characteristic of Springs is based on the physical parameter of springs. Physical parameters used in this research consist of springs and air temperature, total dissolved solid (TDS), and pH (Table 2). The value of each parameter will show the process of the water flow in the subsurface until it reaches the surface. The springs condition and distribution are shown in figure 11.

4.1.1 Temperature

The value of water temperature in the study area has an interval from 31-43.9°C and the average air temperature in the study area is 30.7°C. Those springs are classified as low-medium hot springs (Zhou et al., 2023). Acid Spring and Talaga-2 Spring have relatively higher temperatures than average air temperatures in the study area. Although Acid Spring and Talaga-2 Spring have lower temperatures than the air temperature when collecting data. So, Acid Spring and Talaga-2 Spring were classified into warm spring in this study. Higher temperatures can indicate water comes from deeper aquifers/reservoirs (USGS, 1955). The study area shows Jari Warm Springs as the warmest spring which is the location of in the normal fault zone. So, the geological structure conditions also control the temperature. The temperature value is colder in more simple geological conditions.

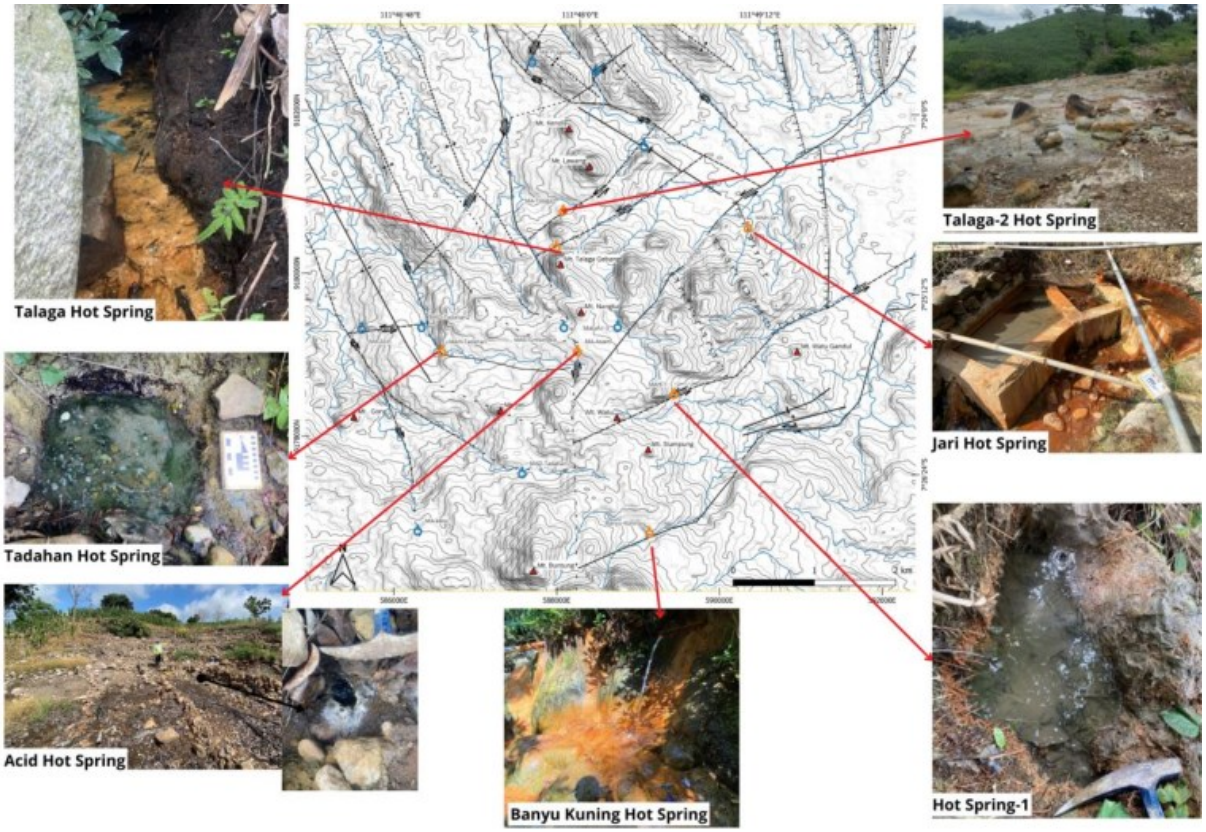

Figure 11: Springs condition and distribution.

4.1.2 Total Dissolved Solid (TDS)

Total dissolved solid shows the amount value of dissolved solids in the water. TDS Value can be classified into fresh water (0-1,000 mg/L); brackish water (1,000-10,000 mg/L); salt water (10,000-100,000 mg/L); brine water (>100,000 mg/L) (Freeze and Cherry, 1979). The TDS value in the study area has intervals from 350-16200 ppm. So, there are 2 freshwater springs, 4 brackish water springs, and 1 saltwater spring. TDS value is also affected by the time of water circulation/ depth of the aquifer and the lithology of the aquifer or reservoir. The aquifer of the springs is identified by the lithology around the spring and the physical characteristics of the spring. In the study area, spring with a wackestone aquifer has a higher TDS value than another aquifer. Based on that value, a spring with a carbonate aquifer will have high TDS value. That is also equal to Cartwright et al. (2017), spring in a marl aquifer (based on Pringgoprawiro and Sukindo (1992), Wackestone Unit equal to marl lithology in Kalibeng Formation) have high TDS value. Acid Spring has the lowest TDS value and low debit with pyroclastic breccia aquifer. Talaga Hot Spring is classified as a freshwater spring with a lava aquifer. But there is a spring with the same lithology but has diverse TDS, this is also affected by the depth of the fault and temperature of the springs. Springs with deeper faults and higher temperatures will have deeper aquifers and higher TDS values in the study area.

4.1.3 pH

pH can indicate dissolved substances in spring. pH is influenced by fluid salinity, temperature, and buffer minerals (Nicholson, 1993). Springs can be classified into 6 types based on pH value, such as very acid spring (pH<2), acid spring (2≤pH<4), light acid spring (4≤pH<6), neutral spring (6≤pH<7.5), light alkali spring (7.5≤pH<9), and alkali spring (9≤pH) (Subtavewung et al., 2005). The pH value in the study area has an interval from 3.95-6.81 with 5.66-6.1 rainwater pH. So, there is 1 acid spring and 6 neutral springs. Acid Spring shows a lower pH value than rainwater. This indicates that another influence makes the water acid. Based on field observations, there a sulfur deposits and vegetation anomalies around Acid Spring. This indicates acid properties come from water with high sulfur content.

Sulfur deposits can come from volcanic origin (inorganic), Bacterial sulfate reductions (organic), thermal decomposition of organic sulfur bearing compound (organic), and thermochemical sulfate reduction (organic) (Ma et al., 2019). This indicates the form of sulfur deposit not just from young vulcanism origin. In the study area, magmatism has an age of 1.8-0.8 million years ago, Pleistocene (Pringgoprawiro and Sukindo, 1992), or classified as inactive or extinct magmatism related to volcanism (McCoy-West et al., 2011 in Moeck, 2014).

Thermochemical sulfate reduction (TSR) became the most influential source of H2S in the sedimentary basin. TSR is made by hydrocarbon and sulfate minerals interaction at >100ºC (Ma et al., 2019). This is because there is a petroleum system in the Kerek Formation (the older formation than Kalibeng Formation or Wackestone Unit) based on Setyowiyoto et al. (2007); and Putra and Praptisih (2017). Wackestone unit can be a source rock in petroleum systems (Setyowiyoto et al., 2007). So, the TSR can be the process of making a sulfur deposit with cubic opaque minerals in petrography analysis of the Wackestone Unit. Thermal decomposition is interpreted as another source of sulfur deposits. Thermal decomposition normally takes place during the heating periods of organic matter and following petroleum formation (Ma et al., 2019). This is shown by the vulcanism in the Pleistocene heated Wackestone Unit and Kerek Formation.

4.2 Factors affecting the formation of springs

Strata and rocks, tectonic structures, geothermal geology, and hydrogeological conditions all have an important impact on the formation of hot springs (Zhou et al.,2023).

4.2.1 Aquifer and Hydrogeological conditions on the formation of hot springs

An Aquifer rock or sediment in a formation, group of formations, or part of a formation that is saturated with water and permeable enough to convey economical amounts of water to wells and springs (Fetter, 2014). The overlay of the aquifer or reservoir is controlled by lithology and geological structure in the study area (Irawan and Puradimaja, 2013). The permeability of lithology in the study area is classified into low and moderate permeability based on Vojtek and Vojtekova (2019) classification. Wackestone, andesite, and claystone have low permeability. Pyroclastic breccia, volcanic avalanche, fragmental sandstone, and packstone-mudstone have moderate permeability. However, at the observation station, there are many fractures in the Wackestone Unit. Fractures will increase the permeability of the rocks. It looks like there are many springs in Wackestone Unit and several resident's groundwater wells.

Recharge area in hydrogeological system is controlled by slope, lithology, and geological structure (Rajaveni et al., 2017). So, the area recharge area potential in study area is in high elevation with flat slope of Pandan Flow Unit and fault zones. Groundwater flows from high to low elevations. The subsurface flow conditions in the study area are interpreted based on the groundwater level of resident's groundwater wells. The water flows from south to north of the study area in the wackestone aquifer. However, the flow will always depend on the orientation of the aquifers.

4.2.2 Impact of structures on the formation of hot springs

The occurrence of a hot spring can be affected by a single fault (regional or local, including normal, or reverse or strike-slip faults) and multiple fault sets including parallel faults, intersecting faults and major faults with descendent faults, and even three-level faults of different scales. A regional fault is usually large and deep, with multiple periods of activity in its evolution. It often plays an important role in heat convection and transmitting groundwaters and is favorable for the formation of hot springs. Sometimes several hot springs exist along a major fault (Zhou et al., 2023). In the study area, the major fault is the Gondang Fault. Gondang Fault controls the appearance of the springs, heat convection for the springs, and transmitting groundwaters.

Identification of structural control on the appearance of hot springs is based on field observations, geological conditions, and fault continuity around the hot springs. Springs can be divided based on the control for appearance of the springs into contact spring, depression spring, fracture spring, fault spring, sinkhole spring, and fracture zone spring (Fetter, 2014). Fault springs generally have high water discharge. However, in the field observations, it is difficult to measure water discharge because in general the springs have more than one discharge point, which means measuring discharge at one point will not be representative. So, in this study interpretation of springs type is based on field observations in the form of qualitative output, lineament interpretation, and physical characteristics of the springs.

There are 2 types of springs in the study area, such as depression spring and fault spring. A spring is formed when the water table reaches a land surface because of a change in topography (Fetter, 2014). Acid Hot Spring is a depression spring in the study area. This spring is characterized in the field by relatively small debit water flow, low TDS value, and moderately steep-steep slope. A spring is created by the movement of two rock units on a fault (Fetter, 2014). Fault springs in the study area consist of Jari Warm Spring, Tadahan Warm Spring, Talaga Warm Spring, Banyu Kuning Warm Spring, and Talaga-2 Warm Spring. These springs are characterized in the field by relatively high debit water flow (there are several discharge spots and several pools), high TDS value, and the continuity of the fault.

4.2.3 Impact of conditions of geothermal geology on the formation of hot springs

Higher hot spring temperatures indicate the water comes from deeper aquifers/reservoirs (USGS, 1995). The heat can come from volcanic or nonvolcanic. The Volcanic heat source of the hot springs also depends on the age of

the magmatism. There are 3 terms of magmatism based on McCoy-West et al. (2011) in Moeck (2014), with active magmatism related to volcanism 0-500 years old, recent magmatism related to volcanism 500–50,000 years old, and inactive or extinct magmatism related to volcanism 450,000 years old. The nonvolcanic heat source can come from the geothermal gradient (Wang et al., 1993; Liu et al., 2015; in Zhou, 2023) and the cooling of the Earth's core and the radioactive heat generation in the upper 20 to 40 km of the Earth's crust. Radioactive heat generation is a product of crustal rocks containing high concentrations of naturally occurring radioactive elements: thorium, potassium, and/or uranium (SMU,2023). Faults will have an important role in this heat source because the fluid will circulate deep within the crust and transport heat to near the surface along permeable faults (Moeck, 2014).

In the study area, the last vulcanism was 1.8-0.8 million years ago (Mount Pandan activities) or included in inactive or extinct magmatism related to volcanism classification. For that reason, volcanic activities will not be the heat source in the study area. Hot springs in the study area were in the continuity of the faults. So, the faults have an important role in the study area because the fault didn't only control the appearance of the springs but also the appearance of the vulcanism. If faults extend to zones above the magma or magma chambers, heat may be easily transported to shallow zones through the faults. Groundwater that circulates deeply through fault zones and is heated indirectly from magma or a magma chamber, may be used as a high temperature hot spring (Moeck, 2014). In the study area, the existence of the gondang fault which is deep enough to create volcanism can be secondary permeability to increase heat flow. Besides that, radiogenic activities also make higher temperatures. In the study area, the Kerek Formation (consisting of alternation sandstone, claystone, tuff, marl, and limestone) will show higher heat production than the Wackestone Unit or Kalibeng Formation (consist of Marl) (Norden & Förster, 2006). So, the heat source in the study area can be dependent on the heat flow, geothermal gradient, and radiogenic heat production. The higher temperature spring can indicate deeper reservoirs or deeper faults or in the fault zone so will have higher heat flow. So, deeper reservoirs (gradient geothermal) and fault zones (secondary permeability to increase heat flow) will have higher temperatures reservoirs in the study area. It can be seen in the Jari Warm Spring, the warmest spring in the study area.

5. CONCEPTUAL MODEL

5.1 A-A' Section

A-A' section shows the conceptual model of Talaga-2 Hot Spring and Talaga Hot Spring (Figure 12). The water flow is controlled by fault and the orientation of the lithology. Talaga-2 Hot Spring has a deeper fault and reservoir based on TDS value. The water flows from south to north of the study area. The fault is interpreted as the permeable zone to be a path for fluid recharge in the reservoir. Krondonan-1 Fault and high topography with a relatively flat slope West of Mount Slumpung are interpreted as the recharge area for Talaga and Talaga-2 Hot Spring. Then the water flows and is heated during the flow process by heat flow. Water flows and passes through faults, then the water comes out as Talaga-2 Hot Spring and Talaga Hot Spring.

5.2 B-B' Section

B-B' section shows the conceptual model of Acid Hot Spring and Banyu Kuning Hot Spring (Figure 13). The water flow is controlled by fault and the orientation of the lithology. Water flows from south to north of the study area in the Pandan Breccia Unit. The recharge area was also controlled by the Senganten-2 Fault. Then, the water flows deeper and follows the lithology orientation. The water flows in the Wackestone Unit and flows to the south of the study area. Water flows and passes through faults, then the water comes out in Banyu Kuning Hot Spring. For Acid Hot Spring, the recharge area is controlled by the Krondonan-2 Fault. Water flows deeper in the Wackestone Unit and is heated during the flow process by heat flow. Because the fault is buried by the Pandan Breccia Unit, the output of the Acid Hot Spring is relatively small and is heavily influenced by the flow of more local springs.

5.3 C-C' Section

C-C' section shows the conceptual model of Jari Hot Spring (Figure 14). The water flow is controlled by fault and the orientation of the lithology. The recharge area was also controlled by the NE-SW fault in the north of Watu Gandul. The water flows through the Wackestone Unit from south to north of the study area. The water then flows through the normal fault zone and is heated during the flow process by heat flow. Water flows and passes through faults, then the water comes out as Jari Hot Spring.

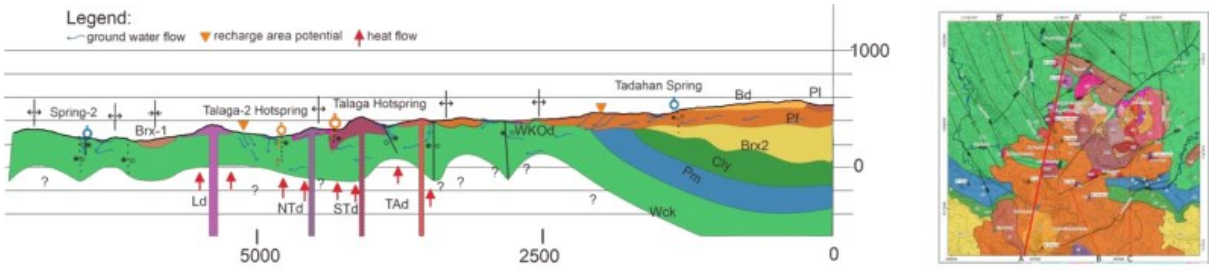

Figure 12: Conceptual model of A-A' section.

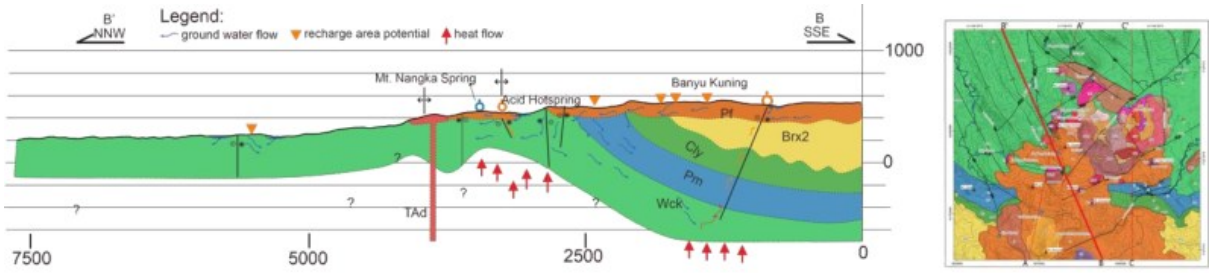

Figure 13: Conceptual model of B-B' section.

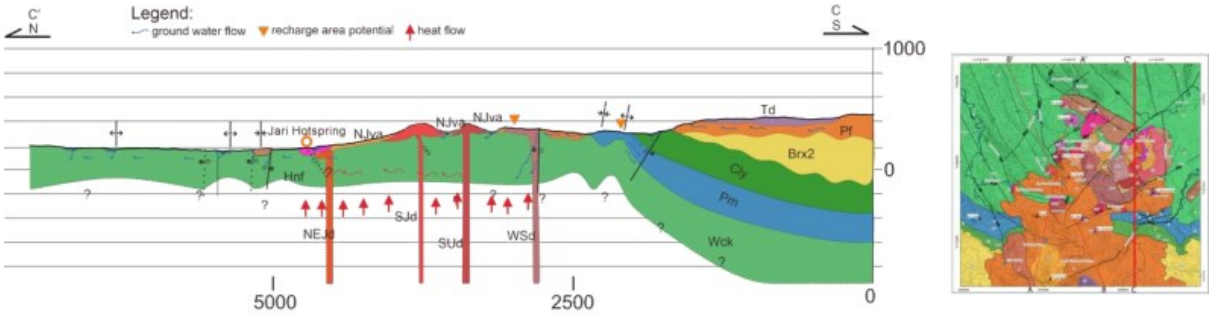

Figure 14: Conceptual model of C-C' section.

6. CONCLUSION

There are 39 informal lithological units in the study area with 5 Crown and 23 Hummock based on vulcanostratigraphy analysis. Left Slip Fault or Gondang Fault (NNW-SSE) is the main fault in the study area. Gondang Fault causes NE-SW Normal Left Slip Fault and Left Normal Slip Fault, NW-SE Right Slip Fault, ENE-WSW Folding, and Normal fault zone in the east of the study area.

There are 7 hot springs in the study area. The springs can be classified into 3 groups, such as fault springs in the Wackestone Unit aquifer with high TDS value and neutral pH, fault springs in the lava dome unit aquifer with lower TDS value than Wackestone Unit aquifer and neutral pH, and depression springs in the Wackestone Unit aquifer with low TDS value and acid pH. Water flows from the south to the north of the study area. Water flow is controlled by faults and lithology orientation. Faults have a dominant influence on the control for appearance of hot springs in the study area. The faults also control the secondary permeability to increase heat flow as the heat source of the hot springs. Radiogenic heat production and gradient geothermal also make the springs have higher temperatures. The fault zone can make better permeability, so we have Jari Hot Spring as the warmest spring in the study area.

REFERENCES

Aridhi, K., Bagga, M.A.O., Abdeljaouad, S., Zargouni, F., and Mercier, E.: Lateral ramp-related folding evidence in the Tellian domain of Tunisia: Tectonic implications. C. R. *Geoscience*, 343, (2011), 360–369.

Burg, Jean-Pierre: Fault, ETH Zurich, Accessed in https://www.files.ethz.ch/structuralgeology/jpb/files/english/3faults.pdf , (2020).

Cartwright, A., Hofmann, H., CurreLl, M.J., and Fifield, L.K.: Decoupling of solutes and water in regional groundwater systems: The Murray Basin, Australia. *Chemical Geology*, **466**, (2017), 466–4.

Choi, P., Lee, S.R., Choi, H., Hwang, J., Kwon, S., Ko, I., and An, G.: Movement history of the Andong Fault System: Geometric and tectonic approaches. *Geosciences Journal*, **6(2)**, (2002), 91-102.

Fetter Jr., C.W.: *Applied Hydrogeology*, 4th Edition, Pearson New International Edition. Pearson Education Limited, (2014).

Freeze, R.A. and Cherry, J.A.: *Groundwater 2nd Edition*, Prentice Hall, Eaglewood, Cliff, NJ, (1979).

Irawan, D. E. and Puradimaja, D. J: *General Hydrogeology Worksheet*, Applied Geology Expertise Group, ITB, (2013).

Jati, W.W., Agna, N., Suryantini, and Muhtar, L.K.: Fracture Characteristics of Mount Pandan Geothermal Complex, East Java, Indonesia, *Proceedings*, World Geothermal Congress 2020+1, (2021).

Ma, X., Zheng, G., Liang, M., Xie, D., Martinelli, G., Sajjad, W., Xu, W., Fan, Q., Li, L., Du, L. and Zhao, Y.: Occurrence and Origin of H2S from Volcanic Reservoirs in Niudong Area of the Santanghu Basin, NW China. *GeofluidsVolume*, Article ID 1279658, (2019), 10 pages.

Maubana, W.M., Maryanto, S., Utami, I.K., and Nadir, A.: Reservoir Magnetic Anomaly at Geothermal Area of Mount Pandan, East Java, Indonesia. *International Journal of Renewable Energy Research*, **Vol.9**, (2019), No.2.

Moeck, I.S.: Catalog of geothermal play types based on geologic controls, *Renewable and Sustainable Energy Reviews*, 37, (2014) 867-882.

Németh, K.: Monogenetic volcanic fields: Origin, sedimentary record, andrelationship with polygenetic volcanism. *The Geological Society of America*, **Special Paper 470**, (2010).

Nicholson, K.: *Geothermal Fluids: Chemistry and Exploration Techniques*, Springer-Verlag, (1995).

Pringgoprawiro, and H., Sukido: Bojongegoro Geological Map 1:100.000, (1992).

Putra, P.S. and Praptisih.: A Re-interpretation of the Kerek Formation in Klantung Area, Kendal, Based on Stratigraphic and Foraminifera Data. *Jurnal dan Sumberdaya Mineral*, (2017).

Rajaveni, S.P., Brindha, K., and Elango, L.: Geological and Geomorphological Controls on Groundwater Occurrence in a Hard Rock Region. *Applied Water Science*, **Vol.7**, (2017), 1377-1389.

Rickard, M.J.: Fault Classification – Discussion. *Geological Society of America Bulletin*, v. 83, (1972), pp. 2545–2546.

Setyowiyoto, J., Datun, M., and Winardi, S.: Geology and Petroleum System Investigation Bancak, Semarang Based on Surface Manifestation. *Media Teknik*, **No.1, Tahun XXIX**, (2007).

SMU, Roy M. Huffington Department of Earth Sciences: What is "Heat Flow". Accessed in https://www.smu.edu/dedman/academics/departments/earth-sciences/research/geothermallab/datamaps/geothermalmapofnorthamerica/what-is-heat-flow, (2023).

Subtavewung, P., Raksaskulwong, M., and Tulyatid, J.: The Characteristic and Classification of Hot Springs in Thailand, *Proceedings*, World Geothermal Congress, (2005).

USGS: Springs of Florida, (1995).

Vojtek, M. and Vojteková, J.: Flood Susceptibility Mapping on a National Scale in Slovakia Using the Analytical Hierarchy Process. *Water*, 11(2), (2019), 364.

Zhou, X., Zhuo, L., Wu, Y., Tao, G., Ma, J., Jiang, Z., Sui, L., Wang, Y., Wang, C., and Cui, J.: Origin of some hot springs as conceptual geothermal models. *Journal of Hydrology*, **624**, (2023), 129927.

Reservoir Fluid Movement Identification using 3-D Inversion Time-lapse Microgravity Monitoring (2015-2023) in the Lahendong Geothermal Field

Lendriadi Agung[1,2], Mohammad Syamsu Rosid[2], Mochamad Tofan Sastranegara[1], Baiq Lola Riandari[1], Anita Fitria Sekar Arumsari[1], and David Paskareinold Timisela[1]

[1]Pertamina Geothermal Energy Tbk, Indonesia
[2]Department of Physics, Faculty of Mathematics and Natural Sciences, Universitas Indonesia, Indonesia

Lendriadi.agung@pertamina.com

Keywords: Fluid, reservoir, microgravity, 3-D inversion, Lahendong

ABSTRACT

Understanding the fluid flow in the reservoir is critical for geothermal utilization. Imbalanced fluid mass during extraction and reinjection caused a decline in the generation of electricity due to a decrease in the quantity of fluid in the reservoir. Time-lapse microgravity monitoring can offer a comprehensive view of fluid movement in the reservoir by observing mass changes over a specific period of time. 3D inversion time-lapse microgravity monitoring can determine the location and depth of mass changes that occur in the reservoir. Annual Microgravity monitoring from 2015-2023 in the Lahendong geothermal field reveals that the majority of the injection fluid flows back into the reservoir through the LHD-51 injection well. Additionally, natural recharge fluid is observed entering the reservoir from an elevation of -500 masl in the southwest area, which has been confirmed by Pressure-Temperature measurement data in the LHD-53 well that show a reversal temperature. Further investigation is required to determine the impact of the natural recharge fluid inflow from the southern region of the Lahendong reservoir.

1. INTRODUCTION

Lahendong geothermal field located about 30 kilometers South of Manado city, the capital of North Sulawasi Province, Indonesia (Figure 1). 80 MW of electricity has been produced from geothermal energy, with UNIT-1, UNIT-2, UNIT-3, and UNIT-4 each generating 20 MW. (Atmojo et al., 2015; Azka et al., 2015; Brehme et al., 2016; Firmansyah et al., 2021; O'sullivan et al., 2023; Permana et al., 2015; Prasetyo et al., 2016; Sambodho et al., 2021; Sumantoro et al., 2015; Yani, 2022; Zahid et al., 2021). In 2001, UNIT-1 initiated operations, followed by UNIT-2 in 2007, UNIT-3 in 2009, and UNIT-4 in 2011. (Koestono et al., 2010; Prabowo et al., 2015; Prasetyo et al., 2016; PT. BURSA EFEK INDONESIA, 2023; Sambodho et al., 2021).

The annual average difference between the fluid extracted and reinjected into the reservoir is estimated to be 3-5 MTon per year since UNIT-4 has been operational(Haq et al., 2019; PT. Pertamina Geothermal Energy, 2024). The result indicates the reservoir experiences a fluid imbalance annually due to geothermal exploitation on the surface, as the fluid extracted exceeds the fluid injected back into the reservoir.

The process of fluid extraction and injection in the reservoir at various well locations suggests that fluid movement will occur within the reservoir. This exploitation process results in the movement of not only the production and injection fluids, but also natural recharge. Recharge is one of the four primary components of a geothermal system, as per Hochstein and Browne (2000). Figure 2 shows conceptual model geothermal system.

Naturally, the reservoir's pressure will fluctuate as a result of mass loss, resulting in the fluid's move from a higher to a lower pressure, as illustrated in Figure 3. In the blue box, there is a loss of mass (ΔM) as a result of fluid extraction during periods 0 to 1 (Figure 3a). Assuming that the fluid extraction conditions stay constant from period 0 to period 2, the mass loss that occurs goes through a shift in location, driving the fluid mass closer to the center (Figure 3b). The mass loss moves further to the left from period 2 to period 3, as illustrated in Figure 3c. This illustrates the fluid's progression from the left to the production well on the right, where it is ultimately extracted. And Figure 3d shows the total mass loss from period 0 to period 3, which demonstrates the fluid mass loss resulting from extraction from production wells during that period.

Naturally, the fluid in the reservoir undergoes movement as a result of the exploitation process, as the geothermal power plant in Lahendong continues to operate. Of course, it is crucial to determine how the geothermal fluid circulates within the reservoir. Barbier (2002) and Rybach (2003) found that sustainability can be achieved in Lahendong by ensuring that the amount extracted is equivalent to or less than the amount replaced. This is because it is associated with geothermal development. In the case of Lahendong, it is evident that the quantity of

fluid extracted exceeded the quantity of fluid returned. However, a natural recharge component is anticipated to compensate for the fluid that was lost as a result of the exploitation.

Consequently, it is crucial to identify how the fluid is transported within the reservoir, whether through extraction, injection back into the reservoir, or natural recharge, which replaces the fluid that is lost in the reservoir. Therefore, it is anticipated that it will be able to offer information on the balance of fluid movement within the reservoir, thereby ensuring the sustainability of geothermal energy utilization for a longer period.

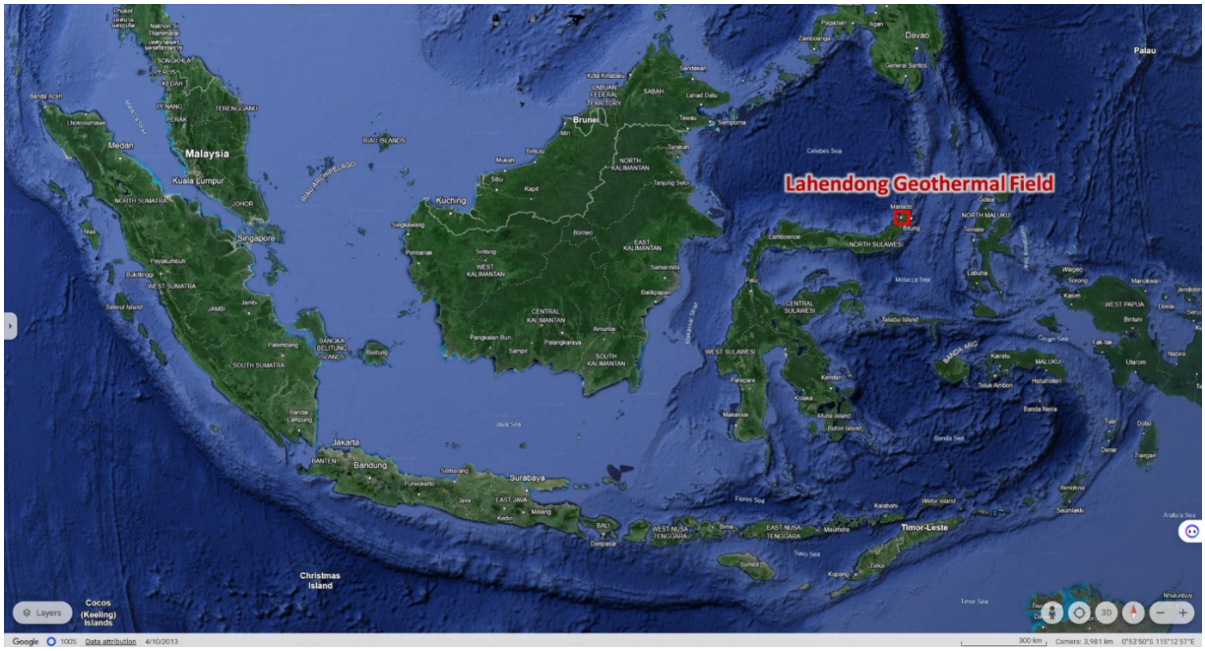

Figure 1: Location of the Lahendong Geothermal Field.

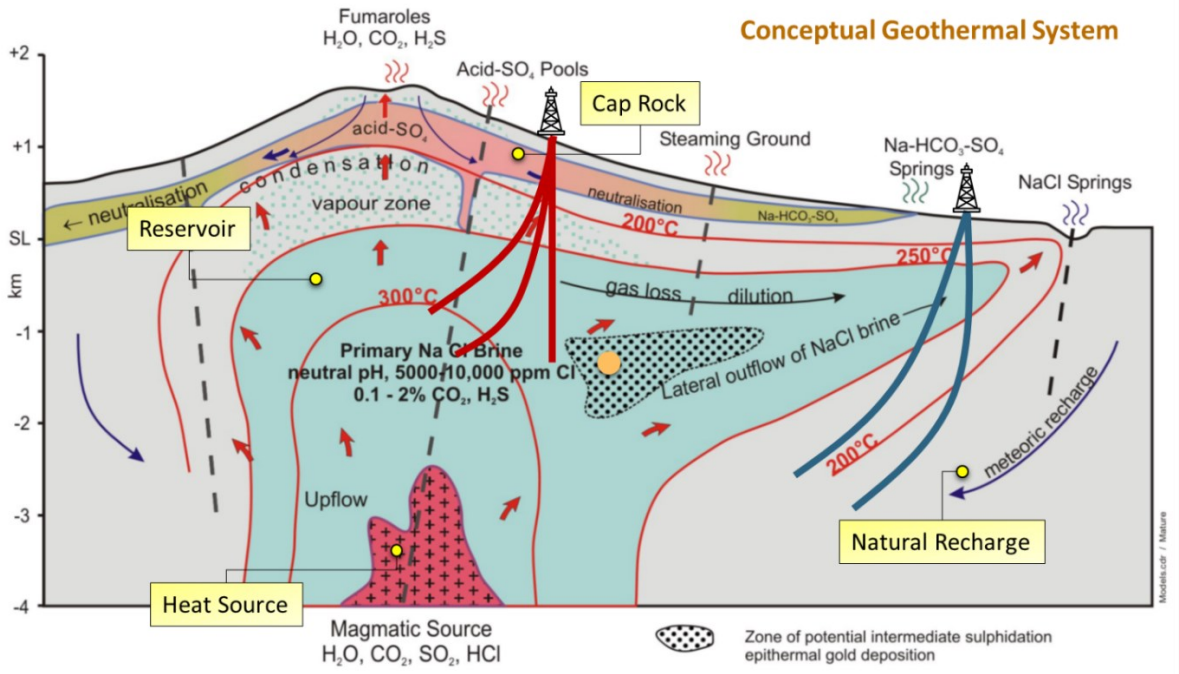

Figure 2: Conceptual model geothermal system (Modified from Bogie et al., 2005).

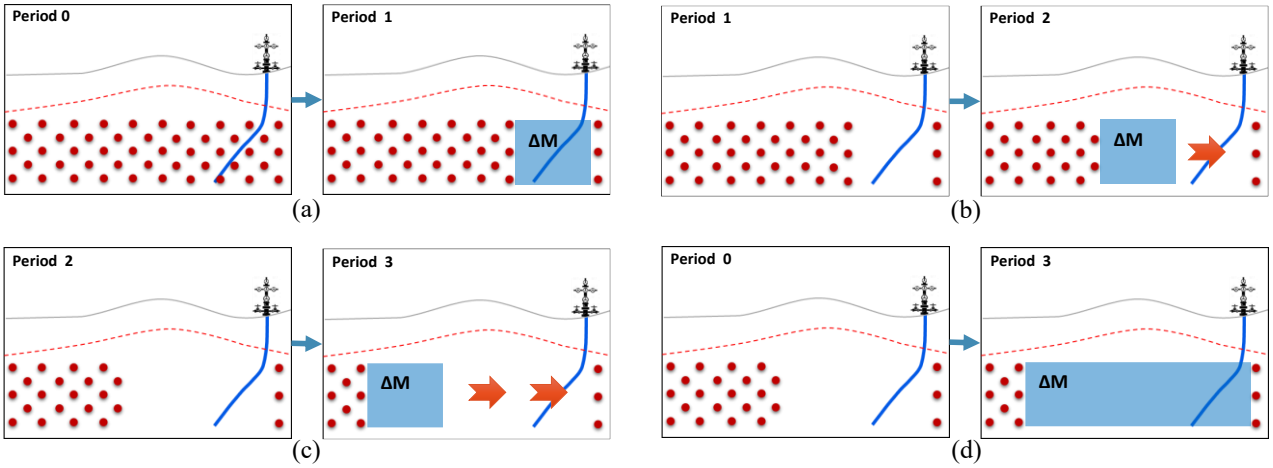

Figure 3: Scematic mass changes during fluid extraction.

2. MATERIAL AND METHOD

Gravity is a geophysical method that has been widely used by researchers to help identify geological structures beneath the surface (Gunadi Putra et al., 2021; Nainggolan et al., 2015; Natasia et al., 2016; Natul & Heliani, 2022; Pertiwi et al., 2023; Rosid et al., 2022, 2023; Sastranegara et al., 2015). However, regarding monitoring changes in mass, modification of this method is required. Differences in gravity values at the same location at different times can help explain differences in mass values that occur between these periods (Agung et al., 2023; Rosid et al., 2021). In the last four decades, time-lapse microgravity monitoring has been widely used in geothermal fields. The identification of fluid movement and mass redistribution in geothermal reservoirs is very important for the sustainability and development of geothermal fields. The studies carried out have explained many causes that might result in changes in gravity in operating geothermal fields (Agung, 2022; Agung et al., 2018; Allis & Hunt, 1986; Apuada & Olivar, 2005; Banos et al., 2020; Haq et al., 2019, 2023; Hunt, 2005; Menzies, 2011; Nishijima et al., 2005; Nordquist et al., 2004; Omollo, 2018; Omollo & Nishijima, 2024; Portier et al., 2021, 2022; Wardhani, 2023).

Gravity changes in micro scale ($\Delta \boldsymbol{g}$) measured on the surface are obtained from the results of gravity measurement readings at different periods between $\boldsymbol{g_{period1}}$ and $\boldsymbol{g_{period2}}$ (Nishijima et al., 2015). The difference between the gravity readings in the two periods describes the mass changes that occurred between those periods.

$$\Delta g = \left(g_{period2} - g_{period1}\right) \tag{1}$$

Hammer (1945) explained that Gauss theorem could be used to calculate mass from residual gravity anomaly data (LaFehr, 1965). The value of gravity in a certain area on the surface of the earth can be quantitatively determined by the value of the total mass beneath it by using the following equation:

$$M = \frac{1}{2\pi G} \iint_{S} \Delta g \, dS \tag{2}$$

where M is the total mass, G is the universal gravitational constant, S is the surface area covering the mass anomaly of interest, and Δg is the relative gravitational acceleration value. In time-lapse microgravity monitoring activities, the Δg value is the difference in gravity readings between two measurement periods.

By knowing the mass change value for each annual period, it is possible to estimate the movement of geothermal fluids that occur in the reservoir. Changes in the total loss or addition of mass resulting from calculations using Gauss theorem can provide an overview of fluid mass transfer from one location to another. This mass change is known from the results of annual time-lapse microgravity monitoring.

The time-lapse microgravity data in Lahendong used is for the period 2015, 2016, 2017, 2018, 2019, 2020, 2021, 2022, up to 2023. Around 118 Benchmark (BM) gravity is routinely monitored every year (Figure 4), and the distance between BM points is ± 200 m. Because UNIT-4 has been operating since 2011, monitoring data that has been carried out routinely since 2015 is assumed to have no significant changes in mass withdrawal; only in June 2017 was there a change in the injection scenario from the LHD-7 well to the LHD-51 well. Apart from that, all Lahendong microgravity time-lapse data has been corrected for the effects of changes in elevation and changes in shallow groundwater levels during each measurement period. So it is assumed that the detected change in gravity is the effect of mass changes that occur only in the reservoir due to exploitation.

The flow rate data for each well is cumulated according to the period the time-lapse microgravity monitoring was carried out. The analysis was carried out during the monitoring period every year and cumulatively for eight years from the beginning of 2015-2023. This was done in the hope of providing an overview of the movement of geothermal fluid changes that occurred in the reservoir during the monitoring period. The results of forward modeling using Gauss Theorm based on flow rate data for each well in Lahendong, show that the gravity changes that occur in Lahendong are estimated to reach -26 µGal (Figure 5), based on a study conducted by Agung et al. (2023), the optimum period for obtaining an overview of fluid mass movements in a reservoir using Scintrex CG-5 or CG-6 is a change in gravity of more than ±25 µGal. Therefore, the monitoring period carried out every year is optimal and is also carried out in the same season.

For each monitoring period, the total mass change is calculated from the results of microgravity monitoring, and a 3-D time-lapse microgravity inversion is carried out to obtain an estimate of the location and depth of the Lahendong reservoir fluid mass change. A detailed schematic flow chart for investigating the characteristics of reservoir fluid movement in Lahendong is shown in Figure 5.

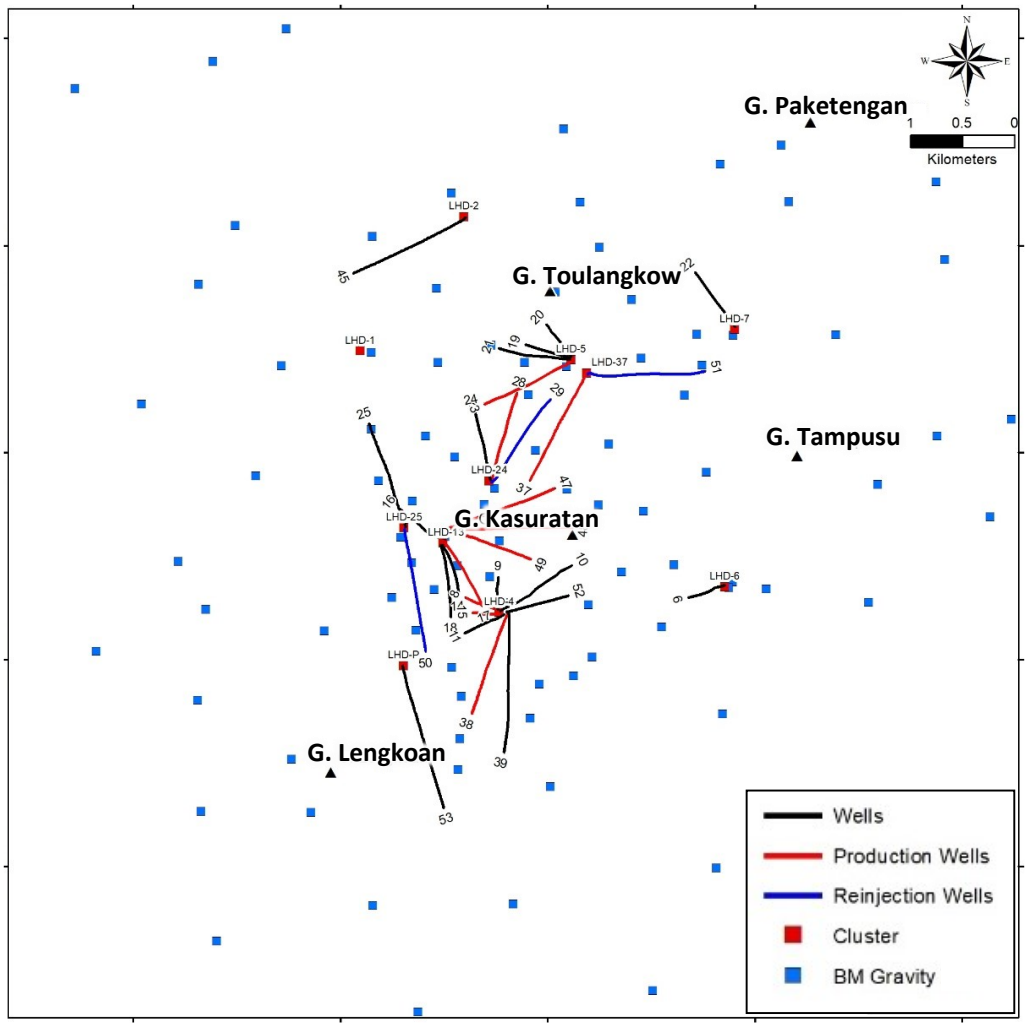

Figure 4: Benchmark microgravity monitoring Lahendong geothermal field.

3-D time-lapse microgravity inversion in Kamojang using the VOXI Modeling Tool in a Geosoft Oasis Montaj cloud and clustered computing module platform (Geosoft, 2024). The Geosoft platform uses the Catercian Cut Cell (CCC) method and an iterative re-weighting inversion algorithm developed by Ingram et al. (2003), and then simplified by Ellis and MacLeod (2013) in order to describe the geometry of the geological surface more efficiently, accurately, and simply than the previous Voxel model results. The iterative re-weighting least squares (IRLS) algorithm approach, which was originally developed by Lawson (1961), is applied to solve optimization problems that may occur iteratively using weighted least squares calculations. Regularization with the misfit function in this iterative inversion is applied to obtain a more stable solution between the observed values and the calculations. Conversely, the extent to which the predicted response matches the observed is influenced by reduced chi-squared misfit (Taylor & Thompson, 1982).

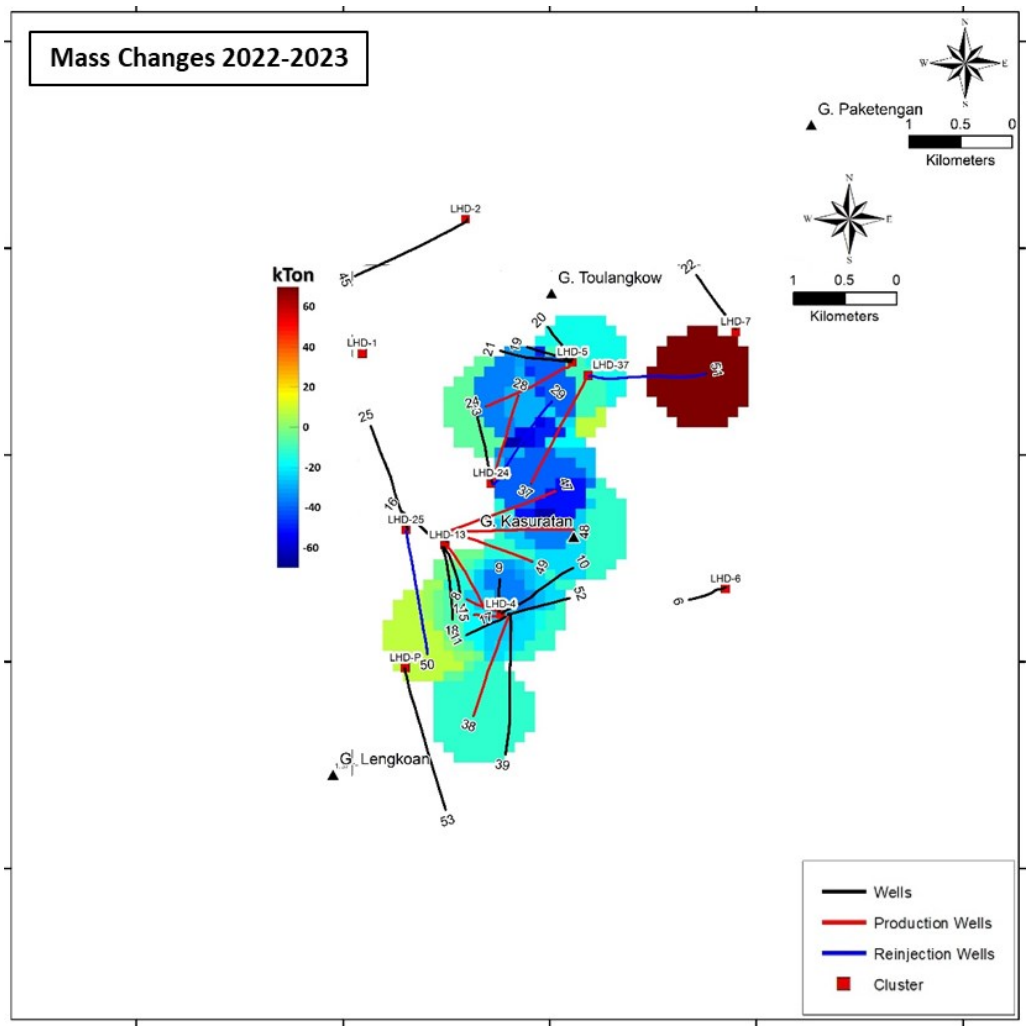

Figure 5: Changes in the mass of production and injection wells in the Lahendong geothermal field over 12 months.

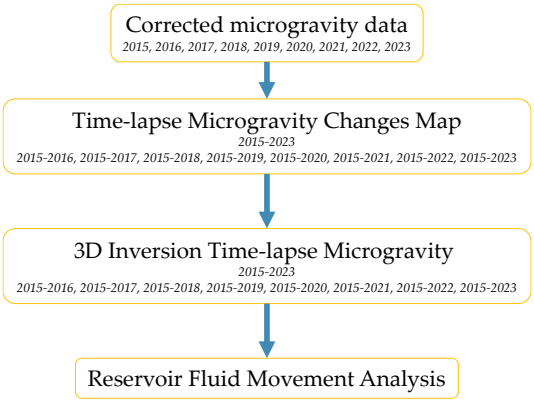

Figure 6: Flow chart investigation of reservoir fluid movement at Lahendong Geothermal Field.

In the 3-D inversion process, the microgravity time-lapse results are only modeled in the reservoir area. Gravity changes that occur near the surface due to the effects of changes in elevation and changes in groundwater levels have been corrected (Allis et al., 2000; Allis & Hunt, 1986). Apart from that, the mass changes that occurred in the Lahendong subsurface over a period of up to eight years are assumed to be only due to changes in fluid mass that occurred in the reservoir. In this very short monitoring period, the rock mass and lithology are considered to have not changed. So the 3-D time-lapse microgravity inversion carried out in Lahendong was only carried out from the top of the reservoir to a depth of around -2000 masl.

From the results of the analysis of gravity change maps during various monitoring periods, and the results of density changes from the results of 3-D inversion modeling, it is hoped that they will be able to describe the distribution of mass changes that occur in the Lahendong reservoir. So it can provide an overview of the fluid movements and dynamics that occur in the reservoir. In this way, it is hoped that we will be able to create a development strategy in the future that will maintain the sustainability of the use of geothermal energy in Lahendong.

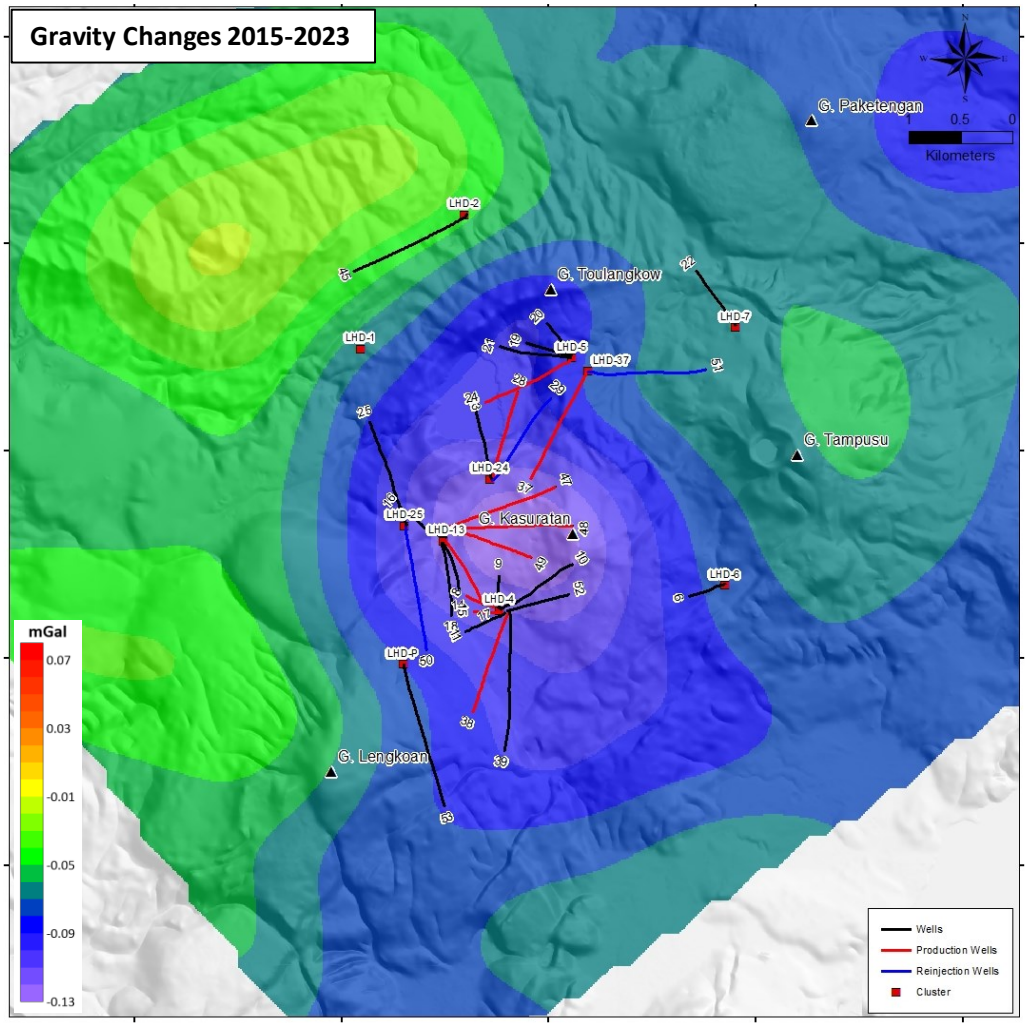

Figure 7: Map of microgravity changes between the 2015–2023 period.

3. RESULT

Figure 7 shows the results of time-lapse microgravity monitoring from 2015–2023, depicting a large decrease in gravity in the zone area near the production wells in Lahendong, which illustrates the occurrence of mass loss in that area. However, interestingly, there is an area in the southern part of the production zone that also experiences a decrease in gravity, meaning that this southern area is also affected by mass extraction in the Lahendong reservoir.

This is also illustrated by the results of annual cumulative gravity monitoring shown in Figure 8, the occurrence of mass loss in the southern area, and the results of time-lapse microgravity monitoring in several periods, including 2015–2016, 2018–2019, and 2021–2022. The loss of mass far from this reservoir also indicates fluid movement from the south towards the Lahendong reservoir.

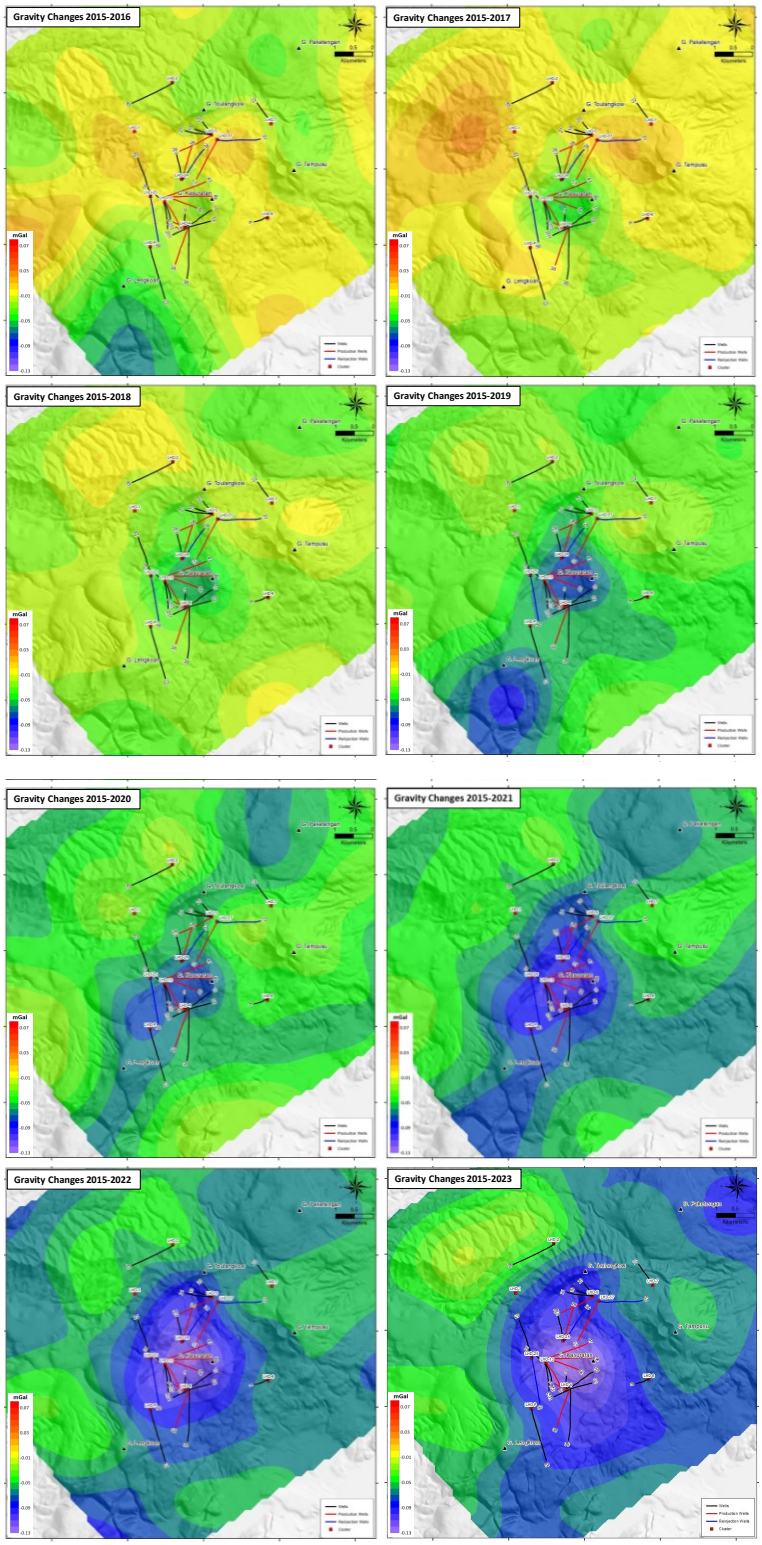

Figure 8: Cumulative map of microgravity changes from 2015 to 2023.

The map of cumulative time-lapse microgravity monitoring results from 2015 to 2023 shown in Figure 8 also provides information that there is an increase in mass in the northern area of the production zone. This is interpreted to be related to production activity in the northern area, originating from wells LHD-7 and LHD-51. This is also in accordance with the map of estimated mass changes resulting from each well, which was previously shown in Figure 5.

To be able to see the position of mass changes both horizontally and vertically, a 3-D inversion was carried out based on the results of time-lapse microgravity monitoring. Because the measured changes in gravity have been

corrected for the effects of changes in elevation and changes in shallow groundwater levels, it is assumed that these measured changes in gravity are only due to the effects of changes in mass in the reservoir. Therefore, the density changes calculated in this 3-D inversion process only originate in the reservoir. The distribution of areas experiencing mass changes in the reservoir in the constraint uses the elevation distribution of the Base of Conductor (BoC) in Lahendong as the Lahendong Top Reservoir. Figure 9 shows the elevation distribution of the BoC in Lahendong, from the BoC results to an elevation of -3000 masl as the basis for the area experiencing mass changes in the Lahendong reservoir due to exploitation.

Cumulatively, the results of 3-D time-lapse microgravity inversion from 2015–2023 show that mass changes occurred at elevations of 500 masl to -3000 masl, with a decrease in density focused in areas near production wells with variations between -1 kg/m^3 and -3 kg/m^3 (Figure 10). From Figure 10, it can also be seen that there is an increase in mass of +1 kg/m^3 to +3 kg/m^3 in the North, Sealtan, and a small part near the LHD-28, LHD-29, and LHD-51 wells. This increase in mass in the northern part may be correlated with injection well activity at LHD-7 and LHD-51, while in the southern part, it may be correlated with the entry of natural recharge in the southern area.

The entry of natural recharge in the southern area is also in accordance with pressure and temperature data from the LHD-53/LHD-P1 well in this area, which indicates the presence of cold fluid entering from the south into the Lahendong reservoir zone. This can also be seen from the results of the 3D inversion time-lapse microgravity shown in Figure 11. The addition of mass in the southern area is slowly entering and approaching the reservoir zone from year to year. However, the effect of the additional mass coming from the south needs to be studied further in order to obtain more comprehensive results regarding the impact on production wells due to the influx of fluid from the south and whether it has a good or bad impact regarding the sustainability of geothermal development in Lahendong, considering the 3D results. The mass inversion that occurs in this southern area is relatively shallow, namely at an elevation of -1000 masl.

The results of the 3D inversion time-lapse Lahendong microgravity shown in Figure 11 also help in identifying fluid movements that occur in the northern part of the Lahendong reservoir. The addition of mass from the north near the LHD-7 and LHD-51 wells, which are approaching the reservoir zone, illustrates the recycling of geothermal injection fluid into the reservoir, so it is hoped that a better balance between production and injection can be achieved. In terms of position, the mass addition that occurs in the northern part is at a deeper elevation, namely at an elevation of -2000 masl. The injection fluid is relatively cooler after being utilized at the surface, and it is hoped that this deeper position of mass addition, when re-injected into the reservoir, will have enough time to be reheated before entering the reservoir and being used for generation.

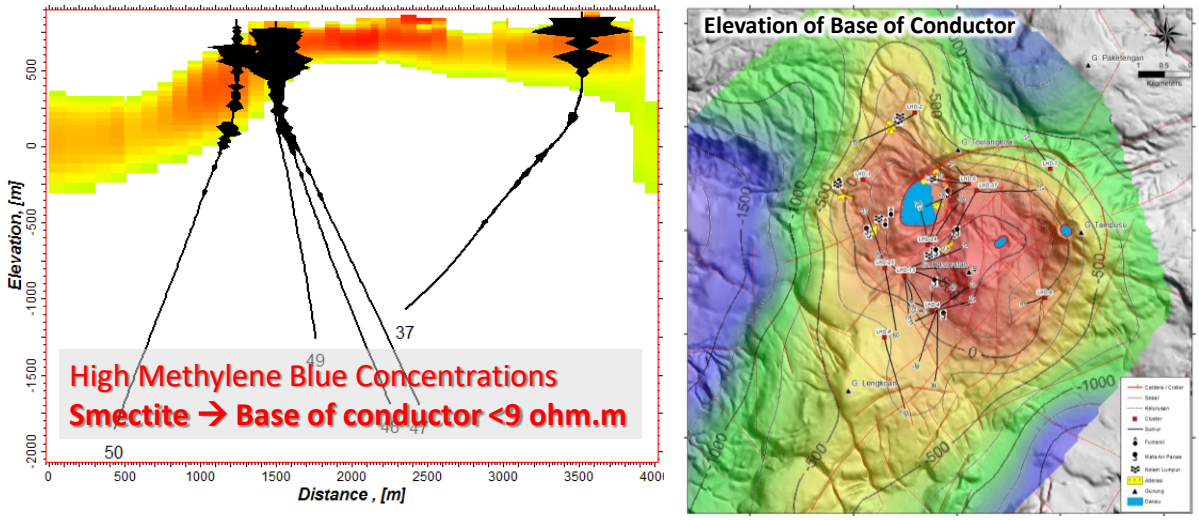

Figure 9: Base of conductor characteristic at Lahendong geothermal Field.

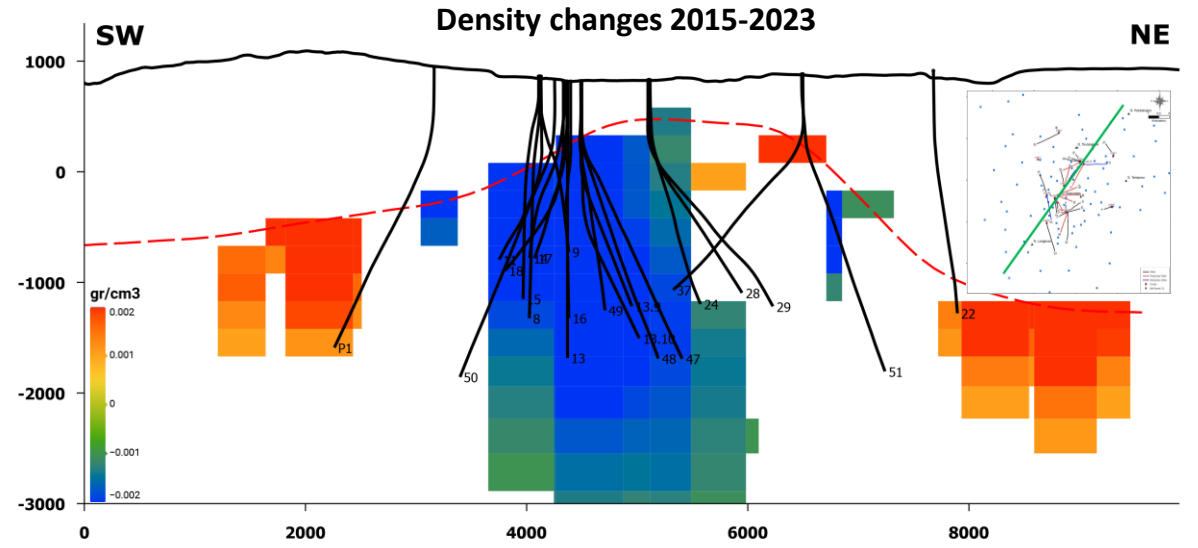

Figure 10: Density changes based on 3D inversion time-lapse microgravity monitoring from 2015-2023.

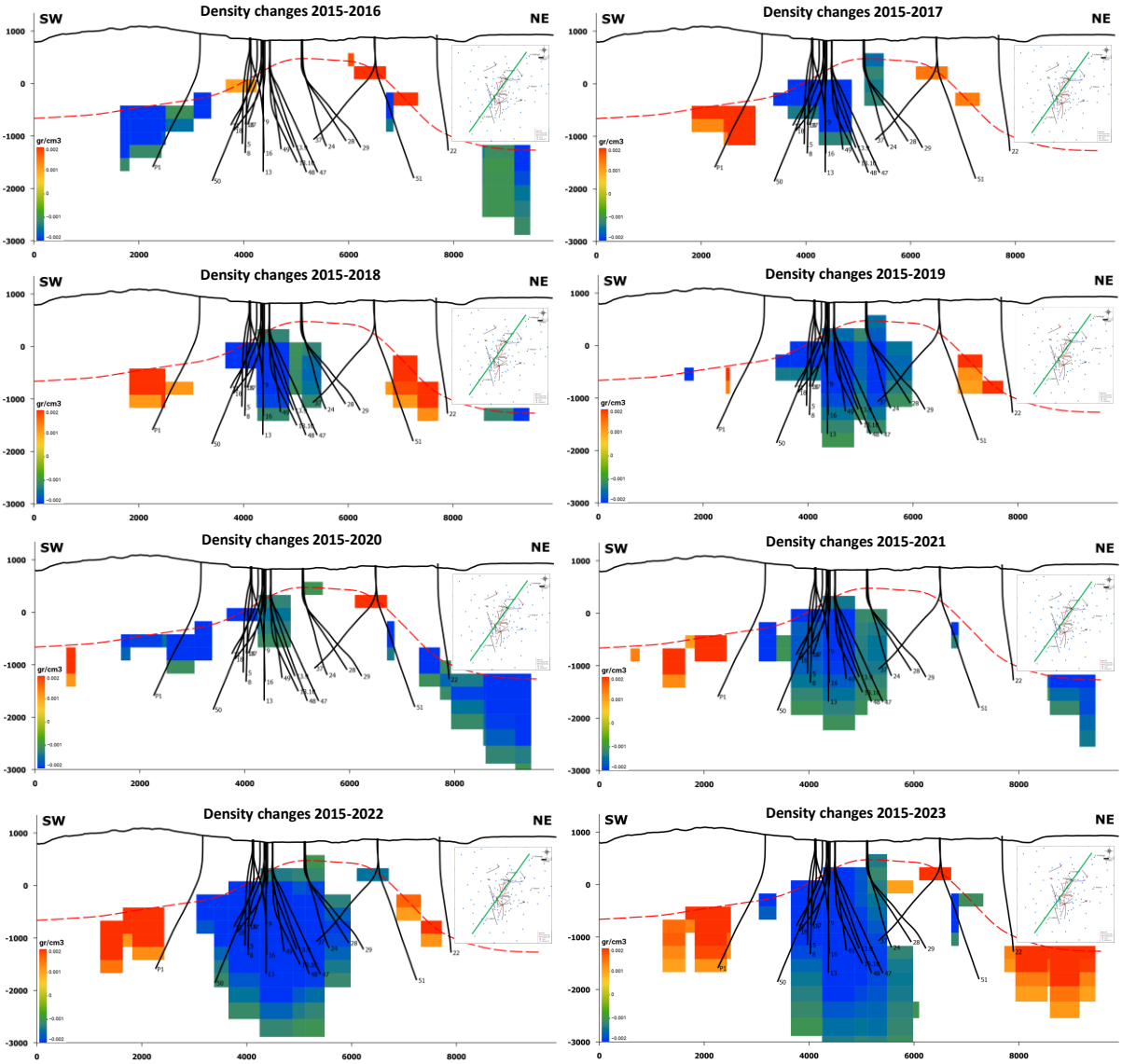

Figure 11: Cumulative annual density changes based on 3D inversion time-lapse microgravity monitoring at Lahendong from 2015-2023.

4. CONCLUSION

An overview of the movement of geothermal fluids in the reservoir can be obtained from the results of time-lapse microgravity monitoring in Lahendong. The position of mass changes in the reservoir, particularly in relation to depth, can be determined through 3D inversion calculations from time-lapse microgravity monitoring. The density decrease in the Lahendong reservoir, which is typically in close proximity to production wells in Lahendong, was observed at elevations ranging from 500 masl to -3000 masl, which is interpreted of mass loss.

The results of 3D inversion time-lapse microgravity monitoring can also be used to identify the dynamics of the injection fluid movement from the LHD-7 and LHD-51 wells. Initially, the injection fluid was detected at an elevation of approximately -2000 masl. Later, the fluid relocated to the production zone at a shallower elevation. The results of 3D inversion time-lapse microgravity monitoring also revealed the movement of natural recharge fluid in the southern part of the Lahendong reservoir. In contrast to injection fluid, the movement of natural recharge fluid in the southern region is characterized by lateral movement at an elevation of approximately -1000 masl. In order to evaluate the impact of the influx of these fluids on the productivity of the reservoir's wells, it is necessary to conduct additional monitoring of the effects of the movement of injection and production fluids.

ACKNOWLEDGMENTS

We express our gratitude on this special occasion to acknowledge the invaluable support provided by the management and geophysics team of the PT. Pertamina Geothermal Energy Tbk during the data collection process, software, and equipment for this study. Further- more, we would like to express our sincere appreciation for the constructive comments provided by the peer reviewer(s) who carefully reviewed and offered insightful feedback on this manuscript.

REFERENCES

Agung, L. (2022). *Identifikasi Pergerakan Fluida Reservoir Menggunakan Metode Time-Lapse Microgravity Monitoring di Lapangan Geothermal Kamojang (Thesis)*. University of Indonesia.

Agung, L., Rosid, M. S., Sastranegara, T., & Haq, F. D. (2023). Period Estimation of Time-Lapse Microgravity Monitoring Using Gauss Theorem – Case Study: Kamojang Geothermal Field. *International Journal of GEOMATE*, 25(112), 1–10. https://doi.org/10.21660/2023.112.4008

Agung, L., Sastranegara, R. M. T., Hendriansyah, T., Nugroho, S. I., Firmansyah, W., Dandari, A., & Raharjo, I. B. (2018). Kamojang Reservoir Mass Changes Revealed from the Application of Gauss Theorem to Microgravity Data during Periods 2016-2014. *Southeast Asian Conference on Geophysics* (SEAGC), 1–12.

Allis, R. G., Gettings, P., & Chapman, D. S. (2000). Precise gravimetry and geothermal reservoir management. *Geothermal Reservoir Engineering*, 25(February 2002), 1–10.

Allis, R. G., & Hunt, T. M. (1986). Analysis of exploitation-induced gravity changes at Wairakei Geothermal Field (New Zealand). *Geophysics*, 51(8), 1647–1660. https://doi.org/10.1190/1.1442214

Apuada, N. A., & Olivar, R. E. R. (2005). Repeat Microgravity and Leveling Surveys at Leyte Geothermal Production Field , North Central Leyte , Philippines. *World Geothermal Congress*, 1–9.

Atmojo, J. P., Widarto, D. S., Kamah, Y., & Bramantyo, E. A. (2015). Heat Source Movements in Lahendong Geothermal Field and Its Affect to The Reservoir Characteristics. *World Geothermal Congress*, April, 1–8.

Azka, G., Suryanto, S., & Yani, A. (2015). Geothermometer, Geoindicator and Isotope Monitoring in Lahendong Wells during 2010- 2012. *World Geothermal Congress*, April, 1–7.

Banos, C. F., Pastor, M. S., Austria, D. C., Monasterial, J. L., Morillo, L. A., & Marteja, V. T. (2020). Repeat Microgravity and Precise Leveling Response to Production in EDC Geothermal Fields, Philippines. *World Geothermal Congress*, 1–9.

Barbier, E. (2002). Geothermal energy technology and current status: an overview. *Renewable and Sustainable Energy Reviews*, 6(1–2), 3–65. https://doi.org/10.1016/S1364-0321(02)00002-3

Bogie, L., Lawless, J. V., Rychargov, S., & Belousov, V. (2005). Magmatic-related Hydrothermal Systems: Classification of the Types of Geothermal Systems and Their Ore Mineralization. *World Geothermal Congress*.

Brehme, M., Blöcher, G., Cacace, M., Deon, F., Moeck, I., Wiegand, B., Kamah, Y., Regenspurg, S., Zimmermann, G., Sauter, M., & Huenges, E. (2016). *Characterizing permeability structures in geothermal reservoirs – A case study in Lahendong. Geothermal Reservoir Engineering*, 2(March), 22–24.

Ellis, R. G., & MacLeod, I. N. (2013). Constrained voxel inversion using the Cartesian cut cell method. *ASEG Extended Abstracts*, 2013(1), 1–4. https://doi.org/10.1071/aseg2013ab222

Firmansyah, W., Prabowo, T., Hananto, B. A., Pasaribu, F., & Silaban, M. S. (2021). Geochemistry Characteristic Monitoring at LHD-α, a Cyclic Geothermal Well in Lahendong Geothermal Field, Indonesia. *World Geothermal Congress*, October, 1–8.

Geosoft. (2024). Voxi - Geophysical Inversion. https://www.seequent.com/products-solutions/geosoft-oasis-montaj/voxi/

Gunadi Putra, U., Jhanesta, W., & Iskandarsyah. (2021). Interpretation of Subsurface Fault Through Multi-Level Second Vertical Derivative Gravitational Data in Bittuang Geothermal Working Area, South Sulawesi, Indonesia. *Journal of Geoscience, Engineering, Environment, and Technology*, 6(4), 184–191. https://doi.org/10.25299/jgeet.2021.6.4.7744

Hammer, S. (1945). Estimating Ore Masses in Gravity Prospecting. Geophysics, 10(1), 50–62. https://doi.org/10.1190/1.1437147

Haq, F. D., Agung, L., Sastranegara, T., Dandari, A., & Hendriansyah, T. (2023). *Geophysical Monitoring for Sustainability of Geothermal Development*. SEG Workshop.

Haq, F. D., Sastranegara, T., Agung, L., Kusuma, A. D., Hendriansyah, T., Fanani, A. F., & Raharjo, I. B. (2019). Production and Reinjection Evaluation on The Basis of 3D Time-lapse Microgravity Inversion. *IOP Conference Series: Earth and Environmental Science*, 318(1), 1–9. https://doi.org/10.1088/1755-1315/318/1/012023

Hochstein, M. P., & Browne, P. R. L. (2000). Surface Manifestations of Geothermal Systems with Volcanic Heat Sources. *Encyclopedia of Volcanoes*, 1, 818–855.

Hunt, T. M. (2005). Using Repeat Microgravity Measurements to Track Reinjection in Liquid-Dominated Fields. *World Geothermal Congress*, 1–6.

Ingram, D. M., Causon, D. M., & Mingham, C. G. (2003). Developments in Cartesian cut cell methods. *Mathematics and Computers in Simulation*, 61(3–6), 561–572. https://doi.org/10.1016/S0378-4754(02)00107-6

Koestono, H., Siahaan, E. E., Silaban, M., & Franzson, H. (2010). Geothermal Model of the Lahendong Geothermal Field, Indonesia. *World Geothermal Congress*, April, 25–29.

LaFehr, T. R. (1965). The estimation of the total amount of anomalous mass by Gauss's theorem. *Journal of Geophysical Research*, 70(8), 1911–1919. https://doi.org/10.1029/jz070i008p01911

Lawson, C. L. (1961). *ph.D Dissertations*. University of California.

Menzies, A. J. (2011). Correlating reservoir pressure changes with production and injection in the Tiwi Geothermal Field, Republic of the Philippines. Transactions - *Geothermal Resources Council*, 35, 1499–1504.

Nainggolan, S. S., Sastranegara, R. M. T., & Raharjo, I. B. (2015). Volcanic Neck of Mount Iyang Argopuro Revealed From Gravity Study. *World Geothermal Congress*, 1–4.

Natasia, N., Syafri, I., Alfadli, M. K., & Arfiansyah, K. (2016). Stratigraphy Seismic and sedimentation Development of Middle Baong Sand, Aru Field, North Sumatera Basin. *Journal of Geoscience, Engineering, Environment, and Technology*, 1(1), 51–58. https://doi.org/10.24273/jgeet.2016.11.7

Natul, A. S., & Heliani, L. S. (2022). A Comparison of Geologic Structure Detection of Sumatera Island Using Goce Satellite Gravity Data and Sgg-Ugm-2 Data. *Journal of Geoscience, Engineering, Environment, and Technology*, 7(3), 95–101. https://doi.org/10.25299/jgeet.2022.7.3.8863

Nishijima, J., Fujimitsu, Y., Ehara, S., Kouno, E., & Yamauchi, M. (2005). Micro-Gravity Monitoring and Repeated GPS Survey at Hatchobaru Geothermal Field , Central Kyushu , Japan. *World Geothermal Congress*, 1–5.

Nishijima, J., Oka, D., Higuchi, S., Fujimitsu, Y., & Takayama, J. (2015). Repeat Microgravity Measurements Using Absolute and Relative Gravimeters for Geothermal Reservoir Monitoring in Ogiri Geothermal Power Plant , South Kyushu , Japan. *World Geothermal Congress*, 1–5.

Nordquist, G., Protacio, J. A. P., & Acuna, J. A. (2004). Precision gravity monitoring of the Bulalo geothermal field, Philippines: Independent checks and constraints on numerical simulation. *Geothermics*, 33(1–2), 37–56. https://doi.org/10.1016/j.geothermics.2003.03.001

O'sullivan, J., Abdurachman, F., Bignall, G., Bromley, C., Dekkers, K., Ghassan, M., Gravatt, M., Hastuti, P., Indra, A., Nugraha, R., Pasaribu, F., Popineau, J., Prasetyo, I., Rai, V., Renaud, T., Riffault, J., Yuniar, D., & O'sullivan, M. (2023). Multidisciplinary collaboration to create a new numerical model of the Lahendong geothermal field. *Geothermal Reservoir Engineering*, 1–15.

Omollo, P. (2018). Precise Micro-Gravity Monitoring of Olkaria Domes Geothermal Field. *African Rift Geothermal Conference*, November, 1–13.

Omollo, P., & Nishijima, J. (2024). Inception of time-lapse micro-gravity monitoring of the great Olkaria geothermal field, Kenya. *Geothermics*, 117(September 2023), 102891. https://doi.org/10.1016/j.geothermics.2023.102891

Permana, T., Mulyanto, & Hartanto, D. B. (2015). Geochemical Changes during 12 Year Exploitation of the Southern Reservoir Zone of Lahendong Geothermal Field, Indonesia. *World Geothermal Congress*, April, 1–6.

Pertiwi, T. B., Daud, Y., & Fahmi, F. (2023). Investigation of Geological Structure Using Magnetotelluric and Gravity Data Optimization on Non Volcanic Geothermal , Bora , Centre of Sulawesi. *Journal of Geoscience, Engineering, Environment, and Technology*, 08(02), 13–17. https://doi.org/10.25299/jgeet.2023.8.02-2.13876

Portier, N., Forster, F., Hinderer, J., Erbas, K., Jousset, P., Drouin, V., Li, S., Sigmundsson, F., Magnússon, I., Hersir, G. P., Ágústsson, K., Guðmundsson, Á., Júlíusson, E., Hjartasson, H., & Bernard, J.-D. (2022). Hybrid Microgravity Monitoring of the Theistareykir Geothermal Reservoir (North Iceland). *Pure and Applied Geophysics*, 179(5), 1935–1964. https://doi.org/10.1007/s00024-022-03018-8

Portier, N., Hinderer, J., Drouin, V., Sigmundsson, F., Schäfer, F., Jousset, P., Erbas, K., Güntner, A., Magnússon, I., Hersir, G. P., Ágústsson, K., & Van, E. D. Z. (2021). Time-lapse Micro-gravity Monitoring of the Theistareykir and Krafla Geothermal Reservoirs (Iceland). *World Geothermal Congress*, 1–11.

Prabowo, T., Yuniar, D. M., Suryanto, S., & Silaban, M. (2015). Tracer Test Implementation and Analysis in Order to Evaluate Reinjection Effects in Lahendong Field. *World Geothermal Congress*, April, 1–6.

Prasetyo, F., O'sullivan, J., & O'sullivan, M. (2016). Inverse Modelling of Lahendong Geothermal Field. New Zealand Geothermal Workshop, November, 1–8.

PT. BURSA EFEK INDONESIA. (2023). *PROSPEKTUS PT PERTAMINA GEOTHERMAL ENERGY TBK* .

PT. Pertamina Geothermal Energy. (2024). *Laporan Monitoring Microgravitasi Lahendong 2024*.

Rosid, M. S., Ali, Y. H., & Ramdhan, M. (2022). Characterization of the Mamasa Earthquake Source Based on Hypocenter Relocation and Gravity Derivative Data Analysis. *International Journal of GEOMATE*, 23(97), 220–227. https://doi.org/10.21660/2022.97.j2375

Rosid, M. S., Nursarifa, S., & Riyanto, A. (2023). Identification of Geological Structures in Sigi Regency, Central Sulawesi Based on Derivative Analysis of Gravity Data. *International Journal of GEOMATE*, 24(103), 26–33. https://doi.org/10.21660/2023.103.3426

Rosid, M. S., Prastama, R. A., Yusuf, M., Daud, Y., & Riyanto, A. (2021). Monitoring of Jakarta Subsidence Applying 4D Microgravity Survey Between 2014 and 2018. *International Journal of GEOMATE*, 20(79), 132–138. https://doi.org/10.21660/2021.79.j2031

Rybach, L. (2003). Geothermal energy: Sustainability and the environment. *Geothermics*, 32(4), 463–470. https://doi.org/10.1016/S0375-6505(03)00057-9

Sambodho, R. P., Nashir, M., Wibisono, B. D., & Toni, A. (2021). Direct Use from Geothermal Brine to Subtitute Conventional Raw Material in Heating Process for Drying Palm Sugar in Lahendong Geothermal Field , Indonesia. *World Geothermal Congress*, October, 2–6.

Sastranegara, T., Nainggolan, S. S., & Raharjo, I. B. (2015). The Application of a Triangular Mesh for Gravity Inversion to Reconstruct Subsurface Geological Structures in the Hululais Geothermal Prospect, Bengkulu. *World Geothermal Congress*, 1–6.

Sumantoro, Z. Z., Yeh, A., O'sullivan, J. P., & O'sullivan, M. J. (2015). Reservoir Modelling of Lahendong Geothermal Field, Sulawesi-Indonesia. *New Zealand Geothermal Workshop*, November, 1–8. https://www.geothermal-energy.org/pdf/IGAstandard/NZGW/2015/121_OSullivan.pdf

Taylor, J. R., & Thompson, W. (1982). *An introduction to error analysis: the study of uncertainties in physical measurements* (Vol 2). University science books.

Wardhani, A. D. K. (2023). *Time-lapse Gravity Monitoring of the Tompaso Geothermal Field in Indonesia from 2006 to 2023* (Issue XV).

Yani, A. (2022). *UPDATE MODEL KONSEPTUAL DAN KAJIAN PEMANFAATAN SUMUR CYCLIC LHD-A UNTUK MENINGKATKAN NILAI KEEKONOMIAN PROYEK PANASBUMI LAPANGAN LAHENDONG - Thesis*. University of Indonesia.

Zahid, A. S., Nashir, M., Gani, V. A., Susilo, B. R., & Kusumah, M. W. (2021). Pipeline Debottlenecking Project to Maintain Steam Supply of Geothermal Power Plant Unit 1-4 at PGE Lahendong before remedial after remedial LHD-47 LHD-48 LHD-47 LHD-48 LHD-49 Pressure Dryness. *World Geothermal Congress*, October, 2–7.

Finding the Correlation Between Electrical Resistivity and Thermal Gradients in Geothermal Fields: A Case Study of Sumani, Way Selabung, and Kadidia

Azralina Maysa Rahayu, Satriya Putra Baskara, Musa Zakariya, Sintia Windhi Niasari, Asep Sugianto, and Tony Rahadinata

azralinamaysa@gmail.com, satriyaputrab@gmail.com, musazakariya0@gmail.com, sintia_windhi@ugm.ac.id, asep.soegie@gmail.com, tony.rahadinata@gmail.com

Keywords: Electrical Resistivity, Gradient Thermal, Sumani, Way Selabung, Kadidia

ABSTRACT

Geothermal field exploration is still not fast due to the high risk of drilling failure (in some fields, it can reach more than 60%). Therefore, additional data, besides magnetotelluric model results, is needed to reduce well drilling failures. One way to decrease drilling failure is by finding the relationship between the electrical resistivity modeling results from Magnetotelluric (MT) data and thermal gradient data from shallow well temperature slope data. This research was conducted in Sumani, Way Selabung, and Kadidia. The preliminary analysis results of the MT cross-section model with well data in the Sumani, Way Selabung, and Kadidia fields show variations in the relationship between electrical resistivity and thermal gradient. In general, the correlation analysis results between electrical resistivity and temperature gradient show an inverse relationship, where an increase in resistivity tends to indicate a decrease in the temperature gradient.

In the Sumani field, the gradient is -1.29 with a coefficient of determination of 0.38. In the Way Selabung field, the gradient is -0.07 with a coefficient of determination of 0.81, and in the Kadidia field, the gradient is -0.0039 with a coefficient of determination of 0.0005. The strongest relationship between the two variables is found in the Way Selabung geothermal field. The variation in temperature gradient values is not only influenced by electrical resistivity values. Several other factors, such as geological conditions, lithology, the amount and type of clay minerals, and water content in the formation, should be considered in this empirical relationship result.

1. INTRODUCTION

1.1 Background

Geothermal energy is a potential renewable energy source alternative to conventional energy sources. Indonesia is one of the countries with the largest geothermal energy potential in the world. Sumani, Way Selabung, and Kadidia geothermal fields are three areas that show significant potential in the exploration and utilization of geothermal energy in Indonesia. The magnetotelluric method is commonly used in geothermal exploration to examine subsurface characteristics. The 2D model of this method can show the electrical resistivity value per depth. A correlation analysis between electrical resistivity and thermal gradient was conducted to support the development of geothermal energy in Indonesia.

1.2 Geology

1.2.1 Sumani

The Sumani geothermal area had lithologies in the form of metamorphic rock units, sedimentary rocks, intrusive rocks, volcanic rocks, and surface deposits. Old (Tertiary) rock units occupied the rocks in the eastern part of the area. The western part of the area generally consisted of younger rock units, except for Meta Limestone, which was exposed in the northwest.

The fault structure in this area generally followed the northwest-southeast direction of the Sumatra fault and the southwest-northeast direction of the fault as a secondary structure. These fault structures controlled the emergence of hot springs at the surface, indicating the presence of geothermal potential at the study site.

The geothermal system in the Sumani area was formed by the residual heat of the magma chamber due to the last volcanic activity of the Tinjau Laut complex during the Pliocene. The residual heat acted as a heat source that heated the subsurface water, which then rose through cracks/fractures and was trapped in a geothermal reservoir. This reservoir was thought to be found in the Meta Limestone rock unit, which was rich in fractures and permeable.

1.2.2 Way Selabung

Based on the tectonic setting, the Way Selabung geothermal field was located in a magmatic arc and right on one of the southern Sumatra fault segments. The constituent rocks in the survey area were dominated by volcanic rocks and clastic sedimentary rocks from the Tertiary to Quaternary ages. The rock units in order from young to old were as follows: Akarjangkang Lava, Sandstone, Asadimana Lava, Pematang Gong Lava, Old Breccia, Ranau Pyroclastic Flow, Sapatuhu Pyroclastic Flow, Ranau Pyroclastic Fall, aai Lava, Bengkong Lava, Pandan Lava, Gedang Lava, Perean Lava, Tebat Gayat Lava, and Aluvium deposits.

The dominant geological structure in the survey area had a northwest-southeast direction pattern that was cut by faults with southwest-northeast and north-south directions. The faults in the survey area were grouped into three main direction patterns: northwest-southeast, north-south, and southwest-northeast. The northwest-southeast fault pattern was cut by other faults with north-south and southwest-northeast patterns that were thought to be younger. The north-south fault pattern followed the Sunda pattern, which formed in the Eocene and was thought to be an old fault. The southwest-northeast fault pattern was in the opposite direction from the Sumatra fault. This fault was thought to be its antithesis.

1.2.3 Kadidia

The Kadidia geothermal area was composed of volcanic products such as lava rocks and andesite breccia. The process of magmatism had produced plutonic granite. This plutonic granite rock was estimated to be from the Plio-Pleistocene era. It intruded on older rock units and was associated with the heat still present in the underlying rock units. At least eight lithologies of plutonic rocks have formed since the formation of the metagranite.

Regionally, the Kadidia geothermal area was controlled by the Palu Koro fault to the west. This fault trended northwest-southeast. Additionally, there was the Koala Rawa basement fault, which trended almost north-south. This fault was suspected to form a permeable zone. In the Kadidia geothermal area, there was a pull-apart mechanism that created a pull-apart basin. This basin was filled with sedimentary materials such as colluvium, lake deposits, alluvium deposits, and alluvial fans.

2. METHODS

2.1 2D Magnetotelluric Inverse Modeling

The data used in this study are *.EDI files were obtained from magnetotelluric measurements in the Sumani, Way Selabung, and Kadidia geothermal fields. An inverse modeling process was then conducted to obtain a model of the resistivity distribution as a function of depth and horizontal distance (2D model). This process was done using WinGlink interpretation software. The 2D electrical resistivity modeling results were analyzed to determine its correlation with the temperature gradient.

2.2 Calculated the thermal gradient

The thermal gradient was calculated at each depth layer with the same electrical resistivity value to determine the correlation between electrical resistivity and thermal gradient. The calculation results were presented as a curve where the electrical resistivity alue was on the x-axis, and the thermal gradient was on the y-axis. The linear regression method obtained a straight-line equation describing the relationship between the two variables. The relation between electrical resistivity and temperature gradient is then correlated with lithological conditions and characteristics based on shallow well data.

3. RESULT AND DISCUSSION

3.1 Result

3.1.1 Sumani

A conductive rock layer is modeled in the 2D resistivity section (Figure 1), thickening towards the northeast. This layer exhibits resistivity values ranging from 2 to 15 Ωm. In the area around the hot spring manifestation, the conductive layer is modeled from the surface to an elevation of -500 meters above sea level.

The SMN1 temperature gradient well is located between points MTSM56 and MTSM50, with an elevation reaching -156 meters above sea level. Six temperature gradient values were obtained by correlating with the same resistivity values (Figure 2). A high-temperature gradient increase, reaching 20.5 ℃/100 m, is observed from the surface to 400 meters above sea level. Subsequently, the temperature gradient significantly decreases to 10.1 ℃/100 m until an elevation of 180 meters above sea level. The temperature gradient then rises again to 10.8 ℃/100 m, reaching an elevation of -156 meters above sea level.

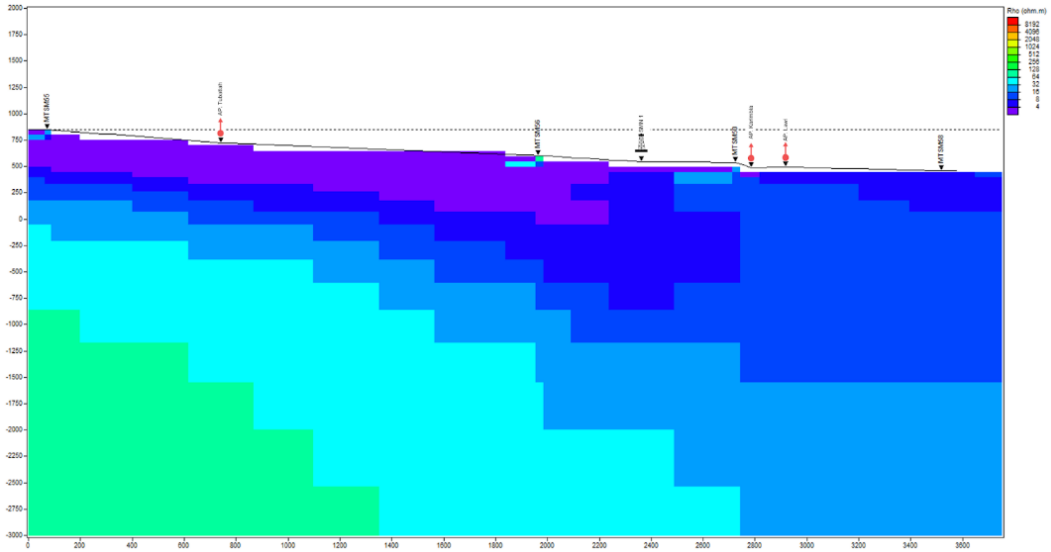

Figure 1: The resistivity model of Sumani geothermal field. The model included magnetotelluric survey points MTSM55, MTSM56, MTSM50, and MTSM58. The SMN1 is location of the temperature gradient well, which is at an elevation of 544 m above sea level and had a depth of 700 m.

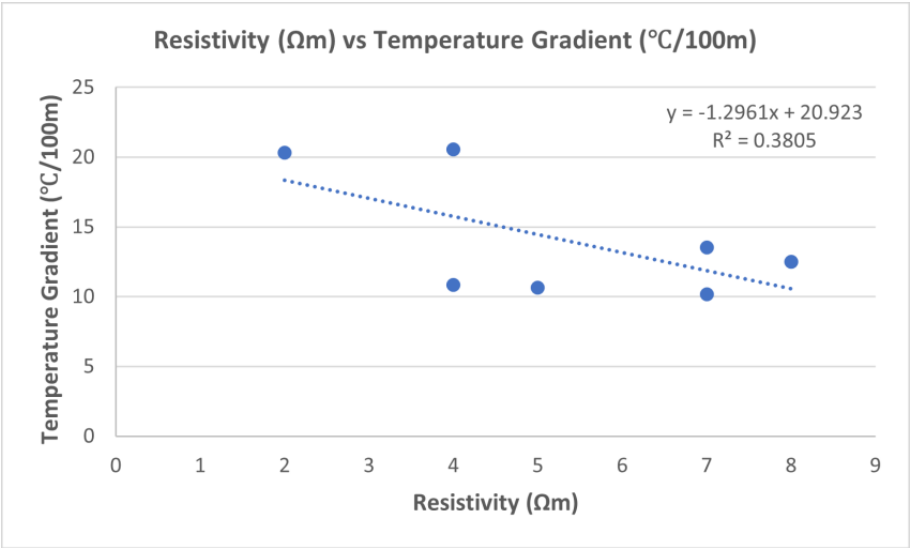

Figure 2: A comparison graph of electrical resistivity values with temperature gradient values per 100 meters showed negative gradient values, indicating that in the Sumani field, as resistivity increases, the temperature gradient decreases.

The 2D resistivity cross-section (Figure 3) shows a layer of rock with low resistivity in the southwest and northeast at a depth of about 550 – 1250 m. This low resistivity is caused by alteration rocks that become the cap rock of the Way Selabung geothermal system. Below the low resistivity zone is a medium resistivity, interpreted as a reservoir zone. To the northeast, the medium resistivity is associated with sedimentary rocks. The high resistivity at the bottom is considered resistive compact sedimentary rock. In contrast, in the southwest, the high resistivity below the medium resistivity layer is considered igneous rock, which is the heat source of the geothermal system.

Temperature slope well WSL1 is located between points MTWS43 and MTWS43A at a depth of 700m to an elevation of -150m above sea level. By correlating the resistivity values, nine temperature gradient values were obtained (Figure 4). The increase in temperature gradient is high, reaching 5.74°C/100 m from elevation 167.9 to 63.5 meter above sea level, while at the surface up to elevation 388.46 meter above sea level, the temperature gradient tends to be low at 1.96-2.05 °C/100 m.

3.1.2 Way Selabung

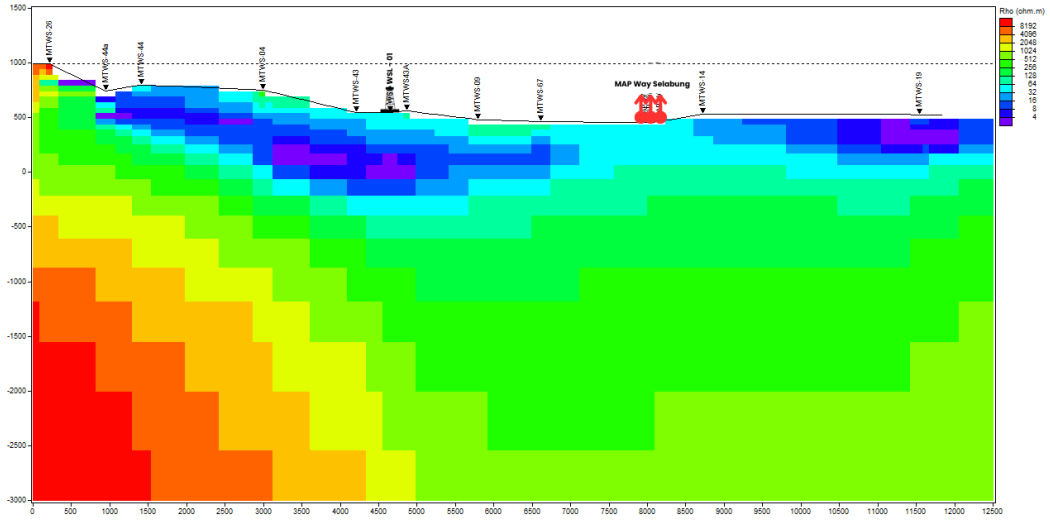

Figure 3: The resistivity model of Way Selabung geothermal field (Line 5). The model included magnetotelluric survey points MTWS-04, MTWS-09, MTWS 14, MTWS-19, MTWS-26, MTWS-43, MTWS-43a, MTWS-44, MTWS-44a, and MTWS-67. The WSL-01 is location of the temperature gradient well, which is at an elevation of 550 m above sea level and had a depth of 700 m.

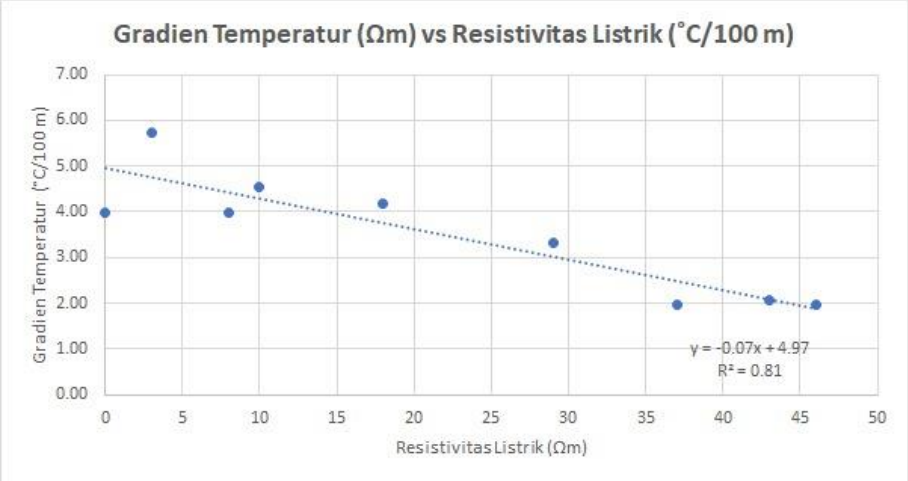

Figure 4: A comparison graph of electrical resistivity values with temperature gradient values per 100 meters showed negative gradient values, indicating that in the Way Selabung field, as resistivity increases, the temperature gradient decreases.

3.1.3 Kadidia

There was a conductive layer in the electrical resistivity model of Kadidia Line 8, which extends from south to north. This layer was located at around 300 meters above sea level. There was a manifestation of a hot spring at point MTKD34. Near this point, there was a temperature gradient well.

The KDD-1 well (Figure 5) had a depth of 700 meters and was situated at an elevation of 632 m. According to the well data, the temperature at the lowest depth was 27 ˚C. At a depth of 700 meters, the temperature was 96.8 ˚C. The temperature gradient value obtained for this well was 12.8 ˚C/100 m.

3.2 Discussion

At the Sumani field, the temperature gradient graph as a function of resistivity is obtained with the linear equation y = -1.3x + 20.92 R2 = 0.38. A moderate negative relationship is observed between electrical resistivity and the temperature gradient. An increase in electrical resistivity tends to be followed by a decrease in the temperature gradient. The coefficient of determination value indicates that approximately 38.05% of the variability in the temperature gradient can be explained by changes in electrical resistivity. Most of the variation in the temperature

gradient is caused by factors other than electrical resistivity, such as variations in lithology types, clay mineral content and type, alteration intensity, water content, and geological structure.

At 495.9 to 398.0 meters above sea level elevations, low resistivity values (2 – 4 Ωm) correspond with high-temperature gradients (20.3 – 20.5 ℃/100m). This correlates with lithologies consisting of Tuff Breccia, Andesite, and Andesite Breccia with weak to moderate alteration intensity. The dominant secondary minerals are clay minerals, including smectite and montmorillonite.

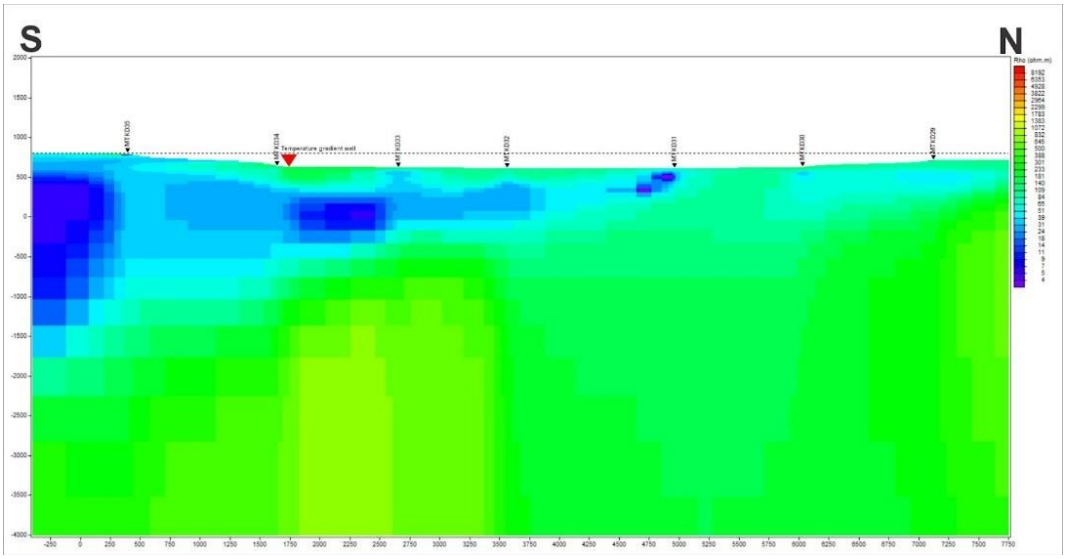

Figure 5: The resistivity model of Kadidia Line 8. The model included magnetotelluric survey points MTKD 35, 34, 33, 32, 30, 29. The red triangle indicated the location of the temperature gradient well, which is at an elevation of 632 m above sea level and had a depth of 700 m.

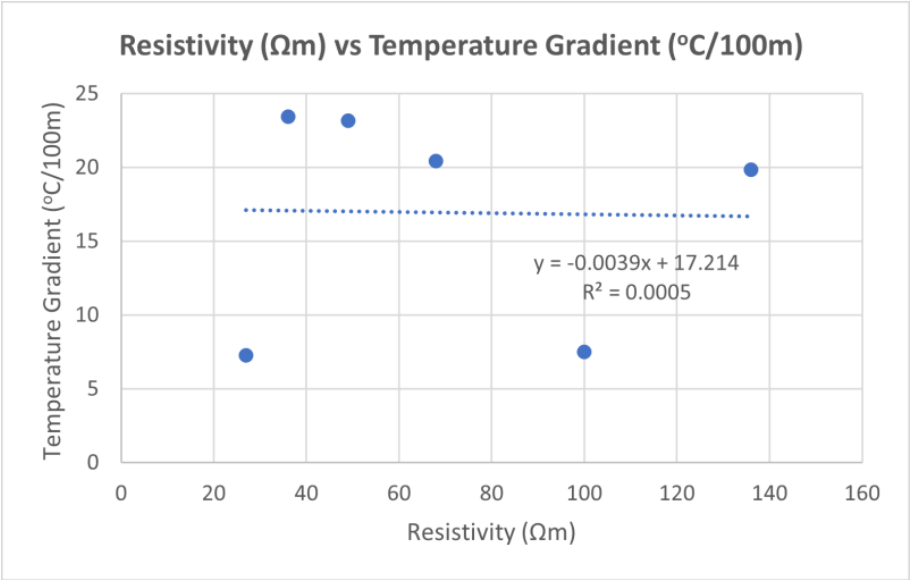

Figure 6: A comparison graph of electrical resistivity values with temperature gradient values per 100 meters showed negative gradient values, indicating that in the Kadidia field, as resistivity increases, the temperature gradient decreases.

At 398.0 to 178.3 meters above sea level, the thermal gradient experiences a significant decrease. This correlates with Ca (Calcite) and Ch (Chlorite) minerals, which are quite dominant. Calcite and Chlorite minerals have a higher specific heat capacity than smectite, significantly decreasing the thermal gradient. At 266.9 meters above sea level elevations to -156 meters above sea level, the resistivity values decrease, which is suspected to be due to contact with water formation in the area.

At the Way Selabung field, a linear equation y = -0.07x + 4.97 R2 = 0.81 is obtained from the temperature gradient graph as a resistivity function. There is an opposite relationship between electrical resistivity and temperature gradient, where an increase in electrical resistivity tends to be followed by a decrease in temperature gradient. The

coefficient of determination shows that about 80% of the variability in temperature gradient can be explained by changes in electrical resistivity. This indicates a strong relationship between the two variables.

At 539.3 to 168 meters above sea level, the resistivity values decreased from 46 Ωm to 10 Ωm. In contrast, the temperature gradient increased from 2˚C/100m to 5.7 ˚C/100m. This corresponds to the increasing intensity of alteration and decreasing Iron Oxide content in the soil, Breccia Tuff, and Tuff lithologies. The temperature gradient decreased to the maximum depth of the well at elevation -137 meters above sea level with a value of 4˚C/100m. The decrease in resistivity value to the bottom of the well reflects the sedimentary rock layer that begins to appear at a depth of 663.9 m.

At the Kadidia geothermal field, the temperature gradient graph (Figure 6) showed the linear equation $y = -0.0039x + 17.214$ with $R^2 = 0.0005$. A negative correlation was shown between the temperature gradient and electrical resistivity values. The higher the resistivity value, the smaller the thermal gradient value.

At a depth of 35 m, the thermal gradient value was 19.8℃/100m with a resistivity value of 135 Ω m. At that depth, the lithology was soil. The alteration level present was classified as weak. Next, at depths down to 181 m, there was a decrease in the thermal gradient value to 7.5 ℃/100m. This correlated with sandstone lithology, which has very low alteration levels. There was also a circulation loss, causing an imbalance between the hydrostatic mud and formation pressure.

At 181 m to 319 m depths, the thermal gradient gradually increased from 20℃/100m to 23℃/100m. The resistivity values decreased from 68 Ωm to 36 Ωm. This correlated with conglomerate lithology interspersed with sandstone and quartz sandstone. The alteration level also increased at these depths. Subsequently, from depths of 319 meters to 700 meters, the thermal gradient value decreased to 7.2℃/100m. The lithology at those depths consisted of alternating breccia, sandstone, claystone, and breccia at the bottom. There was loss circulation below a depth of 550 m, with an increase in the alteration level reaching strong at the bottom of the well.

4. CONCLUSION

The graph comparing temperature gradient values at the Sumani, Way Selabung, and Kadidia geothermal fields showed a negative relationship. When resistivity values decreased, the temperature gradient values increased. Kadidia had the highest gradient value in the comparison graph, while Sumani had the lowest. The differences in gradient values on the resistivity and temperature gradient comparison graph might have been influenced by the type of heat source at each geothermal field. The Sumani field had a notably lower gradient than Kadidia. Way Selabung exhibited intermediate gradient values. Each field's unique geological characteristics likely played a role in these variations.

ACKNOWLEDGEMENT

The author wishes to sincerely thank IIGCE 2024 for the opportunity to write this paper. Special thanks are due to Ms. Sintia for her invaluable guidance and encouragement throughout this process. Her expertise and insights have significantly enhanced the quality of this work. Thanks to Mr. Asep Sugianto and Mr. Tony Rahadinata from PSDMBP for their assistance and support. Their contributions have been vital in the completion of this research. The author values their willingness to offer valuable information and resources.

REFERENCES

Hlaváčová, L., & Juraj, J. K. (2014). *3D Modelling of Geothermal Reservoirs : Case Study from Subtatric Basin in Western Carpathians, Slovaka*. LAP Lambert Academic Publishing.

Kusnadi, D., Risdianto, D., Munandar, A., & Dahlan. (2011). Geologi dan Geokimia Daerah Panas Bumi Wai Selabung Kabupaten OKU Selatan, Sumatera Selatan. *Prosiding Hasil Kegiatan Pusat Sumber Daya Geologi Tahun 2011*. Bandung: Pusat Sumberdaya Geologi.

Rahadinata, T., & Sugianto, A. (n.d.). *Survei Magnetotelurik dan TDEM Daerah Panas Bumi Way Selabung Kabupaten OKU Selatan, Provinsi Sumatera Selatan*. Bandung: Pusat Sumber Daya Geologi.

Rezky, Y., & Simarmata, R. S. (n.d.). *Survei Landaian Suhu Daerah Panas Bumi Sumani*. Bandung: Pusat Sumber Daya Geologi.

Simarmata, R. S., & Munandar, A. (n.d.). *Survei Landaian Suhu Sumur WSL-1*. Bandung: Pusat Sumber Daya Geologi.

Sutarmin, & Daud, Y. (2021). Subsurface Temperature Prediction in Geothermal Field with Neural Network Using 3D MT Data Inversion and Borehole Temperature Data. *AIP Conference Proceedings*. Jakarta: AIP Publishing.

Waples, D. W., & Waples, J. S. (2004). A Review and Evaluation of Specific Heat Capacities of Rocks, Minerals, and Subsurface Fluids. Part 1: Minerals and Nonporous Rocks. *Natural Resources Research*, 97-122.

Wibowo, A. E., Nurhadi, M., Rezky, Y., Hermawan, D., & Setiawan, D. I. (2015, August). Penentuan Kesamaan Reservoir Sistem Panas Bumi Kadidia dan Kadidia Selatan Kabupaten Sigi, Provinsi Sulawesi Tengah Berdasarkan Metoda Geokimia. *Buletin Sumber Daya Geologi*, 10, 54-70. doi:10.47599/bsdg.v10i2.142

Zarkasyi, A., & Nurdin, N. M. (2018). *Survei Magnetotelurik dan TDEM Daerah Panas Bumi Kadidia - Kadidia Selatan, Kabupaten Sigi, Provinsi Sulawesi Tengah*. Bandung: Pusat Sumber Daya Geologi, Badan Geologi, KESDM.

Zarkasyi, A., Muhamad, N., & Rezky, Y. (2015). Survei Magnetotellurik (MT) Daerah Panas Bumi Sumani, Provinsi Sumatera Barat. *Prosiding Hasil Kegiatan Pusat Sumber Daya Geologi Tahun 2016* (pp. 1-10). Bandung: Pusat Sumber Daya Geologi, Badan Geologi, KESDM.

Zarkasyi, A., Rahadinata, T., Suhanto, E., & Widodo, S. (2015). *Investigation of Geothermal Structures of the Kadidia Area, Indonesia, using the Magnetotelluric Method*.

Continuous Development of In-house Laboratory Capabilities of Wayang Windu Geothermal Field

Dwiyogarani Malik, Indra Yudhistira, Nevio M. Kamel,
Dodoh Abdullah, and Galang A. Purnama

Star Energy Geothermal (Wayang Windu), Margamukti,
Kec. Pangalengan, Kabupaten Bandung, Jawa Barat 40378, Indonesia

dwiyogarani.malik@starenergy.co.id

Keywords: Wayang Windu, geothermal laboratory, laboratory accreditation, laboratory analysis, geochemical fluid, laboratory management

ABSTRACT

Wayang Windu Geothermal Field (WWGF) has been operating since 2000. Its successful operation has been significantly supported by the in-house laboratory, which has been functioning since the construction of the first unit. The laboratory provides water and gas analyses as part of Wayang Windu reservoir surveillance and monitoring program in managing reservoir performance and Power Plant Operation. Beyond internal assets, the laboratory also analyzes samples from other companies and commercial laboratories as part of its quality control management, known as the blind test procedure. In 2012, the laboratory was revitalized in alignment with the company's development strategy to achieve an efficient, high-performance facility. Since then, it has expanded its capabilities to analyze major water and gas parameters for reservoir surveillance monitoring, steam purity, environment, domestic needs, and resource assessment for exploration prospects. The laboratory also conducts Hazardous & Non-Hazardous Waste Management during activity. Over the years, this revitalization has maintained high-quality analysis procedures, annual cost savings, and a commitment to becoming a trustworthy laboratory. The laboratory achieved ISO17025 accreditation in 2018 as a testing laboratory under the umbrella of ISO9001. These milestones were not limited to the certification process but also reflected the goal of enhancing human resources alongside facility and equipment capabilities. Most importantly, the continuous development of laboratory management has provided sustainable support for the company's growth.

1. INTRODUCTION

Wayang Windu Geothermal Power Plant is one of Indonesia's biggest operating geothermal fields, currently operated by Star Energy Geothermal (SEG). It started the operation with the first unit in 2000, further expanding its capacity with the 2nd unit in 2006 to generate 227 MW of electricity. The current generation is taken from 28 production wells and 2 injection wells. Among those 28 production wells, 4 of them are two-phase wells. With such power plant operation, the fluid chemistry must be monitored to ensure the safety operating procedure, track the reservoir process, and continuously update the conceptual model. Considering this critical necessity for geothermal operation, Wayang Windu established a non-commercial laboratory, later called as in-house lab, which supports fluid sampling and analysis for internal SEG needs. It is located in the power plant building of Wayang Windu Geothermal Field (WWGF) (Figure 1).

The operation of in-house lab began since the exploration stage in 1997 with limited capabilities, continuously improving over time until able to fully support geochemistry surveillance for more than a decade. Fluid chemistry sampling and analysis that conducted regularly, has become a main scope of in-house lab activities. Monitoring wells for reservoir performance is the primary deliverable which covers more than 50% of the laboratory scope (Figure 2). Power plant is the next client supported by the in-house lab through sampling and analysis conducted in several sampling points in pipeline, scrubbers, and cooling towers. Additional scope for domestic water and environment samples are also covered by the lab.

2. CONTINUOUS IMPROVEMENT OF LABORATORY CAPABILITIES

The geothermal laboratory plays a crucial role in advancing geothermal technology by providing valuable data and insights for continuous improvement and importantly for reservoir management. The facility enables the scientist to analyze and collect samples from the geothermal wells, manifestation, and other locations (surface line, environment, domestic, etc.), monitor changes in fluid chemistry over time, investigate the issues, and develop strategies to improve the performance.

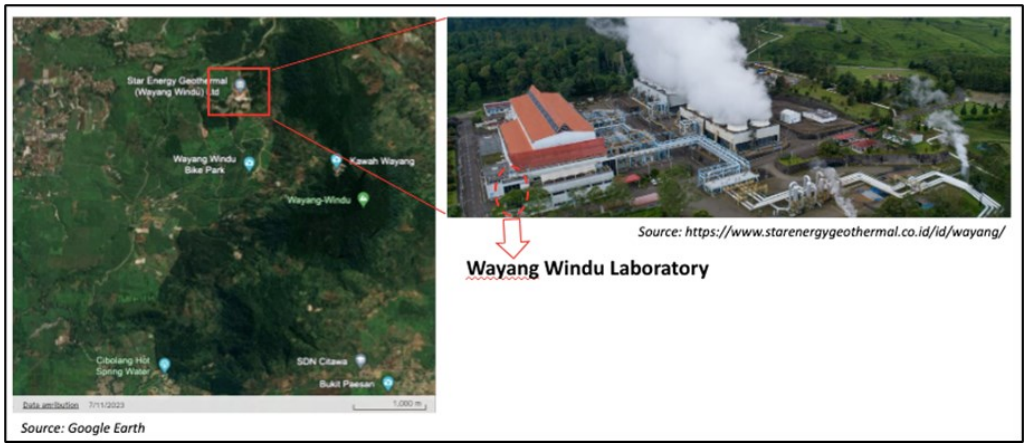

Figure 1: Aerial view of the Wayang Windu Geothermal Field and power plant facilities. Wayang Windu laboratory located inside the main building.

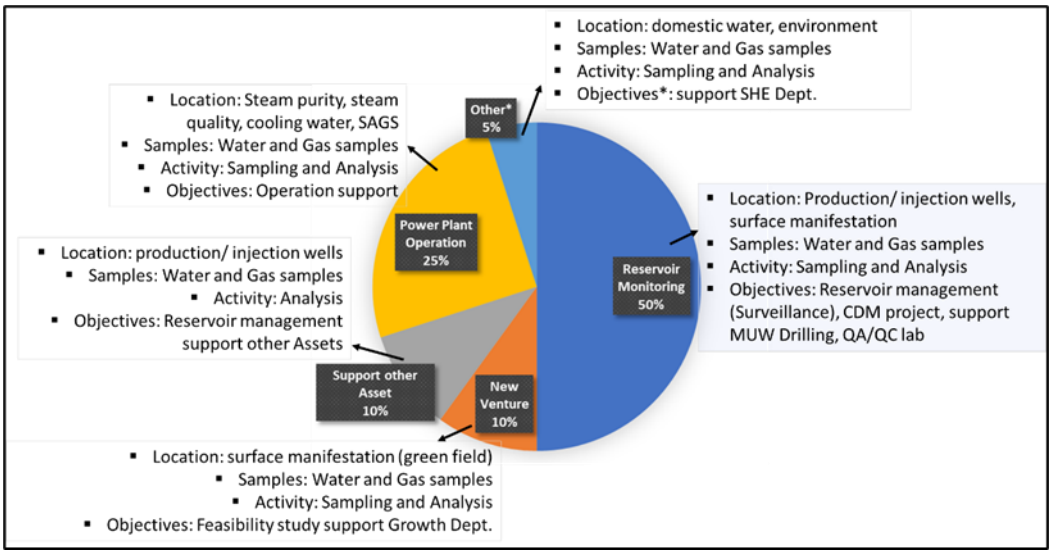

Figure 2: The proportion of scope of services and clients of the in-house laboratory.

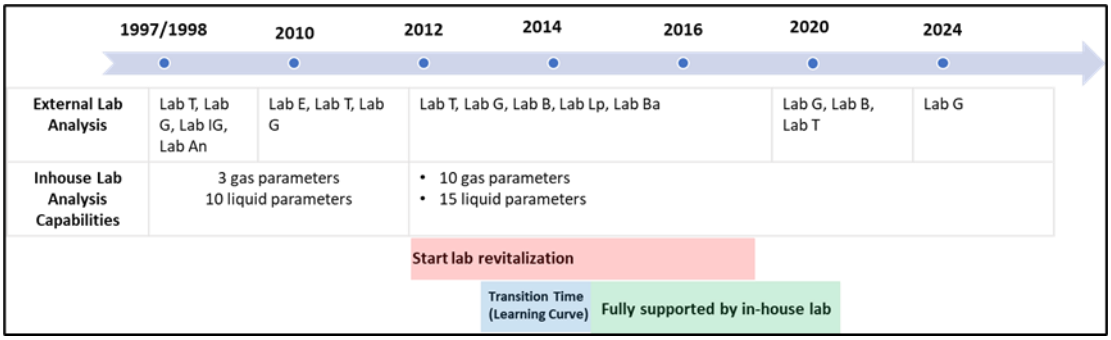

Figure 3: The involvement of external lab was changed overtime, followed by improvement of in-house lab capabilities. The table shows a significant addition of parameters after lab revitalization began, and reduced the number of external laboratories.

With the scope of work majority on the fluid analysis, it becomes crucial that the in-house laboratory establishes a proper management system called Good Laboratory Practice as first stated in The New Zealand Testing Laboratory Registration Act of 1972 (Faridah, 2018). Thus, Wayang Windu Laboratory initiated the Laboratory Revitalization Project in 2012 to implement the good laboratory practice referred to ISO17025 regulation.

Several commercial laboratories involved since the beginning of Wayang Windu Unit-1 which contributed to major improvement of the current processes (Figure 3). It has historically reduced the use of external laboratory services, by adding major equipment like Ion and Gas Chromatograph that significantly contributed to cost savings and increased laboratory personnel laboratory capabilities at the same time. It made the in-house lab add more 7

gas and 5 liquid parameters to analyze (Figure 3), which are the complete parameters necessary for reservoir characterization. However, those commercial labs are positioned as the external QC tool to Wayang Windu laboratory or involved in a blind test procedure (Figure 4).

With the complexities of sampling and analysis activity, the laboratory performance must maintain its quality to get reliable results. Routine calibration and maintenance are crucial actions to keep the equipment in good performance, blind tests and external audits are also considered as the key to good laboratory practice (Faridah, 2018). Those processes were not only considered as a routine, but it is a laboratory management tool to prevent nonconformities, improve, and maintain the quality of the test result.

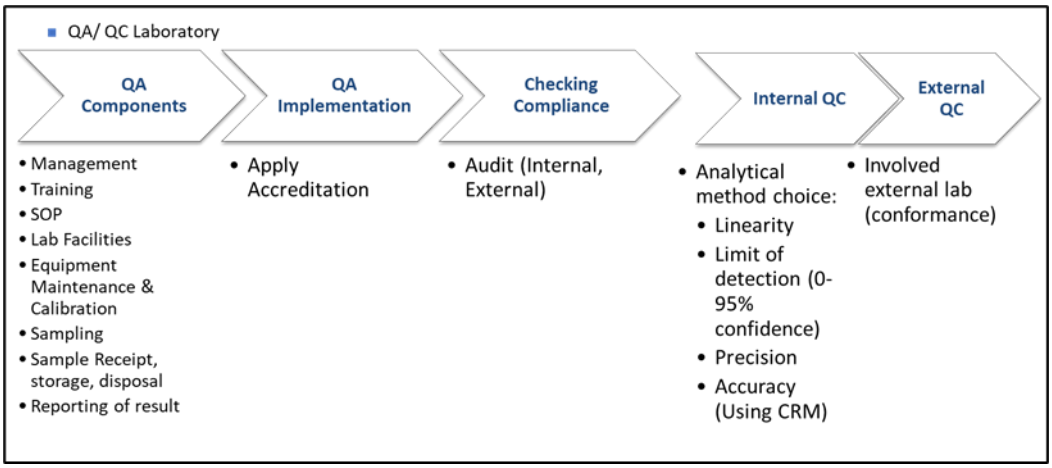

Figure 4: Implemented of the QA and QC methods in Wayang Windu laboratory.

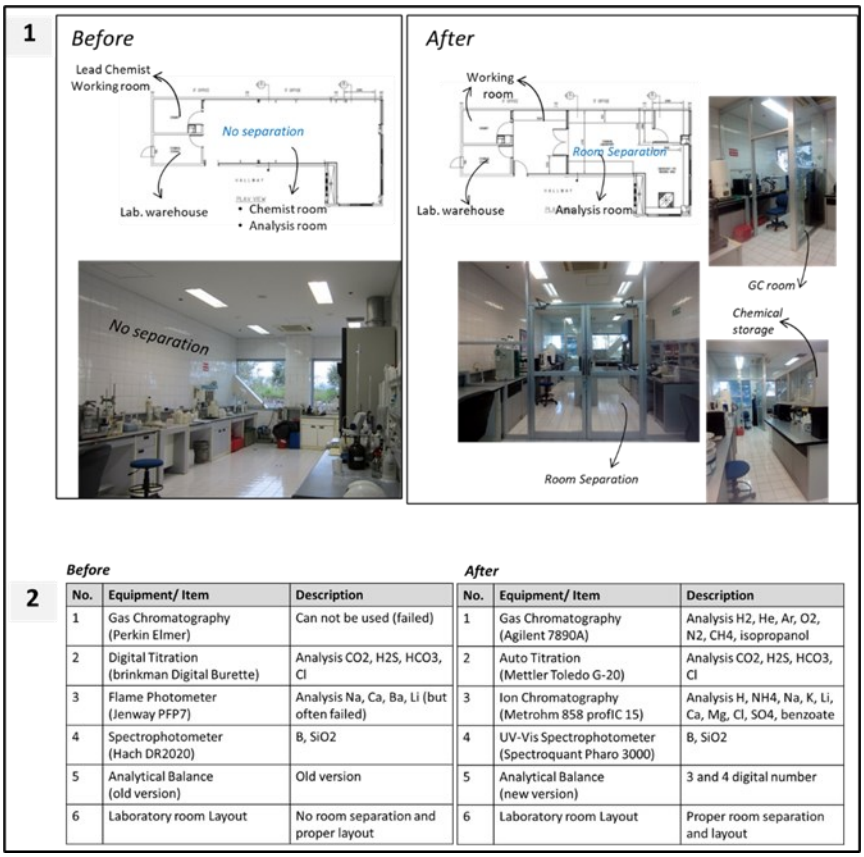

Before

No.	Equipment/ Item	Description
1	Gas Chromatography (Perkin Elmer)	Can not be used (failed)
2	Digital Titration (brinkman Digital Burette)	Analysis CO2, H2S, HCO3, Cl
3	Flame Photometer (Jenway PFP7)	Analysis Na, Ca, Ba, Li (but often failed)
4	Spectrophotometer (Hach DR2020)	B, SiO2
5	Analytical Balance (old version)	Old version
6	Laboratory room Layout	No room separation and proper layout

After

No.	Equipment/ Item	Description
1	Gas Chromatography (Agilent 7890A)	Analysis H2, He, Ar, O2, N2, CH4, isopropanol
2	Auto Titration (Mettler Toledo G-20)	Analysis CO2, H2S, HCO3, Cl
3	Ion Chromatography (Metrohm 858 profIC 15)	Analysis H, NH4, Na, K, Li, Ca, Mg, Cl, SO4, benzoate
4	UV-Vis Spectrophotometer (Spectroquant Pharo 3000)	B, SiO2
5	Analytical Balance (new version)	3 and 4 digital number
6	Laboratory room Layout	Proper room separation and layout

Figure 5: Comparison of before and after laboratory revitalization which involved: 1) laboratory layout changes, 2) additional parameters due to renewal or additional equipment.

2.1 Fluid Analysis

Over the years, Wayang Windu Lab has expanded its analysis as the result of the revitalization process. It is successfully analyzing 15 water parameters and 10 gas parameters following the standard procedures. Those

additional services are the result of the strategic decision in selecting key equipment required to revitalized, such as the installation of Gas and Ion chromatograph equipment. However, the improvement doesn't stop there, but should follow with establishing new procedures, setting up regular maintenance, performing external audits, and manpower skill upgrades. The revitalization also involves laboratory building layout modification as seen in Figure 5. The layout follows the standard regulation of the ISO17025, e.g. room separation has to be clear to store the samples, working room, and confined space for gas chromatography.

This paper shares the critical instruments operate in Wayang Windu laboratory such as Ion Chromatograph (IC) and Gas Chromatograph (GC). Besides, the lab is also equipped with another important instrumentation such as UV-VIS Spectrophotometry, Auto titrator, etc.

1

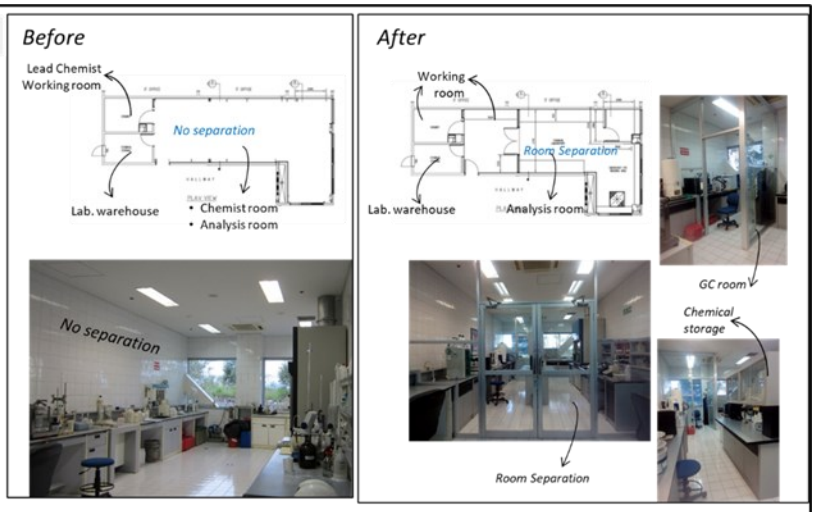

2

Before

No.	Equipment/ Item	Description
1	Gas Chromatography (Perkin Elmer)	Can not be used (failed)
2	Digital Titration (brinkman Digital Burette)	Analysis CO2, H2S, HCO3, Cl
3	Flame Photometer (Jenway PFP7)	Analysis Na, Ca, Ba, Li (but often failed)
4	Spectrophotometer (Hach DR2020)	B, SiO2
5	Analytical Balance (old version)	Old version
6	Laboratory room Layout	No room separation and proper layout

After

No.	Equipment/ Item	Description
1	Gas Chromatography (Agilent 7890A)	Analysis H2, He, Ar, O2, N2, CH4, isopropanol
2	Auto Titration (Mettler Toledo G-20)	Analysis CO2, H2S, HCO3, Cl
3	Ion Chromatography (Metrohm 858 profIC 15)	Analysis H, NH4, Na, K, Li, Ca, Mg, Cl, SO4, benzoate
4	UV-Vis Spectrophotometer (Spectroquant Pharo 3000)	B, SiO2
5	Analytical Balance (new version)	3 and 4 digital number
6	Laboratory room Layout	Proper room separation and layout

Figure 5: Comparison of before and after laboratory revitalization which involved: 1) laboratory layout changes, 2) additional parameters due to renewal or additional equipment.

2.1.1 Ion Chromatograph

The Ion Chromatograph (IC) in Wayang Windu laboratory is an 850 Professional IC-AnCat-MCS (2.850.3030) type, it is one of the model versions of the professional IC line of instruments manufactured by Metrohm company. This equipment is used for the ion chromatographic determination of cations and anions, which take sixty minutes for each sample to analyze. This Professional IC instrument contain the crucial components such as eluent degasser, supressor module, separation column, high pressure pump, conductivity detector, etc. The instrument is also operated with MagIC Net Software, and its automatically recognize the instrument and check its functional readiness (Manual Book 850 Professional IC AnCat). This configuration helps the analyst to conduct their job and avoid analytical errors. Moreover, the advantages for the Wayang Windu laboratory by having Ion Chromatograph are as follow:

a. Accuracy and precision in analysis (short retention time for each ionic compounds)
b. Flexibility an application related and can be adjusted with analysis needs (configuration and method adjustable)
c. Time and cost efficiency

2.1.2 Gas Chromatograph

The Gas Chromatograph (GC) instrument type is the Agilent 7890B to separate a mixture gas compounds into individual components. There are three major steps involved with separating and identifying components of a mixture using GC, such as injecting the sample into GC (Inlet Valve), separating the sample into individual

components (Column), and detecting what compounds were in the sample (Detector). The configuration system uses Agilent's Open Lab software or Masshunter software to automatically recognize and check its functional readiness (Manual Agilent 7890B). Some features are crucial to help Wayang Windu Laboratory for gas analysis, such as:

a. Retention Time Locking (RTL) to maintain exact retention times from injection to injection, column to column, instrument to instrument, and lab to lab.

b. Capillary Flow Technology (CFT) provides unique instrument capabilities, such as multi-dimensional gas chromatography (GC-GC/Deans switch), comprehensive two-dimension gas chromatography (GCxGC) with flow modulation, and backflush at the beginning, middle, or end of the analytical column.

c. Detectors that consist of single filament TCD, auto-ranging FID, and integrated SCD/NCD. The TCD does not require a separate reference gas, does not require manual potentiometer adjustment, and provides a stable baseline with a minimal amount of signal drift. The FID provides the ability to detect and quantitate from parts per billion (ppb) to parts per thousand in a single injection. The integrated SCD/NCD (sulfur or nitrogen chemiluminescence detector) provides low ppb detection, equi-molar response, and quantitation for sulfur or nitrogen contaminants without quenching from matrix.

d. Helium conservation module and alternative carrier gas solutions dramatically reduce the amount of helium used to offer flexibility and cost savings for your laboratory.

Meanwhile, other parts are also supporting the system such as Hydrogen Sensor Module, Large Valve Oven (LVO), Multimode inlet (MMI), Agilent Inert Flow Path, and Low Thermal Mass (LTM) modules.

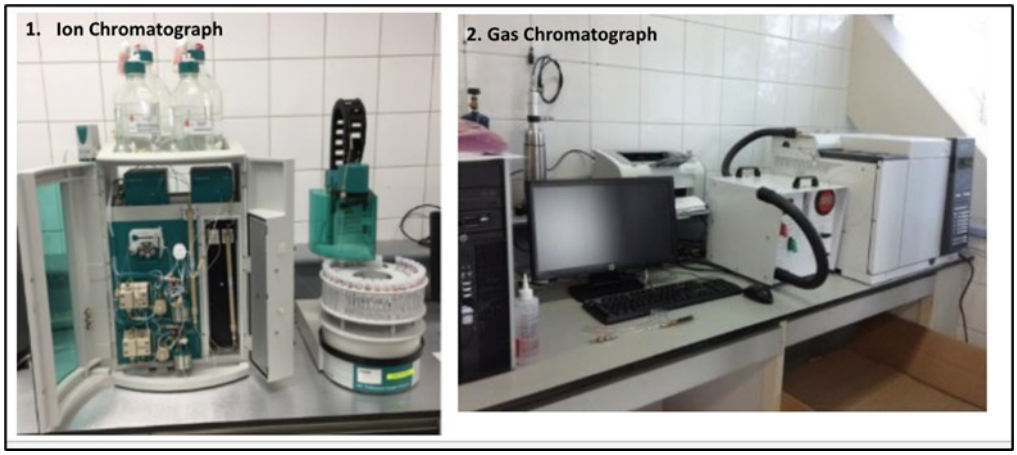

Figure 6: The key equipment installed in Wayang Windu Laboratory for the water and gas analyses : 1) Ion Chromatograph, 2) Gas Chromatograph.

2.2 Equipment calibration and maintenance

Calibration, as defined by ISO/IEC GUIDE 99:2007, establishes a relationship between quantity values and corresponding indications. It involves determining uncertainties associated with measurements. Calibration took to several equipment like IC and GC instrumentation in certain period depend on its type.

The IC instrumentation must be maintained regularly due to routine analysis that is conducted using this instrumentation. Wayang Windu Laboratory established a package of contract with the business partner to perform preventive maintenance service including calibration twice a year. It is crucial to select which part of the instrument that should be maintained or calibrated regularly, that Wayang Windu Lab has selected Filters (inline filter, eluent filter), Pump cleaning (head pump, peristaltic pump, and MSM rotor), Column (conditioning or regeneration), and Leak test.

The GC instrumentation also maintained regularly similar to IC due to routine analysis. Wayang Windu Lab also established the service contract similar to IC to perform preventive maintenance including calibration in three times a year. The preventive maintenance services are recommended to cover activities such as Column conditioning, Gas Standard Injection and calibrated, and Check noise and Drift test.

The output from the services will consist of recommendations regarding the condition of instrumentation, whether there is spare part that should be replaced or keep maintained.

2.3 Internal/ External Audit

The internal audit in Wayang Windu Lab conducted several times and most intense when close to the accreditation process. It collaborates with in-house Management System Department whose regular surveillance audit refers to ISO requirement that also comply with company regulation. The output from the audits are crucial for Wayang Windu Lab as a continuous improvement and enhance the performance.

2.4 Blind Test

A blind test is a procedure to maintain quality by performing analysis involving commercial laboratories or other geothermal field laboratories preferably using the Certified Raw Material (CRM). The result was then compared to check both precision and accuracy. The test started on 2001 since the beginning of Wayang Windu Laboratory operated, and consistently performed in certain period. Figure 7 shows the analyses result in conformities graphs to evaluate historical performance of Wayang Windu Laboratory at various parameters and samples. It shows that Wayang Windu Lab has a consistent result over 60% conformance. Besides, accuracy test evaluated by the repetition of analysis, such as Test #1, 2, and so on. The latest repetition test on 2024 shows a slight discrepancy from the test#1 and 2 which is good to provide the reliable results.

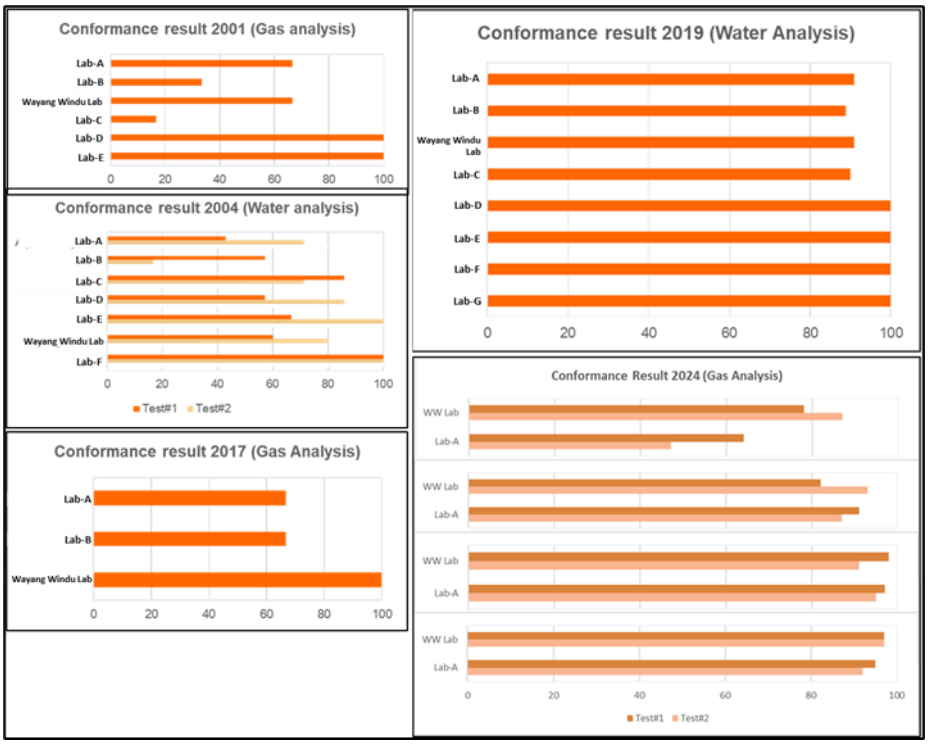

Figure 7: Graphs show the analysis quality represented by conformities. The analyses were taken at various parameters and various commercial and other geothermal field laboratories.

Broadened capabilities were carrying other parties or non-commercial clients such as other geothermal company and institution researchers to participate in a cross reference or blind test. Such activities are good to open and maintain connections and most importantly to open room for improvements. Thousands of samples are the average amount per year that should be conducted by the in-house lab, so that it require more efficient and effective method to accomplish the analysis. Customer satisfaction or feedback form is one the procedures to easily engage the users as stated in ISO17025 guidance. With this approach, Wayang Windu Lab also can maintain the quality of analysis based on customer / client's satisfactory survey and comparation result from another company's clients.

The example in 2023 as seen in Figure 8 is the analysis result in a collaboration test conducted by other geothermal field company. It involves several commercial labs including Wayang Windu Laboratory. The samples taken at other geothermal field from the company and analyzed at each participating labs for complete water parameters. The standardization of the reports are using the Z-scores to evaluate the results. Besides, this method also enables the evaluation to prevent the difference in reference range among laboratories (Duran, 2017). The applied number is within the range of $+2.5 < Z < -2.5$ categorized as acceptance value, and out of that shall be repeated the analysis.

Location	Laboratory	Na (mg/L)	K (mg/L)	Li (mg/L)	Ca (mg/L)	As (mg/L)	Fe (mg/L)	B (mg/L)	SiO_2 (mg/L)	Sampling date
Geothermal Field X	Lab 1	356	97	3.13	<0.04	NA	<0.02	25	933	1/18/2023
	Lab 1	354	106	2.96	2.12	NA	<0.02	27	951	2/4/2023
	Lab 2	304	81.9	2.93	1.49	2.42	0.01	24	873	2/4/2023
	Lab 3	NA	NA	NA	NA	NA	NA	28	1186	1/18/2023
	Lab 3	435	101	3.93	7.79	3.03	<0.01	26	1025	2/4/2023
	Lab 4	350	97	3.43	1.2	NA	NA	60	919	1/18/2023
	Lab 4	364	98	5.72	0.8	NA	NA	577	939	2/4/2023

Z-SCORE Result

Lab	No	Sodium	Potassium	Lithium	Calcium	Boron	Silica
1	1	-0.03	0.00	-0.46	-1.30	-0.43	-0.12
	2	-0.04	0.20	-0.52	0.43	-0.42	-0.07
2	3	-0.33	-0.33	-0.53	0.68	-0.44	-0.29
	4	0.00	0.00	0.00	0.00	0.00	0.00
3	5	0.00	0.00	0.00	0.00	-0.42	0.59
	6	0.44	0.09	1.32	1.19	-0.43	0.14
4	7	-0.06	0.00	-0.34	-0.33	2.40	-0.16
	8	0.02	0.03	0.53	-0.67	1.07	-0.10

Wayang Windu Lab is Lab 4

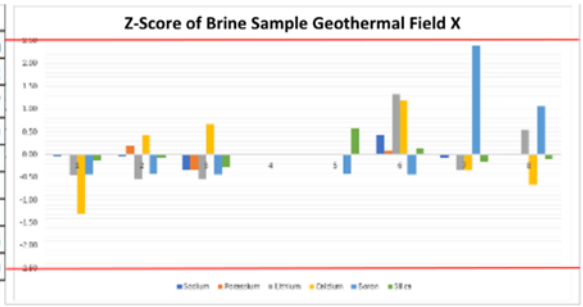

Figure 8: Table above shows the analysis result of each parameter and repetition sample for accuracy test. Table and graph below is a Z-Score result at each parameters. The red line in graphs is the upper and lower range of the Z-Score value, and shows the involved labs including Wayang Windu are within the range (reliable result).

The evaluation of the Z-score shows Wayang Windu lab positioned in-lined with the acceptance value that is similarly to other commercial labs. But the room to improve still exist such as slightly high for Boron analysis in sample#7, even the ranges is acceptable. Overall, those kinds of collaboration are highly important and show that the quality of Wayang Windu Laboratory analysis has a good performance especially for water parameters analysis.

3. THE BENEFITS

The continuous improvement of the in-house lab is a future investment that could be aligned with the future company strategy. The advantage of the laboratory revitalization for more than 10 years in Wayang Windu laboratory was a generous impact on the manpower, services, and company cost-saving. The momentum of laboratory accreditation of ISO17025 in 2018 was considered as a bonus of implementation laboratory revitalization process. By this time, it continues with the cost-saving process. Another advantage is related to manpower or skill upgrade, which is by doing the significant revitalization, it successfully increases independency, manpower skill upgrade, and starts becoming a trustworthy laboratory.

3.1 Accreditation ISO17025

By the process, the lab proposed for the certification and achieved in 2018 tied to ISO 9001. This achievement is not a goal but a bonus from the hardworking yet consistent and continuous effort to maintain the lab performance. Wayang Windu Laboratory has registered fourteen parameters consisting of six gas parameters and eight water parameters as the scope of accreditation which is included in routine analysis conducted in the lab. During accreditation period which starting from 2018 until 2022, Wayang Windu Laboratory is committed to adhere the requirement of ISO 17025 clause with surveillance audit which conducted by Komite Akreditasi Nasional (KAN) as formal representative every year. This is very important as part of maintaining the lab performance including lab personnel abilities, equipment performance or calibration, management contribution and commitment, quality assurance procedure, etc. This approach allows continuous improvement in lab performance based on surveillance finding during external audit by KAN. The benefit of ISO 17025 implementation for laboratory in detail explained as follow (Faridah, 2018):

a. Provide a reference for obtaining formal recognition (accredited) as a competent testing laboratory therefore could improve laboratory's reputation and image.

b. Laboratory management system could improve the consistency of testing and calibration data quality.

c. Facilitate interlaboratory and/or inter-agency collaboration in exchanging information, experience, and harmonization of standards and procedure.

d. Become a baseline for mutual recognition the validity of testing and calibration data on both national and international scales.

3.2 Cost-Saving

Cost saving is one of the benefits directly impacting the company. Since operating the in-house lab, the minimum cost saving can be achieved by at least IDR 200 million / years (see Figure 9). The cost was compared to external analyses, with running operation costs and regular maintenance and calibration. The annual maintenance/ calibration that costs around IDR 50 million/ year is still worth when it compared to a fully external analysis by a commercial lab. Nevertheless, collaboration with other commercial labs is important and needs to be done regularly as part of quality control on a blind test procedure as stated in the Figure 4.

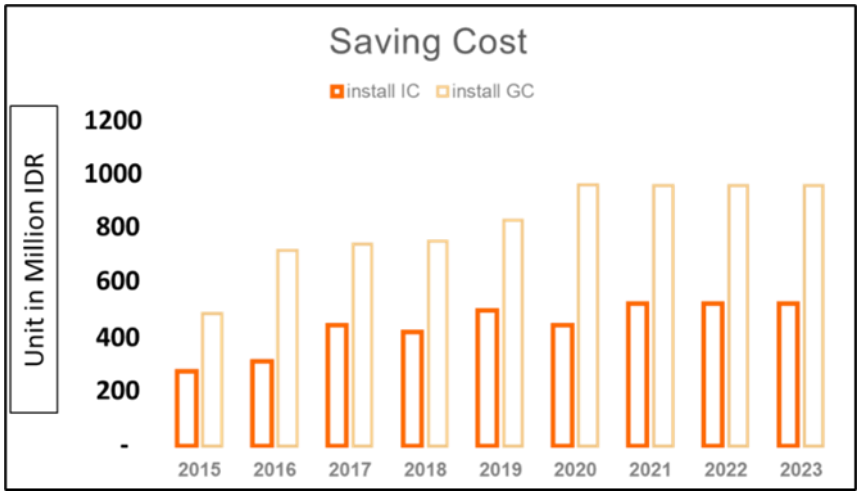

Figure 9: Graph showing cost savings after laboratory revitalization process focusing on installing Ion Chromatograph (IC) and Gas Chromatograph (GC).

4. CONCLUSION

The key points of managing a geothermal fluid laboratory are not only to understand the properties or behavior of the geothermal fluid for reservoir management purposes but also to optimize the efficiency of the operation and most importantly the cost-saving activities. Moreover, managing the laboratory involves implementation of quality control measures to ensure accurate and reliable results. This includes maintaining proper sampling protocols, calibrating the instruments regularly, adhering to safety guidelines for handling hazardous fluid, documenting experimental procedures meticulously, and collaborating with multidisciplinary teams to interpret findings effectively.

The current Wayang Windu Laboratory is continuing the activities as part of the QA/QC lab, including the three-monthly to annual blind tests, equipment calibration and maintenance, and external audit on a call basis. Those activities cost less than half of the equipment prices according to Wayang Windu's condition. It is a worth condition to keep maintaining the current operational cost even if in the future require major equipment renewal such as the more advanced technology of IC and GC.

In summary, managing an in-house laboratory is not an easy task yet not a goal, but it is to develop a ‘culture’ that can create continuous innovation while the base business is running as usual. The continuous laboratory improvement in Wayang Windu is still growing with the settled QA/QC program and is ready to support company strategy.

REFERENCES

Duran I.: Use of Z Score for the Standardization of Laboratory Results Reporting, *Research Gate Publication*, (2017).

Faridah Nur, D., Erawan D., et. al.: Implementasi SNI ISO/IEC 17025:2017 Pernyaratan Umum Kompetensi Laboratorium Pengujian dan Laboratorium Kalibrasi, *Badan Standardisasi Nasional*, Jakarta (2018).

Malik D., et. al.: Laboratory Revitalization Project, *unpublished report*, (2012)

Manual Book: 850 Professional IC AnCat-MCS-2.850.3030

Manual Book: Agilent 7890B Gas Chromatograph Operation Manual

Medina-Pastor P., et. al.: Laboratory Assessment by Combined Z-Score Values in Proficiency Tests, *Analytical and Bioanalytical Chemistry Articles*, (2010)

Unpublished Internal Analysis Report, *UNOCAL*, (2001)

Unpublished Internal Analysis Report, *Mandala Nusantara Limited*, (2014)

Unpublished Internal Analysis Report, *Star Energy Geothermal Wayang Windu*, (2017)

Unpublished Internal Analysis Report, *Star Energy Geothermal Wayang Windu*, (2019)

Unpublished Report, *Geothermal Field X*, (2023)

Unpublished Internal Analysis Report, *Star Energy Geothermal Wayang Windu*, (2024)

https://www.agilent.com/en/product/gas-chromatography/gc-systems/7890b-gc-system#features

https://www.starenergygeothermal.co.id/id/wayang/

The Assessment of The Boundary Reservoir Expansion Based on Magnetotelluric and Wells Data of the Sorik Marapi Geothermal Field in North Sumatra, Indonesia

Keshan Apriliyanthy, Alfiady, Tio Fernando,Wishnu Triananda, and Zammy Sarmiento

keshan.apriliyanthy@ksorka.com

Keywords: Resources Assessments, Magnetotelluric, Wells Data, BOC, TOC, Sorik Marapi

ABSTRACT

It is essential to regularly assess the data obtained during the development of a geothermal field to increase production capacity, particularly in understanding the boundary expansion of the reservoir. One of the key parameters in understanding the reservoir characteristics of the geothermal field is the Top of Reservoir (TOR). During the exploration phase, the base of conductor (BOC) from Magnetotelluric (MT) data is often used as the basis to determine the TOR. However, the actual findings after drilling have shown various ranges of separation between BOC and the commercial TOR. Integrating the MT data with actual drilling data, such as Methylene Blue (MeB) test, alteration mineralogy, and downhole temperature data is crucial.

The wells that were drilled towards a hypothetical upflow exhibit significantly deeper temperature over resistivity (TOR) values compared to BOC, while the wells in the productive outflow show a strong correlation between TOR and BOC. Moving further to the North-East of the Sorik Marapi reservoir, the conductive layer appears thicker, and well data suggest a thick layer of sedimentary rocks. As a result, the conductive layer in the Northern and Eastern areas is interpreted to be associated with the sediment infill of a pull-apart basin, rather than hydrothermal alteration.

It was intended to evaluate reservoir expansion areas for the next development program by combining BOC correlation, alteration mineralogy and downhole temperature to determine the P-10, P-50, and P-90 TOR and their distribution. The end result is used to gain a stronger understanding of the TOR distribution across the field so as to determine the right area in the next development program and minimize the uncertainty in planning drilling targets.

1. INTRODUCTION

Sorik Marapi Geothermal Power (SMGP) is located in North Sumatra, Indonesia, approximately 590 km south of Medan city. It lies within the Mandailing Natal Regency and the nearest major town is Panyabungan, 20 km to the north. The Sorik Marapi concession area has a total area of 629 km2. It encompasses more than 50 km of the Great Sumatran Fault (GSF) zone which is a major geologic tectonic structure that runs the length of Sumatra and controls the location of most of the volcanic and geothermal activity on the island. Apart from being related to the presence of GSF, some surface thermal activity is also associated with the Sorik Marapi volcano (2145 masl), an active andesitic stratovolcano located on the western side of GSF. Phreatic eruptions have occurred several times in recorded history. The volcano has surface solfataric hydrothermal activity in and around the summit crater.

Sorik Marapi power plant currently has installed unit 4 of 160 MW which is on the east flank of Sorik Marapi volcano, where as a whole the Sorik Marapi area has several prospects including Sibanggor, Roburan and Sampuraga. The current development focus is on the Sibanggor prospect, where more than 40 wells from 5 pads have been drilled since 2016, the initial exploration until now development drilling is still ongoing. The results show that the Sorik Marapi field has a geothermal system with neutral pH and high temperature (reaching 320°C from existing pad-T wells that are drilled toward the southwest and south and an indication of potential resources extending to the west of the Sibanggor prospect. Previously, additional geophysical surveys have provided initial guidance for potential southwestward resource expansion before drilling on the Pad-T.

2. GEOTHERMAL CONCEPTUAL MODEL

The Sorik Marapi geothermal field is a typical volcano hosted geothermal system situated along the Great Sumatran Fault (GSF) zone where many commercial geothermal fields are being developed. The Sorik Marapi has a total area of 629 km2 and encompasses more than 50 km of the GSF zone. Temperature as high as 320°C had been encountered from what is inferred to be near the upwelling zone towards the Sorik Marapi volcano – W-SW of wells T-05, T-09, T-11, and A-107.

The models consist of mixtures of fluids and magmatic gases that ascend vertically from the main upwelling zone, at the summit of Mount Sorik Marapi and from there discharge magmatic gases, highly saline fluids with very low pH in Namenek and Siambang thermal areas. Part of the mixture of fluids finds its way laterally and migrates from fractures or faults leading to the Sibanggor Julu and Sibanggor Tonga fumarolic areas. As the fluids migrate, the acidic fluids interact with the rocks and the overlying aquifer forming a mature geothermal system with a neutral pH which is manifested in the thermal springs. The encounter of 320 °C fluid at the latest Pad T wells suggests the presence of a dedicated heat source beneath.

Surface manifestations consisting of fumaroles and vents are distributed fairly along the slopes and into the graben structure in the Sibanggor Julu and Sibanggor Tonga and to as far as 17 kilometers in the Sampuraga lowland with boiling hot springs. It is inferred that the upwelling zone is located in the proximity W-SW of the currently drilled area in Pad A and Pad T. The upwelling is well depicted with a high resistivity anomaly centered within the Sorik Marapi – Sibangor Julu – Sibanggor Tonga areas and overlain by a low resistive layer.

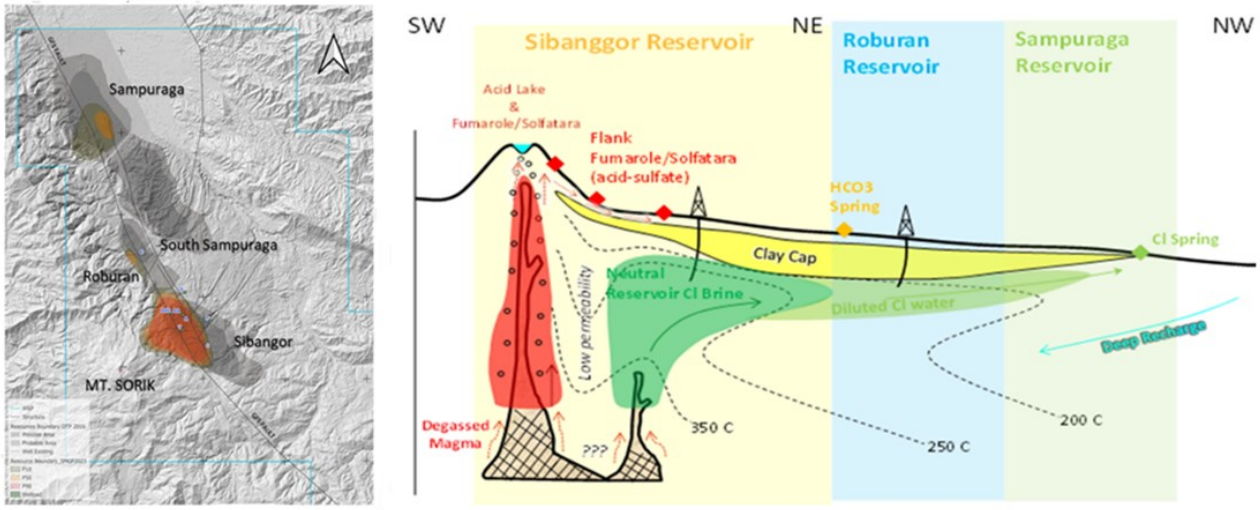

Figure 1: Geothermal conceptual model of Sorik Marapi.

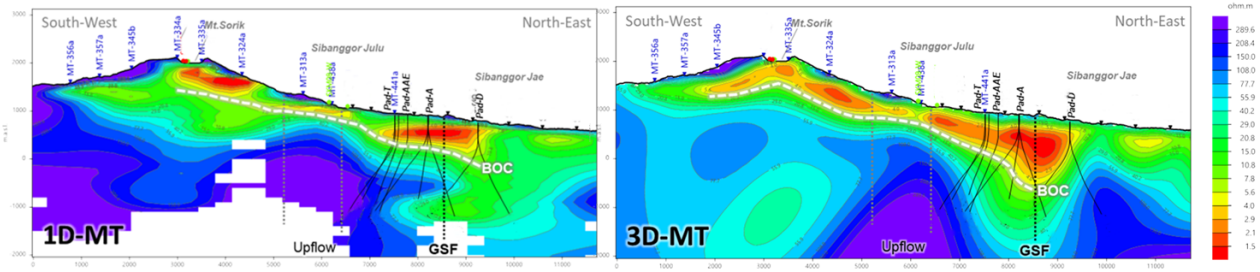

Figure 2: 1D and 3D MT inversion results.

3. MAGNETOTELLURIC RESISTIVITY

The Magnetotelluric (MT) method is an electromagnetic (EM) exploration technique that operates on the principle of passive detection of EM field variations, which induce electric currents in the subsurface. Measurements of electric and magnetic field fluctuations are collected at the surface (Vozoff, 1991). In geothermal exploration, the MT method is widely acknowledged as a valuable geophysical approach for mapping conductive clay cap zones. As a result, MT is frequently employed as a preliminary tool to determine optimal drilling locations in numerous geothermal exploration projects.

3.1 MT Data Processing

MT inversion involves a mathematical approach to create an accurate model of the subsurface resistivity using apparent and phase resistivity data recorded at the surface. It's important to note that the quality of the inversion greatly relies on the quality of the input data, particularly the rho-phase curve. Good input leads to a reliable inversion model, while poor input results in an inaccurate or false inversion model. Before conducting the MT inversion process, it is essential to carry out the classification of MT quality, investigation of sounding curve type,

and correction of static shift. The input data for MT inversion is the apparent resistivity curve, while the output is the true resistivity.

The MT data quality of Sorik Marapi is generally good and acceptable to support 3D inversion and depth-limited 1D inversions used in the interpretation. Based on Figure 2, 1D inversion produces a reliable resistivity model image in the shallower regions and is in good agreement with the base of the conductor (BOC) pattern seen in the 3D inversion. The average 6 Ohm-m value of the BOC in the Sorik Marapi field is also well correlated with the drilling results, particularly evident from the lower boundary of the argillic zone.

Furthermore, the 3D inversion provides a clearer picture of deeper resistivity. It reveals that low resistivity appears to increase in thickness towards the east, indicating an outflow area. Additionally, low resistivity in the eastern part of the GSF influences the sediment formation associated with the pull-apart basin of the GSF. On the western and northeastern flank of Mount Sorik, the low resistivity anomaly seems to diminish under the Sibanggor Julu manifestation, with hot ground alteration, bubbling pools, and acid chloride-sulfate springs indicating the possibility of an upflow zone in this area. This is further supported by the temperatures recorded in wells drilled in that direction, with the hottest temperatures reaching approximately 320 °C.

3.2 Base of Conductor

The conductive zone distribution uses a low resistivity value of 6 Ohm-m which refers to the results of 1D and 3D inversion models, especially in the Sibanggor prospect, an area that has been drilled and is currently being developed. The distribution of Base of Conductor (BOC) showed an updoming pattern that opened from existing Pad A and Pad T in the Sibanggor area around the elevation of 100 masl and up towards Mount Sorik at around 500 masl, where this area is the future well target in planned Pad V which is located inside forestry area. Drilling data on current Pad T wells show the lower part of claycap that ranges from an elevation of 100 - 300 masl as well as the intensity of smectite and illite-smectite minerals. This argillic alteration zone is correlated with the distribution of MeB from drilled wells, the detailed explanation will be described in next section.

The updoming of low conductive anomaly also looks a bit flat towards Mount Sorik (towards Sibanggor Julu and Namenek thermal area) around the elevation of 700 - 900 masl and correlates with the spread of surface manifestations in the form of fumaroles and acid chloride-sulfate springs. In addition, in the Southeastern part of Mount Sorik (towards the Huta Baringin thermal area) there are low conductive anomalies associated with bicarbonate cold springs with an area of BOC at elevation of 1000 - 1400 masl.

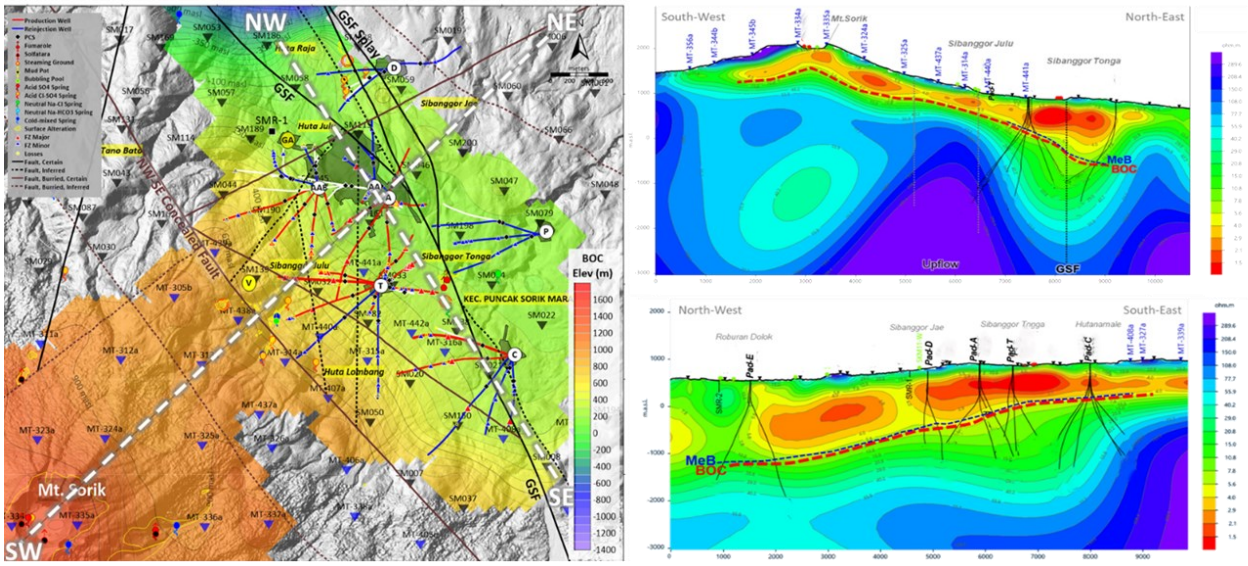

Figure 3: The base of conductor elevation map and 3D MT inversion cross sections with MeB layer. The blue triangle symbol is the MT station surveyed in 2018 and the black triangle symbol MT station was surveyed in 2011.

The wells are in the eastern part of the GSF and also in the northern part such as in Pad P, Pad D, and Pad E are more influenced by volcanic layers mixed with sediment filling which show low resistivity anomalies and low gravity openings which are in the path of the GSF structure. The drilling results in the northern part of the Sibanggor prospect show that under the volcanic layer, there are sedimentary rocks such as tertiary sandstone, limestone, and also thin layers of coal and paleosol. Meanwhile, the BOC in the northern prospects area (Roburan

– Sampuraga) is related by the pull-apart basin structure of GSF, as seen from the deep BOC pattern (around -500 to -1000 masl) and NW-SE oriented.

4. DRILLED WELLS RESULTS

It is important to integrate the MT data with actual drilling data such as Methylene Blue (MeB) test, alteration mineralogy, and downhole temperature data. The wells that drilled towards hypothetical upflow show significantly deeper TOR as compared to BOC while the wells in the productive outflow show a good correlation between TOR and BOC. Further to the northeast of Sorik Marapi reservoir, the conductive layer is thicker and well data suggest a thick layer of sedimentary rocks. As a result, the conductive layer of the Northern area and Eastern area is interpreted to associate with the sediment infill of the pull-apart basin rather than the hydrothermal alteration.

4.1 Lithology

Lithology plays an important role in understanding geothermal systems. Lithology data was acquired from stereoscopic cutting identification and petrography analysis. A total of 46 drilled deep wells have been evaluated and correlated to understand lithology in Sorik Marapi. Stratigraphically, Sorik Marapi consists of seven formations: Paleozoic/Mesozoic Granite, Paleozoic/Mesozoic Metasediments, Tertiary Limestone, Tertiary Sediments, Tertiary Altered Volcanics, Tertiary Limestone, Quaternary-Tertiary Volcanics and Intrusive.

The heat source of Sibanggor prospect (which is found in the Sorik sector and the GSF sector) hypothetically correlates with Quaternary-Tertiary Intrusive. Fine felsic intrusion has been penetrated by wells located at the western side of GSF. Permeability of the reservoir is generally found at metasediments and felsic intrusion. It is suggested that metasediments permeability is influenced by GSF activation, whilst fine felsic intrusion permeability was generated by both fractured areas due to intrusion and also GSF activation. Quaternary-Tertiary Volcanics play at Cap Rock at Sorik Marapi field, especially the Sibanggor prospect. Several wells are drilled to the eastern GSF and penetrate Tertiary Sediments as the basin fills. The evidence of basin fill was also observed when wells at the Northern of Sibanggor were drilled and brought up coal, paleosol, and volcaniclastic sediment to the surface. The basement of Sorik Marapi is high-grade metamorphic rock and granite which are very hard and tight evidence from 2 wells drilled deep to the southwest and penetrated these basement rocks.

The other prospect that was drilled deeply is the Roburan prospect where there are 2 deep wells drilled perpendicular to the GSF and GSF splay. However, poor results were obtained in this area because a thick volcanic claycap layer of about 1200 – 1500 meters followed by a Tertiary sediment layer below it including several paleosol and coal layers indicates that the basin fill sector is getting thicker to the north of the prospect which has a thick and deep of Tertiary sediment product as shown as Figure 4.

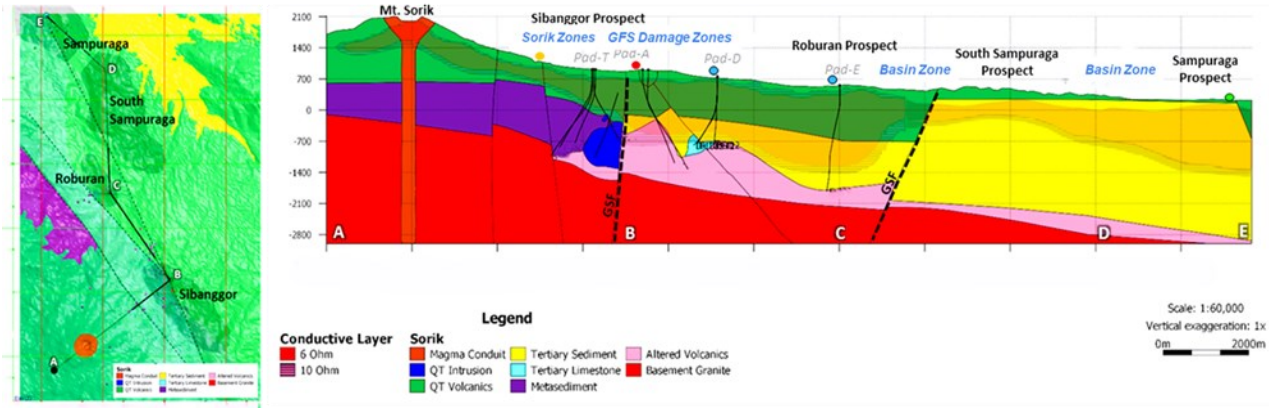

Figure 4: General lithology and distribution of deep wells and prospect locations in the Sorik Marapi field

4.2 Methylene Blue Analysis

Methylene blue (MeB) is an organic dye that shows a high selectivity for adsorption by smectite (swelling) clays in the interlayer site. It has been used to determine the cation exchange of swelling clays since the 1950s (Johnston, 1995 from Harvey, 2000). Geothermal alteration assemblages including smectite or mixed-layer illite-smectite are typically found at temperatures below 200 °C (Harvey, 2000). Because of the very high cation exchange capacity of smectite and mixed layer illite-smectite clays, rocks containing them have very low electrical resistivity (Gunderson, 2000). MeB analyses have routinely been performed for drilled wells in the Sorik Marapi field. It confirms MT's low resistivity anomaly that generally represents the clay cap (Figure 5). The MeB result of drilled wells located at eastern GSF (basin sector) shows a consistent correlation with low resistivity anomaly

(Figure 5), but not with drilled wells at western GSF (GSF sector). This is caused by clay-rich siltstone and sandstone, part of Tertiary Sediment formation, that play role as basin fill of GSF. Some wells drilled to northern Sibanggor have MeB spikes deep below the bottom of clay, suggesting paleosol occurrence as one of the mixed materials at the GSF damage zone and basin fill.

4.3 Alteration Zone

Hydrothermal alteration is a complex process involving mineralogical, chemical, and textural changes, resulting from the interaction of hot aqueous fluids with the rocks through which they circulate, under physio-chemical conditions (Pirajno, 2009). Hydrothermal alteration plays an important role in understanding the geothermal system, as it is the product of hydrothermal activity in the system and it reflects the hydrothermal fluid characteristic. There are factors affecting hydrothermal alteration including temperature, permeability, fluid composition, initial composition of rocks, duration of activity, number of superimposed hydrothermal regimes, and hydrology (Reyes, 1998). Using the petrographic technique, there are several data that can be gleaned including temperature estimation, fluid chemistry, permeability, processes, and thermal history (Reyes, 1998).

Based on mineral assemblage collected from drilled wells data in Sorik Marapi, there are 5 types of alteration zones including Argillic, Transition, Phyllic, Propylitic, and Advanced Argillic; which are derived from the latest alteration sequence. Potassic alteration was possibly observed at two wells drilled toward the southwest (T-07 and AAE-02) at deeper elevation depth, indicating high temperature at the time of formation, with observed patchy - fine grain biotite and k-feldspar alteration minerals. However, at this depth, it may be relict alteration because the Phyllic and Propylitic assemblage is more dominant, with the characteristic of several of these alteration minerals together with epidote which is commonly encapsulated in later quartz, calcite, prehnite, and wairakite.

The argillic zone at Sorik Marapi has various thicknesses from 300 to 500 meters vertical depth (Figure 5). It consists mainly by smectite, accompanied by hematite, pyrite, quartz, and calcite. Sometimes kaolinite and/or low-temperature zeolite are also observed. Phyllic zone is mainly dominated by sericite associated with quartz-pyrite and anhydrite assemblage. The wells drilled towards the upflow or Sorik sector (Figure 5) have thick Phyllic alteration characterized by dominant fracture filled and replaced by anhydrite-quartz-calcite-sericite assemblage that suggested a pressure dropdown at the past which hereafter be a Phyllic zone, this zone becomes impermeable due to fracture sealed and then becomes a gap between bottom of clay and top of the reservoir. Nevertheless, the well drilled to the center shows a consistent trend between the bottom of the clay and the top of the reservoir (Sorik sector at 5).

Propylitic zones of the Sorik Marapi field are mainly defined based on the appearance of continuous epidote, but the results of the petrographic analysis show a texture that characterizes that many epidotes is relict. The latest alteration sequence mostly produces an assemblage of wairakite-adularia-calcite, with some wells also including prehnite as the propylitic assemblage. Advanced argillic was observed at some wells that penetrated GSF splays or minor faults (which are in the Sorik – GSF sectors) (Hendri et.al, 2021). It consists mainly of kaolinite, alunite, diaspore, and pyrophyllite. The appearance of advanced argillic zones suggested shallow acid condensate influx through the GSF splays. Drilled toward the outflow and penetrating GSF, show no propylitic zone (GSF-Basin sector and Basin sector in Figure 5). Although epidote was observed at those wells, it is the product of relict alteration and is contained in sedimentary rocks and old altered volcanic rocks.

5. DISCUSSION

The role of the MT distribution in observing the horizontal and vertical distribution of resistivity, which characterizes the existence of geothermal prospects, is very important before further drilling is carried out. However, before carrying out the mapping of rock resistivity, a hypothetical model based on geology and geochemistry must first be made to find out the general structural patterns, rock regions, and the distribution of manifestations. These are the steps that have been carried out in the Sorik Marapi field, where the low resistive anomaly indicates the spread of this conductive layer starting from Mount Sorik, Sibanggor, Roburan and Sampuraga prospects. However, this conductive layer is not entirely a clay cap which is related to hydrothermal alteration, such as the Roburan prospect, the Sampuraga prospect, and the eastern Sibanggor prospect low resistivity is influenced by mixed Tertiary sediments and located in the

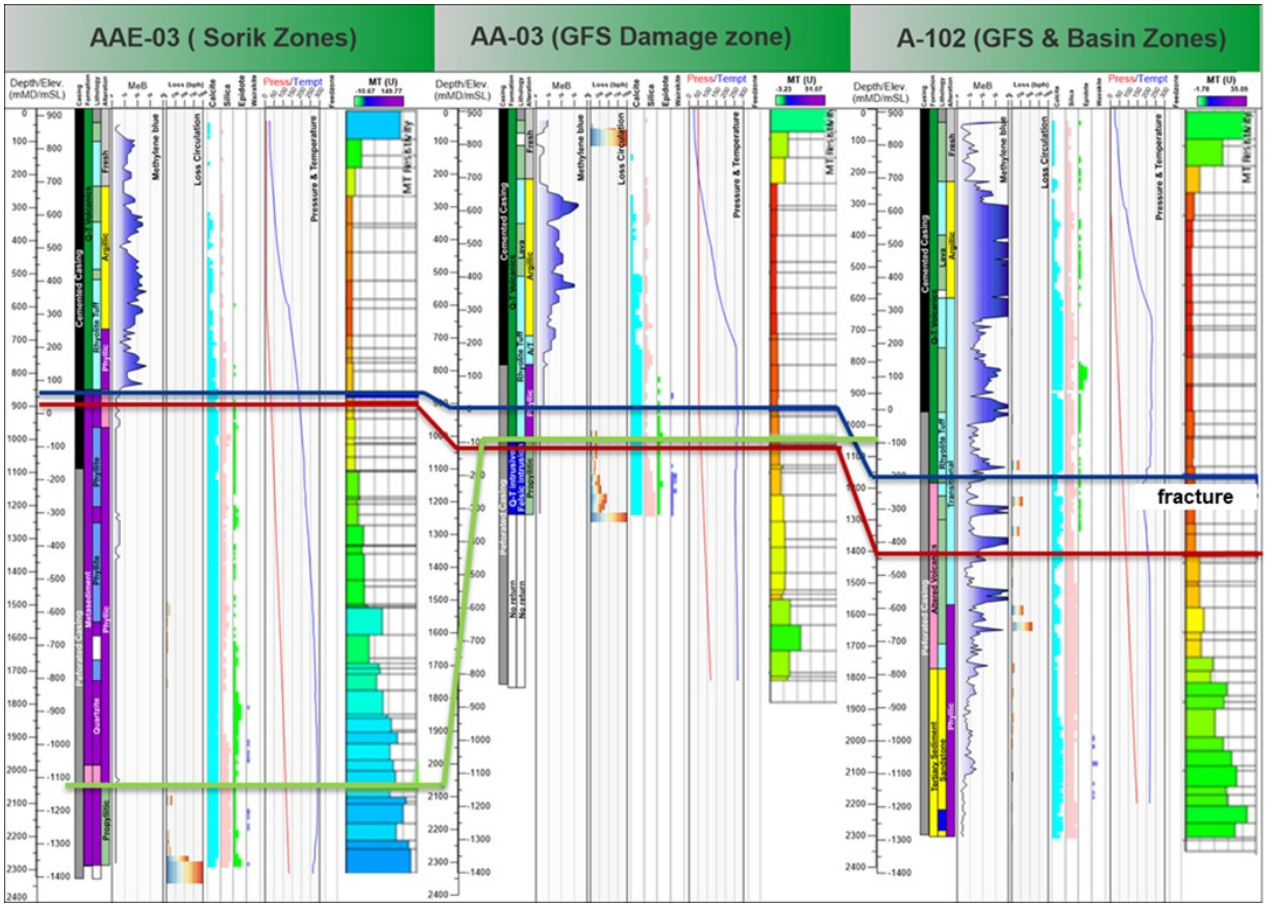

Figure 5: Compiled log of representative well sectors at the same elevation consisting of casing configuration, formation, lithology, alteration type, MeB chart, loss circulation chart, drilling break plot, log of calcite, silica, epidote, wairakite, pressure & temperature chart, feed zone plot and MT resistivity chart.

basin sector. The distribution of low gravity anomalies also supports the structure of this pull-apart basin.

SMGP is involved in the development of several sectors, particularly in the Sibanggor prospect. These sectors are related to low resistivity patterns, feed zone distribution, and TOR distribution patterns. Specifically, they include the Sorik zones, GSF Damage Zones, and Basin Zones. It's worth noting that the most interesting discussion point is the gap between the BOC and TOR in the Sorik Zones.

The low resistivity MT anomaly shows a correlation with the rock units from Quaternary-Tertiary Volcanics and is quite consistent with the distribution of bottom MeB in several zones. Wells drilled to the East and Northeast have thicker low resistivity anomalies. However, the argillic zone thickness is generally the same as an argillic zone of wells drilled toward the Southwest and West (near the upflow zone). The response of low resistivity anomaly from wells drilled to the outflow is caused by the presence of sedimentary rock and old altered volcanic that are rich in smectite. These rocks mean that the drilled wells already penetrated the GSF and basin zones. The TOR in the GSF damage zones appears to have the same correlation as the BOC, this is characterized by the characteristics of the feed zone which is located at a lower elevation that is distributed in felsic intrusion rock and local fracture of damage zone from the GSF structure. The presence of steamcap indications on several wells drilled towards the GSF and there are fumaroles around the Sibanggor Tonga area.

Meanwhile, in the Sorik Zones, the gap between the BOC and TOR is due to indications of alteration of natural boiling minerals presented such as calcite, silica, and anhydrite minerals which fill the factories resulting in an impermeable Phyllic gap. The location of the feed zone is also at deeper elevations and propylitic alteration is also distributed at deeper elevations compared to the wells drilled around the GSF damage zones. The isotherms of the wells drilled at the Sibanggor prospect also show a deep temperature convective trend towards upflow. Only the wells drilled in the upflow direction had temperatures of over 300 °C, such as T-05, T-07, T-09 and T-12.

In the Sorik Zone, the gap between BOC and TOR is caused by changes in the naturally occurring boiling minerals, such as calcite, silica, and anhydrite. These minerals fill the factory, resulting in a Phyllic gap that is impermeable

or becomes a permeable zone at the intrusion contact in the area. The upflow is characterized by an updoming pattern, and the BOC is thinning while the TOR is getting deeper with hotter temperatures, as shown by the isotherm data of wells drilled in the Sibanggor prospect. This data also demonstrates a deep temperature convective trend toward the upflow. Only wells drilled in the upflow direction have temperatures above 300°C, such as T-05, T-07, T-09, and T-12. Therefore, drilling a Step out drill (semi exploration) is necessary to extend the productive reservoir area in this interesting area.

6. CONCLUSIONS

The Sorik Marapi geothermal field (especially the Sibanggor prospect which is currently being developed) is a field located near a vapor core or associated with a magmatic vapor. This is a typical geothermal field in Sumatra which is characterized by a tendency to have a wide gap between the bottom of the conductor (BOC) and the top of the reservoir (TOR) due to boiling and/or condensate percolation, as well as there is Phyllic alteration of mineral assemblies (silica-calcite-anhydrite-sericite) deposited at the mentioned gap as fracture infill. From some of these analyses, it can be integrated that the expansion of prospects in the SMGP field (especially the P-90 TOR as the top of the commercial reservoir) uses an approach such as BOC (low resistivity value of 6 Ohm-m) distribution, MeB trend, appearance of continuous epidote and wairakite minerals, population of propylitic alteration zone, feed zone distribution and isothermal trend as shown a Figure 7.

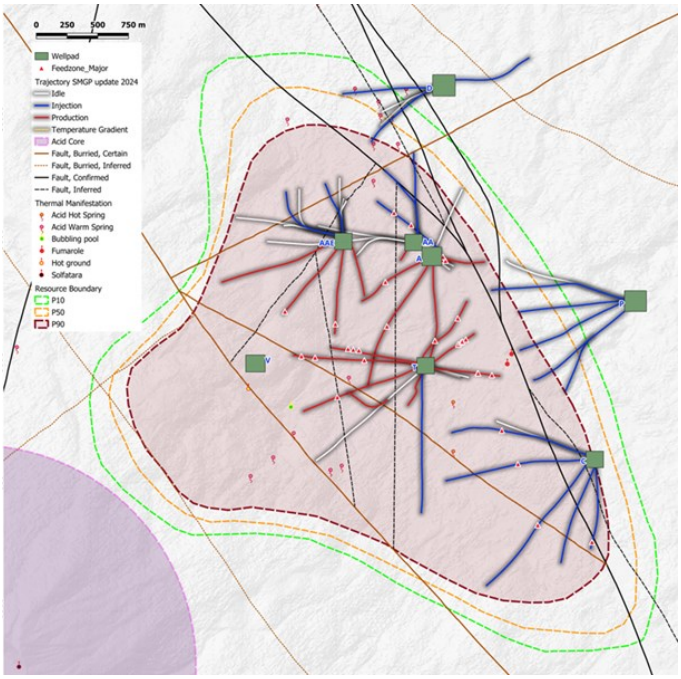

Figure 7: Delineation of P-90, P-50 and P-10 area from Sibangor prospect.

REFERENCES

Cumming, W., Mackie, R.: Resistivity imaging of geothermal resources using 1D, 2D and 3D MT inversion and TDEM static shift correction illustrated by a Glass Mountain case history. *Proceedings*, 7th World Geothermal Congress, Bali, Indonesia (2010).

Cumming, W.: Resource Conceptual Models of Volcano-Hosted Geothermal Reservoirs for Exploration Well Targeting and Resource Capacity Assessment: Construction, Pitfalls and Challenges. Geothermal Resources Council, *Transactions*, v. 40, Davis, California, USA (2016).

Gunderson, R., Cumming, W., Astra, D., and Harvey, C.: Analysis of Smectite Clays in Geothermal Drill Cuttings by The Methylene Blue Method: for Well Site Geothermometry and Resistivity Sounding Correlation. *Proceedings*, 2nd World Geothermal Congress, Beppu-Morioka, Japan (2000).

Harvey, C., Browne, P.: Mixed-Layer Clays in Geothermal Systems and Their Effectiveness as Mineral Geothermometers. *Proceedings*, 2nd World Geothermal Congress, Beppu-Morioka, Japan (2000).

Harvey, C.C., Gunderson, R., and Cumming, W.: Methylene Blue Adsorption: a Real Time Rig Geologist Tool for Estimating Geothermal Reservoir Temperatures and Forecasting Drillhole Stability Problems. *Proceedings* of the New Zealand Geothermal Workshop, Auckland (2000), 151-155.

Hinz, N., Matson, G., Sussman, D., Haizlip, J., Turk, J., Fercho, S., Hendri, R., Siagian, H., Wallis, I., Fishbin, A., Cumming, W., and Letvin, A.: Conceptual Model Update of the Sorik Marapi Geothermal Prospect, Sumatra, Indonesia. Geothermal Resources Council, *Transactions*, v. 45, Davis, California, USA (2021).

Hendri, R., Simamora, S., Siagian, H., Ferdinan, T., Setiawan, J., Simatupang, C., and Pasikki, R.: The important Role of Wairakite at Sorik Marapi Geothermal Field. The 2nd Digital Indonesia International Geothermal Convention, Jakarta, Indonesia (2021).

Hidayat, R., Simatupang, C., Lubis, M. R. S., and Setiawan, J.: The Characteristic of 320 ˚C Geothermal Wells at Sorik Marapi Geothermal Field. The 2nd Digital Indonesia International Geothermal Convention, Jakarta, Indonesia (2021).

Hochstein, M.P., Sudarman, S.: Geothermal resources of Sumatra. Geothermics 22, Elsevier Ltd (1993), 181–200.

Johnston, C. T.: Sorption of organic compound on clay minerals: a surface functional group approach in CMS short course "Organic Pollutants in the Environment" 2-44. Ed. B.L. Sawhney. Clay Minerals Soc. (1995), 197 pp.

Matson, G., Cumming, W., Siagian, H., Hinz, N., Pasikki, R.: Interpretation of Magnetotelluric Resistivity Model of the Sorik Marapi Geothermal Prospect, Sumatra, Indonesia. Geothermal Resources Council, *Transactions*, v. 45, Davis, California, USA (2021).

Mulyani, S., Sarmiento, Z., Chandra, V., Hendri, R., Nasution, S., Hidayat, R., Jhony, J., Sari, P. and Juandi, D.: Calibrated Natural State Model in Sorik Marapi Geothermal Field, Indonesia. International Petroleum Technology Conference, Beijing, China (2019).

Pirajno, F.: Hydrothermal Mineral Deposits, Principles and Fundamental Concepts for the Exploration Geologist. 1992 Edition, Springer, p. 706. Springer (2009).

Reyes, A. G.: Petrology and mineral alteration in hydrothermal systems: From diagenesis to volcanic catastrophes (No. 18). United Nations University, Geothermal Training Programme, New Zealand (2000).

Hendri,R., Simamora,S., Siagian, H. Ferdinan, T., Pasikki. R, Setiawan,J, Simatupang, C., The Important Role of Wairakite at Sorik Marapi Geothermal Field. The 7th Indonesia International Geothermal Convention, Jakarta, Indonesia (2022).

Sanjaya, D., Triananda, W., Pradipta, R, E., Siagian, H., Lubis, R., Simatupang, C., and Pasikki, R.: Fracture Characterization on The Great Sumatran Fault Zone at Sorik Marapi Geothermal Field. The 2nd Digital Indonesia International Geothermal Convention, Jakarta, Indonesia (2021).

Sanjaya, D., Daud, Y., and Siagian, H.: Structure Characterization of Sorik Marapi Field, North Sumatra, Indonesia. The 8th Indonesia International Geothermal Convention, Jakarta, Indonesia (2022).

Soyer, W., Mackie, R., Hallinan, S., Miorelli, F., Pavesi, A., Garanzini, S., Sagala, B., and Siagian, H., 2020. Geophysics over High Enthalpy Fields: Lessons from RLM-3D Magnetotelluric and Joint Inversions. *Proceedings*, 6th World Geothermal Congress, Reykjavik, Iceland (2020).

Vozoff, K.: The Magnetotelluric Method in Electromagnetic Methods in Applied Geophysics, vol. 2B (Tulsa: Nabigihian, M.N., Society of Exploration Geophysicists (1991)), pp 641-711.

Unstable Formation Identification and Potential Drilling Hazard in Geothermal Borehole: Lesson from Sorik Marapi

Tio Ferdinan, Alfiady, Keshan Apriliyanthy, Stephen Simamora, and Zammy Sarmiento

PT Sorik Marapi Geothermal Power Gedung Menara Sentraya Lantai 19 Jl. Iskandarsyah Raya No. 1A, Melawai, Kec. Kebayoran Baru Jakarta Selatan, Daerah Khusus Ibukota Jakarta 12160

tio.ferdinan@ksorka.com, alfiady@ksorka.com, keshan.apriliyanthy@ksorka.com, stephen.simamora@ksorka.com, zammy.sarmiento@ksorka.com

Keywords: unstable formation, geothermal borehole, paleosol, coal

ABSTRACT

Borehole instability has been a common issue in drilling, with geological factor as one of the controllers. Incompetent rock tends to cause sloughing if not treated well, whilst clay-rich rock tends to swell. Those may contribute to drilling problem, even stuck pipe, thus need to be considered as hazard. To understand about expected drilling hazard, identification of unstable formation needs to be done. The identification could be mitigated from geological analysis combine with GIS interpretation, regional geology, and geophysical data. Then, all those hypothesis analyses will be answered by drilling cutting. However, it is quite challenging to identify precise geological information from drill cutting due to its fine size, therefore specific characteristic of drill cutting need to be defined to determine whether its potentially problematic or not. This paper is also intended to share visualization and detail description of unstable formation, which also possibly found problematic in other geothermal fields. Drill cutting was used as real-time initial information when the drilling was undergone. This included rock and mineral characterization through stereo microscope, methylene blue test and cutting size observation. Supporting information acquired including estimated hole size diameter, drilling breaks, parameter anomaly and operation chronology of tag, fill and stuck pipe.

1. INTRODUCTION

The Sorik Marapi Geothermal Field is located about 650 km south-southeast of Medan, the capital city of North Sumatra province and situated within the administrative area of Mandailing Natal district. This field (Sorik Marapi) is located on the lower northeast flank of Sorik Marapi volcano and along a major active strand of the Sumatra Fault System in North Sumatra (Figure 1). Sorik Marapi was initially studied by industry and academia in the 1980s and 1990s (Hochstein & Sudarman, 1993). The first comprehensive geothermal assessment of Sorik Marapi was completed in 2011, and involved geology, geochemistry, and geophysics studies, in addition to drilling three shallow slim wells (SKM, 2011). This assessment concluded that up to 4 possible resource areas were present along discrete parts of the SFS NE of the Sorik Marapi volcanic edifice. Currently Sorik Marapi Geothermal Power (SMGP) has drilled >40 wells in Sibanggor area (southernmost of SKM interpreted area) since 2016 and has proven a ~245° to 325°C and already produced the electricity of 160 MW.

Sorik Marapi geothermal (Figure 2) area is a part of Western Bukit Barisan volcanic range which extends along the length of Sumatran Island. This zone forms a volcanic range separated by graben from the late Mesozoic meta-volcanics and meta-sedimentary which was covered by volcanic sediment of Miocene age. It was then overlain by the quaternary volcanic rocks made up of andesitic to dacitic pyroclastics and lava.

The active Sumatra fault zone runs through the whole length of Sumatra, within the Bukit Barisan, from Banda Aceh to the Sunda Strait, and is paralleled by a line of quaternary volcanoes. The overall shape of Sumatran Fault is sinusoidal, the northern half of which is gently concaved to SW, whereas the southern half is concaved to NE. There is an irregularity in the fault geometry termed “bifurcation”. The Bifurcation started near Sibual-buali and Lubuk Raya towards the Southeast into two principal active strands (Figure 2). The two strands are separated from each other (Natawidjaya, D. H., 2002). The western branch of bifurcation does not rejoin the eastern branch which continued toward the southeast of Sumatra. Sorik Marapi geothermal field lies at the center of the western branch of Sumatran fault. Most of local fault which parallel to NW-SE major fault trend provide less promising permeability except the NE-SW and N-S trend which are believed to provide good permeability in Sorik systems.

The lithologic units in the Sorik Marapi may be summarized into five units based on updated integrated observations from binocular microscope and petrographic analysis which resulted in the identification of several new lithologies and grouped into five formations: 1) Quaternary Intrusions, 2) Quaternary-Tertiary Volcanics, 3) Tertiary Sediments, 4) Mesozoic or Paleozoic granite, and 5) Mesozoic or Paleozoic metasediments (Figure 3).

The potential problem that arises during geothermal well drilling may vary, with frequent issues being lost circulation, stuck pipe, wellbore instability, wellbore reduction, temporary zone closure, cementing job trouble, and a problem related to quality operability, skill, and experience drilling crew. Anadrill (1997) defines a stuck pipe as when the drill string is unable to move up, down, or rotate. A few common causes of stuck pipes are bad hole geometry, poor hole cleaning, and formation problems. In Sorik Marapi Geothermal Field in Sumatera, several wells drilled in Pad XX dealt with reactive and problematic formation, which caused bottom hole assembly (BHA) loss in hole (LIH). Although stuck pipe also occurred at a high percentage at the other pads in the past, the cause was not fully understood, hence the solution could not be defined and the problem could not be properly mitigated. The stuck pipe incidents in Sorik Marapi have allowed the subsurface team to identify and mitigate such a risk.

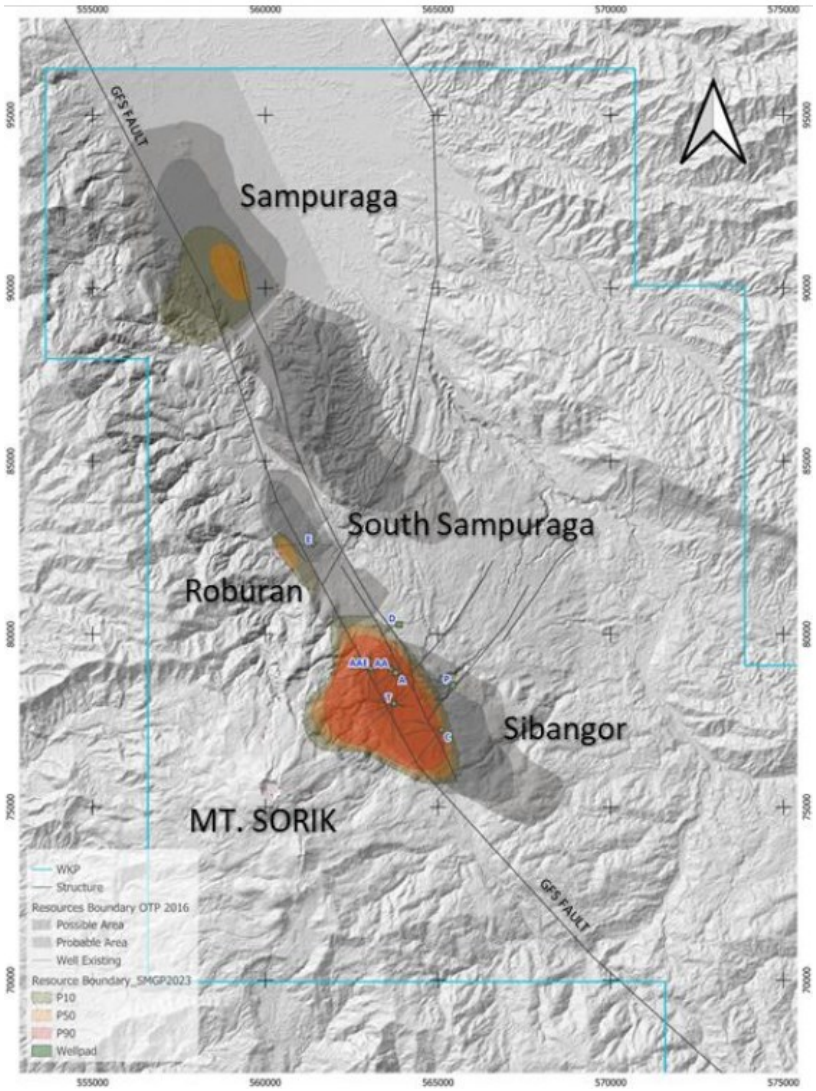

Figure 1: Location map of Sorik Marapi field.

2. METHODOLOGY

2.1 Cutting description

At the rig site, cutting return brought by drilling fluid was regularly sampled every 3 meters. Stereoscope was used to obtain detailed rock and mineral texture, color, size, shape, composition and hardness. Since composition estimation from stereoscope is semi-quantitative, it may differ from each well site geologist, thus modal percentage chart (Shvetsov et al., 1955) was used as reference. Hardness is a bit tricky cause it is qualitative data, especially for specific mineral hardness. For the wells studied, Mohs Scale Hardness Picks was used as it can eliminate handful of possibilities in determining the name of the mineral (Broz et al., 2006).

2.2 Petrography analysis

After studied wells was drilled, several samples from different depth interval were shipped to laboratory. Petrography analysis was performed for 19 samples taken from, 12-1/4" open hole section, the reservoir. Thin section sample preparation and petrography analysis were performed at laboratory. This analysis was conducted to verify cutting description from the rig site and to determine the name of rock and mineral. Besides, it visualizes specific texture that indicate qualitative permeability and semi-quantitatively provides intensity of hydrothermal alteration mineral on cutting samples.

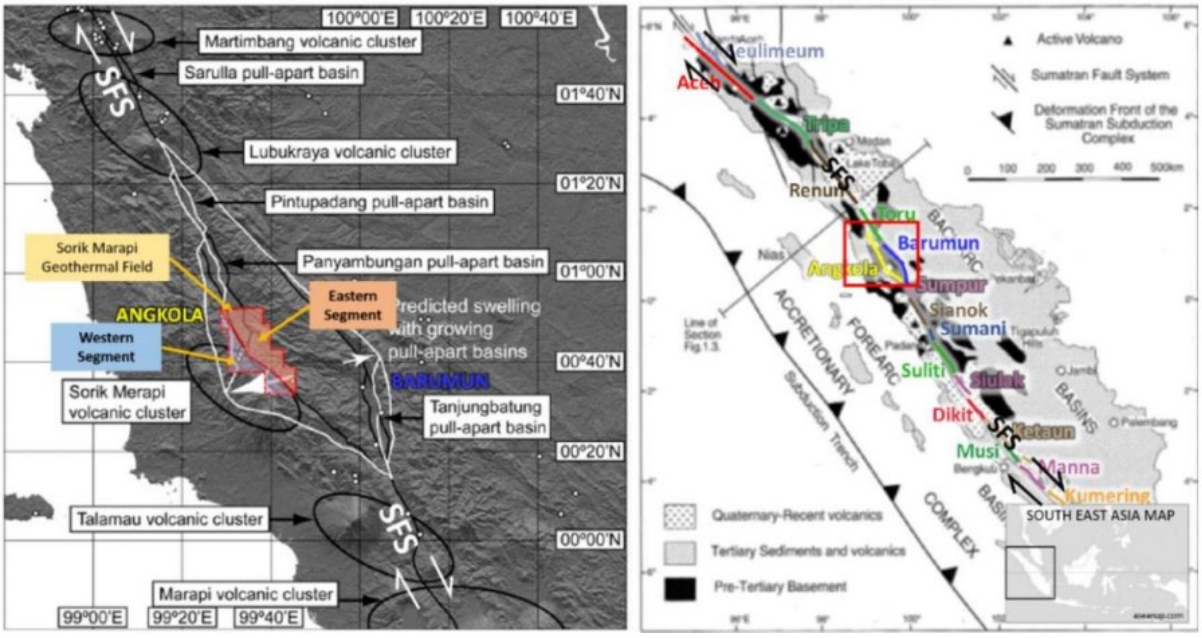

Figure 2: Map of Regional Tectonic setting of Sorik Marapi (left) located along the Sumatran Fault System after Muraoka et al., (2010). GSF segments (right) by (Sieh & Natawidjaja, 2000).

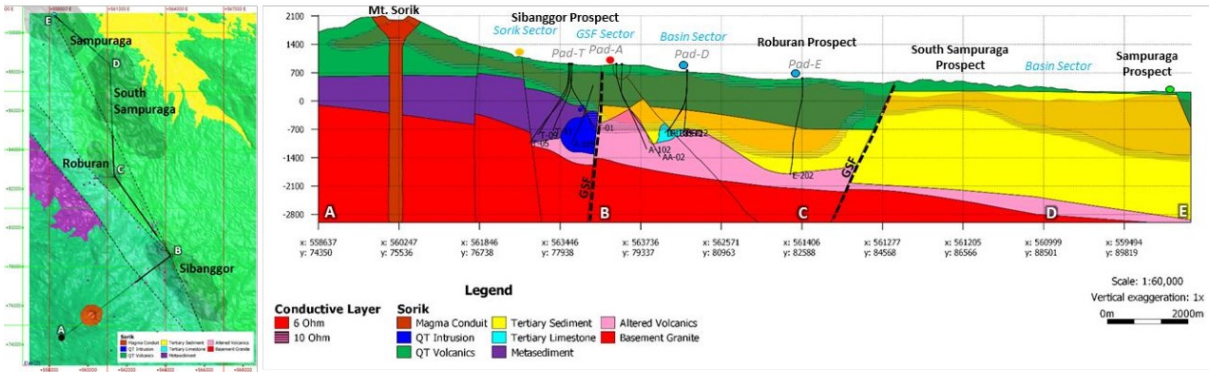

Figure 3: General lithology and distribution of deep wells and prospect locations in the Sorik Marapi field.

2.3 X-Ray Diffraction

X-Ray diffraction analysis (XRD) is a nondestructive technique that provides detailed information about the crystallographic structure, chemical composition, and physical properties of a material. Same as petrography analysis, some samples are selected after the drilling was completed. There is a total of 7 sample chosen for analyze physical properties such as phase composition, crystal structure and orientation of powder, solid and liquid samples.

3. UNSTABLE FORMATION IDENTIFICATION

In Sorik Marapi, there are several lithologies that cause unstable formation, such as paleosol and coal. Based on megascopic analysis, the abundant reddish fragments are suspected to be Paleosol. The fragility is indicative of what was mentioned. It is supported by the presence of hematite, magnetite, and montmorillonite. Paleosol appears in the reservoir zone, and the appearance of paleosol is marked by the presence of MeB spikes in the reservoir zone. Apart from that, there are also coal layers that appear in several Sorik Marapi wells that have the

characteristics of being brittle, black, dull, grainy, don't have a shiny luster (probably low-grade coal), but some fragments have black, shiny, or olive laminae, have 90-degree cleats, and have a wood-like texture.

3.1 Paleosol

In geoscience, paleosol (paleosol in Great Britain and Australia) is an ancient soil that formed in the past. The definition of the term in geology and paleontology is slightly different from its use in soil science.

In geology and paleontology, a paleosol is a former soil preserved by burial underneath either sediments (alluvium or loess) or volcanic deposits (lava flows or volcanic ash), which in the case of older deposits have lithified into rock. In Quaternary geology, sedimentology, paleoclimatology, and geology in general, it is the typical and accepted practice to use the term "paleosol" to designate such "fossil soils" found buried within sedimentary and volcanic deposits exposed in all continents.

In soil science the definition differs slightly: paleosols are soils formed long ago that have no relationship in their chemical and physical characteristics to the present-day climate or vegetation. Such soils are found within extremely old continental cratons, or in small scattered locations in outliers of other ancient rock domains.

Rye & Holland (1998) laid out five criteria for identifying a paleosol. While this was prompted by the need for more stringent identification of Precambrian paleosols, it is applicable to paleosols of any age. The criteria are:

- Formed in situ on bedrock
- soft-sediment deformation at the top of the profile, and
- up-profile changes in chemistry, texture, and mineralogy consistent with terrestrial weathering processes.

In geothermal fields, paleosol is classified as a reactive formation layer and can potentially cause significant hole problems. While drilling previous wells in the formation, the operator experienced five consecutive stuck pipe events and two lost-in-hole (LIH) bottomhole assembly (BHA) incidents that increased drilling time and costs to target depth (TD).

In many of the Indonesian geothermal fields, thin zones of impermeable, dehydrated, fine grained tuffs and paleosols containing a large proportion of smectite clay are routinely found within geothermal reservoirs at temperatures ranging from 200 to 350 C. Smectite in such conditions is inert but, when disturbed by drilling, rock containing it becomes physically unstable.

In Sorik Marapi field, the presence of paleosols near the surface is a common finding in all wells in Sorik Merapi because the layers are still in the argillic alteration zone, which is rich in smectite. Paleosol usually contains argillic minerals (clay content) such as smectite (Daviel et al., 2011), but smectite does not necessarily always indicate the presence of paleosol. When starting to enter the propylitic alteration zone (reservoir area), the percentage of smectite will decay with increasing depth. Among the common clay minerals, smectite has the strongest swelling ability. Problems associated with the swelling clay include caving, sloughing, stuck pipe, bit balling, excessive torque & drag, heaving, suspended drilling activity, and lost revenue.

However, problems will only occur if the presence of this argillic mineral is found in the propylitic zone. This can be indicated as the presence of paleosol in the reservoir zone and when it’s reacted with drilling fluid, which has a high concentration of chemical content, it can be ascertained that swelling will occur and squeeze the drilling pipe which may cause the pipe to be stuck. One way to identify the presence of paleosol in the reservoir is by monitoring through the methylene blue analysis done in cutting as has been implemented in one of Indonesia's geothermal fields. MeB peaks in the reservoir zone may correspond to dehydrated smectite-rich paleosol zones and potentially can cause drilling hazards.

3.1.1 Cutting Analysis

Cuttings are the small pieces of rock that are chipped away by the bit while a well is being drilled. The rock fragments are transported by the mudstream from the bit to the surface where they can be “caught” and analyzed. Identifying paleosols in cuttings is the first thing that can be done before being validated by petrography and XRD analysis. Based on the cutting retrieved in XX-06 well (figure 5) strong evidence of paleosol was observed in these wells, it shows the presence of paleosols that appear in cuttings with the characteristics of dark reddish-brown colour, soft hardness, translucent waxy component (clay-altered lithic/glass), and sedimentary-like brown matrix.There are several ways to identify Paleosol: Cutting analysis, MeB analysis, and Shaker monitoring.

3.1.2 MeB Analysis

The smectite content of the cutting can be detected by Methylene Blue (MeB) analysis (Gunderson et al., 2000). The MeB index is expected to be high when drilling through the clay cap zone. Sihotang (2021) found that smectite clays decrease in the drilling rock cuttings indicated by the MeB index value lower than ten when approaching the top of the transition zone. Figure 6 shows that after passing the clay cap at around depth 1000 mMD, the MeB

index remains constant at around 3. In XX-06 the MeB index observed a sudden increase below the production casing shoe (1500 mMD). As mentioned previously, aerated water was applied once total loss circulation (TLC) was encountered in the reservoir zone and the drill string got stuck not long after. This condition is also similar in XX-07 wells – where a spike reading in MeB was observed below the production casing shoe (1200 mMD).

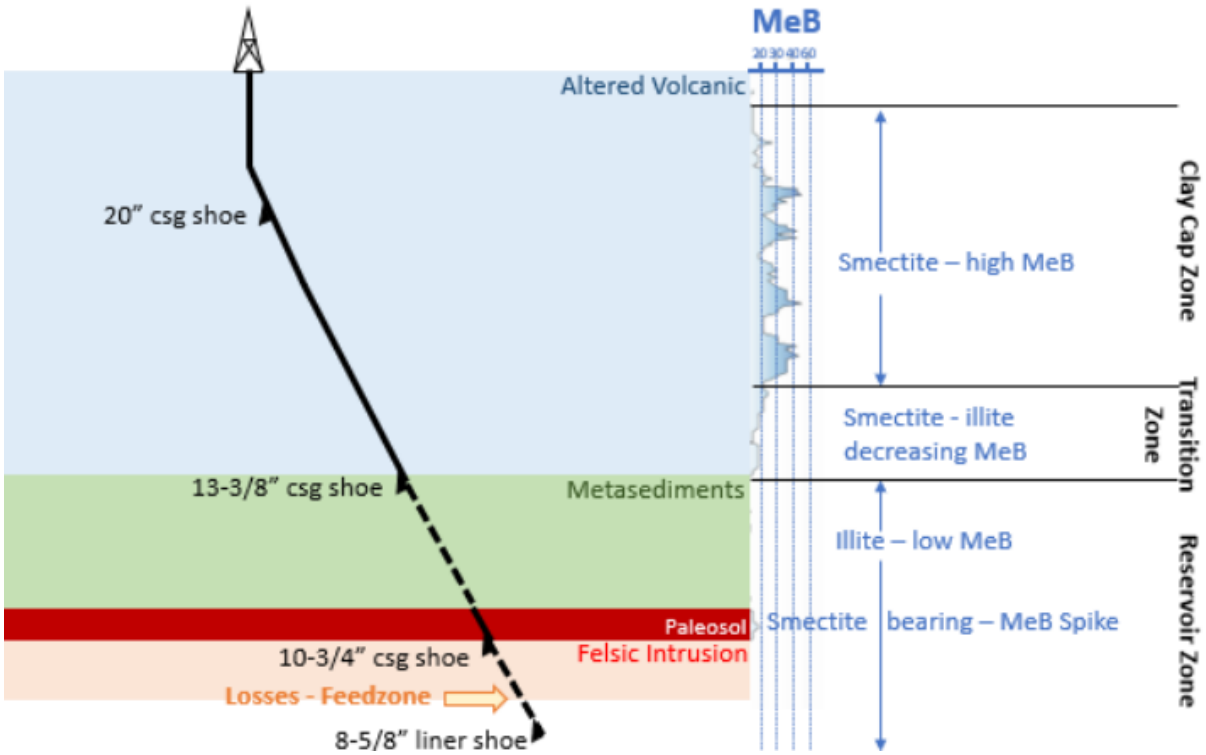

Figure 4: Paleosol illustration in SMGP.

Figure 5: Paleosol on cutting borehole sample.

3.1.3 Shaker Monitoring

As an initiation to analyse the drill cutting faster and in a timely manner, the shaker was periodically monitored, especially when the drilling depth is near a prognosed potential subsurface hazard. At the shaker, paleosol could be assumed if the mud colour turned to reddish-brown and sticky. Some reddish-brown clots are usually observed at the shaker if there is paleosol. However, reddish-brown mud colour does not always indicate paleosol. Hematite-bearing Andesite Lava and Tuff also make the mud colour reddish-brown but are not considered potential subsurface hazards.

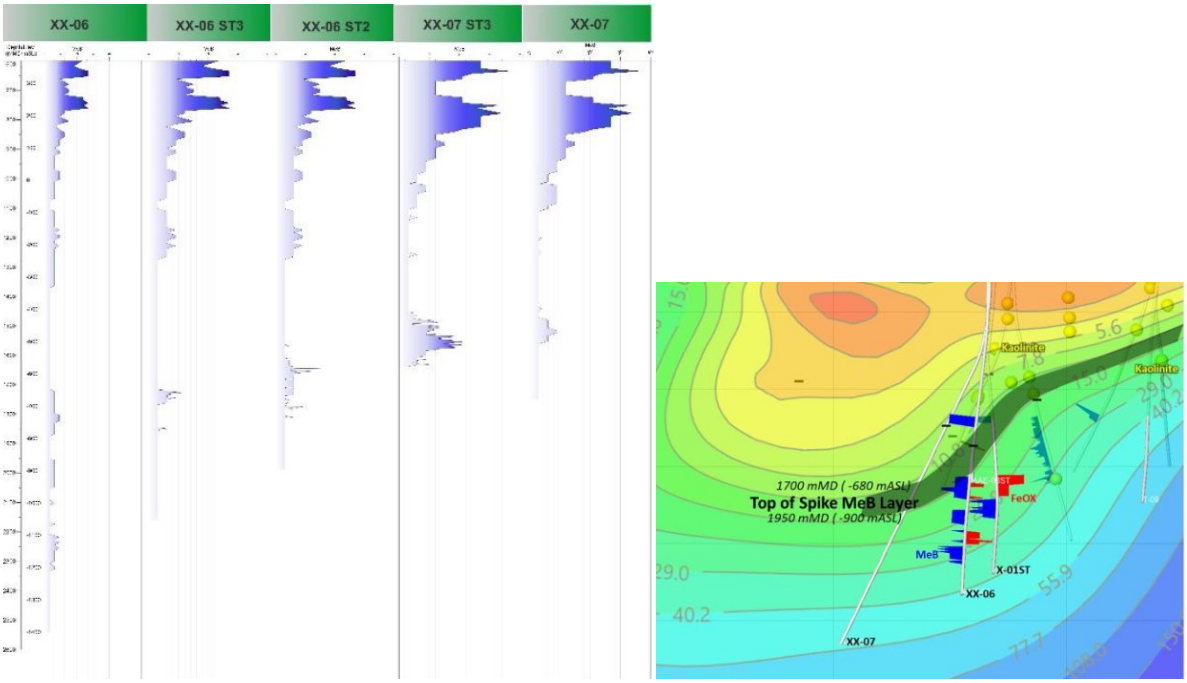

Figure 6: MeB Index of SMGP wells in Pad XX.

Figure 7: Paleosol at shale shaker.

3.2 Coal

Coal is a sedimentary deposit composed predominantly of carbon that is readily combustible. Coal is black or brownish-black, and has a composition that (including inherent moisture) consists of more than 50 percent by weight and more than 70 percent by volume of carbonaceous material. It is formed from plant remains that have been compacted, hardened, chemically altered, andmetamorphosed by heat and pressure over geologic time.

The most common classification is based on rank, referring to the degree of coalification that has occurred. The rank of a coal is determined primarily by the depth of burial and temperature to which the coal was subjected over time. With increasing temperature, peat is converted to lignite, a very soft, low-rank coal. With further increases in temperature, lignite is transformed into subbituminous coal and then into bituminous coal. At even higher temperatures, usually accompanied by intense deformation generated by the folding and faulting of the Earth's crust, anthracites, the highest rank of coal, are produced.

In Sorik Marapi Field, this coal is found in the reservoir in the northern part, where its availability is influenced by the splay of GSF, especially in the northwest part of GSF. This coal thins towards the west and disappears in the east. The splay of this coal is found locally with a thickness of approximately 10 m. This coal becomes a subsurface drilling hazard because of its soft to brittle nature and has many cleavages (flakes) so that the coal interval can become a rubble zone.

There are several ways to mitigate when encountering coal formations in the Sorik field, such as:

1. Separate problematic formation with loss zones
2. Cover problematic formation with blank liner
3. Utilize high performance water-based mud
4. Perform coal drilling procedure
5. Optimize window time (swelling time based on statistic)
6. Proper hole circulation

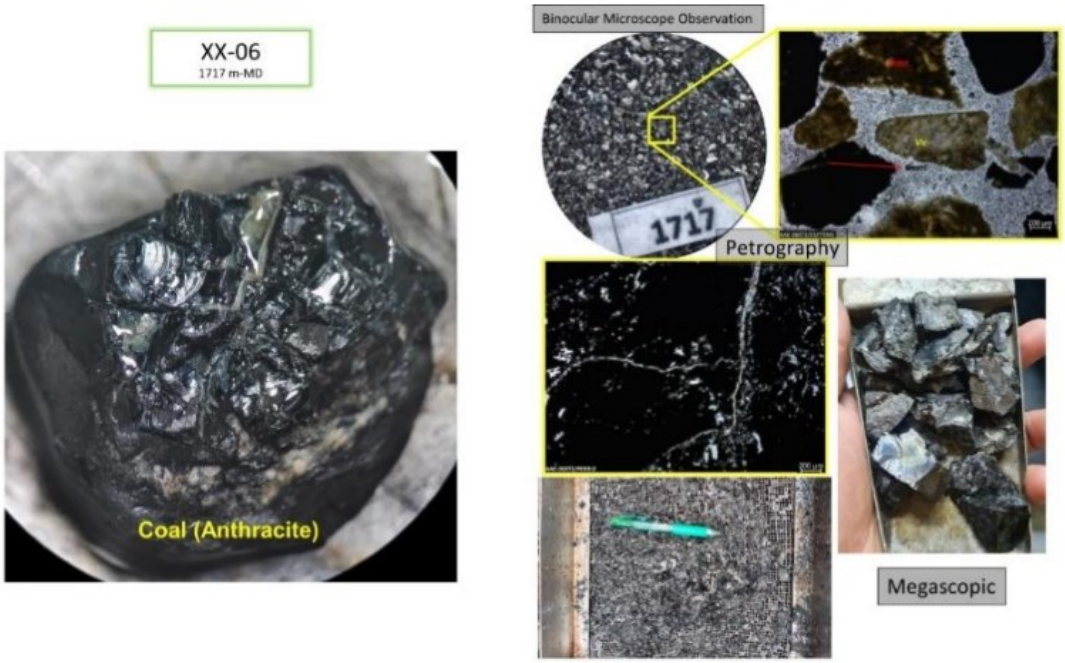

Figure 8: Coal on cutting borehole sample.

4. CONCLUSION

It is concluded that paleosol and coal are the main geological factors in contributing borehole instability in Sorik Marapi. Borehole instability has been a common issue in drilling, with geological factor as one of the controllers. Incompetent rock tends to cause sloughing if not treated well, whilst clay-rich rock has a tendency to swell. Those may contribute to drilling problem, even stuck pipe, thus need to be considered as hazard. In order to understand about expected drilling hazard, identification of unstable formation needs to be done. However, it is quite challenging to identify precise geological information from drill cutting due to its fine size, therefore specific characteristic of drill cutting need to be defined to determine whether its potentially problematic or not. This paper is also intended to share visualization and detail description of unstable formation at Sorik Marapi, which also possibly found problematic in other geothermal fields. Drill cutting was used as real-time initial information when the drilling was undergone. This included rock and mineral characterization through stereo microscope, methylene blue test and cutting size observation. Quick-look also exercised by checking the cutting return at the shale shaker periodically. Supporting information acquired including estimated hole size diameter, drilling breaks, parameter anomaly and operation chronology of tag, fill and stuck pipe.

Suspicion of unstable formation arose against hematite-rich soft fragment with elevated MeB value up to 24, which hereinafter called as Paleosol. In XX-07 well, it causes severe sloughing and swelling as evidenced by continuous abnormal cutting size return at the shale shaker and bigger average diameter hole which checked using hi-vis. The paleosol is the part of Altered Volcanic Formation which consisted of clay-rich intermediate to silicic tuff, lavas, tuffaceous sediment and volcanoclastic sediment that also found as swelling formation. Problem was solved after polyamine applied in drilling fluid system to prevent the swelling process. In XX-06, an even worse unstable formation was observed, namely coal, causing wellbore collapse. Abnormal cutting size up to 6 cm

continuously appear and hole diameter become larger, up to 13.7 inches. High mud weight could overcome the collapsing coal, but failed after loss circulation occur. Casing running problem and stuck pipe happened after penetrating coal. It is concluded that paleosol and coal are the main geological factors in contributing borehole instability in Sorik Marapi.

REFERENCES

Daviel, E., Sanborn, P., Tarnocai, C. and Smith, C.A.S., 2011. Clay mineralogy and chemical properties of argillic horizons in central Yukon paleosols. *Canadian Journal of Soil Science*, 91(1), pp.83-93.

Gunderson, R., Cumming, W., Astra, D. and Harvey, C., 2000, May. Analysis of smectite clays in geothermal drill cuttings by the methylene blue method: for well site geothermometry and resistivity sounding correlation. In *Proceedings World Geothermal Congress* (pp. 1175-1181)

Gürel, A. and Kadir, S., 2006. Geology, mineralogy and origin of clay minerals of the Pliocene fluvial-lacustrine deposits in theCappadocian Volcanic Province, Central Anatolia, Turkey. *Clays and Clay Minerals*, 54(5), pp.555-570.

Sihotang, M., Azis, H., Stimac, J. and Baroek, M., 2021, April. Geology Controlling Factors of the Top Reservoir; Muara Laboh Geothermal System Case Studies. In IOP Conference Series: *Earth and Environmental Science* (Vol. 732, No. 1, p. 012002). IOP Publishing.

Hochstein, M.P., and Sudarman, S., 1993, Geothermal resources of Sumatra, *Geothermics*, v. 22, No. 3, p. 181-200.

Time-Lapse Gravity Monitoring of the Tompaso Geothermal Field in Indonesia from 2016 to 2023

Astha Dandari Kusuma Wardhani[1], R. M. Tofan Sastranegara[1], Gylfi Pall Hersir[2], Egill Arni Gudnason[3], Lendriadi Agung[1], and Fadhilaz Digdaya Haq[1]

[1]PT Pertamina Geothermal Energy Tbk, Jakarta, Indonesia
[2]University of Iceland, Faculty of Earth Sciences, Reykjavik, Iceland
[3]Iceland GeoSurvey (ISOR), Urdarhvarf 8 203 Kopavagur, Iceland

astha.dandari@pertamina.com

Keywords: micro-gravity, gravity, monitoring, geothermal, Tompaso

ABSTRACT

The application of geophysical monitoring techniques is important in geothermal fields as they provide insights into reservoir changes during utilization. One of those techniques is the micro-gravity method which is used to study the mass changes in the reservoir due to fluid extraction and retrieval, represented by gravity changes with time. Seven micro-gravity surveys from 2016 to 2023 have been carried out in Tompaso geothermal field in Indonesia. The first measurement acted as a baseline was done in 2016, which was 4 months prior to the commissioning of the power plant of 2 x 20 MW. This study presents analysis of gravity change, 3-D inversion modelling of the cumulative 7-years time-lapse micro-gravity data and mass change calculation on the basis of 3-D density change model resulted from the inversion modelling. The study revealed that the negative density change area took place in the vicinity of production area which is associated with mass depletion. The study also discovered that the anomalous mass change might correlate with the permeable structures of Tompaso, intersected by the production and reinjection wells. The reservoir mass balance was estimated with the production-reinjection flow rates and time-lapse micro-gravity data. The mass change calculation results on the basis of both 3-D density change model and Gauss's theorem calculation are comparable, which give estimates of the reservoir mass balance. The result shows that the mass balance during the 2016-2023 period is in the range of -24 to -47 Mton which implies that the extracted mass was contributed from the natural recharge of approximately 24 to 47 Mton or 47% to 64% which likely originates from the western-, northern-, and southern part of the field, also indicated by the positive gravity anomaly.

1. INTRODUCTION

The application of geophysical monitoring techniques during geothermal utilization is important because they provide insights into reservoir change during utilization. The physical changes of fluid and reservoir rock properties which are induced by fluid pressure, temperature, and flow rate changes can be detected using e.g., micro-seismic tomography, micro-seismic amplitude attenuation, gravity changes, resistivity and magnetic field changes, remote sensing of surface heat-loss, and ground deformation mapping (Bromley, 2018). The result of geophysical monitoring techniques, in many cases, could also help to improve reservoir simulation models as well as contribute to reservoir management strategy.

Gravity monitoring, or time-lapse gravity, or micro-gravity, has been applied in numerous geothermal producer fields to monitor reservoir change which is represented by gravity changes with time. Mass displacement can cause gravity change by their direct gravitational effect and by deformations at the Earth's surface (Torge, 1989). Mass displacement could be due to natural (tectonic, volcanic) or artificial process of which in this case, is harnessing geothermal fluid. The application of gravity for geothermal reservoir monitoring have been published, such as for Wairakei, New Zealand by Allis and Hunt (1986), Hunt (1995), Hunt and Graham (2009); for Salak, Indonesia by Nordquist et al. (2010); and for Reykjanes, SW-Iceland by Gudnason et al. (2015). Performing the 3-D inversion modeling of gravity monitoring have been successfully applied for Kamojang (Agung et al., 2018) and "US" field (Haq et al., 2019) to evaluate the reservoir mass balance. Gravity monitoring data is also commonly used to validate numerical models since it provides important constraints for reservoir modeling, as have been studied by Protacio et al. (2000) and Nordquist et al. (2004) for Bulalo, Philippines. For better understanding and interpretation of gravity monitoring data, numerous additional data are involved in the analysis, including elevation, groundwater level, downhole data (pressure, temperature, water level), production-reinjection flow rates data, and reservoir numerical model parameter (permeability, porosity, saturation).

The Tompaso geothermal field is a high temperature- two-phase water dominated geothermal system with temperature of 260°-320°C, located in Minahasa District, North Sulawesi Province in Indonesia. The location of

the Tompaso field is displayed on Figure 1. Tompaso belongs to the southern part of the Lahendong geothermal concession, which is owned and managed by PT Pertamina Geothermal Energy, Tbk (PGE). Geologically, it is situated in the northern arm of Sulawesi Island, particularly within Tondano depression which lies within the Sangihe volcanic arc in the Minahasa compartment in the northeastern sector of Sulawesi Island. The volcanic arc is believed to been formed by the subduction of the Molucca sea plate resulting from the collision of Sangihe and Halmahera forearcs (Hamilton, 1979).

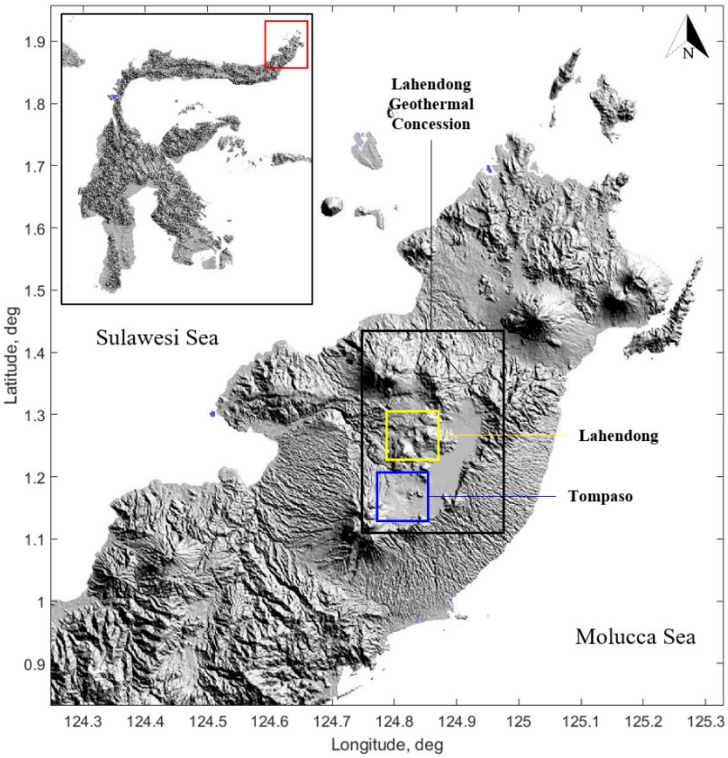

Figure 1: Location of the Tompaso (blue rectangle) and Lahendong (yellow rectangle) geothermal fields in North Sulawesi. The black rectangle shows the Lahendong. geothermal concession. The inset figure shows the Sulawesi Island and the zoomed-in area with a red rectangle.

Tompaso has been generating electricity with an installed capacity of 2 x 20 MWe through two geothermal power plants, Unit 5 & 6 since 2016 (while Unit 1, 2, 3, and 4 are in the Lahendong geothermal field). The Unit 5 and 6 utilize five wells of which all wells are located in Wellpad-C. The hot fluid waste are reinjected to the reservoir through four reinjection wells which are placed in Wellpad-D and E. The location of the wells are shown on Figure 3. The latest geoscientific and reservoir evaluation found the upside potential of Tompaso as confirmed by the recent exploratory wells, hence, PGE intends to develop an additional power plant in the near future.

During 7 years of utilization with continuous production and reinjection, several geophysical monitoring methods such as micro-gravity, elevation changes (ground deformation), and micro-seismics have been carried out in the Tompaso field. In the case of micro-gravity and elevation monitoring, the first measurements were performed in early 2016 prior to the commissioning date, so they serve as a monitoring baseline. Since then, PGE has conducted the data acquisition periodically.

This study presents micro-gravity analysis of the Tompaso geothermal field from 2016 to 2023 to give insight about reservoir changes due to mass displacement during the production and reinjection activities through 3D-density change modelling. The study involved information on production-reinjection flow rates and other supporting data to help the interpretation and to estimate the reservoir mass balance.

2. METHODOLOGY

2.1 Gravity Data

Gravity monitoring is principally performed by repeated measurements at fixed points (benchmarks) within a particular time interval. At the Tompaso geothermal field, gravity measurements for monitoring have been carried out once a year since 2016 until 2023, except in 2020 due to the coronavirus pandemic. The first measurement acting as a baseline was done in May 2016, which is 4 months prior to the commissioning of the power plant in September 2016, followed by new measurements in March the following years. Gravity data were acquired in the

same month each year with the purpose of minimizing the effects of seasonal variations and for periodical analysis and interpretation.

The gravity network used for monitoring in Tompaso covers an area of approximately 90 km^2, of which benchmarks are distributed within the production field, reinjection field, and beyond the reservoir area. The numbers of gravity benchmarks are different between years because benchmarks were added during the following years for better data coverage. The total number of benchmarks were 80 in 2016, 88 in 2017, 108 in 2018 and 2019, and 129 in 2021, 2022, and 2023 (Figure 2). Several benchmarks were lost and destroyed due to unexpected construction work. The gravity monitoring network is depicted in Figure 3. The benchmark TPS-B was assigned as local gravity base point of where all points were tied to, before referenced to the regional benchmark BMKG which was established by the Indonesian Meteorology, Climatology, and Geophysical Agency. The regional benchmark is located about 25 km to the North and is assumed not to be experiencing mass changes or deformation due to geothermal utilization at Tompaso or Lahendong. In addition, it has a known absolute gravity value, hence, it was also used for calibration of the gravimeter. The reference point was measured through repeated data acquisition Base–Regional–Base–Regional–Base and was performed twice which is in the beginning and end of the gravity survey.

The observed gravity data were ensured to be reliable through quality control and correction of tidal effect and drift. Tidal effect is a variation in gravity observations resulting from the attraction of the moon and sun, while drift is a gradual change caused by a heating up of the gravimeter's spring with time. The standard Earth tide correction is applied using Longman's formula which is featured in the gravimeter (Scintrex, 2012). Gravity data at each benchmark were acquired for 15 minutes with recording interval of 30 seconds to ensure stable gravity readings. The gravity data quality control incorporated the standard deviation, tilt, drift, and repeatability at each point. The data show that all the measurement points are of appropriate with an average standard deviation less than 10 µGal, tilt x-y less than 2 arc-sec, drift less than 10 µGal, and repeatability less than 4 µGal.

For the analysis of time-lapse gravity, additional measurements were performed, including precise elevation and groundwater level measurements. The precise elevation measurements were carried out simultaneously with the gravity data acquisition at the same benchmarks. Groundwater level data were collected by measuring the groundwater level at several locations in shallow wells every 1-2 months. The coverage of groundwater level monitoring varies between years as several additional wells were drilled for better data coverage.

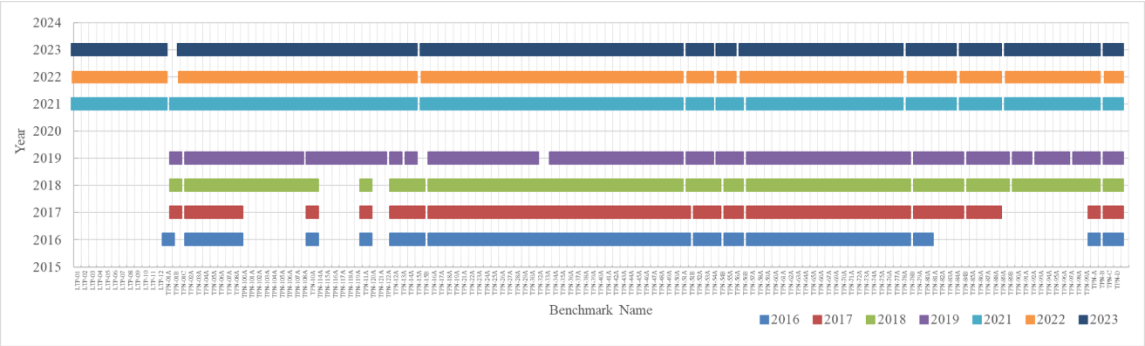

Figure 2: Gravity monitoring benchmarks in 2016 to 2023.

2.2 Production & Reinjection Data

The Tompaso power plant has been generating electricity since September 2016 through Lahendong Unit 5 and 6. The hot fluid has been extracted from five production wells located on well pad C. The production wells are Well-C1, C2, and C3 for Unit 5, and Well-C5 and C6 for Unit 6. Hot fluid is reinjected into the reservoir through four reinjection wells located on well pad D and E which are Well-D1, D2, E1, and E2. The location of the production and reinjection area is shown on Figure 3.

In the analysis of the gravity monitoring data, the extracted- and reinjected mass data from wells are important to estimate the mass balance of the harnessed reservoir. The approximate extracted- and reinjected mass during gravity monitoring periods is shown in Table 1. The extracted mass is defined by negative values corresponding to a mass withdrawal, while the reinjected mass is given as positive values implying a mass retrieval. Until February 2023, the total mass extracted for Unit 5 and 6 was -92.02 Mton. The largest mass was extracted from Well-C5 with mass of -32.01 Mton or 35% of the total extracted mass, followed by Well-C2, C6, C3, and C1. The total reinjected mass was 79.05 Mton which means that 86% of the total extracted mass was reinjected into the reservoir. The largest mass was reinjected through Well-E2 with 30.19 Mton or 38% of the total mass reinjected, followed by Well-E1, D1, and D2. Figure 4 shows the approximate total monthly mass from extraction and reinjection which suggests that in general there is no significant change in the extraction and reinjection scenario

over 7 years of utilization in Tompaso. An enormous extraction mass increase was only observed between November and December 2016 which took place in the beginning of the power plant operation.

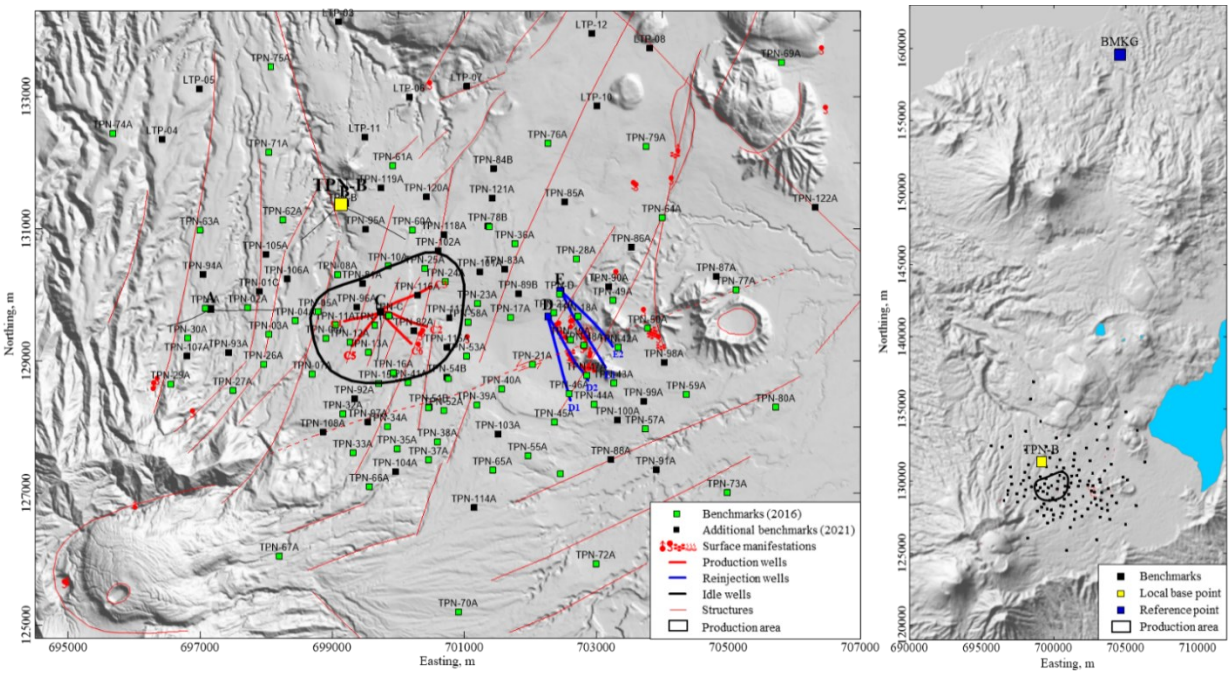

Figure 3: Gravity monitoring benchmarks measured in 2016 (green squares) and additional benchmarks measured in 2021 (black squares) displayed on the left figure, and their location relative to the reference point (blue square) on the right figure. Benchmark TPN-B acted as local gravity base point in the Tompaso field (yellow square).

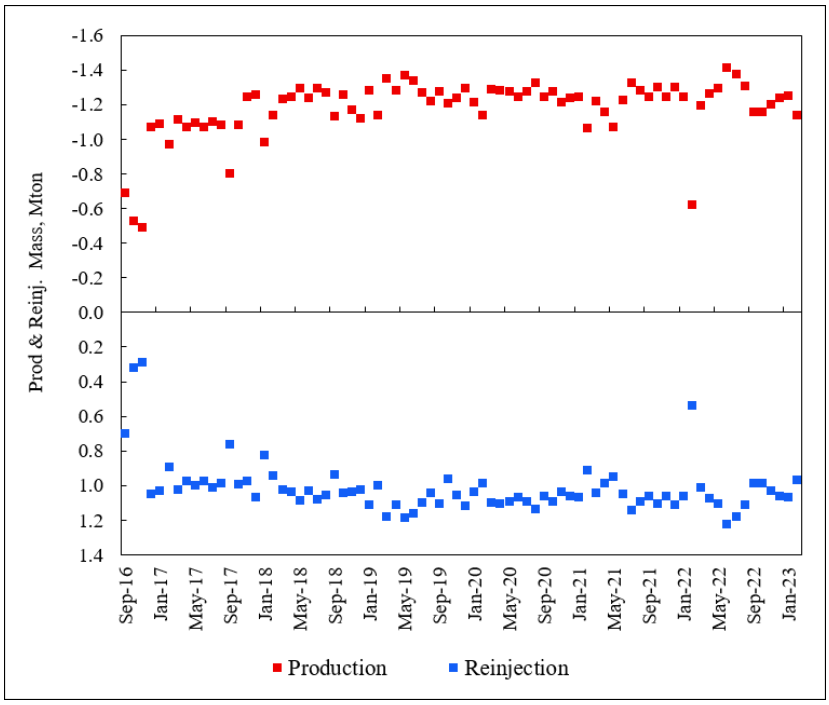

Figure 4: Tompaso geothermal power plant: approximate monthly extraction and reinjection mass in Mton.

2.3 Method

Basically, time-lapse gravity monitoring is a subtraction of observed gravity data at one year from the data of the previous year. Based on yearly data availability as depicted in Figure 2, six periods of observed gravity changes were obtained: 2016-2017 (9 months), 2017-2018 (1 year), 2018-2019 (1 year), 2019-2021 (2 years), 2021-2022 (1 year), and 2022-2023 (1 year). All the measured gravity data are with reference to the reference point BMKG

as the reference point was tied with the base point TPN-B a couple of times during each survey period.

Table 1: Approximate extracted and reinjected mass.

Year	Extracted Mass (Mton)						Reinjected Mass (Mton)				
	Well-C1	Well-C2	Well-C3	Well-C5	Well-C6	Total	Well-D1	Well-D2	Well-E1	Well-E2	Total
2016-2017	-0.68	-0.93	-0.96	-1.52	-0.75	-4.84	0.49	0.53	1.08	2.17	4.27
2017-2018	-1.75	-2.38	-2.22	-4.39	-2.31	-13.06	1.67	1.88	2.92	5.07	11.53
2018-2019	-2.01	-2.72	-2.21	-5.09	-2.66	-14.68	2.50	2.03	2.91	5.02	12.46
2019-2020	-1.83	-3.55	-2.34	-5.16	-2.33	-15.21	2.79	2.77	2.80	4.66	13.02
2020-2021	-1.81	-3.45	-2.29	-5.17	-2.28	-15.00	2.80	2.51	2.95	4.56	12.81
2021-2022	-1.72	-3.08	-2.12	-5.18	-2.15	-14.26	2.76	2.49	2.81	4.12	12.19
2022-2023	-1.79	-3.20	-2.20	-5.50	-2.28	-14.97	2.97	2.41	2.78	4.61	12.77
Total	-11.60	-19.31	-14.34	-32.01	-14.76	-92.02	15.98	14.62	18.26	30.19	79.05
Percentage	13%	21%	16%	35%	16%	100%	20%	18%	23%	38%	100%

In order to capture the gravity effects of mass displacement due to geothermal utilization, the observed gravity changes were corrected for elevation and groundwater level changes. In the case of the effect of elevation changes, the study applied the free-air correction formula to derive the gravity effect due to elevation change δg_h which is given by

$$\delta g_h\,(\mu Gal) = 3.086 \cdot \Delta h \quad (1)$$

where Δh is elevation change in cm. This means that elevation change of 1 cm contributes to a gravity change of 3.086 μGal. The elevation change correction was applied at all benchmarks.

The gravity effect of groundwater level changes can be estimated as a first approximation for uniform changes in homogeneous horizontal layers through a Bouguer plate model (Torge, 1989) of which Bouguer plate reduction δg_b is defined by

$$\delta g_b = 2\,\pi\,G\,\rho\,h \quad (2)$$

where *G* is the Gravitational Constant ($6.67 \cdot 10^{-11}$ $m^3\,kg^{-1}\,s^{-2}$), ρ is density (kg/m^3), and h is thickness (m). By using equation (2), the effect of groundwater level change is given by

$$\delta g_{gw}\,(\mu Gal) = 2\,\pi\,G\,\rho_w\,P\,\Delta h \cdot 10^8 \quad (3)$$

where ρ_w is water density (kg/m^3), P is water-filled pore space (%) and Δh is groundwater level change (m). The water density is assumed to be 1000 kg/m^3. Assuming that the depth to the groundwater is shallow, the porosity is higher than in the reservoir due to less consolidated material. Hence, here, it is assumed that P is around 25% (reasonable value for Tompaso). This means that a groundwater level change of 1 m contributes to a gravity change of ~10 μGal. In this study, one average value was used for every gravity monitoring period to correct for the effect of groundwater level change for the whole area which ranged from -12 μGal to 6 μGal.

The observed gravity changes after being corrected for elevation and groundwater level change were analyzed through; (1) plotting maps and graphs of gravity changes for both the cumulative and each monitoring period, (2) 3-D inversion modelling of gravity changes, (3) mass changes calculation to estimate the reservoir mass balance. The maps of the cumulative observed gravity changes from 2016 to 2023 were plotted using the grid summation technique which allowed the additional data in later years to be included. The gravity change was modelled with a 3-D inversion using VOXI Earth Modelling Extension in Oasis Montaj software (Seequent, 2023) to produce a 3-D density change model.

The total mass change M was then obtained simply by calculating the total of density change of a defined volume, which is given by

$$M = \sum_1^n (\Delta\rho \cdot V) \quad (4)$$

where density change $\Delta\rho$ is expressed in kg/m^3, volume V in m^3, and n is the total number of density changes cube from the 3-D model.

The mass changes on the basis of 3-D density changes model was then validated using Gauss's theorem formula. The amount of mass displacement can be estimated by applying Gauss's flux theorem to gravity data. Even though interpretation of gravity measurements is not unique in determining the distribution of anomalous masses, they can provide an estimate of the total anomalous mass which is corollary of Gauss's flux theorem in potential theory (Parasnis, 1986).

$$M = \frac{1}{2\pi G} \iint \Delta g \, dS \quad (5)$$

$$M = 2.39 \sum (\Delta g \, \Delta S) \quad (6)$$

where Δg is expressed in g.u, the surface area element ΔS in m^2 and M is in 10^3 kg (Mton). The estimate of M in Equation (6) is in some way an underestimate because it is common practices to apply summation in integration over a finite area, while on the contrary, M in equation (5) is over an infinite area (Parasnis, 1986). For Gauss calculation, a MATLAB-based program developed by PGE was used.

Finally, the reservoir mass balance was estimated incorporating the mass change resulting from gravity data and production-reinjection data that considered the percentage of mass recovery from tracer test interpretation.

3. RESULT AND DISCUSSION

3.1 Data Uncertainty

Prior to the analysis, uncertainties were evaluated to ensure the gravity data were acceptable in the analysis and to estimate data uncertainties in general. The uncertainties could be related to the accuracy of gravity and elevation data, benchmark stability, groundwater level change, and reference point. Regarding the accuracy of gravity data, the uncertainty could be given by the mean standard deviation of the measurements, which in this case, is in the range of 1 to 5 μGal, while the uncertainty due to elevation accuracy is between 2 to 5 μGal.

The measurement points should preferably be on a considerably stable bedrock. However, it is difficult to find bedrocks in Tompaso for benchmarks for gravity monitoring due to the soil cover on the surface. Therefore, all measurement points were man-made using concrete which is less firm than bedrock-benchmark. Therefore, they might deform. Such condition could contribute to the uncertainties, although there is no specific technique to assess the uncertainty in these circumstances.

Another factor that contributes to the uncertainty of gravity data in Tompaso is the groundwater level. Besides gravity and precise elevation measurements, ideally, a control point should include the groundwater level measurement to correct its effect. However, such procedures are quite costly. The availability of groundwater level monitoring data from shallow wells are limited to a particular area. As a result, data beyond this area are less reliable than within the area. Due to this limitation, one average value for each period was used to correct the effect of groundwater level change for the whole area which might not be representative at all sites. In addition, the uncertainty of gravity change is also affected by the porosity that is used in the groundwater level change correction, as the effective aquifer porosity is an important parameter that affects the amplitude of gravity change (Bromley, 2018). Based on the data distribution of groundwater level change that has been collected, the uncertainty due to groundwater level change was estimated about 20 μGal.

As discussed earlier, the reference point used in the processing is located at 25 km distance from the Tompaso geothermal area and the data were corrected for the drift and tidal effect. However, due to the reference point's proximity to the ocean which is only about 2.5 km away, the data are possibly affected by residual tidal effects, caused by ocean tidal loading and seismic noise generated from ocean waves. Effect of the ocean tides is one of the largest uncertainties in precise gravimetric measurements and may be corrected for with ocean tide loading models, direct measurement, and removal of a higher order drift function with frequent visits to base stations (Boddice et al., 2018; Orsulic et al., 2019). A study about tidal gravity measurements in Southeast Asia by Melchior et al. (1995) suggests that the oceanic tides contribution to the gravity data at the same reference point used in this study was about 5 μGal.

Based on the uncertainty evaluation as has been described, the total gravity uncertainty is approximately 35 μGal. In this case, the groundwater level change effect has contributed the most in the gravity uncertainty. Therefore, large number and good coverage of groundwater monitoring data are needed for better results.

3.2 Gravity Changes Analysis

The gravity changes between successive monitoring periods (2016-2017, 2017-2018, 2018-2019, 2019-2021, 2021-2022, and 2022-2023 in Tompaso field shows variations in the trend. Considering that there is no significant change in the production-reinjection scenario between years, and all the measurements were done in the same month each year, the gravity change anomaly trend should be quite similar. In this case, such trends could not be found. It might suggest that the gravity measurements detected very small variations. Therefore, to present a more simple understanding, the cumulative gravity change from 2016 to 2023 is analyzed instead. Several data from outer benchmarks are excluded to simplify the interpretation.

The gradual cumulative gravity change from 2016-2023 shows that, despite the uncertainties, in every observation period the trend of cumulative gravity change is consistent, as depicted in Figure 6. The 2016-2017 map shows how gravity changed after 6 months of geothermal production (Figure 6a). In that minimum period, the gravity

change of -50 to 20 μGal is observed, which is acceptable considering the uncertainty of 35 μGal. Moreover, this magnitude is reasonably justified according to study by Agung et al. (2023) that proposed the optimal magnitude of the gravitational-change anomaly to detect which is approximately greater than 25 μgal.

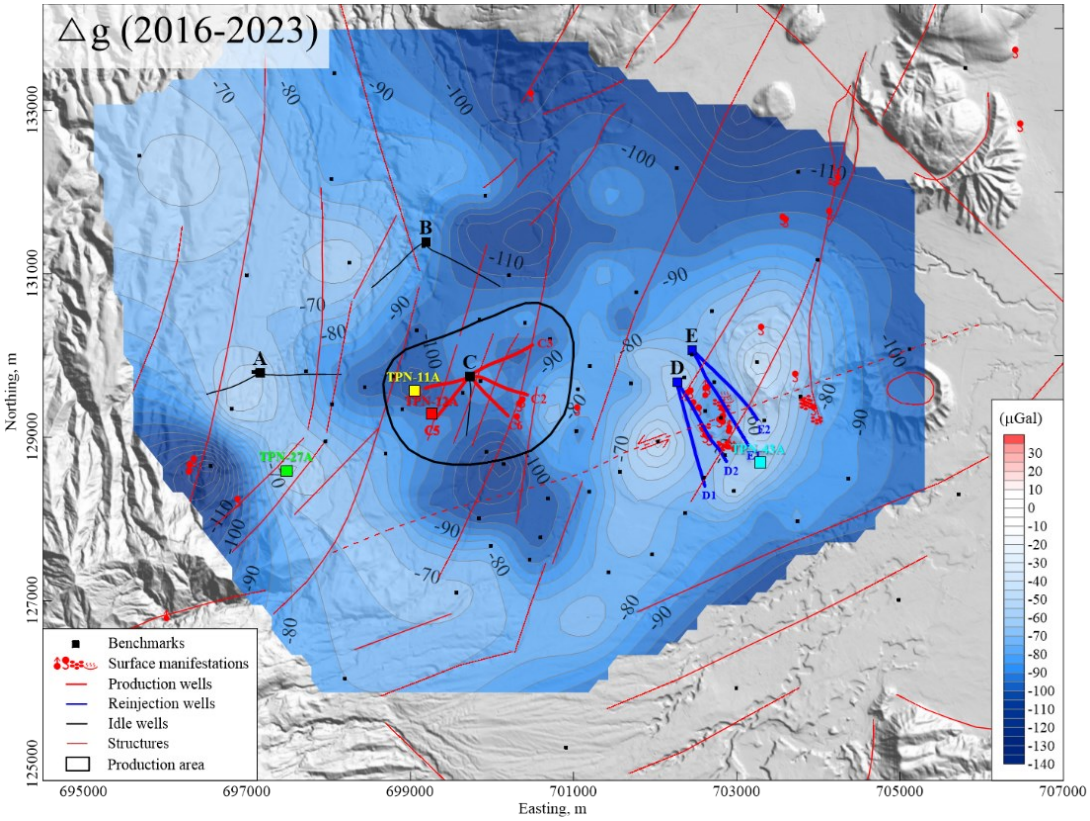

Figure 5: Map of cumulative gravity change of 2016-2023. Benchmark name can be seen in Figure 3. The displayed colored benchmarks (TPN-11A, 12A, 27A, 43A) are discussed further in the study.

The total cumulative gravity change from 2016 to 2023 is negative for the entire area (Figures 5). This could be due to uncertainties, or it could be due to mass changes outside the reservoir. However, the negative gravity changes observed in the northern part of Tompaso are probably affected by geothermal utilization in Lahendong field. Within ~7 years of geothermal utilization, the maximum gravity change reached -80 to -100 μGal in the production area which is comparable with the Reykjanes field in SW-Iceland which experienced a gravity change of -50 μGal during 2 and 4 year periods of production (Gudnason et al., 2015).

Even though negative gravity change takes place in the whole area, the maximum negative gravity anomaly of < -80 μGal is located in and around the production area, which suggests a greater mass depletion with years. The mass depletion might have reached the southern part of the production area as indicated by the extension of the big negative gravity change to the south of the production field. The big negative gravity change is also observed in Bukit Kasih and near reinjection well pad D and E which coincides with the surface geothermal manifestation complex. On the other hand, smaller negative gravity changes are seen around the reinjection area, and in the western to southern part of the Tompaso field. The less negative gravity change around the reinjection area might correspond to the mass retrieval from reinjection fluid in Well-D1, D2, E1, and E2, while the small gravity changes in the western to southern part of Tompaso might be associated with mass supply from outside the reservoir.

The gravity changes at each benchmark were plotted in a graph to give further ideas. The study gave several indications through the graph plots of gravity change at several benchmarks of which this study presents through examples displayed on Figures 7. For instance, the gravity change observed at benchmark TPN-11A (yellow square in Figures 5) that is located in the production area show that in the first phase of production during the 2016-2017 period, significant gravity changes were detected. This is probably due to sudden pressure drawdown and not enough mass support from the surrounding. The gravity changed more gradually in the next periods due to mass balancing process (pressure support). On the other hand, at benchmark TPN-12A (red square in Figures 5) even though it is located within the production field, the gravity changed slightly in the beginning (Figures 7). The observed gravity increase at benchmark 12A might be related to the high permeability zone at the NE-SW Tonsewer Faults that provide fast mass renewal, confirmed by the fact that well C5 delivers the highest mass of

all production wells. The increase of gravity change was also observed during 2017-2018 which implies that there is a quite huge mass inflow in that area.

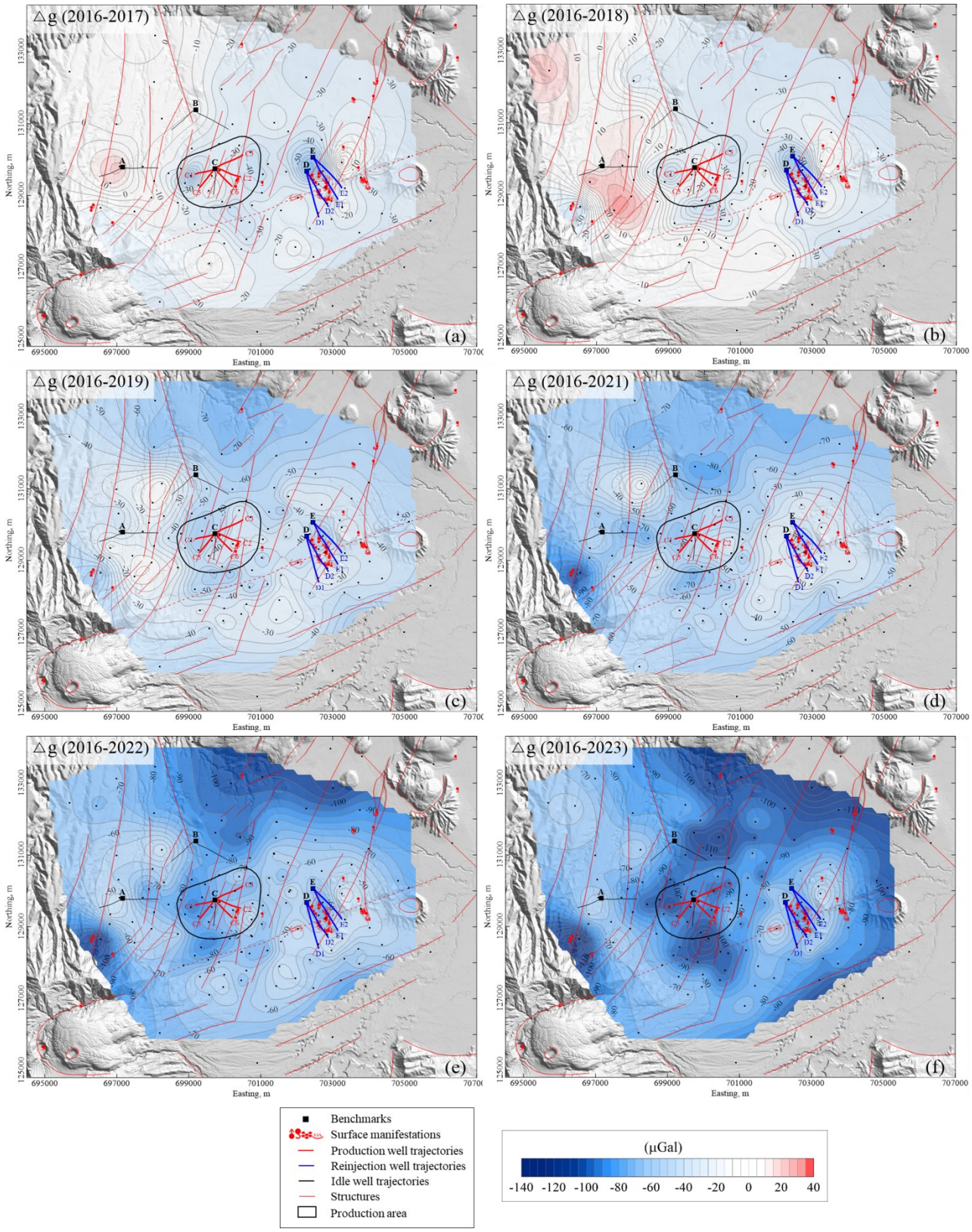

Figure 6: Gradual cumulative gravity changes in Tompaso from 2016 to 2023. Benchmark name can be seen in Figure 3.

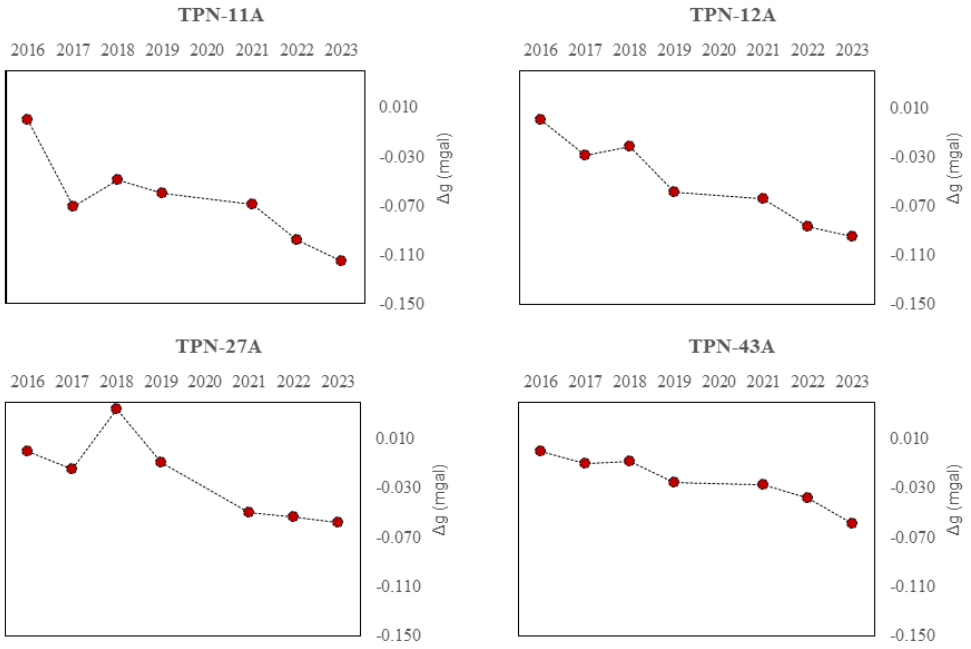

Figure 7: Gravity changes at benchmarks TPS-11A, 12A, 27A and TPN-43A. The location of the benchmarks can be seen in Figure 5.

The high increase of gravity changes during 2017-2018 was also observed clearly in the benchmarks located in the western part of Tompaso field, for example, TPN-27A (green square in Figures 5). Furthermore, the total cumulative gravity changes observed in these benchmarks only reached -50 to -70 μGal which is less than the ones around the production area. These findings suggest that the mass inflow is probably originated from natural recharge which is from the western part of the Tompaso field as indicated by the less negative cumulative gravity changes in that area. In the eastern part, most benchmarks which are located around the reinjection area, for example TPN-43A (blue square in Figures 5) shows gradual gravity change decrease. Furthermore, the total cumulative gravity changes reach -50 to -70 μGal which are comparable with the benchmarks located in the western part. This might correlate with the mass retrieval through reinjection wells D1, D2, E1 and E2.

3.3 The 3-D gravity change modelling

Gravity change modelling was performed to map the density changes in the subsurface. The modelling was performed using VOXI Earth Modelling Extension in the Oasis Montaj software (Seequent, 2023) for 3-D inversion of the cumulative gravity changes from 2016 to 2023. In order to model the gravity anomalies within the reservoir, the bottom of the clay cap was used as top mesh's geometry boundary with the assumption that there are no mass changes in the clay cap. This constraint was applied considering that the gravity change effects at shallow depths have been corrected through the elevation and groundwater level change correction. Hence, the anomaly was assumed to reflect the mass changes in the reservoir where it is located underneath the clay cap.

The inversion result is a 3-D density change model of which in this study is displayed at different depths as shown in Figure 8. The density changes during 2016-2023 are in the range of -0.009 to 0.010 kg/m^3. The result shows that the density change anomalies are well delineated at depths of 500 to 2500 m below sea level (b.sl), where the reservoir zone is found. It implies that the gravity anomalies are caused by the geothermal production-reinjection activity. The negative density change anomaly is observed around the production area which is clearly shown as density change at 1000 to 2500 m b.sl (Figure 8b, 8c, 8d, 8e). It suggests that the mass depletion reached greater depth than the production zone which reaches down to 800 m b.sl. as defined by the deepest production well. On the other side, the positive density change anomalies are detected around the reinjection area, which is interpreted as reinjection mass inflow, found at shallow depth down to 2500 m b.sl. (Figure 8a, 8b, 8c, 8d, 8e) which corresponds to the deepest reinjection well at 2000 m b.sl. The trend of the positive anomaly suggests that the reinjection fluid might flow mostly to the northeast through the NE-SW Totolan-Toraget fault. This interpretation is validated by results from a tracer test that showed interconnection between reinjection wells and manifestation located in the northeast as revealed by recent study (PGE, 2023). Meanwhile, the positive density change anomalies are found in the northern-, western- and southern part which are revealed from shallow depths down to 3000 m b.sl. as response to the natural recharge mass inflow.

Furthermore, the density change model reveals remarkable anomalies, giving further insights into reservoir

behaviour during 2016-2023. One distinctive anomaly is the positive density change observed clearly from 500 to 1000 m b.sl. that occurs in the southwest part of production area and coincides with the trajectory of Well-C5 (Figure 8a, 8b). This positive anomaly could be due to liquid re-saturation caused by recharge inflow into Well-C5 of which the production zone is located from 250 to 750 m b.sl. This interpretation agrees with a preliminary indication that the dryness and enthalpy of Well-C5 were decreasing, possibly as the result of the cold recharge inflow (PGE, 2023). In addition, production geochemistry monitoring data revealed that there is indication of natural recharge influx in Well-C5 as evidenced by the increased magnesium and decreased Non-Condensable Gas (PGE, 2023). This anomaly is also correlated with the gravity change increase in 2017-2018 that is observed at benchmarks TPN-07A, 12A and C which are located near Well-C5. This might be related with the high permeability zone of the NE-SW Tonsewer fault. Another noteworthy anomaly is the negative density change observed from 1000 to 2500 m b.sl. revealed in the south of production Well-C6 (Figure 8b, 8c, 8d, 8e, 8f). The interpretation could be that the production attracted mass from this area where the surrounding has low permeability which causes lack of mass supply leading to a greater depletion.

3.4 Mass Changes and Reservoir Mass Balance

Mass balance estimation was performed based on gravity and extraction-reinjection mass data. Mass change from gravity data was estimated through two methods, one method was through calculation on the basis of density changes resulting from the 3-D model within the defined volume, and the other method was by applying Gauss´s formula to the gravity change. In this study, both methods used the same area which is roughly defined by negative density changes from the 3-D model, interpreted as mass depletion area as depicted in Figure 9. The area used in the calculation excluded the reinjection wells, yet the reinjection mass inflow was taken into account in the mass balance estimation.

Due to uncertainty of the amount of reinjection mass inflow, the mass balance estimation used 2 scenarios for comparison. The first scenario used 25% of the total reinjected mass as indicated by tracer test interpretation regarding mass recovery observed in the production wells. However, this is considered a pessimistic number for mass balance calculation because the defined mass depletion area extended to the northeast and southeast of the production area which is closer to the reinjection wells. Hence, the reinjection fluid inflow in the area was believed to be higher. One hundred percent of reinjection fluid returning to the defined area might be unlikely, therefore, the second scenario used an approximate assumption of 50%. In the case of mass change calculation using density change, several thicknesses were applied; 1000, 1500, 2000, 2500, and 3000 m with the bottom of the clay cap surface used as the top boundary. The result of mass change calculations and mass balance estimations on the basis of density changes is shown in Table 2.

Table 2: Mass balance of 2016-2023 using density change model.

Thickness (m)	Calculated mass change (Mton)	Extracted mass (Mton)	Reinjected mass by 25% (Mton)	Reinjected mass by 50% (Mton)	Mass balance scenario 1 (Mton)[1)]	Mass balance scenario 2 (Mton)[1)]
1000	-8.45				-63.80	-44.04
1500	-17.24				-55.02	-35.25
2000	-25.68	-92.02	19.76	39.53	-46.58	-26.81
2500	-33.29				-38.97	-19.21
3000	-43.63				-28.62	-8.86

[1)] Mass balance = Extracted mass + Reinjected mass – Mass change

In the other method, mass change calculation applied Gauss's formula, given by Equation (6) using MATLAB-based program developed by PGE. Figure 10 shows the surface boundary used for the Gauss´s calculation which is the same area as used in mass changes calculation on the basis of density changes. Table 3 presents the result of the Gauss´s calculation and the mass balance estimation.

Comparing the two methods, both mass balance estimations using the Gauss´s theorem and density changes model show comparable results. From the calculations, it is revealed that the mass balance is negative for the 2016-2023 period. Moreover, the mass balance resulting from Gauss´s calculation for the 2016-2023 period corresponds to a reservoir thickness of 2000 m as revealed from the density change model. The results suggest that there was a natural recharge inflow approximately 24 to 47 Mton that supported the production during ~7 years of operation. The results indicate that the fluid renewal given by the ratio between natural recharge mass and net extracted mass for the 2016-2023 period ranges from 47% to 64%.

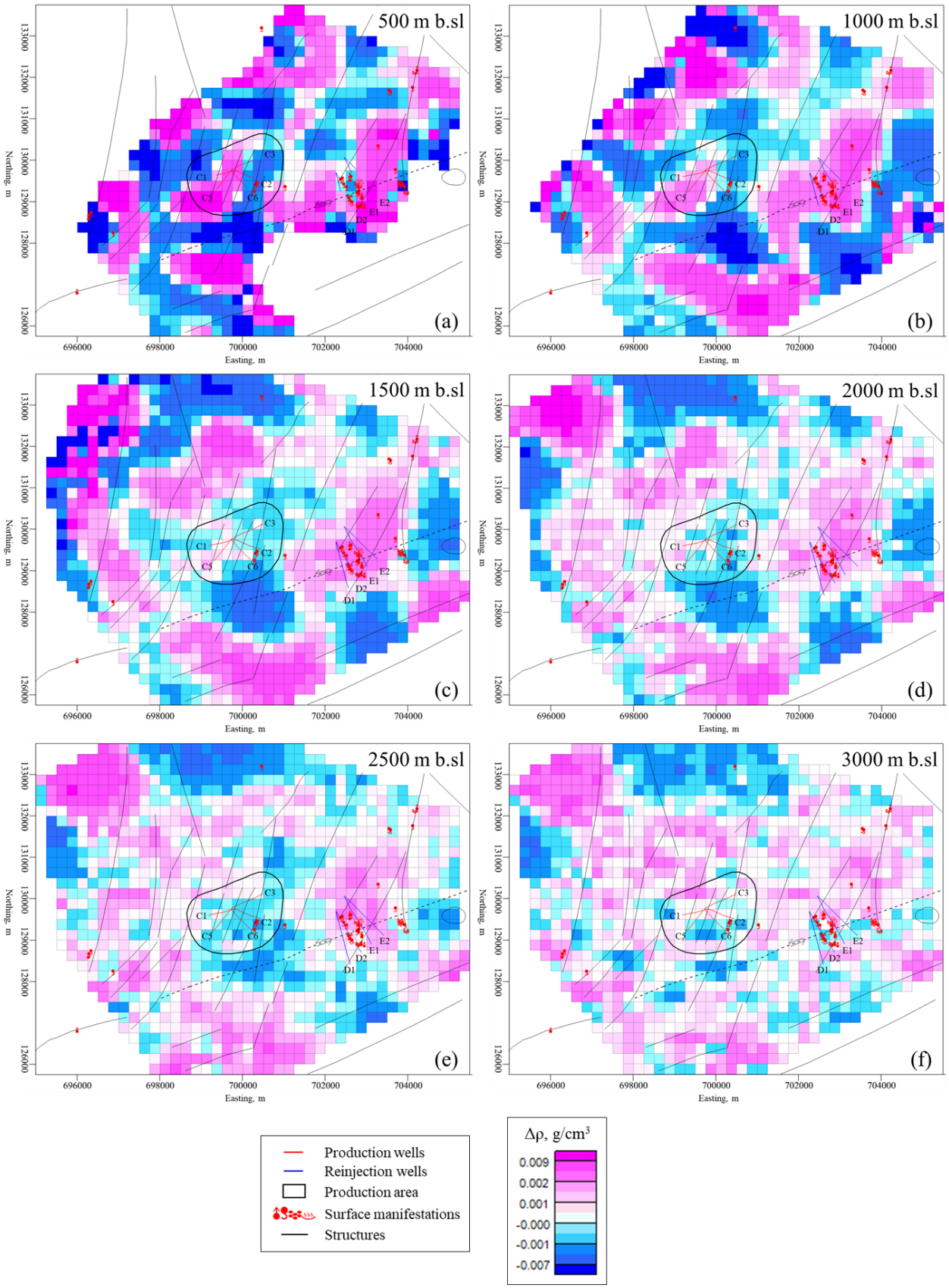

Figure 8: Density change cross-sections for the 2016-2023 period. The negative density change corresponds to mass depletion, while the positive density change is associated with mass gain.

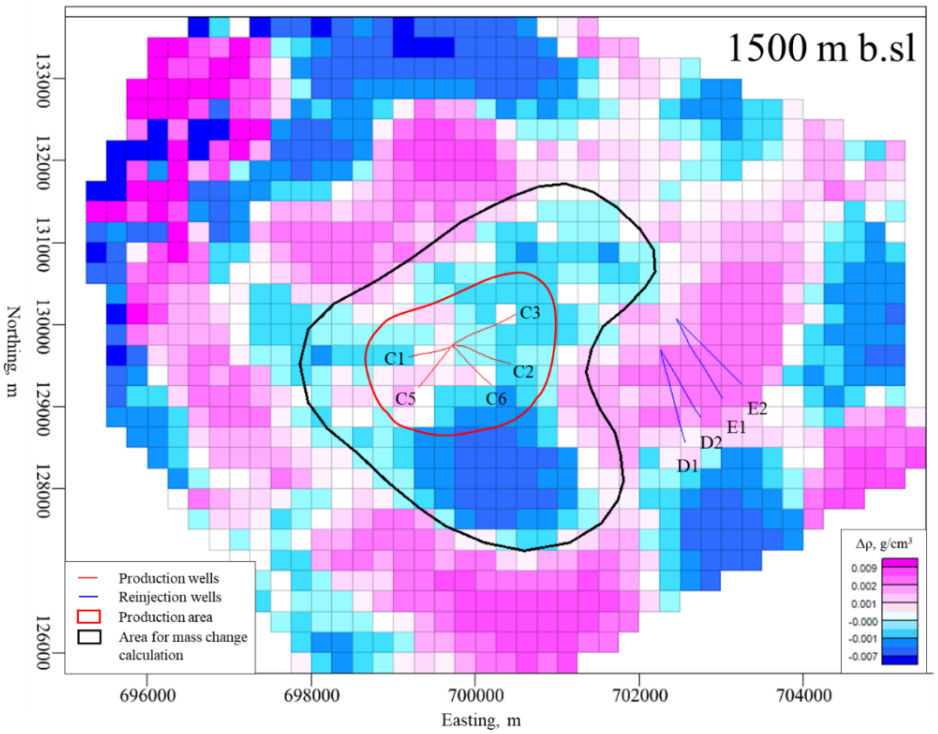

Figure 9: Aea used for mass change calculation.

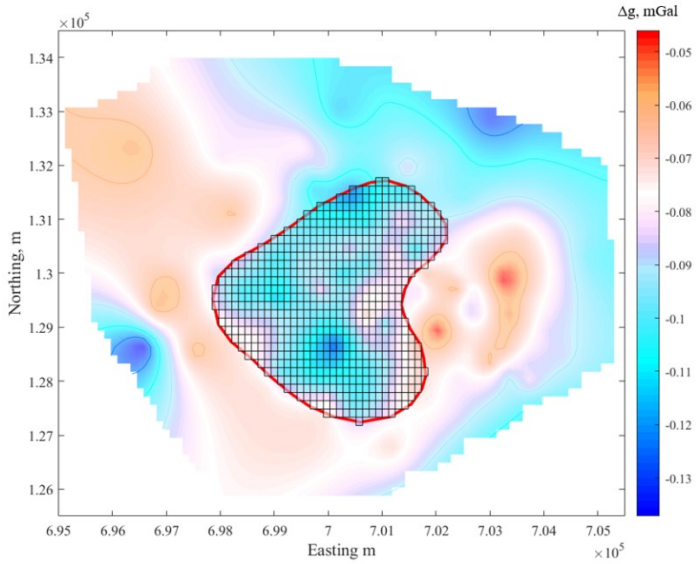

Figure 10: Area used for mass change calculation using Gauss's theorem.

Table 3: Mass balance using Gauss's theorem.

Period	Calculated Gauss mass change (Mton)	Extracted mass (Mton)	Reinjected mass by 25% (Mton)	Reinjected mass by 50% (Mton)	Mass balance scenario 1 (Mton) [1)]	Mass balance scenario 2 (Mton) [1)]
2016-2017[2)]	-8.2	-4.84	1.07	2.14	4.43	5.49
2017-2018	1.97	-13.06	2.88	5.77	-12.14	-9.26
2018-2019	-6.79	-14.68	3.11	6.23	-4.78	-1.66
2019-2021[3)]	-3.74	-30.21	6.46	12.92	-20.01	-13.55
2021-2022	-4.55	-14.26	3.05	6.09	-6.66	-3.61
2022-2023	-6.73	-14.97	3.19	6.38	-5.05	-1.86
2016-2023	-28.04	-92.02	19.76	39.53	-44.22	-24.45

[1)] Mass balance = Extracted mass + Reinjected mass – Calculated Gauss mass change
[2)] 9 months
[3)] 2 years

4. CONCLUSION

The analysis of gravity monitoring data has successfully revealed the reservoir behaviour in Tompaso during geothermal utilization for electricity generation from 2016 to 2023. Through gravity change modelling, it is revealed that the density change anomalies took place from the top of the reservoir down to 2500 m b.sl., which indicates that the anomalies occurred within the reservoir zone. The negative anomaly around the production area is associated with mass depletion and has extended to the southeast and northeast part of the pre-defined production area. The negative anomaly was observed down to 2500 m depth, which indicates that the extracted mass might originate from greater depth. The result also shows that there was an indication of natural recharge influx from the west within the production zone characterized by a positive anomaly as validated by geochemical data. Meanwhile, the reinjection fluid might flow mostly to the northeast as indicated by the trend of the positive anomaly. The anomalous mass change correlates with the most permeable structures in Tompaso trending NE-SW that were intersected by the production and reinjection wells.

Furthermore, mass change calculations using Gauss´s theorem and the density change model show comparable results which give estimates about the reservoir mass balance. The result shows that the mass balance during the 2016-2023 period is in the range of -24 to -47 Mton which implies that the extracted mass was contributed from the natural recharge of approximately 24 to 47 Mton which most likely originates from the western-, northern-, and southern part of the field. The fluid renewal for the 2016-2023 period is in the range of 47% to 64%.

The study also came up with several recommendations for improvement in the future gravity monitoring works in Tompaso. It is recommended to place an additional base point located 5-10 km from the existing outer benchmarks to the west or southwest that must be measured frequently during gravity surveys (preferably twice a day), as the current base point is likely affected by the geothermal activity. The current reference point should also be reconsidered due to its proximity to the ocean. Furthermore, it is suggested to improve the coverage of groundwater monitoring well data because in the Tompaso case the groundwater level changes contribute significantly to the gravity data.

REFERENCES

Agung, L., Rosid, M.S., Sastranegara, R.M.T., and Haq, F.D., Period Estimation of Time-Lapse Microgravity Monitoring Using Gauss Theorem – Case Study: Kamojang Geothermal Field, *International Journal of GEOMATE*, 25, 112, (2023), 11-20.

Agung, L., Sastranegara, R.M.T., Hendriansyah, T., Nugroho, S.I., Firmansyah, W., Dandari, A., and Raharjo, I.B., Kamojang Reservoir Mass Changes Revealed from The Application of Gauss Theorem to Microgravity Data during Periods 2016-2014, *Proceedings The 2nd Southeast Asian Conference on Geophysics (SEAGC)*, Bali, Indonesia, (2018).

Allis, R.G., and Hunt, T.M.: Analysis of Exploitation-Induced Gravity Changes at Wairakei Geothermal Field, *Geophysics*, 51, 8, (1986), 1647-1660.

Boddice, D., Atkins, P., Rodgers, A., Metje, N., Goncharenko, Y., and Chapman, D.: A Novel Approcah to reduce Environmental Noise in Microgravity Measurements Using a Scintrex CG5, *Journal of Applied Geophysics*, 152, (2018), 221-135.

Bromley C.: The Role of Advanced Geophysical Monitoring in Improved Resource Expansion and Make-up Well Drilling Strategy, *Proceedings 43rd Workshop on Geothermal Reservoir Engineering*, Stanford University, California, (2018), 8 pp.

Gudnason, E.Á., Arnaldsson, A., Axelsson, G., Berthet, J.C.C., Halldórsdóttir, S., and Magnússon, I.T.: Analysis and Modelling of Gravity Changes in the Reykjanes Geothermal System in Iceland, During 2004-2010, *Proceedings World Geothermal Congress 2015*, Melbourne, Australia, (2015), 8 pp.

Hamilton, W.B.: Tectonic of The Indonesian Region, *United States Geological Survey*, Washington, (1979), 345 pp.

Haq, F.D., Sastranegara, T., Agung, L., Kusuma, A.D., Hendriansyah, T., Fanani, A.F., and Raharjo, I.B.: Production and Reinjection Evaluation on The Basis of 3-D Time-lapse Microgravity Inversion, *IOP Conf. Ser.: Earth Environ. Sci.*, (2019), 318.

Hunt, T.M.: Microgravity Measurements at Wairakei Geothermal Field, New Zealand; A Review of 30 years data (1961-1991). *Proceedings World Geothermal Congress 1995*, Firenze, Italy, (1995), 6 pp.

Hunt, T.M., and Graham, D.J.: Gravity changes in the Tauhara sector of the Wairakei-Tauhara geothermal field, New Zealand, *Geothermics*, 38, 1, (2009), 108-106.

Melchior, P., Francis, O., and Ducarme, B.: Tidal Gravity Measurements in Southeast Asia, *International Association of Geodesy*, *Symposium Geodesy in Southeast Asia*, USA, (1995), 9493-9507.

Nordquist, G.A., Acuna, J.A., and Stimac, J.: Precision Gravity Modeling and Interpretation at the Salak Geothermal Field, Indonesia, *Proceedings World Geothermal Congress 2010*, Bali, Indonesia, (2010), 8 pp.

Nordquist, G.A., Protacio, J.A.P., and Acuna, J.A.: Precision Gravity Monitoirng of the Bulalo geothermal field, Philippines: Independent Checks and Constrains on Numerical Simulation, *Geothermics*, 33, (2004), 37-56.

Orsulic, O.B., Varga, M., Markovinovic, D., and Basic, T.: LTIde-Matlab/Octave Software Tool for Temporal and Spatial Analysis of Tidal Gravity Acceleration Effects According to Longman Formulas, *Earth Science Informatics*, 12, (2019), 405-414.

Parasnis, D.S.: Principles of Applied Geophysics (Fourth Edition), *Chapman and Hall*, New York, (1986), 412 pp.

PGE: Reservoir Monitoring Assessment Lapangan Tompaso, *Pertamina Geothermal Energy*, unpublished internal report (in Indonesian), (2023).

Protacio, J.A., Golla, G., Nordquist, G., Acuna, J.A., and San Andres, R.B.: Gravity and Elevation Changes in The Bulalo Geothermal Field, Philippines: Independent Checks and Constrains on Numerical Simulation, *Proceedings 22nd New Zealand Geothermal Workshop*, (2000), 5 pp.

Scintrex: CG-5 Scintrex System Operation manual, *Scintrex Limited*, Canada, (2012), 312 pp.

Seequent: VOXI, *website*, https://www.seequent.com/products-solutions/geosoft-oasis-montaj/voxi/, (2023).

Torge, W.: Gravimetry, *De Gruyter*, Berlin, (1989), 465 pp.

Optimalize Geothermal Exploration Potential with Comprehensive Gravity and Landsat Method at Tanggeung Area, West Java, Indonesia

Rahman F, Mawalid A, Fadrian D F, Herlambang K A, Kurniasih, and Pangestu F B

fadhrahman1911@gmail.com, abimawalid10@gmail.com, dhikafaiz@gmail.com, kevinadhiatha@gmail.com, kurniaasih.1219@gmail.com, 11510061@student.upnyk.ac.id

Keywords: Geothermal, Tanggeung, CBA, TSA, 3D Modelling, LST

ABSTRACT

Geothermal energy represents a significant renewable resource potential for Indonesia, especially given its location between volcanic mountains and tectonic plate intersections along the equator. This study focuses on the Tanggeung Area in Cianjur Regency, West Java Province, which holds considerable geothermal potential. Through a combination of geophysical methods and geological analysis, we conducted modeling and characterization of geothermal manifestations in the area.

Previous research in 2009 suggested the presence of geothermal manifestations acting as outflows in Tanggeung. The lithology in the study area is predominantly composed of clay, tuff, and breccia, with the Jampang Bawah formation as the oldest exposed rock. This study utilized geophysical methods, including Complete Bouguer Anomaly (CBA) maps and Trend Surface Analysis (TSA), toidentify geological structures and geothermal anomalies. 3-D modeling results indicated the presence of a clay cap interpreted as breccia, tuff, and andesitic lava from Mount Patuha, as well as reservoir rocks believed to be tuff and sand from the Cibuni River deposits.

Interpretation of geophysical and geological data indicated significant geothermal potential in the Tanggeung area. High gravity anomalies led to the presence of the Jampang Atas formation with tuff breccia, tuff, and andesitic lava rocks from Mount Patuha. Fault analysis and thermal analysis indicated a heat flow from Mount Patuha towards Tanggeung, subsequently giving rise to geothermal manifestations in Leuwilutung.

Validation results using Land Surface Temperature maps and mineral alteration maps supported the findings of geothermal manifestations in Tanggeung. Land Surface Temperature maps showed temperature anomalies consistent with the presence of geothermal manifestations, while mineral alteration maps indicated mineral distribution indicative of rock alteration processes in the area.

Thus, this study provides a significant contribution to understanding geothermal potential in Indonesia, particularly in the Tanggeung Area. These findings have significant implications for the development of renewable energy and the diversification of energy sources, and may serve as a basis for practical steps in utilizing geothermal energy for power generation and other purposes.

1. INTRODUCTION

The utilization of geothermal energy offers more advantages compared to the use of fossil fuels. Geothermal energy is a stable renewable energy alternative, independent of weather or seasonal changes. Geothermal energy sources in Indonesia are widely distributed, with over 300 recorded points from Sabang to Merauke. This potential can be harnessed as a replacement for non-renewable energy sources such as fossil fuels for electricity generation and transportation. Effective utilization of geothermal energy will reduce dependence on conventional energy sources and help address electricity supply issues, which remain a concern for the Indonesian government (Nurwahyudin & Harmoko, 2020).

Geological structures play a crucial role in geothermal systems because features such as faults function as water channels that allow heat movement. However, in geothermal exploration efforts, determining geological structures has limitations. When geological surveys are conducted to identify rock types and geological structures, only those visible on the earth's surface can be detected. Structures covered by sediment layers above are not visible. Therefore, in geothermal exploration, geophysical methods are key to identifying the presence of geothermal systems. Commonly used geophysical methods include resistivity, magnetic, gravity, and electromagnetic techniques. These are preferred over active seismic methods because most geothermal areas are located in volcanic regions where igneous and metamorphic rocks dominate. Additionally, subsurface structures in volcanic areas are generally not layered, making them difficult to detect with active seismic methods.

The research target location is in the Tanggeung area, located in Cianjur Regency, West Java Province. Previous research conducted in 2009 interpreted hot spring data in Tanggeung. The results of this study indicated the presence of manifestations suspected to be the outflow of the Tanggeung area.

The Tanggeung research location is dominated by claystone, tuff, and breccia lithology. By using the gravity method approach, such as the Complete Bouguer Anomaly (CBA) map, residual anomalies, and the Trend Surface Analysis (TSA) map. The results of the TSA map are then correlated with the alteration mineral map and the Land Surface Temperature (LST) map. This study concludes with 3-D modeling of the manifestations and the obtained volume in the Tanggeung Geothermal area, West Java.

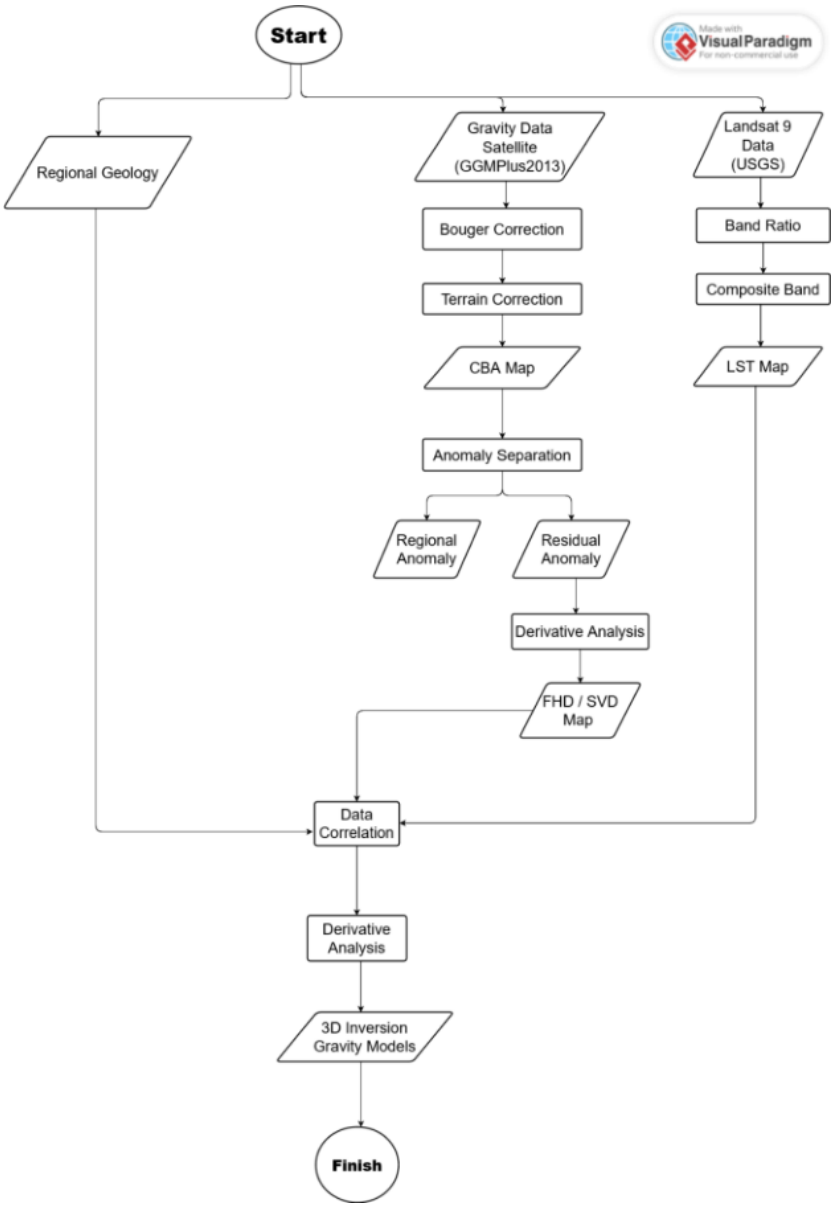

Figure 1: Research Flowchart on Tanggeung Geothermal Area, West Java.

2. METHODOLOGY

The gravity method is a geophysical technique that measures changes in the gravitational field caused by variations in horizontal density below the surface. This method is used to define the architecture of the Earth's crust, identify potential locations for resource exploitation, and build conceptual exploration models for regional Earth characterization. Measurements are taken using a gravimeter, an advanced instrument that measures gravitational acceleration. Gravimeters can be used on the surface or underground if needed (Hinze, Frese, and Saad, 2013).

The presence of a subsurface mass causes a disturbance in the gravitational value, known as a Bouguer anomaly or gravity anomaly. A Complete Bouguer Anomaly (CBA) is derived from gravity data that has undergone various corrections. The equation for CBA is as follows (Telford, Geldart, and Sheriff, 1990):

$$CBA = gobs - g\theta \pm FAC \pm BC + TC \quad (1)$$

Where:

CBA : Complete Bouguer Anomaly (CBA)
gobs : Gravity data obtained from measurement results
gθ : Latitude Correction
FAC : Free Air Correction
BC : Bouguer Correction
TC : Terrain Corection

2.1 Gravity Correction

Gravity methods also include corrections to eliminate noise or additional data obtained from gravity measurements. These corrections are as follows.

2.1.1 Free Air Correction

In geophysics, the free-air gravity anomaly (often referred to as the free-air anomaly) is the gravity anomaly measured after applying a free-air correction. This correction accounts for the elevation at which the measurement was taken, adjusting the gravity measurements to what they would be at a reference level, usually mean sea level or the geoid. Because gravitational values are greatly influenced by distance, it is important to perform an elevation correction from one measurement point to the next. The average value of the free-air gravity gradient is 0.3086 mGal/m or 0.0941 mGal/foot. The following equation can be used to obtain the free-air correction value:

$$FAC = 0.3086\ x\ h \quad (2)$$

Where FAC: Free Air Correction, H: Elevation or height in meters

2.1.2 Terrain Correction

Earth's surface is uneven and wavy according to its topography, So terrain correction is used to level the measuring plane. The formula for field correction is as follows:

$$TC = 0.04193(\rho/n)\ r_2 - r_1 + \sqrt{(r_1^2 + z^2)} - \sqrt{(r_2^2 + z^2)} \quad (3)$$

Where TC: Terrain Correction, ρ : Density of the rock mass, n: The number of segments contained in the zone, r_1: Radius of the inner circle, r_2: Radius of the outer circle, z: The height of a hill or the depth of a valley

2.1.3 Bouger Correction

The Bouguer correction is used to reduce the influence of the gravitational pull of rock mass or material between an observation point and a reference point (mean sea level) when the rock layer is assumed to be infinite. The Bouguer correction formula is as follows:

$$BC = 2\pi G\rho h \quad (4)$$

Where BC: Bouguer Correction, G: Gravitational Constant (6.672 x 10-11 N m2 kg-2), ρ : Rock Density (gr/$cm3$), h: Height above sea level (meter)

2.1 Geology Setting

The oldest rocks exposed in the Tanggeung geothermal area consist of sandstone and claystone, which are part of the Lower Jampang Formation from the Miocene (Tertiary period). Overlying these basement rocks are breccia tuff, tuff, and andesite lava, which belong to the Upper Jampang Formation from the Miocene.

These formations are found along the Cibuni River flow up to the Kadupandak area, which is occupied by alluvial deposits. This area is generally cultivated by the local population for rice paddies, with water sourced from the Cibuni River.

On this geological map, the hot spring manifestations in the "Leuwilutung" area can also be seen. These manifestations are hot springs estimated to be close to the upflow potential of the Tanggeung geothermal area in West Java.

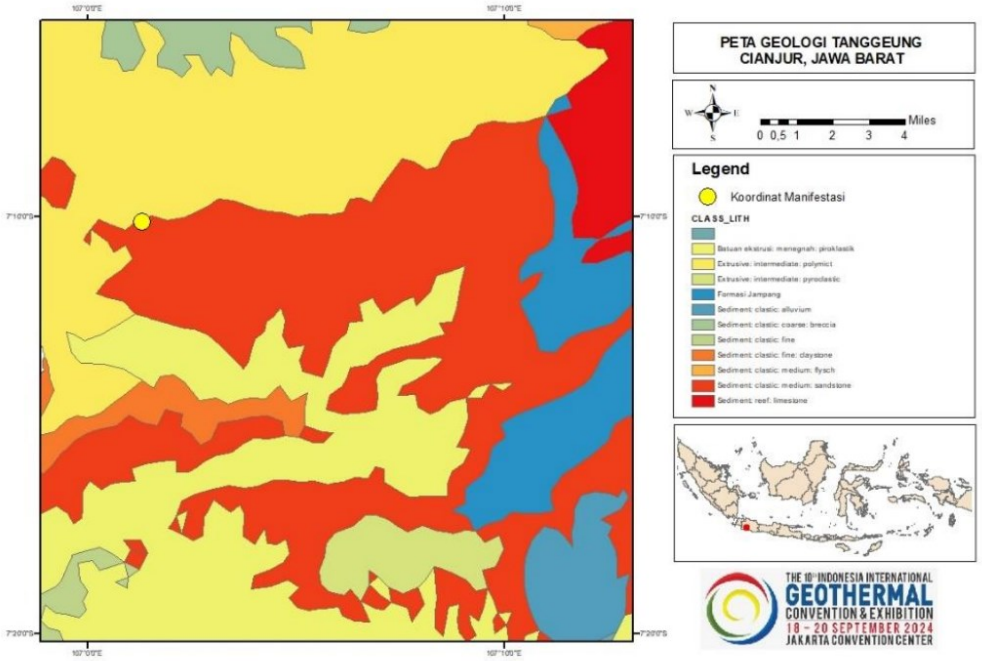

Figure 2: Geology Map of Tanggeung.

2.2 First Horizontal Derivative (FHD)

First Horizontal Derivative (FHD) is the rate of change in gravity horizontally (in the X and Y directions) and is measured in mGal. Sharp changes in anomalies at the contact of bodies will result in maximum FHD values, making it useful for indicating geological structure boundaries based on gravity data. The FHD value is calculated using the following equation:

$$FHD = (g_{(i+1)} - g_i)/\Delta x \quad (5)$$

Where FHD: First Horizontal Derivative (mGal), g: Anomaly (mGal), Δx: The difference in distance along the trajectory

2.3 Land Surface Temperature

Land Surface Temperature (LST) is defined as the temperature condition of the outermost part of an object on the ground surface. LST data can be used for various applications, such as exploration, development, monitoring, and geothermal management, as well as for environmental studies related to geothermal.

Land Surface Temperature (LST) is the ground surface temperature that can be measured using satellite data such as Landsat 8. Landsat 8 has two thermal bands (band 10 and band 11) that record thermal radiation emitted by the earth's surface.

To obtain the final Land Surface Temperature (LST) values, thermal band data processing is required to obtain the Top of Atmosphere (TOA) Radiance, Brightness Temperature (BT), and Land Surface Emissivity (LSE) values (Anandababu et al., 2018).

LST values are converted from satellite temperature values using the following equation:

$$LST = Ts/[1 + (\lambda C_2) \ln e]$$

Where LST: Land surface temperature, Ts: Temperatur satelit, λ: Panjang gelombang satelit citra lansat 8, C2: 14388, e: Emisivitas

2.4 3D Analysis

3-D analysis in gravity methods allows for cubic analysis of gravity data. This technique is useful for various purposes, such as determining the distribution of rocks, identifying geological structures, and making volumetric estimations, such as assessing the potential fluid storage capacity in a given area.

Below is the flowchart of the research conducted in the Tanggeung Geothermal area, West Java.

3. DISCUSSION

3.1 Digital Elevation Model

The topography of the area shows that the research area has a topographical range between 28 to 588 meters above sea level. The southern part of the research area has low topographical values, ranging from 28 to 169.4 meters above sea level, and is dominated by the southern part of the study area, which is suspected to be near the South Java coast in Cianjur, hence the low elevation. Conversely, the central and northern parts of the research area have high topographical values extending eastward, ranging from 177.5 to 588.4 meters above sea level, and are suspected to be hills leading to Mount Patuha from the research location. It can also be seen that the majority of geothermal manifestations are located in areas with medium to high elevation. The manifestation with the highest temperature is located in the upper northern part of the research area, known as the "Leuwilutung" manifestation.

3.2 Complete Bouger Anomaly (CBA)

The Complete Bouguer Anomaly (CBA) map of the study area below shows that the gravity field anomaly values ranging from 157.8 to 203.8 mGal. The high anomaly spreading in the southern part and heading southwest can be interpreted as the Upper Jampang Formation, consisting of breccia tuff, tuff, and andesite lava. These rocks are suspected to originate from the formation in Mount Patuha, extending towards Tanggeung. This high gravity field anomaly ranges between 203.8 and 180.7 mGal. The low gravity field anomalies, with values ranging from 157.8 to 180.7 mGal, are mostly located in the northern part of the research area. This low anomaly correlates with alluvial deposits and sandstone stretching from west to east in the northern part of the study, with the low anomaly area also occupying the manifestation area considered to be the outflow in the research location, namely Leuwilutung.

The CBA map still shows a considerable degree of ambiguity because the anomalies on the map are a combination of residual anomalies (shallow sources) and regional anomalies (deep sources). Therefore, separating the anomalies is still necessary to eliminate this ambiguity.

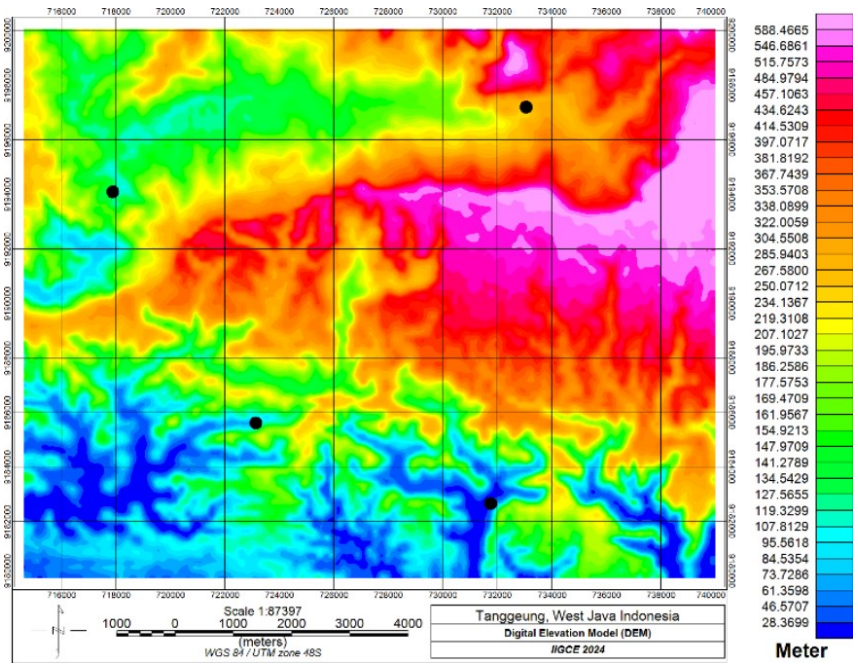

Figure 3: Digital Elevation Model Map.

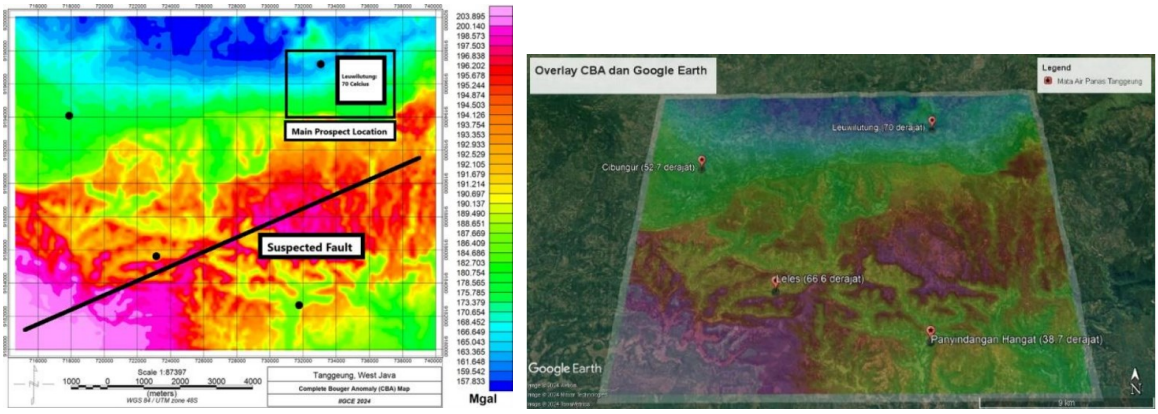

Figure 4: Complete Bouger Anomaly (CBA) Map.

3.3 Regional Gravity Map

After separating the anomalies on the CBA map using a bandpass filter, regional anomalies (deep zone) and residual anomalies (shallow zone) were obtained. On the regional anomaly map, it can be observed that the contours are similar to those on the CBA map. However, the regional anomaly contours appear smoother compared to the CBA map. This is because regional anomalies depict conditions far below the surface, representing layers and rocks in the deep zone. The deep zone in the Tanggeung area shows homogeneous characteristics. The regional anomaly map shows that the gravity anomaly values in the study area range from 158.1 to 203.8 mGal. The relatively high gravity anomalies, ranging from 181.1 to 203.8 mGal, are located in the southern to southwestern parts of the study area. These high anomalies are interpreted as the Upper Jampang Formation, consisting of breccia tuff, tuff, and andesite lava. These rocks are suspected to originate from the formation in Mount Patuha, extending towards Tanggeung. Conversely, the low gravity field anomalies, with values ranging from 158.18 to 179.12 mGal, are mostly located in the northern part of the study area. This low anomaly correlates with alluvial deposits and sandstone stretching from west to east in the northern part of the study. This low anomaly area also occupies the manifestation area considered to be the outflow at the research location, namely Leuwilutung.

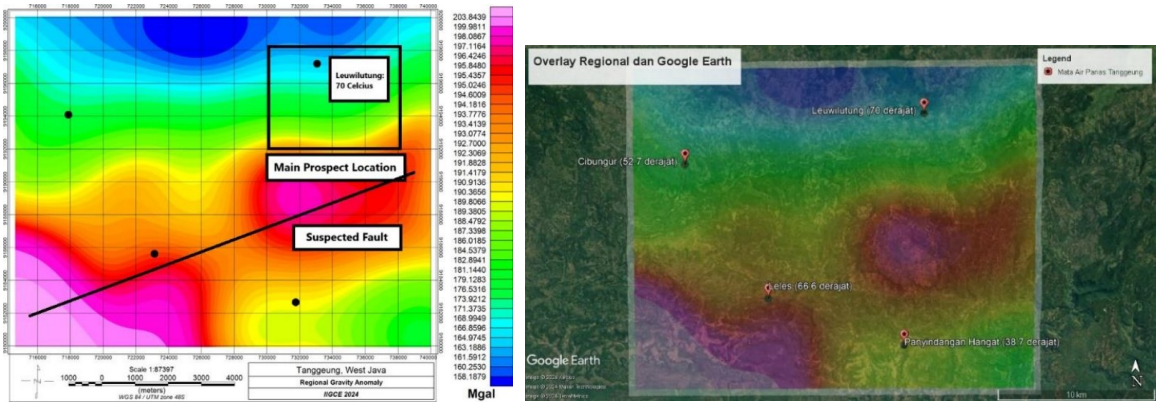

Figure 5: Regional Gravity Map.

The residual anomaly map in the study area shows that the contours exhibit varying degrees of variation. The residual anomaly contours are more diverse and slightly rougher compared to the regional anomalies. This difference arises because residual anomaliesrepresent conditions closer to the surface or shallow subsurface, where the layers and rocks in the shallow zone have heterogeneous properties.

On the residual anomaly map of the study area, gravity anomaly values range from -5.4277 to -4.7858 mGal. The relatively high gravity anomalies, ranging from 5.4277 to 0.6743 mGal, spread in all directions, but there is a noticeable continuity of high anomalies in the central part, which can be considered as faults or rocks with high density such as breccia tuff and andesite lava originating from Mount Patuha and extending towards Tanggeung. Conversely, the low gravity anomalies, with values ranging from 0.6743 to -4.7858 mGal, are mostly located in the northeast, considered as alluvial and tuff deposits because they are near the Cibuni River.

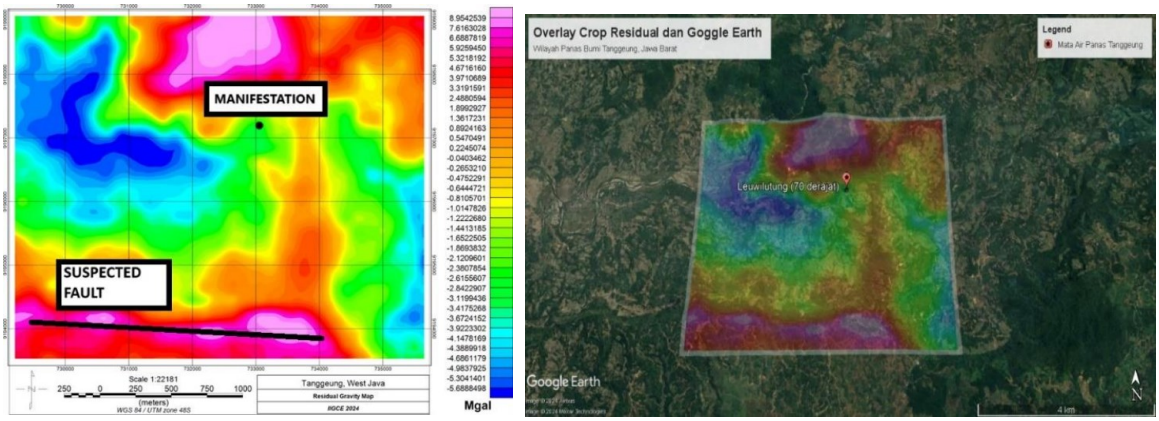

Figure 6: Residual Crop Gravity Map.

The results of the residual map after focusing on the northeast, which has the hottest manifestations with temperatures exceeding 70 degrees celsius, show that in the southern part, there are high gravity anomaly values associated with faults or rocks with high density such as breccia tuff and andesite lava originating from Mount Patuha and extending towards Tanggeung. Additionally, this map shows a flow-like shape moving from the Mount Patuha rocks in the south towards the north. This can be interpreted as a heat flow moving towards the manifestation (outflow) in the north through faults originating from the upflow in the southern part of the study area. The result of the outflow gives rise to the geothermal manifestation known as "Leuwilutung."

This interpretation is further reinforced by the results of trend surface analysis and fault analysis. The trend surface results provide a clear view of the residuals. The TSA results, ranging from order 1 to order 3, with order 3 being the most indicative of the surface, show that the research area is flanked by high-density rocks in all directions. This results in a low anomaly value that is wedged between these high anomalies. This assumption can preliminarily suggest that the area is a basin or a deposition site for tuff rocks, as interpreted by the geological sheet of the study area.

Meanwhile, the fault interpretation is strengthened by the FHD analysis and advanced FHD analysis, which show high values from south to north, clearly indicating a continuity of high anomalies considered to be faults in the research area.

In the cropped FHD map, a clearly visible fault running from west to east is evident, suspected to be a structure originating from Mount Patuha. In the middle, a black dot marks the "Leuwilutung" manifestation. Additionally, there is a path from the major fault in the south leading to the manifestation in the north of the study area. This can be interpreted as a fault that shapes the geothermal structure to be modeled below.

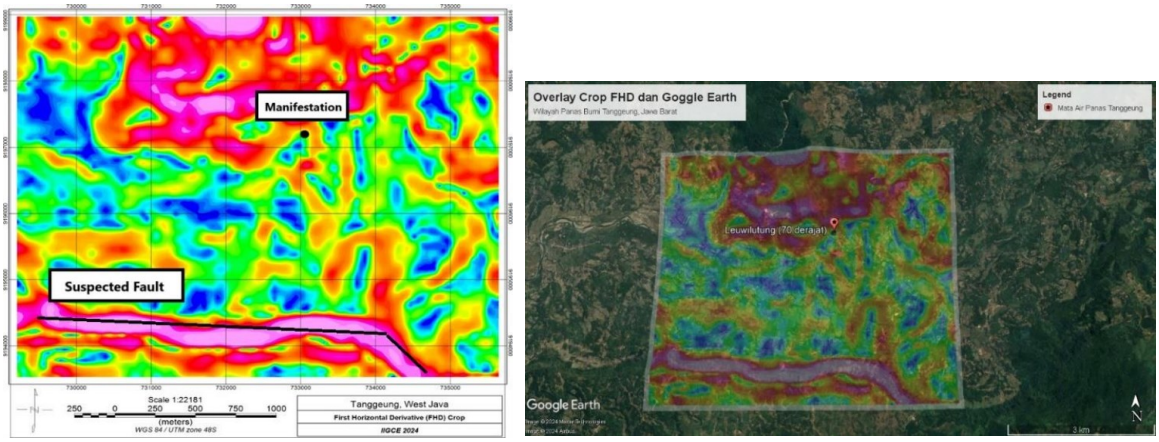

Figure 7: First Horizontal Derivative (FHD) Map.

In order to know where the edge of fault, FHD map will be correlated with the Fast Sigmoid Based Edge Detection (FSED) map. This is an advanced derivative analysis, a fault analysis technique used to identify edges in a fault. The image shows the same area as the cropped FHD map. The edges of the fault are indicated in red, extending from the dominant fault in the south towards the north, leading to the "Leuwilutung" manifestation.

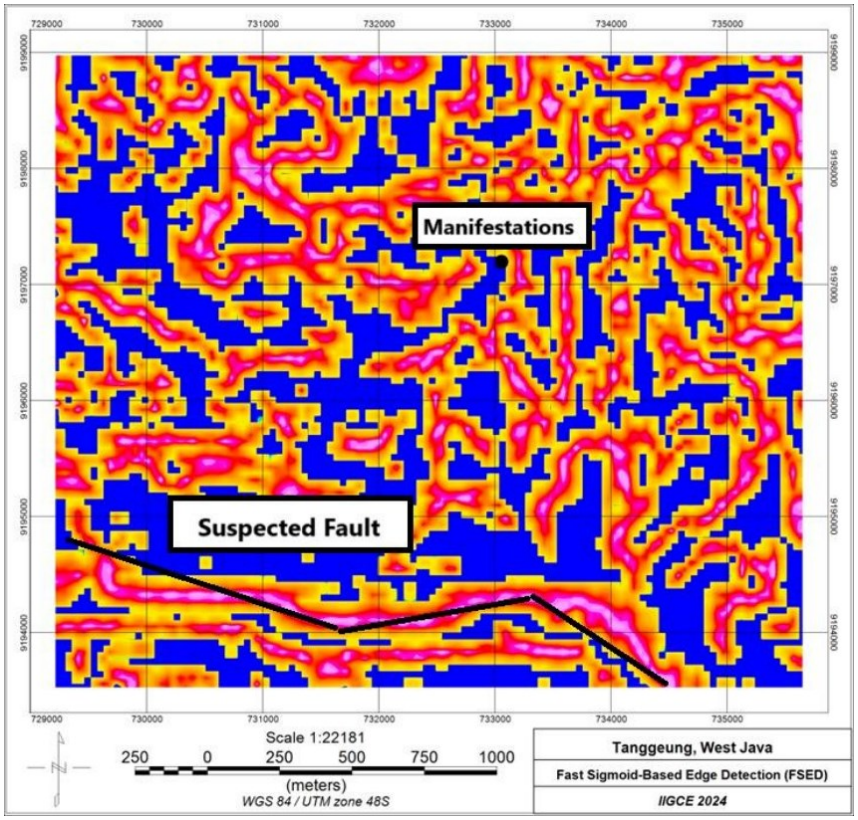

Figure 8: Fast Sigmoid Based Edge Detection (FSED) Map.

3.4 Land Surface Temperature Map

After obtaining and validating the Trend Surface Analysis and fault analysis, additional data is needed to validate that the identified manifestations are accurate points based on the mineral conditions and temperature conditions in the area. The Land Surface Temperature map is used to observe the distribution of temperature and temperature anomalies. Below is the map of the manifestation location at Leuwilutung.

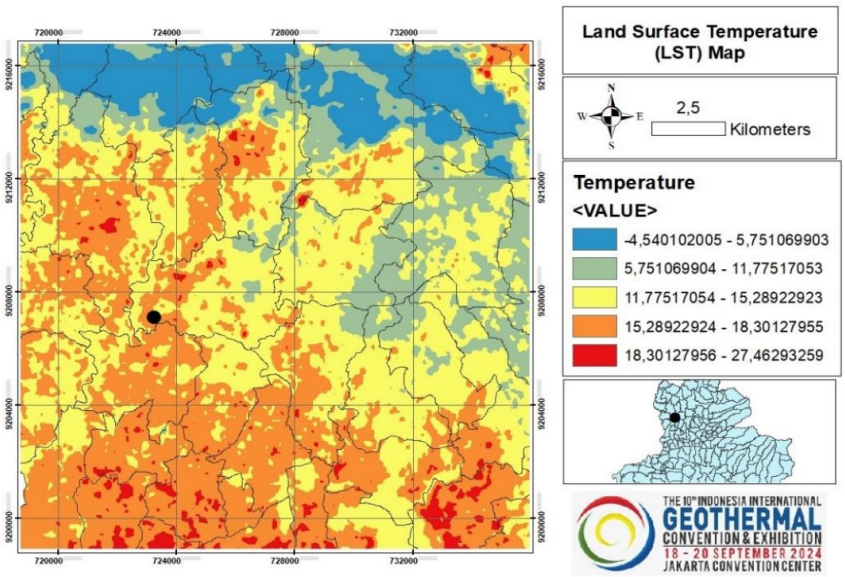

Figure 9: Land Surface Temperature (LST) Map.

It can be seen on the land surface temperature map at the manifestation location that there are notable anomaly values. The majority of the temperatures in the northern part decrease from 15.2 to 11 and down to 5. However, at the manifestation point, marked by a black circular shape, there is an anomaly-colored orange to red in the

northern part, ranging between 15.2 and 27.4℃. Meanwhile, the black color at the southern end represents error and noise. Additionally, the alteration mineral map shows a uniform distribution of clay minerals and iron minerals in the manifestation area, which is an indicator of rock alteration in that region.

3.5 3D-Gravity Map

As mentioned above, the residual map will be made into a 3-D cross-section consisting of three slices, namely A-A', B-B', and C-C', as follows. On average, all slices show the presence of a capping rock considered to be breccia, tuff, and andesite lava from Mount Patuha, with a density value of 2.45 – 2.5 g/cm3 and an average depth of 0 – 700 meters from the surface. Below this, reservoir rock with a density value of 2.4 – 2.3 g/cm3 is deposited, having an average depth of 700 – 1500 meters. The reservoir rock is interpreted as tuff and sandstone.

3.5.1 A-A’ Model

In the 3D gravity model cross-section A - A', oriented west-east, it intersects the Burni Waihlup fumarole in the study area with a depth of more than 2200 meters. In the A-A' modeling, the red-yellow layer at the top is suspected to be the Cap Rock or capping rock layer with a depth of more than 0 - 300 meters. This clay cap is believed to consist of the Pusat Kembar formation, including andesite, dacite, basalt, and pyroclastic rocks rich in clay minerals with a density of about 2.545 - 2.565 g/cm3. The green-blue layer, with a depth of 300 - 1400 meters from the surface, is considered the reservoir system containing alluvium rocks from the Kutacane graben, which are rich in fractures and permeable, having a density of 2.525 - 2.505 g/cm3.

Meanwhile, below the reservoir, at a depth of 1500 – 2200 meters, is suspected to be the Ketambe intrusion formation consisting of granite rocks with a density of 2.545 - 2.565 g/cm3, serving as the heat source for the reservoir above as well as water from the faults in the study area.

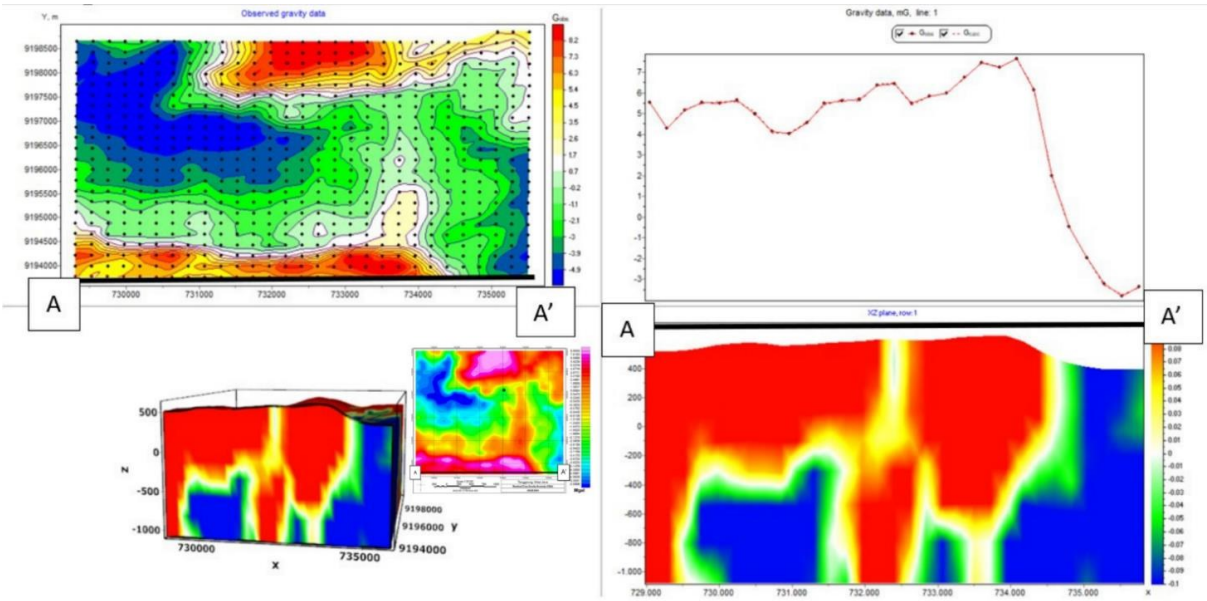

Figure 10: 3D Model Cross-Section A-A’.

3.5.2 B-B’ Model

In the 3D gravity model cross-section B - B', oriented west-east, it is located north of the Burni Waihlup fumarole in the study area with a depth of more than 2200 meters. In the B-B' modeling, the red-yellow layer at the top is suspected to be the Cap Rock or capping rock layer with a depth of more than 0 – 600 meters. This clay cap is believed to consist of the Pusat Kembar formation, including andesite, dacite, basalt, and pyroclastic rocks rich in clay minerals with a density of about 2.545 - 2.565 g/cm³. The green-blue layer, with a depth of 600 - 1000 meters from the surface, is considered the reservoir system containing alluvium rocks from the Kutacane graben, which are rich in fractures and permeable, having a density of 2.525 - 2.505 g/cm³.

Below the reservoir, at a depth of 1000 – 2200 meters, is suspected to be the Ketambe intrusion formation consisting of granite rocks with a density of 2.545 - 2.565 g/cm³, serving as the heat source for the reservoir rocks above as well as water from the faults in the study area.

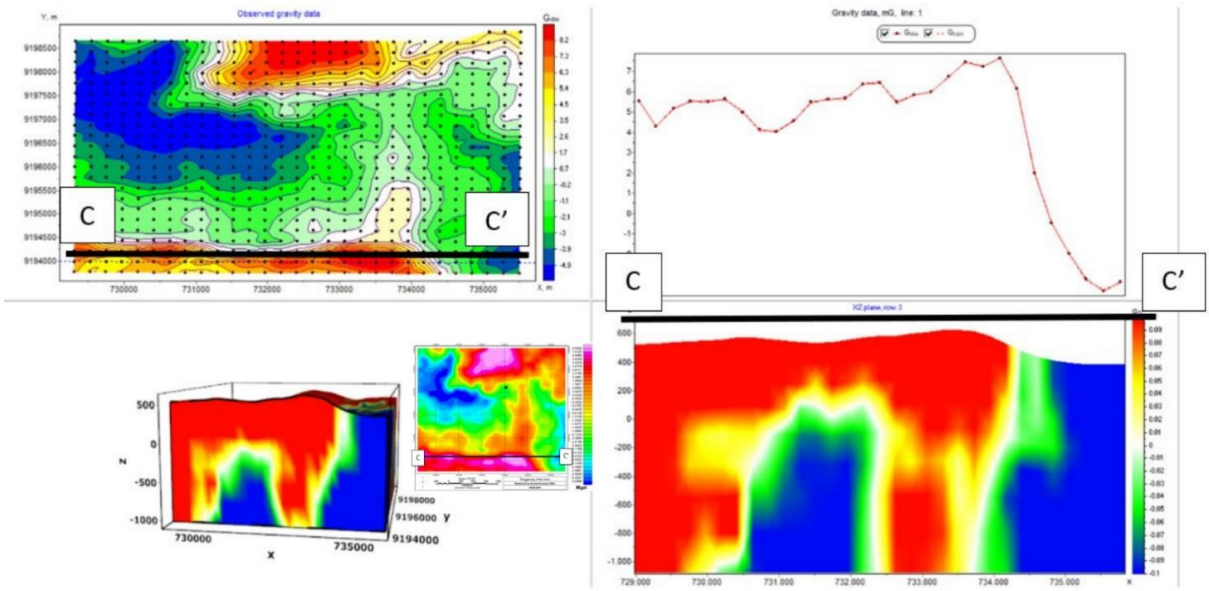

Figure 11: 3D Model Cross-Section B-B'.

3.5.3 C-C' Model

The gravity 3D model cross-section C - C' is a vertical section running north-south, cutting directly through the "Leuwilutung" hot spring in the northern part of the study area, with a depth of over 1400 meters.

In the C-C' model, the red-yellow layer on top is presumed to be the cap rock or sealing layer, with a depth of 0 to 500 meters. This clay cap is thought to consist of breccia, tuff, and andesite lava from Patuha Mount, with a density of 2.45 to 2.5 g/cm³. However, in the northern part of this vertical slice, a blue area can be seen, which may represent the Leuwilutung manifestation in the Tanggeung area.

Below this, the white to green layer indicates the reservoir rock, with a density of 2.4 to 2.3 g/cm³ and an average depth of 600 to 1400 meters. This reservoir rock is interpreted as tuff and sandstone.

The selection of the slicing is based on the absence of significant geothermal structures in the central and northern parts of the study area. The images below show that the central and northern regions are dominated by sedimentary rock deposits, such as tuff and sandstone. This is also interpreted as sediment deposits from rivers, as the study area includes numerous rivers, leading to abundant sediment deposits in the central and northern parts of the study area.

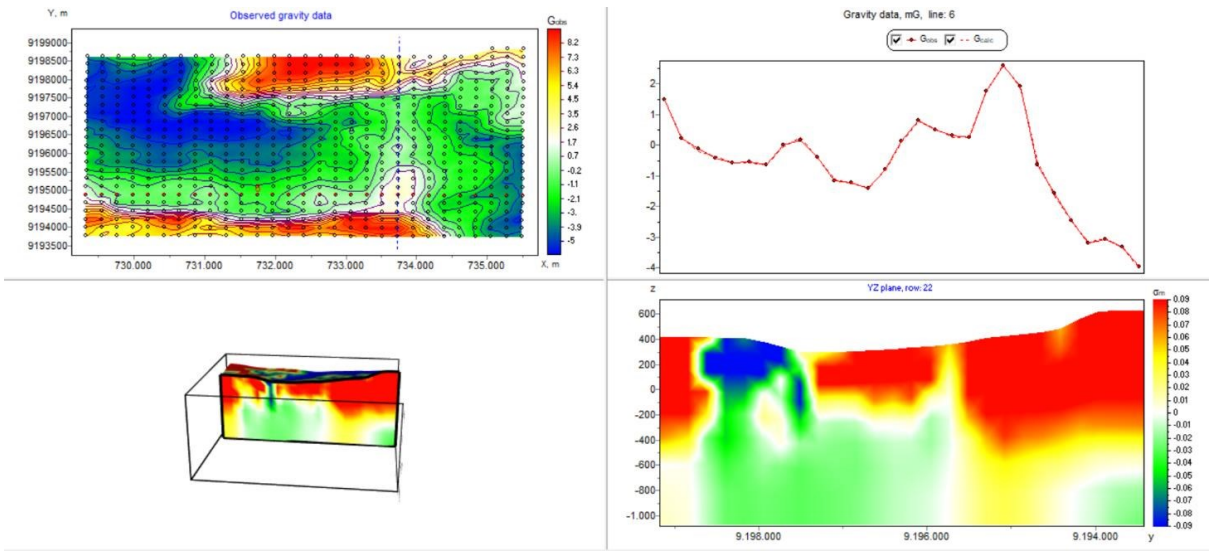

Figure 12: 3D Model Cross-Section C-C'.

3.6 Volumetric Calculation

The 3D inverse modelling of the designated are shown large thickness of breccia stone with density around 2.4-2.7 g/cc that is potential for geothermal storage. Volume of breccia stone on the area is predicted around 9.422-11.215 km3. The model's outcome (Fig X) provides initial insights into the concept of estimated capacity for geothermal storage.

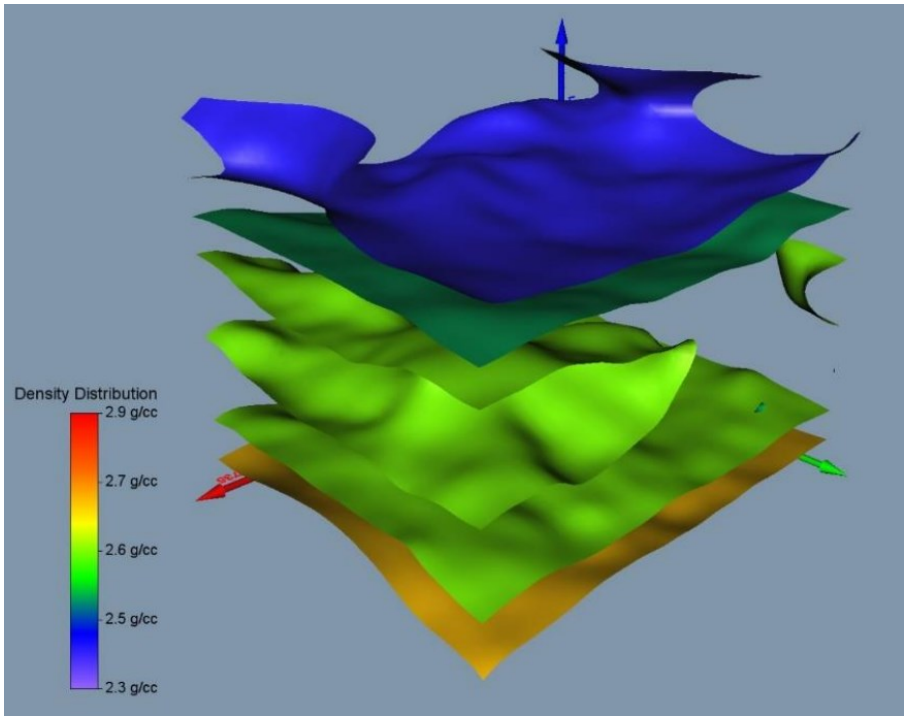

Figure 14: Distribution of Breccia Stone in the Area (Blue = 2.4 g/cc, Light Green = 2.5 g/cc, Light Green – 2.59 g/cc, Yellow = 2.7 g/cc)

4. CONCLUSION

This study shows that the Tanggeung area has significant geothermal potential, as indicated by geothermal manifestations in Leuwilutung, which serve as an outflow from the upflow in the southern part of the study area. Geophysical methods such as resistivity, magnetic, gravity, and electromagnetic have proven effective in identifying geological structures and geothermal potential. Geophysical data analysis reveals high gravity anomalies in the south and southwest, interpreted as the Upper Jampang Formation with rocks such as breccia tuff, tuff, and andesite lava, and low gravity anomalies in the north, interpreted as alluvial deposits and sandstone. A 3D model based on gravity anomaly data shows a clay cap with an average depth of 0 to 700 meters and a reservoir rock of tuff and sandy deposits from the Cibuni River with a density of 2.4 – 2.3 g/cm³ and depths of 700 to 1500 meters. The reservoir volume is estimated to be 9–11 cubic kilometers. These findings can serve as a basis for developing clean and sustainable geothermal energy in the Tanggeung area.

REFERENCES

Hinze, W. J., Von Frese, R. R., Von Frese, R., & Saad, A. H. (2013). Gravity and magnetic exploration: Principles, practices, and applications. Cambridge University Press.

Mussett, Alan & Khan, M. & Button, Sue. (2000). Looking into the Earth: An Introduction to Geological Geophysics. 10.1017/CBO9780511810305.

Telford, W. M., Telford, W. M., Geldart, L. P., & Sheriff, R. E. (1990). Applied geophysics. Cambridge university press.

Anandababu, D., Purushothaman, B. M., & Suresh Babu, S. (2018). Estimation of Land Surface Temperature using LANDSAT 8 Data. International Journal of Advance Research, 4(2), 177–186. www.IJARIIT.com.

Putri, D. A. B., & Harianja, A. K. (2021). Identifikasi prospek panas bumi radiogenik menggunakan landsat-8 dan gravitasi di daerah permis. JGE (Jurnal Geofisika Eksplorasi), 7(1), 52-70.

Ismail, N., Wirja, N., Putri, D. R., Nanda, M., & Faisal, F. (2020). Pemetaan Endapan Mineral Teralterasi Hidrotermal Menggunakan Analisis Citra Landsat 8 di Sekitar Gunung Api Bur Ni Geureudong, Kabupaten Bener Meriah, Aceh. Jurnal Rekayasa Elektrika, 16(2).

Saputri, A. N., Rahmawati, L., & Aziza, A. N. (2022). Pemanfaatan Citra Landsat 8 untuk Mengidentifikasi Keberadaan Heat Flow di Daerah Prospek Panas Bumi Suoh, Lampung Barat. Jurnal Geosains dan Remote Sensing, 3(1), 36-42.

Didit Agus Haryanto (2009). Laporan Akhir Tahun, Potensi Panasbumi Sebagai Sumberdaya Energi Terbarukan Di Kecamatan Tanggeung, Kabupaten Cianjur. Departemen Pendidikan Nasional Universitas Padjadjaran Fakultas Teknik Geologi.

Reservoir Rock of the Lumut Balai Geothermal System Indonesia

Vivi Dewi Mardiana Nusantara, Imam Muhamad Prasetya, Sapto Trianggo Nurseto, and Mulyanto

PT Pertamina Geothermal Energy, Grha Pertamina,
Pertamax Tower 5th floor, Merdeka Timur Street, Jakarta 10110, Indonesia

vivinusantara@pertamina.com

Keywords: Reservoir rock, lateral permeability, breccia, Lumut Balai

ABSTRACT

This study examines the physical properties, composition, dimension, and distribution of the reservoir rock of the Lumut Balai (LMB) geothermal system in Sumatra Indonesia, an extensive geothermal area within a 10 km wide volcanic-hosted caldera. Rock sample and drilling data were analyzed for this study through binocular and petrographic observation, porosity and permeability measurements, and borehole images identification.

The LMB reservoir rock demonstrates favorable grain permeability from the fragment – matrix contact rim in the tuff breccia. This formation permeability contributes significantly to the productive feed points discovered at elevation of 200 to -200 meters. Additionally, the temperature distribution shows close correlation with the tuff breccia and feed point zone, suggesting a vast lateral distribution permeability throughout the caldera.

1. INTRODUCTION

The Lumut Balai (LMB) geothermal system is situated in the active tectonic zone of the Great Sumatran Fault, characterized by tensional faults, horst and depression forming, pull-a-part basins, and series of quaternary volcanic activity. The geothermal system is well-developed within the Old-Lumut Caldera. Quaternary volcanic products dominate the surface rock inside the caldera with andesitic to basaltic composition. The tertiary sediment was marked as the basement formation of the system (Figure 1).

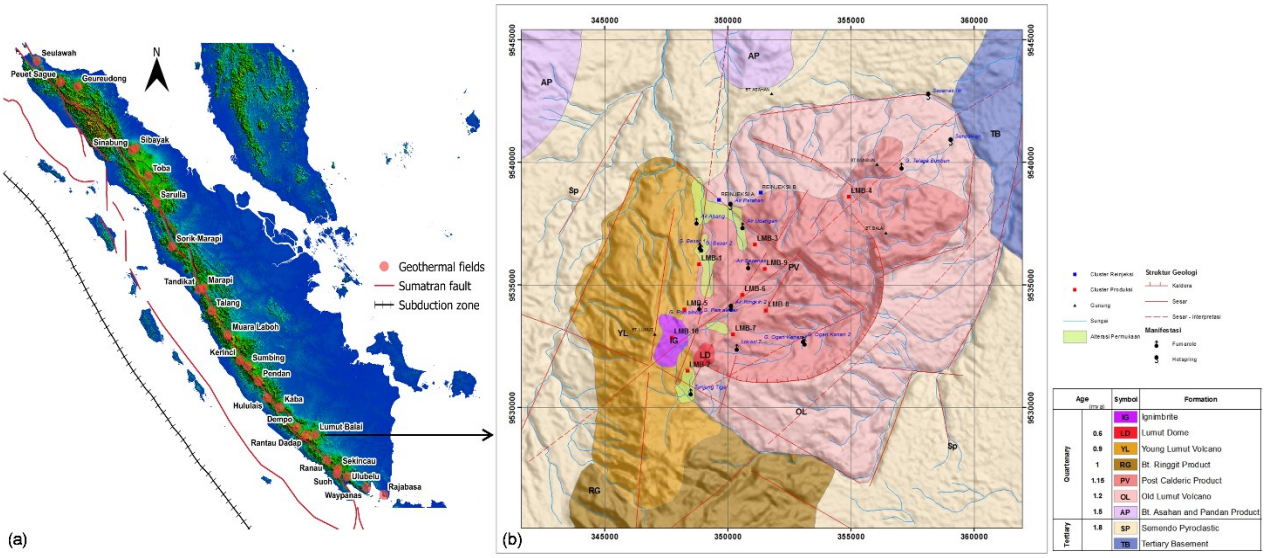

Figure 1: Location of geothermal prospect area along the Great Sumatran Fault (a) and surface geological map of the Lumut Balai Geothermal system (b).

The geothermal system of LMB features a neutral water-dominated reservoir with temperatures ranging from 230 to 260 °C. Productive feed points were discovered near sea level elevation (Yanto, 2021). The reservoir rock associated with feed points, high temperature, and propylitic zone is identified as tuff breccia from the Pre-Old-Lumut Formation product of Old-Lumut Volcano. This favorable volcanic breccia is hydrothermally altered by secondary quartz, calcite, chlorite, epidote, adularia, wairakite, actinolite, and adularia.

2. THE LUMUT BALAI RESERVOIR ROCK

2.1 Physical properties and borehole log

The reservoir rock in LMB is identified as tuff breccia. The rock matrix consists of volcanic glass, tuff, and lapilli, and coarse-sized angular fragments of andesite and basaltic lava act as lithic grains. The poorly-sorted breccia is highly altered with high-temperature secondary mineral assemblage deposition, particularly in between fragments – matrix contact boundaries (Figure 2).

Petrographic observations reveal that intensive secondary mineral deposition occurred in the micro vein network in between grain to grain, grain to matrix, and open vesicles. Secondary quartz, calcite, epidote, and chlorite are the most common minerals found in rock veins. Furthermore, the matrix is altered by scattered fine-grained crystals of chlorite, sericite, epidote, and opaque minerals (Figure 2a and 2b).

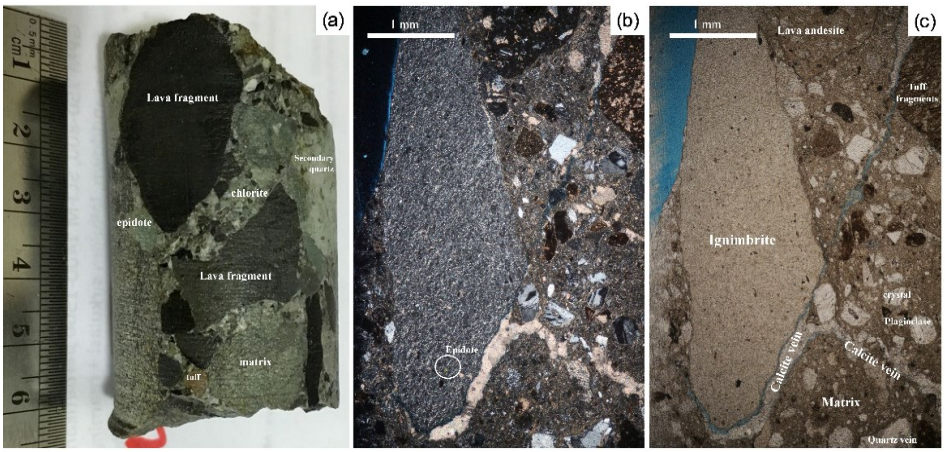

Figure 2: Core sample retrieved from the reservoir zone of LMB system shows fragmental texture in breccia; hand specimen photograph (a), thin section under crossed in polarized view (b), and plane polarized view (c).

Figure 3 illustrates the most prevalent data trend observed in the productive borehole of LMB geothermal system. The tuff breccia is identified as the reservoir rock, due to its strong correlation with the high-temperature alteration zone, measured feed points, and the convective temperature trend in the reservoir.

In a fault-controlled reservoir, the feed points are typically indicated by an immediate high loss rate during steady injection, as seen in the Hululais geothermal field (Arifin, 2020). However, the main feed points in the LMB are found under medium loss conditions (0 to 7 barrel per minute), as demonstrated by Feed Point A (Figure 3). This indicates that Feed Point A is likely associated with an excellent primary permeability of the reservoir rock rather than faulted zone.

Feed Point A, located near sea level, contributes up to 95% of the well's production rate, as confirmed by the production spinner log measurement. Furthermore, the convective temperature trend, indicative of the reservoir zone, is observed at this depth, with temperature reaches 234 °C (Figure 3). On top of that, this borehole successfully generates 6.4 MW of electricity.

2.2 Borehole image

In this study, we cross-validated borehole image data with injectivity/production spinner tests and core samples. Our findings indicate that the typical reservoir rock formation at feed points is strongly associated with fragmental rock, specifically identified as tuff breccia from the core samples.

The tuff breccia interval is characterized by a fine matrix with some conductive, rounded patches, which are interpreted as vesicular structures. These conductive features are believed to represent open spaces filled with conductive minerals, such as clay, or reservoir fluids (Figure 4). Furthermore, spinner test results that this tuff breccia zone contributes for more than 40% of the total injection capacity during the well test. This shows the important role of tuff breccia as a permeable reservoir rock.

2.3 Distribution

The tuff breccia is encountered at relatively similar depths within the caldera, approximately between 200 to -200 meters elevation. Accordingly, all contributive feed points are discovered within the tuff breccia layer. Temperature distribution follows the formation bed and caldera basin, indicating that the reservoir hydrology is controlled by the lateral permeability distribution of tuff breccia in relatively uniform depth (Figure 5).

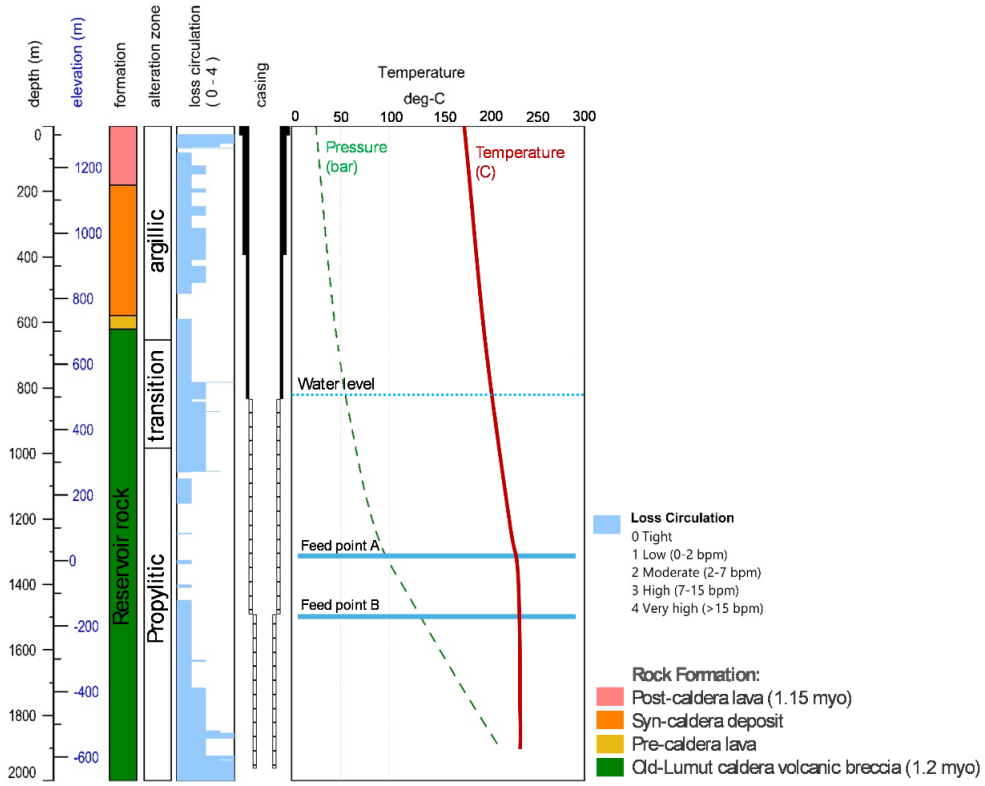

Figure 3: An example of borehole log from producer wells in Lumut Balai geothermal system shows typical association of the feed points with high temperature reservoir zone.

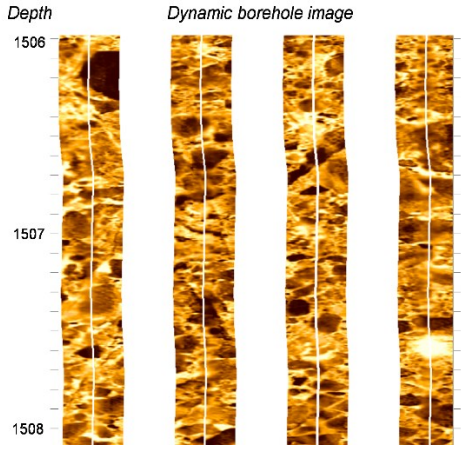

Figure 4: Borehole image of the reservoir rock in Lumut Balai which is associated with the production zone.

3. COMPARISON STUDY

The tuff breccia in LMB is interestingly comparable to the Ulubelu (UBL) reservoir rock. Both fields exhibit a depression-fill mechanism with volcanoclastic deposits; in the case of UBL, the reservoir rock is identified as lapilli tuff (Nusantara, 2021). The reservoir rock is restricted by the caldera rim in LMB, meanwhile it is strongly controlled by the pull a-part basin morphology in UBL. Correspondingly, UBL reservoir rock also shows a favorable lateral primary permeability in its feed points distribution.

We observed and plotted the composition of LMB and UBL core samples into the pyroclastic classification (After Fischer, 1966). Despite sharing a similar fragmental texture, UBL reservoir rock has finer grain size and better sortation than LMB (Figure 6). Nonetheless, both lithologies are effectively contributing to the well's production capacity rate.

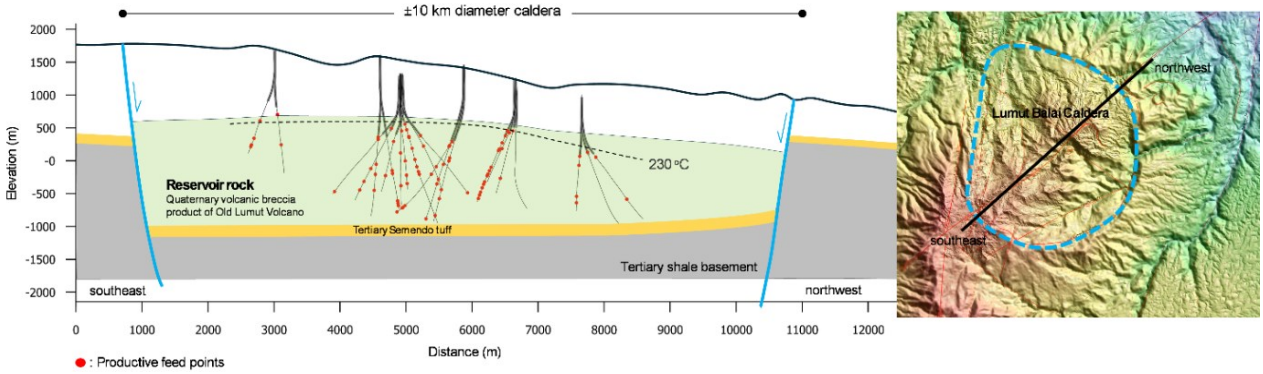

Figure 5: The northeast – southwest profile shows distribution of reservoir rock influences the feed points and temperature lateral extent.

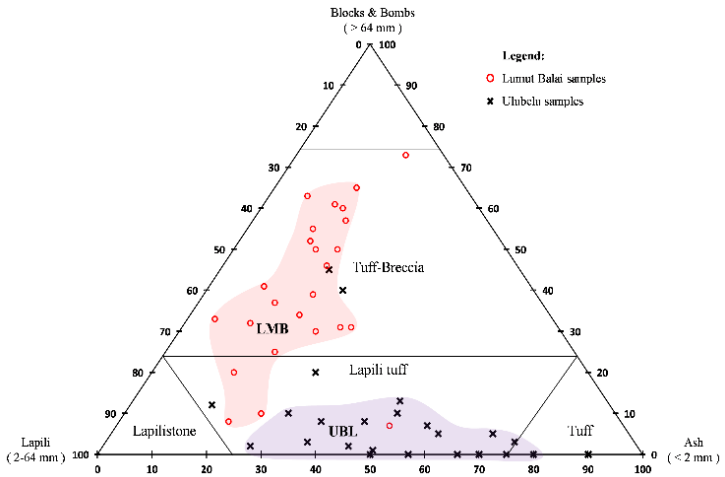

Figure 6: Characterization of reservoir rock in LMB compared to the reservoir rock in UBL geothermal system suggesting a different type of volcanoclastic facies. LMB is composed of tuff breccia and UBL is dominated by lapilli tuff.

Primary permeability and porosity measurements from core samples indicate sufficient initial formation capacity to convey hydrothermal fluid through the lithology layer. Average permeability and porosity measured are 0.37 mD and 4.0 % for LMB, and 0.36 mD and 8.8 % for UBL, respectively. The higher porosity in UBL is attributed to its higher vesicles/ gas escape pores properties in its rock component.

4. CONCLUSION

The LMB geothermal system is influenced by tensional activity inside the caldera that is strongly associated with active volcanism. This combined activity results in the development of tuff breccia as the reservoir rock in LMB geothermal system. The distinctive fragmental texture of LMB reservoir rock promotes significant primary permeability with an extensive lateral distribution, as confirmed by numerous successful boreholes. Consequently, the elevation and thickness of this reservoir rock are crucial factors in well-targeting strategies within this field.

REFERENCES

Arifin, M. T., Nurseto, S.T., Nusantara, V.D.M., Pratama G.R., Marastio, F.E., and Thamrin, M.H.: Feed Zone Evaluation in Hululais Geothermal Field, Bengkulu, Indonesia, Proceedings, 42nd New Zealand Geothermal Workshop, Waitangi (2020).

Firanda, E., Saputra, M.B., and Silaban, M.: The effect of well elevation on production in Lumut Balai field. *Proceedings* World Geothermal Congress 2015, Melbourne (2015).

Fisher, R.V.: Rocks Composed of Volcanic Fragments and Their Classification. *Earth-Science Reviews*, 1, pp 287-298. (1966) doi.org/10.1016/0012-8252(66)90010-9

Nurseto, S.T., Satriani, R.A.J., Thamrin, M.H., and Suryantini.: Productive structural geology in volcanogenic system: A case study of Lumut Balai geothermal field, Indonesia, *Proceedings*, Earth and Environmental Science, (2021), p.732.

Nusantara, V.D.M., Prasetyo, I.M., Pratama, G.R., Alibazah, J. S., Arifin, M.T., Koestono, H., and Thamrin, M.H.: Reservoir rock of Ulubelu geothermal system Indonesia. *Proceedings* World Geothermal Congress 2020+1, Reykjavik, (2021).

Yanto, E., Firanda E., Budiyanto, A., Tiofami, A., and Suranto, H.: Exploitation strategies to minimize decline rate at Lumut Balai area PT Pertamina Geothermal Energy Indonesia. *Proceedings*, 46th Workshop on Geothermal Reservoir Engineering, Stanford University, Stanford, CA (2021).

The Voyage of PGELabs Towards Geothermal Excellence

Losendra Primamas Yonando, Henny Firdaus, Ragil Farhandimas Rizki, Helmi Sopari, M. Iqbal Al Kindi, Teza Permana, Hendra Hadriansyah, Nanda Najih H. A., and Ricsen Halomoan

PT Pertamina Geothermal Energy

losendra.yonando@pertamina.com, henny.firdaus@pertamina.com, ragil.rizki@pertamina.com, helmi.sopari@pertamina.com, muhammad.alkindi@pertamina.com, teza.permana@pertamina.com, hendra.hadriansyah@pertamina.com, nanda.afif@pertamina.com, ricsen.halomoan@pertamina.com

Keywords: laboratory, geothermal laboratory, center of excellence, commercial

ABSTRACT

Laboratory analysis plays a vital role in advancing our understanding of geothermal systems, optimizing resource utilization, and mitigating operational risks. By employing state of-the-art analytical techniques and adhering to rigorous quality standards, researchers and engineers can extract valuable information from geothermal samples to support sustainable and efficient energy production. PGElabs are the pioneer with over 40 years of excellence in geothermal laboratory. Supported by technical experts, advanced instruments, and also guided by ISO/IEC 17025:2017 based laboratory management system, we have developed various methods and standards in terms of sampling, fluid and rock analysis and other special methods so that we contribute to maintaining operational reliability and reservoir sustainability. This paper examines the journey of PGELabs from its initial stage to present condition and also to indicate the pivotal milestone where PT Pertamina Geothermal Energy Tbk (PGE) launched the PGELab to become a commercial geothermal laboratory which is part of PGE's growth story as a center of excellence.

1. INTRODUCTION

PGELabs established in 1983 concurrently with Commercial on Date Unit 1 PT PGE Area Kamojang. PGELabs is a specialized geothermal laboratory which can carry out sampling, chemical analysis of geothermal fluids and rocks/ solids which is equipped with the latest analytical equipment and has been accredited ISO/IEC 17025:2017. Geothermal energy often face challenges associated with resource uncertainty. Successful geothermal production relies heavily on accurate and comprehensive data provided by specialized geothermal laboratories. Through detailed subsurface data and analysis, we can better understand reservoir properties, optimize drilling strategies, and mitigate exploration risks.

PGELabs equipped with advanced geological and geochemical analysis tools will significantly aid in resource assessment and characterization in geothermal energy. As stakeholders deeply involved in the geothermal energy, we wish to underscore the critical importance of geothermal laboratory.

PGELabs, a pioneer with over 40 years of excellence in geothermal laboratory services, offers critical services including Laboratory Analysis, Tracer Tests, and Geothermal Sampling. The laboratory continually develops various methods and standards for sampling, fluid and rock analysis, and other specialized techniques to enhance operational reliability and reservoir sustainability. In 2024, leveraging its extensive experience and international acclaim, PGELabs is set to advance as a commercial entity, marking a significant new phase in its development.

2. OUR SERVICES

PGELabs offers key services such as Laboratory Analysis, Tracer Tests, and Geothermal Sampling. As a specialized geothermal laboratory, PGELabs is equipped with the latest analytical equipment and is accredited to ISO/IEC 17025:2017. This accreditation ensures that we can carry out precise sampling and chemical analysis of geothermal fluids and rocks/solids with the highest level of accuracy and reliability.

2.1 Laboratory Analysis

Laboratory analysis plays a vital role in advancing our understanding of geothermal systems, optimizing resource utilization, and mitigating operational risks. By employing state-of-the-art analytical techniques and adhering to rigorous quality standards, researchers and engineers can extract valuable information from geothermal samples to support sustainable and efficient energy production. Supported by highly qualified and experienced personnel, reliable advanced equipment, and an integrated laboratory management system, PGE laboratories are committed to delivering excellence in every aspect of their work.

Our Expertise:

Fluid analysis

- Geothermal water analysis
- Geothermal gas analysis

Rock Analysis

- Petrography,
- Mineral & scale analysis,
- Fluid inclusion analysis

(a)

(b)

Figure 1: (a) Fluid analysis, (b) Rock analysis.

Figure 2: Tracer test equipment.

2.2 Tracer Test

Tracer tests play a crucial role in advancing our understanding of geothermal systems and optimizing the development and management of geothermal resources for sustainable energy production. Laboratory analysis of tracer samples is essential for elucidating reservoir characteristics, fluid flow dynamics, and heat transfer

processes within geothermal reservoirs. By providing valuable insights into reservoir behavior, tracer test analysis significantly contributes to optimizing reservoir management strategies and enhancing the efficiency and sustainability of geothermal energy production.

Our Expertise:

- Reservoir tracer testing, sampling & analysis
- Chemical tracer flow testing, sampling & analysis

2.3 Geothermal Sampling

Sampling is essential for understanding the composition, temperature, pressure, and other parameters of geothermal reservoirs, which is crucial for assessing the potential for geothermal energy production. PGELabs experienced in conducting geothermal sampling across diverse conditions and locations, we ensure thorough validation and interpretation of sampling data by qualified experts. This expertise and rigorous approach enable us to provide accurate and reliable insights into geothermal resources.

Our Expertise:

- Exploration Geothermal Sampling
- Well Testing Geochemistry Sampling
- Production & Monitoring Sampling

Figure 3: Geothermal sampling activity.

3. OUR TRANSFORMATIONS

PGElabs are the pioneer with over 40 years of excellence in geothermal laboratory. We are always transforming and developing various methods and standards in terms of sampling, fluid and rock analysis and other special methods so that we contribute to maintaining operational reliability and reservoir sustainability.

3.1 Steam Wetness Measurement (2012)

Improving Quality of Steam Wetness Measurement Using Portable Isokinetic and Throttling Calorimeter.

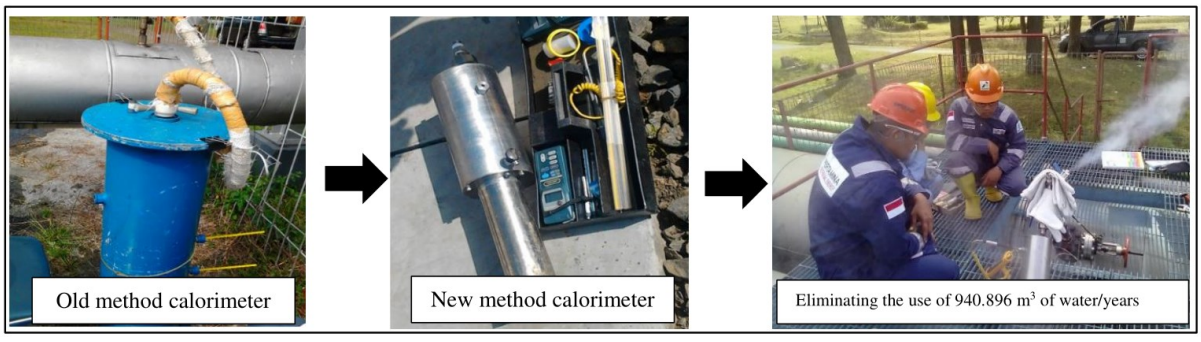

Figure 4: Improving Quality of Steam Wetness Measurement Using Portable Isokinetic and Throttling Calorimeter.

3.2 Superheat Measurement (2012)

Measurement of Superheat Degree in Production Wells Using Mini Probe for Reservoir Monitoring and Evaluation.

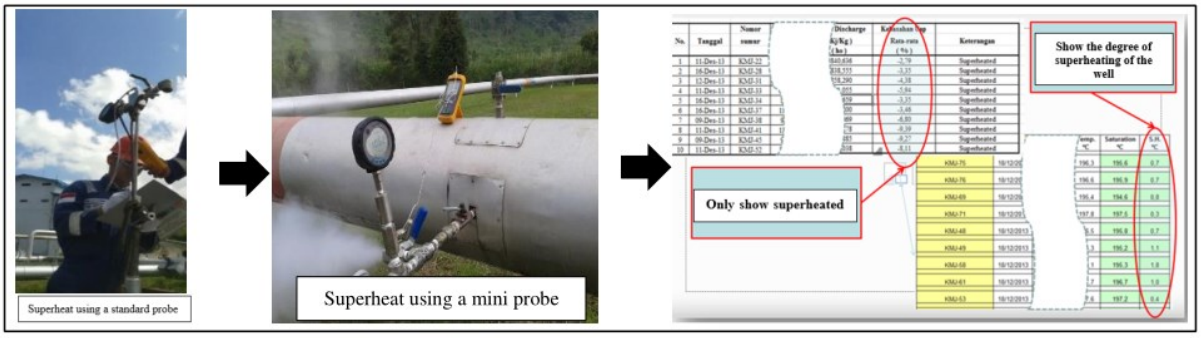

Figure 5: Measurement of Superheat Degree in Production Wells Using Mini Probe for Reservoir Monitoring and Evaluation.

3.3 Fluid Cation Analysis (2013)

Advancing Cation Analysis in Geothermal Fluid: Transition from Conventional Method to ICP-0ES (Inductively Coupled Plasma - Optical Emission Spectroscopy).

PGElabs transitioned from conventional method to ICP-OES (Inductively Coupled Plasma – Optical Emission Spectroscopy) for cation analysis (Na, K, Ca, Mg, Si, Fe, Li, B) in geothermal fluid samples significantly enhances testing quality by delivering more accurate, faster, and consistent results. Unlike manual method, which relies on large quantities of chemical reagents, ICP-OES uses plasma technology to detect cation elements with high sensitivity, even at low concentrations. In addition to improving accuracy, this method also reduces the production of hazardous and toxic waste (B3), supporting more environmentally friendly operations and lowering waste management costs, making it a more efficient and sustainable solution.

Figure 6: ICP-OES (Inductively Coupled Plasma – Optical Emission Spectroscopy).

3.3 Fluid Anion Analysis (2013)

Advancing Anion Analysis in Geothermal Fluid: Transition from Conventional Method to Ion Chromatography.

PGELabs transitioned from conventional method to Ion Chromatography (IC) for anion analysis (F, Cl, SO4) in geothermal fluid samples enhances testing quality by providing more accurate, faster, and consistent results. Unlike manual method, which requires large quantities of chemical reagents, Ion Chromatography uses ion separation technology to detect anion elements with high sensitivity, even in small amounts. In addition to improving accuracy, this method also reduces the production of hazardous and toxic waste (B3), supporting more environmentally friendly operations and lowering waste management costs, making it a more efficient and sustainable solution.

Figure 7: IC (Ion Chromatography).

3.4 Total NCG (Non-Condensable Gas) Measurement (2014)

The Portable total NCG Super Fast at PT PGE for Accelerate the Total NCG Measurement Process.

PGELabs has developed a straightforward tool designed to measure the total amount of Non-Condensable Gases (NCGs) in geothermal steam. The device operates by optimizing the condensation process in a dedicated condenser, where steam is condensed into a container. By measuring the total vapor volume, condensate gas pressure, and condensate volume, it enables precise calculations of the NCG volume. This tool offers several advantages including faster measurement, high accuracy, low cost, portability, ease of handling, simple installation, and being chemical-free and environmentally friendly.

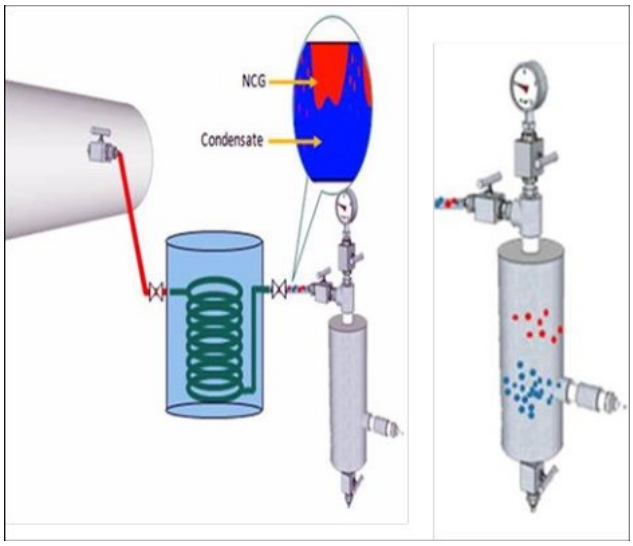

Figure 8: Portable NCG (Non-Condensable Gas).

3.5 Accreditation & Certification ISO/IEC 17025:2017 (2019)

PGElabs is certified and accredited to ISO 17025:2017, reflecting our commitment to transforming and enhancing the quality of our analyses. By adhering to the highest international standards for testing and calibration, we deliver trustworthy and precise results. This accreditation ensures that our laboratory provides reliable and accurate results for a range of tested parameters, including:

- Geothermal condensate (pH , Conductivity, TDS, TSS, Na, K, Ca, Mg, Li, Fe, SiO2, B, NH4, F, Cl)
- Geothermal water (pH, Conductivity, TDS, TSS, Na, K, Ca, Mg, Li, Fe, SiO2, B, NH4, F, Cl, SO4)
- Geothermal gas (steam) (H2, Ar, O2, N2, CH4, CO2, H2S, NH3)
- Geothermal rock
- Geothermal scale.

3.6 Advanced CO2 Gas Analyzer (2020)

Improving the Quality and Quantity of CO2 Testing in Geothermal Steam Samples using the ACID CONVERSION (ACONV) Method.

PGELabs transitioned from conventional acid-base titration to the use of a CO2 Analyzer for analyzing CO2 in Non-Condensable Gas (NCG) samples from geothermal steam has significantly improved the quality of test results by providing more accurate and faster data. The CO2 Analyzer operates automatically with high precision, reducing reliance on operator skill and minimizing the potential for manual errors commonly associated with the traditional method. Additionally, the CO2 Analyzer can process smaller sample volumes more efficiently, allowing for quicker analyses and more consistent, repeatable testing. This enhances overall testing efficiency and supports more effective monitoring of geothermal operations.

Figure 9: Accreditation & Certification ISO/IEC 17025:2017.

Figure 10: CO2 Gas Analyzer.

3.7 Optimization of Anion Sample Preservation (2023)

Improving the Quality of Sulfate Testing in Geothermal Fluid Samples Using the PZACR (Preservetive Zinc Acetate & Conditioning Reagent) PZACR Method (Preservative Zinc Acetate & Conditioning Reagent.

PGELabs has innovated and transformed its processes by incorporating the addition of Zn Acetate for field preservation of samples, which precipitates dissolved H2S, and implementing reagent conditioning during spectroscopic analysis to reduce HCO3 interference. These improvements optimize sulfate testing for brine and injection samples. The PZACR method has extended the holding time for geothermal water samples from 7 days to 43 days. This advancement not only ensures high-quality analysis results but also leads to operational cost

savings, accelerates data delivery, reduces the risk of H2S exposure for analysts, and enhances confidence in the performance of laboratory analysts.

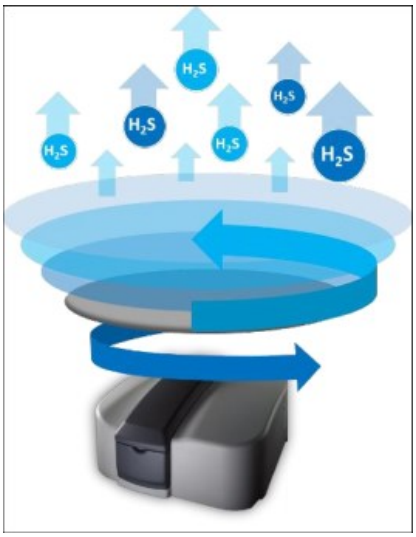

Figure 11: PZACR Method.

Figure 12: Govast (Gas Geothermal Vacuum System).

3.8 NCG (Non-Condensable Gas) Measurement (2023)

Increasing the Effectiveness of Geothermal Gas Sample Testing Preparation Using GOVAST method (Gas Geothermal Vacuum System).

PGELabs has innovated the analysis of geothermal samples by addressing the inefficiencies of direct gas chromatography for concentrations above 100ppb at pressures below 10 kPa. By implementing the GOVAST Gas Geothermal Vacuum System, the laboratory enhanced sample preparation, improving testing precision to an average %RPD of 4.912% and reducing cycle time from 44.58 to 17.34 minutes. This advancement led to substantial cost savings, including reduced external service fees and GC (Gas Chromatography) spare part expenses, a decrease in sample reanalysis from 47.05% to 1.56%, and a reduction in handling hazards.

3.9 NCG (Non-Condensable Gas) Reference Standards (2024)

Production of NCGs Reference Material as a Reference Standard for Geothermal Gas Samples in the Laboratory of PT PGE.

In preparation for its 2024 transition to a commercial laboratory, PGE Laboratory innovated by developing NCGS reference materials to meet ISO/IEC 17025 accreditation requirements. This innovation addresses the lack of available proficiency testing services by creating a unique process for generating reference standards. The procedure involves creating liquid standards for NH3 and CO2, vacuum-sealing them in Giggenbach bottles to prevent contamination, and then injecting these standards into a pre-treatment system for distribution. This advancement has positively impacted the laboratory's performance in quality, cost, delivery, severity, and morale, ultimately leading to successful ISO/IEC 17025 accreditation.

Figure 13: Pre-treatment Reference Standard for Geothermal Gas Samples.

4. CONCLUSION

PGELabs, a pioneer with over 40 years of excellence in geothermal laboratory services, leverages a team of technical experts and advanced instruments to develop a wide array of methods and standards for sampling, fluid, and rock analysis. This expertise ensures the operational reliability of Steamfield Above Ground Systems (SAGS) and power plants, contributing significantly to the sustainable development of geothermal energy in Indonesia. Equipped with the latest sophisticated technology, PGELabs delivers high accuracy and precision in data production, offering comprehensive services throughout all stages of geothermal development. This approach effectively addresses subsurface uncertainty and supports exceptional production quality, fostering the effective and sustainable management of geothermal resources.

PGELabs has received international recognition through ISO 17025:2017 certification, which underscores our commitment to quality assurance in laboratory analysis and sampling. We continuously innovate and transform our processes to enhance the effectiveness and efficiency of our analytical and sampling methods. This dedication to improvement ensures that our results meet the highest standards of quality and precision, reinforcing our role in advancing geothermal energy development with reliable and accurate data.

PGELabs will embark on a new phase of commercialization in 2024, building on its extensive experience and global recognition. This transition represents a significant advancement for the laboratory as it evolves into a commercial entity, leveraging its established expertise and international acclaim to enhance its market presence and expand its service offerings.

REFERENCES

PGELabs Pitchdeck. PGELabs® Your partner toward Geothermal Excellence, (2024).

KAN. Lampiran Sertifikat Akreditasi Laboratorium NO. LP-1320-IDN - SNI ISO/IEC 17025:2017 (ISO/IEC 17025:2017), (2024).

Preliminary Assessment of Critically Stressed Fracture in Lumut Balai and its Effect on Permeability of the Field

Muhammad Tajul Arifin, Sapto Trianggo Nurseto, and Mulyanto

PT Pertamina Geothermal Energy Tbk

muhammad.tajul@pertamina.com

Keywords: Lumut Balai, fracture, permeability

ABSTRACT

Unlike other geothermal fields in Sumatra, which are mostly located near the Great Sumatran Fault, Lumut Balai is situated approximately thirty to forty kilometres away from the fault. This unique location means that the geological structures in Lumut Balai are not directly affected by the movement of the Great Sumatra Fault. However, this situation complicates the assessment of permeable structures in Lumut Balai due to the presence of numerous major geological structures within the field.

To determine which structures direction is permeable, a preliminary slip tendency analysis was conducted. The goal was to identify critically stressed fractures that could serve as easier pathways for fluid flow compared to other fractures. The assessment utilized borehole data from six wells, pressure data and field-wide joint inverted gravity data. Additionally, interpreted feed zone depth data were used to understand the influence of critically stressed fractures on permeability in each well.

The study revealed that critically stressed fractures in Lumut Balai predominantly align with a north-northeast direction, coinciding with several major geological structures in the field. This directional consistency also explains why the hydrology of Lumut Balai flows in specific directions. Furthermore, the assessment found that most of the feed zones with significant contributions are influenced by the occurrence of critically stressed fractures.

By understanding the direction of these fractures from data collected across several wells and integrating it with the field's conceptual model, the assessment could guide decisions on which geological structures to target for future well prognosis.

1. INTRODUCTION

Not all fractures in geothermal fields are permeable, some fractures with certain directions might be more permeable than others, and some of them also could be filled with minerals and block the fluids from passing through the fracture. The permeability provided by fractures is one of the favorable for well targeting, thus efforts on identifying permeable fractures are important work.

Many works have been done in analyzing fractures and their effects on the permeability of a geothermal field, especially in Sumatra, such as in Rantau Dadap & Muara Laboh (Wallis, et al., 2020; Wallis, et al., 2023), Bukit Daun (Ikhwan, et al., 2020), Ulubelu (Nurseto, et al., 2015 and Arifin, et al., 2020), Hululais (Nurseto, et al., 2023, Arifin, et al., 2020), Sorik Marapi (Sanjaya, et al., 2023), Lumut Balai (Nurseteo, et al., 2020, and Kamah, et al., 2010). In general, these publications agree that fault and fractures are one of the main contributors to accommodating fluid flux into the borehole from the reservoir.

The study focuses on Lumut Balai geothermal field which is situated differently compared to the other geothermal fields in Sumatra where most of them are in the proximity of the Great Sumatran Fault. Meanwhile, Lumut Balai geothermal field is located as far as forty kilometers away to the north of Kumering Segment, the closest segment between Lumut Balai and the Great Sumatran Fault (Figure 1.a and 1.b). The geologic structures in Lumut Balai might not be directly influenced by the dextral strike-slip movement of the Great Sumatran Fault, thus complicating the determination of which geologic structures direction are potentially more permeable than the others. To answer this problem, assessment of critically stressed fractures in Lumut Balai is important as these fractures are expected to be hydraulically active due to situated at the appropriate angle to the current stress field, to be mechanically active (Zoback, 2007).

There are 2 publications discussing fractures and permeability as Nurseto, et al., (2020) discussed field-wide productive geological structures and Kamah, et al., (2010) discussed the evaluation of fracture and injectivity in 3 Lumut Balai wells, yet none discusses critically stressed fracture and its effect on permeability.

Thus, the latter sections of this paper cover the data and methodology in determining the critically stressed fracture from 6 wells (Figure 1.c), the analysis of identified critically stressed fracture in wells that is responsible for the permeability of the well, and to some extent its influence on hydrogeology of the Lumut Balai geothermal field.

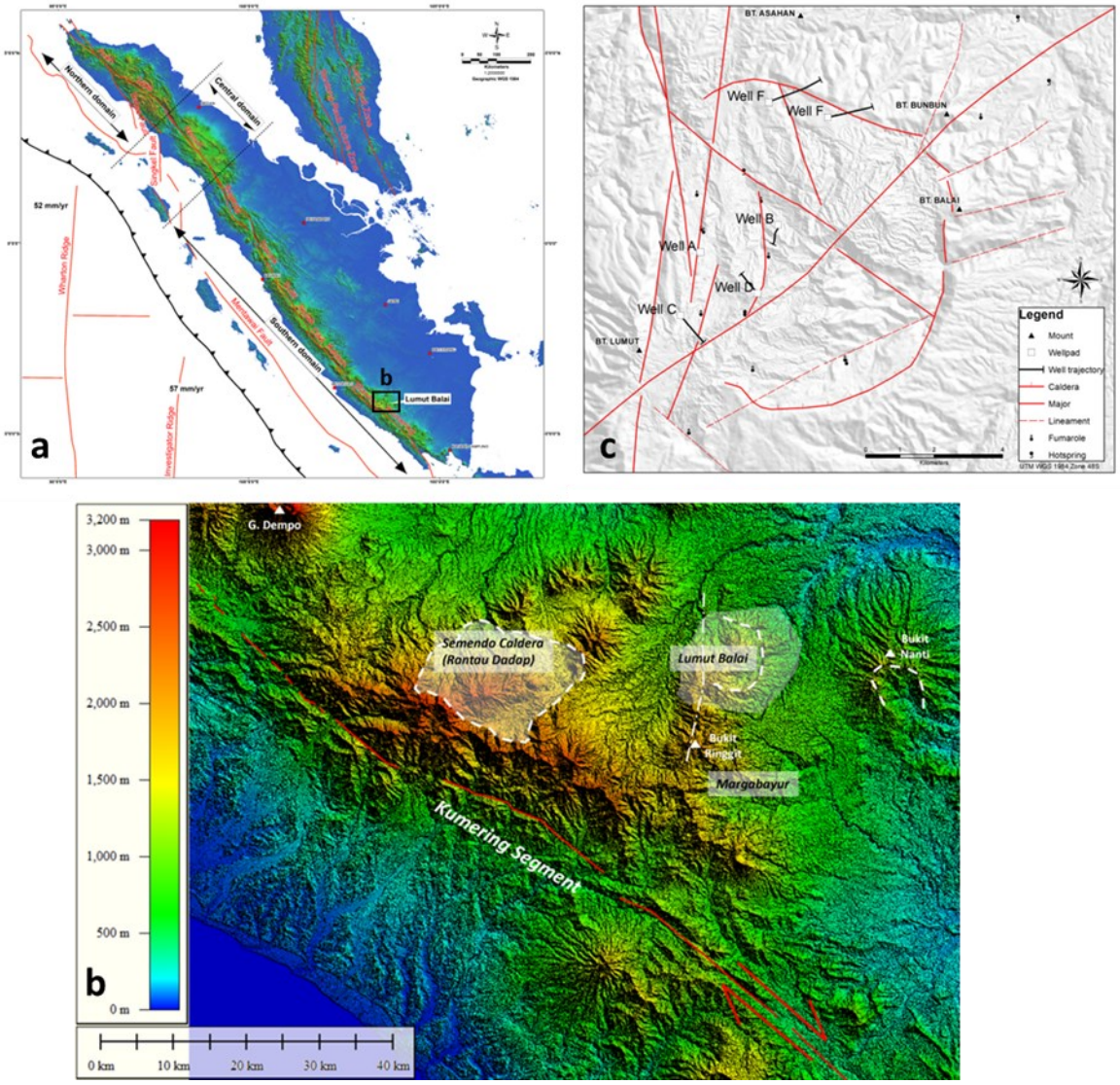

Figure 1: (a & b) Location of Lumut Balai geothermal fields overlain with DEMNAS, regional tectonic setting, Sumatran Faults, and related features (Sieh & Natawidjaja, 2001; Pour, et al., 2016), subdivision of geothermal system in Sumatra (Sutrisno, et.al., 2020). (c) Structural map of Lumut Balai and 6 well distribution used in the study.

2. METHODOLOGY

To analyze which fractures that tend to slip with the direction and magnitude of current the stress field, or critically stressed fractures, the approaches are based on the methods thoroughly explained by Zoback (2007), Wallis et al. (2020), and Ikhwan et al. (2022). The general data and workflow to identify critically stressed fracture are shown in Figure 2, where the datasets that are utilized for preliminary assessment of critically stressed fracture in this study are:

1. Fracture data interpreted on borehole image (micro resistivity or sonic) from 6 wells distributed in the southwest, center, and northern part of the Lumut Balai Caldera (Figure 1.c). Fracture data based on borehole image data is used to analyze the fracture geometry, type, and distribution at depth along the well. As the data used in this study is a micro-resistivity borehole image, the fracture type utilized in the subsequent processes is only the conductive fracture type. This is a generalized type covering all possible conductive fractures such as fault and conductive fracture whether it is continuous or discontinuous. Its conductive nature is interpreted to be filled with water or conductive minerals such as clay, nevertheless,

this feature is the most likely to be permeable. Resistive fracture is not utilized in the analysis due to its being filled and blocked by resistive minerals such as calcite or quartz.

2. Well-test data: pressure and temperature logs. Pressure data is utilized to define the pore pressure around the borehole which is assumed at hydrostatic conditions.
3. Surface gravity data acquisition that has been processed to 3D gravity-MT joint inversion and then converted to density. Density data is utilized to calculate Sv (vertical stress) or overburden.

Maximum horizontal stress orientation is determined based on the average orientation of the drilling-induced tensile fracture (DITF) found in the borehole image data. In a vertical well, the maximum horizontal stress (SHmax) axis could be determined directly by using the strike of drilling-induced tensile fracture when both borehole breakouts and drilling-induced tensile fracture are observed in the well. The DITF is parallel to the SHmax axis, while the borehole breakout is parallel to the direction of minimum horizontal stress (SHmin). Although 1 of 6 of the wells is vertical and has DITF orientation at N 10 E to N 20 E, to honor the sparse distribution of the wells used in this analysis, the average SHmax orientation from 6 wells is at around N 30 E direction which is still reasonable compared to the DITF direction in a vertical well.

The stress regime of Lumut Balai in this study is interpreted to be controlled by a normal stress regime, where the vertical stress is σ1, maximum horizontal stress = σ2, and minimum horizontal stress is σ3. The stress regime determination for this preliminary assessment is based on the condition that Lumut Balai is heavily influenced by its local regime of normal faulting due to the formation of a 9-10 km wide caldera.

After analyzing the fracture distribution at depth, the 1D geomechanics assessment (Sv/Shmin/Shmax calculation in the borehole), and stress regime determination then Fractoolbox (2023) is utilized to calculate slip tendency analysis, convert and plot the fractures with its normal effective stress and the shear stress on 3D Mohr circle. Slip tendency analysis on a 3D Mohr circle utilized $\mu > 0.5$ (shear to stress ratio), where the shear stress acts at the fractures are greater than the normal stress. Fractures that are more likely to be permeable and hydraulically active are the ones with more susceptibility to shearing, hence the current state of shear stress > normal stress at the fractures plane must be met. In convective and high-temperature geothermal systems, the shearing and repeated failures provide a mechanism to prevent the deposition of hydrothermal minerals and maintain the permeability of the fractures (Wallis, et al., 2020, and Ikhwan, et al., 2022).

Lastly, the identified critically stressed fractures at those 6 wells are evaluated against the distribution and magnitude of feed zone data derived from pressure-temperature-spinner (PTS) logs during injection or production. The evaluation demonstrates the influence of critically stressed fractures on the permeability of the well.

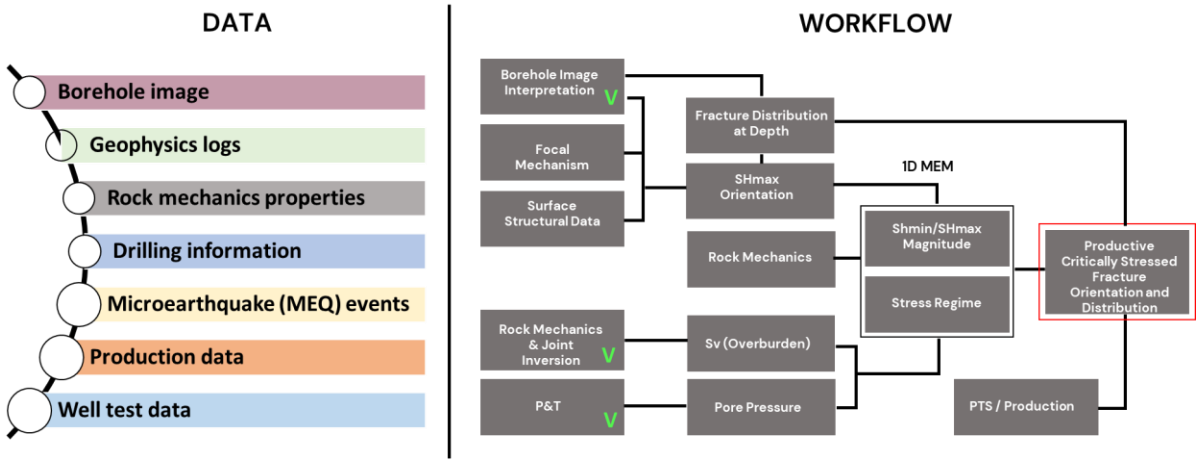

Figure 2: The 1D geomechanics model workflow to identify the critically stressed fracture from the image log data (Ikhwan, et al., 2022). Green marks are the data used in the study.

3. RESULT AND DISCUSSION

The borehole image data acquisition was conducted within the perforated liner sections reflecting the well sections that cover the reservoir zone. Nevertheless, not all the 6 wells reservoir section is covered completely by borehole images, such as the perforated liner 8-5/8" section in Well D and Well E. In addition, some part of the reservoir section in the perforated liner 10-3/4" in Well F is not covered by borehole image data due to wash-out borehole (Figure 3).

The general strike direction of the observed conductive fractures and faults in 5 of 6 wells is dominated by 195-240° (NE-SW) direction with a predominantly high dip angle of 60-80° and a minor relative N-S strike direction

found in Well A (Figure 3). The NNW-SSE strike direction is only observed in Well F as the well is intersected by the relative NNW-SSE direction fault.

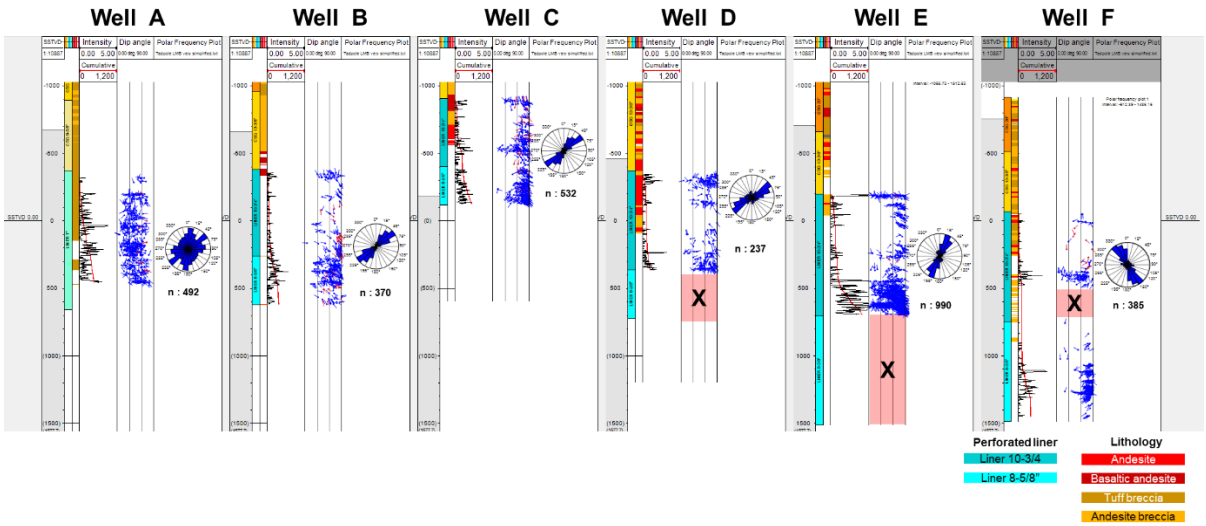

Figure 3: Section of the 6 wells shown in elevation (first column), well sections (second column), lithology (third column), tadpoles and stereonet of the identified conductive fractures (fourth and fifth column). 'X' marks are not covered by the image log.

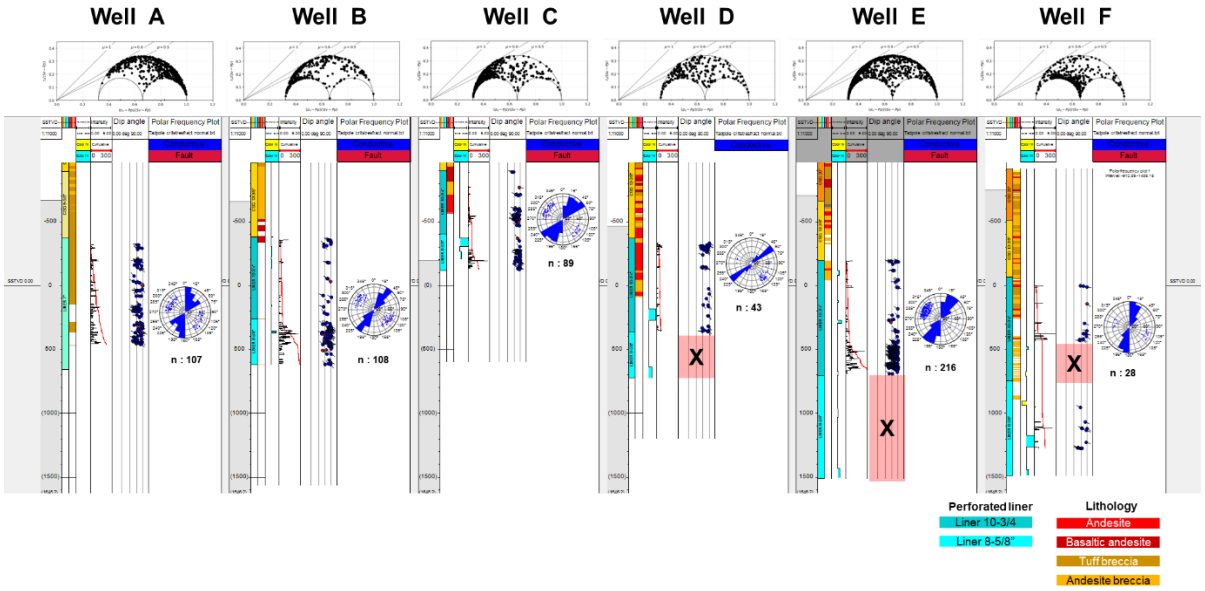

Figure 4: Below the well name is the conductive fractures plotted in 3D Mohr circle. Below the 3D Mohr circle is section of 6 wells shown in elevation (first column), well sections (second column), lithology (third column), tadpoles and stereonet of the identified critically stressed fractures (fourth and fifth column). 'X' marks are not covered by the image log.

After conducting the slip tendency analysis using the above conductive fractures distribution and orientation, there are 591 identified critically stressed fractures from 6 wells which are interpreted to be potentially permeable (Figure 4). These critically stressed fractures are the conductive fractures that are located above the μ 0.5 line within the 3D Mohr circle, reflecting the tendency to slip is greater than the effective normal stress influence. The 3D Mohr circle depicts the conductive fractures with its projected stresses (normal effective stress and the shear stress). The critically stressed fractures observed in these 6 wells have strike direction dominated by 195-225°(NNE-SSW) and dominated by a high dip angle range of 60-80°, mean 62°.

It is noticeable that the fractures population between the conductive fractures and critically stressed fractures are not directly correlated as evidenced in the Well A and Well F. In Well A, the population of conductive fractures in quadrant 2 (NW) and quadrant 4 (SE) are not characterized as critically stressed fractures. Moreover, although

Well F is predominantly comprised of NW-SE conductive fractures, the critically stressed fracture in Well F is dominated by the NNE-SSW direction.

3.1 Influence of critically stressed fractures to the permeability of the well

It is observed that feed zone intervals (third column, after lithology column) coincide with the occurrence of critically stressed fractures in most of the wells, excluding Well A which does not have any PTS data to evaluate the relationship between the observed critically stressed fracture and fluid flux to the well (PTS during production) or to the formation (PTS during injection). More importantly, the major contributor feed zone intervals (light blue bars) in 5 wells are directly influenced by the occurrence of critically stressed fractures cut by the well (Figure 4).

3.1.1 Well B

Out of 532 conductive fractures plotted in the 3D Mohr circle, around 108 fractures are located above the $\mu > 0.5$, which is categorized as critically stressed fractures. The identified critically stressed fracture in Well B formed an NE-SW strike direction (30-45 NE) and has a dip direction facing both NW and SE directions almost equally. Along the borehole depth, in general, the conductive fractures are more intense below the 1300 mTVD along with the 58% fluids injected into the formation.

There are 7 feed zone intervals identified by PTS logs during injection, where the major contributors (>10%) are observed in the 3 intervals. The shallowest major feed zone interval (22%) is not covered by the borehole image data, and thus could not be evaluated control on the permeability at this interval. The other 2 major feed zone intervals (10% and 49% contributions), depicted by numbers 2 and 4, are fracture controlled, suspected heavily influenced by the wide aperture fracture, and coincide with the population of critically stressed fractures around that interval. It is also observed that the 49% feed zone interval is heavily populated with fractures compared to the 10% contributor.

The other 4 minor feed zone intervals (<10% contribution) are interpreted to be more controlled by matrix permeability rather than the fractures. It is also supported by the minimum distribution of the conductive fractures and critically stressed fractures around the 4 minor intervals, as shown by numbers 1 and 3 in Figure 5.

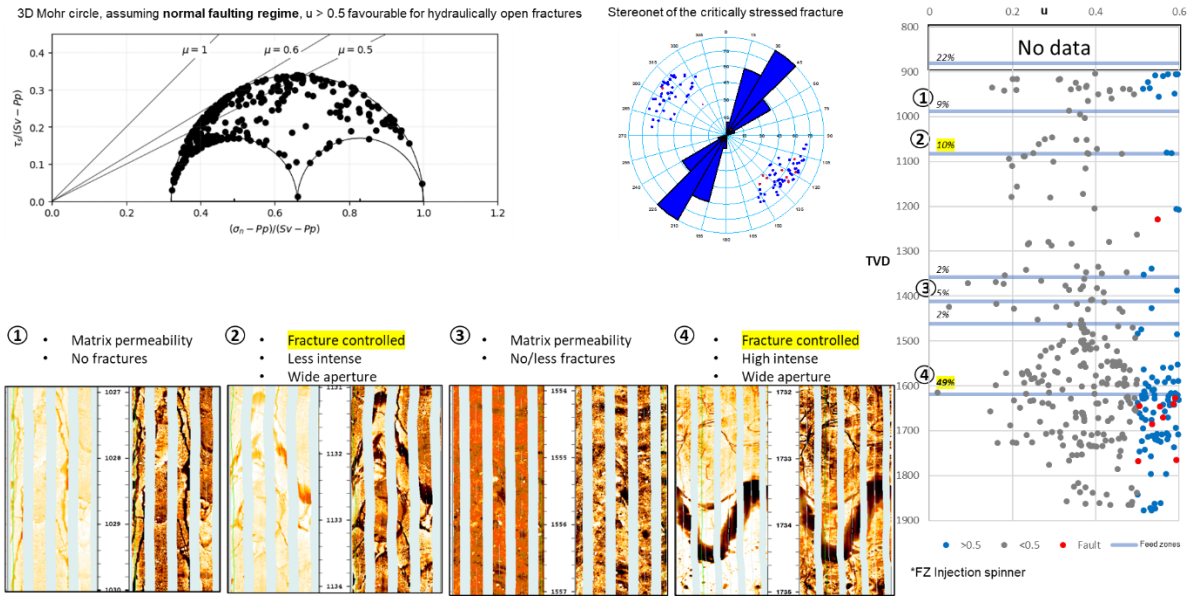

Figure 5: The occurrence of critically stressed fractures with wide aperture and less intensity in Well B contribute heavily to the permeability of the feed zones (highlighted by yellow). Meanwhile the minor feed zones (<10%) are controlled more by matrix permeability. The distribution of the conductive fractures in 3D Mohr circle and stereonet of the critically stressed fractures in Well B. The right chart showed the conductive fractures that have shear to stress ratio < 0.5 are shown by grey points while the critically stressed fractures and faults (> 0.5) are shown in blue and red points. The feed zone intervals are highlighted by light blue rectangular within the same chart and represented by numbers in the fracture distribution chart and in the image log.

3.1.2 Well C

There are 89 out of 532 conductive fractures that are identified as critically stressed fractures in Well C. These critically stressed fractures in Well C are predominantly composed of the 195-240 NE strike fractures (NE-SW) with NW dip direction and much of the fractures are more populated at 1100 to 1600 mTVD depth.

Based on the PTS during injection data, there are only 2 feed zone intervals with 86% (major feed zone) and 14% (minor feed zone) contribution, as shown by numbers 1 and 2 in Figure 6. Both feed zones are interpreted to be controlled by critically stressed fractures identified within each feed zone interval. In the first major feed zone at a depth around 1360 mTVD (86%, number 1), it is interpreted to be heavily influenced by the occurrence of three wide aperture fractures one of them is critically stressed fractured, although fractures population around that interval has less intensity. The latter minor feed zone (14%, number 2) is also influenced by the occurrence of wide aperture conductive fracture that is identified as critically stressed fracture and supported by critically stressed fractures observed around the interval as shown in the borehole image number 2 in Figure 6.

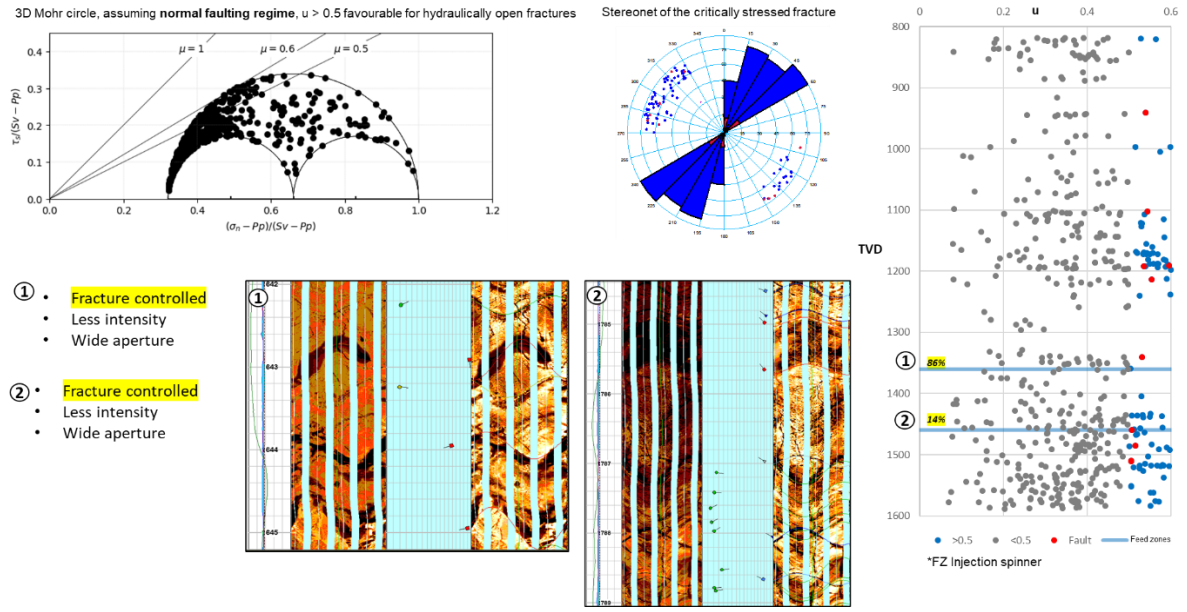

Figure 6: The occurrence of critically stressed fractures with wide aperture and less intensity in Well C contribute heavily to the permeability of the 2 feed zones (highlighted by yellow). The distribution of the conductive fractures in 3D Mohr circle and stereonet of the critically stressed fractures in Well B. The right chart showed the conductive fractures that have shear to stress ratio < 0.5 are shown by grey points while the critically stressed fractures and faults (> 0.5) are shown in blue and red points. The feed zone intervals are highlighted by light blue rectangular within the same chart and represented by numbers in the fracture distribution chart and in the image log.

3.1.3 Well E

This well has PTS log during production and is only covered by borehole image data in the perforated section 10-3/4" (800 to 1800 mTVD) which contains abundant 990 conductive fractures and is mostly located in the interval between 1500 to 1800 mTVD. Only 216 of these conductive fractures are identified as critically stressed fractures that are highly dominated by 195-225 NE strike fractures with their NW dip direction, and only a few fractures have a dip direction at SE (Figure 6).

There are 4 feed zone intervals identified and measured by PTS log during production in the section that is covered by borehole image data, as shown in feed zones number 1 to 4 in Figure 7. Only 1 feed zone interval does not coincide with the occurrence of critically stressed fracture (number 2, with 10% contribution). This feed zone interval is interpreted to be greatly affected by matrix and contact permeability as this interval comprises volcanic breccia with very few fractures.

On the other hand, the other 3 feed zone intervals are interpreted to be not only controlled by fractures (number 1, 3, and 4) but also by matrix/contact permeability (1, and 3). The smaller 6% contribution in the deeper part of the section comprises numerous fractures within the lava andesite (number 4). Around this feed zone interval, there are many of the fractures identified yet do not have any contribution of fluid flux to the well. This interval might comprise fractures that have shallow continuity to the formation. The lithological units within feed zone number 1 with a 17% contribution are almost identical to the feed zone interval number 2. The difference between

the 2 feed zone intervals is the occurrence of critically stressed fractures in feed zone 1 that add more permeability contribution to the fluid flux into the well. The combination of fractures and matrix/contact permeability is also observed in feed zone number 3 with a 41% contribution. This interval coincides with the critically stressed fractures and also many layers of tuff and tuff lapilli which in total greatly contributes to the fluid flux into the well.

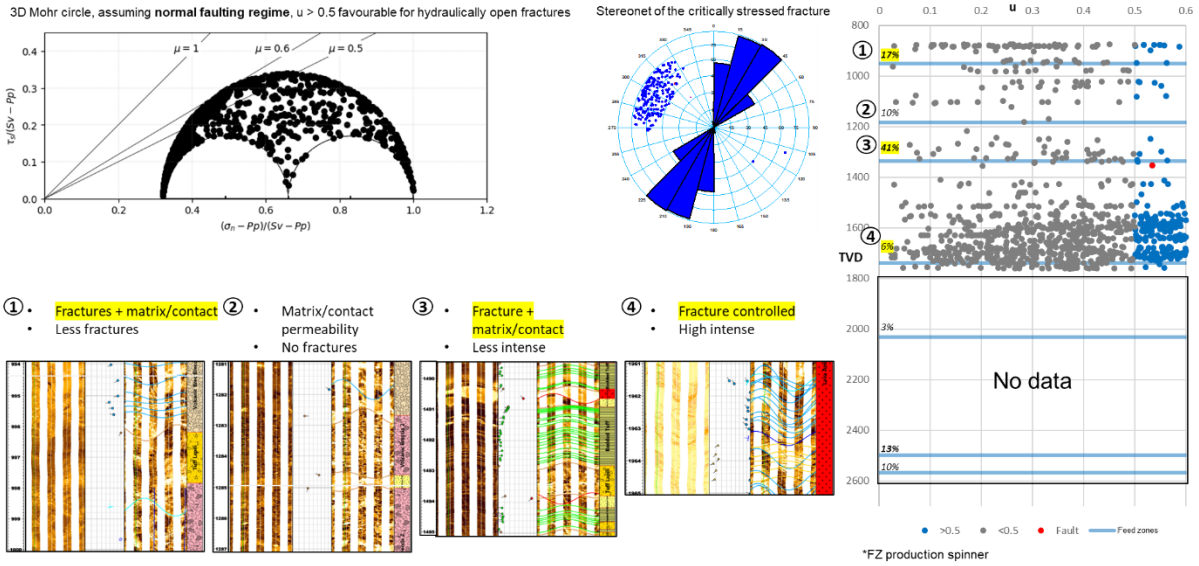

Figure 7: The occurrence of critically stressed fractures with the combination of matrix/contact with less fractures in Well E contribute heavily to the permeability of the number 1 & 3 feed zones while the number 4 is fracture controlled (highlighted by yellow). The distribution of the conductive fractures in 3D Mohr circle and stereonet of the critically stressed fractures in Well B. The right chart showed the conductive fractures that have shear to stress ratio < 0.5 are shown by grey points while the critically stressed fractures and faults (> 0.5) are shown in blue and red points. The feed zone intervals are highlighted by light blue rectangular within the same chart and represented by numbers in the fracture distribution chart and in the image log.

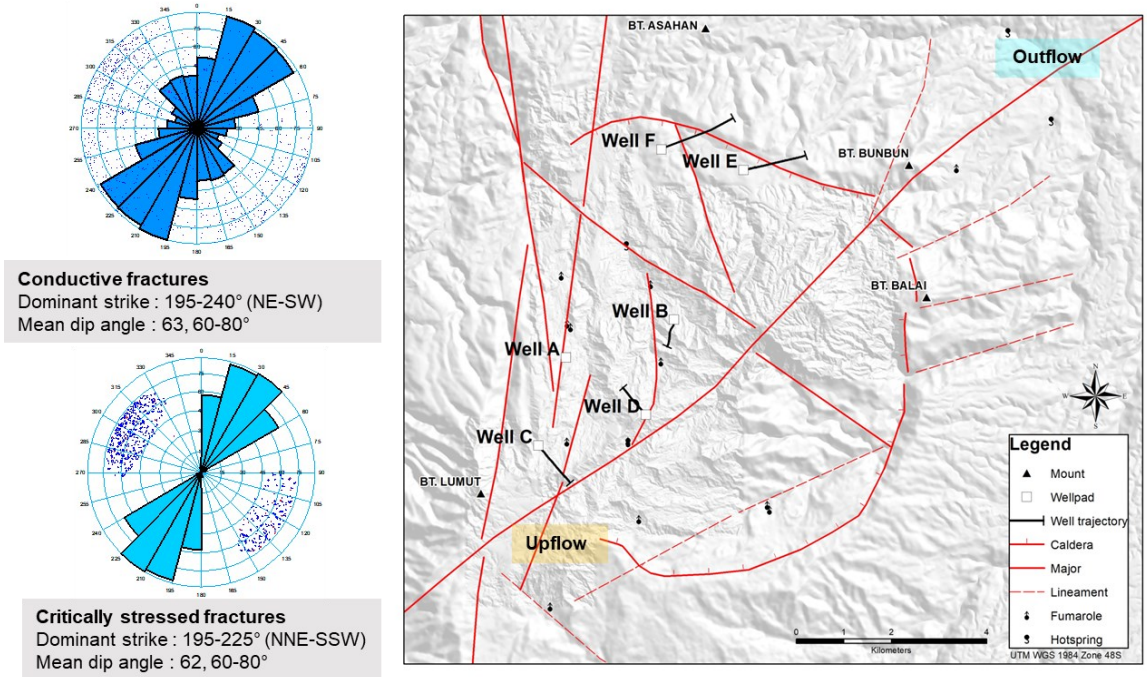

Figure 8: Compilation of conductive fractures and critically stressed fractures depicted in stereonets and its polar demonstrates the domination of NNE-SSW fractures that might influence the hydrology of the fluids from upflow to the outflow in Lumut Balai.

3.2 Field wide permeability contribution

Based on the compilation of conductive fractures from 6 wells, Figure 8 depicted that although the dominant strike of the conductive fractures is NE-SW at around 195-240 NE the other direction of conductive fractures such as N-S, or even the NW-SE are still observed. It is thought that these conductive fractures are the product from the field-wide geological structures that is intersected by the 6 wells. Nevertheless, based on the evaluation above, not all these strike directions contribute to the permeability of each well.

The conductive fractures that have been analysed to be critically stressed fractures are dominated by strike direction of NNE-SSW at around 195 – 225 NE. These are the fractures that responsible to control the permeability at the major feed zone intervals and supported by the primary permeability from the respective lithological units, such as tuff, breccia andesite or lavas or contacts between the lithological boundaries.

The dominant NNE-SSW strike direction of permeable critically stressed fractures support the interpretation of how the fluids move laterally and updip under the caprock from the upflow at the southern end of the Lumut Balai Caldera to the NE outside the Caldera. The outflow area is characterized by chloride hotsprings in Sendawan Ilir, while the upflow area is supported by the evidence of highest temperature well around the upflow area.

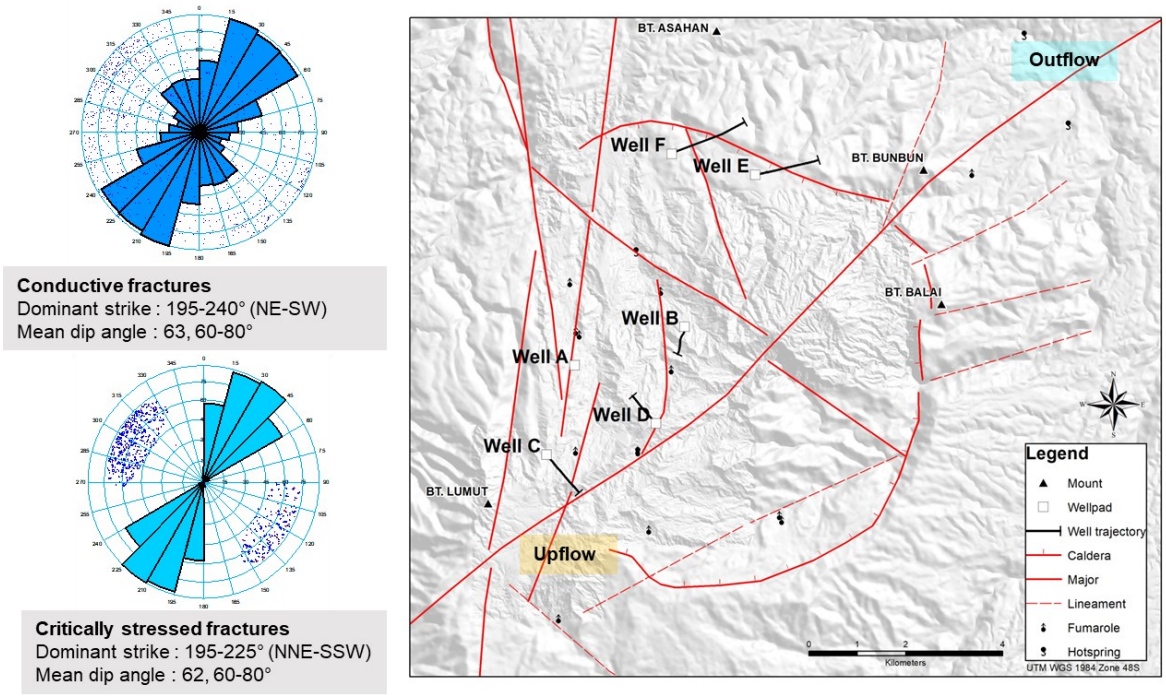

Figure 8: Compilation of conductive fractures and critically stressed fractures depicted in stereonets and its polar demonstrates the domination of NNE-SSW fractures that might influence the hydrology of the fluids from upflow to the outflow in Lumut Balai.

4. CONCLUSION

Identifying potentially permeable geological structures is an important task for geoscientists in the geothermal industry. One way to identify such structures is by analyzing critically stressed fractures using slip tendency analysis

The slip tendency analysis results indicate that critically stressed fractures predominantly strike in the 195°–225° NE (NNE-SSW) direction, which significantly affects the permeability of the feed zone. A feed zone controlled by critically stressed fractures contributes significantly to permeability compared to permeability from lithology or lithological contacts. Moreover, combining critically stressed fractures with other permeability factors further enhances the permeability of the feed zone. The dominant orientation of critically stressed fractures also influences the hydrology from upflow to outflow in Lumut Balai.

Identifying critically stressed fractures and their orientations can assist in well targeting, increasing the possibility of achieving the desired permeability output from a specific geological structure. Additionally, it implies that geological structures with strike directions orthogonal to the critically stressed fractures might be lower permeability. Furthermore, couple of basic data such as focal mechanisms from micro-earthquake events, rock

mechanics measured from petrophysics analysis of the cores and density logging data (if available) could be integrated to measure better Shmin/SHmax magnitude and more precise stress regime determination.

REFERENCES

Arifin, M., T., Prasetyo, I., M., Nusantara, V., D., M., Pratama, G., R., Thamrin, M., H., Koestono, H., (2020), Feed Zones Characterization Based on the Intensity of Faults and Fractures to Reduce Uncertainty of the Future Field Development in Ulubelu Geothermal Field, Lampung, Indonesia, Proceedings, World Geothermal Congress 2020+1, Reykjavik, Iceland.

Arifin, M., T., Nurseto, S., T., Nusantara, V., D., M., Pratama, G., R., Marastio, F., E., Thamrin, M., T., (2020), Feed Zone Evaluation in Hululais Geothermal Field, Bengkulu, Indonesia, Proceedings 42nd New Zealand Geothermal Workshop 24 – 26 November, Auckland, New Zealand.

Fractoolbox (2023) https://github.com/ICWallis/fractoolbox

Ikhwan., M., Wallis., I., C., Rowland, J., V., (2020), Integrated Analysis of Surface and Borehole Data to Construct the Stratigraphy Model of Bukit Daun Field, Indonesia, Proceedings, World Geothermal Congress 2020+1, Reykjavik, Iceland.

Ikhwan, M., Suryanto, S., Tofan, R. M., (2022), Integration of Geoscience, Geomechanics, and Geostatistics Method to Model the Fracture Distribution and Permeability in Naturally Fractured Geothermal Reservoir, Proceedings 44th New Zealand Geothermal Workshop 23 – 25 November, Auckland, New Zealand.

Kamah, Y., M., Hartanto, D., B., Thamrin, M., H., (2010), The Evidence Used in Targeting Wells in a Geothermal Reservoir using Fracture Zone and Erratic Structure at Lumut Balai and Tompaso Geothermal Area, Indonesia, Proceedings, World Geothermal Congress, Bali, Indonesia.

Nurseto, S., T., Arifin, M., T., Prasetyo, I., M., Mulyanto, (2023), Attractive Potential of Geothermal System in Hululais Geothermal Field, Bengkulu, Indonesia, Proceedings: World Geothermal Congress 2023, Beijing, China.

Nurseto, S., T., Satriani, R., A., Thamrin, M., H., (2020), Geology of Lumut Balai Geothermal Field, Proceedings, World Geothermal Congress 2020+1, Reykjavik, Iceland.

Nurseto, S., T., Sardiyanto, Koestono, H., Thamrin, M., H., Kamah, M., Y., (2015), Evaluation of the Productive Geological Structure in Ulubelu Geothermal System, Proceedings: World Geothermal Congress 2015, Melbourne, Australia.

Pour, A. B., Hashim, M., Makoundi, C., Zaw, K., (2016), Structural Mapping of the Bentong-Raub Suture Zone Using PALSAR Remote Sensing Data, Peninsular Malaysia: Implications for Sediment-hosted/Orogenic Gold Mineral Systems Exploration, Resource Geology, Volume 66, Issue 4, p. 368-385.

Sanjaya, D., Triananda, W., Siburian, P., Hartanto, R, (2023), Roles of Borehole Image Logs for Fracture Evaluation and Well Planning in Geothermal Field. A Case Study of Sorik Marapi Field, North Sumatera, Indonesia, GRC Transactions, Vol. 47.

Sieh, K., and Natawidjaja, D., (2000), Neotectonics of the Sumatran fault, Indonesia, Journal of Geophysical Research, Vol 105, No. B12, Pages 28,295-28,326 (2000).

Sutrisno, L., Bonte, D., Daud, Y., Smit, J., Beekman, F., Purwanto, W., Van Wees, J. D., (2021), Regional Characterization of the Sumatran Geothermal Systems, Indonesia, Proceedings: World Geothermal Congress 2020+1, Reykjavik, Iceland.

Wallis, I., Rowland, J., Dempsey, D., Allan, G., Sidik, R., Martikno, R., McLean, K., Sihotang, M., Azis, H., Baroek, M., (2020), Approaches to Imaging Feedzone Diversity with Case Studies from Sumatra, Indonesia and The Taupō Volcanic Zone, New Zealand, Proceedings 42nd New Zealand Geothermal Workshop 24 – 26 November, Auckland, New Zealand.

Wallis, I., C., Dempsey., D., E., Rowland, J., V., (2023), Geologic Controls on Permeability Revealed by Borehole Imaging: Case Studies from Sumatra, Indonesia and the Taupō Volcanic Zone, New Zealand, Proceedings 45th New Zealand Geothermal Workshop 15 - 17 November, Auckland, New Zealand.

Zoback., M., D., (2007), Reservoir Geomechanics, Cambrige University Press.

Fracture Characterization Inside and Outside Salak Geothermal Reservoir

Fanji J. Putra and Yudi Indra Kusumah

Star Energy Geothermal Salak Ltd., Wisma Barito Pacific II 17th Floor, Jakarta 11410, Indonesia

fanji.j.putra@starenergy.co.id

Keywords: Fracture, bore hole images log, Salak, Awibengkok

ABSTRACT

Fractures play an important role at the Salak geothermal field. Previous studies have shown that the majority of permeable entries in Salak are associated with fractures, which are classified as Effective Fractures (EFs). These geological features are responsible for fluid flow in and out of the wellbore. Lithologic contacts have a very limited role in hosting permeable entries. To understand the characteristics of the fractures, borehole image interpretation was conducted on 18 wells, with 12 wells located inside the commercial area and 6 located outside. Subsequently, 3 fracture main parameters were evaluated and compared between inside and outside reservoir, namely, fracture orientation, density, and aperture. The comparison aimed at determining whether fractures outside the reservoir are similar to producing EFs inside the reservoir, or whether they represent a different fracture. Analyses show that some fracture parameters have similar characteristics while others have significant distinctions. Geologic setting and process may cause differences in fracture characteristics. Ultimately, this study is expected to improve well targeting and planning during the drilling of makeup wells and become an input for both static and numerical model.

1. INTRODUCTION

Salak Geothermal Field (also known as Awibengkok) is located in West Java and it is situated 70 km south of Jakarta, the capital of Indonesia (Figure 1; A). It is Indonesia's largest-producing geothermal field with a recent total installed capacity of 381 MWe using six power plants. It consists of 180 MWe from PLN Units 1, 2 & 3, and is mostly provided by two-phase wells located in West Salak area. Star Energy Geothermal Salak supplies the steam to, operates, and produces electricity (201 Mwe) from Units 4, 5 & 6, and mostly using steam cap wells located in East Salak Area (Golla et al, 2020). The Salak geothermal system is a high-temperature water-dominated reservoir with benign chemistry and low-to-moderate NCG content (Acuña et al., 1997). The highest reservoir temperature measured is more than 325 °C, located in the western portion of the production area, and it is interpreted as the main system's upflow. Based on Stimac (2008), the field can be divided into four sectors with distinctive temperatures, fluid chemical signatures, and tracer return patterns. The four sectors have been termed the Western, Central, Eastern, and Far Eastern Cells Conceptual model of the field shows that geothermal fluids generally flow towards the northeast and east-southeast and outflow in the surface thermal manifestations, which are mostly located near the eastern and northern margins of the drilled reservoir (Figure 1B).

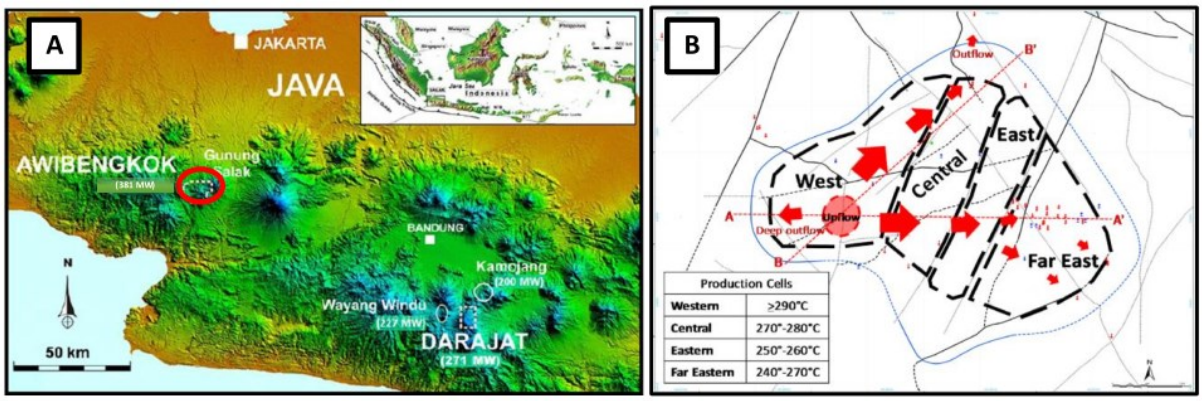

Figure 1: (A) Left: Map of West Java showing major cities and volcanic centers. It is also shown the location of the Salak geothermal field with other geothermal fields in West Java (modified Aprilina et al, 2017); (B) Right: Map showing the conceptual model and the general flow (arrows) of geothermal fluids at the Salak geothermal system under natural-state (pre-exploitation) conditions (Golla et al, 2020).

In past interpretations of fractures from borehole image logs, the stereonet and rose diagram plots that were normally shown depict the general strike and dip orientations of all the discernible open fractures encountered by the well. This paper will deliver more characteristics of the fractures and its comparison between the inside and outside reservoir area. The deliverables of this objective will be used to improve well targeting and input for both static and numerical model parameters.

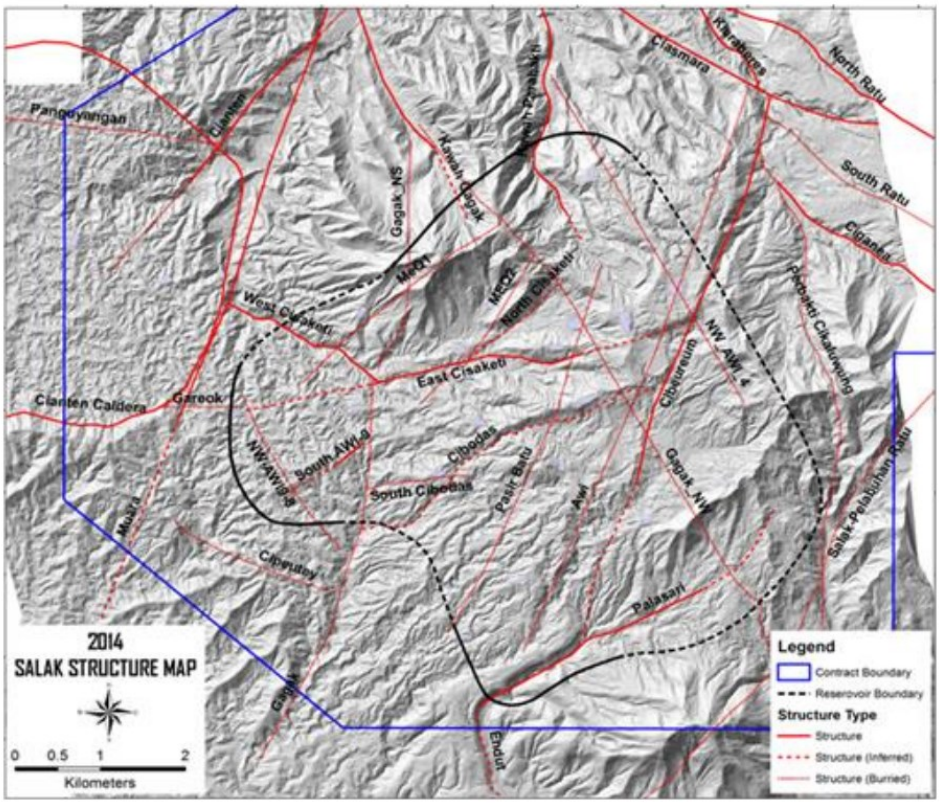

Figure 2: 2014 Salak structural map (Golla et al 2014).

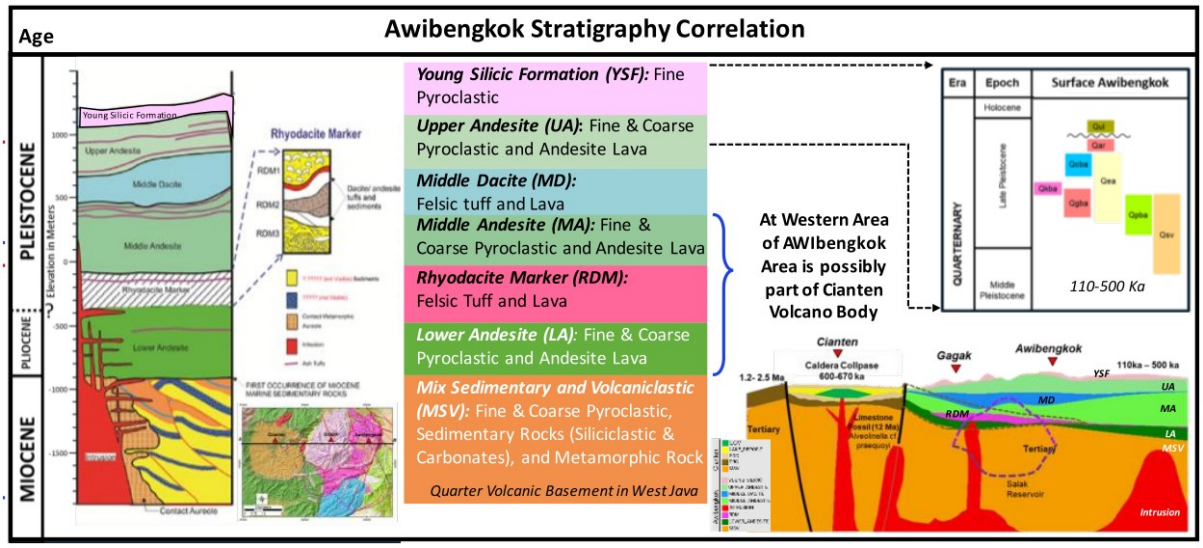

Figure 3: Subsurface stratigraphic section, rock composition and cross section of Awibengkok/Salak Geothermal Field. (modified from Stimac et al, 2007).

2. GEOLOGY OF SALAK GEOTHERMAL FIELD

As typical of most geothermal fields in Indonesia, Salak Geothermal Field is located in the mountains, and it is part of the Taman Nasional Gunung Halimun-Salak with elevations varying between 950-1,500 m above sea level (ASL). The Salak geothermal system is situated in a mountain range comprised of inactive andesitic volcanoes,

with the highest peaks are Gunung Salak, Gagak, Perbakti, and Endut, which lie along the main trend of the Sunda Volcanic Arc which extends from Sumatra to Flores (Hamilton, 1979; Hutchinson, 1989). These peaks border the geothermal field in the east, northwest, southeast, and south, respectively, and give way to lower hilly countries in the north and south (at 600-950 m ASL). The Cianten Caldera, a collapsed andesitic stratocone, lies further to the west with a floor at ~850-950 m ASL (Figures 2 and 3).

Initially, Salak structural map was mainly developed from lineaments interpreted by different workers from aerial photos and satellite imageries and, when possible, augmented with surface field mapping. Unless measured at the surface, most of the structures in the fault model were assumed to dip vertically. Not all these structures (or lineaments) extend deep into the reservoir, and, consequently, affect reservoir permeability and processes. This data subsequently incorporated interpretations from geophysics, geology, geochemistry, and reservoir engineering data. Later on, structural map refinement and validation were conducted by data conditioning to highlight structural relief in the RDM horizon and temperature from well data. Figure 2 below are the result of 2014 Salak structural map refinement (Golla et al ,2014). Salak structure is dominated with NE-SW trend, and it is believed was controlled by West Java the regional stress in West Java (SHmax at N10°E; Tingay et al., 2009). This trend is similar to the general direction of Salak Shmax ($\approx$N24ºE) assuming that the stress regime is extensional (Sugiaman, 2003). This study is corroborated by recent drilling-induced tensile fracture (DTIF) evaluation from borehole image log data denotes that Salak DTIF mostly has NNE-SSW trend. In addition, fault criteria were developed to consistently represent the mapped structures at the surface.

The Salak structures were classified into three general categories, namely:

- **Confirmed**: Structures that were identified at both the surface and confirmed with subsurface data. These structures will be drawn as solid lines and will have a high degree of confidence.
- **Inferred**: Structures that were defined from lineaments from LiDAR or other remote sensing data only. If confirmed by field measurements, these structures will be drawn with solid lines in the structural map but with dashed lines if based on lineaments only.
- **Buried**: Structures that have subsurface evidence/s only and do not correlate with surface lineaments. These structures are drawn as dotted lines and have low degree of confidence.

In term of Stratigraphy, the subsurface rocks at Salak Field are composed of andesitic, basaltic lava, breccia, tuff, and lahar that comprise several long-lived volcanic centers underlying the south-western margin of Gunung Salak Hulen and Lutz (1999; Stimac and Sugiaman (2000). Stimac et al. (2008) divided the subsurface rocks at Salak into four major formations that are thought to represent discrete episodes in the evolution of the western Java segment of the Sunda Volcanic Arc. The “formation” terminology here is used to refer to distinctive time-bounded rock sequences that have not been formally correlated with documented formations on a regional basis. The four major formations, from oldest to youngest, are the (1) Lower Volcanic Formation that consists of Marine Sediments and Volcaniclastics (MSV) and Lower Andesite; (2) Rhyodacite Marker or RDM; (3) Middle Volcanic Formation; and (4) Upper Volcanic Formation. Both the Middle and Upper Volcanic Formations consist of a series of dacitic (at their base) and andesitic rocks overlying each other (Aprilina et al., 2017). In addition, multiple intrusions are spread all over Salak/Awibengkok geothermal field. Figure 3 discerns Awibengkok stratigraphy section.

3. TERMINOLOGY

As in the past, fractures encountered in the borehole image logs were interpreted with the main objective of identifying the fractures that correlate with the permeable entries, evaluating trends exhibited by these fractures, and applying the trends to better understand of geothermal reservoir. Examples of terminology used in Star Energy during the fracture identification are classified as follows (Intani et.al, 2017):

- **Effective Fractures**: These are geologic features that correlate with the PTS-based permeable zones. Normally, these will be high-confidence fractures where the conductive feature is present in all the image log tool pads (i.e., 360° around the borehole). Figure 4 shows a schematic for picking EFs in image log data.
- **Conductive (or Open) Fractures**: These are high-confidence fractures where the electrically conductive fracture trace is present in all the image log tool pads or 360° around the borehole.
- **Partial Open Fractures**: These are fractures where the conductive feature is not found on all the image tool’s pads. The authors tried to follow the 75% (or about 270° around the borehole).

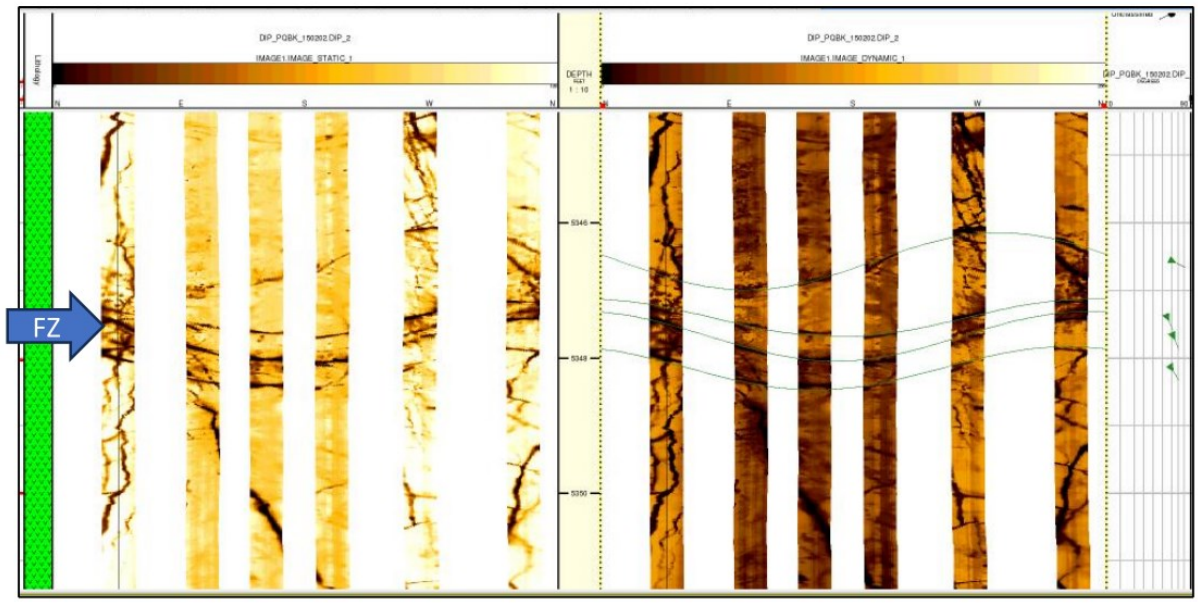

Figure 4: Schematic discerns effective fractures (EFs) picking depend on the location of entry/feedzone (blue arrow). These open/conductive fractures subsequently will be classified as effective fracture (EFs).

4. FRACTURE CHARACTERIZATION INSIDE AND OUTSIDE GEOTHERMAL RESERVOIRS

This section discusses fracture characterization from borehole image interpretation. As mentioned earlier, there is a fracture categorized as Effective Fracture (EFs) because it correlates with a permeable zone, where fluid enters or out from this zone. In some cases, picking the EFs was quite easy because a single, large-aperture fracture stood out at the depth of the production zone. However, there are many cases where no prominent fracture appeared to correspond with the permeable entry. If a single prominent fracture was not present, all fractures within ~10 m of the permeable entry were selected as EFs. Aside from EFs, open (or high-confidence conductive) fractures were also identified from the borehole image logs. Note that the majority of the EFs is composed of "Groups of Fractures" where a certain cluster of fractures was picked to represent the permeable entry because there was no single prominent fracture identified, i.e., the actual % of producing EFs may be lower than shown in figure 5. In Salak commercial area, 82% of permeable entries correlate with EFs composed of a group of fractures, 15% correspond to single fractures, while only 2 permeable zones are related to lithology boundary (figure 5).

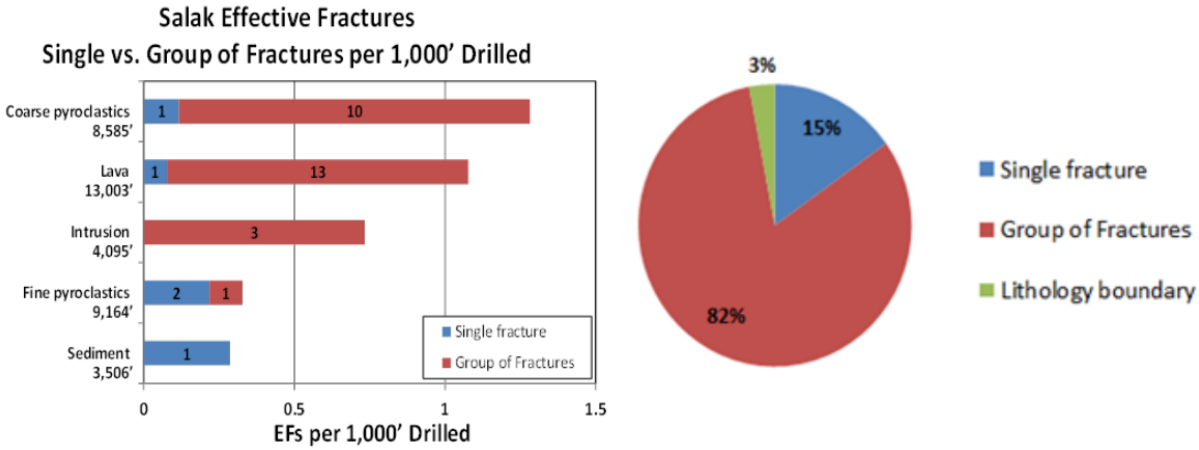

Figure 5: (Right) Pie chart showing the distribution of permeable entries composition: correlate group of fractures (82%), single fractures (15%), lithology boundary (2%). (Left) Chart showing the number of EFs, either as single fracture or group of fractures, in various lithologies. Numbers inside the bars denote the number of EFs/permeable zones.

In Salak fields, there are 18 out of 115 wells with borehole image data. Although only 16% of all Salak wells have image log data, their locations are distributed around the entire Salak main production area (Figure 6). In terms of

location, 12 image log wells are located inside the commercial area, and 6 are located outside. About 50 permeable entries were intersected by these 12 wells, with 31,500 ft /~9600 m (cumulative) of reservoir logged. There are 68% (34 feedzones) of these permeable entries have good-quality image logs that can be interpreted. The remaining 16 permeable zones have no image logs. In the case of Salak, step-out drilling in the Cianten Caldera in the west and at the edge of the commercial reservoir provided the opportunity to collect borehole image data (Figure 6). Effective fractures (EFs) have been identified in some edge wells in the Cianten area. Thus, a one-to-one analysis of Efs inside and outside the Salak reservoir can be conducted. Analysis of these image logs (inside and outside reservoir) revealed about 8,100 open and partial open fractures and only 2% or 141 fractures correlated with permeable zone (EFs). This suggests that only a small percentage of the fractures are produced from the network of open fractures in the geothermal reservoir.

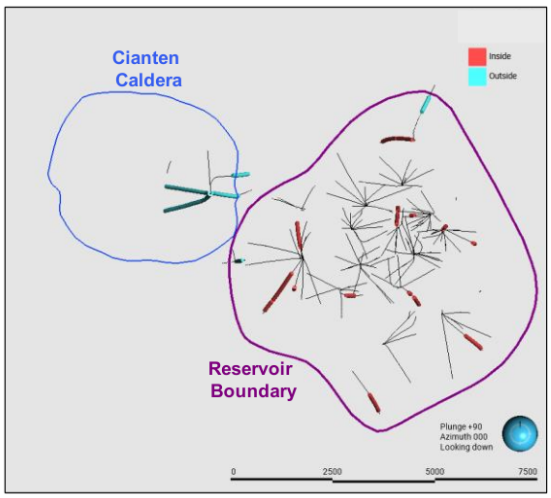

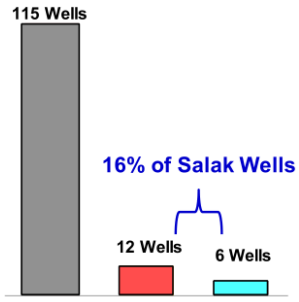

Region	Borehole Image Interval, ft	No. of Open Fractures	No. of Partial Open	No EFs	% of EF from All Open Fractures
Inside Reservoir	~ 31,500	978	3,743	100	10
Outside Reservoir	~23, 400	702	2,674	41	6

Figure 6: (Left) Map showing the location of wells with borehole image logs at Salak. Although only 12 wells (16% of total. wells) are located inside the commercial production area, they are spread out within the production area. The purplepolygon represents the Salak reservoir area. (Right) table shows the numbers of open and EFS inside and outside reservoir.

4.1 Fracture Orientation

Fracture dip azimuth and magnitude scatter plots were generated to determine the general distribution and trends of fractures inside and outside the Salak reservoirs. To remove bias in the plotting, both dip azimuth and magnitude were calibrated to a 0-180° range (Figure 7). If fractures outside the reservoir have dip azimuth >180°, they were normalized/converted to a value between 0° to 180°. Normally, the maximum dip value is 90°; however, fractures that have dip azimuth >180° will have dip magnitudes >90°. For example, a fracture with dip azimuth of 220° and a dip magnitude of 65° will be represented as a fracture with dip magnitude 135° to remove bias. Thus, a dip magnitude of 110° (70°) is steeper than a dip magnitude of 170° (10°). Figure 7 illustrates the normalization of dip azimuth and magnitude into the 0-180° range.

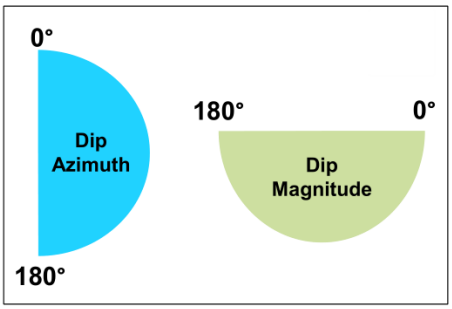

- If measured Dip Azimuth is 210°, the normalized Azimuth = 210°-180° = 30°
- If a fracture has a measured Dip Azimuth >180° and a Dip Magnitude of 70°, the normalized Dip Magnitude = 180°-70° = 110°

Figure 7: Schematic showing the normalization of dip azimuth and magnitude.

At Salak, both open fractures and EFs inside the reservoir have dip azimuth ranging from 50° to 180° with dip magnitude of 60°-120° (figure 8). In terms of dip azimuth, the open fractures and EFs inside the Salak reservoir have an average strike orientation about N22° E and it is very close to the SHmax direction (≈N24° E). For the outside reservoir, both the open fractures and EFs appear to have different dip azimuth ranges with the inside

reservoir (45° to150°), although their dip magnitude range is similar with the fractures inside the reservoir at 70°-120° (figure 8). Other charts used to evaluate the distribution of fractures both inside and outside the Salak are the histogram plots shown in Figures 9 and 10 (dip azimuth and magnitude histogram). In all groups of fractures at Salak, a random (or background; blue highlight) and a dominant set (yellow highlight) of fractures are shown by the histogram charts. The histogram of the dip azimuth of fractures inside the Salak reservoir shows a concentrated population of fractures with an average dip azimuth of 112° or N22° E a strike orientation. This population is very close to the SHmax direction (≈N24° E) or dip azimuth N114°E (top chart: Figure 9). Meanwhile, the concentrated population of fractures outside the Salak reservoir has an average dip azimuth of 90° or a N-S strike orientation (2nd chart in Figure 9) and has wider range (yellow highlight in figure 9 below). A random population of fracture dip magnitude was also identified at Salak inside and outside reservoir (Figure 10). At Salak, the dominant groups of fractures inside and outside the reservoir have very similar average dip magnitudes of 92° and 90°, respectively (Figure 10).

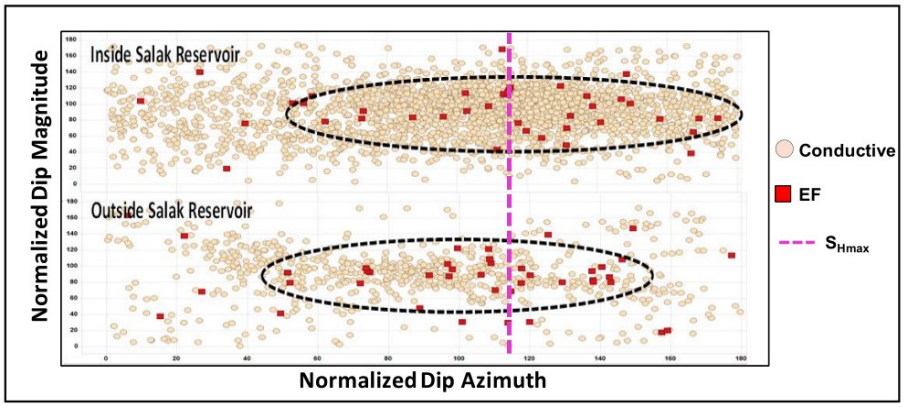

Figure 8: Charts showing scatter plot for the distribution of Conductive (Open) and Effective Fractures inside and outside Salak reservoirs. The strike orientation of the fractures is perpendicular to the dip azimuths shown above.

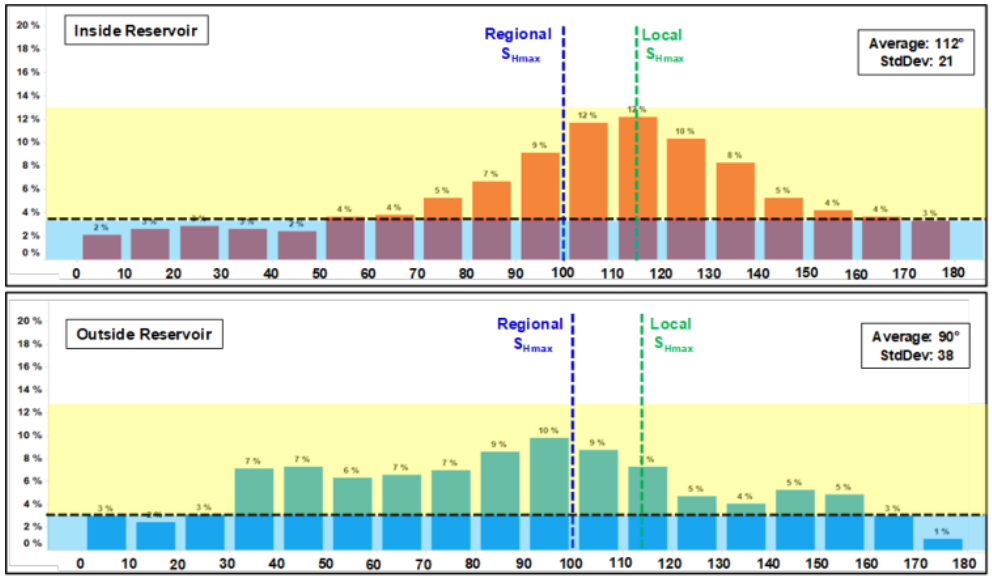

Figure 9: Histograms showing the distribution of dip azimuth of open fractures and EFs inside and outside the Salak reservoirs. The Y-axis denotes the percentage of fractures in one bin divided by all the data. The vertical black dashed lines indicate the SHmax direction in each field while the horizontal black dashed lines are the arbitrarily picked boundary between the random/background and dominant sets of fractures. The strike orientation of the fractures is perpendicular to the dip azimuths shown above.

Besides qualitatively, Salak's aerial distribution of EFs orientation was also evaluated and it can be seen in Figure 11 (Golla et al, 2017). A similar observation is evident at Salak where, cumulatively, the EFs strike mostly within the NE-SW quadrant. The core of the production area (or the Central and East Cells) have slightly more NNE-SSW predominant orientations, while in the West Cell, the EFs exhibit a slightly more ENE-WSW strike

orientation. There may also be slightly more orientational variation in the Far East Cell, although this variation is mostly due to the orientation of fractures associated with the single feed zone logged. The slightly more diverse orientation of the EFs near the eastern edge of the Salak production area. Some factors for the diverse EFs at the edge of the field may be local stresses (Satya and Golla, 2014), presence of nearby eruptive centers etc. Compared to other sectors in reservoir area, outside of reservoir has more variation of EFs orientation.

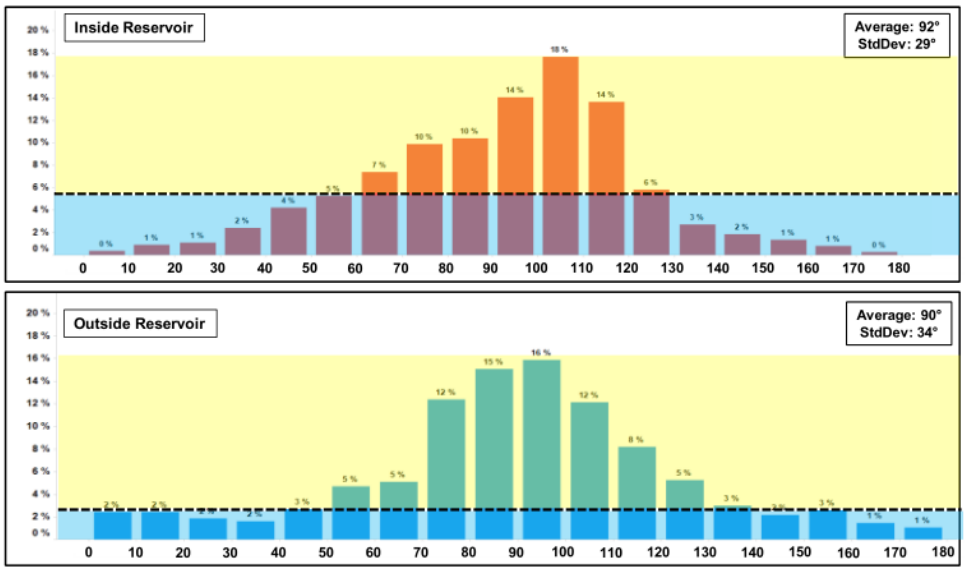

Figure 10: Histograms showing the distribution of dip magnitude of open fractures and EFs inside and outside the Salak reservoirs. The Y-axis denotes the percentage of fractures in one bin divided by all the data. The horizontal black dashed lines are the arbitrarily picked boundary between the random/background and dominant sets of fractures.

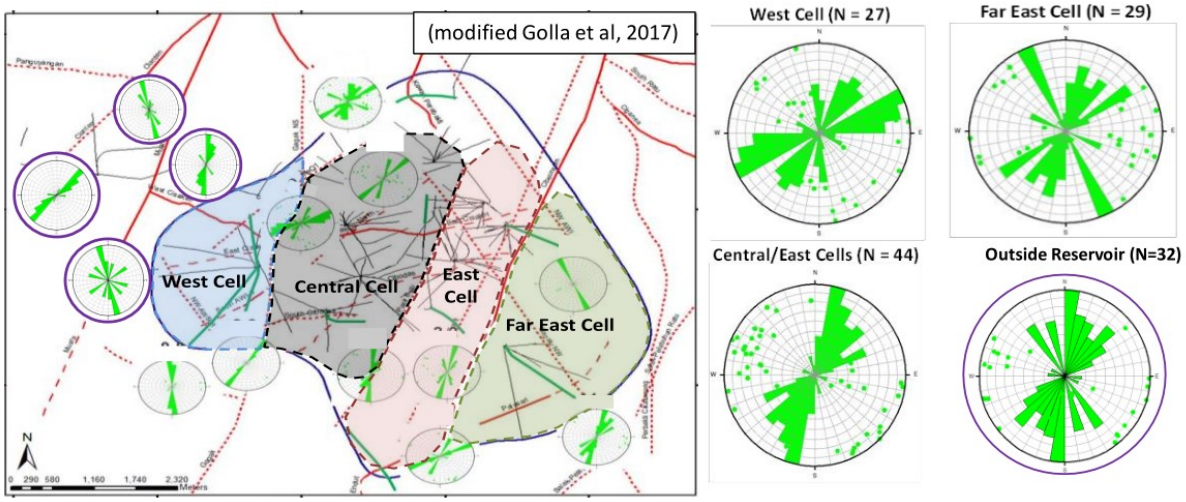

Figure 11: (Left) Map showing the aerial distribution of EFs orientation. (Right) Stereo nets showing the strike orientation, dip azimuth and magnitude (circles) of EFs in each sector of Salak reservoir. Note that outside reservoir stereonet indicates with purple rim color.

4.2 Fracture Density

The next analysis is to evaluate the distribution of fracture density in the different rock types located inside and outside the reservoir, then, test the theory that relatively brittle rocks host more fractures. An apparent increasing trend of open and EFs with depth inside Salak reservoir is demonstrated. The shallower formations have almost similar densities of open and EFs while the deeper Lower Andesite (LA) and MSV Formations host more than half to double the number of fractures (Figure 12). This increasing trend is not demonstrated by the fractures outside the reservoir. The brittle intrusions and andesite lava flows host more open and effective fractures compared with the relatively softer pyroclastic and sedimentary rocks, especially inside the reservoir (Figure 12; left).

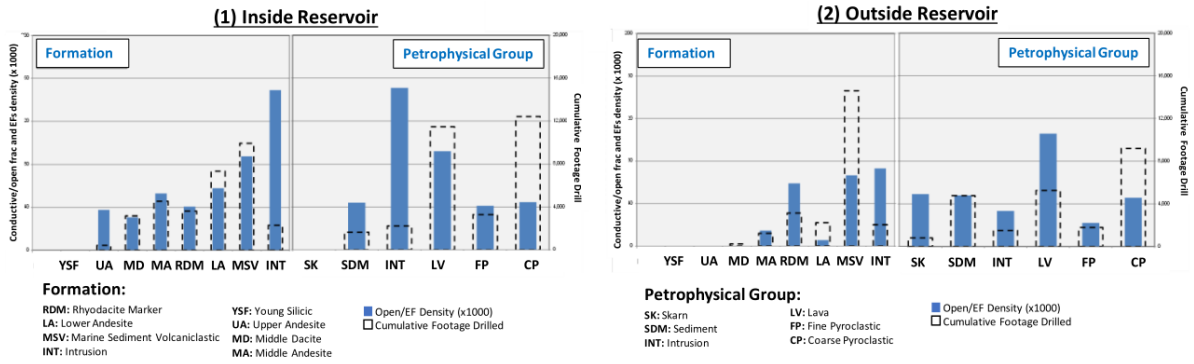

Figure 12: Charts showing the distribution of both Conductive (Open) and Effective Fractures in different formations and petrophysical groups (rock types) located: (1) inside and (2) outside the Salak reservoir. Note that formation, from oldest to youngest, is left to right (YSF to MSV).

Table 1: Fracture Density inside and outside the reservoir.

Area	Borehole Image Logged Interval, ft	Open Fractures Only	Fracture Density Open + Effective Fractures	Effective Fractures Only
Inside Reservoir	31,534	0.064	0.068	0.0027[A]
Outside Reservoir	23,393	0.056	0.057	0.0008[B]

A Excludes borehole image logged interval that did not encounter permeable entries (25,956' only)
B Excludes borehole image logged interval that did not encounter permeable entries (21,417' only)

In general, fracture density for both open and effective fractures inside and outside the Salak reservoir is almost similar (Table 1). If only the Effective Fractures are considered, their density inside the reservoir is about 3 times higher than outside the reservoir. These data show that there are more open fractures inside compared to outside the Salak geothermal reservoirs and this is probably due to the dynamic conditions in the reservoir. The circulating geothermal fluids continuously precipitate and dissolve existing rock minerals which do not happen in static conditions or outside the reservoir. Most of the outside wells in Salak were drilled in the Cianten Caldera where there was once a geothermal system that has since died; thus, this area is possibly now static without active fluid circulation.

4.3 Fracture Aperture

By simple definition, an aperture is an opening, a hole, or a gap in solid materials; therefore, a fracture aperture is the open space in the rock that is occupied by the interpreted fracture. There are some approaches used to estimate fracture aperture. One method that is mostly used to estimate fracture aperture is the calculation by a well-established equation, relating the fracture width to the excess current measured by the imaging tool (Luthi and Souhaité, 1990). Due to the limitation of log data, the aperture of EFs in this study is measured manually by subtracting the depth of the bottom from the top EF surface (Figure 13; left). We acknowledge that this method may yield less accuracy compared to a more general approach. Nevertheless, our goal in employing these techniques is to determine the relative aperture differences both inside and outside the reservoir. The initial measurement generates the apparent aperture because the EF is still influenced by borehole inclination and the EF dip orientation. To get the true aperture, the apparent aperture had to be corrected using β, the angle between the borehole and EF (Figure 13; right).

The table in figure 14 shows the summary of the EF aperture measurement inside and outside of the Salak reservoir. The injection wells drilled outside the Salak reservoir have injecting PTS data; thus, permeable entries and EFs were identified, and EF aperture was measured. S-curves in comparing the distribution of EFs inside and outside the reservoir show significant differences in aperture size (Figure 14; left). It can be discerned by distinct differences of population distribution between the inside and outside reservoir in S-curve. The average aperture of EFs in Salak inside reservoir is about 13 mm and it is almost twice bigger than outside reservoir. Even, the EF apertures in East Salak, mostly steam cap well, is still larger than EF aperture outside the reservoir by almost 20%. In addition, there is an obvious difference in average EF aperture at West and East Salak. The EFs in West Salak have a larger average aperture (>2x) than the EFs in East Salak, and this is probably because brine (in West Salak) will require a larger fracture opening for it to flow out of the matrix. A counterargument to this may be the lower number EFs in West Salak which could bias the average aperture results. The table below in Figure 14 is a tabulation of the comparison of fracture characteristics inside and outside the Salak reservoirs.

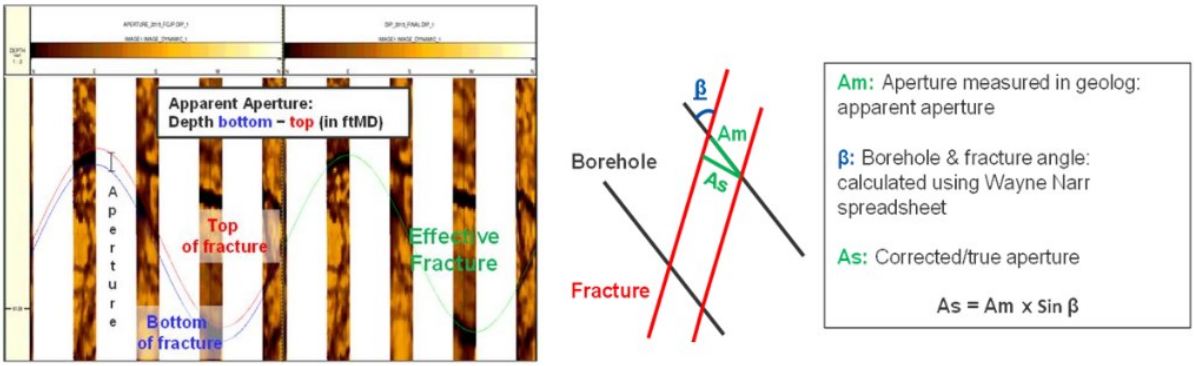

Figure 13: (Left) Borehole image showing the delineated EF and its top and bottom surfaces which were used to manuallymeasure the EF aperture. (Right)Schematic showing β and the formula used to compute for the true aperture.

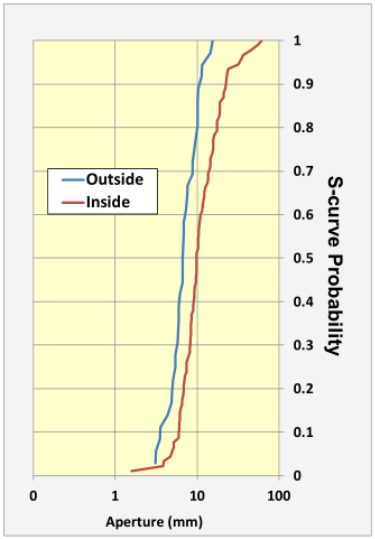

	No. of Data	Min	Average	Max	Std. Dev.
Inside Reservoir	92	1.6	**13.3**	61.8	10.1
East	60	1.6	**9.4**	24.2	4.4
West	32	8.5	**20.6**	61.8	13.2
Outside Reservoir	36	3.1	**7.4**	15.5	3

Figure 14: (Left) S-curve distribution. (Right) Summary table of EF aperture measurement comparison (right).

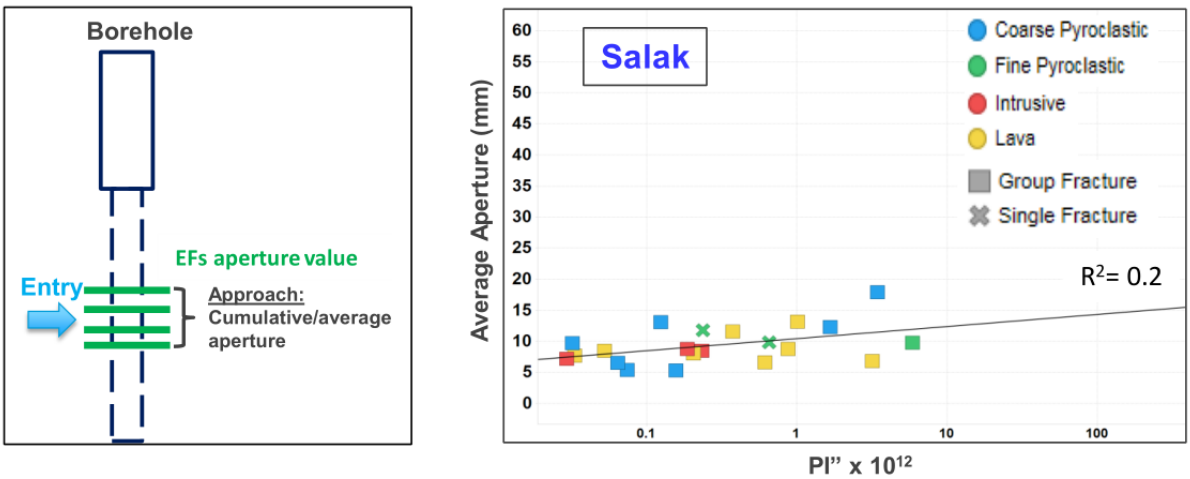

Figure 15: (Left) Illustration of method in evaluating aperture of EFs with permeability. (Right) Cross-plot between average aperture vs permeability (represented by PI').

A working hypothesis that was initially tested was that EF aperture is correlated with permeability, i.e., highly permeable feed zones have larger apertures. In this evaluation, permeability is represented by the productivity index prime value (PI'). There are two ways to use aperture value (cumulative or average aperture value) during aperture vs permeability analysis, as illustrated in Figure 15 (left). As the majority of the permeable zones consist

of Groups of Fractures, the initial analysis considered the cumulative aperture of the Group of Fractures versus the PI' of that particular permeable zone. This approach assumes that all the fractures in the group are producing (which is uncertain). The alternative way of looking at EF aperture is that only one of the fractures in the group is producing; in this case, the average aperture of the group was correlated with the PI' of the permeable zone. The alternative approach was used in this study as it spreads the uncertainty of exactly which fracture is produced in many groups of fractures. The cross-plots between PI and EF aperture at Salak can be looked at in Figure 15 (right). In summary, these cross-plots do not show any strong, direct correlation between the measured EF aperture and PI' as shown by the low R2 (20%). Thus, it seems that permeability is not only controlled by fracture aperture; other influences are fracture connectivity, roughness, etc. Lastly, 5 mm appears to be the smallest EF aperture that can be measured using current software in this current method; there are probably fractures with smaller apertures, but these seem to be not discernible in the software used.

5. DISCUSSION

The general alignment in fracture orientation both inside and outside the Salak geothermal reservoir suggests the presence of a major control on how these fractures were created. It is generally believed that the regional maximum horizontal stress (SHmax) orientation controls the propagation of fractures. In the vicinity of Salak, the general direction of SHmax is ≈N24ºE assuming that the stress regime is extensional (Sugiaman, 2003). The average orientations of fracture dip strike orientation at Salak are generally aligned with the SHmax direction. This interpretation is similar to the results of the analyses of borehole image-derived fractures in other geothermal fields, such as, Dixie Valley, NV (Hickman et al., 1997), Valles Caldera, NM (Nielson et al., 1998), and Wairakei, New Zealand (McLean and McNamara, 2011; McNamara et al., 2016).

In terms of fracture development, local stresses related with volcanism, local faulting, and intrusions may generate a supplementary population to the initial fracture system that is aligned with the regional stress in West Java. Another local control on fracture development appears to be the specific reservoir lithology. This study shows that there are more fractures in the brittle lava flows and intrusive rocks at Salak. Note that these rocks tend to form cooling joints both parallel and perpendicular to their axis of placement; thus, some of the interpreted fractures in borehole image logs are probably inherent. Salak is probably in a transtensional region where both extensional and transtensional shearing are occurring (Fauzi et al., 2015). Transtensional regions are characterized by the presence of both extensional (i.e., normal faults, grabens) and wrench structures (or strike-slip faults); Salak is characterized by both normal and strike-slip structures and lineaments at the surface. This transtensional state is probably responsible for the steeply dipping (>60°) fractures at Salak Fields (Figures 8 and 10). There are no significant differences observed in the fracture dip magnitude inside and outside Salak reservoir, where, both areas have vertical to sub-vertical dips (>60°). The difference is discerned in the fracture orientation/azimuth. Fracture inside reservoir has NNE-SSW trend (N22ºE in average) and it is a similar orientation to Shmax regional (N24ºE), however, some fracture at the edge of the field has diverse orientation and it is inferred due to local stresses, e.g., nearby intrusion (Figure 16A and 16B).

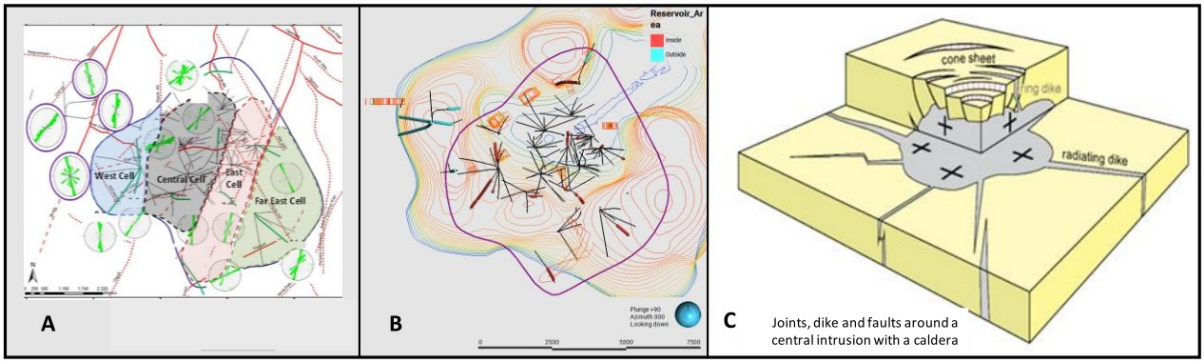

Figure 16: (A)EFs Salak aerial distribution. Note that EFs is mostly has similar orientation with SHmax (NNW-SSW), however, there is diverse of EFs orientation at the edge o the field; (B) Contour line represent of Salak intrusion model. Note that intrusion mostly located in the boundary of Salak Field; (C) Illustration of fracturing inside a caldera (from Burg, 2016). Note that most structures have vertical to sub-vertical dip magnitudes, but the strike azimuth or orientation varies depending on the location within the caldera.

For the outside reservoir, fracture orientation has a wider dominant range and has an average concentration in N-S trend (figure 9). The difference of orientation that occurred in the fracture outside reservoir is inferred due to the location. Most of outside reservoir data comes from well located at the Cianten Caldera, and Caldera geologic setting may generate more variation of fracture orientation with sub-vertical dip as illustrated in Figure 16C. This

figure shows a schematic of the typical fractures (joints) formed in a caldera. Note that the dip magnitude of the fractures is almost similar (or vertical to sub-vertical) but the dip azimuth varies depending on the location within the caldera. Some wells were drilled towards the caldera ring structure, while others were drilled towards the interior of the caldera (Figure 6).

Based on aperture measurement evaluation, aperture EFs inside the Salak reservoir is about twice as larger than effective fractures outside (Figure 14). There are probably many factors that control the fracture aperture size; some obvious mechanisms are (1) compressive stress strength of the general area, (2) fracture azimuth orientation, (3) rock strength, and (4) hydrothermal alteration process. The first mechanism is related to the compressive stress strength difference. Because of the lack of data, it is believed that compressive stress strength is generally the same inside and outside the Salak reservoir. However, brittle rocks will probably break or fracture more than softer rocks as shown by the higher density of fractures in lava flows and intrusion compared with softer pyroclastics and sedimentary rocks. The next mechanism is related to the fracture orientation relative to the regional stress direction. Theoretically, open fractures will be generated if maximum stress (σ1) is parallel to the fracture azimuth (Figure 17). As previously described, the majority of the measured fracture dip azimuth inside the reservoir is parallel with the SHmax orientation; thus, the lower compressive stress inside the reservoir will theoretically generate larger apertures. However, this mechanism does not support actual data which depicts no distinct correlation between aperture size and fracture azimuth (Figure 17). Large fracture aperture should be observed in fractures with 100°-130° azimuth; however, the data shows no distinct patterns in fracture aperture with fracture azimuth.

The last mechanism is hydrothermal alteration and is probably the preferred model to explain the larger effective fracture aperture inside the Salak reservoir. Although the reaction of the circulating geothermal fluids and reservoir rocks may both precipitate and dissolve minerals, it appears that there is more dissolution in rocks with propylitic alteration. Stimac et al. (2004) showed analogues result in Scanning Electron Microscope (SEM) images of the Mat-25 core which indicate that the observed porosity is generated through the destruction of primary porosity and formation of secondary porosity by the hydrothermal system itself as circulating fluids dissolve primary minerals. At Tiwi (Philippines Geothermal Field), total porosity correlates with the abundance of open fractures (Stimac et al., 2004). Furthermore, overburden compaction appears to be likely more extreme for clay-rich formations and poorly consolidated fragmental rocks than for dense lavas. Dense lava flows and intrusive rocks were encountered inside the Salak reservoirs while softer pyroclastics are dominant outside both reservoirs. In addition, mineral precipitation (in particular, silicification) occurs more outside the reservoir and this can reduce fracture aperture. Rock cuttings from the Cianten Caldera wells show abundant secondary silica probably from the cooling geothermal system at Cianten Caldera; also, there was rarely lost mud circulation during the drilling of these wells suggesting fewer open fractures.

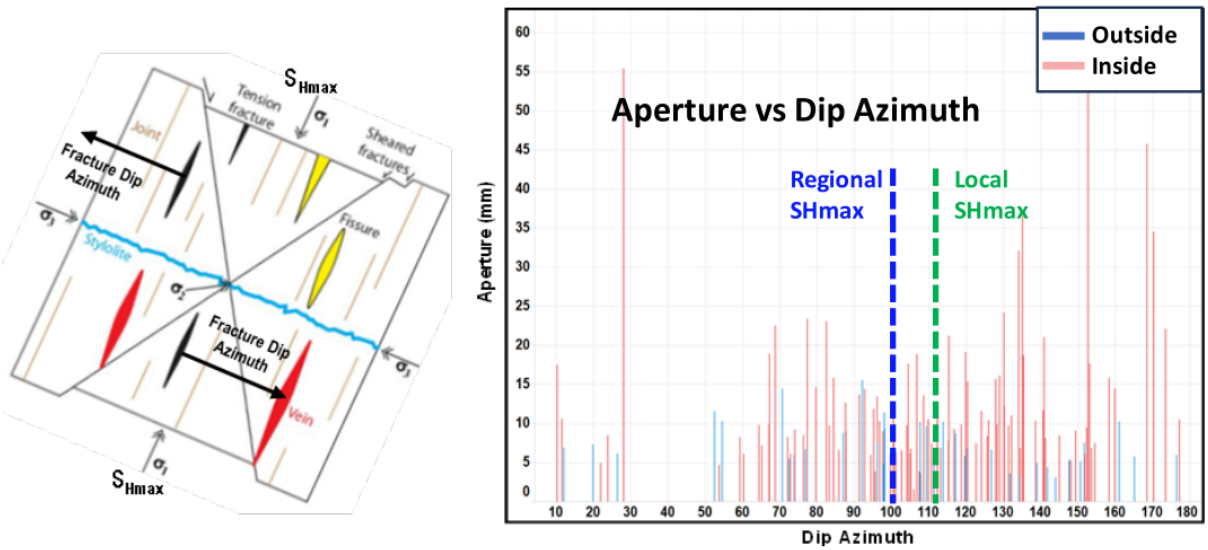

Figure 18: (Left) Schematic showing the illustration of a shear fracture model (modified from Fossen, 2010). Joint, fissure and vein commonly form where σ1 is parallel with fracture plane while stylolites occur where σ1 is perpendicular with the fracture plane. (Right) Chart shows aperture vs. dip azimuth of EFs inside (red) and outside (blue) the Salak reservoir.

In terms of fracture density, conductive/open fracture density is similar between the inside and outside reservoir, where relatively brittle rocks (i.e., lava flows and intrusions) host more fractures than the "softer" pyroclastics and sedimentary rocks. Interestingly, effective fracture (EFs) density discerns that inside reservoir is significantly

higher than outside(~3x). EFs aperture denote that inside reservoir has bigger aperture(~2x) than outside reservoir. According to this evaluation, the inside reservoir has more permeable fractures (i.e., higher EFs density) with larger aperture compared to the outside reservoir, thus, it suggests that fracture connection inside the reservoir is higher than outside.

Based on several observations mentioned in the previous section, there are both similarities and differences in the characteristics of fractures inside and outside the geothermal reservoir. Some of the similar characteristics include the following:

- Two populations of fractures are evident inside and outside the reservoir in terms of fracture orientation (or azimuth), namely, a randomly distributed fracture set and a group that is generally aligned with the SHmax direction.
- Fractures both inside and outside reservoir have vertical to sub-vertical dips (>60°);
- Fracture density discerns that both inside and outside have similar numbers and brittle rocks relatively (i.e., lava flows and intrusions) host more fractures than the "softer" pyroclastics and sedimentary rocks.

Conversely, below are some of the differences in fracture characteristics inside and outside the reservoir:

- Fracture orientation inside reservoir exhibit a narrow range, while fracture outside reservoir has a more varied orientation.
- There are more permeable fractures (i.e., higher EFs density) inside the reservoir.
- EFs inside the Salak reservoir have bigger aperture than those outside.

The differences in geological setting and reservoir process between inside and outside reservoir is apparently cause the differences in fracture characteristics. Table 2 is a summary of characteristics of fracture inside and outside reservoir.

Table 2: The summary of characteristic of fracture inside and outside reservoir.

Parameter		Salak (SHmax N24°E)	
		Inside	Outside
Fracture Orientation	Dip Azimuth	2 populations	2 populations
		Average strike orientation (N22°E) is parallel to SHmax (-2°)	Average strike orientation (N-S) is shifted left of SHmax
		Narrow range	Wider range
	Dip Magnitude	2 populations	2 populations
		Average ~92°	Average ~90°
Fracture Density	Conductive/Open Frac	0.064 (14% more than outside)	0.056
	Open+Effective Frac	0.068 (14% more than outside)	0.057
	Effective Frac	0.0027 (~3x higher than outside)	0.0008
Effective Fracture Aperture, mm		13.3 (~2x bigger than outside)	7.4

Eventually, the result of fracture characterization will be utilized to improve well targeting and planning during the drilling of makeup wells and become an input for the numerical model. Evaluation of open and EFs orientation inside the reservoir is very useful input during developing well trajectory for new Make-up Wells. To optimize well intersection with fracture, well plan trajectory will be generated as much as perpendicular of fracture, thus it is expected to get a higher chance to encounter EFs. In modeling, fracture orientation information will be used to orient the grid in the 3D static model. Also, the evaluation results of fracture density will be used to develop a 3D fracture spacing model. Fracture spacing, an important property, will be used in numerical models to estimate production rates and provide pressure support.

ACKNOWLEDGMENT

The authors would like to thank the management of Star Energy Geothermal Salak Ltd. (SEGS) for supporting this study and granting permission to publish this paper. Massive thanks to SEGS olleagues who contributed to reviewing and improving its contents.

REFERENCES

Acuña, J., Astra, D., Molling, P., Prabowo, H., Stimac, J., Sugiaman, F., Cumming, W., Nordquist, G., Shemeta, J., 1997. Awibengkok 1997 Conceptual Model Summary. *Unpublished Star Energy Geothermal report*, September 1, 1997. pp. 423

Aprilina, N.V., Putra, F.J., Wicaksono, S., Julinawati, T., Tanuwidjaja, R., Hernawan A.: Results of I-I Deep Well: Impact on the Conceptual Model of the Salak Geothermal System. *PROCEEDINGS*, The 5th Indonesia International Geothermal Convention & Exhibition 2017, Cendrawasih Hall - Jakarta Convention Center Indonesia (2017)

Burg, Jean-Pierre, Joints, http://www.files.ethz.ch/structuralgeology/jpb/files/English/4joints.pdf, January 20, 2016, 22 pages.

Fauzi, Ahmad, Permana, Haryadi, Indarto, Sri, and Graffar, E.Z, Regional Structure Control on Geothermal Systems in West Java, Indonesia, *Proceedings*, World Geothermal Congress 2015, Melbourne, Australia, 19-25 April 2015, 7 pages.

Fossen, Haakon, Structural Geology, *Cambridge University Press*, 2010, 480 pages.

Golla, G.U., Putra, F.J., Satya, D.Y., Intani, R.G., Pamurty, N.P., Gunderson, R.P., 2017. Characterization of Permeable Entries and Fractures at the Salak, Darajat, and Mak- Ban Geothermal Reservoirs. *Unpublished Star Energy Geothermal report*, March 30, 2017. pp. 77.

Golla, G.U., Julinawati, T., Putri, R.P., Nordquist, G.A., Libert, F.R.: The Salak Field, Indonesia: On to the next 20 years of production, *Geothermics*, 83, (2020), Article 101715

Hamilton, W., Tectonics of the Indonesian Region, United States Geological Survey Professional *Paper* 1078, 45 pp, 1979.

Hickman, Stephen, Barton, Barton, Zoback, Mark, Morin, Roger, Sass, John, and Benoit, Richard, In-situ Stress and Fracture Permeability in a Fault-Hosted Geothermal Reservoir at Dixie Valley, Nevada, *Geothermal Resources Transactions*, Vol. 21, September/October 1997, pp 181-189.

Hulen, J., Lutz, S.: Alteration mineralogy and zoning in Corehole AWI 1-2, Awibengkok Geothermal Field, West Java, Indonesia. Geothermal Resources Council *TRANSACTIONS* 23, (1999), 19–23.

Hutchinson, C.S., Geological Evolution of South-East Asia, Claredon Press, *Oxford Science Publications, Oxford*, 368 pp, 1989.

Intani, Rindu Grahabhakti, Satya, Drestanta Yudha, Nordquist, Gregg and Golla, Glenn,Permeable Entry Characterization at Darajat Field, West Java., *Proceedings*, The 5th Indonesia International Geothermal Convention & Exhibition (IIGCE) 2017, Jakarta, Indonesia, 2 - 4 August 2017, 4 pages.

Luthi, S.M. and Souhaité, P. Fracture Apertures From Electrical Borehole Scans. *Geophysics* 55,1990. Pp 821–833

McNamara, David D., Bannister, Stephen, Villamor, Pilar, Sepulveda, Fabian, Milicich, Sarah D., Alcaraz, Samantha, and Massiot, Cecile, Exploring Structure and Stress from Depth to Surface in the Wairakei Geothermal Field, New Zealand, *PROCEEDINGS*, 41st Workshop on Geothermal Reservoir Engineering, Stanford University, Stanford, CA, February 22-24, 2016.

Nielson, Dennis L., Barton, Colleen and Keighley, Kelly E., Comparative Study of Fractures in Core and Borehole Televiewer in Well VC-ZB, Valles Caldera, New Mexico, PROCEEDINGS, 23rd Workshop on Geothermal Reservoir Engineering, Stanford University, Stanford, CA, January 26-28, 1998, pp 283-290

Satya, D.Y. and Golla, G., Salak Permeable Entries Characterization: Chevron In-house Presentation, September 29, 2014, 18 pages. Salak Asset Management Team (AMT), 2014 Salak State of the Reservoir, *Chevron In-house Report*, July 2015, 126 pp.

Stimac, James A., Powell, Thomas S., and Golla, Glenn U., Porosity and permeability of the Tiwi geothermal field, Philippines, based on continuous and spot cores, *Geothermics* 33 (2004) 87-107.

Stimac, J., Nordquist G., Suminar, A. and Azwar L.S., 2008. An Overview of the Awibengkok Geothermal System, Indonesia. *Geothermics*, 37, (2008), 300-331.

Stimac, J.A., Sugiaman, F.: The AWI 1-2 Core Research Program Part I: Geologic overview of the Awibengkok Geothermal Field, Indonesia. *Proceedings* World Geothermal Congress 2000, Kyushu-Tohoku, Japan, (2000).

Sugiaman, Frankie, State-of-stress and Wellbore Stability in Awibengkok Field, Unocal *Memorandum*, July 31, 2003, 20 pages.

Tingay, Mark, Morley, Chris, King, Rosalind, Hillis, Richard, Coblentz, David, and Hall, Robert, Present-Day Stress Field of Southeast Asia, Elsevier Journal: *Tectonophysics* 482, June 23, 2009, 12 pages.

Characterization of Fluid Geochemistry from the New Pad in the Westernmost Section of Northern Wayang Windu

Nevio Kamel, Dwiyogarani Malik, Stefano Pentury, and Wintry Dimwani

Star Energy Geothermal, Wisma Barito Pacific II, 17th – 21st floor.
Jl. Let. Jen. S. Parman Kav. 60, Jakarta 11410, Indonesia

nevio.kamel@starenergy.co.id

Keywords: geochemistry, reservoir characterization, surveillance

ABSTRACT

The Wayang Windu Geothermal Field (WWGF) has been operating for over 20 years and is committed to increase the capacity of the power plant should the resource support. Based on the resource assessment, the development needs to cover a larger and deeper area to have sustainable production. The westernmost section has been identified as a promising resource area and approached by the latest drilling campaign in 2021. Pad I, the latest pad in this section, exhibits unique characteristics compared to others. A dry-steam well drilled on this pad, namely I1 produced ~11 kg/s of steam, which is more moderate compared to other dry-steam wells in adjacent pads that produce over 20 kg/s of steam. Concerns have arisen about whether this indicates the well is close to the reservoir's margin, despite a good connectivity to adjacent high-performing wells like D5, D7, and Q6, as observed by chemistry monitoring during drilling. Regular chemistry monitoring sequences, including gas, steam condensate, and stable isotope analysis were conducted to characterize the well. Gas analysis showed NCG levels at 0.8 – 1.0 wt.% in steam, slightly higher than adjacent wells but within the range of the northern reservoir section. In addition, stable isotope analysis indicated enriched composition and positioned close to the surrounding upflow zone. Other findings, such as PT data were consistent, the top of reservoir depth is similar to the adjacent wells, with the presence of a water dead-leg. However, the TFT analysis confronted these results with an enthalpy of around 2786 kJ/kg. Additional analysis using the downhole liquid sample confirmed that the water composition was consistent with the remnant of condensate injectate fluid. Furthermore, a comprehensive saturation model of vapor to liquid (Sv/Sl) was generated to understand the reservoir process occurring in this well which suggested that boiling activity occurs in the reservoir. Based on these indicators, it can be deduced that well I1 is still within the same cell as the northern vapor zone and not located on the reservoir's margin. The current low productivity in this well might be associated with a distinct localized reservoir area associated with the prompter pressure drop than the surrounding wells (Pentury, 2024), which leads to a slower boiling process. Future development strategy still recommends exploring the surrounding areas of Pad I and remaining resources, aligned with frequent surveillance monitoring and comprehensive resource assessment.

1. INTRODUCTION

The Wayang Windu Geothermal Field (WWGF) has been operating for over 20 years with current total installed capacity of 230.5 MWe. Currently, 80% of Wayang Windu production relies on the steam wells, while only 20% comes from the two-phase wells. Based on the resources assessments, the development needs to cover a larger and deeper area to have sustainable production and support WW expansion project. With the success of two big two-phase producers in the 2020-2021 drilling campaign, vertical extension to the reservoir brine is achievable and the two-phase well ratio will keep improving in the future. As for the lateral extension, the westernmost section has been identified as a promising resource area and approached by the latest drilling campaign in 2021.

A new well pad, codenamed I, was constructed in 2020 to cover this area. The result of the drilling in this pad exhibits unique characteristics compared to others. A dry-steam well drilled on this pad, namely I1 produced ~11 kg/s of steam, which is more moderate compared to other dry-steam wells in adjacent pads that produce over 20 kg/s of steam. Concerns have arisen about whether this indicates the well is close to the reservoir's margin, despite a good connectivity to adjacent high-performing wells like D5, D7, and Q6, as observed during drilling activity monitoring. Routine geochemistry fluid monitoring and reservoir data are combined to determine the reservoir characteristic, leading to a recommendation for further development in the area.

2. WELL CHARACTERIZATION

I1 as a dry steam production well monitored through regular chemistry monitoring sequences, including gas, steam condensate, and stable isotope analysis. Gas data is essential in characterizing the well and conceptually locating the area in the geothermal system, whether this area in the productive zones or it is already closer to the margin.

Not only chemistry data, subsurface pressure and temperature data are also vital to understand the reservoir in this western area.

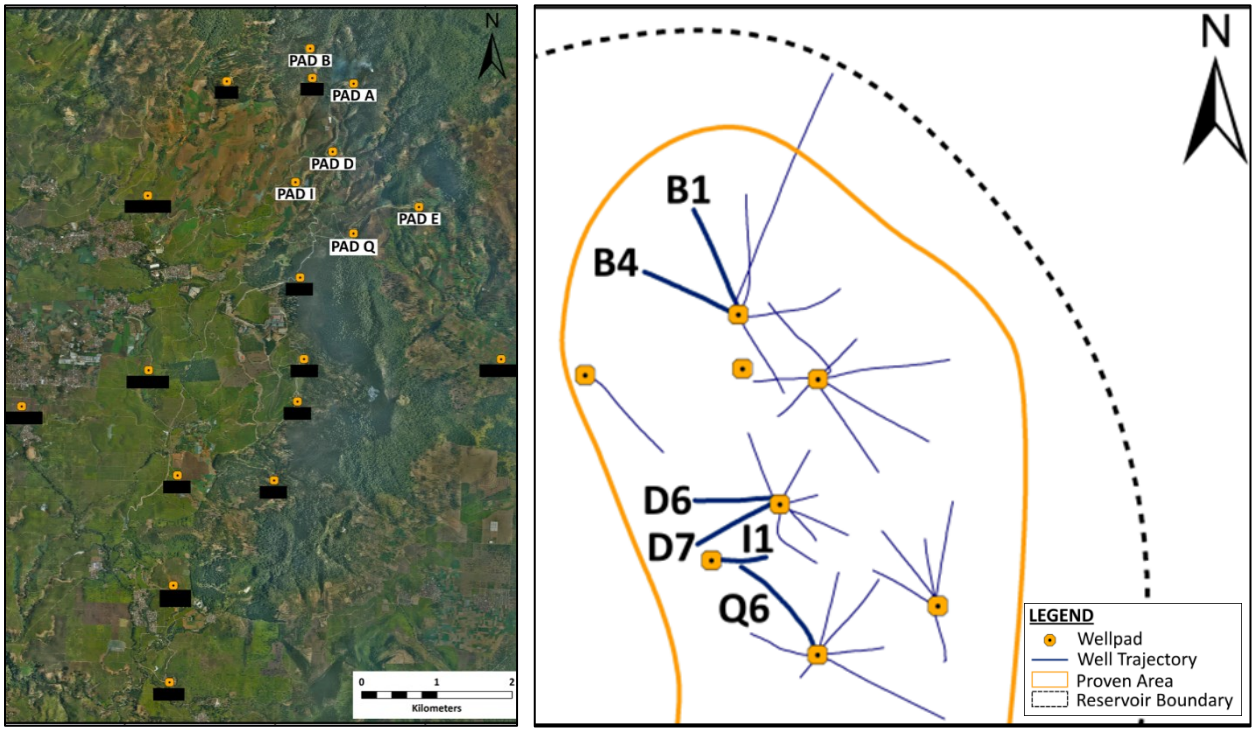

Figure 1: Left: Map of All wellpads in Wayang Windu. Right: Northern area of Wayang Windu with the new I1 well.

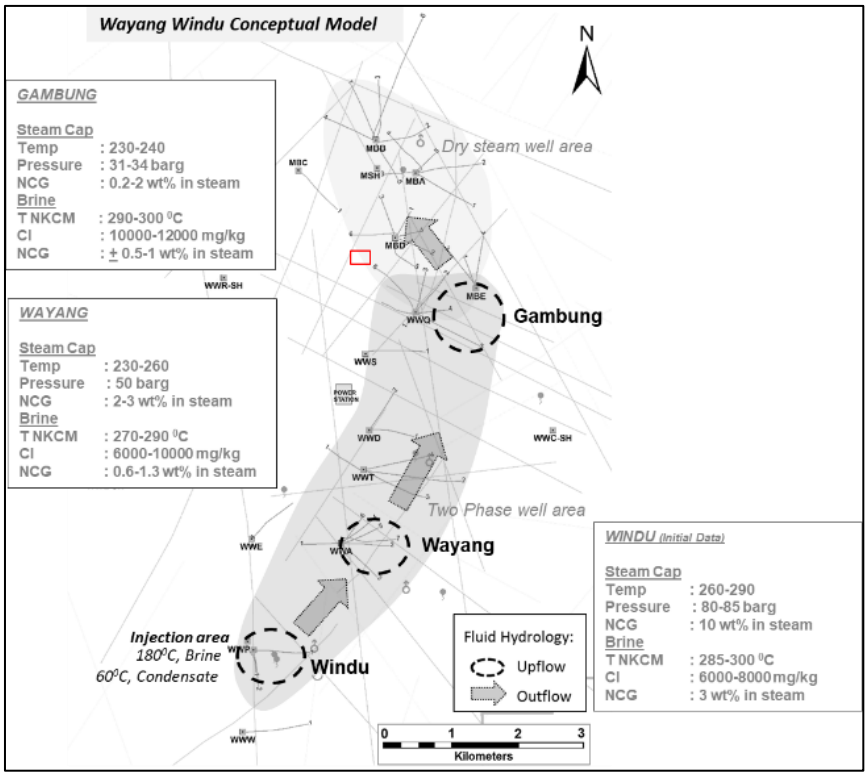

Figure 2: Current Conceptual Model of Wayang Windu Geothermal Field and sector information. There are three uplow areas: Gambung (north), Wayang (central), and Windu (south). Pad I located at the red box (modified from Malik, 2020).

The conceptual model of Wayang Windu has consistently identified three reservoir cells, called Gambung, Wayang, and Windu. The recent model (Figure 2) has shown its sectoral information and the major flow paths. The new pad I was aligned with the current model where it fed by the Gambung reservoir and far from the margin area. However, the analysis on gas and stable isotope composition might be the key parameters in identifying the pad I characteristics and defined the future strategy.

2.1 Gas Analysis

The gas composition analyzed monthly ever since the well started online in mid-2022, including the total Non-Condensable Gas (NCG) and other single gas parameters. The analysis of total NCG will evaluate the general well characteristic in correlation with the recent conceptual model. Considering that this new pad is located further west and semi-exploration, it is expected that the well will be produced from the lateral extension of the Gambung steam cap. The initial prognosis was that the NCG levels would be similar with the closest wells at 0.4-0.6 wt%, however, it had a higher average NCG (as seen in Figure 3) with a stable trend although the value is quite far below the wells that are identified as close-to-margin.

Evaluating the steam composition in the new area is important to involve the behavior of different gas solubility or commonly expressed as the gas ratio. The gas ratio (less soluble gas/ more soluble gas) such as CO_2/H_2S (Figure 3) shows that I1 has a fluctuating trend, which the normal trend of continuous steam formation should follow with decreased CO_2/H_2S as the proportion of the more soluble gas will increase relative to the less-soluble gas (Nicholson, 1993). The observation interprets that pad I has a unique steam formation pattern that shows intermittent pressure changes or even localized permeability, thus making the gas distribution erratic.

Further gas analysis are using CO_2/Ar-H_2/Ar gas ratio grid and FT-CO_2 geothermometer grid. Both cross plots use two geothermometer equations to identify reservoir temperature and the fraction of equilibrium vapor in the sample. Result of the cross plots showing higher temperature on I1 well compared to the surrounding wells. Although in both analyses, the data positioned lower than equilibrated liquid line, which might indicate immature/not fully equilibrated condition (Giggenbach and Goguel, 1989). One possible explanation is continuous extraction on small volume of reservoir section due to localized permeability, limiting contact with the rock in the shallow reservoir section thus not giving the time for equilibration.

2.2 Stable Isotope Analysis

The analysis of stable isotope of ^{18}O and Deuterium has been widely used both for exploration and exploitation. Its implementation on mature vapor-dominated fields, such as the Geysers and Larderello, are observed for its ^{18}O spatial variation (Arnorrsson, 2000). ^{18}O value for deep reservoir fluid is enriched, meanwhile shallow meteoric water has depleted value. This distinctive characteristic helps to identify mixing process between reservoir fluid and meteoric water, which generally interpreted as the relative distance of fluid travelled from deep reservoir feed (upflow) to the meteoric recharge area (outflow).

Stable isotope analyzed from the condensates that are sampled routinely twice a year to characterize the well. Besides, the condensate composition also sampled routinely along with the gas. Result of chemistry analysis on the routine condensate showed no significant mixture of external fluid influx to the wellbore, which implies that the fluid chemistry is the result of reservoir process. Stable isotope analysis also agrees with this observation as all data showed enriched composition and positioned close to the upflow zone, refusing the idea that this well is close to margin as shown by B pad that positioned closer to meteoric water line (Figure 5).

2.3 Pressure Temperature Analysis

Based on PTS data, the top of reservoir depth is similar to the adjacent wells, indicating a connecting and similar system with area in pad D and Q. Initial temperature showed up to 230^{o}C with up to 30 bar pressure. Further analysis interpreted three feed zones in the wellbore, located in around 990, 906, and 880 mASL. This well is a shallow dry steam well with a total depth (TD) that does not exceed the average liquid level of the field, which is approximately 400 meters above sea level (mASL). Therefore, the presence of liquid below approximately 800 mASL in the 2021 PT profile (Figure 6) has been verified as a water dead leg or an accumulation of cooler injected fluid that does not flash, due to the lack of productive fracture zones beneath that depth. This also corresponds to the evidence of the PT spinner profile that shows the increase in RPS only occur on the top of ~800 mASL Chemistry analysis using the downhole liquid sample also confirmed that the water composition was consistent with remnant of condensate injectate fluid. Follow-through tracer flow test (TFT) analysis confirming the water is not producing to the surface, with the results of an enthalpy around 2786 kJ/kg.

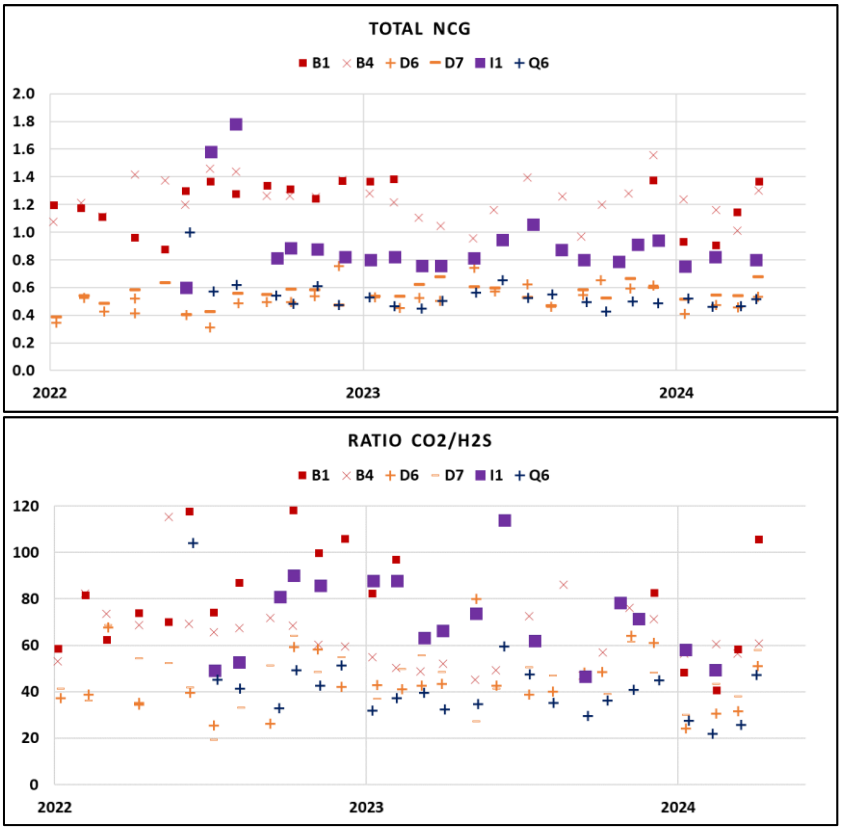

Figure 3: NCG levels at 0.8 – 1.0 wt.% in steam, slightly higher than adjacent wells (Q6, D6, D7) but within the range of the northern reservoir section and not as high as close-to-margin wells (B1, B4).

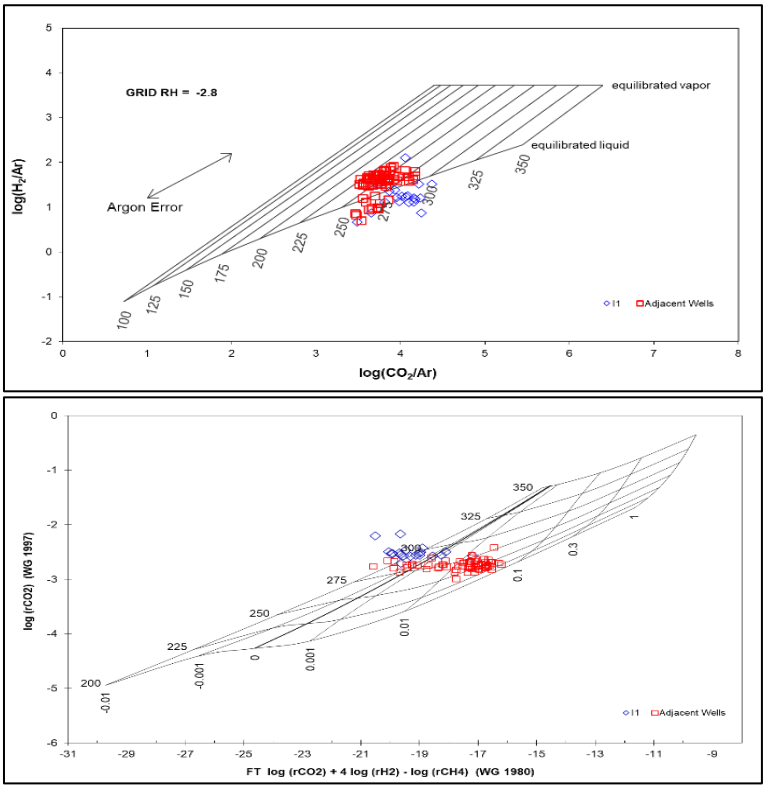

Figure 4: CAR-HAR and FT-CO2 diagram show I1 have higher average temperature than the surrounding wells.

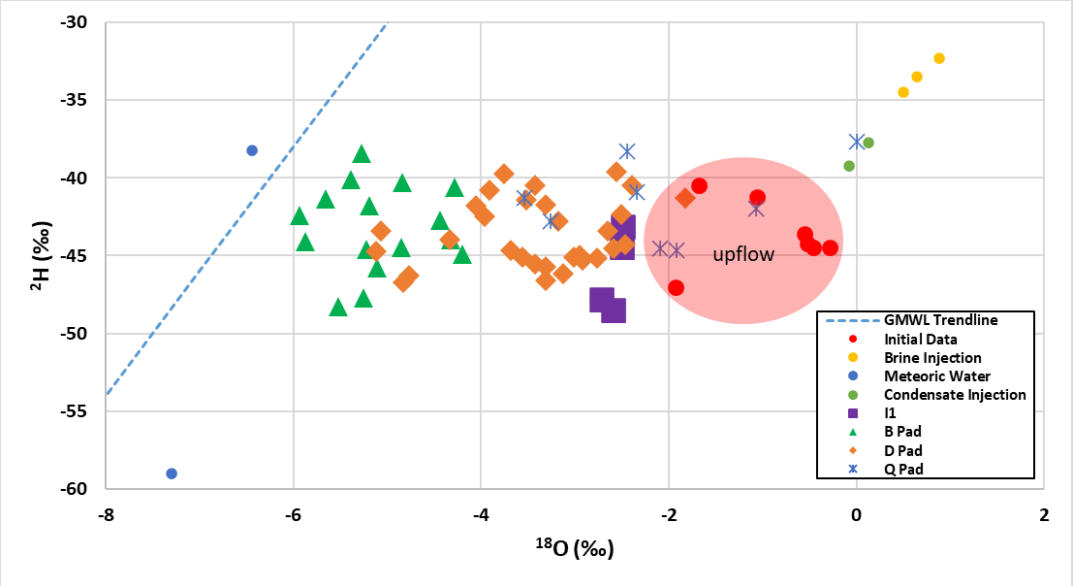

Figure 5: Stable isotope analysis of I1 condensate shows enriched composition.

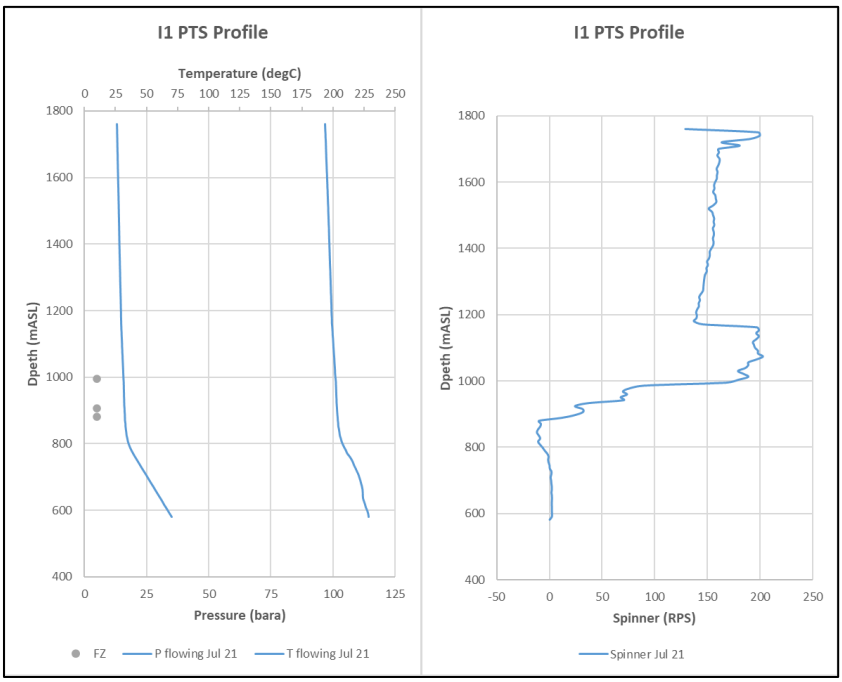

Figure 6: PTS data of I1 well.

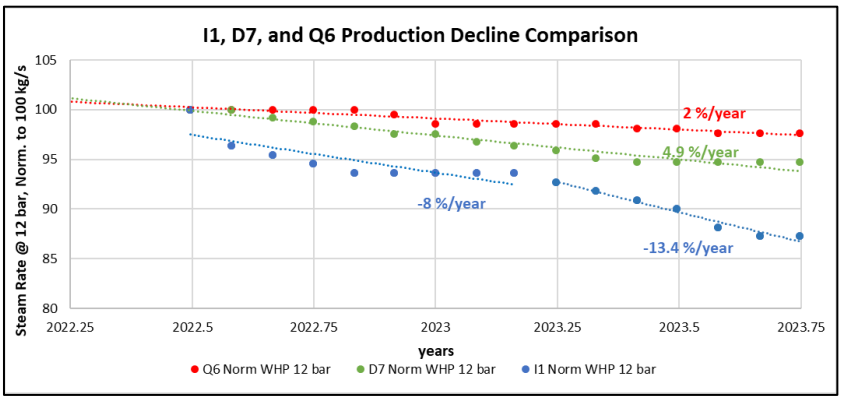

Figure 7: Production decline of well I1 compared to the adjacent wells.

Performance of this well monitored through production and reservoir (steam cap) pressure. I1 well had moderate production in the initial discharge, however it is underperforming in the terms of decline rate. Compared to the adjacent wells that are older and bigger producers, the decline rate of this well is still higher. It has 8% decline in the first year of production and accelerated to 13% per year afterwards, while the surrounding wells Q6 and D7 have only 2% and 5% respectively. Figure 7 show the comparison with normalized 12 bar pressure and 100 kg/s initial steam rate. Similar observation also applies for the reservoir pressure, although initially it has similar magnitude, I1 well have larger pressure decline although producing less than the adjacent wells (Figure 8).

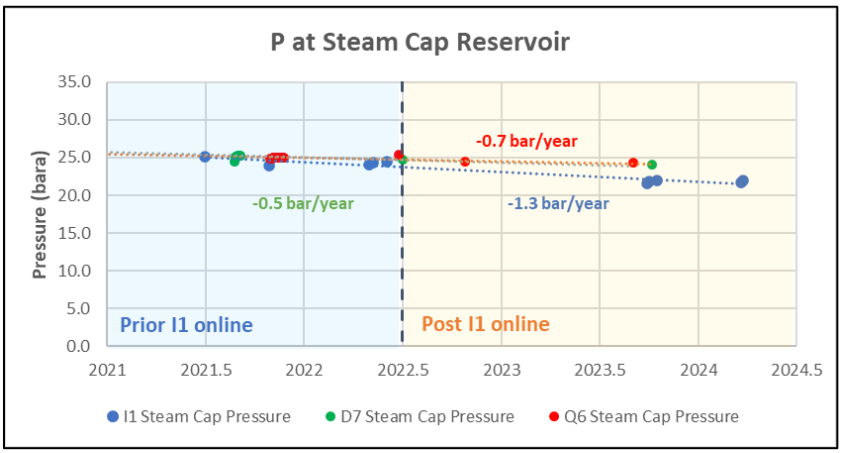

Figure 8: Pressure declines of well I1 compared to the adjacent wells.

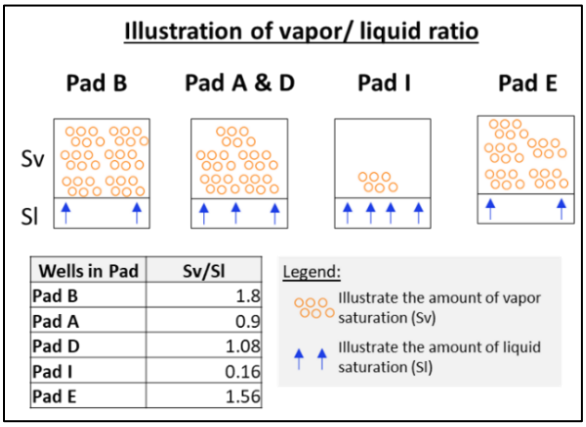

Wells in Pad	Sv/Sl
Pad B	1.8
Pad A	0.9
Pad D	1.08
Pad I	0.16
Pad E	1.56

Figure 9: Saturation model of well pad I compared to the other pads.

2.4 Saturation Model

To further assess the well conceptual resources, a comprehensive saturation model of vapor to liquid (S_v/S_l) from the gas grid reaction generated to understand the reservoir process occurring in the northern part of Wayang Windu. When it monitored continuously including other observation such as volatiles carryover (B, SiO_2, Cl), gas/steam ratio, steam flow, and stable isotope, it gives the benefit to understand vapor dominated wells behavior and a hint to steam reservoir management (D'Amore, 1995). This method also implied in mature vapor dominated field like The Geysers and Larderello.

Application of the vapor/liquid in matrix proportion discussed in this paper is the method to understand the deep process of how gas elements changes reflected by the steam separation process, most importantly in a new pad I. A simple illustration to show the correlation of liquid saturation to physical phenomena in the northern part of Wayang Windu presented in the Figure 9. The fact that B pad is the lowest pressure area, having the most intense boiling means maximum fluid intake into the steam phase, but limited remaining deep recharge, thus increasing degree of superheat and highest Sv/Sl. In contrary, the lowest S_v/S_l ratio reflects the least boiling process in this new pad I. The average value of S_v/S_l (~1) were located in pad A and D where mostly having low superheat and operate at the higher pressure. Those pads are mostly constant high steam suppliers. The pads support the 'balance' characteristic by maintaining the least pressure drop or maintained silica solubility. The physical phenomena reflected by the saturation that pad I has the highest liquid saturation but cannot support the vapor saturation are possibly correlate some parameters affecting the rock matrix, such as local permeability occurring in pad I.

However, the remaining liquid saturation below pad I is still high compared to others, so focusing the production in that area will possibly enhance the boiling area.

3. CONCLUSION

Based on indicators from the data presented above, all evidence narrowed down the interpretation into well I1 is still within the same cell as the northern vapor zone and not located on the reservoir's margin. Resources in this area are confirmed, proven by high temperature in this area. Several geothermometers calculated that I1 even has higher temperature than the adjacent wells. Measured data from PT survey shows temperature of up to 230^{o}C and 30 bar pressure which is reasonable for a dry steam producer. Some notes are that this well has higher pressure drop compared to the adjacent wells. Moderate productivity in this area compared to the adjacent wells might be associated with a distinct localized reservoir area associated with the prompter pressure drop than the surrounding wells (Pentury, 2024), which leads to a slower boiling process. As for the future development strategy, we still recommend exploring the surrounding areas of Pad I, focusing on avoiding the localized permeability around Pad I, going after big permeability potential and maximizing production, along with fit-for-purpose surveillance for comprehensive resource assessment and reservoir characterization.

REFERENCES

Arnorsson, S. (2000), “Isotopic and Chemical Techniques in Geothermal Exploration, Development and Use”, International Atomic Energy Agency, Vienna.

D’Amore, Celati, Calore, (1982), “Fluid Geochemistry Application in Reservoir Engineering (vapor dominated system)”, Proceedings of 8th Workshop Geothermal Reservoir Engineering, Stanford University, California.

D’Amore, F. and Truesdell, A.H. (1995), “Correlation between Liquid Saturation and Physical Phenomena in Vapor-Dominated Geothermal Reservoir”. Proceedings of the World Geothermal Congress, Florence, 18-31 May 1995, 1927-1932

Giggenbach, W.F. and Goguel, R.L. (1989), “Collection and analysis of geothermal and volcanic water and gas discharges,” DSIR report CD 2401, 4th ed., Pentone, New Zealand.

Malik, D., Abidin, Z., Pramono, B. (2020), “Tritium Tracer Injection Test at Wayang Windu Geothermal Field, West Java, Indonesia”, Geothermics 83 (2020) 101718.

Nicholson, K. (1993), “Geothermal Fluids: Chemistry and Exploration Techniques”, Springer-Verlag

Pentury, et. al., (2024), “The Advantages of Simple 3D Numerical Modeling in Characterizing a Localized Reservoir Boundary for New Wellpad Development in Wayang Windu”, Proceedings, The 10th Indonesia International Geothermal Convention & Exhibition (IIGCE) 2024.

Powell, T. (2000), “A Review of Exploration Gas Geothermometry”, Proceedings, 25th Workshop on Geothermal Reservoir Engineering, Stanford University, Stanford, CA, SGP-TR-165.

Powell, T. and Cumming, W. (2010), “Spreadsheets for Geothermal Water and Gas Geochemistry”, Proceedings, 35th Workshop on Geothermal Reservoir Engineering, Stanford University, Stanford, CA, SGP-TR-188.

MT Conductors Below Volcanic Hosted Geothermal Prospects

Friedemann Samrock[1], Wolfgang Soyer[1], Stefano Garanzini[1], Alice Pavesi[1], Randall Mackie[1],
Chevy Iskandar[2], Elfina[2], Inusa Pamusyawara Fauzi[3], Aditya A Juanda[3], and Stephen Halinan[1]

[1]Viridien Group, CGG Eletromagnetics, Italy
[2]PT Geo Dipa Energi, Indonesia
[3]Pertamina Geothermal Energy

Friedemann.Samrock@viridiengroup.com

Keywords: Magnetotelluric, volcanic geothermal systems, deep conductors

ABSTRACT

Elevated temperatures in volcanic geothermal systems result from high heat flow caused by shallow intrusion of magma. Magmatic intrusion acts as the major heat source of the system and drives hydrothermal convection. Understanding the nature and location of magmatic heat sources is therefore relevant for characterizing the geothermal system. Magnetotelluric studies around the world have revealed numerous occurrences of deep electrical conductors below volcanic geothermal prospects. Interpretations of such deep conductors often invoke the presence of magmatic melt and magma derived fluids thereby arguing in favor of interpreting deep conductors as related to the magmatic heat source. However, the architecture of magmatic systems is rather complex and strongly depends on the degree of solidification, residual melt, and volatile content. Electrical resistivity alone does not provide conclusive evidence about the nature of deep conductors. We describe a selection of scenarios and their impact on geothermal reservoir formation: Under favorable conditions magmatic mush reservoirs in the upper crust can remain stable over long geological timescales thereby providing a constant heat supply for a geothermal system. Undesirable situations are encountered when H_2S from degassing magma combines with water to form sulfuric acid brine, a fluid with exceptional high electrical conductivities. Such acidic hydrothermal plumes can form above largely cooled intrusions and make geothermal drilling unattractive. In cases where volcanic eruption happened through sedimentary overburden, deep conductors may also represent buried fluid-bearing sediments, hence being unrelated to magmatic systems and potential heat sources. Therefore, conclusive interpretations of deep conductors require a comprehensive geoscientific approach. First, a detailed understanding of the geological setting, eruptive history and magma evolution is required and, second, integration of various types of geophysical observables is key to understand the internal structure and fundamental petrophysical properties of deep electrical conductors under volcanic geothermal prospects. Here we present case studies from geothermal prospects around the world and provide a classification or grouping for deep conductors based on their geological setting, volcanic history and available well data.

1. INTRODUCTION

Since the beginnings of industrial-scale development of geothermal resources, electrical sounding methods have played an important role in geothermal exploration and for siting drilling targets (Wright et al., 1985). It was recognized early that high-temperature volcanic geothermal reservoirs are often overlain by a pronounced low resistivity layer that is composed of electrically conducting clay minerals, which are produced through hydrothermal alteration (Moskowitz and Norton, 1977). Subsequently, electrical resistivity methods took an important role in geothermal exploration due to their capability to identify and map the extent of the electrically conductive clay “cap”. The clay cap is not only a product of hydrothermal processes and hence a strong indicator for geothermal activity, but it also seals the reservoir top, due to the properties of clays, which swell when in contact with water and form an impermeable layer (Gunderson et al., 2000).

Amongst a variety of active and passive geophysical electromagnetic (EM) sounding techniques, the magnetotelluric (MT) method established itself as a widely used tool in geothermal exploration. MT relies on natural electric and magnetic field variations that originate from global lightning activity and the interaction of the Earth’s geomagnetic field with the solar wind (e.g. Vozoff, 1991). The EM source fields are always present, allowing a short deployment time of measurements systems in the field, and MT easily covers penetration depths relevant for clay cap imaging, reservoir characterization and beyond (e.g. Berktold, 1983; Cumming, 2009; Muñoz, 2013).

In early applications of the MT method in geothermal exploration MT data were generally interpreted using 1D modeling and focused on delineating the clay cap atop the geothermal reservoir (Pellerin et al. 1992, Anderson et al., 2000). 1D imaging of the clay cap is an established application and remains a common method (e.g. Árnason et al. 2010) even after 3D interpretations became feasible with increasing computational capacities. The reason why 1D modelling of MT responses to image the clay cap produces valuable models can be attributed to the strong electrical conductivity signature of the clay cap, which is essentially 1D. Therefore, cross-sections stitched from 1D inversions of the MT responses are still common in geothermal exploration and often used as an initial quality assurance check. Anderson et al. (2000) pointed out that clay cap topography delineated by 1D MT modelling enables the reliable location of geothermal reservoirs, which are encountered under regions of clay cap updoming. 1D models of geothermal areas and prospects often imaged deep electrical conductors below the clay that typically extend from below the clay cap and the geothermal reservoir to greater depths. These deep conductors have been found as early as in studies by Hermance et al. (1976), who interpreted a deep low-resistivity zone beneath Icelandic volcanic prospects as small fractions of basaltic melt. However, quantitative interpretations of deep conductors were hampered by limitations of 1D interpretations of MT data, which provide only a valid approximation for the shallow part near the surface of a volcanic geothermal system. Only in rare cases do MT data obey 1D or even 2D conditions down to larger depths. Owing to their geological nature, volcanic geothermal prospects exhibit strong 3D features that extend from the surface to the lower crust. Deep seated magmatic melt sources feed vertically extensive magmatic pathways that crosscut geological strata and feed shallow melt reservoirs that drive localized hydrothermal fluid flow often hidden under heavily faulted terrain with strong surface topography and steep slopes.

The 3D nature of volcanic geothermal prospects became apparent when 3D MT interpretations of volcanic geothermal prospects provided full-featured 3D images that revealed lateral resistivity variations below the clay cap with vertically extensive transcrustal anomalies raising question about their nature (e.g. Newman et al. 2008, Heise et al. 2015, Hill et al. 2015).

2. METHODS

The MT method is an inductive EM sounding technique especially sensitive to electrical conductors (e.g. Vozoff, 1992). MT relies on measuring time series of the natural electric (**E**) and magnetic (**H**) field variations at a specific location (**r**) at the Earth's surface. In the frequency domain (ω) the electric and magnetic field are related through a complex-valued second-rank tensor Z:

$$\boldsymbol{E}(\boldsymbol{r},\omega) = \begin{pmatrix} C_{11}(\boldsymbol{r}) & C_{12}(\boldsymbol{r}) \\ C_{21}(\boldsymbol{r}) & C_{22}(\boldsymbol{r}) \end{pmatrix} \begin{pmatrix} Z_{xx}(\boldsymbol{r},\omega) & Z_{xy}(\boldsymbol{r},\omega) \\ Z_{yx}(\boldsymbol{r},\omega) & Z_{yy}(\boldsymbol{r},\omega) \end{pmatrix} \boldsymbol{H}(\boldsymbol{r},\omega) \quad (1)$$

Z contains the full 3D information about the electrical resistivity distribution of the subsurface, where lateral information comes from the location (r) and depth information from the frequency (ω). MT electric field data are commonly subject to frequency-independent amplitude changes known as galvanic distortions (e.g. Jiracek, 1990). Distortion is described by a real-valued frequency-independent distortion matrix C. In the ideal case of no distortion present C has the form of the identity matrix and can be omitted from eq. (1).

3D interpretation of MT data requires 3D inverse modelling of the full impedance tensor. In contrast, 1D interpretations of the impedance tensors typically interpret a rotationally invariant of the tensor such as the determinant (Berdichevsky, 1999). For 2D interpretations the impedance tensor is rotated into the direction of geoelectrical strike and only the two modes TE (Zxy) and TM (Zyx) are interpreted. The impedance tensor (eq. 1) can also be affected by galvanic and inductive distortions, which are either caused by small-scale near surface electrical scatterers below the resolution of the data, by pronounced topography (Stark et al., 2013; Käufl et al. 2018), or by a superimposition of both. Concepts to correct for distortions exist for underlying 1D and 2D assumptions (Groom and Bailey, 1989), however, they are strictly speaking not valid for 3D data.

3D inversions can be performed inverting simultaneously for 3D resistivity structure and distortion matrices, with a control parameter that suppresses deviations from the identity matrix, which represents the a priori condition of no distortion (Soyer, 2020). Topographic distortions are addressed by the accurate implementation of topography in the 3D resistivity model (Käufl et al. 2018; Soyer at al., 2019). Another method to bypass distortions is to invert for magnetotelluric phase tensors (e.g. Samrock et al. 2018), a quantity that is unaffected by distortions (Caldwell et al., 2004). 3D inversion of MT data and concepts to address distortion without simplifying assumptions have led to an increasing number of 3D electrical resistivity models of volcanic geothermal prospects that allow interpretations that are consistent with theoretical concepts of the architecture of volcanic geothermal systems and geological models. In the following we present a surface to depth hypothetical model of a volcanic hydrothermal system that builds upon existing models with a stronger focus on deep electrical conductors.

Besides geological causes for deep conductors, non-geological sources must be considered as a possible reason. Data distortion, noise and systematic bias in the MT dead band can lead to geological misinterpretations (Hennessy and Macnae, 2018).

3. COMPREHENSIVE HYPOTHETICAL MODEL OF VOLCANIC HIGH-TEMPERATURE GEOTHERMAL SYSTEMS

The main source of heat in a volcanic high-temperature geothermal system is magmatic activity. Magma is primarily generated through partial melting processes in the Earth's mantle (Grove and Till, 2015). Melt is generated through two main processes: First, by decompression melting at extensional settings such as continental rifts, in the backarc of subduction zones, at midoceanic ridges and by mantle plume activity. The second melt generation process is through a change of composition in the Earth's mantle so that the solidus of the new composition is lower than the present temperature. This process happens e.g. in subduction zones. Magmatic systems are dynamic transcrustal features (Cashman et al., 2017) with a highly complex architecture (Edmonds et al. 2019). Melt eventually reaches the Earth's surface where it erupts in volcanoes or is stored at mid-crustal depths in highly crystalline magmatic mush reservoirs.

Crystal mush reservoirs have relatively small melt fractions and can be in a rheologically locked-up rigid state forming ephemeral systems that undergo increasing solidification through fractional crystallization and degassing (Sparks et al. 2019). Re-melting of crystal mush can be initiated through emplacement of new magma from below at the base of the crystal mush reservoir (Huber at al. 2011). Magma storage in the upper crust drives hydrothermal convection ultimately leading to the formation of a high-temperature geothermal system (Scott et al. 2015). The architecture of such a system in shown in Figure 1. In the following we will describe the individual geological features and their electrical characteristics. The hypothetical model (Fig.1) builds up and expands work by Berktold (1983), Pellerin et al. (1992), Ussher et al. (2000), Andersson et al. (2000), Cumming (2009) and Samrock et al. (2023) amongst others.

Starting from the surface, the shallow depths of volcanic geothermal prospects are typically composed of fresh volcanic material including pumice, ash, and lava flows. This material is mostly dry and characterized by high resistivities. Going deeper, circulating geothermal fluids lead to the formation of the clay cap (feature 1 in Fig. 1). The clay cap forms through alteration along the flow paths of hot circulating fluids that hydrothermally alter the volcanic host rock producing clay minerals such as smectite (Ussher et al. 2000). These clays are characterized by very low electrical resistivities leading to a pronounced electrically conductive layer atop the geothermal reservoir. The clay cap has also a sealing function due to the tendency of clay minerals to hydrate and swell forming an impermeable layer when exposed to water. Hydrothermal alteration is temperature dependent and with increasing temperature clays produced in the argillic alteration regime become hydrothermally unstable. At higher temperatures propylitic alteration takes place with different alteration products such as chlorite and epidote. These minerals are characterized by much higher resistivities leading to an increase in bulk resistivity in the hotter propylitic alteration zone (feature 2 in Fig. 1) below the clay cap. Empirical evidence suggests that the clay cap bottom is marked by the 10Ωm isoline and temperatures of 250°C (Gíslason et al., 2015). Temperatures are hotter in the propylitic alteration zone and in upflow zones that form preferably along geological discontinuities such as faults (Wallis et al. 2017). Since the temperature pattern follows the upflow zones, temperature isosurfaces and hence the argillic alteration front are pushed closer to the land surface leading to the characteristic clay cap updoming above upflow zones (Fig.1; Anderson et al. 2000, Samrock et al. 2023). For a comprehensive database with petrophysical properties, including electrical resistivity, of rock from volcanic geothermal systems see e.g. Scott et al. (2023).

In the following, low resistivity features below the clay cap and the propylitic alteration zone are referred to as deep conductors. Deep conductors can have various origins of which several are described in the following. One reason can be the formation of an acidic hydrothermal plume and a high pyrite concentration. Hydrothermal acid plumes (feature 3 in Fig. 1) form through chemical reactions of sulfur-rich volcanic degassing and water (Byrdina et al. 2018). Byrdina et al. (2018) observed resistivities of acid fluids from Indonesian volcanoes below 0.1Ωm and decreasing resistivities with decreasing pH. Low pH environments also promote the formation of electrically conductive pyrite (FeS_2) by reaction between H_2S-rich fluids and Fe-rich volcanic rock (Levy et al. 2020).

Magma-derived fluids that are exsolved from crystallizing melt tend to migrate upwards due to buoyancy forces and may accumulate in the upper part of an active or cooled magmatic intrusion (feature 4 in Fig. 1). Such magmatic brine lenses can be composed of vapor and brine or even supercritical fluids. Watanabe et al. (2021) presented an empirical model to calculate the electrical conductivity of H_2O-NaCl fluids for pressures up to 200 MPa and temperatures up to 525°C. Their model shows that magmatic brine lenses have low electrical resistivities at the expected temperature and pressure conditions of a high-temperature geothermal system. Tseng et al. (2020) interpreted a deep conductor with resistivities less than 1Ωm below Kusatsu–Shirane volcano, Japan, as pressurized magmatic brine lens, the top of which is sealed by an impermeable layer of precipitated silica and

halite. Magmatic brine lenses are sourced from deeper magma reservoirs that may exist in form of crystal mush reservoirs. Crystal mushes have a crystal fraction of minimum 50 to 60 vol.% which is the mechanical threshold when crystals start touching each other and the melt crystal mixture cannot flow and erupt anymore (Bachmann and Bergantz, 2008). Samrock et al. (2021) coupled laboratory inferred melt electrical conductivity models and thermodynamic modelling of melt evolution and crystal fractionation to constrain electrical conductivities within crystal mush reservoirs. Their models provide interpretations of deep conductors under volcanic geothermal prospects in the Ethiopian rift that agree with thermodynamic equilibrium conditions and consider crystal mush reservoirs as three phase systems that consist of melt, crystals, and a fluid phase. Cordell et al. (2022) used a similar approach to interpret deep conductors and to constrain magma reservoir conditions by integrating thermodynamic petrological models and resistivities within deep conductors.

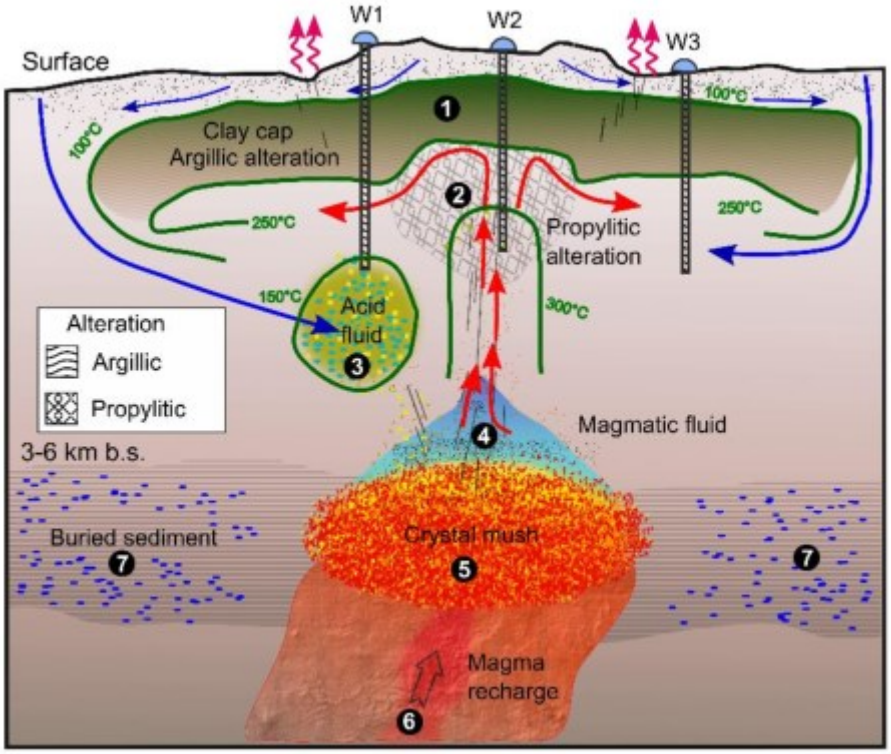

Figure 1: Surface to depth hypothetical model of a volcanic high-temperature geothermal system. The sketch shows the main features of a geothermal system and possible causes for conductive zones below the clay cap. 1) Clay cap: Argillic hydrothermal alteration zone with sealing function atop the reservoir. 2) Propylitic alteration zone below the clay cap, major target for drilling. 3) Acidic hydrothermal plume and formation of pyrite, both form through reaction of sulfur from magmatic degassing with fluids and host rock. 4) Liquid magmatic brine lens with high concentration of dissolved solids. 5) Magmatic reservoir with well interconnected partial melt fraction. 6) Magmatic recharge channel. 7) Buried sedimentary layer.

The upper crustal melt reservoir (feature 5 in Fig. 1) is fed from deeper parental melt sources. Recharge of melt might have ceased or is still ongoing if magmatic melt channels between the upper crustal melt reservoir and the deeper source region of the melt exist (feature 6 in Fig. 1). Active magmatic pathways will appear as deep routed conductors below the volcanic geothermal prospect. As an example, Dambly et al. (2023) presented a multiscale magnetotelluric model of a section in the Ethiopian Rift that shows melt generation and transport from the lower crust up to the near surface below the producing Aluto-Langano geothermal field. In cases where volcanic eruption happens through sedimentary layers, deep conductors can be related to fluid bearing sediments under volcanic cover having no volcanic origin (feature 7 in Fig. 1). This situation is encountered in Sumatra where Tertiary transgressive sediments are embedded between older Mesozoic volcanic units and younger Quaternary volcanic overburden (Barber et al., 2005; Mussofan et al., 2016). Despite not having a volcanic origin, deep sedimentary conductors might be falsely interpreted as magmatic heat source. However, if the geological context is known, sedimentary conductors under volcanic prospects might be target zones for drilling since they are often characterized by high permeabilities and provide good reservoir conditions (Ikhwan et al., 2023).

4. EXAMPLES OF DEEP CONDUCTORS IMAGED UNDER GEOTHERMAL PROSPECTS IN INDONESIA

In our long experience in the field of 3-D MT imaging of volcanic high-temperature geothermal systems, deep conductors appear under about half of volcanic geothermal prospects worldwide, whereas other geothermal fields show no indications for deep conductors (e.g. Soyer at al., 2018). In the following we present vertical sections of 3-D magnetotelluric models from volcanic geothermal fields in Indonesia, where deep conductors have been encountered. A detailed interpretation is beyond the task of this work; however, all three prospects have a long eruptive history and active geothermal surface manifestations. The conductor below Sibayak (Fig. 2) is clearly deep routed, which is indicative of an intrusive origin.

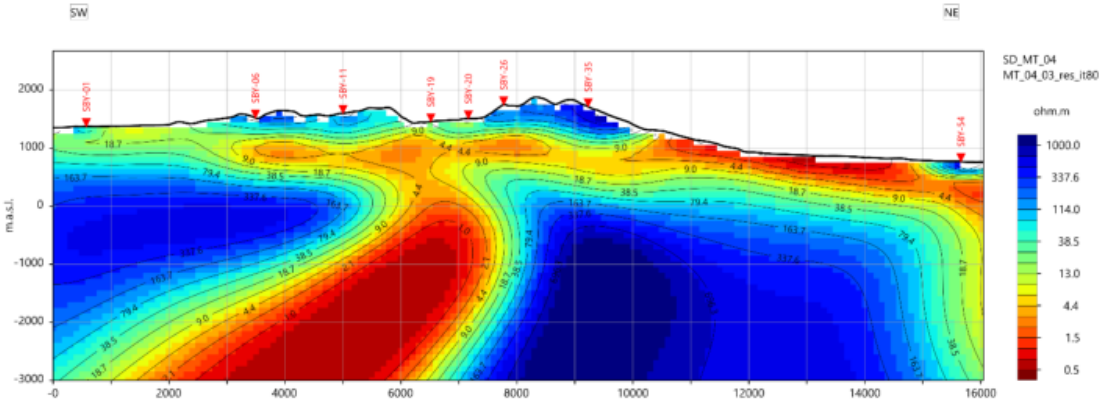

Figure 2: Deep conductor imaged below Sibayak, Indonesia.

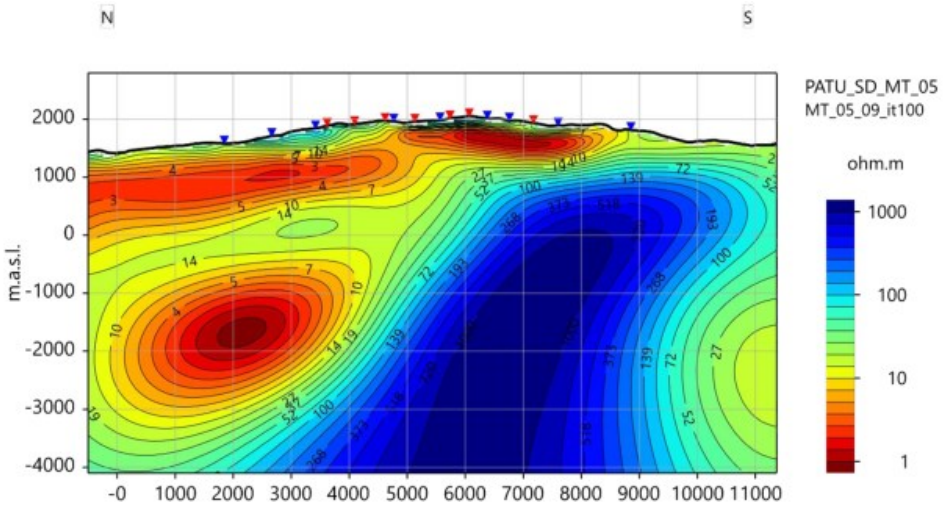

Figure 3: Deep conductor imaged below Patuha, Indonesia.

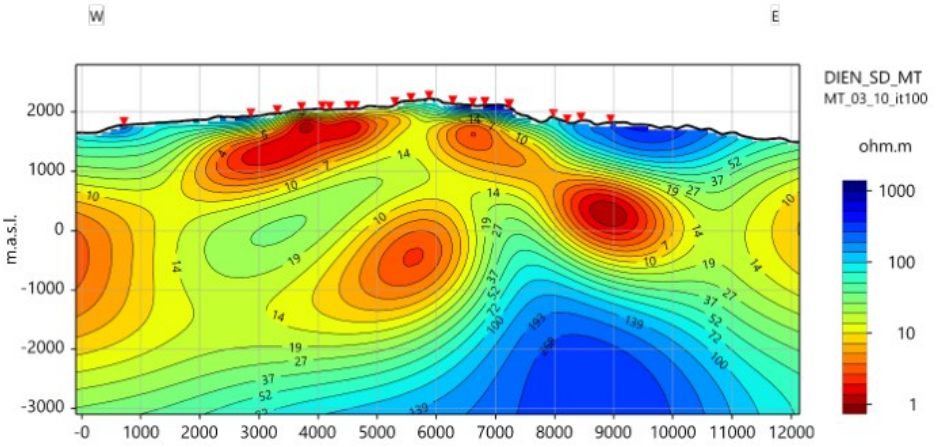

Figure 4: Deep conductor imaged below Dieng, Indonesia.

Geochemical analyses of fluids from Sibayak reveal a dominant magmatic volatile contribution and components of quenched magmatic gases (Fahmi et al., 2020). Sibayak belongs to the Singkut caldera from which Forni et al. (2024) report eruption of crystal-rich magmas and geochemical evidence for long-lived large cumulate crystal mushes.

Not enough data are available from Patuha (Fig. 3) and Dieng (Fig. 4) to provide a conclusive interpretation of the deep conductors. In view of the absence of deep roots and considering the isolated shapes of the deep conductors it could be argued that they represent fluid-rich zones, magmatic brine, or hydrothermal fluid plumes.

5. CONCLUSIONS

Deep conductors under volcanic high-temperature geothermal systems can have many origins that range from magma-related processes and favorable conditions like stable crystal mush reservoirs that represent powerful heat sources to unfavorable conditions like acidic hydrothermal plumes that cause corrosion of geothermal wells and facilities. Even amagmatic causes are possible in cases where volcanic eruption happens through sediments. The described causes for deep conductors provide only a selection, and thus, an incomplete overview. Interpretation of deep conductors requires detailed knowledge of the geological context and eruptive history of the volcanic geothermal prospect. More work is required in the field of melt electrical conductivity models to provide more complete models for composition-dependent melt resistivities. More research is also required to understand bulk resistivities of reactive multiphase magmatic systems that consist of melt, solid, and fluids in different states from liquid to vapor and supercritical. In reactive systems traditional multi-phase mixing laws to derive bulk resistivities do not apply. Finally, yet importantly, the quality of MT data used to derive 3D resistivity models must be critically evaluated and the robustness of deep conductor must be tested. Deep conductors might be artifacts with no geological explanation caused by poor data quality and systematic data bias.

ACKNOWLEDGEMENTS

The authors would like to express their gratitude to PT Geo Dipa Energi and Pertamina Geothermal Energy for the permission to publish the results from the 3D inversion modeling of MT data from Patuha and Dieng (PT Geo Dipa Energi) and Sibayak (Pertamina Geothermal Energy). FS thanks colleagues ETH Zurich for their contributions on the topic.

REFERENCES

Anderson, Errol, Daryl Crosby, and Greg Ussher. Bulls-eye! Simple resistivity imaging to reliably locate the geothermal reservoir. *Proceedings World Geothermal Congress*. 2000.

Árnason, Knútur, Hjálmar Eysteinsson, and Gylfi Páll Hersir. Joint 1D inversion of TEM and MT data and 3D inversion of MT data in the Hengill area, SW Iceland. *Geothermics* 39.1 (2010): 13-34.

Bachmann, O., & Bergantz, G. (2008). The magma reservoirs that feed supereruptions. *Elements*, 4(1), 17-21.

Barber, A.J., Crow, M.J., and Milsom, J.S., Sumatra: Geology, Resources and Tectonic Evolution. Geological Society, London, *Memoirs*, 31 (2005), 290 pp.

Berdichevsky, M. N. Marginal notes on magnetotellurics. *Surveys in Geophysics* 20 (1999): 341-375.

Berktold, A. Electromagnetic studies in geothermal regions. *Geophysical surveys* 6.1 (1983): 173-200.

Byrdina, S., Grandis, H., Sumintadireja, P., Caudron, C., Syahbana, D. K., Naffrechoux, E., ... & Vandemeulebrouck, J. (2018). Structure of the acid hydrothermal system of Papandayan volcano, Indonesia, investigated by geophysical methods. *Journal of Volcanology and Geothermal Research*, 358, 77-86.

Caldwell, T. Grant, Hugh M. Bibby, and Colin Brown. The magnetotelluric phase tensor. *Geophysical Journal International* 158.2 (2004): 457-469.

Cashman, K. V., Sparks, R. S. J., & Blundy, J. D. (2017). Vertically extensive and unstable magmatic systems: a unified view of igneous processes. *Science*, 355(6331), eaag3055.

Cordell, D., Naif, S., Troch, J., & Huber, C. (2022). Constraining magma reservoir conditions by integrating thermodynamic petrological models and bulk resistivity from magnetotellurics. *Geochemistry, Geophysics, Geosystems*, 23(9), e2022GC010455.

Dambly, M. L. T., Samrock, F., Grayver, A. V., & Saar, M. O. (2023). Insights on the interplay of rifting, transcrustal magmatism and formation of geothermal resources in the central segment of the Ethiopian Rift revealed by 3-D magnetotelluric imaging. *Journal of Geophysical Research: Solid Earth*, 128(7), e2022JB025849.

Groom, Ross W., and Richard C. Bailey. Decomposition of magnetotelluric impedance tensors in the presence of local three-dimensional galvanic distortion. *Journal of Geophysical Research: Solid Earth* 94.B2 (1989): 1913-1925.

Grove, T. L., & Till, C. B. (2015). Melting the Earth's Upper Mantle. In *The Encyclopedia of Volcanoes* (pp. 35-47). Academic Press.

Cumming, W. (2009). A conceptual model approach to the geophysical exploration of permeable geothermal reservoirs that considers context and uncertainty. In *SEG International Exposition and Annual Meeting* (pp. SEG-2009). SEG.

Edmonds, M., Cashman, K. V., Holness, M., & Jackson, M. (2019). Architecture and dynamics of magma reservoirs. *Philosophical Transactions of the Royal Society* A, 377(2139), 20180298.

Fahmi, F.L., Giriarso, J.P, Mulyanto, A. P., Thamrin, M. H., Pasaribu, F. (2020). Geochemistry Monitoring of Surface Thermal Manifestation in Sibayak, North Sumatra, Indonesia. *Proceedings World Geothermal Congress*. 2020.

Forni, F., Phua, M., Bernard, O., Fellin, M. G., Oalmann, J., Maden, C., ... & de Maisonneuve, C. B. (2024). Remobilization and eruption of an upper crustal cumulate mush at the Singkut caldera (North Sumatra, Indonesia). *Journal of Volcanology and Geothermal Research*, 445, 107971.

Gíslason, G., Eysteinsson, H., Björnsson, G., & Harðardóttir, V. (2015, April). Results of surface exploration in the Corbetti Geothermal Area, Ethiopia. In *Proceedings World Geothermal Congress*, Melbourne, Australia (pp. 19-25).

Gunderson, Richard, et al. Analysis of smectite clays in geothermal drill cuttings by the methylene blue method: for well site geothermometry and resistivity sounding correlation. *Proceedings World Geothermal Congress*. 2000.

Hennessy, L., & Macnae, J. (2018). Source-dependent bias of sferics in magnetotelluric responses. *Geophysics*, 83(3), E161-E171.

Hermance, J.F., Thayer, R.E. and Bjornsson A.. "The telluric-magnetotelluric method in the regional assessment of geothermal potential." Proc. Second UN Symposium on the Development and Use of Geothermal Resources. Vol. 2. Washington, DC.: *US Government Printing Office*, 1976.

Heise, W., Caldwell, T.G., Bertrand, E.A., Hill, G.J., Bennie, S.L., and Palmer, N.G., 2015, Imaging the deep source of the Rotorua and Waimangu geothermal fields, Taupo Volcanic Zone, New Zealand: *Journal of Volcanology and Geothermal Research*, v. 314, p. 39–48.

Hill, Graham J., et al. Structure of the Tongariro Volcanic system: Insights from magnetotelluric imaging. *Earth and Planetary Science Letters* 432 (2015): 115-125.

Huber, C., Bachmann, O., & Dufek, J. (2011). Thermo-mechanical reactivation of locked crystal mushes: Melting-induced internal fracturing and assimilation processes in magmas. *Earth and Planetary Science Letters*, 304(3-4), 443-454.

Ikhwan, M., Prasetyo, I. M., & Suryanto, S. (2023) The Role of The Hulusimpang Formation in Well-Scale Permeability of The Central-Southern Sumatra Geothermal Fields. *Proceedings World Geothermal Congress* 2023

Jiracek, George R. Near-surface and topographic distortions in electromagnetic induction. *Surveys in geophysics* 11.2 (1990): 163-203.

Käufl, Johannes S., Alexander V. Grayver, and Alexey V. Kuvshinov. Topographic distortions of magnetotelluric transfer functions: a high-resolution 3-D modelling study using real elevation data. *Geophysical Journal International* 215.3 (2018): 1943-1961.

Lévy, L., Maurya, P. K., Fiandaca, G., Bording, T. S., Madsen, L. M., Gailler, L., ... & Árnason, K. (2020). Geo-electrical monitoring of H2S mineralization into pyrite, upon re-injection in basalts at Nesjavellir Geothermal site, Iceland. In *World Geothermal Congress* (Vol. 1).

Pellerin, Louise, Jeffrey M. Johnston, and Gerald W. Hohmann. Evaluation of electromagnetic methods in geothermal exploration. SEG Technical Program Expanded Abstracts 1992. *Society of Exploration Geophysicists*, 1992. 405-408.

Moskowitz, B., and Dennis Norton. A preliminary analysis of intrinsic fluid and rock resistivity in active hydrothermal systems. *Journal of Geophysical Research* 82.36 (1977): 5787-5795.

Munoz, Gerard. Exploring for geothermal resources with electromagnetic methods. *Surveys in geophysics* 35 (2014): 101-122.

Mussofan, W., Sutrisno, L., Ramadhan, I., & Aulia, N. (2016). Geological aspects to constrain geothermal conceptual model: Gunung Rajabasa case study. In *Proceedings* The 4th Indonesia International Geothermal Convention & Exhibition (Vol. 1).

Newman, Gregory A., et al. Three-dimensional magnetotelluric characterization of the Coso geothermal field. *Geothermics* 37.4 (2008): 369-399.

Pellerin, Louise, Jeffrey M. Johnston, and Gerald W. Hohmann. Evaluation of electromagnetic methods in geothermal exploration. *SEG Technical Program Expanded Abstracts* 1992. Society of Exploration Geophysicists, 1992. 405-408.

Samrock, Friedemann, et al. Magnetotelluric image of transcrustal magmatic system beneath the Tulu Moye geothermal prospect in the Ethiopian Rift. *Geophysical Research Letters* 45.23 (2018): 12-847.

Samrock, F., Grayver, A. V., Bachmann, O., Karakas, Ö., & Saar, M. O. (2021). Integrated magnetotelluric and petrological analysis of felsic magma reservoirs: Insights from Ethiopian rift volcanoes. *Earth and Planetary Science Letters*, 559, 116765.

Samrock, Friedemann, et al. Geophysically guided well siting at the Aluto-Langano geothermal reservoir. *Geophysics* 88.5 (2023): WB105-WB114.

Scott, S., Driesner, T., & Weis, P. (2015). Geologic controls on supercritical geothermal resources above magmatic intrusions. *Nature communications*, 6(1), 7837.

Scott, S. W., Lévy, L., Covell, C., Franzson, H., Gibert, B., Valfells, Á., Newson, J., Frolova, J., Júlíusson, E., and Guðjónsdóttir, M. S. (2023). Valgarður: A database of the petrophysical, mineralogical, and chemical properties of Icelandic rocks, *Earth Syst. Sci. Data*, 15, 1165–1195,

Soyer, W., F. Miorelli, and R. L. Mackie. On the Effects of Finite Dipoles in 3-D Magnetotelluric Modeling. 81st *EAGE Conference and Exhibition* 2019. Vol. 2019. No. 1. European Association of Geoscientists & Engineers, 2019.

Soyer, Wolfgang, et al. Geophysics over High Enthalpy Fields: Lessons from RLM-3D Magnetotelluric and Joint Inversions. *Proceedings* World Geothermal Congress. 2020.

Soyer, W., Mackie, R., Hallinan, S., Pavesi, A., Nordquist, G., Suminar, A., ... & Nelson, C. (2018). Geologically consistent multiphysics imaging of the Darajat geothermal steam field. First Break, 36(6), 77-83.

Sparks, R. S. J., Annen, C., Blundy, J. D., Cashman, K. V., Rust, A. C., & Jackson, M. D. (2019). Formation and dynamics of magma reservoirs. *Philosophical Transactions of the Royal society* A, 377(2139), 20180019.

Stark, M. A., et al. Distortion effects on magnetotelluric sounding data investigated by 3D modeling of high-resolution topography. *GRC Transactions* 37 (2013): 521.

Tseng, K. H., Ogawa, Y., Nurhasan, Tank, S. B., Ujihara, N., Honkura, Y., ... & Kanda, W. (2020). Anatomy of active volcanic edifice at the Kusatsu–Shirane volcano, Japan, by magnetotellurics: hydrothermal implications for volcanic unrests. *Earth, Planets and Space*, 72, 1-11.

Ussher, G., Harvey, C., Johnstone, R., & Anderson, E. (2000, May). Understanding the resistivities observed in geothermal systems. In *proceedings* world geothermal congress (pp. 1915-1920). Japan: Kyushu.

Vozoff, K. The Magnetotelluric Method. Electromagnetic Methods in Applied Geophysics: Volume 2, Application, Parts A and B. *Society of Exploration Geophysicists*, 1991. 641-712.

Wallis, I. C., Rowland, J. V., Cumming, W., & Dempsey, D. (2017, November). The subsurface geometry of a natural geothermal reservoir. In *Proceedings* 39th New Zealand Geothermal Workshop (Vol. 21, p. 25). New Zealand: Rotorua.

Watanabe, N., Yamaya, Y., Kitamura, K., & Mogi, T. (2021). Viscosity-dependent empirical formula for electrical conductivity of H2O-NaCl fluids at elevated temperatures and high salinity. *Fluid Phase Equilibria*, 549, 113187.

Wright, Phillip M., et al. State-of-the-art geophysical exploration for geothermal resources. *Geophysics* 50.12 (1985): 2666-2696.

Application of Long Offset Resistivity Tomography for Reservoir Characterization Improvement at The Darajat Geothermal Field, Indonesia

Reka Tanuwidjaja[1], Chris Nelson[1], Bagus Endar B. Nurhandoko[2], and Amalia Nurani[3]

[1]Star Energy Geothermal Darajat, Wisma Barito Pacific II 17th Floor, Jakarta 11410, Indonesia
[2]Physics Department of Institut Teknologi Bandung, ITB Kampus Ganesha, Bandung 40132, Indonesia
[3]Elnusa, Graha Elnusa 17th Floor, Jakarta 12560, Indonesia

reka.tanuwidjaja@starenergy.co.id

Keywords: resistivity tomography, fault imaging, Kendang Fault, MEQ, injection monitoring, Darajat, Indonesia

ABSTRACT

Long Offset Resistivity Tomography has been implemented for the first time in The Darajat Geothermal Field with the objective to image static and dynamic condition of subsurface resistivity structure. The method enables penetration depth of several hundreds to thousands of meters below the surface resulting in strong subsurface resistivity contrast image associated with deep injection fluid distribution. A prominent resistivity anomaly within the reservoir around the main injection well of the field indicates that condensate injection distributed in the deep part of the reservoir. The method also improves the conceptual understanding related to the subsurface extension of a major fault that plays an important role as one of the key geological features of the field, the Kendang Fault.

The subsurface resistivity structure of the field is characterized by a low resistivity from surface to the base of clay cap rock, which represents presence of dominantly smectite alteration mineral. Meanwhile, the underlying reservoir shows a relatively high resistivity signature in comparison to the cap rock. A strong signature of low, instead of high, resistivity in the reservoir near the main injection wells, DRJ-15, is suggesting a deep distribution of condensate injection below the bottom depth of the well. The signature confirms the impacted area of the condensate injection that was previously interpreted from a continuous monitoring of microearthquake (MEQ) that tracks vertically the fluid movement that induced pre-existing fracture at the central area of the field.

The resistivity image suggests that the Kendang Fault has 70° dip angle near the surface. The fault extends into reservoir depth as indicated by information from wells that penetrated the fault. Further evaluation provides information on how the subsurface extension of the fault acts as a fracture driver in the northern section of the reservoir where the sweet spots for production well targeting is located. The interpretation of the resistivity contrast also shows that the alteration tends to be intensive in the east side of the fault where the reservoir is located compared to a relatively fresh rock in the west side of the fault that might also signal the role of the fault as a reservoir boundary of the field.

1. INTRODUCTION

Darajat Geothermal Field is the largest vapor-dominated geothermal system in Indonesia located in West Java, Indonesia, about 230 km southeast of Jakarta (Figure 1). The field has been generating electricity for almost three decades with current operating capacity of 271 MWe from three power plant units. Commercial production began in 1994 with the commissioning of 55 MWe Unit I. The 95 MWe Unit II came online in 2000, followed by Unit III operations in 2007, which after a successful drilling campaign in 2007-2008 had been uprated to final capacity of 121 MWe. The Darajat geothermal system is a high-temperature reservoir with benign chemistry and low non-condensable gas content (<2 wt.%). The system is believed to be associated with the Kendang volcanic complex which is dominantly composed of propylitically-altered andesite lava flows intruded by microdiorite dikes (Rejeki et al. 2010). The dominant geologic structures at Darajat trend NE-SW and NW-SE with minor N-S faults.

Long Offset Resistivity Tomography has been implemented to produce subsurface resistivity model using the assumption that the subsurface rocks possess variation of resistivity values so that geological boundaries or changes in the subsurface rock condition can be identified based on the resistivity signature. If a targeted feature has an electrical resistivity contrast compared to the surrounding rocks, it can be detected by injecting a current and measuring the surface tension through a potential electrode on the surface (Figure 2). The two main objectives of the measurement are to monitor the fluid movement from the injection at DRJ-15 towards nearby production wells and to characterize the Kendang Fault as one of key geological features that often relates to permeable fracture within reservoir. Two measurement lines were designed to achieve these objectives, Line-1 and Line-2 (Figure 3). Line-1 is designed to cross the DRJ-15 from the southeast side and continue extending to the north

side with a total of 3.35 km survey line. This line was intended to image the area near DRJ-15 well TD where the condensate injection is most likely distributed. Meanwhile, Line-2 was intended to image the resistivity contrast due to the presence of the Kendang Fault by conducting a measurement on a 1.6 km of survey line on top of the northern section of the fault.

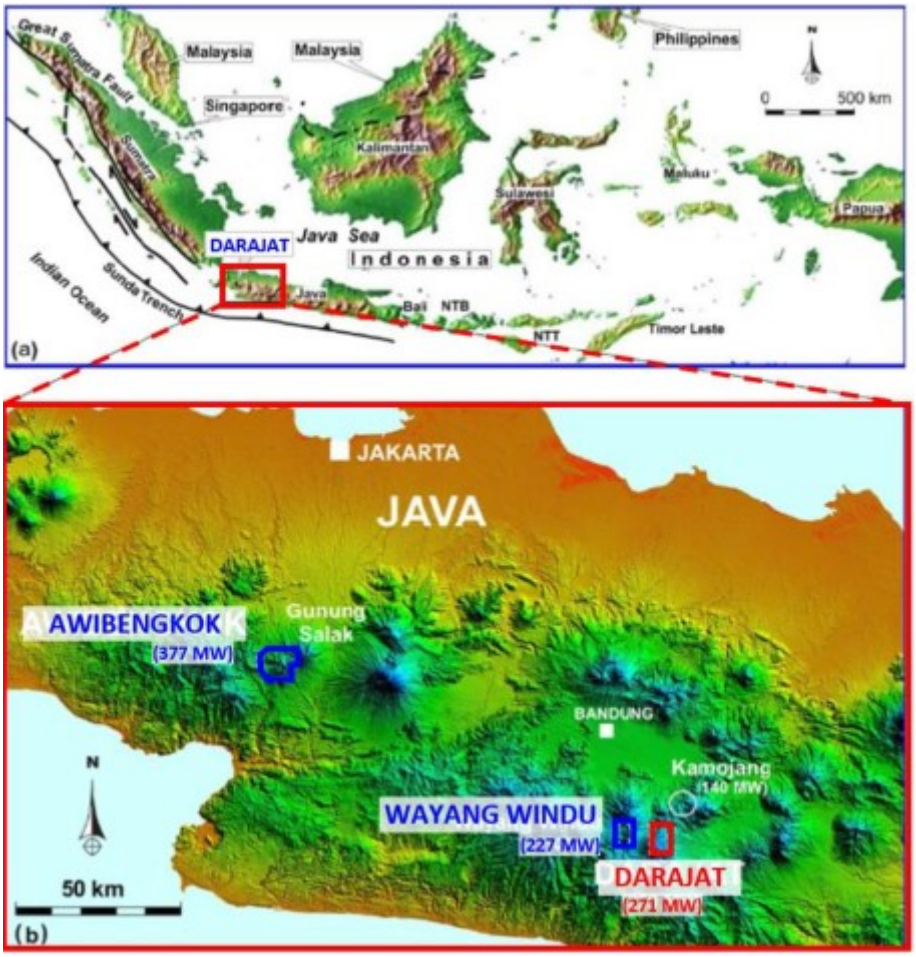

Figure 1: Location map of the Darajat geothermal field in relation to other Star Energy geothermal operations at the Awibengkok (Salak) and Wayang Windu fields.

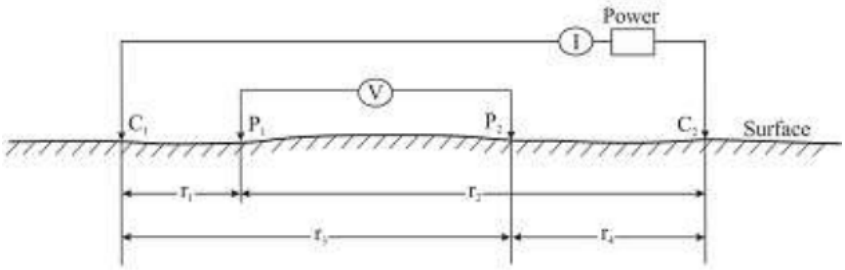

Figure 2: Illustration of tomography resistivity basic configuration measurement with current (C) and potential (P) electrodes, where r is distance between electrodes.

2. CHARACTERIZATION OF INJECTION FLUID DISTRIBUTION IN RESERVOIR

Injection strategy at Darajat has been focused mainly in the central and peripheral area in the northern part of the field. From 2006 to 2011, three wells in the central area were utilized as injection wells. DRJ-15 has been the main injector with an average injection rate of 120 lps (Figure 4A), alongside with DRJ-3 and DRJ-12 that were occasionally utilized as injectors for a short period of time (Figure 5). The DRJ-15 injection provides the pressure support needed by the reservoir, while at the same time the thermal fronts in the vicinity of the well has impacted the stress condition in the reservoir along the fractures. The effect was reflected in the occurrence of MEQ clusters with microseismic activity rate of around 27 events/month, covering an area with 1.5 km radius near DRJ-15.

Figure 5 shows that MEQs were located within a defined volume in the reservoir, but were mostly distributed below the well-TD (i.e. from msl to 2,000 m-bsl). The deep distribution of the MEQs indicates that the injection-induced fracture stimulation is following a vertical trend along the extension of the fracture network below the well-TD.

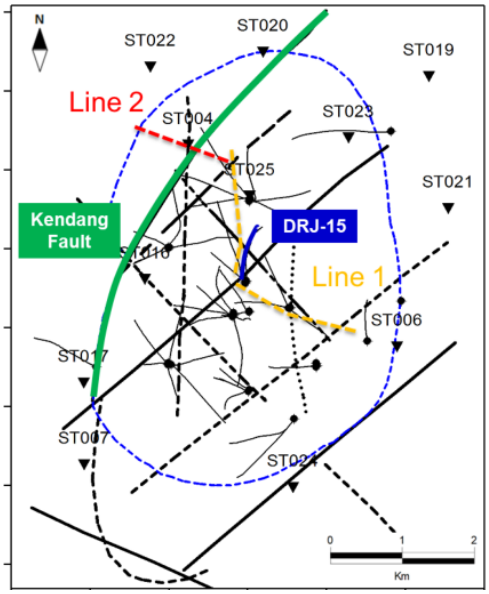

Figure 3: Map of the Darajat Geothermal Field showing reservoir boundary, structure, and drilled wells. Main injection wells, DRJ-15, is in central area (blue highlighted well). Surface expression of Kendang Fault is oriented NE-SW (green highlighted line). Long-offset Resistivity Tomography measurement line represent by Line-1 (yellow dashed line) and Line-2 (red dashed line). The black triangle surrounding the field represent the location of MEQ monitoring station.

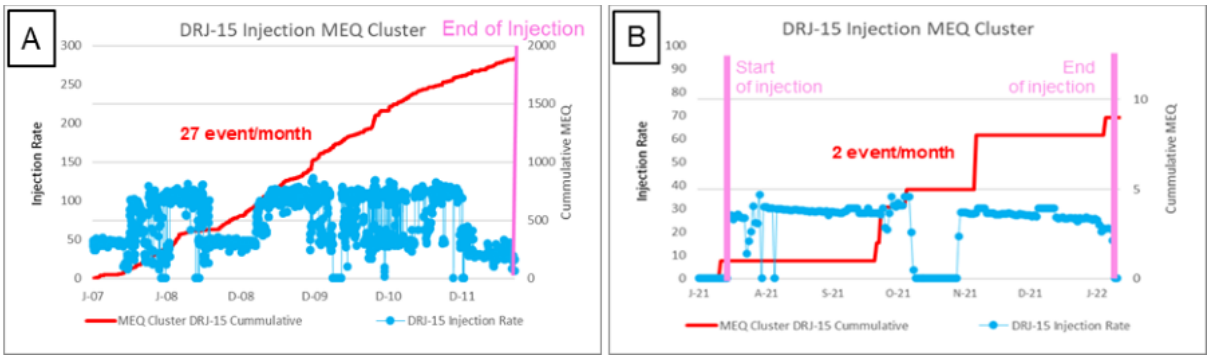

Figure 4: Chart showing the correlation between MEQ activity and injection rates at DRJ-15 in central area during period 2006 to 2011 (A), and 2021 to 2022 (B).

Since late 2011, seismic activity rates near DRJ-15 region had decreased as condensate injection was gradually moved to DRJ-19 in the peripheral area in the northern part of the field to avoid potential injection breakthrough toward the surrounding production wells in the central area. In 2021, DRJ-15 has been re-utilized as an injection well with the objective of providing pressure support to the central production area of the reservoir with a lower injection rate of 30 lps (Figure 4B) to minimize any adverse effect to the nearby production wells. The injection strategy was pursed by considering that the central production area has experienced a larger pressure drop and net-mass drainage from the long-term production activity in the field (Nelson et. al, 2023). Similar to the previous period of DRJ-15 injection, the MEQs tend to occur in the central area and are distributed in the deeper part of reservoir (Figure 5). However, the lower injection rate only results in 2 events/month, thus lowering the confidence level of delineating the area affected by the injection.

To ensure the effectiveness of the lower-rate-injection strategy, it is important to identify a more defined area of where injection fluid might move and re-saturate the reservoir fracture. The resistivity tomography enables to capture the resistivity response as deep as the TD of DRJ-15 with high resolution (Figure 6). the resistivity near the surface shown by a combination of high and low resistivity represents noisy response above the clay cap.

Below this depth, a signature of low resistivity structure represents the clay cap area which is rich with smectite alteration mineral. High smectite content lowers the resistivity, thus the clay cap structure could be delineated. In the central area of Darajat, the low resistivity clay cap structure seems to be disconnected below the DRJ-15 well pad. The observation is consistent with the result of the resistivity image from Magneto-Telluric (MT) survey where the <10 ohm. Meter clay cap structure is showing a lateral disconnection (Figure 7).

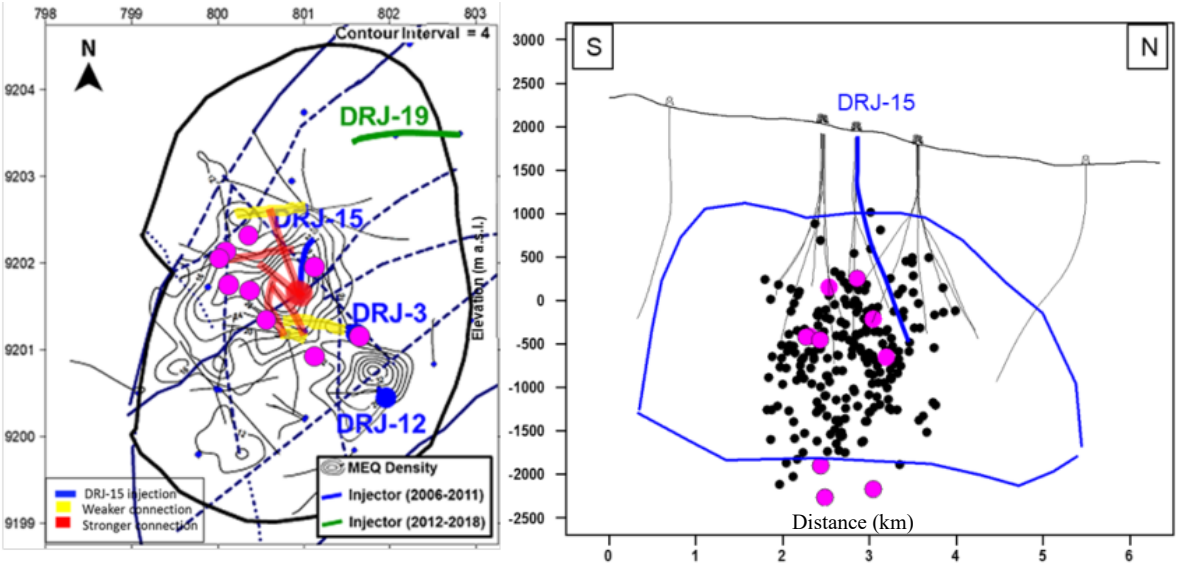

Figure 5: Map showing MEQ event density contour (black) during 120 lps injection vs MEQ event (purple) during 30 lps of injection at DRJ-15. Red and yellow colored well represent nearby well that have strong and weak connection with injection at DRJ-15 (left). Cross-section showing MEQ event (black) during 120 lps injection vs MEQ event (purple) during 30 lps of injection at DRJ-15 (right).

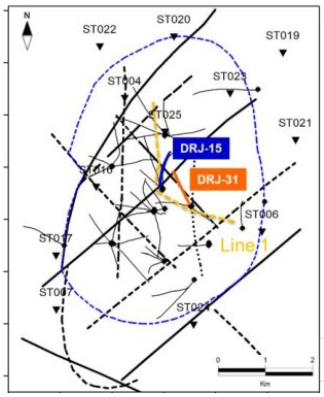

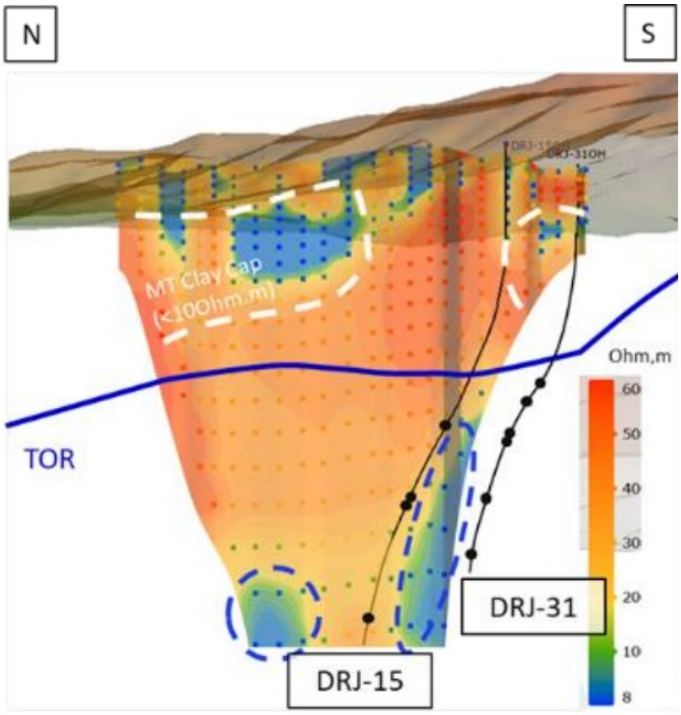

Figure 6:
Maps showing location of measurement Line-1 relative to DRJ-15 injector and DRJ-31 producer well (left). Cross-section showing the resistivity tomography image relative to DRJ-15 and DRJ-31; TOR represents Top of Reservoir, black dots represent permeable entry of the wells, white and blue circled areas highlight clay cap rock and deep low resistivity signature, respectively (right).

Further supporting this observation, a methylene-blue (MeB) analysis result from well cuttings of drilled wells in Darajat confirms this observation as the cuttings in the shallow part of DRJ-15 has lower result of measurement

(< 5 ml/gr) associated with a low composition of smectite alteration minerals (Figure 7). Instead of having a high composition of smectite, this zone shows a strong silicification in tuff and pyroclastic breccia. Below smectite-rich clap cap, the reservoir zone is characterized by the high resistivity signature as seen from MT resistivity image. Consistency is also observed in the resistivity tomography image as the high resistivity structure represents the reservoir zone below the clay cap.

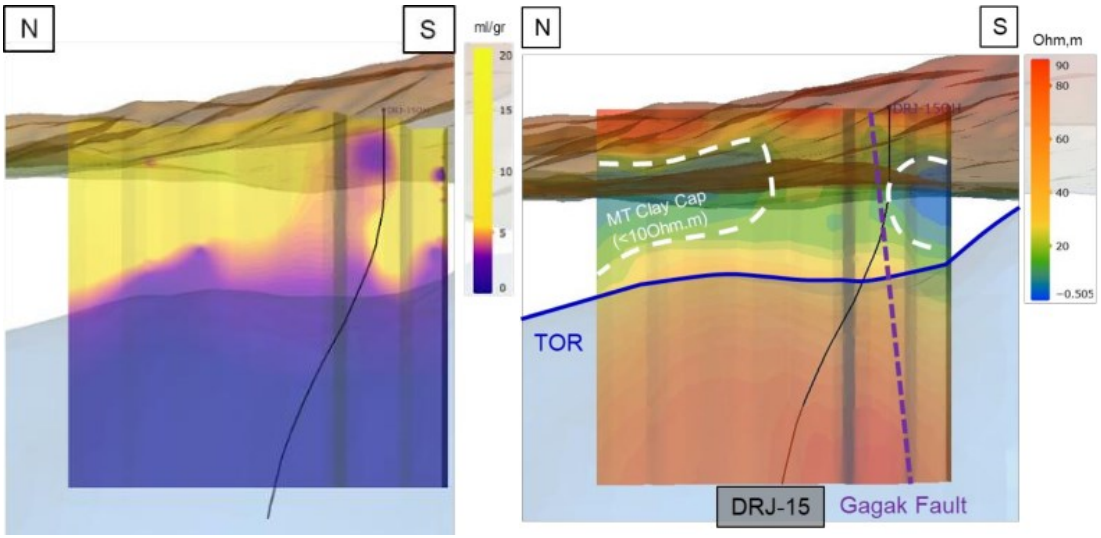

Figure 7: Cross-section showing the MT resistivity image relative to DRJ-15; TOR represents Top of Reservoir, white circled area and purple line highlights the clay cap rock and Gagak Fault, respectively (right). Cross section showing the MeB measurement corresponding with MT cross-section.

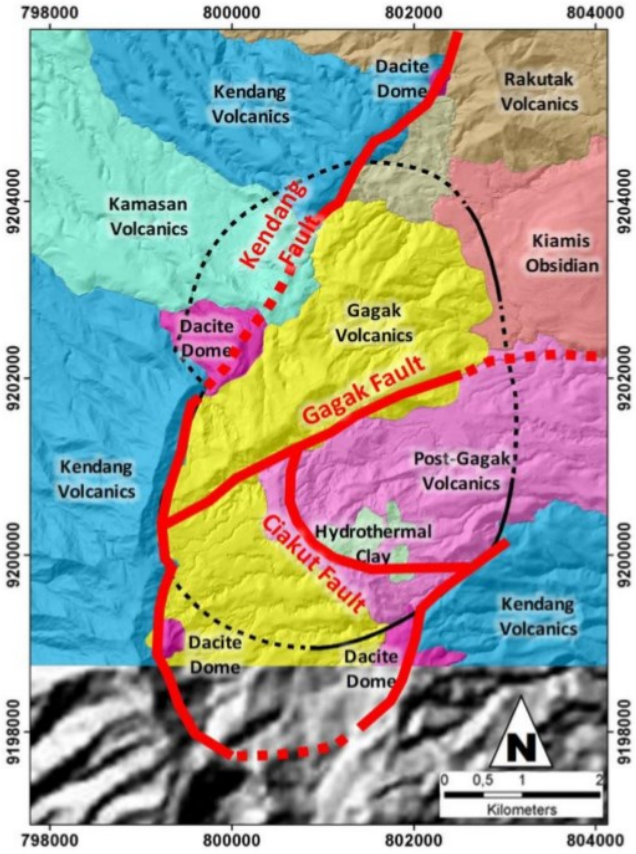

Figure 8: Geological map of Darajat Field showing the interpreted structure based on LiDAR data and offset reservoir rocks; dashed line represents inferred structure section. The Kendang Fault is one of prominent fault observed on surface beside Gagak and Ciakut Fault.

An anomaly is observed in the deep area of the resistivity tomography image. A low resistivity signature occurred near the DRJ-15 well TD where MT resistivity show a relatively uniform signature of high resistivity in the reservoir zone below the clay cap. The difference in the result at this depth is caused by the different characteristic of the measurement point between the two methods. Resistivity tomography provides a better imaging with a high level of detail as a result of more reliable measurement points near DRJ-15 well TD compared to the MT method. The deep low resistivity near DRJ-15 well TD is interpreted to be a response of the liquid phase presence that lower the resistivity response in the zone where the resistivity is expected to be high. Deep low resistivity patch in the north side might indicates a distribution of condensate injected at DRJ-15. It possibly moves deep, as suggested by the MEQ monitoring evaluation, and re-saturates the reservoir fracture toward the north direction. This indicates a good sign since the condensate injection tends to move vertically to the deep part instead of moving directly towards the nearby production wells which could cause an adverse effect for production. Meanwhile in the southern side, elongated low resistivity could be more related to the presence of marginal recharge (MR) that encountered at DRJ-31 production wells. Liquid has been produced from the deep permeable entry of this steam producing well. The distribution of low resistivity that stretched along the depth of DRJ-31 deep permeable entry could help to explain on where MR source could be possibly located.

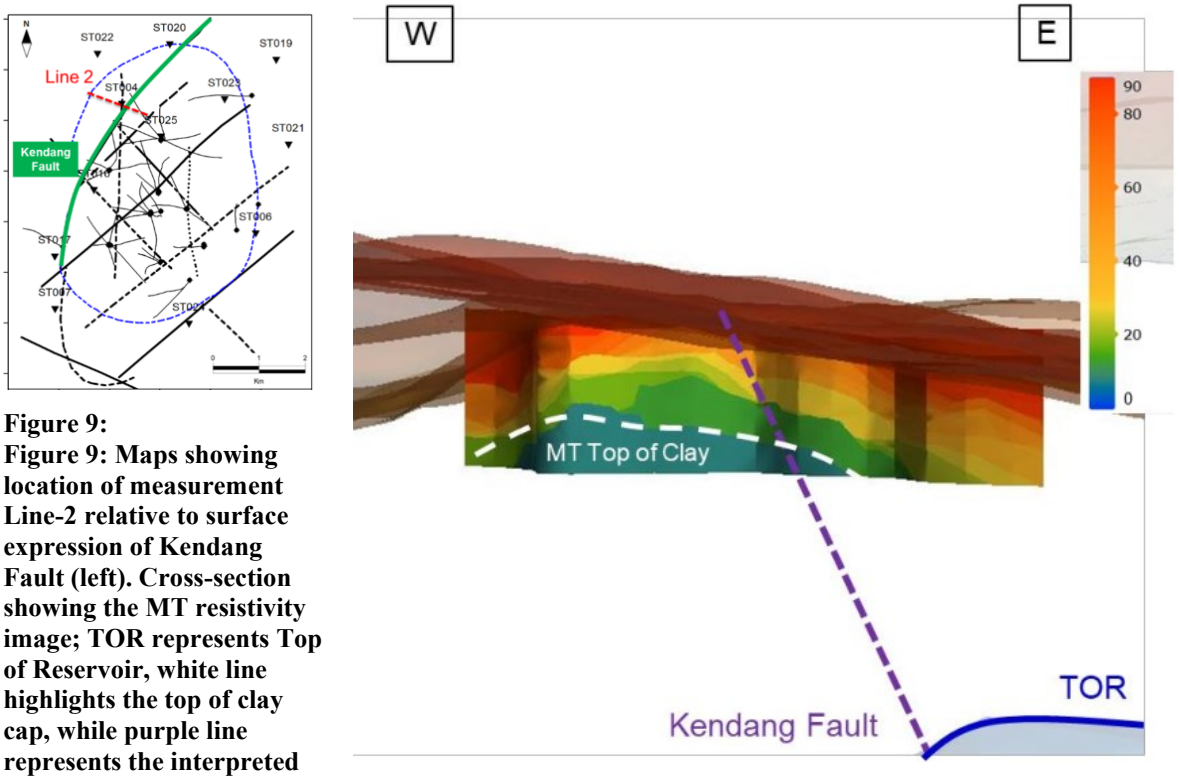

Figure 9:
Figure 9: Maps showing location of measurement Line-2 relative to surface expression of Kendang Fault (left). Cross-section showing the MT resistivity image; TOR represents Top of Reservoir, white line highlights the top of clay cap, while purple line represents the interpreted Kendang Fault extension in subsurface with 70° dip-angle (right).

3. FAULT CHARACTERIZATION

The Kendang Fault is one of the prominent faults observed on the surface besides the Gagak and Ciakut Faults based on the analysis of LiDAR data, drainage patterns, and relative location of eruption centers (Figure 8). The fault is stretched along the western boundary of the Darajat Field with a NE-SW orientation. The surface expression of the fault is prominent in the southern side of the Darajat Field and is inferred in the northern side. Further toward the northeast side, the Kendang Fault extends to the Kamojang Field which may be an indication that it is a section of the ring structure of an earlier volcano (Intani et. al, 2021). Previous evaluation suggests that the Kendang Fault is vertically extending into the reservoir depth as indicated by information from wells that have penetrated the fault. Series of permeable entry zones encountered in penetrating wells indicate a clustering permeable fracture along an interpreted high-angle extension of the fault in the reservoir zone. In the northern side of the field the series of permeable entry zones along the fault are identified as an area where high permeability is distributed.

To better characterize this permeable fracture zone, it is essential to delineate the signature of the Kendang Fault extension in the subsurface. Resistivity tomography enables to capture a resistivity contrast below the surface

expression of the fault in the northern side showing its subsurface signature. The presence of resistivity contrast at Line-2 shows a distinctive separation between high resistivity rocks in the west part and low resistivity in the east side. This result is consistently observed on the implementation of two different measurement configuration: Wenner-Alpha and Wenner-Schlumberger configuration. Both Wenner-Alpha and Wenner-Schlumberger configurations suggest more variation in near surface resistivity, in contract with homogenous layered resistivity model of MT method. The MT resistivity shows a relatively no significant lateral variation, while tomography resistivity shows prominent lateral resistivity contrast (Figure 9).

Resistivity tomography image shows that contact between high and low resistivity coincides with expression of Kendang Fault on the surface. By delineating the contact between resistivity contrast from surface to deeper part, a signature of Kendang Fault with 70° of dip angle could be inferred (Figure 10). This evidence supports the current concept of the high angle Kendang Fault extension in the subsurface. Moreover, the consistent dip angle suggested by resistivity contrast from two configurations of measurement, suggests a better understanding on locating the cluster area of permeable fracture along the Kendang Fault section inside reservoir. Interpretation of resistivity contrast could also suggest that alteration tends to be intensive in the east side of the fault where reservoir is located compared with relatively fresh rock in the west side of the fault. This observation might also signal the role of the fault as a reservoir boundary of the field.

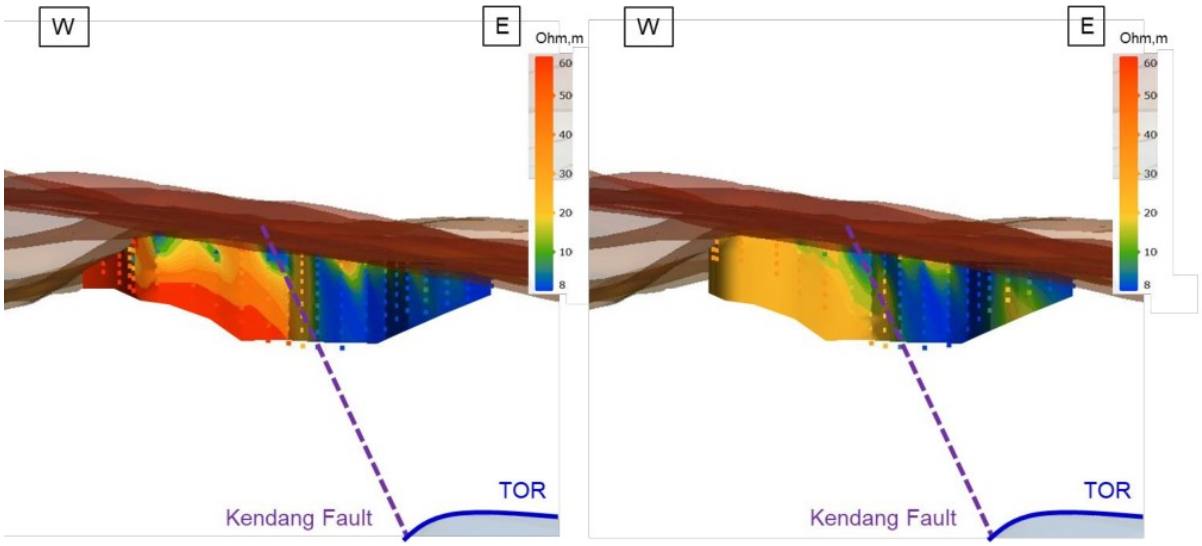

Figure 10: Cross-section showing the resistivity tomography image using Wenner-Alpha (left) and Wenner-Schlumberger (right) configuration. TOR represents Top of Reservoir; purple line highlights the interpreted Kendang Fault extension in subsurface with 70° dip-angle.

4. CONCLUSION

A newly implemented long offset resistivity tomography at the Darajat Filed has provided significant improvements on the learning from the injection monitoring at DRJ-15 and better characterization of the Kendang Fault. The resistivity image produced helps to better understand how the injection at DRJ-15 is distributed in the deeper part and impacting the nearby production wells. This understanding is helpful for the decision-making process of the Darajat Asset Management team for managing the future injection strategy. A time-lapse measurement is encouraged to monitor the evolution of impacted area for long-term injection management strategy. The evaluation of the Kendang Fault signature has also helped in refining the subsurface fault geometry by confirming the high dip angle. This has improved the understanding on the possible highly permeable fractured area along the Kendang Fault inside the reservoir that will be useful for well targeting and the development of the field in the future.

ACKNOWLEDGEMENTS

The authors would like to thank the management of Star Energy Geothermal for allowing publication of this paper. Many thanks to SEGD colleagues, ITB and ELNUSA counterparts who contributed to the development of the charts and figures in this paper, and the hours spent reviewing and improving its contents.

REFERENCES

Intani, R., Syaffitri, Y., Golla, G., Nelson, C., Cita, F., and Ginanjar: The Darajat Geothermal Field, Indonesia, After 24 Years of Production, *Proceedings*, World Geothermal Congress 2020+1, Reykjavik, Iceland (2021).

Nelson, C., Tanuwidjaja, R., Wolfgang, S., Mackie, R., Nordquist, G., and Hallinan, S.: Time-lapse (4D) Microearthquake and Precision Gravity Joint Inversion of the Darajat Geothermal Field, Indonesia, *Proceedings*, World Geothermal Congress 2023, Beijing, China (2023).

Nelson, C., Nordquist, G., Tanuwidjaja, R., and Jupe, A.: Injection-induced Microearthquakes for Reservoir Characterization in Darajat Geothermal Field, Indonesia, *GRC Transactions*, Vol. 42, (2018)

Rejeki, S., Rohrs, D., Nordquist, G., and Fitriyanto, A.: Geologic Conceptual Model Update of the Darajat Geothermal, *Proceedings*, World Geothermal Congress 2010, Bali, Indonesia (2010).

Constructing the Fault from Borehole Image and Drilling Fluid Movement in the Dieng Geothermal Field, Eastern Part of North Serayu Gea-Anticline

Iqbal Maratama, Rizkhy Ridoh Alamsyah, Andhika Putera Utama,
Aditya Yudha Kencana, Zakki Sabiq Purwaka, and Andy Wijaya Atmaja

PT Geo Dipa Energi, Jl. Akses Tol Soroja,
Blok Sumakamanah Parungserab, No.22, Parungserab, Soreang, Bandung

iqbalmrtm@gmail.com

Keywords: fault, borehole image, drilling, geochemistry, permeability, Dieng, geothermal

ABSTRACT

Faults are one of the primary targets in geothermal fields due to the role of the permeability zone in the reservoir. The data representing fault indications on the surface and in the subsurface have the potential to be interrelated. Surface data, such as lidar and surface mapping, can be combined with subsurface well data, such as borehole images and fluid movement, to confirm that a fault has existed.

The drilling campaign has begun in the Sileri area of the Dieng Geothermal Field, with some wells already drilled. Aerated drilling has become a common practice in reservoir sections to ensure that rock cutting reaches the surface or is pushed as far into the formation as possible. The air from the atmosphere enters the wellbore during drilling and may have an impact on the gas chemistry content of the existing well due to the similar permeability pathway from the fault. Evaluation of fluid flow movement during drilling is indicated by an increase in residual gas content as a result of drilling fluid injection into the reservoir. The results of gas monitoring in existing wells will deliver evidence of fault existence, which has previously been interpreted from lidar, geomorphology studies, surface mapping, and, in particular, data borehole images that provide information about fracture orientation, aperture, and fracture type in the well's wall. The primary objective can be obtained by conducting well monitoring and fracture analysis. Gas chemical analysis of CO_2 content, residual gas, NCG, and H_2S was monitored over time from pre-drilling to post-TD. Following that, geochemistry data was evaluated with a fault existence to determine the possibility of a permeable pathway from the fault.

1. INTRODUCTION

Understanding the intricate geological structures beneath geothermal fields is crucial for optimizing resource extraction and ensuring the stability of drilling operations. In this study, we focus on constructing fault systems from borehole images and monitoring the movement of drilling fluids to elucidate well connectivity within the geothermal reservoir of Dieng, Indonesia.

The research framework begins with an overview of the Dieng structure, highlighting its geological significance and the role of surface mapping and Lidar interpretation in preliminary fault identification. Dieng is known for its complex volcanic history, resulting in a dense network of faults and fractures that significantly influence geothermal fluid flow. Surface mapping and Lidar data provide an initial model of these structures, setting the stage for deeper analysis through borehole imaging.

The subsequent steps involve detailed geological structure analysis using borehole images, which offer high-resolution visualizations of the subsurface environment. By examining these images, we can identify fault planes, fracture networks, and other critical features that validate and refine the surface-based structural model. Additionally, monitoring drilling fluid movement between wells helps confirm connectivity within the reservoir. This fluid movement analysis not only supports the existence of the identified faults but also provides insights into their permeability and impact on fluid dynamics. Together, these methods form a comprehensive approach to verifying the geological structures of the Dieng geothermal field, thereby enhancing our understanding and management of this valuable resource.

2. DIENG STRUCTURE OVERVIEW

Java Island is located along the active convergent boundary where the Indo-Australian plate subducts beneath the Eurasian plate. This subduction process has resulted in intense volcanic activity, frequent seismic events, and the formation of various geological structures. The interplay of these tectonic plates has created a dynamic environment, influencing the development of faults, folds, and other structural features. Java's structural

framework is dominated by several major fault systems, including the Java Trench, the Kendeng Zone, and the Meratus Complex.

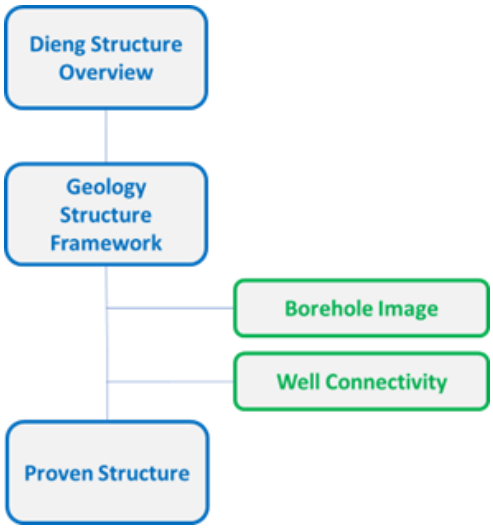

Figure 1: The research framework of this study.

The Dieng Geothermal Field is situated within the complex tectonic setting of the Sunda Arc, a geologically active region characterized by subduction along the convergent boundary between the Australian Plate and the Eurasian Plate. This tectonic interaction has led to the formation of numerous volcanic arcs throughout Indonesia, including the Dieng Plateau, where the geothermal field is located. The area is part of the larger volcanic complex known as the Dieng Volcanic Complex, which is composed of a series of stratovolcanoes and calderas.

The geology of the Dieng Geothermal Field is shaped by this tectonic setting, with volcanic activity playing a significant role in the formation of its geothermal resources. The presence of magma chambers beneath the surface provides a continuous heat source, heating groundwater and creating the conditions necessary for the formation of geothermal reservoirs. Additionally, the tectonic processes associated with subduction contribute to the fracturing and faulting of the crust, creating pathways for the circulation of fluids and enhancing the permeability of the reservoir rocks. This complex interplay of tectonic forces has endowed the Dieng Geothermal Field with its unique geological characteristics, making it a prime location for the extraction of renewable energy resources.

The structural framework of the Dieng Geothermal Field, viewed from a geological perspective, is deeply influenced by the tectonic processes associated with the subduction zone located to the south of Java Island. Subduction occurs when one tectonic plate is forced beneath another, leading to intense geological activity including volcanic eruptions and the formation of structural features such as faults and fractures. In the case of Dieng, this subduction zone plays a pivotal role in shaping the structural landscape of the region.

One prominent structural orientation within the Dieng Geothermal Field is characterized by a north-south alignment of open faults. These faults, resulting from the tectonic stresses associated with the subduction zone, create pathways for the movement of fluids within the Earth's crust. The presence of these faults facilitates the circulation of geothermal fluids, which is crucial for the development of a viable geothermal reservoir.

Another significant structural orientation in the area is aligned along a west-east axis, correlating with the broader subduction process occurring to the south of Java. This structural alignment is indicative of the broader tectonic forces at play, which exert considerable influence on the distribution of geological features and the overall structural framework of the Dieng region. Additionally, the circular structure observed in the Dieng area corresponds to the volcanic activity that has shaped the landscape over time. This circular structure is a manifestation of the volcanic calderas and related volcanic features that characterize the Dieng Volcanic Complex, highlighting the intricate relationship between volcanism and the structural framework of the geothermal field. Overall, the structural framework of the Dieng Geothermal Field reflects the complex interplay of tectonic processes, including subduction-related deformation, faulting, and volcanic activity, which collectively shape the geological characteristics of the region and influence its geothermal potential.

Furthermore, detailed mapping data has identified shear fractures with Northeast-Southwest and Northwest-Southeast trends, indicative of complex shear deformation within the field. These shear fractures, along with the extensional fractures exhibiting North-South and West-East trends, underscore the multi-directional stress regime prevalent in the region.

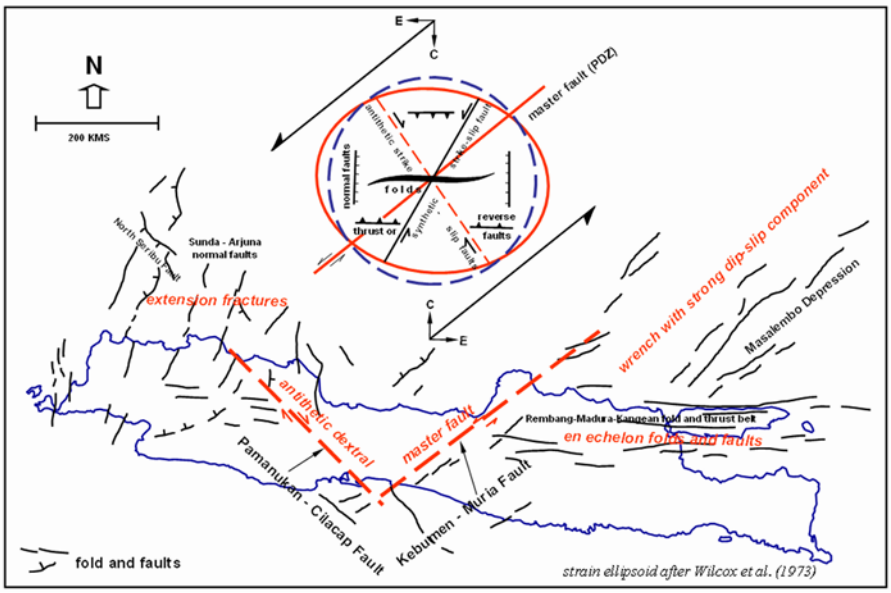

Figure 2: Structural analysis of Java. (Satyana, 2007).

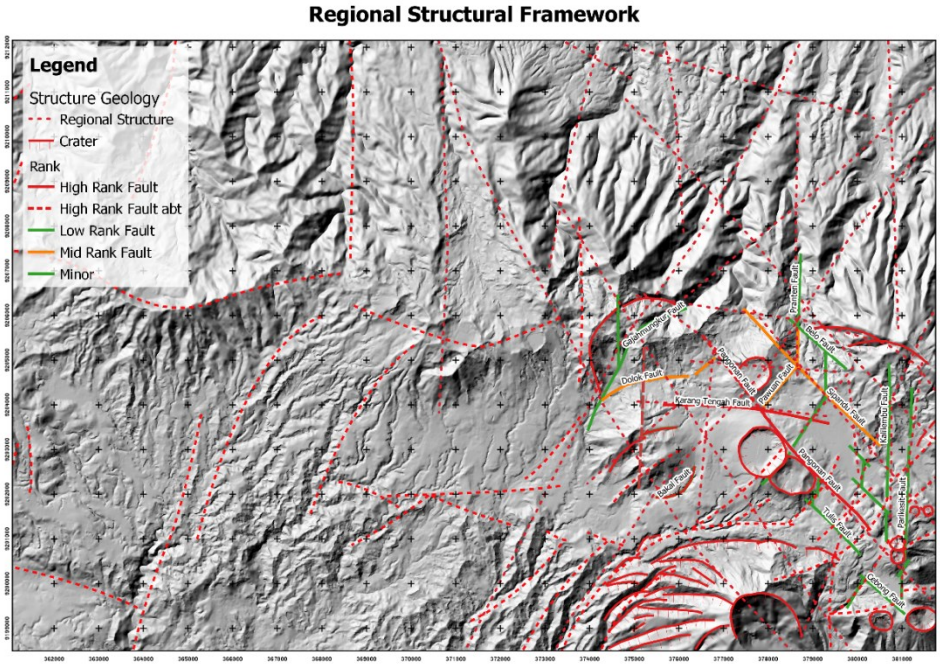

Figure 3: Regional structural framework of Dieng Geothermal.

3. BOREHOLE IMAGE

The analysis of borehole image data from wells 31X, 7Y, and 29X in the Dieng geothermal field provides significant insights into the subsurface fracture systems and supports the existence of faults in the area. Borehole imaging is a crucial technique for visualizing and characterizing fractures and faults, which play a vital role in geothermal fluid movement and reservoir productivity. Borehole images from the three wells reveal various types of fractures, including both open and sealed fractures, as well as a range of fracture orientations. The majority aligns with North-South trends, while some exhibit new and potentially significant orientations.

The borehole image data from these wells not only confirms the existence of previously mapped faults but also reveals new fracture orientations that could indicate additional structural complexity in the Dieng geothermal field. The NW-SE oriented fractures align well with the established fault framework, validating the interpretations made from surface mapping and Lidar data. The identification of N-S oriented fractures, however, introduces new considerations for the geological model of Dieng.

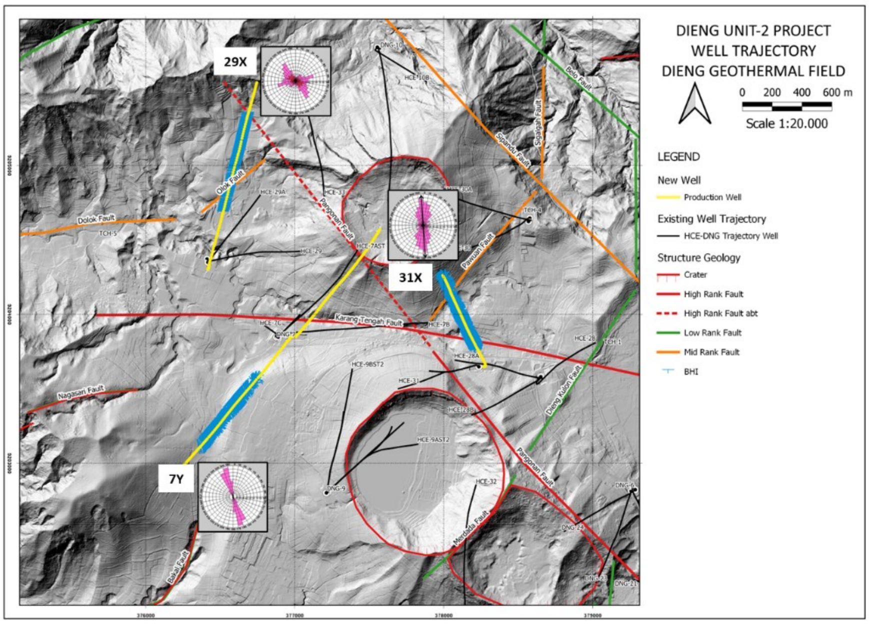

Figure 4: Borehole Image Distribution.

The discovery of N-S oriented fractures in wells 7Y and 31X are particularly intriguing. These fractures may represent a newer set of tectonic activities or localized stress fields. Their presence suggests the possibility of additional permeability pathways, which could influence fluid flow and reservoir dynamics in unexpected ways. This finding warrants further investigation to understand their origin, extent, and impact on the geothermal system.

3.1 Feed Zone-Fracture Orientation

The correlation between feed zones and fracture orientation is a critical aspect of permeability analysis, as it directly impacts the understanding of fluid flow and reservoir connectivity. In the Dieng geothermal field, borehole image data from wells 31X, 7Y, and 29X reveal distinct fracture orientations that correlate with identified feed zones. This section explores the relationship between these orientations and the respective feed zones in each well.

In well 31X, borehole image data predominantly show fractures oriented in a North-South (N-S) direction and E-W orientation (minor). These N-S fractures are closely related to the primary feed zones identified in the well. The alignment of feed zones with N-S fractures suggests that these fractures serve as significant pathways for geothermal fluids. The consistent orientation indicates a dominant stress regime influencing fracture development, facilitating effective fluid flow from the reservoir into the well.

Well 7Y exhibits a more complex fracture orientation pattern, with borehole images revealing both North-South (N-S) and Northwest-Southeast (NW-SE) fractures. These orientations are associated with the distribution of feed zones in the well. The presence of multiple fracture orientations suggests a more intricate stress regime and structural setting, which provides diverse pathways for fluid migration. The correlation between these fracture orientations and feed zones indicates that both N-S and NW-SE fractures contribute significantly to fluid flow into the well.

Lastly, well 29X presents the most varied fracture orientation among the three wells, with fractures-oriented NW-SE, East-West (E-W), and Northeast-Southwest (NE-SW). Borehole image data indicate that these varied orientations correlate with the distribution of feed zones in the well. The diversity in fracture orientations suggests a highly heterogeneous stress environment, which allows for multiple fluid pathways. Each orientation provides a different conduit for fluid flow, enhancing the overall connectivity and fluid recharge within the well.

3.2 New Fault Potential

Recent analysis of the Dieng geothermal field, combining Lidar data, surface lineament mapping, and borehole image interpretations, has suggested the presence of a previously unidentified North-South oriented fault. This section outlines the evidence supporting this new fault hypothesis and its potential implications for the geothermal system. Lidar surveys and surface mapping have revealed a prominent North-South regional lineament in the Dieng area. This lineament extends across the geothermal field and intersects with 29X and 7Y well, indicating significant subsurface structural features. The lineament's orientation and continuity suggest it is a major structural element, potentially representing a fault zone.

Borehole image data from wells 29X and 7Y provide critical subsurface validation for the North-South lineament identified in surface studies. In well 29X, borehole images show significant North-South oriented fractures correlating with feed zones, indicating active fluid flow along these fractures and directly intersecting the identified lineament. Similarly, well 7Y also displays North-South to North northwest-South southeast oriented fractures, reinforcing the continuity of this structural trend.

The correlation between feed zones and North-South fracture orientations further supports the hypothesis of a North-South fault. In both wells 29X and 7Y, the feed zones coincide with North-South fractures, indicating these orientations are crucial for fluid migration within the reservoir. The consistent presence of permeable, North-South oriented fractures in the feed zones suggests that this structural trend is a significant conduit for geothermal fluids.

4. WELL CONNECTIVITY

In the Dieng geothermal field, the connectivity between a new well and existing wells is assessed through the monitoring of gas chemistry during drilling operations. Key gases monitored include CO_2, residual gas, non-condensable gases (NCG), and H_2S. The data indicate that CO_2, residual gas, and NCG are particularly sensitive indicators of drilling fluid influence on the reservoir. This section explains the correlation between the chemistry of these gases and the interaction between drilling fluids and reservoir fluids in a two-phase liquid-dominated geothermal system. CO_2 is a major component of geothermal fluids, often present due to the degassing of magmatic sources and dissolution in reservoir fluids. The introduction of drilling fluids can alter and lead to the decreasing of CO_2 due to mixing process between hydrothermal fluid and drilling fluid. The drilling fluid, particularly during aerated drilling can add air gas, i.e., N_2 and Ar, to the reservoir, therefore there will be an increasing of N_2 and Ar gas, and decreasing of CO_2/N_2 ratio. The total NCG can increase or decrease depends on the drilling fluid mixing proportion.

The interaction between drilling fluids and reservoir fluids can cause shifts in the chemical equilibrium, leading to the release of residual gases. Monitoring these gases helps in understanding the extent of fluid mixing and the resulting chemical reactions. The mixing of drilling fluids with reservoir fluids can increase the partial pressures of NCG, leading to their liberation from the liquid phase. This provides a clear indication of well connectivity and the influence of drilling operations.

In the Dieng geothermal field, which is characterized by a two-phase liquid-dominated system, several chemical reactions can occur when drilling fluids mix with reservoir fluids. The primary reactions of interest involve the dilution of CO_2 and other gases. This reaction is particularly pronounced in areas with high permeability, where fluid mixing is more extensive. The decreased %weight of CO_2 detected in monitoring wells indicates significant interaction between drilling and reservoir fluids, confirming well connectivity. Meanwhile, the influx of drilling fluid into a geothermal reservoir can indeed destabilize the gas chemistry in existing wells due to pressure and temperature changes, chemical reactions, and fluid mixing.

4.1 29X Monitoring

Well 29X and 29 intersected the new fault from the previous interpretation. Drilling activity in well 29X has been observed to correlate with instability in the gas chemistry of nearby existing well 29, particularly regarding non-condensable gases (NCGs) and CO_2 concentrations. Monitoring data from existing well 29 before, during, and after the drilling of well 29X revealed significant variations in the concentrations of NCGs and CO_2. Up-down levels of NCGs were recorded in well 29, indicating a disturbance in the gas equilibrium. The decreasing of CO_2 and NCG during drilling of Well 29X is recorded, indicating there is some connection between Well 29X and 29. After drilling, the gas concentration of the Well 29 back to the normal condition.

4.2 7Y Monitoring

Drilling activities in well 7Y have provided crucial insights into the subsurface geology of the Dieng geothermal field, particularly the presence of a new fault. Monitoring well 7C has shown significant changes in gas chemistry, indicating a correlation with the drilling operations in well 7Y. This section explores the evidence supporting the existence of a new fault based on gas chemistry data from the monitoring wells. Monitoring well 7C has shown a decreasing trend in the concentrations of CO_2 and non-condensable gases (NCGs) during the drilling of well 7Y. However, the monitoring well 29 didn't show the similar pattern. This can be caused by the monitoring of the well 29 is not as frequent as 7C, therefore the gas concentration pattern can't be recognized comprehensively. The decrease in CO_2 and NCG in monitoring well 7C suggests the presence of a new fault intersecting Well 7Y and 7C. The drilling of well 7Y likely intersected a previously unidentified fault. This fault provides a pathway for gases to migrate from deeper reservoir zones to the monitoring wells.

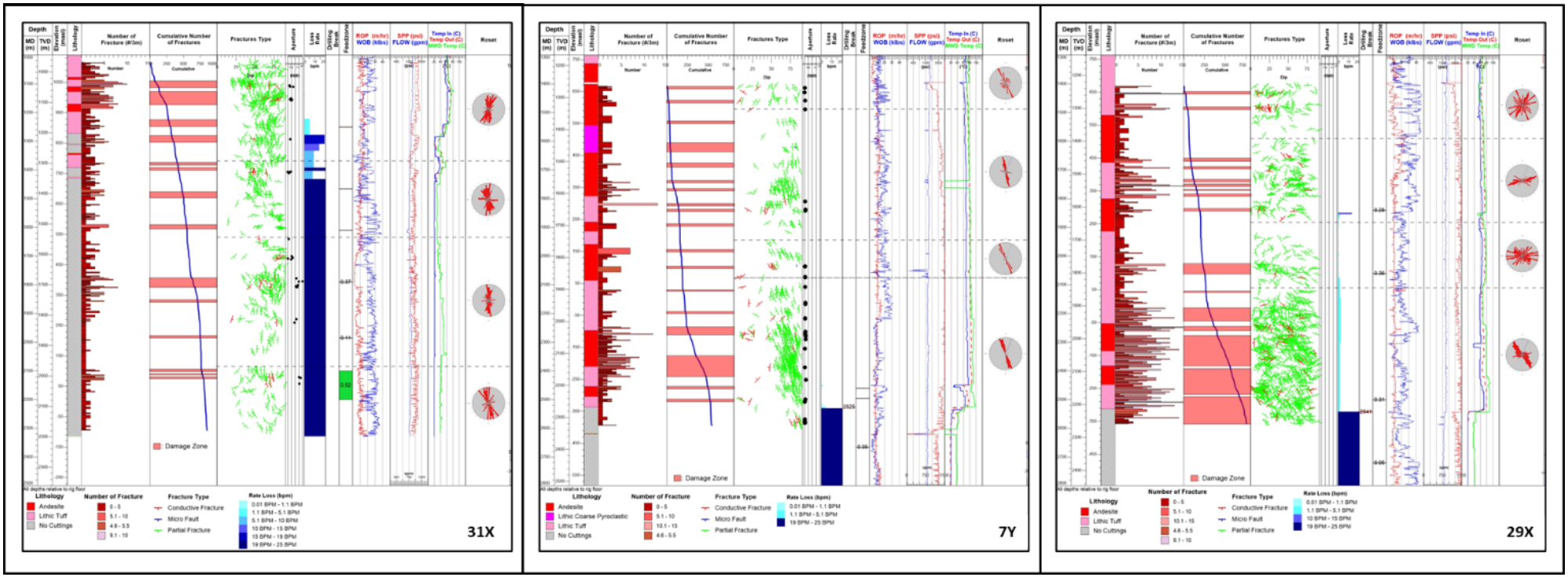

Figure 5: Feed zone fracture orientation.

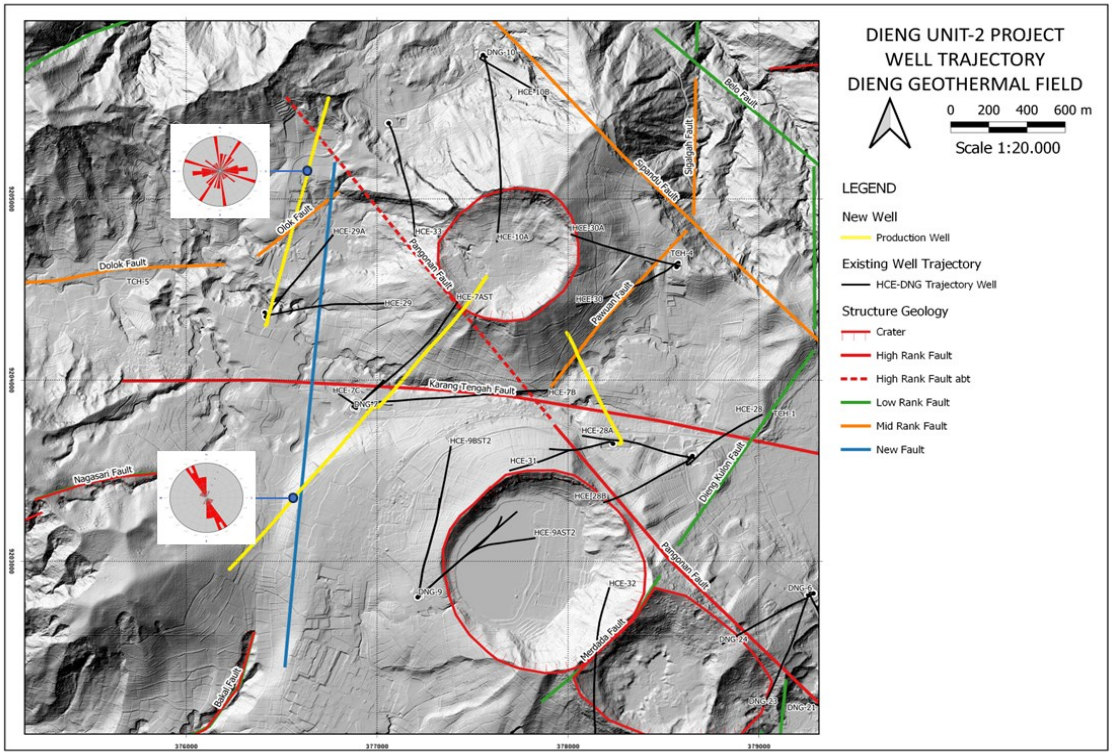

Figure 6: New fault potential.

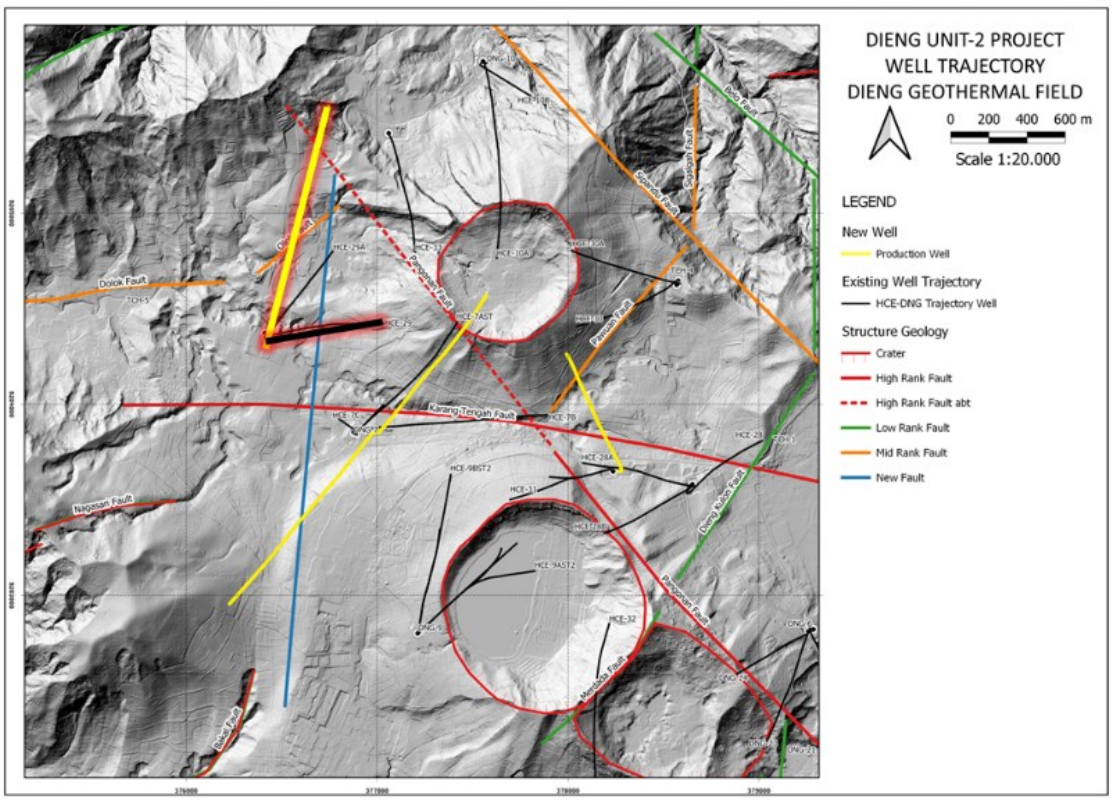

Figure 7: Trajectory of 29X well (glow yellow line) and 29 well (glow black line).

4.3 31X Monitoring

The drilling of well 31X in the Dieng geothermal field was strategically planned to intersect three significant geological features: the Karangtengah fault, the Pawuan fault, and the Pagerkandang volcanic neck damage zone. Neighbor's wells 30, 31, and 28A were used to observe changes in gas chemistry during and after the drilling process. However, during the drilling of Well 31X (February 1 to March 26), the monitoring wells are in the shut

in or bleeding condition due to overhaul of Dieng Unit 1. The complete geochemistry data were obtained on the second week of June. The results provide valuable insights into the subsurface structures and their permeability. Well 30 intersects the Pawuan fault and there is significant changes in CO2 (decreasing), N2 (increasing), Ar (increasing), CO2/N2 ratio (decreasing), and NCG (slight increasing) were observed after the drilling of well 31X. This changes suggests that the Pawuan fault may be act as a significant permeable structure in the Dieng geothermal field and show the connection between Well 31X and 30. The similar pattern is observed in the well 28A and 31 that intersect Karangtengah fault, that shows that this fault probably is a permeable structure and there is connection of well 31X with 28A and 31. This finding indicates sufficient evidence to confirm the existence or influence of the Pawuan and Karangtengah fault on fluid migration and gas transport within the reservoir.

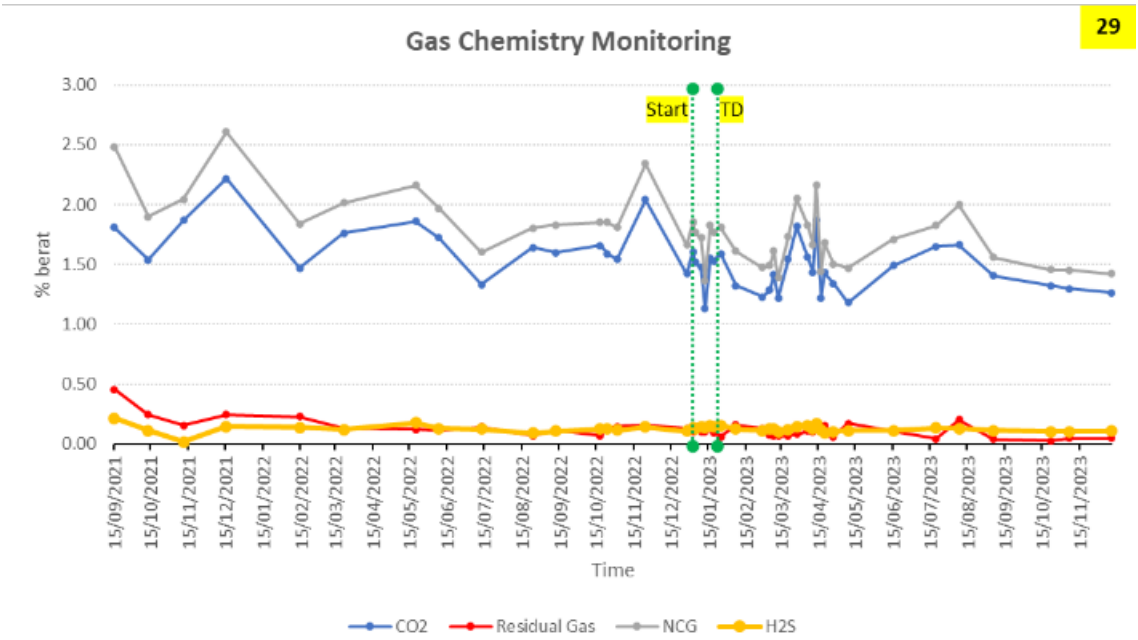

Figure 8: Gas monitoring in the existing well during 29X well drilling.

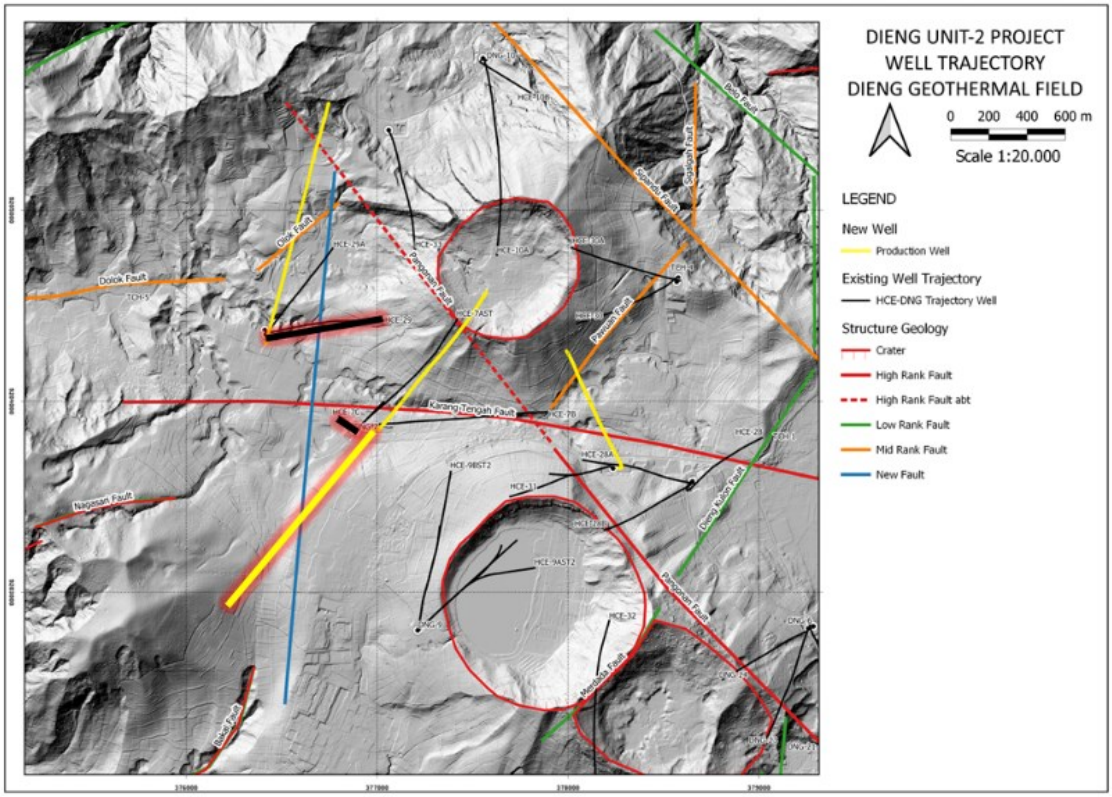

Figure 9: Trajectory of 7Y well (glow yellow line), and 29, 7C well (glow black line).

5. PROVEN STRUCTURE

The identification and characterization of faults in the Dieng geothermal field are crucial for understanding subsurface permeability and optimizing geothermal resource management. Based on surface data, borehole image data, and gas chemistry monitoring from various wells, some faults have been confirmed as significant permeable structures, while others require further investigation. This section summarizes the findings and implications of the existing data.

The integration of surface data, borehole image data, and monitoring well results has led to the confirmation of several key faults as significant permeable structures in the Dieng geothermal field. The newly identified North-South oriented fault, Karangtengah fault, and Pawuan fault have been validated through their impact on gas chemistry. Conversely, Pangonan fault and other remaining structures require further investigation to determine their roles within the geothermal system. Continued data collection and analysis will be essential for fully understanding and optimizing the Dieng geothermal reservoir.

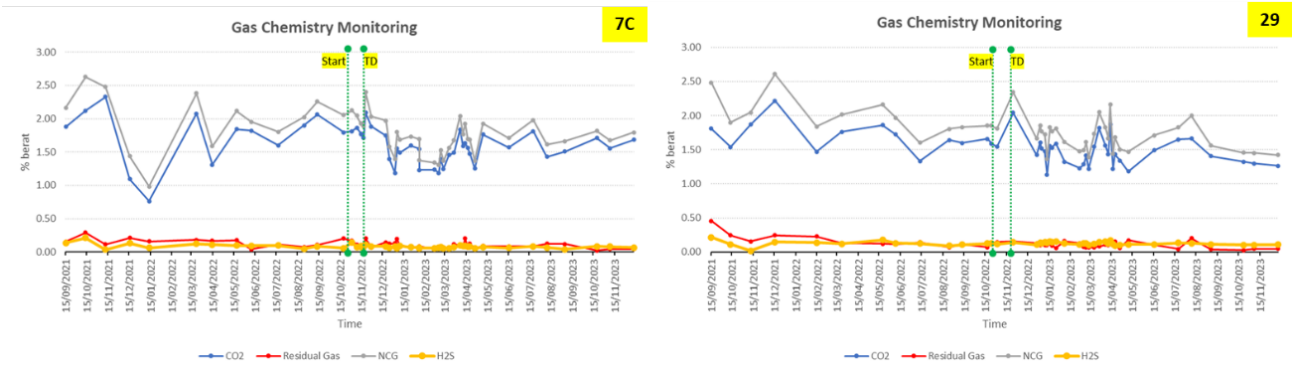

Figure 10: Gas monitoring in the existing wells during 7Y well drilling.

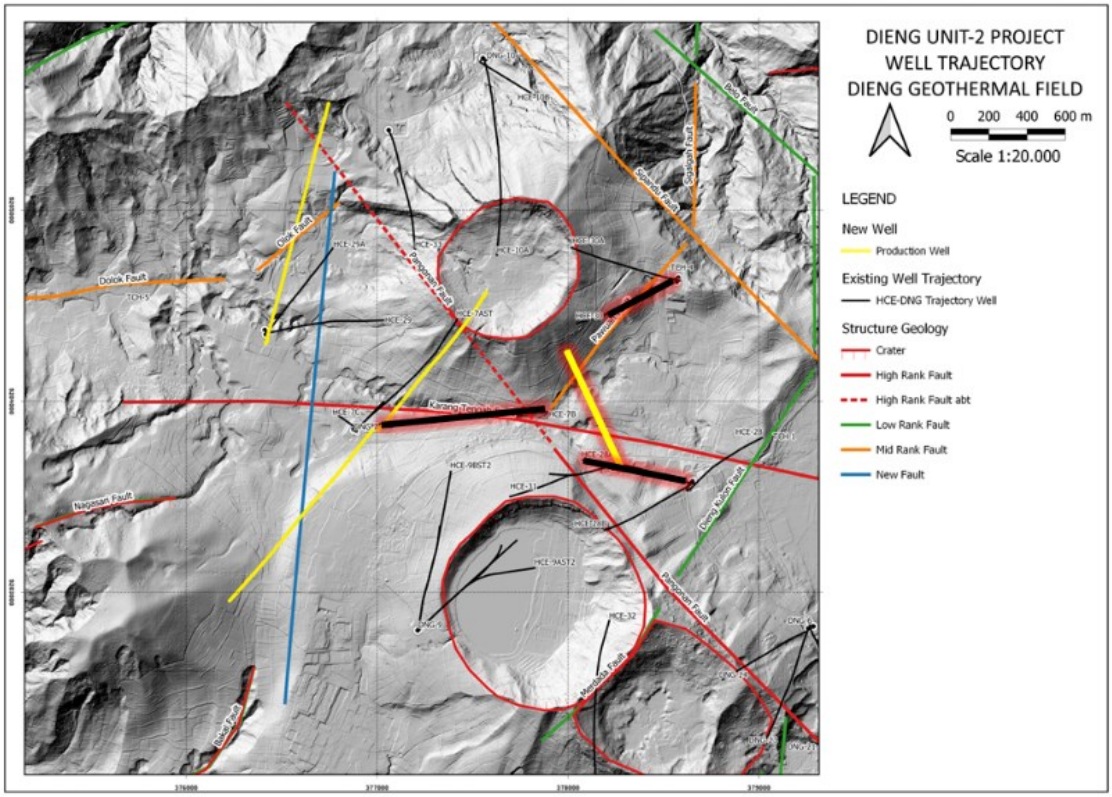

Figure 11: Trajectory of 31X well (glow yellow line), and 28A, 30, and 31 wells (glow black line).

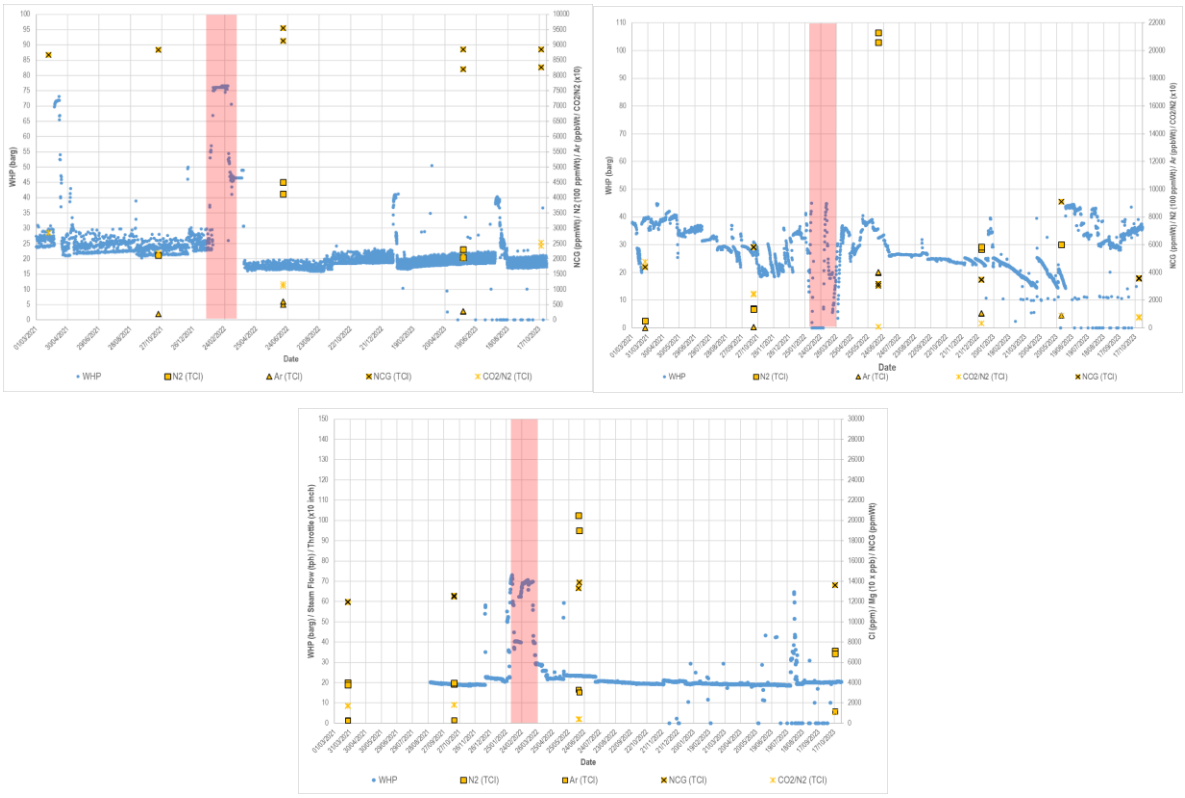

Figure 12: Gas monitoring in the well 28A (left), 30 (right), and 31 (down) during 31X well drilling.

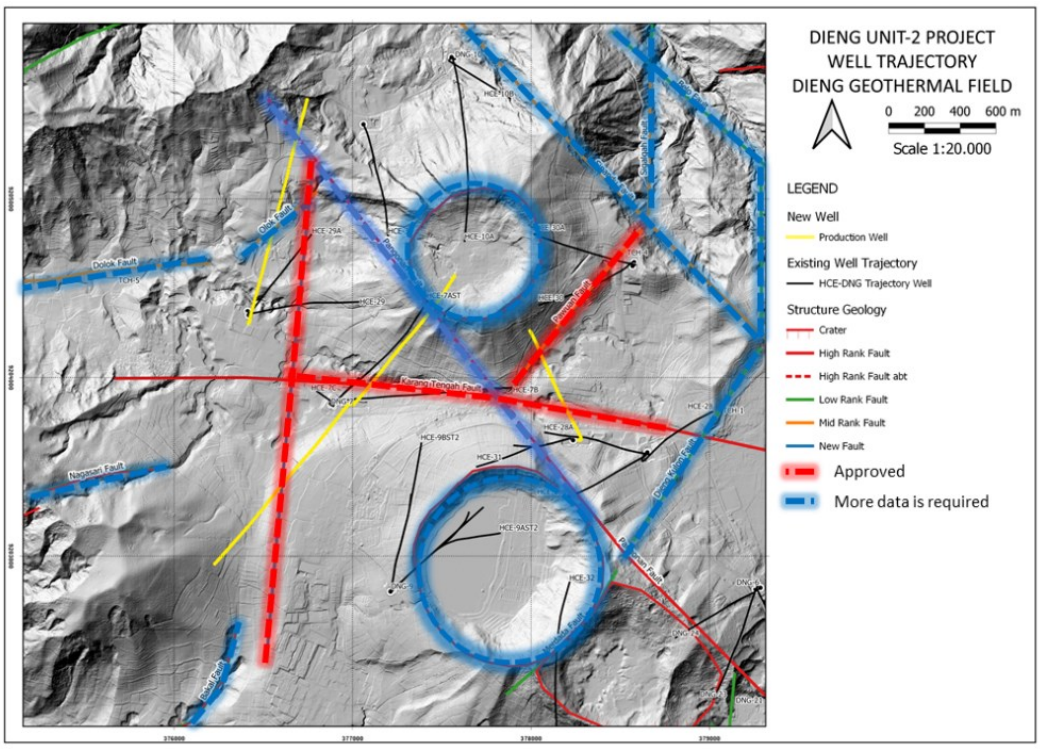

Figure 13: Confirmed fault-based integration data in the research.

6. CONCLUSION

The correlation of surface data, borehole image data, and monitoring chemistry is crucial for accurately proving fault existence and permeability in subsurface geothermal reservoirs. Borehole image data serves as hard evidence for identifying fracture existence and orientation, allowing us to confirm the presence and characteristics of subsurface faults and structures. Monitoring well data, gathered before, during, and after drilling, provides

additional support by revealing patterns of fluid flow and permeability zones, thereby evidencing the connectivity between wells. This comprehensive approach is essential for proving the existence and permeability of faults in the geothermal field.

Furthermore, integrating borehole image data with surface mapping and gas chemistry monitoring creates a robust framework for understanding subsurface dynamics. Borehole images offer direct insights into fracture patterns, which, when correlated with gas chemistry changes observed in monitoring wells, validate the presence of permeable faults. This multi-disciplinary approach not only confirms fault existence but also elucidates the fluid migration pathways within the reservoir.

For future research, it is imperative to incorporate detailed monitoring of pressure and temperature changes. These additional parameters will provide a more nuanced understanding of well connectivity and reservoir characteristics, further enhancing our ability to characterize and manage geothermal resources effectively. This comprehensive monitoring strategy will enable a more detailed and accurate assessment of subsurface structures, improving the overall efficiency and sustainability of geothermal energy production.

REFERENCES

Dieng Subsurface Team: Chemistry Update, *Internal Report* (2024).

Layman, B Erik., Irzarwadi Agus., and Samsudin Warsa.: The Dieng Geothermal Resource, Central Java, Indonesia, Geothermal Resources Council Transactions, (2002), Vol. 26.

LKFT UGM.: Detailed Structural Mapping Lapangan Panas Bumi Dieng, Internal Report, (2013)

Maratama, Iqbal et al: Constructing the Sileri Area's Permeability Distribution Through Integrated Analysis of Surface Fault, Mechanical Zone, and PTS Trend (2024)

Pamungkas, Kharits Jati, et al: The Determination of Fluid Flow Movement from Geochemical Monitoring During Drilling to Prove the Fault Geometry Existence in Patuha Geothermal Area (2024)

Satyana, Awang H.: Central Java, Indonesia-A “Terra Incognita” In Petroleum Exploration: New Considerations on The Tectonic Evolution and Petroleum, Proceedings, Thirty-First Annual Convention and Exhibition, Indonesia Petroleum Association, (2007).

Power Density Assessment of Geothermal Fields in Indonesia

Eko Hari Purwanto and Andi Susmanto

Directorate of Geothermal, Ministry of Energy and Mineral Resources, Jl. Pegangsaan Timur No. 1 Jakarta

eko.hari@esdm.go.id

Keywords: Power Density, Resource Estimation

ABSTRACT

This study evaluates geothermal resource estimation using power density approach. During exploration phase of geothermal development where subsurface data is limited, power density method is frequently utilized by geothermal industry practitioners as an initial resource estimation which is usually expressed in MW/km^2. This technique estimates geothermal resource using the extent of indicative area by statistical means and associates them to other commercially productive fields based on similarities of temperature indication and geological condition.

Power density evaluation in this assessment is carried out on 31 medium and high temperature (>200^{o}C) geothermal fields in Indonesia, in which exploration drilling and/or development drilling are already completed. This enables comparison to be taken place equally between prospects in which geothermal subsurface conditions such as temperature, chemistry and resource dimension are identified and confirmed by exploratory/ development drilling.

This study suggests that medium to high temperature fields in Indonesia exhibit the range of power density from 0,3 to 28,3 MW/km^2. The mean power density in this study is 9,8 MW/km^2. The result is comparatively within the range of findings that has been formulated by Grant and Bixley (2011) whom suggest that typical power density is typically 10-15 MW/km^2 and slightly near from results that have been proposed by Wilmarth and Stimac (2015) which suggested that mean power density distribution from 66 geothermal fields is 15.4 MW/km^2.

This paper proposed that the mean area of proven reserves during exploration and field development phase is 6,5 km^2 and tend to be less than the mean area in production phase which is approximately 16,1 km^2. This is possibly due to increasing number of step-out production wells which may expand proven geothermal delineation area. Meanwhile the power density analysis results for geothermal fields located in different regions in Indonesia indicate that the geothermal fields in Java and Sumatra show a power density of 10.7 to 12.4 MW/km^2. This value is far greater than the power density in the fields located in Sulawesi and Nusa Tenggara, which is 6.7 to 7,2 MW/km^2.

1. INTRODUCTION

1.1 Resource Estimation Importance

Estimation of geothermal resources and reserves is an important stage of activity in geothermal exploration and development. This task is carried out with aims to estimate feasible and commercially-exploitable geothermal prospects and as a technical basis to plan geothermal power plant capacity to be built. Apart from quantifying technical feasibility of geothermal resources, preliminary resource assessment also has a very crucial role in affecting project economics i.e., influencing decision making on project continuance and attracting project funding for further phase of development. The process of estimating geothermal resources and reserves is an iterative process. Generally, updating of geothermal resources and reserves is carried out at almost during important milestones in project implementation which include preliminary survey phase, exploration drilling, feasibility studies and project expansion.

In Indonesia, power density method is one of the resource estimation methods which is used in estimating energy potential, especially in the early stages in preliminary exploration where sufficient geoscientific subsurface data are limited. In Indonesia, several methods of resource and reserve estimations have been standardized in the Indonesian National Standard as follows:

1. Indonesian National Standard 6169:2018 concerning Geothermal Energy Potential Estimation Methods, where this standard regulates the determination of formulas and procedures for each method of estimating geothermal energy potential in Indonesia.
2. Indonesian National Standard 6482:2018 concerning Parameters in Estimating the Potential of Geothermal Energy, where this standard regulates the determination of parameters and values in the methods of estimating the potential of geothermal energy in Indonesia.

3. Indonesian National Standard SNI 6009:2017 concerning Classification of Indonesia's Geothermal Energy Resources and Reserves. This standard explains the purpose of classifying geothermal resources and reserves based on geological, geophysical and geochemical investigations, drilling and reservoir engineering data as shown in Table 1. It is explained from the table that geoscientific data reliability is increasing as geothermal resources changes from speculative resources to proven reserves, where more parameters from well bore are measured and use in estimation. By using this standard, we hope that bankability of geoscientific data can be obtained.

As we observed from the table below, power density method is commonly used to estimate speculative resources where sufficient and detailed geoscientific data is unavailable.

Table 1: Resource classification according to Indonesia National Standard Number 6009 of 2017 modified from BSN (2017).

	RESOURCES CLASSIFICATION				
	SPECULATIVE	HYPOTHETIC	RESERVES		
			POSSIBLE	PROBABLE	PROVEN
Methodology	Geology & geochemistry	Geology, Geochemstry and geophysics (3G)	3G and / or temperature gradient	3G and / or temperature gradient and ≥ 1 exploration well	3G and / or temperature gradient and ≥ 3 exploration well
Map scale	1:100,000	1:50,000	1:25,000 - 1:50,000	1:25,000	1:10,000 - 1:25,000
Temperature estimation	Fluid geothermometer	Fluid geothermometer	Fluid geothermometer	Direct wellbore temperature measurement	Direct wellbore temperature measurement
Fluid chemistry	Surface thermal manifestation	Surface thermal manifestation	Surface thermal manifestation	Direct wellbore measurement and well testing	Direct wellbore measurement and well testing
Resource estimation	Power density	Volumetric stored heat	Volumetric stored heat	Volumetric stored heat	Reservoir simulation

1.2 Power Density Method Overview

Power density method is used to estimate speculative resource potential by means of statistics and to equate the energy potential of a new geothermal field in which the potential is unknown to other developed geothermal fields in which geothermal potential is known, showing sustainable production and has similar geoscientific signatures. Atkinson (2012) explained that power density analysis (MW per km^2) is applied by identifying a developed field with sufficient production history, which has characteristics similar to the field being assessed, and then applied to the field which is being assessed by considering suitable adjustments such as reservoir temperature or plant specific steam consumption.

Grant and Bixley (2011) explains that power density is a method which is frequently used in the early stages of exploration and development to estimate resource capacity based on areal consideration. Proven geothermal area is justified by each successful well within a 1 km circle or square around the well. This area is then multiplied by a power density - typically 10-15 MW/km^2.

Wilmarth and Stimac (2015) suggest that the advantage of estimating geothermal prospects using power density is that it returns a reasonable value immediately, whereas stored heat estimation may also provide certain errors, and numerical simulation may involve longer simulation time and efforts to construct the model but may not be more accurate than power density unless well calibrated by using well temperature and pressure profiles and/or any relevant subsurface geoscientific data.

1.3 Purpose of This Study

This paper aims to provide an overview of power density evaluation of geothermal resources in Indonesia which obtained from 31 medium to high temperature geothermal fields in Indonesia which exploration and/or development drilling have already conducted. This is to provide an even comparison where the fields which will be used as a reference already have temperature, fluid chemistry, geothermal system dimensions confirmed by exploration drilling. We hope that power density result of this study can be used as an initial parameter in estimating geothermal resource for other exploration fields particularly in Indonesia.

2. METHODOLOGY AND CRITERIA IN THIS STUDY

2.1 Power Estimation

In estimating power output for power density, Atkinson (2012) emphasizes the use of sustainable MWe which have been producing for at least 30 years whereas Wilmarth and Stimac (2015) point out net power output especially from fields with long generation histories. This is considered more practical and easily paired with current wellfield configuration. However, power density estimation for small fields is prone to error due to a small uncertainty in output can be a large portion of the output of a small field.

For this study, in order to accommodate more in-depth understanding of geothermal fields that have been explored and currently under development, we use power output from existing power plants, newly commercial operating fields that have been in production for > 2 year (Muara Laboh, Sorik Marapi, Rantau Dedap and Sokoria) and also estimation of proven reserves from brown fields and green fields which are currently being developed. For estimating power output in exploration areas, we use proven reserves data which has been calculated using volumetric and/or reservoir simulation methods and have a P90 probability of success. Thus, we notice that proven reserve is equipped with well data and parameters which accord with Indonesian National Standard because it uses subsurface data which measured directly from the wellbore.

2.2 Area Estimation

Several studies recommend that in order to delineate geothermal prospect area radius maximum from 500 m up to 1000 m buffer/circle around productive wells as proposed by Grant and Bixley (2011) and Wilmarth and Stimac (2015). The area assumption used in this paper is obtained from proven resource calculations that conform with the Indonesian National Standard. With the aims in increasing data reliability and assurance in area measurement, we use area magnitude with the highest probability of success (P90). It is essential that the P90 boundary must be supported by drilling result where the commercially-productive zone is intersected vertically and display reservoir conditions. This assumption is consistent with that made by Atkinson (2012), who suggests that for proved reserves, based on credible analysis, there is a 90% likelihood that the actual value achieved will be greater than or equal to value estimated. However, each company which operates in different fields may use different set of parameters to determine P90 area.

2.3 Reservoir Temperature Estimation

Reservoir temperature estimation use in this study is taken from geoscientific report which already been supported by drilling result and is measured directly from well. However, uncertainty regarding temperature data may be occurred i.e.:

1. Temperature data which collected form geothermal fields are not in similar state (whether it is collected during static or dynamic reservoir condition). Ideally, it should also consider the temperature recovery of the well in the heating-up process.
2. While the other geothermal fields only offer maximum temperature information, some geothermal fields display temperature readings within ranges. This nonconformity of temperature assumptions may have an effect on the power output that was estimated in the earlier stage.

3. RESULTS AND DISCUSSIONS

3.1 Power Density

The power density distribution resulting from 31 prospect populations in 29 geothermal working areas ranges from 0.3 (Tulehu) to 28.3 MW/km^2 (Blawan Ijen), indicating mean value of 9.7 MW/km^2 and standard deviation of 6.6 MW/km^2. The study results display that ~50% of geothermal fields in Indonesia have power density ranges from 6-15 MW (**Figure 1**). These results are in good correlation with several studies which suggest by Grant and Bixley (2011) that typical power density worldwide is typically 10-15 MW/km^2 and slightly near from results that has been proposed by Wilmarth and Stimac (2015) which suggested that mean power density distribution from 66 geothermal fields is 15.4 MW/km^2.

3.2 Geothermal System Type

The vapor-dominated geothermal system fields with reservoir temperature ranges from 239-270 ^{o}C have mean value of 9.6 MW/km^2, whereas liquid dominated fields with reservoir temperature ranges from 235-340 ^{o}C have mean value of 10.7 MW/km^2. This possibly indicates that fields with liquid-dominated characteristics are commercially more optimize in terms of potential energy utilization. This condition is possibly due to brine excess utilization using a bottoming scheme which allows additional power output (i.e., Sorik Marapi, Sokoria, Sarulla and Blawan Ijen) and utilization of low-pressure steam coupled with high-pressure turbines in double flash power plants (i.e., Muaralaboh and Rantau Dedap).

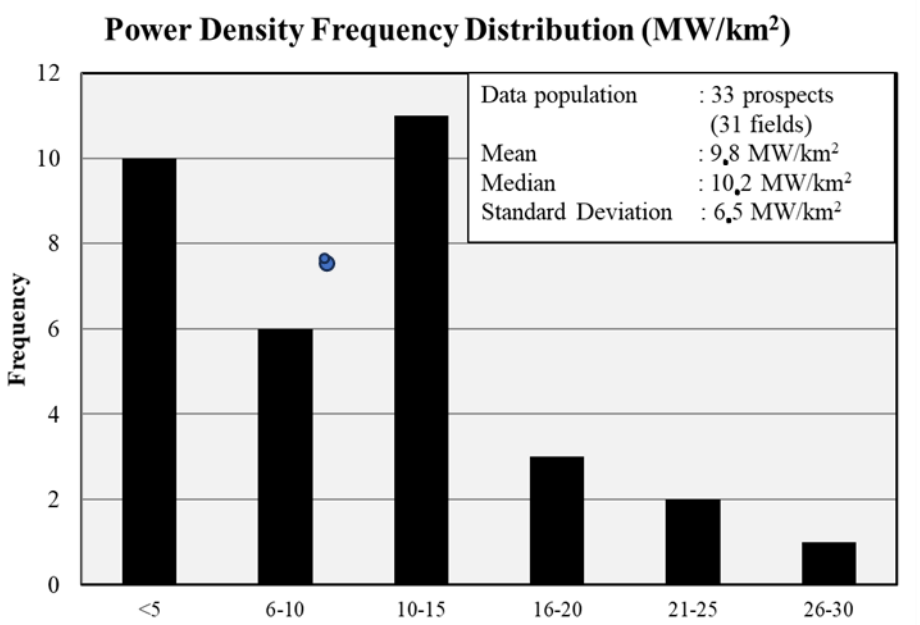

Figure 1: Frequency Distribution of Power Density in Geothermal Fields in Indonesia.

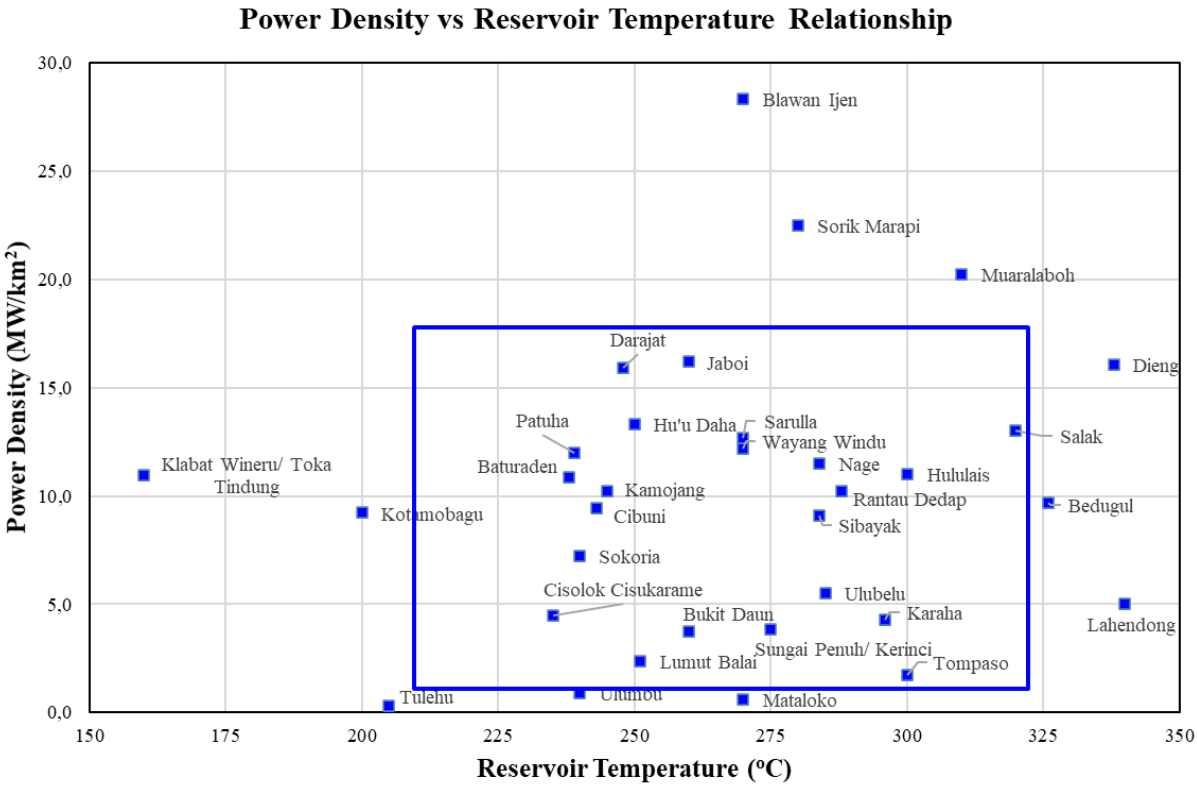

Figure 2: Power Density vs Reservoir Temperatures Plot of Geothermal Fields in Indonesia.

3.3 Relationship with Reservoir Temperature

At least 93% of geothermal fields that have been evaluated in this study are high temperature geothermal fields which have an average power density of ~10 MW/km^2. Power density versus reservoir temperature plot in Figure 2 exhibits scattered data in center and upper right quadrant of the plot. This may indicate certain trend of increasing power density along with the low-gradual rising temperature.

3.4 Indonesia Regional Comparison

Comparison of geothermal power density regionally indicates that geothermal systems on the islands of Java and Sumatra with reservoir temperatures > 235 ºC are areas that have a considerably large average of power density ranges from 10.7 (Sumatera) to 12.4 MW/km^2 (Java) as seen in Table 2. This is possibly due to most field in Java and Sumatera are located in volcano-hosted geothermal system.

Table 2: Regional Comparison of Power Density

Regional	Average Proven Reserve (MW)	Average Proven Area (km^2)	Average Power Density (ºC)	Average Temperature (ºC)
Jawa	146.2	12.3	12.4	267.5
Sumatera	117.9	16.3	10.7	278.5
Bali and Nusa Tenggara	28.5	4.9	7.2	268.3
Sulawesi	71.0	14.0	6.7	250.0
Maluku	2.0	7.0	0.3	205.0

4. CONCLUSIONS AND RECOMMENDATIONS

4.1 Conclusion

Generally, mean power density of geothermal fields in Indonesia are in good agreement and within magnitude with previous studies of ~10 MW/km^2. However, the mean result is slightly lower than previous studies, possibly due to use of P90 area delineation which allows for more accurate power output estimation since it uses the pessimistic case with the higher probability of success. Regional comparison indicates that geothermal systems on the islands of Java and Sumatra, which comprises reservoir temperatures of more than 235 ºC, are areas that have a considerably large average of power density ranges of 10.7-12.4 MW/km^2, compared to other area such as Sulawesi and Nusa Tenggara.

We hope that the results of this study can be used in estimating geothermal resources in Indonesia particularly at pre-detailed exploration stage. This approach is expected to eliminate overestimation of resources assessment.

4.2 Further Works

Sufficient access to comprehensive and thorough geothermal subsurface and engineering production data will allow several aspects to be included further relating to this analysis. Authors would like to suggest several further works as follows:

1. Introducing geoscientific parameters such as geological structure, geothermal system dating and specific geothermal plays to be incorporated in this study. This will allow us to understand the geoscientific correlation with power density.
2. Detailed reservoir temperature both static and dynamic data will provide more provide consistency in the estimation of power output so that it is expected to have an influence on the correlation between power density and reservoir temperature.
3. Proposing new and updated National Guidelines for resource estimation assessment in order to ensure that the techniques employed are consistent and applicable to geothermal areas particularly for low and medium temperatures.

REFERENCES

Atkinson, P.: Proved Geothermal Reserves - Framework and Methodology, Proceedings of the New Zealand Geothermal Workshop 2012, Auckland, New Zealand, 6 pp.

BSN, 2017: Indonesia National Standard number 6009 of 2017 concerning classification of resources and reserves of Indonesia geothermal energy. BSN, Jakarta, Indonesia.

Grant, M.A., and Bixley, P.F., 2011: Geothermal reservoir engineering (2nd ed.). Elsevier, Amsterdam, 359 pp.

Wilmarth, M., and Stimac, J., 2015: Power density in geothermal fields. Proceedings of the World Geothermal Congress 2015, Melbourne, Australia, 7 pp.

Application of NDVI and VARI in Vegetation Monitoring Using GIS and Remote Sensing on Patuha Geothermal Area

Muhammad Gantang Nugraha, Laurentia Mutiara Sani Widyawati,
Agung Maulana, and R. Yulianto K.

PT Geo Dipa Energi

gantang@geodipa.co.id, laurentia@geodipa.co.id, agung@geodipa.co.id, Julianto@geodipa.co.id

Keywords: Remote sensing, GIS, NDVI, VARI, forest, conservation, vegetation, monitoring, geothermal

ABSTRACT

Geothermal projects and power plants are mostly surrounded by forest or conservation area that needs programs to ensure the sustainability of the forest which indirectly affect the sustainability of the geothermal operation. Patuha Geothermal Area managed by PT Geo Dipa Energi (Persero) has 34.900 ha operational area (WKP/Wilayah Kuasa Pengusahaan Panasbumi) which 57% of it is overlaid with conservation forest, protected forest, and production forest. As the company has several programs in forest conservation, continuous monitoring of these forested areas is essential to evaluate the program progress and achievement.

Regarding the forest monitoring, this research focuses on two monitoring tools, Normalized Difference Vegetation Index (NDVI) and Visible Atmospherically Resistant Index (VARI) to assess vegetation/plant health around the Patuha Geothermal Area. Considering the large area or forest and limited monitoring resource, drone/UAV imagery (remote sensing) and digital mapping software (ArcGIS) is used to see either the progress of forest conservation program or if there is any affected plants caused by geothermal activity in different locations. Meanwhile NDVI is a common method which considered the reflectance of the near-infrared band, VARI is more suitable for areas with dust or haze in the air. This study creates the maps based on both NDVI and VARI to get a complete picture of plant health across the geothermal region. Combining this information with mapping software can identify the areas where the healthier plant is.

The results show that compared to VARI, NDVI visualize more detailed plant health result. However, VARI's data patterns strongly resemble those of NDVI. Thus, identifying the plant health by VARI is applicable considering the time efficiency and cost-effective, especially for the early or interim monitoring. While VARI offers a promising alternative, it is important to define certain standard of Health Plant Thresholds of VARI's result because plant health varies across species. In the other hand, NDVI still needed as an initial reference point to support the validation of VARI's results. In Patuha Geothermal Area, NDVI methods used as the initial or baseline data, while for VARI methods used as periodic monitoring tools to collect better data series. With these methods, the forest monitoring of 41 that usually done in xx days, can be done in half a day. This approach using multiple tools will provide fast and valuable information for monitoring the environment and making informed decisions about developing geothermal power while also protecting plants in the Patuha Geothermal Area.

1. INTRODUCTION

PT Geo Dipa Energi (Persero) Unit Patuha is one the Geothermal Power Plant located in West Java, Indonesia. The company is now running 55 MW electricity connected to Java-Madura-Bali electricity grid through Perusahaan Listrik Negara as national electricity company. Geothermal projects and power plants are mostly surrounded by forest or conservation area.. Patuha Geothermal Operation Area (Wilayah Kuasa Pengusahaan Panasbumi) consist of 34.900 ha which 57% of it involves social forestry, conservation forest, protected forest, and production forest.

Vegetation plays a crucial role in geothermal ecosystems, influencing heat transfer, soil stability, and gas emissions. Monitoring vegetation health in these areas is essential to understand the environmental impact of geothermal development and for implementing sustainable management practices. Vegetation in terms of forestry also important for geothermal production sustainability because they conserve groundwater which may contribute the geothermal reservoir recharge. As seen in Figure 1, Patuha Geothermal recharge area is marked by the blue pattern that most of it overlayed with the protected forest zone. Thus, protecting forest is not only benefits the biodiversity conservation, but also maintains the sustainable geothermal operation.

PT Geo Dipa Energi (Persero) Unit Patuha has several programs related to forest conservation, such as revegetation and collaborative forest patrols in the social forestry area. They needs to be monitored periodically to assess the program achievement. Usually the vegetation (plants) health is assessed directly on the dedicated

sampling plot. Therefore, plot-based methods become impracticable in some situations where plants in area are unevenly distributed, or when it is too hard to draw borders in dense vegetation (Buckland, 1993 and White, 2008 in Amagnide, 2021). That traditional field-based methods can be time-consuming and expensive, particularly in large or difficult-to-access areas which risks the results accuracy.

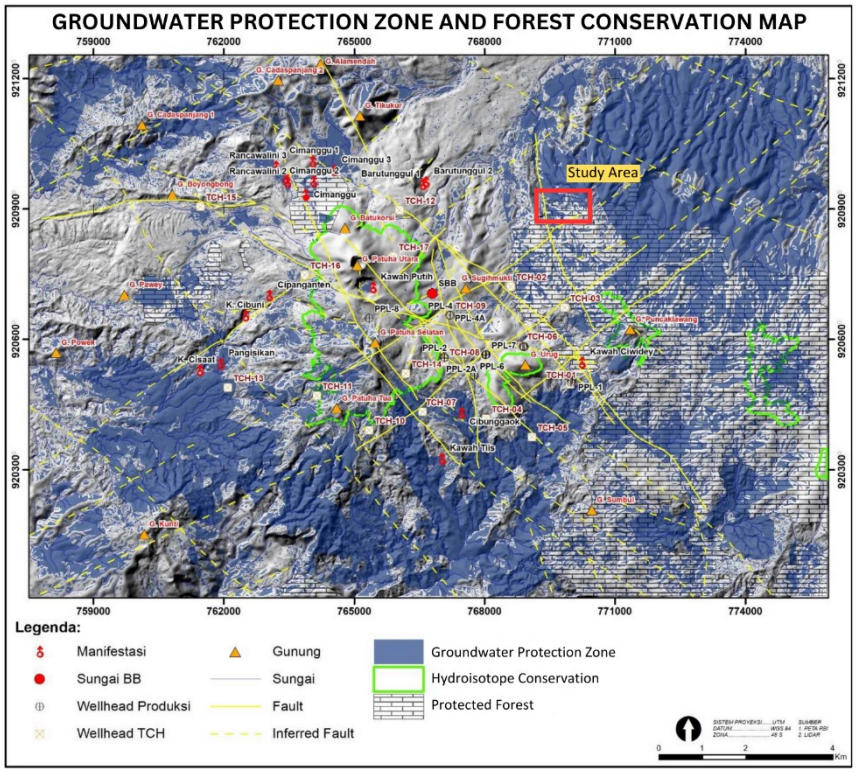

Figure 1: Patuha forestry and groundwater recharge area. (Report Hydrogeology and Recharge Area Patuha, 2023)

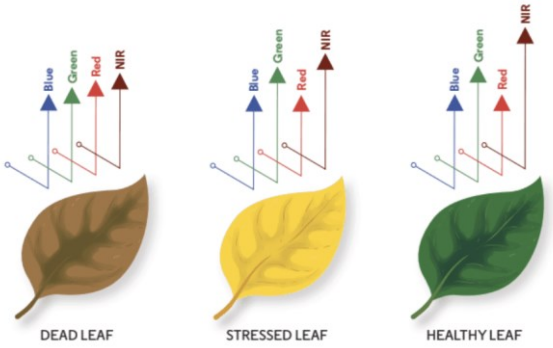

Figure 2: Spectrum/Band to monitoring vegetation health. (Picture from Farmingdynamic.com.)

Remote sensing techniques offer a cost-effective and efficient alternative for monitoring vegetation over large spatial scales. By measuring the amount of light reflected in different parts of the spectrum/bands, scientists developed Normalized Difference Vegetation Index (NDVI) to assess plant health. NDVI is a commonly used vegetation index that takes the difference between the reflectance in the near infrared (NIR) and red wavelengths, and then divides it by their sum. Higher NDVI values indicate healthier vegetation. as seen in the 2 below

This paper aims to compare the effectiveness of NDVI and VARI methods to monitor vegetation health. Both techniques leverage remote sensing data to assess the condition of plant life. By comparing NDVI and VARI, the paper aims to equip readers with a better understanding of these valuable tools for monitoring vegetation health and selecting the most appropriate technique for their specific needs.

2. METHODS

2.1 Study Area

The study focused on a social forestry area near the Patuha Geothermal area, located in Sugihmukti Village, at coordinates 770013 E and 9209376 N, with an elevation ranging from 1,500 to 1,700 meters. The area is planted with various crops, including coffee, lemon, eucalyptus, and others. It is also bordered by the Gunung Tilu conservation forest. This study area is located within a groundwater protection area as seen in Figure 1.

2.2 Research Methodology

The problem and purpose for this study is to compare and recommend the best vegetation monitoring methods by remote sensing technology. Start with determining the study area, followed by data collection, consist of 2 different aerial imaginaries captured by drone equipped with and without NIR camera, and manual vegetation monitoring data in the sample plot. Partial drone data is merged by Agisoft Metashape. Then, the analysis of data is conducted with NDVI and VARI methods with the ArcGIS Pro 3 with the additional module of ArcGIS Pro Deep Learning. The result of NDVI and VARI methods will be compared to the manual sampling report as the confirmatory terms of ability and accuracy.

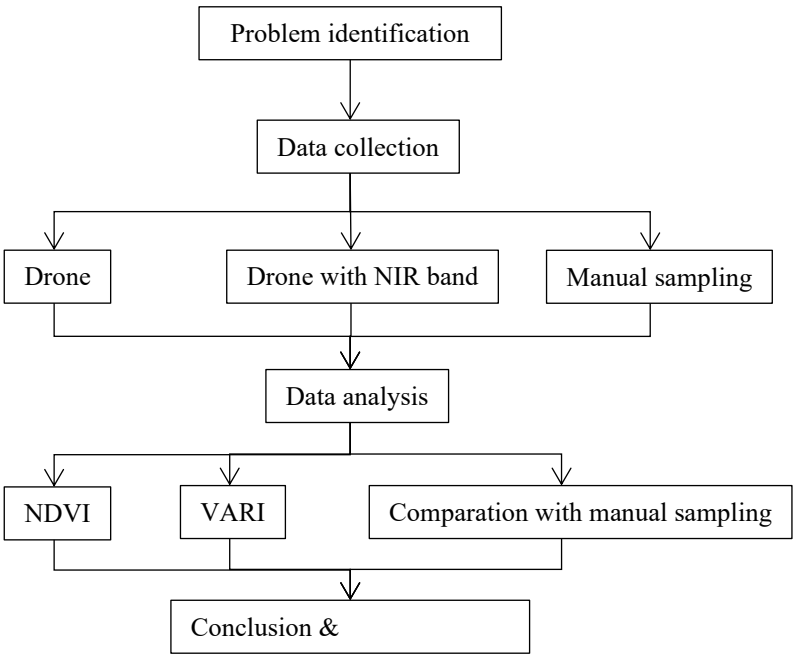

Figure 3: Research methodology.

2.3 Remote Sensing and Geographical Information System

Geographycal Information System(GIS) and remote sensing are powerful tools working together to effectively monitor vegetation health and change over time. These tools have its own benefits, as described below.

2.3.1 Remote Sensing

In the data collection ability, satellites, drones, and airplanes can capture imagery of the Earth's surface. This data comes in various forms, including multispectral (capturing different wavelengths of light) and hyperspectral (capturing a very wide range of wavelengths). Remote sensing data can be further analyzed to define the Vegetation Index, like NDVI. These index leverage the unique spectral reflectance of healthy vegetation to estimate factors like biomass, leaf area, and overall plant health as mention by Jensen, J. R. (2005). By analyzing time series of remotely sensed data, it can identify changes in vegetation cover which usually correspond to drought, deforestation, or agricultural practices. The equipment used in this study are DJI Phantom 4 with NIR camera for NDVI identification and DJI Mavic 2 Pro for VARI identification, to capture the RGB Band. Agisoft Metashape is used to process the drone imagery.

Figure 4: DJI Mavic 2 and DJI Phantom 4 Multispectral .

2.3.2 Geographical Information System (GIS)

GIS used as the spatial data management, this platform can store, manage, and analyze the vast amount of spatial data collected through remote sensing. This analysis ability includes not only the imagery itself but also its response with another information like soil types, topography, and weather data. As a spatial analysis tools, GIS allows users to overlay various data sets to identify spatial patterns and relationships. For example, comparing the areas with declining NDVI with the precipitation data can be used as a tools for assessing drought impacts in certain area GIS able to create informative maps, graphs, and reports that effectively communicate vegetation health trends and changes across a landscape.

In general, the synergy between GIS and remote sensing offers a powerful approach for comprehensive vegetation monitoring, providing valuable insights for sustainable land management practices (Jensen,2005). It can conduct the large scale monitoring which overcoming logistical limitations of field studies, do the time series analysis, allows data integration among the spatial information data, and provides the cost effective methods to monitor large areas. In this study, Arcgis Pro 3.0 software is used to process Drone imagery data consideringits ability to run rapid processing imagery including NDVI and VARI identification

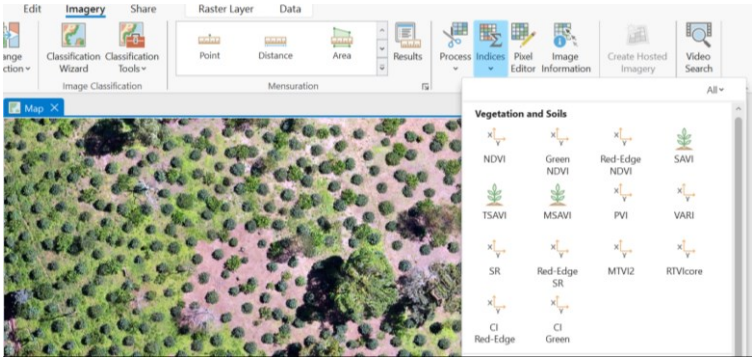

Figure 5: Interface of ArcGIS Pro Tools for Vegetation and soils Monitoring.

2.4 Normalized Difference Vegetation Index (NDVI) and Visible Atmospheric Resistant Index (VARI)

NDVI is a widely used vegetation index that exploits the contrasting reflectance properties of vegetation in the red and Near-infrared (NIR) portions of the electromagnetic spectrum. Healthy vegetation absorbs strongly in the red band and reflects highly in the NIR band. NDVI is calculated using Equation 1.

$$NDVI = \frac{(NIR-Red)}{(NIR+Red)} \quad (1)$$

NDVI values range from -1 to 1, the higher values indicate the denser and healthier vegetation cover. However, NDVI can be sensitive to atmospheric conditions and soil background (Jensen,2005)which may affects its accuracy in certain environments as seen in the Figure 5 below

Figure 5: NDVI Value for Vegetation Health Indicators.

VARI is a modification of NDVI that aims to minimize the influence of atmospheric effects on the index. VARI incorporates a soil adjustment factor to accommodate the background variations. The specific formulation of VARI can be vary, but one common version shown in Equation 2.

$$VARI = \frac{(Green - Red)}{(Green + Red - Blue)} \quad (2)$$

VARI values range depends on the type of plant, generally the higher values indicate the denser and healthier vegetation cover (Gitelson 1996)

Both NDVI and VARI are vegetation indices used in remote sensing to assess vegetation health and cover. They offer valuable insights, but have their own strengths and weaknesses as listed in Table 1 (Nunes 2015).

Table 2: Summarizing the key differences.

Feature	NDVI	VARI
Advantages	Widely used, simple	Less atmospheric impact, less soil background influence
Disadvantages	Sensitive to atmosphere, soil background	Less widely used, variable formula
When to use	Established method, readily available data	Areas with variable atmospheric conditions, areas with sparse vegetation

3. RESULTS AND DISCUSSIONS

In this study, DJI Phantom 4 and DJI Mavic 2 drones were flown at an altitude of 150-200 m above the ground surface, with the same reference point (the same Ground Control Point/GCP). After that, the image data from the drone was processed using Agisoft Metashape to combine the pieces of aerial photographs that had been taken. Figure 6 shows the final result of processed image.

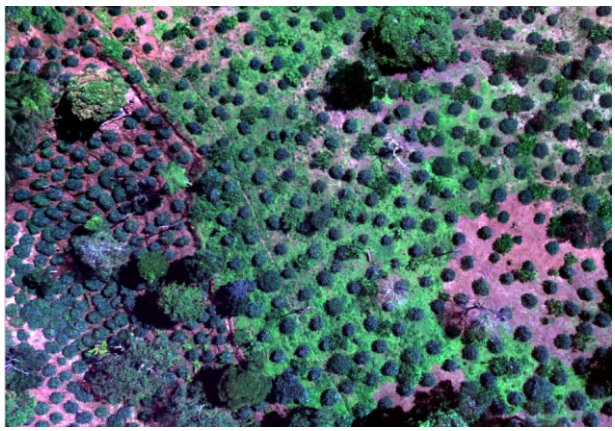

Figure 6: Final result of combined drone image.

Next, the data were processed using ArcGIS Pro 3, it categorized the plant healthy index into 4 classes: Dead Plant, Unhealthy Plant, Moderate Healthy Plant,and Very Healthy Plant, as shown in Figure 6. Refer to Figure 6, VARI only able to detect dead plant to moderate healthy plan. The very healthy plant class is undetected because VARI does not use NIR band to analyze the data.

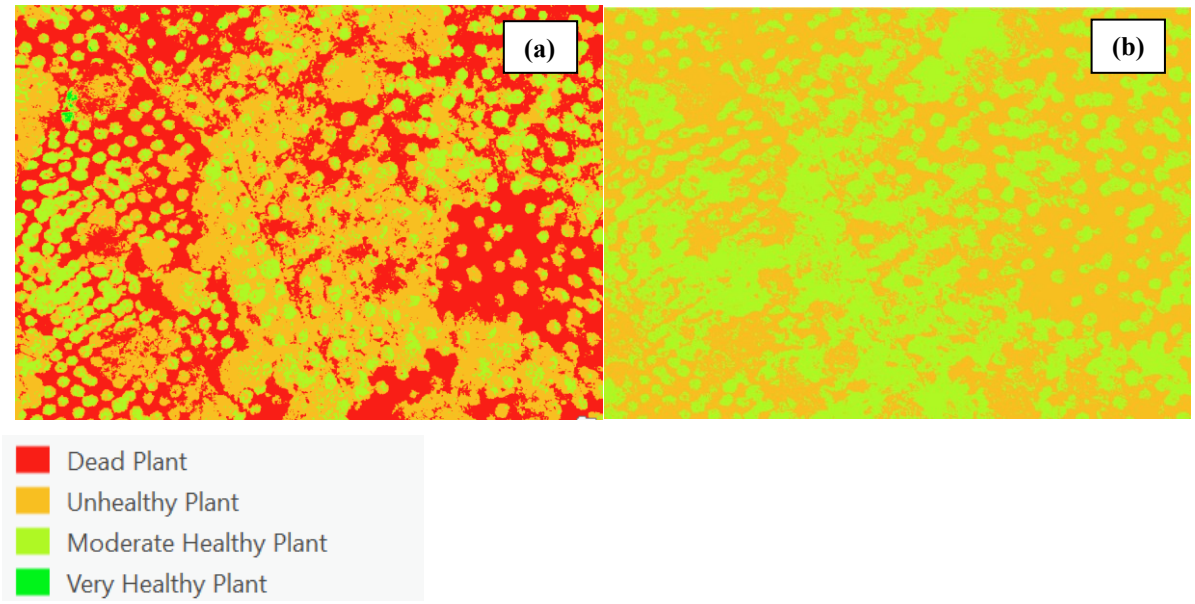

Figure 6: NDVI (a) vs VARI (b) result.

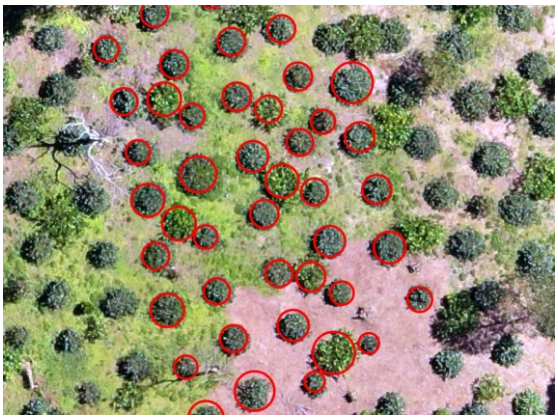

Figure 7: Sampling Point on Block A.

In order to confirm assessment result fromVARI acuracy, samples are taken as the confirmatory of the very healthy plant class, sampling area is located in Block A. The plant marked in red circle on Figure 7 is considered as very healthy plant by manual assessment . This approach allows direct comparison between VARI and NDVI, which established as a benchmark reference point. In addition to this confirmatory approach, ArcGIS Pro Deep Learning is used to enhance plant detection and counting capabilities. By incorporating this sampling technique, will effectively evaluate the precision of VARI in quantifying vegetation health and distribution compared to the well-defined NDVI method, resulted in Figure 8 Furthermore, ArcGIS Pro Deep Learning is used to automate plant identification and enumeration within the Block A, concerning more efficient and objective assessment.

Based on the comparison of NDVI and VARI in Figure 8, NDVI provides a more accurate assessment of vegetation health compared to VARI. NDVI can detect and assess vegetation health, particularly in terms of identifying stress or damage in plants. It utilizes the reflectance of red and near-infrared (NIR) light to determine the photosynthetic activity of plants. VARI, on the other hand, is a relatively new method that utilizes a combination of green and red-light reflectance. While VARI shows promising, NDVI's ability to detect subtle changes in plant health makes it a more reliable.

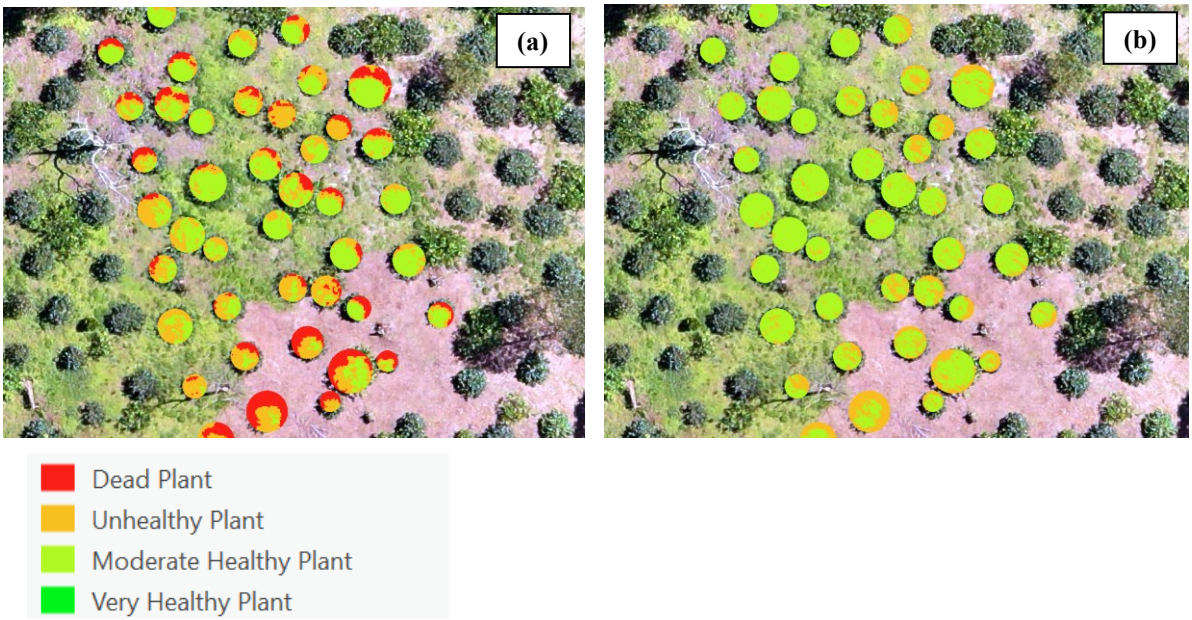

Figure 8: Comparison of NDVI (a) vs VARI (b) Results on Block A.

Figure 8(a) shows that NDVI can effectively identify even partially damaged leaves on moderately unhealthy plants.NDVI's sensitivity to changes in plant health allows it to detect stress or damage even when it is limited to a portion of the plant's leaves. This is particularly important for moderately unhealthy plants, where damage may not be uniformly distributed across the foliage. VARI, while capable of providing general health information, may not be as effective in identifying such localized damage (Figure 8(b)). However, VARI's data patterns closely resemble those of NDVI. Despite VARI's limitations in detecting subtle changes, its overall data patterns exhibit a strong correlation with NDVI results.

In addition regarding the equipment spesification, the affordability of VARI drones allows for frequent monitoring compared to NDVI.VARI drones are generally less expensive than those equipped with NIR sensors required for NDVI measurements. This cost advantage enables more frequent monitoring using VARI, providing a higher temporal resolution for tracking vegetation health changes, and provides more data to conduct the time-series analysis

While VARI offers a promising alternative, it is important to note that standardized health thresholds are yet to be established for VARI. Unlike NDVI, which has well-defined health thresholds for different plant species, VARI lacks standardized guidelines for interpreting its results. This variability necessitates the use of NDVI as an initial reference point and field verification to validate VARI's findings. Considering the variation of plant health for each species, NDVI still needed as an initial reference point and field verification to validate VARI's results. Different plant species exhibit varying ranges of reflectance values that correspond to their health status. Without defining the standard thresholds for each species, VARI's results may be difficult to interpret accurately. Therefore, NDVI methods become a crucial reference point to establish baselines and assess the relative health of plants using VARI. Moreover, field verification is essential to confirm VARI's accuracy and ensure that its results align with actual plant health conditions.

Forest management, or forest conservation monitoring program in particular, needs a balance between quickly monitoring the large areas and getting highly detailed data. For enormous plantations or forest area, flying over the remote sensing technology over the trees equipped with tools like NDVI and VARI gives a general idea of vegetation healthiness across a wide area, even if it is not super precise. In this case, what matters most is the relative size of any affected areas. NDVI might be a better choice than VARI because it uses a specific band to capture chlorophyll health which is NIR sensor, but NDVI cameras on drones are more expensive. The most valuable advantage of using drones with remote sensing for tree health monitoring comes from surveying large areas quickly, especially in remote or steep locations where ground crews would be difficult or dangerous. This study showed they could survey a significant area (over 41 hectares) in just half a day, compared with manual monitoring which can take 7 days.

Choosing Between NDVI and VARI:

- If need a well-established method with abundant data and prioritize simplicity, NDVI might be a good choice.

- If working in an area with variable atmospheric conditions or have sparse vegetation, VARI could offer a more reliable picture of vegetation health.

Ultimately, the best choice depends on your specific needs and the characteristics of study area. Consider factors like:

- Atmospheric conditions: If consistent, NDVI might suffice. For variable conditions, use VARI.
- Vegetation cover: In dense vegetation areas, NDVI might be fine. For sparse vegetation, VARI has an advantage.
- Data availability: Choose the index with readily available data for study area and timeframe.

Additional Considerations:

- Newer, more advanced vegetation indices have been developed that address some limitations of NDVI and VARI. Consider exploring them if needs are specific.
- Combining NDVI or VARI with other remote sensing data (e.g., temperature, soil moisture) can provide a more comprehensive picture of vegetation health.

4. CONCLUSION

Regarding the plant health monitoring in forest conservation program, it can be concludes that NDVI provides more accurate assessment of vegetation health compared to VARI. However, VARI's data patterns still closely resemble those of NDVI but with less detailed. Thus, identifying the plant health by VARI is applicable considering the time efficiency and cost-effective, especially for the early or interim monitoring. While VARI offers a promising alternative, it is important to define certain standard of Health Plant Thresholds of VARI's result because plant health varies across species. In addition, NDVI still needed as an initial reference point in order to conduct the field verification to validate VARI's results. In Patuha Geothermal Area, NDVI methods used as the initial or baseline data, while for VARI methods used as periodic monitoring tools to collect better data series.

REFERENCES

Buckland, S.T., Anderson, D.R., Burnham, K.P. and Laake, J.L. (1993) Distance Sampling Estimating Abundance of Biological Populations

Gitelson, C., Kaufman, Y. J., Merzlyak, M. N., & Yaari, D. (1996). Remote sensing of vegetation fractional cover using red edge reflectance and chlorophyll content. Remote Sensing of Environment, 58(2), 267-278.

Jensen, J. R. (2005). Introductory digital image processing: A remote sensing perspective (3rd ed.). Prentice Hall.

Lunetta, R. S., Young, C. W., Brewer, C. J., & Cole, R. N. (2004). Remote sensing and geographic information systems for natural resources management. Pearson Education Limited. (This book explores applications of remote sensing and GIS in natural resource management, including vegetation)

Myneni, R. B., Ramakrishna, R., Nemani, R. R., & Running, S. W. (1998). Estimation of global vegetation cover content from coarse-resolution satellite data. Journal of Geophysical Research: Atmospheres, 103(D24), 31803-31812.

Nunes, M. A., de Almeida, A. N., Coelho, C. D. B., Carreiras, J. M., & Pereira, A. I. (2015). Monitoring soil erosion in Mediterranean rangelands using high-resolution imagery. Remote Sensing of Environment, 169, 115-127.

Report Hydrogeology and Recharge Area Patuha , (2023)

This page is intentionally left blank

Part 2:
Engineering

This page is intentionally left blank

Integrated Strategy for Increasing Attractiveness and Competitiveness of Geothermal Drilling and Workover Market in Indonesia

M. Rizqi Al Asy'ari[1], Daniel W. Adityatama[1], Nadya Erichatama[1],
Vincentius Adven Brilian[1], Ferdino R Fadhillah[2], Desak Nyoman Inten Apriani[2],
Dorman Purba[2], Astri Indra Mustika[2], and Triwening Larasati[1]

[1]GEOENERGIS, Cibis Nine 11th Floor, Jakarta Selatan 12560, Indonesia
[2]PT Sarana Multi Infrastruktur (Persero), Sahid Sudirman Center 49th floor, Jakarta, Indonesia

rizqialasyari21@gmail.com, rizqialasyari@geoenergis.com

Keywords: geothermal, drilling, market, service company, tender, procurement, attractiveness, competitiveness

ABSTRACT

Indonesia's geothermal drilling demand is projected to increase as necessity for extensive drilling activities for both new projects that in exploration and development, also and maintenance of existing fields, emphasizing the potential market growth. The analysis begins with an overview of the current state of geothermal drilling contractors and rig availability in Indonesia. It notes the competition with the oil and gas industry for drilling rigs, a situation exacerbated by fluctuations in oil prices that can affect the availability and cost of rigs for geothermal drilling. The scarcity of rigs can lead to geothermal operators hiring more expensive, over-capacitated rigs, impacting project economics.

This study advocates for a comprehensive market survey as a foundational step in the procurement process, enabling developers to make informed decisions and select the most efficient procurement strategies. Such surveys help estimate costs accurately and tailor procurement activities to market realities, crucial for enhancing competitiveness and decision-making. To address market competitiveness, this research proposes several strategies, including the development of a centralized integrated vendor database (CIVD) to streamline the tender process, the adoption of well bundling strategies, and ensuring clarity and fairness in payment terms and conditions. Site readiness, clear communication, and stable international currency use for foreign transactions are also recommended to attract more competition and efficiency in the sector.

Furthermore, to increase international participation in Indonesia's geothermal drilling market, the paper suggests promoting local-international partnerships, establishing clear legal frameworks, ensuring transparent and fair operational records, and encouraging technology exchange and R&D collaborations. These strategies aim to create a more open and attractive market for international players, facilitating technology transfer and enhancing overall market dynamism. In conclusion, the research outlines a strategic approach for Indonesia to leverage its geothermal resources more effectively, proposing practical measures to improve market conditions for drilling activities. These strategies are designed to foster a more competitive and attractive environment, encouraging both local and international investment and collaboration in Indonesia's geothermal sector.

1. INTRODUCTION

Indonesia's geothermal resources present significant potential for sustainable energy development with numerous fields invarious stages of exploration and development, making the country a key player in the global renewable energy sector, especially for geothermal energy. This sub-section provides an analysis of Indonesia's geothermal drilling market, correlating the upcoming projects, key contractors, and market dynamics.

The sub-section is also examining the methods used to survey the market, the competitiveness of the Indonesian geothermal sector, and the involvement of international drilling companies. Beyond discussing the research methodologies applied to ensure a comprehensive understanding of the market, this sub-section also delves into strategies to enhance geothermal drilling market competitiveness. This section aims to provide a clear picture of the current market landscape and the opportunities and challenges in Indonesia's geothermal drilling industry.

1.1 Projected Drilling Market Demand: Ongoing and Future Geothermal projects in Indonesia

This sub-section of the report provides a detailed list of the ongoing and planned geothermal projects in Indonesia that mainly based on the RUPTL PLN 2021 – 2030 as the research background of this study. The significance of these information lies not just in their enumeration of projects but in their portrayal of the dynamic nature of Indonesia's geothermal drilling market still large.

Table 1 shows the lists of identified geothermal exploration projects scheduled from 2023 to 2030, detailing their location, managing companies, expected Commercial Operation Dates (COD), and Megawatt (MW) targets. This

exploration phase is critical, as it sets the foundation for future development and commercial exploitation of geothermal resources.

Then, Table 2 shifts the attention to geothermal development projects within the same timeframe. This table provides a more in-depth look at each project, including additional remarks that shed light on their current status and progress. Projects like Jaboi #1 in Aceh and Dieng #2 in Central Java are highlighted with their respective CODs and MW targets, along with notes on their current stages, such as feasibility study reviews or the EPCC process.

In total, there are approximately 25 geothermal fields that in exploration projects and 23 geothermal fields that identified in development projects identified based on RUPTL PLN 2021 - 2030. Some of these projects are anticipated to require extensive drilling activity, indicating a growing market for geothermal drilling in Indonesia. Furthermore, the presence of make-up well and workover projects in existing geothermal fields to sustain operational efficiency and compensate for any declines in production capacity also contributes to the increasing demand in the geothermal drilling market.

1.2 Research Objectives and Methods

The primary objective of this research is to develop and propose integrated strategies aimed at increasing the attractiveness and competitiveness of the geothermal drilling market in Indonesia. This involves analyzing the current state of the market, identifying key challenges, and suggesting practical measures to enhance market dynamics, efficiency, and international participation.

This study seeks to address the following central research question: What integrated strategies can be implemented to enhance the attractiveness and competitiveness of Indonesia's geothermal drilling market?" To support this primary question, the research will explore sub-questions such as:

- How do current market conditions and rig availability impact the competitiveness of geothermal drilling in Indonesia?
- How can market survey help on generating cost estimate and updating the latest condition of current available contractor?
- What kind of strategies for increasing market competitiveness and increasing participation of international drilling companies?

To achieve the research objectives and answer the research questions, a comprehensive and multi-faceted research methodology will be employed, such as literature review, experts consultation and interview, and market research. By employing this comprehensive research methodology, the study aims to provide actionable insights and recommendations that can drive improvements in the geothermal drilling market in Indonesia, making it more attractive and competitive on a global scale.

2. GEOTHERMAL DRILLING CONTRACTORS AT A GLANCE

The objective of this sub-section is to provide an update related to the availability of drilling rigs in Indonesia. This includes cataloguing the rig size, numbers, as well as the typical technical specification which is essential for planning and executing geothermal projects effectively.

2.1 Current Geothermal Drilling Rig Availability in Indonesia at a Glance

The objective of this sub-section is to provide an update related to the availability of drilling rigs in Indonesia. This includes cataloguing the rig size, numbers, as well as the typical technical specification which is essential for planning and executing geothermal projects effectively.

Figure 1 shows the current rig inventory for geothermal project in Indonesia. It is important to acknowledge that this visualization does not encompass the entirety of drilling rigs in the country. The listed rigs and their specifications, as summarized by Hartono (2023), represent only rig list that submitted by identified drilling rig contractors.

Based on current rig contractor that surveyed by Hartono (2023), the most common rig size is 350 horsepower (HP), accounting for 27% of the inventory with 36 rigs. This is followed by the 1500 HP rigs, comprising 25% of the inventory with 20 rigs, highlighting a substantial investment in high-capacity rigs. Notably, rigs with 1000 HP and 2000 HP each make up 12% of the inventory, with 16 rigs available in each category.

Table 1: List of Identified Geothermal Exploration Project 2023 - 2030 (EBTKE, 2023b; PLN, 2021)

No.	Geothermal exploration drilling project	Province	Geothermal Company	COD[1] Target	MW Target	Additional Remarks
1	Atadei #1	East Nusa Tenggara	PT PLN (Persero)	2024	10	-
2	Tulehu	Maluku	PT PLN (Persero)	2025	20	-
3	Songa Wayaua	North Maluku	PT PLN (Persero)	2025	10	-
4	Rajabasa	Lampung	Supreme Energy	2025	220	-
5	Bedugul #1	Bali	Bali Energy Limited	2025	10	-
6	Gn. Ungaran	Central Java	PT Giri Indah Sejahtera	2026	55	-
7	Tangkuban Perahu #1	West Java	PT PLN (Persero)	2026	20	-
8	Tangkuban Perahu #2	West Java	PT PLN (Persero)	2026	20	-
9	Telaga Ngebel	East Java	PT Bakrie Darmakarya Energi	2027	55	-
10	Baturaden #1	Central Java	PT Sejahtera Alam Energy	2028	110	Already drilled 3 (three) explorations well by PT SAE, but did not found any desired exploitable resource
11	Danau Ranau	Lampung and South Sumatra	PT PLN (Persero)	2028	20	-
12	Oka ile ange	East Nusa Tenggara	N/A	2028	10	
13	Kepahiang #1	Bengkulu	PT PLN (Persero)	2028	55	
14	Baturaden #2	Central Java	PT Sejahtera Alam Energy	2029	75	
15	Gn Sirung #1	East Nusa Tenggara	N/A	2029	5	
16	Cisolok -Cisukarame	West java	N/A	2030	20	• Already drilled 1 (one) slimhole well through government drilling program • Tender process starts from October 2023 • IPB (*Izin Panas Bumi*) granted target in 2024
17	Gn. Tampomas	West java	PT Wijaya Karja Jabar Power	2030	45	• Social issues of community rejection • Termination of PT WJP in 2019 • Request from the local government of Sumedang Regency for development • Planned for government drilling in 2025. • Tender process starts from 2027. • IPB (*Izin Panas Bumi*) granted target in 2028
18	Baturaden #3	Central Java	PT Sejahtera Alam Energy	2030	35	
19	Guci	Central Java	PT Spring Energy Sentosa	2030	55	• Returned by PT SES in 2018 • Additional data provided by the Geological Agency in year 2022 for proving a single system with WKP Baturaden
20	Bedugul #2	Bali	Bali Energy Limited	2030	10	
21	Kepahiang #2	Bengkulu	PT PLN (Persero)	2030	110	
22	Bukit Daun	Bengkulu	PT Pertamina Geothermal Energy Tbk	N/A	N/A	
23	Seulawah Agam	Aceh	PT Pertamina Geothermal Energy Tbk	N/A	N/A	

[1] The Commercial Operation Date (COD) targets referenced are derived from the presentation by the EBTKE 20223 and RUPTL PLN for the period 2021-2030. It is important to note that Author has not conducted individual interviews with geothermal developers to obtain updated COD targets. This approach ensures that the data presented is consistent and based on officially published sources, thereby maintaining the accuracy and reliability of the information. However, it also implies that any recent adjustments or updates to COD targets by individual developers may not be reflected in this analysis.

No.	Geothermal exploration drilling project	Province	Geothermal Company	COD[1] Target	MW Target	Additional Remarks
24	Jailolo	North Maluku	N/A	N/A	40	• Returned by Star Energy in 2017 • Licensing n oprogress by Geo Dipa Energi (PT SMI) • Planned for government drilling in 2024 through GEUDP program. • Tender process starts from 2027. • IPB (*Izin Panas Bumi*) granted target in 2028
25	Marana	Central Sulawesi	N/A	N/A	20	• Tender failed in year 2015. • Additional data provided by the Geological Agency in 2021, outside the exploration priority for 2023-2027
26	Suwawa	Gorontalo	N/A	N/A	20	• Offered to state-owned enterprises, but not yet expressing of interest. • Proposed additional data collection by the Geological Agency outside the exploration priority for 2023-2027
27	Gunung Endut	Banten	N/A	N/A	40	• Planned for government drilling in 2026 by Geological Agency • Tender process starts from 2028. • IPB (*Izin Panas Bumi*) granted target in 2029. • Conservation Forest Area (utilization area) • Temperature gradient survey by the Geological Agency in 2023
28	Iyang Argopuro	East Java	N/A	N/A	55	• Returned by PGE in 2014 • Conservation Forest Area
29	Bora Pulu	Central Sulawesi	N/A	N/A	40	• Tender process starts from 2023. • Additional data provided by the Geological Agency in fiscal year 2023. • Potential liquefaction zone • Proposed for tender, but no bidders yet. • Outside the exploration priority for 2023-2027
30	Sembalun	West Nusa Tenggara	N/A	N/A	10	• Results of PSP PLN • Rinjani National Park • Additional data provided by the Geological Agency in 2021, outside the exploration priority for 2023-2027
31	Gunung Pandan	East Java	N/A	N/A	40	• Results of the East Java Provincial Government's PSP
32	Telaga Ranu	North Maluku	N/A	N/A	5	• Results of Star Energy's PSP • Government drilling proposal by PT SMI • Interest shown by ORMAT. • Proposed as a replacement for WKP Bora Pulu to be tendered in year 2023. • IPB (*Izin Panas Bumi*) granted target in 2024.
33	Songgoriti	East Java	N/A	N/A	20	• Planned for government drilling in 2026 by Geological Agency • Tender process starts from 2028. • IPB (*Izin Panas Bumi*) granted target in 2029.
34	Gunung Wilis	East Java	N/A	N/A	20	• Results of MRI Energy 's PSP • Tender failed in year 2016
35	Gunung Galunggung	West Java	N/A	N/A	55	• Results of Energy Kinan International's PSP • Tender failed in year 2016 • Planned for government drilling in 2026 by Geological Agency

No.	Geothermal exploration drilling project	Province	Geothermal Company	COD[1] Target	MW Target	Additional Remarks
						• Tender process starts from 2028.
36	Gunung Ciremai	West Java	N/A	N/A	20	• Returned by Chevron in 2013 • Tender failed in year 2016 • Social issues of community rejection • Additional data provided by the Geological Agency in 2021
37	Lainea	Southeast Sulawesi	N/A	N/A	20	• Tender failed in year 2019. • Proposed additional data collection by the Geological Agency
38	Sumani	West Sumatra	N/A	N/A	20	• Planned for government drilling in 2024 by Geological Agency • Tender process starts from 2026. • IPB (*Izin Panas Bumi*) granted target in 2027.
39	Sipoholon Ria-Ria	North Sumatra	N/A	N/A	20	• WKP established based on the Geological Agency's survey results. • Additional data provided by the Geological Agency in 2022 • Planned for government drilling in 2025 by Geological Agency • Tender process starts from 2027. • IPB (*Izin Panas Bumi*) granted target in 2029.
40	Nage	East Nusa Tenggara	N/A	N/A	20	• Already drilled two (2) wells through government drilling in 2021 by Geological Agency • Tender failed in 2023. • Proposed for re-auction.
41	Wae Sano	East Nusa Tenggara	N/A	N/A	N/A	• Government drilling by PT SMI not implemented due to community rejection. • World Bank withdrawal • PT SMI requests a replacement WKP

Table 2: List of Geothermal Development Project 2023 - 2030 (EBTKE, 2023b; PLN, 2021)

No.	Geothermal development drilling project	Province	Geothermal Company	COD Target[2]	MW Target	Additional Remarks
1	Jaboi #1	Aceh	PT Sabang Geothermal Energy	2023	5	Based on (EBTKE, 2023b), currently still process of Feasibility Study review by the Ministry of Energy and Mineral Resources. The amendment process related to the Extension of the Effective Date (capacity and COD)
2	Dieng #2	Central Java	PT Geo Dipa Energi (Persero)	2023	55	Development drilling already done, waiting for the EPCC power plant process
3	Patuha #2	West Java	PT Geo Dipa Energi (Persero)	2023	55	Development drilling already done, waiting for the EPCC power plant process
4	Lumut Balai #2	South Sumatra	PT Pertamina Geothermal Energy Tbk	2023	55	Still on the EPCC process (PGE, 2023)
5	Sorik Marapi #4	North Sumatra	KS Orka Renewables	2023	50	Preparation for development drilling for unit 4
6	Blawan – Ijen #1	East Java	PT Medco Cahaya Geothermal	2024	35	Ongoing development drilling
7	Cibuni	West Java	PT KopJasa Keahlian Teknosa	2024	10	
8	Sokoria #3	East Nusa Tenggara	KS Orka Renewables	2024	22	
9	Sorik Marapi #5	North Sumatra	KS Orka Renewables	2024	50	
10	Hululais	Bengkulu	PT Pertamina Geothermal Energy Tbk	2025	55	Loan Agreement already secured from JICA (EBTKE, 2023b)
11	Ulumbu #5	East Nusa Tenggara	PT PLN (Persero)	2025	20	Still ongoing review process and additional geoscience survey for expansion project (EBTKE, 2023b)
12	Salak #7	West Java	Star Energy Geothermal	2025	55	-
13	Dieng #3	Central Java	PT Geo Dipa Energi (Persero)	2025	55	-
14	Dieng #4	Central Java	PT Geo Dipa Energi (Persero)	2025	55	-
15	Muara Laboh #2	North Sumatra	Supreme Energy	2025	80	-
16	Rantau Dedap #2	South Sumatra	Supreme Energy	2025	134	-
17	Mataloko	East Nusa Tenggara	PT PLN (Persero)	2025	20	-

[2] The Commercial Operation Date (COD) targets referenced are derived from the presentation by the EBTKE 20223 and RUPTL PLN for the period 2021-2030. It is important to note that Author has not conducted individual interviews with geothermal developers to obtain updated COD targets. This approach ensures that the data presented is consistent and based on officially published sources, thereby maintaining the accuracy and reliability of the information. However, it also implies that any recent adjustments or updates to COD targets by individual developers may not be reflected in this analysis.

No.	Geothermal development drilling project	Province	Geothermal Company	COD Target[2]	MW Target	Additional Remarks
18	Wayang Windu #3	West Java	Star Energy Geothermal	2026	60	-
19	Patuha #3	West Java	PT Geo Dipa Energi (Persero)	2026	55	-
20	Blawan-Ijen #2	East Java	PT Medco Cahaya Geothermal	2026	55	-
21	Jaboi #2	Aceh	PT Sabang Geothemal Energy	2027	2.5	Based on (EBTKE, 2023b), currently still on process of Feasibility Study review by the Ministry of Energy and Mineral Resources. The amendment process related to the Extension of the Effective Date (capacity and COD)
22	Sungai Penuh	Jambi	PT Pertamina Geothermal Energy Tbk	2028	55	-
23	Jaboi #3	Aceh	PT Sabang Geothemal Energy	2030	2.5	-

This diverse range of horsepower availability indicates a robust capability for various drilling/workover demands. The smaller rigs, like the 550 HP constituting 14 rigs, and the 750 HP with 5 rigs, demonstrate versatility in the inventory, ensuring that different drilling requirements can be met efficiently.

This detailed inventory assessment is critical for strategic planning, as it ensures that drilling/workover operations can be matched with appropriate rig capacities, optimizing both performance and cost. The presence of high-capacity rigs in significant numbers also suggests an ability to undertake more demanding drilling operations, which may be required in challenging geothermal developments.

No	Rig Size	No of Rig	%
1	150 HP	1	0.75%
2	250 HP	3	2.26%
3	300 HP	2	1.50%
4	350 HP	36	27.07%
5	400 HP	2	1.50%
6	450 HP	4	3.01%
7	500 HP	2	1.50%
8	550 HP	14	10.53%
9	630 HP	1	0.75%
10	650 HP	3	2.26%
11	700 HP	2	1.50%
12	750 HP	5	3.76%
13	800 HP	4	3.01%
14	1000 HP	16	12.03%
15	1500 HP	20	15.04%
16	1700 HP	1	0.75%
17	1750 HP	1	0.75%
18	2000 HP	16	12.03%
Total Observed Land Rig		133	

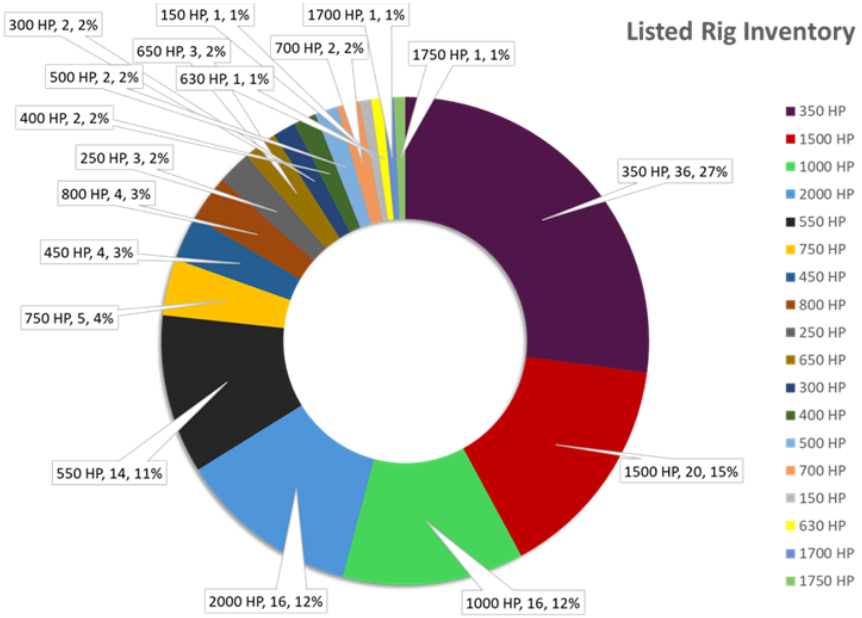

Figure 1: Summary of Current Rig Inventory in Indonesia (Modified from Hartono, 2023)

The Figure 2 shows the typical of required footprint of drilling rig in Indonesia. It presents an overview of the spatial requirements for different rig sizes, a crucial factor in planning and preparing drilling sites. It delineates the length and width dimensions needed for rigs ranging from 750 HP to 3000 HP, converting these into the total area in square meters necessary for the rig setup.

For instance, a 1000 HP rig with two joints necessitates a space measuring 62.4 meters in length and 37.0 meters in width, with typical required area of 2308.8 square meters. This contrasts with the same 1000 HP rig with three joints, which requires a substantially larger area of 3803.8 square meters due to its increased length and width.

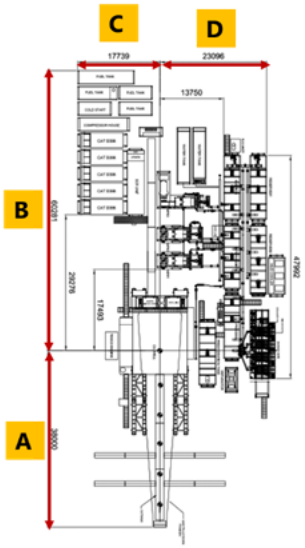

Rig Size	Length, m A + B	Width, m C + D	Area, m2 Only Rig Eq.
750 HP	52.2	35.5	1853.1
750 HP	56.3	17.3	974.0
1000 HP, 1 joint	53.2	47.1	2505.7
1000 HP, 2 joints	**62.4**	**37.0**	**2308.8**
1000 HP, 3 joints	91.0	41.8	**3803.8**
1200 HP, Ideal Rig, 2 Joints	82.9	18.9	**1566.8**
1500 HP	98.2 102.7	40.8 35.0	**4006.6** **3594.5**
1800 HP	82.0	47.7	**3911.4**
2000 HP	89.0	37.0	**3293.0**
3000 HP	62.2	57.8	**3595.2**

- All rig with **3 joints rig mast** → need more **3300 m2**
- Rig with **2 joints Rig mast** → need only **2300 m2** or **30% smaller area**

Figure 2: Summary of Typical Required Footprint for Drilling Rig in Indonesia (Modified from Hartono, 2023)

A noteworthy observation is the comparison between rigs with different mast joint counts: those with three joints require over 3300 square meters, while rigs with two-joint masts demand approximately 30% less space, around 2300 square meters. This information is pivotal for drilling operations where site constraints exist, and it assists in logistical planning, ensuring that the chosen rig will fit within the available area, aligning with the operational and environmental parameters of the project site in Indonesia

From 133 input data of technical specification of drilling rig, Hartono (2023) summarizes the technical rig specification as presented in Table 3. The data are categorized by the rigs' rated drilling depth, mast capacity, rotary table dimensions, mud pump horsepower, mud tank volumes, and Top Drive System (TDS) sizing, offering a comprehensive snapshot of the equipment's capabilities.

Table 3: Rig Specification Summary (Modified from Hartono, 2023)

Capacity (Min-Max)	Unit	650	700-850	1000-1150	1200-1340	1500	1700-1800	2000
Rated Drilling Depth (Written Capacity from Contractors)	Meter	1800	2500 3993	3000 4100	3700 5000	**3500 6095**	**5100 9144**	**3500 6700**
Adjusted Rated Drilling Depth (Based on Hartono, 2023)	Meter	-	1400 2100	**2500 3300**		**3500 6095**	**5100 9144**	**3500 6700**
Mast Capacity (Hook Load)	klbs	350 400	400 500	**440 650**	**441 672**	675 769	850 1000	975 1250
Rotary Table Opening	Inch	17.5 27.5	20.5 27.5	27.5	27.5 37.5	27.5 37.5	37.5	37.5
Rotary Table Height	Meter	**4.9 5.5**	**4.9 7.6**	**5.7 10.25**	**7.71**	6.1 9.1	8.2 9.4	8.2 9.1
Mud Pumps	HP	1000 1300	900 1300	1000 1600	1000 1300	1300 1600	1300 1600	1300 1700
Mud Tanks	Bbls	500 1000	750 1230	1050 1547	1383 2100	1000 2400	1080 1960	1476 1812
TDS Sizing	Ton HP	-	**250 Ton 600 HP**	**350 Ton 800 HP**		**350 Ton 800 - 1000 HP**	**500 Ton 1000 – 1200 HP**	**500 Ton 1000 – 1200 HP**

In the observed capacity brackets, ranging from 650 HP to 2000 HP, the contractors' written capacities are juxtaposed with adjusted depths based on Hartono's 2023 analysis. These adjustments bring to light the practical operational depths, which are notably different from the written specifications. For example, while a rig with a capacity of 700-850 HP is initially rated to reach depths of 2500 meters, Hartono's adjustments indicate a reduced effective depth of 1400 to 2100 meters, which is vital for setting realistic project expectations.

Mast capacities, essential for determining the weight a rig can handle, range from 350 K-Lbs for the lower-end rigs to a substantial 1250 K-Lbs for the highest capacity rigs. This specification is crucial for safety and efficiency considerations during drilling operations.

The rotary table opening, another critical dimension, shows a variation from 17.5 inches (which up to 37.5 inches, impacting the size of the equipment that can be used on the rig. The height of these tables also varies, with some rigs offering up to 10.25 meters, which may influence the choice of rig based on the drilling environment and the spatial constraints of the site.

Mud pumps, which are integral for circulating drilling fluid, show a range in horsepower from 900 to 1700 HP, providing insights into the fluid circulation capabilities of each rig. Similarly, mud tank capacities are delineated, from 500 barrels for the smallest rigs up to 2400 barrels for larger setups, essential for managing the volumes of fluid necessary during the drilling process.

Finally, the TDS sizing, which pertains to the mechanical device used to facilitate the drilling process, is listed, though some entries are not specified. The available data, however, indicate sizes up to 500 tons and power up to 1200 HP, reflecting the operational range of the rigs.

This summary of rig specifications underscores the diversity of drilling equipment available, each with specific features tailored to various drilling requirements. The detailed categorization assists project managers and

technical teams in identifying the appropriate rig for their unique drilling objectives, ensuring that all operational aspects are optimally aligned with the technical demands of geothermal drilling projects.

2.2 Summary of Geothermal Drilling Contractors in Indonesia

Table 4 presents an overview of the geothermal drilling contractors operating in Indonesia. It categorizes these entities based on the type of services, goods, or materials they offer, and briefly explain the potential procurement challenges faced in each type of services, goods or material. It should be noted that the potential contractor or provided in Indonesia that might be unidentified on this study.

A crucial aspect outlined in this sub-section is the potential procurement challenges. These challenges encompass issues related to logistical complexities, quality control, compliance with environmental standards, and the effectiveness of service delivery. Such challenges can significantly impact project timelines and costs, highlighting the need for strategic planning and management in contractor selection and procurement processes.

Table 4: List of Geothermal Drilling Contractors in Indonesia

No.	Type of services, goods, or materials	Potential contractor or provider in Indonesia	Potential procurement challenges
1.	Drilling rig	**STANDARD AND BIG HOLE WELL SIZE (ROTARY RIG):** 1. PT Daya Alam Tehnik Inti (DATI) 2. PT Plumpang Rayah Anugrah (PRA) 3. PT Pertamina Drilling Services Indonesia (PDSI) 4. PT ELNUSA 5. PT Bormindo Nusantara (BORMINDO) 6. PT Asia Petrocom Services (APS) 7. PT Alam Bersemi Sentosa (ABS) 8. PT Apexindo Pratama Duta 9. PT Exspan Petrogas Intranusa (EPI) 10. PT Great Wall Drilling Asia Pacific (GWDC) 11. KS Drilling 12. PT Remaja Bangun Kencana (Rabana) 13. PT Wijaya Bangun Remaja (WBR) 14. PT Eastern Drilling Indonesia Jaya 15. PT Roda Drilling Nusantara (RDN) 16. PT. Tiga Lestari Energi (TLE) 17. PT Harmand Intimarin Indonesia **SLIMHOLE – Small Rotary, Multipurpose and Coring Rig**: 1. PT Petrotec Guna Perkasa 2. PT Boart Longyear 3. PT Integra Oilfield Services 4. PT Bormindo Nusantara 5. Federal International 6. PT Surveyor Indonesia – PT Tridiantara 7. PT Bintang Mandiri Perkasa Drill 8. Iceland Drilling 9. PT Asia Drill Bara Utama 10. PT Bauer Pratama Indonesia 11. PT Parts Sentra Indomandiri 12. PT Asia Petrocom Services (APS)	**STANDARD AND BIG HOLE WELL SIZE** • Rig availability is often defined by the market conditions of the oil and gas industry, which are influenced by fluctuations in oil prices. This market is shared with oil and gas projects, so when oil prices are high, oil and gas companies typically conduct aggressive drilling campaigns to increase production (Purba, et al., 2020a). • Higher oil prices generally lead to not only reduced availability of rigs in the market, but also increasing the rig rental rate. • Rig is the largest cost component in the drilling project, when rig is under IDS leader (Service company) the rate might be higher than usual that lead to significant incremental of drilling cost. • The number of wells might impact significantly to the rig rental rate • Rig company that has experiences in geothermal drilling project are limited. • Several contractors has poor historical safety/environmental records. **SLIMHOLE RIG CHALLENGES** • Experienced coring rig contractors for geothermal projects in Indonesia are limited, hence only a few can meet the technical and safety requirements (for instance, the use of a Blowout Preventer (BOP)). • Importing rigs from abroad faces the challenge of high costs due to the uncertainty in the number of wells to be drilled. Therefore, if the cost of importing these rigs is based solely on a limited number of wells, it will be excessively high.
2.	Directional Drilling	1. Schlumberger 2. Halliburton 3. Scientific Drilling Indonesia (SDI) International 4. Parama Data Unit (PDU) 5. Baker Hughes	• Usually defined by market condition of oil and gas, which influenced by the oil price fluctuation. Most likely, the higher the oil price the less available the reliable unit in the market.

3	Cementing services	1. Schlumberger 2. Halliburton 3. Baker Hughes 4. Duta Wisesa Servisindo (DWS) 5. China Oilfield Services Limited (COSL)	• Usually defined by market condition of oil and gas, which influenced by the oil price fluctuation. Most likely, the higher the oil price the less available the reliable unit in the market. • The company and personnel that has experience in geothermal drilling project are limited.
4	Drilling fluid/mud services	1. MI Swaco - Schlumberger 2. Baroid – Halliburton 3. Baker Hughes 4. PT Huile Indonesia	• Usually defined by market condition of oil and gas, which influenced by the oil price fluctuation. Most likely, the higher the oil price the less available the reliable unit in the market. • The company and personnel that has experience in geothermal drilling project are limited.
5	Mud logging	1. Parama Data Unit (PDU) 2. Pakarti Rekayasa Utama (Parama) 3. PT DHI Excellence Logging (Exlog) 4. Promosindo Midia Tenaga (PMT)	• Usually defined by market condition of oil and gas, which influenced by the oil price fluctuation. Most likely, the higher the oil price the less available the reliable unit in the market.
6	Wireline logging and explosive Handling	1. Schlumberger 2. Halliburton 3. Baker Hughes 4. PT Wahana Kerja Indonesia 5. Tiger Energy 6. Expro 7. NPS 8. SABS	• Usually defined by market condition of oil and gas, which influenced by the oil price fluctuation. Most likely, the higher the oil price the less available the reliable unit in the market. • There are only a few companies that possess logging equipment with high-temperature ratings.
7	Aerated drilling	1. PT Air Drilling Associates (ADA) Indonesia 2. Alfapilar 3. PDSI 4. KAL	• Usually defined by market condition of oil and gas, which influenced by the oil price fluctuation. Air drilling and well testing/stimulation also influenced by oil and gas as air drilling is typically for Managed Pressure Drilling (MPD) operation in oil and gas drilling for underbalance operation • The number of suppliers is limited, with ADA being the current major player and facing limited competition. As a result, the pricing is highly uncompetitive.
8	Casing and liner Provision	1. PT Citra Tubindo TBK (Vallourec) 2. PT Seamless Pipe Indonesia Jaya (SPIJ) / Tenaris 3. PT Tridaya Esa Pakarti 4. PT Telaga Mas Mulia (TMM)	• Usually defined by market condition of oil and gas, which influenced by the oil price fluctuation. Availability of raw material may also impact the price. • Issues arise with domestic content requirements (TKDN) especially when funding comes from international financial institutions, which prohibit local content stipulations during procurement. • Has long lead time. The lead time is estimated 8 – 12 months at the latest for common specification. For special specification such as CRA (Corrosion Resistance Alloy) might take up to 18 months
9	Casing Running	1. PT Carana Bunga Persada 2. PT Varcoindo Bina Jaya 3. PT Indo Kaya Energi	• Usually defined by market condition of oil and gas, which influenced by the oil price fluctuation
10	Casing inspection	1. PT. Sucofindo (Persero) 2. PT. Sekawan Eka Sejati (SES) 3. PT. Grace Technic 4. PT Radiant Utama Interinsco 5. Akura Bina Citra 6. Tuboscope 7. OMS Oilfield Service (OMSOS) 8. PT WIDE & PIN Engineering & Inspection 9. PT Inspektindo Sinergi Persada 10. PT Tridaya Esa Pakarti	• Usually defined by market condition of oil and gas, which influenced by the oil price fluctuation.
11	Fishing and milling Tools	1. Baker Hughes 2. PT Sustraco Adikreasi 3. Schlumberger 4. Expro	• Usually defined by market condition of oil and gas, which influenced by the oil price fluctuation.
12	Drilling Bit	1. National Oilwell Varco (NOV) 2. Baker Hughes 3. Smith – Schlumberger 4. Halliburton 5. Imeco	• Usually defined by market condition of oil and gas, which influenced by the oil price fluctuation. • Some companies do not allow/reluctant to consignment basis agreements, therefore necessitating outright purchases, which in turn impacts efficiency and the total cost
13	H2S Services	1. PDSI 2. Rutledge 3. Dyfco 4. Fergaco Indonesia 5. Total Safety Engineering (TSE) 6. Menara Inti Energi	• Usually defined by market condition of oil and gas, which influenced by the oil price fluctuation.

14	Drilling Waste Management	1. MI Swaco - Schlumberger 2. Scomi Oiltools 3. PPLI 4. HOLCIM	• Usually defined by market condition of oil and gas, which influenced by the oil price fluctuation.
15	Fuel Supply	1. Pertamina 2. PT Berdikari Jaya Bersama 3. Total 4. Shell	• Usually defined by market condition of oil and gas, which influenced by the oil price fluctuation.
16	Well testing and stimulation	1. Thermochem 2. NMS 3. CBN	• Limited players/available contractors
18	Wellhead, Master Valve, X-Mast Tree, and accessories	1. PT Nurman Mitra Sentosa (NMS) 2. Sagatrade 3. DEU (Kyokuto) 4. FMC 5. IKS-TIX 6. Imeco Inter Sarana 7. Wefic Group	• Usually defined by market condition of oil and gas, which influenced by the oil price fluctuation. Availability of raw material may also impact the price. • Has long lead time. The lead time is estimated 8 – 12 months at the latest for common specification. • Issues arise with domestic content requirements (TKDN) especially when funding comes from international financial institutions, which prohibit local content stipulations during procurement.
19	Drilling Insurance	1. Tugu Mandiri 2. Aswata 3. Howden	-
20	Rig Inspection	1. PT. Sucofindo (Persero) 2. PT. Akordia Venatama 3. PT. Ansari Jaya Sakti (AJS) 4. PT. OCS Indonesia 5. Moduresources 6. PT Inspektindo Sinergi Persada 7. PT Indo Yasa Prima 8. PT PJ-Tek Mandiri 9. Applus	• Usually defined by market condition of oil and gas, which influenced by the oil price fluctuation
21	Tubular Inspection	1. Tuboscope 2. Bureau Veritas (BV) 3. OMS Oilfield Service (OMSOS) 4. Akura Bina Citra 5. PT Grace Technic 5. PT Besmindo Andalas Semesta	• Usually defined by market condition of oil and gas, which influenced by the oil price fluctuation

As shown in Figure 6, In the landscape of geothermal exploration in Indonesia, procurement challenges for both standard and big hole rotary rigs, as well as slimhole rigs, present significant hurdles. For the larger rigs, costs are a primary concern, often exacerbated when rigs are under the leadership of Integrated Drilling Services (IDS) providers, which can push rental rates above average. The overall availability of these rigs is closely tied to the fluctuating oil market, with price hikes leading to aggressive drilling in the oil and gas sector and consequent scarcity and cost increases for geothermal projects. Adding to the complexity, there is a scarcity of contractors with a strong track record in both safety and environmental performance in geothermal drilling.

However, because of conventional rotary rig is commonly used in oil and gas industry, so that there is an impact on the geothermal industry regarding rig availability, especially in Indonesia. In Indonesia, it is uncommon for geothermal companies to own and operate the rig and both industries usually rent the rig and crew from a rig company (Purba, et al., 2020).

In line with this research hypothetic, as explained by Gul & Aslanoglu (2018), If there are any significant incremental on oil price and become higher level than before, oil company frequently do massive drilling campaign aggressively to produce the oil and gas from their field. As illustrated in Figure 4, the implication of this kind of condition, there is a high possibility that many oil and gas company will fully occupy rig for their operation.

The recent surge in oil prices has significantly influenced the demand for rig occupation, as exemplified by the drilling campaign of Pertamina Hulu Rokan (PHR). Since 2022, PHR has been conducting drilling and workover activities on a massive and aggressive scale, operating approximately 60 rigs in parallel within their zone/concession area.

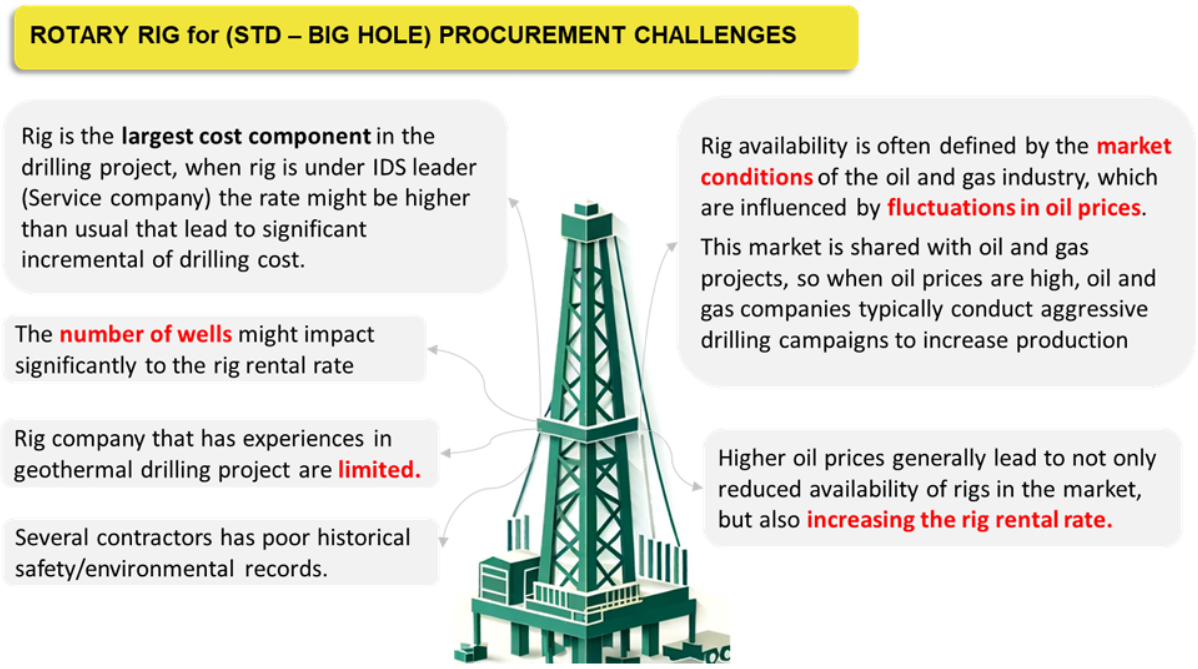

Figure 3: Summary of Rotary Rig Procurement Challenges

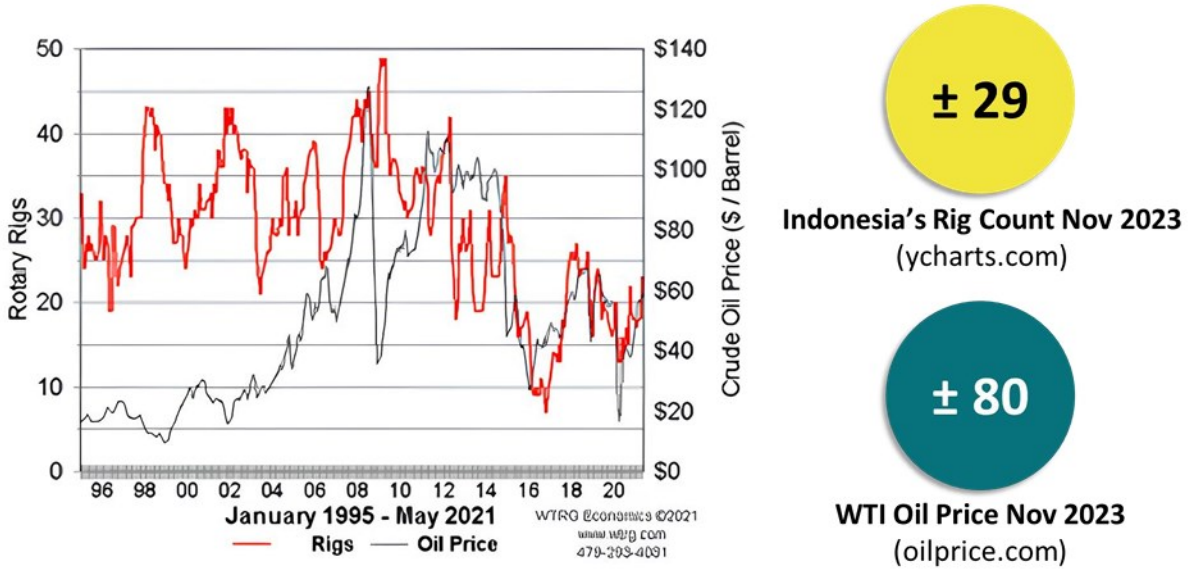

Figure 4: Indonesia's rig count vs oil price. Modified from (Energy Economist, 2021)

Consequently, this situation has created challenges for geothermal companies in securing drilling rigs due to a scarcity and limited availability of proper rig contractors with the suitable capacity required by these companies. Then in such cases, the geothermal company is frequently forced to contract a rig with a capacity greater capacity than required due to a rig availability issue (Purba, et al., 2020).

Conversely, as presented in Figure 5 about slimhole rigs , which are a cost-effective alternative, face their own set of challenges. The pool of contractors with the expertise and equipment to meet the stringent technical and safety standards for geothermal drilling is limited. This situation is further complicated by the high costs associated with importing rigs, a cost that becomes unsustainable if based on a limited number of wells to be drilled.

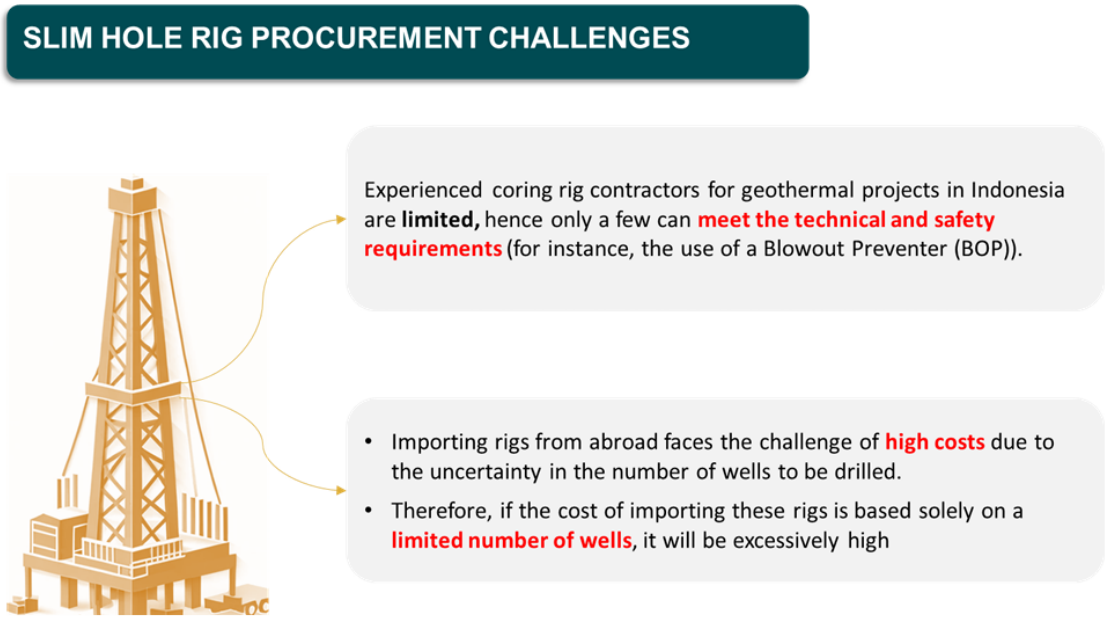

Figure 5: Summary of Slimhole Rig Procurement Challenges (GRG-Geoenergis, 2024)

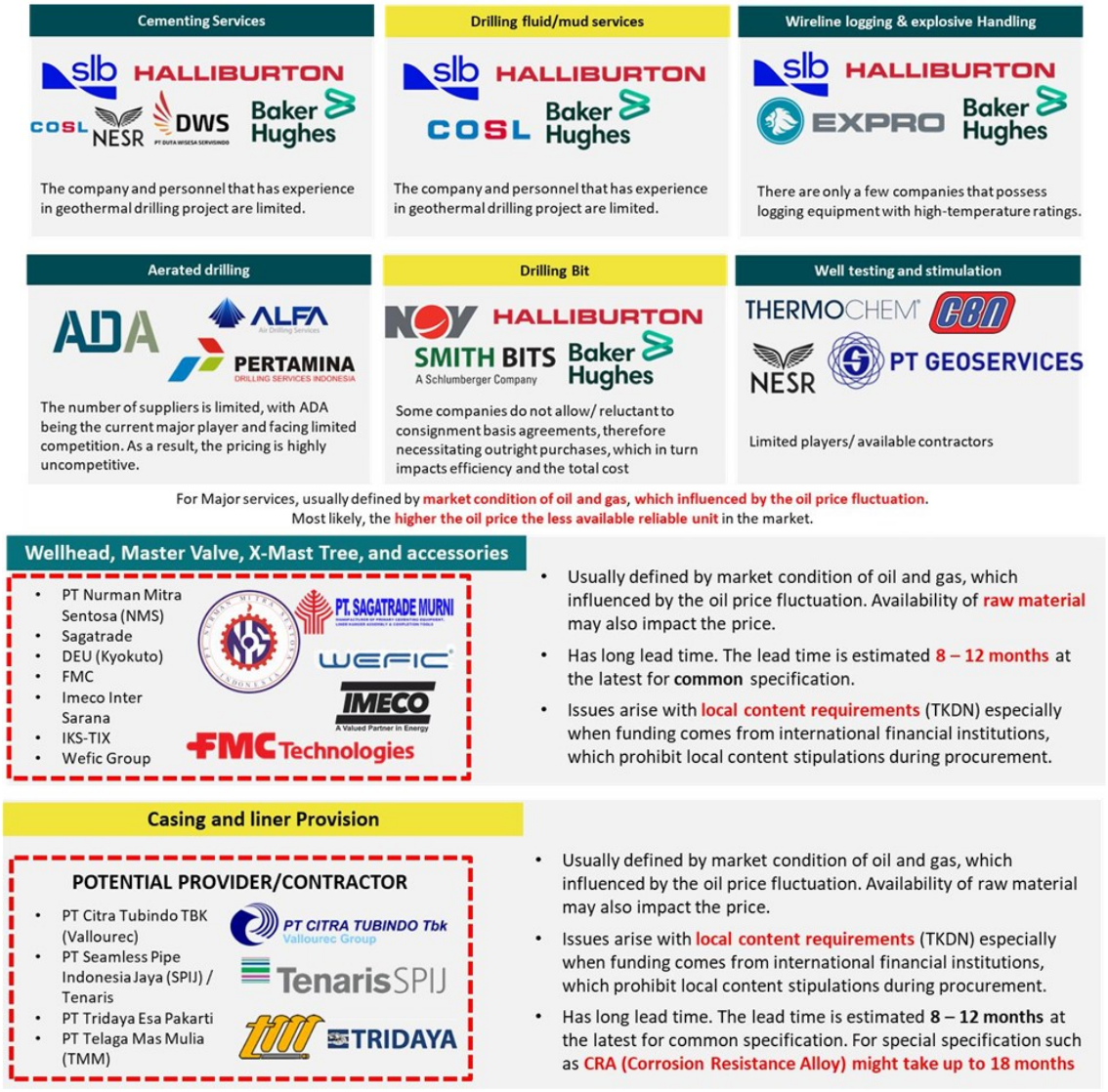

Figure 6: Summary of General Drilling Services Procurement Challenges

Navigating these procurement challenges requires strategic planning and adaptability. Developers must balance the need for cost efficiency with the technical and safety requirements of geothermal drilling, all while operating within a market influenced by the broader energy sector's demands and global price shifts.

The procurement landscape for general drilling services in geothermal exploration presents a multi-faceted challenge as presented in Figure 6, encapsulated by the image detailing the range of services required for a successful operation. Companies such as Schlumberger and Halliburton dominate the space across various service categories, from cementing to drilling fluid services, reflecting a market with limited players. This limited competition is exacerbated by the fact that few companies possess the necessary high-temperature equipment for wireline logging, or have the specific expertise in geothermal projects, further narrowing the options available to developers.

Moreover, the procurement of essential components like drilling bits, well testing, and stimulation services, and even crucial wellhead and x-mass tree accessories, is heavily influenced by the volatile oil market. The fluctuating oil prices not only impact the availability and cost of services but also the reliability of supply. Additionally, the procurement process for casing and liner provision is not immune to these market dynamics, with local content requirements (TKDN) posing additional hurdles, especially when projects are funded by international financial institutions, leading to longer lead times and potential compliance issues.

This procurement environment suggests a need for strategic sourcing, where developers must navigate a complex web of service providers, market conditions, and regulatory requirements to ensure the timely and cost-effective delivery of drilling services.

Based on the analysis in Table 4, Figure 5, and Figure 6 it is observed that several service providers face various challenges during the procurement and tender process for geothermal drilling projects in Indonesia. The procurement and tender challenges are summarized in Figure 7.

Figure 7: Summary of Procurement Challenges in Geothermal Drilling Project

3. MARKET SURYVEY AS THE RELIABLE METHOD FOR INVESTIGATING DRILLING MARKET CONDITION

Market survey for a geothermal drilling/workover project is a comprehensive analysis aimed at gathering and evaluating information pertinent to the drilling sector's current market conditions. This process includes assessing the availability and costs of crucial equipment such as drilling rigs, which are often influenced by the oi price. It also involves the careful evaluation of potential contractors and suppliers, considering their capabilities, financial stability, and adherence to safety and environmental standards.

The market survey is crucial for project planners and decision-makers, as it provides essential insights for informed decision-making regarding equipment procurement, contractor selection, budgeting, and overall risk management, thereby enhancing the likelihood of a project's success.

A critical key to have a successful procurement for the project is by understanding the current market condition as well as the ongoing government regulation related to the procurement process. Strategy of the procurement

process will be easily developed by having a good mapping on those market condition and government procurement regulations. For instance, in the period of low demand due to plunging of oil and gas price, the geothermal company could optimize the contract scopes, remuneration strategy, and performance target leverage to be on geothermal developer company side. Meanwhile, during high demand period it is necessary to balance the leverage in order to attract potential bidders in joining the competitive tender process.

The market survey was conducted with a distinct separation of services deemed critical to the project timeline. For example, certain long lead items (LLI) were identified as top priority and marked as the 1st (first) priority to be completed prior other services. As such, within the methodology of the market survey, priorities are categorized as follows:

1. Long Lead Items, which consist of casing provision, liner hanger, wellhead and master valve, also casing accessories.
2. Drilling rig bundling, usually consist of drilling rig, top drive, H2S, water pump, and heavy equipment.
3. Major drilling services, which usually consist of drilling fluid services, aerated drilling, directional drilling & MWD, cementing services, drilling bit, solid control equipment, mud logging unit, wireline logging, fuel supply.
4. Other supporting services such as casing inspection, tubular inspection, rig inspection, acidizing, well testing, civil work, and others.
5. Logistic and manpower services, which usually consist of project management team and on-site supervision (personnel

The common approach to conducting a market survey involves issuing a Request for Information (RFI) or Request for Quotation (RFQ). The market survey process usually initiates with the establishment/preparation of the well design and drilling program for the basis generating detailed lists of required services and materials. If the technical specifications are not yet determined, a list of potential suppliers or bidders is created to refine the specifications. If the specs are fixed, a technical specification survey is conducted.

Documents are then prepared to engage potential service providers in a market survey. Responses from the survey, in the form of budgetary proposals, are received and compiled into a database. This database is used to create a budgetary estimate, leading to the generation of an Owner Estimate (OE) report, which follows the development of the commercial form and the scope of work. The entire process is designed to ensure that the OE is based on thorough market research and accurate specifications. The workflow is designed to be dynamic, with a continuous loop back to the generation of OE, reflecting the iterative nature of project planning and execution. The common approach of the market survey is illustrated in Figure 8.

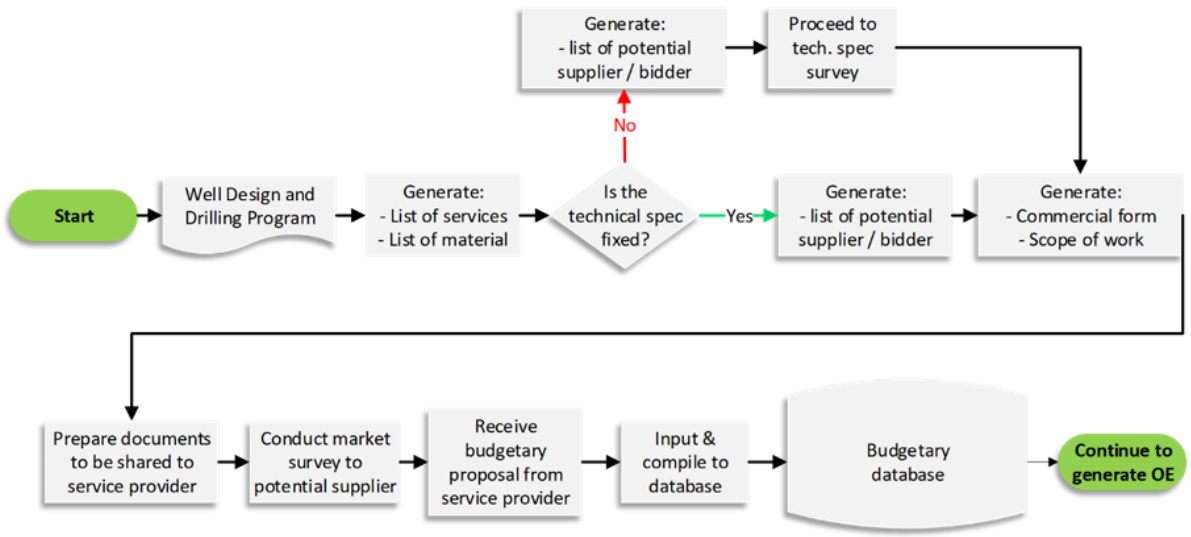

Figure 8: General Market Survey for Generating Engineering / Owner Estimate Workflow for Geothermal Drilling Project

The detail of the market survey methodology for generating engineering / owner estimate is explained below:

1. Obtaining/developing well schematics and general drilling program

This document is prepared by the technical team containing information on well design and drilling activities to be conducted. Some information contained in this document such as the required rig capacity, casing size, casing

shoe depth, Bottom Hole Assembly (BHA) configuration, and so on. This document is the basis used for determining each item in the BEP.

2. Compiling a list of services and materials

The list of services and materials is a document detailing the specifications required for drilling activities. This list is compiled based on the well scheme and the general drilling program previously prepared. At this stage, it is crucial to confirm with the technical team their confidence in the established well scheme and drilling program.

Significant changes in these plans may necessitate changes to the list of services and materials. Should the technical team express low confidence in the existing technical specifications, conducting a technical specification survey may be warranted. Figure 9 is an example of some well materials and well services collected based on well needs.

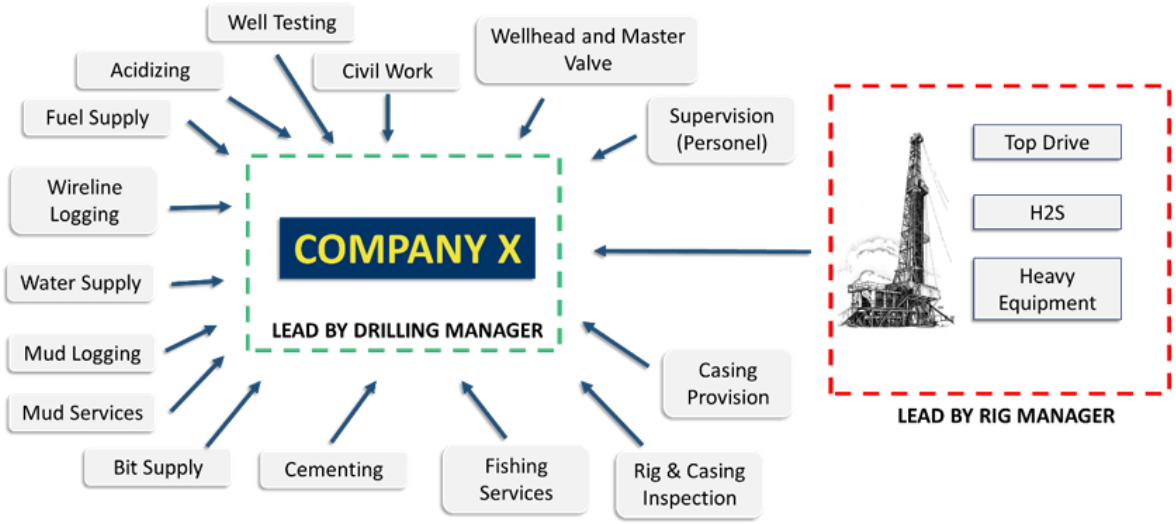

Figure 9: Example of Drilling Services List with Discrete Contract Type

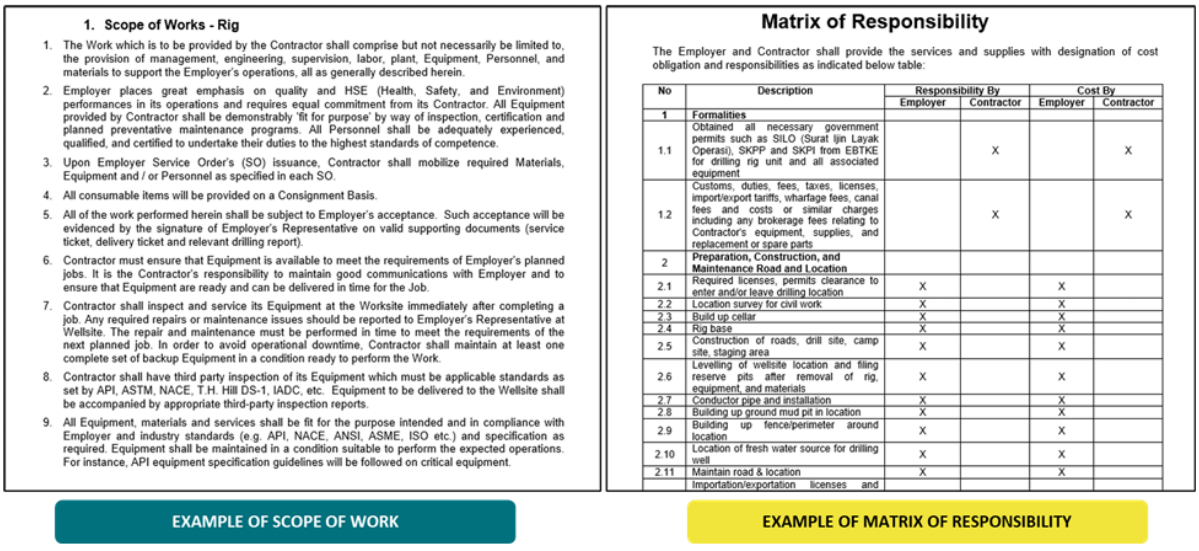

1. Scope of Works - Rig

1. The Work which is to be provided by the Contractor shall comprise but not necessarily be limited to, the provision of management, engineering, supervision, labor, plant, Equipment, Personnel, and materials to support the Employer's operations, all as generally described herein.
2. Employer places great emphasis on quality and HSE (Health, Safety, and Environment) performances in its operations and requires equal commitment from its Contractor. All Equipment provided by Contractor shall be demonstrably 'fit for purpose' by way of inspection, certification and planned preventative maintenance programs. All Personnel shall be adequately experienced, qualified, and certified to undertake their duties to the highest standards of competence.
3. Upon Employer Service Order's (SO) issuance, Contractor shall mobilize required Materials, Equipment and / or Personnel as specified in each SO.
4. All consumable items will be provided on a Consignment Basis.
5. All of the work performed herein shall be subject to Employer's acceptance. Such acceptance will be evidenced by the signature of Employer's Representative on valid supporting documents (service ticket, delivery ticket and relevant drilling report).
6. Contractor must ensure that Equipment is available to meet the requirements of Employer's planned jobs. It is the Contractor's responsibility to maintain good communications with Employer and to ensure that Equipment are ready and can be delivered in time for the Job.
7. Contractor shall inspect and service its Equipment at the Worksite immediately after completing a job. Any required repairs or maintenance issues should be reported to Employer's Representative at Wellsite. The repair and maintenance must be performed in time to meet the requirements of the next planned job. In order to avoid operational downtime, Contractor shall maintain at least one complete set of backup Equipment in a condition ready to perform the Work.
8. Contractor shall have third party inspection of its Equipment which must be applicable standards as set by API, ASTM, NACE, T.H. Hill DS-1, IADC, etc. Equipment to be delivered to the Wellsite shall be accompanied by appropriate third-party inspection reports.
9. All Equipment, materials and services shall be fit for the purpose intended and in compliance with Employer and industry standards (e.g. API, NACE, ANSI, ASME, ISO etc.) and specification as required. Equipment shall be maintained in a condition suitable to perform the expected operations. For instance, API equipment specification guidelines will be followed on critical equipment.

EXAMPLE OF SCOPE OF WORK

Matrix of Responsibility

The Employer and Contractor shall provide the services and supplies with designation of cost obligation and responsibilities as indicated below table:

No	Description	Responsibility By		Cost By	
		Employer	Contractor	Employer	Contractor
1	**Formalities**				
1.1	Obtained all necessary government permits such as SILO (Surat Ijin Layak Operasi), SKPP and SKPI from EBTKE for drilling rig unit and all associated equipment		X		X
1.2	Customs, duties, fees, taxes, licenses, import/export tariffs, wharfage fees, canal fees and costs or similar charges including any brokerage fees relating to Contractor's equipment, supplies, and replacement or spare parts		X		X
2	**Preparation, Construction, and Maintenance Road and Location**				
2.1	Required licenses, permits clearance to enter and/or leave drilling location	X		X	
2.2	Location survey for civil work	X		X	
2.3	Build up cellar	X		X	
2.4	Rig base	X		X	
2.5	Construction of roads, drill site, camp site, staging area	X		X	
2.6	Levelling of wellsite location and filing reserve pits after removal of rig, equipment, and materials	X		X	
2.7	Conductor pipe and installation	X		X	
2.8	Building up ground mud pit in location	X		X	
2.9	Building up fence/perimeter around location	X		X	
2.10	Location of fresh water source for drilling well	X		X	
2.11	Maintain road & location	X		X	
	Importation/exportation licenses and				

EXAMPLE OF MATRIX OF RESPONSIBILITY

Figure 10: Example of rig scope of works (left), Example of contractor's matrix of responsibility (right).

3. Generate list of potential suppliers / bidders

The list is generated by identifying contractors or suppliers who have previously tendered for similar services and materials in drilling activities. Additionally, an evaluation of each available supplier's capacity in the market to fulfill the required services and materials is conducted. The purpose of this stage is to identify potential suppliers likely to participate in the tender process. Table 4 in previous sub-section shows an example list of potential suppliers.

4. Develop Commercial Form and Scope of Work

The commercial form is a document listing the materials required for procurement, detailing the specifications and quantities that suppliers must adhere to. Conversely, the scope of work document outlines the specific tasks or services to be carried out, including information on the minimum requirements and quantities involved. Figure 10 shows the examples of the contents of the scope of work, and Figure 11 show examples of items depicted in the commercial form.

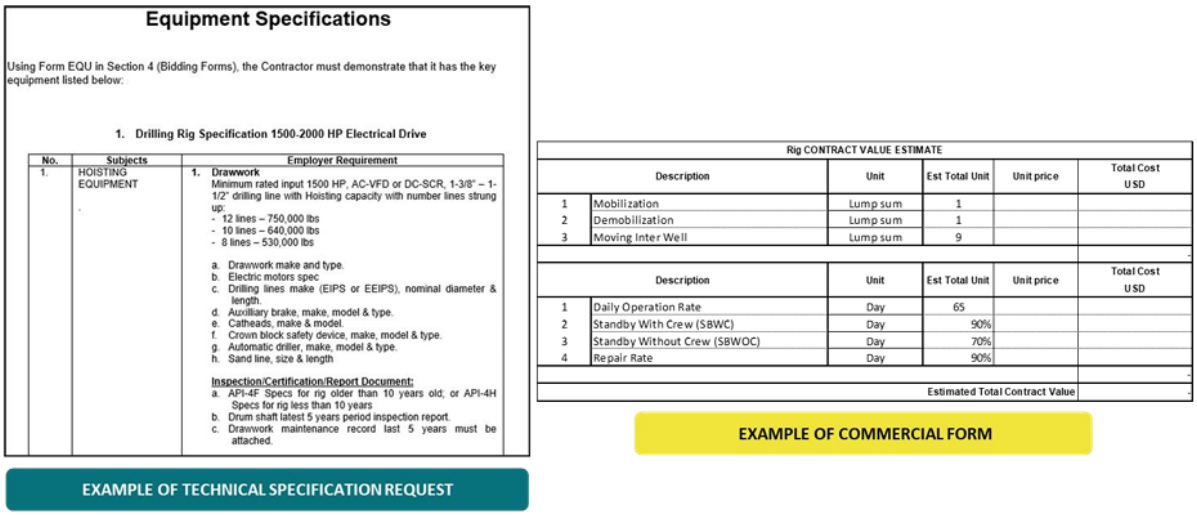

Equipment Specifications

Using Form EQU in Section 4 (Bidding Forms), the Contractor must demonstrate that it has the key equipment listed below:

1. Drilling Rig Specification 1500-2000 HP Electrical Drive

No.	Subjects	Employer Requirement
1.	HOISTING EQUIPMENT	1. Drawwork Minimum rated input 1500 HP, AC-VFD or DC-SCR, 1-3/8" – 1-1/2" drilling line with Hoisting capacity with number lines strung up. - 12 lines – 750,000 lbs - 10 lines – 640,000 lbs - 8 lines – 530,000 lbs a. Drawwork make and type. b. Electric motors spec c. Drilling lines make (EIPS or EEIPS), nominal diameter & length. d. Auxilliary brake, make, model & type. e. Catheads, make & model. f. Crown block safety device, make, model & type. g. Automatic driller, make, model & type. h. Sand line, size & length Inspection/Certification/Report Document: a. API-4F Specs for rig older than 10 years old; or API-4H Specs for rig less than 10 years b. Drum shaft latest 5 years period inspection report. c. Drawwork maintenance record last 5 years must be attached.

EXAMPLE OF TECHNICAL SPECIFICATION REQUEST

Rig CONTRACT VALUE ESTIMATE

	Description	Unit	Est Total Unit	Unit price	Total Cost USD
1	Mobilization	Lump sum	1		
2	Demobilization	Lump sum	1		
3	Moving Inter Well	Lump sum	9		
					-
	Description	Unit	Est Total Unit	Unit price	Total Cost USD
1	Daily Operation Rate	Day	65		
2	Standby With Crew (SBWC)	Day	90%		
3	Standby Without Crew (SBWOC)	Day	70%		
4	Repair Rate	Day	90%		
					-
				Estimated Total Contract Value	-

EXAMPLE OF COMMERCIAL FORM

Figure 11: Example of rig specifications for market survey (left), Example of commercial form for drilling rig (right).

No	Service/Material Provider	Unit	Quantity	Company A Unit Price (IDR)	Company B Unit Price (IDR)	X Company Unit Price (IDR)	Y Company Unit Price (IDR)
I	INTANGIBLE COST						
A.	IDS BUNDLING						
A.1.	Rig Bundling- Mobilisasi dan Demobilisasi (Rig, Top Drive, Mud Logging Unit, H2S, Water Transfer Pump, Milling Tools)						
1	Mobilisasi - Rig & seluruh peralatan pendukung	LS	1				
2	Demobilisasi - Rig & seluruh peralatan pendukung	LS	1				
3	Moving antar wellpad - Rig dan seluruh peralatan pendukung	LS	1				
4	Moving antar well - Rig dan seluruh peralatan pendukung	LS	1				
A.2	Tarif Harian						
	Rig, Top Drive, Mud Logging Unit, Milling Tools, Water Transfer Pump, H2S (equipment dan personel)						
1	Tarif Harian Operasi (THO)	Hari	77.00				
2	Tarif Harian Siaga (THS) - 75% THO	Hari	0				
3	Tarif Harian Rusak (THR)	Hari	0				
3.1	0 - 24 jam setiap 30 hari - 50% THO	Hari	0				
3.2	24 - 48 jam setiap 30 hari - Zero Rate	Hari	0				
4	Tarif Harian Siaga Minimum Crew - 25% THO	Hari	0				
5	Tarif Killing/Quenching	Hari	6				
6	Tarif Milling Engineer (On Call basis)	Hari	17				
A.3	Wireline Logging Services						
1	Wireline Logging - Mobilisasi dan Demobilisasi						
1.1	Mobilisasi - Wireline Logging Unit	LS	1				
1.2	Demobilisasi - Wireline Logging Unit	LS	1				
2	Wireline Logging - Tarif Peralatan & Personel						
2.1	Wireline Logging - Tarif Harian Operasi (THO) *)	Hari	12				
2.2	Wireline Logging - Tarif Harian Siaga (THS) - 50% THO	Hari	65				
2.3	Wireline Logging - Tarif Harian Rusak (THR) - 25% THO	Hari	0				
3	Logging Jobs						
3.1	DHV Job (Black & White)	Job	1				
3.2	CBL Job	Job	1				
3.3	PTS Survey Job	Job	6				
3.4	Caliper Job	job	1				
3.5	MTD Survey Job	Job	1				
A.4	Mud Services						
1	Tarif Mud Engineer	Hari	77.00				

Figure 12: Example of Market Survey Result Database

5. Preparing document for drilling service and material supplier.

This step involves ensuring that the commercial form and scope of work documents for service-material providers are accurate and meet the required information needs. It includes an internal peer-review and re-confirmation with the technical team on specific material-service specifications.

6. Conducting Market Survey

The purpose of the market survey is to gather estimated market prices for the prepared commercial form and scope of work. This involves formal correspondence with listed potential providers, sending them the commercial form and scope of work documents. Providers are expected to reply with price lists that they can accommodate. However, there is a possibility of non-response from some providers, necessitating regular follow-ups by the developer.

7. Compiling Market Survey Database

This database is a compilation of all market survey results. It includes detailed information about the items, responding suppliers, and the prices quoted by them, organized in a table by service-material group. The database's objective is to integrate existing data for easier analysis in subsequent processes. The example of database is illustrated in Figure 12.

8. Generate Cost Estimate

From the market survey results, the budgetary proposal that have been submitted by respondents are utilized for estimating project cost, also known as the Owner Estimate (OE) / Engineering Estimate. The owner estimate is an estimate of the service-material prices used as a guide for budget preparation and procurement in a drilling project. The importance of determining OE for a project is to help evaluating fairness of price value which offered in tender process.

Generating of an owner estimate (OE) involves leveraging data from an existing database to establish reference values and then calculating the individual and total project costs based on the specified quantities and these reference values. The example of owner estimate results is shown in Figure 14. To analyse the updated price list, the market survey data is reviewed to identify the range of prices, taking note of the lowest, median, average, and highest values. Subsequently, an internal analysis is performed to select the appropriate price for inclusion in the owner estimate. The selection of the price can be based on the following consideration:

- The average value from the market survey may be chosen when there is minimal variation in market prices among suppliers for the same item, indicating that the average price is reflective of the market.
- The median value from the market survey might be more appropriate when there is a wide variation in prices among suppliers, which could render an average price calculation inaccurately high.
- Expert team assessments may be preferable when market price data appears anomalous. In such cases, it is advisable to consult prices from several other drilling projects to derive a more representative price point.

If the geothermal developers already has previous drilling contract prior the upcoming drilling campaign, the owner estimate (OE) also require to be compared with previous contract with adjustment inflation rate for sanity check the fairness of current cost estimates. The common approach for inflation rate adjustment is using US PPI Index of Drilling Industry. As shown in Figure 13 as the example for this research, the cumulative inflation rate from 2021 until 2023 is 1.3 (30%) for the drilling industry. Figure 14 and Table 5 shows the example of Engineering Estimate (EE) / Owner Estimate (OE) results of geothermal drilling project.

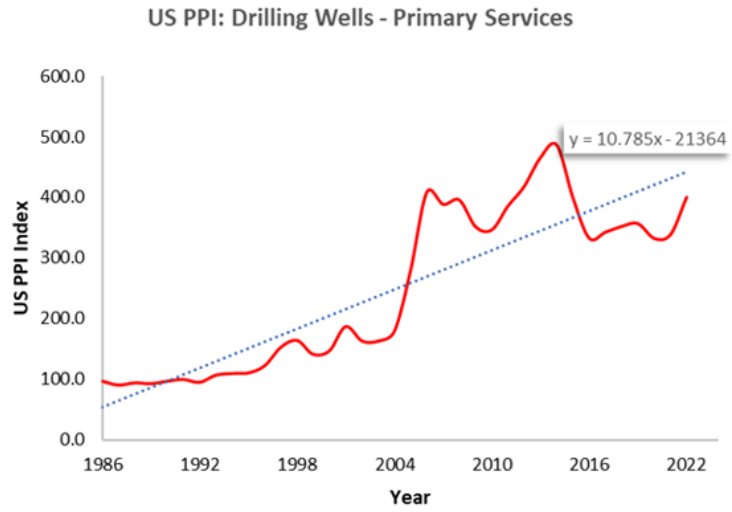

Year	Annual	Index (normalize to 2023)
2020	332.1	1.4
2021	338.2	1.3
2022	399.8	1.1
2023	454.055	1

Figure 13: Inflation Factor from US PPI: Drilling Wells – Primary Services

Figure 14: Example-1 of Cost estimation distribution for each service (Adityatama et al, 2023).

It should be noted the there are several challenges associated with generating an accurate or close enough cost estimate for geothermal drilling in Indonesia such as:

- Geothermal drilling requires various services and materials that may be provided by different companies, complicating the estimation of cost for each service/material.
- The drilling industry is tightly linked to the market condition of the oil & gas industry, which will fluctuate the price of the services and goods for drilling depending on the oil price.

This condition is further aggravated by the absence of any accessible geothermal drilling cost database in Indonesia, in contrast with the oil and gas industry that may have several databases such as IHS Markit's Rushmore for cost estimate and performance benchmark. Those difficulties in generating accurate geothermal drilling cost estimates are problematic as drilling is one of the major cost components in the whole geothermal project.

Moreover, several geothermal developers in Indonesia have their own procurement guidelines that may dictate the tender process to be redone if the cost estimate is way below the price quoted by service companies. The time spent redoing the whole procurement process is disadvantageous to the developers especially in the exploration phase, as the exploration duration is limited by the Government in Indonesia. Therefore, having an accurate cost estimate is crucial to preventing such events.

In short, by performing a comprehensive market survey, the geothermal developers can determine the current market condition and accurate cost estimation, which plays crucial roles in the decision-making process for the best procurement strategy. Additionally, with the selective and progressive method in the market survey, it has narrowed down the bias cost data (if any) for some of the major drilling services contract. The proper market survey can be the basis of remuneration strategy which leads to a cost saving in the project and also helps to fit in the project timeline.

4. VARIOUS STRATEGIES FOR INCREASING GEOTHERMAL DRILLING MARET ATTRACTIVENESS AND COMPETITIVENESS

Building upon the strategies for boosting the competitiveness of the geothermal drilling market, we must also consider the pivotal role that international drilling companies play in advancing this sector. The following section, therefore, shifts focus from domestic competitive enhancements to the global stage, where attracting and retaining international expertise becomes paramount. It explores the strategic factors that make Indonesia's geothermal

market appealing to international entities, thus complementing our overarching goal of fostering a more dynamic and competitive industry. The integration of international players not only broadens the technological and operational horizons but also introduces more advanced practices and standards crucial for the sector's growth.

Table 5: Example-2 of Cost estimation distribution for each service

No	Description	Engineering Estimate Results (Total Cost for 2 wells)	ALA-5 Well (1,400 mMD)	ALA-6 Well (1,800 mMD)
1	**DRILLING SERVICES (Well Cost)**	**$17,387,697**	**$8,282,169**	**$9,105,528**
		Rp260,815,447,580	**Rp124,232,532,580**	**Rp136,582,915,000**
1.1	**DRILLING OPERATIONS**	**$11,831,576**	**$5,643,346**	**$6,188,230**
1.1.1	Contract Rig Bundling (Top Drive, Mud Logging Unit, H2S, Drilling Waste, Heavy Equipment and Transportation, Meals & Accommodation, etc) - Include Mob Demob	$6,216,080	$2,929,628	$3,286,452
1.1.2	Mud, Chemical & Engineering Services and Materials	$652,614	$311,173	$341,441
1.1.3	Drilling Bits	$955,261	$477,631	$477,631
1.1.4	Equipment Rentals (Fishing Equipments)	$274,340	$137,170	$137,170
1.1.5	Directional Drilling and Surveys	$1,094,853	$518,910	$575,943
1.1.6	Geothermal Drilling Services (Aerated Drilling, Welding, and Waste Management)	$1,453,244	$686,316	$766,928
1.1.7	Casing Installation (Casing Running Services and Fill Up Equipment)	$261,755	$130,878	$130,878
1.1.8	Cement, Cementing, and Pump Fees	$479,700	$229,777	$249,923
1.1.9	Miscellaneous (Casing Inspection, Tubular Inspection, and Rig Inspection)	$105,729	$52,864	$52,864
1.1.10	Water System (Water Supply Service & Management)	$338,000	$169,000	$169,000
1.2	**FORMATION EVALUATION**	**$657,787**	**$324,560**	**$333,227**
1.2.1	Coring	$245,687	$122,844	$122,844
1.2.2	Open Hole Electrical Logging Services	$240,500	$115,917	$124,583
1.2.3	Logging Tool Run	$171,600	$85,800	$85,800
1.3	**GENERAL**	**$2,836,254**	**$1,288,497**	**$1,547,757**
1.2.4	Supervision	$447,162	$207,611	$239,551
1.2.5	Insurance	$63,000	$27,000	$36,000
1.2.6	Permits and Fees	$166,358	$76,419	$89,939
1.2.7	Other Transportation	$849,333	$384,667	$464,667
1.2.8	Fuel of Drilling Rig and Associated Services	$1,310,400	$592,800	$717,600
1.4	**TANGIBLES** (Casing, Casing Accessories, Well Equipment Surface, Well Equipment Subsurface, Other Tangible Cost)	**$2,062,080**	$1,025,766	$1,036,314
2	Well Testing Services	Rp500,000,000	Rp250,000,000	Rp250,000,000
3	Civil Work	Rp10,000,000,000	Rp5,000,000,000	Rp5,000,000,000
Total (Rp)		**Rp271,315,447,580**	**Rp129,482,532,580**	**Rp141,832,915,000**
Total (USD)		**USD 18,087,697**	**USD 8,632,169**	**USD 9,455,528**

4.1 Strategies for Increasing Market Competitiveness

The geothermal drilling sector in Indonesia presents unique challenges and opportunities for enhancing market competitiveness. The aim of this sub-section is to evaluate and propose strategies that can intensify competition within Indonesia's geothermal drilling market. This encompasses a thorough assessment of bidding approaches, ranging from discrete to bundled contracts, and their respective impacts on risk and performance.

Additionally, the sub-section seeks to address the significance of updated market surveys tailored to preferred contract types and the importance of timing in the tendering process. Moreover, the potential cost benefits of well bundling and the influence of the number of wells on rig rental rates will be scrutinized. The objective is to equip stakeholders with a clear understanding of the variables that can enhance market dynamics and drive cost-effective procurement.

Figure 15 provide the illustration summary and Table 6 provide the brief explanation of various options to increase geothermal drilling market competitiveness.

4.2 Strategies Strategy for Increasing Participation of International Drilling Companies

The objective of the sub-section is to identify and analyze strategic factors that could enhance the attractiveness of Indonesia's geothermal market to international drilling firms. This will involve examining the impact of contract currencies, the potential cost benefits associated with drilling multiple wells, the readiness of drilling locations, and the reputational considerations of job owners in terms of safety, environmental stewardship, and payment reliability. The sub-section aims to provide actionable insights that could lead to increased international engagement, contributing to the growth and success of Indonesia's geothermal industry. Figure 16 provide the visualization summary and Table 7 provide the brief explanation of various options to increase geothermal drilling market competitiveness.

The Indonesian geothermal drilling market presents significant opportunities amidst its challenges. By implementing strategic initiatives to enhance market competitiveness and attract international participation, Indonesia can leverage its geothermal potential more effectively. Stakeholders, including government bodies, local and international companies, and investors, must collaborate to foster a conducive environment for the growth of this sector.

Figure 15: Summary of Various Options to increase geothermal drilling market competitiveness

Figure 16: Summary of Various Options to increase participation of international drilling companies

Table 6: Various options to increase geothermal drilling market competitiveness.

Strategy	Impact on Market Competitiveness	Benefits	Challenges	Remarks
Develop Open Access Centralized Integrated Vendor Database (CIVD) for Open Tender Announcement of geothermal drilling project	The development of an Open Access Centralized Integrated Vendor Database (CIVD) for open tender announcements in the geothermal drilling projects in Indonesia presents a significant advancement in the procurement process. The CIVD is a widely adopted system within the oil and gas industry, particularly in operations managed by SKK Migas. This platform is renowned for its transparency, providing exhaustive details in tender documentation, including the scope of work, well numbers, drilling depths, and contract specifications. This centralized database streamlines the tender process by providing a single, accessible platform where all necessary procurement information, including prequalification invitations, public auction details, and a comprehensive procurement list, is available. The adoption of the CIVD ensures that all stakeholders have equal access to critical information, thereby facilitating a fair and competitive tendering process.	**Enhanced Transparency and Accessibility:** By centralizing procurement information, the CIVD ensures greater transparency in the tender process. This openness is crucial for maintaining fair competition and allowing all potential vendors equal access to tender information. **Efficiency in Tendering Process:** Streamlines the procurement process, saving time and resources for both developers and vendors. Data Accessibility: Provides easy access to comprehensive tender information, aiding in decision-making. Standardization: Offers a standardized platform for tender announcements, simplifying the procurement process. **Efficiency in Procurement Process:** With all information centralized, the time and effort required to search for tenders, understand requirements, and prepare submissions are significantly reduced. This efficiency is beneficial for both the geothermal developers and the vendors. **Improved Decision-Making:** The CIVD provides geothermal developers with a broad view of available vendors and their capabilities. This comprehensive insight aids in making more informed decisions during the tendering process. **Reduced Risk of Compliance Issues:** A centralized database helps ensure that all vendors accessing the tenders are aware of and comply with the necessary regulatory and legal requirements, reducing the risk of non-compliance in procurement processes. **Facilitation of Market Analysis**: For geothermal developers, the CIVD can be a valuable tool for market analysis, offering insights into the range of available services, pricing trends, and vendor capabilities. This information is crucial for strategic planning and budgeting.	• Transparency and Fairness: Centralized data fosters a more transparent and fair tendering process. • Efficiency in Tendering Process: Streamlines the procurement process, saving time and resources for both developers and vendors. • Data Accessibility: Provides easy access to comprehensive tender information, aiding in decision-making. • Standardization: Offers a standardized platform for tender announcements, simplifying the procurement process.	The development of a CIVD represents a progressive step towards modernizing procurement processes in Indonesia's geothermal sector. This approach aligns with global best practices in tendering and procurement, promoting efficiency, transparency, and competitiveness. Successful implementation requires careful planning, robust technical infrastructure, and ongoing stakeholder engagement to address potential challenges and maximize benefits.

Strategy	Impact on Market Competitiveness	Benefits	Challenges	Remarks
		Level Playing Field: The CIVD ensures all potential contractors, regardless of size or prior engagement with the geothermal sector, have equal access to tender information. This can increase the number of bidders and foster a more competitive environment. **Vendor Visibility:** Smaller or newer vendors, who might otherwise be overlooked, gain visibility in a centralized system. This increased exposure can lead to more diverse and competitive bids. **Quality and Innovation:** With more vendors competing, there's a natural drive towards higher quality and innovation in services offered. Companies may invest more in their capabilities to stand out in a larger pool of vendors. **Cost Effectiveness:** Increased competition often leads to more cost-effective bids for geothermal projects. Developers can benefit from lower prices due to the competitive pressure on vendors.		
Various Contract Bidding Strategy During Tender Process	A clear and well-defined bidding strategy can influence the competitiveness of the geothermal drilling market. By offering various contract types, the market can appeal to a broader range of contractors, each with different preferences and risk appetites. This strategy involves implementing distinct contract models like Discrete, Bundled, Semi-IPM, IPM Day Rate, and Turnkey. Each model caters to different aspects of drilling operations, with varying degrees of risk and control allocated between the developer and the contractor.	The primary benefit of a clear bidding strategy is the attraction of a wider pool of bidders. For instance, discrete contracts, where services and materials are procured separately, tend to be more appealing to providers due to the lower associated risks and clearer scope, thereby reducing the likelihood of performance penalties.	• One of the main challenges is ensuring that the selected bidding strategy aligns with the organization's capability. While discrete contracts may reduce risk, they require the geothermal developer to have a higher level of project management and coordination skills. • Additionally, each type of contract carries its inherent complexities and requires careful consideration of market conditions and project specifics.	It should be noted that discrete contracts are generally more attractive to providers due to the reduced risk. However, this **does not necessarily mean that discrete contracts are always the best option.** The choice of contract type should be based on the geothermal developer's organizational capabilities and the specific requirements of the project. For instance, while discrete contracts might minimize risk, bundled contracts could offer efficiencies of scale and simpler management structures. The selection process should involve a detailed analysis of the project's nature, the developer's expertise, and market conditions to determine the most suitable contract type.

Strategy	Impact on Market Competitiveness	Benefits	Challenges	Remarks
Conduct Market Survey as per Preferred Contract Type Prior to Tender Process	Conducting a market survey tailored to the preferred contract type before initiating the tender process can enhances the competitiveness of the geothermal drilling market. This approach ensures that the tenders reflect current market conditions and pricing, which can lead to more competitive and realistic bids. This strategy involves conducting detailed market surveys for various types of contracts, such as discrete, IPM, or bundled contracts. The survey should focus on gathering current pricing and availability data for services and materials relevant to the specific contract type. The market data collected should be recent to ensure precision and relevance.	A key benefit of this approach is the reduction of risks associated with tender failures due to outdated or irrelevant market data. By aligning the market survey with the contract type, developers can ensure that the prices quoted by contractors accurately represent the market. For discrete contracts, which might generally be lower in cost, such alignment is crucial to ensure budget accuracy especially if geothermal developers are planning to use bundled/IPM contracts.	One of the challenges is ensuring the timeliness and accuracy of the market survey data. Market conditions can change rapidly, making it difficult to maintain up-to-date information. Another challenge is correctly and fairly interpreting the data in the context of different contract types, as costs may vary significantly between discrete, IPM, or bundled contracts.	The more recent and precise the market survey data, the lower the risk of tender failures. It is essential that the contract type is clearly defined so that the contractor's price accurately reflects market conditions. For instance, discrete contract costs may be lower, but if a project is developed using an IPM or bundled contract, the costs from a discrete-only market survey may not be applicable. In such cases, a conservative approach might involve adding an estimated 25%-30% to the total cost of items, materials, and services as gathered from the market survey. This ensures that the owner's estimate is realistic and accounts for potential variations in market conditions across different contract types.
Minimize time gap between market survey and tender process	Maintaining a minimal time gap between conducting the market survey and the bid submission phase can impact the competitiveness of the geothermal drilling market. This approach ensures that the tender process is informed by the most current market data, making the bids more reflective of the current market conditions. This strategy involves closely aligning the timing of market surveys with the initiation of the tender process. It requires efficient planning and execution of market surveys to ensure that the data collected is relevant and immediately applicable for upcoming tenders.	The primary benefit is the increased relevance of market data, which leads to more accurate and competitive bidding. Contractors can base their bids on the latest pricing and availability information, reducing the risk of outdated or inaccurate estimations. This timely alignment can also increase the willingness of contractors to participate in the tender process, as they are assured of current market conditions.	One of the main challenges is the rapid execution and analysis of market surveys without compromising the quality of data collected. Another challenge lies in the coordination between different teams handling the market survey and tender process to ensure seamless integration of data and actions.	The shorter the time gap between the market survey and bid submission, the higher the likelihood of increased participation in tenders. Up-to-date market intelligence directly impacts the accuracy and competitiveness of bids. However, it is crucial to balance the speed of conducting market surveys with the need for comprehensive and reliable data collection. It is essential to have a well-coordinated approach that ensures the market survey data remains relevant throughout the tender process. Streamlining internal processes and communication channels can aid in achieving this synchronization. Careful planning and swift execution are key to maximizing the advantages of this strategy in enhancing market competitiveness.

Strategy	Impact on Market Competitiveness	Benefits	Challenges	Remarks
Well bundling (high number wells that will be drilled in single contract)	Well bundling during the procurement or tender process can substantially enhance market competitiveness in geothermal drilling. By integrating multiple wells into a single tender and campaign, the strategy can lead to more cost-effective bidding and efficient utilization of resources. This strategy involves grouping drilling multiple wells (typically a minimum of five) into a single procurement or tender package. Instead of individual tenders for each well, a bundled approach is adopted, offering multiple wells as a package deal to potential contractors.	One of the key benefits is the potential reduction in unit price, as contractors often offer lower rates for larger volume contracts. This cost efficiency arises from the economies of scale, where the fixed costs of mobilization and setup are spread across multiple wells, thereby reducing the average cost per well. Additionally, well bundling can streamline the procurement process, reducing administrative burdens and time.	A significant challenge is managing the complexity of a bundled tender, which might involve more extensive planning and coordination. Additionally, this approach might limit participation to only those contractors capable of handling multiple wells simultaneously, potentially excluding smaller players from bidding.	The strategy's success largely depends on the careful planning of the bundle size and scope. While larger bundles (more wells) can lead to greater cost savings, they require contractors with sufficient capacity and resources. The strategy also has a notable impact on rig rental rates, with larger contracts often attracting more competitive rates due to the guaranteed volume of work. It's important to balance the advantages of cost savings against the risks of limited contractor participation and the complexities of managing large-scale contracts. Well bundling should be aligned with the capacity and capabilities of the available contractors in the market. A thorough market analysis is essential to determine the optimal number of wells to bundle in a tender to achieve the best balance between cost efficiency and contractor capability.
Drilling site location readiness (well-prepared and accessible)	The readiness of drilling site locations is a crucial factor that impacts the competitiveness of the geothermal drilling market. Ensuring that sites are well-prepared and accessible can streamline project initiation and reduce logistical challenges. This strategy involves thorough site preparation, including ensuring proper access routes, pre-installing necessary infrastructure, and conducting preliminary assessments to facilitate smooth mobilization. It also includes environmental and safety assessments to ensure compliance with regulations.	Ready and accessible sites greatly reduce startup times for drilling projects. By addressing logistical challenges beforehand, contractors can mobilize more efficiently and begin operations sooner. This not only to help to meet the project timeline but also makes bidding for projects more attractive due to reduced initial overheads and uncertainties.	Challenges include the logistics of preparing remote or difficult-to-access sites and ensuring that all preparation work is completed within project timelines and budgets. Inadequate preparation or improper mobilization routes can lead to project delays, resulting in financial losses for both the developer and the contractor.	Site readiness extends beyond mere physical preparation; it encompasses a comprehensive approach to making a site operationally ready. This includes addressing potential social, environmental and regulatory hurdles, ensuring the availability of utilities and services, and preparing for contingencies plan. A well-prepared site attracts more competitive bids as contractors can more accurately estimate costs and timelines without needing to factor in extensive preliminary work. It is critical for project developers to invest time and resources into proper site preparation. Early engagement with contractors can also be beneficial to understand their requirements and challenges. This proactive approach not only enhances market competitiveness by making projects more attractive to bid on but also aligns with best practices for project management, reducing the risk of delays and additional costs.
Using Stable Currency	The choice of currency for contracts can influence the competitiveness of the geothermal drilling market.	By offering contracts in stable currencies, the risk associated with currency fluctuation is minimized.	One of the main challenges is the exposure to currency exchange rate fluctuations, which can impact the actual costs and revenues when converted to the local currency.	The implementation of this strategy requires careful monitoring of global financial markets and an understanding of the implications of using different currencies.

Strategy	Impact on Market Competitiveness	Benefits	Challenges	Remarks
	Utilizing stable and widely accepted currencies can reduce risks associated with currency fluctuations and make contracts more attractive, especially to international contractors. This strategy involves drafting contracts in currencies that are stable and globally recognized, such as the US dollar or the Euro. This choice can be determined based on current financial trends and the currency's stability in the international market.	This stability is particularly appealing to international contractors who operate across various currency zones, as it provides predictability in financial planning and reduces the potential for unexpected losses due to exchange rate changes.	Additionally, depending on the currency chosen, there might be implications for local financial regulations and tax implications.	The benefits of reduced currency risk need to be weighed against potential challenges such as exchange rate volatility and the impact on local financial operations. It is also essential to consider the preferences and capabilities of both local and international contractors when deciding on the contract currency. While opting for stable, widely accepted currencies can make contracts more attractive on the global stage, it is crucial to remain vigilant about the fluctuations in the global financial market and the potential impact on project costs. Regular financial assessments and consultations with financial experts can aid in navigating these complexities, ensuring that the chosen currency strategy aligns with the overall objectives of enhancing market competitiveness in geothermal drilling.
International geothermal drilling contractors' engagement	Engaging international geothermal drilling contractors can enhance the competitiveness of the market. This strategy brings global expertise and experience into the local industry, potentially raising the standard of services offered and fostering a more competitive environment. This involves actively seeking out and encouraging the participation of international drilling contractors. Strategies might include outreach initiatives, partnerships with global drilling firms, participation in international trade shows, and simplifying the entry process for foreign companies.	The main benefit of engaging international contractors is the infusion of global knowledge and advanced drilling techniques into the local market. This can lead to the introduction of more efficient, innovative practices and technologies, enhancing the overall quality and competitiveness of geothermal drilling operations in the region.	One significant challenge is navigating the complex web of international regulations and compliance requirements. Additionally, cultural and operational differences between local and international firms can pose challenges in terms of communication, work styles, and project management. International drilling contractors might have an issue with local content (TKDN) regulation. Then there is import duty that might compromise the economical aspect from international drilling contractor's side if.	A comprehensive approach is required to successfully integrate international contractors into the local market. This includes understanding and adapting to different business cultures, legal requirements, and operational standards. The potential benefits of enhanced service quality and competitiveness need to be balanced against the logistical and regulatory complexities involved in facilitating international participation. While inviting international expertise into the local market can be a powerful catalyst for growth and improvement, it requires a well-thought-out strategy to address the accompanying challenges effectively. Emphasis should be placed on establishing clear communication channels, understanding the nuances of different working cultures, and ensuring regulatory compliance. This approach not only elevates the local market's standards but also fosters a more diverse and dynamic competitive landscape in geothermal drilling. The engagement of international geothermal drilling contractors is crucial for boosting the competitiveness of the geothermal drilling market. The relationship between regulatory protections and operational costs, such as rig day rates and casing rates, significantly affects market dynamics. By reassessing and potentially reducing certain protections, governments can lower these costs, making the market more attractive to international players. This could lead to enhanced efficiency, innovation, and a competitive edge in the global geothermal energy sector.

Strategy	Impact on Market Competitiveness	Benefits	Challenges	Remarks
				Evaluating the impact of protections on unit rates is essential for attracting international contractors and improving market competitiveness. Reducing regulatory barriers could make geothermal projects more financially appealing, encouraging investment and technological advancements. Strategic adjustments in these regulations could foster a more robust, competitive geothermal energy industry worldwide.
Clear Scope of Work and Transparent Communication	Establishing a clear scope of work and maintaining transparent communication can enhances market competitiveness in geothermal drilling. It fosters a trustworthy and efficient procurement environment, which can attract a broader range of contractors and lead to more competitive bids. This strategy involves clearly defining the project's scope of work in tender documents and maintaining open lines of communication with all potential contractors. This can be achieved through regular updates to contractors, invitation for discussions, transparent bidding processes, and providing detailed project specifications.	Clear communication ensures that all parties have a mutual understanding of project requirements, reducing the risk of misunderstandings or misinterpretations. This clarity can lead to more accurate and competitive bids, as contractors can tailor their proposals to precisely match the project's needs. Moreover, it builds trust among contractors, encouraging more companies to participate in the bidding process.	The main challenge lies in maintaining consistent and effective communication across different stages of the procurement process. It requires a dedicated effort to provide timely updates and respond to inquiries, which can be resource-intensive. Additionally, managing a transparent process while adhering to confidentiality and competitive fairness can be complex.	For this strategy to be effective, a well-planned communication protocol must be in place. This includes proactive dissemination of information, structured feedback mechanisms, and the ability to efficiently handle a high volume of inquiries. The scope of work needs to be detailed yet flexible enough to accommodate any unforeseen changes or clarifications. While the benefits of clear and transparent communication are substantial, they hinge on the ability to implement a thorough and structured communication strategy. This involves not only the initial dissemination of information but also ongoing engagement throughout the tendering process. By prioritizing clarity and openness, the geothermal drilling market can foster a more competitive and reliable bidding environment, ultimately leading to more successful project outcomes.
Clear, fair, and transparent payment terms & conditions	Implementing clear, fair, and transparent payment terms and conditions is essential for enhancing market competitiveness in geothermal drilling. This approach can increase confidence in contractors and suppliers, making the market more attractive for both local and international players. The strategy entails developing and clearly communicating payment terms that are equitable	Clear payment terms reduce uncertainty and financial risk for contractors, making bids more competitive and reflective of actual project costs. Transparent and fair payment processes also build trust and credibility in the market, encouraging repeated engagement and long-term relationships with contractors.	One challenge is ensuring that the payment terms are both attractive to contractors and sustainable for the project developers. Balancing prompt payments with the financial management of the project can be complex, particularly in large-scale operations with multiple stakeholders.	A detailed assessment should include evaluating current market standards for payment terms in geothermal drilling, understanding the cash flow requirements of contractors, and aligning them with the project's financial capabilities. Regular reviews and updates to these terms may be necessary to adapt to changing market conditions or project requirements. While setting up clear payment terms is crucial, it is equally important to ensure their consistent application and enforcement. Regular communication regarding payment schedules and prompt resolution of payment-related queries or disputes can further enhance trust and competitiveness in the market. This strategy not only benefits contractors but also aids in maintaining a healthy and competitive market

Strategy	Impact on Market Competitiveness	Benefits	Challenges	Remarks
	and align with industry standards. This includes setting realistic timelines for payment, outlining the process for invoicing, and ensuring that terms are consistent and transparent across all contracts.			environment, fostering growth and innovation in the geothermal drilling sector.

Table 7: Various Options of Increasing Participation of International Drilling Companies

Strategy	Impact on International Participation	Benefits	Challenges	Additional Remarks
Develop Open Access Centralized Integrated Vendor Database (CIVD) for Open Tender Announcement of geothermal drilling project	The establishment of an Open Access Centralized Integrated Vendor Database (CIVD) for announcing open tenders in geothermal drilling projects might be increasing the international participation. This database would serve as a one-stop platform for accessing tender information, making it easier for international companies to identify and compete for opportunities in the geothermal drilling sector. The strategy involves developing a comprehensive, user-friendly, visible, yet easily accessible online database that lists all open tenders related to geothermal drilling projects. This platform should be designed to provide detailed information about each tender, including project specifications, bidding requirements, timelines, and contact details. The database should be regularly updated and made accessible to all potential international bidders.	A centralized vendor database streamlines the tender announcement process, making it more transparent and accessible, especially for international companies unfamiliar with local systems. This can lead to increased competition, potentially resulting in better quality services and cost efficiencies. The platform also serves as a resource for international vendors to understand market needs and tailor their offerings accordingly	Challenges include ensuring the database's security, maintaining up-to-date and accurate information, and promoting the platform to ensure widespread awareness among international companies. Additionally, managing the database requires resources and continuous oversight.	A thorough assessment of the CIVD would involve considering the technical aspects of database management, including data integrity, user interface design, and accessibility. It's also crucial to consider how the platform aligns with international tendering standards and practices to ensure its utility for global vendors. The success of the CIVD hinges on its ability to offer a reliable, comprehensive, and easily navigable source of information. Regular feedback from users, both local and international, can provide insights for continuous improvement, ensuring the database effectively meets the needs of a diverse range of stakeholders. Effective marketing and partnerships with international trade bodies can also help in maximizing its reach and impact, thus boosting international participation in Indonesia's geothermal drilling projects.
Number of wells that will be drilled.	Bundling multiple wells into a single contract can have a significant impact on attracting international drilling companies. Offering contracts for multiple wells can make projects more appealing due to the potential for higher overall profits and more efficient operations. This strategy involves consolidating the drilling of several wells into one contract, rather than tendering each well separately. This can be implemented by outlining a clear plan for the number of wells to be drilled within a specified timeframe and incorporating this into the tendering process.	For drilling contractors, bundled contracts can lead to greater profits as they can optimize resources across multiple wells. From the perspective of the geothermal developer, bundling wells can lead to more competitive unit pricing, as contractors may offer discounts for larger-scale projects. This can result in cost savings and increased efficiency.	The main challenges is ensuring that the contractor has the capacity to handle multiple wells simultaneously. Additionally, managing a larger scale project can be more complex, requiring more robust project management and coordination.	A detailed assessment would include analyzing the capacity of potential contractors to handle multiple wells, assessing the cost benefits of bundling versus individual well contracts, and determining the optimal number of wells to bundle together. This assessment should also consider the logistical and operational implications of drilling multiple wells under one contract. While well bundling can offer financial benefits, it's important for developers to carefully plan and communicate their needs. They should ensure that contractors are fully aware of the scope and scale of the project to avoid any misunderstandings. Additionally, developers should be prepared to manage the complexities that come with larger-scale projects, including increased coordination and resource allocation. The strategy of well bundling can be particularly effective in attracting large international companies that have the capacity and experience to handle extensive projects.
Drilling site location availability and well-prepared	The availability of well-prepared drilling sites and efficient mobilization routes directly impacts the participation of	Well-prepared sites streamline the setup and operations of drilling rigs and services, significantly	One of the primary challenges is the logistical complexity of preparing sites, especially in remote or	A comprehensive assessment would include evaluating the current status of potential drilling sites, identifying the resources needed for preparation, and developing a

Strategy	Impact on International Participation	Benefits	Challenges	Additional Remarks
mobilization route (drilling readiness)	international drilling companies in geothermal projects. Ensuring drilling readiness can make these sites more appealing to international contractors by reducing the likelihood of project delays and logistical challenges. This strategy involves ensuring that the drilling sites, such as well pads, conductors, ponds, etc., are fully prepared before mobilization. It includes developing clear site plans, establishing access routes, and making necessary infrastructural arrangements. This might also entail conducting preliminary assessments to ensure that the sites meet the required standards and are ready for immediate use.	reducing the time and resources needed for mobilization. This efficiency can decrease the likelihood of project delays, making the proposal more attractive to international companies. A ready-to-use site demonstrates project management competence and operational efficiency, essential factors for international contractors.	challenging terrains. Additionally, aligning site preparation with international standards can require significant resources and expertise.	timeline for readiness. It should also involve a detailed analysis of the mobilization requirements specific to different drilling operations and their alignment with international best practices. The more prepared a site is, including the ease of setup for rigs and services, the more attractive it becomes for international contractors. This preparedness not only reduces the risk of delays but also demonstrates a commitment to efficient and effective project management. It's important for developers to understand that the initial investment in site readiness can lead to significant long-term benefits, including attracting reputable international drilling companies.
Job owner safety & enviro record	The safety and environmental record of a job owner (developer) plays a crucial role in attracting international drilling companies. A strong record can significantly enhance a developer's appeal, while a poor history may deter contractors due to concerns over recurring incidents that could damage their reputation and lead to potential blacklisting. This strategy involves maintaining high standards in safety and environmental practices and effectively communicating this track record to potential international contractors. It can include regular safety audits, adherence to international environmental standards, and transparent reporting of safety and environmental performance.	A positive safety and environmental record demonstrates a commitment to best practices, which is highly valued by international contractors. It not only ensures compliance with regulations but also builds trust and credibility, making the developer more attractive to work with.	Maintaining a consistently high safety and environmental standard can be challenging, especially in large-scale and complex geothermal projects. It requires continuous monitoring, investment in safety and environmental management systems, and training for staff.	An in-depth assessment would involve examining the current safety and environmental management practices of the developer, identifying areas for improvement, and benchmarking against international standards. It would also include strategies for effectively communicating these standards to potential international partners. While a strong safety and environmental record can be a significant draw for international contractors, it is important for developers to understand that maintaining these standards is an ongoing process that requires commitment and resources. Developers should also be aware that international companies often have stringent criteria for safety and environmental performance, and meeting these criteria can open up opportunities for collaboration and partnership. It's crucial, therefore, to not only focus on maintaining these standards but also on proactively showcasing them as part of the tendering process to attract the best international talent.
Clear, fair, and transparent payment terms & conditions	Implementing clear, fair, and transparent payment terms and conditions is pivotal in attracting international drilling companies to participate in geothermal drilling projects. This approach assures these companies of financial stability and predictability, which is crucial for their involvement in overseas projects.	Clear payment terms significantly reduce financial uncertainties for international contractors, making them more willing to engage in overseas projects. Consistent and fair payment processes build trust and credibility, making the market more attractive to international	Balancing attractive payment terms for international contractors with the financial realities of the project developers can be challenging. Managing international financial transactions, which may involve different currencies and banking systems, adds another layer of complexity to the process.	An in-depth assessment should consider global best practices for payment terms in the drilling industry, understand the specific financial and cash flow requirements of international companies, and align these with the project's financial planning. It's also important to consider factors such as currency exchange rates, international banking regulations, and potential risks related to international financial transactions.

Strategy	Impact on International Participation	Benefits	Challenges	Additional Remarks
	To ensure effectiveness, the strategy should involve drafting and communicating payment terms that are in line with international standards. This includes specifying payment schedules, defining invoicing procedures, and ensuring contractual terms are transparent and equitable. Regular consultations with international stakeholders can also be beneficial to align these terms with global practices.	players and encouraging long-term business relationships.		Ensuring that payment terms are not only fair but also consistently applied and adhered to is critical. Open communication about payment processes, along with a commitment to resolving any payment issues promptly, will further enhance the attractiveness of the market to international companies. This strategy, while focusing on payment terms, forms part of a broader effort to create a welcoming and reliable business environment for international participants in the geothermal drilling sector.
Job owner payment date record	The payment history of job owners in geothermal drilling projects can impact the willingness of international drilling companies to participate. A track record of timely payments can enhance interest from contractors, while a history of delayed or missed payments may deter them. The strategy involves maintaining a transparent and verifiable record of payment histories for job owners. This could include developing a system for tracking and publicly sharing payment timelines, as well as integrating feedback from contractors on payment experiences. Transparency in payment practices and adherence to contractually agreed terms are key.	A good payment record by the job owner builds trust and confidence among potential contractors, particularly international ones who might be wary of payment risks in foreign markets. Timely payments indicate financial stability and reliability, making the job owner a more attractive partner for future projects.	Challenges include ensuring that all payments are processed on time and in accordance with the terms agreed upon in contracts. Additionally, establishing and maintaining a transparent record system that is accessible and credible can be resource intensive.	An in-depth evaluation of this strategy would consider the existing payment processes and how they can be optimized for transparency and efficiency. It would also look at the potential impacts of payment practices on the reputation of job owners and how this affects their ability to attract international contractors. The assessment should include feedback mechanisms for contractors to report on their payment experiences. While maintaining a positive payment record is crucial, it's equally important for job owners to communicate clearly about any potential delays or issues that might arise. Consistent and open communication regarding payment processes can further bolster the trust of contractors. It's essential for job owners to understand that their payment history not only affects current projects but can also influence their ability to attract skilled contractors for future endeavors. As such, adherence to payment terms is a critical factor in fostering long-term partnerships and ensuring the successful execution of geothermal drilling projects.
Contract Currency	The choice of currency used in contracts can significantly influence the participation of international drilling companies in geothermal projects. Using a widely accepted and stable currency can attract more international players by reducing currency risk and simplifying financial transactions. The strategy involves selecting a currency for contracts that is stable, widely traded, and acceptable to both local and international parties. This could involve using major global currencies like the US Dollar or Euro for international contracts. The decision should be based on current	Using a major global currency reduces the currency risk for international contractors, who may otherwise be hesitant to engage in contracts denominated in a less stable or unfamiliar currency. This also simplifies the financial management for these companies, as they are more likely to have experience dealing in major currencies.	The main challenge is managing the exchange rate fluctuations that can impact project costs and revenues when converting to the local currency. Additionally, there may be legal and regulatory considerations in using foreign currencies for domestic contracts.	A thorough assessment would involve analyzing the potential financial impacts of different currencies, including exchange rate risks and the ease of transaction for international contractors. It would also involve understanding the legal implications and ensuring compliance with local and international financial regulations. While choosing a stable, widely accepted currency can make contracts more attractive to international companies, it's important to continuously monitor global financial markets to understand the implications of using different currencies. Maintaining flexibility in currency choice, while ensuring all parties are comfortable with the arrangement, can be key to successful international partnerships. This strategy, when implemented effectively, can make geothermal drilling projects in the region more accessible and appealing to a global market.

Strategy	Impact on International Participation	Benefits	Challenges	Additional Remarks
	financial trends, currency stability, and the preferences of potential international partners.			
Technology and Knowledge Exchange Programs	Implementing technology and knowledge exchange programs can significantly boost the participation of international drilling companies in geothermal projects. These programs facilitate the sharing of advanced drilling techniques and innovations, making international collaboration more appealing and beneficial. The strategy involves establishing partnerships or agreements with international drilling companies to share technology and expertise. This could include joint ventures, collaborative research projects, workshops, training programs, and conferences. The focus should be on areas where local companies can benefit from international expertise and vice versa.	Such programs enhance the technical capabilities of local geothermal projects, incorporating global best practices and cutting-edge technologies. This mutual exchange fosters an environment of continuous learning and improvement, which is attractive to international companies looking to expand their global footprint. It also strengthens the overall quality and efficiency of geothermal drilling operations.	Challenges include coordinating between different entities with varying operational cultures and technological standards. It also requires significant investment in terms of time and resources to establish and maintain these exchange programs.	A detailed assessment would involve identifying areas where technology and knowledge exchange could be most beneficial. This includes understanding the current gaps in local drilling techniques and the advancements available internationally. The assessment should also include a strategy for implementing these exchange programs in a way that aligns with the goals of both local and international entities. For these programs to be successful, there must be a foundation of mutual trust and a clear understanding of the objectives of both parties. It's important that these exchanges are seen as mutually beneficial, rather than one-sided transfers of knowledge or technology. Effective communication and regular evaluations of the program's impact are crucial to ensure ongoing relevance and value to all stakeholders involved. The ultimate goal is to create a symbiotic relationship that enriches the geothermal drilling sector globally.
Clear Legal and Arbitration Framework	Establishing a clear legal and arbitration framework significantly impacts the participation of international drilling companies in geothermal projects. A well-defined legal structure provides a sense of security and predictability, crucial for international companies considering investment in foreign markets. The strategy involves developing and clearly communicating legal frameworks that govern contracts and dispute resolutions. This includes specifying jurisdictional laws, arbitration procedures, and other legalities in contracts. Ensuring these frameworks align with international legal standards is key.	A clear legal and arbitration framework can reduce perceived risks among international companies, encouraging their involvement. It provides a structured approach to resolving disputes and clarifies legal obligations, leading to a more stable and predictable business environment.	Challenges include ensuring the legal framework is comprehensive yet adaptable to various international legal systems. Balancing the needs of local and international laws and maintaining fairness in legal proceedings can be complex.	A detailed assessment would involve evaluating existing legal frameworks and identifying areas where they might conflict with international standards or fail to provide adequate clarity. This assessment should also consider feedback from international companies on legal barriers they face in foreign markets. While developing a robust legal and arbitration framework, it is crucial to engage with legal experts knowledgeable in both local and international law. Regular reviews and updates to these frameworks may be necessary to keep up with changes in international legal standards. Transparency and clear communication about these legalities are essential to build trust and attract international participants. The objective is to create a legal environment where international companies feel confident to invest and participate in the geothermal drilling market.
Promotion of Local Partnerships (Local-International Hybrid Teams)	Forming local-international hybrid teams can greatly enhance international participation in geothermal drilling projects. This approach promotes a collaborative environment where local knowledge and international expertise converge, making projects more attractive to international companies.	Hybrid teams bring together diverse insights and approaches, leading to more innovative and effective problem-solving. International companies benefit from local knowledge, particularly in navigating regulatory and cultural	The main challenges is managing cultural differences and communication barriers within hybrid teams. It requires a concerted effort to foster an inclusive work culture where all team members feel valued and heard.	A detailed assessment should consider the specific skills and knowledge gaps that can be addressed by international experts. It also involves evaluating the best practices for integrating diverse teams, including training programs, team-building activities, and effective communication strategies.

Strategy	Impact on International Participation	Benefits	Challenges	Additional Remarks
	This strategy involves creating teams that combine the strengths of local and international personnel. This can be achieved through joint ventures, partnerships, or direct hiring. The key is to ensure that these teams are balanced in terms of skills, experience, and cultural perspectives.	landscapes, while local teams gain from the global experience and technical expertise of their international counterparts.		The success of local-international hybrid teams hinges on mutual respect and the willingness to learn from each other. Regular assessments and feedback mechanisms can help identify any issues or areas for improvement. It's also important to establish clear goals and expectations for these teams to ensure they work cohesively towards the project's objectives. By leveraging the strengths of both local and international team members, geothermal drilling projects can achieve higher efficiency, innovation, and success. Hybrid teams, composed of both local and international members, have demonstrated significant success within various geothermal enterprises, including Supreme, Star Energy, and Sarulla Operations Ltd, as well as in service consulting firms such as GRG-Geoenergis, Manvitt-ISOR-Verkis-Rigsis (MVIR group). The primary challenge encountered by these organizations does not pertain to the management of cultural differences but rather to navigating government regulations concerning local content requirements and the acquisition of work permits for foreign personnel.
Global Marketing and Branding of Appeal Reputation of Geothermal Industry in Indonesia	Elevating the global marketing and branding of Indonesia's geothermal industry can significantly influence the participation of international drilling companies. By enhancing the industry's appeal and reputation on a global stage, this strategy can attract more international players seeking lucrative and reputable opportunities. This strategy involves a coordinated marketing effort to highlight Indonesia's geothermal potential, success stories, investment opportunities, and regulatory environment. It could include creating promotional materials, participating in international trade shows, digital marketing campaigns, and fostering media relations to showcase Indonesia's geothermal sector.	Effective global marketing and branding can position Indonesia as a leading destination for geothermal development, attracting international companies with its potential for growth and innovation. It enhances the country's image as a stable, promising market for geothermal investment.	The challenges is creating a marketing campaign that accurately represents the opportunities while addressing any potential concerns of international investors. Additionally, differentiating Indonesia's geothermal market in a competitive global energy sector requires a strategic approach and sustained effort.	A thorough assessment should include analysis of current global perceptions of Indonesia's geothermal industry and identifying key areas for improvement. It should also consider the most effective channels and methods for reaching international audiences, including industry events, digital platforms, and networking opportunities. The global branding and marketing of Indonesia's geothermal industry should not only focus on attracting investment but also on building long-term relationships with international partners. It's important to maintain consistency in messaging and to align marketing efforts with the actual developments and achievements in the sector. Building a strong, appealing brand for the geothermal industry requires collaboration among government bodies, industry players, and marketing experts to ensure a unified and compelling portrayal of Indonesia's geothermal potential on the world stage. The Indonesian government has proactively engaged in the promotion of the country's market advantages at various international platforms, including geothermal conferences and workshops. This effort is aimed at highlighting Indonesia's vast geothermal resources and the potential opportunities for investment and development within this sector.

Strategy	Impact on International Participation	Benefits	Challenges	Additional Remarks
				By doing so, the government not only showcases Indonesia's commitment to renewable energy but also seeks to attract global investors and developers to participate in the exploration and utilization of its geothermal potential. This strategy underscores the government's dedication to fostering sustainable energy resources, contributing to the global transition towards cleaner energy sources while simultaneously stimulating economic growth and development within the country.
R&D Collaboration and Grants	Promoting research and development (R&D) collaboration and offering grants can significantly increase the participation of international drilling companies in geothermal projects. This approach fosters innovation and joint ventures between local and international entities, making the projects more appealing to global companies. The strategy involves setting up collaborative R&D programs and offering grants or incentives for joint research projects between local and international companies. This could include partnerships with universities, research institutions, and industry leaders to develop new technologies or improve existing ones for geothermal drilling.	Collaborative R&D projects bring together diverse expertise, leading to innovative solutions tailored to the unique challenges of geothermal drilling. Grants and incentives make these collaborations financially viable, particularly for international companies looking to invest in new markets. These partnerships can lead to technological advancements, cost reductions, and improved efficiency in drilling operations.	The main challenges include securing funding for R&D initiatives, aligning the interests and goals of different partners, and managing intellectual property rights. Additionally, there may be logistical challenges in coordinating joint projects across different countries.	A detailed assessment should include identifying key areas where R&D could significantly impact geothermal drilling operations. It should also involve evaluating potential partners for collaboration, including their expertise, resources, and compatibility with the project goals. The assessment should consider the financial aspects of such collaborations, including the availability and allocation of grants. While R&D collaboration can lead to significant advancements in the geothermal industry, it requires a long-term commitment and a strategic approach. Transparent communication, clear goal setting, and effective management are crucial for the success of these collaborations. Additionally, promoting these opportunities globally can attract a wider pool of international partners, bringing in fresh perspectives and expertise to the Indonesian geothermal sector.
Enhanced Data Accessibility and Visibility, especially for project tender announcement	Improving data accessibility and visibility, particularly in the context of project tender announcements, can significantly boost the participation of international drilling companies in geothermal projects. Easy access to comprehensive and up-to-date information makes it more convenient for these companies to assess and bid for projects. This strategy involves creating a centralized platform or portal where all relevant data about upcoming tenders and projects are readily available. This includes project specifics, timelines, requirements, and any other pertinent information. Ensuring that this platform is regularly updated and accessible globally is crucial	Enhanced data accessibility allows international companies to make well-informed decisions about participating in tenders. It increases transparency in the tendering process and can lead to more competitive bids from a wider range of international players. Easy access to information also reduces the effort and resources international companies need to invest in preliminary research.	The primary challenge lies in maintaining an up-to-date and comprehensive database, which requires continuous monitoring and updating. Ensuring that the platform is user-friendly and navigable for international users who might not be familiar with local systems or languages is another significant challenge.	A detailed assessment would involve evaluating the current state of data dissemination and identifying gaps in information accessibility. It should also consider the technical requirements for creating and maintaining an international-standard data platform, including language support, user interface design, and data security. While improving data accessibility can significantly aid in attracting international participation, it's important to ensure that the platform complies with international standards of data sharing and privacy. Additionally, promoting this platform through international channels can further increase its visibility, making it an effective tool for drawing global attention to Indonesia's geothermal drilling projects. Regular feedback from users can be invaluable in continuously enhancing the platform's effectiveness.

5. CONCLUSION

Some conclusions that can be drawn from this study can be summarized as follows:

- The analysis reveals substantial growth potential within Indonesia's geothermal drilling market, driven by increasing energy demands and government support for renewable energy. The availability of diverse rig capacities and contractor services highlights a robust infrastructure ready for strategic enhancements.
- Competition with the oil and gas industry for rigs poses a significant challenge, impacting cost and availability. The fluctuating oil prices further exacerbate these issues, necessitating agile and strategic procurement practices.
- Adoption of advanced procurement strategies such as bundled contracts and centralized vendor databases (CIVD) can streamline operations and reduce costs.
- Promoting transparency and fairness in payment terms and conditions is crucial for attracting both local and international competition.
- There's a critical need for fostering local-international partnerships and transparent legal frameworks to attract international drilling companies. Such collaborations can introduce advanced technologies and practices essential for the sector's growth.
- Emphasizing training and development to build local expertise in geothermal drilling will decrease dependence on international talent and strengthen the domestic market's capabilities.

6. RECOMMENDATIONS AND PATH FORWARD

Some recommendations and path forward that can be drawn from this study can be summarized as follows:

1. Enhance Procurement Systems

- Adoption of Centralized Vendor Databases: Streamline the tender process by implementing centralized integrated vendor databases (CIVD), which would improve transparency, reduce procurement times, and lower costs.
- Innovative Contracting Approaches: Encourage the use of bundled contracts and well-bundling strategies to capitalize on economies of scale, potentially lowering costs and enhancing operational efficiency.

2. Foster International Collaboration

- Strengthen International Partnerships: Develop frameworks that facilitate technology transfer and joint ventures with international drilling companies. This can lead to improved technology adoption and innovation in drilling operations.
- Regulatory and Legal Framework Enhancements: Ensure that legal frameworks are conducive to international investment and collaboration, providing clarity and stability that international companies crave.

3. Expand Training and Development

- Invest in Human Capital: Enhance training programs to develop local expertise in advanced geothermal drilling techniques. This investment in human capital will pay dividends in increased operational efficiency and reduced reliance on international expertise.
- Research and Development Focus: Promote R&D collaborations between academia, industry, and government to pioneer advancements in geothermal drilling technologies and practices.

4. Market Dynamics and Competitive Strategies

- Regular Market Surveys: Conduct thorough and regular market surveys to gauge rig availability, service costs, and contractor capabilities, which will aid in timely and effective decision-making.
- Flexibility in Procurement Practices: Adapt procurement strategies in response to market conditions to optimize cost and efficiency, particularly during fluctuations in the oil and gas sector, which impact the geothermal drilling market.

By implementing these recommendations, Indonesia can enhance its position as a leader in geothermal energy, driving both domestic and international investments, while promoting sustainable and economically viable energy solutions. The path forward involves a coordinated effort across multiple facets of the industry to ensure that the potential of Indonesia's geothermal resources is fully realized.

REFERENCES

Adityatama, D.W, Al Asy'ari, M. R., Athalia, J., Fadhillah, F. R., Purba, D.: Proposed Methodology for Generating Geothermal Drilling Cost Estimate in Indonesia: a Case Study in Central Java and West Java. Proceedings World Geothermal Congress 2023 Beijing, China, April 17 – 21, (2023).

EBTKE.: Pengembangan Panas Bumi, Jakarta: Direktorat Panas Bumi. (2023b)

Energy Economist.: Asia Pacific - Oil & Gas Rig Count. [Online]. Available at: http://www.energyeconomist.com/a6257783p/exploration/world/iog/Asia%2520Pacific%2520Oil%2520& %2520Gas%2520R ig%2520Count.html, (2021).

GRG-Geoenergis.: Geothermal Drilling Costs in Indonesia: Statistics, Influencing Factors, Benchmark, and Industry Practices. (unpublished works).

Gul, S. & Aslanoglu, V.: Drilling and Well Completion Cost Analysis of Geothermal Wells in Turkey. Stanford, California, s.n, (2018).

Hartono, Y.: Rig Sizing for Geothermal Well, Bandung, Indonesia: EBTKE, (2023).

PGE.: Proyek Pengembangan - Lumut Balai Unit 2. [Online]. Available at: https://www.pge.pertamina.com/id/proyek pengembangan/lumut-balai-unit-2, (2023).

PLN.: Rancangan Usaha Penyediaan Tenaga Listrik 2021 - 2030, Jakarta: s.n, (2021).

Purba, D. et al.: Geothermal Drilling Cost Optimization in Indonesia: A Discussion of Various Factors. California, IGA, (2020).

United States - Producer Price Index by Industry.: Drilling Oil and Gas Wells, (2023).

Advances in High Temperature Directional Drilling

John Clegg, Peter Harvey, Steve Krase, Gorka Plata, Shraddha Singh, and Matthew White

515 W Greens Road, Suite 316
Houston, TX 77067, United States

jmclegg@hephaeet.com

Keywords: EGS, AGS, unconventional, temperature electronics, sensors, drilling

ABSTRACT

Enhanced and advanced geothermal systems (EGS and AGS) are new methods of creating geothermal installations that will potentially increase electric power production by a factor of greater than 10 when compared with more conventional methods. Many such systems are emerging, and they are attracting a lot of funding and excitement. But compared with conventional hydrothermal wells, they are technically challenging to drill. Accurate well positioning, generally including horizontal wells, will be required for the most advanced well designs to succeed. The oil and gas industry can already drill accurate directional wells and this capability is directly transferable to some of the first EGS and AGS wells because they are likely to be drilled at temperatures familiar to oil and gas drillers. But to make EGS and AGS wells more economically interesting, they will need to be drilled at higher temperatures which are currently beyond the capabilities of oil and gas drilling, completions, and production equipment.

Even the claimed 175°C operating capability of oil and gas technologies is challenging for the economics of geothermal drilling because equipment operated at this maximum temperature limit exhibits low main time between failure and/or service. Therefore, the industry needs a step change in its approach to the temperature capabilities of downhole equipment. This presentation will outline just such an approach to the temperature resistance of the electronics and sensors needed.

Showing in detail a new approach to tool design, it will describe how a combination of component selection, a completely reimagined approach to downhole electronics, and multiple cooling strategies will allow measurement and control to be reliably implemented at higher temperatures, initially above 200°C and ultimately as high as 300°C. This will finally make reliable drilling at high temperature a reality and the presentation will conclude by showing results achieved to date during high temperature testing.

1. INTRODUCTION – UNCONVENTIONAL GEOTHERMAL

Although geothermal wells have been drilled for electric power for more than 100 years, since the first power station was built at Lardarello in Italy in 1924 (Clegg and Krase, 2022), the industry has long been associated with hydrothermal reservoirs, whereby hot fluid is found in naturally fractured formations and can be exploited by drilling wells to transport the hot water and/or steam to the surface. Where such reservoirs exist, they can be a very effective source of heat for power generation, but they are not geographically abundant. They tend to be confined to parts of the world where there is heat close to the surface which itself is combined with said fractured formations and water reservoirs. Unless solved, this geographic confinement would prevent the exploitation of geothermal energy for power at a global scale, with only a small number of "lucky" countries benefiting.

Recently, though, the picture has changed. Numerous different styles of enhanced and advanced geothermal systems (EGS and AGS) have been funded, and some have already been demonstrated at pilot scale. Although the design and principle of operation of each style is unique, they all share one binding characteristic: they create an artificial reservoir instead of relying on a natural, hydrothermal one.

Pioneers such as Fervo and Eavor are demonstrating that EGS and AGS can be made to work, with Fervo demonstrating for the first time that electricity can be reliably generated from an EGS well in Nevada in 2023 (Think Geoenergy, 2023).

Although their modes of operation are very different, both companies, and the vast majority of their potential competitors, rely on accurate directional drilling techniques, placing wells a precise distance apart and in some cases connecting them together at the end, many kilometres below the surface. That might seem like an extraordinarily difficult thing to do, but the directional drilling techniques that have been developed by the oil and gas industry over the last 100 years now allow wells to be placed very accurately (Clegg, 2021).

2. UNCONVENTIONAL OIL AND GAS

In a striking parallel with unconventional geothermal, the unconventional oil and gas industry also emerged by creating artificial reservoirs. In this case, the reservoirs were created by fracturing shale, normally thought of as the source rock for conventional oil and gas reservoirs. The most important of the technologies that enabled unconventional oil and gas wells to be drilled at scale were horizontal drilling and hydraulic fracturing. The directional well profiles that will be required to make unconventional geothermal a success are very similar to those used in unconventional oil and gas: increasingly long horizontal sections to maximise exposure of the well to the premium resource. In the case of oil and gas wells, the premium resource is hydrocarbon. In the case of unconventional geothermal wells, the premium resource is heat. Geometrically, the wells look very similar in either case. The most significant difference is temperature, and this will be discussed further in section 5.

The similarity with unconventional oil and gas is important, because of the cost savings that have been made in that industry over the last 15 years. These cost savings should be directly applicable to the unconventional geothermal industry.

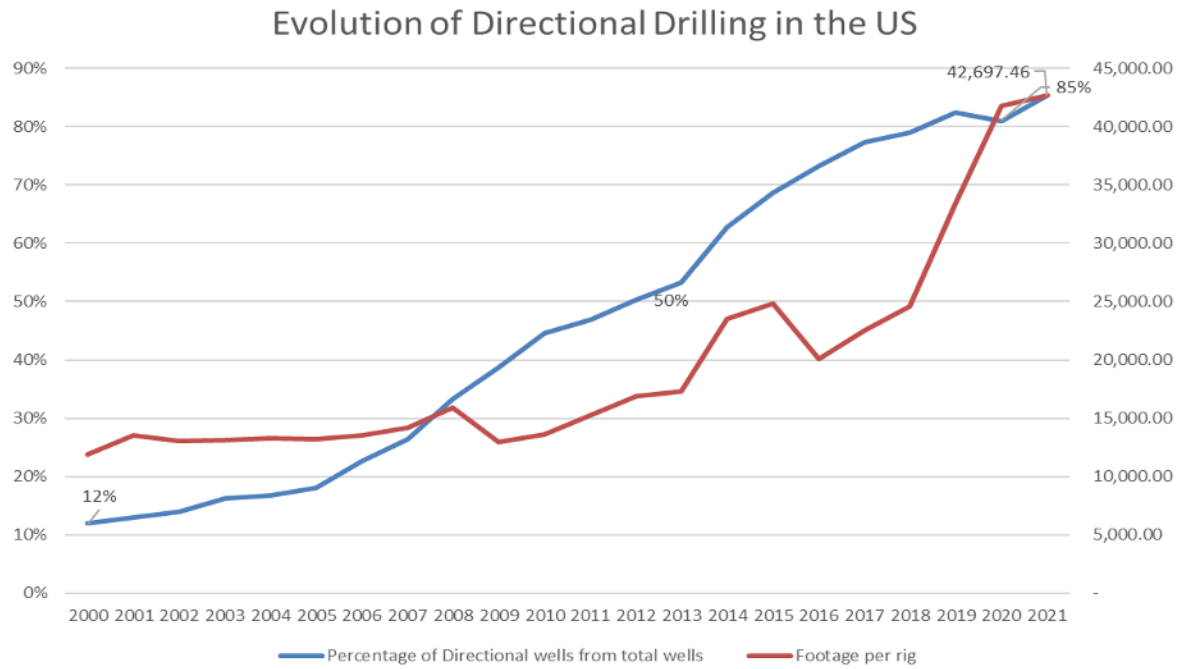

Figure 1: Evolution of the prevalence of directional drilling, and its cost, in the United States.

Figure 1 includes an amalgamation of data from Baker Hughes (bakerhughes.com, n.d.), the United States Energy Information Administration (eia.gov, 2022), and St. Louis Fed (stlouisfed.org, n.d.). It clearly shows how directional drilling has grown from a relatively small niche to the vast majority of wells drilled in the United States during the unconventional shale revolution. It also illustrates how the cost of drilling these wells has come down, with the footage drilled annually per rig increasing by a factor of more than three.

Similar cost savings will be available to the unconventional geothermal industry.

3. TARGETS FOR GEOTHERMAL TO SCALE

In its "Enhanced Geothermal Shot" initiative (energy.gov, n.d.), the United States Department of Energy identified five key areas where technical challenges need to be solved in order to create pathways to a 90% reduction in the cost of EGS by 2035. Two of these are related to subsurface modelling and one to completions and production. The other two are directly related to well construction and include the following specific targets:

- "drill the wellbore at 4X speed"
- "reduce well construction cost by 60%"
- "enable access to 50% more hot rock".

The technology developed for unconventional oil and gas can directly influence these targets. Figure 1 above shows how drilling speed has improved in the unconventional oil and gas industry – the number of feet drilled per rig per year is in inverse proportion to the speed at which the well is drilled. Well construction costs have reduced

in line with this. Additionally, the horizontal drilling techniques pioneered in the unconventional oil and gas industry will allow increasingly long directional or horizontal geothermal wells to be drilled, significantly increasing exposure to hot formations. Based on the progress that the oil and gas industry made over the last 15 years, 50% seems like a very conservative target.

4. UNCONVENTIONAL GEOTHERMAL CASE HISTORIES

There is already evidence that techniques imported from oil and gas drilling are reducing the cost of unconventional geothermal wells.

Results from the Frontier Observatory for Research in Geothermal Energy (FORGE) drilling site in Utah, United States, have shown that drilling speed improved from 14 ft/h to 71 ft/h, a five-fold improvement, between 2017 and 2022, simply by applying oil and gas drilling technologies (US Department of Energy, 2024). The same reference stated that there is still a two-to-three-fold improvement available if the drilling speeds typically achieved in oil and gas can be transferred.

Earlier in 2024 (El-Sadi, *et al*, 2024) Fervo reported significant improvements in drilling performance from their initial wells in Nevada and Utah, United States. Like FORGE, they demonstrated sustained drilling rates of 70 ft/h, resulting from the use of modern drilling techniques imported from the oil and gas industry. Their paper contrasted this with the 25 ft/h baseline estimated by SANDIA (Lowry, et al, 2017) as recently as 2017.

5. THE IMPORTANCE OF TEMPERATURE CAPABILITY

The findings above suggest that the cost targets set by the Department of Energy "Enhanced Geothermal Shot" are very achievable. But as well as reducing the cost of an installation, there are also gains to be found in increasing its value. The leverage of temperature in terms of the value of the well is very high.

A number of scenarios were modelled using the US Department of Energy Geothermal Electricity Technology Evaluation Model (US Department of Energy, 2016). When normalised, they revealed a constant pattern in that the cost of electricity reduces significantly as the temperature of the rock exploited increases. This is clearly shown in Figure 2 below.

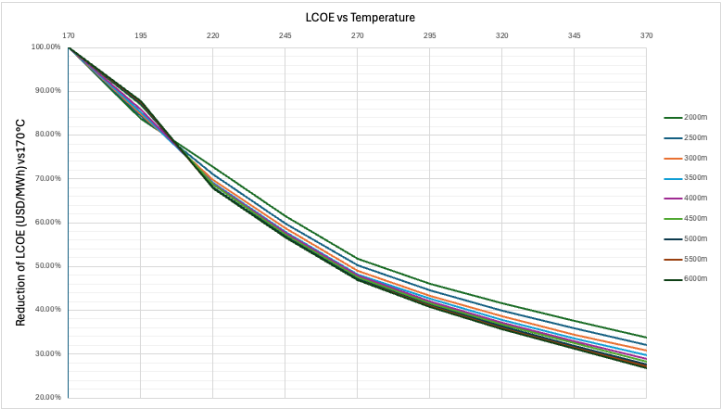

Figure 2: LCOE as a function of reservoir temperature.

The graphs show a consistent and significant reduction in levelized cost of electricity (LCOE) as a result of temperature for EGS systems modelled using GETEM. Results are not shown here for AGS, but increasing temperature has a very similar impact on their economics.

Compared with a baseline (100%) at 170°C, increasing the reservoir temperature to 210°C will reduce the LCOE to approximately 75% of the baseline value. At 300°C, LCOE is only about 30% of baseline. This demonstrates extremely important economic value that will come from deeper and hotter geothermal wells.

170°C was chosen because it is close to the claimed temperature rating of drilling and measurement tools currently used in the oil and gas industry. Typically, this might be 175°C. Occasionally it can be higher, up to 200°C, for a fairly small number of (most likely) expensive tools.

However, this temperature rating is no guarantee that tools will work reliably at such temperatures. The environment in which they are deployed is harsh and difficult, and they often fail prematurely at temperatures lower than their rating.

Research based on drilling a high temperature field in the United States shows a correlation of measurement while drilling (MWD) failures with temperature, but at lower temperatures than would have been expected.

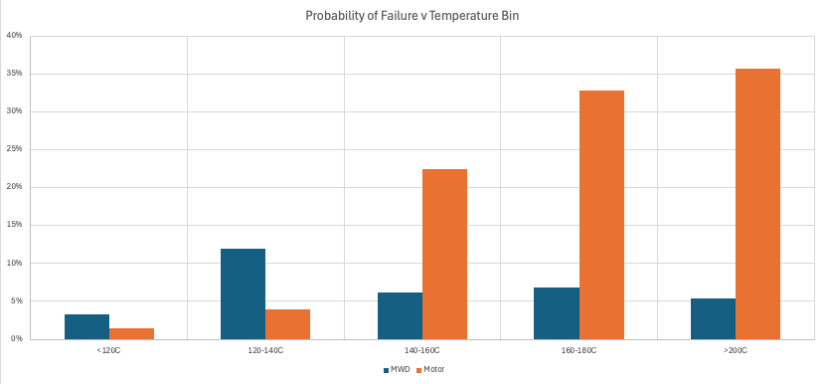

Figure 3: Probability of run terminating failure as a functional temperature.

Rather than working reliably to 175°C, Figure 3 shows that MWD reliability drops off 120°C and 140°C. The picture would probably be worse above 140°C, but for the fact that by then drilling motors, which have a significant elastomeric content in their moulded stators, start to fail even more rapidly than MWD – thereby masking what would otherwise likely be a higher number of run terminating MWD failures at higher temperatures.

This clearly demonstrates the difficulty of drilling at increasingly higher temperatures with equipment directly imported from the oil and gas industry.

6. A HIGH TEMPERATURE DRILLING SYSTEM

Figure 4 shows what a combined high temperature MWD and rotary stable system (RSS) will look like. This drilling system is being developed for operation initially at 210°C, but by 2030 it is anticipated that it will be working reliably at circulating temperatures as high as 300°C.

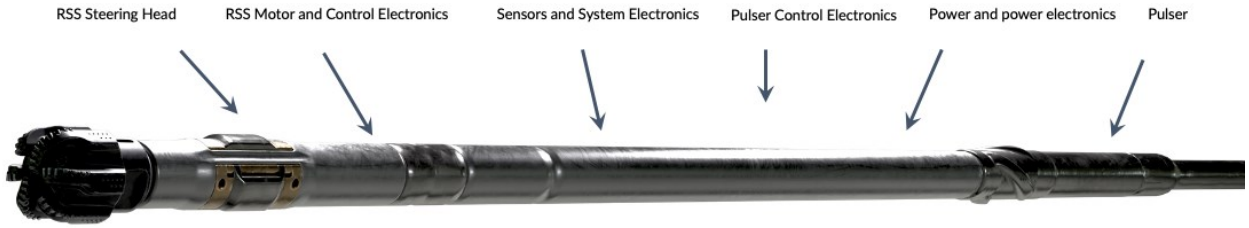

Figure 4: Combined RSS/MWD for high temperature operation.

Closest to the drill bit is the RSS steering head. This can be identical to the type of steering head used in oil and gas wells, with pads and/or pistons that extend once per revolution and urge the bit sideways. However, RSS tools used in oil and gas generally have their own sensor packs and control systems, independent from those used in an adjacent MWD tool – mostly for historic reasons. There is no technical reason why these two set of sensors and electronics cannot be combined. A high temperature drilling tool for geothermal should combine them in order to save on space, cost and technical risk.

Approximately halfway along the tool as illustrated there is a set of sensors and system electronics that is able to measure the direction and inclination of the well, and control a positive mud pulser to send this information to surface. The same sensors can also derive rotational position of the tool and drive electronics that control the steering head. Both the pulser and steering head are controlled with pilot valves that themselves are driven by brushless DC motors.

This drilling assembly can be driven directly from surface, from the top drive, or can be "motorised" in the same way as in oil and gas wells, where a drilling motor is placed above the tool in order to provide additional power downhole. However, conventional mud motors used in oil and gas will suffer at high temperature because of the use of elastomers in their stator assemblies. Options to resolve this include all metal motors (Stefánsson *et al,* 2018) or geared turbines (Jones, Feddema and Sugiura, 2016), both of which can avoid the temperature limitations of the elastomeric stator.

If RSS is not required, the MWD is capable of being used with an oriented directional motor, again very much like oil and gas drilling. As above, the orientation could be of a motor with a metal power section or, again, it could use a geared turbine.

Critical to the success of such a drilling system will be the temperature capability of the sensors and electronics used.

7. A NEW APPROACH TO TEMPERATURE RESILIENCE

Generally, the approach employed to date when attempting to make high temperature drilling and measurement tools has either been to find electronic components that will work at the ambient temperature via a process of screening and selection (Beckwith, 2013) or to try to shield the entire tool from temperature and cool it (Vedum *et al*, 2017 and Stefánsson *et al,* 2018*)*.

Despite many years of trying, the former approach does not appear to capable to get equipment to work reliably above an operating temperature of 200°C. One or two oil and gas manufacturers have managed to get close to 200°C, by using technologies including application specific integrated circuits (ASICs) or multi-chip modules (MCMs). Unfortunately, these approaches suffer from very high non-recurring engineering (NRE) charges, making them unsuitable for products like high temperature drilling tools which are made in low volumes.

A new approach builds on but also modifies these previous attempts. It uses discrete components either selected for or protected from the operating temperature. Discrete components are considered a more cost-effective way of building low volumes of tools. The new approach considers three key requirements:

- Protect the assembly from the external borehole temperature
- Protect components from themselves and efficiently and quickly remove the heat that the components generate internally
- Take the rejected heat from the components to a place where it will do no harm.

This new approach creates a system for mounting boards which allows heat to be removed and rejected quickly. As a first step, it replaces the rectangular printed circuit boards (PCBs) which are ubiquitous in oil and gas drilling and measurement tools, and replaces them with a circular board design. Further, instead of being placed parallel to the axis of the tool, the circular boards are placed normal to the drilling axis in a stack – or perhaps more accurately, in a series of stacks.

The small size of the board means that no component is very far from its edge, and the circular shape tends to promote heat flow, with resistance to radial flow reducing as a function of radial position. The function of the board, and the numerous special materials used in its construction, is to get heat away from vulnerable components as quickly as possible and to the board circumference.

Once at the circumference, the heat can be picked up by a stack of thermally conductive rings which act somewhat like a “thermal superhighway” to take heat away from the board. This “superhighway” could take heat to a pressure vessel which is in contact with drilling fluid flowing past the outside of the tool. This would allow the tool to take advantage of the cooling nature of the drilling fluid, which will almost certainly be at a lower temperature than the formation being drilled. It also allows operation in tandem with technologies like mud chillers and insulated or coated pipe, which can further reduce said temperature of the drilling fluid.

Alternatively, for higher temperature tools, especially as the operating temperature approaches 300°C, the “superhighway “could take heat into a variety of cooling options, which will not be described in this paper. The combination of circular boards and conductive rings lends itself very well to a modular architecture which allows different boards to be treated differently in terms of how they are cooled. By dividing the tool into a small number of stacks of boards, it becomes possible to have very small, compact chambers which can be maintained at different temperatures if necessary. In order for systems to remain cost effective, cooling must be used selectively. Previous projects described above have attempted to cool the whole assembly to the minimum capability of any individual component. This can work for short periods of time, however this approach can be very expensive and power hungry. An alternative approach is to build a series of small chambers and cool each to an appropriate temperature for the weakest component therein. This will avoid cooling a lot of components that do not need it and is much more efficient than maintaining the whole tool at a low temperature.

Figure 5 shows an example of the new generation, high temperature circuit board.

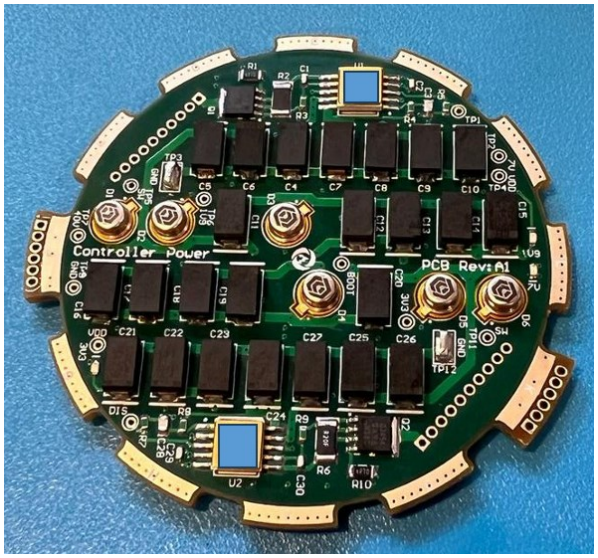

Figure 5: New generation circular PCB.

Figure 6 shows one element of the axial stack of PCBs.

Figure 6: One element of axial PCB stack.

Based on the design of multiple stacks as depicted in Figure 6, thermal modelling has been used to optimize the combination of geometric design and materials selection. As can be appreciated from Figure 7, this modelling has shown that it is possible to keep the temperature of components of the board in a multi-stack assembly within 3.7°C or less of the surrounding environment in an optimized PCB assembly and within 6.5ºC or less of the surrounding environment in a conventional PCB assembly.

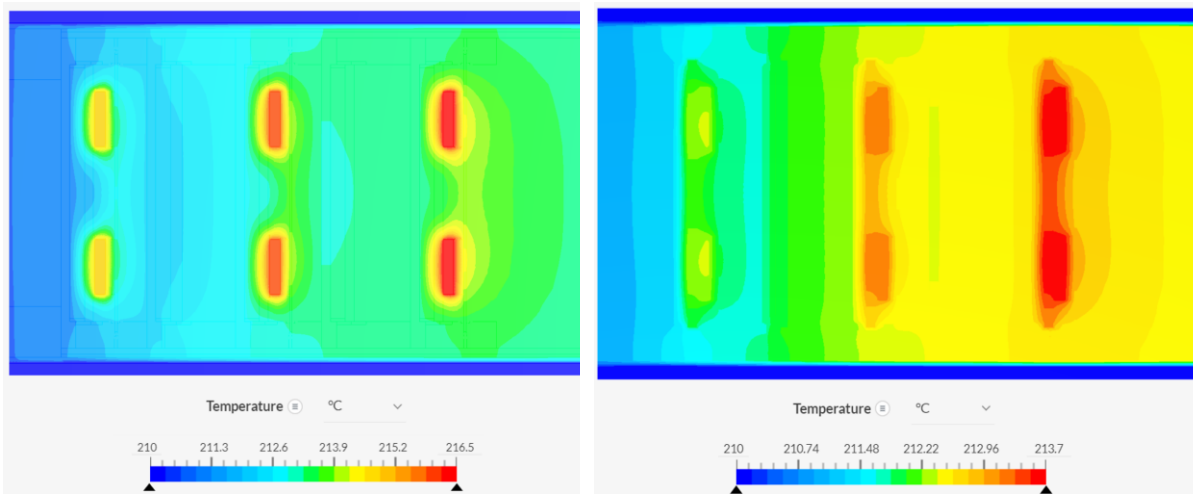

(a) **(b)**

Figure 7: Thermal modelling of a multi-stack using (a) conventional and (b) optimized PCBs.

8. TEST RESULTS

Initial testing has focused on proving "the physics" for a 210°C drilling tool – that is, heat testing components and boards temperatures between 220°C and 230°C for extended periods to make sure that there are no fundamental issues that will prevent components from working – such as leakage or capacitance issues. This testing has proved successful, with components, prototype boards and downhole ready boards heat soaked at these high temperatures for over 500 hours.

Further work will require highly accelerated life testing (HALT) which combines temperature with shock and vibration to fully replicate the downhole conditions that components and boards will see. However, solving problems that might emerge at this stage is simply an engineering challenge. It does not challenge the physics in the way that initial heat testing has already done.

9. CONCLUSIONS

Unconventional geothermal systems (EGS and AGS) bring exciting new possibilities to the geothermal industry and will allow it to scale globally.

They can leverage techniques including directional and horizontal drilling developed for oil and gas and perfected in the unconventional shale boom in the last 15 years.

Those technologies have demonstrated remarkable cost savings in unconventional shale wells that should be directly transferable to geothermal drilling. But the technologies used in oil and gas do not usually work above 175°C and never above 200°C. In fact, it appears that systems tend to have reliability problems someway below their claimed temperature specification capability.

Temperature has a very strong leverage on the economics of unconventional geothermal systems, with modelled LCOE being very strongly dependent on formation temperature.

A high temperature directional drilling system is being developed which avoids the use of elastomers and incorporates new ways of protecting electronics and sensors from temperature. Instead of using long, rectangular PCBs, the new system will use circular PCBs mounted in stacks where the boards are orthogonal to the drilling axis.

This allows three key requirements for temperature management in high-temperature tools to be addressed

- Protect the assembly from the external borehole temperature
- Protect components from themselves and efficiently and quickly remove the heat that the components generate internally
- Take the rejected heat from the components to a place where it will do no harm.

Cooling may be required for operation at high temperatures, but it is not necessary to cool the entire tool – only those components that need it.

Initial test results are very encouraging, and have already shown that a 210°C tool is feasible, with much higher temperature capabilities to follow.

ACKNOWLEDGEMENT

The authors would like to thank the team at Hephae Energy Technology for their support and inspiration.

REFERENCES

Baker Hughes: Rig Count Overview & Summary Count, https://rigcount.bakerhughes.com/ (n.d.)

Beckwith, R.: Downhole Electronic Components: Achieving Performance Reliability, *Journal of Petroleum Technology* (2013).

Clegg, J.: Optimizing Directional Drilling While Simultaneously Maximizing the Whole Life Value of the Well, *SPE-207342-MS*, prepared for presentation at the Abu Dhabi International Petroleum Exhibition & Conference held in Abu Dhabi, UAE (2021).

Clegg, J., and Krase, S.: New-Generation Geothermal Wells – How the Upstream Oil and Gas Industry Can Bring Its Experience to Bear, *IADC/SPE-208747-MS,* presented at the IADC/SPE International Drilling Conference and Exhibition held in Galveston, TX, USA (2022).

El-Sadi, K., Gierke, B., Howard, E., and Gradl, C.: Review Of Drilling Performance In A Horizontal EGS Development, *Proceedings*, 49th Workshop on Geothermal Reservoir Engineering, Stanford University, Stanford, CA, USA (2024).

Federal Reserve Bank of St Louis: Industrial Production: Mining: Drilling Oil and Gas Wells, https://fred.stlouisfed.org/series/IPN213111S (n.d.).

Jones, S., Feddema, C., and Sugiura, J.: A Gear-Reduced Drilling Turbine Provides Game Changing Results: An Alternative to Downhole Positive Displacement Motor, *SPE-178851-MS*, presented at the IADC/SPE Drilling Conference and Exhibition, Fort Worth, TX, USA, (2016).

Lowry, T., Finger, J., Carrigan, C., Foris, A., Kennedy, M., Corbet, T., Doughty, C., Pye, S., and Sonnenthal, E.: GeoVision Analysis: Reservoir Maintenance and Development Task Force Report (GeoVision Analysis Supporting Task Force Report : Reservoir Maintenance and Development). doi:10.2172/1394062 (2017).

Office of Energy Efficiency and Renewable Energy: Enhanced Geothermal Shot, https://www.energy.gov/eere/geothermal/enhanced-geothermal-shot (n.d.).

Stefánsson, A. *et al*.: A 300 Degree Celsius Directional Drilling System, *IADC/SPE-189677-MS,* presented at the SPE/IADC Drilling Conference, Fort Worth, TX, USA (2018).

Think Geoenergy: Fervo Energy Has Announced a Major Milestone With the Successful Drilling, Stimulation, and Testing Results From the Full-Scale EGS Pilot Project in Nevada https://www.thinkgeoenergy.com/fervo-energy-reports-breakthrough-in-field-scale-egs-project-in-nevada/ (2023).

Vedum, J., Røed, M., Kolberg, S., Hjelstuen, M., Liverud, A., and Stamnes, Ø.: Development of a Novel Logging Tool for 450°C Geothermal Wells, *Proceedings*, Conference and Exhibition on High Temperature Electronics Network (HiTEN), Cambridge, UK (2017).

US Department of Energy, Geothermal Technologies Office: Geothermal Electricity Technology Evaluation Model, https://workingincaes.inl.gov/SiteAssets/CAES%20Files/FORGE/inl_ext-16-38751%20GETEM%20User%20Manual%20Final.pdf (2016).

US Department of Energy: Pathways to Commercial Liftoff: Next-Generation Geothermal Power, https://liftoff.energy.gov/wp-content/uploads/2024/03/LIFTOFF_DOE_NextGen_Geothermal_v14.pdf (2024).

US Energy Information Administration: Nearly All New U.S. Crude Oil and Natural Gas Wells Are Horizontal Or Directional, https://www.eia.gov/todayinenergy/detail.php?id=52138 (2022).

Estimating Pressure Drop in Two-Phase Geothermal Fluid Flow

Sanjay Banerjee and Patrick Robinson

MB Century Ltd, 166 Karetoto Road, Wairakei 3384, New Zealand

SBanerjee@mbcentury.com, PRobinson@mbcentury.com

Keywords: Geothermal Two-Phase Flow, Pressure Drop, Homogeneous Flow Model, Separated Flow Model, Harrison Method

ABSTRACT

Estimation of pressure drop in two-phase fluid flow is implicitly a more complex process compared to that for single-phase fluids. Empirical correlations proposed for two-phase pressure drop are based on experiments carried out with air-water mixture in small, horizontal pipelines and do not represent large, cross-country, geothermal two-phase fluid conveying pipelines. The analytical procedure followed in the geothermal industry to predict pressure drop in two-phase pipeline is to apply the available methods and then use correction factors, commonly followed as industry practice based on actual field observations.

Two distinct flow models are commonly used to analyse two-phase flow. In homogeneous flow model, a pseudo single-phase fluid is defined and assumed to be uniformly distributed in the pipe, traveling at a uniform velocity. In separated flow model, the gas and liquid phases are assumed to flow separately within the pipe cross-section. Distinct hydrodynamic and thermal parameters for each phase are determined using void fraction and applied to separate energy equations for each phase, in equilibrium with each other.

The pressure drop in two-phase fluid flow comprises of 3 components — a) frictional, b) acceleration component and c) gravity. The pressure loss predicted as per analytical methods is typically found to underestimate the actual pressure drop in geothermal two-phase pipelines and it is common to apply correction factors to the theoretical results to represent real industrial installations.

Traditionally, spreadsheet-based design tools, based on established theories and correlations proposed for two-phase flow analysis, have been used by geothermal design engineers to estimate pressure losses in geothermal two-phase pipelines. This paper discusses the general theory, assumptions and procedures followed to develop such analytical design tools. The correlations and procedures covered in this report are those proposed by R.F.Harrison (1975) , a graduate student at Auckland University, as part of his Masters thesis and experiments carried out in Wairakei geothermal field, with support and sponsorship of the then Ministry of Works, NZ.

1. INTRODUCTION

The outcome of pressure drop analysis and other key process design parameters, forms the basis for selecting the steamfield development options and determining an appropriate generation facility for geothermal.

Estimating pressure drop in a two-phase geothermal fluid flow, however, involves a somewhat more complex procedure compared to pressure drop in a single-phase fluid flow. Over many decades, there has been extensive research and studies conducted on the mechanism of two-phase (gas & liquid) fluid flow and many papers are available proposing correlations to predict the estimated pressure drop. Most detailed studies relating to geothermal fluids were carried out in small (200 mm or smaller dia), near-horizontal pipes, accompanied by heat transfer. With the increase in implementation of centralized separation plants, two-phase conveying pipelines in modern geothermal plants typically comprise of significantly larger pipes (up to 1.3m diameter) along inclined and nonlinear cross-country routes, often running over several kilometers between wellpads and separation plants. As a result, most of the correlations and equations proposed based on published experimental studies are not directly applicable to modern geothermal two-phase conveying systems. To date, there is no unified methodology for accurately determining pressure losses in large geothermal two-phase pipelines, across range of fluid qualities and flow regimes.

The objective of this paper is to present, in a summarised manner, an overview of the analytical procedure commonly followed by geothermal engineers to estimate two-phase pressure drop. Findings specific to the authors' experience are also shared.

2. ANALYSIS MODELS

Two distinct physical model options are mostly used to analyse and estimate pressure drop in two-phase geothermal fluid flow.

2.1 Homogeneous Flow Model

The homogeneous flow model assumes liquid & gas phases are uniformly distributed across pipe cross-section and travelling with the same velocity. The mixture is treated as an equivalent pseudo single-phase fluid, with suitably defined hydrodynamic and thermal properties.

The homogeneous flow model presents the simplest approach for analysis. However, defining effective physical properties for the equivalent single-phase fluid is difficult and the inaccuracies in assuming the void fraction, mean viscosity and similar critical parameters increase as the flow pattern transitions beyond bubble or stratified regimes. The analysis based on homogeneous flow model tends to overestimate the pressure losses, particularly in the higher ranges of pressure drops.

2.2 Separated Flow Model

In this model liquid & gas phases are assumed to flow separately as continuous phases within pipe cross section, as if in 2 separate pipes. In this approach, the most important parameter is void fraction (α), and using it various other two-phase flow parameters, such as individual phase velocities and mean fluid density, a set of equations is applied for each phase to determine the overall pressure drop.

The separated flow model relies on empirical correlations to determine void fraction, flow regime, and interactions between phases. Results vary significantly depending on the correlation followed. The correlation used by the authors is the so-called Harrison-Freeston method. Harrison, a former graduate student at the Geothermal Institute in Auckland, postulated the correlation in his thesis based on his study of test results by Freeston et al in the Wairakei steam field. It is believed that the pressure drop prediction determined as per Harrison's method generally presents results closest to actual field observations. However, not enough field studies have been conducted to substantiate the hypothesis and the discrepancy between theoretical and actual pressure drop can be significant. The margin of error tends to increase as the flow pattern approaches the slug flow regime.

3. COMMONLY USED PRESSURE DROP CALCULATION METHODOLOGIES

From the conservation of energy principle, the total pressure loss in pipe flow is given by:

$$\Delta P_{Total} = \Delta P_{fr} + \Delta P_{mom} + \Delta P_{gr} \quad (1)$$

Where:

ΔP_{fr} = Pressure losses due to frictional effects
ΔP_{mom} = Pressure losses due to acceleration or change in momentum
ΔP_{gr} = Pressure change due to variation in elevation

Analytical computation of each of the components in Equation 1 above are briefly discussed in sections hereinafter.

3.1 Void Fraction

The void fraction, α is defined as the ratio of cross-sectional area occupied by the vapour phase to the pipe cross section.

$$\alpha = \frac{A_v}{A} = \frac{A_v}{A_v + A_l}, \quad (2)$$

Void fraction is one of the most important parameters for two-phase flow analysis, and many empirical correlations are proposed for determining this. It is, however, safe to state that no single correlation seems to accurately predict void fraction that covers geothermal two-phase flows across all fluid conditions, flow regimes, pipeline sizes & geometries.

A well-known method for two-phase pressure drop estimation, used by the author is the correlation proposed by R.F.Harrison (1977). Harrison used the following empirical equation to determine void fraction, which was based on experimental results found by Butterworth (1975) from tests on horizontal pipelines.

$$\alpha = \frac{1}{1 + \frac{(1-x)}{x}^{0.8} + \frac{\rho_g}{\rho_l}^{0.515}} \quad (3)$$

Another correlation for void fraction determination, which is also often used in two-phase flow analysis, was proposed by Zhao, Lee and Freeston (2000) as a refined and more accurate prediction based on 'seventh power law' of velocity distribution. The empirical correlation is given below and can be solved iteratively for α.

$$\frac{1-\alpha}{\alpha^{7/8}} = \left[\left(\frac{1}{x}-1\right)\cdot\left(\frac{\rho_g}{\rho_l}\right)\cdot\left(\frac{\mu_l}{\mu_g}\right)\right]^{7/8} \quad (4)$$

3.2 Pressure Drop due to Friction and Momentum Changes

Frictional pressure losses are dictated by the interactions between individual phases with the pipe wall and the resulting shear force exerted by the pipe opposing the flow.

Pressure drop due to momentum changes is the result of energy dissipated in the form of acceleration of the two-phase fluid velocity, due to flashing of liquid and expansion of the gas phase.

3.2.1 Separated Flow Model

The Harrison method combines pressure drop components due to frictional and momentum components in following correlation:

$$\Delta P_{mom} + \Delta P_{fr} = \frac{4\cdot\tau_w}{D\times(1-AC)} \quad (5)$$

The wall shear stress is given by

$$\tau_w = 1/2\cdot C_f\cdot\rho_l\cdot {V_l}^2 \quad (6)$$

The wall shear stress can also be expressed in terms of mass flow rate and void fraction, as follows

$$\tau_w = 1/2\cdot C_f\cdot\frac{W^2(1-x)^2}{\rho_l\cdot A^2\cdot(1-\alpha)^2} \quad (7)$$

The acceleration component represents energy losses due to changes in momentum flux and is typically much smaller compared to losses due to frictional and static head components. The term AC in Eqn [5] is. given by -

$$AC = \frac{W^2.x^2}{\alpha\cdot A\cdot P\cdot\rho_g} \quad (8)$$

The wall skin factor for two-phase flow was proposed as follows

$$C_f = 1/4\cdot f_T \quad (9)$$

The friction factor f_T can be graphically selected from a Moody chart. The Colebrook-White equation below estimates the friction factor analytically, based on pipe roughness and Reynold's number. The equation requires iterative solution and can be set-up in Excel based spreadsheet in different options.

$$\frac{1}{\sqrt{f_T}} = -2\log_{10}\left(\frac{\varepsilon/_D}{3.7}+\frac{2.51}{R_e\cdot\sqrt{f_T}}\right) \quad (10)$$

There are many alternative empirical formulae proposed to approximately determine friction factor. Serghides's solution below provides a very high degree of accuracy.

$$A = -2\log_{10}\left(\frac{\varepsilon/_D}{3.7}+\frac{12}{R_e}\right)$$
$$B = -2\log_{10}\left(\frac{\varepsilon/_D}{3.7}+\frac{2.51A}{R_e}\right)$$
$$C = -2\log_{10}\left(\frac{\varepsilon/_D}{3.7}+\frac{2.51B}{R_e}\right)$$
$$f_T = \left\{A-\frac{(B-A)^2}{C-2B+A}\right\}^{-2} \quad (11)$$

The Reynolds number used above is based on liquid phase superficial velocity (theoretical velocity if the entire pipe cross section was occupied by the liquid phase alone), using liquid phase fluid properties, where

$$V_l = W\cdot(1-x)/(\rho_l\cdot A)$$

For commercial steel pipes in geothermal two-phase fluid service, a pipe roughness value upto 0.50 mm is generally used, unless specific data is available.

3.2.2 Homogeneous Flow Model

The Homogeneous method for two phase flow pressure drop is simply the application of the Darcy-Weisbach equation to a pseudo single-phase fluid, defined using the two-phase fluid variables. The pressure drop in terms of metres of head is given by

$$h_L = f_T \cdot \frac{L}{D} \cdot \frac{V^2}{2g} \tag{12}$$

The equivalent two-phase fluid parameters, e.g. dynamic viscosity, density, Reynolds number, are calculated using an equation in the following form:

$$TPV = \frac{1}{\left\{\frac{x}{GV} + \frac{(1-x)}{LV}\right\}} \tag{13}$$

where,

TPV = Two-Phase equivalent variable
GV = Gas Phase variable
LV = Liquid Phase variable

The two-phase Reynolds number for a homogeneous fluid is calculated using the equivalent homogeneous fluid properties. The friction factor for the equivalent homogeneous fluid in turn is calculated using Equation 10 or 11 using the two-phase Reynolds number.

The equations for determining the equivalent two-phase fluid parameters, leading to frictional wall shear stress as per homogeneous flow model are listed as follows,

$$\left.\begin{array}{ll} \text{Dynamic viscosity:} & \mu_{TP} = \frac{1}{\frac{x}{\mu_g} + \frac{(1-x)}{\mu_l}} \\ \text{Mean Velocity:} & V_{TP} = \frac{W}{A} = \frac{4 \cdot W}{\pi \cdot d^2} \\ \text{Fluid density:} & \rho_{TP} = \frac{1}{\frac{x}{\rho_g} + \frac{(1-x)}{\rho_l}} \\ \text{Reynold's Number:} & Re_{TP} = \frac{\rho \cdot V_{TP} \cdot d}{\mu_{TP}} \\ \text{Moody friction factor:} & f_{TP} \\ \text{Harrison Friction factor:} & C_{f_{TP}} = \frac{f_{TP}}{4} \end{array}\right\} \tag{14}$$

where subscript *TP* denotes the variable is the homogeneous two-phase fluid equivalent.

3.3 Equivalent Pipe Length

In addition to frictional losses, the pressure drop along a pipeline is influenced by local energy losses in pipe fittings, valves and other appurtenances. Common practice to account for the pressure losses in valves and pipe fittings is to use "equivalent lengths" of straight pipes that would incur same pressure drops.

Some engineers use published tables from handbooks or suppliers' data listings of equivalent lengths of common fittings and valves. In this method the equivalent lengths of all pipe fittings and valves in terms of straight pipes of same size as the main pipe are separately computed and then added to the length of the straight pipe run. A more popular and convenient methodology for incorporating in a spreadsheet based analytical design tool, is to use the "resistance coefficient" for fittings and valves, based on experimental data provided in CRANE Technical paper 410M. The procedure is discussed below.

The local losses in flow appurtenances can be given by –

$$h_l = K \cdot \frac{V^2}{2g} \tag{15}$$

K is a constant for a given type of valve or fitting, independent of friction factor or Reynolds number.

Comparing equation 15 with Darcy equation 13, the resistance factor for valves and fittings can be expressed in terms of friction factor for fully developed turbulent flow and equivalent pipe length, as follows -

$$K = f_T \cdot \frac{L_{Eq}}{D} \quad (16)$$

Appendix-A of Crane handbook lists representative K values for various valves and fittings in terms of f_T. For example, the equivalent length of a 90º LR elbow is $14f_T$. Substituting the calculated value of friction factor for the given flow conditions, equivalent lengths of various pipe appurtenances are determined and added to the straight length of piping to get the equivalent total pipe length. For special pipe appurtenances, specific resistance factors should be provided by the supplier based on experimental data or other means.

It should be noted that the above discussion and methodology for estimating equivalent length of valves and fittings is based on single phase flow, and its use in two-phase fluid pressure drop calculation is only a reasonable approximation. It is valued as it is easy to implement in analytical design tools. Multipliers to these values based on functions of other fluid properties to improve accuracy have been proposed, but they are not yet implemented in the analysis tools used by the authors.

3.4 Pressure Drop due to Static Head

The gravity component, commonly referred to as Static Head Loss (/gain), represents the change in elevations at the start and end of an inclined pipeline. The pressure drop due to change in elevation is a reversible change (unlike frictional loss), and is given by -

$$\Delta P_{gr} = \rho_m \cdot g . \Delta Z \quad (17)$$

The change in elevation is negative for downhill piping and therefore results in a static head 'gain'. The mean density of the two-phase fluid is dependent on dryness fraction and is determined using established correlations for the chosen analysis model, as explained below.

For Separated flow model,

$$\rho_m = \alpha \cdot \rho_g \cdot (1 - \alpha) . \rho_l \quad (18)$$

For Homogeneous flow model,

$$1/\rho_m = {}^{x}/_{\rho_g} + {}^{(1-x)}/_{\rho_l} \quad (19)$$

For low enthalpy two-phase fluid in downhill piping, the static head gain is often ignored or scaled down.

4. DESIGN TOOLS

Spreadsheet-based design tools, based on the analysis methods described in preceding sections, have been traditionally developed and used by engineers to estimate predicted pressure drop in geothermal two-phase fluid pipeline (Figure 1). The results based on generalised procedure for simplified flow models may not, however, exactly tally with the actual field observations. It is, therefore, a common practice by engineers to include certain "contingency factors" or empirical adjustments to the theoretical analysis results.

In recent years, computer based commercial analysis software packages have become available where one can model the piping network accurately, input the thermodynamic and hydraulic parameters and choose specific correlations to be used for flow analysis. The computer programme then performs the iterative analyses and generates the output, following the same methodology as in the manual spreadsheet.

The outcome of the pressure drop analysis is typically captured in PFD's, together with other key process design parameters, which forms the basis for developing the steamfield and the generation facilities in geothermal developments.

5. CORRECTION FACTORS TO CALCULATED RESULTS

Some considerations for adjustment of theoretical results to predict pressure losses more closely are mentioned below. However, such adjustments are empirical in nature, somewhat subjective and based on discretion of experienced engineers. These can vary according to specific knowledge about flow regimes and fluid characteristics. In brown field developments, actual field measurements from existing two-phase lines should be used to calibrate an analysis model for new assets.

Based on some historical field results in DN400 and DN450 lines, taking the average value of Homogeneous and Harrison pressure loss, following correction factors are generally used by the authors to yield reasonable accuracy against field observations. However, it should be noted that this methodology was derived from specific datasets at limited fluid flows and operating parameters. To further refine the modelling, a greater sample of field data would be beneficial.

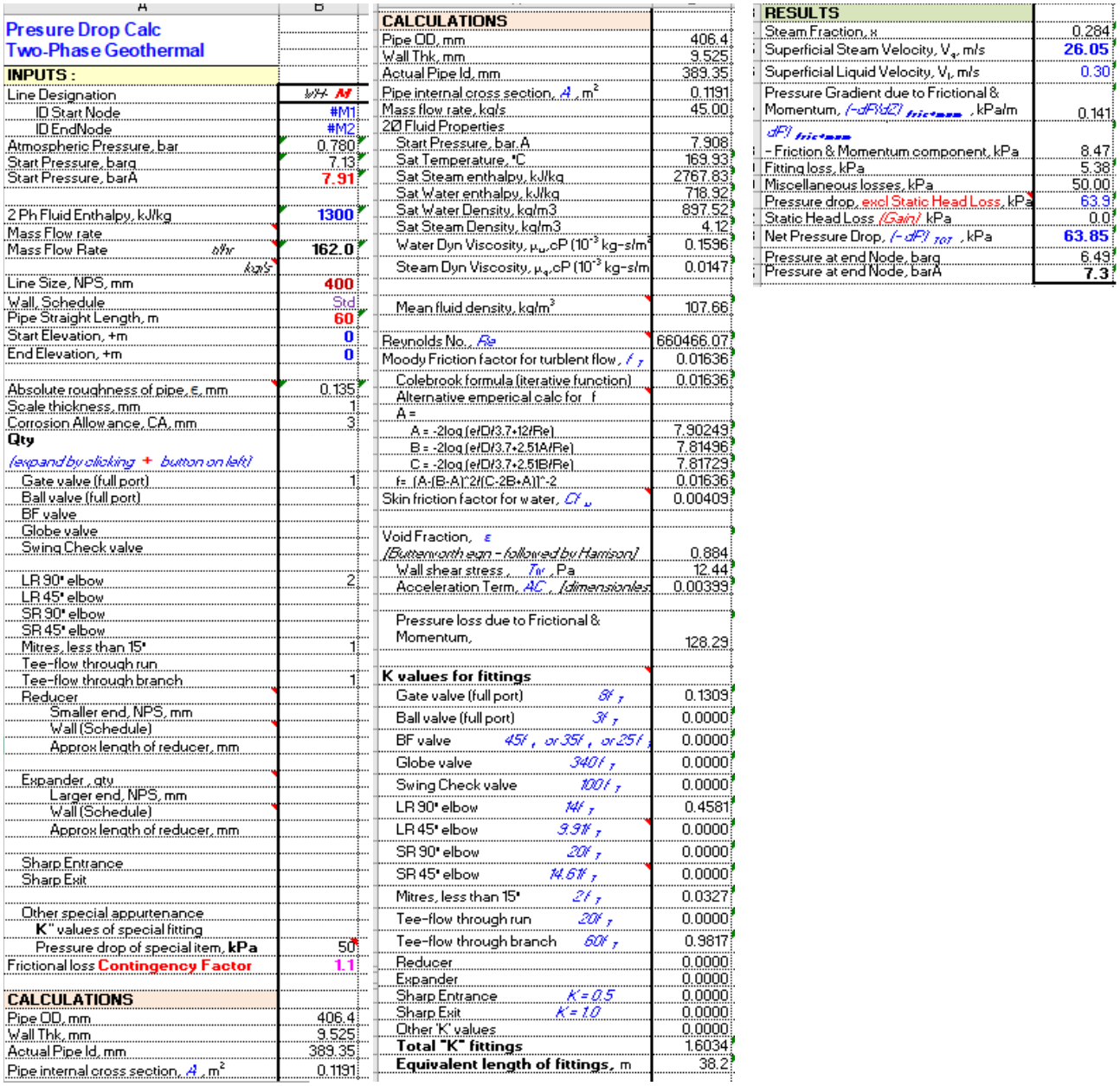

Presure Drop Calc Two-Phase Geothermal	
INPUTS :	
Line Designation	M1 - M2
ID Start Node	#M1
ID EndNode	#M2
Atmospheric Pressure, bar	0.780
Start Pressure, barg	7.13
Start Pressure, barA	**7.91**
2 Ph Fluid Enthalpy, kJ/kg	**1300**
Mass Flow rate	
Mass Flow Rate t/hr	**162.0**
kg/s	
Line Size, NPS, mm	**400**
Wall, Schedule	Std
Pipe Straight Length, m	**60**
Start Elevation, +m	**0**
End Elevation, +m	**0**
Absolute roughness of pipe, ε, mm	0.135
Scale thickness, mm	1
Corrosion Allowance, CA, mm	3
Qty	
(expand by clicking + button on left)	
Gate valve (full port)	1
Ball valve (full port)	
BF valve	
Globe valve	
Swing Check valve	
LR 90° elbow	2
LR 45° elbow	
SR 90° elbow	
SR 45° elbow	
Mitres, less than 15°	1
Tee-flow through run	
Tee-flow through branch	1
Reducer	
Smaller end, NPS, mm	
Wall (Schedule)	
Approx length of reducer, mm	
Expander, qty	
Larger end, NPS, mm	
Wall (Schedule)	
Approx length of reducer, mm	
Sharp Entrance	
Sharp Exit	
Other special appurtenance	
"K" values of special fitting	
Pressure drop of special item, **kPa**	50
Frictional loss **Contingency Factor**	1.1
CALCULATIONS	
Pipe OD, mm	406.4
Wall Thk, mm	9.525
Actual Pipe Id, mm	389.35
Pipe internal cross section, A, m^2	0.1191

CALCULATIONS	
Pipe OD, mm	406.4
Wall Thk, mm	9.525
Actual Pipe Id, mm	389.35
Pipe internal cross section, A, m^2	0.1191
Mass flow rate, kg/s	45.00
2Ø Fluid Properties	
Start Pressure, bar.A	7.908
Sat Temperature, °C	169.93
Sat Steam enthalpy, kJ/kg	2767.83
Sat Water enthalpy, kJ/kg	718.92
Sat Water Density, kg/m3	897.52
Sat Steam Density, kg/m3	4.12
Water Dyn Viscosity, μ_w,cP (10^{-3} kg-s/m)	0.1596
Steam Dyn Viscosity, μ_s,cP (10^{-3} kg-s/m	0.0147
Mean fluid density, kg/m^3	107.66
Reynolds No., Re	660466.07
Moody Friction factor for turblent flow, f_T	0.01636
Colebrook formula (iterative function)	0.01636
Alternative emperical calc for f	
A =	
A = -2log (e/D/3.7+12/Re)	7.90249
B = -2log (e/D/3.7+2.51A/Re)	7.81496
C = -2log (e/D/3.7+2.51B/Re)	7.81729
f= (A-(B-A)^2/(C-2B+A))^-2	0.01636
Skin friction factor for water, Cf_w	0.00409
Void Fraction, ε	
(Butterworth eqn - followed by Harrison)	0.884
Wall shear stress, Tw, Pa	12.44
Acceleration Term, AC, *(dimensionless*	0.00399
Pressure loss due to Frictional & Momentum,	128.29
K values for fittings	
Gate valve (full port) $6f_T$	0.1309
Ball valve (full port) $3f_T$	0.0000
BF valve $45f_T$, or $35f_T$, or $25f_T$	0.0000
Globe valve $340f_T$	0.0000
Swing Check valve $100f_T$	0.0000
LR 90° elbow $14f_T$	0.4581
LR 45° elbow $9.9f_T$	0.0000
SR 90° elbow $20f_T$	0.0000
SR 45° elbow $14.6f_T$	0.0000
Mitres, less than 15° $2f_T$	0.0327
Tee-flow through run $20f_T$	0.0000
Tee-flow through branch $60f_T$	0.9817
Reducer	0.0000
Expander	0.0000
Sharp Entrance $K = 0.5$	0.0000
Sharp Exit $K = 1.0$	0.0000
Other 'K' values	0.0000
Total "K" fittings	1.6034
Equivalent length of fittings, m	38.2

RESULTS	
Steam Fraction, x	0.284
Superficial Steam Velocity, V_s, m/s	**26.05**
Superficial Liquid Velocity, V_l, m/s	0.30
Pressure Gradient due to Frictional & Momentum, $(-dP/dZ)_{friction}$, kPa/m	0.141
$dP)_{friction}$ - Friction & Momentum component, kPa	8.47
Fitting loss, kPa	5.38
Miscellaneous losses, kPa	50.00
Pressure drop, excl Static Head Loss, kPa	63.9
Static Head Loss *(Gain)* kPa	0.0
Net Pressure Drop, $(-dP)_{tot}$, kPa	**63.85**
Pressure at end Node, barg	6.49
Pressure at end Node, barA	**7.3**

Figure 1: Example Spreadsheet Design Tool Showing Inputs and Results for a Single Node.

Table 1: Field Data for Fluid Properties used to Compare Pressure Loss Analysis Results.

Pipe Size (NPS)	Enthalpy (kJ/kg)	Mass (t/h)	Mean Pressure (barg)	Prediict ed Flow regime
450	1208	585	11.4	Slug
400	1221	290	6.3	Annular
400	1280	390	9.6	Annular

The Homogeneous flow model typically underestimates the pressure loss, compared to field observation and a contingency factor of upto 50% (scale up by x1.5) is often applied. The Harrison method using the separated flow model seems to result in more accurate pressure drop in most cases and a smaller contingency factor of 5-10% (scale up by x1.05 – 1.1) is common.

Discretising analysis models is an important aspect of two-phase pressure loss modelling. This is done by breaking a pipeline into smaller segments, and evaluating pressures at consecutive nodes, via an iterative calculation process. Typically, a fixed pressure at a terminal point of the pipeline is required as an input. This could be the flowing wellhead pressure, or a known/required pressure at a junction such as a separation plant. The discretisation process is valuable as it can be used to check convergence of results. Modelling a long pipeline using a single

node can result in significant convergence error, as the two-phase analysis formulae rely on variables which are functions of changing properties over the length of the line, such as steam fraction. In high-flow, transient applications such as emergency dump systems for separated geothermal water, a high resolution of nodes is required as fluid properties change rapidly along the pipe length.

REFERENCES

Butterworth, D. (1975), A comparison of some void-fraction relationships for co-current gas-liquid flow.

Colebrook C.F. and White C.M. (1937), Experiments with Fluid friction roughened pipes.

D.H.Freeston (1980), A Comparison of Experimental Results of Pressure Drop for Two Phase Steam/ Water and Air/ Water Mixtures in a Horizontal Pipe.

Goudar C.T. & Sonnad J.R. (2008), Comparison of the iterative approximations of the Colebrook-White Equation.

Harrison R F. (1977), Geothermal Two-phase Pipe Flow. Wairakei: Chemistry Division DSIR.

Lawrence, C.D (1975), Dealing with two-Phase Flows.

Moody L.F. (1944), Friction Factors for Pipe Flow.

Serghides T.K., Chem Eng, 91 (1984), pp. 63-64, Estimate friction factor accurately.

Spedding & Chen (1980), Two-Phase Flow Pressure Loss Prediction.

Zhao, Lee and Freeston (2000), Geothermal Two-Phase Flow in Horizontal Pipes.

Crane Co., Technical Paper No. 410 M (1982), Flow of Fluids

NOMENCLATURE

A	Pipe Cross Sectional Area (m^2)	V_l	Superficial Liquid Velocity (m/s)
A_l	Liquid Occupied Pipe Area	V_g	Superficial Vapour Velocity (m/s)
A_v	Vapour occupied Pipe Area	W	Two Phase Flow Rate
AC	Acceleration Component	x	Steam Dryness Fraction
C_f	Skin Friction Factor	Z	Relative Elevation (m)
D	Inside Pipe Diameter (m)	α	Cross Sectional Void Fraction
f_T	Friction Factor for Fully Developed Turbulent Flow	Δ	Differential
g	Acceleration Due to Gravity (ms^{-2})	ϵ	Pipe roughness (mm)
K	Flow Resistance Coefficient of a Fitting	ρ_m	Mean Fluid Density (kg/m^3)
L_{eq}	Equivalent Pipe Length of a Fitting (m)	ρ_l	Liquid Phase Density (kg/m^3)
P	Pressure (N/m^2)	ρ_g	Vapour Phase Density (kg/m^3)
Re	Reynolds Number	μ_l	Liquid Phase Dynamic Viscosity (Pa.s)
V	Single Phase Fluid Velocity (m/s)	μ_g	Vapour Phase Dynamic Viscosity (Pa.s)

Monoblock Geothermal Power Plant Study in Dieng Geothermal Working Area

Wahyu Festiawan Nurrochim, Rifki Yogiantara, Herdian Ardi Febrianto, and Andhika Yudiaji

PT Geo Dipa Energi (Persero), Indonesia

wahyufestiawan.n@gmail.com, rifki.yogiantara@geodipa.co.id,
herdian@geodipa.co.id, andhika@geodipa.co.id

Keywords: Geothermal Power Plant, Well Head Generating Power Plant, Geothermal Small Scale Power Plant, Monoblock Geothermal Power Plant, Heat Loss

ABSTRACT

Indonesia's Dieng Geothermal Working Area has 200 MW of geothermal and 580 MW of reserve resources. Currently, PT Geo Dipa Energy has an installed capacity of 60 MWe for its Geothermal Power Plant, which applies single flash systems with a total pipe length of about 8.5 km. The authors aim to study the energy loss from the total potential steam from the production well due to pressure and temperature loss. To address these problems, the authors try to engineer the process using block systems in the geothermal power plant, eliminating energy loss along the pipe systems. The research results indicate that the total pressure and temperature loss, using data from maximum capacity in 2020 compared to current conditions, are about 4.5 bara and 22.43°C, and 2.47 bara and 11.19°C, respectively. Furthermore, using ASPEN HYSYS for modeling and simulation of the block geothermal power plant, it was found that the increase in electricity production was 10.12 MWe and 5.91 MWe, equivalent to 17% - 15% of the existing.

1. INTRODUCTION

The Dieng Geothermal Working Area in Dieng, Central Java, has 200 MW of geothermal and 580 MW of reserve resources (Direktorat Panas Bumi & Ditjen EBTKE, 2017). Dieng has been explored with 47 production wells since 1970: 27 production wells under Pertamina from 1977 to 1993 and 20 production wells under Himpurna California Energy (HCE) from 1995 to 1998 (Layman et al., 2002). In 2019, PT Geo Dipa Energi (Persero) (GDE) renewed the geothermal reservoir data model, resulting in a temperature range of 280–330°C (Ashat et al., 2019) and a water-dominated steam characteristic. The Dieng Geothermal Power Plant (GPP) has an installed capacity of 60 MWe and applies single flash systems technology with multiple separator systems at the well field and power plant area. In 2023–2024, gross production was about 40–45 MWe; in 2020, the full capacity of gross production was achieved at 60 MWe. After almost four years of operation, GPP Dieng has decreased by about 20–25 MWe. This has caused a decline in well production and steam loss along the steam pipeline systems.

Figure 1 shows that seven production wells are separated into several areas, with the total length of the pipe to the power plant being approximately 8.5 km from all production wells. The parameters of well production that can generate maximum capacity in the power plant include an average separator pressure of 12.5 bara, a temperature of 187.5°C, and a total steam flow of 438 t/h. The inlet parameters of the power plant systems are about 7.9 bara pressure, a temperature of 169°C, and a steam flow of 432 t/h. Recently, the parameters from the production wells are about 11 bara on average, with a temperature of 187°C and a steam flow of 316.9 t/h. Additionally, the inlet turbine parameters are 8.8 bara, with a temperature of 173°C and a steam flow of 272 t/h. This shows a steam loss in the piping systems of about 44.63 t/h, or 6.3 MWe power equivalent. Steam loss, changes in pressure, and temperature are caused by friction loss, heat loss, and changes in steam parameters at the well production and inlet turbine conditions. Based on the heat loss calculation formula, the effect of thermal insulation conditions in the steam pipeline network was studied in Cerro Prieto Geothermal Field. The total capacity installed is 720 MWe with 13 operating units. Power plants are fed 165 production wells with two high and low-pressure pipeline networks. The pipeline network length is approximately 140 km, with a diameter of 203.2 to 1219.2 mm (8 inches to 48 inches). All pipes were covered by mineral wool and fiberglass insulation with aluminum or galvanized iron as outer protection. From that condition, heat loss resulted as 136 t/h of condensate or equal to 17.57 MWe electricity power. That value represents about 2.44% of the geothermal field capacity installed (Ovando-Castelar et al., 2012).

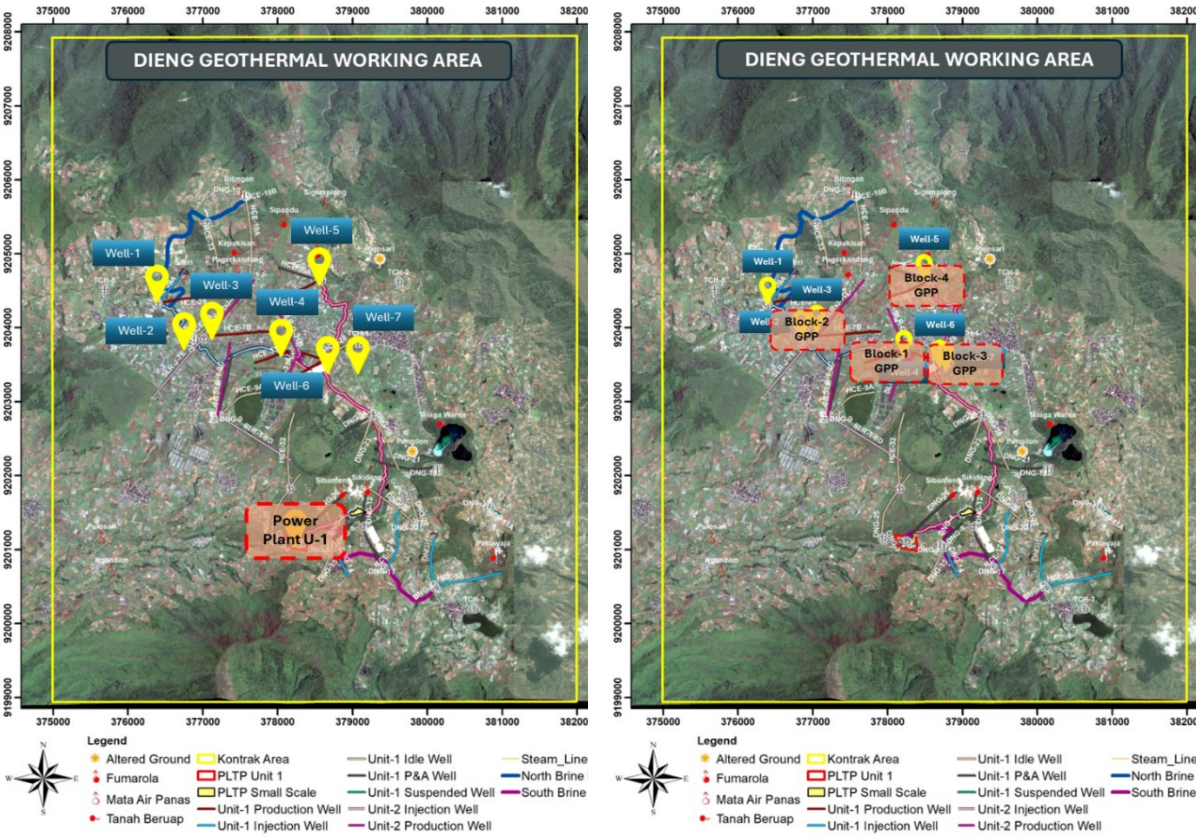

(a) (b)

Figure 1: Production Well of Dieng Geothermal Power Plant: (a) Existing Systems; (b) Block Systems of Geothermal Power Plant (Source: Author's Documentation)

Based on the problems in the piping systems that can affect the geothermal power plants' electricity generation, the author's point of view is to assess the potential of block system geothermal power plants near the production wells. By designing small-scale systems spread across several areas to reduce energy loss along the central steam piping systems and maximize the utilization of geothermal resources. ASPEN HYSYS modeling and simulation are used to create suitable geothermal block power plant systems. The analysis result is to know the potential of electricity generation is before and after the use of geothermal blocks power plant system with existing parameters of production wells condition.

2. ANALYSIS METHOD

2.1 Thermodynamics Power Plant Analysis

The analysis of geothermal power plants is generally based on the first and second laws of thermodynamics. That principle then developed some parameters that are commonly used to analyze geothermal power plant performance, like overall plant efficiency, Net Plant Heat Rate (NPHR), and Specific Steam Consumption (SSC). That approach was developed to adapt to the operational parameters of the geothermal power plant that the system could monitor.

Overall, the plant efficiency of a geothermal power plant is defined by the first law of thermodynamics, which is defined as energy output divided by energy input. Energy output is defined as generator load (W) because it's the product of a geothermal power plant, and energy input is defined as geothermal steam from the production well that is approached by the total mass flow (m) of steam multiplied by the average enthalpy of production (h).

$$plant\ efficiency = \frac{W}{m\ x\ h}\ x\ 100\% \quad (1)$$

Steam-specific consumption (SSC) is the steam consumed to produce a product. In this scope, steam is consumed to produce 1 kW of electricity (Aziz & Juangsa, 2021).

$$SSC = \frac{m}{W\ nett} \quad (2)$$

Based on the literature, SSC in geothermal power plants ranges from 1.8 – 2.22 kg/s per MWe (Gutiérrez Negrín & Lippmann, 2016). This value also informed the technical cost of electricity production in geothermal power plants.

Net plant heat rate is essentially the same as heat rate, which calculates the heat or energy required to generate a system. In this scope, we see the system as a geothermal power plant. So, the energy used is energy from the total flow rate of steam produced by the production well, and the product is electricity generated by the generator. The equation of this parameter is written as:

$$NPHR = \frac{m\ x\ h}{W\ gen} \tag{3}$$

It's important to specify the scope of the system to analyze the performance of the geothermal power plant since it relates to the product of electricity. The gross power product is defined as the generator that loads electricity. Net power is the gross power minus parasitic load. Parasitic load is the energy used to energize auxiliary equipment in a geothermal power plant ((Ozcan & Gokcen, 2013).

$$W_{netto} = W_{gross} - W_{parasitic\ load} = \left([\dot{m}(h_{in} - h_{isen})]\ x\ \eta_{gen}\right) - W_{parasitic\ load} \tag{4}$$

All these parameters can be determined by plant instrumentation system and thermodynamic properties. Generator efficiency is determined by about 98% (Zarrouk & Moon, 2014).

2.2 Pressure and Temperature Drop

A geothermal power plant uses a piping system to deliver steam from the production well to the power plant and deliver the condensate to the re-injection well. Along the piping system, equipment is installed for different functions like valve, reducer, elbow, loop, condensate drain pod, etc. That equipment gains friction loss from fluid inside the pipe. In saturated steam application, high pressure and temperature drops could lead to condensation, decreasing the amount of steam.

Darcy-Weisbach is used to explain the influence of minor losses against pressure drops in piping systems (Department of Energy Fundamentals, 1992).

$$\Delta_p = (f\frac{L}{D} + \sum K)\frac{pV^2}{2} \tag{5}$$

Where f is the friction factor, L is pipe length in m, D is the diameter of the pipe, K is the fitting coefficient, p is the density of the fluid, and V is flow velocity.

To determine the heat loss of the piping system, we used convection and conduction heat transfer approaches (Wang, 2023).

$$\Delta T = (T_i - T_s)\left[1 - exp\left(-\frac{L}{C_p \dot{m} R}\right)\right] + T_s \tag{6}$$

Where T_i is the temperature of fluid inlet condition, T_s is the temperature of the pipe surrounding/ambient, L is pipe length, C_p is the specific heat capacity of fluid, $\dot{m}$ is the mass flow rate of fluid inside the pipe, and R thermal resistance of the pipe. Then, the thermal resistance of the pipe is formulated using the equation below.

$$R = \frac{\ln(D+\delta)/D}{2\pi\lambda} \tag{7}$$

Where D is the pipe's inner diameter, δ is the thickness of pipe insulation, and λ is the thermal conductivity of pipe insulation, which depends on the insulation material.

Using the mathematical heat transfer model, a study in Indonesia's X Geothermal Power Plant to analyze steam pipeline heat (Pudyastuti & Lie, 2020) concluded an adequate discrepancy of about 1.5 – 5.5 % between the model and measurement.

Recent research has shown that the heat loss of geothermal fluid flow in piping systems is relatively negligible (Zarrouk, 2014). In some cases, the heat loss of 80 t/h of steam at 180 °C flows through a 0.4 m diameter pipe along 2.0 km with 8 cm fiberglass pipe insulation thickness and 20 °C ambient temperature. The energy loss is only 0.6%. The following equation can be derived for the above ambient and piping conditions.

$$\eta_{pipe} = 1 - 0.003L_p \tag{8}$$

Where η_{pipe} is the pipe efficiency based on total geothermal energy and L_p is the pipe length in km.

2.3 Scope and Research Flow Framework

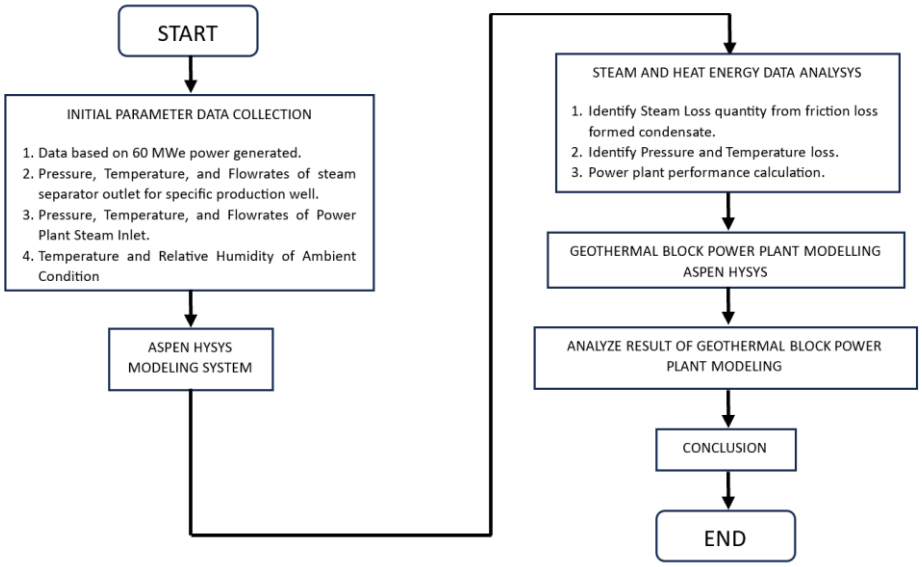

Figure 2: Flow Framework of Research.

Dieng Geothermal Field has seven production wells, and the area is separated from the power plant. Each of them is transported to the Power Plant through a steam pipeline network. This research assesses the potential of geothermal block power plants in block areas of production wells. From the location of the production well and the calculation of pressure drop and heat loss, we divided it into four geothermal blocks. Block-1 (Well-4), Block-2 (Well-1, Well-2, Well-3), Block-3 (Well-6,Well-7), and Block-4 (Well-5). Some research elimination is applied in this research to focus discussion and prevent data bias.

1. Data collected from 2020 operating data parameters at full capacity of production.
2. System scope starts from outlet separator steam until power plant.
3. Subsurface thermal and chemical conditions are neglected.
4. Steady-state condition modeling simulation.
5. The steam dryness of the outlet separator from 2020 data is assumed to be 100%.
6. Turbine efficiency is assumed to be constant at 85% (Zarrouk & Moon, 2014).
7. Pipe insulation condition assumed uniform.
8. The condenser pressure of the geothermal block power plant is assumed to be equal for each block.

First, the researcher collects operational parameters from a Distributed Control System (DCS) for operational parameter data and a Weather Station device for ambient condition data. Operational data collected include pressure, temperature, and mass flow rate of the separator outlet and plant steam inlet. This data is collected based on the full load capacity of the power plant (60 MWe) and current condition. The data was inputted to a Dieng's geothermal power plant system model in ASPEN HYSYS software to simulate the calculation. The simulation results were then collected to identify steam loss, pressure and temperature loss, and power plant calculation. These initial data were then used to model geothermal blocks as specified in the scope of research. The simulation result was used to compare existing plants and identify block geothermal power plant performance.

3. RESULT AND DISCUSSION

The results of performance calculations for the power plant are shown in Table 1. The calculations reveal that the power plant's performance at full capacity conditions (60 MWe) has an NPHR value of 321.25 kJ/kWh higher than the current condition. Furthermore, the total steam usage per 1 MWe of electricity production is also higher by 0.12 t/h or 0.03 kg/s compared to the current condition. The total plant efficiency is lower by about 0.3%, yet both conditions fall within the efficiency range for geothermal power plants worldwide. Additionally, the turbine's isentropic efficiency at both conditions (80.2% and 81.62%) represents the global range for geothermal turbine isentropic efficiency, typically between 60% and 85% (Dickson & Fanelli, 2003). In other words, the performance at full capacity of the power plant and the current conditions still indicate the same plant performance, with no significant decline. The difference in generating power purely comes from the decrease of production wells, parameter conditions at production wells, and the increase in own-use power because of the greater need for supporting equipment.

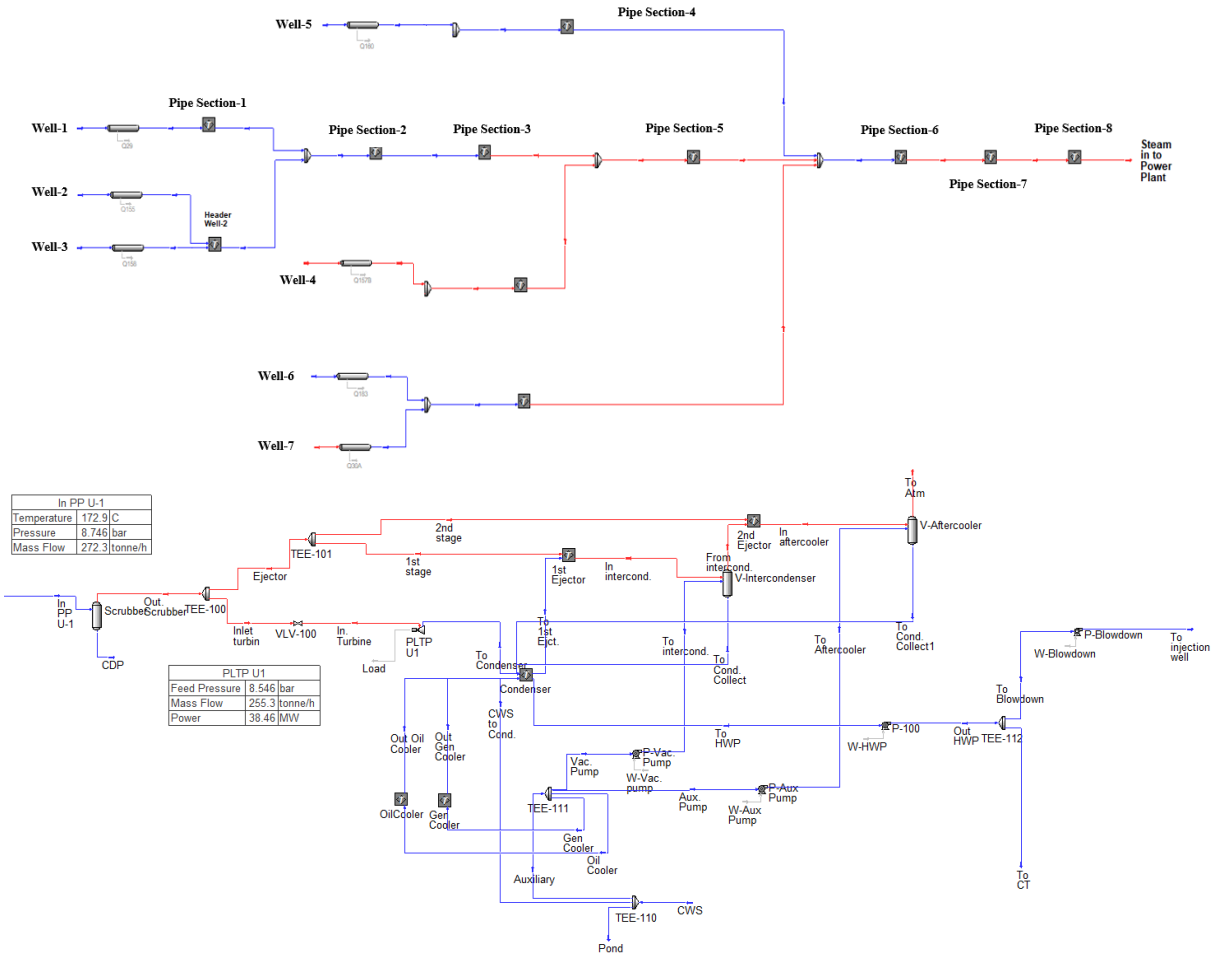

Figure 3: Modeling and Simulation Using ASPEN HYSYS for Well Field and Existing Power Plant Systems.

Table 1: Result Power Plant Summary: (a) Parameter Condition in 2020; (b) Parameter Condition in 2024

POWER PLANT PERFORMANCE SUMMARY UNIT-1

A. PLANT PERFORMANCE

Average			Average		
- GROSS	: 60,09 MW		- NPHR	: 21.382,16 kJ/KWh	
- PS	: 4,81 MW		- SSC	: 7,19 T/h	
- NET	: 55,28 MW		Plant Eff.	: 18,3%	
			PLTP berkisar antara 10% - 20,7% (Zarrouk et al, 2013)		

B. SUMMARY INPUT DATA & MAIN EQUIPMENT PERFORMANCE

Ambient Condition			Steam Quality		
TDB	: 15,29 °C		Dryness	: 99,8%	
TWB	: 13,47 °C		Total NCG contain	: 1,30% Weight	
Plant Parameter			**Turbine Perfomance**		
Total ṁ Steam	: 432,01 T/h		Effeciency	: 80,82 %	
Press. In	: 7,99 bara				
Temp. In	: 169,44 °C		**Cooling Tower Effectiveness**		
ṁ Steam Ejector	: 18,00 T/h		Effectiveness	: 83%	
ṁ Steam Turbin In.	: 414,01 T/h		CT Fan Run	: 18,00 Unit	
Press. In Turbin	: 7,79 bara		CWS	: 17,00 °C	
Temp. In Turbin	: 169,10 °C		CWR	: 34,66 °C	
Press. Out Turbin	: 0,10 bara				
Temp. Out Turbin	: 45,02 °C				

(a)

POWER PLANT PERFORMANCE SUMMARY UNIT-1

A. PLANT PERFORMANCE

Average			Average		
- GROSS	: 38,50 MW		- NPHR	: 21.060,91 kJ/KWh	
- PS	: 3,08 MW		- SSC	: 7,07 T/h	
- NET	: 35,42 MW		Plant Eff.	: 18,6%	
			PLTP berkisar antara 10% - 20,7% (Zarrouk et al, 2013)		

B. SUMMARY INPUT DATA & MAIN EQUIPMENT PERFORMANCE

Ambient Condition			Steam Quality		
TDB	: 15,30 °C		Dryness	: 99,8%	
TWB	: 13,82 °C		Total NCG contain	: 1,32% Weight	
Plant Parameter			**Turbine Perfomance**		
Total ṁ Steam	: 272,30 T/h		Effeciency	: 81,62 %	
Press. In	: 8,83 bara				
Temp. In	: 173,27 °C		**Cooling Tower Effectiveness**		
ṁ Steam Ejector	: 17,00 T/h		Effectiveness	: 77%	
ṁ Steam Turbin In.	: 255,30 T/h		CT Fan Run	: 14,00 Unit	
Press. In Turbin	: 8,63 bara		CWS	: 19,00 °C	
Temp. In Turbin	: 173,00 °C		CWR	: 35,89 °C	
Press. Out Turbin	: 0,09 bara				
Temp. Out Turbin	: 42,42 °C				

(b)

The graph in Figure 4 shows a significant drop in pressure and temperature in pipe sections 4, 5, 6, 7, and 8. Significant pressure drop happens at pipe section 4 and pipe section 6 and each value is about 0,81 bara & 1,7 bara. Further, a considerable temperature drop happened at pipe section 6 about 7,53 °C. The pressure and temperature drop at current conditions are almost similar with data at full capacity of production wells and power plants in 2020. Significant pressure and temperature drop happen at pipe section 6 about 0,72 bara and 3,28 °C. These problems occur because steam from several wells combines into one in the main steam pipe refer to Figure 3, resulting in an increase in the friction loss value due to the increased flow rate. The increased flow rate is directly proportional to the increased amount of steam. Meanwhile, the temperature drop is directly proportional to the pressure drop. This temperature drop is corrected by the specific heat value of the fluid flowing inside the

pipe. Each section's pipeline insulation heat loss was compared with the heat flux unit. In this research, all pipelines used Rockwool pipeline insulation with the assumption all of them are in the good condition and the ambient temperature assumed to be uniform in each area of the pipeline section. The ambient temperature is 15.30 °C, this value is based on the average temperature of Dieng when data is collected. As we can see in Figure 4. If we sum up all heat loss through steam pipelines, total heat loss in 2020 is 100.96 kW and in 2024 total heat loss is equal to 50.83 kW. Each value represents 0.17% and 0.13% of the total load generated by the power plant. This result is smaller than a study of pipeline heat loss with varied condition pipe insulation at the Cerro Prieto Geothermal Field (CPGF) power plant, which represents 2.44% of installed capacity (720 MW_e) (Ovando-Castelar et al., 2012). According to Table 2 there are some pressure drop correlations to pipeline geometry, as seen in Figure 4. The pressure drop of pipe Section 6 is the highest among the others since Section 6 has a 1601.18 m length of pipe with total fittings of 38 units. The amount of that condition increases the total length equivalent. It is stated by the Darcy-Weisbach equation. Pressure drops velocity of fluid multiplied by the total pipe segment, so pipe Section 6 has the highest pressure drop. Refer to Figure 3 although pipe section 2 has the same length and number of fittings as section 6, the pressure drop is lower. This is because pipe section 6 accommodates the total amount of steam from all wells, increasing the steam flow rate and fluid flow velocity.

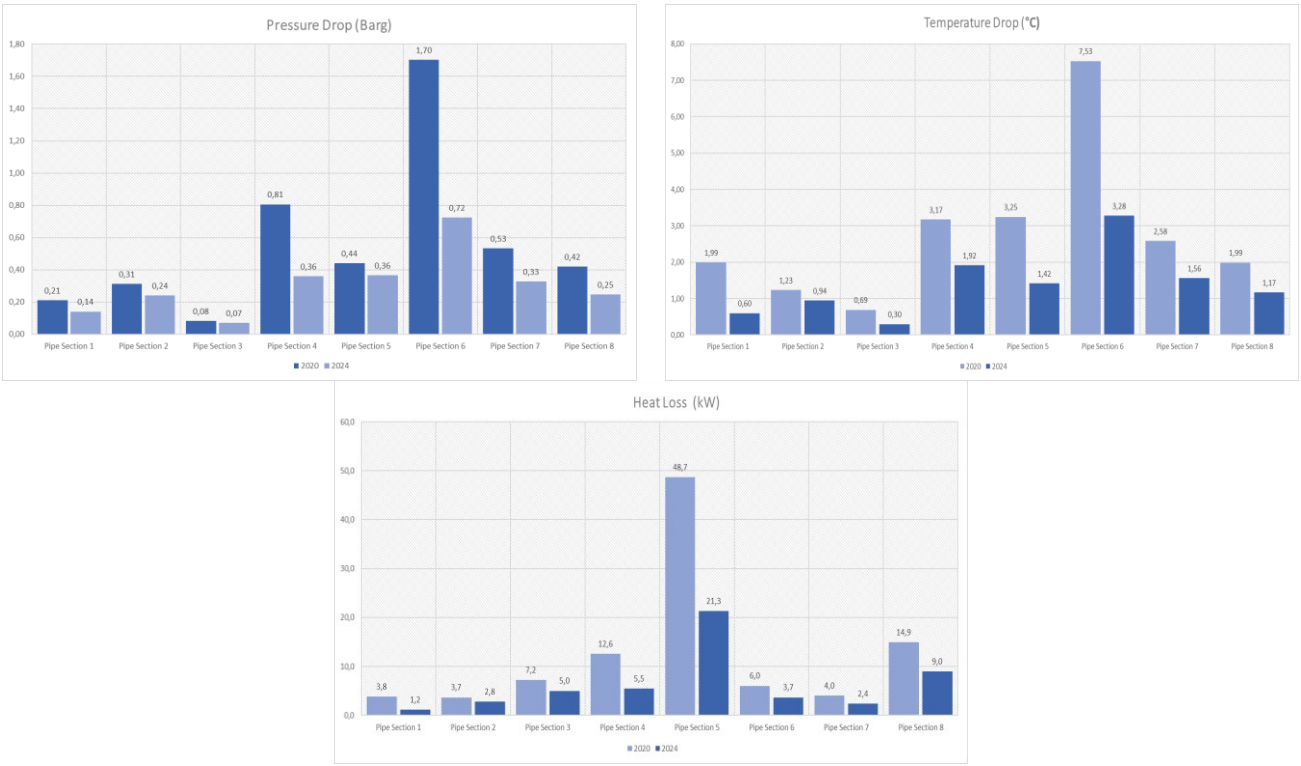

Figure 4: Distribution of Pressure Drop, Temperature Decrease, and Heat Loss.

Table 2: Pipelines Geometry of Existing Geothermal Power Plant.

		Pipe Section 1	Pipe Section 2	Pipe Section 3	Pipe Section 4	Pipe Section 5	Pipe Section 6	Pipe Section 7	Pipe Section 8
Pipe diameter	m	0.381	0.876	0.876	0.575	0.4287	0.876	0.876	0.876
Pipe thickness	m	0.013	0.019	0.019	0.017	0.014	0.019	0.019	0.019
Thermal conductivity pipe	W/m K	45	45	45	45	45	45	45	45
Type of Insulation Pipe		Rockwoll	Rockwoll	Rockwoll	Rockwoll	Rockwoll	Rockwoll	Rockwoll	Rockwoll
Insulation Pipe thickness	m	0.1	0.1	0.1	0.1	0.1	0.1	0.1	0.1
Thermal conductivity insulation	W/m K	0.1	0.1	0.1	0.1	0.1	0.1	0.1	0.1
Pipe length	m	789.861	1926.11	576.52	1535.123	1031.21	1601.18	579.87	504.57
Total Fitting	Unit	38	38	8	87	22	38	19	15

With modeling using ASPEN HYSYS for the Block Geothermal Systems, as shown in Figure 5, 6, 7, and 8, the pressure and temperature drop is insignificant because the friction and heat loss along the pipe are already unavailable. Transferring the steam out separator through the block geothermal system that is not so far from well production can minimize them. Knowing in Tabel 2 that existing and blocked geothermal power plant systems can reduce the steam loss from the well to the power plant. When using the existing system with long central pipe systems in 2020 and 2024 the number of steam losses is 6,36 t/h and 44,64 t/h. Compared with block geothermal systems in 2020 and 2024, the number of steam losses decreases by about 0,39 t//h and 34,05 t/h. Steam loss at both systems in 2024 is still high because one of the parameters of Well 5 is under the saturation condition at the outlet separator. So steam condensation happens along pipe section 4 due to the output parameters of the separator and the number of loops and fittings.

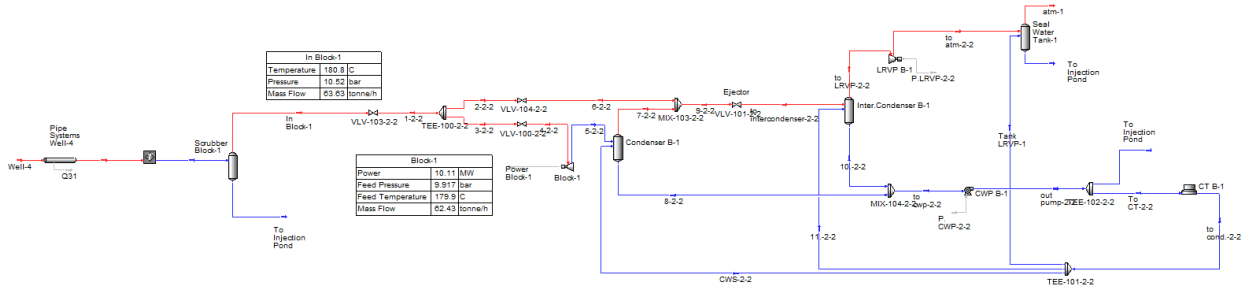

Figure 5: Block-1 Geothermal Power Plant Systems.

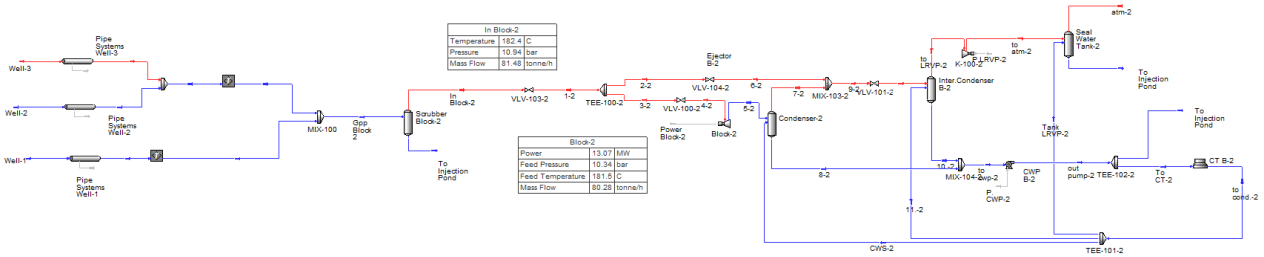

Figure 6: Block-2 Geothermal Power Plant Systems.

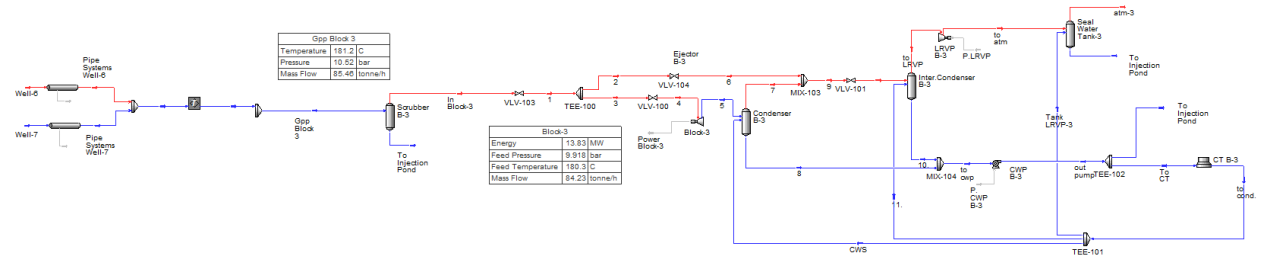

Figure 7: Block-3 Geothermal Power Plant Systems.

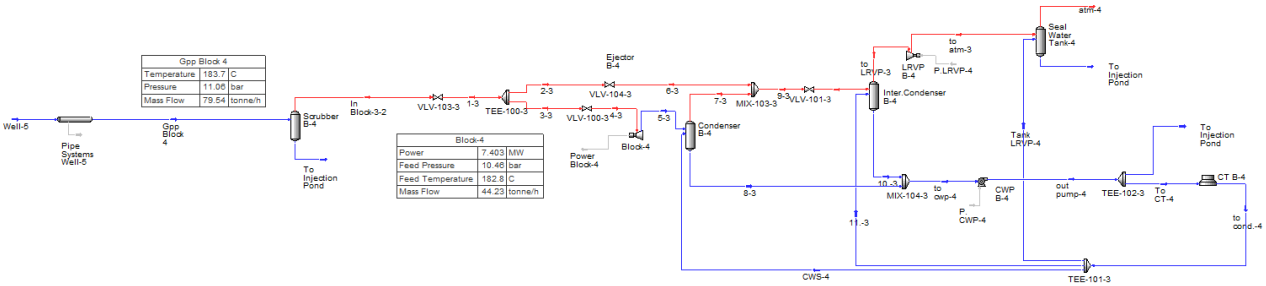

Figure 8: Block-4 Geothermal Power Plant Systems.

Table 3: Overall Power Equivalence Comparison of Existing and Block Geothermal Power Plant Systems.

	2020 Existing Dieng U1 GPP		2020 Block GPP		2024 Existing Dieng U1 GPP		2024 Block GPP	
	Ton/h	**MW**	**Ton/h**	**MW**	**Ton/h**	**MW**	**Ton/h**	**MW**
Steam From Well	**1017,75**	**141,56**	**1027,00**	**165,49**	**811,25**	**114,70**	**804,91**	**128,73**
Steam Outlet Separator	**438,37**	**60,97**	**438,22**	**70,27**	**316,94**	**44,81**	**310,61**	**49,78**
Brine Outlet Separator	**579,38**	**80,59**	**588,78**	**95,22**	**494,30**	**69,89**	**494,30**	**78,94**
Steam Loss	6,36	0,88	0,39	0,06	44,64	**6,31**	34,05	5,37
	1,45%		0,09%		14,09%		10,96%	
Gross Power Plant	**432,01**	**60,09**	**437,83**	**70,21**	**272,30**	**38,50**	**276,56**	**44,41**
Steam Inlet Turbine	**414,01**	**57,59**	**418,23**	**67,15**	**255,30**	**36,10**	**271,76**	**43,64**
Steam Inlet Ejector	18,00	2,50	19,60	3,06	17,00	2,40	4,80	0,77

With the modeling and simulation of the block power plant, it was found that electricity production in 2020 was 70.21 MWe and in 2024 was 44.41 MWe. Compared to the existing power plant design, the opportunity for

increased electricity production using the block system can be identified, with increases of 10.12 MWe and 5.91 MWe for each respective year. This increase in opportunity is obtained by converting energy losses along the pipeline to be directly utilized in the block power plant design. The availability of energy from the wells remains relatively high, with energy availability of 165.49 MWe and 128.73 MWe for 2020 and 2024, equivalent to 42% and 34% being utilized to generate electricity. The brine output from the separator still has energy amounts of 95.2 MWe and 78.94 MWe, or 58% and 66% of the energy remains unutilized and can be converted into electricity. In other words, there is an opportunity or potential to use an integrated combined cycle power plant, thereby increasing the thermal efficiency of the geothermal source.

Table 4: Power Equivalence of Results from Modeling and Simulation for Block Geothermal Power Plant Systems.

2020

	Block-1		Block-3		Block-2		Block-4	
	Ton/h	MW	Ton/h	MW	Ton/h	MW	Ton/h	MW
Steam From Well	**81,99**	**13,84**	**350,58**	**54,09**	**273,95**	**43,99**	**320,48**	**53,57**
Steam Outlet Separator	**79,81**	**13,47**	**198,48**	**30,62**	**84,41**	**13,56**	**75,52**	**12,62**
Brine Outlet Separator	**2,18**	**0,37**	**152,10**	**23,47**	**189,54**	**30,44**	**244,96**	**40,94**
Steam Loss	0,09	**0,01**	0,00	0,00	0,22	0,04	0,08	0,01
	0,11%		0,00%		0,26%		0,10%	
Gross Power Plant	**79,72**	**13,46**	**198,48**	**30,62**	**84,19**	**13,52**	**75,44**	**12,61**
Steam Inlet Turbine	**78,52**	**13,26**	**182,48**	**28,15**	**82,99**	**13,33**	**74,24**	**12,41**
Steam Inlet Ejector	1,20	**0,20**	16,00	2,47	1,20	0,19	1,20	0,20

2024

	Block-1		Block-3		Block-2		Block-4	
	Ton/h	MW	Ton/h	MW	Ton/h	MW	Ton/h	MW
Steam From Well	**68,25**	**10,84**	**184,24**	**30,15**	**227,93**	**36,56**	**324,50**	**51,17**
Steam Outlet Separator	**63,70**	**10,12**	**84,55**	**13,83**	**82,82**	**13,28**	**79,54**	**12,54**
Brine Outlet Separator	**4,55**	**0,72**	**99,69**	**16,31**	**145,11**	**23,28**	**244,96**	**38,63**
Steam Loss	0,07	**0,01**	0,03	0,00	1,34	0,21	32,62	5,14
	0,10%		0,03%		1,62%		41,01%	
Gross Power Plant	**63,63**	**10,11**	**84,52**	**13,83**	**81,48**	**13,07**	**46,92**	**7,40**
Steam Inlet Turbine	**62,43**	**9,92**	**83,32**	**13,63**	**80,28**	**12,88**	**45,72**	**7,21**
Steam Inlet Ejector	1,20	**0,19**	1,20	0,20	1,20	0,19	1,20	0,19

4. CONCLUSION

The research conducted through studying and analyzing the average total pressure and temperature losses during full-capacity generation conditions found them to be 4.5 bara and 22.43°C. In contrast, the current generation conditions are 2.47 bara and 11.19°C. This pressure drop is influenced by the construction of the installed piping system and the amount of steam flowing along the steam pipes to the generator. Increasing the steam flow rate is directly proportional to the fluid or steam flow velocity. Based on the Darcy-Weisbach equation, the flow velocity significantly impacts the pressure drop. The most significant pressure drop occurs in pipe section 6 due to the pipe's construction, which has a length of 1,600 meters and contains 38 fittings.

From the modeling and simulation carried out, the potential for engineering a change in the power generation system to a block geothermal power plant was found, increasing electricity production of 10.12 MWe and 5.91 MWe, or equivalent to 17% - 15% of the existing system, which must transport steam through an 8.5 km long pipe. In other words, using block geothermal power plant technology allows higher electricity production than the existing system.

ACKNOWLEDGEMENT

Our thanks to PT Geo Dipa Energy for supporting this research at Dieng Geothermal Working Area and the data provided.

REFERENCES

Ashat, A., Ridwan, R. H., Prabata, W., Situmorang, J., Adityawan, S., & Ibrahim, R. F. (2019). Numerical simulation update of Dieng geothermal field, Central Java, Indonesia. Proceedings 41st New Zealand Geothermal Workshop, 30(10), 1–8.

Aziz, M., & Juangsa, F. B. (2021). Dry steam power plant: Thermodynamic analysis and system improvement. Thermodynamic Analysis and Optimization of Geothermal Power Plants, 97–111. https://doi.org/10.1016/B978-0-12-821037-6.00015-9

Department of Energy Fundamentals. (1992). Thermodynamics , Heat Transfer , and Fluid Flow Volume 3 of 3 DOE Fundamentals Handbook. Energy, 1(June), 138.

Dickson, M. H., & Fanelli, M. (2003). Geothermal energy: utilization and technology.

Direktorat Panas Bumi, & Ditjen EBTKE. (2017). Potensi Panas Bumi Indonesia (ISBN:9786025039409 (ed.); Jilid 1).

Gutiérrez Negrín, L. C. A., & Lippmann, M. J. (2016). 24 - Mexico: Thirty-three years of production in the Los Azufres geothermal field (R. B. T.-G. P. G. DiPippo (ed.); pp. 717–742). Woodhead Publishing. https://doi.org/https://doi.org/10.1016/B978-0-08-100337-4.00024-3

Layman, E. B., Agus, I., & Warsa, S. (2002). The Dieng Geothermal Resource, Central Java, Indonesia. Transactions - Geothermal Resources Council, January 2002, 573–579.

Ovando-Castelar, R., Martínez-Estrella, J. I., Garciá-Gutiérrez, A., Canchola-Félix, I., Miranda-Herrera, C. A., & Jacobo-Galván, V. P. (2012). Estimation of steam pipeline network heat losses at the cerro prieto geothermal field based on pipeline thermal insulation conditions. Transactions - Geothermal Resources Council, 36 2, 1111–1118.

Ozcan, N. Y., & Gokcen, G. (2013). Performance analysis of single-flash geothermal power plants: Gas removal systems point of view. Geothermal Energy, Technology and Geology, April, 227–260.

Pudyastuti, K., & Lie, N. M. (2020). The analysis of the heat losses in steam pipe lines of the X geothermal field - Indonesia. International Journal of Scientific and Technology Research, 9(3), 1305–1308.

Wang, D. (2023). Heat loss along the pipeline and its control measures. SN Applied Sciences, 5(1). https://doi.org/10.1007/s42452-022-05226-2

Zarrouk, S. J., & Moon, H. (2014). Efficiency of geothermal power plants: A worldwide review. Geothermics, 51, 142–153. https://doi.org/10.1016/j.geothermics.2013.11.001

Drilling Strategies in Red Clay Zone to Manage Iron Oxide Minerals Experience from P-Field, Indonesia

Pradana Vian Prasetyo[1], Didin Chaeruddin Irwansyah[1], Vicki Agustino[1], Dicky Alamsyah[1], Eka Daya Samudera[2], Ingria Yunandra M Arrasy[2], and Budi Setiawan[2]

[1]Rigsis Energi Indonesia, Jakarta, Indonesia
[2]Geo Dipa Energi, Jakarta Indonesia

pradana.prasetyo@rigsis.com

Keywords: Geothermal drilling, red clay, iron oxide, drilling operation

ABSTRACT

Geothermal drilling activities in Indonesia face many challenges especially comes from the formation. One of the challenges is the presence of iron oxide minerals in the red clay zone. Originating from the decomposition of volcanic rocks enriched with iron minerals, red clay exhibits its distinctive reddish hue owing to the omnipresent iron oxide. Hematite (Fe_2O_3) and Magnetite (Fe_3O_4), the predominant iron oxide minerals in geothermal fields, wield considerable influence over the overall mineral composition of reservoir rocks. Encounters with red clay zone which comprise iron oxide minerals during drilling activities necessitate an understanding of their types and abundance, as they can significantly impact the hardness and abrasiveness of subsurface rocks. Mismanagement can result in formation collapse and stuck pipes, thereby elongating drilling time and escalating project costs.

This study offers insights drawn from operational experiences in the P-Field, a noteworthy geothermal site in Indonesia. The discussion encompasses an overview of general iron oxide mineral characteristics and delves into specific strategies for addressing challenges in drilling operations. Emphasis is placed on mud strategies in production zone, defensive drilling methods, the strategic introduction of slightly underbalance drilling by modified ratio of fluid and aerated in the presence of the red clay zone, modify BHA when experiencing high torque in reservoir zone, and the application of economic reservoir zoning. Implementation of these strategies aims to enhance drilling efficiency, mitigate risks, and optimize project costs.

1. INTRODUCTION

Indonesia is one of the countries in the world with greatest geothermal energy potential. According to ESDM (ESDM, 2020), the geothermal potential in Indonesia reached 23,900 Mega Watt (MW). However, the utilization of geothermal in 2022 was still around 2,360 MW according to International Renewable Energy Agency (IRENA, 2023). In order to harnessing the geothermal utilization which still uncovered, drilling project become one of the way to accelerate this matter. Drilling is the one of the way activity for the respective geothermal operator to enhance their business starting from exploration phase to the development wells. Drilling activity is the main way to gain any new discovered of geothermal potential, despite of there are many challenges during the operation and impact on the high cost needed. Therefore, it is necessary to perform the exploration/development drilling and/or workover operation to sustain and/or escalating their operating capacity.

P-field is one of the biggest geothermal field in Indonesia located in West Java, with one unit operating at 55 MW capacity. In order to accelerate their business, a new geothermal power plant is planned to be built in that area which can covered for an additional 55 MW. To support this, the drilling campaign for 12 development wells have been performed started from September 2021 and ended on the March 2024. During the more than two-year drilling campaign, the drilling team faced many challenges, particularly when drilling in reservoir zone. The red clay zone, which contain Iron Oxide mineral, often to be a root cause of drilling problems after they significantly impact regarding the hardness and abrasiveness. This study will explain some drilling strategies to overcome the problems encountered in the red clay formation, providing valuable lessons for other geothermal operators in Indonesia facing similar challenges.

2. OBJECTIVE AND METHODOLOGY

The objective of this study is to discuss the types and characteristics of Iron oxide Minerals in Red Clay zone in P-field during the campaign. Before delving into the details, the drilling performance in P-Field will be explained, with the rate of the well completion being a key parameter for analysis. Additionally, the representation of drilling challenges/problem in reservoir zone will be illustrated using high torque and/or stuck pipe chart for each well. At the end, the drilling strategies during the campaign namely the transformation of mud strategies during drilling in production zone, perform defensive drilling methods, the application of slightly underbalance drilling when

there is an indication of iron oxide, modify BHA when experiencing high torque in reservoir zone particularly, and also the application of economic reservoir zone, are explained into the detail and eventually become a lesson learn and impact to the overall of the drilling campaign.

3. DRILLING CAMPAIGN SUMMARY

P-Field Drilling Campaign had finished to drill 12 big hole development wells. The drilling campaign was started from the rig demobilization in September 2021 and ended in March 2024 as the rig release for last well. As a summary, the project involves one Mobilization, one Demobilization, four Skidding job, seven Moving inter pad. Majority of the wells drilled in four sections: 26" Surface, 17-1/2" Production, 12-1/4" Production Liner and 9-7/8" Production Liner 2 section. However, there are five wells were needed to be drilled until 7-7/8" Production Liner 3 section as the fifth section as contingency plan in order to reach target depth. The drilling depth wells range start from 1506 mMD to 2107 mMD. In terms of drilling days, the duration range within 26 days to 86 days with 53.9 days average. Figure below shows the rate of well completion in P-Field after the campaign.

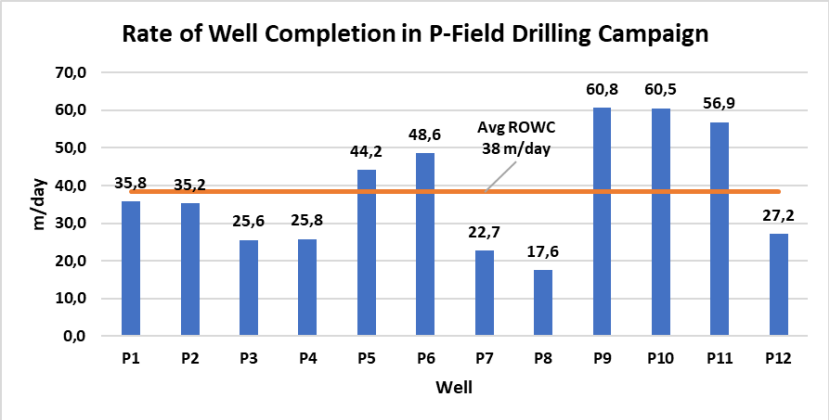

Figure 1: Rate of Well Completion in P-Field.

If looking more detail, there are only five wells which higher than 38 m/day which are P5, P6, P9, P10, and P11. Most of the wells which below average ROWC influenced by hole problem occurred during drilling hence exceed planned days. In addition, drilling campaign generated five wells sidetracked occurred in P3, P4, P7, P8, and P12 which hole problem occurred in these wells specifically. As mentioned above, drilling in Red Clay Zone which contain Iron Oxide mineral generated many drilling problems. The specific explanation of hole problem in Red Clay Zone will discuss in next chapter.

4. RED CLAY FORMATION AND IRON OXIDE MINERALS

Red clay formation is formed by the composition of volcanic rocks that are structured by many of minerals. Iron oxide is one of the mineral composition in red clay formation. Iron Oxide (Fe_2O_3) is composed from the elements between Iron (Fe) and Oxygen (O_2). Hematite/Ferric Oxide (Fe_2O_3) and Magnetite (Fe_3O_4) become the most iron oxide minerals frequently found. Between these types, Hematite/Ferric Oxide is the most iron oxide mineral composition in red clay zone since this kind of mineral has red/brown color which represent the red clay formation. Iron Oxide is a predominant minerals in geothermal fields, wield considerable influence over the overall mineral composition of reservoir rocks in particular. Iron oxide has very unique characteristics with complicated handle. This kind of mineral will react and become rust when meet with oxygen and water. The oxidation process then will occur and cause the solid material, in this case rock, degrade and become brittle. Due to majority of geothermal rocks come from lava which has been deposited from surface over many years, oxidation will occur.

During drilling campaign in P-Field for 3 years, the characteristic of iron oxide minerals have been identified. This type of mineral is reddish and soluble to liquid, particularly when using water in the drilling process. Iron oxide mineral is spreading out in all over P-Field area on two well pads (Pad X & Pad Y) in particular with depth range within 1000 – 1800 m which known as the reservoir zone. Become a soluble and brittle when face the liquid conclude this iron oxide mineral is clearly will affect the hole stability.

5. DRILLING CHALLENGES IN RESERVOIR ZONE

During the drilling campaign in P-Field, stuck pipe incidents accounted for the second highest non-productive time, contributing 699.5 hours or 25.7% of the total NPT. Figure 2 illustrates the high torque and stuck pipe events across all wells in P-Field during drilling campaign.

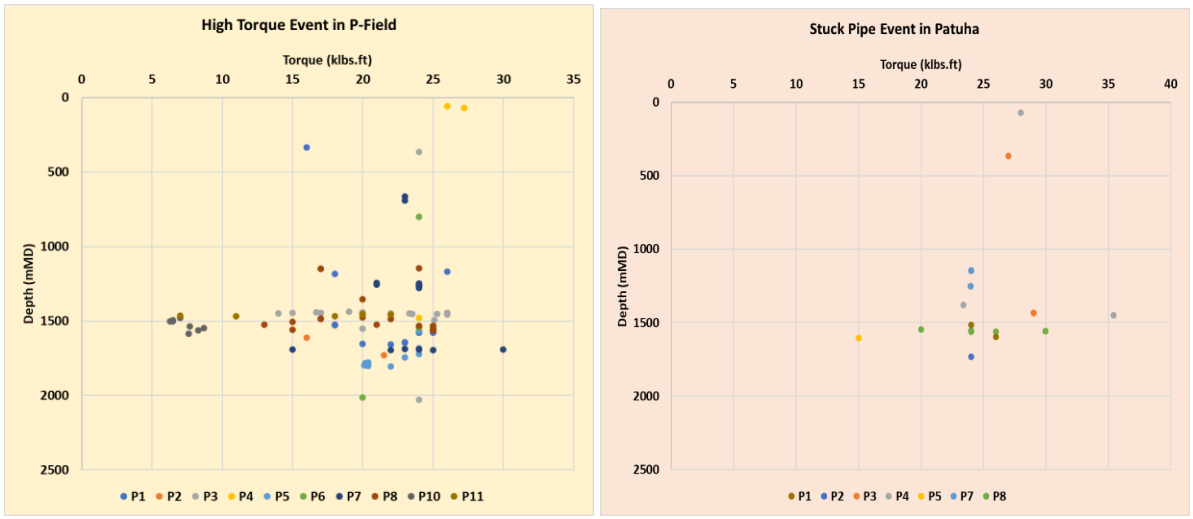

Figure 2: High Torque and Stuck Pipe Distribution in P-Field.

The figure shows that high torque event occurred in all wells with the depth ranging from surface to target depth of 2000 m. However, events most frequent between 1200 m to 2000 m depth, which corresponds to the reservoir zone. High torque events arise due to cuttings and/or formations, which most composed by iron oxide minerals, are not properly circulated to the surface and eventually accumulate below the hole. In addition, since the P-Field reservoir zone does not have a large fault zone to accommodate the cuttings when loss circulation, makes the high torque during drilling happen and stuck pipe then occurred.

Moreover, stuck pipes happen influenced by hole pack off from the formation in most wells. This is particularly problematic in the P-Field reservoir zone, which is composed of red clay formations containing iron oxide minerals that significantly impact formation pack-off. As discussed in the previous chapter, iron oxide minerals fall into three categories, all of which affect formation stability in P-Field. The drilling strategies to optimize handling of iron oxide minerals will be detailed in the following chapter.

6. DRILLING STRATEGIES

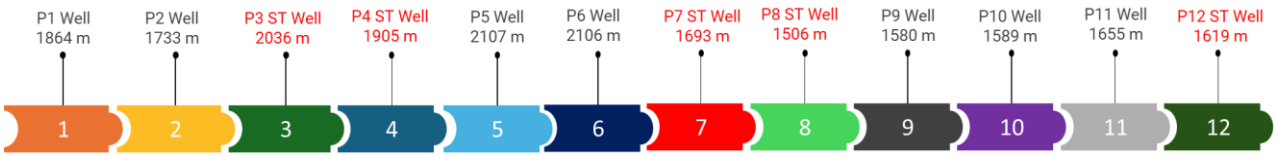

Figure 3: Drilling Journey in P-Field.

Presence of iron oxide mineral in red clay zone become one of the reason hole problem occurred in P-Field. Figure 3 showing the drilling journey in P-Field. Along the campaign, the drilling team continuously learned how the best practice to do the drilling operation since the first and second sidetrack well occurred in P3 & P4 well. The different approaches in terms of drilling operation had been taken to drill in P5 and P6 well. Slightly underbalance drilling and defensive drilling method were applied for the first time and resulting these wells into TD target. However, in the next drilling in P7 and P8 well, since the return condition was PLC and the pad location close to the crater, there was limitation to applied underbalance method, made hole pack off problem occurred suspected by presence of iron oxide in red clay formation. The continuation of drilling problems despite different approaches taken necessitated drilling team to thoroughly review the drilling program. Drilling team concluded that changing mud strategies in production zone, modify drilling BHA when experiencing high torque, maintaining defensive and slightly underbalanced drilling method, and apply the economic reservoir zoning were the best strategies to be applied. The detail of drilling strategies are explained in below.

6.1 Mud Strategies During Drilling in Production Zone

KCl Polymer is the most often mud type used when drilling for 26” section and 17-1/2” section due to these sections possess swelling clay and sticky clay as the drilling hazard. KCl (Potassium Chloride) is effectively used to inhibit clay hydration and generally KCl levels within 3-5%. Moreover, KCl polymer produce sufficient Plastic Viscosity (PV) and Yield Point (YP) as the mud properties which present the ability to lift the cuttings to the surface. Since the drilling in 26” and 17-1/2” are in full return condition mostly and rarely on partial loss event to total loss, this mud system is suitable.

After drilling in 4-5 first well, the team observed that flow return condition when drilling in reservoir zone was partial loss – full return condition instead of total loss. This indicates that the fault in reservoir zone is not large enough. And the presence of iron oxide which soluble and brittle when face the water only and still contain clay washout, can produce more cutting and lead to hole problems. Therefore, drilling team initiate to continue utilized the KCl Polymer mud when drilling in 12-1/4" and 9-7/8" hole section. Nevertheless, it is really noteworthy that KCl polymer mud type is only utilized when the partial loss – full return is still occurred. When encountered partial loss – total loss and the ability of mud mixing is not sufficient, then aerated mud + viscous water be applied. Moreover, in order to prevent high torque, lubricant additives need to be added within 1-2% range either KCl polymer or aerated water + viscous water mud type. Figure 4 explain the decision scheme of mud system in reservoir zone.

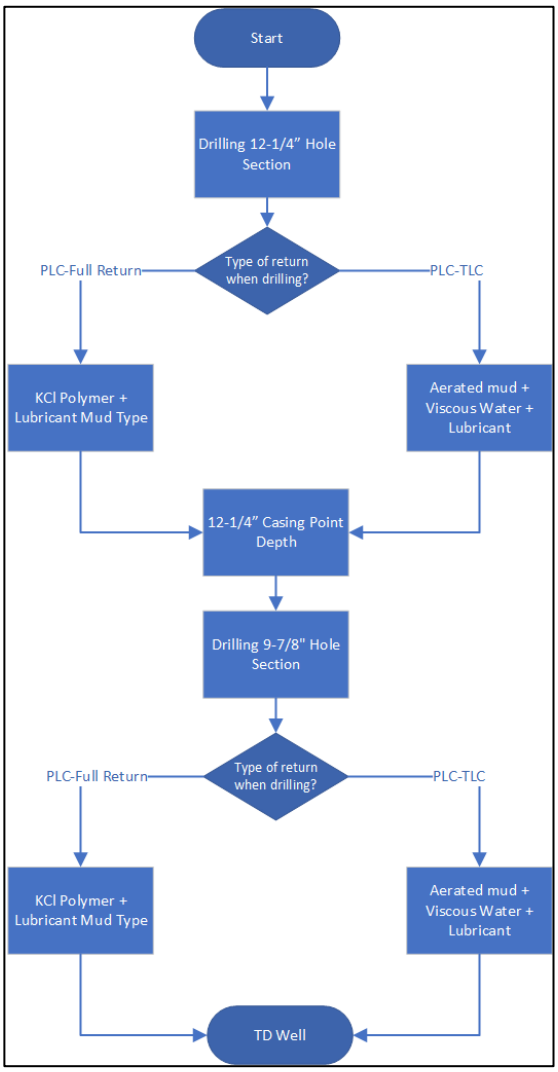

Figure 4: Mud System Selection Scheme.

6.2 Defensive Drilling Method Application

Defensive drilling is another drilling strategies applied in P-Field during the campaign. This method was applied firstly in P5 well and continuously maintained to the last well in P12. The principal of this method is perform drilling along 3-5 m progress. Afterwards, drill string picked up full stand while working pipe and circulate hole. This method is to ensure the wellbore in clean condition after drilled and will not lead to high torque, hence the drilling can reached target as per program. Defensive drilling method generally applied when face the iron oxide minerals. However normal drilling condition was conducted if there is no presence of iron oxide.

6.3 Application of Slightly Underbalance Drilling

As the terms, slightly underbalance drilling is modify the ratio between liquid (water/mud) and aerated mud which makes the mud flowrate lower than air rate in order to prevent iron oxide face the water/liquid. Moreover, since the mud flowrate was reduce, the borehole temperature become slightly hotter and iron oxide minerals is expected to be stable. Since the slightly underbalance drilling influence the pressure in wellbore keep lower than formation

pressure, this make allows cuttings to the surface and keep wellbore in clean condition. The application of aerated mud in slightly underbalance drilling was within 1800-2800 SCFM and influence the foam rate utilization between 8-20 gph. Meanwhile, the liquid ration was keep in 300-500 gpm during drilling.

6.4 Modify BHA in Reservoir Zone

Drilling BHA plays another important role when drilling in P-Field. In the first 4 wells, the directional BHA was always applied from the first to last section. However, stuck pipe occurred in P3 and P4 wells in 12-1/4" section and left the important part of directional BHA in hole which impact on drilling cost. The drilling team, after reviewed the drilling program, agreed to consider the utilization of rotary BHA instead of directional BHA when drilling in reservoir zone. In this case, directional BHA was still become a priority after this type of BHA cand adjust and correct the direction of the well as of reservoir target plan. However, when drilling encountered high torque zone, the replacement from directional BHA to rotary should be performed. From the operation, torque was considered as high when the drill string became difficult to rotate – stalled with the maximum torque was limited into 25 klbs.ft. In addition, since slightly underbalance method was applied in reservoir zone in order to maximize allowing on cuttings to the surface, directional BHA could not accommodate after there was a minimum liquid flowrate requirement from the mud motor and also influence to the temperature. The other objective to utilized rotary BHA in production zone was reduce cost fish and reduce large size of BHA component which impact to the release drill string when stuck. Moreover, even after the high torque and other considerations still occurred during drilling with rotary BHA, decision to utilize slick rotary BHA was conducted.

6.5 Economic reservoir zone

At the time after all drilling strategies had been conducted in reservoir zone (change mud strategies in production zone, defensive drilling method, slightly underbalance drilling, and modify BHA) did not help, then the application of economic reservoir zone become the last option. Economic reservoir zone was applied during the campaign in P-Field start from the P9 to P12 well. This method was conducted during drilling in reservoir zone by set casing shallower in order to prevent hole pack off if the well going deeper particularly when the iron oxide was appear. In this regard, after the well had been set casing using 8-5/8" perforated liner 2, a well completion test then carried out to assess whether the well can produce geothermal fluid. If the well completion test results are good, drilling then will be stopped and that depth. However, if the results are not satisfactory, going deeper the well using 7-7/8" hole section as contingency plan will be continued. Figure 5 shows the detail of drilling strategies during drilling campaign with the results.

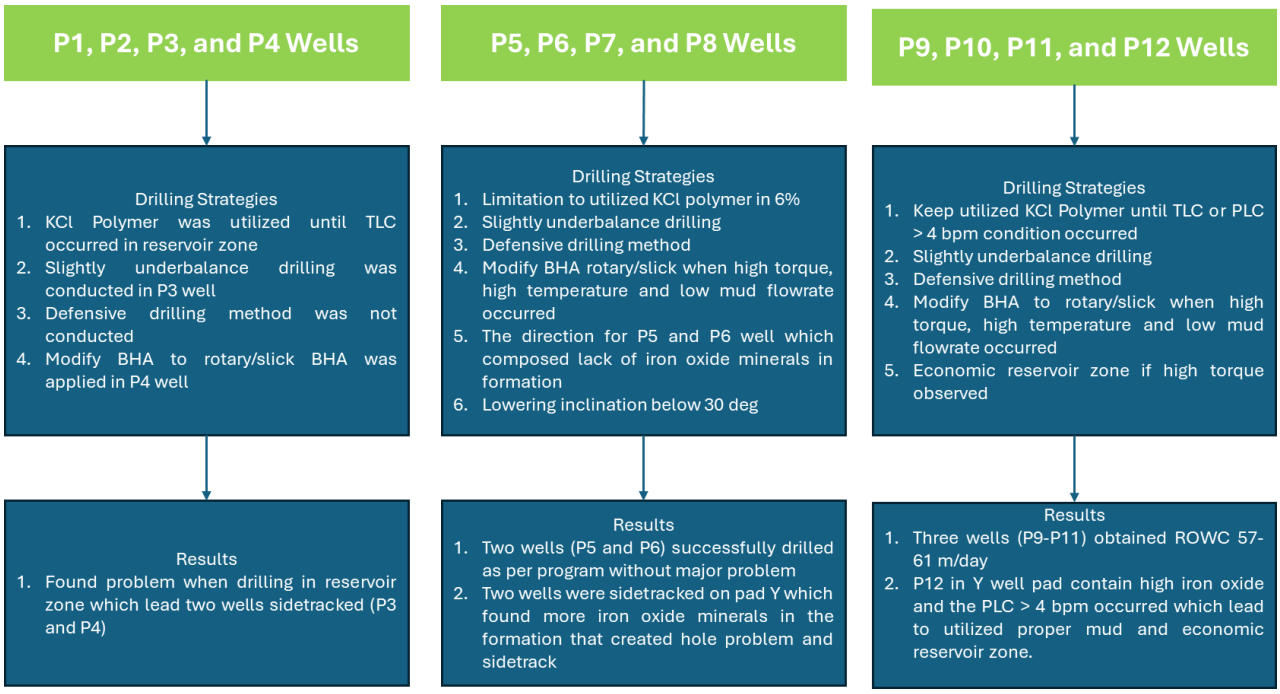

Figure 5: Drilling Strategies with the Result.

As we can see, different drilling approaches were always performed in each of the four wells, resulting in better outcomes. In the first four wells, all wells exceeded the drilling days based on the program, with two wells were sidetracked. Then, in the next four wells, when the defensive drilling method and slightly underbalanced drilling were applied, two wells successfully reached TD (total depth), however P7 and P8 wells experienced sidetrack due to the return condition was PLC and the pad location close to the crater enforced limitation to applied

underbalance method. The peak was in wells P9 to P12, where after a review of the drilling program, only one well exceeded the drilling days and performed a sidetrack.

7. CONCLUSION

Drilling campaign in P-Field resulting 12 development wells had been finished, started from 2021 to 2024. Through three years, many lessons learn were obtained during the campaign, particularly in the drilling operation. The presence of iron oxide minerals in the red clay formation within the reservoir zone presents a challenge for the drilling team to execute the entire well to reach the total depth target. Based on drilling operation, the characteristic of iron oxide minerals have been identified. This type of mineral is reddish and soluble to liquid, particularly when using water in the drilling process, predominantly found in two well pads (Pad X & Pad Y) within the depth range of 1000 – 1800 meters. Consequently, during operations, stuck pipe incidents became one of the largest (NPT) contributor during the drilling campaign, accounting for 699.5 hours or 25.7% of the total NPT. This is understandable as high torque and stuck pipe events mostly occur at depths of 1200 to 2000 meters, which correspond to the reservoir zone. This depth range is also where the red clay zone containing iron oxide is distributed.

During the operation, especially after completing the first four wells, the drilling team then applied another approach, namely Slightly Underbalanced Drilling and Defensive Drilling Method. Both methods successfully brought wells P5 and P6 to reach the expected TD target at depths of 2107 and 2106 meters. However, in the next drilling in P7 and P8 well since the return condition was PLC and the pad location close to the crater, there was limitation to applied underbalance method, made hole pack off problem occurred suspected by presence of iron oxide in red clay formation. The continuation of drilling problems despite different approaches taken necessitated drilling team to thoroughly review the drilling program. Drilling team concluded that changing prudent mud composition and/or system, modify drilling BHA when experiencing high torque, maintaining defensive and slightly underbalanced drilling method, and apply the economic reservoir zoning were the best strategies to be applied.

In terms of applying a mud strategies during drilling in the reservoir under partial loss-full return conditions, a KCl polymer will be used as the mud system to ensure that the cuttings can allow to the surface. A defensive drilling method will also be employed by circulate hole clean and working pipe after drilling 3-5 meters to ensure the wellbore is clean after drilling and to avoid high torque. Slightly underbalanced drilling will also be conducted alongside the defensive drilling method, where the ratio of aerated mud is higher than the liquid. The application of aerated mud in slightly underbalanced drilling ranges from 1800-2800 SCFM, influencing the foam rate utilization between 8-20 gph. Meanwhile, the liquid ratio will be maintained at 300-500 gpm. Modifying the BHA will also be done when high torque is encountered and applied slightly underbalance drilling which influence minimum mud flowrate, by switching from directional to rotary BHA. Moreover, reduce fish cost and reduce large size of BHA component are other objectives to utilized the rotary BHA. However, if this persists, a slick BHA will be used. The economic reservoir zone becomes the last method of the drilling strategy implemented in the P-Field by setting casing shallower to prevent hole packing if the well goes deeper, particularly when iron oxide appears. If the well completion test results are unsatisfactory, then continuing the well deeper using a 7-7/8” hole section as a contingency plan will proceed. The strategies proved successful in the last four wells, which only one well exceeded the drilling days.

REFERENCES

ESDM, K. (2020, March). Potensi Besar Belum Termanfaatkan, 46 Proyek Panas Bumi Siap Dijalankan. Retrieved from Kementrian ESDM: http://www.esdm.go.id/id/berita-unit/direktorat-jenderal-ebtke/potensi-besar-belum-termanfaatkan-46-proyek-panas-bumi-siap-dijalankan.

IRENA. (2023). Renewable Energy Statistic.

Prasetyo, P. Patuha Completion Report, Jakarta (2024)

Samudera, S. Post Drilling Patuha 2 Project, Bintan (2024)

Production Operations Optimization in Patuha Production Well

Adiasa Dewa Pradipta, Ananda Riris Kurnia Pratama,
Andrian Putra Wardana, Budi Santoso, and Hary Darmawan

PT. Geo Dipa Energi (Persero), Aldevco Octagon 2nd Floor.
Jl. Warung Jati Barat No. 75 Jakarta Selatan 12740 Indonesia

adiasa@geodipa.co.id, ananda.pratama@geodipa.co.id,
andrian@geodipa.co.id, budi.s@geodipa.co.id, hary@geodipa.co.id

Keywords: production operations, optimization, well head pressure, trim valve

ABSTRACT

Production operations optimization means various experimental implementation in the field which consider any aspects that might intervene the system in the purpose of obtaining the most optimum operations production. In Patuha Geothermal Field, there is X-7 Well that always gets a spotlight. The well shows an unstable production behavior with the well head pressure declines rapidly. X-7 Well also has calcite scaling problem in wellbore. Well washing usually executed to bring back the performance of X-7 Well before the campaign of well intervention. Well washing is implemented periodically by injecting condensate water for a certain period then shut-in the well until reach its maximum of stable well head pressure then the well online to main system. However, even after the well washing, the well head pressure still declines rapidly. As the result, well washing often forcefully done until the well head pressure equal to main steam line pressure. Due to this condition, the production operations optimization must be implemented. The set of well head pressure and trim valve to steam-in the X-7 well to the main system considering the operations constraint. These will be determined by an upper and a lower limit considering the known data from the well to the main system. The purpose of this optimization is to obtain the most optimal trim-valve opening then the production days getting longer and achieve the most efficient steam production. A 10% trim-valve opening is recommended because it shows the most optimal results in addressing the issues present at X-7 Well.

1. INTRODUCTION

The Patuha Geothermal Field, located southeast of Bandung in West Java, Indonesia, has been in commercial operation since 2014 by producing electricity from vapor dominated steam. Patuha Geothermal Power Plant operates twelve (12) production wells with steam dryness levels ranging from 95% to 98%. The X-7 Well is one of the production wells that contribute to Patuha Unit 1. X-7 Well was drilled in 1997-1998 then subsequently idle due to Indonesia's economic crisis.

During the production process, X-7 Well has exhibited unstable production behavior leading to scaling issues that impact production rates. The ability of the geothermal reservoir to deliver fluids is a success factor in geothermal energy utilization while scaling at pipe connected to production well determines the efficiency of power production. Most common scale in geothermal field are silica and calcite. For example, the serious decline in steam production well in Maori geothermal field is caused by calcite deposit and scale inhibitor is used to prevent precipitation of calcite in the well successfully (Sigfusson and Gunnarson, 2011; Fukoda et.al, 2011; Thorhallsson, 2012). When productions well not perform properly, various well intervention has been implemented such as well head water injection that often conducted at high pressure, intermittent cold-water injection, and well heating up in order to open up the hydrological path to permeable zone (Axelsson et.al, 2006).

In Patuha Geothermal Field, workover and well intervention using Coiled Tubing Unit were conducted multiple times to clean the wellbore from scale and remove any remaining fish with the intention to maintain the production performance of the well, thus minimizing the needs for future well-washing. Well washing is performed at X-7 Well when the well-head pressure almost equal to the main-steam-line pressure and plans for workover or well intervention still scheduled for a later time. Well washing implemented periodically as short-term effort to sustain steam production.

2. METHODOLOGY

Optimization is a time-consuming process that needs numerous stages and considerations from any aspect, often requires repeated efforts to achieve the desired optimum result. Optimization is necessary due to the production behavior of X-7 Well that is being quite unstable. To start, the problem has to clearly defined. Next, literature study is done to gather necessary data and explore the potential solutions. Data collection includes piping specifications to define constraint in this optimization process and historical event data of the well to mapped any

program that has been done previously in the well. Well production data correlate to piping specifications data and historical event data with the output optimization method will be executed in the field, typically through a field trial.

In the field-trial process, data are collected for analysis and evaluation of the field-trial result. It is not always possible to immediately get the right or even the best method. The method needs to be modified or changed if the result is deemed ineffective of implementation in the production operations. The effectiveness of this field-trial process should be carefully and wisely analyzed by comparing it with initial data and previous field-trial data. Geochemical data is essential to corroborate the results of the effectiveness in each field-trial. The end of this optimization is to obtain the most optimal methodology that can be applied to the production operations process in the field, as shown in Figure 1.

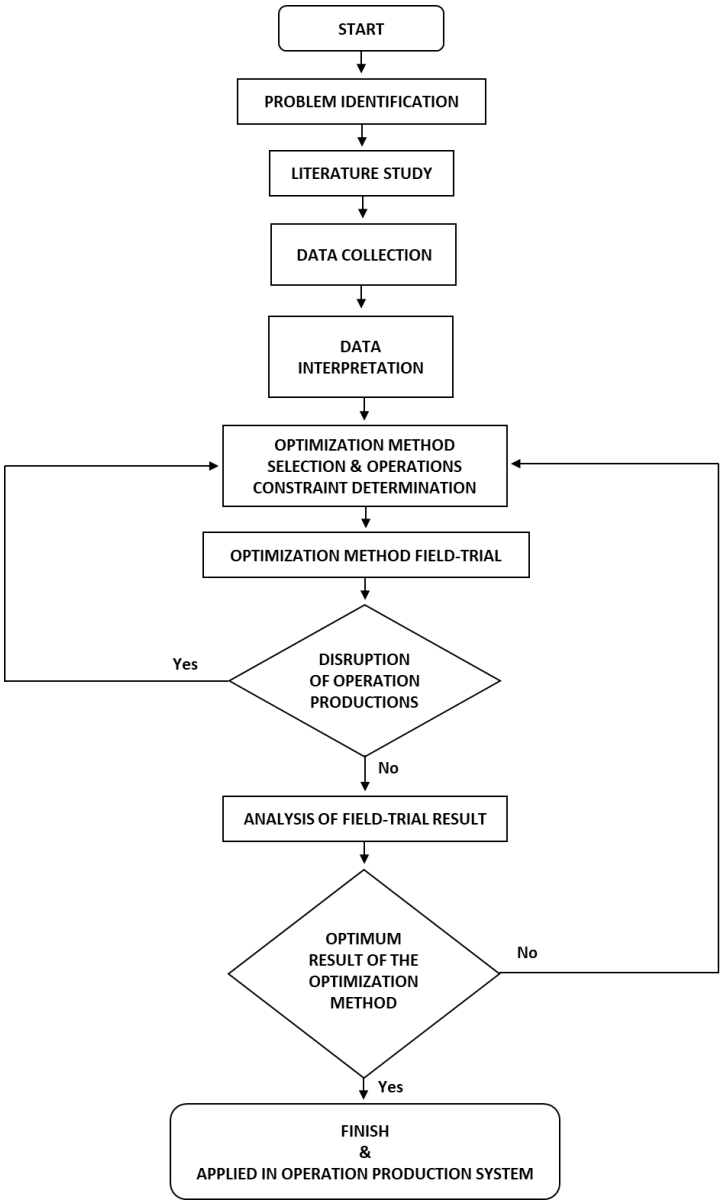

Figure 1: Methodology of the study.

3. CASE STUDY

Workover for X-7 Well was conducted in November 2020, the results were sufficient to supply the steam production. The operation of X-7 was return to normal and the well head pressure declined gradually for about 2.4%/month until it nearly equal to main steam line pressure by January 2022. Well head pressure will equivalent to main steam line pressure unless measures are taken to prevent flow disruption such as blockage or back-pressure. Before this occurrence might happen, the X-7 Well should be out from the main system followed by well washing to restore its performance. After completing the well washing, X-7 Well will be online to the main

system. However, despite the well washing has been done, X-7 Well shows a rapid decline in well-head pressure, approximately 24% per month, eventually almost equal with the main-steam-line pressure. Within less than a month, another well washing is required due to the average monthly decline in well-head pressure of about 40% as shown in Figure 2.

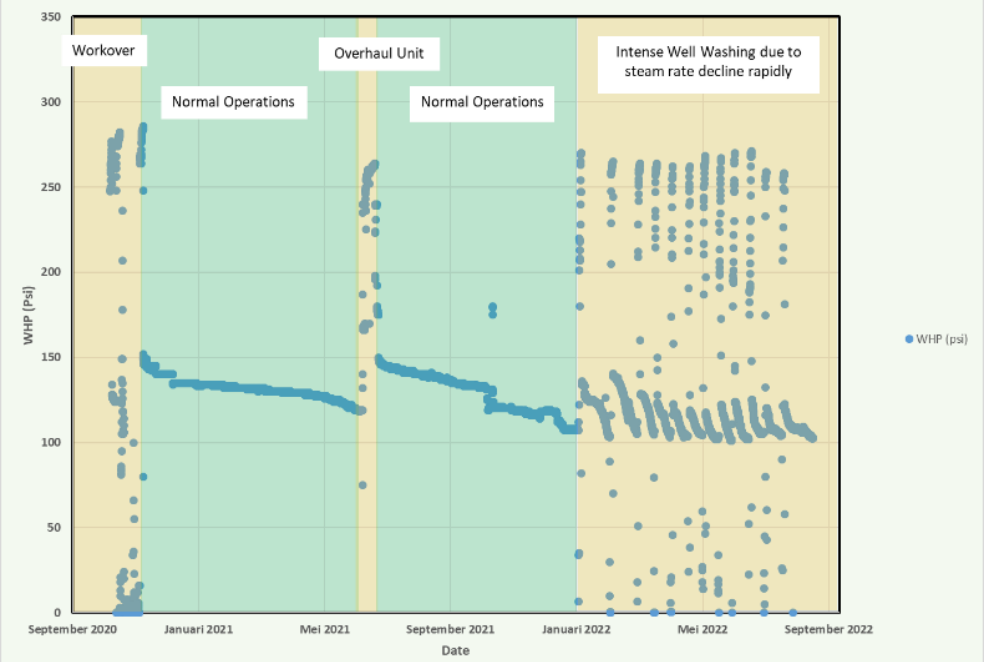

Figure 2: Well Head Pressure X-7 Well Trend after Workover 2020.

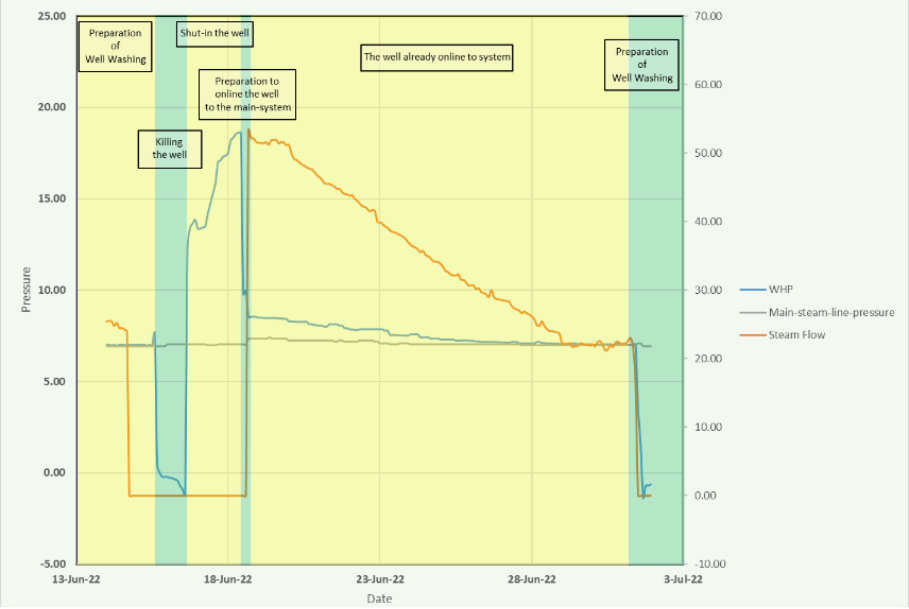

Figure 3: WHP vs Main-Steam-Line-Pressure vs Steam Flow during Well Washing.

3.1 Well Washing

Well washing is the short-term action when the well head pressure declines below the differential pressure restraint to the main steam line pressure with the intention of recovering the performance of the well. Well washing is implemented periodically, conducted by injecting condensate water for a specified duration as part of the program then shut in the well as the program until reaches its maximum shut in well head pressure. Before the well is online to the main system, the steam quality should be checked by using a brass target plate and geochemical analysis as required. If the quality of steam meets the range of its requirement, then the well will be online to the main system.

Well washing is conducted in five stages as shown by Figure 3. The first stage is preparation, since the well head pressure is close to the main steam line pressure, preparation means the pump for killing is in a good condition to

operate and the well will be offline from the system to the silencer. After that, killing the well by condensate water until a vacuum is achieved then condensate water continues to be injected for a certain period and shut-in the well until it reaches its maximum pressure for a certain duration. Next, focuses on preparing to online the well to the main system takes an important role because the steam quality should be checked to ensure it meets the requirements before online to the main system. Finally, the well will be online to the main system to supply the steam production by adjusting the trim valve opening. In every stage of well washing, continuous monitoring is conducted on the wellhead assembly to ensure that there is no leakage during this process. Additionally, monitoring is performed on the casing & wellhead temperatures also wellhead movement.

Table 1: Result of Well Washing after Workover 2020.

Well Wash	Period	WHP DECLINE		Production Days	Trim Valve Opening (%)
		% /day	% /month		
1	Jan-22	0,8%	24%	26,8	40%
2	Feb-22	1,3%	38%	22,9	32%
3	Mar-22	2,3%	68%	12,9	32%
4	Apr-22	2,4%	71%	12,8	34%
5	Apr-22	1,2%	36%	13,8	35%
6	May-22	1,2%	36%	11,8	33%
7	May-22	1,1%	33%	11,8	33%
8	Jun-22	1,9%	57%	9,9	32%
9	Jun-22	1,5%	46%	12,8	32%
10	Jul-22	1,2%	36%	11,7	32%
11	Jul-22	0,8%	24%	14,5	32%
12	Aug-22	0,4%	12%	27,0	32%

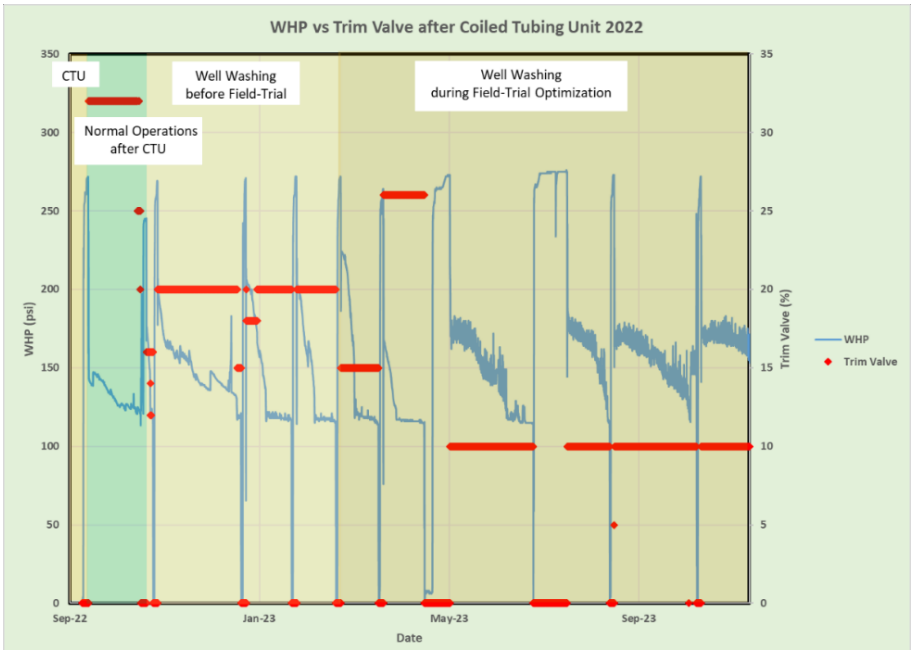

Figure 4: WHP vs Trim Valve after Coiled Tubing Unit 2022.

3.2 Well Head Pressure Decline

After 413 days since the last workover passed and the operation of X-7 Well without conducting any well washing, then the first well washing was finally carried out in January 2022. After the initial well washing, refer to Table 1, the X-7 Well came back online to the main-system with a trim valve opening 40%. However, it only contributes to supply the steam production for 26 days due to a well-head pressure decline of approximately 24% per month, nearly reaching the main-steam-line pressure. After that, a second well washing was necessary, and the well returned online with a trim valve opening 32%, but contributed only 23 days with a well head pressure decline of about 38% per month. Then, well washing was conducted routinely and forcefully at regular intervals. Data shown in Table 1 indicates that the second period well wash with a smaller trim valve opening resulted in shorter production days. Even in the third period, with the same trim valve opening of 32%, production days were further reduced to only 13 days before another well washing was needed. Furthermore, maintaining a relatively constant trim valve opening in subsequent periods around 32%-35% continued to reduce production days, with some

periods lasting only 10 days before requiring another well washing. The X-7 Well demonstrates that increasing the trim valve opening after well washing actually shortens production days, and maintaining a constant trim valve opening leads a continual decrease in production days in each period. This indicates that there is an issue with the X-7 Well, specifically scale growth inside the wellbore that impedes well productivity (Sujarmaitanto, H. et al. 2022). It necessitates a workover or well intervention on this well as a long-term action, similar to the 2020's workover that was previously conducted.

In September 2022, a well intervention using Coiled Tubing Unit was carried out to clean the wellbore of the X-7 Well. After the well intervention was finished, the well was online to the main system for about 32 days. It has to undergo another well washing due to the well head pressure closely equivalent to the main steam line pressure. Then well washing was executed periodically as shown in Figure 4.

4. RESULT AND DISCUSSION

An optimization for X-7 Well is necessary to maximize the production days. Adjusting the trim valve opening is the method to optimize the operations production of X-7 Well so the well washing intensity becomes less frequent and the well can reach its optimal steam production.

4.1 Operations Constraint

The setting of trim valve opening to steam-in the well into the main system must consider operation parameters from the well head, well steam line then main steam line, known as Operations Constraint. These will be determined by upper and lower limit by considering the known data of the wells and the operating parameter correlated to the main system (Donoso, 2022). Well steam line is a line that directly connected from the wellhead to accommodates fluids from a single well before gather to the main steam line. Main steam line is a line that gather all well steam line, thus becoming the main line that transport geothermal fluids to the power plant. Well head pressure and main-steam-line pressure are considered as the limitation in this production optimization. Increasing the trim-valve opening reduces the well head pressure, if this parameter is not carefully managed and exceeds its limits, it can lead to blockage or back-pressure issues. On the other hand, decreasing the trim valve opening increases the well head pressure, which potentially triggers the safety system protection (pressure safety valve and rupture disc) or more serious safety issues if it's not controlled. The maximum well head pressure as the upper limit will be defined lower than the Maximum Allowable Pressure of the well steam line, as shown in Equation 1. The minimum well head pressure as the lower limit will be defined higher than the main steam line's pressure as shown in Equation 2. When reducing the trim-valve opening followed by the increase of well head pressure, it is obligatory to ensure the main steam line pressure does not exceed its maximum design pressure for Pressure Safety Valve, as shown in Equation 4. The minimum main steam line pressure as the lower limit will be defined higher than the well head operating pressure, as shown in Equation 5. The well head operating pressure is defined by a value that is lower than the maximum well head pressure and higher than the minimum well head pressure. These parameters play an important role in the optimization decision making. Any action has to be taken when the well head pressure is near the lower limit or almost equal to the main-steam-line-pressure as well as the upper limit. Specially, the upper limit is beneficial as a guidance to adjust the trim valve when the well has to be online after shut in, to ensure it does not exceed its Maximum Allowable Working Pressure in the well steam line also the design pressure for safety pressure valve in the main steam line.

$$MAWP_{well-steam-line} > WHP_{max} \quad (1)$$

$$P_{operating\ main-steam-line} < WHP_{min} \quad (2)$$

$$MAWP_{well-steam-line} > WHP_{max} \geq WHP_{operating} \geq WHP_{min} > P_{operating\ main-steam-line} \quad (3)$$

$$P_{design\ for\ PSV} > P_{max\ main-steam-line} \quad (4)$$

$$WHP_{operating} > P_{min\ main-steam-line} \quad (5)$$

$$P_{design\ for\ PSV} > P_{max\ main-steam-line} \geq P_{operating\ main-steam-line} \geq P_{min\ main-steam-line} < WHP_{operating} \quad (6)$$

In order to determine the maximum pressure and temperatures as operation constraints, piping design and specification in the steam line have to be considered. Table 2 shows the steam line piping specifications. The constraint set in this optimization is easily illustrated in Figure 5.

Table 2: Steam Line Piping Specification.

Rating	Well Steam Line CLASS 300	PSV at Main Steam Line
Design Pressure	36 barg	11.5 barg (PSV)
Design Temperature Max	250°C	-
Design Temperature Min	15.2°C	-
Operating Flow Temp Max	184.6°C	-
Operating Flow Temp Min	175.5°C	-

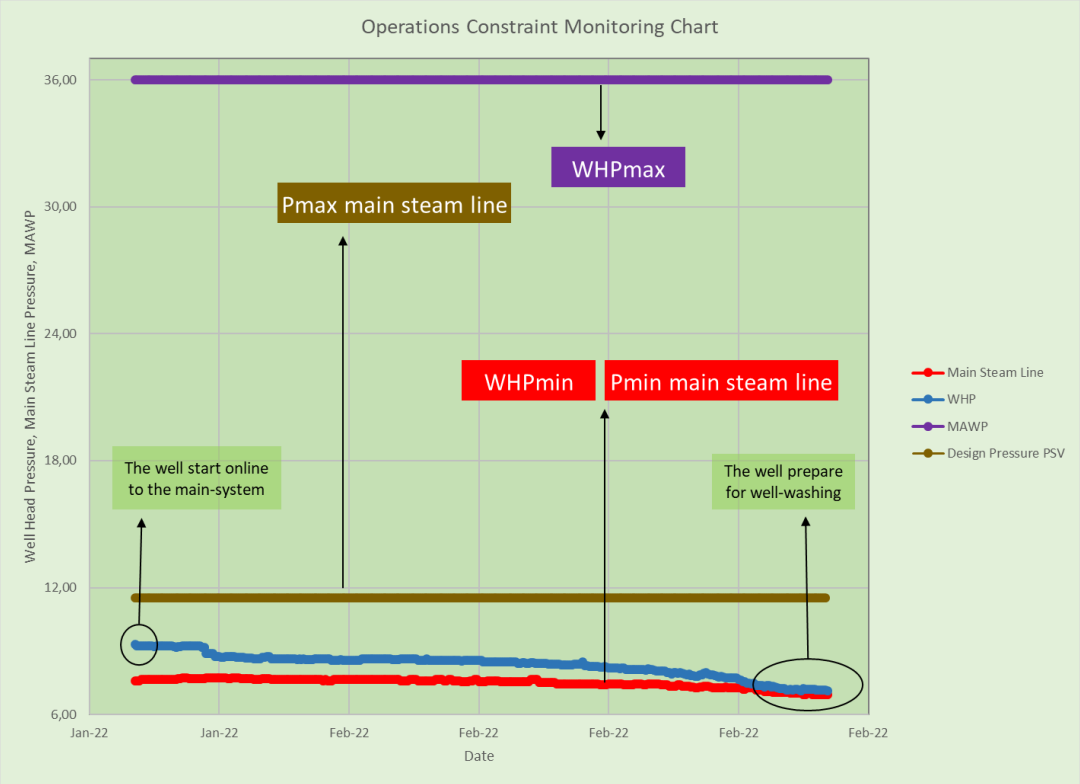

Figure 5: Operations Constraint Monitoring Chart.

4.2 Trim Valve Adjustment

The upper and lower limit in trim valve adjustment cannot be ignored since that are the most important parameters. Adjusting the trim valve opening above 20% requires full attention to the allowable working pressure of the pipe as the upper limit and vice versa.

Table 3: Result of Well Washing after Coiled Tubing Unit. Before Optimization, and During Field-Trial for Optimization.

Well Wash	Period	Trim Valve Opening (%)	WHP Starting (bar)	WHP DECLINE		Production Days	Steam Prod Avg (Tn/hr)	Cum. Steam Prod (Tn)
				% /day	% /month			
13	Nov-22	20%	14.21	0.7%	21%	52.7	26.24	33,114
14	Jan-23	20%	13.76	3.4%	103%	28.7	19.78	13,567
15	Feb-23	20%	15.06	4.2%	125%	24.7	20.57	12,133
16	Mar-23	15%	15.31	4.7%	140%	23.8	16.41	9,255
17	Apr-23	26%	11.63	3.9%	116%	25.8	20.48	12,656
18	May-23	10%	14.14	0.9%	28%	52.6	17.91	22,486
19	Aug-23	10%	15.52	0.6%	17%	51.9	13.01	16,052
20	Oct-23	10%	16.05	0.6%	18%	63.0	12.40	18,767

Before Optimization
Field-Trial for Optimization
Field-Trial for Optimzation

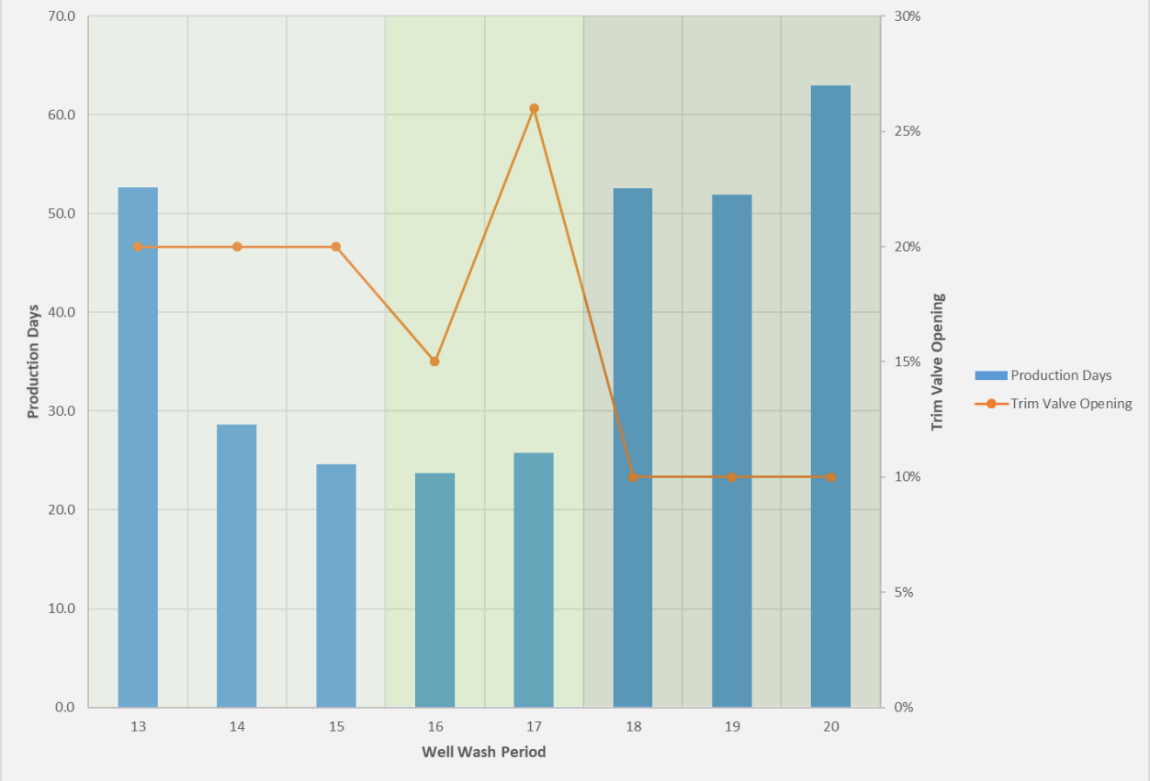

Figure 6: Production Days vs Trim Valve Opening.

The field-trial optimization was executed several times by adjusting trim valve opening with 15% (lower than 20%) and 26% (higher than 20%). The result of these adjustments is shown by Table 3. The trim valve opening at 15% led to shorter production days compared to the trim valve opening at 20% due to higher well head pressure decline with a cumulative steam production falling below expectations. The trim valve opening at 26% resulted in production days and cumulative steam production almost similar to trim valve opening at 20%. In addition, geochemical analysis data as shown in Table 4, indicates several geochemical parameters are sufficiently high and pose a risk of calcite deposition along the wellbore, which may lead to a rapid decline in steam production over a short period of time. Based on the trial result shown in Figure 7, there is no significant difference between 15% and 26% trim valve openings, thus another field trial will be conducted on different trim-valve opening in order to obtain the optimal setting.

Table 4: Geochemical Analysis for X-7 Well.

Well Wash	Period	Trim Valve Opening (%)	pH	Ca (ppm)	HCO3 (ppm)	TDS (ppm)	CSI
13	Nov-22	20%					
14	Jan-23	20%	8.51	5.56	26.93	160.38	0.72
15	Feb-23	20%	7.58	17.7	24.35	183.54	0.75
16	Mar-23	15%	6.52	42.2	29.2	79.79	0.89
17	Apr-23	26%	6.97	21	27.92	228.91	1.2
18	May-23	10%	5.63	4.66	5.66	17.16	-1.18
19	Aug-23	10%	5.39	1.26	13.96	16.02	-1.49
20	Oct-23	10%	5.00	0.79	5.01	15.83	-2.71

Before Optimization
Field-Trial for Optimization
Field-Trial for Optimzation

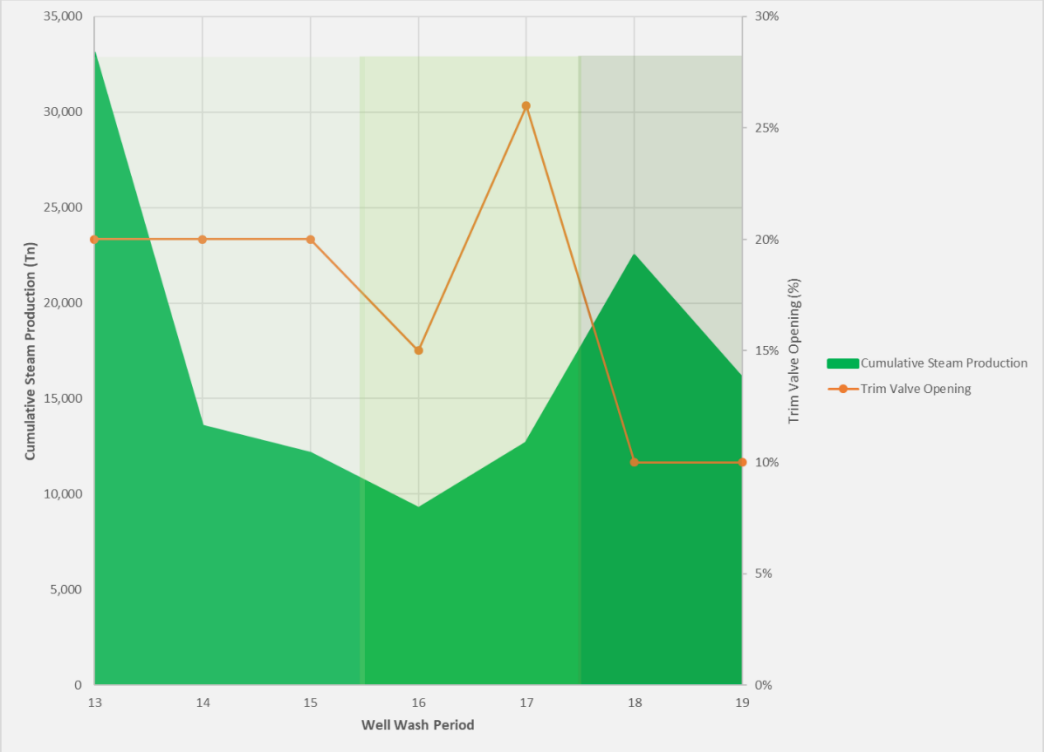

Figure 7: Cumulative Steam Production vs Trim Valve Opening.

The next field-trial was performed by adjusting trim-valve opening at 10%. By adjusting trim valve opening at 10% shows promising result. Thus the 10% trim-valve opening has been decided for next well washing to validate the consistent positive outcomes. Based on the geochemical analysis, the calcite saturation index (CSI) values are negative, indicating a significantly lower risk of calcite deposition. These geochemistry data taken from separated water sample from the well steam line at the top and bottom port sampling points, providing insights into conditions within the wellbore and at the surface. It is also confirmed by the production days which is two times longer and the cumulative steam production increased during that period, the significant results are shown in Table 3 and Table 4 for well wash 18-20.

4.3 Comprehensive Analysis of Field Trial Effectiveness

The result of the field trial has been comprehensively analyzed, encompassing the well production performance throughout its life time or production days and steam production, also geochemical analysis.

Table 5: Optimization Parameters Effectivity Comparison.

Well Wash	Trim Valve Opening (%)	Production Days	Effectiveness by Production Days (%)	Cum. Steam Prod (Ton)	Effectiveness by Cum. Steam Prod (%)	Remarks
13	20%	52.7		33,114		First well wash after Coiled Tubing Unit in 2022
14 & 15	20%	26.67		12,850		
16	15%	23.8	-10.94%	9,255	-19.13%	First field-trial optimization
17	26%	25.8	-3.44%	12,656	2.00%	Second field-trial optimization
18, 19 & 20	10%	55.83	109.38%	19,102	-29.00%	Third field-tial optimization

Before Optimization
Field-Trial for Optimization
Field-Trial for Optimzation

To obtain the most optimum trim valve opening, an effectiveness of production days and cumulative steam production is a crucial parameter that must be considered to formulate recommendations for this problem, as well as the geochemical data as the confirmatory parameters.

Based on the production days for each trim valve opening, the effectiveness that assessed by comparing the data before optimization shows that the result after adjusting trim-valve opening at 10% is up to two times better than trim valve opening at 15% and 26% as shown in Table 5. Therefore, it can be concluded that by comparing to a larger trim-valve opening, a 10% trim-valve opening is recommended because it results in the longest production days that leads to minimize the downtime production of X-7 well. Furthermore, the result of optimizing the production operations of X-7 Well, specifically by reducing the frequency of well washing is crucial to maintain casing integrity. This is because of the high cyclic loads of temperature and pressure changes during well washing can lead to casing damage (Kaldal, S. G. et al, 2012).

Refer to Table 5, on cumulative steam production data, the effectiveness by cumulative steam production is assessed similarly to the calculation for production days. By comparing the effectiveness of cumulative steam production between each trial, a trim-valve opening of 10% shows a slightly lower cumulative production effectiveness compared to larger trim-valve openings, but the difference is not significantly seen when considering its effectiveness in production days.

Based on the geochemical analysis shown on Table 4, a trim-valve opening of 10% indicates relatively low-value geochemical parameters and a CSI value of less than null which indicate a lower risk of calcite scale precipitation. Trim-valve opening of 10% is recommended for X-7 Well production optimization by considering the longer production days, lower well washing frequency, and higher cumulative steam production. The lower risk of calcite precipitation compared to other trim-valve openings and the casing integrity can be more maintained due to less frequent well washing as an additional reason to strengthen the recommendation to solve the issue present in the X-7 well.

5. CONCLUSION

In Patuha Geothermal Field, X-7 Well faced scale growth problem in the wellbore which caused a significant decline in well head pressure. That condition needs periodic well washing to maintain the well performance. The trim-valve opening needs to be controlled at the time X-7 Well needs to be online after well washing shut in. Optimization for this well is an absolute need in order to extend the production lifespan while ensuring optimal output. The optimization was carried out by conducting field trials with various trim-valve openings after completing the well washing by considering operations constraints. Through the analysis & calculations in the field-trial process, trim-valve opening at 10% gives the optimal result and is recommended for X-7 Well operation.

6. RECOMMENDATION

Workover or well intervention is a long-term solution to address this scale growth issue which causes an extreme well-head pressure decline. However, optimization of the production operation is necessary. The optimization processes that were discussed in this paper are possible to be considered as a reference, but need an adjustment to suit both subsurface and surface conditions for each field then the limitation will be identified to conducting the optimization.

REFERENCES

Donoso, Arkaitz Manterola.: Optimization of Geothermal Well Control for a Sustainable Production Strategy using Stock Reservoir Modelling, Reykjavik University, Iceland (2022)

Sujarmaitanto, H. et al.: Calcite Scaling in Vapor-Dominated Well, Patuha Geothermal Field, 8th Indonesia International Geothermal Convention & Exhibition, Jakarta (2022).

Thorhallsson, S., : Common Problems Faced in Geothermal Generation and How to Deal with Them,Short Course on Geothermal Development and Geothermal Well, Santa Tecla, El Salvador, (2012).

Kaldal, S. G. et al : Thermal and Structural Analysis of the Casing in a High Temperature Geothermal Well During Discharge, Proceedings 37th Workshopn on Geothermal Reservoir Engineering, Stanford University, Stanford, California (2012)

Sigfusson, B., and Gunnarson, I,: Scaling Prevention Experiment In The Hellisheidi Power Plant, Iceland,Proceedings, 36th Workshop on Geothermal Reservoir Engineering, Standford University, Standford, CA (2011).

Fukoda, D., Watanabe, M., Maetou, K., Arai, F., Ohta, M., Odagiri, K., and Matsumoto, Y.: Prevention and Dissolution of Anhydrite using Chemical Agents for Production Well at the Maori Geothermal Field, Hokkaido, Japan, Proceedings, International Workshop on Mineral Scaling (2011)

Axelsson, G., Thorhallsson, S., Bjornsson, G., :Stimulation of Geothermal Wells in Basaltick Rock In Iceland, Kartause Ittingen, Zurich, Enhanced Geothermal Innovative Network for Europe, Workhsop 3, Switzerland, (2006).

Unlocking Geothermal Potential: The CaSil Technology

Michael Schweig, James H. Johnston, Thomas Borrmann, and H. Putri Fraser

CaSil Technologies Ltd., PO Box 10-811, Wellington 6143, New Zealand

mschweig@casiltech.com

Keywords: Geothermal, Silica Scaling, CaSil Technology, Calcium Silicate, Silica Extraction, Direct-Use, Reinjection

ABSTRACT

Silica scaling continues to pose a worldwide challenge in the full exploitation of geothermal reservoirs. As dissolved silica precipitates during cooling and steam production, it forms an intractable scale that blocks pipework, heat exchangers and reinjection wells. These deposits significantly lower the efficiency of heat exchangers, resulting in a direct reduction in electricity and revenue generation over time. Regular and costly maintenance is required which leads to plant downtime. Conventional silica scale mitigation techniques are not wholly successful and come with drawbacks such as high cost or corrosion risks.

The innovative and proprietary CaSil technology introduces a disruptive method of transforming dissolved silica entities into a novel calcium silicate (CaSil) product, forming discrete particles that remain suspended and do not adhere to metal surfaces. This process achieves a significant reduction in the silica saturation index to well below 1 within seconds. The robust technology is adaptable to a wide range of brine compositions, regardless of the initial silica concentration, ensuring dependable elimination of silica scaling. Moreover, the CaSil technology facilitates the safe reduction of brine temperatures beyond current limits without inducing any silica scaling. This presents novel business prospects for utilising additional process heat in sectors like greenhouses, aquaculture, or milk powder production, supporting the efforts to decarbonise industrial processes. The CaSil technology can seamlessly integrate with existing geothermal operations, or greenfield plants, offering a versatile solution.

This paper presents updated data from our development plant which was successfully operated across four different geothermal resources in New Zealand. The effectiveness and robustness of the technology which can unlock the full potential of geothermal resources are highlighted. Additionally, data based on laboratory experiments are discussed, addressing the applicability of the technology to high silica, hypersaline geothermal brines such as the Dieng field in Indonesia.

1. INTRODUCTION

1.1 Silica Scaling

The earth's core holds practically inexhaustible amounts of thermal energy. This energy can be extracted to produce electricity in geothermal power stations, particularly in tectonic plate boundary areas with volcanic activity such as the Ring of Fire. Hot water, steam, or a mixture of both is extracted from a natural or artificially created geothermal reservoir. The sourced fluid typically contains a mixture of different minerals in solution, such as chloride-based salts, carbonates, base and precious metals and silica. The specific composition is dependent on the pressure, temperature and rock structure of the resource and varies from location to location. However, steam is required for the technical utilisation, which is produced by reducing the pressure of sourced water in a flash vessel. This causes a portion of the liquid to boil off as steam that can then be used to drive a turbine and produce electricity.

The mass reduction of the liquid phase causes the dissolved chemical species to concentrate in the brine. Additionally, the water temperature decreases to the respective pressure-dependent boiling point. This causes the silica solubility to decrease which is dependent on the fluid temperature. Typically, silica becomes supersaturated after a flashing stage due to the two simultaneously occurring effects and leads to unwanted scaling. The ensuing silica polymerisation process is dependent on the brine pH, salt content and degree of supersaturation. Hypersaline brines in particular suffer from a further significant reduction in silica solubility due to the dissolved salt species. This is a well-documented problem in geothermal resource utilisation and a world-wide challenge (García et al. 2005; Iler 1979; Makrides et al. 1980).

As the silica polymerisation process advances, intractable scale is formed in all process equipment such as pipes, valves, heat exchangers and reinjection wells. This significantly lowers the efficiency of a power plant over time and necessitates costly maintenance and plant downtime. Several mitigation methods have been developed by industry and are used worldwide such as hot reinjection, acid dosing or sequestering agents. However, they can come with significant drawbacks such as a very limited degree of resource usage, corrosion issues or high

operating cost. Additionally, no currently used mitigation technique can fully prevent silica scaling, making regular cleaning and maintenance still a necessity (Gunnarsson and Arnórsson 2005; Thorhallsson 2011; Richardson et al. 2014).

1.2 The CaSil Technology

The Calcium Silicate (CaSil) technology has been developed to address the shortcomings of currently utilised silica scaling mitigation efforts. The technology offers a novel and disruptive solution which can wholly eliminate silica scaling in geothermal resource utilisation. Additionally, significantly lower brine temperatures are possible after the CaSil technology treatment without inducing silica scaling, than with any other commercially available and economical technology. This unlocks the full potential of geothermal resource utilisation for power generation and direct-heat applications. Figure 1 shows a schematic diagram of an exemplary integration of the CaSil technology with a typical geothermal power station. Different implementation methods of the technology are possible depending on the needs of the individual plant.

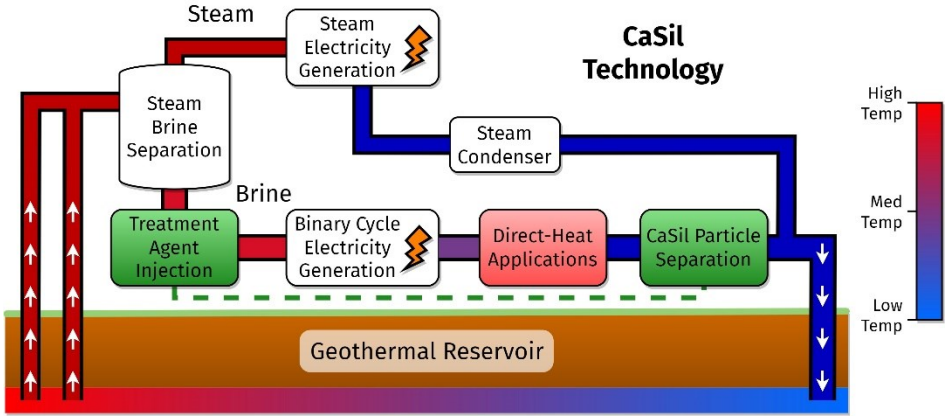

Figure 1: Schematic diagram on an exemplary integration of the CaSil technology in a geothermal power plant with flash and binary cycle.

A treatment agent is injected into the geothermal brine as soon as silica reaches a supersaturated state, which typically occurs after the flashing process. The dissolved silica is rapidly transformed into a novel nanostructured calcium silicate (CaSil) material which does not stick to metal surfaces and has unique chemical and structural properties. The chemical reaction is completed within seconds and forms a colloidal suspension with discrete particles. The suspension can easily flow through pipework and heat exchangers used in a binary cycle plant or for direct-heat applications. Little turbulence is needed to keep all CaSil particles in suspension. Finally, the CaSil is separated as a useful material before brine reinjection.

By transforming the silica, the residual silica concentration in the treated brine is actively lowered which leads to a reduction in the Silica Saturation Index (SSI) to significantly below 1. Silica scaling is effectively prevented at currently common discharge temperatures of geothermal power stations (140-100 °C). This means no scaling can occur after the treatment agent dosing point so all pipework, binary plant heat exchangers and reinjection wells stay clean and fit for purpose. Naturally, this boosts the electricity output of binary plants over time as scaling is eliminated (see section 2.1). Additionally, more heat energy can be extracted safely from the medium temperature brine before an SSI of 1 is re-established, increasing the sales revenue from binary cycle power production. This can be done in additional downstream binary cycle plants or through heat supply to direct-heat applications (see sections 2.2.2 and 2.2.3).

The CaSil technology can be readily installed into existing geothermal power stations or greenfield projects to offer a comprehensive silica scaling prevention technology as well as enable the full utilisation of a geothermal resource.

2. FULLY UNLOCKING GEOTHERMAL RESOURCES THROUGH CASIL

As mentioned before, the CaSil technology significantly lowers the SSI of a given brine well below 1. This enables additional downstream heat utilisation in an economical manner that is currently not possible by any other means. Significantly more value can be created from a geothermal resource by implementing the CaSil technology, depending on the individual resource conditions and site requirements. This can be achieved through additional electricity generation assets, the availability of excess heat for direct-use applications, mineral extraction or the production of environmentally friendly products based on the generated CaSil material.

Through the CaSil technology, the revenue streams of a geothermal power plant can be diversified from just one product (electricity) to a multifaceted industry hub. Each of the individual possible benefits are explained in the following subsections.

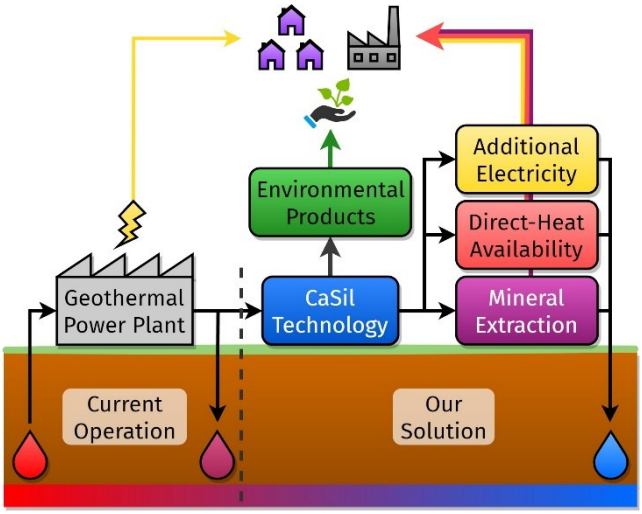

Figure 2: Schematic diagram of the CaSil Technology outputs and possible benefits.

2.1 Enhanced Electricity Generation in Existing Binary Plants

In current operations, binary cycle units experience silica scaling. The mineral deposits reduce the effective heat transfer coefficient and significantly raise the pressure drop across the affected heat exchangers. This results in a gradual reduction in generated power from the unit over time as depicted in Figure 3 (red line). The scaling rate is dependent on the silica concentration and degree of supersaturation. In the example above, a 20 % reduction in power output of a given unit is assumed over a period of 6 months. Once the power output drops below a chosen value (in this case 80 %), the unit is taken out of service and laboriously cleaned. Typically, this includes high pressure water blasting, strong acids or bases, or a combination thereof. Afterwards, the power output returns to 100 %, however, silica scaling will start again immediately and the cycle restarts. Valuable production capacity and revenue is being lost due to this saw-tooth power production profile caused by silica scaling. Additional cost is incurred by the necessary heat exchanger cleaning and plant downtime.

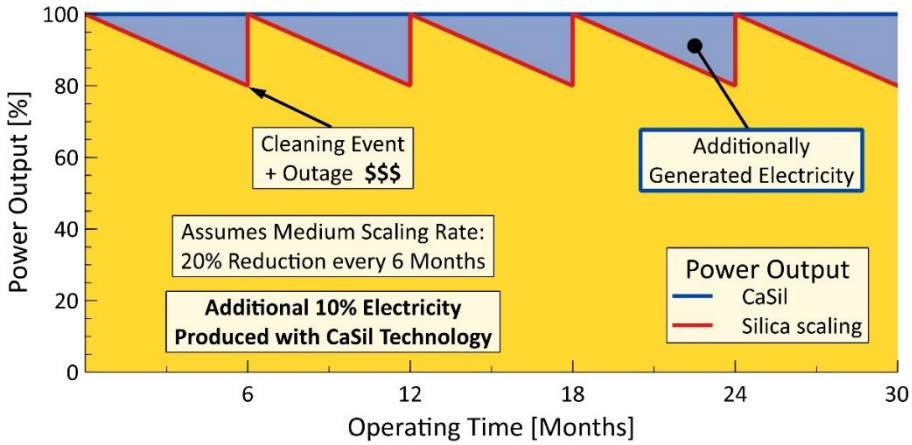

Figure 3: Model power output curve of a typical binary plant affected by silica scaling and enhanced electricity generation enabled by the CaSil technology.

With the CaSil technology, the SSI drops significantly below 1 at common geothermal process temperatures (see also Figure 4). This means that no silica scaling occurs and heat exchangers stay free of depositions. Binary plants can therefore continuously deliver their full power output over time (Figure 3, blue line). This means, that more electricity is generated over time compared to the saw-tooth production profile of a binary unit operating under current conditions. In the depicted example, an additional 10 % of electricity, and therefore revenue, is generated from the same existing asset over time by including the CaSil technology. The amount of additionally generated electricity depends on the individual scaling rate. For severe scaling rates, the amount of additionally generated electricity is estimated to be up to 25 %. Additional benefits are the elimination of strong acids or bases for

cleaning which incur H&S risks around transport, handling and disposal. Furthermore, the financial burden of cleaning services and plant downtime can be eliminated.

2.2 New Downstream Opportunities for Electricity and Direct-Heat Applications

2.2.1 Field Results from CaSil Development Plant

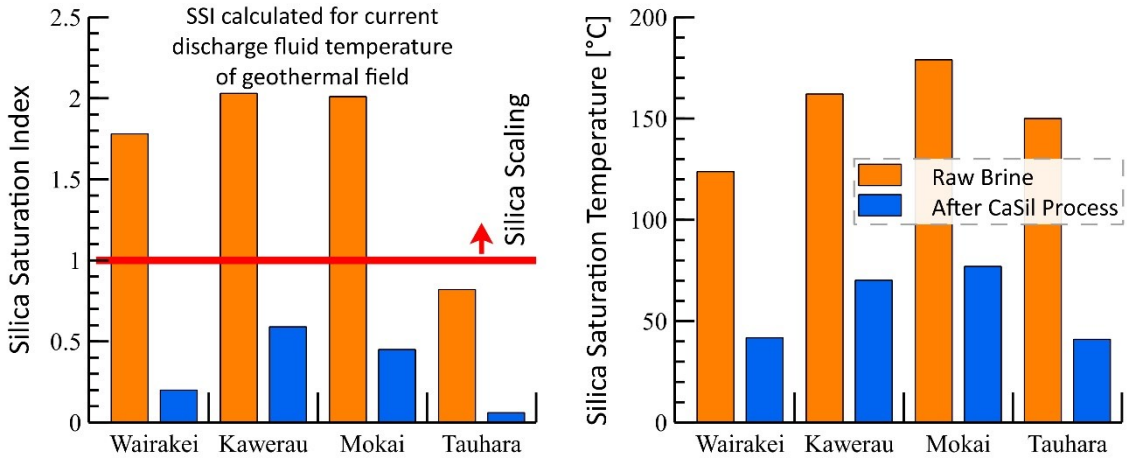

Figure 4: Silica Saturation Index at field discharge temperature and Silica Saturation Temperature for Wairakei, Kawerau, Mokai and Tauhara geothermal fields in New Zealand for sampled raw brine and CaSil treated brine.

The CaSil technology has been successfully proven and demonstrated in different geothermal fields across New Zealand. A continuously operating and fully automated development plant has been designed, built and improved over a number of years which reached its current state of development in 2023, processing up to 3 t/h of geothermal fluid and demonstrating all unit-operations of the technology. The plant was installed at the Wairakei, Kawerau and Mokai geothermal resource for research and development of the technology at the respective fields. Currently, the plant is located at the He Ahi – Eco Business Park near Taupo, New Zealand, which is located on the Tauhara geothermal resource. Field data from the development plant is presented in Figure 4.

The SSI of all fluids is calculated for the current reinjection temperature of each field (left side). In the Wairakei, Kawerau and Mokai fields the sourced raw brines were already supersaturated in silica (SSI > 1) at their respective reinjection temperatures. This means, silica is polymerising and scale formation occurs. At the Tauhara field the fluid is exclusively used for direct-heat applications and currently reinjected at high temperatures. This means the SSI is still below 1. However, as more direct-heat customers establish their presence at the Eco Business Park, more heat will be extracted from the geothermal brine, inevitably leading to an SSI below 1.

After the CaSil treatment the SSI could be significantly reduced below 1 in all these geothermal resources. This means, no more silica scaling occurs at the current reinjection temperatures for each field. In Wairakei, a reduction in SSI from 1.78 to 0.2 was achieved. Similarly, in Kawerau and Mokai the SSI decreased from 2 to 0.6 and 0.45 respectively. The reason for the higher SSI after treatment in Kawerau and Mokai is the significantly more acidic nature of the brines which affects the process chemistry. However, the SSI was still reduced significantly below 1, which cannot be economically achieved by any other means. Changes in the process chemistry are possible to reduce the SSI further if required. In Tauhara, the SSI decreased from 0.8 to 0.06 at the comparatively high current reinjection temperature.

The same results can be seen for the Silica Saturation Temperature (right) which is the fluid temperature at which an SSI = 1 occurs. Significant reductions in the SST after treatment were recorded. In Wairakei, the fluid could be cooled to 42 °C after treatment before silica polymerisation starts again. In Kawerau and Mokai the SST is 70 °C and 77 °C respectively, after the CaSil treatment. At the direct-heat park in Tauhara, the scaling temperature was reduced from 150 °C to 41 °C. For this specific site, the available saleable heat capacity of the park can be increased by up to 60 % by the inclusion of the CaSil technology.

The significant reduction in SST demonstrates the substantial opportunities for geothermal resources for enhanced electricity generation and direct-heat availability for industrial or residential purposes.

2.2.2 Electricity Generation

As detailed in section 2.1, existing binary plants can experience an uplift in power output over time by elimination of the silica scaling problem. However, geothermal resources with severe silica concentrations and scaling rates are unlikely to currently be able to use binary technology. The significant reduction in SSI by the CaSil technology

as detailed in section 2.2.1 allows such power plants to include downstream power production facilities without inducing further silica scaling. Depending on the individual process parameters, this could be a second flash cycle or binary plant unit.

Table 1: Additional electricity that can be produced by a downstream binary plant for exemplary flow rates and current reinjection temperatures. Outlet temperature = 80 °C, c_p = 4.2 kJ/kg*K and η = 12 % assumed.

	Current Reinjection Temperature = Inlet Temperature		
Brine Flow Rate	180 °C	150 °C	130 °C
400 t/h	5.6 MW_{el}	3.9 MW_{el}	2.8 MW_{el}
800 t/h	11.2 MW_{el}	7.8 MW_{el}	5.6 MW_{el}
1200 t/h	16.8 MW_{el}	11.7 MW_{el}	8.4 MW_{el}
2000 t/h	28 MW_{el}	19.6 MW_{el}	14 MW_{el}

Table 1 lists the additional electricity that could be generated by a downstream binary plant for exemplary flow rates and reinjection temperatures, which would be the downstream binary inlet temperature. An outlet temperature of 80 °C and efficiency of 12 % is assumed. Should an additional steam cycle be used instead, the efficiency may be higher accordingly.

Significant uplifts in the overall power generation can be achieved by additional downstream steam cycles or binary plants. Medium sized power plants with 1200 t/h of brine which might currently reinject at 150 °C could generate 11.7 MW_{el} more from the same brine source. For an industry example the Dieng I power plant can be utilised, which is a single flash plant producing 26.9 MW_{el}. Approximately 398 t/h of hot geothermal brine at 182 °C are flashed to atmospheric pressure. Due to the severe silica scaling rates the brine cannot be cooled further in the power generation process. A pond is utilised to precipitate silica before fluid reinjection (Pambudi et al. 2015). Initial laboratory experiments with synthetic and acidified brine from Dieng I confirmed that the CaSil technology can successfully lower the SSI of the brine significantly below 1 (Borrmann et al. 2024). Therefore, approximately 5.7 MW_{el} could be generated from the same resource utilising a downstream binary plant. This assumes an efficiency of 12 % which in an actual plant would likely be higher given the high input temperature of 182 °C. Alternatively, a secondary flash cycle could be used which has a higher efficiency than a binary unit. This combination of CaSil technology and downstream generation asset would boost the power output of Dieng I by at least 21 % simply by utilising the currently unused geothermal brine.

2.2.3 Direct-Heat Uses

Lower temperature brines might not be suitable anymore for further heat extraction (e.g. below 110 °C), or other reasons might exclude the opportunities for the generation of additional electricity detailed in section 2.2.2. In these cases, the supply of direct-heat to industrial or residential customers could be attractive. Naturally, a mix of electricity generation and direct-heat supply can be designed as well, depending on the individual circumstances.

Table 2: Available heat energy for direct-use applications for exemplary flow rates and current reinjection temperatures. Outlet temperature = 80 °C and c_p = 4.2 kJ/kg*K assumed.

	Current Reinjection Temperature		
Brine Flow Rate	150 °C	130 °C	110 °C
200 t/h	16.3 MW_{th}	11.6 MW_{th}	7 MW_{th}
400 t/h	32.6 MW_{th}	23.3 MW_{th}	14 MW_{th}
800 t/h	65.3 MW_{th}	46.6 MW_{th}	28 MW_{th}
1200 t/h	98 MW_{th}	70 MW_{th}	42 MW_{th}

The available heat energy for direct-use applications for exemplary brine flow rates and current reinjection temperatures is presented in Table 2. Even small geothermal plants with only 200 t/h brine flow can supply significant amounts of heat energy for direct-heat applications with medium temperature brines (e.g. 130 °C, 11.6 MW_{th}). Alternatively, larger plants can utilise a portion of their flow for dedicated direct-heat use if the full flow is not required or desired. These opportunities are opened up by the CaSil technology.

Selected examples of direct-heat uses are shown in Figure 5. Additionally, the typically required process temperatures for each application are depicted. For example, horticultural green housing requires process heat in the range of 30-80 °C. Depending on the geographical location of the green house a heat consumption of approximately 1-3 MW_{th}/ha is common (Mertoglu et al. 2003). However, consumption rates larger than 2 MW_{th}/ha occur predominantly in very cold locations. A small geothermal plant with 11.6 MW_{th} dedicated to direct-heat use

could therefore support approximately 5-11 ha of green houses, depending on the geographical location, diversifying the revenue portfolio.

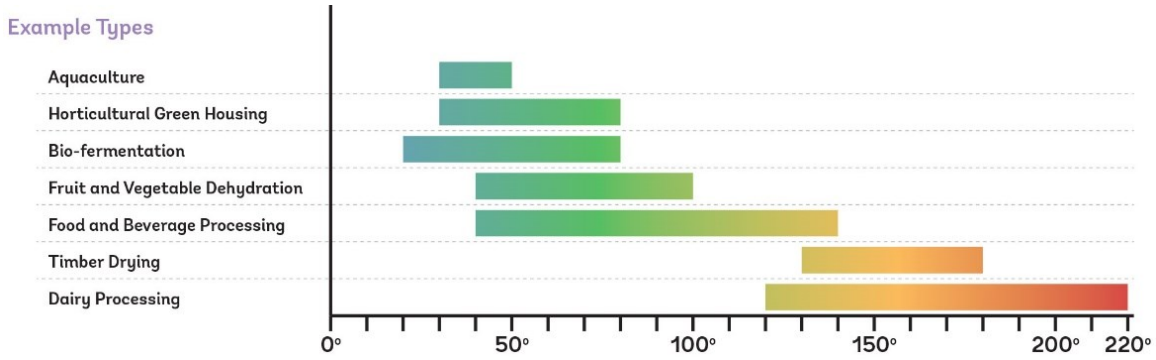

Figure 5: Selected examples of direct-heat uses and required process temperature ranges in °C (Climo et al. 2022).

Process heat from geothermal resources is also low in carbon emissions, with approximately 13 % of the carbon factor compared to natural gas and 7.5 % compared to coal (Climo et al. 2022). This means geothermal can play an important role in the decarbonisation of industry by supplying affordable, clean and always available process heat to industrial or even residential applications. Additionally, direct-heat customers can lower their expenditures by switching to geothermal heat through the lower operating cost compared to coal or gas as well as the reduced carbon emissions for which, depending on location, carbon credits may have to be purchased or a levy paid.

2.3 Mineral Extraction

Geothermal brines contain a cocktail of different species. This includes precious minerals which, if present in sufficient quantity, become financially attractive to extract and process. However, conventional extraction processes typically rely on membranes to concentrate and filter the desired species. In current geothermal plants silica is in a supersaturated state at the point of flashing. Silica polymerises at this point in the process and would consequently severely scale any membranes used for mineral extraction. Therefore, mineral extraction from raw geothermal brines is typically not financially viable due to the high cost incurred through ongoing maintenance and regular capital-intensive replacement of membranes.

Figure 4 showed the significant reduction by the CaSil technology in SSI in the treated brines. This means silica is in a severely undersaturated state. In these process conditions conventional mineral extraction processes can work without membrane fouling from silica and an economical operation is viable.

Laboratory tests were conducted to assess the compatibility of brine mining with the CaSil technology. Most species (e.g. Lithium, Boron, etc.) are not affected by the CaSil treatment, remain in solution and can be extracted downstream of the CaSil process. Other species (e.g. Copper, Zinc, Manganese) are adsorbed by the CaSil material during particle formation and are extracted with the CaSil material in the separation process. The desired minerals can then be further processed.

2.4 Environmental Products

The CaSil material also provides a platform for the development of environmentally beneficial product applications of which a number of applications are in the research and development stage. This is afforded by the unique surface chemistry of the CaSil particles which can be altered by the process chemistry to suit different product application needs.

An attractive application for the CaSil material is the recovery of base metals from waste mining and industrial process streams. As discussed in section 2.3, CaSil adsorbs certain metal ions and is therefore a suitable addition to mining and processing operations to mitigate environmental pollution through mine tailings. Also, the overall efficiency of metal recovery is increased.

2.5 Benefits for Fluid Reinjection

The CaSil technology allows the fluid to be cooled significantly more than is currently possible without inducing any silica scaling. The colder fluid has a higher density which will increase the downhole pressure of the water column, while maintaining the same wellhead pressure. The higher pressure can force more fluid through the porous rock strata, therefore increasing injectivity of the reinjection wells.

Colder fluid is also slightly cooling down the immediate rock strata around the reinjection well. This causes the rock to naturally contract and open more pores and fissures. Analogue, this causes an increase in injectivity of the

wells due to the reduced pressure losses from fluid-rock interactions. This effect can also be observed in well workovers where cooler condensate is injected for prolonged periods of time (Coutts et al. 2018).

Naturally, the reinjection of cooler fluid requires careful field management so no cold spots can develop in the reservoir or breakthroughs occur.

3. CONCLUSION

Silica scaling is the single largest hinderance worldwide in the full utilisation of geothermal resources. The intractable scale blocks pipework, heat exchangers and reinjection wells, lowering the efficiency of the plant, reducing the electricity output and necessitating costly maintenance. Current mitigation efforts fall significantly short of providing a definitive long-term solution to silica scaling. All of them require a trade-off between energy production and required maintenance. Additionally, significant amounts of heat energy are left in the brine and must be discarded due to severe scaling rates at low temperatures.

The CaSil technology is a novel and disruptive technique that uniquely provides a comprehensive silica scale elimination plan for a wide range of geothermal resources. Additionally, the full potential of geothermal energy is unlocked by significantly lowering the silica saturation temperature to unprecedented levels in an economical way. The technology can be readily interfaced with existing geothermal plants or greenfield developments.

Our CaSil development plant has clearly proven the viability and effectiveness of the technology at the Wairakei, Kawerau, Mokai and Tauhara geothermal resources in New Zealand. Silica saturation temperatures as low as 41 °C were achieved in the field.

Geothermal power plants with severe scaling rates which are forced to discharge brine at very high temperatures can benefit significantly from the CaSil technology as the opportunity to use downstream binary plants is unlocked. This can boost the overall electricity generation significantly from the same amount of sourced brine, which is hitherto unobtainable. Electricity generation plants with less severe scaling problems achieve an uplift in performance by eliminating the typical saw-tooth production profile from binary plants due to progressive silica scaling.

Also, significant new business opportunities are unlocked with the sales of heat energy for direct-heat applications such as greenhouses, aquaculture or food product drying. This desirably contributes to the decarbonisation of industry, where geothermal energy can have a significant impact as well. The reduction in SSI also opens the possibility of extracting valuable minerals from the geothermal fluid as conventional membrane extraction processes now become economically viable due to the elimination of scaling/fouling.

Furthermore, benefits for the reinjection system can be achieved by boosting the injectivity of reinjection wells. This is accomplished through the low SSI value of brines and colder fluid temperatures for reinjection. This leads to a denser fluid with higher downhole reinjection pressures as well as a contraction of the rock strata around the well which decreases pressure losses.

ACKNOWLEDGEMENT

The authors would like to acknowledge the New Zealand Ministry of Business, Immigration and Employment for research funding (RTVU2205).

Also, MB Century Ltd for the considerable in-kind support in the pilot scale development of the CaSil technology at Wairakei, Ngati Tuwharetoa Geothermal Assets, the Tuaropaki Trust and Contact Energy Ltd for the opportunity to site the development plant and use of the geothermal brine from the Kawerau, Mokai and Tauhara fields.

REFERENCES

Borrmann, T., Fraser, H. P., Johnston, J. H., Schweig, M., Kardani, I., Singkuang, D., and Sumartha, A. G. A "Case Study of the CaSil Technology at Dieng, Indonesia – Successfully Eliminating Silica Scale." *Proceedings: The 10th Indonesia International Geothermal Convention & Exhibition*, Indonesia, (2024).

Climo, M., Carey, B., and Miller, F. "Action Plan 2022 – 2023; Geoheat Strategy for Aotearoa NZ." *New Zealand Geothermal Association*, (2022).

Coutts, C., Richardson, I., Quinao, J., and Goh, O. "Acid Stimulation of Kawerau Injection Well PK4A Using Hydrofluoric Acid." *Proceedings: 40th New Zealand Geothermal Workshop*, New Zealand, (2018).

García A. V., Thomsen K., and Stenby E. H. “Prediction of mineral scale formation in geothermal and oilfield operations using the extended UNIQUAC model: Part I. Sulfate scaling minerals.” *Geothermics*, 34, (2005), 61-97.

Gunnarsson, I., and Arnórsson, S. “Treatment of Geothermal Waste Water to Prevent Silica Scaling.” *Proceedings: World Geothermal Congress*, Turkey, (2005).

Iler R. K. “The chemistry of silica: Solubility, Polymerization, Colloid and Surface Properties, and Biochemistry.” *John Wiley and Sons*, New York, (1979).

Makrides, A., Turner, M., and Slaughter J. “Condensation of silica from supersaturated silicic acid solutions.” *Journal of Colloid and Interface Science*, 73, (1980), 345-367.

Mertuglo, O., Bakir, N., and Kaya, T. “Geothermal applications in Turkey” *Geothermics*, 32, (2003), 419-428.

Pambudi, N. A., Itoi, R., Jalilinasrabady, S., Sirait, P., and Jaelani, K. “Preliminary analysis of single flash combined with binary system using thermodynamic assessment: a case study of Dieng geothermal power plant.” *International Journal of Sustainable Engineering*, 8, (2015), 258-267.

Richardson I., Addison S., and Lawson R. “Chemistry Challenges in Geothermal Power Generation.” *Proceedings: API Powerchem*, Australia, (2014).

Thorhallsson, S. “Common problems faced in geothermal generation and how to deal with them.” *Short Course on Geothermal Drilling*, Santa Tecla, El Salvador, (2011).

Case Study of the CaSil Technology at Dieng, Indonesia – Successfully Eliminating Silica Scale

Thomas Borrmann[1], H Putri Fraser[1], James Johnston[1], Michael Schweig[1], Ilen Kardani[2], Delvirah Singkuang[2], Ayu Gracia Ade Sumartha[2], Andhika Putera Utama[2], and Aditya Yuda Kencana[2]

[1]CaSil Technologies Ltd, c/- BW Miller Dean, Level 9, 94 Dixon Street, PO Box 11253, Wellington 6142, New Zealand.
[2]PT Geo Dipa Energi, Aldevco Octagon Building 2nd Floor, Jalan Warung Jati Barat Raya No. 75, South Jakarta 12740, Indonesia

tborrmann@casiltech.com

Keywords: Geothermal, Dieng, silica, silica scale, calcium silicate, CaSil, simulated geothermal brine, silica saturation index, electricity generation

ABSTRACT

The CaSil technology is a proprietary innovative new technology that eliminates silica deposition and scaling from geothermal brine, supersaturated in silica. The technology has been developed and successfully demonstrated at development plant scale operation over six years in four New Zealand geothermal fields.

This paper reports an initial study on the application of the CaSil technology to the silica supersaturated, hyper-saline brine from the Dieng geothermal field, Indonesia. Problematic dissolved silica is rapidly captured as a nanostructured calcium silicate material before silica deposition and scaling can occur. This yields a treated brine that can be cooled to unprecedented low temperatures without silica scaling, thereby enabling more heat energy to be accessed and electricity generated from the same brine flow than is currently possible.

Samples of brine from the from the Dieng-1 well that had been acidified after collection were provided by Geo Dipa Energi to CaSil Technologies for analyses and an initial assessment of the suitability of the CaSil technology to prevent silica scaling. Using atomic absorption and UV visible spectroscopies, electrochemistry, and titrations the main constituents of the brine were identified. Based on this, a simulated brine was generated and used to test and identify the potential of the proprietary CaSil technology to reduce silica levels and the Silica Saturation Index, SSI, of this high silica, hyper-saline brine accordingly.

Another intention of these trials was to explore effects from the borate buffer system due to the high boron content of the brine, on the CaSil technology and the reduction of the Silica Saturation Index (SSI) to levels where additional heat can be harnessed and electricity generated without inducing silica scaling. Autoclave reactions were used to simulate field specific high temperature and pressure reaction conditions.

The successful laboratory trials using the simulated brine were confirmed using the Dieng brine samples provided in further experiments. These show the pathway for possible field trials, which promise that by incorporating the CaSil technology, additional heat recovery and electricity generation from the Dieng resource can be achieved without silica scale formation, thereby unlocking the full energy potential and utilisation of this geothermal resource.

1. INTRODUCTION

Geothermal energy is an attractive natural renewable energy resource which can provide large quantities of heat energy for electricity generation and/or direct heating applications. In water dominated high enthalpy fields, the geothermal water (brine) in the subsurface reservoir that is typically about 200-300 ˚C, dissolves rock and sediment minerals in the reservoir rocks releasing silica mainly as the $H_3SiO_4^-$ ion, alkali and alkaline earth metal cations, and anions such as chloride and carbonate into the hot brine.

The superheated brine is piped to the surface where through the steam/water flashing process, about 1/3 of the mass flow is flashed into steam that is used to drive a turbine and generate electricity. The residual 2/3 of the mass flow of the now cooler brine can be used for binary cycle electricity generation or direct heating. The resulting cooling and concentration of the brine leads to silica supersaturation where the solubility of dissolved silica is exceeded, leading to silica polymerisation and problematic silica scaling. The scale undesirably blocks pipes, valves, heat exchangers, other process equipment and reinjection wells. (Borrmann et al 2009, Brown 2011).

Silica scaling severely limits the extent to which the separated brine can be cooled in the binary heat exchangers which in turn limits the amount of electricity generated from the resource. This is a major impediment to the

efficient utilisation of the geothermal resource. Much of the heat energy contained in the separated brine is wastefully reinjected to the reservoir.

Current methods to address silica scaling include acid dosing to lower the pH which slows the silica polymerisation reaction, and the use of sequestering agents to bind the dissolved silica entities. However both these approaches are not particularly effective and silica still scaling persists. Frequent cleaning of heat exchangers and the periodic cleaning of existing reinjection wells or drilling new wells is a common practice (Gunnarsson and Arnórsson 2005).

For higher enthalpy geothermal resources where the brine is heated to higher temperatures in the reservoir, the levels of dissolved silica in the brine are similarly higher. The problem of silica scaling is further increased, and the amount of electricity generated by the binary plant is decreased accordingly. This is particularly the case for the Dieng resource.

1.1 The CaSil Technology

The proprietary CaSil technology, developed by the authors Johnston, Borrmann Schweig and Fraser and owned by CaSil Technologies Ltd, eliminates the world-wide problem of silica scaling and unlocks the full energy potential of a geothermal resource. This is achieved by rapidly capturing the problematic silica species dissolved at supersaturated levels in the separated brine, as a unique proprietary nanostructured calcium silicate (CaSil) product, before silica polymerisation and scaling can occur. The Silica Saturation Index is reduced substantially. The CaSil product is separated continuously from the treated brine and used in various environmentally beneficial applications.

The temperature of the treated brine with this significantly reduced Silica Saturation Index, can be lowered much further than is currently possible with existing practices. This enables significantly more heat energy to be recovered for direct heating applications and more electricity to be generated by the binary cycle process accordingly. In addition, the necessity for cleaning silica scale and associated maintenance requirements is similarly reduced considerably, as is the need for drilling new reinjection wells.

The technology has been developed and successfully demonstrated at pilot plant scale operation over six years in four New Zealand geothermal fields, Wairakei, Kawerau, Mokai and Tauhara, each with different brine compositions and temperatures. This clearly demonstrated the robustness and the wide scale applicability of the technology to different geothermal resources (Johnston et al 2006, Johnston and Borrmann 2017, Schweig et al 2023, 2024)

The CaSil technology is therefore ideally suited for application at the Dieng geothermal resource, Indonesia, where the temperature of the separated brine can currently only be lowered to about 182 ˚C before silica scaling takes place. The CaSil technology reduces the SSI considerably and offers the ability to cool the treated brine to substantially lower temperatures and to enable more electricity to be generated accordingly. This is not possible by the use of acid dosing or sequestering agents.

This paper presents the results of an initial laboratory study on the application of the CaSil technology to prevent silica scaling in the Dieng geothermal brines, using a simulated brine with a composition typical of the high silica, hyper-saline geothermal brine from the Dieng geothermal resource. Also a sample of Dieng-1 brine is included. This work opens up the opportunity for a much wider and in depth field study, using actual Dieng brines.

1.2 The Dieng Geothermal Field

The Dieng geothermal field is one of the most prospected geothermal fields in the Central Java Province, Indonesia, located about 120 km from the province capital Semarang. The area of 63 km^2 in size is located along the Java Trench of the Indo-Australian Plate below the South-East Asian Plate in the volcanic arc, corresponding to the active andesitic volcanism related to the plate subduction. The Dieng area has an estimated field development potential of 400 MWe (Ministry of Energy and Mineral Resources, 2017). It is a high-temperature, hyper-saline field with surface manifestations such as fumaroles, hot springs, and acidic mud pools. These are distributed in the areas of Sileri, Sikidang and Pakuwaja. Sileri is located to the northwest with fluid temperatures around 300 ˚C and acid-sulphate-chloride type hot springs. In the central Sikidang area, fluids at depth are around 300 °C hot and contain high amounts of non-condensable gases (NCGs), mostly CO_2. Sileri and Sikidang are craters that consist of old Dieng volcanic rocks. The upflow areas of the hydrothermal systems are believed to be around Sileri and Sikidang where the fluid flows northeast, and southwest along faults. These faults are the drilling targets for future production wells.

Since 1975, 52 wells have been drilled in Dieng, 27 wells by Pertamina, 20 wells by Himpurna California Energy (HCE) and 5 slim holes for coring. 5 production wells and 4 injection wells are operating for power plant Unit 1. Samples discussed in this article relate to wells HCE 7 and HCE 30. The installed capacity of Unit 1 is 60 MWe and current production is around 55 MWe. In July 1998, this power plant was commissioned by Himpurna

California Energy Limited. After the project was shelved for a while, in 2002, Geo Dipa Energi, a joint venture between PT Perusahaan Listrik Negara (PT PLN) and PT Pertamina, took over the ownership of the Dieng geothermal field. Since 2011, Geo Dipa Energi is a designated state-owned enterprise by Government Regulation no. 62/201.

At Dieng-1, Geo Dipa Energi operates one unit of a single-flash cycle with a capacity of 60 MWe (Ministry of Energy and Mineral Resources, 2017; Kamila et al., 2020). The resource of Dieng-1 is characterized by a water-dominated hyper-saline reservoir with temperatures ranging from 240 to 333 °C (Ministry of Energy and Mineral Resources, 2017; Sudarman and Hochstein, 2017; Nasruddin et al., 2016; Mohammadzadeh et al., 2018). Special attention is paid to the highly problematic issue of silica scaling in the production systems, turbines, and the reinjection system. Deposition of silica scale has been identified widely in Fluid Collection and Reinjection Systems (FCRS), such as in two-phase flow lines, i.e., the separator and the brine line to the reinjection site. These significant scaling problems limit the extent of cooling and the amount of electricity generated, and also adversely affect the operational cost of the Dieng Unit 1 plant. Therefore, a more effective and reliable scaling prevention method is required to ensure future operation, increased resource utilisation efficiency, the and future development of the Dieng geothermal field.

The CaSil Technology is ideally suited to prevent silica scaling in the FCRS to protect the current Geo Dipa Energi assets, enable significantly more electricity to be generated by the binary cycle technology and provide a useful CaSil product for environmentally beneficial applications. This will allow more efficient energy utilisation of the resource and its further expansion.

The chemistry of brines is very field and well specific. The CaSil technology has been shown to prevent silica scaling in four different New Zealand geothermal resources. Building on this success, some preliminary laboratory scale trials using simulated geothermal brines with a composition typical of the Dieng geothermal resource, together with samples of the Dieng brine, have been carried out. The results are presented here.

2. RESULTS AND DISCUSSION

Four acidified samples of brine from the Dieng-1 field were provided by Geo Dipa Energi, Indonesia. These were analysed using the facilities at Victoria University of Wellington, New Zealand (VUW), and also at GNS Science, Taupo, New Zealand for confirmation. The main components (>10 ppm) detected in the brine samples were silica, boron, calcium, arsenic, sodium, potassium, lithium, and chloride. Minor (1 to 10 ppm) elements were manganese, iron, and aluminium. Traces of magnesium, strontium, indium, and germanium were also detected. The samples of brine contained flakes of solid material, which upon digestion released further potassium, silica, and sodium into the brine. These were likely to be mineral fragments from the reservoir rocks. Historically, the brine of the Dieng geothermal field is known to also contain sulfur (measured as sulfate), hydrogen carbonate (bicarbonate), and ammonia. Due to the acidification of the samples, these species were not detected. The acidification step is necessary to reduce the extent to which silica polymerisation takes place following sampling and cooling of the brine, and transportation.

2.1 Analysis of Brine and Preparation of Simulated Brine

Table 1 provides an overview of the range of the major constituents from the historical data, the actual levels measured in the Dieng-1 brine at Victoria University of Wellington, and in the two samples of the simulated brine, Sim 1 and Sim 2.

Table 1: Major constituents of brine collected from the Dieng geothermal field.

	Silica	**Na**	**K**	**Cl**	**B**	**Ca**	**HCO_3^-**	**Li**	**pH**
	ppm	ppm	ppm	ppm	ppm	ppm	ppm	ppm	
Historical data	650 to 950	7k to 11k	2k to 3k	16k to 20k	450 to 700	600 to 900	25 to 45	35 to 65	6 to 6.8
VUW	1175	9000	2542	18k	352	624	n/a	45	<2
Sim 1	1000	8000	2500	18k	450	600	40	45	6.5
Sim 2	1200	8000	2500	18k	450	600	40		6.5

For the following study and the preparation of a simulated brine from Dieng, only the major constituents were considered. Sim 1 and Sim 2 differ in their silica and lithium contents.

Particulates of solid material were also present in the acidified samples from the Dieng field. These were analysed and found to contain silica, borate, potassium, and chloride and were omitted from the simulation. Ammonia, and sulfide were not considered due to their volatile and noxious nature, but will be included in future studies.

The brine simulation faced several challenges: At high pH (>9.5) borate species can precipitate out, and silica and calcium can react to form calcium silicates. Furthermore, at the pH value chosen, silica is supersaturated and will

form silica gel. As discussed below, these challenges were successfully overcome and stable simulated brines were prepared using the constituents in table 2.

Table 2: Stock solutions as source of various elements/species.

	NaCl	KCl	LiCl	As_2O_3 in NaOH	$CaCl_2$	$Na_2B_4O_{17}•10H_2O$	"Na_2SiO_3"	$NaHCO_3$
Target	Na	K	Li	As	Ca	B	Silica	HCO_3^-
Also adds	Cl	Cl	Cl	Na	Cl	Na	Na	Na

Hydrochloric acid was used to adjust the pH, which also adds chloride ions to the solutions thereby assisting in establishing the intended chloride concentrations. Sodium silicate is basic and provided the starting point of the simulated brines. With silica being the main target species of this study, greater care was taken in matching the intended silica levels. The other components were added rapidly to enable speedy processing of the brine due to its tendency to form silica gel. The alkali chlorides, arsenic, and bicarbonate solutions and water were added to the sodium silicate solution first. Then the pH was adjusted to below 9. The borax solution was added, and the pH adjusted to about 6.8. The calcium chloride solution required slight acidification to stabilize it. This slightly acidic solution was added last, and the pH of the final solution adjusted to 6.5 to represent that of Dieng-1 brine. In total 8 brines were prepared. These synthetic brines were analysed to determine the closeness of them to the actual Dieng-1 brine composition.

An overview of how closely the composition of these brines adhered to the planned two simulations is shown in Figure 1. Brines 1 to 3, 7 and 8 were following the Sim 1 composition and brines 4 to 6 of Sim 2. All brines prepared could be used to prepare 2 to 4 samples that were used in the CaSil technology application experiments in parallel, before deposits started to form, with the rest of the brine needing to be discarded. The compositions achieved were mostly within 10 percent of the desired values with some deviating about 20 percent. Lithium was only added to 1 brine, due to limited availability of the source material. Overall, the brines were representative of the compositions targeted and the Dieng-1 brines. Hence, application of the CaSil technology under different operating conditions was attempted for all these brines.

Samples of these prepared brines were taken rapidly and the CaSil agent added. The resulting slurry was stirred for another minute as the CaSil reaction is very rapid, allowed to settle for 2 minutes, and filtered under vacuum. The filtrate was recovered for analysis. The filter cakes were dried at 120 ˚C overnight and weighed to establish yields. Treatments were carried out at room temperature and 70 ˚C at a litre scale, and at 150 and 180˚C in a scaled down approach (250 mL) in an autoclave. The autoclaved samples were cooled down rapidly and quenched to obtain temperature dependent data.

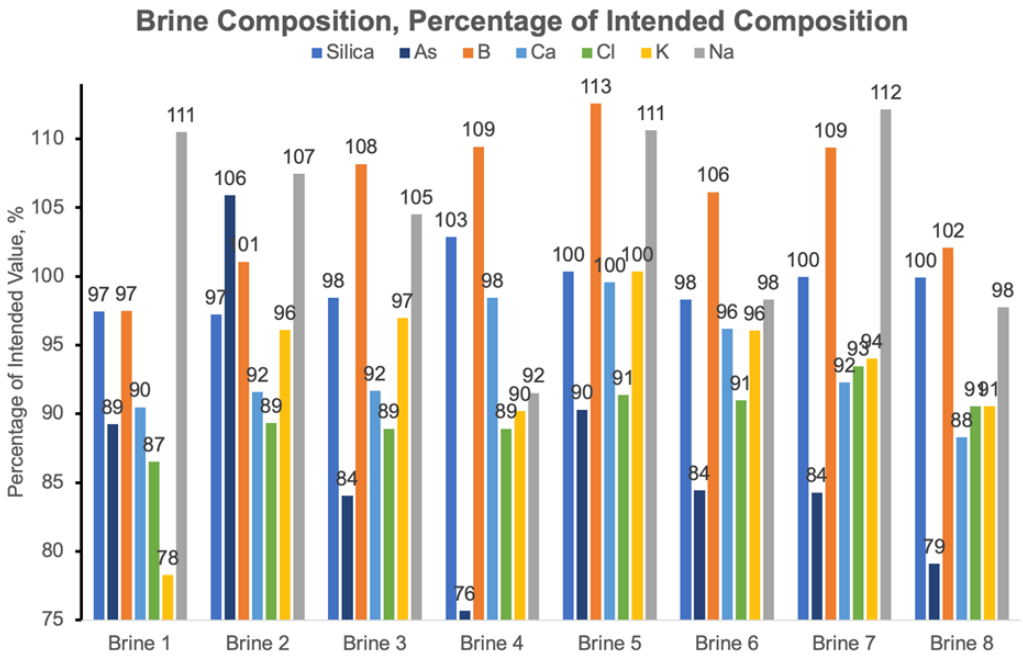

Figure 1: The deviation in the respective compositions of simulated brines from their intended values.

As stated above, the CaSil treatment substantially lowers the Silica Saturation Index (SSI) of geothermal waters by removing silica as a unique nanostructured calcium silicate (CaSil) material. Thereby the CaSil technology enables use of geothermal waters at lower temperatures than currently possible. This laboratory scale work was carried out to ascertain if the CaSil treatment is applicable to the high silica, hyper-saline brines from the Dieng geothermal resource, and any adverse effects of the high levels of borate in the brine. The results presented in Figure 2 show that the residual silica concentration in the treated brine is lowered from the respective initial values of 1000 and 1200 ppm silica to about 150 ppm at room temperature and to about 350 to 450 ppm at 180˚C. The increase in residual silica content with increasing temperature is consistent with the temperature dependent solubility of silica. In all cases the SSI is substantially reduced, allowing the brine to be cooled to much lower temperatures that is currently possible. This desirably confirms the applicability of the CaSil technology to prevent silica scaling at Dieng and thereby enable more electricity to be generated from the existing brine flow (Figure 3).

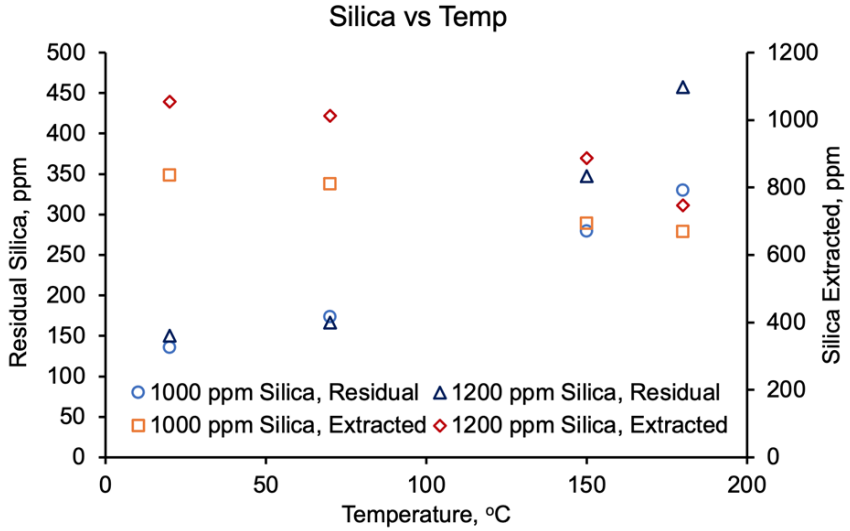

Figure 2: Residual and extracted silica at different temperatures by the CaSil technology.

As the Dieng brines contain high levels of borate, the effect of the borate buffer system on the CaSil technology was investigated. For the simulated Dieng brines, the pH values increased to between 7.7 and 9. It was considered that the presence of the borate in the brine governed this increase in pH, as borate is commonly used in buffer systems (Dubin, 1984). The work here shows that this level of pH increase in the simulated Dieng brines does not affect the CaSil technology.

Using the values for the residual silica concentrations and the pH of the treated brines, the SSI was calculated using the formula published by Brown (2011). Due to the buffering of the pH value, the SSI at room temperature was about 1. However, with increasing temperature the SSI reduced considerably, and very desirably it was as low as 0.3 for the experiments carried out at 180 ˚C. The calculated values of the SSI for following CaSil treatment at different temperatures are shown in Figure 3. These low values of the SSI cannot be achieved by the other methods currently used to address silica scaling. Also pleasingly, no formation of silica gel was observed on cooling of the treated brines to room temperature, even after several days.

The effect of the borate in buffering the pH likely leads to the very low amount of calcium carbonate present in the CaSil product, despite the carbonate/bicarbonate species being present in the simulated brine (see XRD study below). The equilibrium between bicarbonate and carbonate is on the lower side of bicarbonate ($pKa_2 = 10.33$). Therefore, by keeping the pH lower, borate buffer effectively prevents the formation of carbonate ions. This is an interesting finding and invites further investigation.

The application of the CaSil technology in preventing silica scaling as demonstrated here, desirably provides a treated Dieng brine with a very low SSI, that can now be used in downstream recovery of other dissolved minerals including lithium. For these recoveries it needs to be established, if the CaSil technology interferes with any of these species for the Dieng brine. As expected, there was no significant change in the level of lithium before and after the CaSil treatment (less than 1% change which is within the experimental measurement uncertainty). Further work will be carried out in the future to confirm this on actual Dieng brines.

The X-ray diffraction patterns of the CaSil products formed in the process (Figure 4), show the presence of sodium and potassium chlorides. These species could readily be removed from the CaSil products by washing the filter cakes with water, confirming that they originate from trapped pore water in the CaSil filter cakes.

The broad hump in the XRD pattern centered at about 23 °2θ is typical of CaSil, which is amorphous/polycrystalline in nature. Very minor amounts of calcium carbonate in the form of calcite are shown by its main peak at about 30 °2θ. No other calcite peaks are observable. This is a common species that gets trapped in CaSil particulates and is removed with them accordingly. The bicarbonate added to the simulated brine formed this calcite. As, the amount of bicarbonate in the original brine and in the brine following CaSil treatment were very similar, as indicated by titration with acid, the amount of calcite formed was similarly very small. This is a consequence of the borate buffer system detailed above.

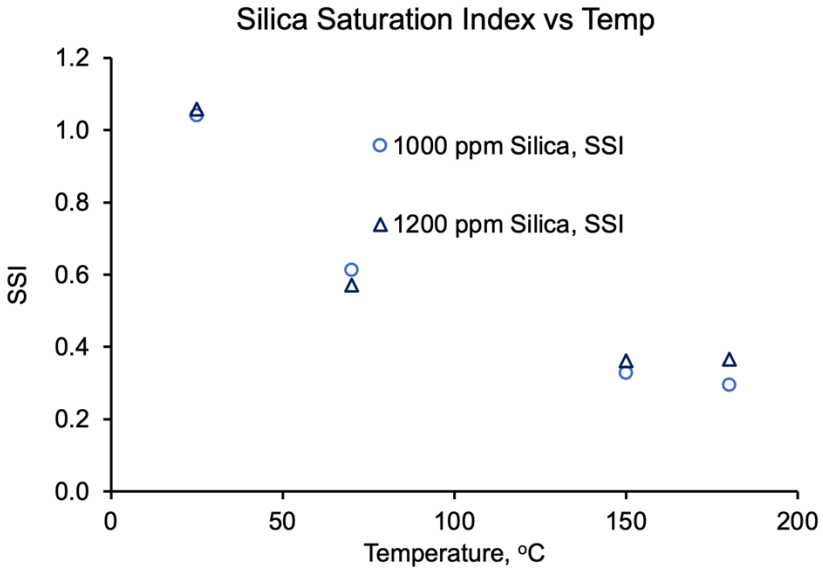

Figure 3: SSI vs temperature for treatment of simulated brines.

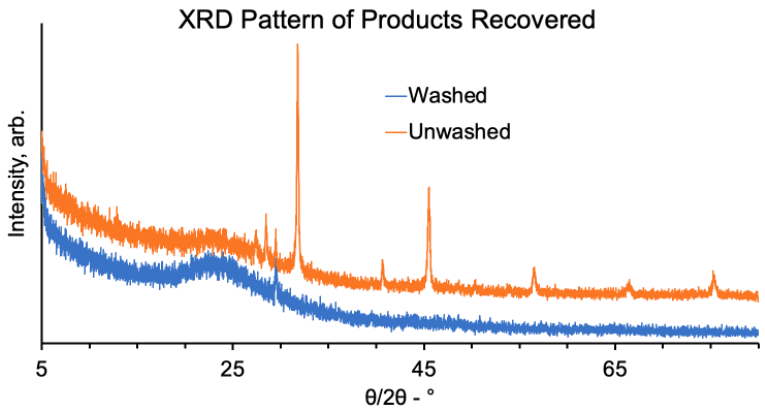

Figure 4: Evidence of salt trapped in the pore water of products.

2.2 Treating Actual Dieng-1 Brine

Encouraged by the findings from the study of simulated brine, a sample from Dieng-1, HCE 7c FA, was treated with the CaSil technology. Prior to treatment, the pH value of the brine sample had to be raised to levels (pH 6.5) comparable to untreated brine. This was accomplished by addition of sodium hydroxide. The supernatant and CaSil product from the treatment of HCE 7c were recovered and analysed. While the CaSil product from the simulated brine was white in color, the HCE 7c CaSil sample was cream colored, which is probably due to the presence of iron and manganese, as they were minor constituents and not incorporated into the simulated brine. Similar discolorations in the presence of iron and manganese have been observed in our previous work. The analysis of the untreated and treated brine from HCE 7c is presented in Table 3.

The most notable and very desirable feature is the substantial removal of silica from Dieng-1 brine, raising of the pH, and consequently substantially lowering the SSI from 9.75 to 0.6. This very clearly demonstrates the effectiveness of the CaSil technology in removing the problematic silica and reducing the SSI to below 1, thereby preventing silica scaling.

Table 3: Comparison of untreated and CaSil treated brine form Dieng-1 HCE 7c.

	Silica	Na	K	Cl	B	Ca	Li	As	pH	SSI
	ppm	ppm	ppm	ppm	ppm	ppm	ppm	ppm		
Untreated	1141	9345	2193	8420	304	514	42	23	6.50	9.75
Treated	77	9528	2117	8200	305	658	43	20	8.83	0.6
Change	-1064	+183	+76	+220	-1	+144	-1	3	+2.33	-9.15

The values for arsenic, boron, chlorine, lithium, potassium, and sodium essentially remained unchanged within the margin of uncertainty. The amount of calcium increased, as is expected from to the CaSil treatment.

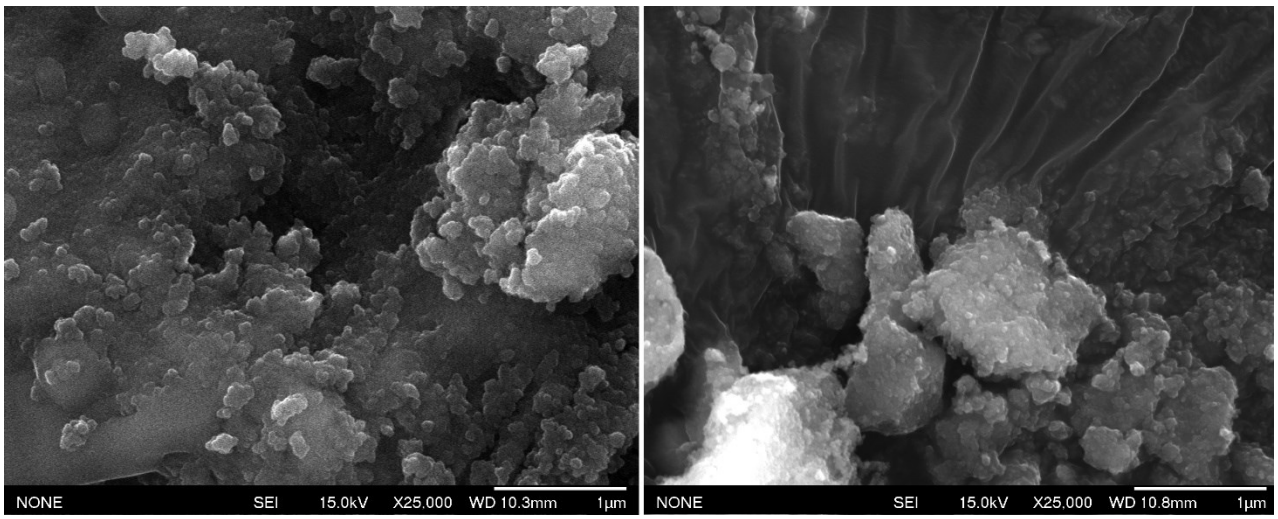

Figure 5: Scanning electron microscope images of simulated CaSil (left) and CaSil recovered from treated HCE 7c (right).

The scanning electronmicroscope images of the CaSil products generated from the simulated brine and the HCE 7c brine (Figure 5) show the products are very similar, and indeed comparable to CaSil products we have generated from many other brines (Borrmann 2009). This result further demonstrates the successful application of the CaSil technology to prevent silica scaling in Dieng brine and to provide a useful CaSil product.

3. CONCLUSIONS

Samples from Dieng-1 brine were provided by Geo Dipa Energi to CaSil Technologies to assess the applicability of the CaSil technology in preventing silica scaling from the brine. The samples and historical data provided by Geo Dipa Energi formed the basis of preparing a simulated brine that was used to carry out the preliminary study presented here. The results clearly show that the CaSil technology substantially reduces the silica content of the simulated brines and also the Dieng-1 brine, thereby lowering the SSI, which in turn prevents silica scaling.

The study also showed that borate present in the brine forms a buffer system that influences the pH change in a way that has not been observed prior to this study. As the Silica Saturation Index is also dependent on the pH, the effect of borate needs to be taken into account in implementing the CaSil technology. However overall, it does not adversely affect the CaSil technology. In the actual brine sample, the effect of borate on the pH was not as pronounced as in the simulated brine samples.

Very little carbonate was captured in the CaSil product despite this species being present in the simulated brine. This could also be due to the presence of the borate buffer. The equilibrium between bicarbonate and carbonate would be on the side of bicarbonate ($pKa_2 = 10.33$). Therefore, by keeping the pH at levels lower than observed for other brines, the borate effectively prevents the formation of carbonate ions, which appears to be necessary to form the usual calcite impurity on the surface of CaSil particles. This is an interesting finding and invites further investigation.

Based on the success of the work using the simulated brines, one of the samples studied in the analysis of Dieng-1 brine was treated by the CaSil technology. This similarly showed the treatment was successful and a CaSil product was produced. The residual silica concentration and pH value meant that the Silica Saturation Index was desirably lowered to 0.6. This low SSI value and the extent of removal of problematic silica from the geothermal brine cannot be achieved by any of the practices currently used to address silica scaling. The distinct advantages of the CaSil technology in preventing silica scaling are clearly demonstrated here.

ACKNOWLEDGEMENTS

This research has been funded by the New Zealand Ministry of Business Innovation and Employment Research (RTVU2205). Also, to Geo Dipa Energi for providing the Dieng-1 samples and allowing us to present this study and results at the IIGCE 2024.

REFERENCES

Borrmann, T., Johnston, J.H., and McBrearty, R.: Nano-Structured Calcium Silicate - A Solution to the Formation of Silica Scale in Geothermal Water, *GRC Transactions*, **33**, (2009), 695-698. https://www.geothermal-library.org/index.php?mode=pubs&action=view&record=1028544

Brown K.: Thermodynamics and kinetics of silica scaling, *Proceedings*, International Workshop on Mineral Scaling, Manila, Philippines, (2011).

Dubin, L.: Silica inhibition: prevention of silica deposition by boric acid/orthorborate ion, *United States Patent*, 4584104, (1984).

Gunnarsson, I. and Arnórsson, S.: Treatment of Geothermal Waste Water to Prevent Silica Scaling. *Proceedings*, World Geothermal Congress 2005. Antalya, Turkey, 24-29 April 2005. International Geothermal Association. (2005). https://www.geothermal-library.org/index.php?mode=pubs&action=view&record=8001229.

Harper, R.T., Thain, I.A., and Johnston, J.H.: Towards the Efficient Utilization of Geothermal Resources, *Geothermics*, **21**, (5/6), (1992), 641-651. https://doi.org/10.1016/0375-6505(92)90017-4.

Johnston, J.H., Borrmann, T., and McFarlane, A.J.: Nano-structured Calcium Silicate, Functionalised Forms Thereof, Preparation and Uses. *NZ Patent Specification* No. 537747, (2006).

Johnston, J.H. and Borrmann, T.: Nanostructured Calcium Silicate Hydrate – A Potential Solution to Problematic Silica Deposition from Geothermal Brine and a Useful Product. *New Zealand Geothermal Workshop, Rotorua,* 22-24, (2017).

Kamila, Z., Kaya, E., and Zarrouk, S.J.: Reinjection in geothermal fields: An updated worldwide review 2020, *Geothermics*, **89**, (2020), 101970. https://doi.org/10.1016/j.geothermics.2020.101970.

Ministry of Energy and Mineral Resources: Potensi Panas Bumi Indonesia Jilid 1. Kementerian Energi dan Sumber Daya Mineral, Ministry of Energy and Mineral Resources, Jakarta, Indonesia (2017).

Mohammadzadeh, S., Jalilinasrabady, S., Fujii, H., and Pambudi, N.A.: Classification of geothermal resources in Indonesia by applying exergy concept, *Renew. Sustain. Energy Rev.*, **93**, (2018), 499–506. https://doi.org/10.1016/j.rser.2018.05.018.

Nasruddin, N., Alhamid, M.I., Daud, Y., Surachman, A., and Sugiyono, A.: Potential of geothermal energy for electricity generation in Indonesia: A review, *Renew. Sustain. Energy Rev.* **53**, (2016), 733–740. https://doi.org/10.1016/j.rser.2015.09.032.

Schweig, M., Johnston, J.H., Borrmann, T., and Fraser, Update, H.P.: On the CaSil Technology: Economically Solving the Worldwide Problem of Silica Scaling and Enabling Unprecedented Low Temperature Direct-Heat Extraction and Electricity Generation Utilisation. *GRC Transactions,* Vol. 47, (2023) 2733-2744.

Schweig, M., Johnston, J.H., Borrmann, T., and Fraser, Update, H.P.: Unlocking Geothermal Potential: The CaSil Technology. *Proceedings: The 10th Indonesia International Geothermal Convention & Exhibition*, Indonesia, (2024).

Sudarman, S., and Hochstein, M.P.: History of Geothermal Exploration in Indonesia (1970-2010), *Proceedings 36th New Zealand Geothermal Workshop 24 - 26 November 2014*, Auckland, New Zealand (2014).

Comparative Analysis of Steam Flowmeters for Enhanced Geothermal Power Plant Performance

U. Anang Ischak

Star Energy Geothermal
Wisma Barito Pacific II 17th - 21st Floor, Jl. Letjen S. Parman Kav 60, Jakarta 11410, Indonesia

uaischak@starenergy.co.id

Keywords: geothermal power plants, steam flow measurement, flowmeter selection, performance optimization

ABSTRACT

Accurate steam flow measurement is crucial for optimizing geothermal power plant performance. This paper delves into the selection of steam flowmeters for geothermal applications, providing a comprehensive comparison of various flowmeter types based on technical parameters such as measurement accuracy, pressure drop, maintenance needs, installation complexity, fluid compatibility, and scaling potential. The discussion covers understanding steam flow conditions, specific challenges encountered in geothermal environments, and the latest advancements in flowmeter technologies tailored to the unique demands of geothermal processes.

Through comprehensive analysis and comparative studies, this paper offers valuable insights into the factors to consider when choosing the optimal flowmeter for enhancing the performance and reliability of steam flow measurement systems in geothermal power plants. Venturi, Orifice and Annubar flowmeters offer simplicity and more cost-effective but have limitations in accuracy and involve pressure drop impacts. Vortex flowmeters propose several advantages over traditional differential pressure flowmeters, particularly in applications involving wet steam or fluctuating flow rates. Coriolis flowmeters provide high accuracy, but they are more expensive and sensitive to vibrations. Ultrasonic and Magnetic flowmeters offer non-intrusive measurement, but their accuracy can be affected by steam properties and flow conditions. Additionally, this paper explores the advantages and limitations of other flowmeter types, providing a comprehensive overview of the available options for geothermal steam flow measurement.

The selection of a steam flowmeter should be based on a thorough evaluation of the plant's requirements, considering factors like flowmeter specifications, such as measurement accuracy, pressure drop, maintenance requirement, installation complexity, fluid compatibility, scaling risk and other potential considerations. This paper provides a valuable framework for selecting the most suitable steam flowmeter to optimize geothermal power plant performance and ensure reliable operation.

1. INTRODUCTION

Indonesia is a country with geothermal resources accounting for 40% of the world's total geothermal energy, showcasing significant potential for renewable energy sources. Despite this vast potential, the utilization of geothermal energy began only 20 years ago, and as of now, Indonesia has tapped into just 4-5% of its geothermal capacity. The country, particularly in non-Java islands, is facing a substantial increase in electricity demand, necessitating additional power generation each year. Currently, the installed capacity of geothermal power plants is approximately 2.3 GW out of a total national capacity of around 83.8 GW. The Government of Indonesia expects geothermal to play an increasingly important role as a renewable energy source.

In partnership with two state-owned companies, Pertamina and Perusahaan Listrik Nasional (PLN), Star Energy Geothermal (SEG) operates three geothermal power plant assets in West Java with a total capacity of 886 MW. The Darajat geothermal power plant in Garut Regency generates 274.5 MW, consisting of Unit 2 (97.5 MW), Unit 3 (122 MW), and supplying steam to Unit 1 PLN to produce 55 MW of electricity. The Salak geothermal power plant in Sukabumi Regency generates 381 MW, consisting of Units 4, 5, and 6 (each producing 67 MW) and supplying steam to Units 1, 2, and 3 PLN (each producing 60 MW of electricity). The Wayang Windu geothermal power plant in Pengalengan Regency generates 230.5 MW, consisting of Unit 1 (113.5 MW) and Unit 2 (117 MW).

To support the safe, reliable, and efficient operation of all its geothermal power plant assets, SEG currently employs steam flowmeters in both the Resource Production Facility (RPF) and the Power Generation Facility (PGF). At Darajat, which features steam-dominated resources, venturi tubes and orifice plates are used for steam flow measurement. The venturi flowmeters are installed in the main steam system within the PGF, while orifice flowmeters are commonly implemented in the auxiliary steam systems of the PGF and also in the RPF. Meanwhile, at Salak and Wayang Windu, where wet geothermal resources are prevalent, venturi tubes and

annubar flowmeters are more commonly used. Venturi flowmeters are utilized for steam measurement in the main steam systems of the PGF, while annubar flowmeters are installed in both the main steam and auxiliary steam systems within the PGF, as well as in the RPF, particularly downstream of the separators.

SEG is actively expanding its geothermal power generation capacity. To optimize existing plants and extend their operational life, the company is retrofitting existing units at Darajat, Wayang Windu, and Salak with advanced steam turbine equipment and Balance of Plant (BOP) technologies. Additionally, several new plants are under development, including the Salak Binary Plant (15 MW), expected to be operational this year, with Wayang Windu Unit 3 and Salak Unit 7 following in the next few years. SEG is also exploring new geothermal areas, such as in South Sekincau and Hamiding. These combined efforts aim to achieve the 1,200 MW generation target by 2028 through a mix of new plants, exploration endeavors, and implementing advanced technology in existing facilities to optimize performance and ensure continued safe and reliable operations.

This technology deployment of various flowmeters ensures that each type of geothermal resource and facility setup is accurately monitored and managed, contributing to the overall operational excellence of the plants. Through these efforts, SEG is not only expanding its capacity but also enhancing the reliability and performance of its geothermal power generation, aligning with the national goal of increasing the role of renewable energy in Indonesia's power sector.

2. SIGNIFICANCE OF STEAM FLOWMETERS IN GEOTHERMAL APPLICATIONS

This paper delves into the critical role of accurate steam flow measurement in optimizing performance and ensuring safety within geothermal power plants. It presents a comparison of various steam flowmeter technologies employed in geothermal applications. By understanding the significance of steam flowmeters, the diverse measurement techniques available, and the challenges encountered in geothermal environments, plant operators can make informed decisions when selecting the most suitable flowmeter technology for their specific needs.

Steam flowmeters are instrumental in ensuring efficient and reliable operation of geothermal power plants by providing real-time data on steam flow rates. This information is critical for three primary functions:

- **Optimizing Power Generation:** Precise steam flow measurements enable plant operators to fine-tune turbine operation. This allows for maximizing power output while minimizing energy losses through efficient steam utilization.
- **Ensuring Plant Reliability:** Flowmeters act as integral reliability components by continuously monitoring steam flow rates. Real-time data allows for detection of anomalies and potential process changes, such as unexpected pressure drops or flow fluctuations, enabling operators to take immediate action.
- **Improving Plant Efficiency:** By tracking steam flow through different stages of the power generation process, plant managers can identify areas for efficiency enhancement. This can lead to reduced operational costs and minimized sub-surface resources impact through optimized steam supply utilization.

2.1 Challenges in Steam Flow Measurement for Geothermal Applications

Measuring steam flow in geothermal environments presents unique challenges:

- **Steam Conditions:** Unlike traditional steam applications, geothermal steam often contains liquid droplets and impurities. Not all flowmeters are capable of handling this fluid process flow accurately. The chosen technology must be suitable for measuring this special steam conditions.
- **Harsh Environment:** Geothermal fluids can be highly corrosive due to the presence of dissolved minerals, and steam flow can reach high velocities, leading to potential erosion. Flowmeters must be constructed from materials that are both corrosion-resistant and suitable for withstanding high-velocity flow to ensure long-term reliable performance and maintain measurement accuracy.
- **Varying Flow Rates:** Geothermal steam flow rates can fluctuate significantly depending on reservoir conditions and power generation demands. The chosen flowmeter technology must have a wide dynamic range to accommodate these variations and provide accurate measurements across the entire operating spectrum.
- **Steam Temperatures and Pressures:** Flowmeters must be constructed from robust and temperature-resistant materials suitable for these conditions to ensure long-term reliable performance

2.2 Diverse Steam Flowmeter Technologies

Geothermal power plants utilize a variety of steam flowmeter technologies as follows:

- **Differential Pressure (DP) Flowmeters:** These are the most common type due to their simplicity and affordability. They measure the pressure difference across a restriction (orifice plate, venturi tube, or annubar) in the steam flow path. This pressure difference is proportional to the flow rate, providing a reliable and relatively inexpensive measurement method. Including to this flowmeter type is annubar flowmeters, also known as averaging pitot tubes.
- **Vortex Flowmeters:** These flowmeters employ vortices generated by a bluff body (typically a triangular prism) placed in the flow stream. As steam flows past the bluff body, vortices are shed at a frequency proportional to the flow rate. This non-intrusive measurement technique offers high accuracy and a wide flow range, making it suitable for diverse geothermal applications.
- **Coriolis Flowmeters:** These flowmeters utilize the Coriolis force to measure mass flow rate. As steam flows through a vibrating tube, the Coriolis force causes the tube to twist slightly. The frequency of this twisting motion is directly proportional to the mass flow rate. While offering high accuracy and direct mass flow measurement, Coriolis flowmeters are generally more expensive and more sensitive to vibrations compared to other technologies.
- **Ultrasonic Flowmeters:** These flowmeters employ ultrasonic waves to measure the transit time of the waves across the steam flow path. The difference in transit time between upstream and downstream measurements is proportional to the flow velocity. This non-intrusive technique offers high accuracy and is well-suited for wet steam conditions.
- **Magnetic Flowmeters:** These measurement devices are also known as electromagnetic flowmeters, operate based on the principle of electromagnetic induction. As conductive steam flows through a magnetic field, a voltage is generated proportional to the flow velocity.

By understanding the significance of steam flowmeters, the diverse measurement techniques available, and the challenges encountered in geothermal environments, this paper equips plant operators and engineers with the knowledge necessary to select the optimal flowmeter technology for their specific geothermal power plant application. Several sections below will discuss various steam flowmeter options suitable for geothermal power plant applications. Each section will also examine the specifications of the flowmeters, including measurement accuracy, pressure drop, maintenance requirement, installation complexity, fluid compatibility, scaling risk and other potential considerations.

3. DIFFERENTIAL PRESSURE (DP) FLOWMETERS

Differential pressure (DP) flowmeters operate based on Bernoulli's principle, which relates fluid velocity to pressure. As steam flows through a restriction its velocity increases as it passes through the narrowed section, causing a corresponding decrease in pressure. The pressure difference (ΔP) is measured across the restriction and is proportional to the square root of the flow rate. This section discusses the different types, operating principles, installation considerations, advantages, and drawbacks of DP flowmeters for steam flow measurement in geothermal applications. DP flowmeters encompass a variety of designs, each tailored to specific applications. Below are the most widely used type of flowmeter in geothermal power plant applications:

- **Orifice Plates:** These are the most common DP flowmeters, featuring a thin plate with a central orifice that creates a pressure differential proportional to flow rate.
- **Venturi Tubes:** These devices utilize a tapered throat section to induce a pressure differential, offering better accuracy compared to orifice plates.
- **Annubar:** These flowmeter also known as averaging pitot tubes. They offer several advantages over traditional DP flowmeters, particularly in applications requiring very low pressure-drop or involving fluctuated flow rates.

3.1 Orifice Plates

Orifice flowmeters are widely used devices for measuring fluid flow rates in various industries, including geothermal power plants. They operate based on the principle of differential pressure, where a restriction (orifice plate) is inserted into the flow stream, causing a pressure drop that is proportional to the flow rate.

3.1.1 Orifice Plate Specifications

The accuracy of orifice meters is influenced by several factors, including fluid properties, pipe configuration, orifice dimensions (beta ratio), Reynolds number, and correction factors. Optimal performance is typically

achieved with beta ratios between 0.35 and 0.6. However, under specific conditions, beta ratios outside this range may be used, though they come with increased measurement uncertainty. The overall accuracy ranges from ±0.5 to ±5%.

Orifice plate specifications are detailed in standards such as API MPMS Chapter 14.3 and include several key aspects. The thickness of the orifice plate is crucial and depends on the line size, with a minimum thickness of 1/8 inch for lines under 10 inches and 1/4 inch for larger lines. The flatness of the plate is also critical, with the maximum deviation from flatness calculated based on the orifice and pipe diameters. Additionally, the surface roughness of the plate should not exceed 50 micro inches to ensure accurate measurements. The upstream edge of the plate must be a sharp square-edge that does not have any burrs, as these imperfections can increase measurement uncertainty. Proper centering of the orifice bore within the pipe is essential, especially for custody measurement applications, where stricter tolerances are required.

The materials used for orifice plates are typically corrosion-resistant, such as stainless steel (304SS, 316SS), Monel, or other alloys, depending on the service conditions. The location of pressure taps, which can be flange, corner, or radius taps, is another important factor influenced by flow conditions, pipe size, cost, and required accuracy. For piping specifications, the latest revisions of standards like ISO 5167 outline the requirements for the design of the pipe section preceding and following an orifice plate, known as the meter run. This section of the piping system must establish a stable and predictable flow profile before the fluid encounters the orifice. Key factors influencing meter run design include pipe diameter, fluid properties, flow rate, and desired accuracy.

Generally, a minimum of ten pipe diameters of straight pipe is recommended upstream of the orifice, with an optimal length of 25 to 30 diameters. Downstream, a minimum of five pipe diameters is typically required, but eight to ten diameters are preferred for better accuracy. However, these are just guidelines, and the actual requirements can vary based on specific conditions. Factors such as the presence of valves, elbows, or other fittings near the orifice can influence the necessary straight pipe lengths. Additionally, fluids with high viscosity or those containing suspended solids may necessitate longer meter runs. To further enhance the flow profile and reduce required straight pipe lengths, flow conditioners like straightener vanes can be employed.

Installing an orifice flowmeter can be relatively straightforward, but precise alignment and adherence to piping specifications are crucial. The corrosive nature of geothermal fluids necessitates the use of compatible materials for the orifice plate and other components. While orifice flowmeters generally require minimal maintenance, regular inspections are essential to identify potential issues such as erosion, corrosion, or blockage. The orifice plate, pressure taps, and sensing lines should be checked for any abnormalities. In geothermal applications, where scaling is a common problem, additional cleaning or chemical treatment might be necessary to maintain meter performance.

Although orifice flowmeters are commonly used to measure steam flow rates in geothermal power plants, their application presents specific challenges. A primary concern is the pressure drop induced by the orifice, which can reduce system efficiency. To ensure accurate measurements, careful installation and adherence to piping guidelines are crucial. The corrosive nature of geothermal fluids necessitates the use of corrosion-resistant materials and regular inspection to prevent scaling and maintain performance. Additionally, factors such as flow profile, cavitation, and velocity can impact the accuracy of orifice flowmeters in geothermal environments.

3.1.2 Orifice Bores

Orifice plates come in various configurations of orifice bores, including concentric, eccentric, multi-hole and segmental designs, each suited for specific fluid conditions and applications. The concentric bore design is the most common and is ideal for measuring clean fluids like steam, gas, water, air, and clean liquids. The eccentric bore design is used for liquids containing gas, allowing the gas to pass through the orifice bore located at the top of the pipe. The segmental bore design is suited for liquids with solids, with an opening that allows solids to pass freely. Segmental bore orifice plates are often preferred over eccentric plates for measuring suspended solids in liquids and gases. Recently, multi-hole bore orifice plates have been developed, offering a wider range of applicable Reynolds numbers and requiring shorter meter run lengths compared to eccentric and segmental designs. However, data for eccentric and segmental plates is limited and outdated, with concentric orifice meters generally providing more accurate measurements. Figure 1 provides the picture of orifice bores.

For geothermal steam measurement, the concentric design is generally the most widely used type of orifice plate. The primary reasons for selecting the concentric design include:

1. Simplicity: Its simple and symmetrical design makes it easier to manufacture, install, and calibrate.
2. Accuracy: Available data and research indicate that the concentric design provides better accuracy compared to other designs, especially for single-phase fluids like steam.
3. Standardization: The concentric design is widely adopted, leading to more established industry standards and practices.

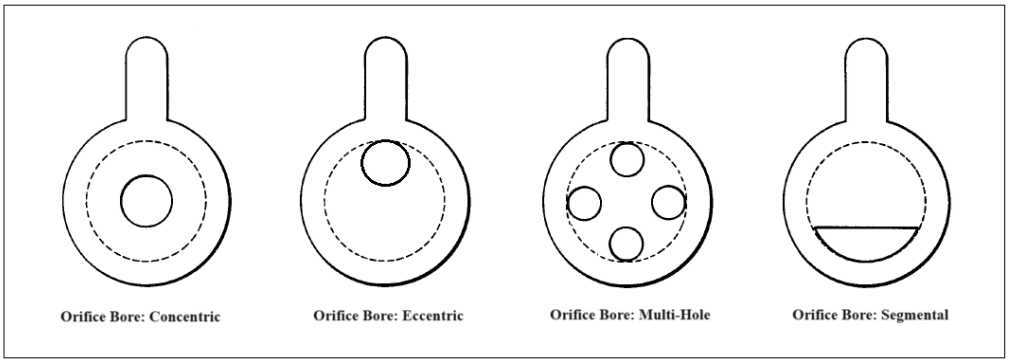

Figure 1: Various Orifice Bores.

Other orifice plate designs, such as eccentric, segmental, and multi-hole, are typically better suited for fluids containing solid particles or multiphase mixtures. For relatively clean steam, the concentric design is often sufficient. While other factors such as fluid conditions, required accuracy, and cost should be considered, the concentric design remains the preferred choice for most geothermal steam measurement applications.

3.2 Venturi Tubes

Venturi flowmeters are widely utilized in various industries including geothermal power plants, operated based on the principle of differential pressure. As the fluid passes through a narrowed section of the tube, its velocity increases while pressure drops. This pressure difference is then used to calculate the flow rate. Compared to orifice meters, venturi flowmeters typically offer a broader flow range and better measurement accuracy. This is primarily due to the carefully designed converging and diverging sections of the venturi tube, which help to maintain a stable and predictable flow profile, thus reducing the chances of measurement errors. The accuracy of venturi meters usually ranges from ±0.5% to ±3% of the actual flow rate, depending on factors such as the Reynolds number, fluid properties, and adherence to manufacturing tolerances. Figure 2 provides the schematic of venturi tube.

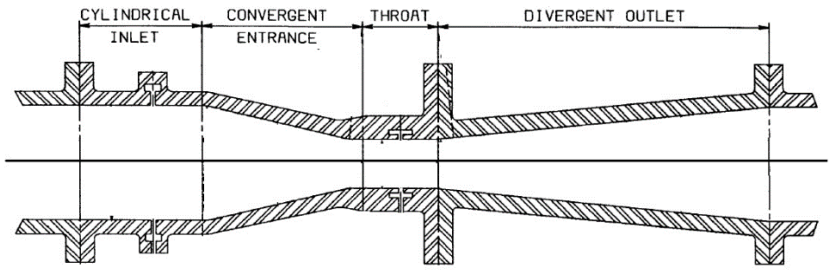

Figure 2: Venturi Tube.

One of the key advantages of venturi flowmeters is their relatively low pressure-drop. The gradual expansion of the fluid through the diverging section of the venturi tube minimizes energy losses, resulting in a permanent head loss that typically ranges from 10% to 14% of the measured differential pressure. This characteristic makes venturi flowmeters particularly appealing for geothermal applications, where maintaining system pressure is critical for efficiency. Additionally, the reduced pressure-drop compared to other differential pressure devices, like orifice plates, contributes to overall system energy savings, making venturi meters a more energy-efficient choice. Figure 3 compares the overall pressure loss through several DP flowmeter primary elements.

In terms of fluid compatibility, venturi flowmeters are versatile and can handle a wide range of fluids, including gases, liquids, and slurries. This makes them suitable for the challenging conditions found in geothermal power plants, where fluids can be highly corrosive or contain suspended solids. To ensure long-term durability and performance, materials like stainless steel, high-strength alloys, and ceramic coatings are often used in the fabrication of venturi tubes. Although the potential for scaling is lower in venturi meters due to their smooth flow path and larger cross-sectional area, it remains a concern in geothermal applications with high mineral content. Regular inspections and cleaning are recommended to prevent scaling, particularly in the throat area, which is more susceptible to build-up.

The installation of venturi flowmeters requires careful consideration of space and pipe configuration. While they generally require shorter upstream and downstream straight runs compared to orifice meters, typically 5 to 10 pipe

diameters upstream and 2 to 5 diameters downstream. The larger physical size of venturi tubes means that they take up more space and can be more complex to install. Proper alignment and adherence to these installation guidelines are essential to ensure accurate measurements. Despite the initial complexity, venturi flowmeters are known for their low maintenance needs, making them a cost-effective choice in the long run. Regular maintenance, including inspections for erosion, corrosion, or scaling, is crucial to maintain optimal performance, especially in harsh geothermal environments.

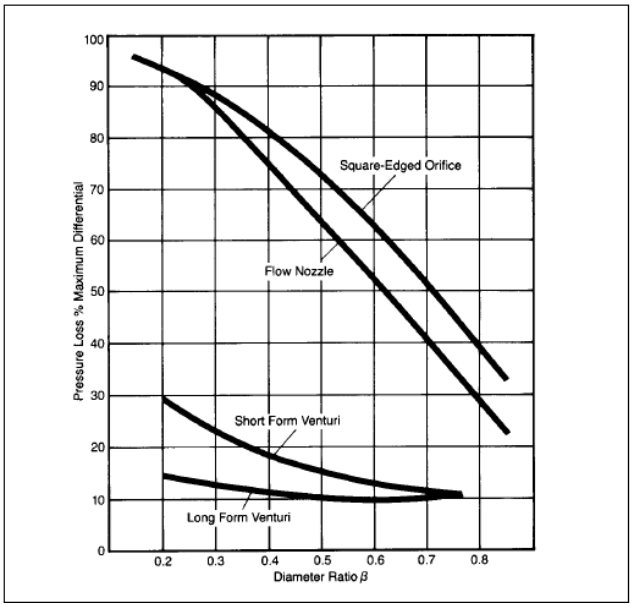

Figure 3: Pressure Loss vs. Diameter Ratio (Beta).

In conclusion, venturi flowmeters offer a robust and reliable solution for measuring flow rates in geothermal power plants. Their high accuracy, low pressure-drops, and minimal maintenance requirements make them well-suited to the demanding conditions of geothermal applications. While they may come with a higher initial cost and installation complexity compared to other flowmeter types, the benefits they provide in terms of durability, energy efficiency, and long-term reliability often justify the investment. By carefully considering factors such as fluid compatibility, scaling risk, and installation requirements, venturi flowmeters can significantly contribute to the efficient operation of geothermal power plants.

3.3 Annubar

Annubar steam flowmeters, also known as averaging Pitot tubes, are a type of differential pressure flowmeter designed to measure the flow of steam and other fluids in various industrial applications, including geothermal power plants. These flowmeters operate on the principle of differential pressure, where the flow velocity is determined by measuring the difference in pressure between the upstream and downstream sides of the sensor. The annubar design features multiple pressure-sensing ports along the length of the tube, which average the flow profile across the pipe, resulting in a more accurate measurement of the flow rate. Figure 4 provides the measurement principles of annubar flowmeters.

One of the key advantages of annubar flowmeters is their accuracy, which can range from ±1% to ±2% of the actual flow rate, depending on the specific model and installation conditions. This accuracy is influenced by factors such as the Reynolds number, fluid properties, and the installation environment. In geothermal power plants, where precise steam flow measurement is crucial for efficient operation, the accuracy of annubar flowmeters makes them a reliable choice. However, achieving optimal accuracy requires careful attention to installation and calibration procedures, as any misalignment or improper positioning can lead to measurement errors.

In terms of pressure drop, annubar flowmeters typically exhibit a very low pressure-drop compared to other differential pressure flowmeters like orifice plates. This lower pressure-drop is due to the streamlined design of the annubar sensor, which minimizes disruption to the flow and reduces energy losses. For geothermal applications, where maintaining system pressure is essential, this characteristic is particularly beneficial, as it helps preserve the overall efficiency of the power plant. The lower pressure-drop also means that less energy is required to maintain the desired flow rate, contributing to overall cost savings in the operation of the plant.

Maintenance requirements for annubar flowmeters are generally low, making them an attractive option for geothermal power plants. These meters are often equipped with retractable insertion devices that allow for inspection or repair without interrupting the flow. The annubar sensor, typically constructed from corrosion-resistant materials such as stainless steel or high-strength alloys, ensures durability even in harsh environments. However, regular inspections are necessary to check for any signs of wear, corrosion, or scaling, especially in geothermal applications where the steam may contain impurities that can deposit on the sensor over time. Fouling can affect the accuracy of the flow measurement and should be addressed promptly through cleaning or chemical treatment.

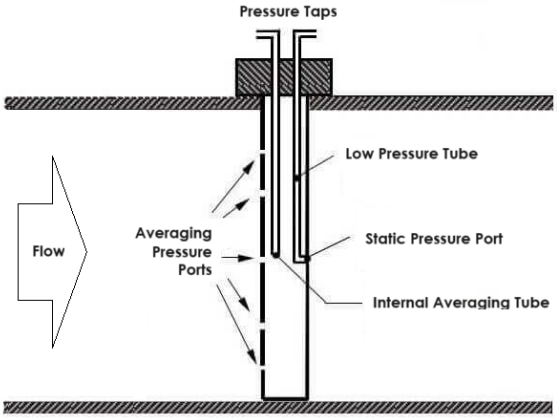

Figure 4: Measurement Principle of Annubar (Averaging Pitot Tubes).

The installation complexity of annubar flowmeters is relatively moderate compared to other differential pressure flowmeter types. These flowmeters are generally easier to install than orifice plates, as they do not require extensive straight pipe runs upstream and downstream of the sensor. However, proper alignment and positioning of the annubar sensor within the pipe are critical to ensuring accurate measurements. In geothermal power plants, where space may be limited, the compact design of the Annubar flowmeter can be advantageous, allowing for installation in areas where larger flowmeters might not fit. Additionally, the ability to install Annubar flowmeters in existing pipelines with minimal modifications makes them a flexible option for both new installations and retrofits.

Another consideration in using annubar flowmeters is the risk of resonance vibration. A vibration force perpendicular to the flow stream can occur due to the shedding of alternate vortices. It is important to check the frequency of this shedding against the natural resonance frequency of the sensor. A failed Annubar sensor could potentially enter and damage downstream equipment, so opposite-side support should be considered, especially for large line sizes.

Fluid compatibility is another important factor for annubar flowmeters, particularly in geothermal applications. The materials used in constructing the annubar sensor must be compatible with the steam and other fluids in the system. In geothermal power plants, where steam may be corrosive or contain particulate matter, selecting the appropriate materials is crucial for ensuring long-term reliability and performance. Stainless steel, high-strength alloys, and other corrosion-resistant materials are commonly used to withstand the harsh conditions found in geothermal environments.

Scaling potential is a significant concern in geothermal applications, where steam often contains dissolved minerals that can precipitate and form deposits on the surfaces of the flowmeter. While annubar flowmeters are less prone to scaling than some other flowmeter types due to their smooth design and minimal surface area, scaling can still occur, particularly in the pressure-sensing ports. Regular maintenance and cleaning are essential to prevent scaling from affecting the accuracy of the flow measurements. In some cases, chemical treatments or the use of anti-scaling agents may be necessary to keep the flowmeter functioning optimally.

Another factor to consider when using annubar flowmeters in geothermal power plants is the potential for cavitation and erosion. High-velocity steam flows can lead to cavitation, where vapor bubbles form and collapse, potentially damaging the sensor and other components. To mitigate this risk, it is important to ensure that the flowmeter is installed in a location where the steam velocity is within acceptable limits and that the sensor is designed to withstand the operating conditions. Additionally, using erosion-resistant materials can help extend the lifespan of the flowmeter in environments where particulate matter is present.

In summary, annubar flowmeters have emerged as a valuable option for steam flow measurement in geothermal power plants, particularly in applications where non-intrusive measurement, very low pressure-drop, wide flow

range, and accuracy are critical. Their ability to handle fluid compatibility and fluctuating flow rates makes them well-suited for geothermal environments. However, their higher cost, sensitivity to installation, risks of resonance vibration, and potential issues with fouling require careful consideration when selecting a flowmeter technology for geothermal applications.

3.4 Summary of DP Flowmeters

Differential Pressure (DP) flowmeters, including orifice plates, venturi tubes, and annubar flowmeters, are commonly used in geothermal steam measurement due to their reliability and established industry standards. Each type of DP flowmeter has distinct characteristics, advantages, and limitations that make them suitable for specific applications within geothermal power plants.

DP flowmeters offer a range of options for steam measurement in geothermal power plants, each with its own set of strengths and weaknesses. Orifice plates are cost-effective and simple but suffer from higher pressure-drops and potential accuracy issues. Venturi tubes provide a good balance between accuracy and pressure-drop, making them suitable for maintaining system efficiency, though they come with higher installation complexity. Annubar flowmeters combine low pressure-drop with ease of installation, though they require careful handling to avoid issues like vibration and fouling. The choice between these options depends on the specific requirements of the geothermal application, including the need for accuracy, pressure management, ease of installation, and long-term maintenance.

4. VORTEX FLOWMETERS

Vortex flowmeters are a popular choice for steam measurement in various industrial applications, including geothermal power plants, due to their robustness, reliability, and relatively low maintenance requirements. These flowmeters operate on the principle of vortex shedding, where an obstruction or bluff body placed in the flow path causes vortices to form alternately on each side of the bluff body. The frequency of these vortices is directly proportional to the flow velocity, allowing the flowmeter to calculate the volumetric flow rate. Vortex flowmeters are particularly well-suited for measuring the flow of steam, gases, and liquids, offering a versatile solution for geothermal power plant applications. Figure 5 describes the measurement principle of vortex flowmeters.

One of the primary advantages of vortex flowmeters is their accuracy, which typically ranges from ±0.75% to ±2% of the reading, depending on the specific model and the flow conditions. This level of accuracy is generally sufficient for most steam measurement applications in geothermal power plants, where precise flow measurement is critical for efficient plant operation. The accuracy of vortex flowmeters can be affected by factors such as fluid density, viscosity, and velocity (max 250 fps for steam and gases). Considering this limitation, vortex meters require minimum Reynolds number typically ranging from 10,000 to 40,000 for common shape of bluff body. However, modern designs often include compensation algorithms to account for these variables for enhancing measurement reliability.

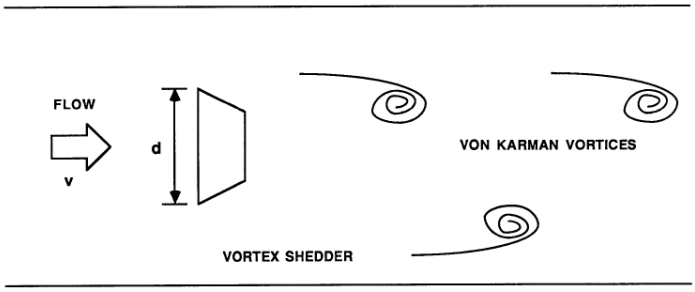

Figure 5: Measurement Principle of Vortex Flowmeter.

Vortex flowmeters also have the advantage of a relatively low pressure-drop compared to other flow measurement technologies like orifice plates. The pressure drop across a vortex flowmeter is mainly due to the presence of the bluff body in the flow path, which is designed to minimize flow disruption while still generating vortices. This low pressure-drop is beneficial in geothermal power plants, where maintaining system pressure is essential for operational efficiency. By minimizing energy losses, vortex flowmeters contribute to the overall energy efficiency of the plant.

Maintenance requirements for vortex flowmeters are relatively low, making them an attractive option for geothermal power plants. The design of vortex flowmeters is inherently simple, with no moving parts that can wear out or fail over time. This simplicity reduces the need for regular maintenance and makes vortex flowmeters more reliable in the long term. However, periodic inspections are still necessary to ensure that the bluff body and

the sensors are free from any buildup of deposits or scaling, which can occur in geothermal applications due to the presence of minerals in the steam.

Installation of vortex flowmeters is relatively straightforward, but it is important to follow specific guidelines to ensure accurate measurements. Vortex flowmeters require a certain length of straight pipe upstream and downstream of the meter to ensure a stable flow profile. Typically, 15 to 50 pipe diameters depend on the piping elements upstream of meter and 5 to 10 pipe diameters downstream are recommended. In geothermal power plants, where space can be limited, careful consideration must be given to the placement of the flowmeter to meet these requirements without compromising the overall system design.

Fluid compatibility is another important factor to consider when selecting vortex flowmeters for geothermal applications. The materials used in the construction of the flowmeter must be compatible with the steam and any impurities present in the fluid. In geothermal environments, where the steam can be corrosive or contain particulate matter, selecting the appropriate materials is crucial to ensure the longevity and reliability of the flowmeter. Common materials include stainless steel and high-grade alloys that offer resistance to corrosion and erosion.

Scaling risk is a significant concern in geothermal power plants due to the high mineral content of the steam. While vortex flowmeters are generally less prone to scaling than some other flowmeter types, scaling can still occur on the bluff body or in the sensor area, leading to inaccuracies in flow measurement. Regular cleaning and maintenance are necessary to prevent scaling from affecting the performance of the flowmeter. In some cases, the use of anti-scaling agents or chemical treatments may be required to keep the flowmeter operating at optimal performance levels.

Vortex flowmeters are also known for their versatility in handling a wide range of flow rates, making them suitable for geothermal power plants with varying steam output. The ability to accurately measure both low and high flow rates without requiring recalibration or significant adjustments is a key benefit of vortex flowmeters. This versatility makes them a reliable choice for geothermal applications, where steam flow can fluctuate based on operational demands.

In summary, vortex flowmeters are a robust and reliable choice for steam measurement in geothermal power plants, offering a good balance of accuracy, low pressure drop, and minimal maintenance requirements. Their versatility in handling different flow rates, combined with their compatibility with corrosive and particulate-laden fluids, makes them well-suited for the challenging conditions found in geothermal environments. However, careful attention to installation, fluid compatibility, and scaling potential is necessary to ensure the long-term performance and reliability of vortex flowmeters in these applications. The installed cost of vortex meters through 4 inch is typically less than for orifice meters. Vortex meters 6 inches and larger may have higher costs than orifice meters.

5. CORIOLIS FLOWMETERS

Coriolis flowmeters are widely recognized for their high precision and versatility in various industrial applications, including steam measurement in geothermal power plants. These meters operate on the principle of the Coriolis effect, where the mass flow rate is determined by measuring the phase shift caused by the fluid's inertia as it flows through vibrating tubes. This direct measurement of mass flow, rather than volume flow, allows for extremely accurate and reliable readings, which is particularly valuable in geothermal steam applications where precise flow measurement is crucial for efficient power generation. Figure 6 describes the measurement principle of Coriolis flowmeters.

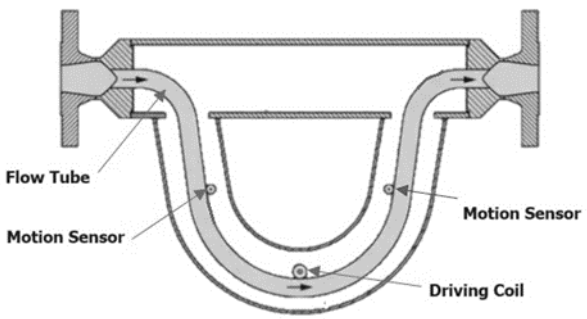

Figure 6: Measurement Principle of Coriolis Flowmeter.

One of the most significant advantages of Coriolis flowmeters is their exceptional measurement accuracy, often within ±0.1% to ±0.2% of the actual mass flow rate. This level of precision makes them one of the most accurate flow measurement technologies available, far surpassing other types such as orifice plates or vortex flowmeters. This accuracy is maintained even under varying process conditions, including changes in temperature, pressure, and flow rate, making Coriolis meters particularly well-suited for the dynamic environments often encountered in several industries.

In terms of pressure drop, Coriolis flowmeters typically exhibit a high pressure-drop compared to other flow measurement technologies. The pressure drop is primarily a function of the tube geometry and the density and viscosity of the fluid. While the pressure drop in Coriolis meters is generally higher than that in annubar or venturi flowmeters, it is often lower than that in orifice plates, making it a balanced choice in terms of energy efficiency. In geothermal applications, where maintaining system pressure is essential, the moderate pressure-drop of Coriolis meters is usually acceptable, especially when balanced against their accuracy and other benefits.

Coriolis flowmeters are known for their relatively low maintenance requirements, which is a significant advantage in geothermal power plants where equipment accessibility can be challenging. The design of these meters, with no moving parts and minimal internal components, reduces the likelihood of wear and tear. However, regular inspections are recommended to ensure the integrity of the vibrating tubes, especially in environments with corrosive or abrasive fluids, such as geothermal steam. Over time, buildup or scaling inside the tubes can occur, potentially affecting the meter's performance, so periodic cleaning or chemical treatment may be necessary to maintain optimal operation.

Installation complexity is another factor to consider when implementing Coriolis flowmeters in geothermal power plants. While these meters are relatively easy to install compared to more complex systems like venturi tubes, they do require careful alignment and mounting to ensure accurate readings. The installation process must account for factors such as vibration isolation, as external vibrations can interfere with the meter's operation. Coriolis meters installation is also sensitive to electromagnetic interference, so sensor unit should be located at least 0.6 m from large transformer of motors. Higher fluid temperature should be considered, since flow tube assembly limits operating temperature within ranges -240°C to 204°C. Additionally, the need for straight pipe runs upstream and downstream of the meter is minimal, which can simplify installation in constrained spaces commonly found in geothermal facilities.

Fluid compatibility is a critical consideration for Coriolis flowmeters, particularly in geothermal applications where steam can contain various impurities, such as dissolved minerals and gases. The materials used in the construction of Coriolis meters must be selected to withstand these harsh conditions. Common materials include stainless steel and other high-strength alloys, which offer resistance to corrosion and erosion. In cases where the steam contains particularly aggressive chemicals, specialized coatings or materials may be required to ensure long-term durability.

In geothermal steam applications, scaling is a significant concern for Coriolis flowmeters due to the high mineral content in the steam, which can lead to the deposition of solids on the internal surfaces, particularly in the small size of flow tubes of the meter. This risk is heightened in the bends and junctions where fluid velocity changes, potentially reducing measurement accuracy and causing blockages. To mitigate this, regular maintenance, including inspections and cleaning, as well as the use of anti-scaling agents or chemical treatments, is essential to ensure reliable operation and maintain the accuracy of steam flow measurements in geothermal power plants.

Coriolis flowmeters are widely regarded as a robust and reliable choice for steam measurement in geothermal power plants, but they come with certain trade-offs. Their initial cost is generally higher than that of other flow measurement technologies, such as orifice plates or venturi meters. However, this higher upfront investment is often justified by their superior accuracy, lower maintenance requirements, and long-term reliability. Selecting the optimal flowmeter requires a comprehensive evaluation of all factors, not just measurement accuracy, to ensure the best balance of performance and cost-effectiveness.

Finally, it is important to consider the potential for process disruptions when using Coriolis flowmeters in geothermal power plants. While these meters are generally very reliable, any issues with the vibrating tubes, such as damage or fouling and sensitivity to electromagnetic interference, can lead to measurement inaccuracies or even meter failure. Therefore, it is essential to have a robust maintenance and monitoring program in place to detect and address any potential issues before they impact plant operations. This proactive approach can help ensure that the Coriolis meters continue to provide accurate and reliable steam flow measurements, contributing to the overall efficiency and effectiveness of the geothermal power plant.

6. ULTRASONIC FLOWMETERS

Ultrasonic flowmeters are increasingly being adopted in geothermal power plants for steam measurement due to their non-intrusive design, high accuracy, and low pressure-drop characteristics. These flowmeters operate based on the principle of measuring the transit time or Doppler shift of ultrasonic signals as they pass through the steam. By analyzing the time, it takes for ultrasonic waves to travel between sensors, the flow rate of the steam can be determined with high precision. Figure 7 describes the measurement principles of ultrasonic flowmeters using transit time and Doppler effect.

In terms of measurement accuracy, ultrasonic flowmeters are known for their high accuracy, typically within ±0.5% to ±2% of the actual flow rate. This accuracy is largely unaffected by changes in steam density, pressure, or temperature, making them particularly suitable for the variable conditions often found in geothermal power plants. However, the accuracy can be influenced by the homogeneity of the steam flow, as ultrasonic signals require a clear path through the fluid. Any presence of condensate, air bubble, particulate matter, or large temperature gradients can affect the readings, necessitating careful monitoring and calibration to ensure optimal performance.

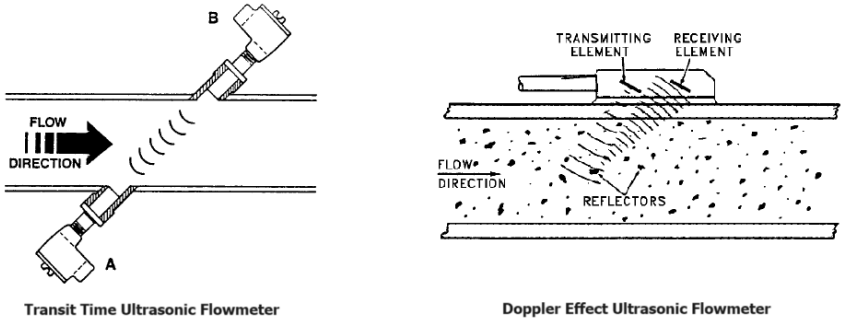

Figure 7: Measurement Principles of Ultrasonic Flowmeter.

One of the standout features of ultrasonic flowmeters is their negligible pressure drop. Unlike traditional flowmeters that rely on obstructions or constrictions in the flow path, ultrasonic flowmeters are non-intrusive and do not disrupt the flow of steam. This characteristic is crucial in geothermal power plants, where maintaining system pressure is vital for efficient operation. The lack of pressure drop also translates to energy savings, as there is no need to compensate for the losses typically associated with other flow measurement technologies.

When it comes to maintenance requirements, ultrasonic flowmeters are relatively low maintenance compared to mechanical flowmeters. Since there are no moving parts or direct contact with the steam, wear and tear are minimized, leading to longer service intervals and reduced maintenance costs. However, regular inspections are still necessary to ensure that the sensors are clean and functioning correctly. In geothermal environments, where steam can contain impurities and scaling is a common issue, periodic cleaning of the sensors is essential to maintain accuracy and prevent any buildup that could interfere with the ultrasonic signals.

The installation complexity of ultrasonic flowmeters can vary depending on the specific design and application. Clamp-on ultrasonic flowmeters, which are attached externally to the pipe, offer the advantage of easy installation without the need for pipe modifications or process shutdowns. However, clamp-on sensor requires special attention to ensure solid acoustic contact with the pipe wall through the use of conducting grease or gel material. In contrast, inline ultrasonic flowmeters, which require installation directly into the pipeline, may involve more complex procedures, including precise alignment and calibration. Ultrasonic flowmeters require a minimum straight pipe (meter run) from valves, tees, elbows, pumps, compressors, etc., to meet performance specifications. Typically, 10 to 20 diameters upstream and 5 diameters downstream are required. Upstream length requirement can be reduced by installing flow conditioners. Despite this, the installation of ultrasonic flowmeters is generally less invasive than that of other flowmeter types, making them an attractive option for both new installations and retrofits in geothermal power plants.

Fluid compatibility is another critical factor in the use of ultrasonic flowmeters in geothermal applications. These flowmeters are highly versatile and can be used with a wide range of fluids, including steam. However, the presence of non-uniform steam flow, such as droplets or solid particles, can affect the transmission of ultrasonic signals. It is important to ensure that the steam is as homogenous as possible to achieve accurate measurements. In geothermal power plants, where steam quality can vary, proper steam conditioning and monitoring are essential to optimize the performance of ultrasonic flowmeters.

Scaling potential is a concern in geothermal applications due to the high mineral content of the steam. While ultrasonic flowmeters are less prone to scaling than some other types of flowmeters, the buildup of scale on the sensors can still occur over time, particularly in harsh geothermal environments. Regular maintenance and cleaning, as well as the use of anti-scaling agents, can help mitigate this issue. Additionally, selecting flowmeters with robust sensor designs that can withstand scaling and corrosion is crucial for long-term reliability.

The ability to measure bidirectional flow is another advantage of ultrasonic flowmeters, making them particularly useful in complex geothermal power plant systems where steam flow may need to be measured in both directions. This feature enhances their versatility and allows for more comprehensive monitoring and control of the steam flow throughout the plant.

In summary, ultrasonic flowmeters offer a compelling solution for steam measurement in geothermal power plants, combining high accuracy, low pressure-drop, and minimal maintenance requirements. Their non-intrusive design and adaptability to various installation scenarios make them suitable for both new and existing installations. However, to maximize their effectiveness, careful consideration must be given to factors such as steam homogeneity, sensor maintenance, and scaling risk. When properly selected and maintained, ultrasonic flowmeters can provide reliable and accurate steam flow measurements, contributing to the overall efficiency and performance of geothermal power plants.

7. MAGNETIC FLOWMETERS

Magnetic flowmeters, also known as electromagnetic flowmeters, measure volumetric liquid flow rate. Its fundamental operating principle is based on Faraday's law of electromagnetic induction. The voltage induced across any conductor, as it moves through a magnetic field at right angles to the lines of flux, is proportional to the velocity of that conductor. The magnetic flowmeters commonly used in various industrial applications for measuring the flow of conductive fluids. However, their application in steam measurement, particularly in geothermal power plants, is less common due to the specific challenges posed by steam as a fluid. Despite these challenges, magnetic flowmeters can still be considered for certain steam measurement applications, provided that the right specifications and special requirements are considered. Figure 8 describes the measurement principles of magnetic flowmeters.

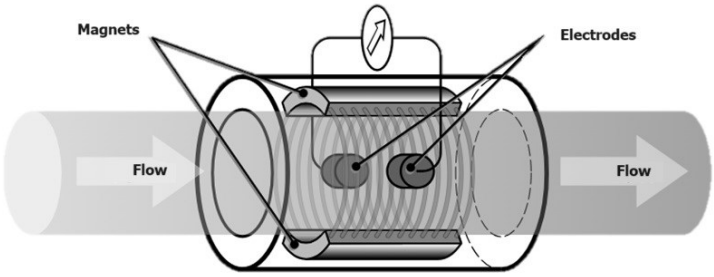

Figure 8: Measurement Principles of Magnetic Flowmeter.

One of the primary advantages of magnetic flowmeters is their high accuracy, which typically ranges from ±0.2% to ±1.0% of the actual flow rate. This level of accuracy is particularly valuable in geothermal power plants, where precise measurement of steam flow is crucial for optimizing plant efficiency and ensuring accurate billing in commercial applications. However, it is important to note that magnetic flowmeters require the fluid to be electrically conductive, which is not the case with steam. As a result, special considerations, such as using a conductive fluid in a two-phase flow system or employing alternative technologies, must be made when considering magnetic flowmeters for steam.

In terms of pressure drop, magnetic flowmeters have a distinct advantage over other types of flowmeters, such as orifice plates or venturi tubes. Since they do not have any moving parts or obstructions in the flow path, the pressure drop across a magnetic flowmeter is negligible. This characteristic is beneficial in geothermal power plants, where maintaining system pressure is critical for efficient operation. The low pressure-drop associated with magnetic flowmeters helps to minimize energy losses and maintain the overall efficiency of the plant.

Maintenance requirements for magnetic flowmeters are generally low, making them an attractive option for geothermal power plants. The absence of moving parts reduces the likelihood of mechanical wear and tear, leading to longer service intervals and lower maintenance costs. However, in geothermal applications, where the steam may contain impurities such as dissolved minerals or particulates, regular inspections and cleaning may still be necessary to prevent fouling of the flowmeter's electrodes. Ensuring that the electrodes remain clean and free from deposits is essential for maintaining accurate measurements over time.

The installation complexity of magnetic flowmeters is relatively straightforward compared to other flowmeter types. Magnetic flowmeters can be installed in both horizontal and vertical piping configurations, provided that the pipe is completely filled with the fluid being measured. In geothermal power plants, where space and piping configurations can vary, this flexibility in installation is advantageous. However, it is important to ensure that the flowmeter is properly grounded and that the installation adheres to manufacturer guidelines to avoid issues such as electrical noise interference, which can affect measurement accuracy.

Fluid compatibility is a critical consideration when selecting a flowmeter for geothermal steam measurement. While magnetic flowmeters are well-suited for measuring the flow of conductive liquids, their application in steam measurement is very limited due to the non-conductive nature of steam. In geothermal power plants, where the steam may contain a high level of dissolved solids or other impurities, these impurities can potentially render the steam conductive, allowing for the use of magnetic flowmeters in certain cases. However, this approach requires careful analysis of the steam's properties and may not be suitable for all applications.

Scaling risk is a concern in geothermal applications, where the steam often contains minerals that can precipitate and form deposits on the flowmeter's electrodes. These deposits can interfere with the flowmeter's ability to accurately measure flow and can lead to maintenance issues over time. To mitigate scaling, regular cleaning and the use of anti-scaling agents may be necessary. Additionally, selecting materials for the flowmeter that are resistant to scaling and corrosion, such as certain alloys or coatings, can help to extend the flowmeter's lifespan in harsh geothermal environments.

Another consideration for using magnetic flowmeters in geothermal power plants is the potential impact of temperature and pressure on the flowmeter's performance. Geothermal steam is typically at high temperatures and pressures, which can affect the materials used in the flowmeter and the overall measurement accuracy. Ensuring that the flowmeter is rated for the specific temperature and pressure conditions of the geothermal application is crucial for reliable operation. Additionally, the flowmeter should be calibrated to account for any temperature or pressure variations that may occur during operation.

In summary, while magnetic flowmeters are not commonly used for steam measurement in geothermal power plants due to the non-conductive nature of steam, they can still be considered for certain applications where the steam contains sufficient impurities to render it conductive. Their high accuracy, low pressure-drop, and minimal maintenance requirements make them an attractive option, provided that the specific challenges of geothermal steam measurement are addressed. Careful consideration of factors such as fluid compatibility, scaling risk, and installation complexity is essential to ensure the successful application of magnetic flowmeters in geothermal environments.

8. DISCUSSION

Steam flow measurement plays a critical role in the operation of geothermal power plants, ensuring efficiency, reliability, and overall effectiveness. Steam flowmeters are essential tools that provide real-time data on steam flow rates, which is vital for optimizing power generation, maintaining plant reliability, and enhancing operational efficiency. Accurate steam flow measurements enable operators to fine-tune turbine operations, promptly address anomalies or fluctuations, and identify opportunities for efficiency improvements, thereby reducing operational costs and optimizing the use of steam resources.

However, measuring steam flow in geothermal environments presents unique challenges. The presence of liquid droplets, impurities, and corrosive fluids within the steam requires flowmeters that are specifically designed to handle these harsh conditions. The selected flowmeters must be constructed from corrosion-resistant materials capable of withstanding high-velocity flows while maintaining accuracy. Additionally, they must be able to accommodate varying flow rates and endure the high temperatures and pressures typical of geothermal steam, ensuring consistent and reliable performance under diverse operating conditions.

The comparison chart (Table 1) outlines the key factors to consider -accuracy, pressure drop, maintenance requirements, installation complexity, fluid compatibility, scaling risk, and cost- when selecting steam flowmeters for geothermal power plants.

Table 1: Key Factors for Selecting Steam Flowmeters in Geothermal Power Plants.

Flowmeter	Accuracy	Pressure Drop	Maintenance	Installation	Fluid Compatibility	Scaling Risk	Cost
Orifice	±0.5% to ±5%	Moderate	Low	Low	Applicable	Low	Low
Venturi	±0.5% to ±3%	Low	Low	Low to Moderate	Applicable	Low	Moderate
Annubar	±1% to ±2%	Very Low	Low to Moderate	Low to Moderate	Applicable	Low to Moderate	Low

Vortex	±0.75% to ±2%	Low	Low	Low	Applicable	Low to Moderate	Moderate
Coriolis	±0.1% to ±0.2%	High	Low	Low	Applicable with Note (1)	High	High
Ultrasonic	±0.5% to ±2%	Very Low	Low	Low	Applicable with Note (2)	Low	Moderate
Magnetic	±0.2% to ±1.0%	Very Low	Low	Low	Not Applicable	Low	High

Note:
(1). Manufacturer to be consulted for certain pipe size, special steam conditions and other potential interferences.
(2). Significant solids or impurities flowing through the meter may affect to signal degradation.

Given the complexities and challenges inherent in geothermal environments, selecting the appropriate steam flowmeter requires careful consideration of these factors. The above chart provides a general comparison to aid in the initial selection process. However, specific operating conditions, process requirements, or unique circumstances may necessitate deviations from these general guidelines. In such cases, engineers should consult applicable industrial standards and seek guidance from manufacturers to ensure that the selected flowmeter meets the specific needs of the geothermal power plant.

9. FORWARD PLAN

To further refine the selection and implementation of steam flowmeters in geothermal power plants, a comprehensive forward plan is essential. This plan should encompass several key areas as follows:

- **Quantitative Analysis and Performance Evaluation:** The first step in the forward plan is to conduct a thorough quantitative analysis of the existing flowmeter performance across all geothermal power plant assets. This analysis should focus on measuring the accuracy, reliability, and efficiency of the current steam flowmeters under varying operational conditions. Important parameters such as measurement accuracy, pressure drop, maintenance frequency, and operational costs should be tracked and compared across different types of flowmeters. This data will provide a solid foundation for assessing the effectiveness of current technologies and identifying areas where improvements can be made.
- **Vendor Input and Detailed Specifications:** Engaging with flowmeter vendors is crucial for obtaining detailed specifications, understanding the latest technological advancements, and gathering budgetary information for potential upgrades or new installations. Vendors should be consulted to provide tailored recommendations based on the specific conditions of each geothermal site, including steam quality, flow rate variability, and environmental challenges. This input will help in refining the flowmeter selection criteria and ensuring that the chosen technologies align with the operational needs of the plants. Additionally, obtaining budgetary estimates will facilitate financial planning and decision-making for future investments in flow measurement technology.
- **Evaluation of Company Best Practices:** A review of the company's best practices in steam flow measurement should be conducted to identify successful strategies and lessons learned from past experiences. This review should include case studies from existing geothermal sites, focusing on the effectiveness of different flowmeter technologies in enhancing plant performance. Insights gained from these practices can be used to develop standardized procedures for flowmeter selection, installation, and maintenance across all geothermal assets. Sharing these best practices internally will ensure consistency in operations and help avoid common pitfalls associated with steam flow measurement.
- **Integration with Future Geothermal Development Plans**: The forward plan should be aligned with the company's future geothermal development plans. As new geothermal fields are explored and additional power generation capacity is brought online, the selection and deployment of steam flowmeters must be integrated into the overall project planning. This includes early-stage engineering design, budgeting, and procurement processes to ensure that the most suitable flow measurement technologies are selected for new installations. Moreover, as the company expands its geothermal footprint, there should be an emphasis on adopting innovative flowmeter technologies that offer enhanced accuracy, lower maintenance, and better adaptability to the unique challenges of geothermal steam.

Following this forward plan will ensure that steam flow measurement systems are optimized for current operations while being well-prepared for future geothermal developments. This proactive approach will enhance the long-term efficiency, reliability, and sustainability of geothermal power generation.

10. SUMMARY

Effective steam flow measurement is crucial for the efficient and reliable operation of geothermal power plants. Steam flowmeters provide the real-time data necessary to optimize turbine operations, detect process anomalies, and enhance overall plant efficiency. Accurate steam flow measurement allows operators to fine-tune power generation processes, ensuring that energy output is maximized while minimizing waste and operational costs. Given the unique challenges presented by geothermal steam, such as the presence of liquid droplets, impurities, and corrosive substances, selecting the right flowmeter is a critical decision that directly impacts plant performance.

In geothermal environments, the harsh conditions require flowmeters that are robust and capable of maintaining accuracy under specific temperatures, pressures, and varying flow rates. The materials used must resist corrosion and erosion, ensuring long-term reliability and consistent performance. Flowmeters like Coriolis, Venturi, Vortex, and Ultrasonic meters each offer specific advantages, such as high accuracy, low maintenance requirements, and suitability for varying operational conditions. However, each technology also presents trade-offs, such as the higher initial costs associated with certain flowmeters or the moderate scaling risks in specific applications. Although magnetic flowmeters offer high accuracy and very low pressure drop, they are not applicable for geothermal steam measurement due to their incompatibility with geothermal steam.

Venturi tubes, annubar, and orifice plates are the most commonly used flowmeters in geothermal applications, each offering distinct benefits suited to geothermal steam measurement. Venturi tubes are valued for their low pressure drop and reliability at high velocities, making them cost-effective. Annubar flowmeters excel in accuracy and minimal pressure drop, especially in fluctuating flow rates. Orifice plates, though prone to higher pressure loss, are cost-effective and standardized, with proven reliability. Supported by industry standards, these flowmeters balance accuracy, maintenance, and installation complexity, making them well-suited for geothermal environments. Their proven track record and cost-effectiveness solidify their preference for steam flow measurement in geothermal plants.

Ultimately, the selection of steam flowmeters in geothermal power plants should be guided by a comprehensive analysis of the plant's specific requirements, operating conditions, and long-term goals. Engineers must weigh the benefits and trade-offs of each technology, consult with manufacturers, and adhere to industry standards to ensure that the chosen flowmeter meets the operational demands of the plant. By carefully considering these factors, geothermal power plants can achieve optimal performance, reliability, and efficiency in steam flow measurement, contributing to the broader goal of sustainable energy production.

REFERENCES

Auliya, M.F., and Setiawan, A.: Main Steam Flowmeter Review U400, U500 and U600, Star Energy Geothermal (2021).

Auliya, M.F., and Setiawan, A.: Venturi Inspection Report, Star Energy Geothermal (2021).

Baker Hughes: Steam Flow Measurement in Geothermal Power Plants: A comparative study of different flowmeter technologies, Baker Hughes. https://www.bakerhughes.com/panametrics/success-stories/steam-flow-measurement-geothermal-power-plant.

Chevron.: Instrumentation and Control Manual – Flow Measurement, Chevron, USA (2016).

Chevron Geothermal Indonesia: Darajat Power Plant Unit 2 & Unit 3 System Description Rev. 1, Chevron Geothermal Indonesia (2016).

Chevron Geothermal Indonesia: Resource Production Facility System Description Rev. 1, Chevron Geothermal Indonesia (2016).

Chevron Geothermal Salak: Salak Power Generation Facility Unit 400, 500 and 600 System Description Rev. 1, Chevron Geothermal Salak (2015).

Magma Nusantara Limited: Descriptive Manual for Power Station - Wayang Windu Geothermal Power Project, Magma Nusantara Limited (2000).

Ischak, U.A., and Kurniawan, I.: Geothermal Power Plant Retrofit to Optimize Generation: A Case Study from Salak Unit 4/5/6, Proceedings, 49th Workshop on Geothermal Reservoir Engineering, Stanford University, Stanford, California (2024).

Yokogawa Electric Corporation: Steam Flow Measurement in Geothermal Power Plants, Yokogawa Electric Corporation https://www.yokogawa.com/us/industries/renewable-energy/geothermal-power/.

Condition Based Lubrication Drives Down Maintenance Costs and Downtime Cost in Patuha Geothermal

Raka Anugrah Pratama, Andisyah Purdanto, and Yanuar Ramdhani

PT Geodipa Energi

raka@geodipa.co.id, andisyah@geodipa.co.id, yanuar@geodipa.co.id

Keywords: Lubrication, Maintenance, Condition Monitoring

ABSTRACT

Abnormal wear is the opposite of good health for machinery. A high wear rate implies poor machinery health. 6%–7% of the gross national product is required to repair the damage caused by mechanical wear, Rabinowicz, E.(2008). Abnormal wear is one of the damages caused by poor lubrication. The end result of poor lubrication and contamination control is often an unnecessarily high downtime and a high cost of business, such as unacceptable levels of downtime and lost revenue, high energy consumption, and high usage of consumable parts. To overcome these challenges, modern maintenance principles are based on the application of equipment condition monitoring techniques. One of these techniques is condition-based lubrication using offsite oil analysis, which is designed to keep track of the health of lubricants as well the equipment. The methodology used before implementing a condition-based lubrication oil analysis program is critical machine selection, selection and testing of lubricant parameters, data analysis, and maintenance decision support. To illustrate the benefits of implementing condition-based lubrication, a case study of lubrication system on steam turbine, lubrication system on hot well pump and lubrication system on cooling tower gearbox is presented. In this case study, wear, contamination, and chemistry were analysed. The result of the analysis shows that rotating pressure vessel oxidation test (RPVOT) on the lubrication system of steam turbines is decreasing, it is in line with the aging of lubricant. With this method, the right maintenance decision protected the steam turbine from catastrophic failure. Furthermore, condition-based lubricant oil analysis has succeeded in extending the oil change of the lubrication system on the hot well pump and cooling tower gearbox. There are many hidden costs of failure due to poor lubrication and hidden costs of an oil change that have influenced companies to find a more efficient approach to keeping oil healthy and reliable, including downtime costs and maintenance costs. Therefore, a condition-based lubricant program will help to determine when an oil change is necessary and can assist in analysing lubrication-induced damage that could result in equipment breakdown.

1. INTRODUCTION

PT Geo Dipa Energy geothermal working area is located in Patuha, West Java Province. Geothermal powerplant consist of major system such as main steam system, circulating water system, auxiliary water system, gas extraction system, and condensate drain system. The equipment on the system have a lubrication system. Lubrication oil is used to reduce wear, improving machine reliability and reduce economic cost associated with possible future unplanned maintenance. Therefore, an oil lubrication system should be monitored regularly and the oil should be replaced in time to extend the period over which the machine operating in a healthy state. In a modern maintenance technology, condition monitoring especially lubrication analysis plays a crucial role in optimizing the machine activities, as a part of an effective maintenance policy. Lubricant oil analysis has an important rule to drive down maintenance cost and downtime cost because there are many hidden cost of failure due to poor lubrication. The primary purpose of lubricant oil analysis is to register any abnormalities of oil parameters of the machine before the functional breakdown occurs. Oil analysis have a many parameter, main parameter consist of viscosity, water content, solid particle content, and total acid number. Another parameter can be applied according to operational of equipment. Rotating vessel oxidation test is an additional of lubricant test beside the main parameter. RVPOT is a test that determines the oxidation stability of an oil and it is a more proactive approach because can respond to pending problem before permanent harm is done to the oil or machine. The test is ideal for large oil volume with low make up fluid requirements and also severe duty application. In this paper, we present a condition based maintenance lubricant oil analysis to drives down maintenance and down time cost by conducting regular check adjusted to the lubricant capacity of each equipment, adding lubricant alarm limit and lubricant critical limit on the equipment. also improve to some equipment for supporting this program. Condition based lubrication is expected to reduce maintenance cost and operational cost due to equipment breakdown.

1.1 Predictive Maintenance

Maintenance is concerned with keeping an asset in a good working condition so that the asset may be used to its full productive capacity, Ramesh,G., and O'hanlon, T (2013). Predictive maintenance is one of the management maintenance method. Predictive maintenance. The common premise of predictive maintenance is that regular monitoring of the actual mechanical condition, operating efficiency, and other indicators of the operating condition of machine-trains and process system will provide the data required to ensure the maximum interval between repairs and minimize the number and cost of unscheduled outages created by machine – train failures, Keith,R. (2018). A comprehensive predictive maintenance management program uses an effective tools, vibration monitoring, thermography, oil analysis, sound level ultrasonic, partial discharge, and corona detection. All of the equipment to obtain the actual operating condition of plant system based on actual data.

1.2 Lubricating Oil Analysis

Now it is one of the most important component of condition based maintenance is lubricating oil analysis. Oil analysis can provide information about machine condition. The object of oil analysis is to determine an assets mechanical wear condition, lubricant condition, and the contamination on lubricant. Simply, oil analysis is a routine activity for analysis oil health. Machine wear analysis is the analysis of particle in the oil. Contaminant in oil can be in solid or liquid form. Solid contaminants such as sand and dirt. Lubricant condition should be monitored, one key oil properties for lubricant condition is viscosity. In rotating machines, oxidation and acidity of the oil are monitored to determine if the oil is still fit for use and to prevent corrosion. As a predictive maintenance tool, lubricating oil analysis can be used to schedule oil change intervals based on the actual condition of oil. in midsize to large plants, a reduction in the number of oil changes can amount to a considerable annual reduction in maintenance costs.

2. METHODOLOGY

This study incorporated a case study from the major equipment in Patuha Geothermal Powerplant consist of steam turbine lubrication system, hot well pump lubrication system, and cooling tower gearbox lubrication system. This study concerned on improving machine reliability and reduce breakdown level due to poor lubrication so maintenance cost and breakdown cost can be reduced. Figure 1, illustrated several steps to be taken in the methodology.

Research method start with identifying the problem that occur in lubrication system of steam turbine, hot well pump and cooling tower gearbox. After that conduct a literary study to find the best method of condition based maintenance oil analysis. The result of the literary study were applied to the critical machine selection, in this section machine should be categorized as a critical machine level use maintenance priority index (MPI) with system equipment reliability prioritization (SERP). Selection and testing lubricant parameter based on equipment condition. Steam turbine have a different testing parameter with other equipment because steam turbine use a large oil capacity. After the data is obtained, the next step is analyze the data, create an alarm limit and critical limit also improve lubrication maintenance method. so maintenance team can makes a decision on maintenance strategy such as topping up turbine lubricant for increasing the additive level of oil, drives down the rate of oil aging and extend the interval for oil change with several kind of lubrication maintenance strategy.

2.1 Critical Machine Selection

Since the Patuha Geothermal Powerplant had numerous equipment. The first phase of the study involved selection of the critical machine type amongst them. To assist in selecting the critical machines, several factors among others were considered and evaluated. First, does the machine failure significantly affect the productivity of company. Second, does the machine service imply high cost and the last, does the machine have a high complexity level (Karanovic,2018). After the consideration of all the aforementioned factors, steam turbine should be conduct lubrication test more complex than routine test, RVPOT should be include on lubricant analysis. Different with hot well pump and cooling tower gearbox, they used only routine test for lubricant analysis.

2.2 Selection and testing lubricant parameter

The chemistry related testing lubricant parameters are viscosity and total acid number. Steam turbine have more complicated testing parameters. Routine test and rotating pressure vessels to determine the oxidation stability of their oils. Lubrication testing parameters additionally include water content and particle content as contamination parameter. Steam turbine have more complex testing parameter, using routine test and determination of oxidation stability of steam turbine oils by rotating pressure vessel. Beside the testing lubricant parameter, sampling frequency must be considered, machinery manufactures will often suggest a sampling interval, but that should only be a rough guideline. The equipment asset owner is the best judge of sampling interval include safety risk, criticality of equipment, operating condition, how costly is a failure in repair cost or lost production and what is

the failure history. Steam turbine and hot well pump use quarterly sampling frequency for cooling tower gearbox use semiannually sampling frequency.

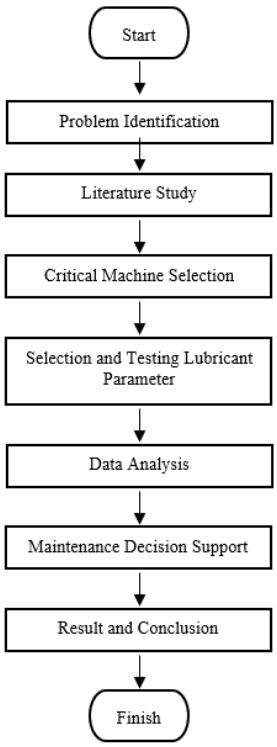

Figure 1: Research Method Flow Diagram.

2.2.1 Viscosity

Viscosity is the most important physical property of a lubricant. Viscosity is an oil's resistance to flow and shear. The correct balance between high viscosity for load carrying and low viscosity for ease of circulation must be considered for any lubricant and its application oil provide benefits in addition to lubrication and its is vital that it be able to flow under all condition. Excessively low viscosity will reduce the oil film strength, weakening its ability to prevent metal to metal contact. Excessively high viscosity reducing its ability to lubricated. The viscosity of oil impacted by temperature variation, additives, water contamination, thermal and oxidation degradation. Considering the most important physical property of a lubricant is viscosity, any change in viscosity higher or lower than cautionary limit, should be investigated, these change of chemical characteristic of oil like oxidation, evaporation, and thermal cracking of oil molecules. The increase viscosity leads to high internal friction affected to raise the lubricant temperature and energy losses over time, while if the viscosity decrease lowest that lower cautionary limit, offer less lubricity and low fil thickness that contribute to the high wear on the lubricated parts. Standard used for testing oil viscosity is ASTM D 445.

2.2.2 Total Acid Number

TAN or total acid number values are commonly used to measure degradation of machine lubricants in order to avoid machine wear, corrosion, varnish, clogged filters and other problems. Degradation of a lubricant caused by the breakdown of chemical component in the oil which result in the formation of acidic by products, formed by chemical reaction between oil base and additive component. Its lead to corrosion of oil wetted machine parts and the formation of varnish and sludge which can quickly clog oil filters. Standard used for testing oil total acid number is ASTM D 974.

2.2.3 Water Content

Water is the second most destructive contaminant. Water promotes change in chemical and physical properties in mineral oils and some synthetic such as acid formation, viscosity change, varnish, and sludge beside that water encourages aeration problems such as foaming and air entrainment and for viscosity effects water leads to stable emulsions, higher viscosity and non newtonian properties. Water contaminant have a three type. First dissolved water, the molecules dispersed one by one throughout the oil like. Second, emulsified water, microscopic globules of water dispersed in stable suspension in the oil. And the last free water, water that readily settles to tank/sump bottom. Standard used for testing oil water content is Karl Fischer.

2.2.4 Particle count

The vigilant practice of monitoring particles in oil effectively tracks the cause of wear and the effect of wear. In this test, high particle counts indicate that machinery may be wearing abnormally or that failures may occur because oof temporarily or permanently blocked orifices. Standard used for testing particle count is ISO 4406.

2.3 Data Analysis

In this method data analysis play an important rule in root cause failure analysis if the equipment breakdown caused by poor lubrication and help maintenance team to make a decision of maintenance or repair. The first of all, collecting, categorizing and evaluating all design and operating manuals including schematic are required to understand the complexity of equipment. Operating parameter also need to be considered, reflect the minimum requirement for operating the equipment this include operating temperature, lubricant requirements, filtration requirement and other parameters that directly or indirectly impact reliability and life cycle cost. Oil sampling location should be identified for each piece of equipment to allow trouble free, repetitive, and representative so that the good data will be obtained. To compare the data, fresh oil baseline must serve as a reference point, lubricant and additive packages might change over time, thus updating lubrication targets and alarm should take these change. The last step is database development, which involves organizing equipment data and information also collecting data along with the equipment specific targets and alarm.

2.4 Maintenance Decision Support

To take a maintenance decision support, in this method the most sophisticated use of oil analysis data and reports will aid strategic with scatter gram . Identify the types of equipment that breakdown most, extend oil drain with minimal risk by finding the threshold where severity level spike and make purchasing decisions based on which makes and models perform the longest before replacement is required, target for saving maintenance cost and reduce downtime cost expected to be accomplished.

3. RESULT AND DISCUSSION

In this section, the result data is presented with case studies related to the lubricant analysis. Advantage lubricant analysis for reducing maintenance cost and for reducing the downtime cost following to the methodology in section 2. The case studies include aging on steam turbines lubricant, Improve replacement oil schedule on Hot Well Pump from time based maintenance to the condition based maintenance, and upgrade base oil material on cooling tower due to high temperature operational.

3.1 Aging on Steam Turbines Lubricant

Lubricant on steam turbine, oil flowing through the bearing absorbs heat from the journal as the shaft carries it over the upper half of the lining. Steam turbine operate on a family of lubricating oil known as R&O oils (Rust & Oxidation inhibited oil). the rotating pressure vessel oxidation test (RPVOT) is a test that determines the oxidation stability of an oil, RVPOT measure the actual resistance to oil oxidation. The RVPOT value drops to 144 after 6 years of operations.

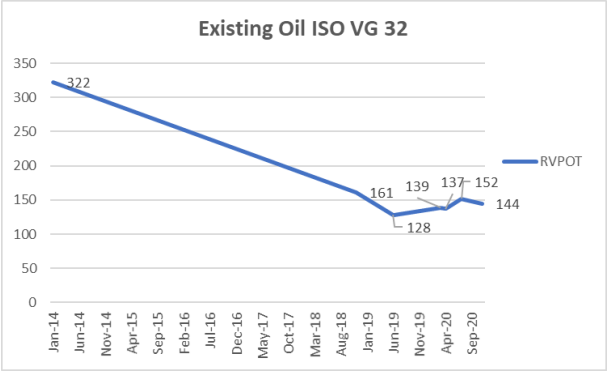

Figure 2: Trend Existing Oil ISO VG 32.

Based on figure 2. A sign of oil oxidation appears when the RVPOT value decreases. It can cause damage to the lubrication system in the future. To avoid this case, management decide to replace steam turbine oil with a higher RVPOT value. More RVPOT value can slow down the rate of oil oxidation and oil aging. Comparison of the specifications between the manual operation, the existing oil and the new oil may be seen in figure 3.

As a result, extend oil life and avoid a sudden damage. If no replacement is carried out, the risk of maintenance costs and downtime costs as follows, Total Downtime for six days plant shutdown is equal with downtime cost IDR 11,772,596. Cost for material oil and purifier task is IDR 600,000,000. If management doesn't take action in

this case, total losses cost will reach IDR 12,327,596,246. Based on analytical data and troubleshooting, management take an action to replace oil with the higher RVPOT and perform oil analysis quarterly. Oil replacement was carried out during the overhaul 2021. Based on Figure 4, during the monitoring period of steam turbines lubricant from 2021, Parameter in a normal condition. Viscosity did not significantly changes. In this research recommended alarm limit for viscosity change with percentage deviation from baseline, +5% for upper cautionary, -5% for lower cautionary, +10% for upper critical, -10% for lower critical. The second test is total acid number, TAN value moved within the recommended tolerance for steam turbine lubricant, Less than 0.5 mgKHO/g.

Aspect	Manual Operation	Existing Oil (Brand A ISO VG 32)	New Oil (Brand B ISO VG 32)
Kinematic Viscosity @40degC	28.8 cSt - 35.2 cSt	31.2 cSt	30 cSt
Viscosity Index	≥ 95	105	117
Flash Point	≥190° C	226° C	228° C
Pour Point	≥-10°C	-20°C	-30°C
Neutralization Value	≤ 0.3 (mg KOH/g)	-	0.1 (mg KOH/g)
Rust Prevention Test	Shall Pass	Pass	Pass
RVPOT		322 minutes	1000 minutes

Figure 3: Comparison of Oil Specification.

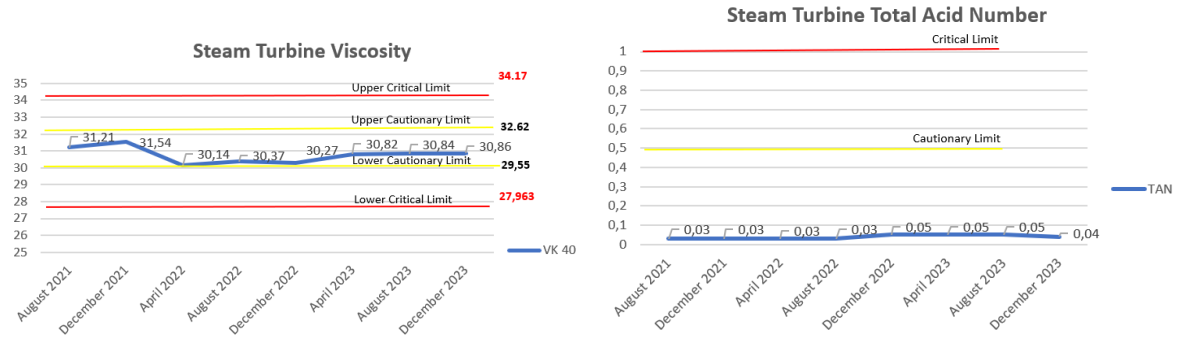

Figure 4: Trend of viscosity and TAN values change on Steam Turbine.

In line with other parameter, water content keeps on track below the alarm limit, in a lubricating system, the two most harmful phases are free and emulsified water. In a journal bearing on steam turbine, the incompressibility of water relative to oil can result in a loss of the hydrodynamic oil film that in turn leads to excessive wear. As little as one percent water in oil can reduce the life expectancy of journal bearing by as much as 90% (Hannon, 2022). The standard of water content on steam turbine is less than 500 ppm.

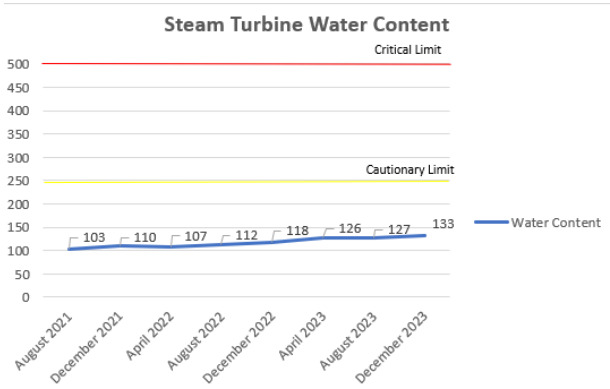

Figure 5: Trend of Water Content on Steam Turbine.

Since 2021, According to the figure 6. RVPOT value remains at 1360 and higher. RVPOT still corresponds to the value of the new oil analyzed. Performing RVPOT testing is recommended to be part of a complete test slate to helping evaluate condition of the fluid and the analysis should be supported with limit tip alarm limit and caution limit for early detection failure on lubricating system. Limit tip for cautionary limit is baseline RVPOT x 0.5 and limit tip for critical limit is baseline RVPOT x 0.4.

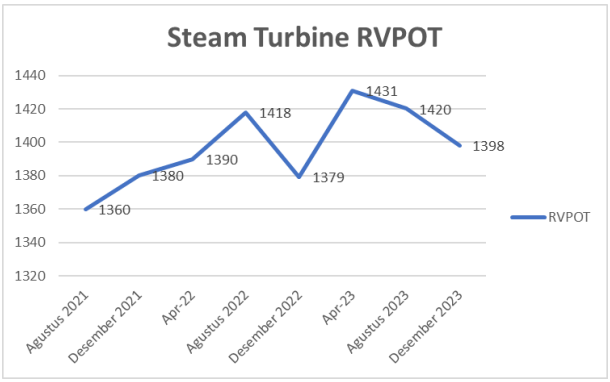

Figure 6: Trend of Steam Turbine RVPOT.

Considering of aging oil are associated with solid particle oil contamination. The solid particle test should be performed. During the research, the solid particle content did not significantly change and mostly constant within the permitted limits, solid particle content value from august 2021 to December 2023 according to the ISO 4406 solid particle test is 16/14/11 and it has not changed after 3 years of operation.

3.2 Improving oil replacement schedule on hot well pump from time based maintenance to the condition based maintenance.

According to the manual instruction maintenance hot well pump, oil filling of the motor hot well pump is changing every years, no matter what the condition of lubricant. Hot well pump oil analysis can't be performed because the sampling port on hot well pump is not available. For improving predictive maintenance task, sampling port should be installed, sampling port plays an important role in oil analysis program design repeatability data. Lubricant properties that can be used for oil drain according to condition based use viscosity properties, water content, Total acid number and solid particle content. The research mission is improving the oil replacement schedule and the two-year mission involved sampling and evaluating the lubricant every four months. if the oil drain carried out every year, resulting in 4 hours of downtime. If the production loss that occur is 60 MW/h, total production loss is 100 MW when performed oil replacement for each equipment. Patuha geothermal powerplant use two hot well pump with 100 % operation method. total maintenance cost and downtime cost that can be saved is IDR 723,840,000. the material for oil replacement that can be saved is IDR 10,000,000. In addition, this program can reduce the risk of waste oil due to replacing or drain oil according to the condition based lubricant. According to the figure 7. During monitoring the research since 2021, four main parameters in a good condition. Viscosity value didn't significantly change. Same as limit tip viscosity value on steam turbine, Hot well pump use alarm limit for viscosity change with percentage deviation from baseline, +5% for upper cautionary, -5% for lower cautionary, +10% for upper critical, -10% for lower critical. The second test is total acid number, the value TAN remains in a normal condition and less than the cautionary limit.

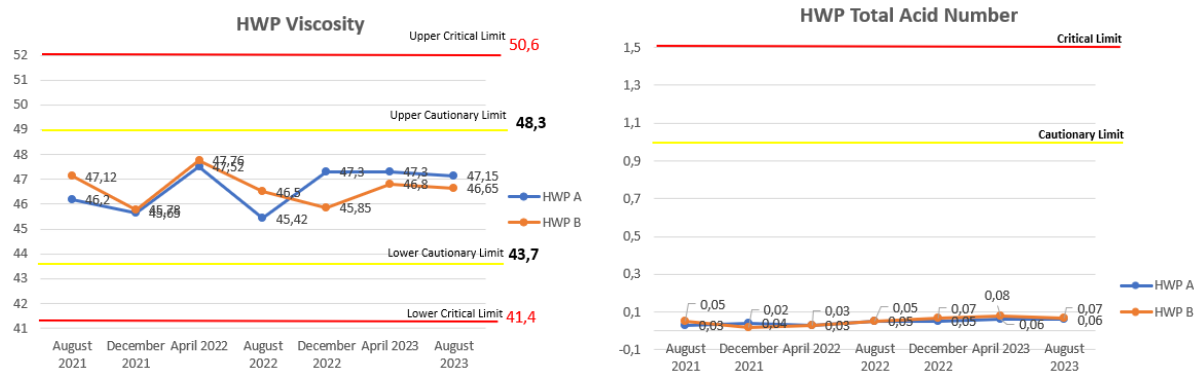

Figure 7: Trend of viscosity and TAN values change on Hot Well Pump.

The water content and solid particle content of the lubricant are the next to parameters to be examined. Under normal conditions during the experiment, the water contents was constant at 200 ppm, which is less than the 500 ppm cautionary limit for both hot well pumps A and B.

Solid particle content "hot well pump A" better one step particle contaminant than "hot well pump B", According to the ISO 4406, solid particle content for "hot well pump A" is 17/15/12, meanwhile "hot well pump B" has a 18/16/13. Even though the value are different, both equipment still in a good condition, Seen from the viscosity

value and TAN value didn't change significant. Because solid particle content is one of the contaminants that can increase a viscosity and total acid number in line with an aging oil.

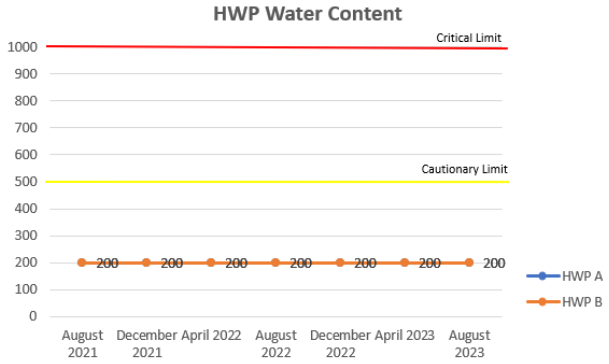

Figure 8: Trend of Hot Well Pump Water Content.

3.3 Improving base oil material on cooling tower gearbox because of high temperature operational.

Cooling tower is a specialized heat exchanger in which air and water are brought into direct contact with each other in order to reduce the water temperature. One of the Main equipment in cooling tower is Gearbox. Gearboxes are available in a variety of design and reduction ratios to accommodate the different fan speeds and horsepower of cooling towers. Gearbox that used in Patuha Geothermal Powerplant reduce rotation per minutes from 3000 RPM to 112 RPM. In accordance to the visual inspection result. Temperature of gearbox lubricant reach a maximum value above 82ºC and when inspect the internal gear, varnish formation starting to appear. Several corrective actions have been taken, but the oil temperature is still high. At this elevated temperature, viscosity to decrease, the lubricant film to become thinner, an acceleration in abrasion and scuffing conditions, the oil to age sooner, the additives to deplete quicker, an acceleration of corrosion, and the formation of sludge and varnish. The fluid film needs to be thick enough at operating temperature to separate the surface even under load, however, they should not be so thick that the parts have difficulty moving due to the viscous lubricant. The Arrhenius law states that with every increase of 10ºC in a lubricant's base temperature, oil life is halved (Whitby, 2022). Based on figure 9 & figure 10 below. the results of oil analysis, there was an increase value in water content and total acid number.

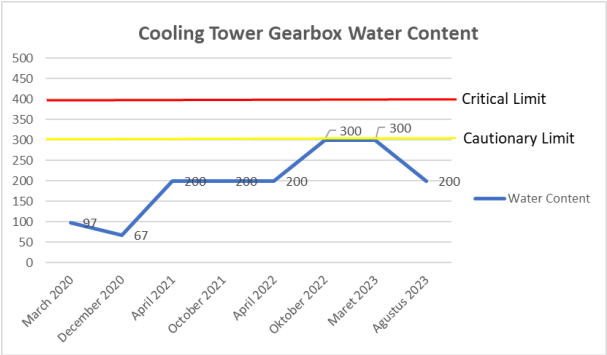

Figure 9: Trending Water Content on Gearbox.

Water content value continues to increase from 97 PPM to 300 PPM reached cautionary limit. In accordance with the result, management decide to take good corrective action starting with troubleshooting cause water system can be increases in the lubricating system. The presence of water in a lubricating oil can cause the progress of oxidation to increase tenfold, resulting in premature aging of the oil, particularly in the presence of catalytic metals such as copper, lead and tin. in addition, Certain additives such as sulfurous anti wear and extreme pressure type additives and phenolic antioxidants are readily hydrolyzed by water, resulting in both additive mortality and the formation of acidic by-products. Currently cooling tower gearbox use additive Extreme Pressure. Solid particle content for gearbox cooling tower according to the ISO 4406 is 20/18/15. Solid particle contaminant like dirt, metal particles, soft insoluble, and soot can affect to the change oil chemistry oxidation and additive depletion. In addition, chemically attacks machine surface one of the is adherent varnish. During the research period, TAN value moved within the recommended tolerance, however the trending of TAN is increasing. Most of acids in lubricating system are product of oil oxidation process or aging. Oxidation is the permanent degradation of a lubricant by chemical reactions involving oxygen. As oxidation progresses long chain molecules are produced, which lead to sludge, tars and varnish. Acids are produced which leads to corrosion.

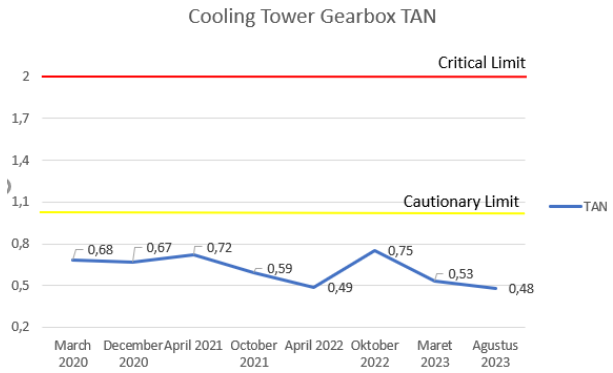

Figure 10: Trending Gearbox Total Acid Number.

From troubleshooting result, proactive maintenance was carried out. After that, execute study literature associated with lubricating system on cooling tower gearbox. In manual specification and standard, viscosity grade should be use ISO VG 220 complete with rust and oxidation additive but without extreme pressure additive. In case the temperature above 82° C, base material of oil must be use synthetic for base material of oil. Due to synthetic lubricant offer advantages of extended service life, a broader operational temperature range, reduce friction, and the ability to maintain a higher film strength which can extend service of life of the gear drive. Considering to the result of oil analysis and study literature about maintenance manual of gearbox cooling tower. Management decide to improving base material of oil from mineral oil to synthetic oil made from polyalphaolefins base stock. This is intended to reduce working temperature because the synthetic base has advantages in viscosity index and thermal oxidative stability. The viscosity index of an oil is the term used to express an oil's resistance to viscosity change as the temperature change. An oil that thins out significantly as its temperature increases is said to have a low viscosity index. An oil whose viscosity does not change significantly as its is heated up is said to have high VI. If the oils viscosity is to high with a low potential shear rate, the internal resistance to flow will increase the temperature dramatically, causing an overheated condition, which can also cause a breakdown of the oil film and may cause oxidation of the oil. beside that oil with lower viscosity and high potential shear rate must still maintain a sufficient oil film, it's quite apparent that as temperature rise, the oil film may fail and metal to metal contact may occur.

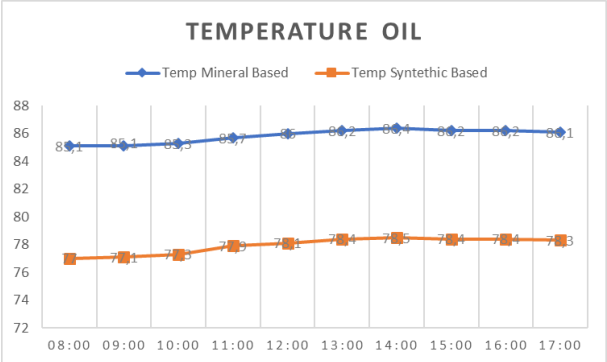

Figure 11: Temperature Oil Comparison.

After oil replacement has been done, there is a decrease in oil temperature around 6°C – 8°C. with these result the new oil expected to decrease the rate of oxidation and acid number, so that can extend service of life of the gear drive oil. Related to water content and solid particle contamination, management decide to install desiccant breathers. The desiccant breather can control of dirt and moisture ingress. A gearbox breakdown may happen if management keeps using mineral base oil and the operating temperature rises above 82°C. Potential maintenance cost and downtime cost as follows: IDR 200,000<000 for recondition the gear drives and 8 hours of downtime for cooling tower gearbox replacement. Eight hours of downtime results in a output loss of megawatts. Meanwhile total lost income up to IDR 11,440,000. this improvement is expected to extend replacement oil schedule from semiannually to every 2 years. It can be achieved if management perform oil analysis to determinant the condition of oil. perform oil replacement every two years can provide economically benefit as Figure 12.

According to the figure 12. The cost saving that can be obtained if management perform every two years oil replacement compared with semiannually oil replacement are IDR 19,208,106 for single unit cooling tower. The program can save around IDR 48,020,285 every years and IDR 96,040,530 every two years, if it's implemented for five units of the cooling tower. In addition to the financial aspect, there are several advantages that have an

impact on safety and the environment. The Impact on safety is increasing total safe working hours, this is related to work accident that may occur when conducting oil replacement. The impact on the environment is decreasing total oil waste. and also, the most important thing when base material has been upgraded to the synthetic based is all about operation and oil parameters. Gearbox can operate optimally according to the standard working temperature below 80^{o}C and prevent the gearbox from sudden damage which will impact to the maintenance costs and downtime costs.

Aspect	Mineral Oil	Synthetic
Period	2 Years	2 Years
Oil Replacement	4 times	1 times
Total Production Lost	IDR 25,472,261	IDR 6,368,155
Oil Replacement Cost	IDR 14,176,000	IDR 17,072,000
Waste Oil Processing Cost	IDR 4,000,000	IDR 1,000,000
Total Cost For 1 unit cooling tower	IDR 43,648,261	IDR 24,440,155
Total Cost For 5 unit Cooling tower	IDR 218,241,305	IDR 122,200,775

Figure 12: Table Comparison of oil replacement costs.

4. CONCLUSION

The poor lubrication and contamination control plays a key role in high downtime and high cost of business. such as unacceptable levels of downtime and lost revenue, high energy consumption, and high usage of consumable parts. To overcome these challenge this paper studies about condition based lubrication program. This program enables a user to have confidence in the quality of the lubricants in each machine and to help analyze the condition of the machine in its current state. Condition based lubricant can be used to determine when lubricant needs to be changed, so that its inferior properties of performance doesn't not impact the useful life of the machine. For achieving excellence in condition based lubricant program, analyzing the result of the routine test, using cautionary limits and critical limits, using trend graphs, will enable machines or equipment and system to be monitored effectively to determine both lubricant service lifetime. In this research three cases study were observed to prove that maintenance costs and downtime cost can decrease when implementing a condition based lubrication program. In the case of oil aging on steam turbine due to oil degradation, condition based monitoring oil analysis works in the troubleshooting process, problem solving and decision making. In addition, oil analysis can assist in continues improvement such as in the case of improving base oil material on cooling tower gearbox and extend service life of oil in hot well pump. The three cases studies above can reduce maintenance cost and downtime cost up to IDR 13,099,456,511. Establishing an effective condition base lubrication can start with small aspect, establish the methods, correct lubricant sampling methods and comprehensive testing are important for accurate data, data analysis with tip limit standard, reporting and corrective action, and then gradually expand the program integration with other condition monitoring program, expand the program as the cost-benefits become clear. The management should be commits and support, so that condition based lubrication program can running properly and can give benefit for the company.

REFERENCES

Keith, M : Maintenance Engineering Handbook Seventh Edition, Mc Graw Hill, New York (2008)

Ramesh,G., and O'hanlon, T. : Maintenance and Reliability Best Practices, Industrial Press, Inc., 989 Avenue Of the America, NY(2013)

Keith, M. : An Introduction To Predictive Maintenance 2nd ed., Elsevier Science, United States of America (2002).

Whitby, R.D : Lubricant Analysis And Condition Monitoring, CRC Press Broken Sound Parkway NW, United State Of America (2022)

Zhao, Y : Oil Analysis Handbook 3rd Edition, Spectro Scientific inc, Massachusset USA (2017)

Noria : Fundamentals of Machinery Lubrication, Noria Corporation, Tusla OK (2013)

Livingstone,G , Ameye J, & Thompson, B : Rethinking Condition Monitoring Strategies For Today's Turbine Oils, Noria Corporation, Tusla OK (2010)

Fitch, J : The effects of temperature on lubricants, Noria Coorporation, Tusla OK (2007)

NOMENCLATURE

Measurement Units

kW	kilowatts
MW	megawatts
cSt	centistoke
ppm	part per milion

Abbreviations

PdM	Predictive Maintenance
CBM	Condition Based Maintenance
ASTM	American Standard Testing and Material
ISO	International Standard Organization
MPI	Maintenance Priority Index
SERP	System Equipment Reliability Prioritization
HWP	Hot Well Pump
RVPOT	Rotating Pressure Vessel Oxidation Test
VI	Viscosity Index
TAN	Total Acid Number
R&O	Rust & Oxidation Inhibitor
IDR	Indonesian Rupiah

Geothermal Champaign a Success Story of GRE Pipe for Downhole Casing in Geothermal Well

Nico Riyanto

P.T. FUTURE PIPE INDUSTRIES, Talavera Office Park 8th floor, South Jakarta, Indonesia

n.riyanto@futurepipe.com

Keywords: GRE Pipe, Direct Use, District Heating, Composite Pipe

ABSTRACT

Glass Reinforced Epoxy (GRE) pipe is a composite material made of glass fibre filament and polymer resin that used as a binder. The usage of this material is mainly to substitute metallic material against corrosive environment such as water, CO2 and H2S. The main advantages of GRE pipe for geothermal application are its ability to maintain the flow without scaling and less maintenance required during the lifetime. However, there are also some limitations as of today on what GRE pipe can provide, especially on the temperature limit that can only reach up to 100°C and pressure up to 3000 psi. Most of the application of composite pipe is for the cooling tower pipeline system in geothermal power plant where it requires low temperature and pressure, but used as alternative of metallic pipe which might corroded over the lifetime.

This paper will provide the detail of GRE pipe for district heating in Champigny, France that has low enthalpy and water dominated reservoir. Compared to common steel pipe, GRE pipe can provide better OPEX that require less maintenance and work-over for the well. Furthermore, we might foresee the application of GRE pipe for different application in geothermal sector in Indonesia for its direct use such as agriculture, tourism, hospital, and other potential application that only require low enthalpy reservoir type.

1. INTRODUCTION

1.1 Glass reinforced pipe types

Glass reinforced pipe is type of composite pipe that use the glass fiber and plastic resin to create dense structure material with high resistance against corrosive fluid that might appear using metallic material. There are several types of glass composite pipe depending on the resin types and each of type has different application and advantages. Below is a short introduction of glass reinforced pipe.

Table 1: Types of Composite Resin and Its Application.

Resin Type	Advantages	Application
Glass Reinforced **Epoxy** (GRE)	High resistance against water, brine, H2S and gas	Pressure rate up to 3000 psi, Temperature rate up to 100°C
Glass Reinforced **Polyester** (GRP)	High resistance against water and brine	Pressure rate up to 60 bar, Temperature rate up to 60°C
Glass Reinforced **Vinylester** (GRV)	Better chemical resistance than Epoxy material	Pressure rate up to 60 bar, Temperature rate up to 100°C

The main material for fiber glass composite pipe is the silica filament fiber which provide the mechanical strength needed, while the resin is used as the binder of the filament and to distribute the load evenly throughout the filament structure. Depending on the degree of winding angle of filament wound, it will provide different characteristic of structural strength. Commonly GRE pipe is produced with winding of 55° to reach its optimum strength of 2:1 burst and tensile strength.

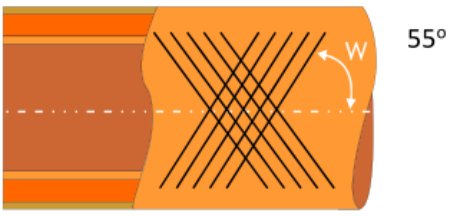

Figure 1: Winding Angle of Pipe Wall Construction.

1.2 Composite pipe manufacturing process and jointing system

Commonly there are several types of manufacturing depending on the application and desired structural strength:

1.2.1 Helical winding:

The silica fiber filament is dipped into the bucket full of resin as a binder. The filament is then winded with winding angle 55° around the mandrel as mould until it reached the desired thickness. The pipe then heated at temperature up to 160°C to cure the resin until harden. This type of manufacturing process normally produce glass reinforced epoxy (GRE), glass reinforced polyester (GRP) or glass reinforced vynilester (GRV). Due to the mandrel available, the pipe dimension can be produced up to 48inch.

1.2.2 Continuous winding:

Using chopped fiber glass that pour into the mandrel. Resin and topcoat material then added on top of the fiber glass. Sometimes silica sand also added to increase the stiffness. Normally using polyester or Vynilester resin type that is self-cured once mixed. The pipe diameter that can be produced by this process from DN 300 up to DN 4000 which it has high productivity rate for larger diameter than helical winding process.

Once manufactured, the pipe will be jointed depending on the design and condition. There are several types of jointing system for composite pipe as per figure 2 depending on each application such as the design pressure requirement and field utilization. The mechanical joint, such as thread and couple joint, integral joint, and flange joint, have better mechanical strength compared to the other types of joint. However, the strength is compensated with the need of thicker pipes than adhesive or lamination joint.

Figure 2: Helical winding machine.

1.3 Composite pipe application and advantages

The main application of composite pipe is used as an alternative solution of corrosive environment that can't be overcame by metallic material such as carbon steel and stainless-steel material. There are several advantages of composite pipes compare to other metallic materials such as:

- Longer lifetime up to 30 – 50 years design lifetime since it's not corroded overtime.
- Less maintenance required since no scale build-up and no corrosion appear during the life application that leads to less operation expense.
- Less weight than metallic material which leads to better logistics and delivery process to remote area.

Due to those advantages, the application is various even more for the application that has high water content which is the main factor of corrosion for metallic material. One of the potential usages is the geothermal well for production casing and we had one example of success story in Champigny Sur Marne, France for the application of GRE pipe casing with high water content and high salinity which highly corrosive for carbon steel material.

Figure 3: Continuous winding machine.

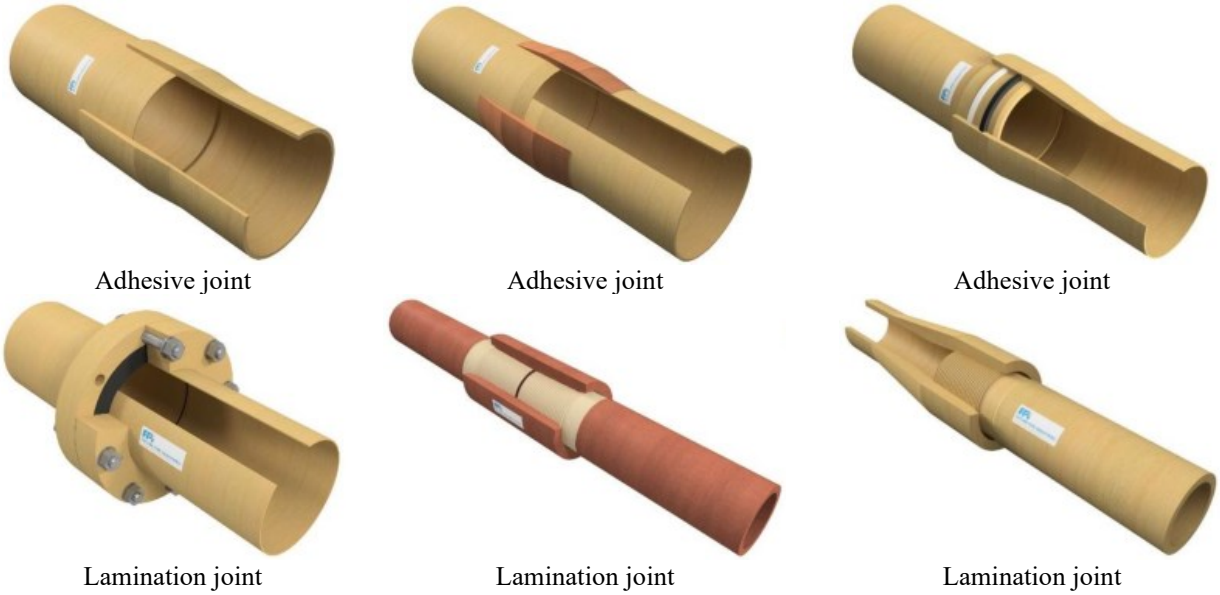

Figure 4: Types of jointing system for composite pipe.

2. GEOTHERMAL CHAMPIGNY-SUR-MARNE PROJECT OVERVIEW

2.1 Project Background

Group Coriance is a French company that focusing to achieve green energy provide for communal and industrial application. The company has been established since 1998 as subsidiary of Gaz de France to operate geothermal networks for Meaux (41km east from Paris) and Fresnes (12km south from Paris). One of the main services is direct heating using geothermal energy for the habitant area and for industrial application. Since then the company also provide other source of energies such as biogas, biomass, and energy recovery from the industrial area below are several projects that has been done:

- Geothermal for district heating 10 projects
- Biomass for power plant and heating 18 projects

- Biogas 1 project and
- Energy recovery from biomass and waste treatment 4 projects

2.2 Well parameter and casing design

The project was done in 2023 operated by Group Coriance in France who is operated to provide heating network in the area. The initial project was done in 1983 for the first geothermal well in Champigny Sur Marne and it has been operated as heat source for 5,477 habitants which account for 75% of the heating by renewable energy. The characteristic of the reservoir as per table 2 below.

Table 2: Well parameter. Bureau de Recherches Geologiques et Minieres (1984).

Description	Remarks
Bottom Hole Temperature	80°C – 90°C
Well Head Temperature	68°C – 72°C
Injection Well Temperature	40°C
Total depth	1,805m
Production rate	350 m3/h water dominated
Fluid type	high water salinity 150 g/L of equivalent NaCl (common sea water at 35 g/L NaCl)
Reservoir formation	limestone with 14% porosity

Future Pipe Industries supplied the material of casing GRE pipe to General Tubular Services Gmbh as the sub-contractor which running the downhole casing pipe. There are 2 wells drilled for this project which are production and reinjection well, the well schematics of the 2 wells are similar as summarized in the table 3.

Table 3: Casing design.

Casing Section	Casing Specification
Conductor Casing	18-5/8” 87.5# K55 Buttress Connection, Depth 130m
Intermediate Casing	13-3/8” GRE pipe 750psi 4RD connection, Depth 400m
Production Casing	10” GRE pipe 1000psi 4RD connection, Depth 1000m
Production Casing liner	7-5/8” GRE pipe 1000psi 4RD connection, Depth up to 1800m

2.3 Rig running process

The connection type offered is 4RD connection type which is a FPI’s patented connection that has 4 thread per inch (TPI) on the thread profile for faster rig running and better mechanical strength. Considering the pipe wall thickness of GRE pipe is thicker than metallic pipe, the hole section and OD diameter of pipe should be determined further to get a better clearance. Future Pipe Industries also in coordination with running services to design several accessories equipment such as cross over, centralizer and other downhole equipment to be compatible with GRE pipe. Another solution to reduce the clearance is to use carbon filament rooving that has better mechanical strength and temperature resistance than silica filament rooving. Using this material as a coupler can reduce the pipe wall thickness significantly.

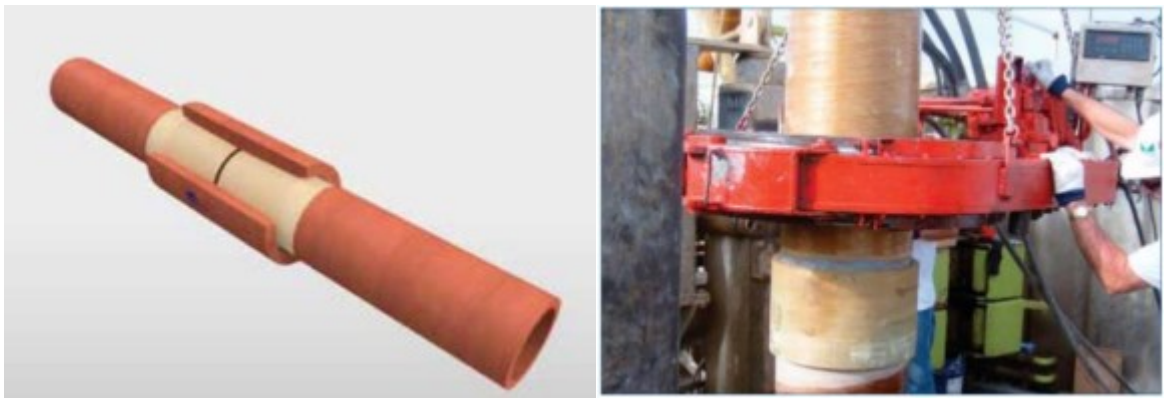

Figure 5: GRE pipe with thread and couple connection (left) and rig Running on the field (right).

Figure 6: Application of thread sealant on pin and box.

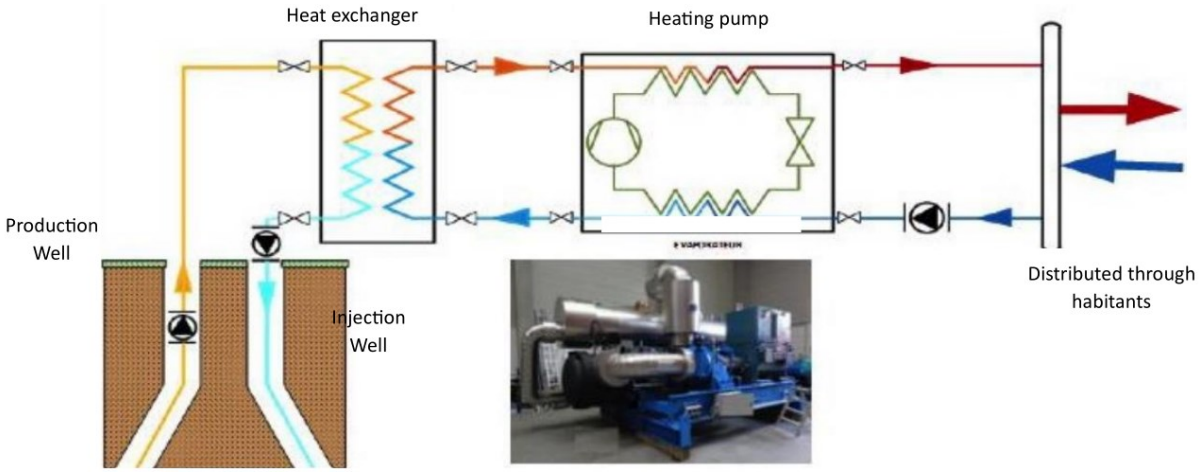

Figure 7: Project layout.

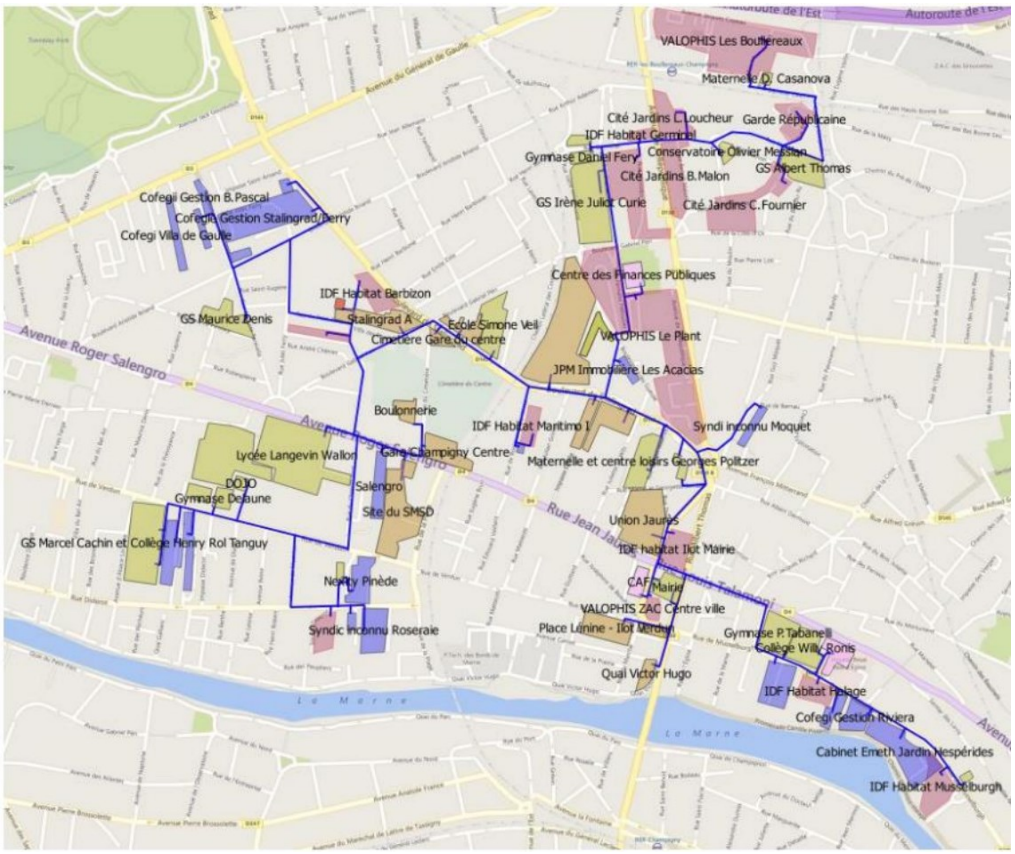

Figure 8: Pipeline distribution around the habitant (up to 9km pipeline).

The running process of GRE pipe is a little bit different compared to common metallic pipe. Normally metallic pipe require grease to be applied to reduce friction, while GRE pipe require sealant on thread for permanent casing application to increase the jointing strength. The thread sealant should be applied on both pin and box and combed evenly throughout the thread surface.

2.4 Project layout and result

The production fluid is then circulated into the heat exchanger which then the heat will be circulated with heating pump to habitants in the area. The production fluid will be reinjected into the earth to be circulated and maintain the pore pressure. Figure 7 and figure 8 describes the project layout and the heating distribution throughout the habitants.

The project is quite successful that it reduces the carbon emission by 9,500 tonnes of CO2 each year compared to common natural gas heating source. The use of GRE pipe material is also reducing the maintenance and workover required during operation which also leads to increase the productivity rate of the well. Since the successful project in 2023, FPI received another continuous order from Groupe Coriance for another field for similar application in France in 2024.

3. POTENTIAL USE OF COMPOSITE PIPE IN INDONESIA GEOTHERMAL

3.1 Direct use potential application

Indonesia geothermal application is mainly for power generation since its location is within the ring of fire. The common temperature required for power generation application in Indonesia can reach above 250°C which is too high for composite pipe to reach. However, there are several potential applications for low enthalpy geothermal that can be used for direct use other than communal heating such as agriculture, fishery, hospital, and recreation. Below are some example and application based on the temperature of production well:

- **Aquaculture and fish farming**. Maintaining specific water temperature is a challenge in aquaculture and fish farming industry where it can impact the yield rate and quality of fish produced. Low enthalpy geothermal well with temperature range between 30°C – 50°C can be a solution for this application since the temperature can be maintained 24/7 with very low carbon footprint. Indonesia as maritime country has high potential for this application since it has wide biodiversity that can harness further the potential and improve the quality.
- **Industrial processes**. Several industries will require heating such as food drying, pasteurization and sterilization which require heating process. Geothermal energy can be used and integrated in the process to reduce the use of electricity that heavily used in the application. Several industries such as food processing, pulp and paper, textile manufacturer can be benefited for such application. Even though the initial capex is high, the operation and maintenance required with geothermal will provide better total operating cost. The temperature required for this application is various from 50°C for drying and washing, up to 120°C for sterilization.
- **Greenhouse cultivation**. This application is similar to aquaculture, greenhouse cultivation can benefit further with the well maintained and controlled temperature from geothermal well. The optimal temperature maintained by geothermal heat source can increase the crop yield, growth and provide uniform produce. Several countries such as Netherland has embraced this application to increase their agricultural cultivation such as potato, tulips, etc which is quite important for 4 seasons countries such as Netherland to be able to maintain the optimum temperature throughout the year. Indonesia can also be benefited further with this application to increase the crop yield on the lack-fertilized field. Furthermore, with the current condition of global warming, where the temperature has increased significantly and extended dry season throughout the year, this can impact the production.

The economics of scale for those applications needs to be determined further since the utilization is not to generate power, then it needs to convert the equivalent to the power replacement. However, the recent study shows that between 2010 to 2020, the application of direct use geothermal has increased from 400 petajoule/year to 1,000 petajoule/year which increase over doubled in the duration of 10 years. Most of it used for district heating (80%), bath and recreation (15%), and agriculture and industry (5%). The main driver of this increments due to several factors such as:

- Sustainable and clean energy
- Reliable 24/7 throughout the year
- Affordable in the rural area
- Independent heat source

There are several challenges to realize the direct use of geothermal as per below:

- High CAPEX that upfront that needs to be prepared. The highest factors are drilling process and equipment, infrastructure and heating distribution.
- High OPEX which include maintenance and potential workover during the life cycle of the well is also another challenge that need to be addressed.
- Geothermal wells are very dependent on the location of the heat source. Green field will require exploration process to understand the geological structure which an additional cost that might not be recovered if the location is not suitable.
- Some countries or location has cheaper substitute source of energy such as fossil fuels, solar energy, or wind energy that might generate higher energy source.

Figure 9: GRE pipe as cement stinger application in oil and gas field.

3.2 Other potential application of composite pipe in geothermal sector

There are other applications of composite for geothermal sector which can be a better choice compared to common metallic pipe. Below summarize the application and advantages with composite pipe compared to metallic pipe:

- **Cooling tower in power plant**. Operating temperature can be up to 70ºC and dimension requirement up to 1.8m will be challenging to install when using metallic pipe. Not to mention the production of large diameter pipe is expensive, the logistic and installation process in remote area will increase the cost even more. Additionally, the fluid water for the cooling tower can heavily corroded when using common steel pipe that increase the cost for repair and replacement during the life cycle which add the operation cost.
- **Reinjection pipeline**. The reinjection pipeline from power plant to the water injection well can provide additional benefit by using composite pipe. There are 2 main benefits for this application.
    - The installation process of GRE pipe is easier even in the remote and mountainous area due to its density is only 25% of steel pipe density. This can lead to better loading and unloading on the site, faster process, and better safety risk.
    - Corrosive resistance of composite pipe against water can provide better operational cost (less maintenance and inspection) which lead to lesser frequency of shut down the well due to inspection, maintenance, and replacement process.
- **Cement stinger**. Geothermal well normally require high permeability to assure the heat flow and production of steam are promising. This condition is quite challenging with cementing process where imperfect cementation can cause collapse built-up which can damage the casing pipe and lead to pipe failure, even more in Indonesia which has high temperature up to 350ºC. Therefore, one of the solutions is to use quickset cement type that can easily harden once set-up. The challenge of quickset cement type is it can harden inside the pipe ID and can causes stuck on the pipe (normally drill pipe), this leads to problem to retrieve the pipe and fishing, even more it can lead to abandoning the pipe. Composite pipe

can be a solution for this application since the pipe can be used as sacrificial pipe that can reduce the rig running time when there is a pipe stuck inside the well. Whenever the quick-set cement hardens inside the pipe, composite pipe can be drilled-out (penetration rate up to 80ft/hour) and the well can continue for the next stage of operation.

4. CONCLUSION

The application of composite material in geothermal sector has several advantages due to its high corrosion resistance against water and brine water which can reduce the operational expense compared to conventional steel pipes due to its frequent maintenance and inspection. However, there are several limitations of glass fiber composite pipe in geothermal sector which is the high temperature. Up to today the application of glass fiber composite pipe can only reach up to 100ºC of operation temperature, which is very low for geothermal well for power generation which can reach up to 350ºC (highest record can reach 400ºC).

There are several other applications where composite pipe is suitable option such as:

- Direct use geothermal well which has operation temperature up to 100oC.
- Cement stinger for quickset cement type to reduce the risk of well abandon.
- Reinjection pipeline from sumpit or power plant to injection well.
- Cooling tower in geothermal plant which can provide better value due to its corrosive resistance and lightweight.

Based on the result of geothermal application in Champigny which shows high potential application, there is also some potential application of direct use of geothermal in Indonesia. There are several studies that shows its potential, but the main challenge is how to articulate the economics of scale from conventional energy source to geothermal source.

REFERENCES

Al Asy'ari, M., Adityatama, D., Brilian, V., Erichatama, N., Purba, D.: Beyond Electricity: Geothermal Direct Use Business Models and Potential Applications in Indonesia. PROCEEDINGS, 49th Workshop on Geothermal Reservoir Engineering Stanford University. Stanford, California: Stanford University. 2024.

Aljuzayri, M., Corona, M., Franco, M., Alzlfawi, A., et. al.: Curing Total Losses Via Placement of Aggressive Cement Recipe Trough Sacrificial Fiberglass Pipe, SPE-216975-MS, Paper presented at the ADIPEC, Abu Dhabi, 2 – 5 October 2023.

Bureau de Recherches Geologiques et Minieres: Projet Geothermique De Champigny-Sur-Marne. Paris. 1984.

Mission Regionale d'Autorite Environnementale: Avis délibéré en date du 3 septembre 2020 de la Mission régionale d'autorité environnementale d'Île-de-France sur la réalisation d'un doublet géothermique dit "Champigny-sur-Marne/Rousseau" à l'aquifère du Dogger, dans le cadre de la demande d'autorisation d'ouverture de travaux miniers géothermiques sur la commune de Champigny-sur-Marne (94). Paris. 2020.

U.S. Department of Energy: Geothermal Technologies Program. Energy Efficiency and Renewable Energy, Washington, 2004.

World Bank Group: Direct Utilization of Geothermal Resources, ESMAP Technical Report 21/22. Washington. 2022.

Avoiding Stuck Pipe Incident Through Effective Management of Metasedimentary Rocks in Geothermal Drilling

Gatra Kusuma, Umar Sidiq, Rully Putradi,
Komang Wisnu, Wahyu Sutresno, Tesha, Timora, and Hargi

Pertamina Geothermal Energy - SLB

GKusuma@slb.com, umar.sidiq@pertamina.com, rully.putradi@pertamina.com,
kmurti@slb.com, wahyu.sutresno@pertamina.com

Keywords: metasediment, geothermal drilling, stuck pipe, fracture, cost, drilling

ABSTRACT

Drilling formation along with fracture network and metasedimentary rocks in accessing reservoir process is known as the one of the greatest challenging tasks in Sumatra geothermal drilling operations. The associated formation risks in drilling operations causes total loss of circulation, well control problems, hole instability, drilling dynamic issues and several stuck pipe incidents that lead to loss in hole BHA. With the understanding that the interaction between each element within the drilling operation system, including rock mechanics, drilling parameters and drilling fluid properties, can be known well by each work function. Unfortunately, in the process of achieving the goal and hitting the target there are still shortcomings in understanding the behavioral differences of penetrated formation.

Operations safely is a key factor in making the entire process safe, economical, and environmentally friendly. Indeed, the primary objective is to overcome these risks and necessary to ensure the borehole can be drilled safely and meet the Well objectives/target. The concern arises regarding the phenomenon that occurs is the difficulty in estimating drilling mud due to fluid's transmissibility is very unpredictable. Considerable non-productive time has been recorded due to hole cleaning issue and packing-off then causing stuck pipe event. In addition, partial to total loss circulation occurs when drilling reservoirs section adding the complexity of the problem. Realizing that continuing to drill development wells using conventional drilling practices in the same manner and expecting different results is not a solution. Hence, drilling development well in the same field will repeat the same problems to be occurred.

The objective of this study is eliminating stuck pipe events and enhancing drilling efficiency, particularly in wells where metasedimentary formations are present. By collecting data from offset wells to design and build qualitative parameters to ensure drilling operations run flawlessly. Design begins with selection process review of available information in the area based on the results of sonic logs, lithology, and subsurface modeling to get the best offset well candidate. The categories on which information is collected must have empirical correlation to fill in zones of missing and/or poor-quality result well. The emerged empirical correlation will be developed to obtain strategic needs. Every single element in the drilling function from trajectory, bottom hole assembly, drilling parameters, remedial work and escalation plans resulted in successful and safe drilling of metasedimentary formation moreover reduce drilling time and being ahead of plan in recent wells.

1. INTRODUCTION

In several areas of Sumatra where geothermal drilling operations take place, metasedimentary rocks are commonly encountered when drilling through the reservoir section. In general, metasedimentary rocks are metamorphic rocks that originate from the transformation of sedimentary rocks under conditions of high temperature and pressure deep in the earth's crust. They are characterized by features such as foliation, where mineral grains align in parallel layers. These rocks exhibit varying degrees of hardness, abrasiveness, and structural integrity depending on their specific type.

The identified characteristics of metasedimentary formations will notably impact drilling operations. Formation hardness and abrasive nature of metasedimentary rocks can lead to accelerated wear on drilling tools and equipment, increasing the risk of mechanical failure and operational downtime. Additionally, the presence of foliation planes in metasedimentary rocks creates planes of weakness where rocks can cleave or fracture easily, potentially causing instability in the wellbore and increasing the likelihood of stuck pipe incidents.

Stuck pipe incidents in metasedimentary formations often occur due to abrupt changes in rock hardness, encountering foliation planes, or inadequate drilling practices. To prevent and mitigate these challenges, thorough geological assessment and planning are essential before drilling commences. Employing appropriate drilling techniques and equipment, such as robust drilling fluids and wellbore stability analysis, helps manage the variable

conditions encountered in metasedimentary formations. Continuous monitoring of drilling parameters and real-time data analysis can aid in early detection of potential issues, allowing for prompt adjustments to drilling operations to prevent stuck pipe incidents. Furthermore, investing in advanced technologies and training programs that focus on geomechanically understanding and drilling optimization contributes to safer and more efficient drilling practices in metasedimentary environments.

2. PROBLEM AND CHALLENGE

Geothermal drilling presents unique challenges and risks. If not effectively managed, these risks can lead to high impact event, i.e stuck pipe, which prolongs the drilling process. This extended duration directly increases costs due to higher consumption of resources such as consumables, drilling mud, and bottom hole assembly. Additionally, encountering obstacles such as wells failing to reach target reservoir depths adds to these costs.

In figure 1 illustrates that high impact events and additional time during drilling account for around 50% of the total time spent in the process. Majority of these issues stem from unpredictable conditions within the drilling holes, resulting in significant time losses categorized as high impact event. The dynamic changes in drilling hole conditions especially in reservoir section with the exist of metasediment formation necessitate rapid decision-making. The metasediment formation in this field is the main factor causing stuck pipes incident. The efforts to free the pipe and conduct new drilling process(side track) take a very long time with an uncertain success rate. Therefore, accurate field data is crucial to support agile and informed decision-making throughout the drilling operation.

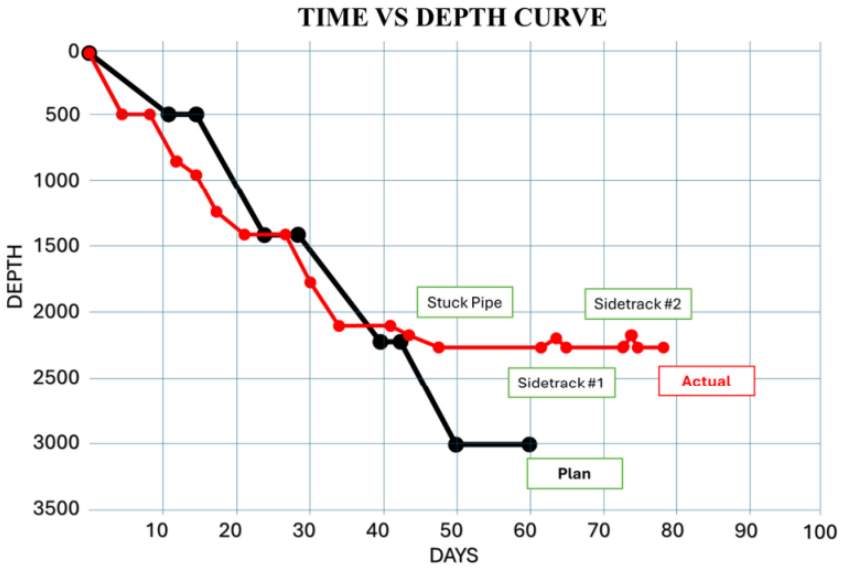

Figure 1: Time vs Depth Curve.

Knowing which processes consume the most time is crucial because inefficiencies can lead to significant additional costs. Stuck pipe and remedial action exacerbate these costs and contribute to company losses that must be addressed. Based on the background above, the main focus of this research is the need to improve the operational model due to the negative impacts caused by these challenges. The development of this model aims to minimize or eliminate the impact, thereby reducing its detrimental effects and enhancing the overall effectiveness of the drilling process.

2.1 Stuck pipe and Hole Problems

Drilling operations encounter numerous challenges due to highly dynamic conditions, resulting in increased effort, time, and implementation costs. For instance, the red curve in figure 1 illustrating actual time which shows no progress in depth increase over consecutive days, highlighting significant inefficiencies. Failing to reach the target depth underscores a clear discrepancy between the objective and actual performance.

Target implementation time or working days during drilling activities for the development of the Well based on the Program were completed within 60 days, however the actual implementation was 89.25 days. Meanwhile, the target depth achieved is shallower than the 3000m as per initial program, namely 2274m. The decision to complete drilling at a depth of 2274 m was due to the many drilling problems occurred. The main problem that caused the delay in drilling time for the subject well was the presence of a metasedimentary zone which prone to collapse and lead pack off at a depth of 2220 to 2274m which resulted in frequent stuck pipe event and require sidetrack drilling.

2.2 Prolonged Flat Time

Basically, the well construction involves two primary phases: on bottom drilling and flat time, where the depth of the hole remains unchanged. Activities during flat time include tripping, casing and liner installation, cementing, etc. These activities contribute significantly to the total time spent as clearly shown in figure 2 where the portion of time breakdown is dominated by flat time. Therefore, any problem during these activities can extend the overall well conditioning time or vice versa, problems during drilling will create additional sequence for flat time activities. Proper strategy at the planning stage, thorough preparation, and clear procedural instructions are essential to optimize flat time activities and reduce such potential delays.

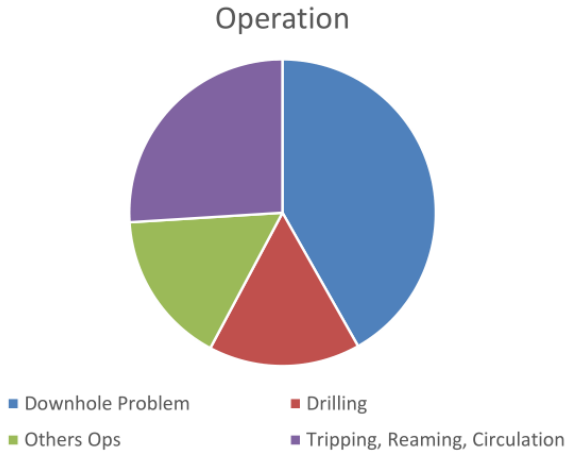

Figure 2: Operation Breakdown.

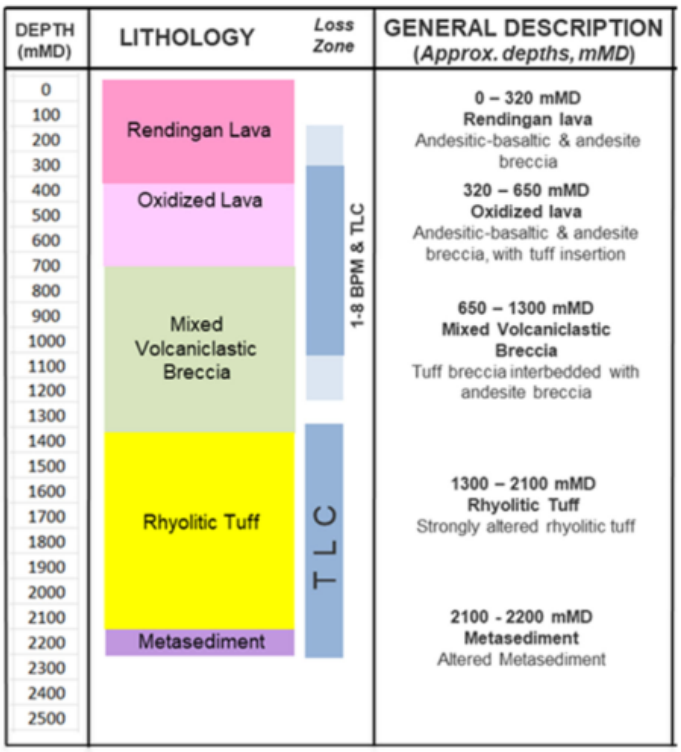

Figure 3: Formation Prognostic.

These operational hurdles severely impede the company's ability to achieve its goals efficiently. Figure 2 illustrates this with a significant percentage of work dedicated to unproductive activity, sidetracking and making a new path. This discrepancy underscores the need to explore the pack off phenomenon and devise strategies to address it. Thus, it is expected that inefficient activities which led remedial actions required to address issues is avoidable.

3. METHODOLOGY

Drilling for geothermal energy in Indonesia poses significant challenges, primarily due to widespread reservoirs with loss circulation during drilling. These fields are located in varied geological environments across the country, each posing distinct challenges for drilling activities. Stretching from North Sumatra to East Java, these geothermal fields can experience severe loss circulation, sometimes leading to complete losses.

3.1 Risk Identification

To successfully drilling and reach target through sedimentary rocks environments, specific strategy needs to be addressed in planning stage to overcome and reduce the severity of impact based on risk identification.

Registered risk include:

- Prognostic data: Identifying the concern depth of metasedimentary rocks presence during drilling and its respective hole section are derived from subsurface data as shown in Figure 3.
- Drilling Parameter: Utilizing offset well data to identify the implication of applied parameter within concern depth interval.
- BHA Configuration: Reassessing used BHA drilling that adding potential and/or limitation issue while penetrating the problem zone.

3.2 Planning and Simulation

The derived simulation from prognostic profiles and optimized using offset well data provides a detailed circulation ECD profile during drilling operations, as illustrated in Figure 4. The most accurate/precise simulation results play a critical role in assessing the feasibility of drilling strategies and equipment funding for successful geothermal drilling operations. By obtaining information related to ECD expectations obtained during the drilling process, drilling parameters can be monitored and adjusted during the next execution phase. The obtained ECD value will be used as a benchmark to be achieved during penetration of metasedimentary formations.

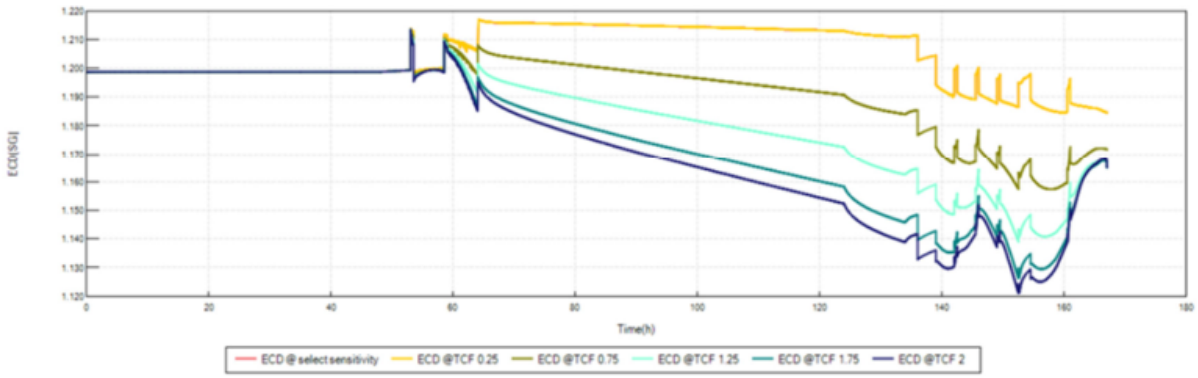

Figure 4: Prediction and Simulation ECD Profile.

By leveraging advanced modeling techniques, such as those integrating historical data from offset wells, drilling engineer and stakeholders can make better decisions that mitigate risks and optimize operational efficiency. Based on Thermal Calibration Factor(TCF) sensitivity, predicted ECD value will help executor during drilling.

Furthermore, these precise simulations not only enhance operational planning but also contribute to cost-effectiveness and project viability. This proactive approach not only instills confidence in stakeholder and executor of robust simulation methodologies remains essential for driving innovation and achieving sustainable success in geothermal drilling.

3.3 Drilling Strategies in through metasediment

Effective drilling strategies are essential when operating in metasedimentary reservoir sections. One approach is to use a combination of high-viscosity drilling mud and aerated fluids to increase the carrying cutting capability. The expected ECD value from simulation results becomes the basis of information/parameters to adjust drilling parameters by monitoring real-time ECD from the MWD tool. By having this practice, the fluid in the annulus able to maintain borehole integrity and prevent cuttings from falling/pack into BHA, thus drilling process going safely and smoothly to the intended target depth.

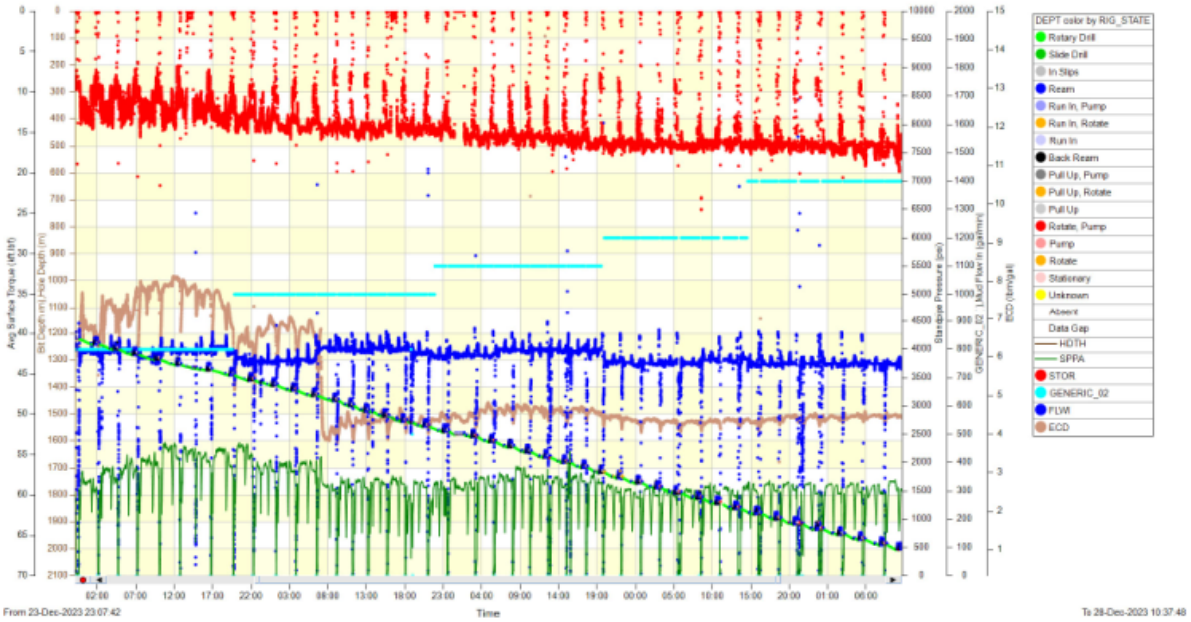

Figure 5: Drilling Parameter Monitoring.

Another strategy involves intermittent drilling, where the operation is paused periodically to allow the cutting away from BHA, thereby extending the operational flawlessly. Specific drilling practices must be implemented, which practices include:

- Circulation Management: Maintaining an optimal mud circulation rate to allow cutting move up to surface and going to fracture/loos zone.
- Monitoring: Continuous monitoring of surface and downhole measurements to anticipate and address potential problem before they occur.
- Adaptive Strategies: Implementing flexible drilling strategies that can be adjusted based on real-time data from the drilling operation as shown in Figure 5.

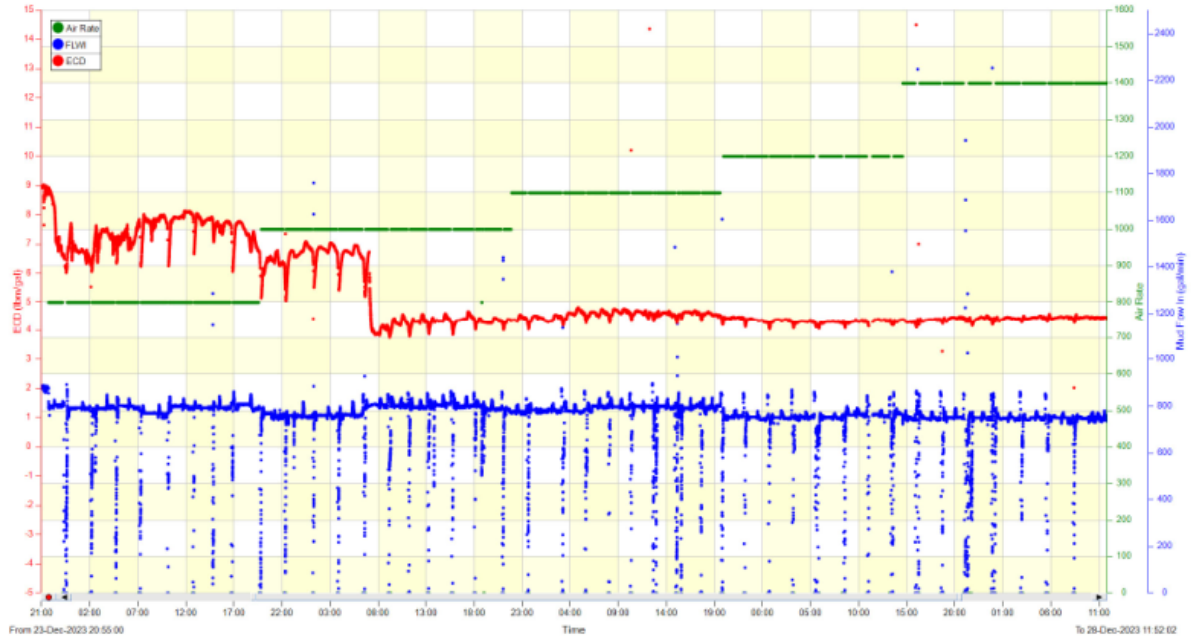

Figure 6: Managing Down Hole Pressure.

4. RESULT AND DISCUSSION

4.1 Actual Circulating ECD Profile

Field data shows that maintaining an optimal ECD profile is crucial for the success of geothermal drilling operations especially in penetrating sedimentary rocks as shown at Figure 6

By carefully managing the circulation rate, combination on pump rate of Mud and Air it is possible to keep the down hole pressure or ECD in the wellbore within a range that is safe for drilling operation. This practice helps in confirming the surface measurements and downhole condition which is annular around the BHA.

4.2 Supporting Operation

To ensure smooth and efficient drilling operations, it is essential to have clear contract requirements that support the use of downhole measurements to support drilling operation. These requirements should include provisions for:

- Downhole Annulus Pressure: Agreements on using and monitoring parameter based on downhole measurements as a surface reading confirmation.
- Operational Flexibility: Allowances for adaptive drilling strategies based on real-time data.
- Plan to action: Clear instruction and procedure from the stakeholder to the executor.

4.3 Operational Efficiency

- Eliminate Non-Productive Time (NPT): Stuck pipe event and side tracking can lead to significant non-productive time (NPT), where drilling operations are halted for remedial working. This not only increases operational costs but also delays project timelines. As an implementation result can be seen in Figure 7 where the actual progress much faster compare to the plan with 19days save time.

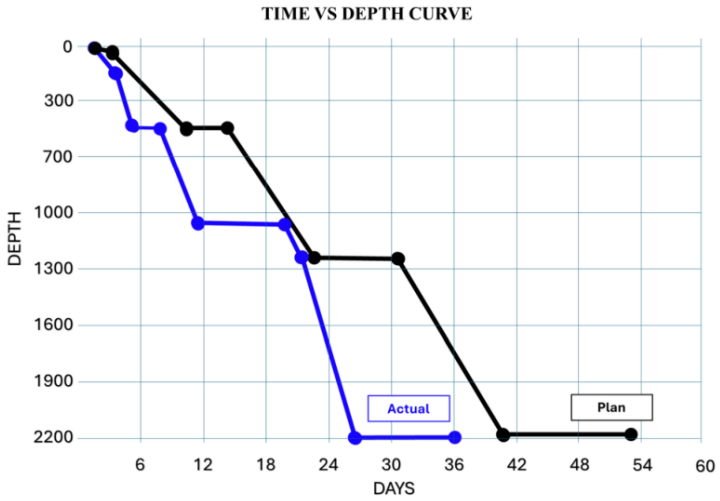

Figure 7: Operational Efficiency.

- Parameter Adjustment: Managing the metasedimentary drilling requires effective combination strategies, such as optimizing aerated mud circulation rates and using downhole pressure sensor. These measures are essential to maintain the integrity of the annulus so as not to complicate the drilling process and increase operational complexity.

5. CONCLUSION

Geothermal drilling in losses circulation with metasedimentary rock presents unique challenges that require innovative approaches and robust risk mitigation strategies. While complex drilling environment necessitate the exploration of alternative methods, using downhole measurements offer reliability with specific drilling practices provides a viable solution, enabling efficient and safe operations while controlling costs. By having engineered approach, integrated simulation, monitoring and implementing comprehensive risk mitigation strategies, it is possible to overcome the challenges of geothermal drilling through sedimentary rocks.

REFERENCES

Kiran, Raj. Application of machine learning and well log attributes in geothermal drilling. 2022. doi.org/10.1016/j.geothermics.2022.102355

R Pessier and M Fear, “Quantifying common drilling problems with mechanical specific energy and a bit-specific coefficient of sliding friction”, SPE paper no. 24584, presented at 67th SPE Annual Technical Conference and Exhibition, Washington, DC (Oct 1992).

Rehm, B., McClendon, R., & Miglierini, G. (2009, January). Circulating fluid losses during drilling operations. In SPE/IADC Drilling Conference and Exhibition. Society of Petroleum Engineers.

Zhu, Shuo. Intelligent Prediction of Stuck Pipe Using Combined Data-Driven and Knowledge-Driven Model. May 2022Applied Sciences 12(10):5282. DOI:10.3390/app12105282

A Value to Reduce Overall Geothermal Cost – Unified Well Construction

Gatra Kusuma, Ridha Budi, Doddy Darmawan, Komang Wisnu, Aufy, Hargi, and Timora

Star Energy Geothermal - SLB

GKusuma@slb.com, ridha.nugraha@starenergy.co.id,
doddy@starenergy.co.id, kmurti@slb.com, anvg@starenergy.co.id

Keywords: geothermal drilling, optimization, cost reduction, performance drilling, cost, drilling

ABSTRACT

The very aggressive development of geothermal assets requires innovative solutions to overcome the complexity of the drilling process. As global interest in environmentally friendly energy increases, geothermal challenges need to be addressed. The unique challenges often faced in geothermal drilling are harsh environments, fractured formations, and highly dynamic operations. Short drill bit life, low penetration rates, and equipment failure are common problems, coupled with reduced drilling fluid properties and difficulty in managing mud systems.

Understanding and mitigating these technical challenges is critical to minimizing risk and increasing economic viability. Experience and knowledge from the oil and gas industry is invaluable in dealing with drilling challenges. While some strategies may prove effective, others lead to inflated costs. Adapting drilling methodologies and systems to the unique geothermal environment is critical to optimizing drilling projects and controlling costs. especially demanding drilling conditions require great effort, energy and strategic thinking.

This paper highlights the value of unified well construction for managing and consulting in improving drilling performance and reducing costs. During a three-year Geothermal Project in West Java, Indonesia, 70-75% reduction in well costs per meter resulted in millions of dollars in savings through knowledge management and accelerated learning.

1. INTRODUCTION

There has been a steep increased in drilling activity happening over the past years in search of geothermal energy. As the search for new and continues friendly environmental energy, of course operators will increasingly move towards drilling with more challenging well trajectories toachieve their objectives and led operators to a more complex drilling environment. Drilling in unique environments and complex well designs will need a huge concern from technical, environmental and economic risks. Historically speaking, too much time was spent to deal with stuck pipes event before results in lost in holes (LIH). To pursue efficient and effective geothermal drilling operations, new approaches need to be introduced to this industrial climate.

Dealing with challenging environments requires integration on every single element to fulfill its objectives. The idea is to improve process by having all service requirement, increase response time to potential problems before they occur and finally cost reduction. The collaboration come up with the main goal to improve service quality. By providing a real-time data and support for 24/7 connection as a part of unified solution process made huge improvement on service quality. This must be achieved by defining operational workflows that utilize integration data and information to bring improvement in place on each phase: plans, execution, evaluation stages. Discussion of the operational framework and background and the role of technology to support operational performance will be described in this paper.

2. PROBLEM AND CHALLENGE

The risk of geothermal drilling will turn into a problem and become non-productive time (NPT) if it is not prevented and mitigated properly. Increasing the drilling process will directly increase drilling cost.

As can be seen in Figure 1 Drilling Time Distribution, unplanned events and Non-Productive Time (NPT) reaches 45.3% of the total time. The uncertainty in geothermal drilling makes the decision-making process very dynamic. Making fast and precise decisions in this dynamic process certainly requires support in the form of good information from the field. Analyzing on time allocation during drilling process, providing a breakdown to highlight durations for activities such as drilling, tripping, casing, cementing, logging, and others. Understanding these time distributions is crucial because inefficiencies can lead to significant cost escalations. Issues such as low Rate of Penetration (ROP), stuck pipe incidents, loss circulation, and flat time exacerbate these challenges, contributing to financial losses for the company.

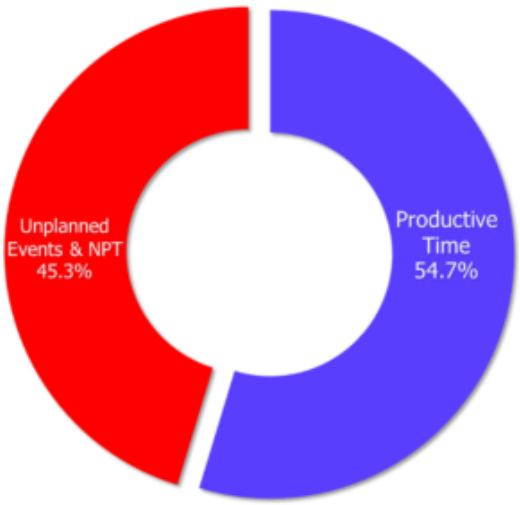

Figure 1: Drilling Time Distribution on Previous Campaign.

Given this context, the primary focus of this research is to enhance the operational model. This model aims to swiftly mitigate Non-Productive Time (NPT), thereby reducing its adverse effects and enhancing overall drilling efficiency. The research will delve into several key areas to address fundamental issues.

2.1 Hard and Abrasive Formation

The hardness and abrasiveness of geothermal formations significantly influence various aspects of drilling operations. Issues such as slow Rate of Penetration (ROP) and equipment damage are common due to the characteristics of rocks in geothermal environments. These factors not only slow down drilling progress but also escalate costs. Equipment damage can necessitate replacements and being more complicated when stuck pipe happen. Increasing the need for costly remedial measures in terms of time, money, and energy.

Figure 2: Drilling Bit Condition, Left: Pre-Run and Right: Post-Run.

Figure 2 illustrates the real contrast in drilling bit condition before and after use, highlighting the frequent occurrence of tool failures that reduce ROP and require operational consideration or replace Bottom Hole Assembly (BHA) components. Despising many mitigation efforts, attempting optimal results is still difficult to achieve. Overcoming these ongoing challenges is especially in geothermal drilling environment. Therefore, a comprehensive evaluation is essential, combining mathematical modeling through simulation results and empirical research based on historical data.

2.2 Stuck pipe and Hole Problems

The challenges encountered in each drilling operation poses significant barriers to the company's effective goal attainment. Figure 3, the Previous Campaign Drilling Curve, vividly illustrates the diverse patterns in drilling performance, encompassing variations in slopes and final depth outcomes. Discrepancies in slowdowns and unmet depth targets across different wells underscore the array of issues encountered during drilling, resulting in inconsistent overall performance.

As previously elucidated, the significant prevalence of problems arising from uncertain drilling conditions results in extensive time consumption and Non-Productive Time (NPT) during the drilling process, classified as unplanned. For instance, the yellow curve representing Well-E displays the most pronounced and deepest curve among all wells, indicating a notable deviation from the performance of other wells. None of the wells achieved the slope and depth reached by Well-E, highlighting a misalignment between the objective function and actual accomplishments.

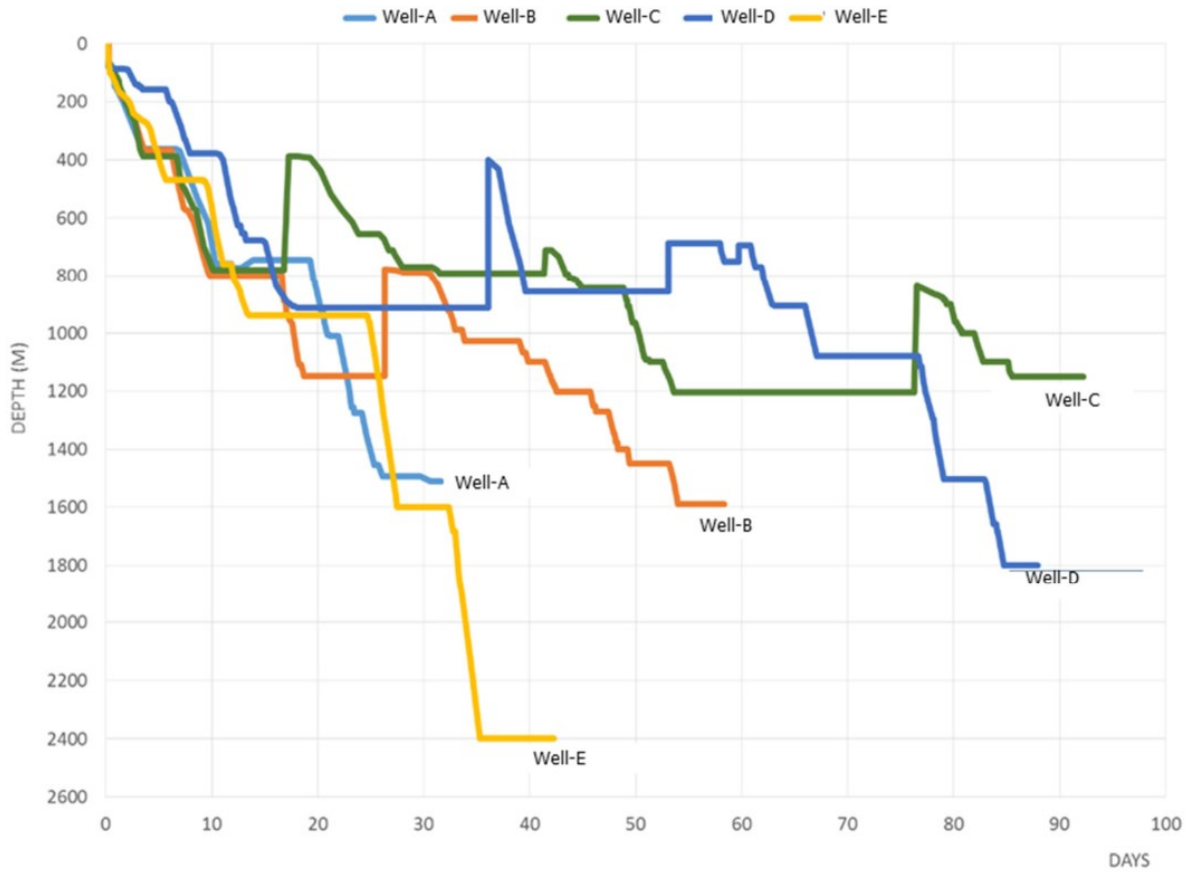

Figure 3: Previous Campaign Drilling Curve.

This discrepancy underscores the need to explore the factors contributing to this phenomenon and devise strategies to address it, a topic which will be elaborated upon in the subsequent chapter utilizing the previously outlined methodology.

2.3 Drilling in Total Lost Circulation

A critical risk associated with geothermal drilling is lost circulation. This often results in significant losses of mud, making it exceptionally challenging to remedy the situation using lost circulation materials or even cement plug job. The formation characteristics consist of fracture propagation which is subsequent to lost circulation. This challenge is further compounded maintaining wellbore stability in formations with micro-network fractures poses considerable challenges during drilling. The penetration of drilling fluid into these fractures fails to equilibrate the pore pressure with the mud pressure, leading the fluid level to drop and fail mud pressure support from overbalance. Therefore, cuttings-induced pack-off over the Bottom Hole Assembly (BHA) can be happen during making up new connection due to insufficient annular pressure. This scenario has been observed repeatedly when drilling fluid fails to suspend cuttings, ultimately culminating in a stuck pipe event.

2.4 Prolonged Flat Time

Essentially, well construction encompasses two main phases which are drilling (on bottom) and flat time, where no advancement occurs in hole depth. As previously mentioned, flat time activities encompass various operations such as pipe tripping, casing and liner installations, cementing, BOP and wellhead handling, pressure testing, and completions-significantly contributing to the overall time allocation. This downtime, often resulting from challenges outside the drilling operation, heightens risks such as failure during casing/liner installation and completion.

Another critical aspect of well construction, characterized by substantial the “unseen" loss time, occurs during flat times. As evidenced in the preceding discussion, particularly in Figure 3 Drilling Curve, several wells exhibit prolonged flat times, depicted by a horizontal line indicating no depth increase over time. Consequently, any issues arising during these activities can prolong the average time required to condition the well. Rig performance, meticulous planning, comprehensive preparation, and clarity in low-level instructions are paramount in optimizing flat time activities. Therefore, this paper will elucidate strategies for reducing flat time to enhance performance and minimize costs.

3. SOLUTION

Star Energy Geothermal has implemented a comprehensive strategy following extensive consultations with technical experts from its service providers to optimize resources across systems, technology, and workforce. The primary objective is to tackle drilling challenges, address issues with loss circulation and implement best practices to ensure geothermal drilling process are safe, efficient, and cost-effective. Consequently, these solutions enable expedited drilling operations without constraints, effectively resolving existing issues.

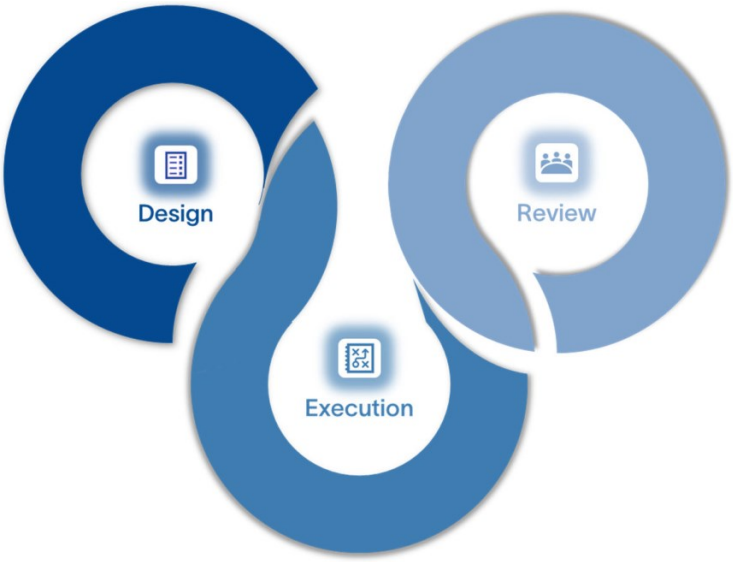

Figure 4: Improvement Cycle.

The improvement initiatives encompass three fundamental phases: design, execution, and review, detailed in Figure 4. Each phase yields substantial information and data crucial for developing strategies and bridging operational gaps. In the design stage, the process begins with establishing a Risk Register to proactively identify potential issues. Subsequently, potential problem scenarios are modeled for the subject well using data from offset and similar wells in term of geological prognosis, accompanied by comprehensive solutions and lessons learned. Further analysis will refine initial best practices to uncover opportunities for enhancement and improvement.

Once the strategy and program are finalized in the design stage, real-time monitoring of all operations ensures adherence to the plan and enables immediate support for swift resolution of any deviations caused by unforeseen challenges. Specifically, the proposed solutions for mitigating loss circulation, hole instability issues led to stuck pipe and optimizing drilling processes empower operators to minimize risks, enhance performance, and achieve safer operation.

4. MANAGING THE CHALLENGES

Significant advancement in drilling operations, showcasing the successful implementation of proven technological solutions and integration services resulting from enhanced cognitive capabilities within the improvement cycle.

The achievement is underpinned by five core pillars: Key Performance Indicators (KPIs), Historical Performance analysis, Performance Improvement plans, Implementation Strategy, and Performance Lookback as shown in Figure5. This discussion will elucidate how optimizing each of these critical components has contributed to this remarkable progress.

Figure 5: Managing the Challenges.

Table 1: Drilling Well Objectives.

Objectives	Information
Value Based Well Objective (VBWO)	Maintain well control at all times.
	Meet or exceed P50 initial expected steam rate at commercial wellhead pressure
	Meet or exceed project economic of positive NPV
	Complete well hook-up one month after flow test and put the well on-line right after well hook-up commissioning.
	Complete the well within AFE days and budget.
	Characterize the well as per plan i.e. completion test, flow test, geological data
	Flow test within five days on availability of SIMOPS permission otherwise after rig move
Health, Safety, & Environment (HSE)	No LTI'S (lost time injuries).
	No environmental incidents, spills and minimum environment impact.
	No major or catastrophic service quality incident.
	Incident and injury free operation (IIFO) .

4.1 Key Performance Index

To enhance overall asset investment efficiency, the focus is on assessing and drilling complex wells aimed at boosting well productivity. This involves strategically selecting existing locations or those with minimal footprint, optimizing resource usage and concerning environmental impact. Collaboration among function plays a crucial role in enhancing collective capabilities, aimed at achieving more economical drilling costs for future geothermal operations. By pooling resources and expertise, operators can leverage shared knowledge and technologies to streamline processes and reduce operational expenses.

Efforts to enhance drilling efficiency and minimize environmental impacts are central to this collaborative approach. As depicted in Table 1, Key Performance Index are translated into specific objectives for each well drilling activity. Through collaborative initiatives, operators can explore innovative drilling techniques and technologies that enhance operational efficiency while prioritizing sustainability. This collective endeavor not only facilitates cost-effective development of geothermal resources but also promotes responsible management of natural resources. By aligning strategies and leveraging collaborative advantages, operators can pave the way for sustainable growth in geothermal energy production, simultaneously driving economic benefits and environmental sustainability.

4.2 Historical Performance and Performance Lookback

In the domain of drilling operations, data derived from offset wells plays a pivotal role as a foundational reference throughout the stages of design and implementation. This dataset offers critical insights into a spectrum of parameters that exert influence over drilling conditions. These insights are instrumental in preemptively identifying potential challenges, such as risks of circulation loss or drilling breaks, which can significantly impact operational efficiency and safety. Moreover, the data aids in strategizing effective responses to unforeseen issues that may arise during operations, such as managing cuttings during pipe landing and casing operations, and addressing downtime for repairs, such as the installation of Blowout Preventer (BOP) connections and reaming activities.

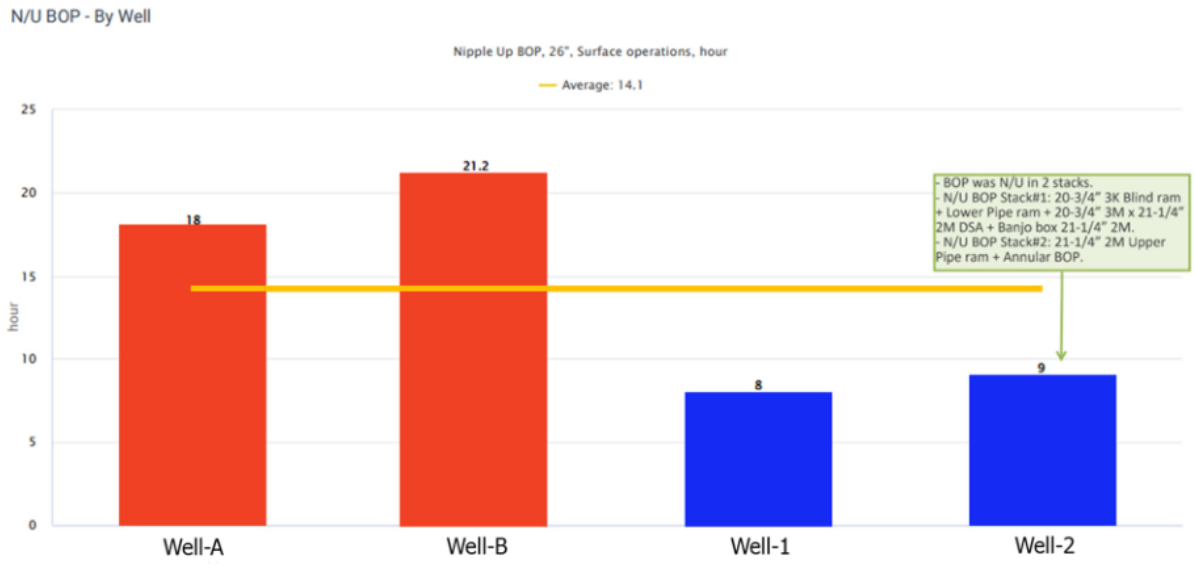

Figure 6: Improvement of N/U BOP.

Leveraging offset well data allows drilling engineers can proactively anticipate complications and develop solutions that mitigate risks while optimizing operational outcomes, as illustrated in Figure 6 which highlights improvements in process efficiency. Through effective utilization of historical data, engineers enhance decision-making processes, streamline operations, and uphold rigorous safety protocols. This proactive approach ensures that drilling activities proceed smoothly, minimizing disruptions and maximizing productivity. Ultimately, integrating comprehensive data analysis from offset wells plays a crucial role in achieving operational excellence and resilience in the dynamic field of drilling operations.

4.3 Performance Improvement Plan and Implementation

Following the thorough completing comprehensive identification and measurement processes outlined earlier, the collaborative teams engineering and drilling operations initiate strategic interventions using precise principles and methodologies. These actions are aimed at effectively addressing inefficiencies and unlocking opportunities for enhancing performance. In response to identified operational shortcomings and instances of downtime, comprehensive strategies have been meticulously formulated to bolster drilling performance across all operational

domains. These initiatives encompass a comprehensive approach that integrates process improvement, technology integration, and procedure optimization. This holistic strategy aims to maximize operational efficiency and minimize disruption, addressing both immediate and intermediate time frames.

4.3.1 Immediate Within 6 Month

In the realm of drilling operations, the data from offset wells serves as invaluable reference throughout both the design and execution stages. These datasets provide crucial insights into various parameters that influence drilling conditions. By analyzing how these parameters behaved in past operations, engineers gain a clearer understanding of expected outcomes and potential challenges. This historical data is particularly critical during the monitoring phase, where real-time data is consistently benchmarked against established standards from offset wells. This comparison enables Real-time Decision Center (RTDC) engineers to promptly identify and evaluate any deviations or anomalies occurring at depth, as depicted in Figure 7 which illustrates deviations in well trajectory. Through continuous comparison and real-time monitoring, early detection of deviations allows for swift decision-making regarding necessary solutions. These insights facilitate proactive adjustments, ensuring operational continuity and minimizing risks associated with unforeseen drilling conditions.

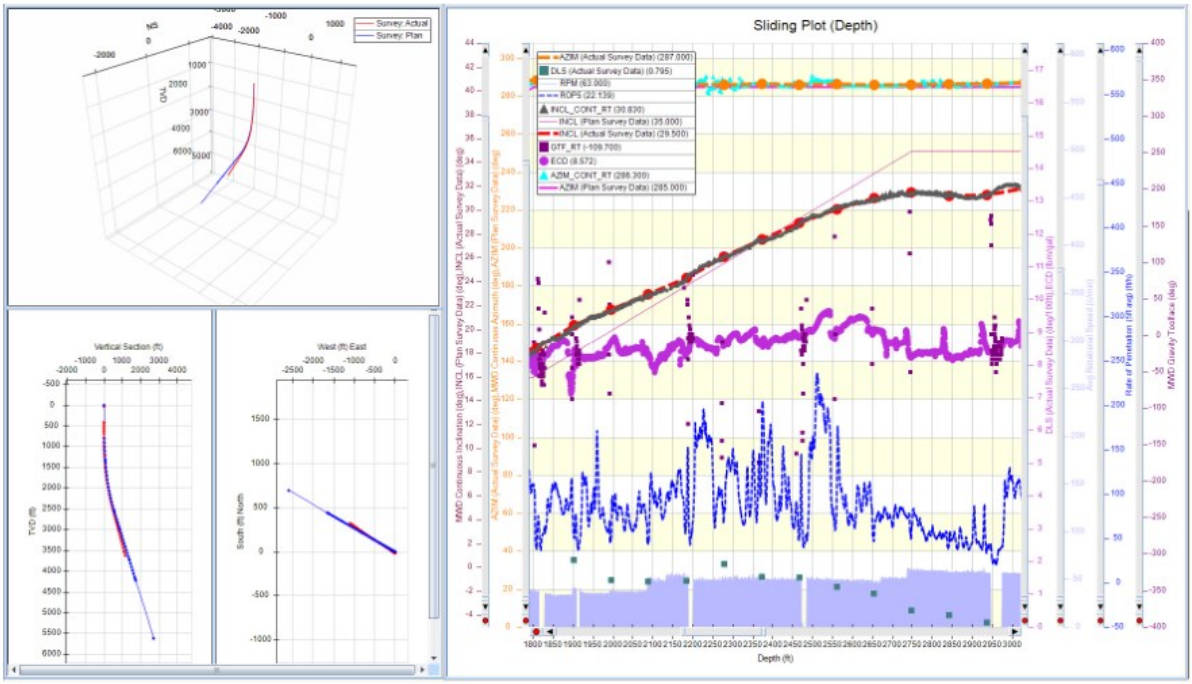

Figure 7: Real-Time Trajectory Monitoring.

This visual representation not only facilitates rapid identification of anomalies but also enhances the precision of decision-making processes. Engineers can promptly correlate observed data trends with known benchmarks, swiftly diagnosing any discrepancies and taking appropriate corrective measures. This proactive approach not only enhances operational efficiency but also reduces potential downtime and optimizes resource utilization. The monitoring plot derived from real-time data as shown in Figure 7 provides a clear visualization of trajectory adjustments and their feasibility. Assessing the likelihood of achieving desired trajectories and identifying potential challenges could expedite decision-making throughout drilling operations. Leveraging insights from offset well data empowers engineers to effectively navigate complexities and uphold stringent standards of safety, efficiency, and performance in geothermal operations. This integrated approach ensures that operational objectives are met with precision while minimizing risks and maximizing operational success.

4.3.2 Intermediate 1 – 2 Years

The improvement strategies developed are meticulously introduced to stakeholders and higher-level management, ensuring they are aligned with organizational objectives and project goals. This involves comprehensive communication and detailed presentations that methodically outline the potential impact and benefits strategies. This collaborative effort aims to cultivate a shared understanding and commitment among all stakeholders, setting the stage for seamless execution by the project implementation team. Translating these strategies into actionable steps, the teams are well-positioned to implement effective solutions that not only address current inefficiencies but also establish a pathway towards sustained operational excellence in drilling operations.

Intermediate improvement plan makes decision makers and the teams deal with hard system changes, fundamental changes, not only changing on the form of procedures or strategies. The improvement plan on the basic elements requires costs and a long process so that it is targeted with a time span of 1-2 years of improvement. Therefore, when considering well design, several critical factors are taken into account to optimize performance and mitigate risks. Anticipating subsurface hazards is crucial, as it involves thorough geological and geophysical assessments to identify potential challenges such as underbalance formation pressures, loss circulation, or hard and abrasive formations that impact to service quality as shown in Figure 8. Dropping tendency is shown in Figure 8 as the result of stabilizer worn out that led to near miss accident by missing the target.

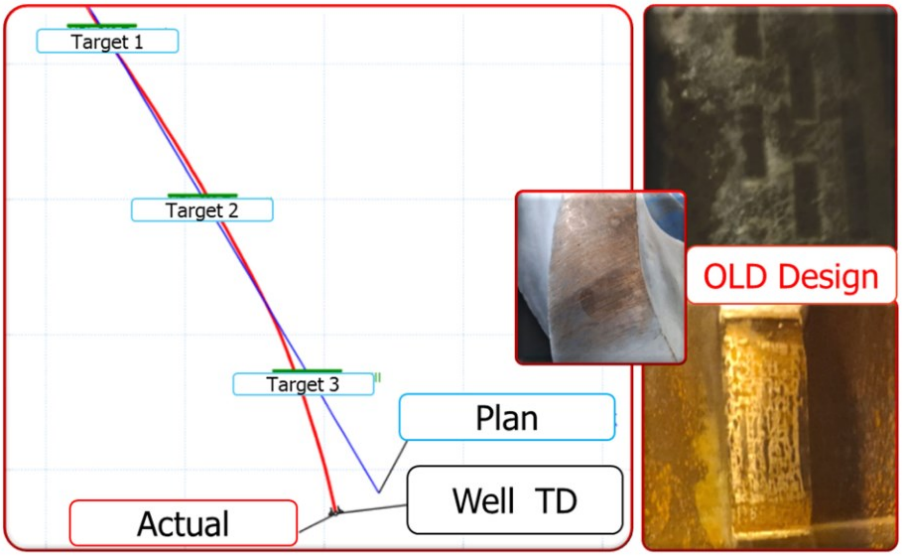

Figure 8: Equipment Deformation and Consequence.

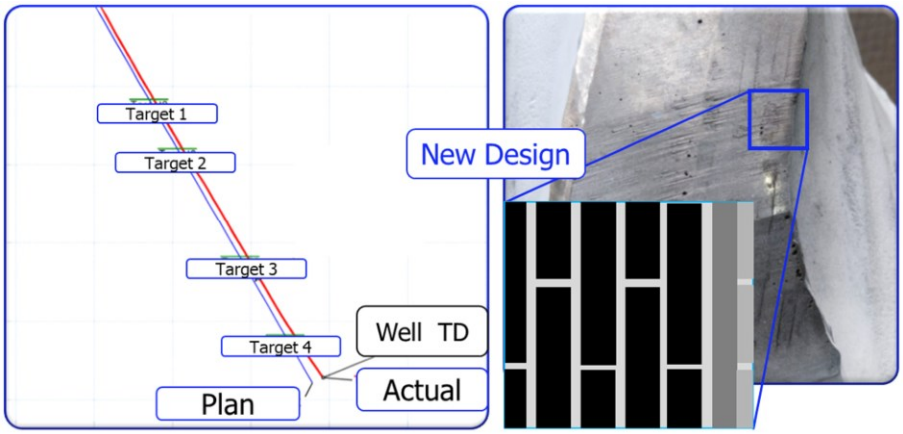

Figure 9: Quality Assurance through Innovative Design.

Improvement has been addressed with careful consideration is given to depth, formation hardness, and well trajectory requirements to ensure service quality guarantee. Increasing drilling efficiency involves adapting equipment protection designs for abrasive formations and implementing advanced drilling techniques, which contribute to increasing penetration rates and guaranteeing the quality of services provided as shown in Figure 9. Additionally, selecting appropriate drilling equipment protection plays a vital role in preventing drilling problems, ensuring robust equipment no drop tendency is shown and all targets are hit without any exception in term of efficient drilling operations.

In conclusion, integrating these advanced strategies and technologies into drilling operations not only improves immediate efficiency but also lays the groundwork for long-term success. By focusing on meticulous planning, stakeholder alignment, and leveraging cutting-edge technologies, drilling teams can navigate challenges effectively, achieve operational excellence, and uphold high standards of safety and performance in geothermal and other drilling operations.

5. RESULT

Building up a strong organizational capability is crucial for achieving continuous improvement in drilling operations. This entails leveraging advanced technologies such as real-time monitoring systems and enhancing cognitive skills. Efforts are also focused on enhancing overall asset investment efficiency through the assessment and drilling of complex wells aimed at increasing productivity.

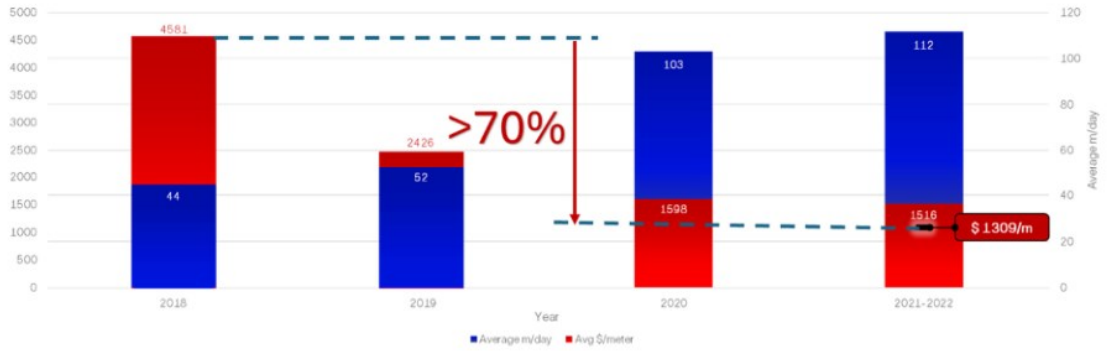

Figure 10: Reduction in Well Cost per Meter.

These initiatives embody a holistic approach to optimizing operational efficiency, reducing expenses, and ensuring long-term sustainability in geothermal drilling practices. This is exemplified by the fastest and most cost-effective drilling of geothermal wells in Indonesia over the past five years, as depicted in Figure 10. The learning curve and improvements achieved in this campaign are clearly shown, with drilling costs per meter decreasing by 70-75% and drilling speed increasing. Collaborative efforts among operators further enhance capabilities, aiming to achieve more cost-effective drilling operations in future geothermal developments.

ACKNOWLEDGEMENT

This successful implementation of systems, technology, and integration by Star Energy Geothermal demonstrates that Integrated Well Construction is a viable solution for the entire geothermal industry. The author extends sincere gratitude to Star Energy Geothermal for their invaluable support of this research. We are grateful for their permission to publish this paper and commend their dedication to advancing sustainable geothermal drilling. Special thanks are also due to the field and office personnel, including SEG and SLB crews, wellsite supervisors, and workshop personnel, whose contributions were instrumental in achieving this success.

REFERENCES

"DOX Single Point Analysis -Torque and Drag BasicConcept in Correlation with API RP 7G" (Content ID6042882).

Fridleifsson, Ingvar B. The possible role and contribution of geothermal energy to the mitigation of climate change. IPCC Geothermal. 2008

Lavrov, A. Lost circulation: mechanisms and solutions. Gulf Professional Publishing. 2016

M. Radov et al. Enhancing Production from High-Enthalpy Geothermal Wells with New Electric Submersible Pump Technology. Electric Submersible Pumps Symposium held in The Woodlands, Texas, USA, 2–6 October. 2023

N.C Meany. Method and apparatus for determining potential interfacial severity for a formation.

Nahun Vega, “Drilling Efficiency Through MSE” IPM Project Optimization, and Decision Making

P.A.Curry. New Method Of Representing Rock Properties Over Entire Bit Run Improves Computer Generated Bit Recommendations. SPE/IADC Drilling Conf. Dallas. 2004

R Pessier. Quantifying common drilling problems with mechanical specific energy and a bit-specific coefficient of sliding friction. SPE paper no. 24584. Washington DC. 1992

Rehm, B. Circulating fluid losses during drilling operations. In SPE/IADC Drilling Conference and Exhibition. Society of Petroleum Engineers. 2009

SPE-110563-PP. Improving the Value of Real-Time Drilling Data To Aid Collaboration, Drilling

SPE-172740. The Implementation Of Real Time Data Drilling Decision Centre (RTTDC) in Kuwait

Geo-LOK Casing Hanger: A Superior Alternative to Conventional Cementing in Deep Geothermal Wells

Kevin Gray[1], Daria Ivakhnenko[1], Ben Adams[1], Zander McDougall[2], and Garry Stephen[2]

[1]Black Reiver Consulting EURL, 16 Rue Anatole France, Quillan, 11500, France
[2]OSI Renewables, Heartlands Business Park, Whitburn, EH47 0SF

kevin.gray@blackreiver.com, daria.ivakhnenko@blackreiver.com,
ben.adams@blackreiver.com, zander.mcdougall@osirenewables.com

Keywords: geothermal drilling, optimization, cost reduction, performance drilling, cost, drilling

ABSTRACT

The technology, widely used in tension leg platform (TLP) applications for oil and gas wells, holds immense potential if adopted in deep geothermal wells. Its implementation could lead to significant reductions in well construction costs, bolster long-term well integrity, and enhance the life-long thermal performance of the wells, thereby painting a promising financial picture. The paper introduces a technology that has already demonstrated its global reach and long-term reliability in its current application (Wybro and Chaison, 1995). However, its use in geothermal wells could revolutionise standard well design methodologies and cost assumptions, sparking further research and development in the industry.

Traditionally, geothermal well construction requires that the casing strings be cemented back to the surface to manage the axial compressive loads on the casing body and casing couplings caused by thermal expansion, which would otherwise lead to premature loss of well integrity (Arbad et al., 2022; Finger and Blankenship, 2010; Teodoriu and Falcone, 2009). With the repurposing of the existing technology, the requirement for the entire annulus to be cemented will be removed, as the unique design allows casing expansion to be accommodated without increasing the axial compressive load. Removing the requirement to cement the annulus to the surface presents considerable technical and financial opportunities over the entire well life cycle. In geothermal well construction, managing the axial compressive loads at the surface considerably reduces the casing costs, as the traditional primary approach to managing collapse, in addition to a fully cemented annulus, is to increase the tubular wall thickness. This approach is especially costly in reservoir-dependent (hydrothermal) wells as the aggressive corrosive environments created by the production of geothermal brines often require high-cost corrosion-resistant tubulars (Belayneh and Tantuoyir, 2021). The maintenance of the casing-to-casing annulus allows the potential for lifelong, continuous automated surveillance of the integrity of the primary production conduit, which is not currently possible with traditional geothermal well construction methodologies.

The instigation of continuous well integrity surveillance, made possible by the proposed approach, offers the opportunity to reduce monitoring and maintenance intervals, and it is likely that the need to schedule periodic well shut down to allow wall thickness checks will be reduced as the annulus can be under continual surveillance and action taken at first appearance of a leak path (NORSOK, 2013). The proposed approach allows a reduced cementing requirement, lowers cementing costs, and minimises exposure to cementing risks, as only a minimal conventional annulus cement job will be sufficient to manage well integrity. Removing the need to cement the entire length of the casing allows consideration of using externally insulated casings and sleeves on the uncemented section of the production casing. This lower loss of heat to shallower, thermally parasitic formations will allow production wellhead temperatures to be higher, with a consequent lifelong improvement in the well's thermal performance.(Adams, 1991; Belayneh and Tantuoyir, 2021) From an Environmental Social Governmance (ESG) standpoint, a conventional 'cut and pull' abandonment approach at the end of the wells' life. For lifetime carbon footprint assessment (Energy Sector Management Assistance Program (ESMAP), 2012), this method allows the recovered steel from the abandoned well to offset the well's energy footprint, thereby reducing the lifetime carbon impact of the well construction process. Reducing the carbon footprint of a geothermal well further improves the technology's contribution to improving the geothermal project's net sustainability and environmental benefits.

1. INTRODUCTION

In higher enthalpy geothermal wells, the most, widely adopted methodology for managing the compressive casing loads caused by the thermal expansion of the casing string is conventionally placed annular cementing (Sanyal and Urmeneta, 2005; Mulders, 2006), filling the entire annulus back to the surface. This approach is often combined with selecting casings with higher wall thicknesses.

Cementing the annulus back to the surface is not without difficulties (Teodoriu et al., 2022). Managing cement slurry losses and ensuring high-quality, void- and leak-path-free cement placement can be challenging in some geological environments, especially those that are highly fractured or have high bulk permeabilities Typical of reservoir-dependent (hydrothermal) geothermal wells.

Figure 1: Original application as a Tendon Top Connector Assembly.

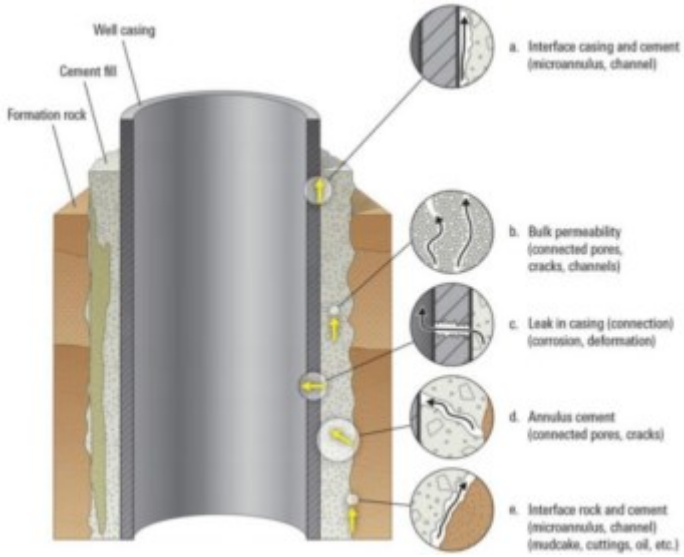

Figure 2: Poorly executed cementing operations can lead to Potential Leak paths, including channelling, micro annuli, and poor mud cake removal. (https://www.slb.com/-/media/files/well-intervention/industry-article/201705-os-bdt-promill-north-sea).

In such geological conditions, cementing will likely not be completed successfully (Figure 2) without the need for some form of tertiary loss control measures, which leads to more complex cementing operations, more expensive slurry designs, and higher material consumption.

The need for highly specialised metallurgies for tubular goods, such as Corrosion-Resistant Alloys (CRA) required as large-diameter high-weight casing rather than the lighter small-diameter production tubing used for oil and gas wells, adds to the project's financial, organisational, and logistical burden.

The long lead times and high cost of the specialised alloys required to assure well integrity by minimising corrosion effects over the long-anticipated operational life of geothermal wells must be considered in the early stages of project planning. These high well-construction costs can often inhibit project feasibility. Cementing the annulus to the surface also sacrifices the ability to add annulus surveillance capability to the well and prevents the well operator from immediately identifying a production leak. Within wells with a fully cemented annulus, casing

leaks of geothermal brines can go unnoticed for long periods of time, risking contaminating shallow aquifers. This problem has affected many early pioneering geothermal projects.

In order to minimise the risk of developing corrosion and leak paths, the traditional approach uses monitoring tools such as multi-finger calliper (MFC) and ultrasonic (USIT) logging to determine the residual casing wall thickness over the length of the casing string. Deploying these highly specialised logging tools is also associated with additional costs, not just for the tools themselves but with the shutdown of production flow whilst the well is prepared for logging.

A high-quality cement-to-formation bond, without any void spaces or potential fluid pathways, is critical for axial load management and avoiding collapse risk due to trapped fluid expansion. In deep geothermal wells, this also causes a higher heat loss to the formation in the shallow sections of the well due to their lower temperature and, hence, can be regarded as a loss of production. (figure 3)

In a geothermal well cemented to the surface, the operator has limited options for running insulated coatings on the production casing. This limitation has a considerable lifetime impact on the economic return of the entire project.

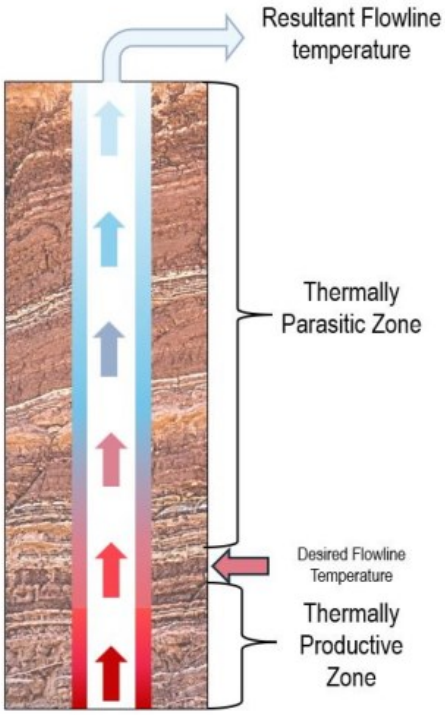

Figure 3: Thermally Productive and Thermally Parasitic zones in a geothermal well (Black Reiver Thermal Modeling Service).

Another consideration of the fully cemented annulus is that if there is a need for well recompletion, side-tracking (or abandonment), a simple "cut-and-pull" approach to recover the casing string is no longer an option. In some cases, this can render the well unrecoverable, resulting in the need to redrill the entire well or section.

The high heat transfer coefficient of the cement in the 'overburden', thermally parasitic well section leads to considerable heat losses to the surrounding rocks. (Asadia et al., 2018) The heating of shallower formations over the operational life of the well creates the potential for changing the stress regime acting around the wellbore. Thermally-induced geo-mechanical changes to the formation around the wellbore may cause numerous issues with wellbore integrity and stability, from simple loss of the cement to formation bond up to the casing collapsing. These effects will become more significant as the industry pushes towards higher enthalpy wells.

In addition to the geomechanical effects of shallow formation warming, changing the temperature of the shallow well sections and potentially transferring the heat to the aquifers is considered 'an act of pollution' in some regulatory jurisdictions. (Blum et al., 2021) It may be associated with significant financial sanctions for projects adversely impacting aquifer temperatures.

2. AN ALTERNATIVE METHOD

Geo-LOK Technology might be considered an innovative approach to tubing/casing hanger systems for deep geothermal wells. However, the technology is not new for the drilling industry in general, as it has been successfully used for many years for tendon tensioning in floating tension leg offshore platforms (TLPs). Geo-LOK technology represents a potentially significant advancement in tubing and casing hanger systems, particularly in deep, high-enthalpy geothermal wells. This section explores the mechanics and benefits of the Geo-LOK system, comparing it with conventional methods and highlighting its impact on well integrity and performance.

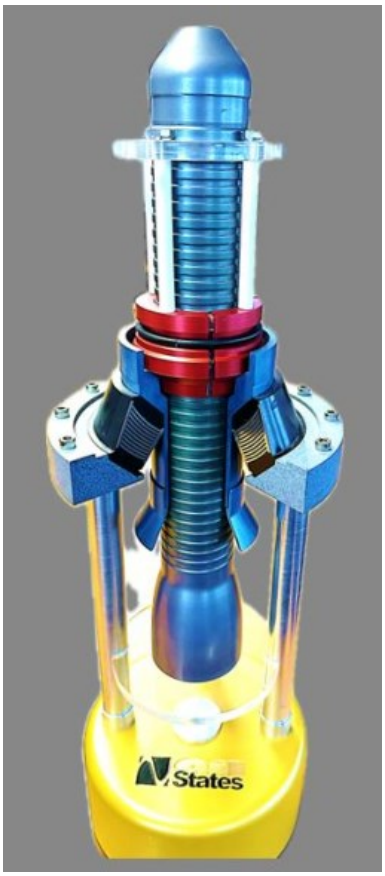

Figure 4: Simplified model of Geo-LOK operating principles (Image credit Black Reiver Consulting).

3. DESIGN AND FUNCTIONALITY OF GEO-LOK

Geo-LOK is an adaptive tubing/casing hanger system specifically engineered to accommodate the string's axial expansion without imposing an additional compressive load on the casing and its connections. Its design allows for the axial extension of the tubular string during the heating phase of geothermal operations. In contrast to conventional methods (Bellarby, 2009), which often struggle to cope with the increased compressive load on the string, Geo-LOK provides for a controlled axial movement.

4. MECHANISM OF ACTION

Geo-LOK (figure 4) supports the tubular string expansion in increments, effectively adapting to the axial growth of the tubular string. This incremental support ensures the string remains stable and well-supported throughout the heating and cooling cycles. When a geothermal well using a Geo-LOK hanger is cooled and the tubular string contracts, Geo-LOK facilitates a controlled mechanical release of the increased tension, preventing over-tensioning of the tubular string and its connections. This ability to control the axial stress in the production string allows for maintaining structural integrity without annular cementing to the surface and without requiring increased wall thickness tubulars.

5. ADDRESSING AXIAL STRESS CHALLENGES

For deep geothermal wells, excessive compression due to string expansion during the production phase and excessive tension during the cooling phase present significant challenges for casing design.

These cyclic thermal-induced stresses are a common source of failure of casing strings in existing geothermal wells. Traditional mitigation techniques, such as cementing the annulus to the surface and choosing tubulars with thicker walls, often fail to fully address these issues in a technically feasible or financially acceptable manner. This failure often leads to compromised well integrity and/or reduced operational efficiency being imposed on the well at the design stage.

6. ADVANTAGES OF GEO-LOK TECHNOLOGY

While effective in some applications, traditional cementing of the annulus to the surface often fails to address the unique challenges posed by the extreme temperature variations typical in higher enthalpy, deep geothermal wells. With its adaptive and supportive design, Geo-LOK technology offers a superior, better-value alternative that also permits a considerable improvement in the thermal performance over the life of the well.

Among the potential advantages of Geo-LOK application in deep geothermal wells, the authors can list the following:

6.1 Axial Stress Management

Geo-LOK minimises the risk of excessive compressive and tensile stresses being placed on the production conduit by varying operational conditions in the well. Allowing controlled axial growth and contraction avoids these stress variations, removing the potential for damage to the casing and its connections and reducing the potential for failure of the casing to cement bond.

6.2 Enhanced Well Integrity With Lower Costs

Geo-LOK technology enhances the overall integrity and longevity of geothermal wells primarily by mitigating the effects of thermal-induced stresses on the casing string and the annular cement barrier, reducing the potential for failure.

The use of Geo-LOK technology allows the simple instrumentation of the annulus of the production conduit with continuous pressure measurement sensors, equipped with upper, lower and rate of change state alarms. This permits instantaneous identification and notification of potentially damaging leak paths that may allow geothermal brines to contaminate surface sweet-water aquifers.

The ability to demonstrate continuous well surveillance may be sufficient to satisfy regulators that the periodic monitoring of the well using specialised logging cased hole techniques, such as MFC and Ultra-Sonic Imaging (USI) Tools for residual casing wall thickness assessment is not required or may be performed with a much longer interval between monitoring interventions. This considerably reduces ongoing well maintenance and regulatory compliance costs.

Table 1: Thermal model inputs for a simplified mono-bore well (Ben Adams, Black Reiver Consulting, Thermal Modeling Service).

Model Inputs	
Hole Diameter	12.25"
Casing OD	9 5/8"
Casing ID	8 5/8"
Insulation Thickness	0.015 m
Surface Temperature	10 degC
Bottomhole Temperature	120 degC
Formation Density	2700 kg/m3
Fluid Density	997 kg/m3
Fluid Specific Heat	790 J/(kg.K)
Formation Specific Heat	4180 K.kg/K
Thermal Conductivity of Casing	45 W/(m.K)
Thermal Conductivity of Cement	1.2 W/(m.K)
Thermal Conductivity of Annular Fluid	0.594 W/(m.K)
Thermal Conductivity of Casing Insulation	0.05 - 0.1 W/(m.K)
TVD	2500 m
Fluid Inflow Temperature	120 degC

6.3 Reduction Of Heat Loss To Formation

One key benefit of Geo-LOK technology is its ability to minimise heat loss to the formations in thermally parasitic sections of the well. By providing a barrier with a lower heat exchange coefficient than cement, Geo-LOK helps maintain the well's thermal efficiency, which is critical for optimising geothermal energy production. To illustrate this further Black Reiver Consulting ran a number of thermal scenarios on the same theoretical well (Table 1) using our in-house thermal model.

From these models, it was possible to evaluate the increased thermal power available from the same well completed with a conventional cemented to the surface annulus (Scenario 1), a Geo-LOK well with a fluid-filled annulus (Scenario 2) and two Geo- OK wells where due to the preserved ability to insulate the external surface of the casing, it had been insulated with materials of differing thermal conductivity. The thermal conductivity of the 2 insulations was modelled with a high TC example at 0.1 and a low TC example at 0.05. The basic design of the well was a simplified 2500m deep monobore well cased with 9 5/8" casing and a maximum BHT of 120°C.

The model was run over a range of flow rates taken after 5 years of operation to show instantaneous gain in power of the three scenarios using Geo-LOK. (Tables 2 and 3) This flowrate sensitivity analysis was done under the well conditions as simulated after 5 years of continuous operation. This was done in order to moderate the gains shown in the initial years and present a more conservative picture of the thermal benefits of removing the annular cement.

Table 2: Conventional cemented annulus well compared to flowing wellhead temperatures and gain in thermal power from a Geo-LOK well with fluid in the annulus. (Ben Adams, Black Reiver Consulting, Thermal Modeling Service)

Conventional Cemented Annulus		Geo-LOK with Fluid in Annulus		
Flow Rate (L/s)	WHT (degC)	WHT (degC)	Δ degC	Gain in thermal power (kW)
2.0	80.7	83.5	2.8	23.3
4.0	97.4	99.2	1.9	31.1
6.0	104.1	105.5	1.4	34.1
8.0	107.8	108.9	1.1	36.1
10.0	110.1	111.0	0.9	37.2
15.0	113.3	113.9	0.6	38.2
20.0	114.9	115.4	0.5	39.3
30.0	116.6	116.9	0.3	40.1
40.0	117.4	117.6	0.2	40.1
50.0	117.9	118.1	0.2	39.7
60.0	118.3	118.4	0.2	40.1
70.0	118.5	118.7	0.1	41.0
80.0	118.7	118.8	0.1	40.1
90.0	118.8	119.0	0.1	41.4
100.0	119.0	119.1	0.1	41.8

Table 3: Flowing wellhead temperatures and gain in thermal power from a Geo-LOK well with externally insulated casing. Data is relative to the conventional well model presented in Table 2. (Ben Adams, Black Reiver Consulting, Thermal Modeling Service)

Geo-LOK with External Casing Insulation (Insulation TC = 0.1 W/m/K				Geo-LOK with External Casing Insulation (Insulation TC = 0.05 W/m/K		
Flow Rate (L/s)	WHT (degC)	Δ degC	Gain in thermal power (kW)	WHT (degC)	Δ degC	Gain in thermal power (kW)
2.0	92.6	12.0	99.9	99.0	18.3	153.2
4.0	105.0	7.6	127.6	108.8	11.4	190.6
6.0	109.7	5.5	138.7	112.3	8.2	205.4
8.0	112.1	4.3	144.8	114.2	6.4	213.3
10.0	113.6	3.6	148.4	115.3	5.2	218.2
15.0	115.7	2.5	153.6	116.8	3.6	225.1
20.0	116.8	1.9	156.3	117.6	2.7	229.1
30.0	117.8	1.3	159.3	118.4	1.9	232.0
40.0	118.4	1.0	160.5	118.8	1.4	234.1
50.0	118.7	0.8	160.9	119.0	1.1	234.1
60.0	118.9	0.6	160.5	119.2	0.9	235.8
70.0	119.1	0.5	160.9	119.3	0.8	234.1
80.0	119.2	0.5	163.9	119.4	0.7	237.4
90.0	119.3	0.4	161.8	119.5	0.6	237.0
100.0	119.3	0.4	163.0	119.5	0.6	238.3

The model was also run at a constant 20 l/s flowrate over an anticipated 30-year operational well life to show a potential lifetime increase in total thermal return. (Table 4)

Whilst it is beyond the scope of this paper to assign direct monetary values to the achievable, increased power outputs, it would be easy to calculate the value of an individual project if given the applicable energy feed-in tariffs and power conversion efficiencies. It is sufficient to say that the value of this increase is significant.

6.4. Cost Reduction in Drilling and Casing

Geo-LOK reduces the overall drilling and casing costs by lessening the dependency on thicker-walled, high-cost corrosion-resistant tubulars. The drilling rig specification for any specific well is often defined by the hoisting requirements of the heaviest casing string. The ability to reduce casing string weight by running lighter, lower wall thickness tubulars can considerably reduce the drilling rig hook-load requirement and the additional drilling costs associated with larger capacity rigs.

6.5 Cementing Costs

Geo-LOK reduces the amount of cement required for well construction, simplifies the cement placement, and eliminates the need for high-cost lightweight and low-viscosity slurries. By decreasing the need to cement the annulus to the surface, the technology lowers the bottom hole pressures experienced during cemening, increasing the probability of successful, loss-free cement placement. The removal of annular cement from the lower temperature sections of the well also removes the casing collapse risk associated with the heating of the trapped fluid in voids or channels behind the casing due to poor cement placement. This, in turn, substantially reduces the need for expensive cement placement evaluation logging.

Table 4: Flowing wellhead temperatures and gain in thermal power from a Geo-LOK well with externally insulated casing shown on a time basis over a 30-year operational lifespan. BHT = 120°C (Ben Adams, Black Reiver Consulting, Thermal Modeling Service)

	Conventional Cemented Annulus	Geo-LOK with External Casing Insulation (Insulation TC = 0.05 W/m/K		
Time Step (yrs)	WHT (degC)	WHT (degC)	Δ degC	Gain in thermal power (kW)
0.1	112.4	117.2	4.8	403.0
0.5	113.7	117.4	3.7	306.0
1.0	114.1	117.5	3.3	279.2
2.0	114.5	117.5	3.1	255.0
3.0	114.7	117.6	2.9	242.4
4.0	114.8	117.6	2.8	234.9
5.0	114.9	117.6	2.7	229.1
6.0	115.0	117.6	2.7	223.2
7.0	115.0	117.7	2.6	219.9
8.0	115.1	117.7	2.6	216.5
9.0	115.1	117.7	2.6	214.0
10.0	115.2	117.7	2.5	211.5
11.0	115.2	117.7	2.5	209.0
12.0	115.2	117.7	2.5	206.5
13.0	115.3	117.7	2.5	204.8
14.0	115.3	117.7	2.4	204.0
15.0	115.3	117.7	2.4	201.5
16.0	115.3	117.7	2.4	200.6
17.0	115.3	117.7	2.4	199.0
18.0	115.4	117.7	2.4	198.1
19.0	115.4	117.7	2.4	196.5
20.0	115.4	117.7	2.3	195.6
21.0	115.4	117.7	2.3	194.8
22.0	115.4	117.7	2.3	193.1
23.0	115.4	117.8	2.3	193.1
24.0	115.5	117.8	2.3	192.3
25.0	115.5	117.8	2.3	190.6
26.0	115.5	117.8	2.3	190.6
27.0	115.5	117.8	2.3	189.8
28.0	115.5	117.8	2.3	188.9
29.0	115.5	117.8	2.3	188.1
30.0	115.5	117.8	2.2	187.3

6.6 Enhanced Abandonment Processes

Geo-LOK technology simplifies the abandonment process of geothermal wells. A fully cemented casing string left in the well requires section milling to permit the currently accepted abandonment standards, a time-consuming and costly process. In contrast, Geo-LOK enables a more efficient, easy and cost-effective "cut-and-pull" approach to be adopted. This is especially true in hard rock geothermal applications where long-term maintenance of a full wellbore is assured. This ability to fully recover the bulk of the casing back from the well, as previously mentioned, also allows the offsetting of the carbon footprint of the recovered alloys, improving the lifetime ESG profile of the well.

7. CONCLUSION

The Geo-LOK casing hanger technology represents a potentially significant advancement in geothermal well construction, offering a promising solution to the challenges and limitations of conventional cementing methods. Its unique ability to manage axial stresses without the need for full-length annulus cementing brings both technical and economic benefits. These include substantial cost reductions in casing and cementing, improved well integrity assurance, and enhanced thermal performance of geothermal wells.

Geo-LOK technology offers substantial benefits across financial, operational, and environmental aspects when considered as an alternative to conventional cementing for deep geothermal wells. Financially, it reduces cementing, casing, logging, and abandonment costs, making well construction and operation more cost-effective. Operationally, it enables continuous annulus surveillance and real-time management of well integrity, reducing monitoring intervals. This further improves the economic performance of the well.

Environmentally, Geo-LOK supports more sustainable well abandonment practices, minimizes heat loss of the produced fluids, and lowers the carbon footprint of geothermal projects. Moving forward from this paper, the adoption of Geo-LOK technology needs to be fully validated across the full 'ecosystem' of geothermal environments; the authors encourage further research and field trials. This will not only enhance understanding of the technology but also pave the way for continuous improvement and optimization in the industry.

REFERENCES

Adams, J. (1991). How to design for annulus fluid heat-up. *SPE Paper 22871*. Presented at the 66th Annual Technical Conference and Exhibition of the Society of Petroleum Engineers, Dallas, TX.

Belayneh, M., & Tantuoyir, M. M. (2021). Geothermal well design for efficient energy extraction and long-term integrity. *International Journal of Engineering Research and Technology*, 14(12), 1223–1234.

Blum, P., Menberg, K., Koch, F., Benz, S. A., Tissen, C., Hemmerle, H., & Bayer, P. (2021). Is thermal use of groundwater a pollution? *Journal of Contaminant Hydrology*, 239, 103791. https://doi.org/10.1016/j.jconhyd.2021.103791

Carvalho, M. R., Forjaz, V. H., & Almeida, C. (2006). Chemical composition of deep hydrothermal fluids in the Ribeira Grande geothermal field (São Miguel, Azores). *Journal of Volcanology and Geothermal Research*, 156(1-2), 116-134.

Energy Sector Management Assistance Program (ESMAP). (2012). Greenhouse gases from geothermal power production. *ESMAP Technical Report* 009/16. Washington, DC: World Bank.

Finger, J., & Blankenship, D. (2010). *Handbook of best practices for geothermal drilling*. Sandia National Laboratories, Albuquerque, NM.

Asadia, I., Shafigha, P., Abu Hassana, Z. F. B., & Mahyuddina, N. B. (2018). Thermal conductivity of concrete – *A review. Journal of Building Engineering*, 20, 81-93.

Bellarby, J. (2009). *Well Completion Design*, Volume 56. ISBN: 9780444532107.

Mulders, F. (2006). Studies on wellbore integrity. *Proceedings* of the 2nd Wellbore Integrity Network Meeting, Princeton, New Jersey.

NORSOK D-010. (2013). *Well integrity in drilling and well operations*. Rev 4.

Sanyal, S. K., & Urmeneta, N. (2005). Thirtieth Workshop on Geothermal Reservoir Engineering. In *Proceedings*: Thirtieth Workshop on Geothermal Reservoir Engineering: January 31-February 2, 2005. Stanford, California; Stanford University.

Teodoriu, C., & Falcone, G. (2009). Comparing completion design in hydrocarbon and geothermal wells: The need to evaluate the integrity of casing connections subject to thermal stresses. *Geothermics*, 38(2), 238-246.

Teodoriu, C., Esquitin, Y., & Vasques, R. (2022). 47th Workshop on Geothermal Reservoir Engineering. In 47th *Workshop* on Geothermal Reservoir Engineering 2022: Online, 7-9 February 2022*. Stanford, California; Stanford Geothermal Program.

Wybro, P. G., & Chaison, M. (1995). *Cost-effective TLP installation methods and tendon top connectors*. United States: N. p., 1995. Web.

Arbad, N., Emadi, H., & Watson, M. (2022). A comprehensive review of geothermal cementing from well integrity perspective. *Journal of Petroleum Science and Engineering*, 217, 110869. https://doi.org/10.1016/j.petrol.2022.110869

Reliability Analysis of Pressure Transmitter Integration with Flow Switch for Enhanced Seal Water System Performance in LRVP Systems at Geothermal Power Plants Kamojang

Muhammad Indjra Dije, Ales Daniel, Fikrul Jihad, and Luhung Pravubinantaka

Pertamina Geothermal Energy

muhammad.dije@pertamina.com, ales.daniel@pertamina.com,
fikrul.jihad@pertamina.com, luhung@pertamina.com

Keywords: Liquid Ring Vacuum Pump (LRVP), Flow Switch (FS), Pressure Transmitter (PT), Reliability

ABSTRACT

Non-Condensable Gas (NCG) is a natural component of geothermal fluids in the form of a gas matter that is unable to undergo a condensation process in a cooling water system. NCG could interfere with the heat transfer process inside a condenser by raising its internal vessel temperature, resulting in reduced turbine efficiency. In principle, the liquid ring vacuum pump (LRVP) is a compressor that compresses NCGs before distributing it to the cooling tower, as a part of the cooling water process. The seal water system inside an LRVP is transferred by an Auxiliary Cooling Water Pump (ACWP), creating a sealing ring that works both as a gas compressor and as a prevention against foreign fluids that interfere with the pump's process. A fault in the seal water system can cause serious problems, such as overheating, corrosion, or reduced performance. As this seal water system holds a major role in the LRVP system, it is necessary to maintain both safe and reliable implementation of the instrumentation and control system. Kamojang Geothermal Power Plant Unit IV uses a flow switch as a detector to ensure proper operation of the seal water flow system and as a permission for activating or tripping the LRVP. The Power Plant experienced three plant trips between 2016 and 2023, due to some false signals transmitted by the flow switch. The addition of a pressure transmitter in parallel with the flow switch was proposed to enhance reliability. Data from turbine trip failures due to flow switch issues were analyzed to determine the Mean Time Between Failures (MTBF) and system reliability. The parallel configuration aimed to improve the cooling water system's dependability. Results indicate a significant reliability improvement, with the new system achieving a reliability of 0.92 compared to 0.37 for the existing system over 3.5 years, demonstrating a 0.55 increase.

1. INTRODUCTION

Geothermal Power Plant (GPP) holds its remarkable use of dry steam from the earth's reservoir to generate electricity by propelling the steam turbine. As one of Indonesia's oldest geothermal producers, PT Pertamina Geothermal Energy Tbk (PGE) has generated 235 MW of total power generated, with Kamojang Geothermal Power Plant Unit IV as one of the pioneers of Pertamina's owned GPP (Dwikorianto, Hendriansyah, Sastranegara, & Nugroho, 2018). The GPP extracts the dry steam that powers the coupled turbine-generator with power generated at 60 MW, where the steam is condensed into a condenser and processed into a cooling water process. The condensed steam then being reinjected into a reinjection well, which plays a vital role in both sustaining its geothermal reservoir quality and producing a low emission byproduct. Albeit for its well-known low-emission power plant, Kamojang Geothermal Power Plant Unit IV still produces a relatively low gas emission known as the NCG.

NCG is a type of gas unable to undergo a condensation process in a cooling water system. CO2 and H2S gas have the greatest percentage of content in the NCG produced. To remove the NCG from the system, the Gas Extraction System holds a vital role in the circulation process. The removal process has been automated into several sequences of operation between LRVP and Ejector (Novtafiani, Adhikihal, & Zaki Hamidi, 2018). By creating a vacuum chamber in the suction port, the NCGs are transported and then discharged through a discharged port with pressure from the impeller. To create a vacuum chamber inside the LRVP, an ACWP discharged the sealing water into the LRVP to create a seal water system. However, there have been some operational issues reports regarding the flow control system from ACWP into LRVP, resulting in the cooling water system's reliability.

When determining the seal water performance in LRVP systems, one of the sensors used is the flow switch (FS). which then decides the logic system of a GPP. However, it became crucial since it caused several power plant failures since 2016. The main factor is the sensor being installed as the sole component to monitor the sealing water flow from ACWP to LRVP, which increases the probability of a failure to occur. As this raises a new concern of a single sensor use in the system, a new system should be taken out to enhance the LRVP's performance, defined through a mathematical prediction that describes the system's reliability.

This paper discusses the re-evaluation of the flow control system's reliability from ACWP to LRVP from commissioning until the recent operation in 2023. Additionally, a pressure transmitter is installed on the same line as the flow switch to monitor the sealing water flow to the LRVP as the new modification, ensuring sufficient cooling water supply. The current study aims to investigate the effect of a logical modification towards increment on the reliability of a cooling water system in GPP. Based on its evidence of the new modification, the result can directly improve the further development and operation of other GPP in Indonesia. Furthermore, the result can also predict the foreseeable future of the repair time of the LRVP systems in the Kamojang Area.

2. METHODS

The objective of this paper is to enhance the power plant's reliability by resolving issues caused by false signals from the flow switch. Identification of the system and data collection were conducted to support the reliability analysis of the system using an exponential distribution.

The assumptions used in this paper are as follows:

- All parameters are statistically independent
- Exponential distribution is taken for all repair activities
- After repair/replacement unit works as new
- Flow switch and Pressure transmitter work in parallel and fail with a constant rate

The failure data for turbine trips caused by flow switch failure were gathered from PGE's internal records from commissioning until the recent operation in 2023. Based on the collected data, the system's MTBF (Mean Time Between Failures) value is determined, which is then utilized to determine the reliability function of the existing system.

A pressure transmitter is then added as an additional criterion to enhance the system's reliability. The MTBF value used for the pressure transmitter is based on references from previous research. The pressure transmitter is configured in parallel with the flow switch. The reliability values of the existing system and the new system implementation are then compared to assess the improvement in reliability achieved.

2.1 System Description

In principle, LRVP is a compressor that compresses NCGs before distributing it to the cooling tower, as a part of the cooling water process. The seal water system inside the LRVP is transferred by an ACWP, creating a sealing ring that works both as a gas compressor and as a prevention against foreign fluids interfering with pump's process.

Flow Switch is a mechanical switch that is switched on or off in response to the flow or non-flow of a fluid such as air or water (Mcrill, 2017). The flow switch in this system functions as a safety feature for the LRVP pump, ensuring that the sealing water line receives the appropriate water supply.

Figure 1 shows the Process Flow Diagram (PFD) of the geothermal power plant and details the process of FS as an indicator that water from the cooling water supply has flowed into the LRVP sealing water process. This component is considered to have failed if it is unable to monitor the flow through the sealing water process in the LRVP.

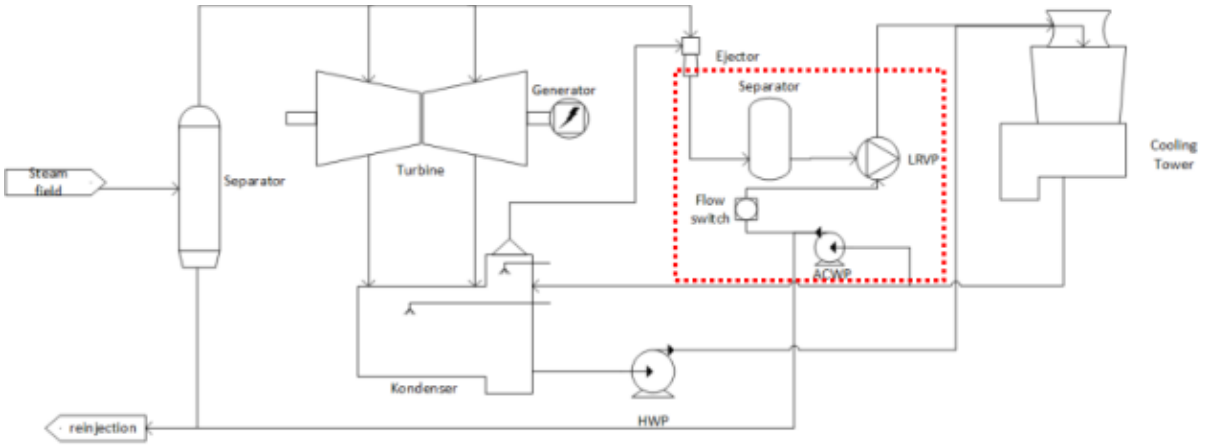

Figure 1: PFD of GPP and existing system details.

The following is the interlock and control diagram that causes the LRVP to trip.

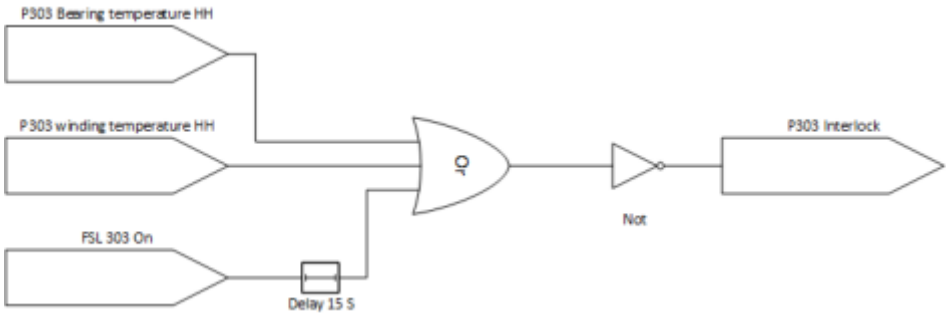

Figure 2: Interlock and control diagram of existing system.

According to the schematic above, the LRVP can trip under three conditions: the bearing motor's high-high temperature, the winding motor's high-high temperature, or the flow switch being active for more than 15 seconds. The LRVP will trip if any one of these conditions is true.

2.2 Reliability

Reliability is the probability of a device performing its purpose adequately for the period intended under the given operating condition. Reliability engineering covers both qualitative and quantitative aspects, aiming for reliable system design to achieve reliability targets (Biniwale & Choudhary, 2023). The quantitative method is developed using maintenance data regarding to each component's time to failure and time to repair. Reliability is calculated using the formula below.

$$R(t) = 1 - F(t) = \int_0^\infty f(t)dt \tag{1}$$

2.2.1 Mean Time Between Failure

Mean Time Before Failure (MTBF) is a measure of the reliability of an asset or an equipment. It is calculated through as follows:

$$MTBF \approx \int_0^T T \times f(x)dx \tag{2}$$

With T as the time to failure of a system. Since the value of MTBF is almost equal to the time that is expected from the failure of an equipment (Calixto, Eduardo et al., 2016) or called Mean Time to Failure (MTTF), we can assume that:

$$MTBF \approx MTTF \tag{3}$$

As MTTF is defined through an arithmetic average, the MTBF can be calculated simply as its best practice through the equation as follows:

$$MTBF = \frac{Operating\ Time}{Number\ of\ Failures} \tag{4}$$

The MTBF can be calculated as the operating time of an asset, divided by the number of failures over time. As an inverse of MTBF, a failure rate can be defined through the following equations:

$$\lambda = \frac{f}{T} \tag{5}$$

With failure rate denoted by Lambda (λ) is a number that is constant for as long as the useful life of an asset (Ramesh, 2013). The failure rate is a very important tool for the reliability of an asset. Some can also expect a variety of failure rates over time, depending on the different times of failure in a system.

2.2.2 Reliability of Exponential Distribution

The Exponential distribution is one of the most widely used in reliability problems. The very reason behind the popularity of this distribution can be attributed primarily to the fact that it is used to model the time to failure of components and systems with a constant failure rate, a situation that is often realistic (Hungund & Patil, 2014). The reliability is given below.

$$R(t) = e^{-\lambda t} \tag{6}$$

2.3 Reliability Block Diagram (RBD)

While calculating the system reliability is necessary to predict the repair time, an evaluation through subsystems is one of the crucial factors when determining the Reliability Density Function. It is important to specify first the boundaries of a system, continued with defining the logic of a system using the Reliability Block Diagram (RBD). The RBD method is divided into two types of systems, with respectively series and parallel block model (Calixto, 2016).

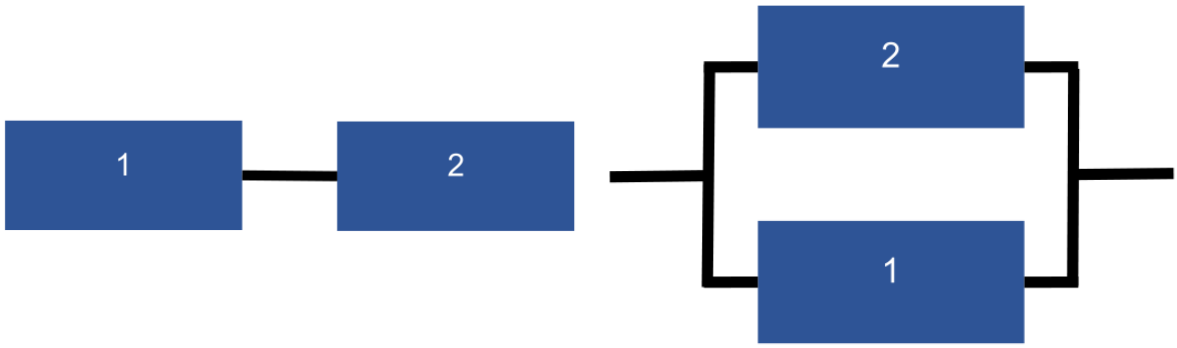

Figure 3: (a) Series and (b) Parallel block model

The series block model explains that when one piece of equipment fails, it causes a system loss of production. Whereas the parallel block model represents that it needs two or more pieces of equipment to fail in a system. Both the series and parallel block models are described mathematically by the following equations:

$$R(T) = R1(T) \times R2(T) \tag{7}$$

$$R(T) = 1 - \Big(\big(1 - R1(T)\big) \times \big(1 - R2(T)\big)\Big) \tag{8}$$

In reliability engineering, using a parallel configuration for system components is a common method to enhance overall system reliability. This approach leverages redundancy, meaning that multiple components perform the same function, thereby increasing the chances of system success even if one component fails (Menčík, 2016)

2.4 New System Implementation

In the new system, a pressure transmitter is added after the flow switch. A pressure transmitter is a device designed to measure pressure in liquids, gases, or fluids and convert this pressure into an electrical signal that can be used for monitoring and control purposes (Volonterio, 2023).

Both the flow switch and the pressure transmitter are placed in the sealing water line that supplies water to the LRVP. If the pressure detected by the pressure transmitter is below the predetermined threshold, the system will identify that the water flow is insufficient.

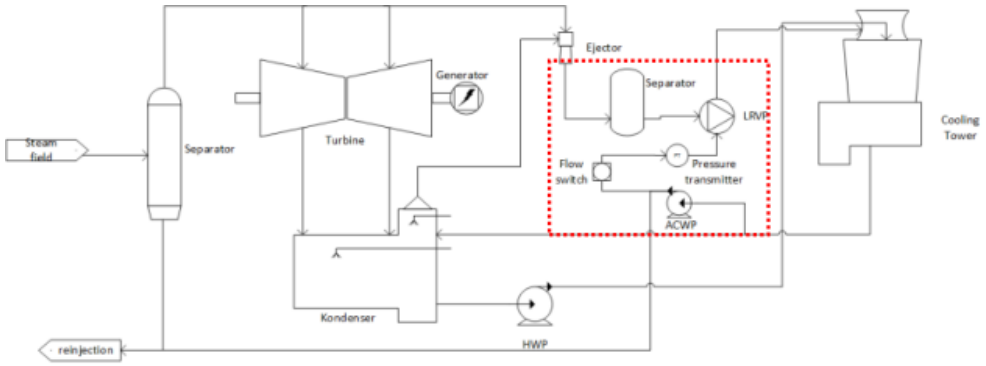

Figure 4: PFD of GPP and new system implementation.

The following is the interlock and control diagram for the new system that causes LRVP to trip.

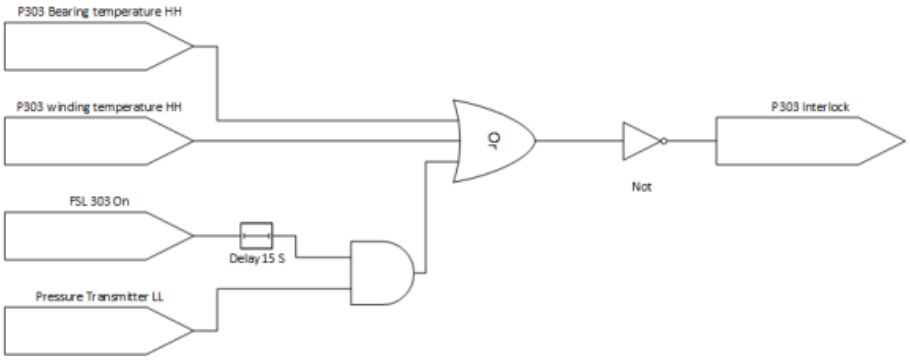

Figure 5: Interlock and control diagram existing system.

According to the schematic above, the LRVP can trip under three conditions: the bearing motor's high-high temperature, the winding motor's high-high temperature, or both of these conditions are met: the flow switch is active for more than 15 seconds and the pressure transmitter reads LL. The LRVP will trip if any one of these conditions is true.

If the pressure transmitter detects pressure below the set limit, the system will activate protection mechanisms. A low pressure reading from the transmitter will send an alarm to operations for further action, while a low-low pressure reading will trigger the LRVP, considering the flow switch is also activated.

3. RESULT AND DISCUSSION

The Power Plant experienced three plant trips between 2016 and 2023, due to false signals transmitted by the flow switch which are as follows,

Table 1: Plant trip by false signal.

Trip date	Repair Duration	Cause
Saturday, 30 January 2016	8 hours	False signal from flow switch
Saturday, 25 August 2018		
Monday, 13 March 2023		

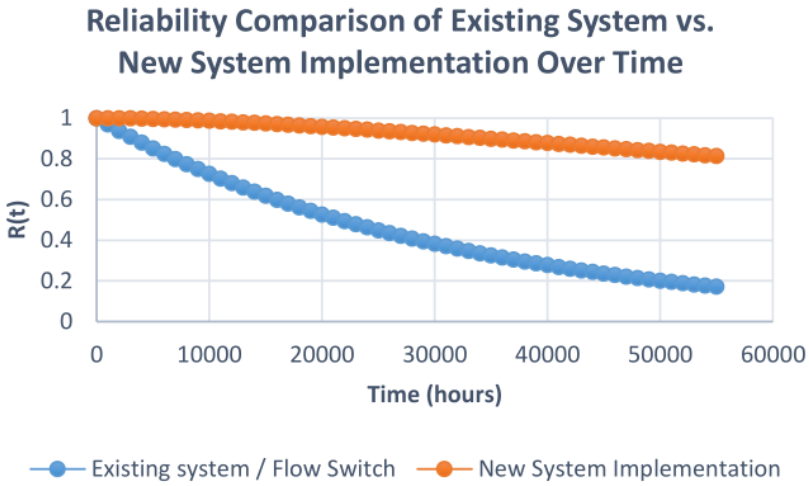

Figure 6: Reliability comparison.

Based on the data above, the Mean Time Between Failures (MTBF) is calculated to be approximately 31188 hours or 1299.5 days or equivalent to 3.5 years. Substitute the value into equation (5) and (6) resulting in the reliability function over time as shown in figure 6 for t = 3.5 years, the reliability value obtained is 0.37.

Reddy et al. (2016) in their research concluded that the smart pressure transmitter has an MTBF of 215509 hours or 8979.5 days. By substituting this value into the equation (5) and (6), reliability over time is obtained. This value is then combined with the reliability of the flow switch over time using a parallel system $R(T)FS//R(T)PT$ to improve the system reliability, resulting in the combined system reliability as shown in figure 6 for t = 3.5 years, the reliability value obtained is 0.92.

The blue line illustrates the reliability of the existing system, which uses a flow switch as the sole component for monitoring the sealing water flow to the LRVP. The orange line represents the new system implementation, which adds a pressure transmitter in parallel with the flow switch to enhance system reliability.

The existing system shows an exponential decrease in dependability with time, consistent with the exponential distribution theory often used to model the time between failures for electronic components. This decay indicates that the system's reliability decreases significantly as time progresses, reflecting a higher likelihood of system failure over an extended period. Initially, the reliability is at 1 (or 100%) but decreases progressively as time increases. This indicates that the probability of the flow switch functioning without failure decreases significantly over time.

The new system implementation also shows an exponential decrease in dependability with time. The reliability also starts at 1 (or 100%) but decreases much more slowly compared to the existing system. The combined system maintains a higher reliability over a longer period. As illustrated in the reliability graph, the new system implementation with the parallel configuration (flow switch and pressure transmitter) shows a much slower decline in reliability over time compared to the existing system with only the flow switch.

4. CONCLUSION

Implementing a highly reliable pressure transmitter in parallel with the flow switch greatly enhances the reliability of the system. The reliability of the existing system and new system implementation of 3.5 years is found to be 0.37 and 0.92 respectively thus, the difference between these values amounts to 0.55. The implementation of a parallel configuration in the cooling water system LRVP (flow switch and pressure transmitter) at the GPP has demonstrated a substantial improvement in system reliability, ensuring more stable and dependable operations over time.

REFERENCES

Biniwale, D., & Choudhary, S.: RELIABILITY ANALYSIS : A REVIEW, Solovyov Studies ISPU (2023)..

Calixto, E.: Gas and oil reliability engineering: modeling and analysis, Gulf Professional Publishing (2016).

Dwikorianto, T., Hendriansyah, T., Sastranegara, R., & Nugroho, S.: Evaluation study on the effect of production and fluid reinjection towards reservoir using micro gravity in Kamojang geothermal field, Journal of Physics: Conference Series (2018).

Hungund, C., & Patil, S.: RELIABILITY ANALYSIS OF THERMAL POWER GENERATING UNITS BASED ON WORKING HOURS. Journal of Reliability and Statistical Studies, (2014), 13-123.

Mcrill, D.: Sciencing. Retrieved from Sciencing: https://sciencing.com/purpose-flow-switch-6457925.html (2017, April 25)

Menčík, J.: Concise Reliability for Engineers, IntechOpen (2016).

Novtafiani, S., Adhikihal, S., & Zaki Hamidi, E.: Perancangan Automasi Hotwell Pump dan Gas Extraction System di PLTP Unit IV PT Pertamina Geothermal Energy Area Kamojang, Proceedings, Seminar Nasional Teknik Elektro UIN Sunan Gunung Djati, (2018), 97-108.

Ramesh, G.: Workbook to Accompany Maintenance & Reliability Best Practices 2nd Edition, Industrial Press (2013).

Reddy, Y., Narne, R., Santhosh, T., Gopika, V., & Shreshta, N.: Reliability prediction of smart pressure transmitter for use NPPs, Int J Syst Assur Eng Manag (2016).

Volonterio, E.: ABB. Retrieved from ABB: https://new.abb.com/products/measurement-products/measurement-products-blog/what-is-a-pressure-transmitter (2023, May 23).

Upgrading Bently Navada 3300 to 3500: A Case Study of Wayang Windu Unit 1 Geothermal Power Plant

Khansa Ambar Purbaranti, Teja Prasetya, Muhammad Ichsan, and U. Anang Ischak

Star Energy

Khansa.AmbarPurbaranti@starenergy.co.id, Teja.Prasetya@starenergy.co.id, m.ichsan@starenergy.co.id, uaischak@starenergy.co.id

Keywords: Upgrade, Bently Nevada 3300, Bently Nevada 3500, Case Study, Wayang Windu Unit-1

ABSTRACT

The upgrading of condition monitoring systems is crucial for enhancing the performance and reliability of geothermal power plants. This paper presents a case study on the upgrade from Bently Nevada 3300 to Bently Nevada 3500 at Wayang Windu Unit 1 in 2023. The decision to upgrade was primarily driven by the obsolescence of spare parts and services associated with the older system, as well as the desire to leverage the benefits offered by Bently Nevada 3500. The scope of work covered the Turbine-Generator and Hotwell Pump equipment, two critical components of the geothermal power plant.

Moreover, the transition to Bently Nevada 3500 empowered Wayang Windu Unit 1 with advanced monitoring capabilities, improved reliability, and enhanced performance inherent in the newer system. Bently Nevada 3500's outstanding data acquisition and processing capabilities, including increased channel count and faster processing speed, facilitated more comprehensive machine monitoring and fault detection. Furthermore, the upgraded system introduced a modern graphical user interface and sophisticated data management tools, improving the user experience and streamlining data storage, retrieval, and analysis. Additionally, the modular design of Bently Nevada 3500 ensured flexibility and scalability, while its future-proof technology ensured compatibility with emerging advancements.

This paper delves into the benefits and challenges encountered throughout the upgrade process, beside the invaluable lessons learned and best practices identified for future projects. Through a thorough analysis, this case study offers valuable insights into the significance of condition monitoring system upgrades in geothermal power plants. It highlights the importance of transitioning to Bently Nevada 3500 to optimize reliability, efficiency, and operational readiness in geothermal power generation.

1. INTRODUCTION

Star Energy Geothermal operates three different locations of Geothermal Power Plant at West Java with total capacity 886 MW (see Figure 1). Star Energy Geothermal (Wayang Windu), Ltd generates 230.5 MW, consist of two units 1 x 113.5 MW and 1 x 117 MW. Star Energy Geothermal Salak, Ltd (SEGS) generates 381 MW consist of 3 x 67 MW and supply steam to PLN to produce 3 x 60 MW electricity. While Star Energy Geothermal Darajat II, Limited (SEGD) generates 274.5 MW consists of 219.5 MW as well as to supply steam to PLN to produce 1 x 55 MW electricity.

Star Energy Geothermal (Wayang Windu) Limited operates 230.5 MW of electricity capacity. Star Energy Geothermal (Wayang Windu) Limited has exclusive right until 2039 to develop contract area under Joint Operation Contract with PT Pertamina Geothermal Energy (PGE) and sale of electricity up to 400 MW under Energy Sales Contract with PGE & PLN.

SEGWW is located 40 km south of Bandung in West Java and operates a total of 230.5 MW for the Java-Madura-Bali grid. The first Unit (113,5 MW) at Wayang Windu was completed in 1999 and, since 2000, has been producing at full capacity with an availability rate of over 98%. At the time of its installation, Unit 1 was the largest geothermal turbine in the world. On March 2nd, 2009, the then Indonesian Minister of Energy and Resources officially inaugurated Wayang Windu Unit 2, which has a generation capacity of 117 MW from a single turbine.

Three critical assets in Wayang Windu Unit-1 are moniored by supervisory instrument, Turbine, Generator and Hot Well Pump. The FUJI 110 MW steam turbine is directly coupled to the FUJI two-pole 137.5 13.8 kV generator. The steam turbine is a single casing, double-flow, reaction type with eight stages in each flow. Its type is single casing, dual flow, dual exhaust, condensing. It has eight blading stages with rated gross output of 110 MW, its rated steam pressure and temperature are 10.2 bara and 180.7 deg C, its back pressure at exhaust is 110 mbar absolute, its pressure relief device operating pressure is 0.5 barg, the direction of rotation is clockwise

viewed from the generator side. The critical speed of turbine rotor is 1950 rpm and the critical speeds for turbine free standing blades are 2750 and 3230 rpm.

Figure 1: Star Energy Geothermal Plant locations at West Java, Indonesia.

The generator is three phase 50Hz FTLRI type air cooled with forced air-cooling using water. Its terminal voltage is 13,8 kV, its line current 5753 A, its insulation class is F (stator & rotor), its power factor is 0.8 lagging, its rotating speed is 3000 rpm with brushless excitation, it has two poles. Its rotor critical speeds below synchronous speed are 1156 rpm for generator shaft and 1450 rpm for combined unit. Its rotor critical speed above synchronous speed are 3588 rpm for generator shaft and 3950 rpm combined unit.

The condenser cooling water and condensed turbine exhaust steam collects in the condenser hotwell as condensate. Two 50% duty hotwell pumps remove condensate from the hotwell and deliver it to the cooling tower. The hotwell pump is from DMW corporation with vertical centrifugal canned type.

Mechanical failure especially in Turbine-Generator of power plant is what should be avoided, because it is not only can cause loss of production but also can be catastrophic. Continuously monitoring critical asset parameters such as vibration, temperature, speed, and numerous other condition indicators is a proven method for anticipating and preventing mechanical failures – proven in tens of thousands of industrial facilities around the world by delivering tangible benefits such as: Improved protection from catastrophic failures, better machinery reliability/availability, fewer process interruptions, enhanced maintenance/outage planning, lower maintenance and repair costs, longer intervals between outages, reduced insurance premiums. (Baker Hughes -2020) Critical asset parameters at Wayang Windu Unit-1 are supervised by Bently Nevada System, auto shut-down protection is also provided for several conditions which are turbine differential expansion very high, turbine/generator bearing vibration very high, turbine/generator bearing metal temperature very high, and thrust failure. Overspeed in turbine is supervised by six speed sensors, three of them are the input for F/V converter and alarm setter to be the input for overspeed protection, two of the sensors are the input for Woodward, one of the sensors as the input to DCS for indicator.

Before the upgrade, Bently Nevada 3300 was used and below are the detail of the T-G and also HWP supervisory system in Wayang Windu U-1.

Temperature Monitoring

Existing temperature monitoring of WW Turbine-Generator consist of temperature sensors, temperature monitor, and relay module. Refer to Tavle 1,2, and 3.

Turbine Speed Monitoring

Existing turbine speed monitoring of WW Turbine-Generator consist of speed sensors, frequency to voltage converter, and relay module. Refer to Table 3 and 4.

Turbine Keyphasor

Existing turbine keyphasor monitoring system consist of position detector, extension cable, proximitor, system monitor, and DC Power supply. Refer to Table 5 and 6.

Table 1: Instrument Configuration for Temperature Monitoring.

No.	Element	Description	Remarks
1.	Sensor	RTD temperature sensor (Redundant) Sensor Connection	PT100 M10
2.	Module	Temperature Monitor Relay Module Module Configuration	With local digital indication U1: 3300/35-12-01-00-00 Bently With hard contact: High and High-High Protection Panel Rack Configuration
3.	Output	Analog Modbus	DC4-20mA (Hardwire to DCS) Not connected

Table 2: Instrument Operating Range for Temperature Monitoring.

No.	Name	Scale Range	Unit		Normal Value	Design Value	Alarm	Manufacturer (Installed)	Connection To
1.	Turbine Thrust Brg. Mtl. Temp. (Front)	0-200	ºC		90	120	H: ≥100ºC HH: ≥120 ºC	Okazaki R35	Temp. Monitor CH 1
2.	Turbine Thrust Brg. Mtl. Temp. (Rear)	0-200	ºC		90	120	H: ≥100ºC HH: ≥120 ºC	Okazaki R35	Temp. Monitor CH 2

No.	Name	Scale Range	Unit	Normal Value	Design Value	Alarm	Manufacturer (Installed)	Connection To
3.	Turbine Brg. Mtl. Temp. (Front)	0-200	ºC	90	120	H: ≥100ºC HH: ≥120 ºC	Okazaki R35	Temp. Monitor CH 3
4.	Turbine Brg. Mtl. Temp. (Rear)	0-200	ºC	90	120	H: ≥100ºC HH: ≥120 ºC	Okazaki R35	Temp. Monitor CH 4
5.	Gen. Brg. Metal Temp. (T-Side)	0-150	ºC	90	125	H: ≥100ºC HH: ≥120 ºC	Okazaki R35SP	Temp. Monitor CH 5
6.	Gen. Brg. Metal Temp. (E-Side)	0-150	ºC	90	125	H: ≥100ºC HH: ≥120 ºC	Okazaki R35SP	Temp. Monitor CH 6

Table 3: Instrument Configuration.

No.	Element	Description	Remarks
1.	Sensor	MPU	Pulse
2.	Module	Amplifier Module Speed Converter Module	For governor speed input (2 sensors), for indicator (1 sensor) For DCS (1 sensor), for Protection Relay (3 sensors)
3.	Output	Analog Relay Modbus	DC4-20mA (Hardwire to DCS) Protection Relay Not available

Table 4: Instrument Operating Range.

No.	Name	Scale Range	Unit	Model	Manufacturer	Connection to
1.	Turbine Speed	0-3600	Rpm	MP-930	Ono Sokki	IC Amplifier → Governor Woodward 505D
2.	Turbine Speed	0-3600	Rpm	MP-930	Ono Sokki	IC Amplifier → Governor Woodward 505D
3.	Turbine Speed	0-3600	Rpm	MP-930	Ono Sokki	Speed Amplifier → F/V Converter → DCS
4.	Turbine Speed	0-3600	Rpm	MP-930	Ono Sokki	F/V Converter → Alarm Setter
5.	Turbine Speed	0-3600	Rpm	MP-930	Ono Sokki	F/V Converter → Alarm Setter
6.	Turbine Speed	0-3600	Rpm	MP-930	Ono Sokki	F/V Converter → Alarm Setter

Table 5: Instrument Configuration.

No.	Element	Description	Remarks
1.	Sensor	8mm Probe Sensor Connection	Voltage. Bently 330104-00-04-10-02-00 M8
2.	Cable	Extension Cable	
3.	Module	Proximitor System Monitor Power Supply 3300 Weatherproof housing	Bently Nevada 330200-50-00 (Unit-1) Bently Nevada 3300/03-01-00 3300/14-01-20-00 3300/05-26-00-00
4.	Output	Analog Relay	NA NA

Table 6: Instrument Operating Range.

No.	Name	Scale Range	Unit	Normal Value	Design Value	Alarm
1.	Key Phasor	0-3600	Rpm	(-)	(-)	(-)

Table 7: Instrument Configuration.

No.	Element	Description	Remarks
1.	Sensor	8mm Probe Sensor Connection	Voltage Bently 330104-00-04-10-02-00 M8
2.	Cable	Extension Cable	Bently 330130-040-01-00
3.	Module	Proximitor System Monitor Power Supply	Bently Nevada 330100-50-00 (Unit-1) Bently Nevada 3300/16-13-01-00-00 3300/14-01-20-00
4.	Output	Analog Relay Buffer Output	DC4-20mA (hardwire to DCS) Dry Contact for Alarm: High and High-High Protection BNC Connection

Table 8: Instrument Operating Range.

No.	Name	Scale Range	Unit	Normal Value	Design Value	Alarm	Connection to
1.	Turbine Shaft Vibration (Front1)	0-200	µm			Turbine Front Bearing Vib H: ≥100 µm	Vibration Proximitor Turbine Shaft Vibration (Front1)
2.	Turbine Shaft Vibration (Front2)	0-200	µm			Turbine Front Bearing Vib HH: ≥146 µm	Vibration Proximitor Turbine Shaft Vibration (Front2)
3.	Turbine Shaft Vibration (Rear1)	0-200	µm			Turbine Rear Bearing Vib H: ≥100 µm	Vibration Proximitor Turbine Shaft Vibration (Rear1)
4.	Turbine Shaft Vibration (Rear2)	0-200	µm			Turbine Rear Bearing Vib HH: ≥146 µm	Vibration Proximitor Turbine Shaft Vibration (Rear2)
5.	Generator Shaft Vibration (T-Side1)	0-200	µm			Gen T-Side Bearing Vib H: ≥100 µm	Vibration Proximitor Generator Shaft Vibration (T-Side1)
6.	Generator Shaft Vibration (T-Side2)	0-200	µm			Gen T-Side Vib HH: ≥146 µm	Vibration Proximitor Generator Shaft Vibration (T-Side2)
7.	Generator Shaft Vibration (E-Side1)	0-200	µm			Gen E-Side Bearing Vib H: ≥100 µm	Vibration Proximitor Generator Shaft Vibration (E-Side1)
8.	Generator Shaft Vibration (E-Side2)	0-200	µm			Gen E-Side Vib HH: ≥146 µm	Vibration Proximitor Generator Shaft Vibration (E-Side2)

Turbine-Generator Bearing Vibration

Existing Turbine-Generator bearing vibration monitoring system consist of 8mm Probe, extension cable, proximitor, dual vibration monitor, and relay modules. Refer to Table 7 and 8.

Turbine Shaft Thrust Displacement

Existing Turbine Shaft Thrust Displacement Monitoring System consist of position detector, extension cable, proximitor, and dual thrust position monitor, and relay modules. The outputs of dual thrust position monitor are connected to DCS through DC4-20mA cable. Refer to Table 9 and 10.

Table 9: Instrument Configuration.

No.	Element	Description	Remarks
1.	Sensor	8mm Probe Sensor Connection	Voltage Bently 330104-00-04-10-02-00 M8
2.	Cable	Extension Cable	Bently 330130-040-01-00
3.	Module	Proximitor System Monitor	Bently Nevada 330100-50-00 (Unit-1) Bently Nevada Dual Thrust Position Monitor 3300/20-12-01-01-00-00
4.	Output	Analog Relay	DC4-20mA (hardwire to DCS) Dry Contact for Alarm: High, Low, High-High, and Low-Low Protection

Table 10: Instrument Operating Range.

No.	Name	Scale Range	Unit	Normal Value	Design Value	Alarm	Connection To
1	Turbine Thrust Displacement	-1 - +1	Mm			H ≥ +0.5mm L ≤ -0.5mm HH ≥ +1.0mm LL ≤ -1.0mm	Proximitor → Position Monitor
2	Turbine Thrust Displacement	-1 - +1	Mm				Proximitor → Position Monitor

Turbine Shaft Differential Expansion

Existing Turbine Shaft Differential Expansion Monitoring System consist of position detector, extension cable, proximitor, 25mm Differential Expansion Transducer, special differential expansion monitor. Refer to Table 11 and 12.

Table 11: Instrument Configuration.

No.	Element	Description	Remarks
1.	Sensor	7200 11mm Probe (diff. expansion A&B) Sensor Connection 25mm Diff. Expansion Transducer Sensor Connection	Voltage. Bently 19048-00-20-10-02 M11 Bently. 102242-00-07-50-01 M25
2.	Cable	Extension Cable	Bently 24710-040-00
3.	Module	Proximitor System Monitor	Bently Nevada 19049-03 (Unit-1) Ramp Differential Bently Nevada (3300/46-XX-01-01-00) Full Scale:2-0-12mm, Single 4° Ramp Dual Differential Bently Nevada 3300/45-XX-XX-01-00 (ChannelA: Full Scale 4.5-0-7.5mm 25DE Probe; ChannelB: Full Scale 6-0-10mm)
4.	Output	Analog Relay	DC4-20mA (hardwire to DCS) Dry Contact for Alarm: High-High Protection

Table 12: Instrument Operating Range.

No.	Name	Scale Range	Unit	Normal Value	Design Value	Alarm	Connection to
1.	Turbine Differential Expansion A	2-0-12	Mm			VH: ≥ +5.0 mm ≥ -3.0 mm	Turbine Differential Expansion A Proximitor
2.	Turbine Differential Expansion B	6-0-10	Mm				Turbine Differential Expansion B Proximitor
3.	Turbine Differential Expansion C	4.5-0-7.5	Mm			VH: ≥ +5.0 mm ≥ -3.0 mm	Terminal Box

Hotwell Pump Vibration Monitoring

Existing Hotwell Pump (HWP) Vibration Monitoring System consist of velomitor piezo-velocity sensor, interconnecting cable, velocity transducer housing, dual velocity monitor, connector protector kit, connector protector pack, isolator. Refer to Table 13 and 14.

Table 13: Instrument Configuration.

No.	Element	Description	Remarks
1.	Sensor	Velomitor piezo-velocity sensor	Bently 330500-01-00
2.	Cable	Interconnecting Cable Connector protector kit Connector protector pack Isolator	Bently 89477-17 40113-02 40180-02 19094-01
3.	Module	Velocity Transducer Housing Dual Velocity Monitor	Bently Nevada 21128-02-01 (Unit-1) Bently Nevada 3300/55-03-14-14-00-00-05-00
4.	Output	Analog Relay	DC4-20mA (hardwire to DCS) Dry Contact for Alarm: High

Table 14: Instrument Operating Range.

No.	Name	Scale Range	Unit	Normal Value	Design Value	Alarm	Connection to
1.	HWP (A) X Vibration	0-200	µm			H ≥150 µm	HWP (A) X Vibration Proximitor
2.	HWP (A) Y Vibration	0-200	µm			H≥150 µm	HWP (A) Y Vibration Proximitor
3.	HWP (B) X Vibration	0-200	µm			H≥150 µm	HWP (B) X Vibration Proximitor
4.	HWP (B) Y Vibration	0-200	µm			H≥150 µm	HWP (B) Y Vibration Proximitor

Obsolescence of Bently Nevada 3300

As mentioned above, most of the T-G parameters in Wayang Windu Unit-1 are supervised by Bently Nevada system, before Wayang Windu Unit-1 Shutdown and Turn-Around (SDTA) on August 2023, Bently Nevada 3300 was still used while on March 2014 it is classified as obsolete, meaning the product has no (or limited) support and is not recommended for continued use in a machinery protection application (Phase 5). In fact, limited repairs were possible only until 2017. Before the upgrade, Wayang Windu mitigated the issue if BN 3300 fails with the spare of BN 3300 modules in Darajat site.

BN 3300 was upgraded to BN 3500 on WW U-1 SDTA in 2023, after its commissioning in WW U-1 on September 2023, BN 3500 is still in lifecycle phase 1 and 2, BN 3500 will be in lifecycle phase 1 and 2 until 2024 ~ 2027, then it will be in phase 3 for 5 to 8 years. After this period, the system will transition to phase 4 and it will stay in phase 4 as long as Bently Nevada is able to procure the necessary components to perform repairs. These dates are estimates based on Bently Nevada's current planning and market conditions, actual dates of lifecycle changes may vary depending on industry and business conditions in the future as some components used to manufacture and/or repair systems can become unavailable. Bently Nevada Asset Condition Monitoring hardware utilized a life cycle management program consisting of five phases as described below.

- Phase 1: Product Release

Hardware is released for sale with full support including ongoing enhancements, custom modifications, new spare parts, and full repair capabilities.

- Phase 2: Mature Product

Same as Phase 1 except that no new enhancements are planned. Custom modifications are still available but discouraged. A notification of last time to buy new systems is typically issued several months before transitioning to Phase 3.

- Phase 3: Spares Only

Product is no longer available for new installations and no new custom modifications are available. New spare parts (including those for existing custom modifications) are still available. New spare parts (including those for existing custom modifications) are still available, and repair and support are provided as in Phases 1 and 2. A notification of last time to buy spare parts is typically issued several months before transitioning to Phase 4.

- Phase 4: No Spares, Limited Support

New spare parts are no longer available, and support is limited to repair, exchange, or remanufacture (subject to component availability). Notice of last date to repair is typically issued several months before transitioning to Phase 5.

- Phase 5: Obsolete

The product has no or limited support and is not recommended for continued use in a machinery protection application. Customers are advised to migrate to an appropriate replacement product with the assistance of their Bently Nevada sales professional.

2. UPGRADE OF BENTLY NEVADA 3300 TO BENTLY NEVADA 3500 IN WAYANG WINDU UNIT-1

Wayang Windu Unit-1 (WW-1) had been using Bently Nevada (BN) 3300 to monitor its Turbine-Generator (T-G) parameters since WW-1 commissioning in 2000. In 2017, Bently Nevada announced that Turbine Supervisory Instrument (TSI) BN 3300 is obsolete, and Bently Nevada will no longer support spare parts and services for this model.

In case failure of BN 3300, the turbine and generator will be unprotected and potentially lead to LPO due to spare part unavailability. Lead time for typically new version of TSI is 24 weeks after PO or will potentially result in large financial losses of around USD$47.4 M. Obsolete BN 3300 was upgraded with Bently Nevada 3500 to get full support on the technical and the spare parts from OEM.

This upgrade project covered Bently Nevada 3500 material purchasing, services such as engineering and detail design, setting, testing, installation on Unit 1 during 2023 Shut Down and Turn Around (SDTA) and commissioning.

The procurement process was started in Q4-2022 to meet the schedule for new turbine supervisory instrument installation during WW-1 SDTA in Q3-2023.

2.1 Scope of Upgrade

The supervised parameters of Wayang Windu U-1 T-G and Hot Well Pump (HWP) parameters are Turbine Thrust Bearing Metal Temperature, Turbine Bearing Metal Temperature, Generator Bearing Metal Temperature, T-G Shaft Vibration, Turbine Differential Expansion, Turbine Shaft Thrust Displacement, Keyphasor and HWP Vibration.

The installation service of new rack of Bently Nevada 3500 Vibration Monitor was including panel BN 3300 dismantling, front cubicle panel's modification as the dimension of BN 3300 and BN 3500 is different. BN 3500 vibration monitor installation, configuration & verification, and loop check/signal verification.

2.2 Challenge and Lesson Learnt of the Upgrade

As stated, the upgrade from Bently Nevada 3300 monitoring system to Bently Nevada 3500 monitoring system was done during Outage of Wayang Windu Unit-1 on August 2023. This 2023 Outage has a target of 12 days completion, so the upgrade process is needed to be finished under 12 days. SEG challenged the service contractor to do the installation within 6 days, the mutual understanding of it as a challenge and not for the maximum budgeting for contractor's man-power is needed for both the contract owner and the contractor.

The other lesson learnt from this upgrade project are to ask the contractor to provide a drawing and bill of material even for the smallest modification task. Involve maintenance team since engineering phase, ensure maintenance team is informed of all the details of modification.

2.3 The Advantage of Using Bently Nevada 3500

The 3500 is the result of decades of experience in the condition monitoring & protection field. With features like 1X, 2X, not 1X variables, extensive fault tolerant design, RF immunity, ease of configuration, etc. – the 3500 is an improvement on the 3300 in almost every way. And with a standardized 19" size and 4-channel cards that are less than an inch wide, the channel density possible in a 3500 is far greater than a 3300. Several application-specific monitors are also available (recip compressor, hydro, aeroderivative gas turbine, etc.), making it the ideal solution for all your condition monitoring & protection needs. (Baker Hughes)

The 3500 Series Machinery Monitoring System is also designed to communicate directly with System 1® software for state-of-the-art machinery condition monitoring & diagnostic capabilities. This ensures that along with industry trusted machinery protection, we also have access to effective machinery condition monitoring tools, so you are well informed about the health of your machines. Understanding their condition allows us to more effectively plan maintenance cycles and optimize planned down time for these critical assets. 3500 series is also easy to be configured using configuration software and the modules are hot swappable.

Table 15: The material scope of the upgrade and several differences between modules of BN 3300 and modules of BN3500 also the description of each BN 3500 modules.

No.	Parameter as input	Modules in BN3300	Modules in BN3500	Remarks
1.	Turbine Thrust Bearing Metal Temperature (Front)	3300/35	3500/61 Temperature Monitor	Both 3300/35 and 3500/61 are 6-channel temperature monitor. 3500/61 accepts both RTD and TC temperature inputs. It compares the input against user-programmable alarm setpoints. 3500/61 provides recorder outputs for each of its six channels.
2.	Turbine Thrust Bearing Metal Temperature (Rear)			
3.	Turbine Bearing Metal Temperature (Front)			
4.	Turbine Bearing Metal Temperature (Rear)			
5.	Generator Bearing Metal Temperature (T-Side)			
6.	Generator Bearing Metal Temperature (E-Side)			
7.	Turbine Shaft Vibration (Front 1)	3300/16 Dual Vibration Monitor	3500/42M Proximity Module	3300/16 module provides 2 channels, 3500/42M module provides 4 channels
8.	Turbine Shaft Vibration (Front 2)			
9.	Turbine Shaft Vibration (Rear 1)	3300/16 Dual Vibration Monitor		
10.	Turbine Shaft Vibration (Rear 2)			
11.	Generator Shaft Vibration (T-Side 1)	3300/16 Dual Vibration Monitor	3500/42M Proximity Module	
12.	Generator Shaft Vibration (T-Side 2)			
13.	Generator Shaft Vibration (E-Side 1)	3300/16 Dual Vibration Monitor		
14.	Generator Shaft Vibration (E-Side 2)			
15.	Turbine Thrust Displacement	3300/20 Dual Thrust Monitor	3500/42M Proximity Module	
16.	Turbine Thrust Displacement			
17.	Turbine Shaft Differential Expansion A	3300/46 Ramp Differential Expansion	3500/45 Position Module	3500/45 accepts input from proximity transducers, Rotary Position Transducers (RPTs), DC Linear Variable Differential Transformers (DC LVDTs), AC Linear Differential Transformers (AC LVDTs), and rotary potentiometers.
18.	Turbine Shaft Differential Expansion B			
19.	Turbine Shaft Differential Expansion C	3300/45 Dual Differential Expansion		
20.	NA	3300/14 DC Power Supply	3500/15 Low Voltage DC Power Supply	
21.	NA	(-)	3500/15 AC Power Supply	Back-up Power Supply in BN3500 rack
22.	NA	(-)	3500/22M TDI Module	The interface between 3500 monitoring system and the advanced System 1

				Optimization and Diagnostic Platform.
23.	Keyphasor	3300/03 System Monitor	3500/25 Keyphasor Module	Receives signal from proximity probes or magnetic pickups and converts the signals to digital Keyphasor© signals. Keyphasor© signal is used to measure shaft rotative speed and vector parameters such as 1X vibration amplitude and phase
24.	NA	3300 Weatherproof Housing	3500/05 19-inch Rack	19-inch rack has 14 available module slots. The rack is designed to hold all monitor modules to communicate with one another and for the power supplies to distribute power to each module as required.
25.	NA	(-)	3500/33 Relay Module 16 Channel	Each relay utilized on the Relay Module includes "Alarm Drive Logic". The Alarm Drive Logic is programmed using AND and OR logic (Boolean), and can utilize alarming inputs (alerts and dangers) from any monitor channel or any combination of monitor channels in the rack. This Alarm Drive Logic is programmed using the 3500 Rack Configuration Software to meet the specific needs of the application.
26.	NA	(-)	3500/92 Comm Gateway Ethernet	It provides extensive communication capabilities of all rack monitored values and statuses for integration with process control and other automation systems using both Ethernet TCP/IP and serial (RS232/RS422/RS485) communications capabilities. It also permits Ethernet communications with 3500 Rack Configuration Software and Data Acquisition Software.
27.	NA	(-)	3500/94M VGA Display	Delivers real-time values and current machine status at the machine and in the control room. The 3500/94M provides a real-time window into the machine health and instrumentation condition.
28.	NA	(-)	3500 Rack Config Software	
29.	NA	(-)	Engineering Laptop for Configuration	

3. CONCLUSION

Wayang Windu Unit-1has upgraded its turbine supervisory instrument to Bently Nevada 3500 Monitoring System on August 2023. It is still on lifecycle phase 1 and 2. Bently Nevada 3500 is the monitoring system which can be configured easily, it has better GUI and it can connect to system 1 to provide owner with effective machinery condition monitoring.

REFERENCES

Baker Hughes: 2021 Statement of 3500 Monitor System Lifecylce Support

Fuji Electric: Descriptive Manual of Power Station Wayang Windu Unit-1

https://www.bakerhughes.com/bently-nevada/orbit-home/orbit-article/so-you-have-3300-rack-now-what

https://www.baritorenewables.co.id/en/our-business

Turbine Supervisory Instrument Wayang Windu Unit-1

Instrument List, Instrument Loop Diagram, Schematic Drawing Wayang Windu Unit-1

Inconsistent Quality of Class G Cements

Ramil Joseph L. Bunac[1] and Lawrence Diehm Weber[2]

[1]14F 6750 Bldg, Ayala Avenue, Makati City, Philippines
[2]Riverside, Ca. 92504, USA

RBunac@pgpc.com.ph, DRBC@pgpc.com.ph

Keywords: API, Class G Cement, Cement Quality

ABSTRACT

The industry standard for cement and materials for well cementing in the petrol and natural gas industries is the API Monogram, API Spec 10A / ISO 10426. While the specifications set forth in this document are an excellent benchmark for commonly used oil well cements such as Class G cement, there are limitations to the specification's ability to ensure the desired and necessary level of performance for specific and varying cementing applications encountered in well cementing. Commonly recognized problems and the resulting primary performance factors of concern are early gelation of the cement and poor response to available chemical additives. These concerns are especially true for geothermal cementing operations, which differ from oil and gas operations in multiple ways, such as relatively low placement temperatures for various casing strings but with exceedingly elevated temperature conditions once wells are placed in production mode. Loss circulation while drilling and cementing is also a common and major challenge in most geothermal fields and without acceptable cement properties the cost of curing such losses can be substantial due to consumption of large quantities of cement and chemicals, plus the additional rig time required for such operations. Experience with many of the API Class G cements manufactured in the Asia Pacific suggests that early gelation is indeed a common problem in this region.

Production of oil well cement is a relatively small portion of the cement manufacturing industry and recent pandemic induced supply chain disruptions, coupled with an increasing demand for construction cement as economies reopened, resulted in limited availability of Class G cement in SE Asia. This has been further hampered by the fact that oil and gas operations are more predominate in the region and thus the manufacture of Class G cement is geared more to their needs and well conditions and thus the manufacturers have little incentive to make available Class G cement which is more suited to geothermal cementing operations. Importation of optimal quality Class G cement from other regions is an option but geographically isolated geothermal locations such as the Philippines are subject to significant logistical and economic barriers.

Presented in this paper is a technical background of API Class G cements as well as laboratory data detailing variations in performance of Class G cement available from regional suppliers and variations between batches of cement sourced from the same supplier. This paper documents a case history of the challenges faced by one operator in conducting cementing operations for geothermal wells in the Philippines geothermal environment with regionally available API monogramed Class G cement. This case history also includes the negative impact on performance and cost of cementing operations that less-than-optimal cement can have over a multi-year drilling campaign.

1. INTRODUCTION

1.1 Basics of Cementing

Cement is one of the most important components for drilling and completing a geothermal well. Its applications include cementing the casing strings in position, thereby providing mechanical support, corrosion protection, thermal isolation and long-term zonal isolation within the wellbore. Additionally, it is used for plug cementing operations to shut-off or control lost circulation while drilling, to provide a solid base for sidetracking operations and other remedial operations such as top-up jobs for when the desired top of cement is not achieved or when losses occurs during primary cement job on liners necessitating liner top "squeezes" and for shoe squeezes when the required seal is not achieved on the primary job.

The first application of cement in well drilling industry is recognized to have occurred in 1903 when Frank F. Hill with Union Oil Co. mixed and dumped 50 sacks of Portland cement into a well to shut off a water flow in a California oilwell. Portland cement has remained the dominant type of cement until today. Modern oilwell cementing began in 1910 when A. A. Perkins introduced his 2-plug cementing technique. As drilling became more advanced allowing drilling of deeper wells the increasingly difficult down hole conditions with high temperatures and pressures presented challenges for cementing operations. In the 1920's, techniques were tried, such as adding tons of ice to the drilling mud to cool down the wellbore before cementing. However, these

procedures had limited success which then gave rise to the development of special cement additives that could alter the cement slurry properties to allow placement of cement under the diverse range of well conditions. The use of geothermal resources has been existence for thousands of years for warmth, cleansing and as a mineral source. Use of geothermal surface sources became increasing common in the mid-nineteenth century with transportation of the heat by pipelines with the first geothermal power plant being established in 1904 in Lardarello, Italy. The first drilling and cementing of geothermal wells began in 1921 at The Geysers field in California. Demands for improved performance of the cement in ever increasing difficult down hole conditions such as temperature and pressure as the procedures employed in the 1920's such as adding tons of ice to the drilling mud in attempt to cool down the wellbore were not completely successful. This gave rise to the development of special additives to control the cement slurry properties required for cementing.

1.2 Brief History on API Specifications

Initial methods for testing and evaluating available cements utilized the ASTM (American Society of Testing and Methods) test methods for construction cement. The American Petroleum Institute soon recognized that the ASTM test methods were inadequate for well cementing applications and established the first committee to study cements in 1937. This resulted in the proposed API Code 32 in 1940, later to become API RP10B, adopted as the standard for well cement testing methodology in 1956. The actual Specification for Oilwell Cements (formerly API Standard 10A) was introduced in 1953 and since 1955, any manufacturer wishing to use the API monogram must undertake to make cement according to the relevant specifications detailed in Specification 10A.

Oilwell consumption of portland cement represents only a fraction of a percent of total world cement production, and geothermal consumption of cement is only a fraction of that used in oil and gas operations. Thus, the common well cements are generally derived from the same clinker as construction cements of the appropriate “type”. They may be ground to a different degree of fineness in certain cases so that they pass the additional tests prescribed by the API but, otherwise, they are essentially the same. Thus, most of the major “classes” of API cement are analogous, or very similar, to the various “types” of cement used in the construction industry.

Of the various types or 'classes' of API cement (Figure 1.) the most common one in use outside North America is Class G, a basic sulphate-resistant cement that can be modified with specific additives to perform at the extreme depths typical of today’s oilwells. While API Class G is available in the Asia Pacific region, the number of API Monogram manufacturers is very limited in comparison to construction cement manufacturers which are common and plentiful in most every country in the region due to the high cement demand of the construction market.

This is particularly true in countries such as the Philippines where API oilwell cement must be imported or where local regulations impose heavy tariffs on foreign goods.

1.3 Cement Performance Issues

When water is added to cement a series of reactions takes place that results in the formation of the final set product. These reactions are essentially the same for all Portland cements varying only in the rate at which they occur. This is dependent on the proportions of each phase present and the average particle size of the cement powder.

Class G Specification:
The product obtained by grinding Portland cement clinker, consisting essentially of hydraulic calcium silicates, usually contains one or more forms of calcium sulfate as an interground addition. No additions other than calcium sulfate or water, or both, shall be inter- ground or blended with clinker during manufacture of Class G well cement. This product is intended for use as a basic well cement. It is available in moderate sulfate-resistant (MSR) and high sulfate-resistant (HSR) Grades.

Intended Application:
Intended for use as a neat cement from the surface to 8,000 feet, or to 200F BHST, without additives. When modified with additives, this cement can be used for most well applications both shallow and deep. This cement is manufactured under stringent requirements for chemical content and physical performance tests.

Figure 1: API Classification for Class G Cement.

The chemical reactions involved in setting are complex and still the subject of much conjecture. However, for a simple system like neat cement powder plus distilled water as used for the API Specification test, the setting process is straightforward despite the complex reactions involved. In such circumstances the factors affecting setting time are temperature, chemical composition, including gypsum content and particle size distribution.

Such ideal conditions are never encountered in the field, however, where logistics dictate the use of mixing waters of varying quality, and well status necessitates the use of retarders or other materials to achieve the desired properties of a cement slurry. Mixing energy, shear rates and heat-up rates, due to specific equipment and well configurations, can all influence cement behavior. Also, cements are particularly susceptible to environmental

conditions such as ambient temperature and humidity, so their storage and transportation are key factors in controlling their behavior, particularly in the Tropics. But it is in their response to additives under actual field conditions, that cements display their greatest variation.

One of the more common problems seen in the well drilling industry is that of cement gelation. Gelation can be defined as a premature viscosification or a gel-strength buildup of the cement slurry. This can have significant consequences for field operations and may be so severe as to cause job failure. Due to its often-unpredictable nature, the phenomenon of cement gelation is difficult to deal with, along with the fact that it may occur under a variety of field conditions. It may occur immediately after mixing or as the cement slurry is subjected to temperature increases during pumping. Gelation often occurs under conditions of limited shear or during static conditions such as for planned or unplanned shutdowns during a cement job. The fact that the physio-chemical basis of gelation is complex, it can occur under a broad spectrum of conditions. Some of factors involved include the chemical composition of the cement powder itself, its fineness, its microstructure, the mix water quality, the types (if any) of additive used, the rate of heat flux into the slurry as well as the final temperature to which the slurry is exposed.

2. CEMENT MANUFACTURE

2.1 Manufacturing Process

Cements are industrial products and therefore subject to variations in composition and properties. These variations can be minimized by careful selection and grading of raw materials and by close attention to the proportioning of the raw materials and process control during manufacture. Portland cement is a complex mixture of heterogeneous inorganic compounds. The principal phases that can be identified are Tricalcium silicate (C_3S), Dicalcium silicate (C_2S), Tricalcium aluminate (C_3A) and Tetracalcium aluminoferrite (C_4AF), the proportions of these vary with the class of cement. Associated with these are also relatively minor quantities of Magnesium Oxide (MgO) and gypsum ($CaSO_4.2H_2O$).

The manufacturing process involves the 'burning' of a mixture of calcareous and argillaceous materials in a rotary kiln and subsequently grinding the product to a fine powder. The calcareous materials are usually forms of calcium carbonate (seashells, limestone, chalk) and are effectively the source of lime for the reaction. The argillaceous materials provide silica and may come in the form of clays, shales or silica rock. Bauxite (Aluminum oxide) and iron ore are also added to provide aluminum and iron where the source rocks are low in these elements.

The raw materials are first run through crushers and stored, eventually being transferred to the raw material grinding mills where they are combined in appropriate weight proportions. The mixture is passed through the grinders multiple times until it is ground to the required fineness. Once this fineness has been attained the raw meal is pumped to air-blending silos and from there via a weigh feeder is transported to the cyclone system where it is preheated to approximately 400ºC by the hot gases coming from the kiln. After entering the kiln itself, the raw meal passes through a series of temperature zones as summarized in Table 1.

Table 1: Cement Manufacturing Process.

Zone	Temperature of Material	Physical and Chemical Changes
1.Preheating zone	400 - 550 ºC	Driving off impurities continues
2.Calcining zone	550 - 1000 ºC	Carbonates decompose to oxides
3.Sintering zone	1000 - 1450 ºC	Oxides combine to form clinker minerals and modules of clinker form due to partial melting
4.Outlet zone	1450 - 1200 ºC	Cooling begins

2.2 Variations in Composition and Properties

The rate of movement of the material from inlet to outlet is dictated by the slope and rotation of the kiln. The resultant product called clinker exits at the lower end of the kiln through a grate cooler and is then transported to the clinker storage facility. Once the clinkehas cooled and it is time to proceed with the final processing the clinker is mixed with a specific quantity of gypsum and ground to a fine powder in a ball mill. The output from the ball mill is then fed to an air separator such that coarse particles being recirculated. Cements containing too high a proportion of coarse particles have a reduced rate of hydration, high free water level and a delayed development of compressive strength. Cements which contain excessive quantities of fines typically exhibit poor rheological properties and frequently require the addition of large amounts of additives to provide effective retardation. By proper adjustment of the feed to the mill and air separator, the fineness is controlled.

2.3 Cement Property Issues

During the grinding process, the temperature of the material rises above the boiling point of water. This causes the gypsum (CaSO4.2H2O) added to be partially dehydrated to hemihydrate (CaSO4.½H2O Plaster of Paris) and anhydrite (CaSO4). Such a change can induce a phenomenon known as 'false set' a premature thickening when the cement is mixed with water, which is obviously undesirable. This dehydration of gypsum is reduced by maintaining the temperature of the cement within prescribed limits and by spraying water into the mill. After grinding the meal, the process of cement manufacture is complete, and the product is pneumatically transferred to a silo for storage.

3. CEMENT QUALITY

3.1 API Specifications

All batches of raw materials should be analyzed chemically before use and from the grinders and to the kiln. Such analysis should be carried out on a strict schedule (every 1-3 hours) during manufacture. Analysis of the clinker is more detailed and includes estimations of free lime and sulphate while the final product, the cement itself, must be subjected to additional physical tests such as sieve analysis and specific surface area determine (Blaine fineness). In choosing between available class G cements, the primary performance factors of concern are retarder response and early gelation of the cement. The chemical and physical properties of cement determining these performance factors include tricalcium aluminate (C3A) content, fines content and free lime. For most cement slurry applications, acceptable performance requires minimization of these three properties. In many cement purchase contracts, the cementing service company and/or the operating company specifies an API class G cement of high sulfate resistance with its lower limitation (3.0% maximum) on tricalcium aluminate content. Fines content and free lime concentration contribute to the problems but neither one is addressed directly by API specifications (Table 2.)

Table 2: API Cement Manufacturing Specifications.

Description	API Specification Class G HSR
Silicon Dioxide (SiO3)	n/a
Aluminum dioxide (Al2O3)	n/a
Ferric Oxide (Fe2O3)	n/a
Magnesium Oxide (MgO)	max. 6.0 %
Sulfur Trioxide (SO3)	max. 3.0 %
Tricalcium Silicate (C3S)	max. 65 % / min 48 %
Tricalcium Aluminate (C3A)	max. 3.0%
C4AF+2*C3A	max. 24 %
Loss on Ignition	max. 3.0 %
Insoluble Residue	max. 0.75 %
Total Alkali (%Na2O+0.658*K2O)	max. 0.75 %
Blaine Finness (m2 / kg)	n/a
Autoclave Expansion (%)	n/a

Finally, all necessary API Specification tests (Table 3), including determinations of free water, thickening time per Schedule 5, soundness and compressive strength, must be conducted and this information recorded on a report.

Table 3: API Cement Slurry Performance Specifications.

Description	Summarized API Specification
Thickening Time	More than 90, less than 120 min, tested at 125 F, schedule 5 API, 1.9 SG, 44% water
Consistency	Less than 30 Bc during 15-30 min. of the stirring period, tested at 125 F, schedule 5 API, 1.9 SG, 44% water
Free Water	Less than 3.5ml/250ml @ 80 F
Compressive Strength	> 300 psi after 8 Hours @ 100 F > 1500 psi after 8 Hours @ 140 F

3.2 Potential Problems Not Detected by API Tests

Cements from different manufacturers or even different batches from the same manufacture which even though they may pass the API specifications, often exhibit wide differences in performance when exposed to various mixing, pumping and wellbore conditions in addition to response to various additives and additive concentrations.

Given this fact, it is always preferable to identify and choose the available API cement which best fits operational needs and conditions and then continue to monitor the performance of each new batch. Such an approach helps detect potential problematic batches of cement and allows designs to be modified, if necessary. This strategy can dramatically reduce the number of unsuccessful cement jobs, but it does have limitations.

Table 4: API Cement Slurry Specification Testing.

Supply 1, Lot 3	Supply 1, Lot 6
Thickening Time S/N: Single Cell Set Conditions – Set hard Consistency: 40 Bc – 01:22 hr:mn; 70 Bc – 01:52 hr:mn; 100 Bc – 01:59 hr:mn Thickening Time Chart 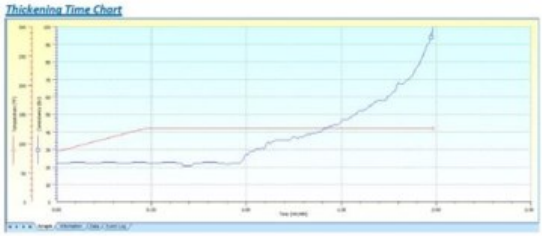 TESTING SPECIFICATION Test Item: Appearance – Unit: – Specification: Free Powder Flow – Results: Free Powder Flow Thickening Time – Unit: minutes – Specification: 90-120 – Results: 119 Consistency during the 15 mins to 30 mins stirring period – Unit: Bc – Specification: Max. 30 – Results: 22	Thickening Time S/N: Single Cell Set Conditions – Set hard Consistency: 40 Bc – 01:03 hr:mn; 70 Bc – 01:29 hr:mn; 100 Bc – 01:43 hr:mn Thickening Time Chart 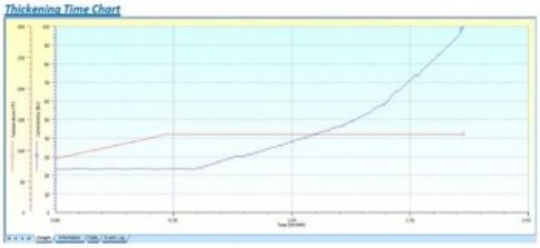 TESTING SPECIFICATION Test Item: Appearance – Unit: – Specification: Free Powder Flow – Results: Free Powder Flow Thickening Time – Unit: minutes – Specification: 90-120 – Results: 103 Consistency during the 15 mins to 30 mins stirring period – Unit: Bc – Specification: Max. 30 – Results: 24

Table 5: Variation between 2 different lots of cement of exact same slurry design.

Supply 1, Lot 3 16.0 ppg Tieback Design	Supply 1, Lot 5 16.0 ppg Tieback Design
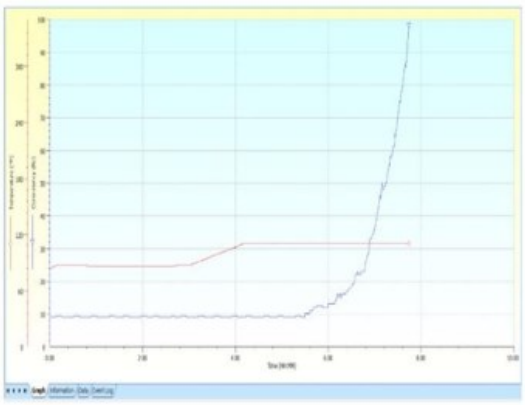	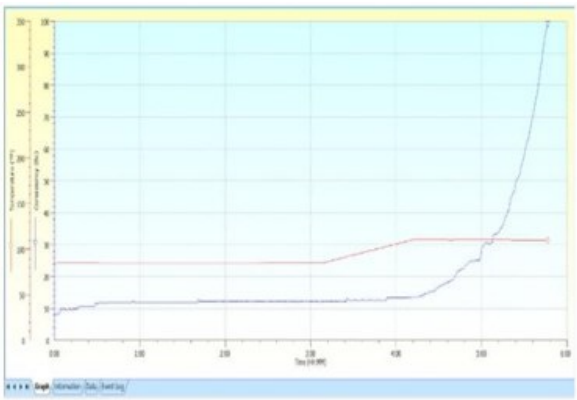
Consistency: 40 Bc – 04:05 hr:mn – 110 °F 70 Bc – 04:31 hr:mn – 110 °F Batch Mix Time – 03:00 hr:mn – 88 °F Thickening time does not include Batch mix time	Consistency: 40 Bc – 02:18 hr:mn – 110 °F 70 Bc – 02:36 hr:mn – 110 °F Batch Mix Time – 03:00 hr:mn – 88 °F Thickening time does not include Batch mix time
(2 hour batch mix time)	(2 hour batch mix time) 2 hour decrease in Thickening Time due to new lot of cement

The behavior of cements which pass the API Specification tests may vary greatly when mixed at densities and temperatures different than that specified in the API Specification Tests, and with the addition of chemical additives. Experience with some API cements and most construction cements manufactured in Asia Pacific has found that early gelation is a common problem. At best, the API Class G Specification tests may provide some insight into the gelation tendencies of a given cement. Quite often this problem is not identified until additional testing is conducted as some cement designs may perform as required regardless of the cement being used whereas others can be drastically impacted by differences in the cement supply. Table 4 presents two different batches of

cement which both meet API Specifications. Note that for Lot 3, the thickening time result is approaching the upper limit of the specification and Lot 6 has a shorter thickening time than Lot 3 but well within specification. Table 5 shows how these two different Lots of cement behave differently in an actual cement slurry design. Lot 6 exhibits a two-hour shorter Thickening Time for the exact same slurry design.

Thus, thickening charts become an important record of the cement's potential for problems. Figures 2. and 3. Illustrate types of undesirable setting behavior because of gelation of the cement slurry as observed by the Thickening Time charts and observations of the cement slurry condition after removal from the consistometer and opening of the cement slurry test cup and removal of the paddle assembly.

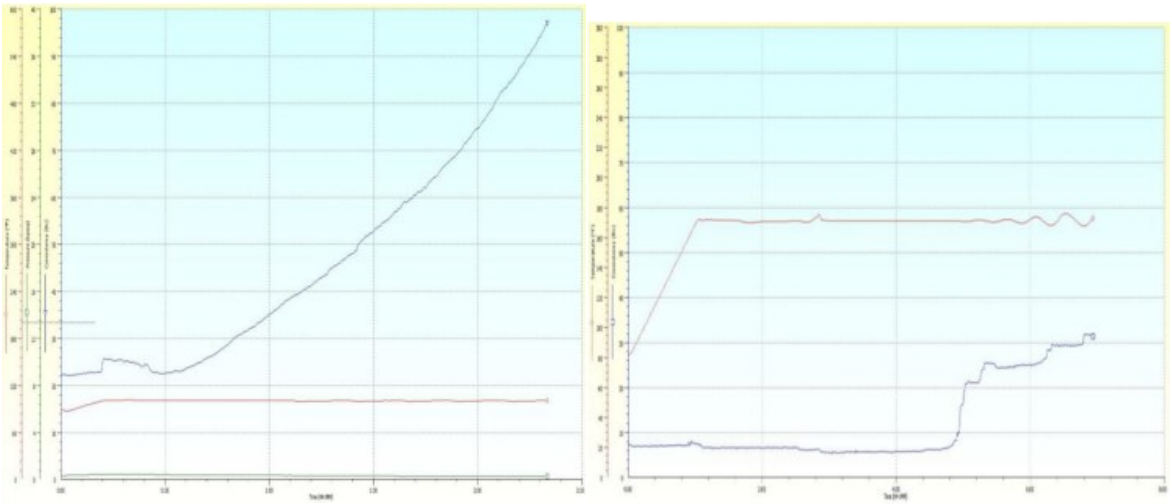

Figure 2: Thickening Time Charts with indication of Cement Gelation.

Figure 3: Slurry Test cup pictures showing gelation as exhibited by cement forming around the center of the consistometer cup paddle due to less mixing energy.

4. CASE STUDY PHILIPPINES

4.1 Cement Availability Issues

The Philippine Geothermal Production Company (PGPC) is engaged in an ongoing well drilling campaign and in addition to the supply disruptions in recent years, the rising demand for construction cement has seemingly impacted the quality of the Class G cement available in the region. Experience with API Class G cements manufactured in Asia Pacific suggests that early gelation of cement for certain cement slurry designs is indeed a common problem in this region. For the regionally predominate oil and gas operations and wellbore conditions that can be quite different than for geothermal operational conditions, the regionally available cement is generally quite acceptable. As geothermal operations are relatively small, it is postulated that the manufacturers have little incentive to produce a separate stock of cement which is more suited to geothermal cementing operations. Currently, there are only three Class G cement suppliers used for most geothermal well cementing operations in the region. Importation of Class G cement has been considered but the high import taxes, transportation costs and logistics present a significant barrier to sourcing Class G cement from outside the region.

From 2020 through most of 2022, the supply of cement provided to PGPC through its cementing services provider came primarily from one supplier. This cement performed reasonably well in both cement additive response and consistency from batch to batch, allowing cement slurry designs to be extended to 14.0 ppg without addition of lightweight additives and to be mixed at 16.0 ppg for Tieback operations and 16.4+ ppg kick off plugs. Reactivity of this cement source was somewhat on the high end for a class G cement but presented no significant gelation

problems. This allowed PGPC to develop very effective lost circulation designs. With the performance of the cement supply remaining fairly consistent between batches cement designs we were able to be further optimized in both performance and cost.

4.2 Performance Issues

A summary of the cement supply is provided in Table 6.

Table 6: Cement Supply and Lot Numbers.

Well No	Cement Source	Lot #	Remarks
1	Supply 1	Lot 1	Meets API specifications, works well with all cement slurry designs and is consistent from lot to lot
2	Supply 1	Lot 1	
3	Supply 1	Lot 2	
4	Supply 1	Lot 2	
5	Supply 1	Lot 2	
6	Supply 2	Lot 1	Cement provides excellent performance, requiring least amount of additives
7	Supply 2	Lot 1	
8	Supply 2	Lot 1	
9	Supply 1	Lot 3	Similar to prior Supply 1 batches
10	Supply 1	Lot 4	More reactive than previous batches, requiring higher concentration of retarder to achieve required Thickening Times
11	Supply 1	Lot 5	Similar to Lot 4, slightly more reactive
12	Supply 1	Lot 6	Very different from previous batch. High gelation tendencies required excessive amount of lab testing and increased chemical additives
13	Supply 3	Lot 1	Less reactive than initial Supply 1 Lots but exhibiting tertiary gelation for lightweight designs. Unable to achieve design requirements with available chemical additives. Fairly consistent between the 2 Lots that were utilized
14	Supply 3	Lot 1	
15	Supply 3	Lot 2	
16	Supply 3	Lot 2	

Towards the end of the first 9 or 10 wells, the cement from Supplier #1 became more reactive and began to cause concerns over gelation issues. This did not significantly impact any of the primary cementing except for the 16.0ppg tieback design which is the most critical cement job as any failure in placement of a 100% continuous cement sheath between casing can range from costly remedial operations and loss of production to complete loss of the well. A shortening of the thickening time with the new cement (Table 5.) was managed by adjustments in additive concentrations. For lost circulation plugs, the gelation exhibited by this batch of cement was beneficial for the desired high early gelation and faster set times. Due to concerns about the cement quality from this supplier, an alternate source was identified, but in the interim while awaiting shipment, the current cement supply was used for the next well(s).

Going to the next field location with plans for three wells, the starting point for cement designs was based on the designs which became standard after the first 11 wells. A new batch of cement from Supply 1 (Lot 6) had been received and tested according to API Spec. 10A. Though this new shipment of cement met API Specifications, given the prior experience with shortened thickening time of the 16.0 ppg Tieback design, it was also tested with the tieback design to confirm performance acceptability. Thickening Time results were found to be consistent with previous cement supplies and thus the new lot was considered acceptable. Operations proceeded accordingly until confirmation testing of the cement blended for the surface casing job with cement design of 14.0ppg revealed that this new Lot was significantly different. This batch of cement, when mixed at the standard 14.0ppg density for the standard surface casing design, exhibited both early and latent gelation problems. Thickening times would not build while mixing and the cement slurry would quickly become unpumpable with any shutdown in mixing. As shown in Fig 4 and Fig. 5 below, the thickening time charts did exhibit the typical and expected increase in viscosity as measured in the standard cementing measurement of bc. (Bearden Units). Upon opening of the slurry cup, it was found that the cement had gelled up around the paddle which is a clear indication of a gelation problem.

Multiple slurry design changes were made in attempt to correct the gelation problem, but no solution was found in time and to not delay operations it was decided to forego the fluid loss control and just focus on obtaining a design with acceptable pump time and rheological properties.

Cement designs for subsequent liner jobs were similarly impacted by the cement quality (Figs 6 and 7) but in attempting to correct the gelation problem resulted in an additional problem of slurry instability.

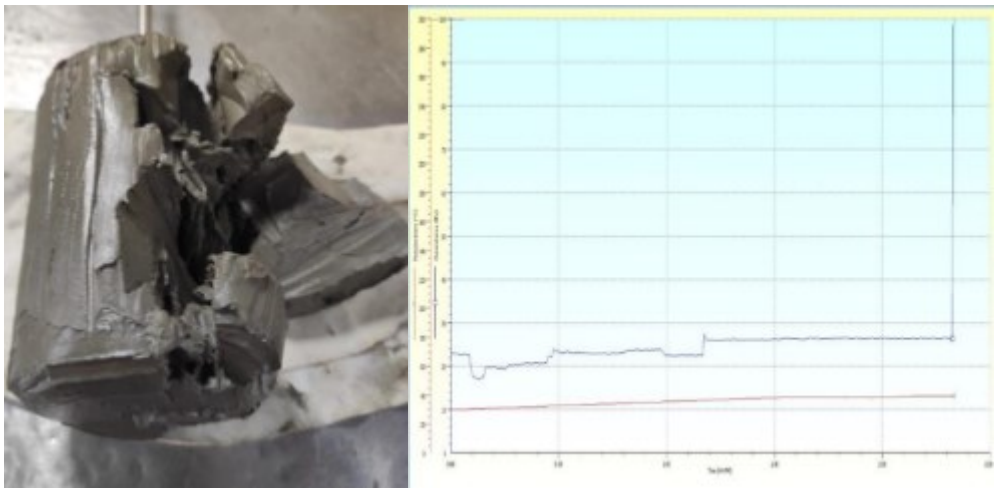

Figure 4: Surface Casing - Thickening time chart and picture after removal from slurry cup.

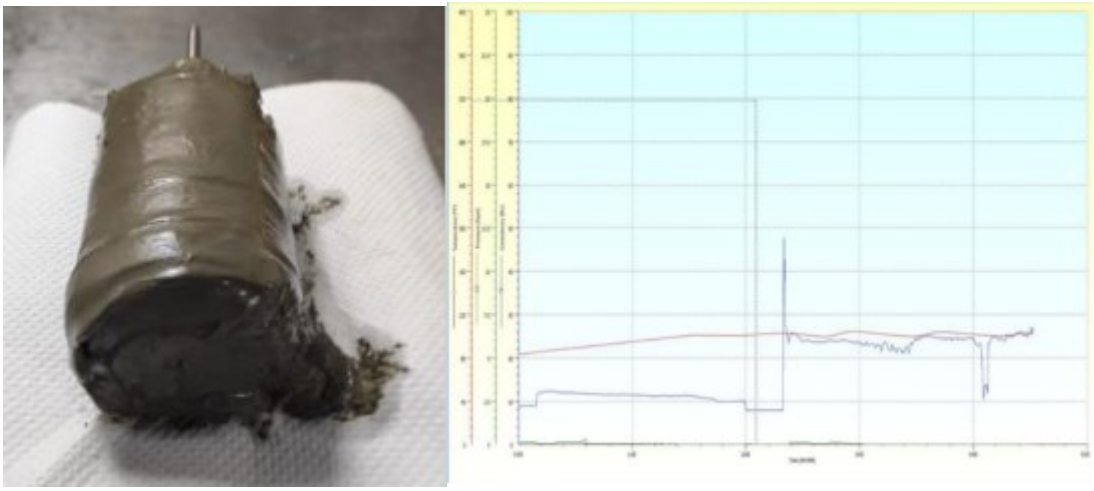

Figure 5: Surface Casing - Attempts to correct this gelation resulted in unstable cement slurries.

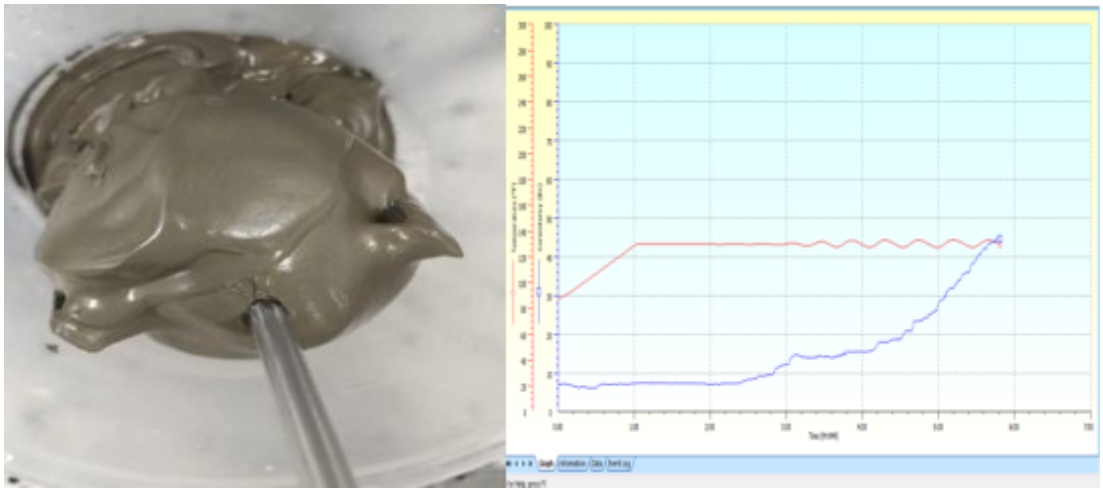

Figure 6: Intermediate Liner – Temperature oscillation caused by slurry gelation.

It was possible after a significant amount of lab testing to meet specifications and achieve manageable though less than desirable designs for the Liner jobs by incorporating a costly amount of microsilica additive to help stabilize the cement slurry. In total, over 100 lab designs had to be tested in search of acceptable cement slurry designs with this batch of cement. Based on the performance of this batch of cement from Supplier #1 and the fact that a

new supply of cement from Supplier #3 was now in stock, it was decided not to use this Lot#7 cement for any primary cement jobs on the next wells and to discontinue sourcing any cement from Supplier #1. Before placing the order for Class G cement from Supplier #3, API specification testing and confirmation testing of the 16.0ppg Tieback design found that this cement supply would be acceptable. Unfortunately, this was before the experience that a cement that would be acceptable for a cement slurry density of 16.0ppg may not be acceptable at all for a 14.0ppg cement slurry density.

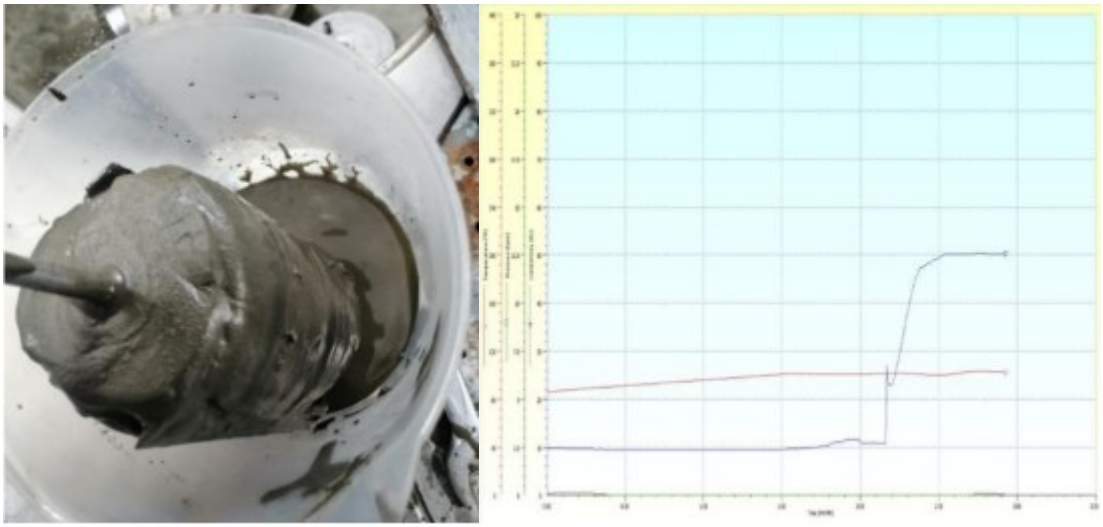

Figure 7: Deep Liner – slurry unable to set evenly.

Testing of this newly arrived cement supply #3 for the 14.0ppg surface casing, 14.0ppg liners and 15.0ppg lost circulation plugs found that this cement behaved exactly opposite of the previous cement supply. This new supply of cement exhibited low reactivity at lower temperatures and had some latent gelation issues. Placement temperature for the surface casing cement operations is typically 100oF to 110oF due to relatively shallow setting depth, continuous pumping of fluids downhole to combat loss circulation and the fact cementing is done via inner string method. Intermediate liner cementing temperatures are typically 130oF to 150oF. Even with the addition of accelerators it was not possible to get 14.0ppg designs that exhibit proper thickening time curves. In general, the normal gelation in the cement hydration process did not take place while being stirred in the HPHT consistometer and attempts to cure this problem ended with the cement setting around the shaft of the mixing paddle but remaining liquid towards the outer edge where the mixing energy was somewhat less (Fig. 8).

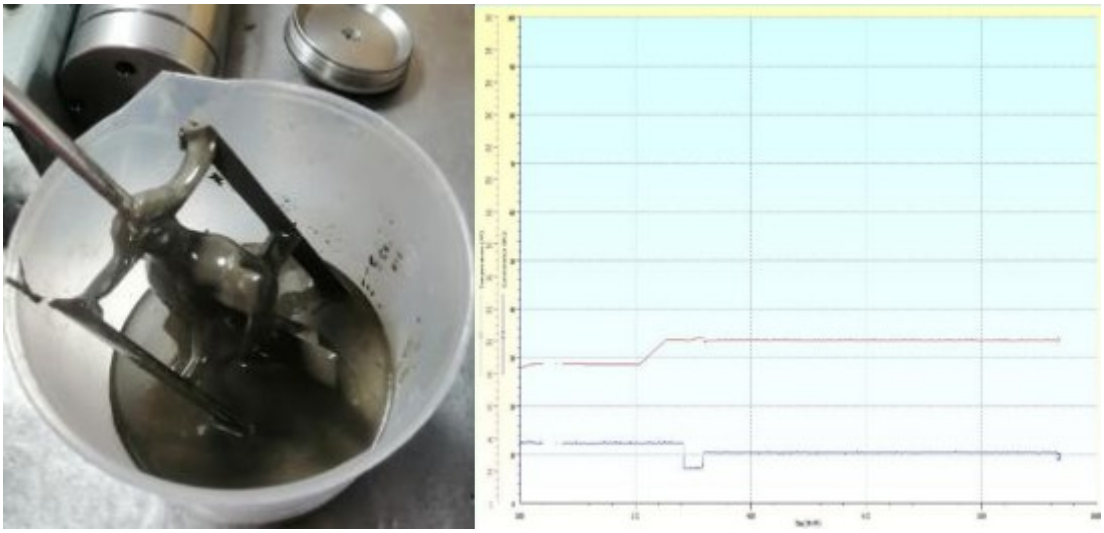

Figure 8: 14.0ppg Surface casing Pilot test using samples of Supply #3.

After a multitude of tests of using currently available chemical additives, the only effective means to accelerate and stabilize the hydration process was to increase the densities of the 14.0ppg cement designs to 14.5ppg and to add a costly stabilizer type additive. The remaining cement Supply #1 was kept on hand for lost circulation plugs however this became an operational risk to keep two very different cements on location given the possibility that field crew may inadvertently use the wrong cement for a given job.

Given the performance of cement supply #3, samples of the latest batch of Class G cement were obtained from supplier #2 as that cement had previously proven of acceptable quality. Unfortunately, even though it met API Specifications, it was found that the cement from that source had also become very reactive with gelation problems similar to Lot 6 from supplier #1. The exact reason for the change in quality of Class G cement from both Supplier #1 and Supplier #2, is not known but it is most likely due to a change in the raw materials. Also, it is worth noting that faster setting cement with shorter gel times is generally desirable for construction cement and as previously stated, construction cement is the primary product of cement manufacturers.

4.3 Cost Impact

Upon the successful completion of the 16 well drilling campaign, the cementing cost per job per well was compiled and organized for comparison of the different cement supply. Do take note that the first 11 wells were drilled in a different field from an earlier campaign (2020-2022) and the latter was most recent (2022-2023)

A discernible trend emerges during the first 11 well drilling campaign, a gradual decline in pricing signifying a favorable cost-effectiveness for the cementing process. As mentioned in Table 4, wells 1 - 5 came from supplier 1, and wells 6 - 8 is from supplier 2. The reason for getting cement from supplier #2 was due to supply chain disruption and with supplier 1 being unable to manufacture on time, nonetheless, the cement from supplier 2 behaved similarly to the prior supplier. Wells 9 – 11 is from supplier 1 as well and no significant changes in cost were observed. In the following campaign starting with Well 12, operations switched to a fresh supply of cement from supplier #1. This led to a notable rise in costs, largely attributed to the quality of the cement. Transitioning to a newly arrived G Cement provided by supplier #3 starting from Well 13 did not alleviate the cost concerns, as this time, the cement proved to be less reactive compared to previous batches. Consequently, despite the change in suppliers and cement batches, the cementing costs for the second campaign significantly exceeded those of the first 11 wells, with some costs even doubling. The most evident case in this drilling campaign for the cost impact of the cement supply is during the cementing of the liner strings. This is best exemplified by the 13-3/8" intermediate liners as this casing string were run in every well (Fig.11).

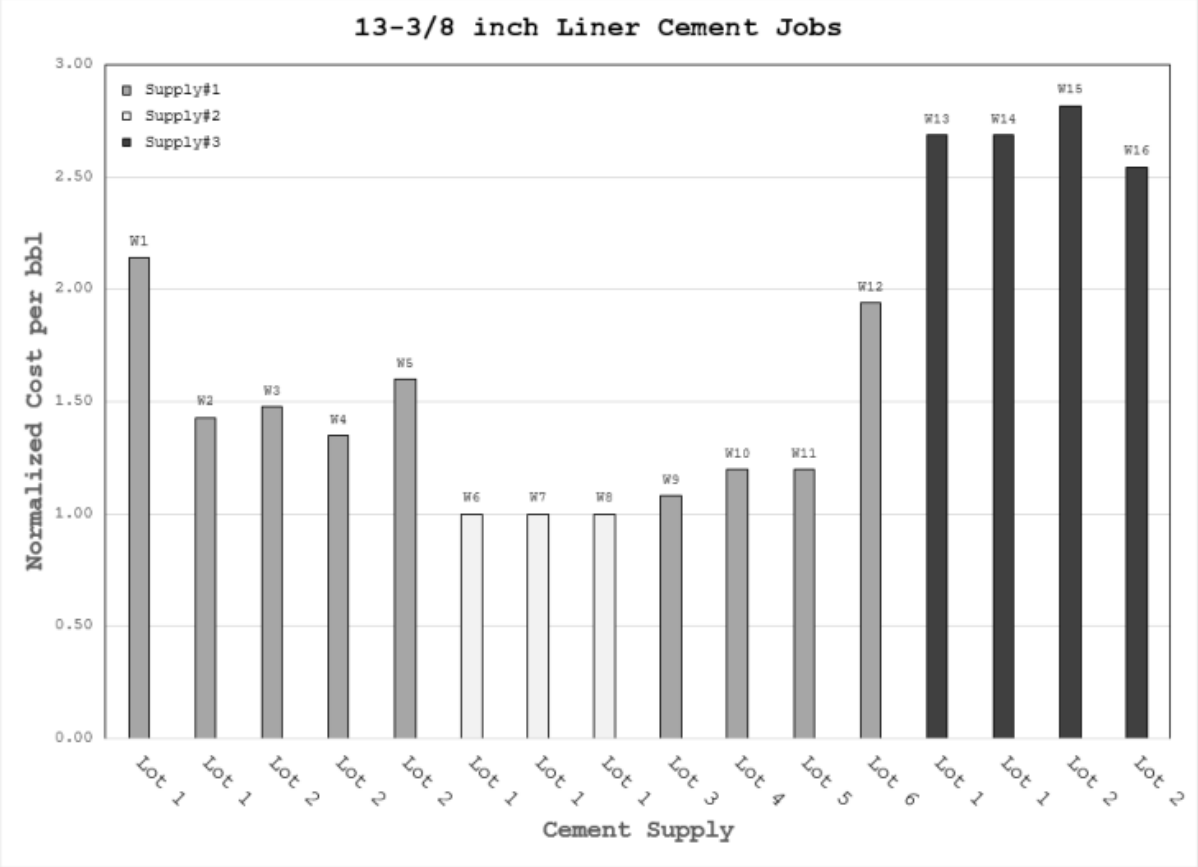

Figure 9: 13-3/8" Intermediate Casing (Wells Vs. Cost/Barrel).

5. CONCLUSION

Production of cement is one of the main and most important industries worldwide. Its primary use as a binding agent for concrete that is one of the most frequently used materials for civil construction projects, can be

considered the backbone for development. While its application for well cementing is equally important, the fact remains that this usage of cement is relatively minor in comparison especially for geothermal cementing operations which are small compared to oil and gas operations. This is further complicated by the fact that the raw materials vary in chemical make-up and what may be acceptable for use in concrete, may not be as suitable for geothermal well cementing. API standards have long provided a benchmark for ensuring cement manufactured to its specifications are generally suitable for well cementing. However, as observed in PGPC's geothermal operations, there can be a significant distinction between cement that is merely adequate and that of which delivers exceptional performance for any given supply and batch.

To better ensure a cement supply which is optimal and to improve cement consistency from lot to lot, one recommendation is to engage an open line of communication with the cement manufacturer to convey the cement properties that are needed for geothermal operations. This would ideally include witnessing API specification testing conducted at the cement manufacturing facility as a first step in the screening process for acceptance of any lot of cement. In addition to API specification tests, testing of actual cement designs planned for all casing strings should be conducted by the cementing service provider to ensure that the cement meets not only the API specifications but is applicable for the intended geothermal operations. Aside from the manufacturing process, packaging, shipping, handling and storage should be considered to ensure the quality of the cement from point of manufacture to point of use. Procedures should minimize the risk of exposure to contaminants, environmental factors (moisture, etc.) and ensure that the cement is delivered and maintained in the same condition as it was at the point of origin. Furthermore, additional tests may be taken per new batch that has arrived to confirm consistency with the tests from the point of origin.

In summary, cement quality is a critical factor that dictates the success of a cementing operation. High-quality cement is essential to ensure the ability to formulate cost effective cement slurry designs that are mixable, pumpable and meets all performance requirements to ensure the formation of a strong, stable, and impermeable barrier in the wellbore, particularly in demanding applications such as geothermal operations. Conversely, poor cement quality may result in costly cement designs or the inability to design a slurry which meets performance requirements and thereby increase the potential for job failures requiring costly remedial operations and the potential for failures in well integrity and long-term performance. All in all, API specifications may serve as an overall guide in controlling quality and acceptability of well cements, but additional controls as suggested in this paper are often necessary to further prevent cement quality issues for geothermal operations.

REFERENCES

Bourgoyne Jr., A., Chenevert, M., Millhelm, K., and Young Jr., F.S.: Cements, Applied Drilling Engineering, SPE Textbook Series Vol 2, Society of Petroleum Engineers, Richardson, TX (1986).

Cements and Materials for Well Cementing, API Specification 10A, 25th Edition, (2019).

Dahegaokar A. D., and Dudhe A. D.: Physical & Chemical Properties of Cement – A Study, International Journal of Creative Research Thoughts, Vol 2, Issue 11, Chandrapur, India (November 2023).

Panagoda, Sanuja & Ranasinghe, Hansa & Perera, Vishwa & Sandunika, Irukshi & Tilanka, Gemal & Alwis, Saneeka & Dilka, Shashini. Cement Manufacturing Process and Its Environmental Impact. 43. 161-168. (2023)

Selvan P. S.: Excessive Retardation in Concrete, International Journal of Creative Research Thoughts, Vol 7, Issue 2, Chennai, India (March 2021).

Tamas, F. D. Acceleration and Retardation of Portland Cement Hydration by Additives, Central Insitute of Building Material Research, Budapest, Hungary.

Debottlenecking Ulubelu: Optimizing Steam Supply

A.H. Fauzi, A. Kuswantoro, I. Solikhin, A.T. Putra,
M. Rofii, H.B. Setyawan, and M.W. Kusumah

PT Pertamina Geothermal Energy, Jl. Muara Dua, Kec. Ulubelu, Kab. Tanggamus, Lampung 35379

abdul.hfauzi@pertamina.com, ade.tputra@pertamina.com

Keywords: Debottlenecking, Steam Supply

ABSTRACT

Pertamina Geothermal Energy Area Geothermal Ulubelu supplies steam to PLN - Indonesia Power plants and its own power plants with a total installed capacity of 220 MW (4X55MW). There are a total of 30 production wells owned by PGE Ulubelu to fulfill the steam demand. Based on production test data and well histories, if all potential production wells can supply the system, the expected power generation can reach at least 4 x 50 MW. Steam supply shortages are due to decreased production well capacity and wells that cannot supply into the system due to various reasons. One of them is a bottleneck on the pipeline side. A study and simulation are conducted before the debottlenecking process. Debottlenecking is done by changing the configuration in the system supply to the plant by adding new pipeline and separator so that the steam supply provided is optimal. The wells that previously couldn't supply steam to the system (UBL-38 and UBL-45) can now supply steam to the system again and additional steam supply of a total of 18 MW was obtained after debottlenecking. From the series of processes conducted, it can be concluded that increasing steam supply can be achieved not only by drilling new wells but also by optimizing production well facilities from upstream to downstream, considering various aspects and utilizing well data owned with relatively lower costs.

1. INTRODUCTION

Indonesia continues to strive for net zero emissions, a situation where the amount of carbon released does not exceed what is absorbed by the earth, as part of its efforts to maintain the earth's climate balance (Nabila, 2022). This is being pursued through various strategic steps, one of which is increasing the utilization of new and renewable energy (NRE). The target for NRE's share in the national energy mix is to reach 39% by 2040 and 66% by 2060. One potential energy source is geothermal energy, where Indonesia possesses about 40% of the world's geothermal energy or approximately 28,617 MW, although its utilization is still very low. The low utilization of geothermal energy is due to several factors such as high exploration risks, varying economic feasibility of geothermal power plants, locations intersecting with conservation areas, issues in setting electricity sale tariffs, and social issues (Anindya, 2023).

PT Pertamina, through its subholding Pertamina Geothermal Energy, actively contributes to maximizing Indonesia's geothermal potential by harnessing geothermal energy to produce electricity. One of Pertamina Geothermal Energy's working areas is the Ulubelu area in Lampung province, with a total installed capacity of 4 x 55 MW. Units 1 and 2 belong to PT PLN with a steam sale business scheme, while units 3 and 4 operate on an electricity sale business scheme. A total of 186 MW out of 641 MW (29%) of the generation capacity in Lampung province is supplied by steam and electricity produced by Pertamina Geothermal Energy Ulubelu Area. Although the energy contribution percentage in Lampung province is relatively high, this capacity has not reached the target of installed capacity due to several factors that need to be analyzed to take the most appropriate action.

PT Pertamina Geothermal Energy began steam production in 2012, which was then supplied to PT PLN's power plants units 1 and 2 to generate electricity. In 2016, PGE started independently producing electricity at unit 3, followed by unit 4 in 2017. During the early steam production period from 2012-2015, there was a decrease in production capacity at units 1 and 2. From 2016 to 2022, total generation increased with the addition of new power plant units 3 & 4, but the maximum production capacity of each individual plant decreased. Out of the installed capacity of 55 MW, the highest generation per unit only reached 4 x 50 MW in 2019, with 20 operational wells out of a total of 28 production wells. This condition could be influenced by both internal factors such as upstream (steam supply) and downstream (plant performance) issues, as well as external factors like climate change due to global warming. Rising temperatures each year affect generation because the power plant type is condensing pressure, meaning temperature increases impact cooling and the achievable vacuum.

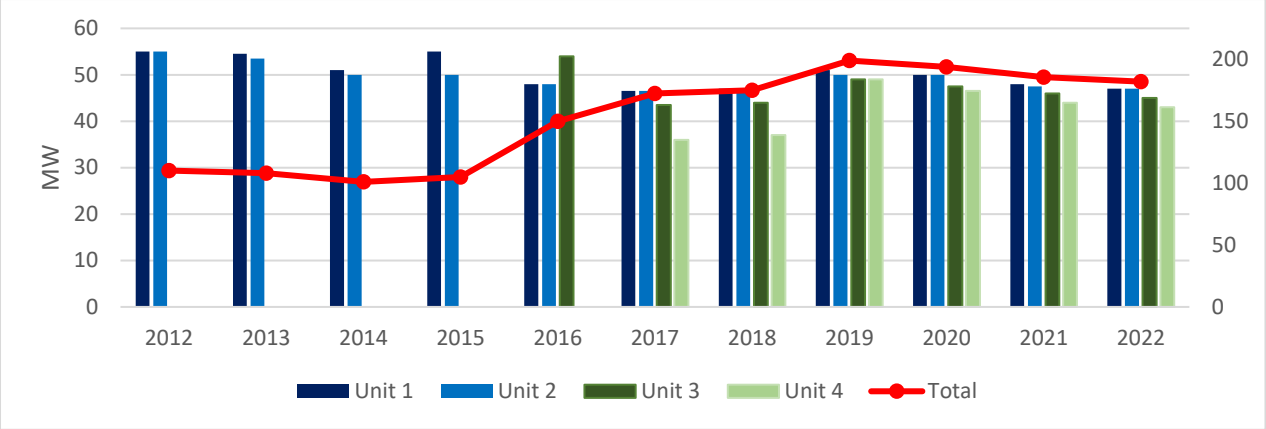

Figure 1: Power Plants Capacity from 2016-2022.

On the upstream side, it was found that with the same number of production wells, the capacity achieved decreased. Production well declines occur over time and can vary significantly (Sanyal, 2000). In the Ulubelu geothermal field, production well capacity declines at a rate of 5%. To compensate for this, new wells are drilled to achieve maximum production capacity. There were an additional 2 production wells by 2022, but this was not sufficient to meet the steam supply needs. Even with these additional wells, total generation in 2022 was lower than in 2019.

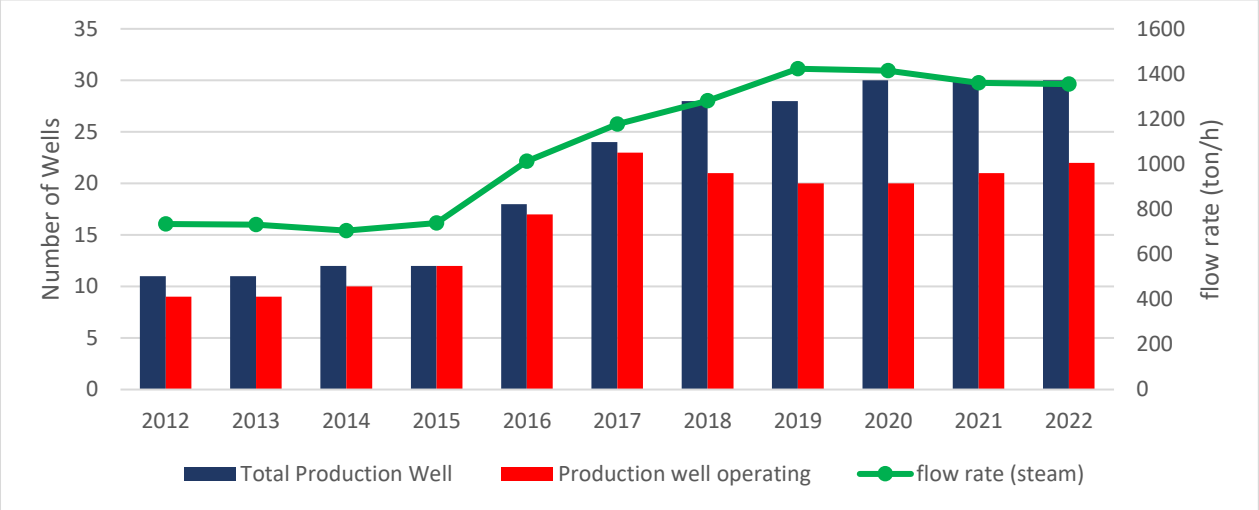

Figure 2: Production Well from 2016-2022.

2. METHOD AND RESULT

PGE monitors production and reinjection wells through Tracer Flow Tests (TFT). These tests are crucial not only for subsurface studies but also for measuring the flow rate of geothermal two-phase fluids, which is then used to determine the capacity of geothermal production wells through various approaches (Axelsson, 2013). The latest test results indicate that the total capacity of all production wells is equivalent to 206.84 MW. This shows that the plant's capacity can still be optimized through certain steps to at least reach the highest generation ever achieved, 4 x 55 MW or 200 MW.

In 2022, PGE Ulubelu had a total of 30 production wells, but only 22 could be connected to the system. Wells UBL-12, UBL-16, UBL-29, and UBL-30 were shut-in due to low pressure and could not enter the system, while well UBL-27 was tentatively connected due to its interference with UBL-56. When both wells were operated simultaneously, a pressure drop occurred in UBL-56, and the pressure in UBL-27 progressively decreased from the initial system entry until it fell below the header pressure. Wells in cluster I could not enter the system because the flow pressure in the pipes from cluster J was much higher than the flow from cluster I at the tie-in point between clusters J and I, preventing cluster I from entering the central separator. This condition was considered a bottleneck that needed to be addressed.

Table 1: Well Production Capacity of Ulubelu Field.

Cluster	Well	Capacity (MW)	Cluster	Well	Capacity (MW)
B	UBL - 02	6.00	H	UBL - 25	8.00
	UBL - 03	4.00		UBL - 26	8.50
	UBL - 15	10.00		UBL - 28	5.50
	UBL - 16	0.00		UBL - 30	0.00
	UBL - 55 (B8)	10.00	G	UBL - 29	3.00
C	UBL - 05	6.60		UBL - 31	4.00
	UBL - 06	0.00		UBL - 48 (G5)	6.24
	UBL - 07	6.00	I	UBL - 34 (I1)	0.00
	UBL - 08	6.00		UBL - 38 (I2)	8.00
	UBL - 27	0.00		UBL - 45 (I3)	4.00
	UBL - 56 (C6)	4.00	J	UBL - 51 (J1)	19.00
D	UBL - 11	10.00		UBL - 53 (J2)	23.00
	UBL - 12	0.00		UBL - 54 (J3)	17.00
	UBL - 14	5.00	K	UBL - 43 (K2)	6.00
	UBL - D5	18.00		UBL - 50 (K4)	9.00

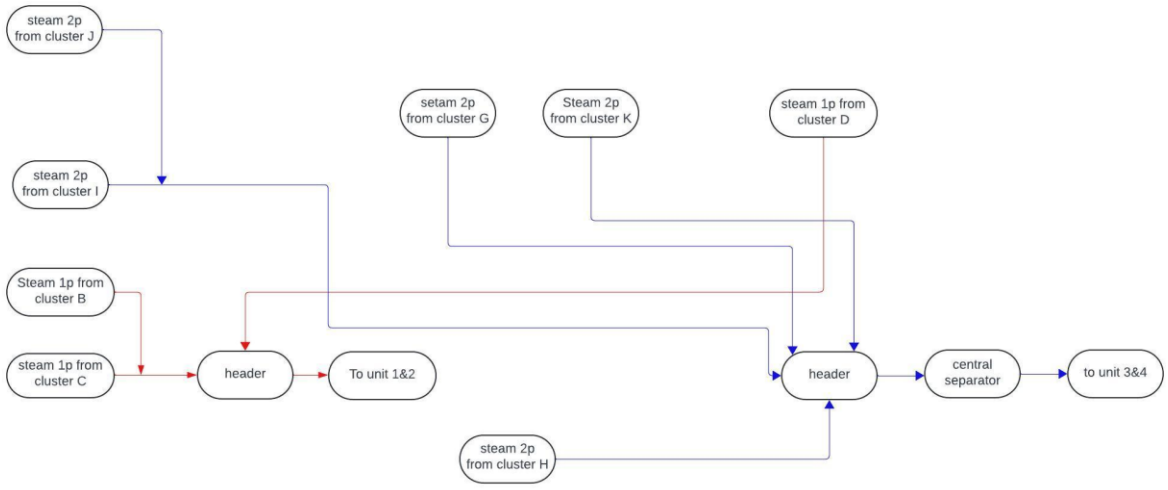

Figure 3: SAGS Configuration before Debottlenecking.

Debottlenecking efforts began with simulation modeling using Aspen Hysys software with the NRTL (Non-Random Two-Liquid) fluid package. This choice was made because the simulation involves not only water but also carbon dioxide as a non-condensable gas. The NRTL fluid package was selected to provide the best correlation for this complex system. The simulation was conducted under conditions where wells in cluster I could enter the system. The simulation results required changes to the production system route and the addition of a separator.

Wells from cluster I would re-enter the system to supply steam to units 3 and 4, while steam from cluster J, initially using the cluster I route, would be redirected to a new separator and through a new route supplying units 1, 2, 3, and 4, with a dominant supply to units 1 and 2. The addition of a separator is necessary for the wells in cluster J due to the limited design capacity of the separator in units 1 and 2, which could create new issues for the wells in clusters B and C if they are combined through a two-phase flow route. With the new route specifically created for the wells in cluster J, there will be a pressure reduction in the cluster I route, allowing the wells in cluster I to re-enter the system and flow towards units 3 and 4. However, on the other hand, the steam supply to units 3 and 4 decreases because the flow from cluster J wells is no longer maximized towards units 3 and 4, and there is an increase in flow to units 1 and 2. Additionally, a new route was added so that steam from cluster D could flow to

supply units 3 and 4, helping to compensate for the steam shortfall due to the route changes in the cluster J wells. Dividing the flow and adding new routes would reduce pressure in the existing routes, allowing wells to optimize their supply to the system.

The simulation results were implemented and completed in early February 2023. Post-debottlenecking, generation increased by 18 MW. This increase was due to wells in cluster I entering the system as per the simulation results, bringing the total number of production wells in the system to 24. Comparing post-debottlenecking generation with TFT analysis results, the actual plant capacity reached 97%.

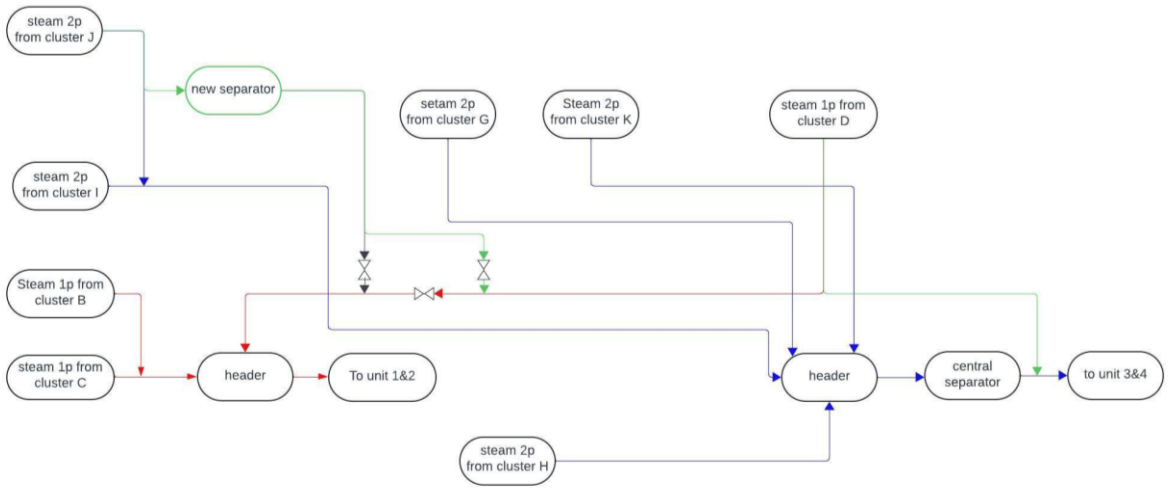

Figure 4: SAGS Configuration After Debottlenecking.

Table 2: Comparison of Before and After Debottlenecking.

Component	Before Debottlenecking	After Debottlenecking
Total Capacity (MW)	182	200
Total Production Well	30	30
Operated Production Well	22	24

3. CONCLUSION

The bottleneck in the Ulubelu geothermal field was due to the SAGS configuration, preventing all potential wells from supplying the system. Debottlenecking involved reconfiguring the SAGS by modifying the steam route and adding a new separator. The occurrence of bottlenecks in steam configuration can be prevented by utilizing more comprehensive data related to the geothermal field and the production wells that will be operated, as well as through a comprehensive approach and operational planning. However, in practice, geothermal development is often carried out in stages due to high costs, which means that the necessary data is not always available in full during the early construction phase. Additionally, changes in production well conditions and discrepancies between estimated well potential and actual conditions after drilling often require adjustments in approach and planning to maximize the available potential. Therefore, the implementation of predictive technology and scenario-based planning becomes crucial to addressing these challenges, with the aim of optimizing resources and preventing operational bottlenecks in the future.

REFERENCES

Adiwardhana, Anindya & Institute, Pertamina. Peningkatan Peran Energi Geothermal dalam Periode Transisi Energi [The Increasing Role of Geothermal Energy in the Energy Transition Period]. 8. 77-87. (2023).

Axelsson, G.. Tracer tests in geothermal resource management. EPJ Web of Conferences, 50, 02001.(2013).

Nabila, Z.P. Pemerintah Indonesia Menuju Target Net Zero Emission (NZE) Tahun 2060 dengan Variable Renewable Energy (VRE) di Indonesia [Indonesian Government Towards Net Zero Emission (NZE) Target by 2060 with Variable Renewable Energy (VRE) in Indonesia]. Jurnal Ilmu Sosial, Vol 2 No. 2 Indonesia (2022)

Sanyal, Subir & Butler, Steven & Brown, Philip & Goyal, Keshav & Box, Tom. An Investigation of Productivity and Pressure Decline Trends in Geothermal Steam Reservoirs. Proceedings. World Geothermal Congress, Japan (2000).

Sanyal, Subir & Tait, Ann & Klein, Christopher & Butler, Steven & Lovekin, James & Brown, Philip & Sudarman, Sayogi & Sulaiman, Syafei. Assessment of Steam Supply for the Expansion of Generation Capacity from 140 to 200 MW, Kamojang Geothermal Field, West Java, Indonesia. Proceedings. World Geothermal Congress, Japan (2000).

Lesson Learned from a Forced Outage on April 14, 2024: Improving System Reliability in Power Generation Plants by eliminating nuisance trip due to improper setting of motor protection – A Case Study of Geothermal Power Plant Lumut Balai Unit 1

Surya H Silitonga, Muhammad Habib, Indrayanto, Erwandi Yanto, Edward Prananta Barus, Aris Kurniawan, and Catur Hendro Utomo Sukristiono

Graha Pertamina, Pertamax Tower, 7th Floor, Jalan Medan Merdeka Timur No. 11-13, Jakarta 10110, Indonesia

surya.silitonga@pertamina.com

Keywords: Power Generation, Forced outage, System reliability, Motor protection, Transmission line fault, negative sequence current

ABSTRACT

This paper discusses the lessons learned from a forced outage (FO) incident experienced at Geothermal Power Plant (GPP) Lumut Balai Unit 1 on April 14, 2024. The FO was triggered by a lightning strike on the 150 kV transmission lines from the GPP to the Tanah Abang Substation (owned by PLN) used to deliver electricity production to customers. The strike occurred at 16.7 km and 19.8 km from the GPP and activated the 87L protection relay which triggered Auto-reclose 150 kV CB operated on phase R. This, in turn, caused all motors on the medium voltage 6.3 kV system (HWP A & B, LRVP A & B, CT FAN A to F) to trip due to an unbalanced system on the Grid detected by its negative sequence current (46) relay.

Through detailed analysis of the event, including root cause analysis and examination of system protection settings, valuable lessons were identified to improve system reliability and prevent similar incidents in the future. The focus was particularly on motor protection during unbalanced system faults on the Transmission Line.

It was found that the delay time of the unbalance relay for the medium voltage (MV) motors in GPP Lumut Balai Unit 1 had been set for 1 second. However, according to IEEE Std C37.96-2012, the recommended standard value should be 10 seconds with a pickup value of 15%. This deviation caused the unbalanced relay protection in the GPP to operate prematurely during single phase grid disturbances or during Auto-reclose 150kV CB Operated, where the deadtime of recloser is only 1 second. When the unbalance system was detected, the relay operated within 1 second, causing all motors on the medium voltage 6.3 kV system to trip, resulting in the turbine trip and the opening of Circuit Breaker 52G. The 3-hour forced outage at PLTP AG Lumut Balai resulted in an Equivalent Availability Factor (EAF) loss of 0.07% and an Equivalent Forced Outage Rate (EFOR) increase of 0.034%.This overly sensitive unbalance relay protection setting caused unnecessary trips. Evaluating the delay time according to IEEE standards for the unbalance relay is essential to prevent the unit from experiencing unnecessary protection trips. This paper emphasizes the importance of proper relay settings and adherence to industry standards such as IEEE Std C37.96-2012. Recommendations for enhancing system protection and reliability in power generation plants are provided.

1. INTRODUCTION

Protecting induction motors in power plants is paramount to maintaining operational reliability and efficiency. According to IEEE Std C37.96-2012, a critical protective relay used is the motor unbalance relay, which safeguards equipment against current and voltage imbalances. This relay ensures that motors operate within acceptable operating limits, preventing potential damage and outages.

This study focuses on identifying the root cause of a forced outage that occurred at the Lumut Balai Geothermal Power Plant on April 14, 2024. The objectives are to determine the underlying issues, propose solutions to prevent recurrence, and evaluate whether the relay setting and coordination are in compliance with IEEE Std C37.96-2012. By addressing these aspects, the study aims to enhance not only reliability of the motor but also reliability and availability of the Lumut Balai's Geothermal power plant.

2. TRANSMISSION LINE PROTECTION SYSTEM

Transmission lines are the backbone of the power grid, whose main function is transferring electricity power from a source to a load point over long distances. The role of transmission line protection is to detect and isolate faults with high selectivity, so that faults in one line are isolated without causing disruption to the rest of the system. The necessity for precise transmission line settings arises from the need to maintain the stability and efficiency of the power grid, preventing issues such as voltage drops, power outages, and energy inefficiencies since transmission line protection failure is one of the leading causes of power system collapse, and blackout.

Distance and differential relays are the two most commonly used transmission line protection methods. Traditionally, both use fundamental-frequency voltages and/or currents to protect transmission lines as shown on Figure 1. Two sources represent the grid on the sending and receiving sides. There are distance and differential relays in each bus with a voltage transformer (VT), current transformer (CT) and circuit breaker (CB). The relays get the relevant measurement from the VT and CT, take decisions based on the available data and send the trip signal to the CB. In the case of the differential relay, there is necessarily a communication channel between the two line terminals.

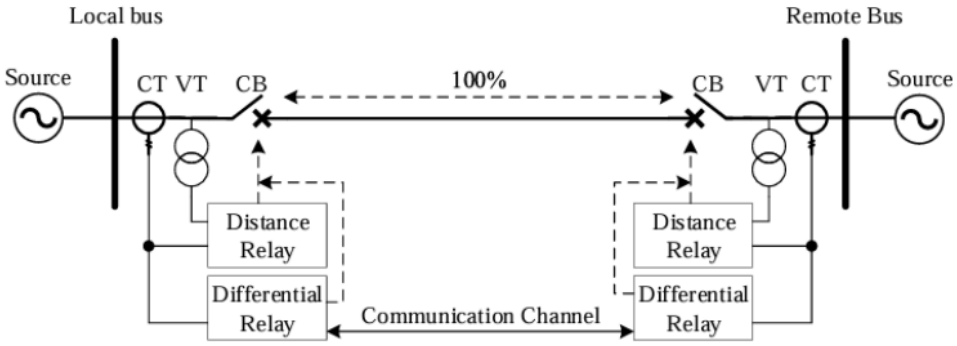

Figure 1: Single Line Diagram Protection of Transmission Line.

2.1 Distance Relay Protection

Distance relay protection is a widely used method for protecting transmission lines. It can work with measurements from the relay's location, without communicating with the other line terminal, and is relatively simple to implement in numerical relays. A distance relay calculates fault impedance from the local measurement of voltage and current, and compares this with a preset impedance to determine whether the fault is within its operating region or not as Figure no 1. The fault distance is inferred from the impedance, as the electrical characteristics of a transmission line relate its length to its impedance, hence the name distance protection.

Distance relay protection is a non-unit type of protection, its protection zone is not strictly limited within the protected line segment. Distance relays are designed to operate with different zones. The zone 1 is usually set at around 80% of the line length, usually set to be instantaneous (no deliberate delay). The zone 2 and the zone 3 are usually set at 120% and 220% of the line length, with added delay. Zone 2 ensures that the protected line is entirely covered, in case of faults beyond zone 1. Its delay gives time for a fault just beyond the line end to be cleared by protection relays closer to the fault. Zone 3, where used, provides a backup to other protection relays.

2.2 Differential Protection

Differential protection operates on Kirchhoff's current law, that the total current entering the protected zone should be equal to the current leaving it under normal conditions. As shown on Figure 1, differential protection, therefore, requires fast communication between two terminals of the protected line for transmitting measurement data. It is a unit-type protection, provides excellent selectivity, and is immune to many different system changes. However, practically, differential protection always needs backup protection due to the possibility of communication channel failure.

2.3 Transmission Line Setting

For the protection system of the Transmission Line, we use Micom P545 Agile as the brand and type of the relay. This protection relay has 2 activated functions, which is Distance Relay (21) and Line Differential Current (87L). Furthermore, the autoreclose function is set on this relay based on the sending of 87L.

2.3.1 Distance Relay Setting

The 150kV Lumut Balai substation is connected to the 150kV Transmission line Tanah Abang Substation by using two (2) lines, line 1 and line 2. The estimated length of the transmission line around 19.3km as shown in Figure 2.

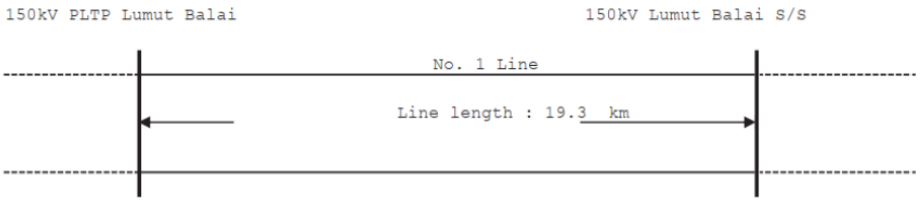

Figure 2: 150kV Transmission Line Lumut Balai unit-1.

Line impedance of 150kV Lumut Balai unit-1 to the 150kV Transmission Line Tanah Abang :

- Z1 (Positive sequence impedance): 4.67 ∠ 74.73842883 Ω
- Z0 (Negative sequence impedance) : 28.88 ∠ 72.18920452 Ω
- Zm (Mutual impedance) : 6.07 ∠80.98023335 Ω
- Source impedance (Zs) : 2.75 Ω
- Minimum fault current : 5589.66A

These setting was programmed to the Micom P545 Agile as shown on Table 1.

Table 1: Line Parameters.

Address	Name	Value
GROUP 1 LINE PARAMETERS		
30.02	Line Length	19.3 km
30.03	Line Impedance	4.7 Ohm
30.04	Line Angle	74.7 deg
30.05	kZN Res Comp	1.71
30.06	kZN Res Angle	-3.04deg
30.07	Mutual Comp	Disabled
30.0B	Phase Sequence	Standard ABC
30.0C	Tripping Mode	1/3 Pole
30.10	Line Charging Y	0 sec

Setting group of CT and VT can be found on Table 2, where the CT ratio is 600/5 A and VT ratio is 150kV/100V.

Table 2: CT & VT Setting.

Address	Name	Value
CT AND VT RATIOS		
0A.01	Main VT Primary	150 kV
0A.02	Main VT Sec'y	100 V
0A.03	C/S VT Primary	150 kV
0A.04	C/S VT Secondary	100 V
0A.07	Phase CT Primary	600 A
0A.08	Phase CT Sec'y	5 A
0A.0B	SEF CT Primary	600 A
0A.0C	SEF CT Secondary	5 A
0A.0D	MComp CT Primary	600 A
0A.0E	MComp CT Sec'y	5 A
0A.0F	C/S Input	BN
0A.10	Main VT Location	Line
0A.11	CT Polarity	Standard
0A.13	SEF CT Polarity	Standard
0A.14	M CT Polarity	Standard
0A.18	VT Connected	Yes

Based on the engineering design calculation, the distance relay have 3 different zone protection, Z1 with reach 0.299 ∠ 74.739 ohm, Z2 with reach 0.449 ∠ 74.739 ohm and Z3 with its reach 0.815 ∠ 74.739 ohm as shown on Table 3.

Table 3: Distance relay Protection Setting Element.

Address	Name	Value
GROUP 1 DISTANCE ELEMENTS		
32.01	PHASE DISTANCE	
32.02	Z1 Ph. Reach	0.299 ohm
32.03	Z1 Ph. Angle	74.739 deg
32.07	R1 Ph. Resistive	3.45 ohm
32.08	Z1 Tilt Top Line	0 deg
32.09	Z1 Sensit. Iph>1	4.1 A
32.10	Z2 Ph. Reach	0.449 ohm
32.11	Z2 Ph. Angle	74.739 deg
32.15	R2 Ph. Resistive	3.45 ohm
32.16	Z2 Tilt Top Line	0 deg
32.17	Z2 Sensit. Iph>2	4.1 A
32.20	Z3 Ph. Reach	0.815 ohm
32.21	Z3 Ph. Angle	74.739 ohm
32.25	R3 Ph. Res. Fwd	3.45 ohm
32.27	Z3 Tilt Top Line	0 deg
32.28	Z3 Sensit. Iph>3	4.1 A

Basic scheme mode for the distance relay is standard setting with definite time. Time delay for Z1 is 0 second (instantaneous), time delay for Z2 is 0.4 second and time delay for Z3 is 1.2 second as shown on Table 4.

Table 4: Distance relay Protection Scheme Logic.

Address	Name	Value
GROUP 1 SCHEME LOGIC		
34.01	BASIC SCHEME	
34.02	Basic Scheme Mode	Standard
34.08	Zone 1 Tripping	Phase & Ground
34.09	tZ1 Ph. Delay	0s
34.0A	tZ1 Gnd. Delay	0s
34.10	Zone 2 Tripping	Phase & Ground
34.11	tZ2 Ph. Delay	0.4s
34.12	tZ2 Gnd Delay	0.4s
34.18	Zone 3 Tripping	Phase & Ground
34.19	tZ3 Ph. Delay	1.2 s
34.1A	tZ3. Gnd. Delay	1.2 s

2.3.2 Line Differential Current Setting

On a per-phase basis, the current inputs at each protected terminal are measured and communicated to devices at the other protected terminals. This allows for fault detection and tripping initiation, if necessary. At each device in the scheme, the remote current measurements received through the communication links are processed and compared with the local signals. This comparison allows the derivation of the differential current and bias current values on a per-phase basis.

The differential and bias currents are then compared against a tripping criterion defined by a dual-slope characteristic, as shown in Figure 3.

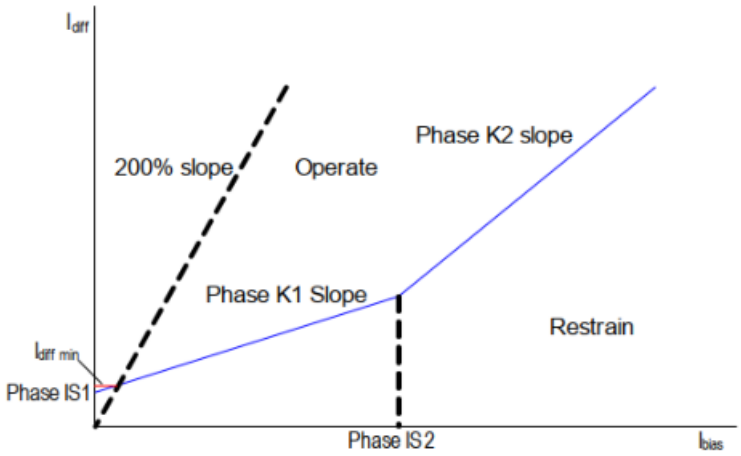

Figure 3: Dual slope current differential bias characteristic.

Refer to Figure 3 above, the phase current differential characteristic is defined by four settings:

- **Phase Is1**: The basic differential current setting which determines the minimum pick-up level of the protection.
- **Phase k1**: The lower percentage bias setting used when the bias current is below the Phase Is2 setting. This provides stability for small CT mismatches, while ensuring good sensitivity to resistive faults under heavy load conditions.
- **Phase Is2**: A bias current threshold setting, above which the higher percentage bias setting Phase k2 is used.
- **Phase k2**: The higher percentage bias setting used to improve protection stability under heavy through fault current conditions.

The tripping criteria is defined by the bias characteristic graph. Basically if the differential current is above the line, the protection will trip. If it is below, the protection will restrain. Final setting of line differential current protection can be found on Table 5.

Line Circuit Breaker (CB). After the temporary fault is cleared, then the 150kV Line CB will close again. If the fault is not cleared or if a permanent fault is detected then the 79 Final trip will trigger Lockout relay (86-1) to work and open permanently 150kV Line CB. These two functions will give some event on the Sequence of Event (SOE) on the Distributed Control System (DCS) as shown on Table 6.

Table 5: Line Differential Current Setting.

Address	Name	Value
GROUP 1 PHASE DIFF		
33.01	Phase Diff	Enabled
33.06	Phase Is1	1 A
33.07	Phase Is2	10 A
33.08	Phase k1	30.00%
33.09	Phase k2	150.00%
33.0A	Phase Char	DT
33.0B	Phase Time Delay	0 s
33.0E	PIT Time	200.0 ms
33.0F	Ph CT Correction	1
33.10	Compensation	None
33.17	PIT I selection	Remote
33.3F	NEUTRAL DIFF	
33.40	In Diff	Disable
33.41	In Diff Time	0 s
33.42	In Diff Is1	0.1 A
33.43	In Diff Is2	10 A
33.60	Ph Diff Stub Bus	Disable

When 87L detects any fault on the Transmission Line, it will trigger Autoreclose (79) work to open the 150kV

Table 6: Logic Scheme of Line Differential Current & Autoreclose.

Device	Function	CB			86-1	86-2	94	79	DCS
		TC-1	TC-2	Block	-K861	-K862	-K941	-F871	(SOE)
P545	87L	x						x	x
	79 Final Trip	x			x				x

3. MOTOR UNBALANCE PROTECTION

3.1 Working Principle & Type of Relay

The most common cause of unbalance for three-phase motors is the loss of phase resulting from an open fuse, circuit breaker, connector, or damaged conductor. Unbalances in other connected loads can also affect the motor. A voltage unbalance of 3.5% can produce a 25% or greater increase in motor temperature. This results primarily from negative sequences produced by the unbalance.

Unbalanced currents cause excessive heating in motor rotors due to opposing magnetic fields in parts of the rotor of either synchronous or induction motors that can result from excessive unbalanced (negative-sequence) currents. This current produces flux in the motor air gap rotating in the opposite direction to the actual motor direction. The relative effect is essentially double-frequency current in the rotor. Higher resistance in the rotor further increases heating, and negative-sequence impedance remains essentially at locked-rotor value. Thus, high current and high resistance compound the heating effect. Derating guidelines for unbalanced voltage are provided in NEMA MG-1, Part 20 and Part 21, respectively. Negative-sequence currents reduce the available accelerating torque.

Several types of relays are available to provide phase unbalance protection, including single phasing. Most of these relays are described in Chapter 4 of IEEE Std 242-2001 (IEEE Buff Book™) and in IEEE Std C37.96™-2012. list common protection relay that being used as follows :

a. Phase current unbalance (Device 46).

   This relay protects against unbalanced currents in a polyphase circuit. Mechanical phase current unbalance relays are induction disk devices that detect unbalance in the currents in the three phases. These relays inherently have a time delay. Occasionally, a timer is used to obtain additional delay. Because this relay cannot protect for unbalances less than 25%, its selection is questionable except for complete loss of one phase. Unfortunately, this device shares the same device number as the negative sequence overcurrent relay (Device 46) in item d).

b. Phase current unbalance high resistance ground (HRG) (Device 46).

   In high-resistance grounded (HRG) systems, setting a current unbalance relay (Device 46) to trip can cause unwanted tripping during ground faults. While some low-voltage (LV) protection relays have a blocking function to prevent this, if the Device 46 lacks such a function, it's recommended to use it for alarm only.

c. Reverse-phase (Device 46).

   This relay protects aganninst reversed phase sequence in a polyphase circuit. This relay is rarely used for motor unbalance protection.

d. Negative sequence overcurrent (Device 46).

A negative sequence overcurrent relay is a time over-current relay with extremely inverse characteristics that operates at very small levels of negative sequence current. Settings are available to alarm before trip and to trip upon a limit of I22t.

e. Negative sequence voltage (Device 47).

Because negative sequence voltage relays operate instantaneously on negative sequence overvoltage, some external time delay might be necessary.

f. Voltage balance (Device 60).

The voltage balance (60) element compares voltage sources to determine if there is a difference in voltage, i.e., for VTs determining if both input sources are present or if there is an open fuse losing one source. If a source is not present, then the output of this element blocks (removes permission) from tripping or starting elements. The voltage balance 60 relay is an older method than voltage-unbalance 47 protection, which is based on sequence components

3.2 Relay Selection & Setting

Geothermal Power Plant Lumut Balai unit-1 is designed to use the negative sequence current (46) as the unbalanced protection of the Medium Voltage (MV) motor. The negative sequence current is contributed by the motor or system when :

1. An unbalance voltage condition exist (e.g., open-phase conditions, single-phase faults, or unbalance load)
2. Stator coil cutout occurs during a repair
3. There are shorted turn in the stator winding

These negative-sequence currents induce double line-frequency current that flow in the damper or rotor parts. Final setting of 46 Relay protection of the MV motor are shown on Figure 4.

46 : Negative sequence current / unbalance

Element activity : On

Setting group
- Tripping curve : Definite time
- Threshold current : 15 % of IB
- Delay : 1000 ms

Tripping behavior

Output O1 - Type : Normally Open

Output O1 - Mode : Pulse

Latching : Yes

Activate output O1 : Yes

Trigger fault recording : With

Activate indicators : L9

Figure 4: Parameter setting of relay 46 (negative sequence current).

The setting curve has a definite time, when the negative sequence current is exceeding its setting value (15% of Ib) then the relay will work after 1 second as its delay time of the protection relay.

4. RELIABILITY AND AVAILABILITY OF POWER PLANT

The reliability and availability of power plants, as indicated by metrics like EAF and EFOR, are crucial for ensuring consistent and efficient power generation. By focusing on these metrics, power plant operators can improve performance, reduce costs, and ensure a stable supply of electricity.

4.1 EAF (Equivalent Availability Factor)

The Equivalent Availability Factor (EAF) for a power plant is a measure of the reliability and availability of the plant to generate electricity over a specific period of time. It is typically expressed as a percentage and is calculated based on the actual availability of the plant compared to its maximum potential availability under ideal conditions.

$$EAF = \frac{Availabe\ Hours}{Period\ Hours} \text{x } 100\% \quad (1)$$

- Available Hours = The total number of hours during which the power plant is ready to operate (Total hours in the period - Production loss hours).
- Period Hours = Total hours in the observation period.

4.2 EFOR (Equivalent Forced Outage Rate)

EFOR is Equivalent Forced Outage Rate. It is a metric used in the energy and power generation industry to measure the reliability and availability of a power plant or a specific unit within the plant. EFOR specifically focuses on the rate of forced outages experienced by the unit or plant

$$EFOR = \frac{Forced\ Outage\ Hours}{Total\ Available\ Hours} \text{x } 100\% \quad (2)$$

- Forced Outage Hours = Total hours during which the unit or plant was unavailable due to forced outages.
- Total Available Hours = Total operational hours during the same period.

5. PLANT INTERLOCK

The steam turbine and steam turbine generator are provided with the protection system to prevent unsafe conditions during normal or emergency operation. To ensure the safety operation of the plant, interlock between the steam turbine control system and steam turbine generator control system is designed to shut the plant down automatically. The basic concept of interlock between steam turbine control system and steam turbine generator control system is as shown below :

5.1 Initiation of steam turbine generator protection system

When the Generator Protection System is initiated, the steam turbine and generator are automatically tripped immediately.

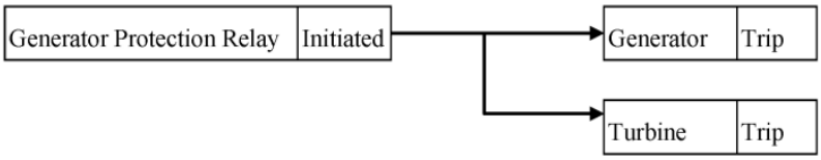

Figure 5: Generator Protection Trip Command.

As shown in Figure 5, both Generator and Steam Turbine will automatically trip when the Generator Protection Relay detects any internal or external fault that might cause damage to the Generator. List of Generator Protection Relay Function is refer to the electrical interlock diagram which is consist of several relay like Generator Differential (87G), 3rd Harmonic Neutral Undervoltage (27TN), Neutral Overvoltage (59N), VT Fuse Loss (60F), Generator Loss of Field (40G), Generator Reverse Power (32G), Generator Out of Step (78G), Generator Negative Sequence (46G), Generator Over Excitation (24V/F), Generator Overvoltage (59G) and AVR Protection.

5.2 Initiation of steam turbine protection system.

When the turbine protection system is initiated, the steam turbine generator is automatically tripped immediately.

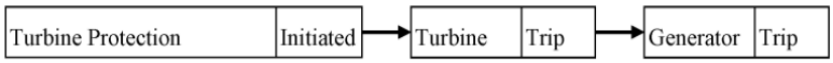

Figure 6: Turbine Protection Trip Command.

As shown in Figure 6, when turbine protection detects any anomalies that exceed its operation limit then the turbine will trip and then this signal will be sent as input for the generator trip. The turbine protection consists of following protection such as D-EHC Heavy fault, Turbine overspeed, Both Hot Water Pump trip, Condenser vacuum low low, etc.

6. FORCED OUTAGE REPORT AND ANALYSIS

Forced Outage Report & Analysis delves into the critical process of documenting and analyzing these unplanned outages. By systematically recording and scrutinizing forced outages, power plant operators and engineers can identify underlying causes, assess the impact on plant performance, and develop strategies to prevent future occurrences.

6.1 Sequence of Events turbine trip

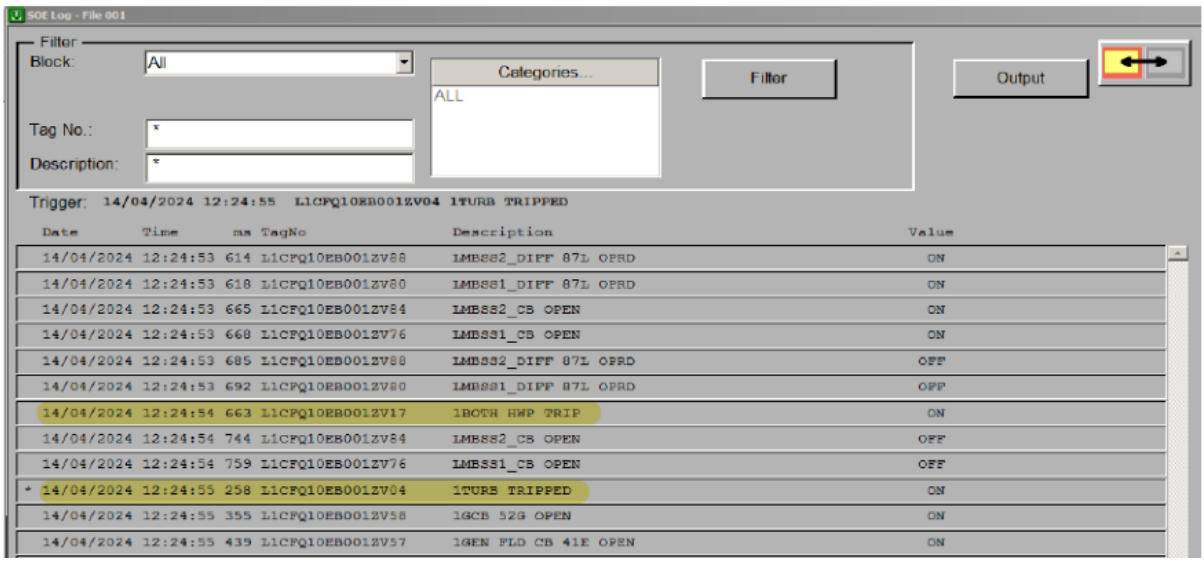

Figure 7: Tosmap SOE (Sequence Of Event) Turbine tripped.

The Sequence of Events (SOE) log in Figure 7 indicates that on April 14, 2024, at approximately 12:24:55, there was a disturbance on phase R of the 150V transmission line, as evidenced by the actions taken by the protection systems (87L operated) and 150kV CB line open. The specific event "1TB TRIPPED" signifies a major issue that triggered a series of protective measures. In response to the detected anomaly, the corresponding 150kV line circuit breakers (LMBSS1_CB and LMBSS2_CB) were opened to isolate the fault and protect the system. The repeated switching of these circuit breakers due to activation of the reclosure function caused further protective actions, including the "BOTH HWP TRIP" Ultimately, these protective measures culminated in the "1TB TRIPPED" event, signifying that the turbine was tripped to prevent damage and maintain the integrity of the whole system.

6.2 Root Cause Analysis

Lumut Balai Geothermal Power Plant experienced a turbine trip due to an external disturbance on the both phaseR of 150kV Transmission Line 1 and 2, this 1 phase fault caused by lightning strike produced a voltage drop and a current spike on the 150kV side phase R and neutral side. This triggered the operation of the Line Differential (87L) relay, leading to the tripping of all motors on the 6.3kV medium voltage side (HWP, LRVP, CT FAN) due to motor unbalance. Consequently, the tripping of both HWP motors caused the MSV and MCV to fully close, resulting in a turbine trip and the opening of breaker 52G as per Plant interlock diagram and PLTP Unit 1 entered a backfeeding condition.

When the lighting strike happened, voltage drop happened and automatically high current occurred on phase R of both transmission line 1 and Line 2. The Line Differential Relay on Line 1 and Line 2 detected the fault and attempted to mitigate the anomaly in the grid by activating the auto-reclose function.`

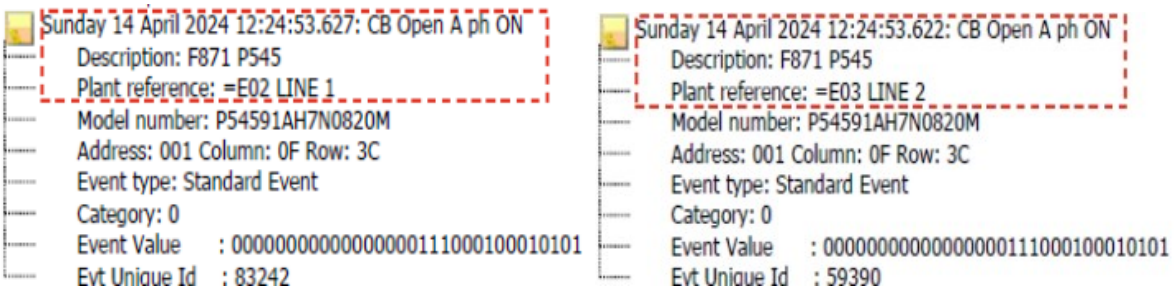

Figure 8: Auto reclose at line 1 and line 2.

As shown on Figure 8, the autoreclose is working to open 150kV Line CB Phase R on Sunday April 12, 2024 at 12:24:53:627 for line 1 and 12:24:53:622 for line 2. The autoreclose worked due to the external fault that was detected by the 87L relay.

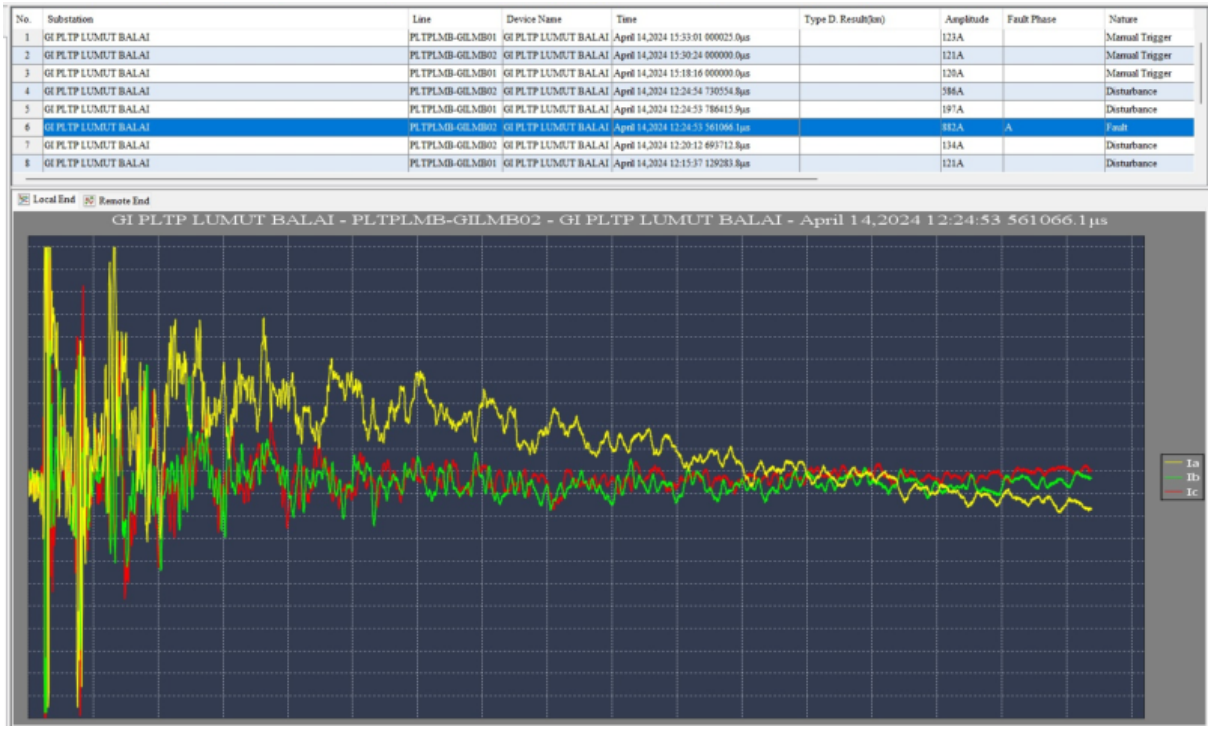

Figure 9: True Travelling Wave - failed in Phase A.

Based on Figure 9, it can be seen that there is an anomaly in phase R, with the value of the current spiking significantly at 12:24:53.

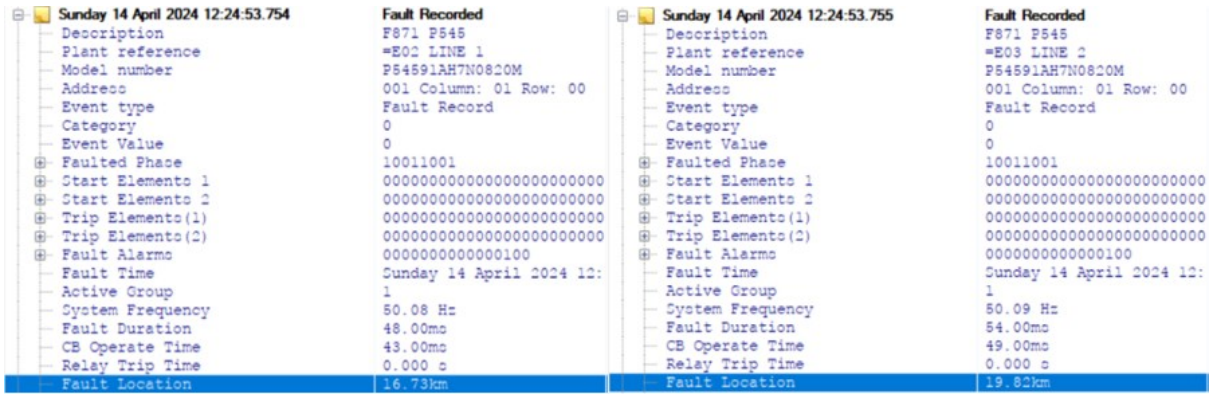

Figure 10: Fault Location.

In the Figure 10, From the data analysis of Micom Agile 150 kV line, auto reclose occurred on Line 1 due to a fault on phase R (CB Open A ph ON) at 12:24:53.627 with a fault location at km 16.73. Similarly, on Line 2, auto reclose also occurred on phase R (CB Open A ph ON) at 12:24:53.622 with a fault location at km 19.82. Based on the fault location, the distance relay protection also detects this fault, however since the location is not in Zone 1 for both lines then it needs additional time delay for the protection relay to be operated.

During the operation of the line differential (87L) protection system, which attempted to clear the fault by activating auto reclose on single phase R, the recloser's dead time setting is 1 second as shown on Figure 11.

Therefore, the auto-recloser waits for 1 second after detecting the first fault to determine if it's temporary or permanent. However, during this waiting period, an anomaly (unbalanced current) occurs on the medium voltage (MV) system. This anomaly is detected by the negative sequence current (46) relay protecting the MV motor. Since the unbalanced current reaches the relay's setting value and the 1-second time delay elapses, all motors on the MV side trip abruptly due to the motor unbalance protection.

Subsequently, tripping of both hot water pumps triggers the turbine to trip as well. This chain reaction results in an undesired forced outage at the Lumut Balai Geothermal Power Plant (PLTP). This outage could have been avoided if the time delay setting for the negative sequence current (46) relay on the MV motor had been longer than the dead time of the auto-recloser.

GROUP 1 AUTORECLOSE		
AR Mode	AR 1/3P	49.51
AR Shots	1	49.59
AR Skip Shot 1	Disabled	49.5A
Multi Phase AR	Allow Autoclose	49.5C
Discrim Time	500.0 ms	49.5D
CB IS Time	5.000 s	49.60
CB IS MemoryTime	500.0 ms	49.61
DT Start by Prot	Protection Reset	49.62
3PDTStart WhenLD	Disabled	49.63
DTStart by CB Op	Disabled	49.64
3P AR Dead Time	1.000 s	49.67
3P AR DT Shot 1	3.000 s	49.68
3P AR DT Shot 2	60.00 s	49.69
3P AR DT Shot 3	60.00 s	49.6A
3P AR DT Shot 4	60.00 s	49.6B

Figure 11: Setting Group of Autoreclose.

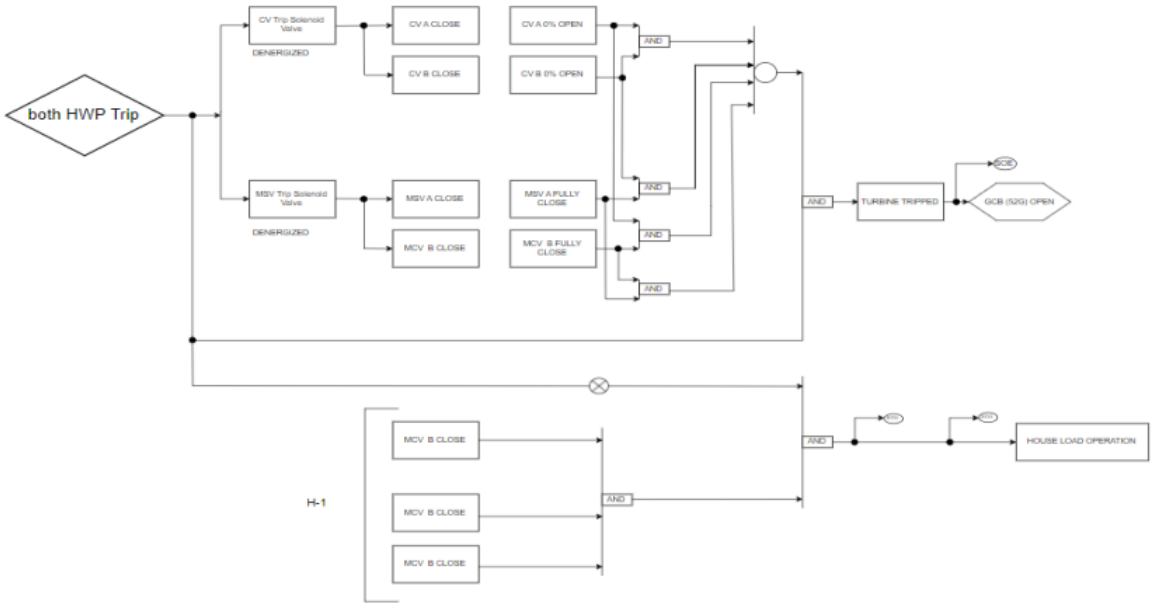

Figure 12: Plant Interlock both HWP trip.

According to the IEEE standard C37.96-2012, a delay time of 10 seconds is recommended for the motor unbalance relay. Ensuring proper coordination and setting alignment between upstream protection relays, such as the auto-recloser and the motor unbalance relay, is crucial to minimize unnecessary outages and ensure reliable operation of the power system.

From the plant interlock in Figure 12, it can be seen that when both hot water pumps trip, it will de-energized the main stop valve (MSV) and main control valve (MCV). This subsequently causes the turbine to trip and the opening of 52G, resulting in the Lumut Balai Geothermal Power Plant experiencing backfeed due to the disturbance.

Figure 13 shows a graphical representation of the simultaneous operation of auto reclose and the motor unbalance relay. When the line differential protection activates auto reclose to address the disturbance, the motor unbalance relay simultaneously detects the disturbance and begins its countdown.

As shown in Figure 13, a disturbance occurred on phase R Line 1 on Sunday, April 14, 2024, at 12:24:53.627 and auto reclose was active for a duration of 1.128 seconds. The differential currents, particularly IA Differential, exhibit a very high peak value (5476.385), indicating a significant imbalance or fault in phase R. The differential currents for phases B and C are relatively low, signifying that the primary issue lies within phase R.

As shown in Figure 14, a disturbance occurred on phase R Line 2 on Sunday, April 14, 2024, at 12:24:53.624 and auto reclose was active for a duration of 1.118 seconds. The differential currents, particularly IA Differential, exhibit a very high peak value (5259.318), indicating a significant imbalance or fault in phase R. The differential currents for phases B and C are relatively low, signifying that the primary issue lies within phase R.

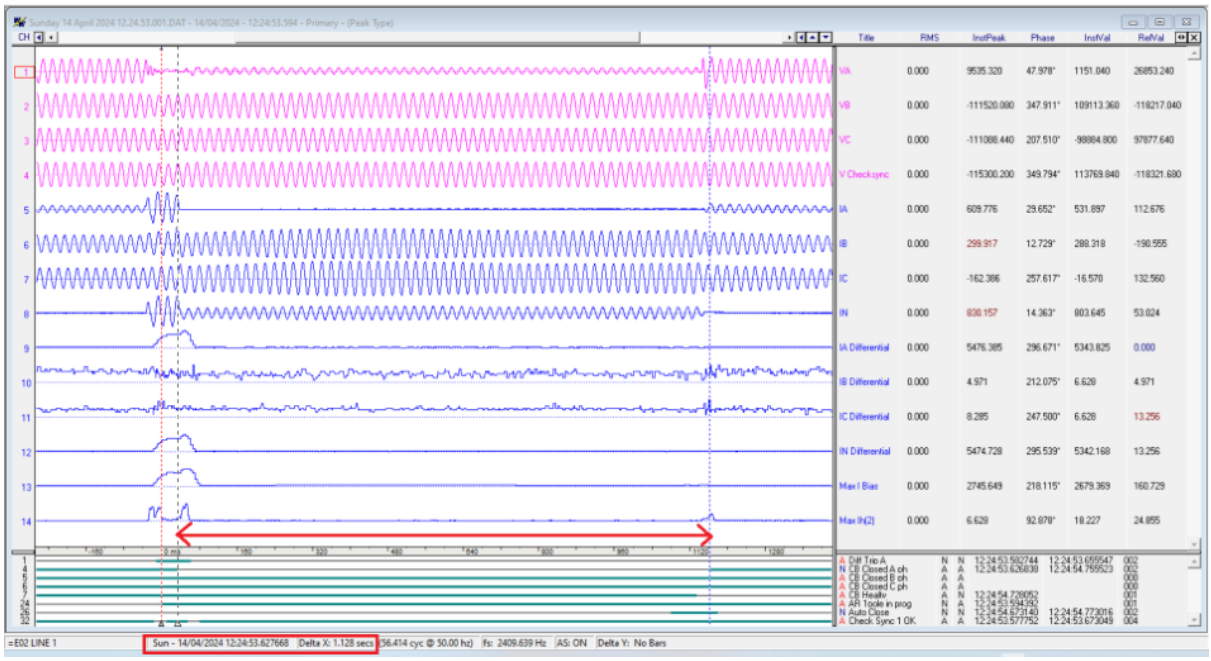

Figure 13: Auto reclose at Line 1 (87L).

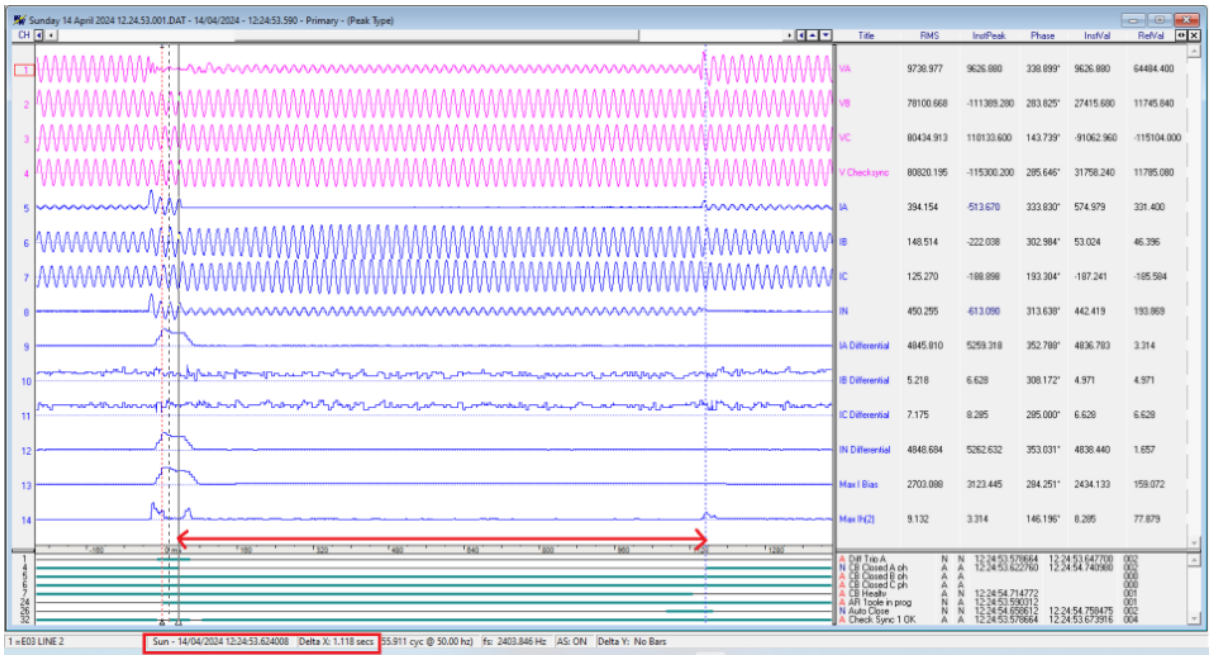

Figure 14: Auto reclose at Line 2 (87L).

As shown in Figure 15 of Hot Well Pump A, it appears there is unbalanced current in the system due to auto reclose on the phase R of the Transmission Line. The current on each phase R, S and T are uncontrollable at that time, unbalanced currents cause excessive heating in motor rotors due to opposing magnetic fields in parts of the rotor of induction motors that can result from excessive unbalanced (negative-sequence) currents. This current produces flux in the motor air gap rotating in the opposite direction to the actual motor direction. However, we need to understand that the condition will damage the motor if only the negative sequence current is high and also occur in a long duration exceeding the limit from the Manufacturer or any International Standard.

Similar to Figure 15, the HWP motor B also experiences the same condition (unbalance current on the MV system) during auto reclose on the 150kV Transmission line in Figure 16..

From the waveform data for Transmission Line 1 & 2, HWP A & B, we can conclude that when a lightning strike occurs and a disturbance happens on the grid, the protection relays, including the line differential relay and the motor unbalance relay, operate almost simultaneously. The line differential relay attempts to clear the disturbance

on the grid by activating the auto-reclose function, while the motor unbalance relay works to secure the equipment by responding to the motor unbalance condition setting.

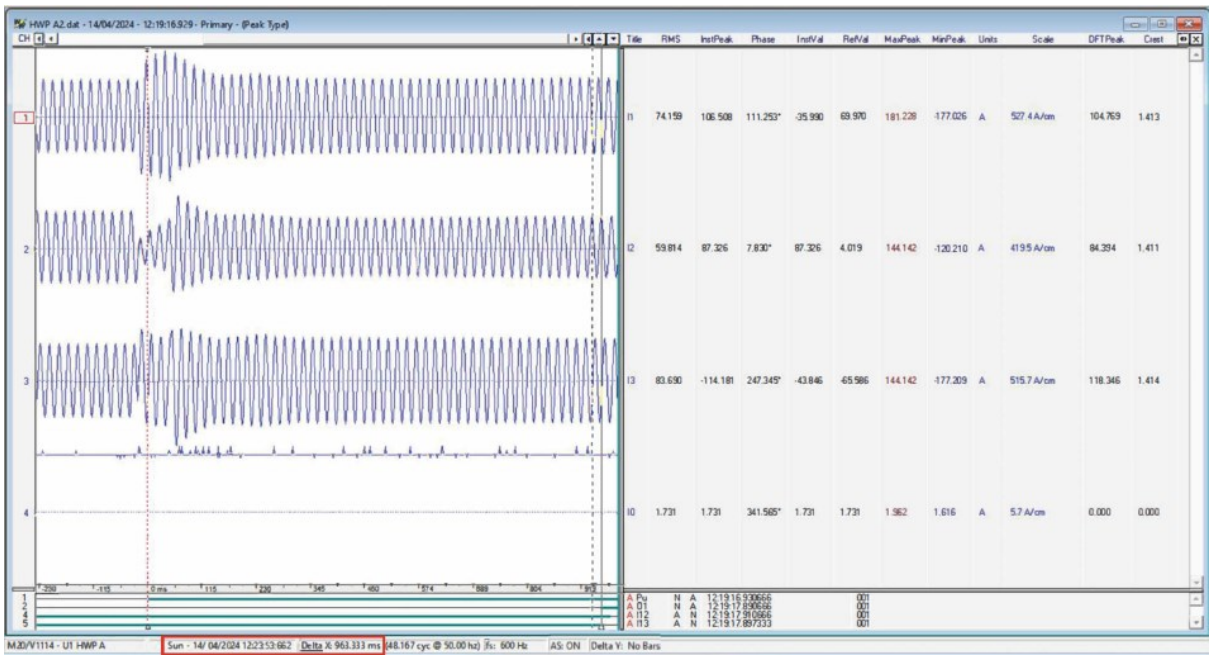

Figure 15: Motor unbalance at HWP A.

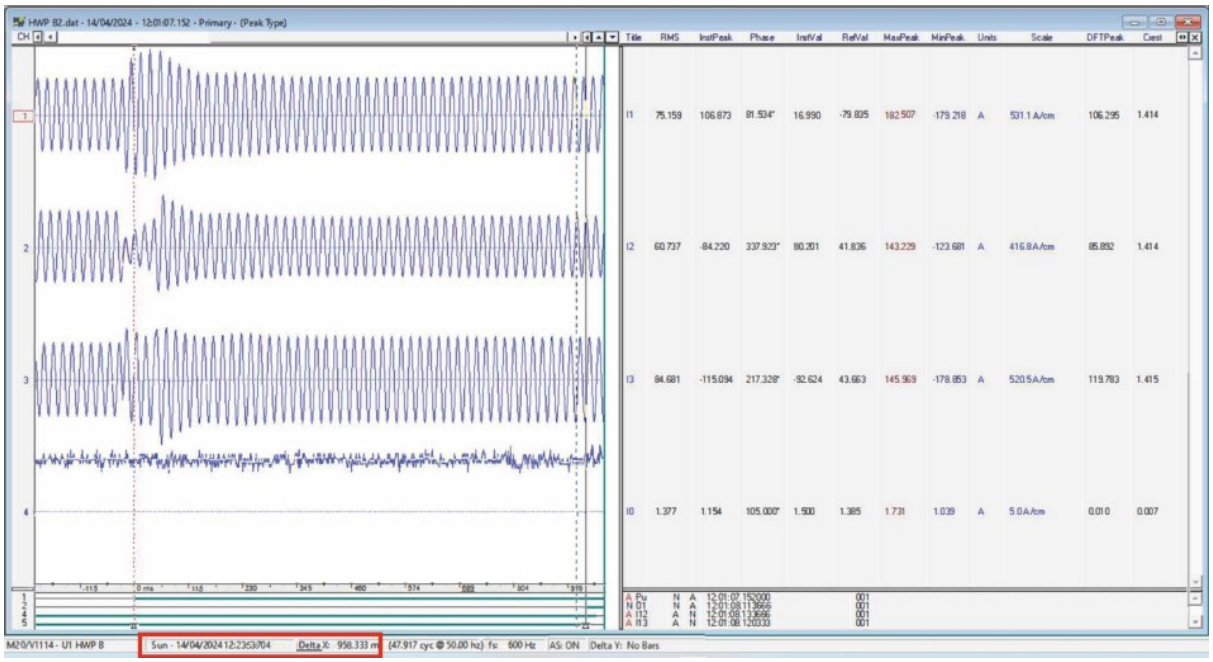

Figure 16: Motor unbalance at HWP B.

Equipment	Event	Start	Stop	Process time	Status	Plant Interlock
Transmission Line#1	Auto reclose Line#1 CB Phase A Open	12:24:53:627	12:24:54:756	1128 ms	CB Close	none
Transmission Line#2	Auto reclose Line#2 CB Phase A Open	12:24:53:622	12:24:54:741	1118 ms	CB Close	none
HWP A	Motor Unbalance	12:24:53:662	12:24:54:663	963.33 ms	HWP A Trip	Turbine Tripped 12:24:55:258
HWP B	Motor Unbalance	12:24:53:704	12:24:54:663	958.33 ms	HWP B Trip	

Figure 17: Table event of auto reclose and unbalance.

6.3 Business impact of the outage

As a result of this incident, the Lumut Balai Geothermal Power Plant experienced a total downtime of 3 hours. This downtime reduced the Equivalent Availability Factor (EAF) by 0.07% and increased the Equivalent Forced Outage Rate (EFOR) by 0.034%. The estimated lost revenue amounted to IDR 191,472,442. This event underscores the critical importance of maintaining robust and reliable systems. By swiftly addressing such

challenges, we reinforce our commitment to operational excellence and uphold our company image as a dependable and resilient energy provider dedicated to sustainability and customer satisfaction.

7. IMPROVEMENT PROGRAM

The current setting for motor unbalance protection on the medium voltage (MV) motors is 15% of rated current (Ib) with a delay time of 1 second (definite time curve). and after conducting an extensive literature review , about relay coordination, sequence of events, O&M also According to the IEEE C37.96-2012 standard, the pick-up current setting already meets the requirement. However, the 1-second time delay is too fast and cannot accommodate any temporary voltage or current imbalances on the grid (known as "swing") that can occur during single-phase auto reclose operations. This overly sensitive unbalance relay protection setting caused unnecessary trips. The new value for the delay time is set to 10 seconds (definite time curve) based on the recommendations from the IEEE C37.96-2012 standard. This new time delay will provide proper protection for the motors in case of any real unbalanced condition (e.g., broken circuit components like cables, windings, or fuses) while preventing unnecessary tripping due to grid swings, unbalanced current transformer burdens, etc.

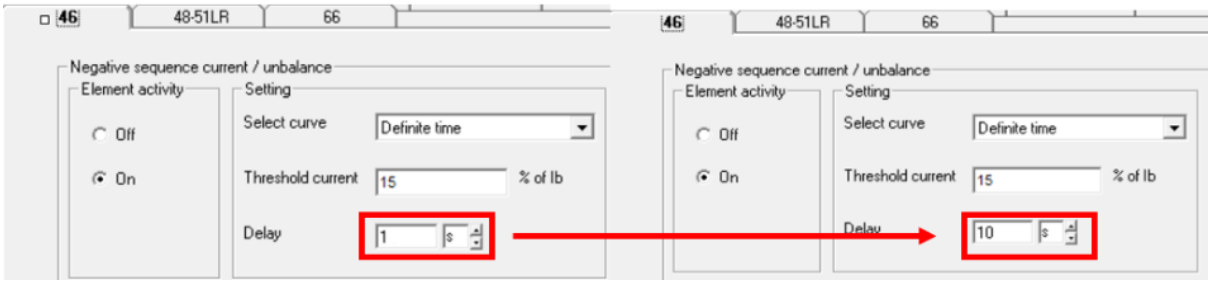

Figure 18: Delay time motor unbalance from 1s to 10s.

As shown in Figure 18, we modify the time delay of the negative sequence current (46) relay on the MV motor from 1 second to 10 second. Evaluating the delay time according to IEEE standards for the unbalanced relay is essential to prevent the unit from experiencing unnecessary protection trips and miss coordination with the upstream protection relay.

8. CONCLUSION

The unplanned outage at the Lumut Balai Geothermal Power Plant (PLTP) resulted from the simultaneous operation of the line differential relay's auto-reclose function and the motor unbalance relay, both configured with identical delay times. During the auto-reclose cycle, the motor unbalance relay detected phase differences, triggering unnecessary tripping of the motors even though the line fault had been cleared by the line differential relay. This unnecessary tripping can lead to increased downtime and potential equipment stress.

To prevent future occurrences and improve overall system reliability, we implemented a staggered delay time strategy between the line differential relay and the motor unbalance relay. This enhanced coordination between the protective devices minimizes the likelihood of unnecessary motor trips.

Following the IEEE C37.96-2012 standard, we adjusted the motor unbalance relay's delay time from 1 second to 10 seconds. This change ensures proper coordination, preventing unnecessary trips and enhancing system reliability. We expect this adjustment to eliminate similar incidents in the future, leading to a projected increase in Equivalent Availability Factor (EAF) by 0.07% and a reduction in Equivalent Forced Outage Rate (EFOR) by 0.034%.

ACKNOWLEDGEMENT

The authors would like to express their gratitude to Pertamina Geothermal Energy Lumut Balai for granting permission to share the data used in this study.

REFERENCES

Hoq, Md Tanbir. (2023). Distance Protection of Transmission Lines with High Levels of Series Compensation: A study on frequency and time domain communication independent distance protection for series compensated lines. Doctoral thesis, KTH Royal Institute of Technology.

IEEE Std 3004.8-2016. Recommended Practice for Motor Protection in Industrial and Commercial Power Systems. Institute of Electrical and Electronics Engineers.

IEEE Std C37.96-2012. Guide for AC Motor Protection. Institute of Electrical and Electronics Engineers.

IEEE std C37.113-2015.Guide for Protective Relay Application to Transmission Line.

Nirupma Sharma, Aparna Acharya, Irene Jacob, Sumanth Yamujala, Vikas Gupta, and Rohit Bhakar. (2021). Major Blackouts of the Decade: Underlying Causes, Recommendations and Arising Challenges. In International Conference on Power Systems (ICPS), pages 1–6, Kharagpur, India, 2021. IEEE. doi:10.1109/ICPS52420.2021.9670166. ISSN: 2691-0233.

Toshiba. (2019b). Plant Interlock Diagram (Electrical). Toshiba (internal document).

Toshiba. (2019c). Classroom Lecture for Toshiba Steam Turbine Control System. Toshiba (internal document).

Energy Efficiency Potential at Steam Ejector 60% of Patuha Geothermal Power Plant Unit 1

Audi Ardika Paundratama, Ananda Riris Kurnia Pratama, and Muhammad Abdurrahman Saleh

PT. Geo Dipa Energi (Persero), Aldevco Octagon 2nd Floor.
Jl. Warung Jati Barat No. 75 Jakarta Selatan 12740 Indonesia

audi@geodipa.co.id, ananda.pratama@geodipa.co.id, abdurrahman.s@geodipa.co.id

Keywords: Ejector, Control Valve, Power Plant Generation

ABSTRACT

Indonesia has 40% of the world's potential geothermal resources, estimated at 28,000 megawatts (MW). Patuha Geothermal Power Plant is one of the power plants that have been established in Indonesia and operated under PT. Geo Dipa Energi (Persero). Patuha Geothermal Power Plant has a capacity of 1 x 60 MW. One of the factors that contributes to power plant efficiency is Non Condensable Gas (NCG) content, like CO2 and H2S that can commonly can be found at steam compositions coming from geothermal wells. Patuha Geothermal Power Plant uses Gas Removal System that consisting of an ejector and liquid ring vacuum pump (LRVP). Gas Removal System has the function to extracting NCG accumulation and exhaust it into the atmosphere. Current operational condition at Patuha GRS system is a combination of 60 % ejector and one Liquid Ring Vacuum Pump in service. Meanwhile, on daily operating condition of Patuha power generation on each day can fluctuate depending on several factors, such as demand that has been determined by the grid dispatcher or production well capabilities producing steam, so that here Patuha Power Plant can operate in fluctuate condition and not always in full load capacity considering Patuha Power Plant is a power generation system that is following system in the national grid. So this condition is an opportunity for Patuha Geothermal Power Plant to increase energy efficiency by reducing the use of motive steam on the ejector system which is controlled based on the load conditions of the generator without affecting the ejector design. The consumption of motive steam used in ejector has the potential to be excessive because there is no control system that can regulate the steam motive flow to the ejector using a control valve. In general, the impact that occurs from the current operating base of the gas removal system consist of a 60% ejector in service without using a flow control valve (FCV) on motive steam line, is the excess of motive steam, which the motive steam should be able used to help the generation load on the generator turbine when there is not much steam production from the well. The solution for Patuha Geothermal Power Plant is to add a flow control valve to the motive steam line in the 60% ejector.

1. INTRODUCTION

Geothermal energy is a renewable energy with a stable characteristic for generating electricity and is used as the base load for power generation on national grid electricity. Geothermal power plants operate like other thermal power plants, using the rankine cycle principle. Steam as the working fluid will expand through turbines, which are coupled with generators to convert kinetic thermal energy to electrical energy. Indonesia has 40% of the world's potential geothermal energy resource, estimated at 28,000 MW. Patuha Geothermal Power Plant is one of those commercially operated by PT Geo Dipa Energi (Persero) with an installed capacity of 1 x 60 MW. Patuha Geothermal Power Plant is a dry steam power plant with characteristic vapor dominance, and there is little gaseous content such as carbon dioxide, hydrogen sulfide, methane, and others (Dipippo 2016). Non-condensable gas in geothermal power plants is one factor contributing to plant performance efficiency; otherwise, the NCG needs further handling to dissipate to prevent increasing condenser pressure and affecting turbine output. The influence Non Condensable Gas caused reduce geothermal fluid can be extracted in energy conversion, for each 1% NCG increase turbine losses 0,86% at inlet due to decreasing turbine inlet temperature (Gocken and Yildrim, 2008). Commonly, geothermal power plants use a gas removal system consisting of an ejector and a liquid ring vacuum pump (LRVP). Before the production well was completely drilled, the GPP surface facility design had already started due to the uncertainty of geofluid properties during the early stages; therefore, the sizing equipment gas removal system (GRS) used two to three times the actual condition (Yamin W et al., 2020). The principle operation ejector-based Bernoulli is that the accelerating high-pressure motive steam through the nozzle will be converted to velocity energy and sucking NCG at the lower pressure suction side. Currently, the Patuha Geothermal Power Plant GRS system is using a combination hybrid system operation with a 60% ejector and one liquid ring vacuum pump (LRVP) in service. The NCG content in the Patuha geothermal field, based on analysis during initial operation, was about 1.09%–1.14% by weight of total steam supply, and there was a decline to 0.68% by weight average NCG content in 2022. The daily operation flow consumption of steam as motive steam to gas removal system is 7.01 t/h and the inlet pressure is 7.79 bar. This condition means the means the motive steam pressure is

too high from the minimum inlet pressure and could potentially be reduced. Reducing the waste of disposed energy is significantly important to improving geothermal power plant performance (Pambudi et al., 2014). The motive steam to get the optimum point was to be set as close to the critical pressure limit (choked flow) as possible and obtain the highest efficiency (Hanafi et al., 2015). The suction load of the ejector will decrease if the motive steam supply pressure is greater than 20%–30%. In the above design, this condition causes too much steam to expand across the nozzle (Lines and Smith, 2000). This study aims to present a potential improvement in plant performance efficiency at the Patuha Geothermal Power Plant based on the current operating mode. To maximize potential excessive motive steam at 60% ejector, existing optimization will be carried out by installing an additional flow control valve (FCV).

2. METHOD

2.1 Research Methods

This study was conducted to determine the potential reduction of flow motive steam consumption that can be used in ejector 60% on gas removal systems (GRS). Research methods start with identifying the current pattern of the operating mode gas removal system (GRS), then conduct data collection to find the data design and operating ejector 60%, after that conduct a literary study to find the best methods to calculate related current ejector 60% steam consumption end ejector 60% design steam consumption. In this study we use data comparison between design steam ejector and operation data, the result of the literary study are applied to the determine the potential to reduce of motive steam consumption ejector 60%. After the data is obtained, the next step is to analyze minimum steam flow rate on motive steam ejector 60% and analyze opening flow control valve (FCV) on motive steam to obtain desired minimum motive steam flow rate. The flow diagram show on the Figure 1.

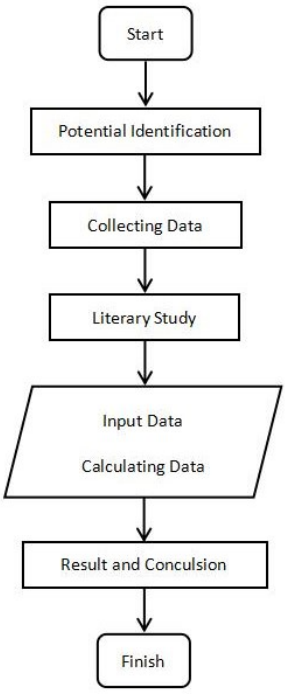

Figure 1: Research Methods Diagram.

2.2 Data Collecting Methods

2.2.1 Overview Gas Removal System

To remove NCG from the condenser and discharge it to atmosphere the most commonly Geothermal Power Plant used steam jet ejector, two or more stage ejectors can be arranged to get greater compression. In two stages system to condense the first stage motive steam and prior to ensure in the second stages only handles non condensable gas an inter condenser are used. A hybrid system operation are used to increase efficiency and reduce motive steam consumption, the gas removal system used Liquid Ring Vacuum Pump combiner with steam jet ejector (R.B. Swandaru, 2006). Figure 2 show the simplified process flow diagram gas removal system are used patuha geothermal power plant. The ejector is designed to operate at a specified steam pressure, ejector manufacturers summarize critical data on a ejector data design and performance curve. Table 1 shows ejector data design for a single stage ejector and figure 3 shows on a performance curve for a single stage ejector. On the y-axis of this curve is suction pressure bar absolute (bar A). On the x-axis is the water vapor equivalent load (kg/hr).

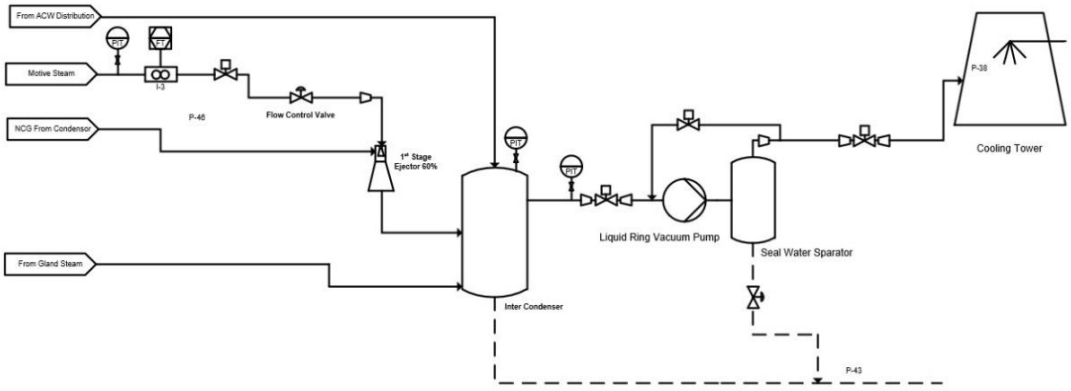

Figure 2: Process Flow Gas Removal System.

Table 1: Ejector Data Design.

Ejector Stage	30% Y-Stage	40% Y-Stage
60% Y-Stage	Suction Load Air kg/h	57.5
76.5	115	Suction Load NCG kg/h
3501.5	4669	7003
Suction Load Water Vapour kg/h	691.5	922
1383	Suction Pressure Bar (a)	0.0921
0.0921	0.0921	Discharge Pressure Bar (a)
0.298	0.298	0.298
Operating Steam Pressure (minimum) Psi (g)	7.8	7.8
7.8	Operating Steam Temperature ℃	169
169	169	Steam Flow kg/h
4539	6067	9101

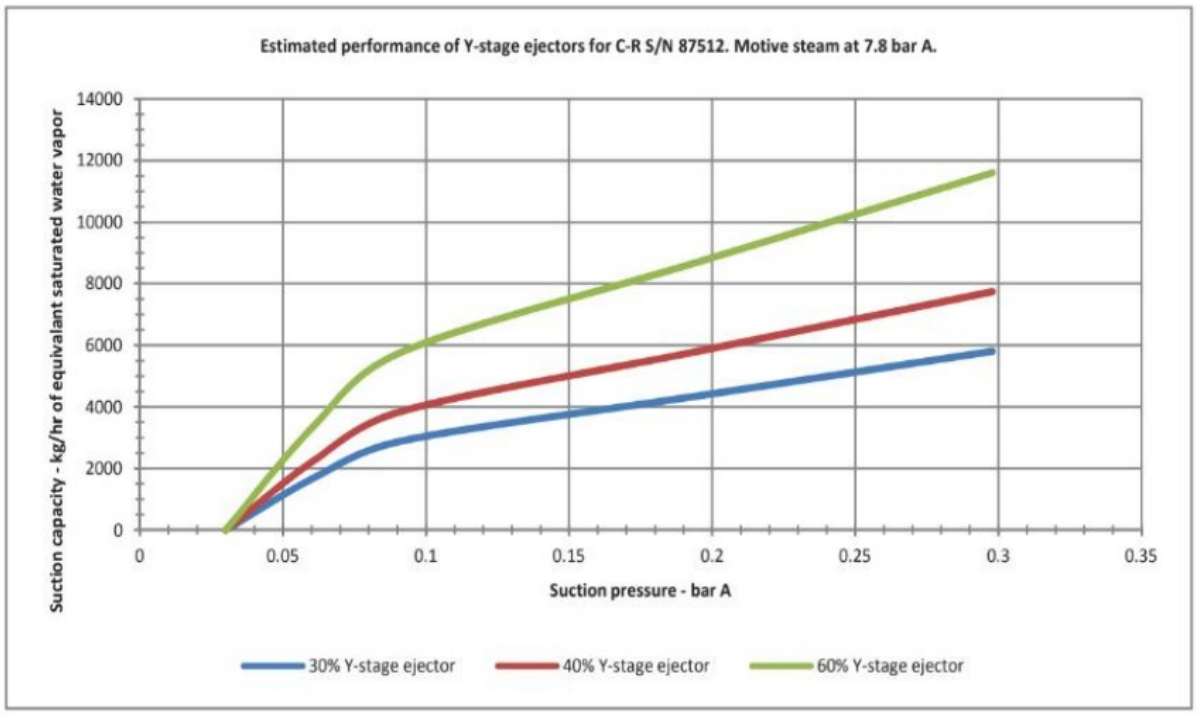

Figure 3: Performance Curve For a Single Stage Ejector.

2.2.2 Operating Data Ejector

Currently operating mode gas removal system at Patuha Geothermal Power Plant is using hybrid combination system, depend on vacuum condenser with one 60 % ejector and one liquid vacuum pump (LRVP).The initial sampling result of NCG content based on first performance test at 2014 is about 1.09% - 1.14% by weight of total steam supply show on table 2 and there was decline to 0.68 % by weight average NCG content at 2022 show on table 3.

Table 2: NCG Analysis Result On Initial Performance Test 2014.

Date Time	GSA/Steam Ratio (ppm by Weight)
24/09/2014 12:00	1.14%
24/09/2014 15:00	1.12%
24/09/2014 19:00	1.09%

Table 3: NCG Analysis Result at 2022.

Date	GSA/Steam Ratio (ppm by Weight)
31/12/2012	0.68%

The current daily operation flow rate steam as motive steam to ejector 60% is average 7.019 t/h at 2022 show on table 4 and consumption of motive steam used in ejectors in service has the potential to be excessive due to there is a decrease in the total of Non Condensable Gas (NCG) and the flow motive steam required for the ejector potentially to be reduced.

Table 4: Average Steam Flow Rate at 2022.

Month	Steam Flow (t/h)
January	6.91
February	6.96
March	6.88
April	6.82
May	6.73
June	6.70
July	6.67
August	6.75
September	6.77
October	7.8
November	7.62
December	7.62

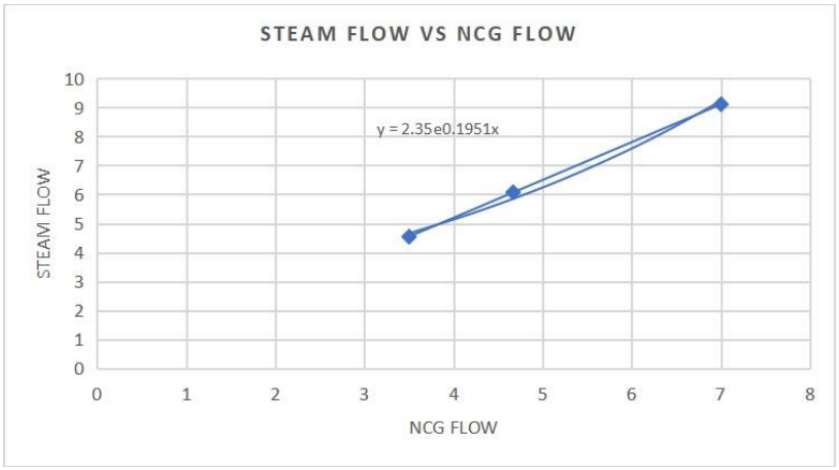

Figure 4: Function Relation Ratio Steam Flow and NCG Flow.

3.RESULT AND DISCUSSION

To analyze and calculate the motive steam flow rate required for the 60% steam ejector, are using the procedure of a function equation ratio based on the total suction load called the non-condensable gas (NCG) flow rate design and the motive steam flow rate design shown in Figure 4. In line with the decrease in NCG content average in 2014, the steam flow rate will also decrease. The steam consumption of a single-stage ejector is dependent on the mass flowrate (and molecular weight) of the gas to be handled (Bandoro, 2006). Meanwhile, also have to consider that the minimum suction pressure should not decrease below the minimum operating steam pressure of the ejector. Thus, the ratio between a suction load and motive steam flow rate can be determined by the equation.

$$y=2.35e0.1951x \quad (1)$$

Condition operation motive steam consumption was higher than the process requirement based on design, manufacture, and NCG content conditions. Based on the result of the study comparison design on steam ejector 60% with actual condition operation to obtain plant performance, we suggest the Flow Control Valve is possible to install to reduce excessive motive steam and give the optimum startup operation to control steam flow to ejector 60% depend on vacuum condenser and prevent over vacuum that cause turbine rolling when vacuum up operation and give the optimum startup without use ejector 30% or 40% to initial build up vacuum on condenser. Optimum operation flow control valve between 65% and 70% considered NCG content from steam. In this condition, we can reduce motive steam to 2.6-3.2 T/h as shown in figure 5. Based on the assumption that all excessive steam will flow through the steam turbine, the increased output of the steam turbine is approximately 300–400 KWH with the current steam-specific consumption (SSC).

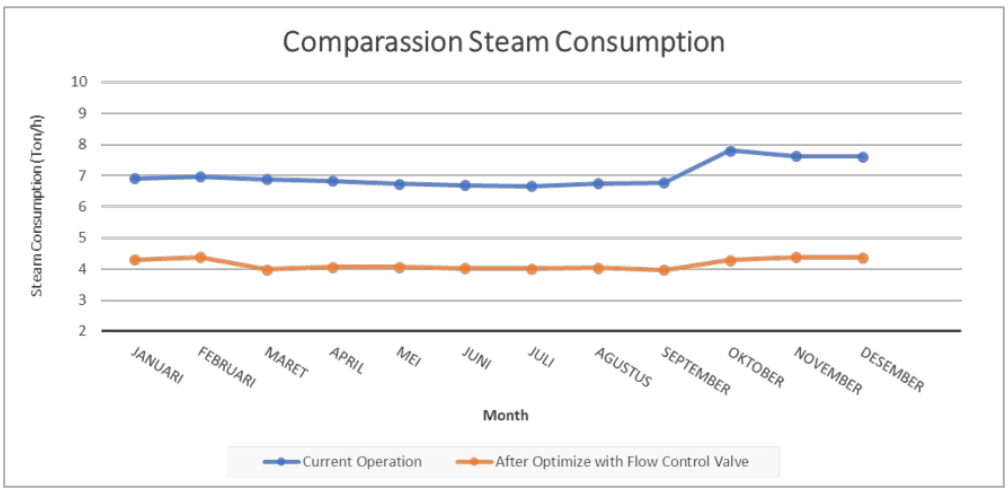

Figure 5: Comparison Steam Consumption.

REFERENCES

DiPippo, R., 2007, Geothermal Power Plants – Principles, Applications, Case Studies and Environmental Impact. Massachusetts: Butterworth – Heinemann.

Ejector Instalation, Operation, and Maintenance Manual Corporation: CROLL – REYNOLDS CO., INC.

Gokcen, G. and Yildrim, N. 2008, Effect of Non Condensable Gas on Geothermal Power Plant Performance. Case study : Kizildere Geothermal Power Plant – Turkey, Int. J. Exergy vol. 5 Nos 5/6.

Hanafi, A. s., Mostafaa, g., Waheed, A., and Fathy, A., 2015 1-D Mathematical Modelling and CFD Investigation on Supersonic Steam Ejector in MEDD – TVC. The 7th International Conference on Applied energy – ICAE 2015. Abu Dhabi: Energy Procedia, 75, 3239 –3252.

Lines, J. R. and Smith, R. T., 2000, Ejector System Troubleshooting. Corporation: https://www.graham-mfg.com/usr/pdf/TechLibVacuum/216.PDF

Ozcan, Y. N., and Gokcen, G. 2009, Thermodynamic assessment of gas removal system for single – flash geothermal power plant, Applied Thermal engineering, 29 (14-15), 3246- 3253.

R. B. Swandaru, 2006, Thermodynamic analysis of preliminary design of power plant Unit 1 Patuha, West Java, Indonesia, Report of The United Nation University Geothermal Training Programme, Reykjavik, Iceland, Report No: 7 pp 83 – 37.

Wibisono, Y., Makertihartha, N., and Rizkiana, J., 2020, Evaluation on Energy Efficiency Improvement in Geothermal Power Plant with The Application of Load – based Gas Removal System and Cooling Water Pump Control System. Research article/Vol. 14 No 1, pp. 30 – 46.

DRJ-31 Scrubbing Facility to Sustain Darajat Unit-1 Steam Supply

Surya Eko, Kalih Sholli, Wibisono, Sigit Winarno, Irfan Ismail, and Asiawan Hanindito

Star Energy

suko@starenergy.co.id, klrz@starenergy.co.id, qwaa@starenergy.co.id, tctb@starenergy.co.id, mair@starenergy.co.id, ayyv@starenergy.co.id

Keywords: Separator, Wet steam, Pipeline, Steam quality

ABSTRACT

Darajat Unit-1 steam supply comes from North Sector (60%) and South Sector (40%) areas. As some of the South sector wells have repetitive wellbore issues, Unit-1 steam supply dependency on North Sector is growing. This dependence intensified following a landslide in the South Sector (Cikupakan) on November 19, 2021, disrupting steam flow from Pad 4. Backup from Unit-2 wells (Pad-18) was required, potentially jeopardizing Unit-2's steam buffer and generation capacity in the long run.

To maintain steam supply to Unit-1 without interrupting Unit-2 steam supply, One of the mitigations is by reactivating the currently inactive wells i.e. DRJ-31 well. The well was put offline after latest sampling performed in May 2018 shows that the dryness possible was 95.37%.

Additional steam-liquid separation process is required in DRJ-31 pipeline to remove 4.63% liquid content from the produced steam. The separated steam would be directed to Unit-1, while the separated liquid would be flowed into the zero discharge condensate reinjection system. A dedicated separator was chosen due to its scheduling flexibility (not requiring Unit-1 shutdown for installation) and cost-effectiveness.

The dedicated separator was designed according to ASME Sec VIII Div 1 (2019 ed.) standards. Unlike typical wellpad separators, the DRJ-31 separator utilizes a fast-acting LCV (level control valve) to ensure a minimal liquid level inside the vessel. This approach obviates the requirement for a loop seal, which conventionally necessitates a vessel skirt height of up to 7 meters. Fabrication, installation, and commissioning of the separator were completed over a span of 10 months, from June 2021 to March 2022. Performance testing was conducted to find optimum delta pressure which resulted in highest possible steam quality (min 99%) and the most optimum steam flowrate, with dryness reaching up to 99.8% at specific wellhead pressure and flow rate.

Since its reactivation in February 2022, DRJ-31 has consistently delivered an average steam flow rate of 10.9 kg/s, equivalent to the production of approximately one makeup well. As of the latest operation report, DRJ- 31 is currently producing 15 kg/s of steam at WHP of 13 barg. This successful re-activation enhances Unit- 1's steam supply security and reduces reliance on Unit-2 wells.

1. INTRODUCTION

Darajat unit-I steam supply is maintained by group of wells in North and South Sectors, i.e. DRJ-7, DRJ-9, DRJ-10, DRJ-11, DRJ-31 in North area and DRJ-8, DRJ-13, DRJ-34 in South area. North area wells supports around 60% of steam delivered to Unit-1, while the rest (40%) comes from South area wells. As most of the Southern wells are known to have repetitive wellbore issue (e.g. scaling), Unit-1 steam supply dependency on Northern wells production is growing over time.

Since 19 September 2021, steam supply from South Sector has been significantly reduced due to landslide at Cigupakan area, damaging some south sector's steam pipeline and cut off steam supply from Pad 4. This has caused redirection of around 32 kg/s Pad-18 steam (normally fed into Unit-II) to Unit-I via Pad-9 junction line (north sector). This condition impacts in reduction of Unit-II steam buffer which can threaten Unit's capability to fulfill long term business plan target.

To maintain steam supply to Unit-1 without interrupting Unit-2 steam supply, One of the mitigations is by reactivating the currently inactive wells i.e. DRJ-31 well. The well was last opened for production to Unit-I in July 2016, supplying 7 kg/s steam (equal to 3.5 MW) at 10% valve opening. The well was then put offline after latest steam quality sampling performed in May 2018 shows that the dryness possible was 95.37%.

Additional steam-liquid separation process is required in DRJ-31 pipeline to remove 4.63% liquid content from the produced steam. The separated steam would be directed to Unit-1, while the separated liquid would be flowed into the zero discharge condensate reinjection system. A dedicated separator was chosen due to its scheduling flexibility (not requiring Unit-1 shutdown for installation) and cost-effectiveness.

2. PROJECT COMPLETION DATA

DRJ-31 separator installation project was started in Q3 2021 and finished in Q1 2022. Scope of project include separator fabrication, pipeline & pipe support modification, electrical & instrument work, and commissioning of DRJ-31 separator. The dedicated separator was designed according to ASME Sec VIII Div 1 (2019 ed.) standards with design basis for separator capacity of: 15 kg/s (WHP 14.2 barg) inlet fluid flowrate at 95.37% steam quality, while the pipeline was designed according to ASME B31.3.

2.1 Facility Arrangement

Before installation DRJ-31 separator, steam from well DRJ-31 flows directly to Pad-3 steam header to supply to Unit-1 Darajat. After installation DRJ-31 separator, in normal operation, wet steam from well DRJ-31 flows through Separator. The outlet steam flows to Pad-3 header to supply to Unit-I Darajat, while separated liquid flows to condensate reinjection system, as shown in Fig.1.

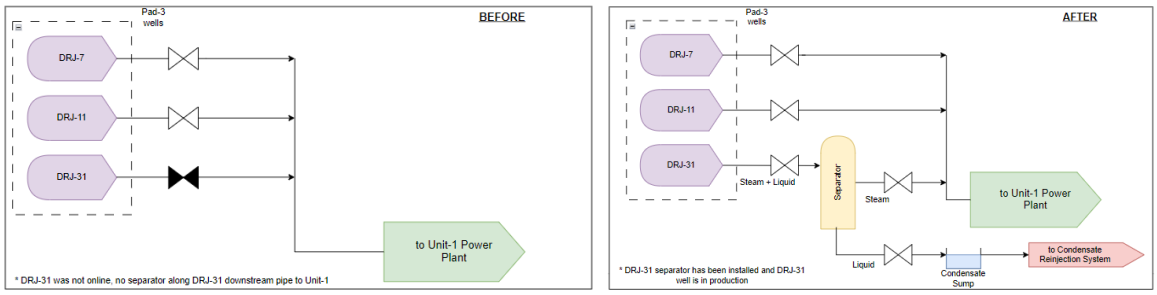

Figure 1: Schematic diagram of Pad-3 Steam Pipeline Arrangement (Before and After DRJ-31 Separator Installation Project).

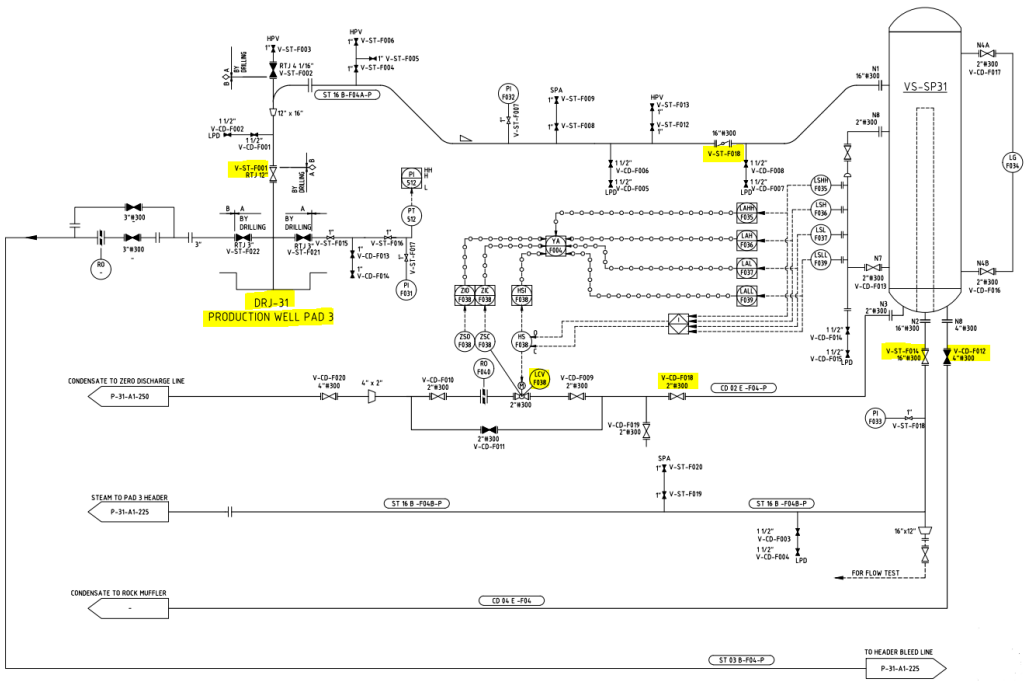

Figure 2: P&ID DRJ-31 Production Well.

2.2 General System Description

DRJ-31 wellhead separator (VS-SP31) is Vertical Bottom Outlet type separator. Separation process works by using centrifugal force of fluid spinning inside the separator. Steam-liquid mixture in contact with vessel's wall causes vapor-liquid separation where liquid drops to the bottom of the vessel, while vapor/steam and gas exits through a standpipe extending up inside the vessel.

As shown in Fig.2, the wellhead separator receives mixture of steam and liquid from the wellhead production flowline. A manually operated FCV (V-ST-F018) located in the flow line controls the flow rate from the well to the separator. The manual operated valve is 16-in butterfly valve and normally is set at certain opening to maintain wellhead pressure based on reservoir management team requirement.

The FCV has a master valve on its upstream side (V-ST-F001) so that the FCV and vessel can be shut-down for maintenance. Downstream of the vessel is also equipped with isolation valves (V-CD-F018, V-ST-F014, and V-CD-F012) to allow for vessel inspection/maintenance.

The FCV has a master valve on its upstream side (V-ST-F001) so that the FCV and vessel can be shut-down for maintenance. Downstream of the vessel is also equipped with isolation valves (V-CD-F018, V-ST-F014, and V-CD-F012) to allow for vessel inspection/maintenance.

Liquid level inside the vessel is controlled/maintained by LCV-F038. During normal operation, liquid level shall be maintained between LSL-LSH. Liquid level control is needed to seal the liquid (condensate) system from steam system. This is to allow small pressure change during operation without affecting the separation efficiency of the separator, or causing risk of hammering due to gas/vapor blow-by to liquid line.

LCV-F038 operates in "on/off" mode by motorized actuator that functions open and close the valve to maintain separator loop seal liquid level between LSL-LSH in about 340 mm. Level switches LSH-F036 and LSL-F037 are provided to detect/sense liquid at low and high level for LCV activation. When the condensate liquid level in the separator reaches the high level switch (LSH-F036), the relay circuit de-energizes the CLOSE command and energizes the OPEN command to the LCVF038 which holds it open and allows the condensate to drain from the separator liquid loop seal.

The level control valve is also used for start-up of the separator system. During this operation, the LCV is controlled locally by the operator, who monitors separator level on the level gauge and adjusts the LCV position to suit. During vessel startup, mixture of steam and liquid from the well is discharged from the separator, through the valve V-CD-F012, to existing rock muffler in Pad 3.

3. DRJ-31 SEPARATOR PERFORMANCE TEST

Performance testing was conducted to find optimum delta pressure which resulted in highest possible steam quality (min 99%) and the most optimum steam flowrate, with dryness reaching up to 99.8% at specific wellhead pressure and flow rate. The work steps is to test separation performance in several wellhead pressures: 14, 16, 18, and 20 barg, by maintaining separator pressure at 12 barg, slightly higher than Pad-3 header pressure, then measuring steam quality outlet separator at each wellhead pressure. WHP is set by adjusting V-ST-F018 (flow line BV) and separator pressure is set by throttling 16" BV at temporary flow test line to Rock Muffler. Steam flowrate is measured by using orifice installed at temporary flow test line between 1-½" LPD and the 16" BV. Steam quality will be measured on temporary flow test line (separator outlet).

Separation performance (in term of outlet dryness) as a function of pressure difference (ΔP) between well head and separator is shown in the following chart:

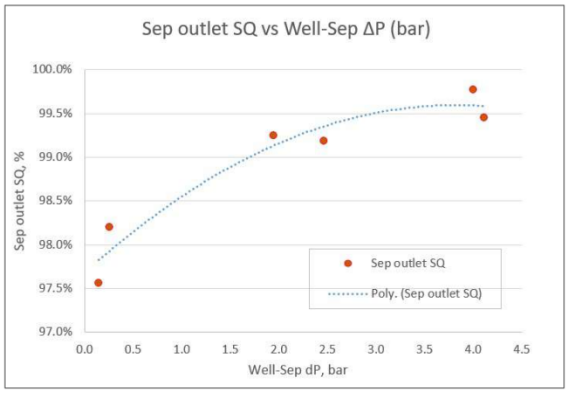

Figure 3: DRJ-31 Separator Outlet Steam Quality vs Well-Separator dP.

The plot shows that higher ΔP impact in higher steam dryness outlet separator which indicating substantial effect of flashing across FCV to the decrease of steam wetness. Although high ΔP requires higher wellhead pressure (i.e. with ΔP 4 bar and Separator Pressure 12 barg, WHP will be 16 barg), wherein it means wetter steam from well, flashing (JT effect) combined with separation process is able to compensate it and produce higher SQ steam from separator. DRJ-31 Separator predicted performance within 12-16 barg wellhead pressure range, at 12 barg operating pressure, is summarized in Table 1.

Steam quality higher than 99% can be obtained by operating the well at 14 barg and separator 12 barg pressures, with steam flowrate 11.12 kg/s. The steam flowrate is 4 kg/s (~ 2MW equivalent) higher than it is at WHP 15.75

barg. Test results evaluation suggest that DRJ-31 Separator is ready for service in support of Unit-I steam supply management.

Table 1: DRJ-31 Well and Separation System Predicted Performance at 12 barg Separator Pressure.

WHP, barg	SQ Steam from Well, %	SQ Sep Outlet, %	Steam from Separator Flowrate, kg/s
12	93.4%	98.2%	13.01
12.25	93.5%	98.3%	12.93
12.5	93.5%	98.4%	12.81
12.75	93.6%	98.6%	12.65
13	93.6%	98.7%	12.44
13.25	93.5%	98.8%	12.18
13.5	93.5%	98.9%	11.87
13.75	93.4%	99.0%	11.52
14	93.2%	99.1%	11.12
14.25	93.0%	99.2%	10.68
14.5	92.8%	99.3%	10.18
14.75	92.6%	99.4%	9.65
15	92.3%	99.5%	9.06
15.25	92.0%	99.6%	8.43
15.5	91.6%	99.7%	7.75
15.75	91.3%	99.8%	7.03
16	90.8%	99.8%	6.26

Since its reactivation in February 2022, DRJ-31 has consistently delivered an average steam flow rate of 10.9 kg/s, equivalent to the production of approximately one makeup well. As of the latest operation report, DRJ- 31 is currently producing 15 kg/s of steam at WHP of 13 barg. This successful re-activation enhances Unit- 1's steam supply security and reduces reliance on Unit-2 wells.

4. CONCLUSION

DRJ-31 separator installation was done with design basis of 95.37% and total steam flowrate from well at 15 kg/s (WHP 14.2 barg). In normal operation, wet steam from well DRJ-31 flows through separator. Outlet steam flows to Pad-3 header to supply to Unit-1 Darajat, while separated liquid flows to condensate reinjection system header line in Pad-3. From the performance test, highest steam quality achieved was 99.8% obtained at DRJ-31 WHP 15.8 barg and separator pressure of 11.8 barg; while the lowest WHP to get steam dryness outlet separator > 99% is at 14 barg. Test results evaluation suggest that DRJ-31 separator is ready for service in support of Unit-1 steam supply management.

REFERENCES

Sadiq J. Zarrouk, Munggang H. Purnanto: Geothermal steam-water separators: Design overview, *Geothermics*, **53**, (2015), 236-254.

Star Energy Geothermal Darajat II, Ltd., Project Turn-Over Report DRJ-31 Scrubbing Facility, (2022), Unpublished internal company document.

The Study of Safety Integrity Level (SIL) using A Layer of Protection Analysis (LOPA) Method in Geothermal Steam Field PT XYZ

Putri Shavira, Efrata Pratenta Meliala, Adi Suparyanto, dan Wahyu Agung Pramudito

putrishavira11@gmail.com, efrata.meliala@yahoo.com,
adisuparyanto68@gmail.com, wahyu.agung@universitaspertamina.ac.id

Keywords: SIL, LOPA, Geothermal, Steam Field, Operational Risk

ABSTRACT

In 2021, geothermal utilization in Indonesia was approximately 9% of the total geothermal potential capacity in the country. PT XYZ is one of the geothermal industries in Indonesia that operates water-dominated geothermal fluids. Geothermal fluids operate in monitoring of pressure, temperature, flow, and enthalpy, which create operational risks that need to be addressed and developed in a safe manner. One of the risk mitigation developments is Safety Integrity Level (SIL).

This study aims to evaluate the Safety Integrity Level (SIL) at the two phases of Geothermal Steam Field Facilities PT XYZ by using the Layer of Protection Analysis (LOPA) method. A quantitative method was used to evaluate the design and actual operation using LOPA in 2023. As a result, information on the SIL value can be used to determine an improvement program to enhance the SIL value according to the company's needs and provide information for the development of new facility designs if necessary.

1. INTRODUCTION

Electrical power is one of the most important needs since it is potentially utilized in a variety of applications, including manufacturing, healthcare, and other daily needs. Currently, fossil fuels are the most common source of electric power. In Indonesia, electricity accounts for 69% of total fossil energy use, while Renewable Energy used for 31% (CNN Indonesia, 2022). Geothermal energy is one of the renewable energy sources that can be used to generate electricity in Indonesia. Indonesia is located in the Ring of Fire region, which is marked by numerous volcanoes and high seismic activity, gives it significant geothermal potential. Indonesia's geothermal potential is 11,073 MW, with reserves of 17,506 MW scattered across 331 places from Sabang to Merauke (no date). With its enormous geothermal potential, it can be used to generate electricity to fulfil increasing demands. One of geothermal fields in a certain area produces a fluid consisting of a two-phase fluid, steam and brine. The two-phase fluid must first be separated into steam and brine using separator and other supporting equipment to power the turbine. The two-phase steam field facilities operate at high temperatures, pressures, and flow rates, which increases the potential of failure or accidents. Steam production facilities must consider aspects of safety and workplace security. As a result, efforts are required to reduce the risk of failure by improving the Safety Integrity Level (SIL). SIL is a safety level that reduces the risk of failure, which can be determined using the layer of protection analysis method. The LOPA method can identify and evaluate the existing protection layers in a two-phase steam field to mitigate risk. LOPA can quantitatively evaluate the efficiency of each protective layer using the Probability Failure on Demand (PFD) value, which helps in determining the SIL classification of geothermal facilities in two-phase steam fields (Marszal & Scharpf 2002). Currently, there are two-phase steam field geothermal facilities that have not concern about SIL because the geothermal field still apply the proven methods or are manually operated by operators. As a result of using proven methods, there are many instances of failure that can lead to production interrupts and loss production due to maintenance activities. In the two-phase steam field, the system is evaluated to determine which SIL values can be improved. By evaluating and implementing SIL in geothermal facilities of the two-phase steam field, it is expected to enhance safety levels and reduce production losses due to failures.

2. LITERATURE REVIEW

2.1 Safety Integrity Level (SIL)

The Safety Integrity Level (SIL) is a safety level of a Safety Instrumented System (SIS) used to reduce process risk. SIL is separated into four levels, each of which describes the amount of safety protection provided by a procedure. SIL 1 is the lowest level; SIL 4 is the highest. A process's SIL value indicates how accurate a component's security level is. SIL is often assessed using a risk analysis approach known as Layer of Protection Analysis (LOPA).

SIL is confirmed by computing the Probability Failure on Demand average (PFDavg) for each system component. PFDavg is the average likelihood that a SIF will be unable to execute a security function. The failure rate (λ), or the number of failures in a unit of time, influences the value of PFDavg. Once the PFDavg value of a component has been obtained, the SIL level may be derived using IEC 61508 as stated in Table 1.

Tabel 1: Safety Integrity Level (IEC 61508).

Safety Integrity Level (SIL)	Average Probability Failure on Demand (PFD_{avg})
4	0.00001 – 0.0001
3	0.0001 – 0.001
2	0.001 – 0.01
1	0.01 – 0.1

2.2 Hazard and Operability Studies (HAZOP)

Hazard and Operability (HAZOP) is the study of equipment dangers in real-world production operations. HAZOP seeks to detect possible adverse events that might endanger or disrupt operations, such as hazards to people's safety and potential harm to assets, the environment, and reputation. The discovered threats are reported on the HAZOP worksheet, together with any actions for further investigation and appropriate supporting information (Salaheldine Darwish et al. 2020).

A team of specialists with expertise, experience, and responsibility for the processes and components to be studied conducts HAZOP analysis. When evaluating the study, the facilities to be examined are separated into different sections with specific limits known as nodes, based on the complexity of the system and the natural separation in ratings, pump absorption, drainage pipelines, tanks, and so on.

In the study, HAZOP employed a guide word to assist the design team in identifying failure scenarios in a process that might lead to risk and operational issues. Following a node-based identification using a guide word, a review will be performed by looking at the cause, which is the cause of the deviation, the consequence, which is the result of a process, and the safeguards, which are the layer of protection that prevents the occurrence of a consequence.

2.3 Layer of Protection Analysis (LOPA)

Layer of Protection Analysis (LOPA) is a risk analysis approach that uses basic criteria to define and analyze hazards semi-quantitatively, as well as to create a layer of protection to deal with process risks. LOPA is a risk assessment that necessitates the identification of additional risks, namely the Hazard and Operability Study (HAZOP). LOPA is used to assess if the protective layer and other measures necessary are enough to address the probability of failure and to establish the layer's degree of safety (Studi et al., n.d.).

The major goal of the LOPA approach is to verify that a proper protection layer is in place, reducing the possibility of an accident and calculating the safety level of the protective layers. In a hazard scenario, one or more protective layers are necessary, depending on the complexity of the industrial process and the severity of the danger. The layers on the LOPA are structured like onion structure, as seen in Figure 1.

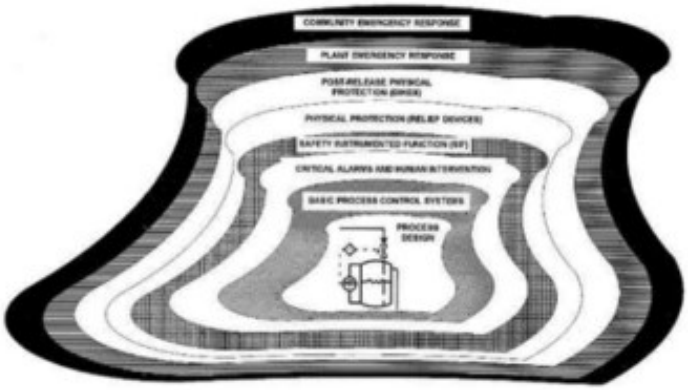

Figure 1: Protection Layer Against Possible Accidents (American Institute of Chemical Engineers. Center for Chemical Process Safety. 2001).

The protective system on the LOPA has the following protective layer:

1. Basic Process Control System
2. Critical Alarms and Human Intervention
3. Safety Instrumented Function (SIF)

4. Physical Protection (Relief Devices)
5. Post-release Physical Protection
6. Plant Emergency Response
7. Community Emergency Response

3. RESEARCH TYPE AND METHOD

3.1 Independent Protection Layer (IPL)

IPL are identified from two-phase steam field geothermal facilities to determine the Probability Failure on Demand (PFD) value for each protection layer. Without protection layers, the PFD value will be set to 1. If there are protection layers, the PFD value for that layer can be determined using existing references. One reference that can be used to determine the PFD value when there is protection layer is the CCPS 2001. However, there are some data within the company that can be used to determine the PFD value. Table 2 below shows the PFD value of each IPL.

Tabel 2: PFD Value for IPL (American Institute of Chemical Engineers. Center for Chemical Process Safety. 2001).

No.	IPL	PFD
1	Basic process control system, if not related to the initial cause considered	0.1
2	Alarm operator with enough time to respond	0.1
3	Relief valve	0.01
4	Rupture disk	0.01
5	Flame/detonation arrestors	0.01
6	bund/dike	0.01
7	Underground drainage system	0.01
8	Open vent	0.01
9	Fireproofing	0.01
10	Blast-wall/bunker	0.001
11	Redundant	0.01 (maximum credit)
12	Different backup tool	0.01 – 0.001
13	Other event	Based on experience
14	SIS with SIL 1	0.1 – 0.01
15	SIS with SIL 2	0.01 – 0.001
16	SIS with SIL 3	0.001 – 0.0001
17	Internal mechanical security trips independent of SIS	0.1 – 0.001
18	A Non-Return Valve (NRV) or check valve	0.1
19	"Inherently Safe" Design	0.01

The equation for determining PFD based on SIS may be configured in different ways. There is a system 1oo1 having one source (Willey & Sons 2010), as illustrated in the following equation 1.

$$PFD_{avg} = \lambda^{DU} \times T_i/2 \quad (1)$$

Where:

λ^{DU} = Failure Rate Dangerous
T_i = Time Interval
PFD = Probability Failure on Demand

3.2 Target Mitigated Event Likelihood (TMEL) Identification

In the LOPA method, first find the TMEL value to determine the PFD value. The TMEL is a value determined by the management of the company to reduce the likelihood of hazard emerging as a result of a consequence. TMEL values are shown in Table 3.

3.3 Initiating Event Frequency (IEF)

Determining the Initiating Event Frequency (IEF) is a necessary step to calculate the LOPA GAP value. The events that occur must result in consequences affecting all safeguards. The frequency of an event must consider background aspects such as the frequency of the operation mode corresponding to the scenario. Generally, the frequency of IEF is expressed in events per year, although other units such as per 106 hours are also used. Initiating events are grouped into three categories: external events, equipment failure, and human failure.

External failures include natural phenomena such as earthquakes, tornadoes, floods, and events originating from fires or explosions at adjacent facilities. Equipment failures can be further classified into control system failures

and mechanical failures, which include software bugs, corrosion, and defects. Human failures encompass operational errors, maintenance errors, and program errors. Table 4 below shows the IEF values used to determine the LOPA GAP.

Tabel 3: Target Mitigated Event Likelihood Value.

Severity Level	Safety Consequence	Target Mitigated Event Likelihood
CA	Single first aid injury	0.03
CB	Multiple first aid injuries	0.003
CC	Single disabling injury or multiple serious injuries	0.0003
CD	Single on-site fatality	0.00003
CE	More than one and up to three on-site fatalities	0.00001

Tabel 4: Initiating Event Frequency Value (American Institute of Chemical Engineers. Center for Chemical Process Safety. 2001).

Initiating Event	Frequency Range from Literature (per year)	Example of a Value Chosen by a Company for Use in LOPA (per year)
Pressure vessel residual failure	10^{-5} to 10^{-7}	1 to 10^{-6}
Piping residual failure—100 m—Full Breach	10^{-5} to 10^{-6}	1 to 10^{-5}
Piping leak (10% section)—100 m	10^{-3} to 10^{-4}	1 to 10^{-3}
Atmospheric tank failure	10^{-3} to 10^{-5}	1 to 10^{-3}
Gasket/packing blowout	10^{-2} to 10^{-6}	1 to 10^{-2}
Turbine/diesel engine overspeed with casing breach	10^{-3} to 10^{-4}	1 to 10^{-4}
Third party intervention (external impact by backhoe, vehicle, etc)	10^{-2} to 10^{-4}	1 to 10^{-2}
Crane load drop	10^{-3} to 10^{-4} per lift	1 to 10^{-4} per lift
Lightning strike	10^{-3} to 10^{-4}	1 to 10^{-3}
Safety valve opens spuriously	10^{-2} to 10^{-4}	1 to 10-2
Cooling water failure	1 to 10^{-2}	1 to 10^{-1}
Pump seal failure	10^{-1} to 10^{-2}	1 to 10^{-1}
Unloading/loading hose failure	1 to 10^{-2}	1 to 10^{-1}
BPCS instrument loop failure Note: IEC 61511 limit is more than 1×10^{-5}/hr or 8.76×10^{-2}/yr (IEC, 2001)	1 to 10^{-2}	1 to 10^{-1}
Regulator failure	1 to 10^{-1}	1 to 10^{-1}
Small external fire (aggregate causes)	10^{-1} to 10^{-2}	1 to 10^{-1}
Large external fire (aggregate causes)	10^{-2} to 10^{-3}	1 to 10^{-2}
LOTO (lock-out tag-out) procedure failure overall failure of a multiple-element process	10^{-3} to 10^{-4} per opportunity	1 to 10^{-3} per opportunity
Operator failure (to execute routine procedure, assuming well trained, unstressed, not fatigued)	10^{-1} to 10^{-3} per opportunity	1 to 10^{-3} per opportunity

3.4 Target Mitigated Event Frequency (TMEF)

Target Mitigated Event Frequency (TMEF) is a target of the probability of the occurrence of a hazard. The value can be determined on the basis of the severity of the hazardous event that can be defined using the following 2 equation.

$$TMEF = UEF_1 \times PFD_{tot1} + UEF_2 \times PFD_{tot2} + \cdots \quad (2)$$

Where:

TMEF = Target Mitigated Event Frequency

UEF = Unmitigated Event Frequency
PFD = Probability Failure on Demand

TMEF can be determined by knowing the UEF and PFD_{total} values of each initiating cause.

3.5 Determine Safety Integrity Level (SIL)

SIL is a safety level of the Safety Instrumented System (SIS) as an attempt to reduce risk in a process. SIL can be determined by reviewing SIL classification using the LOPA method, determining TMEL values, and determining the TMEF values to obtain a gap. The gap obtained is used as the primary reference for the SIF to be designed and evaluated. Target SIL guidelines require a gap specified with the PFD LOPA gap. The value of the PFD on the LOPA gap can be determined using the equation 3 as follows:

$$PFD_{gap} = TMEL/TMEF \quad (3)$$

After determining the PFD_{gap} value, the level of SIL can be determined according to IEC 61508 according to Table 1. After performing SIL classification using the LOPA method and determining the degree of SIL, SIL verification was undertaken to verify if the current instrument meet the SIL classification level.

4. MODELLING, CALCULATION, AND ANALYSIS

Figure 2 is a flowchart that explains the workflow of SIL evaluation on Geothermal Steam Field using the LOPA method.

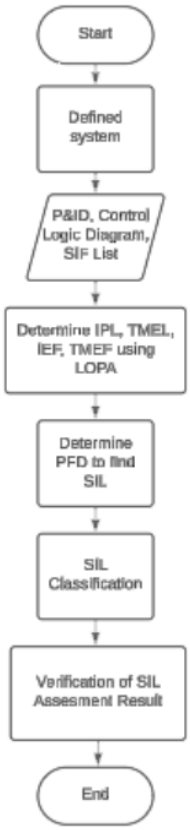

Figure 2: Flowchart SIL Evaluation on Geothermal Steam Field using LOPA Method.

4.1 SIF List Determination

To perform SIL classification processes on geothermal field steam facilities, two phases are selected based on the highest HAZOP risk and the failure in the field based on discussions and interviews. The SIF list was derived from the P&ID and Control Logic Diagram by analyzing the sensor, logic solver, and final element components in the two-phase steam field. Figure 3 shows the P&ID used to define List 1 SIF as a sample.

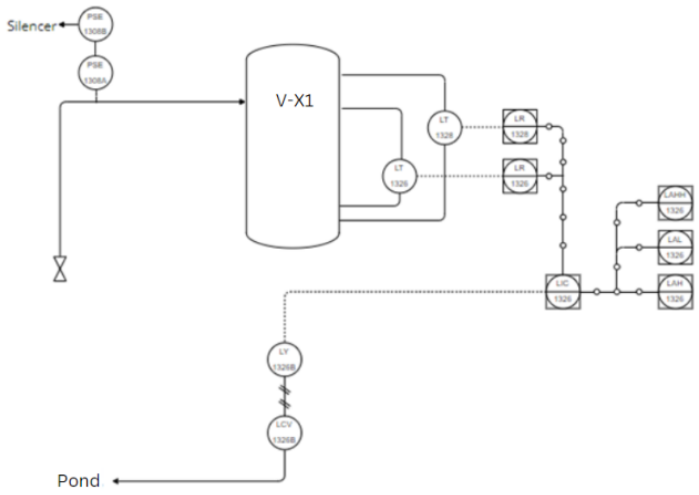

Figure 3: P&ID V-X1.

Based on the P&ID in Figure 3 can be determined SIF List as in Table 5.

Tabel 5: SIF List.

No.	SIF	Design Intent	Initiator
1	[SIF] High High Level in Wellhead Separator V-X1	To prevent overfilling of Wellhead Separator V-X1	01-LAHH-1326
2	[SIF] High High level in Wellhead Separator V-X2	To prevent overfilling of Wellhead Separator V-X2	01-LAHH-1426
3	[SIF] High High Level in Wellhead Separator V-X3	To prevent overfilling of Wellhead Separator V-X3	01-LAHH-1726
4	[SIF] High High Level in Wellhead Separator V-X4	To prevent overfilling of Wellhead Separator V-X4	01-LAHH-1826
5	[SIF] High High Level in Wellhead Separator V-X5	To prevent overfilling of Wellhead Separator V-X5	01-LAHH-1926
6	[SIF] High High Level in Wellhead Separator V-X6	To prevent overfilling of Wellhead Separator V-X6	01-LAHH-2012A
7	[SIF] High High Level in Wellhead Separator V-X7	To prevent overfilling of Wellhead Separator V-X7	01-LAHH-2112A
8	[SIF] High High Level in Wellhead Separator V-X8	To prevent overfilling of Wellhead Separator V-X8	01-LAHH-2212A
9	[SIF] High High Level in Wellhead Separator V-X9	To prevent overfilling of Wellhead Separator V-X9	01-LAHH-2312A
10	[SIF] High High Level in Wellhead Separator V-X10	To prevent overfilling of Wellhead Separator V-X10	01-LAHH-4012A
11	[SIF] High High Level in Wellhead Separator V-X11	To prevent overfilling of Wellhead Separator V-X11	01-LAHH-4112A
12	[SIF] High High Level in Wellhead Separator V-X12	To prevent overfilling of Wellhead Separator V-X12	LAHH-6001
13	[SIF] High High Level in Wellhead Separator V-X13	To prevent overfilling of Wellhead Separator V-X13w	LAHH-5012

4.2 SIL Classification

SIL classification is use to conduct SIL approaches to two-phase steam field geothermal facilities in order to obtain SIL values from the LOPA gap. The process of SIL classifications is based on cause and consequence in the HAZOP. To determine the SIL value of the Lopa gap, the Target Mitigated Event Likelihood (TMEL) values obtained from consequences, Initiating Event Frequency (IEF), Probability Failure on Demand (PFD) on initiating cause, and Independent Protection Layer (IPL) based on the Center for Chemical Process Safety (CCPS) to determine PFD_{Avg} values. After determining the PFD_{Avg} value, the SIL value can be calculated for the LOPA gap.

Take a sample for the calculation of SIL classification which is SIF list 1. In doing SIL Classification this is done determination of consequence of HAZOP first to determine the value of TMEL. Which is obtained TMEL on SIF

List 1 obtains 0.00001. After determining the TMEL value, the Unmitigated Event Frequency (UEF) value of each initiating cause is obtained as in Table 6.

Tabel 6: IEF Value and UEF from Initiating Cause.

No.	Initiating Cause	IEF (Event per yr)	Conditional Modifiers		UEF (Event per yr)
			Description	Prob	
1	More flow from upstream (Wellhead) due to increasing productivity of reservoir	1	Operation mode	0.1	0.1
2	High Silica scale formation at separator (for prolonged time)	0.4	Operation mode	0.1	0.04
3	LCV accidently close due to instrument air off due to compressor off	0.1	Operation mode	0.1	0.01

From Table 6, it is known that the value of IEF can be determined based on Table 3. The value of the IEF at the initiating cause of the first is worth 1 because at the time of production produced on SIF list 1 increases is a natural cause, which is the case naturally from the reservoir.

$$UEF = IEF \times Prob$$

$$UEF_1 = 0.1$$

Then the IEF rating on the second initiating cause is 0.4 because based on the data obtained from the agency during the interview, silica-related interference occurs as many as 4 times a year. So, the UEF value can be determined with the completion as follows.

$$UEF = IEF \times Prob$$

$$UEF_2 = 0.04$$

Then the IEF value on the third initiating cause is 0.1 according to Table 6. So, the UEF value can be determined by completion as follows.

$$UEF = IEF \times Prob$$

$$UEF_3 = 0.01$$

The total PFD value for each IPL is then determined to establish the SIL classification by adding all IPLs from each starting cause, as shown in Table 7.

Tabel 7: PFD Value from each IPL.

No.	Initiating Cause	Independent Protection Layers (IPLs)			
		IPL Description	Type of IPL	PFD	IPL Description
1	More flow from upstream (Wellhead) due to increasing productivity of reservoir	Rupture Disc (e.g. PSE-1308A, PSE-1308B)	Physical Protection	0.01	1E-07
		[SIF] High High level alarm on separator V-X1 (e.g. LAHH-1326)	SIF	1	
		[Alarm] High Level alarm on separator V-X1 (e.g. LAH-1326) to alert operator for opening bypass valve	Alarm and Operator Response	0.1	
		Rupture Disc (e.g. PSE-1332)	Physical Protection	0.01	
		Condensate Drain Port	Physical Protection	0.01	
2	High Silica scale formation at	Acid Injection available	Human Intervention	0.1	1E-03
		Automatic Condensate Drain Port	Physical Protection	0.01	

No.	Initiating Cause	Independent Protection Layers (IPLs)			
		IPL Description	Type of IPL	PFD	IPL Description
	separator (for prolonged time)				
3	LCV accidently close due to instrument air off due to compressor off	[SIF] High High level alarm on separator V-X1 (e.g. LAHH-1326)	SIF	1	1E-01
		[Alarm] High Level alarm on separator V-X1 (e.g. LAH-1326) to alert operator for opening bypass valve	Alarm and Operator Response	0.1	

Based on Table 4, the PFD_{total} value of each initiating cause is obtained, so the TMEF value can be determined using the equation 2 as follows.

$$TMEF = 0.00104$$

Once the TMEF value is known, then the PFD_{gap} value can be determined by dividing the TMEL value by the previously specified TMEF using the equation 3 as follows.

$$PFD_{gap} = 0.0096$$

By knowing the PFD_{gap} value of SIF list 1, then the level of SIL can be classified according to Table 1. The PFD_{gap} value obtained is 0.0096 so the SIL level is SIL 2.

Then the calculation is done in the same way up to the 13th SIF list to determine the SIL classification. Table 8 shows PFD_{gap} values obtained from 13 SIF surveys.

Tabel 8:Table PFD_{gap} for 13th SIF Review.

No	SIF	Probability Failure on Demand (PFD) Lopa GAP	SIL Classification
1	Separator V-X1	0.0096	SIL 2
2	Separator V-X2	0.0096	SIL 2
3	Separator V-X3	0.0096	SIL 2
4	Separator V-X4	0.0096	SIL 2
5	Separator V-X5	0.0096	SIL 2
6	Separator V-X6	0.0096	SIL 2
7	Separator V-X7	0.0096	SIL 2
8	Separator V-X8	0.0096	SIL 2
9	Separator V-X9	0.0096	SIL 2
10	Separator V-X10	0.0096	SIL 2
11	Separator V-X11	0.0096	SIL 2
12	Separator V-X12	0.0096	SIL 2
13	Separator V-X13	0.0096	SIL 2

4.3 SIL Verification

After doing SIL classification, perform SIL verification by determining the type of sensor, logic, and actuator used on each separator and arrangement of PFD sensors. Then determine the architectural constrain and carry out certification from manufacturing based on the sensor used so that SIL values on SIL verification can be determined and compared with the SIL value obtained on LOPA gap.

PFD SIL calculation is performed to determine the SIL level in order to verify whether the SIL classification value requires additional components, replaces the component with the corresponding PFD value, or there is a problem with redundancy. Table 9 shows the data obtained from the search for certification and manufacturing data based on the components used.

Based on Table 9, the average PFD value for the Rosemount transmitter level sensor is obtained using the equation 1 with a time interval of 1 year.

$$PFD_{avg} = 0.000018396$$

Here is a calculation of PFD_{avg} for logic solver using equation 1 with time intervals of 1 year.

$$PFD_{avg} = 0.0001752$$

Here's a calculation of the PFD_{avg} for the LCV actuator using equation 1 with a time interval of 1 year.

$$PFD_{avg} = 0.00097674$$

After obtaining PFD_{avg} values from each sensor, logic solver, and actuator, the overall PFD_{avg} value may be determined the following formula.

$$PFD_{avg} = 0.0013359$$

A total PFD_{avg} value of 0.0013359 is obtained, which is based on the provisions of IEC 61511 and CCPS 2001, the SIF review list 1 is included in SIL 2. This means that the SIL value between SIL classification and SIL verification is the same so that no component needs to be replaced with the corresponding PFD value.

The steps subsequently continue up to SIF list 13, determining SIL verification. Table 10 The following table shows the PFD_{gap} values obtained from 13 SIF evaluations.

Tabel 9: PFD SIL Calculation SIF 1.

Component	Brand	SIL Certificate	Configures SIF	Failure Rate	PFD
Level Transmitter LT-1326	Rosemount 115X/205X	SIL 2	1oo1	4.2E-08	0.00018396
Logic Solver	Triconex/ Tricon	SIL 2	1oo1	4E-08	0.0001752
Level Control Valve LCV-1326B	Neles	SIL 3	1oo1	2.2E-07	0..00097674
PFD average					0.0013359

Table 10: PFD table for the 13th SIF review.

No	SIF	Probability Failure on Demand (PFD)	SIL Verification
1	Separator V-X1	0.0013359	SIL 2
2	Separator V-X2	0.0013359	SIL 2
3	Separator V-X3	0.0013359	SIL 2
4	Separator V-X4	0.0013359	SIL 2
5	Separator V-X5	0.0013359	SIL 2
6	Separator V-X6	0.0013359	SIL 2
7	Separator V-X7	0.0013359	SIL 2
8	Separator V-X8	0.0013359	SIL 2
9	Separator V-X9	0.0013359	SIL 2
10	Separator V-X10	0.0013359	SIL 2
11	Separator V-X11	0.0013359	SIL 2
12	Separator V-X12	0.005006	SIL 2
13	Separator V-X13	0.005006	SIL 2

4.4 Verification of SIL Assessment Result

The SIL evaluation, which included SIL classification based on CCPS SIL standards calculations and SIL verification based on certification of each sensor, actuator, and final element component, resulted in SIL 2 for 13 SIF reviews. This SIL 2 can be validated against existing literature, such as CCPS, and compared to the institution's P&ID, which has been updated to meet the necessary criteria. In addition, a field expert verified the SIL evaluation results.

Achieving SIL 2 for 13 SIF evaluations in the two-phase geothermal steam field was considered adequate. SIL levels depend on operational patterns, and geothermal systems cannot have identical operations to those in oil & gas or petrochemical industries. At the institution where the SIL evaluation was conducted, the system classification is SIL 2, but some components used are certified SIL 3. Thus, SIL 2 is sufficient for the operational pattern, but the geothermal industry has not yet made SIL mandatory. Therefore, SIL requirements still depend on the needs of each company or institution.

5. CONCLUSION

Based on the data analysis and discussions conducted to evaluate the SIL level at the two-phase steam field geothermal facilities, the following conclusions can be drawn:

1. Based on the analysis performed for the SIL classification process using the LOPA method, it was determined that the target safety level for the two-phase steam field geothermal facilities in the 13 SIF evaluation is SIL 2.
2. With the SIL evaluation conducted, the proposed improvement program is to perform maintenance at least once a year, as estimated by the SIL analysis. This includes maintenance of sensors, actuators, final elements, and the wiring system in the two-phase steam field.
3. SIL evaluations using the LOPA method can be utilized in the geothermal industry to consider process safety and continuous improvement, consequently improving operational safety using logic control technology and reducing the probability of failure that impacts opportunity loss.

REFERENCES

American Institute of Chemical Engineers. Center for Chemical Process Safety., 2001, *Layer of protection analysis : simplified process risk assessment*, Center for Chemical Process Safety of the American Institute of Chemical Engineers.

Marszal, E.M. & Scharpf, E.William., 2002, *Safety integrity level selection : systematic methods including layer of protection analysis*, Instrumentation, Systems, and Automation Society.

Salaheldine Darwish, A., Salem Mansour, M., Farag, H. & Ezzat, K.H., 2020, 'Applying LOPA and fuzzy logic to identify SIL requirement for safety critical functions in a direct reduction iron industry', *Alexandria Engineering Journal*, 59(5), 3575–3585.

Studi, P., Keselamatan, T., Kerja -Ppns, K., Rosyidiin, A.F., Nugroho, A., Amrullah, H.N., Teknik, Jurusan, Kapal, P., Kerja, K., Perkapalan, P., Surabaya, N., Teknik, Jalan & Kampus, K., no date, *Proceeding 2nd Conference on Safety Engineering and Its Application*, ANALISIS RISIKO DENGAN METODE LAYER OF PROTECTION ANALYSIS PADA REACTOR PLATFORMING DI INDUSTRI PETROKIMIA.

Willey, A.J. & Sons, 2010, *GUIDELINES FOR PROCESS SAFETY ACQUISITION EVALUATION AND POST MERGER INTEGRATION*.

DEN , 6 Feb. 2023, *DEN: RI Masih Bergantung pada Energi Fosil sampai 2050*.

Kementerian ESDM RI , 6 Feb. 2023, Kementerian ESDM RI - Media Center - Arsip Berita - *Kini Indonesia Menjadi Produsen Listrik Panas Bumi Terbesar Kedua Dunia*.

The First Bullhead Acidizing in Silangkitang Production Well

Irfan Hamzah[1], Ayu A. Utami[1], Daniel Wilson[2], Grandy Danakusumah[1], Arsyan H. Sasoni[2], Zaky Mubarok[1], Albertus Ivan[3], Aditya Hernawan[1], Riza Pasikki[1], and Nur Choiri Amin[2]

[1]Sarulla Operations Ltd., The Energy Building, 7th Fl., South Jakarta, 12190
[2]PT. Solenis Technologies Indonesia, Bidakara Tower 1, Jl. Gatot Subroto 71-73, Tebet, South Jakarta, 12870
[3]Medco Geothermal Sarulla, The Energy Building, 8th Fl., South Jakarta, 12190

irfan.hamzah@sarulla-geothermal.com

Keywords: acidizing, bullhead, calcite, scaling, Silangkitang, well stimulation

ABSTRACT

SIL1-2, an exploration well drilled in 1997, is in Silangkitang Geothermal Field. With minor reservoir pressure and enthalpy drop, the wellbore-size constrained SIL1-2 was initially produced at a stable mass rate in the first three years of production. The well performance showed a significant decline trend in the following years due to a combination of wellbore and near-wellbore calcite scaling. Several trials of wellbore clean-out have been done since 2020 to recover well performance, one of which left the presence of fish in hole. The inaccessible wellbore of SIL1-2 creates complexity, from minimum downhole information to limited options of any well intervention options. Through risk assessment, the acid bullhead stimulation method was considered the only viable option to restore well capacity, considering the presence of fish, feed zones that are located below the top of the fish, the uncertainty of fishing job due to slim hole completion, good wellbore and wellhead integrity. Bullhead stimulation was aimed to dissolve the scale deposits in both wellbore and near wellbore; sweep out the solution to formation, bind, and prevent the dissolved Ca^{2+} ions from being redeposited, expecting permeability improvement in formation. The rock formation (core sample), as the only solid sample reference, underwent laboratory testing with acid and alkali-based chemicals. The bullhead stimulation at SIL1-2 has successfully improved the production capacity, while it also practically reduced equipment needed and loss generation as compared to other well-stimulation methods ever tried.

1. INTRODUCTION

The Silangkitang (SIL) geothermal field, one of four known geothermal prospects within the Sibualbuali Working Area, is in Pahae Jae, North Tapanuli Regency, North Sumatera Province, Indonesia. SIL is a fault-controlled geothermal system that is situated along the Great Sumatera Fault (GSF). A 110 MW Geothermal Combined Cycle Power Plant, consisting of a backpressure steam turbine and binary units, is operated by Sarulla Operation Ltd. (SOL). This technology allows nearly 100% reinjection, maintaining the sustainability of the field. The current production and injection strategy is maintained by four production wells, located in the center of the field, and seven injection wells, distributed in the northwestern and southeastern parts of the field (Figure 1). UNOCAL, who was initially granted to conduct the exploration and development, drilled five exploration wells in the late 1990s. SIL1-2, one out of three wells drilled relatively perpendicular to the GSF, encounters good permeability with a fluid temperature of more than 300°C. SIL1-2 well deliverability is categorized as wellbore-size limited, and it's actively being used as a production well to date. It initially produced ~ 420 t/hr of the total mass rate at 22barg operating WHP, with an average enthalpy of 1360J/g. The well generated approximately 18MWe stably supplied to the power plant, from early commissioning in March 2017 to December 2019, before continuously showing a high decline rate of ~45-50%/ year. A high decline rate is not expected as the reservoir pressure shows relatively minor pressure drawdown since early production. The well has been continuously operated at minimum allowable Wellhead Pressure (WHP) to sustain the generation.

During a regular static Pressure Temperature (PT) survey performed in early 2020, the well was observed to have shallower accessibility by ~1900 ft as compared to its total depth of 7644 ft.MD, indicating the presence of an obstruction. An attempt to clear the obstruction was run by using Coil Tubing (CT) mechanical cleanout within the same year. The scale deposit was observed around the top of the 7" production casing. Unfortunately, after clearing the whole 7" casing, ~3750ft long of 1 ¾" CT was lost in hole. The well intervention activity was categorized as unsuccessful, with CT fish left in hole and zero production recovery. An additional well intervention was continued by performing fishing in March 2021. Nearly half of the CT length was retrieved and well performance recovered temporarily to its ideal capacity, before the new high declining trend (Figure 2).

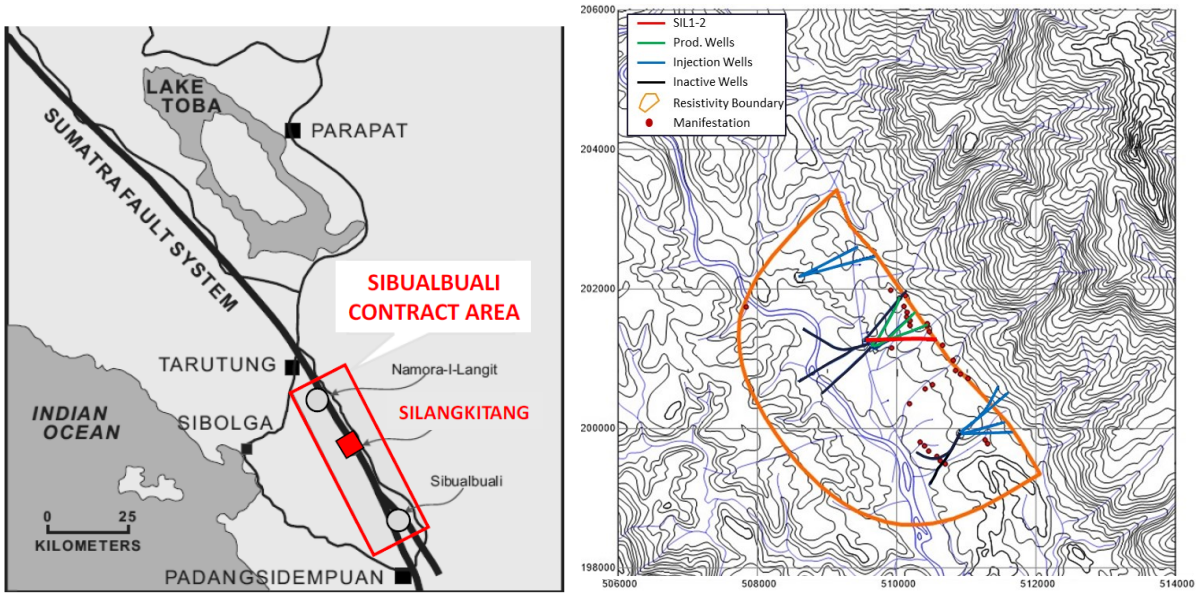

Figure 1: Location map of Silangkitang and wells distribution map (adapted from Satya et al., 2021).

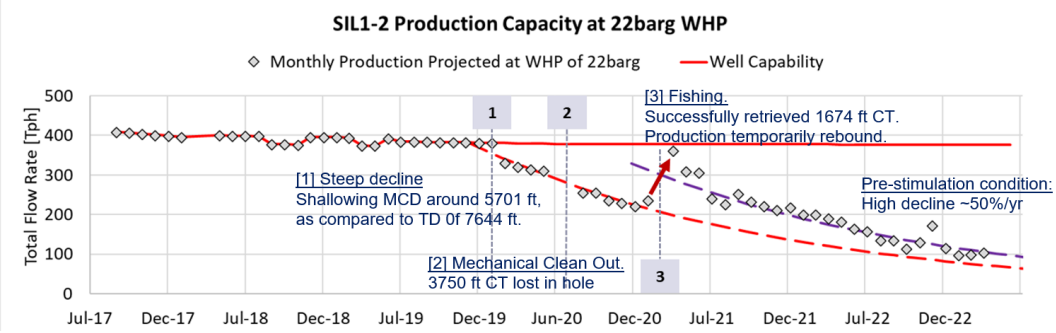

Figure 2: SIL1-2 normalized production capacity at minimum allowable WHP and its sequential observation.

2. PRE-STIMULATION ASSESSMENT

2.1 Geochemistry Assessment

Sets of geochemistry data were taken regularly as part of well monitoring activities. To complete the well performance evaluation and the scaling potential assessment, the geochemistry data were simulated with the WATCH aqueous speciation program (Arnorsson, et al., 1982) to identify the type of scale (mineral). The initial flowing chemistry data of SIL1-2 was collected during December 2017 and this is assumed to be the baseline and equilibrium condition of the well. The simulation was focused on the retrograded solubility minerals such as calcite and anhydrite. The SI (log Q/K) of calcite from the baseline data is 0.21 and it's slightly above the theoretical SI (log Q/K = 0). This information, however, strongly indicates the calcite scaling potential. Years after the well was in production, the SI of calcite was observed to be higher than the initial, suggesting the likelihood of calcite deposition over time starting from the reservoir or near wellbore conditions (Figure 3). On the other hand, anhydrite remains undersaturated over time. The possible causes of scaling deposition may be attributed to factors such as low operating pressure conditions that create deeper flashing points. The equilibrium state of the fluid is disturbed and the dissolved CO_2, when it flashes, degassing and causing the calcite to be precipitated (Kaya et al., 2010; Satman et al., 1999).

2.2 Wellbore Assessment

The wellbore accessibility of SIL1-2 was restricted by two objects, i.e., scale deposit and CT fish left in hole. The top of fish was estimated at ~5667ft.MD and assumed to be extended irregularly to the bottomhole. The identified feedzones of SIL1-2 are located below the top of the fish, at 6383 and 6883ft.MD, both lie in 5" and 3.5" perforated liner, respectively (Figure 4). Considering the presence of fish, running any PT/PTS log to assess the wellbore dynamics is a non-viable option. The pre-acid stimulation flow rate based on the tracer flow test in December 2023 yields about 89 t/hr total at a minimum allowable WHP of 20barg.

These two conditions imply that the possibility of conducting conventional downhole acid treatment becomes impractical and an immediate cleanout treatment must be performed before the FZ is blocked by scale. The only feasible option to recover the well performance is by bullhead stimulation, where all chemicals are pumped from the surface through the wellhead.

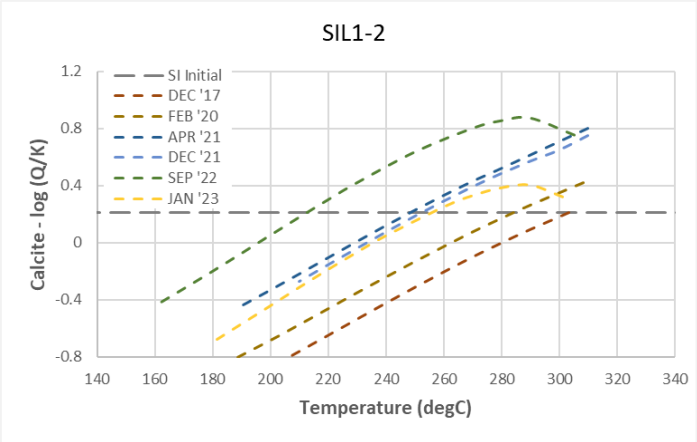

Figure 3: Calcite oversaturation in the wellbore of SIL1-2 based on monitoring data simulated in adiabatic cooling conditions.

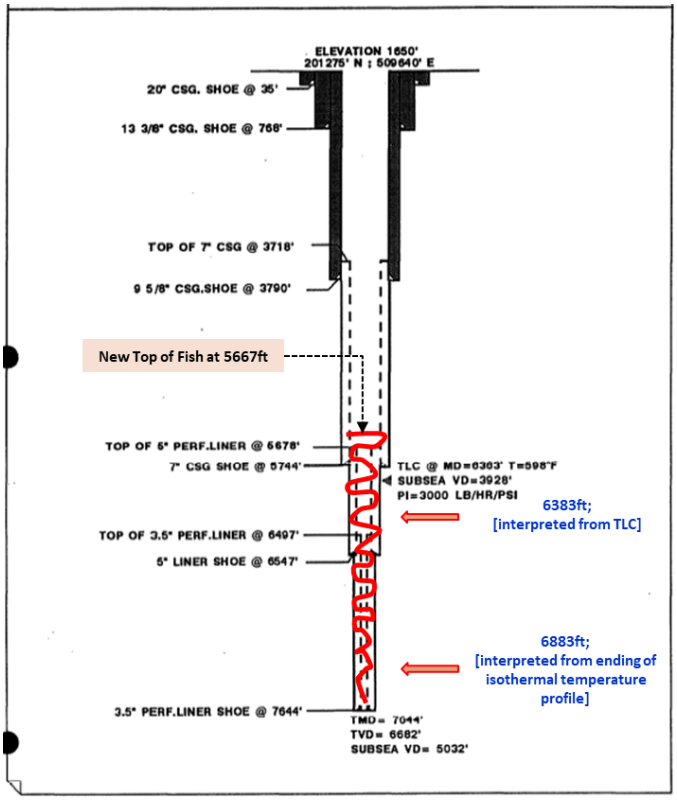

Figure 4: Well casing configuration and accessibility.

3. BULLHEAD ACIDIZING PROGRAM

3.1 Chemical Selection and Delivery

Due to the inaccessibility of the wellbore, there was no scale sample retrieved from SIL1-2 well. The type of scale was estimated by chemical simulations and references from nearby well that showed similar behavior, i.e., calcite oversaturation, drop pressure and mass flow, and possible injection breakthrough. In the nearby well case, the calcite scale deposit was successfully cleaned out with acetic acid. It is also well known that HCl is suitable and applied for dissolving calcite deposits in geothermal production wells (McLean et al., 2021; Kaya et al., 2010).

The bullhead acidizing method is demonstrated in other fields, solving and treating both calcite and silica(te) deposits. In Domo San Pedro, the implementation of acid bullhead was used successfully to treat calcite and silica

scaling in the wellbore and formation, improving about 351% of well performance (Rodriguez, et al., 2021). The chemicals they used as dissolver are HCl and formic acid (calcite), and alkaline solutions (silicate). A similar case was also demonstrated in the Wairakei geothermal field where a combination of acid and caustic was used to remove both calcite and silica in the production well. The chemical treatment can deliver 100% well capacity recovery (McLean et al., 2021). The bullhead acidizing method was also successfully demonstrated in Kawerau injection well, dissolving the silica scaling in near wellbore formation with Hydrofluoric Acid (HF) and formic acid, resulting in higher injection capacity (Goh et al., 2020).

Corresponding to the above examples, an idea was raised to improve in situ permeability by conducting solubility tests on the (deposited) secondary minerals in fractures/veins/veinlets. Two core samples, which were described as having mainly silica (quartz) and minor calcite in fractures, analog as SIL1-2 feedzone depths underwent dissolution test with repeated steps of alkaline – acid – alkaline- acid solutions. The acid solution is mainly composed of hydrochloric acid, and the alkaline solution is mainly composed of caustic. The weight loss (%solubility) of the two rock samples was 9 and 12.3%, respectively. Although the main dissolution agent is the acid, the result allowed permeability improvement by enhancing the dissolution rate. This, however, determined the type of chemicals used for the cleanout program, which are a combination of acid, alkali, and chelating agents. The acid solution, as developed by SOLENIS, is blended with a food-grade base corrosion inhibitor that would work up to 200°C and it is safer from an environmental perspective.

The bullhead acidizing method has several benefits as compared to the CT method, including but not limited to the following:

- Simplification of the whole job sequence: no high-pressure pumping unit, no lifting equipment during the job, etc.
- Increasing the pumping rate, having higher pumping rate could:
    - Prevent the well from being heated up which consequently reduces the corrosion inhibitor failure (exceed temperature rating).
    - It may increase the formation coverage, more chemical-scale reactions.
    - When a chelating agent is used, a higher rate may improve the dissolution rate. Rose et al. (2010) studied that a higher injection rate can improve the dissolution rate by 4.5% and extend the radial penetration.
- No downhole equipment, no lost-in-hole risk.

3.2 Executed Program

The bullhead acid stimulation program was divided into four steps and completed successfully within three days of operations. The first step is to quench the well with fresh water to create a vacuum condition before acid injection. The second step is to inject the acid solution of GS1127 to dissolve and flush the scale in the wellbore. This second process concluded with condensate displacement and continued with overnight quenching to allow further soaking time. The third step involves alkaline treatment with alkali GS1014 and additive of GS1824. This phase attempts to improve the formation's permeability and bind the dissolved Ca^{2+} ions by adding the additive (redeposition prevention). The fourth and last step is to inject the GS1127 which aims to dissolve the remaining calcite in the reservoir. The executed program is summarized as follows (Figure 5):

4. RESULT AND DISCUSSION

4.1 Well Capacity Improvement

After four days of shut-in, the well SIL1-2 flowed back to the plant system. To increase measurement accuracy, the single-phase flowmeter at the outlet of the separator is set as the main parameter. At stabilized ~27 barg WHP of SIL1-2, the total mass rate in the separator was increased by 292 t/hr (Figure 6). Figure 7 shows the deliverability curve of SIL1-2 pre- and post-bullhead acidizing. The total flow rate of SIL1-2 post-acid stimulation is ~420 t/hr at 22 barg WHP or equivalent to its initial capacity. The target generation of SIL is recovered post-acid stimulation of SIL1-2, and even better, can be optimized to slightly above the initial power plant design. Considering less operational complexity, minimum operational downtime, and removal risks of downhole intervention, the bullhead acidizing method offers a more attractive solution than the other past successfully applied chemical well stimulations in SIL, i.e., CT, rig.

Step One - Well Killing
- Killing the well with 160 – 320 lpm fresh water. Vacuum condition prior acid injection.
- Well turned to ~0 barg in 6.5 hours.

Step Two - Treatment within the Wellbore (Acid Dosing)
- To dissolve and flush scale in the wellbore, GS1127 was injected thru crown valve.
- 30 m^3 at high rate of 1200 lpm, another 30 m^3 with lower rate of 360 lpm.
- Displaced with 240 lpm condensate for 20 mins to push remaining acid in wellbore to formation.
- Switched and quenched the well with 240 lpm of river water from backside, allowed overnight reaction/soak time.

Step Three - Treatment within the Formation (Alkaline Dosing)
- Injected the 20 m^3 of GS1014 with GS1824 at 2666 lpm, attempted for formation permeability improvement and bind Ca^{2+} ion, prevent redeposition, i.e., calcite, possible silica/quartz dissolution.
- Displaced with condensate for 1 hr before moving the third step.

Step Four – Treatment within the Formation (Acid Dosing)
- Tuned to 1800 lpm (condensate + acid) and injected remaining 40m^3 of GS1127. Attempted to push away the acid out to the formation and dissolves remaining calcite in reservoir.
- Displace with 3x wellbore volume at 2500 lpm for 1 hr.
- Well shut-in and heating up.

Figure 5: Summary of the executed chemical cleanout program.

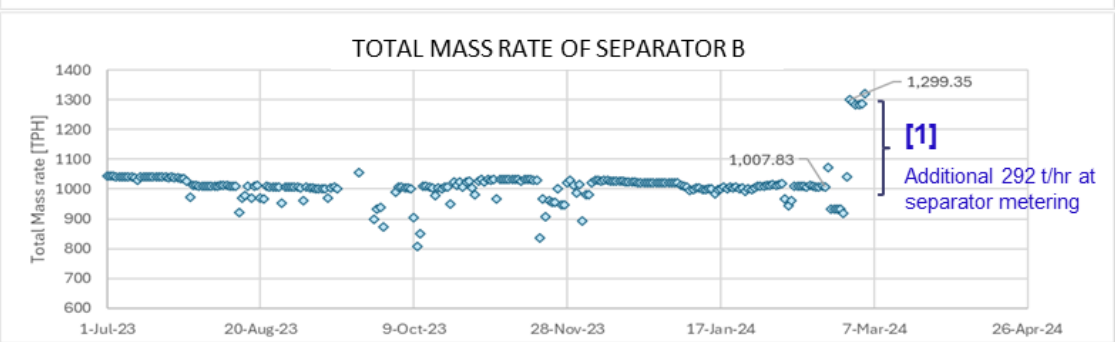

Figure 6: The observed mass rate increment at the production separator after the stimulation is completed.

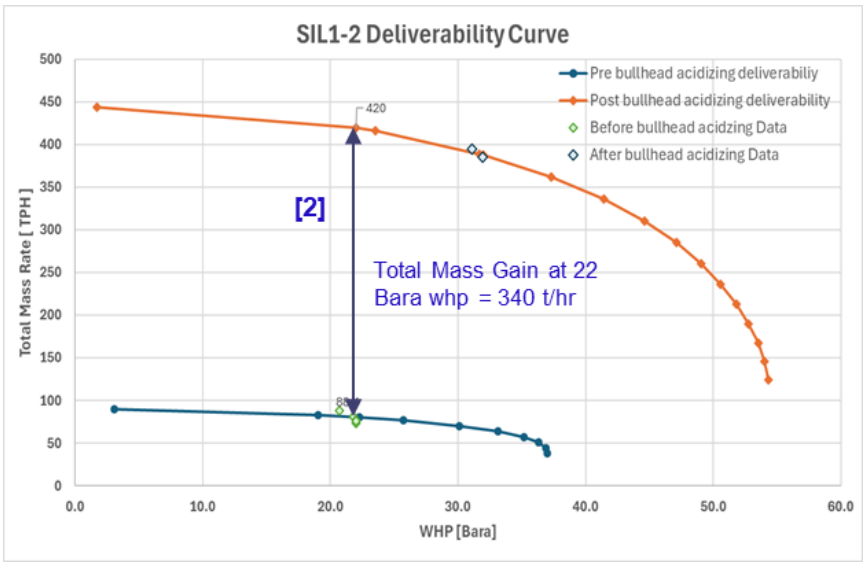

Figure 7: Post-acidizing updated deliverability curve of SIL1-2 which shows a 340 t/hr improvement (normalized to 22 barg).

4.2 Well post-stimulation Observation

Regardless of the methodology, chemical selections, and capacity improvement, the repetition of scaling deposition in SIL's production well is unavoidable. The repetition of deposition may be caused by the nature of the fluid that is oversaturated with respect to calcite and/or the consequences of the operating conditions. Confirmed by the latest chemistry data (April 2024) of SIL1-2 and exercised using different degassing coefficients in the WATCH program, suggesting the oversaturation of the fluid to calcite above 280°C or starting from the reservoir condition (Figure 8). After a cumulative four months of production, the well already shows a declining trend in mass rates. At 22 barg, SIL1-2 delivers about ±300 t/hr (Figure 9). Although the decline trend may be flattened, the well is expected to require similar well stimulation in the future.

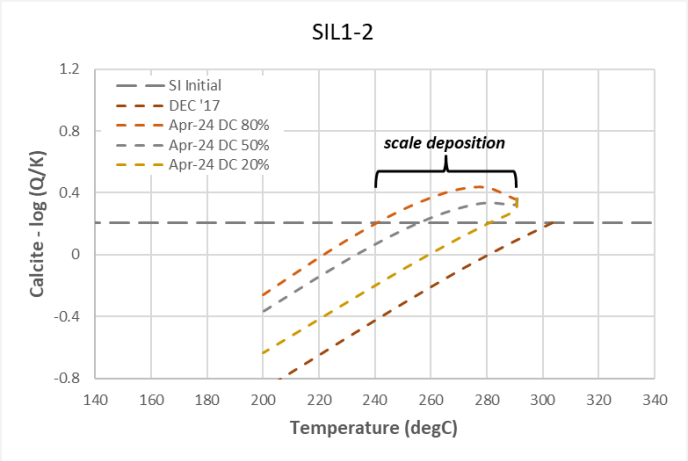

Figure 8: Post-acidizing WATCH simulation showing possible scaling deposition starting from reservoir up to wellbore conditions (or in the range of flowing temperature).

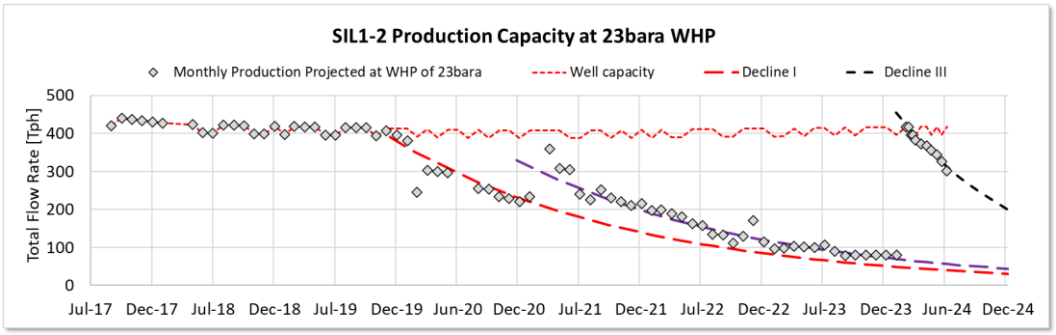

Figure 1. Updated decline trend of SIL1-2.

5. CONCLUSION

The bullhead acidizing successfully recovered the initial mass rate capacity of the SIL1-2 well. Although no methodology could confirm the permeability improvement, the combination of acid and alkali injection was considered to dissolve the calcite scale deposits in both the wellbore and the near wellbore. Further decline of the well is likely due to operating conditions and the produced reservoir fluid characteristics of which such deposition is inevitable. Though future well stimulation is expected, SIL1-2 is in an ongoing long-term observation, always fine-tuned for optimum operating conditions. Based on this result, bullhead acidizing is one methodology that has been proven in SIL and will be considered for any future well stimulations.

ACKNOWLEDGEMENTS

The authors wish to thank Sarulla Operations Ltd. for enabling this work and permission to publish this information, and to all team working members who were involved in this project.

REFERENCES

Arnorsson, S., Sigurdsson, S., Svavarsson, H.: The chemistry of geothermal waters in Iceland. I. Calculation of aqueous speciation from 0° to 370°C, *Geochimica et Cosmochimica Acta*, 46, (1982), 1513-1532.

Goh, O., Richardson, I., and Siega, F.: Acid Stimulation of Kawerau Injection Well KA44 Using Hydrofluoric Acid and Formic Acid, *Proceedings,* 45th Workshop in Geothermal Engineering, Stanford University, Stanford, California (2020).

Kaya, T., Parlaktuna, M., Demirci, N., Guney, A., Dedeoglu, V., Kaya, R.: Effectiveness of the Acidizing and Mechanical Reaming of Geothermal Production Well in Kizildere Geothermal Well in 2009, *Proceedings*, World Geothermal Congress, Bali, Indonesia (2010).

McLean, K., Wilson, D., Muller, L., Bluemle, M.: Chemical Removal of Formation Scale in Geothermal Production Wells, *Proceedings*, 43rd New Zealand Geothermal Workshop, Te Papa, Wellington, New Zealand (2021).

Rodriguez, E., Ocampo, F., Reyes, V., Avalos, D., Garcia, J., Muller, L.: Wellbore Calcite and Silica Deposition Issues and Solutions: A Case Study at Domo San Pedro, *Proceedings,* World Geothermal Congress, Reykjavik, Iceland (2021).

Rose, P. E., Xu, T., Fayer, S., Pruess, K.: Chemical Stimulation for EGS: the Use of Chelating Agents at High pH for the Simultaneous Dissolution of Calcium Carbonate, Silicas, and Silicates, *Proceedings*, World Geothermal Congress, Bali, Indonesia (2010).

Satman, A., Ugur, Z., Onur, M.: The effect of calcite deposition on geothermal inflow performance, *Geothermics*, 28, (1999), 425-444.

Satya, D., Suryantini, Astra, D.: Geology Assessment of Permeability Distribution in Silangkitang Geothermal Field, North Sumatra, Indonesia, *Proceedings*, ITB International Geothermal Workshop, Bandung, Indonesia (2021).

Dieng 2 Drilling Campaign Success Story

Marzuki Nyakmat[1], Zakki Sabiq Purwaka[1], Budi Setiawan[1], Ingria Yunandra M. Arrasy[1], Jarot Pambudi[1], Adiwibowo Sitompul[1], and Didin Chaerudin Irwansyah[2]

[1]Geo Dipa Energi
[2]Rigsis Energi Indonesia

marzuki@geodipa.co.id

Keywords: geothermal drilling, drilling performance, geothermal drilling campaign

ABSTRACT

Geo Dipa Energi (GDE) had successfully completed Dieng 2 Drilling Campaign to prepare and supply the generation of new Dieng 2 Power Plant rated 55 MWe. The drilling campaign involved the drilling of 10 wells and additional workover operation for one well. The campaign was successfully finished within the initial planned time although the project is started lately, and one additional workover operation could be performed. In the end of the project, GDE achieved Drilling Days, Depth and Cost within plan and budget, showcasing the project's success. To achieve these targets, several improvements were continuously conducted from the first well to the last well drilled, which will be detailed in this paper. The other achievements that related to safety and drilling operation will also be described. To measure the drilling performance, GDE used ROWC (Rate of Well Completion), CPM (Cost per Meter) and NPT (Non-Productive Time) parameter. These parameters combination will demonstrate how the drilling execution was keep improving. This paper will also present a comparison of the Dieng 2 Campaign with another campaign executed by several geothermal operators in Indonesia. Moreover, valuable lessons learned and drilling strategy during the project execution, which are crucial for future drilling campaigns, will also be shared.

1. INTRODUCTION

Geo Dipa Energi (GDE) is one of the geothermal operators in Indonesia who operates two fields: Dieng and Patuha. The Dieng field currently has an electrical generation capacity of 60 MW, while Patuha has 55 MW. GDE is expanding its generation capacity by constructing a new power plant with a capacity of 55 MW in the Dieng Field. This power plant is named Dieng 2 Power Plant. To meet the steam requirements for this new power plant, 6 new production wells and 4 new injection wells are required. Therefore, GDE has successfully conducted Dieng 2 (D2) Drilling Campaign to drill wells for the Dieng 2 power plant. In addition to drilling activities, there was an additional workover operation performed for the first well drilled in the campaign. In the other hand, D2 drilling campaign is the first drilling campaign conducted by GDE as an Indonesian geothermal operator.

2. DIENG 2 DRILLING CAMPAIGN

To carry out D2 drilling campaign, GDE utilized a 1500 hp rig. Furthermore, approximately 20 service companies were involved, including directional drilling, cementing, drilling mud, casing running, and other related services. The contract system to bundle these service companies was semi-IPM contract system. Under this system, several service companies are bound by a framework contract, while others are tied to separate contracts. The typical well schematic of well drilled in D2 drilling campaign is shown by Figure 1.

2.1 Drilling Days Performance

Overall, D2 Drilling Campaign was completed 91 days ahead of the planned campaign duration, including rig movement and an additional workover activity. This excellent performance was achieved through evaluations and improvement meeting conducted for each well to be drilled, including post-drilling meetings, pre-spud meetings, and stuck pipe prevention meetings with the involved service companies. The detailed drilling time for each well can be seen in Figure 2.

Out of the 11 activities performed, 8 were executed successfully ahead of the planned schedule. Among the 3 activities that slightly exceeded the planned time, one was the workover operation, which unexpectedly required more time despite no significant technical problems. Meanwhile, the other two activities, drilling well #2 and #9, faced challenges due to a fishing job in well #1 and a stuck pipe incident that necessitated a sidetrack in well #9.

2.2 Drilling Depth Performance

The success rate of the well depth in reaching its target is 99%. The success rate of the drilling depth describes the comparison between the actual and planned cumulative depth. Eight wells succeeded to reach or even exceed their target depth. Only two wells did not achieve the target depth due to a stuck pipe that left a fish in hole for

well #2 and the drillstring weight almost reached the tensile strength of drillpipe for sidetracking in well #9, making the hole cannot be drilled deeper.

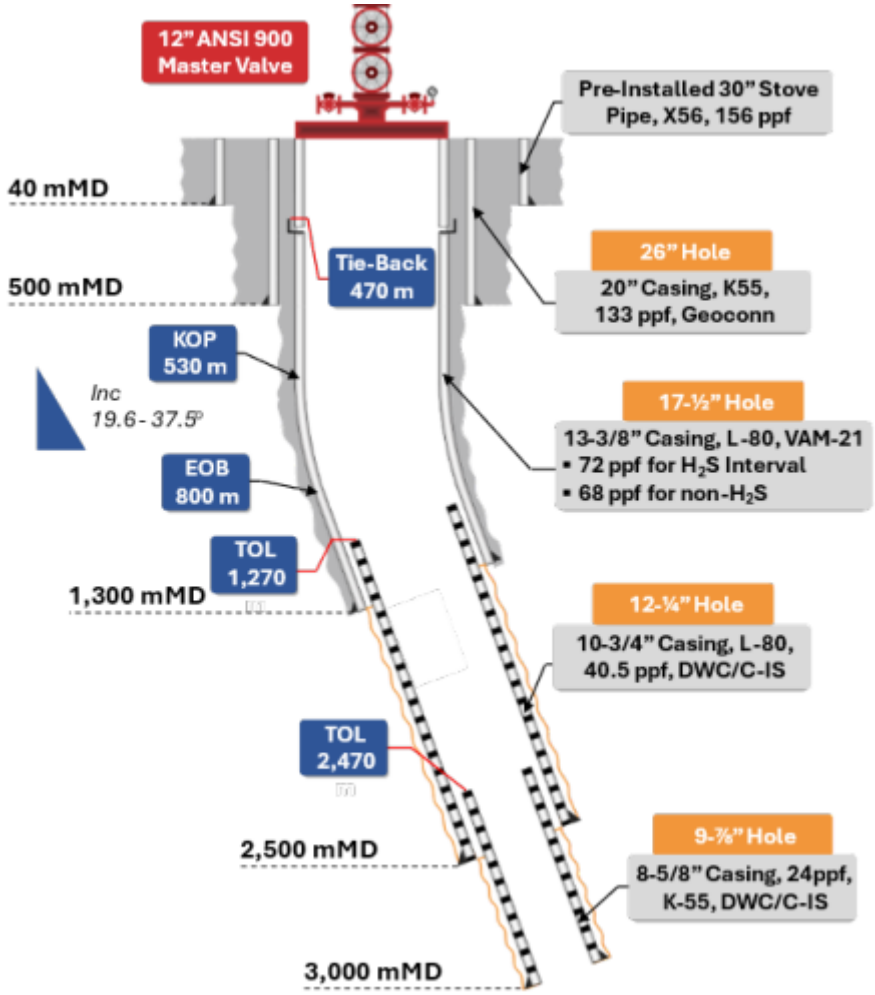

Figure 1: Typical Well Schematic of D2 Drilling Campaign.

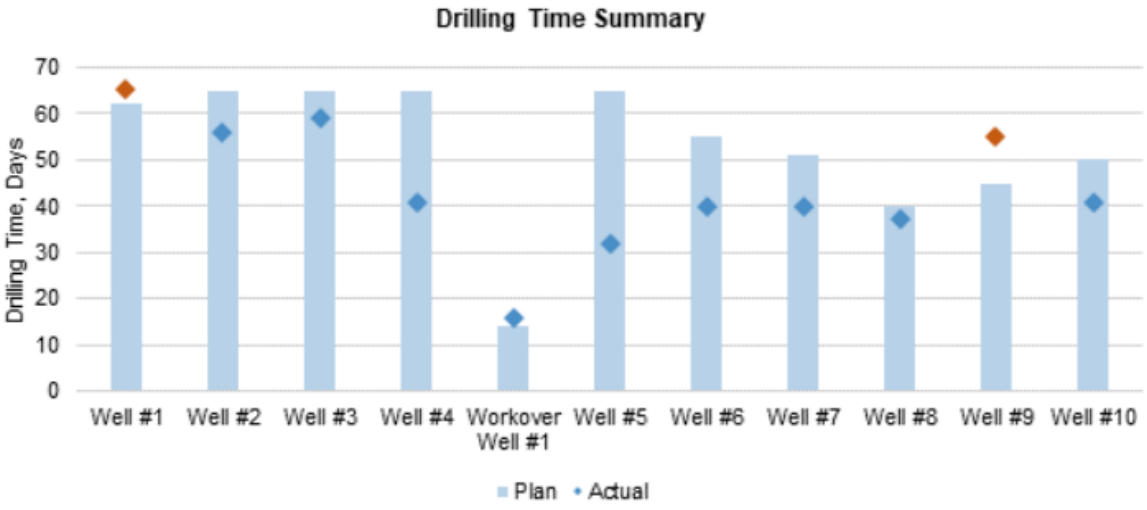

Figure 2: Drilling Time Summary Chart.

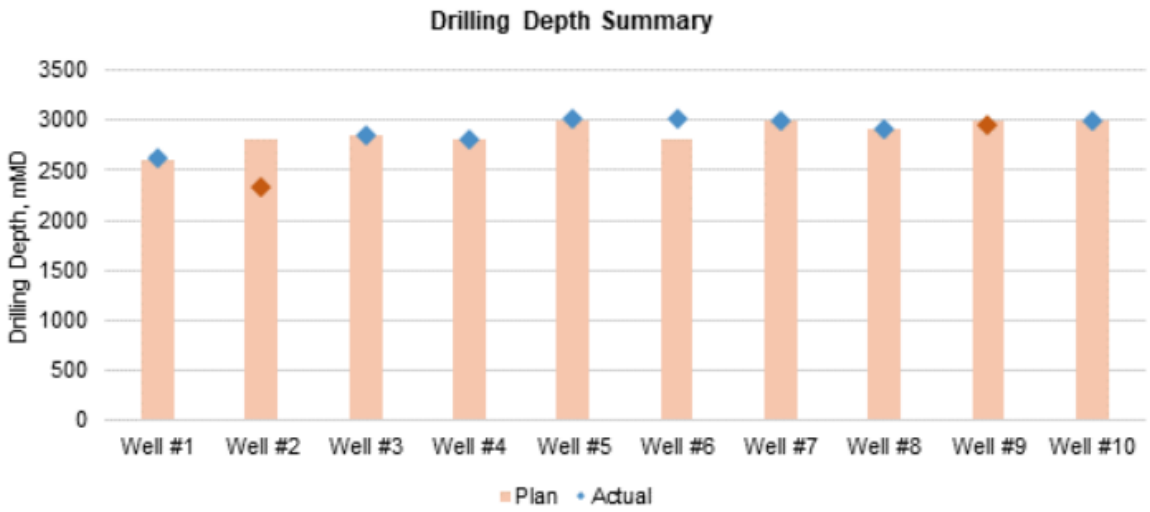

Figure 3: Drilling Depth Summary Chart.

2.3 Drilling Cost Performance

The cost efficiency of drilling correlates with the success of the two previous parameters. The cumulative final drilling cost incurred during the D2 Drilling Campaign remains below the planned cost, reaching only 95%. From all 11 operations, 7 wells succeeded to achieve final cost below the planned.

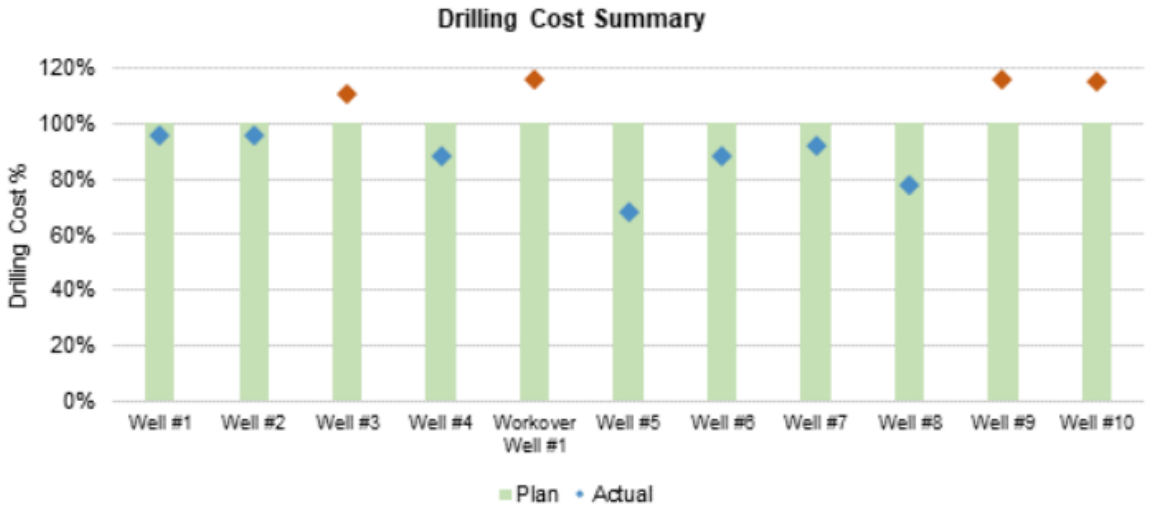

Figure 4: Drilling Cost Summary Chart.

When compared to the allocated investment, the drilling expenses are even lower at 86%. This translates to a significant 14% savings, which is commendable. The average cost rate per depth in D2 Campaign is 2,038 USD/m. Furthermore, the six producer wells drilled are estimated to generate power up to 97 MW collectively, resulting cost rate at 670,599 USD/MW. This rate is below the planned rate at 1,000,000 USD/MW.

2.4 Overall Drilling Performance

The drilling performance of Dieng 2 campaign is measured with Drilling Depth, Rate of Well Completion (ROWC), Cost per Meter (CPM) and Non-Productive Time (NPT) Parameters. Drilling depth is the deepest bit depth of the last wellbore instead of the last casing run depth. Below is the summary of ROWC, CPM and NPT of D2 Campaign. The benchmark data is gathered from 224 geothermal wells in Indonesia from another geothermal operator companies.

- **ROWC** is the average of depth deepening in a day and stated in m/day. The higher the value, the better the drilling performance. The average ROWC of D2 Campaign is 61.19 m/day, much better than the average ROWC of geothermal drilling in Indonesia in 45 m/day (drilling data by EBTKE interval 2009-2022).

- **CPM** is the average final cost (without movement cost) spent per meter drilled and stated in USD/m. The lower the value, the better the drilling performance. The average CPM of D2 Campaign is 2,038 USD/m, much better than the average CPM of geothermal drilling in Indonesia in 2,700 USD/m (drilling data by EBTKE interval 2009-2022).
- **NPT** is the time spent for unplanned operation (based on GDE's rules) experienced compared to the total drilling time. Low NPT value means good drilling execution. The average NPT value of D2 campaign is 8.35%, lower than the maximum NPT target at 10%.

Figure 5 shows the ROWC, CPM ad NPT record of each well in D2 Drilling Campaign.

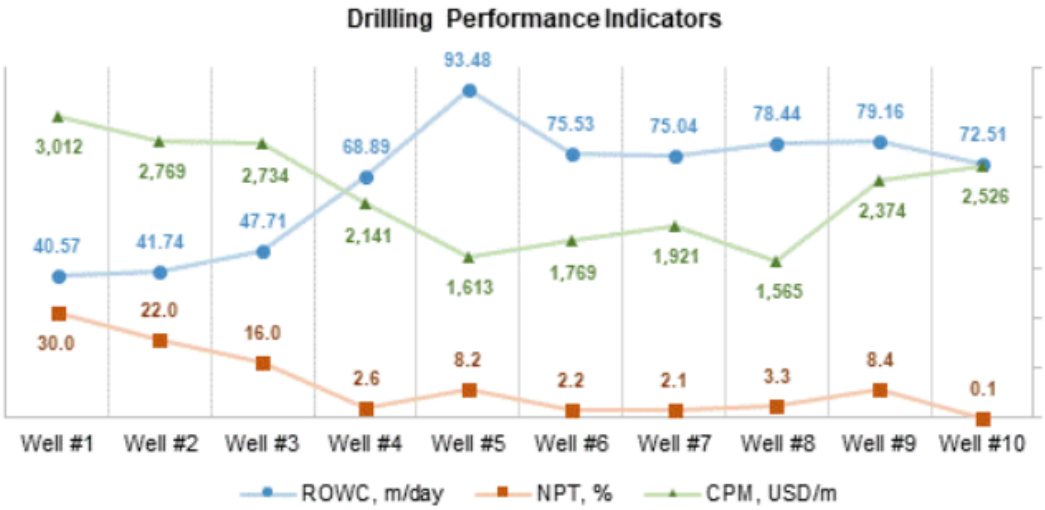

Figure 5: Drilling Performance Indicators Chart.

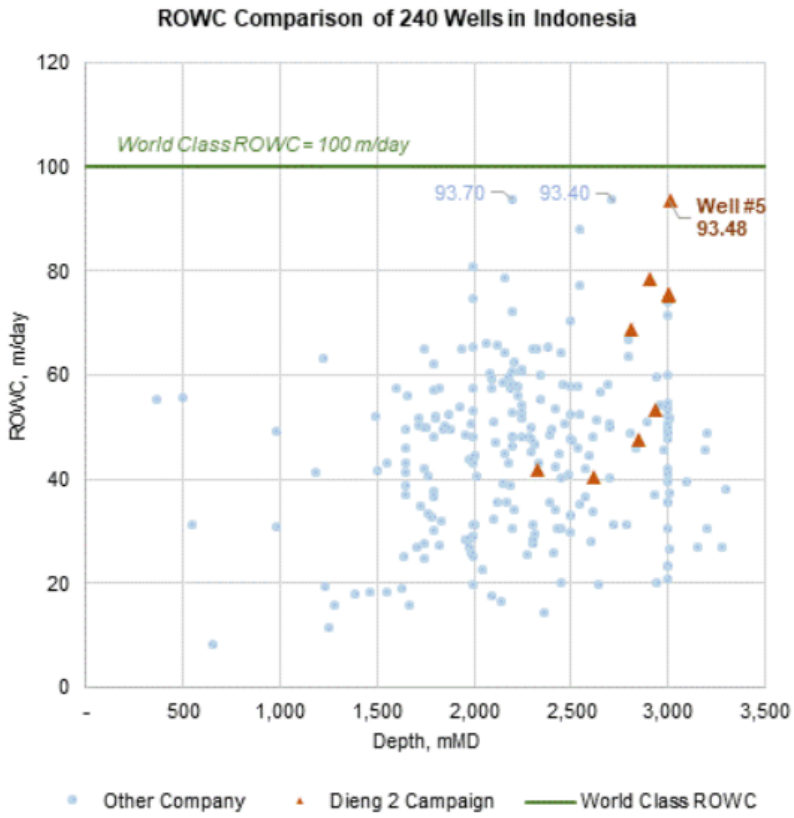

Figure 6: ROWC Comparison of 240 Geothermal Wells in Indonesia.

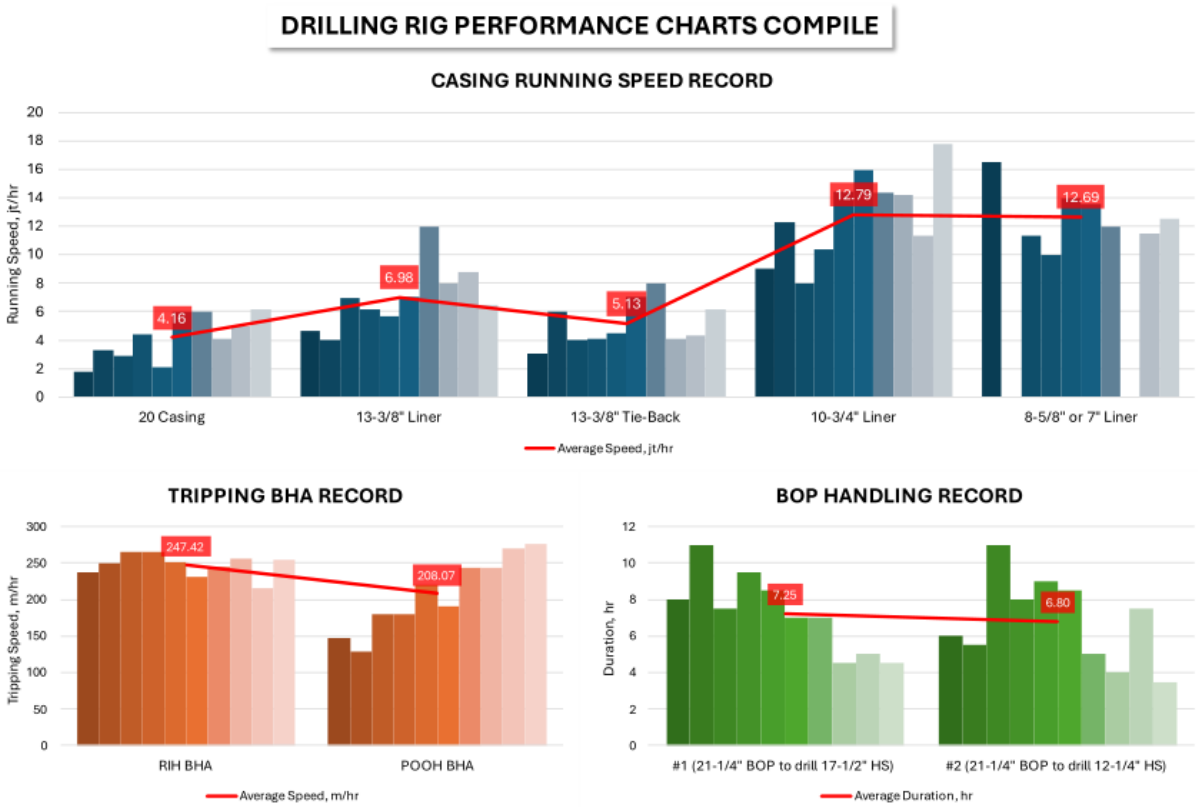

Figure 7: Drilling Rig Performance.

Excellent drilling campaign has been performed during Dieng 2 Project in term of ROWC, CPM, and NPT. By taking attention to the ROWC, it is important to note that 8 out of 10 wells recorded value above 45 m/day. The only 2 wells that were not reaching 45 m/day are the 2 first drilled well when the learning curve was just being started. The peak of ROWC value was gained in the Well #5 with 93.48 m/day. The decreasing trend value of CPM from the first well to the last well demonstrates an outstanding learning curve. From NPT side, 7 out of 10 wells record NPT value below 10% to qualify the drilling operation objective. The last well records only 0.1% of NPT which shows once again a good learning curve.

2.5 Other Achievements

During the D2 Drilling Campaign, several other outstanding achievements were attained in terms of safety and drilling operations. Some of these accomplishments are:

- Zero Recordable Accident in 1,362,474 hours (702 days) without incident as the commitment of Geo Dipa Energi for safety operation.
- Second best ROWC in Indonesian geothermal drilling record with 93.48 m/day in Well #5 as shown in Figure 6.
- Long 12-1/4" open hole section at Well #7 with 1,471 m and was successfully running 10-3/4" perforated liner to bottom.
- High daily Rate of Penetration (ROP) at Well #5 with 324 m drilling depth progress in a day.

3. VALUABLE LESSON LEARNED AND DRILLING STRATEGY

Here are some of the key factors that significantly contributed to the success of drilling operations in Dieng, particularly in terms of drilling timeline, cost efficiency, and operational excellence.

- The selection of high-quality service companies with high qualification, especially for the drilling rig provider which demonstrated by rapid duration of mobilization, moving/skidding, demobilization, tripping time, BOP handling, casing running and also the low value of Non-Productive Time (NPT). The drilling rig performance is shown in Figure 7.
- Efficient contract value resulting from grouping several service companies into a single rig bundling within the semi-IPM contract scheme.

- Competent planning and operational supervision achieved by highly skilled office drilling team that has been involved in several drilling campaigns previously and the selection of highly experienced man power or field drilling team to execute the plan.
- Appropriate drilling fluid design which was achieved by conducting Inhibitive Tests. This test provided a solution to address bit balling issues caused by sticky clay. This involved using a drilling fluid formulation combining KCl, PHPA, and lubricant, resulting in high penetration rates and eliminating the need for frequent bit and BHA trips for cleaning.
- Performance-based drill bit selection system. Three drilling bit providers were participated in D2 drilling campaign and evaluated based on maximum drillable depth, cost per foot, and rate of penetration (ROP).

4. CONCLUSION

GDE has successfully completed their first ever drilling campaign as an Indonesian geothermal operator, Dieng 2 Drilling Campaign, for the supply of steam to the new Dieng 2 Power Plant. The drilling campaign was completed 91 days ahead of schedule, achieving 99% of the planned drilling depth and saving 5% of the planned costs. Beyond the technical aspects, GDE also recorded 1,362,474 hours (702 days) of Zero Recordable Accidents, demonstrating their commitment to safety. Another achievement from this drilling campaign was achieving the second-best Rate of Well Completion (ROWC) in Indonesia with a rate of 93.48 m/day during the drilling of Well #5. Additionally, they successfully drilled the longest 12-1/4” open hole section in Indonesia at Well #7 (1,471 m) while successfully running 10-3/4” perforated liner to the bottom. Well #5 also had the best daily Rate of Penetration (ROP) with 324 m of drilling depth progress in a single day. These successes were attributed to various efforts, including selecting high-quality services with high qualifications, efficient contract value, competent planning and supervision, appropriate drilling fluid design, and a performance-based drill bit selection system.

REFERENCES

EBTKE: Drilling Performance Record in Indonesia, Jakarta (2022).

Irwansyah, D.: Dieng Completion Report, Jakarta (2023).

Sabiq, Z.: Post Drilling Dieng 2 Project, Bali (2023).

Acid Jetting Treatment for Scaled Up Production Well

Gamal Hastriansyah, Benedict Amandus Hananto, Dhanie Marstiga Yuniar, and Fernando Pasaribu

PT Pertamina Geothermal Energy Tbk. Grha Pertamina – Pertamax Tower,
Medan Merdeka Timur 11-13, Gambir, Jakarta Pusat

gamal.h@pertamina.com

Keywords: : production well, scaling, hole cleaning, acidizing

ABSTRACT

Production well 8C4, operational for five years, experienced a significant decline in performance, from 55 kg/s at 14.7 bar to 55 kg/s at 9.6 bar. Analysis of routine fluid samples revealed that calcite oversaturation occurred when temperatures exceeded 140°C within the wellbore. In response, an intervention involving jetting and acid treatment was initiated. Leveraging completion test data and insights from pre-job testing, the intervention strategy was tailored for optimal results. The implementation of the acid jetting treatment yielded promising outcomes, with a notable 65% increase in steam production.

1. INTRODUCTION

Well 8C4 was fully drilled in 2009, reaching a depth of 1755 meters with big hole configuration. Loss of circulation began at 1189 meters, and the injectivity index is in the range of hundreds (kg/s/bar). The reservoir fluid is in a compressed liquid state with a temperature of 264℃. During a separator flow test, it was confirmed that the well produces fluid at a rate of 120 kg/s at 15.2 bar pressure, with a flowing enthalpy of 1100 kJ/kg. Since 2012, the well has been supplying steam to a power plant. The specific configuration of the well is detailed in Figure 1.

1.1 Production trend

In 2012, the initial production from the well was impressive, yielding 468 tons per hour of total mass flow at 13.9 barg, which generated 9.87 megawatts of electricity. By 2017, production had decreased to 188 tons per hour of total mass flow at 9.32 barg, resulting in 3.44 megawatts of electricity. Despite the reduction in production rate over the years, the flowing enthalpy and static reservoir pressure have remained stable, indicating sustained performance without decline.

The deliverability output curve, modeled elliptically, effectively illustrates the discharge performance of the well. Despite consistent reservoir pressure and flowing enthalpy, significant drops in production occurred between 2012 and 2013, as well as between 2013 and 2014. However, from 2014 to 2017, there were no major fluctuations in production levels. This stable phase in production contrasts sharply with the earlier years, as depicted by the elliptical model on the deliverability output curve in Figure 2.

The high Calcite Scaling Index as seen in Figure 3, caused calcium scale deposition when the well produced exceeded 140°C, prompted a Go-Devil survey (sizes 8", 5", and 3") in the UBL-8/C4 well. During the survey, soft tagging was observed at a depth of 859 mMD. Subsequent analysis revealed a severe reduction in liner diameter, from 10 inches to 3 inches (Hastriansyah, 2018). A small sample retrieved by the Go-Devil was dissolved in hydrochloric acid (HCl) for analysis. X-ray diffraction conducted on a neighboring well at a depth of 845 mMD confirmed the presence of calcite scale.

1.2 Pressure and Temperature Measurement

Downhole pressure and temperature are routinely monitored in production wells whenever feasible. Figure 4 illustrates the PT profile between 2010 and 2016, showing no significant decline in either pressure or temperature.

2. HOLE CLEANING

A hole cleaning operation involving a jetting tool and acidizing was scheduled for well 8C4. Due to the continuous operation of the well, an integrity check could only be conducted as part of the hole cleaning procedure. As part of this process, a basic well condition survey was introduced, which included deploying a go-devil, a scale catcher, conducting injection PTS (Pressure, Temperature, and Spinner), and performing a gross permeability test throughout the well cleaning program.

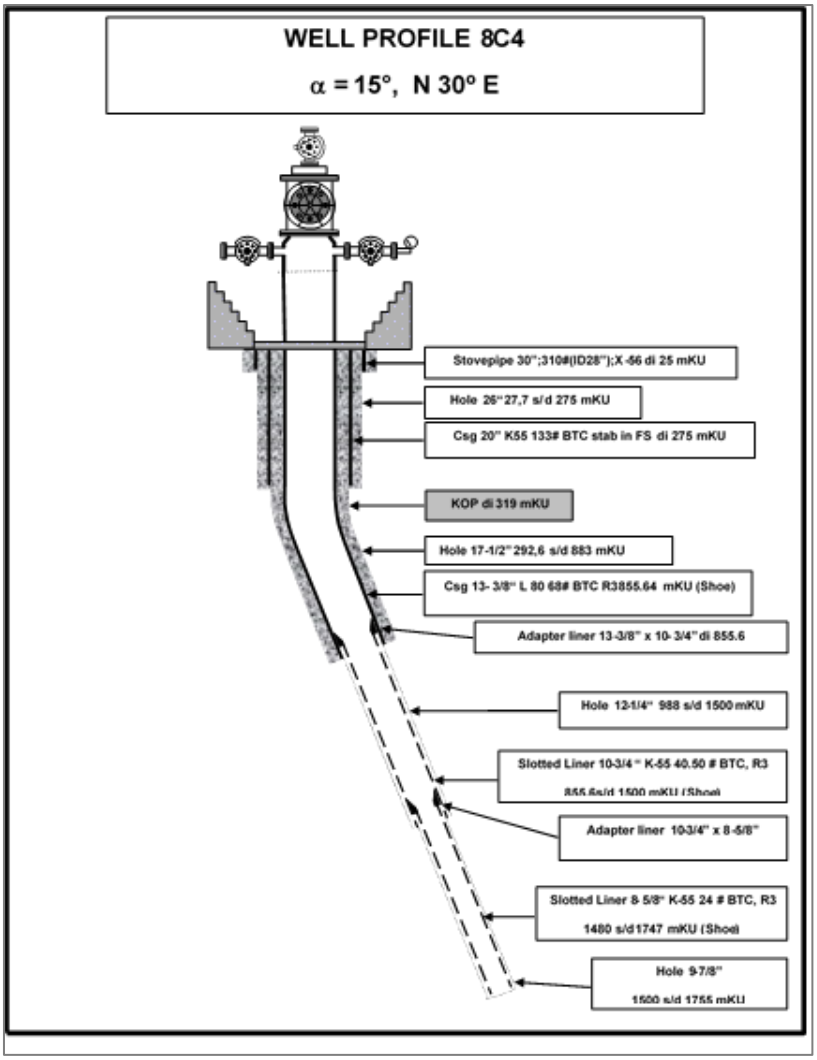

Figure 1: Well Configuration 8C4.

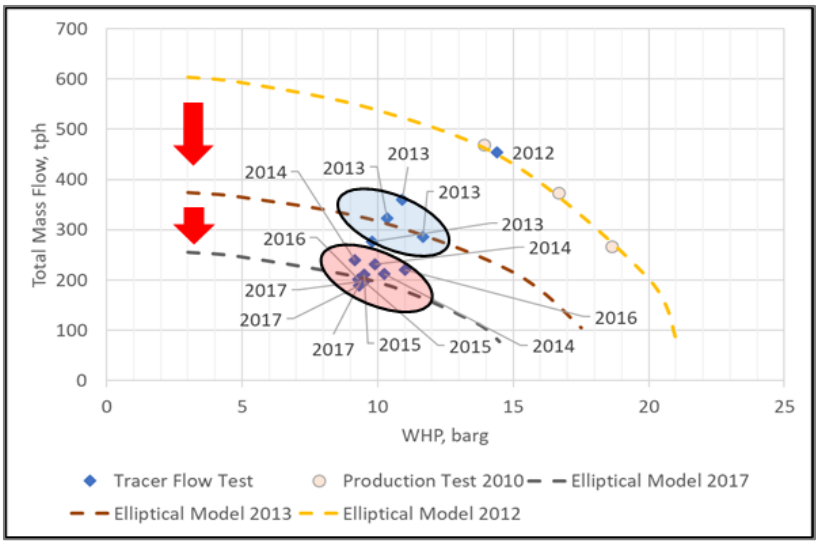

Figure 2: Deliverability Output Curve 8C4.

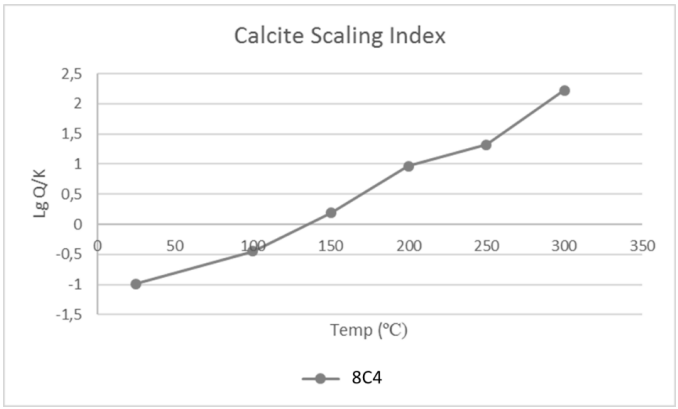

Figure 3: Well 8C4 Calcite Scaling Index.

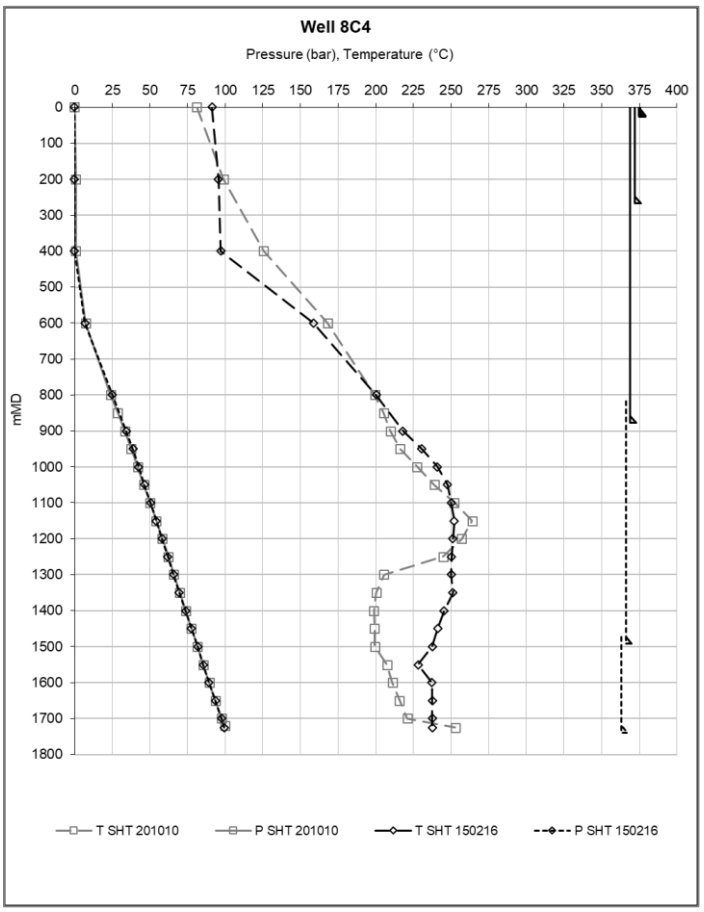

Figure 4: Well 8C4 Shut In P&T Profile.

2.1 Acid Design

For sandstone acidizing operations, the preferred acid type is mud acid, which combines hydrochloric acid (HCl) and hydrofluoric acid (HF). The acid should demonstrate a solubility range of 50% to 70% based on laboratory testing, ensuring effective dissolution of mineral deposits within the sandstone formation (see Table 1 for Acid Design in well 8C4**)**. During operations, a coiled tubing with a diameter of 2-7/8 inches is utilized, allowing for precise acid delivery. The total injection rate is maintained at 10 barrels per minute (bpm), optimizing the treatment process to enhance reservoir permeability and production efficiency.

Permeability is directly correlated with volume, highlighting the need to consider its implications. For high permeability reservoirs, the suggested fluid volumes range from 160 gal/m to 500 gal/m for preflush (PF) and 250 gal/m to 500 gal/m for main flush (MF). Additionally, the reaction's harmful effects on metal must be considered. Acidic fluids (AF) can be used to produce HF solutions and are less toxic than HF, as liquids are safer to handle and reduce the need for manual handling. AF exhibit moderate to high solubility with minerals such as feldspar, illite, smectite, chlorite, calcite, and kaolinite.

Table 1: Acid Design.

Type	Product	Volume
Pre-Flush	9% HCl	200 gal/m
Main Flush	14% HCl – 22% Ammonium Fluoride	400 gal/m
Post Flush	Water	400 gal/m
Additive	Corrosion Inhibitor Iron Control Agent Friction Reducer	

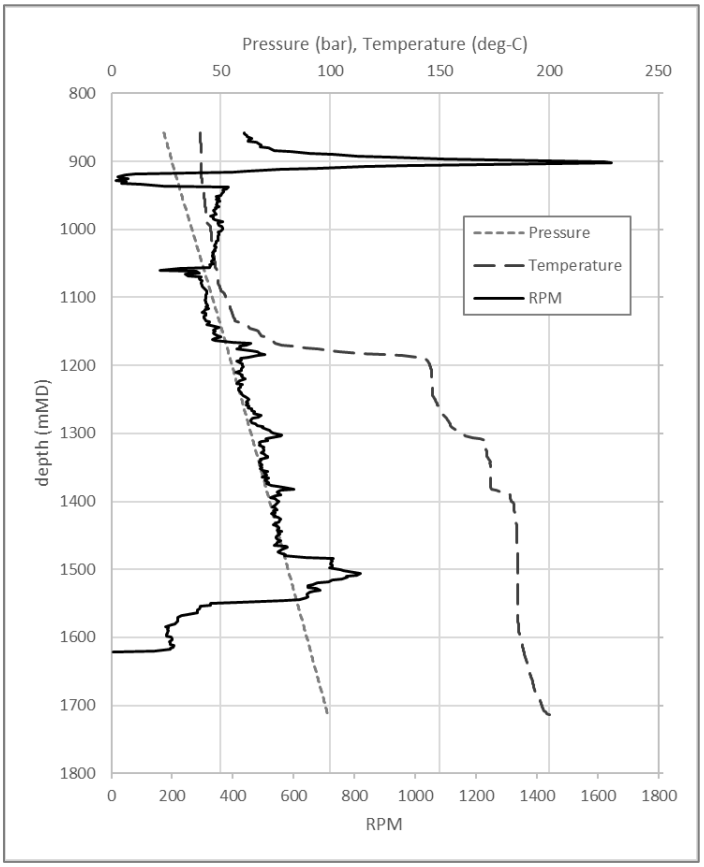

Figure 5: Injection PTS data.

Table 2: Acidizing Result Comparison.

	Total flow (tph)	Steam flow (tph)	Generation (Mwe)
Pre acid	188	28	**3.4**
Post acid	392	46	**5.7**

Corrosion inhibitors play a crucial role in protecting coiled tubing and wellbore from corrosion. Iron control agents are essential for reacting with dissolved metal ions to prevent solids precipitation, thereby maintaining the integrity of the system. Additionally, friction reducers are utilized to decrease injection pressure in coiled tubing, enhancing the efficiency and safety of the injection process.

2.2 Acidizing Operation

The process begins with Step I, where quenching is conducted at a rate of 10 BPM (barrels per minute). In Step II, the equipment is run into the hole until it reaches the target depth. However, the operation cannot penetrate below 896 meters. To address this, acid is pumped using a jetting nozzle, successfully achieving penetration. In Step III, acid is injected at a rate of 5 BPM, with annulus water being pumped at the same rate. Unfortunately, the

injection PTS data (Figure 5) exceeds the maximum temperature for the corrosion inhibitor, necessitating the dumping of acid at 1100 mMD.

3. CALCULATION, RESULT, AND DISCUSSION

The results of the operation were a mix of significant improvements and some drawbacks. On the positive side, steam flow improved by an impressive 165% (see Table 2), and discharge performance recovered, approaching the levels specified in the Output Curve Model from the year 2012 (Figure 6). However, there was a reduction in enthalpy, which decreased from 1026 kJ/kg to 980 kJ/kg. This indicates a slight decline in the energy content per unit mass, which might impact the overall efficiency despite the gains in flow and discharge performance.

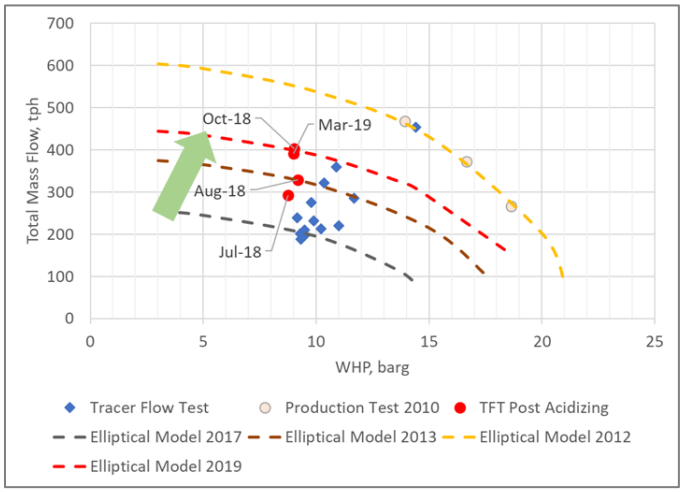

Figure 6: Deliverability Curve After Acidizing.

4. CONCLUSION

Well UBL-8/C4 had calcite scaling deposition in the wellbore and fine migration problems. Acidizing stimulation using Sandstone Acid was successfully performed in this geothermal well, which recovered its discharge performance. Consequently, the steam production of UBL-8/C4 increased by 1.65 times, from 27.5 ton/hr (3.4 MWe) to 45.5 ton/hr (5.7 MWe).

ACKNOWLEDGEMENT

The authors wish to thank the management of PT Pertamina Geothermal Energy Tbk. for the permission to publish this paper. Discussion with Reservoir team members are very much appreciated.

REFERENCES

Grant, M. and Bixley, P.: Geothermal Reservoir Engineering 2nd Edition, Academic Press (2011).

Hastriansyah, G.: Reservoir Monitoring Report, Internal Report (2017).

Hastriansyah, G. et al.: Determination of Wellbore Scale Thickness Using Analyses of Injection Spinner Data, *Proceedings*, The 6th Indonesia International Geothermal Convention & Exhibition (IIGCE) 2018.

Marastio, F. et al.: Well Screening, Design, Treatment and Evaluation of Acidizing in Geothermal Reservoir – A Case Study: 8C4 & 45I3, Forum Hulu Pertamina (2019)

Pertamina Geothermal Energy: Laporan Well Completion Test Sumur 8C4, Internal Report (2009).

Pertamina Geothermal Energy: Laporan Kegiatan Uji Produksi Sumur 8C4, Internal Report (2010).

Pertamina Geothermal Energy: Laporan Kegiatan Hole Cleaning Sumur 8C4, Internal Report (2018).

Saptadji, N.M.: Teknik Panas Bumi, *Penerbit ITB* (2001).

Yuniar, D. M., et al.: Ulubelu, First Year Monitoring, *Proceedings*, World Geothermal Congress, Melbourne (2015).

Production Optimization Priorities Using the Analytical Hierarchy Process to Enhance Well Capacity in the Geothermal "X" Field

Muhammad Thasril, Efrata Pratenta Meliala, and Aditya Tirta Pratama

muhammad.thasril@student.sgu.ac.id, efrata.meliala@student.sgu.ac.id, saditya.pratama@sgu.ac.id

Keywords: Geothermal, Multicriteria Decision-Making, Production Optimization, Analytical Hierarchy Process

ABSTRACT

Geothermal power plants in Indonesia generally have a capacity of around 55 MWe. The steam from the production well is transported to the power plant through a steam gathering system. However, natural decreases in the production well's capacity can be occurred due to several factors such as wellbore and reservoir issues. Monitoring various factors can help identify these issues, guiding future planning for well optimization program such as optimizing WHP, well investigation, well intervention, workover or drilling programs to maintain production capacity. This paper explores a data-driven approach to prioritize well optimization activities in geothermal field "X" using the Analytical Hierarchy Process (AHP). AHP is a multicriteria decision-making tool that enables the consideration of various factors influencing such as wellhead pressure, steam flow, cost and lesson learn of production optimization. The methodology involves identifying these key criteria, constructing pairwise comparison matrices to quantify their relative importance, and deriving weightings for each factor. Subsequently, different well of are evaluated based on their impact on the weighted criteria. Finally, an AHP-based developed for decision analysis aimed at establishing an overall priority ranking of nine production wells and support management decisions regarding the next production optimization strategies.

1. INTRODUCTION

Geothermal power plants play a crucial role in Indonesia's energy sector. As one of the prominent companies engaged in energy production in Indonesia, PT. XYZ has been actively involved in sustainable energy generation. One of its geothermal fields is responsible for extracting steam and brine from geothermal reservoirs and transporting them to the power plant for electricity generation. The Geothermal "X" Field has nine production wells, and monitoring and mantaining the production capacity of these wells is essential for sustained energy production. Many factors like wellbore integrity, reservoir depletion, and operational challenges can lead to a natural decline in the production capacity of geothermal wells over time (Dewi et al., 2020). To address these challenges, Production enhancement activities, such as well workovers, interventions, and drilling new wells, play a crucial role in maintaining the production capacity of the Geothermal "X" Field.

Based on the company's historical data, the pany has i activities to minimize the gap between target and realization, and has shown a positive trend in closing this gap, as shown in Figure 1. However, after 2021, the gap has widened.

According to the other data, the gap between the target and realization for electricity generation from the Geothermal "X" Field had exhibited a positive trend in closing until 2021. However, this gap has widened after 2021. Additionally, the gap in the equivalent availability factor decreased to 16.1% in 2021 but has since become wider, indicating the need for the company to implement measures to increase steam supply and close this gap, as shown in Figure 2.

To address this challenge, the company needs to develop a comprehensive strategy to prioritize its well optimization efforts. The Analytical Hierarchy Process (AHP) is a multi-criteria decision-making tool that can be effectively utilized to evaluate and prioritize different well optimization techniques based on their impact on key criteria such as wellhead pressure, steam flow, cost, and success ratio from the past of production enhancement such as workover, well intervention, additional/upgrading facilities. Therefore, this study aims to apply the Analytical Hierarchy Process (AHP) to analyze the decision-making process in prioritizing well optimization activities for the Geothermal "X" Field to maintain its production capacity. By ishing an overall priority ranking of production wells, the company can effectively manage resources and prioritize activities such as workover, well interventions, or additional/upgrading facilities. This will ultimately contribute to ensuring the long-term inability of its by existing assets, which is assumed to be more attractive than drilling a new well.

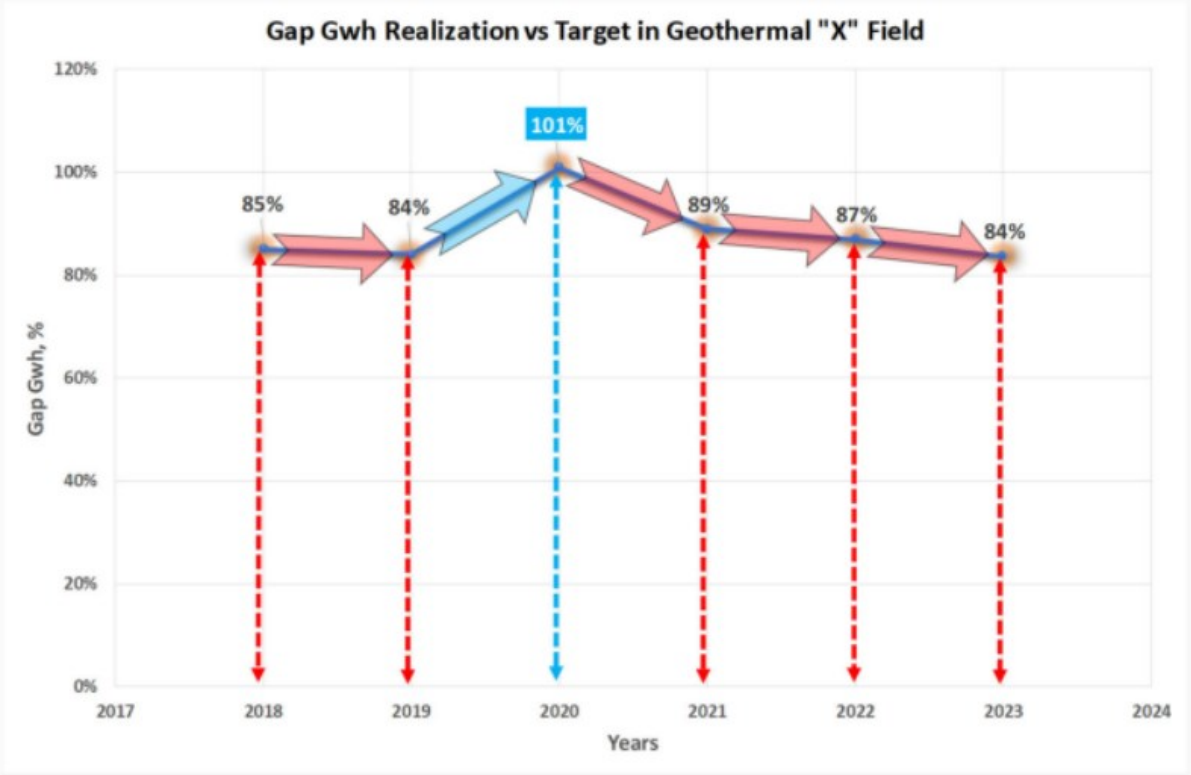

Figure 1: Gap Analysis Gwh Target vs Realization in "X" Field (PT.XYZ, 2024).

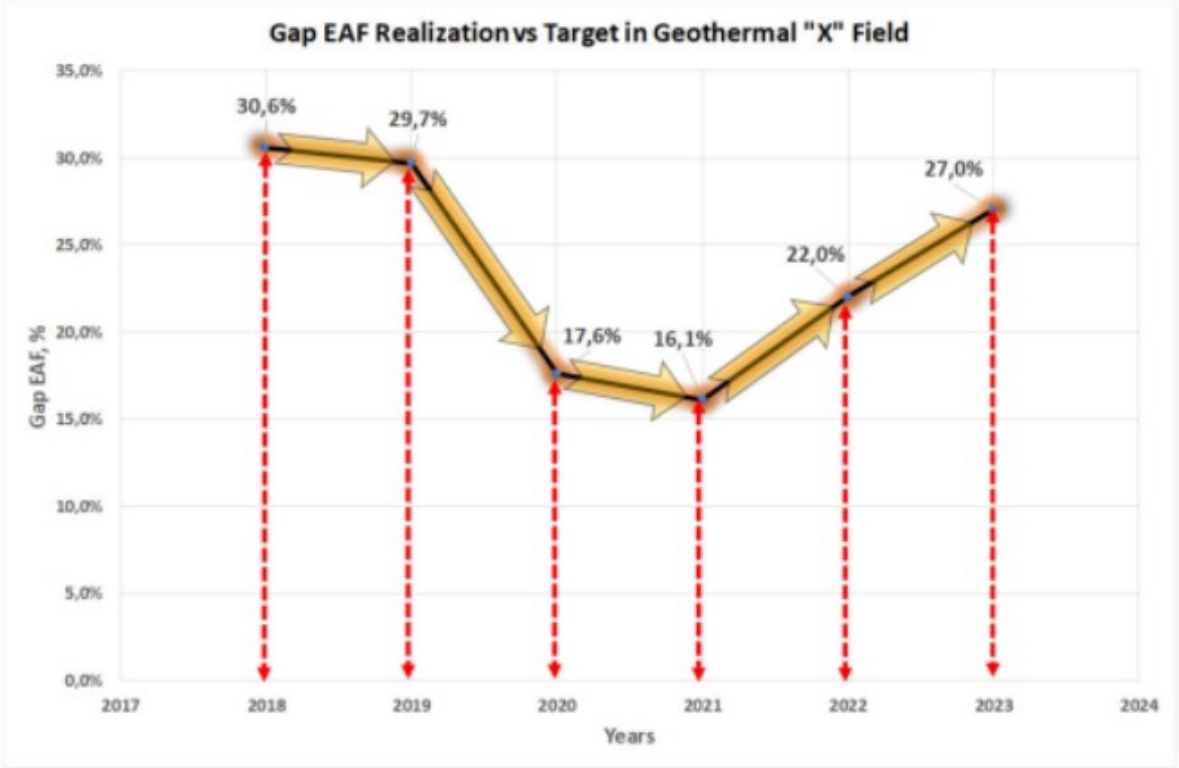

Figure 2: Gap Analysis Equivalent Availability Factor (EAF) in Geothermal "X" Field (PT.XYZ, 2024).

2. Literature Review

2.1 Analytic Hierarchy Program (AHP)

Decision analysis is based on axiomatic decision theory and it incorporates! insights from the study of decision-making (Cui et al., 2021). Multi-Criteria Decision Making (MCDM) is a comprehensive, multidimensional approach to address decision-making challenges across various fields, seeking the most favorable alternative by considering all relevant criteria. This method employs powerful tools to analyze complex decision-making problems in different domains (Afandi, 2018). The Analytical Hierarchy Process (AHP) is a traditional MCDM techni that bines both qualitative and quantitative analyses (Liu et al., 2020). It helps in the overall selection process by breaking down a complex issue into a hierarchical structure of goals, criteria, and alternatives (Sharma & Gandhi, 2008). AHP organizes and analyzes complex decisions, allowing decision-makers to compare and prioritize different alternatives based on multiple, often conflicting criteria. It is particularly effective in situations involving subjectivity and is well-suited for problems where decision criteria can be organized hierarchically into sub-criteria (Tuzmen & Sipahi, 2011). Developed by Thomas Saaty in the 1970s, AHP involves several steps (Emawan et al., 2021): constructing a hierarchical model with the objective, alternatives, and evaluation criteria; assigning weights to the criteria through pairwise comparisons; synthesizing judgments to establish priorities; assessing the consistency of these judgments using an ratio; and making the final decision based on the results. For example, a study by Simorangkir & Pratama (2023) integrates AHP with the whale optimization algorithm to determine the best energy source and important components before optimizing them. Febrianto et al. (2022) used AHP to select the right training material for mechanics, finding that the highest -ranked option was the Komatsu model unit with preventive maintenance training materials. Similarly, Budiman & Pratama (2022) employed AHP to decide which secondhand plastic injection molding machine to purchase, concluding that the Potenza PT350 was the best option to meet customer demand with a 300-ton capacity.

To make comparisons, we need a scale of numbers that indicates how many times more important or dominant one element is over another element as shown in Table 1.

Table 1: Scale Instrument for Pairwise Comparison Data Collection Method, Tools & Technique Interpretation.

Intensity of Importance	Definition
1	Equal Importance
3	Moderate Importance
5	Strong Importance
7	Very Strong Importance
9	Extreme Importance
Intensities of 2, 4, 6, and 8 can be used to express the level of intermediate values	

The AHP assigns a weight to each evaluation criterion based on the decision maker's pairwise comparisons. A higher weight indicates greater importance of the corresponding criterion. For each criterion, AHP then scores the options according to the decision maker's pairwise comparisons of the options relative to that criterion. A higher score reflects better performance conceming the specific criterion. Finally, AHP combines the criteria weights and option scores to determine a global score for each option, resulting in an overall ranking. The global score for an option is a weighted sum of the scores it received for all criteria.

2.2 Criteria Parameter

The main criteria parameters in the Analytical Hierarchy Process (AHP) include:

a. Wellhead Pressure (WHP)

Wellhead pressure is a crucial indicator of the well's production capacity (Qin et al., 2013), monitoring and maintaining wellhead pressure is essential for sustained energy production (Carson & Mansure, 1982). Declining wellhead pressure can be a signal of reservoir depletion or well integrity issues, requiring optimization measures (Al-Dulaijan et al., 2013). In this study, the tools and technique to enhance the quality of user's judgement is the gap between actual condition and average wellhead pressure within a year data approach.

b. Steam Flow

Steam flow rate is another critical parameter in maintaining the power plant's energy production. The steam flow rate from a production well directly impacts the power generation capacity of the geothermal power plant. Optimizing steam flow is critical for maintaining the overall production capacity. According to Dwikorianto et al., (2010), the steam flow rate is a key parameter in geothermal power plant operations, as it determines the

amount of electricity that can be generated. Maintaining and optimizing the steam flow from production wells is essential for sustaining the power generation capacity of the geothermal fi field. In this study, the tools and technique to enhance the quality of user's judgement is using the gap between actual steam flow and the target flow rate data approach.

c. Cost

The cost associated with well optimization activities is a crucial consideration in the decision-making process. This includes the costs of well workover, well intervention, or additional/ upgrading facilities. The cost factor should be evaluated in terms of the financial impact and feasibility of the proposed optimization measures. Selecting the most cost-effective solutions that can effectively improve production capacity is essential for maintaining the overall profitability and sustainability of the geothermal operations. In this study, the tools and technique to estimate the cost is based on the three- point estimation PERT (Program ion and Review Technique) approach. This involves optimistic, pessimistic, and most likely cost scenarios to obtain a more accurate and realistic cost estimate for the well optimization activities.

d. Success Ratio

The success ratio of the well optimization activities is another important criterion in the decision-making process. The success ratio of production enhancement activities, such as well workovers, well interventions or additional/upgrading facilities, is a critical factor in the decision making process for prioritizing well optimization efforts. The success ratio reflects the historical performance and effectiveness of these activities in improving well productivity and maintaining production capacity. A high success ratio indicates that the proposed optimization measures are more likely to achieve the desired outcomes, making them more attractive options for the company to prioritize. Conversely, a low success ratio may suggest the need for more thorough evaluation or alternative approaches to ensure the long-term sustainability of the geothermal operations. In this study, the tools and technique to measure the success ratio is based on the historical data of past production enhancement activities and or well investigation data in the Geothermal "X" Field and or well investigation data. User judgement will rely on this data to enhance the quality of input of this Analytical Hierarchy Process (AHP) Application.

3. METHODOLOGY

Methodology of this research is combining data quantitative and qualitative approach which is a conceptual framework of this study can be shown at Figure 3.

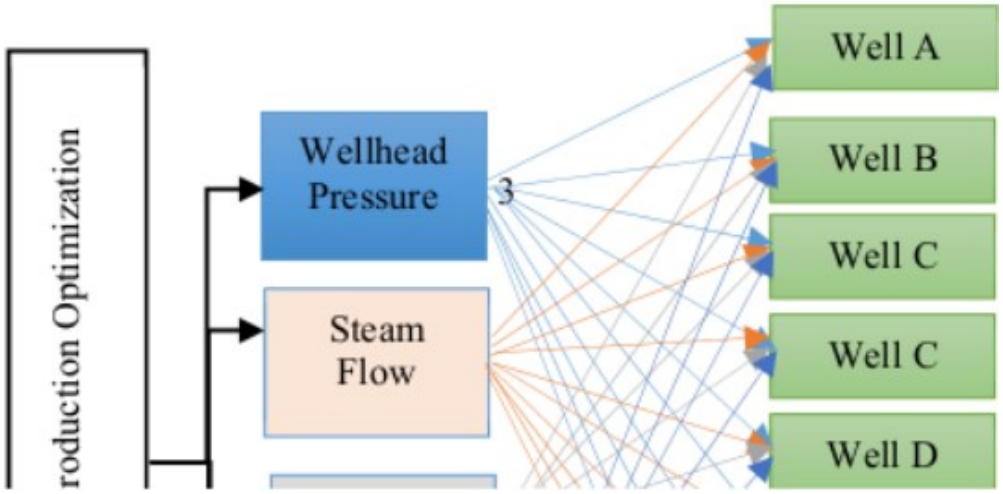

Figure 3: Conceptual framework AHP Well Intervention Priority in "X" Field at PT. XYZ.

Based on those conceptual frameworks, the data collected in this study was created in Table 2. Most of data is based on expert judgement, data analytical, and three-point estimation PERT that come from **unpublished check sheets** owned by an expert in PT. XYZ. The result from expert will interpreted to the level of Fundamental Scale for Pairwise Comparisons either linear regression if using data driven for tools & technique interpretation or verbal judgement if using expert judgement (Saaty, 1987).

Table 2: Data Collection Method, Tools & Technique Interpretation.

No.	Level Judgment	Tools & Technique Interpretation	Remarks
1	Wellhead Pressure	Expert Judgement	
2	Steam flow	Expert Judgement	
3	Cost	Expert Judgement	
4	Success Ratio	Expert Judgement	
5	Wellhead Pressure comparison each alternative	Data Analytical	Gap of WHP Actual vs Average 1 year calculation by Users compare with each alternative
6	Steam flow comparison each alternative	Data Analytical	Gap of Steam Flow Actual vs Average 1 year by Users compare with each alternative
7	Cost comparison each alternative	Three-point estimation PERT	Gap Based on judgement users for pessimistic, optimistic and most likely in regards cost of well treatment compare with each alternative
8	Success ratio comparison each alternative	Data Analytical	Expert Judgement based on historical well for well treatment, well investigation and or well surveillance data compare with each alternative

4, RESULT AND ANALYSIS

4.1 Result of Decision Criteria

Based on tools & technique interpretation from Table 2, the result of level importance in decision criteria can be shown in Table 3.

Table 3: Result Pairwise Comparison in Decision Criteria.

	Cost	Steam flow	Success Ratio	WHP
Cost	1.0	1.0	0.1	1.0
Steam flow	1.0	1.0	0.1	2.0
Success Ratio	9.0	9.0	1.0	9.0
WHP	1.0	0.5	0.1	1.0

According to Table 3, the priority and level consistency shown acceptable as per Table 4.

Table 4: Result the Priority and Level Consistency in Decision Criteria.

Decision Criteria	Priority	Consistency Ratio	Degree of Consistency
Cost	0.083	0.023	Acceptable
Steamflow	0.102		
Success Ratio	0.744		
WHP	0.072		

4.2 Result of Alternative and Overall Goal

After decision criteria, the next step evaluation is to get overall goal based on decision criteria compare with all alternatives. Based on Table 2, the result of level importance, consistency ratio and degree of consistency for WHP, Steam Flow, Cost, and Success Ration can be shown in Table 5, Table 6, Table 7, and Table 8, respectively.

Table 5: Result of WHP in Comparison Each Alternative.

Well	A	B	C	D	E	F	G	H	I	Consistency Ratio	Degree of Consistency
A	1.0	9.0	7.0	9.0	9.0	9.0	9.0	6.0	5.0	0.026	Acceptable
B	0.1	1.0	0.3	1.0	1.0	1.0	1.0	0.3	0.2		
C	0.1	3.0	1.0	4.0	4.0	4.0	4.0	0.5	0.3		
D	0.1	1.0	0.3	1.0	1.0	1.0	1.0	0.3	0.2		
E	0.1	1.0	0.3	1.0	1.0	1.0	1.0	0.3	0.2		

Well	A	B	C	D	E	F	G	H	I	Consistency Ratio	Degree of Consistency
F	0.1	1.0	0.3	1.0	1.0	1.0	1.0	0.3	0.2		
G	0.1	1.0	0.3	1.0	1.0	1.0	1.0	0.3	0.2		
H	0.2	4.0	2.0	4.0	4.0	4.0	4.0	1.0	1.0		
I	0.2	5.0	3.0	5.0	5.0	5.0	5.0	1.0	1.0		

Table 6: Result of Steam Flow in Comparison Each Alternative.

Well	A	B	C	D	E	F	G	H	I	Consistency Ratio	Degree of Consistency
A	1.0	9.0	8.0	9.0	9.0	0.2	8.0	9.0	0.3		
B	0.1	1.0	1.0	1.0	1.0	0.1	0.5	1.0	0.1		
C	0.1	1.0	1.0	1.0	1.0	0.2	1.0	1.0	0.1		
D	0.1	1.0	1.0	1.0	1.0	0.1	0.5	1.0	0.1		
E	0.1	1.0	1.0	1.0	1.0	0.1	0.5	1.0	0.1	0.043	Acceptable
F	5.0	9.0	9.0	9.0	9.0	1.0	8.0	9.0	2.0		
G	0.1	2.0	1.0	2.0	2.0	0.1	1.0	2.0	0.1		
H	0.1	1.0	1.0	1.0	1.0	0.1	0.5	1.0	0.1		
I	4.0	8.0	8.0	8.0	8.0	0.5	8.0	8.0	1.0		

Table 7: Result of Cost in Comparison Each Alternative.

Well	A	B	C	D	E	F	G	H	I	Consistency Ratio	Degree of Consistency
A	1.0	4.0	4.0	6.0	9.0	1.0	4.0	1.0	40		
B	0.3	1.0	1.0	4.0	9.0	0.2	1.0	0.2	1.0		
C	0.3	1.0	1.0	3.0	9.0	0.2	1.0	0.2	1.0		
D	0.2	0.3	0.3	1.0	7.0	0.1	0.3	0.1	0.3		
E	0.1	0.1	0.1	0.1	1.0	0.1	0.2	0.1	0.2	0.050	Acceptable
F	1.0	6.0	6.0	9.0	9.0	1.0	4.0	1.0	4.0		
G	0.3	1.0	1.0	3.0	6.0	0.3	1.0	0.2	1.0		
H	1.0	5.0	6.0	8.0	9.0	1.0	6.0	1.0	4.0		
I	0.3	1.0	1.0	3.0	2.0	0.3	1.0	0.3	1.0		

Table 8: Result of Success Ratio in Comparison Each Alternative.

Well	A	B	C	D	E	F	G	H	I	Consistency Ratio	Degree of Consistency
A	1.0	0.1	0.3	0.3	1.0	9.0	0.3	1.0	0.2		
B	7.0	1.0	4.0	4.0	5.0	9.0	4.0	5.0	2.0		
C	3.0	0.3	1.0	1.0	2.0	9.0	1.0	2.0	0.3		
D	3.0	0.3	1.0	1.0	2.0	9.0	1.0	2.0	0.3		
E	1.0	0.2	0.5	0.5	1.0	9.0	0.3	1.0	0.2	0.047	Acceptable
F	0.1	0.1	0.1	0.1	0.1	1.0	0.2	0.2	0.1		
G	3.0	0.3	1.0	1.0	3.0	6.0	1.0	2.0	0.3		
H	1.0	0.2	0.5	0.5	1.0	5.0	0.5	1.0	0.2		
I	6.0	0.5	4.0	4.0	2.0	8.0	4.0	6.0	1.0		

Therefore, all alternative comparison each decision criteria are acceptable, and the final result of overall goal can be shown in Table 9.

Table 9: Result of Priority Alternative Well.

AHP Ranking		
Alternative Well	**Priority**	**Rank**
A	0.107022896	3
B	0.236364806	1
C	0.086976542	4

AHP Ranking		
Alternative Well	**Priority**	**Rank**
D	0.07917817	6
E	0.04796491	9
F	0.068157793	8
G	0.084137718	5
H	0.070116459	7
I	0.220080706	2

4. CONCLUSION

Production optimization is a critical task for geothermal companies to optimize and continuously improve on their assets. The AHP approach allows the company to systematically evaluate and prioritize the production well optimization options based on key criteria such as wellhead pressure, steam flow, cost, and success ratio. The final result of the Analytical Hierarchy Process tells us that the top 3 wells that need to optimization are Well B, Well I, and Well A. However, if the company needs to maximize its capacity and the cost still feasible, it may add Well C and Well G as shown in the Table 9 as alternative solutions.

Optimizing Performance of LP-Separator and Brine ORC Using Brine Reinjection System (BRS) Pumps in the 15 MW Combined Double Flash and Binary System at PT. Sorik Marapi Geothermal Power

Hary Sumantry Aka, Guntur G. Lintang, Ezi Haili Ananta, Dedy Setiawan, and Ali Sahid

PT. Sorik Marapi Geothermal Power, Mandailing Natal, South Sumatera, Indonesia

harysumantryaka@gmail.com

Keywords: Optimizing, Brine Reinjection System (BRS) Pump, LP-Separator, Brine ORC

ABSTRACT

The 15 MW Combined Double-Flash and Binary system utilizes 2-phase geofluid (steam and brine) from two production wells, Well T-01 and Well T-02, with a steamfield facility consisting of an HP-Separator, LP-Separator, and Brine Reinjection System (BRS) Pumps (BRSP-01 and BRSP-02), and a power plant facility consisting of a Steam Expander (SE-07), Steam ORC (ORC-16), and Brine ORC (ORC-15). The Double-Flash system uses the hot brine from the first separation by the HP-Separator to be re-flashed (second separation) using the LP-Separator to produce additional steam. Meanwhile, the Binary system uses the exhaust steam from SE-07 for ORC-16 and the hot brine from the LP-Separator for ORC-15. ORC-15 utilizes the heat from the brine after the second separation from the LP-Separator to heat the working fluid (R245fa) using heat exchanger equipment (pre-heater and evaporator) to vaporize the working fluid and drive the working fluid expander to generate electricity. The operation of the LP-Separator and ORC-15 is connected to the operation of the BRS Pump. The brine from the HP-Separator is pumped to the LP-Separator using BRSP-01, and the brine from the LP-Separator is pumped to ORC-15 using BRSP-02. The BRS Pump is a brine pump used for pumping hot brine at a specific pressure and brine rate, controlled by a variable frequency drive (VFD). This allows the operator to regulate the discharge pressure and brine rate entering the LP-Separator and ORC-15. Thus, the operator can optimize the process using the BRS Pump to achieve optimal pressure and brine rate settings to produce an optimal steam fraction (steam rate) in the LP-Separator and optimal power generation from ORC-15. Additionally, a higher discharge pressure will make the brine more saturated, and the SSI value will be lower than without using the BRS Pump, reducing the potential for scaling formation along the brine line from the HP-Separator to the LP-Separator and the brine line from the LP-Separator to the ORC-15 Outlet. By optimizing BRSP-01, the LP-Separator steam fraction value will increase by 0.6629% to 3.1080% (using BRSP-01) compared to 3.0875% (without BRSP-01). This results in a total power generation increase of 0.0604% to 11466.2443 kW (using BRSP-01) compared to 11459.3174 kW (without BRSP-01). Optimizing BRSP-02 will increase the power generation of ORC-15 by 0.5774% to 1409.7176 kW (using BRSP-02) compared to 1401.6246 kW (without BRSP-02. Furthermore, the potential for scaling formation along the brine line from the HP-Separator to the LP-Separator can be minimized because the discharge pressure is above the saturation pressure, i.e., 8.94 barg (Pressure saturation is 6.61 bar), and the SSI value decreases by 0.0534% to 1.1238 (using BRSP-01) compared to 1.1244 (without BRSP-01). Along the brine line from the LP-Separator to the ORC-15 Outlet, the discharge pressure is 17.32 barg (Pressure saturation is 4.30 bar), and the SSI value decreases by 0.2749% to 1.3460 (using BRSP-02) compared to 1.3497 (without BRSP-02).

1. INTRODUCTION

The Combined Double Flash and Binary system is a advance geothermal energy conversion system that combines double flash and binary conversion systems. The double flash system performs a flashing process or separation of steam and brine from a 2-phase geofluid through two separation stages. The 2-phase geofluid from the production well undergoes the first separation (first flash/separated) using an HP-Separator. The brine from the HP-Separator, which still has a high temperature and contains steam fraction, holds the potential to produce additional steam for the steam expander/turbine. Therefore, the brine undergoes a second separation process using an LP-Separator (second flash/separated). The binary system is a power generation system that uses heat from brine or steam to transfer heat to a working fluid (secondary fluid) using heat exchanger equipment (preheater and evaporator). This process produce vapor from the working fluid, which drives the working fluid expander/turbine to generate electricity.

The 15 MW system in Sorik Marapi using the Combined Double Flash and Binary system, utilizing geofluid from two production wells, Well Production T-01 and T-02. Geofluid from the production wells flows to the HP-Separator for the first flash process. The brine from the HP-Separator is then directed to the LP-Separator for the second flash process, transported using the Brine Reinjection System (BRS) Pump or BRSP at a specific pressure

and flow rate. The BRSP can be controlled by the operator as the pump motor is equipped with a variable frequency drive (VFD), allowing the frequency of the BRSP to be set according to the discharge pressure and system flow rate. After the second flash, the brine from the LP-Separator is not immediately reinjected but instead directed to the Brine ORC (Binary System) or ORC-15. The brine from the LP-Separator still has a high temperature and can be utilized as a heat source for heat transfer with the working fluid in ORC-15. The brine from the LP-Separator is directed to ORC-15 using BRSP-02, with the pressure and flow rate adjusted to match the working pressure and flow rate of ORC-15. Afterward, the brine from ORC-15 flows to the reinjection system line.

From the explanation above, the BRSP plays a crucial role in the operation of the 15 MW Combined Double Flash and Binary system, particularly for the LP-Separator and Brine ORC. This is because the BRSP functions to maintain the pressure and flow rate of brine along the brine line. Therefore, using the BRSP allows optimization of the output from the LP-Separator and Brine ORC by determining the optimal discharge pressure from BRSP-01 and BRSP-02 entering the LP-Separator and Brine ORC. The discharge pressure at the LP-Separator will control the inlet of the LP-Separator, resulting in different steam fraction values for each pressure setting. By optimizing the discharge pressure with BRSP-01, the most optimal steam fraction value can be achieved. An optimal steam fraction will produce an optimal steam rate and ultimately generate the most optimal power from the Steam Expander (SE-07) and Steam ORC (ORC-16). Furthermore, optimizing ORC-15 using BRSP-02 will determine the optimal discharge pressure to achieve optimal power generation from ORC-15. In addition to achieve optimal thermodynamic processes, BRSP optimization also influences the potential for scaling formation in the brine line from the HP-Separator to the LP-Separator (BRSP-01) and the brine line from the LP-Separator to ORC-15 (BRSP-02). Scaling potential in the brine line is affected by the pressure and temperature of the brine line. The brine line temperature will indicate the saturation pressure, where if the pressure line is below the saturation pressure, the brine will have the potential to undergo flashing, increasing silica concentration due to the brine becoming more concentrated and raising the SSI value. Therefore, the pressure line must be maintained above the saturation pressure to keep the brine in a saturated state, reducing the flashing process and minimizing the scaling potential in the brine line. Using the BRSP, the brine line pressure can be stably set above the saturation pressure, reducing the potential for scaling in the brine line.

Optimizing discharge pressure and flow rate using BRSP for the LP-Separator and ORC-15 is crucial for maximizing total power generation and reducing the potential for scaling formation in the brine line, ensuring the entire system operates optimally. Therefore, this paper will explain the optimal BRSP discharge pressure values for optimizing the output of the LP-Separator and Brine ORC using thermodynamic simulation methods. The optimization results will compare the values with and without using BRSP in the 15 MW Combined Double Flash and Binary system at Sorik Marapi.

2. BASIC THEORY

2.1 Double Flash

In this system, two geofluid separation processes are used the HP-Separator and LP-Separator. Additionally, two types of steam expanders/turbines are employed the HP-Steam Expander and the LP-Steam Expander, which are coupled with a single generator.

2.1.1 Steam Fraction Analysis of LP-Separator

The brine from the discharge of the BRSP-01 (6), which still has a hot temperature, will flow to the LP-Separator (7) to extract additional steam from the hot brine that can still be flashed because it still has a steam fraction (x7). The thermodynamic process that occurs in stage 6-7 is isenthalpic, where there is no enthalpy loss in the process. Therefore, the formula for this process is as follows:

$$h_6 = h_7 \quad (1)$$

At the LP-Separator (7), the steam fraction value (x_7) is given by:

$$h_6 = h_{f7} + x_7 . h_{fg7} \quad (2)$$

$$X_7 = (h_6 - h_{f7})/h_{fg7} \quad (3)$$

2.1.2 Steam Rate and Power Generation of LP Steam Expander

Steam rate from LP-Separator can calculate with this equation

$$m_{lps} = (1 - x_2) . x_7 . m_{total} = m_8 \quad (4)$$

And to calculate the brine rate from LP-Separator use this equation

$$m_{lpb} = (1 - x_2) . (1 - x_7) . m_{total} = m_{11} \quad (5)$$

The power output by the two stages is quantified through the mass flow rate, as well as the amount of brine for reinjection and the amount of waste heat from the condenser. The isentropic efficiency and power of the LP-Steam Expander can be expressed in the same way as the single-flash turbine.

$$\eta_{lpt} = (h_9 - h_{10})/(h_{10} - h_{10s}) \quad (6)$$

$$W_{lpt} = m_s \,.\, (h_8 - h_5) = (1 - x_2) \,.\, x_7 \,.\, m_{total} \,.\, \eta_t \,.\, (h_8 - h_{5s}) \quad (7)$$

2.2 Brine Organic Rankine Cycle (ORC)

2.2.1 Heat Transfer

The analysis of the heat exchanger where the geothermal brine transfers some of its thermal energy to the working fluid is another straightforward application of the principles of thermodynamics and mass conservation. Considering the entire package as the thermodynamic system, the governing equation is:

• Brine ORC (Stage a/u – c/w dan Stage 13a/13b – 14a/14b: heat transfer)

$$m_{brine} \,.\, (h_{13a/13b} - h_{14a/14b}) = m_{wf\ exp.1/exp.2} \,.\, (h_{a/u} - h_{c/w}) \quad (8)$$

$$m_{wf\ exp.1/exp.2} = m_{steam}.(h_{13a/13b} - h_{14a/14b})/(h_{a/u} - h_{c/w}) \quad (9)$$

2.2.2 Power Generation

With the usual assumptions of negligible potential and kinetic energy terms, along with steady, adiabatic operation, the power is determined from

• Brine ORC (Stage a/u – b/v: Isentropic)

The brine from BRSP-02 LP-Separator (13) will transfer heat to the working fluid, causing it to undergo a phase change into vapor with high thermal energy content. At this stage, an isentropic process occurs, and the applicable formula is as follows:

$$W_{t\ exp.1/exp.2} = m_{wf} \,.\, (h_{a/u} - h_{b/v}) = m_{wf} \,.\, \eta_t \,.\, (h_{a/u} - h_{b/v}) \quad (10)$$

2.3 Brine Reinjection System (BRS) Pump

The Brine Reinjection System (BRS) Pump, or BRSP, is a centrifugal pump used to pump hot brine from the HP or LP-Separator to the next system. BRSP consists of BRSP-01, which pumps hot brine from the HP-Separator to the LP-Separator, and BRSP-02, which pumps brine from the LP-Separator to the Brine ORC and the reinjection system.

2.3.1 Basic theory of Centrifugal Pump

An increase in the fluid pressure from the pump inlet to its outlet is created when the pump is in operation. This pressure difference drives the fluid through the system or plant. The centrifugal pump creates an increase in pressure by transferring mechanical energy from the motor to the fluid through the rotating impeller. The fluid flows from the inlet to the impeller center and out along its blades. The centrifugal force hereby increases the fluid velocity and also consequently transforming the kinetic energy in to pressure.

2.3.2 Thermodynamics Pump Theory

In the HP-Separator, there are centrifugal pumps named BRSP-01, which function to increase the pressure of brine from the HP-Separator to the LP-Separator. Besides that, centrifugal pump also use to increase pressure of the brine from LP-Separator to Brine ORC using BRSP-02.

2.3.3 Stage 3-6 (BRSP-01: Isentropic) and Stage 11-13 (BRSP-02: Isentropic)

The brine from the HP-Separator (3) enters the suction of the BRSP-01 and then pumped towards the LP-Separator. This Brine Pump functions to pump the hot brine towards the LP-Separator with a controlled pressure and flow rate according to the system's requirements. The enthalpy value of the brine entering the LP-Separator is the enthalpy value at stage 6 (discharge), which is the brine that has been pumped, not the enthalpy value at stage 3 (suction).

The brine from the LP-Separator (11) enters the suction of the BRSP-02 and then be pumped towards the Brine ORC. This Brine Pump's function is to pump the brine to the Brine ORC by increasing the pressure according to the working pressure inlet of the Brine ORC, ensuring that the brine remains saturated and will reducing the potential formation of silica in the Brine ORC, although not significantly. The enthalpy value of the brine entering the Brine ORC is the enthalpy value at stage 13, not the enthalpy value at stage 11.

The definition of pump efficiency is similar to that of a turbine, but the numerator is the isentropic work. Here is the formula to determine the enthalpy value at discharge of the BRSP (6 and 13):

$$h_{6/13} = h_{f3/11} + (h_{6s/13s} - h_{f3/11})/\eta_{BRSP-01/02} \quad (11)$$

The isentropic value of the Brine Pump (6s) can be determined using the following formula:

$$h_{6s/13s} = h_{f3/11} + v_{3/11}(P_{6s/13s} - P_{3/11})$$

Where v3/11 is the specific volume of the brine at the suction of the BRSP-01/02, which can be determined using the density value of the brine.

$$v_{3/11} = 1/\rho_{f3/11} \quad (12)$$

2.4 Scaling Potential in Brine Line

2.4.1 SSI Analysis

The essential parameter in terms of silica deposition is silica saturation index (SSI). SSI is the ratio between the concentration of silica in solution and the solubility of amorphous silica under the same conditions, or if formulated.

$$SSI = concentration\ of\ silica\ in\ solution\ /\ concentration\ solubility\ of\ amorphous\ silica \quad (13)$$

The SSI parameter can be used to estimate the probability of silica scaling as follows:

- If SSI > 1, the fluid is in a supersaturated condition, and silica deposition is possible.
- If SSI = 1, the fluid is in a saturated condition.
- If SSI < 1, the fluid is in an undersaturated condition, thus silica deposition is unlikely to occur

2.4.2 Pressure Saturation and Flashing Process

Geothermal fluids can exist either in liquid or vapor depending on the pressure and temperature conditions affecting them. The fluid remains in a liquid state only at a specific pressure, its temperature is below the boiling point or saturation temperature. The fluid exists in vapor at a specific pressure, its temperature exceeds the boiling point of water or saturation temperature.

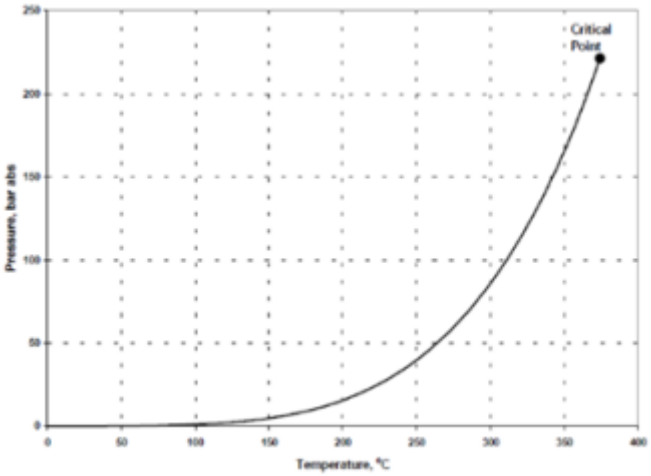

Figure 1: Relationship between Saturation Temperature and Pressure.

The curve in Figure 1 is called the saturation curve. Above the saturation curve, where the temperature is higher than the saturation temperature, only vapor phase exists within the system. In this state, the vapor is called superheated steam. Below the saturation curve, where the temperature is lower than the saturation temperature, only liquid phase exists within the system. In this state, the liquid phase is referred to as compressed liquid.

3. METHODOLOGY

3.1 Working Process

The working process implementation in this paper is as follows:

a. Creating Process Flow Diagram (PFD) and T-S Diagram
b. Data Collection:
   - Steam Field Data (Production Well Data, HP-Separator, BRSP-01, LP-Separator, and BRSP-02)
   - Power Plant Data (SE-07, Steam ORC (ORC-16), and Brine ORC (ORC-5))
   - TFT data (Steam Rate and Brine Rate)

c. Thermodynamics Analysis (Fluid Properties and Heat & Mass Balance)
   - Optimizing using BRSP-01 for LP-Separator and BRSP-02 for Brine ORC
   - Steam field Analysis
   - Power Generation Analysis (SE-07, Steam ORC (ORC-16), and Brine ORC (ORC-16))
   - Pressure saturation analysis
   - SSI Analysis

d. Result Discussion

3.2 Thermodynamics Properties

The geofluid from the Production Well is in the form of two-phase steam and brine, the Water Saturated thermodynamics properties are used. In determining thermodynamics properties for steam and brine, the author uses NIST Reference Fluid Thermodynamic and Transport Properties—REFPROP Version 9.1 The working fluid used in Steam ORC and Brine ORC is Refrigerant R245fa, and the thermodynamic properties of R245fa are determined using data from NIST Reference Fluid Thermodynamic and Transport Properties—REFPROP Version 9.1 The air humidity use in Evaporative Cooling Condenser (ECC) Analysis especially Air Cooler, and the thermodynamic properties of Air Humidity are determined using data CoolProp-Version 6.4.1.0.

4. DATA

4.1 Process Flow Diagram (PFD)

4.1.1 Process Flow Diagram of Double Flash

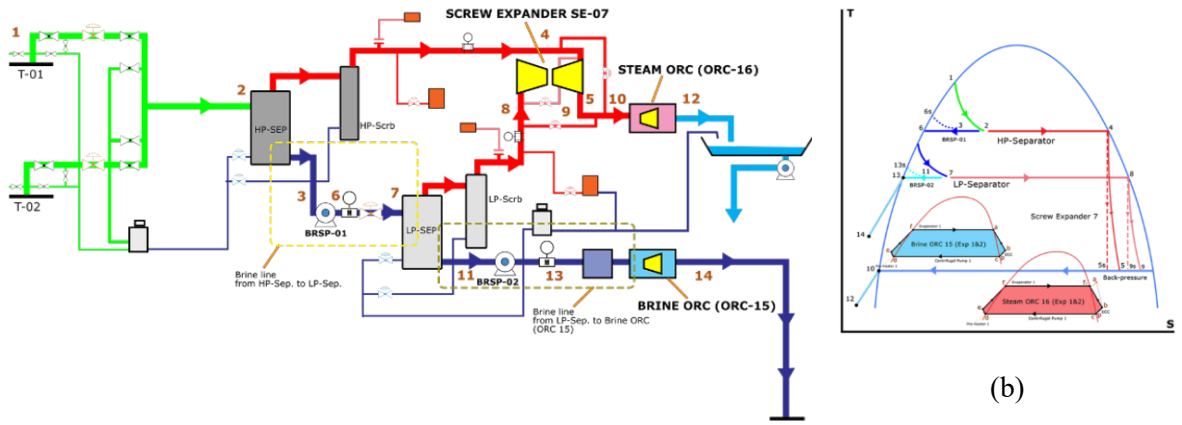

(a) (b)

Figure 2: Combined Double Flash and Binary (Steam ORC and Brine ORC): Process Flow Diagram (a) T-S Diagram (b).

(a) (b)

Figure 3: Steam Expander (SE-07) (a) Steam ORC (ORC-16) (b).

Figure 2 illustrates this process starting from the Production Well (1) such as T-01 and T-02, where two-phase geofluid flows to the HP-Separator (2) for steam-brine separation. The steam separated from the HP-Separator and HP-Scrubber (2) will flow to the HP Steam Expander-generator (4) to generate electricity and the brine from the HP-Separator (3) will enter the suction of the BRSP-01 and then pumped towards the LP-Separator (7) for double flash process to extract additional steam from the hot brine that can still be flashed because it still contains a steam fraction (x7). The steam separated from the LP-Separator and LP-Scrubber flows to the LP-Steam Expander to generate electricity again and the brine from the LP-Separator (11) will enter the suction of the BRSP-02 and then pumped towards the Brine ORC (13).

4.1.2 Process Flow Diagram of Brine ORC

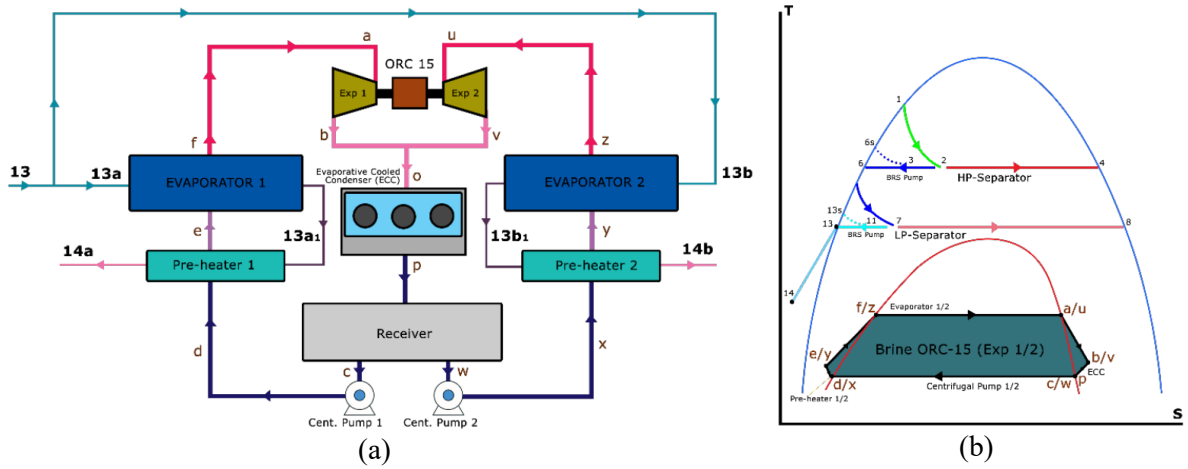

(a) (b)

Figure 4: Brine ORC: PFD (a), T-S Diagram (b).

Figure 5: Brine ORC (ORC-15).

Figure 4 illustrates the process where brine discharged from BRSP-02 at the LP-Separator is pumped with a pressure around 17 barg towards the Brine ORC. This brine retains a high temperature value around 145°C and a high enthalpy value (hf), indicating its potential for heat transfer with the working fluid to generate electricity again. There are three main processes: the Brine in ORC-15 process, which is the hot brine pumped by BRSP-02. The second part is the Binary loop Exp-1, which is the binary system for Exp-1 consisting of states a-f, and the third part is the Binary loop Exp-2, which is the binary system for Exp-2 consisting of states u-z. And finally the process will continuesly and make a thermal cycle. For condensing vapor R245fa in ORC-15 using Evaporative Cooled Condenser (ECC) especially Air Cooler.

4.1.3 Process Flow Diagram of BRSP

In Figure 6, it shows a simple process flow diagram of the Brine Reinjection System (BRS) Pump (BRSP) in the 15 MW Combined Double Flash and Binary (Brine ORC) system. Here, the hot brine separated from the HP-Separator flows towards the suction of BRSP-01 (Stage 3), which then pumps it towards the LP-Separator (Stages 6-7) with a specified discharge pressure and flow rate. BRSP-01 functions to pump the hot brine towards the LP-

Separator while controlling the pressure and flow rate using a Variable Frequency Drive (VFD) to adjust the pump frequency and discharge control valve. Before entering the LP-Separator, the inlet pressure to the LP-Separator is controlled by a control valve (CV) to lower the pressure, thereby initiating the second flashing process in the LP-Separator. Subsequently, the brine separated from the LP-Separator flows to the suction of BRSP-02, which then pumps it towards the Brine ORC (ORC-15) (Stages 11-13) and further into the reinjection system. Thus, from the diagram above, there are three types of brine lines: the brine line from the HP-Separator to the LP-Separator, the brine line from the LP-Separator to Brine ORC-15, and the brine line from the Outlet ORC-15 to the reinjection system. BRSP-02 functions to pump the brine to ORC-15 by increasing the

pressure according to the inlet working pressure of ORC-15, ensuring the brine remains in a saturated condition and minimizes the potential formation of silica in the Brine ORC, albeit not significantly. BRSP-02 is essential for increasing the pressure in the line, as the Brine ORC (ORC-15) reduces pressure due to the heat transfer process between the brine and the refrigerant in the heat exchanger (preheater and evaporator). Therefore, BRSP will maintain the pressure in the reinjection system above the saturation pressure.

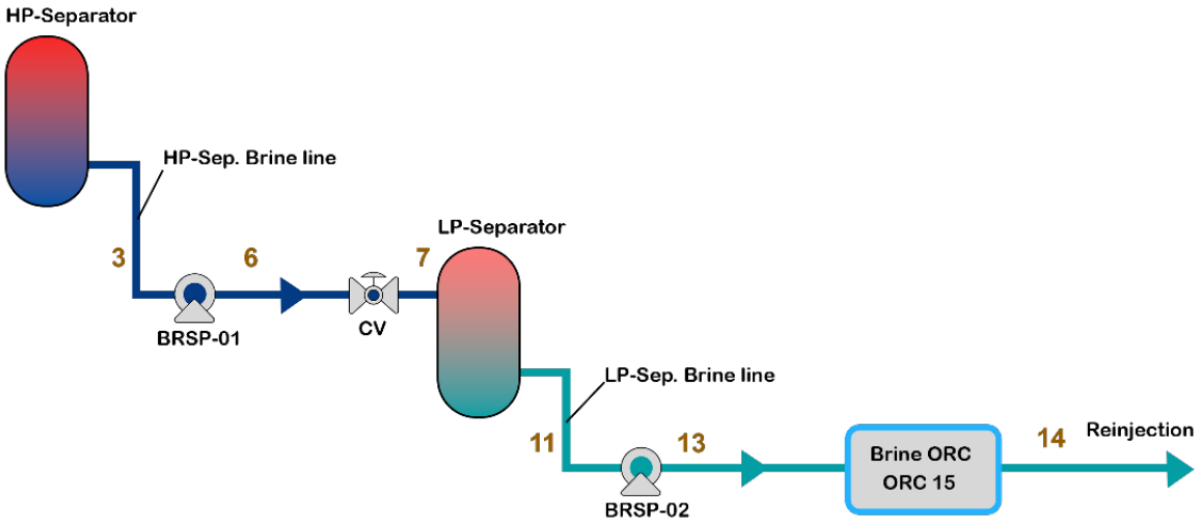

Figure 6: PFD BRSP-01 dan BRSP-02.

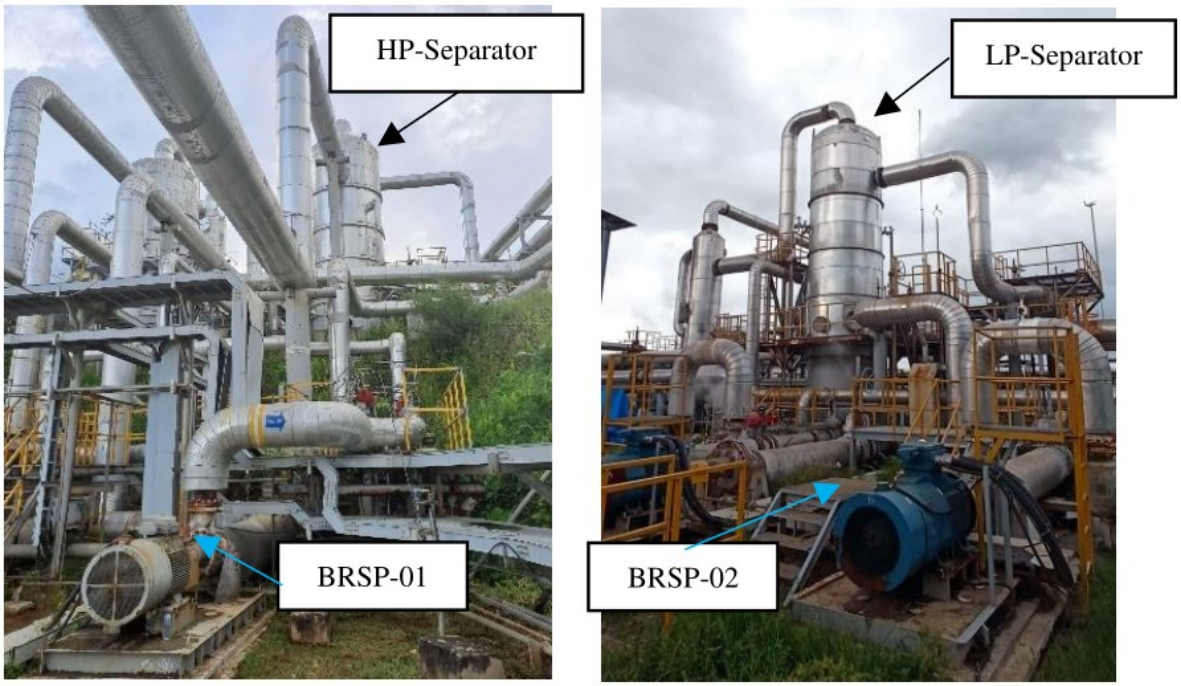

Figure 7: HP-Separator and BRSP-01 (a); LP-Separator and BRSP-02 (b).

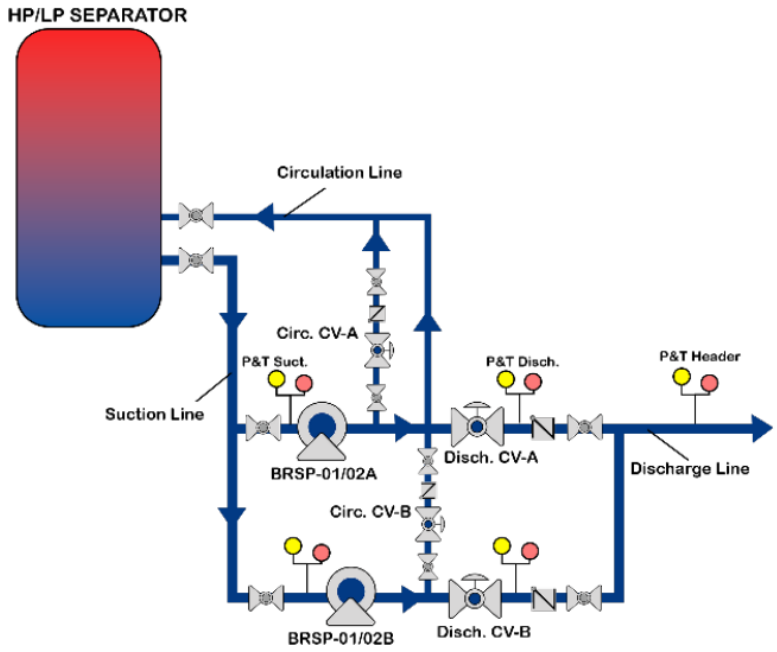

Figure 8: Configuration of the Brine Reinjection System (BRS) Pump (BRSP).

In Figure 8, it illustrates the configuration of the Brine Reinjection System (BRS) Pump equipment. BRSP of The HP and LP-Separators operate in parallel, requiring two BRSP pumps to ensure redundancy: while one BRSP (a) is running, the other BRSP (b) remains on standby. Additionally, in cases where the Brine ORC requires a higher brine consumption and the Brine Reinjection System Pump (BRSP) is operating with insufficient brine flow, a second BRSP will be activated alongside the first to increase the brine rate, thereby meeting the higher brine consumption demands of the Brine ORC. This setup allows for seamless backup in case of issues with one BRSP, facilitating maintenance without disrupting the system. Additionally, there are three main lines in the BRSP: the suction line, discharge line, and circulation line. The suction line transports brine from the HP/LP-Separator to the suction of BRSP-01/BRSP-02. The discharge line serves as the brine discharge line from the BRSP, pumping brine to either the LP-Separator or Brine ORC system. The circulation line pumps brine back to the HP/LP Separator under certain process conditions, such as during separator level decreases or during BRSP changeovers. To control brine flow within the BRSP system, control valves (CVs) are employed, namely the Discharge CV and Circulation CV. These CVs facilitate easy changeover of BRSP operations by operators. Moreover, to prevent backflow during BRSP changeovers, check valves are installed in the discharge and circulation lines. For monitoring operational parameters, Pressure and Temperature transmitters are integrated into the BRSP system.

4.2 Operation Data

The data processed for calculations in this paper is the actual operational data based on Fluid Collection and Reinjection (FCRS) data in August 2022. The FCRS data are shown in Table 1, 2, and 3. The specification and operation data of BRSP are shown in Table 4, 5, and 6.

5. RESULT

5.1 Heat and Mass Balance of LP Separator, Brine ORC and BRSP

Table 7 shows the Heat and Mass balance and SSI analysis of the brine line system from HP-Separator to LP-Separator, brine line from LP-Separator to ORC-15, and brine line from Outlet ORC-15 to the reinjection system.

Table 7 shows that stage 6 represents brine entering the LP-Separator using BRSP-01 with a discharge pressure of 9.94 bar, a temperature of 162.76 ℃, and a brine rate of 112.83 kg/s. The brine enthalpy entering the LP-Separator is 687.65 kJ/kg (stage 6). By comparing stage 6 with stage 3 as the suction of BRSP-01, it can be seen that the enthalpy value of stage 6 is higher than stage 3 (687.22 kJ/kg). This is due to the increased discharge pressure of BRSP-01. For the brine line from the LP-Separator to ORC-15, there is also a difference between stage 11 and stage 13. At stage 11, as the brine suction of BRSP-02, the discharge pressure is 4.79 bar, the temperature is 146.30 ℃ with 616.23 kJ/kg brine enthalpy value. At stage 13, as the brine discharge of BRSP-02, the discharge pressure is 18.32 bar, the temperature is 146.58 ℃, and the brine rate is 109.32 kg/s. The brine rate of the LP-Separator is lower compared to the HP-Separator because part of the steam content from the HP-Separator brine rate has been separated, thus reducing the brine rate flowing to ORC-15. The enthalpy value entering ORC-15 as

the heat source for heat transfer is 618.33 kJ/kg (stage 13). This enthalpy is used by ORC-15 to heat the working fluid, which is the R245fa refrigerant. Meanwhile, the temperature of the brine line, after its heat has been utilized by ORC-15, will drop to 72.39 ℃ with a pressure of 8.80 bar and a brine enthalpy of 303.10 kJ/kg.

Table 1: Assumption Data.

Unit	
Eff. Steam Expander	82%
Eff. BRSP	70%
Eff. Wf Expander (Brine ORC)	75%
Eff. Cent. Pump (Brine ORC)	70%
Eff. Fan ECC (Brine ORC)	70%

Table 2: Operation Data of Double Flash.

Op. Param.	HP-Separator	LP-Separator
P inlet, barg	6.20	7.94
T inlet, °C	164.70	161.70
P out, barg	5.20	3.25
T out, °C	162.10	145.50

Table 3: Operation Data of Brine ORC.

OP. Parameter	Brine ORC (ORC 15)	
Eta Exp	75%	
Eta Cfg Pump	70%	
Eta Fan Ecc	70%	
HEAT SOURCE (BRINE FROM LP-SEPARATOR)		
	EXP-01	***EXP-02***
T in_Brine, °C	146.58	146.58
P in_Brine, Mpa	1.60	1.50
T out_Brine, °C	111.00	76.00
P out_Brine, Mpa	0.88	0.88
m total_brine, kg/s	***109.32***	
m_brine, kg/s	84.73	24.60
WORKING FLUID (R245fa)		
T_eva, °c	82.00	84.00
T_cond, °C	48.00	49.00
Superheater, °C	5.00	5.00
subcooling, °C	15.00	15.00
Pinch point ain all HX, °C	13.00	13.00

Table 4: Specification Data of BRSP.

Specifications:	BRSP-01	BRSP-02
Motor		
Power, kw	1.1	250
Voltage, v	380	380
Current, A	2.6	465
Speed, r/min	1400	1490
Freq, hz	50	50
Pump		
Q, m3/h	490	418
H, m	52	135
n, r/min	1480	1450
MAWT, degC	200	168
MAWP, Mpa	4	3

Table 5: Operation Data of BRSP-01 HP-Separator to LP-Separator.

Time	Freq., Hz	P. Disch., Barg	Temp., °C	Flow Rate, Ton/hr
3:00 AM	33.6	9.46	166.7	89.4
9:00 AM	33.5	9.46	166.7	89.4
3:00 PM	31.7	9.21	166.6	305.7
9:00 PM	33.9	9.45	166.7	226.7

Table 6: Operation Data of BRSP-02 LP-Separator to Brine ORC (ORC-15).

Time	Freq., Hz	P. Disch., Barg	Temp., °C	Flow Rate, Ton/hr
3:00 AM	48.1	16.56	148.1	351.1
9:00 AM	48.2	16.56	148.1	351.1
3:00 PM	47.9	16.34	147.7	351.6
9:00 PM	48.0	16.57	148.1	347.6

5.2 Optimizing Using Brine Reinjection System (BRS) Pumpa (BRSP)

5.2.1 Optimizing BRSP-01

The optimization of BRSP-01 involves optimizing the discharge pressure of BRSP-01 at the HP-Separator so that the inlet pressure before the CV LP-Separator operates around 9-10 barg. With such discharge pressure and CV LP inlet pressure, the brine enthalpy value at the inlet of the LP-Separator will increase due to the increased discharge pressure. Therefore, based on thermodynamic calculations, BRSP-01 can enhance the steam fraction in the LP-Separator.

a. Optimization of LP-Separator

Figure 9 shows that by optimally operating the discharge pressure of BRSP-01 for the inlet pressure before the CV LP-Separator with a recommended pressure of 9.94 bar, the steam fraction will increase from 3.08753% (with a BRSP-01 suction pressure of 7.19 bar) to 3.10800%, or an increase of 0.66299%. The increase in steam fraction means that the steam rate produced by the LP-Separator ill increase from 3.4836 kg/s (12.5412 t/h) to 3.5067 kg/s

(12.6243 t/h), or an increase of 0.0831 t/h. The results of this optimization calculation are very feasible to apply, as the current operating system still has potential for further optimization, considering that the BRSP-01 specification can operate at a pressure of 4 MPa (40 bar) and the working pressure of the LP-Separator is 1.1 MPa (11 bar). Although the output of the LP-Separator does not increase significantly, with this discharge pressure, the BRSP-01 and LP-Separator can operate optimally according to equipment specifications. This increase in steam rate will cause the brine rate of the LP-Separator to decrease from 100.2889 kg/s (361.0397 t/h) to 100.2058 kg/s (360.7405 t/h). This is because, with a higher discharge pressure, the steam flashing from the brine will increase, resulting in a lower brine rate entering ORC-15 compared to the brine rate of the HP-Separator.

Table 7: Heat & Mass Balance and SSI Analysis of Brine Line BRSP-01 and BRSP-02.

Stage no.	Unit	3	6	11	13	14
Descriptions		*Brine phase form HP-Sep. to Suction BRSP-01*	*Brine phase discharge BRSP-01 to LP-Sep.*	*Brine phase form LP-Sep. to Suction BRSP-02*	*Brine phase discharge BRSP-02 to Brine ORC*	*Brine phase outlet Brine ORC to reinjection system*
Geofluid Type		*Single Phase Brine*	*Single Phase Brine*	*Single Phase Brine*	*Single Phase Brine*	*Single Phase Brine*
Steam Fraction		0.00%	0.00%	0.00%	0.00%	0.00%
Temperature	°C	162.10	162.76	146.30	146.58	72.39
Temperature Saturation	°C	166.04	179.62	150.23	207.99	174.41
Pressure	bar a	7.19	9.94	4.79	18.32	8.80
Pressure Saturation	bar a	6.52	6.63	4.31	4.34	0.35
Mass Flow	kg/s	112.83	112.83	109.32	109.32	109.32
Enthalpy	kJ/kg	687.22	687.65	616.23	618.33	303.10
Entrophy	kJ/kg.K	1.97	1.97	1.80	1.81	0.98
Density	kg/m3	904.83	904.83	920.46	920.46	976.73
Silica Concentration	ppm	781.85	781.85	806.93	806.93	806.93
SSI		1.1243	1.1238	1.3496	1.3460	3.1862

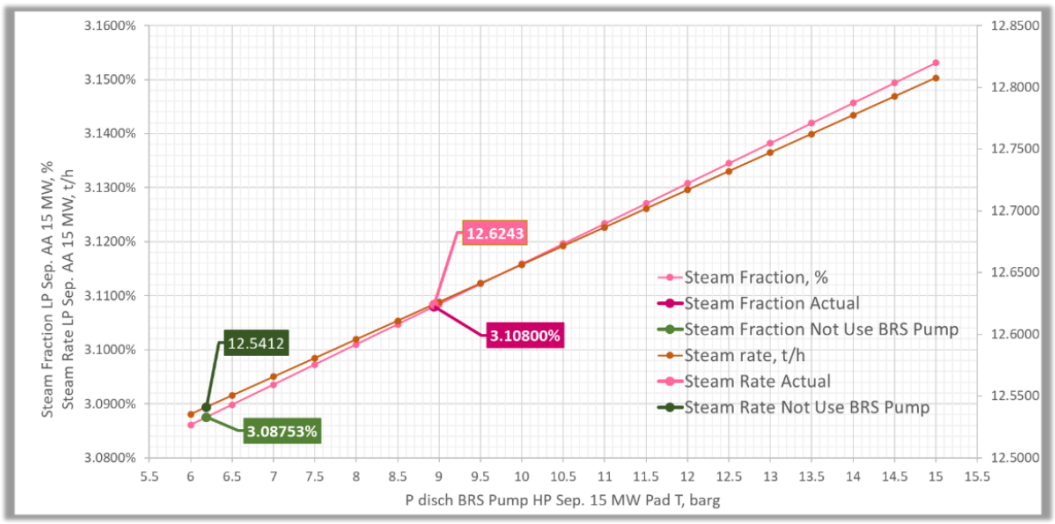

Figure 9: Optimizing BRSP-01: Steam Fraction and Steam Rate Analysis of LP-Separator.

b. Optimization of Power Generation

With the increase in steam fraction from the LP-Separator, the power generation from Steam Expander-07, Steam ORC (ORC-16), and Brine ORC (ORC-15) will change. This can be seen from the graph results in Figure 10. SE-7 will increase from 5427.6233 kW to 5430.9453 kW (an increase of 0.0612% or 3.3320 kW), resulting in an increase in Thermal Efficiency from 4.21485% to 4.21743% and Utilization Efficiency from 14.61649% to 14.62544%. Meanwhile, the power generation of ORC-15 will decrease from 1410.0154 kW to 1409.7176 Kw (a decrease of 0.0211% or 0.2987 kW), resulting in a Thermal Efficiency of Brine ORC of 4.1016% and a Utilization Efficiency of 15.2697%. As for the power generation of ORC-16, it will increase from 4621.6787 kW to 4625.5815 kW (an increase of 0.0844% or 3.9028 kW), resulting in a Thermal Efficiency of Steam ORC of

5.4199% and a Utilization Efficiency of 71.0551%. From the results, an increase in steam fraction will lead to higher power generation in both the Steam Expander (SE-07) and the Steam ORC (ORC-16) due to the increased steam supply rate. However, this increase in steam rate will result in a decrease in the brine rate, thereby reducing the brine supply to the Brine ORC (ORC-15) and consequently lowering its power generation. The changes in power generation will directly affect the thermal efficiency and utilization efficiency. As power generation increases, both thermal efficiency and utilization efficiency will rise, and vice versa.

c. Pressure Saturation Analysis of Brine Line

With optimal discharge pressure, the brine will become more saturated and can reduce the flashing process along the brine line due to pressure loss along the pipe. This can decrease the silica concentration and the SSI value.

The saturation pressure of the brine line from the HP-Separator to the LP-Separator is 6.63 bar with a brine line temperature of 162.76 ℃, and the operating pressure of BRSP-01 is 9.94 bar. Based on the graph in Figure 11, the operating pressure of BRSP-01 will operate at a pressure above the saturation pressure, thus keeping the brine in a saturated condition. However, if the operating pressure of the brine line falls below the saturation pressure, flashing will occur in the brine, making it more concentrated due to the steam flashing out from the brine. This will cause the silica concentration and SSI to increase, especially since the brine line will experience pressure loss along the line. Therefore, the brine line pressure must be maintained above the saturation pressure using BRSP-01. If the brine line pressure suddenly drops below the saturation pressure, hammering will occur. This happens due to the sudden flashing of the brine. The subsequent hammering effect is very dangerous as it can damage the brine line facilities.

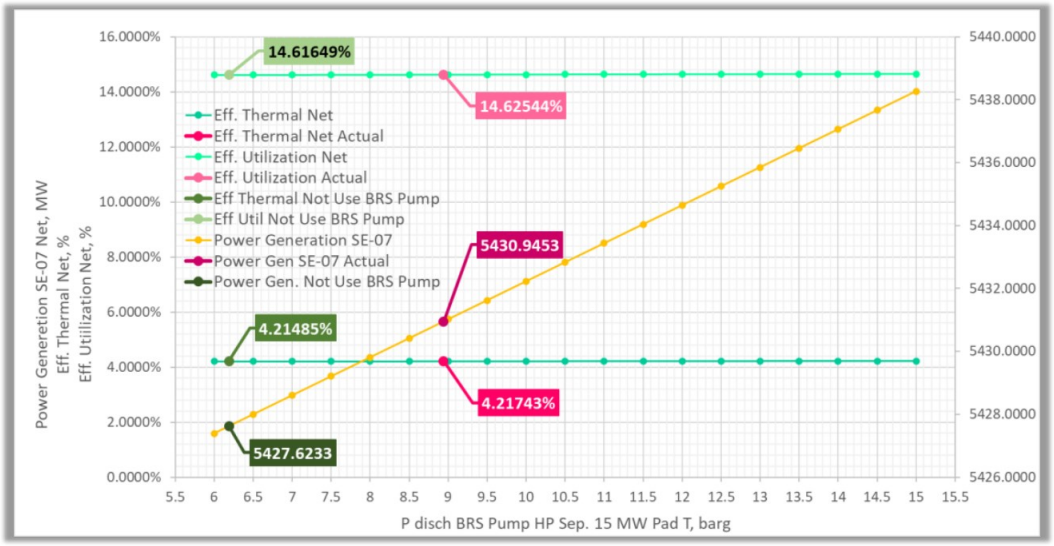

(a)

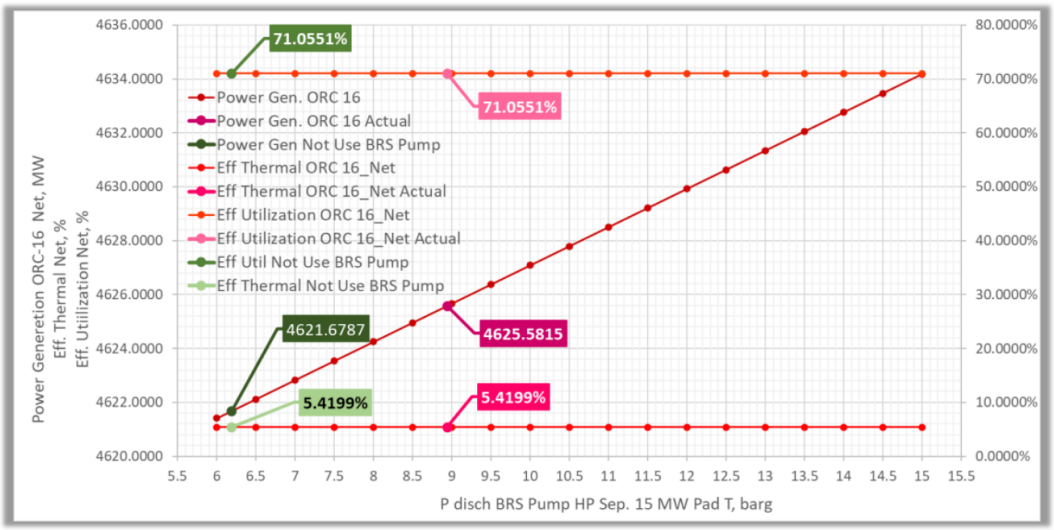

(b)

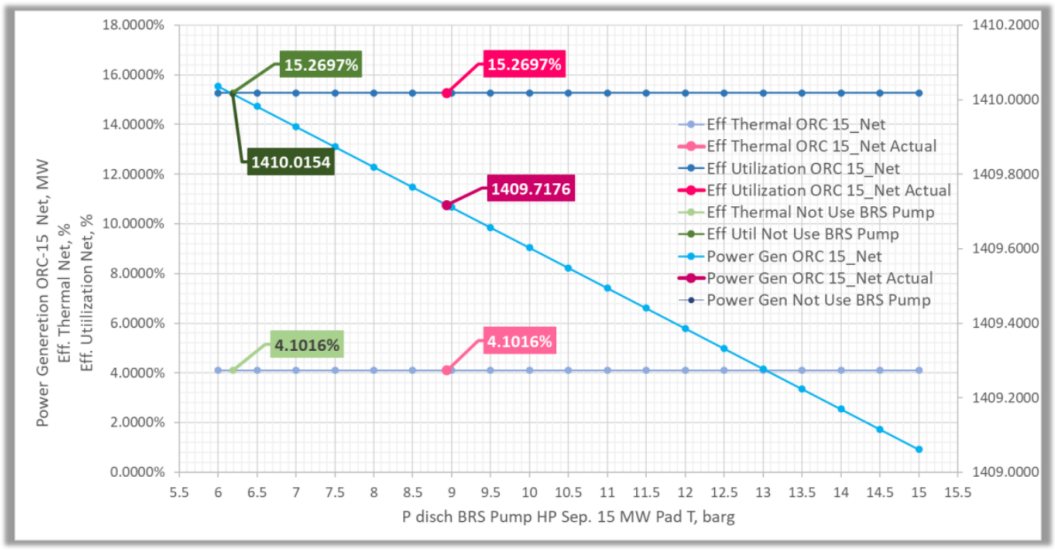

(c)

Figure 10: Optimizing BRSP-01: Power Generation SE-07 (a), ORC-16 (b) and ORC-15 (c).

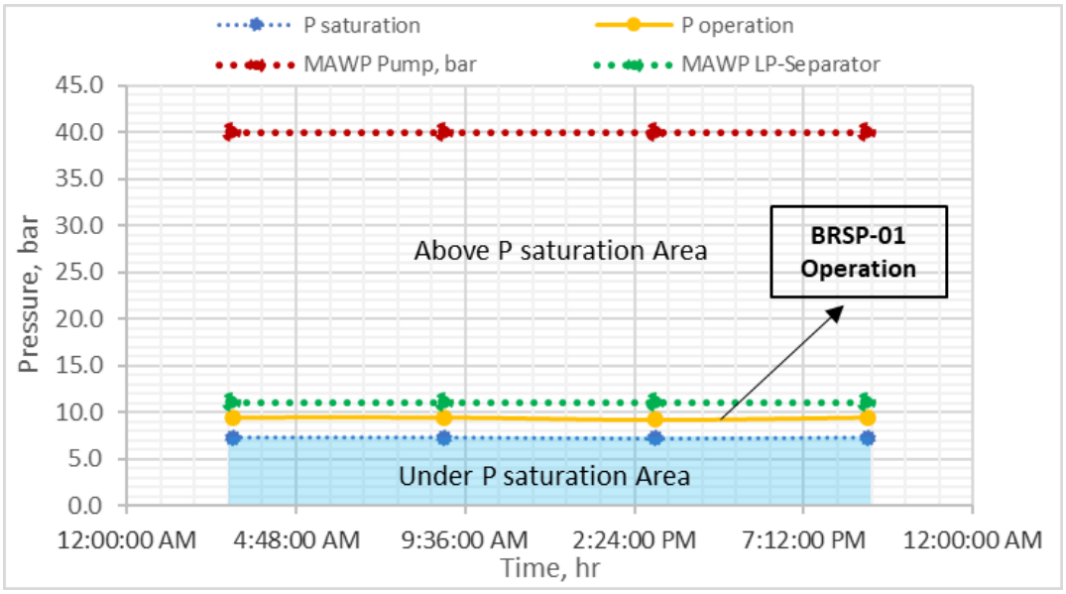

Figure 11: Optimizing BRSP-01: Pressure Saturation Analysis.

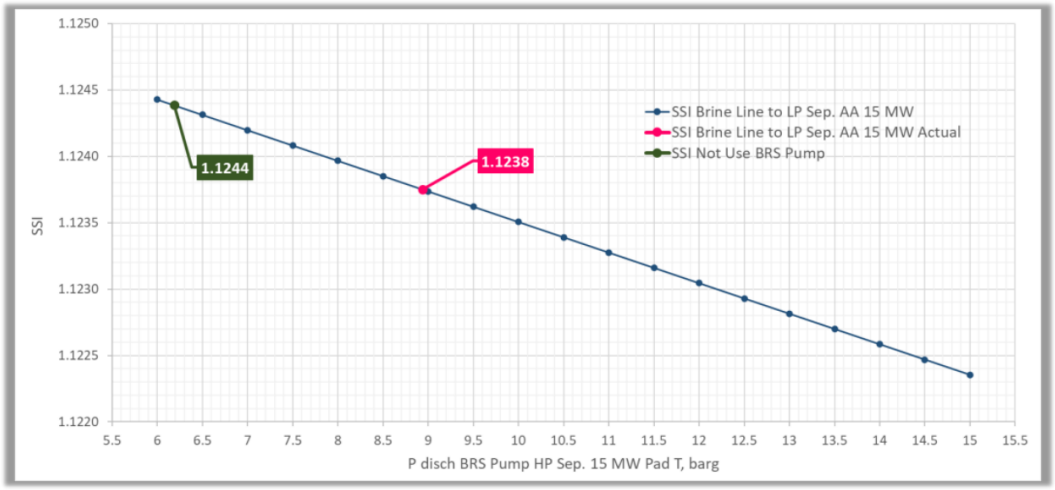

Figure 12: SSI Analysis of Brine Line from HP-Separator to LP-Separator.

d. SSI Analysis

The SSI analysis of the brine line from the HP-Separator to the LP-Separator is shown in Figure 12. In Figure 12, it is shown that with a discharge pressure of BRSP-01 of 8.94 barg, the SSI value decreases from 1.1244 without BRSP-01 (with a BRSP-01 suction pressure of 6.19 barg) to 1.1238, a decrease of 0.0006 (0.0534% decrease). This decrease in SSI is due to the increased discharge pressure, which leads to an increase in brine enthalpy. With the increase in brine enthalpy, the temperature rises from 162.10 ℃ to 162.76 ℃. Additionally, one of the factors influencing silica concentration is temperature; higher temperatures result in higher silica concentration calculations (Amorphous Silica Index). Thus, compared to the silica concentration sample (Silica Solution), the SSI value decreases. Conversely, if the brine line temperature decreases, the SSI value increases, and the potential for scaling also increases. Despite the optimization of BRSP-01 resulting in a slight decrease in the SSI value, it can still significantly reduce the potential for scaling along the brine line, considering the pressure loss from the HP-Separator to the LP-Separator. With BRSP-01, the SSI value in the brine line remains stable (does not increase) due to reduced pressure loss, thereby reducing the potential for scaling in the brine line.

5.2.2 Optimizing BRSP-02

BRSP-02 Optimization involves optimizing the discharge pressure of BRSP-02 at the LP-Separator so that the inlet pressure of Brine ORC (ORC-15) can operate around 17-19 barg. With this discharge pressure and ORC-15 inlet pressure, it will increase the brine enthalpy value at the inlet of ORC-15 as a heat source due to the increased inlet pressure. This, in thermodynamic and heat transfer calculations, can enhance the power generation of ORC-15.

a. Optimization of Power Generation

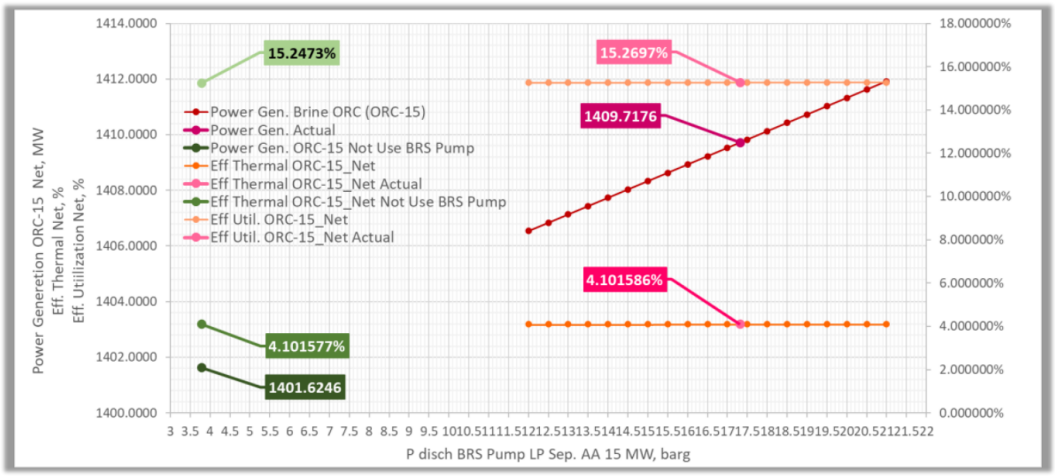

Figure 13: Optimizing BRSP-02: Power Generation ORC-15.

With the optimization of BRSP-02, the power generation of ORC-15 will increase by approximately 0.5574%, from 1401.6246 kW to 1409.7176 kW (Figure 13), an increase of 8.0930 kW. This results in the Thermal Efficiency of Brine ORC increasing from 4.101577% to 4.101586% and the Utilization Efficiency increasing from 15.2473% to 15.2697%. With BRSP-02 optimization, it is possible to maintain stable power generation of ORC-15 despite a decrease in brine rate due to the increased steam fraction from the LP-Separator after the previous optimization of BRSP-01. This optimization calculation shows promising application potential because BRSP-02 is not yet operating optimally, given its MAWP of 3 MPa (30 bar) and the working pressure inlet of ORC-15 at 2 MPa (20 bar). These specifications indicate that there is still room to optimize the processes of BRSP-02 and ORC-15 according to their respective working pressures.

b. Pressure Saturation Analysis of Brine Line

The saturation pressure of the brine line from the HP-Separator to the LP-Separator is 4.34 bar with a line temperature of 146.58 ℃, while the operating pressure using BRSP-02 is 18.32 bar. With this operating pressure, according to Figure 14, the pressure is above the saturation pressure, meaning the brine is in a saturated condition, thereby preventing flashing of the brine before it enters ORC-15. If flashing occurs in the brine before entering ORC-15, the brine will become more concentrated due to the steam released from the brine, leading to an increase in silica concentration and SSI values. Additionally, the heat transfer processes in the preheater and evaporator of ORC-15 will reduce the pressure and temperature of the brine line, further increasing silica concentration and SSI values after exiting ORC-15. Therefore, to minimize scaling formation in the preheater and evaporator, the inlet pressure of ORC-15 must be maintained above the saturation pressure so that silica concentration does not increase

before entering ORC-15. Meanwhile, the saturation pressure of the brine line from the outlet of ORC-15 to the reinjection system is 0.35 bar with a line temperature of 72.39 ℃, and the operating pressure is 8.8 bar. With this operating pressure, the pressure is above the saturation pressure, ensuring the brine remains in a saturated condition.

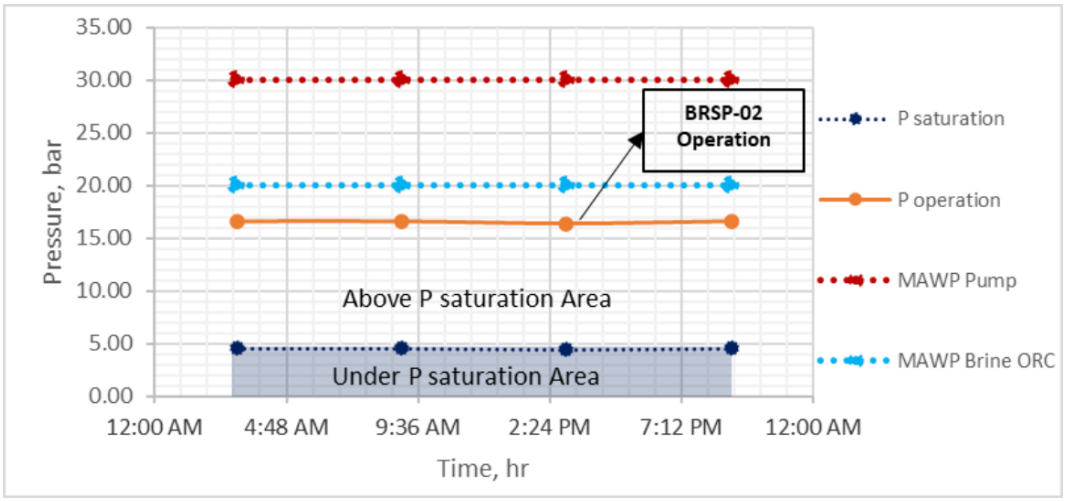

Figure 14: Optimizing BRSP-02: Pressure Saturation Analysis.

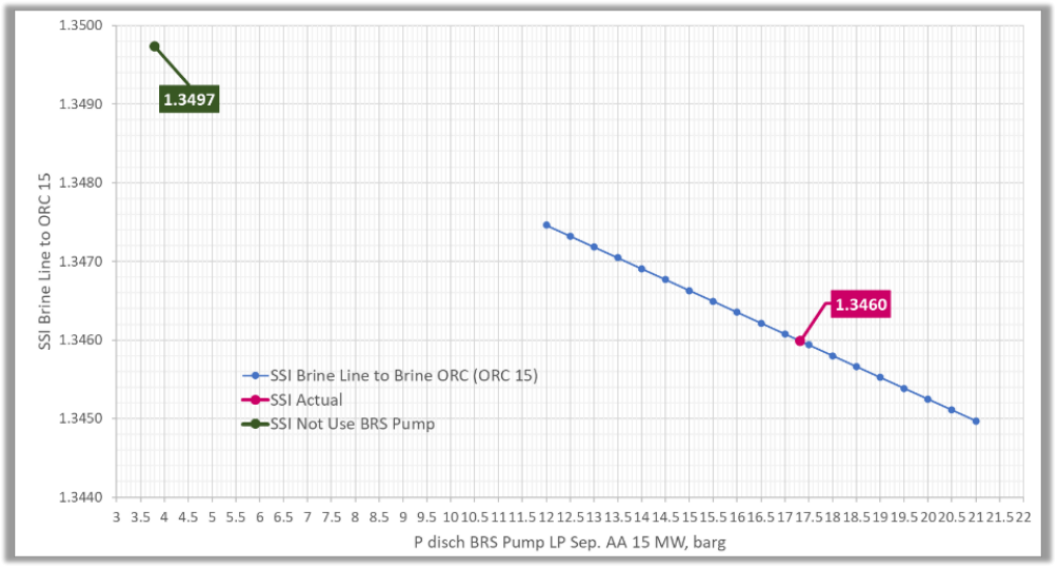

Figure 15: SSI Analysis of Brine Line from LP-Separator to Brine ORC (ORC-15).

c. SSI Analysis

The SSI value on the brine line from the LP-Separator to ORC-15 is 1.3497, which is higher compared to the SSI value on the brine line from the HP-Separator to the LP-Separator, which is 1.124. This is because the brine rate from the LP-Separator is lower compared to the brine rate from the HP-Separator due to the steam being flashed back by the LP-Separator. Additionally, the temperature of the brine line with BRSP-02 is lower compared to the temperature with BRSP-01, at 146.58 ℃ compared to 162.10 ℃ (BRSP-01). This lower brine rate and temperature will cause the brine to become more concentrated, leading to a higher silica concentration and consequently increasing the SSI value compared to BRSP-01.

With BRSP-02 optimization, it can maintain the SSI value of the brine line stable and prevent it from increasing. In Figure 15, it shows that with a BRSP-02 discharge pressure of 17.32 barg, it will reduce the SSI value from 1.3497 with the brine line pressure without BRSP-02 (BRSP-02 suction pressure) of 3.79 barg to 1.3460, or a decrease of about 0.0037 (a decrease of 0.2749%). The temperature rises from 146.30 ℃ to 146.58 ℃. Although this reduction in SSI value is not very significant, it can still reduce the potential for scaling formation both in the brine line at the ORC-15 inlet and in the loop heat exchanger pipes (pre-heater and evaporator). Once the brine has absorbed its heat, the pressure and temperature of the ORC-15 outlet towards the brine line reinjection system

will decrease to 8.80 barg and 72.39 ℃. With this decrease in temperature, the SSI value will increase compared to the ORC-15 brine line. Therefore, BRSP-02 plays a crucial role in maintaining the brine line pressure above saturation pressure to prevent an increase in SSI values in the brine line reinjection system.

5. DISCUSSION

Optimizing the Brine Reinjection System (BRS) Pump (BRSP) can enhance the total power generation generated by the 15 MW Combined Double Flash and Binary System. Additionally, maintaining the brine line pressure above saturation pressure can minimize the potential for scaling formation. BRSP-01 is a pump designed to transfer brine from the HP-Separator to the LP-Separator at a specific discharge pressure. Optimizing BRSP-01 will impact the total power generation of the combined SE-07 power generation, Steam ORC (ORC-16), and Brine ORC (ORC-15).

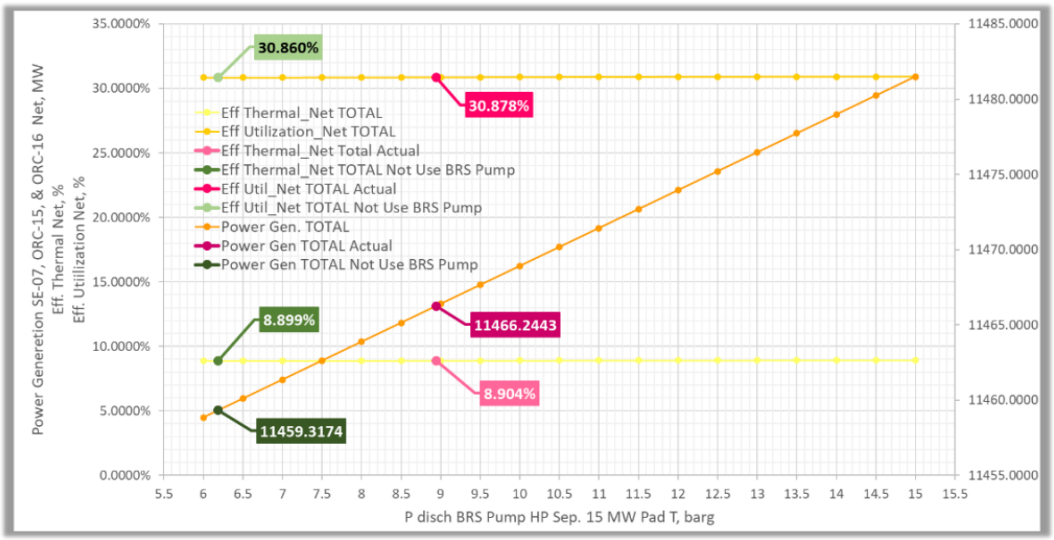

Figure 16: Optimizing BRSP-01: Total Power Generation of SE-07, ORC-15, and ORC-16.

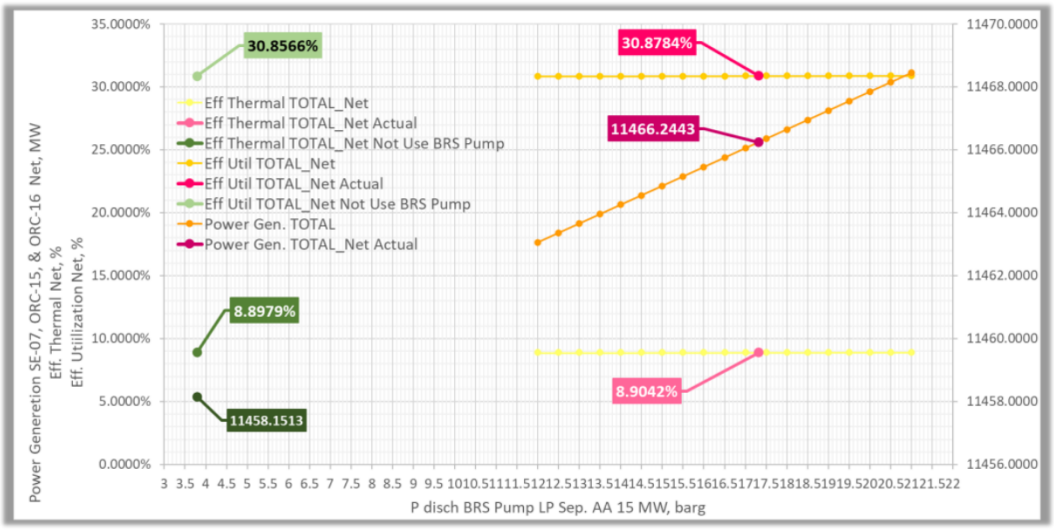

Figure 17: Optimizing BRSP-02: Total Power Generation of SE-07, ORC-15, and ORC-16.

Based on Figure 16, the differences in total power generation, thermal efficiency, and utilization efficiency can be observed between operation pressures without BRSP-01 and with BRSP-01. Using BRSP-01 at an operation pressure of 8.94 barg results in a total power generation of 11466.2443 kW. This value is higher compared to operating without BRSP-01, which yields 11459.3174 kW. The increase in total power generation with BRSP-01 compared to without BRSP-01 is 0.0604% or approximately 6.9269 kW. With the increase in total power generation, the total thermal efficiency will also rise from 8.899% to 8.904%. Similarly, the total utilization efficiency will increase from 30.860% to 30.878%. Although the increase in total power generation with a discharge pressure of 8.94 barg is not significant, the discharge pressure can still be increased since the maximum

working pressure before the CV LP-Separator is 11 barg, indicating further optimization potential with a higher discharge pressure from BRSP-01 to achieve greater total power generation.

In addition to optimize BRSP-01, this system also needs to be optimized with BRSP-02. Because as the steam fraction from the LP-Separator increases, the brine rate from BRSP-02 will decrease. Based on Figure 17. Above, the differences in total power generation, thermal efficiency, and utilization efficiency can be observed between operation pressures without BRSP-02 and with BRSP-02. Using BRSP-02 at an operation pressure of 17.32 barg results in a total power generation of 11466.2443 kW. This value is higher compared to operating without BRSP-02, which yields 11458.1513 kW, an increase of approximately 8.0930 kW. The increase in total power generation with BRSP-02 compared to without BRSP-02 is 0.0703%. With the increase in total power generation, the total thermal efficiency will also rise from 8.8979% to 8.904%. Similarly, the utilization efficiency will increase from 30.8566% to 30.8784%. Although the increase in total power generation is not significantly with a discharge pressure of 8.94 barg, the discharge pressure can still be increased since the maximum working pressure inlet Brine ORC (ORC-15) is 20 barg.

In addition to influence total power generation, the optimization of BRSP-01 and BRSP-02 can also minimize scaling potential in the brine line from HP-Separator to LP-Separator, from LP-Separator to Brine ORC (ORC-15), and from the outlet of ORC-15 to the reinjection system.

Figure 18 shows the SSI values for each brine line in this system. The SSI value for the brine line from HP-Separator to LP-Separator using BRSP-01 is 1.1238 with a temperature of 162.76 ℃. This value is lower compared to not using BRSP-01, which is 1.1243 with a temperature of 162.70 ℃. Next, the SSI value for the brine line from LP-Separator to ORC-15 using BRSP-02 is 1.3460 with a temperature of 146.58 ℃. This value is lower compared to not using BRSP-02, which is 1.3496 with a temperature of 146.30 ℃. Meanwhile, the SSI value for the brine line from the outlet of ORC-15 to the reinjection system is 3.1862 with a temperature of 72.39 ℃. With SSI values above 1 for each brine line, scaling potential remains present. Optimizing BRSP is not significantly the primary method to prevent scaling formation, but BRSP functions to maintain the brine line in a saturated condition so that scaling potential does not increase due to pressure and temperature drops along the brine line. To effectively prevent scaling in the brine line, the optimal method currently is to maintain the brine line temperature above 180 ℃. At this temperature, the SSI value would be < 1 or within the no scaling potential area. However, because the 15 MW system uses a Combined Double Flash and Binary conversion system where the heat from brine is maximally utilized for electricity generation, it causes the brine line temperature to remain low (<100 ℃). The lower the Brine ORC outlet temperature, the greater the power generation obtained. This means that more heat from the brine is transferred to the working fluid, which will increase the SSI value to greater than 1, and the potential for scaling formation becomes higher. With this conversion system, increasing the brine line temperature by more than 100 ℃ is challenging. If the outlet temperature of Brine ORC increases, it indicates suboptimal heat transfer, resulting in decreased power generation of Brine ORC and potential issues such as scaling in the loop pipe heat exchangers (pre-heater and evaporator). Therefore, the most effective current method to prevent scaling in the brine line is to use additional chemical treatment such as scale inhibitors injected into the brine line before entering LP-Separator and Brine ORC.

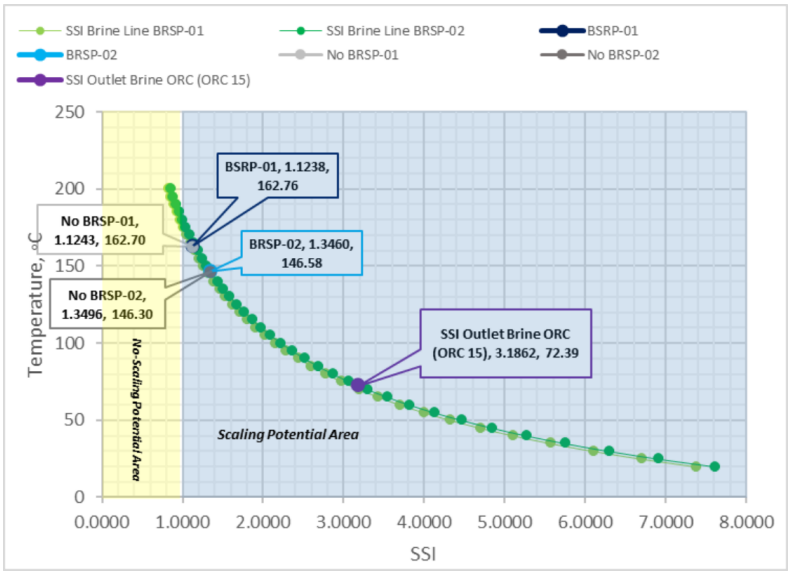

Figure 18: Optimizing BRSP-01 and BRSP-02: SSI Analysis.

6. CONCLUSION

The conclusions in this paper are as follows:

1. By optimizing BRSP-01, the brine enthalpy discharge value will increase based on the increase in discharge pressure, from 687.22 kJ/kg (P suct: 6.19 barg) to 687.65 kJ/kg (P disch: 8.94 barg). Meanwhile, the brine enthalpy value for BRSP-02 optimization increases from 616.23 kJ/kg (P suct: 3.79 barg) to 618.33 kJ/kg (P disch: 17.32 barg).
2. The steam fraction produced by the LP-Separator will increase from 3.08753% to 3.10800% using BRSP-01. Thus, the steam rate of the LP-Separator increase from 3.4836 kg/s (12.5412 t/h) to 3.5067 kg/s (12.6243 t/h), and the brine rate decrease from 100.2889 kg/s (361.0397 t/h) to 100.2058 kg/s (360.7405 t/h).
3. Total power generation will increase from 11459.3174 kW to 11466.2443 kW (a 0.0604% increase) with BRSP-01 optimization, while with BRSP-02 optimization, ORC-15 power generation will increase from 1401.6246 kW to 1409.7176 kW (a 0.5574% increase), resulting in total power generation increasing from 11458.1513 kW to 11466.2443 kW (a 0.0703% increase).
4. The saturation pressure of the brine line from HP-Separator to LP-Separator is 6.63 bara (Temperature: 162.76 ℃) with BRSP-01 operating pressure at 9.94 bara, while the saturation pressure of the brine line from LP-Separator to Brine ORC is 4.34 bara (Temperature: 146.58 ℃) with BRSP-02 operating pressure at 18.32 bara, and the saturation pressure of the brine line outlet from Brine ORC to the reinjection system is 0.35 bara (Temperature: 72.39 ℃) with reinjection system operating pressure at 8.8 bara.
5. The SSI value for the brine line from HP-Separator to LP-Separator decrease by 0.0534%, from 1.1244 (without BRSP-01) to 1.1238 (using BRSP-01) with temperature at 162.76 ℃, while the SSI value for the brine line from LP-Separator to ORC-15 decrease by 0.2749%, from 1.3497 (without BRSP-02) to 1.3460 (using BRSP-02) with temperature at 146.58 ℃, and the SSI value for the brine line from ORC-15 to reinjection system increase to 3.1862 due to the outlet temperature dropping to 72.39℃.
6. Optimizing BRSP-01 and BRSP-02 will increase the steam fraction and total power generation, albeit not significantly. By optimizing the discharge pressure, BRSP-01 and BRSP-02 operation can be optimized, enhancing the output of the LP-Separator and Brine ORC. Meanwhile, the SSI values will decrease, albeit not significantly, as BRSP helps maintain pressure above saturation and prevents SSI values from rising due to pressure and temperature drops along the brine line.

ACKNOWLEDGEMENT

The author would like to express sincere gratitude to Mr. Richard Alexander for his generous support throughout the research process and for his invaluable guidance, expertise, and contributions to this paper.

REFERENCES

DiPippo, R.: Extraction turbines and feed-heating in geothermal binary plants: A thermodynamic performance assessment. Kidlington, UK: Elsevier (2024)

DiPippo, R.: Geothermal power plants. Principles, applications, case studies and environmental impact, Kidlington, UK: Elsevier (2008)

Grundfos: The Centrifugal Pump, Department of Structural and Fluid Mechanics Grundfos Research and Technology, Denmark

Karingithi, Cyrus W: Chemical Geothermometers for Geothermal Exploration, Presented at Short Course IV on Exploration for Geothermal Resources, organized by UNU-GTP, KenGen and GDC, at Lake Naivasha, Kenya (2009)

Khasani. et al.: Hydraulic Analysis of Brine Reinjection Pump Systems at Dieng Geothermal Field, Central Java, Proceedings Indonesia International Geothermal Convention & Exhibition 2014, Jakarta Convention Center Indonesia (2014)

Pratama, Heru Berian and Koike, Katsuaki: Thermodynamic model-based specification of optimal geothermal power generation system for high-temperature liquid-dominated reservoirs using flash and flash-binary cycles, Elsevier (2024)

Saptaji, Nenny, Ashat, Ali and Taha, Dimas: Teknik Produksi Geotermal. Bandung: ITB Press, (2023).

Saptaji, Nenny: Teknik Geotermal. Bandung: ITB Press, (2018).

Surindra, Mochamad Denny. et al.: Comparison of the Utilization of 110 ◦C and 120 ◦C Heat Sources in a Geothermal Energy System Using Organic Rankine Cycle (ORC) with R245fa, R123, and Mixed-Ratio Fluids as Working Fluids. Processes 2019, 7, 113; doi:10.3390/pr7020113 (2019)

Slim–Core Hole Drilling Best Practices, Lessons Learned and Improvement Plan to Increase The Probability of Success in Reaching Exploration Objectives

Tommy Souvanir, Hadi Permana, Sahat Nainggolan, Subur Arianto,
Jefri Marthias, Andri Burnama, and Seto Tanimo

PT. Ormat Geothermal Indonesia

tsouvanir@ormat.com, hadi.abdi.permana@gmail.com, sahat.nainggolan2@gmail.com,
subur.arianto@gmail.com, andriburnama@gmail.com, stanimo@ormat.com

Keywords: exploration, slim-core hole, geothermal

ABSTRACT

The Indonesian government continues to set optimistic targets for Geothermal expansion in terms of capacity and ratio of geothermal to electrical energy sources, while the reality remains lower than the aim. The absence of geothermal exploration is not due to a scarcity of new opportunities; there are plenty of fresh prospects waiting to be explored, but rather is due to longer time and higher expense. In the most cases, the time and cost efficiency of new prospect investigation is still a big challenge, with exploration taking more than 6 years and resulting in substantial costs, making the project's economics less appealing. Exploration drilling is a crucial activity that has contributed to inefficiency in terms of time and expense; it is a complicated issue, and the Indonesia market has yet to develop a best practice to address the challenge of effective and efficient exploration drilling. In theory, slim-core hole drilling is one of the best methods for conducting effective and efficient exploration drilling because it is a compact operation that requires very little preparation and support, it can provide the most critical information for reserve confirmation, and it has the lowest cost impact to get out of the concession. However, in the case of recent exploration drilling, the drilling time is significantly longer than the target time, the actual cost exceeds the budget, and the success ratio is low in comparison to the objectives, and as a result, Indonesia geothermal practitioners are beginning to question the use of slim-core hole drilling exploration solutions. This paper, based on the author's and the exploration drilling team's direct experience with one of the most recent slim-hole exploration drillings in Indonesia, will attempt to share the best practices and lessons learned, as well as insight into coring activity and improvement plan to increase the probability of success. By implementing the best practices and mitigating lessons learned, the success ratio of slim-core hole to meet the objectives will increase. Based on the recent slim hole drilling, most of them were targeting in the range of 60 days of drilling time and approximately USD 1.2 million in drilling costs, which have a good chance of being met if the best practices and lessons learned are implemented. The combination of the improvement plan and learning curve reduction strategy may result in the slim-core hole being more effective and efficient, the drilling days less than 60 days and the drilling cost less than USD 1 million can be easily accomplished. With the historical of slim-core hole drilling in Indonesia, it is not an invention, it only requires innovation to become a viable option.

1. INTRODUCTION

1.1 Indonesia Geothermal Exploration

Geothermal exploration continues to be significantly lower than the expected target, resulting in new geothermal in term of the number and capacity are not achieved. The exploration took longer time for the execution and most of them have a longer an idle time in between the stages that's impacted to the project economic, there are a lot an invisible and indirect cost keep piled up during the slow progress, and with the idle time will delay the return of the investment if the project is feasible and decided to be continued to the development stage, if the project is not feasible, the idle time will extend the sunk cost duration and it has huge concern for the investor on their investment. A longer time for the investment return combined with the uncertainty of possible total investment cost are a big concern for the investor to enter the geothermal market, or to continue and add their investment in geothermal industry.

The reserve confirmation is the exploration aim, refer to SNI 6009 – 2017 in Figure 1, the process will start with speculative and hypothetic study and then follow with reserve assessment to identify a possible reserve, to simulate a probable reserve and to calculate a proven reserve.

Figure 2 illustrates an example of geothermal exploration with prolonged execution process. It took more than twenty (20) years to complete the reserve confirmation, starting with an early study for project financing, followed by a geoscience study, and ending with initial and additional exploratory drilling. And the latest status of this concession is waiting for development execution. if just reflecting to this case and there isn't an innovation to

bring the process become time effective and cost efficient, and then Indonesian geothermal growth always behind the expected.

GEOTHERMAL RESERVE CONFIRMATION (REF SNI 6009-2017)

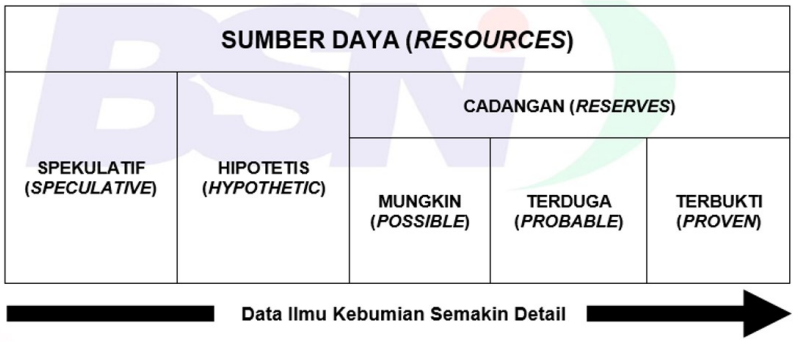

Figure 1: Geothermal reserve confirmation (Ref SNI 6009-2017).

CASE EXAMPLE – EXPLORATION PREPARATION TO EXECUTION

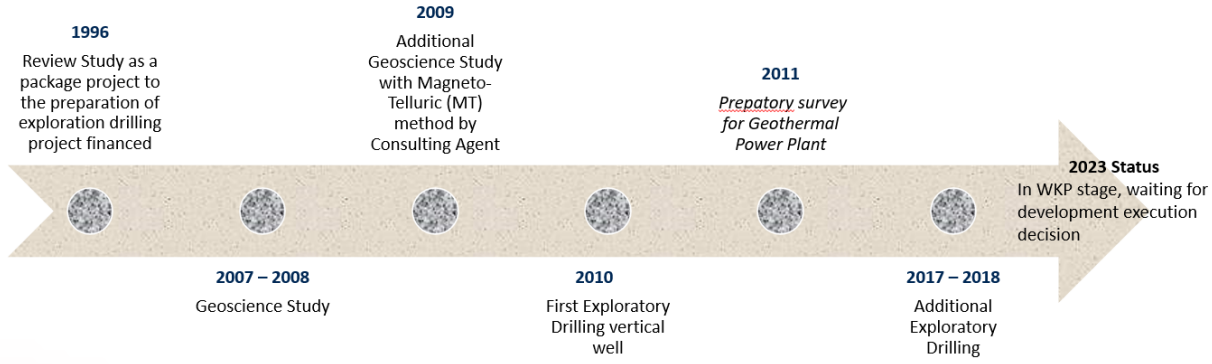

Figure 2: An example of geothermal exploration with prolonged execution process.

The innovation to bring the efficiency with an effective exploration should be able to demonstrate the reserve, to get as much sub surface information as feasible, the probable reserve in a timely and cost-effective manner, and reduce the cost impact to get out of the concession.

Given that exploration drilling is the ultimate activity for reserve confirmation in geothermal projects, it's crucial to adopt options that ensure cost efficiency, time effectiveness, and provide key information for reserve confirmation. Using slim-core hole drilling, in the theory, can a viable option for exploration drilling, offering a less expensive, compact, and lean approach to gather initial subsurface data and confirm the reserve.

1.1 Indonesia Geothermal slim-core hole historical performance

A slim-core hole is not a something new for Indonesia Geothermal exploration as illustrated in Figure 3 for the historical summary, back to the early state of Indonesia geothermal Industry in between 1994 – 1998, two (2) big geothermal fields in Indonesia, Sarulla and Darajat had performed slim-core hole exploration drilling campaign with a good result in term of performance and reserve confirmation. In Sarulla, in between approximately 1994 until 1997, from nine (9) exploration wells were drilled, Six (6) were slim-core hole wells with three (3) of them were deviated well. With the limited information of those wells, and only having the final well schematic from the old well report, so there is no information about the days and cost, however there is an interesting information for the well depths were in the range 6662 ftMD or 2029 mMD to 8000 ftMD or 2436 mMD which are deeper than the target depth of all exploration wells that's recently drilled and planned to drill.

Darajat has a good documentation on the slim-core hole drilling performance, referred to riza et all, proceeding 20th NZ Geothermal Workshop 1998 publicity, within two years, six (6) slim-core holes successfully drilled with a good performance to meet the objectives. The project was very successful obtaining a valuable sub surface information to answer the probable reserve in a timely and cost-effective manner and adopted the best practices from other previous project in Sarulla to reduce the learning curve while keep continuing capture the best practices and lesson learned to improve the learning curve. The well depths were in the range of 4402 ftMD or 1340 mMD and 7578 ftMD or 2308 mMD, with the average drilling time was 61 days includes with two wells were experienced the stuck pipe and sidetracked. The program was started with DRJ S1 drilling, the drilling was

completed in 51 days for 4402 ftMD and 1,340 mMD, it was a good starting for the first well that's revealed the project team capability to manage the learning curve, on the next well the performance continuously improved, the number of drilling days is improved along with the well depth deeper, even for two wells that experienced with stuck pipe and end up with sidetrack, it's indicated the team had significant lesson learned on the second event, the decision to solve the problem more faster and efficient in the second well if compare than the first well, in DRJ S-2 the total drilling days was 85 days to drilled 4730 ftMD or 1441 mMD with number days for the stuck pipe event and sidetracking about 13.3 days, whilst in DRJ S-6 the total drilling days was 58 days to drilled 6273 ftMD or 1911 mMD with number days for the stuck pipe event and sidetracking about 5 days. Based on an interview with one of project team who were involved in Darajat slim-hole core, the after-action review and individual well lookback were two key activities performed to lower the learning curve and improve the performance.

Figure 3: Indonesia slim-core hole historical.

Recent geothermal exploration in Indonesia has experienced major problems that diverge completely from expected advantages. In the decade, about six (6) exploration drilling using slim-core hole have resulted in excessive cost overruns, significant project time delays and other problem such as unpaid invoices, labor strikes due to delayed salary payments and contract fulfillment failure.

Start with Ijen exploration that was executed in 2016 until the last slim-core hole in 2022 at Klabat wineru, the drilling days to complete one well extremely longer than the target day, with the target days less than 60 days, the execution end up with delays up to close to four times of the target. With the excessive delays, the well cost became exceeded the budgets and the project spending became overruns because of the direct and in direct cost were ramping up a long with the additional days. however, with the delays and overruns, the target depth range to be drilled were able to achieve and this is an important note that's informing the planned target depth still within the design limit of slim – core hole rig equipment.

In the following time performance of the last two slim – core hole drilling, clearly non-related drilling was the major contribution to the total time performance. In Hu'u drilling in figure 04 obviously the drilling progress were stopped because of equipment problems and non-technical issues, from 193 days of spud to rig release, the planned days only 26.9 % or 51.9 days. even though the performance was not satisfied, but if we normalized the total time without NPT and unplanned event, the performance to drill 922m days with 51.9 days is still aligned with the historical performance at Darajat.

In klabat Wineru drilling as illustrate in figure 05 that's the starting drilling about the same with Hu'u. from 204.7 days of spud to released, the planned days only 28 % or 52 days. Same with Hu'u, the drilling performance were very slow progress with a lot of stopped that caused by equipment problems. With all the obstacles, the well can be drilled to 985 mMD of 1000 mMD the target depth, which if the time performance normalized without the NPT, the team performance also aligned with the historical of darajat's performance.

An interesting fact of recent slim – core hole drilling is that from six of slim-core hole drillings, Three (3) of them were drilled by same rig contractor which are Nage, Hu'u and Klabat Wineru, and for Ijen, even though it was drilled with different rig company, the majority of the management were the same as the rig contractor in nage, Hu'u and Klabat Wineru. In Ijen, they wasn't used a brand new rig, but in Nage, Hu'u and Klabat Wineru, they brough three (3) a brand new rigs, which the equipment problems shouldn't be an issue, however in reality all of

those operation have a same problem of the equipment reliability. Some reason behind the equipment problems were lack of engineering design on rig auxiliary equipment selection that's lead to in compatible equipment and un operable the equipment, procuring of an used and nonstandard equipment, none of preventive maintenance plan combined with not ready with the spare parts, and bad contractual with the rig manufacture for after sales support. Unpreparedness and a lack of experience have significantly impacted drilling operations, even though the rig contractor has already hired experienced professional crews to mitigate operation problems, but without a good system, financial and non-financial support, those are not working.

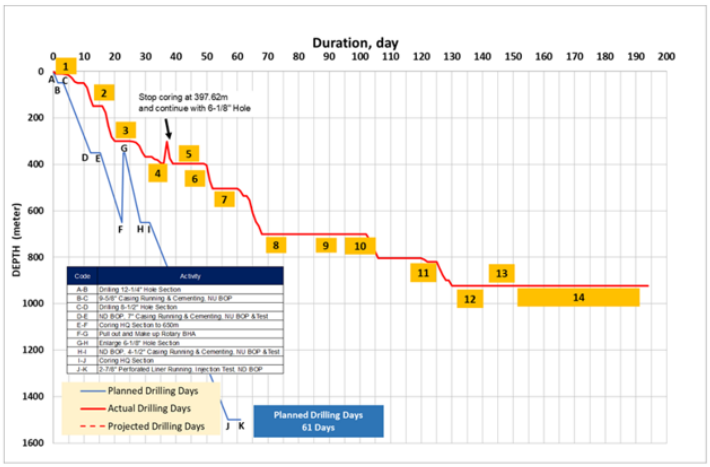

No.	Depth	Duration	Problem
1	10 m 13 m 16 m 28 m	± 7 days	A. Leaking on surface section. - Required to re-set riser and cement job - 3 times Grouting Job with cement B. Problem with Mud Pump
2	149.67m	± 3.5 days	Loss circulation starts at 143.6 m. Pumped LCM and Set 2 cement plugs
3	282.30m	± 3.3 days	Loss Circulation starts at 282.3m Pumped 2x Cement Plug
4	367.19m	± 2 days	Waiting on Thrust Bearing and TDS Crossover
5	397.62m	± 2 days	Hole Problem - Hole instability issue
6	397.62m	± 5 days	Waiting on Mud Pump Spare Part since 4th June 22 @ 12:00 hrs
7	504.89m	± 6.64 days	- Pull out of hole bit due to high torque - Incident on 15th Jun '22, back to operation on 21 June @21:30
8 & 10	701m	± 19 days	- Hard reaming during running in hole - Casing running stop at 372m and requirement to pull out casing - BHA trip to condition the hole - Cementing Plug stabilization
9	701m	11 days	Stop Operation due to community issue since 12th July 2022 @ 14:00 hrs until 23 July 2022 @ 14:00 hrs
11	805 m	5.5 days	Stop Operation due to waiting on spareparts (wireline winch drum) since 13th August 2022 @ 15:00 hrs.
12	922.65 m	on-going	NQ Pipe left in hole
13	922.65 m	10.75 days	Problem with Saver sub, waiting on equipment Pipe drop and fishing 2 times
14	922.65 m	33 days (on going)	Continue Fishing NQ Left in hole since 12th Sept

Total NPT = 109.8 Days

AFE Days : 61 Days
Actual Days : 193 Days
Normalized W/O NPT: 83.2 Days

	Time Distribution of HDH-NA-1			
Units	**NPT**	**Unplanned**	**Planned**	**TOTAL**
Hours	905.50	2485.75	1246.25	4637.50
Days	37.7	103.6	51.9	193.23
Percentage	19.5%	53.6%	26.9%	100%

Figure 4: Hu'u slim-core hole performance drilling.

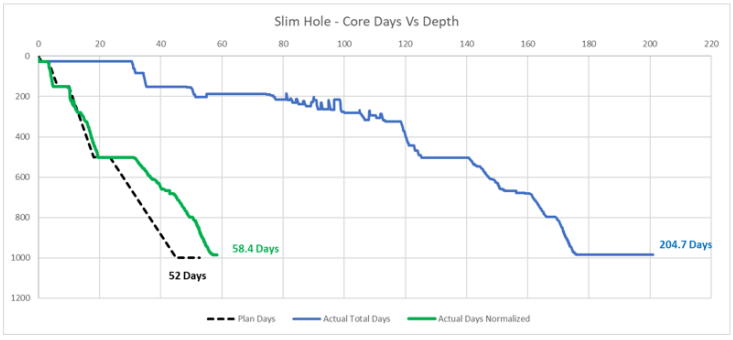

NPT Breakdown

Section	NPT	NPT Days	Event Summary
MOB	0%	0.00	
Drill conductor hole	56%	0.52	Problem on Mud Pump No.02, Rig Genset No.02 and main rig system
Set conductor casing	0%	0.00	
Install WH and BOP	0%	0.00	
Drill with 8-1/2" to 150 m	92%	33.75	Top Drive Problem - Leak at the swivel. EPIROC Rig Problem - rig enginee, drilling consule, pipe skate. Open Hole Loss Circulation Plug I.
Set and Cement 7" Casing	0%	0.00	
Install HW and BOP	78%	7.29	EPIROC Rig Problem - CAN Bus issue, drilling parameter issue
Drill with 6-1/2" Bit to 500 m	87%	66.77	Open Hole Loss Circulation Plug II to XII. Waiting on Mud Material. Rig Top Drive Failure. Rig Mud Pump Problem.
Set & cement 4-1/2" casing	46%	2.19	Waiting on Cementing Mareial
Install HW and BOP and test	0%	0.00	
Drill HQ rod to Well Td	52%	35.52	HQ Rod Stuck in hole. NQ String Dropped to hole and fishing operation. Crew strike due to payment problem.
Evaluate hole	19%	0.19	
Run liner	0%	0.00	
Rig down	0%	0.00	
Total:	71%	146.27	

AFE Days : 52 Days
Actual Days : 204.7 Days
Total NPT : 146.2 Days
Normalized W/O NPT: 58.4 Days

Figure 5: Klabat Wineru slim-core hole performance drilling.

Although the drilling performance did not meet the target time, there were numerous lessons learned and best practices identified that can be used to improve the likelihood of the success next slim-core hole drilling. The understanding of difference between rotary drilling and coring operation is one of fundamental learnings, because most of drilling professional and practicians are very well known with rotary drilling operation, however for slim-core hole updated knowledges almost none because of the time gap between the last slim-core hole drillings back in 1998 until recently drillings and the slim-core hole drilling only use in the initial exploration. In the additional exploration and development state, slim-core hole is no longer used, the slim hole until big hole drilling design are used. Normally the coring is operated a lot in mining, and the interaction between geothermal drilling and mining also almost none, so it's also lead for the coring drilling has no information about slim-core hole drilling for Geothermal exploration. The following is summary of differentiate between rotary drilling and coring operation.

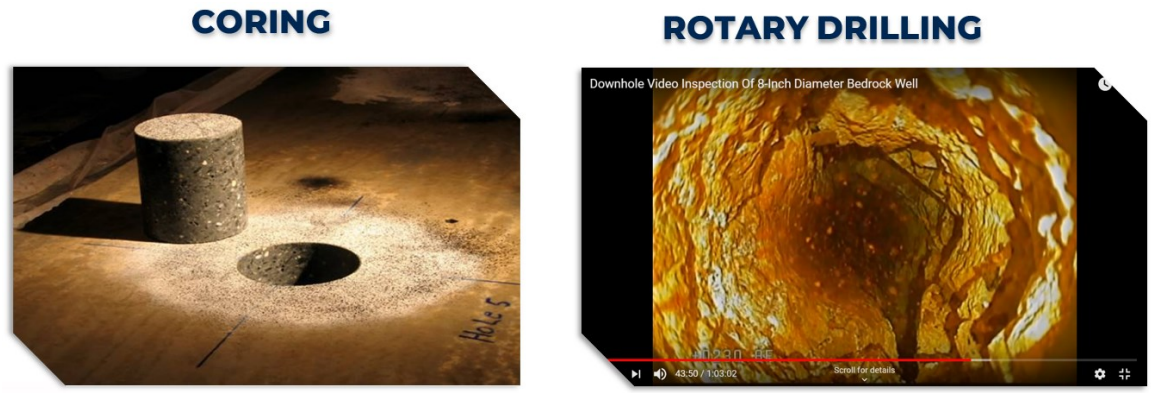

Figure 6: The core hole shape vs rotary drilling shape.

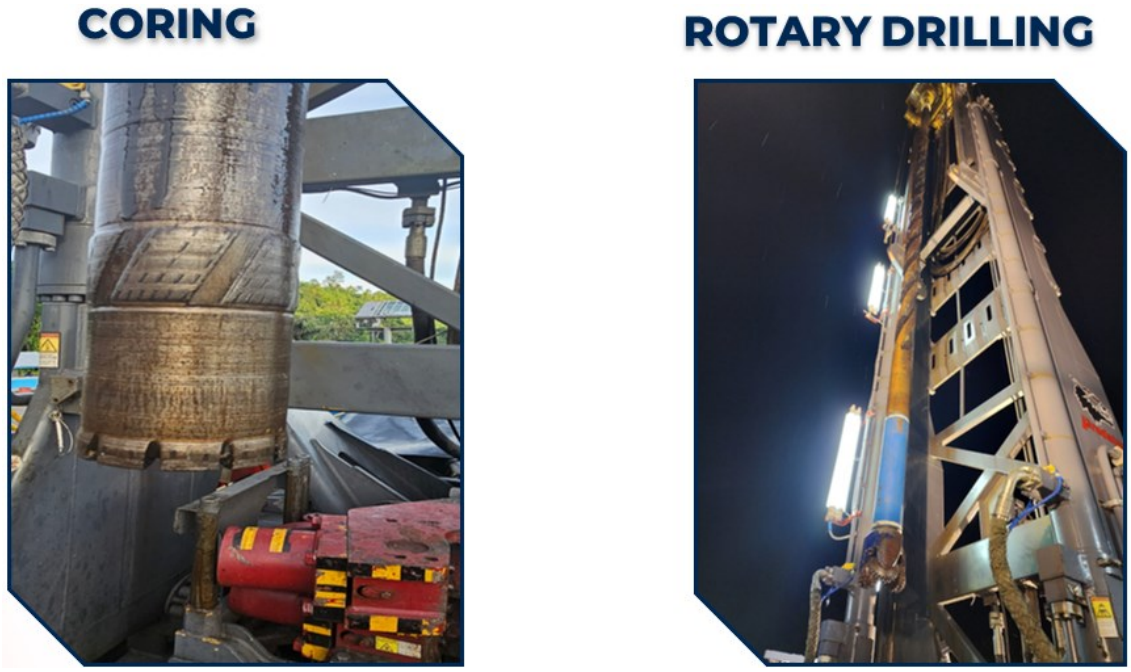

Figure 7: the core hole BHA vs rotary drilling BHA.

2. ROTARY DRILLING VERSUS CORE DRILLING

The following Figures 6 is to compare the shape of core hole versus rotary drilling, and it's very clear the different shape between those, the core hole has smooth rounded shape and in gauge while rotary drilling hole more to rough shape and more to over gauge. The explanation why it being a different shape because of different mechanism as can see in the Table 1.

The coring making a hole using a core head which the size almost the same the pipe that's usually called rod, the coring BHA has slick and straight configuration while rotary drilling BHA making hole using drill bit with the size bigger than the drill pipe, the rotary drilling BHA has size down from the bit to BHA component such as stabilizer, drill collar, and to the drill pipe sizes as can see in figure.07 of coring BHA and rotary drilling BHA.

Table 1: Differentiating Coring and Rotary Drilling mechanisms.

	CORING	ROTARY DRILLING
Formation cut	Polishing	Crushing and shearing
Dominant force	More to the rotation	More to Weight, assisted by rotation
Torque	Low	High
Vibration	Less	More vibrate
Weight on bit	Very low WOB	Higher WOB
Cutting size	Very fine	Rough and bigger
Hole shape	In gauge	Slightly over gauge
Bit	Core head	Drill bit
BHA Geometry	Slick and straight	Size down from bit to the pipe
Circulation	High pressure and low flow rate	High flow rate and relatively low pressure

Table 2: Differentiating Coring and Rotary drilling stuck pipe recovery.

	ROTARY DRILLING	CORING
Stuck pipe mechanism	Pack off/Bridge off, Differential Sticking, Wellbore Geometry	
Stuck pipe recovery	• Pipe severing • Fishing out or side tracking	• Continue drilling with a smaller core size • Cleaning out the annulus with a slightly larger core size • Side tracking
Stuck pipe severing	Explosive (Common) Mechanical cutter Both are using wireline	Mechanical cutter run with smaller rod

To cut the formation, the coring assembly polishing the rock using rotation as dominant force with the weight only to maintain the contact with formation while rotary drilling crushing and shearing the rock using weight with the assist of the rotation. The polishing is resulted in in gauge and smooth hole shape with produced very fine cutting while rotary drilling has slightly over gauge and rough hole with the cutting size roughly and bigger. The coring parameter is low torque and less vibration if compared with rotary drilling. The circulation of coring has high pressure with low flowrate is because of small annulus clearance and very fine cutting while rotary drilling circulation usually high flow rate with the pressure relatively low because of bigger annulus clearance that's required more volume to fill it.

The slim-core hole drilling operation includes rotary drilling and continuous coring, the conductor, surface or intermediate, and production holes are drill with rotary drilling, after the production casing is set and cemented, and permanent wellhead and master valve installed, continuous coring is using to drill the well to the target depth.

Another key learning is the stuck pipe recovery practices for the core hole. The stuck pipe mechanism for both rotary drilling and coring are the same, but stuck pipe recovery and stuck pipe severing in coring has differentiate with rotary drilling as can see in Table 2. There is an option to clean out the pack off annulus with a slightly larger core size but most of the time if the attempt to free the rod is failed, the rod is cut with mechanical cutter that's run with the smaller rod. After the rod is cut, which normally right below the wellhead to maintain small clearance in the anulus to keep the rod stable to core smaller hole.

In addition to the understanding of coring basic concept and stuck pipe recovery practice, another key learning in slim-core hole drilling as follow.

3. SLIM-CORE HOLE DRILLING KEY LEARNING

3.1 Well objective – scale of priority

Well-defined drilling objectives are crucial for good planning, efficient resource allocation, and proper risk mitigation to deliver the project safely and successfully. Adding too many objectives can increase complexity and drag down the project. To meet increasing complexity, mitigation should be increased, and most of the time, the project team was unaware that the invisible project cost had risen dramatically. The most important aspect of determining exploration drilling objectives is setting reserve confirmation objectives, which frequently trap the project team with overly ambitious goals, resulting in higher risk due to high uncertainty conditions and exceeding the design technical limit.

The following table 03 is an example of additional objective during defining well objective of the initial exploration, without the additional objective, the option can be varied, and the slim-core hole is one of the preferred option, however after the additional objective added, the slim-core may have design limit issue, and if still continue with this option, additional mitigation is required, which most of the time the project team did not realized such mitigations had burdened the project cost before the project performed with the consequence of the risk also rose. Most of the time, the project team is too focused on the success scenario and forgets that exploration has a flip of unsuccess risk, with the additional mitigation costs and increasing the complexity. The cost consequence is also automatically high if the exploration result is unfavorable and must be halted, and it becomes a sunk cost that affects the financing of the future project and makes the economics of geothermal project unattractive.

Table 3: An example of additional objective during defining well objective of the initial exploration.

Category	Definition	Additional Objective
PSPE Objectives	Determine Probable Reserve (ref SNI 6009-2017)	• Confirming Probable Reserve Calculation can be used as reference to develop first 20 MW without doing more exploration • Confirming field development strategy • After IPB awarded, Company is able directly to drill 40 kg/s steam production well and 1 brine injector well with capacity of 120 MW and 1 condensate well with capacity of
	▪ Obtaining geological, geochemistry, and geophysics survey data	
	▪ Drill 1 (one) exploration well	
	▪ Able to prove geothermal conceptual model	
	▪ Able to estimate reservoir dimension	
	▪ Able to determine reservoir rock characteristic	
	▪ Able to determine reservoir fluid characteristic	

3.2 Well control – a realistic risk assumption and mitigation

The key risk of an exploration drilling well control which has huge uncertainty and being a big challenge for the project team to do a precise projection of anticipate pressure and temperature with the absence of the offset well and sub surface information. Most of the time, to address this uncertainty the project team come up with very conservative estimation that's lead to excessive mitigations to mitigate all possible conditions, which this is the safest way, but there is a consequence to drilling cost, the economics of project and the technical design limits. The additional mitigations affect not only the mitigation cost, but also to the complexity of well design, drilling equipment set up and the execution time. During the operation, more time will be required to ensure that all the mitigations are in place.

In recently slim-core hole drilling, to mitigate all potential predicted pressure and temperature, a larger and bigger BOP and wellhead stack were required, and to accommodate the installation of wellhead and BOP stacks, the sub structure was modified become a taller and wider. The modification was not just stopped at the substructure, but the other rig equipment was needed to adjust to fit with a modified substructure, such as pipe rack adjustment to be leveled with the new platform elevation, high pressure and low-pressure circulation line adjustment for re-alignment, electrical line re-set up, and so on, and those modifications were not only increased the preparation cost but also the dimension of equipment that's affected to the complexity of handling and mobilization.

To address this challenge, the project team should be innovative to keep the economics of project and ensure the well always secured. The well control risk of anticipate pressure and temperature need to be assessed with realistic number instead of very conservative approach. To prevent the very low likelihood and highest severe well control risk consequences, in addition to the maximum mitigations within the design limit, project team can innovate with decision point mitigation by setting minimum acceptance criteria for reservoir drilling instead of just focusing to the total depth, especially for the first well drilled. When minimum acceptances are fulfilled, the drilling can put

on hold for observation while drilling for the next well and then resumed for deepening if necessary. With the updated sub surface data from the first well drilling, the uncertainty of well control risk will be reduced, risk mitigation can be reassessed to more effective and efficient, well depth can be revisited and adjusted accordingly, and drilling practices can be improved to be more optimized. This initiative ensures all the hazards are always within the design limit of mitigation, and that mitigation costs are kept low due to the rig's compact size for mobility.

3.3 A reliable project drilling team with extensive role and responsibilities

With Preliminary Survey and Exploration License (PSPE) scheme legislation for recent geothermal exploration, there is increased pressure to deliver the exploration project cost-effectively and on schedule because all spending is done by the license holder. Having a dependable exploration team is one of the most crucial components in the success of geothermal exploration drilling operations. Because exploratory projects are typically short in duration, have a wide range of work scopes, and are cost sensitive, the project drilling team must be small, multitasking, problem solver, fast learning, collaborative, and have extended roles and responsibilities.

Slim-core hole drilling as the initial exploration, which combines rotary and coring drilling, requires a project drilling team with a combination of rotary and coring drilling knowledge, as well as multi-project type, roles, and exploration experience, to face all possible challenges during the exploration drilling process.

3.4 Well design – Design limit Optimization

In most circumstances, too many and complex objectives also had impacted on well design, and most of the time, the project team was trapped in this situation where they pushed the limit instead of optimizing the design limit. Given that slim-core hole drilling is an initial exploratory step, and the basic rig equipment design is for continuous coring, the project team must understand the design limit of the equipment in order optimize the coring capability to reach the target depth slim-core hole. What happened recently of the failure of slim-core hole can be caused by the practices of the project team and rig contractor to push the design limit coring rig by modifying rig equipment, with the assumption it could be extended the hole depth and increased the hole size of the rotary drilling for conductor until production hole and reduce the interval depth the coring because of most of the team perception of the continuous coring will take longer time and high risk of stuck pipe if compare than rotary drilling. however, in recently actual slim-core hole performance, with reliable equipment and experience personnel, coring performance can match with rotary drilling and less stuck pipe events.

3.5 Rig and equipment selection – standard equipment optimization and minimize the modification

The modification of rig equipment in slim-core hole drilling projects, when not properly engineered and lacking professional and experienced personnel involvement, could be led to significant risks. These include the potential for incompatible and inoperable equipment, as has been observed in many recent projects. Combined with issues such as inadequate preventive maintenance and poor availability of critical spare parts, these problems often lead to stopped drilling progress. To mitigate these risks, it's essential for project team and rig contractor to focus on proper equipment use and maintenance, optimize design limits rather than modifying equipment.

3.6 Rig contractor selection – proven experience and track record

The key lesson learned of recent slim-core hole is that the incompetence of rig contractors has significantly impacted the success of exploration projects. An underperforming rig contractor can cause delays in drilling progress, which is a critical activity in exploration. Once drilling fails, the entire project is at risk of failure. To mitigate these risks, it's essential to ensure the competence and reliability of rig contractors.

Given that most of the top ten rig coring companies operate in Indonesia as shown in figure 08, it should theoretically not be difficult to find competent and professional rig contractor for geothermal exploration using slim-core hole drilling. What the project team should do is meet with top coring companies to discuss project goals and expectations, and then select a preferred contractor by selecting organizations that offer the best combination of competence, dependability, and cost-effectiveness.

4. SLIM-CORE HOLE COST PROJECTION

If all the lessons learned are addressed and the best practices are followed, which is not a rocket science, slim-core hole drilling will likely be less expensive that other initial exploration options. According to white et all, deep slim-core hole for geothermal exploration, GRC transaction, 2010 , the actual drilling performance for a 1500 m deep continuously cored and subsequently hole opened slim hole is typically 60 – 65 days, which is nearly twice of that standard geothermal production well of the same depth, and cost US$ 1.3-1.8, whereas a standard diameter geothermal production well this deep might cost 3-4 times as much at about US$5-6 million or more.

Assuming the mitigation strategy is already in place, we can determine whether white et al's anticipated time and cost are still applicable in the current Indonesian market. Using core rig capacity of 300 – 450 HP and a daily rig

cost US$ 23 per house power as referred to SK APMI 2017 Tarif harian operasi drilling (THO) onshore, the daily spread cost will be approximately US$ 20,7 K – US$ 31 K, and if the plan for slim-core hole is to drill 1500 meters with the target days is 60 days, the well cost may be US$ 1.24 – 1.86 million, which is consistent with White et all. Estimated.

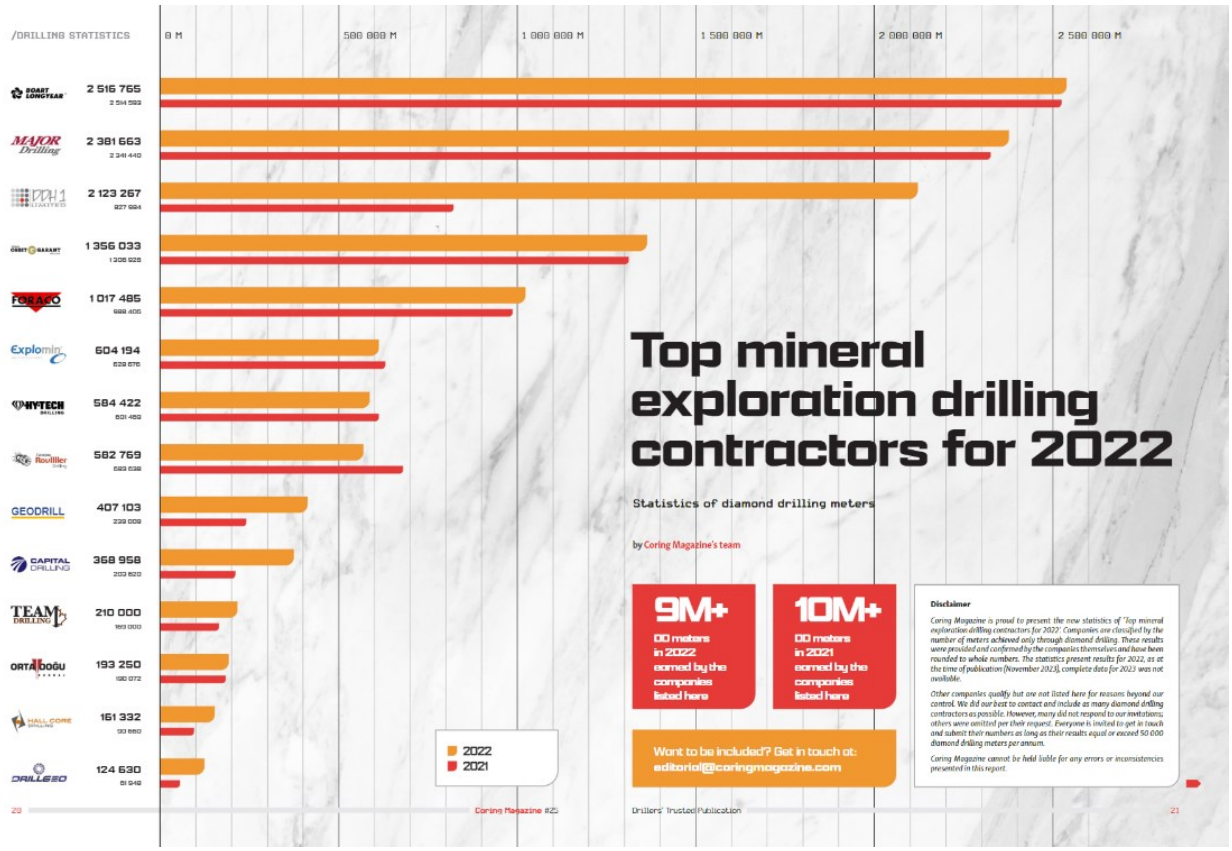

Figure 8: Top ten rig coring companies.

	WELL COST PROJECTION
Rig Capacity	300 HP – 450 HP
Daily Rig cost (* USD 23 /HP)	USD 6,900 – USD 10,350
Daily spread cost	USD 20,700 – USD 31,050
Drilling days	60 Days
Well depth	1500 m
Well cost	USD 1.24 Million – 1.86 Million

* SK APMI 2017, Tarif Harian Operasi Drilling (THO) onshore of USD 19 – USD 23 per HP

Figure 9: Well cost projection.

5. CONCLUSION

The slim-core hole was effectively conducted in the early stages of Indonesia geothermal exploration, yielding positive results in terms of performance and reserve confirmation, confirming the slim-core hole as the best alternative for performing effective and efficient initial exploration. By leveraging historical successes, understanding the critical differences between drilling operations, prioritizing well objectives, assembling a reliable exploration team, optimizing well design, selecting the right equipment and contractors, and implementing best practices and mitigation strategies, the goal of efficient and cost-effective slim-core hole drilling in geothermal exploration high likelihood to be achieved, and the aim of slim-core hole drilling to 1500 m within 60 days at a cost of around US$1.2 million remains realistic. The successful of slim-core hole execution will be

advantageous to enhance number of reserve confirmation of long list geothermal prospects, which can accelerate Indonesia geothermal growth.

REFERENCES

Coring magazine, driller's trusted publication coring ISSN 2367-847X, #25, 11/23, coringmagazine.com (2023).

Direktorat Panas bumi,: Lesson learned Pengeboran Sumur Slim Hole, Ministry of Energy and Mineral Resources, (2023)

Hu'u project drilling team : Operasional pengeboran slim hole PSPE Hu,u Daha, *Proceeding*, Forum group discussion Slim hole drilling , Jakarta (2022).

Indonesia project drilling team : TTG 2-1 performance tracker, OGI, Jakarta (2022).

Komite teknis 27-05, Panas Bumi : SNI 6009 : 2017 Klasifikasi sunmber daya dan cadangan energi panas bumi Indonesia, BSNI, Jakarta (2017).

Riza, and Berry, B : Slimhole drilling experience a tDarajat Geothermal Field, West Java, Indonesia, Proceeding, 20th NZ Geothermal Workshop 1998, Amoseas Indonesia Inc, Jakarta (1998).

Unocal Sarulla project drilling team: Sarulla well schematic, Unocal-Sarulla, (1994-1998).

The Approach of Rock Muffler Design for a Typical 55 MW Net of Geothermal Power Plant in Indonesia

Nursanty E. Banjarnahor, Agung W. Mukti, Agus Hendrayana, Fadil A. Lubis, Muhammad Tito Setiawan, Denis D. Pamungkas, Aqmal N. Kusuma, and Rezky Maulana Yusuf

PT. Geo Dipa Energi, Parungserab, Soreang, Bandung Regency, West Java 40922

santy@geodipa.co.id, agungw@geodipa.co.id, denis@geodipa.co.id, tito@geodipa.co.id, fadil@geodipa.co.id, maulana.rezky@geodipa.co.id

Keywords: rock muffler, design, geothermal power plant

ABSTRACT

The approach for designing a rock muffler of a typical 55 MW capacity geothermal power plant in Indonesia is elaborated in this paper. The rock muffler runs as the facility for venting steam in the event of the power plant shut down or emergency cases. Based on historical production data of existing 60 MW gross capacity power plant, the rock muffler may accommodate approximately 400 tons per hour of steam. The objective of this paper is to give the approach of the rock muffler design that needs to meet the requirements for typical 55 MW net power plant in Indonesia. The noise level limit allowed in the residential area is 55 dB during day time and 45 dB during night time. With the site-specific approach, the findings are the dimension of the rock muffler recommended using 6.5 m height of the structure with 5.5 m height of scoria rocks filling. On the other side, the recommended length and width of rock muffler is 18 m x 8 m. In this dimension approach, the highest noise modeling results in approx. 41 dB at the receptor with approx. 700 m straight line. Furthermore, the paper gives the examples and approach of calculations for sizing of a rock muffler in geothermal power plant.

1. INTRODUCTION

Indonesia has enormous geothermal potential as per data published by the Government of Indonesia. One of the development phases of a geothermal power plant is designing the equipment using an engineering approach to get the dimension of equipment. In geothermal power plants and steam above ground systems (SAGS), rock mufflers serve as critical safety and operational components. Their primary function is to safely vent steam during planned shutdowns, unplanned outages, and emergency scenarios. The design of a rock muffler necessitates rigorous calculations that take into account the site ambience conditions, geothermal fluid characteristic, related regulation, and applicable standards. The objective of this paper is to give the approach of the rock muffler design that needs to meet the requirements for typical 55 MW net or 60 MW gross power plant in Indonesia. . The pipeline and diffuser are sizing and design based on mass flow rate for 55-69 MWgross generation of Geothermal power plant.

2. CODES AND STANDARDS

To meet the requirements for a typical 55 MW net power plant in Indonesia, the design of the rock muffler shall consider applicable codes and standards, including but not limited to those specified in Table 1 Applicable Codes and Standards.

Table 1: Applicable Codes and Standards.

No	Code and Standard	Description
1	API 5L	Specification for Line Pipe
2	ASME B31.1	Power Piping
3	ASME B16.5	Pipe Flange and Flanged Fittings
4	ASME B15.47 Series-A	For Large Diameter Flanges
5	ASME B36.10	Welded and Seamless Wrought Steel Pipe
6	API 598	Valve Testing
7	API RP 521	Pressure Relieving and Depressuring Systems
8	API 600 Series	Valve
9	SNI 2847-2019	Structural Concrete Requirements for Buildings
10	SNI 1727-2018	Minimum Loads for Designing Buildings and Other Structures
11	SNI 1726-2019	Earthquake Resistance Design for Buildings and Non-Buildings
12	SNI 8460-2017	Geotechnical Design Requirements

Both for National or Local Government to maintain production facilities and local environment from defects and pollution (air, water, sound, etc.), the designer shall follow applicable regulations from Indonesia Government, including but not limited to those specified in Table 2.

Table 2: Applicable Government Regulations.

No	Regulations	Description
1	Decree of the State Minister of Environmental No.48 year 1996	Concerning the Noise Level Standards
2	President Decree No. 76 year 2000	Operation of Geothermal Resources for Power Generation
3	Decree of the State Minister of Environmental No110 year 2003	Guidelines on Stipulation of Accommodating Capacity of Load of Water pollution in Water Sources
4	International Finance Corporation (IFC) World Bank (WB) Environmental, Health and Safety (EHS) year 2007	General Guidelines for Noise Level Standards which 55dB (decibel) for day, 45dB for night, and 3dB increment

Table 3: Parameter of Assumption.

Parameters	Value	Unit
Environmental		
Dry bulb temperature	21	ºC
Wet bulb temperature	19	ºC
Site Elevation	1932	masl
Rainfall	179	mm/year
Wind	From North – East to South – West Wind gusts > 3.6 – 8.8 for less than 20% time	m/s
Seismic	0.29	g
Atmospheric Pressure	0.797	bara
Geothermal Fluids		
Fluid	Saturated Steam	-
Mass Flow	400 – 500	tph
SSC (steam specific consumption)	7.2	ton/mw hr
Generation	55-69	MW
Upstream Pressure	9.7	bara
Enthalpy	2735 – 2776	kJ/kg
Steam Fraction	0.98 – 1	-
Temperature	180	ºC
Scoria Rock		
Density	2550	Kg/m^3
Porosity	25	%
Average Diameter	200	mm

3. ASSUMPTION AND CALCULATIONS

3.1 Assumption Data

The assumptions used in this hydraulic analysis are homogenous rock dimensions with shape assumed nearly to perfect sphere. In designing the rock muffler, there are some criteria with engineering and environmental aspects that need to be considered as follows:

- Design lifetime for 30 years.
- Design shall provide accessibility for operator and engineer to operate and maintenance activities.
- Design shall follow the latest standard that still apply and shall have flexibility and reliability.

Proper material selection for long term operation, minimum maintenance due to corrosion and erosion effect, noise emission and proximity to inhabited area, noise limitation should not exceed 55 dB and 45 dB at 100 meters distance. There are several data for environmental, fluids, and scoria rock that will be used for calculation of the rock muffler design as shown in Table 3 with all units in Metric system.

3.2 Calculations

The calculation will consist of discharge flowrates, sonic velocity, hole sizing, drag force, and noise prediction.

- Environmental: Upstream pressure, atmospheric pressure
- Assumption: Mass flow rate for 60 MW gross (SSC = 7.2 ton/ MWh), Steam fraction (Inlet scrubber)
- Steam properties: Density, Specific volume, Molecular mass, compressibility factor (Z), heat capacity constant volume (CV), heat capacity constant pressure (CP), Universal gas constant (R)

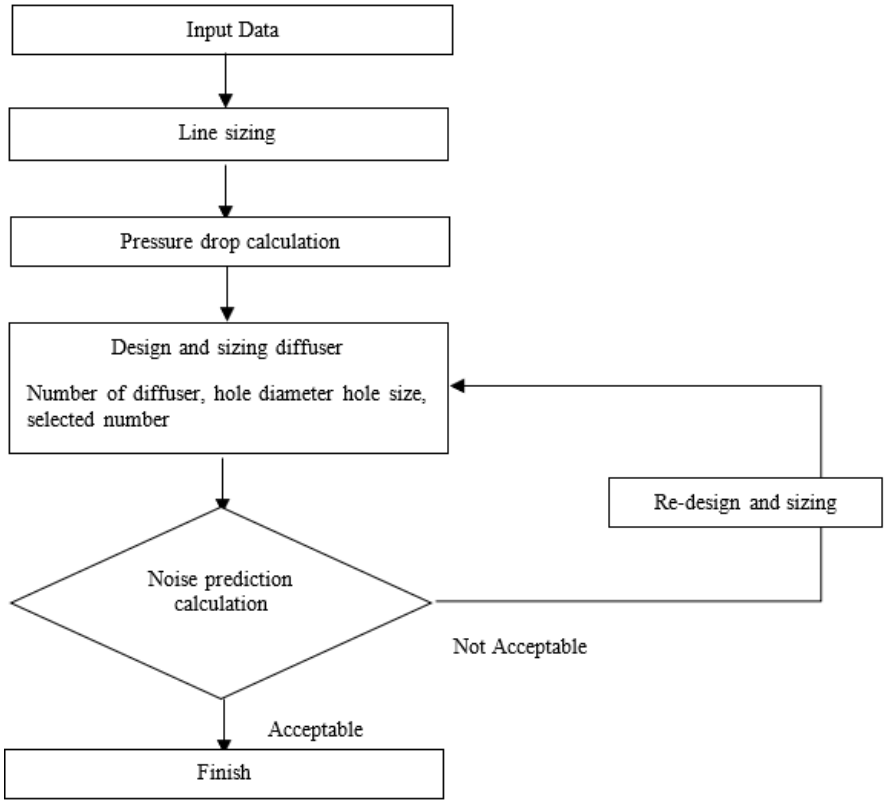

Figure 1: Flowchart.

The compressible fluid flow through the nozzle and orifice can be calculated based on Verma and Pruess (1976)] (equation 2-24), with the following formula:

$$q = YCA\sqrt{\frac{2\Delta p}{\rho}} \quad (1)$$

where

q = Flow rate (kg/hr),

Y = expansion factor,

C = flow coefficient for orifice and nozzle

Δp = pressure differentiation between upstream and downstream (bar),

A = hole area (m^2)

ρ = fluid density (kg/m^3)

Steam sonic velocity can be calculated based on Crane Co [4] (equation 3-8), with the following formula.

$$v_s = 316.2\sqrt{\gamma\, P\, V} \quad (2)$$

where

υ_s = Steam sonic velocity,

γ = Specific *heat ratio* (Cp/Cv),

P = Pressure (bar.a)

V = Specific voulme (m^3/kg)

Hole sizing can be calculated based on discharge flowrate calculation divided by the number of holes. To reduce noise steam sonic velocity limitation should not exceed 0.3 mach based on IEC 60534-8-3 [7]. The drag force value are needed to determine the drag resistance of rock, Drag force can be calculated based on Perry's handbook [5] (equation 6-227) with the following formula (3).

$$F_D = \frac{C_D\, Ap\, \rho\, u^2}{2} \tag{3}$$

where

F_D = drag force

C_D = drag coefficient

C = flow coefficient for orifice and nozzle

A_p = particle cross section area (m^2)

ρ = fluid density (kg/m^3)

elative velocity between particles. Then the noise prediction can be calculated based on silencer Application [5] with the following formula (4).

$$L_W = 17\, W + 50\, log\ T\ - 85\, dB \tag{4}$$

where

L_w = noise level outlet diffuser (dB)

W = steam mass flow outlet

P = diffuser holes (lb/h)

T = upstream temperature (deg R).

Pressure drop calculated using prediction of steam flow pressure drop which is through packed beds of rock layer can be calculated by using Ergun's Equation [10] as follow formula (5)

$$\frac{\Delta P}{L} = \frac{150(1-\varepsilon)^2 \mu U}{\varepsilon^3 {D_p}^2} + \frac{7(1-\varepsilon)\rho U^2}{\varepsilon^3 D_p} \tag{5}$$

Where

$\frac{\Delta P}{L}$ = pressure drop per length (bar/m),

ε = rock porosity

μ = dynamic viscosity of the fluid

U = Superficial bed velocity (m/s),

D_p, = diameter of Particle (m),

ρ = Density of the fluid (kg/m^3).

4. RESULTS AND DISCUSSION

The results section will include the calculated values for discharge flowrates, sonic velocity, hole sizing, drag force, noise prediction, and pressure drop as Table 4.

The material for use with maximum operating temperature (MOT) shall be established greater than or equal to the operating temperature. The design temperature at least 10° C above the MOT. The design temperature shall be rounded up to nearest 5°C increment. In designing the rock muffler unit for geothermal applications considered various specifications and materials to ensure optimal performance and durability. The noise levels were a critical consideration, with the design ensuring a noise level of 85 dB at the outlet diffuser and 35 dB at the outlet of the rock muffler. It is acceptable noise level as mentioned in the regulation, the noise in receptor or nearest community is 45 in night time. This comprehensive design ensures that the rock muffler unit will perform effectively under the specified conditions, with careful consideration given to material selection especially for rocks, noise reduction, and structural integrity. The selection of materials, and dimension will lead to the noise level approach as stated in the previous section. It is recommended to lead this desain to noise modeling if required to ensure the noise data is acceptable by the requirements and regulations. Following Figure 2: The proposed drawing of rock muffler can describe about the rock muffler proposed design using the approach.

Table 4: Results.

No	Description	Results
1	Material used for diffuser pipe	API 5L Grade B
2	Pipe size for diffuser pipe	24 in
3	Pipe wall thickness	12.7 mm
4	Schedule	XS
5	Length of diffuser	10,000 mm
6	Amount of holes	704
7	Diameter of holes	40 mm
8	Structure	6.5 m height of the structure with 5.5 m height of scoria rocks filling
9	Dimension of rock muffler	18 m x 8 m
10	The noise levels	85 dB at the outlet diffuser and 35 dB at the outlet of the rock muffler
11	The total weight for the rock muffler unit	estimated around is 265,500.3 kg

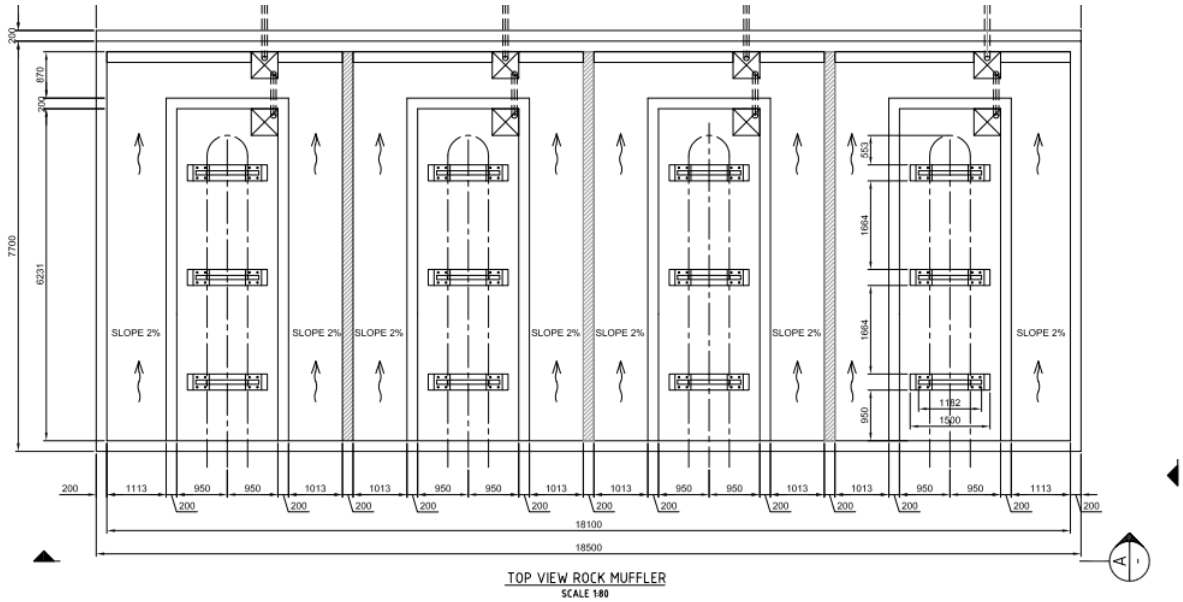

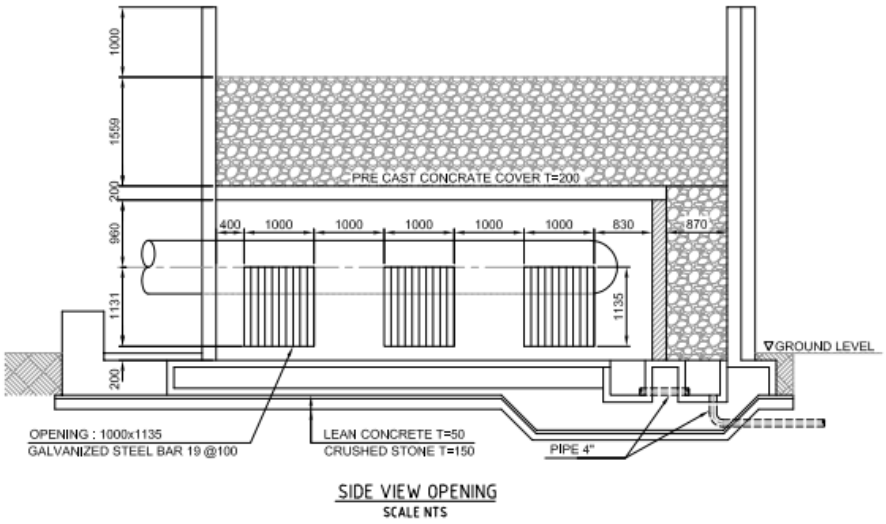

Figure 2: The proposed drawing of rock muffler.

5. CONCLUSION AND RECOMMENDATION

The rock muffler equipment is one of the significant parts of geothermal utilization for emergencies to ensure the flow of steam for emergencies to the air meets regulations in terms of noise level and safety concerns. The approach of a typical 55 MW net or 60 MW gross capacity production geothermal power plant is elaborated in this paper. The rock muffler runs as the facility for venting steam in the event of the power plant shut down. Based on historical production data capacity of the rock muffler may accommodate approximately 400 tons per hour of steam. The objective of this paper is to give the approach of how to design the rock muffler that needs to meet the requirement of regulation, in this case, the Government of Indonesia. The noise level limit allowed in the residential area is 55 dB. In this case, noise modeling may be required to ensure compliance. Current calculation findings are the dimension of the rock muffler recommended using 6.5 m height of the structure with 5.5 m height of scoria rocks filling. On the other side, the recommended length and width of rock muffler is 18 m x 8 m. In this dimension approach, the highest noise modeling results in approx 41 dB at the receptor with a distance of approx 700 m straight line.

REFERENCES

Crane Co. (n.d.). Technical Paper No. 410M: Flow of Fluids through Valves, Fittings, and Pipe.

Cummins, J.R., and Golden, B.G. (n.d.). Silencer Application Handbook.

Davies, E.: Noise and Vibration. In Plant Engineer's Reference Book. (2002).

Jamie, T., et al.: Evaluation of Pressure Drop and Particle Sphericity for an Air Rock Bed Thermal Energy Storage System. Energy Procedia, 57 UK: Elsevier Ltd, (2013). 633–642.

Michael, T. Sound Engineer's Pocket Book. (2000).

Perry, R.H., and Green, D.W. (n.d.). Perry's Chemical Engineers' Handbook.

IEC 60534-8-3. Industrial-process control valves – Part 8-3: Noise considerations – Control valve aerodynamic noise prediction method

A Drilling Learning Curve Continuous Improvement and Immediate Corrective Action

Muhammad I, Tommy S, and Seto T

PT. Ormat Geothermal Indonesia

tsouvanir@ormat.com, muhirfan@ormat.com, stanimo@ormat.com

Keywords: Learning curve, Geothermal exploration, Geothermal drilling

ABSTRACT

Every new drilling campaign has a learning curve that affects performance, even if it is a development drilling and numerous drilling campaigns have been completed. The learning curve of probabilistic exploration will be longer due to a lack of subsurface hazard knowledge and no offset well data use as a reference, which will increase the risk assumption. The learning curve will also be influenced by the presence of new parties in each drilling campaign, such as new contractor, equipment, or personnel. The ability to shorten the learning curve will automatically improve time and cost efficiency.

This paper will discuss daily drilling continuous improvement and immediate corrective action methodologies that have successfully lowered the learning curve of drilling exploration, resulting in increasing time and cost efficiency. In addition to efficiency, best practices and lessons learned were documented and could be utilized in the next well drilling, and an improvement plan initiative were identified to ensure the continuity of efficiency.

1. INTRODUCTION

Even though geothermal drilling Indonesia has been performed for many years, there was a pause in between drilling campaigns, which can be only a couple of years but can also be more than ten years. The reason for the pause was that the target well to be drilled has already been achieved to supply the steam as per the target, but there was also observation time required before moving to development stage from the exploration. A vacuum situation between drilling campaign causes the learning curve break, the learning curve begins over the campaign is resumed, lengthier vacuum drilling results in longer learning curves.

The learning curve in exploration drilling should be longer than the development drilling because of in absence of sub surface information and offset well, which will increase the risk profile and require additional safeguard to be identified and mitigation plan to be established. The learning curve delays were also contributed by the first time set up and the introduction of new parties such as new contractor, new equipment, new crews, all of which need more time for familiarity and effective coordination and communication.

The learning curve has impact to the performance and economics of project, the ability to shorten the learning curve is one critical aspect in delivering successful projects. The sensitivity and urgency of the learning curve increase with the size of drilling project. For smaller and shorter drilling projects which a restricted time and budget, reducing the learning curve is essential, and most geothermal exploration projects are small and short. Even while the learning curve in the development drilling project is not as sensitive as that in exploration drilling, it is still critical to maintain the project improving over the time. The development drilling learning curve can be shorter than the exploration because of the best practices and lessons learned from the preceding project already there.

2. GEOTHERMAL DRILLING PROJECT PREPARATION TO EXECUTION

Geothermal drilling campaign project will begin with the collaborative work by multidisciplinary project team to prepare comprehensive project plan, with the detailed drilling plan as the key deliverable. Once the plan is included in the budget approved by management, the project team will handover drilling program to drilling team for the execution, and once handed over, the drilling time and learning curves are begins. The drilling team will be responsible for carrying out the drilling according to the drilling program and within the budget. Because exploratory drilling is the ultimate activity in the exploration projects, with assigned budget exceeding 80% of the total project budget, effective drilling execution time and cost expenditure within the budget will increase the exploration project's chance of success. One of the most difficult aspects of drilling execution is reducing the learning curve while maintaining safety and standards. The ability to manage the learning curve efficiently has a significant impact on time and expense budgets. With 24 hours and 7 days of drilling operation, the learning curve should be reduced continually, at the activity level, and with immediate corrective action.

3. LEARNING CURVE CONTINUOUS IMPROVEMENT AND IMMEDIATE CORRECTIVE ACTION

Drilling execution consist of numerous series and concurrent activities that be grouped into preparation, execution, and evaluation. To reduce the learning curve as quickly as feasible, a learning curve plan must be developed prior to drilling execution preparation, a learning initiatives implementation strategy must be established during execution, and the identified learning initiatives must be documented for evaluation. Figure 1 depicts the learning curve continuous improvement and immediate corrective action were designed and implemented by the authors and drilling team, which successfully lowered the learning curve for exploration drilling execution.

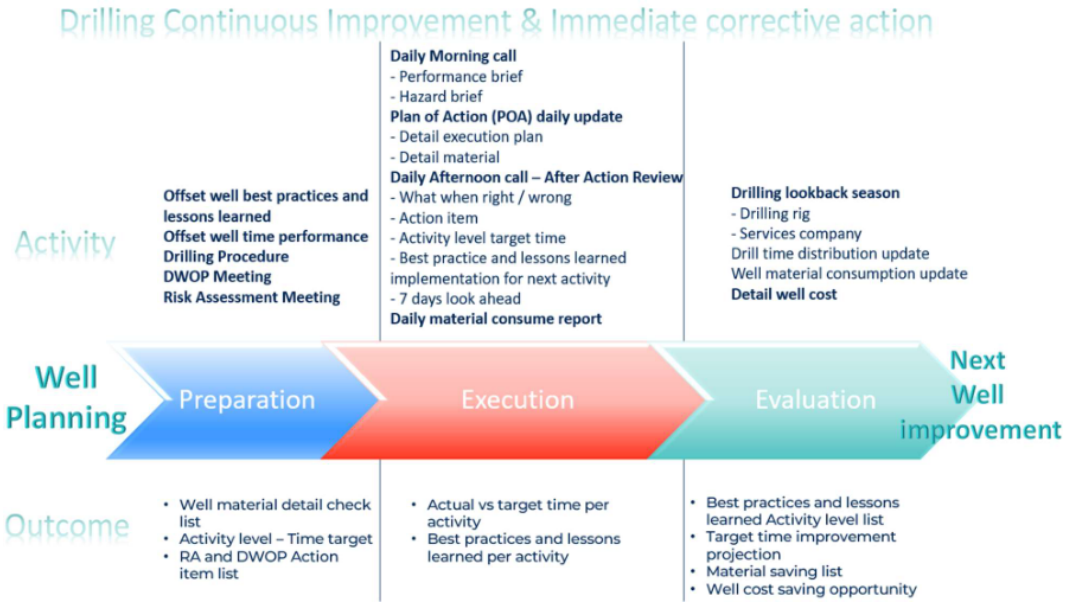

Figure 1: The learning curve continuous improvement and immediate corrective action.

3.1 Drilling Execution Preparation

Drilling execution preparation was optimized to prepare a good learning improvement plan. Through offset well review, all the best practices and lessons learned initiatives were identified and listed to be embedded in the drilling procedure, and the base line time performance of each activity were identified to be set as the execution detail time target. The identified best practices and lessons learned were also used to mitigate all identified risks, as detailed in the risk assessment document.

In the absence of an offset well in the first well of the exploration drilling, the analog well for best practices and lessons learned was selected from Indonesia geothermal well drilling practices, while the base line time performance to calculate the drilling time target was taken from the recent wells drilled by selected drilling rig and services.

In the Risk Assessment (RA) meeting, the mitigation of all identified risks were shared and assessed by all groups involved in the execution to verify all mitigation are practicable and can be implemented prior to the execution at the activity level. While in Drilling Well On Paper (DWOP), the detail drilling procedure includes best practices, the lessons learn mitigation, the detail well material, and the execution detail time targets was reviewed in length and collaboratively with big group to ensure that it is adequate, realistic, and understandable.

All the action items from risk assessment and DWOP meeting were listed, along with the person in charge and target time, and will be carried out as part of the drilling detail execution plan.

3.2 Drilling Execution After Action Review

In drilling execution, well material detail checklist was revisited regularly on daily basis, both before and after the job execution, the detail target time was monitored and reviewed per activity level, and the action item list from RA and DWOP was checked on regular basis before the activity was performed to ensure that all the action items were completed prior to the job.

During drilling execution, in daily morning call that was usually attended by a large group of project drilling team and all involved party representatives, in addition to daily progress reporting and operation discussion, a performance brief session was conducted to compare the actual performance with the target time and gather the best practices and lessons learned from the big group. The drilling hazard briefing was also conducted to ensure

that all mitigation plans for potential hazards in place, as well as to assess the effectiveness of the job's mitigation strategy.

The Plan Of Action (POA) was updated on a daily basis by drilling supervisor in collaboration with the onsite team, and it comprises specific material, services, and support for each activity to ensure that the drilling execution plan is followed accurately and that no human error occurs. The POA was discussed in a daily afternoon call between the drilling engineering team and the drilling operation team as part of After-action review. During this conference, it was examined what when right or wrong in last 12 hours, as well as best practices, lessons learned, and action items for the next 24 hour's work. The activity level target time was ran through to update the 7 days look ahead time. The list of best practices and lessons is constantly updated based on what identified in that day's discussion, and it will be carried over to the drilling evaluation.

3.3 Drilling Execution Evaluation

With the action item review in daily basis during execution, almost none further evaluation was required after the first well was drilled, the team only needed to double check the completeness of the documentation of best practices and lessons learned from the daily drilling execution through drilling lookback season.

During the lookback season, which was attended by all parties involved in the drilling execution, the drilling engineering team shared the drilling performance, including best practices, lessons learned, and sensitivity analysis of the perfect well target, while the rig contractor and each segment of the services company prepared and presented their individual lookbacks. The drilling lookback should be performed before finalizing the next well drilling program to ensure that it is updated with the first well's best practices and lessons learned, target time improvement projection, material saving list and well cost savings opportunity list.

4. DRILLING EXPLORATION LEARNING CURVE IMPROVEMENT

With a detailed learning curve continuous improvement plan and the consistency of project drilling team in the plan implementation, the challenge drilling learning curve has been successfully answered as seen in Figure 2. In the first well, the project team has successfully completed the drilling of the big hole in less than average for the first geothermal exploration well with the big hole design in Indonesia from 2010 to 2023.

With the second well's improvement plan updated with best practices and lessons learned, target time improvement projection, material saving list and well cost savings opportunity list from the first well, the project drilling team successfully completed the drilling two (2) times faster and 31% less cost than the first well and still exceeding the average time of the second geothermal exploration well in Indonesia.

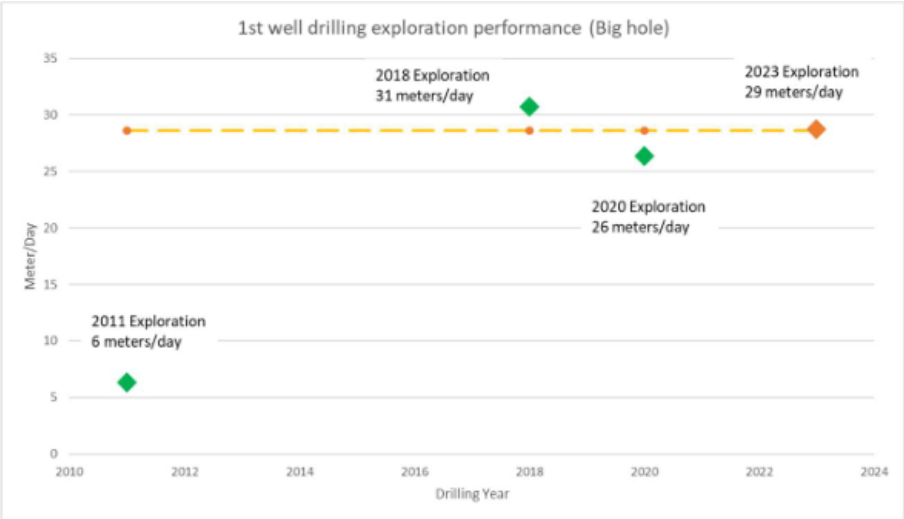

Figure 2: 1st Well drilling exploration.

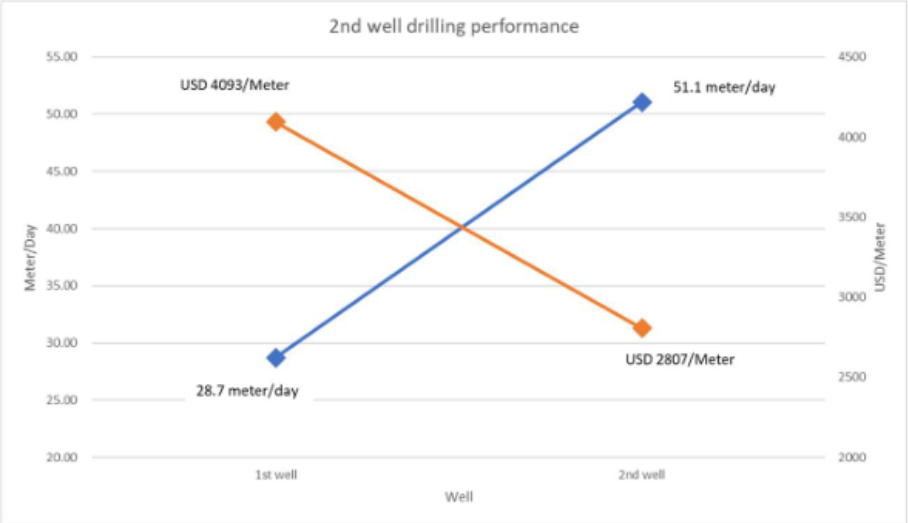

Figure 3: 2nd Well drilling performance.

5. CONCLUSIONS

Drilling learning curves challenges is always there, and they have become more challenging in the exploration well because of the absence of the information as offset, paired with the first operation set up of equipment and organization. With a good detail plan is crucial to the success, the consistency of plan implementation will increase the likelihood of success, close monitoring with immediate corrective action will keeps focus on the center of the target, and team collaboration and coordination increases efficiency have successfully reduced the learning curve of drilling exploration.

REFERENCES

Indoensia project drilling team, Wapsalit project drilling lookback, Ormat Geothermal Indonesia, Jakarta, (2023).

Muhammad, I., Tommy, S. Drilling performance benchmarking study, Ormat Geothermal Indonesia, Jakarta, (2023).

The Influence of Quicklime (CaO) Addition on pH and Silica Recovery in Brine of Dieng Geothermal Plant Indonesia

Desy Hikmatul Siami and Jilda Sofiana Dewi

UGM

desyhikmatulsiami@mail.ugm.ac.id, jildasofianadewi@mail.ugm.ac.id

Keywords: Brine, CaO, Dieng Geothermal Plant, Silica

ABSTRACT

Indonesia is located in a strategic location with volcanoes which makes the country the world's largest geothermal storage. One of the geothermal sources in Indonesia is Dieng. The Dieng geothermal field has a high silica content from the brine around 1065-1400 mg/L SiO2/kg geothermal brine, but the presence of silica is one of the most significant problems in geothermal power plants. Recovery of supersaturated silica in brines is a good method to eliminate scale precipitation. The use of CaO has a practical advantage in removing dissolved silica from the brines. This research focuses on removing dissolved silica using CaO from the brine's Dieng Geothermal Plant. CaO was added as a flocculant with concentrations of 0.5, 1, 5, and 10 g/L. The retention time varied as 0, 15, 30, and 60 minutes. In the case of CaO addition, silica recovery rates increased with the amount of CaO added. These results indicate that addition of CaO can be used for silica recovery from geothermal brine at the Dieng Geothermal.

1. INTRODUCTION

Indonesia is one of the countries that has a lot of benefits from finding alternative energy to replace fossil fuel energy. Compared with all countries in the world, Indonesia has the greatest potential to further develop geothermal energy because Indonesia has the largest geothermal resources in the world. In other words, Indonesia has 40% of the world's geothermal resource potential but only 4% has been utilized (Ministry of Energy and Mineral Resources, 2023). Geothermal energy can develop in Indonesia because Indonesia's geography is dominated by volcanoes. This volcano was formed due to the subduction zone between the Eurasian Plate and the Indo-Australian Plate. The Dieng geothermal field has become a Geothermal Working Area which has an area of around 63 km2 and has a type of system in a two-phase reservoir which is dominated by the liquid phase with a temperature of around 240 °C – 333 °C (Prasetio et al., 2010). According to Boedihardi, et al (1991), the type of Dieng geothermal reservoir system was two-phase, dominated by the liquid phase, and provided information regarding the existence of three prospect areas in the geothermal field in Dieng, namely Sileri, Sikidang-Merdada, and Pakuwaja (Figure 1).

In the liquid phase characteristics, the Dieng geothermal field has a high silica content from the brine (Pambudi, N.A., 2015). The presence of silica is one of the most significant problems in geothermal power plants (Al Radi et al., 2022). The concentration of silica in geothermal fluids is controlled by the solubility and precipitation of different silica minerals. Silica occurs in various forms or polymorphs such as quartz, chalcedony, cristobalite, opal, and amorphous silica, each of which shows variations in solubility (Nicholson, 1993). In the Dieng geothermal field, there is a type of amorphous silica found in the silica scaling process of 90-98% (Jenie et al., 2018). Because silica has reactive properties, it dissolves easily with water, so the higher the temperature, the greater the solubility concentration. The solubility of various scales in geothermal systems has been reported in a specific order: amorphous silica has the highest solubility, followed by aluminum scale, and then ferric silicate scale (Juhri, et al., 2023). This ranking indicates that amorphous silica dissolves more readily in geothermal brine compared to the other types of scales. Understanding this solubility hierarchy is crucial for developing effective strategies for scale management and prevention in geothermal plants. By targeting the most soluble scales, such as amorphous silica, with appropriate chemical treatments or operational adjustments, it is possible to mitigate scaling issues more efficiently and maintain optimal performance in geothermal energy extraction processes.

Juhri, et al., (2023) showns the mineralogical composition of samples labeled OC-S, BR-S, and TP-S, with specific attention to amorphous silica (AS) content using X-ray diffraction (XRD) in Figure 2. The broad humps observed in the regions marked "AS" indicate the presence of amorphous silica in all three samples, as amorphous materials lack the distinct, sharp peaks typical of crystalline structures. The patterns also show peaks corresponding to various other minerals such as sphalerite, galena, pyrite, magnetite, and halite, identified by different symbols. These peaks suggest that, in addition to amorphous silica, the samples contain crystalline phases of these minerals.

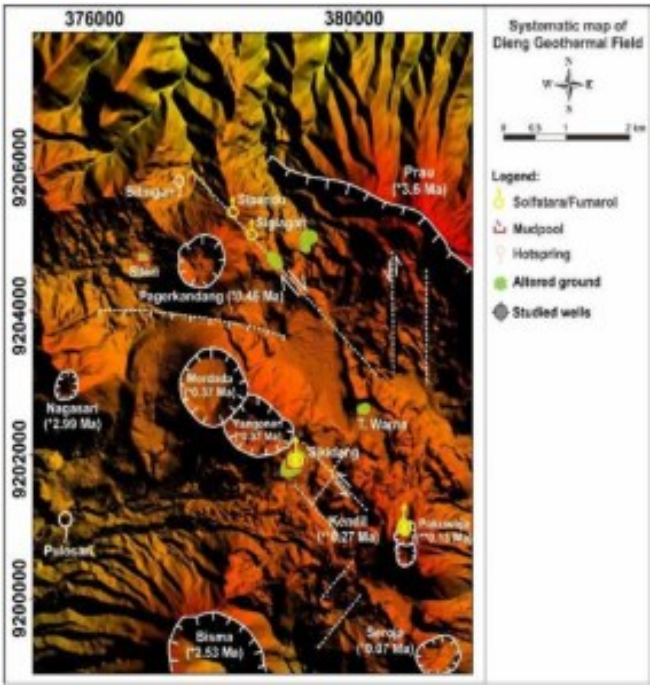

Figure 1: Dieng plateau volcanic area (Shalihin et al., 2020).

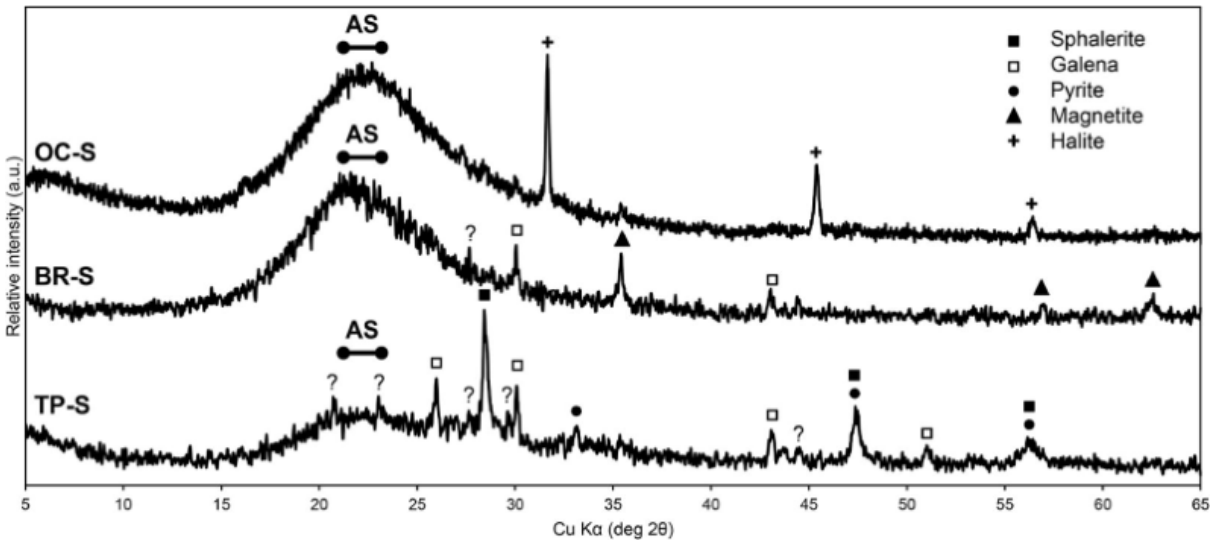

Figure 2. XRD patterns of the scale samples of the Dieng geothermal power plant (Juhri, et al., 2023).

Large concentrations of silica cause scaling in geothermal steam production well pipes and brine injection line pipes. Scaling occurs because of the presence of silica, which originates from salt mineral deposits dissolved in the water. As the concentration of silica increases, it can form a crust that obstructs the fluid flow process within the pipes. This blockage can significantly impair the efficiency and functionality of the geothermal system, leading to increased maintenance costs and operational challenges. The presence of crust and brine from the separation process represents a potential waste product that can be reused, thereby enhancing its utility value. For instance, silica from geothermal brine can be repurposed as adsorbents, used in the field of building materials, the synthetic materials industry, or further processed into nanomaterial-based products. This approach not only addresses the issue of scaling but also aligns with sustainable waste management practices, contributing to the overall efficiency and environmental friendliness of geothermal energy production (Asadi & Norouzbeigi, 2018; Syabani et al., 2020). To be able to utilize silica (SiO2), it is necessary to have a recovery process or recover pure silica from solidified geothermal waste. The recovery results can be further processed into downstream products. Silica downstream products are widely used in various sectors such as civil and construction, cleaning products, pharmaceuticals, and cosmetics. Silica is also the main precursor for various types of inorganic and organometallic materials (Terzioglu et al. 2013).

Recovery of supersaturated silica in brines is a good method to eliminate scale precipitation. The use of CaO has a practical advantage, for it is inexpensive and effective in removing dissolved silica from the brines. This research focuses on removing dissolved silica using CaO from the brine's Dieng Geothermal Plant.

2. METHODS

In this study, brine samples were obtained from the Dieng Geothermal Plant. The chemical reagents to recover supersaturated silica were quicklime (CaO). A total of 850 mL brine was collected in a teflon beaker and kept at 90 ◦C in a water bath. After keeping the brine at 90 ◦C for a given retention time 15, 30, and 60 min, CaO was added as a flocculant and stirred. The concentration of CaO was 0.5, 1, and 5 g/L. After adding the chemicals, the sample water was collected and filtered through a 0.2-µm membrane filter, then filtrate followed by chemical analysis of total silicic acids using a spectrophotometer (Ueda., et.al., 2022). Table 1 shown the data collection matrix for this research.

Table 1: Data Collection Matrix.

Retaining Time (min)	Code Sample		
	0.5g CaO	1g CaO	5g CaO
15	Sample 1	Sample 4	Sample 7
30	Sample 2	Sample 5	Sample 8
60	Sample 3	Sample 6	Sample 9

Table 2: Chemical composition of brine Dieng geothermal power plant.

Element	Concentration (ppm)
SiO_2	1065 – 1400
Cl	21200 – 28400
SO_4	74.4
Li	40-60
Na	8340 – 11460
K	2520 – 3340
Mg	0.5
Ca	440 – 860
HCO_3	25.0
Fe	1.35
Al	0.01

3. RESULT AND DISCUSSION

The general chemical characteristics of brine, such as chemical elements, their concentrations, and total dissolved solids, are key for understanding how brines form and their economic values. According to the Mineral Resources Handbook, for water bodies, a salinity value (total dissolved solids) (TDS) of less than 1 g/L is classified as fresh water, 1–3 g/L as brackish water, 3–10 g/L as salt water, 10 ‑ 50 g/L as saline water, and a salinity value of ⩾50 g/L as brine. The average salinity of seawater is 35 g/L (saline water) (Liu et al., 2023). As brine salinity increases, the contents of some components increase or decrease. For example, in the brine of the Kunteyi salt lake in the Qaidam Basin, the potassium and magnesium contents increase with increasing salinity, but the sodium and chloride contents decrease rapidly after the salinity reaches 340 g/L, as a result of sodium chloride crystallization. In addition, the calcium concentration decreases with increasing salinity, due to gypsum precipitation. The contents of some minor and trace elements, such as lithium and boron, generally increase with increasing salinity (Liu et al., 2023).

The formation of silica scaling in the brine injection pipeline is controlled by the chemical and thermodynamic properties of amorphous silica (Pambudi, et al., 2015). During the brine injection process, heat transfer occurs as the brine flows through the injection pipe. This process is exothermic, meaning the system releases heat to the surroundings because the brine's temperature is higher than that of the environment. The heat transfer process causes a distribution of brine temperature as it flows along the injection pipeline. The chemical attribute of amorphous silica that significantly impacts scaling formation is its saturation solubility in relation to temperature. The variation in brine temperature during the injection process leads to a decrease in the saturation solubility of amorphous silica along the injection route. Brine contains cations such as K^+, Ca^{2+} , Na^+, Mg^{2+}, Li^+, B^{3+}, Rb^{2+} , and Cs^{2+}, as well as anions such as SO_4^{2-} , Cl^-, HCO_3^-, CO_3^{2-}, NO_3^-, Br^-, and I^-, which are valuable elements (Liu

et al., 2023). Chemical analysis of anions and cations in brine at the Dieng geothermal power plant shown in Table 1 (Juhri, et al., 2019 and Pambudi, et al., 2015).

Table 2 presents the chemical composition of the brine from the Dieng geothermal power plant. The concentration of each element is measured in parts per million (ppm). Silicon dioxide (SiO2) ranges from 1065 to 1400 ppm. Silica is commonly found in geothermal brine and can lead to scaling in equipment if concentrations are high. Chloride (Cl) is found in high concentrations, ranging from 21200 to 28400 ppm, indicating the high salinity of the brine. Sulfate (SO4) has a concentration of 74.4 ppm, an important component though present in lower amounts compared to chloride. Lithium (Li) concentrations range from 40 to 60 ppm, valuable for its use in battery production. Sodium (Na) is another major cation in the brine, with concentrations between 8340 and 11460 ppm. Potassium (K) ranges from 2520 to 3340 ppm, another significant cation. Magnesium (Mg) is found in very low concentrations at 0.5 ppm. Calcium (Ca) ranges from 440 to 860 ppm and can contribute to scaling when reacting with carbonates or sulfates. Bicarbonate (HCO3) has a concentration of 25.0 ppm, indicating dissolved carbonates which can also lead to scaling. Iron (Fe) is present at 1.35 ppm and can cause corrosion issues in equipment if found in higher concentrations. Finally, aluminum (Al) is found in very low concentrations at 0.01 ppm.

3.1. Behavior of silicic acid in brine

Silicic acid (H_4SiO_4) in geothermal brine exhibits complex behavior influenced by several factors such as temperature, pH, concentration, and the presence of other ions. Silicic acid has limited solubility in water and remains in its monomeric form at lower concentrations. However, as the concentration increases, particularly in geothermal brine, it tends to polymerize into larger molecules like dimers, trimers, and colloidal silica particles, leading to the formation of silica deposits or scaling. The temperature in geothermal environments significantly affects this process; higher temperatures accelerate the polymerization of silicic acid, resulting in faster silica scale formation on surfaces like pipes, turbines, and heat exchangers. The pH of the brine also plays a crucial role in determining the speciation of silicic acid. At neutral to slightly acidic pH, it remains mostly monomeric, whereas in more alkaline conditions, it deprotonates to form silicate anions, which are less likely to polymerize. Additionally, the ionic strength of the brine, influenced bythe presence of ions such as sodium, calcium, and magnesium, can either inhibit or promote polymerization depending on their concentrations and interactions with silicic acid. Silica scaling poses a significant operational challenge in geothermal power plants by reducing efficiency, increasing maintenance costs, and causing downtime. Various strategies are employed to mitigate silica scaling, including pH adjustment, the use of chemical inhibitors, regular mechanical removal of deposits, and gradual cooling of the brine to prevent rapid polymerization. Understanding the behavior of silicic acid in brine is essential for efficient geothermal power plant operation, enabling the management of factors that influence silicic acid behavior to minimize the negative impact of silica scaling and maintain optimal system performance.

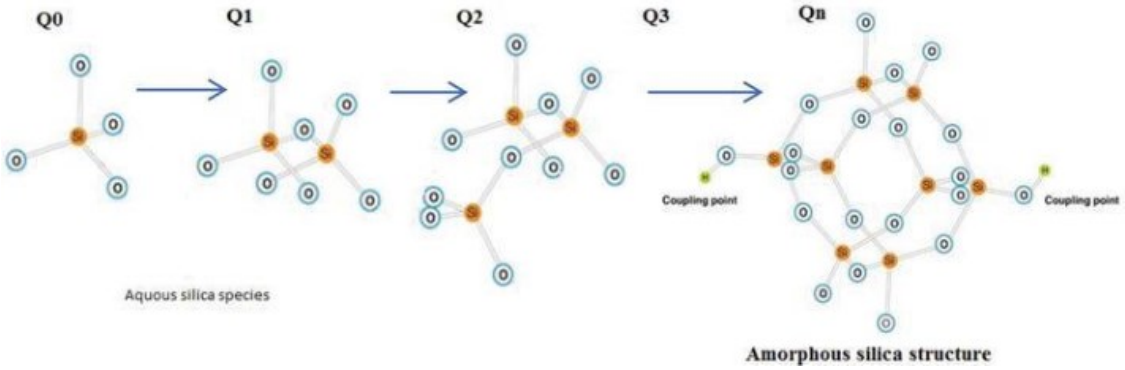

Figure 3: Mechanism of dissolved silica species (Q0 < Q1 < Q2 < Q3 aggregation) polymerisation into amorphous silica structure (Luvenich, 2020).

Dissolved silica species polymerisation path or aqueous silica solubility showns in Figure 3. The process begins with monomeric silica species (Q0), which are individual silicon atoms bonded to hydroxyl groups. These monomers can polymerize to form dimers (Q1), trimers, and eventually larger oligomers (Q2), as the silicon atoms bond together through siloxane bonds (Si-O-Si). As the polymerization continues, the oligomers grow into larger structures (Q3) through further condensation reactions. Finally, these increasingly complex structures aggregate to form amorphous silica (Qn), a non-crystalline, random network of silica. This process involves coupling points where the individual silica species join, leading to the formation of the extensive, interconnected network characteristic of amorphous silica.

3.2. CaO addition to brine

The addition of calcium oxide (CaO) plays a crucial role in enhancing silica recovery. When CaO is introduced into the brine, it reacts with dissolved silica species to form calcium silicate compounds. This reaction promotes

the precipitation of silica, converting it from its dissolved state into a solid form that can be more easily removed from the solution. During the entire retention time, the total concentration of silicic acid in the brine decreased immediately after the addition of CaO. The concentration of silicic acid decreased by around 34% upon addition of 5g CaO at a retention time of 60 min. The total concentration of silicic acid at the Dieng Geothermal Plant was reduced to less than 350 mg/L by adding 5 g/L CaO at a retention time of 60 min. The target silicic acid concentration in the treated brine is about 380 mg/L, which is the solubility of amorphous silica (Fournier, 1977). So in this study the recovery of silicic acid was in accordance with the solubility limit of amorphous silica.

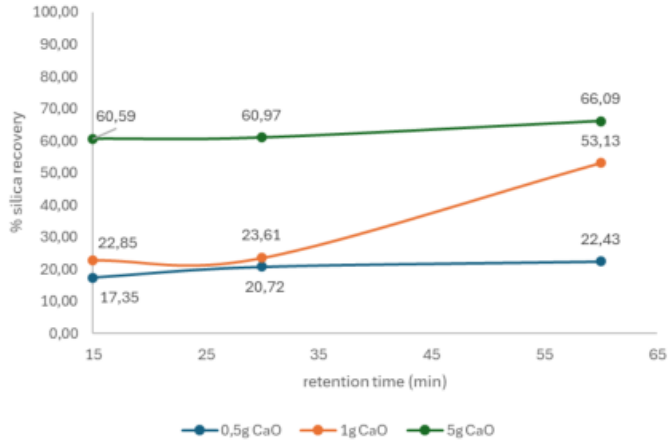

Figure 4: Percentage of silica recovery at various residence times.

The Figure 4 illustrates the effect of CaO addition on silica recovery at three different CaO concentrations (0.5g, 1g, and 5g) over retention times of 15, 30, and 60 minutes. The recovery of silica increases slightly from 17.35% to 22.43% at 0.5g CaO, more significantly from 20.72% to 53.13% at 1g CaO, and from 60.97% to 66.09% at 5g CaO. This trend suggests that higher concentrations of CaO and longer retention times both contribute to increased silica recovery. The underlying reason for this behavior lies in the chemical interactions between CaO and silica. Calcium oxide (CaO) can react with dissolved silica in the brine to form calcium silicate compounds, which precipitate out of the solution. Higher concentrations of CaO provide more reactant available to interact with silica, leading to a greater amount of silica being precipitated and thus recovered. Additionally, longer retention times allow more time for these chemical reactions to occur and for the precipitated silica to settle out, further enhancing recovery. Therefore, both the amount of CaO and the retention time are crucial factors in maximizing silica recovery from geothermal brine.

The addition of CaO increases the pH of the brine, further driving the polymerization and precipitation processes. When 5 g/L CaO is added, the pH increases to about 10. This indicates that returning the treated brine through the reinjection well requires adjusting the pH to neutral or slightly alkaline by adding acid to suppress the reaction between the treated brine and surrounding rocks in the reservoir. As the pH rises, silicic acid deprotonates and forms silicate anions, which readily combine with calcium ions (Ca^{2+}) provided by the CaO. This reaction leads to the formation of calcium silicate hydrates, which precipitate out of the solution. In the neutral pH regions, $SiO_2aq/H_3SiO_4^-$ (or $SiO_2aq/Si(OH)_3O^-$) mol ratios are approximately 1/1000, decrease with increasing pH and are almost unity at pH >10 ($H_3SiO_4^-$ is the dominant species). For Ca species, Ca^{2+} ions are always the dominant ones (Ca^{2+} /$CaCl^+$ mol ratios are always~1.2), and Ca^{2+}/ $H_3SiO_4^-$ and $CaCl^+$/ $H_3SiO_4^-$ mol ratios become 10.5 (Ueda et al., 2003). These results demonstrate that Ca reacts with SiO_2 and $H_3SiO_4^-$ and that the surface of the silica deposits is covered by the dominant species in the brines, i.e. $H_3SiO_4^-$ at pH <10.5, and Ca^{2+} and/or $CaCl^+$ at pH >10.5.

At a pH of 6.77 in these brines, it was observed that the amount of silica extracted from geothermal brines increased. Thomas (1992) noted that raising the pH by adding NaOH to Hawaiian geothermal brines with SiO2 and Ca concentrations of 700 and 500 mg/l, respectively, led to a reduction in total silica levels. Significant silica deposition in the brines occurred at pH levels exceeding 10 (Kato et al., 2003). Table 3 presents findings from the addition of quicklime without pH adjustment. Increasing the reagent concentration resulted in a decrease in the total silica concentration of the brines, with pH levels rising from 6.71 to 11.74 due to the generation of OH- ions through the addition of quicklime ranging from 0.5 to 5 g/l, respectively. Similar outcomes were observed at the Mokai geothermal plant in New Zealand, where most silica could be removed from the brines at pH levels exceeding 11 (Ueda et al., 2003).

The recovery of silica through the addition of CaO is a strategic approach that addresses both operational efficiency and maintenance concerns in geothermal power plants. By facilitating the precipitation of silica, CaO effectively reduces the concentration of dissolved silica in the brine, thereby mitigating the risk of silica scaling. This scaling can otherwise lead to significant performance degradation of the plant's equipment, such as heat

exchangers, turbines, and pipes, due to the accumulation of amorphous silica deposits. The precipitated calcium silicate can be easily separated from the brine through filtration or sedimentation processes, ensuring that the brine entering the geothermal system is much cleaner and less likely to cause scaling.

Table 3: Effect of adding quicklime (CaO) on pH.

Code	pH
Sample 1	6.71
Sample 2	7.57
Sample 3	8.17
Sample 4	7.77
Sample 5	8.11
Sample 6	9.34
Sample 7	9.37
Sample 8	10.74
Sample 9	11.74

Moreover, this method of silica recovery preserves the integrity of the geothermal infrastructure. By continuously removing silica from the brine, the lifespan of the equipment is extended, and the frequency of maintenance shutdowns is reduced. This results in more consistent energy production and lower operational costs. Additionally, the recovered silica, in the form of calcium silicate, has potential applications in various industries, such as construction and materials science, providing an opportunity for resource recycling and value addition.

4. CONCLUSION

In conclusion, adding CaO for silica recovery is an effective method to prevent scaling and maintain the efficiency of geothermal power plants. Silica recovery shows a slight increase from 17.35% to 22.43% with 0.5g of CaO, a more significant rise from 20.72% to 53.13% with 1g of CaO, and from 60.97% to 66.09% with 5g of CaO. This pattern indicates that higher CaO concentrations and longer retention times enhance silica recovery. By exploiting the chemical interactions between CaO and dissolved silica, geothermal plants can improve performance, reduce maintenance costs, and potentially generate valuable by-products. For future research, it is recommended to conduct silica recovery using a series of test circulations or a closed-loop system to better simulate the actual process in a geothermal power plant.

ACKNOWLEDGEMENT

Thanks to Geo Dipa Plant Dieng and LPDP Kelurahan Universitas Gadjah Mada that have taken part to commit and contribute to this sustainable project, and all individuals who have contributed by providing insights and corrections.

REFERENCES

Al Radi, M., Adil Al-Isawi, O., Abdelghafar, A. A., Fayez Abu Qiyas, A., AlMallahi, M., Khanafer, K., and Assad, M. E. H. (2022). Recent progress, economic potential, and environmental benefits of mineral recovery geothermal brine treatment systems. Arabian Journal of Geosciences, 15(9). https://doi.org/10.1007/s12517-022-10115-4.

Asadi, Z., and Norouzbeigi, R. (2018). Synthesis of colloidal nanosilica from waste glass powder as a low cost precursor. Ceramics International, 44(18), 22692–22697. https://doi.org/10.1016/j.ceramint.2018.09.050.

Boedihardi, M., Suranto, and Sudarman, S. (1991). Evaluation of the dieng geothermal field: review of development strategy. Proceedings 20th Indonesian Petroleum Association. https://doi.org/10.29118/ipa.1483.347.361.

Elders, W. A., and Moore, J. N. (2016). Geology of geothermal resources. In Geothermal Power Generation: Developments and Innovation. Elsevier Ltd. https://doi.org/10.1016/B978-0-08-100337-4.00002-4.

Jenie, S. N. A., Ghaisani, A., Ningrum, Y. P., Kristiani, A., Aulia, F., & Petrus, H. T. M. B. (2018). Preparation of silica nanoparticles from geothermal sludge via sol-gel method. AIP Conference Proceedings, 1–6. https://doi.org/10.1063/1.5064968.

Juhri, Saefudin., Yonezu, Kotaru., Yokoyama, Takushi., Nurpratama, M. Istiawan., Harijoko, Agung., (2019). Formation Mechanism of Silica Scale in Dieng Geothermal Power Plant, Indonesia. Conference: 41st New Zealand Geothermal Workshop.

Juhri, S., Yonezu, K., Harijoko, A., Nurpratama, M. I., & Yokoyama, T. (2023). Diverse scale deposition in response to the change in chemical properties of geothermal water at the Dieng geothermal power plant, Indonesia. Geothermics, 111, 102717.

Kato, K., Ueda, A., Mogi, K., Nakazawa, H., & Shimizu, K. (2003). Silica recovery from Sumikawa and Ohnuma geothermal brines (Japan) by addition of CaO and cationic precipitants in a newly developed seed circulation device. Geothermics, 32(3), 239–273. https://doi.org/10.1016/S0375-6505(03)00019-1

Liu, C., Lowenstein, T. K., Wang, A., Zheng, C., & Yu, J. (2023). Annual Review of Environment and Resources Brine: Genesis and Sustainable Resource Recovery Worldwide. 48, 371–394. https://doi.org/10.1146/annurev-environ-112621-

Nicholson, K. (1993). Geothermal fluids, chemistry and exploration techniques. Springer Verlag.

Pambudi, N. A., Itoi, R., Yamashiro, R., Alam, B. Y. C. S., Tusara, L., Jalilinasrabady, S., and Khasani, J. (2015). The behavior of silica in geothermal brine from Dieng geothermal power plant, Indonesia. Geothermics, 54, 109-114, https://doi.org/10.1016/j.geothermics.2014.12.003

Prasetio, R., Abidin, Z., and Yulizar, Y. (2010). Isotope and Gas Geochemistry of Dieng Geothermal Field, Indonesia Isotope and Gas Geochemistry of Dieng Geothermal Field, Indonesia. Proceedings World Geothermal Congress 2010.

Shalihin, M. G. J., Utami, P., and Nurpratama, M. I. (2020). The Subsurface Geology and Hydrothermal Alteration of the Dieng Geothermal Field, Central Java: A Progress Report. IOP Conference Series: Earth and Environmental Science, 417(1). https://doi.org/10.1088/1755-1315/417/1/012010.

Syabani, M. W., Ina, A., Indri, H., and Yayat, I. S. (2020). Silica from geothermal waste as reinforcing filler in artificial leather. Key Engineering Materials, 849 KEM, 78– 83. https://doi.org/10.4028/www.scientific.net/KEM.849.78.

Terzioglu, P., Yucel, S., Rababah, T. M., and Özçimen, D. (2013). Characterization of wheat hull and wheat hull ash as a potential source of SiO2, BioResources 8(2),4406-4420. https://doi.org/10.15376/biores.8.3.4406-4420.

Ueda, A., Ozawa, A., Unami, S., Kusakabe, M., Hirayama, N., Mogi, K., Ikeda, M., Yokoyama, T., and Yonezu, K. (2022). Recovery of silica from saline geothermal brine at the Yamagawa Power Plant for inhibition of scale formation by batch- and circulation-tests using cationic flocculant and quicklime. Geothermics, 99, 102312. https://doi.org/10.1016/j.geothermics.2021.102312.

Improving Geothermal ORC Capacity by Using Chemical Method to Remove Silica Deposit

Radhitya E Pradipta[1], Ryan Hidayat[1], Mona Natalia Siahaan[2], and Gabriel Mendoza[2]

[1]KS Orka Renewable
[2]Nalco Ecolab

radhitya.pradipta@ksorka.com, ryan.hidayat@ksorka.com,
gabriel.mendoza@ecolab.com, monanatalia.siahaan@ecolab.com

Keywords: Organic Rankine Cyle, Silica Deposition, Cleaning

ABSTRACT

The development of ORC (Organic Rankine Cycle) technology at Sorik Merapi Geothermal Field represents a significant advance in the utilization of geothermal energy. The ORC technology from Kaishan Group can extract more energy from brine. However, the ORC operations are challenged by rapidly changing operational conditions, particularly fluctuations regarding temperature and pressure. These changes can lead to technical issues, including the formation of silica scale deposits within ORC tubing, which adversely affect the ORC's performance and longevity. Scale deposit may cause lower heat exchange process in the system which have necessitate shutdowns for cleaning the tubing. This also effects on efficiency and reliability of the ORC.

To overcome this challenge, chemical methods have been implemented at Sorik Merapi. This method involves dissolving the scale deposits into smaller deposits, even reducing into monomeric silica form. The cleaning procedure includes identifying the suitable chemical and soaking it in the Heat Exchanger tubing before continuing with mechanical cleaning out with water.

The result of this method has been promising. It has effectively restored the heat transfer efficiency and recover the brine flow inside the tubing. The ability to perform cleaning efficiently and with minimal operation disruption ensures that the ORC system can maintain high performance and reliability.

1. INTRODUCTION

Sorik Marapi Geothermal Power project is located in Mandailing Natal regency, North Sumatra. Total generation until January 2024 is 160 MWe. The utilization of Brine ORC (Organic Rankine Cycle) namely ORC-XV begins in June 2021 during unit 2 commissioning. Dengan installed brine ORC-XV from Kaishan Group adds generation 2.5 MW with flow rate 380-400 M3/hr. The brine ORC transfers the heat from the brine to the secondary fluid medium which cause the brine temperature to reduce from 143°C to 75°C. With this energy extraction, reduction in temperature, and the chemistry in the brine, the silica saturation index will increase from 1.11 to 2.41 which indicates that silica scaling and deposition potential will increase during the extraction process, as amorphous silica has prograde solubility with regards to temperature (Fournier and Rowe, 1977).

In extracting geothermal energy, particularly in brine ORC system, silica has long been a critical factor that limits the energy extraction from geothermal fluid. Silica deposition forms a highly insulative that reduce the heat transfer. At severe condition, the silica deposition can hinder the fluid flow to the brine ORC system and reduce injectivity in the reinjection well. The layer that formed, apart from being insulative, it also very tenacious and difficult to remove.

The silica deposition is the result of multiple coexisting chemical reactions and processes in the geothermal fluid: direct deposition of monomeric silica, co-precipitation with other minerals and ions (mostly metals), and monomeric silica polymerization (Gill and Jacobs, 2018). Many chemical and physical parameters, such as the concentration of silica and other minerals, temperature (Fournier et al., 1983), Setiawan et al., 2019), binary unit design (Grassiani, 2000), acidity (Addison, et al., 2015), and others, influence these reactions and processes. To stop silica deposition, every reaction, process, and variable needs to be managed at the same time.

It cannot be denied that even though silica inhibitors are used, the silica scale will still be formed, therefore clean-out is carried out using combination of chemical and mechanical methods to remove scaling in the heat exchanger tubing if generation lower than 80% compared to original performance.

2. METHODOLOGY

Silica (SiO_2) exists in a number of different forms. Quartz (crystalline silica) is one of the most abundant minerals in the Earth's crust and exists as such in the geothermal reservoir, while it is normally precipitated in surface

equipment as amorphous (non-amorphous) silica. As is the case for most minerals, amorphous silica has prograde solubility with regards to temperature (Fournier and Rowe, 1977) as shown in the equation: *log C = -731/T + 4.52,* where C and T are silica concentration and temperature, respectively. Because of this, amorphous silica is one of the most ubiquitous minerals found in geothermal heat exchangers (Zarrouk, 2019). The difference in the solubility of quartz and amorphous silica (see Figure 1) allows the operationality of geothermal power development, otherwise any temperature decrease will lead to silica scaling immediately (Brown, 2011).

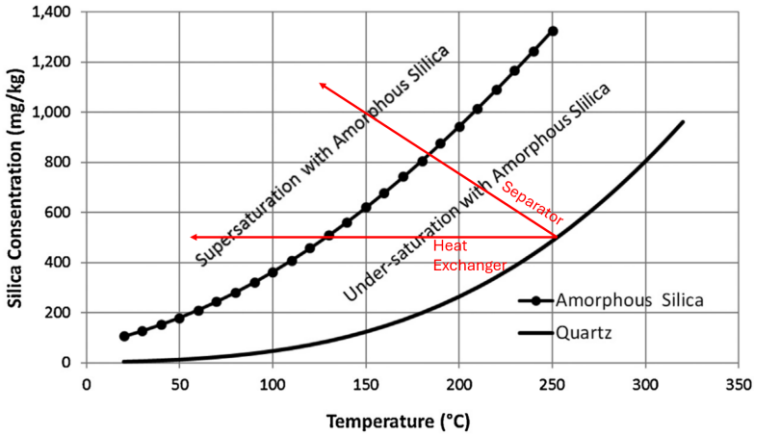

Figure 1: Solubility of quartz and amorphous silica with temperature (Modified from Zarrouk et al., 2014).

One of the most widely used method to prevent silica scale deposition is pH-modification (reduction) which retards the precipitation and deposition of amorphous silica in surface facilities (Gallup, 2011). It is considered a cost-effective approach in dealing with silica scaling. Another scale control method is by using of polymeric silica inhibitors which has the advantage of lower corrosion rates compared to the former. Silica inhibitors can be considered at brines where high silica concentration drives scale formation (Finster et al, 2015). Several tests in the laboratory and in the field were done by geothermal industry experts in the past (Mejorada et al., 2000; Baltazar et al., 2014; Gill and Jacobs, 2018). These studies showed field testing is one of the keys to determine and effectively implement a working and economical method to minimize silica scaling.

Despite efforts to mitigate silica deposition, clean-out of geothermal pipelines and heat exchangers are still needed periodically. Silica deposition leads to deterioration of heat transfer and reduction in power generation of ORC units. Candido and Zarrouk (2017) studied different cleaning methods accounting for both technical and economic aspects to be applied in a binary plant in the Philippines. The methods involved water blasting, mechanical cleaning, chemical cleaning (using HCl, HF acid and inhibitor) or a combination of these.

Caustic solution can also dissolve silica scales and calcite scales in the presence of a chelating agent was shown by some studies (Xu et al., 2009; Rose et al, 2010) in laboratory experiments and in simulation software. This is also in line with the experiments conducted by Lichti et al. (2000) in Ohaaki that silica scaling can be prevented by increasing the pH of the brine using alkali solution. Caustic soda was also shown to be able to disilicate geothermal brine in the experiment by Gallup (2003). This is because solubility of silica increases at higher pH, where the weak silicic acid (H_4SiO4) dissociates to H^+ and H_2SiO4^- ion at very high pH (Brown, 2011). The solubility of amorphous silica as a function of pH is illustrated in the graph below:

The graph in Figure 2 shows that the solubility of amorphous silica sharply increases as the pH increases. The abovementioned studies show that combination of caustic chemicals and thermally stable chelating agents can be effective approach to mineral dissolution or chemical cleanout in geothermal. In this paper, chemical clean-out was also implemented using NaOH and chelating agent to dissolve the silica deposits in the ORC. The method is done by injecting chemicals inside the heat exchangers, soaking, disposing it, then repeating the process until the clean-out is complete. The main equipment and tools used are chemical dosing pump, chemical tank, hose, and NaOH IBC tank. The key parameters monitored are pH, temperature, pressure, silica concentration and conductivity.

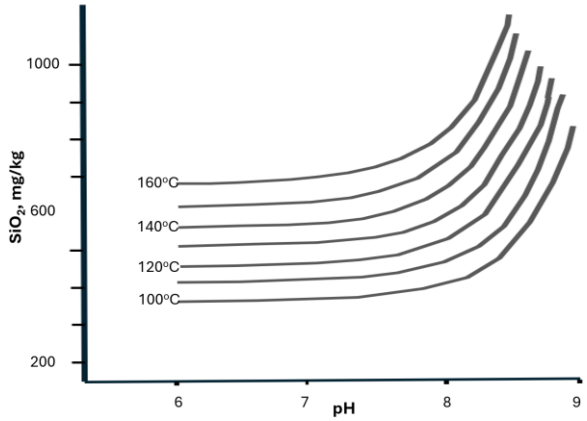

Figure 2: Solubility of amorphous silica with pH (Modified from Brown et al., 2011).

The cleaning process was started by filling the system with hot brine, followed up by turning on the heater and circulation pump. It is critical to keep the temperature within 70-80°C to reduce risk of coagulation of particles. NaOH was then injected until pH reached and stabilized at 12-13, followed by chemical dosing. Soaking of the heat exchangers was done for about six hours before flushing as certain silica concentration and conductivity thresholds were reached. This process was repeated until silica concentration in the solution dropped to the original concentration in the brine. The whole chemical cleanout was run for 36 to 48 hours per ORC. More details in the method are discussed in the Clean Out Program section in this paper.

3. PLANT OPERATING CONDITION

The Brine ORC-XV plant captures the energy from the geothermal brine that collected from two production wells. The plan diagram can be seen Figure 1. The chemistry and thermodynamic properties from each production well can be seen in Table 1.

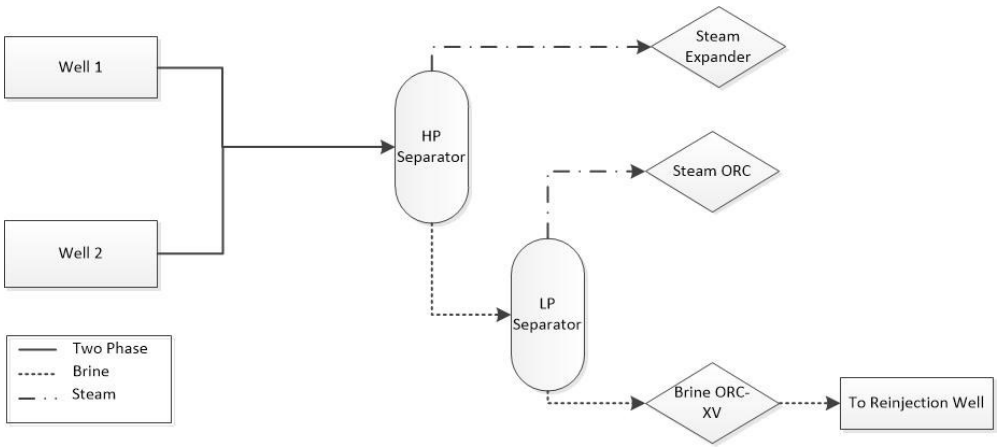

Figure 3: Sorik Marapi Geothermal Field Unit-2 ORC Plant Diagram.

Table 1: Sorik Marapi Geothermal Field Unit-2 ORC Plant Production Well Properties.

Parameter	Well 1	Well 2
Enthalpy (kJ/kg)	1044	1122
Flow Rate (ton/hour)	270	226
Sampling Temperature (0C)	167	167
pH at 250C	8.4	8.5
Silica (ppm)	555	610
Aluminum (ppm)	0.79	0.86

As can be seen in Figure 1, there are three High Pressure separators and one Low Pressure separator. The steam from all HP separators will be combined and sent to Steam Screw Expander. The brine from HP separator combine with two phase fluid from Well 1 and 2 separated once more in LP separator. The brine from LP Separator sent to brine ORC, while the steam go to Screw Expander and the excess team going to Steam ORC. Based on the

operating condition in each separator, the chemical properties and operating condition at the brine ORC inlet can be seen in Table 2.

Table 2: Sorik Marapi Geothermal Field Unit-2 ORC Plant Chemistry & Operating Condition.

Parameter	Brine ORC
Inlet Temperature (^{0}C)	144
Outlet Temperature (^{0}C)	75
Flow Rate (ton/hour)	380-400
Silica (ppm)	~647

Based on the profile temperature in the Brine ORC, we used the formula from Fornier and Rowe, 1977 to simulate the silica saturation index (SSI) based on Amorphous silica solubility, to understand the degree of scaling in the system. The result of simulation can be seen in Figure 4.

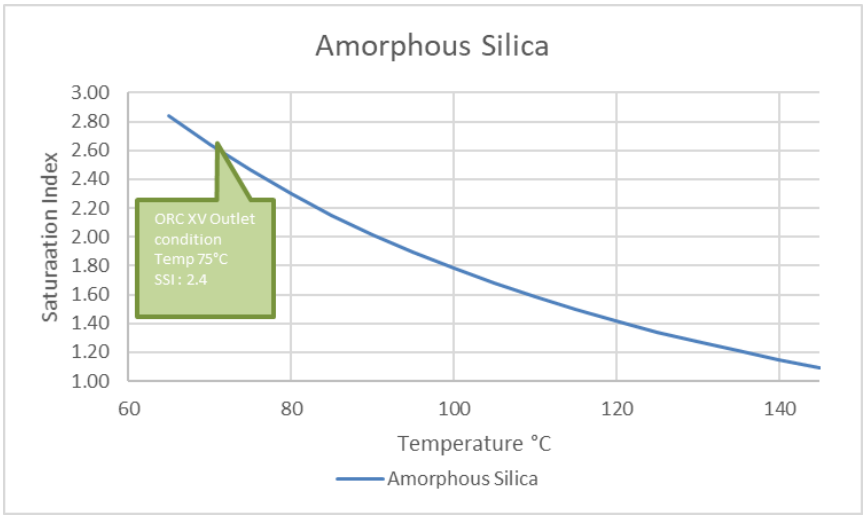

Figure 4: Silica Saturation Index at Brine ORC-XV.

From the Figure 4, it can be seen that the brine at 90^{o}C is in supersaturated condition (SSI 2.09). Therefore, the silica scaling is inevitable and must be mitigated to maintain the heat transfer rate.

4. SILICA INHIBITOR IMPLEMENTATION RESULT

Silica inhibitor has been implemented to prevent silica scale formed in Heat exchanger. The system is closely monitored to determine the effectiveness of this program. The lead parameters that monitored are brine ORC differential pressure, monomeric silica at the inlet and outlet of brine ORC (%polymerization), and the lag parameter is generation.

4.1 Lead Parameter

Monitoring the lead parameter conducted on daily basic. Monomeric silica analysis can be used to determine the silica deposition rate in the system. If well maintained in the monomeric form, the system's deposition rate will be reduced. The monomeric silica analysis can be used to optimize the inhibitor dosage according to requirements because it is done on-site. The inhibitor dosage is deemed sufficient to prevent polymerization if the monomeric silica at the brine ORC outlet is kept at a value of more than 90% of the brine ORC inlet silica concentration (<10% polymerization) as the result,the silica polymerization is able to maintained below 10% with average polymerization is 5.8%.

Delta temperature is obtained from subtracting the inlet temperature from the outlet temperature. The delta temperature will increase as the result of scale, the heat extraction is not in the optimized caused by silica scaling forming in the tubbing. Monitoring delta temperature shows the temperature can be maintained.

Similar with delta temperature, Delta pressure is obtained by subtracting the inlet pressure and outlet pressure. If scaling takes into account the delta pressure, it will increase as the result of blocked tube by scaling silica in the heat exchanger. The Figure 3 suggest that delta pressure is well maintained in a range.

4.2 Lag Parameter

Generation is a lag parameter to determine the success of silica inhibitor treatment. Unlike lead parameter which can be monitored on daily basic and corrective action taken immediately. The generation will be affected if scaling has been formed in Heat exchanger.

Even though the lead parameters show that everything is on target, it cannot be denied that silica scale still forms. However, with management using silica inhibitor chemicals to prevent scale, the generation is able to maintain 80% of its initial capacity. In the case of ORC-XV, modifications were made in October because the source was divided into SMGP U-4 , thus the maximum generation could not return to the condition in February.

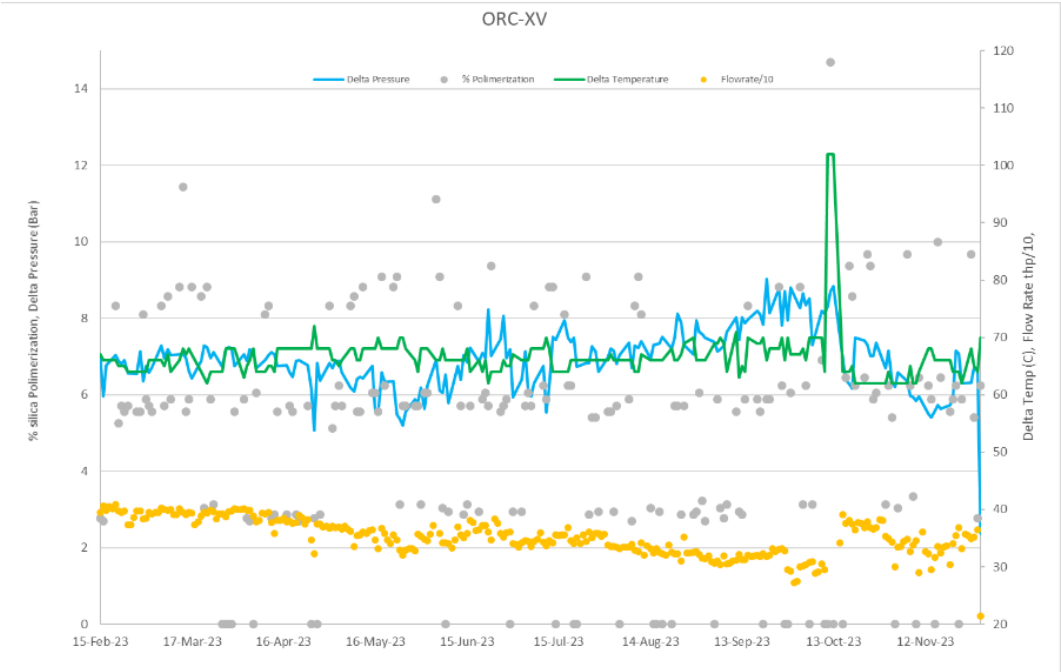

Figure 5: ORC-XV Lead Parameter.

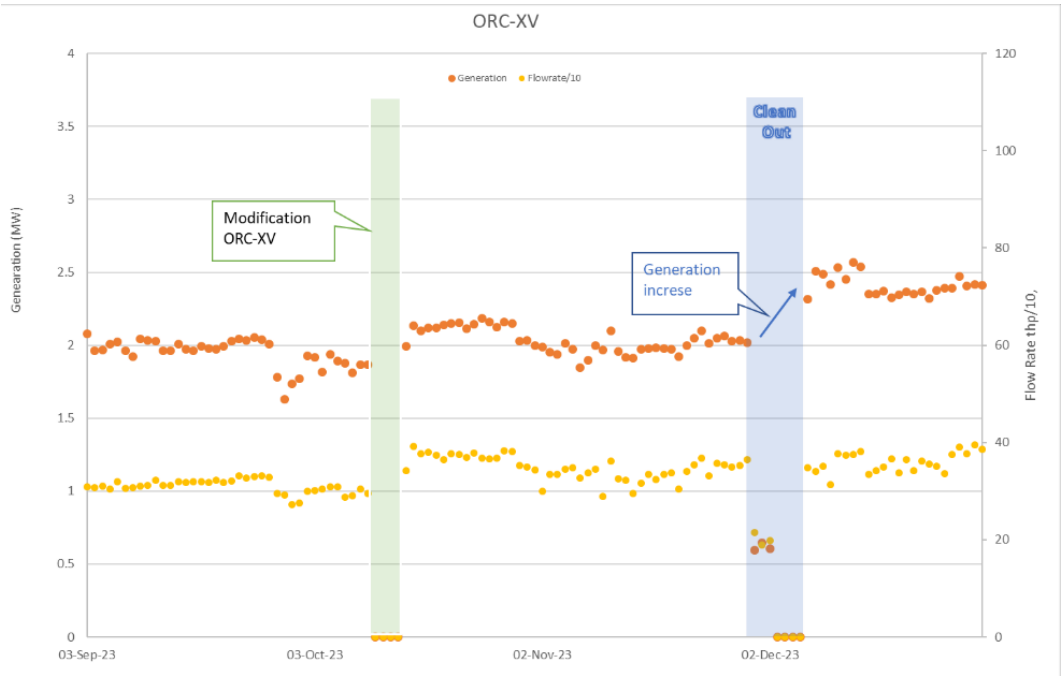

Figure 6: ORC-XV Lag Parameter.

5. CLEAN OUT PROGRAMS

The clean out program carried out is a hybrid using chemical and mechanical. Chemical is carried out first before opening the cover or head of the heat exchanger. The chemical used uses NaOH and cleating agent to dissolve complex silica deposits (T.R McCartney, etc, 2017). The mechanism process is begins with the mixed scale formation in metal surfaces meet with chemical dissolver to become smaller deposit chipping, polymeric silica, monomeric silica, metal silicates and metal ions. It acts as a nucleus for seeding reaction promoting scaling and deposition in the downstream. Increase scaling deposition tendency.

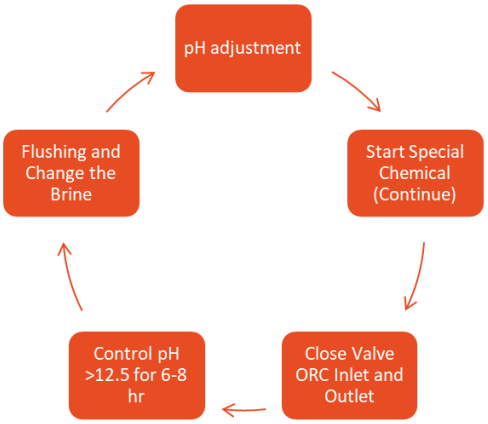

Figure 7: Chemical Clean Out Method.

Chemical clean out is used by the soaking method where NaOH plus cleaning agent chemical is injected into the system and the chemical is routinely replaced when it is saturated (Figure 7). Chemical clean out is carried out for ± 36 hours. During the clean out program, several parameters are monitored, namely pH, electric conductivity (EC) and silica.

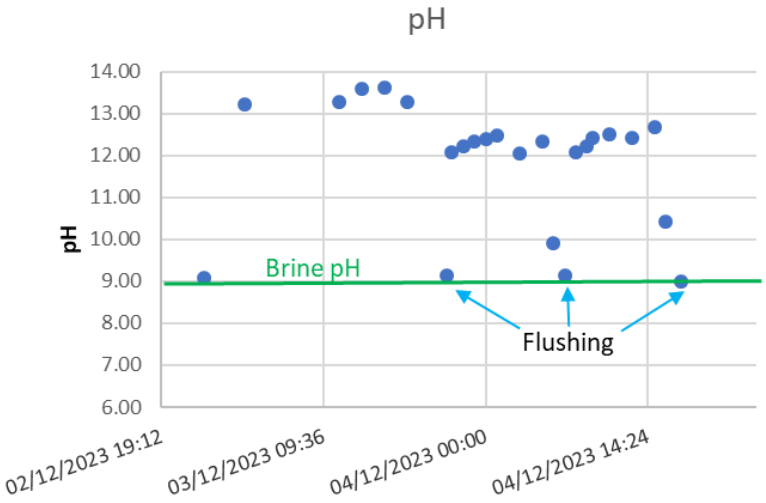

Figure 8: Online Clean out pH monitoring.

The original pH of brine is 8.8, thus during clean out we need to increase the pH to achieve above 12 therefore the cleaning agent, as dissolving chemical is able to dissolve silica. During clean out activity, there were three times to replace chemicals, this is show by the fluid pH being below 10 in the Figure 8. A high EC value indicates that the silica has been dissolved and if the value is stable, it means that the chemical is no longer able to dissolve the silica so it must be replaced, due to limitation of measuring instrument, the maximum EC value is 200,000 ms. Silica concentration monitoring is carried out to ensure that the silica is too high. A high silica value indicates that the chemical clean out has succeeded in dissolving the silica (Figure 9), the silica concentration as baseline is ~660 ppm and during clean out silica increase up to 2,100 ppm.

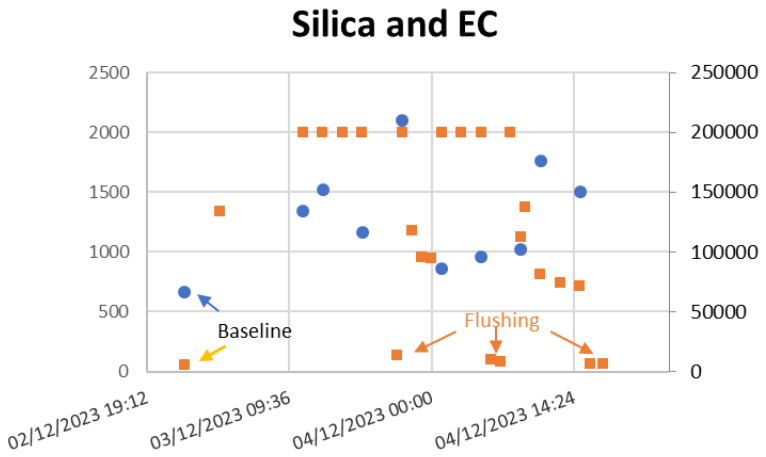

Figure 9: Online Clean out Silica and EC Monitoring.

After the chemical clean out is finished, the mechanical clean out was carried out to remove the silica that has fallen out and clean up the remaining scaling residue. After cleaning out the generation rebounded to the state before the scale occurred, in the case of ORC XV the generation increase was 0.4 MW.

6. CONCLUSION

Managing the silica scale at Sorik Marapi was implemented by using a chemical silica inhibitor to prevent silica, the results show that for approximately a year the generation was able to maintain 80% of the original design at SSI 2.4. A hybrid clean out using offline chemical and mechanical methods is carried out if the scaling has been formed with a lag parameter in generation. The result of clean out the generation is able to rebound to near original design.

REFERENCES

Addison, S., Brown, K., von Hirtz, P., Gallup, D., Winick, J., Siega, F., & Gresham, T. (2015). Brine Silica Management at Mighty River Power. *World Geothermal Congress*. New Zealand.

Andritsos, N., Karabelas, A., & Koutsoukos, P. (2002). Scale formation in Geothermal Power Plants. (pp. 179-189). international summer school on direct application of geothermal energy.

Borrman, T., Schweig, M., Cairns, M. J., Johnston, J. H., & Gray, A. K. (2018). Removing silica from geothermal water - Year One of Pilot Plant Operation with a Focus on Carbonate and Silica Analysis. *Proceedings 40th New Zealand Geothermal Workshop*.

Brown, K. (2011). Thermodynamics and kinetics of silica scaling. *Proceedings International Workshop on Mineral Scaling 2011*. Manilla.

Brown, K. (2013). *Mineral Scaling in geothermal power production*. Reykjavik, Iceland: UNU-GTP.

Fertani-Gmati, M., Brahim, K., Khattech, I., & Jemal, M. (2014). Thermochemistry and kinetics of silica dissolution in NaOH solutions: Effect of the alkali concentration. Elsevier, 58-67.

Fournier, R. O., & Rowe, J. J. (1977). The solubility of amorphousilica in water at high temperatures and high pressures. *American Mineralogis*, 1052-1056.

Fournier, R., & Williams, M. O. (1983). Calculation of Amorphous Silica solubilities at 25 C to 300 C. *Publication of an Organization other than the US Geological Survey*, 587-596.

Fukuda, D., Watanabe, M., Arai, F., Sasaki, S., Sako, O., Matsumoto, Y., & Yamazaki, S. (25-29 April 2010). Removal of Anhydrite and Mg-Silicate Scales from Production Wells Using Chemical Agents at the Mori Geothermal Field in Hokkaido, Japan: An Application of Chemical Well Stimulation. *Proceedings World Geothermal Congress 2010*. Bali, Indonesia.

Gabelich, C. J., Chen, W. R., Yun, T. I., Coffey, B. M., & Suffet, I. ". (2005). The role of dissolved aluminum in silica chemistry. In *Desalination* 180 (pp. 307-319). Elsevier.

Gallup, D. L. (1997). Alumunium Silicate Scale Formation and Inhibition: Scale Characterization and Laboratory Experiments. *Geothermics*, 483-499.

Gallup, D. L. (2011). pH Modification Scale Control Technology. *Proceedings International Workshop on Mineral Scaling*. Manilla.

Gill, J. S., & Jacobs, G. T. (2018). Managing Silica Deposits in Geothermal Power Plants- Pros and Cons of pH Mod versus Silica Inhibitor. *GRC Transactions*; Vol 42.

Grassiani, M. (2000). Siliceous Scaling Aspects of Geothermal Power Generation Using Binary Cycle Heat Recovery. *Proceedings World Geothermal Congress*. Kyushu - Tohoku, Japan.

Hassan, H. (2022). *Utilization of Thermal Potential of Abandoned Wells*. India: Elsevier.

Hochstein, M. P. (1990). Classification and Assesment of Geothermal Resources. *Dickson MH and Fanelli M (eds) Small geothermal resources* (pp. 31-59). Rome: Italy.

Lokarev, A., Stepanova, E., Ogay, M., Kovtun, E., Morozov, Y., Makiyeva, M., & Nam, N. (2020). Possibility of using thermal water from the Nizhne-Paratunskiye springs of Kamchatka to create pharmaceutical and cosmeceutical compositions. *Farmacevticheskoe delo i tehnologija lekarstv (Pharmacy and Pharmaceutical Technology)*.

McCartney, T., Gharaibeh, S., & Roxanne, S. (2017). Improved Methods for Removal of Silicate Deposits. *Heat Exchanger Fouling and Cleaning*. www.heatexchanger-fouling.com.

Monterozo, F. E., Gica, G. R., & Mantri, D. (2022). Recovery of Reinjection Well Capacity Using Online Scale Dissolution. *The 8th Indonesia International Geothermal Convention & Exhibition (IIGCE)*. Jakarta.

Nalco Water Handbook. (2018). *Nalco Water Handbook*. McGraw Hill.

Setiawan, F. A., Rahayuningsih, E., Petrus, H. M., Nurpratama, M. I., & Perdana, I. (2019). Kinetic of Silica Precipitation in Geothermal Brine with Seeds Addition: Minimizing Silica Scaling in a Cold Re-Injection System. *Geothermal Energy*.

Todd, M. A., & Bluemle, M. J. (2022). Formation and mitigation of mineral scaling in geothermal power plants. In *Water-Formed Deposits* (pp. 269-282). Elsevier.

Ueda, A., Kato, K., Mogi, K., Mroczek, E., & Thain, I. (2003). Silica removal from Mokai, New Zealand, geothermal brine by treatment with lime and a cationic precipitant. *Geothermics*, 47-61.

Yanto, E., Halimzikri, M. A., Budiyanto, A., Tiofami, A., Khasani, D., & Suranto, H. (February 15-17, 2021). The Importance of Cooling Water Treatment System at Lumut Balai Geothermal Power Plant. *PROCEEDINGS, 46th Workshop on Geothermal Reservoir Engineering*. Stanford, California: Stanford University.

Zarrouk, S. J., Woodhurst, B. C., & Morris, C. (2014). Silica scaling in geothermal heat exchangers and its impact on pressure drop and performance: Wairakei binary plant, New Zealand. In Geothermics 51 (pp. 445-459). *Geothermics*.

Zhang, L., Geng, S., Chao, J., Yang, L., & Zhao, Z. (2022). Scaling and blockage risk in geothermal reinjection wellbore: Experiment. *Journal of Petroleum Science and Engineering*; Elsevier.

UBL-M.3 Sidetrack to Recover Geological Prognosis

Rivaldi Azhar Ramadhani and Fariz Grahadiningrat

Pertamina Geothermal Energy, Grha Pertamina – Pertamax Tower 8th Floor
Jakarta Pusat, DKI Jakarta, 10110, Indonesia

rivaldi.ramadhani@pertamina.com, fariz.grahadiningrat@pertamina.com

Keywords: Geothermal Drilling, Geothermal Cementing, Sidetrack, Well Recovery, Well Integrity

ABSTRACT

Realizing the target of 1 GW installed geothermal capacity is the main goal and commitment of PERTAMINA Geothermal Energy Tbk. (PGE) to maximize the potential of renewable energy in Indonesia. This goal inevitably comes with various challenges, both technological and commercial, including drilling activities that play a crucial role in accelerating the realization of this target.

One of the major challenges faced by PGE occurred during the PGE Drilling Campaign at well UBL-M.3, where a downhole problem arose involving the stuck of Running Tools and the drill pipe during the cementing process in the 17.5" Hole Section. This issue was caused by a technical error related to the timing of pulling up the running tool with the thickening time of the cement.

Given that UBL-M.3 is a high-stakes well with significant gigawatt potential, all possible efforts were made to recover the well. These efforts included Working Pipe to release the stuck assembly, Mechanical Back Off to reduce the length of the fish to facilitate the fishing process, Running OEDP Jetting Tools, Rotary Shoe, and Guide Shoe to grind-out the cement around the fish with jetting effects, and eventually, deciding to perform a 20” Casing Sidetrack Open Window.

There were many debates and challenges to overcome in executing the Sidetrack Open Window process, ranging from procurement issues and limited availability of tools, long delivery times for equipment, well integrity issues, high index directional drilling challenges, and most critically, the lack of experience with sidetracking 20” casing in geothermal wells operated in Indonesia.

This paper will discuss the process and long journey of the Success Story of the 20” Casing Sidetrack Open Window in well UBL-M.3, and the lessons learned to prevent similar issues in the future, thereby facilitating smoother drilling operations.

1. INTRODUCTION

The Ulubelu Geothermal Area is located in the Tanggamus Regency of Lampung Province, within the Pulau Panggung District, approximately 100 km west of Bandar Lampung. The area can be accessed by a four-wheeled vehicle via a paved road from Bandar Lampung to the Pulau Panggung District, followed by a roughly 15 km stretch of rocky and partially paved road towards Ulubelu.

Geoscience and reservoir studies have revealed that the reservoir zone in the northern sector, which is close to the upflow zone, contains high-enthalpy fluid (2600 kJ/kg) and high temperature (270 – 280°C), along with high non-condensable gas (NCG) content (1.4-1.7 wt%) but moderate permeability (300-900 lpm/ksc). Nearly all wells in this zone exhibit relatively high production outputs between 18-30 MW with high dryness (50-90%). However, there is a possibility that the reservoir characteristics could align with the wetter cluster I or K due to the location of M in between them. These makeup wells are also intended to replace the loss or decline in production from these wells.

The top of the reservoir in the northern sector is located around sea level. The depth of the feed zones in this sector has been well mapped using PTS injection and production data. Generally, productive feed zones are found at depths ranging from -150 to -750 meters above sea level. The permeability control of the reservoir is influenced by fracture zones-oriented NW-SE and NNW-SSE (Karangrejo Fault trend) and the lateral permeability of the matrix in the Rhyolitic Tuff formation.

UBL-M.3 is one of the well which are drilled in the PGE Ulubelu area. This well is considered a crucial and concluding well of the PGE Drilling Campaign 2023-2024 in the PGE Ulubelu Area. It is a directional makeup well with four hole sections: 36", 26", 17.5", and 12.25". The well has a total depth of 2156 mMD, a kick-off point at 150 mMD, a hole direction of N 49 E, and four targets located at depths of 1315 mMD, 1755 mMD, 1942 mMD, and 2068 mMD.

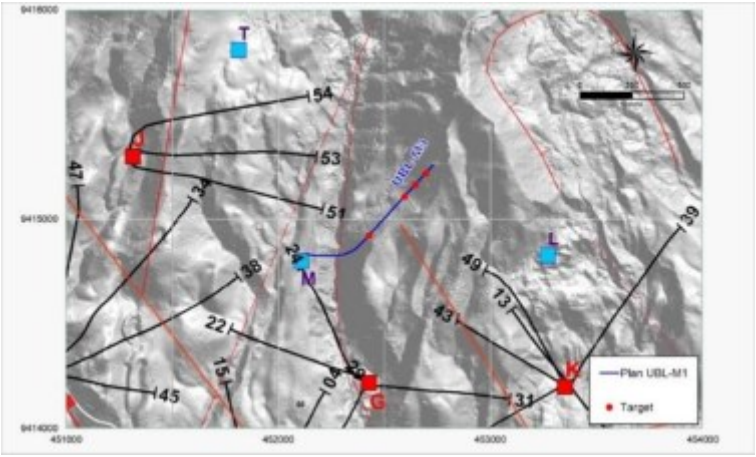

Figure 1: UBL-M.3 Well Targeting Map.

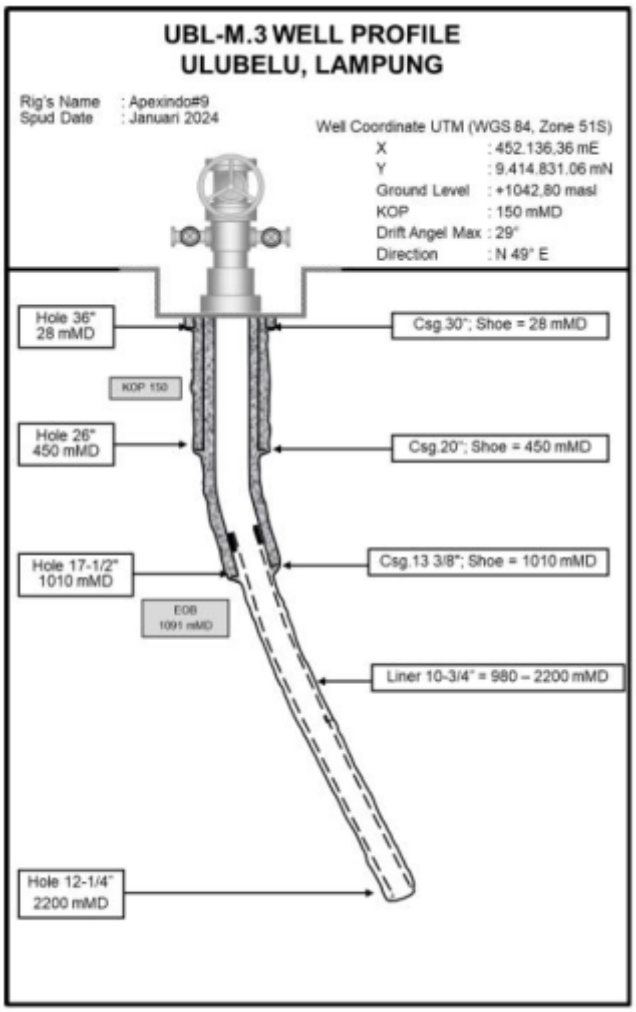

Figure 2: UBL-M.3 Well Profile.

Well UBL-M.3 commenced drilling at 21:30 WIB on January 16, 2024. In actual operations, the drilling proceeded smoothly starting with the 36" Hole Section (0 - 28.5 mMD), which took 39.5 working-hours. This included the formation drilling, reaming, trips (B/O and L/D), circulation and conditioning of the hole, WOC, cutting of the 30" stove pipe, installation of the 29.5" bottom flange and the 30" x 1000 psi diverter, and performing the diverter function test.

Similarly, the 26" Hole Section (28.5 - 449 mMD) also progressed smoothly, taking 123 working-hours. This involved formation drilling, trips, circulation and conditioning of the hole, installation of the 20" casing,

cementing of the 20" casing, WOC, installation and function testing of the 21.25 x 2000 psi BOP, cutting off the casing, and other related activities.

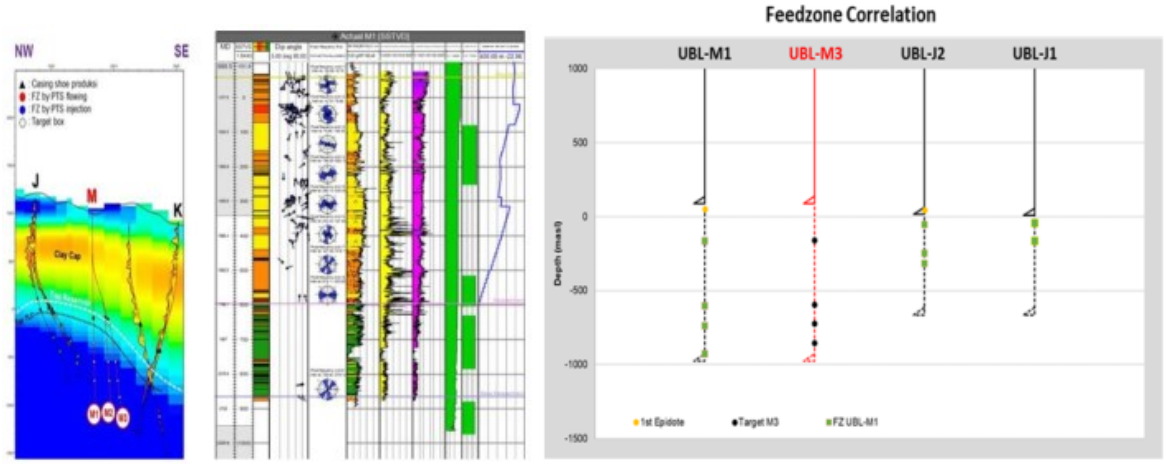

Target	Keterangan	mMD	mKT	X	Y	Z
Target-1	Korelasi feedzone sumur UBL-51	1291	1215	452,459.76	9,414,901.90	-162
Target-2	Korelasi feedzone sumur UBL-51; 53; 54 & Fracture model	1786	1648	452,640.84	9,415,059.31	-595
Target-3	Korelasi feedzone sumur UBL-51, 53, Fault Kr. Rejo & Fracture model	1935	1778	452,695.16	9,415,106.53	-724
Target-4	Korelasi feedzone sumur UBL-43, Fault Kr. Rejo & Fracture model	2083	1908	452,749.48	9,415,153.75	-855

Figure 3: Feedzone Correlation and Distribution for UBL-M.3 Well Targetting.

The issue encountered with Well UBL-M.3, which will be discussed furthermore in the next section of this paper, occurred during cementing operations in the 17.5" Hole Section (449 - 1004 mMD).

2. RELATED WORK

Based on the previous study and experience, cementing, either it was in Geothermal or in Oil and Gas, is one of the most critical steps to done in drilling operation. Cementing is a key and essential part of the wellbore construction process (Lootens, 2004) and the integrity of the well construction depends to its cementing (Ridha et al., 2010), also cementing is the key to ensure the safety of the well and durability (Pourafshary et al., 2009 ; Ershadi et al., 2011)

Cementing techniques invlolve the deployment of cement slurry on the Geothermal Well annulus and casing to provide proper zonal isolation. The target is to completely hinder fluids in the well from Interacting from one part to another, provide an anchor for the casing, prevent corrosion of the Casing, prevent shock loads during drilling, prevent blowouts, plug off vugular zones or fractures, and the last is for Abandonment (Anaele et al., 2020).

Geothermal Cementing is one of the most challenging steps in Geothermal Drilling Operation. Besides of its criticality, the environment in geothermal is classified as High Pressure and High Temperature (HPHT). One of the cementing parameter, Thickening Time is affected by High Temperature. Thickening Time (TT) test was performed using a High-Pressure- High-Temperature (HPHT) Consistometer rated at a pressure of up to 206.8 MPa (30,000 psi) and temperatures of up to 204 deg-C (400 deg-F).

The cement slurry was mixed according to API procedures and then placed in a slurry cup into the consistometer for testing. The testing pressure and temperature were controlled to simulate the conditions the slurry will encounter in the well. The test concluded when the slurry reached a consistency considered unpumpable in the well. The time it takes the cement slurries to reach 40Bc, 70Bc and 100Bc consistency were recorded (Anon,1997 and 2013). The test was done at 80 deg-F, 100 deg-F, 120 deg-F, 140 deg-F and 160 deg F. From this study, it was shown that at constant concentration, increase in temperature leads to decrease in thickening time and leads to the faster setting of the cement slurry. (Anaele et al., 2020).

The issue of UBL-M.3 occurred during cementing operations in the 17.5" Hole Section while pulling the running tools and conducting drill pipe out of the hole after the first step of tieback cementing was completed. The chronology began with the process of pulling them out from 386 – 250 mMD and circulating the displacement

cement with a flow rate of 500 GPM and stand pipe pressure of 0 psi, with the water return obtained from the cementing process. The process of pulling the running tools and conducting drill pipe continue from depth 250 mMD – 241 mMD.

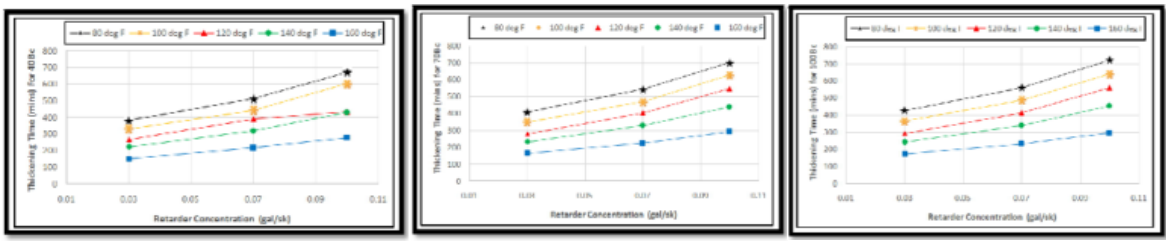

Figure 4: The Effect of Temperature on the Thickening Time at 40 Bc, 70Bc and 100 Bc.

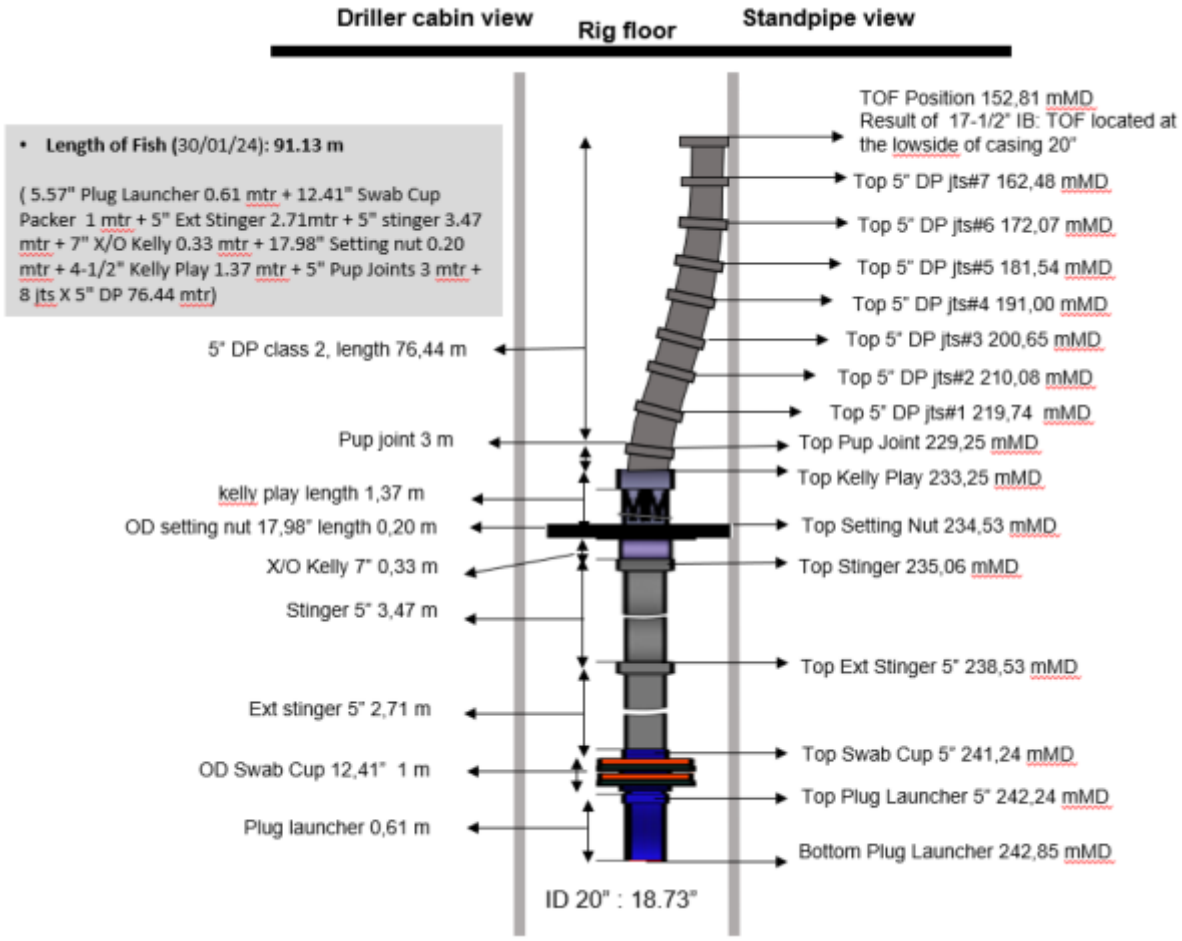

Figure 5: Running Tool Fish Illustration (Initial Condition).

While the pulling process is conducted at 241 mMD, drag overpull was found ranging from 40 – 110 klbs (the normal P/U is 60 klbs). Continued the effort to pull with reciprocating at interval 241-240 mMD, with a pulling force of 330-335 klbs, while pumping with a flow rate of 1210 gpm and stand pipe pressure of 380-415 psi. Tried rotating with a torque limit of 30-32 klbsft, but it was still unsuccessful.

The next plan, the decision to mechanically blind backed off the 5" drill pipe is taken with the string weight positioned at 70 klbs, setting torque to 32 klbsft, RPM 1-2, with two left turns achieving a torque of 28 klbsft. Lifted the assembly, pulling up weight of 50 klbs (indicating the 5" drill pipe had disconnected). Continued pulling the drill pipe assembly to the surface (retrieved 18 joints of 5" drill pipe).

There are several probable causes back then when the stuck of running tools is happened, caused by the early cement set. This early cement set caused by the dynamic condition of the borehole of UBL-M.3, therefore the Thickening Time is set earlier than the program. The combination between the high uncertainty of the subsurface condition (such as anomaly temperature increase, etc), which may lead to the unmatched chemical composition

of cement with its condition, causes the anomaly in the thickening time of the cement. The composition of the cement should have match with the dynamic condition of the well itself.

The other causes is the pumping speed when the cementing operation conducted. Due to the technical difficulties of the pumping speed while cementing, the cementing coverage to annulus isn't ideal enough. The cement that already set at the lowside solidified faster than the upper side while the cementing process hasn't done, and eventually causes the stuck running tools.

Finally, after all those efforts above are done with nothing in result, eventually the team decided to do the contingency plan consists of Fishing and Well Intervention Operations and Sidetrack Drilling.

3. METHODOLOGY

3.1 Fishing and Well Intervention Operations

Fishing and Well Intervention is the first option that the team decided to use to overcome this problem after all the jarring efforts are resulting none. These methods are done by the teamwork of all the parties that responsible and in charge for the Fishing and Well Intervention processes from Pertamina Geothermal Energy itself, PDSI-WIS (Pertamina Drilling Services Indonesia – Wellbore Integrity Solutions) from Fishing Services, and also Apexindo (APX-09) as the Rig Contractor.

The equipment provided by all the parties, whether from the Fishing and Well Intervention Tools, Drilling Bit, Drilling Accessories, and others. The journey of the well and geological recovery is not easy. There are so many trials and errors that done, using the combination between the equipment provided by PGE, PDSI-WIS and Apexindo itself, that summarized into the flowchart below until the team decided to do the accidental Sidetrack Drilling to Recover the Geological Prognosis at UBL-M3.

These activities in total spent about 858.5 Hrs of total NPT 1026.5 hours, contributed to the 46.48% of the total NPT percentage 55.58% from the whole drilling operation activity at UBL-M3 well. Therefore, the main contributor of the biggest NPT percentage contribution comes from the 17.5" Hole Section drilling activity due to this stuck running tools.

3.2 Sidetrack Drilling

After all the long journey and trial & errors of the Fishing Operation and Well Intervention activity have no success results, the team eventually decided to do the Sidetrack Drilling. Sidetrack Drilling at UBL-M3 well journey is not an easy thing to do. There are so many considerations, pros and cons and also debates and challenges to overcome in executing the Sidetrack Open Window process such as:

1. Procurement issues and limited availability of tools
2. Long delivery times for equipment
3. Well integrity issues
4. High index directional drilling challenge
5. Lack of experience with Sidetracking 20" Casing in geothermal wells operated in Indonesia.

For the technical of drilling operation itself whenever the decision to do the sidetrack is taken, there are no technical issues that faced by the team. All the sidetrack drilling operation working smoothly and so does the safety a spect.

4. RESULTS

Sidetrack Drilling of the UBL-M.3 Well commenced on March, 9th 2024 at 1:30 a.m. from depth 264 mMD (Hole Section 17.5"). The sidetrack drilling operation applies drilling parameter as the same normal Drilling Operation previously, such as WOB 5-30 klbs, FR 700-800 gpm, SPP 1400 – 1800 psi, etc. The sidetrack operation process are going smoothly, and finally reached the Total Depth of 2152 mMD at March, 29th 2024 at 19:00 a.m. The total amount of days needed to successfully conduct the Sidetrack Drilling from the depth where the running tools stuck until 2152 mMD is 20.72 days or approximately 497.5 hours of operation.

For the procurement isues and limited availability of tools, it contributed to a minor amount of NPT approximately 4-5 days due to the special requirements of tool to do the sidetrack activity. For Well Integrity issues, all the works are done safely whether is it from the Drilling aspect or the Geological aspect. There are no significant difference of formation lithology between the initial prognosis and the actual sidetrack operation. The geologist perform a real time analysis from the actual cutting that came out from the shale shaker, and found no difference prior to the previous prognosis. High index directional drilling challenge also can be overcomed safely without any issues.

Figure 6: Fishing and Well Intervention Operations Summary Flowchart.

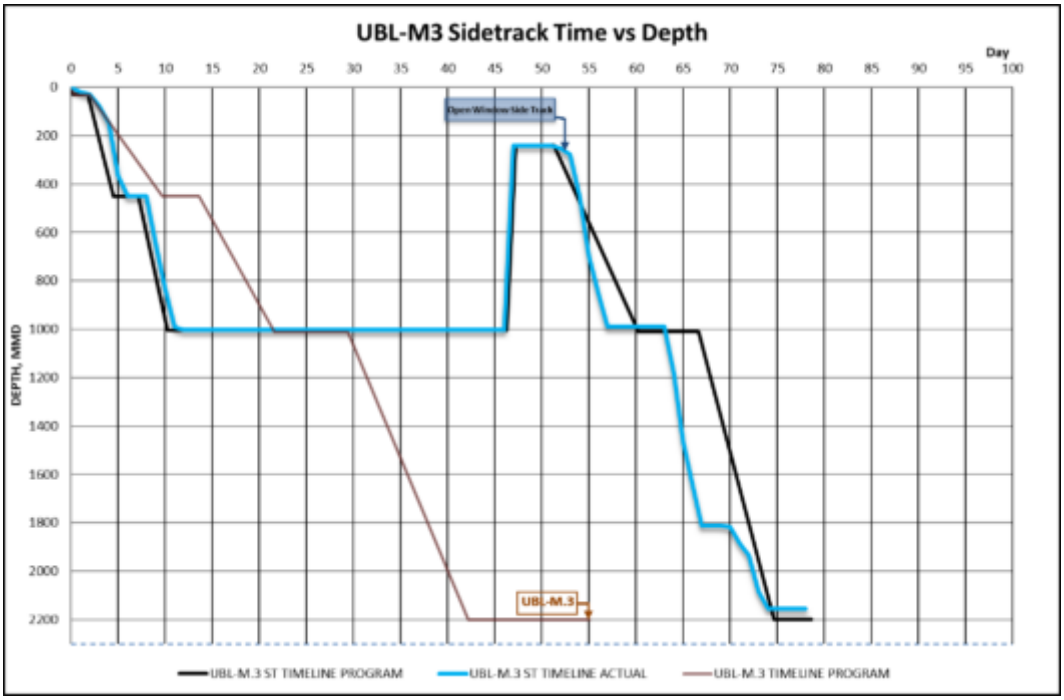

Figure 7: Time vs Depth UBL-M3 ST Graph.

5. DISCUSSION

Sidetrack Drilling of the UBL-M.3 Well all done in total amount of days needed to successfully is 20.72 days or approximately 497.5 hours of operation. The total amount of the UBL-M.3 days already included with the other NPT while the sidetrack operation is ongoing. The NPT breakdown besides the Fishing Operation are:

a. Well Control Operation (68.5 hours)
b. Other Services Problem (22.5 hours)

c. Circulating System Reparation (19 hours)
d. Directional Services Problem (9.5 hours)
e. Repair Power System (3.5 hours)
f. Wireline Services Problem (3.5 hours)
g. Aerated Drilling Services Problem (1.5 hours)
h. Location Problem (2 hours)

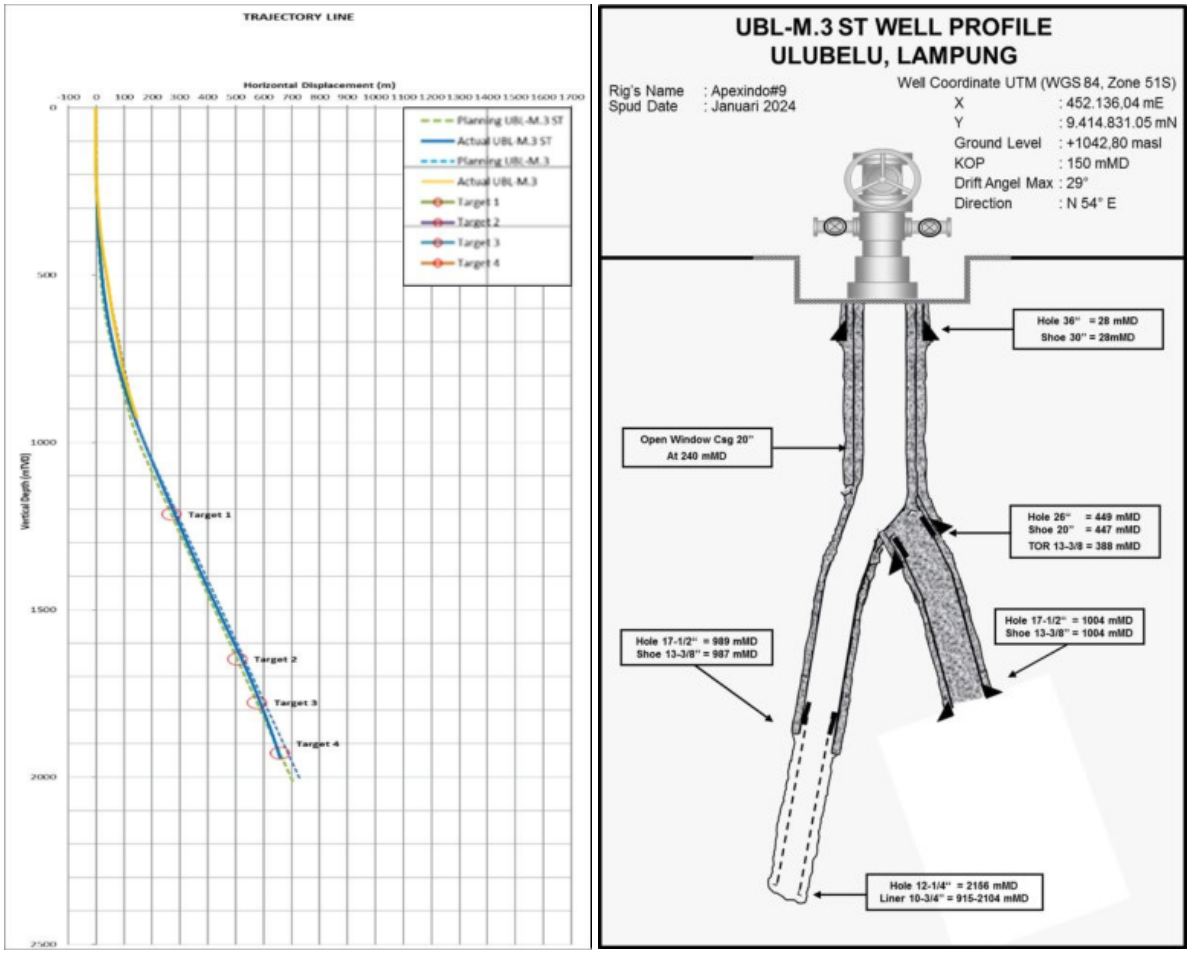

Figure 8: Well Trajectory Path & Well Schematic of UBL-M.3 Sidetrack.

Based on this data, while the sidetrack operation is ongoing, there are no major issues that related to the sidetrack operation itself. The Well Control Operation problem happened due to a steam kick while the drilling formation process is going through. This problem can be done by increasing the water volume pumping to annulus, the usage of aerated drilling and other well control efforts that usually done while there is a steam kick happened at a geothermal well. The other NPT whether from the Rig System or from the services company are just a minor technical difficulties that can be solved within under 24 hours.

6. CONCLUSION

As already mentioned previous earlier for the cons of this operation, Sidetrack is a massive and critical decision that should be considered by any Geothermal Company especially when the drilling operation are facing the unwanted downhole problems, and in this paper is the cementing process. It is known that major technical difficulties or any other unwanted accident are inevitable, especially when it comes to the dynamic condition of the subsurface, that cannot be precisely preedicted.

The biggest consideration of Pertamina Geothermal Energy to do this operation is the lack of sidetracking 20" Casing experience in geothermal wells operated in Indonesia, because this could be a do-or-die process due to a lack of experience and can lead to a bigger problem or even abandon the hole itself.

The teamwork and hardwork between Pertamina Geothermal Energy and all the Services Company that contributed to the UBL-M3 drilling operation are two key of success to do this complicated sidetrack 20" Casing experience that rarely done in Indonesia and should be given an enormous appreciation

The lesson that can be learned from this sidetrack operations are:

a. Always be critical and mindful whenever the critical steps in drilling are going to be executed such as Cementing Process and any other steps that considered to be important, critical or even dangerous
b. Reanalyzing the cementing process before the operation is going to be done, whether it was the material aspect such as the chemical addition, the composition of the cement to match it with the downhole condition or subsurface condition based on the drilling program prognosis to minimize the uncertainty of downhole condition, or the cementing operation process such as the pumping rate of the cement so that the coverage of the cement in the annulus will be perfect.
c. Reanalyzing the drilling operation process whenever the cementing process is going through such as the circulation process or pulling the drill string out of hole while waiting the Thickening Time process of the cement itself, and other activity.

ACKNOWLEDGEMENT

We would like to extend our deepest gratitude to the individuals and teams who have made significant contributions to the success of this project. First and foremost, we thank Mr. Tesha, Vice President of Drilling and Services, for his visionary leadership and unwavering support. We are immensely grateful to Mr. Radianto Ritamawan, Manager of Drilling Operation & WO/WI, whose expertise and guidance have been invaluable throughout the drilling process. We also express our sincere appreciation to Mr. Wahyu Sutresno, Manager of Drilling Planning & Support, for his meticulous planning and strategic insights. Special thanks to Mr. Fery Malau, the Assistant Manager of Drilling Operation, for his dedicated efforts and operational oversight. Our heartfelt thanks to Mr. Umar Sidiq, Drilling Engineer, for his technical acumen and problem-solving skills. We also acknowledge the entire Pertamina Geothermal Energy Drilling Team for their hard work and collaboration. We are grateful to the Pertamina Geothermal Energy Area Ulubelu team for their on-site support and operational assistance. Special recognition goes to the UBL-M3 Drilling Team for their perseverance and commitment in overcoming the challenges faced during this project. Lastly, we thank the UBL-M3 Rig Contractor and Services Company Team for their professionalism and expertise, which were crucial in achieving the project milestones. This project would not have been possible without the collective efforts and dedication of all these individuals and teams.

REFERENCES

American Petroleum Institute (API): Recommended Practice 10B for Testing Well Cements. American Petroleum Institute, Washington DC, USA (1997)

Anaele, J., and Otaraku, I.: Effect of Temperature on the Thickening Time Property of Cement Slurry, Proceedings, The International Journal of Science & Technoledge, Port-Harcourt University, Port Harcourt, Nigeria. (2020)

B, Akin S: Utilization of Supplementary Cementitious Materials in Geothermal Well Cementing, Proceedings. Thirty-Eighth Workshop on Geothermal Reservoir Engineering Stanford University, California. (2013)

Gabolde, G., Nguyen, J.P: Drilling Data Handbook – Seventh Edition". Institut Francais du Pétrole Publications. (1999) Recommended Practice 13B-2: Recommended Practice Standard Procedure for Field Testing oil-Based Drilling Fluid, Third Edition February (1998).

Joel, O. F: The Secondary Effects of Lignosulphonate Cement Retarder on Cement Slurry Properties. Journal of Engineering and Applied Sciences 4: 1-7.(2009)

Lootens D., He´braud P., Le´colier E.and van Damme H. (2004): Gelation, shear-thinning and shear-thickening in cement slurries. Oil and Gas Sci. Technol.59, 1, 3140.

Montes, A et al.: Stuck Pipe Prediction in Utah FORGE Geothemal Wells, Proceedings, SPE Annual Technical Conference and Exhibition, San Antonio, Texas, USA. (2023)

Pourafshary P, Azimipour S. S, Motamedi P, Samet M and Taheri S. A. (2009): Priority Assessment of Investment in Development of Nanotechnology in Upstream Petroleum Industry.-Society of Petroleum Engineers, Saudia Arabia Section Technical Symposium, Saudi Arabia

Ridha S., Sonny Irawan S., Bambang Ari W and Jasamai M.: ''Conductivity Dispersion Characteristic of Oilwell Cement Slurry during Early Hydration''. International Journal of Engineering & Technology IJET-IJENS Vol:10 No:06.(2010)

Rotich, M.: An Unconventional Directional Sidetrack of a Geothermal Well: Menengai Well MW15A, Geothermal Development Company, Menengai, Kenya. (2022)

Salam K.K, Arinkoola A.O, Ajagbe B.and Sanni O: ‘’Evaluation of Thickening Time of Oil Field Class G Cement Slurry at High Temperature and Pressure using Experimental Design’’ International Journal of Engineering Sciences 2: 361-367. (2013)

Southon.,J Gorbachev.: Drilling Geothermal Wells Efficiently, With Special Reference To The Mutnovsky Geothermal Power Project. Geoterm JSC and Philippines Geothermal Incorporated (2003)

V. Ebadi. T, Rabani. A.R, Ershadi L., Soltanian H.: The Effect of Nano silica on Cement Matrix Permeability in Oil Well to Decrease the Pollution of Receptive Environment. International Journal of Environmental Science and Development, Vol. 2, No. 2, April (2011)

Zhang, j et al.: Research and Application of Old Well Sidetracking Technology in Dagang Oilfield, Proceedings, International Field Exploration and Development Converence, Xi’an, China (2022)

Achievement of Drilling Incident Free Operation by Implementing of Safety Behavior Method

Fachrul Subarkah, Budi Santoso, and Mangojak Siagian

Star Energy Geothermal, Wisma Barito Pacific II, 17th – 21st Floor,
Jl. Letjen S. Parman Kav. 60, Jakarta Barat 11410, Indonesia

fsub@starenergy.co.id

Keywords: drilling, safety behavior, safety culture, risk management, incident free operation

ABSTRACT

Successful safety behavior must take place in several well-controlled stages, beginning with capturing an individual's attention to the fact that a change of safety behavior attitude is needed; and by convincing that individual that his currently held attitude is wrong or inappropriate to the situation.

Star Energy Geothermal Drilling Team took a proactive approach to manage anticipated and emerging safety behavior issues. A good example of this approach is the adaptation of the Incident Free Operation (IFO) method through the implementing of Drilling IFO concept, fostering Safety Culture and applying Behavior-Based Safety (BBS) observation at drilling operation site. Utilizing data from daily BBS observation, safety concerns are prioritized using daily and weekly priority scales to improve the safety culture, focusing on both safe person and safe condition strategies, which directly correlate with workplace behavior. 'Safe person' strategies, in particular address individuals' risk perceptions and should be considered in the risk assessment process. Similar to BBS cards, applying the COACH Cards method by Parker Wellbore Indonesia as Drilling Contractor aids in analyzing safety behavior challenges, such as, unsafe act, behavior and deviation from Standard Operating Procedures (SOP's). To address these challenges, an extensive IFO program and integration of new safety culture findings, facilitates the refinement of safety concept in the field. Key updates also include increased understanding of Coach Cards terms and their application. These insights and the updated conceptual understanding of the BBS Coach Cards have provided a credible identifying of the performance trend to have the necessary confidence to improve safety culture performance.

The Drilling Team Leadership need to place greater emphasis on human behavior at work and would benefit greatly from training in areas of behavior which can contribute to unsafe situations, unsafe conditions, and accidents. Both Drilling Team Leadership Management and Employee attitudes vary dramatically with respect to safety and risk management. The effective development and promotion of health and safety by Leadership is an important feature of the health and safety culture of any organization.

1. INTRODUCTION

Behavior is translated from English "behavior" and is often used in everyday language, but the notion of behavior is often interpreted differently from one person to another. In general, behavior is all actions or actions carried out by living things (Notoatmojdo, 1985). Behavior is also often interpreted as an action or activity displayed by a person concerning others and the surrounding environment (Syaaf, 2007).

Behavior is an actual activity observed directly or indirectly through attitudes and actions. However, it does not mean that behavior can only be seen from the perspective or actions (Notoatmodjo, 1985). According to Notoatmojdo (1985), behavior is a person's psychic reaction to his environment in the form of active or real action and passive state or unreal action. The American Encyclopedia of Introduction to Health Behavioral Science defines behavior as an organism's reaction to its environment. New behavior will occur when something is needed to cause a response, called a stimulus. Thus, a particular stimulus will produce a specific behavior as well.

Understanding behavior that is very diverse and plural requires an understanding that is always related and cannot be separated from its contextuality. Because the behavior displayed by a person can occur at different times but in the same situation, or appear in other cases, relatively not too much additional time (Notoatmodjo, 1985).

Habits, values, and use of resources in a society or group will produce a pattern of life (way of life) which is generally called culture. In the book, Notoatmodjo (2007) says behavior is one aspect of culture, and then culture profoundly influences this behavior. Human behavior is a balance between the driving forces and the restraining forces. Furthermore, the behavior can change if there is an imbalance between the two parties within a person so that there is a possibility of behavioral changes in a person, namely the increase of the driving force, the restraining points decrease, or the driving force decreases and the restraining force increases (Lewin, 1970).

Borman and Motowidlo (1993) distinguish **Safety Behavior** at the individual level into two categories, namely safety compliance and safety participation. **Safety Compliance** is defined as the main activity that individuals must perform to maintain safety in the workplace, including compliance with work procedures and the use of personal protective equipment (PPE). On the other hand, **Safety Participation** is defined as behavior that does not directly contribute to safety activities but will help the work environment to remain safe. Some examples of safety participation are attending safety meetings and helping co-workers solve work safety problems. It can say that behavior is the result of a person's efforts achieved with abilities and actions in certain situations, so that behavior is the result of a link between safety behavior efforts and the ability to carry out their duties. Therefore, behavior is essential to know about the employee's performance. A leader will use the job description as a benchmark by carrying out such an assessment. If the execution of the work matches or exceeds the job description, it means that the job is carried out successfully. Therefore, behavior is the essential thing used to know about the employee's performance.

Safety Behavior applies task behavior in the workplace (Griffin and Neal, 2000). Safety Behavior is task behavior and contextual behavior, Borman and Motowidlo, (1993) in (Griffin and Neal, (2000) namely individual compliance and participation in safety maintenance activities in the workplace. As feedback, employees should be aware of the importance of safety for themselves and for the company he works for.

Safety Behavior in work safety, which is directly related to employee behavior in working for individual safety, is closely related to the safety culture and safety knowledge because the company's current safety culture can affect employee health. With high work safety knowledge, employees can understand the meaning of work safety well. And the most crucial component in maintaining the safety of life and safety of work equipment is knowledge of the use of safety equipment for employees where the impact that can fill from safety behavior for the company is work productivity (Wardani, 2013).

Safety behavior is related to Safety in the workplace to minimize workplace accidents. Sahab (1997) says that failure in carrying out Safety Missions is due to a lack of motivation to work safely. He also noted that Safety Communication is needed to encourage behavior change to motivate them to work safely. One of the factors that can relate to Occupational Safety and Health (OSH) is the Predisposing Factor. The predisposing factors in this analysis include five sub-variables: knowledge, training, attitudes, motivation, and communication.

Behavior-Based Safety (BBS) provides robust positive results when applied in organizations seeking to reduce employee injuries due to at-risk / unsafe behaviors. Primary techniques in BBS include peer observation and feedback, training and education sessions, behavior-based incentives, prompts, and goal setting (Geller, 2001; Krause, Robin, and Knipling, 1999). Almost all prior BBS research has been applied in work settings where employees can systematically observe the safe versus at-risk / unsafe behavior of their co-workers. BBS programs are advantageous because they are easy to implement, are easy to teach, and can be implemented in the setting where the problem occurs (Daniels, 1999; Geller, 2001). BBS programs have been successfully used to increase safety related work behaviors in a variety of organizational settings, including drilling operation.

While BBS focuses on workers' safety-related behaviors, this focus does not imply a one-dimensional (i.e., behavioral) view towards safety. In fact, Geller (2001) and Krause (1997) believe safety interventions that focus exclusively on reducing at-risk safety-related work behaviors without acknowledging the system in which they occur will have modest long-term success. Comprehensive BBS programs focus on three interdependent factors (person, behavior, and environment) in an organization's safety system.

2. JOURNEY TO APPLY BBS – COACH CARDS OBSERVATION

Star Energy Geothermal Drilling Team took a proactive approach to manage anticipated and emerging Safety Behavior issues. A good example of this approach is the adaptation of the Incident Free Operation (IFO) method through the implementing of Drilling IFO concept, fostering Safety Culture and applying Behavior-Based Safety (BBS) observation at drilling operation site. Utilizing data from daily BBS observation, safety concerns are prioritized using daily and weekly priority scales to improve the Safety Culture, focusing on both safe person and safe condition strategies, which directly correlate with workplace behavior. 'Safe person' strategies, in particular address individuals' risk perceptions and should be considered in the risk assessment process. Similar to BBS cards, applying the **COACH Cards** observation method aids in analyzing Safety Behavior challenges, such as, unsafe act, unsafe behavior and including deviation from Standard Operating Procedures (SOP's).

The development of a proper safety management system requires continual attention to three domains, namely the environment (equipment, tools, and housekeeping), the person, (knowledge, skills, abilities, intelligence, and personality) and behavior (Geller, 1998a and 1998b). The behavioral safety approach which introduces a planned schedule of events that combine to create an overall continuous improvement intervention (Krause, 1995).

A behavior-based program targets specific are unsafe behaviors. The focus of the program is on that small proportion of unsafe behavior that is responsible for most of the accidents. The unsafe behavior identified in the process is written onto a checklist in a system where employees observe each other. Behavior-Based Safety is based on observational data collection which is applied using COACH Card method. The higher the number of observations, the more reliable the data. According to the Heisenberg Uncertainty Principle, the very act of observing and measuring people's safety behavior alters the behavior of those being observed (Cooper, 2000). This analysis is aimed at assessing for implementation of a Behavior-Based Safety Coach Card intervention plan amongst drilling operation workers in the Star Energy Geothermal drilling site.

3. DATA COLLECTION PROCEDURE

The instrument employed for data collection was the BBS Coach Card checklists, requiring the workers to either tick box “safe‟, or “unsafe‟ for each condition and behavior type item listed. Baseline data were established with respect to respondents’ behavioral safety trend. This was to track their level of safe behavior or unsafe behavior over time during 24/7 operations.

3.1 Participants

The drilling operation workers at Star Energy Geothermal comprising of Company Man (Drilling Site Manager), Rig Superintendent, Drilling Technicians, HSE Reps, Toolpusher, Drillers, Derrickman, Floorman, Cementing Supervisor & Team, Mud Engineer, Crane Operator, Drivers, Welder, Material Man, Warehouse Man, Paramedic, Directional Drillers, Casing Crew, H2S Engineer, and etc. at project sites, were included in the analysis and not only one or some portions (sections). The following activities were carried out by these workers: Mobilization, Rig-Up/Down, Drilling, Mud Mixing, Running Casing, Cementing, Well Completion and etc. at drilling site.

3.2 Coach Card Checklist

The checklist administered with respect to these observations were behavioral based. It consists of seven (7) segments and has a completion time of approximately 5-10 minutes for each card. The segments include Workplace Exposures, PPE, Tools & Equipment, Environmental, Policies & Procedures, and Personal State of Mind – in COACH Cards terminology The checklists were of simple design, requiring the workers to either tick box “safe‟, or “unsafe‟ for each condition and behavior type item listed then following by describe observation. Those completing the peer-observation checklist on other workers‟ actions were advised to ask for the reason the unsafe act had occurred, direct coach or reinforce if safe. Drilling HSE Reps team members at the end of the daily workday (Day and Night Shift) collected completed these COACH Cards checklists and descriptions. These checklists were either placed into election type boxes scattered around the site, or handed back directly to the Drilling HSE Reps, or often via work group team leaders.

4. DATA ANALYSIS

The observation data analysis was used for collecting responses from the subject selected from the daily observation cards. It assessed different employees' perceptions and opinions regarding how strongly they believe them and others within the organization support safety, measures employee perceptions of many formal safety management systems and those instances of behavior which directly or indirectly impact on the safety of others. It was designed in a multiple thick box format upfront side card and describe the observation on the backside card. The Step 1 and 2 choose thick box that apply had statements in the 7 segment and following by summary notes of describe the observation.

The data analysis is to identify the major significant intervention observations among the respondents in terms of improvement in behavioral safety was to develop a simple chart that fits the collected data defining the relationship between respondents’ perception of unsafe behavior and percentage safe behavioral practices at the workplace.

The purpose of this analysis was to explore workers, supervisors, and all team member perceptions of safety behavior at work in Star Energy Geothermal drilling operation and identify the factors that discourage safe behaviors. Using quantitative and qualitative approach based on COACH Cards data and conventional content analysis to interpret the data, this analysis found the most cited the contributory factors to exhibit unsafe behaviors were:

- inadequate direct supervision,
- unsafe workplace conditions,
- workers’ perceptions, skills, and training,
- broader organizational factors.
- unsafe behavior and human error are important contributors to dangerous incidents and occupational injuries.

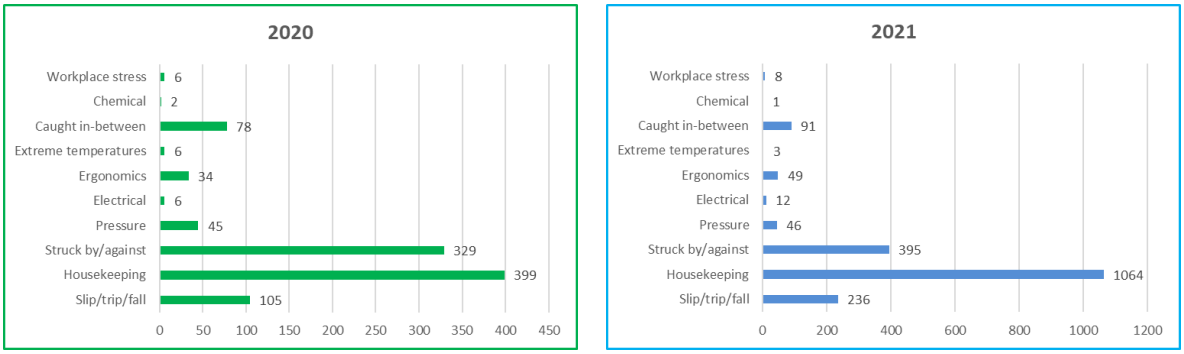

a) b)

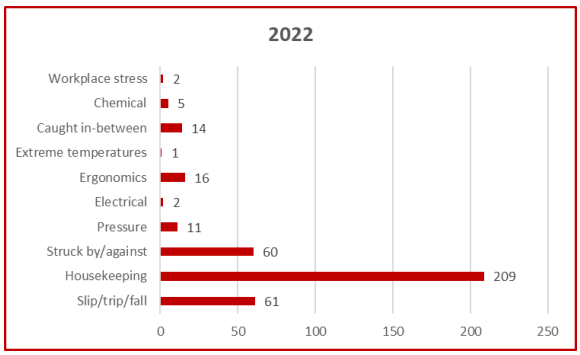

c)

Figure 1: a, b and c, Unsafe Behavior findings record based on the Workplace Exposure factor analysis within 2020 – 2022 COACH Cards data collected.

Table 1: SHE Performance of Star Energy Geothermal Drilling Make Up Well (MUW) Program 2018 - 2022.

Data	Wayang Windu	Darajat	Wayang Windu	Salak	Darajat	Total
Safe Man Hours	374,886	615,664	530,179	457,032	436,068	2,413,829
Safe KM Driven	279,878	459,465	359,589	319,451	295,495	1,713, 878
BOBS	17,243	20,008	14,814	15,463	15,323	82,851
Permit to Work	3,775	7,235	5,566	5,236	4,749	26,561
JSA	4,357	8,227	5,567	5,236	4,749	28,136
PJSM	4,357	8,288	5,607	4,466	4,749	27,467
SHE Inspection	258	864	885	939	909	3,855
SHE Drill	68	86	55	52	59	320

Table 2: Accumulative Data Summary of 2018-2022 Drilling SHE Performance.

2,413,829 Man-Hours Free LTI (= 3,6 Years)	**1,713,878** Safe Km Driven
26,561 Permit To Work	**28,136** Job Safety Analysis
82,851 BBS Observation Cards	**3,855** SHE Inspections

5. RESULTS

On the chart Figure 1 a, b and c, Unsafe Behavior based on the Workplace Exposure factor analysis within 3 years collected COACH Card data present the symmetric plots of the observed Workplace Exposure parameters against responses from respondents Coach Cards by drilling workers, respectively. This figure presents the Workplace Exposure observation reflecting the resultant factors trend of Top Three factors of Unsafe Behaviors. Furthermore, this Figures also present plots of percentage risk of workers based on observations card and checklist describe analysis.

Star Energy Geothermal Drilling Team took a proactive approach to manage anticipated and emerging safety behavior issues. A good example of this approach is the adaptation of the Incident Free Operation (IFO) method through the implementing of Drilling IFO concept. Table 1 and 2 above stated the SHE Performance was achieved accumulative **2,413,878 Man-hours Free LTI or 3.6 years Free LTI**. And the COACH Cards observation accumulative were **82,851 cards** as record of Safety Behaviors during SEG Drilling Make Up Well Program in 2018 – 2022.

This achievement was consisting of both Drilling Team Leadership Management and Employee (workers on drilling site) attitudes vary dramatically with respect to safety, risk management and IFO concept. The effective development and promotion of health, environment and safety improvement by Leadership is an important feature of the Safety Culture and Performance of organization which was confirmed that SEG Drilling Team on the 4th Stage position in the Bradley Curve in Figure 2 below:

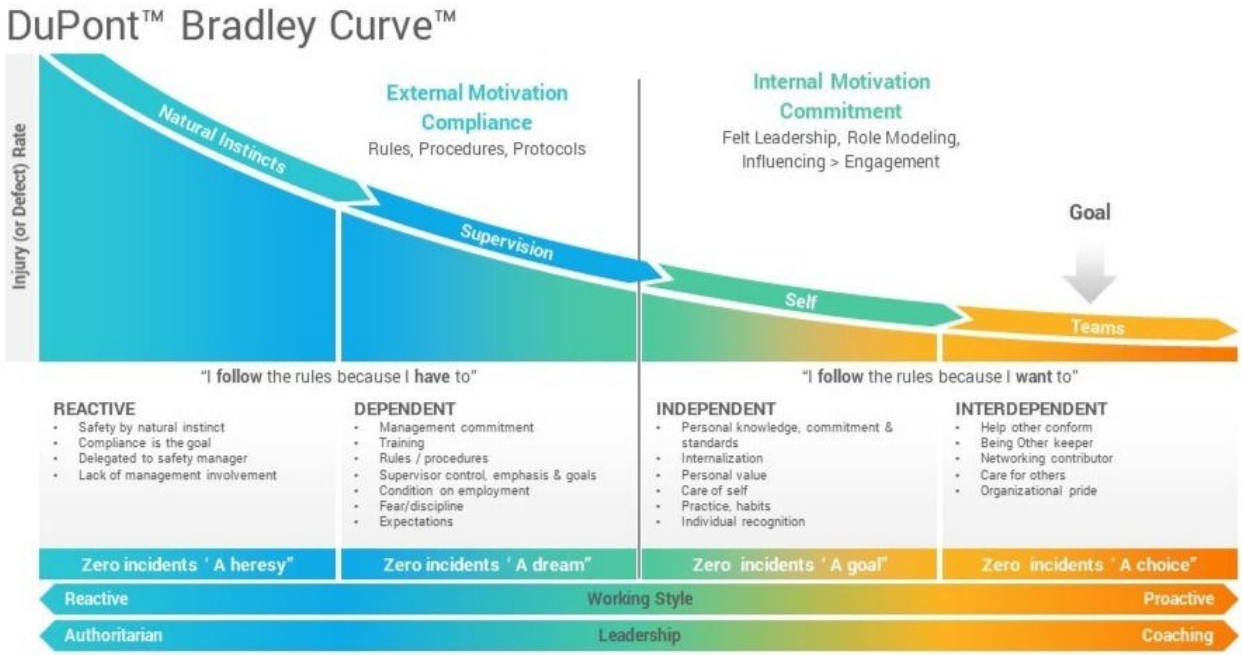

Figure 2: The DuPont Bradley Curve.The Bradley Curve was created by DuPont in 1995 to try and benchmark notions of culture and performance in relationship to safety. The DuPont Bradley Curve depicts four stages of safety culture. A company's culture can be attributed to any one of these stages and then developed to reach others. Companies with frequent accidents are in the First Stage. At the other end of the spectrum, in the Fourth Stage, are companies where accidents are rare or do not occur at all. Two interim stages lie between the first and the fourth stage. Each stage is characterized by a behavioral basis in relation to occupational safety. This is based on a key question: What is the foundation to prevent accidents - natural instincts, rules and supervision, responsibility, or shared responsibility.

The way Star Energy Geothermal Drilling Team organizations act out their safety management systems and how systems operate in drilling operations were includes safety culture, safety leadership and safety behavior fit modification which was categorized in **4th Stage** position on the DuPont Bradley Curve as the Goal achievement:

- Internal Motivation Commitment
- I follow the rules because I want to
- Interdependent Stage
- Zero Incidents A Choice, Proactive Working Style, and Leadership Coaching

5. CONCLUSION AND RECOMMENDATION

5.1 Conclusion

Based on the results of this analysis, the following conclusion can be drawn:

1) The findings of this analysis suggest the implementation of the behavior-based safety program lowered the number of recordable safety incidents in the drilling site.

2) Behavior-based feedback increased percentage safe scores from baseline to intervention, and these improvements were maintained for the various groups of drilling workers at the various team involved.

3) The Behavioral Based Safety process using Coach Cards observation at SEG Drilling Operational site, showed Top Three a baseline data of "unsafe behavior" of Workplace Exposures during data quantitative in **2020 – 2022** Drilling MUW observation cards record, to be significantly high in Figure 1 a, b and c:

- Housekeeping factors (399, 1064, 209 cases),
- Struck by/against factors (329, 395, 60 cases)
- Slip/trip/fall factors (105, 236, 61 cases).

5.2 Recommendation

1) For a more proactive safety culture, a behavioral based safety program can be maintained; by peer-to-peer observation of workers safe and unsafe behavior; direct coaching and giving feedback, thereby gaining trust, and improving on the safety behavior, safety culture and performance.

2) Hand and fingers Injury Prevention program should be established periodically, as Workplace Exposure for Struck by/against statistics at work were contributed as the Second of Top Three Unsafe Behaviors record.

3) Allocation of resources (operational cost, additional times consume and method), as regards finding of observation factors data for Workplace Exposure Slip/trip/fall and Housekeeping on drilling site are mandatory to improve the best selective solutions. If these were not applied, it will be leading to the high contributed factor of Unsafe Behavior recorded on sites.

4) The drilling operation workers feel that skills in Safety Culture are not shown, so drilling rig contractor and service company must provide more things that support improving or strengthening Safety Behavior. Therefore, the drilling rig contractor and service company must maximize the applicable rules to improve Safety Behavior.

REFERENCES

Cooper MD (2000). Towards a model of safety culture. Safety Sci., 36(2): 111-136.

Fleming, M. Safety Culture Maturity Model; HSE Offshore Technology Report 2000/049 Sudbury, UK, 2000; pp. 3–7. Minerals 2013, 3-72.

Geller ES (1998a). Principles of behavior-based safety. Proceeding of The American Society of Safety Engineers Behavioral Safety Symposium, Light Up Safety in the New Millennium (p. 1324). Des Plaines, IL: American Society of Safety Engineers.

Geller ES (1998b). Understanding behavior-based safety: Step-by-step methods to improve your workplace (2nd ed.). Neenah, WI: J. J. Keller and Associates.

Geller ES and Williams JH (2001). Behavior-Based Intervention for Occupational Safety. Journal of Safety Research.

Geller ES and Williams JH (2001). Keys to behavior-based safety from safety performance solutions. Rockville, MD: Government Institutes.

Geller, S. 2004. The “big five” and you: How personality traits can affect behavior. Industrial Safety & Hygiene News, 38(7): 12.

Gul M, Ak MF. A comparative outline for quantifying risk ratings in occupational health and safety risk assessment. J Clean Prod. 2018.

Krieger GR and Montgomery JF (1997). Accident prevention manual. Springfield, IL: National Safety Council.

Lardner, R. Towards a Mature Safety Culture. Presented at the Institute of Chemical Engineers Annual Conference, Manchester, UK, 2002

Ministry of Health of the Republic of Indonesia, 2015, 1 Worker in the World Dies Every 15 Seconds Due to a Work-Accident. (http://www.depkes.go.id/article/view/201411030005/1-orang-pekerja-in-the-world-diesevery-15-seconds-dueto-a-workaccident.html#sthash.o3CKTFE6.dpuf).Neal, A., & Griffin, M.A. 2006. A study of the lagged relationships among safety climate, safety motivation, safety behavior, and accidents at the individual and group levels. Journal of Applied Psychology, 91(4): 946–953.

Notoatmodjo, S. (2003). Health Education and Behavior, Rineka Cipta, Jakarta.

Peterson RS, Smith DB, Martorana PV, Owens PD. The impact of chief executive officer personality on top management team dynamics: one mechanism by which leadership affects organizational performance. J Appl Psychol. 2003;88(5):795.

Step Change in Safety. Changing Minds: A Practical Guide for Behavioral Change in the Oil & Gas Industry. Step Change in Safety Website Available online: http://www.stepchangeinsafety.net/knowledgecentre/publications/publication.cfm/publicationid/16

Xue Y, Fan Y, Xie X. Relation between senior managers' safety leadership and safety behavior in the Chinese petrochemical industry. J Loss Prev Process Ind. 2020;104142

Zahiri Harsini A, Ghofranipour F, Sanaeinasab H, Amin Shokravi F. A randomised controlled trial of an educational intervention to promote safe behaviours in petrochemical workers: a study protocol. BMC Public Health2019;19(1):776. https://doi.org/10.1186/s12889-019-7126-1

Darajat H_2S Abatement System for Well Production Test

Sigit Winarno, Wibisono, Thomas Agus Bayu Prasetyo, Windu Hasta Bayu,
Irfan Ismail, Endik Sudarman, and Diah Ayu Pramesti

Star Energy Geothermal, Wisma Barito Pacific II, 17th – 21st Floor,
Jl. Letjen S. Parman Kav. 60, Jakarta Barat 11410, Indonesia

sigit.winarno@starenergy.co.id, wibisono@starenergy.co.id, thomas.agus@starenergy.co.id,
winduhasta.bayu@starenergy.co.id, irfan.ismail@starenergy.co.id, essx@starenergy.co.id,
diahayupramesti@gmail.com

Keywords: H_2S abatement system, flow test, production test, zeolite, caustic soda, NaOH

ABSTRACT

Geothermal power offers a significant advantage over traditional fossil fuel plants by producing lower emissions. However, geothermal fluids can still contain dissolved non-condensable gases (NCG) like H_2S, which poses environmental and safety concerns. Effective abatement systems are crucial to address these challenges and ensure the responsible development of geothermal resources.

Star Energy prioritizes safety, health, environment, community protection, and efficient geothermal operations. In line with this commitment, we have developed and successfully tested a H_2S abatement system, complying with Ministry of Energy and Mineral Resources regulations on pre-requisite for newly drilled wells production test.

This system utilizes a compact tower scrubber with a two-stage treatment process. H_2S Scrubbing with diluted Sodium Hydroxide (NaOH): A dilution of 48% NaOH solution is sprayed countercurrent to the H_2S flow, effectively neutralizing the gas through a chemical reaction. A circulating system replenishes the NaOH solution, and a mist eliminator minimizes caustic carryover, preventing potential skin irritation. Small size – high cation exchange capacity zeolite (Aluminum Silicate with CEC > 100 meq. /100g) is packed within the tower to further capture H_2S through a physical adsorption process. The zeolite's small size optimizes contact surface area for efficient adsorption.

The system's effectiveness was demonstrated during function test and a bleed trial on well DRJ-41. Initial H_2S concentrations of 200 ppm were reduced to zero within minutes, showcasing the system's ability to both adsorb and neutralize H_2S. Furthermore, H_2S levels in the surrounding area remained at 0 ppm throughout the bleeding process, confirming the system's success in mitigating potential environmental and health risks.

Star Energy's Darajat H_2S abatement system exemplifies our dedication to responsible geothermal development. This successful implementation paves the way for safe and efficient utilization of geothermal resources while minimizing environmental impact. We commit to advancing technology and best practices for a cleaner and more sustainable future.

1. INTRODUCTION

Aligned with Star Energy Geothermal Darajat objective to support development of geothermal resources, a Make Up Well drilling project was planned and executed during February - July 2022 to maintain steam supply for Darajat powerplant Unit-2 and Unit-3. Upon completion of each well drilling, a well production test is planned as a mean to measure well productivity. During this test, fluids produced from the well are flowed through flow test line to rock muffler. Included in the fluid produced is NCG (Non-Condensable Gas), e.g., CO_2, CH_4, H_2S which accumulated at upper part of wellbore during well heating period (post well drilling completion and prior well flow test). These gases – especially H_2S – brought with it safety concern due to its poisonous nature.

A series of incidents involving H_2S gas release during well drilling/well production tests in geothermal field operated by other developers occurred in January – March 2022 period. These incidents led to investigations which resulted in EBTKE (Directorate General of New, Renewable Energy and Energy Conservation) – a part of GOI Ministry of Energy and Mineral Resources - issuing additional requirement for an H_2S abatement system/procedure in place for a well production test project. The system should be placed to neutralize H_2S gas accumulation flown from well in a way that H_2S gas discharged from well to surroundings is maintained at zero ppm, or at least at acceptable minimum safety level.

This pre-requisite for an H_2S abatement system in a well flow test operation presented a challenge worth taking in return for a safer operation. Darajat team – consists of Asset Management, Power Plant Operation and Facility

Engineering team – were working on literature study on H_2S abatement system, as well as gaining knowledge and sharing lessons learned with personnel at the Kamojang geothermal field, operated by PT Pertamina Geothermal Energy, on their H_2S abatement system design for well flow test operation.

The design process continued with main idea of utilizing 48% NaOH solution (as learned from Kamojang geothermal field) combined with zeolite packed inside H_2S scrubbing tower. The H_2S gas flow from well will undergo adsorption by zeolite rock and chemical reaction with 48% NaOH solution inside scrubbing tower. These processes are accommodated inside scrubbing tower, in which the inflow of H_2S gas is controlled/throttled to avoid H_2S gas and NaOH solution carry over – out to surroundings. The process should finish with steam flown out from scrubbing tower mist eliminator as all the H_2S gas accumulation has all been neutralized and then the well is declared safe for flow production test operation.

2. DESIGN

The objective of this phase was to design a system accommodating a circulation of 48% NaOH solution countercurrent to the H_2S flow inside a zeolite-packed tower, in which the flowing H_2S gas will undergo process of adsorption by zeolite rock and chemical reaction with 48% NaOH solution.

2.1 Process Flow Diagram

The process of H_2S gas neutralization by NaOH and adsorption by zeolite is described as follow:

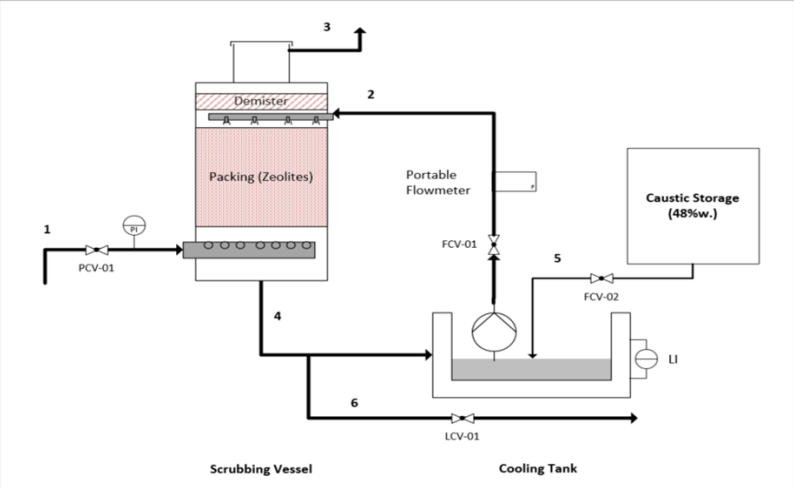

Figure 1: Process flow diagram for H_2S gas neutralization by NaOH and adsorption by zeolite in a scrubbing tower.

The process commences with (1) flowing steam containing H_2S gas from well to scrubbing tower inlet through a throttled 3" line. A valve is installed to control the flow rate. The incoming steam flows upward through zeolite-packed bed where adsorption process occurs. (2) NaOH solution is pumped from cooling tank up to scrubbing tower top, where it is sprayed countercurrent to the steam flow. The NaOH solution neutralizes H_2S gas in the steam flow. (3) The neutralized steam flows out of scrubbing tower through demister. Demister/mist eliminator is installed to minimize NaOH carryover to avoid potential irritation. (4) Reaction residue flows through drain line back to cooling tank. (5) Make-up NaOH is supplied from storage tank to replenish NaOH solution. (6) Once H_2S gas content is neutralized and leaving steam flow coming out of the scrubbing tower, Reaction residues is then drained to nearest sump to be pumped into re-injection well.

2.1.1 H_2S gas neutralization by NaOH

As shown in the process flow diagram above, process no. 2 involves H_2S gas neutralization by countercurrent flow of NaOH solution. The reaction that occurs between NaOH and H_2S is as follow:

$$NaOH + H_2S \rightarrow NaHS + H_2O \quad (1)$$

$$NaHS + NaOH \rightarrow Na_2S + H_2O \quad (2)$$

The amount of NaOH that is readily available in relation to the amount of H_2S that is scraped into the solution determines the extent of reactions 2.1 and 2.2 (Mamrosh et al., 2014). The progression of reaction 2.1 to reaction 2.2 is encouraged when there are higher levels of NaOH present compared to the sulfide that is present. The NCG and H_2S content used as basis of design comes from previous well production test conducted in Darajat geothermal field is as follow:

Table 1: NCG content reference for H_2S abatement system design.

Well Reference	NCG in Total Flow (wt.%)	H_2S in Total Flow (wt.%)	H_2S in Total NCG (wt.%)
DRJ-A	3.6	0.10	2.83
DRJ-B	7	0.09	1.2

The data used as basis of design is from DRJ-B where the well production is categorized as standard or normal in Darajat (at a range of 10 kg/s – 20 kg/s steam flow rate), thus is considered more representative to model the future well production tests condition. The data from well A is considered not representative since the well steam flow rate is low (below 1 kg/s). Mass balance calculation made based on neutralization reaction and reference data shown in table 1 is shown below.

Non-Condensable Gas mass fraction $= 7wt.\%$

Steam (H_2O) mass fraction $= 100\ wt.\% - 7\ wt.\% = 93\ wt.\%$

H_2S mass fraction $= 0.09\ wt.\%$

Assuming total flow through well through 2" scrubbing tower inlet pipe $= 1\ kg/s$

Then,

Steam (H_2O) mass flow rate $= 93\ wt.\% \times 1kg/s = 0.93\ kg/s$

Non-Condensable Gas mass flow rate $= 7\ wt.\% \times 1kg/s = 0.07\ kg/s$

H_2S mass flow rate $= 0.09wt.\% \times 1kg/s = 0.0009\ kg/s$

$= 0.0009\ kg/s \times 34.1kg/kg.mol$

$= 0.0000257\ kg.mol/s$

$= 0.0257\ mol/s$

Assuming selective reaction to H_2S with 50% NaOH excess above stoichiometry requirement:

$2NaOH + H_2S \rightarrow Na_2S + 2H_2O$

NaOH mass flow rate $= 2 \times 0.0257\ mol/s = 0.05\ mol/s$

NaOH with 50% excess $= 0.05\ mol/s \times (1 + 50\%) = 0.077\ mol/s$

$= 0.077\ mol/s \times 39.997kg/kg.mol$

$= 0.003\ kg/s$

Table 2: Mass balance calculation for H_2S reaction with 50% excess NaOH.

Component	2NaOH (aq)	H_2S (g)	Na_2S (aq)	$2H_2O$ (aq)	UoM
Initial	0.0770	0.0257			mol/s
Reaction	-0.0462	-0.0231	0.0231	0.046	mol/s
Residue	0.0308	0.0026	0.0231	0.046	mol/s
Mass Rate	0.0012	0.0001	0.0018	0.001	kg/s

From calculation above, the H_2S gas flow rate is reduced from 0.0009 kg/s down to 0.0001 kg/s, indicating 90% H_2S gas neutralization efficiency.

Calculating NaOH 48 wt.% requirement in 1 liter solution (NaOH density 1.5 kg/l):

NaOH 48 wt.% flow rate $= 0.003\ kg/s \div (48\% \times 1.5\ kg/l) = 0.004\ l/s$

NaOH 48 wt.% mass rate $= 0.00641\ kg/s$

Calculating NaOH 32 wt.% requirement in 1 liter solution (NaOH density 1.3 kg/l):

NaOH 32 wt.% flow rate $= 0.003\ kg/s \div (32\% \times 1.3\ kg/l) = 0.007\ l/s$

NaOH 32 wt.% mass rate $= 0.00962\ kg/s$

From calculation above, the required NaOH 32 wt.% for the H_2S neutralization reaction is 0.00962 kg/s.

Simulation the reaction using DWSIM for wellhead condition at 13 barg (194.4ºC saturation temperature), 2.5 barg scrubbing tower inlet pressure and 1 barg outlet pressure, we get:

Table 3: DWSIM simulation for well DRJ-B H_2S neutralization with 50% excess NaOH.

Stream	UoM	1	2	3	4
		DRJ-B Bleed	NaOH 32 wt.%	Outlet Vapor	Drain
Temperature	ºC	194.4	50.0	100.0	100.0
Pressure	bar	2.5	2.5	1.0	1.0
Mass Flow	kg/s	1.0	0.00962	1.0	0.02359
Volumetric Flow	m^3/d	71,496.0	0.76	141,167.0	2.1
H_2S Concentration	ppm	900.0	-	90.7	0.9

The summary of mass balance calculation for process flow diagram (Figure 1) is shown in Table 4.

The calculation shows that the neutralization process utilizing countercurrent flow of NaOH solution should reduce the H_2S gas concentration from 900 ppm down to 91 ppm, equal to 90% reduction of H_2S gas concentration. Nonetheless, a 91 ppm of H_2S gas concentration is considered poisonous. According to the National Institute for Occupational Safety and Health (NIOSH) Recommended Exposure Limit (REL), the acceptable level of hydrogen sulfide exposure is 10 ppm, while U.S. Occupational Safety and Health Administration (OSHA) Permissible Exposure Limit (PEL) stated that the acceptable level is in between 10 ppm - 50 ppm depends on the activity. Thus, additional compound could be added into the system to neutralize or absorb the remaining 10% of H_2S gas concentration. Team decided to add natural zeolite rock into the system to further increase H_2S gas neutralization.

Table 4: Mass balance calculation summary for process flow diagram.

Stream	UoM	1	2	3	4	5	6
Description		Fluids from well	NaOH to Scrubber	Outlet Vapor	Liquid from scrubber	Make-up NaOH	Liquid Disposal
Pressure	bara	2.5	2.5	1	1	1	1
Temperature	ºC	194.4	48.7	100	85	25	85
Mass Flowrate							
Total	kg/s	1	0.0096	0.99	0.024	0.0058	0.0198
H_2O	kg/s	0.93	0.0065	0.91	0.019	0.0030	0.0178
NCG:							
CO_2	kg/s	0.07	0.0000	0.069	0	0	0
H_2S	kg/s	0.00088	0	0.00009	2E-08	0	2E-08
NaOH	kg/s	0	0.003	0	0.001	0.0028	0.00099
Na_2S	kg/s	0	0	0.00028	0.0012	0	0.00099
Vol Flowrate	m^3/d		0.76		2.06	0.34	1.5
Concentration:							
NaOH	wt.%	0	32%	0	5%	48%	5%
H_2S	wt.%	0.09%	0	0.01%	0.0001%	0	0.0001%
	ppm	900	0	91	0.91	0	0.91

2.1.2 H_2S gas adsorption by natural zeolite

The tetrahedron is the fundamental building component of the zeolite framework, having a silicon or aluminum atom at its center and four oxygen atoms at its vertices. The negative charge of the framework is defined by the substitution of Si4+ by Al3+, which is compensated by monovalent or divalent cations placed together with water.

The most conserved and stable component is the aluminosilicate framework, which specifies the structural type. Water molecules can exist in voids of huge cavities and be bonded via aqueous bridges between framework ions and exchangeable ions. Water can also act as a bridge between two exchangeable cations.

Zeolites and adsorbates interact strongly. Different diffusion and polarity characteristics of adsorbates interact with the zeolite framework differently and are thus distinguished by certain zeolite kinds (Kamarudin et al., 2007). Because of their open, cage-like structures, high cation exchange capacities, large internal surface areas, variable aggregate sizes, and high permeability features, zeolites have diverse commercial uses such as highly selective adsorbents, ion exchangers, and highly active catalysts (Sand and Mumpton, 1978).

The reaction mechanism that occurs in removing H_2S by using zeolites is as follows (Sigot et al., 2015).

$$H_2S(g) \rightarrow H_2S(ads) \quad (3)$$

Reaction 3 occurs when the hydrogen sulfide is adsorbed at zeolites surface. After that, the hydrogen sulfide experienced dissolution in water contain in zeolites pores as seen in equation 4:

$$H_2S(ads) \rightarrow H_2S(aq) \quad (4)$$

$$H_2S(aq) + H_2O(l) \rightarrow HS(aq)^- + H_3O(aq)^+ \quad (5)$$

$$HS(aq)^- + O(ads) \rightarrow S(ads) + OH(aq)^- \quad (6)$$

$$xS(ads) \rightarrow Sx(ads) \quad (7)$$

Equation 5 indicates the dissociation of hydrogen sulfide in the water film. After that, the HS- undergoes oxidation with adsorbed oxygen as seen in equation 6. Furthermore, in equation 7 occurs the formation of cyclic sulfur polymers.

Zeolites have pores that allow molecules with smaller diameters to be adsorbed, whereas molecules with bigger diameters cannot pass through these pores. This is an appealing adsorptive property for eliminating pollutants from natural gas such as hydrogen sulfide, carbon dioxide, and moisture (Abdirakhimov et al., 2022). Thus, the addition of zeolite into the system to further decrease H_2S gas content – below acceptable exposure safety limit.

2.2 Scrubbing Tower Design

To accommodate the two process – i.e., H_2S gas neutralization by NaOH and H_2S gas adsorption by natural zeolite, a scrubbing tower is designed. The design objective of scrubbing tower is to estimate minimum scrubbing tower diameter and height that would allow for the calculated speeds of load and flood in tower of filling. This way, the H_2S gas flow will have sufficient retention time inside scrubbing tower to react with NaOH and zeolite. As initial guess, the scrubbing tower diameter and height will resemble the dimension of available flash tank in Darajat geothermal field. This is done to optimize material usage and to minimize construction time. In this case, the size of available flash tank is around 1.029 m in diameter and about 3.875 m in height.

2.2.1 Scrubbing Tower Diameter

The minimum required diameter is calculated using packed tower flood correlation to estimate the speed of loading and flooding in scrubbing tower.

Packed bed diameter calculation:

Column inside diameter (ID) $= 40.5\ in = 1.029\ m$

Column surface area (A) $= 0.25\ \times \pi \times (1.029\ m)^2 = 0.831\ m^2$

Referring to Table 3, mass flow rate of steam mixture and NaOH are 1 kg/s and 0.00962 kg/s, respectively. Density of steam mixture and NaOH are 1.21 kg/m^3 and 1,300 kg/m^3 with viscosity of 0.45 cP.

Steam mixture flux (G) $= (1\ kg/s\ \times\ 3600\ s/hr)/(0.831\ m^2\ ) = 4{,}331.5\ kg/m^2.hr$

NaOH mixture flux (L) $= (0.00962\ kg/s\ \times\ 3600\ s/hr)/(0.831\ m^2\ ) = 41.7\ kg/m^2.hr$

Calculating x and y for packed tower flood correlation:

$$x = \frac{L}{G}\sqrt{\left(\frac{\rho_G}{\rho_L}\right)} = \frac{41.7\ kg/m^2.hr}{4{,}331.5\ kg/m^2.hr}\sqrt{\left(\frac{1.21 kg/m^3}{1{,}300 kg/m^3}\right)} = 2.93 \times 10^{-4}$$

Using the calculated x value above and with extrapolation, the y value can be found using correlation below (Joaquin, Gabriel, Jesus, 2016):

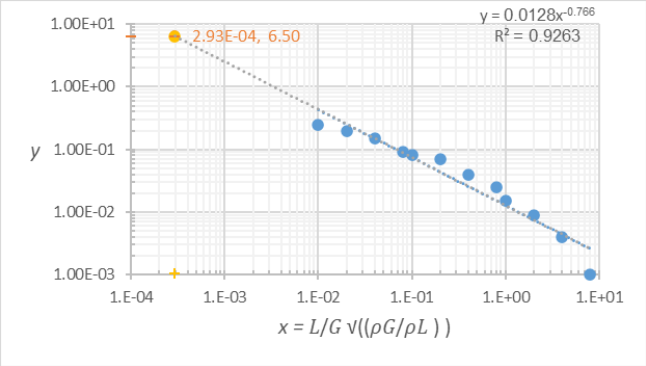

Figure 2: Packed tower flood correlation for *x* and *y*.

From correlation above, the *y* value is used to calculate *G flooding* with assumption:

Zeolite filler bulk density $= 1{,}600\ kg/m^3$

Zeolite filler surface area $= 800{,}000\ m^2/kg$

Zeolite filler porosity $= 0.75$

Surface area of dry filler$= 800{,}000\ m^2/kg \div 1{,}600\ kg/m^3 = 500 m^2/m^3$

With $g = 1.27 \times 10^8 m/hr^2$, then:

$$G_{flooding} = \sqrt{\frac{6.5 \times 1.27 \times 10^8 \times 1.21 \frac{kg}{m^3} \times 1{,}300 \frac{kg}{m^3}}{(0.45\ cp)^{0.2} \times \left(\frac{500 \frac{m^2}{m^3}}{0.75^3}\right)}} = 35{,}857.35\ kg/m^2.hr$$

$$G\ to\ G_{flooding}\ ratio = \frac{G_{steam\ mixture}}{G_{flooding}} = \frac{4{,}331.5\ kg/m^2.hr}{35{,}857.35\ kg/m^2.hr} = 0.12 = 12\%$$

Gas flow assuming 60% flooding $= 60\% \times 35{,}857.35\ kg/m^2.hr = 21{,}514.41\ kg/m^2.hr$

Minimum required scrubber area $= \frac{1 kg/s \times \frac{3{,}600\ s}{1\ hr}}{21{,}514.41\ kg/m^2.hr} = 0.17\ m^2$

Minimum required scrubber diameter $= \sqrt{\frac{0.17 m^2}{0.25\ \pi}} = 0.46\ m$

Adding 30% safety factor for scrubber diameter, then:

Minimum required scrubber diameter $= 0.46\ m \times (1 + 30\%) = 0.6\ m = 24\ in$

From this calculation, available material diameter ($40.5\ in = 1.029\ m$) is above minimum requirement ($24\ in = 0.6\ m$), considered sufficient diameter for the scrubbing tower.

2.2.2 Scrubbing Tower Height

Minimum scrubbing tower height is calculated as follow:

Assuming diffusivity value for H_2S and NaOH:

$D_A = DH_2S = 3.51 \times 10^{-9} m^2/s$

$D_B = DNaOH = 1.4 \times 10^{-9} m^2/s$

Assuming Henry constant for H_2S, $HH_2S = 25\ bar.m^3/kmol$

Assuming mass transfer coefficient for liquid phase and gas phase:

Liquid phase mass transfer coefficient $k_{AL} = 1.2 \times 10^{-4} m/s$

Gas phase mass transfer coefficient $k_{GA} = 2.6 \times 10^{-2} kmol/bar.m^2 s$

Kinetic reaction constant $K = 9.5 \times 10^3 m^3/kmol.s$

Then calculating Liquid to Gas mass flow rate ratio by using mass balance calculation in Table 3:

$$\frac{G}{L} = \frac{0.00962\ kg/s}{1\ kg/s} = 0.01$$

Also from Table 3, calculating NaOH concentration, $C_B = \frac{0.077\ mol/s}{0.004\ l/s} = 18\ mol/l$

Then to check the effects of reaction kinetics we can calculate Hatta Moduli:

$$M_H = \sqrt{\frac{DH_2S \times K \times C_B}{k_{GA} \times HH_2S}} = \sqrt{\frac{3.51 \times 10^{-9} m^2/s \times 9.5 \times 10^3 m^3/kmol.s \times 18\ mol/l}{2.6 \times 10^{-2} kmol/bar.m^2 s \times 25\ bar.m^3/kmol}} = 0.03$$

For very low Hatta Moduli (M_H below 1) is met that $E \approx 1 + \frac{{M_H}^2}{3} \approx 1 + \frac{(0.03)^2}{3} = 1.0003$

The condition of neglecting kinetic is that $E > 5M_H$, which is:

$E > 5M_H$

$\leftrightarrow 1.0003 > 5 \times 0.03$

$\leftrightarrow 1.0003 > 0.15$

Thus, the kinetics do not affect the reaction.

To calculate the scrubbing tower height, first we calculate:

$$\frac{1}{K_{GA}} = \frac{1}{A \times k_{GA}} + \frac{HH_2S}{A \times \sqrt{K \times C_B \times DH_2S}}$$

$$= \frac{1}{500 m^2/m^3 \times 2.6 \times 10^{-2} kmol/bar.m^2 s} + \frac{25\ bar.m^3/kmol}{500 m^2/m^3 \times \sqrt{9.5 \times 10^3 m^3/kmol.s \times 18\ mol/l \times 3.51 \times 10^{-9} m^2/s}}$$

$$= 2.12\ bar.m^4.s/kmol$$

According to Robert E. Treybal, the pressure drop for an absorber should be around 200 N/m^2– 400 N/m^2 (Treybal, 1980), thus we may take $\Delta P = 400\ N/m^2 = 0.004\ bara$

$\Delta P \times Z = Pa$; while $Z = \frac{G_m}{K_{G \times A \times P}} \int_{y2}^{y1} \frac{dy}{y - ye}$. With known parameters below:

Molar gas flow rate per unit cross sectional area: $G_m = \frac{53.2194}{1{,}000 \times 0.831\ m^2} = 0.064\ kmol/s.m^2$

Gas phase mass transfer coefficient: $k_{GA} = 2.6 \times 10^{-2} kmol/bar.m^2 s$

Surface area of dry filler per unit volume: $a = 500 m^2/m^3$

For iteration process, we use Z initial guess = 2.4 m. Then:

$$Pa = \Delta P \times Z = 400 \frac{N}{m^2} \times 2.4\ m \times 10^{-5} = 0.0094\ bara$$

$$H_{0G} = \frac{G_m}{k_{GA}.a.Pa} = \frac{0.064\ kmol/s.m^2}{2.6 \times 10^{-2} kmol/bar.m^2 s \times 500 m^2/m^3 \times 0.0094\ bara} = 0.52m$$

While the scrubber tower height Z, is also defined as:

$Z = H_{0G} \times N_{0G}$, we need to find the values of H_{0G} and N_{0G}.

$$N_{0G} = \frac{1}{1 - \left(\frac{m_{Gm}}{L_m}\right)} \times ln\left[\left(1 - \frac{m_{Gm}}{L_m}\right)\frac{y_1}{y_2} + \frac{m_{Gm}}{L_m}\right]$$

Colburn (Colburn, 1969) suggested that the optimum value of $\frac{m_{Gm}}{L_m}$ is between 0.7 – 0.8. For this case we take:

$$\frac{m_{Gm}}{L_m} = 0.7$$

For ratio of mol fraction of solute in gas phase at bottom and top, from Table 2 data we get: $\frac{y_1}{y_2} = \frac{0.0257}{0.0026} = 10$

Then we can use the following correlation (or N_{0G} formula above) to find N_{0G}:

$$N_{0G} = \frac{1}{1-(0.7)} \times ln[(1-0.7)10 + 0.7] = 4.36$$

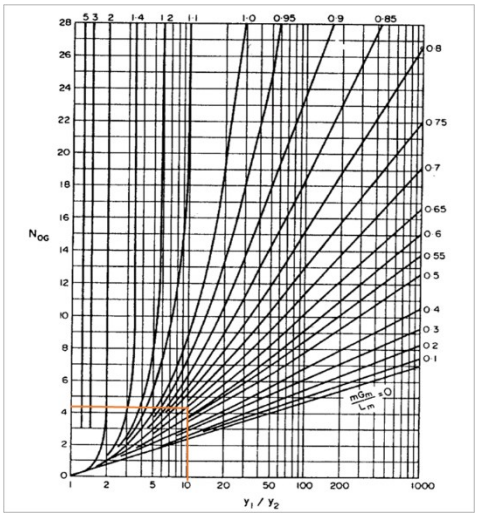

Figure 3: Packed tower flood correlation for $\frac{y_1}{y_2}$, $\frac{m_{Gm}}{L_m}$, and N_{0G}.

Now we can calculate scrubber tower height *Z*:

$$Z = H_{0G} \times N_{0G} = 0.52m \times 4.36 = 2.28m$$

Adding 10% safety factor for scrubber tower height we get $Z = 2.28m \times (1 + 10\%) = 2.5m$

From above calculation we find that the height of available material (3.875 m) is above minimum required height (2.5 m), thus is considered sufficient to accommodate tower flooding. Below is the calculated design for the minimum required diameter and minimum required height for the scrubbing tower:

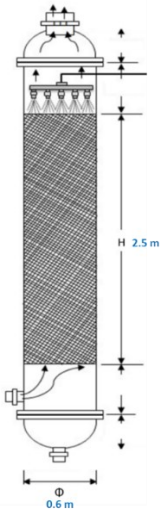

Figure 4: Calculated minimum required diameter and minimum required height for scrubbing tower.

3. IMPLEMENTATION

Construction was commenced with the idea of optimizing available material in Darajat geothermal field while also fulfilling design requirement for technical, environment and safety concern. Several reasons to progress with

this idea included efficiency. By utilizing available materials, we avoided procurement lead time, which could potentially delay the new well production tests and commissioning of the wells. Below is general arrangement drawing for scrubbing tower:

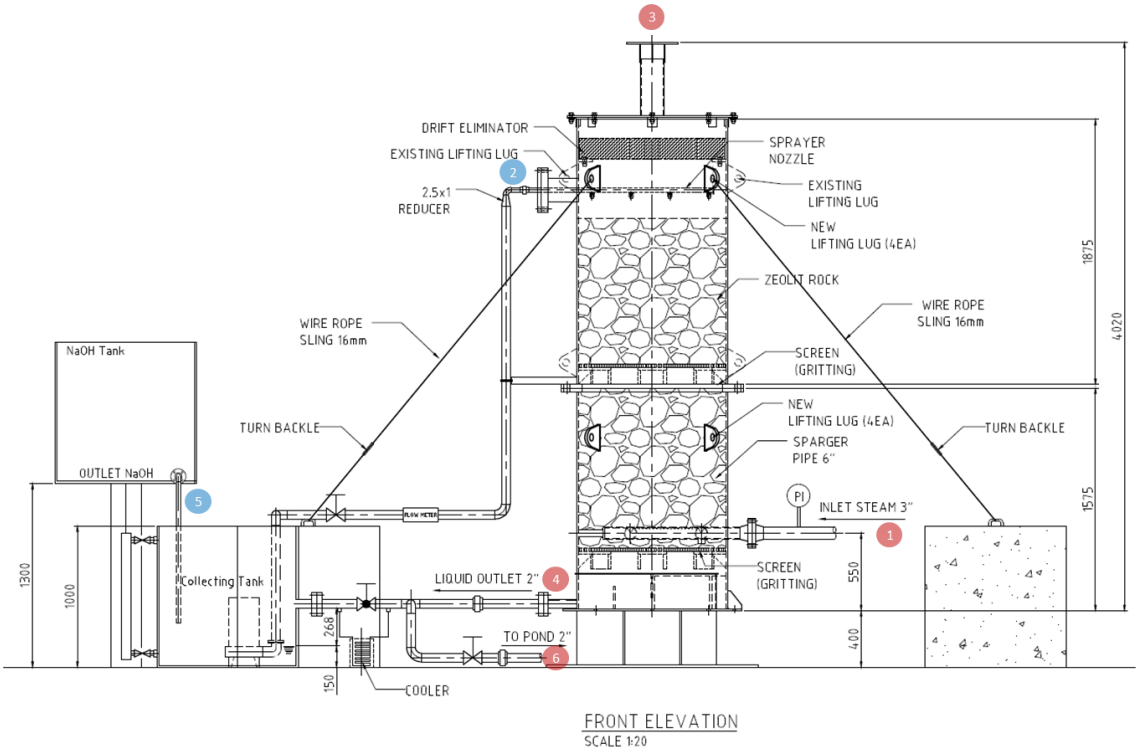

Figure 5: General arrangement drawing for scrubbing tower.

Figure 6: Construction phase.

The construction phase started at the end of March 2022, approximately two weeks after EBTKE issued regulations for an additional H_2S abatement system on March 12, 2022, and about one week after a sharing session with PT. Pertamina Geothermal Energy – Kamojang, a neighboring geothermal field that shares similar field characteristics. The construction was completed in around six weeks in early May 2022 and soon after the completion, a pilot test was conducted on 13 May 2022 on well DRJ-B.

The test was witnessed by EBTKE inspector for well production test and was supported by medical team, FERT (Fire and Emergency Rescue Team) and Security team for environment and safety concern. The test started with water circulation test inside scrubbing tower to ensure pumps were working well. Then, after preparing a solution of NaOH 48wt.% and water (in a volume ratio of 1:2), with 600 liters of NaOH 48wt.% and 1,200 liters of water, the pH was measured at 13.The process continued with re-circulation of NaOH and water solution through scrubbing tower and back to circulating tank. Once the system function test completed, the steam mixture from well DRJ-B was opened through 3" bleed line, 2" scrubbing tower inlet and into packed scrubbing tower. During

the test, operators wore SCBA (Self Contained Breathing Apparatus) and H_2S gas was monitored using portable H_2S gas detector and multi-gas detector.

Figure 7: Pilot test on well DRJ-B.

The accumulated H_2S gas concentration from well DRJ-B prior to the test was measured at 200 ppm. After approximately 30 – 60 minutes, steam came out from scrubbing tower outlet after all H_2S accumulation was adsorbed by zeolite pack and NaOH solution. During the test, the H_2S gas concentration at 0 m – 100 m radius from scrubbing tower was measured at 0 ppm. This shows that the scrubbing tower system was working effectively in binding H_2S.

Post the test, the used NaOH solution was drained through drain line into sump. The sump fluid was then pumped into condensate line and then to injection well. The portable scrubbing tower system was dismantled and moved to next location for another well production test. As shown in Table 5 below, the system was working well during well DRJ-C production test.

Table 5: H_2S scrubbing tower performance during well DRJ-C production test.

Time	H_2S (ppm)	CO (ppm)
09:43	0	181
10:00	0	37
10:31	0	16
10:40	0	0

4. PROCESS OPTIMIZATION

During 2022 make up well drilling campaign, five wells were drilled. All of the wells were treated using an H_2S scrubbing tower system during the initial phase of the well production test to neutralize H_2S gas accumulation. Improvements were made on the H_2S scrubbing tower system through well #1 to well #5 production test to make the system safer and more effective. The improvements made were the change of circulating line from rigid pipe to a flexible hose, improvements on pump electrical panel, NaOH circulation tank top cover, iteration of NaOH 48 wt.% volume used in solution and zeolite rock re-use through washing and boiling. The optimization of NaOH 48 wt.% and zeolite rock are described in below sub-sections.

4.1 NaOH Optimization

The data processing is conducted to determine the optimum concentration of NaOH to absorb non-condensable gas contained in wells. There are 5 concentrations of NaOH, some of them were chosen from literature data and the other were determined by choosing the closest interval. The trial was conducted by using the predetermined NaOH solution to absorb non-condensable gas in gas removal system of Unit-3 in Star Energy Geothermal Darajat II for 72-96 hours. After that, the solutions that have been in contact with non-condensable gas were researched its pH and absorbance to determine the best NaOH concentration. The flowchart of determination of NaOH concentration is presented in Figure 8.

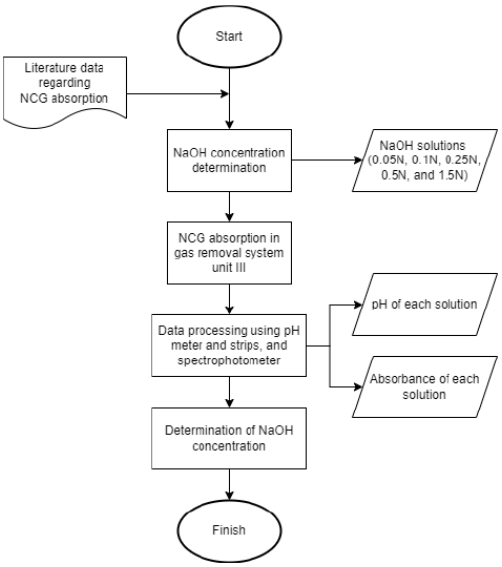

Figure 8: NaOH concentration determination flowchart.

Following the research conducted by Bontozoglou and Karabelas (1993), the selected NaOH concentrations were 0.05N, 0.5N, and 1.5N. The experiment was done by flowing the non-condensable gas from gas removal system unit III into the tube and leaving it to react for 72 hours. From the detector, the value of H2S detected was greater than or equal to 200 ppm with the inlet pressure was 1.173 mbar.

Figure 9: NaOH 0.05N after 72 hours contact.

Figure 10: NaOH 0.5N after 72 hours contact.

Figure 11: NaOH 1.5N after 72 hours contact.

Physically, the NaOH with 0.05N concentration gave cloudy appearance and a little amount of NaS solid was also discovered as it can be seen in Figure 9. On the other hand, the 0.5N NaOH solution gave a significant difference in terms of color. From the Figure 10, the appearance of solid NaS is more visible as it precipitated in the bottom of the tube. The biggest concentration, in this case is 1.5N, gave a stronger yellow color than the 0.5N as well as had more NaS precipitation in the bottom of the tube. From these trials, it can be concluded that the higher the concentration of NaOH will give stronger yellow color and more precipitation will be formed.

Considering the price of NaOH is currently high, the goal is to determine the lowest concentration of NaOH that can achieve satisfactory absorption.. Therefore, trials with 0.1N and 0.25N NaOH were conducted. However, due to a certain condition, the absorption process cannot be done in 72 hours, thus a monitoring was conducted in 24 hours and 96 hours.

As it can be seen from Figure 12 and Figure 14, the 0.1N concentration did not give any significant change in terms of color, however a small amount of precipitation was formed. Contrary to the previous concentration, 0.25N of NaOH offered a slightly yellow color of solution as well as formation of solid Na2S as it can be seen in Figure 13 and Figure 15.

The higher the concentration of NaOH will result in more Na2S precipitation. The pH of each solution was measured using pH meter. The result can be seen in Table 6.

Figure 12: NaOH 0.1N after 24 hours contact.

Figure 13: NaOH 0.25N after 24 hours contact.

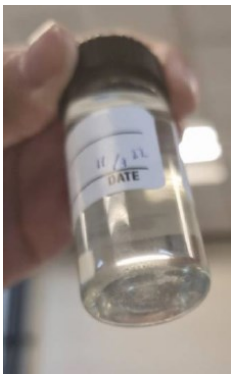

Figure 14: NaOH 0.1N after 96 hours contact.

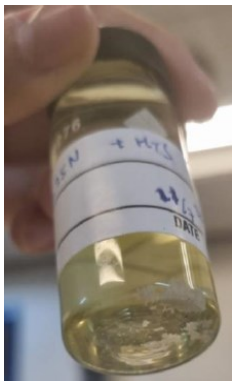

Figure 15: NaOH 0.25N after 96 hours contact.

Table 6: Initial and final pH of various NaOH concentrations.

NaOH Concentration (N)	Initial Theoretical pH	Initial Actual pH	Final Actual pH
0.05	12.70	11.63	8.62
0.1	13.00	13.11	7.84
0.25	13.40	13.54	7.02
0.5	13.70	13.90	8.88
1.5	14.18	13.96	8.26

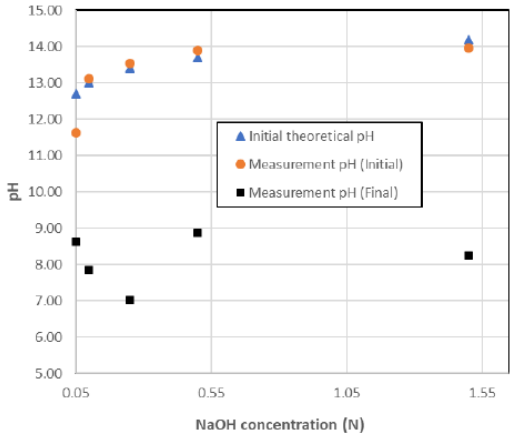

Figure 16: pH of various NaOH concentrations.

It is shown that gas in gas removal system unit III contains with acid gas due to the decrease of pH from more than 11 to in the range of 7 to 8. Compared to the other concentrations, the final pH of 0.05N and 0.5N were bigger; more than 8.5. This might be because the pH measurement was not conducted directly after the samples were taken. This will result in the evaporation of acid gas and thus pH to increase.

On the other hand, the absorbance of each sample was also determined by using spectrophotometer. The obtained data for various concentrations of NaOH is presented in Table 7.

Table 7: Spectrophotometer data of various concentrations of NaOH.

	λ_{440}	λ_{465}	λ_{546}	λ_{590}	Absorbance	%Transmittance
0.05N	0.093	0.085	0.070	0.065	0.313	0.731
0.1N	0.156	0.141	0.106	0.100	0.503	0.605
0.25N	0.783	0.283	0.054	0.053	1.178	0.308
0.5N	0.175	0.072	0.024	0.022	0.293	0.746
1.5N	2.282	0.792	0.106	0.100	3.281	0.038

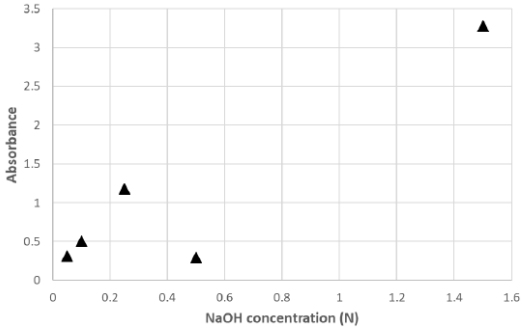

Figure 17: Absorbance of various concentrations of NaOH.

Due to some limitations that occurred in the laboratory, the spectrophotometer can only be used for measuring the absorbance of each concentration by using multiwavelength. Table 7 shows the absorbance of each solution tends to increase when the concentration of NaOH becomes higher. It is proven by the Lambert-Beer law in which the absorbance is linear as it shows in equation below:

$$A = abc = -logT$$

Where A indicates the absorbance, a is the molar absorptivity, b is the path length, and c is the concentration of the sample.

The high value of absorbance indicates that there is absorption in the solution. The higher the concentration of NaOH will result in higher absorbance which leads to more effective absorption. However, the exact chemical compound contained in the sample cannot be determined as it needs to be tested with certain reagents. Since there was a limitation in terms of having all necessary reagents to detect sulfide, the action could not be performed. Therefore, it could only be concluded that something was absorbed by NaOH, but the exact compound was unknown.

There is a depletion in the absorbance of 0.5N of NaOH as seen in Figure 17. This might be because the solution was tested before the other solutions. Thus, resulting in evaporation of absorbed NCG especially H_2S content.

4.2 Zeolite Optimization

The zeolite used in this research were natural zeolite, and zeolite which have been used for well bleeding of well DRJ-C. The zeolite were experienced in 2 treatments, which are with and without boiling.

Figure 18: DRJ-C ex-use zeolite without boiling.

Figure 19: Aquadest of DRJ-C ex-use zeolite with boiling.

Figure 20: Aquadest of natural zeolites with boiling.

Physically, the color of aquadest of DRJ-C ex-use zeolite with boiling was yellowish transparent, while the aquadest of natural zeolite was a little cloudy. The aquadest of DRJ-C ex-use zeolite without boiling had darker color and in certain sides, the dark color of zeolite turned into its original color as seen in Figure 21 below. This phenomenon was also proven that the DRJ-C zeolite were boiled.

The spectrophotoscopy and pH strips data are presented in Table 8.

Figure 21: Original and DRJ-C zeolite after boiling comparison.

Table 8: Spectrophotometer pH data of zeolite.

	λ440	λ465	λ546	λ590	Absorbance	pH
DRJ-D zeolite without boiling	0.181	0.17	0.143	0.133	0.627	6
DRJ-D zeolite with boiling	0.105	0.081	0.041	0.031	0.258	6.5
Natural zeolite with boiling	0.137	0.126	0.1	0.091	0.455	7

Theoretically, the boiled sample has higher absorbance due to the presence of heat will make the reaction occurs faster. The different result to the theory might be due to redeposition. The exact activity in zeolite cannot be seen with naked eyes and specialized instruments are needed. Compounds that previously were adsorbed by the zeolite and then released due to high temperature or being rinsed re-enter the different pores of zeolite. Since the absorbance measurement was conducted by measuring the aquadest, then the particles or compounds that have been re-entered the zeolite as redeposition cannot be measured.

On the field implementation, the boiling of zeolite was provided by exothermic reaction between NaOH solution and H_2S gas. The reaction releases heat that boils zeolite rock inside scrubbing tower. This results in faster reaction/adsorption of H_2S gas by zeolite rocks.

Zeolite fulfill the characteristics of gas adsorption such as the accessibility of the molecules, and pore network system. As zeolite are three-dimensional, thus the pore blockage to the adsorption sites can be prevented (Kamarudin et al., 2007). The high value of cation exchange capacity (CEC) of used zeolites (>100) also led to high number of negative charge and more cations that can be detained (Mengel, 1914). In addition, the natural zeolite have been widely employed as adsorbents in separation and purification procedures due to their excellent cation-exchange ability and molecular sieve capabilities.

Due to their high cation-exchange ability as well as to the molecular sieve properties, natural zeolite have been widely used as adsorbents in separation and purification processes in the past decades (Wang and Peng, 2009).

5. CONCLUSION

The conclusions that can be obtained from the described work on H_2S abatement system are as follows:

1. High concentration of NaOH will result in faster equilibrium state, thus resulting in more Na_2S precipitation.
2. The effective absorption and optimum concentration of NaOH is 0.25N by considering the price and environmental perspective. Smaller NaOH volume is cheaper, and the more neutral the final pH of drained fluid, the more environmentally friendly it is.
3. Presence of zeolite will increase the effectivity of abatement system due to its ability to adsorb H_2S. The presence of zeolite pack provides more retention time for H_2S gas to react with NaOH solution. In the other hand, the exothermic reaction between NaOH solution and H_2S gas provides heat that boils zeolite rock, resulted in faster adsorption of H_2S gas by zeolite rock.
4. The H_2S abatement system is considered effective as H_2S gas absorbents can adsorb H_2S gas from new wells.
5. The design, parameter, and composition of abatement have met the requirement of EBTKE letter no. 2.E/EK.04/DEP.T/2022

REFERENCES

Abdirakhimov, M.; Al-Rashed, M. H.; Wójcik, J., “Recent Attempts on the Removal of H2S from Various Gas Mixtures Using Zeolites and Waste-Based Adsorbents”, Energies 15 (2022), 5391.

Bhatia, S. C., “Advanced Renewable Energy Systems”, Woodhead Publishing India, India, 2014.

Bontozoglou, V.; Karabelas, A. J., "Simultaneous Absorption of H2S and CO2 in NaOH Solutions: Experimental and Numerical Study of the Performance of a Short-Time Contactor", Industrial & Engineering Chemistry Research 32 (1993), 165-172.

Fajrian, H., "Insiden Berulang PLTP Sorik Marapi, DPR Sarankan Cabut Izin Operasi", katadata.co.id (2022), https://katadata.co.id/happyfajrian/ekonomi-hijau/628b5f7c5ae82/insiden-berulang-pltp-sorik-marapi-dpr-sarankan-cabut-izin-operasi, Accessed 25 July 2022.

Guittara, P., "Kebocoran Gas PLTP Sorik Marapi Berulang, Ini Kata Manajemen", CNBC Indonesia (2022), https://www.cnbcindonesia.com/news/20220427110933-4-335267/kebocoran-gas-pltp-sorik-marapi-berulang-ini-kata-manajemen, Accessed 25 July 2022.

Humas EBTKE, "Respon Kementerian ESDM Atas Kejadian Well Kick di Proyek Panas Bumi Sorik Marapi", Direktorat Jenderal Energi Baru Terbarukan dan Konservasi Energi (EBTKE) (2022), https://ebtke.esdm.go.id/post/2022/04/25/3154/respon.kementerian.esdm.atas.kejadian.well.kick.di.proyek.panas.bumi.sorik.marapi, Accessed 25 July 2022.

Kamarudin, K. S. N.; Mat, H. B.; Hamdan, H., "Zeolite as Natural Gas Adsorbents", Thesis, Universiti Teknologi Malaysia, 2007.

Kompas, "3 Fakta Insiden Berujung Maut di PLTP Dieng, Geo Dipa Pastikan Bukan karena Ledakan Salah Satu Sumur", Kompas.com (2022), https://yogyakarta.kompas.com/read/2022/03/13/092000678/3-fakta-insiden-berujung-maut-di-pltp-dieng-geo-dipa-pastikan-bukan?page=all., Accessed 25 July 2022.

Liputan6, "Viral Sumur Panas Bumi di Dieng Meledak Tewaskan Pekerja, Ini Penjelasan Geo Dipa", Liputan6.com (2022), https://www.liputan6.com/regional/read/4909968/viral-sumur-panas-bumi-di-dieng-meledak-tewaskan-pekerja-ini-penjelasan-geo-dipa, Accessed 25 July 2022.

National Center for Biotechnology Information, "Sodium Hydroxide", PubChem (2022), https://pubchem.ncbi.nlm.nih.gov/compound/Sodium-hydroxide, Accessed 13 August 2022.

Rodríguez, E.; Harvey, W. S.; Ásbjörnsson, E. J., "Review of H2S Abatement Methods in Geothermal Plants", Thirty-Eighth Workshop on Geothermal Reservoir Engineering (2014), Stanford-United States.

Sigot, L.; Ducom, G.; Germain, P., "Adsorption of hydrogen sulfide (H2S) on zeolite (Z): Retention mechanism", Chemical Engineering Journal 287 (2016), 47-53.

Steffen, "Density of Sodium Hydroxide", Steffen's Chemistry Pages (2018), https://wissen.science-and-fun.de/chemistry/chemistry/density-tables/density-of-sodium-hydroxide/, Accessed 25 July 2022.

Tamada, S.; Boki, K., "Properties of Various Adsorbents for Removal of Hydrogen Sulfide Gas", Chemical and Pharmaceutical Bulletin 22 (1974), 2701-2709. Wang, S.; Peng, Y., "Natural zeolites as effective adsorbents in water and waste water treatment", Chemical Engineering Journal 156 (2010), 11-24. James, R.; Gould, T., "Bleeding Characteristics of Geothermal Well", Twelfth Workshop on Geothermal Reservoir Engineering (1987), Stanford-United States.

Prasetyo, T. A. B., "Rekayasa Zeolite Alam Bayah dengan Penambahan Larutan FeCl3·6H2O dan Proses Ultrasonik Sebagai Kandidat Adsorben Gas H2S", Doctoral Thesis, Universitas Indonesia, 2019.

https://www.researchgate.net/figure/Physical-Properties-of-Pure-Natural-Zeolite_tbl1_316658971 (zeolite density)

http://nopr.niscair.res.in/bitstream/123456789/9528/1/IJCT%2011%285%29%20704-709.pdf (zeolite surface area)

https://www.researchgate.net/figure/Bulk-Density-and-Total-Porosity-for-Varying-Zeolite-and-Silica-Contents_tbl1_320221805 (zeolite porosity)

https://acreditacion.uni.edu.pe/wpcontent/uploads/2017/05/Design-of-a-NaSH-Production-Plant-Using-H2S.pdf (packed tower design)

https://ceng.tu.edu.iq/ched/images/lectures/chemlec/st4/c1/EQUIPMENT_DESIGN_LECTURE_25%20mass%20transfer%20equipment%203.pdf (packed bed height calculation)

Total Loss Plugging Optimization in 26 Hole Section Using High-Vis + Cement

Ade Dwi Prasetyo and Rivaldi Azhar Ramadhani

Pertamina Geothermal Energy
Grha Pertamina – Pertamax Tower 8th Floor
Jakarta Pusat, DKI Jakarta, 10110, Indonesia

mk.ade.prasetyo@pertamina.com

Keywords: Geothermal Drilling, Geothermal Cementing, Drilling Fluid, Loss Optimization, Lost Circulation Material

ABSTRACT

In geothermal well drilling, things do not always go smoothly as planned. One of the problems in drilling operations is lost circulation, which is the loss of drilling fluid into the formation, preventing the drilling fluid from circulating back to the surface completely. This issue has the potential to become a significant problem, particularly when it occurs in a 26" section, both operational days and costs. ement plug is a method used to prevent lost circulation by pumping cement to the depth where the lost circulation is occurring. However, it often requires multiple cement plug attempts to address the lost circulation effectively, especially since lost circulation in the 26" section is often found to be due to large fractures or faults.

Several previous attempts have been already done at one of the previous wells at PGE (TPS-P2.1) by using only cement plugs and lost circulation materials, resulting unsatisfactory results. As the time passes by, also with further analysis between drilling engineering, drilling fluids and cementing aspects, an optimal cement design was developed in this case for the lost circulation mitigation method, specifically for the 26" section, by combining high-viscosity drilling mud and cement. This method was applied in well TPS-P2.1 and it needed only one cement plug attempt to address lost circulation in the 26" section, indicating it was more effective compared to the methods used in the previous well.

The success-ratio of this method was analyzed through laboratory testing, which involved mixing high-viscosity drilling mud with cement. The laboratory results showed a rapid physical change in the cement mixture when combined with high-viscosity mud, causing it to thicken quickly and form a solid mixture. This analysis demonstrated that the method is more effective because the rapid physical change of the pumped fluid for the cement plug can seal the lost circulation path, making it a more efficient solution for mitigating lost circulation.

This paper will explore the extensive process and journey behind the successful mitigation of total losses in the 26" section of the TPS-P2.1 well. Moreover, it will highlight the lessons learned to prevent similar issues in future operations, ensuring smoother and more optimized drilling operation processes.

1. INTRODUCTION

The Lahendong PGE Area is one of the areas of Pertamina Geothermal Energy that has generated significant installed capacity to benefit Indonesia, particularly in supplying electricity to the North Sulawesi and Gorontalo regions. Starting from 2001, which marked a milestone in the development of geothermal energy in eastern Indonesia, PGE began operating geothermal power plants commercially in the Lahendong working area, North Sulawesi Province.

Pertamina Geothermal Energy main goal, is to be the World Class Green Energy Company with largest geothermal capacity globally. One of the short term goal is to reach the 1 GW installed capacity all across indonesia. One of he process that has to be done and gone through is drilling and exploration process itself, and Lahendong is becoming one of the biggest potential investor and contributor to make this happen. During the drilling campaign of PGE at 2023-2024 timeframe, Lahendong had one of the most wells drilled compared to other areas during that timeframe such as Kamojang or Ulubelu, and one of the Lahendong wells that drilled that time is TPS-P2.1

TPS-P2.1 is the second of two exploration wells in the Lahendong 7&8 project. Well TPS-P2.1 is a directional big hole exploration well with a final depth of 2919 mMD and a total duration of 45 days. This well will be utilized as a production well to support the development plan of PLTP LHD unit 7&8 in the Tompaso field, Lahendong geothermal area. Below is the well profile of well TPS-P2.1

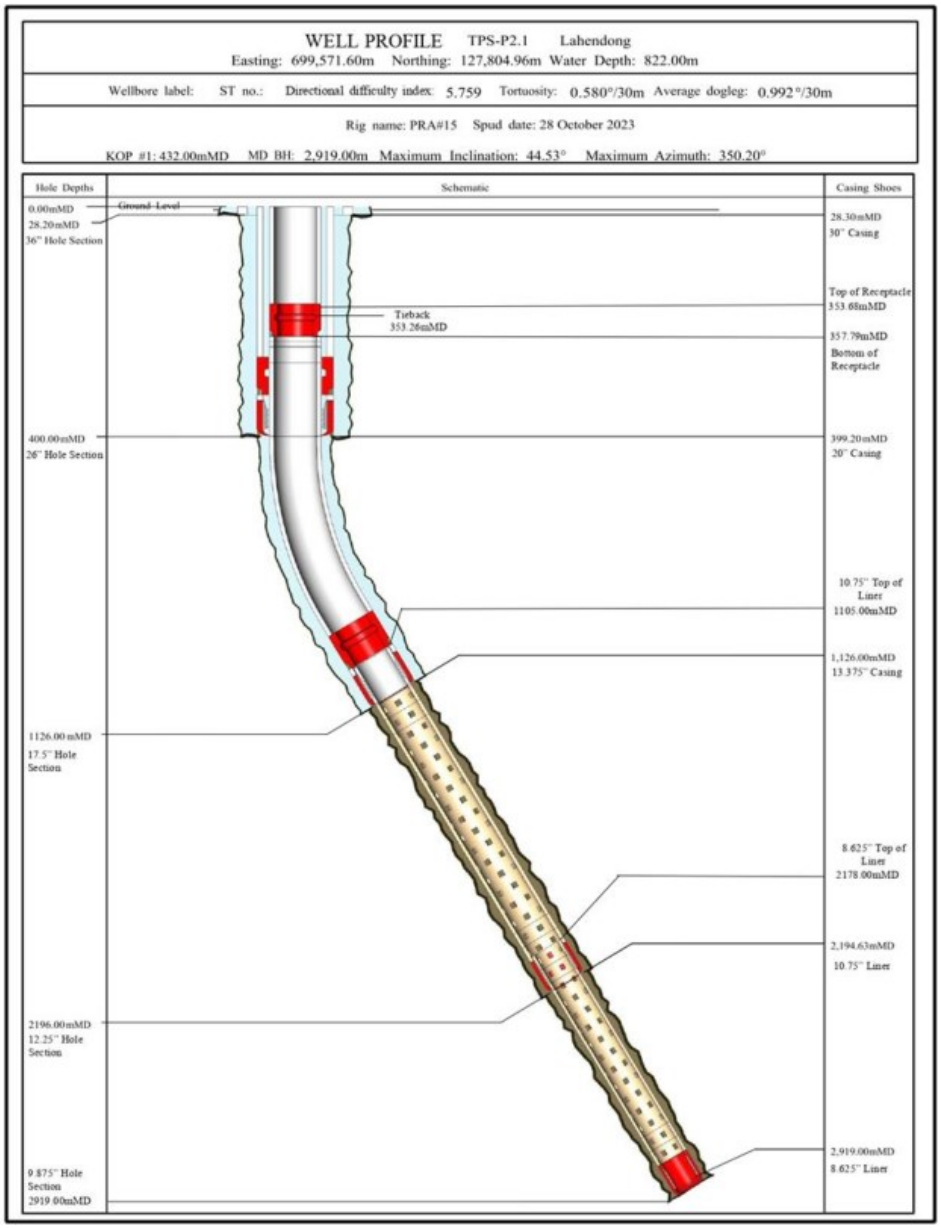

Figure 1: TPS-P2.1 Well Schematic.

2. RELATED WORK

The Concept of drilling in Geothermal and Oil and Gas is slightly different. Drilling, when it was conducted in Oil and Gas whenever loss condition is encountereed during drilling, the process should be done cautiously because the loss condition in oil and gas can lead into kick and even blowout without proper well control action. Therefore, in oil and gas the preparation of kill mud weight should be prepared well while the loss condition or even kick is encountered during the drilling operation.

While in Geothermal, whenever the loss condition is encountered, that means the reservoir is going to be achieved at a certain depth especially whenver we already set at a production depth based on reservoir and geological prognosis. But the danger of kick in geothermal is still can be faced when we encountered the loss condition at the early depth, especially ate early hole section (36" or 26"). The kick that will be happened is the steam kick and one of the most dangerous substances is the Hydrogen Sulfide gas if the steam kick happened, and it also can lead into a blowout such as drilling operation in oil and gas.

During the drilling of well TPS-P2.1 with a 26" trajectory at a depth of 58 mMD, total loss circulation (TLC) was encountered. Previously, in the first exploration well (TPS-A.1), a similar issue occurred where during the drilling of the 26" trajectory at a depth of 39 mMD, TLC was encountered. To mitigate the TLC, a cement plug was

applied using cement and natural LCM a total of 12 times. However, this effort was not successful in mitigating the TLC, so blind drilling was performed until the casing point of the 26" trajectory depth.

Therefore the background of this history will be one of the reason why this paper will explain furthermore about the analysis until the new method to cure the losses at early stage at TPS-P2.1 especially at Hole Section 26" is invented, which is the HighMent, the combination of High-Vis Mud and Cement to combat and cure the losses at the early depth, to achieve a smoother drilling process.

Table 1: Sequence Cure Losses at TPS-A.1 Well.

CEMENT PLUG JOB DI TPS-A.1					
NO	PLUG	TANGGAL JOB	VOLUME	TAGGED	KETERANGAN
1	Plug Material #1	29 Juni 2023	5M^3	-	- Jerami 5 Karung - Sekam Padi 3 Karung - Batu Bata 1000 pcs - 12 Batang pisang berukuran 10-15 cm
2	Cement Plug #1	29 Juni 2023	210 bbls	35 mMD	15.8 ppg, UCA 500 (9h : 30m)
3	Plug Material #2	30 Juni 2023	3M^3	-	- Cacahan Batang Pisang 2 BB - Jerami 7 Karung, - Sekam Padi 11 Karung
4	Cement Plug #2	30 Juni 2023	200 bbls	25 mMD	15.8 ppg, UCA 500 (9h : 30m)
5	Plug Material #3	1 Juli 2023	5M^3	-	- Cacahan Batang Pisang 3 BB - Jerami 6 Karung - Bata Merah 180 Pcs - LCM Medium 10 Sack
6	Cement Plug #3	1 Juli 2023	300 bbls	76 mMD	15.8 ppg, UCA 500 (8h : 10m)
7	Plug Material #4	2 Juli 2023	8M^3	72 mMD	- 25 Batang pisang berukuran 30-40 cm - Batu Bata 600 Pcs - Pasir 2 BB, - Bentonite (18 sack) Bola
8	Plug Material #5	2 Juli 2023	3M^3	45 mMD	- 5 Batang pisang berukuran 30-40 cm - Serbuk kayu 3 Karung - Bentonite (2 Sack)
9	Cement Plug #4	3 Juli 2023	150 bbls	35 mMD	15.8 ppg, UCA 500 (6h : 55m)
10	Cement Plug #5	3 Juli 2023	91 bbls	15 mMD	15.8 ppg, UCA 500 (6h : 55m)
11	Cement Plug #6	5 Juli 2023	100 bbls	35 mMD	15.8 ppg, UCA 500 (6h : 55m)
12	Cement Plug #7	5 Juli 2023	200 bbls	39 mMD	15.8 ppg, UCA 500 (6h : 55m)

In previous drilled wells especially in Tompaso Area, numerous attempts have been done to cure severe losses specifically for the 26" section. Methods by using only cement plugs and lost circulation materials prove to have unsatisfactory result. Due to the severe losses normal conventional lost circulation materials are no use and to overcome this challenge alternative solution is needed.

With further analysis between drilling engineering, drilling fluids and cementing aspects, an optimal cement design was developed in this case for the lost circulation mitigation method, specifically for the 26" section, by combining high-viscosity drilling mud and cement.

3. METHODOLOGY

3.1 High-Viscosity Drilling Mud Design

The hi-vis mud used is optimized to maximize its viscosity while still allowing it to be pumped using a rig pump. The purpose of maximizing the mud's viscosity is to act as a cushion, so when the hi-vis mud is pumped into the well where TLC occurs, it is hoped that it will not immediately enter/disappear into the fractures.

3.2 Cement Design

To combat severe losses due to cavernous formation it was proposed to have cement slurry with high viscosity and rapid gel development properties. Cement with these properties can reduce its fluidity properties once it entered the loss formation and pumping is stopped, hence improving sealing thief zone and mitigate loss formation.

Cement slurry is tested at 30ºC by testing the rheological properties, thickening time, and the compressive strength with an ultrasonic cement analyser. These tests are run to have cement that is mixable and pumpable during cementing job and after cementing job have rapid gel development once it is static, indicated by early strength development during static time.

3.3 High-Viscosity Drilling Mud and Cement Mixture

In lab high-viscosity drilling mud and cement was hand-mixed with 1:1 by volume mixture to observe the fluid profile during intermixing. This mixture has high viscosity that rheological properties can not be tested by rheometer.

Table 2: Design Mud Hi-Vis.

MUD PROPERTIES		SPECIFICATION	Initial Result
Mud Weight	ppg	-	8.4
Funnel Viscosity	sec/qt	>200	245
Reading @ 120°F 600	rpm		94
Reading @ 120°F 300	rpm		75
Reading @ 120°F 200	rpm		65
Reading @ 120°F 100	rpm		55
Reading @ 120°F 6	rpm		26
Reading @ 120°F 3	rpm		23
PV	cp	-	19
YP	lbs/100 ft2	>55	56
Gel Strength 10" @ 120°F	lbs/100 ft2	-	23
Gel Strength 10' @ 120°F	lbs/100 ft2	-	33

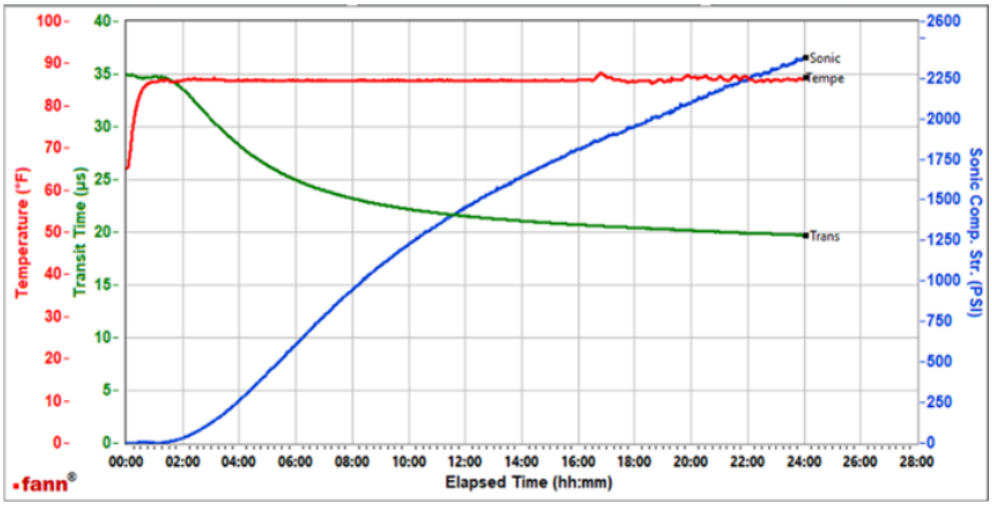

Figure 2: Ultrasonic Compressive Analyzer Chart.

Table 3: Ultrasonic Compressive Analyser Test Result.

BHST (°C)/BHCT(°C)	30/30
Density (ppg)	15.8
Time to Reach 50 psi (hh:mm)	02:15
Time to Reach 100 psi (hh:mm)	02:47
Time to Reach 500 psi (hh:mm)	05:23

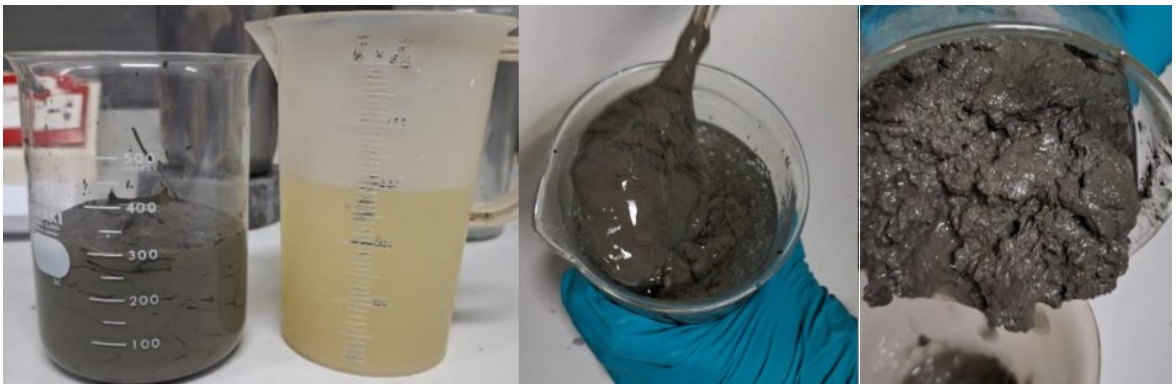

Figure 3: High-Viscosity Drilling Mud and Cement Mixture.

3.4 Cementing Job

Cementing plug job were performed with open-ended DP to reduce friction pressure from viscosity of mud and cement. Open-eneded DP was set around 30" conductor shoe.

During cementing job 200 bbl of high-viscosity drilling mud was pumped ahead of 200 bbls of 15.8 ppg cement slurry. 200 bbl is equal to hole volume with 100% excess. Throughout cementing job no return was observed even with high excess volume.

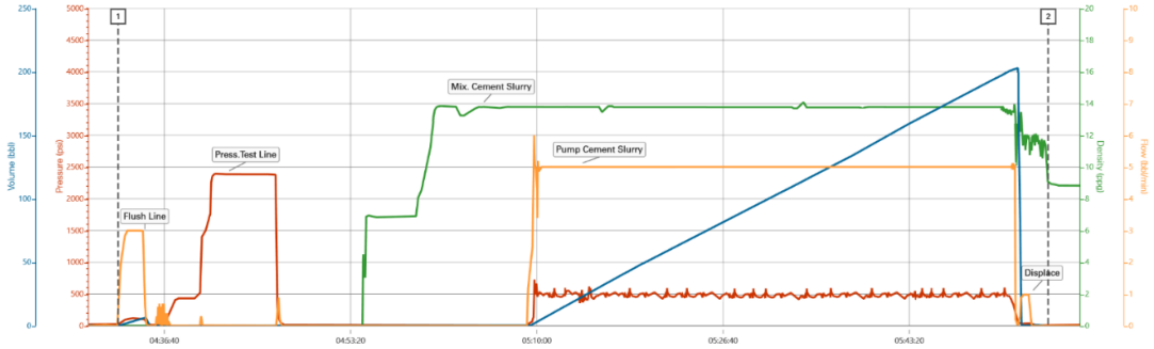

Figure 4: Cementing Plug Job Chart.

4. RESULTS

After WOC for 7.5 hours, cement was tagged at 30m. The cement plug was drilled out, and no losses were observed during and after drilling out the cement, meaning that the job was successfully completed up to the 20" casing point. Additionally, no losses were encountered during the cementing of the 20" casing.

5. DISCUSSION

The Combat Total Loss experiment by using High Vis + Cement at Trajectory 26" is one of the most creative and innovative breakthrough to cure the losses. One of the main advantages of this innovation is there is no need to do a new mixture or create a big amount of trial and error by using new chemical that never used at geothermal drilling operation especially in Pertamina Geothermal Energy.

High Vis and Cement is absolutely available in Pertamina Geothermal Drilling operation because these two materials are a critical and essential materials that used for cementing and drilling mud. The simplicity of the chemical to create a high percentage of effectiveness is truly a genius work to be done.

Based on this data, while the cement plug is performed with open-ended DP to reduce friction pressure with 200 bbl of High Vis Drilling mud pumped ahead of 200 bbls of 15.8 ppg cement slurry (200 bbl is equal to hole volume with 100% excess), there are no major issues that related to the combat loss operation itself, and the loss is cured.

6. CONCLUSION

Geothermal Cementing, until recent days, is still considered as one of the most critical and tricky steps. The prognosis about Loss Condition prediction and fractures prediction about losses at per depth as per analyzed at prognosis always cannot be 100% accurate. The downhole uncertainty is still a major problem to be considered because the nature is so unpredictable, including in geothermal downhole condition.

The biggest consideration of Pertamina Geothermal Energy to do this operation is because the endless and ineffective loss circulation can lead into NPT and increase of massive amount of drilling operation cost, especially in daily rig costs, cement plugs and of course loss circulation material. Therefore, this study needs to be analyzed and applied to every well, because this method is proven to be more effective than usual loss circulation material.

Combining high-viscosity drilling mud and cement has been proven effective in treating loss circulation in the 26-inch outer diameter (OH) surface section, especially in the Tompaso Area. The purpose of using this high-viscosity and cement for the cement plug is to seal off fracture paths/loss zones so that a large volume is not required if total loss circulation (TLC) is encountered, particularly in geothermal wells where TLC is often found in the 26" section. This method can be a new breakthrough to be implemented whenever the loss at early depth will be encountered in any geothermal wells.

The lesson that can be learned from this combat loss operations are:

a. Always be critical and innovative to do an experiment to invent the most innovative and efficient way whenever the combat loss at early section is encountered to reduce and optimized the daily operation costs
b. Reanalyzing the combat loss process before the operation is going to be done, whether it was the material aspect such as the loss circulation material addition, the composition of the LCM to match it with the downhole condition or subsurface condition based on the drilling program prognosis to minimize the uncertainty of downhole condition.
c. Don't only use and repeating the same method to cure the loss that has a big uncertainty, because it will resulting in a waste of time (NPT)

ACKNOWLEDGEMENT

We deeply appreciate the contributions of everyone involved in this project's success. We extend our sincere gratitude to Mr. Tesha, Vice President of Drilling and Services, for his exceptional leadership and unwavering support. Mr. Radianto Ritamawan, Manager of Drilling Operation & WO/WI, has provided invaluable expertise and guidance throughout the drilling process. Special recognition goes to Mr. Wahyu Sutresno, Manager of Drilling Planning & Support, for his meticulous planning and strategic insights, and to Mr. Fery Malau, Assistant Manager of Drilling Operation, for his dedicated efforts and oversight. Our heartfelt thanks go to Mr. Ade Dwi Prasetyo, Drilling Engineer, for his technical proficiency and problem-solving skills, and to the entire Pertamina Geothermal Energy Drilling Team for their hard work and collaboration. We are grateful to the Pertamina Geothermal Energy Area Lahendong team for their on-site support and operational assistance. We commend the TPS-P2.1 Drilling Team for their perseverance and commitment in overcoming project challenges. Lastly, we acknowledge the professionalism and expertise of the TPS-P2.1 Rig Contractor and Services Company Team especially the cementing services, whose contributions were instrumental in achieving project milestones. This project's success is a testament to the collective efforts and dedication of these exceptional individuals and teams.

REFERENCES

Canson, B.E: Lost Circulation Treatments for Naturally Fractured, Vugular, or Cavernous Formations. Presented at the SPE/IADC Drilling Conference, New Orleans, Louisiana, 6–8 March. SPE-13440-MS. https://doi.org/10.2118/13440-MS (1985)

Nayberg, T. M. and Petty, B. R: Laboratory Study of Lost Circulation Materials for use in Both Oil-base and Water-base Drilling Muds. SPE Drilling Engineering. Vol. 2, pp. 229–236. http://dx.doi.org/10.2118/14723-PA (1986)

Jadhav, R. and Patil S:. Acid-Soluble Thixotropic Cement System for Lost Circulation Challenges. Presented at the Abu Dhabi International Petroleum Exhibition & Conference, Abu Dhabi, UAE, 12–15 November. SPE-193168-MS. https://doi.org/10.2118/193168-MS (2018)

Steam Turbine Casing Leak Issue and On-site Repair Process

Rasyid, Andrianto, and Hepy

PT Sulzer Indonesia

rasyid.aziz @sulzer.com, andrianto.hapsoro@sulzer.com, hepy.hanipa@sulzer.com

Keywords: Steam leakage, casing on-site repair, Laser Metal Deposition (LMD)

ABSTRACT

This paper details the on-site repair work performed on the high-pressure (HP) casing split line of the 11 MW Steam Turbine casing in East Java. Commissioned to address casing leakage issues, the scope of work included assessing the flatness, gap, and contact of the split line surfaces, performing weld build-up for dimensional restoration using the Laser Metal Deposition (LMD) method, and completing on-site final machining. The repair outcomes demonstrated effective sealing of the steam pathway at the contact surface. High-temperature sealant was applied to optimize surface sealing performance.

1. INTRODUCTION

Sulzer was commissioned to address casing leakage issues on the high-pressure (HP) casing split line of a 11 MW Steam Turbine unit. The issue of leakage along the casing split line has persisted since the previous overhaul of the unit, where it was temporarily addressed using sealant. The turbine casing consists of two parts: the HP casing and the LP casing. Both casings are joined together with bolts, forming the assembled casing, with the joint located in the midsection. Each casing comprises upper and lower halves.

Indications of the leakage issue are marked by the absence of contact between the upper and lower casing surfaces along the split line area. Visible gaps and leaks have been identified at distinct points, as indicated by the blue ink in Figure 1 and Figure 2.

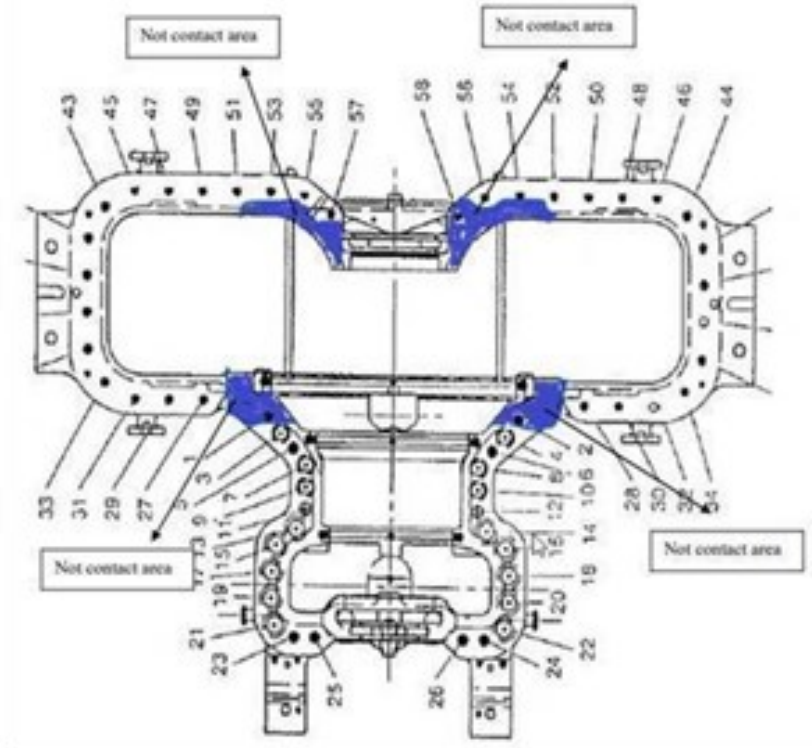

Figure 1: Non-contact area schematic on HP & LP casing split line surface captured during previous overhaul work.

Figure 2: Contact check result indicating non-contact area on lower casing split line.

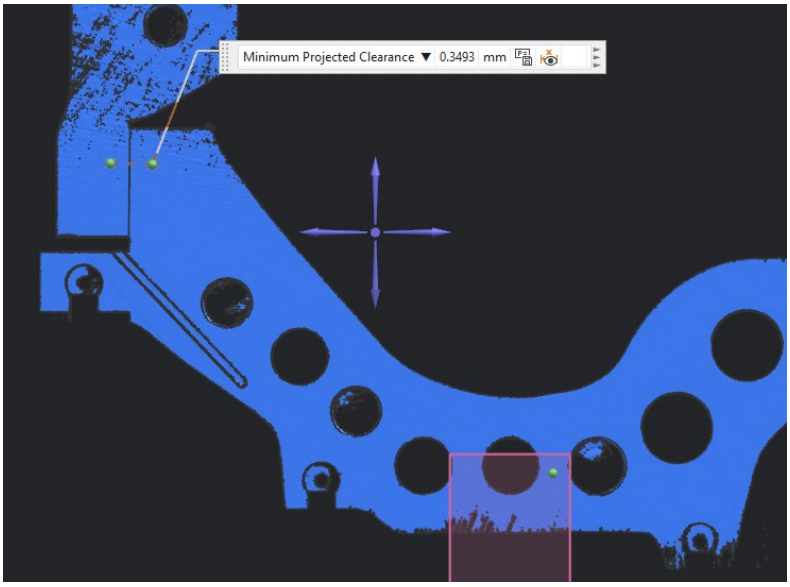

Figure 3: Uneven surface condition between the HP lower casing (left) to the LP lower casing (right).

2. REPAIR PREPARATION

There are two main challenges in completing the repair. The first challenge involves obtaining accurate assessment of the flatness of split line surfaces for both the upper and lower casings. This information is critical for final machining process to ensure effective contact in closing the leakage gaps. To achieve the highest accuracy possible, in addition to gap and contact inspections (with all bolts tightened), flatness check was conducted using portable vertical milling machine and 3D scanner.

The second challenge is to employ a dimensional restoration method that avoids significant side effects, such as distortion to critical dimensions like the casing inside diameter, split line, and casing bolt holes. To mitigate this risk, Laser Metal Deposition (LMD) was utilized, which is a low heat input restoration method.

It was observed the leaking issue on the turbine casing is primarily due to casing distortion, with a minor contribution from erosion or steam cuts. A thorough investigation is required to identify the root cause of the casing distortion. One potential scenario under consideration is the suspicion that the bolt joining the HP and LP casing may have loosened during operation. This potential loosening could lead to the HP casing (both upper and

lower halves) sliding downward relative to the LP casing, creating gaps as indicated in Figure 3. The specific reasons behind the bolt loosening remain unknown and further investigation is required.

Laser Metal Deposition (LMD) weld build-up was prepared and executed on the non-contact area and specifically targeted the lower casing due to practical and time constraint. The concept involved building up the non-contact surface by LMD and subsequently machining it until the contact and non-contact surfaces were leveled. Inconel powder, a material commonly used in geothermal applications for its superior corrosion and erosion resistance compared to the typical turbine casing material, was utilized. This approach enhances the integrity and reliability of the casing during operation.

A portable vertical milling machine was prepared to perform on-site machining with schematic shown in Figure 4. Since the HP casing was sliding downward relative to the LP casing, the lower half HP casing surface became positioned below the lower half LP casing surface level. Due to this suspicion, the plan was to use the LP casing surface as a datum for machining.

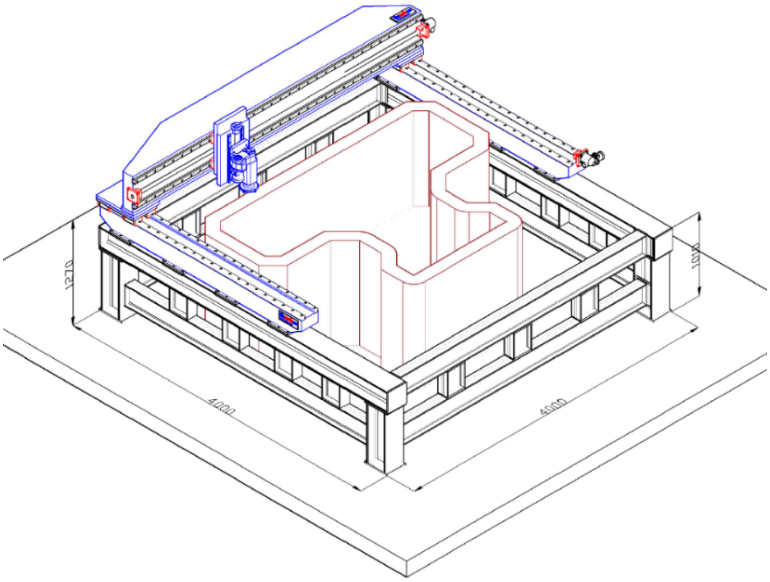

Figure 4: Schematic of portable vertical milling machine.

Figure 5: LMD build-up process on lower casing split line surfaces.

2.1 Initial Attempt Result

The initial repair attempt, which involved LMD build-up and machining, was performed on the lower casing split line surface, as shown in Figure 5 and Figure 6. Following the repair, contact, gap, and flatness checks were conducted to evaluate the results. During this phase, it was possible to perform gap check from the internal side of the casing. The results of the contact check are displayed in Figure 7.

Figure 6: On-site machining process on lower casing split line surfaces.

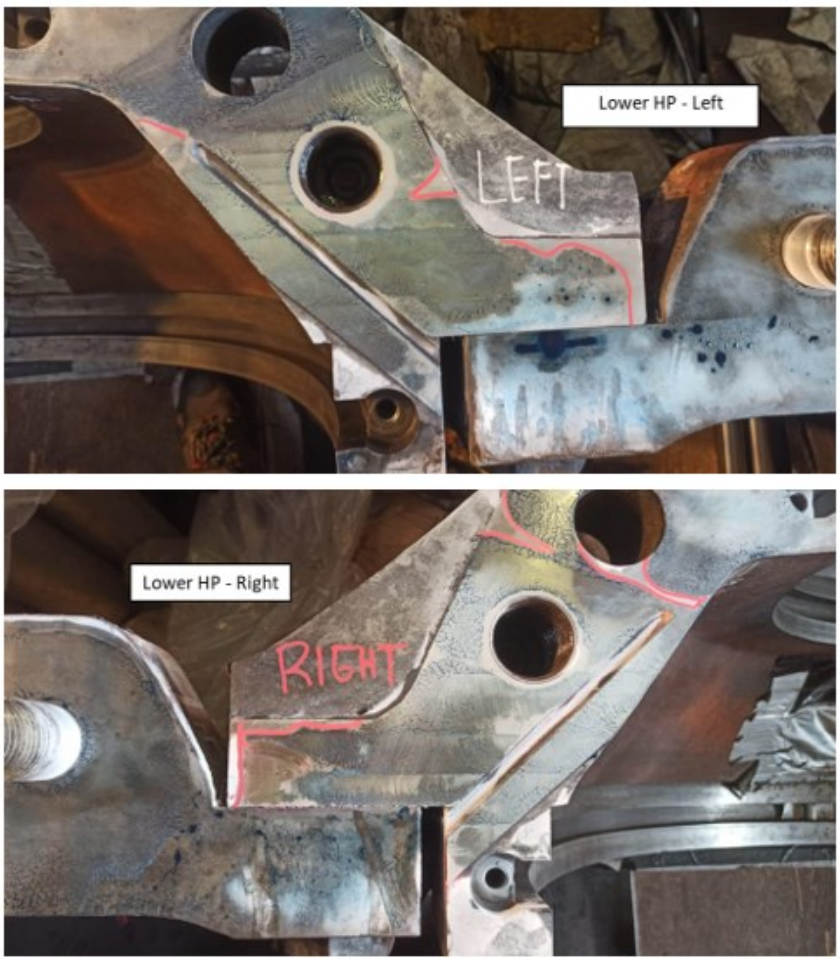

Figure 7: Initial repair attempt contact check results.

Several observations were made based on inspection results:

- The previous non-contact area on HP casing surface has now achieved contact.
- The LP casing surface away from the bolt hole area exhibited weak or was entirely non-contact.

Second repair attempt will be conducted according to the following plan:

- Further build-up LP casing surface that exhibited weak or entirely non-contact
- Shift the machining reference datum to the LP casing surface near the bolt hole area, which has strong contact.

2.2 Second Attempt Result

Several observations were made based on inspection results after second attempt repair:

- Certain areas are still lack of contact as shown in Figure 8.
- Upon conducting gap check with feeler gauge from internal side of the LP casing, a 0.03 mm thick feeler gauge cannot enter certain split line surfaces with weak contact.

As a result of these conditions, following conclusions were drawn:

- Contact classifications were defined, as shown in Figure 8.
- Since the upper-half HP is also observed to be sliding downward, the final machining target on the lower casing should compensate the contour of the upper half HP casing.
- The upper half LP casing surface displays a slope from outward to inward, resulting in larger gaps compared to those formed on the HP casing.
- The upper casing appears to have some degree of uneven surface at random locations.

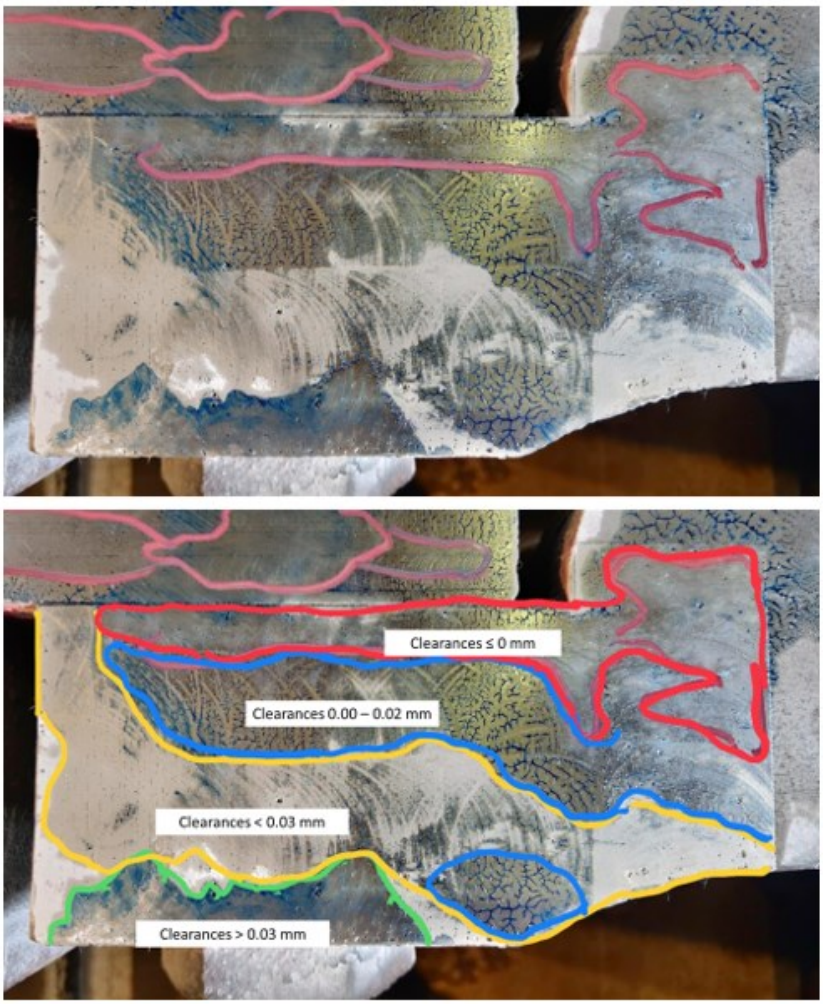

Figure 8: Classification of contact surfaces. Green mark indicates borderline of 0.03 mm feeler gauge penetration.

Following the above conclusions, below repair strategy is planned:

- Conduct rough cutting to a thickness of 0.05 mm in the area below the upper half HP casing.
- Perform rough cutting to a thickness of 0.2 mm in the area below the upper half LP casing.
- Following the rough cutting process, manual finishing was carried out by hand to achieve contact between the lower and upper half casing. The finishing involved stoning, polishing, and dressing. Every after each finishing iteration, contact check will be conducted to evaluate the result.

2.3 Final Attempt Result

LMD build-up was once again performed on the still non-contact area, followed by machining and series of iterations of manual finishing and inspection. While the general idea of the process is to make the majority of non-contact surface become contact, the more important objective is to block the steam pathway from reaching the outside of the casing.

Final contact check result is shown in Figure 9:. Certain areas suspected to have clearances of up to 0.03 mm were observed and subsequently addressed using high-temperature sealing.

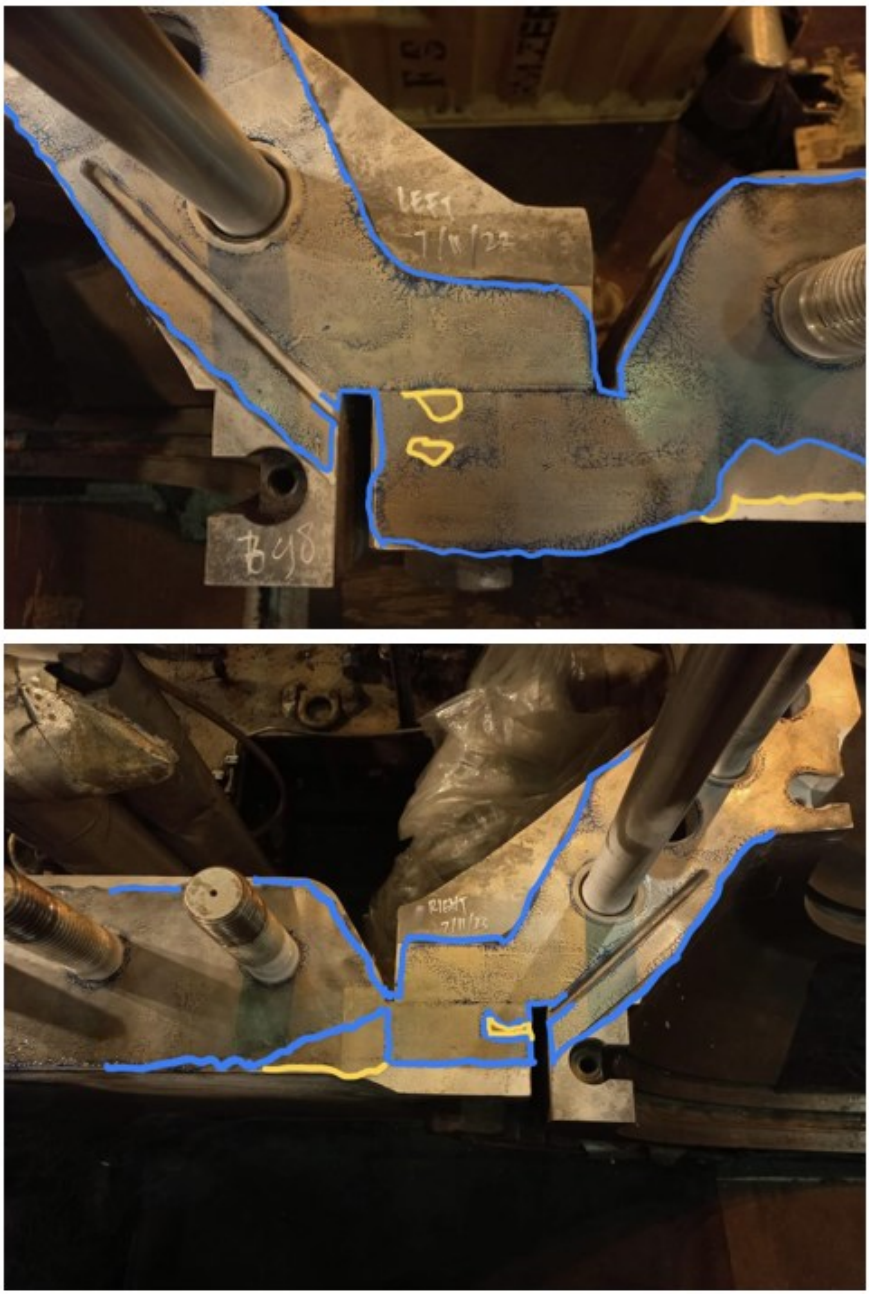

Figure 9: 3rd repair attempt contact check result .

Based on inspection results of repair final attempt, following conclusions were drawn:

- The steam pathway is already sealed as shown in Figure 9. Contact check comparison is shown in Figure 10.
- Certain areas that are suspected to have clearances of up to 0.03 mm are observed. While these particular areas do not compromise the sealing of steam pathway, they have also been addressed through high temperature sealing.

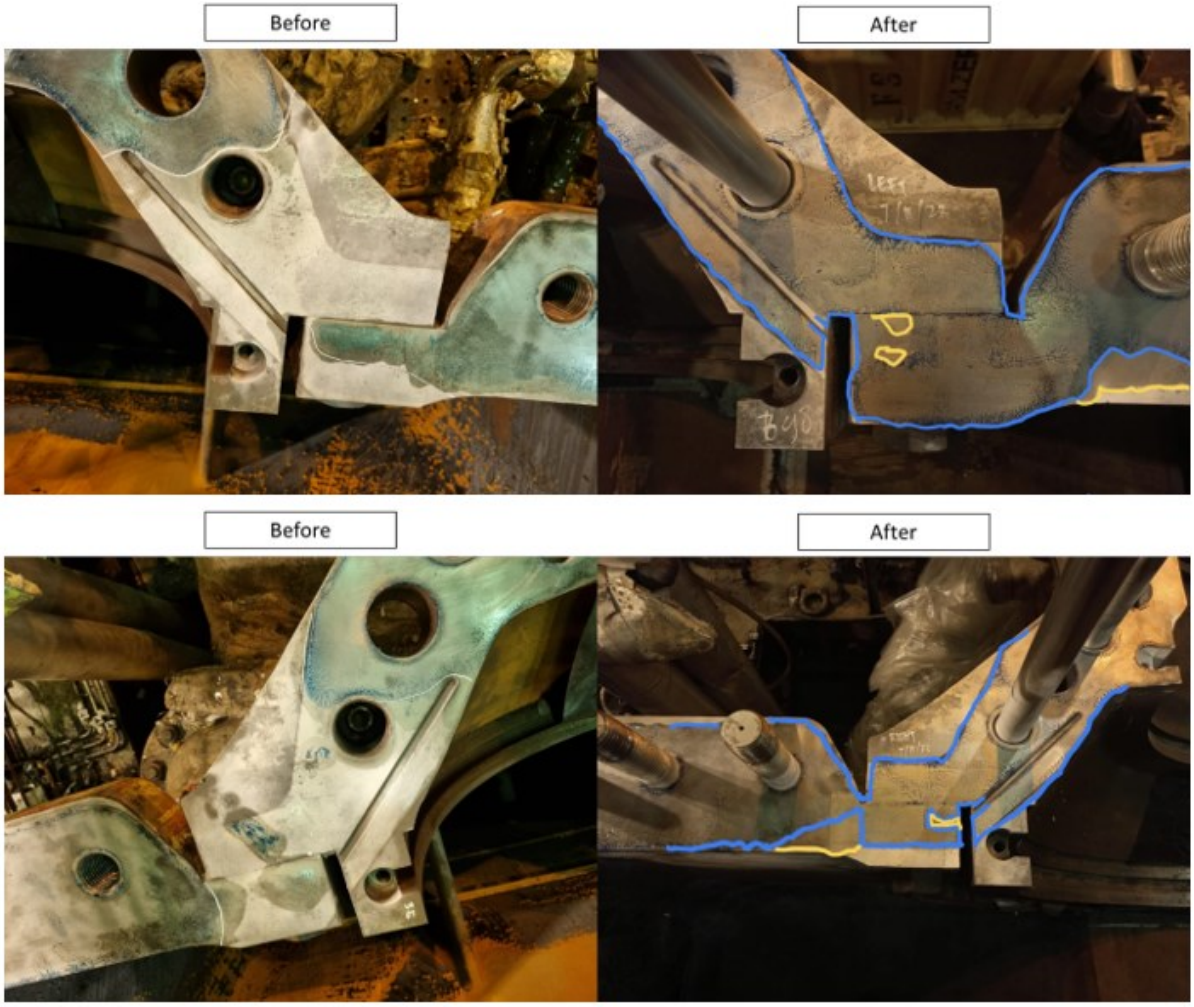

Figure 10: Contact check result comparison before and after repair.

3. CONCLUSION

With the steam path sealed, the leakage issue in the turbine casing has been resolved. The repair process was completed on time and fit for purpose. Through the application of LMD, it becomes evident that the significant risk of casing distortion as a side effect of dimensional restoration method can be avoided.

The on-site machining process, which accelerates the repair duration, contributes to the prompt installation of the rotor, thereby enabling customers to quickly resume their production operations. Consequently, this allows them to recover lost production time during the downtime period.

REFERENCES

Sulzer Indonesia Internal Documentation & Reports

Pardhi, Yogiraj: Laser metal deposition – developing new materials, *Sulzer White Paper,* (2022).

Optimizing Open Cooling Tower Water Treatment in Star Energy Geothermal Darajat (SEGD) Unit-2 and Unit-3 Power Plants: A Five-Year Performance Review

Tania Retno Kinasih, Wibisono Yamin, Ghina Thifal Ramadhani Eka Putri,
Oscar Satria Ganda, Indra Kurniawan, Hasan Arief Supriatman,
Dedi Kusnadi, and Bobby Nugroho Wicaksono

TROK@starenergy.co.id, wibisono@starenergy.co.id, GTRE@starenergy.co.id, oscar.ganda@starenergy.co.id, inkurni@starenergy.co.id, hsmj@starenergy.co.id, dekusna@starenergy.co.id, bobby.wicaksono@ecolab.com

Keywords: Cooling Tower Water Management, Non-oxiding Biocides, Geothermal Power Plant, Long-term Optimization

ABSTRACT

Effective cooling water management is vital for geothermal power plants, ensuring optimal performance and minimizing corrosion, scaling, and fouling within the heat transfer system. This paper presents a rigorous five-year evaluation of open cooling water treatment strategies implemented at Darajat Units 2 and 3. Geothermal cooling water treatment faces unique challenges due to complex water chemistry. Factors like temperature, flowrate, non-condensable gas (NCG) content, and organic bacterial presence significantly influence treatment efficacy. In the case of Darajat Unit-2 and Unit-3, high ammonia and sulfate levels provide sustenance for microbial growth. To address these complexities, SEGD have developed and optimized a tailored treatment program incorporating biocides, dispersants, and corrosion inhibitors. This multi-pronged approach effectively controls microbial growth within the cooling water system. Following a five-year treatment period, key parameters like Total Aerobic Bacteria (TAB) have been maintained below 10,000 cfu/ml, Sulfate-Reducing Bacteria (SRB) below 325 cfu/ml, and fungal presence has been significantly reduced. Our findings emphasize the critical role of long-term cooling water treatment in geothermal power plant operations. Effective management strategies directly impact plant efficiency, reliability, and environmental sustainability. Notably, the successful utilization of non-oxidizing biocides has minimized microbial growth and prevented foaming. This paper underscores the importance of continued treatment optimization to address the unique challenges inherent to geothermal cooling waters. By doing so, SEGD can ensure the long-term viability of geothermal energy as a clean and renewable power source.

1. INTRODUCTION

1.1 Cooling Systems

The Darajat Power Plants, Unit 2 and Unit 3, exemplify the potential of geothermal energy. Situated at Gunung Darajat, Garut, West Java, Indonesia, these facilities house 96 MW and 121 MW (gross) capacity steam turbine-generators, respectively, within a single building at 1723 m asl. By utilizing a dry steam geothermal resource and transmitting electricity to the national grid, SEGD provides a clean and reliable energy source to the region. Key features of the plant include surface condensers, hybrid gas removal systems, and crossflow cooling towers, highlighting the technology employed in geothermal power generation.

Cooling water systems are integral to geothermal power plants, enabling steam condensation and waste heat dissipation. However, the efficiency of these systems, particularly the cooling towers, hinges on effective water treatment. Untreated cooling water can lead to scaling, corrosion, and biological fouling, which hamper heat transfer efficiency and damage equipment. Implementing appropriate treatment methods ensures optimal water quality, promoting high operational efficiency, extended equipment life, and reduced environmental impact.

In the Darajat Power Plants, a steam condensing and cooling system is essential for achieving acceptable plant cycle efficiency. Due to the absence of a large water body nearby, cooling towers serve as the primary source of cooling water. The condensed steam is also source of make-up water for the cooling system, compensating for water loss due to evaporation. Notably, normal plant operation results in a surplus of make-up water, with the excess directed to the condensate injection system. Both Unit 2 and Unit 3 utilize two cooling systems: an open-loop circulating water (CW) system and a closed-loop component cooling water (CCW) system.

Figure 1: Aerial Photograph of Darajat Power Plant Units 2 and 3. (From top to bottom: the interface area, cooling towers, and the power generation building)

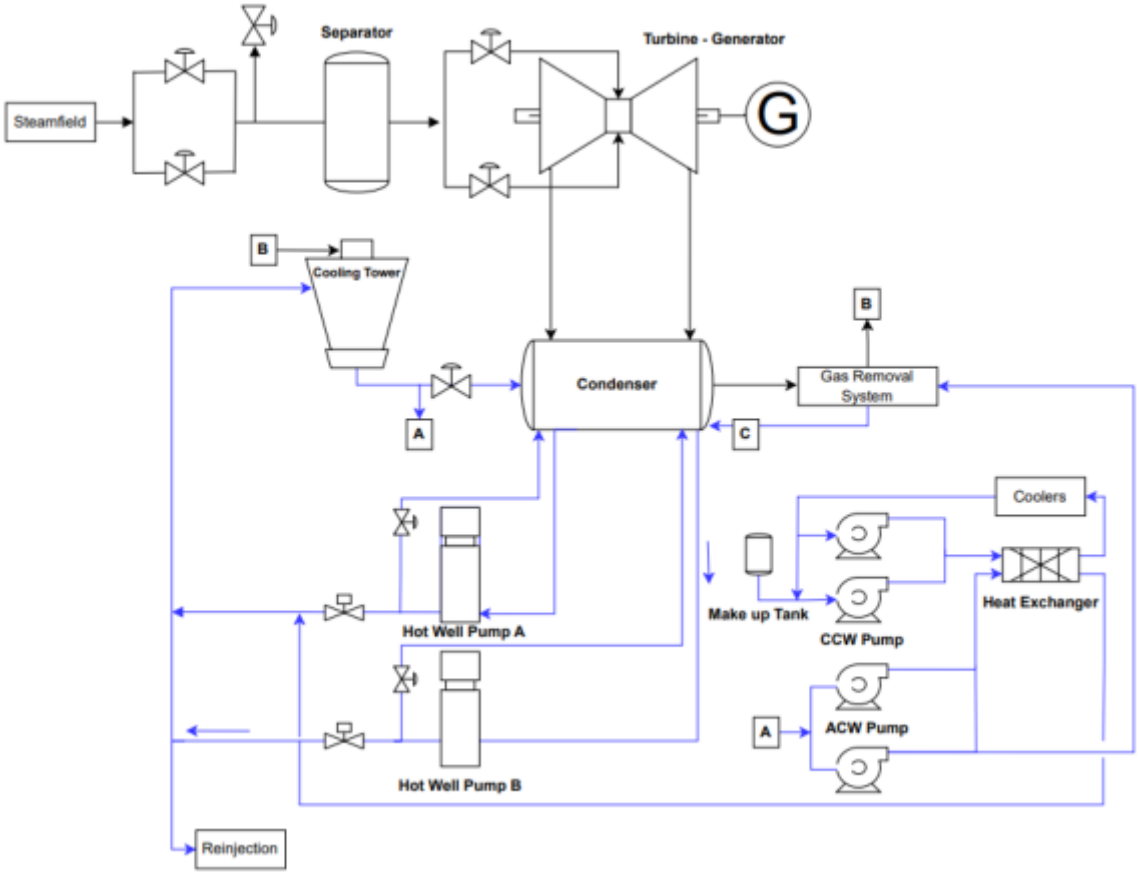

Figure 2: Open loop circulating water systems of Darajat Unit-2 and Unit-3.

The open-loop CW system is an evaporative cooling cycle designed to condense steam turbine exhaust and cool auxiliary plant systems. Hotwell pumps transfer hot water from the condenser to the cooling tower, where it is cooled through evaporation and returned to the condenser.

At each unit, steam exhaust from the turbine is cooled in direct contact with main condensers. Cooling water is drawn in by the condenser vacuum and sprayed into the condenser. A control valve regulates cooling water flow. Two hotwell pumps transport circulating water from the condenser to the crossflow cooling tower, where it is cooled by evaporation. The tower is designed for optimal performance at 100% plant load at 15.5°C wet bulb temperature. Flow regulating valves balance flow to the cooling tower hot basin. Cooling tower fans draw air through the tower splash bar fill, cooling the circulating water, which collects in the cooling tower basin.

The component cooling water (CCW) system of each unit is a secondary fresh water closed loop circuit that supplies all heat exchangers not supplied by the circulating water system, including lube oil, generator air, hotwell pump motors, and air compressor coolers. The closed-loop system minimizes fouling of the associated equipment heat exchangers. Two 100% duty pumps circulate water throughout the loop. The system rejects heat through two 100% duty titanium plate heat exchangers to auxiliary cooling water.

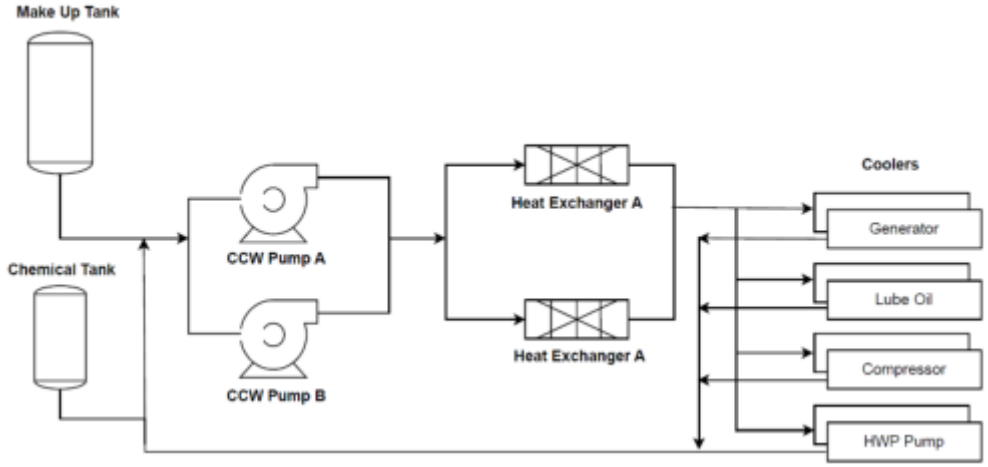

Figure 3: Closed-loop Component Cooling Water (CCW) system of Darajat Unit-2 and Unit-3.

The component cooling water head tank provides sufficient net positive suction head for the CCW pumps. The head tank also is set such that the pressure in the CCW system is greater than the pressure in the open loop cooling system, so that any leaks in the heat exchanger will not introduce geothermal condensate into the predominantly carbon steel CCW system. Makeup water is provided from domestic water.

1.2. Chemical Dosing System

Geothermal fluids, characterized by their unique chemical composition and varying thermodynamic conditions, pose inherent challenges to the operational integrity of geothermal power plants. The presence of soluble species and dissolved gases within these fluids can lead to scaling (fouling) and corrosion of metallic surfaces in contact, thereby necessitating chemical treatment strategies tailored to each specific geothermal site.

Corrosion, a pervasive issue in geothermal facilities, can manifest in various forms across the production well, surface equipment, piping, steam turbine, reinjection line, and other components interacting with geothermal fluids. The severity of corrosion is exacerbated by site-specific factors such as elevated concentrations of corrosive agents (H2S, Cl-, SO42-, CO2), high temperatures, and cathodic reactions with metal surfaces. In severe cases, corrosion can induce catastrophic equipment failures, exemplified by pipe ruptures or bursts, with potential ramifications for safety, health, the environment, and surrounding communities. Moreover, the degradation of equipment due to corrosion can significantly impact plant reliability, leading to increased downtime (Loss Production Opportunity) and escalating operational costs for corrective measures.

The Chemical Dosing System is designed to control the microbiological activity and pH of the circulating water, auxiliary cooling water, and condensate reinjection systems to maintain their optimum performance and material protection. The cooling water chemistry will be controlled and monitored by measuring pH, conductivity, microbiological count, and blowdown rate. Cooling water is treated with a mastered injection of biocide for microbiological control, caustic soda solution for pH control and corrosion inhibitor for corrosion control specially for the reinjection line and wells.

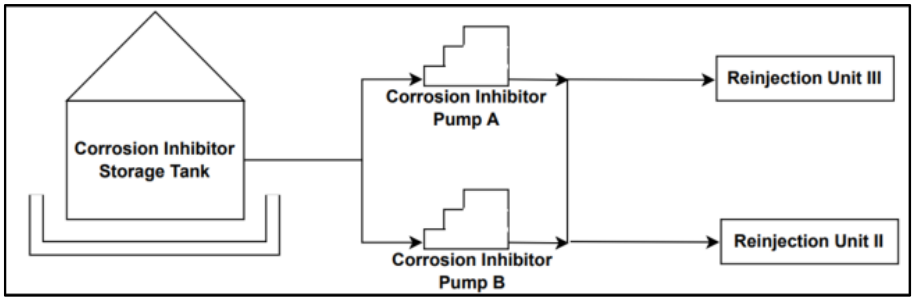

Figure 4: Chemical Dosing System.

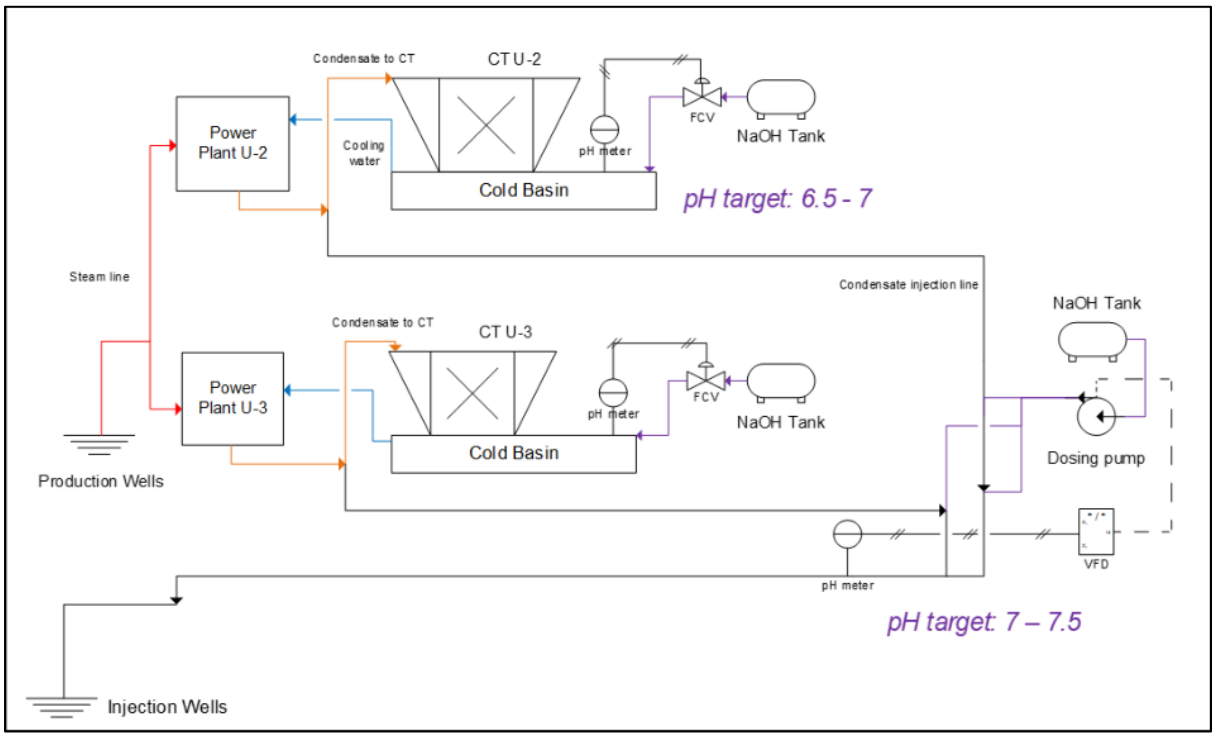

Figure 5: Caustic Soda Dosing System.

The caustic soda dosing system can raise the pH of condensate circulated within the power plant from its natural level of 3.5 to within the range 6.5 to 7. It can also raise the pH of reinjection condensate to 7 – 7.5. The existing biocide system consists of two 100% capacity pumps and two biocide tanks. Discharge lines to the cooling towers are cross connected by additional piping to be able to add biocide to both unit's cooling tower. Microbiological control is monitored through manual and visual cooling system inspections and microbiological plate counts. System inspections provide evaluation of sessile organisms and cooling system conditions. Performance criteria are established using inspection results along with the microbiological plate count data.

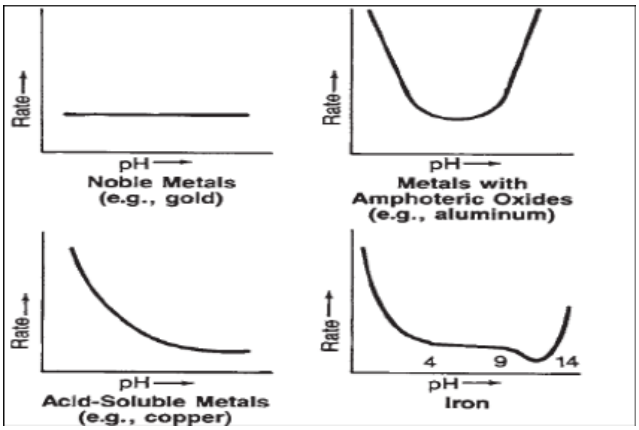

Figure 6: General Influence of pH on Corrosion Rate.

Given the complex interplay of factors influencing the performance of cooling water systems in geothermal power plants, this paper presents a comprehensive five-year review of the open cooling water treatment strategies implemented at Units 2 and 3. By analyzing the operational data, chemical treatment methodologies, and lessons learned, this study aims to provide valuable insights into the challenges and best practices for maintaining efficient and reliable cooling water systems in geothermal power generation facilities.

2. CHALLENGES OF GEOTHERMAL COOLING WATER TREATMENT

2.1 Challenges in Unit-2 and Unit-3 Plants Open Cooling Systems

Open cooling water systems in geothermal power plants face four primary challenges: corrosion, scale, fouling, and microbiological contamination. If left unaddressed, these issues can lead to reduced heat transfer efficiency, equipment failures, and even plant shutdowns, resulting in lost production opportunities and increased maintenance costs.

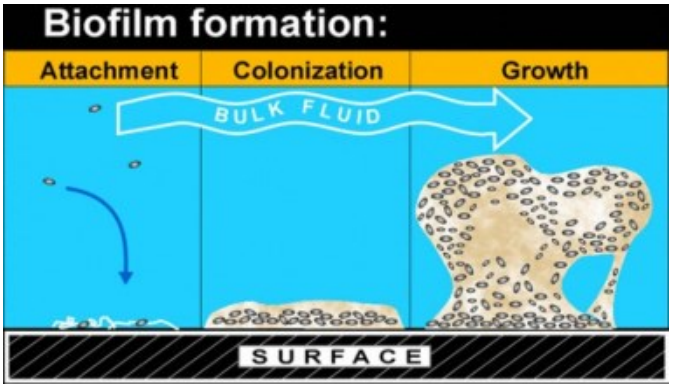

Figure 7: Progression stages of growth of a bacterial biofilm. (Kashef, et al. 2017)

Microbiological growth poses a significant challenge in geothermal power plant cooling water treatment due to the high levels of nutrients, particularly sulfur and ammonia, present in the condensate used as cooling water makeup. These nutrients create an ideal environment for the proliferation of microorganisms, which can cause a variety of problems:

1. Aerobic Slime Formers

Ubiquitous in the environment, these bacteria readily colonize open systems, adhering to surfaces throughout the cooling circuit, including heat exchangers. Encapsulated in slime layers, they form biofilms that impede heat transfer and may promote corrosion.

2. Anaerobic Corrosive Bacteria (e.g., Sulfate-Reducing Bacteria)

These bacteria utilize sulfate ions, producing hydrogen sulfide as a metabolic byproduct. This highly corrosive acid generates sludge, contributing to fouling and corrosion in the cooling tower basin and downstream equipment.

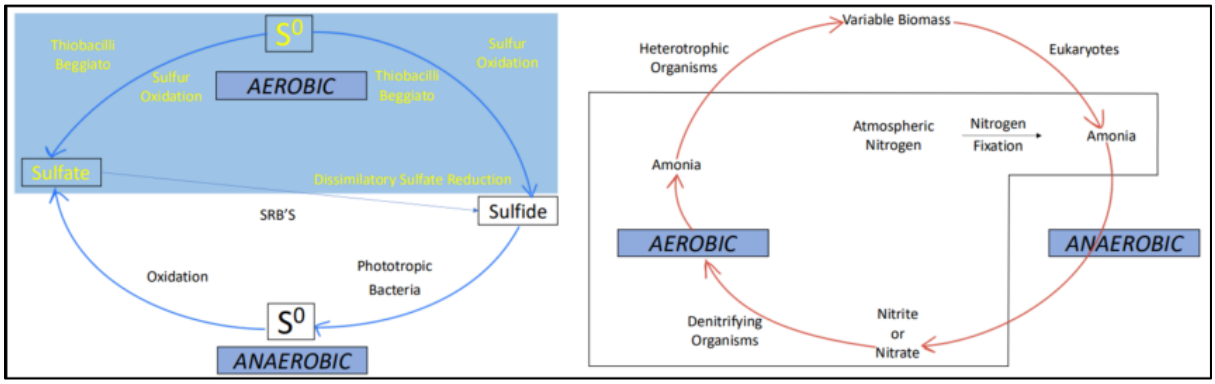

Figure 8: Microbiological Transformations of Sulfur and Nitrogen in Geothermal Systems. (Nalco Water Handbook, 2018)

3. Nitrifying Bacteria

Nitrifying bacteria metabolize ammonia, converting it to nitrates, a process implicated in corrosion and scaling in systems susceptible to ammonia contamination.

4. Algae

Flourishing in sunlight, algae mainly colonize open cooling tower decks, causing plugging of distribution decks. Excessive growth can lead to detachment and subsequent fouling of heat exchangers.

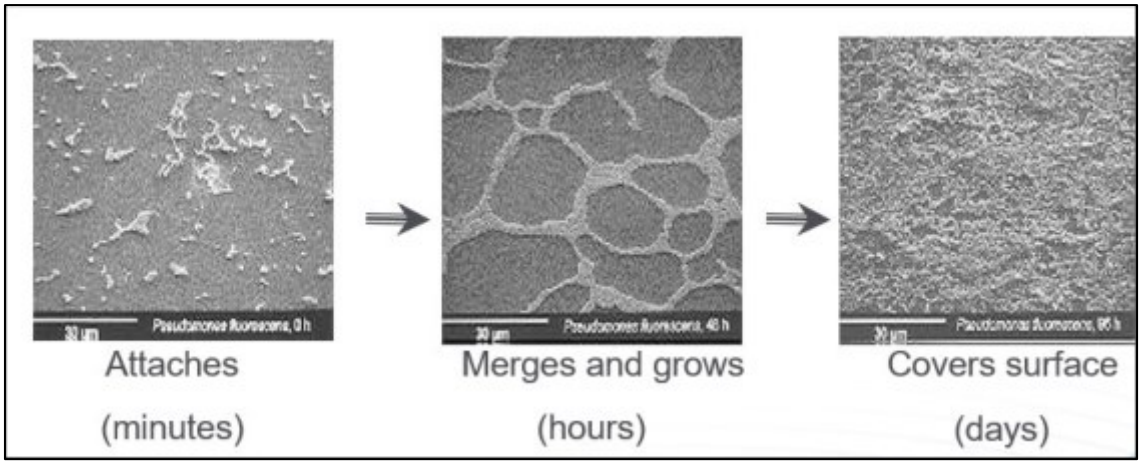

Figure 9: Microbiological growth in metal (Nalco Water Handbook, 2018).

The presence of these diverse microorganisms necessitates continuous chemical treatment to maintain the operational efficiency, integrity, and longevity of cooling system components.

While the Unit 2 and Unit 3 cooling system predominantly employs corrosion-resistant materials such as stainless steel (SS), fiberglass-reinforced plastic (FRP), and ceramics, minimizing corrosion risk remains a priority for maximizing equipment lifespan and maintaining system integrity. Corrosion management practices, adhering to equipment design specifications, are implemented to mitigate potential corrosion issues.

2.2 Challenges in Unit-2 and Unit-3 Plants Closed Cooling Systems

Closed recirculating cooling systems in geothermal power plants, while generally considered more stable than open systems, are nonetheless susceptible to corrosion, fouling, and microbiological growth. These issues are interdependent, as corrosion can be exacerbated by fouling and microbial activity, leading to a cascade of problems that can compromise system efficiency and longevity.

1. Corrosion

In closed systems, the absence of blowdown for removing corrosion products can lead to the accumulation of suspended solids, increasing the risk of clogging, erosion, and localized corrosion under deposits. Oxygen ingresses through makeup water or air leakage, along with the deposition of solids, can further accelerate corrosion processes.

2. Fouling

Fouling deposits, composed of suspended solids, scaling products, corrosion byproducts, and microbial growth, can hinder system performance by obstructing valves, orifices, and recirculating lines. The build-up of foulants can also impede heat transfer, reducing overall system efficiency.

3. Microbiological Growth

Microbial activity can thrive in closed systems due to the introduction of oxygen, debris, and nutrients from various sources, including makeup water, process leaks, and open make-up water tanks. Microbial growth contributes to fouling, corrosion, and impaired heat transfer due to the formation of insulating biofilms.

The specific treatment requirements for the closed-loop cooling system are informed by the presence of carbon steel components within the circuit, necessitating targeted strategies to mitigate corrosion and fouling risks.

Table 1: Specification of Unit-2 and Unit-3 closed-loop system.

PARAMETER	UoM	CCW Unit 2	CCW Unit 3
Total System Volume	m^3	7	7
Recirculating Rate	m^3/hr	477	466
Material		Carbon Steel, Copper	Carbon Steel, Copper

2.3 Challenges in Condensate Reinjection Lines

Maintaining the heat and mass balance of geothermal power plants necessitates the continuous reinjection of condensate into the reservoir. However, this process presents operational challenges, particularly corrosion in reinjection lines, which can significantly impact plant reliability and potentially lead to environmental concerns.

In the Darajat geothermal field, a 4.5 km, 12-inch carbon steel pipe transports condensate from the power plants to the reinjection well (Pad-19). Any disruption to this system, such as leaks or damage requiring offline repairs, necessitates unit shutdowns, impacting power generation and revenue. Additionally, leaks in the reinjection line, which traverses through community plantation areas, pose environmental risks due to potential liquid spills.

Figure 10: Condensate Reinjection Piping (under Steam Pipeline).

Table 2: Specification of PLTP Darajat Condensate Reinjection Lines.

PARAMETER	UoM	Value
Distance	km	4.5
Temperature	°C	40 – 50
Total Condensate	lps	130
Pipeline Material	-	Carbon Steel

Due to the pipeline's considerable length and associated costs, complete replacement with corrosion-resistant materials, such as stainless steel, is not economically feasible. Therefore, the company has employed a more cost-effective mitigation strategy: the application of chemical corrosion inhibitors. This approach effectively mitigates the risks of corrosion-induced leaks and subsequent environmental damage, while ensuring the continued operation and integrity of the reinjection system. Given the financial and environmental implications, ensuring the integrity and availability of the reinjection system is crucial.

Four primary factors influence the type, rate, and inhibitor selection for corrosion mitigation in reinjection systems: temperature, dissolved solids concentration, pH, and dissolved oxygen concentration. Understanding these parameters is key to developing effective corrosion management strategies that ensure the longevity and reliability of reinjection infrastructure in geothermal power plants.

3. METHODOLOGY

3.1 Chemical Treatment Selection in Geothermal Cooling Systems

Selecting the appropriate chemical treatment for geothermal cooling systems is crucial to ensure optimal performance, minimize corrosion and fouling, and maintain operational efficiency. This section discusses the selection process for both condensate reinjection and open and closed cooling systems, highlighting the specific challenges and treatment options in the context of the SEGD geothermal power plant.

3.1.1 Open Cooling System – Microbial Growth Control

Microbiological growth in open cooling systems can lead to fouling, corrosion, and reduced heat transfer efficiency. Non-oxidizing and oxidizing biocides are commonly used to control microbial growth, each with distinct characteristics:

Table 3: Characteristic of non-oxidizing and oxidizing biocides.

PARAMETER	Non-Oxidizing Biocides	Oxiding Biocides
Consumption of Contaminants (H_2S & NH_3)	Not consumed, less reactive	Consumed, very reactive
Halogen Demand Consideration	No issue	Requires careful management of halogen demand to maintain free residual chlorine (FRC) levels between 0.2 - 0.5 ppm
Microbiological Control	Excellent	Less effective
Chemical Consumption	Lower	Consumed, very reactive

To address the challenge of microbial growth in the open cooling system, a comprehensive biocide selection process was undertaken. Given the superior performance of non-oxidizing biocides in geothermal applications, the focus was on evaluating different non-oxidizing biocides against the SEGD's specific microbial growth targets:

- Total Aerobic Bacteria (TAB): < 10,000 cfu/mL
- Sulfate-Reducing Bacteria (SRB): < 325 cfu/mL

Laboratory tests were conducted to assess the efficacy of various non-oxidizing biocides in controlling TAB and SRB populations. The test results indicated that biocide N7330 exhibited the highest efficacy, consistently achieving near-complete removal of TAB and a significant reduction in SRB levels, surpassing the SEGD targets. Based on the laboratory findings, N7330 was selected as the optimal biocide for microbial control in the SEGD open cooling system. Field implementation has further validated this choice, with actual performance data consistently demonstrating effective control of microbial growth within the specified targets. The biocide dosage is adjusted as needed to maintain optimal performance, facilitated by a performance-based contract with the chemical supplier.

3.1.2 Closed Loop Cooling System – Corrosion Control

Corrosion is the deterioration of materials, typically metals, caused by chemical reactions with their environment. This process often leads to component failure. Essentially, corrosion reverses the extractive metallurgy process, returning the metal to a more thermodynamically stable compound form. Several factors influence corrosion, including:

- Metal properties: Position in the galvanic series, purity, surface layer characteristics, and corrosion product properties.
- Corrosive environment properties: Concentration, stress, erosion, and temperature.

Corrosion generally involves a chemical reaction between the metal and its surroundings (like oxygen or water), producing more stable compounds. The flow of electrons from the less noble metal (anode) to the more noble metal (cathode) drives the corrosion of the less noble metal. (Kumat et al., 2021).

Closed recirculating cooling systems are effectively protected from corrosion through the application of various chemical inhibitors. Among the most widely utilized are passive film-forming inhibitors, including PSO-based treatments, Boron-nitrite formulations, and molybdate blends.

In these closed systems, complete corrosion prevention is achieved by maintaining higher inhibitor concentrations, a practice proven to be more cost-effective than in open recirculating systems due to reduced water loss and lower chemical consumption. Preventing corrosion is of paramount importance in closed loops, as the accumulation of insoluble corrosion products can lead to fouling, flow restrictions, and accelerated localized corrosion.

The primary objective of corrosion control in closed systems is to establish near-complete (approaching 100%) protection for all metal surfaces. Effective treatment programs, when diligently monitored and maintained, can closely achieve this goal. Common Corrosion Inhibitors in Closed-Loop Cooling Systems:

1. Phospinosuccinic Oligimer (PSO-Based)

PSO is a type of corrosion inhibitor known for its effectiveness in forming a protective film on metal surfaces. This film acts as a barrier against corrosive agents, preventing or slowing down the corrosion process by forming

a protective layer at the anode, the site where metal corrosion typically begins. This helps to prevent further metal loss.

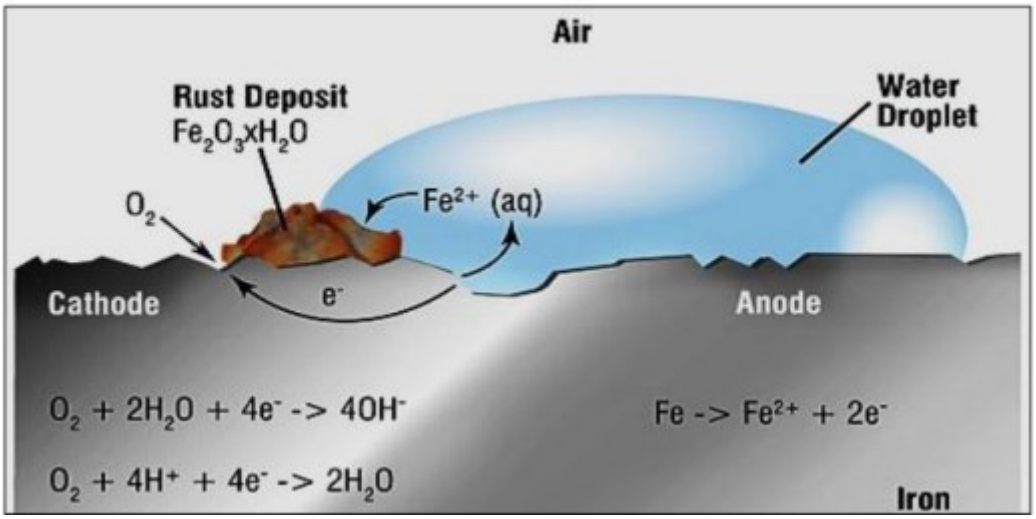

Figure 11: Mechanism of corrosion in metal (Aljamali et al., 2019).

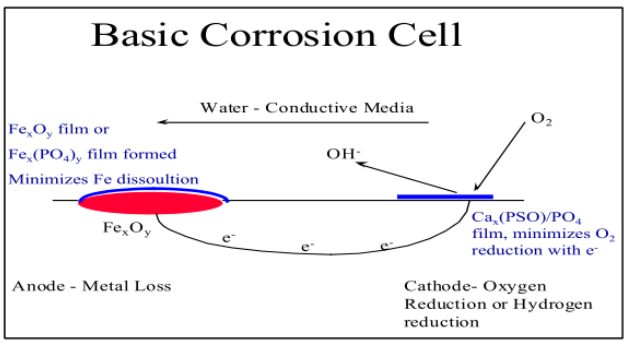

Figure 12: PSO-Based Corrosion Inhibition Mechanism (Nalco Water Handbook, 2018).

2. Boron-Nitrite Based

Boron-nitride (BN) is increasingly being explored as a component in corrosion inhibitor formulations. It exists in various forms, including hexagonal boron nitride (h-BN) and cubic boron nitride (c-BN). This chemical encourages the formation of a thin, protective film of iron oxide on metal surfaces, effectively shielding the metal from corrosive elements and minimizing metal loss.

3. Molybdate Blends

Molybdate blends typically contain molybdate ions along with other inhibitors. Molybdate ions form a protective film on metal surfaces by reacting with the metal itself and with corrosion products. This film is often described as a "self-healing" layer, meaning it can repair itself if damaged.

To assess the efficacy of various corrosion control chemicals for the closed-loop cooling system, laboratory tests were conducted. The performance of three chemicals was evaluated: a blank (untreated) sample, TRAC-109, and a molybdate-based inhibitor. The SEGD target corrosion rate for the closed-loop system is ⩽10 mpy (mils per year).

Table 4: Comparative Study of Corrosion Inhibition Effectiveness.

No	Sample Code	Dosage (ppm)	Corrosion Rate (mpy)	Iron Concentration (ppm)		
				Initial	Final	Additional
1	Blank	-	1.87	0.423	23.148	22.725
2	TRAC-109	2000	0	0.423	0.429	0.006
3	Molybdate Base	800	1.19	0.423	15.072	14.649

The results demonstrated that TRAC-109, at a dosage of 2000 ppm, completely inhibited corrosion, achieving a corrosion rate of 0 mpy and minimal iron concentration increase. The molybdate-based inhibitor, while reducing corrosion compared to the blank, did not meet the SEGD target.

Based on these findings, TRAC-109 was selected as the most effective corrosion inhibitor for the SEGD closed-loop cooling system. In field applications, the dosage of TRAC-109 is adjusted to maintain the target corrosion rate, ensuring optimal performance and longevity of the system.

3.1.3 Condensate Reinjection System – Corrosion Control

Corrosion attack that occurs within a geothermal plant may result in severe equipment damage whether in the production well, surface equipment and piping, steam turbine, reinjection line and all the equipment which handle condensate, steam, and condensate/steam mixtures. There are 4 (four) main factors influenced the corrosion type, rate and inhibitors type use in surface/reinjection system of geothermal plant:

1. Temperature
2. Dissolved Solids concentration
3. pH
4. Dissolved Oxygen concentration

High corrosion potential and aggressive attack in the steam and condensate often cause catastrophic failure, low reliability, and high total operating cost in geothermal plant. In the past corrosion has been dealt with by using corrosion resistant materials and nowadays corrosion inhibitor application is one of the most cost-effective solutions.

Corrosion control is a prominent part of maintaining a cooling water system (Nalco Water Handbook, 2018). It can be the most complex to solve; thus, it is important to observe all the possible parameters for control. A complete solution involves a combination of possible ways to minimize corrosion. They are:

1. Use of corrosion resistant materials, such as stainless steel, copper-nickel alloys, or plastic.
2. Use of coatings such as paint, epoxy coatings, and metal cladding.
3. Cathodic protection.
4. Sacrificial anodes reduce corrosive attack.
5. Application of chemical corrosion inhibitors.

In reinjection systems, corrosion can significantly impact pipe and wellbore lifespan, leading to costly repairs and downtime. Nalco 3DT129, a multifunctional corrosion and scale inhibitor, has been effectively used to mitigate this issue. By forming a protective film on metal surfaces, it acts as a barrier against corrosive elements in the water, reducing metal loss and extending the life of critical equipment. This chemical is well-suited for low hardness/low alkalinity environments and is often used with a dispersant polymer to enhance protection and ensure optimal performance. Injecting 3DT129 so far has succeeded in protecting the reinjection line through possibility of corrosion.

3.2. Parameter Monitoring

To monitor the parameters, there are some indicators that we need to observe. We divide the control parameters into two indicators:

Table 5: Key Indicators of Control Parameters for Cooling System Performance Evaluation.

Leading In dicator	**Lagging Indicator**
Water chemistry	SSC (specific steam consumption)
Bacterial count	Approach temperature
Filler Weight	Cooling system efficiency
Temperature data	Cooling water temperature

3.2.1 Leading Indicator

Leading indicators are proactive measures that can predict future performance and potential issues in the cooling water system. They often indicate conditions that could lead to problems if not addressed promptly. For example, monitoring water chemistry parameters like pH, conductivity, sulfate, iron, and microbiological content is crucial for preventing scaling, corrosion, and biofouling. Deviations from the optimal range can signal the need for adjustments in the treatment program, thus preventing issues such as reduced heat transfer efficiency or equipment damage, which are reflected in lagging indicators like temperature data.

The following are Key Performance Indicators for open loop cooling water treatment:

Table 6: Key Performance Indicators for open loop cooling water treatment.

Parameters	Value	Unit
pH	6.5 - 7	
Total Aerobic Bacteria	10,000	cfu/mL
SRB	325	cfu/mL
Turbidity	<5	NTU
Total Suspended Solids	<5	mg/L
Total Alkalinity	<100	mg/L as CaCO3
Free Chlorine	<1	mg/L as C12
Chloride	<10	mg/L as CCl
Total Hardness	<30	mg/L as CaCO3
Total Dissolved Solids	<200	mg/L as NaCl
Total Iron	<0.5	mg/L as Fe
Dissolved Silica	<10	mg/L as SiO2

3.2.2 Lagging Indicator

Lagging indicators reflect past performance and are used to measure the impact of the treatment program over time. These reactive measures provide data on the outcomes of various operational conditions and maintenance practices. For instance, Specific Steam Consumption (SSC) measures the steam used per unit of electricity generated, with higher values indicating inefficiencies in the cooling system or potential steam leaks. An increase in SSC can trigger investigations into cooling system performance and maintenance needs. Additionally, Approach Temperature, the difference between the cooling water outlet temperature and the ambient wet-bulb temperature, is a key indicator of heat exchange efficiency. A higher approach temperature can signal fouling or inefficiencies in the heat exchanger. Other lagging indicators include overall cooling system efficiency, encompassing factors like heat transfer rates, energy consumption, and operational uptime. Monitoring these lagging indicators helps identify areas for improvement and evaluate the effectiveness of the implemented treatment program over time.

4. RESULTS AND DISCUSSION

4.1 Leading Indicators

During five years of treatment, the challenge found in the cooling water SEGD is the common problem in most cooling water systems, such as microbial, increasing sulfate, and corrosion. High ammonia and sulfate are the cause of increased microbial growth. Increasing sulfate can be caused due to an increase in NCG levels. And the corrosion may happen due to increased level of dissolved oxygen in the basin. The presence of algae, sulfur, and mud (dead bacteria) can inhibit the performance of cooling water.

The chart below illustrates the effectiveness of the implemented biocide treatment program in controlling leading indicators such as Total Aerobic Bacteria (TAB), Sulfate-Reducing Bacteria (SRB), Total Suspended Solids (TSS), Total Dissolved Solids (TDS), Total Alkanity, Turbidity, Total Iron, Dissolved Silica levels within the open cooling water system. The data covers approximately five years, presenting leading indicator counts before and after treatment at both Cooling Water 2 (CW2) and Cooling Water 3 (CW3). The results consistently demonstrate attainment of the target leading indicator limits as shown in Figure 13.

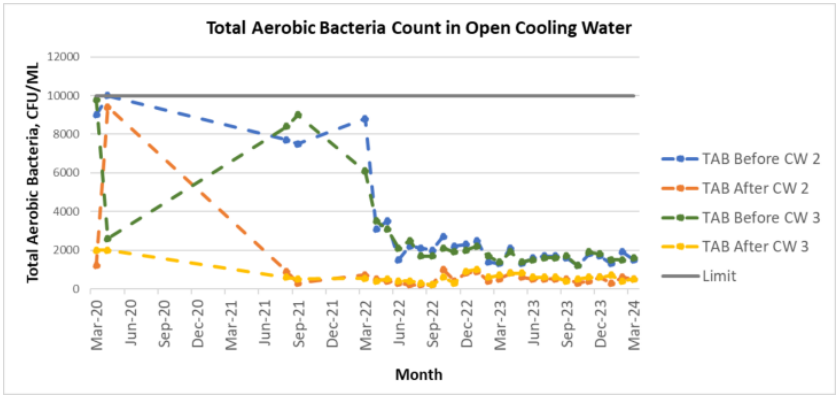

Figure 13: Total Aerobic Count in Unit-2 & Unit-3 Open Cooling Water.

The chart shows a significant decrease in Total Aerobic Bacteria (TAB) after the implementation of the cooling water (CW) treatment in both Unit-2 and Unit-3. The TAB count consistently remained below the specified limit after treatment, indicating the effectiveness of the chemical dosing system in controlling bacterial growth in the open cooling water. Overall, the CW treatment successfully maintained the TAB count within the desired range, ensuring the system's efficient and safe operation.

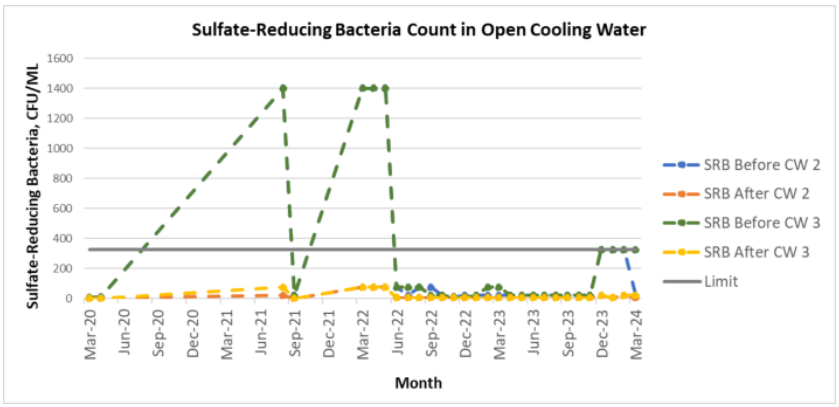

Figure 14: Sulfate-Reducing Bacteria in Unit-2 & Unit-3 Open Cooling Water.

The data indicates a significant reduction in Sulfate-Reducing Bacteria (SRB) after the implementation of the cooling water (CW) treatment in both Unit-2 and Unit-3. While SRB counts fluctuated before treatment, they consistently remained below the specified limit after treatment, highlighting the effectiveness of the CW treatment.

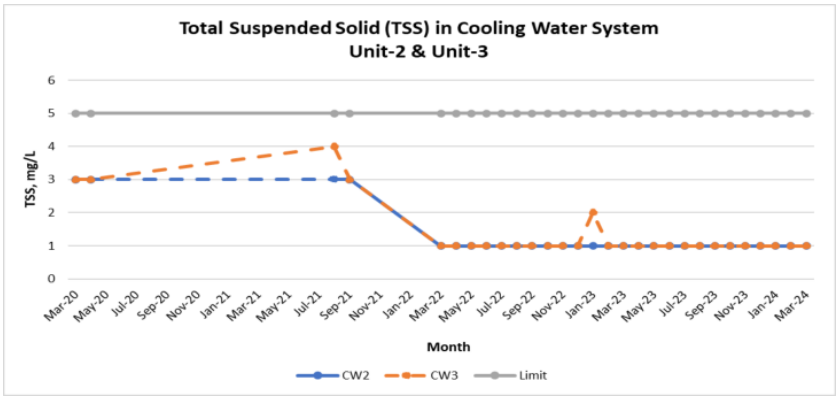

Figure 15: Total Suspended Solid (TSS) count in Unit-2 & Unit-3 Open Cooling Water.

Historical data shows a significant reduction in Total Suspendd Solids (TSS) in both cooling water systems after January 2022. Both systems consistently remained below the specified limit (4 mg/L) from January 2022 to March 2024, indicating the effectiveness of the treatment in controlling TSS levels.

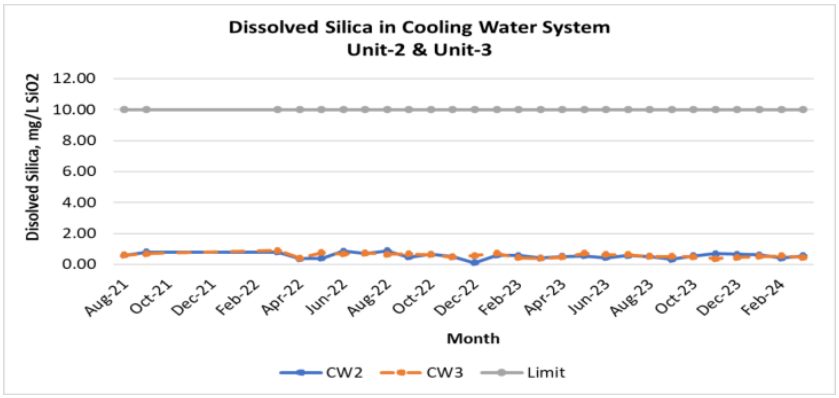

Figure 16: Total Dissolved Solid (TDS) count in Unit-2 & Unit-3 Open Cooling Water.

Figure 16 indicates a significant decrease in Total Dissolved Solids (TDS) levels in both cooling water systems after January 2022. Both systems consistently maintained TDS levels below the 200 mg/L limit after this period,

signifying the effectiveness of the implemented treatment in controlling TDS. In contrast, Figure 17 shows that turbidity levels in both systems have remained consistently low throughout the entire monitoring period, well below the 5 NTU limit, suggesting that turbidity has not been a significant concern in these cooling water systems.

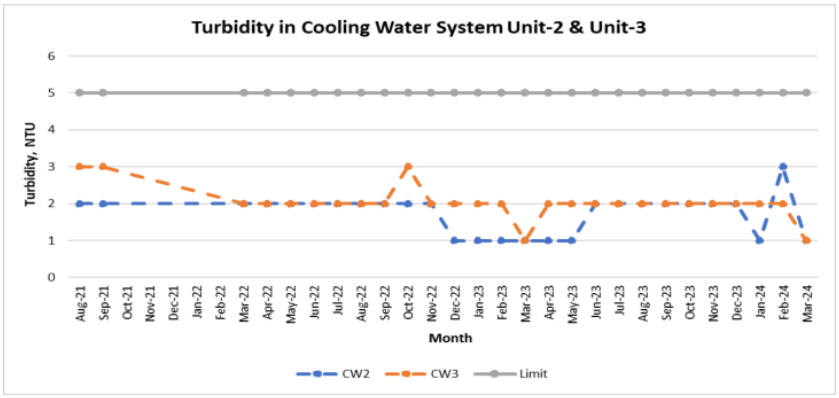

Figure 17: Turbidity in Unit-2 & Unit-3 Open Cooling Water.

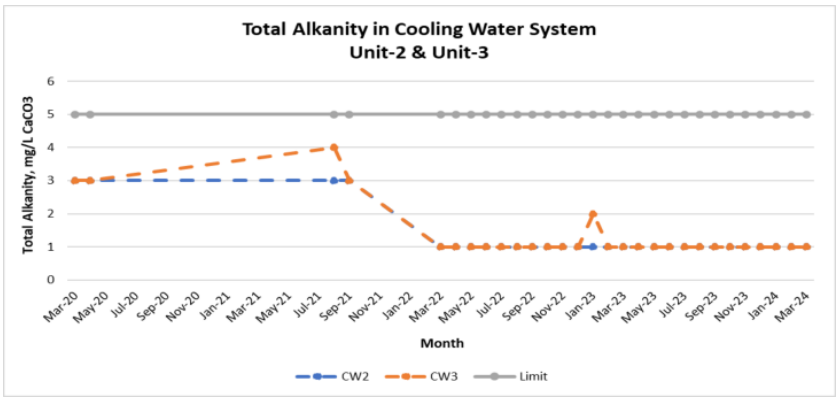

Figure 18: Total Alkanity count in Unit-2 & Unit-3 Open Cooling Water.

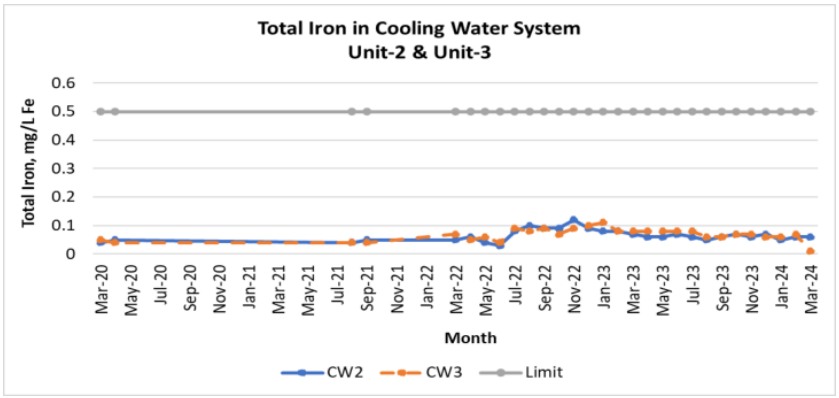

Figure 19: Total iron in Unit-2 & Unit-3 Open Cooling Water.

Figure 19 shows a significant decrease in Total Iron levels in both Unit-2 and Unit-3 after the implementation of the cooling water (CW) treatment in March 2020. The Total Iron levels have remained consistently below the 0.5 mg/L limit since then while Dissolved Silica levels as shown in Figure 20 have remained consistently below the 10 mg/L limit. These indicate the effectiveness of the CW treatment in controlling iron and silica deposition in the cooling water systems.

Based on the performance above, it is shown that TAB, SRB, and fungi can be reduced below the threshold during five years treatment. This microbial is important to be suppressed with non-oxidizing biocide as the outgrowth of bacteria can reduce cooling water performance and not causing foaming in the basin and condenser. Foaming is affected by clogging the filler which can impact increasing approach temperature.

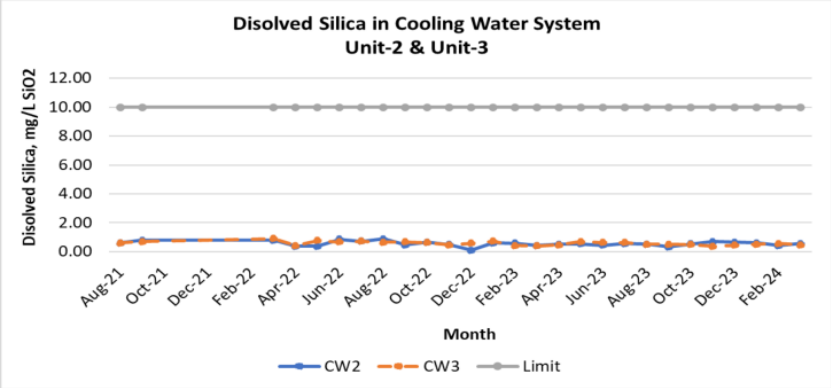

Figure 20: Dissolved Silica in Unit-2 & Unit-3 Open Cooling Water.

Non-oxidizing biocides are often chosen over oxidizing biocides due to their cost-effectiveness. Here are a few reasons for this preference:

1. Lower Dosage Requirements

Non-oxidizing biocides generally require lower dosages to achieve the same level of microbial control, leading to cost savings on the quantity of chemical used.

2. Extended Residual Effect

These biocides tend to have a longer residual effect, meaning they remain active in the system for a longer period. This reduces the frequency of application, thereby lowering overall treatment costs.

3. Equipment Longevity

Non-oxidizing biocides are less corrosive compared to oxidizing biocides, which can prolong the life of equipment and infrastructure, reducing maintenance and replacement costs. Non-oxidizing biocides is also didn't impact to the water chemistry, unlike the cleaning chemical.

4. Reduced By-product Formation

They produce fewer harmful by-products during their use, which can decrease the need for additional treatments and the handling of hazardous waste, contributing to cost savings in waste management and environmental compliance.

5. Compatibility with Other Chemicals

Non-oxidizing biocides often have better compatibility with other chemicals used in industrial processes, minimizing the risk of adverse reactions and the need for additional corrective treatments.

In summary, the implemented cooling water (CW) treatment has effectively controlled various parameters in both units, including significant reductions in bacteria, solids, iron, and silica. This successful control has prevented corrosion, equipment damage, and

ensured safe and efficient operation. Additionally, the use of non-oxidizing biocides has proven cost-effective, reducing chemical usage and overall costs.

4.2 Lagging Indicators

Lagging indicators provide valuable insights into the past performance of the cooling water system and the effectiveness of the treatment program. During five years of treatment, lagging indicators such as steam consumption, cooling tower efficiency, and cooling water temperatures are used to evaluate the historical performance of the cooling water system. These metrics serve as benchmarks for identifying areas requiring improvement and assessing the efficacy of the treatment program.

The steam consumption rate, defined as the steam mass flow per unit power output (kg/s/MW), is a critical performance indicator for power plants. Figure 21 illustrates the effectiveness of the cooling water system treatment program as one of important factors in maintaining steam consumption rates within the desired range for Units 2 and 3 over five years. The data shows that steam consumption rates for both units generally remained below the lower limit during this period. Occasional instances of exceeding the upper limit were attributed to issues with the Liquid Ring Vacuum Pump, which necessitated switching to a standby ejector system requiring additional steam. Conversely, instances of falling below the lower limit occurred during steam flow meter calibration.

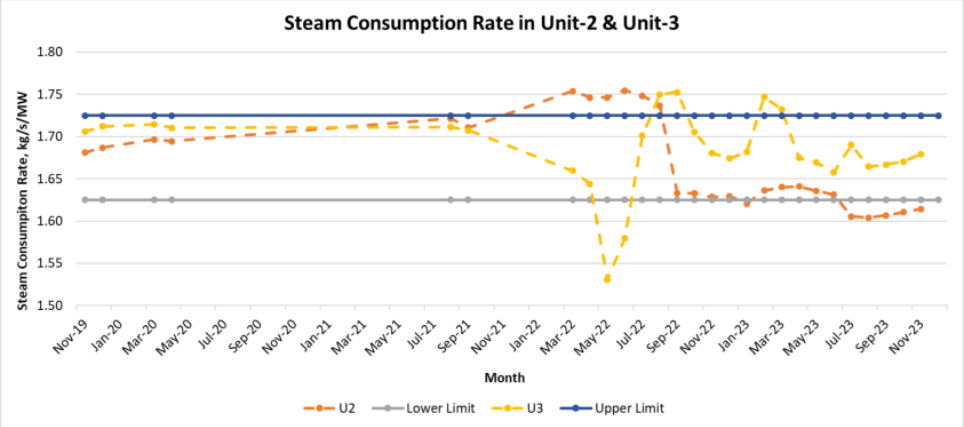

Figure 21: Steam Consumption Rate in Unit-2 & Unit-3.

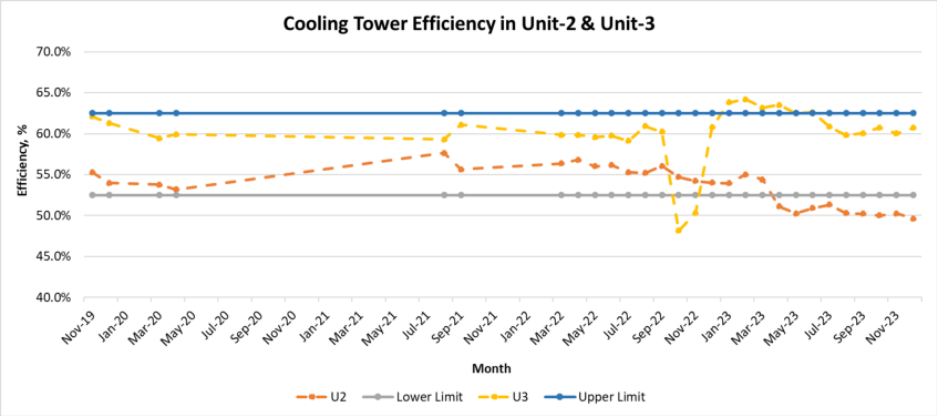

Figure 22: Cooling Tower Efficiency in Unit-2 & Unit-3.

Figure 22 illustrates the impact of the cooling water system treatment program on the efficiency of cooling towers in Units 2 and 3 over a five-year period. Overall, both units maintained cooling tower efficiencies above the minimum threshold throughout the observation period. Instances where efficiency dipped below the lower limit coincided with scheduled online maintenance of the cooling tower fan motors, which were performed alternately for each unit. This data suggests that the cooling water system treatment program has been effective in sustaining optimal cooling tower performance in both Units 2 and 3.

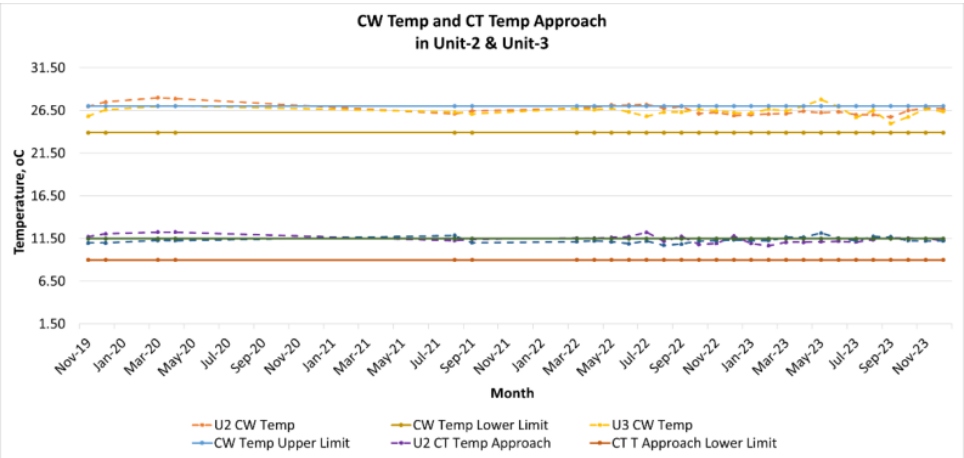

Figure 23: CW Temp, CT Temp Range, CT Temp Approach in Unit-2 & Unit-3.

Figure 23 illustrates the impact of the cooling water system treatment program on the cooling water temperature and approach of cooling towers in Units 2 and 3 over a five-year period. Overall, both units maintained cooling water temperature and approached within the expected range (CW temperature between 23.9 to 27°C and Approach between 9 to 11.5°C) throughout the observation period. Instances where CW temperature and approach

exceeded the upper limit coincided with scheduled online maintenance of the cooling tower fan motors, as discussed previously.

The cooling water treatment program helps maintain the cooling water temperature at the outlet of the cooling tower by preventing the buildup of scale, deposits, and microbiological growth. These factors can hinder heat transfer efficiency, leading to increased cooling water temperatures. By controlling these issues, the treatment program ensures optimal heat exchange between the cooling water and the ambient air, resulting in the desired outlet temperature. Additionally, the program may include corrosion inhibitors that protect the cooling tower components, further contributing to efficient operation and consistent temperature control.

5. CONCLUSION AND RECOMMENDATION

Based on the analysis conducted, the following conclusion can be drawn:

1. The cooling water treatment program has successfully controlled microbial growth, scale, corrosion, and other fouling issues in SEGD Units 2 and 3, leading to improved system performance and efficiency.
2. The use of non-oxidizing biocides has been instrumental in maintaining microbial control without adverse effects on water chemistry or equipment.
3. Long-term monitoring and a comprehensive treatment strategy incorporating biocides, dispersants, and corrosion inhibitors are crucial for sustaining optimal cooling system performance and longevity.
4. Maintaining cooling water parameters within specified limits has resulted in significant benefits, including reduced corrosion, improved operational efficiency, and cost savings through decreased chemical usage and equipment maintenance.
5. The implemented program has successfully addressed challenges such as increased sulfate and corrosion, ensuring the continued reliable operation of the cooling water systems.
6. The program's effectiveness is further validated by the consistently acceptable levels of lagging indicators like steam consumption, cooling tower efficiency, and water temperature.
7. By preventing the buildup of scale, deposits, and microbiological growth, the program has maintained optimal cooling water temperature, maximizing heat transfer efficiency.

Overall, the five-year data demonstrates the cooling water treatment program's success in optimizing system performance, reducing costs, and ensuring long-term operational reliability.

The following recommendations are proposed to further enhance the performance and efficiency of the cooling water system in SEGD units 2 and 3:

1. Implement online monitoring of condenser performance and utilize sulfur dispersants in the cooling water system to further enhance plant efficiency and water quality.
2. Continue the comprehensive cooling water treatment program, incorporating regular monitoring and adjustments as needed, to ensure long-term system reliability and cost-effectiveness.

REFERENCES

Aljamali, N. M., Mohsin, N. M. B., & H, N. A. (2019). Review on Corrosion and Rust Inhibition of Machines in Chemical Engineering Field. International Journal of Thermodynamics and Chemical Kinetics, 5(1), 15-22.

Ecolab International Indonesia. (2024). Personal Service Report. PT. Ecolab International Indonesia.

Kashef, N., Huang, Y.-Y., & Hamblin, M. R. (2017). Advances in antimicrobial photodynamic inactivation at the nanoscale. Nanophotonics, 6(5), 1-19

Kumar, S., Harsimran, S., & Rakesh, K. (2021). Overview of corrosion and its control: A critical review. Proceedings on Engineering Sciences, 3(1), 13-24. doi: 10.24874/PES03.01.002

Nalco Water Handbook. (2018). Nalco Water Handbook. McGraw Hill.

Pratikno, H. (2015). Aging Treatment to Increase the Erosion-Corrosion Resistance of AA6063 Alloys for Marine Application. Procedia Earth and Planetary Science, 14, 41-46.

Ridha, M., Fonna, S., Huzni, S., Israr, & Ariffin, A. K. (2010). The development of particle swarm optimization (PSO) for boundary element inverse analysis to identify rebar corrosion. Seminar Nasional Tahunan Teknik Mesin (SNTTM) ke-9,

Verma, C., Quraishi, M. A., & Rhee, K. Y. (2022). Aqueous phase polymeric corrosion inhibitors: Recent advancements and future opportunities. Journal of Molecular Liquids, 348, 118-387.

Yanto, E., Halimzikri, M. A., Budiyanto, A., Tiofami, A., Khasani, D., & Suranto, H. (February 15-17, 2021). The Importance of Cooling Water Treatment System at Lumut Balai Geothermal Power Plant. PROCEEDINGS, 46th Workshop on Geothermal Reservoir Engineering. Stanford, California: Stanford University.

Towards Sustainable Power Generation: Optimizing Chemical Dosing System for Stable pH and Reduced Corrosion Rate at PLTP Darajat II Through the Use of Metering Pump and Non-Contact Transmitter

Laila Sifha Urrohma, Toto Juniandri, Komar Wardana, Feriza Lukman,
Muhammad Ichsan, Oscar Satria Ganda, and Tania Retno Kinasih

Star Energy Geothermal, JI. Letjen. S. Parman Kav. 60 Jakarta 11410, Indonesia

laila.urrohma@starenergy.co.id

Keywords: Chemical dosing system, PLTP Darajat II, NaOH fluctuations, Condensate pH, Metering pump, Ultrasonic level transmitter

ABSTRACT

The chemical dosing system at PLTP Darajat II currently faces challenges in maintaining condensate pH, leading to inefficiency and corrosion issues. The control valve system used to deliver NaOH solution to neutralize condensate water causes significant fluctuations in NaOH solution flow, resulting in up to five times the daily requirement being wasted. This occurs due to the strong influence of the NaOH solution level in the tank on the flow rate from the control valve. Additionally, the small (1-inch) valve is prone to freezing the NaOH solution in cold temperatures ($10° - 11°C$), hindering or stopping the flow. Moreover, NaOH level measurement in the tank still uses a level gauge that is not monitored by the DCS, leading to undetected NaOH solution depletion during flow fluctuations. The current chemical dosing system causes condensate pH at PLTP Darajat II unstable which results in a severe corrosion rate on the injection pipe of 32 mpy as measured on the corrosion coupon. Such a high corrosion rate will cause pipe leaks, infrastructure damage, and disruption of PLTP operations. Leaks in condensate pipe will cause spills that pollute the surrounding environment, adversely affecting ecosystems and public health due to the presence of heavy metals such as arsenic, sulfide, boron, and mercury. This pollution has the potential to cause social conflict and violates Indonesian government regulations, particularly Law No. 32 of 2009 on Environmental Protection and Management, which can result in criminal penalties and fines.

The corrosion rate on the injection pipe can be reduced by maintaining a stable flow rate of NaOH, which can be achieved by using a metering pump. A metering pump allows for more precise and stable flow control, minimizing NaOH fluctuations and waste as it is not affected by the NaOH level. This study will evaluate the effectiveness of a metering pump for a chemical dosing system with field trials. This study will also evaluate the metering pump control system with MATLAB simulation. Furthermore, the use of NaOH concentration of 48% makes maintenance of level gauge difficult and hazardous. Therefore, this study will also provide a comparative analysis between non-contact transmitters (i.e., ultrasonic) and level gauge (currently in use). The combination of a metering pump and non-contact transmitter on the chemical dosing system at PLTP Darajat II will minimize NaOH fluctuations, prevent waste, and ensure stable condensate pH. Effective implementation of this system will protect infrastructure, preserve the environment, and ensure regulatory compliance, allowing the PLTP to continue its contribution to sustainable and environmentally friendly renewable energy.

1. INTRODUCTION

Corrosion is a significant challenge in the infrastructure of geothermal power plant pipelines, particularly in PLTP Darajat II. The presence of acidic condensate water due to the presence of $CO2$ and $H2S$ is a major factor contributing to the corrosion rate (Tang et al., 2015; Buzăianu et al., 2016). To address this issue, PLTP Darajat II employs a chemical dosing system. This system injects sodium hydroxide (NaOH) solution to neutralize the acidity of the condensate water, thereby reducing the corrosion rate. However, in practice, the chemical dosing system at PLTP Darajat II experiences several operational constraints that lead to non-optimal and fluctuating NaOH solution consumption. This has repercussions not only on the economic side but also on the effectiveness of condensate pH control, ultimately affecting the corrosion rate.

The dosing system at PLTP Darajat II is a multi-stage system with two treatment stages (Fig. 1). The first treatment is carried out at the cooling basin cooling tower (downstream of cooling tower) before the condensate is sent to the power plant. The target pH for this system is 6.2. In this first treatment, NaOH flow is controlled by a control valve, by which the opening is regulated by a pH transmitter using feedback control. The second treatment is performed at the condenser outlet. The condensate water leaving the condenser is divided into two streams one to the cooling tower and one to the injection well. The second dosing treatment is carried out along the pipeline to the injection well, where the target pH is 7. In this second treatment, NaOH flow is controlled by a metering pump, by which the pump speed is regulated by a pH transmitter using feedback control. Despite having a multi-stage

control system, the corrosion rate at PLTP Darajat II reaching up to 32 mpy as measured on the corrosion coupon, which falls into the severe category (NACE SP0775, 2013). The failure to achieve the desired pH has been considered as one of key contributing factors to the high corrosion rate at PLTP Darajat II.

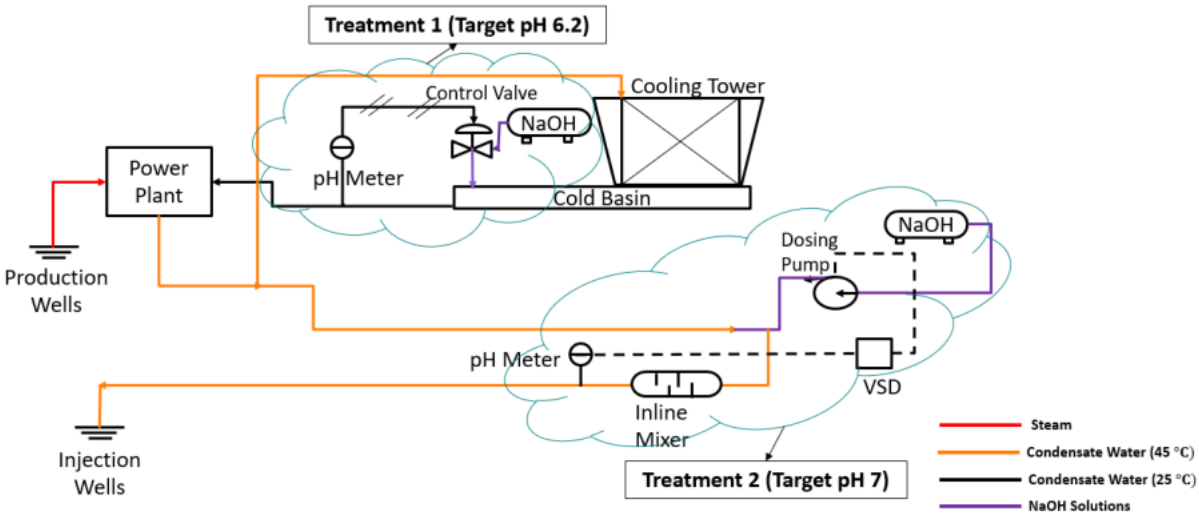

Figure 1: Chemical dosing system at PLTP Darajat II.

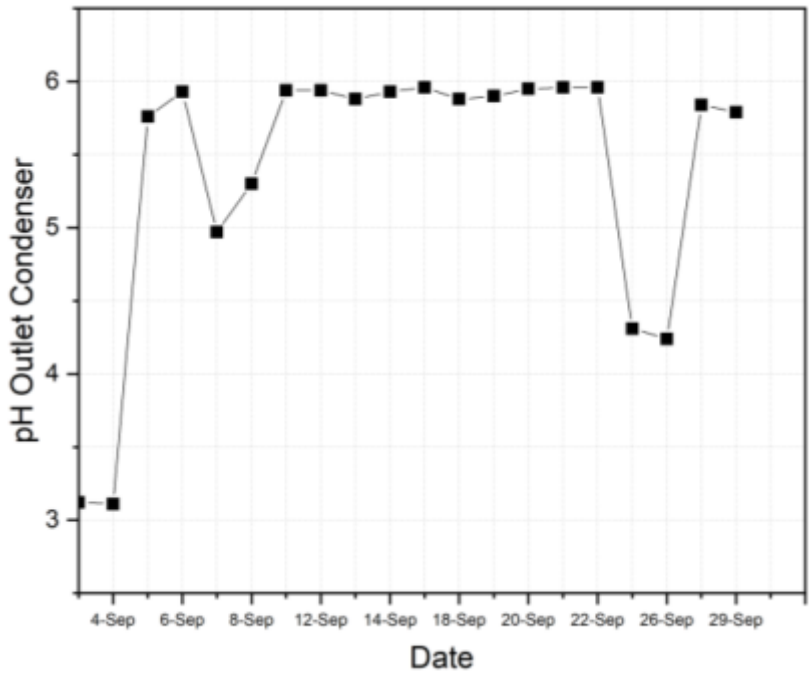

Figure 2: pH outlet condenser on December 2023.

One of the problems that hinders the achievement of the desired pH is the limitation in the chemical dosing system, particularly in the first treatment stage. This system utilizes gravity to deliver NaOH. Consequently, the flow of NaOH fluid varies even at a fixed valve opening. This variation in NaOH flow depends on the level of NaOH in the storage tank. Variations in NaOH flowrate are influenced by Torricelli's law, the higher the NaOH level in the storage tank, the faster the NaOH flowrate (Fox et al., 2011). Additionally, since NaOH tends to freeze at temperatures close to 10-11°C, this freezing also impedes the flow rate of NaOH (Hou, 1942). Meanwhile, the ambient temperature in the PLTP Darajat II environment can reach 8.4 °C.

Furthermore, the control system of the chemical dosing system at PLTP Darajat II still employs conditional control. For instance, if the pH read by the pH transmitter is 6, the valve opening is 80%. The conditional control system at PLTP Darajat II only utilizes three condition variations pH 6, pH 6.1, and pH 6.2. The use of these three pH conditions is ineffective since the condenser outlet pH varies daily ranging from 3.11-5.96 (Fig. 2). Additionally, the NaOH level is still monitored using a level gauge that is not integrated into the DCS. Consequently, during long holidays and SDTA, NaOH depletion is not uncommon.

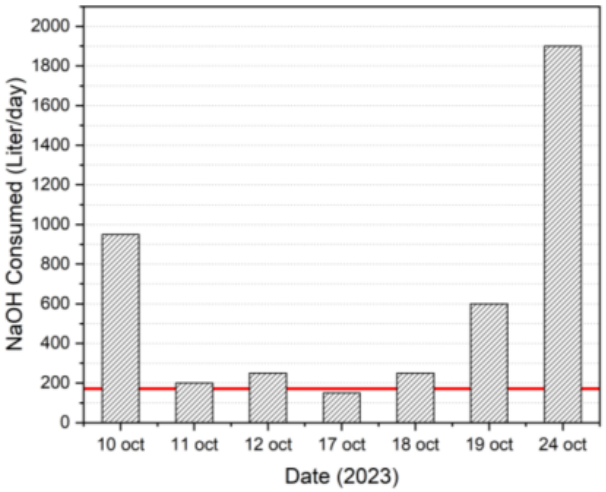

Figure 3: Consumption of NaOH for 7 days in the month of October 2023.

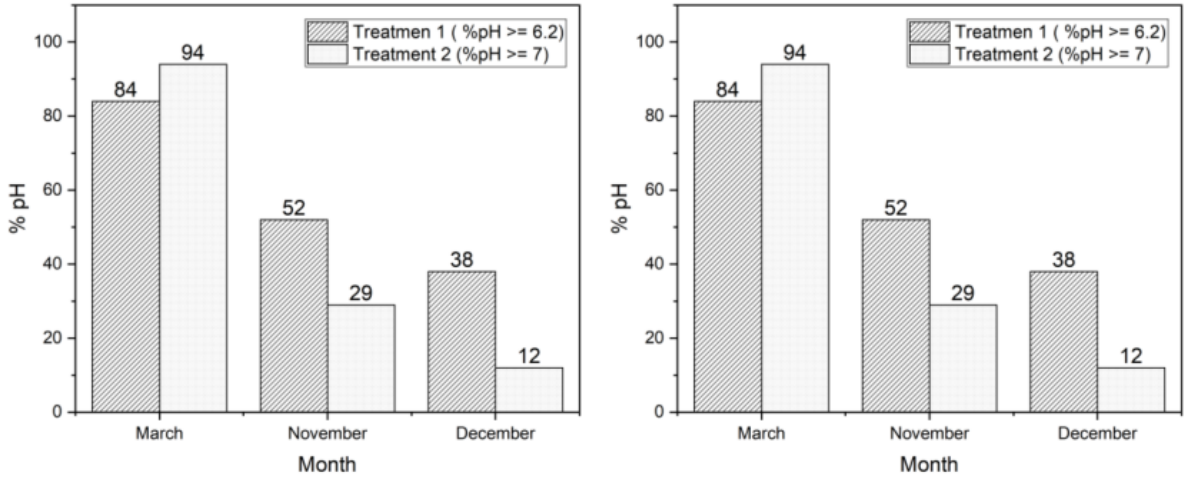

Figure 4: (a) Correlation between the pH value in treatment stage 1 and in treatment stage 2 in the year 2023, (b) Corrosion rate in the year 2023.

The combination of these three issues has detrimental consequences for the economics and reliability of the equipment. From an economic standpoint, based on data collected over seven days (Fig. 3), NaOH consumption exhibits both excesses and deficiencies, as indicated by the graph fluctuating above and below the red line. The excess consumption of 3,118 liters over seven days results in a loss of $893.76. Conversely, insufficient NaOH consumption leads to inadequate condensate water pH control, resulting in a high corrosion rate at PLTP Darajat II, which can lead to reduced expected lifetime of the pipes. Figure (4) shows that if the pH obtained in treatment 1 does not reach 6.2, then the pH obtained in the second treatment has the possibility of not reaching 7. These conditions ultimately leading to an increase in the corrosion rate. Moreover, this high corrosion rate has the potential to cause pipe leaks, which could lead to condensate contamination of the environment due to the presence of heavy metals such as arsenic, sulfide, boron, and mercury (Ellis, 1997). The potential for condensate contamination of the environment could result in violations of Regulation 32 of 2009 on Environmental Protection and Management, potentially leading to fines and imprisonment.

To achieve pH stability in a chemical dosing system, a stable flow rate of NaOH is essential. However, in practice, maintaining a constant flow rate is often challenging due to the influence of Torricelli's law from the NaOH tank and low ambient temperatures. To mitigate these conditions, appropriate valves and metering pumps are necessary. This study aims to analyze the effectiveness of the valves and metering pumps currently used in the chemical dosing system at PLTP Darajat II by utilizing operational data collected over 1.5 years. Additionally, an analysis will be conducted on the existing control system and a simulation using MATLAB software to evaluate the effectiveness of the control system on treatment 1 when using a metering pump and PI control. The study will conclude which between the valves and metering pumps is most suitable for the dosing system. Moreover, due to

frequent NaOH depletion during long holidays and SDTA, a comparative study will also be conducted to determine the most suitable level transmitter for the NaOH storage tank.

2. METHOD

2.1 Method for analyzing valve and metering pump

A comprehensive study was conducted to evaluate the effectiveness of a control valve and a metering pump in delivering NaOH solution within a chemical dosing system. Field data was collected from PLTP Darajat II over 1.5 years, encompassing normal power plant operations from January 2023 to July 2024. Two types of equipment were analyzed an EZ Fisher control valve (1 inch) with a pneumatic actuator for the valve and a peristaltic pump type Boyser AMP 10 B with an electric motor actuator for the metering pump. The control valve data exhibited greater variation compared to the peristaltic pump data. The control valve data was analyzed for valve opening variations of 30%, 40%, 70%, and 80%, while the peristaltic pump data was analyzed for variations of 22% and 33%. Additionally, the peristaltic pump was subjected to field trials with data variations of 22%, 30%, 33%, 40%, and 50%.

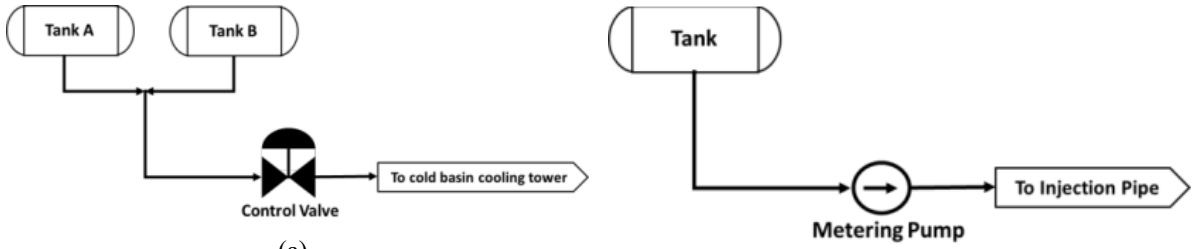

Figure 5: (a) Treatment 1 with double interconnected NaOH tank system, (b) Treatment 2 with single tank.

Treatment 1 used an interconnected double NaOH tank system, while treatment 2 used a single tank (Fig.5). To consider the slight variation in liquid level in the double tank system, the average liquid level was calculated and used as the representative NaOH level in the analysis. For the single tank in treatment 2, the liquid level was used directly. The collected data was analyzed using mean (equation 1) and standard deviation (equation 2).

$$\bar{x} = \frac{\sum_{i=1}^{n} x_i}{n} \quad (1)$$

$$SD = \sqrt{\frac{1}{n}\sum_{i=1}^{n}(x_i - \bar{x})^2} \quad (2)$$

Here,
$\bar{x}$: Mean
SD : Standard Deviation
x_i : Individual data point
N : Total number of data points

2.2 Method for analyzing the control system of a valve and a metering pump

To analyze the control system for control valves and metering pumps, two approaches can be taken. The first approach involves analyzing the existing control system at PLTP Darajat II to determine whether the current system effectively controls the pH. The second approach involves simulating the control system using MATLAB software to observe the pH response in treatment 1 when employing a metering pump with PI control.

In the existing control system at PLTP Darajat II, the control valve (treatment 1) is regulated using conditional control (if-else), where the valve opening depends on three pH variations: 6, 6.1, and 6.2. On the other hand, the metering pump (treatment 2) is controlled using a PI controller. The analysis will focus on the response of the final elements (valve and metering pump) and the resulting pH response for both control systems implemented at PLTP Darajat II. Subsequently, MATLAB simulation will be conducted to examine the pH response in treatment 1 under the control of a metering pump and PI controller.

MATLAB Design Simulations

In the PLTP Darajat II, the mixing of condensate water and NaOH is carried out within an inline mixer. The inline mixer is a device that combines acidic and basic solutions by injecting the solutions into a pipe in a continuous

process (Fig. 6). Therefore, in this control simulation, an inline mixer system will be employed using Equation (3) (Lee & Choi, 2000).

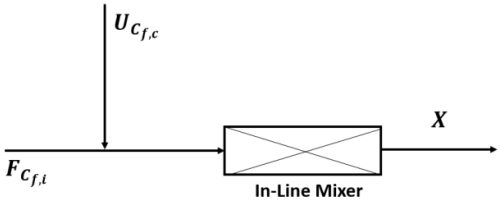

Figure 6: In-line mixer for mixing of acid and base solutions.

$$x_i(t) = \frac{Fc_{f,i}}{F + u(t-\theta)} + \frac{u(t-\theta)c_{c,i}}{F + u(t-\theta)}, \quad i = 1,2,3,\ldots,n \tag{3}$$

Here,

F : Flowrate of the influent stream
$c_{f,i}$: Total ion concentration of the *i*-th component in the influent stream
$c_{c,i}$: Total ion concentration of the *i*-th component in the titrating stream
u : Flowrate of the titrating stream
θ : Time delay due to the in-line mixer
x_i : Total ion concentration of the ith component in the effluent stream of in-line mixer

Furthermore, in this simulation, the neutralization process is assumed to be very fast, resulting in the output of the inline mixer being in equilibrium. Consequently, the pH can be calculated under this condition using Equation (4) (Wright et al., 1992). Additionally, this control simulation assumes the use of strong monoprotic and mono-hydroxyl acids and bases, namely HCl and NaOH.

$$\sum_{i=1}^{n} x_i(t) A_i\big(z_1(t)\big) + z_1(t) - K_w/z_1(t) = 0$$
$$pH_1 = -\log_{10}(z_1(t)) \tag{4}$$

Where $Ai(z)$ is, for an m-proatic acid,

$$A_i(z) = \frac{m + (m-1)z/K_{i,m} + \cdots + z^{m-1}/K_{i,m}K_{i,m-1}\ldots K_{i,2}}{1 + z/K_{i,m} + \cdots + z^{m}/K_{i,m}K_{i,m-1}\ldots K_{i,1}}$$

And, $Ai(z)$ for an m-hydroxyl base,

$$A_i(z) = \frac{mz^m + (m-1)K_w z^{m-1}/K_{i,m} + \cdots + {K_w}^{m-1} z/K_{i,m}K_{i,m-1}\ldots K_{i,2}}{z^m + K_w z^{m-1}/K_{i,m} + \cdots + {K_w}^{m}/K_{i,m}K_{i,m-1}\ldots K_{i,1}}$$

Here,

$Ai(z)$: Nonlinear function
m : Number of hydrogen ion or hydroxide ion which can be released
n : Number of components
Kw : Dissociation constant of water
Ki : Dissociation constant of the i-th component
z : Hydrogen ion concentration, in the in-line mixer

Due to its high accuracy of up to 1% in flow delivery, the flowrate of the metering pump is considered linear for the simulation (Garcia & De Godoy, 2011). Additionally, the pump dynamics are assumed to be very fast, and therefore the frictional forces within the pump are neglected. The pump design is illustrated in Figure 7.

The simulation of treatment 1, which employs a metering pump and PI control, utilizes HCl as a simplified representation of condensate water. This simplification was adopted to facilitate mathematical modeling. However, this simulation still uses some of the existing parameters at PLTP Darajat II such as 18 M NaOH and a condensate flow rate of approximately 3447 liter/s. The control system model is illustrated in Figure 8.

2.3 Method for the comparative study of contact and non-contact transmitters

A literature review was conducted to perform a comparative study for selecting the appropriate contact or non-contact transmitter for measuring NaOH level in the tank. The literature was analyzed based on several parameters

of accuracy, installation, maintenance, cost, environmental impact, calibration, sensitivity, interference, safety, measurement range, and suitability for NaOH.

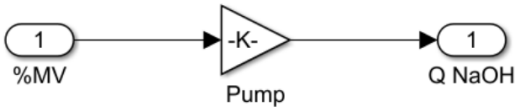

Figure 7: Model of the pump.

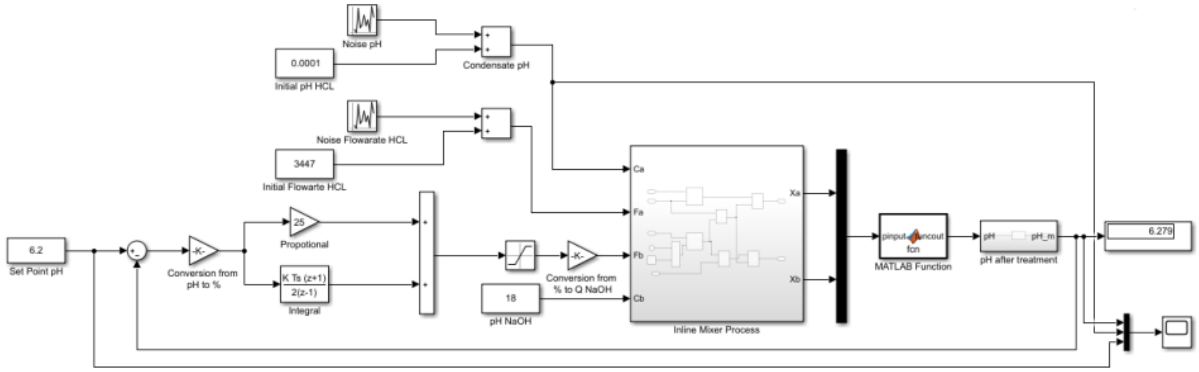

Figure 8: Modelling the pH neutralization plant in MATLAB Simulink for treatment 1 when using a metering pump and PI control.

3. RESULT AND DISCUSSION

3.1 Analyzing Valve and Dosing Pump Effectiveness in Flowing NaOH

Despite the multi-stage chemical dosing system employed at the PLTP Darajat II, the corrosion rate, particularly on the carbon steel injection pipes, has reached severe levels. Consequently, this study aims to analyze the effectiveness of valve and peristaltic pumps in the NaOH dosing system of PLTP Darajat II. The data utilized in this study was collected during normal power plant operation.

In first treatment stage of the PLTP Darajat II chemical dosing system, gravity is employed to deliver NaOH. The control valve then regulates the NaOH flow. Various valve opening percentages have been implemented, including 30%, 40%, 70%, and 80%. As illustrated in Figure 9, the NaOH flow rate is inconsistent for the same valve opening percentage, regardless of whether the valve is opened at 30%, 40%, 70%, or 80%. This indicates fluctuations in NaOH flow. Further observation reveals that the NaOH flow rate fluctuation follows the NaOH level in the tank. The higher the NaOH level in the tank, the faster the NaOH flow rate. This phenomenon can be explained by Torricelli's Law. This law, an application of Bernoulli's principle, states that the fluid flow velocity is directly proportional to the square root of the fluid height. In other words, the higher the fluid is above the orifice, the greater the flow velocity. This can be understood because the higher fluid possesses greater gravitational potential energy, which is converted into kinetic energy as the fluid flows out of the orifice (Fox et al., 2011).

Apart from the influence of the NaOH level in the tank, Figure 10 demonstrates that the NaOH flow rate can also vary for the same NaOH level and valve opening percentage. The potential cause of this variation in NaOH flow rate is NaOH solidification within the valve or flow pipe, which impedes the flow rate. NaOH solidification is a frequent occurrence at PLTP Darajat II due to its mountainous location, where nighttime temperatures can reach 8.4 degrees Celsius, the freezing point of NaOH. Additionally, the unstable flow rate is another factor contributing to NaOH solidification. Unstable flow is often accompanied by pressure and flow velocity fluctuations. When the flow becomes slow or even stops momentarily, the NaOH within the pipe and control valve is more susceptible to reaching the low ambient temperature, particularly when the ambient temperature approaches or falls below the NaOH freezing point.

An examination of NaOH consumption data for valve opening percentages of 30%, 40%, 70%, and 80% in Figure 11 and Table 1 reveals that valve opening variation does not result in a significant difference in NaOH utilization. Theoretically, a larger valve opening should lead to a higher NaOH consumption rate. For instance, valve opening at 80% should result in higher NaOH consumption; however, the actual consumption is often similar to that of 70% and 40% valve openings. Furthermore, the standard deviation values also indicate significant variation in daily NaOH consumption, with daily consumption deviations reaching 406 liters from the average daily consumption. This high standard deviation demonstrates that daily NaOH consumption using the control valve is

highly variable and inconsistent, making it impossible to accurately predict daily consumption. This is likely due to NaOH solidification within the pipes and the NaOH level in the tank, which hinders the control valve's ability to effectively regulate the NaOH flow rate.

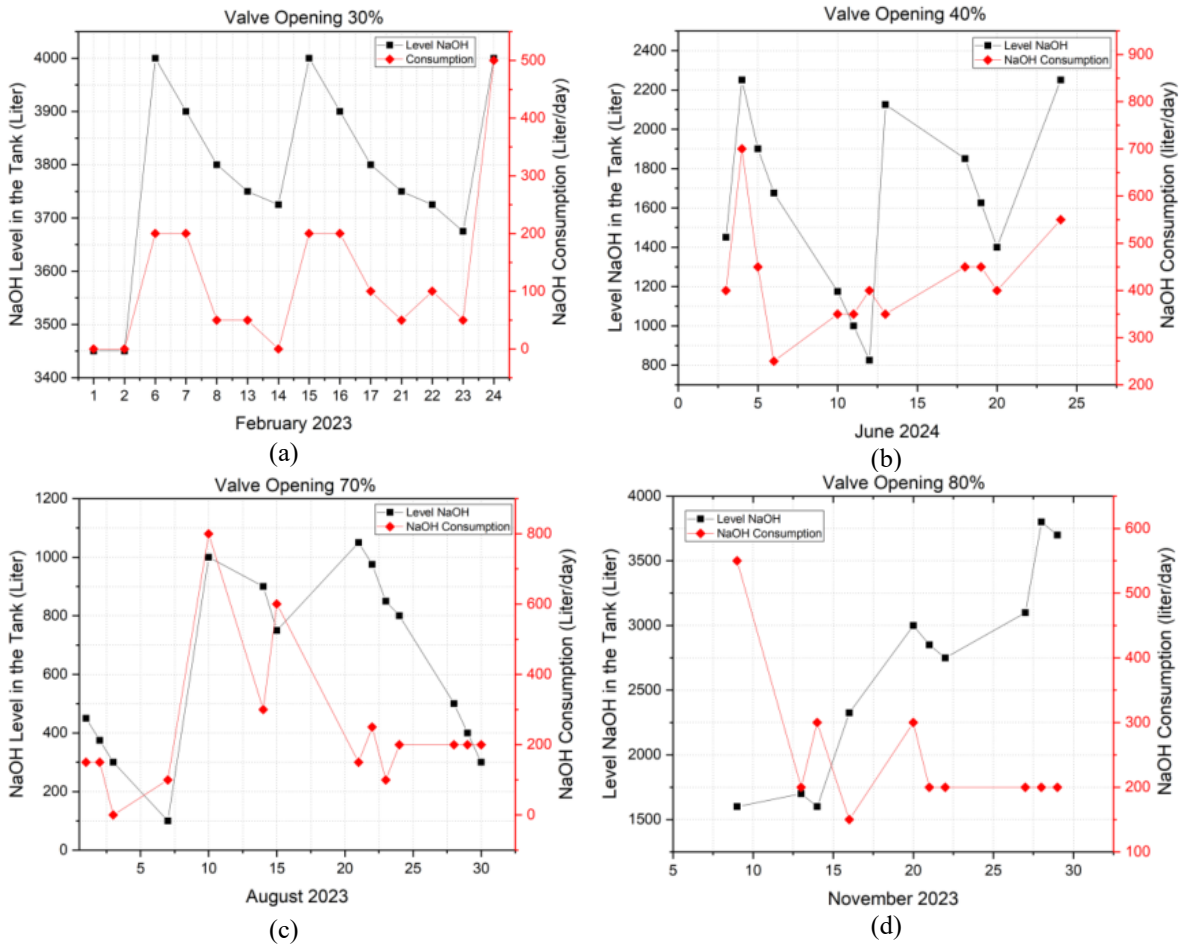

Figure 9: Relationship of the NaOH level in the tank to the daily consumption of NaOH (a) 30% valve open, (b) 40% valve open, (c) 70% valve open, (d) 80% valve open.

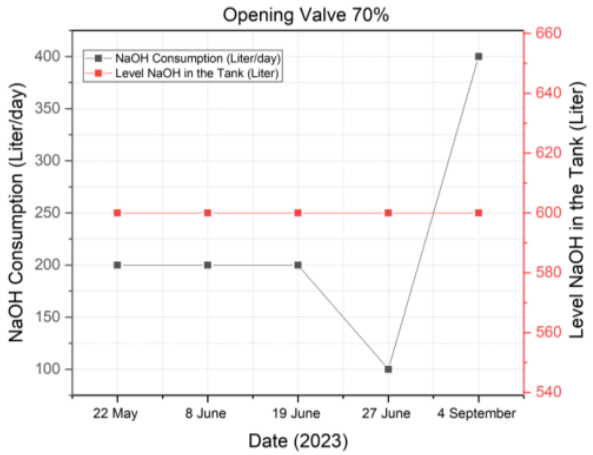

Figure 10: NaOH consumed at 70% valve opened on different days.

Table 1: Mean and standard deviation of NaOH consumption for 30%, 40%, 70%, and 80% valve opening variations.

Opening Valve	**30%**	**40%**	**70%**	**80%**
Days	26 days	16 days	82 days	39 days
Mean	144 liters	344 liters	246 liters	372 liters
Standard deviations	127 liters	176 liters	118 liters	406 liters

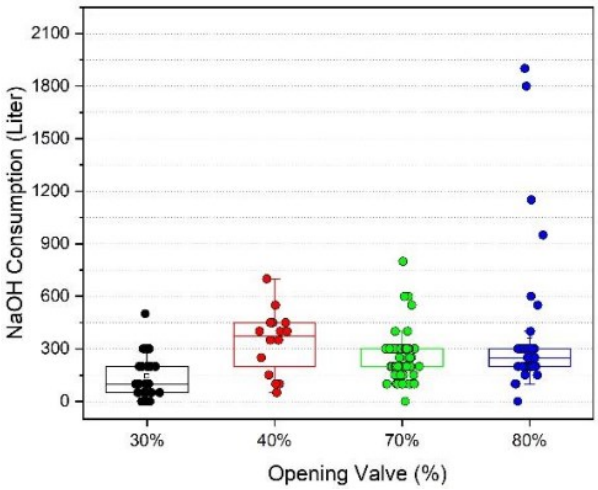

Figure 11: Rate of consumption of NaOH for variations in valve opening of 30 %, 40 %, 70 % and 80 %.

In second treatment stage, a peristaltic metering pump was employed. Field trial testing was conducted at motor speeds of 22%, 30%, 33%, 40%, and 50%. The data obtained in Figure 12 demonstrates a linear relationship between motor speed and NaOH consumption. The faster the motor speed, the higher the daily NaOH consumption.

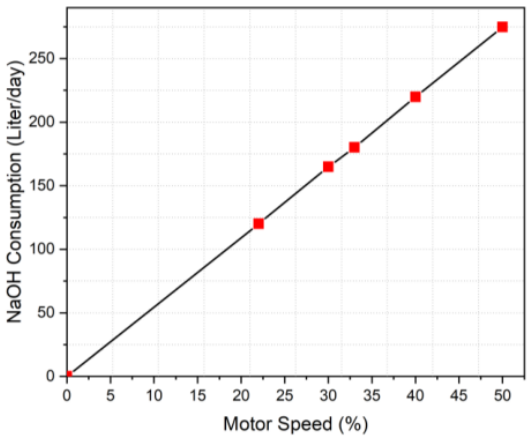

Figure 12: Relationship between the speed of the motor and NaOH consumption (field trial).

An analysis of the peristaltic pump's effectiveness using pump speed variations of 22% and 33% was conducted. Data from Figure 13 indicates that variations in the NaOH tank level do not influence NaOH consumption. Additionally, when using the peristaltic pump, solidification within the flow pipe is rare due to the stable flow, which reduces the contact time between NaOH and the low ambient temperature, thereby minimizing the risk of solidification. Figure 13 further demonstrates that the peristaltic pump delivers NaOH with stability and consistency, resulting in a significant reduction in NaOH consumption variation.

This study highlights the significant flow fluctuations experienced by the valve in the NaOH dosing system at PLTP Darajat II, influenced by the NaOH level in the tank and NaOH solidification phenomena. Conversely, the peristaltic pump exhibits superior stability and accuracy, demonstrating a linear relationship between motor speed and NaOH consumption while minimizing the impact of tank level variations and solidification. Therefore, the peristaltic pump is more strongly recommended for dosing applications that demand high precision and consistency.

Figure 14 is the response of the existing control system at PLTP Darajat II, the orange graph represents the response of the control valve and metering pump, while the blue graph represents the pH response generated by the control system. The pH response produced by the control valve (treatment 1) exhibits an unstable pH value at the setpoint with an average error of 1.24±1.1 pH (Fig. 14(a)). This significant error can be attributed to the system employing feedback control with conditional control, which utilizes only three pH conditions: at pH < 6, the valve opens 80%; at pH < 6.1, the valve opens 35%; and at pH > 6.2, the valve closes. Consequently, this conditional control system is similar to an on/off control system. On/off control systems do not consider how close the measured value is to the setpoint. On/off control systems only react to whether the output value is higher or lower

than the setpoint, causing the system to oscillate around the setpoint, often with a considerable amplitude, leading to a large error value. In addition to conditional control, the oscillation is also caused by the control valve utilizing gravity to flow NaOH. As discussed in section 3.1, at the same opening valve, the NaOH consumption rate varies due to the Torricelli law.

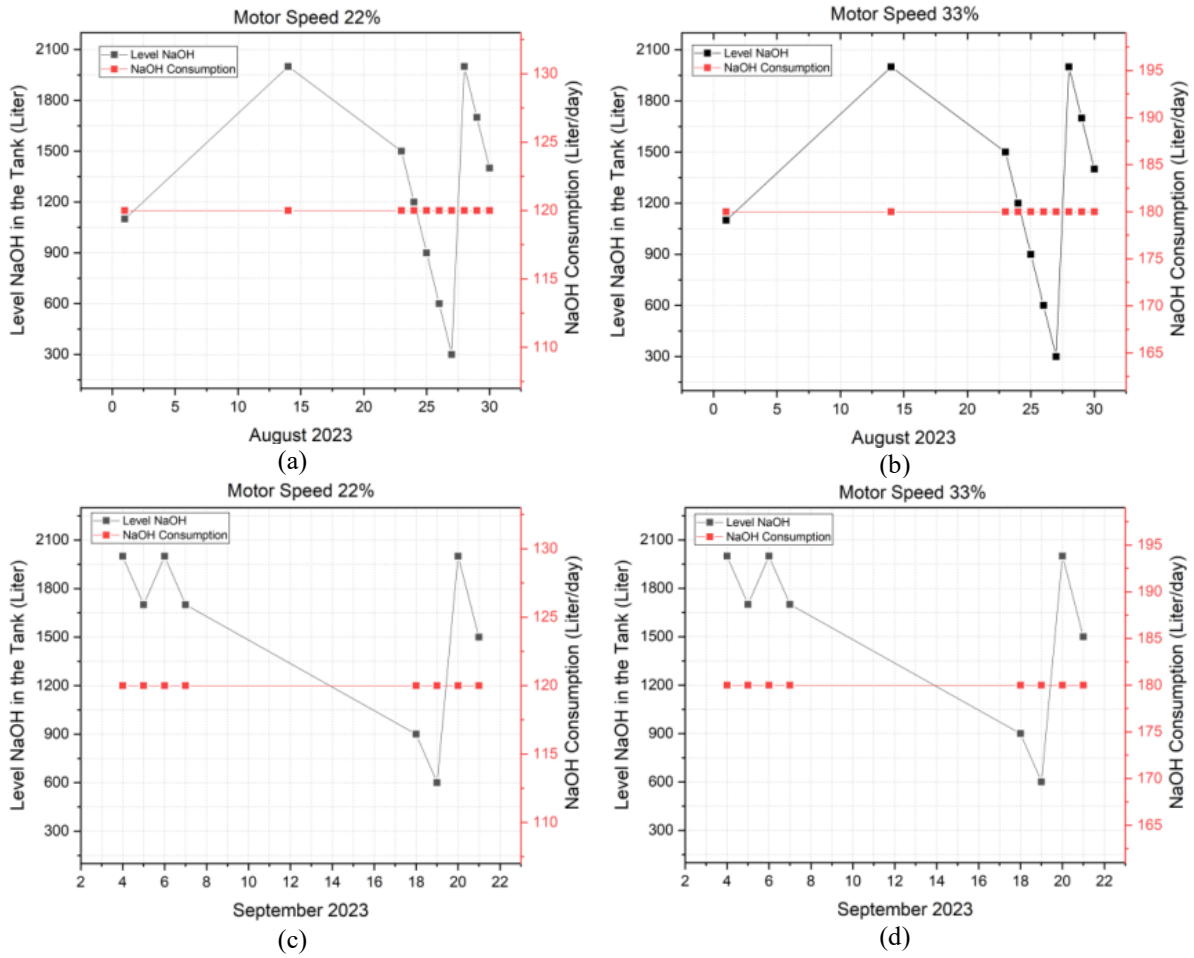

Figure 13: Relationship between NaOH level in tank and daily NaOH consumption (a) 22% motor speed in August, (b) 33% motor speed in August, (c) 22% motor speed in September, (d) 33% motor speed in September.

3.2 Analyzing the effectiveness of system control of valves and metering pumps in delivering NaOH

Subsequently, for the metering pump (treatment 2), utilizing feedback control with a PI controller, the pH remains stable at the setpoint with an average error of 0.06±0.05 pH (Fig. 14(b)). The relatively small error is attributed to the PI controller's (Proportional-Integral controller) ability to more smoothly control the process. The proportional portion of the PI controller responds to changes in the measured value relative to the setpoint, while the integral portion accumulates the error over time and adjusts the output to gradually eliminate the error. This enables the PI controller to stabilize the system closer to the setpoint with smaller oscillations and a lower error.

Therefore, since the pH produced in treatment 1 is unstable and oscillatory, to achieve a more stable pH, it is recommended to replace the valve with a metering pump to produce more accurate dosing and to modify the control system with feedback control utilizing a PI controller (Fig. 15).

Furthermore, a pH control simulation was conducted in accordance with the design in Figure 15, assuming the use of a strong acid (HCl) and a strong base (NaOH) to simplify the derivation of the system equation for simulation. The simulation results using MATLAB software are presented in Figure 16. Based on the simulation results, it is evident that under varying pre-treatment pH conditions, if a chemical dosing system with PI control is applied, the pH setpoint (pH 6.2) is achieved with an average error of 0.05±0.06 pH. Although the simulation results are not entirely representative due to the ideal conditions and the use of a strong acid, the simulation results demonstrate that employing a PI controller can yield a more stable pH when applied to treatment 1.

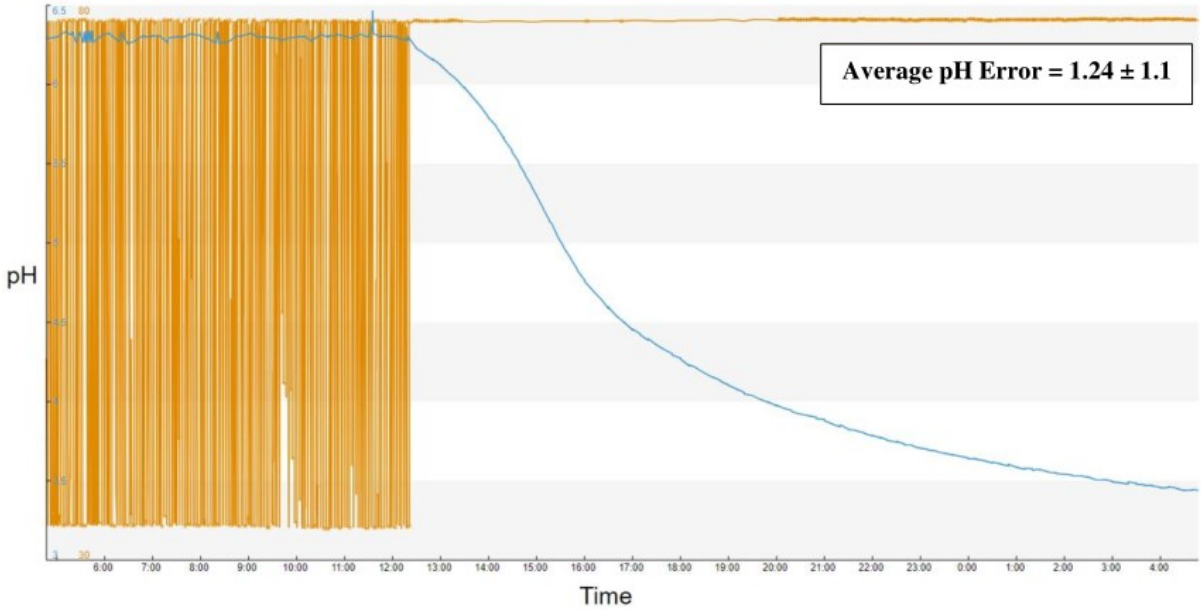

(a)

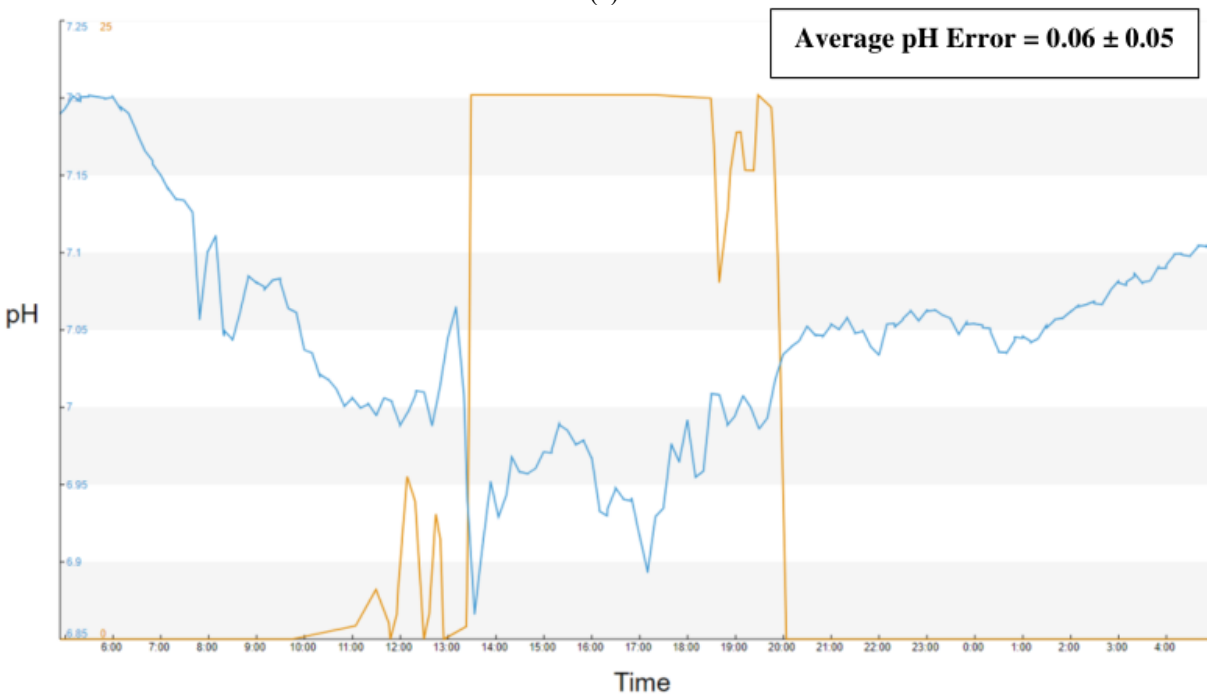

(b)

Figure 14: Response of the existing control system at PLTP Darajat II, orange line represents the response of the control valve and metering pump & blue line represents the pH response (a) Response of control valve and pH output in treatment 1, (b) Response of peristaltic pump and pH output in treatment 2.

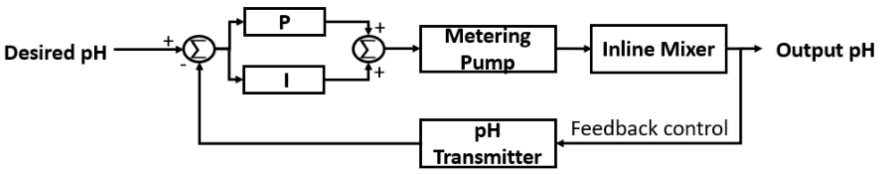

Figure 15: Design of system control block diagram for treatment 1 when using metering pump and PI control.

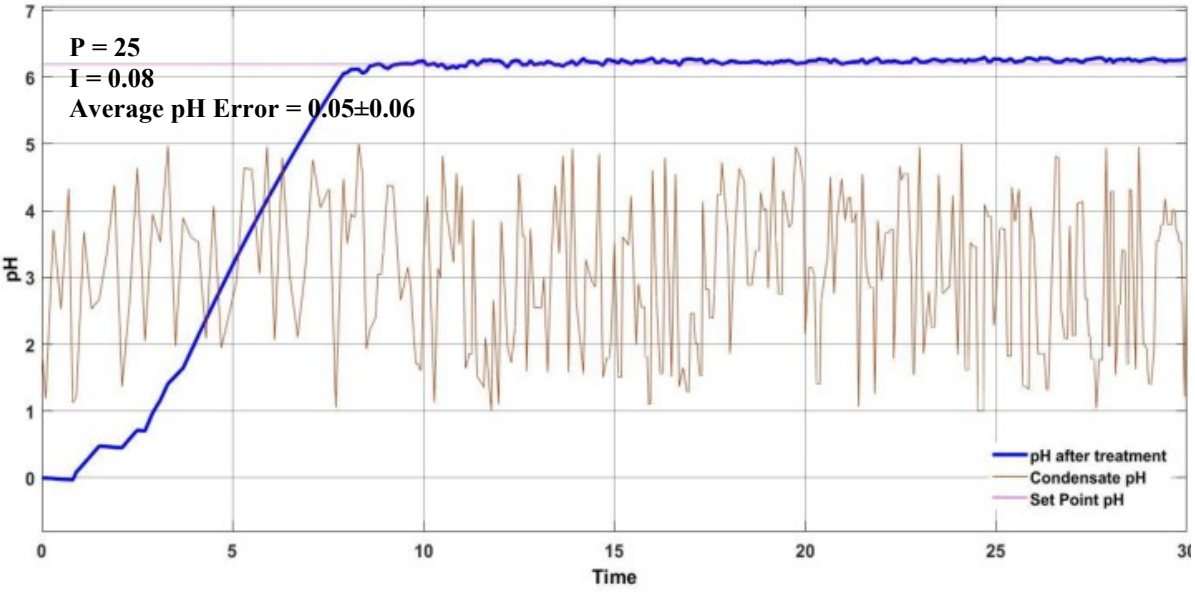

Figure 16: Results of a MATLAB Simulink simulation of treatment 1 when using a dosing pump and a PI control system.

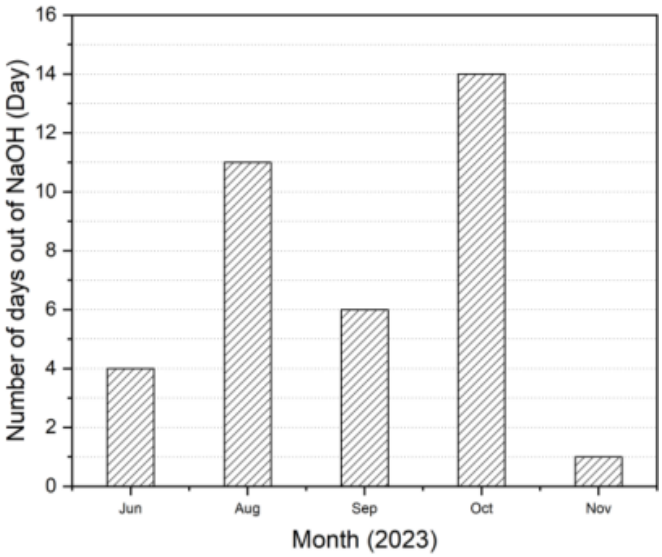

Figure 17: Duration of running out of NaOH for a period of 5 months.

3.3 Comparative analysis of contact and non-contact level transmitters

In power plant operations, the pH of condensate water is not stable but fluctuates depending on steam conditions. This variability leads to unpredictable daily NaOH consumption, emphasizing the importance of NaOH level monitoring to prevent depletion. Figure 17 illustrates a 5-month NaOH depletion incident at PLTP Darajat II due to the use of non-integrated level measurement devices with the DCS. As a result, manual level checks were required, leading to frequent NaOH depletion during long weekends or SDTA periods. During these times, NaOH consumption is high and unpredictable, and other tasks often take priority, hindering proper level monitoring. Therefore, employing a level transmitter for NaOH monitoring is crucial to provide timely low-level alerts, ensuring timely NaOH delivery.

Various level transmitters are available; however, due to the highly concentrated and corrosive nature of NaOH solutions, a comparative study between non-contact and contact transmitters is essential, as shown in Table 2. Based on the Table 2, contact transmitters perform well for NaOH applications when using corrosion-resistant materials. However, they require frequent maintenance to prevent fouling and corrosion. While accuracy and initial costs are relatively favorable, long-term costs may be higher due to maintenance requirements. In contrast, non-contact transmitters are better suited for this application as they are unaffected by the corrosive properties of NaOH. Therefore, the preferred level transmitter for this application is a non-contact transmitter. The specific non-contact transmitters to be analyzed are ultrasonic, radar, and laser.

Table 2: Comparative study of contact and non-contact level transmitters (Lipták, 2003; Eccles, 2018).

Parameter	Contact Transmitter	Non-Contact Transmitter
Principle	Direct contact with the liquid	No direct contact with the liquid
Common Types	Float, Capacitive, Conductive, Hydrostatic	Ultrasonic, Radar (Microwave), Laser
Accuracy	Generally high, depends on the technology	High, but can be affected by environmental conditions
Installation	Requires penetration into the tank or vessel	Installed externally, no tank penetration needed
Maintenance	Higher maintenance due to potential fouling and corrosion	Lower maintenance, no direct contact with corrosive liquid
Suitability for NaOH	Must use materials resistant to NaOH corrosion (e.g., PTFE, stainless steel)	Not affected by NaOH corrosion since no direct contact
Cost	Generally lower initial cost ($100 – 1000)	Higher initial cost, but lower long-term maintenance ($100 – over 1000)
Environmental Impact	Potential leakage and contamination risk	No risk of contamination due to leakage
Calibration	Requires periodic calibration	Less frequent calibration, depending on the model
Sensitivity to Obstructions	Less sensitive, but float type can be affected by debris	Can be affected by foam, vapor, and obstructions in the signal path

Table 3: Comparative study of non-contact level transmitters (Lipták, 2003; Navaratne, 2023; Peterson, 2023).

Parameter	Ultrasonic	Radar (Microwave)	Laser
Operating Principle	Sound waves reflect off the liquid surface	Microwave signals reflect off the liquid surface	Laser beams reflect off the liquid surface
Accuracy	High, but can be affected by temperature and gas composition in the tank	Very high, less affected by temperature and gas composition	Very high, but can be affected by vapor and airborne particles
Measurement Range	Up to 10 meters	Up to 30 meters	Up to 100 meters
Installation	Easy to install on top of the tank	Easy to install on top of the tank	Requires precise alignment for optimal accuracy
Maintenance	Low, but sensor can be affected by dirt or buildup	Very low, sensor protected from dirt	Low, but lens must remain clean
Environmental Resistance	Less resistant to harsh environments and temperature changes	Very resistant to harsh environments and temperature changes	Moderate, can be affected by vapor and dust
Cost	More affordable than radar or laser ($100 – 1000)	More expensive than ultrasonic ($300 – over 1000)	Most expensive among the three (Over $1000)
Calibration	Requires periodic calibration	Less frequent calibration, depending on the model	Requires periodic calibration
Interference	Can be affected by foam, turbulence, and deposits on the sensor surface	Less affected by foam or turbulence	Can be affected by vapor, particles, and atmospheric conditions
Safety	Safe for use in various conditions	Safe and can be used in extreme conditions	Safe, but potential laser hazards must be considered

According to the comparative table in Table 3, for measuring NaOH level in a stable tank (without temperature changes, gas, turbulence, or foam changes), an ultrasonic transmitter is an excellent and economical choice. This

transmitter offers sufficient accuracy and lower costs under stable conditions. However, if higher accuracy is required and sufficient budget is available, a radar (microwave) transmitter is an excellent choice with superior accuracy and reliability. Laser transmitters can be considered for applications requiring very long-range measurement or very high accuracy, although these may not be necessary under stable conditions.

4. CONCLUSION

Based on the conducted analysis, the following conclusions can be drawn :

1. In the PLTP Darajat II, the NaOH flow controlled by valves shows significant fluctuations and often freezes due to low temperatures, while the NaOH flow controlled by the metering pump is more stable and consistent. Then, conditional logic-based control on the valve control results in rough and unstable control, while PI control on the dosing pump provides smoother and more precise adjustments.
2. The simulation results obtained from MATLAB Simulink show that by replacing the valve with a metering pump and using a PI controller, treatment 1 will be able to maintain a stable pH at the desired pH.
3. The use of non-contact level transmitters is strongly recommended for NaOH applications as they are unaffected by the corrosive nature of NaOH and require minimal maintenance. For measuring NaOH level in stable tanks (without temperature changes, gas, turbulence, or foam fluctuations), ultrasonic transmitters represent an excellent and economical choice.

RECOMMENDATIONS

Based on the analysis conducted, the following recommendations are proposed to enhance the stability and precision of pH and NaOH consumption in the chemical dosing system:

1. Implement metering pump with PI control for chemical dosing system: For precise and stable control of pH and NaOH consumption, it is recommended to employ a metering pump equipped with PI (Proportional-Integral) control.
2. Ultrasonic transmitter for level monitoring: For level monitoring of NaOH, the utilization of a non-contact ultrasonic transmitter is suggested when the tank conditions are stable (free from temperature changes, gas, turbulence, and foam) and an economical transmitter is desired.

REFERENCES

Buzăianu, A. et al. (2016) ‘Some analysis of major impact of geothermal fluid components in power plant equipment’, IOP Conference Series: Materials Science and Engineering, 133, p. 012043. doi:10.1088/1757-899x/133/1/012043.

Eccles, A. (2018) Sodium hydroxide storage tanks & specifications, Protank. Available at: https://www.protank.com/sodium- hydroxide (Accessed: 08 July 2024).

Ellis, A.J. (1977) ‘Geothermal Fluid Chemistry and human health’, Geothermics, 6(3–4), pp. 175–182. doi:10.1016/0375-6505(77)90026-8.

Fox, R. W., McDonald, A. T., & Pritchard, P. J. (2011). Introduction to Fluid Mechanics. John Wiley & Sons.

Garcia, C. and De Godoy, R.J. (2011) ‘Modelling and simulation of ph neutralization plant including the process instrumentation’, Applications of MATLAB in Science and Engineering [Preprint]. doi:10.5772/24718.

Lee, J. and Choi, J.Y. (2000) ‘In-line mixer for feedforward control and adaptive feedback control of ph processes’, Chemical Engineering Science, 55(7), pp. 1337–1345. doi:10.1016/s0009-2509(99)00407-8.

Lipták, B.G. (2003) Process measurement and analysis. Boca Raton, Fla: CRC Press.

Melling, P. J., & Thomson, P. (2000). Industrial Process Control: Advances in Instrumentation and Control. Wiley-IEEE Press

Navaratne, S. (2023) A guide to choosing Ultrasonic, radar or submersible tech for Level Monitoring, ellenex. Available at: Available at: https:// www.ellenex.com/post/sensors-unleashed-a-guide-to-ultrasonic-radar-and-submersible-tech (Accessed: 08 July 2024).

Peterson, S. (2023) Radar vs. ultrasonic level sensors, Endress+Hauser. Available at: https://endressprocessautomation.com/radar-vs-ultrasonic-sensors-fit-for-purpose-technology/ (Accessed: 08 July 2024).

NACE SP0775-2013, “Preparation, Installation, Analysis, and Interpretation of Corrosion Coupons in Oilfield Operations” (Houston, TX: NACE International, 2013).

Tang, D. -Z. et al. (2015) ‘Effect of ph value on corrosion of carbon steel under an applied alternating current’, Materials and Corrosion, 66(12), pp. 1467–1479. doi:10.1002/maco.201508365.

T. P. HOU, "Manufacture of Soda Ash," 2nd Ed. N.Y., Reinhold Publishing Corp., 1942. From Industrial Engineering Chemistry, Vol. 46, No 11, p. 2401.

Wright, R.A. et al. (1992) ‘Control of an industrial ph process using the strong acid equivalent’, 1992 American Control Conference [Preprint]. doi:10.23919/acc.1992.4792142.

100% Coring Recovery in a High-Angle Well of Dieng Plateau's Geothermal Formation with a Combined Anti-Jamming System and Full-Closure System in One Assembly

Benny Richard Wales[1], Triadi Herwasto Aribowo[1], Kurnia D. Huway[1], Arif Hudiman[1], Budi Setiawan[2], Yudi Hartono[2], and Zakki[2]

[1]NOV, Kawasan Taman Tekno Blok C No.1, Tangerang Selatan
[2]Geodipa Energi, Soreang, Bandung

Benny.Wales@nov.com Triadi.aribowo@nov.com Kurnia.darmawan@nov.com Arif.Hudiman@nov.com Yudi.Hartono@geodipa.co.id Budi.setiawan@geodipa.co.id Zakki@geodipa.co.id

Keywords: Drilling, Coring, Geothermal, High angle well

ABSTRACT

The Dieng Plateau in central Java, Indonesia, forms the floor of the caldera complex on the Dieng volcanic complex. This complex consists of stratovolcanoes, craters, and Pleistocene to Holocene-age volcanic cones that store natural wealth in the form of geothermal energy. For drilling within the Dieng area, the operator requires coring to check the distribution of diorite intrusion at the Merdada crater and Pagar Kendang volcanic necks.

The hard yet brittle formation presents a significant challenge to the coring process, particularly with the standard conventional system, as the core may slide and fall from the inner barrel assembly when pulling the coring assembly out of the hole. The challenge is further increased by the total loss circulation condition, which is preferred as the coring point zone. This means there are no pressure readings available, which would typically be used as one of the indications or coring parameters to spot any anomalies. Additionally, backside pumping is required to maintain the well's hydrostatic pressure to mitigate any steam kick while coring is in progress. Thus, more challenges arise.

To overcome the challenges, a full-closure system technology with a double-catcher assembly—comprising the clam shell catcher and the spring catcher—is required. However, this technology alone is insufficient in geothermal applications due to the type of non-cemented formation profile, which causes core jamming and results in very low to zero penetration during coring. To remedy this issue, an additional system, known as the Anti-Jamming System, is required. This system can alleviate internal friction within the core barrel assembly, specifically at the inner barrel assembly.

This paper provides detailed information about how the combination of anti-jamming system technology and full-closure system technology, along with certain key procedures, strategies, and lessons learned from the initial well, could mitigate the potential hazards or risks of a coring job in a geothermal application. Based on the recent coring operations in three wells, all coring jobs have successfully achieved 100% core recovery in the Dieng area with superior performance.

1. INTRODUCTION

PT Geodipa Energi is exploring the Dieng Plateau geothermal field onshore Indonesia **(**Figure 1**).** The Dieng area contains 10 core wells planned from June 2021 to May 2023; however, not all wells are cored, mainly because of the wellbore situation. This paper will discuss three core wells: Q-1, T-1, and T-2. All three are directional wells drilled using PT Plumpang Raya Anugrah's PRA-09, a 1,500-hp land rig.

Dieng Plateau's 9-7/8-in. hole section consists of interbedded formations of minerals, including illite, chlorite, first continuous epidote, wairakite, phrenite, and calcite, as shown in Figure 2. Diorite formations are known to be highly altered microdiorite intrusion; secondary mineral assemblages consist of epidote, actinolite, sericite, and an expected medium to hard andesite layer with possible high borehole temperature.

All three wells (Q-1, T-1, and T-2) were expected and considered to be hard or very hard formations that are non-cemented with high permeability formation profiles. Thus, the fluid loss circulating zone is the preferred depth for coring. Coring in non-cemented volcanic formations carries significant risks, such as core slip-off, core jamming, and milling of the core. Fortunately, these issues are frequently detectable at the surface gauge through two key parameters: torque and penetration rate (ROP). Standpipe pressure is ineffective because it would be zero at the total fluid loss zone.

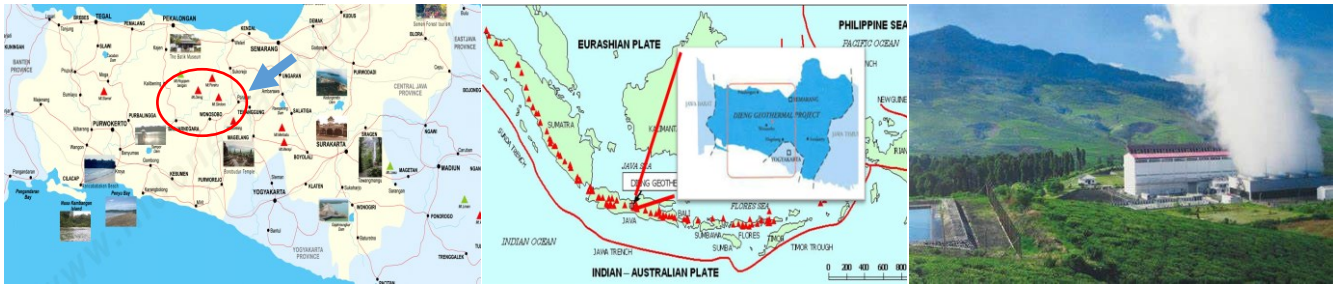

Figure 1: Well location.

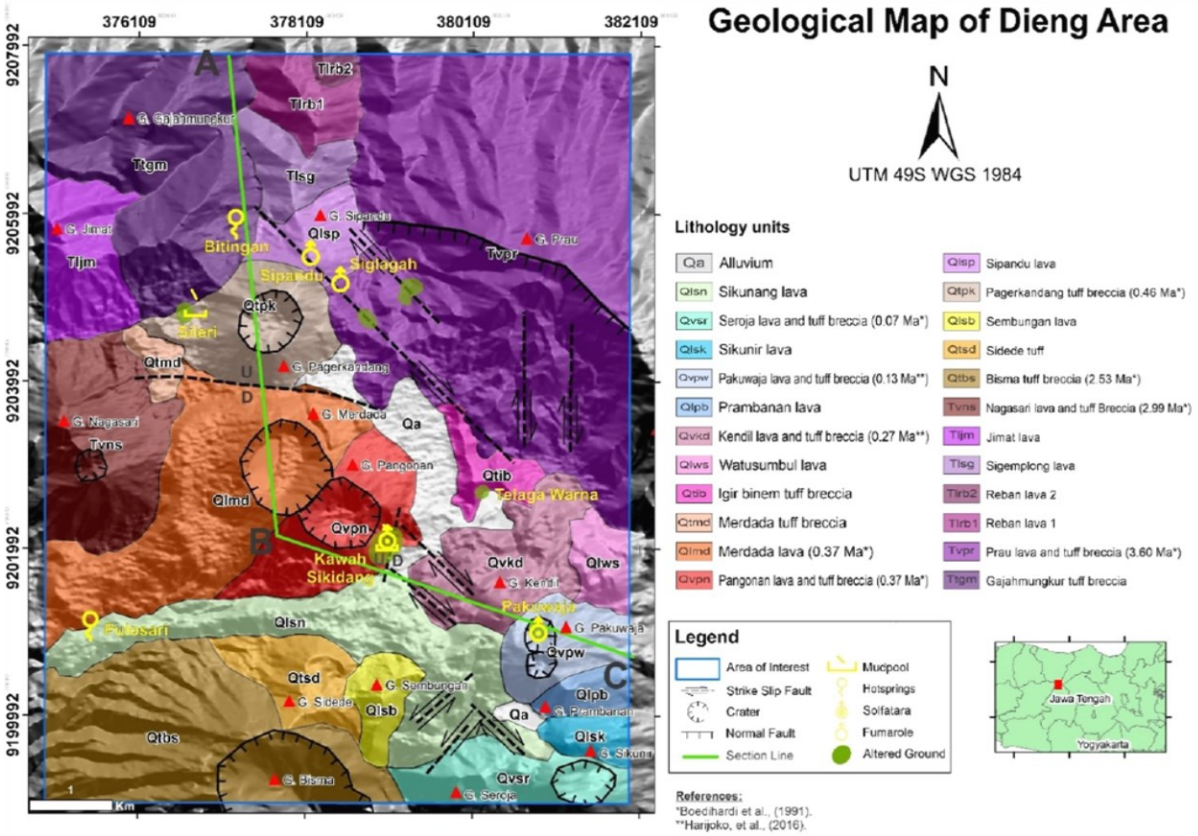

Figure 2: Geological map of Dieng Plateau (Ref. SGP-TR-223).

To mitigate or potentially eliminate the risks or expected hazards, both the operator and coring services contractor held technical meetings. They decided that the full closure system would be the main system for the core wells, as stipulated in the contract. Certain key parameters were also discussed and finalized in a written coring program.

Q-1 was the first well to core that had an issue with core jamming, and no penetration could be made despite changing a few key coring parameters. Due to the core jamming and the lack of decent core samples for analysis, the Q-1 well was deemed unsuccessful. Core samples are required to determine further planning of the Dieng Plateau area of the steam reservoir. Thus, all the lessons learned from the Q-1 well (Jan 2022) were then applied to the T-1 well (June 2022) and the T-2 well (July 2022). The T-1 and T-2 wells were then considered successful coring operations in terms of core quality and core length quantity for a 1x9m run. As a result, the T-1 and T-2 wells of the Dieng Plateau area serve as the basis for this paper.

2. CORE OBJECTIVES

The target was to check the distribution of Diorite Intrusion at Merdada crater and Pagar kendang volcanic neck. Coring procedures and programs were designed to obtain core samples with minimal to no mechanical damage from coring downhole until core retrieval, surface handling, and core packaging. Thorough preparations are crucial for achieving optimal results in any coring operation. The following key factors were considered:

- Coring tools type, completeness, condition, and assembly as per manual.
- Core head selection to achieve the best core quality and ROP.

- Inner barrel type of material and condition are based on the bottomhole parameter.
- Surface handling equipment completeness and condition.
- Core packaging items' completeness and condition.
- Coring bottomhole assembly (BHA) analysis on torque and drag parameter limitations.
- Apply lessons learned from previous wells in a nearby area.
- Other components at the surface that may be additional factors to consider, for example, air and fluid combination, etc.

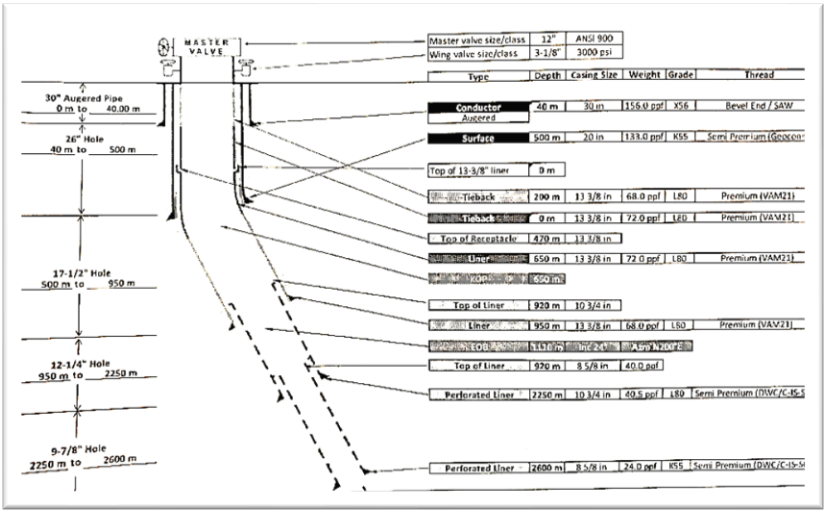

Figure 3: Well schematic of Q-1.

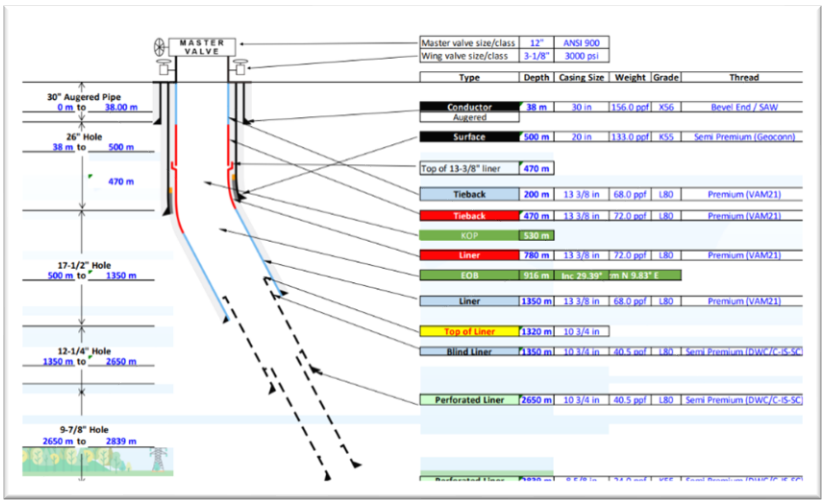

Figure 4: Well schematic of T-1.

3. EQUIPMENT IMPLEMENTATION

The non-cemented hard formations are problematic because:

- Jam when entering the barrel because of a non-cemented profile like boulders in many shapes.
- Fracture from the catcher forces.
- Fracture from column weight and vibrations.
- Slide out while retrieving barrel to surface.

Due to the risks mentioned above, a standalone single-spring conventional catcher will not be able to catch or grab the non-cemented but hard formations, especially while pulling the core barrel assembly out of the hole. Thus, the contract initially stated the use of a full closure system as part of the coring process solution, as shown in Figure 6.

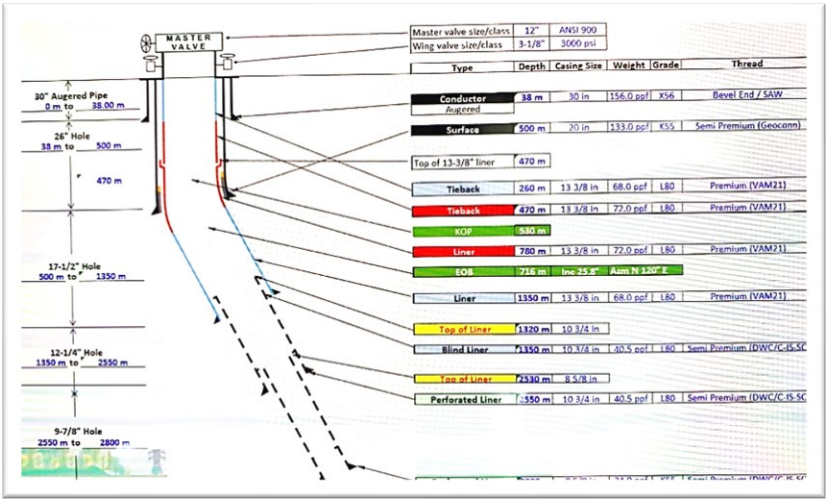

Figure 5: Well schematic of T-2.

3.1 Full Closure System

A full closure system, or the dual-core catcher system with a full closure mechanism, is designed for any applications related to unconsolidated formations, where poor core recovery is anticipated due to low rock strengths and/or when non-cemented fractured formations may potentially jam when only using a conventional catcher system. A full closure system is optimal when seeking to avoid short core runs, unscheduled trips, and loss of critical core data in unconsolidated formations. Given the profile of the aforementioned volcanic formation—which is non-cemented, as proven by a total fluid loss zone at the coring point depth—the formation category fits with the system's design and usage. The system is designed to prevent any core sample from falling and slipping out of the inner barrel assembly while pulling the core barrel assembly out of the hole.

Figure 6 shows the dual-core catcher system with a full closure mechanism, which enables the capture and recovery of the non-cemented formations that cannot be effectively retrieved using conventional equipment.

The following are the features and benefits of the dual-core catcher system with full closure:

- Complete capture – Full closure catcher system completely retains the core, even in problematic formations.
- Backup catcher – Secondary spring catcher secures core in place for cemented formation.
- Slick entry – Unobstructed entry prevents jamming.
- Efficient shearing – High-energy activation of clam shells cleanly shears core.
- At-will activation – Hydraulic drop ball system does not rely on inner barrel weight, allowing targeted activation.

The Full-Closure Core Catcher System enables full retrieval of unconsolidated, friable, fractured, and non-cemented formations. The system allows a smooth and unobstructed entry of the core into the barrel. At the conclusion of coring, the system is activated to release a pair of spring-loaded shells (*clam shell catcher*), securing the core in the inner tube. The shells prevent the core from falling out of the barrel while lifting the core barrel system off-bottom and out of the hole.

3.2 Anti-Jamming System

Core jamming is the main issue in geothermal applications that needs to be dealt with as well. While this anti-jamming system was not available within the contract for the Q-1 well, lessons learned and subsequent evaluations persuaded the client to implement it for the T-1 and T-2 wells.

This system—compatible with the Full Closure System—is designed to minimize and eliminate core jamming within the system for a certain number of times, depending on where core jamming occurs.

Liner anti-jamming was installed on the telescopic shoe and then located inside the aluminum inner barrel. If core jamming occurs near the friction holes, the friction holes will shear, as they are the weak point for releasing the friction building up within the inner diameter of the liner anti-jamming.

Figure 6: Dual-core catcher system with full closure.

Components of Full Closure System

The installing process is started by a drop ball sub connected to kelly/top drive at the surface (4-1/2-in. IF connections, with usage to drop activation ball already within the sub, without a need to disconnect drill pipe to drop the activation ball, coring BHA still at on-bottom depth).

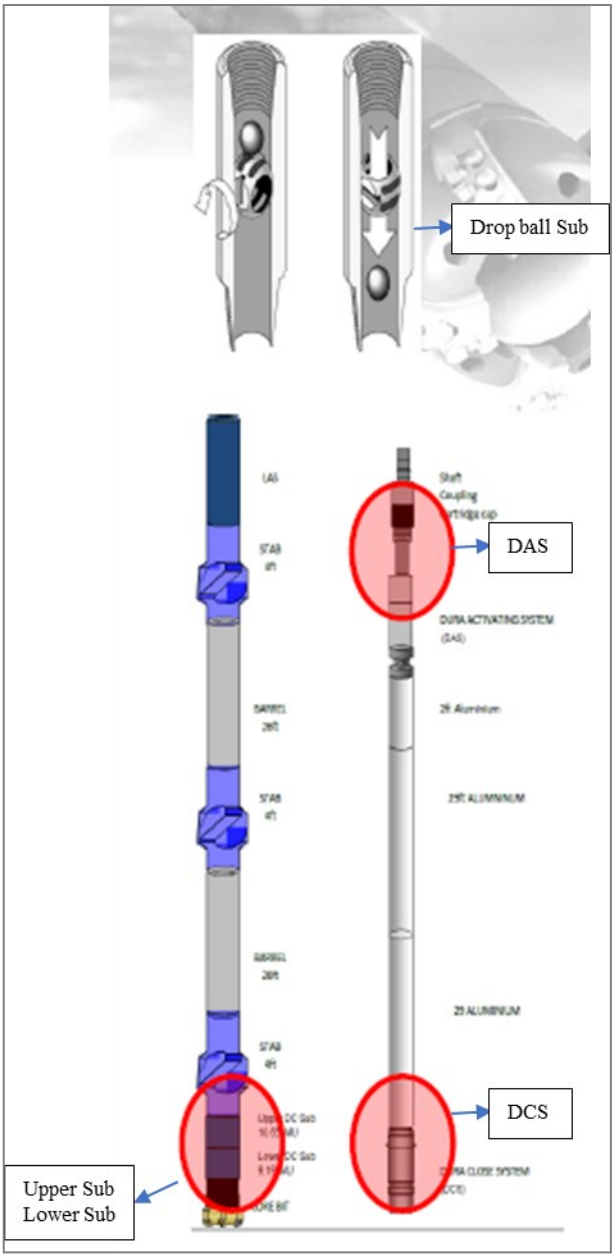

Figure 7: Added components *(in Red)* to the conventional core barrel to convert the standard conventional system into a full closure system.

3.3 Full Closure System Activation Steps

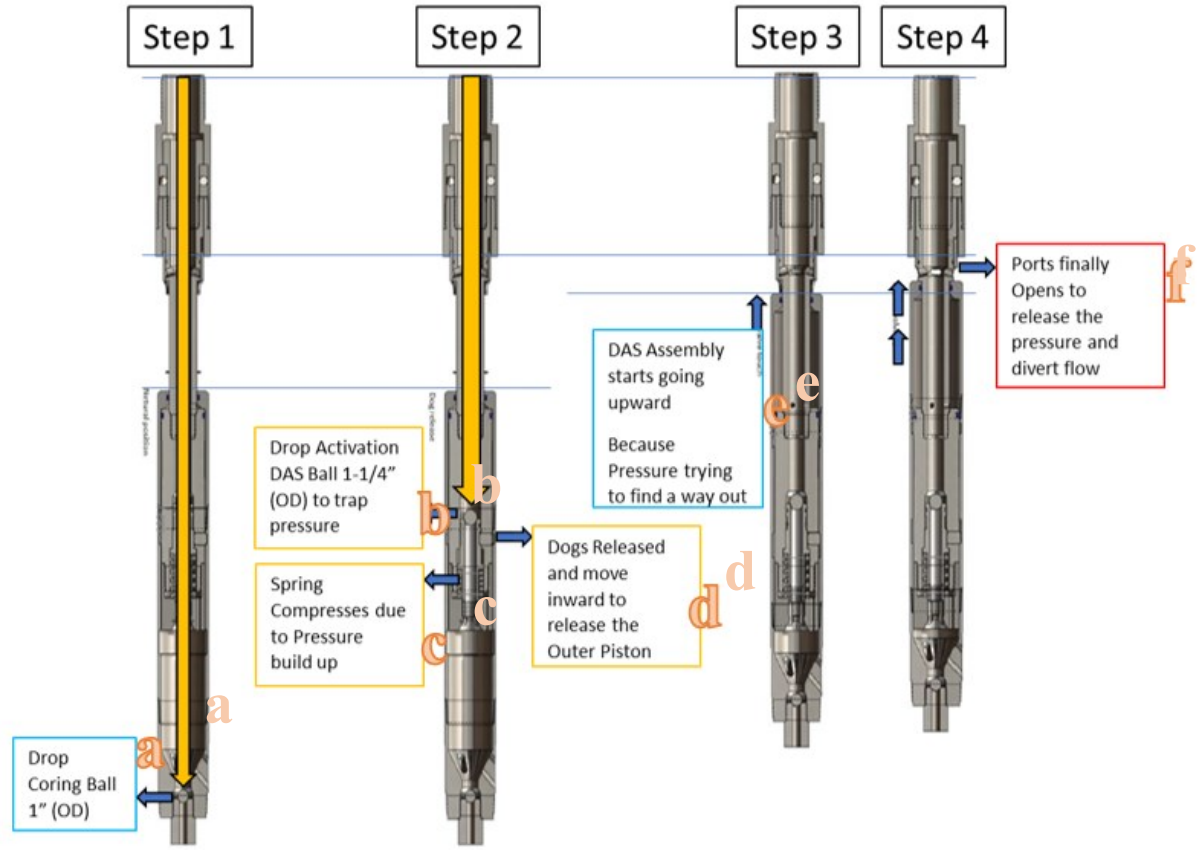

Figure 8: Top section (DAS).

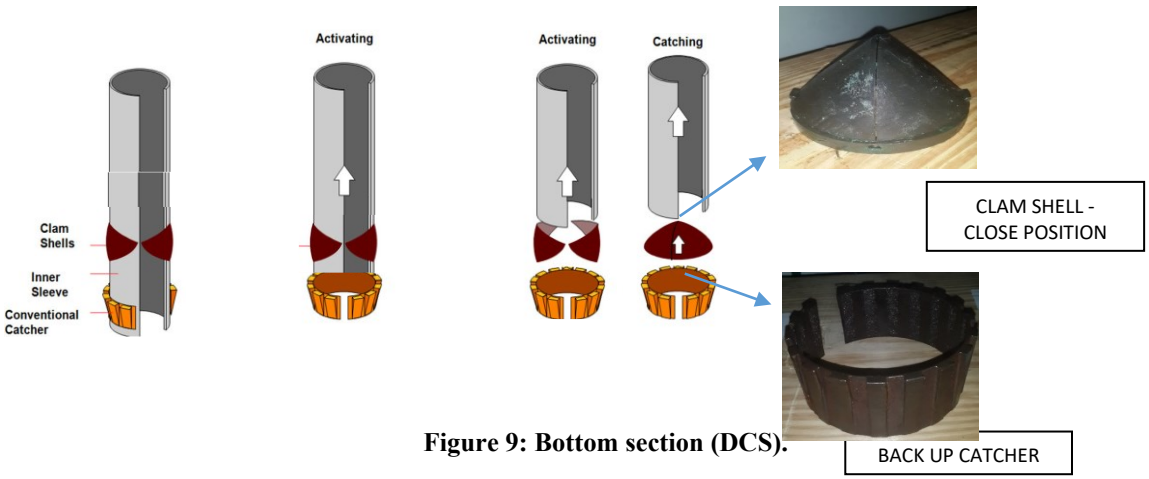

Figure 9: Bottom section (DCS).

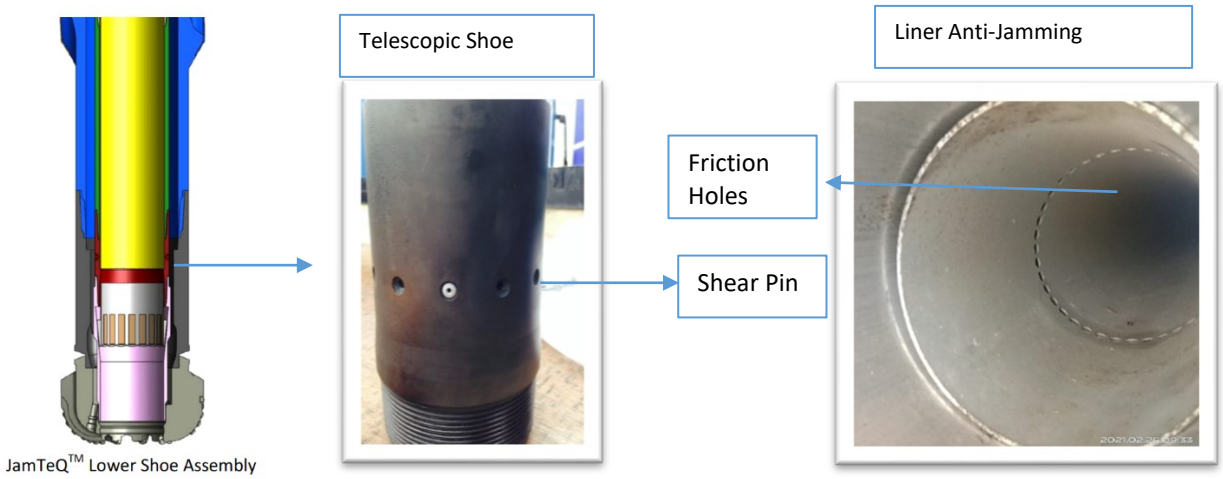

Figure 10: Anti-jamming system components.

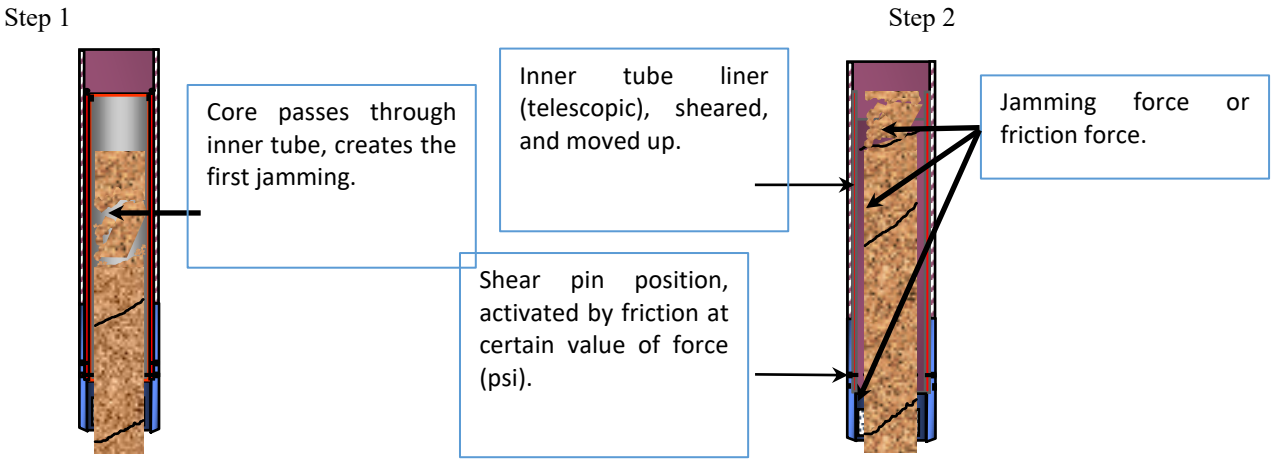

Figure 11: Anti-jamming activation steps.

The system activates downhole by the friction force; thus, it is not seen at the surface gauge parameter. Proof will be notified upon the core reaching the surface, and the liner anti-jamming will be spotted at a certain meterage of the inner barrel, either the liner still located at the bottom, middle, or top of the inner barrel along with the core sample. After the cutting process of the inner barrel with core and liner, the evidence will be seen clearly.

3.4 Core Head

At the Q-1 well, there is a high awareness of the core jamming anomaly in this type of formation. However, the contract with the client restricted the coring service provider from using only a standard conventional *or* full closure system. Given these constraints, core head selection was crucial. Applying general theory related to ROP, diamond and impregnated diamond core heads were not applicable to the project. Instead, a polycrystalline diamond compact (PDC) core head was selected. The chosen PDC core head had a design optimized for a good penetration rate and a medium number of cutters. This moderately aggressive core head design was recommended as the best available solution to minimize the chance of core jamming.

For Q-1, the 8-1/2-in. PDC core head steel body with seven blades and 13-mm (3D ION) cutters **(Figure 10).** This core head was selected because the shaped cutter design (3D ION) recently launched for geothermal applications, and its features support the best ROP mindset, based on the rule of thumb theory in drill bit designs, such as:

- Fewer blades equal aggressivity prior to better ROP
- Fewer blades equal bigger junk slot (10.240 $in.^2$) for better cleaning, which would help in ROP
- Bigger cutter size equals deeper depth of cut, which would increase ROP
- Seven bigger nozzles (14/32-in.) generate 0.249 $hp/in.^2$

For the T-1 and T-2 wells, the 8-1/2-in. PDC core head steel body with nine blades and 13-mm cutters. This core head was selected because the design supports the best stabilization mindset; thus, it has been proven to help reduce the chance of core jamming. Its features include:

- More blades equates to less aggressivity in ROP, reducing torque and vibration
- More blades equate to smaller junk slot (8.740 in.^{2}) and higher stability in hole
- Smaller cutter size equates to durability in hard formation, able to grind in high rotation
- Nine smaller nozzles (12/32-in.) generate a higher 0.279 hp/in.^{2} that helps in ROP downhole

Figure 12: 8-1/2-in. x 4-in. 713 PDC core head (3D ION).

Figure 13: 8-1/2-in. x 4-in. 913 PDC core head (4DXC ION).

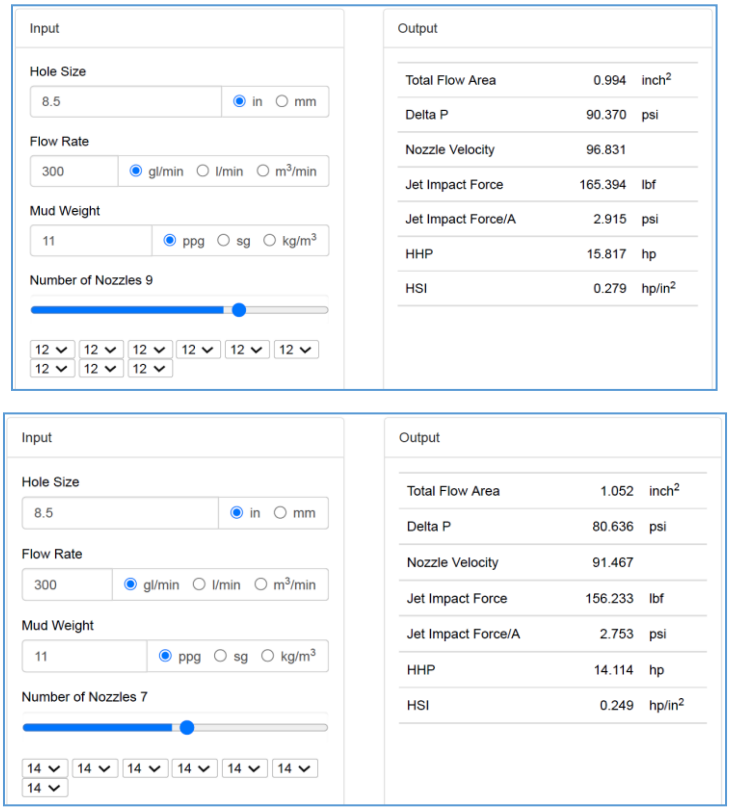

8-1/2-in. 913

8-1/2-in. 713

Figure 14: Core head capabilities value (TFA, Velocity, JIF, HSI).

A few feature differences between the core head used at T-1 and T-2 (8-1/2-in. 913S) and the core head used at Q-1 (8-1/2-in. 713S) are:

- Core head 8-1/2-in. x 4-in. 913S has a better durability value in abrasiveness and a higher temperature limit because of the latest 4DXC ION cutter.
- Core head 8-1/2-in. x 4-in. 913S has a higher horsepower hydraulics per square inch (HHSI) value of 0.279 hp/in.^{2}, compared to core head 8-1/2-in. x 713, with an HHSI value of 0.249 hp/in.^{2}. Higher HHSI equates to better ROP.
- Core head 8-1/2-in. x 4-in. 913S has a smaller-size (12/32-in. OD) port nozzle, resulting in a higher jet impact force value of 165.394 lbf compared to 156.233 lbf from the 8-1/2-in. x4 in. 713S core head. Core head 713 was initially chosen for Q-1 due to fewer blades, with a bigger junk slot area for cleaning as the main reason.

4. RUN RESULTS

4.1 Coring Operation with the Full Closure System in the Q-1 well

On the first run at the Q-1 well, a 9-m core was planned and then ran from 2,260.6 m MD to 2,262.17 m MD (**Cored 1.5 m**). However, the core run was unsuccessful, with 0.65 m/43% recovery. From this run, we could identify the root cause and apply the lessons learned to the next well.

The first well parameters (Q-1 well) with recovery 0.65 m/43%:

1. Flow Rate: 250 gpm
2. WOB: 4–30 klbs
3. RPM: 60–90
4. Torque: 9–13 kft/lb (off bottom 11 kft/lbs)
5. SPP: 0 psi

4.2 The COMBO Full Closure System and Anti-Jamming System in the T-1 well

In the second run at the T-1 well, a 9-m core was planned and then ran from 2,463m MD to 2,471 m MD (**Cored 8.7 m**). The coring run was successful with 6.25 m/71.84% recovery. The root cause and all lessons learned were implemented on the next well.

The second well parameters (T-1 well) with recovery 6.25 m/71.84%:

1. Flow Rate: 300 gpm
2. WOB: 4–25 klbs
3. RPM: 60–90
4. Torque: 19–23 kft/lbs (off bottom 21 kft/lbs)
5. SPP: 0 psi

4.3 The COMBO Full Closure System and Anti-Jamming System in the T-2 well

A combination of the Anti-Jamming System and Full Closure System was also used to cut core in the T-2 well, building on a few lessons learned from the T-1 well. The key changes made included adjusting parameters and adding lubricant to the fluid program during the coring operation. The run was successful, achieving 100% core recovery of 8.43 m core from 2,570 m MD to 2,578.43 m MD.

The third run parameters (T-2 well) with recovery 8.43 m/100%:

1. Flow Rate: 300 gpm
2. WOB: 4–18 klbs
3. RPM: 60–80
4. Torque: 12–15 (off bottom 13 kft/lbs)
5. SPP: 0 psi

Figures 15 and 16 illustrate the core process, from making up the coring BHA to handling the core on the ground and packing the core.

5. OPERATIONAL CONSIDERATIONS/LESSONS LEARNED

- The combination of the Anti-Jamming System and Full Closure System has proven to be crucial in the success of the T-1 well and even more so at the T-2 well coring operation.
- Analysis of the three wells (Q-1, T-1, and T-2) revealed significant differences in procedures, informed by lessons learned and optimizations implemented at the next wells.

- Core jamming was the main issue during coring at the geothermal applications, not just the non-cemented formations that may cause the core to fall off from the inner barrel assembly. Core jamming occurred at the Q-1 well.

Make-Up Coring BHA Make-Up DAS Make-Up Inner Barrel Assembly

Figure 15: Make-up coring BHA combo full closure and anti-jamming system.

Core Marking and Condition of Inner Cutting the Core Packaging the Core

Figure 16: Core marking to packaging the core at the T-2 well.

- The coring flow rate is crucial for successful core retrieval in geothermal applications. The use of lubricant increased the elimination and success of the coring operation at the T-2 well. Other parameters may need to be adjusted on-site, as engineers must react to changes in the penetration rate.
- The combination of the aluminium inner barrel and the anti-jamming liner tube proved to be suitable and applicable and is highly recommended for coring operations with similar well profiles near the T-1 and T-2 wells.
- Key anomalies to closely monitor are:
    - Torque values: An on-bottom parameter torque value equal to or less than the off-bottom parameter torque value indicates core jamming.
    - ROP: A penetration rate of less than 10 fph, down to 0 fph, indicates core jamming.
    - Pressure: No pressure at geothermal applications, as coring point depth is preferred at either severe or, most likely, total fluid loss zones.

ACKNOWLEDGEMENTS

The authors would like to give gratitude to all the representatives involved in these projects, whose efforts contributed to the exceptional core quality and core length achieved at the T-1 and T-2 wells. The success of these wells is attributed to the use of the combined Anti-Jamming System and Full Closure System in one assembly run. The authors would also like to thank the Geodipa Energy Management and Coring Service Provider Director for the permission to present and publish this paper.

REFERENCES

The Geology and Geothermal System of the Dieng Geothermal Field, Central Java, Indonesia – SGP-TR-223

Coring at Extreme Temperatures, Design and Operation of a Core Barrel for the Iceland Deep Drilling Project – PWGC2010

Evaluating the Opportunity of Using General Motor Condition Monitoring in Early Failure Detection to Reduce the Frequency of Vibration Analysis by Applying Matthew Correlation Coefficient Method

Muhammad Dhafier Mu'afa, Laila Sifha Urrohma, Firas Irfansyah Kurniawan, Toto Juniandri, Sekti Setiono, Fauzan, and Andry Hudarojat

Star Energy Geothermal, Jl. Letjen S. Parman Kav. 60 Jakarta 11410, Indonesia

muhammad.muafa@starenergy.co.id

Keywords: Predictive Maintenance, General Motor Condition Monitoring, Vibration Analysis, Geothermal Power Plant, Cost Efficiency, Early Failure Detection

ABSTRACT

In geothermal power plants, Hot Well Pump (HWP), Component Cooling Water Pump (CCWP), Auxiliary Cooling Water Pump (ACWP), Liquid Ring Vacuum Pump (LRVP), and Cooling Tower Fan (CTF) are commonly driven by electric motors and considered as critical equipment. Therefore, motor mechanical faults such as misalignment, bearing problems, transmission element problems, and loose foundation can lead to equipment failure and Loss Production Opportunities (LPO). Therefore, appropriate Predictive Maintenance (PdM) of the motor is necessary to prevent such failures through condition monitoring. At PLTP Darajat II, motor condition monitoring activities like Vibration Analysis (VA) and General Motor Condition Monitoring (GMCM) are performed on those equipment. VA is a condition monitoring method to identify mechanical faults by evaluating the vibration frequency and amplitude from its frequency-domain vibration data. Meanwhile, GMCM is a new method that can identify both mechanical and electrical faults on a motor by measuring its terminal voltage and current. However, GMCM and VA measurement at the same time is considered to be cost-inefficient due to similar purposes. This study aims to enhance PdM cost-efficiency by investigating GMCM's effectiveness for early mechanical failure detection and exploring the possibility of reducing VA frequency for motor-driven equipment. The Matthew Correlation Coefficient (MCC) method is used to compare GMCM and VA data from HWP, CCWP, ACWP, LRVP, and CTF at PLTP Darajat II. Currently, VA is the most commonly used method to detect mechanical faults on motors. Hence, VA diagnostics data is used as a reference, with GMCM as a comparison. The number of samples used in this study is 41 with confidence level and margin of error value of 88% and 12.13%, respectively. The samples are obtained from GMCM and VA of those equipment within the same period of month, ensuring similar motor operating conditions. The results demonstrate a weak and negative correlation between the results of GMCM and VA (MCC = -0.307). GMCM exhibits low sensitivity and F1 score of 17% and 7%, respectively. The values demonstrate that GMCM often failed to detect motor mechanical faults similar to VA. Additionally, its low specificity (40%) and accuracy (37%) values, highlight its inability to accurately identify the non-faulty motors. These findings suggest that GMCM is currently not a viable replacement for VA in mechanical fault detection. More VA and GMCM samples can be added to improve the confidence level and margin of error used in the MCC. Further research is also necessary to improve GMCM's performance before considering it as an alternative to reduce VA frequency for motor-driven equipment.

1. INTRODUCTION

In a Geothermal Power Plant, electric motors play an important role in electricity production. Hot Well Pump (HWP), Component Cooling Water Pump (CCWP), Auxiliary Cooling Water Pump (ACWP), Liquid Ring Vacuum Pump (LRVP), and Cooling Tower Fan (CTF), which are considered as critical equipment, are commonly driven by electric motors. Failure of those equipment may result in Loss Production Opportunity (LPO) which has significant technical and economic consequences, such as lower plant availability-reliability factor and decrease in revenue, respectively. A predictive maintenance strategy that can prevent unforeseen failures on equipment is commonly known as condition monitoring. This strategy involves regular checking on an equipment to detect early signs of wear and potential failures that come along. In much bigger picture, condition monitoring can be implemented to ensure the reliability of a power plant. Even though there are additional expenses that have to be incurred along with the implementation of condition monitoring, these costs are significantly much lower compared to the cost of equipment replacement or the amount of LPO.

Vibration Analysis (VA) and General Motor Condition Monitoring (GMCM) are two condition monitoring methods that are used in PLTP Darajat II for motor driven equipment, such as HWP, CCWP, ACWP, LRVP, and CTF. Each method has its own approaches and advantages. VA (Vibration Analysis) and GMCM (General Motor Condition Monitoring) are methods used for condition monitoring to detect mechanical faults in motor-driven

equipment, such as those mentioned above. However, at the PLTP Salak and PLTP Wayang Windu, only VA is employed for the condition monitoring of these equipment.

VA is a process of analyzing anomalies and monitoring change from the established vibration signature of a motor driven equipment. The vibration of motor is characterized by its frequency, amplitude, and intensity. VA is a well-established and widely used method for identifying anomalies, such as mechanical faults in electric motors. VA can detect a range of mechanical faults such as misalignment, imbalance, bearing wear, and other mechanical problems. For instance, misalignment typically results from a combination of radial and axial components, while bearing wear often produces vibration spikes in high frequency.

On the other hand, GMCM offers a newer condition monitoring technology that can provide a more integrated approach for motor condition assessment. Unlike VA, which is predominantly mechanical, GMCM integrates both electrical and mechanical fault detection. GMCM can provide insights regarding the electrical and mechanical faults by measuring and analyzing the electric motor's terminal current. GMCM uses advanced algorithms to analyze the motor's electrical signal, enabling the detection of anomalies that might not be apparent through VA alone.

Currently, VA is the most used condition monitoring method, especially to detect mechanical faults on motors since the reliability of GMCM on detecting mechanical faults still remains under evaluation. At PLTP Darajat II, where both VA and GMCM are currently employed, the effectiveness of GMCM on early detecting mechanical faults is currently being evaluated by comparing it to the VA results. If GMCM is proven to be as effective as VA on detecting mechanical faults, GMCM can be considered to be installed online while reducing the VA frequency for motor-driven equipment at the same time. This strategy is expected to enhance the overall reliability and efficiency of predictive maintenance (PdM) programs in PLTP Darajat II. This paper will answer how effective GMCM can detect mechanical faults on motor-driven equipment in accordance with VA by using the Matthew Correlation Coefficients (MCC) approach.

2. LITERATURE REVIEW

2.1 Vibration Analysis

Vibration analysis (VA) is a powerful and effective predictive maintenance method utilized to detect mechanical faults by analyzing the vibration patterns of a machine (Mobley, 2002; Minette et al., 2016). Machine vibrations can be represented in various forms, including displacement, velocity, and acceleration (Chu et al., 2024). Displacement describes the distance of movement of the measurement point, velocity describes how fast a movement is, and acceleration describes the change in velocity in a given time unit. Vibration analysis can be performed on both time waveform and frequency spectrum of the vibration signal. Vibration signal's frequency spectrum is obtained by applying Fourier Transform to the signal's time waveform.

Time domain vibration analysis can be performed using parameters such as root mean square (RMS), standard deviation, peak amplitude, kurtosis, crest factor, slope, and many others (Yadav et al., 2020). An example of time domain vibration analysis interpretation can be seen in Figure 1(a) below. In addition to time domain analysis, frequency spectrum analysis is highly recommended for real-world vibration analysis applications, especially for rotating machinery. Frequency analysis decomposes the time waveform and represents the repetition of vibration patterns, allowing the investigation of frequency components corresponding to each component (Chu et al., 2024). Frequency domain vibration analysis is superior to time domain vibration analysis on detecting abnormal vibration patterns, since it allows the identification of specific frequencies associated with specific components or phenomena, such as machine rotation frequency, gear tooth frequency, or bearing damage frequency, which cannot be done in the time domain. An example of frequency domain vibration analysis interpretation can be seen in Figure 1(b).

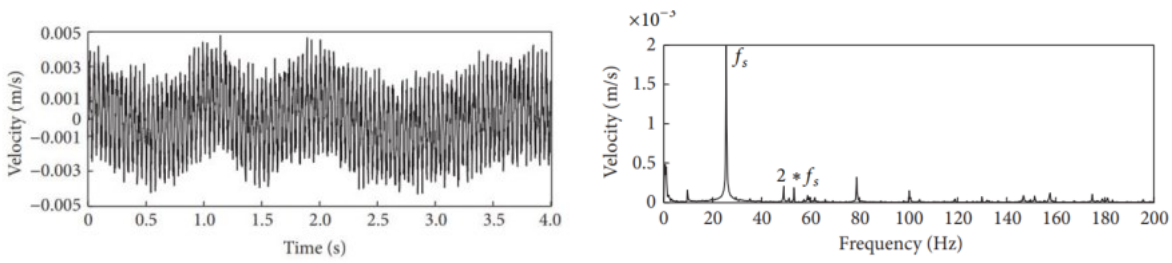

(a) (b)

Figure 1: (a) Waveforms in Time Domain, (b) Waveforms in Frequency Domain (Patel et al., 2014).

2.2 General Motor Condition Monitoring (GMCM)

General Motor Condition Monitoring (GMCM) is a revolutionary technology that utilizes a single toolkit to detect both mechanical and electrical faults. Additionally, GMCM provides corrective recommendations upon detecting any malfunctions. Based on their installation method, GMCM can be categorized into two types: permanently installed and portable toolkit. In practice, portable GMCM toolkit is more preferrable to be utilized due to its better transportability and operability. This portability of GMCM toolkit can facilitate the evaluation of all 3-phase AC motors operating under low to medium voltage conditions, regardless of their specifications.

This portable and versatile toolkit empowers power plant to analyze the condition of all its motors. Operating the GMCM toolkit is straightforward and does not require specialized personnel for fault analysis. The toolkit independently identifies faults using an internal motor fault database and model, eliminating the need for trend data analysis. This database-driven approach enables fault detection within an hour, from measurement to report generation.

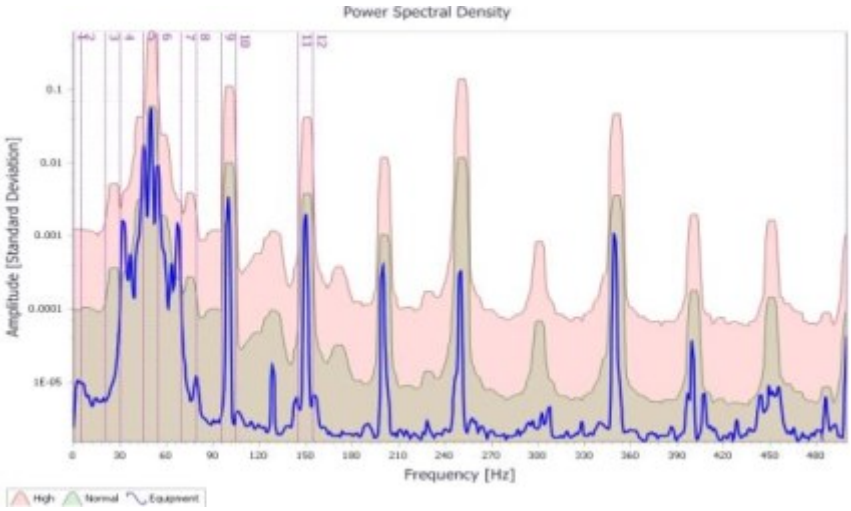

Figure 2: Comparison of Measured Power Spectral Density (PSD) of an Equipment (Blue Line) with PSD from GMCM Database. (Red and Green Lines) (Star Energy Geothermal, 2023)

The GMCM procedure begins with measuring the current at the motor terminals. This time-domain current data is then transformed into power spectral density (PSD) to analyze motor faults. The resulting PSD graph is compared to standard PSD graphs within the GMCM toolkit to determine the type of fault (Figure 2). The entire process, from time-domain to PSD transformation and motor condition assessment, is performed within the toolkit, limiting human involvement to setting up the equipment for current data acquisition.

2.3 Matthew Correlation Coefficient (MCC)

The Matthews Correlation Coefficient (MCC) is a statistical measurement utilized to evaluate the quality of binary classifications (Chicco et al., 2021). It has the advantage of being reliable even when the data used is imbalanced (Chicco & Jurman, 2020). MCC represents the correlation between observed and predicted results, resulting in a value between -1 and 1 (Chicco et al., 2021). An MCC value of 1 indicates perfect prediction, occurring when the model's predictions align with the actual truth labels. Meanwhile, an MCC value of 0 indicates that the model's predictions are no better than random chance, and the model performs the same as flipping a coin. In other words, it has no discriminatory ability. An MCC value of -1 indicates perfect inverse prediction, occurring when the model's predictions are completely opposite to the actual labels. For example, if the model predicts all positive samples as negative and vice versa, the model will result in a -1 MCC value. Since MCC is a binary classification, a confusion matrix (Figure 3) is used to represent how many elements are correctly predicted and how many are incorrectly classified. Figure 3 shows four terms:

1. The actual positives that are correctly predicted positives are called true positives (TP).
2. The actual positives that are wrongly predicted negatives are called false negatives (FN).
3. The actual negatives that are correctly predicted negatives are called true negatives (TN).

The actual negatives that are w Figure 4 illustrates the process of the research conducted in this paper. First, data from GMCM and VA testing on the same equipment and at close intervals is collected. Next, a confusion matrix is determined, which will then be used to evaluate the Matthew Correlation Coefficient (MCC) score. Once the confusion matrix results are obtained, MCC, Sensitivity, Specificity, Accuracy, and F1 score are calculated. The results of the survey/research can be visualized using a ROC curve. Finally, before drawing conclusions, a confidence level shall be determined to indicate the quality of the survey results.

4. rongly predicted positives are called false positives (FP).

Figure 3: Confusion Matrix (De Diego et al, 2022).

The MCC calculation can be done using equation (1) (De Diego et al., 2022).

$$MCC = \frac{TP\ x\ TN - FP\ x\ FN}{\sqrt{(TP + FP)(TP + FN)(TN + FP)(TN + FN)}} \quad (1)$$

In addition to the MCC method, there are several other statistical methods that can be used to evaluate the quality of binary classification, including sensitivity, specificity, accuracy, and F1 Score (Rainio et al., 2024). Sensitivity is a measure of the model's ability to correctly identify actual machine failure events (true positives). High sensitivity means the model rarely misses actual machine failures (true positives). The sensitivity calculation can be done using equation (2).

$$Sensitivity = \frac{TP}{FN + TP} \quad (2)$$

Specificity is a measure of the model's ability to correctly identify healthy machine signals (true negatives). High specificity means the model rarely misclassifies healthy signals as machine failures (false negatives). The specificity calculation can be done using equation (3).

$$Specitifity = \frac{TN}{FP + TN} \quad (3)$$

Accuracy is the proportion of overall correct model predictions (true positives and true negatives) divided by the total predictions. High overall accuracy indicates good model performance, but it should be considered along with sensitivity and specificity depending on the context. The accuracy calculation can be done using equation (4).

$$Accuracy = \frac{TP + TN}{TP + TN + FP + FN} \quad (4)$$

F1 Score is a combined metric that combines sensitivity and specificity into a single score. High F1 Score indicates a good balance between sensitivity and specificity. The F1 Score calculation can be done using equation (5).

$$F1\ score = \frac{2 \times Sensitivity \times Specificity}{Sensitivity + Specificity} \quad (5)$$

3. METHODOLOGY

Figure 4 illustrates the process of the research conducted in this paper. First, data from GMCM and VA testing on the same equipment and at close intervals is collected. Next, a confusion matrix is determined, which will then be used to evaluate the Matthew Correlation Coefficient (MCC) score. Once the confusion matrix results are obtained, MCC, Sensitivity, Specificity, Accuracy, and F1 score are calculated. The results of the survey/research can be visualized using a ROC curve. Finally, before drawing conclusions, a confidence level shall be determined to indicate the quality of the survey results.

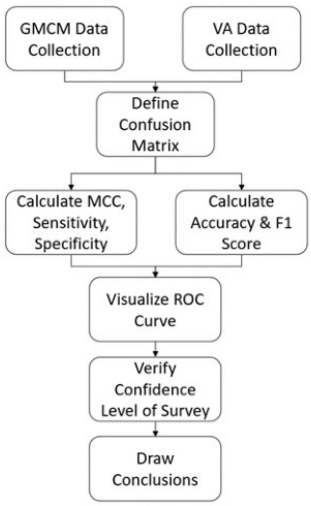

Figure 4: Research Methodology.

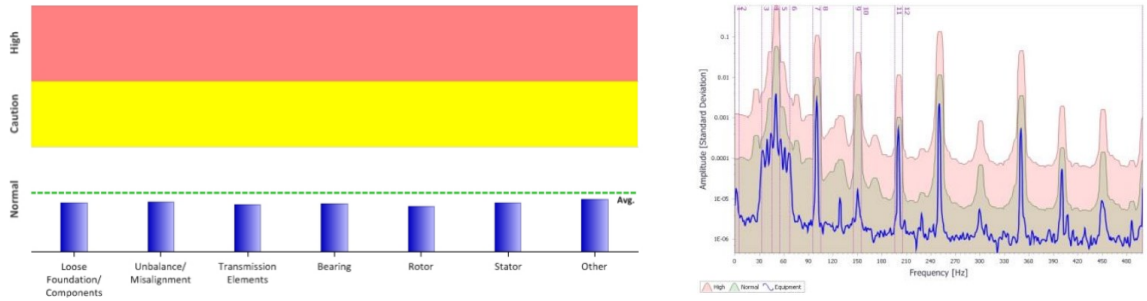

(a) (b)

Figure 5: (a) GMCM Results in Normal Condition, (b) Power Spectral Density in Normal Condition (Star Energy Geothermal, 2023).

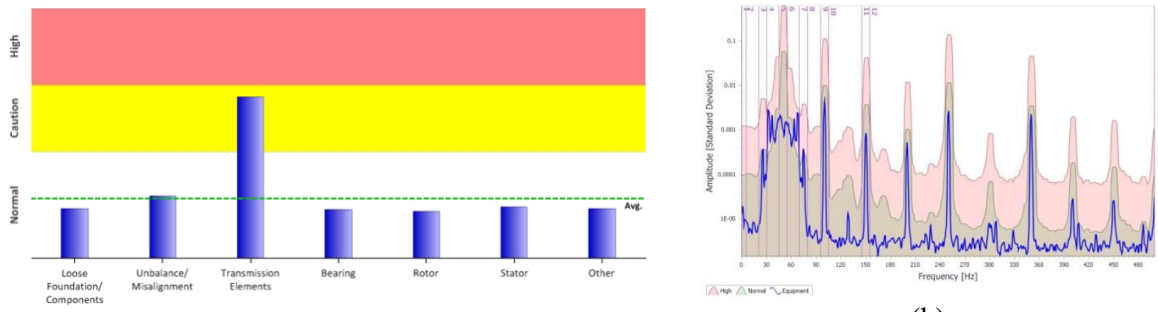

(a) (b)

Figure 6: (a) GMCM Results in Anomaly Condition, (b) Power Spectral Density in Anomaly Condition (Star Energy Geothermal, 2023).

The GMCM data were collected by measuring the current at the motor terminals using a clamp ampere meter. This method involves capturing the current signals directly, which initially are represented in the time domain. To gain deeper insights into the motor's operational characteristics, these time-domain signals were transformed into the frequency domain using techniques such as Fourier analysis. This transformation allows for a detailed examination of the signal's frequency components, which are critical for diagnosing the motor's performance and detecting potential issues.

Figure 5 shows one of the GMCM tests performed on the Hot Well Pump 3A, for example. In this test, the GMCM analysis indicated that the Hot Well Pump 3A is functioning normally. This conclusion is derived from analyzing the amplitude of the Power Spectral Density (PSD) at different frequencies. The PSD provides a representation of how the power of the current signal is distributed across various frequency components. To evaluate the operating condition of the Hot Well Pump 3A, the PSD obtained from its current measurements was compared to a benchmark PSD model. By comparing the pump's PSD to this standard model, it was possible to identify any deviations or anomalies that might suggest underlying issues with the equipment.

The General Motor Condition Monitoring (GMCM) indicates an anomaly or fault when the amplitude of the Power Spectral Density (PSD) of the measured current exceeds a threshold set by the model. GMCM can detect various mechanical faults such as loose foundations or components, unbalance or misalignment, issues with transmission elements, and bearing wear as shown in Figure 6 (a). It can also identify electrical faults like broken rotors and stator issues. Each type of fault is characterized by specific frequencies and amplitudes. Figure 6 shows an example of GMCM detecting an anomaly in a Liquid Ring Vacuum Pump U3.

In the context of Vibration Analysis (VA) testing, velocity measurements were carried out at several critical points on the Hot Well Pump 3A, for example. These measurements were taken in the horizontal, vertical, and axial directions to capture a comprehensive picture of the motor and pump vibrational behavior. Velocity measurements were taken in units of mm/s peak. To assess the severity of the detected vibrations, it is essential to classify the motor and pump according to recognized standards. For this purpose, the ISO 10816-1:1995 standard is used for motors, providing guidelines on evaluating mechanical vibrations in various machine components. Additionally, the ISO 10816-7:2009 standard applies to pumps, specifying the acceptable vibration severity levels for different pump types. This classification is critical for determining the acceptable vibration thresholds and for assessing whether the observed vibration levels fall within safe operating limits. If the vibration levels exceed the predefined acceptable limits, it could signal the need for further analysis or intervention to prevent potential damage or operational failure. Table 2 shows that Hot Well Pump 3A works on normal operation.

Table 1: ISO 10816 Standards for Motor & Pump (ISO 10816, 1995).

Standard	A	B	C	D
Motor	0.4 – 2.54	2.54 – 6.36	6.36 – 15.8	15.8 – 63.65
Pump	< 4.95	4.95 – 7.07	7.07 – 10.75	> 10.75

Table 2: VA Results for Motor & Pump in Normal Condition (Star Energy Geothermal, 2023).

Point	Value	Units	Standard by ISO 10816-1
Motor Outboard Y Direction	1.327	mm/Sec	A
Motor Outboard X Direction	0.838	mm/Sec	A
Motor Outboard Axial	2.091	mm/Sec	A
Motor Inboard Y Direction	0.633	mm/Sec	A
Motor Inboard X Direction	0.472	mm/Sec	A
Motor Inboard Axial	1.185	mm/Sec	A
Pump Inboard Y Direction	1.803	mm/Sec	A
Pump Inboard X Direction	2.397	mm/Sec	A
Pump Inboard Axial	1.006	mm/Sec	A
Foundation Y Direction	0.179	mm/Sec	A
Foundation X Direction	0.224	mm/Sec	A
Foundation Axial Direction	0.236	mm/Sec	A

If the vibration velocity measurements exceed the thresholds defined by these standards, it suggests that the equipment may be experiencing operational issues that could lead to further mechanical damage or failure. In the example of the Liquid Ring Vacuum Pump U3, high vibration levels were detected specifically at the Shaft Inboard Axial position, indicating potential problems.

Table 3: VA Results for Motor & Pump in Anomaly Condition (Star Energy Geothermal, 2023).

Point	Value	Units	Standard by ISO 10816-1
Motor Outboard Vertical	1.985	mm/Sec	A
Motor Outboard Horizontal	2.389	mm/Sec	A
Motor Inboard Vertical	1.915	mm/Sec	A
Motor Inboard Horizontal	2.352	mm/Sec	A
Motor Inboard Axial	2.188	mm/Sec	A
GB Input Shaft Inboard Vertical	3.952	mm/Sec	B
GB Input Shaft Inboard Horizontal	4.955	mm/Sec	B
GB Input Shaft Outboard Vertical	6.449	mm/Sec	C
GB Input Shaft Outboard Horizontal	5.261	mm/Sec	B
GB Int Shaft Inboard Vertical	4.732	mm/Sec	B
GB Int Shaft Inboard Axial	8.327	mm/Sec	C
GB Int Shaft Outboard Vertical	5.399	mm/Sec	B

Point	Value	Units	Standard by ISO 10816-1
GB Output Shaft Inboard Vertical	4.095	mm/Sec	B
GB Output Shaft Inboard Horizontal	3.334	mm/Sec	B
GB Output Shaft Outboard Vertical	2.968	mm/Sec	B
GB Output Shaft Outboard Horizontal	3.934	mm/Sec	B
GB Output Shaft Outboard Axial	5.197	mm/Sec	B
Pump Inboard Vertical	4.507	mm/Sec	B
Pump Inboard Horizontal	3.840	mm/Sec	B
Pump Inboard Axial	4.134	mm/Sec	B
Pump Outboard Vertical	3.910	mm/Sec	B
Pump Outboard Horizontal	3.911	mm/Sec	B

To determine the correlation between GMCM testing and VA, the Matthew Correlation Coefficient (MCC) statistical method is used by comparing the test results for each motor-driven equipment. VA data serves as the baseline to validate the GMCM because VA is a long-established and proven method. In this evaluation, 41 sets of VA and GMCM measurement data from Hot Well Pump (HWP), Component Cooling Water Pump (CCWP), Auxiliary Cooling Water Pump (ACWP), Liquid Ring Vacuum Pump (LRVP), and Cooling Tower Fan (CTF) were collected from 2022 until 2024. The measurements and health analysis of these equipment based on VA and GMCM were conducted nearly simultaneous, ensuring that the equipment was in similar conditions both externally and internally. In the MCC evaluation metrics, the results are categorized into four groups: True Positive (TP), False Negative (FN), False Positive (FP), and True Negative (TN). Table 4 shows the confusion matrix between VA & GMCM testing to identify the evaluation metrics group and Table 5 shows some results of the comparison of GMCM and VA data.

Table 4: VA & GMCM Confusion Matrix.

Vibration Analysis (VA)	General Motor Condition Monitoring (GMCM)	Results
Fault	Fault	True Positive (TP)
Fault	No Fault	False Negative (FN)
No Fault	Fault	False Positive (FP)
No Fault	No Fault	True Negative (TN)

Table 5: Results of VA & GMCM Correlation Evaluation.

Motor Driven Equipment	VA Results	GMCM Results	Remarks
Liquid Ring Vacuum Pump U2	B	Normal	True Negative
Liquid Ring Vacuum Pump U3	C	Caution	True Positive
Cooling Tower Fan U3	B	High	False Positive
Auxiliary Cooling Water Pump	C	Normal	False Negative

4. RESULT AND DISCUSSION

They obtained 41 VA and GMCM testing data on the same motor-driven equipment. From these data, there were 14 True Negatives, 1 True Positive, 5 False Negatives, and 21 False Positives (Table 6). These data were then applied to calculate the Matthew Correlation Coefficient (MCC). These numbers are crucial for calculating the Matthew Correlation Coefficient (MCC), which is used to evaluate how well the methods (VA and GMCM) correlate with each other in identifying the equipment's condition (normal or faulty).

From Table 7, the MCC (Matthews Correlation Coefficient) value obtained is -0.3071. This value indicates that the relationship between GMCM (General Motor Condition Monitoring) and VA (Vibration Analysis) in detecting mechanical faults is weak and negative. This suggests that the predictions made by GMCM for detecting mechanical faults tend to not align with the results from VA. Additionally, to provide a more comprehensive understanding of GMCM's effectiveness in detecting mechanical faults, other evaluation metrics were assessed. Based on the data in Table 7, GMCM has a sensitivity of 17% and an F1 score of 7%, indicating that GMCM is not sensitive enough in detecting the presence of mechanical faults, meaning it tends to miss many mechanical faults. Furthermore, with a specificity of 40% and an accuracy of 37%, GMCM is not accurate in identifying motors that are not faulty.

Table 6: VA & GMCM Confusion Matrix Results.

Confusion Matrix	Value
True Negative (TN)	14
True Positive (TP)	1
False Negative (FN)	5
False Positive (FP)	21

Table 7: Calculation Results of MCC, Sensitivity, Specificity, Accuracy, and F1 Score.

Parameter	Value
Matthew Correlation Coefficient	-0.3071
Sensitivity	17%
Specificity	40%
Accuracy	37%
F1 Score	7%

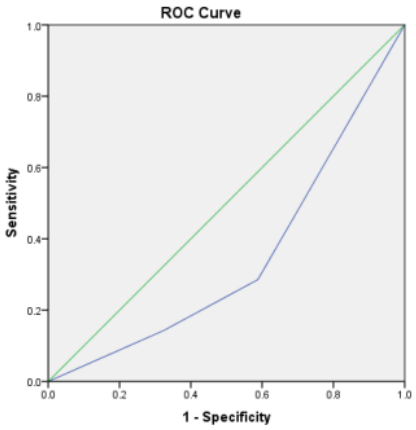

Figure 7: ROC Curve.

Furthermore, ROC curve analysis was conducted to evaluate the effectiveness of the GMCM (General Motor Condition Monitoring) model in identifying actual mechanical faults (sensitivity) and how well GMCM avoids identifying the absence of mechanical faults as mechanical faults (specificity). Based on Figure 7, the area under the ROC curve (AUC) is 0.345, indicating that the performance of GMCM in detecting the presence of mechanical faults falls below the unsatisfactory threshold. This suggests that the GMCM method cannot effectively distinguish between the presence and absence of mechanical faults. From various evaluation metrics conducted above, it is evident that the performance of GMCM in detecting mechanical faults is still low. Therefore, for now, if GMCM is to beused to reduce the number of VA measurements, it needs to be reconsidered due to the low sensitivity and specificity values of GMCM.

When assessing the Matthew Correlation Coefficient (MCC), the confidence level plays a crucial role in gauging the certainty of the evaluation results. It indicates how closely the MCC calculated from a sample reflects the true value within the entire population. The confidence level, typically presented as a percentage, represents the probability that the calculated confidence interval accurately contains the actual MCC. This metric is essential for understanding how reliable and precise the MCC estimate is from the sample data. By providing insights into the expected range of values, confidence levels aid in making well-informed and confident decisions regarding the correlation between variables.

Based on the selected values, the sample size n and the margin of error E are determined Equation 6, 7, and 8.

$$x = Z\left(\frac{c}{100}\right)^2 r(1-r) \tag{6}$$

$$n = Nx/((N-1)E^2 + x)) \tag{7}$$

$$E = \sqrt{\frac{(N-n)x}{n(N-1)}} \tag{8}$$

Where the N is population size, r is the fraction of responses that interested in, and $Z(c/100)$ is the critical value for the confidence level c. The margin of error E is the level of error that represents the acceptable degree of uncertainty in survey results. For instance, if 90% of the respondents say "yes" and only 10% say "no". To achieve a lower margin of error, a larger sample size is necessary. The confidence level represents the degree of uncertainty that can be accepted in the survey. For instance, if a survey includes 20 yes-no questions and is set a 95% confidence level, it means that for one of these questions (about 1 in 20), the percentage of "yes" answers will probably differ from the true population percentage by more than margin of error. The "true answer" represents the actual percentage that would be obtained if every individual in the population were surveyed. Achieving a higher confidence level requires a larger sample size.

To determine the confidence level and margin of error, a sample size n of 41 and a fraction of responses r of 0.5 (a conservative assumption) were used. Calculation of x shown in Equation 9.

$$x = (1.5548)20.5(1 - 0.5) = 0.6041 \tag{9}$$

A Z-value of 1.5548 was used, assuming that with a sample size n of 41, an 88% confidence level can be achieved. This assumption was validated by calculating the sample size n to match the relationship between the confidence level c and the given sample size.

The calculation process shown in Equation 10.

$$n = \frac{20000\ x\ 0.6041}{(20000 - 1)\ x\ (0.12)^2\ x + 0.6041} = 41.87 \tag{10}$$

Thus, the required sample size was calculated to be approximately 41.87. Since this closely aligns with the available sample size of 41, it can be concluded that the confidence level is 88%.

Calculation of margin of error E shown in Equation 11.

$$E = \sqrt{\frac{(20000 - 41)0.6041}{41(20000 - 1)}} = 0.1213 = 12.13\% \tag{11}$$

Hence, with 41 data points for VA and GMCM, a confidence level of 88% and a margin of error of 12.13% were obtained. To achieve a more accurate survey result, typically a confidence level of 95% with a margin of error of 5% is preferred, where a higher confidence level and a smaller margin of error will yield better survey results. To achieve the confidence level and margin of error values mentioned above, 377 samples of VA and GMCM testing would be needed.

5. CONCLUSION

Based on the sampling and testing of 41 data points, it was concluded that there is no significant positive or negative correlation between VA (Vibration Analysis) and GMCM (General Motor Condition Monitoring); their results appear to be largely random. This conclusion was drawn with a confidence level c of 88% and a margin of error E of 12.13%. To achieve a higher confidence level c of 95% and reduce the margin of error E to 5%, 377 samples and tests would be required for both VA and GMCM at PLTP Darajat II. Therefore, with the current confidence level and margin of error, further sampling and testing data are necessary for researching the correlation between VA and GMCM, while maintaining the frequency of VA testing on HWP, CCWP, ACWP, LRVP, and CTF.

REFERENCES

Chicco, D., Tötsch, N. and Jurman, G. (2021) 'The Matthews Correlation Coefficient (MCC) is more reliable than balanced accuracy, bookmaker informedness, and markedness in two-class confusion matrix evaluation', BioData Mining, 14(1). doi:10.1186/s13040-021-00244-z.

Chicco, D. and Jurman, G. (2020) 'The advantages of the Matthews correlation coefficient (MCC) over F1 score and accuracy in binary classification evaluation', BMC Genomics, 21(1). doi:10.1186/s12864-019-6413-7.

Chu, T. et al. (2024) 'A review of vibration analysis and its applications', Heliyon, 10(5). doi:10.1016/j.heliyon.2024.e26282.

De Diego, I.M. et al. (2022) 'General Performance Score for Classification Problems', Applied Intelligence, 52(10), pp. 12049–12063. doi:10.1007/s10489-021-03041-7.

International Organization for Standardization (1995). ISO 10816-1: Mechanical vibration – Evaluation of machine vibration by measurements on non-rotating parts – Part 1: General guidelines. Geneva: ISO.

Mobley, R.K. (2002) An introduction to predictive maintenance. Amsterdam: Butterworth-Heinemann.

Minette, R.S. et al. (2016) 'Experimental modal analysis of electrical submersible pumps', Ocean Engineering, 124, pp. 168–179. doi:10.1016/j.oceaneng.2016.07.054.

Patel, V.N., Tandon, N. and Pandey, R.K. (2014) 'Experimental study for vibration behaviors of locally defective deep groove ball bearings under Dynamic Radial Load', Advances in Acoustics and Vibration, 2014, pp. 1–7. doi:10.1155/2014/271346.

Rainio, O., Teuho, J. and Klén, R. (2024) 'Evaluation metrics and statistical tests for machine learning', Scientific Reports, 14(1). doi:10.1038/s41598-024-56706-x.

Star Energy Geothermal. (2023) 'Technical Report General Motor Condition Monitoring', PLTP Darajat II.

Star Energy Geothermal. (2023) 'Technical Report Vibration Analysis', PLTP Darajat II.

Yadav, O.P. and Pahuja, G.L. (2020) 'Bearing Health Assessment using time domain analysis of vibration signal', International Journal of Image, Graphics and Signal Processing, 12(3), pp. 27–40. doi:10.5815/ijigsp.2020.03.04.

Power Redundancy Strategy for Darajat Geothermal S1 and S4 Wellpads Using Photovoltaic-Battery System to Increase Plant Reliability

Firas Irfansyah Kurniawan, Toto Juniandri, Agustiawan, Febrian Tommy,
Asiawan Hanindito, Nixon Manik1, and Asep Cahyana Suarsa

Star Energy Geothermal, Wisma Barito Pacific II, 17th — 21st floor,
Jl. Letjen S. Parman Kav. 60 Jakarta 11410, Indonesia

Firas.Kurniawan@starenergy.co.id, tjey@starenergy.co.id; eops@starenergy.co.id,
febrian.tommy@starenergy.co.id, ayyv@starenergy.co.id, nixon.manik@starenergy.co.id,
ascahya@starenergy.co.id

Keywords: Power Redundancy, Geothermal Power Plant, Photovoltaic, Battery

ABSTRACT

In October 2022, Darajat II Geothermal Power Plant Unit 2 (DRJ U2) was shutdown due to planned overhaul. Two weeks into the shutdown, Darajat II Geothermal Power Plant Unit 3 (DRJ U3) tripped due to High-High level of condensate at Unit 3 separator that resulted in Loss Production Opportunity (LPO) with estimated total amount of 120k USD. Based on the Root-Cause Analysis (RCA) result, the trip was caused by loss of power supply to Automatic Drain Pot (ADP) and other instrumentation devices in Pad S1 and S4 area. These two pads were put into service in 2020 and powered by DRJ U2 through 6.3 kV common service bus. The power redundancy for Pad S1 and Pad S4 is designed to be provided by DRJ U3 through online power maneuver into the 6.3 kV common service bus. Meanwhile, the online power maneuver could not be performed because DRJ U2, 6.3 kV common service bus, and DRJ U3 were unable to synchronize. Based on the RCA result, a portable diesel generator set was prepared as a backup power supply to mitigate the loss of power supply to Pad S1 and S4. The power maneuver was then successfully performed manually, allowing Pad S1 and S4 to be powered by DRJ U3. The portable diesel generator set was still prepared as a stand-by power supply in case of a power supply failure from DRJ U3 to Pad S1 and S4 occurs. Portable diesel generator set was chosen since the existing DC UPS of ADP needs to be charged to provide continuous power supply. Meanwhile, the portable diesel generator set has many drawbacks such as fluctuating fuel prices, lack of auto power transfer ability, and a relatively high carbon footprint. With the increase of Photovoltaic-Battery's (PV-Battery) technology, this paper evaluates the use of PV-battery system as a greener stand-by power supply alternative with the auto start capability, and can also to be operated as a house load compensator for existing Pad S1 and S4, new condensate re-injection pump, and future house load around the wellpads area. Comparative study between PV-battery system and diesel generator as stand-by power supply alternatives is also provided in this paper. This study shows that the proposed PV-battery system can provide better operability, better maintainability, better reliability, greener, and slightly more economical stand-by power supply alternative for Pad S1 and S4.

1. INTRODUCTION

In a multi-unit power plant, power maneuver or bus transfer system is commonly employed to continuous power plant operation by preventing critical power plant auxiliaries system to trip when the primary power source shutdown due to disturbances or maintenance activities (Kansara, 2017). On the other words, power maneuver system is employed to provide power redundancy for critical power plant house load system by switching the power supply from one source to another. Ideally, the power maneuver is performed online where the source transfer is initiated at the Distributed Control System (DCS) by operator. This method is usually known as online power maneuver or fast bus transfer system.

Unfortunately, that was not the case in Darajat II Geothermal Power Plant Unit 2 (DRJ U2) and Unit 3 (DRJ U3). Back in October 2022, DRJ U2 was shutdown due to planned overhaul, which is commonly known as Shutdown Turnaround (SDTA). Two weeks into the shutdown, DRJ U3, which was operating normally, tripped unplannedly due to High-High level of condensate at its separator. This accident resulted in Loss Production Opportunity (LPO) with estimated total amount of 120k USD. Besides LPO, an accident such this unplanned trip also decreases the availability and reliability factor of power plant, since the power plant was not able to generate electricity for about several hours due to forced outages. Based on the Root-Cause Analysis (RCA) result, it was identified that the High-High level of condensate was caused by loss of power supply to Automatic Drain Pot (ADP) and other instrumentation devices in Pad S1 and S4 area. For additional information, Pad S1 and S4 were put into service in 2020 as steam production facilities for DRJ U3.

Power of Pad S1 and S4 has been supplied by DRJ U2 since the first time those two wellpads were put into service. When DRJ U2 shutdown, online power maneuver was supposed to be performed by switching electrical load from DRJ U2 to DRJ U3 on the 6.3 kV common service bus in order to provide power redundancy for Darajat S1 and S4 wellpads. There are two online power maneuver methods that can be used on the Darajat 6.3 kV common service bus, namely bumpless transfer (make-before-break) and override. Bumpless transfer will cause a brief parallel connection between U2 and U3, before one of them is opened. Meanwhile, override will cause U2 and U3 a continuous parallel connection between U2 and U3. Unfortunately, these online power maneuver methods could not be performed at that time. Then, the power maneuver was tried to be performed manually using break-before-make method. A portable generator set is prepared to be utilized as a backup power supply for Pad S1 and S4 in case of a failure in the manual power maneuver execution. Fortunately, the manual power maneuver was successfully performed right before the latest DRJ U2 SDTA in May 2024. For additional information, power maneuver or bus transfer between DRJ U2 and DRJ U3 6.3 kV system has never successfully performed since the common service bus 6.3 kV was operated for the first time in 2009. Since the manual power maneuver has only been performed once, the portable diesel generator set is still prepared as a stand-by power supply in case of a power supply failure from DRJ U3 to Pad S1 and S4 occurs. However, a portable diesel generator set has several drawbacks such as fluctuating fuel prices (Lau et al, 2015; Zhu et al., 2018; Farnoosh, 2022), lack of auto power transfer ability, and greenhouse gas emissions (Jakhrani et al., 2012; Yilmaz and Dincer, 2017; Barbosa et al., 2021).

This paper shows that PV-battery system is a doable stand-by power supply alternative other than diesel generator set, which both can be utilized in a geothermal power plant to prevent unplanned trip during power maneuver. This paper also reveals several benefits that can be obtained from the utilization of PV-battery system as a stand-by power supply, which can not be obtained by diesel generator set utilization such as increasing asset revenue due to its houseload compensating ability and boosting company image due to its “greener” power generation process. Even though a PV-battery system takes longer installation time and may not be yielding significant economic benefits if compared to a diesel generator, its overall benefits make the PV-battery system worth to be considered as a stand-by power supply alternative in a geothermal power plant.

2. LITERATURE REVIEW

(Reshid, Majid and Muhammad, 2014) state that power redundancy strategy can be classified as an important aspect in a power plant operation to ensure its performance and reliability. Power redundancy refers to the availability of the backup power supply to replace the primary power supply during a disturbance. Power redundancy failure, especially on critical system or equipment in a power plant, can cause problems such as unplanned unit shutdown, which can furtherly lead to Loss of Production Opportunity (LPO) and decrease in unit reliability factor. According to ISO 3997-9 (Farhat, 2021), reliability factor is defined as complement of the Forced Outage Rate (FOR) which is considered as one of the indicators used to evaluate the performance of a power plant, based on SPLN K7 001:2007 about Indikator Kinerja Pembangkit (Power Plant Performance Indicators).

Regarding to the idea of proposed power redundancy strategy, a study by (Hwang, Tongsopit and Kittner, 2023) has shown that replacing diesel backup generators to PV-plus-storage microgrids in one building not only able to increase or maintain its reliability, but would also save public expenditure cost and reduce CO2 emissions. A study by (Thomsen et al., 2019) also shows that a PV array and battery storage system could maximize reliability, and also could be a cost-effective replacement for diesel generators at remote locations, with the fuel savings quickly outweigh the initial cost.

Regarding to the strategy implementation, several research have discussed the implementation of PV system in a geothermal power plant area through the studies about the combination of geothermal power plant and PV system. (Zhou et al., 2011) explored the potential benefits from utilizing solar energy resources for a solar heating system in a Organic Rankine Cycle (ORC) or binary geothermal power plant, which resulted in increasing thermal efficiency and net power output. (Hameed et al., 2019) also studied the utilization of PV system to supply power for injection pumps and feed pumps, and to provide additional heat for the working fluid in a binary geothermal power plant. That study resulted in power plant efficiency improvement by 35%. Furthermore, a study by (Vidyanandan, 2017) shows that the efficiency and power output of a PV cell will be higher in lower module temperature. If module temperature falls below 25oC, the efficiency will increase about 0.5% per degree Celsius increase of temperature. It can be comfortably said that the proposed PV-Battery system is suitable enough to be implemented in Darajat geothermal area, which is located in highlands with relatively low air temperature around 16.44oC. Based on global horizontal irradiation (GHI) and air temperature data in proposed location, also based on the normal operating cell temperature (NOCT) of the chosen PV module, the estimated module temperature is around 21°C (Duffie and Beckman, 2013).

3. METHODOLOGY

Electrical loads in Darajat Pad S1 and S4 are supplied by S4-SS Substation which is located in Pad S1. The S4-SS substation consists of a 125 kVA two-winding transformer (S4-T1), which currently is utilized to step-down 6.3 kV from the common service bus into 400V. The single line diagram and load demand of S4-SS substation are shown below in Figure 1 and Table 1, respectively.

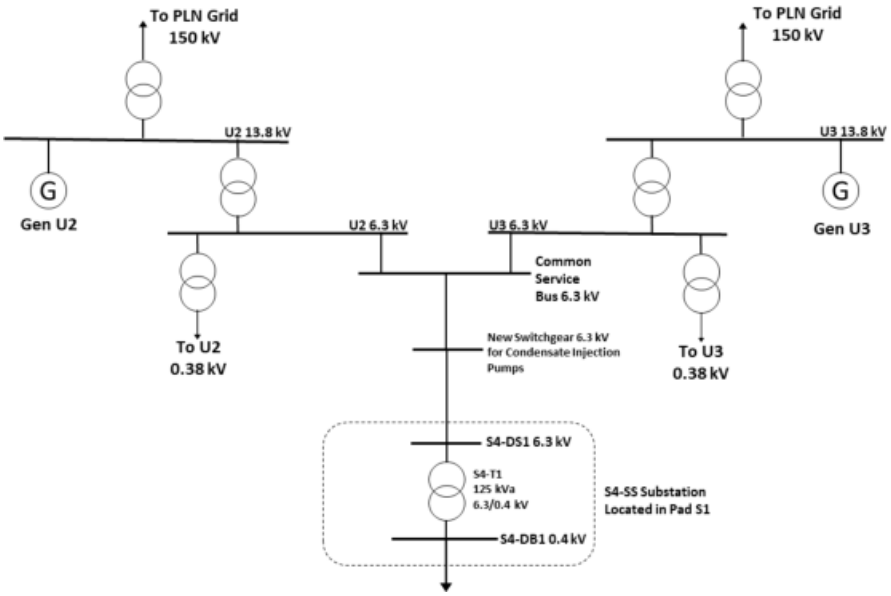

Figure 1: Single Line Diagram of Pad S1 and S4 Power Supply.

Table 1: Load Demand in S4-SS Substation.

Load Demand	Power Consumed (kW)
Auxiliary Control Supply (ADP, Phase Fault Relay, Surge Protection, and External Lights Control)	0.8
Control Panel (PLC)	0.5
Space Heater	0.2
Lighting	1.5
Total	**3**

The most concerning load in in S4-SS substation is the auxiliary control supply which supply power the valve actuator of ADP K001. Therefore, when a loss of power supply occurred like what happened in October 2022, the ADP will not be able to work automatically. Hence, there will be less liquid separation/disposal in pipelines, which leads to higher liquid carry over to downstream equipment of DRJ U3 steam production system. In order to prevent such thing for the upcoming DRJ U2 SDTA, Darajat Team has prepared a 10 kVA diesel generator set to be located in the S4-SS substation to substitute the role of S4-T1 transformer in supplying power to the S4-DB1, in case a failure regarding to the newly-tried manual power maneuver occurs. As mentioned in the earlier section, the utilization of this diesel generator set comes along with several drawbacks.

In this section, the idea of using PV-Battery system to replace portable diesel generator set as a stand-by power supply alternative for Pad S1 and S4 will be reviewed through a compact comparative study. The comparative study will be conducted by considering two different point of views, quality and economy. From a quality point of view, the comparative study will be conducted by considering several aspects such as system design, installation time, operability, maintainability, reliability, and its environmental impact during operation. The results will be portrayed through a strategy table in order to examine the advantages and disadvantages between those two alternatives. Meanwhile, several economical aspects such as Levelized Cost of Energy (LCOE), Net Present Value (NPV), and payback period of those two alternatives are considered to compare them from economical point of view.

3.1 Strategy table

Strategy table is a decision-making tool that provides a visual framework to help choose between two or more alternatives by considering multiple factors. The strategy table used in this study can be seen in Table 2 below. The results of each assessment will be stated in “High,” “Medium,” and “Low,” where “High” represents the best

result and “Low” represents the worst. The assessment results will be categorized as "High," "Medium," and "Low," with "High" indicating the best outcome and "Low" the worst. A plus symbol (+) indicates the proposed solution outperforms the existing solution in a specific aspect. Conversely, a delta symbol (Δ) will indicate areas where the existing solution is superior. If the proposed solution possess more plus symbols than delta, it will be identified as more preferrable stand-by power supply alternatives for Pad S1 and S4.

Table 2: Strategy Table.

	Alternative 1 (Existing)	Alternative 2 (Proposed)	Remarks (+/Δ)
Aspect 1	Low	High	+
Aspect 2	High	Medium	Δ
Aspect 3, etc...	Low	Medium	+

3.2 Levelized Cost of Energy (LCOE)

Levelized cost of energy (LCOE) is defined as the discounted lifetime cost of ownership and use of a generation asset which is converted into an equivalent unit of cost of generation in price per energy unit. LCOE can also be expressed as the ratio of the total costs of a power plant to the total amount of electricity expected to be generated over the plant’s lifetime, which both are expressed in net present value terms (UK Department for Business Energy and Industrial Strategy, 2020). According to the Department of Business, Energy, and Industrial Energy of United Kingdom, LCOE calculation is shown below (Eq. 1).

$$LCOE = \frac{Capital\ Investment\ Cost\ +\ \sum_{t=1}^{n} \frac{O\&M\ Cost\ +\ Fuel\ Cost}{(1+d)^t}}{\sum_{t=1}^{n} \frac{Et}{(1+d)^t}} \quad (1)$$

where E_t is the annual energy generation of the power plant expressed in kWh.

Value of LCOE is widely used as a comparative measurement between alternative sources of energy since it can be determined as the minimum price or break-even price at which energy must be sold to adequately compensate a project’s suppliers, employees and investors for their contributions within a period of time (Massachusetts Institute of Technology, 2007); UK Department for Business Energy and Industrial Strategy, 2020). With this comparison method, an alternative with smaller LCOE will be identified as more preferrable stand-by power supply alternatives.

3.3 Cash Flow Analysis

Cash flow analysis is an economical analysis process of examining and evaluating a company’s inflows and outflows of cash over a specific period of time. Cash flow analysis consists of several parameters calculation such as Net Present Value (NPV), Internal Rate of Return (IRR), and Payback Period. The cash flow is calculated by subtracting cash inflows or benefits, with cash outflows or cost. In this study, investment cost and annual O&M cost of the proposed PV-Battery system is considered as annual cash out flows. Meanwhile, capital investment cost, additional revenue, O&M cost reduction, and fuel cost reduction between the proposed PV-battery system and existing diesel generator set is considered as annual cash inflows.

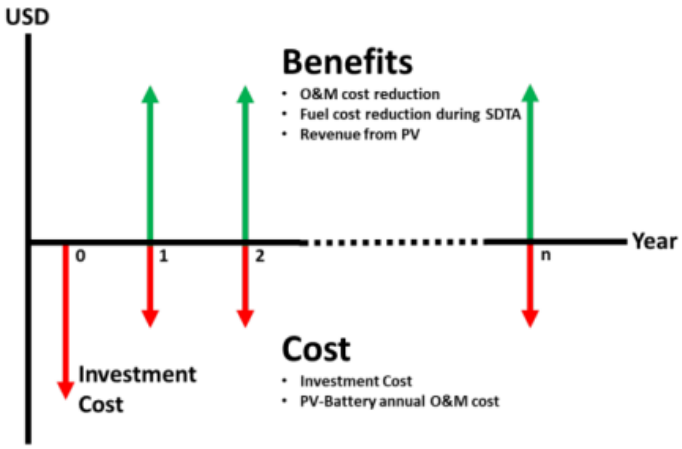

Figure 2. Cash Flow Model.

NPV is commonly used to estimate if a project is economically feasible to be executed or not, by predicting if its financial return will be more than the current investment or not. The project financial return is calculated by summing each year's discounted cash flow with the investment expenditure (Shou, 2022). The expression of NPV calculation is shown in Eq. 2 below:

$$NPV = -CF_0 + \frac{CF_1}{(1+d)^1} + \frac{CF_2}{(1+d)^2} + \cdots + \frac{CF_n}{(1+d)^n} \quad (2)$$

where $CF_{(t)}$ is the net cash flow in period t, d is discount rate, and n is the project lifetime. If the proposed alternative's NPV is positive, it can be identified that the project is economically feasible to be executed.

It represents the discount rate at which the NPV of an investment or project equals zero. In other words, IRR can be identified as the rate of return at which the present value of future cash flows equals to the initial investment. Meanwhile, the payback period is the length of time or years it takes to recover the investment cost from the discounted cash flows. The proposed alternative's IRR is considered to be acceptable when it exceeds the required discount rate set by the company of investor, while the payback period is considered to be acceptable if it takes less than the project lifetime.

LCOE, NPV, IRR, and Payback Period are calculated based on several parameters such as the investment cost, annual O&M cost, fuel cost, annual revenue, annual energy generation, and project lifetime, and discount rate which values can be seen in Table 3.

Table 3: Economic Analysis Parameters.

	Diesel Generator set	PV-Battery
Investment Cost (USD)	7437	8500
Annual O&M Cost (USD)	1124	238
Fuel Cost (USD)*	8367	-
Annual Energy Generation (kWh)**	28280	8800
Annual Revenue (USD)	-	645
Project Lifetime (years)	15	15
Discount Rate (%)	10%	x

*Fuel cost of diesel generator set if operated only during DRJ U2 SDTA (30 days) to supply Pad S1 & S4
**Annual energy generation of diesel generator set if operated to supply Pad S1 & S4 for a whole year

The investment cost and annual O&M cost are gathered from disclosed asset's and manufacturer's information. The calculation of diesel generator set fuel cost can be seen below in Eq. 3 and Eq. 4, respectively, with the fuel price is assumed to be the same as Pertamina Dex prices for West Java Area which is 0.93 USD/liter.

$$Fuel\ Cost = Load\ (\%) \times Fuel\ Consumption\ at\ 100\%\ Load\ (ltr/h\ ) \times Operating\ Time\ (h) \times Fuel\ Price\ (USD/ltr) \quad (3)$$

$$Fuel\ Cost = (3kW/8kW) \times 2.74\ (ltr/h) \times 720\ h \times 0.93\ (USD/ltr) = 688\ USD \quad (4)$$

Calculation of diesel generator set annual energy generation can be seen below in Eq. 5 and Eq. 6, respectively.

$$Annual\ Energy\ Generation_{DG} = Load\ (kW) \times Operating\ Time\ (h) \quad (5)$$

$$Annual\ Energy\ Generation_{DG} = 3\ kW \times 8760\ h = 28280\ kWh \quad (6)$$

The calculation of annual revenue and annual energy generation of proposed PV-battery system can be seen later in 4.1.2 PV-Battery. The project lifetime is assumed to be 15 years according to the shortest equipment lifetime in the proposed PV-battery system, which is the battery module. Lastly, the discount rate is assumed as 10% according to company's best practice.

4. ANALYSIS

4.1 System Design

The existing stand-by power supply for Pad S1 and S4 consists of a portable 10 kVA diesel generator set, while the proposed PV-battery system will consist of a 5.95 kWp PV system and an energy storage system with 5 kW maximum capacity.

4.1.1 Diesel Generator Set

The existing diesel generator set has a total 8 kW capacity consists of one unit of HARTECH 10KVA Silent Type (HT10Y). The generator set display and its technical specification are shown below in Figure 3 and Table 4, respectively.

Figure 3: HARTECH 10 kVA Silent Type (HT10Y).

Table 4: Technical Specification of Diesel Generator Set.

Parameter	Specification
Power Output	10 kVA / 8 kW
Voltage Output	220 VAC (1Ph), 380 VAC (3Ph)
Current	15.19 A
PF	0.8
Frequency	50 Hz
Fuel Capacity	45 Ltr
Fuel Consumption	2.74 Ltr/hr (100% Load) 2.05 Ltr/hr (75% Load)

The diesel generator set is located in Pad S1, beside the prefabricated S4-SS substation, where the diesel generator set will substitute the role of S4-T1 transformer in supplying power for all loads in S4-DB1, which includes the ADP. The system design is quite simple since it is only consisting of one equipment. System design and interconnection of diesel generator as stand-by power supply for Pad S1 and S4 is shown in Figure 4 below:

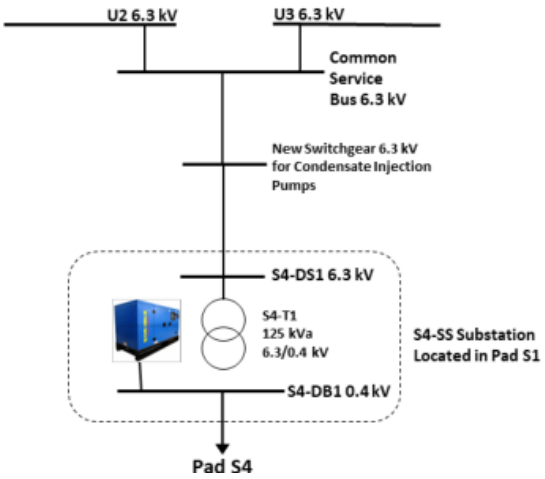

Figure 4: Diesel Generator Set System Design and Interconnection.

4.1.2 PV-Battery

The proposed PV-Battery system will consist of PV modules, three-phase hybrid PV inverter, energy storage system, and smart power/energy meter. The PV system will be roof-mounted with 5.9 kWp capacity consisting of 14 units of TrinaSolar Vertex S TSM-DE09R module with nominal power of 425 W. This module is chosen because it meets the specification needed and qualify the local content requirement. PV modules configuration will be divided into 2 strings, consist of 7 modules each, which will be installed in two orientations with azimuth angle of 135o and 315o, and tilt angle of 15o. Another source of energy, the energy storage system, will have a total capacity of 5 kW which consists of a unit of Huawei LUNA2000-5KW-C0 power module and a unit of

Huawei LUNA2000-5-E0 5 kWh battery module. The energy storage system technical specification is shown in Table. The product display and technical specification of designated PV module and energy storage system are shown in Figure 5, Table 5, and Table 6, respectively.

(a) (b)

Figure 5: (a) PV Module (TrinaSolar Vertex S TSM-DE09R), (b) Energy Storage System (Huawei LUNA2000-5KW-CO Power Module and LUNA2000-5-EO Battery Module).

Table 5: Technical Specification of PV Module.

Parameter	Specification
Solar Cells	Monocrystalline
Module Dimensions / Weight	1762 x 1134 x 30 mm / 21.8 kg
Peak Power (PMAX)	425 Wp
Maximum Power Voltage (VMPP)	42.2 V
Maximum Power Current (IMPP)	10.08 A
Open Circuit Voltage (VOC)	50.2 V
Short Circuit Current (ISC)	10.61 A
Module Efficiency	21.3 %
Operating Temperature	-40~+85°C

Table 6: Technical Specification of Energy Storage System.

Parameter	Specification
Battery Module Energy	5 kWh
Peak Output Power	3.5 kW in 10s
Operating Voltage Range	600 – 900 V

Both PV system and energy storage system will be connected to Huawei SUN2000-5KTL-M1 three-phase hybrid inverter with rated output power of 5 kW. The proposed system is also equipped with a unit of Huawei DTSU666-H smart energy meter. The product display and technical specification of the hybrid inverter and smart energy meter are shown in Figure 6, Table 7, and Table 8, respectively.

This proposed system design does not require to open any space since it is roof-mounted. However, it still requires some civil works for PV module roof mounting, earthing system, and for equipment installation. The proposed PV-Battery system location and design are shown in Figure 7.

(a) (b)

Figure 6: (a) Hybrid Inverter (Huawei SUN2000-5KTL-M1), (b) Smart Energy Meter (Huawei DTSU666-H).

Table 7: Technical Specification of Hybrid Inverter.

Parameter		Specification
Input (PV)	Max. PV Power Input	7500 Wp
	Operating Voltage Range	140 V ~ 980 V
	Max Input Current per MPPT	11 A
	Max Short Circuit Current	15 A
	No. of MPPT	2
Input (Battery)	Compatible Battery	5kWh – 30 kWh
	Operating Voltage Range	600 V ~ 980 V
	Max Operating Current	16.7 A
Output	Rated Output Power	5000 W
	Rated Output Voltage	380 VAC (3-phase)
	Rated Frequency	50 Hz / 60 Hz
	Max Output Current	8.5 A
	Power Factor	0.8 Lag to 0.8 Lead (Adjustable)

Table 8: Technical Specification of Smart Energy Meter.

Parameter	Specification
Line Voltage Measurement Range	304 Vac ~ 399 Vac
Phase Voltage Measurement Rang	176 Vac ~ 288 Vac
Current Measurement Range	0 ~ 100 A
Voltage and Current Measurement Accuracy	± 0.5%
Power and Energy Measurement Accuracy	± 1%
Frequency Measurement Accuracy	± 0.01 Hz

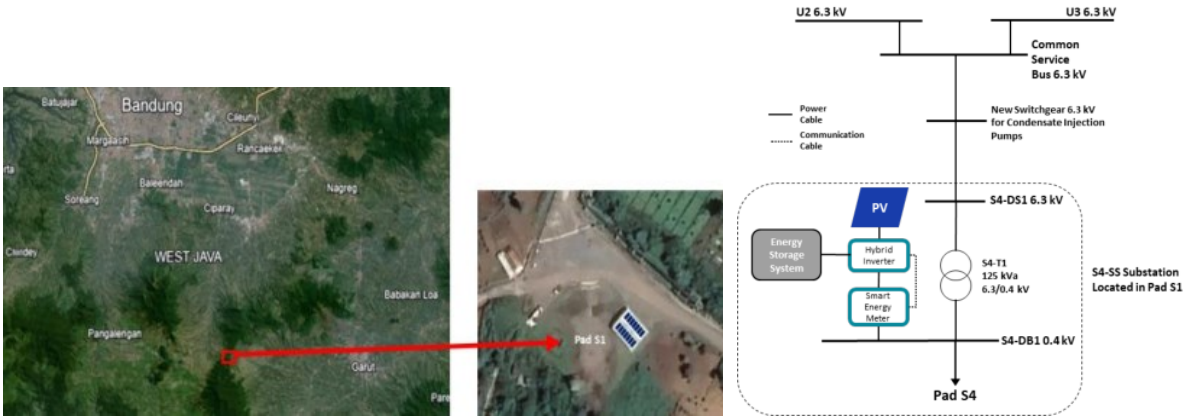

(a) (b)

Figure 7: (a) Proposed PV-Battery System Location; (b) Proposed PV-Battery System Design and Interconnection.

Furthermore, the proposed PV-battery system can generate annual revenue unlike the diesel generator, since the proposed system is connected to the power plant house load system, so it is able to supply excess electricity to compensate house loads. The simulation was performed using PVsyst software to determine the 5.95 kWp PV-without-battery system electricity production for a year. The simulation was performed in Darajat Pad S1 location, with Global Horizontal Irradiation (GHI) of 1546 kWh/m2/year. The roof-mounted PV modules plane orientation was adjusted in accordance with the S4-SS substation roof construction. PV module degradation, module losses, inverter losses, and wiring losses are also included in the calculation. According to the simulation result portrayed in the loss diagram, the PV itself can be expected to produce electricity up to 7.3 MWh per year.

If the battery is assumed to operate and discharge 85% of its power capacity each day, it can be obtained that the energy storage system itself can produce electricity up to 1.5 MWh per year. In total, the proposed PV-Battery system can be expected to produce electricity and increase Darajat net generation up to 8.8 MWh per year, with assumed 0.6% degradation per year based on the manufacturer's claim. Based on Peraturan Presiden Republik Indonesia No. 112 Tahun 2022, electricity price of a 95 MW geothermal power plant which has neem operated for more than 10 years such as DRJ U2 is assumed as 0.0735 kWh/year. Hence, the expected amount of produced electricity can increase the revenue up to 645 USD each year.

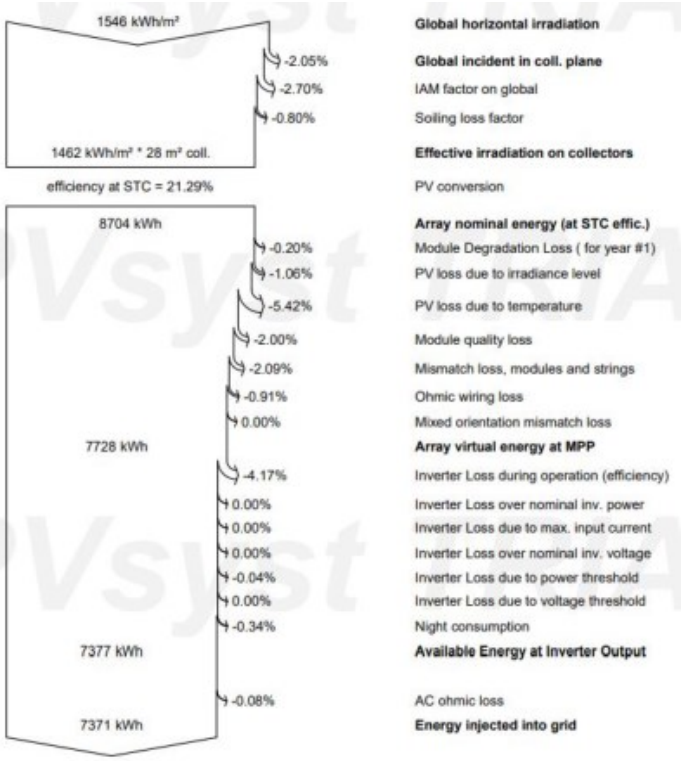

Figure 8: Loss Diagram of PV System.

4.2 Installation Time

The estimated installation time of the proposed PV-Battery system is 500 minutes longer than the installation time of the diesel generator set. The installation time estimation of the proposed PV-Battery system is conducted by assuming that all equipment and materials had arrived at the warehouse in the basecamp area, which is located 3.7 km away from the designated installation location (Pad S1). Detail of installation time estimation between two alternatives can be seen in Table 9.

4.3 Operability

4.3.1 Diesel Generator Set

the diesel generator set is not equipped with auto-start ability because it is designed to be portable and can be moved to different locations as needed. Hence it must be installed and started manually. Furthermore, if the diesel generator set is running out of fuel, it must be stopped first manually through the local switch and push button. The diesel generator set must be cooled down for about 5 minutes before it is fueled up. After the generator set is fueled up, it has to be started again and warmed up for about 5 minutes before it is loaded and operated again. The diesel generator set can only be used to supply power for loads under the S4-SS substation in loss of power plant supply worse condition such as power maneuver failure during SDTA or line fault. Since the power demand will be continuous, so the diesel generator set has to be operated continuously, which requires a quite large amount of fuels.

Table 9: Installation Time Estimation.

Diesel Generator Set		PV-Battery System	
Actions	**Estimated Time (Minutes)**	**Actions**	**Estimated Time (Minutes)**
3 km delivery from MTCE Tool Room to Pad S1 (including lifting and rigging)	40	3.7 km delivery from warehouse to Pad S1(including loading and unloading)	50
Connecting power cables	15	Mounting system installation	90
Fueling up	5	Equipment installation	180
Warming up	5	Cable connection	120
		System inspection, testing, and commissioning	120
Total	**70**	**Total**	**560**

4.3.2 PV-Battery System

The proposed PV-Battery system will utilize a hybrid inverter which makes the system can operate with (on-grid) or without (off-grid) power plant house load system connection. The proposed system also has several features which makes the system can operate under several conditions such as normal condition, loss of power plant supply during sunlight, and loss of power plant supply during no sunlight. During normal condition, the proposed system can operate to supply power to Pad S4 under S4-SS substation.

During normal condition where the connection or power supply from power plant is available, the excess power generated from PV is utilized to charge the battery module in energy storage system, and to supply the new condensate reinjection pump on the new switchgear 6.3 kV. The energy storage system (battery) can be operated in two operating modes, time-based and kWh-based. In time-based operation mode, the energy storage system will only supply power during specified time of the day. Meanwhile in kWh-based operation mode, the energy storage system will adjust its power supply according to the energy reading from the smart energy meter. When the PV is unable to generate required power due to the absence of sunlight, the energy storage system will cover the battery will cover the lack of power required by Pad S4. After the battery has been fully discharged or has been discharged below its designated State-of-Charge (SOC) percentage, the power plant house load system will take over the energy storage system to supply power to Pad S4. The operation schematic of the proposed PV-battery system during normal condition can be seen in Figure 9.

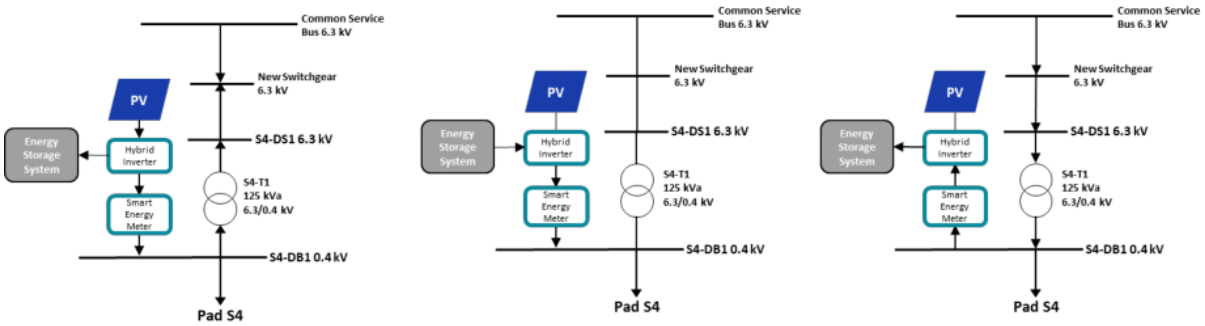

Figure 9: PV-Battey System Operation During Normal Condition.

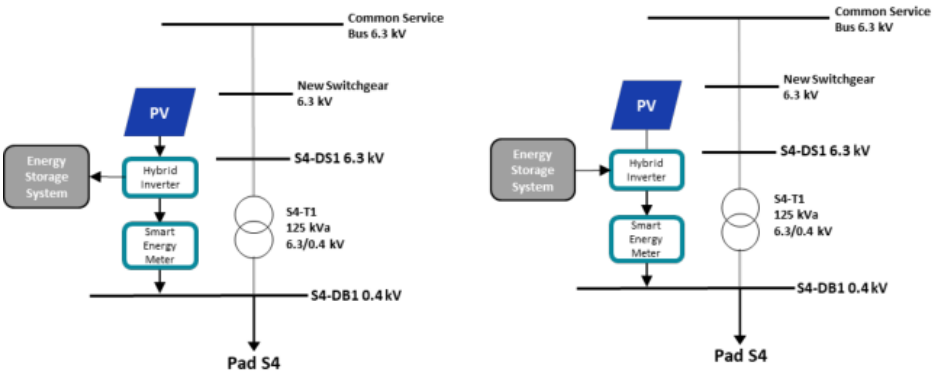

Figure 10: PV-Battery System During loss of Power Plant Supply Condition.

During loss of power plant supply condition such as manual power maneuver activity, power maneuver failure, or even worse line fault, PV will generate and supply power to Pad S4 where the excess power is utilized to charge the battery module in energy storage system. When there is not enough sunlight to generate enough power required by Pad S4, the electrical loads in Pad S4 will fully rely on the energy storage system until it runs out. The operation schematic of the proposed PV-battery system during loss of power plant supply condition can be seen in Figure 10.

In worse condition such as power maneuver failure during SDTA or line fault, where electrical loads in Pad S4 demand continuous power supply for much longer period, the energy storage system will supply power to loads under the S4-SS substation load. In this situation, the power will also be used to charge the battery in ADP's UPS DC system, which consists of 2x12V 38 Ah Valve Regulated Lead Acid (VRLA) battery, in order to substitute the role of PV-battery system as ADP power supply when there is absence of sunlight and the battery in energy storage system runs out.

4.4 Maintainability

In Darajat, several maintenance activities are performed on the diesel generator set every month. The PM activities includes equipment cleaning and checking on several parameters and equipment such as oil engine level, radiator water coolant level, air filter condition, v-belt condition, battery electrolyte, hose and tubing clamp condition, bolts mounting engine, oil engine pressure, engine temperature, engine rpm, pump pressure, abnormal noise, and leaks of oil or clamp hose or tubing. The engine oil, fuel filter, and oil filter also have to be changed or replaced every year.

Meanwhile, according to the manufacturer manual, the proposed PV-Battery system requires less maintenance activities compared to a diesel generator set. the maintenance activities requirement only includes monthly visual equipment and parameter inspection, monthly PV module cleaning, and annual electrical testing such as grounding resistance, PV open circuit voltage, DC cable insulation resistance, AC cable insulation resistance.

4.5 Reliability

Both diesel generator set and PV-Battery system possess high reliability value of 99%. However, the reliability of a diesel generator set is expected to be decreasing over outage and storing period.

4.5.1 Diesel Generator Set

Since the reliability of portable diesel generator set has not been assessed due its limited operating hours, reliability assessment of the diesel generator set in this paper utilized a study by (Marqusee, Ericson and Jenket, 2021) that assessed the impact and reliability of a emergency diesel generator on supplying critical loads. From the study, it can be summarized that a well-maintained EDG has a reliability between 92% and 96% for providing backup power for four days of outage, between 90% and 95% for one-week outage, and between 75% and 87% for a two weeks outage. In addition, long-term storage of diesel has a risk of microbial growth due to its limited shelf life, so diesel generators may experience a system failure if the fuel is not replaced every 6–12 months to maintain quality (Hwang, Tongsopit and Kittner, 2023).

4.5.2 PV-Battery System

High reliable operation is demanded in this proposed PV-Battery system. Inverter is identified as one of the most critical components in the system, whose failures can lead to a total loss of electricity production of the system. The manufacturer, Huawei, claims that the SUN2000-5KTL-M1 has high reliability number up to 99.9%. Furthermore, a study by (Sangwongwanich et al., 2018) reveals that the reliability of an inverter can be improved by battery utilization.

4.6 Environmental Impact During Operation

Increasing trend of renewable energy has never been separated from the environmental issues posed by conventional energy sources such as fossil fuels. Global warming has been the biggest environmental issue which caused by greenhouse gas emissions released from fossil-fueled engines, such as diesel generators, to the atmosphere. It is widely known that diesel generator emits greenhouse gases, such as carbon dioxide (CO2), due to the utilization of fossil fuels as its source of energy. The consumption of 1 liter diesel fuels (solar) emits around 2.4—2.8 kgCO2 (Jakhrani et al., 2012), which means that the existing diesel generator will emit around 59 kgCO2 per day if it is being utilized as a backup power supply for Pad S1 and S4, which is equal to 0.8 kgCO2 per kWh. Besides CO2, diesel generator also emits air pollutants such as sulfur dioxide (SO2), Carbon Monoxide (CO), and particulate matter (PM) (Hwang, Tongsopit and Kittner, 2023; Ahmed et al., 2020) which have negative impacts on human health. Meanwhile, The carbon footprint and pollutants of PV-battery solar systems that is emitted during operation is negligible (Bošnjaković et al., 2023). Meanwhile, about 98% of greenhouse gases and pollutant from non-renewable energy generator are emitted during the operation phase (Bošnjaković et al., 2023).

4.7 Levelized Cost of Energy (LCOE)

With 15 years of project lifetime, the expected LCOE of diesel generator set and PV-battery system is 0.439 USD/kWh and 0.296 USD/kWh, respectively. The detail calculation of diesel generator set and proposed PV-battery system LCOE can be seen in Eq. 7 and Eq. 8, respectively.

$$LCOE = \frac{7437 + \sum_{t=1}^{15} \frac{1124+8367}{(1+0.1)^{15}}}{\sum_{t=1}^{15} \frac{26280}{(1+0.1)^{15}}} = 0.439\ USD/kWh \quad (7)$$

$$LCOE = \frac{8500 + \sum_{t=1}^{15} \frac{238}{(1+0.1)^{15}}}{\sum_{t=1}^{15} \frac{8800}{(1+0.1)^{15}}} = 0.296\ USD/kWh \quad (8)$$

4.8 Cash Flow Analysis

Cash flow analysis was conducted by assuming the inflation rate for revenue, O&M cost, and fuel cost is 3%, geothermal income tax is assumed as 34% (based on Peraturan Menteri Keuangan Republik Indonesia No. 179/PMK.011 Tahun 2013), and DRJ U2 SDTA is assumed to be held once every 3 years with 30 period of days. The cash flow analysis is also conducted with assumption that the funds used for this project's investment come without any loans from external sources. Hence, the interest rate on loans is assumed as zero. The cash flow analysis calculation result shows that the proposed PV-battery system project possesses a positive NPV value of 652.49 USD, IRR value of 11.2%, and payback period of 14 years which is less than the project's expected lifetime.

5. RESULTS AND DISCUSSIONS

5.1 Strategy Table Result

The filled-up strategy table, which can be seen in Table 10, shows that even though the PV-battery system requires longer installation time than the existing portable diesel generator set, it proposes a better operability, more maintainable, more reliable, and greener stand-by power supply alternatives for Pad S1 and S4, which can also compensate power plant house loads to increase asset's revenue.

Table 10: Strategy Table Result.

	Portable Diesel Generator Set	PV-Battery	Remarks (+/Δ)
System Design	Medium	High	+
Installation Time	High	Medium	Δ
Operability	Low	High	+
Maintainability	Medium	High	+
Reliability	Medium	High	+
Environmental Impact During Operation	Low	High	+

5.2 LCOE and Cash Flow Analysis Result

From the LCOE calculation results, it can be identified that the proposed PV-Battery system still possesses smaller LCOE than diesel generator set, despite its higher investment cost and lower energy production. Meanwhile, cash flow analysis results show that the utilization of PV-battery system as a stand-by power supply for Pad S1 and S4 will not provide much benefits if compared to a diesel generator set from an economical point of view. This lack of benefits occur due to Indonesia's high geothermal income tax, which leads to decrease in project's annual net income. Changes in regulations related to renewable energy, especially geothermal energy, may increase interests from companies or investors to enhance the integration of renewable energy sources to replace fossil fuel-based energy sources. However, economical benefits from this project, may vary in different geothermal power plant locations, since higher electricity price will result in better NPV, IRR, and Payback Period.

6. CONCLUSION

In providing a stand-by power supply for Pad S1 and S4 to prevent unplanned trip during DRJ U2 and DRJ U3 power maneuver, PV-battery system is considered to be a doable stand-by power supply alternative other than diesel generator set. Despite its longer installation time and insignificant economic benefits if compared to the diesel generator set, proposed PV-battery system can offer a stand-by power supply alternative with better operability, maintainability, reliability, and less environmental impact during its operation which can lead to a better company image. However, the economical benefits from PV-battery system can be improved by change in regulation, such as tax reduction or renewable energy integration obligatory, or by executing the project in a geothermal power plant with higher electricity price.

REFERENCES

Ahmed, W.K. et al. (2020) 'Environmental Impact of Using Generators in the University of Technology in Baghdad, Iraq', *Journal of Thermal Engineering*, 6(6), pp. 272–281. doi:10.18186/THERMAL.822496.

Barbosa, R. et al. (2021) 'Variable Speed Diesel Electric Generators: Technologies, Benefits, Limitations, Impact on Greenhouse Gases Emissions and Fuel Efficiency', *Journal of Energy and Power Technology*, 4(1), pp. 1–1. doi:10.21926/jept.2201003.

Bošnjaković, M. et al. (2023) 'Environmental Impact of PV Power Systems', *Sustainability (Switzerland),* 15(15), pp. 1–26. doi:10.3390/su151511888.

Duffie, J.A. and Beckman, W.A. (2013) *Solar Engineering of Thermal Processes*. John Wiley & Sons, Inc. doi:10.1002/9781118671603.

Farhat, H. (2021) 'Chapter 4 - Maintenance: Availability and reliability', *Operation, Maintenance, and Repair of Land-Based Gas Turbines*, pp. 89–106. doi:https://doi.org/10.1016/B978-0-12-821834-1.00009-5.

Farnoosh, A. (2022) 'Power Generation from Coal, Oil, Gas, and Biofuels', *The Palgrave Handbook of International Energy Economics*, pp. 111–130. doi:10.1007/978-3-030-86884-0_6.

Hameed, Z. et al. (2019) 'Hybrid System of Geothermal Power Generation Using Abandoned Oil/Gas Bores Assisted by the Power of Solar Plates', *Proceedings of 2019 the 7th International Conference on Smart Energy Grid Engineering, SEGE 2019*, pp. 246–249. doi:10.1109/SEGE.2019.8859821.

Hwang, S., Tongsopit, S. and Kittner, N. (2023) 'Transitioning from diesel backup generators to PV-plus-storage microgrids in California public buildings', *Sustainable Production and Consumption*, 38(April), pp. 252–265. doi:10.1016/j.spc.2023.04.001.

Jakhrani, A.Q. et al. (2012) 'Estimation of carbon footprints from diesel generator emissions', *Proceedings of the 2012 International Conference in Green and Ubiquitous Technology, GUT 2012*, pp. 78–81. doi:10.1109/GUT.2012.6344193.

K.V Vidyanandan (2017) 'An Overview of Factors Affecting the Performance of Solar PV Systems', *Energy Scan*, (27), pp. 2–8.

Kansara, V.K. (2017) 'Bi-directional fast bus transfer scheme for three interconnected busbars', *2017 6th International Conference on Computer Applications in Electrical Engineering - Recent Advances, CERA 2017*, 2018-Janua, pp. 47–50. doi:10.1109/CERA.2017.8343299.

Lau, K.Y. et al (2015) 'Photovoltaic systems for Malaysian islands: Effects of interest rates, diesel prices and load sizes', *Energy*, 83, pp. 204–216. doi:https://doi.org/10.1016/j.energy.2015.02.015.

Marqusee, J., Ericson, S. and Jenket, D. (2021) 'Impact of emergency diesel generator reliability on microgrids and building-tied systems', *Applied Energy*, 285. doi:https://doi.org/10.1016/j.apenergy.2021.116437.

Massachusetts Institute of Technology (2007) *The Future of Coal: An Interdisciplinary MIT Study*. doi:10.2469/faj.v10.n4.77.

Reshid, M.N., Majid, M.A.A. and Muhammad, M. (2014) 'Evaluation of redundancy for power generating unit in a cogeneration power plant', *MATEC Web of Conferences*, 13. doi:10.1051/matecconf/20141303010.

Sangwongwanich, A. et al. (2018) 'Reliability Assessment of PV Inverters with Battery Systems Considering PV Self-Consumption and Battery Sizing', *2018 IEEE Energy Conversion Congress and Exposition, ECCE 2018*, pp. 7284–7291. doi:10.1109/ECCE.2018.8557479.

Shou, T. (2022) 'A Literature Review on the Net Present Value (NPV) Valuation Method', *Proceedings of the 2022 2nd International Conference on Enterprise Management and Economic Development (ICEMED 2022)*, 656(Icemed), pp. 826–830. doi:10.2991/aebmr.k.220603.135.

Thomsen, N. et al. (2019) 'A sustainable prototype for renewable energy: Optimized prime-power generator solar array replacement', *International Journal of Energy Production and Management*, 4(1), pp. 28–39. doi:10.2495/EQ-V4-N1-28-39.

UK Department for Business Energy and Industrial Strategy (2020) *Electricity Generation Cost Report 2020, BEIS Electricity Generation Cost Report*. Available at: https://assets.publishing.service.gov.uk/government/uploads/system/uploads/attachment_data/file/911817/electricity-generation-cost-report-2020.pdf.

Yilmaz, S. and Dincer, F. (2017) 'Optimal design of hybrid PV-Diesel-Battery systems for isolated lands: A case study for Kilis, Turkey', *Renewable and Sustainable Energy Reviews*, 77, pp. 344–352. doi:https://doi.org/10.1016/j.rser.2017.04.037.

Zhou, C. et al. (2011) 'a Feasibility Study on Hybrid Solar-Geothermal Power Generation', *New Zealand Geothermal Workshop*, (November), pp. 1–6.

Zhu, L. et al. (2018) 'The Impact of the Relationship Between Operational Cost and Oil Prices on Economic Assessment in Oil and Gas Industry', *Springer Proceedings in Business and Economics*, pp. 83–89. doi:10.1007/978-3-319-72745-5_9.

Darajat Unit II Generator Lifetime Assessment

Agustiawan, Agus Riyadi, and Febrian Tommy

Star Energy Geothermal, Wisma Barito Pacific II, 17th — 21st floor,
Jl. Letjen S. Parman Kav. 60 Jakarta 11410, Indonesia

eops@starenergy.co.id, agus.riyadi@starenergy.co.id, febrian.tommy@starenergy.co.id

Keywords: Geothermal Power Plant, Generator, Lifetime Assessment, Condition Indicator

ABSTRACT

Star Energy Geothermal Darajat Power Plant Unit 2 is a geothermal power plant located in Garut Area, 40 km south of Bandung, West Java Indonesia which operated by Star Energy Geothermal Darajat II, Limited. This geothermal power plant consists of turbine and generator as main equipment to produce the electricity. Generator equipment has nominal capacity 100.76 MVA and has been operated for more than 20 years. A comprehensive Lifetime Assessment (LTA) was conducted in 2022 to evaluate the generator current condition, estimate its remaining operational lifetime, and inform maintenance strategies. The LTA adhered to the K5.007.2020 SPLN "Pedoman Asessmen Generator" standard. Electrical tests of the rotor and stator were a primary focus in assessing the generator's health. Condition Indicators (CI) and Data Indicators (DI) were also evaluated to estimate the remaining useful life of the generator. The assessment determined lifetime of 24 years for the generator. Importantly, the LTA identified the potential to extend this lifetime through targeted repairs to the circuit ring brazing and cooling system. The results of this LTA will be instrumental in guiding Star Energy Geothermal Darajat II, Limited, in planning maintenance and repair activities. This proactive approach will help ensure the generator continued reliable operation and maximize its contribution to the power plant's output.

1. INTRODUCTION

Unit 2 Darajat Generator has been operated more than 20 years with capacity 100.76MVA. The subsequent data outlines its technical specifications.

Table 1: Darajat Unit 2 Generator Specification.

Generator Synchronous	
Type	FTLRI 524/60-2
Output	100706 kVA
Frequency	50Hz
Voltage	13800V
Current	4213A
Speed	3000rpm
Ex. Voltage	415V
Phase	3
Ex. Current	784A
Standard	IEC34-3(1988)

Darajat Unit 2 Generator functionality relies on the seamless interaction of its rotor, stator, and various accessories. Over time, all these components are susceptible to performance degradation. Since these components are critical and their failure can lead to reduced output, unplanned outage and loss production opportunity consequences. A proactive Lifetime Assessment (LTA) strategy is necessary to avoid such risks. The LTA is also helps determine the most appropriate maintenance steps for continued generator health. The LTA is expected to be determined a lifetime and a guideline for determine appropriateness operation on intervals inspection, repair decision nor replacement. Moreover, LTA is employed to increase the service life of equipment nearing the end of its design specified as mandated by ESDM Regulation No. 33 of 2021, Appendix V (J)(6).

2. METHODOLOGY

The condition assessment of Darajat Unit 2 Generator follows the guidelines established in the SPLN standard K5.007.2020, titled "Generator Assessment Guidelines." This standardized approach ensures a consistent and comprehensive evaluation of the generator health. The standard utilizes a comprehensive assessment Table 2 that evaluates various generator components based on specific criteria.

Figure 1: Darajat Unit 2 Generator.

Table 2: Overall Assessment Criteria for Generator Components.

Generator Components	Visual Inspection [a]	Age [b]	Technology Level [c]	Operation Limit [d]	Stator Electrical Test [e]	Rotor Electrical Test [f]	Stator Core Test [g]	Maintenance [h]	Data Quality [i]	Weighting Factor
Stator						NA	NA			3.0
Stator core					NA	NA				1.5
Rotor					NA		NA			2.5
Cooling System					NA	NA	NA			2.0
Neutral Grounding					NA	NA	NA			0.5
Bearing					NA	NA	NA			1.5
Casing Stator					NA	NA	NA			0.5
Generator Shaft					NA	NA	NA			1.0
Brush Rigging					NA	NA	NA			1.0
Oil System					NA	NA	NA			1.0
Weighting for Condition Parameters	1.0	2.0	1.0	1.0	3.0	2.5	1.0	1.5	Data Quality (DI)	
Condition Indicator (CI)										

[a] Visual inspection value (see Table 2.), [b] Age value (see Table 3.)
[c] Technology level value (see Table 4.), [d] Operation limit value (see Table 5.)
[e] Stator electrical test value (see Table 6.), [f] Rotor electrical test value (see Table 7.)
[g] Stator core test value (see Table 8.), [h] Maintenance value (see Table 9.)
[i] Data quality value (see Table 10.)

Generator health is assessed by evaluating each component. This includes the stator, stator core, rotor, cooling system, neutral grounding system, bearings, stator casing, generator shaft, brush rigging and oil system. The assessment considers several factors: visual inspection, age, technology level, operating limit, maintenance history. Electrical testing is only performed on the stator and rotor to get more detailed health data. All this information is then used in a formula to calculate a Condition Indicator (CI) for the entire generator. This CI value provides a single score that reflects the overall health and lifetime of the generator.

$$CI = \frac{\sum_{K=1,M}^{J=1,N} SC(K,J)xF(K)xF(J)}{\sum_{K=1,M}^{J=1,N} F(K)x(F(J)} \quad (1)$$

The system assigns a quality score to each component. This score is then combined with a weighting factor specific to that component. The resulting value, called the Data Indicator (DI), is calculated by multiplying the quality score by the weighting factor.

$$DI = \frac{\sum_{K=1,M} SD(K)xF(K)}{\sum_{K=1,M} F(K)} \quad (2)$$

where M, K, J, SC(K, J), F(J), SD(K), F(K) are total part which related on generators, identification part no. generator (from 1 until M), no. identify condition parameters (from 1 to 8, depending on condition physical, age, and etc), weighted values for parameter conditions, value weighting parameters condition, data quality score for each part given by the assessor based on the rating quality data each component, weighting factor for part / item defined by level interest to overall component condition, respectively.

The lifetime of the generator is calculated by comparing its current health indicator (CI) with its condition maximum condition value of assessment of all 10 (5.28). The difference between these values is then multiplied by the generator's design specifications (30 years) to determine how much longer it can operate effectively.

$$\text{Lifetime} = \left[\frac{CI}{5.28} \text{ x } 100\%\right] \text{x Design Life Specification} \quad (3)$$

These tables offer a breakdown of various factors affecting generator condition. The information within them is then consolidated into Table 1.

The visual condition of a generator, assessed through a thorough inspection, offers valuable insights into its overall health and reliability. Stator winding insulation, a critical factor in generator performance, can be indirectly evaluated through visual inspection. Signs like loose components, corona discharge (often appearing as a faint glow), and adherence of dust, dirt, or grease can indicate potential overheating and warrant further investigation. These visual observations, when combined with other diagnostic techniques, can help establish the generator's health and predict potential problems before they escalate.

Table 3: Visual inspection value.

Visual Rating of Generator Condition (rotor pull out condition)		**Effect**	**Score**
Very clean	All conditions look clean, both stator and rotor	No real defects	9 – 10
Clean	An inspection revealed clean stator end windings, wedges, and core despite the presence of oil seepage within the generator stator	Some defects are obvious and do not affect function	7 – 8
Fairly Clean	The condition of one of the stator end windings looks dirty, there is oil seepage on the inside of the stator, several areas show corona, there is looseness in the wedges and spacers and medium dust air filters	Moderate damage with adequate function and several operational indicators can show more than limited values, an influence on reduced operation, checking seals related to cooling air, and replacing filters	4 – 6
Dirty	The condition of the end winding, wedges, brush holder, diode rectifier looks dirty and there is seepage of lubricating oil on the inside of the stator and the air filter has thick dust	Serious damage, at least in the seal section, has a large clearance, extensive corona, looseness in the wedges and spacers, several operating indicators show values that are more than the limit, thus affecting the decrease. operation, generator conditioning for testing	1-3
Very Dirty	The end winding, wedges, brush holder, diode rectifier, and generator body are covered in thick dust as well as the condition of the lubricating oil leaking on the inside of the stator, filter. thick dusty air	Serious damage, there is dirt that resembles grease on the winding insulation, extensive corona, the generator cannot be tested, the generator does not function long	0

Table 4: Age value.

Generator Life Rating				Score
Age of generator stator/insulation	**Generator stator core age**	**Age of generator rotor/insulation**	**Age of generator components (bearings, coolant)**	
< 5 years	< 5 years	< 5 years	< 5 years	10
5 – 10 years	5 – 15 years	5 – 10 years	5 – 8 years	9
10 – 15 years	15 – 30 years	10 – 15 years	8 – 12 years	7-8
15 – 20 years	> 30 years	15 – 20 years	12 – 15 years	5-6
20 – 25 years		20 – 25 years	15 – 20 years	3-4
25 – 30 years		25 – 30 years	20 – 25 years	2
> 30 years		> 30 years	> 25 years	1

Table 5: Technology level value.

Level of insulation technology used	Score
Class H	10
Class F	7 - 9
Class B	4 - 6
Class A	1 - 3

Table 6: Operation limit value.

Operation limit	Score
The design standards have not changed, and the original plant design has no operational constraints	8 - 10
Minimum restrictions: temperature, vibration, and coolant leaks	5 – 7
Moderate limitations: shorts between windings, changes in structural defects and rotor ground faults	3 – 4
Severe limitations: the generator can no longer operate, has significant degradation, limiting performance and reliability if operated	0 – 2

Table 7: Stator electrical test value.

Stator electrical test	Score
All measurement results are within the applicable limits (commissioning, manual book, standard reference) and are low partial with an increase in measurement results of <2% to the design value	9 - 10
All measurement results are within the applicable limits (commissioning, manual book, standard reference) and are low partial with an increase in measurement results of <5% to the design value	7 - 8
Some measurement results exceed the applicable limits, such as: IR, PI and PD	5 - 6
The limits for the IR, PI, PD and Tan Delta measurement results exceed the applicable limits	1 - 4
All measurement result value limits have passed	0

Table 8: Rotor electrical test value.

Rotor electrical test	Score
All measurement results are within the applicable limits (commissioning, manual book, standard reference) with an increase in measurement results of <2% to the design value	8 - 10
All measurement results are within the applicable limits (commissioning, manual book, standard reference) and with an increase in measurement results of <5% to the design value	5 – 7
The measurement result value exceeds the applicable limits	1 – 4
Rotor short between turns	0

Table 9: Stator core test value.

Operating with a defective condition	Score
ELCID testing with low flux did not show any anomalies	10
ELCID testing with low flux shows small abnormal area values	5 – 9
ELCID testing with low flux shows large areas of abnormal values,	1 – 4
Operating with a defective condition	0

Table 10: Maintenance value.

Number of corrective maintenances	Score
Minimum level (normal conditions): routine preventive maintenance with minor work, routine cleaning and testing carried out on recommended frequency.	9 – 10
Low level: routine corrective maintenance with light work, for example: repairs that can be completed during a unit outage, preventive maintenance that is scheduled periodically basic (e.g., cleaning cooling tubes, cooling system maintenance)	5 – 7
Medium level: some unit maintenance that requires time for the unit to be turned off as a preventative maintenance measure, for example tightening bolt connection on winding, cleaning cooling system)	3 – 4
Significant level: additional and corrective maintenance work is required, resulting in a forced shutdown, such as: oil leaks in bearings, coolant gas leaks, overheating temperature	0 – 2

Table 11: Data quality value.

Data Availability and Data Accuracy	Score
High. Generator maintenance policies and procedures are followed by operation, routine checks, tests, and measurements are carried out at a normal frequency. Required data and information are available for team assessment through all available means, possible and visual inspection interviews with experienced generating units.	8 - 10
Medium. One or more of the routine examinations, tests and measurements completed within the normal 6–24-month frequency, or a fraction of the required data information and documents not available to the assessment team.	5 – 7
Low. One or more of the routine examinations, tests and measurements completed in the past 24-36 months is normal frequency, or several results not available.	3 – 4
Low. One or more required inspection tests and measurements completed >36 months past normal frequency, as of results not available.	0 – 2

3. RESULTS AND DISCUSSION

The generator began Commercial Operation Date (COD) on June 1, 2000, resulting in an approximate age of 22 years at the time of LTA implementation in 2022. A major overhaul, including stator and core rewinding, was necessary in 2013 due to equipment failure. The generator rotor was subsequently replaced in 2016 to address excessive vibration. For the purpose of lifetime assessment calculations in the "Age" column Table 13, replaced components like stators and rotors are considered to have been restored to a 'new' condition.Table 12 outlines the age criteria evaluation. Table 13 are observations that were made during the Darajat Unit 2 Generator condition assessment.

Table 12: Generator component Age criteria evaluation.

No	Part	Note	Age (Years)	Score
1	Stator	Rewinding = 2013	10	9
2	Stator Core	Rewinding = 2013	10	9
3	Rotor	New Rotor = 2016	7	9
4	Cooling System	1998	25	5
5	Neutral Grounding	1998	25	5
6	Bearing	2016	7	9
7	Casing Stator	1998	25	5
8	Generator Shaft	New Rotor = 2016	7	9
9	Brush Rigging	Maintained Annually	x	9
10	Oil System	Maintained Annually	x	9

Table 13 highlights several key observations regarding the generator condition that warrant further investigation:

1. Neutral Grounding (Circuit Ring) Visual Inspection

The visual inspection of the neutral grounding system, particularly the circuit ring area, resulted in a score of 6, which is lower than the scores assigned to other generator components. This discrepancy is attributed to discoloration observed on the circuit ring. Discoloration may indicate brazing neutral bar issue, potentially impacting component lifetime.

2. Stator Operation Limit

Data analysis indicates elevated temperatures in the windings of the Darajat Unit 2 Generator. Notably, the winding temperature rises to 120°C under full load conditions. The operational temperature of the circuit ring falls within a range of 140°C to 150°C. Given the observed winding temperature and the typical operating range of the circuit ring (140°C – 150°C), the current operating limit for the stator is assigned a value of 6. This value likely signifies a cause for concern, as it suggests potential proximity to the stator safe operating limits.

Table 13: Result of Darajat Unit 2 Generator evaluation.

Generator Components	Visual Inspection	Age	Technology Level	Operation Limit	Stator Electrical Test	Rotor Electrical Test	Stator Core Test	Maintenance	Data Quality SD(K)	Weighting Factor
Stator	9	9	8	6	8			8	8	**3.0**
Stator core	9	9	8	8			10	8	8	**1.5**
Rotor	9	9	8	8		10		8	8	**2.5**
Cooling System	9	5	8	8				7	8	**2.0**
Neutral Grounding	9	5	8	8				8	8	**0.5**
Bearing	9	9	8	8				8	8	**1.5**
Casing Stator	9	5	8	8				8	8	**0.5**
Generator Shaft	9	9	8	8				8	8	**1.0**
Brush Rigging	9	9	8	8				8	8	**1.0**
Oil System	9	9	8	8				8	8	**1.0**
Weighting for Condition Parameters (FJ)	**1.0**	**2.0**	**1.0**	**1.0**	**3.0**	**2.5**	**1.0**	**1.5**	**Data Quality (DI)**	**108.62**
									Condition Indicator (CI)	**4.82**

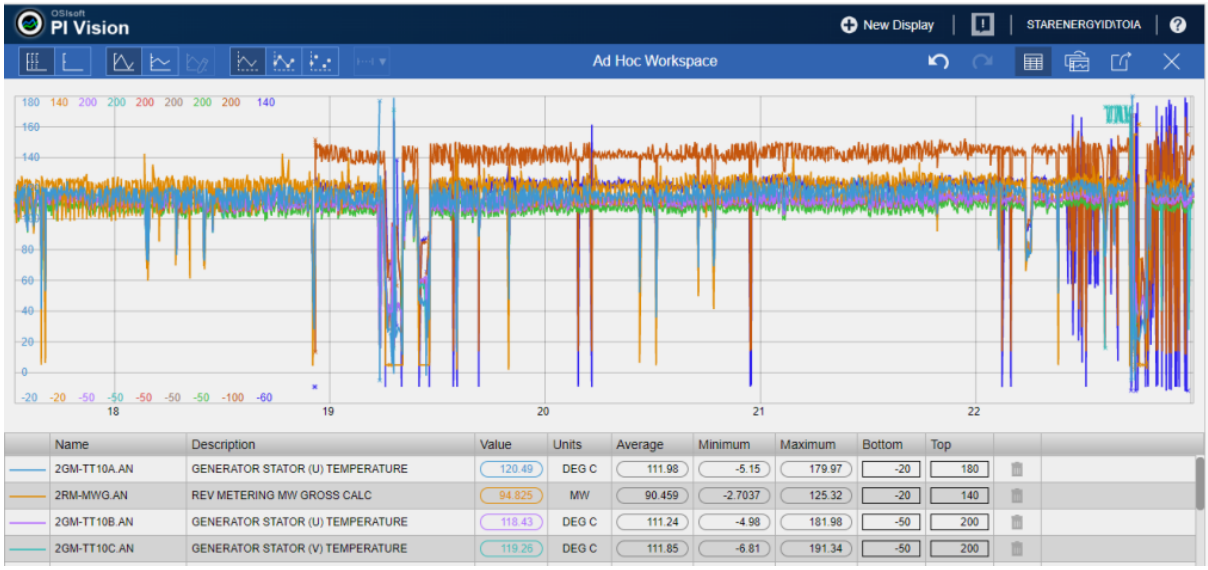

Figure 2: Operation data of Darajat Unit 2 Generator.

4. CONCLUSION AND RECOMMENDATION

4.1 Conclusion

While the initial lifetime estimate suggests the Darajat Unit 2 Generator could potentially function for another 27 years based on its design age (refer to previous sections for details on calculation method), certain observations necessitate further attention to ensure it reaches its full lifetime potential.

As highlighted in Table 13. (or mention the specific section if different), the visual inspection of the neutral grounding system, particularly the circuit ring area, revealed a concerning condition (discoloration). These observations suggest potential with brazing neutral bar issue. Additionally, data analysis indicates elevated temperatures in the windings, particularly under full load conditions. These observations suggest potential issues with the winding insulation degradation and dust accumulation.

4.2 Recommendations

Therefore, to achieve generation with Reliability Factor (RF) 99.59% and Availability Factor (AF) 99.09% and to maximize the generator lifetime estimated 27 years of operation since the last assessment, it is recommended to:

1. Prioritize maintenance of the neutral bar and circuit ring brazing. This could involve further visual inspection, x-ray testing, and potential repairs or replacements as needed.
2. Prioritize maintenance of the winding insulation. This could involve further visual inspection, partial discharge camera corona, partial discharge probe and potential repair for insulation degradation as needed.
3. Inspection during overhaul included a comprehensive evaluation of generator components, employing tests such as insulation resistance, winding resistance, tan delta, ELCID, bump, wedge analysis, core flux test, repetitive surge oscilloscope (RSO), and AC impedance/pole drop.
4. Predictive maintenance activities included continuous monitoring and analysis of winding and circuit ring temperatures using PI Vision, online partial discharge (PD) analysis, end winding vibration analysis, and flux probe measurements.

REFERENCES

Generatortech: Air-gap flux probe, Remote Data Analysis System

IRIS Power LP: Endwinding Vibration Monitoring, Evatracll

IRIS Power LP: Partial Discharge Monitoring, EMC Assembly 16kV

MARATHON GENERATOR: Insulation System Thermal Life Expectancy vs Total Operating Temperature

PERMEN ESDM: Nomor 33 Tahun 2021 Tentang, K3 PPLH dan Kaidah Teknis Panas Bumi Untuk Pemanfaatannya Tidak Langsung

PJBS: Report Lifetime Generator Darajat II, Limited (SEGD II), Garut (2022)

SPLN: K5.007.2020 Guidelines Assessment Generator Condition, incl in it

Design of Steam Wash System as Deposition Prevention Method on Geothermal Turbine

Bakhtiar Zaid Ariadji[1], Tubagus Ahmad Fauzi Soelaiman[2], Firman Bagja Juangsa[2], Yusniar Ully Andrianingtyas[1], Hanifah Bagus Sulistyardi[1], and Rahmad Harahap[1]

[1]PT. Pertamina Geothermal Energy Tbk
[2]Institut Teknologi Bandung

bakhtiar.ariadji@pertamina.com

Keywords: superheated steam, steam wash, deposition, wheel chamber pressure

ABSTRACT

Vapor-dominated geothermal systems have their benefits and drawbacks when it comes to the power plant and steam above ground system (SAGS) facilities. SAGS of vapor-dominated geothermal systems are known to be less complicated due to the lack of brine production. But due to this very condition, plus the large amount of cooling fluid being wasted in the cooling tower to the air, one of the problems in dry steam power plants is the lack of fluid being injected back into the reservoir. The reservoir will continuously produce steam but with no addition of fluid from reinjection, the volume of fluid in the reservoir will be reduced. This can cause a rapid decline in well production, and can also result in the production of superheated steam. Superheated steam carries two major threats regarding the reliability of the power plant, which are chlorine carry over from reservoir that can cause corrosion along the pipeline, and impurities being carried into the turbine as the result of no steam condensation along the pipeline or scrubber, in which the condensed steam and impurities are supposed to be ejected from the system through condensate traps. The impurities then will be deposited on the high pressure stages of the turbine which have the highest pressure drop along the steam path. Deposition of impurities on the high pressure stages of the turbine can be indicated by the increase of wheel chamber pressure (WCP) at certain flowrate.

In this research, steam wash system was designed as an effort to prevent deposition in geothermal turbines. In the steam wash system, the temperature of superheated steam at a pressure of 7.7 bar abs with a mass flow rate of 80 kg/s is reduced from 173.835°C to saturation temperature using injection water with a temperature of 25°C and a pressure of 8.7 bar abs with a flow rate of 0.3757-0.3814 kg/s, or around 0.5% of the mass flow rate of superheated steam. This design can decrease impurities consentration from 2.86 ppm to 2.33 ppm. Water treatment plant is also designed to fulfill the required specification of injection water, which requires 2,923.07 W of electricity to operate. Apart from that, the economics of the steam wash system have been compared with the Business as Usual (BAU) scheme, where until 2045 the implementation of the steam wash system has a profit value of IDR 116,421,802,990.63 greater than the BAU scheme.

1. INTRODUCTION

In a dry steam geothermal power plant system, impurities such as silica and chloride carried by steam from the reservoir will be removed through the condensate trap or scrubber when the steam undergoes condensation. In cases which the steam condition is superheated, there is a chance that steam condensation will not occur along the pipeline or scrubber. When the largest pressure drop occurs in the first stage of the turbine, the steam will begin to condense so there is a chance that impurities will be deposited on the first stage of the turbine. Deposit buildup in the first stage of the turbine can be indicated through the deviation of wheel chamber pressure (WCP) from the design pressure according to the steam flow rate.

In geothermal fields with superheated steam, it is necessary to carry out wet scrubbing so that the steam can become a mixture of two phases, so that impurities can be removed through condensate that forms along the pipeline and disposed of through steam traps and scrubbers (Chauhan, 2019). Several methods of wet scrubbing can be used to improve steam purity, such as the application of a scrubbing line and steam wash. Scrubbing lines are segments of pipe that have a large diameter to reduce speed and promote condensation by reducing the thickness of the insulation (Mubarok and Zarrouk, 2016). The length of the scrubbing line is an important parameter because the condensate that is formed takes time to fall to the bottom of the pipe (Arifien, et al., 2015). Steam washing increases steam purity through two stages. The first stage is injecting water to reduce the temperature of the superheated steam. The second stage is the removal of impurities through condensate which is formed and removed through a steam trap and scrubber. In this case, the injected water has two roles, namely helping to separate the liquid phase from the vapor, which causes heavier droplets so that they can be removed from the vapor stream, and by capturing semi-volatile material with the liquid phase, so that it can be removed

via degreasing equipment. water (Richardson, et al., 2014). The mass flow rate of the injection water is approximately 0.5-2% of the mass flow rate of steam (Morris, et al., 2019). The amount of injection water should not be too much, because it can cause the steam to be too wet after the injection water is injected, thus increasing the risk of wear on the turbine components (Sakai, 2022). In addition, injection water must not contain oxygen so as not to cause pitting corrosion in production facilities (Villa Jr, et al., 2005). Between the scrubbing line and steam wash methods, the steam wash method is superior because its operation is more flexible, it can follow the conditions of the steam that will enter the turbine. The objective of this paper is to design a steam wash system that can remove impurities from superheated geothermal fluid, so that it can improve the reliability of the geothermal power plant.

2. METHODS

The design of a steam wash system is divided into several stages, including calculating the heat loss to the environment, calculating the injection water flow rate requirement, calculating the condensate formed, and calculating the water treatment plant specification. Apart from that, flow simulations and economic analysis were also carried out. The data used in the calculation is obtained from one of the dry steam geothermal power plant in Indonesia.

2.1 Calculation of Heat Loss to the Environment

To be able to calculate the amount of condensate formed after superheated steam becomes saturated steam after mixing with injection water, it is necessary to calculate the heat transfer from the steam in the pipe to the ambient air. The illustration can be seen in Figure 1, and the thermal circuit can be seen in Figure 2.

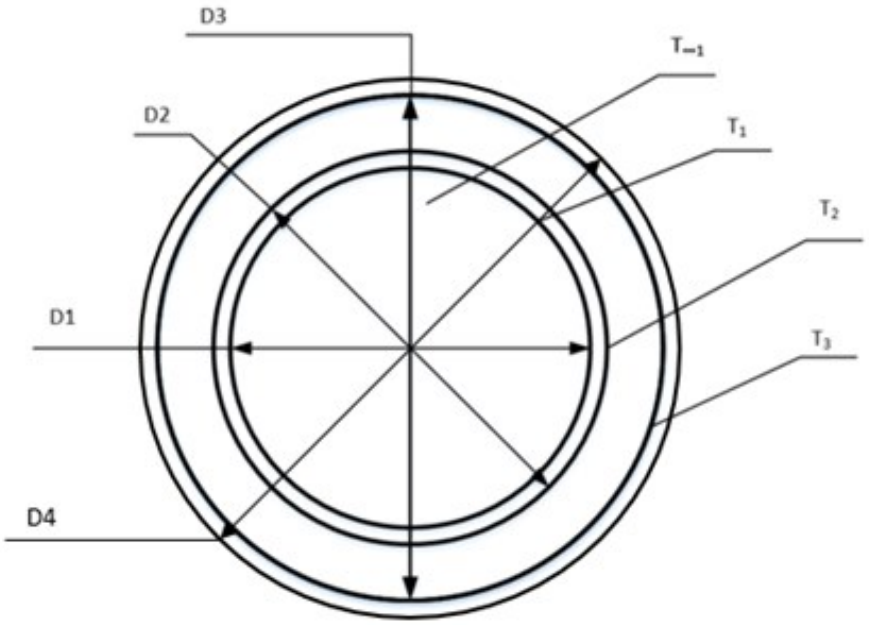

Figure 1: Heat transfer from steam to environment.

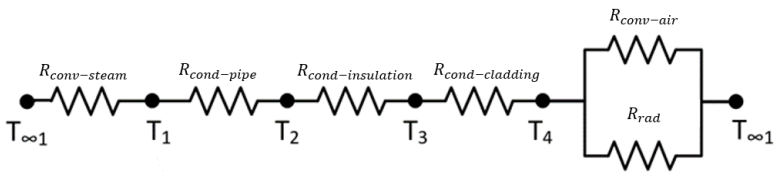

Figure 2: Thermal resistance circuit.

With the temperature on the outside of the cladding determined for safety reasons in operation and in accordance with the thermal resistance series above, the following equation is obtained (Bergman, 2011):

$$Q_{loss} = \frac{T_{\infty 1} - T_4}{R_{konv-uap} + R_{kond-pipa} + R_{kond-insulasi} + R_{kond-cladding}} \quad (1)$$

$$Q_{loss} = \frac{T_{\infty 1} - T_3}{\frac{1}{h_{uap}.A_1} + \frac{ln\,(R_2/R_1)}{2.\pi.k_{pipa}.L} + \frac{ln\,(R_3/R_2)}{2.\pi.k_{insulasi}.L} + \frac{ln\,(R_3/R_2)}{2.\pi.k_{cladding}.L}} \quad (2)$$

The value of h_{steam} is obtained from the following equation:

$$h_{uap} = \frac{Nu_{D_{uap}}.k_{uap}}{D_1} \quad (3)$$

$$Nu_{D_{uap}} = 0{,}023\ .\ {Re_D}^{4/5}.Pr^n \quad (4)$$

$$Re_D = \frac{\rho.VD_1}{\mu} \quad (5)$$

Equation 4 which is used to obtain the Nusselts Number has conditions including flow in a round pipe, turbulent flow, fully developed, $0.6 \leq Pr \leq 160$, $Re \geq 10{,}000$, $(L/D) \geq 10$, and $n = 0.3$ for $Ts < Tm$ (Bergman, 2011). The data used in this calculation can be seen in Table 1.

Table 1: Material and steam data as a basis for calculating heat loss to the environment.

	Parameter	Symbol	Value
Pipe	Size		32 inch
	Schedule		XS
	Thickness		12.7 mm
	Inner Diameter	D1	787.6 mm
	Inner Radius	R1	393.8 mm
	Outer Diameter	D2	813 mm
	Outer Radius	R2	406.5 mm
	Thermal Conductivity	k_{pipe}	54 W/m.K
Insulation	Type		Calcium Silicate
	Thickness		50 mm
	Outer Diameter	D3	913 mm
	Outer Radius	R3	456.5 mm
	Thermal Conductivity	$k_{insulation}$	0.057 W/m.K
Cladding	Thickness		0.8 mm
	Thermal Conductivity	$k_{cladding}$	237 W/m.K
	Surface Temperature	T_3	45°C
Steam	Temperature	$T_{\infty 1}$	168.835°C
	Pressure	$P_{\infty 1}$	6.85 barg
	Mass Flowrate	$\dot{m}$	80 kg/s
	Density	ρ	4.013 kg/m^3
	Viscosity	μ	1.464 x 10^{-5} N. s/m^2
	Specific Heat	c_p	2.5855 kJ/kg.K
	Thermal Conductivity	k_{steam}	0.03455 W/m.K
	Prandtl Number	Pr	1.0955

2.2 Calculation of the Injection Water Flow Rate Requirement

After the heat loss to the environment is calculated, the need for injection water to reduce the temperature of superheated steam can be calculated using the energy and mass balance equation with the assumptions that the condition is in steady state, no work to or from the system, and kinetic and potential energy are ignored. from those assumptions, these equations are obtained (Moran, et al., 2010):

$$\dot{Q}_{loss} + (\dot{m}_1 h_1 + \dot{m}_2 h_2) = \dot{m}_3 h_3 \quad (6)$$

$$\dot{m}_1 + \dot{m}_2 = \dot{m}_3 \quad (7)$$

The value of $\dot{Q}_{loss}$ varies with the distance which is assumed to be the distance required until mixing between superheated steam and injection water has been completed. The longer the mixing distance, the less the injection water needed. Calculations are carried out using the data in Tables 2 and 3 to find the mass flow rate of injection water and steam downstream of the injection point using Equations 6 and 7 according to variations in the selected mixing distance.

2.3 Calculation of the Formed Condensate Flow Rate

The schematic of the steam wash system can be seen in Figure 3.

X in the figure describes the distance from the injection point to the point where mixing is complete. The criteria for mixing to be completed are where there is no difference in temperature, speed and density between the steam

and the injected water. Calculation of the mass flow rate of condensate formed can be done by dividing the heat value loss to the environment by the vaporization enthalpy of the steam. Apart from that, a simulation was also carried out using Aspen Plus software to calculate the amount of condensate formed in the steam trap and scrubber. The parameters entered in the model created in Aspen Plus software can be seen in Table 4. The mass flow rate of the condensate formed is calculated using equation 8.

$$\dot{m}_{condensate} = \frac{Distance\ of\ Pipie.\ Q_{loss}}{h_{vaporization}} \quad (8)$$

Tabel 2: Known parameters.

Known Parameters	Value	Unit
Superheated Steam Pressure (Upstream)	7.7	bar a
Temperatur Uap Superheated Steam Temperature (Upstream)	174	°C
Superheated Steam Mass Flow Rate (Upstream)	288	Tonne/h
Atmospheric Pressure	0.85	bar a

Tabel 3: Set parameters.

Set Parameters	Value	Unit
Injection Water Pressure	8.7	bar a
Injection Water Temperature	25	°C
Steam Pressure (Downstream)	7.7	bar a
Steam Temperature (Downstream)	168.835	°C

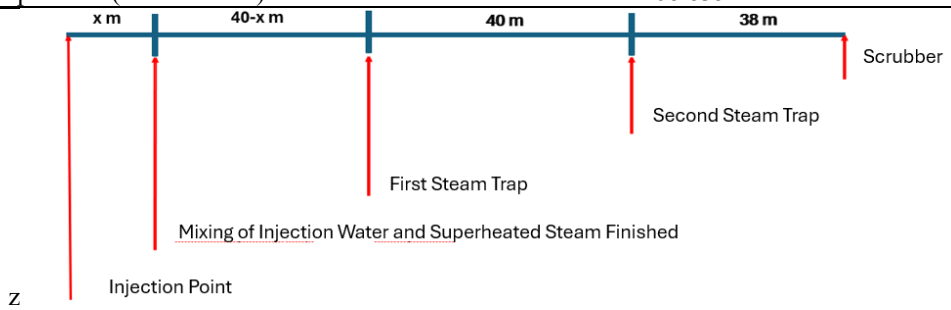

Figure 3: Distance from injection point to steam trap and scrubber.

Table 4: Input parameter for steam condensation simulation.

Component	Parameter	Value	Unit
Superheated Steam	Mass Flow Rate	80	kg/s
	Temperature	173.835	°C
	Pressure	7.7	Bar a
Injection Water	Mass Flow Rate	According to calculation results	
	Temperature	25	°C
	Pressure	8.7	Bar a
Pipe	Distance from Injection Point to the First Steam Trap	40	m
	Distance from the First Steam Trap to the Second Steam Trap	40	m
	Distance from the Second Steam Trap to Scrubber	38	m
	Heat Loss	According to calculation results	

Table 5: Concentration and solubility of materials contained in the steam.

Ion	ppm	Solubility (PubChem, 2024)
Chloride Ion	0.05	6.3 mg/ml steam
Sulfate Ion	0.88	28.1 g/g steam
Sodium Ion	0.03	36 g/100g steam
Kalium Ion	0.08	100 mg/ml steam
Calcium Ion	0.04	74.5 g/100ml steam
Magnesium Ion	0.02	73.8 g/100ml steam
Lithium Ion	0.01	76.9 g/100ml steam
Total Iron	0.02	-
Fluoride Ion	0.05	0.00169 mg/ml steam

Ion	ppm	Solubility (PubChem, 2024)
Boron	1.66	-
Silica	0.02	-

The approach taken to calculate the amount of material content that can be carried away by the condensate is divided into two stages. The first stage is to calculate the solubility of the material contained in the condensate. The second stage is to calculate the minimum horizontal distance required for condensate droplets to descend from the highest point in the pipe to the bottom of the pipe. The assumption used in this approach is that the impurity material contained in the steam will dissolve completely in the condensate that has formed, in accordance with the limited solubility value of the material. Therefore, it can be assumed that condensate droplets that will fall from the highest point in the pipe to the bottom of the pipe will contain all dissolved material. The concentration and solubility value of each material contained in the steam can be seen in Table 5.

Single droplet model is used for calculating the minimum distance required for condensate droplets to descend from the highest point in the pipe to the bottom of the pipe (Arifien, et al., 2015). The schematic of the model can be seen in Figure 4. The equations used in this model are as follows (Mubarok and Zarrouk, 2016 & Arnold and Stewart, 2008):

$$V_t = 0{,}0036\sqrt{\frac{d_p(\rho_l-\rho_g)}{C_d\rho_g}} \quad (9)$$

$$C_d = \frac{24}{Re} + \frac{3}{Re^{0,5}} + 0{,}34 \quad (10)$$

$$Re = 0{,}001\frac{\rho_g d_p V_t}{\mu} \quad (11)$$

$$t_s = \frac{h}{V_t} = \frac{L}{V_s} \quad (12)$$

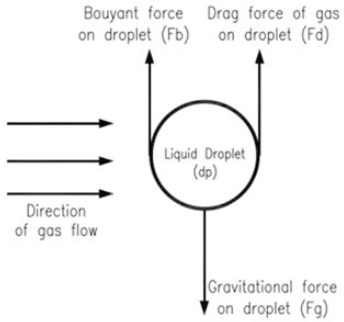

Figure 4: Single droplet model (Arifien, et al., 2015).

2.4 Calculation of Water Treatment Plant Specification

After the injection system is designed, the water treatment plant is designed. Because of the injection water is sourced from the cooling tower basin, the quality of which can be seen in Table 6, has lots impuries that does not meet the recommended values or limits for injection water determined from the turbine Operation & Maintenance Manual, a water treatment plant is needed so that The injection water quality can meet the recommended values and limits.

Table 6: Recommended Values, Limit Values, and Water Quality Data

Parameter	Recommended Values	Limit Values	Water Quality from Cooling Tower Basin
pH	≥ 5.0 ≤ 10.0	≥ 4.0 ≤ 10.0	6.5
TDS	≤ 0.5 ppm	≤ 5 ppm	96.42 ppm
SS	≤ 0.1 ppm	≤ 1 ppm	N/A
Chloride Ion	≤ 0.1 ppm	≤ 1 ppm	0.546 ppm
Sulfate Ion	≤ 0.1 ppm	≤ 1 ppm	4.207 ppm
Sodium Ion	≤ 0.1 ppm	≤ 1 ppm	5.217 ppm
Kalium Ion	≤ 0.1 ppm	≤ 1 ppm	4.275 ppm
Calcium Ion	≤ 0.1 ppm	≤ 1 ppm	40.241 ppm
Fluoride Ion	≤ 0.1 ppm	≤ 1 ppm	0
Arsenic	≤ 0.1 ppm	≤ 1 ppm	N/A

Parameter	Recommended Values	Limit Values	Water Quality from Cooling Tower Basin
Boron	≤ 0.5 ppm	≤ 5 ppm	N/A
Silica	≤ 0.1 ppm	≤ 1 ppm	N/A
Total Iron	≤ 0.1 ppm	≤ 1 ppm	N/A
Oxygen	≤ 0.01 ppm	≤ 0.1 ppm	9.09 ppm

Design of the water treatment plant for the reverse osmosis membrane section is using Water Application Value Engine (WAVE) software. In order to provide storage reserves in the tank before entering the injection system, the mass flow rate of water that needs to be produced from the water treatment plant is determined to be greater than the injection water requirement. The size of the tank is arranged in such a way that it can retain water for a certain time interval.

The oxygen content value in the cooling tower basin water exceeds the recommended limit value, so treatment is carried out by mixing hydrazine to reduce the oxygen content of the water to be injected, which meets the following chemical equation:

$$N_2H_4 + O_2 \rightarrow N_2 + 2H_2O$$

From this equation, the amount of hydrazine needed to reduce the oxygen level in the water to be injected can be calculated. The schematic of the water treatment plant can be seen in Figure 5.

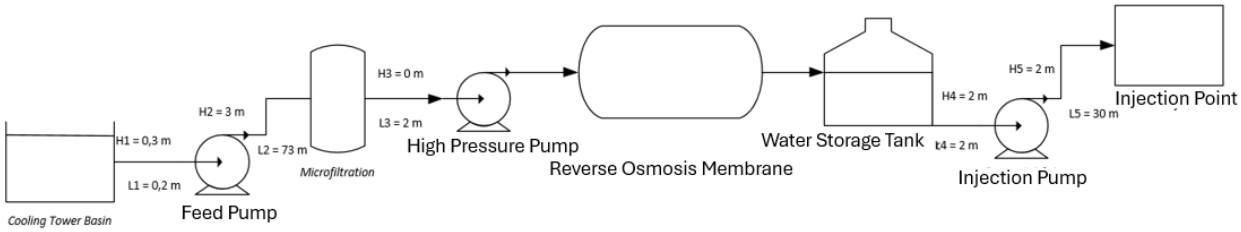

Figure 5: Schematic of Water Treatment Plant.

The input data and assumptions used to calculate pump specifications are as follows:

- Injection water temperature: 25°C
- Atmospheric pressure: 850 mBar
- Density of water: 995.7 kg/m^3
- Gravitational Acceleration: 9.81 m/s^2
- Microfiltration works at a pressure of 1 barg (Van Der Bruggen, 2018)
- The pressure drop across the microfiltration filter is 0.5 barg (Gao, 2022)

The equations used to calculate pump specifications are as follows:

$$P = \rho . g . Q . H \quad (13)$$

$$H = \frac{(P_{Discharge} - P_{Suction})}{\rho . g} \quad (14)$$

$$P_{Suction} = P_{surface\_suction} + P_{static\_suction} - \Delta P_{friction\_suction} \quad (15)$$

$$P_{Discharge} = P_{surface\_discharge} + P_{static\_discharge} + \Delta P_{friction\_discharge} \quad (16)$$

$$P_{static\_suction/discharge} = \rho . g . h_{static\_suction/discharge} \quad (17)$$

$$\Delta P_{friction\_suction/discharge} = f . \left(\frac{L}{D}\right) . \left(\rho \frac{V^2}{2}\right) \quad (18)$$

$$\frac{1}{\sqrt{f}} = -2 \log_{10} \left(\frac{\varepsilon}{3{,}7D} + \frac{2{,}51}{Re\sqrt{f}}\right) \text{ for } Re > 4000 \quad (19)$$

2.5 Flow Simulation

As a visualization of the calculation results, a flow simulation is carried out by entering input parameters from the calculation results of the heat heat loss and the required mass flow rate of the injected water. Flow simulations were carried out using Ansys Fluent software. The boundary conditions specified as input are the speed and temperature of the superheated steam, the speed and temperature of the injection water, and the pipe wall temperature.

2.6 Economic Analysis

An economic analysis was carried out on the installation of a steam wash system over the remaining life of the available generator, which was then compared to the Business as Usual (BAU) scheme. In the BAU scheme, there is no intervention in the deposition process in the turbine, resulting in suboptimal generation over time, which can then be returned to optimal conditions by cleaning at a Major Overhaul every two years. The data and assumptions used in economic analysis are as follows:

- Power plant production capacity is 35 MW.
- For schemes using steam wash it is assumed to be produced at full load throughout the year.
- The price of electricity is 8.25 US cents per kWh.
- The USD to IDR exchange rate is IDR 15,500.00 for 1 USD.
- Power plant will be operated until 2045.
- Operational costs incurred come from the use of hydrazine as an oxygen scavenger.
- Maintenance Outage is carried out every 2 years for 14 days for both schemes.
- In the Business as Usual (BAU) scheme, if an increase in wheel chamber pressure occurs because it exceeds certain limits, the steam mass flow rate must be reduced so that the wheel chamber pressure is within the permitted limits in accordance with the applicable operating guidelines.

3. RESULTS AND DISCUSSION

3.1 Heat Loss to the Environment

The results of the calculation of heat wasted on the environment can be seen in Table 7. It can be seen that the heat loss per meter of pipe length is 379.63 W. This value can then be used as a basis for calculating injection water requirements based on the distance required until mixing is complete. Apart from that, this value is used as input data in the Aspen Plus simulation to simulate condensation that occurs in pipes.

Table 7: Heat Loss to the Environment.

Parameter	Symbol	Value
Diameter	D1	0.813 m
Area	A	0.519 m^2
Fluid Velocity	V	38.404 m/s
Reynolds Number	Re_D	8557219.192
Nusselts Number	$Nu_{D_{steam}}$	12280.88985
Heat Transfer Coefficient	h_1	521.972 $W/m^2 . K$
Contact Surface Area	A_1	2474.318 m^2 per meter
Convection Thermal Resistance	$R_{conv-steam}$	7.743 x 10^{-7} $W/m . K$
Pipe Conduction Thermal Resistance	$R_{cond-pipe}$	9.355 x 10^{-5} $W/m . K$
Insulation Conduction Thermal Resistance	$R_{cond-insulation}$	0.3239 $W/m . K$
Cladding Conduction Thermal Resistance	$R_{cond-cladding}$	1.75 x 10^{-6} $W/m . K$
Heat Loss	Q_{loss}	379.63 W per meter

3.2 Injection Water Flow Rate

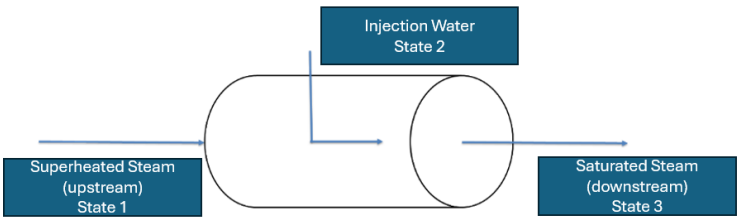

Figure 6: Schematic of Steam Wash Injection.

The scheme for water injection into superheated steam can be seen in Figure 6. The calculation results for injection water mass flow rate requirements are shown in Table 8.

It can be seen that to reduce the temperature of superheated steam at a rate of 80 kg/s from 173.835°C to the saturation temperature at 168.835°C at a pressure of 7.7 bar a requires water injection with a temperature of 25°C and a pressure of 8.7 bar a varying between 0 .3757-0.3814 kg/s according to the distance between the injection point until the mixing is complete, which is varied between 0-40 meters. The range of ratios of the value of the

mass flow rate of injection water to the mass flow rate of steam is between 0.470-0.477%, which is a very small difference, so a precise control system is needed to be able to produce steam with the appropriate values for each parameter.

Table 8: Results of Injection Water Mass Flow Rate Requirement Calculation.

		Parameter	Unit	State		
				1	2	3
		Temperature	°C	173.835	25	168.835
		Pressure	bar a	7.7	8.7	7.7
		Enthalpy	kJ/kg	2777.83	126.53	2766.73
Mixing Distance (m)	0				0.3814	80.3814
	1				0.3812	80.3812
	5				0.3807	80.3807
	10	Mass Flow Rate	kg/s	80	0.3799	80.3799
	20				0.3785	80.3785
	30				0.3771	80.3771
	40				0.3757	80.3757

3.3 Condensate Flow Rate

The steam wash system model has been created using Aspen Plus as can be seen in Figure 7.

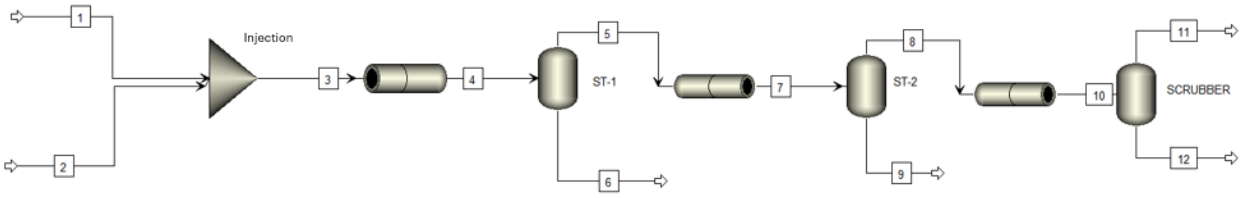

Figure 7: Model of Steam Wash Model.

The state of each flow are obtained using the model in Figure 7. In this model the input parameters are included as in Table 4 as well as the mass flow rate of injected water and heat loss to the environment which have been calculated previously. The simulation results can be seen in Table 9. It can be seen that the total condensate formed is 0.0096 kg/s or 34.72 kg/h, with details of 0.0032 kg/s in the first steam trap, 0.0033 kg /s on the second steam trap, and 0.0031 kg/s on the scrubber. From these results, the mass flow rate of the condensate formed is much less than the mass flow rate of the incoming injection water, so it can be concluded that there is an increase in the mass flow rate of fluid entering the turbine. Therefore, an approach was taken using the solubility of the contained material to ensure that the impurity material contained in the superheated steam could be carried out by the condensate formed through the steam trap and scrubber.

The mass flow rate limit of each contained material that can be dissolved in condensate water is obtained using the solubility data of the contained material from Table 5 and the calculation results of the condensate formed, the value of which can be seen in Table 10. Then, this value is compared with the flow rate the mass of each material contained, so that it can be concluded that almost all of the material contained can be dissolved in the condensate, except for sulfate ions and fluoride ions of which the remaining 102.64 g/h and 10.09 g/h respectively will be carried away. to the turbine. In addition, materials such as total iron, boron, and silica cannot be dissolved in the condensate.

The next stage is to calculate the distance required for the condensate droplets at the highest position in the pipe to be able to descend to the bottom of the pipe. This aims to illustrate the possibility of condensate formed along the pipe being able to descend to the bottom of the pipe and be removed through steam traps and scrubbers located at several points on the pipe route as in Figure 3. The minimum distance required for condensate droplets at the highest position in the pipe to be able to descend to the bottom of the pipe is greatly influenced by the diameter of the droplet formed as written in Equations 9 to 12. The calculation results can be seen in the graph in Figure 8. With the distance between the points injection and the first steam trap and the distance between the first steam trap and the second steam trap is 40 meters, the minimum diameter of the condensate droplet is 272 μm. Meanwhile, for condensation formed after the second steam trap, the minimum diameter of the condensate droplets is 282 μm so that all the condensate droplets formed can fall to the bottom of the pipe and be removed through a scrubber which is 38 meters from the second steam trap.

Table 9: Results of Process Simulation.

Parameter		Temperature (°C)	Pressure (Bar)	Mass Flow Rate(kg/s)
State	1	173.835	7.7	80
	2	25	8.7	0.3814
	3	168.83	7.7	80.3814
	4	168.72	7.68	80.3814
	5	168.72	7.68	80.3782
	6	168.72	7.68	0.0032
	7	168.62	7.66	80.3732
	8	168.62	7.66	80.3749
	9	168.62	7.66	0.0033
	10	168.52	7.64	80.3749
	11	168.52	7.64	80.3717
	12	168.52	7.64	0.0031

Tabel 10: Results of Material Solubility on Steam Flow After Steam Wash Injection.

Ion	Mass flow rate limit in which the ion is dissolvable	Mass Flow Rate after Injection	Details
Chloride Ion	81,13 g/h	10,15 g/h	Completely dissolved
Sulfate Ion	25,76 g/h	179,91 g/h	102,64 g/h left
Sodium Ion	4166,68 g/h	14,91 g/h	Completely dissolved
Kalium Ion	1287,80 g/h	40,33 g/h	Completely dissolved
Calcium Ion	9594,11 g/h	20,04 g/h	Completely dissolved
Magnesium Ion	9503,96 g/h	9,92 g/h	Completely dissolved
Lithium Ion	9903,18 g/h	4,96 g/h	Completely dissolved
Total Iron	-	9,92 g/h	Not dissolved
Fluoride Ion	0,02 g/h	10,15 g/h	10,09 g/h left
Boron	-	478,08 g/h	Not dissolved
Silica	-	5,76 g/h	Not dissolved

3.4 Water Treatment Plant Specification

From the calculation results of the mass flow rate requirement for injection water of 0.3814 kg/s, or 1.38 m^3/h, it is determined that the volume flow rate of water entering the water storage tank is 4.5 m^3/h so that injection water can be stored, so the water treatment plant does not need to operate all the time. Assuming the RO membrane has a recovery rate of 75%, the volume flow rate of water entering the water treatment plant is 6 m^3/h. These values along with the water quality from the cooling tower basin as in Table 6 were entered into the WAVE software so that results were obtained as can be seen in Table 11.

Then, to calculate the size of the water storage tank, a minimum retention time of 8 hours is determined, so the minimum tank size is 11.03 m^3. Therefore, the water storage tank specifications are determined as follows:

- Tank diameter: 3 meters
- Tank height: 2 meters
- Tank volume: 14.14 m^3

With this volume of water storage tank, the water retention time in the tank during use of the injection system is 10.25 hours. After the water volume in the tank decreases and approaches empty because the water is used for steam wash injection, the water conditioning system operates again and refills the tank for 4.53 hours with the injection process continuing.

With an oxygen content in the injection water of 9.09 ppm, 0.935 kg of 35% hydrazine is needed per day to evacuate all the oxygen in the injection water so as not to cause corrosion in the system.

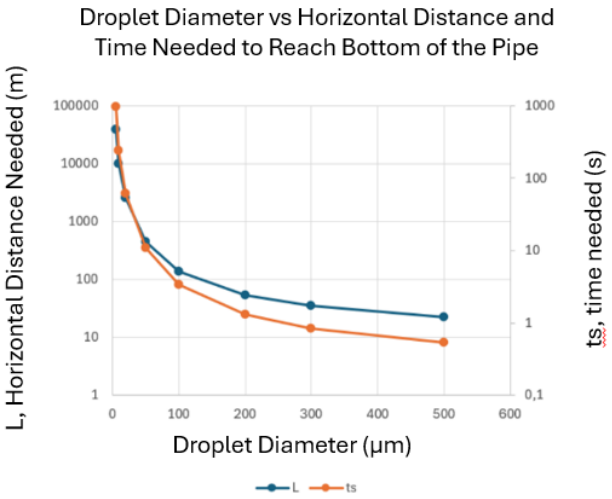

dp (μm)	5	10	20	50	100	200	300	500
L (m)	39422,1	9931,43	2537,11	446,98	138,17	53,67	34,7	22,07
ts (s)	958,81	241,55	61,71	10,87	3,36	1,31	0,84	0,54

Figure 8: The Effect of Droplet Size on the Horizontal Distance and the Time Required for the Droplet to Descend to the Bottom of the Pipe.

Table 11: Calculation Result of Water Treatment Plant Specification.

Parameter	Value	Unit
TDS of Source Water	96.39	Ppm
Volumetric Flow Rate of Source Water	6	m^3/h
TDS of Permeate Water	4.94	Ppm
Volumetric Flow Rate of Permeate Water	4.5	m^3/h
TDS of Concentrate Water	371.8	Ppm
Volumetric Flow Rate of Concentrate Water	1.5	m^3/h
Discharge Pressure of High Pressure Pump	7	Bar
Chloride Ion	0.0	ppm
Sulfate Ion	0.02	ppm
Sodium Ion	0.04	ppm
Kalium Ion	0.96	ppm
Calcium Ion	0.29	ppm

The calculation results regarding pump specifications can be seen in Table 12. In a water treatment plant, the greatest power requirement comes from the pump. In this system the total power requirement is 2,923.07 W.

Table 12: Calculation Result of Pump Specification.

No	Pump	Differential Pressure (m)	Hydraulic Power (W)
1	Feed Pump	14.52	236.87
2	High Pressure Pump	75.09	1,225.33
3	Injection Pump	89.53	1,460.87

3.5 Results of Flow Simulation

In carrying out flow simulations, a mesh of the flow in the pipe has been created covering the flow in the pipe along 30 meters from the injection point to find the point where mixing between the injected water and superheated steam has been completed. The criterion for mixing to be complete is where there is no difference in temperature, speed and density between the steam and the injected water. In this simulation, the number of elements used was 239,397, and the number of spots was 241,292.

The flow simulation results in the form of velocity contours can be seen in Figures 9 and 10. It can be seen in Figures 9 that the velocity contours in the area around the injection point are slower up to a distance of around 4

meters, after which the flow has the same velocity profile. Apart from that, it can be seen in Figure 10 that the water volume fraction has reached 0 percent at a distance of around 0.3 meters from the injection point, which illustrates that all of the injected water has changed phase to steam.

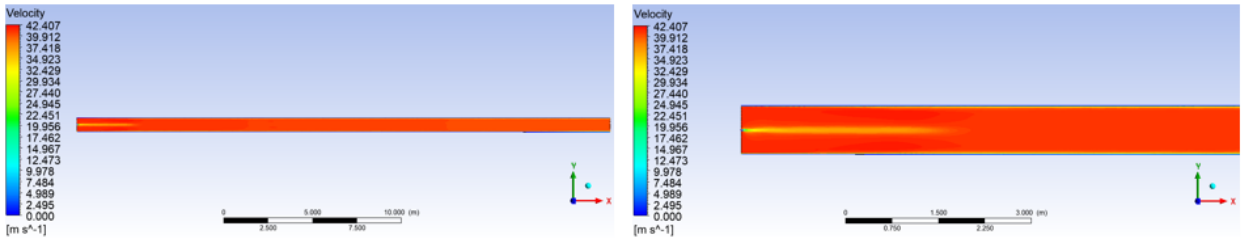

Figure 9: (a) Velocity Profile on 0-30 Meter from Injection Point and (b) Velocity Profile on Injection Point.

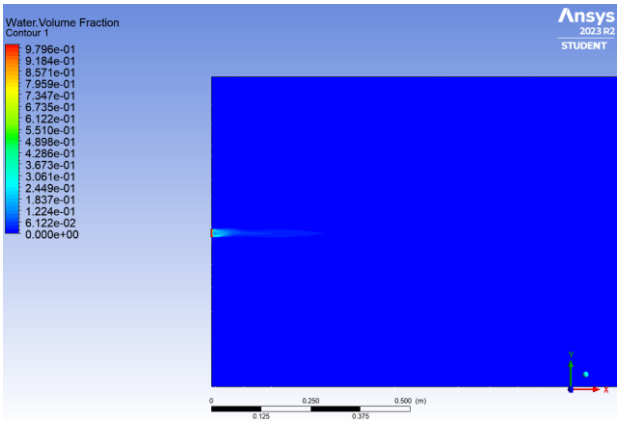

Figure 10: Volume Fraction Profile of Steam on Injection Point.

3.6 Results of Economic Analysis

The capital costs of a steam wash system consist of the capital costs of components consisting of a nozzle and a water treatment plant which includes a water storage tank, feed pump, high pressure pump, injection pump, RO membrane, and oxygen scavenger system. The capital costs of each component were obtained from offers from various companies which were then compared to obtain an estimated capital cost of the steam wash system of IDR 1,820,862,507.00. Operational costs for the steam wash system are related to the use of 35% hydrazine as an oxygen scavenger which requires an amount of 0.935 kg per day or 341.415 kg per year, which is estimated to cost IDR 47,798,061.90 per year.

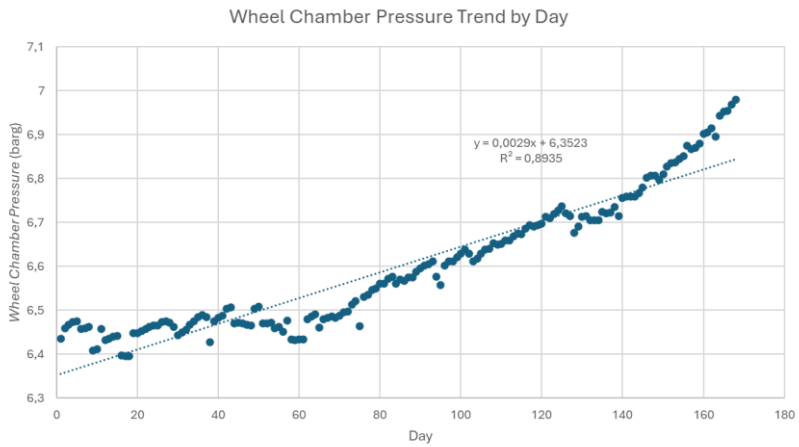

Figure 11: Wheel Chamber Pressure Trend By Day.

In the Business as Usual (BAU) scheme, the plant operation is modeled in accordance with the wheel chamber pressure increase modeling. From previous operational data, a graph of the increase in wheel chamber pressure is obtained as in Figure 11. From this graph, an equation is obtained that describes the increase in wheel chamber pressure per day, where the increase will continue until the maximum value that can be operated. In this condition, according to the turbine operation & maintenance manual, the steam mass flow rate entering the turbine must be reduced so that the wheel chamber pressure value is at the maximum value at the upper limit of the steam mass flow rate. Reducing the steam mass flow rate causes a decrease in generation. This decline in generation occurred until periodic maintenance outages were carried out every 2 years. Figure 12 explains the operational modeling results of the BAU scheme.

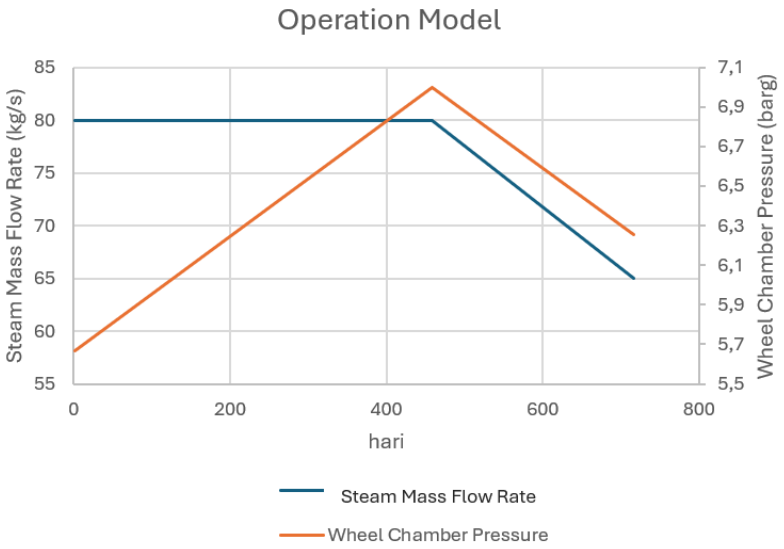

Figure 12: Operation Model Results of BAU Scheme.

Until 2045, the steam wash scheme gets a Net Present Value (NPV) of IDR 3,711,527,813,835.86, while the BAU scheme gets an NPV of IDR 3,595,106,010,845.23, so that using the steam wash system provides a profit of IDR 116. 421,802,990.63 compared to if the deposition problem was only resolved by mechanical cleaning every maintenance outage every 2 years.

4. CONCLUSIONS

The steam wash system has been designed to prevent deposition on the turbine caused by impurities contained in the steam. In a system where the steam is in a superheated condition, the steam temperature needs to be lowered to the saturated steam temperature so that the steam can then be condensed. To reduce the temperature of superheated steam at a pressure of 7.7 bar abs with a mass flow rate of 80 kg/s, injection water with a temperature of 25°C and a pressure of 8.7 bar abs is required as much as 0.3757-0.3814 kg/s, or about 0.5% of the mass of superheated steam. Variations in the mass flow rate of injection water are caused by differences in distance from the injection point to the point of complete mixing. The total power required for the water conditioning system that supplies injection water is 2923.07 W, where this system can produce injection water with Total Dissolved Solids of 4.94 ppm. In addition, there is a conditioned water storage tank that can retain water for 10.25 hours during operation of the steam wash system, and can be fully filled in 4.53 hours with the injection process still running.

Using the steam wash system until 2045 provides a profit of IDR 116,421,802,990.63 compared to if the deposition problem was only resolved by mechanical cleaning every maintenance outage every 2 years, during which period derating would occur due to the buildup of deposition on the turbine.

REFERENCES

Arifien, B. N., Zarrouk, S. J., and Kurniawan, W.: Scrubbing lines in geothermal power generation systems, *Proceedings*, 37th New Zealand Geothermal Workshop (2015).

Arnold, K. and Stewart, M.: Gas-liquid and Liquid-liquid Separators. Gulf Professional Publishing (2008).

Bergman, T. L.: Fundamentals of heat and mass transfer, John Wiley & Sons, New York (2011).

Chauhan, V.: Superheated steam scrubbing and untilization for power generation, *Ph.D Thesis*, Reykjavik University (2019).

Gao, S., Zhong, C., and Wang, Z.: A model describing the pressure drops across the membrane and cake layers for constant flux cross-flow microfiltration process, *Journal of Environmental Chemical Engineering*, **10**(3), (2022), 107984.

Moran, M. J., Shapiro, H. N., Boettner, D. D., and Bailey, M. B.: Fundamentals of engineering thermodynamics, John Wiley & Sons, New York (2010).

Morris, C. J., Mroczek, E. K., and Misa, T. N.: Geothermal steam condition performance monitoring, *Geothermics*, **81**, (2019), 101-112.

Mubarok, M. H. and Zarrouk, S. J.: Steam-field design overview of the Ulubelu geothermal project, indonesia, *Proceedings*, 38th New Zealand Geothermal Workshop, 23, 25. (2016).

National Library of Medicine. https://pubchem.ncbi.nlm.nih.gov/, Downloaded at July 15 2024.

Richardson, I., Addison, S., and Lawson, R.: Chemistry challenges in geothermal power generation, API Powerchem Australia (2014).

Sakai, Y.: Advanced geothermal steam turbines, Advances in Steam Turbines for Modern Power Plants, Woodhead Publishing, (2022), 549-586.

Van der Bruggen, B.: Microfiltration, ultrafiltration, nanofiltration, reverse osmosis, and forward osmosis, *Fundamental Modelling of Membrane Systems*, (2018), 25-70.

Villa Jr, R. R., Isip, J. L., Peñaranda, J. R. S., Salonga, N. D., Rubin, D. B., Bontia, U. R. P., and Saw, V. S.: Methods of Removing Solids from the Discharge of Steam Dominated Wells in Leyte Geothermal Production Field, Philippines, *Proceedings,* World Geothermal Congress 2005 (2005).

NOMENCLATURE

C_d	:	Drag coefficient
d_p	:	Droplet diameter (m)
h	:	Distance from droplet to bottom of pipe (m)
L	:	Horizontal distance needed (m)
μ	:	Steam viscosity (cP)
Q_{loss}	:	Heat loss to the environment (W per meter)
Re	:	Reynolds Number
ρ_g	:	Density of steam (kg/m3)
t_s	:	Time needed for droplet from the top to the bottom of pipe (s)
V_s	:	Steam velocity (m/s)
V_t	:	Terminal velocity of droplet (m/s)

Application of Rock Muffler Concept in Addressing Well Testing Challenges in Patuha-2 Geothermal Expansion Project, West Java, Indonesia

Nurlianto Sadji[1], Asum Sumama[1], Randy Wijaya Atmaja[2], Dito Sukarno[2], Siti Olivinia Yusra[2], Rudy Martikno[2], and Ramonchito Cedric M. Malate[3]

[1]PT JACOBS, Talavera Bldg., Jakarta Indonesia
[2]PT Geo Dipa Energi (Persero), Jakarta, Indonesia
[3]JACOBS New Zealand, Level 2 Carlaw Park, 12-16 Nicholls Lane, Auckland New Zealand

nurlianto.sadji@jacobs.com

Keywords: Patuha Geothermal Field, well testing, noise level

ABSTRACT

PT Geo Dipa Energi GDE (Persero) has embarked on the expansion of Patuha Geothermal Field in West Java, Indonesia in January 2022 based on the updated resource assessment and reservoir modelling of greater Patuha resource, follow on geoscientific studies and feasibility update of Patuha project. The expansion program called for drilling of twelve (12) production wells to support the 55 MWe Patuha-2 power plant. The drilling campaign was successfully completed in March 2024, but the programmed production well testing activities encountered a few challenges that presented some difficulties in proving the capacity of the wells.

Well testing of Patuha-2 steam wells has been programmed to generally meet the prescribed environmental, safety and social standards related to H_2S gas emissions, Brine Carry-Over (BCO) and Nosie levels that could potentially affect the nearby households/vegetation. The discharge of the wells could also potentially present some level of mineral (calcite) deposition like calcite scaling in a Patuha-1 production well. This paper discusses the modifications made to the current Atmospheric well test facility component with the application of Rock Muffler concept in addressing the BCO and Noise level issues. Additional modification using Palm Fibers to further control the BCO were successfully implemented. Discharge testing of the wells using the abovementioned novel solutions successfully addressed the BCO and noise level issues.

1. INTRODUCTION

The steam dominated Patuha Geothermal Field is in West Java province of Indonesia and about 50 kilometers southwest from Bandung city. The Indonesian government assigned PT Geo Dipa Energi (GDE) in 2002 to continue development of Patuha after the financial crisis in 1998. GDE constructed the surface gathering system in 2011 and commissioned the first 55 MWe Patuha-1 power plant in September 2014. GDE has lately embarked on the 55 MWe Patuha-2 expansion and started the drilling campaign in December 2021.

Discharge testing of Patuha-2 production wells is expected to produce single phase/dry steam fluid at the wellhead that requires measurement of enthalpy of the fluid mixture as well as the total mass flow. Here, the James Lip pressure method is initially planned to be employed in calculating the discharge enthalpy and flows using the Low-Emission Compact Muffler (LECM) unit. The programmed well testing activities encountered some challenges in addressing noise levels and Brine Carry-Over (BCO). The performance of LECM was found to be less effective in managing these issues that made GDE examine the application of portable rock muffler technology.

1.1 Low Emission Compact Muffler (LECM)

The LECM well testing unit developed by Thermochem has proven to be a robust system that provides good flow rate and enthalpy measurements for geothermal production well flow tests. The LECM units have been verified to yield good enthalpy and brine flow measurements from Mag Flow Meters on the outlet of the LECM, as well as the internal LECM unit design with baffles in the lower container and mist eliminator pads on the upper stack to improve separation efficiency and reduce brine carryover out of the top of the LECM unit.

In Patuha, a 20 ft LECM was employed as atmospheric separator for well flow testing with some modifications, where the James tube is then replaced by an orifice plate and Mag Flow Meters with the expected small amount of brine component in the discharge fluid. Figure 1 shows the schematic layout of the LECM while Figure 2 shows the modified schematic of the LECM.

1.2 Low Emission Rock Muffler Container (LERMC)

The Low Emission Rock Muffler Container is normally used to vent steam to atmosphere under pressure control for well testing purposes. Here, the bottom part of the LECM was modified where the inlet pipe into the LERMC is connected to a header pipe with several perforated pipes attached to the header to uniformly distribute the discharge fluid and flow separation is achieved. Several layers of rocks are placed on top of the discharge pipes inside the bottom rock muffler container. This configuration will ensure the steam will pass through the rock layers and exit to the atmosphere.

The upper component of the LECM was also modified with the installation of Palm fibers to reinforce the Mist Pads that were damaged during initial flow tests of Patuha wells. Figure 3 shows the schematic layout of the Low Emission Rock Muffler Container while Figure 4 shows the modified schematic layout of LECM.

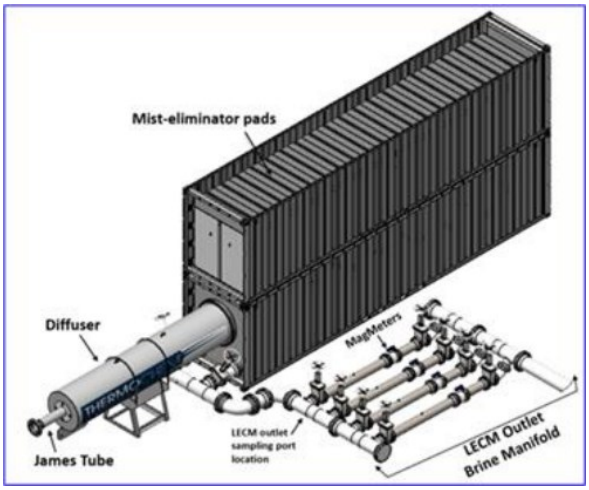

Figure 1: Schematic of the LECM components, including James tube, diffuser, mist eliminator pads, LECM outlet brine manifold, location of LECM brine outlet sampling port, and Mag Flow Meters.

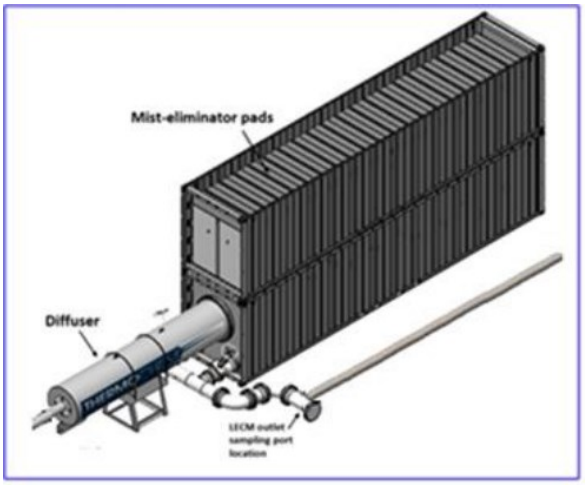

Figure 2: Schematic of the LECM components, dummy James-tube, diffuser, mist eliminator pads, LECM outlet brine outlet sampling port.

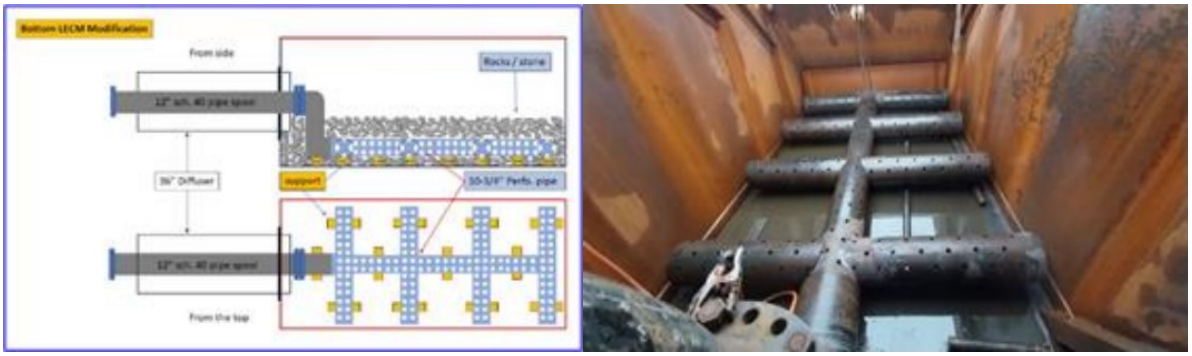

Figure 3: Schematic of the modified bottom part of LECM with the installation of rock muffler components.

1.3 Low Emission Rock Muffler Container Design Criteria

There are some engineering and environmental criteria to be considered in designing the Low Emission Rock Muffler Container (LERMC). The engineering criteria are as follows:

a. Flow capacity should be considered to avoid erosion effect and choke effect (covered by flow velocity analysis study).
b. Proper material selection for long term operation (covered by mechanical strength analysis study).
c. The foundation of rock muffler unit must be able to withstand weight load of rocks.
d. The pipe should be easy to maintain due to corrosion and erosion effect.

The environmental criteria are as follows:

a. Noise emission and proximity to inhabited areas.

b. The potential for accumulation of Non-Condensable Gas (NCG) including hazardous concentrations of H2S in the system.
c. The need to avoid steam clouds drifting over access roads, transmission lines, and local communities.

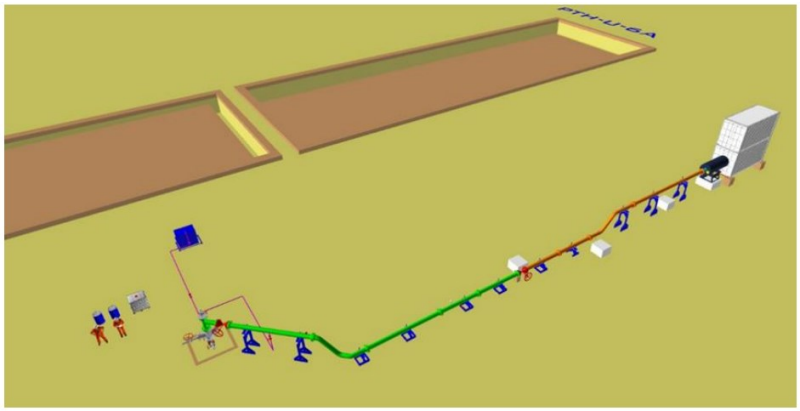

Figure 4: Well Testing Schematic using Rock Muffler.

2. PATUHA WELL TESTING PROGRAM

Horizontal discharge testing is conducted on Patuha-2 production wells to measure the discharge fluid characteristic and fluid chemistry with the aim of establishing their production characteristics. The atmospheric silencer testing method is generally the acceptable and preferable technique of testing production wells because of its low cost and simple installation. Separating the water and steam phases in a cyclone separator (pressurized) and measuring the two phases (while contained within pipelines) separately is generally considered an accurate method of testing the output of a production well.

More recently, the Low Emission Compact Muffler (LECM) is being used to replace the cyclone separator and address brine carryover during discharge test. The application of tracer flow testing (TFT) method can also be an option in establishing well flows during horizontal discharge test. The TFT method was initially developed for the on-line measurement of brine and steam flows and total enthalpy within a pipeline carrying two-phase geothermal fluid.

The well testing process at Patuha was initially designed for single phase/dry steam wells. The Patuha-2 wells are tested using a Low Emission Compact Muffler unit that allows the anticipated brine component to be separated from the steam and collected in a well site disposal pond while the steam is discharged directly into the atmospheric separator. The initial discharge of the Patuha-2 wells contained some drilling debris and good amount of brine that presented some challenges in addressing Brine Carry Over (BCO). Noise emission is generally acceptable for the single-phase discharge, but the noise levels become a concern after dry steam discharge follows, which also becomes an issue to the surrounding community.

The application of a Low Emission Rock Muffler Container was then evaluated to address the above issues especially the increased noise emission levels. The inlet pipe, complete with the header and perforated pipes, were fabricated and installed inside the container. The tank was then filled with porous rocks to reduce the produced noise level. This work can be conducted in short time using available materials in the field and can meet the standard criteria of environmental aspects.

3. ENGINEERING CALCULATIONS

The process design of Rock Muffler Container considers two methods of analyses namely:

3.1 Fluid Velocity Analysis

For pipe sizing, velocity analysis is conducted to ensure fluid velocity will not cause pipeline erosion which will shorten operating life of the pipeline. For orifice hole/perforation sizing, velocity analysis is also conducted to obtain the required pressure for the steam to pass through the holes with specified mass flow rate. Another consideration is that the rock muffler will exhaust steam which has certain mass flow rate and velocity to drag/carry the rocks. Therefore, the drag force produced should not exceed the force exerted by the rocks due to gravity to make sure the rocks will not be blown away from the rock muffler container.

For Patuha well PTH-X-1 well testing case, by assuming the median pipe pressure rate during well testing line to be 18.6 bars in 12” Flowline Sch. 40 API 5L Gr. B pipe with mass flow rate is 20 kg/s, the calculated steam velocity is around 36.5 m/s. This fluid velocity is below the maximum velocity limit for dry steam of 60 m/s.

Hence, the calculated velocity is considered acceptable considering the short term well testing duration. Routine intensive pipe thickness monitoring was also conducted to assure the pipeline reliability.

Orifice hole sizing was performed iteratively. With upstream pressure of 3.56 bara at the header pipe and downstream pressure of 2.97 bara, the diameter of hole (perforations) is measured at 27 mm with total mass flow rate is 20 kg/s (or 72.27 ton/hr.) for estimated total of 600 holes. The velocity in each hole is estimated at about 62.68 m/s (see calculation in Table 1).

Assuming the surface area of rock muffler tank is 20% and using Coefficient of Drag (Cd) of 2 and rock density of 2,500 kg/m3 with diameter (sphere type) of 200 mm, the calculated drag force is 5.3 N. This drag force is still much lower than rock's gravity force of 102.7 N. Further calculation is conducted using smaller rock diameter of 20 mm; the calculated drag force is about 0.05 N. This drag force is still lower than rock's gravity force of 0.10 N (see calculation in Table 2). Thus, it is concluded that the rocks will not be blown away from the tank for diameter greater than 20 mm.

Table 1: Calculation results for velocity analysis.

Description		Unit
Beta	0.7	
C	0.61	
Upstream P	3.56	barg
Downstream P	2.97	barg
Delta P dP	0.59	barg
Pressure Ratio dP/P	0.45	
Y straight line	0.84	
Specific volume	1.076	m3/kg
Diameter of Hole	27	mm
Flow per hole	0.036	m3/sec
Flow per hole	0.120	ton/hr
Velocity in hole	62.68	m/sec
Flow required	72.27	ton/hr
Hole made	600	ea

Table 2: Calculation results for drag force. (From Amri Zein et.al., 2010).

Description	For d = 200mm	Unit	For d = 20mm	Unit
Steam Flow	144.00	t/hr	144.00	t/hr
Area of centre portion	20.00	m2	20.00	m2
Cd	2.00	kgm/s2	2.00	kgm/s2
Plain velocity	3.39	m/s	3.39	m/s
Open Area	0.20		0.20	
Velocity	16.94	m/s	16.94	m/s
Steam Density	0.59	kg/m3	0.59	kg/m3
Diameter sphere (Rock)	0.20	m	0.02	m
Rock Density	2,500.00	kg/m3	2,500.00	kg/m3
Gravity	9.81	m/s2	9.81	m/s2
Drag	5.32	N	0.05	N
Gravity Force	102.74	N	0.10	N

3.2 Strength Analysis

Strength analysis was also conducted to ensure a fluid pressure below the limit of design pressure to have a long operating life. Pipe bursting pressure of 10.3/4 inch Grade K 55, #40.5 ppf is 1580 psi or 108.93 bar, which is much higher than shut in pressure of well PTH-X-1 (18.6 bar).

4. LOW EMMISSION ROCK MUFFLER CONTAINER VS LOW EMMISION COMPACT MUFFLER

The main issue with the flow test of PTH-X-1 is its proximity to the nearby household community (areal distance ~1 km) that would likely present concern on elevated noise emission levels during discharge test. GDE has then

implemented the use of Rock Muffler Container to address the issue. The bottom part of the LECM was then modified where the 12" inlet pipe was connected to a header pipe with several perforated pipes attached to the header. Several layers of rocks are then placed on top of the discharge pipes inside the bottom rock muffler container.

The performance of LERMC was evaluated by comparing the following discharge parameters against the parameters obtained from the previous discharge test of well PTH-Z-1 using the 20 ft LECM:

a. Noise Measurement
b. Exposure of Brine Carry Over

The noise levels recorded during PTH-X-1 discharge using the rock muffler LERMC ranged from about 69 to 88 dBA within 10 meters radial distance as summarized in Table 3 below. The noise levels obtained during PTH-Z-1 discharge using LECM ranged from 98 to 109 dBA which were much higher than noise levels using LERMC.

Table 3: Comparison of noise level monitoring results.

Day No	1	2	3	4	5	6	7	8	9	10	11	12	13	14	15	16	17
LERMC noise (dB)	83.7	77.6	69.3	69.2	71.8	80.4	72.1	84.1	81.3	85.2	82.3	78.4	85.1	86.4	87.8	85.5	88.5
LECM noise (dB)	102.3	104.2	97.9	105.1	105.2	106.2	108.8	107.1	105.4	106.6	105.2	105.4	105.7	105.0	105.2	105.2	104.0

The noise level measurements in the nearby community during PTH-X-1 discharge was found to be below 60 dBA which is much lower than the prescribed WHO noise level threshold at around 85 dBA during daytime. Figure 5 below summarizes the noise level monitoring during PTH-X-1 (LERMC) and PTH-Z-1 (LECM) discharge test.

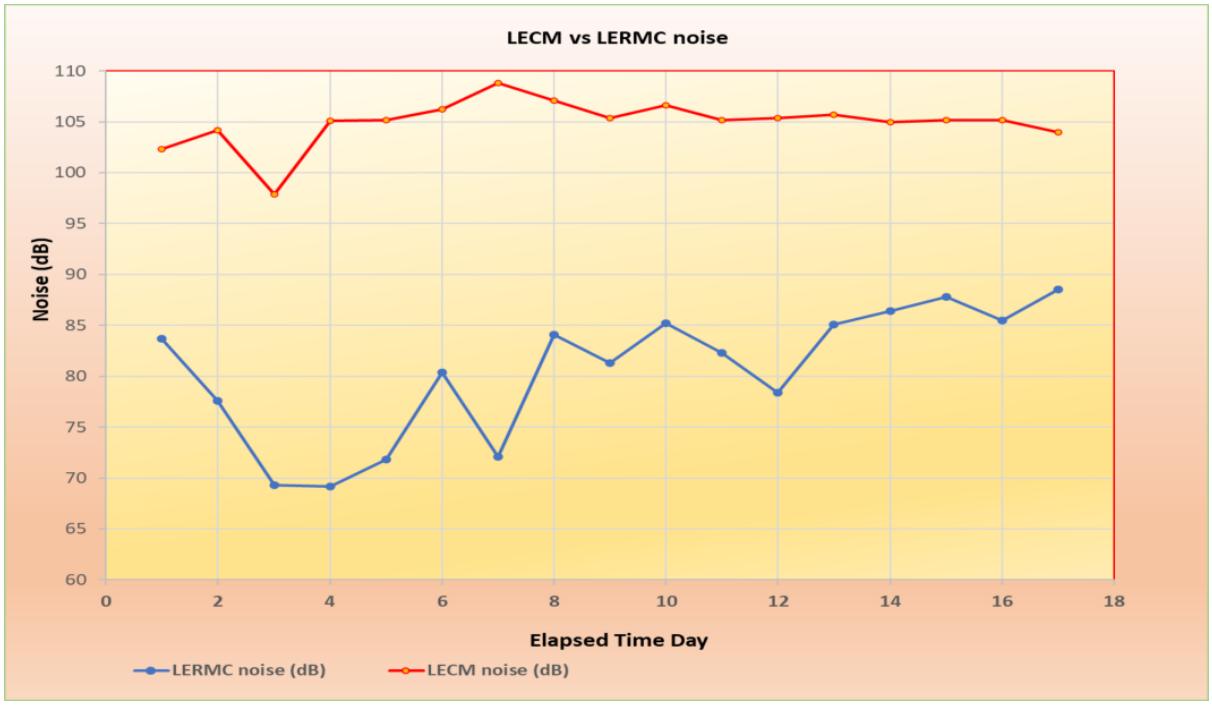

Figure 5: Noise level comparison plot.

Exposure of Brine Carry Over (BCO) was also evaluated, during PTH-Z-1 discharge test using LECM. BCO was observed within 20-to-30-meter radius of LECM. The BCO observed during PTH-X-1 flow test using LERMC is within 5 to 10 meters radial distance. The results obtained may not be conclusive since other factors such as wind speed and direction may likely affect the BCO evaluation.

5. PALM FIBER OPTION TO ADDRESS BCO

The upper component of LECM includes the Mist Pads to address the Brine Carry Over during the well discharge tests in Patuha. The Mist Pads become damaged, and its performance deteriorated after several Patuha wells tested that prompted GDE to examine other options to address BCO. The use of Palm fibers was tested and the upper LECM component was modified to accommodate the Palm fibers. Application of Palm fibers provided good control of BCO with succeeding discharge tests. Figure 6 below shows the typical Palm fiber installation undertaken during the Patuha well discharge tests.

Figure 6: Typical Palm fiber installation during Patuha well discharge test.

6. SUMMARY AND CONCLUSION

Discharge testing of Patuha-2 production wells using the abovementioned novel solutions successfully addressed the Brine Carry Over (BCO) and Noise level emission issues.

Some conclusions and recommendation are made for this study as follows:

a. The Rock Muffler Container (LERMC) can be used for well testing purposes in dry steam wells. The fluid velocity limits should be considered, which depends on well flow capacity. Further study of container rock muffler design is recommended.
b. The Rock Muffler Container (LERMC) can effectively reduce Noise emission levels and Brine carry over.
c. Application of Palm fibers to replace the Mist Pads was successfully implemented. The cost-effectiveness of using Palm fibers against the Mist Pads was successfully demonstrated apart from its single advantage to be ecofriendly.

ACKNOWLEDGEMENT

The authors wish to thank PT GeoDipa Energi (Persero) for the support and permission to publish this work. The authors also thank PT Jacobs Indonesia for the support.

REFERENCES

American Petroleum Institute. API Specification 5L, Specification for Line Pipe, 43rd Edition, 2004.

Amri Zein, Paul A. Taylor, Yudi Indrinanto, Heribertus Dwiyudha: Portable Rock Muffler Tank for Well Testing Purpose. Proceedings World Geothermal Congress 2010. Bali, Indonesia, 25-29 April 2010.

Easley Elizabeth, Nurlianto Sadji, and Winahyu Setyo Utami: Geothermal Well Testing Using a New Atmospheric Separator and Metering System in Sarulla. PROCEEDINGS, The 6th Indonesia International Geothermal Convention & Exhibition (IIGCE), Jakarta, Indonesia, 5-8 September 2018.

Grant, M.A and Bixley, P.F. “Geothermal Reservoir Engineering” 2nd edition book, Elsevier, 2001.

Analysis Of NCG, TDS, Wetness, Cl, Si0$_2$, And Na Parameters to Maintain The Quality Of 2 Phase Steam Gathering Line

Ahmad A. and Bayan I

Ahmadariza07@gmail.com, bindriyani29@gmail.com

Keywords: Steam Gathering, Steam Geothermal, Wetness, Non-Condensable Gas (NCG), Total Dissolved Solid (TDS), Contents Cl, Contents SiO_2

ABSTRACT

Geothermal energy is an important renewable energy source in reducing dependence on fossil fuels. Based on the fluid phase in the reservoir, geothermal systems are divided into single phase systems (vapor dominated) and two phase systems (water dominated). In the Dieng field, it is included in the two phase fluid system (water dominated) which contains 60% liquid phase (brine) and 40% steam phase. The PLTP generation system is a generation system that utilizes geothermal energy in the form of steam. The steam used to rotate the turbine contains chemical elements that cause scale, corrosion and erosion on the turbine. This steam will experience a decrease in pressure, temperature, enthalpy and chemical content. Steam quality is defined as a physical aspect which includes temperature (superheat), dryness (water content in a liquid state), and non-condensable gas content. High levels of impurities in the steam will reduce the purity level of the steam. It is necessary to analyze the quality of steam to get good steam. Monitoring parameters starts when steam flows to the turbine and condenser. When steam is flowed to the turbine, parameters such as Wetness, Non-Condensable Gas (NCG), Cl and SiO_2 content, Na content, total dissolved solid (TDS) will be obtained. Total dissolved solids (TDS). Then a standard will be obtained to maintain the quality of geothermal steam. If the NCG value is below 2% then it can be said that the steam quality can be used well. If the steam has a small solids content below 300 then the TDS value is said to be safe and unlikely to cause corrosion. If the steam parameters contain Cl and SiO_2 which have values below 1 ppm, the steam quality is said to be good for society. Likewise, with a Na content that has a value below 0.1 ppm, if the steam has a small Na content, the steam is said to be good. If steam has a Wetness value of less than 1% then the steam is said to contain little water.

1. INTRODUCTION

Geothermal comes from the words Geo which means earth and Therm which means heat. Geothermal energy itself is an environmentally friendly energy source that comes from the heat contained in hot water, water vapor and rocks along with their associated minerals and other gases, all of which cannot be separated genetically in a geothermal system and to utilize them requires several stages. processing.

The hot fluid will press against the surrounding rock to find a gap or way out and release the pressure. Because the pressure is higher than the pressure at the surface, the fluid will move up through the cracks. The fluid will come out as a surface manifestation. Based on the fluid phase in the reservoir, geothermal systems are divided into single phase systems (vapor dominated) and two phase systems (water dominated). In the Dieng field, it is included in the two phase fluid system (water dominated) which contains a water dominated system which is 60% liquid phase (brine) and a vapor dominated system which is 40% steam phase.

Geothermal energy is an alternative energy that has great potential to be developed in the future, especially for use as electricity generation energy, replacing dependence on the use of hydrocarbon energy sources whose reserves are decreasing day by day. Indonesia has geothermal resources reaching 40% of the world's potential and is a renewable energy source and environmentally friendly energy in its production stage. The Dieng geothermal field began to be developed in 1990. The installed power plant with a capacity of 60 MW began operating in 1998. There are 3 prospect areas in the Dieng geothermal field, Sileri, Sikidang and Pakuwaja.

Steam field project owned by PT. Geo Dipa Energi, located in Dieng, is a geothermal company operated to produce electrical power. In the geothermal processing process, of course there are many installations and pipe networks used for various geothermal production activities, one of which is the distribution pipe as a medium for transporting steam and brine.

PLTP Unit I Dieng has 44 production wells including injection wells, however, due to limitations in some wells which are no longer able to produce steam or damage to the reservoir, only 8 wells are operated as steam suppliers with an installed production capacity of 60 MW, whereas for PLTP's own injection wells The Dieng unit has 8 injection wells. On average, these production wells have a depth of around 3000 m below the earth's surface.

Each well has a different wellhead pressure ranging from 20 - 45 bar, and is capable of producing steam with different capacities. To be able to drive the turbine driving the generator requires steam that is really clean and has the lowest possible humidity level so that it is not damaging to the turbine. Because the quality of the steam produced by the Dieng production well is very low, a very complex steam processing system is needed starting from the production well, steam separation, gathering system, to the power plant.

Basically, geothermal production equipment is very important in the ongoing geothermal production to be transported to the power plant to act as a generator and power plant driver.

2. THEORY REVIEW

2.1 Steam Production Components

The steam production components here are equipment or construction related to steam production from geothermal sources. The equipment and construction include:

a) Production Well

A production well is a well that produces geothermal steam at a depth of around 3000 m below the ground surface. This well produces wet steam which still contains water so it must be separated using a separator.

b) S-bend

The S-bend functions to flow two-phase fluid from the production well to the throttle valve.

c) Throttle Valve

The throttle valve functions to regulate the flow rate and at the same time to regulate the pressure at the wellhead. The purpose of regulating pressure through the throttle valve is to prevent scaling in the wellbore. Throttle valve opening is adjusted to SSI (Silica Saturated Index).

d) Two-Phase Flow Pipe

This pipe functions to convey two-phase fluid originating from the well to the separator. This pipe has various sizes, namely: 12", 16" and 18".

e) Rupture Disk

The rupture disk functions as a safety measure if excess pressure occurs in the pipe located before the separator and in the separator. The rupture disk will break if the pressure exceeds the set pressure and the fluid will flow directly to the AFT/free silencer so that the pipe is safe from damage.

f) By Pass Valve

The function of the by pass valve is to flow two-phase fluid directly to the AFT/silencer when the well is opened or when it is about to operate, namely to check the cleanliness of the fluid before it flows to the separator. Fluid is considered clean if the results of brine sampling analysis meet existing standards, especially chloride (Cl) analysis.

g) Separator

The separator functions to separate the two-phase fluid from the production well into a vapor phase and a liquid phase. When the 2-phase fluid enters the separator, the steam will rise to the top while the brine will fall to the bottom. The steam formed is used to drive the turbine through a gathering system. The brine will be pumped by a brine pump to be injected back into the earth. The type of separator used here is a cyclone separator with a working pressure ranging from 10-14 bar.

h) Dump Valve

The function of the dump valve is to maintain the brine level in the separator according to the set point. If the dump valve experiences problems, it will fail to close which will flow to the AFT/silencer.

i) Acid Pump

The acid pump functions to pump acid into the brine through a nozzle located downstream of the separator. The acid used is sulfuric acid (H_2SO_4). This acid functions to maintain the pH of the brine between 4.7-5.2, thereby slowing down the deposition of silica in the brine distribution pipe.

j) Seal Water Pump

The water pump seal functions to pump water into the flow pipe which is paired in series with the acid pump to dilute the acid and is used as a mechanical seal water pump.

k) Atmospheric Flash Tank (AFT)/Silencer

The Atmospheric Flash Tank (AFT) or silencer functions to reduce the level of noise resulting from the production process, to flash the brine so that low pressure brine is obtained and to control the flow of fluid to be discharged. On the inside of the AFT there is a plate which is useful as a sound dampener.

l) *Kanal*/Ditch

The canals or ditches in the pad function as a place to drain the brine originating from the AFT. The brine that comes out will experience a decrease in temperature and pressure, when the temperature and pressure decrease there will be a separation of silica and brine.

m) *Balong* (Pond)

Balong or pond is used to accommodate the brine that comes out of the AFT/silencer. Brine from each pad in the batang (pond) is distributed using a brine pump to be re-injected through the injection well.

n) Silica Holding Area

Silica from the *balong* (pond) in each pad is deposited and then taken and stored in a silica reservoir. The reservoir has a filter which functions to filter the brine that enters the silica. The filtered brine is pumped to pond 29 and then injected into DNG-10 and HCE 29-A.

o) Condensate Drop Port (CDP)

The condensate drop port (CDP) is a place to dispose of condensate formed along the steam distribution on the steam line to the power plant. CDP also functions to release condensate to keep the steam quality dry until it reaches the turbine. CDP has several components such as a chamber, 1.5" and 2" valves, and a steam trap. The chamber functions to collect the condensate that is formed. The steam trap functions to automatically release condensate as a place for water vapor (condensate) output.

p) Condenser

The condenser is a tube-shaped device filled with water which functions to cool the brine by using tubing which has a spiral shape to ensure cooling occurs during brine sampling.

2.2 Steam and Brine Distribution Components

The steam and brine distribution components here are equipment related to the distribution of the results of the separation separator. This equipment includes:

a) Injection Pump (Brine Pump)

The brine pump functions to flow the brine resulting from the separation from the separator to the pond.

b) Booster Pump

A booster pump is a pump used to increase brine pressure which is installed in series with the brine pump. This pump is only used if the discharge pressure from the brine pump is insufficient.

c) Steam Line

A steam line is a pipe-shaped medium for flowing steam from a production well to a turbine which is usually 36” in size.

2.3 Supporting Components

Supporting components here are equipment or construction related to the process of generating power from the steam produced. The equipment and construction include:

a) Wellhead

A wellhead or what is usually called a well head is surface well control equipment made of steel which forms a seal system which is useful for preventing bursts or leaks of well fluid to the surface. This wellhead functions to control the flow rate of the well, monitor well head pressure, and act as a support for the casing string. In this well head there are several parts as follows:

1) Annulus Valve

The function of the annulus valve is to determine whether the production casing is leaking or not. In this component, a manometer is installed which functions to see the pressure in the valve annulus.

2) Wing Valve/Side Valve

The wing valve or side valve functions for well bleeding, which means that when the well is not producing, it does not emit steam from the top. This wing valve is used to release steam so that it does not die, because if it dies it will experience steam condensation which causes the steam to decrease in temperature so that the bowels of the earth will not reach the perfect boiling point. Apart from that, the wing valve also functions as a wellhead pressure indicator.

3) Angle Valve

The angle valve functions as a way for injection fluid to enter when well logging is carried out. When logging, the production well needs to be killed first so that no fluid will flow to the surface. Apart from that, this angle valve also functions as a wellhead pressure indicator.

4) Master Valve

The master valve is composed of an upper master valve and a lower master valve. This master valve functions to open and close the well fluid flow. The master valve is a type of gate valve, so the master valve is always 100% open (fully open) or 100% closed (fully closed). The master valve must not be left half open because there will be turbulence in the flow which can cause erosion at the corners of the gate.

5) Flow-T

Flow-T is a component that functions to direct fluid flow from the master valve to the s-bend.

6) Crown/Top Valve

The crown/top valve functions as a well survey route. Used for well maintenance, pressure and temperature measurements, and well logging.

b) Mixing Tee

Mixing Tee functions as a mixture of acid and clean water (seal water).

c) Weirbox

The Weirbox functions to roughly determine the flow rate of the production fluid and the quality of the fluid. There are 3 types of weirboxes that are often used, namely: rectangular, suppressed, triangular. The type often used in Dieng Unit I is the rectangular weirbox type. Currently the weirbox is no longer used because of the large amount of silica that has deposited.

d) Valves

A valve is a component that functions to control flow and pressure in a system. In general, the types of valves used, especially at PLTP Dieng, are gate valves, ball valves and check valves.

e) Sumur Injeksi

Injection wells function to inject cooled brine into the bowels of the earth. This is done by keeping the cycle in the bowels of the earth running, so that the Dieng PLTP process can continue to produce.

2.4 Electric Power Plant Component

Power generation components here are equipment or construction related to the process of generating power from the steam produced. The equipment and construction include:

a) Rock Muffler

A rock muffler is a block-shaped structure containing rocks which functions as a safeguard for steam from excessive pressure before it enters the power plant, as well as reducing noise that occurs when steam is emitted.

b) Scrubber

A scrubber is a tool that has the same function as a separator, namely as a final separator before the steam enters the turbine, as well as as a steam purifier. The purpose of this separation in the scrubber is to separate the steam from the water that is still carried during the distribution of steam in the steam line. By using a scrubber, it is hoped that the steam entering the turbine is truly dry steam that is free from the liquid phase.

c) Demister

A demister is a tool in the form of a cylindrical tube and inside it there is a grid to eliminate water droplets and solid particles contained in the steam. This component functions as a filter for particles that are still carried by the steam, so that the steam entering the turbine is completely dry. This is done as an effort to avoid vibration, erosion and scale formation processes on the turbine.

d) Turbin

The turbine functions to drive a generator using steam power from a production well that has been processed first.

e) Governor

The governor functions to control the steam entering the turbine. By controlling the amount of steam entering the turbine, the turbine rotation can also be adjusted to either increase or decrease. The governor consists of two components, the first to measure or detect speed, the second to translate this measurement into movement at the governor output to control equipment that regulates the amount of steam entering the turbine.

f) Generator

The generator functions to produce electricity from the rotation of the turbine. The generator used has an installed capacity of 60 MW, frequency of 50-60 Hz and rotation speed of 3000 rpm.

g) Transformator

A transformer is equipment used to increase or decrease voltage. 15kV/150kV step up transformer and 150kV/15kV step down transformer. This transformer has two functions, when the generator is on, the transformer functions to step up or increase the voltage from 15kV to 150kV. If the generator is being overhauled or is not operating, the transformer functions to step down or reduce the voltage obtained from PLN by 150kV to 15kV.

h) Main Condenser

The steam that has been used to drive the turbine is fed into the condenser which functions to condense the steam that has been used to rotate the turbine. The condensation process is carried out by mixing the steam coming out of the turbine with cooling water directly. Cooling water is obtained from the cooling tower which is sprayed at the top of the main condenser.

i) Steam Ejector

This component functions to maintain vacuum conditions in the condenser by sucking in non-condensable gas (NCG) or gas that cannot be condensed in the main condenser and expelling it through the cooling tower by being sucked in by the fan and expelled into the open air.

j) Hot Well Pump

This pump is very vital for use in power plants. This pump is directly connected to the main condenser, namely to drain condensate with a temperature of 33°C to be cooled to the cooling tower. The amount of condensate with a volume of around ±5,400,000 liters requires a pump with a very large capacity to move it, especially since the steam supply from the turbine runs continuously so that to keep the main condenser vacuum (with a water level of around 40% of the total volume), the condensate must be moved , this is done because the condensed steam will increase the volume of the condensate.

k) Cooling Tower

The type of cooling tower used is a mechanical draft cooling tower. In a mechanical draft cooling tower, hot water from the condenser is sprayed on a wooden structure in layers called fill. When passing through the fil, heat transfer occurs from the hot water to the air (at the top of the cooling tower there is a fan). The cooling tower used has 9 pairs of fans.

2.5 Geothermal Power Plants

The electricity generation process at the Dieng PLTP has several stages, namely separating steam and brine in the separator, removing moisture from the steam (moisture remover) in the scrubber, then the steam is passed to the turbine and produces electricity in the generator. Steam quality plays an important role in geothermal power plants. High levels of impurities in the steam will reduce the level of purity of the steam. If the steam used to rotate the turbine contains impurities, it is likely that the turbine will experience corrosion so that the rotation of the turbine rotor connected to the generator does not work optimally, which will result in the generator's output power not being optimal. Therefore, it is necessary to analyze the quality of steam to get good steam.

In geothermal power plants (PLTP), various types of fluids such as hot water, hot steam, salt solutions, organic fluids, supercritical CO2, and hydrocarbon fluids are used based on the geological characteristics and temperature of the PLTP location to produce electrical energy.

PLTP Dieng is a Geothermal Power Plant located in the tourist area of Dieng, Central Java. Dieng PLTP is one of several PLTPs owned by PT Geo Dipa Energi (Persero), a company operating in the geothermal energy sector in Indonesia. PLTP Dieng has a capacity of 60 MW and consists of two units, namely Unit 1 and Unit 2. Unit 1 has been operating since 2011, while Unit 2 is currently under construction and is expected to be operational in 2024.

In an effort to increase the use of geothermal energy in Indonesia, the government is targeting increasing the role of geothermal energy in the energy mix for electricity generation from 5% to 11% by 2025. This is in line with the vision of PT Geo Dipa Energi (Persero) to become a thermal energy company leading earth in Indonesia and contributing to national energy security.

The type of PLTP development in Dieng uses the flash PLTP type. PLTP Flash Steam uses hot water mixed with steam from a geothermal reservoir as a working fluid. This hot water has a temperature higher than its boiling point at atmospheric pressure. When this hot water is drawn to the surface and the pressure is reduced, it boils and turns into steam. The steam produced is used to drive turbines and electric generators.

Flash PLTP is more flexible than dry PLTP. The advantage is that it can be used in areas with geothermal sources that contain hot fluids, even in areas with lower geothermal temperatures.

The steam that flows into the turbine then moves the turbine rotor and spins the generator. The electric charge is also generated from the rotation of the magnet in the generator and the electricity flows through copper cables to the transformer where the voltage is increased before being distributed to homes. After the steam works in the turbine, the remaining steam from the turbine (exhaust steam) which has lowered pressure and temperature will flow to the condenser to be condensed (water steam). Main steam comes out of the turbine along with the NCG (Non Condensable Gas) contained in it. The condensation process is assisted by cooling water to speed up the phase change process. Meanwhile, NCG from the condenser is pulled by the ejector towards the intercondensor and then cooled using cooling water by spray which is pumped by the ACWP (Auxiliary Cooling Water Pump) from the cooling tower.

The condensate from the condenser is then pumped by the HWP (Hot Well Pump) to the cooling tower. If the water level in the cooling tower is excessive, it will be channeled to the injection well to increase natural filling of the reservoir to maintain reservoir pressure and extract more heat from the hot reservoir.

2.6 Steam Quality

The PLTP generation system is a generation system that utilizes geothermal energy in the form of steam. The steam is obtained from wells that have been made by Pertamina. Steam from the well is channeled to the steam receiving header, which functions to ensure that the steam supply does not experience disruption even if there is a change in supply from the production well. The steam is channeled to a separator to separate solid substances, silica and water spots carried in it. This is to avoid vibration, erosion and scale formation on the turbine which will rotate the generator.

The quality of geothermal steam is no less than boiler steam. Under the same pressure conditions, geothermal steam is usually drier than boiler steam due to its superheated nature. General parameters of steam quality are Wetness, Non-Condensable Gas (NCG), Cl and SiO2 content, Na content, total dissolved solid (TDS). Total dissolved solid (TDS) is the total amount of substances dissolved in water. The dissolved solids or salt content of water present as ions increases the electrical conductivity of water. The higher the conductivity, the greater the potential for corrosion. A higher value of total dissolved solids will reduce the rate of heat transfer, increase scale deposits and will increase heat loss (Kamal, 2019).

Steam quality is defined as a physical aspect which includes temperature (saturated), dryness (water content in liquid condition), and non-condensable gas content. High levels of impurities in the steam will reduce the purity level of the steam (<1). Taking into account the decrease in pressure and temperature which will have an impact on reducing the MW produced and allow condensation to occur in the steam flow pipe which will result in corrosion of the turbine which will endanger the continued operation of the geothermal plant.

The steam used to rotate the turbine contains chemical elements that cause scale, corrosion and erosion on the turbine. This steam will experience a decrease in pressure, temperature, enthalpy and chemical content. Steam quality is defined as a physical aspect which includes temperature (superheat), dryness (water content in a liquid state), and non-condensable gas content. High levels of impurities in the steam will reduce the purity level of the steam. Geothermal steam contains many minerals such as salt, silica, sodium and other minerals. Most of the decline that occurs in steam is behind the decline in steam quality (Triyana, 2016).

To calculate steam quality, use the equation (Muharrir & Hajar, 2019):

$$x = \frac{s1 - sf}{sg - sf} \quad (1$$

Where :

x = Steam Quality, S1 = Entropy Value Steam Pressure Entry of turbin, sf = Entropy values saturated liquid Steam pressure out Turbine, SG = Entropy values saturated vapor vapor vapor pressure out of turbine.

Entropy is a thermodynamic quantity that functions to measure energy in units of temperature that cannot be used to do work. The entropy of a closed system will always increase and in heat transfer conditions the heat energy will move from components at high temperature to components at low temperature. To determine the enthalpy and entropy values of the steam used in the generating system in this research, you can use a saturated steam table. If the pressure or temperature data is inaccurate, it is necessary to interpolate the data. In this research, data interpolation can be used, which is intended to determine a value that is between two known values. This interpolation is based on comparative theory. In this study, comparisons were made between the steam pressure value entering the turbine and the enthalpy of saturated vapor (h1), the value of the steam pressure entering the turbine with the entropy of saturated vapor (s1), the value of the steam pressure leaving the turbine with the enthalpy of saturated liquid (hf), the steam exiting pressure. turbine with saturated vapor enthalpy (hg), turbine exit steam pressure with saturated liquid entropy (sf), and turbine exit steam pressure with saturated vapor entropy (sg).

3. RESEARCH METHODOLOGY

3.1 Introduction

By reviewing related and relevant literature, both literature from the company and outside the company, interviews and field observations at the company.

3.2 Data Collection

The data required is standard parameter monitoring data from the fluid laboratory.

3.3 Data Analysis

To maintain steam quality, it is also necessary to analyze the parameters that are monitored. One way to maintain steam quality can be seen from measuring the efficiency of the separator which can be done by comparing the chloride (Cl) content between steam and brine. Checking chloride levels in steam and brine is carried out using the Mohr argentometric titration method and analysis of chloride (Cl) content is carried out in the laboratory. The smaller the concentration of chloride that dissolves or is carried away by the steam, the better the working efficiency of the separator as a separation tool to produce good quality steam. Table 1 is the standards for monitoring steam quality parameters. Optimizing and maintaining steam quality can be seen based on standards set by the laboratory.

Table 1: Steam Quality Standards.

Parameter	Geothermal Steam
Non-Condensable Gas (NSG)	Less than 2%
Steam Wetness	Less than 1%
Cl Content	Less than 1 ppm
SiO2 Content	Less than 1 ppm
Na Content	Less than 0,1 ppm
Total Dissolved Solid (TDS)	Less than 300

4. DISCUSSION

As can be seen in the picture, monitoring parameters starts when steam flows to the turbine and condenser. When steam is flowed to the turbine, parameters such as Wetness, Non-Condensable Gas (NCG), Cl and SiO_2 content, Na content, total dissolved solid (TDS) will be obtained. Total dissolved solids (TDS). Then a standard will be obtained to maintain the quality of geothermal steam. If the NCG value is below 2% then it can be said that the steam quality can be used well. If the steam has a small solids content below 300 then the TDS value is said to be safe and unlikely to cause corrosion. If the steam parameters contain Cl and SiO_2 which have values below 1 ppm, the steam quality is said to be good for society. Likewise, with a Na content that has a value below 0.1 ppm, if the steam has a small Na content, the steam is said to be good. If steam has a Wetness value of less than 1% then the steam is said to contain little water. Steam temperature is also an important factor the quality of a geothermal well.

The higher the steam temperature, the better the quality. From the observation results, the steam temperature was quite stable for each well. Laboratory analysis of well condensate samples (SCS) shows that the anion and cation content is relatively stable. The concentration of silica in well fluid is still far below the solubility of silica at temperatures above 100oC, but developments must still be monitored. An increase in the Sulphate/Chloride ratio can indicate the entry of water resulting from steam heating into the reservoir.

REFERENCES

Agus Adhi, Ardy Kusumma, Dedi Nugroho, Analisa Efisiensi Kinerja Generator G-101 pada Pembangkit Listrik Tenaga Panas Bumi; Jurnal Transistor EI, Universitas Oslam Sultan Agung, Semarang, 2022.

Boedihardi, M., Suranto, Sudarman, S., Evaluation of the Dieng Geothermal Field; Review of Development Strategy, Proceeding Indonesian Petroleum Association 20th Annual Convention, Indonesia (1991).

DiPippo, R., 2008: Geothermal power plants: Principles, applications, case studies and environmental impact (2nd edition). Butterworth-Heinemann (Elsevier), Oxford, 520 pp.

Dr. Páll Valdimarsson, Geothermal power plant cycles and main components, UNU-GTP and LaGeo, in Santa Tecla, El Salvador, January 16-22, 2011.

Gudmundur Kjartansson, Low Pressure Flash-Steam Cycle at Hellisheidi-Selection Based on Comparison Study of Power Cycles, Utilizing Geothermal Brine, Proceedings World Geothermal Congress 2010, Bali, Indonesia, 25-29 April 2010.

Karlsdottir et al., Comparison of Methods for Utilization of Geothermal Brine for Power Production, World Geothermal Congress 2010, Bali, Indonesia.

PT. Geo Dipa Energi (Persero) Internal Report, Detail Geological Mapping of Dieng Field. Unpublished report for PT Geo Dipa Energi (Persero) (2013).

PT. Geo Dipa Energi (Persero) Internal Report, Detail Well Targeting, Subsurface Project Development and Execution Process (SPDEP) Phase 2, Unpublished report for PT Geo Dipa Energy (Persero) (2021)

PT. Geo Dipa Energi (Persero) Internal Report, Development Drilling Plan, Unpublished report for PT Geo Dipa Energi (Persero) (2019).

PT. Geo Dipa Energi (Persero) Internal Report, Dieng and Patuha Expansion Feasibility Study, Unpublished report for PT Geo Dipa Energi (Persero) (2019)

PT. Geo Dipa Energi (Persero) Internal Report, Dieng Completion Report: Drilling Performance Workshop, Completion Report, Unpublished report for PT Geo Dipa Energi (Persero) (2019)

PT. Geo Dipa Energi (Persero) Internal Report, Resource Target Area of Dieng, Subsurface Project Development and Execution Process (SPDEP) Phase 1, Unpublished report for PT Geo Dipa Energy (Persero) (2020)

Van Bemmelen, R. W., Geologi of Indonesia vol. IA, Second Edition, Martinus Nijhoff/The Hague, Belanda. p. 29, 595, 615-616. (1970)

Successful Drilling Campaign at Karaha Bodas Geothermal Field: Overcoming Challenges and Optimizing Performance

Edyson, Priozky Purba, Gatra Kusuma, and Fery Malau

Pertamina Geothermal Energy

mk.edyson@pertamina.com, priozky.purba@pertamina.com,
GKusuma@slb.com, fery.malau@pertamina.com

Keywords: Geothermal Well, Drilling Engineering, Drilling Operations, Pipe Stuck, NPT

ABSTRACT

In the dynamic landscape of geothermal energy production, Karaha Bodas stands as a significant asset within the portfolio of PGE. Despite its importance, the power plant at Karaha Bodas has faced challenges, notably a high reservoir decline rate of 24% since 2019. The PGE drilling campaign of 2023-2024 initially targeted the drilling of only a single well in the Talaga Area, namely the TLG-3.4 well. Well TLG–3.4 aimed towards the western side, where the fracture network is predominantly composed of pyroclastic rocks, fault models, and lateral permeability, with a planned total depth (TD) of 2400 mMD. However, the drilling operation encountered significant challenges, including a stuck pipe and Lost in Hole (LIH) at a depth of 2189 mMD within the 12-1/4" hole section. Despite these challenges, the well managed to recover three out of four drilling targets. Encouraged by the promising results from logging surveys, PGE Management decided to expedite the drilling campaign by adding the TLG-3.5 well to the schedule. Targeting a similar direction as TLG-3.4, the TLG-3.5 well aimed to leverage on the potential identified in its predecessor while striving for optimal outcomes and embracing the challenge of reaching the planned target depth. With approximately only one month of preparation, the PGE Drilling Team conducted a thorough internal evaluation to address operational and engineering concerns from the stuck pipe incident in TLG-3.4. This paper presents the success story of the PGE Drilling Team in the drilling of the TLG-3.5 well, achieving the target total depth without encountering a stuck pipe and minimizing Non-Productive Time (NPT) to a remarkable 0.35%, compared to TLG-3.4's NPT of 15.74%. It underscores the resilience, adaptability, and technical prowess demonstrated in overcoming obstacles and advancing geothermal exploration in Karaha Bodas.

1. INTRODUCTION

In the GWA (Geothermal Working Area) Karaha-Cakrabuana located in West Java, Indonesia, there is a geothermal prospect known as Karaha-Talaga Bodas. Within this prospect, GGGR (Geological, Geophysical, Geochemical, and Reservoir) studies and drilling have been conducted. Based on the GGGR study, the reservoir is divided into three areas, each with different characteristics. The southern part (Talaga) is a reservoir area with acidic reservoir fluid. The central part (Karaha) is a reservoir area with neutral pH fluid. The northern part (G. Putri) is a reservoir area with medium temperature and low permeability. Based on the reserve calculations using the volumetric heat stored method, it is concluded that the proven reserves of the Karaha geothermal prospect are 30 MW. Geothermal system of Karaha–Talaga Bodas is partially vapor-dominated and fracture-controlled, situated in the northern area of the Galunggung Volcano.

Currently, there is only one power plant unit in this region, commissioned in 2018. The Karaha Power Plant, operated by PT Pertamina Geothermal Energy Tbk, has installed capacity of 30 MW, contributing substantially to the region's energy needs. Despite its importance, the power plant at Karaha Bodas has faced challenges, notably a high reservoir decline rate of 24% since 2019 due to several subsurface issues such as very acidic reservoir fluid, scalling problem, well integrity concerns, and other complications.

Despite these intricate challenges, PGE perseveres in continuously seeking strategic solutions to restore the Karaha Power Plant to its original production capacity. As part of the solution, initially a single make–up well, named TLG–3.4 will be drilled in the Karaha area during PGE 2023 – 2024 drilling campaign. TLG–3.4 well aimed towards the western side, where the fracture network is predominantly composed of pyroclastic rocks, fault models, and lateral permeability, with a planned total depth (TD) of 2400 mMD. Unfortunately, it didn't turn out smoothly according to plan. During the drilling operation, challenges such as rig equipment problem, water supply shortage, slow rate of penetration (ROP), and pipe stuck were encountered. The Non-Productive Time (NPT) for this well amounted to 170 hours, with 100 hours due to pipe stuck incidents, 46 hours due to shortage of water supply, 20 hours due to rig equipment failure, and 3.5 hours due to aerated drilling equipment failure. The financial loss due to the pipe stuck incidents is estimated to be around 1.1 million USD for compensating the BHA equipment left in the wellbore, along with an additional 500,000 USD in daily operational costs for the efforts to

free the stuck pipe. With an NPT of 170 hours, or approximately 15.7% of the total drilling duration and the final total depth (TD) that could be reached only 1940 mMD due to pipe stuck and lost in hole event, there are many aspects that need to be mitigated and improved to ensure that future well drilling in the Karaha-Talaga Bodas area can be conducted more effectively and efficiently.

Despite these incidents, the well managed to recover three out of four reservoir targets with promising logging surveys results. With this good news, PGE Management decided to expedite the drilling campaign by adding the TLG–3.5 well to the schedule. Targeting a similar direction as TLG–3.4, the TLG–3.5 well aimed to leverage on the potential identified in its predecessor and enhance steam supply to Karaha Power Plant Unit 1. With approximately only one month of preparation, the PGE Drilling Team conducted a thorough internal evaluation to address operational and engineering concerns from the stuck pipe incident in TLG-3.5.

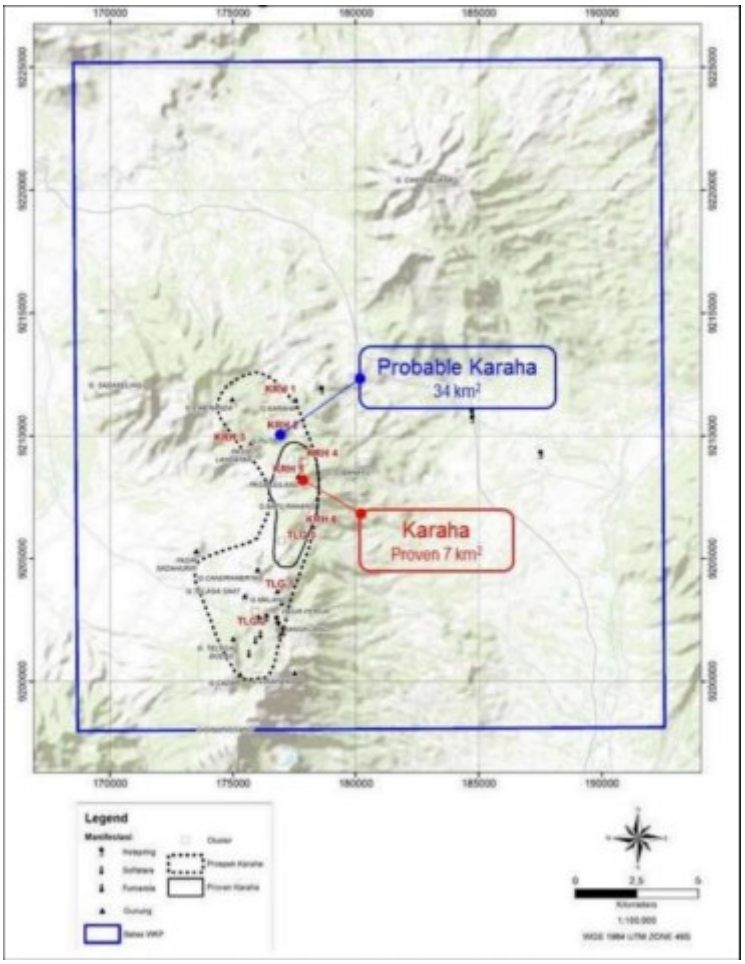

Figure 1: Geothermal Reserve Map of Geothermal Working Area (GWA) Karaha-Cakrabuana.

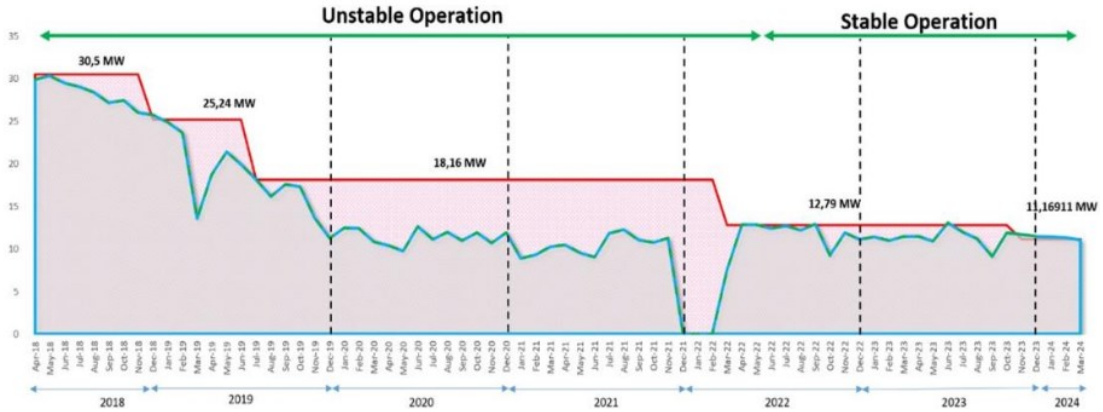

Figure 2: Electricy Production Realization of Karaha Power Plant.

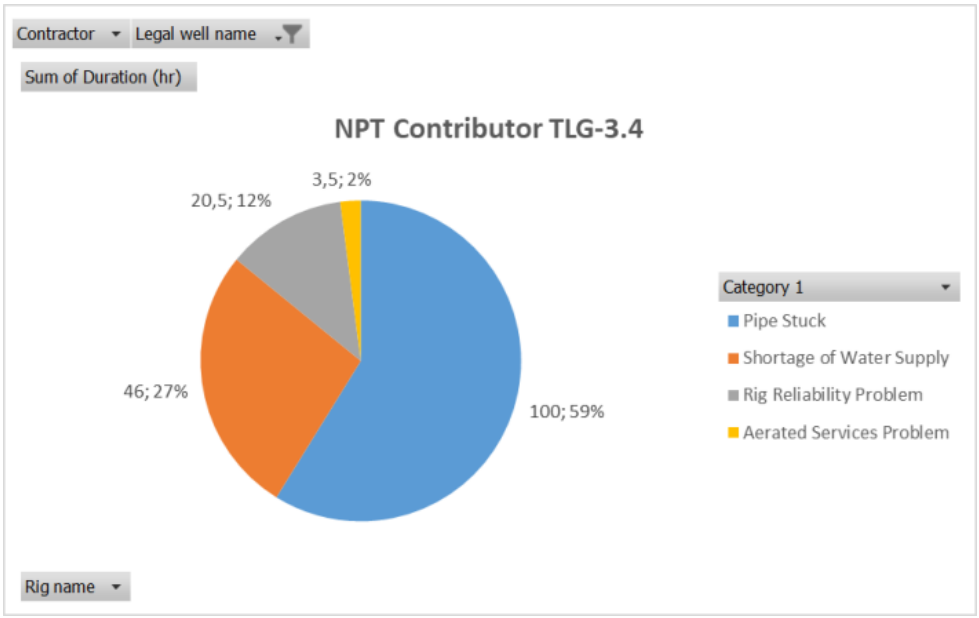

Figure 3: NPT Contributor TLG-3.4 Well.

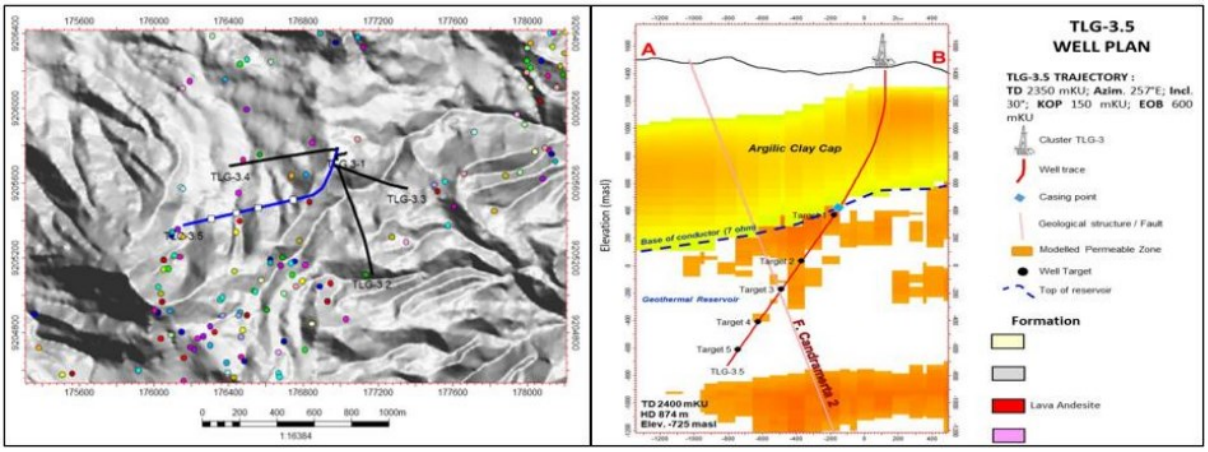

Figure 4: Target Map of Drilling TLG-3.5 Well.

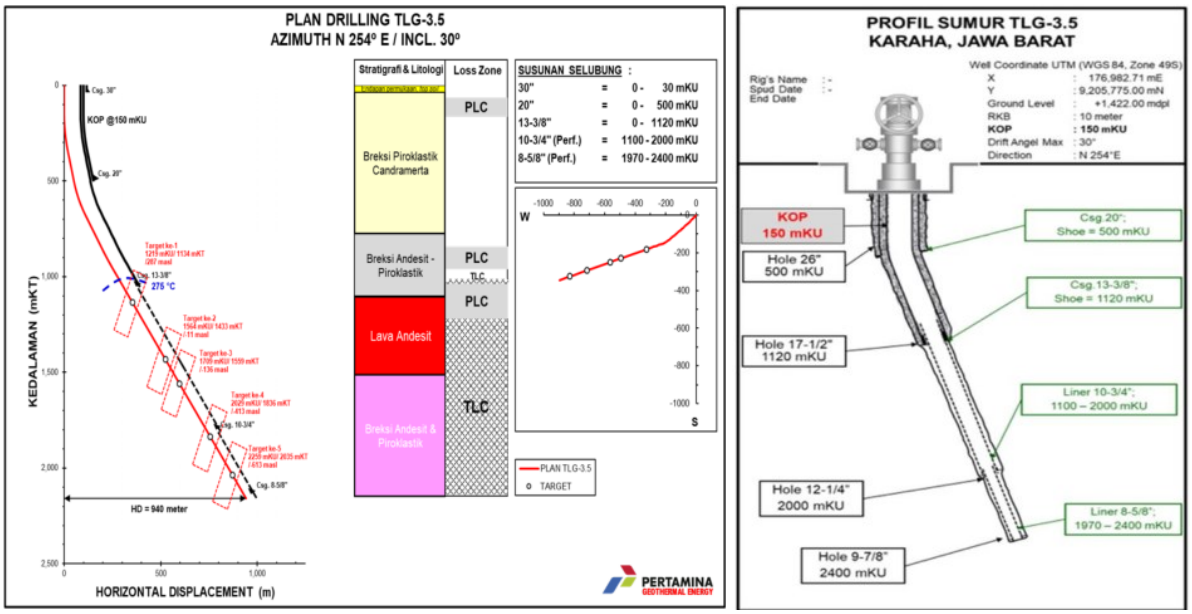

Figure 5: Directional Drilling & Well Profile Plan TLG-3.5 Well.

With well budget allocation and planned drilling time similar to TLG-3.4, the TLG-3.5 well is designed as big hole well type with 5 hole sections (36", 26", 17-1/2", 12-1/4", 9-7/8") and total depth (TD) of 2400 mMD.

2. KARAHA BODAS KEY CHALLENGES

2.1 Short Preparation Time For Materials And Documents

Originally there were no plans to drill the TLG-3.5 well during the 2023-2024 drilling campaign which made this a significant shift in strategy. The decision to drill the TLG-3.5 well was made on short notice due to the promising steam potential discovered in the TLG-3.4 well. PGE management recognized the opportunity to optimize mobilization costs and accelerate the fulfillment of steam supply needs, so they decided to move forward with the TLG-3.5 well immediately after the completion of TLG-3.4. As a result, the PGE drilling team faced the challenge of preparing for this new well in a compressed timeline of approximately 1.5 months, starting from scratch. The compressed timeframe presented several challenges:

- **Budget Administration**: The allocation and approval of the budget for TLG-3.5 had to be fast-tracked. This required intense coordination between the drilling team and PGE's financial department to ensure that funds were made available without delay. Streamlining the budget administration process was crucial to prevent any bottlenecks that could hinder the timely commencement of drilling operations.
- **Prognosis & Drilling Program Development**: Developing a comprehensive drilling prognosis and program under such tight deadlines was another significant hurdle. The drilling team had to quickly analyze the data from TLG-3.4, incorporate lessons learned, and create an optimized drilling plan for TLG-3.5. This involved rapid decision-making and close collaboration between geologists, engineers, and operational planners to ensure that all potential risks were addressed and that the well design was both robust and efficient.
- **Procurement and Supply Chain Management of Drilling Materials**: Procuring drilling materials and equipment, which is usually a time-consuming process, needed to be expedited. The team had to quickly secure various items, from casing and accessories to bits, within a short timeframe. To address this, team decided to transfer several drilling materials from other PGE areas to speed up the process.

Despite these challenges, the PGE drilling team managed to spud the TLG-3.5 well on schedule. This achievement was made possible through intense collaboration across departments, the acceleration of key processes, and the team's ability to adapt quickly to changing circumstances.

2.2 Limited Water Supply

Due to its geographical location, the Karaha-Talaga Bodas area is situated in a mountainous region, which presents several challenges related to water availability. The region's limited water sources are heavily dependent on rainfall, making water supply unpredictable and variable. Additionally, local communities rely on these water sources for their daily needs, further straining the availability of water for industrial use. Given these constraints, drilling activities in the Karaha-Talaga Bodas area are typically scheduled only during the rainy season (November – January). Water supply is critical in geothermal drilling operations for several reasons. It is essential for lifting drilling cuttings, cooling various bottom hole assembly (BHA) tools, preventing well kicks, and maintaining overall drilling efficiency. Inadequate water supply can lead to significant operational issues, including delays in drilling, increased costs, higher risks of equipment failure, and other safety hazards.

In the existing water line system of the region, two operational water sources are available for drilling purposes: Pancuran 7 and Talaga-2. However, the water from these sources has certain limitations. Due to their proximity to the crater, the water is acidic and sulfuric. These properties can pose additional challenges, such as corrosive effects on equipment and potential complications in managing water quality during drilling operations.

2.3 Absrasive Formation

In geothermal drilling, abrasive formations refer to geological layers or rock formations that contain hard, abrasive minerals such as quartz, feldspar, or volcanic rocks. These minerals are particularly challenging for drilling operations due to their hardness and abrasive nature, which leads to significant wear and tear on drilling equipment. As a result, drilling through these formations often results in increased maintenance costs, slower drilling progress, and a higher likelihood of equipment failure. The TLG cluster, specifically within the 12-1/4" hole sections, is known to have abrasive formations. Based on drilling history and lithology studies, this section is predominantly composed of Lava Andesite formations that have undergone significant alteration, with silica and total mineral content ranging from 60% to 79%. This high level of alteration makes the rock even more challenging to drill through.

Given these difficulties, the type of drill bit used becomes critically important. Different type of bits can produce varying types of cuttings and result in different hole geometries, which can either facilitate or hinder the drilling process in such abrasive environments. Therefore, selecting the appropriate bit and precisely designing the Bottom

Hole Assembly (BHA) are essential to successfully navigating these challenging formations, so that the drilling operation can penetrate abrasive zones efficiently, minimizing downtime and reducing costs while maintaining the integrity of the wellbore and equipment.

2.4 Pipe Stuck TLG-3.4

During the drilling operation of the TLG-3.4 well, the team encountered significant challenges with two times of pipe stuck incidents. which occurred at depths of 1937 and 2195 mMD. The first pipe stuck incident occurred at a depth of 1937 mMD after the initial appearance of Total Loss Circulation (TLC) at 1915 mMD in the 12-1/4" hole section. Fortunately, the issue was resolved after several jarring jobs, allowing the drill string to be freed from the stuck point. The team then decided to pull the drill string to the surface and replace the Bottom Hole Assembly (BHA) with a new one. The second pipe stuck incident occurred at a depth of 2195 mMD in the 12-1/4" hole section. Unfortunately, this issue could not be resolved despite several jarring jobs, leading to the decision to perform a mechanical back-off. Multiple attempts were made to fish the BHA left in the wellbore, but these efforts were unsuccessful, resulting in the loss of the entire Bottom Hole Assembly (BHA) within the well. This incident not only caused considerable cost overruns but also significantly extended the drilling time, as the team had to manage the aftermath of the stuck pipe and replace the lost equipment. Due to this pipe stuck event, The Non-Productive Time (NPT) amounted to a total of 100 hours, severely impacting the overall efficiency of the drilling operation. The illustration of this pipe stuck incident is shown in Figure 6.

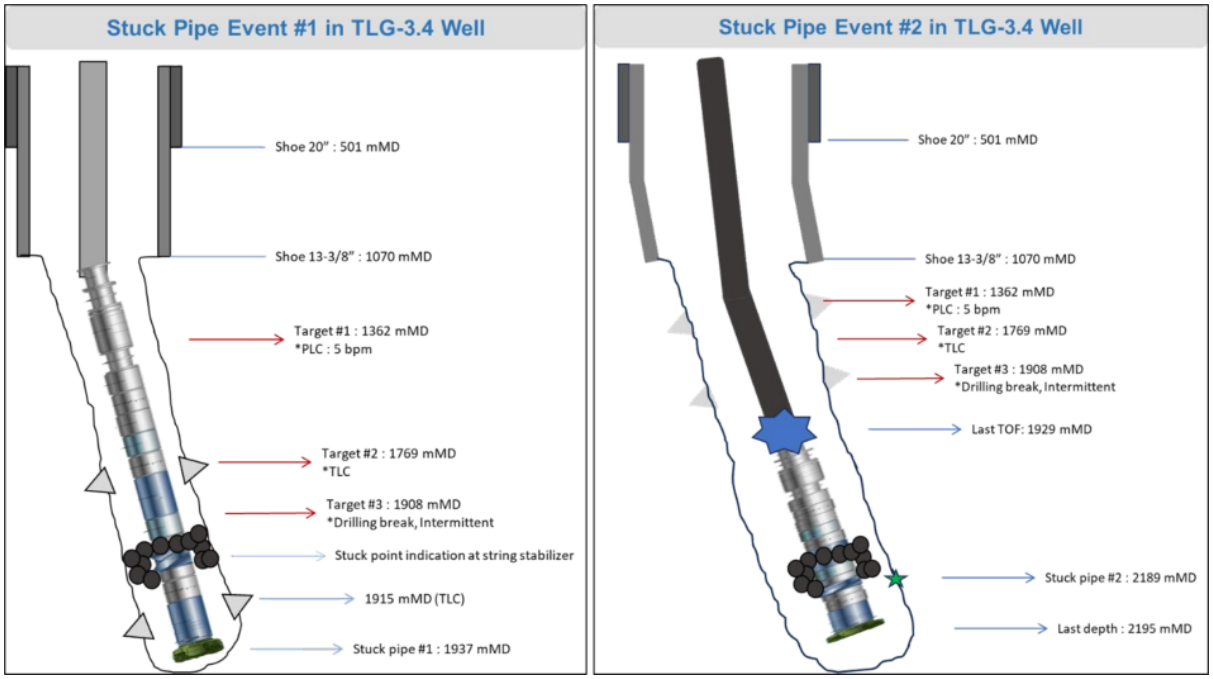

Figure 6: Pipe Stuck Ilustration of TLG-3.4 Well.

Several factors have been identified as root causes of the pipe stuck incidents in the TLG-3.4 well, particularly in the zone with total loss circulation. These issues include ineffective hole cleaning, excessive sliding drilling, and inadequate control of drilling parameters.

- **Ineffective Hole Cleaning**: The practice of hole cleaning in the TLG-3.4 well was insufficiently executed under total loss circulation condition, resulting in a significant build-up of cuttings and debris within the wellbore. As these materials gather, they can obstruct the path of the drill pipe, creating a situation where the pipe may become stuck in the wellbore. This issue was clearly shown by the Torque and Drag chart of TLG-3.4 well, which displayed anomalies and deviations from the expected simulation chart, as shown in Figure 7.
- **Excessive Sliding Drilling**: The frequent use of sliding drilling under total loss circulation conditions can contribute to pipe stuck event because the drill pipe moves along the wellbore without surface rotation, reducing the hurling effect on cuttings compared to rotating drilling mode.
- **Inadequate Control of Drilling Parameters**: Drilling parameters such as weight on bit (WOB), rotation speed (rpm), and rate of penetration (ROP) must be controlled, especially under total loss circulation conditions. This is to ensure that the volume of cuttings produced does not exceed the capacity for removing them from the wellbore. Failure to manage these parameters effectively can also lead to pipe stuck events.

With the root causes identified, the PGE drilling team will focus on improving hole cleaning practices, optimizing drilling techniques, and better controlling drilling parameters. These measures are intended to significantly reduce the risk of pipe sticking in future well drilling operations.

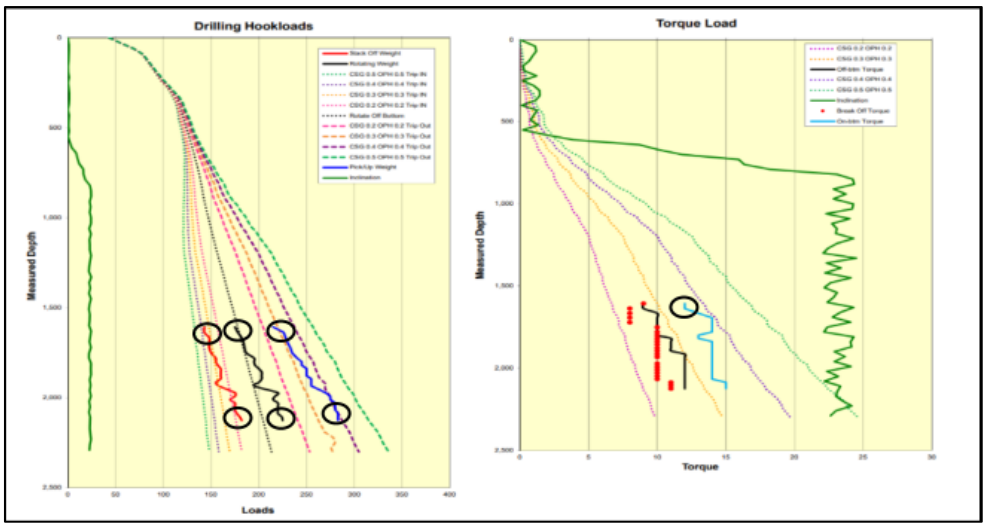

Figure 7: Torque and Drag Chart TLG-3.4 Well.

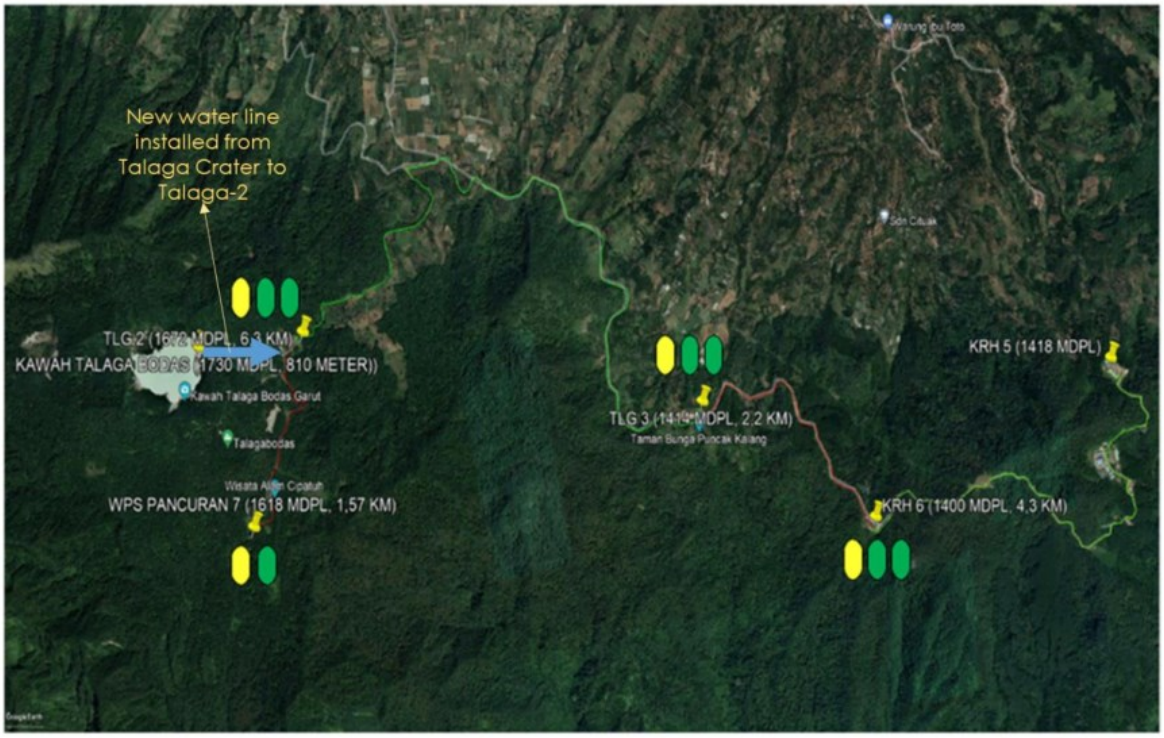

Figure 8: New Water Line System for TLG-3.5 Well.

3. KARAHA BODAS KEY SUCCESS

3.1 Water Supply Strategic Improvement

In the case of the TLG-3.4 well, the PGE Drilling Team encountered a shortage of water supply when drilling under total circulation condition in 12-1/4" hole section. Even though it was the rainy season, the main water source can't supply the required minimum flow rate of 1200 GPM, which was essential for continuing drilling. The insufficient water supply posed a risk to the drilling operation, making it necessary to halt drilling until the water supply could be restored to adequate levels. As a result of this issue, Non-Productive Time (NPT) accumulated to 46 hours. This is the second largest contributor to NPT in this well after the pipe stuck issue. The water supply for the TLG-3.4 drilling operation depended to WPS Pancoran 7 and Talaga 2. However, these sources were inadequate for providing the necessary flow rate for effective drilling. Approximately 1 kilometer

from WPS Talaga 2, there is a large reservoir known as Talaga-Bodas Crater. Despite its proximity and potential, this water source had never been utilized, and a water line connecting it to the drilling site had not been installed. To address this challenge and prevent similar issues in future operations, the PGE Drilling Team came up with an idea to improve water supply reliability by tapping a new water line system that bypassed directly from Talaga Crater to Talaga 2 using 6" pipe. This improvement allows for a stable water flow rate of 1200 GPM into the wellbore because the Talaga-2 water source has larger capacity to accommodate larger volumes compared to Pancuran 7. However, the water reaching the drilling site still had acidic and sulfuric properties, making it unsuitable for direct use. Therefore, the water was first collected in the rig's active tank, where it underwent treatment with KOH (potassium hydroxide) to neutralize the acidity and make it safe for equipments in drilling operations.

3.2 Trajectory & BHA Design Improvement

The TLG-3.5 was designed as a 3D well with a J-shaped trajectory, which had a maximum inclination of 30° and was oriented to an azimuth of 254°. The KOP (Kick-off Point) was designed to start at a depth of 150 mMD, and the End of Build (EOB) was expected to be completed before reaching the Total Loss Circulation (TLC) zone, thereby minimizing the need for corrections or sliding drilling in the TLC zone. Based on the root causes and lessons learned from the TLG-3.4 well, the following improvements have been made regarding trajectory and BHA design:

Casing Point Adjustment: Initially, TLG-3.4 well was designed with a casing point of 10-3/4" at a depth of 2400 mMD to maximize the steam potential from the existing feed zone. However, the appearance of erratic torque in the 12-1/4" section indicated that continuing drilling under these conditions posed a significant risk of pipe stuck. Thus, the casing point for the 10-3/4" casing of TLG-3.5 well was adjusted to 2100 mMD. After that, drilling continued with a 9-7/8" section to reach the total depth (TD).

TLG-3.4 Well Design

No	Hole Size / Section (in)	Section Length (m)	Casing Size (in)	Casing Point Depth (mMD)	Casing Type
1	36	30	30	30	Stove Pipe
2	26	500	20	500	Intermediate
3	17-1/2	785	13-3/8	1285	Production
4	12-1/4	1015	10-3/4	2300	Perforated Liner
5	9-7/8	400	8-5/8	2700	Perforated Liner

TLG-3.5 Well Design

No	Hole Size / Section (in)	Section Length (m)	Casing Size (in)	Casing Point Depth (mMD)	Casing Type
1	36	30	30	30	Stove Pipe
2	26	500	20	500	Intermediate
3	17-1/2	620	13-3/8	1120	Production
4	12-1/4	980	10-3/4	2100	Perforated Liner
5	9-7/8	300	8-5/8	2400	Perforated Liner

Figure 9: Casing Point Adjustment.

Bit Run for 12-1/4" Section TLG-3.4 Well

Number of Runs	Merk	IADC	Dull Grade In	Dull Grade Out	Depth In (mMD)	Depth Out (mMD)	Drilling Meterage (m)	Bit Hours (hrs)	ROP avg (mnt/mtr)	ROP avg (mtr/hrs)	WOB avg (klbs)	Reason to POOH
1st	Smith	716	New Bit	2-3-WT-S-X-1/8-BT-BHA	1070	1578	508	58,9	6,96	8,62	27,7	Slow ROP
2nd	Smith	537	New Bit	2-4-WT-C-E-1/8-CT-BHA	1578	1937	359	35,44	5,92	10,13	40,6	After pipe stuck and jarring job event
3rd	Smith	435	New Bit	Lost in Hole	1937	2195	258	19,45	4,52	13,26	35,3	Lost in Hole

Bit Run for 12-1/4" Section TLG-3.5 Well

Number of Runs	Merk	IADC	Dull Grade In	Dull Grade Out	Depth In (mMD)	Depth Out (mMD)	Drilling Meterage (m)	Bit Hours (hrs)	ROP avg (mnt/mtr)	ROP avg (mtr/hrs)	WOB avg (klbs)	Reason to POOH
1st	Smith	537	New Bit	4-8-BT-G-E-1/8-LT-HR	1111	1547	436	56,83	7,82	7,67	33,8	Due to max krev achieved
2nd	Smith	517	New Bit	3-1-WT-A-E-1/16-BT-HR	1547	1959	412	42,02	6,12	9,80	23,6	Due to max krev achieved
3rd	Smith	537	New Bit	1-1-WT-A-E-I-NO-TD	1959	2100	141	15,69	6,68	8,99	28,2	Reached CP

Figure 10: Bit Run for TLG-3.4 & TLG-3.5 Well.

- **Trajectory Tendency Management**: In TLG-3.4, drilling in the 12-1/4" hole section exhibited a tendency to drift left due to drilling through fracture zones. The main target for both TLG-3.4 and TLG-3.5 was directed to the main fault. When the well intersected the main fault, the direction was further affected by the fault's dip, causing a stronger leftward tendency. To address this challenge, the drilling engineer adjusted the strategy for drilling this section by aligning the directional work to the right side of the directional plan. This strategy aimed to minimize the need for corrections or sliding drilling in the reservoir section. Since it was identified that TLG-3.4 got stuck prior to correcting or sliding in the reservoir section.
- **Jar Setting Modification**: To accommodate a wider range of WOB (Weight on Bit) during drilling of the 12-1/4" section, the team decided to replace several 5" HWDP (Heavy Weight Drill Pipe) below the jar with severals 6-1/2" DC (Drill Collar), increasing the weight below the jar by 5 to 10 klbs. The additional WOB also improved efficiency for penetrating abrasive formations compared to TLG-3.4.
- **Bit Selection**: Because of bit stock availability, the bit selection for the TLG-3.4 well involved using two types: PDC (Polycrystalline Diamond Compact) and TCI (Tungsten Carbide Insert) Tri-Cone Bit. Both types of bits have different cutting mechanisms. The PDC bit uses a mechanism with a fixed, shear-cutting action that is effective in softer formations but can wear down more quickly in abrasive

conditions. On the other hand, the TCI bit employs a rotary, impact-cutting mechanism that is more durable and suited for harder, abrasive formations. In addition, this led to inconsistencies in the type of cuttings produced, variations in hole geometry, and the formation of ledges along the well trajectory. To address these issues in the TLG-3.5 well, the team decided to use a single bit type, TCI bit. This strategy helps ensure a more uniform and accurate hole shape, which is crucial for successful drilling operations and minimizing additional downhole challenges.

3.3 Drilling Parameter Gameplan

Offset wells data plays a pivotal role across design and execution phases. These datasets offer essential insights into parameters shaping drilling conditions. Analyzing past operational behaviors provides engineers with a clearer view of anticipated outcomes and potential challenges. When designing wells, several critical factors are considered to optimize performance and mitigate risks.

MD	SWOB MIN	SWOB MIN	SWOB MAX	SWOB MAX	SRPM MIN	SRPM MIN	SRPM MAX	SRPM MAX	FLWI MIN	FLWI MIN	FLWI MAX	FLWI MAX	DIFF PRESS MIN	DIFF PRESS MIN	DIFF PRESS MAX	DIFF PRESS MAX
m	*Klbf*	*Klbf*	*Klbf*	*Klbf*	*c/min*	*c/min*	*c/min*	*c/min*	*gal/min*	*gal/min*	*gal/min*	*gal/min*	*psi*	*psi*	*psi*	*psi*
1100	15	20	30	35	30	40	50	60	800	850	880	900	20	50	100	200
1300	15	20	30	35	30	40	50	60	800	850	880	900	20	50	100	200
1500	15	20	30	35	30	40	50	60	800	850	880	900	20	50	100	200
1700	15	20	30	35	30	40	50	60	800	850	880	900	20	50	100	200
2100	15	20	30	35	30	40	50	60	800	850	880	900	20	50	100	200

Figure 11: Optimum Operating Window.

Foreseeing subsurface hazards is paramount, involving comprehensive geological and geophysical assessments to identify potential challenges such as unbalanced formation pressures, lost circulation, or hard, abrasive formations that can impact service quality. Through meticulous planning and strategic measures, all these risks were effectively managed, ensuring operations followed trajectory plans precisely, achieving targets safely and efficiently. As shown in Figure 12, optimum parameters were established based on this data and were implemented during the operation, demonstrating enhanced performance and successful drilling outcomes in the TLG-3.5 well. This improvisational effort aims to cultivate mutual understanding and commitment among stakeholders, paving the way for seamless implementation by the project team. By translating these strategies into actionable steps, these teams are poised to execute effective solutions that not only address current inefficiencies but also establish a pathway to sustainable operational excellence in drilling operations. During monitoring phases, this historical data becomes crucial as real-time metrics are continuously compared against established benchmarks from offset wells.

3.4 Hole Cleaning Practice

In this section, concerns and best practices related to hole cleaning under total loss circulation conditions (17-1/2", 12-1/4", & 9-7/8" Hole Section) will be described. These best practices has been applied in drilling the TGL-3.5 well, which is part of the lessons learned from TLG-3.4. Drilling under total loss circulation conditions is a tricky and challenging job because we can't be exactly sure whether the produced cuttings have been safely transported to secure zone or not. The objective of drilling under total loss conditions is not to bring the cuttings to the surface but to lift them to the disposal zone (fracture) or at least as high as possible away from the BHA area, which has the smallest clearance to the wellbore. Without good hole cleaning practices, drilling cannot proceed and may cause pipe stuck issue. In addition, total loss conditions can result in an insufficient hydrostatic column in the wellbore, potentially causing a well or steam kick. Therefore, here are some best practices to ensure effective hole cleaning in the wellbore:

- Perform wash and ream 3 times after reaching stand down depth or before making the next DP connection.
- Conduct air bypass before doing connection for the next string at depth of 1 jts off bottom.
- Execute two times Hi-Vis with sweeps per DP stands
- Apply 1 joints off-bottom during drilling in total loss conditions.
- Ensure connection time does not exceed 5 minutes.
- Maintain ROP within safe range to ensure that the cuttings we produce are balanced with our lifting capacity.
- Use two float subs in the DP assembly to avoid kick through the string.
- At the first occurrence of total loss circulation, observe the well's reaction. If a well kick occurs, begin preparations to pump water via the annulus. Pump water within safe range via annulus to mitigate the risk of well kick from the annulus.
- Apply adequate water flowrate (gpm) and air flowrate (scfm) according to the drilling program, ensuring the total mixture flowrate does not exceed an equivalent of 900 gpm (limitation of 8" mud motor).

- Use foam and corrosion inhibitors (with formula as per drilling program) during aerated drilling to assist with cuttings lifting and prevent corrosion on the tubular string.
- If sliding drilling is unavoidable during total loss conditions, polish the hole along the slide interval (raise the string 1-2 m above the initial slide interval without rotation, then continue rotating the string until the last drilling depth).
- After TD is reached, do wiper trip drill string until the last casing point depth.

3.5 Drilling Parameter Real Time Monitoring

Real-time monitoring of drilling parameters refers to the continuous and immediate observation of various indicators during the drilling operation such as WOB, ROP, RPM, and torque. The real-time monitoring system must be accessible and monitored directly both of personnels in the field and engineer at the head office so that immediate adjustments can be made in case of operational changes and anomalies, enhancing operational efficiency, enabling data-driven decision-making, ensuring compliance with regulations, and facilitating continuous improvement across department in the future. For instance, during the drilling of the 12-1/4" and 9-7/8" hole sections under challenging total loss circulation conditions, real-time monitoring provided immediate feedback on the effectiveness of hole cleaning practices. Any deviations in the expected performance, such as a drop in ROP or an unexpected increase in torque, could be quickly addressed by adjusting drilling parameters or implementing corrective actions like additional wash and ream cycles, additional sweep Hi-Vis, or lowering drilling parameter. Additionally, the data collected in real-time served as a valuable resource for post-drilling analysis, contributing to continuous improvement in drilling practices and strategies.

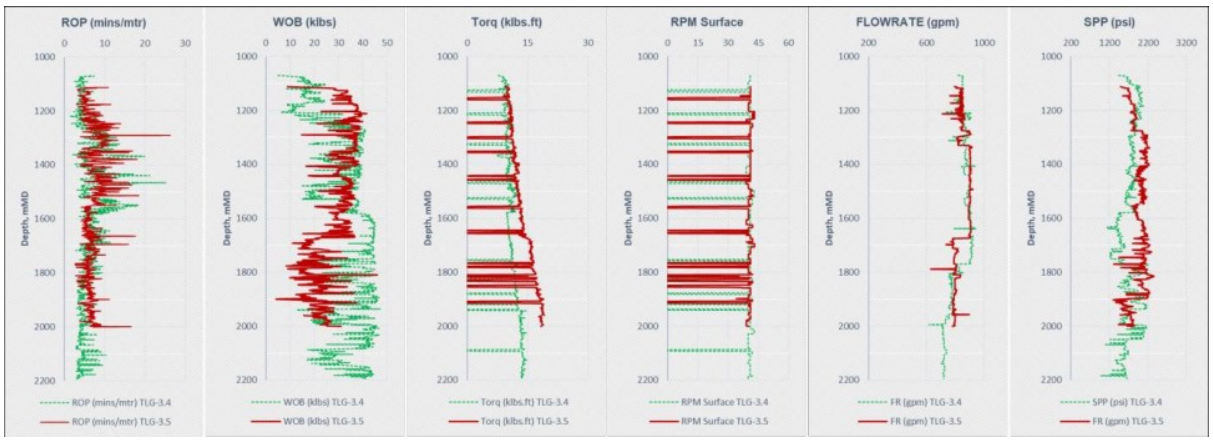

Figure 12: Drilling Parameter Real Time Monitoring TLG-3.5.

Another parameter that needs to be monitored is the Torque and Drag Chart. Torque refers to the rotational force required to turn the drill string and bit, while drag refers to the frictional resistance that the drill string encounters as it moves through the wellbore. Both parameters are crucial for assessing wellbore conditions and understanding whether the drill string is experiencing excessive torque or if cuttings are not being effectively removed. If the torque values exceed expected levels, it describes that the drill string is encountering more resistance than anticipated. This could be due to inadequate hole cleaning, leading to the accumulation of cuttings or other debris that causes friction. By monitoring the torque values in real time, the drilling team can identify if the drill string is experiencing excessive torque and take corrective actions to mitigate the issue. This can be seen in Figure 14, marked in red circle. Starting at a depth of 1800 mMD, the values for pick up, slack off, rotating weight, on-bottom, and off-bottom torque showed excessive increases. Then, drilling was halted to normalize parameters and consider continuing drilling until the casing point at 2100 mMD with close monitoring.

4. RESULTS AND DISCUSSIONS

As a result of implementing the various lessons learned and best practices from previous operations, the TLG-3.5 well was successfully completed in both a timely and cost-effective manner. The well reached its target depth of 2403 mMD as planned, with no incidents of pipe stuck, steam kicks, or other significant downhole issues. This successful execution led to substantial cost savings, amounting to approximately 30% of the planned budget, and the project was finished 29% ahead of the scheduled timeline. The non-productive time (NPT) for this project was exceptionally low, totaling only 3.5 hours, which constitutes just 0.35% of the total drilling days. This NPT was due to the overheating of check valves from aerated drilling equipment, but the issue was quickly troubleshooted. In comparison to other wells drilled within the TLG cluster, the TLG-3.5 well has the best NPT and drilling time performance to date. In addition, all of 5 reservoir targets were hit within the center-to-center distance coverage.

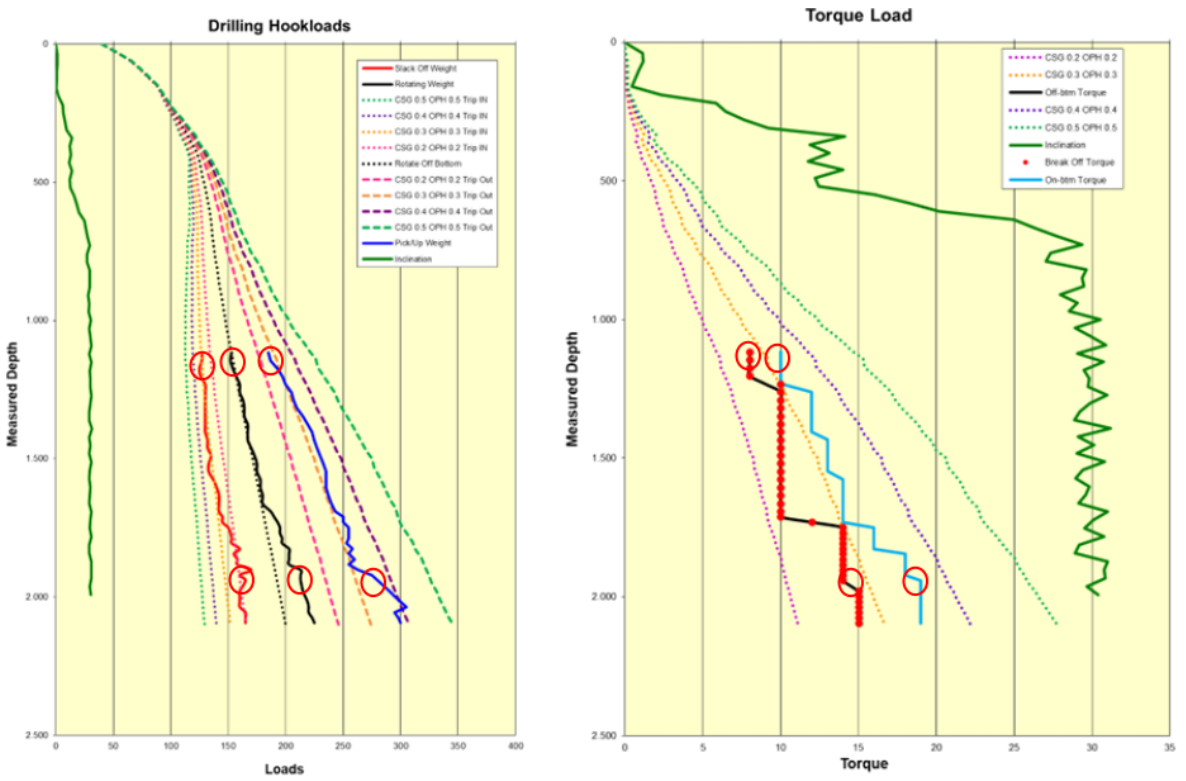

Figure 13: Torque and Drag Chart TLG-3.5.

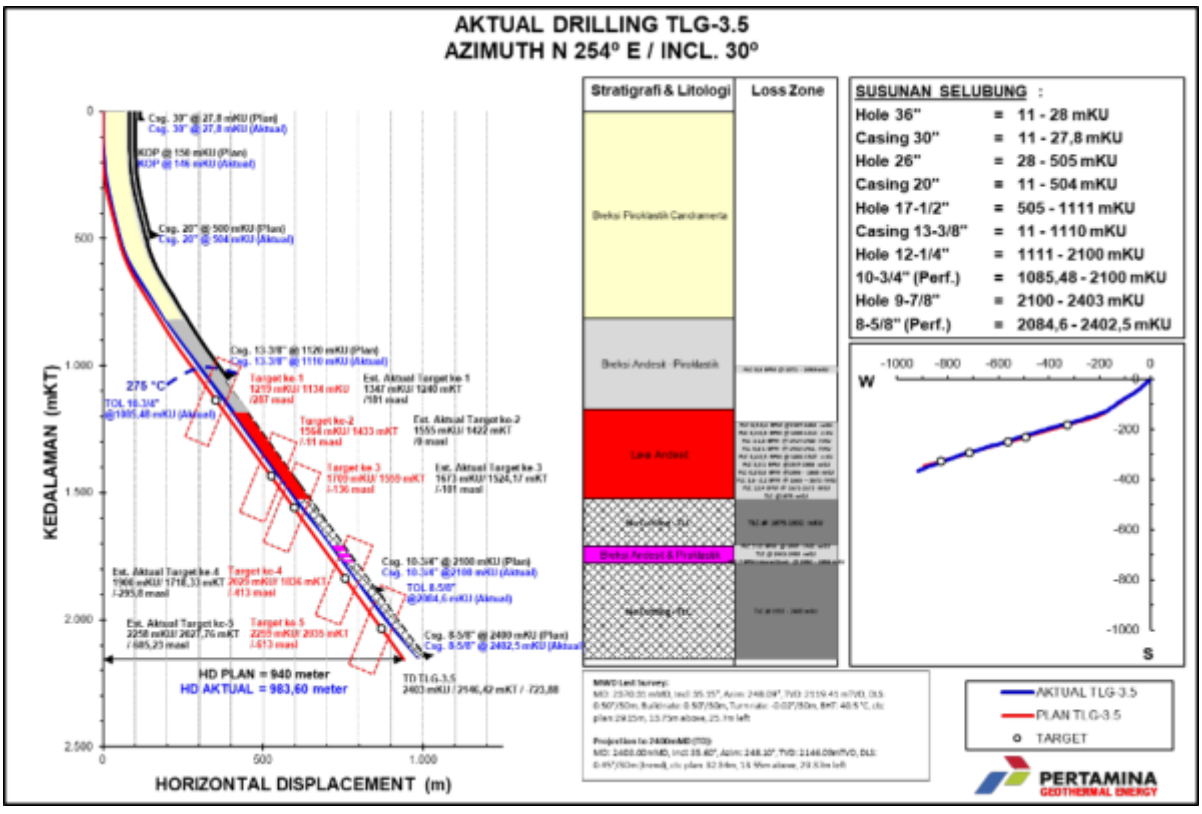

Figure 14: Actual Well Profile & Lithology - TLG-3.5.

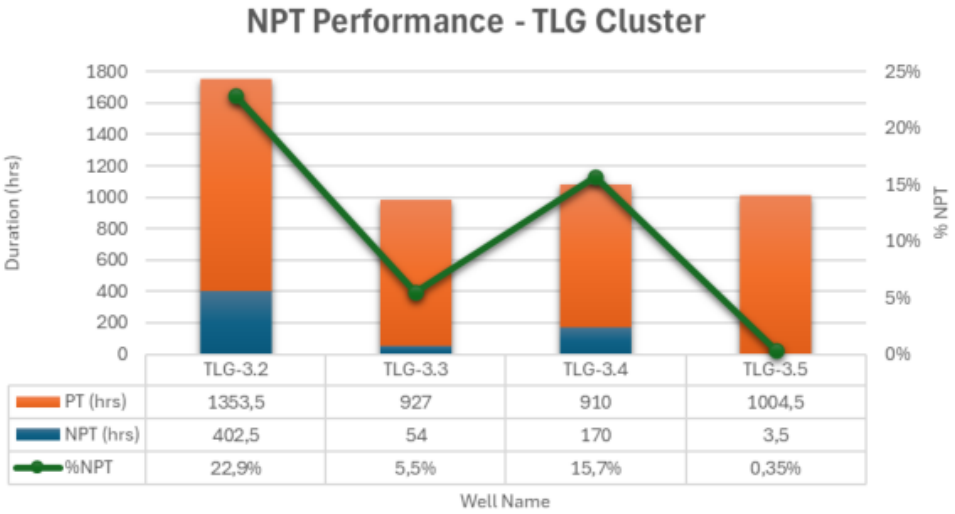

Figure 15: NPT Performance - TLG Cluster.

Based on logging surveys and reservoir simulation, the TLG-3.5 well has the potential to supply steam in line with the P50 target. With this potential addition, it is hoped that the TLG-3.5 well can be a key to the puzzle for restoring the Karaha Power Plant to its original production capacity

5. CONCLUSIONS

The success story of drilling the TLG–3.5 well is a result of comprehensive and in-depth collaboration between drilling engineering and drilling operations, as well as the lessons learned from the TLG–3.4 well. The unconformities encountered during the drilling of the TLG–3.4 well were not viewed as setbacks but rather as valuable experiences for drilling better wells in the future. From a drilling engineering perspective, the factors that contributed for preparing a comprehensive drilling program for TLG–3.5 drilling are as follows:

- Detecting and mitigating all drilling hazards to anticipate and prevent undesired problems during the operation
- Redesigning the wellbore trajectory and BHA tally to accommodate the existing limitations in the reservoir
- Determining the most optimal drilling parameters for each section to achieve the best drilling performance

On the other hand, drilling operations play an important role in ensuring that the actual drilling sequences proceeds according to the plan determined by all stakeholders, as follows:

- Ensure the reliability and suitability of all rig equipment and service companies before drilling operations commence to minimize unnecessary non-productive time (NPT).
- Review hole cleaning practices and ensure they are executed as planned to ensure the cuttings produced during drilling are lifted to safe area in order to prevent pipe stuck issues.
- Close monitor drilling parameters in real-time to immediately intervene and rectify any anomalies during drilling operations.

The drilling design and best practices used at the TLG–3.5 well will serve as a reference for the TLG-3.6 well, the next makeup well in the cluster. For the geothermal industry, the author hopes that the success story of drilling the TLG-3.5 well will serve as an inspiration and milestone in geothermal well drilling and reservoir development.

REFERENCES

Aromaharmuzi A. (2015). ”Pertamina Geothermal Energy Drilling Campaign”, Proceeding World Geothermal Congress 2015, Melbourne.

Finger J. and Blankenship D. (2010). “Handbook of Best Practices for Drilling”. Sandi National Laboratories, New Mexico.

PGE Drilling Team. (2023). “Drilling Program TLG-3.4”, PT Pertamina Geothermal Energy, Jakarta.

PGE Drilling Team. (2023). “Drilling Program TLG-3.5”, PT Pertamina Geothermal Energy, Jakarta.

PGE Drilling Team. (2023). “Final Well Report TLG-3.4”, PT Pertamina Geothermal Energy, Jakarta.

PGE Drilling Team. (2023). “Final Well Report TLG-3.5”, PT Pertamina Geothermal Energy, Jakarta.

Nemcok, M et al. (2006). “Controls on the Karaha–Talaga Bodas geothermal reservoir, Indonesia”, Geothermics Vol 36, USA.

Rawan M. (2018). “Drilling Planning and Operation of Deepest Geothermal Well in Asia”. 43rd Workshop on Geothermal Reservoir Engineering, California

Rigorous Calculation for PSV Liquid Thermal Expansion in Cooling Water Service of Inter Condenser in Geothermal Operation

Wijaya Jatmiko Putro and Wibisono Yamin

PT Star Energy

wjot@starenergy.co.id, qwaa@starenergy.co.id

Keywords: thermal expansion, PSV

ABSTRACT

This paper presents a rigorous analysis of the adequacy of Pressure Safety Valve (PSV) capacity for thermal expansion scenarios in the cooling water service of an inter condenser within a geothermal operation. Conventional calculations for PSV capacity were reviewed and found to lack consideration of critical factors such as variable heat transfer rates, temperature-dependent fluid properties, and manufacturer-specific empirical formulas. To address these limitations, a rigorous calculation approach was employed, incorporating dynamic simulations and detailed heat transfer reduction phenomena. The results indicate that while conventional calculations suggest the current PSV is inadequate, rigorous calculations demonstrate that the PSV capacity is sufficient to handle the required relief rates. The study concludes that the existing PSV does not require upgrading and recommends further Hazard and Operability (HAZOP) studies to assess the necessity and scenarios for PSV deployment. This analysis underscores the importance of considering real-world phenomena and manufacturer-specific data in PSV sizing and selection.

1. INTRODUCTION

Pressure Safety Valves (PSVs) are critical components in geothermal operations, ensuring the safe release of excess pressure to prevent equipment damage and potential hazards. This study focuses on the adequacy of PSV-YYY, which protects the inter condenser in a geothermal cooling water system. The inter condenser, a key component in the geothermal process, transfers heat from non-condensable gases (NCG) and steam to cooling water. The PSV is designed to relieve pressure caused by thermal expansion of the cooling water, which can occur if the cooling water flow is blocked while the hot side remains active.

Conventional calculations for PSV capacity often rely on simplified assumptions, such as constant heat transfer rates and fixed fluid properties, which may not accurately reflect real-world conditions. This study revisits these calculations, incorporating a more rigorous approach that accounts for variable heat transfer rates, temperature-dependent fluid properties, and manufacturer-specific empirical formulas. The goal is to verify whether the current PSV capacity is adequate for the thermal expansion scenario and to identify any potential need for PSV upgrades.

Conventional calculations have been done to check the capacity adequacy of PSV-YYY. Review for that calculation is conducted to verify calculation result. From the review, there are some items that need to be considered for adequacy check of PSV. Those items are shown in Table 1.

Considering those items, further calculation was conducted. There are 2 types of calculation:

a. Rigorous calculation is conducted to get maximum and realistic result that match that real phenomenon.
b. Conventional calculation by applying maximum heat exchanger duty during operation and leakage factor is conducted as per discussion with Facility Engineering Team and Technical Authority Process.

Comparison of calculation results is summarized in Table 2.

Table 1: Required Items to be Considered for PSV Calculation.

Item	Consideration
Heat Transfer Rate	The heat transfer rate is not fixed. As the cold side fluid temperature is increasing and reach temperature of hot side, heat transfer rate will decrease accordingly since driving force for heat transfer is temperature difference
Cold Side Fluid Properties Changed	Cold side fluid (cooling water) has significant difference of properties at different temperatures. Therefore, calculation need to be conducted at any point temperature to achieve all possible highest required relief rate
Formula by Manufacturer	The manufacturer has its own empirical formula. As per API 520, it is recommended to conduct calculation by using valve manufacturer formula (Kd value by manufacturer)

Table 2: Calculation Result of Adequacy Check of PSV.

Item	PSV-YYY
Conventional Calculation	
Required Flowrate [USGPM]	22.6
Current PSV Flowrate Capacity [USGPM]	17.7
Current PSV Status	Not Adequate
Rigorous Calculation	
Required Flowrate [USGPM]	19.1
Current PSV Flowrate Capacity [USGPM]	20.1
Current PSV Status	Adequate

Therefore, the PSV is not required to be changed or upgraded for current usage. As per discussion, it is found that there is less likely PSV will pop due to thermal expansion scenario. Therefore, it is recommended to conduct further HAZOP study to assess the requirement and scenario of those PSV.

2. GENERAL INFORMATION

This report covers the review of adequacy check of current PSV capacity. Information regarding PSV and its protected equipment is shown in table 3 and table 4 below:

Table 3: Information of PSV.

PSV Item	Value / Remark
Protected Equipment	Inter Condenser
Set Pressure [barg]	5.85
Over Pressure [%]	10
Relief Pressure [barg]	6.44
Back Pressure [barg]	0 (to atmosphere)
Orifice Area [mm2]	47.74
Manufacturer	Crosby
Type	3990

Table 4: Information of Protected Equipment.

Protected Equipment	Inter Condenser
Maximum Heat Exchange [Watt]	15,852,654
Hot fluid	
Fluid name	NCG – Steam
Mass flow [kg/hr]	30,048
Inlet Temperature [C]	96.5
Outlet Temperature [C]	43.3
Inlet Pressure [barg]	-0.5445
Outlet Pressure [barg]	-0.5685
Protected Equipment	**Inter Condenser**
Cold fluid	
Fluid name	Cooling Water
Mass flow [kg/hr]	1,209,535
Inlet Temperature [C]	27.2
Outlet Temperature [C]	38.5
Inlet Pressure [barg]	4.15
Outlet Pressure [barg]	4.10
Shell (Hot side)	
OD [m]	1.092
Length [m]	7.315
Tube (Cold side)	
OD [mm]	19
ID [mm]	17.27
Length [m]	7.315
Quantity [ea]	1598

Protected Equipment	Inter Condenser
Volume [m3] (include margin 50%)	4.11
Design Pressure [barg]	6.86

All value is using SI unit. However, for convenience reason, flowrate calculation result is shown in field unit [USGPM] since value in SI unit [m3/s] shown is very small value.

2.1 Assumption

- Heat transfer is reduced with linear approximation as per equation for jacketed vessel with isothermal heating medium.
- No heat loss from system to environment vice versa.
- Perfect mixing of cooling water after heated by steam.
- Sudden relief once there is volume expansion.
- Atmospheric pressure is 0.85 bara.
- The volume of cooling water that is directly affected by heat transfer is the volume of cooling water at tubing plus 50% design margin.

2.2 General Calculation Procedure

The required relieving rate is not easy to determine. Since every application is for a relieving liquid, the required relieving rate is small; specifying an oversized device is, therefore, reasonable. A nominal diameter NPS 3/4 × NPS 1 relief valve is commonly used. If there is reason to believe that this size is not adequate, the procedure in API 521 section 4.4.12.3 can be applied.

If the fluid properties vary significantly with temperature, the worst-case temperature should be used. Alternatively, API-521 also recommends conducting more Rigorous calculation methods that include temperature-dependent fluid properties can be used to optimize the size of the relief device.

In this review, 2 types of calculation were conducted:

1. Rigorous calculation is conducted to get maximum and realistic result that match that real phenomenon.
2. Conventional calculation by applying maximum heat exchanger duty during operation and leakage factor is conducted as per discussion with Facility Engineering Team and Technical Authority Process.

2.3 Methodology for the Calculation

The methodology for the calculation was followed from API 521-2014 section 4.4.12 (Hydraulic Expansion) and API 520 section 5.8 (Sizing for Liquid Relief). All constants and factors must be evaluated in the standard which included Expansion rates for sizing of relief devices that protect against thermal expansion was calculated using equation from API 521, section 4.4.12.3 as below:

$$q = \frac{\alpha_v \cdot \phi}{1000 d \cdot c}$$

ASME allowable accumulation pressure of which 10% is chosen for the pressure relief device. The cross-sectional area of each pressure relief device was determined from the selected size orifice area in pressure safety valve specification.

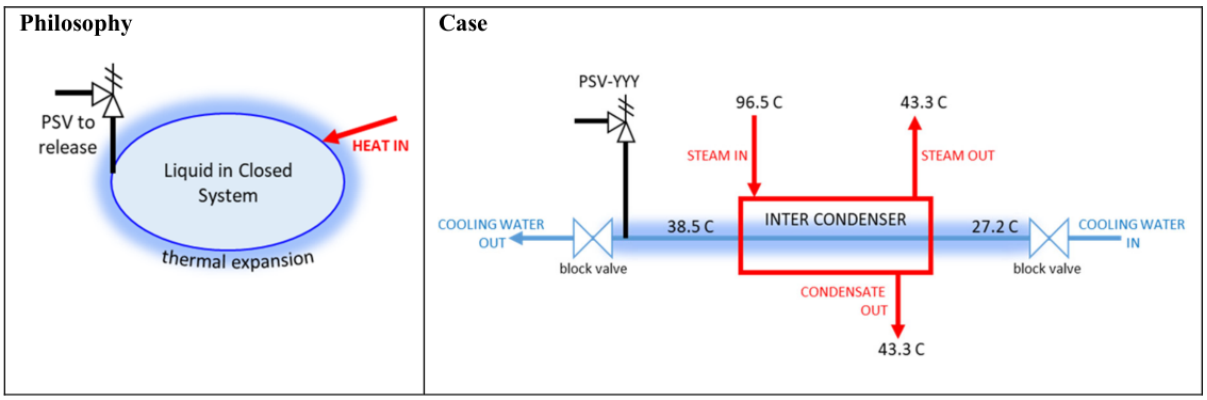

Figure 1: Simplified Diagram of Thermal Expansion Scenario.

3. DISCUSSION AND ANALYSIS

3.1 Relief scenario

As per API 521 there are 14 possible relief scenarios. However, there is only 1 possible relief scenario, thermal expansion, which could occur in this system. Other relief scenarios such as blocked outlet, for instance, will not occur since tube side design pressure 6.86 barg, while maximum service water pump (AWP) discharge pressure is only 4.34 barg. (Muskan, 2015). Thermal expansion could occur due to an exchanger is blocked in on the cold side with flow in the hot side as described in figure 1. Blocked cold side is described in yellow highlight.

3.2 Heat Transfer

In the heat exchanger, heat is transferred from hot fluid (steam) to cold fluid (cooling water). When cooling water is blocked, the temperature of cooling water will increase until reach the inlet steam temperature. Once the temperature of cooling water reaches the temperature of inlet steam, thermal equilibrium is established, and heat transfer will be stop since driving force of heat transfer is temperature difference. (Rates of Heat Transfer, n.d.) Since there is blocked cooling water, heat transfer profile is applying equation for batch heating process: jacketed vessel with isothermal heating medium as per Perry Chemical Engineering Handbook 8ed-(2008), equation 11-35.

$$\ln (T_1 - t_1)/(T_1 - t_2) = UA\Theta/Mc$$

Where:

T1 is temperature of incoming hot fluid (constant) [^oC]
t1 is temperature of cold fluid at beginning of period [^oC]
t2 is temperature of cold fluid at end of period [^{oC}]
U is coefficient of heat transfer [W/m^2 C]
A is heat-transfer surface [m^2]
Θ is time [s]
M is mass of fluid being heated [kg]
c is specific heats of cold fluids [J/kg C]

The heat transfer profile is shown in Figure 2 and Figure 3 for Inter Condenser A/B and After Condenser respectively.

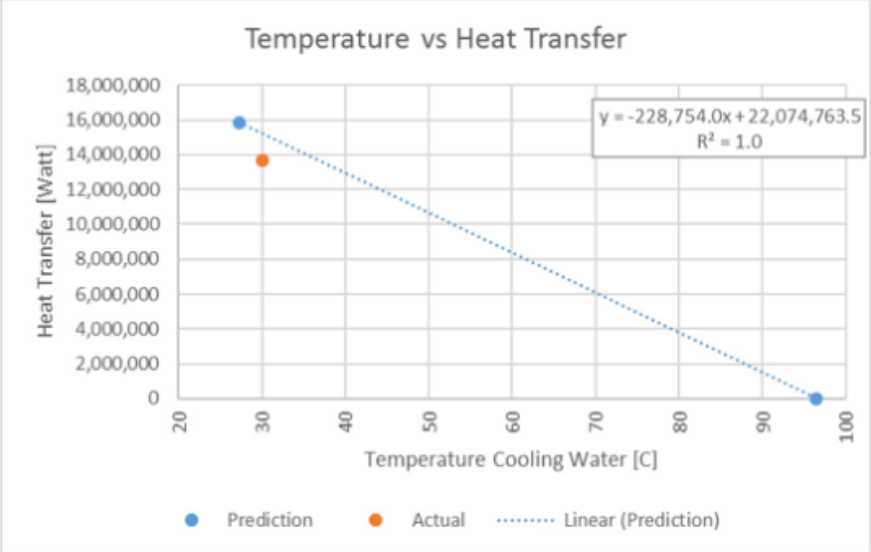

Figure 2: Profile of Temperature vs Heat Transfer for Inter Condenser (related to PSV-YYY).

By considering heat transfer reduction, the temperature profile of blocked cooling water (CW) that is heated by steam is shown in Figure 3 for Inter Condenser. Figure 3 also shows the comparison of temperature profile where there is constant heat transfer is applied.

Figure 3 shows that reduced heat rate is more representing real condition, where cooling water temperature will always below or maximum same with steam temperature. While constant heat rate shows something odd where at some point, cooling water temperature could reach higher than steam temperature.

Conventional calculation did not consider heat transfer reduction. Conventional calculation is applied constant heat transfer (design duty of heat exchanger) in all temperature and time. Heat Transfer reduction applied for Rigorous calculation as this condition is more match with real phenomena.

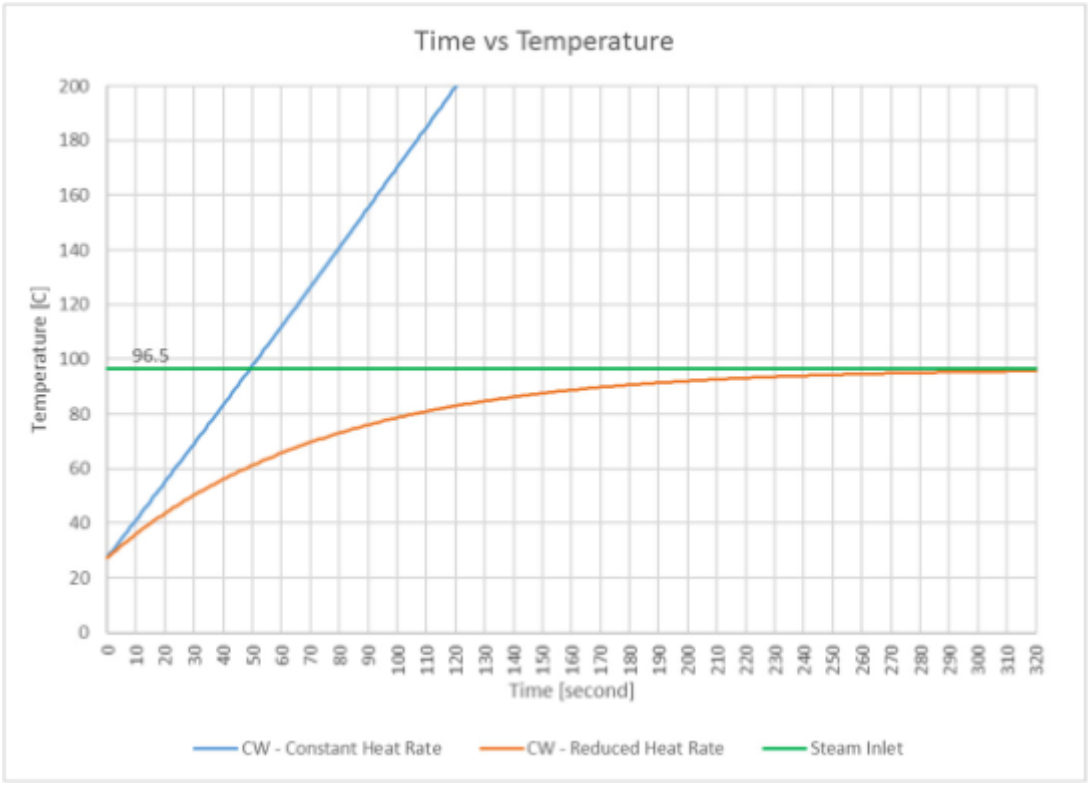

Figure 3: Profile of Time vs Cooling Water Temperature for Inter Condenser (related to PSV-YYY).

3.3 Cold Side Fluid Properties Changed

Cooling Water (Cold Side Fluid) has significant difference of properties at different temperatures. Specific gravity, cubic expansion coefficient, and heat capacity of water are shown in Figure 4, Figure 5, and Figure 6 respectively.

Conventional calculation was only conducted at 1 point which is in 38.5 ^{o}C for PSV YYY. In this review, Rigorous calculation is conducted in all possible temperature ranges, to get maximum and realistic value of relief rate.

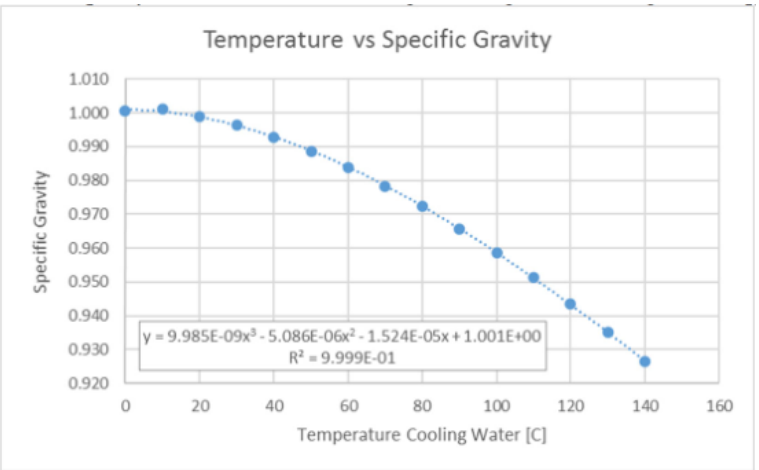

Figure 4: Profile of Temperature vs Density of Cooling Water.

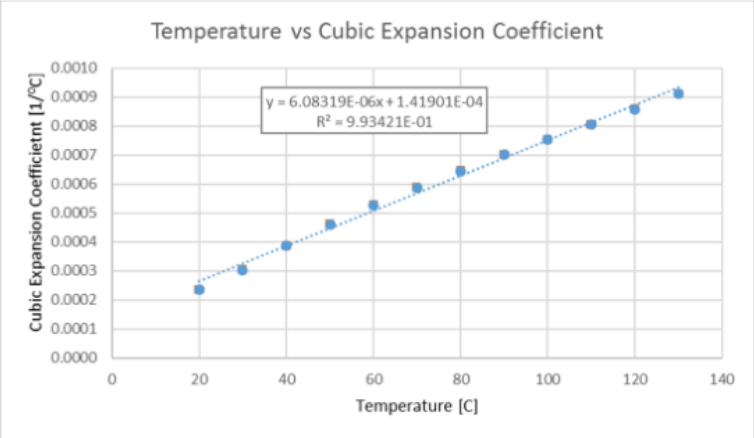

Figure 5: Profile of Temperature vs Cubic Expansion Coefficient of Cooling Water.

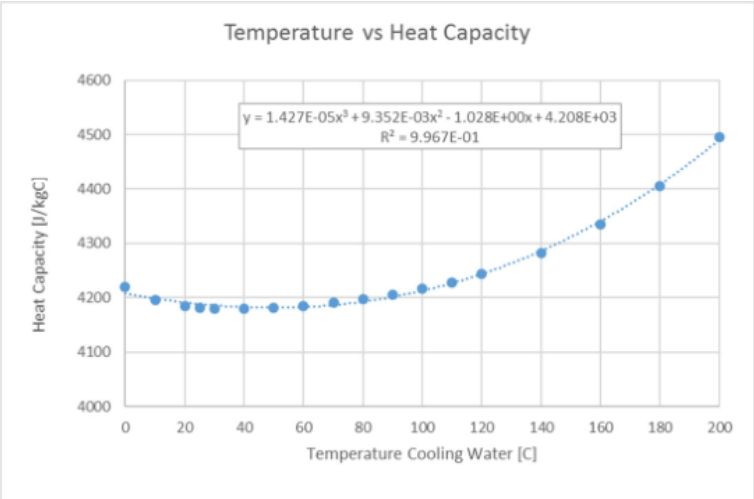

Figure 6: Profile of Temperature vs Heat Capacity of Cooling Water.

3.4 Formula by Manufacturer

General formula for PSV flowrate capacity per API 520 section 5.8.1.3 page 76 is defined as formula below:

$$Q = \frac{A \,.\, \boldsymbol{Kd} \,.\, Kw.Kc \,.\, Kv}{11.78} \sqrt{\frac{\Delta P}{G}}$$

Where:

Q is PSV flowrate capacity, L/min
A is effective discharge area, mm2
Kd is coefficient of discharge that should be obtained from valve manufacturer. For preliminary sizing, a value of 0.65 can be used.
Kw is correction due to backpressure
Kc is combination correction factor for installation with a rupture disk
Kv is correction factor due to viscosity
ΔP is differential pressure, kPa. Differential pressure = set pressure + over pressure – back pressure
G is specific gravity of the liquid

All coefficients are the same for both API and Vendor equation, except for Kd. API is recommending value Kd 0.65 for preliminary sizing, while CROSBY equation is applying value Kd 0.74 (Crosby® Pressure Relief Valve Engineering Handbook, 1997). However, API recommends using Kd value from valve manufacturer, while Conventional calculation is still using preliminary Kd value of 0.65.

3.5 Pressure and Temperature Rise

As the cold fluid is being heated by steam, the cold fluid temperature will increase. As the temperature rises, pressure will increase accordingly. Pressure will increase from operating temperature until reaches the set point of PSV, and PSV will start to open to release pressure. Pressure rise formula is defined in below equation:

$$p_2 = p_1 + \frac{(T_2 - T_1)(\alpha_v - 3\alpha_l) - \left(\frac{q_{ll} \cdot t}{V}\right)}{\chi + \left(\frac{d}{2E \cdot \delta_W}\right)(2.5 - 2\mu)}$$

Where

p_2 is the final gauge pressure of blocked-in, liquid-full equipment, expressed in kPa (psig);

p_1 is the initial gauge pressure of blocked-in, liquid-full equipment, expressed in kPa (psig);

T_2 is the final temperature of blocked-in, liquid-full equipment, expressed in °C (°F);

T_1 is the initial temperature of blocked-in, liquid-full equipment, expressed in °C (°F);

α_v is the cubic expansion coefficient of the liquid, expressed in 1/°C (1/°F);

α_l is the linear expansion coefficient of metal wall, expressed in 1/°C (1/°F);

χ is the isothermal compressibility coefficient of the liquid, expressed in 1/kPa (1/psi);

d is the internal pipe diameter, expressed in m (in.);

E is the modulus of elasticity for the metal wall at T_2, expressed in kPa (psi);

δ_W is the metal wall thickness, expressed in m (in.);

μ is Poisson's ratio, usually 0.3;

q_{ll} is the liquid leakage rate across the block valve seat (usually taken as 0), expressed in m^3/s ($in.^3/s$);

t is the elapsed time for leakage, expressed in seconds;

V is the pipe volume, expressed in m^3 ($in.^3$).

From the equation P1, P2, and T1 are known variables. By modification of the equation, T2 can be calculated.

3.6 Calculation Result

3.6.1 Conventional Calculation.

Calculation result conducted by Conventional is summarized in table 5 below:

Table 5: Result of Adequacy Check of PSV by Conventional Calculation.

Item	PSV-YYY
Initial Temperature Cooling Water start blocked in [C]	38.50
Temperature Cooling Water at Required Relief [C]	38.72
Heat Transfer at Required Relief Rate [Watt] (note 1)	15,852,654
Kd (note 2)	0.65
Required Flowrate [USGPM]	22.6
Current PSV Flowrate Capacity [USGPM]	17.7

Notes:

1. Apply design duty of heat exchanger
2. Apply preliminary Kd value

From the above calculation result, it is shown that current PSV capacity is lower than required flow rate which means current PSV is not enough to handle relieving scenario.

3.6.2 Rigorous Calculation

Rigorous calculation is applying dynamic simulation and rigorous calculation to achieve maximum relief rate by considering heat transfer reduction phenomenon and cold fluid properties change.

Calculation is conducted in all possible range of cooling water temperature (27.2 – 96.5 C for PSV-YYY) depending on how fast valve closing. Calculation result is summarized in Table 6,

Table 6: Result of Adequacy Check of PSV by Rigorous Calculation.

Item	Remark / Value
Initial Temperature Cooling Water start blocked in [C]	(note 1)
Temperature Cooling Water at Required Relief Rate [C]	37.53 (note 1)
Heat Transfer at Required Relief Rate [Watt] (note 2)	13,490,596
Kd (note 3)	0.74
Required Flowrate [USGPM]	19.1
Current PSV Flowrate Capacity [USGPM]	20.1

Notes:

1. Cooling water could be blocked at any possible range of cooling water temperature.
2. Apply heat transfer at maximum relief rate result of rigorous calculation as per Figure. 7 and Figure 8.
3. Apply Kd value from Manufacturer

Detail calculation result of relief rate for each PSV by applying Rigorous calculation is shown in Figure 7 and 8.

From the above calculation result, it is shown that relief rate is not fixed at all time. Relief rate increases until reaches maximum and then decreasing until reach zero. From the above calculation result, it is shown that relief rate reach maximum at some point of cooling temperature and reach zero at maximum cooling water temperature. At maximum temperature of cooling water, temperature of cooling water is same with temperature of steam where thermal equilibrium is reached so that there is no heat transfer and consequently no liquid expansion. From the above calculation result, it is shown that current PSV capacity is higher than required flow rate.

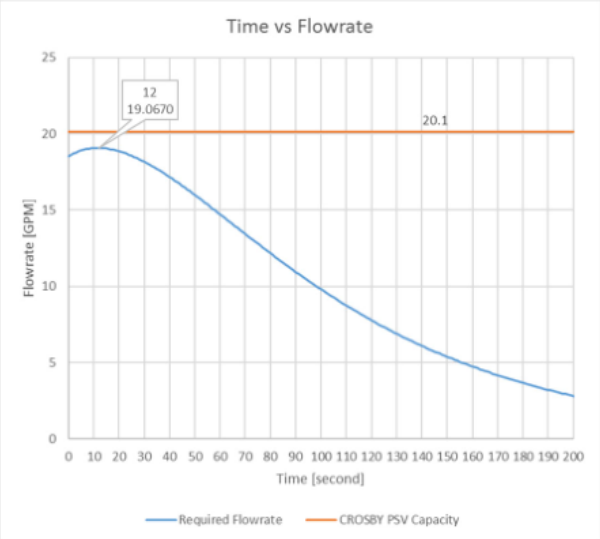

Figure 7: Profile of Time vs Required Flowrate and PSV Flowrate Capacity for PSV-YYY.

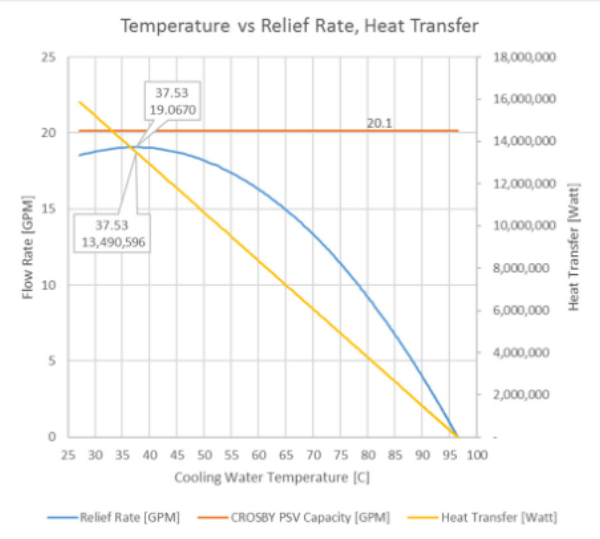

Figure 8: Profile of Temperature vs Required Flowrate and PSV Flowrate Capacity for PSV-YYY.

4. CONCLUSION AND RECOMMENDATION

4.1 Conclusion

As per the above analysis, there are some points that need to be considered for sizing PSV with thermal expansion case for an exchanger that blocked in on the cold side with flow in the hot side. Those consideration are summarized in table 7.

By considering those above aspects. Further calculation for PSV adequacy check was conducted. A comparison of calculation method and result is shown in Table 8 and 9 respectively.

From the calculation result, it is concluded that PSV-YYY is still adequate to accommodate thermal expansion of blocked cooling water at heat exchanger due to heated by steam.

4.2 Recommendation

PSV-YYY is still adequate to accommodate relief rate of protected equipment due to thermal expansion scenario. Therefore, this PSV is not required to be changed or upgraded for current usage. As per discussion, it is found that there is less likely PSV will pop due to thermal expansion scenario. Therefore, it is recommended to conduct further HAZOP study to assess the requirement and scenario of this PSV.

Table 7: Required Items to be Considered for PSV Calculation.

Item	Consideration
Heat Transfer Rate	The heat transfer rate is not fixed. As the cold side fluid temperature is increasing and reach temperature of hot side, heat transfer rate will decrease accordingly since driving force for heat transfer is temperature difference
Cold Side Fluid Properties Changed	Cold side fluid (cooling water) has significant difference of properties at different temperatures. Therefore, calculation need to be conducted at any point temperature to achieve all possible highest required relief rate
Formula by Manufacturer	The manufacturer has its own empirical formula. As per API 520, it is recommended to conduct calculation by using valve manufacturer formula (Kd value by manufacturer)

Table 8: Comparison of PSV Calculation Method.

Item	Conventional Calculation	Rigorous Calculation
Heat transfer	Constant heat transfer by applying heat exchanger design duty	Applying heat transfer reduction by assuming system as batch heating process for jacketed vessel with isothermal heating medium
Initial blocked temperature	Calculation conducted at 1 point temperature: 38.5 ºC	Calculation conducted at all possible temperature range: 27.2 – 96.5 ºC
Kd value	Apply preliminary value	Apply value from manufacturer

Table 9: Comparison of PSV Calculation Result.

Item	Remark
Conventional Calculation	
Required Flowrate [USGPM]	22.6
Current PSV Flowrate Capacity [USGPM]	17.7
Current PSV Status	Not Adequate
Rigorous Calculation	
Required Flowrate [USGPM]	19.1
Current PSV Flowrate Capacity [USGPM]	20.1
Current PSV Status	Adequate

REFERENCES

American Petroleum Institute. (2014). Pressure-relieving and Depressuring Systems. API STANDARD 521 SIXTH EDITION.

American Petroleum Institute. (2014). Sizing, Selection, and Installation of Pressure-relieving Devices; Part I—Sizing and Selection. API STANDARD 520 NINTH EDITION.

Crosby® Pressure Relief Valve Engineering Handbook. (1997). Crosby Valve Inc.

Daniel, F. (1996, September 19). Shell and Tube Heat Exchanger Specification Sheet - Inter Condenser.

Muskan, A. (2015). Power Generation Facility Unit 400, 500 and 600 System Description. Jakarta: Chevron Geothermal Salak.

Perry, R., & Green, D. (2008). Perry's Chemical Engineers' Handbook. McGraw-Hill.

Rates of Heat Transfer. (n.d.). Retrieved from https://www.physicsclassroom.com/class/thermalP/Lesson-1/Rates-of-Heat-Transfer

USA Industries, Inc. (2020). Industrial Charts & Tables. Retrieved from https://www.usaindustries.com/charts-and-tables/birmingham-wire-gauge-bwg-boiler-condenser-tube-size-chart.php

Implementing Deep Learning for Self-Diagnostic of Cooling Tower Fan Motor Vibration at Wayang Windu Geothermal Power Plant

Syahrizal Faried Roosydi, Burhan Syahputra, Iman Kustaman,
Toto Juniandri, and Mochamad Bhakti Prasastia

PT Star Energy

Syahrizal.Faried@starenergy.co.id

Keywords: Geothermal Power Plant, Deep Learning, Cooling Tower Fan Motor, Data Analysis

ABSTRACT

Geothermal power plants represent a significant renewable energy source with considerable potential in Indonesia. One critical process within the geothermal industry involves the cooling of condensate water using cooling towers, which involve large rotating equipment comprising fans and motors, leading to high vibrations occurs in the cooling tower, which can affect the performance of the geothermal power plant generation. In the Wayang Windu power plant, occasional reductions in generation load occur due to cooling tower issues. This is attributed to the suboptimal functioning of the cooling tower. In Wayang Windu case, a decrease in load commonly occurs by approximately 0.5 – 2 MW per fan, but it will increase exponentially whenever more than one fan is affected. The loss of a fan reduces cooling capacity and efficiency of the condenser unit. Cooler water allows for more efficient condensation, which enhances the efficiency of the thermodynamic cycle. Those cases can lead to Loss of Production Opportunities (LPO). Therefore, motor measurement and analysis play a critical role in diagnosing cooling tower faults. In Wayang Windu, data analysis of motors on the cooling tower is conducted using internal resources without the assistance of third-party engineering services. As a result, Wayang Windu possesses raw data for motor analysis, comprising vibration data for each motor, along with analysis reports in managing motor conditions. Therefore, there is potential to enhance the existing system's efficiency by applying artificial intelligence through the development of deep learning that studies the existing trends and reports. The amount of data available for creating deep learning models includes cooling tower motor data from 2019 to 2024, with a sampling time of 500 milliseconds. This approach is expected to shorten data analysis and report generation time which usually takes minimum 2-4 days from data collecting to analysis, thereby achieving time efficiency, and increasing the reliability of the system due to continuous condition-based maintenance implementation. Deep learning techniques have gained popularity for condition-based maintenance applications due to the promulgation of industrial data globally, expediting the optimization of maintenance activities by monitoring assets. The utilization of Deep learning algorithms in developing anomaly detection model based on instrument data has been applied across various industries. This research discusses the application of deep learning algorithms to create auto-detection models for motor analysis on geothermal power plant cooling towers. Incorporating deep learning enables the transformation of condition-based maintenance, converting conventional reporting analysis, which is time-consuming, into an instant process. Deep learning enables swift and firsthand analysis of real-time sensor data, which can immediately provide text-based warnings to the PC workbench when undesirable occurrences arise. This research can provide comprehension of how deep learning application enhance instant analysis in geothermal power plant cooling tower, offering a solution to enhance the current safety measures with condition-based maintenance method, enabling prompt and direct actions when undesired conditions occur.

1. INTRODUCTION

One of the critical components of geothermal power plants is the cooling tower. Cooling towers are employed to condense steam on the low-pressure side of the turbine, optimizing electrical generation efficiency (Sarmago et al.,2001). Cooling towers utilize electric motors to drive fans that facilitate the heat exchange process, a crucial function in maintaining the operational stability and efficiency of the plant. The presence of large rotating equipment and their elevated placement within the tower structure, such as the wooden structure standing for about 24 years in one of the cooling towers at Wayang Windu, poses significant challenges, contributing to potentially high vibrations in the tower. As a result Over the past years, vibration levels in the Wayang Windu cooling tower were classified between Zone B (okay) & C (alert) in normal operation according to ISO 108613. This vibration environment is critical as it directly affects the equipment's condition and performance.

The performance of cooling towers directly influences the overall efficiency of geothermal power plants. For instance, in the Wayang Windu case, a failure in a single cooling tower cell can result in a load reduction of approximately 0.5 to 2 MW. This reduction becomes exponentially greater with multiple cell failures, leading to a substantial drop in overall load when up to eight cells are non-operational. This potential for load reduction underscores the importance of maintaining the optimal operation of cooling tower cells. Proper maintenance of

cooling towers is crucial not only for sustaining the power plant's output but also for ensuring its economic viability. The failure of multiple cells can lead to a cascade effect, where the plant's efficiency deteriorates rapidly, causing increased operational costs and reduced power availability.

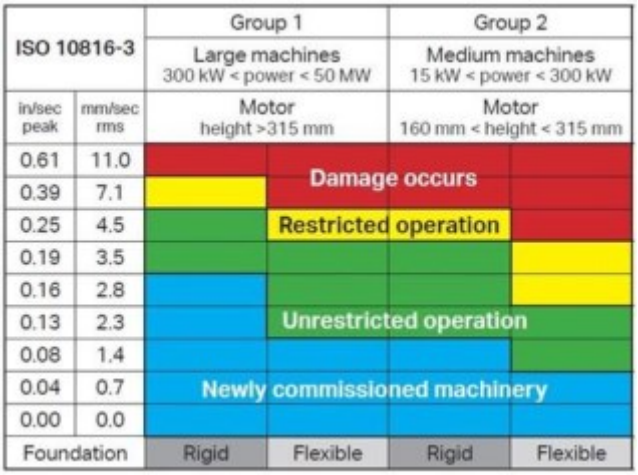

Figure 1: ISO 10816-3 Standard.

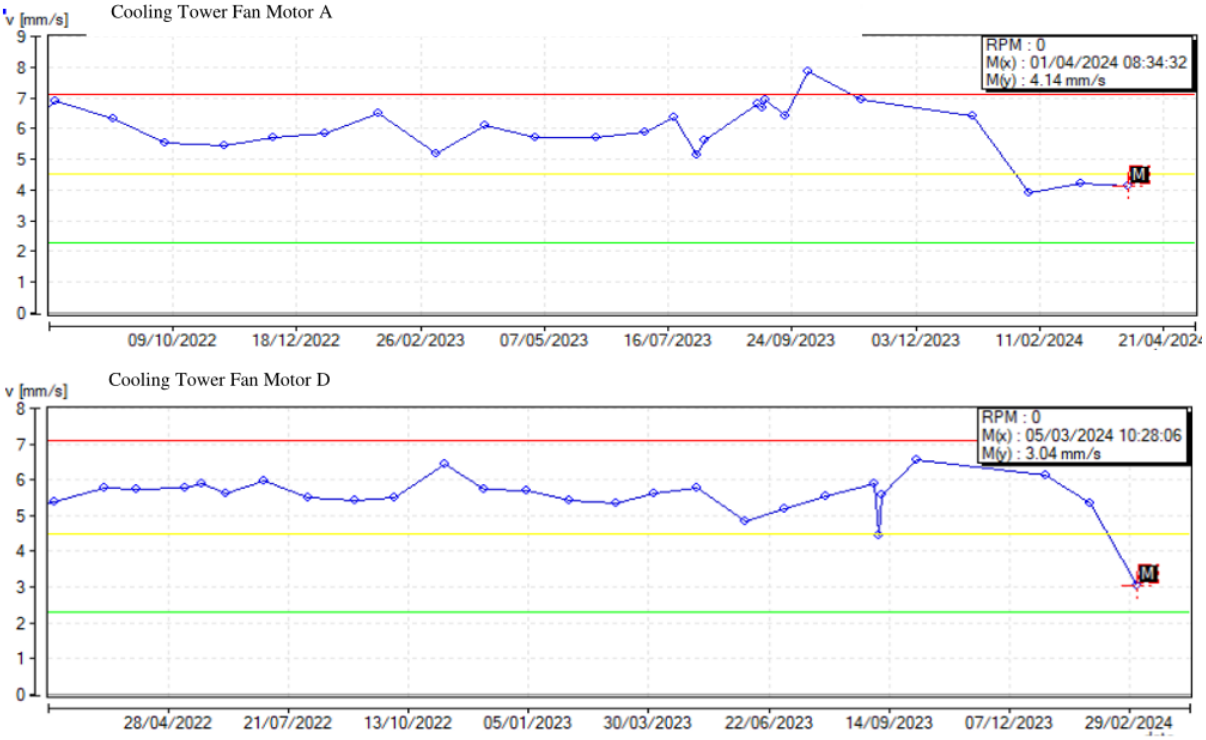

Figure 2: Overall Velocity Vibration of the Electric Motor Cooling Tower.

One method to maintain the performance of cooling towers involves preparing a monthly report for geothermal power plants to evaluate the condition of each piece of equipment. This report is known as the P2RM (Powerplant Performance Reliability and Maintainability). The report contains detailed analyses where the analyst looks for symptoms, behaviors, and patterns that recur over time. These details are compiled, outlined in the report, and published at the end of each month. This report explains all measurements, whether the equipment is operating under normal conditions or not. The analyst translates the measurement data to identify potential failures in the equipment being analyzed, highlighting parts that may fail. This process involves manual data collection, data entry into a work computer, performing manual analysis on the data and report generation to assess the condition of the motor or gearbox in the cooling tower.

In the 21st century, New Industry 4.0 is driven by the integration of cyber-physical systems and advanced computing infrastructures like AI, big data, data analytics, cloud computing, and IoT platforms (Lee et al., 2019). Various studies explore different Artificial Intelligence methods for predictive maintenance across diverse systems, aiming to optimize maintenance strategies in industrial applications (Nchekwube et al., 2022). These

technologies significantly enhance the precision and effectiveness of predictive maintenance systems, making them more autonomous and adaptable in complex operational environments (Ucar et al., 2024). Data-driven intelligent predictive maintenance (IPdM) addresses the pressing need to predict equipment failures and reduce unplanned downtime (Wang et al., 2023). Deep learning, a subset of AI, plays a crucial role by training algorithms to detect patterns in large datasets, improving the accuracy and timeliness of failure predictions. The application of deep learning in data analysis shows considerable potential to enhance maintenance processes, offering insights that can lead to more efficient operations (Mohammadi et al., 2018). The application of artificial intelligence in condition monitoring systems, specifically using deep learning (DL) algorithms for intelligent identification and prediction in industrial facilities, can significantly enhance productivity by reducing the required man-hours (Kraus et al., 2020). This results in a decreased time span in the analysis process, leading to better allocation of human resources. Moreover, if this process can be streamlined seamlessly, continuous predictive maintenance can be implemented, allowing for the constant prediction of equipment failures. This enables the early detection of potential issues, ensuring timely interventions and minimizing downtime.

The integration of deep learning into the maintenance procedures of cooling towers at geothermal power plants has the potential to transform condition-based maintenance practices. Prior to adopting deep learning, maintenance efforts were largely manual and time consuming. By Implementing deep learning, the maintenance process becomes more efficient. This paper aims to highlight the synergy between historical equipment data derived from reports compiled by capable people that have already observed the equipment for over several years and artificial intelligence in geothermal industry. By integrating these insights, the AI system aims to replicate the maintenance team's decisions that used to take time in reporting to be instantaneous, thereby increasing the productivity of manhours in operations at geothermal power plants.

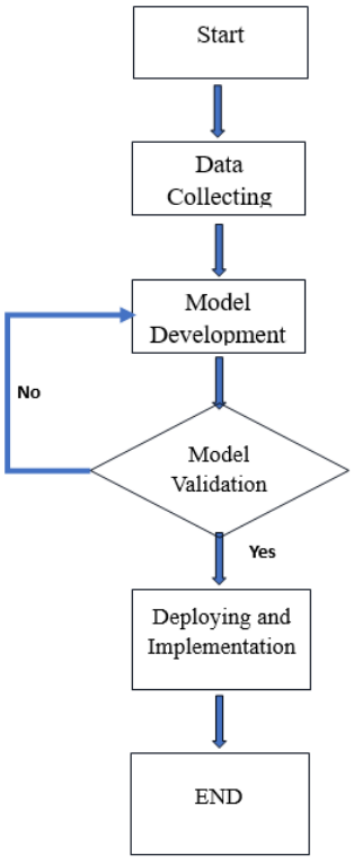

Figure 3: Process Flowchart.

2. METHODOLOGY

In this paper, we propose the development of an intelligent system for anomaly and fault detection in electric motors used in cooling towers. The flowchart outlining the development process is illustrated in Figure 3.

2.1 Data Collection and Processing

The data used in this paper's methodology for implementing artificial intelligence for fault detection comes from Baldor electric motors, which are manufactured with an RPM of 1485 and operate at a frequency of 50 Hz. This

data set comprises vibration data collected from 8 motors installed in a cooling tower. Each motor was carefully monitored to gather comprehensive vibration data, ensuring a diverse and representative sample of operational conditions. All data was obtained through manual measurements taken at various critical points on the drive end and non-drive end of each motor, covering horizontal, axial, and vertical axes. These measurements provide a multi-dimensional view of the motors' vibration characteristics, capturing any anomalies or deviations that may indicate potential faults. The detailed data collection points for each motor on all axes can be seen in Figure 4.

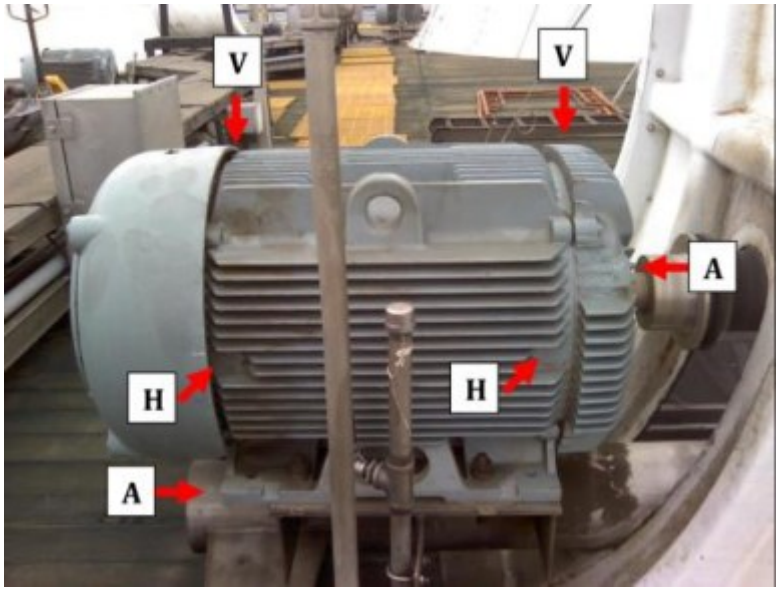

Figure 4: Data Collection Points for Electric Motor.

Each data sample has a duration of 500 ms, with measurements taken monthly over a span of 5 years from 2019 to 2024. The displacement data obtained is transformed into velocity and bearing envelope acceleration, which are then converted from time series to frequency series. Based on ISO 10816, the overall amplitude of the motor ranges from 0 to 5 Hz to 1000 Hz. In the Wayang Windu best practice, frequencies in the range of 0 to 1600 Hz will be used as input for the artificial intelligence model. Following data collection, the dataset was classified based on the motor's condition, with analysis reports conducted by the Condition based Maintenance (CbM) team Wayang Windu team serving as references for determining motor conditions. Classification and labeling were restricted to three categories: motors in normal condition, motors showing anomalies but still acceptable for operation, and motors exhibiting anomalies indicative of potential failure.

The selection of these three categories is based on the diverse possibilities of failure conditions, where each failure type does not have enough samples for artificial intelligence modeling. This presents potential for further development to classify each failure type individually, enabling identification of every possible failure. However, given the current data constraints, it will be necessary to augment the data for each failure type using various transformations. This will create variations from the original data and increase the amount of failure data for each type of failure which will be interesting for further development. Examples of input data for each label can be observed in figure 5 to Figure 10.

After classifying the vibration data into velocity and bearing envelope acceleration categories, a comprehensive dataset was compiled, consisting of 2,805 data points for velocity and 2,501 data points for bearing envelope acceleration. These data points were meticulously collected and analyzed to capture variations across different operational conditions of the motors. The specific breakdown of this dataset, including detailed statistics and distributions for both velocity and bearing envelope acceleration measurements, can be found in Table 1.

Table 1: Original Data Distribution for each label.

Label Category	Velocity	Bearing Envelope
Healthy	960	835
Acceptable	900	819
Potential Failure	945	847
Total	2.805	2.501

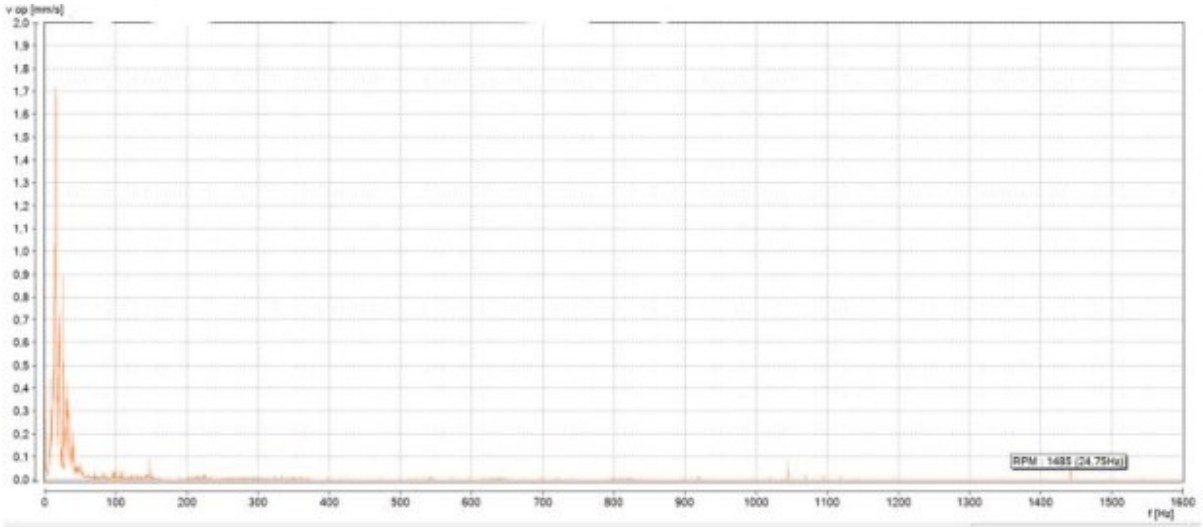

Figure 5: Velocity Domain Normal Condition.

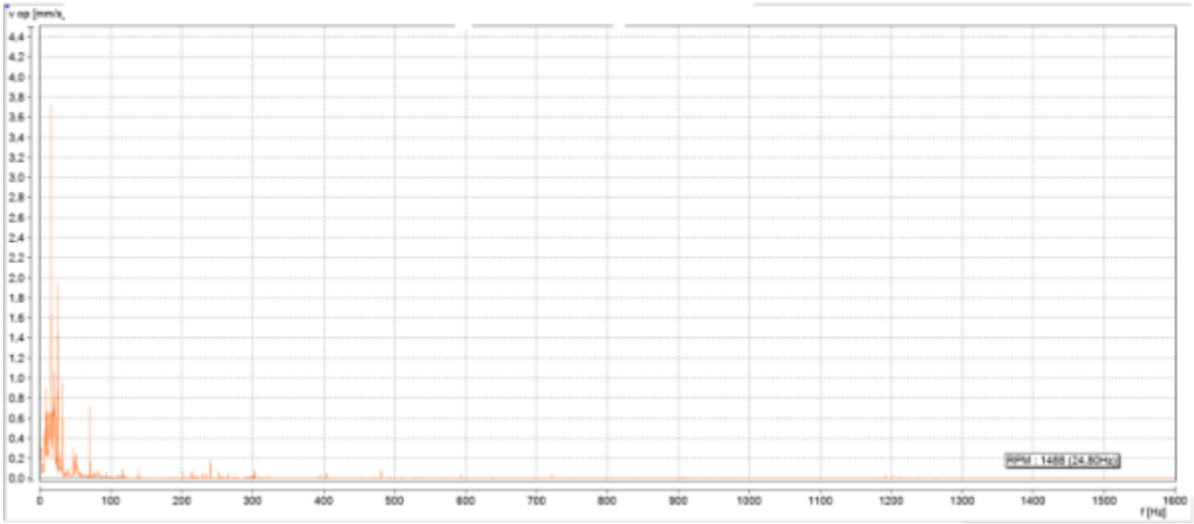

Figure 6: Velocity Domain Quite High in 1x Order but still Acceptable.

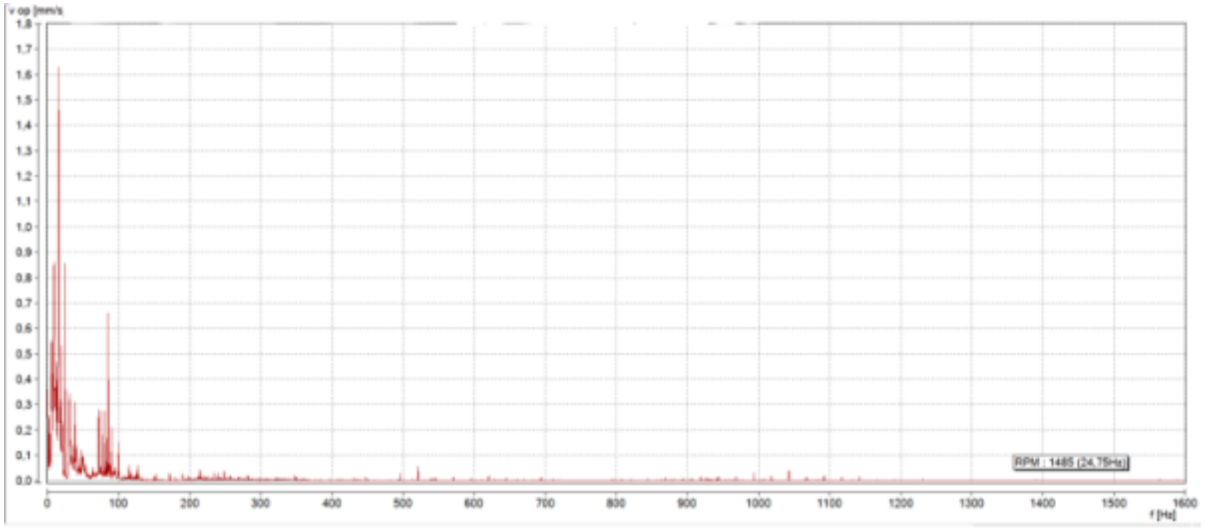

Figure 7: Velocity Domain Potential Failure indicates early defect on both bearings and mechanical looseness.

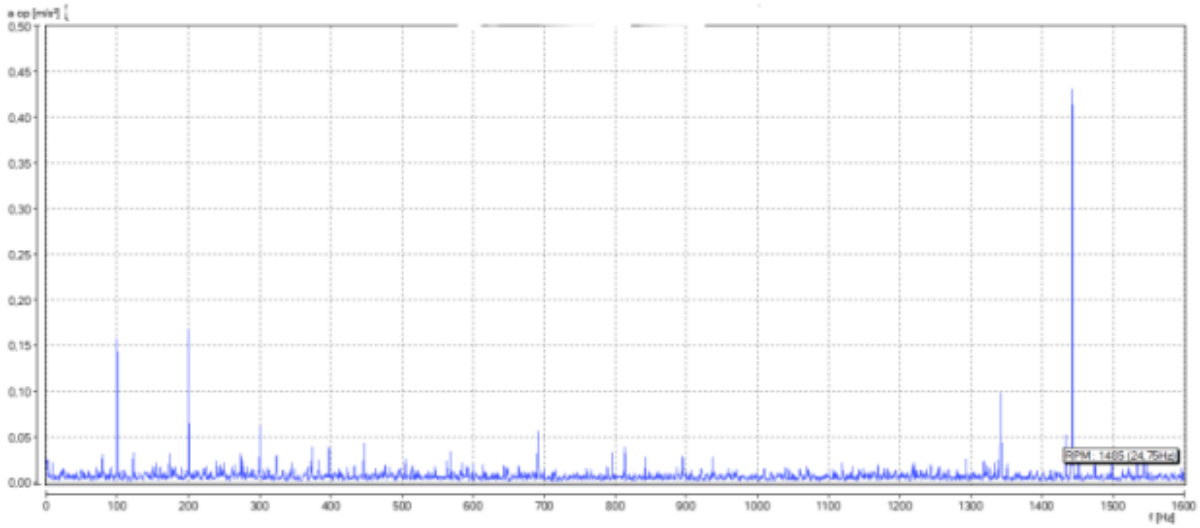

Figure 8: Bearing Envelope Acceleration Domain: Normal Condition.

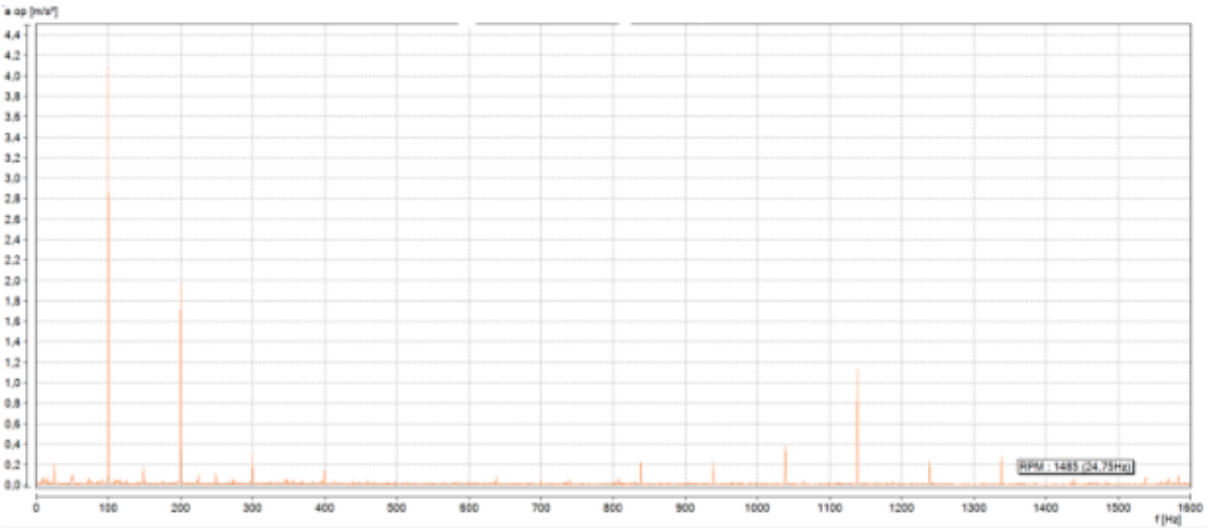

Figure 9: Bearing Envelope Acceleration Domain: Electrical Noise Symptom Detected in 100 Hz but Still Acceptable.

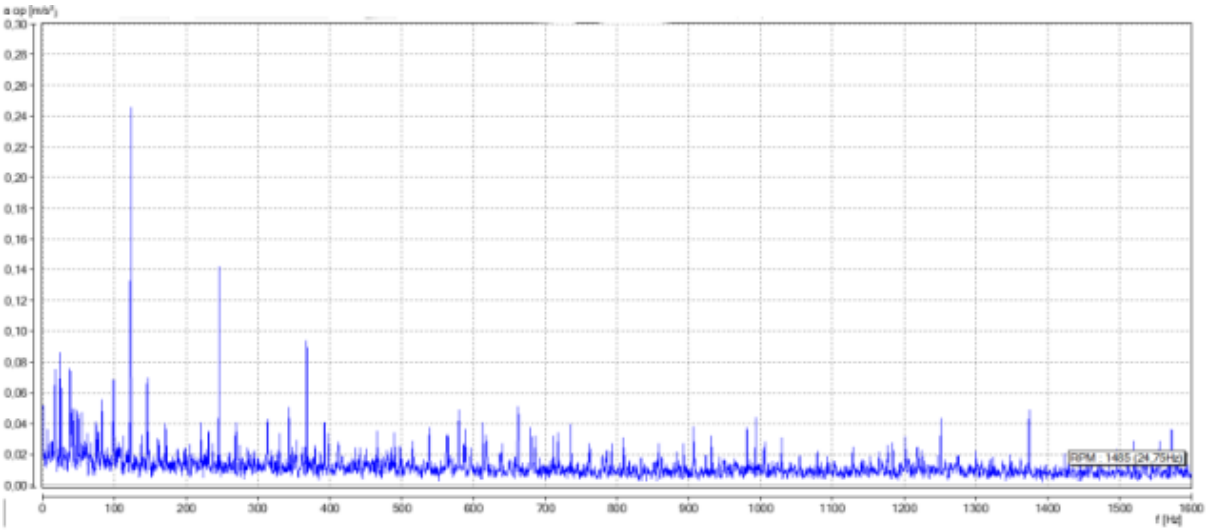

Figure 10: Bearing Envelope Acceleration Domain: Potential Failure Because Bearing Defect Frequency Detected.

The data categorized into three classes exhibit significant variation due to the diverse conditions grouped under each label. For instance, within the failure category, different failure modes such as misalignment and bearing defects each with distinct patterns are combined under a single label. This complexity also applies to the other labels. To address potential underfitting in the model for each label, it is crucial to increase the amount of data that shares similar variations and patterns. Following the data collection process, data augmentation is implemented to generate additional data with comparable variations. One approach widely adopted in existing research is the application of Gaussian noise and data scaling for augmentation. (Victor & Ali, 2024) Specifically, Gaussian noise with a standard deviation of 0.03 is introduced to add minor perturbations to the data, while scaling is performed within the range of -0.02 to 0.02. These methods help to create augmented data that retains the essential characteristics of the original data while introducing slight variations. An example of the augmented data compared to the original data is presented in Figure 11 and Figure 12.

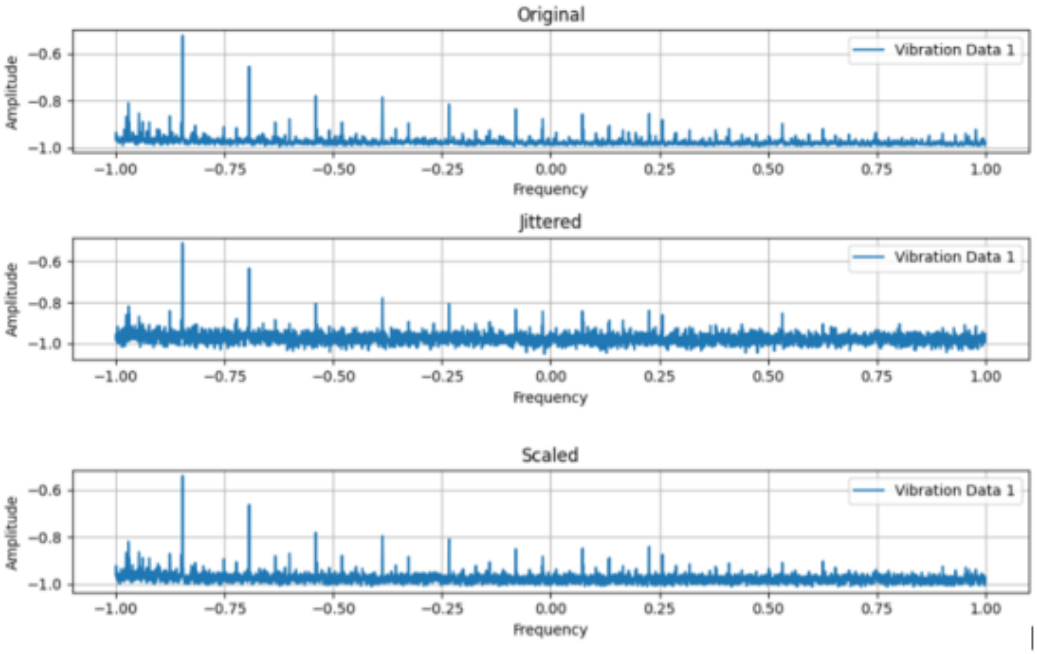

Figure 11: Example of Bearing Envelope Acceleration Original Data and its Augmentation version.

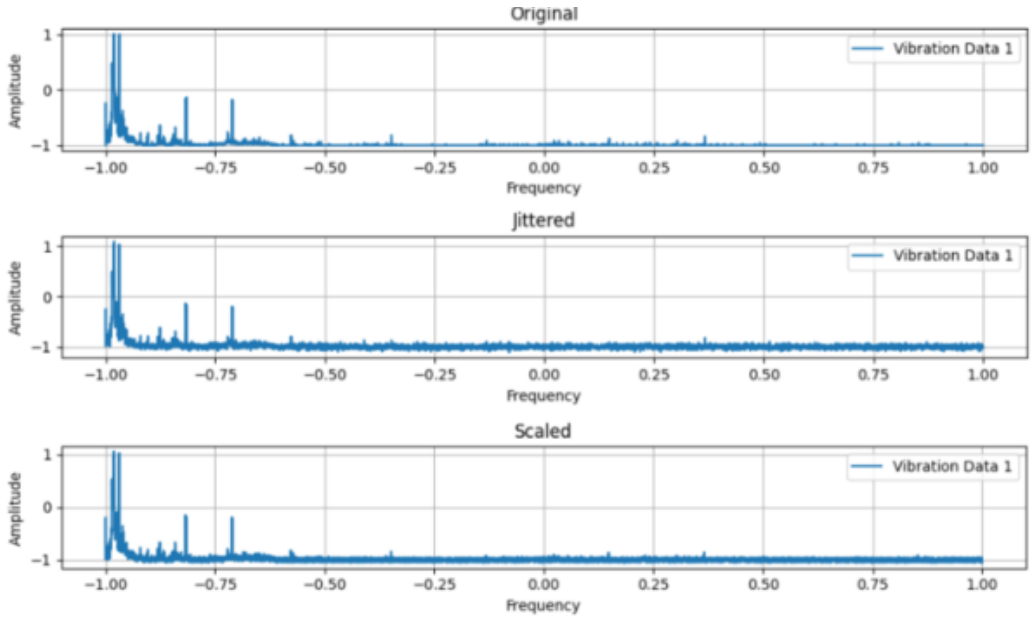

Figure 12: Example of Velocity Original Data and its Augmentation version.

Consequently, the total dataset used as input for the artificial intelligence model will be tripled compared to the original data, as shown in Table 2.

Table 2: Data Distribution for each label.

Label Category	Velocity	Bearing Envelope
Healthy	2880	2505
Acceptable	2700	2457
Potential Failure	2835	2541
Total	8415	7503

2.2 Model Development

This section details the methodology employed in the development of the artificial intelligence model. Initially, vibration data were collected and transformed into the velocity and bearing envelope acceleration domains. Subsequently, the data were converted from time series into the frequency domain to extract crucial parameters. Following these transformations, normalization was applied to standardize the frequency domain data within the range of -1 to 1, thereby enhancing model performance. The normalized vibration data were then structured into arrays consisting of frequency values and their corresponding measurements. This step is pivotal as it facilitates the capture of intricate patterns inherent in vibration signals. The dataset utilized for this process was derived from vibrations recorded across eight motors, serving as primary inputs for training the artificial intelligence model. Next, the dataset was partitioned into two subsets: training data and validation data. This segregation is imperative to mitigate overfitting, a phenomenon where the model performs excessively well on training data but fails to generalize to unseen data. Based on best practice data splitting for train and test an 80:20 split ratio was selected, allocating 80% of the dataset for training and reserving 20% for validation and testing purposes.

The model development was executed in a Python environment utilizing the PyTorch library, a robust framework for constructing artificial intelligence models. The development process encompassed several steps:

1. Selecting Appropriate Architectures: Identifying and choosing artificial intelligence architectures best suited for the classification task. In this research, two machine learning models and two deep learning models are selected. The two machine learning models used are Decision Tree and Random Forest, while the deep learning models chosen is Residual Network 1D. Separable CNN1D is selected for its faster training, lower memory requirements, and potentially superior performance in tasks like time series analysis by breaking down convolutions into efficient steps, making it suitable for intricate pattern recognition tasks (Pazos et al., 2024).
2. Tuning Training Parameters: Systematically adjusting hyperparameters such as learning rate, batch size, and the number of epochs is crucial to optimize the performance of the model. This process involves fine-tuning these parameters to find the optimal combination that maximizes the model's accuracy and efficiency in classifying vibration data.
3. Optimizing the Model: Implementing techniques such as regularization and dropout is essential to mitigate overfitting and improve the model's ability to generalize. Regularization techniques help in preventing the model from memorizing noise or irrelevant details in the training data, thereby enhancing its robustness when applied to new, unseen data. Dropout, on the other hand, aids in reducing interdependent learning among neurons during training, promoting better generalization and preventing the model from becoming too specialized to the training dataset.

2.3 Model Validation

Next, Deep learning model and machine learning model algorithms are developed to compare their performance in classifying vibration signals into three categories based on the available data. The analysis results from previous P2RM reports are used as a basis to validate the developed artificial intelligence models. This involves comparing metrics such as confusion matrix, accuracy, precision, recall, and F1 score of these models with the reported outcomes. By leveraging these documented results, a comparison is made to evaluate how well the models classify the conditions of motors in cooling towers based on vibration data (Lee et al., 2021). This approach ensures a comprehensive analysis and confirms the models' capability in effectively detecting anomalies and faults. One of the commonly used tools in predictive analysis is the confusion matrix, which evaluates the performance of classification-based models. It provides a summarized table of the number of correct and incorrect predictions made by the classifier. A confusion matrix is an N x N table used for assessing the performance of a classification model. By visualizing the confusion matrix, one can determine the model's accuracy by examining the diagonal values, which represent the number of correct classifications. Confusion matrix consists of TP (true positive), TN (true negative), FP (false positive), and FN (false negative) are terms used in the evaluation of the models. These terms help measure how accurately the models classify vibration data from cooling tower motors. TP represents cases where the model correctly identifies a condition as positive (correctly detects an issue), TN represents correctly identified non-issues, FP indicates cases where the model incorrectly flags a non-issue as an issue, and FN shows cases where an actual issue is missed by the model.

From the confusion matrix, we can calculate various performance metrics: Accuracy measures the proportion of correct predictions made by the model out of all predictions and is expressed as a percentage (%). It provides an overall indication of the model's performance by evaluating how often the model makes correct predictions across both positive and negative classes. The formula for calculating accuracy is given by Equation (1).

$$Accuracy = \frac{TP + TN}{TP + TN + FP + FN} \tag{1}$$

Precision computes and estimates the number of positive classes that are correctly identified as truly positive among all instances that were predicted as positive. The formula for calculating precision is given by Equation (2).

$$Precision = \frac{TP}{TP + FP} \tag{2}$$

Sensitivity, also known as recall, measures and predicts the number of positive classes in the dataset by determining the proportion of actual positive instances that are correctly identified by the model. The formula for calculating sensitivity is given by Equation (3).

$$Sensitivity = \frac{TP}{TP + FN} \tag{3}$$

The F1 score is the harmonic mean of precision and recall, providing a balanced measure that considers both the precision (the accuracy of positive predictions) and sensitivity (the ability to identify all positive instances). The F1 score is expressed mathematically as shown in Equation (4), where a higher F1 score indicates a better balance between precision and recall.

$$F1\ Score = \frac{2\ .Precision.Sensitivity}{Precision + Sensitivity} \tag{4}$$

An ROC curve (receiver operating characteristic curve) is a graph showing the performance of a classification model at all classification thresholds. This graph plots two parameters, the true positive rate (TPR) vs false positive rate (FPR) (Fawcett, 2006). The equation for true positive rate is same as sensitivity or equation (3) and the equation for the false positive rate is given by equation 5.

$$FPR = \frac{FP}{FP + TN} \tag{5}$$

ROC graphs are an excellent tool for visualizing and assessing classifiers. They offer a more comprehensive measure of classification performance compared to scalar metrics like accuracy, precision, sensitivity etc. This is because they separate classifier performance from class imbalance and errors (Fawcett, 2006).

This methodology ensures a thorough approach to analyzing and classifying vibration data, crucial for enhancing the detection of anomalies and faults in cooling tower motors. By achieving high scores in these metrics' accuracy, precision, recall, and F1 score the models demonstrate their reliability in effectively assessing the motors' conditions based on vibration data. This validation approach not only strengthens the analysis process but also builds upon insights gained from previous P2RM studies. It leverages prior knowledge to improve the models' capability to identify and predict potential issues.

2.4 Deploying and Implementation

After validating the model, the next step is to implement Artificial intelligence into the existing maintenance process. There are two methods available for implementing AI models into maintenance operations in the geothermal industry. The essence of these methods depends on the approach to vibration data acquisition. One method involves manual collection of data, which is then fed into an AI model for instant analysis. Alternatively, the AI model can be integrated with a continuous condition monitoring system. The first method is generally easier to implement but may be constrained by its reliance on time-based data collection systems. In contrast, the second method facilitates the establishment of a continuous condition-based maintenance system but requires modification of the existing monitoring system.

Deploying artificial intelligence model to existing condition monitoring system involves a structured series of steps to ensure it operates efficiently and effectively. Initially, data collection begins with sensors and monitoring devices attached to the equipment, capturing parameters like vibration that indicate its operational state. This data is then securely transmitted to a centralized storage system, typically cloud-based or a dedicated local database.

Next, the raw data undergoes preprocessing to eliminate noise, handle outliers, and standardize formats. This critical step enhances data quality and ensures consistency across datasets. Following preprocessing, feature extraction identifies significant patterns from the data, essential for the accuracy of the AI models. The trained AI model is then deployed to continuously analyze real-time data, detecting anomalies and predicting potential equipment failures. Results from the model are interpreted by the condition analysis module, which assesses the equipment's health status. An alert system promptly notifies maintenance personnel of detected anomalies or predicted failures, enabling timely intervention and minimizing unexpected downtimes.

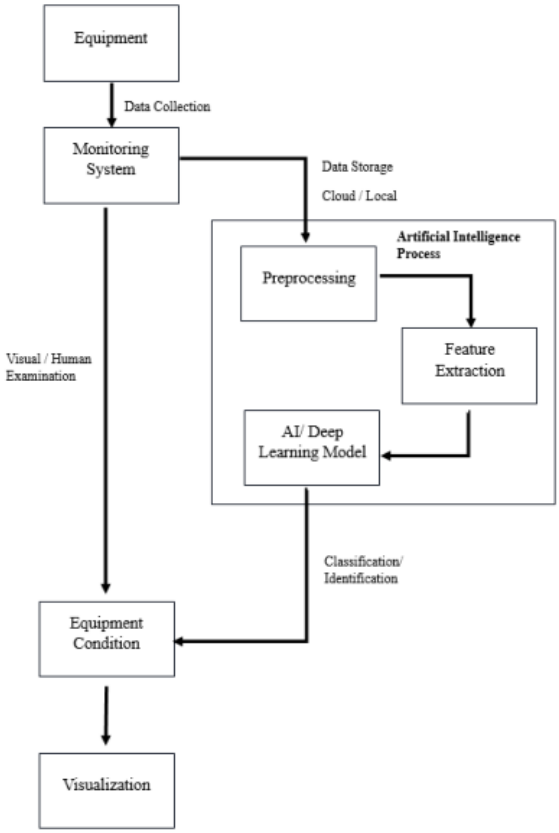

Figure 13: Implementation Scenario for Continuous Monitoring.

Visualization tools, such as dashboards and reports, are employed to provide users with real-time insights and historical data analysis. These tools simplify decision-making by presenting complex data in a user-friendly format. Additionally, a supervisory role ensures that decision-making processes are guided effectively, enabling the condition-based maintenance team to maximize system performance through continuous monitoring. In conclusion, deploying an AI -based condition monitoring system involves a holistic approach from initial data collection to continuous learning aimed at optimizing equipment performance. The diagram of the implementation process can be seen in Figure 13.

3. RESULT AND DISCUSSION

After completing model development and data preprocessing, the artificial intelligence model will undergo rigorous testing to accurately identify and classify motor conditions. This testing phase is crucial to assess how well the model performs in real-world scenarios. The analysis results will be validated using several key performance metrics, including a confusion matrix, accuracy, precision, recall, and F1 Score. These metrics provide a comprehensive evaluation of the model's ability to correctly classify different motor conditions.

It's important to note that the dataset used includes a wide range of possibilities for both failure conditions and acceptable operating conditions in the equipment. This variability in the data reflects diverse scenarios and conditions that motors may encounter in practical use. Such diversity can significantly impact the performance of the artificial intelligence model, influencing its ability to generalize across different types of anomalies and operational states. The performance results for each model and architecture, including these metrics, are summarized in table 3, providing a clear comparison of their effectiveness in fault detection and classification tasks.

Table 3:Artificial Intelligence Model performance comparation.

Model	Validation Accuracy	
	Velocity	Bearing Envelope Acceleration
Separable CNN1D	95.37%	91.59%
Random Forrest	84%	80 %
Decision Tree	79%	74 %

Based on the analysis presented in Table 2, the deep learning model demonstrates better accuracy than the machine learning model, highlighting its ability to learn the vibration patterns of the equipment. Among the deep learning models, the Separable CNN1D model stands out as the most accurate, effectively distinguishing between normal operating conditions, acceptable anomalies, and potential failure scenarios. Its robust performance in classifying these distinct motor conditions is particularly noteworthy, highlighting its capability to reliably identify subtle patterns and variations in vibration data indicative of different operational states.

The detailed performance metrics to this model can be found in Table 4 for velocity and Table 5 for bearing envelope acceleration domain. This selection is grounded in the Separable CNN1D model's exceptional performance metrics, which include high accuracy, precision, recall, and F1 Score.

Table 4: Separable CNN1D Velocity Frequency domain.

Label	Precision	Sensitivity	F1-Score
Healthy	0.9397	0.9449	0.9423
Acceptable	0.9428	0.9475	0.9451
Potential Failure	0.9762	0.9671	0.9716

Table 5: Separable CNN1D Bearing Envelope Acceleration Frequency Domain.

Label	Precision	Sensitivity	F1-Score
Healthy	0.9293	0.882	0.9050
Acceptable	0.9214	0.9395	0.9303
Potential Failure	0.8982	0.9212	0.9096

Furthermore, the performance of the model also visually uses confusion matrix and receiver operating characteristics parameter that shown in Figure 14 and Figure 15.

Where class 0 is equipment in normal condition, class 1 is equipment exhibiting acceptable condition, and class 2 is equipment exhibiting potential failure.

The experimental results demonstrate that the implemented deep learning approach effectively predicts the vibration conditions of cooling tower motors at geothermal power plants. Analysis of the training and validation loss graphs indicates that the model is not overfitting and performs well, achieving an accuracy exceeding 90% for two parameters. Currently, the model classifies motor equipment conditions into three categories: normal condition, acceptable, and potential failure condition.

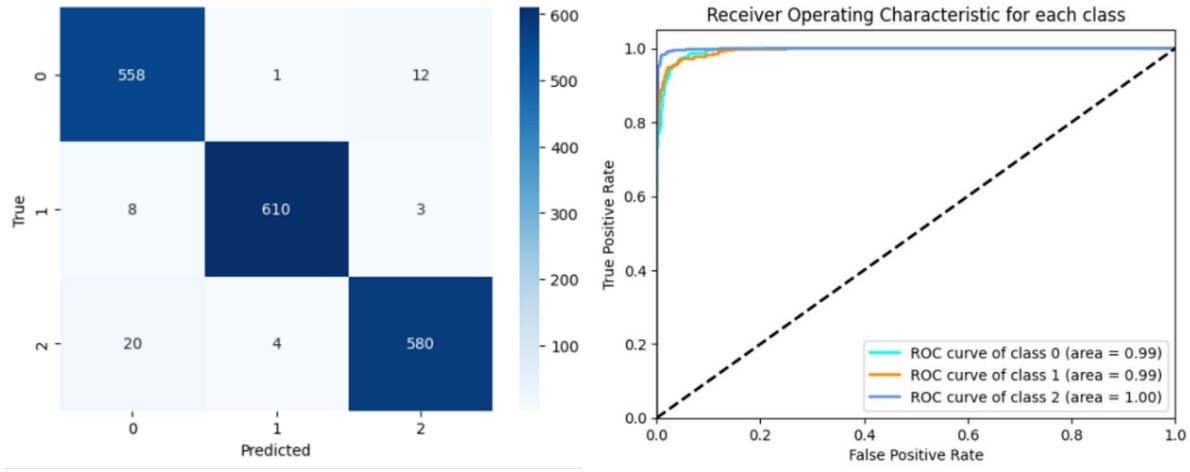

(a) (b)

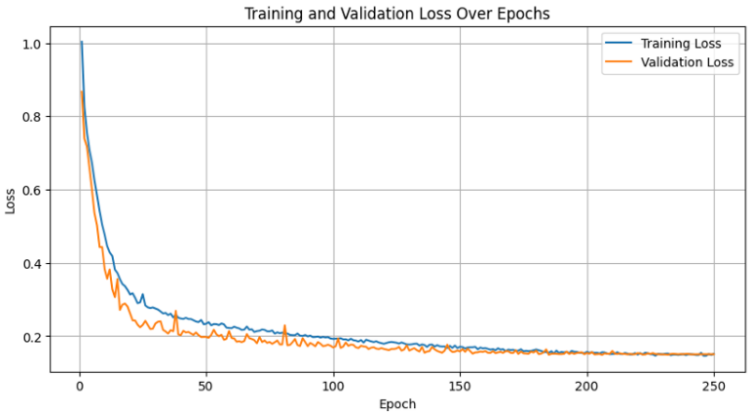

(c)

Figure 14: (a) Confusion Matrix Separable CNN1D Velocity Domain (b) ROC Graph Separable CNN1D Velocity Domain (c) Training Loss vs Validation Loss Graph Velocity Domain.

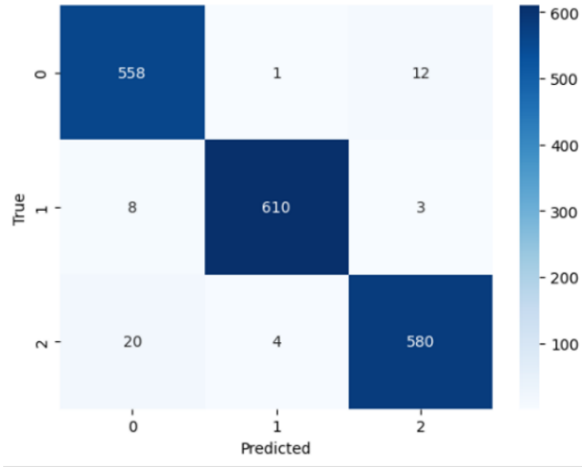

(a)

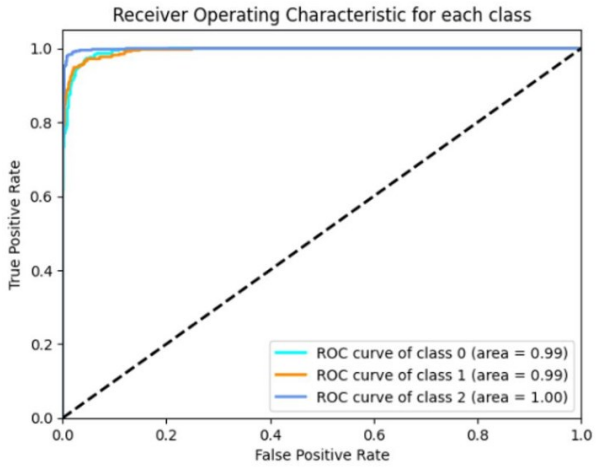

(b)

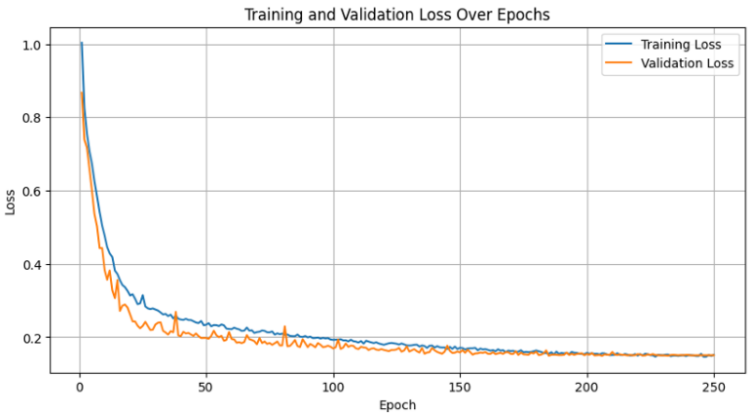

(c)

Figure 15: (a) Confusion Matrix Separable CNN1D Bearing Envelope Acceleration Domain (b) ROC Graph Separable CNN1D Bearing Envelope Acceleration Domain (c) Training Loss vs Validation Loss Graph Bearing Envelope.

For now, implementation still involves manually inputting vibration data into the deep learning model for classification. To facilitate this process, a simple graphical user interface (GUI) was created to ease data input. The user will input the data, which has already been gathered using a Handled vibration instrument. After that, the deep learning model will classify the condition of the equipment. Examples of the user interface and the output of the user interface of deep learning model are shown in Figure 16.

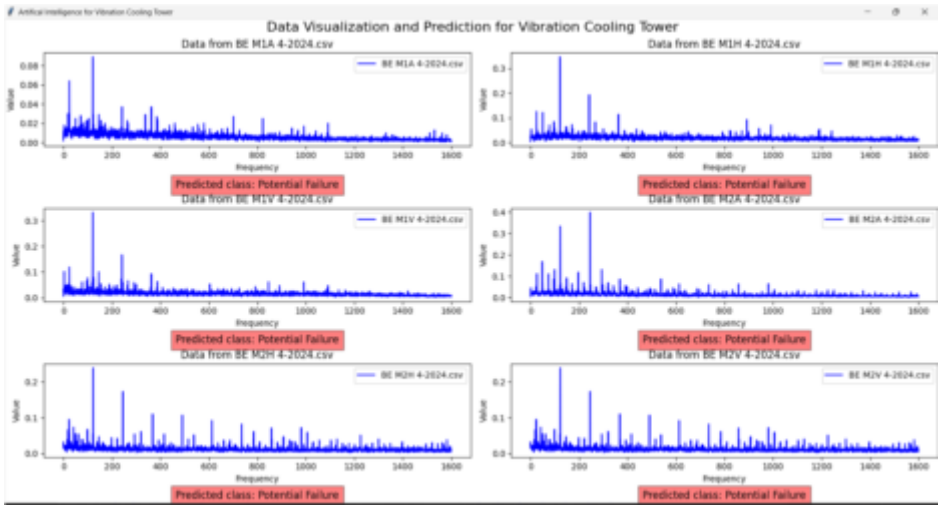

Figure 16: Example of user interface for Deep Learning Vibration Analysis.

Integrating deep learning to continuous monitoring of condition-based maintenance into the geothermal power plant's condition monitoring system remains challenging due to necessary modifications to the existing infrastructure. Nevertheless, this research offers valuable insights into applying deep learning for condition monitoring systems. These insights lay the groundwork for integrating artificial intelligence in the Wayang Windu geothermal power plant, enhancing productivity by automating time-consuming manual processes into instantaneous ones. This transformation reduces the manual workload on human resources, shifting their role from performing manual analyses to supervising decisions made by automated systems. Consequently, this approach minimizes the man-hours required for each condition-based maintenance cycle, optimizing the allocation of human resources.

4. CONCLUSION

The implementation of deep learning for diagnosing vibrations in cooling tower fan motors at the Geothermal Power Plant has shown promising results. The models achieved an accuracy of 95.37% for classifying vibration in the velocity frequency domain and 91.59% in the bearing envelope acceleration frequency domain. These findings demonstrate the effectiveness of deep learning in assessing the motor's condition based on historical data. Currently, the models can classify three conditions: normal operation, acceptable anomalies, and potential failures. The integration of artificial intelligence, specifically deep learning, into condition monitoring systems requires further exploration to ensure seamless and reliable implementation. This includes accurately diagnosing complex equipment failures and integrating with existing monitoring processes in the geothermal industry. Deep learning has proven effective in classifying motor conditions, paving the way for automated condition-based maintenance or intelligent condition-based maintenance. This automation improves productivity in data analysis, reducing downtime and enhancing overall cooling tower operational efficiency. As the dataset continues to grow and the models are refined further, we anticipate improvements in condition-based accuracy and diagnostic capabilities. This solidifies the role of deep learning as a powerful tool in industrial maintenance, especially geothermal, supporting continuous advancements in condition-based maintenance strategies.

5. FUTURE DEVELOPMENT

Deep learning holds significant promise for future development, provided we have sufficient data for training. As datasets for vibration analysis grow and diversify, it will become increasingly feasible to identify specific issues such as misalignment, bearing defects, and other types of failures. Moreover, leveraging current data trends, artificial intelligence can also estimate the remaining life of equipment until failure. This progress will greatly enhance the diagnostic capabilities of systems, leading to more precise maintenance recommendations that can be acted upon promptly. Additionally, techniques such as data augmentation can simulate failures without damaging equipment, enabling us to refine our failure categories beyond the current three to more detailed classifications.

Furthermore, with adequate data, artificial intelligence can be applied to other equipment and systems. The potential for artificial intelligence in geothermal power plants is particularly vast, with numerous possibilities yet to be explored. This research represents an initial step toward harnessing artificial intelligence to turn challenges into opportunities, ultimately achieving unprecedented levels of productivity.

REFERENCES

Fawcett, T. (2006) 'An introduction to ROC analysis', Pattern Recognition Letters, 27(8), pp. 861–874. doi:10.1016/j.patrec.2005.10.010.

Kraus, M., Feuerriegel, S. and Oztekin, A. (2020) 'Deep Learning in Business Analytics and Operations Research: Models, applications and managerial implications', European Journal of Operational Research, 281(3), pp. 628–641. doi:10.1016/j.ejor.2019.09.018.

Lee, W.J. et al. (2019) 'Predictive maintenance of machine tool systems using artificial intelligence techniques applied to machine condition data', Procedia CIRP, 80, pp. 506–511. doi: 10.1016/j.procir.2018.12.019.

Lee, S. et al. (2021) 'A study on deep learning application of vibration data and visualization of defects for predictive maintenance of gravity acceleration equipment', Applied Sciences, 11(4), p. 1564. doi:10.3390/app11041564.

Mohammadi, M. et al. (2018) 'Deep learning for IOT big data and Streaming Analytics: A survey', IEEE Communications Surveys & Tutorials, 20(4), pp. 2923–2960. doi:10.1109/comst.2018.2844341.

Nchekwube, D.C. et al. (2022) 'Predictive maintenance of industrial equipment using Deep Learning: From sensory data to remaining useful life estimation', 2022 IEEE International Conference on Metrology for Extended Reality, Artificial Intelligence and Neural Engineering (MetroXRAINE) [Preprint]. doi:10.1109/metroxraine54828.2022.9967582.

Paolanti, M. et al. (2018) 'Machine Learning Approach for predictive maintenance in industry 4.0', 2018 14th IEEE/ASME International Conference on Mechatronic and Embedded Systems and Applications (MESA) [Preprint]. doi:10.1109/mesa.2018.8449150.

Pazos, J.F. et al. (2024) 1D separable convolutional neural network architecture for stellar classification based on spectral characteristics [Preprint]. doi:10.36227/techrxiv.171838514.45528307/v1.

Sarmago, W. et al. (2001) 'An Innovative Approach To Treating Geothermal Power Enerating Cooling Water System In The Philippines', The 5th Inaga Annual Scientific Conference & Exhibitions.

Ucar, A., Karakose, M. and Kırımça, N. (2024) 'Artificial Intelligence for predictive maintenance applications: Key components, trustworthiness, and future trends', Applied Sciences, 14(2), p. 898. doi:10.3390/app14020898.

Victor, A.O. and Ali, M.I. (2024) 'Enhancing time series data predictions: A survey of augmentation techniques and model performances', Proceedings of the 2024 Australasian Computer Science Week [Preprint]. doi:10.1145/3641142.3641143.

Wang, H. et al. (2023) 'Deep-learning-enabled predictive maintenance in industrial internet of things: Methods, applications, and challenges', IEEE Systems Journal, 17(2), pp. 2602–2615. doi:10.1109/jsyst.2022.3193200.

Bhakti Twist Phenomenon on an Old and or Refurbished Turbine Rotor

Mochamad Bhakti Prasastia Utama and Indra Wening Maharsi

PT Star Energy

bhakti_tech@yahoo.com, indraweningmaharsi@starenergy.co.id

Keywords: CSI Analyzer 2130, VibExpert, Vibration, Frequency, Spectrum, Waveform, Crack, Twist, Turbine Rotor, Segregate Unbalance, System-1, PI System

ABSTRACT

Most Vibration Analysts in the world agree that looseness is one of the five most common causes of breakdowns that result in excessive engine vibration, along with eccentricity, unbalance, and misalignment. The best solution to the looseness problem is to install the machine properly. But how if we found non-harmonic (independently) 5x or 6x or 7x or 8x, etc. on the old and/or refurbished turbine rotors a device designed to have the same reaction frequency as the dominant vibration direction of the structure itself that will counteract the initial motion? Vibrations from the machine will form a signal that can be detected by the CSI Analyzer 2130 tool to produce a vibration signal. The signal can be analyzed as damage to the machine from this vibration. As the damage done to the Turbine Rotors base frames. The study analyzed vibrational signals in damaged Base frames by monitoring the times of 50 Hz spectrum signals at 250 Hz to 400 Hz, the difference was seen in the shape of the spectral signal and vibrational waveform. In addition, the overall value also shows an increase in the Turbine Rotors Side. The overall value produced on the turbine casing can reach more than 15 mm/sec RMS on the turbine horizontal side. In contrast to the system under normal conditions with an overall value of 1.433 mm/sec RMS. The overall value of the damaged system has exceeded the vibration limit of 7.5 mm/sec RMS.

1. INTRODUCTION

The mechanical vibrations generated from the machine come from the internal high- speed rotating activity of the system itself, so the vibration symptom has a frequency that cannot be felt significantly by the human senses. One of the machines which a high-speed rotation with a stable vibration frequency is a Turbine Rotor. The Turbine The turbine rotor receives high-pressure steam or hot water from the geothermal reservoir. As this fluid passes through the turbine blades, it expands, and its pressure drops. This expansion causes the rotor to spin, converting the thermal energy of the fluid into rotational mechanical energy. And all the indications of a problem at the Turbine Rotor will determine from the fault frequency of vibration produced by the magnitude. The objective of this study is to get benefit by employing vibration signal analysis to anticipate and assess potential damage to the Turbine Rotor, thereby fostering proactive measures against unforeseen harm resulting from the 'Bhakti Twist Phenomenon'.

2. LITERATURE

Vibration analysis is one of the methodologies usually used in performing predictive techniques for Rotating Equipment (rotating machines). This technique utilizes the characteristics of the vibration generated by a rotating machine. Some of the defects that often appear on rotating machines are base-frames defects (resonance), unbalance, and misalignment. Each failure defects cases have its specific characteristics in the generated vibration signal pattern. There are three main parameters analysis should we concerned with vibration analysis performing, namely amplitude, frequency, and phase.

Amplitude is the size or magnitude of the vibration signal generated or identified as the magnitude of the generated force by the vibration. The higher the indicated amplitude, the greater the disturbance that occurs. The magnitude scale of the amplitude depends on the type of engine and its damage. The increase in amplitude at specific faults frequencies identifies the suspects of disturbances in the engine. By knowing the frequency when the machine vibrates, precision observation can determine the cause or source of the problem.

Measurement trending will send information about the increasing level of engine vibration. When the engine vibration level increases beyond the baseline signal, it is necessary to carry out special handling on the engine. Baseline data is a collection of data obtained through measurements when the machine is operating stably. The baseline data serves as a comparison of measurement data to determine the engine condition. Meanwhile, to classify the level of damage or severity of the large turbo machinery, several standards are used to evaluate damage, Vibration Standard:

Mechanical vibration — Evaluation of machine vibration by measurements on non-rotating parts, part 2 : Land-based steam turbines and generators in excess of 50 MW with normal operating speeds of 1500 r/min, 1800 r/min, 3000 r/min and 3600 r/min.

Zone boundary	Shaft rotational speed r/min			
	1 500	1 800	3 000	3 600
	Peak-to-peak relative displacement of shaft µm			
A/B	100	90	80	75
B/C	200	185	165	150
C/D	320	290	260	240

Figure 1: ISO 7919-2:2001.

Special-Purpose Steam Turbines for Petroleum, Chemical and Gas Industry Services:

2.8.5.5 During the shop test of the machine, assembled with the balanced rotor, operating at its maximum continuous speed or at any other speed within the specified operating speed range, the peak-to-peak amplitude of unfiltered vibration in any plane, measured on the shaft adjacent and relative to each radial bearing, shall not exceed the value calculated from Equation 6 or 25 micrometers (1.0 mil), whichever is less:

$$A = 25.4\sqrt{\frac{12,000}{N}} \qquad (6)$$

In U.S. Customary units,

$$A = \sqrt{\frac{12,000}{N}}$$

Where:

A = amplitude of unfiltered vibration, in micrometers (mils) peak to peak.
N = maximum continuous speed, in revolutions per minute.

At any speed greater than the maximum continuous speed, up to and including the trip speed of the driver, the vibration shall not exceed 150 percent of the maximum value recorded at the maximum continuous speed.

Figure 2: API STANDARD 612.

In this case:
N = 3000 RPM

$$A = 25.4 \times \sqrt{\frac{12000}{3000}} = 50.8 \mu m \text{ p-p}$$

Most Japan Manufacture Standard:
Warning Level : 125 microns
Fault Level : 250 microns

Mechanical vibration — Evaluation of machine vibration by measurements on non-rotating parts,

Part 2: Land-based steam turbines and generators more than 50 MW with normal operating speeds of 1500 r/min, 1800 r/min, 3000 r/min and 3600 r/min.

Zone boundary	Shaft rotational speed r/min	
	1 500 or 1 800	3 000 or 3 600
	R.m.s. vibration velocity mm/s	
A/B	2,8	3,8
B/C	5,3	7,5
C/D	8,5	11,8

NOTE 1 These values relate to steady-state operating conditions at rated speed for the recommended measurement locations (see Figure 1). They apply to radial vibration measurements on all bearings and to axial vibration measurements on thrust bearings.

NOTE 2 These values are valid for steam turbines and generators mounted on rigid and flexible foundations. However, in general, vibration magnitudes observed on machines on massive concrete foundations are lower than those for machines with more flexible foundations.

Figure 3: API ISO 10816-2.

3. METHODOLOGY

The method used in this research is to take vibration signals with the CSI Analyzer 2130 and System-1 on the vertical, horizontal, and axial Turbine Rotors. The procedure is as follows:

1. Turbine Rotor in operating condition with a rotating speed of 3000 RPM, measured using a CSI Analyzer 2130, VibeExpert, and Bently Nevada Module.
2. Measurement of vibration signals using this tool on the vertical, horizontal, and axial on each inboard side and also by using proximity probes.
3. After obtaining a vibration signal indicating damage to the inboard side, the data is entered into the AMS Suite software database: Machinery Health Manager, Omni trend and System-1.
4. The next measurement on the system uses a monitoring signal on the Normal Averaging amplitude value at maximum frequency = 1000 Hz.

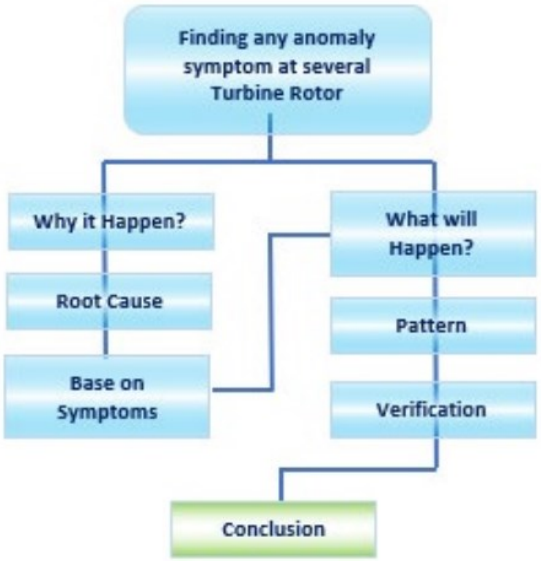

Figure 4: Workflow.

4. DATA ACQUISITION

Data Collecting -Correct and accurate data collection will be helpful in the process of analyzing research results. The data collection method also determines the quality of the data obtained. In this study, researchers took data directly by observing several data of trending, Orbits, waveform, and spectrum patterns of the damage on the system.

After more than 20 years of working with turbo machinery systems, I have discovered a trend indicating that older or improperly refurbished turbine rotors tend to exhibit symptoms akin to looseness. However, unlike typical looseness, these symptoms are synchronous but not harmonics.

Rotor Turbine Outboard Horizontal

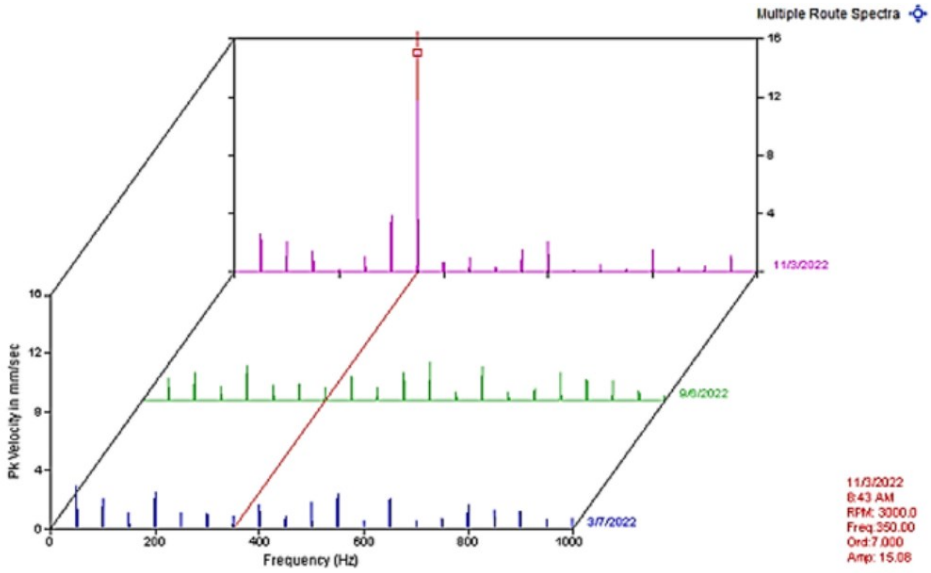

Figure 4: Spectrum shown 7X at Turbine Rotor.

Spectrum shown that 7X pattern at refurbished rotor turbine was occur, maybe it's acceptable for overall value but 15 mm/sec is too high for a single pattern. Vice versa to the previous, inboard side also shown that 7X pattern at refurbished rotor turbine was occur, maybe it's acceptable for overall value but 17 mm/sec is too high for a single pattern. On another Geothermal Plant and different manufacture, Rotor Spectrum after 8 years of operation shown increasing at 6X order.

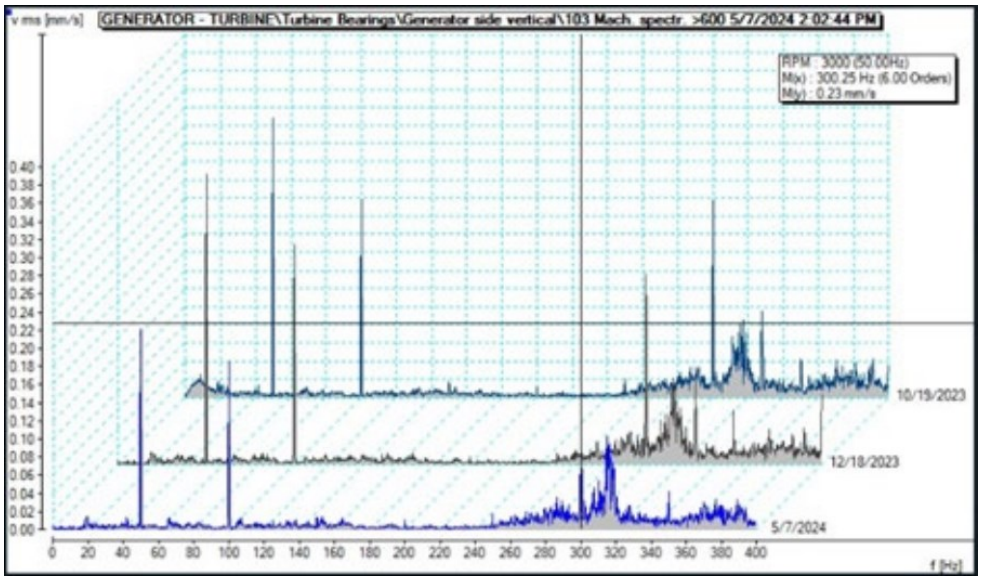

Figure 5: Spectrum shown 6X at Turbine Rotor after 8 years of operation.

And then the other Rotor Spectrum after 12 years of operation on another Geothermal Plant and different manufacture, also shown increasing at 6X order.

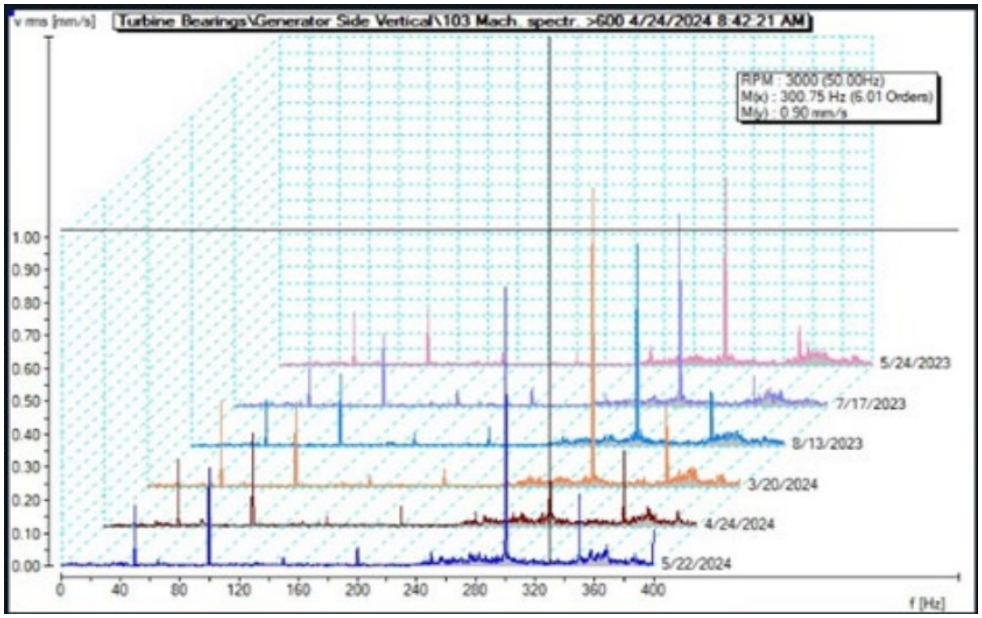

Figure 6: Spectrum shown 6X at Turbine Rotor after 12 years of operation.

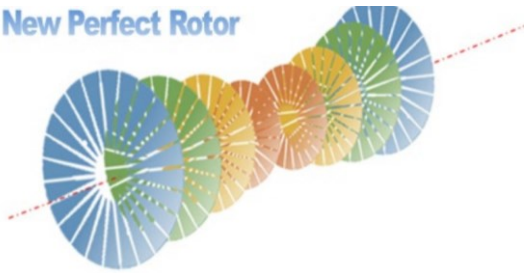

Figure 7: Illustration of the New Turbine Rotor.

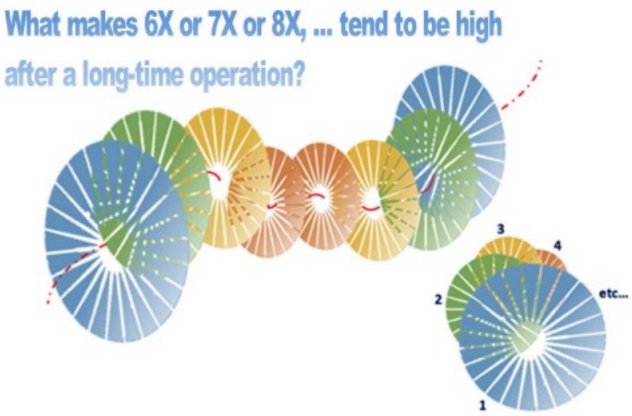

Figure 8: Illustration of the Turbine Rotor after a long-time operation.

5. DATA ANALYSIS

So, the question is, “What has happened to the mentioned rotors above?” The hypothesis regarding this phenomenon posits that it arises from the twist effect induced by 'segregated unbalance', which develops and accumulates over its operational lifespan.

Performing balancing operations may effectively reduce vibration amplitudes by compensating for overall vector forces. However, it cannot eliminate the phenomenon of 'segregated unbalance'. The next analysis is to determine, what will happen then or how harmful the twist phenomenon to the equipment? A cascade plot, in the context of vibration analysis, typically refers to a type of spectrogram or frequency-time plot. It displays how the spectral content of vibration signals changes over time or with varying operational conditions.

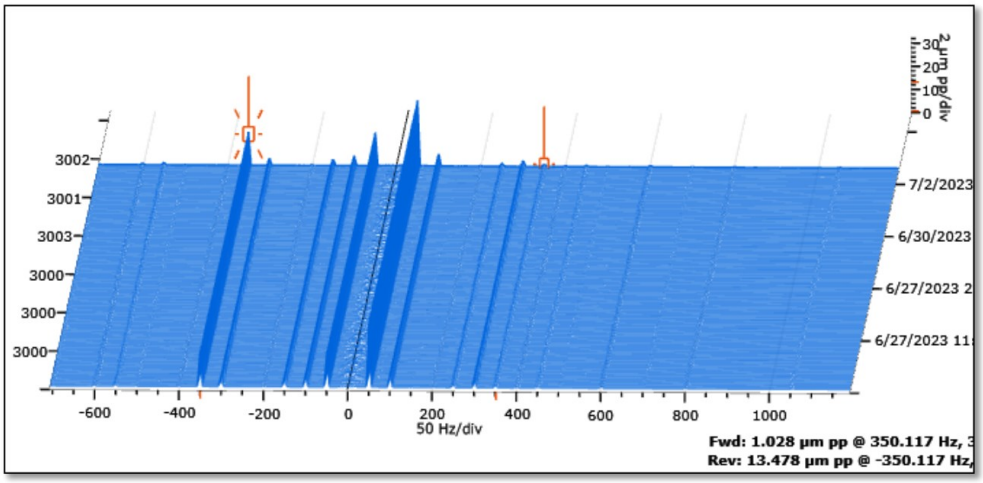

Figure 9: Cascade Plot of Full Spectrums.

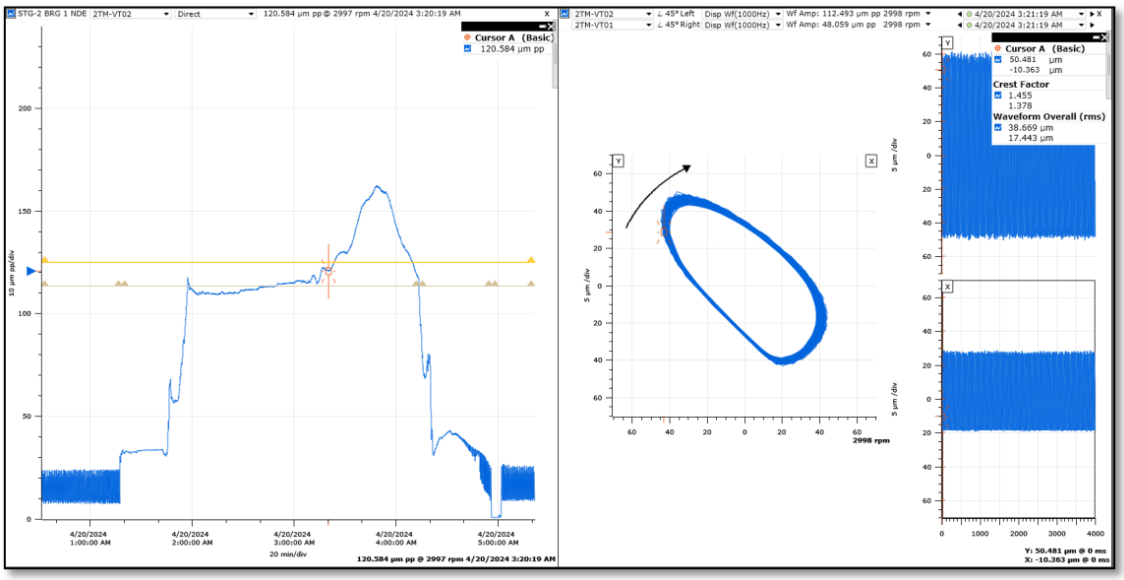

Figure 10: Trending and Orbit.

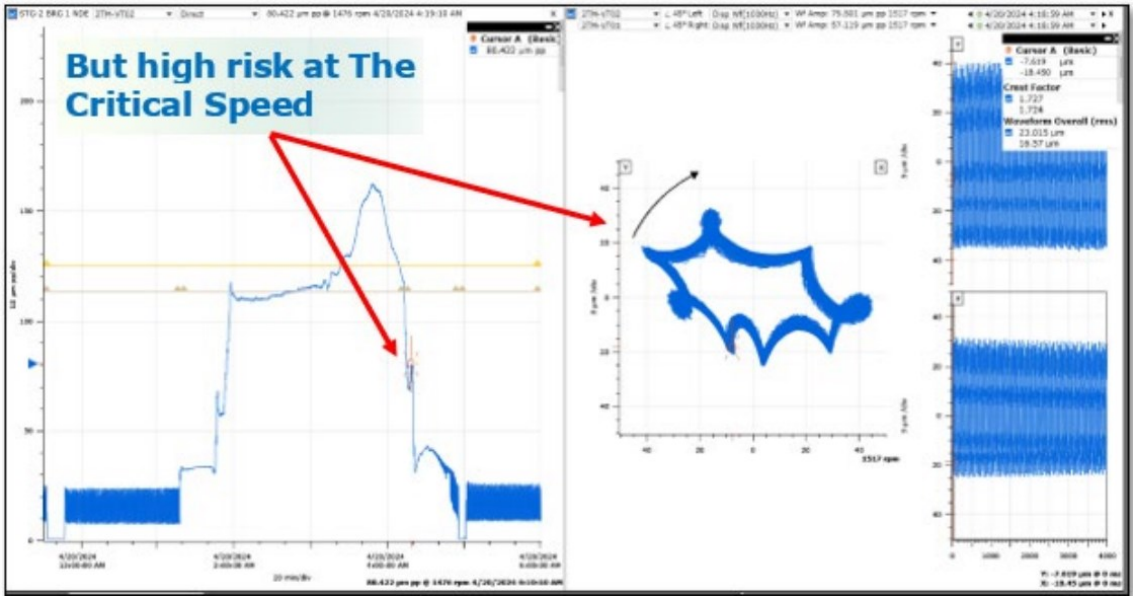

Figure 11: Trending and Orbit.

Cascade plot shows symptoms frequency on the horizontal axis and time on the vertical axis. The plot is formed by plotting successive spectra side by side, showing how frequency components evolve over time or with changes in operating conditions and it's shows that 7x were dominated in reverse spectrum area, which mean it can generate partial reverse orbits.

And as we all know that Increased reverse orbit correlates with heightened risk of turbine rotor rubbing occurrences and generate the Newkirk Effect. The new kirk effect occurs due to the high heat and mechanical pressure generated during rubbing due to high friction, which can cause atoms to migrate from the base metal to the regions subjected to high heat and pressure. This phenomenon can alter the chemical composition of the metal around the weld area, potentially affecting its mechanical properties and corrosion resistance.

The data shows that orbit seems good at normal operation by using Fmax 1000 Hz. Even though the amplitudes are too high but overall shape still look like a normal acceptable eclipse.

There is the potential for turbine rotors to experience operational challenges during start-up or shutdown periods. 'The Twist Phenomenon' can generate and amplify the overall vibration amplitude. In many cases, the rotor eccentricity increases significantly, and the rotor will bow more rapidly just before turbine failure occurs.

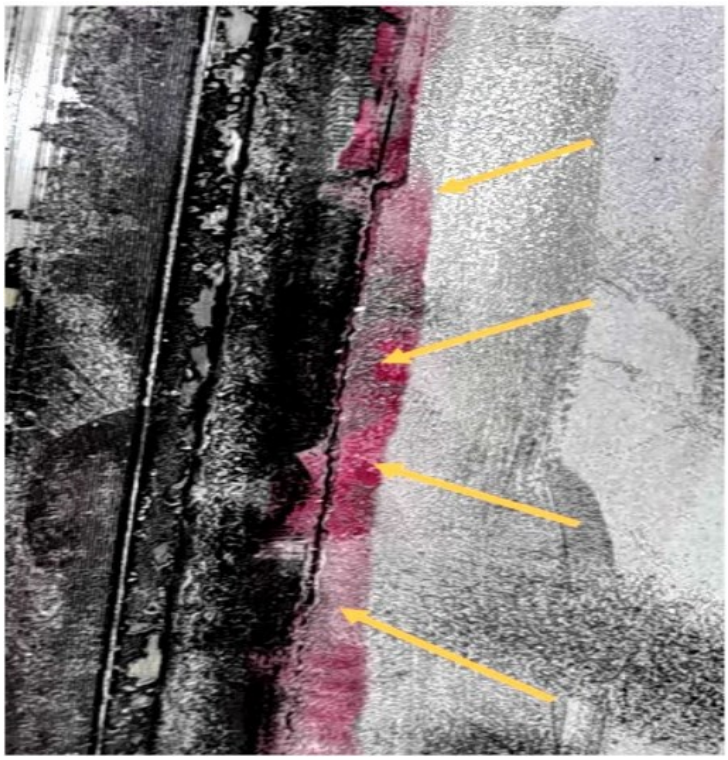

Figure 12: Rotor Crack.

Nearly two years after the detection of the Bhakti Twist Phenomenon at one of Indonesia's largest geothermal power plants, the turbine rotor has ultimately ceased to function.

6. CONCLUSION

If we found non-harmonic (independently) 5x or 6x or 7x or 8x, etc. on the old and/or refurbished turbine rotors a device designed to have the same reaction frequency as the dominant vibration direction of the structure itself that will counteract the initial motion. As the objective of this study is to employ vibration signal analysis to anticipate and assess potential damage to the Turbine Rotor, thereby fostering proactive measures against unforeseen harm resulting from the 'Bhakti Twist Phenomenon'. The results of the research on the Turbine Rotor symptom's, the following conclusions are drawn:

1. Cascade plot of full spectrum can reveal potential problem of Bhakti Twist Phenomenon.
2. Bhakti Twist Phenomenon can generate new kirk effect occurs due to the high heat and mechanical pressure generated during rubbing due to high friction, which can cause atoms to migrate from the base metal to the regions subjected to high heat and pressure.
3. Bhakti Twist Phenomenon increasing the potential for turbine rotors to experience operational challenges during start-up or shutdown periods.

4. Bhakti Twist Phenomenon' can generate and amplify the overall vibration amplitude. In many cases, the rotor eccentricity increases significantly, and the rotor will bow more rapidly just before turbine failure occurs.
5. Monitoring the Bhakti Twist Phenomenon provides benefits by allowing for the anticipation and assessment of potential damage to the turbine rotor, thereby enabling proactive actions to prevent unexpected damage.

REFERENCES

Agilent Technologies: The fundamentals of Signature Analysis. Note: 243

Bently Nevada – Machinery Diagnostic (2023)

ISO 10816: Mechanical vibration -- Evaluation of machine vibration (2014)

Mackay, Steve: Practical Machinery of Vibration Analysis and Predictive Maintenance. Oxford: Elsevier (2024).

S Ralph Buscarello: Practical Solutions to Machinery and Maintenance Vibration Problems, Chapter 1, Basic Information. Section 1 What to Look For, Most of the Time

How to Avoid Derating by Installing Tune Mass Dynamic Absorber

Mochamad Bhakti Prasastia Utama and Indra Wening Maharsi

PT Star Energy

bhakti_tech@yahoo.com, indraweningmaharsi@starenergy.co.id

Keywords: CSI Analyzer 2130, Vibration, Frequency, Spectrum, Waveform, Deformation, Hot Well Pump, Resonance, Dynamic Absorber

ABSTRACT

Most Vibration Analysts in the world agree that resonance is one of the five most common causes of breakdowns that result in excessive engine vibration, along with eccentricity, unbalance, and misalignment. The best solution to solve the resonance problem is to install the machine properly. Another possible temporary solution to solve the resonance problem is to install a dynamic absorber, a device designed to have the same reaction frequency as the dominant vibration direction of the structure itself that will counteract the initial motion. Based on ISO 10816-1-1995 standard, the SEGD U2 Hot Well Pump operation severity level shall be less than 6.36 mm/sec-peak and must be shut down when it reaches 15.8 mm/sec-peak. Meanwhile, vibration amplitude rapidly increased and fluctuated at 13.6 mm/sec-peak and tended to be high which was caused by imbalance, Cavitation, and Resonance due to improper structure. Shutting down the Hot Well Pump will impact to de-rating of the power plant by up to 60% of power production or equals to US$ 178,700 per day. Installing Tune Mas Dynamic Absorber (TMDA) on SEGD U2 Hot Well Pump successfully reduced vibration significantly, avoided de-rating, and saved electrical power production for several months.

1. INTRODUCTION

The mechanical vibrations generated from the machine come from the internal high- speed rotating activity of the system itself, so the vibration symptom has a frequency that cannot be felt significantly by the human senses. One of the machines which a high-speed rotation with a stable vibration frequency is a Hot Well Pump. The Hot Well Pump aims to inject the volume of water to the system. The impeller element itself is generally placed in the pump which held by the stools to support the rotation force of the system. And all the indications of a problem at the Hot Well Pump will determine from the fault frequency of vibration produced by the magnitude.

The purpose of this paper is to determine the damage to the Hot Well Pump with vibration signal analysis and how to solve it according to the condition that surrounded by H2S enclosure and zero downtime issue, during Covid-19 pandemic period based on real experience.

2. LITERATURE

Vibration analysis is one of the methodologies usually used in performing predictive techniques for Rotating Equipment (rotating machines). This technique utilizes the characteristics of the vibration generated by a rotating machine. Some of the defects that often appear on rotating machines are base-frames defects (resonance), unbalance, and misalignment. Each failure defects cases has its specific characteristics in the generated vibration signal pattern. There are three main parameters analysis should we concerned with vibration analysis performing, namely amplitude, frequency, and phase.

Amplitude is the size or magnitude of the vibration signal generated or identified as the magnitude of the generated force by the vibration. The higher the indicated amplitude, the greater the disturbance that occurs. The magnitude scale of the amplitude depends on the type of engine and its damage. The increase in amplitude at specific faults frequencies identifies the suspects of disturbances in the engine. By knowing the frequency when the machine vibrates, precision observation can determine the cause or source of the problem.

Measurement trending will send information about the increasing level of engine vibration. When the engine vibration level increases beyond the baseline signal, it is necessary to carry out special handling on the engine. Baseline data is a collection of data obtained through measurements when the machine is operating stably. The baseline data serves as a comparison of measurement data to determine the engine condition.

Meanwhile, to classify the level of damage or severity of the rotating machine, one of the standards is used to evaluate damage based on the class and type is ISO- 10816.

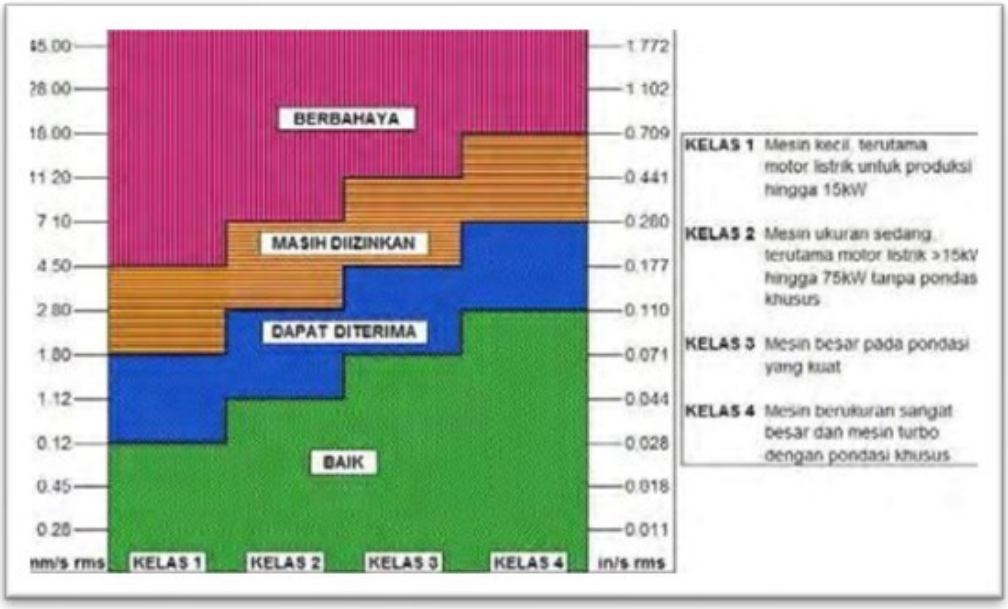

Figure 1: ISO 10816-1.

3. METHODOLOGY

The method used in this research is to take vibration signals with the CSI Analyzer 2130 and T-Wave on the vertical, horizontal, and axial Hot Well Pumps. The procedure is as follows:

1. Hot Well Pump in operating condition with a rotating speed of 750 RPM, measured using a CSI Analyzer 2130.
2. Measurement of vibration signals using this tool on the vertical, horizontal, axial, and peakvue on each inboard side.
3. After obtaining a vibration signal indicating damage to the inboard side, the data is entered into the AMS Suite software database: Machinery Health Manager.
4. The next measurement on the system uses a monitoring signal on the Normal Averaging amplitude value at maximum frequency = 1000 Hz.

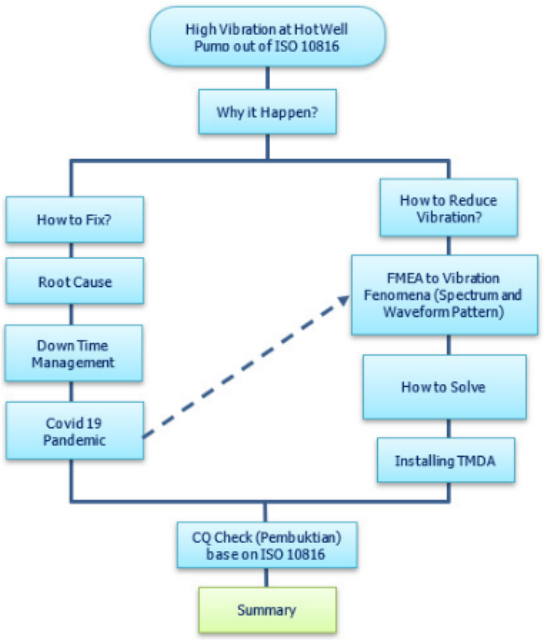

Figure 2: Workflow.

4. DATA ACQUISITION

Data Collecting -Correct and accurate data collection will be helpful in the process of analyzing research results. The data collection method also determines the quality of the data obtained. In this study, researchers took data directly by observing several data of trending, waveform, and spectrum patterns of the damage on the system.

Overall vibration amplitude data shown acceptable value except for Motor Outboard Y Axis, and it's looks so directional especially at Y direction.

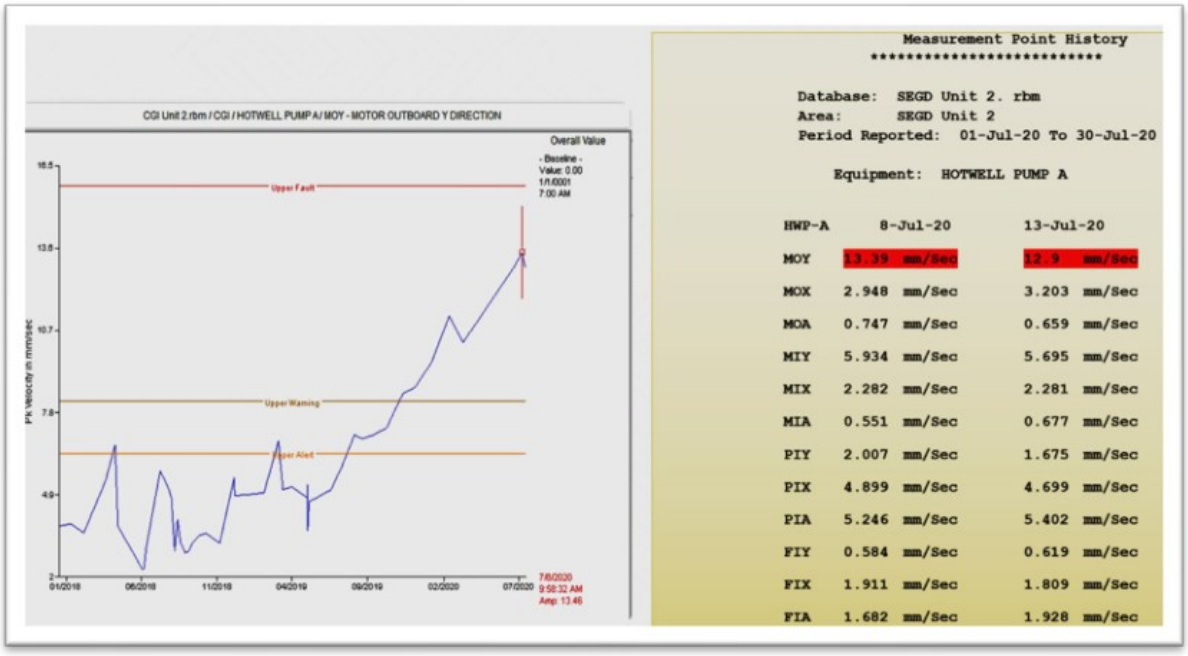

Figure 3: Overall data of HWP.

5. DATA ANALYSIS

The graph of the measurement results on the vertical direction of the outboard motor side, shown in the spectrum and waveform vibration signals. This spectrum and waveform signal indicates that the vertical outboard vibration signal is out of ISO-10816 severity. Coast down Analysis and Bump test are the way to confirm the phenomenon of resonance.

Both Coast down and bump test analysis shown that critical speed or natural frequencies approximately at 10Hz -12.5Hz, which mean it's too close to the operational rotating speed (750 RPM).

The SEGD U2 Hot Well Pump operation severity level shall be less than 6.36 mm/sec-peak and must be shut down when it reaches 15.8 mm/sec-peak. Meanwhile, vibration amplitude rapidly increased and fluctuated at 13.6 mm/sec-peak and tended to be high which was caused by imbalance, Cavitation, and Resonance due to improper structure. Shutting down the Hot Well Pump will impact to de-rating of the power plant by up to 60% of power production or equals to US$ 178,700 x 60% per day.

Since we found that vibration at Hot Well Pump was generated by 12.5 Hz and dominated by vertical axis or 'Y' direction, and it's confirmed as resonance effect, so we need to reduce the amplitude. Natural frequency is a root of Stiffness (k) divided by mass (M):

$$Nf = \sqrt{\frac{k}{M}}$$

Hence, we can change the stiffness of the HWP structure, or we can change the mass of the HWP structure, but there's another way to solve this problem by installing TMDA.

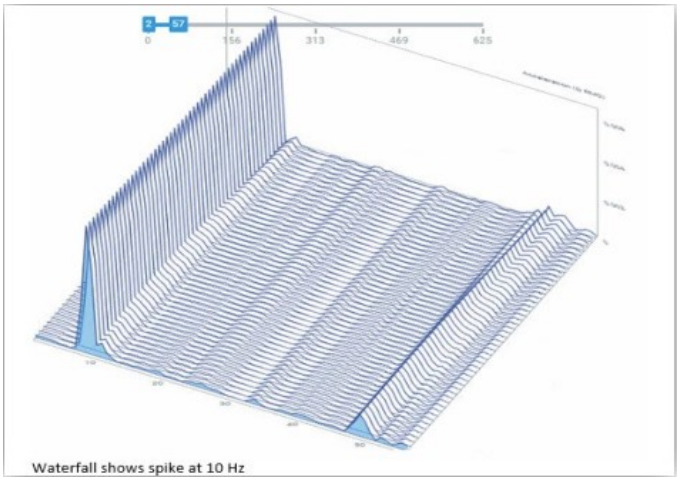

Figure 4: Coast down of HWP.

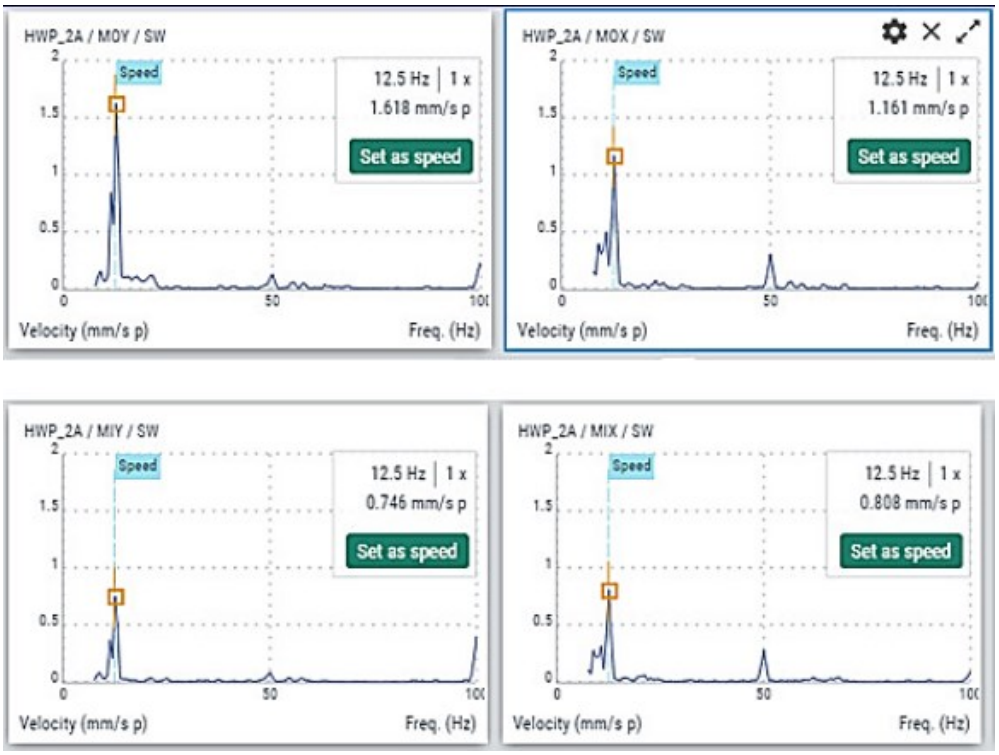

Figure 5: Bump Test Analysis.

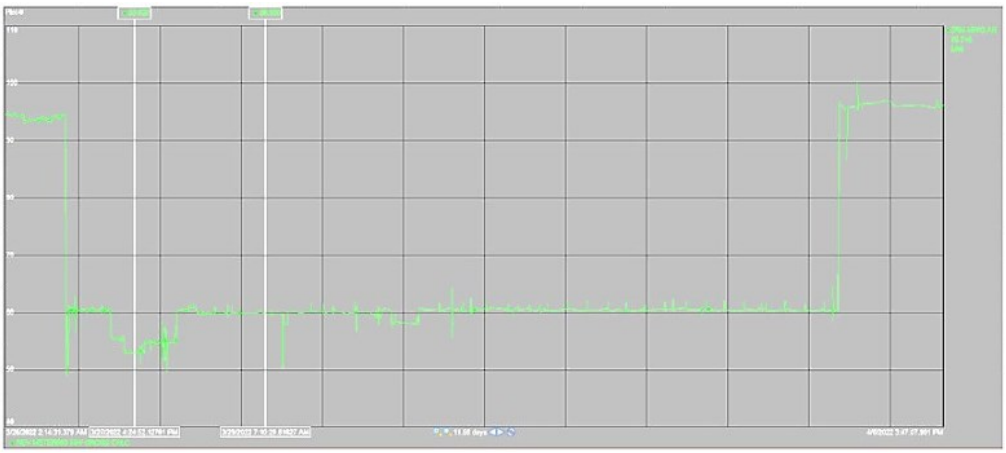

Figure 6: Generation by using single HWP Only.

6. VERIFICATION AND SOLUTION (CALCULATION METHODOLOGY)

By utilizing two degrees of freedom equation, then the next step is entering identify data into the calculation formula:

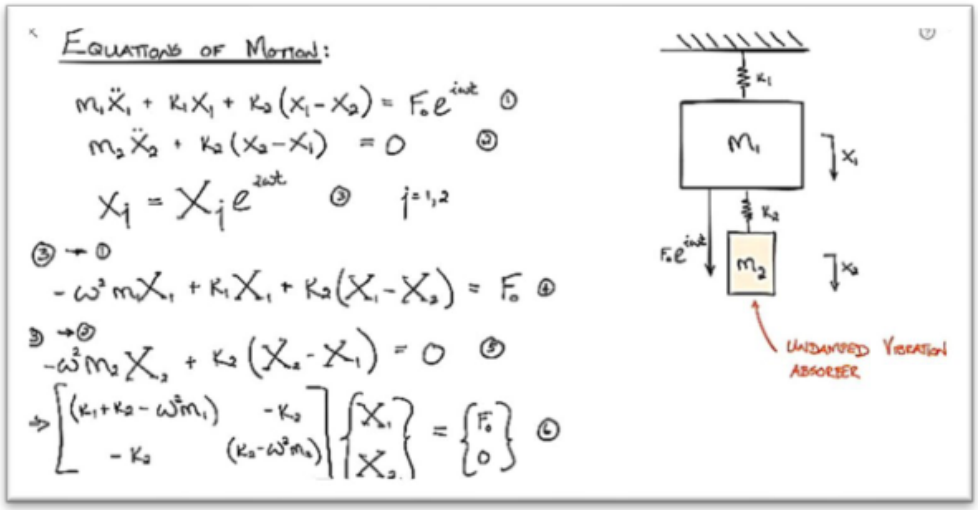

Figure 7: Two degree of freedom formula without damping.

$M\ddot{X}1 + k1X + k2\ (X2 - X1) - Fa \sin \omega t$ (1)

$m\ddot{X}2 + k2\ (X2 - X1) = 0$ (2)

Put X1 = Asin ωt and X = B2 sin ωt it's mean Ẍ1 = rees-ω² Asin ωt and Ẍ2 =-ω² B sin ωt Subtitute to equations (1) dan (2)

$k1 + k2 - M\omega^2)\ A - k2B = F$ (3)

$-k2A + (k2 - m\omega^2)\ B = 0$ (4)

Hence:

$$A = \frac{F_a\,(k_2 - m\omega 2)}{(k_1 + k_2 - M\omega 2)\,(k_2 - m\omega 2) - k_2 2}$$

So, to counter all resultant of force in Hot Well Pump with mass M, then the number of A needs to the limit of zero, A

□0, then k2 = mω² or ω² = k2/m = k1 /M.

→ ***k1/M = k2/m or f1 = f2 ….*** (Seto. William W 1985)

It's hard for us to estimate the mass of the Hot Well Pump on the site, but there are two keys that we can use to solve the problem:

1. First, we got the magnitude.
2. Second, we have the number of frequencies (12.5 Hz)

Since f1 = f2, then what we've to do now is find the tunning to create a 12.5 Hz

Dynamic Absorber to counter the force with 12.5 Hz of frequency. Here we adopt the journal of Randy Fox in Entek IRD International Corp. Houston, TX to create a simple Dynamic Absorbers:

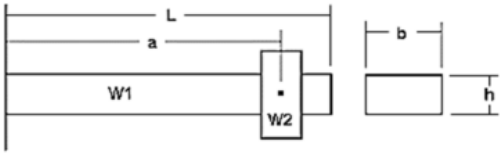

$$W2 = \frac{(2.114 \times 10^5)\ E\ I}{N_f^2\ (3a^2L - a^3)} - \frac{0.75\ w\ L}{3a^2L - a^3}$$

WHERE: N_f = DESIRED NATURAL FREQUENCY (CPM)

w = WEIGHT PER INCH OF SPRING (lbs) = b x h x d

E = MODULUS OF ELASTICITY

STEEL = 29,000,000 psi
ALUMINUM = 10,000,000 PSI
COPPER = 16,000,000 PSI
IRON = 18,000,000 PSI

$I = \frac{b\,(h^3)}{12}$ MOMENT OF INERTIA FOR RECTANGULAR CROSS SECTION "b" and "h" dimensions in inches

W2 = REQUIRED WEIGHT IN POUNDS (lbs)

DENSITIES (d): STEEL = 0.282 lbs/in^3

ALUMINUM = 0.099 lbs/in^3

COPPER = 0.321 lbs/in^3

IRON = 0.260 lbs/in^3

Figure 8: Simple Dynamic Absorbers.

Then the next step is simulating the formula above into the excel program to calculate the dimension of dynamic absorber that we need:

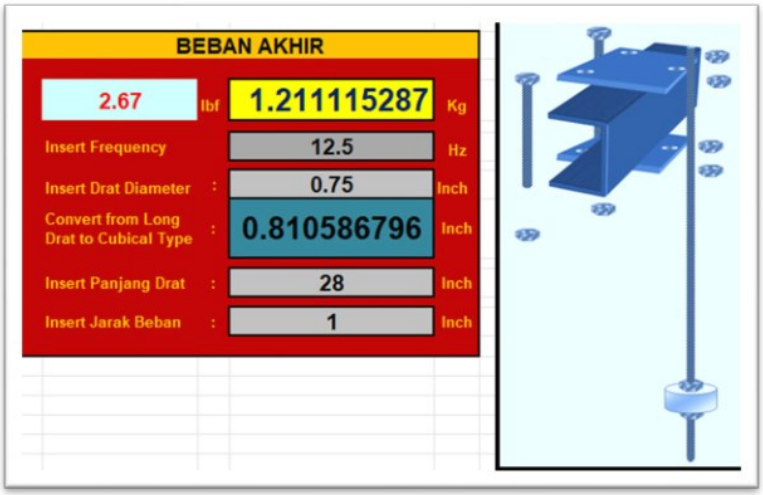

Figure 9: Simple dimension of TMDA.

Iron bar with a pendulum (weight) was chosen as the construction of the Dynamic Absorber as shown in the picture below, here in after the Dynamic Absorber Trial is named Dynamic Absorber Trial-1 (DAT-1).

Figure 10: Installed of TMDA Trial-1 (DAT-1).

As the result, all vibration value at Hot Well Pump tends to decrease after Dynamic Absorber Installation and this also confirms and proves the truth of the Failure Analysis first hypothesis regarding the cause of the alleged damage at Hot Well Pump.

Data -The presentation of research data is in the form of spectrum graphs and vibration signal waveforms from the research process on damaged Hot Well Pump Stuhl and after installed TMDA.

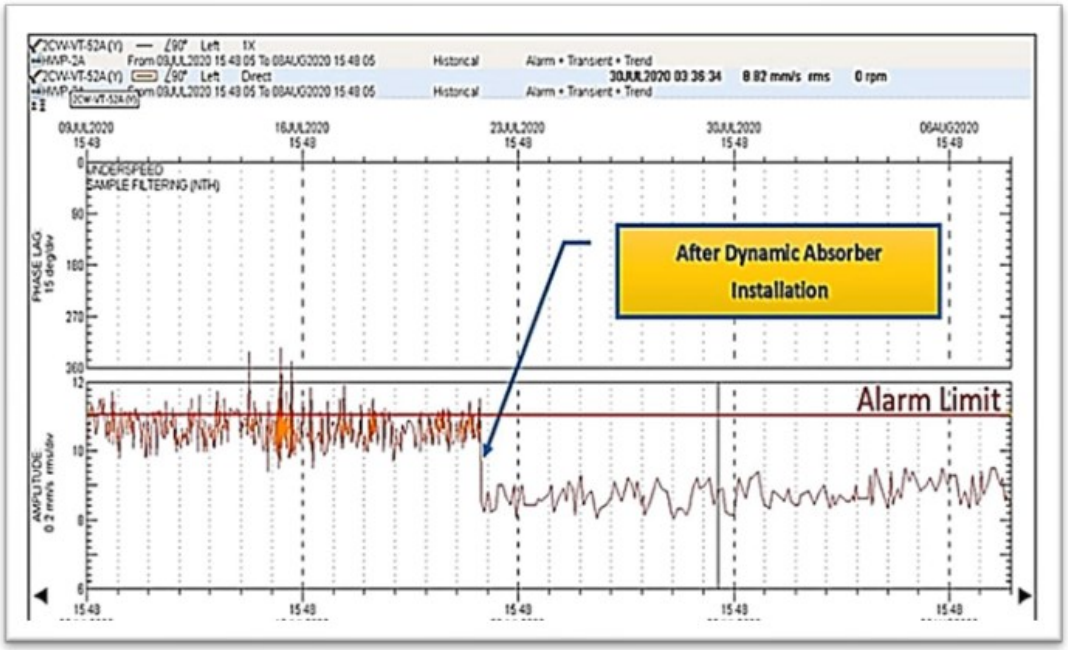

Figure 11: Vibration Amplitude After Installed TMDA.

Figure 12 confirming at the time of dynamic absorber installation according to the recommendations, that the overall vibration tends to decrease.

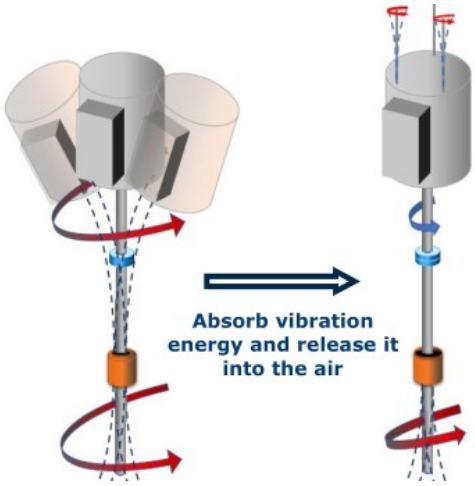

Figure 12: TMDA Absorb vibration energy and release it into the air.

7. CONCLUSION

The best solution to solve the resonance problem is to install the machine properly. Another possible temporary solution to solve the resonance problem is to install a dynamic absorber, a device designed to have the same reaction frequency as the dominant vibration direction of the structure itself that will counteract the initial motion.

As the purpose of this paper is to determine the damage to the Hot Well Pump with vibration signal analysis and how to solve it according to the condition that surrounded by H2S enclosure and zero downtime issue, during Covid-19 pandemic period. The results of the research on the Hot Well Pump symptom's, the following conclusions are drawn:

1. Vibration analysis can produce failure diagnosis stages in the machine that been occurred due to the interaction between vibration and improper quality of the structure.
2. The cause of the Hot Well Pump failure is due to initial deformation that caused by resonance, confirmed by Coast down analysis and Bump test result.
3. In the case of resonance, the accuracy of the absorber dynamic personal frequency value is the most influential factor in reducing the machine vibration amplitude value.
4. Installing the TMDA on the hot well pump has been shown to reduce the vibration amplitude by up to 30%, thereby avoiding a loss of more than USD 26 million per year during the COVID-19 pandemic.

REFERENCES

Agilent Technologies: The fundamentals of Signature Analysis. Note: 243

Heinz P. Bloch – Elsevier: Practical Machinery Vibration Analysis & Predictive Maintenance

ISO 10816: Mechanical vibration -- Evaluation of machine vibration (2014)

Mackay, Steve: Practical Machinery of Vibration Analysis and Predictive Maintenance. Oxford: Elsevier (2024).

Randy Fox: Dynamic Absorbers for Solving Resonance Problems, Entek IRD International Corp. Houston, TX

S Ralph Buscarello: Practical Solutions to Machinery and Maintenance Vibration Problems, Chapter 1, Basic Information. Section 1 What to Look For, Most of the Time

Tiara Vibrasindo Pratama: Pemrosesan Sinyal. Jakarta: Tiara Reliability Solution (2005).

Utilization of Refurbished PDC Bit in Geothermal Drilling in Sumatera: Performance Review and Lessons Learned

Triadi Herwasto Aribowo, Mada Amatori Sutan, Arif Hudiman, Juliana Phan, Rahmad Febdiansyah Bas, and Kurnia Darmawan Huway

NOV, Kawasan Taman Tekno Blok C No.1, South Tangerang

Triadi.Aribowo@nov.com Mada.Sutan@nov.com Arif.Hudiman@nov.com Juliana.Phan@nov.com Rahmad.FebdiasyahBas@nov.com Kurnia.Darmwan@nov.com

Keywords: Drilling Performance, Drill Bits, Refurbished PDC Bits, Geothermal

ABSTRACT

The cost of drilling typically constitutes a significant portion of the total cost of a geothermal power project. On average, drilling costs can account for about 30% to 50% of the total cost. The percentage can vary depending on several factors, including the depth and complexity of the drilling, the geological conditions, the type of geothermal system being installed, and the location of the project.

Reducing drilling costs is critical to making geothermal projects more economically viable. Several strategies and technological advancements have been implemented to reduce the costs, including lowering drilling equipment costs. One visible way to reduce drilling equipment costs is through refurbishment.

Recent advancements in Polycrystalline Diamond Compact (PDC) drill bits have made them widely used in geothermal drilling applications due to their improved performance compared to Roller Cone (RC) bits. The PDC bit can also improve cost efficiency through repairability. However, how does the refurbished PDC bit perform in geothermal drilling? This paper provides a performance review of several refurbished bit runs in geothermal drilling in Sumatera, along with key lessons learned from the bit design that could contribute to optimal performance and cost-effectiveness.

1. INTRODUCTION

The cost of drilling wells represents a significant portion of the overall expenses in geothermal energy projects. One key area that contributes a significant amount to the production cost is the drilling process (Sugiura et al., 2021). And the drilling cost can account for up to 50% of the capital cost of developing a representative 50-megawatt (MW) geothermal plant (Tester et al., 2006). As the industry strives to make geothermal energy a more viable and competitive option, reducing these drilling costs has become a primary focus.

To address the high costs associated with drilling, several strategies have been proposed and implemented. These strategies range from optimizing drilling techniques to enhancing the performance and longevity of drilling equipment. Among these strategies, one particularly effective approach is the repair or refurbishment of polycrystalline diamond compact (PDC) drill bits.

Practically, the PDC bit is more feasible to repair as it was made from replaceable materials as long as the body itself was still in good condition with some criteria compared to Roller Cone (RC) bits or hybrid bits that combine PDC and Roller Cone (Aribowo et al., 2023).

Rather than incurring the substantial costs of purchasing new PDC drill bits, repairing and reconditioning used bits also offers a cost-effective alternative. This practice not only extends the service life of the drill bits but also significantly reduces the overall drilling expenditures. By focusing on the repair of PDC drill bits, geothermal projects can achieve substantial cost savings while maintaining operational efficiency and effectiveness.

The question now is how the refurbished PDC will perform in geothermal drilling. Will it be the same as the new bits in terms of achieving its targets? This paper evaluates several refurbished bit runs in geothermal drilling in Sumatera, along with key lessons learned from the bit design that could contribute to optimal performance and cost-effectiveness.

2. PDC REFURBISHED BIT

Refurbishing drill bits is often much cheaper than purchasing new ones. This can result in significant cost savings, especially in industries where drill bits are used extensively, especially in geothermal drilling.

The PDC refurbishment process is basically to restore the bit condition to its prime condition after the bit passes through several criteria, such as no severe erosion, excessive damage on the bit body or cutter pocket, and less than 2/16-in. undergauge (Aribowo et al., 2023). The bit is then going to the main process, as shown in Figure 1.

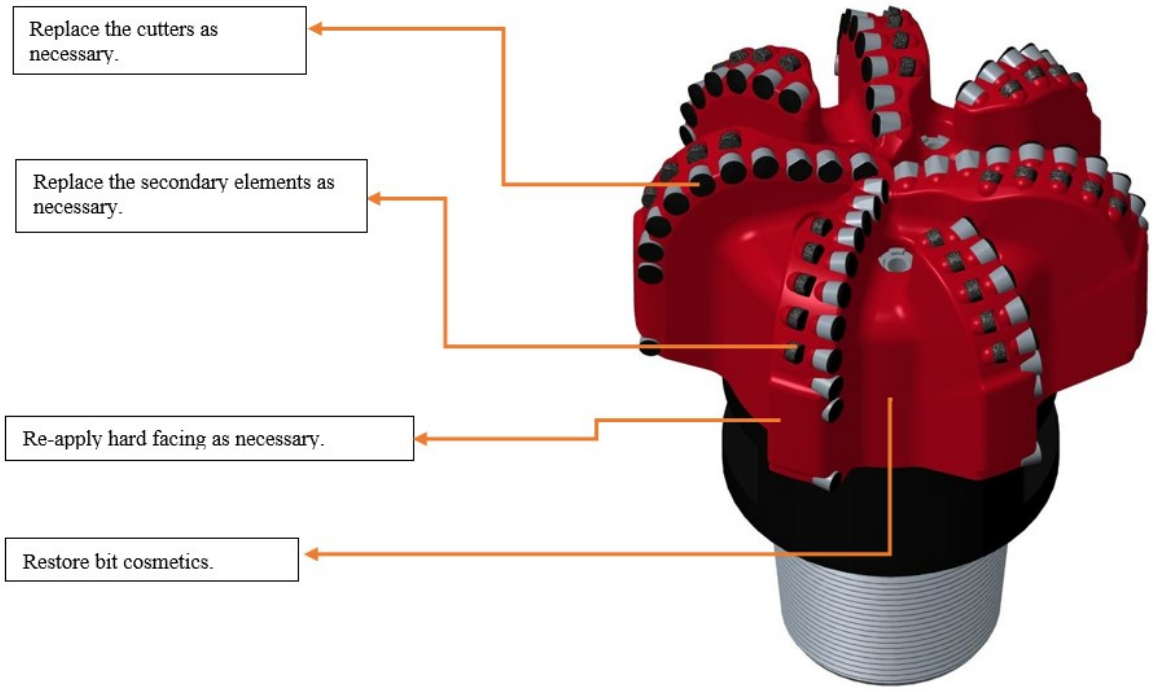

Figure 1: PDC bit refurbishment main process.

Proper refurbishment can significantly extend the life of a drill bit. By repairing worn and damaged PDC cutters, a refurbished bit can perform almost like new, thereby maximizing the return on the initial investment.

3. METHODS IN PERFORMANCE REVIEW OF REFURBISHED PDC BIT

As known, refurbished drill bits are less expensive than new ones. By ensuring that refurbished bits perform well, companies can reduce costs significantly without compromising on drilling efficiency. There are several methods and indicators for reviewing the performance of refurbished PDC bits:

1. **Bit Performance**: The assessment of refurbished bit performance can be seen from several runs and its parameters, including total interval drilled, rate of penetration (ROP), and reason pulled. A well-refurbished drill bit can maintain or even improve its performance. This ensures that the drilling process remains efficient and effective, reducing downtime and increasing productivity.
2. **Repair Quality**: One indication of an optimal repair process that adheres to high-quality standards is the absence of lost cutters. A lost cutter indicates a poor repair process, as the cutter is completely gone from the cutter pocket. This typically occurs when the braze bond fails to retain the carbide substrate. Figure 2 shows an example of a lost cutter on the PDC bit.

Figure 2: Example of a lost cutter on PDC bit.

In addition to the above indicators, evaluating the performance of refurbished bits introduces new design criteria, which will improve their repair capabilities and reliability for continued use.

4. RUN PERFORMANCE OF REFURBISHED PDC BITS

The performance review was taken from one of the major geothermal operators in Sumatera. Several refurbished PDC bits, consisting of 17.5-in., 12.25-in., and 9.875-in. sizes, were run. This data is intended to serve as reference material for the performance of refurbished bits, provide insights into whether poor bit performance is due to poor repair quality or not, and guide the optimization of bit design to ensure continued use.

4.1 The 17.5-in. PDC Refurbished Bits

One type of 17.5-in. FTKC76 bit has already been run in several geothermal wells in Sumatera. Based on the bit record, the 17.5-in. FTKC76 serial number A1 had been refurbished two times, and it was used to drill about 300- to almost 1,000-m intervals. The bit drilled a volcanic rock such as andesite lava, rhyolite, and tuff in directional wells with a mud motor assembly. In summary, the refurbished bit that ran in the XA-03 and XP-117 wells demonstrated a very good performance compared to the new ones. Although it was a refurbished bit, the final average ROP achieved was between 10 m/hr and 14.6 m/hr, or around 50% faster than the new one. In terms of bit performance, it can be concluded that a refurbished bit does not downgrade the performance; instead, it is similar or even improves the performance.

The second 17.5-in. FTKC76 serial number B1 was refurbished once and run in the XV-01 well. The bit was picked up to continue drilling the entire 17.5-in. interval after the previous bit was pulled out due to penetration rate and bit hours. However, it only drilled 195 m before experiencing a hole problem that led to pulling out of the hole. In terms of bit performance, the bit achieved an average ROP of 7.62 m/hr, which was considered moderate as the drilling was controlled due to a hole issue. Table 1 shows the whole run record for the 17.5-in. PDC716 refurbished bit, including serial numbers A1 and B1, along with new ones for comparison.

Table 1: Run performance results of the 17.5-in refurbished PDC bit.

Well	Size (in.)	Bit Type	SN / Status	Depth In (m)	Depth Out (m)	Interval (m)	ROP (m/hr)	Rig Dull Grading
XP-119	17.5	FTKC76	A1 / New Bit	400	1,215	815	9.31	0-1-WT-S-X-I-PN-PR
XA-03	17.5	FTKC76	A1 / Refurbished #1	405	775	370	14.62	0-1-WT-S-X-I-NO-TD
XP-117	17.5	FTKC76	A1 / Refurbished #2	400	1,350	950	10.0	1-4-BT-G-X-1-NO-TD
XP-118	17.5	FTKC76	B1 / New Bit	394	1,351	957	10.35	1-1-WT-A-X-I-BT-TD
XV-01	17.5	FTKC76	B1 / Refurbished #1	1,226	1,421	195	7.62	1-3-CT-S-X-3-BT/PN-HP

Figures 3 and 4 show the dull condition of the 17.5-in. FTKC76 serial number A1 for the second and third runs in refurbished condition.

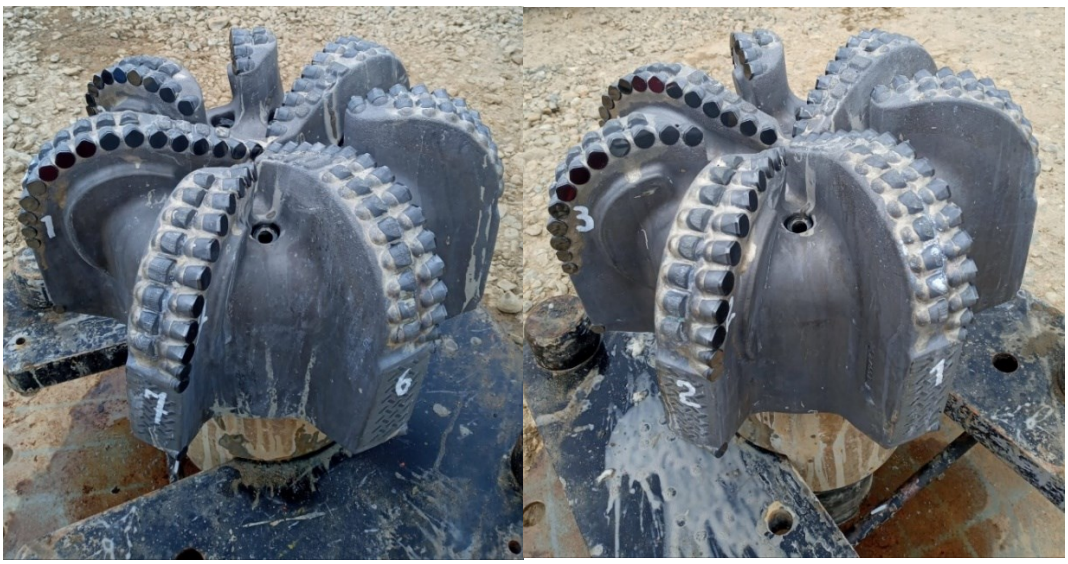

Figure 3: The dull condition of the 17.5-in. refurbished bit run in the XA-03 well.

Figure 4: The dull condition of the 17.5-in. refurbished bit run in the XP-117 well.

Figure 5: The dull condition of the 17.5-in. refurbished bit run in the XV-01 well.

Reviewing the dull condition of the 17.5-in. FTKC76-A1, none of them are indicating any lost cutter condition. The last run in SP-117 well shows that the major dull condition is mostly broken cutters (BT) and worn cutters (WT) on the secondary elements, which are not related to the poor repair quality. The broken cutters are most likely due to the high impact. In terms of gauge durability, the bit got wear and slightly chipped, resulting in an undergauge of 1/16 in. Based on the repair criteria, the bit should still be in repairable condition.

Figure 5 shows the dull condition of the 17.5-in. FTKC76 serial number B1 refurbished bit.

In terms of bit durability, the dull condition of the 17.5-in. FTKC76 serial number B1 run in the XV-01 well is still considered in acceptable condition. There are no indications of lost cutters, only broken cutters, indicating no major issues with the bit's repair quality. Looking at the dull grading measurement, it was reported that the bit got 3/16-in. undergauge. According to the acceptable refurbishment criteria, the repairable condition should not be more than 2/16-in. undergauge. Therefore, the 3/16-in. undergauge exceeds the acceptable limit for continued repairability.

4.2 The 12.25-in. PDC Refurbished Bits

Data records reveal that PDC bits have dominated several geothermal wells drilled in Sumatera. Based on the 12.25-in. bit record, seven refurbished bits were run, with one able to be rerun in a different well. Table 2 shows all 12.25-in. bit runs for refurbished bits, including the new ones, for comparison.

The refurbished bits tend to have shorter intervals, as most were picked up to continue after a previous run failed to finish the section. In terms of ROP, the bits were very competitive, ranging from 5 m/hr to 16 m/hr, indicating the varying challenges and characteristics of each well. However, most of the bits could finish the section to total depth (TD).

Table 2: Run performance results of the 12.25-in. refurbished PDC bit.

Well	Size (in.)	Bit Type	SN / Status	Depth In (m)	Depth Out (m)	Interval (m)	ROP (m/hr)	Bit wear
XT-09	12.25	FTKC76	A07 / New Bit	1,441	2,100	659	7.31	1-2-WT-S-X-I-NO-TD
XT-10	12.25	FTKC76	A07 / Refurbished	892	1,100	208	16.00	1-2-WT-A-X-2-BT-TD
XT-03L2	12.25	FTC76	A63 / New Bit	810	1,279	469	19.14	1-2-BT-G-X-I-NO-BHA
XT-03L3	12.25	FTC76	A63 / Rerun Bit	874	1,000	126	11.45	1-2-WT-G-X-I-BT-TD
XAAE-08	12.25	FTC76	A63 / Refurbished	2,000	2,157	157	13.66	1-3-BT-G/S-X-I-CT-TD
XP-119	12.25	FTKC76	A98 / New Bit	1,700	2,305	605	12.17	0-1-WT-S-X-I-NO-TD
XAAE-06	12.25	FTKC76	A98 / Refurbished	1,287	1,466	179	5.52	1-2-WT-S-X-1-CT-PR
XAAE-03	12.25	FTKC76	A27 / New Bit	1,501	2,200	699	11.15	1-2-WT-S/G-X-1-CT-TD
XAAE-06ST2	12.25	FTKC76	A27 / Refurbished	1,466	1,730	264	6.00	0-1-WT-S-X-I-BU-BHA
XAAE-06ST2	12.25	FTKC76	A27 / Refurbished Rerun	1,730	1,858	128	6.61	1-1-WT-A-X-I-NO-TD
XAA-01	12.25	FTKC76	A02 / New Bit	1,337	1,655	318	9.09	1-3-WT-S-X-1-BT-TQ
XP-117	12.25	FTKC76	A02 / Refurbished	1,650	1,749	99	5.13	2-3-BT-S-X-1-CT-PR
XP-118	12.25	FTC76	A37 / New Bit	1,739	2,577	838	9.96	1-2-WT-S-X-I-CT-TD
XV-03	12.25	FTC76	A37 / Refurbished	2,100	2,550	450	5.51	1-3-WT-S-X-2-BT-TD

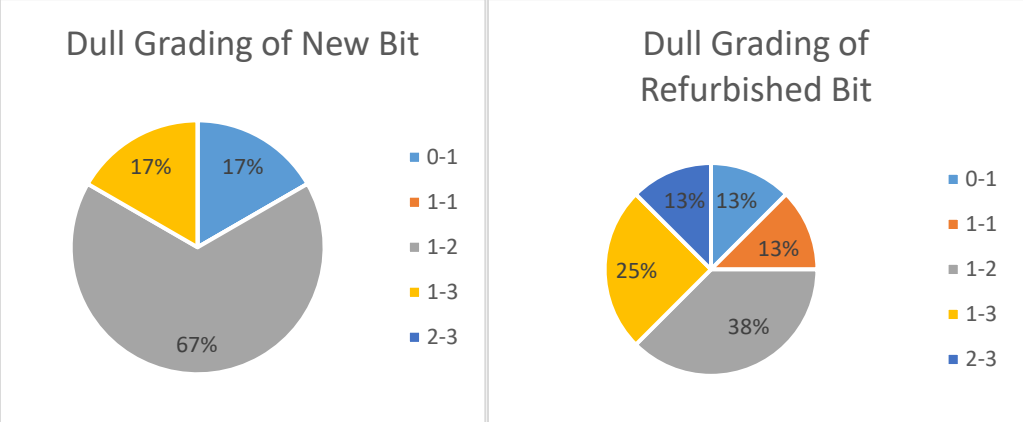

Figure 6: The dull grading percentage of the 12.25-in. new and refurbished conditions.

Figure 6 shows the major dull condition to represent the bit durability. The percentage of dull grading results showed similarity in the highest dull grading percentage with 1-2. Again, this data shows that refurbished bits can perform comparably to the new bits.

The dull pictures of the 12.25-in. FTKC76 refurbished bit run in the XT-10 well, as shown in Figure 7, show that the cutting structure has very minimal wear. However, based on the gauge measurement, the bit got 2/16-in. undergauge, with several broken cutters and wear on the gauge pads.

The12.25-in. FTC76 refurbished bit run in the XV-03 well had similar results. The bit was picked up to finish the section with a total interval of 450 m, as the previous bit could not complete the section due to penetration rate and bit hours. The bit got significant wear on the gauge and several broken cutters on the gauge area, leading to a 2/16-in. undergauge, as shown in Figure 8. This finding necessitates a step change in the bit's durability to

potentially enhance the bit in future designs, particularly in the gauge area. Improving gauge protection will lead to extending the life of a drill bit for continued use.

Figure 7: The dull pictures of the 12.25-in. FTKC76 refurbished bit run in the XT-10 well.

Figure 8: The dull pictures of the 12.25-in. FTC76 refurbished bit run in the XV-03 well.

Figure 9: The dull pictures of the 12.25-in. FTC76 refurbished bit run in the XV-03 well.

4.3 The 9.875-in. PDC Refurbished Bits

Based on the run record, only one 9.875-in. bit was used in geothermal drilling in Sumatera. Initially, the bit completed a 750-m interval to TD in the XAA-01 well. After this run, several worn cutters were observed in all areas. These worn cutters were subsequently replaced with new ones, and the refurbished bit was deployed to drill the entire 9.875-in. section in the XV-03 well. The results showed that the bit completed the section to TD with an average ROP of 6.12 m/hr. Performance-wise, the refurbished bit demonstrated strong capabilities by achieving TD in a single run. Although the ROP was slower than the new ones, this is suspected to be due to factors beyond the bit itself, as the dull was still rated at 1-1-WT. Figure 9 shows the dull pictures of the 9.875-in. FTKC76 refurbished bit after running in the XV-03 well.

Table 3: Run performance results of the 9.875-in. refurbished PDC bit.

Well	Size (in.)	Bit Type	SN / Status	Depth In (m)	Depth Out (m)	Interval (m)	ROP (m/hr)	Rig Dull Grading
XAA-01	9.875	FTKC76	A92 / New Bit	1,800	2,550	750	8.20	1-1-WT-A-X-I-CT-TD
XV-03	9.875	FTKC76	A92 / Refurbished	2,550	2,750	200	6.12	1-1-WT-A-X-I-CT-TD

5. NOTABLE PERFORMANCE, LESSONS LEARNED, AND FUTURE WORK

The following highlights the notable performances of the refurbished bits:

1. The 17.5-in. FTKC76 refurbished bit drilled a cumulative interval of 950 m and achieved a good ROP of 10 m/hr despite being in the second refurbished condition.
2. The 12.25-in. FTC76 refurbished bit drilled the longest interval, 450 m to TD, in the challenging XV-03 well.
3. The 9.875-in. FTKC76 refurbished bit drilled the entire section from shoe to shoe and still came out in excellent dull condition 1-1-WT.

The lessons learned from the above performance runs indicate that there are still bits with good cutting structures in the face but have undergauge. Undergauge is crucial as it is a part of the bit body. Once the bit got significant undergauge (more than 2/16 in.), it can no longer be repaired.

The standard gauge protection for the PDC bit uses *Thermally Stable Polycrystalline* (TSP) material on the gauge pads. Once the bit gets undergauge more than 2/16 in., its gauge durability may decrease as there is only a little to no TSP material remaining. In the repair process, installing TSP material can be complex and difficult, unlike just applying hard facing. As a result, modifications to the bit design, particularly on the gauge pads, may be necessary for the continued use of a refurbished bit.

Replacing TSP material with a PDC dome insert as gauge protection in future bit designs improves wear resistance. Furthermore, the PDC dome insert is a more changeable component in the repair process, increasing the likelihood of continuous bit refurbishment. **Figure 10** shows the new bit design featuring improved gauge protection with PDC dome inserts for future refurbishment.

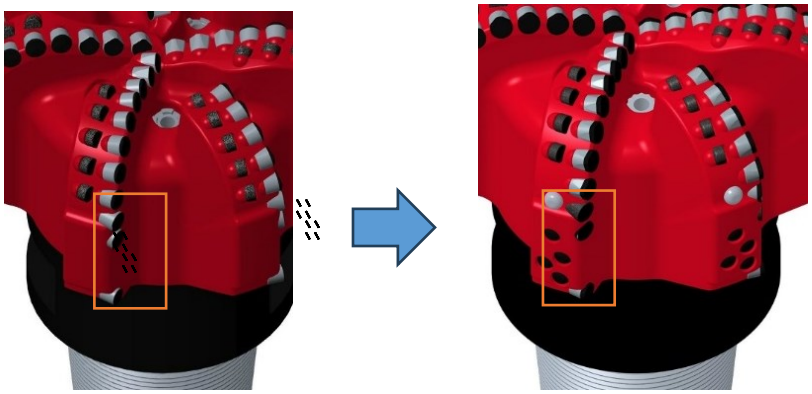

Figure 10. The new bit design for improved gauge durability and repair capabilities.

6. CONCLUSION

Following the performance review of all refurbished bits runs in geothermal Sumatera, it was concluded that the refurbished bits could maintain or even deliver better performance than the new ones. Most of the bits achieved the drilling targets without downgrading their performance, although some bits might come out with 1-3 or 2-3.

However, general observation found that the most refurbished bit was also able to complete the section to TD with good dull grading.

There are no findings to suggest that the refurbished bits suffered from poor repair quality, as indicated by the absence of major dull conditions or lost PDC cutters.

In future work, installing PDC dome inserts on the gauge pads is expected to reduce the undergauge issues. This modification will also improve repair capabilities, as these components are more changeable. Secondly, supporting software for the refurbishment process, where we store the dull data, is beneficially required. The data can be used to observe the dull trend and help in future design iterations.

In summary, implementing refurbished bits remains beneficial for ensuring an efficient and effective drilling process. Their good durability allowed the bits to be run multiple times, resulting in:

- Reduced drilling costs.
- Better inventory management.
- Lowered carbon emissions and collaborative efforts toward global decarbonization objectives.

REFERENCES

Aribowo, T.H., Phan, J..: An Approach to Using PDC Refurbished Bits Delivers Effective Bit Utilization in Geothermal Drilling, *Proceedings,* The 9th Indonesia International Geothermal Convention & Exhibition (IIGCE) 2023.

Sugiura, M. J., Lopez, R., Borjas, F., Jones, S., McLennan, J., Winkler, D..: Oil and Gas Drilling Optimization Technologies Applied Successfully to Unconventional Geothermal Well Drilling, *Proceedings*, SPE Annual Technical Conference and Exhibition, Dubai, UAE. 2021. SPE-205965-MS. https://doi.org/10.2118/205965-MS

Tester, J. W., B. J. Anderson, A. S. Batchelor, D. D. Blackwell, R. DiPippo, E. M. Drake, J. Garnish, B. J. Livesay, M. C. Moore, K. Nichols, S. Petty, M. N. Taksoz and R. W. J. Veatch. 2006. “The Future of Geothermal Energy, Impact of Enhanced Geothermal Systems (EGS) on the United States in the 21st Century.” Massachusetts Institute of Technology and Idaho National Laboratory. INL/EXT-06-11746. https://www1.eere.energy.gov/geothermal/pdfs/future_geo_energy.pdf

The Use of PE100 Polyethylene to Minimise Condensate Pipeline Corrosion at The Star Energy Wayang Windu Geothermal Power Plant

Amos Tay[1] and Alex Kartono[2]

[1]Borouge, One George Street, 18-01 Singapore 049145
[2]Borouge, Revenue Tower 19F, District 8, Jl. Jendral Sudirman Kav 52-53 (SCBD), Jakarta Selatan 12190

amos.tay@borouge.com; alex.kartono@borouge.com

Keywords: corrosion free, condensate pipeline, polyethylene, PE100

ABSTRACT

The Wayang Windu geothermal plant, which is owned and operated by Star Energy, was initially completed in 1999 and today generates up to 227MW of electricity using the natural hot fluids from a reservoir deep beneath. Steam which is used to generate the electricity using steam turbines, will be returned to the underground reservoir through pipelines and injection wells after it has cooled and condensed. Unfortunately, the condensate is very corrosive due to high levels of dissolved solids and the relatively high condensate temperatures, which typically reaches 50°C. In addition, the Wayang Windu pipelines are laid in a hilly region and flow under gravity, which makes them prone to erosion. Therefore, the corrosion and erosion of the steel pipelines carrying the condensate cannot be avoided and after some years in operation, regular repairs are necessary due to leakages. Eventually, the steel pipelines need to be replaced.

After nearly 15 years of operation, half the length of the condensate pipelines at Wayang Windu had been extensively repaired, and this section was due to be replaced. Instead of replacing it with another steel pipeline, Star Energy's engineering team decided to explore other pipeline materials that are less prone to corrosion. The availability of polyethylene (PE) pipe systems in Southeast Asia has greatly increased over the past two decades, giving engineers new options for consideration. Additionally, the region has gradually adopted the use of specifically engineered PE100 pipe grade materials that comply with the requirements of international standards. Having reviewed the options, the Star Energy team decided to install a single 400 mm OD SDR 11 PE100 above ground pipeline in order to evaluate the performance of this material in a new application, together with identifying the practical challenges in constructing such a pipeline.

This paper will describe the above in more detail, while explaining the design and installation process the Star Energy team, together with their contractors and suppliers, went through. It will also detail the lessons that they learnt while working on the project.

1. INTRODUCTION

The first Wayang Windu geothermal plant was built in 1999 by Star Energy 40 km south of Bandung, West Java, to generate 110 MW of electricity using the earth's natural high-temperature fluids, as shown in Figure 1. A second 117 MW unit was added in 2009 and the facility, shown in Figure 2, which now has a capacity of 227 MW. It is operated under a joint operating agreement between Star Energy and Indonesia's state-owned oil and gas company PERTAMINA. This gives Star Energy the right to generate up to 400 MW of electricity on an area of 12,960 hectares for a period of 42 years. The sale of generated electricity to state-owned electricity company PLN and its delivery into the West Java grid is governed by an Energy Sales Agreement.

Thermal energy from the earth is extracted in the form of geothermal fluids from deep underground reservoirs through multiple production wells. This steam and brine mixture is sent to a cyclone separator where it is separated, and the steam is sent to the power plant. The brine is returned to the reservoir through a backsplash well to maintain pressure and extend the reservoir's life. The steam is passed through a turbine to generate electricity, condensed and sent to a cooling tower. The hot condensate is cooled in the cooling tower and some of the cooled water is returned to the condenser to condense the steam. Excess condensate is returned to the reservoir through a condensate injection well.

Similar to other geothermal plants, Wayang Windu has kilometers of pipeline that transport condensate – essentially brine that corrodes steel pipes. The focus of this technical article is on the replacement of some steel condensate injection pipelines with PE pipes.

2. PROJECT BACKGROUND

The original 16-inch steel condensate injection pipeline runs from the power plant interface to the injection wellpads WWF and WWP, shown in Figure 1 and in more detail in Figure 3. The figure also shows part of the route of the injection pipeline, which is approximately 7,750 m long.

Figure 1: Map showing the location and layout of the Wayang Windu Geothermal Power Plant.

Figure 2: View of the Wayang Windu Geothermal Power Plant showing the generating house and cooling towers.

Originally, carbon steel was used for the pipelines because of a lack of alternative materials and the expectation that corrosion would not be a major problem since the condensate had most of its oxygen removed by the power plant's condensers before entering the pipeline. The pipelines were designed as pressure pipelines with a maximum flow rate of 177 kg/s (just under 175 l/s) at a velocity of 1.5 m/s, but much of the pipeline operates in open channel flow conditions at much higher velocities and minimum pressures. The reason is that the gradient from the power plant to the injection well is steep. A portion of this is shown in Figure 4.

After commissioning in 1999, the pipeline was inspected periodically. In 2010, it was discovered that the pipe walls had thinned significantly and were leaking, especially in the first uphill half of the pipeline, where open

channel flow conditions prevailed. Although to a lesser extent, corrosion also occurred in the pressurised rear portion of the pipeline.

Since 2011, the Star Energy team initiated a series of temporary measures to address the leak. This includes spot repairing leaks, replacing badly corroded pipe spools, limiting low rates and rotating pipes where practical. This final step was done to move the thin walled, more corroded sections from the bottom of the pipe to the top. From this final mitigation, it is clear that the level of corrosion, resulting wall thinning and leakage along the base of the pipeline are significantly more severe, at least along the sections where open channel flow conditions were prevalent.

A failure analysis of a 4 km mountain section of the pipeline revealed that the pipeline was subjected to a combination of corrosion and erosion. Visual inspection of the defective pipe spool revealed directional metal loss with significant wall thinning along the base of the pipeline. Figure 5 shows a typical defective pipe and Figure 6 shows how the corrosion products have been eroded from the pipe invert. Erosion occurred when steep open channel flow conditions existed along the section of the pipeline, resulting in very high flow velocities. These sometimes exceeded the erosion limit, releasing corrosion products that were providing some protection to the underlying steel.

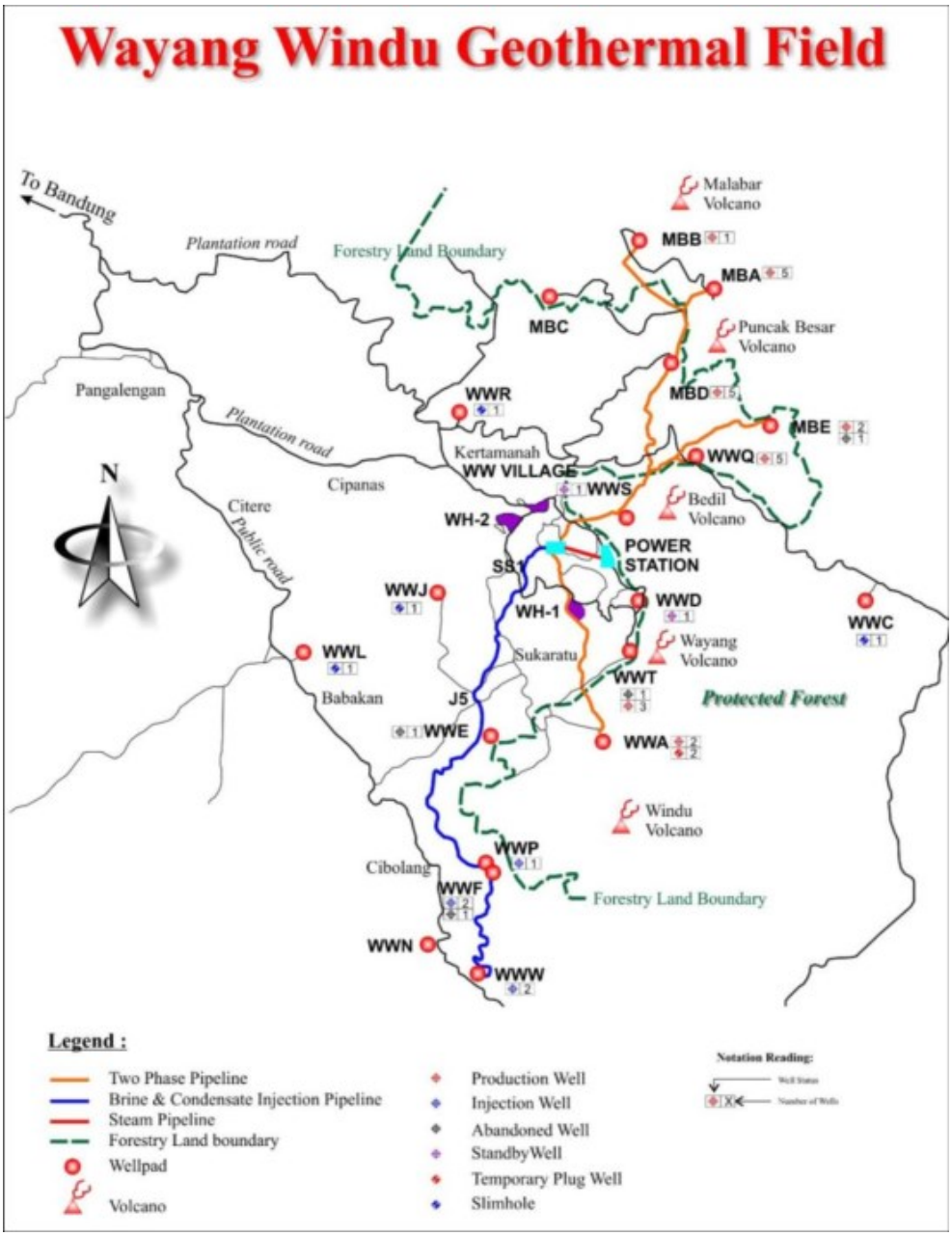

Figure 3: Plan of the Wayang Windu Geothermal Field showing the blue condensate injection pipeline, the first half of which was replaced under the project.

Figure 4: View of the Geothermal Power Plan showing the condensate pipeline replaced under the project.

Figure 5: View of a badly corroded steel pipe taken from the section replaced under the project.

Figure 6: Internal view showing where corrosion products have been scoured by erosion.

Despite mitigation measures implemented on site, the condition of the condensate pipeline continues to deteriorate, with 5 to 8 significant leaks per year. Hence, in 2012, Star Energy decided to replace the first 4 km of the condensate pipeline and commissioned an engineering firm to conduct a feasibility study.

3. FEASIBILITY STUDY

The feasibility study was undertaken by PT Gago Engineering, a Bandung based engineering consultancy specialising in the energy sector.

The feasibility study was titled "Condensate Pipe Replacement Using Non-Steel Base Material". It comprised three key sections, namely non-metallic pipe material selection, process design and piping design.

As the title suggests, Star Energy had already decided to explore the use of non-metallic pipe materials to avoid the well-known corrosion problem. The material selection process looked at the use of the following materials:

- High Density Polyethylene (HDPE)
- Polyvinylidene Fluoride (PVDF)
- Polypropylene (PP)
- Chlorinated Polyvinyl Chloride (CPVC)

To get a subjective look at each material, their relative performance against each of the following parameters was assessed:

- Mechanical strength
- Water and chemical resistance
- Erosion resistance
- UV degradation
- Ease and effectiveness of jointing systems
- Maintainability
- Total installed cost

When selecting the material, it was determined that each of the four polymer pipe materials was more or less suitable for the intended application at an operating temperature of 50°C and pressure of up to 12 bar and that none of them would suffer from corrosion.

It was found that locally available PP is not suitable for above-ground installation as it is exposed to sunlight and degraded by ultraviolet (UV) radiation. This effect can be slowed by adding UV stabilisers, but the only long term-term solution is to permanently coat the pipeline, which is not practical.

The same is true for CPVC, with the added complication that CPVC has very poor resistance to ammonia and limited resistance to most amines, even at ambient temperature. This is due to the high reactivity of amines with chlorine, which strips the chlorine from the CPVC, which weakens the material and leads to failure.

PVDF is an excellent all-purpose pipe material that can be used in temperatures up to 140°C and has excellent UV resistance. This material is typically used for demanding applications in the chemical industry, but it is only available in sizes up to 225 mm OD (Outer Diameter) because it is at least five times more expensive than HDPE.

In the manufacture of HDPE pressure pipe systems, ISO (International Organization for Standardization) and European standards only allow the use of pre-compounded PE80 and PE100 materials. Such materials can be fully protected from UV degradation by the dispersion of carbon black (2-2.5% by mass) throughout the resin and can be used at operating temperatures of up to 60°C. As shown in Figure 7, they also have very good abrasion resistance, an important property considering the erosion of existing steel pipelines due to high flow velocities.

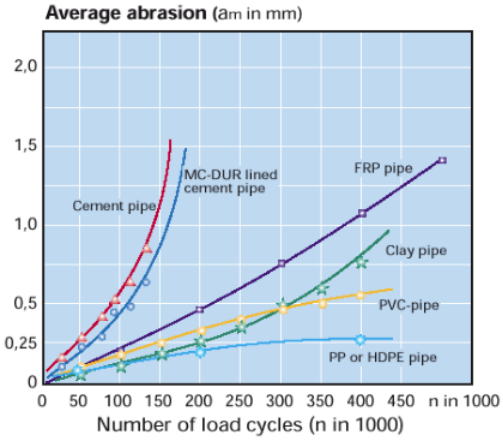

Figure 7: Chart showing abrasion (erosion) rates measured using Darmstadt Test.

With regards to jointing, CPVC pipes are jointed either with rubber rings or cemented joints. Whilst PP pipes can be jointed using butt fusion welding, but at that point of time only pipes with spigot and socket rubber ring joint are available in Indonesia. Both PVDF and HDPE can be jointed by butt fusion welding, effectively creating a continuous pipe with no seams.

The feasibility study concluded that while PVDF was the material of choice, PE100 (HDPE) offered the best cost-performance balance for this application and was adopted for the pipeline replacement project. The study also compared the estimated replacement costs of the PE100 pipeline with that of carbon steel pipeline. Despite PE100 having a lower cost per unit weight, the difference between the two materials was found to be relatively small, especially at lower operating temperatures, when considering the higher density and hoop stress capacity of carbon steel. The most significant difference was for the installation cost, with PE100 averaging about 60% lower than that of carbon steel.

3.1 Detailed design

Detailed planning was also undertaken by PT Dago Engineering and essentially involved designing an above ground PE100 pipeline mounted on prefabricated concrete supports running alongside the existing carbon steel pipeline.

The consultancy was apparently unaware of the ISO 15494 standard, which covers the design of plastic piping systems for industrial applications and therefore the design was developed using a combination of ASME B31.3, the code for process piping, along with information taken from several sources concerning the design of PE100 pipe systems.

The pipeline itself comprised a PE100 pipe with 400 mm OD SDR 11 (Standard Dimension Ratio, is the ratio of the pipe outside diameter divided by its minimum wall thickness and determines the pipe pressure rating) with a minimum wall thickness of 36.3 mm. At a temperature of 20°C, such a pipeline would have a design pressure of 16 bar (232 psi) but at a temperature of 50°C this should be reduced to 9.8 bar using the temperature derating factor given in ISO 4427 Part 1. This was considered more than sufficient considering this section of pipeline being replaced was operating under free-flowing conditions and at minimal pressure.

The design also called for the PE100 pipes and fittings to be butt fusion welded together whenever possible to effectively create a continuous pipeline with no seams. It should be noted that PE100 has a thermal coefficient of expansion of 0.18 mm/m/°C, more than 15 times that of carbon steel, this continuity required the provision of expansion loops at regular intervals.

3.2 Construction and commissioning

Following the completion of the detailed design and after going through a tendering process, the contract to supply and install the new PE100 pipeline was awarded to PT Wirana Jayatama Abadi, a Jakarta-based general contractor that principally works in the energy sector.

The manufacture and supply of the PE100 pipes and fittings was sub-contracted to PT Indopipe (now owned by PT Wahana Duta Jaya Rucika), a company based in Surabaya with over 10 years' experience and can produce pipes up to 1000 mm OD. All pipes and fittings were produced using the BorSafeTM HE3490-LS and BorSafeTM HE3490-LS-H PE100 pipe grades manufactured in the United Arab Emirates by Borouge. Both materials have long track records of being used for industrial pipeline applications and have been used to produce pipes and fittings of up to 2000 mm OD.

Following the contract award in August 2013, construction work started in November. As the new pipeline was to be laid alongside the existing one, as shown in Figure 8 and 10, the route was straightforward with a repetitive construction process comprising the following steps:

- Supply of materials to site
- Production of the precast concrete pipe supports
- Laying out of pipes and fittings along the pipeline route
- Installation of the pipe supports
- Jointing and installation of the pipes and fittings

Delivery and installation of the new 3,750 m pipeline was completed within 8 months and proven to be a significantly easier exercise than installing a new steel pipeline, partly because the PE pipeline had no lining or coating system that need to be completed after butt fusion welding.

Figure 8: The new PE100 condensate pipeline as it passes through the tea plantation.

Figure 9: A butt fusion joint on the condensate pipeline showing the QA system markings.

The Star Energy team implemented a simple quality control system for managing the jointing of the pipe sections to form the pipeline. Figure 9 shows an example of the quality control table that was marked on the pipe beside each butt fusion joint. The date indicates when the joint was made, while JN gives the joint number for record purposes on the project welding map. VC indicates that the joint has passed a visual check of parameters such as the pipe ends being square, cleanliness during butt fusion and the weld bead width being within tolerance. BFP on the fourth row stands for Butt Fusion Parameters and shows parameters such as the fusion pressure, temperature and heating time were within the required tolerances. Following pressure tests, the new pipeline was commissioned on 16 July 2014 and to date has been operational for over a decade without incident.

Figure 10: A view along the completed pipeline showing the precast concrete saddles.

4. LESSONS LEARNT

The following is a brief summary of the observations and lessons learnt by the project team during the design, construction and subsequent operation of the new PE100 pipeline.

4.1 Pipeline design

- Designers should be familiar with the pipe material properties, particularly the relationship between operating temperatures, hoop stresses and service life. If necessary, technical support should be sought from the PE100 resin manufacturer for technical assistance.
- The PE pipe grades supplied throughout Asia follow the ISO rather the ASTM (American Society for Testing and Materials) International. Therefore, designers should use ISO standards such as ISO 4427 and ISO 15494 whenever practical, and make sure there are no contradictions where reference is made to both ISO and ASTM.
- As the pipeline was laid through tea plantations, the Star Energy team was concerned with accidental damage due to agricultural activities. Where external surface damage of pipeline is a concern, either during installation or operation, Borouge recommends that designers specify the use of a High Stress Crack Resistant (HSCR) PE100 grade, such as BorSafeTM HE3490-LS-H. These materials have a very high resistant to the formation crack, initiated from external damages, and growth of cracks through the pipe wall.
- With regards to tapping and connections, designers need to be aware of the differences between how these are achieved on steel and PE pipelines and should not overlook the use of electrofusion (EF) tees and tapping saddles.

4.2 Jointing and installation

- The contractor and supervising engineering must implement a comprehensive quality assurance programme to ensure that jointing is undertaken in accordance with the ISO standards. It is recommended that all butt fusion and EF jointing machines have a data storage and export function to allow all the welding parameters to be reviewed by both the contractor and supervising engineer.
- As with the welding of steel pipelines, the fusion jointing of PE100 pipelines should be performed by properly trained and certified personnel. Only a few locally trained personnel with extensive experience in butt fusion jointing were available to work on the project and this limited the effectiveness of the quality assurance programme.
- Borouge recommends, as a minimum, the person managing the contractor's site jointing team and one member of the site supervision team to be trained, examined and certified in accordance with an internationally recognised PE pipe jointing qualification such as the German GW330.
- Once the logistics are properly arranged, the delivery, jointing and installation of PE pipes is a relatively fast process, as there is no requirement to complete the coating or lining of the pipeline after jointing.
- As mentioned earlier, there are a wide range of fittings that are available for PE pipelines and contractors need to be familiar with their availability and correct installation. Many of these fittings are produced using injection molding process and need to be imported from overseas.

4.3 Operation, maintenance and monitoring

- The use of PE100 for the condensate pipeline has removed the risk of corrosion, together with the associated costly, time consuming and disruptive monitoring and repair activities.
- Whilst the Star Energy team were very familiar with operating steel pipe systems, they had no experience in using PE pipe systems and therefore encountered some difficulty in developing an inspection, monitoring and preventive maintenance programmes. Pipe producers and the PE100 resin manufacturer should be able to provide information on failure mechanisms and give their recommendations on inspection and maintenance programmes etc.
- Small diameter tapping for instrumentation, off-takes and sampling can be installed using EF tapping saddles. These are fusion welded to the exterior surface of the pipeline whilst it is in operation and contain a cutting head, allowing a 'hot-tapping' to be undertaken, thereby minimising operational disruption.

5. CONCLUSION

To the best knowledge of the authors, the Wayang Windu project is the first project where PE100 pipeline has been installed to serve as a condensate return pipeline at a geothermal power plant.

This was surprising, likely because many engineers believed that PE100 is not suitable for use at high temperatures and pressures. They are unaware of example that such pipe systems have been used for over 15 years in the Sultanate of Oman to carry out very aggressive water and crude oil mixtures that have a constant temperature of

50°C. Such systems operate at pressures of up to 10 bar and in an environment where exposed pipe surface temperatures can reach 80°C.

In this paper, the authors have shown how a PE100 pipe system can be used for geothermal pipe applications at temperatures of up to 50°C. The authors also tried to provide some useful technical advice on the design and implementation of such projects, particularly when it comes to the lessons learnt during the process. The documentation of this project has been done to encourage other geothermal power plant owners, operators and designers to consider the use of PE100 pipe systems for lower temperature applications, such as condensate pipelines.

REFERENCES

Wedgner, A., Zatnika, G. G., & Mulyono, S. (2016). The Wayang Windu Geothermal Power Plant: First ever use of PE100 for a condensate pipeline. Plastic Pipes Conference Association, Berlin, Germany. Retrieved from https://www.pe100plus.com/PPCA/The-wayang-windu-geothermal-power-plant-First-ever-use-of-PE100-for-a-condensate-pipeline-p1596.html

Evaluating the Effectiveness of Cooling Tower Fillpack Replacement for Improved Condenser Performance and Power Generation in Wayang Windu Unit-2 Geothermal Plant

Wahyu Danumulyo, Anton Purwakusumah, and Indra Wening Maharsi

WDGC@Starenergy.co.id, Anton.Purwakusumah@Starenergy.co.id, indraweningmaharsi@Starenergy.co.id

Keywords: Cooling Tower, Performance, Condenser Pressure, Power Generation

ABSTRACT

As heat transfer equipment the performance of cooling towers is mainly affected by the effective heat transfer area which may deteriorate due to fouling. The effect of decreased performance in Cooling tower also comes into effect in the condenser that leads to reduction in power generation. This paper will discuss the evaluation performance method using in house calculation of condenser modeling and Cooling Tower performance evaluation using four-point Tchebycheff method. Common remedial actions applied are cooling tower fill-pack replacement and condenser nozzle cleaning. Means that the remedial action based on condenser performance evaluation that continues with calculation of impacted power generation will drive the economic benefit resulting from the remedial action. Following the techno economic analysis it was found that the benefit from restoring power generation capacity could have positive gain in terms of financial benefit.

1. INTRODUCTION

In order to maintain performance of a single flash geothermal power plant it is crucial to keep the cooling water system in its best performance. Cooling water systems provide condensation process of exhaust steam turbine in subcooled condition to be fully condensed thus providing maximum vacuum condition leading to maximum power generation by creating as much as delta pressure of inlet and outlet of the turbine. Common problem in aging cooling tower is fouling on heat transfer surface media that reduces its effectiveness and the problem could be delivered to condenser and this condition lead to reduction of maximum capacity of single flash geothermal power plants such in Wayang Windu.

2. SINGLE FLASH GEOTHERMAL PLANT COOLING SYSTEM PERFORMANCE

There are three major components in a single flash geothermal power plant cooling water system which is condenser, cooling water circulation transfer pump (hot well pump) and cooling tower. This paper mainly focuses on performance of cooling tower and condenser that play a key role in power generation. Meanwhile Hotwell pump deteriorating performance could be straightforwardly identified by comparing its current performance against original performance and/or performance curve.

2.1 Cooling Tower Performance

Wayang Windu geothermal power plant uses the countercurrent type of cooling tower as the following schematic (Figure 1).

The predominant factor to maintain cooling tower performance is the available surface area. Wayang Windu uses a countercurrent cooling tower where the main medium for heat transfer is cooling tower fill-pack. Because of impurities in cooling water that mainly consist of silica, sulfur, calcite or other minerals it may form scaling and reduce effective heat transfer area for cooling process. If scaling happened then water spray from nozzle will make a phenomena like water fall where ideally the water falling down shall be distributed evenly. Overall heat transfer process as function of effective surface area for heat transfer process as the following:

$$Q = K * S * (hw-ha) \quad (1)$$

- Q = total heat transfer Btu/h
- K = Overall enthalpy transfer coefficient lb/hr.ft^2
- S = Heat Transfer surface area ft^2 where S equal to a x V
  - a → area of transfer surface per unit of tower volume (ft^2/ft^3)
  - V → effective tower volume ft^3
- hw = enthalpy of air-water vapor mixture at the bulk water temperature, Btu/lb dry air
- ha = enthalpy of air-water vapor mixture at the wet bulb temperature, Btu/lb dry air

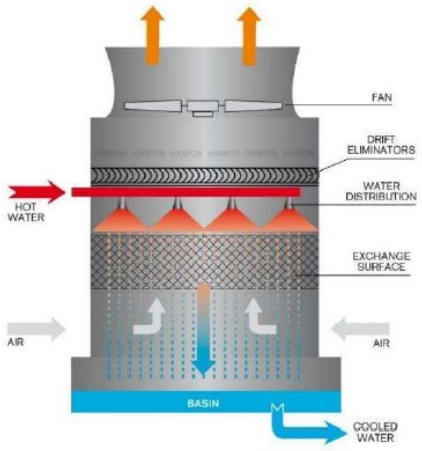

Figure 1: Schematic of Counter Current Flow Cooling Tower as Used in Wayang Windu Geothermal Plant.

Application to small element of heat transfer surface area ds then giving :

$dQ = d[K*S*(hw-ha)] = K*(hw-ha)*dS$ (2)

Water side	Air side
Q = Cw * L * Cooling Range dQ = d[Cw*L*(tw2-tw1) dQ = Cw * L * d (tw) …(3)	Q = G * (ha2 – ha1) dQ = d[G * (ha2 – ha1)] dQ = G d(ha) …(4)
K*(hw-ha)*dS = Cw * L * d (tw) $dS = \frac{\frac{L}{K}\frac{Cw}{(hw-ha)}}{} dtw$ $S = \frac{L}{K}\frac{cw}{(hw-ha)}\int_{tw1}^{tw2} tw$ $\frac{KS}{L} = \frac{KaV}{L} = \frac{Cw}{hw-ha}\int_{tw1}^{tw2} tw$	K*(hw-ha)*dS = G d(ha) $dS = \frac{G}{K}\frac{d(ha)}{(hw-ha)}$ $S = \frac{G}{K}\int_{ha1}^{ha2}\frac{d(ha)}{(hw-ha)}$ $\frac{KS}{L} = \frac{KaV}{L} = \frac{G}{L}\int_{ha1}^{ha2}\frac{d(ha)}{(hw-ha)}$

Where

Cw = specific heat of water (BTU/lb)
L = water mass flow rate (lb/hr)
G = Air mass flow rate (lb/hr)

Meanwhile the KaV/L is known as “Merkel Number” or NTU. Where NTU is “Number of Transfer Unit” independent factor from the tower size and fill configuration. From the above equation, plotting NTU vs L/G gives what is known as “demand curve”. NTU also showing “tower demand curve”.

$$NTU = \frac{KS}{L} = \frac{KaV}{L} = \frac{G}{L}\int_{ha1}^{ha2}\frac{d(ha)}{(hw-ha)}$$

The KaV/L value can be obtained from the Cooling Tower datasheet provided by the manufacturer. Subsequently, if the Merkle Number or KaV/L from actual data falls below the original values, a comparison can be made to determine the extent of the cooling tower's performance deterioration. Using the latest Merkle number values, the estimated cooling water temperature flowing to the condenser can then be calculated.

A decreasing trend in NTU values indicates a decline in cooling tower performance, signaling the potential need for corrective measures like replacing the fill-pack. However, since temperature variations can affect NTU, it's essential to collect and average data over time. This averaged data can then be used for an economic analysis to determine if fill-pack replacement is justified. Alternatively, referring to historical data on cooling water temperature improvements after previous fill-pack replacements may also help in decision-making.

Table 1: Current WW U-2 Merkle Number by Original Design.

Parameter	Value	Unit		Parameter	Value	Unit
Dry bulb Temp	73.4	F		Hot Water Temp	44.20	^{0}C
Dry bulb Temp	23	^{0}C		Hot Water Temp	111.56	F
Wet bulb Temp	62.6	F		Cold Water Temp	22.50	^{0}C
Wet bulb Temp	17	^{0}C		Cold Water Temp	72.50	F
Altitude	1,740	M		L/G Ratio	0.99	
				Cooling Range	39.06	F
				Air Enthalpy	35.38	BTU/lb

Water side				Air side			
Descriptions	**tw(^{0}C)**	**hw (KJ/kg)**	**hw (Btu/lb)**	**Description**	**ha (Btu/Lb)**	**hw-ha**	**1/(hw-ha)**
tw_1 + 0.1 x Range	26.41	110.64	47.57	ha_1 + 0.1 x L/G x Range	39.25	8.32	0.12
tw_1 + 0.4 x Range	38.12	159.61	68.62	ha_1 + 0.4 x L/G x Range	50.87	17.75	0.06
tw_1 + 0.6 x Range	45.94	192.26	82.66	ha_1 + 0.6 x L/G x Range	58.62	24.03	0.04
tw_1 + 0.9 x Range	57.65	241.27	103.73	ha_1 + 0.9 x L/G x Range	70.25	33.48	0.03
						Sum of 1/(hw-ha)	0.25
				NTU = Sum of 1/(hw-ha)/4* Range= **K AV/L**			**2.42**

From the calculation model using four point Tchebycheff method as described in Table 1, we can calculate current NTU and compare it with design. Furthermore we might also estimate cooling water outlet temperature using NTU value that we had already found by using iteration process. The estimated cooling water temperature could then be used for condenser calculation as describe in the next part of this paper.

The four-point Tchebycheff method, illustrated in Table 1, allows for the calculation of current NTU. This calculated value can then be compared to the design NTU to assess performance. Additionally, an iterative process using the obtained NTU value enables the estimation of the cooling water outlet temperature. This estimated temperature will subsequently be used for condenser calculations, as detailed in the following section of this paper.

2.2 Condenser Performance

All the steam exhaust from the turbine in Wayang Windu power plant where it has direct condenser type for the main condenser exhaust steam from turbine contacted directly with cooling water from cooling tower basin using spray nozzles. However as seen in figure 2, the main condenser also use to collect and cooled down hot fluid that comes from utilities such as Liquid ring vacuum pump, auxiliary cooling water pump or other equipment a part of balance of plant such as steam ejector. Motive steam used in downcomer of steam ejector were collected in bottom flow of inter and after condenser then they flows directly to bottom part of condenser and take part in achieving equilibrium state of condenser.

In the Wayang Windu power plant, utilizing a direct condenser configuration, all turbine exhaust steam directly contacts cooling water from the cooling tower basin via spray nozzles within the main condenser. Additionally, as depicted in Figure 2, the main condenser serves to cool down hot fluid discharges from utilities (e.g., liquid ring vacuum pumps, auxiliary cooling water pumps) and balance of plant equipment (e.g., steam ejectors). Motive steam from the steam ejector downcomer is collected in the inter-condenser bottom flow, subsequently entering the main condenser's bottom section, contributing to the overall condenser equilibrium.

A common challenge in the geothermal industry is the lack of access to detailed condenser equilibrium calculations, which are often proprietary information held by manufacturers. This necessitates the development of in-house calculation methods to accurately estimate condenser equilibrium and, subsequently, condenser pressure. A viable approach involves utilizing heat transfer principles, where the cooling fluid (cooling water from the cooling tower) experiences an increase in enthalpy and temperature, while the cooled fluid transfers its heat, resulting in a decrease in both enthalpy and temperature, as illustrated in Table 1.

Input data used for calculation merely the turbine exhaust temperature, cooling water temperature and flow into condenser which is also cooling water from utilities as part of balance of plant as stated in figure 2. Main cooling water from cooling tower basin as major flow contributor. Meanwhile additional flow to main condenser from balance of plant are coming from ACWP (Auxiliary Cooling Water Pump), LRVP (Liquid Ring Vacuum Pump), Inter and after condenser drain in GRS (Gas Removal System). The spreadsheet developed for calculation then use to iterate equilibrium of temperature value where the convergence result showing zero sum of enthalpy which correspondent to condenser pressure in equilibrium that take into effect to power generation output from turbine.

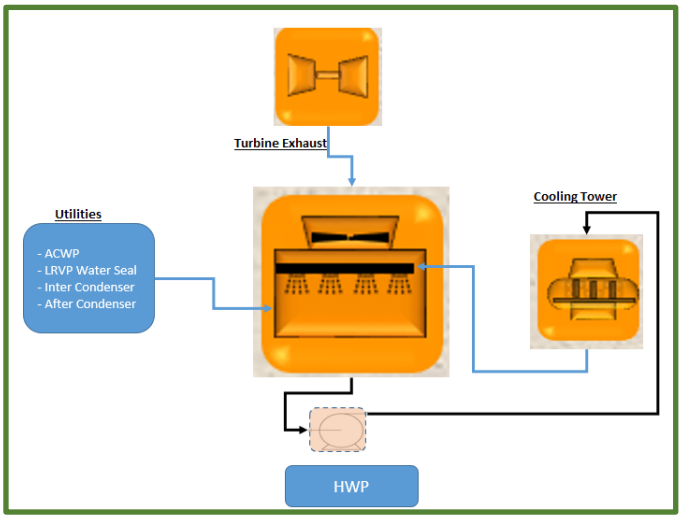

Figure 2: Direct Contact Mass Balance in Wayang Windu Geothermal Plant.

Figure 3: Megawatt Benefit of Cooling Tower Fillpack Replacement and Condenser Nozzle Cleaning.

3. PERFORMANCE EVALUATION RESULT AND TECHNO ECONOMIC IMPACT

Following the replacement of all eight cooling tower (CT) cells, the cooling water outlet temperature was analyzed using data collected over four years. The original design specified a CT outlet temperature of 22°C. However, with the new cells and a wet bulb temperature of 17°C (same as design), the final outlet temperature is around 24.5°C.

To assess if this lower temperature is sufficient to achieve the original design condenser pressure of 0.1 bara, a condenser performance evaluation was conducted. Further analysis, utilizing material and heat balance calculations, indicates that due to excess condenser capacity, the desired 0.1 bara pressure is achievable even with the increased cooling water temperature compare to original design.

It was found that merely from calculation and collected data that a decrease of 1^0C in cooling water outlet of cooling tower will shift the equilibrium in condenser that lead to increase of power generation around 1.2 MW that could be represented from figure 3 by comparing purple wedges (power generation increase) and green

wedges of the curve (CT outlet temperature decrease) along with completion of all 8 cells of CT fillpack. Meanwhile red wedges in the curve of figure 3 showing do nothing possible case in effect to the power generation (in MW). However the red wedge seem linear in the early phase due to power demand actual from buyer that is not maximum that lead to reduce in actual power generation did not take into significant effect as remaining capacity of cooling otwer still able to handle the required demand by user (PLN) which not reach maximum load due to decrease of power demand in Jawa Bali areas at that time.

Table 2: In House Calculation for Equilibrium in Condenser.

	T_{in} cond_	T out	TTD	P condenser	Actual P Cond
	52.43	50.84	1.6	0.129	0.120064
	Total enthalpi differential				
	Cooling Load	Steam + Cooling water utilities	Cooling Water from CT	Cooling Load	
	Condensation process	-1.49E+09	1.50E+09	Condensation process	
	Cooling Temp process	-5.82E+06		Cooling Temp process	
	Total Heat transfer in condenser	**-1.50E+09**	**1.50E+09**	Total Heat transfer in condenser	

Process Fluid	unit	in	out	Delta Enthalpi		Process Fluid	unit	in	out
Steam				**0.00**		**Cooling Water**		**in**	**Out**
Total Flowrate	**kg/h**	**767,268**	**767,268**			**Total Flowrate**	**kg/h**	**17,227,908**	**17,227,908**
Pressure	bara	0.13	0.13			Pressure	bara	0.85	0.13
Temperature	C	52.43	52.43			**Temperature**	**C**	**30**	
SQ	%	0.82	0			CW temp increase			50.84
Enthalpy Condensation	KJ/Kg	2165.58	219.42			Enthalpy	KJ/Kg	125.74	212.75
Total Enthalpi	KJ/H	1.66E+09	1.68E+08	**-1.49E+09**	**1.50E+09**			2.17E+09	3.67E+09
Temperature	C	**52.43**	50.84						
Enthalpy Decrease Temp	KJ/Kg	219.42	212.75						
Total Enthalpi	KJ/H	1.68E+08	1.63E+08	**-5.12E+06**					
Utilities									
Pressure	bara	0.8	0.12						
Temperature	C	51	50.84						
Total Flowrate	kg/h	1,026,480	1,026,480						
Enthalpy	KJ/Kg	213.44	212.75						
Total Enthalpi	KJ/H	2.19E+08	2.18E+08	**-7.06E+05**					

4. CONCLUSION

The evaluation of cooling tower performance and condenser, followed by remedial actions such as cooling tower fill-pack replacement and condenser nozzle cleaning, along with techno-economic analysis, leads to several conclusions:

1. Every 1°C increase in cooling water temperature results in an approximate 0.008 bara increase in condenser pressure, causing a power generation impairment of about 1.2 MW at the Wayang Windu U-2 geothermal power plant.
2. The in-house calculation approach provides acceptable results for actual condenser pressure, with a variation of 5%. This method proves valuable for predicting power generation and evaluating economic benefits.

REFERENCES

DiPippo, R.: Geothermal Power Plants, Vol 7, *Handbook,* (2012).

Hyungsul, Moon and Zarrouk, Sadiq J.: Efficiency of Geothermal Power Plants : A Worldwide Review, *Proceedings*, New Zealand Geothermal Workshop, November (2012).

Kern, Donald Q.: Process Heat Transfer, Hand Book. New York, N.Y. April (1950).

Cooling Tower Thermal Design Manual, Daeil Aqua Co. Ltd (2003).

FUJI Electric : Wayang Windu Cooling Tower Operation Manual. (2010).

Marley Termal Science publication : Variable Flow Over Cooling Towers. TR-014, September (2017).

Zein, Amri., Taylor, A. Paul., Dwiyudha, Heribertus : Modification of Condenser Nozzle and Cooling Tower Exit Screen to Increase Condenser Performance, *Proceedings,* World Geothermal Congress, April (2010).

From Lab to Field: A Review of The Scaling Phenomenon in Geothermal

Hande Sile, Duygu Disci, Argyro Spinthaki, and Ugur Kaymakci

Kurita Europe GmbH, Mannheim, Germany

Keywords: Geothermal, scaling, downhole scaling, water treatment, anti-scalant, inhibitor

ABSTRACT

Geothermal energy is a renewable and clean source of power that can provide electricity and heat for various industries as a key transition to achieving net zero emission targets. However, geothermal utilization faces a major challenge: scaling. Scaling is the formation and accumulation of mineral deposits which reduces the efficiency and sustainability of the geothermal system leads to an increase in operational and maintenance cost.

The scaling phenomenon is related to the reservoir characteristics and the harsh conditions of the process designed to extract more energy from the geothermal source. The geothermal fluid contains dissolved minerals that are in chemical equilibrium at the reservoir depth with corresponding pressure and temperature. When the fluid moves to the surface from bottomhole through the wellbore, the thermodynamic conditions change, and some minerals become supersaturated and tend to precipitate and deposit on the walls of the production wells. The most common scaling minerals are carbonates seen in the downhole.

Scaling can have detrimental impacts on the production wells, such as reducing the well diameter and the flow rate, triggering the corrosion and erosion on the casings and wellhead assembly, causing additional cost for well stimulation and workover operations.

Scaling solutions dedicated to geothermal technology start from the production well and are distinctively constituted regarding the surface conditions until the re-injection well. This study highlights global cases showing the benefits of effective water treatment in preventing scaling in geothermal systems. The demonstrations will include lab studies and following field applications.

1. INTRODUCTION

Geothermal energy is a solid candidate to make green energy transitions all around the world. It is renewable but not free of challenges. The natural problems that majorly appear in both explorational and operational periods can be listed as organic and inorganic precipitation (scaling), corrosion, and erosion. All these natural challenges are required to be treated due to their potential damage to almost all the parts of the process.

Geothermal systems can be classified according to distinct aspects such as reservoir thermodynamics, geological setting, utilization characteristics, and process type, etc. Based on the reservoir temperature, they are classified as low, medium, and high temperature geothermal systems.

Liquid-dominated and vapor-dominated geothermal systems refer to the physical state of geothermal flow in the reservoir (Bodvarsson, 1964; Axelsson and Gunnlaugsson, 2000). Utilization of this hot media at surface can be grouped into two parts as direct use and power generation. The type of heat extraction process is determined by the source capacity.

All types of geothermal fluids tend to create significant problems related with their specific chemistry. Depending on this specific chemistry, scaling, corrosion and even both can be faced at the same time. The variations in temperature, pH, non-condensable gas (NCG) content, permeability, rock types of the formation and hydrothermal activities change the composition of water which ends up with high degree of diversity in mineralization (Jamero and Zarrouk, 2016). It goes forward with co-precipitation turning into the most challenging mechanism for scale forming along the industrial processes.

Scaling forms at various locations within the process under different physical and chemical conditions:

- Downhole scaling in the well: due to the sudden pH change around boiling/flashing depth with changing in temperature (T) and pressure (P)
- Scaling at surface facilities: due to the sudden P changes regarding the mechanical design and flow regime
- Scaling in plant area: due to the cool-down of geothermal brine during the heat transfer in heat exchangers
- Scaling in re-injection process: due to the low process temperature

The prevalent deposit types encountered in geothermal are carbonates, silica and silicates, sulfides, and sulphates. Carbonates are majorly calcite and dolomite and minorly aragonite since fractured marble is widely distributed on subsurface as a rock formation for low-to-medium enthalpy geothermal reservoirs. Carbonate and silica mineralization also influenced by magnesium level in the system. Silica tends to form as amorphous silica (SiO_2) which may also co-precipitate with metal-silicates like Mg, K, Al-silicates. Sulphates precipitate as Ca-sulphate and Ba-sulphate in barite form. Sulfides occur in the form of many phases, and are usually in well-crystallized form (Corsi, 1986). Pb, Zn, Fe, Cu, As dominate the frequently observed deposits of sulfides while antimony-sulfide can be distinguished as the most specific scale type in geothermal deposition in stibnite mineral. All these scaling formations may cause considerable damage which lead to decrease in efficiency and total energy output, increase in downtime and maintenance, resulting in loss of energy and high operational costs.

There are different methodologies to control scale forming and protect geothermal facilities. The efficiency of each method is related to the process conditions, scaling mechanism, fluid content and project feasibility. This paper aims to indicate successful achievements in the field applications of inhibition and dispersion method against common scale ranges. Composed treatment programs which are applied to different process designs are supported by initial laboratory studies to ensure material compatibility, thermal stability, and desired performance rate for significant problems of the related geothermal fields.

2. METHODS

Geothermal is a unique process with harsh physical and chemical dynamics that create challenges to mimic in the lab conditions: elevated temperature, high pressure, high salinity, high amount of NCG, etc. Therefore, all the lab test results would require confirmation with industrial applications in the field. Kurita's technical team demonstrated standardized lab test concepts to get an initial approach of the viable solutions to be confirmed with the field trials.

Two comparative approaches are presented to reveal scaling cases in geothermal: laboratory tests and field applications.

2.1 Lab-scale tests

Several experimental methods are conducted to validate stability and performance of geothermal inhibitors in lab-scale.

2.1.1 Differential Scale Loop (DSL)

The Differential Scale Loop (DSL) is an automated versatile device to examine the precipitation and deposition tendency of scale (especially $CaCO_3$) under elevated temperature and pressure, e.g., simulated geothermal conditions. The apparatus includes a capillary tubing loop, oven equipped with the loop, pump and brine control unit for dosing, and PC control (Figure 1).

Pumping of the geothermal brine to scale loop as blank and/or treated with anti-scalant at different concentrations indicates a trend of differential pressure within the capillary loop. The evaluation of ΔP versus time corresponds with anti-scaling performance of related inhibitor at simulated elevated temperatures.

Figure 1: Showing the equipment setting of DSL in operation. From right to left oven equipped with scale loop, dosing unit and computer.

2.1.2 Beaker Tests for Antimony-Sulfide Dispersion

Principle: Tests are conducted in a brine of defined quality by in-situ precipitation of antimony sulfide and particle growth observation in presence and absence of chemical additives. Antimony sulfide formation and precipitation is highly pH-dependent, thus careful pH control is rendered crucial.

Trial brine composition: Test water is made by dissolving stock solutions into DI-water (Figure 2).

Ions	mg/L	mol/m³
Ca^{2+}	91.97	2.29
Mg^{2+}	12.1	0.50
Na^{+}	85.1	3.70
Cl^{-}	162.5	4.58
SO_4^{2-}	47.9	0.50
HCO^{3-}	225.9	3.70

Figure 2: The content of artificial brine simulated like geothermal conditions.

Dispersant stock solutions are prepared as 1000 ppm as actives, pH is adjusted to 6.3 and dosed in each trial. Common test dispersant concentrations are: 1, 1.86, 3, 7.75 and 15 ppm as actives.

Procedure: Tests are done with an antimony sulfide concentration of 20 ppm. 2L test water are prepared. After stirring 5.74 mL of Antimony (III) chloride – solution is added, and pH is adjusted to 6.3 (+/- 0.1) with sodium hydroxide and/or hydrochloric acid. In seven beakers, the calculated amount of dispersant is added. The 8th beaker is the control experiment (absence of dispersant). In each beaker 250 mL of test water are added the solutions are stirred at 300 rpm. 68.8 µL sodium sulfide solution 5% are added in each test beaker. This is the initiating moment of the experiment. After 15 min the beakers are removed from the stirring plate and placed in a row with a white background. A photo of all beakers is captured immediately after 22 hours.

2.2 Field Trials

By using the promising results from laboratory experiments, several field trials distributed around various geographies are conducted to confirm the performance of products at in-situ conditions. Kuritherm™ product range is dedicated to geothermal applications to avoid several types of inorganic and organic precipitation in the system.

2.2.1 Downhole Treatment

Background: A binary cycle geothermal power plant (GPP) suffered from carbonate and silica scaling in production wells and metal-silicate deposits in separation station at the surface. System data analyzed and the mechanism of scaling form examined.

Process conditions: Product is dosed to the 170 tph total mass flow rate of two-phase flow from the well. The capillary tubing is set around 2000 m depth for chemical injection.

Actions: Samples are collected from the outlet of accumulation tank located upstream of brine transfer pump through a condenser. Coupon monitoring ports are located at the production line near wellhead (two-phase flow) and downstream of separation (single-phase flow). Dosage optimization trial is performed for 1 week duration starting with the high dosage rate of 8 ppm.

2.2.2 Dispersion of Stibnite in ORC (Organic Rankine Cycle) Unit

Background: A binary GPP suffered from antimony-sulfide deposition as stibnite form in the heat exchangers of ORC unit. Especially in preheaters where the highest ΔT occurs to maintain desired heat capacity; the heavy scaling causes dramatic increase of ΔP in the heat exchangers. Scaling proceeds in re-injection lines and brine injection pump units (BIP) additionally. Not only the frequent maintenance periods but also less power generation result in higher operational costs for the plant.

Process conditions: The trial of new antimony-sulfide stabilizer is dosed at the upstream of ORC unit (inlet of the vaporizer) to protect the heat exchangers and re-injection facilities. The total flow rate of brine is approximately 800 tph and the outlet temperature of plant area is around 70 ^{o}C which is considered as re-injection temperature.

Actions: An exclusive Kuritherm™ product that contains organic polymers effective on sulfide stabilization and dispersion is tested for stibnite inhibition for more than 8 months at several dosage rates. Optimization studies completed and stabile treatment program is set for plant area. The sampling ports are at the inlet of ORC unit and outlet of Preheater under trial. ΔP is monitored to evaluate performance parallel to regular coupon controls.

3. RESULTS AND DISCUSSION

3.1 Stibnite Dispersion Lab Test Results

One of the Kuritherm™ state-of-the-art solutions can act as an effective dispersant of Antimony (III) sulfide scaling. Despite the widely conducted research on carbonate and silicate scaling, studies concerning the mitigation strategies towards antimony sulfide are limited. Presented indicate the effect of a new polymeric anti-scalant as a successful antimony sulfide stabilizer, Additional to the laboratory results, the superior efficiency of this product will be demonstrated with physical parameters observed during plant application. Demonstration to a test series with the best of candidates are shown below (Figure 3).

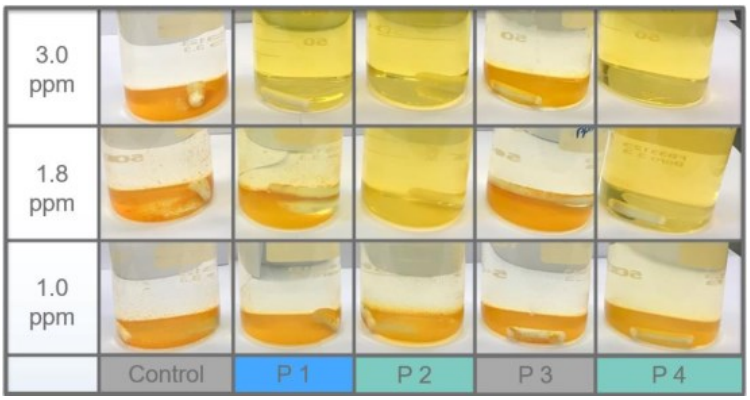

Figure 3: Showing the results of beaker test for antimony sulfide dispersion. P4 ≥ P2 > P1 ≥ P3 ≥ Control.

The evolution of precipitation in a variety of polymer concentrations in real-time pictures against the Control are presented. Upon experiment initiation, there are not any differences between the Control and the dispersant-containing solutions visually. The system is monitored for up to the first 22 hours after initiation of trial and the results shown in Figure 5 are evaluated. While conventional inhibition methods are rendered challenges of such insoluble scales, dispersion can be a very efficient alternative approach e.g., P4 and P2 (Figure 3).

3.2 Downhole Treatment Results

The trial is completed in 1 week including the steps of dosage optimization, sampling, and monitoring of product performance at related locations in the process. The coupons were checked physically every day and re-assembled to the pipelines without any cleaning. No scaling is observed on the wellhead coupon belonging to two-phase flow area (Figure 4). Some Mg-silicate traces are observed on the separation station coupon belong to the single-phase flow (Figure 5) which might be seen because of cleaning effect in the separation station.

Figure 4: The initial status of the coupons at the first day of trial with scale. Coupon on the left is at wellhead, the right at the outlet of accumulation tank.

Figure 5: The clean coupons from the last day of the trial. Coupon on the left is at wellhead, the right at the outlet of accumulation tank.

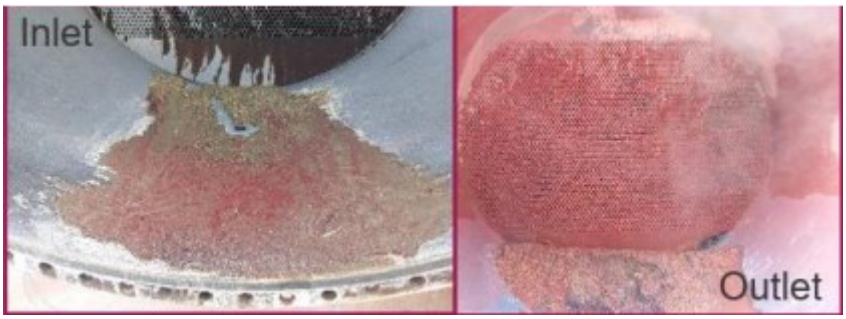

Figure 6: The cross-section view of a shell-and-tube heat exchanger (preheater) before the application of Kuritherm™ treatment program. The inlet on the left and outlet on the right show antimony-sulfide precipitation within the tubes.

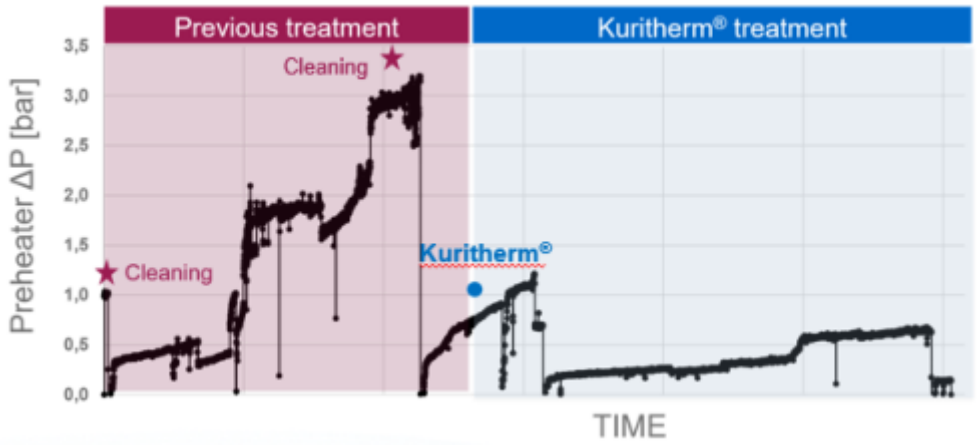

Figure 7: The trend of ΔP of the heat exchanger in ORC unit versus time. After a strong cleaning operation ΔP increases in a noticeably abbreviated time due to the fast scaling shown at the left side of the graph. Once the second cleaning operation is performed, Kuritherm™ treatment started and ΔP gets stabile even for a longer term shown at the right side of the graph.

The in-situ XRF analysis of deposits by using hand-held size mobile device at site show the distribution of inorganic components of scale in ratio. Dominant content of the deposit at wellhead coupons are determined as carbonate and silica scaling while metal-silicates are determined on the surface coupon.

The trends of results from regular chemical analysis are evaluated during the trial. Total Hardness (ppm $CaCO_3$) and Silica (SiO_2) values tend to increase at the initial phase of trial and become stabile by time until the last day.

3.3 Stibnite Dispersion Field Results

An effective stabilizer with particular dispersion effect is developed to inhibit antimony-sulfide precipitation in geothermal surface systems. The initial observations from the inside of heat exchanger reveal the critical status of equipment before treatment. The metal surface of heat exchangers where the heat transfer should occur, totally covered by reddish-blackish stibnite deposits. (Figure 6).

The stibnite scaling is hard to remove by any chemical or mechanical cleaning operation due to the common co-precipitation of silica and silicate minerals. Even at these challenging conditions, the new development of stibnite inhibitor presented promising results in the field trial which confirmed by the plant data monitoring and regular analysis (Figure 7).

Kuritherm™ stabilization and dispersion effect against stibnite and co-precipitated minerals such as metal-silicates verified by the long-term low ΔP values in the preheater. Less maintenance periods and more heat transfer bring saving in energy and cost.

4. SUMMARY AND CONCLUSION

Scaling is observed as a natural challenge in geothermal utilizations. What makes geothermal approach essential is considering it that starts in the production site and ends in the re-injection. The presented laboratory studies and field results subject to support controlling of major scaling issues faced in various regions under the operation of different geothermal technologies.

Two case studies were presented to compare successful lab test methods with their corresponding field applications. Carbonate precipatation is one of the common scaling problems in downhole conditions. That is why DSL equipment is used to simulate these conditions and check the scaling tendency. The field results which are monitored by well-determined KPI's confirmed the DSL results by achieving similar successful results of Kuritherm™ product. Additionally, a full study of product development for stibnite scaling control is examined starting from the research phase in lab. Initial field application results show that the product significantly increased the production efficiency in the plant by avoiding decrease in the heat transfer of preheaters.

The featured outcomes are listed below:

- The downhole scaling inhibition is monitored by wellhead coupon control as a visual observation together with periodic chemical analysis of hardness to keep track of precipitated levels in the well if any exist. A proper downhole treatment is able to control not only the scaling on the walls of the wellbore components but also the equipment at surface under two-phase flow conditions.
- The combination of inhibition and dispersion effect provides continuous protection of geothermal systems from variety of mineralization that occurs due to the co-precipitation mechanism.
- Antimony sulfide as a significant scaling type for geothermal is hard to inhibit and remove from the process. The stability and performance of a new development for stibnite stabilization is confirmed by the field results which show a parallel behavior observed during the laboratory tests.

REFERENCES

Axelsson, G., and Gunnlaugsson, E. (convenors) "Long-Term Monitoring of High- and Low-Enthalpy Fields Under Exploitation." *World Geothermal Congress 2000 Short Course*, International Geothermal Association, Kokonoe, Kyushu District, Japan, (2000), 226.

Bödvarsson, G. "Physical Characteristics of Natural Heat Sources in Iceland." *Proceedings: UN Conference on New Sources of Energy, Volume 2: Geothermal Energy, Rome, Italy*, United Nations, New York, (1964), 82-89.

Corsi, R. "Scaling and Corrosion in Geothermal Equipment: Problems and Preventive Measures." *Geothermics*, Vol. 15, No. 5/6, (1986), 839-856.

Jamero, J., and Zarrouk, S., J. "Mineral Scaling in Geothermal Two-Phase Pipelines." *Proceedings 38th New Zealand Geothermal Workshop*, Auckland, New Zealand, 23 - 25 November (2016).

Current Practices to Manage Silica-based Scaling in Geothermal Operations

Duygu Disci, Argyro Spinthaki, Ugur Kaymakci, and Hande Sile

Kurita Europe GmbH, Mannheim, Germany

Keywords: Silica, metal silicate, geothermal, scale prevention, inhibitors, solubility

ABSTRACT

Biofouling, scale precipitation, and corrosion can jeopardize the integrity of water treatment facilities and the efficiency of the plant, with scale and corrosion particularly posing significant challenges to geothermal systems. Downhole applications are severely affected due to brine characteristics, high ionic concentrations, high temperatures and the common presence of dissolved gases. While both problems can occur separately, they can also be commonly identified together (under deposit corrosion/pitting). Common scale types in geothermal systems are mainly carbonates, sulphides, and silica and silicates. Silica and metal silicate precipitation is especially in geographies like Turkey, New Zealand, and Indonesia cause severe problems and must be tackled with state-of-the-art mitigation strategies.

For improved plant efficiency and to avoid fatal material failures in any part of the massive installations, finding the proper treatment program has a vital role. While traditional approaches, such as acidic treatment and caustic applications are used, the safety risks can be significant and strict measures should be followed to avoid equipment damage in case e.g. proper dosing is not applied. Therefore, the focus and efforts of the scientific community over the past decades have been devoted to the utilization of different chemical additives such as polyacrylate based polymers and phosphonates for the mitigation of such issues. In this paper Kurita's approach will be presented to solve issues of scaling especially towards silicates commonly seen in geothermal plants.

1. INTRODUCTION

Silica is one most of the most widely encountered compounds in geosphere where the nature takes its source to generate heat and power through geothermal brine. While this compound has a vital role in several industrial and biological applications, the reason why it is widely mentioned in geothermal applications are due to its ability and affinity to form chemical bonds at various physical conditions such within a geothermal plant. These so-called deposits are formed due to the polycondensation of silicate particles to form amorphous silica and/or as metal silicate when different metal ions are involved in the brine, such as magnesium, aluminium, manganese, calcium, and iron.

Metal silicates bear some structural similarities to silica (such as the SiO4 tetrahedra) but present a vast number of differences in their composition, structural chemistry, and formation processes. It is worth mentioning that the composition of the nine rock-forming minerals reveals that they all belong to the silicate group of minerals, whose basic building block is the SiO4 tetrahedron. Metal silicates form in waters with high silica and low salinity contents in the presence of certain metal ions. Iron and magnesium silicates exhibit low solubilities in low enthalpy brines, while aluminium silicate usually precipitates in fluids of higher temperatures.

There are several kinds of such additives, named scale inhibitors, depending on the nature of the scale to be inhibited. Such scale inhibitors are usually either polymeric in nature, or smaller molecules, such as phosphonates. Scale inhibitors are widely applied in water governed systems in order to reduce system cleanings, shut - downs and to prevent system malfunctions. The quest for the ideal scale/deposition inhibitor is still on-going and unfortunately, a "universal" scale inhibitor is not available yet, due to each scale having its own idiosyncrasies and thus requiring special treatment. Several system variables must be considered in the process to ensure the proper selection of the scale inhibitor. These include system pH, supersaturation, presence (or absence) of oxidizing biocides, inhibitor tolerance to hardness, temperature, and potential of composite scale formation. In our studies in order to find the proper mitigation technique, a proper lab method for each scale has been investigated. From our extensive studies we can summarize the conditions of precipitation for widely encountered metal silicates (Table 1).

Among those detailed studies, this paper is focused on experimental and field results regarding Aluminium silicate based scales.

Table 1: Solubility Characteristics of the commonly encountered metal silicates.

Scale Type	pH range of induced precipitation	Temperature Characteristics
Amorphous Silica	5 - 9	Normal Solubility
Magnesium Silicate	> 8.5	Inverse Solubility
Aluminium Silicate	5.5 - 8.5	Normal Solubility
Iron Silicate	5 - 9	Inverse Solubility
Manganese silicate	Under Study	Inverse Solubility

2. AL-SILICATE INHIBITION EXPERIMENTAL METHODS

Principle: This experimental protocol concerns inhibitor evaluation against aluminium-silicate scaling. It focuses on trial conditions that are commonly encountered in water treatment fields worldwide. The purpose is to identify chemical additives that will prevent the scale precipitation through threshold inhibition mechanisms.

Stock Solutions: The sodium silicate solution (solution A) used in all experiments containing 1000 ppm silicate, expressed as ppm SiO_2, is prepared by dissolving 4.08 g of $Na_2SiO_3 \cdot 5H_2O$ in 1 L of deionized water. A 10.000 ppm Al^{3+} solution (solution B) is prepared by dissolving 8.948 g of aluminum chloride in 100 mL of DI water.

Procedure: 50 or 80 mL of solution A (for a final concentration of 500 or 800 ppm silicic acid) and 49 or 19 mL respectively of DI water are placed in each flask, stirring is initiated at 250 rpm and the solutions are heated up to 70°C with well-sealed caps. When the desired temperature is reached, the calculated amount of inhibitors are added. One beaker serves as the control experiment (absence of inhibitor). Additionally, 0.125 or 0.2 mL of solution B are added to all beakers (for final aluminum concentrations 12.5 or 20 ppm respectively), the pH is adjusted to 7 (±0.08), caps are sealed, stirring speed is lowered to 150 rpm and this is the initiating moment of the experiment. After 3 and 24 hours, the following measurements took place: molybdate – reactive silica, total silica, soluble aluminum, and turbidity.

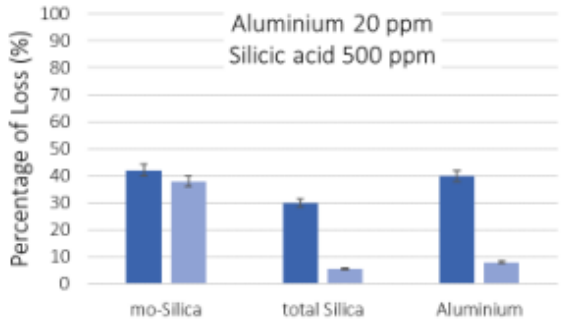

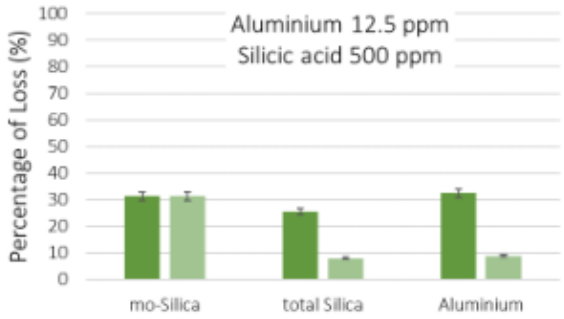

Figure 1: (left) and Figure 2 (right): Stabilization of silica and aluminum species leading to decrease in aluminum silicate scale precipitation (increasing Al3+).

3. FIELD TRIALS, SILICA AND SILICATE INHIBITION AT SURFACE

Background: A triple-flash GPP suffered from heavy amorphous silica and different types of metal-silicate precipitation at critical parts of the plant. The heavy scales decrease the power output and cause additional downtime. A possible number of deposits was calculated and estimated as 470 kg/h at 2000 tph mass flow rate in the process.

Process conditions: The physical parameters of High-Pressure (HP), Intermediate-Pressure (IP) and Low-Pressure (LP) flashing stations are examined in terms of P, T, and flow rate conditions. Products are dosed on averagely 2000 tph brine flow rate. The re-injection temperature is below 120 oC which makes the geothermal brine super-saturated with the silica content above 500 ppm in the system.

Actions: Different silica and silicate inhibitors which are customized as a functional product line, Kuritherm™, dosed at several injection points. The treatment program is composed to existing data and scaling simulations. During the field trial, chemical analysis, scaling coupon check, in-situ XRF analysis, online scaling sensors and physical observations are considered as performance monitoring tools. The existing data set of 1 year monitoring is reviewed to make a proper technical evaluation.

The interesting observation from these trials was the negligible difference in the soluble silica results with or without product, a clear stabilization effect in total silica and soluble aluminium is marked. These are promising results considering that aluminum can act as the catalyst of this reaction (Figure 1 and Figure 2).

4. AL-SILICATE INHIBITION EXPERIMENTAL RESULTS AND DISCUSSION

This work starts with revealing the true nature of the so-called “aluminium silicate”, through a series of bench-top synthesis experiments under various conditions and complete physicochemical characterization. The research proceeds with developing the control strategies to be implemented for its mitigation starting from beaker tests and working the way up all the way to pilot plant and field trial tests. Selected results of additives present potential as stabilizing agents, by complexing the aluminum species, and preventing “aluminium silicate” scale formation.

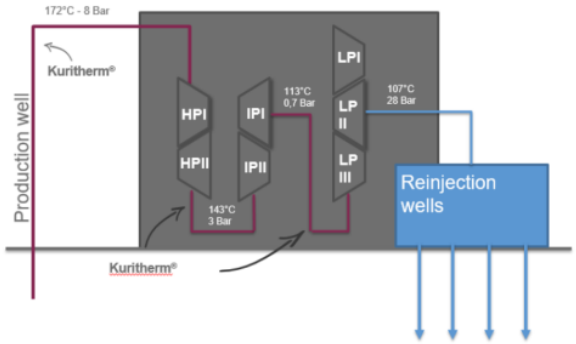

Figure 3: The general overview of process flow scheme of the triple-flash GPP with applied treatment program.

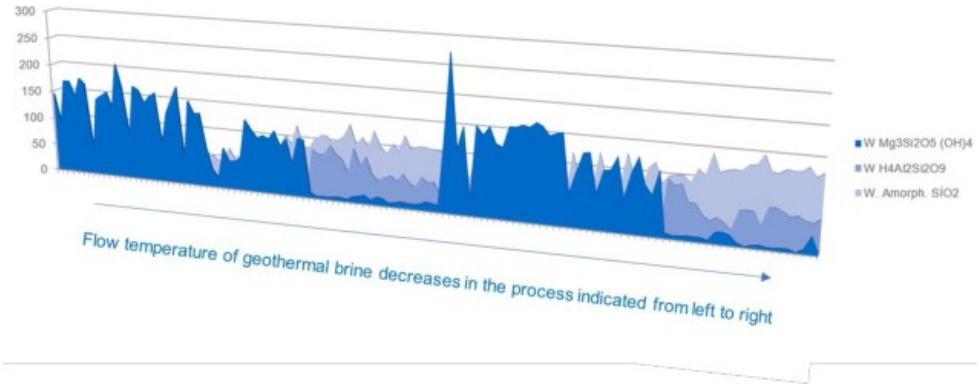

Figure 4: The XRF analysis of silica and silicate deposits from various parts of the process in GPP. From left to right the flow T decreases and the form of the deposit changes accordingly. Magnesium silicate tends to precipitate at high T while at lower T metal silicates such as Al, and K-silicate co-precipitate. Around the re-injection area where the lowest T is observed, the mechanism of scaling turns into creating amorphous silica.

Figure 5: The progress of improvement in product performance over time: the coupon above has traces of metal-silicates and silica deposits and the coupon below indicates the results of a more efficient treatment.

5. FIELD RESULTS

Steam-flash geothermal systems are exposed to dramatic P-T changes in the process. The chemical equilibria of two-phase flow coming from production well including NCG (Non-Condensable Gases) and high amount of dissolved minerals disturbed at the HP, IP, and LP levels of separation and requires individual treatment concept (Figure 3).

The kinetics of silica polymerization are overly sensitive to the temperature and pH variations in the system. Therefore, the form of the scale changes immediately on a dynamic T profile. From high T to low T environment which is recorded from HP to LP flashing vessels, the mineral composition of silica and silicate deposits starts to be evolved as it is verified with the XRF analysis of related scale layers (Figure 4).

Several products from Kuritherm™ solution portfolio are tried to retard silica polymerization process and to induce dispersion within the geothermal flow. The improvement of treatment programs over time can be seen on periodic coupon monitoring at different ports (Figure 5).

The observations of coupon monitoring are correlated with online scaling sensors which provide instant non-stop data within the pipeline. Inhibition of metal-silicates successfully verified and amorphous silica is dispersed by the effect of strong treatment program.

6. SUMMARY AND CONCLUSIONS

Scale and deposit mitigation has been at the epicentre of research for an extended period of time and research on this subject holds enormous potential. There is plenty of room for further growth, from different additives that can be evaluated against unwanted precipitation to altering and improving the evaluation methods.

A proper treatment is a key to keep the geothermal plants sustainable by protecting the equipment, lowering the production loses and increasing the heat transfer efficiency by lowering the scaling tendency. As seen in this paper a proper chemistry is necessary to obtain these conditions in the plant. The quest for the ideal scale/deposition inhibitor is still on-going and unfortunately, a “universal” scale inhibitor is not available yet, due to each scale having its own idiosyncrasies and thus requiring special treatment.

Silica and silicate precipitation is a complex genesis and needed to be treated regarding the individual characteristics of process and fluid chemistry. Long term monitoring applications verify the performance of executed treatment program.

REFERENCES

Demadis, K. D., Spinthaki, A., Kamaratou, M., Petratos, G., Matheis, J., Disci-Zayed, D., & Hater, W. (2019). Control of metal silicate scaling by chemical additives. In *Proceedings of Corrosion 2019*, NACE International, Paper No. 12863.

Demadis, K. D., Spinthaki, A., Petratos, G., Matheis, J., Disci-Zayed, D., & Hater, W. (2020). Metal sulfide scale inhibitors. In *Proceedings of Corrosion 2020*, NACE International, Paper No. C2020-14459.

Kamaratou, M., Spinthaki, A., Disci, D., & Demadis, K. D. (2024). Chemical control of ferric silicate scaling by phosphonate additives under geothermal stresses. *Geothermics, 123*, Article 103119.

Kamaratou, M., Spinthaki, A., Disci, D., & Demadis, K. D. (2024). Ferric silicate precipitates relevant to geothermal systems: Delineation of their complex formation. *Geothermics, 123*, Article 103118.

Spinthaki, A., Kamaratou, M., Matheis, J., Disci, D., Hater, W., & Demadis, K. D. (2021). The precipitation of “aluminum silicate” under geothermal stresses: Identifying its idiosyncrasies. *Geothermics, 92*, Article 102060.

Spinthaki, A., Kamaratou, M., Disci, D., Hater, W., & Demadis, K. D. (2023). Inhibition of aluminum silicate scaling by phosphonate additives under geothermal stresses. *Geothermics, 111*, Article 102690.

Spinthaki, A., Matheis, J., Hater, W., & Demadis, K. D. (2018). Antiscalant-driven inhibition and stabilization of “magnesium silicate” under geothermal stresses: The role of magnesium–phosphonate coordination chemistry. *Energy & Fuels, 32*(11), 11395–11405.

Spinthaki, A., Petratos, G., Matheis, J., Hater, W., & Demadis, K. D. (2018). The precipitation of magnesium silicate under geothermal stresses. Part 1: Formation and characterization. *Geothermics, 74*, 81–91.

This page is intentionally left blank

Part 3:
Resource Management

This page is intentionally left blank

Brine Management & Reinjection System for Dieng Two-Phase Fluid Geothermal Field

Akbar Putra, Hendra Ardi Kurniawan, Bhaskara Aji Pawitra,
Sarbeni Rangkuti, and Herdian Ardi Febrianto

PT Geo Dipa Energi (PERSERO), Aldevco Octagon Building, Indonesia

akbar.putra@geodipa.co.id

Keywords: Manual Cleaning, Scaling, Brine, Two-Phase Geothermal Field, Dieng

ABSTRACT

PT. Geo Dipa Energi (PERSERO) operates Dieng geothermal field with two-phase production fluid type. The production fluid characteristics are; 30% dryness level, up to 183 degrees Celsius temperature, 11 bar pressure, and contains dissolved Silica up to 1070-ppm concentration. The decrease in temperature and pressure on the surface facilities causes the initially dissolved Silica substance to condense into a solid and stick to the medium it passes through, this is usually known as “Scaling” phenomenon. To maintain asset operations, environment and subsurface water balance, a brine management system is needed at the Dieng geothermal field.

This case study was carried out by the Maintenance Department, PT. Geo Dipa Energi (Unit Dieng) in 2024. The output of this study is a best practice for brine management system from the surface to the subsurface in the Dieng geothermal field facility that is economical, environmentally friendly and can be applied on a scheduled basis to support company power generation business process.

This study method was carried out by collecting production fluid data for all wellpads in Dieng geothermal field, existing piping system & maintenance schedule, and costs incurred by different cleaning methods. The data is then subjected to comparative analysis both in safety, technical and financing terms to produce optimal and economical practices according to current conditions.

The results of study and field practice shows that the use of manual cleaning techniques in brine management & reinjection system is the most optimal and economical for Dieng geothermal field existing facility. This method is recommended for application in current two-phase Dieng geothermal field facility and other geothermal fields with similar conditions.

1. INTRODUCTION

1.1 Dieng Geothermal Field

The Dieng Steam Field is one of many geothermal fields to generate electricity, which is currently operated by PT Geo Dipa Energi (PERSERO). The Dieng Geothermal Steam Field is located 98 km from the west of Semarang city center.

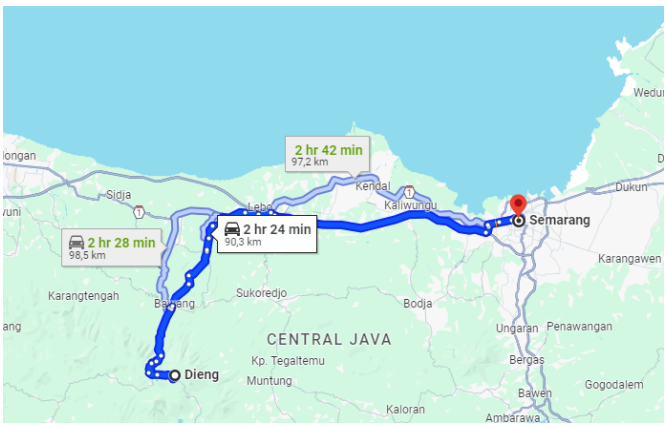

Figure 1: Dieng Geothermal Field is located in Central Java (Google.com/maps).

The first drilling well DNG-1 in the Dieng geothermal field was carried out in 1977 under the management of PT Pertamina and completed at 1978. In early 1990s, Dieng field development right was granted to HCE (Himpurna California Energy Ltd.). In 2002, the development right of the Dieng Field was granted to PT Geo Dipa Energi (PERSERO) and on September 2002 Dieng Unit 1 started to operate commercially (Sirait, et al., 2015). Currently Dieng Unit 1 and the small scale power plant produce around 52 MW.

1.2 Dieng Geothermal Field Production Fluid

The Dieng geothermal field operates with 7 online production wells, 5 injection wells. In June 2024. The production fluid is a 2-phase type with 70% brine and 30% steam. Field data shows a brine production rate of 438 TPH (Tons per hour) or 1,916 GPM (Gallons per Minute).

Table 1: Dieng Geothermal Field Brine Production 30th June 2024.

	Brine Production Rate	
Production Well	Ton / Hour	Gallon / Minutes
HCE-7B	20	87,5
HCE-7C	60	262,5
HCE-29	18	78,75
HCE-28A	13	56,875
HCE-28B	24	105
HCE-31	5	21,875
HCE-30	208	910
Condensate Power Plant	90	393,75
Total	438	1916,25

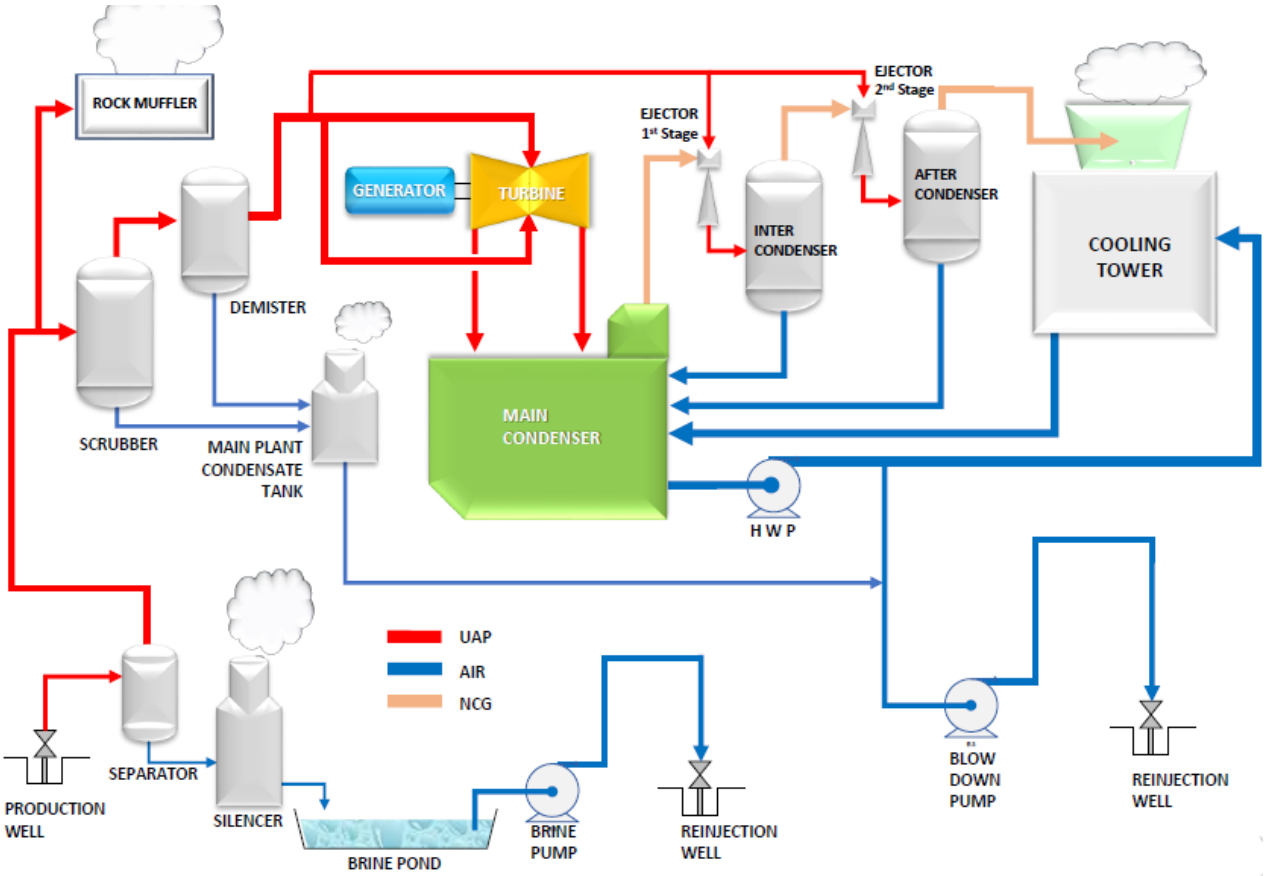

Figure 2: Dieng Geothermal Production System.

Production fluid from the Dieng field geothermal well is channeled to a separator system to separate the two types of production fluid phases. The steam phase resulting from the separation will flow to the generating turbine to rotate the generator turbine which produces electricity. The brine will flow into the flashing system AFT (Atmoshperic Flash Tank) or Silencer, open canal and pond to reduce pressure, temperature and noise. The brine then flowed with the help of a mechanical pump to re-enter the piping system which continue to reinjection wells. 5 reinjection wells were used to inject a total of 2,110 GPM. Brine produced from the Dieng geothermal field is classified as having high silica content. In the 2-phase pipe from the well head, the brine composition was found as in Table 3 (Juhri et. al., 2001).

Table 2: Dieng Geothermal Field Brine Injection 30th June 2024.

Injection Well	Brine Injection Rate (GPM)	Note
SLR-G-29B	710	
HCE-29A	750	Northern Injection
DNG-14	250	
DNG-15	200	
HCE-5A	200	Southern Injection
Total	2110	

Table 3: Sample from HCE-30 at Two Phase Line showing Dieng Geothermal Water characteristic. (Juhri et. Al., 2001).

Chemical Composition	Concentration (ppm)
Cl	21.200,0
SiO4	74,4
HCO3	25,0
Na	10.249,0
K	2.817,0
Ca	708,8
Mg	0,5
SiO2	1.064,5
Al	0,0
Fe	1,4

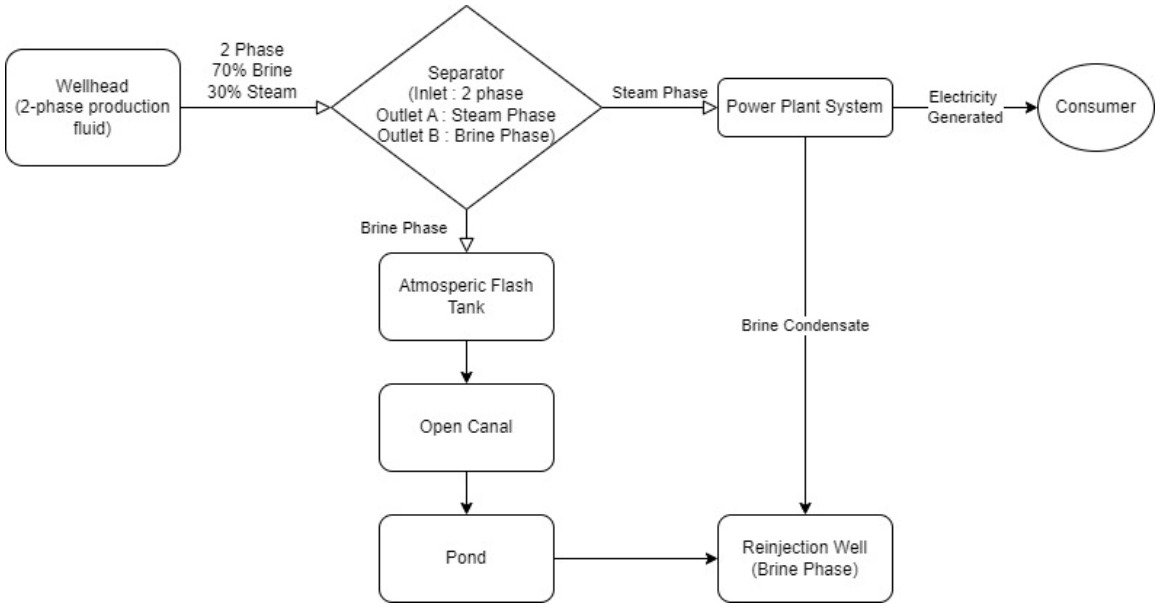

Figure 3: Dieng Geothermal Field Brine System.

The production fluid from the geothermal wellhead has a pressure of 11 bar and a temperature of 183 degrees Celsius. The brine that flows through the system at Wellpad Dieng experiences a significant drop in temperature until at the open pond the brine temperature is only 90 degrees Celsius.

1.3 Dieng Geothermal Field Piping Facilities

Piping facilities in the Dieng geothermal field are used as a fluid transportation medium. The fluids transported include 2-phase fluids (brine & steam), steam, brine and condensate. Piping facilities use 2 types of pipes, welded pipes and flange to flange pipes.

At wellpads, flange-to-flange type piping facilities are used to transport 2-phase fluid from the wellhead to the separator, then from the separator to the Atmosperic Flash Tank and to SAGS (Steam Above Ground System). At brine lines system that connect between Wellpads, the use of 8", 12", and 16" welded pipes are common practice with some use of 8" flange to flange type pipes. The specification of the pipe are Carbon Steel material with 40 schedule.

Figure 4: Dieng Geothermal Pond & Open canal system.

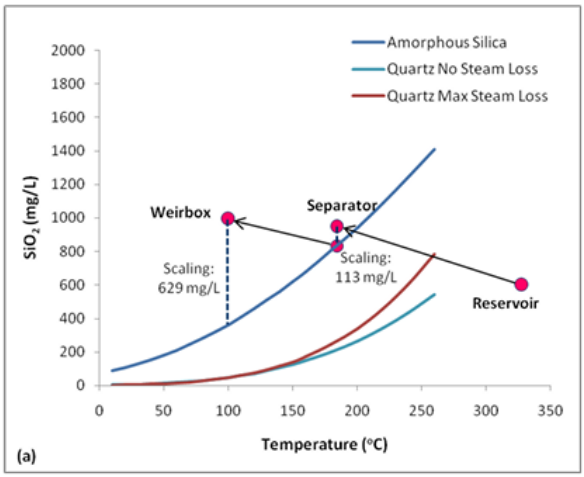

Figure 5: a) Amorphous Silica Saturation Curve of Dieng Geothermal Well. (Utami et. al., 2014). b) Silica Deposition on pipeline.

Table 4: Dieng Geothermal Brine Line Piping Facilities.

No	Type of Pipe	Material	Size (inch)	Total Count (lines)	Total Length (meters)	Sub total Length by type	Proportion
1	Flange to Flange	Carbon Steel Schedule 40	8"	11	12.072	12.072	24%
2	Welded	Carbon Steel Schedule 40	8"	23	29.826	37.560	76%
3	Welded	Carbon Steel Schedule 40	12"	2	2.358		
4	Welded	Carbon Steel Schedule 40	16"	5	5.376		

1.4 Maintenance schedule.

Company's Maintenance Division carries out routine maintenance on Dieng geothermal field assets, including the piping system used for brine management & reinjection. The difference in pressure between points on the pipeline indicates a disturbance causing the pipe did not function properly. The pressure drop will become greater as time goes by, the inspection and maintenance need to be carried out to return the pipe to its original condition. Maintenance aims to ensure that piping facilities remain reliable to support maximum and environmentally safe geothermal electricity generation operations.

2. LITERATURE REVIEW

2.1 Deposition of Silica

One of the chemical components that can be found in brine is dissolved silica. The silica solubility as presented by Amorphous Silica Saturation Curve are scaled with increase of Temperature and pH. The decrease of temperature will decrease the silica solubility forcing the excess dissolved silica to be deposited at the piping medium until it reaches the saturation limit.

At the beginning, the silica solubility is relatively high on reservoir until the wellhead (183 degree celcius). As the brine moves to lower temperature at the weirbox (98 degree celcius), the dissolved silica concentration is

higher than the solubility of amorphous silica. Thus, would potentially form the solid silica deposition (Utami et. al., 2014).

Silica Saturation Index (SSI) is Dissolved Silica Concentration divided by Solubility of Amorphous Silica, by first taking a brine sample to determine the silica content in the brine and determine the operating temperature (F. Dwiputra et al., 2022).

The SSI value is determined by the following equation :

$$SSI = \frac{Dissolved\ Silica\ Concentration}{Solubility\ of\ Amorphous\ Silica}$$

The occurrence of silica scaling can be predicted by the SSI value provided that SSI > 1 means silica scaling is possible, SSI < 1 then silica scaling is not possible. The Dissolved Silica Concentration was determined by laboratory tests using the Direct Nitrous Oxide-Acetylene Flame Method. The Solubility of Amorphous Silica is determined by the following equation :

$$Log\ C = -\frac{731}{T} + 4{,}52$$

Where,

C =Solubility of Amorphous Silica (mg/kg)

T = Absolute temperature (K)

Below are the calculation result and simulation from brine chemistry for Silica Saturation Index in Dieng Geothermal Well.

Table 5: Silica Concentration & Silica Saturation Index (SSI) for Dieng Geothermal Well sample (F. Dwiputra et. al., 2022).

Parameter	*Flashing*	*Line 2 Single Flash*			
	Separator 1	*Inlet Holdup vessel* 2	*Holdup vessel* 2-A	*Holdup vessel* 2-B	*Holdup vessel* 2-C
Temperature °C)	215,6	210,6	206,8	202,4	200,2
Temperature (K)	488,75	483,75	479,95	475,55	473,35
Silica Total (mg/kg)	1116	1126	1108	1116	1110
Silica Amorf (mg/kg)	1057,66	1020,68	992,94	961,24	945,56
SSI	1,055	1,103	1,116	1,161	1,174
Titik Sampel	S01	S21	S22	S23	S24

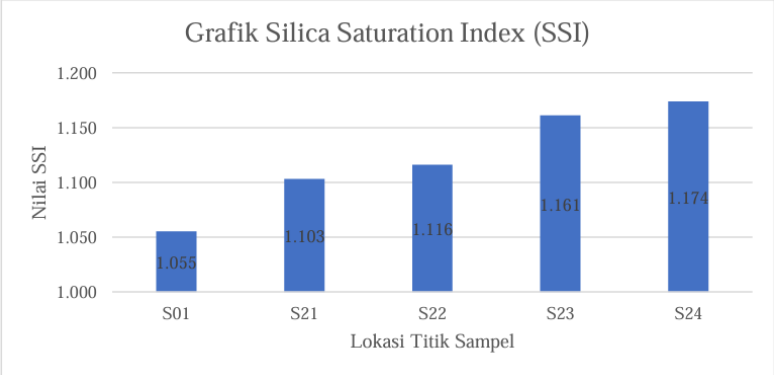

Figure 6: SSI Graphic for Dieng Geothermal Well sample (F. Dwiputra et. al., 2022).

Silica deposition can take the form of a solid material that sticks to the piping media it passes through. Over time, the buildup of silica causes the internal diameter of the pipe to narrower.

2.2 Welding Pipe Connection

One of the most common practices used to connect pipes is using welding method. The welding process is where the two ends of the pipe are connected using a heating application. This type of connection is permanent and

requires cutting to separate the pipe later on. The welding connection method is applied without using connection fittings or bolting.

There are several types of welding methods for pipe connections, including: 1) Butt Weld, which is a welding method by bringing the two ends of the pipe together without touching each other and making a connection. This welding method is the simplest and easiest to apply in various situations. 2) Lap Weld, is a welding method by bringing two pipes together with one of them squeezing the other and then welding. 3) Plug Weld, is a welding method by inserting one pipe into another.

Figure 7: Butt Weld application on pipe.

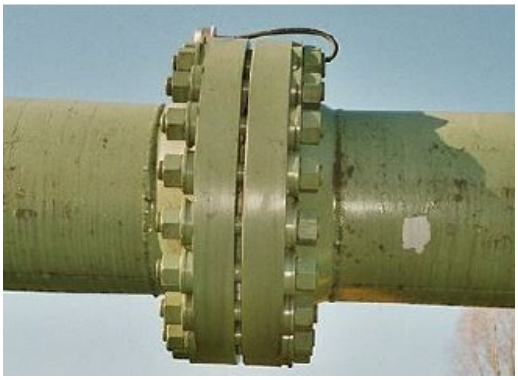

Figure 8: Flange to Flange connection on pipe.

Connection using the welding method has several advantages including; 1) There are rarely or no leaks at all. 2) cheaper costs when compared to flange to flange connections. 3) Easy to apply insulation material and requires less material. 4) More resistant to vibration. 5) easier to repair without risk of losing fittings.

Connection using the welding method also has several disadvantages including; 1) Requires Welding personnel expertise. 2) The use of heat in welding has the potential to affect the characteristics of the pipe material. 3) Does not provide room for expansion. 4) Requires longer time for the Inspection process. 4) Require penetrant test for leakage.

2.3 Flange to Flange Pipe Connection

Apart from connecting pipes using the welding method, the flange to flange method can also be applied to piping systems. Connection using this method requires 3 main components, including; Bolts, Gaskets and Pipe Flange. This type of connection is a temporary / non-permanent connection.

A flange is a connection between pipes that functions as a base for using bolts in the connection. Flange is needed in a pair so that it can be connected from each end of the pipe. Bolts are components used to provide compressive pressure on the flange to flange connection system. There are several types of bolts that are commonly used, including Stud Bolts and Machine Bolts. Gaskets are components that provide a sealing function to pipe connections. The gasket will be pressed from both sides and is usually a type of silicon and stainless steel material. Gaskets should only be used once and not for reuse to avoid leaks at the Flange to Flange connection.

The advantages of the Flange to flange connection method include: 1) The connection is much faster than the welded type. 2) Suitable for use when the pipe will be paired with other equipment. 3) Easier for the dismantle and assembly for maintenance purposes.

The disadvantages of the Flange to flange method include; 1) A leak test needs to be carried out to ensure that there are no leaks at the flange to flange connection. 2) Requires more expensive costs compared to the welding

type because of the flange and gasket material. 3) Less resistant to vibration systems. 4) Use of damaged gaskets may result in leaks. 5) requires tension to produce effective sealing.

Table 6: Comparison of Welded Connection & Flange to Flange connection on pipe.

No.	Parameter	Pipe Connection	
		Welded	Flange to Flange
1	Cost required	Low	High
2	Duration required for Connecting & Dismantling	High	Low
3	Resistance to Vibration	High	Low
4	Require specific skilled personnel	Yes	No
5	Potential heating damage to material	Yes	No
6	Potential tension damage on material	No	Yes

Figure 9: Temporary Office.

Figure 10: Partial trim on Dieng Brine line.

Figure 11: Manual cleaning silica deposition on Dieng Brine line.

Figure 12: NDT Penetrant test after Manual Cleaning process on Dieng Brine line.

2.4 Manual Cleaning for Silica Deposition

Manual Cleaning Method is the simplest and the earliest method that has been used. This method only uses simple mechanical equipment such as hammers, rod, and spades. Manual cleaning of silica can be done according to the welded type of pipe and flange to flange type of pipe connection.

Preparation for manual cleaning method includes; Permit to work approval, material dan tools mobilization, schedule acceptance and initial field survey. A temporary office is required for temporary placement of material, tools, and documentation. The temporary office should be placed in such way that allow ease access from any cleaning points.

Preparation for manual cleaning method includes; Permit to work approval, material dan tools mobilization, schedule acceptance and initial field survey. A temporary office is required for temporary placement of material, tools, and documentation. The temporary office should be placed in such way that allow ease access from any cleaning points.

Personnel required in manual cleaning method are consisted of Site Coordinator, Safety Man, Welder, Pipe Fitter, and helper. Aside from the specific personnel required for welding and fitting pipe, the personnel specifically for manual cleaning is mainly unskilled and helper.

The main step of Manual cleaning method is consisted of 3 substep such as; Dismantling pipe, Manual Cleaning, Reassembly and testing connection pipe. Dismantling pipe for welded connection type will cut the pipe for each 6 meters, while for flanged pipe only by removing studbolts. If cutting or dismantling flange pipe is not accessible due to field condition, Lap Patch can be secondary alternative. The lap patch will partly trim the body of pipe, allowing manual cleaning without dismantling pipe connection.

Manual Cleaning for brine line can be done after making sure the dismantling or partial trimming process completed. After making sure the thickness of silica deposition then the cleaning process can be begin with.

Manual Cleaning starts with hammering process using 5 kgs hammer toward the body of pipe which will result the detachment of solid silica deposition from the internal pipe wall. The solid silica will be taken out using spades or rods. This process can be done repetitively until the internal pipe completely clean from silica solid. After that, the silica solid will be transported using bags and vehicle to designated place for further process / utilization.

After making sure the cleaning process done, all left to do is reassembling of the pipe body. For welding type connection, the welding procedure specification (WPS) should follow API 1104 and ASME Sec IX standard alongside with approved Procedure Qualification Record (PQR). For Flange to flange type connection, reassembling should follow bolting and using new gaskets. During connection of each end, the other end should be plugged using temporary plug to avoid any external solid to accidentally enter the clean pipe.

The manual cleaning process will ends with leakage testing using NDT Penetrant test for welding type or leakage test for flange to flange connection.

The manual cleaning process has several advantages such as; 1) Low cost as it only requires unskilled personnel and simple mechanical tools. 2) This method can be used effectively for small footprints during application. 3) This method allow the silica cleaning process to be manageable and avoid scattering to surrounding. 4) The use of simple task and equipment also making this process classified as low risk task avoiding pressure and temperature risk.

The main disadvantage of manual cleaning technique is its requires long duration as the process is mainly manual and labour works. Other disadvantage is potential physical damage or material deformation to pipe body due to hammering in long time. This can be resulted in thinning of pipe wall thickness and lower its strength. The use of routine wall thickness inspection is needed for extra precaution other than replacing with the new pipe all along.

2.5 Waterjetting Cleaning for Silica Deposition

The waterjetting method of silica cleaning uses water pressure to remove precipitated silica and considered a more advanced method for cleaning. Water is jetted using up to 20.000 psi pressure through equipment nozzle of the waterjetting equipment to be directed to the scaling pipe. The steps for waterjetting silica cleaning work are essentially same as manual cleaning except for the execution part where manual method hammering and using spades is replaced by jetting of pressurized water.

Waterjetting technique requires additional special jetting equipment and competent jetter and operator personnel. The use of water as jetting media also requires the sufficient water source to be easily accessible and connected to jetting equipment. Waterjetting technique also required temporary water containment equipped with filtration method to separate the water and the silica. The water can be used afterward.

Figure 13: Waterjetting for silica deposition line Dieng Geothermal field.

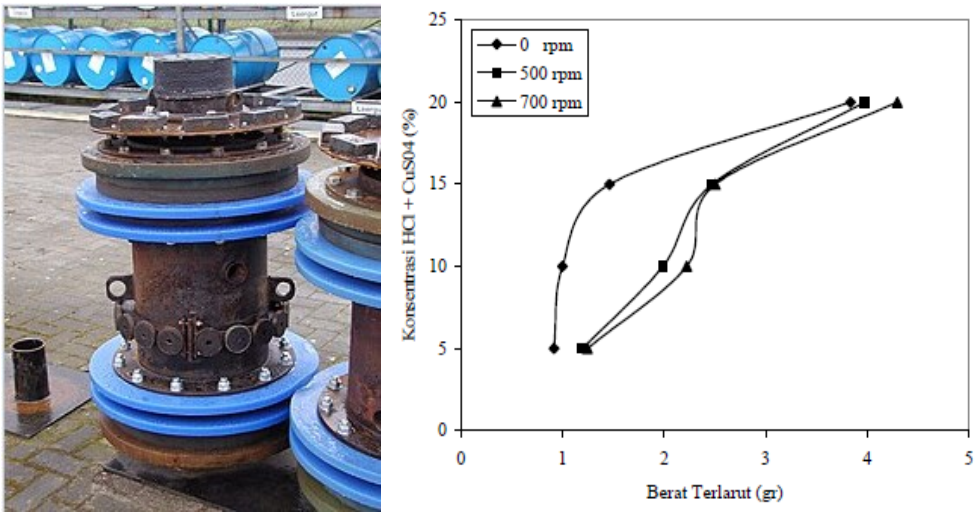

Figure 14: a) Pigging devices. b) HCL & CuSO4 concentration influence to dissolved scale (Syahri et. al., 2008) .

Waterjetting technique has the main advantage of completing the task much faster than using manual cleaning process. While the disadvantage of this technique are; 1) Higher cost as it requires additional equipment & skilled personnel. 2) require wide area to accommodate placement of waterjetting equipment. 3) require water supply. 4) potential environmental damage as the jetting result of high pressure water and silica scattering around. 4) higher risk as it consist of pressurized water work.

The Waterjetting techniques is suitable for advanced facilities such as the use of flange to flange connection pipe due to its short duration required for connection and dismantling, the use of dedicated cleaning yard for safer and allow cleaning of many pipe in very short time, also any means of transporting pipe from its location to the cleaning yard. The use of waterjetting technique on welded pipe connection is limited by the time requires for cutting and welding the pipe, this can result in longer equipment rent thus further increase the maintenance total cost.

2.6 Other cleaning methods: Pigging & Chemical Addition

Pigging requires "pigs" to be inserted into pipelines to perform cleaning activities. The pig was placed in one end of pipeline and pushed through the line by the product flow. It scrapes the insides of pipe as it travels, removing dirt and debris as it goes. This method is done without stopping the flow of product in the pipeline.

The use of chemicals to mitigate scaling can be used by injecting scale inhibitor chemicals. The use of chemicals includes HCl, CuSO4 and a mixture of HCL & CuSO4. The working principle of scale inhibitors is by forming complex compounds between scale inhibitors and scale-forming elements. The complex compound formed will dissolve in water, thereby blocking the growth of large crystals. Besides that, it can be used to prevent scale crystals from sticking to the pipe walls (Syahri et. al., 2008).

3. METHODOLOGY

The method used in this research is comparative analysis of multiple alternatives to determine the most suitable solution for the problem. This include stating the scope of the discussed problem, gathering required case data, determining the root of the problem and objective, researching potential alternatives, determining important parameters, testing alternatives resulting on quantitative and qualitative parameters, comparing tested alternatives data parameter, scoring, determining most suitable method based on scoring, completing with what-if situation and summarize the whole process to produce recommendation.

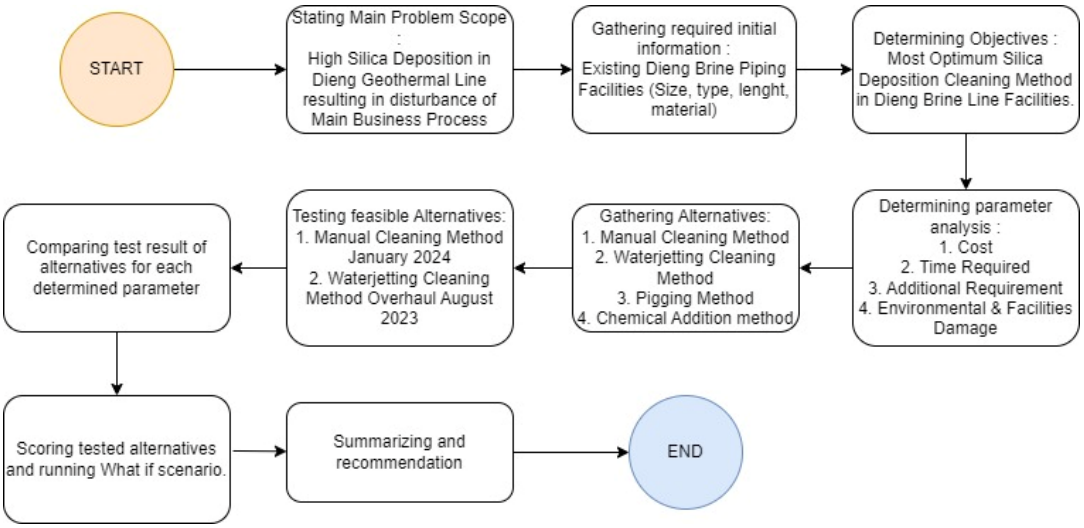

Figure 15: Comparative Analysis for Dieng Geothermal Brine Management & Reinjection System solution.

4. RESULT AND ANALYSIS

The main objective is to find the most suitable method in term of economical, safety, environmental and practical maintenance schedule to be applied to solve dieng geothermal deposition piping system. There are 4 potential alternatives which will be evaluated based on important parameters such as: 1) The total cost per meter of cleaning pipe, 2) The time required to complete pipe cleaning process, 3) The HSSE aspect including safety for the worker and surrounding and the effect to the environment. 4) The potential damage for piping facilities in the future. 5) the field feasibility.

Feasibility of each solutions should be assessed to eliminate any non-practical solution for current condition and objective. Based on 4 potential solution, the perquisites can be breakdown as below:

Table 7: Pre-Eliminary assessment of solution feasibility.

No	Cleaning Method	Compatibility of cleaning massive silica solid deposotion	Compatibility for non flowing condition	Result of Assessment
1	Manual Cleaning	V	V	Feasible
2	Water Jet Cleaning	V	V	Feasible
3	Pigging Method	V	X	Not Feasible
4	Chemical Addition Method	X	V	Not Feasible

Based on the assessment above, it was decided to continue with comparing the manual cleaning method and the water jet cleaning method.

4.1 Manual cleaning application for deposited silica pipeline system in Dieng Geothermal field.

Pipeline cleaning process using Manual Cleaning method is applied in 5 different scenarios in Dieng Geothermal pipeline system that prone to silica deposition problem. The cleaning process applied in full welded type of pipeline system as well as the mixed one with flanged type connection. The piping system is consisted of 8", 12" and 16" size of diameter. Manual cleaning application applied to brine line with hard silica deposition condition.

Table 8: Manual Cleaning Application Summary.

No.	Method	Total Cost	Pipe Connection	Pipe Size	Total Joint	Total Length (m)	Cost (Rp/m)	Time (hr)	AVG Speed (m/hr)	Silica Hardness Level	Safety & Environmental Aspects	Side Effect
1	Manual Cleaning	Rp 273.227.200	48% Flanged 52% Welded	8"	799	4794	Rp 56.993,58	255	18,8	Hard (Brine Line)	Labour Physical injury	Potential deformation on pipe body
2	Manual Cleaning	Rp 226.436.000	41% Flanged 59% Welded	8"	686	4116	Rp 55.013,61	172,5	23,9	Hard (Brine Line)	Labour Physical injury	Potential deformation on pipe body
3	Manual Cleaning	Rp 1.900.000.000	26% Flanged 74% Welded	8", 12", & 16"	4087	24522	Rp 77.481,45	1852,5	13,2	Hard (Brine Line)	Labour Physical injury	Potential deformation on pipe body
4	Manual Cleaning	Rp 116.882.500	Welded	8" & 16"	398	2388	Rp 48.945,77	105	22,7	Hard (Brine Line)	Labour Physical injury	Potential deformation on pipe body
5	Manual Cleaning	Rp 1.650.000.000	26% Flanged 74% Welded	8", 12", & 16"	2962	17772	Rp 92.842,67	1852,5	9,6	Hard (Brine Line)	Labour Physical injury	Potential deformation on pipe body

Total cost	total length (m)	cost Rp/m	Total Duration (hr)	Speed (m/hr)
Rp 4.166.545.700,00	53.592,00	Rp 77.745,67	4237,5	12,65

Table 9: Water jet Cleaning Application Summary.

No.	Method	Total Cost	Pipe Connection	Pipe Size	Total Joint	Total Length (m)	Cost (Rp/m)	Time (hr)	AVG Speed (m/hr)	Silica Hardness Level	Safety & Environmental Aspects	Side Effect
1	Water jet Cleaning	Rp 216.698.002	Flange to flange	10", 16", 18", & 20"	13	78	Rp 2.778.179,51	36	2,2	Very hard (2-phase)	Risk Pressure, Silica Scatter	Water Supply
2	Water jet Cleaning	Rp 390.000.000	Flange to flange	18" & 25"	24	146	Rp 2.671.232,88	46,2	3,2	Very hard (2-phase)	Risk Pressure, Silica Scatter	Water Supply

Total cost	total length (m)	cost Rp/m	Total Duration (hr)	Speed (m/hr)
Rp 606.698.002,00	224	Rp 2.708.473,22	82,2	2,7

A total of Rp 4.166.545.700 was required to clean a total 53.592 meters pipeline manually. This conclude the average cost of cleaning is Rp 77.745 per meter. The duration required is 4237,4 hrs thus the average speed of Manual cleaning process is 12,7 meters / hr.

The application of manual cleaning has side effects on both personnel safety and piping facilities. As the job is mainly hard labour, the potential risk of work is physical injuries due to falling objects and exhaustion. The piping

facilities suffers from hammering process could lead into deformation and lowering the strength in long run. Using manual cleaning on any line which operate in high temp and pressure could lead into early failure of the pipe.

The process is very simple that this method can be used for any brine line which very close to community farm, doesn't provide water supply and wide area to do work. While using manual cleaning can be flexible to do in any place, cleaning a very hard type of silica deposition on two phase line wellpad requires much longer time and can cause potential delay on business process.

4.2 Water Jet cleaning application for deposited silica pipeline system in Dieng Geothermal field.

Water Jet cleaning application is applied in 2 different scenarios in Dieng Geothermal Field piping system. The cleaning process is appied to full flanged pipe connection with varied diameter of 10", 16", 18", 20" and 25". The silica hardness level was very hard due to its located on two phase piping system.

A total of Rp 606.698.002 was required to clean a total 224 meters pipeline using Water Jet. This conclude the average cost of cleaning is Rp 2.708.473 per meter. The duration required is 82,2 hrs, thus the average speed of Water Jet cleaning process is 2,7 meters / hr.

The application of water jet cleaning has side effects on both personnel safety and environmental surrounding. As the job is pressurized water technique, the potential risk of work is injuries due to high pressure flow. The early precaution should be taken to make sure the job is done safely and eliminate the accident potential as much as possible. The surrounding environment suffers from scattering of silica. Housekeeping process should be included and additional rug needed to contain the silica.

The process is advanced that this method can be used to break down very hard silica such as in two phase line or any lower hardness silica. While using water jet cleaning can be flexible to do in any level of silica hardness, using this method requires a lot more equipment to begin with. The need of water supply and potential scattering of silica hinders this method to be used near community farm such as brine line. The use of this method can optimalized by several option such as; 1) Preparing a dedicated cleaning station which close to water supply and away from community. 2) a dedicated vehicle for transportation. 3) a full 100% flanged type connection of piping system as it align with speed of dismantling and practical re-assembly.

4.3 Water Jet cleaning and Manual Cleaning application comparison in Dieng Geothermal field.

Result of both cleaning method application on geothermal piping system can be measured by the cost and the speed of the process. The manual cleaning process proved to require less budget than using waterjet cleaning. This mainly caused due to its difference technology used. The cost of water jet equipment rent, skilled operator and personnel, water supply and power supply all resulted on high total cost to use Water Jet cleaning method. The ratio of cost between Manual Cleaning and Water Jet Cleaning is 1:35, which means that using water jet cleaning method to clean deposited silica pipeline is 35x more expensive than the manual cleaning.

Figure 16: Comparison of a) cost & b) speed of Manual dan Water Jet Cleaning method.

The result of speed conclude that manual cleaning is faster than water jet cleaning. The ratio is 1:5, which means cleaning manually is 5x faster than using water jet for given condition. This is related to the hardness level of silica scale target. The harder the silica deposition, the more power it required to detach from internal pipe diameter. Using manual cleaning method on brine line which has hard level of silica is proved faster than using Water Jet cleaning on very hard silica deposition at two phase line Wellpad. While speed and cost is used for

quantitatively evaluate both method characteristic, the field practice can be optimized by considering practical and future qualitative concern.

Table 10: Qualitative Comparison Manual dan Water Jet Cleaning method.

Cleaning Method	Accessibility	Area Footprint	Power	Personnel Risk	Environment Risk	Facilities Damage	Best Application
Manual	High Can easily reach brine line location	Small Only for personnel & hand tools	Low Limited to soft to hard silica deposit	Low Only manual labour and gravity	Low Silica fragment can be contained easily	High Physical Deformation	**Brine Line**, which : 1. Away from water supply 2. Soft to hard Silica 3. Low operating pressure line 4. Near civil community 5. Small area
Water Jet	Low Requires area with water supply	Large Require wide area for equpment placement	High Can easily clean very hard silica deposit	High Pressurized water	High Silica fragment scatters around	Low to N.A	**2-phase wellpad line**, which : 1. Equipped with water pond 2. Very hard silica deposit 3. High operating pressure line 4. Separated from community 5. Wide area

Considering accessibility, area, power, personnel risk, environment risk and facilities damage the use of most optimum cleaning method can be determined accordingly. Manual Cleaning method is best used on Brine line due to accessibility, soft to hard silica, low operating pressure line which lower the risk of physical deformation due to hammering, away from water supply, near people and small area of job.

While manual cleaning is best to be used on brine line, the Water jet cleaning is best use on Wellpad 2-phase line. The use of hammering on 2 phase line will very much damage the pipe body and potentially fail in the near future as it operate with extreme pressure and temperature. This risk can be easily eliminated by using water jet technique. The silica on two phase line Wellpad is closer to wellhead and usually deposit very hard silica on pipe, the use of manual cleaning requires too much duration to be applied on this case and potentially delay the upcoming maintenance schedule. This risk can also easily eliminated by using waterjet technique.

This conclude that to achieve best outcome of cleaning deposited silica in Dieng geothermal piping system, the use of both Manual Cleaning and Water Jet cleaning is required. Manual Cleaning can be used on Brine Line and Water Jet Cleaning should be used on 2 phase Wellpad line. By combining these two methods, piping system can be cleaned with most optimum budget, technical application, and environmental concern.

5. CONCLUSION

By combining Manual cleaning and water jet cleaning method on Dieng Geothermal Piping system, company can effectively and efficiently cleaned silica deposition on both Brine line and 2 phase line by considering cost, technical application, Safety, environment and facilities aspects. Manual cleaning method is best to be used on Brine line while Water Jet cleaning is best to be used on 2-phase line.

Manual cleaning method costs lower to operate than waterjet cleaning with 1:35 ratio. Manual cleaning needs Rp. 77.746 per meter cleaned, while Water Jet cleaning costs Rp 2.708.473 per meter cleaned. The speed of manual cleaning comparing to waterjet is 1:5 ratio for current Dieng existing facilities application.

For further research, Water Jet cleaning should be tested its application on Brine line deposited silica. Due to lower hardness of silica level on Brine line than 2-phase line, the use of waterjet technique on brine line should yield much faster speed.

The use of pigging and chemical addition method to clean deposited silica should be studied deeper to achieve practical level.

ACKNOWLEDGEMENT

The authors would like to thank the management of PT Geo Dipa Energi for the permission to publish this paper. The authors will retain sole responsibility for any errors of interpretation.

REFERENCES

Dwiputra, F.: Analisis Silica Saturation Index di Jalur Brine Production Optimization Unit Lapangan Panas Bumi Dieng. Prosiding, UNJ, Indonesia (2022).

Juhri, S.: Study on Silica Scaling at Open Canal System, Dieng Geothermal Power Plant, Indonesia. Proceedings World Geothermal Congress Reykjavik, Iceland (2021).

Sirait, P.: Reservoir Modeling for Development Capacity of Dieng Geothermal Field. PROCEEDINGS, Fourtieth Workshop on Geothermal Reservoir Engineering Stanford University, Stanford, California (2015).

Syahril, M.: SCALE TREATMENT PADA PIPA DISTRIBUSI CRUDE OIL SECARA KIMIAWI. ISBN: 978-979-3980-15-7 Yogyakarta (2008).

Utami, W.: The Effect of Temperature and pH on the Formation of Silica Scaling of Dieng Geothermal Field, Central Java, Indonesia. PROCEEDINGS, Thirty-Ninth Workshop on Geothermal Reservoir Engineering Stanford University, Stanford, California (2014).

Application of Geochemistry Monitoring for reservoir surveillance at Sorik Marapi Geothermal Field

Radhitya E Pradipta[1], Ryan Hidayat[1], M Yamin Nasution[1],
Zosimo Sarmiento[1], Jill Haizlip[2], and Zachary Brown[2]

[1]KS Orka – Sorik Marapi Geothermal Power
[2]Geologica Geothermal Group

radhitya.pradipta@ksorka.com, ryan.hidayat@ksorka.com, Muhammad.yamin@ksorka.com,
zammy.sarmiento@ksorka.com, jhaizlip@geologica.net, zbrown@geologica.net

Keywords: TFT, NCG, Reservoir Surveillance, Geochemistry

ABSTRACT

The Sorik Marapi Geothermal Power (SMGP) field is a high enthalpy liquid dominated geothermal system which currently utilizes 15 production wells to support 160 MW gross capacity. A geochemistry surveillance program has been in place since the start of power generating operations in late 2019 monitoring the geochemical reservoir response in correlation with mass extraction and injection.

The geochemistry field monitoring consists of weekly geochemical measurements at production wells: gas/steam using a wet gas meter, and field measurements of chloride, silica, pH, and, conductivity for steam and brine monitoring. This field monitoring produces instant results as the measurements are done on site at Sorik Marapi. During the same time period, quarterly geochemiscal samples of produced fluids from each well are collected for more comprehensive laboratory analysis including non-condensable gas speciation of steam samples, and anion-cation , stable water isotope and total silica concentrations in brine. Mass flow rates measured at multiple-well separators and at the power plant inlets are supplemented with tracer flow test (TFT) data at individual wells and separators measuring steam and brine flow rates which produce, and enthalpy and total discharge data from calculations.

In this paper, we document how the geochemical surveillance programs captured reservoir changes over time and correlate these changes with production and injection data over the same period. Using temporal and spatial plots, the geochemistry data informs the evolution of the reservoir over time including; the development of a steam cap in portions of the reservoir, the impact of drilling activities, injection breakthrough, and related changes to the operational strategy. The interpretation from weekly monitoring is validated with quarterly sampling and the quality of weekly dataset and monitoring program is assessed in the context of other operational and geoscientific datasets providing a vital data set indicating real time reservoir response to production and injection which has been important for managing the reservoir.

1. INTRODUCTION

Sorik Marapi geothermal field license Area in northwestern Sumatera, located 650 km south-southeast of Medan. Sorik Marapi Geothermal Power (PT. SMGP) has geothermal concession that covers an 629 km2 area, The geothermal system was defined based on a generally N-S elongate magnetotelluric (MT) low resistivity anomaly (~6 km2) ad a wide distribution of warm to boiling hot springs and fumaroles primarily centered along the Sumateran Fault System (SFS) and extending west into the summit crater of Sorik Marapi Volcano (Figure 1) (Geologica, 2024).

The geothermal area lies within a depression zone which is a part of pull-apart basin caused by the displacement of Great Sumatran Fault Zone (GSFZ).

The active fault GSFZ appears to control the permeability, possible intrusive heat source and stratigraphy observed within the Sorik Marapi geothermal field. The stratigraphic sequence includes thick sequence of Quaternary volcanics overlying the older metamorphic, volcanic, metavolcanic and intrusive rocks which form the basement west of GSF. On the eastern side of GSFZ, the metasediments and sedimentary rocks are present shallower than on the western side. Existing fractures based on identification of feed zones within the wells appear to be related to displacement along the GSFZ. The presence of this range of geologic and geophysical features and the high number of surface manifestations and mass discharged from these features is a strong indication of a high temperature fault-controlled geothermal system (Hinz et al., 2021).

There are more than 40 wells drilled in the Sorik Marapi concession. Providing steam and hot brine for the power plants, SMGP drilled from Pad A (7 wells), pad T (10 wells), pad AA (3 wells), pad AAE (6 wells), and the most

recent pad V (3 wells). The primarily injection is provided from pad P (4 wells including one with multilateral wells), Pad C (5 wells) and Pad D (3 wells) (Figure 2)

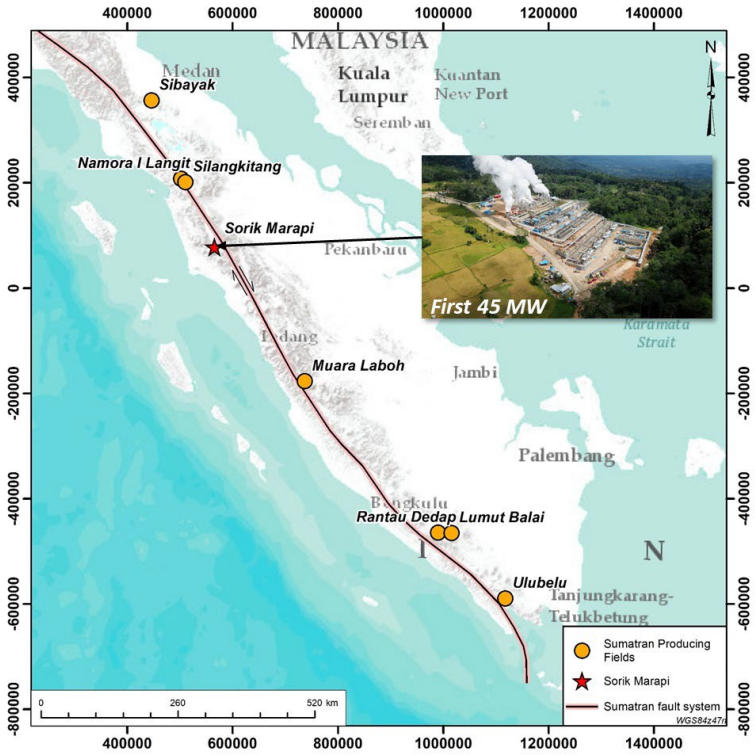

Figure 1: Sorik Marapi Location on Sumatera relative to other geothermal fields.

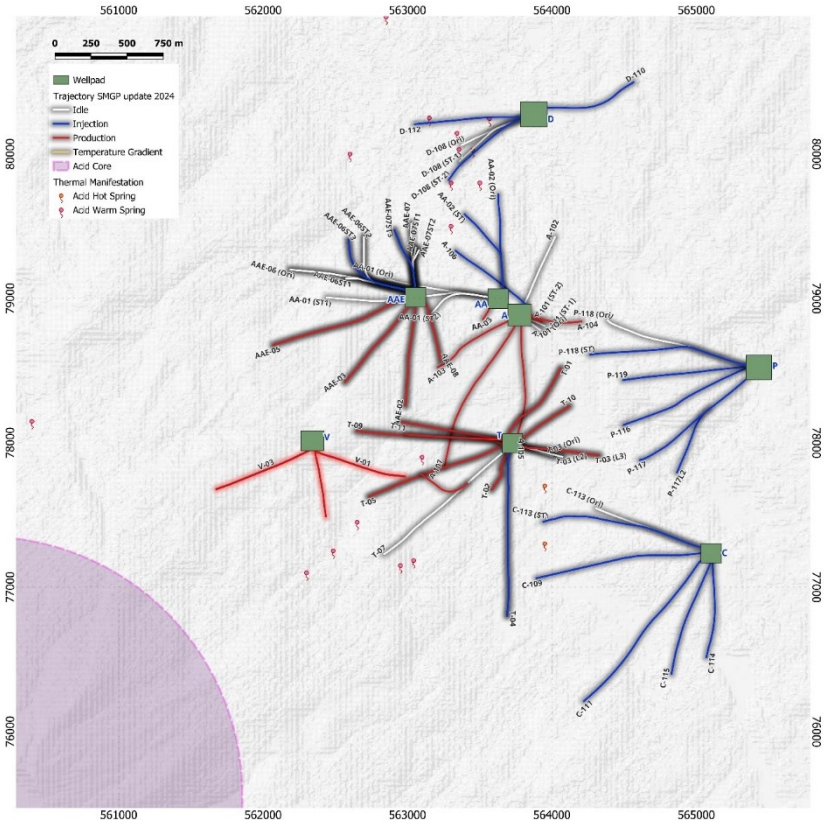

Figure 2: Production and Injection wells with feed zones drilled within the currently developed Sorik Marapi Geothermal Reservoir.

Geothermal brine and steam samples a from production wells have been sampled every 2 weeks and analyzed for gas/steam (steam sample) and pH, electrical conductivity, silica (SiO_2) and chloride (Cl) (brine sample) as a part of reservoir surveillance to understand reservoir conditions. Additional geochemical surveillance programs such as quarterly sampling and tracer flow testing (TFT) (Hirtz, 2001), full non-condensible gas (NCG) analysis of steam, full anion-cation analysis of brine, and stable water isotope analysis were established to validate and supplement weekly monitoring (Figure 3). TFT data allows the geochemistry of the total discharge (representing the reservoir fluids averaged over multiple feed zones if they exist) to be calculated for individual wells and enables comparison of geochemical monitoring and individual well performance.

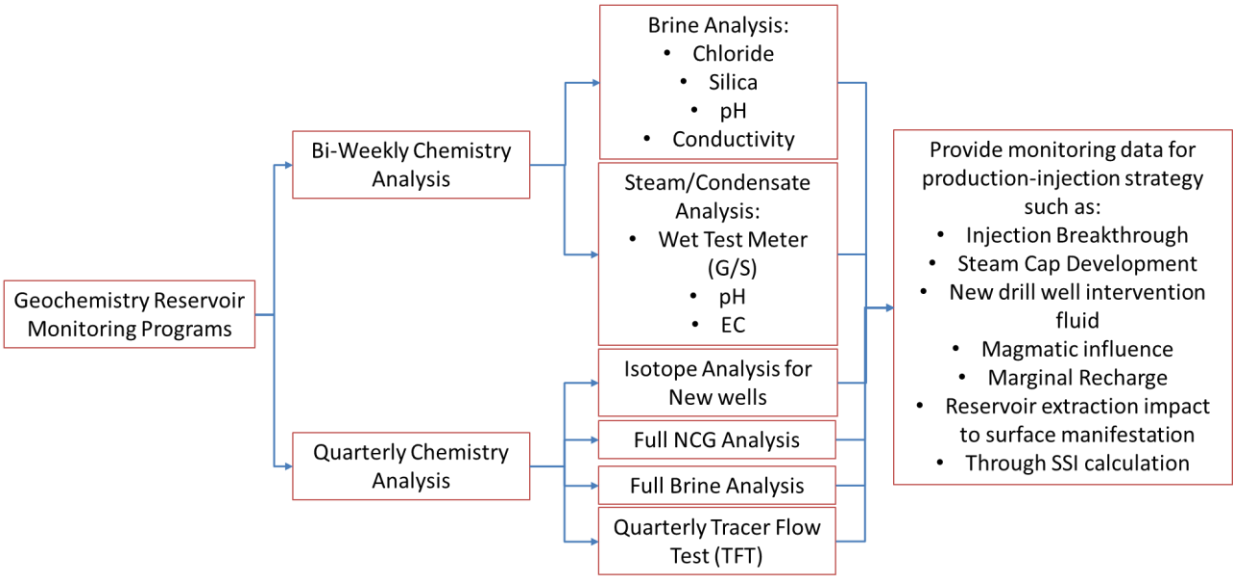

Figure 3: SMGP Surveillance Programs.

Problem	Enthalpy	NCG	Chloride	Silica
Injection Break through	↓	↓	↑	↑
Meteoric Water Break through	↓	↓	↓	↓
Reservoir Cooling	↓	↓	↓	↓
Steam Cap	↑	↑	↓	↓

Figure 4: Bi-weekly Chemistry Analysis at SMGP .

2. SURVEILLENCE PROGRAMS

2.1 Bi-weekly

The geochemical monitoring at SMGP consists of bi-weekly field measurements of steam and brine: gas/steam (G/S) using a wet gas meter in steam samples, and field measurements of chloride, silica, pH, and, conductivity in brine samples collected at operating production wells (Pad A, Pad T, Pad AA, Pad AAE). Initially, weekly samples were collected at steam and brine outlets of high pressure separators which combined flows from one or two wells, in order to use the separator flows to estimated total enthalpy and correct to reservoir conditions. Subsequently, sampling was changed to wellheads using a small sampling separator.

Figure 4 shows the problem identification within SMGP bi-weekly chemistry monitoring program. To confirm trends indicated by bi-weekly monitoring, quarterly geochemical sampling and analysis of brine and steam and TFT from individual wells is performed. This approach is applicable in Sorik Marapi field and might be similar with the other water dominated field.

The silica concentration in brine is important for controlling brine treatment for silica scale control in geothermal power plants or reinjection line/wells with low discharge temperatures, especially in high-temperature volcanic geothermal settings. The basis of chemical brine treatment for silica scale mitigation depends on silica concentration, pH and brine flowrates.

2.2 Quarterly geochemical sampling, analysis and TFT

More comprehensive quarterly geochemical monitoring includes tracer flow test (TFT) (Hirtz, 2001) measurements of enthalpy and steam and brine flow, laboratory analyses of non-condensable gas primary species concentrations in steam samples, anion-cation laboratory analysis of brine, and stable isotope analysis of steam and brine at the new wells (Figure 3) The data are collected and stored in a geochemical database for evaluation over time and comparison with baseline or initial fluid chemistry. While bi-weekly monitoring data are primarily used as measured to evaluate trends, quarterly laboratory analyses are corrected to reservoir conditions based on sampling conditions and reservoir enthalpy of the individual well. The main purpose of quarterly geochemistry sampling and analysis is to confirm and further explore the reservoir behavior indicated by the bi-weekly chemistry, validate trends and assess additional reservoir conditions related to production and injection from the more detailed chemistry.

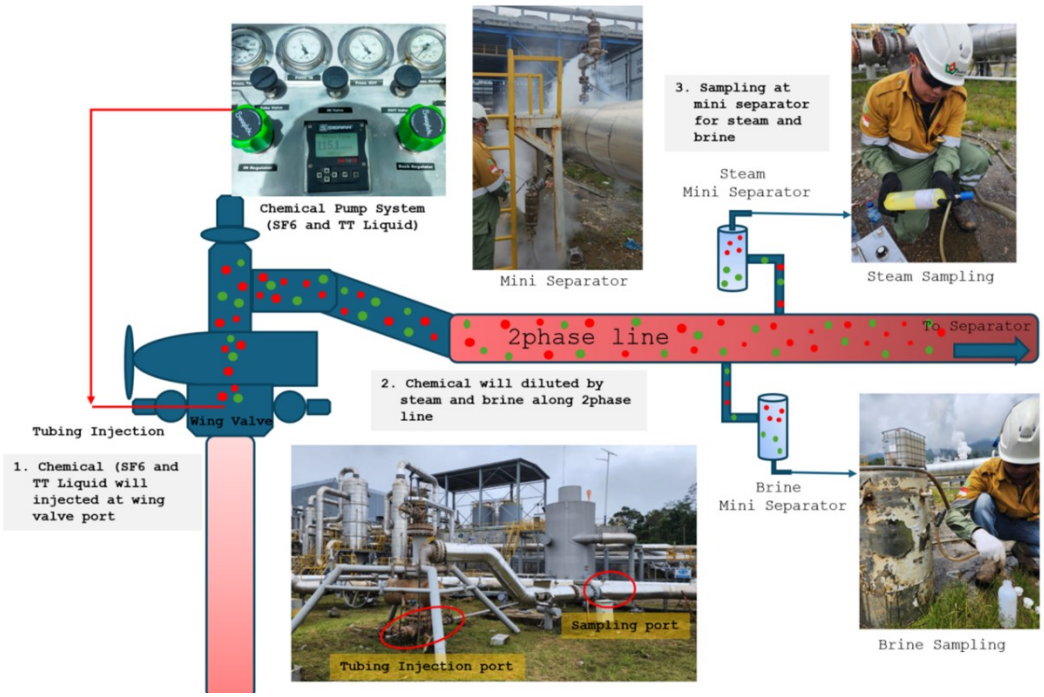

Figure 5: TFT field sampling.

During TFT testing (Figure 5), the injection of chemical in two-phase line allows the determination of steam and brine mass by the dilution of tracer chemical injected. This method is performed without disrupting the production conditions, thus the generation is not effected. TFT allows measurement of the individual well performance of mass flow of steam and brine at specific pressures and temperatures from which enthalpy and total mass flow are calculated. TFT testing frequency has varied from lower frequency (once a year) to higher frequency (3-4 times a years). Current plans include conducting more TFT tests as a part of reservoir monitoring, as a comparison with installed metering, and to allow construction of output curves and Pressure-Temperature- Spinner (PTS) analysis at specific flow rates. The enthalpy data from TFT results were used to interpret geochemical data by calculating the chemistry of the reservoir fluid before boiling (to calculate the chemistry of the total discharge).

There are three main step to conducting he TFT and quarterly geochemical sampling and analysis programs; sampling preparation, field sampling, and laboratories analysis. The sampling preparation includes giggenbach bottle preparationand tracer liquid calibration.

Field sampling requires a chemical injection location, chemical dilution, and sampling at specific, documented conditions. In SMGP, the tracer is injected into the wing valve. 3/8” tubing is inserted into the middle of pipe for ensuring the chemical injection. The minimum distance between injection port and sampling port is 20 pipe diameters to achieve proper mixing. The steam is sampled from a vertical port at the top of the line and the brine is sampled from a port at a 45^{o} from the bottom of the pipe The mini separator is installed at each port to separate steam and brine, then each fluid is cooled in a dedicated condenser/cooler to ensure that there is no flashing and then sampled.

The specific of tracer flow test at Sorik Marapi was the sampling location were less than 20 pipe diameters and located before FCV, thus, to operate this TFT equipment and result need more calibration data. The sampling strategy was to take as many data, then select the result based on data distribution.

Production and injection monitoring data of SMGP are documented in daily production and daily injection reports These reports record wellhead pressure (WHP), wellhead temperature (WHT), flow control valve position (FCV%) for each production well, separator steam mass flows, brine mass flows, separator temperature and pressure, and total mass flow (TMF) and temperature and pressure for injection wells. One or multiple wells flow to each high-pressure separator. Some wells which have a lower flowing wellhead pressure flow to low pressure separators. Therefore, TMF and enthalpy for production are measured as steam flow and brine flow at a separator pressure, which can be combined to estimate total production. For example, flow from wells A-105 and A-107 combine into separator HP-105 and the steam flow and brine flow from this separator is measured continuously but not the individual wells. Mass flow rates measured at the separators have been supplemented with TFT data which may include steam rate, brine rate, and enthalpy data for total discharge calculation. Based on the production and injection monitoring data, the timing of major operational changes, such as changes in injection, can be identified. Major changes in operations can be compared with geochemical monitoring data over time to identify potential changes in the reservoir, indicated by chemistry.

3. STUDY CASE SORIK MARAPI

3.1 Baseline Geochemical Condition

Initial well testing and production indicated the SMGP wellfield produced fluids over a range of flow rates (~100-500 tph) from a reservoir between <260 ˚C and 290˚C (enthalpy from ~1100 to ~1300 kJ/kg) primarily from Quaternary to Tertiary volcanics and intrusives and older metasediments. Later drilling produced higher flow rates to over 600 tph and enthalpies to nearly 1500 kJ/kg. Analysis of baseline (initial well tests 2017 – 2020) samples indicate that all Sorik Marapi wells, except those on Pad D from which there is no well test data, produce a Na-Cl type fluid with relatively low noncondensable gas (NCG) of ~400 mg/kg (corrected to reservoir conditions) from a single geothermal system. Initial reservoir fluid concentrations include ~500 – 600 mg/kg Cl (reservoir corrected), Cl/B ratio ~23, and clustering of data points on cation and anion trilinear plots (Figure 6 and figure 7). Note that hotter and cooler wells group close together, especially in cations controlled by temperature-sensitive reactions.

Initially, produced fluids from wells in the hottest portion of the Sorik Marapi reservoir (i.e., likely to be closest to the upflow, Pad T) are characterized by higher SiO_2 ~630 mg/kg versus field-wide average of 530 mg/kg, and higher NCG, ~960 mg/kg (reservoir corrected), but about the same concentration of Cl (650 mg/kg in upflow zone and 670 mg/kg field-wide average. Groupings of wells with deeper, hotter feedzones (mostly on Pad T) can be seen in cation and anion trilinear plots of baseline chemistry (6 and 7). The anion and cation concentrations of all wells plot in a group suggesting that under baseline conditions, anion concentrations (Cl, HCO_3 and SO_4) as well as cation Na, Ca and K concentrations (but to a lesser extent) were similar in wells of different temperatures, with the exception of wells adjacent to the upflow near Pad T, and therefore lower temperatures were initially unlikely to be related to unequilibrated mixing with cold meteoric water.

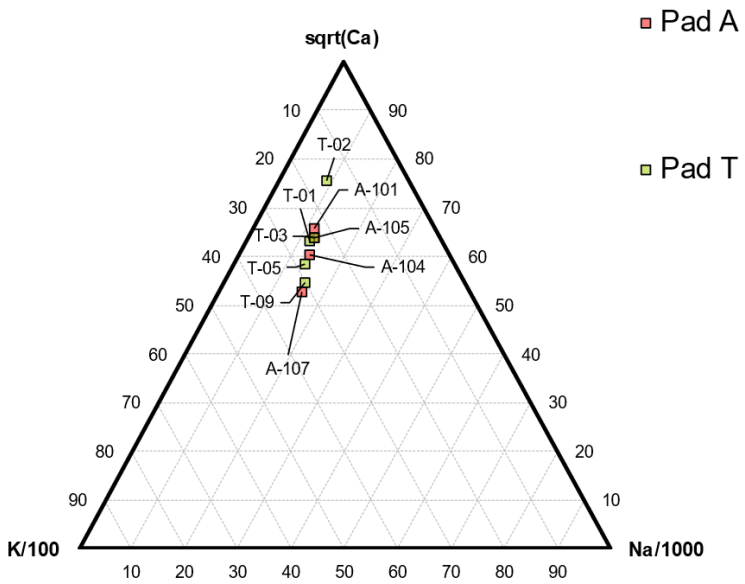

Figure 6: Cation trilinear plot of baseline (2017 – 2020) Pad A and Pad T geochemical samples. Note the temperature dependent mixing trend with T-09 and A-107 as the hot end members.

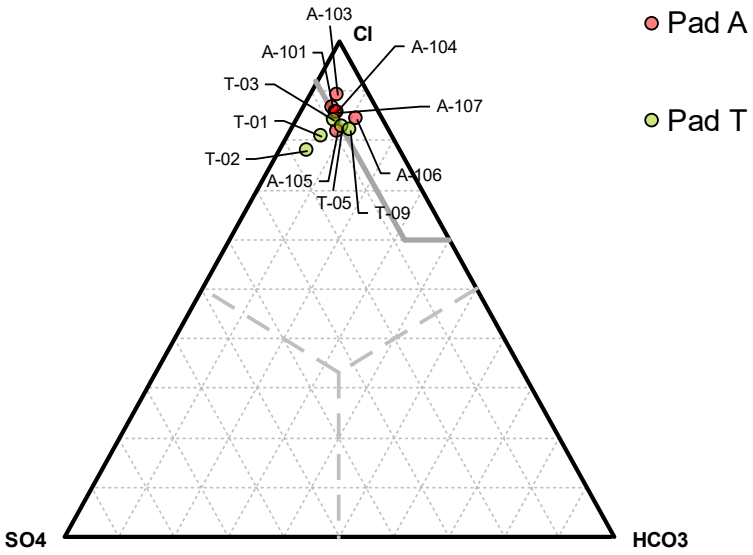

Figure 7: Anion trilinear plot of baseline (2017 – 2020) Pad A and Pad T geochemical samples.

Baseline laboratory gas analyses indicate reservoir NCG concentrations range from ~400 – 1000 mg/kg, with an average ~428 mg/kg NCG in the total fluid (reservoir corrected). Baseline NCG concentrations show two groups: One group has > ~600 mg/kg and while the other has < ~600 mg/kg. Wells with higher NCG concentrations (T-09, A-107, T-05 average >800 mg/kg) are characterized by higher H_2S (T-09, A-107, T-05 average ~200 mg/kg H_2S whereas the fieldwide average is ~100 mg/kg in the reservoir). Wells with higher NCG and H_2S, deeper feedzones, higher measured temperatures, and are likely to be closer to the upflow.

3.2 Geochemical trends, Interpretation, and Operational Impact

Temporal geochemical trends in Sorik Marapi production fluid shows the fluid chemistry and reservoir condition have changed over the last ~4 years of production and injection operations. As in other liquid-dominated geothermal fields under exploitation, chloride (Cl) and non-condensable gas (NCG) can vary between production and injection. In this paper, we will only discuss pad A production wells. Pad A has 5 production wells: A-101, A-103, A-104, A-105, and A-107 (Fig 8) and A-106 as backup injector wells.

3.3.1 Injection Tracking

Geochemical and enthalpy changes indicate that in-field waste brine injection at A-106 lead to chemical and possible thermal injection breakthrough to production wells at SMGP. While the greatest effects are observed in Pad A wells our analysis indicates that the impact of injection on production is widespread. Laboratory analyses suggested fluid geochemistry from Pad A wells was initially relatively stable until mid-2021 (8). Increasing Cl and decreasing NCG in Pad A wells occurred after March 2021 to early-2022, concurrent with high rates of injection into well A-106. After A-106 injection was reduced and eventually ceased in mid-2022, Cl concentrations declined or stabilized to mid-2023. Changes in bi-weekly field measurements of geochemical parameters (Cl, G/S (G/S representsNCG), SiO_2) in A (and T pad) wells appear to coincide with injection into A-106, which began in late May 2021 and increased through June 2021, then decreased in mid-2022 and was reduced to zero by the end of July 2022

Observed geochemical changes in production wells do not correlate directly with injection into other wells on C, T, and P Pads, and the overall injection rates into these wells (e.g., C-111, C-114, P-116, P-118, P-119, T-04, and T-07) are much less than A-106 injection rates during the same time period. Comparing laboratory Cl data from A pad wells to injection flow rates at SMGP over time prior to June 2021, indicates limited correlation between injected and produced fluid until A-106 injection began in June 2021.

Magnesium (Mg) concentrations decreased from an average ~0.023 to 0.004 mg/kg with many wells having concentrations too low for laboratory detection, indicating it is unlikely that meteoric waters (typically, high in HCO3 and Mg) are currently being pulled into the geothermal reservoir. Consistent with Cl increases, NCG concentrations in Pad A wells decreased over the same time period; both indicative of injection breakthrough. After A-106 injection was decreased and discontinued, NCG concentrations in most wells recovered to pre-A-106 levels.

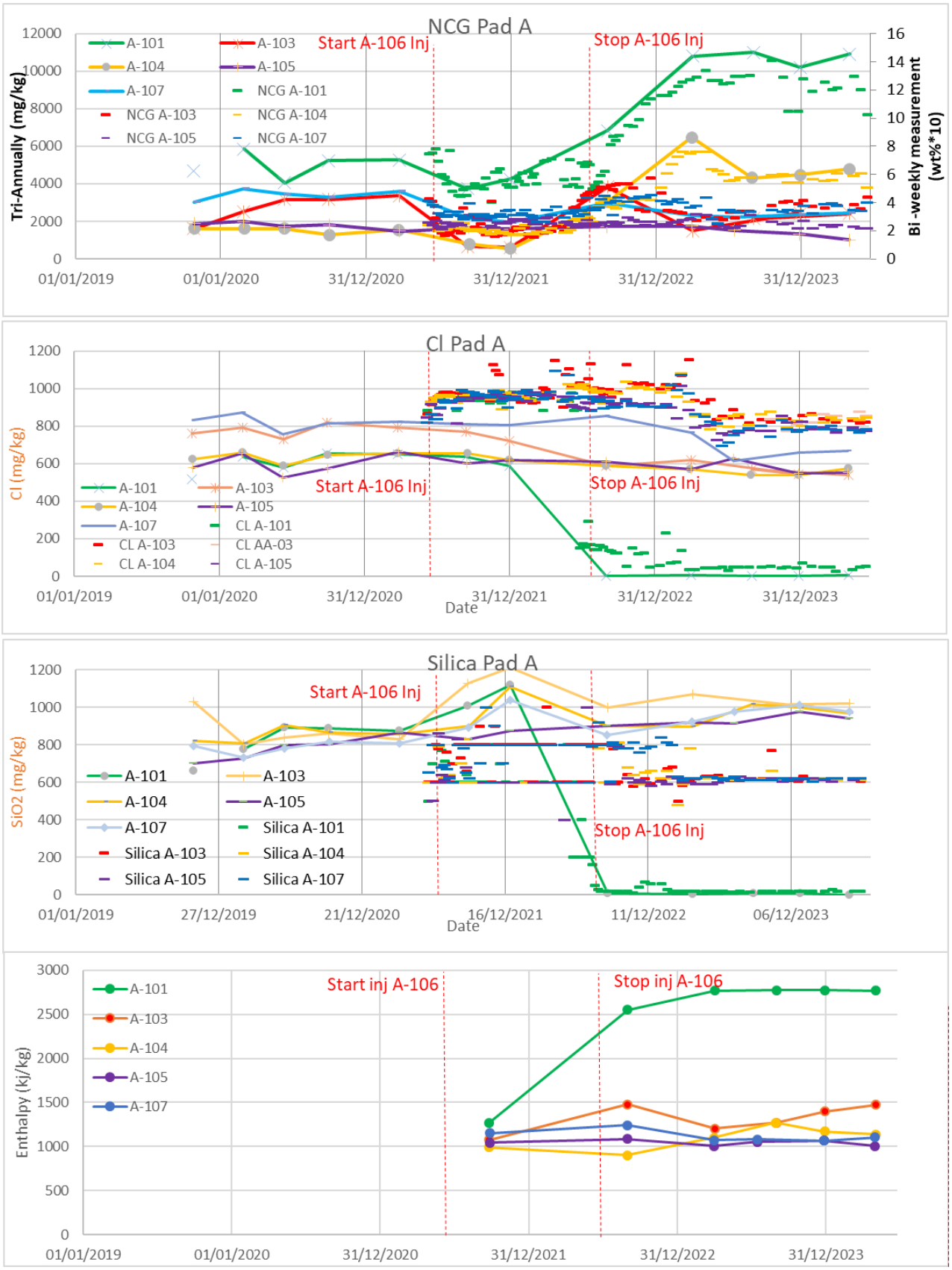

Figure 8: Bi-weekly sampling compared with Quarterly sampling.

3.3.2 Boiling, Excess Steam and Development of a Steam Cap

After recovering from being suppressed by injection breakthrough, total NCG concentrations increased from 2022 to 2023 with especially high increases in A-101 and A-104, and a slight increase in A-103 (Figure 8). Field geochemical data for A-101 indicates a large increase in NCG concentrations and sharp declines in Cl and SiO2 beginning in mid-2022 which correlate with the changes observed in laboratory geochemical data (8). The increases in NCG correlate with increases in enthalpy (from TFT) at A-101, and to a lesser extent A-103 and A-104 since injection into A-106 was curtailed. It appears that A-101 has begun producing near 100% steam since mid-2022 (when A-106 injection stopped) with a high flowing enthalpy of ~2500 kJ/kg. The original pressure-temperature surveys from initial flow tests from this well also indicated a possible steam zone. Liquid samples from this well, when collected, appear to be steam condensate (very low Cl and SiO2 concentrations). A-101 has the shallowest fluid entry of pad A wells and while the increases in NCG and enthalpy suggest development of a steam cap, the recent stabilization in A-104 suggests the steam cap may be limited. Note that one Pad A well, A-105, showed no decrease or increase in NCG or enthalpy.

4. CONCLUSION

The geochemical monitoring program at Sorik Marapi Geothermal field successfully monitoring key reservoir processes such as injection breakthrough and development of a steam zone in some wells and stabilization in other wells. While the quarterly geochemical monitoring with enthalpy measurements using TFT confirmed the field data, the field monitoring allowed for real time results enabling reservoir management to address issues including modification of injection strategy. After modifying injection strategy, the SMGP geochemical monitoring program was able to confirm recovery of production wells from the adverse impacts of injection breakthrough.

Sorik Marapi geochemistry programs was designed for a geothermal liquid dominated field with double flash brine ORC; the field chemistry used differences in Cl (higher concentration in injecton) and NCG (lower concentration in injection) between production and injection due to the flash system and steam loss. These program, especially the field measurements, should be adapted to the field as needed for different types of surface facilities The Bi-weekly field monitoring may be modified if the surface facilities change, wellfield production and injection strategies change and the parameters differentiating production and injection fluids change

REFERENCES

Carver, C., and Hidayat, R., 2020, The fluid geochemistry of the Sorik Marapi geothermal reservoir: GRC Transactions 44

Geologica, 2024, Resource Update of the Sorik Marapi Geothermal Project, Technical report to Sorik Marapi Geothermal Power, 07 June. (Unpublish)

Henley, R.Ws, Truesdell, A.H.. and Barton, P.B., 1984,“Fuiid-Mineral Equilibria in Hydrothermal Systems, Reviews in Economic Geology, Volume 1, Society of Economic Geologists.

Hidayat, R., Hendri, R., and Chandra, V., 2019, An Overview Geochemistry In Sorik Marapi Geothermal Field. The 7th Indonesia International Geothermal Convention & Exhibition (IIGCE) 2019

Hinz, N., Matson, G., Sussman, D., Haizlip, J., Turk, J., Carver, C., Fercho, S., Hendri, R., Siagian, H., Fishbin, A., Cumming, W.B., Letvin, A., and Milton, A., 2021, Conceptual Model Update of the Sorik Marapi Geothermal Prospect, Sumatra, Indonesia. GRC Transactions 45.

Hirtz, P.N., Kunzman, R. J. Broaddus, M.L., Barbita, J.A,, 2001, Developments in tracer flow testing for geothermal production engineering, Geothermics, Volume 30 Issue 6, December 2001, p 727-745.

Sarmiento, Z, and SMGP Staff, 2024, Resource Development and Performance Update: Sorik Marapi Geothermal Field, Madailing Natal, Panyambungan, North Sumatra, Proprietary Report, 24 pages.

Modelling Non-Condensable Gas Reinjection Geochemical Dynamics in Geothermal Fields: A Case Study of Ngā Tamariki, New Zealand

Yeftamikha Siahaan[1], Eylem Kaya[1], Dale E. Altar[1], John Mering[2], Denni Subekti[2], Ayu Utami[2], Roxanne Atayde[2], Kelly Melia[2], and Fabian Sepulveda[2]

[1]University of Auckland, Auckland, New Zealand
[2]Mercury Energy Ltd., New Zealand

yyef541@aucklanduni.ac.nz

Keywords: reactive transport model, TOUGHREACT, NCG reinjection, Ngā Tamariki

ABSTRACT

Ngā Tamariki geothermal field is located in the Taupo Volcanic Zone (TVZ), New Zealand, with current electricity production of 85 MWe from four binary units. To minimise the carbon emission, non-condensable gas (NCG) from one of their units has been injected back into the reservoir through reinjection wells.

Ngā Tamariki is operated with 100% reinjection distributed across north and south reinjection areas. A 1D radial multiple interacting continua (MINC) model was set up using TOUGHREACT v.4.13 to simulate chemical and mineralogical reactions occurring in the reservoir near the north reinjection area. The model calibration process aimed to simulate the reinjection history of the well using integrated geochemical and flow modelling. The model focuses on the reservoir rock near the NM9 reinjection well, which receives the most NCG injections, extending to the nearest production well (NM7), which is located ~1 – 1.5 km to the southeast. Several scenarios, ranging from 0% to 50% NCG reinjection rates, were investigated. The analysis included diagnostics for assessing mineral dissolution and precipitation and their overall effect on the reservoir porosity and permeability.

The 1D-radial model shows porosity-permeability increases near the reinjection well and decreases in the outer part. This trend was mainly due to the dissolution and precipitation trends of calcite and anhydrite. Different NCG reinjection scenarios show variations in calcite dissolution. A higher amount of NCG reinjection gives a higher dissolution of calcite near the wellbore due to the lower pH of the injection fluid. The porosity, permeability, and volume fraction of other minerals did not show any significant changes within different NCG reinjection scenarios.

1. INTRODUCTION

Geothermal is considered a clean source of energy, particularly when compared to fossil fuels. The average operational emission intensity of geothermal power plants in New Zealand is 76 $gCO_{2\text{-}eq}$/kWh. This is significantly lower than natural gas power plants, which release 390 $gCO_{2\text{-}eq}$/kWh (combined cycle) and 525 $gCO_{2\text{-}eq}$/kWh (open cycle), and coal power plants, which release 955 $gCO_{2\text{-}eq}$/kWh (Mclean & Richardson, 2019). Geothermal power plants emit various gases known as non-condensable gases (NCGs), of which CO2 is the main component. These NCG emissions from geothermal operations can be decreased by injecting them back into the reservoir. NCG reinjection could give positive impacts such as reservoir recharge, pressure support, steam production improvement, and permeability enhancement. However, it could also give negative impacts, such as a porosity and permeability decrease, NCG breakthrough to nearby production wells, and NCG leakage to the surface (Kaya & Zarrouk, 2017).

Several geothermal fields in the world have implemented NCG reinjection, including Hellisheidi (Aradóttir et al., 2015; Ratouis et al., 2022), Kızıldere (Erol et al., 2022), Umurlu (Yücetaş et al., 2018), Hijiori (Yanagisawa, 2010), Ogachi (Kaieda et al., 2009), and Coso (Kolar et al., 2015). In New Zealand, NCG reinjection has also been applied at Te Huka (Ruiz et al., 2021), Ngāwhā (Mclean et al., 2023), and Ngā Tamariki (Abd Ghafar et al., 2022). Te Huka and Ngāwhā have been reinjected with 100% of the NCG, while Ngā Tamariki has been reinjected with 25% of it (Mclean et al., 2023). While most of the fields have found no problems, several NCG reinjection projects have encountered issues, including scaling in production lines in Hijiori (Yanagisawa et al., 2007), CO_2 increases in the produced fluid in Ogachi (Pistone et al., 2011; Kaieda et al., 2009), and increases in operational costs in Coso (Kolar et al., 2015).

The Ngā Tamariki geothermal field is located in the Taupo Volcanic Zone (TVZ), New Zealand, producing 85 MWe from four binary units (Figure 1). Ngā Tamariki has a deep and hot reservoir (260-285°C), near-neutral fluid, high content of chloride (900-1000 mg/kg), with domination of meteoric water (Chambefort et al., 2016). There are three production wells and four reinjection wells. The reinjection wells are located in the south and north of the field, while the production wells are located in the centre of the field.

NCG reinjection has been implemented in Ngā Tamariki since mid-October 2021 (Abd Ghafar et al., 2022). NCG from one of the binary units, which constitutes 25% of the total NCG of the plants, is injected mainly into NM9, located in the northern part of the field. The NCG is dissolved together with the brine before the reinjection well. Abd Ghafar et al. (2022) reported that there were no issues found in Ngā Tamariki after almost one year of NCG reinjection. While the effect on the reservoir remains uncertain, a reactive transport model could provide a clearer understanding of how mineral solubility, porosity, and permeability in the reservoir might be affected. This paper will focus on the results of the 1D-radial model.

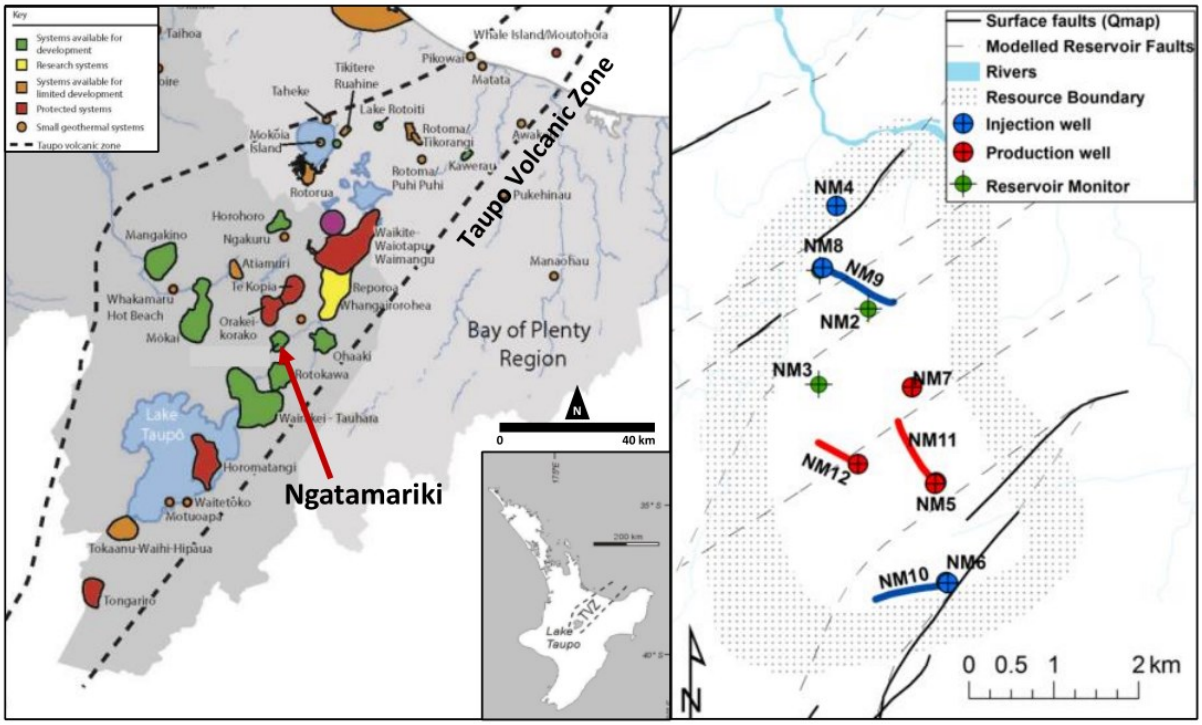

Figure 1: Left: Location of Ngā Tamariki geothermal field in the Taupo Volcanic Zone (TVZ), New Zealand (modified from Luketina et al., 2021); Right: Location of wells and resistivity boundary in Ngā Tamariki geothermal field (Quinao et al., 2017).

2. METHODOLOGY

2.1 Reactive Transport Model

The reactive transport model in this research was created using TOUGHREACT v.4.13 (Sonnenthal et al., 2021). TOUGHREACT is a programme for conducting numerical simulations that can simulate chemically reactive non-isothermal multiphase flow fluids in porous and fractured rock formations (Xu et al., 2006). It was developed by incorporating thermal-physical-geochemical conditions into the TOUGH2 simulator, enhancing its capability to model the interactions between fluids and rock matrices in complex geological systems under reservoir conditions. Numerous subsurface thermophysical and chemical processes are considered across a broad range of temperature, pressure, ionic strength, water saturation, pH, and Eh conditions. Mineral and fluid interaction can occur under equilibrium conditions or with kinetic rates. The simulation can be used to predict how the porosity and permeability of the formation change over time based on the precipitation and dissolution processes.

Additional chemistry calculations were also conducted using a separate programme called PHREEQC (Parkhurst & Appelo, 2013), a programme by the U.S. Geological Survey (USGS). PyTOUGH (Croucher, 2023) was used to create the model's grid, while TIM (Yeh et al., 2013) was used to visualise the grid structure.

2.2 Model Setup and Parameters

2.2.1 Model setup

A 1D-radial model of the first and major feedzone (FZ#1 in Figure 2) of the NM9 reinjection well was created to understand the chemical and mineralogical (volume fraction change) response of the reservoir to the NCG reinjection implementation. Figure 2 shows the stratigraphy, pressure and temperature (PT) data, and production casing depth with the location of the feedzones. The parameters used in the 1D-radial model followed the feedzone parameters, namely a thickness of 29.6 metres (rounded up to 30 metres) and pressure and temperature of the feedzone following the PT data. The model was constructed with two parts: the reservoir and the outer parts

(Figure 2). The reservoir part was created using multiple interacting continua (MINC) for a radius of 3 km. The outer part was created using a single porosity approach with a total radius of 50 km to prevent boundary effects. The injection rate followed the daily injection rate data of NM9, proportionate to the contribution of the feedzone.

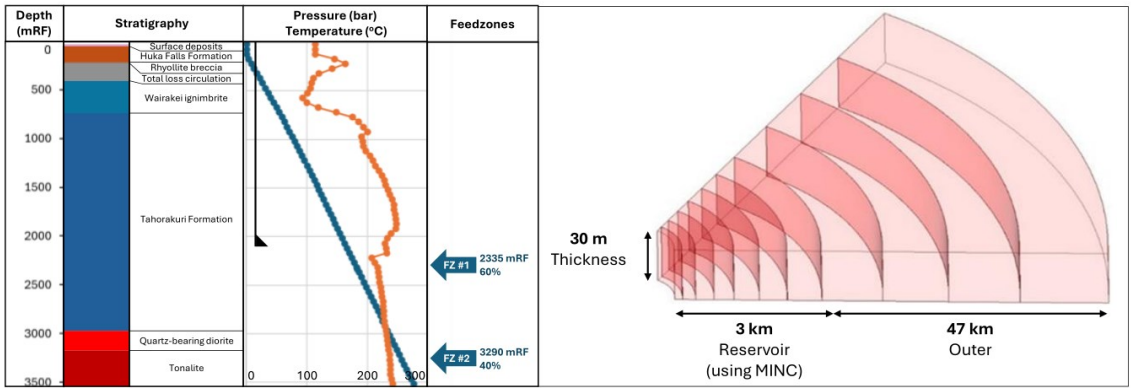

Figure 2: Left: NM9 stratigraphy log with PT data, production casing depth, and feedzone depth (compiled from Lewis et al. (2013) and Mercury (personal communication, February 2, 2024)); Right: An unscaled illustration of the 1D-radial model.

2.2.2 Fluid chemistry

The fluid chemistry used in the model was the reservoir and injection chemistry. The reservoir fluid chemistry data was obtained from the produced fluid chemistry of the nearest production well, NM7. This data was corrected to reflect the reservoir conditions using quartz geothermometer calculations. The pH of the reservoir chemistry was calculated using PHREEQC. The injected fluid chemistry consists of a mixture of brine and condensate, and the NCG chemistry data were calculated using the mass balance calculations. Furthermore, the bicarbonate (HCO_3^-) concentration was recalculated following the field pH measurements using PHREEQC. The fluid and NCG chemistry data are then combined and input into PHREEQC to get the pH for each model scenario. The reservoir and injected fluid chemistry used in this model can be seen in Tables 1 and 2, respectively.

Table 1: Reservoir-corrected produced fluid chemistry of NM7 (Mercury, personal communication, February 2, 2024).

	Concentration (ppm)	
Date	1/15/2019	8/2/2021
Fluid		
pH	6.119	6.149
Na^+	504.6	485.8
Cl^-	842.0	837.4
HCO_3^-	38.2	34.3
Ca^{2+}	2.6	2.6
SO_4^{2-}	7.4	9.0
Mg^{2+}	0.01	0.01
Fe^{2+}	0.01	0.02
K^+	112.6	108.1
$SiO_{2(aq)}$	623.1	642.3
AlO_2^-	0.3	0.2
Gas		
CO_2	2013.5	1904.7
H_2S	38.2	70.4
CH_4	21.5	18.3
H_2	0.1	0.1

2.2.3 Volume fraction of minerals

The volume fraction of minerals was determined following analysis by Sewell (2022) and from the NM9 geological report by Lewis et al. (2013) at the depth location of the feedzone. Table 3 shows the volume fraction of minerals used in the model. Although some of the minerals are initially not found in the mineralogy data, namely amorphous silica, chalcedony, smectite, and montmorillonite, they were still input into the model with a volume fraction of 0% to know the precipitation possibility of these minerals.

Table 2: Injected fluid chemistry. Besides the recalculated pH and bicarbonate, the chemistry data was obtained from Mercury (personal communication, February 2, 2024).

	Concentration (ppm)		
	0%	**25%**	**50%**
Fluid			
pH	5.52	5.23	5.08
Na^+	501.0	501.0	501.0
Cl^-	931.0	931.0	931.0
HCO_3^-	101.9	101.9	101.9
Ca^{2+}	2.9	2.9	2.9
SO_4^{2-}	10.3	10.3	10.3
Mg^{2+}	0.0	0.0	0.0
Fe^{2+}	0.5	0.5	0.5
K^+	107.0	107.0	107.0
$SiO_{2(aq)}$	688.0	688.0	688.0
AlO_2^-	0.8	0.8	0.8
Gas			
CO_2	533.2	928.6	1324.1
H_2S	66.2	75.1	84.0
CH_4	4.0	8.1	12.2
H_2	0.00001	0.00001	0.00001

2.2.4 Reactive surface area (RSA) of minerals

The RSA of the minerals was calculated using the same methodology reported in the TOUGHREACT module (Sonnenthal et al., 2021), which was calculated for each mineral for the fracture and matrix domains. The result of the calculation and the RSA used in the model can be seen in Table 3.

Table 3: Volume fraction and calculated RSA for each mineral.

Minerals	**Volume fraction**	**RSA (m^2/m^3)**	**RSA/1000**
Quartz	50%	1.414E+02	1.414E-01
Albite	2%	5.655E+00	5.655E-03
Calcite	7%	1.979E+01	1.979E-02
Chlorite	2%	5.655E+00	5.655E-03
Pyrite	2%	5.655E+00	5.655E-03
Illite	12%	3.393E+01	3.393E-02
Kaolinite	7%	1.979E+01	1.979E-02
Anhydrite	5%	1.414E+01	1.414E-02
Pyrophyllite	7%	1.979E+01	1.979E-02
Am-silica	0%	3.142E+02	3.142E-01
Chalcedony	0%	3.142E+02	3.142E-01
Smectite	0%	3.142E+02	3.142E-01
Montmorillonite	0%	3.142E+02	3.142E-01
Matrix	-	4.440E+03	-

2.2.5 Chemical reaction of minerals

The chemical reaction of minerals, with their related parameters, could affect the behaviour of the minerals. All minerals were assigned with kinetic reactions in this model. Table 4 shows the rate constants, activation energies, and rate laws for each mineral, which were mainly sourced from Altar & Kaya (2020), Palandri & Kharaka (2004), and Xu et al. (2007).

In the thermodynamic database of TOUGHREACT, the dissolution reaction of each mineral was also input. These chemical reactions were beneficial in determining which chemical species would affect the behaviour of minerals. Table 5 shows the summary of the chemical species associated with the minerals.

Table 4: Kinetic reaction parameters for minerals consisted of rate constants, activation energies, and rate laws (Altar & Kaya, 2020; Xu et al., 2007; and Palandri & Kharaka, 2004).

Mineral	Dissolution			Precipitation		
	Log k_{25}	E_a	Rate law	Log k_{25}	E_a	Rate law
Quartz	-13.99	87.7		-9.42	49.8	$a_{SiO_{2(aq)}}$
Albite	-10.16	65.0	$a_{H^+}^{0.457}$			
	-12.56	69.8				
	-15.60	71.0	$a_{H^+}^{-0.527}$			
Calcite	-0.30	14.4	$a_{H^+}^{\square}$	-2.15	51.9	$a_{Ca^{2+}}^{\square} a_{HCO_3^-}^{\square}$
	-5.81	23.5				
Chlorite	-11.11	88.0	$a_{H^+}^{0.5}$			
Pyrite	-4.55	56.9				
Illite	-12.60	14.0				
Kaolinite	-13.18	22.2				
Smectite	-12.78	35.0				
Montmorillonite	-14.41	48.0				
Anhydrite	-3.19	14.3				
Pyrophyllite	-12.40	29.0				
Amorphous silica				-9.42	49.8	$a_{SiO_{2(aq)}}$
Chalcedony				-9.42	49.8	$a_{SiO_{2(aq)}}$

Table 5: Summary of chemical species of each mineral's chemical reaction.

Mineral	Chemical species
Albite	Na^+, $SiO_{2(aq)}$, AlO_2^-
Calcite	H^+, Ca^{2+}, HCO_3^-
Chlorite	H^+, $SiO_{2(aq)}$, Fe^{2+}, Mg^{2+}, H_2O, AlO_2^-
Pyrite	$H_{2(aq)}$, H^+, Fe^{2+}, $H_2S_{(aq)}$
Illite	H^+, Mg^{2+}, K^+, $SiO_{2(aq)}$, H_2O, AlO_2^-
Kaolinite	H^+, $SiO_{2(aq)}$, H_2O, AlO_2^-
Anhydrite	Ca^{2+}, SO_4^{2-}
Pyrophyllite	H^+, $SiO_{2(aq)}$, AlO_2^-
Quartz	$SiO_{2(aq)}$
Am-silica	$SiO_{2(aq)}$
Chalcedony	$SiO_{2(aq)}$
Smectite	H_2O, Ca^{2+}, H^+, Mg^{2+}, $SiO_{2(aq)}$, AlO_2^-
Montmorillonite	H^+, Ca^{2+}, K^+, Na^+, Mg^{2+}, H_2O, $SiO_{2(aq)}$, AlO_2^-

2.3 Model scenarios

This research aims to investigate the differences between several NCG reinjection scenarios, namely 0% NCG reinjection, 25% NCG reinjection, and 50% NCG reinjection. The modelling period covers three periods: before NCG reinjection (2013-2021), current NCG

reinjection (2021-2024), and future NCG reinjection (2024-2034). A summary of the scenarios used in the model can be seen in Table 6.

Table 6: Scenarios that are being used in the model.

Period	Scenario 1: 0% NCG reinjection	Scenario 2: 25% NCG reinjection	Scenario 3: 50% NCG reinjection
Before NCG reinjection (2013-2021)	No additional NCG injection (only passive)	No additional NCG injection	No additional NCG injection
Current NCG reinjection (2021-2024)		25% NCG injection	25% NCG injection
Future NCG reinjection (2024-2034)			50% NCG injection

3. RESULTS AND DISCUSSION

3.1 Calibration Results

Calibration was conducted to ensure the model's parameters accurately represented field conditions. This was conducted by comparing the model results with measured parameters, e.g. pressure and chemistry concentration trends.

3.1.1 Pressure calibration

The initial pressure from the model was very high compared to the pressure from PT data. This high-pressure result was attributed to the thin layer thickness and the low permeability of the fracture. Modifications to the layer thickness or permeability were necessary to mitigate this pressure difference. It was decided not to change the thickness as it would differ from the condition of the feedzone being modelled. Instead, the permeability was modified to a higher value. This is a reasonable approach as the permeability data provided by Mercury (personal communication, February 2, 2024) represented the permeability of the rock medium in the reservoir, whereas only the feedzone being modelled is expected to have a much higher permeability. Therefore, the permeability values were increased by a factor of 5.5.

The pressure comparison can be seen in Figure 3. The model's result from the first grid of the radial model shows a close alignment with the pressure from PT data. The comparison between the model's results with wellhead pressure (WHP) also shows a similar trend, although not entirely identical. It was difficult to achieve a similar trend with WHP as the model represents only one feedzone group, while WHP is affected by all of the feedzones and processes inside the wellbore as well as from the potential connection to nearby production and reinjection wells.

The pressure data in Figure 3 also shows that the PT data and WHP do not change dramatically over time, which may indicate that there is no significant permeability loss or precipitation around the wellbore. This is valid even when the injection rate increased in early 2021. It seems that there is no significant injectivity loss in this well.

3.1.2 Chemistry calibration

Chemistry calibration was also conducted by comparing several chemical species, namely chloride (Cl^-), sulphate (SO_4^{2-}), and bicarbonate (HCO_3^-). Chemical concentrations from the grid corresponding to the location of NM7 were compared with chemical concentrations from field data under reservoir conditions. The grid of NM7 was chosen by using the closest distance between the modelled feedzone of NM9 to the NM7 well, measured using TIM for visualising the well's trajectories.

The model gives a chloride value of around 910 ppm, which closely matches the field value of around 850 ppm. Sulphate concentration from the model was relatively high, at around 300 ppm, while the field data is only around 10 ppm. Bicarbonate concentration from the model also shows a higher value, around 150 ppm, which is higher than the field data of 40 ppm. Introducing a natural flux with a rate of 3.5E-5 kg/s.m2 and water enthalpy at reservoir temperature was considered to observe its effect on the model's sulphate and bicarbonate value. After a natural flux was introduced, the sulphate and bicarbonate concentrations from the model decreased to around 40 ppm and 90 ppm, respectively. The comparison of the chemical concentrations can be seen in Figure 4.

Further reducing these concentrations would require reducing the injection rate and increasing the natural flux rate. However, these adjustments were not conducted to prevent further deviation of the model from the reservoir conditions and potential interference with other chemistry calibrations. Notably, minerals associated with sulphate and bicarbonate, such as anhydrite and calcite, are more likely to be overestimated. This difference between model and field data could be due to the distance between NM9 and NM7. They may have been too close for choosing the grid. Using a longer distance would result in lower concentrations.

3.2 Effects on the volume fraction of minerals

Each mineral demonstrates unique behaviour depending on its chemical reaction parameters, including the kinetic rate constant, activation energy, assigned reactive surface area, and reaction with different chemical species. Different NCG reinjection scenarios were also expected to give distinct results because of variations in their injection chemistry, particularly in gas composition and pH (Table 2).

This section will discuss the trends in several minerals within the radial distance at the end of the simulations with all scenarios. The focus will be on the changes in each mineral's volume fraction in the fracture domain. Therefore, the results in Figure 5 represent the mineral's volume fraction in the fracture.

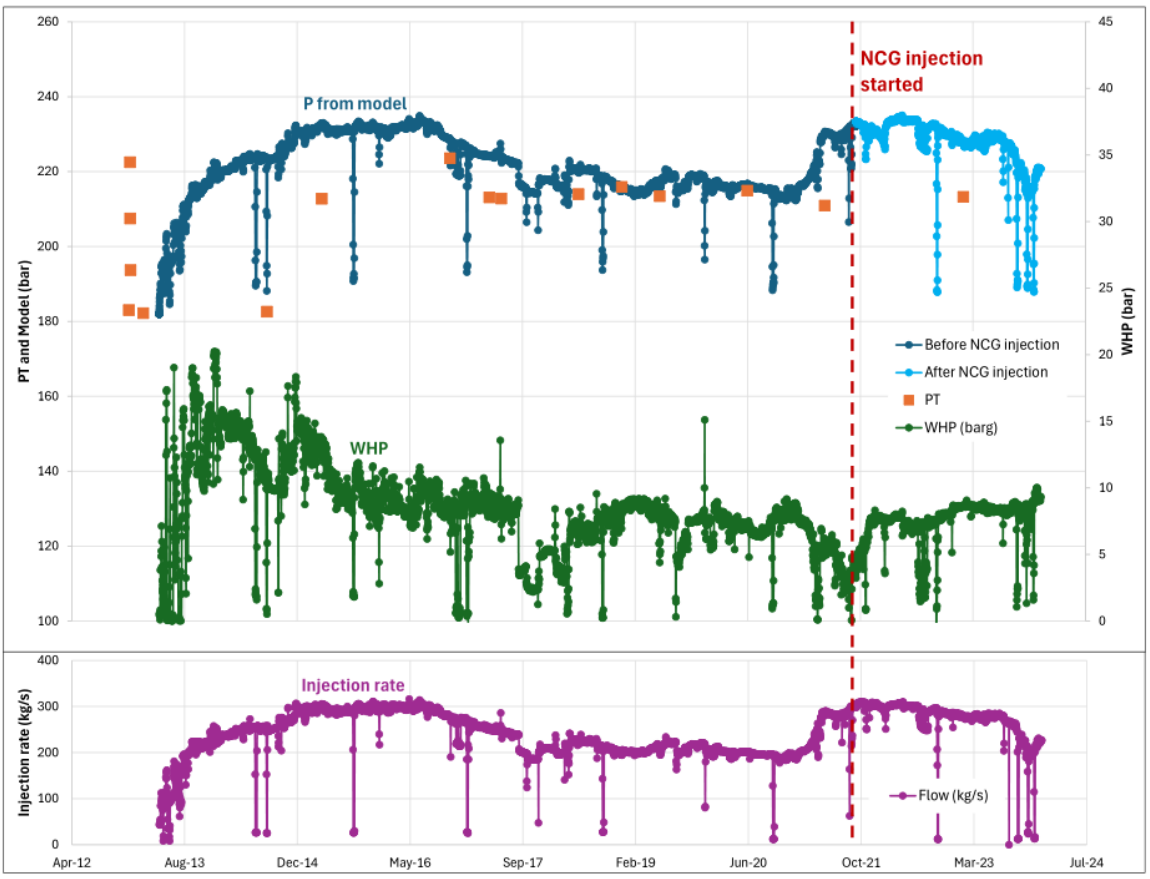

Figure 3: Pressure comparison between the model's result, PT logging data, and WHP with injection rate plotted below the pressure comparison.

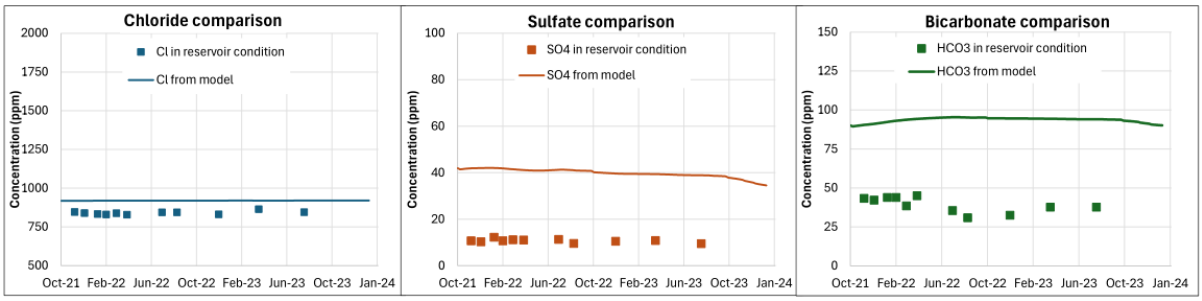

Figure 4: Chemical concentration comparison between the model's result and field data in reservoir condition.

The result of calcite is given in Figure 5A. Calcite shows a dissolving trend within around 1000 m near the wellbore, as indicated by a decrease in its volume fraction. Beyond 1000 m, calcite shows minimal precipitation to no change. This precipitation was due to the presence of calcium ions in both the injected fluid and the reservoir. The comparison between different NCG reinjection scenarios shows that only calcite gives different results with different NCG reinjection scenarios (Figure 5A). An increase in the NCG reinjection amount leads to higher CO2 and subsequently lowers the pH (Table 2). The lower pH promotes calcite dissolution in the near wellbore area, contributing to an increase in porosity and permeability.

Anhydrite shows a dissolving trend around 800 m from the injection well (Figure 5B). After 800 m, anhydrite shows a precipitation trend. The precipitation's magnitude is much higher than the calcite's precipitation trend. This trend of anhydrite shows that the dissolved anhydrite in the near wellbore is precipitating in the outer area. This anhydrite precipitation also aligns with the evidence of anhydrite scaling found in the adjacent monitoring well NM2 (Buscarlet et al., 2016). Anhydrite shows similar results across different NCG reinjection scenarios (Figure 5B). Despite variations in H2S concentrations among different NCG reinjection scenarios (Table 6), it does not appear to affect the anhydrite precipitation. Anhydrite formation requires calcium (Ca2+) and sulphate (SO42-). According to the reaction in Equation (1) below, H2S would need to be oxidised to become SO42-. This

reaction was input into the model's thermodynamic database. Due to the field's closed system without any contact with the atmosphere, no oxygen was found in the system.

$$H_2S + 2O_2 = SO_4^{2-} + 2H^+ \quad (1)$$

Pyrite only shows precipitation near the wellbore (Figure 5C). Different NCG reinjection scenarios yield similar results, as the variation in H2S injection is very small (Table 2). Amorphous silica shows slight precipitation (Figure 5D), while quartz does not change significantly despite its high-volume fraction. It shows insignificant dissolution in the near wellbore and precipitation in the outer area. This slow change was due to its low rate constant (Table 4). Clay minerals, namely kaolinite and smectite, show a precipitation trend near the wellbore. Some minerals do not show any or minimal changes in the model (below 0.01% of change), namely albite, chalcedony, chlorite, pyrophyllite, illite, and montmorillonite. Although if looked at closely, some of the minerals show a precipitation trend near the wellbore, such as chalcedony, illite, and montmorillonite, and some others show a dissolution trend, such as albite and chlorite, it was decided to neglect it as the changes were not significant. Pyrophyllite, on the other hand, shows no change in its volume fraction.

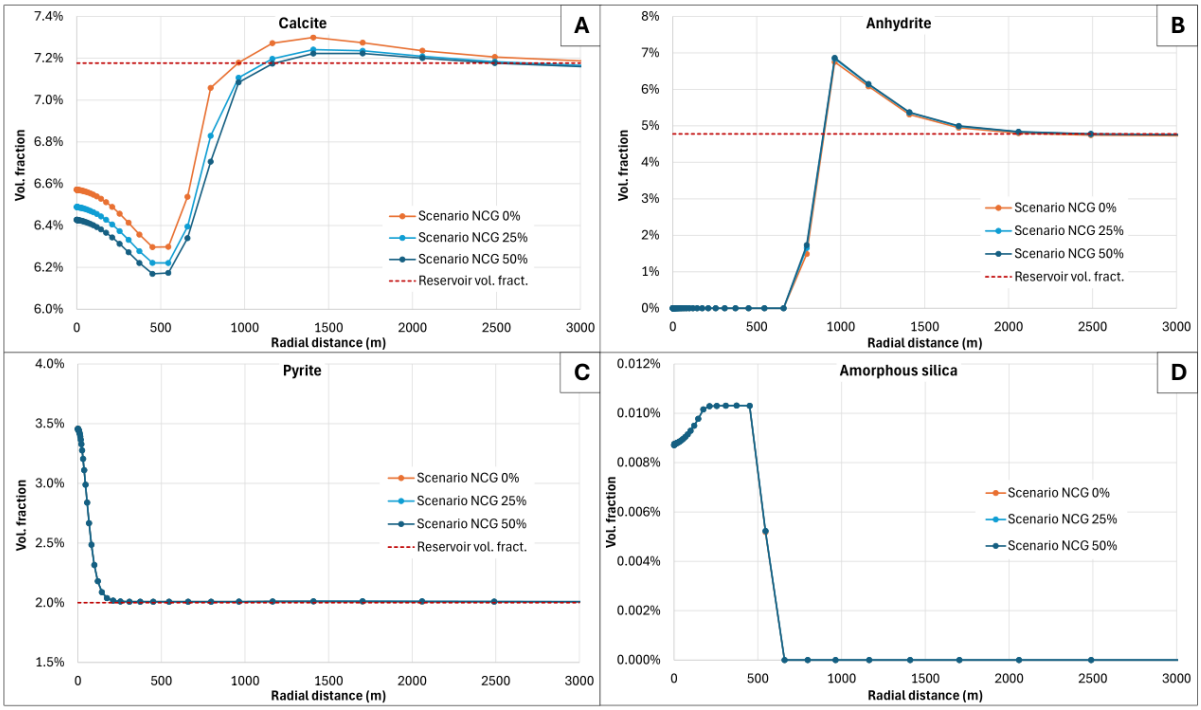

Figure 5: Volume fraction change within radial distance of calcite, anhydrite, pyrite, and amorphous silica at the end of the model's running time in 2034.

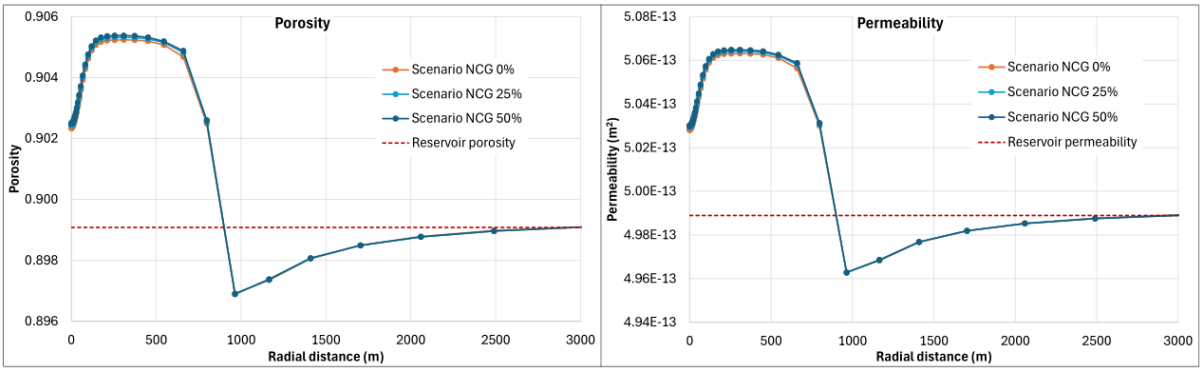

Figure 6: Porosity (left) and permeability (right) value within the radial distance at the end of the model's running time in 2034.

3.3 Effects on porosity and permeability

Changes in the mineral volume fraction contribute to the porosity and permeability of the rock. Porosity and permeability within the radial distance at the end of the model's run time in 2034 can be seen in Figure 6. Both porosity and permeability show a similar trend, increasing from the wellbore to around 900 m and decreasing in

the later part. Calcite and anhydrite are two main minerals affecting porosity and permeability trends. The dissolution of calcite and anhydrite in the near wellbore area increases the porosity and permeability. In the outer area, anhydrite precipitation decreases the porosity and permeability.

3.4 Effects on chemical concentration

The chemical concentration and minerals' volume fractions influence each other. A high concentration of specific chemical species may result in the deposition of certain minerals and, subsequently, a decrease in the chemical concentration. The dissolution of minerals can lead to an increase in some chemical concentrations. The relationship between chemical concentrations and minerals'volume fraction is governed by the mineral's kinetic reaction parameters (Table 4) and the chemical reactions (Table 5). This section will further discuss several key minerals undergoing significant changes, such as calcite, anhydrite, and pyrite, and their interactions with chemical concentrations (Figure 7).

3.4.1 Calcite

Calcite is mainly affected by pH, bicarbonate, carbon dioxide, and calcium concentration. This is because the chemical reaction of calcite was affected by these components in their kinetic reactions (Table 4) and chemical reactions (Table 5). pH, bicarbonate, and carbon dioxide are interrelated through the equilibrium reaction of Equation (2). The calcite dissolution reaction is shown in Equation (3). Both equations are input into the thermodynamic database of TOUGHREACT.

$$CO_{2(aq)} + H_2O \rightleftharpoons H^+ + HCO_3^- \quad (2)$$

$$Calcite + H^+ \rightleftharpoons Ca^{2+} + HCO_3^- \quad (3)$$

Figure 7 shows the relation between calcite and related chemical concentrations. According to the equilibrium reaction of dissolved carbon dioxide and bicarbonate (Equation 2), an increase in dissolved carbon dioxide would decrease the pH, favouring calcite dissolution. The dissolution of calcite, in turn, would increase the calcium and bicarbonate concentration. Due to the increase of bicarbonate, the dissolved carbon dioxide would decrease to fulfil the equilibrium condition of Equation (2). Dreybrodt et al. (1997) mentioned that the reaction described in Equation (2) limits the precipitation rate of calcite due to its slow kinetics.

The bicarbonate concentration increases until saturation conditions are reached, at this point, calcite dissolution stops, followed by a small precipitation of calcite. Due to its retrograde solubility (Zarrouk & McLean, 2019), calcite precipitation is also affected by the temperatures, which will increase towards the outer parts of the wellbore. The solubility of calcite was assigned in the thermodynamic database. Calcite precipitation is also followed by a decrease in bicarbonate and calcium concentrations, following Equation (3).

3.4.2 Anhydrite

Anhydrite is affected by calcium and sulphate concentrations, as detailed in its kinetic reaction (Table 4) and chemical reaction (Table 5). Figure 7 is plotted to better understand the relationship between anhydrite and related chemical concentrations. According to Equation (4), anhydrite dissolves and increases calcium and sulphate concentrations near the wellbore. This increase continues until calcium and sulphate reach oversaturation, at which point anhydrite precipitates. Temperature also affects the precipitation of anhydrite, following the retrograde solubility of anhydrite (Zarrouk & McLean, 2019).

$$Anhydrite \rightleftharpoons Ca^{2+} + SO_4^{2-} \quad (4)$$

As explained in section 3.2, different NCG reinjection scenarios with varying hydrogen sulphide concentrations do not affect the precipitation of anhydrite. This is due to the need for oxygen to oxidise the hydrogen sulphide into sulphate that is needed to form anhydrite (Equation 1).

3.4.3 Pyrite

According to its chemical reaction, Pyrite is affected mainly by iron and hydrogen sulphide (Table 5 and Equation 5). Due to its fast kinetic rate (Table 4), pyrite only precipitates near the wellbore, followed by the decreasing trend of iron and hydrogen sulphide (Figure 7).

$$Pyrite + H_{2(aq)} + 2H^+ \rightleftharpoons Fe^{2+} + H_2S_{(aq)} \quad (5)$$

3.5 Effects throughout times

To better understand how each NCG reinjection scenario affects the overall volume fraction, the net change through time for the future model at NM9 (first grid) and at the estimation of NM7 were plotted (Figure 8). Based on the charts, an increase in net volume fraction happened in both NM9 and NM7 wells, with a slightly higher increase in NM7. Different NCG reinjection scenarios gave different results only in NM9, where increased NCG would lower the net volume fraction increase.

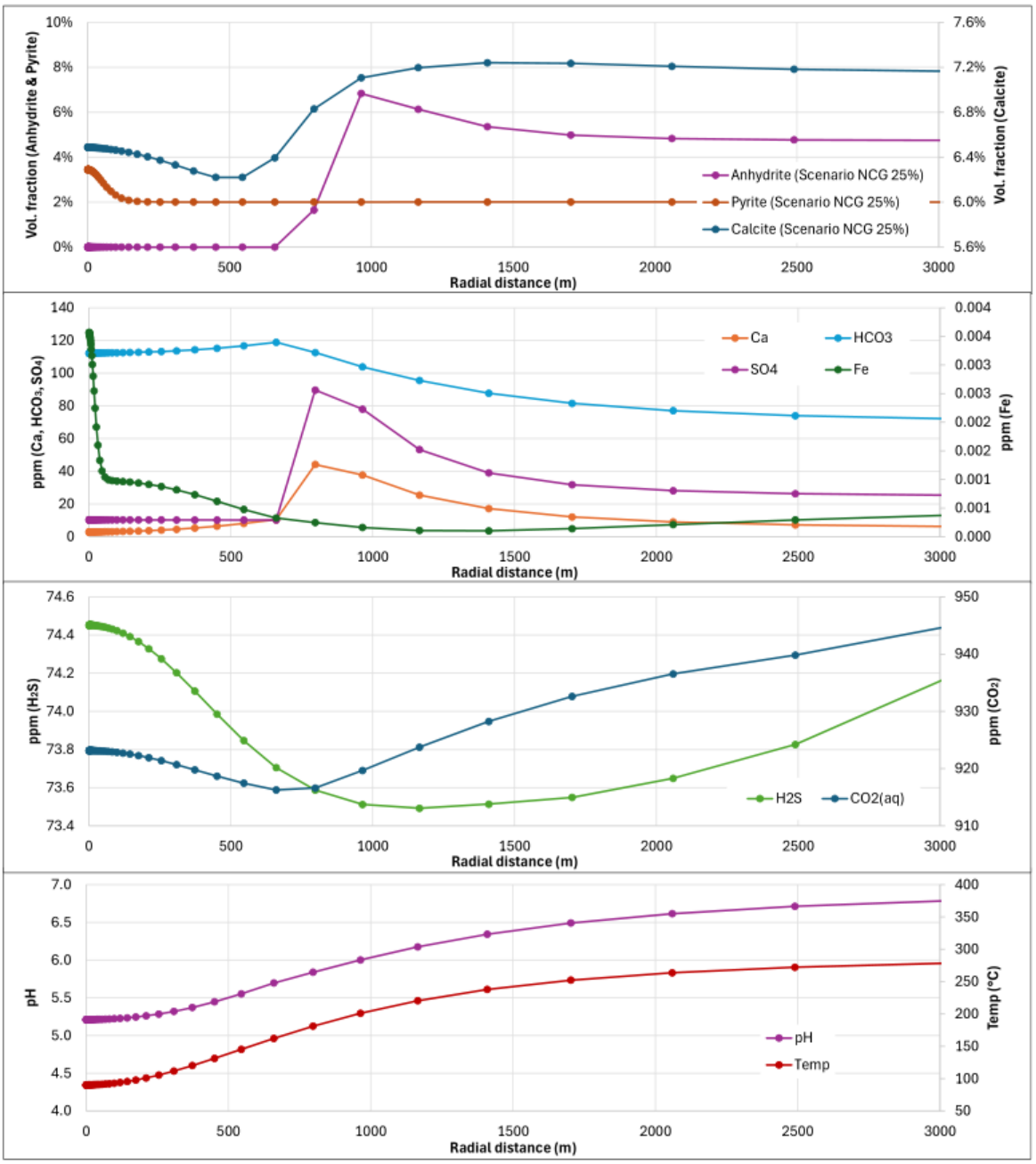

Figure 7: Volume fraction trend of calcite, anhydrite, and pyrite with related chemical species concentrations (Ca, HCO3-, SO42-, Fe, H2S, and CO2), pH, and temperature within the radial distance from the wellbore.

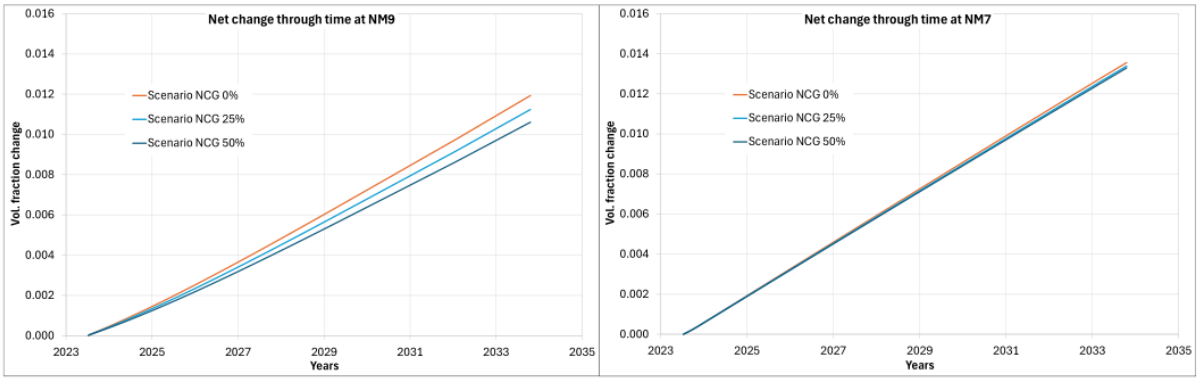

Figure 8: Left: net change through time at NM9; Right: net change through time at NM7.

4. CONCLUSION

The reactive transport models presented in this work evaluate the effects of the NCG reinjection on the Ngā Tamariki reservoir. The NCG is mainly reinjected to NM9 reinjection well located in the northern part of the Ngā Tamariki geothermal field. The nearest production well, NM7, was also included in the model to evaluate whether NCG reinjection has any influence on production.

The 1D-radial model shows a varying trend of porosity and permeability along the radial distance. Near the NM9 wellbore, porosity and permeability increase, mainly due to the dissolution of calcite and anhydrite. Conversely, the porosity and permeability decrease in the outer region due to anhydrite precipitation. Different NCG reinjection scenarios of 0%, 25%, and 50% of NCG reinjection were also modelled. These scenarios did not show significant differences in porosity and permeability. However, calcite dissolution showed differences for each scenario. Higher amounts of NCG reinjection resulted in increased calcite dissolution in the vicinity of the wellbore due to the lower pH of the injection fluid. On the other hand, anhydrite distribution did not show any significant variations across the different NCG reinjection scenarios. The increase of H2S concentrations did not affect the precipitation of anhydrite as the additional H2S is not oxidised to SO42- due to anoxic conditions in the reservoir.

ACKNOWLEDGEMENT

The authors would like to thank Mercury NZ Ltd. for the provision of field data, permission to publish, and for the support and discussions during this research. We also thank the NZ Ministry of Business, Innovation and Employment for funding the work through the MBIE Research Programme: UOAX2211 “Reversing Carbon Emissions in the Geothermal Energy Industry: Template for Emission-Intensive Industries” projects.

REFERENCES

Abd Ghafar, S., Allan, G., Ferguson, A., Siega, F., Rivera, M., & Murphy, B. (2022). Non Condensable Gas Reinjection Trial at Ngatamariki Geothermal Power Plant. *Proceedings 44th New Zealand Geothermal Workshop*.

Altar, D. E., & Kaya, E. (2020). Numerical modelling of the interaction between geothermal injectate-non condensable gas solutions and greywacke. *International Journal of Greenhouse Gas Control*, 94. https://doi.org/10.1016/j.ijggc.2019.102922

Aradóttir, E. S. P., Gunnarsson, I., Sigfússon, B., Gunnarsson, G., Júliusson, B. M., Gunnlaugsson, E., Sigurdardóttir, H., Arnarson, M. T., & Sonnenthal, E. (2015). Toward Cleaner Geothermal Energy Utilization: Capturing and Sequestering CO2 and H2S Emissions from Geothermal Power Plants. *Transport in Porous Media*, 108(1), 61–84. https://doi.org/10.1007/s11242-014-0316-5

Buscarlet, E., Richardson, I., Addison, S., Moon, H., & Quinao, J. (2016, November 23). Geochemical modelling of plant and reservoir processes at the Ngatamariki geothermal field. *Proceedings 38th New Zealand Geothermal Workshop*.

Chambefort, I., Buscarlet, E., Wallis, I. C., Sewell, S., & Wilmarth, M. (2016). Ngatamariki Geothermal Field, New Zealand: Geology, geophysics, chemistry and conceptual model. *Geothermics*, 59, 266–280. https://doi.org/10.1016/j.geothermics.2015.07.011

Croucher, A. (2023). *PyTOUGH user’s guide*.

Dreybrodt, W., Eisenlohr, L., Madry, B., & Ringer, S. (1997). Precipitation kinetics of calcite in the system CaCO3 - H2O - CO2: The conversion to CO2 by the slow process H+ + HCO3- → CO2 + H2O as a rate limiting step. *Geochimica et Cosmochimica Acta*, 61(18), 3897–3904. https://doi.org/10.1016/s0016-7037(97)00201-9

Erol, S., Akın, T., Başer, A., Saraçoğlu, Ö., & Akın, S. (2022). Fluid-CO2 injection impact in a geothermal reservoir: Evaluation with 3-D reactive transport modeling. *Geothermics*, 98. https://doi.org/10.1016/j.geothermics.2021.102271

Kaieda, H., Ueda, A., Kubota, K., Wakahama, H., Mito, S., Sugiyama, K., Ozawa, A., Kuroda, Y., Sato, H., Yajima, T., Kato, K., Ito, H., Ohsumi, T., Kaji, Y., & Tokumaru, T. (2009). Field experiments for studying on CO2 sequestration in solid minerals at the Ogachi HDR geothermal site, Japan. *Proceedings, Thirty-Fourth Workshop on Geothermal Reservoir Engineering*.

Kaya, E., & Zarrouk, S. J. (2017). Reinjection of greenhouse gases into geothermal reservoirs. *International Journal of Greenhouse Gas Control*, 67, 111–129. https://doi.org/10.1016/j.ijggc.2017.10.015

Kolar, M., Osgood, S., & Echt, W. (2015). Coso Case Study: 22 Years of Reliable Sulfur Removal. In *GRC Transactions* (Vol. 39).

Lewis, B., Chambefort, I., Rae, A. J., & Sanders, F. (2013). Geology of Well NM9, *Ngatamariki Geothermal Field*.

Mclean, K., Montague, T., Alcaraz, S., Daysh, S., Doorman, P., Luketina, K., Tsui, K., White, B., & Zarrouk, S. J. (2023, April 17). 2020-2023 New Zealand Country Update. *Proceedings World Geothermal Congress 2023*. https://www.nzgeothermal.org.nz/news--

Mclean, K., & Richardson, I. (2019, November 23). Greenhouse gas emissions from New Zealand geothermal power generation in context. *Proceedings 38th New Zealand Geothermal Workshop*.

Palandri, J. L., & Kharaka, Y. K. (2004). *A compilation of rate parameters of water-mineral interaction kinetics for application to geochemical modeling*.

Parkhurst, David. L., & Appelo, C. A. J. (2013). *Description of Input and Examples for PHREEQC Version 3-A Computer Program for Speciation, Batch-Reaction, One-Dimensional Transport, and Inverse Geochemical Calculations*. http://www.hydrochemistry.eu

Pistone, S., Stacey, R., & Horne, R. (2011). The significance of CO2 solubility in geothermal reservoirs. *Proceedings, Thirty-Sixth Workshop on Geothermal Reservoir Engineering*.

Ratouis, T. M. P., Snæbjörnsdóttir, S., Voigt, M. J., Sigfússon, B., Gunnarsson, G., Aradóttir, E. S., & Hjörleifsdóttir, V. (2022). Carbfix 2: A transport model of long-term CO2 and H2S injection into basaltic rocks at Hellisheidi, SW-Iceland. *International Journal of Greenhouse Gas Control*, 114. https://doi.org/10.1016/j.ijggc.2022.103586

Ruiz, N. C., Mclean, K., Richardson, I., Misa, T., Ferguson, A., Altar, D. E., & Kaya, E. (2021, November 23). Passive NCG reinjection at Te Huka geothermal binary power plant. *Proceedings 43rd New Zealand Geothermal Workshop*.

Sewell, S. (2022). *Geologic controls on seismic velocity from well logs and seismic tomography at the Rotokawa and Ngatamariki Geothermal Fields, New Zealand*. Victoria University of Wellington.

Sonnenthal, E., Spycher, N., Xu, T., & Zheng, L. (2021). *TOUGHREACT V4.13-OMP & TReactMech V1.0*.

Xu, T., Apps, J. A., Pruess, K., & Yamamoto, H. (2007). Numerical modeling of injection and mineral trapping of CO2 with H2S and SO2 in a sandstone formation. *Chemical Geology*, 242(3–4), 319–346. https://doi.org/10.1016/j.chemgeo.2007.03.022

Xu, T., Sonnenthal, E., Spycher, N., & Pruess, K. (2006). TOUGHREACT - A simulation program for non-isothermal multiphase reactive geochemical transport in variably saturated geologic media: Applications to geothermal injectivity and CO2 geological sequestration. *Computers and Geosciences*, 32(2), 145–165. https://doi.org/10.1016/j.cageo.2005.06.014

Yanagisawa, N. (2010). Ca and CO 2 Transport and Scaling in the Hijiori HDR System, Japan. *Proceedings World Geothermal Congress*, 25–29.

Yanagisawa, N., Matsunaga, I., & Sugita, H. (2007). Estimation of mineral transportation in HDR circulation test. *Proceedings, Thirty-Second Workshop on Geothermal Reservoir Engineering*.

Yeh, A., Croucher, A. E., & O'sullivan, M. J. (2013). TIM-yet another graphical tool for TOUGH2. *35th New Zealand Geothermal Workshop*.

Yücetaş, İ., Ergiçay, N., & Akın, S. (2018). Carbon Dioxide Injection Field Pilot in Umurlu Geothermal Field, Turkey. In *GRC Transactions* (Vol. 42).

Zarrouk, S. J., & McLean, K. (2019). Operation and management of geothermal wells. *Geothermal Well Test Analysis*, 217–255. https://doi.org/10.1016/B978-0-12-814946-1.00009-8

Transient Heat Conduction Modelling for Slim and Large Diameter Geothermal Well: A Case Study from Okuaizu Field, Tohoku, Japan

Ken Prabowo

Baker Hughes

Keywords: Transient Heat Conduction, Geothermal Well Modelling, Pressure and Temperature Survey (PTS), Thermal Conductivity Calibration

ABSTRACT

Japan is set to triple its geothermal power generation to 1.6 GW by 2030. Due to the Strategic Energy Plan and emergence of Advanced Geothermal System, there has been increasing focus on small-scale plants (<7.5 MW) that offers shorter development timeline and minimum environmental impact assessment. Unlike the traditional focus on high temperature sources, the situation may require past exploration well to be revisited. Amongst the data are pressure and temperature profiles that plays a pivotal role in locating & characterizing potential feed zones, designing well & facility and most importantly determining project feasibility. However, geological complexity of the island poses a challenge in terms of acquiring and apprehending the temperature profile.

This paper is meant to show how transient heat conduction modelling is able to be utilized to better understand the temperature gradient from PTS survey both in slim hole and large diameter well. The slim holes have measurement from different time and meant to calibrate the heat conduction parameters including the bottom hole temperature and formation heat transmissivity. The selected larger hole diameter wellbore has fluctuations in the PTS survey and the transient temperature modelling is meant to eliminate the conducted heat and give insight into other possible heat transmission mechanism such as convection.

The result shows the workflow can match the temperature in shallow T-1 and deeper OA-1 by a margin of <5%. While in larger diameter wellbore such as N-17t and N-18t, the temperature profile was able to match the trend especially in the shallow section while the lower zones seem to be influenced by convection that increases the temperature beyond the temperature conduction model. The convection zones could be further matched by increasing the thermal conductivity to represent heat exchange through fluid. In conclusion, the workflow could be further utilized to better understand PTS survey and bring more insight that ultimately would help in developing the geothermal fields.

1. INTRODUCTION

Pressure and temperature survey or PTS are performed frequently in a geothermal operation. From time to time, measurement with fluctuating gradient that deviates from the linear geothermal gradient are encountered. More than often, these “fluctuations” are ignored even though the subsurface temperature distribution has a far-reaching consequence to exploration and development strategy of a geothermal asset. Heat conduction modelling could be utilized to gain better understanding of the temperature gradient and this paper is meant to evaluate and showcase how this near wellbore physics could be utilized to improve our understanding on wellbore dynamics.

2. METHODOLOGY

The basis of thermal flux is based on one dimensional Fourier’s Law that could be formulated as below.

$$\frac{Q}{\Delta t} = -kA\frac{\Delta T}{\Delta x}$$

Q is the net heat (energy) transfer, Δt is the time taken, ΔT is the difference in temperature between the cold and hot sides, Δx is the thickness of the material conducting heat (distance between hot and cold sides), k is the thermal conductivity, and A is the surface area of the surface emitting heat.

The paper utilize in house software that has adapted the heat flux equation to wellbore condition. Surface emitting heat is calculated based on the inputted wellbore schematics and thermal conductivities of each heat conducting material are defined separately as shown in Figure 1.

Overall wellbore simulation could be illustrated in Figure 2. Geothermal gradient are assumed to be constant leaving the fluid temperature in the wellbore to be solved through the iterations. For this exercise, transient simulation would be performed for maximum duration of 5 days.

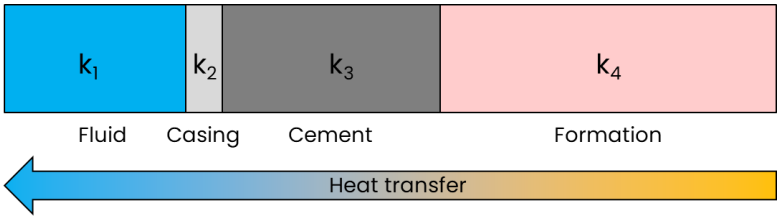

Figure 1: Heat flow patch from formation to wellbore with different heat conductivity.

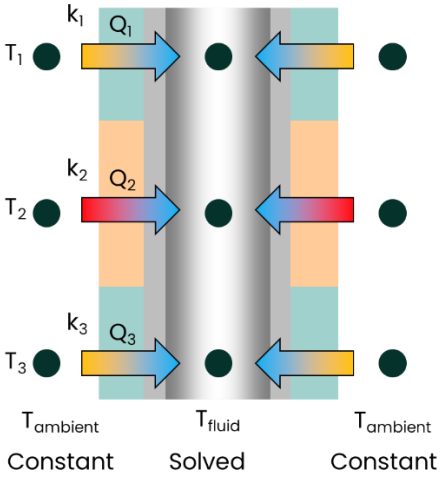

Figure 2: Illustration of 1D heat flux model with constant temperature and fluid temperature to be solved.

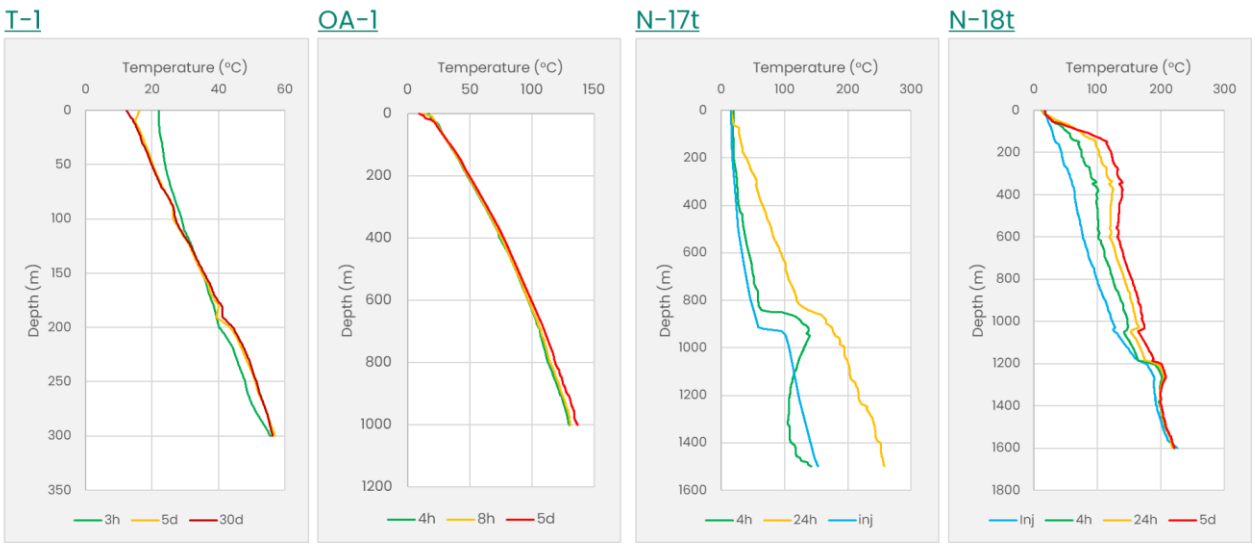

Figure 3: PTS surveys from T-1, OA-1, N-17t and N-18t.

3. OKAIZU FIELD OVERVIEW

The Okuaizu Geothermal Field is located approximately 35 km southwest of the active volcano Mt. Bandai. The field has been extensively studied since 1974. The commercial power station has started operation on 1995 with capacity of 65 MW. There are publicly available and suitable dataset for this research. The dataset includes completion, well trajectory, stratigraphy & production/injection history. There are four well that has been selected based on the hole size and distinct pressure measurement: slim hole: T-1 & OA-1 and large diameter wellbore: N-17t & N-18t. The digitized PTS surveys from Garg & Combs (2002) are shown in Figure 3. PTS surveys from these well would be used to calibrate the heat flux model.

4. RESULT

4.1 T-1 Slim Hole

T-1 is a slim hole with a depth of 300 meter. Available PTS survey are done within 3 hours, 5 days and 30 days. The trend indicates a single linear geothermal gradient. Measured temperature can be matched using default thermal conductivity of 1.3 BTU/(hr.ft.°F). Surface or near surface temperature initially comes from the injection inlet and it shifted to geothermal gradient after the operation stops. The temperature stabilized after approximately 12 hours. Prior to reaching state of equilibrium (such as measurement in the third hours), temperature in wellbore has not reflected the geothermal gradient of the formation.

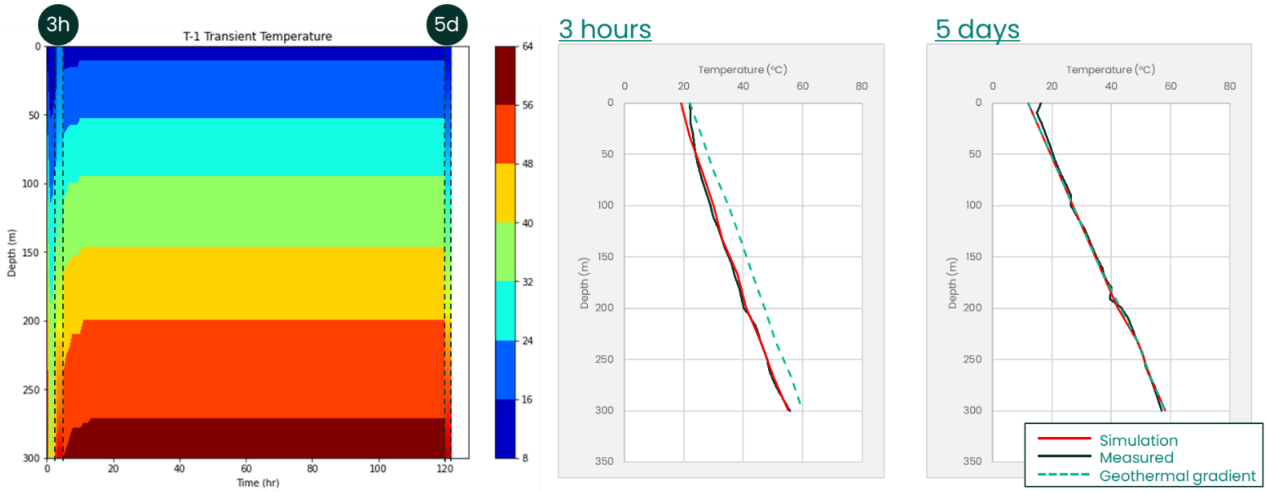

Figure 4: Transient temperature result for T-1.

4.2 OA-1 Slim Hole

OA-1 is a slim hole with a depth of 1,000 meter. Available PTS survey was done in 4 hours, 8 hours and 5 days. The curving temperature along the wellbore indicates changes in geothermal gradient. The measure temperature could be matched by using default thermal conductivity and three different temperature gradients. The temperature stabilized after approximately 100 hours.

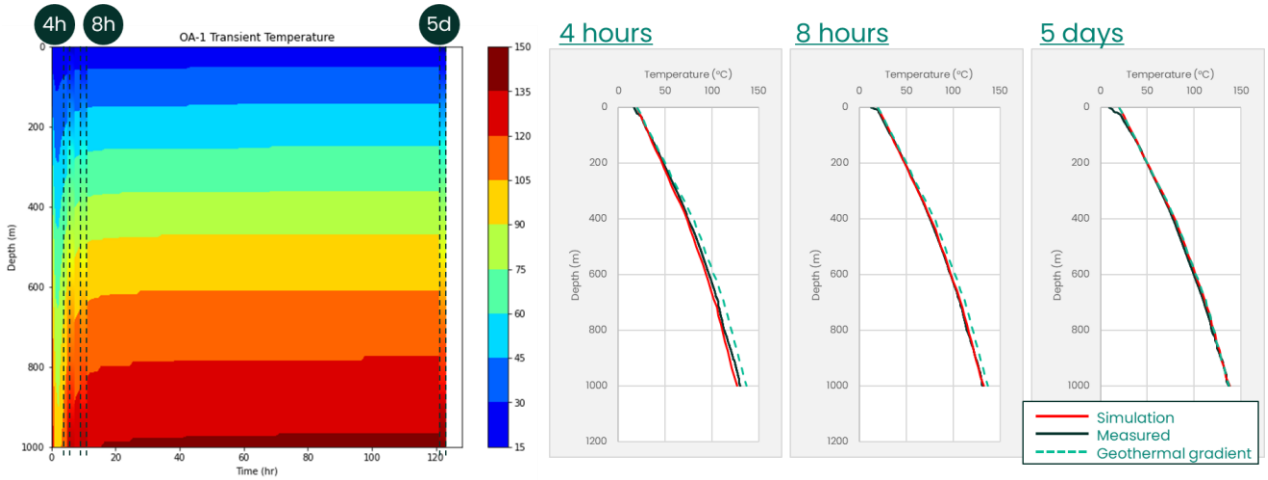

Figure 5: Transient temperature result for OA-1.

4.3 N-17t Large Hole

N-17t is a large diameter deviated well with a depth of 1,500 meter. Available PTS survey is done during injection, 4 hours and 24 hours. Abrupt shift in the bottom section of the well indicates convection. In order to match the measured temperature, the thermal conductivity was increased to 50 BTU/(hr.ft.°F) and the initial geothermal gradient was split into two different gradients. The temperature has yet to be stabilized after approximately 24 hours of shut in.

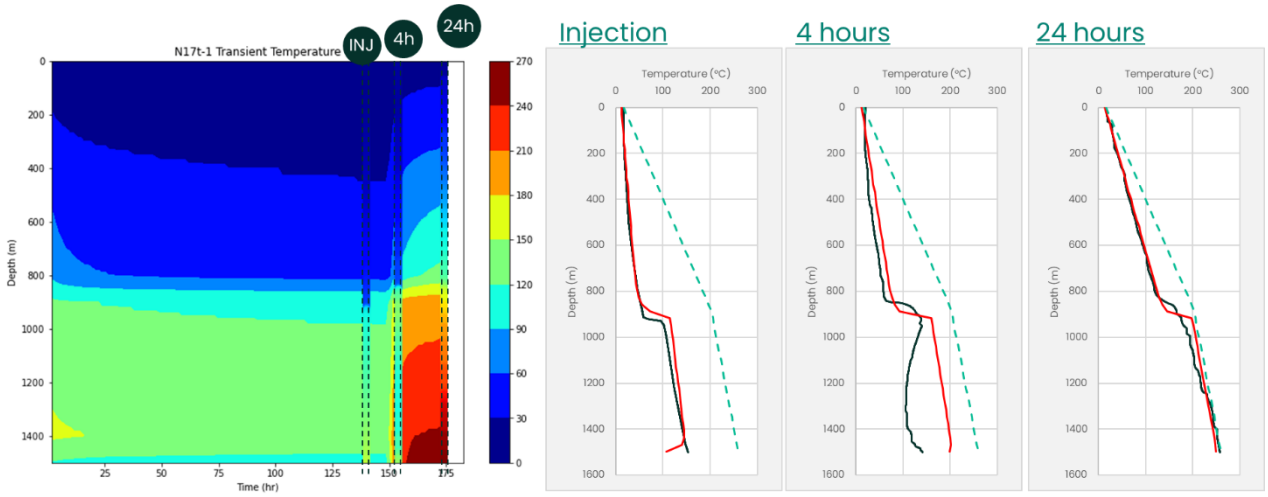

Figure 6: Transient temperature result for N-17t.

4.4 N-18t Large Hole

N-18t is a large diameter deviated well with a depth of 1,600 meter. Available PTS survey is done during injection, 8 hours, 24 hours, 60 hours and 5 days. Fluctuating temperature in the top and bottom section of the well indicates changes in geothermal gradient. The top temperature could be matched by adjusting the geothermal gradient to match the curve shape. In order to calibrate the temperature during injection and shut in, the thermal conductivity also needed to be increased to be at least 50 BTU/(hr.ft.°F) in the concave sections.

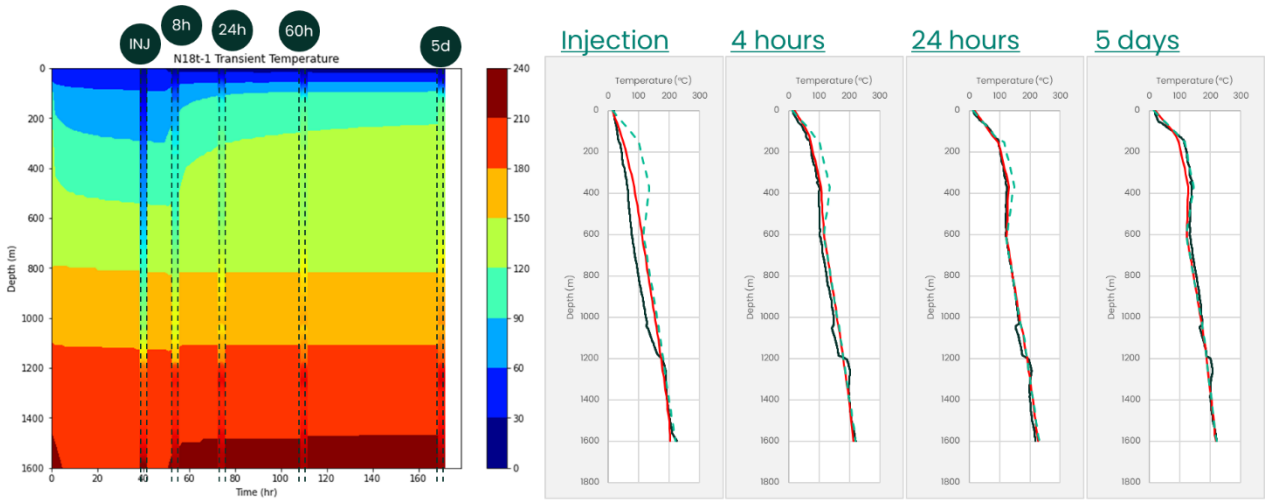

Figure 7: Transient temperature result for N-18t.

5. CONCLUSION

1. The heat conductivity model is based 1D Fourier's Law.
2. Okaizu geothermal field in Japan is selected due to widely available dataset.
3. Four wells were selected to be digitized and used for this exercise:
   - Slim hole: T-1 & OA-1
   - Large diameter wellbore: N-17t & N-18t
4. The simulation was able to simulate and match the measured temperature in slim hole that has minimum fluid movement (heat conduction dominated).
5. The large wellbore in this exercise indicates presence of convection. The thermal conductivity of the fluctuating interval was increased to better match the measured temperature.
6. Benefits of deploying this workflow:
   - Accurately estimate true geothermal gradient from short shut-in time or even shallow slim hole.
   - Strategically plan PTS survey interval.
   - Better understanding of full wellbore dynamics and its operating envelope.
   - Gain better insight on formation properties specifically thermal conductivity and storativity.

REFERENCES

Sabodh K. Garg, Jim Combs. (2002). A Study of Production/Injection Data from Slim Holes and Large-Diameter Wells at the Okuaizu Geothermal Field, Tohoku, Japan. Idaho National Engineering and Environmental Laboratory

The Advantages of Simple 3D Numerical Modeling in Characterizing a Localized Reservoir Boundary for New Wellpad Development in Wayang Windu

Stefano Pentury, Mulyadi, Deoky Pandu Dewanto, and Meiyanto Joko Purnomo

Star Energy Geothermal Wayang Windu, Jakarta

stefano.pentury@starenergy.co.id

Keywords: geothermal reservoir characterization,reservoir simulation, TOUGH2 simulator

ABSTRACT

The Wayang Windu field has maintained its steam supply above the power plant demand from the start of commercial operations in 2000 until the present time. There are currently 32 active producers, five of which are new wells drilled in 2021. Those new wells were drilled from three distinct well pads within the proven reservoir area, with one steam well located at a new well pad in the northern reservoir sector, known as MBI-X well. Despite its good performance, MBI-X has exhibited a relatively higher pressure decline than its neighbor wells. As a result, MBI-X might be associated with a distinct reservoir localized area that is relatively less connected to the adjacent higher production wells. An analytical pressure transient analysis confirmed that MBI-X lies in a confined boundary configuration resembling an intersecting fault, ranging approximately 200-300 m in distance. Despite this, pressure transient analysis could not determine which intersect faults confine the reservoir. To provide some insight, a simple 3D numerical process model has been developed using TOUGH2 simulator with a dimension of 1600x1600x1600 m, involving MBI-X as well as the other two most nearby wells, WWQ-X and MBD-X. Expectedly, this approach can assist earth scientists and engineers during the well targeting process for new make-up wells (MUW), especially within MBI's pad, where there will be plenty of make-up wells to drill in the upcoming Wayang Windu drilling campaign.

1. INTRODUCTION

Located approximately 40 km south of Bandung, Wayang Windu field has consistently been one of the largest geothermal producer in Indonesia for more than 20 years, providing up to 230.5 MW of electricity. The Wayang Windu reservoir is a high-terrain geothermal system that has relatively high temperature (250-320 degC) which has been described as a transitional zone between vapor dominated system from the top of reservoir at 1200 mASL until 400 mASL and liquid dominated system that follows. Wayang Windu has maintained its strong steam production, with an extraction primarily sourced from the steam cap northern area, followed by the central liquid area; meanwhile the injection wells have strategically been placed in the southern area. Up to this point, not much exploitation has been executed in the north-west part of the field, although microgravity survey indicates a reduction in gravity which might imply for strong connection to the main extraction area. In 2021, there were six wells located in four different wellpads drilled in the Wayang Windu field, bringing the total number of wells to 65, of which 32 are active producers. Amongst of the four wellpads, there is a new well pad called MBI located in the north-west, which consists of only 1 well, named MBI-X. As there will be additional wells to drill in the next drilling campaign, the objective of this paper is to perform reservoir characterization including the MBI region. This MBI pad is important because it represents the new beginning to explore more productive zone on the way to the westside.Furthermore, the Pressure Temperature Spinner (PTS) analysis and drilling breaks indicate that MBI-X has three feed zones (FZ) at about 990, 906, and 880 mASL.. With a total depth (TD) no greater than the field's average liquid level at about 400 mASL, MBI-X ought to be a steam (vapor dominated) well. Therefore, based on Figure 1, it is verified that the liquid beneath ~800 mASL in the 2021 PT profile (left graph) is water dead leg; an accumulated colder injected fluid that is not flashing since there is no productive FZ below that depth. This also corresponds to the evidence of no spinner change below 800 mASL.

On the other hand, although MBI-X has showed a decent initial performance, it is underperformed shown by a more accelerated decline compared to the most nearby wells, MBD-X and WWQ-X that have been actively produced for 5 years and 8 years, respectively. Figure 2 shows the production performance of MBI-X in comparison to MBD-X and WWQ-X. To make the comparison more apparent, the steam rate has been normalized to 12 bar of wellhead pressure and initial value is set to 100 kg/s. According to figure 2, MBD-X and WWQ-X have both been able to maintain productions at 2% and 5% annually, respectively. MBI-X, on the other hand, experiences a sharper decline with a rate of 8 %/year in the first year of production, then it accelerated to 13.4 %/year afterwards.

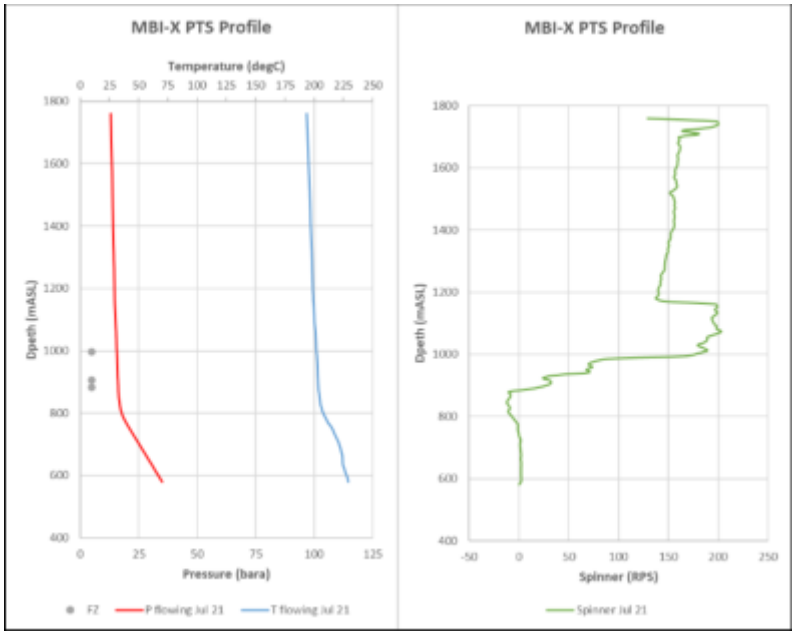

Figure 1: MBI-X PTS profile and FZ information.

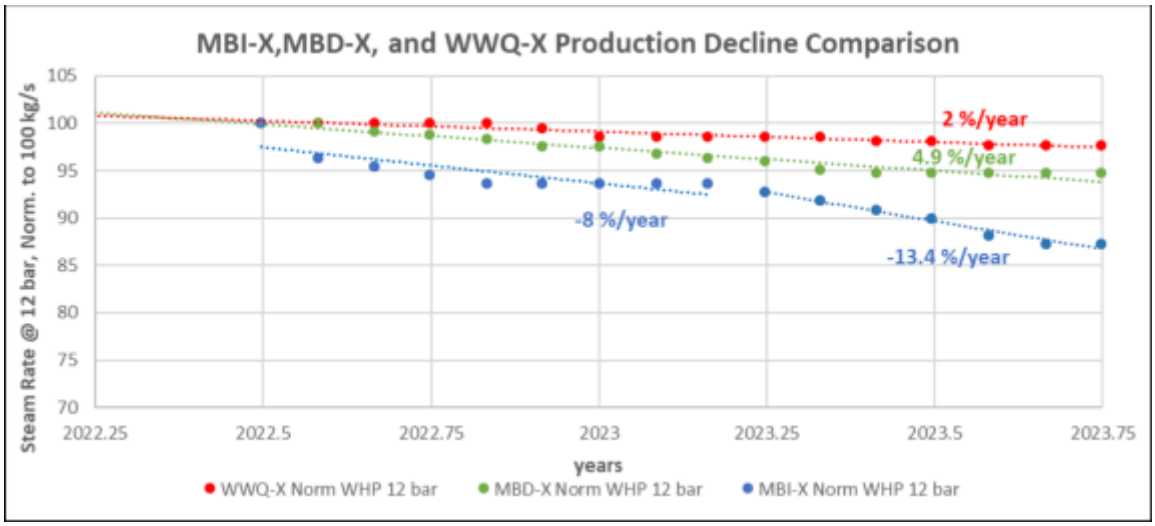

Figure 2: Production Performance of MBI-X comparing to its nearby wells.

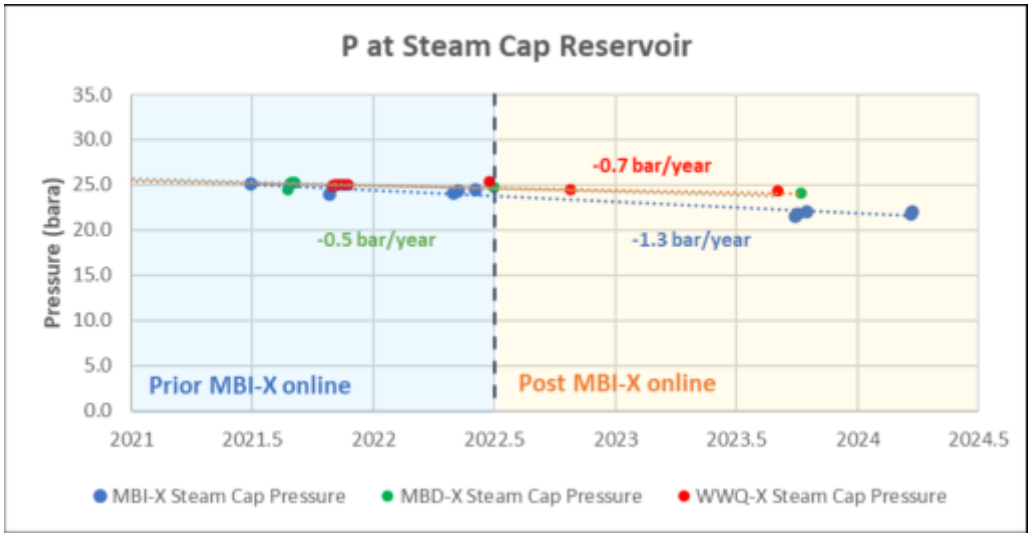

Figure 3: Pressure Response of MBI-X comparing to its nearby wells.

Meanwhile for the reservoir pressure within the steam cap area, MBI, WWQ, and MBD wells tends to have similar magnitude in the beginning. Corresponding to the higher production decline of MBI-X than MBD-X and WWQ-X, the pressure of this well also shows a larger pressure drop overtime, lying at 1.3 bar/year. Figure 3 shows how distinct the pressure of MBI-X performs against MBD-X and WWQ-X.

Due to a different steam production and reservoir pressure response with only short FZ distance to its neighbor wells ranging from ~274 to 627 m, MBI-X might be located in a local confined reservoir area that is separated from MBD-X and WWQ-X reservoir. Despite that, prior to the online of MBI-X on July 2022, the reservoir pressure still shows the same declining trend as MBD-X and WWQ-X for a year of monitoring. Therefore, it is most likely that MBI-X still has a weak connection toward MBD-X and WWQ-X and does not separate completely. Given that, an initiative to assess MBI-X's boundary condition through Pressure Transient Analysis (PTA) has been implemented.

PTA is a powerful tool that can be used to identify crucial parameters including reservoir boundary type alongside with the distance approximation. The reservoir boundary type can be identified through the derivative pressure and differential pressure curve extracted by various well-testing pressure responses such as build-up test, injection test, fall-off test, or production test. Nevertheless, it is essential that the response duration must be long enough just to ensure that it reaches the reservoir boundary, in conjunction with the good pressure response quality for better interpretation. The huff and puff program was executed in October 2023 consists of series of well tests including build-up test, injection test, and fall-off test that can be used for pressure transient analysis. Among of those series of well tests, it appears that there were 1 build-up (before 1st cycle) and 1 injection test (during 1st cycle) that had a sufficient duration and quite good quality data. Even though there was no direct measurement of the bottom hole pressure during huff and puff, the well head pressure was monitored continuously and could represent steam cap pressure properly. After doing pressure transient analysis with various sensitivities and trial and errors on the well-head pressure profiles, the best model that fit was either homogeneous or dual porosity slab with boundary type of intersecting faults. For instance, figure 4 shows the pressure transient analysis result of the build-up test pre-1st cycle.

Figure 4 shows an uptrend profile of both the derivative curve and the differential pressure curve at the late period, indicating that MBI-X has a limited reservoir boundary. Both Homogeneous and Dual Porosity model conclude the reservoir boundary to be as intersecting faults with similar distance at around ~200 m from the MBI-X's feedzones. Corresponding to the previously developed structure interpretation, the confined boundary that restricts MBI-X's area might be resulting from the damaged zone of Bedil-Gambung Fault and Cibitung Splay Fault, which propagated with a buffer of 100 m outwards, linear with the green dots shown in figure 5.

Therefore, the structural interpretation in figure 5 will be used as a guide to create the 3D static model; the aim of this model is to validate the local compartment of MBI-X and to provide a clear picture on how the key static properties distribute throughout the region.

2. MODEL SETUP

A simple 3D numerical process model has been created using TOUGH2 simulator; which is a widely used numerical simulator in the geothermal industry for modelling subsurface fluid and heat flow processes in porous and fractured media. The model was created with a simple dimension of 1600x1600x1600 m that covers MBI-X alongside with its two neighboring wells, MBD-X and WWQ-X. The grid size should be as small as possible in the focus area to create a more refined profile; with finer size focusing in MBI-X area (50 m in distance) and more coarser outward with a distance ranging from 200 m to 300 m in size as shown by figure 6.

Majority of static properties had been set referring to the Wayang Windu full field model developed by Pasikki et al (2020), which was properly calibrated to the measured data. The uppermost model is expected to represent the top of reservoir at the elevation of 1200 mASL, connected to the atmosphere with a distance of 537 meters from the interface (based on average actual topography). While the bottom part of the model is at an elevation of -400 mASL, which is linked to a 300 degC hot plate at a distance of 2200 m. An upflow with rate of 5 kg/s and enthalpy of 1500 kJ/kg is attached at the bottom part of the model, then, a deliverability outflow with PI of 1e-12 m3 is attached at the middle side of the model. These configurations for the upflow and outflow were determined through several trial and errors. In the meantime, the summarized of the initial rock properties is shown in Table 1 and illustrated in Figure 7.

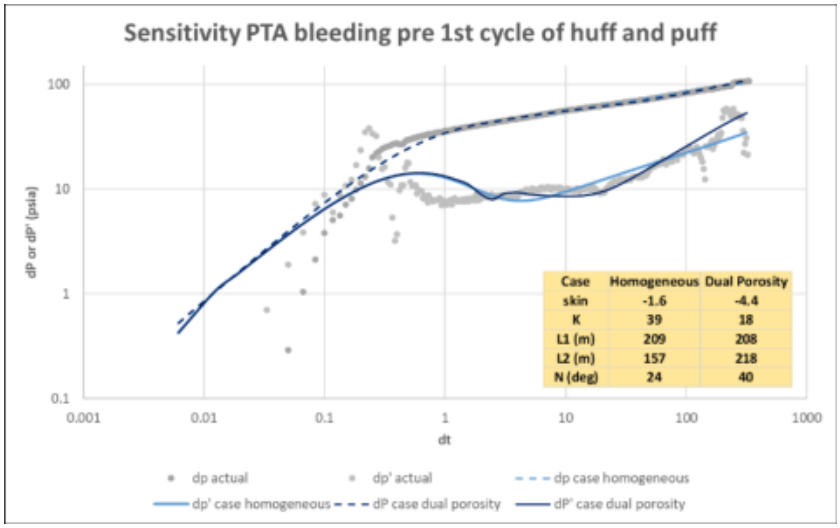

Figure 4: PTA MBI-X Analaytical Result.

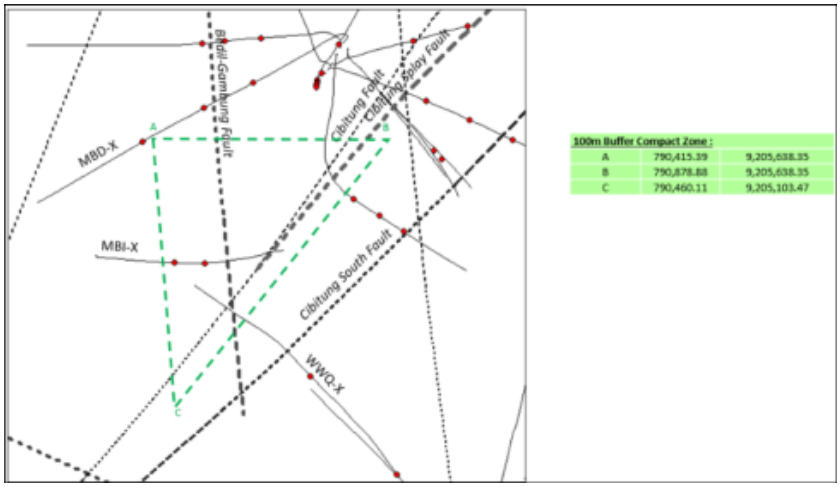

Figure 5: Structural Interpretation of the Localized area.

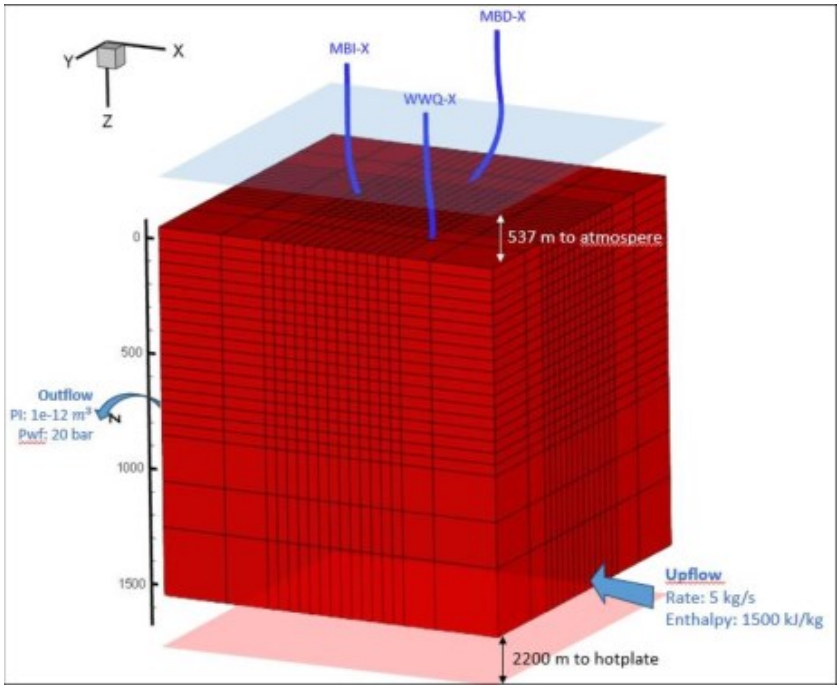

Figure 6: Model Geometry and Boundary Information.

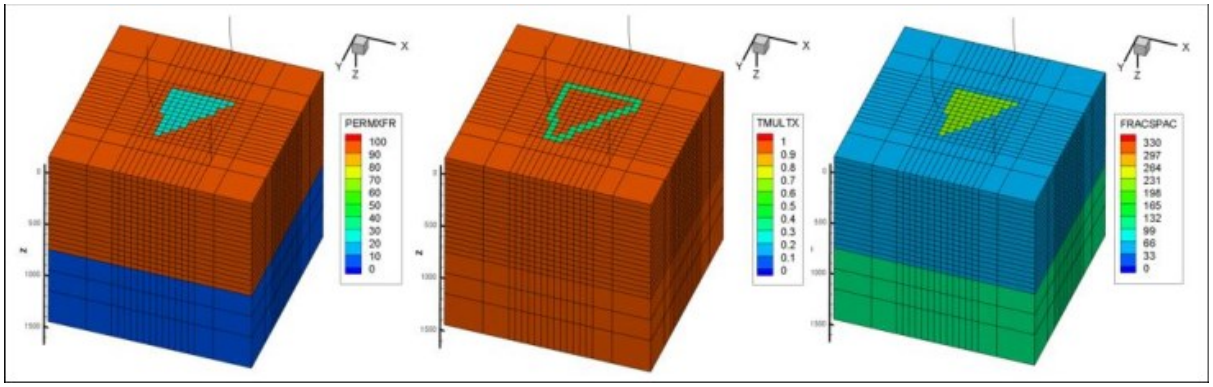

Figure 7: Reservoir Properties of the 3D model.

Table 1: Initial Rock Properties of the Model.

Static Properties	Value	Remarks
Fracture Permeability X,Y,Z	• Within MBI-X: 30 mD • Outward MBI-X: 100 mD	• Refer to PI" formula and PTA calculation • Based on Wayang Windu full field model
Transmissivity multiplier X,Y,Z	Surrounding MBI-X: 0.3	Create it as if a barrier capturing smaller volume; The barrier is not fully closed leaving a fraction of 30%.
Fracture spacing	• Within MBI-X: 220 m • Outward MBI-X steam cap area: 50 m • Outward MBI-X liquid area: 110 m	• To make the MBI-X to have a smaller fracture-matrix interaction • Based on Wayang Windu full field model • Based on Wayang Windu full field model
Matrix Permeability X,Y,Z	5 µD	Based on Wayang Windu full field model
Fracture Porosity	50% with 2% bulk volume	
Matrix Porosity	7% with 98% bulk volume	

In particular, the local area of MBI-X is differentiated by three parameters, such as fracture permeability, transmissivity multiplier, and fracture spacing; where the distribution itself refers to the structure interpretation as discussed in the previous section. Moreover, the faults confined the area of MBI-X is assumed to have 0-degree dip angle due to several uncertainties that can occur in the actual condition. At the same time, the applied fracture permeability refers to the Darcy equation with corrected PI toward enthalpy and pressure corresponds to the thermodynamic state, published by Pasikki et al (2017). Using equation (1) and with parameters of; total calibrated PI" of MBI-X at 4.83E-12 m3, well radius (rw) based on actual condition at 0.26 m, drainage radius (re) to be assumed at 500 m, and the thickness (h) is assumed as the height between the top of liner (TOL) and the deepest feedzone at 213 m, a fracture permeability (k) about ~30 mD is obtained. This is the fracture permeability used for MBI-X's local area in the model.

$$k = PI" \; x \; \frac{\ln\left(\frac{re}{rw}\right) - \frac{1}{2}}{2\pi h} \qquad (1)$$

Likewise, the transmissivity multiplier is set to be modest, assumed to be 30% in this case, to indicate a weak connection between MBI-X to MBD-X and WWQ-X.

3. SIMULATION RESULTS

3.1. Initial State Model

The fundamental step in reservoir modeling is to ensure that the model is aligned with the actual initial condition, which can be achieved by changing the configuration of boundary condition to match the model's pressure and temperature throughout the elevation. In this case, the actual initial condition to be matched refers to the first stabilized PT static survey of MBI-X that took place after completion of drilling campaign in June 2021. By setting the start-time of the model as entirely liquid, the model is run for 47500 years to reach pseudo-steady state

condition. Figure 8 exhibits the matching result between the model and the actual measured data with respect to MBI-X, MBD-X, and WWQ-X.

In overall, the initial state model shows good match in term of pressure and temperature with the actual data of MBI-X and the two nearby wells. The higher actual liquid column in MBI-X is more caused by the existence of a non-evaporated fluid post-drilling (water dead leg).

3.2. History Matching Model

The history matching procedure is used for an additional calibration once the initial state model has been verified to fit the real data. The history matching process is carried out in a separate model using INCON (initial condition) corresponds to the end time of the initial state model, and run until early of 2024. The historical shut-in well head pressure (SI WHP) or the steam cap reservoir pressure is the parameter to be matched; The simulated SI WHP can be calculated by using exponential regression from the reservoir pressure of the steam cap block, with a slope of -4.9718 x 10-5 bar/m referencing to the study of Acuna and Pasaribu (2010). Thus, since the wells have been operated dynamically with variety of WHP throughout the time, the pressure response from the model that will be looked at only occurs while shut-in condition which can be represented by the peak of solid line seen in figure 9.

Initially, the applied static properties shown in table 1 does not give a proper match in the history matching, given that the MBI-X pressure decline in the model is still not sharp enough comparing to the actual measured data. This indicates that the recharge for MBI-X is still large enough to maintain its pressure overtime. Hence, the transmissivity multiplier must be further reduced to minimize the lateral recharge from the surroundings, as well as increasing the fracture spacing to limit the recharge from the matrix. On contrary, the fracture permeability does not significantly impact the pressure decline overtime but has a stronger effect on the pressure drawdown and build-up during the dynamic changes of the wells.

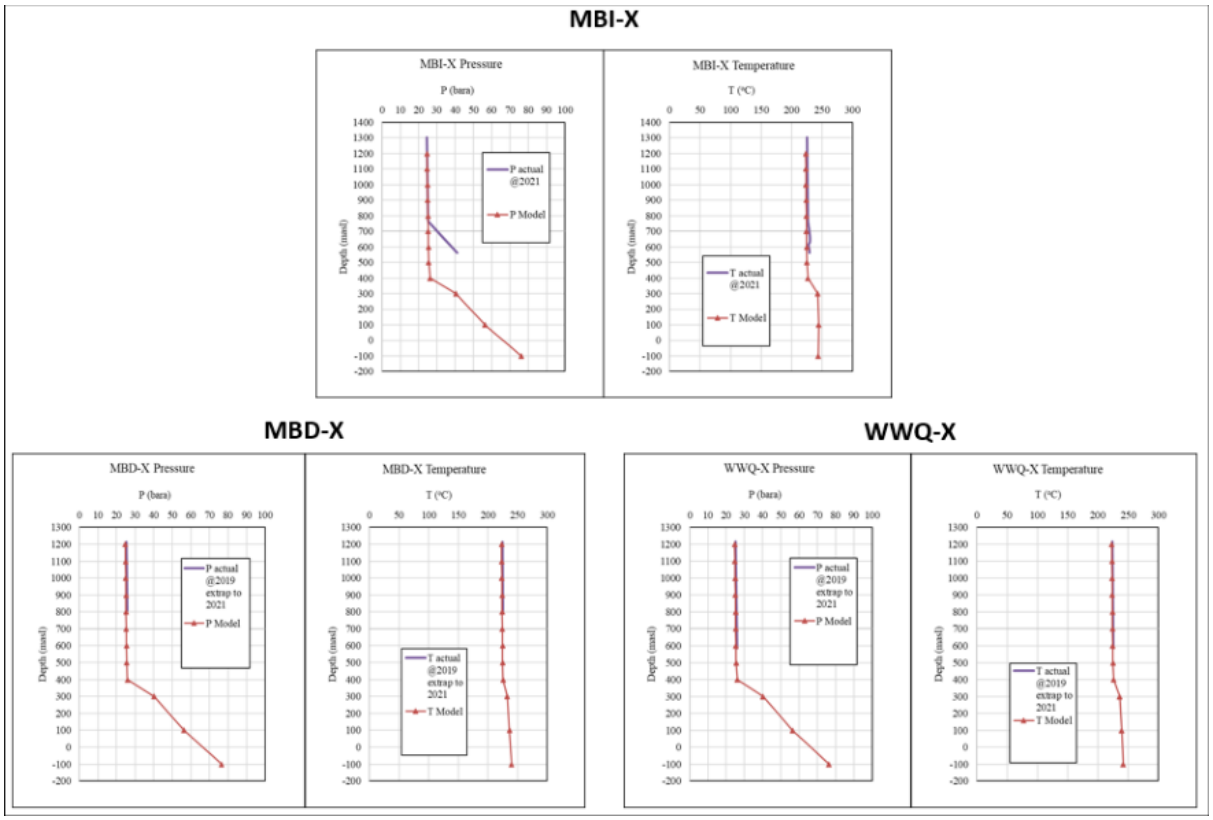

Figure 8: Initial State Model Result.

Figure 9 illustrates how a model with new transmissivity multiplier and fracture spacing given in table 2 produces the best results for MBI-X after several trials to match the actual data. However, in comparison to MBI-X's result, the WWQ-X and MBD-X results still show less accuracy in the history matching. This might be because the model only partially accounts for their two reservoirs.

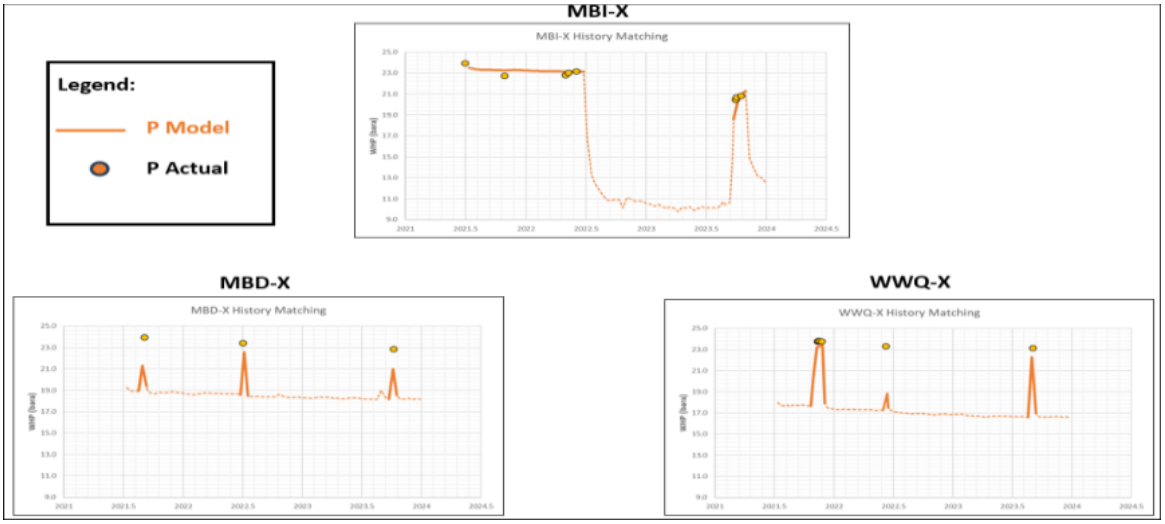

Figure 9: History Matching Model Result.

Table 2: Final Rock Properties of the Model.

Static Properties	Value	Remarks
Fracture Permeability X,Y,Z	• Within MBI-X: 30 mD • Outward MBI-X: 100 mD	The same as Initial Properties in Table 1
Transmissivity multiplier X,Y,Z	Surrounding MBI-X: 1%	Reduced from 30% to 1%
Fracture spacing	• Within MBI-X: 330 m • Outward MBI-X steam cap area: 50 m • Outward MBI-X liquid area: 110 m	Only increasing within MBI-X from 220 to 330 m
Matrix Permeability X,Y,Z	5 µD	The same as Initial Properties in Table 1
Fracture Porosity	50% with 2% bulk volume	
Matrix Porosity	7% with 98% bulk volume	

To gain a better understanding on how several parameters affect the pressure response over time, sensitivity analysis is developed and explained in detail. The sensitivity analysis focusses to see the effect of parameters that have a control in the mass transfer and heat transfer both on the intra block (i.e., fracture spacing) and on the inter block (i.e., fracture permeability and transmissivity multiplier). Furthermore, the sensitivity analysis will give a conclusion which of these parameters that have the biggest impact in the history matching process.

3.2.1 Transmissivity multiplier sensitivity analysis

Transmissivity multiplier is responsible in controlling both anisotropic permeability and the thickness in a specified block, meaning that the lower transmissivity multiplier can create a more flow restriction throughout the porous medium. Usually, this parameter is used to apply reservoir heterogeneity such as making local compartment areas and barriers. In this model, it is designed to enclose the MBI-X area as if it has its own localized bounded reservoir with lower drainage volume as shown in figure 7. Corresponding to figure 10, the smaller the transmissivity multiplier, the weaker the connection between MBI-X to MBD-X's and WWQ-X's reservoir. It causes more pressure drop during production and less pressure rebound during shut in as impact of less pressure support from the surrounding reservoir.

3.2.2 Fracture spacing sensitivity analysis

In contrast, fracture spacing is one parameter that can control the intra-block mass and heat transfer between the fracture and the matrix. The larger the fracture spacing, the less plentiful the series of fractures throughout the block, allowing for minor matrix-fracture mass and heat exchange, which creates less recharge coming from the matrix. Thus, the reservoir pressure should have become less sustainable in the long run. According to Lippman et al (1985), fracture spacing can be varied and can reach a value up to 1640 ft or 500 m. Since fracture spacing

of 330 m is sufficiently large, the other two parameter that is used for the sensitivity analysis are less, which are 60 m and 220 m. Figure 11 proves by applying smaller fracture spacing within MBI-X area, it gives MBI-X's pressure to decline more gradually as time passes.

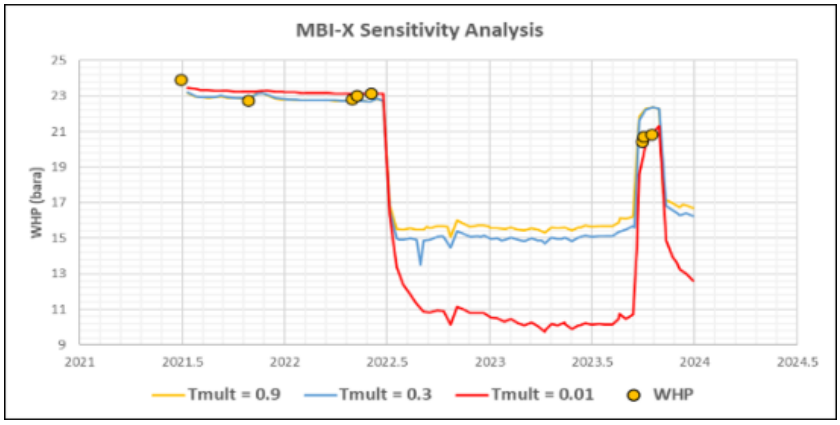

Figure 10: Transmissivity multiplier Sensitivity Analysis.

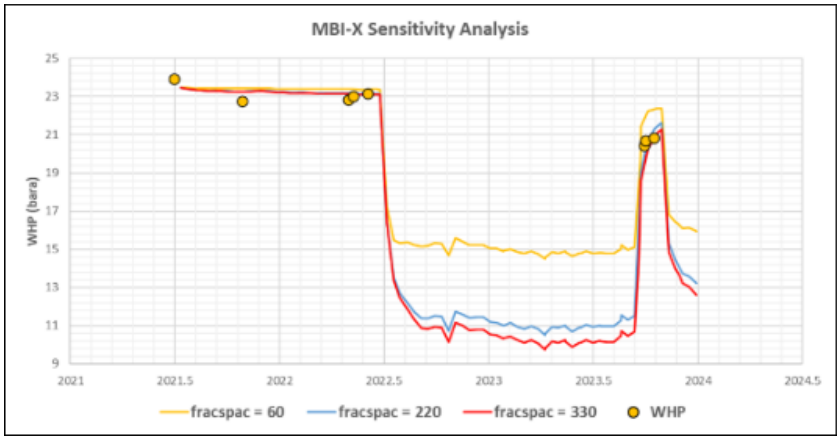

Figure 11: Fracture spacing Sensitivity Analysis.

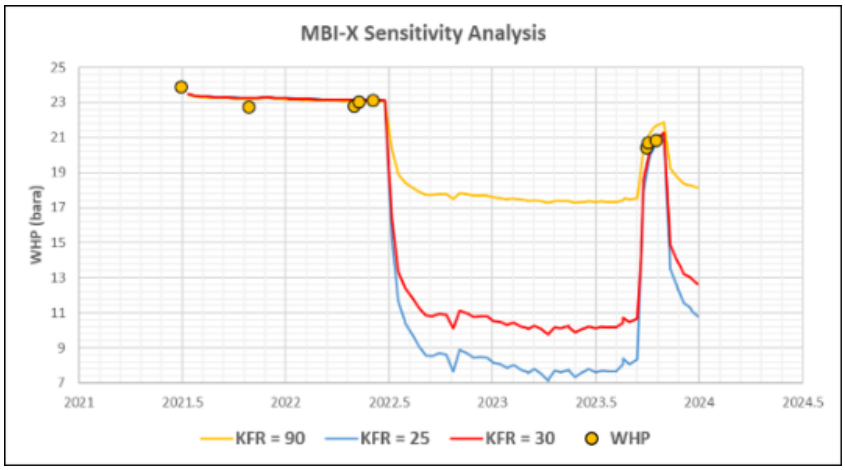

Figure 12: Fracture Permeability Sensitivity Analysis.

3.2.3 Fracture Permeability sensitivity analysis

Furthermore, fracture permeability manages to control the ability for a fluid between fractures internally. Even though, there is also an interaction between fracture and matrix, the fluid movement between these two is dominantly controlled by the matrix permeabilities, especially when the fracture has only 2% of the bulk volume. Figure 12 shows the sensitivity analysis in fracture permeability from 25 to 90 mD. Based on figure 12, it is clear that adjusting fracture permeability affects the pressure drawdown and build up during flowing and shut-in periods, respectively, instead of pressure decline over time itself. The small effect on the pressure over time is due to insignificant contribution of the fracture properties toward the intrablock fracture-matrix along with the

continuously limited recharge between inter-blocks due to the very small transmissivity that surrounds the drainage volume of MBI-X.

Therefore, amongst these three parameters, transmissivity multiplier and fracture spacing are the two parameters that give the most impact in the pressure decline while shut-in overtime. However both parameters must be combined in order to get the best match with the actual data. Eventually, it can give a sense that MBI-X reservoir tends to have a local enclosed reservoir with lesser series of fractures.

4. CONCLUSION

Amidst the tremendous performance of Wayang Windu field over 20 years of production, there is one newly drilled well, MBI-X whose performance differs to the neighboring wells (MBD-X and WWQ-X) despite relatively close distance. This has been proven from the pressure and production response of MBI-X that has declined more promptly compared with the two nearby wells. In addition, Pressure Transient Analysis (PTA) is carried out and can confirm that MBI-X's reservoir is finite, constrained by impermeable faults with approximately 200 meters in distance. However, PTA could not give a clear insight where these faults are located.

Reservoir Simulation has some advantages in tackling those uncertainties; not only it can confirm that one well MBI-X is located in a local finite area, but it can also give an insight on how the structure looks like. The outcome of this simulation has a crucial role to plot the next MUW in the upcoming drilling campaigns, especially at the surroundings of MBI-X since it has a prospective connectivity to the main production area according to various kinds of surveillance activity. After conducting a sensitivity analysis on numerous parameters in the numerical model, it is validated that MBI-X has a lower drainage volume after applying very low transmissivity multiplier in every corner of the area, and has fewer series of fractures by increasing the fracture spacing. Although lower fracture permeability may contribute to a slight effect in the reservoir pressure, the model suggests that the variance in MBI-X performance is primarily driven by changes in the reservoir volume and the counts of fracture.

In conclusion, validation through this simple process model can bring a valuable guidance for well targeting to not go toward the area. Based on this analysis, the area needs to avoid can be approximately up to ~124,000 m2 which is within the 100 m buffer damaged zone from Bedil-Gambung and Cibitung Splay Fault. However, in terms of the elevation, the confined boundary can only be confirmed in the steam cap zone with 0 degrees of dip angle due to the unavailability data in the liquid zone. Yet, this result is not definitive, and future make-up well (MUW) campaign must also contribute to validate the local compartment area. Continued data monitoring must be done to get the model closer to an imitation of the actual condition, especially on the lateral extension; this can be supported by kinds of activities such as drilling more brine toward that area and gathering more geochemistry and geophysical data.

5. REFERENCES

Acuna, J. A., and Pasaribu, F.: Improved Method for Decline Analysis of Dry Steam Wells, Proceedings, World Geothermal Congress Bali, Indonesia (2010).

Lippman, M. J., Bodvarsson, G.S., and Gaulke, S. W., Enthalpy Transients in Fractured Two-Phase Geothermal Systems (1985).

Pasikki, R. G., Bratakusuma B., and Mulyadi.: Numerical Model of Wayang Windu Geothermal System to Optimize Production Strategy, Proceedings, World Geothermal (WGC), Reykjavik, Iceland (2020).

Pasikki, R. G., Peter, and Libert, F.: Impact of Enthalpy and Pressure Change to Geothermal Inflow Performance Relationship,

Proceedings, 5th Indonesia International Geothermal Convention & Exhibition (IIGCE), Jakarta, Indonesia (2017).

Utilizing Numerical Pressure Transient Analysis across Diverse Well Challenges in the Wayang Windu Field

Stefano Pentury and Mulyadi

Star Energy Geothermal Wayang Windu, Jakarta

stefano.pentury@starenergy.co.id

Keywords: Pressure Transient Analysis, reservoir simulation, TOUGH2 simulator, fall off tests

ABSTRACT

Pressure transient analysis (PTA) is a very powerful tool in the oil and gas industry that allows us to acquire reservoir parameters such as permeability, reservoir boundary, and skin factor in a more efficient manner. This valuable information serves as a guide for assessing the extent of drainage areas, providing initial structural insights, and informing decisions related to well stimulation. However, the common analytical method for PTA is designed more for an isothermal well, which means that it might not be reliable in non-isothermal wells like geothermal wells. Hence, in this study, alternatives of creating a 2D or 3D numerical model that incorporates phase changes and heat flow is applied, with the model is created radially using logarithmically spaced radius with the TOUGH2 simulator. While the common analytical method can also be utilized in geothermal wells in the end, the results can be deviating as it does not involve the effect of temperature that amends the PVT data of the fluid (e.g density and viscosity). This is proven from this study as the skin factor often overestimated, potentially leading to misinterpretations in the degree of scale that damages the reservoir. On the other hand, this numerical method can also be more versatile while it comes to non-ideal data inputs, such as when encountering pressure bumps resembling of steam inflow during the early of fall of test. By that reason, this study also shows the example to overcome such a challenge.

1. INTRODUCTION

1.1 Background

In the oil and gas industry, PTA has been trusted for many years as one of the fastest methods to identify some reservoir parameters such as skin factor, reservoir permeability, and reservoir boundary or the drainage area. Two main inputs for PTA are the profile of pressure and flow/mass rate while changing the wellbore condition. The well condition changes can be varying such as changing from production to shut-in (build-up test), shut-in to production (drawdown test), shut-in to injection (injection test), and injection to shut-in (fall-off test). The profile used for the analysis can be in a form of single test, changing from 1 condition to another or by including several multi-rate tests or what it is so called as the superposition. The application is mostly done through analytical approaches involving mathematical correlations, with semi-log curve and log-log derivative type curve being the two most widely used approaches. The concept in either approaches is mainly the same, where the pressure as the time flow/mass rate changes, have been converted into a semi-log or log-log curve in particular ways, then it gives several variables (e.g. slope, or Pd, td, Cd, etc) that can be used to calculate the reservoir parameter such as skin factor and permeability. However, in some contexts, the reservoir condition can be complex such as having a finite boundary in a specific geometry, more heterogeneous, or fuggy which need more advanced formulation. But, the PTA on those cases can be easily done nowadays with an analytical PTA software.

Despite of the widely used of analytical PTA software in the oil and gas reservoir, this software might not be reliable in the geothermal reservoir. The reason is simply because all the mathematical correlations provided in this software is only applicable in an isothermal condition as it does not accommodate the fluid properties changes (e.g. density, viscosity, etc) due to the thermal changes. Kaya et al (2019) demonstrate that performing PTA using analytical PTA software can lead to a significant overestimation of reservoir properties, particularly the skin factor. This overestimation can mislead interpretations regarding the presence and scale of skin in the reservoir.This must be carefully taken into account, as positive skin factor ($s>0$) can lead the decision to conduct several types of workover project that can costs up to thousands or even million of dollars. With this condition, expertise such as McLean and Zarrouk (2016), have found a new approach through a numerical modeling so the PTA can be done in the geothermal reservoir with more accurate and reliable results. The numerical modeling is executed using a simulator that involves the thermal changes or thermodynamic conditions that is called as TOUGH2; as the model is created radially with 1 layer starting from a block size with the smallest radius in the middle, considered as the well, and becomes logarithmically larger toward the reservoir for a smaller running time.

Wayang Windu field, located in South Bandung, Indonesia, is one of the largest geothermal producers in the world. As of 2024, it generates electricity with a capacity of up to 230.5 MW and plans to expand its generation capacity in the coming years.In this study, one until two wells with different condition is used to conduct PTA, especially with numerical approach along with the assessment to its reliability compared to the analytical approach. The study starts from showing how the numerical model has been set up, showing the results and sensitivity analysis, and the comparison to the analytical approach. In addition, one from the two wells used, has a unique condition where there is an anomaly pressure bump due to the presence of steam inflow at the fall-off test profile; thus, this study also shows the application of numerical PTA in this non-ideal condition.

1.2 Study Case

For geothermal reservoir, sometimes fall off test and injection test are the two out of four tests that are more suitable, as the build up test and drawdown test can let the steam inflow to set the pressure profile apart from ideal. Thus, for this study, it uses fall off test for as the input of the model. There are two cases used for numerical PTA with TOUGH2, which are MBA-X with an ideal pressure profile where there is no any disturbance during the data acquisition, and WWA-X with a non-ideal pressure profile due to the presence of steam inflow; the study in MBA-X is more robust which includes sensitivity of several variables, while WWA-X only acts as an additional case showing on how to handle with non-ideal input. Before setting up the model for each case, a brief background on MBA-X and WWA-X is provided in the following section.

MBA-X is one of the steam wells that is located in the northern main production area with a current production and initial production at 7 kg/s and 13 kg/s, respectively. The drilling of this well had been completed on Jan 2019 with a total depth (TD) of 1480 mMD. However, after being produced for several years, the maximum clearance depth (MCD) got shallower which is now lying at 1220 m. Preliminary assessment suggests the shallowing MCD is due to rubble formation build-up and it can be the main reason for the production to drop ~6 kg/s. By this reason, an initiative to do PTA in this well has been carried out to see if there is also a flow assurance issue within the reservoir aside the one that takes place in the wellbore as result of the rubble formation. Fall off test along with PTS injection have been conducted on Dec 2022 (injection rate: 48 kg/s). According to the PTS injection result, there are two inflows observed at 1160 m and 970 m above sea level, indicated by the temperature and spinner response. In addition, inferring the steam inflow can disturb the ideal fall-off test pressure profile, the pressure at the logging hanging depth closed to the MCD has no steam inflow (injection pressure > shut-in pressure); so, there is no issue to start the fall-off test in that particular depth. Figure 1 and 2 shows the MBA-X's PTS profile. On the other hand, figure 2 shows the MBA-X's Fall Off Test Profile, started from injecting a condensate at 48 kg/s, then it stopped letting the pressure to fall off until it reaches the reservoir (shut-in) pressure. This Fall Off test profile, which is the one that will be used to calibrate the model.

In another scenario, WWA-X production also tends to drop quite promptly 10 months after the well online from the start. Although the production transient effect might be the main cause here, conducting PTA to see the flow assurance issue within the reservoir can be one good solution, especially to WWA-X as one of the biggest two-phase producers in Wayang Windu field (current production 25 kg/s). The same as MBA-X, the PTA is executed through the data from Fall Off test and it takes place on September 2022 alongside PTS injection.

However, during the implementation of PTS injection, the temperature response still shows a gradual increase as it goes deeper towards the MCD, meaning there is still a possibility of steam inflow to exists and can disturb the Fall Off test pressure response (see figure 3). Consequently, the steam inflow did disturb the Fall Off Test and the profile can be seen in figure 3. Last but not least, in terms of the testing period, the fall off test is still at the early stage (wellbore storage) since it can be continued due to the steam inflow and an operational issue.

2. DESIGN STRUCTURE

2.1 MBA-X numerical design structure

For MBA-X, referencing from the study of McLean and Zarrouk (2016), a single-layer radial model has been developed, with a block of smaller radius representing the well located in the center of the model, which then spatially extends logarithmically towards the reservoir. The case has been done in two discrete models; one that is the condition changes from shut-in to injection (injection test) with a period about 1 day, the other is when it changes from the injection to shut-in (fall-off test) for 4 days. In addition, the grids are classified into three lithologies as each lithology has its own properties, which are the well, the skin (near-wellbore) area, and the reservoir area as can be seen in figure 4.

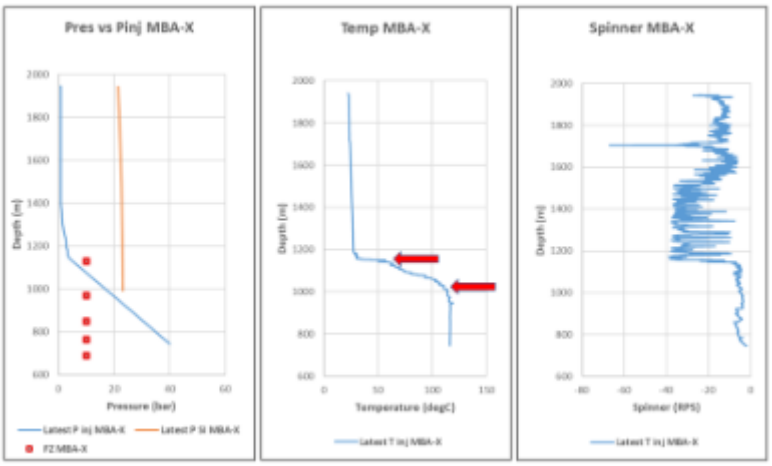

Figure 1: MBA-X's PTS profile.

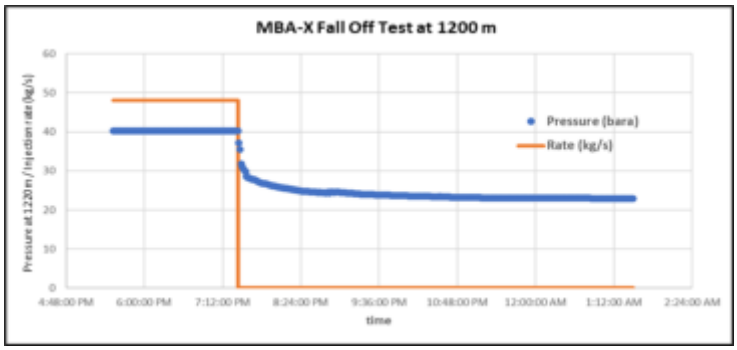

Figure 2: MBA-X's Fall Off Test Profile.

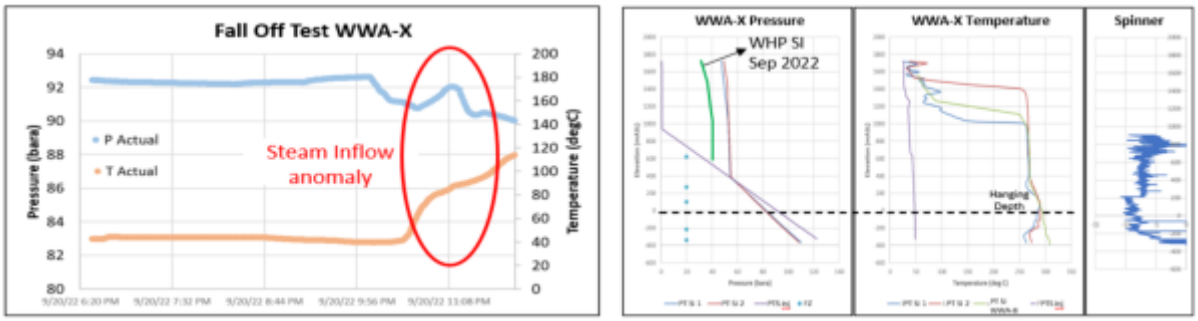

Figure 3. WWA-X's Fall Off Test Profile (left) and PTS profile (right).

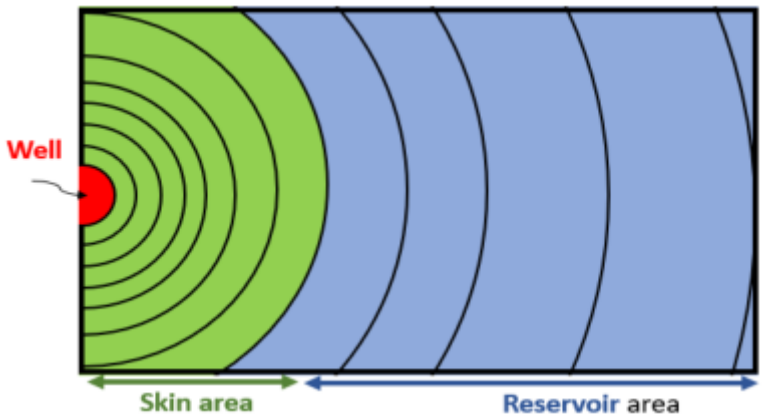

Figure 4: the grid model of PTA MBA-X numerical model.

In addition, since there is no any boundary seen in the pressure profile, the radius of reservoir is designed spatially large with no impermeable boundary in the end; meanwhile the skin does not extend far from the wellbore lying at 4 m in radius. The model has a total of 100 blocks consists of 15 blocks up to the end of the skin area, and 85 blocks applied on the rest of the reservoir. Although in an ideal case, the porosity of a well must be 100%, it can create instability in the TOUGH2 simulator; so, the porosity is applied with a high number as possible, such as 90%. The permeability assigned in the model will act as the MBA-X's true permeability which will then be compared to the analytical PTA. On the other hand, by knowing both skin permeability and reservoir permeability, the skin factor can be estimated simply with a common skin factor formula that is derived from mathematical models describing fluid flow in porous media as follows:

$$s = \left(\frac{kres}{ksin} - 1\right)\ln\left(\frac{rskin}{rwell}\right) \quad (1)$$

The well block is also being applied with a rock compressibility or can be called a well compressibility to accommodate the wellbore storage effect in the wellbore. The compressibility of the well, as well as the skin and reservoir permeability, incorporates values determined through extensive calibration or sensitivity analysis to align with the pressure derivative type curve created; the sensitivity study is also provided in later section. In summary, table 1 shows the detailed inputs of the reservoir model including the reservoir parameters after sensitivity study.

Table 1: MBA-X's assigned reservoir parameters and injection parameters.

Properties	Value	Remarks
h (thickness) | Depth reference @ 1200 m	300 m	Based on actual thickness from TOL to MCD
well radius (rw)	0.22 m	Based on actual
skin radius (rs)	4 m	Logarithmically spaced radius that consists of 14 blocks
reservoir radius (rres)	100,000 m	Logarithmically spaced radius that consists of 85 blocks
Ø Reservoir	10% (single porosity)	
Ø Well	90%	
Well Compressibility (Ct)	9 x 10^{-8} Pa^{-1}	For capture wellbore storage
Initial P reservoir	22.88 bar	From PT Shut-in
Initial T reservoir	219 degC	From PT Shut-in
Calibrated skin permeability	16 mD	Based on calibration/sensitivity study
Calibrated res permeabiliy	10 mD	Based on calibration/sensitivity study
Injection rate	48 kg/s	
Enthalpy of Mass in	546 kJ/kg	Refer to the T mixture during Fall-off test

2.2 WWA-X numerical design structure

WWA-X's model framework is much more complex than MBA-X as the radial model must be created in 3D, containing at least three layers to accommodate several zones such as steam zone, boiling zone, and brine zone. In this model, 5 layers are created as the first two layer act as the steam zone with thickness of 400 m, then the following 2 layers as the boiling zone thickens at 300 m, and finally the rest 200 m layer as liquid zone as can be seen in figure 5.

The concept WWA-X radial model is generally the same as MBA-X, but only it is built more in a 3D model consisting more than 1 layer. The way the water being injected into the model is also treated different to MBA-X's model, where the water at 30 kg/s is injected through an extra cell that will go down quite straightly toward the three well blocks underneath. Whereas for the steam zone blocks (400 meters at the top of the model), it is made to have higher lateral permeability so it can go straight to the liquid zone through the well blocks that have higher Z permeability. To simulate the steam to entering the liquid layer can be a challenge and full of uncertainty; the concept that previously discussed is just one way to make the steam so it can enter the liquid zone. The details of the assigned properties can be seen in the table 2.

Unlike the well testing in MBA-X that use a single test, WWA-X well testing consists of several multi-rate injection tests before implementing the fall off test. Those multi-rate tests are included as the field data to be matched with the model; the well testing in WWA-X can be seen in figure 6. Lastly, the depth reference to extract the injection and fall-off test pressure refers to -16 mASL, which is the deepest layer corresponds to the model.

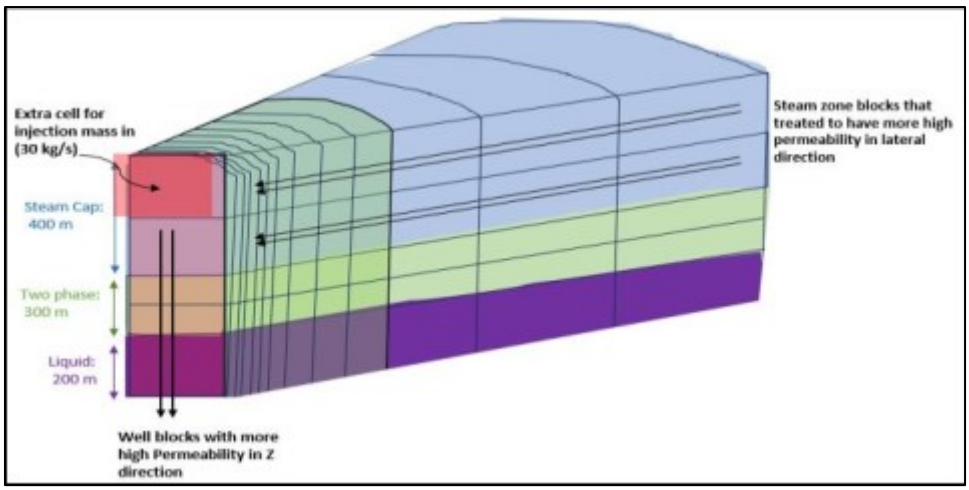

Figure 5. the grid model of PTA WWA-X Model (Additional Case).

Table 2: WWA-X's assigned reservoir parameters and injection parameters.

Properties	Value	Remarks
h (thickness)	900 m (400 m of steam cap, 300 m of boiling, and 200 m of liquid)	Based on actual thickness and PT SI survey
r skin (steam cap, boiling, liquid)	14 m, 24 m, 24 m	
Ø Reservoir	20% (single porosity)	
Ø Well	90%	
Well Compressibility (Ct)	6 x 10-8 Pa-1	For capture wellbore storage
Initial P reservoir (layers: 2 steam cap, 1 boiling, 1 liquid)	54, 54, 61, 71, 85 bara	From PT Shut-in
Initial T reservoir (layers: 2 steam cap, 1 boiling, 1 liquid)	269, 270, 276, 286, 288 degC	From PT Shut-in
Calibrated skin permeability (layers: 2 steam cap, 1 boiling, 1 liquid)	250 mD for all	Based on calibration/sensitivity study
Calibrated res permeabiliy (layers: 2 steam cap, 1 boiling, 1 liquid)	50, 50, 30, 10, 10 mD	Based on calibration/sensitivity study
Injection rate	30 kg/s	
Enthalpy of Mass in	159 kJ/kg	Refer to the T mixture during Fall-off test

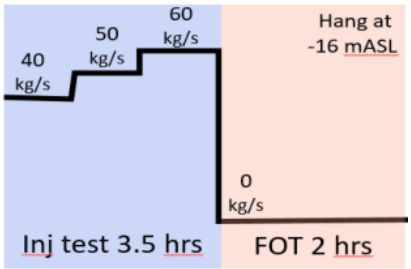

Figure 6: WWA-X multi-rate tests and fall-off test.

2.3 Analytical PTA

Furthermore, for the analytical PTA, the pressure derivative curve that is once created by the model is then being used as the same derivative curve to estimate the skin factor and the permeability through the analytical PTA software. However, the reservoir distance will not be the parameter to be compared in this case, as the pressure profile still shows an infinite acting behavior for MBA-X, and it is even still in the wellbore storage stage for WWA-X. Ideally, the fluid properties of water should have changed as the temperature changes. One complexity in the analytical PTA is that the temperature is a fixed parameter, meaning the viscosity and density will also be fixed. Figure 9 shows the relationship of both viscosity and density vs temperature developed by Alambra (2022).

As a result of figure 7, it creates a confusion which temperature should be chosen in the analytical PTA since MBA-X has a temperature ranging from 129 degC (injected) to 220 degC (reservoir temperature). Thus, in order to be more moderate, the temperature applied is the average between the two which is ~170 deg C, creating the viscosity to be ~0.2 cP according to figure 7.

3. RESULTS AND ANALYSIS

3.1 Final Result of PTA MBA-X

After doing sensitivity study of several parameters, the best match is the model with well's grid rock compressibility of 9 x 10^{-8} Pa^{-1}, alongside with skin permeability and reservoir permeability of 18 mD and 11 mD, respectively, similarly what is showed in table 1 in the previous section. By using those permeabilities and formula 1 as described in the section 2, it gives an approximate skin factor of -1.1; this confirms MBA-X does not have a wellbore damage in the reservoir and no need to be stimulated (s<0). Figure 7 illustrates the comparison between the model and field data in regards of the pressure profile, temperature profile, and the derivative pressure curve.

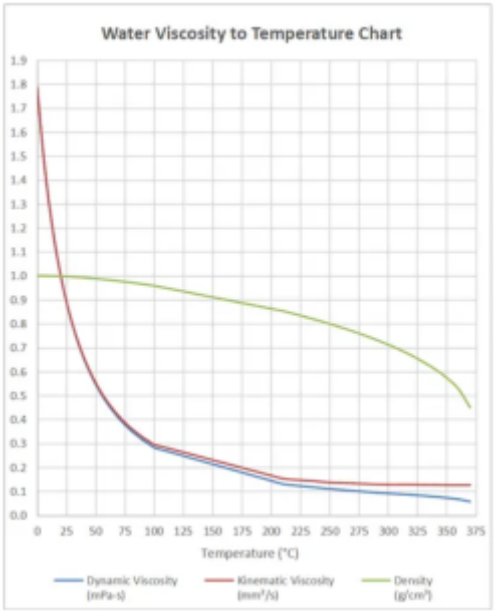

Figure 7: Relationship of water viscosity and density vs Temperature, Alambra (2022).

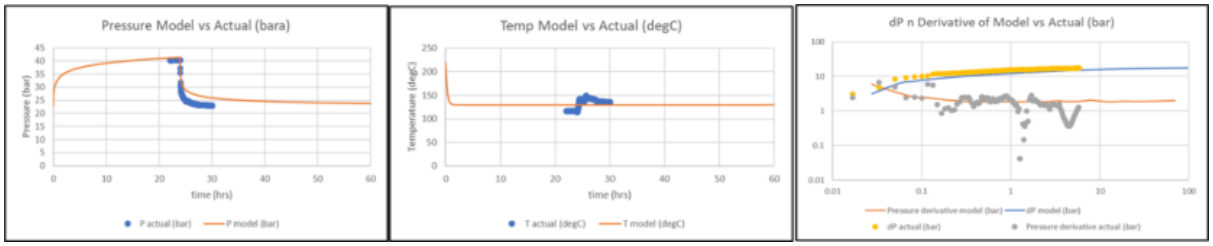

Figure 8: PTA MBA-X Model vs Actual Results.

According to figure 8, the pressure and temperature of the model generally matches the measured data. Since the 1 layered model has no mass outs such as outflow in a form of extra cell or production, it barely covers the heated-up temperature (temperature increase) corresponding to the temperature field data during fall-off test as seen in figure 8. Due to that reason, the enthalpy of injection is set to be the water enthalpy that has been mixed with steam inflow during the fall-off test (546 kJ/kg), creating it is much more matched with the late-time temperature. The conversion from pressure profile to the derivative curve and pressure drop on the right graph of figure 8, which is the orange line and blue line, respectively, is supported by the conversion feature in a PTA analytical software; those two graphs resulting a satisfactory match with the measured data. The good match of this comes after making several adjustments/sensitivities in the well compressibility, and skin factor. Thus, the next sub-section will discuss the effect of well compressibility and skin factor changes alongside with the other parameters.

3.2 Sensitivity Study of PTA MBA-X

The parameters used for the sensitivity analysis are layer thickness, well-block compressibility, temperature injection, well radius, and skin factor, where every one of them can be illustrated in figure 9. Transmissivity or the overall flow capacity which is denoted as k.h is one of the most important parameters to be monitored. Thus, when thickness (h) decreases for a given permeability, it surely decreases the flow capacity allowing the pressure drop to be larger alongside with the increase of the derivative curve. On the other hand, in the dynamic sense, higher well block compressibility (considered as wellbore storage) allows a higher compression into the fluid resulting it to move slower in response. This makes the pressure drop and derivative curve become delayed and shifted more to the right side. Similarly to the reservoir thickness, the well radius is also the other parameter that controls the volume. But, unlike the reservoir thickness that covers the entire reservoir, well radius only covers the small part within the well-block. This creates the result of sensitivity is the same with thickness where the higher the wellbore radius, the larger the pressure drop and derivative curve, but only it has insignificant effect. The skin factor and injection/mixing temperature are two important parameters that show a similar response in the sensitivity analysis. Both, the increase of skin factor and the decrease of mixing temperature, produces a higher hump at the early stage of the derivative curve profile.

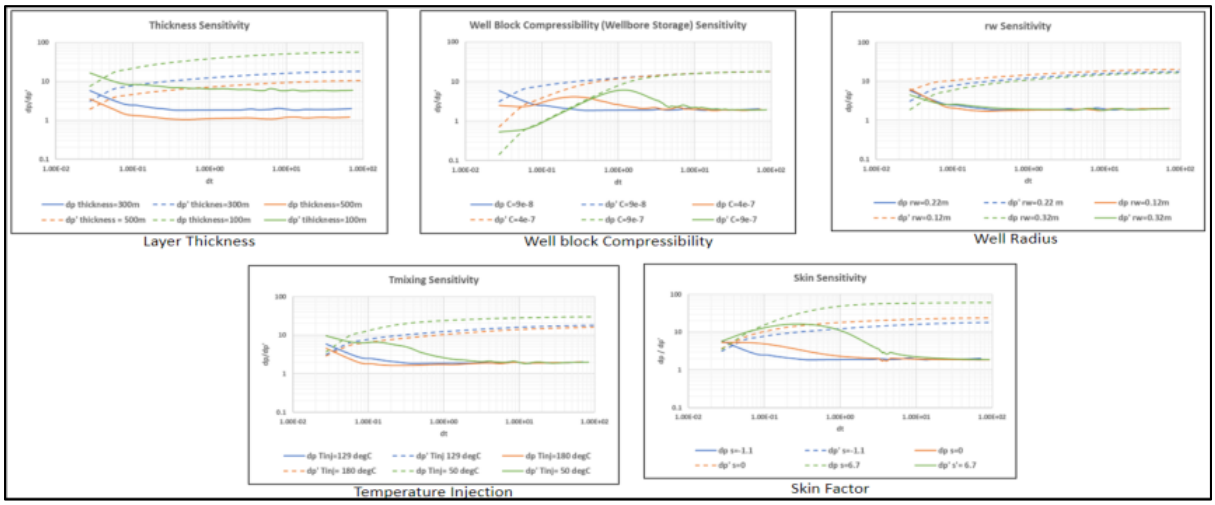

Figure 9: PTA MBA-X Model Sensitivity Analysis.

Table 3: Skin Sensitivity Analysis of MBA-X Model.

Numerical skin factor	Analytical skin factor	Numerical K (mD)	Numerical K (mD)
-1.1 (matched)	0.2	10	16.8
0	1.5	10	15.5
6.7	7	10	9.4

Table 4: Temperature Sensitivity Analysis of MBA-X Model.

Model Temp (degC)	Model skin factor	Analytical skin factor	Model K (mD)	Analytical K (mD)
129 (matched)	-1.1	0.2	10	16.8
50	-1.1	3	10	15.3
180	-1.1	-0.5	10	16.8

Table 3 and table 4 shows the comparison results between the numerical model and analytical approach with respect of the skin factor and the injection temperature, respectively.

Based on the three scenarios of skin sensitivity analysis (-1.1, 0, and 6.7), all the three shows an overestimation of skin factor. On the other hand, the slight difference of the permeability is more derived from the uncertainty of the applied viscosity in the analytical approach.

Moreover, since the decrease of injection/mixing temperature also makes a higher hump at the early stage of the pressure derivative curve, it can mislead the analytical PTA interpretating as an increase in the skin factor. This is proven from the table 4, especially when the mixing temperature being 50 degC, the analytical PTA concludes a positive skin factor even though it should have been a clean formation.

3.3 Final Result of PTA WWA-X (Additional Case)

Different to MBA-X, WWA-X does not have analytical PTA to be matched with as the very early time response in the pressure profile can produce a lot of uncertainty while determining the results.

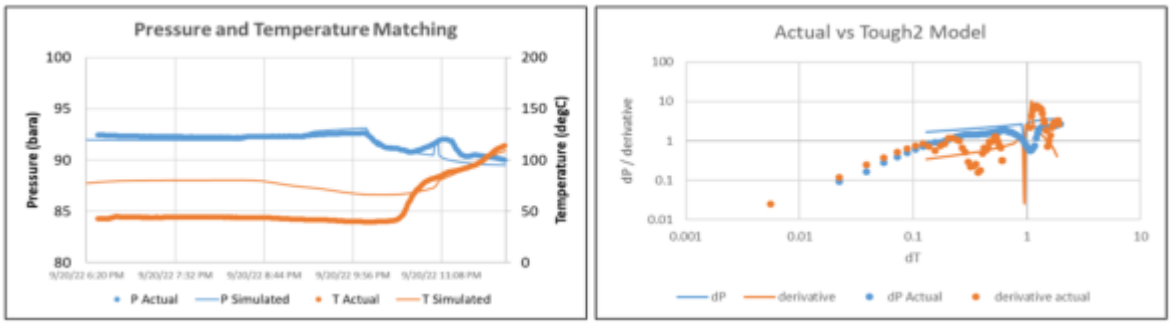

Figure 10: PTA WWA-X Model vs Actual Results.

To have a limited fall-off test pressure response (stopped at the early stage) together with acquiring a pressure bump due to steam inflow anomaly, makes the numerical modeling be somewhat more challenging. Moreover, creating a model with multiple layers may prevent pressure and temperature stabilization. Corresponding to the result seen in figure 10, the pressure overall shows a good match with the measured data. The model also depicts the pressure bump due to the steam inflow with the right timing, yet not the duration which is possibly due to the instability in TOUGH2 when it comes to an extremely low temperature or vacuum condition. This pressure bump has heavily been controlled by the reservoir permeability in the steam cap and it is also responsible to the slightly overmatch of the temperature profile; where the increase of steam cap reservoir's permeability allows the pressure bump to be more seen, yet the temperature becomes larger. Then, with those permeabilities, it creates a skin factor as -4.5 (clean formation) with derivative curve as can be seen on the figure 10.

4. CONCLUSION AND RECOMMENDATION

4.1 Conclusion

This paper shows the application of numerical PTA in a couple of Wayang Windu wells with one well whose result is compared with the common analytical approach. As a result, application of PTA using numerical and process model is something that will be high interest for geothermal reservoir since it has accommodated the thermodynamic system or the changing of fluid properties due to thermal change. Based on this study, also consistent with the study of Kaya et al (2019), the skin factor calculated by the analytical approach is mostly overestimated in every case which surely can mislead the decision of workover that can spend thousands of dollars or more. For example, as lowering the injection/mixing temperature has the same response as the increase of skin, it can conclude the reservoir to have a wellbore damage in a form of scale/skin regardless how clean the reservoir is. In addition, numerical PTA at times can be more versatile than the analytical approach for geothermal reservoir. To put it another way, it can be used to match a non-ideal pressure profile such as having a pressure bump due to the presence of steam inflow at the early stage of the fall-off test in particular two-phase well. However, in this context, it must be made by at least 3 layers that consists of steam cap, boiling, and liquid zone, where the pressure and temperature might not be stabilized as the initial state condition.

4.2 Recommendation

Implementing Fall-Off Test in a geothermal well must be extremely careful, especially when it deals with a steam well or well whose feedzone/series of fractures is many. Thus, it needs a deeper assessment while setting the hanging depth, such as ensuring there is no inflow indicated by comparison between injection pressure and shut-in pressure, or set it at a point where it has stabletemperature profile. In addition, in spite of the more reliable result from the simplified PTA numerical model in this study, the thermal effect is only responsible to the change of fluid properties. Meanwhile, on an actual case, the thermal effect can affect the rock properties such as rock matrix expansion that can reduce the pore size. Therefore, it is suggested to consider this for a more accurate and representative results in the future.

REFERENCES

Alambra, K.: Water Viscosity Calculator (2022).

Kaya, E., Adityatama, D, and Zarrouk, S J.: Investigation of pressure transient analysis methods for single-phase and CO2-rich geothermal reservoirs, *Department of Engineering Science, University of Auckland, Auckland*, New Zealand (2019).

McLean, K. and Zarrouk, S. J.: Presusre transient analysis of geothermal wells: A framework for numerical modelling, *Department of Engineering Science, University of Auckland*, Auckland, New Zealand (2016).

A Conceptual Model of Maritaing Geothermal Green Field Prospect Area in East Nusa Tenggara, Indonesia Using Numerical Modelling

Armando Ariakta Aloanis, John O'Sullivan, and Michael Gravatt

Geothermal Institute, University of Auckland, Auckland 1010, New Zealand

aalo689@aucklanduni.ac.nz

Keywords: 3D Conceptual Model, Geothermal Reservoir Modelling, Natural State Simulation, Maritaing

ABSTRACT

Maritaing is one of the potential geothermal areas in the eastern part of Indonesia, located in Alor Island, East Nusa Tenggara. Previous studies indicate that the green field has 17 MW of hypothetical resources. This study aims to create a conceptual model of the geothermal prospect area by combining geology, geophysics, and geochemistry data. The model is built based on a digitalized conceptual model using Leapfrog and a natural state model through numerical modelling using AUTOUGH2. Furthermore, the natural state model is calibrated by matching the temperature of the top of the reservoir from geothermometer data and surface manifestations. In accordance with the parameters obtained from the numerical modelling, a new conceptual model of the Maritaing geothermal prospect area successfully represents the heat and mass flow of the system.

1. INTRODUCTION

The Maritaing geothermal area is one of the potential fields that is situated on Alor Island, East Nusa Tenggara province. The field is located at 800 km from the Ulumbu field and about 700 km from the Maritaing area. The field is about 5 km away from the port. Preliminary studies have been conducted regarding its geology, geophysics and geochemistry (Rahadinata et al., 2017; Setiawan et al., 2015; Supriyadi et al., 2015). The system was confirmed to have a chloride-content hot spring, which is presumed to be in the up-flow zone. There are also several warm springs spread around the eastern and southern parts of the field (Supriyadi et al., 2015). The prospect area is 3 km^2 and the temperature of the reservoir is estimated to be 200°C.

This paper objective is to present an updated conceptual model of Maritaing reservoir through calibrating a natural state numerical model using AUTOUGH2 that tightly coupled with 3D digital conceptual model of the Maritaing field in Leapfrog Geothermal. The 3D digital conceptual model was based on previous tentative conceptual model and involving data of geological, geophysical surveys and geochemical studies. Several steps were conducted to build the 3D conceptual model including set up the structures, rock types, alteration rock, and surface features. This 3D conceptual model was used as the basis for the numerical reservoir model. The calibration of the natural state model was according to the geothermometer and surface features data.

Figure 1: Location of the Maritaing Geothermal Field on Alor Island, East Nusa Tenggara, Indonesia, modified from maps.google.com.

2. FIELD INFORMATION

2.1 Geological Setting

The study by Setiawan et al. (2015) highlights the fact that the Maritaing geothermal field mainly consists of surface deposits, volcanic rocks and sedimentary rocks. Surface deposits which formed in this field are alluvium and lake deposits. The volcanic rocks mainly consist of andesite lava and pyroclastic flows. Conglomerates and limestone are the sedimentary rocks in the field. According to Noya et al. (1997), the Alor formation is composed of lavas and breccia, interspersed with tuff. The lavas include hornblende andesite, biotite hornblende andesite,

hyalo andesite, and pyroxene basalt. Strong alteration, mineralization, and sheeting joint structures are evident in specific areas.

The sequence of stratigraphic layers, starting from the oldest and going through to the youngest formation, including Katuwusi andesite lava, Katuwusi pyroclastics, Worakena andesite lava, Koya-Koya andesite lava, Koya-Koya pyroclastic, Inukamang andesite lava, Pakmana andesite lava, Meriaka andesite lava, Kunatena pyroclastic, Bulamaka andesite lava, Karitemang dacite lava, lake deposit, Karitemang pyroclastic-1, Karitemang pyroclastic-2, conglomerate, limestone and alluvium (Setiawan et al., 2015). Figure 2 depicts the distribution of rock formations on a geological map.

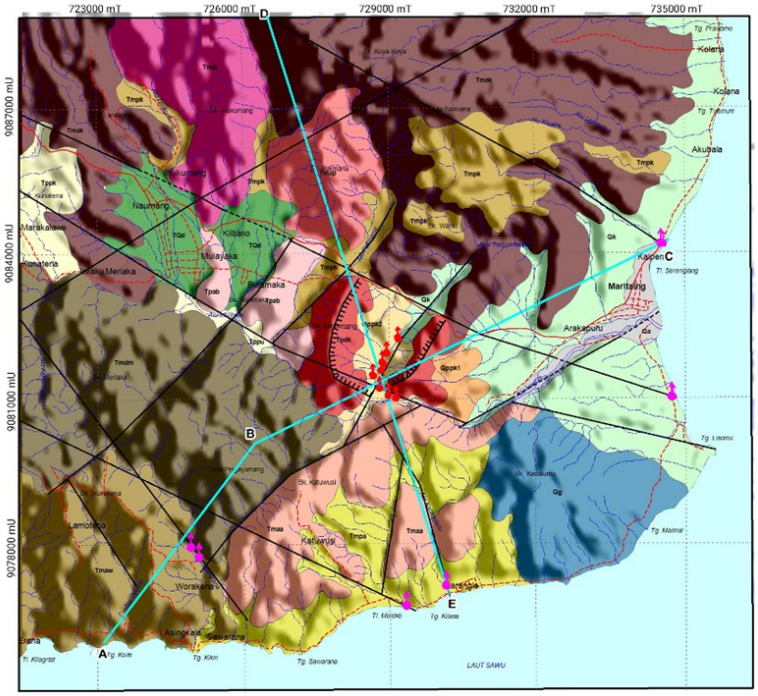

Figure 2: Geological map of the Maritaing geothermal field (Setiawan et al., 2015).

2.2 Geophysical Surveys

Various resistivity and gravity measurements have been carried out to determine the prospect areas (Rahadinata et al., 2017; Supriyadi et al., 2015). Gravity measurements were conducted in a closed polygon manner where each measurement always begins and ends with a measurement at the base point. The method has the ability to provide structural information in prospect areas. The Audio Magnetotelluric (AMT) measuring the response of the electric field and magnetic field to natural variations in the electromagnetic field with a frequency range from 0.1 Hz to 10 kHz was also applied. Low resistance values in a geothermal system identify zones of altered rock which serve as a caprock to prevent hot fluids from reaching the surface (Supriyadi et al., 2015).

Recent Magnetotelluric (MT) and Time Domain Electromagnetics (TDEM) surveys conducted by Rahadinata et al. (2017) aimed to gain subsurface data with more focus on the surrounding geothermal prospect area. TDEM and MT measurements were conducted at 42 points, which covers the entire estimated potential area. The TDEM distribution points were designed to be utilised for MT data correction. The distributions of resistivity values at different depths are shown in Figure 3.

At depths of 100 m and 250 m, conductive zones with resistivity <10 Ohm·m observed around the Maritaing hot spring location. They form a closed and extensive southwest-northeast pattern that corresponds with the geological structure presumed to control manifestations in the survey area. This conductive zone is believed to act as the cap rock layer for the Maritaing geothermal system. In comparison, low resistivity values in the south and east at 250 m depth are expected due to the sedimentary rocks that are not revealed at the ground surface. At 500 m depth, certain conductive zones around the manifestation begin transforming into a higher resistivity zone, which is believed to be a transition zone between cap rock and reservoir. Medium resistivity values start to emerge around the surface features at a depth of 750 m and extend to a depth of 1000 m and are thought to correspond to the reservoir of the system (Rahadinata et al., 2017).

The cross-sections of the third and fourth tracks that intersected the area of surface features are shown in Figure 4. Both tracks show the existence of a conductive layer throughout the zone of surface features, extending

approximately 500 m from the surface and presumed to be the cap rock. A medium resistivity zone with 20-150 Ohm·m is assumed to be the reservoir. Meanwhile, the medium resistivity values outside the prospect area are believed to correspond to the pyroclastic Koya-Koya (Rahadinata et al., 2017).

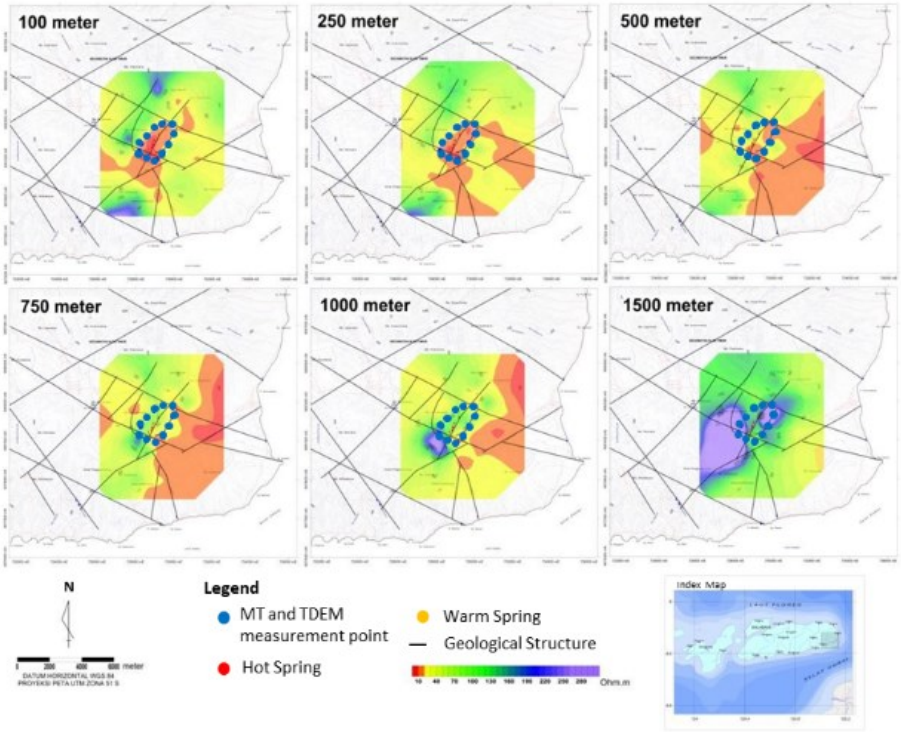

Figure 3: Resistivity maps for different depths 100 m, 250 m, 500 m, 750 m, 1000 m, 1500 m (Rahadinata et al., 2017).

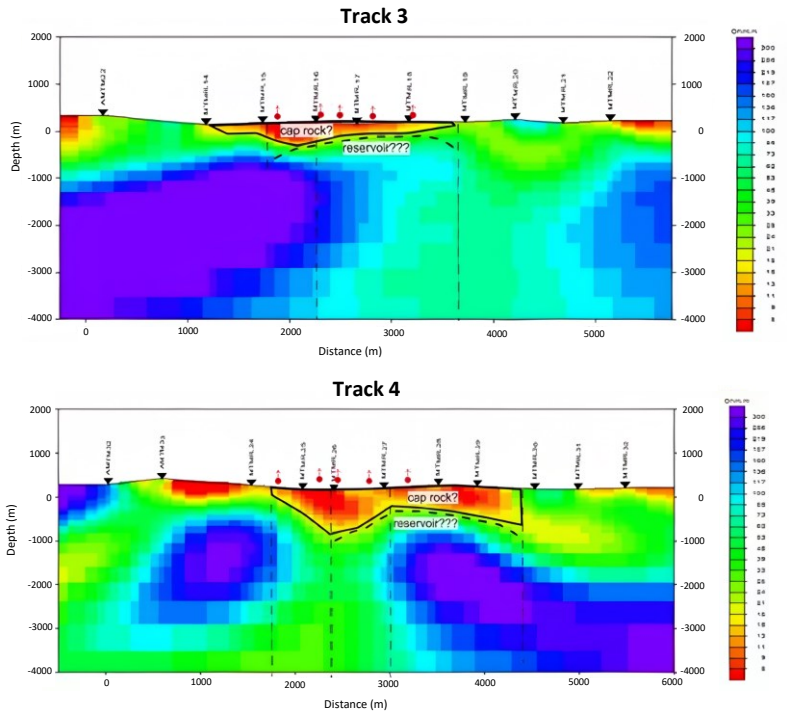

Figure 4: Cross-section display of MT measurements along track 3 and track 4 (Rahadinata et al., 2017).

2.3 Geochemical Studies

Nine water samples were analysed from hot springs and warm springs in the Maritaing geothermal system (Setiawan et al., 2015). The temperatures of the features range from 58° - 81ºC, and they are of chloride and chloride-bicarbonate type (Direktorat Panas Bumi, 2017). As shown by the ternary Cl-SO_4-HCO_3 plot in Figure 6, Kura hot springs, along with Alakalela and Mabata warm springs, are of chloride type. High silica content and the existence of silica sinter indicate that the hot fluid originates from the reservoir with little mixing with groundwater. The mixing of hot fluid and seawater is thought to happen at both Alakalela and Mabata warm springs, which appear on the beach. Additionally, intensive mixing of hot fluid with ground water, condensate water or carbonate rock is believed to be happening at other warm bicarbonate springs (Setiawan et al., 2015).

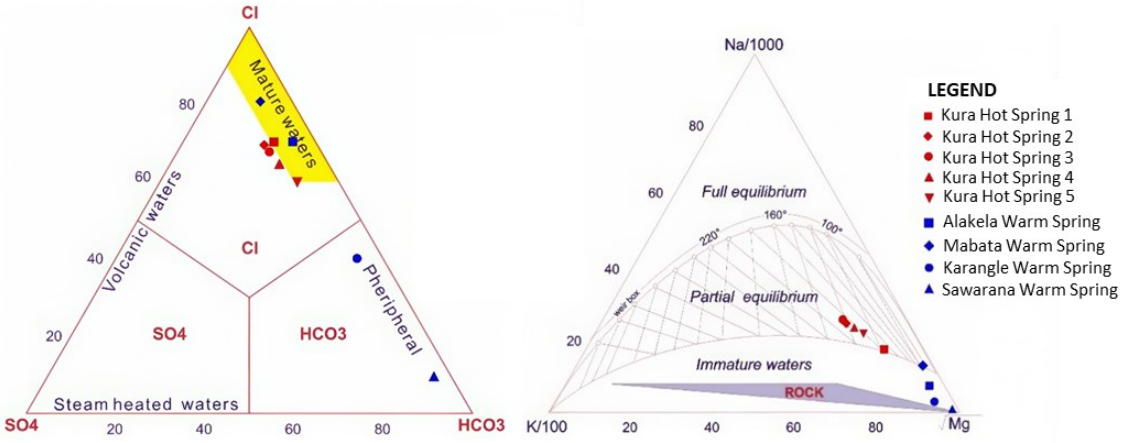

Figure 5: Ternary Cl-SO4-HCO3 diagram (left) and ternary Na-K-Mg diagram (right) (Setiawan et al., 2015).

2.4 Tentative Conceptual Model

Setiawan et al. (2015) developed a tentative conceptual model for Maritaing hydrothermal system, which was used to develop the 3D conceptual model for the current study. The tentative conceptual model is depicted in Figure 6.

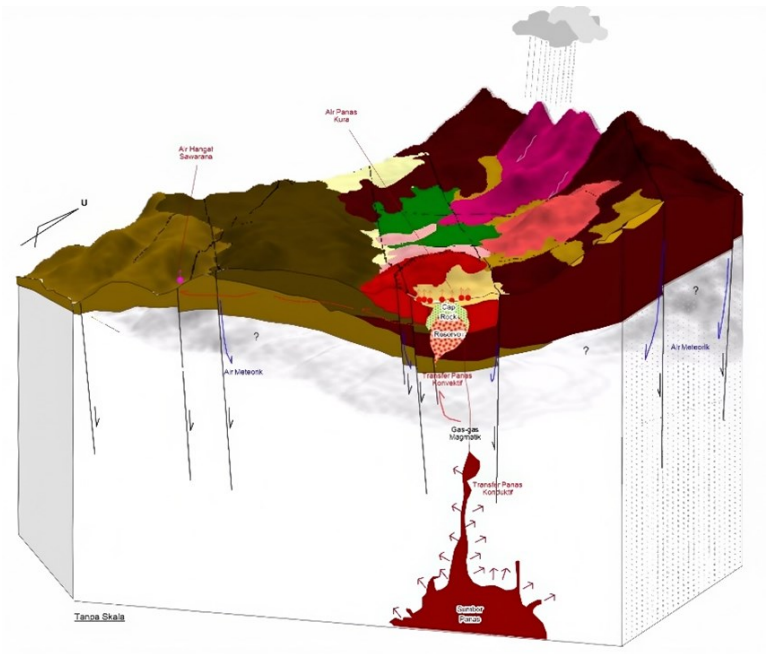

Figure 6: Tentative conceptual model (Setiawan et al., 2015).

The geothermal system in Maritaing is believed to be linked with young magmatic activity within the weak zone of the Maritaing Depression, characterized by volcanic rocks with an intensive fault system and supported by a substantial fluid supply from the north and south of the depression in a medium terrain setting. Meteoric water infiltrates the rainwater catchment areas in the north and south of the Maritaing Depression through permeable

zones. The residual heat from magmatic rocks around Mt. Karitemang has heated the meteoric water, forming the reservoir. The Maritaing reservoir is expected to be an intensively fractured system in volcanic rocks, consisting of tertiary lavas and breccias that have experienced repeated tectonic activities (Setiawan et al., 2015).

Alteration rock, which serves as the impermeable layer (cap rock), has been formed as a consequence of the interaction between hot fluid and the surrounding rocks. The cap rock layer of the system is assumed to be *montmorillonite* clay formed from an argillic-type alteration process of tertiary volcanic rocks (Setiawan et al., 2015).

The hot fluids, along with dissolved elements, accumulate in the reservoir around Karitemang Hill and move convectively to the surface through faults. These hot fluids emerge on the surface at the hot spring manifestations in the Kura area. Simultaneously, the warm springs formed further east and south are believed to have travelled laterally through faults from the Maritaing geothermal system before emerging (Setiawan et al., 2015).

3. 3-D CONCEPTUAL MODEL

3.1 Geological Model

Establishing geological model started by extracting X, Y, and Z coordinate points and imported to Leapfrog in order to set up the topography of the model. The area extends for 40 km around the surface features at Mt. Karitemang, which is believed to be the centre of the geothermal system. Large area gives ability of the reservoir to contain large-scale convective system and its surrounding meteoric charge. The rock stratigraphy and fault structure are set by digitising the boundary of each formation, horizontally and vertically according to the geology map. Table 1 gives the summary of stratigraphy units in the Maritaing geothermal area.

Table 1: Summary of the stratigraphy units in the Maritaing geothermal system.

Rock Units	Abbreviation	Geologic Age
Alluvium	Qa	Holocene
Limestone	Qg	Pleistocene
Conglomerate	Qk	Pleistocene
Karitemang Pyroclastics 2	Qppk2	Pleistocene
Karitemang Pyroclastics 1	Qppk1	Pleistocene
Lake Deposit	Tqd	Pleistocene
Karitemang Dacite Lavas	Tpdk	Pliocene
Bulamaka Andesite Lavas	Tpab	Pliocene
Kunatena Pyroclastic	Tppk	Pliocene
Meriaka Andesite Lavas	Tmam	Late Miocene
Pakmana Andesite Lavas	Tmap	Late Miocene
Inukamang Andesite Lavas	Tmai	Late Miocene
Koya-Koya Pyroclastics	Tmpk	Late Miocene
Koya-Koya Andesite Lavas	Tmak	Late Miocene
Worakena Andesite Lavas	Tmaw	Late Miocene
Katuwusi Pyroclastics	Tmpa	Late Miocene
Katuwusi Andesite Lavas	Tmaa	Late Miocene

As indicated in Table 1, the geological periods are categorised into three epochs, namely: Late Miocene, Pliocene, Pleistocene, and Holocene. The late Miocene includes the following formations (bottom to top): Katuwusi Andesite Lavas (Tmaa) alongside with Koya-Koya Andesite Lavas (Tmak), Inukamang Andesite Lavas, and Pakmana Andesite Lavas which are pyroxene andesite type lavas from Late Miocene. In addition, for the rock units in Late Miocene, Meriaka Andesite Lavas is of hornblende andesite type. The pyroclastics rock unit in the Late Miocene consists of Katuwusi Pyroclastics, which are composed of lapilli tuff and tuff breccia, and Koya-Koya Pyroclastics in the form of a breccia (Setiawan et al., 2015).

During the Pliocene epoch, volcanic rocks continued to form in the Maritaing depression zone. The rock units are Kunatena Pyroclastics (Tppk), Bulamaka Andesite Lavas (Tpab), and Karitemang Dacite Lavas (Tpdk). Kunatena pyroclastic deposits (Tppk) consist of tuff breccia with andesite and dacite fragments. Bulamaka andesite lava

(Tpab) is pyroxene andesite with fine fractures filled with quartz. Karitemang dacite lava (Tpdk) forms the crater structure of Karitemang Ridge, where the Kura hot springs are situated (Setiawan et al., 2015).

In the Pleistocene epoch, Lake Deposits (Tqd) in the form of conglomerate and sandstone from volcanic rock fragments were formed throughout the depression zone of Maritaing. Simultaneously, Volcanic activity from Mt. Karitemang led to the formation of Karitemang Pyroclastic 1 (Qppk1) in the eastern part of the crater. Following this, the Karitemang Pyroclastics 2 (Qppk2) formed within the crater and extended southwards. Both pyroclastic rock units are made up of tuff breccia with andesite and dacite fragments (Setiawan et al., 2015). A conglomerate rock unit in the form of sandstone and conglomerate was formed in the eastern part of the field, simultaneously with a Limestone rock unit in the southeast. Continuous deposition of an Alluvium rock unit (Qa) in the form of surface deposits has occurred along the mouth of the Irawuri River (Setiawan et al., 2015).

For the structural model, there are fifteen faults that are assumed to intersect each rock unit vertically 90º. In addition, certain faults are extended laterally. These assumptions were made since there are no data constraints and they help to optimise the fluid pathways and help with calibration of the numerical model. To facilitate calibration, the rock types for faults with a NW-SE orientation are named A to H and faults with a NE-SW orientation are named T to Z.

The NE-SW fault around Mt. Karitemang is expected to control the Kura hot spring features. Meanwhile, the NW-SE fault that crosscuts Mt. Karitemang controls the surface features in the southern part of the area of interest. These are expected to be the main faults that control the geothermal system at Maritaing.

3.2 Alteration Model

To build the alteration model, resistivity measurement data from the Geology Agency of Indonesia were imported along with the resistivity map (Figure 3) and the MT cross sections (Figure 4). They play an essential role in setting the boundaries, laterally and vertically, of the clay cap. It is believed that the clay cap consists of low permeability clays formed by the alteration process. The polylines method was also utilised to define the form of the clay cap. It appears that an up-dome formation is present beneath the northern part of the clay cap, leading to a thicker zone in the southern area. Additionally, the clay cap is exposed to the surface in the west area. Although the alteration model has a high uncertainty due to the interpretation applied, the model is able to be tested on the numerical model through the calibration process. Combined model of the geological and alteration model in Leapfrog is shown in in Figure 7.

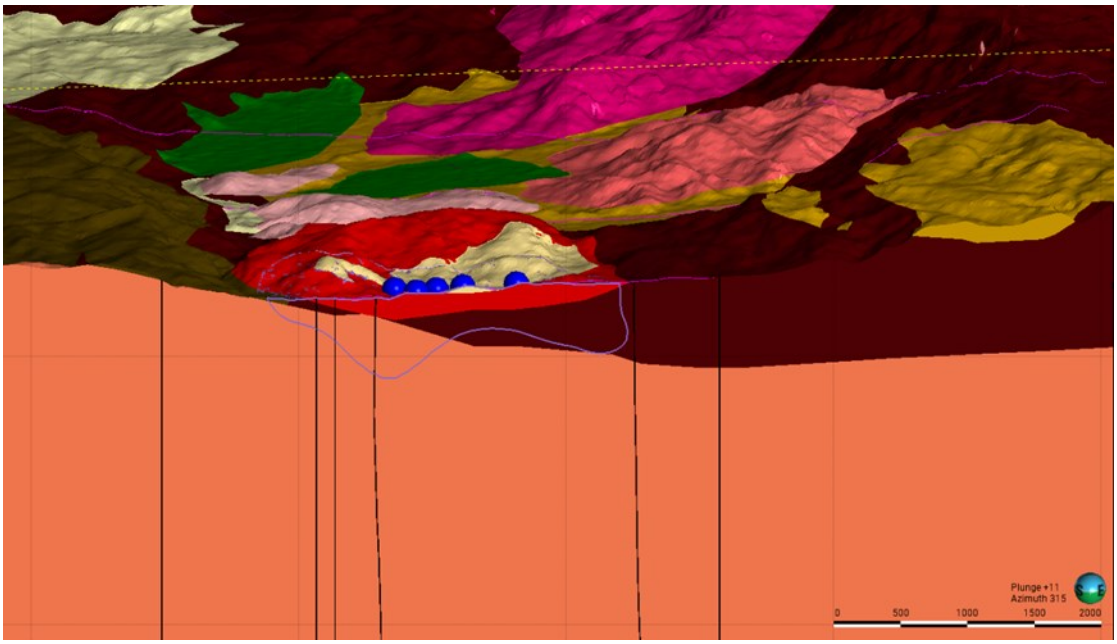

Figure 7: Combined digital conceptual model including geological, structural and alteration models. The black lines represent the faults while the purple line depicts the alteration zone.

4. NUMERICAL MODEL

4.1 Model Grid Setup

The initial model grid was created to be consistent with the Leapfrog model. The grid is oriented 26° from the azimuth to align with the main faults, facilitating model calibration. The model grid covers an area of 13 X 12 km

and the grid is comprised of 12,008 blocks. The largest blocks are 800 m X 800 m, with vertical thickness ranging from 500 m at the base to 100 m near the surface. In areas of interest, a smaller block size was set for better resolution.

The rock types of the blocks were automatically matched to the formations, structures and alterations in the Leapfrog model, allowing seamless integration using PyTOUGH scripts (Popineau et al., 2018). O'Sullivan et al. (2023) explain the rock-type naming convention related to the geology, structures and alteration zones. Figure 8 depicts the grid layout area imported into Leapfrog. The model tries to match the location and boundary of each formation, as shown by the colour of the blocks.

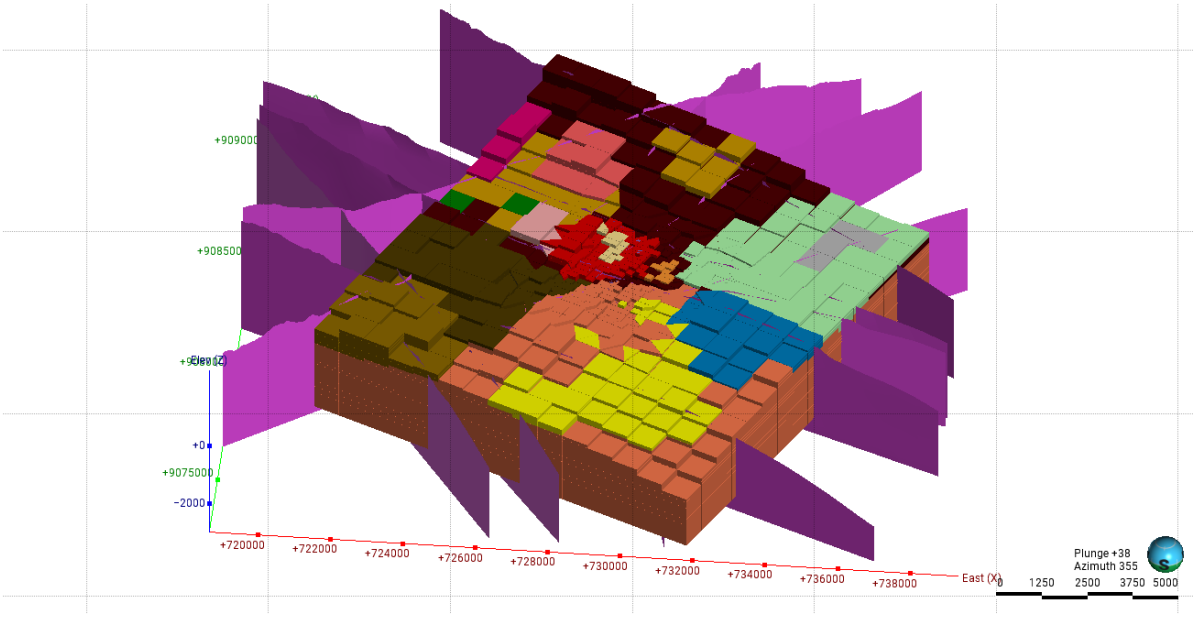

Figure 8: Grid Layout for Maritaing geothermal field in Leapfrog. The colour of the blocks represents the lithology, while the magenta-coloured planes are the faults.

4.2 Boundary Condition

Top boundary: The top boundary of the model is defined by the ground surface and dry atmospheric conditions are set, with a pressure of 1 bar and a temperature of 15ºC. The EOS3 equation of the state module in TOUGH2 provides the thermophysical properties of water and air for the mass and energy balance equations (Pruess et al., 1999). Moreover, the module allows the vadose zone to be included above the water table, at pressures close to the atmospheric pressure (O'Sullivan & O'Sullivan, 2016). A high permeability at the top layer was assigned to allow rainwater infiltration, which then flows from the higher elevation following the topography. An annual rainfall of 800 mm per annum with a 10% rate of infiltration was implemented.

Side boundary: The model has a no-flow side boundary condition implemented for the natural state because the model is sufficiently large to include the entire whole convective geothermal system without any side flows.

Base boundary: A uniform background heat flux of 64 mW/m² was applied to the base boundary. Furthermore, a total mass upflow of 33 kg/s with an enthalpy of 1200 kJ/kg of hot mass was injected into eight blocks, situated under the NE-SW fault around the Kura surface features.

5. NATURAL STATE SIMULATION

5.1 Model Calibration

Calibrating a model is a repetitive process required to ensure the reliability of the fit of the model to the data. A model that has been through calibration is expected to represent the real reservoir and field condition as precisely as possible. In calibration, changing one or several parameters affects several model results concurrently. Manual model calibration is generally a widely used method to improve a model (O'Sullivan et al., 2016) and was implemented in this study.

For calibrating this model, the parameters adjusted were the hot mass injected at the base of the model and the permeabilities of the rock types controlling the fluid flow. Permeabilities were adjusted, taking account of the

lithology and fault structures. High permeabilities were assigned to certain shallow structures, allowing some hot fluid to flow to the surface, matching the real surface features in certain areas.

In order to attain steady-state conditions, the model was run for 5 X 10^{13} seconds for each step of calibration. The 33 kg/s of hot mass was injected into the 5 blocks, concentrated under the NE-SW fault near Kura hot springs. It is expected that this fault mainly controls the upflow in the Maritaing geothermal field. On the other hand, the NW-SW fault which crosscuts Mt. Karitemang allows the fluid to flow to the northwest and southwest. Geological rules are consistently implemented on the different formations and faults. They allow an increased permeability along the strike and vertically up the dip of faults and a decreased permeability across the strike of the fault. Thus, anisotropic permeabilities are used for each rock type to represent the characteristics of the faults. Meanwhile, isotropic permeabilities are implemented for the base rock types as the baseline for adjusting the permeabilities of the faults.

Additionally, the altered clay cap is assumed to serve as a fluid barrier, restricting flow to the surface. Low permeabilities are assigned to certain blocks, representing the shape of the clay cap. Due to the irregular dome shape of the cap, the fluid flow from depth is forced to disperse underneath the cap.

Attaining a good match to data for downhole temperatures is a benchmark in the successful calibration of a natural state model. However, the well drilling stage has not been conducted since Maritaing field is categorized as a greenfield. Therefore, the calibration of the model was believed to be successful when several conditions were met, such as the temperature under the clay cap achieved the constraint temperature of around 200°C and, the model illustrates a significant amount of heat reaching the surface in zones where surface features occur, and the fluid flow in the model follows reasonable pathways.

5.2 Natural State Model

The natural state model was successfully calibrated by matching the estimated temperatures of the clay cap and the surface features data. Surface features used as reference for the model are in locations such as Kura River for the hot springs (KUA01, KUA02, KUA03, KUA04, KUA05) and for the warm springs in Alakalela (ALK01), Mabata (MBT01), Karangle (KRL01), and Sawarana (SWA01). Most of the surface features, especially surface features in Kura River area are chloride-type hot springs, indicating that the area is an upflow zone. The surface features outside Kura River are thought to result from the lateral flow of the fluid, indicating they are in an outflow zone.

The temperature under the clay cap was constrained to be 200°C as the result of geothermometer data and the expected temperature at which the rock is altered. The large size of the blocks is the reason why the temperature does not exactly match 200°C underneath the clay cap. Figure 18 and Figure 19 show temperatures on NE-SW and E-W oriented slices, respectively.

Upflow zones are identified, matching the temperature isotherm of 200ºC below the clay cap and the existence of hot springs of chloride type near the Kura River (KUA01, KUA02, KUA03, KUA04 and KUA05). The outflow zone is indicated by the locations of warm springs of bicarbonate type, such as KRL01 and ALK01. Additionally, the higher elevation zone in Figure 21 acts as the recharge zone for meteoric water.

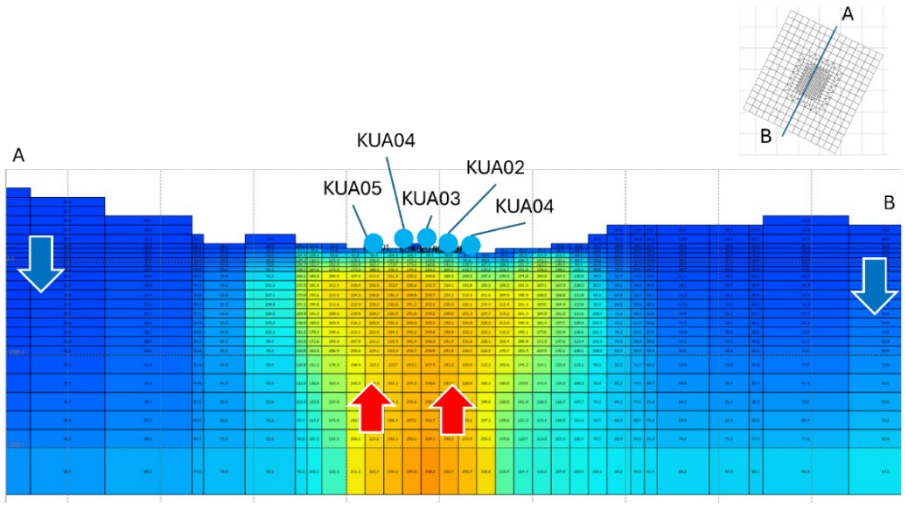

Figure 9: NE-SW oriented slice of temperature plotted with TIM. Red arrows depict the upflow, while blue arrows illustrate the recharge.

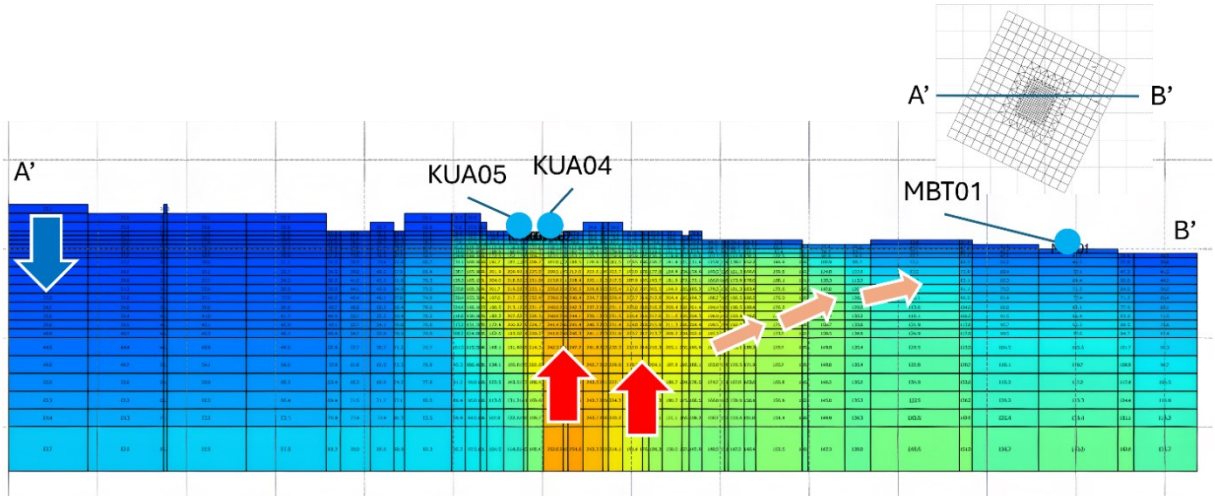

Figure 10: E-W oriented slice of temperature plotted with TIM. Red arrows depict the upflow, orange arrows depict the outflow while the blue arrow depicts the recharge.

6. UPDATED CONCEPTUAL MODEL

Based on the calibration result, an updated conceptual model of the Maritaing geothermal field is proposed. The plan view of the conceptual model with the fault are shown in Figure 11.

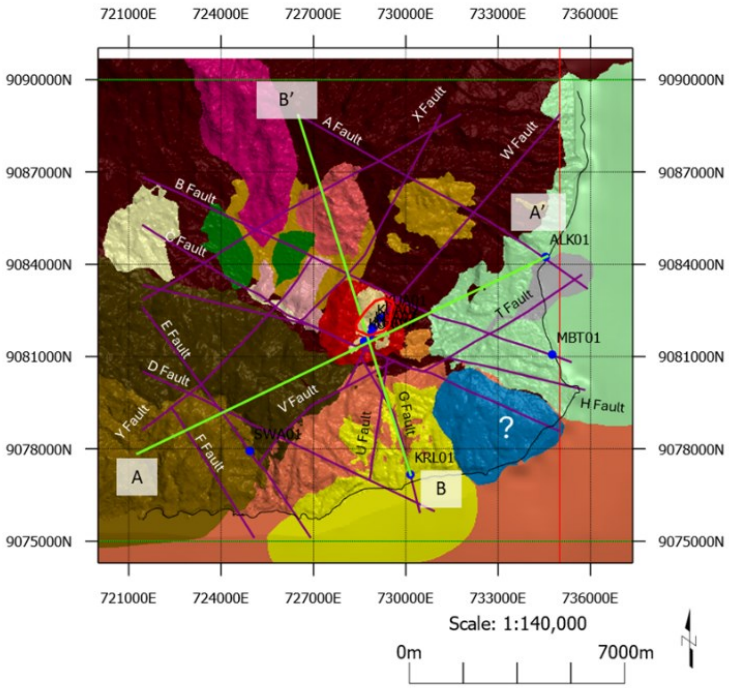

Figure 11: Plan view of the updated conceptual model, showing the fault lines (purple), surface features (blue dot), section lines of cross section images A-A' (Figure 23) and B-B' (Figure 24) (green lines)

Based on the interpretation of Magnetotelluric data, the altered zone is situated around the Kura hot springs. The possible heat is expected to rise directly under the Kura hot spring through the W fault (red line). B Fault is expected to act as the barrier of the fluid, restraining further flow to the NE, but cause the mass flow to the SE direction, resulting in Mabata warm spring (MBT01). Additional pathways of the fluid are expected to flow along the C fault, following the topography elevation. A low permeability area is estimated to lie on the western part of the Tmaw formation since the calibration results show less mass flow infiltration of the reservoir through the formation. Meanwhile, the north area of the field, where most of the Tmak formation lies, serves as the recharge area for the reservoir.

The slices of the updated conceptual model are shown in Figure 12.

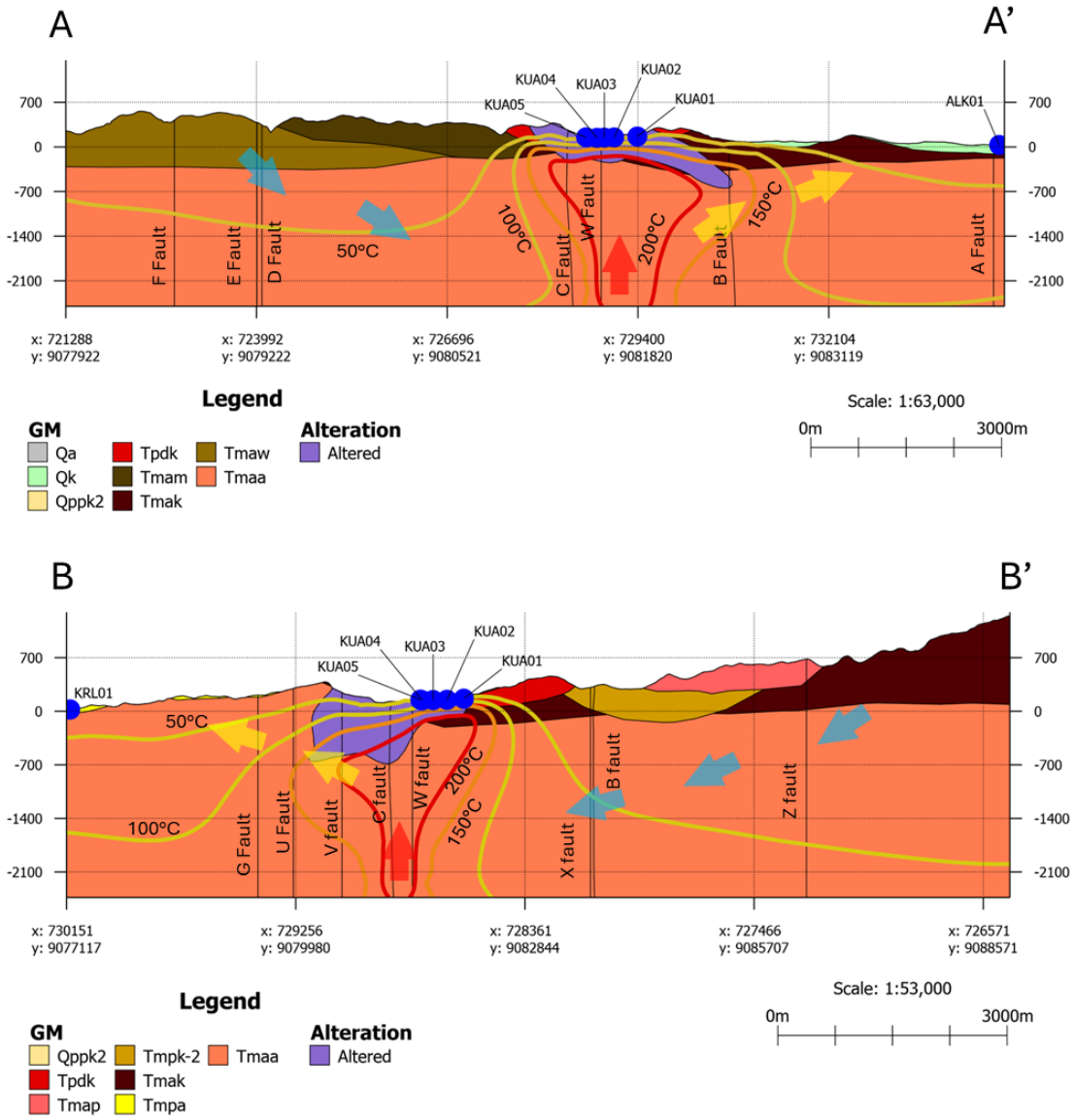

Figure 12: Proposed conceptual model of Maritaing geothermal field based on numerical modelling. The top part shows the A-A' and the bottom part shows the slice B-B', from the figure 22. The red arrow parti is upflow, the yellow arrow is the outflow while the blue arrow is the recharge

From slice A-A', the upflow comes beneath the Kura hot springs through the W Fault. The mass outflow goes to the NE part of the field, resulting in the existence of the Alakalela surface feature (ALK01). The recharge water comes from the SW part of the Maritaing, the infiltration water is relatively small based on the calibrated model. Similarly, the slice B-B' shows the upflow that goes through the W fault. The outflow travels laterally in the NE direction of the Maritaing, leading to the existence of the Karangle surface feature (KRL01). The main recharge zone is identified from the northern part of the Maritaing through the Tmak formation.

It can be shown the 200°C isotherm describes the estimated reservoir area. It is apparent that the Tmaa formation serves as the host rock for the reservoir. The altered rock was exposed to the surface for the western part of the alteration zone, resulting in a dome shape at the north-east part of the clay cap. The thickness of the clay cap ranges from 400 to 700 m. It appears that the W fault along with the C fault located around the Kura hot springs controls the Maritaing system.

7. CONCLUSION

This study has been successfully developed conceptual model based on 3D digital conceptual model and numerical model of Maritaing field. The calibration process yielded a good match based on the geothermometer data

temperature constraint of the geothermometer result and surface features data. The 3D digital conceptual model and natural state in numerical model are able to update the tentative conceptual model of the field, where the heat sources are estimated to be located below the Kura hot springs. Establishing the digital conceptual model in Leapfrog geothermal made the numerical model consistent with the available data and able to ease the modelling process.

ACKNOWLEDGEMENTS

The authors would like to acknowledge EBTKE and Geology Agency of Indonesia in providing the necessary data, and also to Seequent in providing the access to build the 3D digital conceptual model. Authors would like to give thanks to LPDP or Indonesia Endowment Fund to support the research project.

REFERENCES

Direktorat Panas Bumi. (2017). *Potensi Panas Bumi Jilid 2*. EBTKE.

O'Sullivan, J., Cantwell, A., Archer, R., O'Sullivan, M., Williams, B., & Krom, T. (2016). A New Geothermal Modelling Workflow Using Leapfrog and TOUGH2. *African Rift Geothermal Confer*ence, Addis Ababa, Ethiopia.

O'Sullivan, J., Popineau, J., Gravatt, M., Renaud, T., Riffault, J., Croucher, A., Yeh, A., & O'Sullivan, M. (2023). An integrated, mesh-independent geothermal modelling framework. *Environmental Modelling & Software*, 163, 105666. https://doi.org/https://doi.org/10.1016/j.envsoft.2023.105666

Popineau, J., O'Sullivan, J., O'Sullivan, M. J., Archer, R., & Williams, B. (2018). *An integrated Leapfrog/TOUGH2 workflow for a geothermal production modelling*.

Rahadinata, T., Zarkasyi, A., & Dewi, R. (2017). *Survei Magnetotellurik (MT) dan Time Domain Elektromagnetics (TDEM) Daerah Panas Bumi Maritaing, Kabupaten Alor, Provinsi Nusa Tenggara Timur*

Setiawan, D. l., Wibowo, A. E. A., & Hermawan, D. (2015). *Geologi dan Geokimia Panas Bumi Daerah Maritaing Kabupaten Alor, Provinsi Nusa Tenggara Timur*

Supriyadi, Y., Takodama, I., & Nurdin, N. M. (2015). *Survei Terpadu Gaya Berat dan Audio Magnetotelluric (AMT) Daerah Panas Bumi Maritaing, Kabupaten Alor, Provinsi Nusa Tenggara Timur*

2023 Microearthquake Monitoring Result as Part of Reservoir Monitoring in Namora-I-Langit Geothermal Field

Yuris Ramadhan[1], Grandy B Danakusumah[1], Irfan Hamzah[1],
David Sahara[2], and Aditya Hernawan[1]

[1]Sarulla Operation Ltd., 7th Floor the Energy Building, SCBD Lot 11A Jakarta 12190, Indonesia
[2]Global Geophysics Research Group, Institut Teknologi Bandung, Jalan Ganesha No. 10, Bandung, 40132, Indonesia

Yuris.ramadhan@sarulla-geothermal.com

Keywords: Namora-I-Langit, Microearthquake, Reservoir Monitoring

ABSTRACT

Sarulla Operation Ltd. has been operating the Namora-I-Langit geothermal field since 2017. The field that is located in North Sumatra is part of the liquid-dominated reservoir within the Great Sumatran Fault segment. Since 2020, 18 seismic equipment has been deployed to support the reservoir monitoring from the microearthquake events in Namora-I-Langit and the neighbours' field in Silangkitang. The purpose in this study is to describe the current 2023 monitoring result in Namora-I-Langit field in relation to the reservoir process including the injection movement, drilling result, and the overall reservoir changes. Simultaneously, the possible faults/ fractures distribution can be observed and used for the future development plan. Currently, 2558 seismic events have been recorded over the 2023 timeframe, with an average of 4-7 occurrence each day as a baseline. However, some increasing seismic rates are recorded and may correlate with the operations, like the injection process, well drilling, well surveillance, and other activities. In addition, large earthquakes with epicentres in Tarutung region were recorded during monitoring in August 2023. To improve the seismic location, hypocentre relocation and waveform cross-corelation were utilized to minimize the residual travel time and pinpoint more exact position.

The results so far are quite consistent with the interpretation of injection channel which runs from eastern part from NIL3N injection wells to the south and west from production wells. Another conclusion from the recent WJR1-2 well drilling shows that the northern NIL area has an aseismic zone that been identified as permeable locations. Meanwhile the concentrated seismic event around Great Sumatran Fault may show the barrier zone that separates the NIL field from the tight zone on the eastern side of the Hutajulu Fault. Tomography and focal mechanism model were conducted to support the monitoring evaluation. Resulting in some consistent interpretation of reservoir geometry and fault direction. However, the model has considerable uncertainty due to the data distribution and limitation. Finally, the monitoring survey plans to continue in 2024 with certain improvements, such as the station relocation, velocity model, and the resolution boundary for tomography model. Some ideas for running the time lapse (4D) tomography or Ambient Noise Tomography are also considered as part of the future improvement.

1. INTRODUCTION

Sarulla Operation Ltd (SOL) has been given the right to operate power generation from Geothermal field in Sarulla contract block, North Sumatran Province. Currently, the total installed capacity 330 MW generates from Namora-I-Langit (NIL) and Silangkitang (SIL) geothermal fields under a single Contract as part of a Joint Operating Contract (JOC) with Pertamina. However, this study will be focused on monitoring the reservoir performance at Namora-I-Langit field from a geophysical perspective.

The geological background from Namora-I-Langit is a volcanic complex at the northwest end of the Sarulla contract block. The complex consists of two volcanic products from andesitic to rhyolitic lavas and tuffs. Namora-I-Langit also situated around the Great Sumatra Fault (Tor Sibohi and Hutajulu Faults) that makes the permeability is dependent on the fracture development around the area (Figure 1 (left)). Whilst the presence of geothermal activity manifested from thermal features such as fumaroles, acid sulfate springs, neutral Cl-sulfate-bicarbonate hot springs, gas seeps, and numerous warm bicarbonate springs covering an area of about 30 km2 (Gunderson et al., 2000). The field is currently operated with the high temperature system and produced from a two-phase fluid from the wells.

Starting from 2020. MEQ Monitoring has been initiated in Both NIL and SIL to understand the dynamic reservoir process in response to exploitation activity (injection movement, reservoir geometry). The total area for both NIL and SIL is ±224 km^2 covered by total of 18 seismometer-geophones (Yudha et al., 2021). The other advantage from MEQ Monitoring study is the characterisation of fractures/fault distribution along the field. The result is

useful for reservoir characterization and reservoir management plan (development strategy and well targeting). Another purpose beside the resource monitoring is as input for shareholder on potential hazard (large earthquake) and environmental issue related to geothermal activities (safe operation).

2. METHODOLOGY

Sarulla Operation Ltd has operated maximum 18 seismometers dedicated to monitor the reservoir development. The tools are using the shallow burial geophone from Geotech and equipped with SMART24R recorder and GPS to get the optimum tools performance. For the operation, the battery is equipped for the tools and needs to be replaced every 1-2 weeks for the charging.

Calibration and tool setting up were done before installed by synchronizing all the equipment to ensure the tools will run together. Then all the instruments were installed at each microseismic station location. The network arrays for the stations are shown in Figure 1 (right). The distribution is not ideal due to the accessibility to reach the high side location of Great Sumatran Fault and the security purposes. During monitoring from 2020 – 2023. Several 1D velocity model has been improved from previous model by using only events with high accuracy, azimuthal Gap < 180, and Immediate vicinity of Sumatran Fault & excluding mountains area. Velocity model has been stable and constant after June 2021. For data QC, wadati diagram was used to present the linear correlation and predict the uncertainty of waveform phase arrival time and the ratio of Vp/Vs. In average shows normal Vp/Vs trend of the rock ~ 1.713 + 0.011 with Total P-S pairs= 32.10. Therefore, using this diagram, the best practice for determining good correlation or good picking of P-wave and S-wave should be within the gradient value.

The normal Hypocenter determination is using the Nonlinear calculation, but to minimize the residual of "pair events" instead of "single events", the relative relocation (HypoDD) and waveform cross-correlation (WCC) were performed as it common applied for local scale, e.g. geothermal, underground mining. While, to obtain the Magnitude was determined using duration magnitude and Length/duration using the coda wave with the average Magnitude around 0.5-1. Later, the Hypocenter relocation & waveform cross-correlation has improved the travel time residual (RMS) and narrow the uncertainty to become ~ 100 m (x, y, z) correspond to 0.02 s RMS misfit.

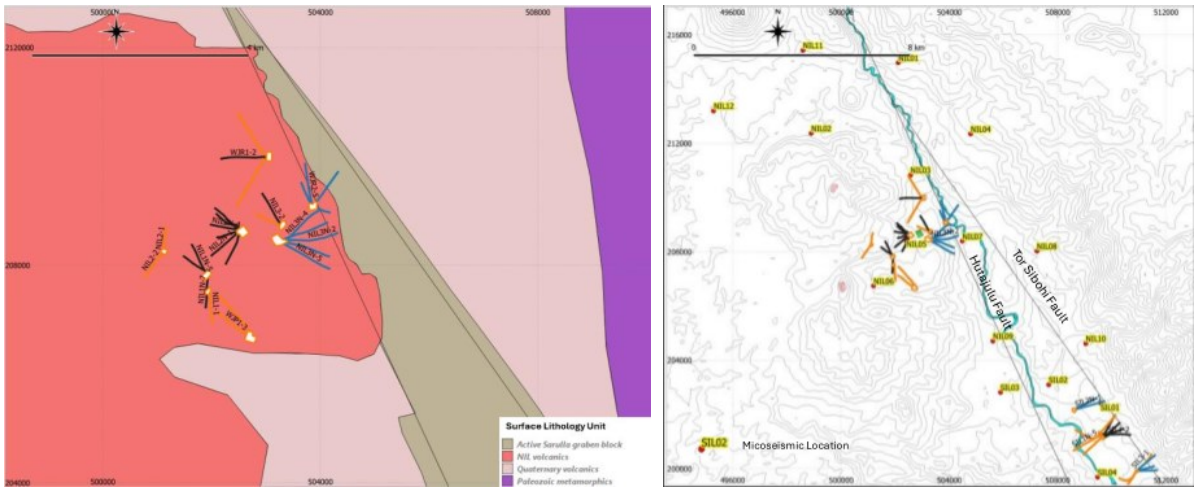

Figure 1: (left) Surface Stratigraphy and Regional fault Map and (right) Seismometer distribution including in Neighborhood field (SIL) with background topography and regional fault.

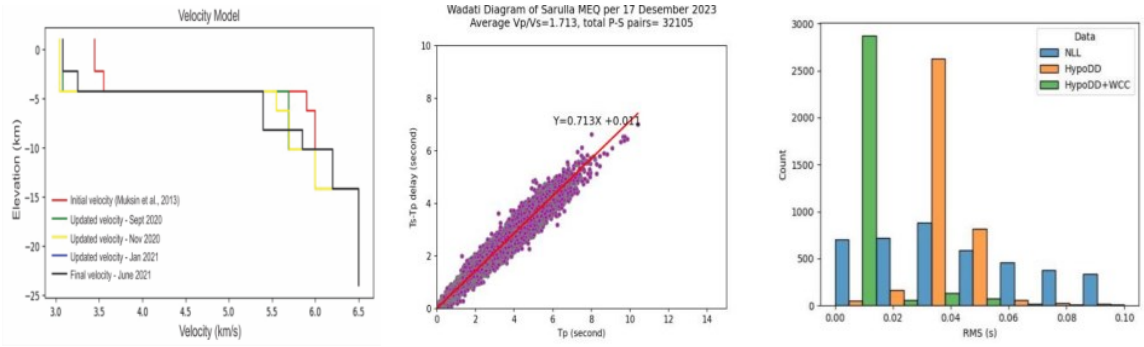

Figure 2: (a) Current 1D velocity model compared with previous model and (b) Wadati Diagram (c) RMS calculations from NLL, HypoDD, and HypoDD + WCC.

3. MEQ MONITORING RESULT

In 2023 Monitoring, 2558 seismic events were picked, covering around ±224 km^2 of NIL and SIL area. During the measurement, there were an average 4-7 event/day occurred as a background for both areas. Some increasing seismic trends are associated with outage/curtailment, well drilling, surveillance, and acidizing (workover). Some of the activities will be further explained in this chapter. While the high event rates also occurred in 2023 and interpreted from major earthquake with epicenters in Tarutung represent on red dashed lines. However, for the confidence level, only 418 seismic events will be presented on the general map from HypoDD+WCC relocation events.

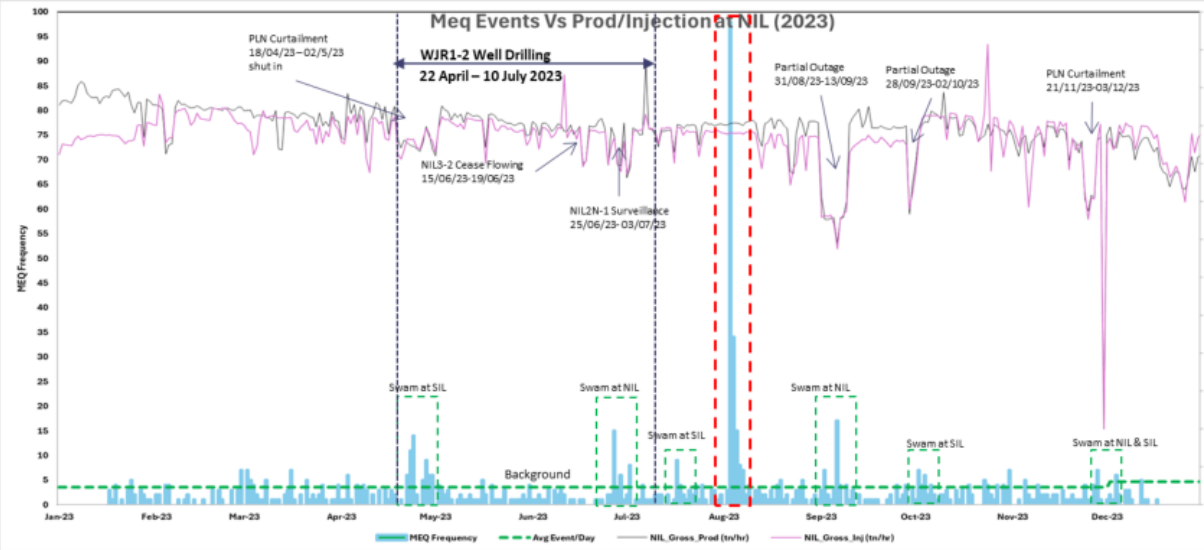

Figure 3: Production and Injection volume (tn/hr) at NIL compared with the MEQ frequency.

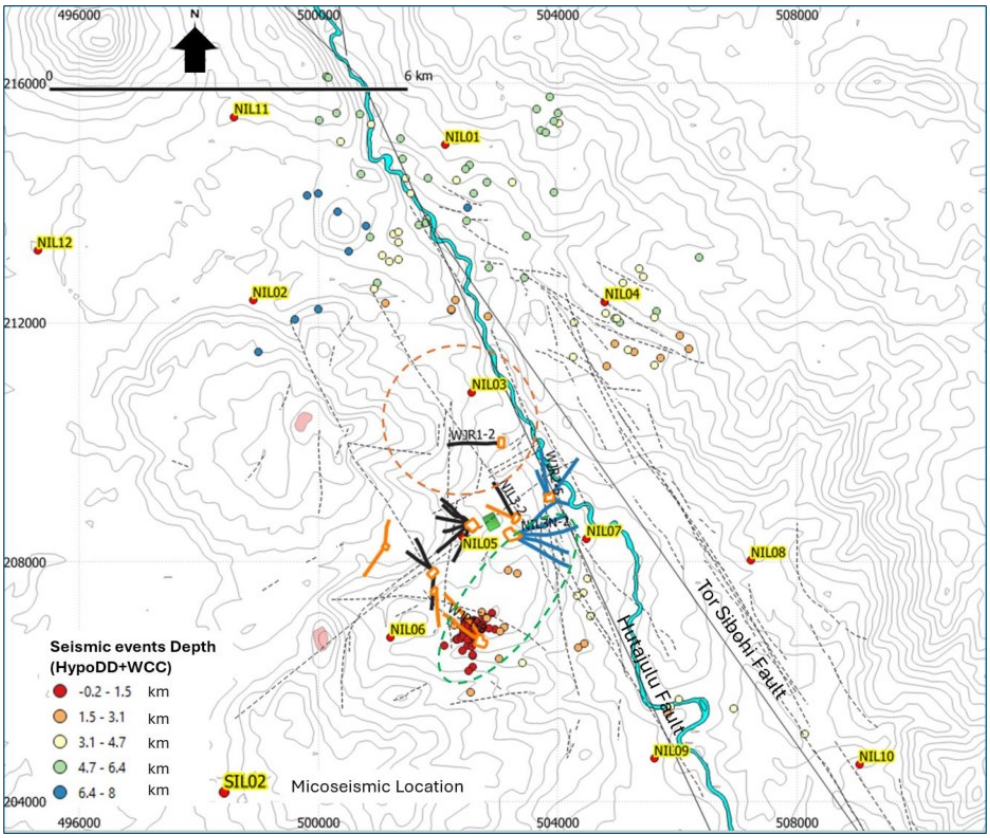

Figure 4: MeQ event distributions (HypoDD + WCC) with background topography contour in grey lines, MEQ station on red dotted symbol, and more detail faults in black dashed lines. The orange dashed circle represents the WJR1-2 well area and green dashed ellipsoid represents NIL injection movement.

3.1 WJR1-2 Well Drilling and NIL Injection Movement.

Sarulla Operation Ltd. has initiated the drilling campaign program to restore the steam recovery in Namora-I-Langit Field. The campaign will be in staged, with one well drilled in 2023 and two wells planned for 2025, all in northern region (Figure 4). WJR1-2 is the first well drilled between 22 April 2023 and 10 July 2023, and it has intersected the reservoir section and penetrating total loss condition (TLC) on 20 June 2023 (Figure 3).

During the drilling in reservoir/ TLC, no significant swarm events around WJR1-2 wells (Figure 4). However, the events are increased in the northern part and along Great Sumatran Fault after TLC condition. This might be because the pressure injection necessary to induce seismic event is still smaller than fracture gradient surrounding the wellbore. Or the area though to be permeable enough resulted in no event being recorded (aseismic area), yet the fluid still be indicated to flow direct to north area through the Great Sumatran Fault (Hutajulu Fault). This assumption provide weight to the idea that the northern part of Namora-I-Langit is still potentially exploitable.

Meanwhile, certain seismic occurrences may be attributed to operational changes, in particular to the injection location and the rate. The major changes for the injection rate had occurred in 2022. There was an injection maneuver from seven wells in two different pads into two wells in same pad and the injection scheme will continuing through 2023 (Figure 4).

Based on observation, some seismic pathway seen from NIL3N well to WJP (green dashed line). This NE-SW trend may relate to the fracture/injection path. However, compared with previous year before the maneuver, the event frequency seems slightly decreased. Some anomalies were seen on WJP pad area (red dots on south corner). These seismic events occurred rapidly in shallow level. This is interpreted whether the events derived from injection wells (blue line) or there is a natural downflow from shallow level.

3.2 2023 Tarutung Earthquake

The MEQ monitoring shows an increase in seismic occurrence, not only in shallow level from geothermal process, but also in deeper sections that related to natural earthquake. Figure 3 depicts the relationship between the rapid increase of MEQ frequency with more than 100 events in August 2023 and the natural earthquake occurrence. Based on the comparison with BMKG data, 33 seismic events recorded on 3rd of August 2023 on BMKG stations with magnitude 1.9-2.8 Richter Scale with penetration depth around 2- 3 km from surface.

Meanwhile, in the same time SOL has recorded a total of 106 seismic occurrences between 3 and 6 August 2023, with depths ranging from 5-7 km and magnitude less than 1 order. The seismic events which are centered on the east side of Great Sumatran Fault (Figure 5) reflect an extension of the larger seismic event from 2022 earthquake and are thought to be an ancient fault reactivation from the Great Sumatran Fault movement. This evidence is supporting the SOL data for earthquake mitigation plan for the future development.

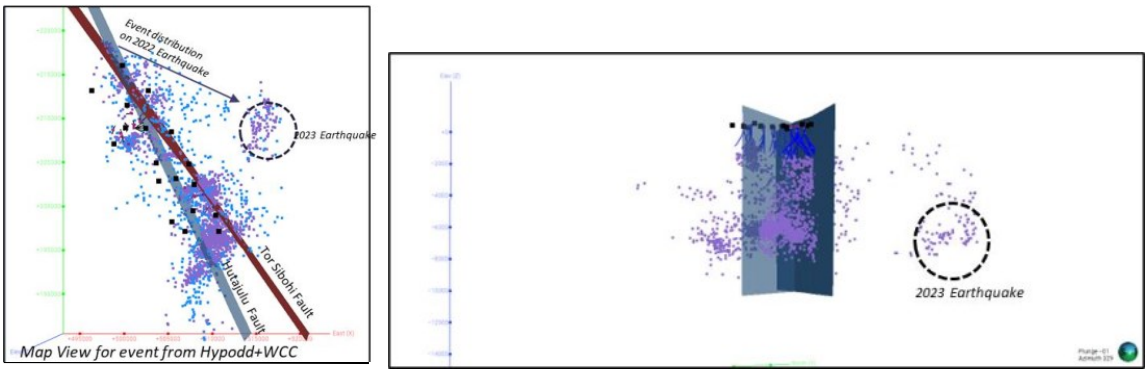

Figure 5: (left) Map view and (right) Cross Section for seismic event distribution from HypoDD+WCC analysis from 2020 – 2023 with focus on black dashed line for 2023 Earthquake in August.

3.3 Tomography and Focal Mechanism

Advanced processing such as tomography inversion and focal mechanism has been performed on the 2023 data. The color scale in Figure 6 shows for Vp and Vs represents a relative perturbation value compared to the initial 1D model, while Vp/Vs color scale shows an absolute number. P-wave velocity is commonly used to determine properties like the type of rock, porosity, and the presence of fluids. S-waves only travel through solids and are sensitive to shear modulus, so they are used to determine the rigidity of the material they travel through. The ratio of the Vp/Vs can provide insights into the present of fluid. A higher Vp/Vs ratio may indicate the presence of fluids in the rock, as fluids can significantly slow down S-waves more than P-waves. Based on the tomography modeling, NW-SE and NE-SW alignment of high velocity anomaly (Vp) were seen and may be associated with Sumatran Fault (Tor Sibohi Fault) as boundary and compartment location (south of WJP wells may have tight

permeability). While several low velocity (Vp and Vs) zones around the WJR1 area indicate highly fractured zone and the fluid/ steam zone also correlated in the southern part with the high Vp/Vs value around those area. In line with the figure, the focal mechanism around 0 – 2200 masl was exhibited, together with tomography. The result shows the possible orientation of the fault plane and slip on fault plane. Based on the beach ball trend, NIL area has act as normal fault - indicate tension zone with trend dominant parallel with major fault.

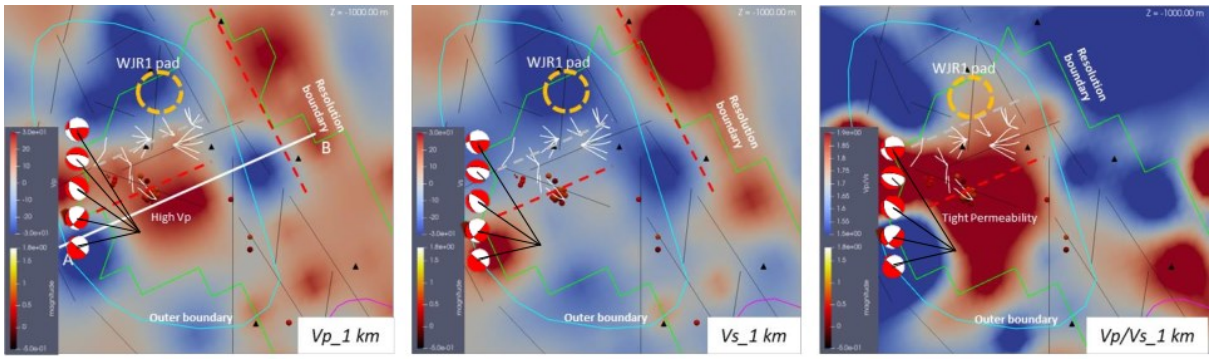

Figure 6: Map from tomography model from VP, VS, and ratio of VP/VS at 1 km depth. The heat color represents the values from low to high and the beach ball represents the location and trend of focal mechanism.

4. CONCLUSION AND RECOMMENDATION

Microearthquake events in Namora-I-Langit occurred from tectonic movement along Great Sumatran Fault or from local reservoir process/operation. Based on the comparison with the MEQ frequency, some increasing seismic trends proved to be coincided with those activity such as, outage/curtailment, well drilling, surveillance, acidizing (workover), and the rapid increase is related to natural earthquake.

Some examples of MEQ monitoring results in 2023 include the injection channel from in NIL location, which seems to be dominant to south-west within the compartment. This is consistent with surface structure and well data findings. However, no notable swarm events were observed during WJR1-2 drilling. Possibly the area is highly permeable or in aseismic zone. Finally, in addition to the shallow process, a natural earthquake around reported near Tarutung area, which was connected with BMKG data and interpreted as the re-activation of the ancient fault based on the movement of Great Sumatran Fault. These examples demonstrate how MEQ monitoring may help to support the reservoir monitoring, particularly beyond the well area.

Some advance processing was also studied and can support the general look for area with low permeability and general NW-SE trend from Great Sumatran Fault. However, the current model has some limitations and create some uncertainty. Based on the considerations, relocation some station to the West area, update velocity model, and improve resolution boundary will be improved in 2024 in order to raise data confidence and helps to identify the resource boundaries better. Some ideas for running the time lapse (4D) tomography or Ambient Noise Tomography (ANT) are also considered as part of the future improvement. In the meantime, the current result will be used as an input for reservoir characterization (conceptual model and resource boundary) & management (injection strategy, etc.), and assess the structure interpretation.

REFERENCES

Gunderson, Richard, et al. "Exploration results in the Sarulla block, north Sumatra, Indonesia." *Proceedings of the World Geothermal Congress, Japan*. 2000.

Satya, Drestanta Yudha, David Sahara, and Doddy Astra. "Preliminary Result of Microearthquake Monitoring at Namora-I-Langit and Silangkitang, Sarulla, North Sumatra, Indonesia." *IOP Conference Series: Earth and Environmental Science*. Vol. 1014. No. 1. IOP Publishing, 2022.

Mustika Bumi Indonesia, *Final Report for MEQ Monitoring Period 2020 – 2023 in NIL-SIL Geothermal Field* (Unpublished). Jakarta, 2024.

Analysis of Thermal Breakthrough Using Tracer Test in Geothermal Well W Field

Wily Rustam, Armando Ariakta Aloanis, Rivaldo Maurizio Tambahani, and Ricardo Kandoli

Department of Geothermal Engineering, Faculty of Mining and Petroleum Engineering, Bandung Institute of Technology, Ganesha Street No. 10, Lebak Siliwangi, Coblong, Bandung City, West Java, 40132, Indonesia

wilyrustam@gmail.com

Keywords: Tracer test, thermal breakthrough, temperature decline

ABSTRACT

Production and injection wells are crucial to geothermal power plants, with their use varying due to reservoir differences. These variations are understood through tests, like tracer tests, which involve mixing injection water with a tracer at a specific temperature to study reservoir properties. In this context, Naphthalene disulfonate (NDS) tracers were used in four injection wells: Well I-1 with 2.6 NDS; I-2 with 1.5 NDS; I-3 with 2.7 NDS; and I-4 with 1.6 NDS. The highest NDS detection was 2.6 in Well A, followed by 1.6 in Well I-4. Starting January 21, 2020, 1150 tph of 150-152°C water mixed with NDS was injected. This resulted in a temperature drop of 10°C in Well A and 15°C in Well B, with initial temperatures at 195°C and 184°C, respectively. Predicted temperatures after 2500 days are 185°C for Well A and 164°C for Well B, significantly affected by the 600m (A to I-1) and 700m (B to I-4) distance between injection and production wells. By 2034, Well A is expected to breakthrough, and by 2028, Well B.

1. INTRODUCTION

Geothermal resources can be accessed at a depth of 4-5 kilometers, exhibiting temperatures that span a range of 200 degrees Celsius. The injection of water into an injection well via fractures in hot rocks results in the generation of steam or hot water, which can be harnessed to drive turbines for the purpose of electricity generation. Water may be located at specific depths or exist within the reservoir, thereby transforming it into a geothermal reservoir (Johnston et al., 2011). The energy derived from the surface surpasses the inherent thermal heat flux, thereby causing a decline in temperature of the reservoir over time. The gradual impact on production wells is anticipated as a result of thermal breakthrough, whereby even cold water can eventually be extracted (Nottebohm et al., 2012). The Ahuachapan Field in El Salvador experienced a thermal drawdown of 30 degrees Celsius over a period of four years. Furthermore, it has been observed that in the Palinpinon Field located in the Philippines, a thermal drawdown of 50 degrees Celsius has occurred over a period of four years subsequent to the implementation of injection. In year 5, a thermal breakthrough is induced, thereby emphasizing the significance of conducting a tracer test. One of the primary objectives of this test is to ascertain the correlation between injection wells and production wells (Axelsson, Björnsson, et al., 2005). (Axelsson et al., 2005; Kaya, Zarrouk, & O'Sullivan, 2011) suggest that in order to mitigate this phenomenon, a water reinjection process is implemented, along with measures to prevent the depletion of water in geothermal reservoirs, thereby facilitating repeated cycles. A viable approach to examine this phenomenon is through the utilization of a tracer test. The assessment of mass movement in geothermal reservoirs is a conventional technique that can serve as a valuable instrument for the regulation of production and injection activities. The conducted tests reveal a correlation between injection and production wells, thereby enabling the identification of the most favorable placement for these wells (Suzuki et al., 2014). The utilization of the tracer test has been established as a potent technique for the purpose of characterizing geothermal reservoirs throughout time. These devices are utilized for the purpose of monitoring fluid flow and approximating the duration of fluid retention within reservoirs (Nottebohm et al., 2012).

Thus, the present investigation aims to conduct a thermal drawdown analysis by means of a tracer test on production well A and production well B located in Field W. The present analysis aims to ascertain the thermal breakthrough. The present study's favorable outcome is anticipated to provide a foundation for comprehending fluid dynamics within the reservoir and devising strategies for ascertaining the placement of production or injection wells, along with future production schemes. Geothermal energy has a potential estimated at approximately 5000 EJ (exajoules) per annum, as determined through engineering calculations. Nevertheless, in order to harness such a quantity of energy, one must possess the necessary capability and technological advancements. Despite having a generating potential of 28.1 MW, geothermal power plants have not been extensively utilized in Indonesia. Therefore, it is imperative to undertake measures aimed at optimizing their utilization (Melysa & Fitrianti, 2015). In the context of geothermal exploitation, the ongoing production of energy may result in thermal breakthrough and consequent energy loss. To address this issue, the reinjection of water is implemented to establish a recurring cycle (Plummer et al., 2011). Kaya et al. (2011) have identified several

advantages associated with re-injection. An ecologically sustainable approach to the management of brine and condensate disposal and separation. This process facilitates the replenishment of the reservoir and mitigates the decline in reservoir pressure. The utilization of a reduced amount of gas in the steam enhances the efficiency of the generator. There is a need to enhance the output of hot water and energy generated. The comprehension of the mean velocity, dispersion, and fluid flow volume within the reservoir and tracer is essential (Bjarkason, 2014).

Injection wells are a necessary component for re-injection activities. However, in practical application, the re-production of injected water can be a time-consuming process, leading to significant uncertainty. As such, it is imperative to identify strategies to mitigate this challenge. The comprehensive nature of data collected from various fields such as exploration, geology, geophysics, geochemistry, and reservoir characteristics facilitates the examination of pertinent issues. This data can be incorporated into a simulation model to forecast the flow of the reservoir. Furthermore, the examination of concerns raised can be aided by conducting tests on geothermal wells, such as the tracer test (Maier et al., 2014). A tracer test is a type of well test that is conducted in conjunction with the reinjection of water that has been infused with a tracer substance. The purpose of this test is to ascertain the properties of a geothermal reservoir. As per Axelsson's (2013) findings, certain prerequisites must be met for a substance to qualify as a suitable tracer during a tracer test. The tracer can be detected in reservoirs even at lower concentrations upon injection. The tracer does not undergo any reaction or absorption by the reservoir rock. The tracer exhibits stable temperature under reservoir conditions, inexpensive, simple to evaluate and eco-friendly.

As per Lake's (2007) publication, the primary objective of the tracer test is to assess the correlation between injection and production wells. An additional aim is to assess the efficiency of the sweep and determine the overall volume of pores. At the outset, the process of conducting tracer tests necessitated a greater amount of time for larger quantities owing to the dissipation of tracer elements and loss of temperature. The employment of naturally occurring tracers such as chloride and ammonia has been supplanted by the utilization of an artificial tracer, namely tritium. Naphthalene-1-sulfonic acid (a) is a chemical compound characterized by the molecular formula $C_{10}H_7SO_3H$. The aforementioned compound is devoid of color, exhibits solubility in water, and finds extensive application in the dye manufacturing sector. Four distinct chemical compounds derived from naphthalene-1-sulfonic acid are utilized as tracer variants and are blended with the injection water. The aforementioned chemical entities include naphthalene-2,6-disulfonic acid (b), naphthalene-1,5-disulfonic acid (c), naphthalene-2,7-disulfonic acid (d), and naphthalene-1,6-disulfonic acid (e). Thermal breakthrough refers to a phenomenon whereby the production temperature of a well decreases to the point where it is no longer economically viable, resulting in the production of cold water. This phenomenon can be attributed to various parameters, as noted by Rijn (2018). The parameters of interest include distance, flow rate, reservoir thickness, reservoir rock density, specific heat of reservoir rock, depth, and injection temperature.

The proposed final project entails conducting a research study aimed at analyzing temperature drops and thermal breakthroughs through the utilization of a tracer test. The primary objective of this investigation is to establish the correlation between production wells and injection wells. The utilization of tracer tests has been employed for several years as a potent technique for the characterization of geothermal reservoirs. The material's stability under geothermal conditions and its non-reactivity with reservoir rocks are crucial factors for its practical application. The tracer utilized must possess the capability of being detected in low concentrations, while also being non-toxic to both the environment and human beings (Nottebohm et al., 2012).

2. MATERIAL AND METHOD

2.1 Data for Calculating Thermal Drawdown

In order to conduct thermal drawdown calculations aimed at assessing temperature fluctuations resulting from production activities, certain data is necessary. As per the study conducted by Reidus et al. (2019), the utilized data is presented Table 1.

Table 1: Data.

No	Data	Explanation
1	Temperature (T)	$T_{path,i}$; T_{inj}
2	Flow Rate (Q)	Q_{inj} & Q_{prod}
3	Fraction of tracer	ppm
4	Time (t)	Function of time
5	Additional data	

2.2 Calculation of Thermal Drawdown

The present study outlines the methodology employed for processing the thermal drawdown calculation data acquired from the geothermal well. The thermal drawdown formula proposed by Reimus et al. (2019) was utilized

for this purpose. Retrieve tabulated data from Excel pertaining to tracer test outcomes and associated supporting data. The computation of thermal drawdown can be achieved by utilizing the subsequent equation:

$$\Delta T = T_{Prod,f} - T_{Prod,i} = -f \frac{Q_{inj}}{Q_{prod}} (T_{path,i} - T_{inj}) \quad (1)$$

Symbol	Definition
ΔT	Change in production temperature.
Tprod,f	Final production temperature.
Tprod,i	Initial production temperature.
Qinj	Injection flow rate (mass or volume per unit time).
Qprod	Production flow rate (mass or volume per unit time).
Tpath,i	Initial temperature along the path between injection and production points.
Tinj	Injection temperature.

The equation is analytical, derived from first principles or assumptions about the system. It represents a relationship between temperature changes and fluid flow rates in the system. Key assumptions:

- The equation assumes steady-state conditions, meaning the system has reached a point where variables do not change with time.
- The flow rates Qinj and Qprod are constant over the period considered.
- The temperature difference Tpath, i−Tinj represents the driving force for heat exchange between the injected fluid and the surrounding environment.
- The fraction f is assumed to be constant and may encapsulate the efficiency of the heat transfer process, considering factors like reservoir characteristics or wellbore conditions.

3. RESULT AND DISCUSSION

The present study examines the phenomenon of temperature reduction in geothermal fluids, which can be attributed to production activities and may persist until a thermal breakthrough is achieved. The subject of investigation pertains to a geothermal field that comprises two phases and commenced drilling operations on October 15, 2016. The temperature of the fluid emanating from the wellhead exhibits a range of 155 ºC to 200 ºC. At present, there exist six operational production wells that cater to the energy demands of power plants. The tracer test was initiated on January 21, 2020 and data was collected and documented until July 7, 2020. Four distinct NDS tracers were employed and subsequently introduced into four separate reinjection wells, specifically identified as the I-1 Well employs the utilization of certain techniques or methods. 2.6 NDS, the I-2 Well employs certain techniques or methods. 1.5 NDS, the I-3 well is utilized for various purposes. 2.7 NDS, the I-4 well employs. 1.6 NDS.

Based on the production data, it can be inferred that production wells A and B exhibit favorable performance. The primary focus of this thesis will be on the two wells in question. Production well A is the well in closest proximity to reinjection well I-1, as depicted in Figure 1. The assertion is corroborated by the significant yield of 2.6 NDS in the operational well A, as illustrated in Figure 1. Furthermore, it is noteworthy that production well B exhibited a significant yield of 2.6 NDS, succeeded by a yield of 1.6 NDS. The reason for this is that production well B is in close proximity to the reinjection wells I-4. The results obtained from Tracer 2.6 NDS indicate a twofold increase in peak returns observed in production wells A and B. This observation provides valuable insights into the fluid dynamics and the time taken for the injection water to reach the production well. The aforementioned visual representation can be observed in Figure 1 and Figure 2.

This result is corroborated by Rijn's (2018) research, which posited that the spacing between wells is a critical factor impacting the likelihood of a breakthrough event. In instances where the spacing between wells measures 1500 meters, the temperature variation observed over a period of 50 years has registered a mere 0.1 ºC. The tracer distribution map appended to this document reveals that the spatial separation between production wells I-1 and production wells A is 600 meters, while the distance between reinjection wells I-4 and production wells B is 700 meters. Given that the inter-well spacing is below 1500 meters, it is probable that a breakthrough would transpire earlier than anticipated.

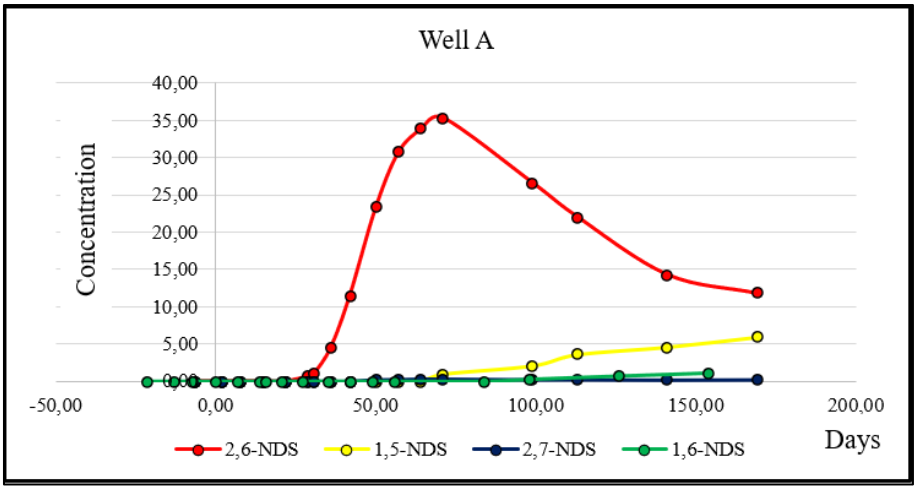

Figure 1: NDS Concentration from Tracer Test in Well A.

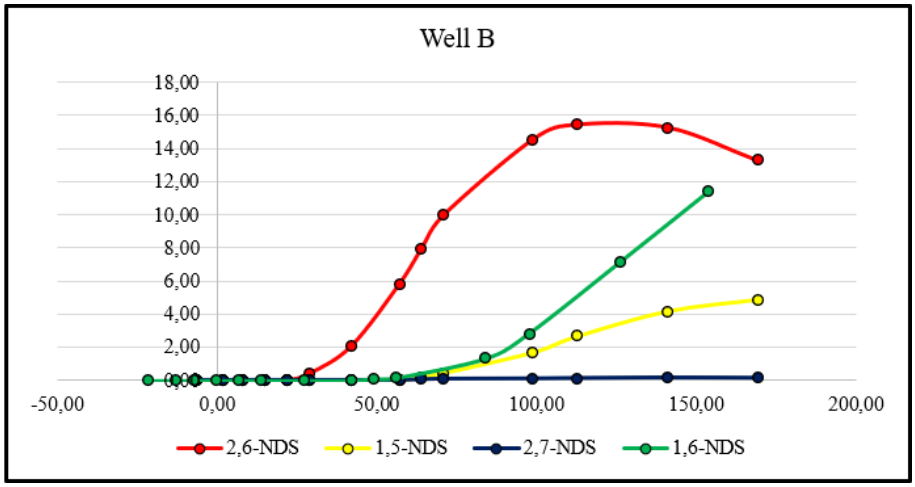

Figure 2: DS Concentration from Tracer Test in Well B.

As per the findings of Hidayat et al. (2019), it has been established that the principal source of geothermal fluid emanates from a specific production well, namely well C. The maximum temperature of the fluid recorded in this well has been determined to be 200 ºC. The temperature differential between production well A and well C is 5 ºC, whereas production well B exhibits a temperature differential of 15 ºC. The temperature decrease in well A can be computed by means of the subsequent equation, as inferred from the conducted tracer testing.

$$\Delta T = -f \frac{Q_{inj}}{Q_{prod}} (T_{path,i} - T_{inj}) \quad (2)$$

$$\Delta T = (-0.1) \frac{1150\ tph}{449\ tph} (191 - 150\ °C) \quad (3)$$

$$\Delta T = -10\ °C$$

This is further corroborated by the forecasted reduction in temperature observed in well A. According to Figure 3, a reduction of 10 ºC is anticipated to transpire in 2027, specifically 2500 days subsequent to the implementation of the tracer test. The calculation of the temperature drop in well B can be derived from the tracer testing results, utilizing the subsequent equation:

$$\Delta T = -f \frac{Q_{inj}}{Q_{prod}} (T_{path,i} - T_{inj}) \quad (4)$$

$$\Delta T = (-0.1) \frac{1150\ tph}{554\ tph} (184 - 150\ °C) \quad (5)$$

$$\Delta T = -7.06\ °C$$

This assertion is further corroborated by the forecasted reduction in temperature within borehole B. Nevertheless, the observed reduction in temperature was not 7.06 ºC, but rather 15 ºC over a span of 2500 days. The observed

disparity can be attributed to the proximity of the reinjection wells, which has resulted in a rapid decline of production well B.

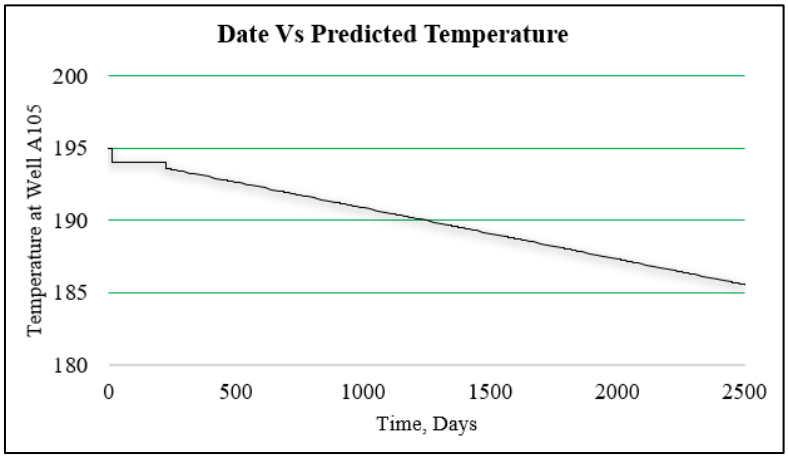

Figure 3: Prediction of Temperature in Well A.

Based on the given information regarding the decrease in temperature, it can be inferred that a reduction of 10 ºC will occur after a period of 6.8 years, equivalent to 2500 days. The thermal breakthrough in well A can be predicted by factoring in the condition that the temperature remains above 160 ºC. In January 2020, the temperature recorded in well A was 195 ºC. The temperature drop calculation indicates that it took approximately 35 ºC for the temperature to decrease, which is equivalent to 3.5 times the initial temperature. Thus, based on the available data, it can be inferred that the anticipated thermal breakthrough is likely to transpire in 2044, which is approximately 23.8 years from the present time.

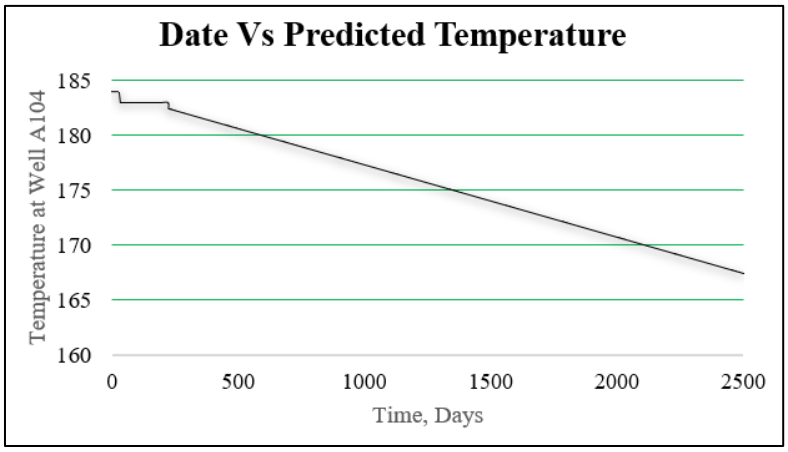

Figure 4: Prediction of Temperature in Well B.

The temperature of well B at the outset of January 2020 was recorded as 184 ºC. Subsequently, it was observed that the temperature experienced a decline of approximately 24 ºC. This value is equivalent to 1.5 times the result obtained from the computation of the temperature drop as described earlier. Thus, it is anticipated that a thermal breakthrough may transpire in 2028, which is eight years from now.

The aforementioned forecast is substantiated by the production scenario of the enterprise, which has remained unchanged subsequent to the execution of the tracer test. In the event of a modification in the given circumstances, it is plausible for a thermal breakthrough to either decelerate or accelerate. Various strategies can be employed to postpone the onset of thermal breakthrough, such as upholding the injection temperature, minimizing the frequency of injection rates, increasing the separation distance between injection and production wells, and implementing other relevant measures.

4. CONCLUSION

The proximity of production wells A to injection wells I-1 and production wells B to injection wells I-4 results in a more rapid decrease in temperature due to inadequate or insufficient time for the geothermal fluid to undergo maturation and subsequent production. The temperature of production well A decreased by 10 ºC, while that of production well B decreased by 15ºC. The proximity of the production and injection wells was found to have

influenced this temperature reduction. The projected occurrence of a thermal breakthrough in production well A is estimated to be in the year 2044, whereas in production well B, it is anticipated to occur in 2028. Given the limitations of the present study, it is anticipated that forthcoming investigations will employ a reservoir simulation model that closely approximates the W field to elucidate the dynamics of geothermal fluid flow. Additionally, it is recommended that tracer return data be recorded over extended periods for alternative injection wells to establish their interconnectivity with production wells. In order to expand its knowledge beyond the injection wells I-1 and I-4, it is imperative to undertake further research and analysis. In order to mitigate the swift thermal drawdown, it is necessary to either shut down existing injection wells or introduce new ones at a specific distance.

REFERENCES

Axelsson, G., Björnsson, G., & Montalvo, F. (2005). Quantitative Interpretation of Tracer Test Data. *World Geothermal Congress*, April, 24–29.

Axelsson, G., Grímur Björnsson, & Montalvo, F. (2005). Quantitative Interpretation of Tracer Test Data. *Transactions - Geothermal Resources Council*, April, 513–519.

Bjarkason, E. K. (2014). *Predicting Thermal Drawdown in Geothermal Systems Using Interwell Tracer Tests*.

Johnston, I. W., Narsilio, G. A., & Colls, S. (2011). Emerging geothermal energy technologies. *KSCE Journal of Civil Engineering*, 15(4), 643–653. https://doi.org/10.1007/s12205-011-0005-7

Kaya, E., Zarrouk, S. J., & O'Sullivan, M. J. (2011). Reinjection in geothermal fields: A review of worldwide experience. *Renewable and Sustainable Energy Reviews*, 15(1), 47–68. https://doi.org/10.1016/j.rser.2010.07.032

Maier, F., Schaffer, M., & Licha, T. (2014). Temperature determination using thermo-sensitive tracers: Experimental validation in an isothermal column heat exchanger. *Geothermics*, 53, 533–539.

Melysa, R., & Fitrianti. (2015). Analisis Potensi Daya Listrik Pada Sumur Produksi Panas Bumi Dengan Menggunakan Metode Back Pressure Pada Unit XY. *Journal of Earth Energy Engineering*, 4(2), 30–37.

Nottebohm, M., Licha, T., & Sauter, M. (2012). Tracer design for tracking thermal fronts in geothermal reservoirs. *Geothermics*, 43, 37–44.

Plummer, M. A., Palmer, C. D., Mattson, E. D., & Hull, L. C. (2011). A Reactive Tracer Analysis Method for Monitoring Thermal Drawdown in Geothermal Reservoirs. *Thirty-Sixth Workshop on Geothermal Reservoir Engineering*, 5.

Suzuki, A., Niibori, Y., Fomin, S. A., Chugunov, V. A., & Hashida, T. (2014). Fractional derivative-based tracer analysis method for the characterization of mass transport in fractured geothermal reservoirs. *Geothermics*, 53, 125–132.

Quantification of Feedzone Contribution Based on PTS Flowing Survey on Wells JTG-3 and GMB-2 Karaha Geothermal Field

Ryandra S. Dharmawan, Welayaturromadhona, and Riska L. Sari

Petroleum Engineering Department, Faculty of Engineering, University of Jember, Jember, Indonesia

ryandrasatyadharmawan06@gmail.com

Keywords: Geothermal, Feedzone, Massrate, PTS Flowing

ABSTRACT

The Karaha Geothermal Field or Karaha Field is an active production field owned by PT Pertamina Geothermal Energy which has production problems, namely scaling of corrosion residue caused by the presence of acid content in this field's reservoir. This research aims to determine the production potential of the JTG-3 and GMB-2 wells in the Karaha Field which was obtained from the result of the PTS flowing survey and from geochemical samples. The research began by reviewing and analyse PTS flowing data and well configuration data which was obtained from the drilling process, those data are used to determine the condition of the wells and reservoir.

The result show that there has been a decrease in production figures at JTG-3 well from 102 t/hr mass rate with a dryness of 37% in 2018 to 43 t/hr mass rate with a dryness of 29% in 2022. Apart from that, GMB-2 well does not have the latest production data. However, in 2019 production reached 64 t/hr mass rate, which is much higher than the JTG-3 well considering that the GMB-2 well is a single phase well were the dryness will be assumed to be 100%. Later on, the result of electricity production potential also showed that were in line with the steam mass rate contained in each well, whre the GMB-2 well recorded the highest potential. Afterwards, from the result of the water sample analysis carried out, it can be seen that the wells studied experienced scaling problems, supported by the result of the fluid velocity curve which showed turbulent result. The scaling that occurred in the wells at the Karaha Field was Fe Scaling, which is a residue resulting from corrosion, and SiO2 which is mainly found in 2-phase wells with low dryness.

1. INTRODUCTION

Pressure, temperature, and spinner (PTS) surveys conducted under flowing conditions are essential procedures as the resultant data is invaluable for determining a well's fluid production capacity. Furthermore, these surveys assist in identifying the number of feed zones and assessing each feed zone's ability to channel fluid from the reservoir into the well. The collected data can also highlight potential issues within the well or the reservoir, exemplified by the challenges encountered in the JTG-3 and GMB-2 wells in the Karaha Geothermal Field.

This field faces a significant issue of declining production due to the acid content from the heat source intruding into the reservoir. Such acid intrusion can compromise the well's stability, causing damage to the well liners, leading to scaling, and subsequently reducing production over time. To address these challenges, this research involved collecting well water samples to analyse the fluid content. This analysis aims to identify the problematic constituents affecting well production and to establish benchmarks for mitigating these production issues. The research workflow is illustrated in Figure 1.

2. PTS FLOWING SURVEY

The pressure, temperature, and spinner measurements in this study were conducted on wells JTG-3 and GMB-2, with a total of three sets of data obtained from measurements taken in 2018 and 2022 for well JTG-3 and in 2019 for well GMB-2. Variations in cable speed were applied at two different speeds for each measurement to determine the slope used in calculating fluid velocity. Figure 2 illustrates the implementation of downhole logging.

The raw data obtained directly indicated the location of each feed zone, marked by a significant increase in spinner frequency as shown in figure 3. However, it is important to note that an increase in spinner frequency does not always indicate a feed zone position. The spinner's response to the fluid can also be influenced by the roughness of the surface it traverses and the casing ID. As a result, anomalies in the spinner response can be observed at different casing joints and areas with high roughness.

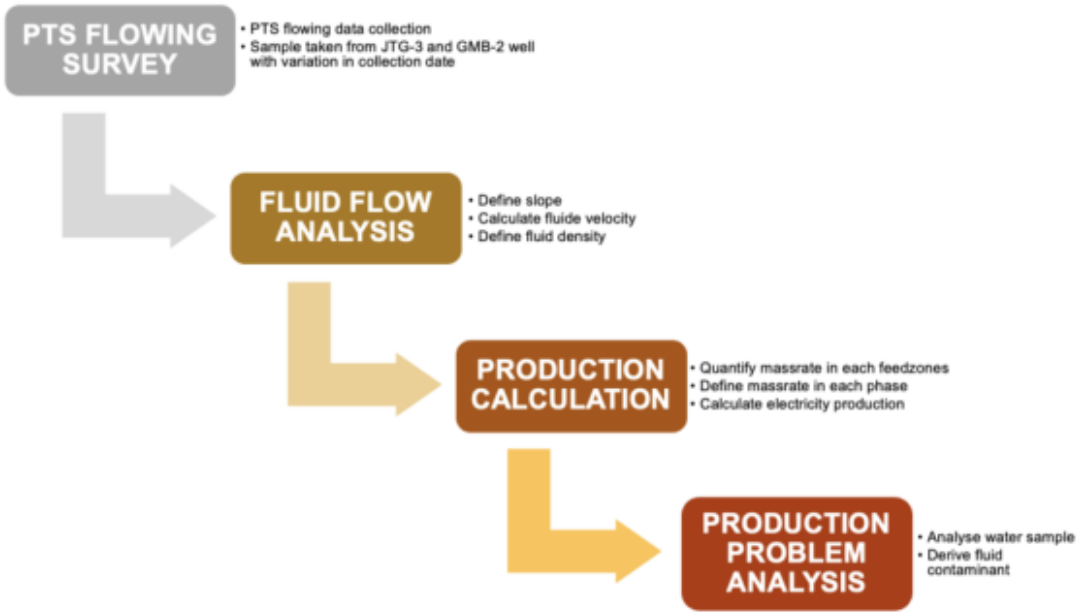

Figure 1: Detailed Workflow Implemented in the Research for Quantify Feedzone Fluid Production and Analyse Production Problem.

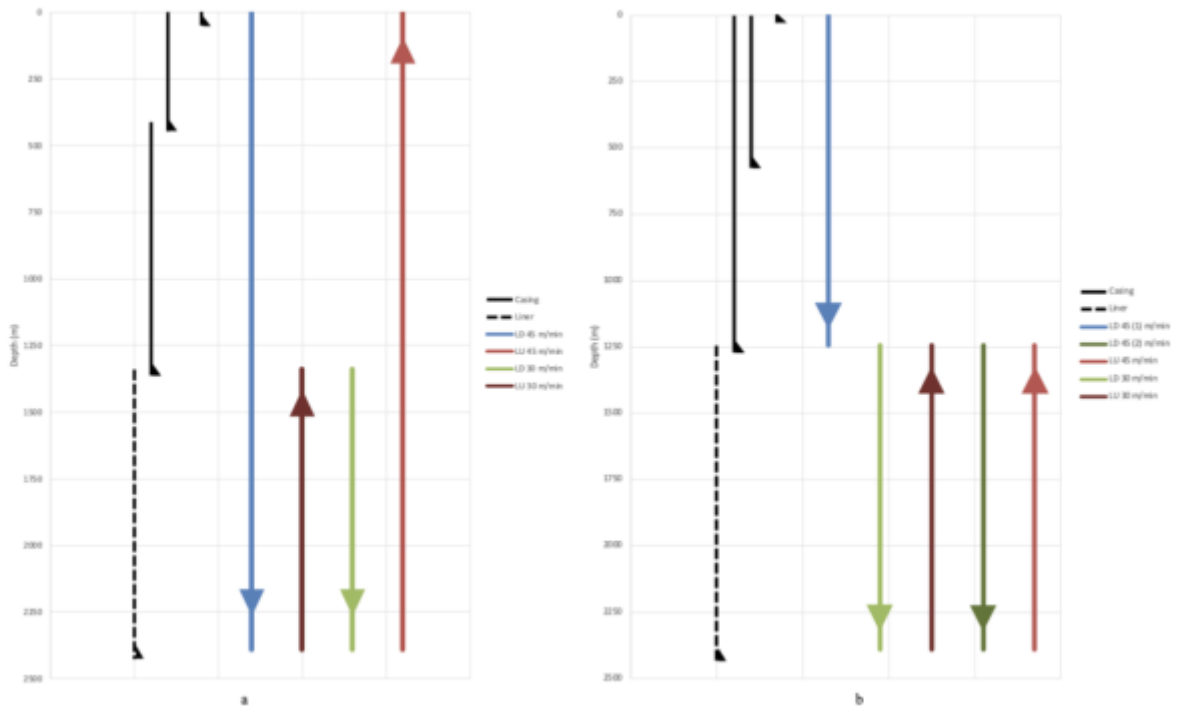

Figure 2: Illustration of the PTS flowing procedure, a) well JTG-3, b) well GMB-2.

3. FLUID FLOW ANALYSIS

Analysis of fluid flow patterns can be conducted by examining the fluid velocity curve. To determine fluid velocity, calculations based on spinner frequency and cable speed are necessary. Therefore, the slope is calculated using the following equation:

$$slope = \frac{V_t}{f} \quad (1)$$

Where Vt and f represent the cable speed and spinner frequency, respectively. The calculated slope results can be observed in Figure 4.

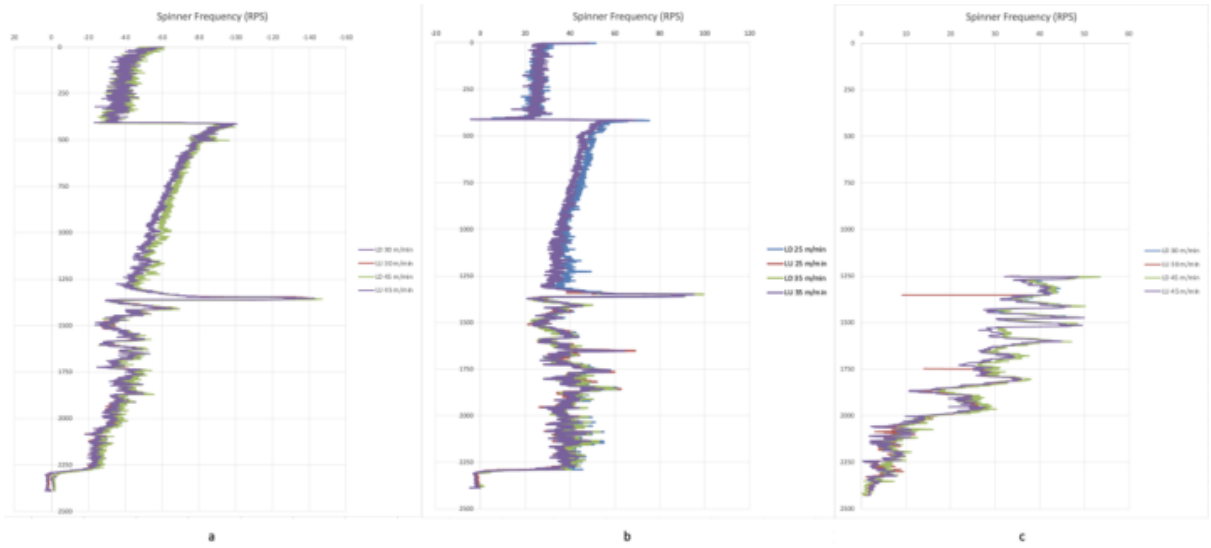

Figure 3: Spinner frequency curves, a) well JTG-3 (2018), b) well JTG-3 (2022), c) well GMB-2 (2019).

Figure 4: Slope observed, a) well JTG-3 (2018), b) well JTG-3 (2022), c) well GMB-2 (2019).

The slope is determined based on dominant data anomalies present in the curve. Subsequently, the determined slope value is used to compute fluid velocity based on the equation 2.

$$Vf = (f \times slope) - Vt \quad (2)$$

Here, Vf represents the fluid velocity. Grant & Bixley (2011) explain that anomalies in fluid flow patterns can be observed from the fluid velocity curve. More turbulent fluid flow is indicated by higher deviations in flow pattern anomalies, as demonstrated in the fluid velocity calculations for wells JTG-3 and GMB-2 shown in Figure 5.

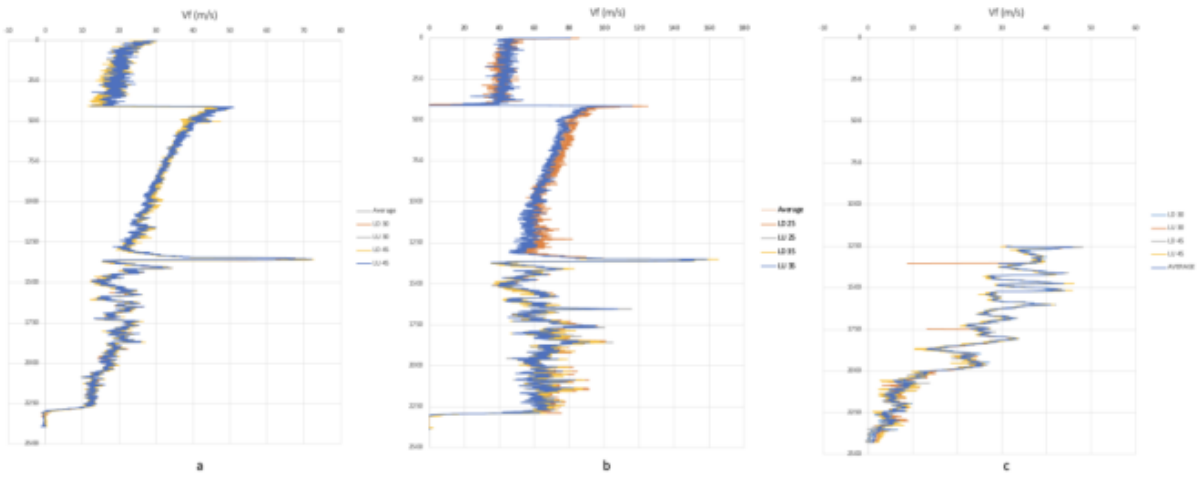

Figure 5: Fluid velocity curve, a) well JTG-3 (2018), b) well JTG-3 (2022), c) well GMB-2 (2019).

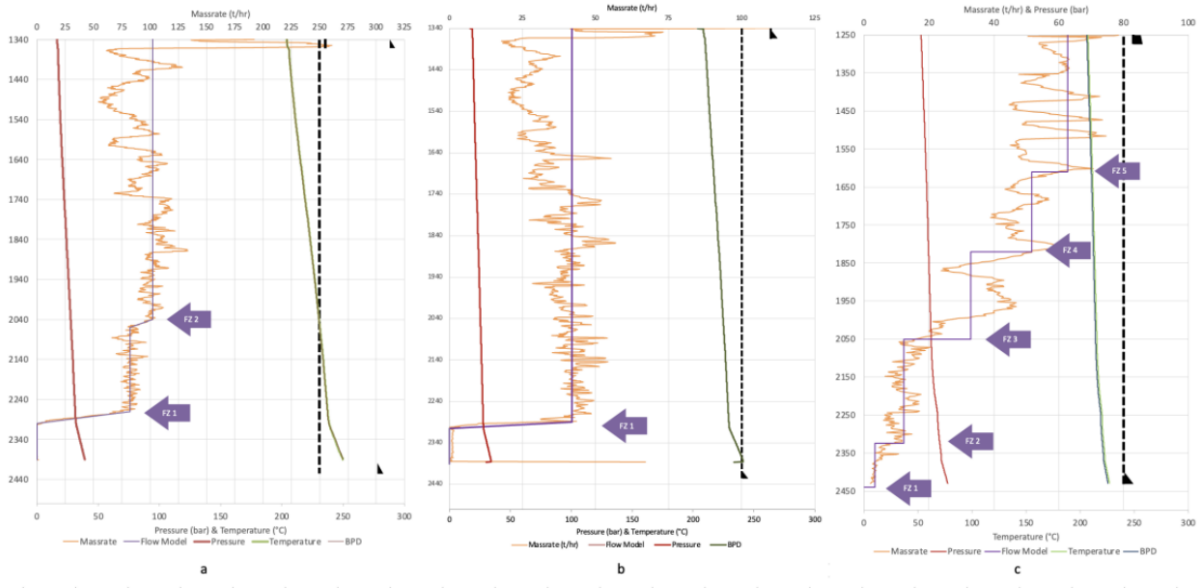

Figure 6: Mass rate curves with feedzone mark, a) well JTG-3 (2018), b) well JTG-3 (2022), c) well GMB-2 (2019).

The flow conditions in well JTG-3 tend to be more laminar, with significantly lower deviations compared to well GMB-2. However, in 2022, the flow conditions in well JTG-3 became increasingly turbulent, although not more turbulent than in well GMB-2.

4. PRODUCTION QUANTIFICATION

When calculating the production capacity of a geothermal well, the primary metric is the well's steam production. This is because the luid used to drive the turbine and generate electricity must be in the vapor phase. The key indicator of steam production is the mass flow rate of the fluid.

4.1 Mass Rate & Feedzone Contribution

Mass rate is the ultimate outcome of the PTS flowing survey, providing an indication of the well's production rate as elucidated by Buscato (2012). Unlike flow rate, which compares the fluid flow in volume per unit time, mass rate compares the fluid flow in mass per unit time, typically expressed in kg/s or t/hr. The distinction between mass rate and fluid velocity lies in the adjustments for casing diameter and fluid density, as defined equation 3.

$$\dot{m} = V_f \rho \left(\frac{\pi}{4} ID\ Casing^2\right) \quad (3)$$

Where $\dot{\mathbf{m}}$ and $\boldsymbol{\rho}$ is the mass rate and fluid density. The total mass rate measured for well JTG-3 in 2018 was 102 t/hr. In 2022, the total mass rate for the same well was 43 t/hr, while well GMB-2 had a total mass rate of 64 t/hr

in 2019. These results will be validated by examining TFT data corresponding to the PTS survey dates. Upon calculation and plotting the mass rate curve, the productive permeable zone, commonly referred to as the feed zone, should become apparent. This zone possesses high permeability, allowing geothermal fluid to flow from the formation into the well. The feed zone can be identified from the mass rate curve at the lower sections of the well (along the liner) by observing anomalies in mass rate changes. The location of the feed zones for each well data set can be seen in the figure 6.

Subsequently, the contribution of each feed zone will be quantified to ascertain the percentage contribution of each feed zone to the total well production using equation 4.

$$\%\ contribution = \frac{\dot{m}_1 - \dot{m}_0}{\dot{m}} \times 100\% \quad (4)$$

The contributions of each feed zone in each well are detailed in Table 1. The loss of the feed zone at a depth of 2060 m-MD in well JTG-3 has a significant impact on the fluid composition within both the well and the reservoir. Therefore, a further analysis of the fluid composition, reviewing the geochemical data of the well, is necessary.

Table 1: Each Feedzones Contribution.

Well	Measurement Date	Feedzone	Contribution (%)
JTG-3	2018	FZ-1	80.6
		FZ-2	19.4
	2022	FZ-1	100
GMB-2	2019	FZ-1	5.3
		FZ-2	11.6
		FZ-3	35.6
		FZ-4	29.8
		FZ-5	17.7

4.2 Production Potential

In the production process, after the fluid is extracted from the well, it enters a separator to divide it into vapor and liquid phases, since only the vapor phase is utilized to drive the turbine. The separated liquid phase then passes through a weir box to measure its mass rate, after which it is reinjected into the reservoir via a reinjection well. The mass rate of the brine passing through the weir box can

be determined, and by subtracting the known brine mass rate from the total mass rate, the steam mass rate can be ascertained. The mass rates of each phase can be calculated using equation 5 and 6.

$$\dot{m}_b = 2.362\left(C_d\ tan\frac{\theta}{2}\ h^{5/2}\right)\rho \quad (5)$$

$$\dot{m}\,s = \dot{m} - \dot{m}\,b \quad (6)$$

and the dryness can be calculated using the following equation:

$$dryness = \frac{\dot{m}_s}{\dot{m}} \times 100\% \quad (7)$$

where ṁ b, ṁ s, Cd, θ and h is brine mass rate, steam mass rate, dischange coefficient, v-notch angle and brine height in v-notch. With a v-notch angle of 90° and a discharge coefficient of 0.9, the calculated mass rates of each phase and their corresponding dryness are presented in Table 2.

Table 2: Result of the mass rate calculation for each phase.

Well	Measurement Date	h (m)	Massrate (t/hr)			Dryness
			Total	Brine	Steam	
JTG-3	2018	0.145	102	64	38	37%
	2022	0.15	43	30	13	29%
GMB-2	2019	-	64	-	64	100%

After all the steam is separated from the liquid phase, the steam enters the turbine to drive it. The turbine is connected to a generator that produces electricity. The electrical output from each well can be calculated based on the well's production mass rate and the specific steam consumption (SSC) of the turbine. In this study, the SSC of the turbine according to field specifications is 8 kg/MW-s. The calculated production capacity from each test is detailed in Table 3.

Table 3: Electricity production potential based on each test result.

Well	Measurement Date	$\dot{m}s$ (kg/s)	SSC (kg/MW-s)	Electricity Production (MW)
JTG-3	2018	10.5	8	1.31
	2022	3.6	8	0.45
GMB-2	2019	17.7	8	2.22

5. PROBLEM ANALYSIS

The issue of declining production at the Karaha Field is critical and warrants thorough investigation to identify the underlying causes. To this end, the productivity index (PI) of this field will be examined to elucidate the production decline in wells JTG-3 and GMB-2, as well as through the analysis of water samples from these wells.

5.1 Productivity Index

Wells can be classified into two categories: productive and non-productive. Musnal & Melisa (2016) assert that the capacity of a geothermal fluid accumulation in the reservoir to be extracted is contingent upon the reservoir's productivity. Consequently, a comparison is made between the well's production rate and the reservoir pressure, a value known as the productivity index (PI). According to Brown (1997), PI can be measured by comparing the bottomhole flowing pressure (Pwf) with the static well pressure (Ps) and the produced fluid, which expressed in equation 8.

$$PI = \frac{\dot{m}}{Ps - Pwf} \tag{8}$$

The PI calculation results for well JTG-3 and GMB-2 with its feedzones are presented in Table 4.

The PI data for well JTG-3, derived from measurements taken in 2018 and 2022, reveals a decline in PI in 2022, indicative of a reduction in well productivity. According to Wahyudityo et al. (2013), this necessitates the collection of well water samples to analyse the chemical content within the well, as well JTG-3 is a two-phase well with low dryness, rendering it susceptible to scaling, which can diminish well productivity. Furthermore, the PI data for well GMB-2 yielded a value of 0.86, which is considered quite satisfactory for a single-phase steam well, as it is assumed that all produced fluid will be utilised to drive the turbine. In contrast, well JTG-3, being a two-phase well with low dryness, undergoes a separation process, resulting in a smaller quantity of steam produced compared to a single-phase steam well.

Table 4: PI in each wells and its feedzones.

Well	Measurement date	Ps (bara)	Pwf (bara)	Feedzone	PI (kg/s.bar^{-1})	
					Feedzone	Well
JTG-3	1 Aug 2018	99.4	39.7	FZ-1	1.38	1.71
				FZ-2	0.33	
	9 Dec 2022	99.4	34.3	FZ-1	0.64	0.64
GMB-2	20 Mar 2019	50	50	FZ-1	0.05	0.86
				FZ-2	0.10	
				FZ-3	0.31	
				FZ-4	0.26	
				FZ-5	0.15	

5.2 Water Sample Analysis

The Karaha Field is indicated to have acidic content caused by the intrusion of magmatic fluids into the reservoir. This is evidenced by the closure of exploration wells in the Talaga Bodas Area. Although the issue of acidic content is common in geothermal fields, it is essential to collect fluid samples from the wells for chemical analysis. Additionally, several wells in this field are two-phase with low dryness, increasing the potential for scaling. The Cl-SO4-HCO3 diagram is shown in Figure 7.

A sample taken from a well must contain a high chloride (Cl) content, as Cl is the element that binds reservoir water, also known as mature waters. This water is the result of heating meteoric water by the heat source, but it does not necessarily contain the sulphate (SO4) element present in the heat source. The heat source and the reservoir must have a boundary separating them to prevent acidic sulphate from the heat source (volcanic waters) from contaminating the reservoir fluid. The indication of volcanic waters entering the reservoir is a shift in the well water sample point from the mature waters area near the Cl peak towards the volcanic waters area on the SO4 axis.

In essence, the currently active wells in the Karaha field are still considered free from volcanic water contamination. However, a closer examination reveals a shift in the GMB-2 well sample point towards SO4 compared to the JTG-3 well sample, which is precisely at the Cl peak. Although this shift is not significant and remains within the mature waters area, there is a trend of increasing SO4 concentration as samples are taken further north in this field. This supports the theory of magmatic fluid intrusion contaminating the northern reservoir, corroborated by the pH samples shown in Table 5.

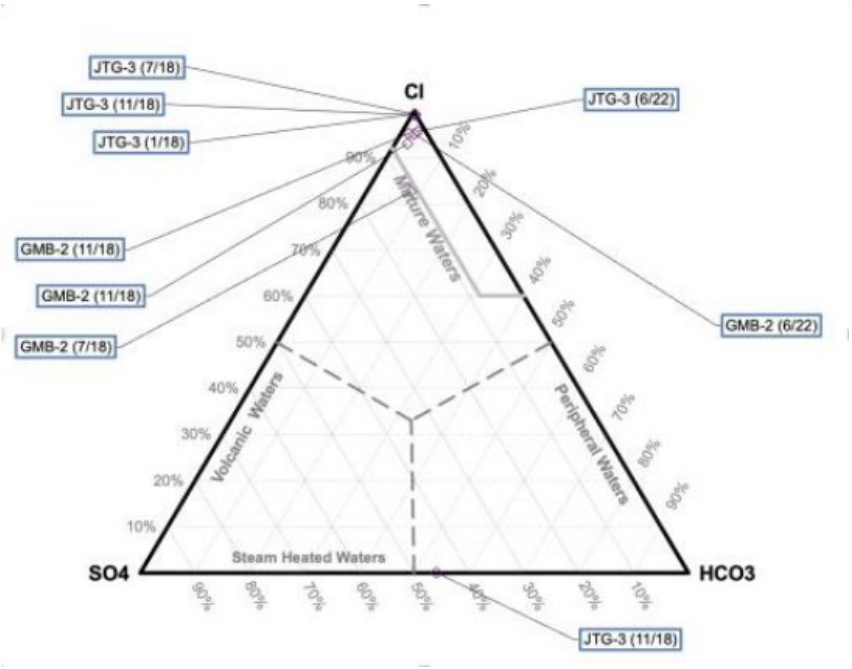

Figure 7: Cl-SO4-HCO3 diagram.

Table 5: pH data from well water samples JTG-3 and GMB-2.

Well	Sample Collection Date	pH
JTG-3	17 July 2018	7.5
	22 June 2022	7.2
GMB-2	7 November 2019	6.2
	23 June 2022	5.9

Table 6: Fe concentration in wells JTG-3 and GMB-2.

Well	Sample Collection Date	pH
JTG-3	17 July 2018	0.01
	22 June 2022	0.11
GMB-2	7 November 2019	0.02
	23 June 2022	0.35

With more acidic conditions observed in well GMB-2, which is located in the northern area of the field, compared to well JTG-3 in the southern area, a downward trend in pH is apparent. This aligns with the increase in acidic sulphate concentration, which will inevitably affect the production process of wells situated further north, such as well GMB-2. Higher acid content accelerates corrosion of the slotted liner used in the wells. The presence of Fe metal in the well water samples further evidences this corrosion, as shown in Table 6.

The highest concentration of Fe metal is found in well GMB-2, consistent with higher sulphate content and lower pH in this well. Unfortunately, there are no recent data for well GMB-2, so the corrosion rate in this well cannot be determined. Additionally, well JTG-3 also shows the presence of Fe metal, albeit at lower concentrations, but an increase in Fe metal concentration is observed from samples taken in 2018 compared to those in 2022. The residue from corrosion of the liner then moves with the fluid flow in the well.

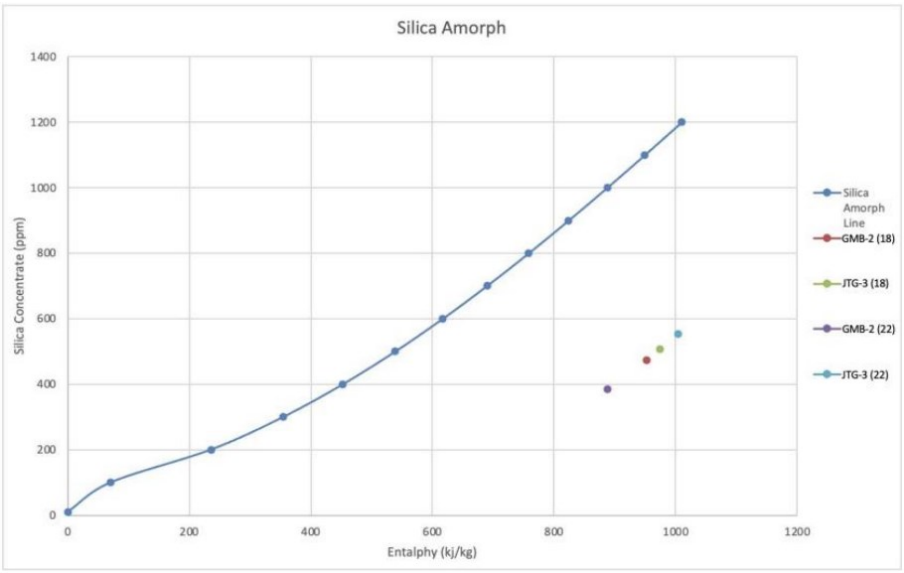

Figure 8: Silica amorph curve.

There is also SiO2 content in these wells, indicated through calculations with the silica amorph curve shown in Figure 8. The four sample points below the silica amorph line indicate that the silica content in these wells is still within acceptable limits. However, SiO2 will adhere to the casing and liner walls, causing scaling.

Well JTG-3 has a higher silica concentration than well GMB-2 because well JTG-3 is a two-phase well with low dryness, containing significantly more brine than well GMB-2. The higher the brine content, the greater the potential for SiO2 scaling. In the case of these two wells, the SiO2 present adheres to the well walls, serving as a medium for Fe metal corrosion residue to adhere as well, resulting in scaling composed of a mixture of SiO2 and Fe metal. Well JTG-3 has a lower Fe content due to lower sulphate concentration but higher SiO2 content due to more brine, which is the opposite of the condition in well GMB-2. Scaling in Karaha Field wells will undoubtedly cause production declines, as seen in Figure 6, and financial losses for the field.

6. CONCLUSION

Based on the result exercise, the following conclusion can be drawn:

1. Based on the fluid velocity curve, the results indicate turbulent flow patterns in both wells. However, the flow in well GMB-2 is deemed more turbulent compared to well JTG-3 due to the higher deviation observed in the curve for well GMB-2.
2. The electricity production derived from well JTG-3 based on the PTS flowing survey was 1.31 MW in 2018 and 0.45 MW in 2022, whereas the electricity production from well GMB-2 was 2.22 MW in 2019. This is based on the mass rate obtained from the PTS flowing survey, which was 102 t/hr in 2018 and 43 t/hr in 2022 for well JTG-3, and 64 t/hr for well GMB-2 in 2019.
3. According to the geochemical water sample review, well JTG-3 is assessed to contain less acid compared to well GMB-2, as evidenced by the lower pH and SO4 concentration. This results in a higher rate of corrosion and scaling from corrosion residues in well GMB-2. Conversely, well JTG-3 has a higher SiO2 concentration, affecting silica scale formation. Therefore, while well GMB-2 faces more severe issues related to acid-induced scaling, considering the actual production phase and silica solubility, well JTG-3 is likely to experience a greater production decline compared to well GMB-2.

In subsequent research, it is recommended to review PTS injection data to enhance the reliability of the findings. Additionally, it is advised to examine the latest PTS flowing data from well GMB-2 to enable a comparison of fluid velocity curves. Given that the PTS flowing test is conducted to ascertain the properties of the feedzone, data processing should focus exclusively on the data indicated along the liner, as it is assumed that no further feedzone exists once the casing is reached. Furthermore, a detailed study on the issues of acidity and scaling in this field is necessary to optimise production at the Karaha Field.

ACKNOWLEDGEMENT

The authors would like to express their appreciation to PT Pertamina Geothermal Energy for access to field data and continuous support.

REFERENCES

Brown, K. E. (1997). *The Technology of Artificial Lift Methods* (Vol. 4). PennWell Books.

Buscato, N. M. (2012). *QUANTIFYING FEED ZONE CONTRIBUTIONS FROM PRESSURE-TEMPERATURE-SPINNER DATA AND PRESSURE TRANSIENT ANALYSIS USING WELLTESTER*. https://api.semanticscholar.org/CorpusID:110104054

Grant, M. A., & Bixley, P. F. (2011). Chapter 4 - Interpretation of Downhole Measurements. Dalam M. A. Grant & P. F. Bixley (Ed.), *Geothermal Reservoir Engineering (Second Edition)* (hlm. 61–74). Academic Press. https://doi.org/https://doi.org/10.1016/B978-0-12-383880-3.10004-6

Musnal, A., & Melisa, R. (2016). Perhitungan Analisis Sistem Nodal Untuk Menentukan Laju Alir Minyak Dengan Meningkatkan Range Efesiensi Electric Submercible Pump Pada Sumur di Lapangan Minyak PT. BOB. BSP - Pertamina Hulu. *Journal of Earth Energy Engineering*, 5(1), 42–51. https://doi.org/10.22549/jeee.v5i1.460

Wahyudityo, R., Harto, A. W., & Suryopratomo, K. (2013). *Analisis Scaling Silika pada Pipa Injeksi Brine di Lapangan Panas Bumi Dieng dengan Studi Kasus di PT. Geo Dipa Energi*. https://api.semanticscholar.org/CorpusID:100678477

Positive Impact of Reinjection Infill on Geothermal Field Pressure Support

Fabiola Pardede, Wishnu Triananda, Rivan Yuono, Ryan Hidayat, and Radhitya Pradipta

PT Sorik Marapi Geothermal Power, Menara Sentraya 19th Fl., Jl. Iskandarsyah Raya No. 1A, Jakarta Selatan

fabiola.pardede@ksorka.com

Keywords: Sorik Marapi, reservoir surveillance, reinjection, reservoir, pressure, temperature, downhole, flowing

ABSTRACT

Observations of downhole pressure and temperature in Sorik Marapi geothermal production wells has shown indications of reinjection impacts on continuously flowing wells. The cooling impact was observed from the temperature reversal observed in the flowing wellbore profile, which was not previously seen during testing. Injection infill began in 2021 to provide more pressure support in productive reservoir. The shift in injection strategy partially away from infill zone conducted in 2022 shows that the productive reservoir still impacted with pressure support while reducing negative cooling impact. From the second quarter of 2023, brine rate output of production well AA showed a declining trend. By mid-2024, the rate of decline in brine mass flow production had eased with further improvement potential. The continuation of injection strategy away from within production zone showed improvement in nearby production well's flowing performance. These downhole surveys and production data analysis provides sufficient indication and insights for field-wide resource optimization.

1. INTRODUCTION

Sorik Marapi reservoir, developed by PT Sorik Marapi Geothermal Power as a project under KS Orka Renewables Pte. Ltd (KSO - a Singapore based company), is one of the liquid-dominated geothermal fields situated in Sumatran Fault damage zone, specifically in Mandailing Natal Regency. Until mid-2024, Sorik Marapi has been exploited and developed aggressively in four phases since 2019, producing up to 1100 kg/s of total mass flow rate consisting of steam and brine for the dual-flash system and combined-cycle modular power generation technology by Kaishan. One of the major challenges faced in liquid-dominated geothermal field such as Sorik Marapi pertains to effectively managing the fluid reinjection strategy. To address this concern, multiple work related to reservoir tracer testing, routine surface wellhead data monitoring, routine geochemistry sampling and monitoring, tracer flow tests samplings, and downhole surveys are conducted among other possible testing and surveys to characterize well and reservoir. Observations discussed in this study had resulted in a proactive intervention in the existing reinjection strategy not only to protect the main production zone from negative cooling impact but also to drive a properly provided active reservoir pressure support.

This study is aimed to investigate the effect of specific reinjection strategy implemented within Sorik Marapi main production zone using interpretations of short-term downhole pressure and temperature surveys. Sorik Marapi main reservoir has observed a trend of two-phase expansion, related to Sorik Marapi fluid saturation and enthalpy measured at surface. Sample data of production wells-fluid enthalpy at the subsurface had been identified at an estimated averaged value ~1070 kJ/kg with an increasing enthalpy trend over the recorded history. The observed increase in production enthalpy as a result of two-phase fluid expansion was anticipated, because Sorik Marapi had continued to increase field-wide mass extraction rate with each completion of phase development.

Abundant knowledge and understanding were gained throughout the period of reinjection and production monitoring. Discrete interpretations from downhole survey data were obtained by Sorik Marapi Geothermal Power's in-house logging team using in-house logging truck and facilities are incorporated into the specific evaluation of infill reinjection strategy. Observations of downhole pressure and temperature in flowing surveys had shown indications of reinjection impacts, in which negative cooling impact confirms the observed decline in brine mass flow production.

2. REINJECTION STRATEGY AND RESERVOIR RESPONSE

2.1 Reinjection in Sorik Marapi Geothermal Field

Liquid-dominated Sorik Marapi reservoir has been continuously accepting continuous stream of mixed brine and condensate since production began in 2019. The reinjection strategy has evolved with Sorik Marapi's four phase developments up to mid-2024, in terms of reinjection temperature, total mass injected, and reinjection location. The source of reinjection into Sorik Marapi reservoir since 2019 has been situationally mixed with fresh water from drilling fluid waste from the concurrent drilling activities, which is estimated to have contributed as much as <1% of the total water volume injected up to mid-2024. As the drilling waste contribution had been relatively

little and intermittent compared with the overall brine and condensate injectate, the injectate chemistry changes due to drilling activity has been disregarded in this study which could be for potential future study.

Reinjection temperature in Sorik Marapi is equal to the mixed rejected temperature outlet from binary cycle modules and condensate outlet from the hybrid evaporative-cooled condenser. Throughout Sorik Marapi's four phase development, rejected temperature from power generator outlet averaged from 80°C to 90°C, depending on the amount of brine being utilized into the system. In general, excess brine supply allows for higher brine mass flow rate as heat source into the heat exchangers and therefore exits the brine Organic Rankine Cycle (ORC) system with an elevated rejection temperature.

Additionally, excess brine supply that do not enter the heat exchanger system will be bypassed to join the brine outlet from system to the reinjection line, which therefore increases the overall injectate temperature that is being accepted by Sorik Marapi reservoir. Increased reinjection temperature causes a downward shift of overall injectors injection capacity curve, and therefore requiring an adjustment in the reinjection strategy. Excess brine supply in Sorik Marapi occurs intermittently as newly drilled wells were being flow tested or brine utilization awaits for the upcoming phase development. By mid-2024, the injectate temperature within Sorik Marapi overall reinjection line and wellheads remain stable at the measured average of 80°to 86°C.

For the purpose of this study, the reinjection activity which targeted location within proximity of Sorik Marapi main production zone is mainly called infill reinjection. Historically, reinjection infill in Sorik Marapi had been actively conducted on several injectors located in different well pads, where major production wells also exist in the same corresponding well pads.

2.1.1 Reinjection Infill at Well ZZ

In particular, an infill reinjection well so called well ZZ, is of great interest for Sorik Marapi's reservoir characterization due to its uniqueness in presenting immediate reinjection impact to production wells within its proximity. Well ZZ is a single infill injector located in well pad ABZ which had been injecting mixed brine and condensate since mid-2021, with main objective of supporting Sorik Marapi's second phase development reinjection demand.

Injection well ZZ demonstrated an outstanding injection acceptance capacity while flow testing the well had confirmed that it remained a low performing producer, even for Sorik Marapi's standard. The opportunity of utilizing high injection capacity in well ZZ posed risk and challenges on managing Sorik Marapi's reservoir.

In response to this challenge, a well-executed monitoring routine program at surface and downhole was initiated to safely enable well ZZ as an infill injector. It is important to note that infill injector ZZ is located in the same well pad, well pad ABZ, as major production wells, including production well AA and well BB.

2.1.2 Reinjection Infill Strategy Remains Successful in Several Injectors

In the course of high-rate reinjection infill at well ZZ, production well AA within the proximity exhibits rapid performance decline observed from declining flowing wellhead pressure, declined total mass output, and confirmed by decreased non-condensable gas (NCG) content. As well ZZ eventually reduced injection rate and eventually stop injecting in 2024, well ZZ availability is maintained as an injector for the long term strategy planning or future field management strategy.

Nevertheless, the indicative success by far of reinjection infill can be attributed to the infill injectors other than well ZZ in Sorik Marapi. These infill injectors had been actively accepting mixed brine and condensate as injectate since mid-2021 and remained so up to early 2024. Further monitoring and evaluation is imposed into these other infill injectors with similar attentiveness as to the previously discussed well ZZ to ensure that the reinjection strategy is proper according to Sorik Marapi development phase. It is possible that future reinjection strategy would imposes shifting in infill injection strategy away to peripheral, according to Sorik Marapi's reservoir response to the planned fifth phase development.

2.2 Downhole Pressure and Temperature Observations

Downhole pressure and temperature profiles were measured during flowing condition to Sorik Marapi power plant system. At least two production wells in Sorik Marapi had demonstrated pressure support within the productive area due to infill reinjection. The effectiveness of reinjection infill not also indicated by lack of pressure drawdown observed, but also lack of thermal breakthrough to the nearby producers.

The analysis of the two production wells presented in this study, so called well AA and well BB, have consistently demonstrated the absence of reservoir pressure drawdown, offering strong assurance that reinjection infill in Sorik Marapi is functioning intended. Nevertheless, the strategic approach still require careful implementation as a concerning development of cooling impact was observed in specific well AA. This observation serves as a

reminder of the importance vigilant downhole reservoir surveillance and swift active response measures in maintaining the productivity of geothermal field.

Well AA stands as a vital active production well, contributing both steam and brine for the Sorik Marapi screw expanders, steam ORCs, and brine ORCs, which has a capacity of ~4.9 MW. Since its commissioning in 2019, well AA had been actively feeding supply into Sorik Marapi's power generation system.

For well AA, diagnosing its declined performance has highlighted the exhibition of cooling impact due to reinjection returns in Sorik Marapi. Production well AA had been continuously producing > 24 kg/s total mass flow rate for 5 years, discharged at wellhead pressure >11 bara. Comparison of well AA flowing temperature profiles well AA is shown in Figure 1 below, with surveys conducted in 2021 and 2024. Flowing profile in 2024 observes a window of temperature reversal measured from depth 1300 – 1700 mMD. The temperature deflection in flowing survey well AA in 2024 is observed from ~8 to 30°C, while previous 2021 survey observed fully-saturated temperature profile from top to bottomhole.

Remarkably, no cooling impact was observed in the downhole flowing survey of production well BB, within the proximity of the infill reinjection well ZZ. Production well BB had been continuously producing > 98 kg/s total mass flow rate for 5 years, discharged at wellhead pressure >11 bara. Comparison of flowing temperature profiles well BB is shown in Figure 2 below, with surveys conducted in 2021 and 2024. Flowing pressure profile in 2024 observes a higher wellbore flowing pressure at the bottomhole. There are differences observed in the temperature profile of well BB, in which the temperature profile follows fully saturation profile as a function of fluid pressure throughout bottom up of the hole.

Based on internal report analysis, the productivity performance as a function of permeability had not experience any significant changes in both wells AA and BB. Trianandra (2024). The well integrity and treatment remains similar for both production wells throughout 2021 until 2024, without any wellbore obstruction nor intervention applied.

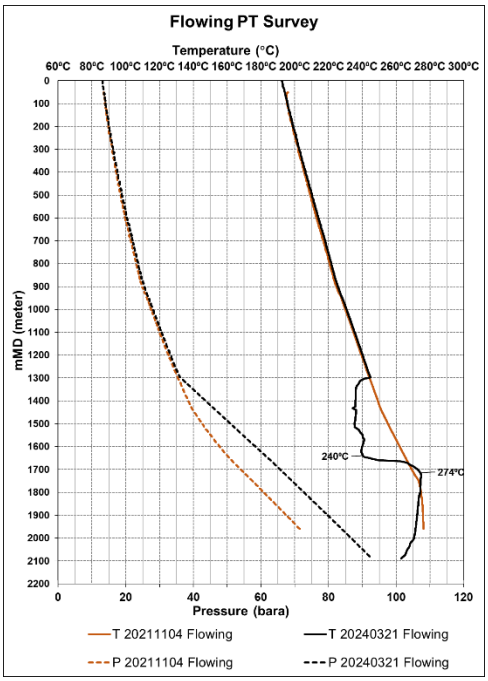

Figure 1: Comparison of Pressure Temperature surveys of flowing well AA in 2021 and 2024.

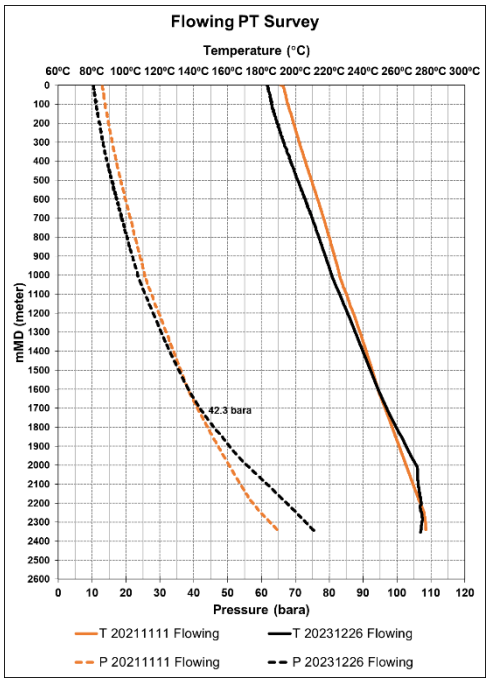

Figure 2: Comparison of Pressure Temperature surveys of flowing well BB in 2021 and 2024.

2.3 Impact of Reinjection

The shift in reinjection strategy to partially divert main production zone reinjection to across production zone boundary was conducted in 2022. Initiating the reinjection diversion was triggered by the rapid decline of wellhead pressure and production supply observed on well AA. This specific action is termed partial as it consists of targeted diversion of reinjection from a specific injector ZZ, while other wells injecting within main production zone remained unchanged.

As newly drilled wells were commissioned with excess hot brine into the Sorik Marapi reinjection system, well ZZ was initially designated to accept mixed brine and condensate at noticeably higher flow rate beginning in

early-2022. Well ZZ high injection capacity availability leads it to be the main objective of accommodating higher capacity reinjection required for the hot reinjection overall demand.

Rapid performance decline which was observed in well AA was analyzed and eventually understood as a direct cooling impact from the high-rate infill injection imposed on the nearby injector well ZZ. After the observation of rapid decline at well AA, a stop injection was imposed to the injection at well ZZ once plausible. The window of beginning injection at well ZZ until executing the reinjection shift away was imposed within several months which may likely to have avoided detrimental impact on Sorik Marapi reservoir long term utilization.

3. CONCLUSION

Even though analysis and interpretation of data collected during Sorik Marapi reinjection infill is still on going at the time of writing of this study, available results are highly positive. On the one hand, negative cooling impact or rapid production decline is not expected in production wells during long term injection in the current partially infill injection strategy. On the other hand, steam and brine production from Sorik Marapi field may be supported by the partially infill reinjection strategy, by maintaining stable pressure drawdown.

Similarities in well AA and BB were observed in the positive impact of reinjection infill as flowing pressure support to improve nearby production well's flowing performance. The shift in injection strategy partially away from infill well ZZ conducted in 2022 shows that it is likely that Sorik Marapi productive reservoir is still impacted with pressure support while reducing negative cooling impact.

The Sorik Marapi continued development will significantly affect reservoir fluid pressure and temperature balance, as well as its geochemistry. The optimized strategy in the upcoming term may differ significantly from the current discussion. Therefore, it may be concluded that reservoir surveillance by downhole surveys is important for Sorik Marapi field management, with additional allowance of flexibility to optimize the extraction and reinjection strategy.

REFERENCES

Sarmiento, Z., et al: Update on the Exploration and Development Drilling at the Sorik Marapi Geothermal Field, North Sumatra, Indonesia, *Proceedings,* 5th Indonesia Internation Geothermal Convention & Exhibition, Jakarta, Indonesia (2017).

Triananda, W., et al: Well AA Performance Update, *PT Sorik Marapi Geothermal Power*, (2024).

Navigating Geothermal Challenges: A Decision Framework for Successful Well and Reservoir Interventions

Kennard Maturgo, John Gilliland, Martin Pujol, Neale Young, and Nadia Domanski

JRG Energy Consultants Ltd, PO Box 42246, Auckland 1745, New Zealand

ken.maturgo@jrgenergy.com

Keywords: Intervention, wellbore simulation, cost-benefit analysis, risk assessment, decision matrix tool

ABSTRACT

Continuous exploitation of two-phase geothermal reservoirs often encounters challenges such as mineral scaling, pressure drawdown and thermal breakthrough. These challenges can abruptly affect production, reduce a well's effective lifetime or increase the overall project expenses required to achieve sustainability of a geothermal resource. Several well and reservoir interventions like scaling inhibition, broaching, acid treatment, mechanical workovers using coiled tubing and reinjection optimisation have proven to be successful in mitigating the negative effects of these challenges. However, the probability of success is not guaranteed and therefore, the economic benefits are unique for each solution. This variability, along with changing priorities and preferences such as lesser budget allocation for geothermal subsurface maintenance compared to other asset maintenance activities, makes it challenging for geothermal production managers to make informed decisions regarding well and reservoir intervention activities.

In this paper, a decision matrix tool is established to prioritise the approach for each well and reservoir intervention based on technical, financial and risk factors. Wellbore simulation is used as a tool in predicting outcomes such as productivity enhancement and capacity gain, while a cost-benefit analysis is also done to provide the initial ranking. To finalise the assessment, risks based on operational perspective are considered against the overall ratings. Lastly, the decision matrix tool is applied to case studies showing the sensitivity of factors in determining the likelihood of success for each well and reservoir intervention.

1. INTRODUCTION

Geothermal energy production particularly for electric power generation are unique for every location and operation. It is common that the maintenance of steam fields and power stations becomes challenging due to dynamic changes in reservoir processes, which include pressure drawdown and thermal breakthrough among others. The former usually occurs faster in high-enthalpy fields and can be mitigated by optimum reinjection. However, the latter could be more difficult to manage when the reinjected fluids result to invasive cooling and dwelling in the reservoir. These issues often lead to changes in pH, temperature and ion concentration due to flashing, and alteration of fluid composition resulting to mineral scaling either in the wellbore or reservoir formations. As a result, operating expenses attributed to intervention increase and accumulate over time.

Managing the expectations in addressing these challenges effectively start with meticulous planning based on the combination of technical evaluation and experience. Parameters such as production and injection rates frequently indicate the need for intervention to recover or optimise the well capacity, while selection of the desired solution considers the overall program and operational duration. It is critical to assess downhole conditions by determining the type and size of mineral scale, as well as any casing issues that may impede the progress of intervention operations (Erichatama, Adityatama, Al Asy'ari, & Purba, 2024). Though various well and reservoir interventions like scale inhibition, broaching, acid treatment and mechanical workovers have proven to be effective, the probability of success remains variable and makes economic benefits highly dependent on the skills and experience of people involved. As a result, the decision-making process becomes complicated with the equally important consideration of other necessary asset maintenance activities that also affects the cost in operating the geothermal field.

With the aid of an *Intervention Decision Matrix Tool*, geothermal production managers will be able to visualise the relative benefits and risks of each well and reservoir intervention for successful navigation towards mitigating geothermal challenges. This would also allow quick delineation of best options supporting timely decision-making that could save time and efforts from designing multiple solutions.

2. METHODOLOGY

The success of well and reservoir interventions is difficult to predict. It could be based on priorities or preferences of asset owners depending on historical experience and available budget. Technical prognosis, financial projection

and risk rating are the key considerations in reducing bias for selecting the most suitable intervention after downhole information and condition have been reviewed. The decision matrix tool that can be used to prioritise the well and reservoir interventions applicable for a particular scenario has a straightforward process (Figure 1). It starts with wellbore simulation to predict possible capacity recovery from implementing the interventions, followed by a cost-benefit analysis that covers the revenue from electricity sales and costs attributed to the intervention and opportunity losses. The next step is to evaluate the uncertainties based on perceived risks of each intervention relative to one another in the context of addressing a particular scenario. Risk ratings would differ between the wellbore and reservoir scaling scenarios. The probability of success for each intervention is estimated and a Monte Carlo simulation is applied to determine the confidence level of having the likelihood that an intervention will succeed. Once the success factors are scored, the ranking may be used to suggest a course of action in selecting the most viable intervention.

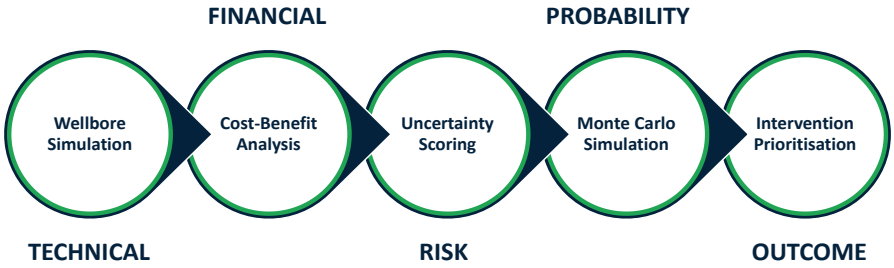

Figure 1: Decision matrix tool framework for well and reservoir interventions.

2.1 Success Rating

A four-point scale with scores from 0 to 3 is used to evaluate each factor: (a) technical, (b) financial, and (c) risk. The technical factor considers well deviation, casing condition, age of well and scale location. If the anticipated mineral scaling is inside the wellbore, it is important to consider the hardness, interval, diameter and deviation at point of the scales. The financial factor is based on the present value ratio of costs and benefits from implementing the intervention for 5 years. Costs include the expenses to conduct the intervention and opportunity losses while the production capacity is declining, and the missed revenue if the baseline capacity is not achieved by the potential maximum output recovery. Lastly, the risk factors are relative to the interventions and scaling problem. The operational risks of interventions being considered are safety, schedule, supply chain, structure of the team and stakeholder obligations. Hence, an intervention may have a different score for the issue on scaling inside the wellbore compared to scaling in the reservoir formations. Also, weights are imposed on each factor for sensitivity analysis. With the weighted factors in place, the success rate is then calculated using the Equation below:

$$S = \frac{Tx+Fy-Rz}{Tx+Fy} \quad (1)$$

where *S, T, F, R* are the success rate, factor scores for technical, financial and risk with corresponding weights *x, y, z,* respectively.

2.2 Monte Carlo Simulation

The success rate may become insufficient at times when decision makers have different priorities. In the case of an operating geothermal field, maintenance activities for assets other than the subsurface are usually given higher priority due to being the recurring cost drivers. This often results in reduced budget for well and reservoir interventions leading to more future expense such as drilling a new well. To supplement the calculated success rate, a probabilistic approach using Monte Carlo simulation is incorporated to consider random variability in the results. Since the success of interventions are highly dependent on the activity program and schedule, the PERT probability distribution is used in simulating the confidence level. The Program Evaluation and Review Technique (PERT) analysis is ideally used for activities with defined duration with variables regarded as independent of each other (Hajdu & Bokor, 2014). In the case studies, success rates of each intervention are treated independently to predict their individual confidence levels.

3. CASE STUDY

A hypothetical production well is created using *Gudrun* from the Volsung software package. The model is a deviated well consisting of standard 9-5/8" production casing and 7" liner with 3 feed zones. Table 1 summarises the baseline well and reservoir parameters used while Figure 2 shows the wellbore schematic from the Gudrun graphical user interface.

Table 1: Summary of basic well parameters used in the wellbore model.

Well Parameters	Value
Total Depth	3,000 mMD
Deviation	11°
Production Casing	9-5/8" (40 lbs/ft; 0.05mm rugosity)
Production Liner	7" (23 lbs/ft; no rugosity)
Feed Zones	1,500 mMD / 1,800 mMD / 3,000 mMD
Maximum Bottomhole Pressure	120 bar
Maximum Bottomhole Temperature	325°C at 3,000 mMD

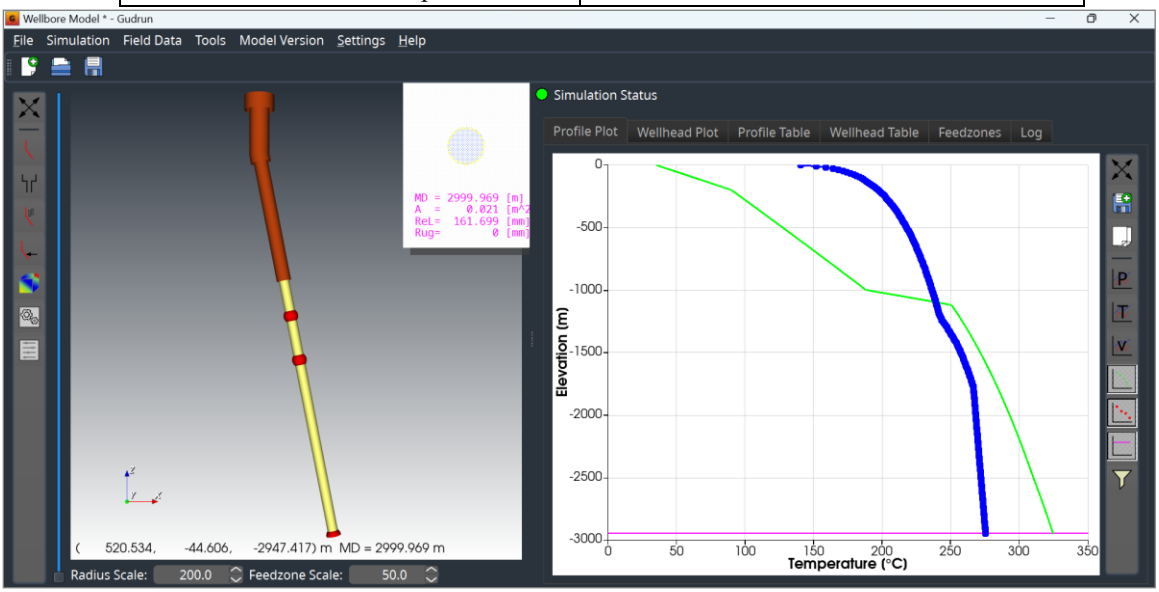

Figure 2: Graphical user interface of Gudrun showing a representation of the wellbore model created.

Table 2: Assumptions for wellbore scaling scenario.

Indicators	Baseline	Assumption
Downhole Condition	No issues	5" opening remains at 1,500m; 2" opening remains at 1,800m; no known casing defects
Scale Information	None	1-meter interval at the 11° deviated liner just above the 1,500 mMD and 1,800 mMD feed zones; aged calcite
Total Mass Flow	42 kg/s	24 kg/s
Enthalpy	1953 kJ/kg	1935 kJ/kg
Power Potential	12.8 MWe	7.2 MWe

3.1 Wellbore Scaling

Geothermal well output declines naturally due to reservoir pressure drawdown but an abrupt loss indicates that there is a worse cause usually attributed to mineral scaling or casing damage. The former can be easily resolved with well interventions such as broaching and work overs using coiled tubing or drilling rig. Options to increase the chance of success also include acid treatment by bullheading and pumping through a drill string or coil tubing. The most common mineral scaling issue is due to calcite, which occurs mainly at the flash point in the wellbore. If not addressed, it will continuously aggravate as the flash point moves when the wellbore internal diameter decreases over time (Wilson, Aranas, Bixley, Anderson, & Patterson, 2015; Wilson, Gilliland & Austin, 2015). Table 2 shows the changes between baseline and wellbore scaling conditions assumed for the case study. The wellbore model was evaluated based on the remaining diameter of the production liner where the flash point occurred, and thus scaling. The obstruction in this model is more severe at the middle feed zone (1,800 mMD) as compared to the shallower feed zone (1,500 mMD), which resulted to about 5-MW decrease in electric power potential of the well.

3.2 Reservoir Scaling

Compared to scaling inside the wellbore, the production output decrease could be slower when scales deposit in the reservoir formation. In the case of calcite, it may also deposit in the reservoir when carbon dioxide (CO_2) separates from the fluid solution along with other triggers like high pH and over-saturation of calcium ions as well as carbonate minerals (Akin, et al., 2015). Intervention options become limited to acid treatment by bullheading and pumping through a drill string or coil tubing unlike in wellbore scaling scenario wherein you can opt for the cheaper mechanical cleanout. Table 3 shows the changes between baseline and reservoir scaling conditions assumed for the case study. The wellbore model was evaluated based on the reduction of productivity index at the middle feed zone (1,800 mMD). The focus of the model is the effect of reduced permeability due to scaling in the formation, thus skin factor is not considered. In this scenario, the permeability of the feed zone at 1,800 mMD was significantly affected by reservoir scaling and resulted to a decrease in productivity index from 2.0 to 0.1 kg/s-bar. Although the reduction in electric power potential is almost the same as the wellbore scaling scenario, the perceptible change is on the enthalpy having a relatively lower value. In a real scenario, one possible interpretation could be that the reservoir scaling may have been caused by reinjection returns with fluids that have been over-saturated with calcium.

Table 3: Assumptions for reservoir scaling scenario.

Indicators	Baseline	Assumption
Downhole Condition	No issues	Productivity index of the feed zone at 1,800 mMD decreased from 2.0 to 0.1 kg/s-bar
Scale Information	None	Scaling in the reservoir formation affecting the permeability of the feed zone at 1,800 mMD
Total Mass Flow	42 kg/s	24 kg/s
Enthalpy	1953 kJ/kg	1918 kJ/kg
Power Potential	12.8 MWe	7.0 MWe

Table 4: Wellbore scaling scenario – predicted best outcomes from simulation and other considerations.

Intervention	Maximum Recovery, MWe	Post-intervention Power, MWe	Assumption
Broaching	4.8	11.9	Wellbore simulation – 100% cleared 1,500 mMD; 50% cleared 1,800 mMD
Mechanical Cleanout (Coiled Tubing)	5.2	12.4	More cleared scales than broaching due to more sophisticated downhole tools
Mechanical Cleanout (Drilling Rig)	5.4	12.6	More cleared scales than coiled tubing due to more rotation and weight on bit
Acid Treatment (Bullhead)	4.8	11.9	Assumed the same outcome as broaching; acid pumping instead of mechanical cleanout
Acid Treatment (Coiled Tubing)	5.4	12.6	Better outcome than bullheading due to reaching the target zone for acid treatment
Acid Treatment (Drilling Rig)	5.7	12.8	Better outcome than using a coiled tubing due to more weight on bit in case of need for mechanical cleanout
Acid Treatment (Drilling Rig) and Scaling Inhibition	5.7	12.8	Same as acid treatment using drilling rig

4. DISCUSSION AND RESULTS

The success rates of each intervention option are evaluated independently between the wellbore scaling and reservoir scaling scenarios due to the difference in scale locations. Mechanical cleanout is not applicable for reservoir scaling but acid treatment can be suitable to either case. Additionally, scaling inhibition is considered in

the wellbore scaling scenario to test its viability if selected from other well intervention options. Table 4 and Table 5 summarise the best possible outcomes of each intervention in terms of maximum increase in power potential. For the wellbore scaling scenario, acid treatment using a drilling rig has the highest recovered output mainly due to its combined capability to pump acid at the specific target zone and drill-out scales with more weight and capability to rotate than of the coiled tubing.

Table 5: Reservoir scaling scenario – predicted best outcomes from wellbore simulation and other considerations.

Intervention	Potential Recovery, MWe	Recovered Power, MWe	Assumption
Acid Treatment (Bullhead)	4.1	11.2	Wellbore simulation – 50% recovery of productivity index at 1,800 mMD feed zone (from 0.1 to 1.0 kg/s-bar)
Acid Treatment (Coiled Tubing)	5.3	12.4	Better outcome than bullheading due to reaching the target zone for acid treatment
Acid Treatment (Drilling Rig)	5.3	12.4	Better outcome than using a coiled tubing due to more weight on bit in case of need for mechanical cleanout

Table 6: Initial ranking of interventions for wellbore scaling scenario.

Intervention	Technical	Financial	Subtotal	Ranking
Broaching	2.20	2.63	2.42	7th
Mechanical Cleanout (Coiled Tubing)	2.20	2.74	2.47	5th
Mechanical Cleanout (Drilling Rig)	2.20	2.71	2.46	6th
Acid Treatment (Bullhead)	2.70	2.46	2.58	4th
Acid Treatment (Coiled Tubing)	2.95	2.59	2.77	3rd
Acid Treatment (Drilling Rig)	3.00	2.61	2.80	2nd
Acid Treatment (Drilling Rig) and Scaling Inhibition	2.70	3.00	2.85	1st

Table 7: Initial ranking of interventions for reservoir scaling scenario.

Intervention	Technical	Financial	Subtotal	Ranking
Acid Treatment (Bullhead)	2.70	2.48	2.59	3rd
Acid Treatment (Coiled Tubing)	2.95	2.40	2.67	1st
Acid Treatment (Drilling Rig)	3.00	2.32	2.66	2nd

4.1 Preliminary Ranking

Based only on technical and financial factors that are treated equally important, an initial ranking is obtained to show a preliminary comparison for each well and reservoir intervention. Table 6 shows that the most attractive intervention for wellbore scaling would be acid treatment using a drilling rig with scaling inhibition afterwards. This is mainly because the well output is maintained at maximum potential annually despite the required initial expense for an acid treatment to ensure that the wellbore is clear prior to installation of a scaling inhibition system. In the case of reservoir scaling, the most attractive intervention is acid treatment using coiled tubing (Table 7). The reason for coiled tubing to lead the scores in acid treatment for reservoir scaling is because of the cheaper cost compared to using a drilling rig for the same capability of being able to pump acid at the specific target zone that bullheading may not achieve.

4.2 Sensitivity Analysis

Calculating the success rating of the interventions provides further justification for possible plans of action. If the decision maker is a person who is technically inclined, the selection process would be biased to factors (i.e., downhole condition and scale information) that will drive the success during operations. Meanwhile, decision makers who safeguard the financial aspects would highly consider the cost-benefit analysis outcome. An organisation's current circumstance usually dictates the preference during selection and makes it difficult for production managers to amplify their decisions. There are cases when the urgency to execute an intervention takes over the financial aspects, while there are also occasions when budget is a constraint.

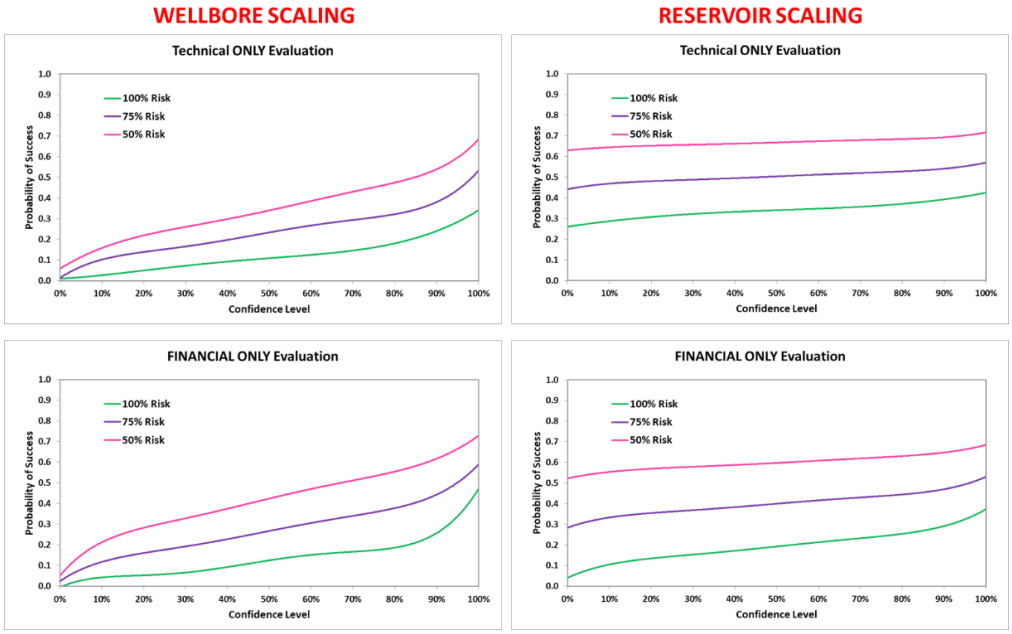

Figure 3: Probability of success and confidence level at various risk magnitude for scaling interventions based on technical and financial scoring only.

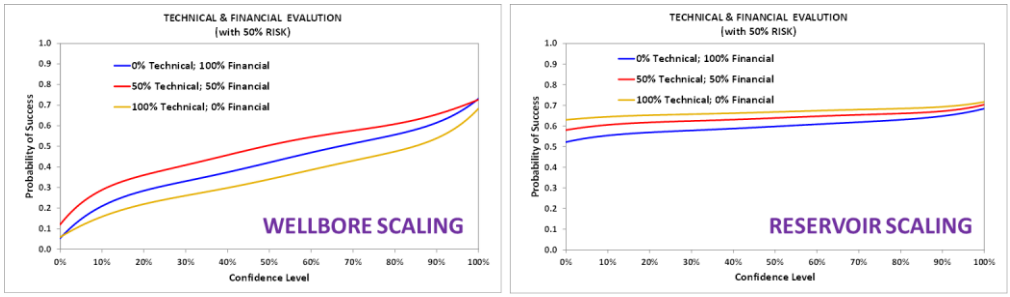

Figure 4: Probability of success and confidence level at various technical and financial magnitudes with 50% risk for scaling interventions.

Applying the Monte Carlo simulation helps define the confidence level based on historical trends or events, which can be correlated with the success rate. Figure 3 shows that the probability of success increases as the risk factors are reduced whether the assessment is biased to the technical or financial aspects. Moreover, the probability of success is more sensitive to the increase in confidence level of a decision maker in the wellbore scaling scenario possibly because there are more intervention options available than in the reservoir scaling scenario. If the risk factors are presumed mitigated by 50%, the wellbore scaling scenario suggests that having a balanced view between technical and financial factors is most desirable followed by giving more weight to financial factors while the reservoir scaling scenario indicates that the best outcome is more dependent on the technical factors (Figure 4).

4.3 Success and Confidence

Integrating the success rates and confidence levels with the preliminary ranking changes the impression on well and reservoir interventions. However, the values should not be treated as absolute figures to conclude which intervention is better since the calculations and assumptions were based on the best outcome considering potential maximum electric power output recovered and absence of issues during execution despite the risk factors. Table

8 summarises the estimated success rates and confidence levels at 50% weight each of the technical, financial and risk factors specific to the parameters in the case studies. Mechanical cleanout using a drilling rig has a negligible success rate due to the risk factors scoring higher than the technical and financial factors, but the confidence level of having this value is only 25%. This means that there is still a 75% opportunity that the success rate could be higher by significantly mitigating the risk factors.

Table 8: Success rates and confidence levels at 50% weight on each of the factors specific to the case studies.

Intervention	Success Rate	Confidence Level
Broaching	0.74	100%
Mechanical Cleanout (Coiled Tubing)	0.55	61%
Mechanical Cleanout (Drilling Rig)	Nil	25%
Acid Treatment (Bullhead)	0.56 – 0.71	66% – 96%
Acid Treatment (Coiled Tubing)	0.55 – 0.63	32% – 62%
Acid Treatment (Drilling Rig)	0.51 – 0.58	1% – 52%
Acid Treatment (Drilling Rig) and Scaling Inhibition	0.52	54%

5. CONCLUSION AND FUTURE WORK

The *Intervention Decision Matrix Tool* is a chain of steps that builds the framework for the selection of fit-for-purpose well and reservoir interventions. It is a quantitative approach to providing justification for decision makers and is an ongoing development envisaged to be an "input-output" spreadsheet deck and eventually may further become an application or software for the geothermal energy industry.

REFERENCES

Akin, S., Yildirim, N., Yazman, M., Karadağ, M., Seçkin, C., Tonguç, E., . . . Yarim, H. (2015). Coiled Tubing Acid Stimulation of Alaşehir Geothermal Field, Turkey. *Proceedings World Geothermal Congress 2015*. Melbourne, Australia.

Erichatama, N., Adityatama, D., Al Asy'ari, M. R., & Purba, D. (2024). Enhancing Geothermal Well Workover Planning Through Data-Driven Performance Evaluation. *PROCEEDINGS, 49th Workshop on Geothermal Reservoir Engineering. Stanford University*, Stanford, California.

Hajdu, M., & Bokor, O. (2014). The Effects of Different Activity Distributions on Project Duration in PERT Networks. *27th IPMA World Congress*. Elsevier Ltd.

Wilson, D., Aranas, M., Bixley, P., Anderson, J., & Patterson, D. (2015). Application of Coiled Tubing for Live Well Workovers. *Proceedings 37th New Zealand Geothermal Workshop*. Taupo, New Zealand.

Wilson, D., Gilliland, J., & Austin, A. (2015). Broaching: An Effective Method of Well Intervention for Calcite Scale Removal. *Proceedings World Geothermal Congress 2015*. Melbourne, Australia.

Targeting Two-Phase Steam Dominated Reservoir in Hot Water Geothermal System in Ulubelu Geothermal Field, Lampung, Indonesia

Imam M. Prasetyo, M. Ikhwan, Anita Fithriah S. A., Anjani Puspadianti,
M. Permadi Sugiarto, M, R. M. Tofan S., and Teguh Prabowo

PT. Pertamina Geothermal Energy

imam.pras@pertamina.com

Keywords: Ulubelu, steam sustainability, two-phase reservoir, hot water geothermal system, updoming structure, clay cap

ABSTRACT

The Ulubelu geothermal field, operated by PT. Pertamina Geothermal Energy Tbk. (PGE), is located in Lampung Province at the southern tip of Sumatera Island. Geologically, the field is situated within a Quaternary volcano-tectonic depression characterized by a strong caldera environment that predates post-caldera tectonic activity (Prasetyo, 2023). It lies approximately 15-20 km from the Sumatera Fault System (SFS) and exhibits a slightly different trend (NNW-SSE) than the SFS. Currently, the Ulubelu field generates up to 220 MW of electricity from four 55 MW steam plants. To ensure sustainable steam supply and counteract reservoir performance decline, Ulubelu Field has planned regular drilling campaigns for make-up wells.

Since 2014, two years after the initial production of Units 1 and 2, make-up wells have been drilled to supply steam to the Ulubelu Geothermal Power Plants (GPP). Due to the limited current well targeting area and significant well interference, PGE opted to drill delineation wells to the north of the central production area. This designated area, within the inferred upflow zone of Mt. Rendingan crater, was identified as a promising site for field expansion based on geoscientific and reservoir data. The area features a classic volcano-hosted geothermal system with an updoming clay cap structure near the volcanic edifice.

Between 2018 and 2024, six wells were drilled from two wellpads (UBL-J & UBL-M) in the northern area. The first three wells were drilled sequentially from Pad UBL-J to confirm the hypothesized upflow and the existence of a two-phase reservoir beneath Mt. Rendingan crater. The results were promising, revealing a two-phase reservoir with temperatures around 260-280°C and enthalpies of 2400-2800 kJ/kg, yielding substantial output. Subsequently, three more wells were successfully drilled from Pad UBL-M to exploit the northern production area east of Pad UBL-J, showing similar characteristics.

Targeting the northern area with the MT-Resistivity updoming structure beneath Mt. Rendingan crater has proven valuable for sustaining steam availability in the Ulubelu field. The productivity in this two-phase steam-dominated reservoir is generally high. However, as steam-dominated reservoirs tend to experience rapid decline in production, rigorous reservoir monitoring is essential to manage fluid production effectively.

1. INTRODUCTION

The Ulubelu geothermal field, located in Tanggamus Regency, Lampung Province, at the southernmost part of Sumatra Island, generates up to 220 MW of electricity through four 55 MW condensing steam plants. The geothermal power plant installation began in 2012 with the commercial generation of units 1 and 2, while units 3 and 4 went online in 2016 and 2017, respectively. Since then, a total of 62 wells, including production, injection, and make-up wells, have been drilled in the Ulubelu field.

The decline in reservoir performance during geothermal field exploitation is common and can be attributed to various factors, such as decreased reservoir pressure and wellbore issues (e.g., scaling and restrictions). To maintain a sustainable steam supply to the geothermal power plant (GPP) and counteract the decline in reservoir performance, well interventions and drilling of make-up wells are typically conducted. PGE has planned and executed a series of well interventions and a make-up well drilling campaign. Between 2018 and 2024, PGE drilled 12 wells from new wellpads, specifically UBL-J and UBL-M.

Generally, make-up well will optimize the existing area of production. However, due to limited availability of space both at surface and subsurface, new area of production need to be delineate. The strong candidate to target is the upper-north area where the previous wells drilled and integrated geoscience data show near-upflow zone area with high productivity potential.

2. ULUBELU GEOTHERMAL SYSTEM

Ulubelu Geothermal Field lies on the southern tip of the Sumatera Fault System with an NW-SE trend. It is physiographically located within Bukit Barisan Mountain Range (Figure 2.1). The Sumatera Fault System is believed to have a close relationship with the volcanism along Bukit Barisan Mountain Range. The segmented Sumatera Fault limits the southern part of Sumatera Island by the Semangko Segment. It corresponds to the dextral slip movement of oblique convergence plates beneath Sumatera Island that terminates at Teluk Semangko. It also exhibits several fault splays and prominent pull-apart basins (Suoh Sekincau). The field is located around 15-20 km from Semangko Fault and has a slightly different trend from Semangko Fault (NNW- SSE).

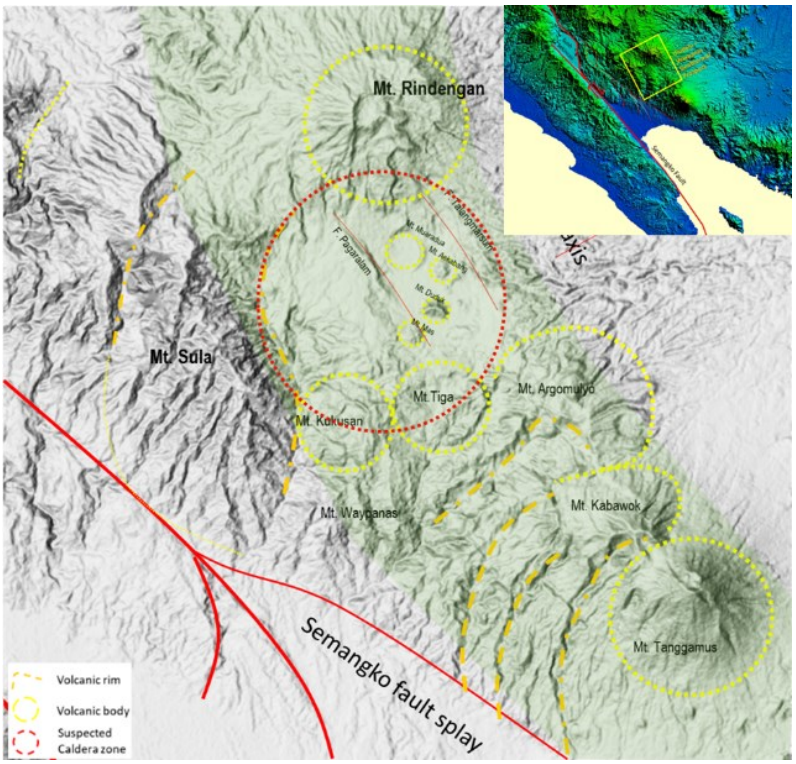

Figure 1: Location of the Ulubelu field at southern tip of Sumater near the Semangko segment.

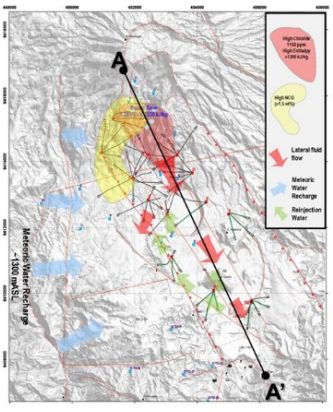

Hydrology model of Ulubelu System

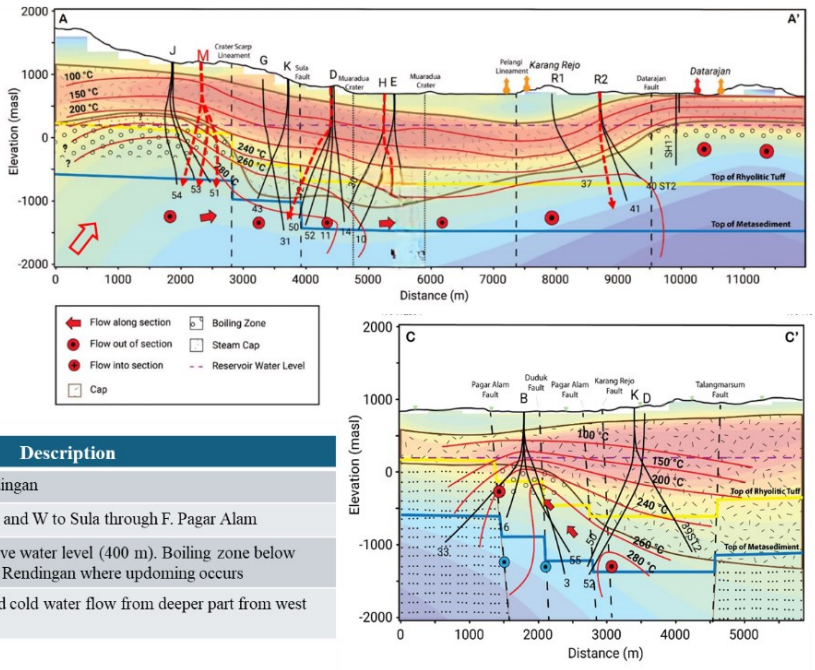

Elements	Description
Upflow	Fluid rise beneath Mt. Rendingan
Outflow	Flows SE towards datarajan and W to Sula through F. Pagar Alam
Clay Cap	Firm clay cap generally above water level (400 m). Boiling zone below clay cap exhibits below Mt. Rendingan where updoming occurs
Cold water flow	Pagar Alam Fault introduced cold water flow from deeper part from west

Figure 2: Summary of Ulubelu field's hydrology.

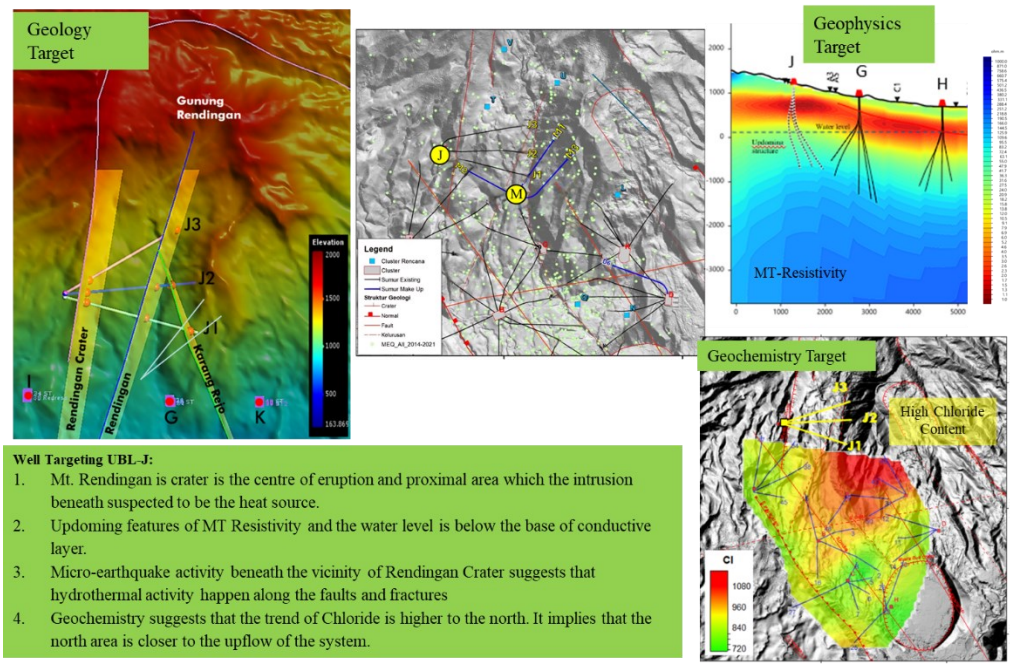

Figure 3: Rationales behind targeting the upper-north area (Mt. Rendingan's crater) of Ulubelu field.

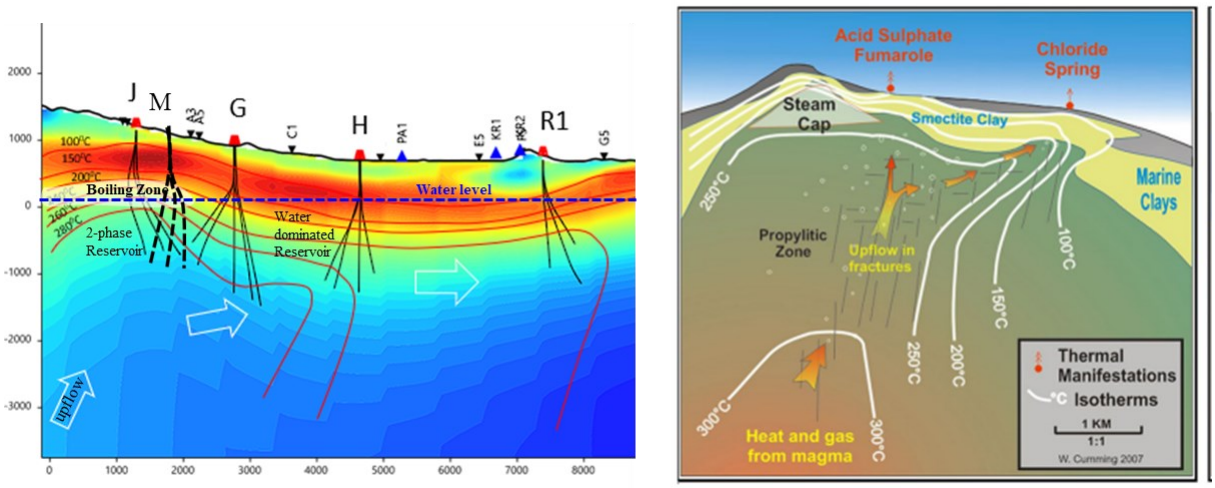

Figure 4: NW-SE MT-Resistivity structure of Ulubelu Field. Comparison of MT-Resistivity model of Ulubelu with the volcanic-hosted geothermal system as described by Cumming (2016). The updoming feature and water level below the base of conductive layer provide hint of two-phase reservoir existence.

The hydrology of Ulubelu field is postulated arise beneath G. Rindengan high and moves away laterally to the lower elevation through NW-SE geological structure (Pagar Alam, Duduk, Karangrejo Faults) and permeable Rhyolitic Tuff Unit. The geothermal fluid is benign and has chloride content of 1200-1300 mg/kg with temperature at the upflow up to 285°C. As it moves away from the upflow zone, it becomes more diluted and lower in temperature. The reversal temperature profile from wells in the west suggests that there are fluid outflows from deep reservoir to the shallower reservoir to the west. It also suggests that cooler deep fluid may also intruded from west to east from Pagar Alam to the graben. The outflow characterized by its high permeability, lower temperature, more dilute chemistry and temperature reversal profile. The temperature reversal profile shows particularly in wells that intersecting the Pagar Alam Fault.

Firm clay cap recorded by MT Resistivity model extent along NW-SE graben. It exhibits updoming structure in the north area beneath Mt. Rendingan and thicker to south east. The NE-SW MT-Resistivity structure exhibit thickening to the east. This implies that the reservoir is deeper in the east. The tilted geometry of the reservoir seems to be controlled by deposition of rhyolitic tuff units along the graben structure. This feature in the north-east acts as deep upflow that rise toward shallower aquifer toward SW.

3. TARGETTING TWO-PHASE RESERVOIR ZONE

In 2018, PT Pertamina Geothermal Energy (PGE) initiated a make-up wells drilling campaign to maintain steam supply to geothermal power plant (GPP). A major challenge of this campaign was the limited area available for drilling both surface and subsurface. To address this, a detailed analysis of integrated subsurface data was conducted, leading to the decision to delineate the upper-north area towards the Rendingan crater for additional well placements. Some of the rationales drilling to the upper-north area are :

1. Mt. Rendingan is crater is the centre of eruption and proximal area which the intrusion beneath suspected to be the heat source.
2. Updoming features of MT Resistivity and the water level is below the base of conductive layer.
3. Micro-earthquake activity beneath the vicinity of Rendingan Crater suggests that hydrothermal activity happen along the faults and fractures.
4. Geochemistry suggests that the trend of Chloride is higher to the north. It implies that the north area is closer to the upflow of the system.

Identifying a two-phase steam-dominated system within a predominantly water-dominated geothermal field may seem counter-intuitive. However, certain geological and geophysical indicators can provide critical insights.

1. Updoming of MT-Resistivity Structure: Magnetotelluric (MT) resistivity surveys, which measure the earth's natural electromagnetic fields, can reveal subsurface structures. An updoming resistivity structure indicates regions with concentrated heat and fluid flow, suggesting high permeability and significant heat transfer in volcanic geothermal systems.
2. Thinning of the Clay Cap: The thickness of the clay cap, a low-permeability layer, is crucial in geothermal systems. Thinning but highly conductive beneath a volcanic center due to thermal buoyancy facilitates the upward migration of hot water. When this heated water encounters the base of the clay cap, it can spread laterally, potentially forming steam-dominated zone if boiling conditions are met.
3. Water Table Position: A water table located below the base of the conductive layer (typically associated with the clay cap) strongly indicates a two-phase reservoir. This condition implies that pressure and temperature conditions support the coexistence of liquid and steam phases.

Ulubelu field's NW-SE MT-Resistivity cross-section provides insight of the subsurface structure. The model exhibits updoming structure beneath Mt. Rindengan and thickening of clay cap to the SE. Pressure measurement from previously drilled wells indicates water level throughout the field. The water level in Ulubelu generally has same elevation indicating that it is within the same hydrology and no compartmented reservoir. It is located beneath the clay cap on Mt. Rendingan suggesting that two-phase reservoir potentially exist during the initial stage of well-targeting.

4. RESULT FROM DRILLING

The delineation of the upper-north extension towards Mt. Rindingan began from pad UBL-J. PGE prepared three sequential wells in pad UBL-J, with one well drilled from the existing pad (UBL-D) between the first and second wells of UBL-J. This strategy allowed flexibility to evaluate the results from UBL-J1 before deciding to drill two more wells in UBL-J.

The UBL-J drilling campaign commenced in early 2018 with UBL-J1 and concluded with the third well (UBL-J3) in August 2018. All wells were directional, targeting the eastern region inside the Rindingan Crater, reaching total depths between 2100-2200 mMD or approximately -650 to -700 mRSL. The Top of Reservoir (ToR) is located between 100 mRSL and sea level, with major feed zones between -100 to -500 mRSL.

Well completion tests were conducted to understand the reservoir characteristics in the area. The gross permeability tests from the UBL-J wells indicated injectivity indices ranging from 280-900 lpm/ksc. By April, the wells had heated up to static temperatures, recording average maximum temperatures of 260-280°C. Interestingly, the Boiling Point Depth curve between sea level and -500 mRSL aligned with the convective profile of the UBL-J wells, suggesting the existence of a boiling zone near the UBL-J wells.

Well testing commenced with UBL-J1 in 2019 and continued sequentially with UBL-J2 and UBL-J3 in the same year. The results from UBL-J1 were promising, exhibiting dry steam with a dryness of averaging above 90% and enthalpy of 2400-2800 kJ/kg. This marked the discovery of the first two-phase steam-dominated reservoir in the PGE field in the Sumatra region.

In 2022, PGE initiated another drilling campaign to expand the upper-north Ulubelu area. Wellpad UBL-M was constructed east of UBL-J, targeting the eastern extension area from UBL-J where the two-phase steam-dominated reservoir was discovered. The campaign started in 2022 with the drilling of UBL-M1. Following the same strategy, the rig was moved to another well in an existing pad while UBL-M1 was being evaluated before proceeding with

the drilling of UBL-M2 and UBL-M3. The results from UBL-M1 were also encouraging, confirming the presence of a two-phase reservoir in the area east of the UBL-J wells.The summary of drilling result can be seen in Table1.

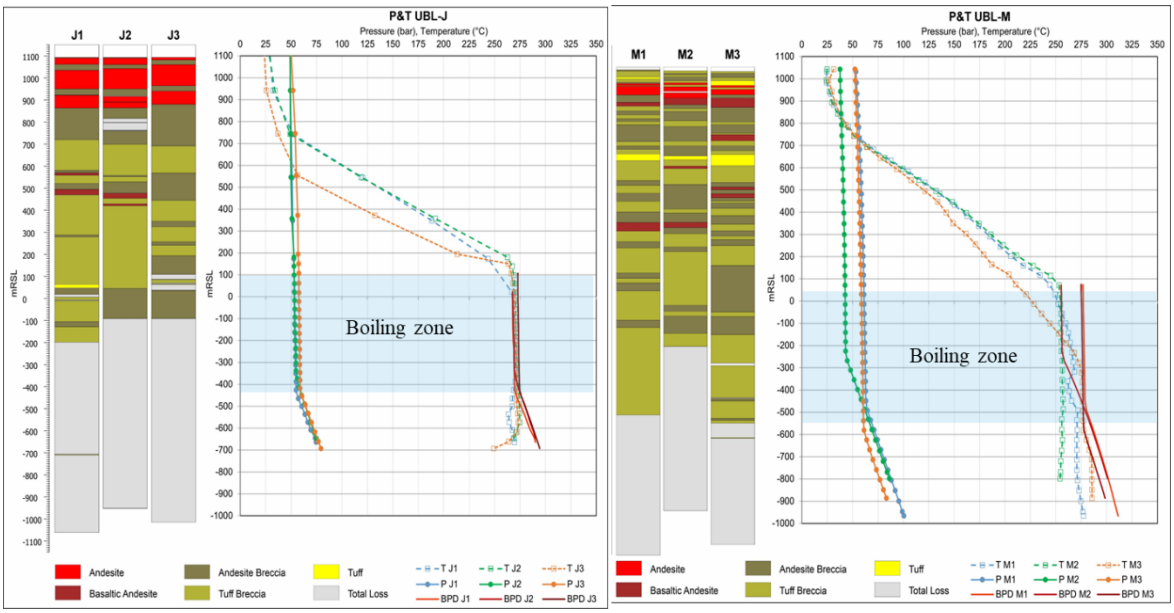

Figure 5: Composite log of static PT measurements and borehole geology of UBL-J and UBL-M wells.

Table 1: Summary of well testing from UBL-J and UBL-M production test. It exhibits overall high dryness and high productivity in upper-north area.

Well	WHP (barg)	Throttle Valve (%)	Dryness	Enthalpy (kJ/kg)	Steam flow rate (t/hr)
J1	23.5	40	1	2801	159.5
J2	25	40	1	2786	338.2
J3	20.6	47	0.89	2569.9	196
M1	25.0	25	0.82	2400.9	88.2

5. CONCLUSION AND RECOMMENDATION

Targeting the upper-north area with the MT-Resistivity updoming structure beneath the Mt. Rindingan crater has proven valuable for sustaining steam availability in the Ulubelu field. The depth of the water table provides insight into the field's thermodynamics and, together with the updoming MT-Resistivity profile, can indicate the presence of a steam cap. This method can also help predict whether the reservoir will be two-phase or water-dominated with low dryness, in addition to geochemical plots.

The overall productivity in this two-phase steam-dominated reservoir is generally high. However, as steam-dominated reservoirs exploitation tend to experience rapid declines in production, rigorous reservoir monitoring is essential. One pitfall in targeting this feature, as mentioned by Cumming (2016), is the need for caution when there are no strong indications of thermal manifestations such as fumaroles at the surface (hidden geothermal systems). This absence may reflect relict alteration with past high-temperature propylitic alteration recorded by MT-Resistivity. A thorough examination of the field's geology, identification of the rock's age, and the possibility of metamorphic rock exposure at the surface can strongly indicate a fossil geothermal system, which is significantly cooler in recent times.

REFERENCES

Cumming, W. Resource conceptual model of volcano-hosted geothermal reservoirs for exploration well targeting and resource capacity assessment: construction, pitfalls and challenges. Geothermal Resources Council Transactions, Vol. 40, 2016.

Cumming, W. Geothermal resource conceptual models using surface exploration data. Proc. 34th Workshop on Geothermal Reservoir Engineering, Stanford University, Stanford, California, February 9-11, 2009.

Koestono, H., Prasetyo, I.M., Nusantara, V.D.M, Thamrin, M.H., Silaban, M,. Subsurface geology of the north sector of Ulubelu geothermal field, Lampung, Indonesia. *Proc. World Geothermal Congress 2020+1.,* Reykjavik, Iceland, April-October 2021

Nurseto, S.T., Sardiyanto, Koestono, H., Thamrin, M.H., Kamah, M.Y. Evaluation of the productive geological structure in Ulubelu Geothermal System. *Proc. World Geothermal Congress 2015,* Melbourne, Australia, 19-25 April 2015.

Prabowo, T., Yuniar, D.M., Sugiharto, M.P., Fanani, A.F., Saputra, M.B. Well Production Test Reports : UBL-J1, UBL-J2, UBL-J3, UBL-M1, Internal Report, PT. Pertamina Geothermal Energy.

Prasetyo, I.M, Nainggolan, S.S, Nurseto, S.T., Mulyanto, Hastuti, P. Pieces of evidences of tectonically dissected caldera setting that controls the Ulubelu-Waypanas Geothermal System. *Proc. World Geothermal Congress 2023*, Beijing, China, October 2023

Prasetyo, I.M., Koestono, H., Sardiyanto, Yuniar, D.M., Hastuti, P., Adi, T., 2018. Ulubelu Geothermal Field Conceptual Model Update, Internal Report, Dec. 2018, PT. Pertamina Geothermal Energy.

Thermochem, 2022. Capacity of the Ulubelu geothermal reservoir to sustain PT, Pertamina Geothermal Energy's Development Strategy, Internal Report, May 2023, PT. Pertamina Geothermal Energy.

Production Improvement as Result of Injection Breakthrough Recovery: Case Study Sorik Marapi Geothermal Field, Indonesia

Wishnu Triananda, Fabiola Pardede, Rivan Tri Yuono,
Keshan Apriliyanthy, Radhitya Pradipta, and Ryan Hidayat

KS Orka Renewables Pte. Ltd., Menara Sentraya 19th floor,
Jl. Iskandarsyah Raya No. 1A, Melawai, Jakarta Selatan

wishnu.triananda@ksorka.com

Keywords: Geothermal Reservoir, Production, Injection Breakthrough, Injection Recovery

ABSTRACT

Reinjection of produced brine allows a sustainable geothermal field operation. It also helps to avoid environmental waste while minimizing reservoir pressure decline that can affect well productivity. However, in some fields injection of produced brine could cause catastrophic circumstances. In particular at the field that uses a binary system, where the rejection temperature can be as low as 65-100˚C. This condition can be worst in fractured controlled reservoirs in which fracture or fault becomes a toll-way of reinjection water. As a result, the injection breakthrough occurs prematurely causing a production decline.

Well-B is an infill producer well that was drilled to provide steam and brine for power plant generation. Despite having a good permeability as well as pressure region, this well performs very poorly with cycling wellhead pressure behavior as shown by the initial flow test activity. Meanwhile, Well-A is a good injector that accepts 95°C brine up to ~1000 tph.

Amalgamating several data such as daily monitoring data, pressure-temperature surveys, geochemistry observation, and geology yields a quite concluding outcome. The analysis shows there is indeed certain connectivity between those wells that cause thermal breakthroughs. Therefore, several actions were taken to overcome the situation such as managing the injection rate of the injection well while shutting in the production well to allow heating up. Moreover, during the well flows, the well production opening is kept as low as possible to avoid cooling. The practice yields a fruitful outcome, the performance rebound, evidenced by a sustained flow with higher discharge pressure (higher MDP) with the absence of cycling behavior.

1. INTRODUCTION

Sorik Marapi geothermal field is a project of PT. Sorik Marapi Geothermal Power (SMGP), a subsidiary of KS Orka Renewables Pte Ltd. that located in Mandailing Natal Regency, North Sumatra. From its 15 active production wells and 18 Injection wells, Sorik Marapi currently delivers 160 MW of electricity to supply the North Sumatra PLN grid.

Sorik Marapi implements the double-flashed binary ORC (Organic Rankine Cycle) system on its power plant to optimize the generation. However, utilizing this strategy can either be beneficial or drawback to the reservoir due to its rejection temperature can be as low as 65-100˚C.

Well-B is an infill producer well that was drilled to provide steam and brine for power plant generation. Despite having a good permeability as well as pressure region, this well performs very poorly with cycling wellhead pressure behavior as shown by the initial flow test activity. Meanwhile, Well-A is a good injector that accepts 95°C brine up to ~1000 tph. This paper discusses the impact of injection operation in the Sorik Marapi geothermal field and its influence on the nearby production well.

2. WELL-B CHARACTERISTIC AND INITIAL FLOW TEST

Well-B is an infill well that was drilled towards the southwest and reached a total depth of 1750 m-MD. Partial loss circulation (PLC) started to occur at a depth of ~950 m-MD in the 12-1/4” hole section, which was later followed by the total loss circulation (TLC) up to 240 tph at ~1250 m-MD (SMGP, 2021a).

A completion test was done soon after drilling was completed to identify well potential productivity. The Pressure Temperature Spinner (PTS) survey indicated that the majority of the injected fluid was leaving the wellbore from the shallow feed zone around 950-1050 m-MD (SMGP, 2021b). The occurrence of permeable zones in this well is also supported by the presence of fractures through the borehole image logging (SMGP, 2021c). Based on the completion test data, if the well is heated up to 270°C the maximum discharge pressure (MDP) of Well-B can reach up to 20 bara.

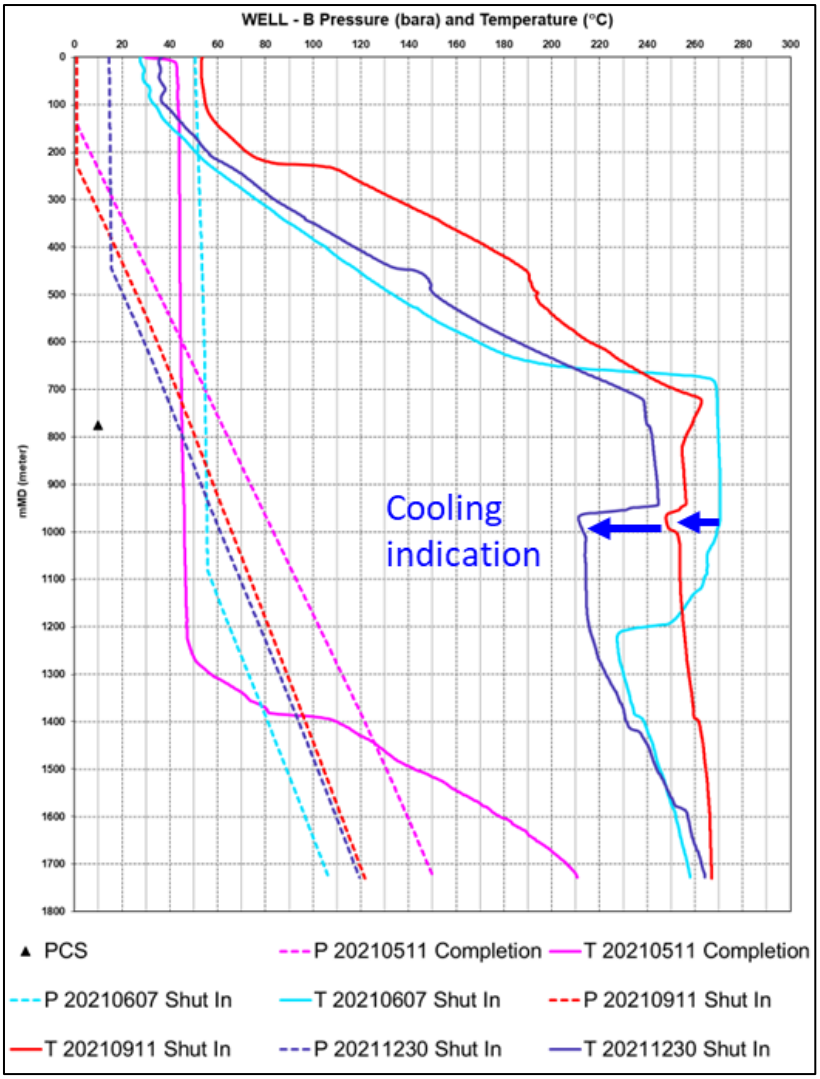

Figure 1: Well-B Heat Up Profiles showing cooling at shallow permeable zone.

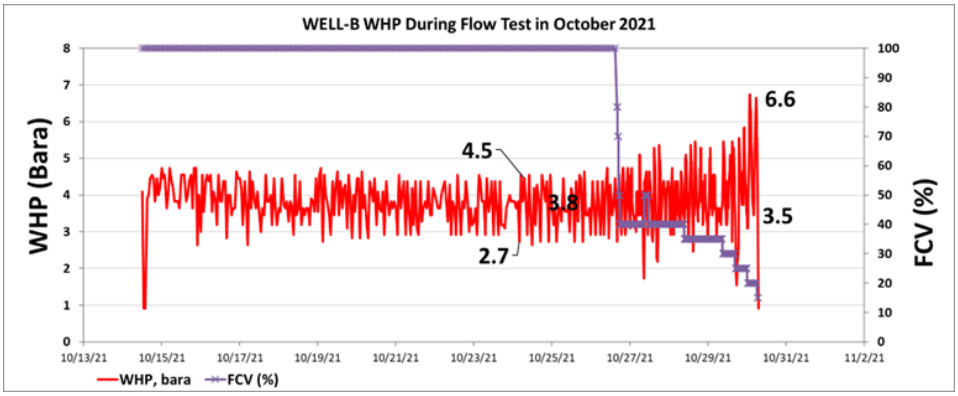

Figure 2: The Wellhead Pressure (WHP) of Well-B During October 2021 Flow Test.

Several shut-in surveys were performed after drilling to observe the heating-up process as shown in Figure 1. On the June 2021 heat-up survey (light-blue line in Figure 1), the temperature around the permeable zones was up to 270°C with an unheated section around the TLC depth. However, on the August 2021 survey (red line in Figure 1), whilst the deep unheated section was absent, well temperature decreased as a function of time, and slight temperature deflection was also noticed at a depth of ~950 m-MD.

The initial flow test was successfully conducted in October 2021 through air-capped stimulation. However, the well flowed with lower wellhead pressure (WHP) than expected and showed cycling behavior. Figure 2 shows

the oscillation of wellhead pressure clearly exhibited at various well opening with larger amplitude at lower Flow Control Valve (FCV) opening.

Cycling is normally caused by the presence of two significant feeds of different enthalpy and permeability (Grant & Bixley, 2011). Well-B stopped flowing at FCV of ~15% noted by the drop of WHP yielding MDP of ~6 bar. Afterward, Well-B was left shut in to heat up.

Post-flowing PT survey was conducted two months after the flow (December 2021), where temperature up to 50°C cooler than the June 2021 survey was observed (dark-blue line in Figure 2). The deflection temperature occurred at a depth below 950 m-MD where the major feedzone is located. A well discharge that purposely accelerated the heating-up process by discharging any left drilling fluid and materials, but insinuated cooling was happening on this well.

3. COOLING SOURCE INVESTIGATION

The causes of cooling phenomenon were investigated and nearby injection is one of the suspects. The upper feed zone of Well-B (the biggest fracture aperture from the image log) directly connects with the shallow entry of Well-A via the fault (Figure 3). Karmila et al (2021) stated that faults can be one of the contributors to the cooling risk of producer well, although there is a considerable distance between production and injection.

Prior to the Well-B flow test, the aforementioned Well-A was injected at a quite high rate up to ~1000 tph. Continuous high injection and pressure drawdown could cause adequate hydrostatic pressure to allow the injected fluid to be pushed toward the shallow wide aperture feed zone of Well-B.

A recommendation was made by reducing the injection rate to a minimum, even stopping the injection temporarily to effectively enhance energy recovery.

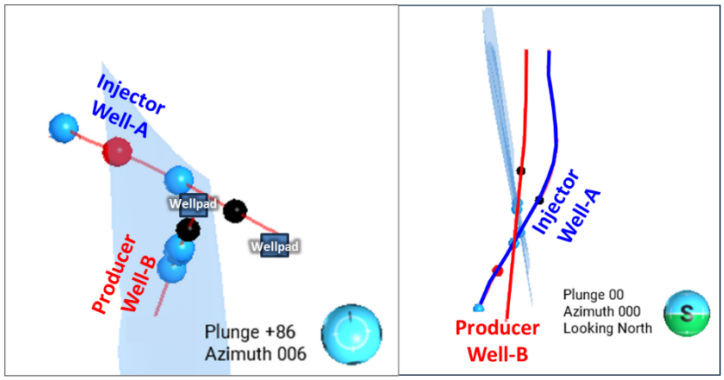

Figure 3: 3D section of fault (blue plane) that intersects the feed zones of Well-A and Well-B.

4. WELL-B PRODUCTION REBOUND

The heating-up process of Well-B took place over the period of 22 months with the latter 14 months of stop to low injection of Well-A. Comparing the PT shut-in in December 2021 with the latest PT shut-in in August 2023 (green line in Figure 4), Well-B shows a considerable heating-up process up to ~40°C. The previous cooling or temperature reversal at the shallow zone is absent. This indicates the applied injection strategy yields a positive response.

The second flow test was conducted in August 2023 to observe the heat-up process. Well-B was pre-compressed to 30 barg in preparation for air-cap discharge. During compress, sudden WHP built up to ~40 barg observed, and Well-B was directly released to the rock diffuser through the bleed line. At WHP of ~16 barg, the wellhead temperature (WHT) increased and the flow was diverted to the silencer through the production line.

Figure 5 depicts the wellhead pressure (WHP) during the flow test. Cycling WHP was observed at the beginning before it stabilized at ~3.7 barg with an MDP of ~5 barg at 19.9% FCV. After ~13 days flowing, remarkably WHP upsurge was observed from 5 barg to 17 barg, which later stabilized at ~14 barg yielding the highest MDP of Well-B. Afterward, flowing PTS was conducted to assess any potential improvement. Based on the analysis, the absence of previous cooling allows for the well rebound productivity. A significant enthalpy increase is observed at the shallow feed zone, resulting in a higher overall flowing enthalpy of the well.

Currently, the well has a sustainable flow and is connected to the power plant to boost the field generation at lower FCV opening to avoid any possibility of similar thermal breakthrough.

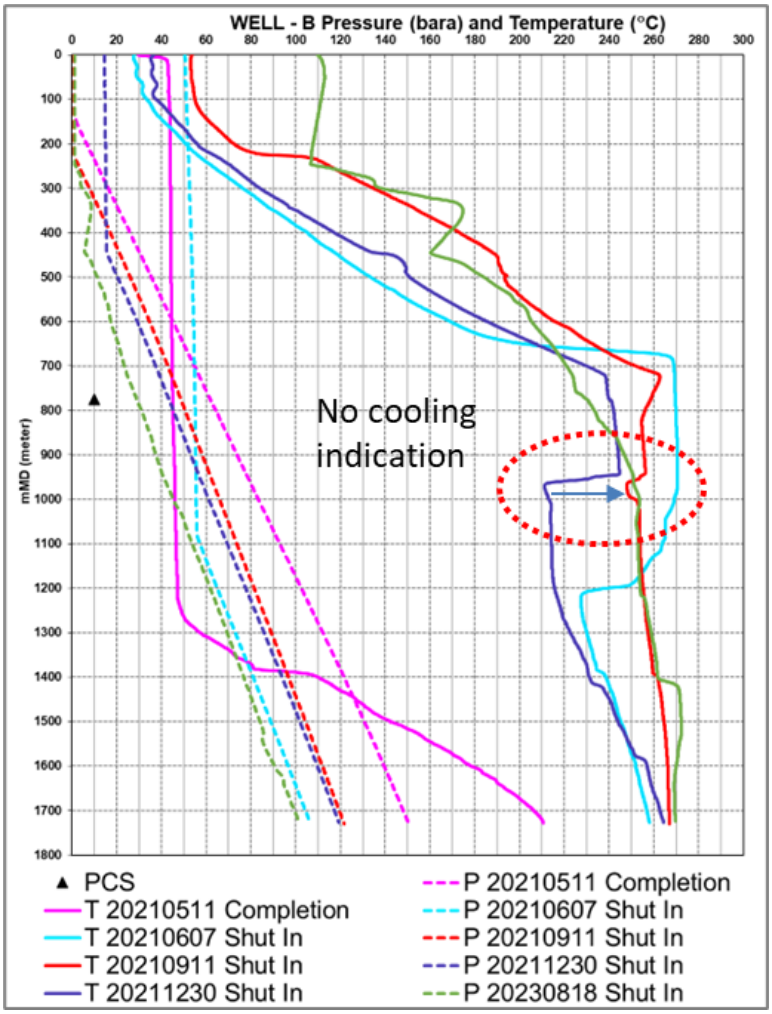

Figure 4: PT Profile after 22 months heating up process (green line).

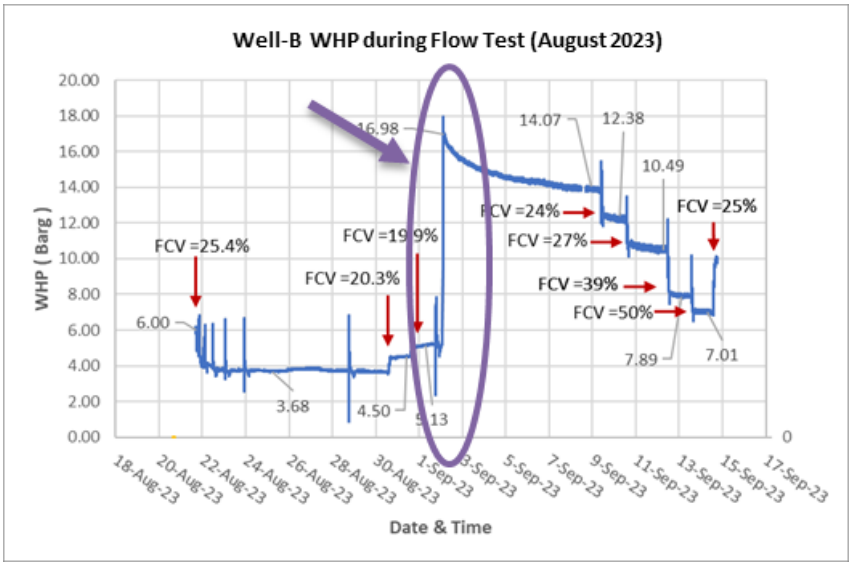

Figure 5: Wellhead Pressure (WHP) of Well-B during flow test in August 2023. Sudden WHP upsurged during flow at a similar FCV opening.

5. CONCLUSION

Good management of reinjection strategy has been proven to assist in sustainable geothermal field operation. Reinjection is required not only to comply with environmental regulations but also to allow better reservoir performance by providing pressure support and minimizing cooling from thermal breakthroughs.

Amalgamating several data such as daily monitoring data, pressure-temperature surveys, geochemistry observation, and geology may assist the reinjection strategy. The analysis shows there is indeed certain connectivity between Well-A and Well-B those that cause thermal breakthroughs resulting in poor performance of Well-B.

Therefore, several actions were taken to overcome the situation such as managing the injection rate of the injection well while shutting in the production well to minimize pressure difference between both wells thus helping accelerate the heating-up in the production well. Moreover, intervention during the well flows, such as keeping the well production opening as low as possible to reduce pressure sink in the production well area had successfully avoid further cooling. The practice yields a fruitful outcome, based on Well A result the performance rebound, evidenced by a sustained flow with higher discharge pressure (higher MDP) with the absence of cycling behavior.

REFERENCES

Grant, M., & Bixley, P.:Geothermal Reservoir Engineering – 2nd Edition. *In NASPA Journal (Vol. 42, Issue 4),* (2011).

Kamila, Z., Kaya, E., & Zarrouk, S. J.: Reinjection in geothermal fields: An updated worldwide review 2020. *Geothermics, 89(October 2020),* (2021). https://doi.org/10.1016/j.geothermics.2020.101970

SMGP: AA-03 End of Well Report, *Unpublished Report,* (2021a).

SMGP: AA-03 Completion Test Report, *Unpublished Report,* (2021b).

SMGP.: AA-03 XRMI Interpretation Report, *Unpublished Report* (2021c).

The Analysis of Sokoria MTB A-03 Well Performance Post-Shallow Wellbore Perforation

Rivan Tri Yuono, Fabiola Pardede, and Wishnu Triananda

KS Orka Renewables Pte. Ltd., Menara Sentraya 19th floor,
Jl. Iskandarsyah Raya No. 1A, Melawai, Jakarta Selatan

rivan.yuono@ksorka.com

Keywords: Sokoria, Production Well, Wellbore Perforation, Injectivity Index

ABSTRACT

Sokoria geothermal field has produced 8 MW of electricity from two units since July 2023. PT Sokoria Geothermal Indonesia, a subsidiary of KS Orka Renewables Pte Ltd, developed the field. So far 4 production wells and 3 injection wells have been drilled to maintain steam supply for generation. MTB A-03 is one of 4 wells that act as a production well to operate 8 MW generation in Sokoria Geothermal Power Plant. The well has a maximum temperature of 190-200 °C at stabilized conditions. The well is the only one that produces neutral fluid from the initial flow and does not need to use NaOH treatment like other wells.

The post-completion test in MTB A-03 well revealed the presence of a shallow feed zone behind the cemented 9 5/8" casing in the well at approximately ~800-900 m depth, where further analysis observed this feed zone as an additional production zone. That feed zone also had the highest temperature profile. To optimize the flow rate, such a zone had to be perforated. As a result, a production path was created from the production zone into the wellbore. Water loss tests were conducted along each step of the operation as a reference for future analyses.

The wellbore perforation resulted in an overall increase of 6 times of injectivity index for MTB A-03 well. Currently, the well is operating at WHP 2.8 Bar and WHT 138 °C. Along with MTB A-04 well, both are supplying steam to the Sokoria Power Plant unit-2 with a capacity of 3 MW.

1. INTRODUCTION

The Sokoria geothermal field is a project developed by PT Sokoria Geothermal Indonesia, a subsidiary of KS Orka Renewables Pte Ltd. This field is located at Flores Island, East Nusa Tenggara Province, Indonesia. Sokoria Geothermal Indonesia (SGI) has produced 8 MW of electricity from 4 production wells. The first commissioning was conducted in March 2022 and continued with the second commissioning in July 2023. PT Sokoria Geothermal Indonesia was the first developer who applied combined steam and brine binary technology. This is applicable in the island setting countries, especially in Indonesia where many but small geothermal resources or markets have been identified. This technology has several advantages, including:

- Utilize low-pressure wells (2 - 4 bar)
- Reduce heat and pressure loss in pipelines
- Closed loop system thus minimizing the potential for emissions
- Applying the appropriate technology for pH and scale treatment
- Smaller construction (footprint) area
- Relatively shorter construction duration

Sarmiento et al. (2019) explained that Sokoria geothermal field is a typical volcano-hosted geothermal system associated with a heat source from magma underneath Mount Kelimutu. An attempt to mitigate the risks associated with the presence of acidic and magmatic fluids at the three lakes at its summit has been made by drilling the first five wells several kilometers from the summit craters, where either a separate upflow or a lateral deep outflow of the summit system is found. The temperatures encountered by wells are consistent with those predicted by the gas geothermometer (220-260 °C) and a higher pH (4.2- 5.7) was encountered than those from the lakes. The base of the electrically conductive layer and the depth of the transition zone between the clay cap and the reservoir have been consistent with the drilling results, where the top of the reservoir (200-220 °C) is delineated at elevation 400 to 500 m mASL. The Sokoria geothermal field is a single-phase water-dominated reservoir that discharges fluids with medium enthalpy (850-950 kJ/kg) close to the feed zone temperatures measured in the wells. WHP ranges from 3 to 5.4 Bara based on the results of the brief discharge tests.

Well MTB A-03 is the third deep exploratory well completed in the Sokoria geothermal field. This standard well was spudded on cellar 3 of Pad A and was deviated to explore the postulated deep neutral geothermal reservoir at the Sokoria prospect area. The well was spudded on 13th February 2018 and achieved total depth (TD) on 21^{s}t

March 2018, the bore reached a TD of 2072 mMD. MTB A-03 completion was performed safely on 23-24 Jan 2024. Injection PT-Spinner, multi-rate II tests, pressure fall-off, and static PT have been successfully performed to identify the location of the permeable zone, injectivity index, and near wellbore characteristic of MTB A-03. Permeable zones of MTB A-03 are identified from the analysis consistent with the evidence of PLC and TLC during drilling.

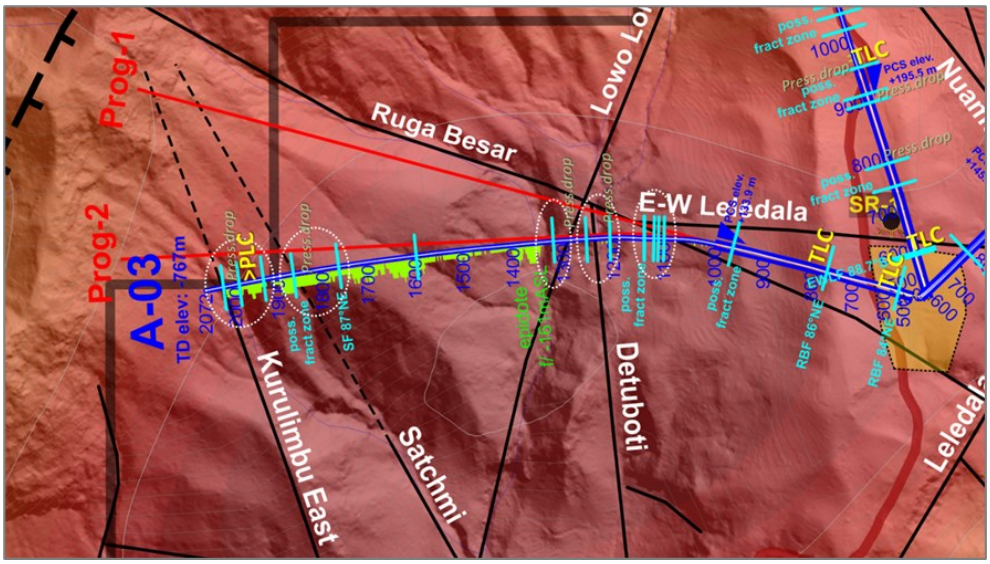

Figure 1: Faults target of MTB A-03 well.

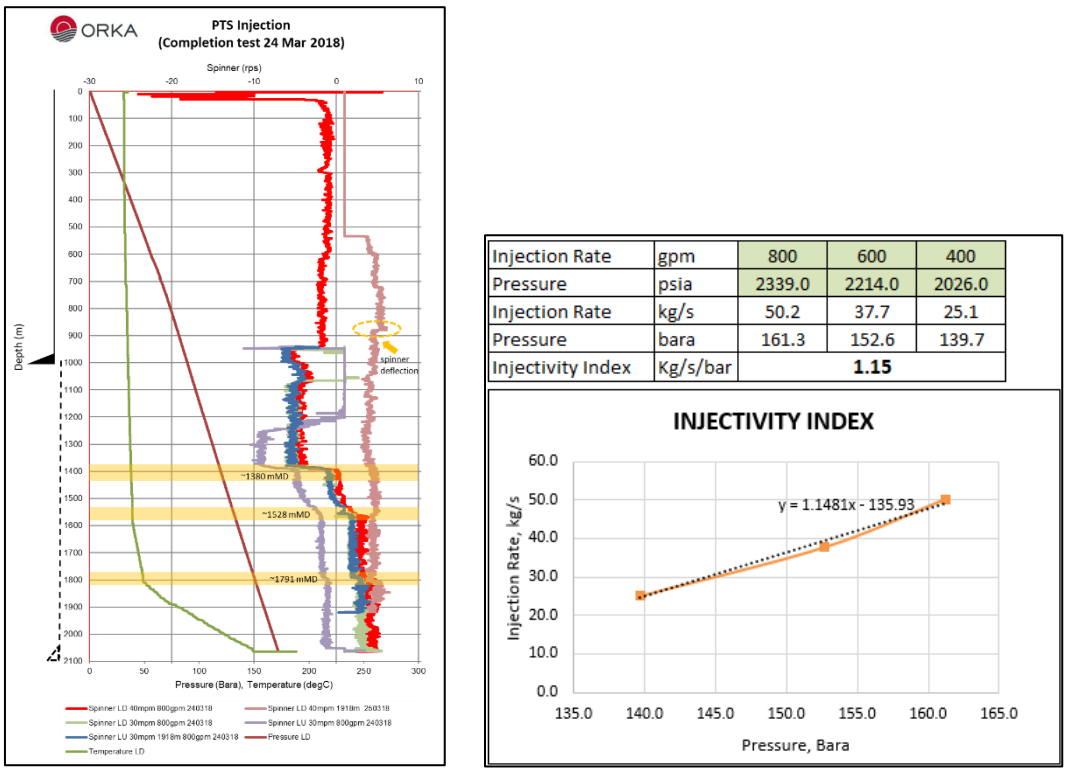

Figure 2: PTS Injection and Calculated Injectivity Index of MTB A-03 well.

2. WELL CHARACTERIZATIONS

2.1 Completion Test (2018)

Three feed zones were estimated according to this PTS survey, the feed zone at 1791 m correlated with Satchmi Fault 87° NE at 1761 mMD, and the appearance of epidote with a moderate abundant amount which indicates the presence of high-temperature minerals, then other feed zones indicated at 1460 m and 1570 m. Spinner deflection was also observed at a range of ~800 - 900 mMD inside the production casing.

The injectivity test was conducted during this completion test. The well was subjected to 3 different pump rates (800 GPM, 600 GPM, and 400 GPM) with the PTS tool set at 1918 m. The injectivity index was calculated by plotting the measured pressure taken at the end of each pump rate against the injection rate. Tabulated in the table above is the data used in calculating the well's injectivity index. The calculated injectivity index of the well is 1.15 kg/s/bar, indicating that MTB A-03 has low permeability (Internal Report, 2018).

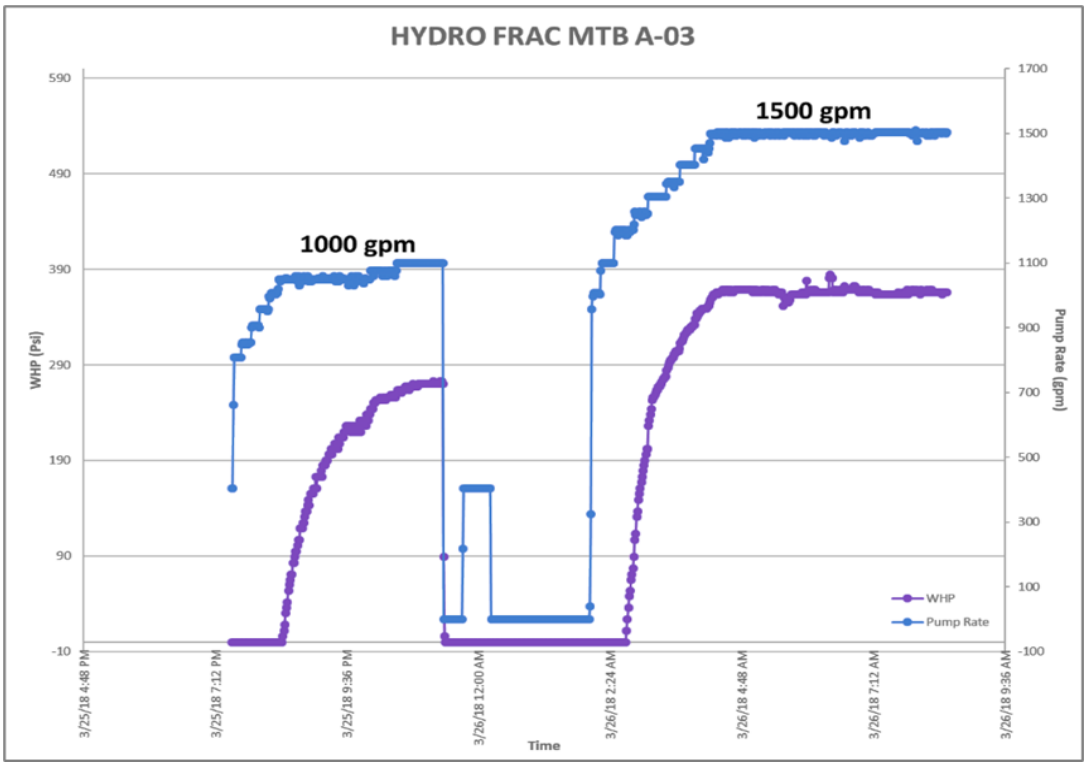

Figure 3: Hydro-fracture test on MTB A-03 well.

2.2 Hydro-Fracturing Test (2018)

Hydro-fracturing test was conducted to increase productivity or injectivity index, by pumping pressure to the reservoir by injecting water for at least 6 hours while pumping at the maximum rate that the well can take without building so much pressure at the wellhead, e.g. 500 psi. The objective is to give the well a chance again in case some fractures are plugged with cuttings and drilling fluids which could be opened at high pressures. This will be done after completing the PFO. Note that WHP remains zero at pumping rates of 800, 600, and 400 GPM.

The hydro-fracturing test was conducted at MTB A-03 by injecting water with a 1500 GPM pump rate for 13 hours. When injecting water with pump rates of 850 GPM and 950 psi, WHP was still at 0 psi. WHP slightly increased to 113 psi and stabilized at 226 psi after increasing the pump rate to 1000 GPM. The pump rate was later increased to 1500 GPM, and wellhead pressure also increased and stabilized at 366 psi for about 6 hours of pumping.

2.3 Heat-up Surveys (2019)

Several heat-up surveys were performed from day 1 after the completion test until 30 days after the well shut-in. Based on PT days 30, the highest temperature increase is observed at 750 mMD, reaching 223°C. This depth is located inside the production casing. Temperature deflection also was observed at a range of ~800-900 mMD. This depth confirms the spinner deflection which is identified from PTS injection data. Meanwhile, the permeable zones (1461, 1570, and 1761 mMD) also show a heating-up profile with temperatures of 202 °C, 173 °C, and 199 °C, respectively.

The pressure control point (PCP) or "pivot" pressure is a strong indication of the feed zone location in the well. This indicates a strong connection to the reservoir at this depth, which keeps the pressure constant at this depth, while it changes above and below due to changes in the density of the fluid column as the temperature increases in the well (Zarrouk, et al 2019). In wells that have multiple feed zones, like MTB A-03, the PCP will generally be located in between the feed zones. For these wells there will usually be associated internal wellbore flow between zones resulting from the pressure differences (Grant, 2011).

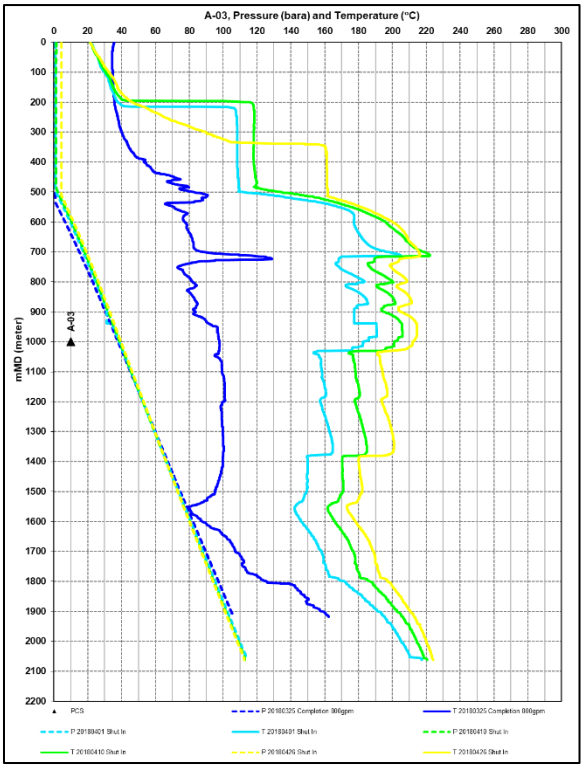

Figure 4: Pressure and Temperature profiles of MTB A-03 well during cold water injection and heat-up.

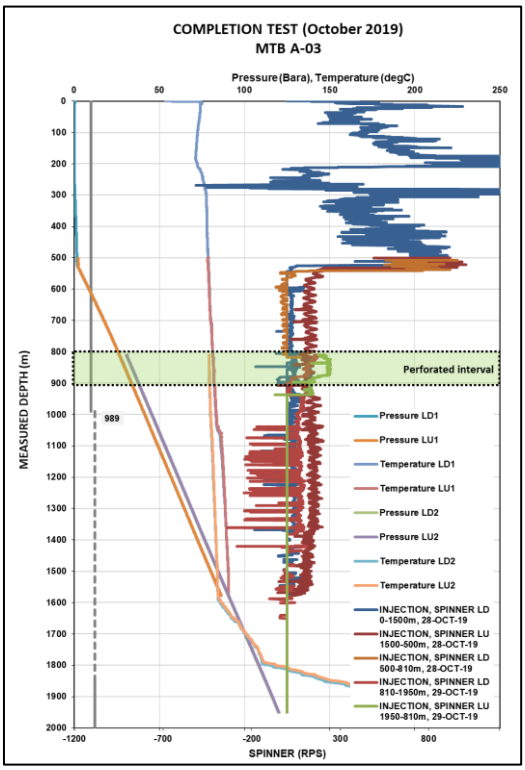

Pressure		Injection Rate	
bara	psia	gpm	kg/s
26.75	387.908	200.00	12.60
28.11	407.665	400.00	25.20
30.57	443.333	600.00	37.80

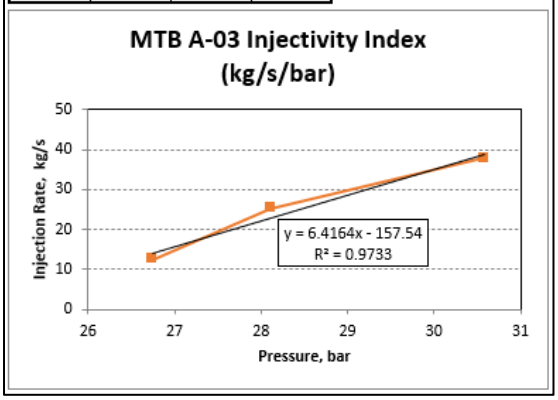

Figure 5: PTS Injection and Calculated Injectivity Index of MTB A-03 well after perforation job.

Figure 4 shows heating profiles in MTB A-03. The pressures from a pivot at 1150-1250 mMD between the two feed zones were identified by the injection profiles. There are permeable zones at ~800-900 mMD and 1461 and 1570 mMD. The upper zones inflow during the heating period, with a downflow to the lower zone. This internal

flow rapidly heats the well, and in 30 days the inflow at ~800-900 mMD has heated the well up to 223 °C. Part of the wellbore remains below the lower feed zones and is heating more slowly.

2.4 Completion Test Post Perforation Job (2019)

The previous analysis states that there was an indication of a shallow feed zone at a range of ~800-900 mMD. The location is inside the 9-5/8" production casing. To optimize the flow rate, such a zone had to be perforated. Perforation operation was completed with a total of 100 m perforated from the bottom of the production casing. The 2nd completion test was conducted to observe well characteristics qualitatively and quantitatively after the perforation job. The stages are the same as before, starting from dummy run, and PTS injection and ending with PT shut-in for 8 hours.

The result of the completion test in October 2019 showed an improvement of the Injectivity Index to 6.4 kg/s/bar or an increase 6 times larger than the previous injectivity index in March 2018. There is no change in MCD (maximum clear depth) during the completion test which indicates that no problems were found with wellbore integrity after perforation activity.

3. WELL PERFORMANCE

3.1 Output Test

MTB A-03 was discharged for the first time on 13th December 2019 through an air compression technique to stimulate the flow. This well was discharged for 126 days or almost 5 months before being switched to shut-in condition on 30 April 2020. The horizontal discharge method has been implemented in MTB A-03 to reduce the effects of direct exposure from geothermal fluid to the environment. Two-phase fluid has flowed to the atmospheric separator through the short-closed pipeline. In the separator, steam has been flashed to the atmosphere and brine has been flowed to the flash tank. The calculated enthalpy and total mass flow rate from the flow test are presented in Fig. 6. The well has an average WHP and total mass rate of 3.2 Bara and 16 kg/s respectively at 100% FCV opening.

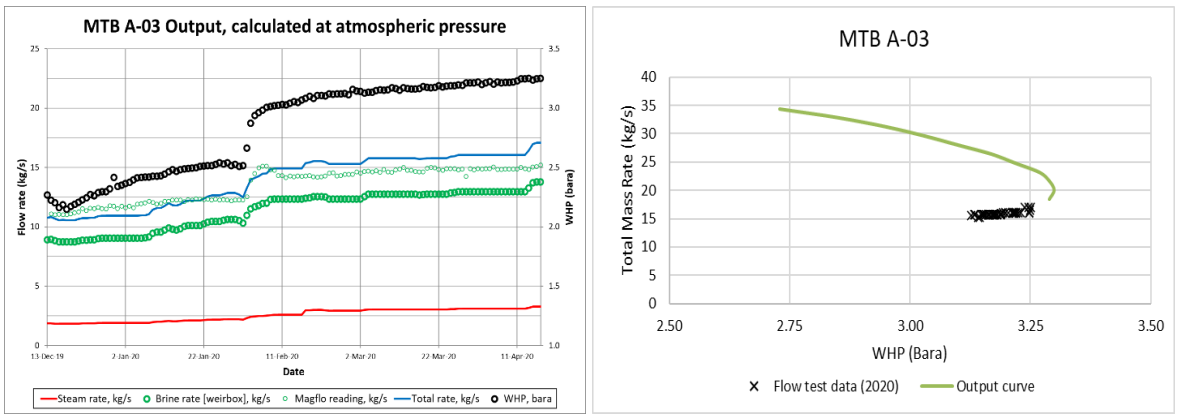

Figure 6: MTB A-03 flow test data (2019-2020) and estimated output curve.

The second test was performed on 7 December 2022 to assess well performance while nearby wells were online to the system. The test only lasted for 10 hours. The well appears to flow at a higher WHP (~4.8 Bara) and total mass rate (~21 kg/s), compared to the previous flow test (2019-2020). Discharge enthalpy is about 850 kJ/kg and pH after 10 hours flowing is 6.6 without caustic treatment. The flow test result concluded there was no observable impact from A-03 discharge to the flowing WHP of nearby wells. The flowing PTS also was conducted two times in December 2019 and February 2020. Figure 7 below compares the 2020 flowing survey with the previous log in December 2019. The temperature was observed to have increased by 9 °C in the perforated zone and ~15 °C in the production area (above 1400 mMD). Based on the analysis, flowing mass enthalpy is estimated at ~850 kJ/kg.

3.2 Online to Modular Power Plant

Currently, Sokoria Geothermal Indonesia operates 2 generation (modular power plant) units with a capacity of 8 MW, with a total development of 30 MW which is being planned in the following years. MTB A-03 is one of the wells supplying steam and brine for power plant unit 2 which is actively operating in July 2023. Wellhead pressure (WHP) and wellhead temperature (WHT) are stabilized at 2.8 Bar and 138 °C, respectively with 40% FCV opening. MTB A-03 has been continuously flowing with a neutral pH and no scaling issues since the middle of 2023. The estimated production of MTB A-03 is equal to ~1.5 MW at current WHP.

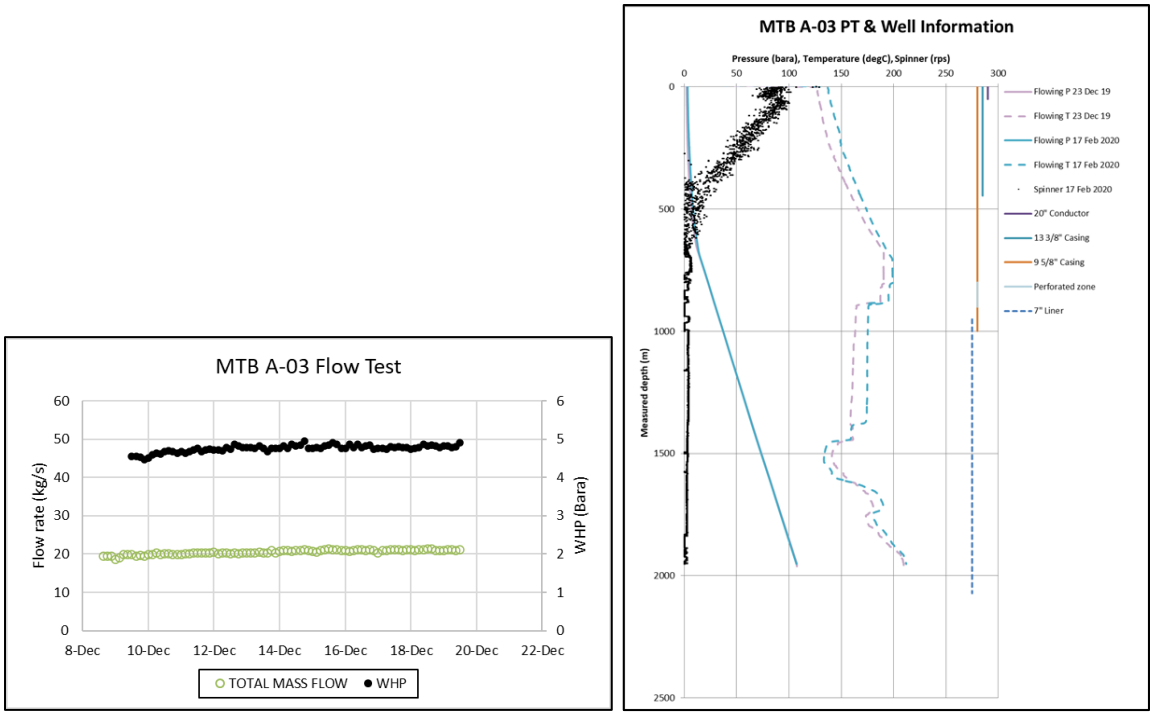

Figure 7: Flow test and PTS data of MTB A-03 Well in 2022.

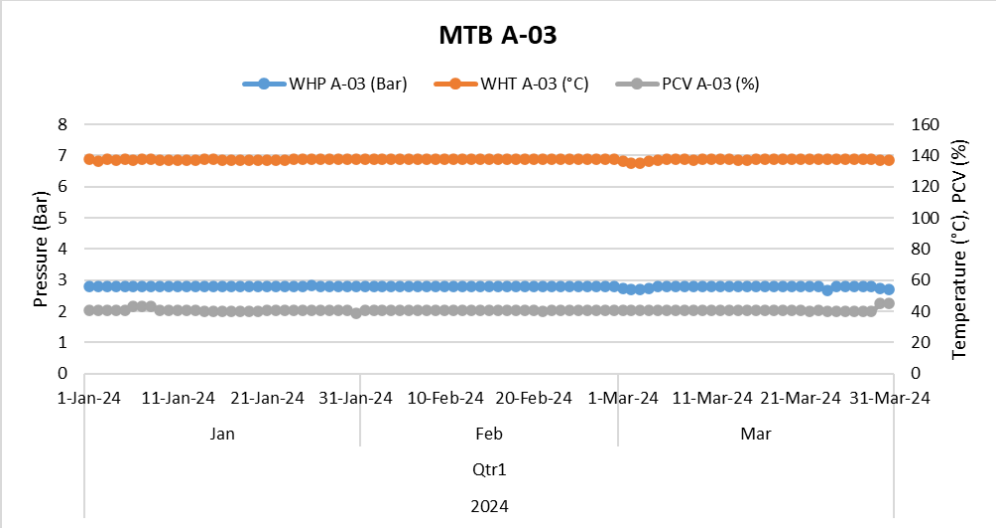

Figure 8: MTB A-03 well performance since online to system.

4. CONCLUSIONS

The conclusions that can be summarized from this study are as follows:

1. MTB A-03 well performance has progressed after carrying out several activities and analyses, mainly due to the perforation job that opens the production zone at shallow depth.
2. The resulting test in October 2019 showed an improvement in the Injectivity Index to 6.4 kg/s/bar or an increase 6 times larger than the previous injectivity index in March 2018.
3. MTB A-03 was discharged for the first time in December 2019. The well has an average WHP and total mass rate of 3.2 Bara and 16 kg/s respectively at 100% FCV opening.
4. The well appears to flow at a higher WHP (~4.8 Bara) and total mass rate (~21 kg/s), compared to the previous flow test (2019-2020). Discharge enthalpy is about 850 kJ/kg and pH after 10 hours flowing is 6.6 without caustic treatment.
5. The flow test result concluded no observable impact from A-03 discharge to the flowing WHP of nearby wells. The temperature was observed to have increased by 9 °C in the perforated zone and ~15 °C in the

production area (above 1400 mMD). Furthermore, there is a temperature deflection at the perforation zone (~800-900 m depth). Based on the analysis, flowing mass enthalpy is estimated at ~850 kJ/kg.

6. MTB A-03 has been continuously flowing with a neutral pH and no scaling issues since the middle of 2023. The estimated production of MTB A-03 is equal to ~1.5 MW at WHP 2.8 bar and WHT 138 °C.

REFERENCES

Grant, Malcolm A., et al. 2011. Geothermal reservoir engineering – 2nd Edition. Academic Press.

Sarmiento, Z., Sagala, Birean, S., and Siagian, H.: The Sokoria geothermal system, Flores Island, Indonesia, *Geothermics*, (2019).

Sokoria Geologist Team, 2018: Completion geology well report MTB A-03. KS Orka Renewables Pte. Ltd., Internal Report.

Zarrouk, S. J. and McLean, K. (2019): Geothermal well test analysis: fundamentals, applications, and advanced techniques. 1st edition, Elsevier.

Analysis of Most Common Problems in Brine Injection Pump: Lesson Learned from Geothermal Dieng Site

Rizky Himawan, Hendra Ardi Kurniawan, and Ramdani Alfan Subekti

PT Geo Dipa Energi (Persero) Unit Dieng, Jalan Raya Dieng Batur, Wonosobo, Central Java

rizky.himawan@geodipa.co.id

Keywords: Brine pump, reliability, maintenance standard

ABSTRACT

Dieng Geothermal Field is a geothermal field with water-dominated reservoir characteristics where injection strategy plays a crucial role in maintaining operational continuity. One aspect of the injection strategy is preparing reliable brine injection equipment. Based on historical data, vertical pumps as brine injection equipment experience breakdowns at least 4 times a year. The primary objective of this paper was to conduct a comprehensive analysis of the factors impacting the reliability of vertical pumps. The study started by collecting preventive and predictive maintenance data, process review, and evaluating about maintenance standards. The vibration analysis data as a part of the predictive maintenance item shows that the most common problems identified are misalignment, bearing problem, bend shaft, unbalance and cavitation. Several improvements were taken to reduce corrective action and improve vertical pump reliability related to Dieng's Site characteristics. This study involved several improvements to enhance the reliability of a brine injection pump. Improvements that were taken included process limitation, design analysis, maintenance procedure, and precision installation process. Furthermore, this paper can become a reference for another geothermal field in order to resolve the brine injection pump reliability problem and make some improvements to achieve high effectiveness of maintenance action.

1. INTRODUCTION

Dieng Geothermal Field is located in the Dieng Plateu, which is geothermal working area managed by PT Geo Dipa Energi (Persero). Dieng Geothermal Field has potential of up to 400 MW. Currently, PT Geo Dipa Energi (Persero) operates two geothermal power plants, namely Dieng Unit 1 for 60 MW and Dieng Small Scale for 10 MW. Based on the steam characteristics in Dieng Geothermal Field, which has water-dominated steam characteristics, there are some brine managements that should be carried out to support stable power plant operation. One of the most critical equipment to ensure that system can run well is brine pump. The reliability of brine pump in steam field area will indirectly affect the overall electricity generation process. But the actual reliability still low, so there should be an analysis about what makes the brine pump reliability is low.

Brine management in Dieng Site mostly uses vertical pump type. Based on (Kurniawan et al., n.d.) maintenance data shows that the vertical pump reliability shows the most effective and efficient than horizontal pump type depending on the maintenance time and maintenance cost.

2. BRINE PUMP IN DIENG SITE

The injection well, which is higher than the production well, requires Dieng to carry out a pumping process so that the brine fluid can flow to the injection well. Strategy in brine management is important because maintaining smooth operations means you must be able to maintain pond levels to prevent overflow. If the pond overflows, environmental issues will arise, the consequences of which will mean having to lower the well opening, which will directly reduce the generating capacity of the power plant. In fact, if the brine gets out of control, it could result in well shut-in, which means there is no generation process at the power plant.

The complex condition of brine, which has a lot of mineral content, including silica which has the potential to cause surface facility brine management to become plugging, makes brine management a critical aspect in managing geothermal power plants in the Dieng. Brine management in Dieng Site need reliable pump for stable operation. Maintenance history shows that the breakdown event of vertical brine pump is still quite high. The lifetime of brine vertical pump is mostly not more than 3 months. There are many breakdowns of pump happened in every month. Data shows us the disbursement of the breakdown event in every month. This condition needs to be evaluated.

The condition of the vertical brine pump should be evaluated to reach better reliability. Maintenance strategies, like Preventive Maintenance, Predictive Maintenance and other type of maintenance should be evaluated. Proactive maintenance should be performed because of its low cost and great impact to the equipment.

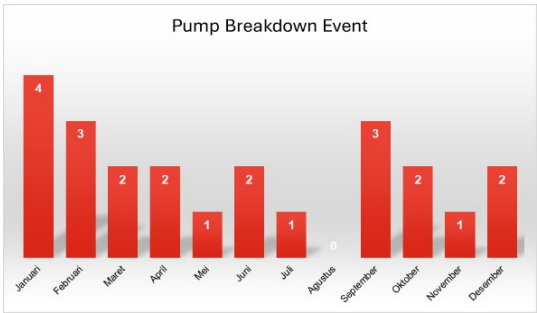

Figure 1: Existing Pump Breakdown Event Condition.

2.1 Probability Causes

Several cause that probably happen are cavitation, misalignment, bearing problem, bend shaft, unbalance, etc. All types of failure cause should be assessed to see which type of failure most contribute to pump breakdown, or pump short lifetime.

2.1.1 Unbalance and Bend Shaft

The vertical pump construction at the Dieng Site has a multistage impeller and long shaft construction. With multistage impeller construction, it increases the potential that unbalance could occur in more than 2 planes, especially if the number of stages is more than 2, such as at the Dieng Site, there can be 3, 4, 5 or 7 stages.

Unbalance occurs because there is excess mass on one or more sides, the amount of which is outside the established standards. Unbalance is a condition where a shaft's geometric centerline and mass centerline do not coincide. Each machine and type of use has different standards for unbalance. ISO 1940-1 is a standard that determines the amount of residual unbalance mass that is permitted according to its use. Unbalance is the most frequented abnormal vibration profile seen in rotating machinery and is instigated during assemblage, maintenance or fabrication (Spagnol & Wu, 2016).

With a long shaft construction, it is also possible for shaft deflection to occur, which if there is excessive external force, can result in shaft bending. This cannot be avoided considering that with a certain diameter and length, the shaft relatively has low rigidity characteristics.

2.1.2 Cavitation

Cavitation is a topic that is often discussed considering that it is a condition that is often found in centrifugal pumps. The condition of the brine, which still has a relatively high temperature, has the potential to cause bubbles to form when there is less flow in the suction area. Cavitation is a commonly natural phenomenon caused by local pressure being lower than the saturated vapor pressure, resulting in the formation of steam pockets. These pockets aggregate and collapse with the flow of fluid, not only disrupting the stable flow state but also generating considerable noise and causing damage to nearby surfaces (Xie et al., 2024). The design of the suction line also determines whether there are significant restrictions from the pond to the pump inlet, considering that the fluid being pumped also has the potential to cause the line to become a dead end after a certain amount of time in operation.

2.1.3 Misalignment

Cases of misalignment also often occur when installing motors and pumps but are more common in horizontal pumps. Horizontal pumps are generally equipped with a groove between the pump head connection and the motor, so that there is minimal misalignment. However, sometimes it needs to be verified further, considering that the surface flatness on the pump head could shift/out of tolerance.

This case of misalignment needs to be considered, especially if the coupling construction is a rigid coupling type. Moreover, most vertical pumps at the Dieng Site have a running speed of 3000 rpm, so based on ANSI/ASA standards the permitted tolerances are quite tight.

2.1.4 Bearing Problem

Bearings on vertical pumps are rolling bearings and plain bearings. Rolling bearings are usually used in motors and for upper pumps. Meanwhile, for the middle to lower part of the pump, which is in direct contact with the fluid, usually uses a plain bearing. The type of plain bearing material used for vertical pumps at the Dieng Site is carbon bushing.

2.2 Existing Maintenance Condition

In this paper, the writer collects all data about maintenance action that has been taken every day to solve or facing the vertical pump condition. As an illustration, the process of recording the performance of each equipment is still done manually, so that if a failure occurs, it will be difficult to detect the root cause, because the data availability is minimal.

2.2.1 Preventive Maintenance

Preventative (or periodic) maintenance where maintenance is based on the length of the operating period (Simm et al., 2016). The mechanical team has a preventive maintenance schedule for existing vertical pumps. Scheduled preventive steps include a daily visual check routine, clean up, tightening and painting if necessary. Then, given the existing conditions, an overhaul is scheduled every 3 months. However, this schedule often shifts, or is not implemented due to frequent breakdowns that occur.

2.2.2 Predictive Maintenance

Predictive maintenance strategies have led to the need for machinery condition monitoring. Condition monitoring can be defined as monitoring the physical parameters associated with the operation of the machine, such as vibration, temperature or pressure, to determine the operational condition of the machine (Simm et al., 2016). Predictive maintenance in Dieng Site is carried out only by taking the overall value from vibrations. Then, recording is done manually. This makes it difficult when data is needed at any time, because the data is spread across each worker. Then, trends cannot be carried out to evaluate whether there is an increase in vibration parameters, or anomalies in other parameters such as pressure, current and temperature.

2.3 Existing Process Condition

The current condition is that the only protection available is overload on the motor. The absence of other protection, such as level switches/sensors, pressure sensors, and vibration sensors makes it difficult to detect anomalous conditions early. This condition also allows the pump to run without liquid due to a low pond level, or the pump to continue running even though the vibration conditions are high, or even to continue running even though no pressure is produced.

3. ANALYSIS AND IMPROVEMENT ACTION

This analysis was carried out to find out what could possibly be improved to increase the reliability of the vertical pump at the Dieng Site. This analysis is based on the condition of existing equipment, maintenance procedures that have been carried out, design standards used, quality checks that have been implemented, as well as paying attention to operational requirements. Improvement actions taken are in accordance with financial capabilities and ease of realizing these improvements.

3.1 Review the Root Cause

Currently, the Dieng Site has a Vibration Analyzer, so it can be used to evaluate all rotating equipment in Dieng. The author has collected data as evidence to analyze the source of the problems currently occurring. The author has summarized and written down several findings that occurred at the vertical pump at the Dieng Site, and at this time the author only discusses the problems that mostly occur at the Dieng Site, where if most of these problems are resolved, hopefully, it can increase the reliability of the vertical pump at the Dieng Site significantly.

The author evaluated the pumps that were running and looked at the history of damage that had occurred and found that the majority of vertical pumps that were currently running experienced misalignment, bearing problems, bend shaft, unbalance and cavitation. The Pareto Chart can be seen in figure 2.

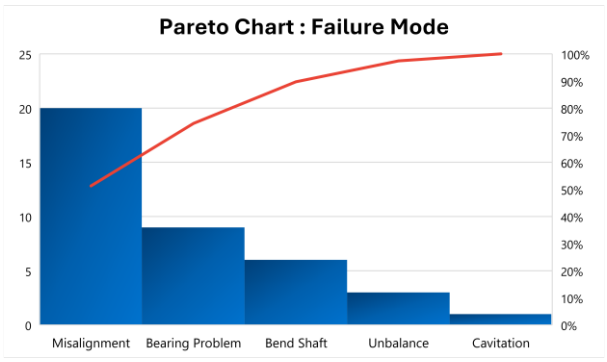

Figure 2: Pareto Chart Failure Mode Vertical Pump.

3.1.1 Misalignment

A common problem (estimated to cause over 70% of vibration problems in rotating machinery is shaft misalignment(Simm et al., 2016). The number of catastrophic cases at the Dieng Site, especially broken shafts in the coupling area, is an interesting aspect for analysis. The current condition is very detrimental because it has the potential for derating, and high repair costs will arise. Then, the vertical pump design in Dieng uses grooves, which rely on adjustments to the grooves between parts/components to ensure the straightness of the installation. With this design, the existing installation procedure does not require an alignment process when installing the coupling and installing the motor to the pump head.

Figure 3: Catastrophic Failure due to Misalignment.

However, with repeated incidents of damage, it provides chances for analysis as to whether the pump currently running is still in one axis (aligned) condition. So, with existing predictive tools, in the form of a vibration analyzer, an evaluation of the running condition of the pumps is carried out. Unfortunately, the author found that there were symptoms of misalignment in running pumps as much as 51%. One example of vibration reading results that show symptoms of misalignment can be shown in figure 4.

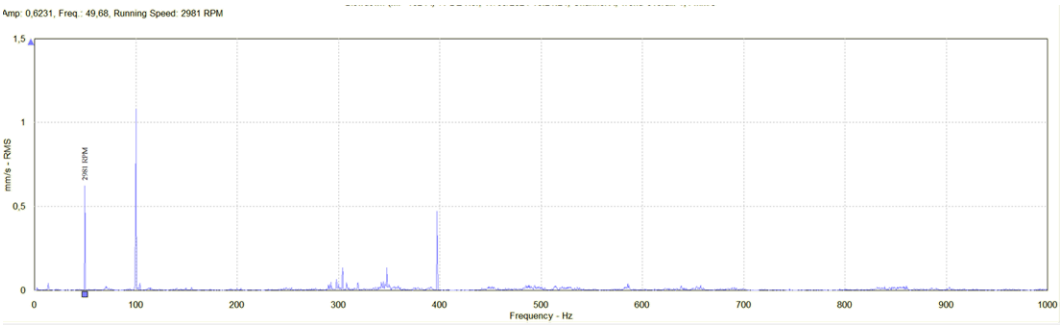

Figure 4: Vibration Spectrum Pattern of Misalignment.

After reviewing it, the condition of the groove used as a reference to ensure the installation process was carried out correctly, and that the results were straight between the coupling, pump and motor parts, had experienced wear. So, when installation is carried out without adjustments, it has the potential to cause misalignment.

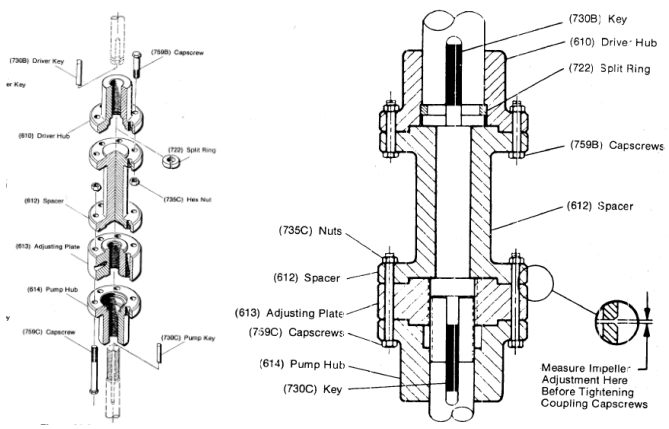

Figure 5: Vertical Pump Coupling Design.

Therefore, it is necessary to add an adjuster to carry out alignment, with worn conditions, meaning there is still space to carry out re-alignment. So, we no longer rely on existing grooves, but the alignment process is still carried out to ensure that the installation process complies with existing standards. The standard currently used is ANSI/ASA S2.75-2017, the maximum misalignment value is determined by the running speed and the type of coupling used.

An illustration of the clutch arrangement that may occur under existing conditions can be seen in figure 6. Where it is very possible for the clutch components to be installed not on one axis, which will cause misalignment and influence high vibration and low pump reliability.

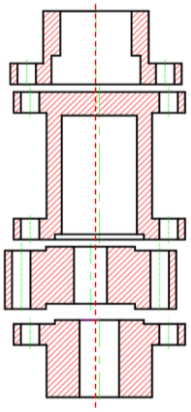

Figure 6: Coupling Misalignment Illustration.

Figure 7: Excessive Wear in Carbon Bushing Vertical Pump.

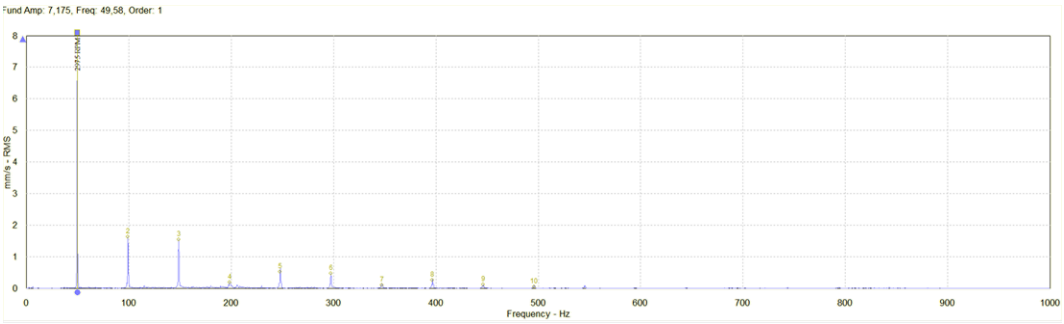

Figure 8: Vibration Spectrum Pattern of Rotating Looseness.

3.1.2 Bearing Problem

Vertical pump designs generally use plain bearings/bushings as bearings in the pump area. This is because this bearing will be in direct contact with fluid, where typical rolling bearings are not applicable for this function. The plain bearings/bushings used have several types of materials, such as bronze, carbon graphite, etc. In the vertical pump at the Dieng Site, the type of bushing material used is carbon graphite, where this material has resistance to very high temperatures, and produces low friction.

Considering the plain bearing/bushing used, clearance is an important parameter to test whether the bearing is still suitable for use or not. If there is excessive clearance, it will increase the space for the shaft to move, which will cause the pump to run with high vibration conditions. In vibration analysis, this can be categorized as mechanical looseness, where the characteristic is that there are harmonics at 1x the running speed. If over clearance is not detected, and there is no vibration sensor as protection, then this condition can have fatal consequences, namely

metal to metal contact can occur, when the carbon bushing is completely worn. If this is allowed to continue, it will result in catastrophic failure.

The author has carried out an evaluation for all pumps running in the Dieng Site area and found that there are several conditions where there is already over clearance for pumps that are still operating.

In this condition, a strategy is needed by carrying out routine monitoring, if over clearance has occurred, mechanical rotating looseness symptoms will arise, where the trend can be seen to determine the right time to carry out repairs.

3.1.3 Unbalance / Bend Shaft

Having a multistage impeller construction and long shaft construction, makes the vertical pump prone to unbalance or bending of the shaft. Ideally, each impeller should be balanced individually before assembly is carried out, then final balancing will be carried out after all the impellers have been installed. However, because it does not have balancing equipment, and demands that the pump must be ready to be installed again in a short time, the balancing process was not carried out.

With a long shaft, the potential for the shaft to bend due to excessive force when installing the coupling is also a factor that needs to be evaluated. Not carrying out run out on the shaft before, after the coupling shaft installation process, and after the assembly process means that the same quality for each pump cannot be always achieved.

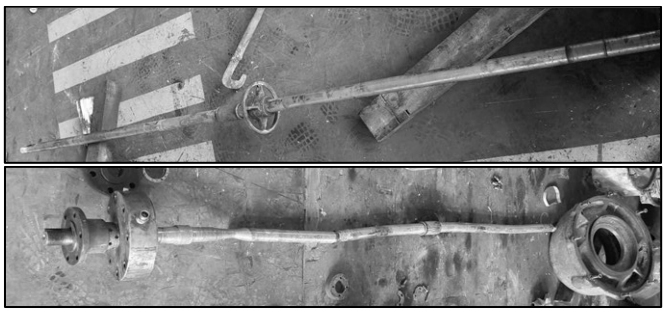

Figure 9: Catastrophic Failure due to Bend Shaft.

The author tried to evaluate the condition of the running pumps, and it was found that around 23% of the pumps operating at the Dieng Site experienced unbalance/bend shaft conditions with varying severity. The following is evident from one of the pumps operating in the steam field area.

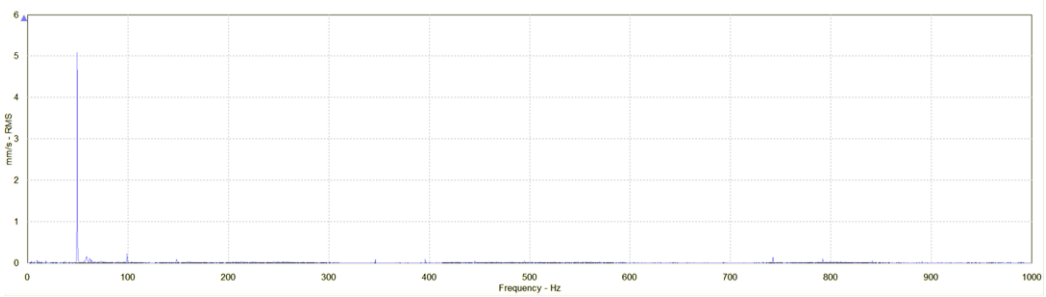

Figure 10: Vibration Spectrum Pattern of Unbalance/Bend Shaft.

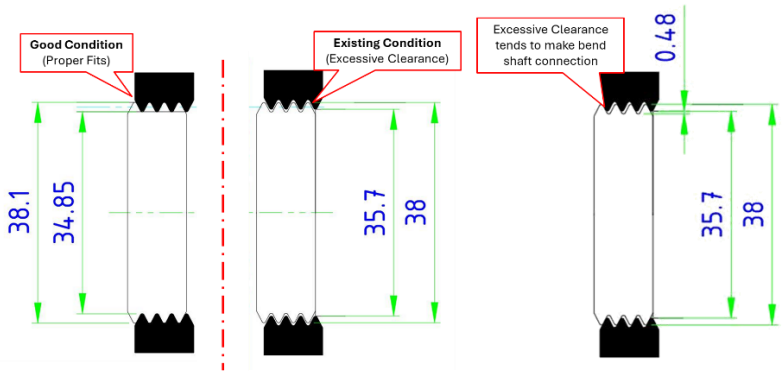

Figure 11: Shaft Coupling Thread Clearance Analysis.

Because the symptoms are the same, namely dominant at 1X running speed, so in the vertical pump it is difficult to distinguish whether there is an unbalance condition in the rotating part of the vertical pump, or whether a shaft bend is occurring. This can be minimized if we eliminate one of the symptoms. For example, if a run out has been carried out, and it is confirmed that the shaft is straight, then it can be ascertained that the condition that is occurring is unbalance in the pump's rotating part assembly.

Because there is no balancing machine, one of the actions that can be used for evaluation is the run out of the pump shaft, pump shaft coupling, and installation process. The author found that there was over clearance in the pump shaft coupling thread connection. Illustrations can be seen in figure 11.

Over clearance conditions in the coupling and pump shaft connections tend to cause the resulting pump shaft connection to become bent. This can affect the overall quality of the assembly, because if the coupling which should be able to connect the two shafts straight is not aligned, it will provide excessive force on the shaft itself, which will result in the shaft bending.

3.1.4 Cavitation

The condition of the brine content in the pond at the Dieng Site requires cleaning every 2 or 3 months, considering that the silica deposits that occur in the cooling pond are quite massive during that time. The open condition of the cooling pond, which is used as a suction pump, really allows restrictions to occur on the strainer, or even on the suction bell. The author found several incidents, where when the pump was damaged, and an inspection was carried out foreign material was found covering the suction bell as seen in the figure 12. So, this condition allows the pump to remain in running condition even though the incoming fluid is insufficient or even no fluid at all, considering that there is no other protection other than motor overload.

Figure 12: Foreign Material in Suction Bell Vertical Pump.

The author tried to evaluate the condition of the pumps that were running and found that there were several pumps that were running in cavitation conditions. Apart from foreign materials, manual operation sometimes increases the human error factor, in the form of allowing the pump to continue running even though the cooling pond is at a low level. One of the author's findings through vibration analysis can be seen in figure 13.

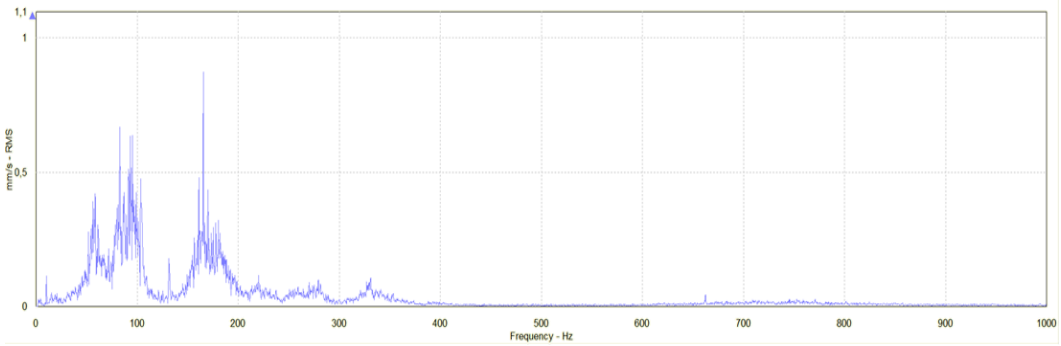

Figure 13: Vibration Spectrum Pattern of Cavitation.

So, under these conditions, there is a real potential for cavitation to occur due to the lack of flow in the suction bell and suction line. This needs to be of particular concern to the operations division which carries out routine patrol checks every day. If a cavitation condition is found, mitigation needs to be carried out to prevent the pump from continuously running in a cavitation condition, which will influence pump damage.

Some indications that can easily be recognized if cavitation occurs are the cavitation noise signal is random, and its spectral structure is unique. The liquid-loaded noise signal is promising for detecting cavitation (Liu et al., 2023), Then, there are pressure pulsations due to cavitation that can be easily seen on pressure gauge (Liu et al., 2023). Vibration increases in the blade pass frequency area and random noise increases (Liu et al., 2023). Then,

the level is in low condition, remembering that if there is a head decrease of 3% it increases the possibility of cavitation (Kazi et al., 2011)

3.2 Improvement Action

3.2.1 Alignment and Run Out Installation Procedure

Considering that the condition of the pump component grooves is worn, it is necessary to carry out an alignment procedure for each motor, pump and clutch installation. The current condition of the head does not have an adjuster to precisely adjust the position of the motor and pump. So, modifications have been made in the form of an adjuster installed on the pump head to regulate the straightness of the motor installation on the pump head.

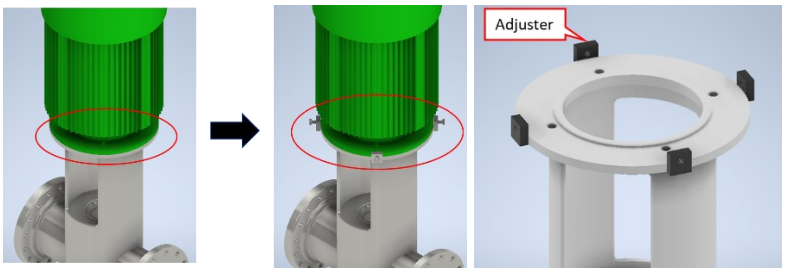

Figure 14: Adjuster Modification for Alignment Process.

Then, before alignment is carried out, several procedural steps need to be carried out, namely:

a. Run out of motor shaft and coupling
   This is done to evaluate whether the motor shaft is still straight or not. Then run out of the motor coupling also needs to be done, to determine whether the coupling is still in good condition and installed with the appropriate clearance. Because, if there is over clearance it will cause the center between the motor shaft geometry and the motor coupling to shift, and this will definitely affect the subsequent alignment process.
b. Run out of pump shaft and coupling
   This needs to be done when the pump is in good condition after full assembly has been carried out in the workshop. This is used to confirm whether the pump shaft and coupling are installed precisely. This can be done with a dial indicator while the pump is still horizontal. It is necessary to check the installation of the coupling and shaft, which is often found that the axis between the shaft and coupling has shifted due to over clearance and inappropriate feather key dimensions.
c. Alignment between pump head and motor
   This can be done after the head pump assembly has been installed in its place, and the motor has sat on the head pump. The alignment process is important considering that the groove between the pump head and motor has experienced wear and tear, which still provides enough space to shift, so that the position of the pump and motor axes are in the same axis/alignment.
d. Alignment between motor coupling and spacer
   The coupling alignment process needs to be carried out considering that the coupling arrangement used is a rigid type of clutch, and the running speed is quite high, namely 3000 rpm, so that if we refer to ANSI/ASA standards the tolerances are quite tight. If you review the existing design, the coupling arrangement is long, which involves spacers and adjusting nuts, so the coupling alignment process needs to be done with precision, because if one of the arrangements is wrong, it will affect the subsequent alignment process and the alignment process.
e. Axial play settings
   Axial play is used to ensure that the axial position of all rotating parts does not come into contact with static parts when operating. In vertical pump construction, there is an adjusting nut that can be used to regulate axial play precisely. This process can be carried out using a vernier caliper.
f. Coupling installation
   After the alignment process is complete, you can continue with the process of installing the clutch bolts. However, you need to pay attention to the order of tightening, remembering that the alignment process needs to be maintained so as not to change the settings that have been made.
g. Final run out checks
   After the coupling bolt tightening process is carried out according to the torque, the next step is to ensure that the entire alignment process has been carried out properly and correctly. So, it is necessary to carry out a final run out of the pump shaft, remembering that if the alignment process has been carried out correctly, it will produce a good run out too. However, if the alignment process is not carried out properly, it will result in the clutch arrangement and connections between motor and pump components resulting in run outs outside the standard (out of tolerance).

3.2.2 Re-design Pump Shaft Coupling

The thread in the pump shaft clutch connection uses a smooth thread design. The thread construction used is Whitworth which has a pitch design of 55° (Simmons et al., 2020). If you look in more detail, in thread construction there are major and minor diameters that need to be met. Considering that the threads currently used are not standard, it is necessary to carry out a detailed analysis of the major and minor diameters of the thread. When the analysis was carried out, minor and major discrepancies were found, so it was necessary to standardize the drawing thread to avoid bending of the shaft after connection.

Standard Shaft Coupling Thread Data		
Pitch Diameter	:	35,39 mm
Major Diameter	:	38,1 mm
Minor Diameter	:	32,68 mm
Pitch	:	2.54 mm

Figure 15: Standard Shaft Coupling Thread Data.

Standard shaft coupling data in figure 15 provide complete data for fabrication shaft coupling vertical pump in Dieng Site. It designs for better shaft connection, and avoid the bend shaft condition due to loose clearance between shaft and coupling shaft. Detail design can be viewed in figure 16.

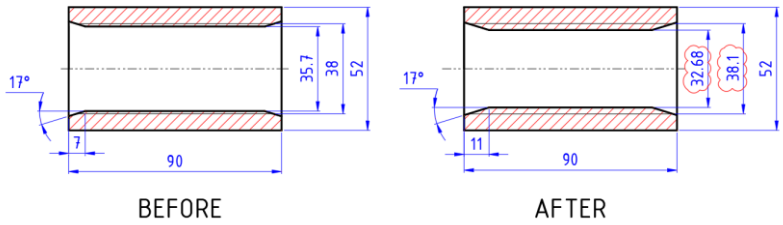

Figure 16: Standard Shaft Coupling Final Design.

Figure 17: Installation of Level Transmitter.

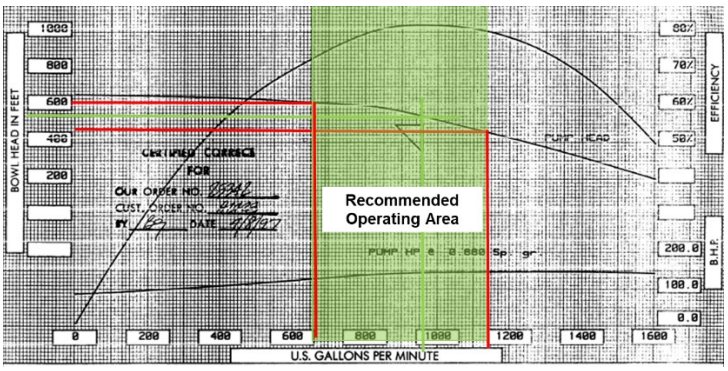

Figure 18: Recommended Operating Area based on Pump Performance Curve.

3.2.3 Installation of Level Switch/Level Transmitter and Process Limitation

To overcome the condition that the pump continues to run even without liquid conditions, which will result in cavitation conditions that will damage the pump, so one of the improvements that has been made is to install a level switch as additional protection when the pump is running in low level conditions.

Then, the operating process greatly influences the overall performance of the equipment, so it is necessary to review the process limitations for each pump. Several literatures say that the recommended pump operation is 70% - 120% of BEP. So, the author collects all pump performance curves, to ensure that the pump continues to work within permitted conditions.

3.3 Improvement Result

After implementing all the improvement actions in the discussion above, observations are then carried out within one year, which can be compared with the conditions before the improvement. The historical results show that there has been a reduction in breakdown events of up to 74%. In Figure 19, the trendline tends to decrease, indicating that there is a trend towards improving the reliability of the vertical pump.

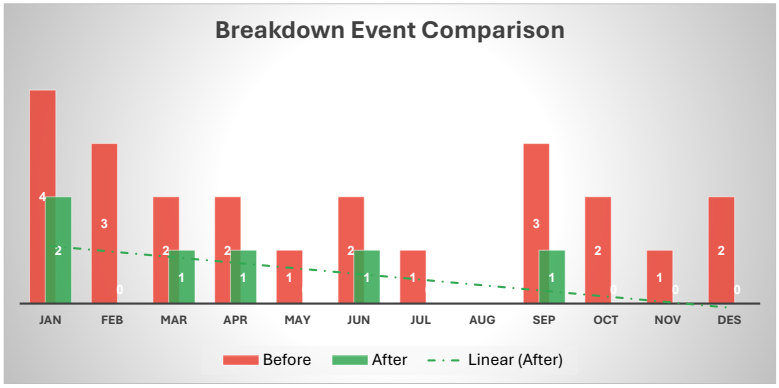

Figure 19: Breakdown Event Comparison After Improvement Action.

4. CONCLUSION

Based on data collection and maintenance history review, the biggest causes of damage are misalignment with 51%, bearing problem with 23%, bend shaft with 15%, unbalance with 8% and cavitation with 3%. Improvements that have been carried out are in the form of alignment assessments and applications, and run out checks for vertical pumps, re-designing threads of coupling shafts, adding level switches or level transmitters, as well as input for the operations team regarding process limitations in pump operation.

REFERENCES

Himpurna California Energy. (1997). Dieng Geothermal Project Unit 1 (Vol. 4 and 7). Dieng Geothermal Project Data Book. Himpurna California Energy, LTD.

Kazi, S. N., Al-Arabi, A. A. B., Selim, S. M. A., Saidur, R., & Duffy, G. G. (2011). Detection of Cavitation in Centrifugal Pumps. *Australian Journal of Basic and Applied Sciences*, 5(10), 1260–1267.

Kurniawan, H. A., Arifin, M., & Sutrisno, B. (n.d.). *Brine Injection Pump Operation and Maintenance Actions (A Lesson Learned from Dieng Geothermal Field)*.

Liu, X., Mou, J., Xu, X., Qiu, Z., & Dong, B. (2023). A Review of Pump Cavitation Fault Detection Methods Based on Different Signals. In Processes (Vol. 11, Issue 7). Multidisciplinary Digital Publishing Institute (MDPI). https://doi.org/10.3390/pr11072007

Ludeca. (2024). Using ANSI Shaft Alignment Tolerances to Help Solve Base-Bound and Bolt-Bound Situations. https://ludeca.com/blog/alignment/11528/using-ansi-shaft-alignment-tolerances-to-help-solve-base-bound-and-bolt-bound-situations/

Simm, A., Wang, Q., Huang, S., & Zhao, W. (2016). Laser based measurement for the monitoring of shaft misalignment. *Measurement: Journal of the International Measurement Confederation*, 87, 104–116. https://doi.org/10.1016/j.measurement.2016.02.034

Simmons, C. H., Maguire, D. E., & Phelps, N. (2020). Screw threads and conventional representations. In *Manual of Engineering Drawing* (pp. 207–219). Elsevier. https://doi.org/10.1016/b978-0-12-818482-0.00017-7

Spagnol, J. P., & Wu, H. (2016). Rotor Vibration under the Coupled Effects of Mass Unbalance and Asymmetric Bearings. *Applied Mechanics and Materials*, 846, 199–204. https://doi.org/10.4028/www.scientific.net/amm.846.199

Xie, H., Luo, X. Q., Feng, J. J., Zhu, G. J., & Li, C. H. (2024). Application of three cavitation models in centrifugal pump cavitation flow simulation. *Journal of Physics: Conference Series*, 2707(1). https://doi.org/10.1088/1742-6596/2707/1/012141

Application Transient Analysis at Later Stages of Production

Ahmad Fahmi Fanani, M Afif Habiburrahman, Dennis Grey,
Dhanie Marstiga Yuniar, and Fernando Pasaribu

PT Pertamina (Persero)

ahmad.fanani@pertamina.com, mafif.habiburrahman@pertamina.com,
mk.dennis.grey@mitrakerja.pertamina.com, Dhanie.marstiga@pertamina.com,
Fernando.pasaribu@pertamina.com

Keywords: reservoir characteristics, pressure transient analysis, pressure build-up

ABSTRACT

Kamojang, one of the biggest and oldest geothermal fields in the world, has been actively producing for more than 40 years. The key to maintaining productivity is to understand that reservoir characteristics change occasionally. One way to evaluate the change in the reservoir is through pressure transient analysis (PTA). A fall-off test (FOT) is performed during the completion test to acquire pressure transient data. Furthermore, since Kamojang is a single-vapor phase field, a pressure build-up test (PBU) is performed during the production phase to acquire additional pressure transient data and get more information about the reservoir. The pressure transient data is evaluated using commercial software to capture the changes in reservoir characteristics during the production period, such as transmissibility and skin factor, in each well.

1. INTRODUCTION

Kamojang is located in Ibun District, approximately 40 km from Bandung, West Java, with an elevation of around 1500 meters above sea level. The reservoir is classified as a single-vapor-phase reservoir. Currently, total vapor production is comparable to 235 MWe, complemented by six power plant units. Now, Kamojang has 97 wells along the production period from 1974 to 2024 (63 production wells, 9 injection wells, 16 monitoring wells, and 9 abandoned wells). With such high levels of output, reservoir management is essential for maintaining reservoir performance. One approach to reservoir management is to monitor the reservoir and determine its features using pressure transient analysis.

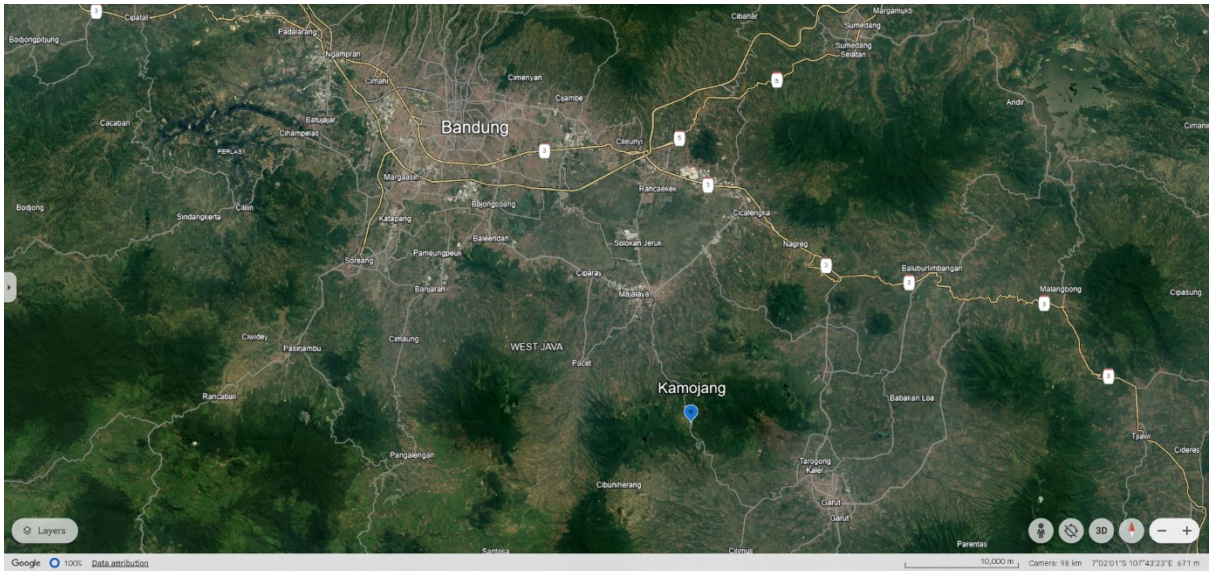

Figure 2: Kamojang Location from Google Earth (Google, 2024).

Pressure transient analysis (PTA) is the process of analyzing the resulting pressure and flow data set by matching the data to an analytical or numerical model of the well and reservoir. Data collection typically involves four types of tests: drawdown, build-up, injection, and fall-off tests (Zarrouk & McLean, 2019). However, with geothermal, only two types of tests are practicable to implement: build-up and fall-off tests, because thermal shock along the pipe does not occur during the test. A study was conducted to capture the reservoir parameters of a geothermal reservoir in Turkey utilizing both pressure build-up and fall-of-test methods (Aydin, Merey, & Akin, 2024). In this scenario, to monitor reservoir characteristics throughout vapor production in Kamojang, PTA is performed

on build-up test data, which can be repeated on a regular basis. To monitor reservoir parameters, it is preferable to use build-up test data rather than fall-of-test (FOT), which is often performed only once throughout the well completion test period. For those reasons, only build-up test data is used in this paper to depict the changes in reservoir characteristics in Kamojang during the production period.

The primary purpose of PTA is to gather reservoir data with some typical outcomes, including reservoir transmissivity (kh), skin factor (s), initial reservoir pressure (Pi), and other parameters indicating reservoir size and boundaries. This analysis plays a crucial part in reservoir management. For example, knowing the properties surrounding the wellbore, such as skin and permeability, can help with decision-making when developing a workover/well intervention strategy. Other than that, the characterization of the permeability system can also be helpful in determining the location of the new make-up well. With that being said, PTA takes a big part in taking care of reservoir management system.

In Kamojang, pressure build-up tests are conducted by shutting down the well after a certain amount of production time to allow the reservoir pressure to return to its static shut-in point if possible. From 2009 until 2023, pressure build-up tests were performed often, which necessitated a complete investigation of reservoir characterization. However, in this study, PBU tests were performed in most of production wells to provide a thorough understanding of reservoir attributes using the same pressure transient test method. However, not all of that data can be examined using pressure transient analysis due to pressure instability and other issues that may arise throughout the test. This study will provide PTA for some wells that can be evaluated because the tests were performed several times in previous years to capture more understanding of reservoir properties along the production period.

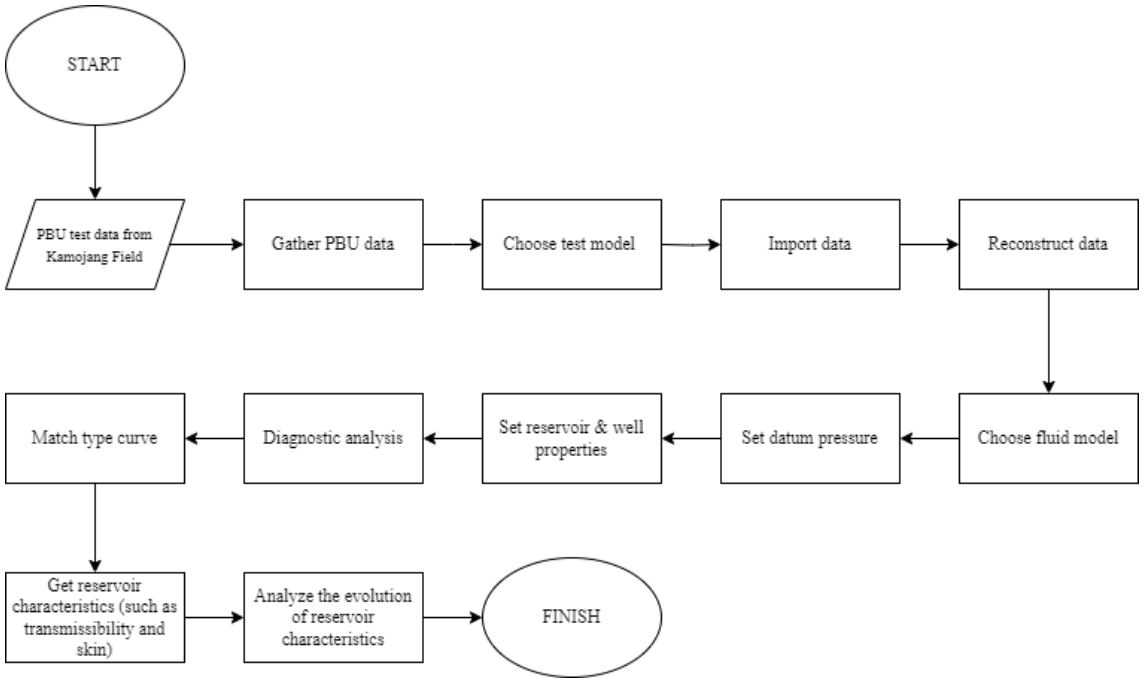

Figure 2: Methodology for the study.

2. METHODOLOGY

For this study, transient data sets were acquired by creating pressure disturbances in the production well through a shut-in method by monitoring wellhead pressure (pressure build-up test). The analysis will cover pressure transient analysis for several production wells, as these tests were conducted multiple times in previous years to track changes in reservoir properties over the production period. The employment of computers to match models to well-tested data was inevitable. Reservoir features can be approximated at an early age by utilizing software and inverse modeling to match transient data (Earlougher, R.C., & Kersch, 1972). With the development of PTA, in this study, reservoir characteristics will be modeled using existing well data with the aid of WellTest 2019.1 software (IHS Markit, 2019). A detailed description of the study methodology is illustrated in Figure 2.

After obtaining the transient data, the appropriate build-up test model will be selected, and then this data will be imported into the software. These datasets will be quite numerous (it can be more than 10,000 data points). Therefore, to ensure an optimal data volume of less than 5000 data points, data reconstruction is necessary using a data filtering method involving logarithmic points per cycle or arithmetic time steps tailored to meet the

requirement. If necessary, this data reconstruction allows adjustments to the shut-in period, which may differ from the well closure time data.

Fluid properties are important in reservoir characterization modeling because they apply to geothermal fluids at high temperatures, which might change their own properties and, as a result, pressure disturbance responses. Aside from fluid parameters, reservoir and well properties influence these responses. As a result, inputs obtained from PT survey monitoring data are critical, augmented as needed by assumptions tailored to reservoir conditions. These data inputs are essential to obtaining the right analysis of our reservoir characteristics.

Once all input data is consistent with reservoir conditions, additional analysis is required to ascertain reservoir characteristics. Following that, diagnostic analysis is performed to help detect several effects throughout the pressure transient: wellbore storage effects, reservoir radial flow, and boundary effects (pseudo-steady state). Understanding these phases aids in the early stages of type curve matching. Type curve matching can be aided by making alterations to predetermined parameters. Furthermore, automated matching methods can be done by iterating parameters like permeability, skin, wellbore storage, reservoir boundaries, and so on to ensure that they match the reservoir model. After all processes have been completed the reservoir parameters matched with the type curve will be used as outputs for subsequent analysis. This analysis will involve comparing data from the same wells across different years. These results will serve as the foundation for understanding the evolution of reservoir characteristics through PTA.

3. RESULTS AND DISCUSSIONS

Pressure transient studies were performed on 61 wells in the KMJ field, including FOT and PBU tests. Only 31 wells underwent the PBU test more than once. Wells with PBU data from two time periods, 2009-2012 and 2019-2023, were chosen for this study, totaling seven wells (which are KMJ-A, KMJ-B, KMJ-C, KMJ-D, KMJ-E, KMJ-F, and KMJ-G). This analytical constraint was designed to generalize the research findings and examine the impact of production on reservoir properties such as transmissibility and skin over a given time period.

The geological structure map of the Kamojang revealed that the wells are directed towards two structural fault boundaries, notably Kendang and Laksana faults. The PTA is used to identify the properties of these geological structural boundaries. The geological structure map of Kamojang shows that KMJ-C, KMJ-E, and KMJ-G are oriented toward the Kendang Fault. Meanwhile, KMJ-D and KMJ-F are pointing toward the Laksana Fault. Furthermore, KMJ-A is oriented toward the northeast, while KMJ-B is oriented toward the north. In Figure 3, a well distribution map of Kamojang is shown.

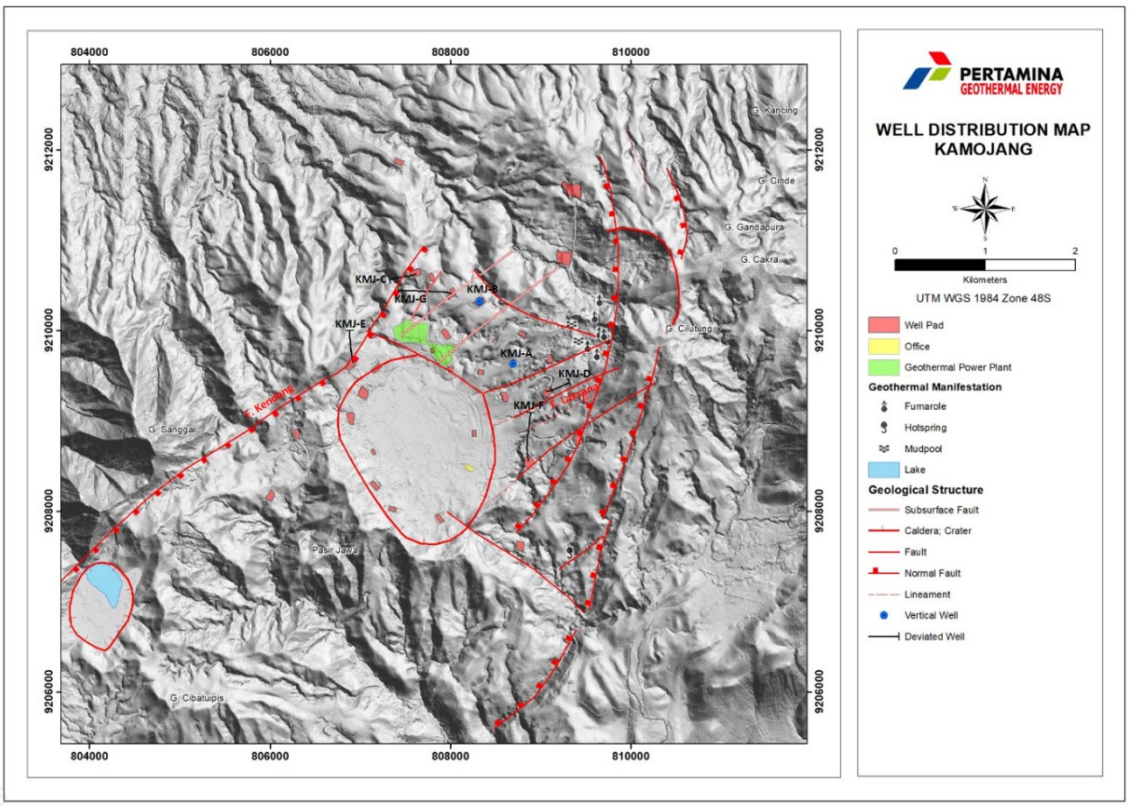

Figure 3: Well Distribution Map of Kamojang.

In the figures below (Figure 4, Figure 5, and Figure 6), log-log plots for the wells directed towards the Kendang Fault are presented. The analyses of these three figures indicate a similarity in reservoir characteristics, where the pressure transient characteristics still act as an infinite-acting reservoir. The pressure derivative plot at the late time reveals that the pressure response is constant, with no increase or drop. Based on this evidence, it may be argued that these wells do not respond to possible boundaries at the Kendang Fault, implying that the structure is still acting as a reservoir. Furthermore, it is also probable that the duration of the pressure build-up test was insufficient to see the boundary effects of the Kendang Fault.

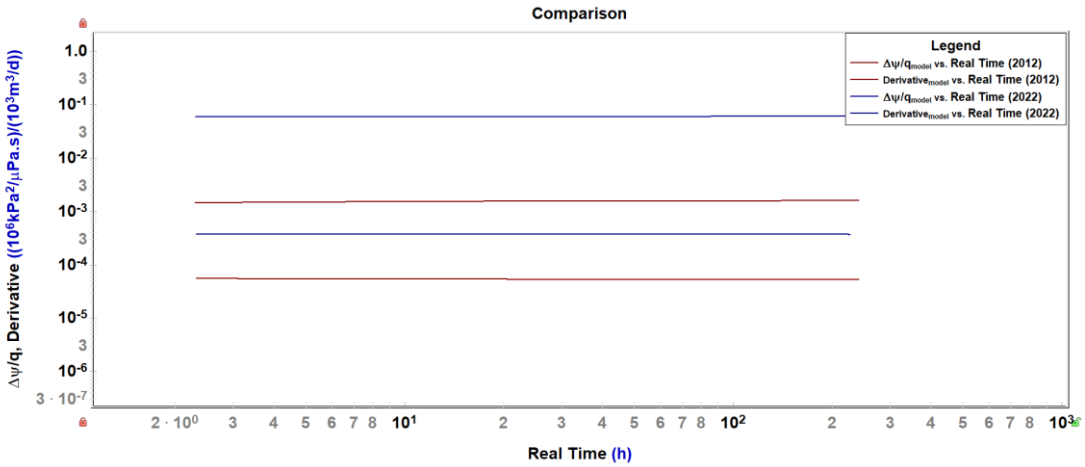

Figure 4: Pressure Build-Up (PBU) Comparison Plot in KMJ-C.

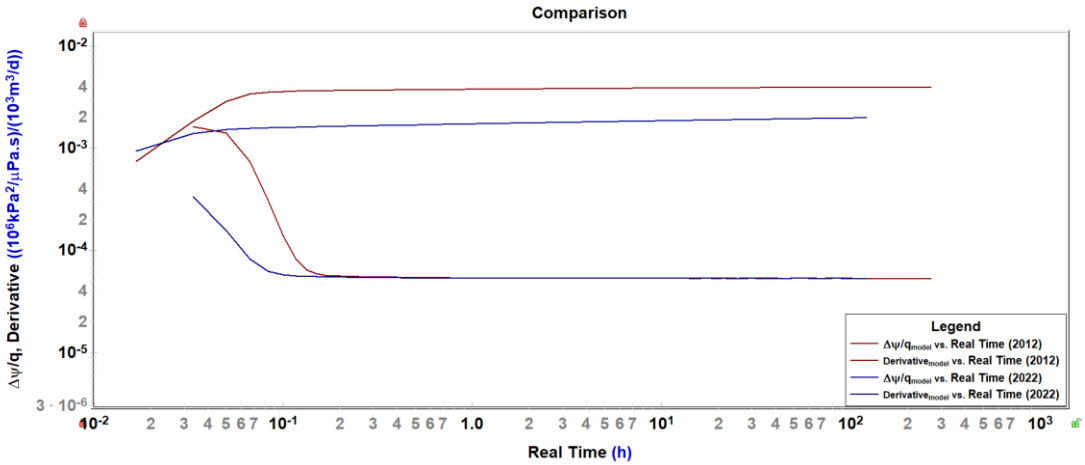

Figure 5: Pressure Build-Up (PBU) Comparison Plot in KMJ-E.

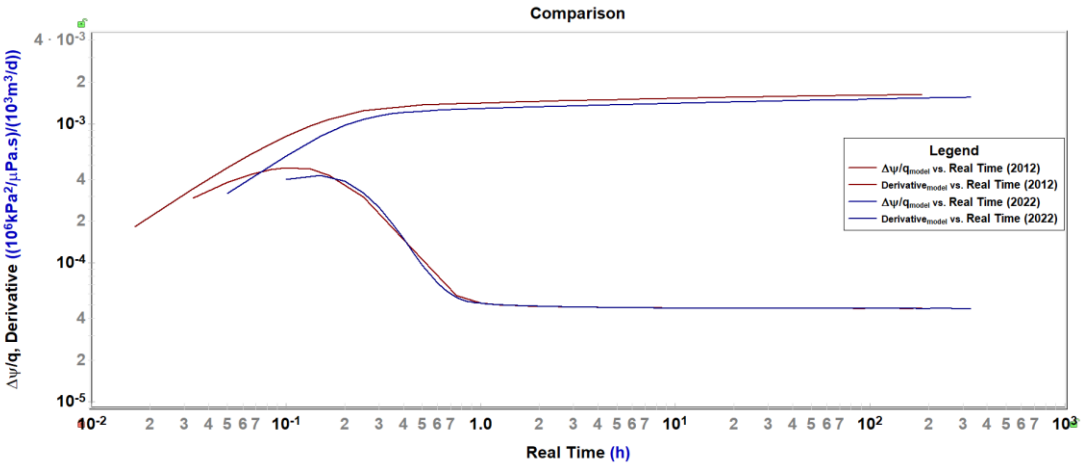

Figure 6: Pressure Build-Up (PBU) Comparison Plot in KMJ-G.

For the wells directed towards the Laksana Fault, the log-log plots are represented in Figure 7 and Figure 8. The PBU (Pressure Build-Up) results indicate the presence of a no-flow boundary for these wells, although it cannot be immediately confirmed due to the need for a drawdown test, which is essential for verifying the boundary characteristics (Zarrouk & McLean, 2019). However, conducting a drawdown test in a geothermal field is challenging due to issues related to thermal shock and the potential need for discharge stimulation to enable fluid flow from the wells. In well KMJ-D, the heat boundary can be relatively determined due to the presence of a radial flow pattern indicated by the pressure response on the pressure derivative plot before it rises. On the other hand, in well KMJ-F, the heat boundary is relatively difficult to determine because the radial flow pattern is not reflected before any disturbance to the reservoir pressure response occurs.

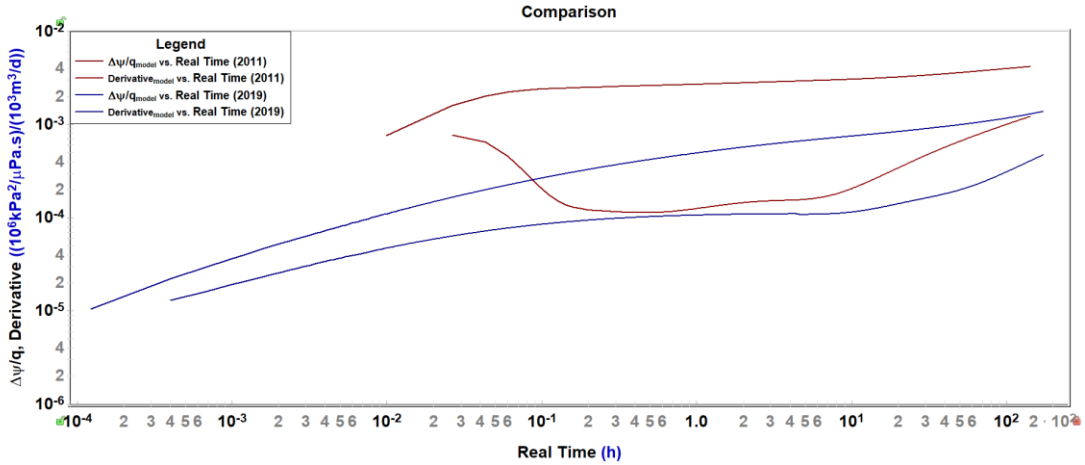

Figure 7: Pressure Build-Up (PBU) Comparison Plot in KMJ-D.

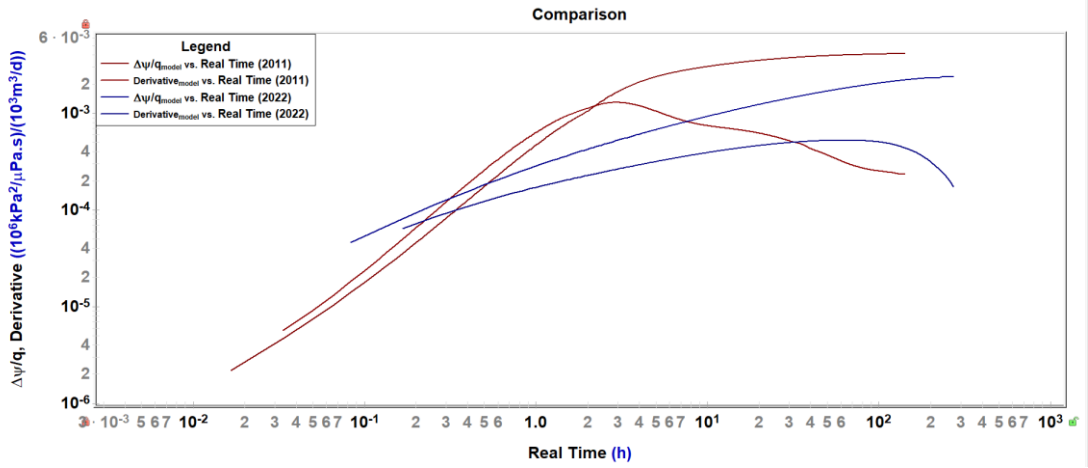

Figure 8: Pressure Build-Up (PBU) Comparison Plot in KMJ-F.

The log-log plot profile for well KMJ-A (Figure 9) shows a constant pressure boundary, which is a reservoir state in which the reservoir pressure remains constant at a set distance from the well (unaffected by production or injection). This boundary can be circular or linear with a constant pressure profile and a decreasing derivative profile. The pressure transient profile for well KMJ-B shows that pressure transients are controlled by flow within narrow and wide fractures (Figure 10). This signifies that the flow is linear, rather than radial. The width of the fracture will cause differences in the pressure and pressure derivative profiles. However, in order to further understand these features, additional pressure transient test are required (drawdown tests), which are typically difficult to implement in geothermal wells.

The results of the seven PTA for the seven wells are summarized in Table 1. From these results, it is observed that in the absence of significant changes in transmissibility during the production period, there is a numerical decrease in the skin value over approximately 10 years of production in these wells. This suggests that numerically, there appears to be an "improvement" in the near-wellbore condition. However, it cannot be conclusively stated that the decrease in skin value represents an actual "improvement" in near-wellbore conditions, as no well stimulation treatments were performed during this period. Instead, this could indicate that the decline in reservoir pressure is the main factor affecting the reservoir characteristics in the Kamojang field.

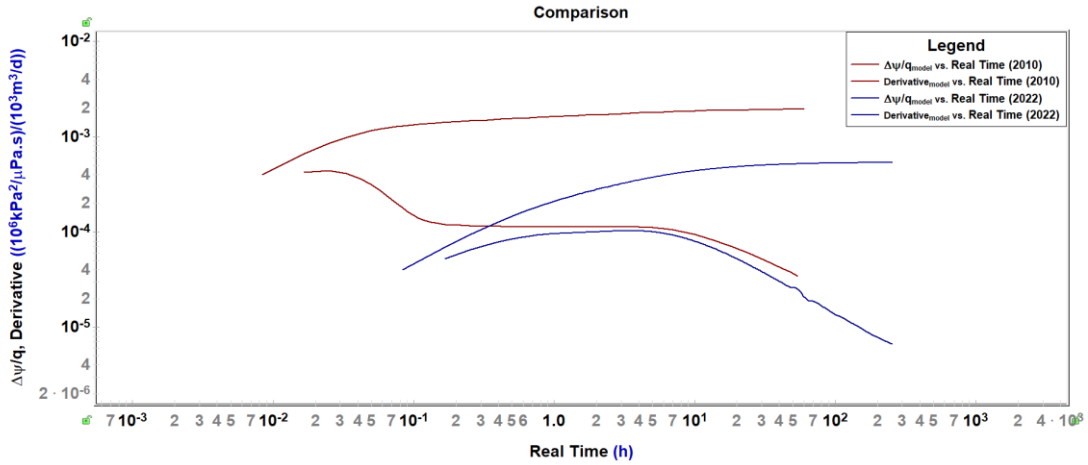

Figure 9: Pressure Build-Up (PBU) Comparison Plot in KMJ-A.

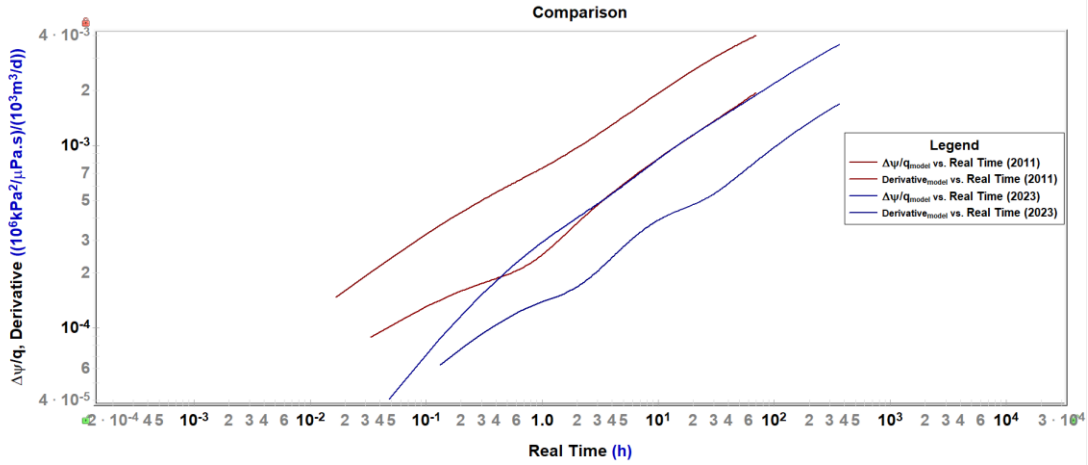

Figure 10: Pressure Build-Up (PBU) Comparison Plot in KMJ-B.

Table 1: Reservoir Characteristics Summary in Kamojang.

Well	First Period		Second Period	
	kh (D.m)	S	kh (D.m)	S
KMJ-A	2.7	2.5	2.7	-3.8
KMJ-B	1.03	-3	1.03	-3.93
KMJ-C	6	8	0.85	74
KMJ-D	2.8	7	2.8	-2.6
KMJ-E	6	30	6	12
KMJ-F	0.4	-3	0.35	-4.86
KMJ-G	6.3	9.8	6.3	8.75

4. CONCLUSION

Through pressure transient analysis (PTA), changes in reservoir characteristics at the Kamojang field have been observed over several years, specifically between the periods 2009-2012 and 2019-2023. PTA plays a crucial role in reservoir management by helping identify changes in factors such as transmissivity and skin factors.

The results of PTA on several wells showed a numerical decrease in skin value, which might indicate an "improvement" in near-wellbore conditions, even though no well stimulation treatments were performed. However, this decrease is more likely due to the natural decline in reservoir pressure over time.

The analysis also identified that certain wells are directed toward structural geological boundaries, such as the Kendang and Laksana Faults. Wells directed toward the Kendang Fault exhibit reservoir characteristics that still

act as an Infinite Reservoir, while wells directed toward the Laksana Fault suggest the presence of a possible no-flow boundary.

In summary, this study provides valuable insights into reservoir characteristics in the Kamojang field and highlights the importance of continuous monitoring and thorough analysis for effective reservoir management.

5. RECOMMENDATION

In the Kamojang region, it is essential to conduct tests on these wells to obtain comprehensive reservoir characterizations across the entire area. These tests should not only be performed but also be carried out correctly and with adequate time to ensure the accuracy and reliability of the data. This will enable a more accurate assessment of the geothermal potential and support informed decision-making for future development and management strategies.

REFERENCES

Aydin, H., Merey, S., & Akin, S. (2024). Pressure Transient Analysis of Alaşehir Geothermal Reservoir. *Workshop on Geothermal Reservoir Engineering*. California: Stanford University.

Earlougher, J., R.C., & Kersch, M. (1972). Field examples of automatic transient test analysis. *J. Pet. Technol*, 1271-1277.

Google. (2024, July). Google Earth Project. Retrieved from https://earth.google.com/web/search/PT.+PGE+Area+Kamojang,+Laksana,+Bandung+Regency,+West+Java/@-7.03369701,107.72313419,671.40088813a,98030.75789167d,30y,0h,0t,0r/data=CigiJgokCUIAyhG88RrAERtMz1JNSB3AGQ-XcdJKHltAIYqn_2IDzVpAOgMKATA

IHS Markit. (2019). Retrieved from https://www.spglobal.com/commodityinsights/en/ci/products/welltest-reserve-pta-software.html

Zarrouk, S. J., & McLean, K. (2019). Geothermal Well Test Analysis. Auckland: Elsevier.

Formulation and Technical Implementation of Gazsol (Gas Abatement System with Zeolite and Sodium Hydroxide Liquid) for Geothermal Well Production Test in Kamojang Field

Nanda Najih Habibil Afif, Muhammad Iqbal Alkindi, Efrizal, Yanuaris Dwi Cahyono, Hendrik Kurniawan Sinaga, Hanifah Bagus Sulistyardi, and Teza Permana

PT. Pertamina Geothermal Energy Tbk.

nanda.afif@pertamina.com, muhammad.alkindi@pertamina.com, efrizal@pertamina.com, muhammad.alkindi@pertamina.com, hendrik.sinaga@pertamina.com, hanifah@pertamina.com, teza.permana@pertamina.com

Keywords: Gazsol, geothermal, production test, H_2S, zeolite

ABSTRACT

This initiative by PT Pertamina Geothermal Energy (PGE) addresses a critical issue in geothermal well testing within national geothermal industry, specifically in 2022. During this period, high-risk incidents in some companies (other than PGE) led to several fatalities and numerous medical treatment cases linked to hydrogen sulfide (H_2S) gas exposure. The project aimed to prevent such hazardous exposures by developing an effective, efficient, and standardized gas abatement system. The solution, termed Gazsol (Gas Abatement System using Zeolite and Sodium Hydroxide Liquid), is designed to neutralize the accumulation of toxic gases during geothermal well production test. The necessity for this system arises from regulatory directives by the Directorate General of New Renewable Energy and Energy Conservation (EBTKE), which mandates gas abatement systems in all geothermal well testing activities to prevent fatalities and serious incidents similar to past occurrences in Indonesia. Gazsol represents a modification and development of existing technology, utilizing specific materials to effectively neutralize toxic gases. The implementation of this system has demonstrated significant improvements. The complete elimination of H_2S exposure during gas release has been achieved, along with the reduction in operational cost, the punctuality of well testing schedule, the absence of TRIR–NoA incident, and the adherence of positive moral perception from the community and well testing operator. Gazsol has been standardized and recognized for its replicability, setting a new benchmark for safety and efficiency in geothermal energy production.

1. INTRODUCTION

Geothermal energy, a sustainable and renewable resource, has been gaining increased attention as a viable alternative to conventional fossil fuels. It offers a clean, low-emission source of energy that can significantly reduce our carbon footprint and combat climate change. However, the development and utilization of geothermal resources are not without challenges, particularly concerning the safety and environmental impact of production processes (Bertani, 2016). The recent events in Indonesia's geothermal sector underscore the need for rigorous safety protocols and advanced technological solutions to mitigate potential hazards.

In March 2022, PT. Pertamina Geothermal Energy (PGE) Kamojang's proposal for production testing was put on hold for several days by the Directorate General of New Renewable Energy and Energy Conservation (Ditjen EBTKE). This suspension was primarily due to the alarming number of Notices of Accident (NoA) and Total Recordable Incident Rate (TRIR), which included six fatalities and 89 medical treatment cases within the first three months of 2022. These incidents were attributed to toxic gas exposure during the activation of wells for production testing at PT. Sorik Marapi and PT. Geo Dipa Energi. The victims included both workers and local community members, highlighting the risks associated with geothermal operations (Upstream Online, 2022).

Non-condensable gases (NCGs) like hydrogen sulfide (H_2S) and carbon dioxide (CO_2) can accumulate in geothermal wells during a shut-in position due to natural geothermal reservoir dynamics. When the well is shut in, the flow of geothermal fluids stops, causing pressure to build up within the well. This pressure increase causes NCGs to migrate from deeper high-pressure zones towards the wellbore. Without fluid movement, these gases exsolve from the geothermal fluids and concentrate in the wellbore, reaching hazardous levels (Rodriguez et al., 2014). Figure 1 illustrates NCG accumulation scheme within a geothermal well compared with the Pressure-Temperature logging profile after a distinctive shut-in period in a vapor-dominated reservoir in Kamojang field.

In response to these incidents, in 2022 the Director General of EBTKE issued a circular mandating the use of gas abatement systems in all production testing activities. However, there is currently no standard, optimal, and measurable gas abatement system for geothermal wells in PGE or even in Indonesia. The dominant reasons for

this gap include the reliance on estimates for materials used, lack of accommodation for varying concentrations of toxic gases, and the design of gas abatement equipment based on individual user assumptions without considering specific formulations. Furthermore, there is an absence of specialized formulations or calculations that can effectively address the varying concentrations of toxic gases. Regarding to Rodriguez et al. (2014), effective gas abatement systems should incorporate precise formulations and calculations to handle the specific gas concentrations encountered in geothermal operations.

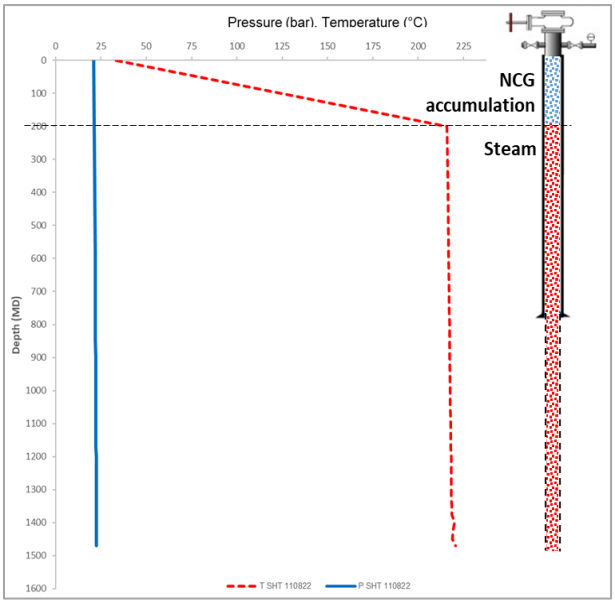

Figure 1: The illustration of the NCG accumulation scheme within a geothermal well compared with the Pressure-Temperature logging profile after a distinctive shut-in period in a vapor-dominated reservoir in Kamojang field.

The highlight of issues faced by PGE Kamojang prior to implementing innovations during gas abatement process was the unspecified quantity of NaOH used during the gas abatement, leading to ultra-excessive usage of NaOH. This excessive use not only resulted in the production of a substantial amount of liquid waste but also significantly increased the expenses due to the high cost of NaOH for geothermal industry purposes. Before the innovation, gas abatement process could add up the liquid waste as many as 2200 liters from post-NaOH usage. On other hand, the high amount of NaOH use could give the adverse effects of NaOH dispersion to the air, including black spots, itchy skin, and stinging eyes within a radius of up to 200 meters. This phenomenon could happen due to the absence of a standard gas abatement system, resulting in redundancy and ambiguity during the formulation of materials. Furthermore, the lack of a properly dimensioned gas abatement system led to the use of excessive amounts of NaOH, or in other circumstances (other than PGE), resulted in an inadequate amount of materials to absorb toxic substances from being released into environment.

The demanding need for a standardized gas abatement system in geothermal operations is definite. Such a system should be capable of handling different concentrations of toxic gases, ensuring the safety of both well testing operators and the surrounding communities. This paper aims to explore the current challenges in developing an effective gas abatement system for geothermal wells and propose potential solutions based on best practices from other industries. By addressing these issues, PGE Kamojang proposed Gazsol, a new system that combines natural zeolite and sodium hydroxide liquid with a specific abatement atmospheric flash tank. This formulation approach ensures the necessary amount of used material to respond to the different characteristics of geothermal wells effectively.

2. METHODS

2.1 Zeolite for H_2S Adsorption

Zeolites, due to their unique structural and chemical properties, have proven to be highly effective for the adsorption of hydrogen sulfide (H_2S), a toxic and corrosive gas. Structurally, zeolites are characterized by their three-dimensional microporous framework composed of silica (SiO_2) and alumina (Al_2O_3) tetrahedra, linked by oxygen atoms. This framework forms a crystalline lattice with a vast network of uniformly sized pores and cavities, providing an extensive surface area conducive to adsorption. The large surface area and high pore volume allow zeolites to trap and hold a significant amount of gas molecules, making them highly efficient at adsorbing H_2S (Georgiadis et al., 2021).

Natural zeolites are described with the following chemical formula (Coombs et al., 1998).

$$\left(M_x^+, M_y^{2+}\right)\left[Al_{(x+2y)}\ Si_{n-(x+2y)}O_{2n}\right] \times mH_2O \quad (1)$$

Where M_x^+ are monovalent values with stoichiometry x, M_y^{2+} are divalent values with stoichiometry y, [$Al_{(x+2y)}$ $Si_{n-(x+2y)}O_{2n}$] is structural cations, and *m* is the number of water molecules in the structure (Čejka and van Bekkum, 2005).

The mechanism of H_2S adsorption by zeolites involves both physical and chemical adsorption processes. In physical adsorption, H_2S molecules are attracted to the internal surfaces of the pores through weak van der Waals forces. When a gas stream containing H_2S passes through the zeolite, the H_2S molecules are drawn to the internal pore surfaces and become adsorbed. This process is facilitated by the uniformity of the pore sizes, which ensures selective adsorption of H_2S molecules while excluding larger molecules that may be present in the gas stream (Breck, 1974).

When impurities come into contact with a zeolite, the hydrogen sulfide molecules can react with these cations to form metal sulfides, effectively removing compound such as H_2S from the gas phase. The mechanism can be represented as follows:

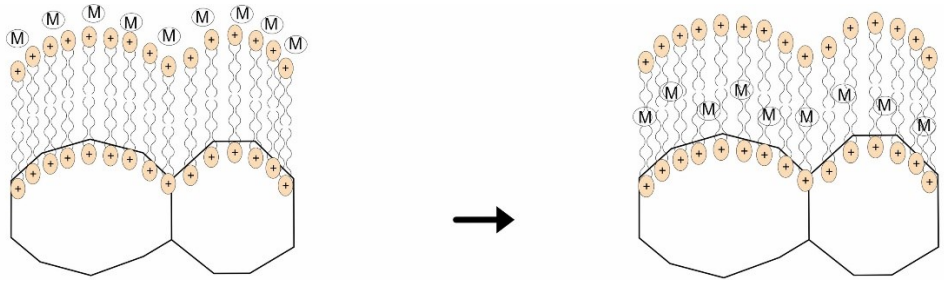

Figure 2: A scheme for principal mechanisms of adsorption of heavy metals with natural zeolites under electrostatic interaction (Velarde, L., et al., 2023).

One of the significant advantages of using zeolites for H_2S adsorption is their regenerability. After a zeolite becomes saturated with H_2S, it can be regenerated through various methods, such as heating or exposure to a vacuum. This regeneration process desorbs the adsorbed H_2S molecules, restoring the zeolite's adsorption capacity and allowing it to be reused multiple times. This regenerability not only extends the lifespan of the zeolite but also reduces operational costs and waste generation, making zeolites a sustainable choice for long-term use.

2.2 NaOH for H_2S Adsorption

The adsorption of hydrogen sulfide using sodium hydroxide (NaOH) is an efficient method for removing this toxic and corrosive gas from various industrial and environmental contexts. The mechanism involves a series of chemical reactions that result in the conversion of H_2S into harmless compounds. This process is primarily driven by the strong basic nature of NaOH, which facilitates the absorption and neutralization of H_2S (Rodriguez et al., 2014).

When H_2S gas comes into contact with an aqueous solution of NaOH, a neutralization reaction occurs. The hydroxide ions (OH^-) from NaOH react with the hydrogen sulfide gas (H_2S) in a two-step process. In the first step, H_2S dissolves in water to form hydrogen ions (H^+) and bisulfide ions (HS^-):

$$H_2S \leftrightarrow H^+ + HS^- \quad (2)$$

This reaction is an equilibrium process, meaning that it can proceed in both directions. The second step involves the reaction of bisulfide ions with hydroxide ions to form sulfide ions (S^{2-}):

$$HS^- + OH^- \rightarrow S_2^- + H_2O \quad (3)$$

The overall reaction can be represented as:

$$H_2S + 2NaOH \rightarrow Na_2S + 2H_2O \quad (4)$$

In this process, H_2S is effectively removed from the gas phase and converted into sodium sulfide (Na_2S) in the aqueous phase. The formation of water (H_2O) as a byproduct further contributes to the neutralization process.

The efficiency of H_2S adsorption using NaOH depends on several factors, including the concentration of NaOH, the temperature, the contact time between the gas and the liquid, and the pH of the solution. A higher concentration of NaOH increases the availability of hydroxide ions, thereby enhancing the reaction rate and the overall

adsorption capacity. The optimal pH for this reaction is typically above 10, where NaOH is fully dissociated, providing a high concentration of OH^- ions.

Temperature also plays a crucial role in the adsorption process. Higher temperatures generally increase the reaction rate, but extremely high temperatures can lead to the decomposition of Na_2S, thereby reducing the efficiency of H_2S removal. Additionally, sufficient contact time between H_2S and NaOH ensures that the gas has ample opportunity to dissolve in the aqueous phase and react with the hydroxide ions (Rodriguez et al., 2014).

The application of sodium hydroxide (NaOH) for hydrogen sulfide (H_2S) adsorption is widely utilized across various industries, including natural gas processing, wastewater treatment, and biogas purification. For instance, in natural gas processing, the removal of H_2S is crucial to prevent corrosion in pipelines and equipment, ensuring compliance with safety and environmental regulations. Similarly, in wastewater treatment, NaOH is used to eliminate H_2S odors and prevent the formation of sulfuric acid, which can damage infrastructure (Awe et al., 2017).

2.3 Considered Variables for Gas Abatement Formula Approach

To approach the required amount of material for H_2S abatement in a geothermal well, several key variables must be considered. Here's a detailed explanation of each variable:

2.3.1 Geothermal Well Casing Dimension

The dimensions of the geothermal well casing play a crucial role in determining the volume and pressure of the geothermal fluids being extracted. These dimensions include the diameter and depth of the casing:

- The diameter of the well casing affects the flow rate of geothermal fluids. A larger diameter allows for a higher flow rate, which can result in a greater volume of H_2S and other gases being extracted.
- The depth of the well influences the temperature and pressure of the geothermal fluids. Higher temperatures can increase the solubility and concentration of gases like H_2S in the fluid.

By understanding these dimensions, we can estimate the volume of geothermal fluid and the associated gas emissions, which is essential for calculating the amount of material required for H_2S abatement.

2.3.2 Gas Chemistry Ratio and Composition

The gas chemistry ratio and composition, particularly the ratio of H_2S to other gases, are critical in determining the abatement strategy. Common gases in geothermal wells include H_2S, CO_2, CH_4, and N_2. The ratio and composition can vary significantly between wells.

- H_2S Ratio: The proportion of H2S relative to other gases such as CO_2 and CH_4 must be determined. For instance, if the gas composition is 70% CO_2, 20% H_2S, and 10% CH_4, the abatement system must primarily target H_2S.
- Total Gas Composition: Understanding the total gas composition helps in designing the abatement system to handle not only H_2S but also other gases that may impact the efficiency of the abatement materials (e.g., NaOH and zeolite).

2.3.3 Concentration of NaOH and Zeolite

The concentration of NaOH (sodium hydroxide) and zeolite used in the abatement process is pivotal in ensuring the effective removal of H_2S from geothermal fluids. NaOH neutralizes H_2S through a chemical reaction that forms sodium sulfide (Na_2S) and water. The concentration of the NaOH solution must be sufficiently high to react with all the H_2S present. Typically, this concentration is determined based on stoichiometric calculations considering the amount of H_2S, with the required concentration calculated from the molar ratio of NaOH to H_2S.

Zeolite serves as an adsorbent material capable of capturing H_2S molecules. The concentration and quantity of zeolite required depend on its adsorption capacity and the volume of gas passing through it. Zeolite effectively traps H_2S molecules within its porous structure, making it an essential component in the abatement process. To ensure the effectiveness of zeolite in H_2S abatement, it is essential to conduct thorough material characterization to determine its concentration and actual presence within natural rock formations. Microscopic analysis and X-ray diffraction (XRD) are critical techniques used to obtain these data. The observation under microscope allows qualitative examination of rock samples to identify mineral composition and texture, while XRD provides precise information on the crystalline structure and quantitative mineralogical composition. Together, these analyses offer a comprehensive understanding of the zeolite content, ensuring its efficacy in the H_2S abatement process.

2.3.4 Design of Flash Tank

The design of the flash tank is integral to the effectiveness of the H_2S abatement process. The flash tank allows the geothermal fluid to depressurize, separating steam from liquid. Proper design ensures efficient contact between H_2S and NaOH.

- *Dimensions of flash tank*: the size and volume of the flash tank are crucial as they determine the residence time of the geothermal fluids and gases within the tank. Sufficient residence time is essential to ensure that NaOH has adequate opportunity to effectively neutralize H_2S. A properly sized flash tank allows for the optimal interaction between the NaOH solution and the H_2S gas, enhancing the efficiency of the abatement process.
- *Dispersion Pipe*: this part within the flash tank plays a vital role in uniformly distributing the NaOH solution throughout the tank. This uniform distribution ensures maximum contact between the NaOH solution and the H_2S gas. The design, placement, and configuration of the dispersion pipe directly affect the interaction efficiency, enabling thorough mixing and effective neutralization of H_2S.
- *Minimum amount of NaOH*: the dimensions of the flash tank and the flow rate of geothermal fluids are key factors in determining the minimum amount of NaOH required for complete neutralization of H_2S. The tank must be large enough to provide sufficient mixing and reaction time between the NaOH solution and the H_2S gas. Proper tank design ensures that the NaOH solution can interact effectively with the H_2S, ensuring complete abatement and preventing any untreated gas from escaping.

3. RESULTS

3.1 Zeolite Characterization

This section will discuss the results of characterizing natural zeolite rock using X-Ray Diffraction (XRD) and microscopic analysis. The graph in Figure 3 is a crucial component of the analysis, displaying the XRD pattern of the zeolite rock. The x-axis represents the 2-theta (deg) values, while the y-axis shows the intensity (cps) of the diffraction peaks. These peaks are indicative of the crystalline phases present in the sample. The superimposed red and blue lines highlight the peaks corresponding to specific minerals, with annotations for heulandite and mordenite clearly marked. The analysis results are summarized, confirming the identification of heulandite and mordenite as the primary zeolite minerals within the natural rock sample. This confirmation is crucial as it validates the presence of these minerals, which are known for their significant industrial and environmental applications due to their adsorptive properties.

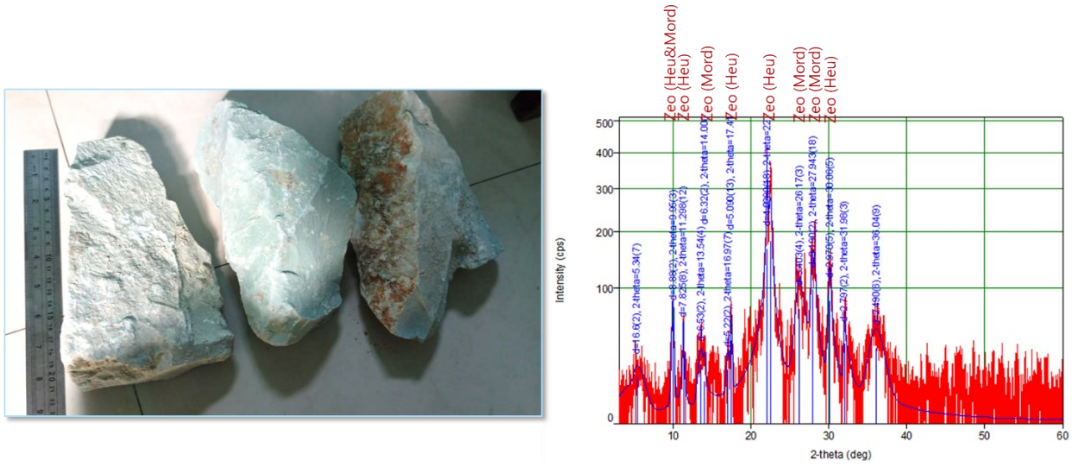

Figure 3: (left) photograph on the left side showcases the natural zeolite rocks that were selected for the study, providing a visual context for the material being analyzed; (right) the graph of XRD analysis result using graph method.

Figure 4 provides an in-depth analysis of the zeolitic rock under thin section observation using reflecting microscope. The primary focus is on determining the abundance and distribution of zeolite minerals within the rock sample. The microscopic analysis reveals that the base rock is identified as lithic tuff, a type of volcanic rock composed of consolidated volcanic ash and fragments. The findings indicate a significant alteration of the lithic tuff by zeolite minerals, transforming its original composition. The analysis confirms that zeolite minerals are prevalent in the rock.

Additionally, a comparator chart from the BC Ministry of Forestry (1997) is included, which serves as a reference for estimating the abundance of zeolite minerals within the thin sections. This chart provides visual aids for comparing different percentages of mineral abundance, assisting in the qualitative quantification of zeolite content, with an abundance ranging between 30-40%.

Overall, the microscopic analysis complements the previous XRD characterization by providing a visual confirmation of the zeolite minerals within the natural rock. The combined use of XRD and thin section offers a comprehensive understanding of the zeolitic rock's mineralogical composition, confirming the presence and

significant abundance of heulandite and mordenite. For further data processing, this data would contribute significantly in providing zeolite abundance data during formulation stage and calculation of required abatement materials.

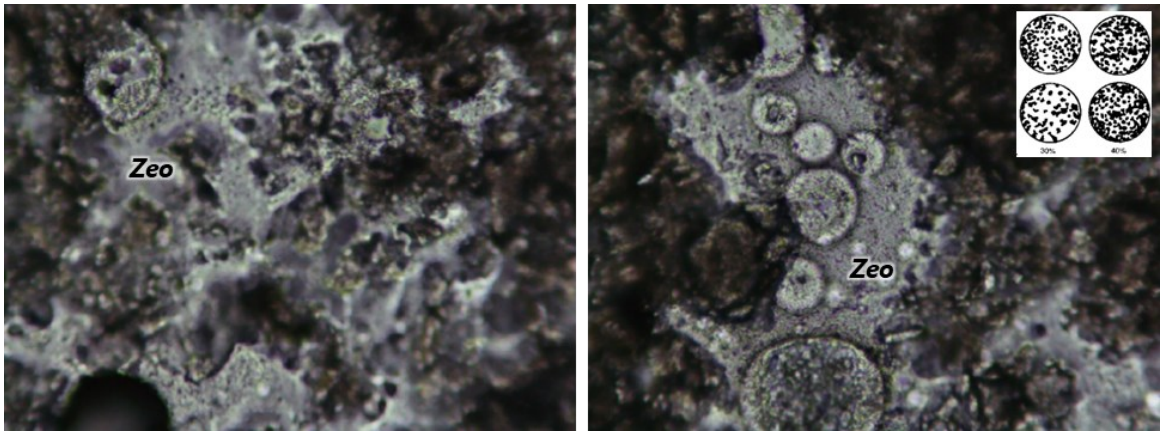

Figure 4: Photographs of zeolite rock under 100x magnification using reflecting microscope, zeolite mineral within the rock section provided by white greenish object with granulose texture.

3.2 Natural Zeolite Adsorption to H_2S: Experiment Result

The provided graph illustrates the relationship between the concentration of hydrogen sulfide (H_2S) over time in comparison to the background concentration of H_2S. Notably, the ratio between these concentrations begins to stabilize at around the 1300-second mark, indicating that the adsorption process reaches a point of equilibrium.

Based on the experiment, the ability of the zeolite to adsorb H_2S is quantified as 1667 ppm H_2S per square meter of zeolite area or equivalent with 2532.5 mg/Nm^3 per meter square of zeolite surface area. This high adsorbance capacity demonstrates the effectiveness of zeolite in capturing and retaining H_2S molecules, which is essential for applications in environments where H_2S buildup poses a risk. This high adsorption capacity underscores the remarkable effectiveness of zeolite in capturing and retaining H_2S molecules. Such a significant adsorbance capacity is particularly essential for applications in geothermal well testing activity.

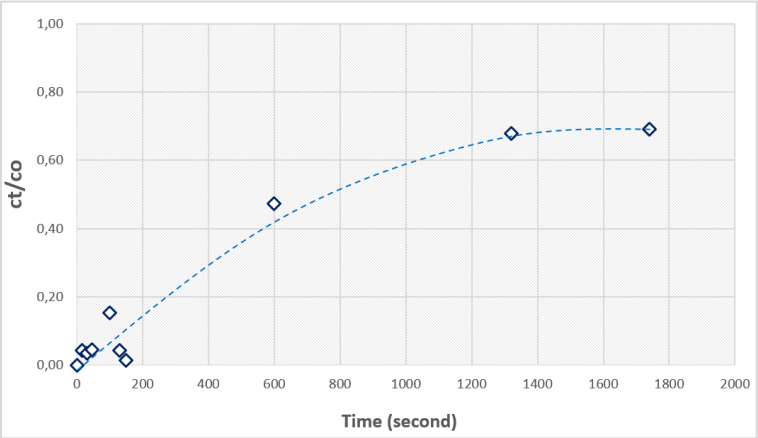

Figure 5: The image appears the graph related to the ratio between the concentration of H_2S over time compared to the background concentration of H_2S. Begins at 1300-second point, the trend of the ratio turned to stationary.

The stationary trend observed in the graph after 1300 seconds suggests that the zeolite has reached its maximum adsorption capacity under the given conditions. This information is vital for optimizing the use of zeolite in practical applications, as it helps to determine the appropriate amount and surface area of zeolite required to achieve desired levels of H_2S removal. Consequently, this contributes to more efficient and cost-effective gas abatement process.

3.3 Gazsol Technical Design

3.3.1 Configuration

The below image depicts the technical configuration of Gazsol application designed for gas abatement in Kamojang field, preceding geothermal well production test. The illustration highlights main setup that includes several crucial components starting from the wellhead and extending to Gazsol flash tank.

Figure 6: Technical configuration of Gazsol application for gas abatement process preceding geothermal well production test: (A) master valve, (B) top valve, (C) side valve, (D) tandem side valve, (E) casing head, (F) gas abatement pipe, (G) gas dispersion pipe, (H) main body flash tank, (J) steel wire rope, (K) hefty concrete cube.

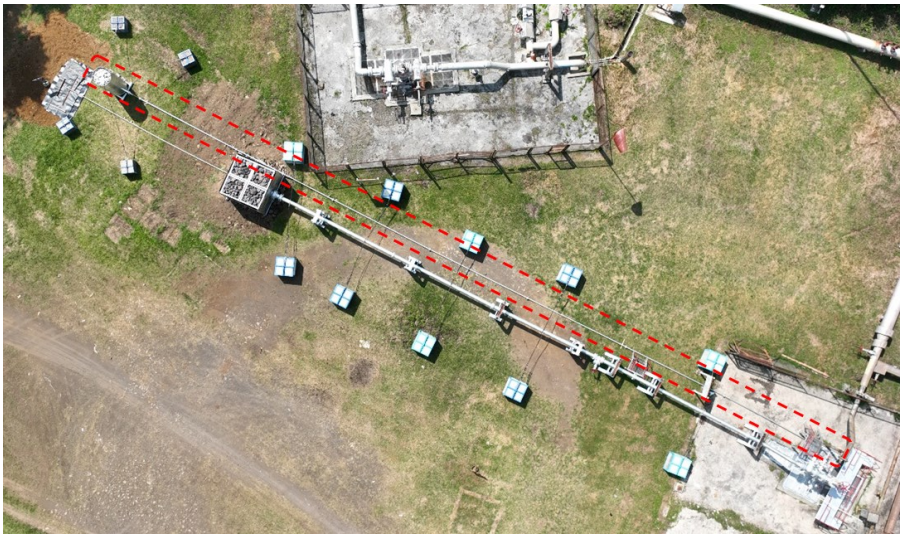

Figure 7: Bird's-eye view of Gazsol implementation in the Kamojang geothermal field for the purpose of geothermal well testing. The dotted red line outlines the real configuration of Gazsol, spanning from the wellhead assembly through the side valve, then being connected by gas abatement pipe into the Gazsol main body flash tank.

At the wellhead, the master valve (labeled A) is prominently featured. This valve plays a critical role in controlling the flow of geothermal steam and gas from the well. Above the master valve is the top valve (B), which provides an additional access into the well from the top side. The side valve (C) and tandem side valve (D) facilitate the diversion of gas from the main flow path. The casing head (E) serves as a transition point between the wellhead and the surface piping, ensuring a secure and stable connection. From the casing head, the gas abatement pipe (F) extends horizontally, acting as a conduit for the gas to be transported away from the wellhead.

The gas accumulation from the subsurface enters the gas dispersion pipe (G), which is connected to the main body flash tank (H). This tank is a critical component of the Gazsol system, designed to handle and neutralize the gas by allowing it to dissipate safely. The flash tank's robust structure ensures that the gas is contained and treated effectively. Supporting the system, a steel wire rope (J) is used to stabilize and secure the components, ensuring they remain in place during operation. Additionally, a hefty concrete cube (K) provides a solid foundation, preventing any movement or displacement of the equipment.

This configuration allows for the efficient accumulation and redirection of gas from the top part of the geothermal casing. The gas flows from the side valve into the gas abatement system, where it is safely managed and neutralized. This setup is essential for maintaining safety and efficiency during geothermal well testing, ensuring that any gas emissions are properly handled before production test begins.

3.3.2 Flash Tank

Figure 8 provides a detailed technical design for a Gazsol atmospheric flash tank, illustrating its main components and operational flow. The primary structure of the flash tank includes a main body, inspection ladder, inlet pipe, perforated dispersion pipe, NaOH drainage pipe, and the zeolite bucket.

The gas accumulation process begins at the inlet pipe, where the gas enters the flash tank. From there, the gas moves into the slotted dispersion pipe, which evenly distributes the gas within the tank. This dispersion ensures that the gas floats upward efficiently, passing through the slotted bucket base. As the gas ascends, it interacts with the zeolite rocks inside the bucket, initiating the adsorption reaction. The zeolite effectively captures and retains the H_2S molecules, demonstrating its high adsorption capacity. This process is crucial for environments where H_2S buildup poses a risk, as it ensures that harmful gases are adequately treated and removed. Besides that, zeolit stacks in the upper part of the tank also helps in retaining the NaOH dispersion effect to the air.

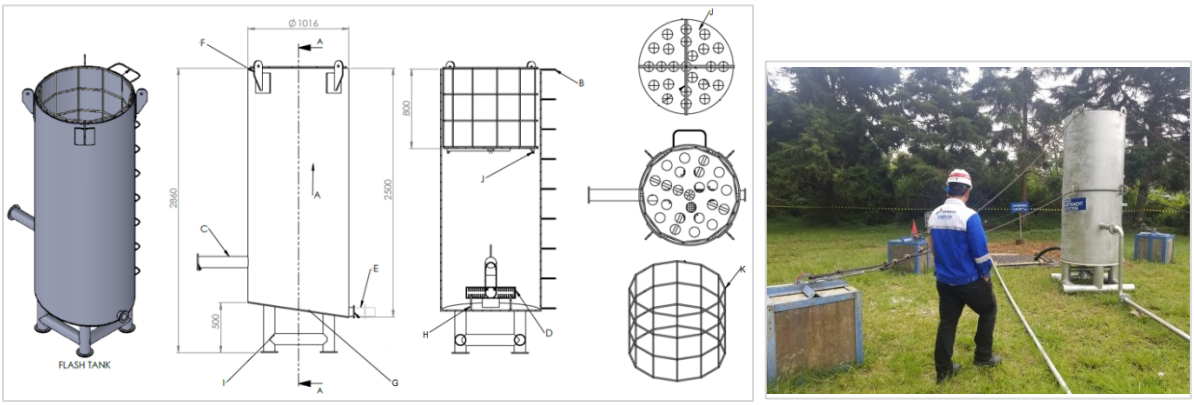

Figure 8: (left side picture) technical design for a Gazsol atmospheric flash tank: (A) main body, (B) inspection ladder, (C) inlet pipe, (D) perforated dispersion pipe, (E) NaOH drainage pipe, (F) zeolite bucket holder, (G) inclined-base, (H) support for dispersion pipe, (I) main body support, (J) enforced slotted metal for bucket base, (L) zeolite bucket; (right side picture) Gazsol has been applied for geothermal well production, anchored by hefty concrete cube, as it was being inspected by the EBTKE inspector (the man in the picture).

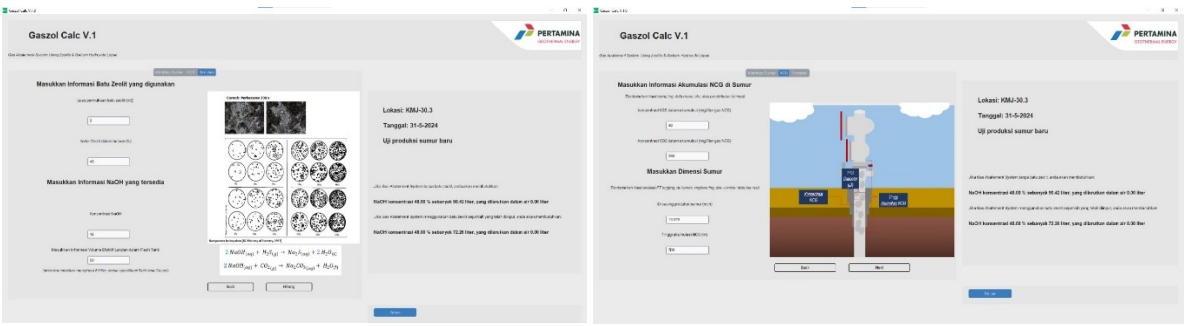

Figure 9: Gazsol Calc interface, a simple application to formulate the quantity of sodium hydroxide and zeolitic rock for gas abatement system.

The design also highlights key structural elements like the inclined base, which allows for the efficient drainage of NaOH after the abatement system has processed the gas. Additionally, the support systems for the dispersion pipe and the main body ensure the stability and proper functioning of the flash tank.

Overall, the design showcases the ample approach to gas treatment within the Gazsol flash tank, emphasizing the efficiency and effectiveness of its components in handling H_2S adsorption.

The flash tank was outlined by several assumptions and calculations for determining the flash tank's appropriate dimensions and operational parameters. Key parameters in the table include line pressure, enthalpy of steam, AFT pressure, steam velocity, steam dynamic viscosity, and water density, among other relevant physical properties and calculations essential for the apparatus's functionality. The flash tank detailed pressure design wall thickness according to ASME B31.1 Power Piping standards, regarding to weld joint quality factor, design temperature, weld joint strength reduction factor, material allowable stress, and manufacturing tolerances.

3.4 "Gazsol Calc": A Formulation to Quantify Abatement Materials

Figure 9 showcases the Gazsol Calc application, a simple tool meticulously developed through a series of sequential experiments by PGE using Python. This tool is designed to determine the precise quantities of materials required for an effective gas abatement system, focusing specifically on zeolitic rock and sodium hydroxide (NaOH). Both of these components are essential in the gas abatement process, which is critical for maintaining safety and efficiency during geothermal production test. The application integrates complex calculations and scientific principles to ensure accurate and reliable data, providing a significant advantage for professionals in the geothermal industry.

The Gazsol Calc interface is presented in a user-friendly manner, beginning with a introductory that outlines the purpose and capabilities of the application. Users are prompted to enter detailed well data, including the well name, date, relevant notes, and any specific conditions at the well site. This initial input form is crucial as it ensures that the subsequent calculations are tailored to the unique parameters of each geothermal well, allowing for highly customized and precise estimations. The interface also includes visual aids and detailed instructions to guide users through the data entry process, making it accessible even to those who may not be experts in the field.

One of the key capabilities of the Gazsol Calc is its ability to calculate the required amount of zeolitic rock based on its abundance at the site. This feature ensures that the use of natural resources is optimized, reducing waste and improving the overall efficiency of the gas abatement process. Additionally, the application can determine the necessary quantity of sodium hydroxide (NaOH) needed, if required, for the process. This is particularly important as NaOH is a critical chemical in neutralizing and managing gas emissions, and its precise measurement is essential for safety and effectiveness. Furthermore, the application computes the effective concentration of NaOH to be used, ensuring that the chemical is used in the most efficient manner possible, thereby minimizing costs and environmental impact.

3.5 Environment Monitoring During Gas Abatement Process Using Gazsol

Figure 10: Environment monitoring during gas abatement system in geothermal well X, the red dotted circle indicates the radii of observation during gas abatement process.

Observation point	Noise	H2S (ppm)	CO (ppm)	Dispersion effect of NaOH	Complaint	Observation point	Noise	H2S (ppm)	CO (ppm)	Dispersion effect of NaOH	Complaint
TP 1	70 dB	2	0	None	None	TP 4	65 dB	5	0	None	None
TP 2	8.7 dB	7	0	None	None	TP 5	45 dB	0	0	None	None
TP 3	63.6 dB	0	0	None	None	TP 6	45 dB	0	0	None	None

Figure 11: The recap of environment monitoring during well production test of geothermal well X, Kamojang Field.

The tabular data in Figure 11 provides a comprehensive recap of the environmental monitoring results. It details the observations recorded at each monitoring point, including noise levels, concentrations of hydrogen sulfide and carbon monoxide, the dispersion effect of NaOH, and any community assessment. For instance, at TP-1, noise

levels were recorded at 70 dB, with H2S concentration at 2 ppm and CO at 0 ppm. There were no noted effects of NaOH dispersion or community complaints at this point.

Similarly, at TP-2, noise levels were significantly lower at 8.7 dB, but CO levels were higher at 7 ppm, while H_2S remained at 0 ppm. Like TP-1, no dispersion effect of NaOH or community complaints were reported. At TP-3, noise levels were measured at 63.6 dB, with both H2S and CO concentrations at 0 ppm, and again, no issues with NaOH dispersion or community concerns. Further observation points, TP-4, TP-5, and TP-6, show varied noise levels, with TP-4 recording 65 dB and TP-5 and TP-6 both at 45 dB. At TP-4, H2S levels were 5 ppm, while CO remained at 0 ppm. Neither TP-5 nor TP-6 showed any significant levels of H_2S or CO, nor any impact from NaOH dispersion or community complaints.

Overall, this detailed monitoring effort provides crucial data that helps in evaluating the environmental impact of the gas abatement system using Gazsol in place at geothermal well. The consistent documentation of noise levels, gas concentrations, and community feedback plays an essential role in ensuring the environmental safety and operational integrity of the geothermal field activities, especially during gas abatement process using Gazsol.

4. CONCLUSION

The formulation and technical engineering design for gas abatement system in Kamojang field that further being implemented and termed as “Gazsol” has led to significant benefits within the geothermal operation. The combination of zeolitic rock and sodium hydroxide, packed in distinctive design and dimension of flash tank, then being formulated under quantitative approach derived from some steps of experiments, can result in notable five points of view:

- Quality: the use of the Gazsol system led to the reduction of hydrogen sulfide (H_2S) emissions from >500 ppm to 0 ppm (under STP), significantly enhancing air quality in the geothermal field and eliminating serious health and environmental risks.
- Cost: operational costs associated with the gas abatement process were drastically reduced from approximately Rp61.25 million per year to Rp3.2 million per year, reflecting a 95% savings. This reduction was achieved by optimizing the amount of NaOH used, avoiding unnecessary expenditure, and making the process much more cost-effective.
- Delivery: project deliveries improved as the new gas abatement system eliminated delays caused by the lack of preparedness in managing gas emissions. The implementation of a standard system with clear material formulations led to projects being completed on time and on schedule, demonstrating enhanced efficiency and reliability.
- Safety: the gas abatement process safety has been improved vastly with Gazsol. The amount of NaOH waste was reduced from 2200 liters to 75 liters, a 96.7% reduction. The system also eliminated adverse effects of NaOH dispersion, within a 200-meter radius, significantly enhancing the work environment's convenience.
- Moral: 100% of personnel now feeling safe and comfortable while performing their duties, compared to 71% feeling unsafe previously. This increase in morale is a direct result of the improved safety and working conditions brought about by the new gas abatement system.

For further development, it is recommended to conduct comprehensive observations of the zeolitic rock under various physical conditions such as temperature and pressure to understand their impact on various geothermal environment. Additionally, further studies should focus on optimizing the flash tank design to enhance its efficiency and effectiveness. The development of the Gazsol Calc application should also be advanced, taking into consideration the need for an improved user interface, better replicability, and wider accessibility, ensuring that the application is user-friendly and can be easily adopted across different geothermal sites.

REFERENCES

Awe, O.W., Zhao, Y., Nzihou, A., Minh, D.P., & Lyczko, N. 2017. A review of Biogas Utilisation, Purification and Upgrading Technologies. *Waste and Biomass Valorization,* 8, 267–283. https://doi.org/10.1007/s12649-016-9826-4.

Bertani, R. 2016. Geothermal Power Generation in the World 2010-2014 Update Report. *Geothermics*, 60, 31-43. https://doi.org/10.1016/j.geothermics.2015.11.003.

Breck, D. W. 1974. *Zeolite Molecular Sieves: Structure, Chemistry, and Use*. New York: John Wiley & Sons.

Čejka, J. and Bekkum, H. van. 2005. *Zeolites and Ordered Mesoporous materials: Progress and Prospects*. first ed., Elsevier.

Coombs, D.S., Armbruster, A., Artioli, G., Colella, C., Galli, E., Grice, J.D., Liebau, F., Mandarino, J.A., Minato, H., Nickel, E.H., Passaglia, E., Peacor, D.R., Quartieri, S., Rinaldi, R., Ross, M., Sheppard, R.A., Tillmanns, E., Vezzalini, G. 1998. Recommended nomenclature for zeolite minerals: report of the subcommittee on zeolites of the international mineralogical association, commission on new minerals and mineral names. *Mineral. Mag*., 62 (4) (1998), pp. 533-571, 10.1180/002646198547800.

Curković, L., Cerjan-Stefanović, Š., & Filipan, T. (1997). Metal ion exchange by natural and modified zeolites. *Water Research*, 31(6), 1379-1382. doi:10.1016/S0043-1354(96)00403-2

Georgiadis, AG., Charisiou, Nikolaos D., Gaber, Safa., Polychronopoulou, Kyriaki., Yentekakis, Ioannis V., and Goula, Maria A. Adsorption of Hydrogen Sulfide at Low Temperatures Using an Industrial Molecular Sieve: An Experimental and Theoretical Study. *ACS Omega* 2021 6 (23), 14774-14787 DOI: 10.1021/acsomega.0c06157.

Huang, X., Zhao, L., & Gao, Y. (2016). "Adsorption Mechanism of Hydrogen Sulfide by Sodium Hydroxide Solution." *Chemical Engineering Journal*, 290, 53-59.

Mishra, P., & Tiwari, S. K. (2020). *Zeolites: Applications in adsorption and catalysis*. In S. S. Ray, & M. Ramalingam (Eds.), Advanced Applications and Current Research of Zeolites. London: Elsevier. doi:10.1016/B978-0-12-816514-6.00001-5.

Rodriguez, E., Harvey, WS., and Ásbjörnsson, EJ. 2014. Review of H2S Abatement Methods in Geothermal Plants. Stanford University. *Proceeding, Thirty-Eighth Workshop on Geothermal Reservoir Engineering Stanford University*, Stanford, California, February 24-26, 2014 SGP-TR-202.

Upstream Online News. 2022. https://www.upstreamonline.com/safety/fatal-incident-at-indonesian-geothermal-plant/2-1-1185978.

Velarde, Lisbania., Nabavi, Mohammad Sadegh., Escalera, Edwin., Antti, Marta-Lena., Akhtar, Farid. 2023. Adsorption of heavy metals on natural zeolites: A review. *Chemosphere* Volume 328, July 2023, 138508, Elsevier, https://doi.org/10.1016/j.chemosphere.2023.138508.

Evaluating Reinjection Efficiency in The Kamojang Geothermal Field Using Gas and Isotope Chemistry Data

Baiq Lolla Riandari, Ristio Effendi, and R. Mochamad Tofan S

PT. Pertamina Geothermal Energy Tbk.

Baiq.Riandari@pertamina.com, Ristio.Efendi@pertamina.com, rmtofans@pertamina.com

Keywords: geochemistry, geoindicator, kamojang, vapour dominated, superheat

ABSTRACT

The Kamojang Geothermal Field, located in West Java Province, Indonesia, is the oldest and one of the most significant steam-dominated geothermal fields in the country, managed by PT. Pertamina Geothermal Energy (PGE). Since the first exploration in 1918 by the Dutch East Indies government, the field has undergone extensive development, culminating in a current installed capacity of 235 MW. This paper evaluates the efficiency of reinjection processes in the Kamojang field, employing gas and isotope chemistry data collected since 2017. Reinjection is critical for maintaining reservoir pressure and ensuring sustainable production. Since 2019, reinjection has been conducted through 6 reinjection wells, However, wellbore issues have led to the cessation of reinjection in KMJ-21 and KMJ-55, reducing the number of active reinjection wells. This reduction requires efficient management strategies to optimize reinjection volumes and maintain reservoir stability.

The reinjection process will affect the composition of the production well fluid due to differences in the composition and temperature of the reinjection fluid compared to the reservoir fluid, ultimately altering the production well fluid. Therefore, monitoring these geoindicators, including isotopes and superheat, helps assess the effectiveness of reinjection in production wells and aids in optimizing reinjection strategies. The study concludes that while reinjection processes influence gas fractionation and isotope distribution in the Kamojang field, the reduction in reinjection wells has not yet led to matrix steam production. However, current reinjection levels are insufficient to prevent superheat increases, indicating the need for enhanced reinjection strategies. Continuous monitoring and targeted management are essential for optimizing reinjection efficiency and sustaining geothermal energy production in the Kamojang Geothermal Field.

1. INTRODUCTION

Kamojang Geothermal Field is located in Bandung and Garut Regencies, West Java Province. Owned by PT. Pertamina Geothermal Energy, it is the oldest geothermal field in Indonesia. This field is also one of the steam-dominated geothermal prospects in Indonesia. The first efforts to explore geothermal energy sources in Indonesia were conducted in the Kamojang Crater area by the Dutch East Indies government in 1918, with the drilling of five shallow wells. One of these Dutch exploratory geothermal wells, known as Kawah Kareta or well KMJ-3, which has a depth of approximately 60 meters, still emits steam to this day.

During the period from 1971 to 1979, a collaboration between Indonesia and New Zealand led to the drilling of 14 wells (KMJ-6 to KMJ-20) in the Kamojang Geothermal Prospect. The geothermal potential of Kamojang was proven to be viable for electricity generation, marked by the operation of a small-scale Mono Block turbine of 0.25 MW, utilizing steam from a single production well, KMJ-6. This Mono Block marked the initial momentum for the utilization of geothermal energy for electricity generation in Indonesia. The development period of Kamojang geothermal energy continued into the commercialization stage, signified by the commercial operation date (COD) of Unit 1 in 1983, with a capacity of 30 MW, followed by the COD of Units 2 and 3 in 1987, each with a capacity of 2 x 55 MW. This was achieved through a Steam Sale and Purchase Agreement (PJBU) business scheme between Pertamina and PT. Indonesia Power, a subsidiary of PLN.

Pertamina has continuously conducted further exploration to optimize the utilization of geothermal potential in Kamojang, successfully increasing capacity and constructing Geothermal Power Plant (PLTP) Unit 4 with a capacity of 60 MW in 2008 and Unit 5 with a capacity of 35 MW in 2015. These developments were implemented through a Total Project Electricity Sale and Purchase Agreement (PJBL) business scheme between PT. Pertamina Geothermal Energy (PGE) and PT. Indonesia Power. Thus, the Kamojang PLTP has been operating for more than 40 years and currently has an installed capacity of 235 MW with five generating units, supported by approximately 97 geothermal wells consisting of 63 production wells, 9 reinjection wells, 16 monitoring wells, and several abandoned wells.

Figure 1: Location Map of Kamojang Geothermal Field.

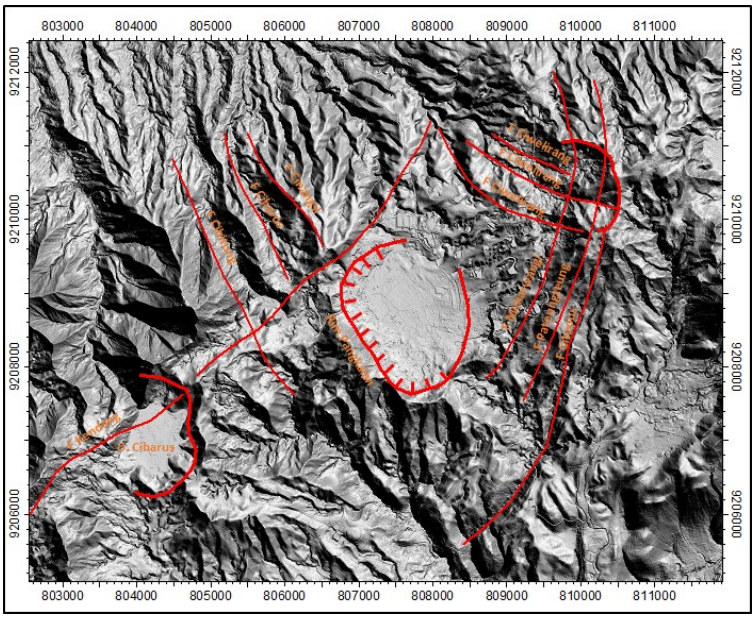

Figure 2: Geological Structure Map of the Kamojang Geothermal Field.

2. THE GEOLOGY OF THE KAMOJANG GEOTHERMAL FIELD

The Kamojang area is situated at the center of a volcanic mountain range oriented WestSouthwest-EastNortheast (WSW-ENE) Regionally, volcanic activity in this area has occurred since the Pleistocene era. Volcanic eruptions along fracture lines are associated with the WSW-ENE fault system. The sequence of volcanism from the oldest (WSW) to the youngest (ENE) includes Mount Rakutak, the Ciharus Complex, the Pangkalan Complex, the Gandapura Complex, the Masigit Complex, and the Guntur Complex. The reservoir rocks in the Kamojang Geothermal Field consist of interbedded pyroclastic and andesitic lava with some basaltic andesite and lacustrine tuff (Utami, 2000). Information from production wells indicates that the subsurface geology of the Kamojang Field is composed of altered andesite, altered pyroclastic rocks, and altered basaltic andesite, as demonstrated by the analysis of core samples and cuttings from the observed wells.

The geological structures in the Kamojang Geothermal Prospect are identified based on satellite image analysis, subsurface data from drilling, and geophysical measurements. Generally, the structures in Kamojang consist of:

- Circular collapse structures, such as the Pangkalan rim/caldera and other smaller circular structures seen at Lake Ciharus and around the summit of Mount Rakutak.
- The Ciharus Block Structure group, oriented NW-SE.
- Normal faults, oriented NE-SW to nearly north-south, including the Mekarwangi Fault, Citepus Fault, and Pateungteung Fault, located in the eastern part.
- The Ciwelirang normal fault, oriented NW-SE, located in the northern part of the Kamojang Geothermal Prospect.

In general, the wells drilled around the Pangkalan Caldera structure, the NW-SE normal fault structure in the Ciharus block, and the nearly north-south structures in the KWK area, such as the Mekarwangi Fault, Pateungteung Fault, and Citepus Fault, are productive wells. Good permeability in the younger NE-SW to nearly north-south faults is also indicated by the presence of massive manifestations such as craters, fumaroles, and hot springs in the NE area associated with these faults

3. GEOCHEMICAL CHARACTERISTICS OF KAMOJANG GEOTHERMAL FIELD

As previously mentioned, Kamojang is a steam-dominated geothermal field, so unlike two-phase fields, geochemical monitoring in this field is more focused on gas observations in wells. Sampling in Kamojang is conducted three times a year, and the analysis is carried out in the internal PGE laboratory located in the Kamojang area. In this paper, the discussion of geochemistry and monitoring of Kamojang will only use data obtained since 2017.

Kamojang itself has a relatively low gas/steam ratio, averaging less than 1% wt or 10,000 ppmW, and this ratio is evenly distributed throughout the Kamojang area. High NCG values are found in several wells at the edge of the field, assumed to be caused by condensation, and in the eastern part, assumed to be related to the production of fresh matrix steam with a higher gas content. The main gas composition in NCG in Kamojang is CO2, which reaches more than 80% dry gas, followed by H2S. This composition is not much different from other PGE-owned geothermal fields. In the ternary diagram plot of N2-Ar-CO2, the wells in the Kamojang field do not have magmatic influence because the plot position is not on the magmatic line and tend to originate from brine with neutral fluids.

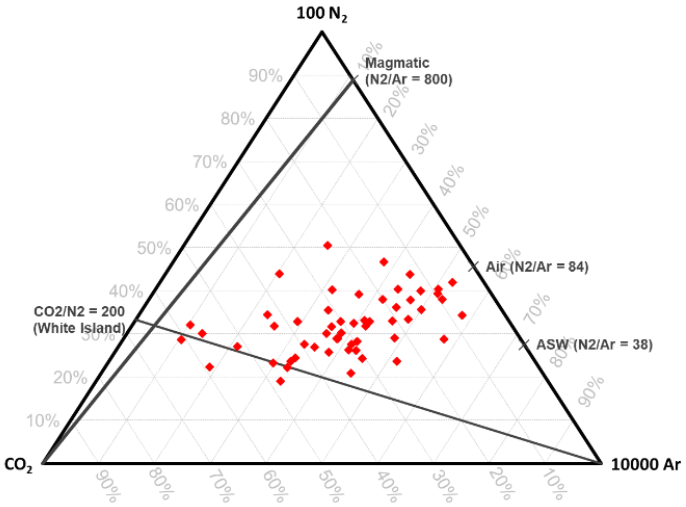

Figure 3: The ternary diagram of N2-CO2-Ar for production wells in the Kamojang field shows that the wells in the Kamojang area are not affected by magmatic fluids.

The manifestations of the Kamojang field consist of fumaroles and hot springs, mostly located in the northeast part and associated with the NE-SW to nearly north-south trending Pateungteung fault. Hot springs are also found on the rim of the Pangkalan caldera and in the southeast part of the Kamojang field. The hot spring manifestations in Kamojang consist of sulfate water and bicarbonate water. Bicarbonate water appears in the southwest (Ciharus) and southeast (Citepus) areas, assumed to be associated with the outflow zone. The Ciharus manifestation is associated with the Kendang Fault, and the Citepus manifestation is linked to the Kamojang recharge zone.

4. REINJECTION IN THE KAMOJANG FIELD

Since 2019, reinjection in the Kamojang Field has been carried out through 6 reinjection wells: KMJ-20, KMJ-21, KMJ-32, KMJ-35, KMJ-39, and KMJ-55, which are distributed throughout the Kamojang Field and are expected to cover the entire area. The fluid re-injected at Kamojang consists of condensate from the six power plants in the area, with the current total injection rate averaging around 4,000 liters per minute, or approximately 240 tons per hour. These reinjection wells are crucial for maintaining the overall mass balance within the Kamojang reservoir because vapor-dominated systems are characterized by tightly sealed reservoir boundaries, so the natural recharge of liquid tends to be minimal. Ensuring a balance between the fluid extracted and re-injected into the reservoir is vital to prevent excessive depletion in certain production zones, which could disrupt the long-term sustainability of the reservoir

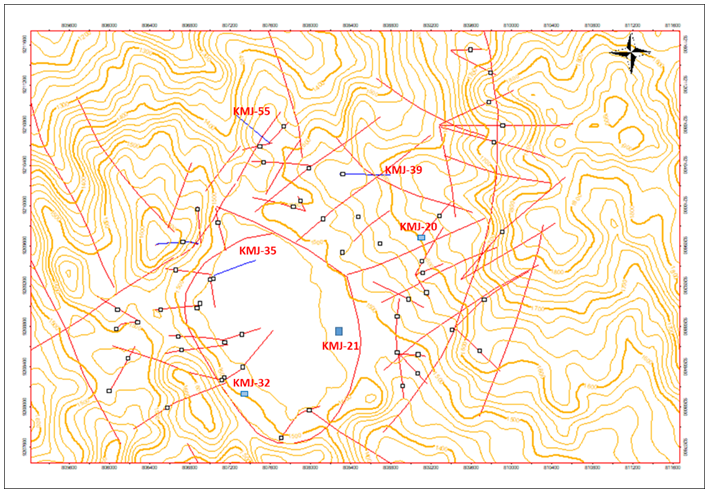

Figure 4: Map of Reinjection Wells in the Kamojang Geothermal Field.

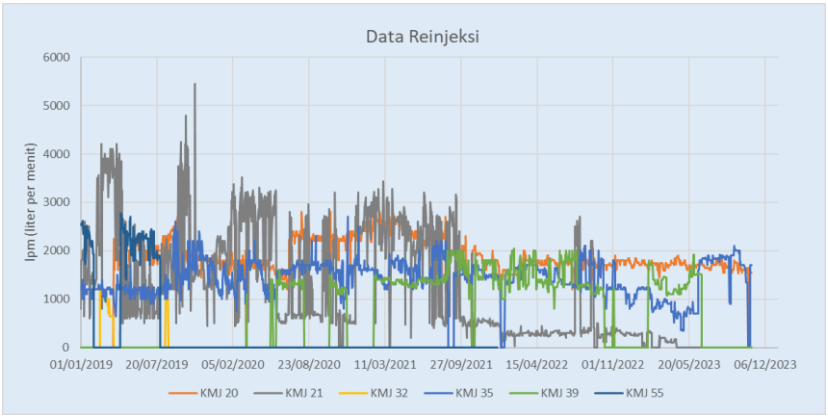

Figure 5: Graph of the reinjection volume of reinjection wells in Kamojang showing the dynamics of reinjection volume and the active reinjection wells in Kamojang from 2019 to 2023.

The dynamics of reinjection volumes in the Kamojang Field can be seen in figure 5. At the end of 2019, KMJ-32 and KMJ-55 stop operating due to wellbore issues as evidenced by their sudden drop to zero reinjection rates. Initially, KMJ-21 had the highest reinjection volume among all wells, but starting in 2021, its volume gradually declined due to wellbore problems that reduced the well's reinjection capacity. This trend is visible as a consistent decrease in KMJ-21's reinjection rate. Currently, the operating reinjection wells in the Kamojang Field are KMJ-20, KMJ-35, and KMJ-39 underscores the need for targeted management strategies to optimize reinjection efficiency and maintain reservoir pressure effectively.

5. GEOINDICATOR DYNAMICS DUE TO THE REINJECTION RETURN PROCESS

The reinjection process in geothermal fields significantly influences the chemical composition as well as chemical geoindicators, which are critical for understanding reservoir behavior. Reinjection of cooled geothermal fluids, especially condensate in steam-dominated geothermal fields, back into the reservoir not only helps maintain pressure but also affects various geoindicators such as temperature and chemical composition since condensate has a different chemical composition compared to the reservoir fluids. These changes can provide insights into the reservoir's response to reinjection, highlighting areas of enhanced permeability and potential thermal breakthroughs. Monitoring these geoindicators allows for the optimization of reinjection strategies, ensuring efficient resource utilization and long-term stability of geothermal energy production. In the Kamojang Geothermal Field, the strategic placement of reinjection wells and continuous monitoring of geoindicators are essential practices for maintaining reservoir health and optimizing energy output. With the reduction of reinjection wells in the Kamojang Field, monitoring these geoindicators becomes increasingly important to assess whether the remaining reinjection wells and their reinjection volumes are sufficient to maintain the Kamojang reservoir, or if the effects of the reduction in the number of reinjection wells have started to appear in Kamojang.

5.1 Superheat

Superheat occurs when the fluid's temperature exceeds its saturation temperature at a given pressure, specifically the pressure at the time of measurement. In a geothermal system, superheat conditions are assumed to arise when the reservoir is depleted of liquid, causing the existing steam to be continuously heated by a heat source above its boiling point. An increase in the superheat value of a well indicates a deficiency in reinjection mass. If this condition persists, the continuous loss of steam mass will result in a detrimental loss of pressure support. Additionally, superheat conditions can lead to various wellbore issues, including an increased risk of corrosion and scaling. Therefore, superheat is a crucial parameter monitored during geothermal field activities, especially in Kamojang. With the reduction in reinjection wells in Kamojang, superheat has become an essential indicator to determine whether a well is receiving sufficient mass from reinjection. Additionally, the overall adequacy of reinjection in the Kamojang field can be assessed by observing the trend of superheat over the years.

Superheat measurements have been carried out in Kamojang since 2016. The superheat measurements conducted are surface superheat measurements. This method is chosen because it is more efficient and can be performed periodically. Additionally, flowing PTS surveys were also examined to assess downhole superheat and compare it with wellhead superheat measurements. Generally, the review indicated that wellhead superheat data reasonably represented the level of superheat occurring in the field. Although monitoring has been conducted since 2016, the intensive increase in superheat began in 2019 and has continued to rise until now. The trend shows that the highest measured superheat values generally occur in the western and central areas of the field, which have experienced the longest production history and greatest pressure drawdown. The highest superheat observed is above 15 degrees. In 2021, superheat expanded to the southwestern part, even though this area contains the injection well KMJ-35, indicating that the support from reinjection fluids is no longer sufficient to maintain the reservoir in this zone. As of 2023, superheat in Kamojang has shown a continuously increasing trend, particularly in areas with superheat above 15 degrees, which has extended toward the northeast following the decrease in reinjection fluid volume in well KMJ-21. This indicates that the reduction in reinjection wells in Kamojang has had a negative impact on wells connected to the reinjection wells that have ceased operation.

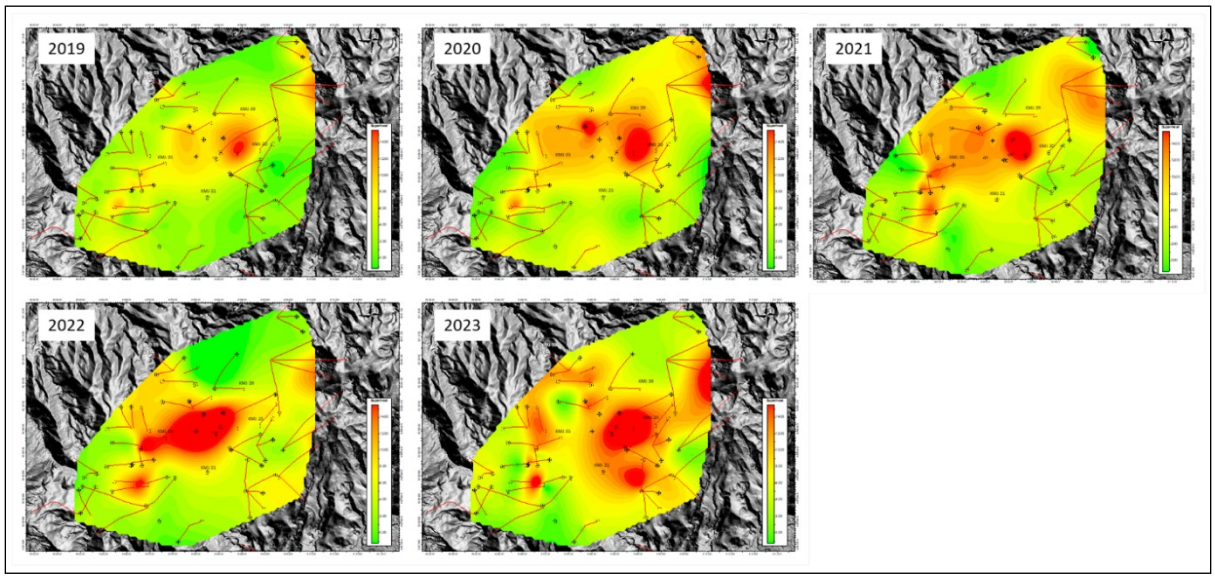

Figure 6:. Superheat Distribution Map in the Kamojang Geothermal Field. It is evident that over the years, the area affected by superheat has progressively expanded.

Unlike other parts of the field, the northeast area has a shorter production history. Additionally, due to the location of these wells along the structural alignment, it has resulted in low to moderate superheat production. The southeastern area of the field has the highest measured reservoir pressures and consistently shows some of the lowest observed superheat values in the field, typically less than 5 °C. The pattern of sustained low superheat values in the southeast supports the interpretation that this area may partly be producing fresh reservoir matrix steam from the east. Another area of sustained low superheat is observed in the southwestern margin of the field, which is likely related primarily to the influence of injection fluids and potentially minor recharge along the Kendang fault zone.

5.2 Gas Equilibrium

At equilibrium, concentrations of gases in reservoir steam and liquid are different because gases partition strongly into the steam. If reservoir liquid vaporizes during production and this steam mixes with the original reservoir

steam, gas concentrations in the mixture will not correspond to equilibrium in either liquid or steam (Truesdell, 1993). However, the fractionation of the original reservoir steam present in the produced fluid (represented as Y), which has mixed with vaporized liquid, can be determined by combining gas equilibrium and gas solubility equations on opposing axes. This approach not only provides the Y value but also determines the temperature of the fluid. The Y value, or fractionation, ranges from 0 to 1, where Y = 0 indicates that the entire sample originated from the boiling of reservoir liquid, while Y = 1 signifies that the sample represents pre-existing reservoir steam

In the Kamojang field, the steam fraction is calculated using the D'Amore gas geothermometer, which involves reactions where CH_4 and H_2O combine to produce CO_2 and H_2, a process known as the Fischer-Tropsch (FT) reaction and also the reaction where H_2 and H_2O combine with pyrite (FeS_2) to form H_2S and magnetite, represented as HSH. There are three equilibrium states considered in this reaction, known as HSH1, HSH2, and HSH3. However, in the Kamojang area, we will only use FT-HSH2, as it is the most applicable and provides the most accurate temperature readings for this field.

Based on the plot of the FT-HSH2 geothermometer grid, the Y values in the Kamojang field range from 0.02 (indicating fluids mostly composed of recently boiled liquid) to 0.3 (indicating fluids mixed with reservoir steam). Wells with the highest Y values are located in the southeast, which indicates more production of original matrix steam, in comparison to wells in the west and the early-developed central parts of the field, which yield lower Y values, indicating depletion of the original matrix steam and production from reservoir liquid. Additionally, the gas geothermometer values from the Kamojang wells can be determined, which range between 250-275°C.

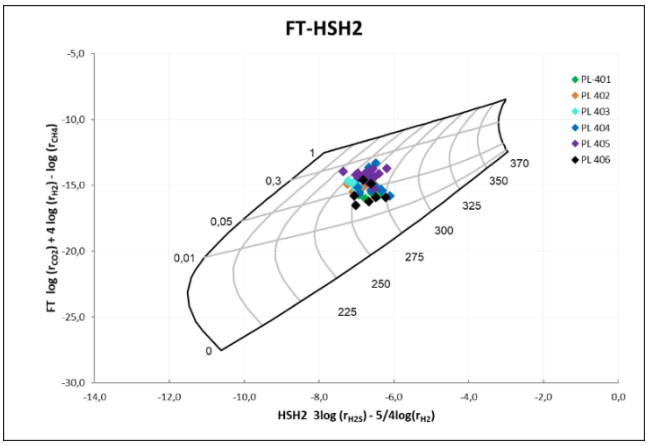

Figure 7: Gas geothermometer FT-HSH 2 for wells in Kamojang shows that the wells in Kamojang have varying Y values and temperatures ranging from 250 to 275°C.

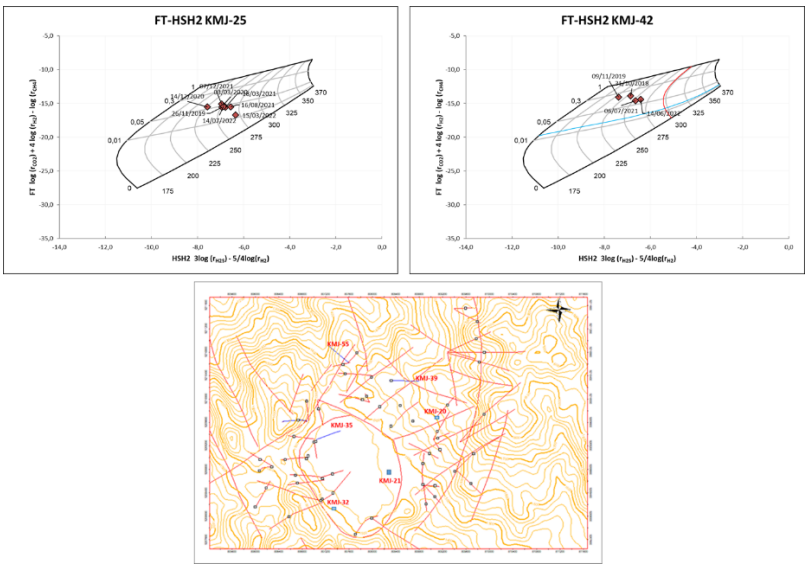

Figure 8: Geothermometer grid FT-HSH 2 from wells KMJ-42 and KMJ-25 experienced changes in gas fractionation throughout 2017-2023. These changes are assumed to be due to condensation, either by recharge fluid or reinjection condensate.

During the exploitation process, changes in Y values can occur due to the reinjection process, which causes the reinjection fluid to be produced in greater quantities, resulting in an increase in vaporized liquid and a decrease in the percentage of reservoir steam. Alternatively, the process of reservoir dry-up can reduce the vaporized liquid and make the original reservoir steam more dominant. Considering these factors, monitoring of Y values in the Kamojang Field is conducted to observe whether there are changes in these values in the wells in Kamojang.

Based on the monitoring results of all wells in Kamojang, only two wells exhibited a shift in Y values, indicating a change in gas fractionation in the produced wells, namely KMJ-42 and KMJ-25. In well KMJ-42, an increase in temperature was observed alongside a decrease in the Y value. This phenomenon is assumed to be caused by the production of more vaporized liquid, while the temperature increase itself can be attributed to the oxidation conditions of H2S. Well KMJ-42 is located on the western edge of the Kamojang Field, which is a recharge zone for this field, suggesting that the change in gas fractionation in this well is likely influenced by natural recharge.

In contrast, well KMJ-25 is not situated on the edge of the field but is very close to the injection well KMJ-39. The Y value in this well also experienced a decrease to 0.01, which is characteristic of a fluid mostly composed of recently boiled liquid. Additionally, the well's temperature showed an increase, attributed to the oxidation of H2S. Based on the analysis of this graph, it is assumed that well KMJ-25 is significantly influenced by the injection fluid from the nearby injection well, KMJ-39.

Apart from these two wells, there have been no significant changes in gas fractionation in the wells of the Kamojang Field, whether caused by condensation or the dry-out process. Therefore, it can be concluded that the reduction in the number of injection wells and the volume of injection fluid has not yet caused the wells in Kamojang to produce greater percentage of matrix steam.

5.3 NH_3

One of the key parameters for identifying injection returns is the trend of rising NH_3 levels in dry gas. This is also observed as an increase in NH_3 compared to less soluble gases like CO_2 and H_2S. The rise in NH_3 levels is linked to the increased production of boiled injection fluids. Due to NH_3's high solubility in liquid water, it is likely that some of this gas dissolves in condensing steam in the wellbore and then remains in the steam condensate as it cools at the surface before reinjection. Therefore, samples with a high proportion of "injectate" would exhibit higher NH_3 concentrations than the typical well fluid (Lowenstern, 1999).

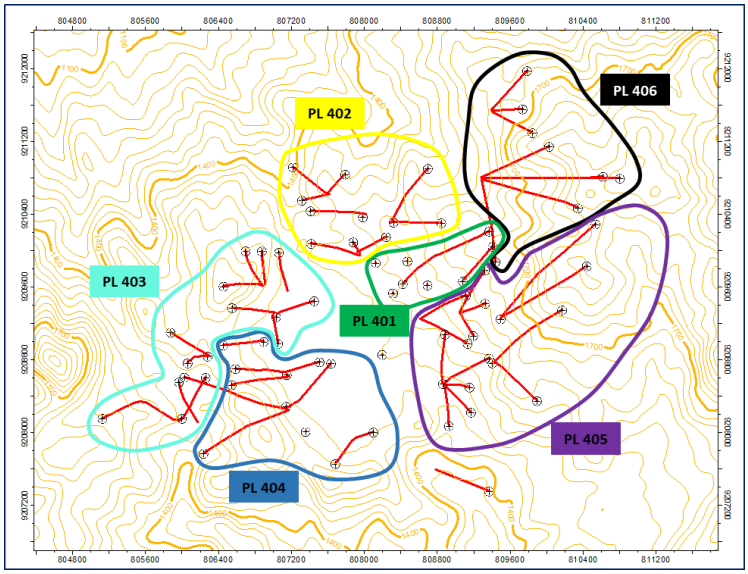

Figure 9: The wells in Kamojang are divided into several clusters based on the turbines they support. Unit PL 401, PL 402, PL 403, and PL 404 support PLTP Units 1, 2, and 3, while PL 405 supports PLTP Unit 4, and PL 406 supports PLTP Unit 5.

PL-402 wells exhibit the strongest signatures of injection-derived steam while wells in the PL-401 area, near the fumaroles and several injection wells, display a range of NH3 signatures. This suggests that wells in this region are sensitive to the injection strategy used for the numerous nearby injection wells. In the western part of the field (PL-403 and PL-404), wells show moderate to strong injection return signatures. This is expected due to the area's long production history and the lowest reservoir pressure. Many wells in PL-403 and PL-404 with more moderate NH3 signatures are offset from the Kendang fault, while those with the strongest NH3 signatures are located closer to the fault.

Wells in the PL-405 area, especially on the eastern side of the sector, show the lowest impact from injectate in the field, indicated by the lower NH3 distribution. Wells in PL-405 generally produce very low injection tracer returns. This is interpreted to be due to the higher pressures in the PL-405 sector. Tracer injected in wells on the boundary of PL-405 (such as injection well KMJ-21) might preferentially travels parallel to the primary NE-SW fracture direction, or towards areas of lower pressure once in the vapor state.NH3 signatures in PL-406 show two distinct clusters. Most wells exhibit stronger NH3 signatures, but two wells in the south end of the PL-406 sector (KMJ-88 and KMJ-89), which have a trajectory to the northeast, show distinctly lower NH3 signatures similar to those in the PL-405 area. This may be due to the proximity of KMJ-88 and KMJ-89 to the higher pressures in PL-405 and their location further off the structural strike from the injection wells. Based on NH3 monitoring, it can be determined that the reinjection fluid reaches the wells in Kamojang to varying degrees. Compared to the previously discussed superheat pattern, the NH3 signature shows a correlation between reinjection fluid and superheat values. PL-402, which has a high NH3 signature indicating a strong connection with the reinjection well, shows a lower degree of superheat compared to other areas. Similarly, PL-403 and PL-404 initially exhibited low superheat and high NH3 signatures, although superheat in these areas eventually increased. An exception occurs only in the PL-405 area, where the low superheat is more due to the support from the original matrix steam rather than reinjection support.

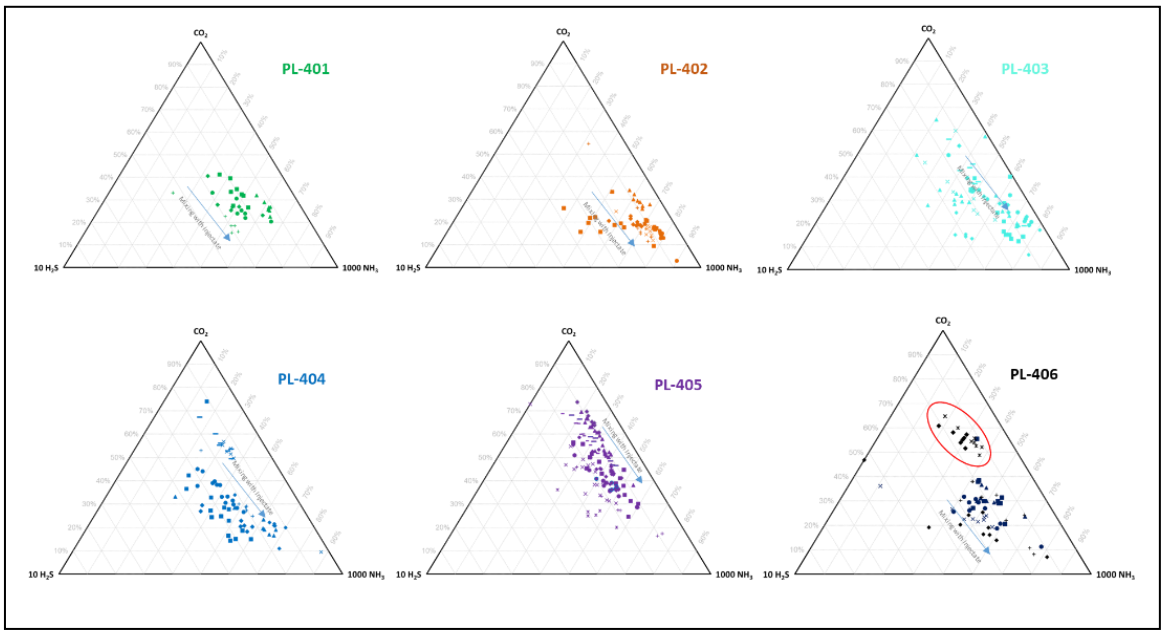

Figure 10: Ternary diagram showing the distribution of soluble gases including H2S, CO2, and NH3, with trends of increasing NH3 attributed to breakthrough of injection fluids. The red circles indicate wells KMJ-88 and KMJ-89, which have a slightly different pattern compared to other wells in PL-406 due to their closer proximity to the PL-405.

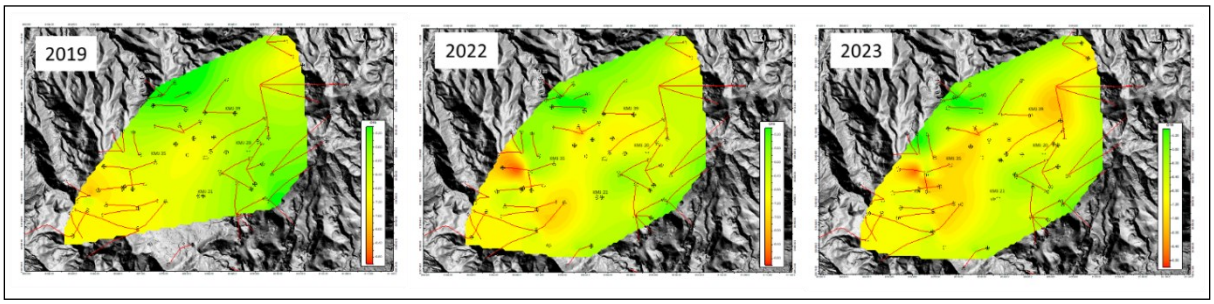

Figure 11: Isotope Distribution Map in the Kamojang Geothermal Field.

5.4 Isotope

Stable isotopes, particularly oxygen-18 (^{18}O), are valuable parameters for monitoring geothermal systems. This is because changes in stable isotope values can reflect the ongoing processes in geothermal fluids. It is well-known that the ^{18}O isotope in geothermal fluids tends to be more enriched compared to local meteoric water. This enrichment occurs due to water-rock interactions, where oxygen exchanges between rocks and fluids, leading to a higher concentration of the isotope in the liquid phase. When geothermal fluids mix with meteoric water, the

isotope values can be affected. Since meteoric water generally has lower ^{18}O values, any mixing would result in a lower ^{18}O value in the geothermal fluid compared to its original value. In addition to natural recharge mixing, reinjection breakthrough is another factor influencing isotope values. The reinjection water, typically condensate from the cooling tower, has undergone evaporation, making its isotope values highly enriched. If a well is affected by reinjected fluids, its ^{18}O isotope values will be significantly more enriched compared to surrounding wells. Given these characteristics, stable isotopes are essential parameters in the geochemical fluid monitoring process conducted in the Kamojang Area.

Generally, the ^{18}O isotope patterns in the Kamojang Geothermal Field for the years 2019, 2022, and 2023 are closely related to the active injection wells at the time the data was collected. The ^{18}O isotope pattern in 2019 differs slightly from that in 2022, with the central part of the field appearing more depleted than in the following years. This difference is because the injection well KMJ-39, located in the central part of the field, only began operations in 2020, and the enrichment pattern only becomes apparent in the maps for 2022 and 2023. Based on the ^{18}O isotope distribution maps above, it is evident that enriched isotopes are present in wells with good connectivity to the injection wells, while depleted isotopes are found on the edges of the field, associated with a supply of fluid more depleted in isotopes, such as natural recharge or areas not connected to the injection wells. Additionally, the isotope patterns in the Kamojang field also seem to correlate with the superheat pattern, where areas with enriched isotopes, such as PL-402 in the northwest, PL-405 in the southwest, and areas around the injection wells, also have lower superheat compared to surrounding areas. In contrast, areas with depleted isotopes, such as the central part of the field, also correlate with higher superheat values. An exception occurs in the western and southwestern parts, where depleted isotopes correlate with recharge influence associated with the Kendang fault. From this observation, it can be concluded that the ^{18}O isotope can be used to monitor the reach of reinjection fluids in the wells of Kamojang, as it closely matches the superheat pattern in this field.

5. CONCLUSION

Superheat measurements indicate a significant increase beginning in 2019, with the highest values observed in the western and central areas, correlating with prolonged production and substantial pressure drawdown. Superheat values have continued to rise, particularly in areas with superheat above 15 degrees, which has extended toward the northeast following the decrease in reinjection fluid volume in well KMJ-21. This suggests that the reduction in reinjection wells in Kamojang has negatively impacted wells connected to the reinjection wells that have ceased operation.

However, based on gas equilibrium, this has not yet caused the Kamojang wells to produce higher matrix steam, indicating that the Kamojang reservoir can still support field exploitation. The connectivity between reinjection wells and production wells is actually quite good, as evidenced by monitoring of NH3 and 18O isotopes, which shows a strong correlation between some areas and reinjection wells, marked by a strong NH3 signature and enriched isotopes in the PL-402, PL-401, PL-403, and PL-404 areas. Nevertheless, these areas have still shown an increase in superheat, indicating that the rise in superheat is more likely due to a lack of reinjection fluid rather than poor connectivity with reinjection wells.

REFERENCES

Beall, J.J., NH3 as a natural tracer for injected condensate: *Geothermal Resources Council Transactions*, v. 17, p. 215-219 (1993)

D'Amore, F., and Truesdell, A.H., Calculation of geothermal reservoir temperatures and steam fraction from gas compositions: *in* 1985 *International Symposium on Geothermal Energy: Geothermal Resources Council Transactions*, v. 9, pt. 1,p. 305-310. (1985)

Lowenstern, J.B., Janik, C.J., Fahlquist, L.S., and Johnson, L.S.: *Gas and Isotope Geochemistry of 81 Steam Samples from Wells in The Geysers Geothermal Field, Sonoma and Lake Counties, California*, U.S.A., U.S. Geological Survey Open-File Report 99-304 (1999)

Klein,C.W.,Enedy,S.,Butler.S.J., and Morrow,J.W.:Injection Returns and Evolution of Non-Condensible Gases at the NCPA Geysers Wellfield,California, *GRC Transactions*, Vol 33 (2000)

Powell, T.: A Review of Exploration Gas Geothermometry, *Proceedings, 25th Workshop on Geothermal Reservoir Engineering*, Stanford University, Stanford, CA (2000)

Thermochem Indonesia, PT.: Capacity of the Kamojang Geothermal Reservoir to sustain PT Pertamina Geothermal Energy's Development Strategy, *Confidential report*,2022

Truesdell, A., Enedy, S., and Smith, B.: Geochemical Studies of Reservoir Processes in the NCPA Field of The Geysers, *Proceedings, 18th Workshop on Geothermal Reservoir Engineering*, Stanford University, Stanford, CA (1993)

Truesdell, A.H., Box, W.T., Jr., and Haizlip, J.R., 1987, A geochemical overview of The Geysers (California) geothermal reservoir, *in* M.K. Horn, ed., *Transactions 4th Circum-Pacific Energy and Mineral Resources Conference*, Singapore, August 1986, p. 487-499 (reprinted *in* C. Stone, ed., 1992, Geothermal Resources Council Special Report Number 17, p. 121-132.).

Truesdell, A.H., and White, D.E., Production of superheated steam from vapor-dominated geothermal reservoirs: *Geothermics*, v. 2, p. 154-173 (1973)

Utami, P.: Characteristics of the Kamojang Geothermal Reservoir (West Java) as Revealed by Its Hydrothermal Alteration Mineralogy, *Proceedings, 25th Workshop on Geothermal Reservoir Engineering*, Stanford University, Stanford, CA (2000)

3D Density Change Model to Support Well Targeting in Steam Cap Area: A Case Study on the Salak Geothermal Field, Indonesia

Azizatun Azimmah, Muhamad Wildan Perdana, and Yudi Indra Kusumah

PT. Star Energy

Azizatun.Azimmah@starenergy.co.id

Keywords: Density change model, Microgravity inversion, geophysics, geothermal

ABSTRACT

Geothermal well targeting can be challenging due to the unpredictable nature of subsurface conditions, which may lead to drilling unproductive wells. To address these uncertainties, implementation of advanced technology and refinement of subsurface models are essential. This study aims to highlight the possibility of using a density model based on gravity data measurement to improve the targeting of geothermal makeup well drilling, particularly when aiming for steam cap reservoir. Implementing this method is expected to increase efficiency and cost-effectiveness, as demonstrated in the Salak field.

Microgravity/precision gravity has been measured in Salak from 1994 to 2020 for routine reservoir surveillance conducted every 3 to 4 years. Our methodology involved refining Free Air Gravity (FAG) measurements using radial basis functions and applying microgravity inversion techniques to develop density change models spanning from 2005 to 2020. Reservoir boundaries and water level elevation data serve as constraints for the microgravity inversion process. Outside the designated reservoir boundary and beneath estimated water levels, adjustments during microgravity inversions were limited, allowing only for minor perturbations. It is believed that the detectable density changes observed by microgravity surveys primarily originated from fluid phase alterations in two-phase geothermal fields induced by geothermal exploitation activities.

To effectively target wells, it's important to identify the "sweet spots" within the reservoir. This requires combining data on reservoir properties with a conceptual understanding of the reservoir itself. One of the important “sweet spots” characteristics in targeting steam cap reservoir is steam cap distribution. The distribution of steam cap can be obtained from the Pressure Temperature (PT) dataset but limited spatially to the distribution of existing wells in Salak. The density change model generated based on microgravity inversion can be useful in areas where there is high uncertainty due to lack of PT data. By interpreting gravity decline, which is largely due to density changes resulting from the development of the two-phase zone in Salak, the 3D density change model can identify areas of steam cap development, delineates zones with potential interconnected fractures and relatively favorable mass depletion rate. Such insights are pivotal for guiding decision-making processes regarding the targeting and development of steam wells in Salak Field. This model has also been shown to have good correlations with steam cap pressure, well production/injection data, and tracer test results, which validates its accuracy and reliability.

1. INTRODUCTION

The Salak geothermal field, with an installed capacity of 381 Mwe, is located in West Java, Indonesia, approximately 70 kilometers south of Jakarta (Figure 1). This location places the field within a region known for its geothermal potential due to its tectonic and volcanic activity. The geothermal field benefits from this geologically active setting, which is conducive to the development of geothermal resources. The Salak field has been in operation for 30 years, making it one of the longest-running geothermal projects in Indonesia. During these three decades, the field has undergone numerous development and optimization efforts to ensure its productivity and sustainability.

The Salak geothermal system is a high-temperature water-dominated reservoir with benign chemistry and low-to-moderate NCG content (Acuña et al., 1997). With its 30 years of operation, the Salak reservoir currently shows distinctive attributes across its eastern and western sectors: Eastern Salak region is noticeably characterized by a developed steam cap zone allowing most of the producing well in this region to be steam dominated, whereas western Salak area is characterized by liquid-dominated production wells.

The process of managing the reservoir to sustain the required generation possesses challenges, particularly in geothermal makeup well targeting. The main challenge is the unpredictable nature of subsurface conditions, which can lead to the drilling of target wells that do not yield the expected result. Addressing these challenges requires the integration of advanced technology and more reliable subsurface models. Modern advancements in

geophysical methods, data processing, and computational modeling offer new approaches to better understand and estimate subsurface conditions.

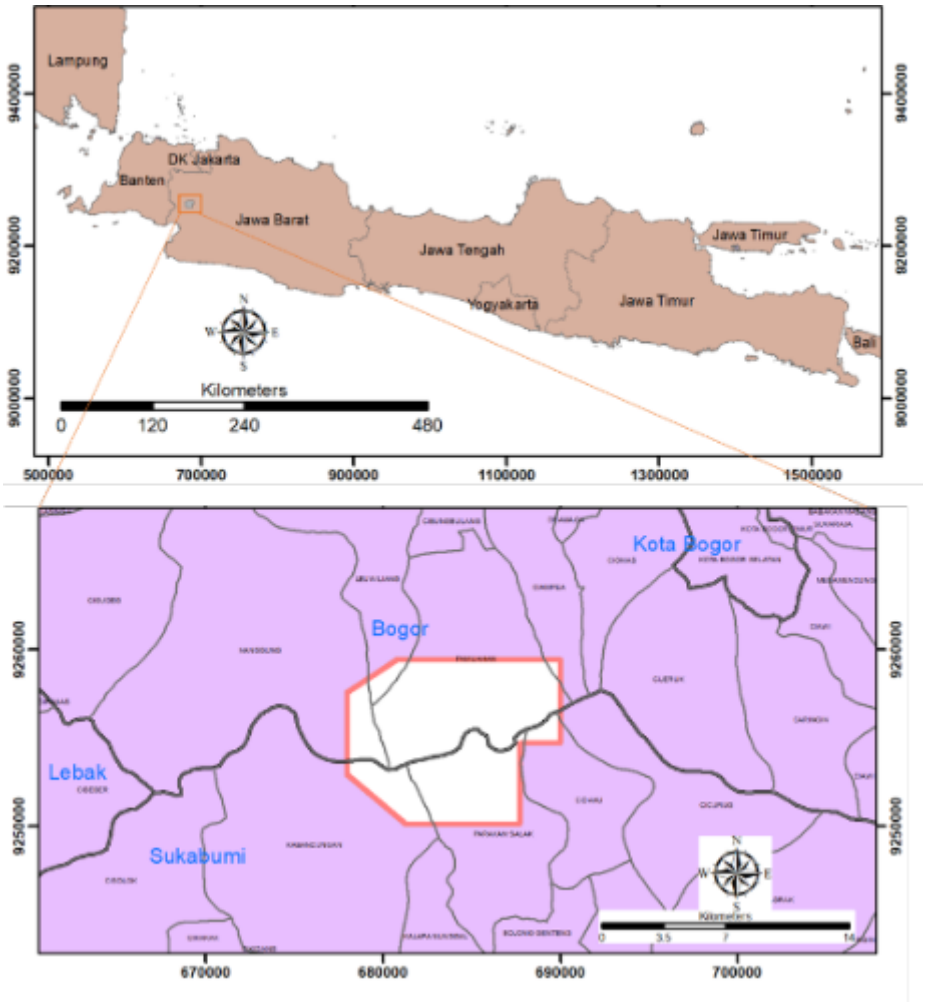

Figure 1: Location of Salak Geothermal Field Working Area (within red polygon).

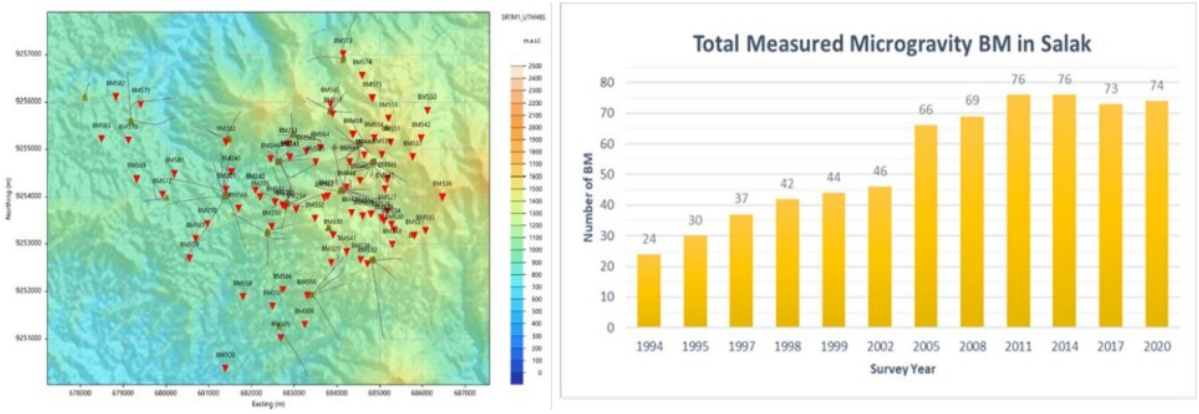

Figure 2: Benchmarks location in Salak Field (left) and the number of measured BM in each survey (right).

One of common geophysical techniques for reservoir monitoring is precision gravity and leveling survey which aim to measure subtle changes in the Earth's gravitational field inferring the changes in the reservoir net mass over particular time intervals. This survey is conducted by measuring variations in the Earth's gravitational field at distributed surface points called benchmark or BM (Figure 2) (CGG, 2021), revealing changes in subsurface mass distribution. Such variations are particularly useful in geothermal fields, where the extraction and reinjection of fluids can cause changes in subsurface density. From 1994 to 1999, precision gravity and leveling survey were

conducted annually, however since then, considering the rate of changes in the measured gravitational acceleration, the interval was optimized to be conducted every 3-year interval (Figure 2).

This study investigates the potential of using a density model to support the targeting of geothermal makeup well drilling, with a focus on steam cap well target. By refining subsurface models with detailed density data, this study aims to reduce uncertainty in well placement, thereby increasing the likelihood of intersecting productive zones and optimizing resource extraction.

2. METHODOLOGY

The methodology employed in this study involves refining Free Air Gravity (FAG) measurements, performing 3D inversion on the microgravity data and interpreting the inverted density change model. FAG measurements provide initial gravity data corrected for the elevation of the measurement point. In this study, Radial Basis Functions (RBF) were utilized to smooth the FAG data, minimizing the effect of outliers.

Following the refinement of the FAG data, microgravity inversion techniques were applied to develop detailed three-dimensional density change models. Microgravity inversion process inverts surface gravity measurements into subsurface density distributions. The 3D modeling mesh is of regular 100m x 100m x 100m cell size extending from 1,600 to -4,100 mASL elevation. A homogeneous density changes values of zero is used as the starting model (CGG, 2021).

For time windows of density change models, it was decided to use the delta density during 2005–2020 and 2011–2020 for investigation. The 2005 and 2011 surveys are used as baseline for these two time-windows, respectively, in accordance with BMs number and distribution.

To ensure the accuracy of the density change models, several constraints and assumptions were incorporated. Reservoir boundaries and elevation of steam-water contact in the reservoir were used as primary constraints during the inversion process. Outside the designated reservoir boundary and below estimated water levels, adjustments during microgravity inversions were limited to minor perturbations. The primary driver of the detectable density changes observed in the Salak field is believed to be fluid phase changes within the two-phase geothermal reservoir. As a typical two-phase system, Salak reservoir consists of both liquid and steam zone. The extraction, injection, and natural recharge processes in a producing geothermal field can lead to changes in the proportions of liquid and steam phases, altering the overall density of the reservoir rocks. These changes in density are detectable at the surface using sensitive gravimetric instruments. In the Salak field, the observed density changes are thought to be induced by geothermal activities, such as fluid extraction and reinjection, which alter the distribution and behavior of fluids within the reservoir.

The interpretation of the model includes how density change model correlates with other data, validate whether this model supports previous findings from other studies in Salak and how to utilize this model to support well targeting.

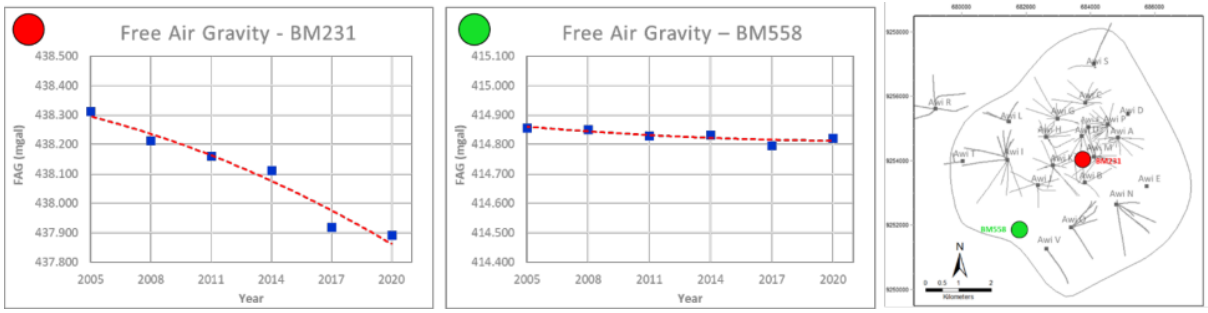

Figure 3: FAG trend overtime in region impacted by Salak production activities (BM 231) and region with minimum impact from Salak production activities (BM558).

3. RESULTS AND DISCUSSION

The observed decline in gravity measurements within the Salak geothermal field has been interpreted as a result of density changes primarily associated with the development of a two-phase zone. The development of such zones typically leads to a reduction in liquid saturation within both the rock matrix and the fracture network which decreases the overall density of the subsurface materials and eventually detectable as a decline in gravity measurements. In Salak Field, highest gravity decline is observed in BM 231 (Figure 3) which is located in the center part of reservoir between Awi M and Awi B pad. This part of the field is presumed to experience largest reservoir compaction due to continuous mass extraction from Salak producing wells. In contrary, BM that is

located far from production area, BM558, very low decline in FAG was observed suggesting no significant impact from Salak production.

Figure 4 and Figure 5 show density change occurring in Salak at 200 mASL. Over time, the density evolution model delineates three distinct zones: (1) areas characterized by a decrease in density attributed to production activities such as mass extraction leading to phase changes denoted by blue to red region in the map (e.g., water to steam, generally occurred in shallow reservoir section), with minimal influence from mass recharge sources; (2) areas exhibiting a slight increase in density due to the influence of mass recharge sources, notably injection activities and marginal recharge processes involving mass influx and cooling (denoted by greyish region in the map); and (3) areas where no density change is observed (denoted by white region). The latter is presumably associated with the following reasons: the absence of phase changes, insufficient extraction or recharge to change the density, resultant of both extraction and recharge nullifying each other's impact, other reason would possibly be related to data unavailability due to the lack of BM in this region. Understanding the reservoir process happening in Salak would assist in determining the more accurate explanation when interpreting this region.

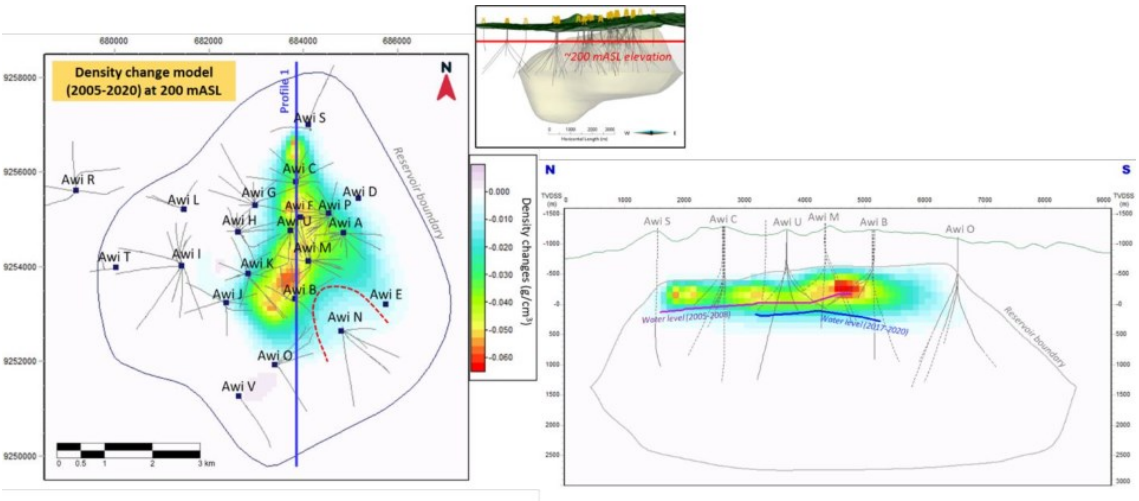

Figure 4: Density change between 2005-2020 at 200 mASL elevation and the north-south cross section relative to water level from different period.

Density changes model between 2005 and 2020 is shown in Figure 4. The most significant density decline occurred near AWI M and AWI B, likely due to continuous extraction since the early stages of production in the eastern part of the Salak field. Another substantial decrease in density is observed in the northern area following extraction from AWI C wells. The widespread density decrease in the eastern, northern, and central production wells of Salak indicates that mass extraction exceeds recharge rates, thereby could not sufficiently compensate for the total mass loss produced by the wells.

Between 2011 and 2020 (Figure 6), the most significant and noticeable decline in density occurred in the northern part of the Salak field near AWI C. The relationship between high mass extraction rates and density changes was also examined (Figure 7). Analysis of cumulative extracted mass during 2011-2020 indicates that AWI C extracted a greater amount of mass compared to other well pads. However, despite the high cumulative production, AWI A and AWI P exhibit relatively low-density changes. This anomaly suggests that well AWI A and AWI P receives substantial pressure support from potentially marginal recharge and injection breakthrough from the southeast injectors, specifically from wells AWI N and AWI O, which mitigate the density reduction that would typically accompany high mass extraction.

These findings signify the sensitivity of the density model to the field's operational dynamics. In both models, the decrease in density does not extend westward in Salak, as the impact of production from western wells was counterbalanced by additional mass injection from AWI I. Furthermore, a distinct "bent feature" (red dashed line) observed in the southeastern part of Salak suggests two possible causes: impact from injection operations at AWI N and O, and/or the absence of production wells in that specific area. Tracer tests conducted in Salak (Figure 7) confirm the occurrence of injection breakthrough from injection wells reaching and affecting production wells in the field.

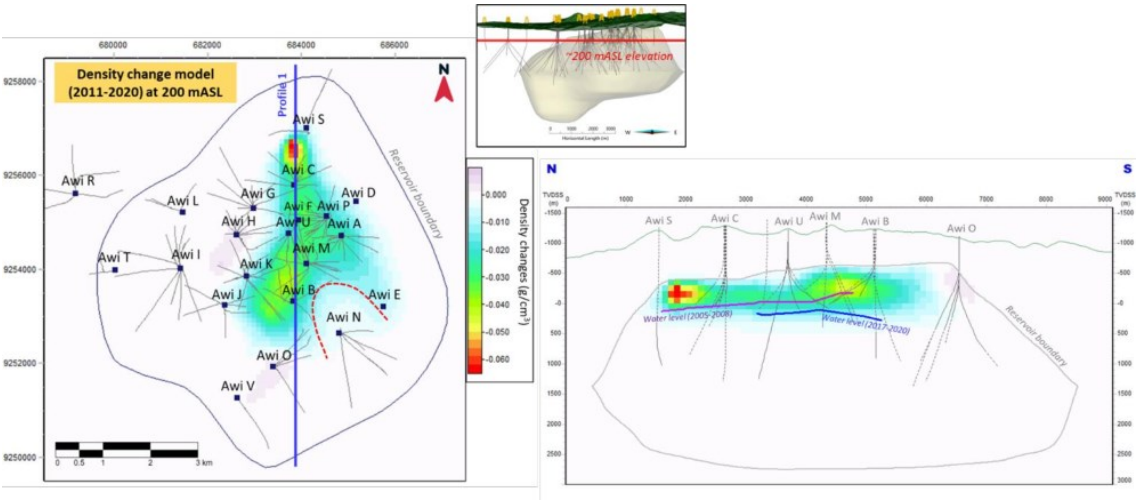

Figure 5: Density change between 2011-2020 at 200 mASL elevation and the north-south cross section relative to water level from different period.

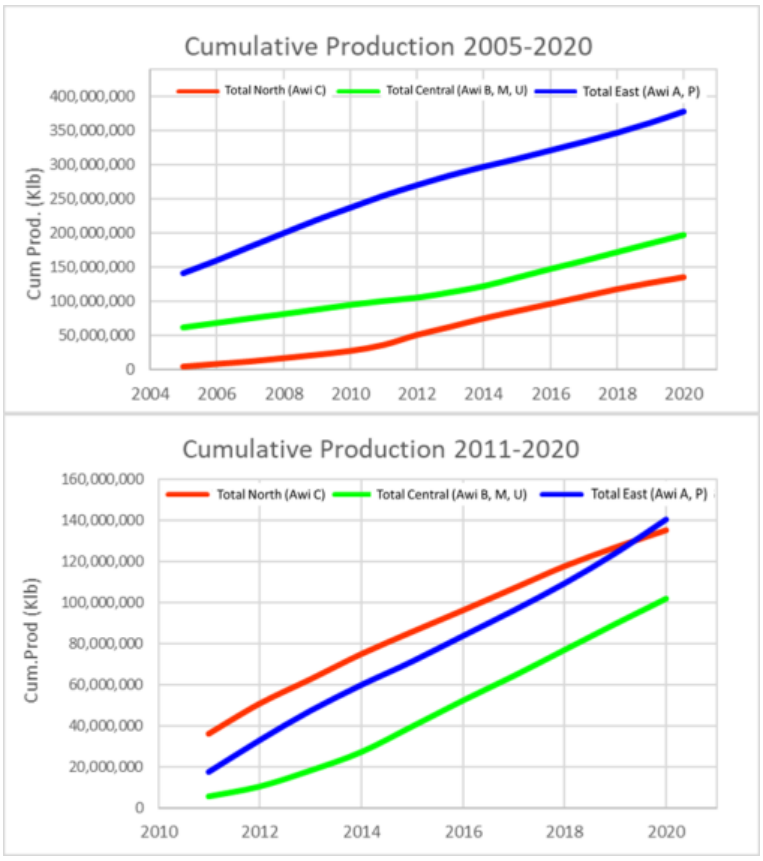

Figure 6: Total cumulative production of Pad Awi C (northern part of reservoir), Pad Awi B, M, U (central part of reservoir) and Pad Awi A, P (eastern part of reservoir) within different time windows.

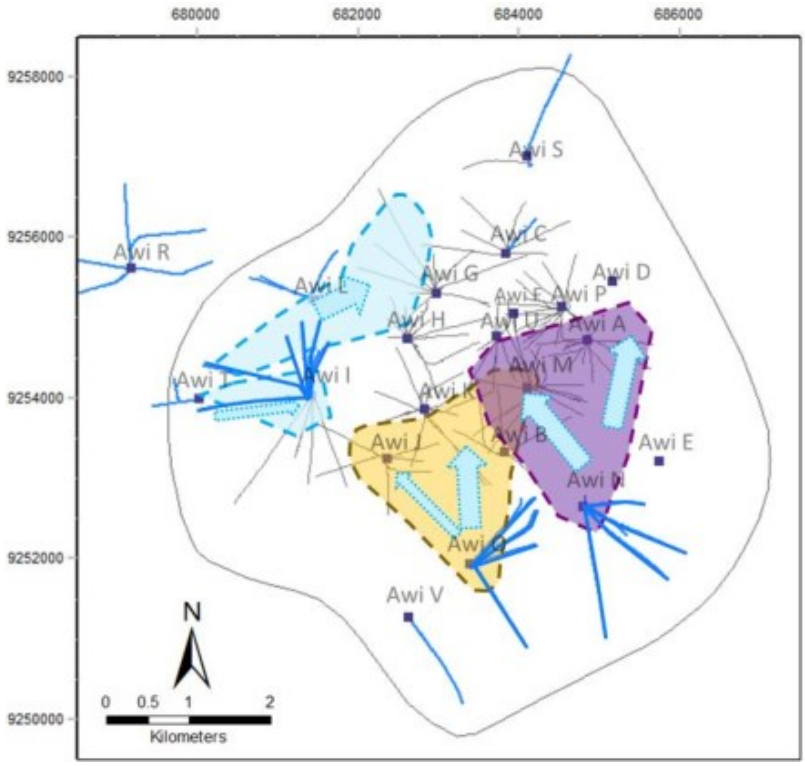

Figure 7: Illustration of 2009 Salak Tracer Test study results, modified from Abdurrachman et., al. (2014).

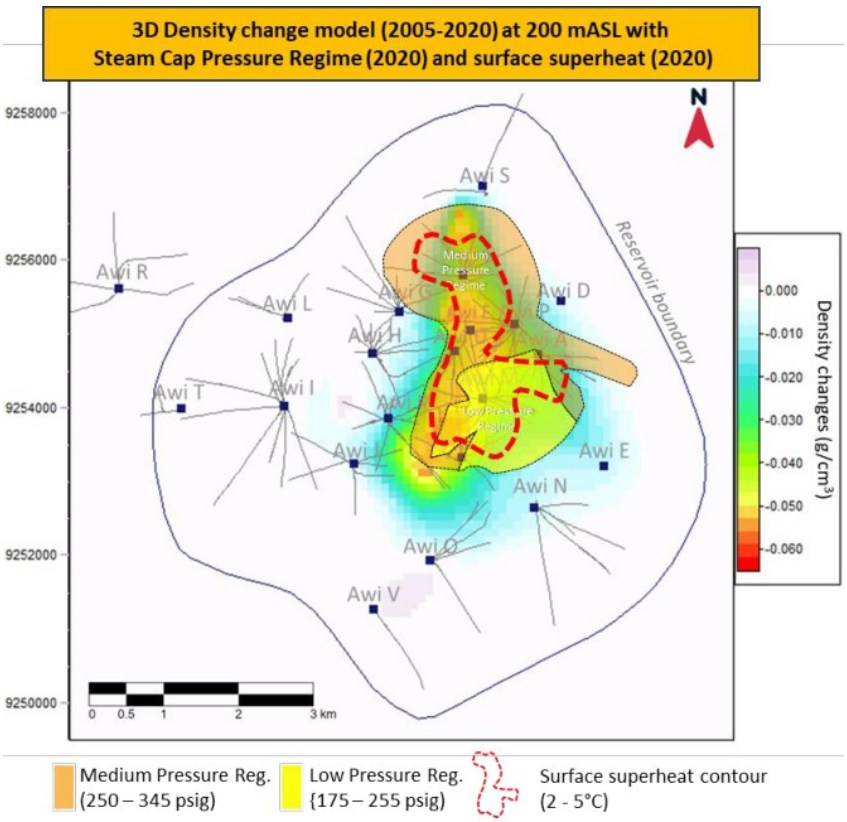

Figure 8: Density change model relative to steam cap pressure regime and surface superheat data in Salak.

Negative density changes observed through microgravity surveys exhibit a strong spatial correlation with areas subjected to steam cap pressure regimes and recorded surface superheat (Figure 8). The maximum observed changes in density are notably located within zones identified as having low and medium steam cap pressure

regimes, indicating significant fluid extraction and phase change activities in these areas. The surface superheat map identifies areas where surface temperatures exceed their saturation levels. Although not perfectly aligned, these regions of surface superheat correspond fairly with the areas showing density decreases as detected by density model. Confirmation of these correlations requires the availability of downhole superheat data.

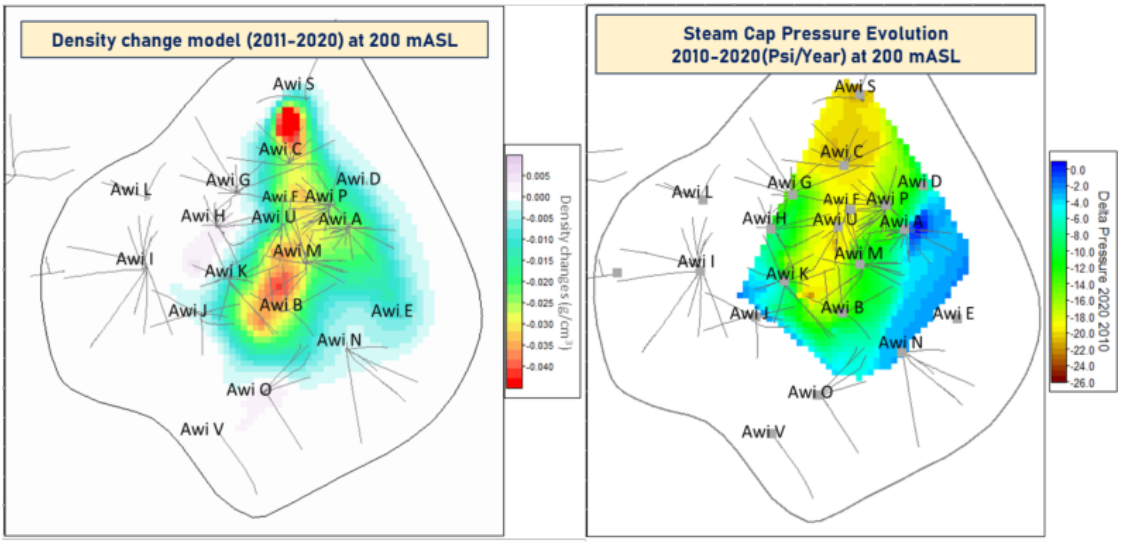

Figure 9: Density change model in comparison with steam cap pressure evolution showing relatively similar trend.

Further analysis of density changes over a shorter period, specifically from 2011 to 2020, reinforces the observed correlation between density changes and steam cap pressure evolution (Figure 9). The comparison suggests that the areas experiencing the most significant density reductions correspond well with the regions undergoing steam cap pressure evolution from numerical model. The density change model shows good correlation, in which during 2010 to 2020, steam cap pressure decline map shows major decline in both Awi C and north of Awi B.

Effective geothermal well targeting necessitates the identification of "sweet spots" within the reservoir. These zones are particularly favorable for drilling due to their high permeability, pressure, and temperature conditions. Identifying these zones requires a combination of detailed data on reservoir properties and a robust conceptual understanding of reservoir dynamics. One of the critical characteristics of these sweet spots, especially when targeting steam cap reservoirs, is the distribution of the steam cap itself.

Data on steam cap distribution can be derived from various sources, including Pressure Temperature (PT) datasets. PT data provide valuable information on the pressure and temperature conditions within the reservoir, which can be used to infer the presence and extent of steam caps. The density change model generated from this study is particularly useful in areas with high uncertainty due to a lack of direct PT data. With the help of density change models, a more comprehensive representation of areas where steam caps are likely to be present in the reservoir can be generated.

Regions exhibiting significant decreases in density are presumed to denote highly productive areas with extensive interconnected fractures. These areas have experienced substantial fluid extraction, leading to a pronounced reduction in subsurface mass. Such regions are typically less impacted by injection or marginal recharge (IB/MR), making them prime targets for further development. The higher density decrease in these zones indicates their potential for sustained production due to the presence of a well-connected fracture network facilitating efficient fluid flow. Nevertheless, targeting areas for makeup well should always consider the sustainability of targeted well production. Avoiding areas with highest density decline but still showing interconnected fracture to promote sustainability and balance out the extracted region would also be a good option to consider.

Areas with increasing density features should be approached with caution as they are potentially impacted by mass recharge sources, including injection and marginal recharge. The increased density in these areas suggests that the natural or artificial recharge processes are replenishing the reservoir, which may hinder the steam cap development.

It is important to note that areas lacking significant density decreases do not necessarily indicate an absence of productive potential or interconnected fractures. Such regions might still possess the capability to become productive but may currently exhibit less extraction activity or be influenced by mass recharge processes. The

presence of less density decrease could be attributed to lower extraction rates, indicating that the area has not yet reached its full production potential.

4. CONCLUSION

The insights gained from this study suggest that the density change model could serve as a robust indicator for identifying steam cap development areas, delineating zones with potential interconnected fractures and relatively favorable mass depletion rate. Such insights are pivotal for guiding decision-making processes regarding the targeting and development of steam wells in Salak Field. This model has also been shown to have good correlations with steam cap pressure, well production/injection data, and tracer test results, which validates its accuracy and reliability.

REFERENCES

Abdurachman, F., Aprilina, N.V., Hernawan, A., Kusumah, Y.I., Libert, F., Nelson, C., Paramitasari, H., Pasaribu, H., Putra, F.J., Ryder, A., Satya, D.Y., Simatupang, C., Tanuwidjaja, R., Wicaksono, S., Golla, G., Rejeki, S.; *2014 Salak State of the Reservoir*. SEGS In-House Report, October 15 (2015).

Acuña, J.A., Stimac, J., Sirad-Azwar, L., Pasikki, R.G.: Reservoir Management at Awibengkok Geothermal Field, West Java, Indonesia, *Geothermics* (2008).

CGG Electromagnetics (Italy): *4D Inversion Modeling of Microearthquake Monitoring and Time-lapse Gravity in Salak Geothermal Field*, Project Final Internal Report (2021).

Resource Assessment of Papandayan Geothermal Field, West Java, Indonesia

Winnie Tandri Alia, John O'Sullivan, and Michael Gravatt

Department of Engineering Science, The University of Auckland, Private Bag 90210, Auckland, New Zealand

tandrialia@gmail.com

Keywords: Geothermal, Papandayan, 3D Geological Model, Conceptual Model, Reservoir Numerical Modelling, Natural State Model, Uncertainty Quantification, Resource Assessment

ABSTRACT

Papandayan geothermal field in West Java is one of Indonesia's Geothermal Field with a mean estimated potential output of 21 MW. An assessment of the Papandayan resource using a new numerical model including uncertainty quantification is presented in this study. Following the method developed by the Geothermal Institute at the University of Auckland, a new 3D geological model was constructed based on public sources and data from The Directorate-General of New Renewable Energy and Energy Conservation in Indonesia (EBTKE). The construction of the 3D geological model involved the integration of geology, geophysics, geochemical and spatial data through Leapfrog Energy. The 3D geological model illustrates the aspects such as the geological structures, rock types, water level and thermal features. Using an integrated modelling approach, the new digital conceptual model was used to create a new reservoir model following best practices.

The natural state model was simulated using both AUTOUGH2 and Waiwera to assure compatibility with industry standard TOUGH2 while also enabling quick calibration and uncertainty quantification through cloud computing. To calibrate the model, the permeability distribution of the rocks and the deep flow boundary condition are adjusted. For uncertainty quantification, a large number of models (1000 samples) were generated and run. The parallelized geothermal simulators like Waiwera which was developed by the University of Auckland in cooperation with GNS science (Croucher A. , et al., 2020) can accelerate this process dramatically. The next step is to condition each natural state model using the temperature distribution based on the clay cap and applying an Approximate Bayesian Computation Method (ABC). Once the ensemble of models had been filtered, a novel method was used to run maximum potential scenarios for each model. in this research, future production assumed a binary power plant for 25 years. The results of this resource assessment give the mean estimate (P50) of net power output potential for Papandayan at 18.5 MW, the P90 at 12.3 MW and the P10 at 28.4 MW.

1. INTRODUCTION

Geographically, Mount Papandayan is a stratovolcano that rises from 1,100 to 2,665 meters above sea level. The site is at 107.44'00" east and 7.19'00" south between Bandung and Garut District, West Java province. The last eruption of Mt Papandayan was in 2002, making it an active volcano. (Sulastri et al., 2014). Papandayan geothermal studies started in the late 1990s with geology and geochemistry research. The study covered lithology mapping, geologic structure, and alteration. Additionally, it involved locating, collecting, and examining fluid from thermal features (Nasution, 2008). Thermal features include solfataras, fumaroles, mud pools, steaming ground, hot springs, and large alteration zones, ranging in temperature from 55 to 260 °C, mostly being SO_4-type waters (Nasution, 2008). Several Geophysical surveys have been conducted to complement geothermal studies, as recorded in several publications (Nasution, 2008; Nurhasan, 2012; Geology Institution, 2018; Diba, 2021). In 2019, the Indonesia Geological Agency assessed the geothermal potential in Papandayan using the stored heat method, resulting in in a mean estimate of 21 MW of geothermal power. Considering these findings, Papandayan presents a promising prospect for geothermal energy.

The Indonesian archipelago has 40% of the world's geothermal reserves. Approximately 23.36 GW of geothermal potential is estimated by the Directorate General of Geology and Mineral Resources, with utilization only reaching 10% (Alhusni, 2022). Indonesia has a longstanding ambition to increase geothermal energy production to achieve the country's energy sustainability goals. According to the National Energy General Plan 2021-2030, Indonesia aims to produce an additional 870 MW of geothermal power by 2025, and by 2021-2030, geothermal power capacity is expected to reach 3,355 MW. Supporting these projections requires a comprehensive and robust exploration phase of green fields, which include the Papandayan. According to Nugraha (2017), the geothermal potential at Papandayan is quite attractive due to its location in West Java, an area with significant geothermal potential. The region's geological and tectonic conditions, along with successful nearby geothermal projects like Kamojang and Darajat, enhance Papandayan's appeal for development. These factors suggest that the existing exploration data for Papandayan should be examined more closely to capitalize on its potential.

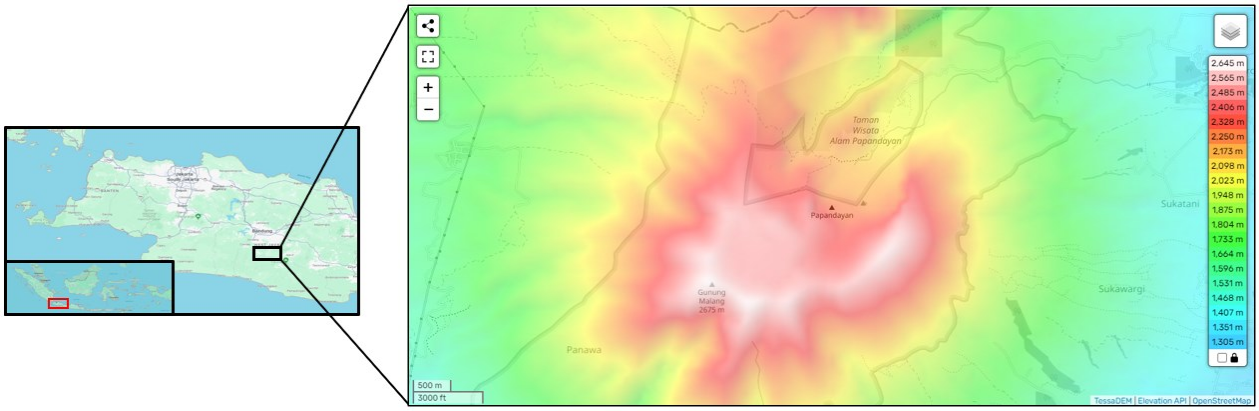

Figure 1: Location and topography map of Papandayan area modified from Google maps and topographic-map.com/Papandayan.

To advance beyond the current exploration stage, a better understanding of the Papandayan geothermal system is necessary. The process involves developing a 3D digital conceptual model and a numerical reservoir model. A 3D digital conceptual model visually represents the Papandayan geological system and geothermal system, while a numerical reservoir model provides a better understanding of Papandayan subsurface conditions. The numerical reservoir model calibration process can test different conceptual representations despite limited subsurface data. Additionally, numerical models of reservoirs developed during the exploration can be enhanced with downhole data as it is acquired. A numerical model calibrated with the downhole data provides invaluable insights for supporting drilling and well-testing operations. Nevertheless, resource assessments remain valuable at any stage of a geothermal project, particularly during exploration.

The first stage of this research was to create a 3D digital conceptual model of the Papandayan field using Leapfrog Energy. The 3D digital conceptual model was designed based on the relevant structural features, types of rocks, and thermal features of Papandayan. Papandayan's conceptual model provides the basis for 3D geological and reservoir models. The conceptual model combines geological, geophysical, and geochemistry data (3G) to describe physical mechanisms influencing fluid and heat flow in the Papandayan geothermal system. A 3D geological model was then used to generate a numerical reservoir model. This numerical model captures the natural state of the system and provides a starting point for a simulating the future production of the reservoir before exploitation. The clay cap can be interpreted from geophysical studies, is used to calibrate the numerical reservoir model with the reservoir assumed to be approximately 190-200°C at this location.

The numerical reservoir model is simulated with AUTOUGH2, while Waiwera is used for quick calibration and uncertainty quantification through cloud computing. Both geothermal simulators are utilized to ensure compatibility with the industry standard TOUGH2. To calibrate the numerical modelling, adjustments are made to the permeability and porosity of rocks and the mass flow. For uncertainty quantification, a large number of models (1000 samples) are generated and run. Parallelized geothermal simulators like Waiwera, which the University of Auckland developed in cooperation with GNS science (Croucher A. , et al., 2020), accelerate this process by exploiting cluster compute nodes. The next step is to condition the steady state model and temperature for the clay cap. In this process, the Approximate Bayesian computation method (ABC) is used. Following the acceptance of the steady state model based on geophysical data, a novel method was used to estimate and run maximum potential production scenarios. For this research, a future production scenario of a typical binary power plant was projected for 25 years.

2. GEOLOGICAL SETTING

MT Papandayan Volcanic Area is categorized into quaternary volcanic systems, identified by the presence of quaternary volcanic deposits in the vicinity of the eruption center (Sulastri, 2014). There are three geological structures on Mt. Papandayan: area morphology, fault structure and crater structure. Firstly, morphology of this area is characterized by steep slopes and mountains which dominate the landscape (Figure 2). Secondly, fault structure which most fault structures were found near Tegal Alun-Alun Crater, Mt. Nangklak, Mt. Walirang, Mas Crater, and on the volcano's northwest and southeast slopes (Figure 3). There are two normal faults with fault directions of NW-SE and NE-SW, respectively. In addition, there are three attributes that characterize normal faults: topographic lineaments, brecciation, and crushed zones. Lastly, several craters exhibit this structure, including Brungbrung Crater, Manuk Crater, Mas Crater, Tegal Alun-Alun Crater, Nangklak Crater, and Baru Crater (Sulastri, 2014).

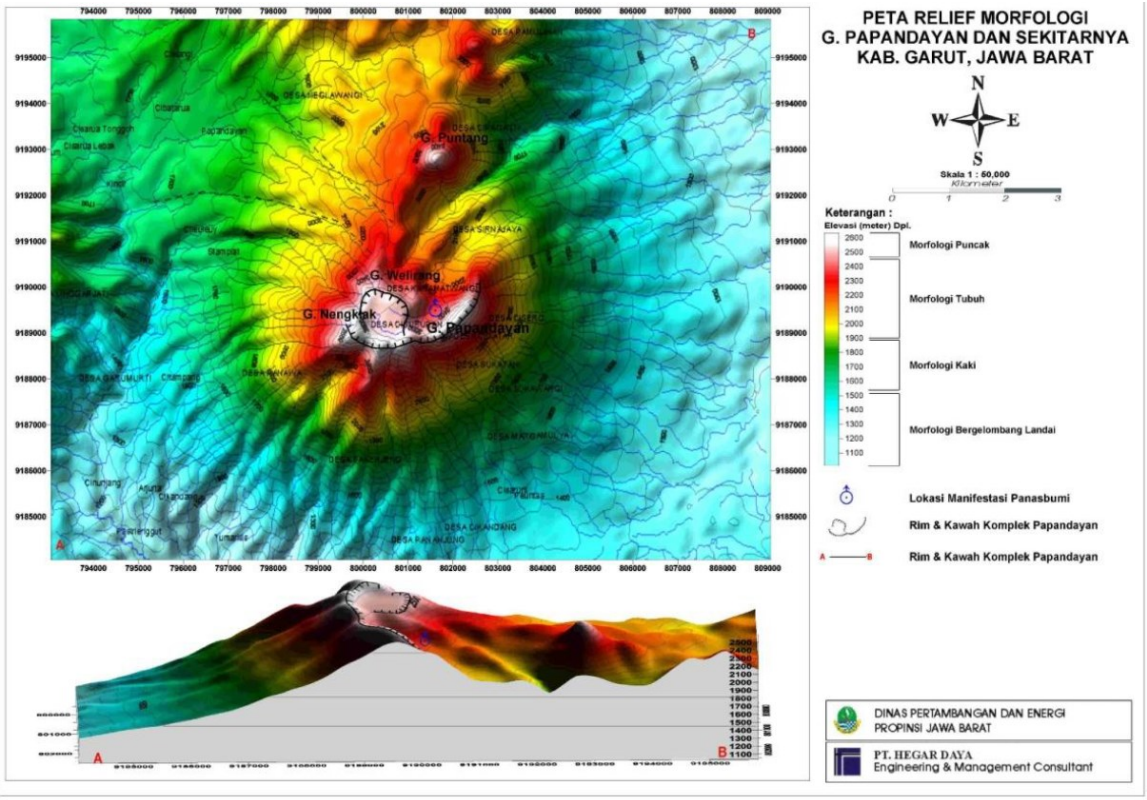

Figure 2: Morphology map of Papandayan Mountain (Geology Institution, 2018).

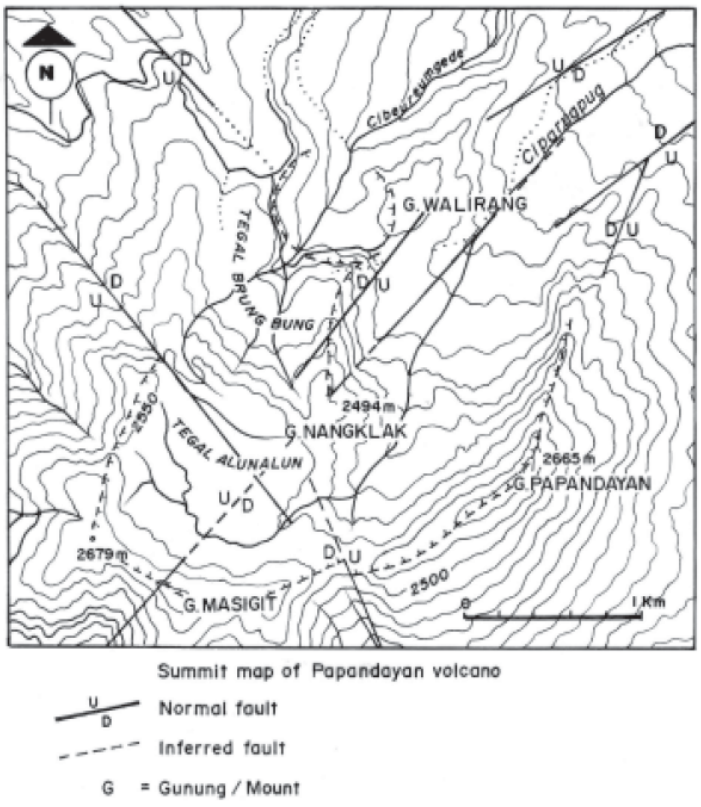

Figure 3: Geological Structure in Mt Papandayan and surrounding Area (Sulastri, 2014).

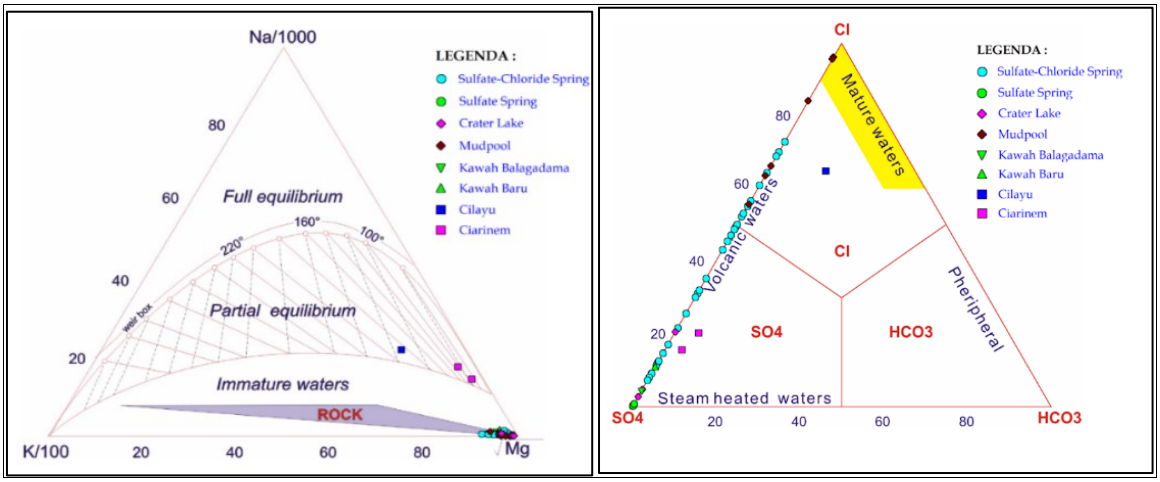

Figure 4: Water chemistry analysis.

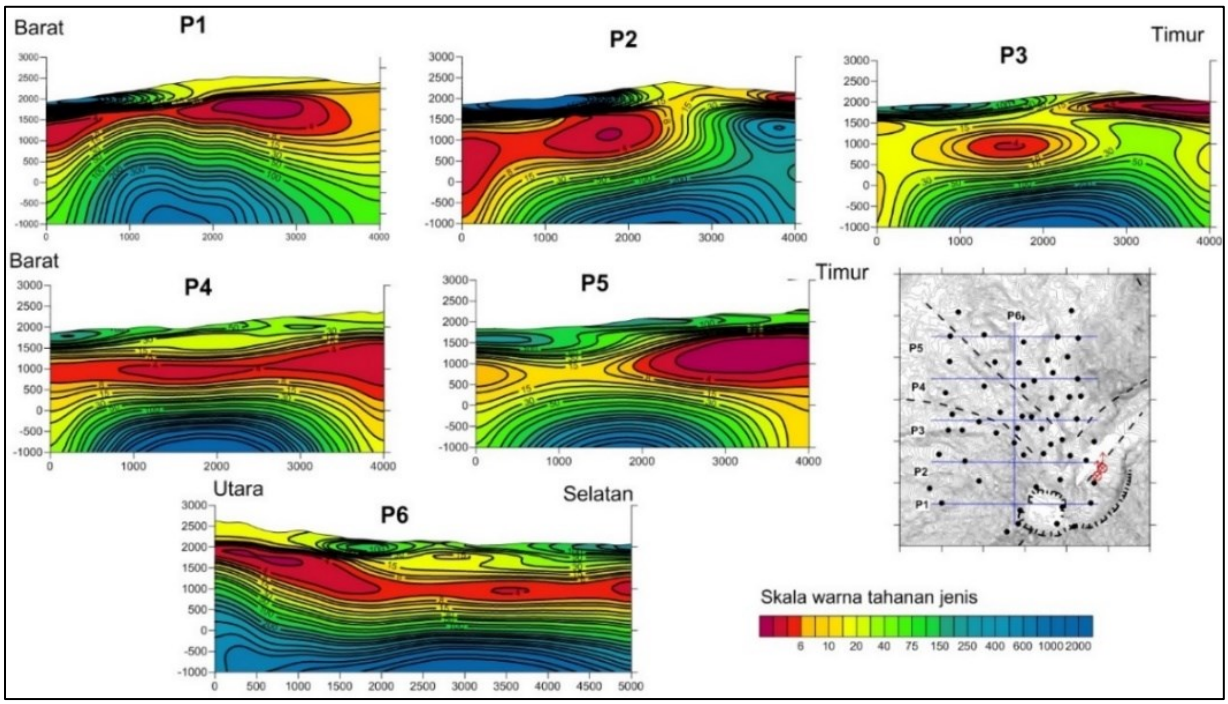

Figure 5: Magnetotelluric cross section maps of Papandayan (Geology Institution, 2018).

3. GEOCHEMISTRY STUDY

In accordance with geochemical analysis, Papandayan lava has a silica content of 55% (Sulastri, 2014). Accordingly, the values of SiO_2 variation in volcanoes are classified as medium-K andesite (Maitre, 1989). With regards to water chemistry analysis, Cl-SO_4-HCO_3 triangle diagram has been plotted showing that all water samples in the Papandayan area are located in volcanic waters which show manifestations that appear on the surface associated with Papandayan volcanic activity. Except for the Cilayu and Ciarinem, Volcanic water or steam heated waters in water samples indicate surface or near-surface steam interaction. Hot spring which are in the steam heated water zone (located far to the south outside the Papandayan prospect area). Meanwhile the Mg content in The Na-K-Mg triangle diagram shows that the appearance of water manifestations in the Papandayan complex is strongly influences by surface water. Additionally, Gas geothermometry result of Papandayan Reservoir is 240 -250 ℃ (Geology Institution, 2018; Maitre, 1989).

November 2002 was marked by an explosive eruption. The result was the formation of Kawah Baru. Volcanic eruptions that occurred up to 2002 tend to be more explosive. South-to-north displacement centres of eruption are controlled by structure. There are five large craters on Mount Papandayan that contain active thermal manifestations of fumaroles and springs. Several fumaroles and hot springs are active within the craters of Mount Papandayan. Fumarole discharges range in temperature from 90°C to 260°C, primarily containing H2O, CO2, and H2S (Sulastri, 2014).

4. GEOPHYSICAL SURVEY

Low resistivity anomalies (from Magnetotellluric survey) associated with altered rocks are distributed in the south-southeast (Tegal Alun), east (hot springs – Papandayan crater) and central areas. In Tegal Alun area, low resistance altered rocks of < 8 ohm begin to be modelled at a depth of around. 500 – 1500 m. In the eastern area or around the Papandayan craters, this altered rocks layer begins to be modelled from the surface to a depth of around 500 m. Meanwhile, in the middle area, the new altered rocks are modelled at a depth of around 800-1500 m. The low-resistivity rock < 8 ohm is thought to be clay cap for the Papandayan geothermal system (Geology Institution, 2018).

The clay cap is modelled with varying dimension but generally has a thickness of around 500-1000 m. The distributions pattern is based on lateral and vertical result starting from the southern area of Tegal Alun, the eastern area (Papandayan crater) and the central area of the investigation, meanwhile the low values in the north-northeast are not yet definitely part of clay cap based on its geological setting (Geology Institution, 2018).

The rock layer with a medium resistivity value ranging from 10-50 ohm is estimated as a reservoir rock layer. This layer lies beneath a low-resistivity rock layer, which is a type of impermeable rock, likely serving as clay cap. The peak of this reservoir rock begins to appear at depth at around 1400-1500 m in the southern (Tegal-Alun) and central part. Meanwhile, in the eastern area (Papandayan crater), this medium resistivity type of rock layer is modelled to be shallower, namely 500-750 m (Geology Institution, 2018).

5. CONCEPTUAL MODEL

A hydrothermal conceptual has been developed (Geology Institutional, 2018) as an initial concept for creating 3D conceptualizations. A detailed structural and geophysical study was incorporated with the previous model to represent the whole system. The new conceptual models as can been seen in Figure 6.

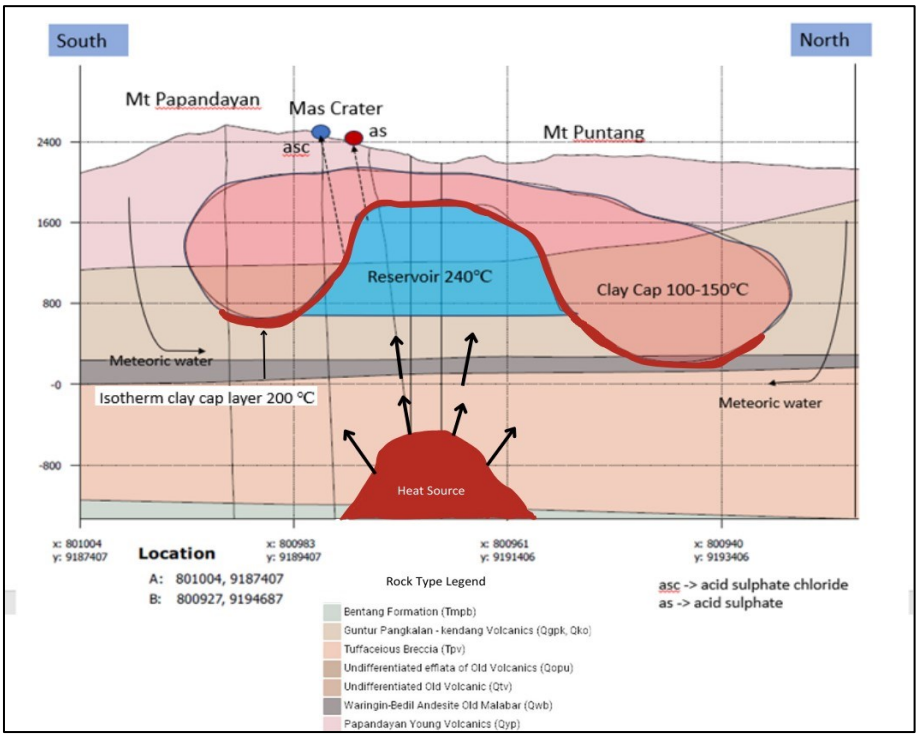

Figure 6: Conceptual Model of Papandayan Geothermal Field.

Papandayan geothermal power, sourced from ongoing volcanic activity, presents a notable volcanic risk. This is supported by magnetotellurics (MT) measurement data showing high resistivity values (> 200 ohm-m) extending continuously to a depth of over 3 km beneath the Mas Crater (Institution Geology, 2018). The heat source from magma chamber raises the temperature of the overlaying permeable rocks. This hot rock interacts with both deep, hot fluids and meteoric water. Fault structures and fractures act as pathways for this fluid movement, allowing it to rise towards the surface (Mahzari, 2021).

Magnetotellurics (MT) data indicate the presence of geothermal reservoirs with resistivity values ranging from 10 to 100 ohm-m and thicknesses of 750 to 100 m. Based on geological conditions, the reservoir rock is likely fractured volcanic rock, similar to the Darajat Reservoir, with estimated temperatures reaching up to 240°C

(Geology Institution, 2018). The reservoir age is believed to date back to the Quaternary Pleistocene and consists of efflata and andesitic-to-basaltic lavas. MT data suggests the reservoir depth varies from 500-750 m in the eastern part (Papandayan Crater) to 1400-1500 m in the southern part (Tegal Alun) (Geology Institution, 2018).

The geothermal fluid is concentrated in the Mas Crater and are characterized by an acidic water and acidic sulphate-chlorite composition (Mazot, 2008). These acidic surface manifestations, exhibit temperatures ranging 23°C to 91°C with an average 57°C (Birdina, 2018). The acidity likely originates from oxidation of hydrogen sulphide (H_2S) gas and the reaction of sulphur dioxide (SO_2) with water vapor. While the full origin of the fluids remains under investigation, the presence of altered rocks and cold water with a pH of 4 suggest ongoing geothermal activity in the Papandayan area (Geology Institution, 2018).

Steam-heated alteration are evident on the surface around the Mas Crater. These white-coloured rocks, composed kaolinite and illite clays, reflect them influence of acidic fluids interacting with magmatic fluids (Geology Institution, 2018). Additionally, low resistivity values low values (< 10 ohm-m) measured at the bottom of Tegal Alun, from a depth of 500 m to1500 m, suggest the presence of clay minerals (likely smectite) formed by hot fluid alteration of the surrounding rocks (Geology Institution, 2018).

6. 3D DIGITAL CONCEPTUAL MODEL

A 3D digital conceptual model of Papandayan was developed utilizing Leapfrog Energy. The model in this study is constructed using information, as shown in Table 1. The 3D digital conceptual model as was developed by specifying both rock formation units and fault structures, and an alteration model was constructed based on and geophysical data. The altered and unaltered volumes of the two models were then combined into a new 3-dimensional model as and be seen in Figure 8.

Table 1: An overview of data for 3D Digital Conceptual Model of Papandayan.

Type of Data	Function	Remark
Coordinate and Elevation (XYZ) Data	Create topography of Papandayan area and surrounding field	Based on public satellite data
Geological Map	Setting up Papandayan Stratigraphy on plane view	Based on public data
Geological cross-section map	Setting up Papandayan stratigraphy according to depth	Based on public data
Geophysical and Geochemistry data	Evaluating 3D Geology model with Geophysics and Geochemistry data	Based on public data and from EBTKE

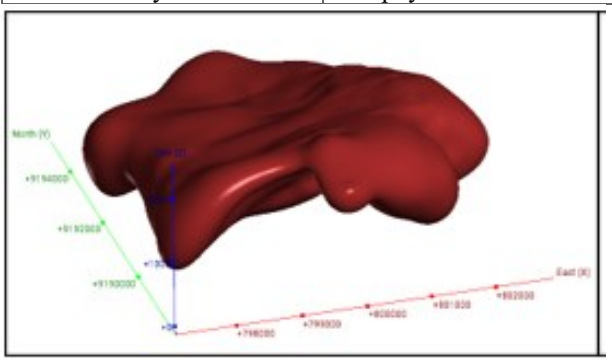

Figure 7: Alteration Model.

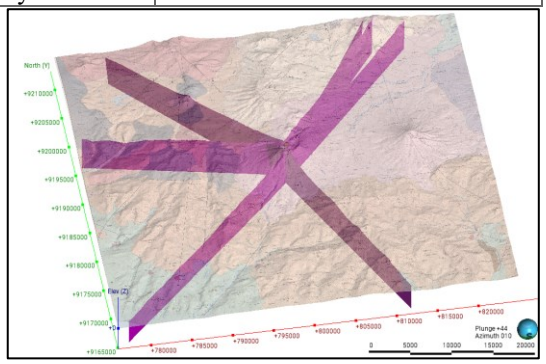

Figure 8: Fault Structure.

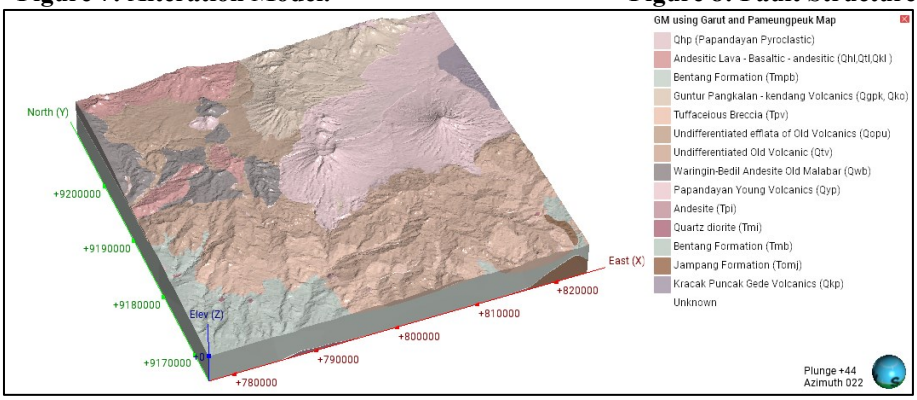

Figure 9: 3D Geological Model of Papandayan.

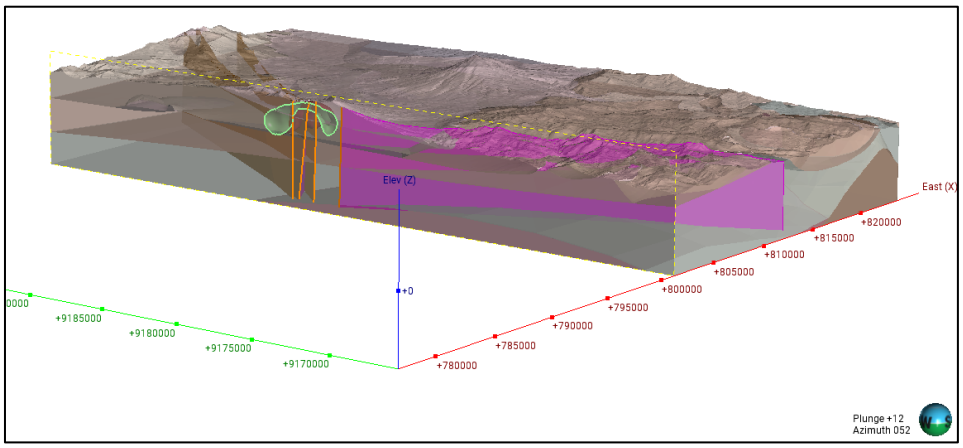

Figure 10: The Outcome of the 3D Digital Conceptual Model of Papandayan on North – South Slice (Combined model of Geology, Faults and Alteration Zone).

7. NUMERICAL MODELLING

7.1 Reservoir Model Grid Setup

In this stage of the project, the AUTOUGH2 grid is implemented in Leapfrog Energy using a 3D Geological model. 49,112 blocks make up the AUTOUGH2 grid, which measures 15.8 km by 16 km (Figure 10). The blocks are 800 m x 800 m with a vertical thickness varies between 500 m at the base and decreasing to 100 m closer to the surface. The grid is refined more in the potential area (Papandayan) with blocks 200 m x 200 m. By using this grid as the reservoir setting up, a natural state condition will be simulated. Leapfrog Energy automatically assigns rock types, saving significant effort by eliminating the tedious task of manually inputting lithology data into the reservoir model. In addition, each time the geological model is modified, Leapfrog Energy instantly updates AUTOUGH2.

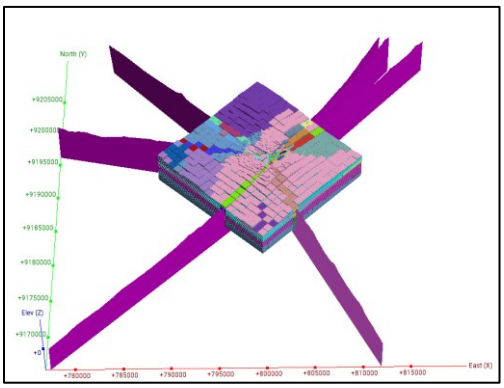

Figure 11: 3D view of Reservoir grid with orientation follows faults direction.

7.2 Boundary Condition

7.2.1 Top Boundary

At top of the model, Ground Surface is assigned as top of model. At this case dry atmospheric conditions are assigned at the top surface of field with the pressure of 1 bar and range temperature 12-28.2 °C. An annual rainfall of Papandayan area 3321 mm/year (Weather and Climate, 2020) and an infiltration rate of 10% are used in the analysis. High permeability was applied to the block's surface to facilitate rainwater flow to lower elevations because of the topography. The equation of state of water and air (EOS 3) is used in this case.

7.2.2 Side Boundary

No-flow boundary condition at the side was used as the model considers the entire convective geothermal system without side flows. It's assumed that the boundaries are far enough away that the flows at the boundary do not affect the flows of the geothermal system.

7.2.3 Base Boundary

80 mW/m^2 is the background heat flux at the base boundary. This heat flux indicates the up-flow zone under MT Papandayan. In addition, hot mass was fed into 12 blocks with a total up flow of 44 kg/s and enthalpy 1400 KJ/kg located under NW-SE faults which cross Mt Papandayan.

8. NATURAL STATE MODEL PAPANDAYAN

The natural state model was run using AUTOUGH2 geothermal simulator and successfully calibrated based on the bottom clay cap temperature isotherm of 200℃. The propylitic alteration zone occurred at the temperatures between 200°C - 300°C and produced altered rock including chlorite, epidote, quartz, pyrites, carbonate, and zeolites including prehnite and wairakite. As shallow formations cool below 230°C, argillic alteration occurs. Clay cap minerals are formed, including smectite, illite, and mixed smetite-illite clays (Mielke, Prieto, Bignall, & Sass, 2015). Natural state model ran for approximately 5x10^{13} seconds. The model reaches steady state at this point. Temperature consistency is evident in the dome area of the clay cap. The dome structure is of primary interest for drilling since it implies that the dome structure enables geothermal fluid to accumulate, making it more concentrated and accessible.

Papandayan Geothermal when reaching steady state. The calibrated model applied a deep up flow condition at the bottom of the model with a total mass flow rate 44 kg/s and an enthalpy of 1400 KJ/kg. The deep up flow in the calibrated model was focused along NW-SE faults which is consistent with the conceptual model as described in Figure 6. In the NW-SE direction as can be seen in Figure 12, three faults serve as the main heat transfer conduit from the depth to the reservoir and enable wider clay cap formation. Meanwhile, faults in the NE-SW directions also affect the Papandayan geothermal system. These faults mainly act as barriers to prevent fluid from flowing in the SE direction. This is necessary since naturally fluid preferentially due to topography changes.

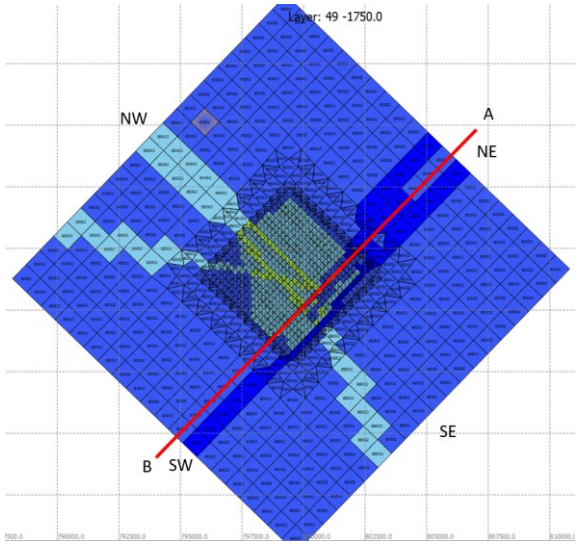

Figure 12: Fault Structure at bottom layer of reservoir grid (Visualization in Tim).

Permeability values for each rock type are calibrated parameter and values are within the range set by publication (Mielke, Prieto, Bignall, & Sass, 2015). The adjusted permeabilities are ensured to follow the geological rule. The clay cap was set at layers 6 to 36 based on the 3D Magnetotellurics Survey, with permeability ranging between 0.1 and 0.3 md. Meanwhile, the reservoir zone beneath the Caprock consists of Quaternary Holocene Papandayan Young Volcanics, Quaternary Pleistocene Guntur-Pangkalan and Kendang volcanics, Quaternary Pleistocene Waringin-Bedil Andesite old Malabar, and Tertiary Pliocene Tuffaceous Breccia Rocks. A range of 0.5 md to 300 md has been assigned to the permeability of reservoir rocks. Reservoirs generally have high permeability so that hot fluids can flow from deep formations and meteoric water can recharge. For the faults, permeability along the faults is greater than permeability across the fault. Vertical permeability (k3) is always set higher than k1 and k2 for the intersection part. In addition, the permeability of the rocks outside of the reservoir is designed to be lower than the reservoir area to confine the heat and prevent it from escaping.

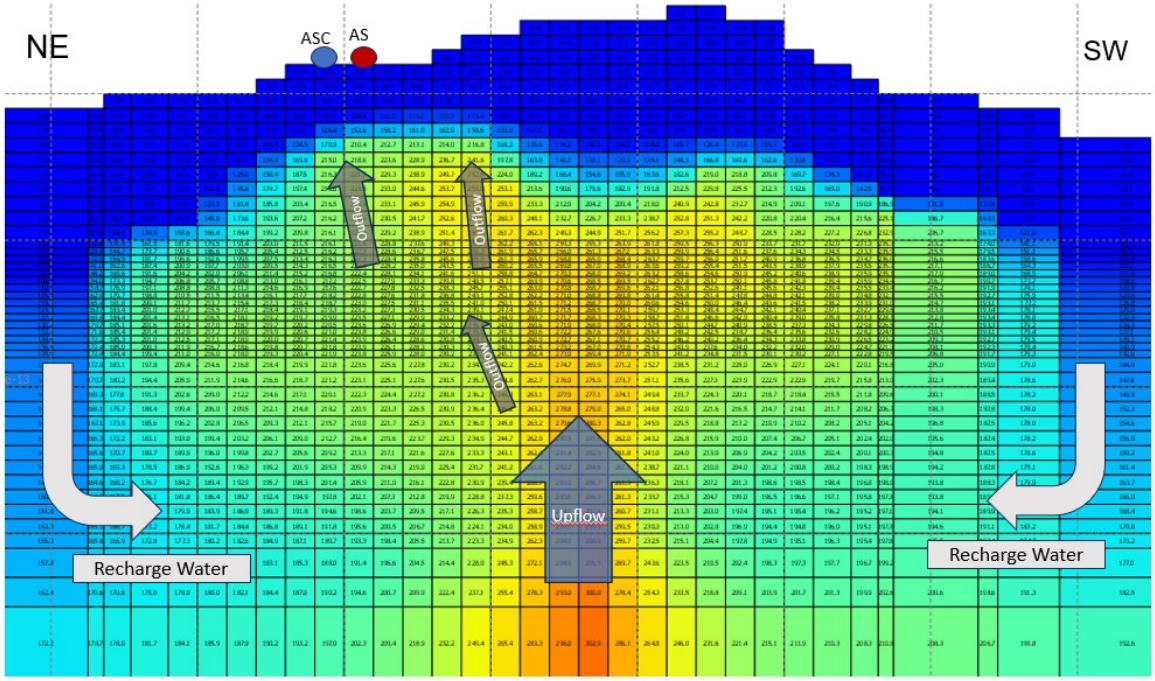

Figure 13: Temperature distribution for steady state for natural state simulation (Visualization in Tim). The slice is taken from Point A to B as per figure 12.

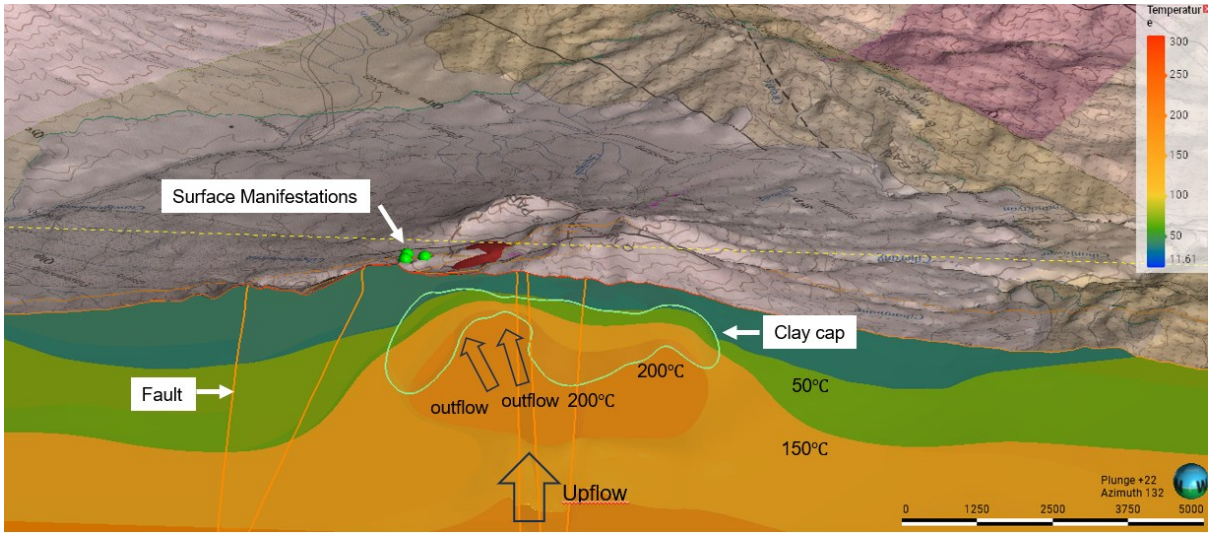

Figure 14: Temperature distribution for steady state for natural state simulation (Visualization in Leapfrog).

9. RESOURCE ASSESSMENT

9.1 Model Generation for Uncertainty Quantification

Model generation for uncertainty quantification are based on geology, structural setting, alteration data, and potential locations of deep up flows (Dekkers, et al., 2022). Based on a random distribution of parameters, the resources assessment method generates unconditioned sample models (prior distribution) that are predefined within a reasonable range of their permeability and porosity as well as their magnitudes of up flow. A probability density function was used to sample the total up flow, with the calibrated-up flow as the mean, as shown in Figure 15. In the first trial, a mean value of 44 kg/s total up flow was obtained by manually calibrating the natural state model, which is used for the uncertainty quantification. Selected blocks by the model calibration are then placed at faults in the bottom layer to distribute the total up flow according to a Gaussian distribution. Figure 16 illustrates variations in total up flow sources at bottom layer of model samples (-1750 masl).

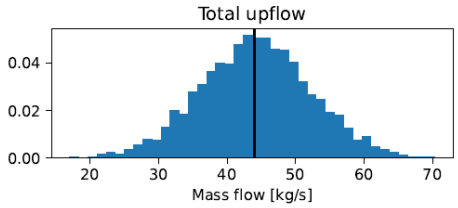

Figure 15: Total Up flow Distribution.

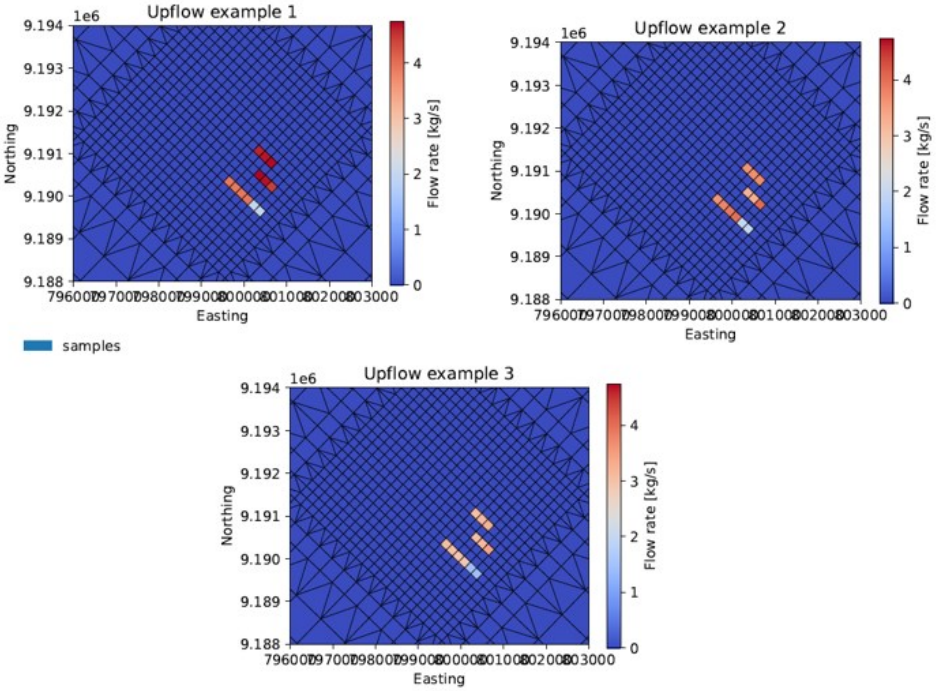

Figure 16: Three examples of up flow distribution at deep up flow sources located at bottom of the sample models' layer 49 (-1750 masL).

Depending on the location of the rock types, e.g., near the surface, deeper, or close to the clay cap, the prior mean rock permeabilities vary. The permeability of the rocks is determined by a combination of the formation permeabilities (base rocks) and modifiers due to structural setting. The modifier is a multiplier factor for calculating the permeability of fault rocks and is based on geological rules. Fault rock permeability should be multiplied by at least 1 along the fault strike and vertical direction. The purpose is to prevent the permeability from decreasing compared to its base rock in those directions. A higher permeability is also expected in the vertical direction of the intersection fault rock. Alternatively, the multiplier for fault rock permeability across the strike of the fault should be maintained to or lower 1 (Beer, et al., 2023). The same principle applies to clay cap permeability, which should have a lower permeability than the corresponding base rock, so the multiplier should be set at 1 or less. Figure 17 depicts examples of permeability in basement rocks (BH001) and how the permeability modifier is assigned to the fault (BH001) that cuts through the basement rocks. The permeability along the fault is k1, the permeability across the fault is k2, and the permeability vertically is k3. The k2 multiplier is lower than 1, and hence the fault rock permeability across the fault is decreasing. Conversely, k1 and k3 modifiers are greater than 1, increasing rock permeability in the k1 and k3 direction.

9.2 Alteration Model Conditioning

By applying Approximate Bayesian Computation (ABC), the steady-state models are filtered based on the temperature and location of the clay cap) (Beamont, 2019). The ABC method is implemented using the *ccandu* (corresponding to conditional composition and uncertainty quantification) Python package developed by the University of Auckland (Croucher A. , et al., 2020). A filtered model with its block distribution can be seen in Figure 18.

The selected block locations are mainly concentrated underneath clay cap dome in the filtered model. Those blocks represent more likely to reach temperatures around 190°C. Clay cap outer blocks away from the dome are not considered because of the uncertainty of the MT inversion at depth and clay cap edge. There are 100 samples that have been filtered down using this clay cap condition.

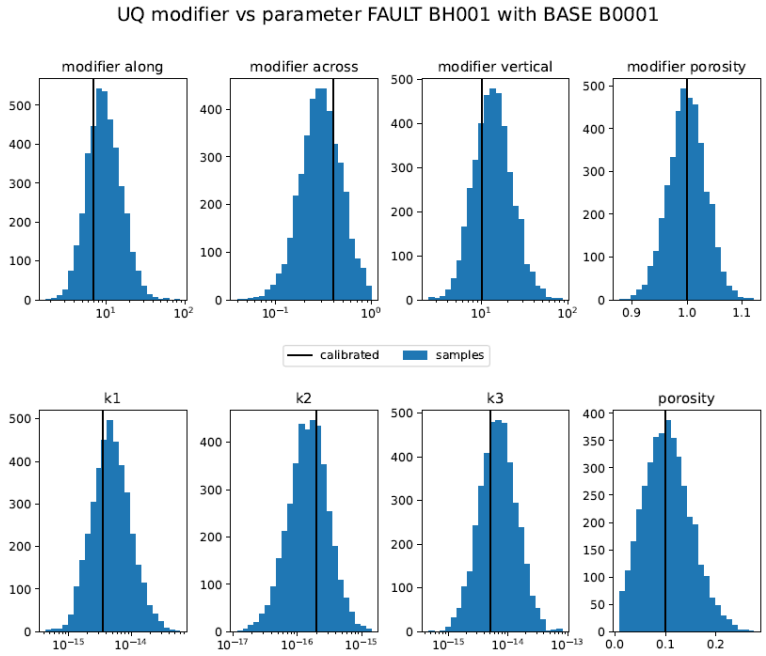

Figure 17: Permeability and Modifier Distribution of Fault BH001.

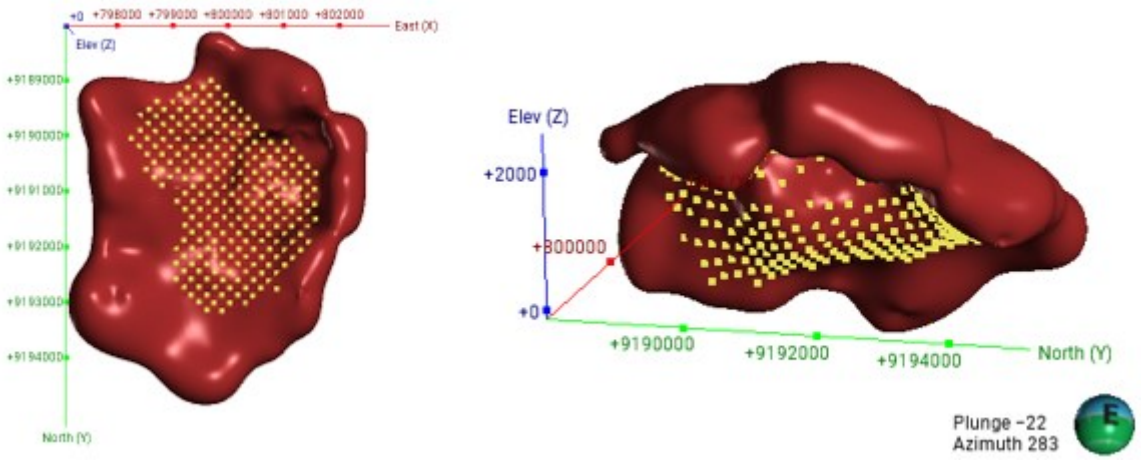

Figure 18: Block samples distribution used for conditioning the models. Down view (left) and angle up view (right).

Comparison between the unfiltered and filtered temperature distributions obtained directly beneath the clay cap is demonstrated in Figure 19. The bright red line is the calibrated model meanwhile the black dashed line indicated filtered model. Blocks under the clay cap are filtered using the ABC method based on 190°C temperature.

9.3 Power Output

In total, 1000 sample models were generated. A total of 100% of the sample models converged to a natural state (NS) when simulated using NeSI (the New Zealand eScience Infrastructure) high-performance computing facility. An average of 2-3 minutes was required to run the model on a single node (40 CPUs). Based on the clay cap temperature distribution, converged samples were conditioned to produce 100 acceptable models for the future scenario (FS). One future scenario sample took about 12 minutes to run using NeSI. The running process is fully parallelizable, and by using 100 nodes with 40 CPUs each, we can accelerate the process. The time run 1000 natural state samples and 100 future scenario samples, excluding setup and postprocessing, can be done within 1 hour, depending on the resources available.

The future scenario was based on a binary power plant using 15% thermal to electrical power efficiency. The net power output in MWe comes from the following equation.

$$Net\ Power\ Output = \left(Enthalphy_{Prod} - Enthalphy_{Inj}\right) x\ \ production\ mass\ flow\ rate\ x\ 15\%\ thermal\ efficiency$$

Figure 20 displays the consolidated results from the selected 100 samples over 25 years of production, detailing power output, gross thermal output, mass flow rate, injection mass flow rate, and enthalpy. According to the resource assessment result, Papandayan's geothermal potential is at least 12.3 MWe (P90) over this period. This means that 90% of the sample models achieve at least this power output. Moreover, the assessment indicates a potential of approximately 18.5 MWe (P50) and 28.4 MWe (P10), representing the reservoir's probable and possible power potentials, respectively.

With this condition steam production is at least 90 kg/s, the production enthalpy is stable at least 1050 KJ/kg for the full simulation, and injection enthalpy is constant at 335 KJ/kg (equal to 80°C liquid water). In addition, a reinjection mass flow rate of over 100 kg/s with at least 70 % Injection mass fraction is assumed to be necessary to achieve this production level.

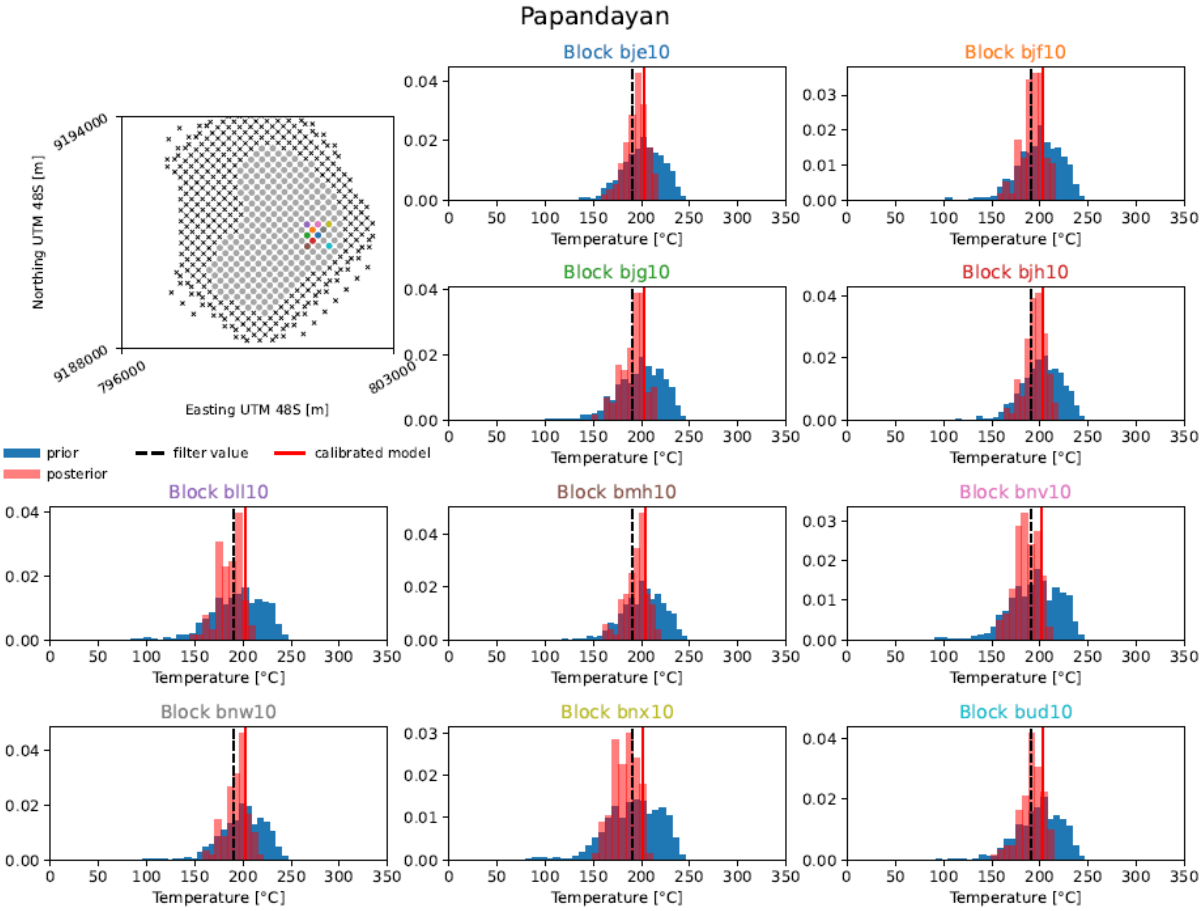

Figure 19: Temperature distributions of 10 selected blocks located directly below the clay cap, unfiltered (blue) and filtered (red).

10. CONCLUSION

Papandayan geothermal field in West Java, Indonesia, has been assessed for its resource potential. Results were obtained by considering the new, 3D natural state model produced using limited public sources and data from The Directorate-General of New Renewable Energy and Energy Conservation in Indonesia (EBTKE). Using an ensemble of acceptable sample models, the resource assessment enhances understanding the potential heat source and the permeability distribution. The approach is expected to give an accurate resource estimate by using the available data.

The natural state model was calibrated to 44 kg/s of up-flow mass rate coupled with an enthalpy of 1400 KJ/kg. The deep up-flow blocks are located across NW-SE faults, and the hot fluid originating from these blocks is capped by an alteration zone. A Magnetotellurics survey cross-section maps were integrated with 3D point data to estimate the alteration zone. Utilizing a high-performance computing facility, 1000 alternative models were generated and simulated, then filtered based on the temperature beneath the clay cap. After filtering, the top 100 most probable sample models were obtained using Approximate Bayesian Computation (ABC). These models

were used to estimate power output for 25 years of simulated production that gives a P10/P50/P90 uncertainty estimates.

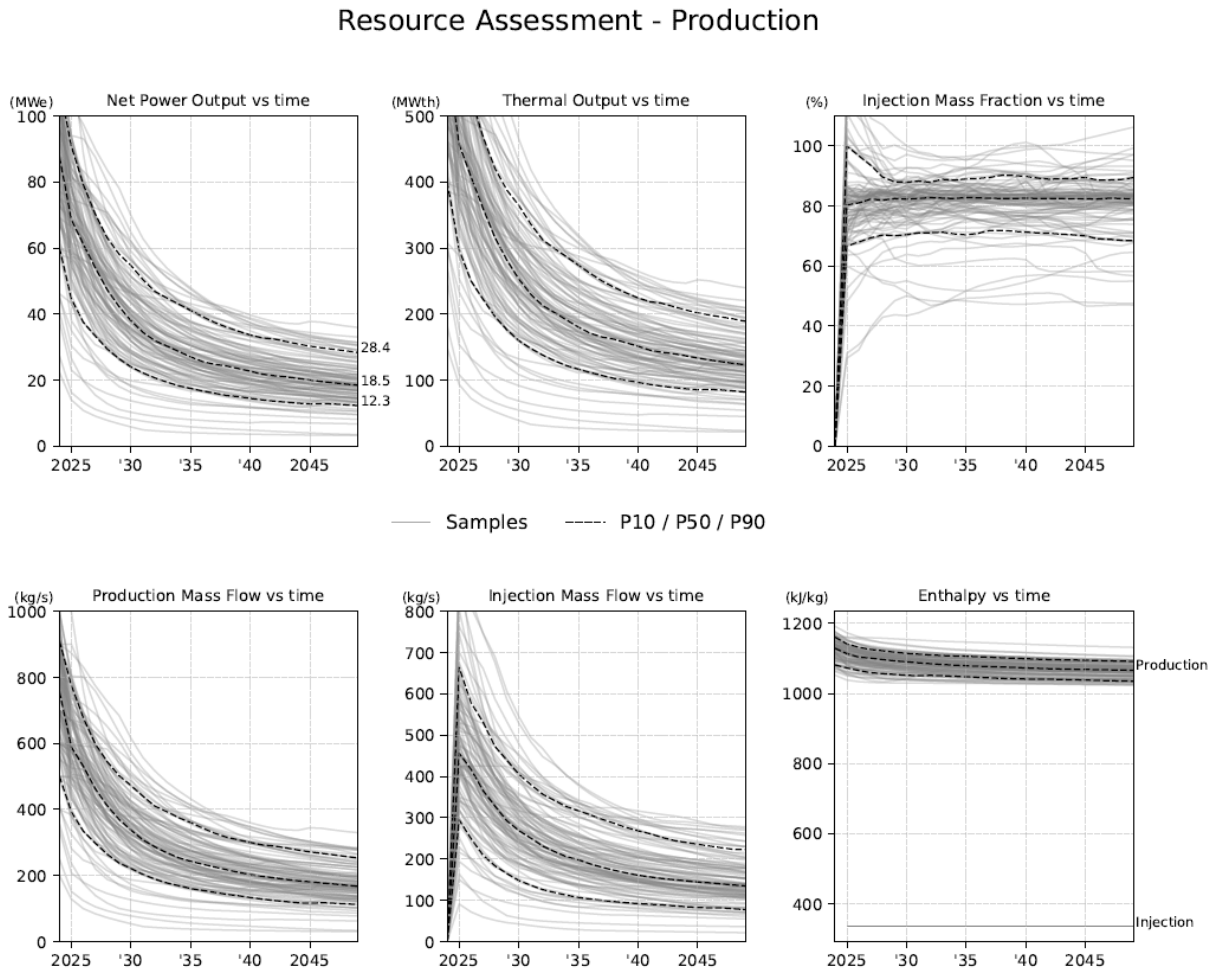

Figure 20: Papandayan Geothermal Field's total resource potential. Graphs from left to right, top to bottom, show estimated thermal power output, steam flow rate, mass flow of production, injection mass flow, and enthalpy for 25 years of production.

The results of the uncertainty quantification of Papandayan resource potential of at least 12.3 Mwe (P90). This potential is close to the estimate of the Indonesia Geology Institution made using the stored heat calculation method, in which the P90 is 16 MWe. By incorporating reservoir physics and realistic energy extraction, we have performed a resource assessment using more detailed parameters and a more realistic representation of the uncertainties.

To increase the confidence of the research study, it is recommended that a more robust geoscience study should be conducted to have an enhanced understanding of the lithology, surface manifestations, and coverage of the alteration zone. Downhole measurements are also valuable in calibrating the model and will reduce uncertainty. A resource assessment based on this study's methodology is very beneficial since it provides a realistic estimate of the resource based on available data, and it can easily be updated based on new field measurements or existing well data. Through seamless operation between the modelling tools, it is possible to modify existing models to be compatible with updated data in a straightforward and intuitive manner. Additionally, stakeholders are more likely to have confidence in the economic viability when more accurate assessments are conducted due to more realistic assumptions.

ACKNOWLEDGEMENT

We acknowledge the support of Indonesia EBTKE (The Directorate-General of New Renewable Energy and Energy Conservation) for providing support of the data and Seequent though the generous license provided for LEAPFROG Energy. In addition, Author would like to say grateful message for LPDP (Indonesia Endowment Fund for Education Agency) for granting the scholarship and supporting the first author financially during master study period.

REFERENCES

Alhusni, H. (2022). *Geothermal Business Outlook in Indonesia*. California: Proceedings. 48th Workshop on Geothermal Reservoir Engineering.

Beamont, M. (2019). *Approximate Bayesian Computation. Annual Review of Statistics and Its Application*. 379-403.

Beer, d. A., Gravatt, M. J., Renaud, T., Nicholson, R., Maclaren, O. J., Dekkers, K., & O'Sullivan, P. J. (2023). Geologically Consistent Prior Parameter Distributions for Uncertainty Quantification of Geothermal Reservoirs. *Proceeding, 48th Workshop Geothermal Reservoir Engineering*.

Birdina, S. (2018). Structure of The Acid Hydrothermal System of Papandayan Volcano. *Journal of Volcanology and Geothermal Research*.

Croucher , A., O'Sullivan , J. P., Sullivan, M., Yeh, J., Burnell, J., & Kissling , W. (2020). Waiwera: A parallel open-source geothermal flow simulator. *Computers & Geoscience*.

Dekkers, K., Gravatt, M., Maclaern, O. J., Nicholson, R., Nugraha, R., O'Sullivan, M., . . . O'Sullivan, J. P. (2022). Resource Assessment : Estimating the potential of a Geothermal Reservoir. *Proceeeding 47th Workshop on Geothermal Reservoir Engineering*.

Geology Institution, I. (2018). *Final Report of Magnetotelluric (MT) and Time Domain Electromagnetic (TDEM) Papandayan Geothermal Field, Garut West Java*. Garut: PSDMP.

Mahzari, P. (2021). Characterizing fluid flow paths in Hellisheidi geothermal field using detailed fault mapping and stress-dependent permeability. *Geothermics*.

Maitre, L. (1989). *A Classification of Igneous Rocks and Glossary of terms:Recommendation of International union of Geological union of Geological Sciences Subcomission on the Systematics of Igneous Rocks*. Blackwell Scientific Publication.

Mazot, A. (2008). Chemical evolution of thermal waters and changes in the hydrothermal system of Papandayan Volcano (West Java, Indonesia) after November 2002 eruption. *Journal of Volcanology and Geothermal Research*.

Mielke, P., Prieto, A., Bignall, G., & Sass, I. (2015). Effect of Hydrothermal Alteration on Rock Properties in The Tauhara Geothermal Field . *Proceeding World Geothermal Congress 2015*.

Nasution, A. (2008). GEOTHERMAL GEOPHYSICAL STUDY OF MT. PAPANDAYAN,. *Proceedings of the 8th Asian Geothermal Symposium*, December 9-10, 2008.

Nugraha, H. S. (2017). A Study on the Impacts of Incentives to the Geothermal Energy Electricity Price in Indonesia using Production-based Cost Approach. *Proceeding the 5th Indonesia Geothermal Convention & Exhibition (IIGCE) 2017*.

Sulastri, M. (2014). Geothermal Development Potential of Papandayan Volcano, Garut City, West Java Province Through Geochemical Analysis Study & Field Activity. *Proceedings Indonesia International Geothermal Convention & Exhibition 2014*, 5.

Weather and Climate. (2020). Retrieved from https://weather-and-climate.com/average-monthly-precipitation-Rainfall,garut-west-java-id,Indonesia.

Sizing and Optimizing Resources: A Decision Support System Applied to Lithium Extraction for Indonesia Geothermal Brine

Esty Mustika Suud[1], Suryantini[1,2], and Herbert Lubis[3]

[1]Geothermal Master Program, Faculty of Mining and Petroleum Engineering, ITB, Bandung, Indonesia
[2]Applied Geology Research Group, Faculty of Earth Science and Technology, ITB, Bandung, Indonesia
[3]Alumnus Sarulla Geothermal Project and Member of Indonesia Renewable Energy Society, Indonesia

estymustikas@gmail.com, herbert.lubis@gmail.com

Keywords: Sizing, Optimization, Resources, Geothermal Brine

ABSTRACT

This paper is the continuation of our previous paper, namely, Review of Lithium Extraction Suitable for Indonesia Geothermal Brine. In the competitive and growing lithium extraction from geothermal brine, efficiency plays a crucial role. Activities and its associate resources must be efficiently scheduled in order to maintain satisfactory production, reducing operational costs. However, this is still a critical and difficult task. This paper presents a decision support system including three scenarios such as direct lithium extraction only, direct silica extraction only, and hybrid extraction of both lithium and silica. The decision support system will determine the most robust among those three scenarios. A successful application of this decision support system will be executed by lithium and or silica extraction system over 10 years or more of time horizon. With direct lithium and or silica extraction sizing and scheduling results that will be implemented in the company, this case study deals with investments in the order of hundred millions of dollars.

1. INTRODUCTION

Lithium is the cornerstone of energy transition because of the following two reasons, the first reason is that it has the key ingredient in batteries for electric cars and renewable power storage, making it a critical commodity for the energy transition to reduce emissions of greenhouse gases. And the second reason is that Lithium is a big enabler of the energy transition from a battery perspective as we move to electric vehicles and add energy storage to electricity grids, allowing for greater penetration of renewables. As a result, lithium is increasingly being seen as a critical mineral by governments, where they want to secure supplies for that transition, and that has made it an increasingly important commodity. In line with this cornerstone of energy transition, Indonesia is committed to achieve Net Zero Emissions by 2060 or earlier and is beginning to put in place the policies and frameworks that can help reach this target while moving towards advanced economy status.

Lithium is an alkali metal that typically occurs in brine as LiCl. This LiCl solution is concentrated and purified through various processes and is then converted to high-purity Lithium Carbonate Li_2CO_3 and/or Lithium Hydroxide Monohydrate $LiOHH_2O$ commercial products. In the produced geothermal brines, consisted of the following chemical components such as Li, Fe, Si, Ca, Mg, Na and may include additional components such as K, B, Al, Sr, Mn, Cu, Ba, Zn, Ni, Cr.

Silica is one of the most common components of geothermal fluids and it is an important material for development of renewable energy, namely it is the main component for silicon solar cell. Silica is also used in applications in rubber, plastics, paint, paper, ceramics, pharmaceuticals, pesticides, chemical and odor absorbents, and adhesive industries.

Due to its importance and high investments for manufacturing both for instance high-purity Lithium Carbonate (Li_2CO_3) and or silica (SiO_2) crystalline nano-powder, these industries present an enormous potential of growth. To fully sized and optimized the development of these potentials are critical and simulated using a decision support system such as capital budgeting and investment for a decision making process.

The next sections in this paper present the desk study of decision support system with inputs such as Capital Expenditure (CAPEX), Operational Expenditures (OPEX), and Working Capital. A specification of Financial Model (Excel) is developed as a basis for calculating Net Present Value Finally, a conclusion is made with based on Financial Model for Capital Budgeting and Investment.

2. DESK STUDY OF DECISION SUPPORT SYSTEM

Direct Lithium Extraction (DLE) Adsorption is a commercial technology possibly could be adapted and suitable to Indonesia Geothermal Fields for the following reasons it has a fifty-year development and implementation

history, practiced commercially in South America for 26 years and recently in China, higher lithium recovery, lower water and chemicals consumption, shorter lead time to production, minimal footprint, potential for no carbon emissions, and an additional revenue stream from unused brine resources for geothermal power producers.

Adsorption is the most developed DLE technology globally, using adsorbents to adhere to the lithium for selective removal. Some sorbents developed can recover >90% of the lithium present, including recently tested lithium aluminium layered double hydroxide chloride sorbent, or LDH (Lithium-Aluminium Double Hydroxide Chloride). During more recent testing, the LDH sorbent was made by intercalating (inserting) aluminium hydroxide with lithium chloride, which made several $[LiAl_2(OH)_6]^+$ layers in the sorbent. These layers were separated by water molecules and hydroxide ions that created spacing requirements to allow lithium chloride to enter more readily than other ions, such as sodium and potassium. After the sorbent was loaded with the lithium chloride, it was washed with a diluted lithium chloride stream to remove unwanted ions, then washed a second time to unload the lithium chloride.

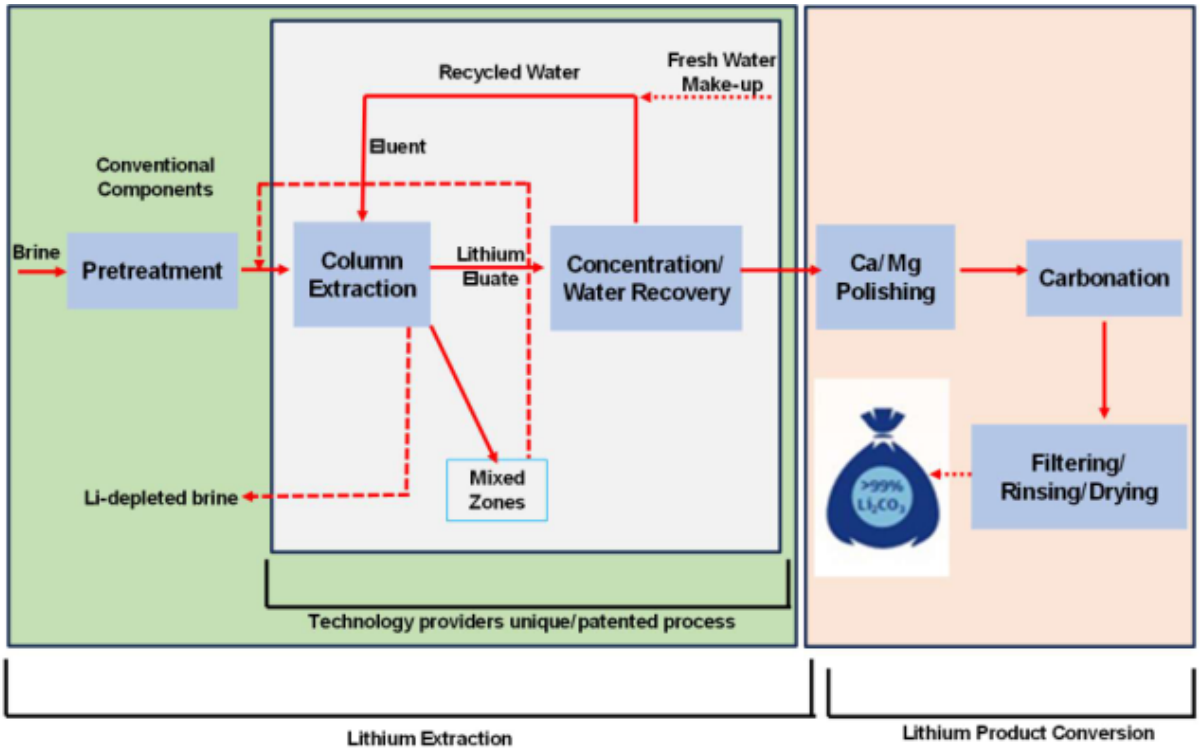

Figure 1: DLE Flow Chart (Goldman Sachss, 2023).

Pre-Feasibility Study and/or Pilot Scale in the Technical Feasibility Study of Direct Lithium Extraction (DLE), with reasonable assumptions, can provide guidance for estimating costs of lithium extraction from geothermal brines. The following table summarizes report in National Renewable Energy Laboratory (NREL) US Department of Energy in May 2021 (Warren, 2021) on DLE Project Economics. Capital Expenditures (CAPEX) are a company's major, long-term expenses while operating expenses are a company's day-to-day expenses. Examples of CAPEX include physical assets, such as buildings, equipment, machinery, and vehicles. Operating Expenses (OPEX), refer to the costs that a business incurs through its normal day-to-day operations. Examples of OPEX include employee salaries, rent, utilities, and property taxes. Working Capital is a financial metric that indicates the difference between a company's current assets and current liabilities. It is the day-to-day cash that a company needs to run business operations. Working capital helps plan for future needs and ensure the company has enough cash and cash equivalents to meet short-term obligations, such as unpaid taxes and short-term debt.

The main focus of this present study was limited to understanding techniques and costs made publicly available by companies with projects advanced to stages of development and investment that require formal reporting to pertinent institutions. These projects were focused on geothermal, salar (brine from salt-flat or lakebed), oilfield, and evaporite brines, all of which were informative for estimating costs of lithium extraction from geothermal brines. Eventually, a specific geothermal fluid will require a best-lithium extraction processes, or combination of processes, based on fluid composition and physical and chemical requirements related to power generation and reservoir management. The authors have researched that far for CAPEX, OPEX, and Working Capital of adsorption DLE from geothermal brines in the public domain. And there have not been any case studies from companies that have researched it to date. It is all still under research. And as such that is an issue that needs to

be added to this paper for further research. But for financial modeling with the specification in Figure 2, let us assume for adsorption DLE from geothermal brine for lithium factory at 2,000 ton/year CAPEX $ 60 million, OPEX $ 6,000/ton, and Working Capital $ 4 million.

By using decision support system like excel financial model, sizing and optimizing geothermal brines for Lithium Factory can be done with sensitivity analysis.

The technology for silica extraction from geothermal brine (Nursanto et l., 2023) is presented in Figure 3 Block Flow Diagram of Silica Plant.

Table 1: Summary of DLE Project Economics.

Company	SRI International	Vulcan Energy Resource	Standard Lithium	E3 Metals Corp	Anson Resources	Pure Energy Minerals	Lake Resources
Project	Salton Sea	Upper Rhine Valley	Lanxess Smackover	Clearwater	Paradox Stage 3 (Li)*	Clayton Valley	Kachi
Location	California, USA	SW Germany	Arkansas, USA	Alberta, Canada	Utah, USA	Nevada, USA	Argentina
Document	DOE, CEC reports	PFS	PEA	PEA	PEA	PEA	PFS
Brine type	Geothermal	Geothermal	Evaporite (Br tail brine)	Oilfield	Evaporite	Evaporite	Salar
Resource (1,000 kg LCE)	NA	15,850,000	3,140,000	2,200,000	192,000	217,700	1,010,000
Lithium concentration (mg/L)	400	181	168	74.6	100–500	65–221	289
Production (mt/yr)	20,000**	40,000	20,900	20,000	15,000	11,500	25,500
Production cost ($/mt)	3,845	3,217***	4,319	3,656****	4,545	3,217*****	4,178
CAPEX ($1,000)	52,300	1,287,600	437,162	602,000	120,000	358,601	544,000
OPEX ($1,000/yr)	76,900	128,688	90,259	73,200	68,180	36,516	106,539
Modeled product price ($/mt)	12,000	14,925	13,550	15,160	13,000	12,267	11,000
Pre-tax IRR (%)	268	31	41.8	32	106	24	25
Technology	Ion exchange	Adsorption	Ion exchange	Ion exchange	Ion exchange	Solvent extraction******	Ion exchange
Lithium recovery	90%	90%	90%	>90%	75%	90%	83.20%
Product	Li2CO3	LiOH·H2O	Li2CO3	LiOH·H2O	Li2CO3	LiOH·H2O	Li2CO3
Comments	Bench-scale testing and ASPEN modeling of hybrid sorbent with nanostructured manganese oxide embedded within Li-imprinted polymer beads using synthetic brine.	Known geothermal resource with measured chemistry and temperature. Bench-scale testing of two commercially available adsorbents using Upper Rhine Valley brine.	Bench- and mini-pilot-scale confirmation of process using ceramic adsorbent and crystallization process to convert concentrated LiCl into high-purity Li2CO3.	Bench-scale testing demonstrated high Li selectivity and recovery. Full process yet to be tested.	Multi-stage development with stage 3 producing 60,000 mt/yr NaBr and 15,000 mt/yr Li2CO3. Production cost reported as All-in Sustaining Cost.	Bench-scale testing of brine and synthetic equivalents informed the solvent extraction process developed by Tenova.	Nano-coated, porous ion exchange beads, tailored composition, and continuous column process.

*Estimated based on lithium component of operations; Phase 3 PEA retracted in June 2020 due to amounts of inferred resources. This does not affect estimates of CAPEX and OPEX.
**Estimated commercial production with costs and performance informed by bench-scale experiments and ASPEN modeling (Ventura et al. 2020).
***Euro to USD exchange rate 1.2; $3,656/mt Li2CO3.
****$4,155/mt Li2CO3

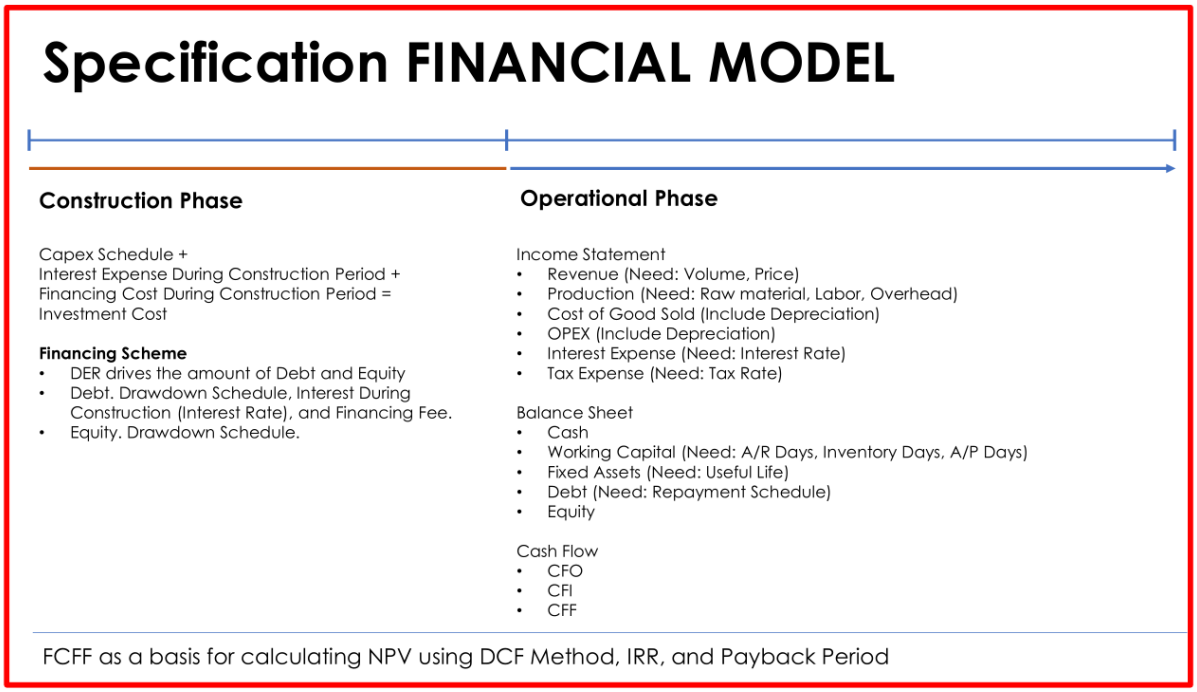

Figure 2: Specification For FINANCIAL MODEL.

DER – Debt to Equity Ratio
FCFF – Free Cash Flow to Firm
NPV – Net Present Value
DCF – Discounted Cash Flow
IRR – Internal Rate of Return

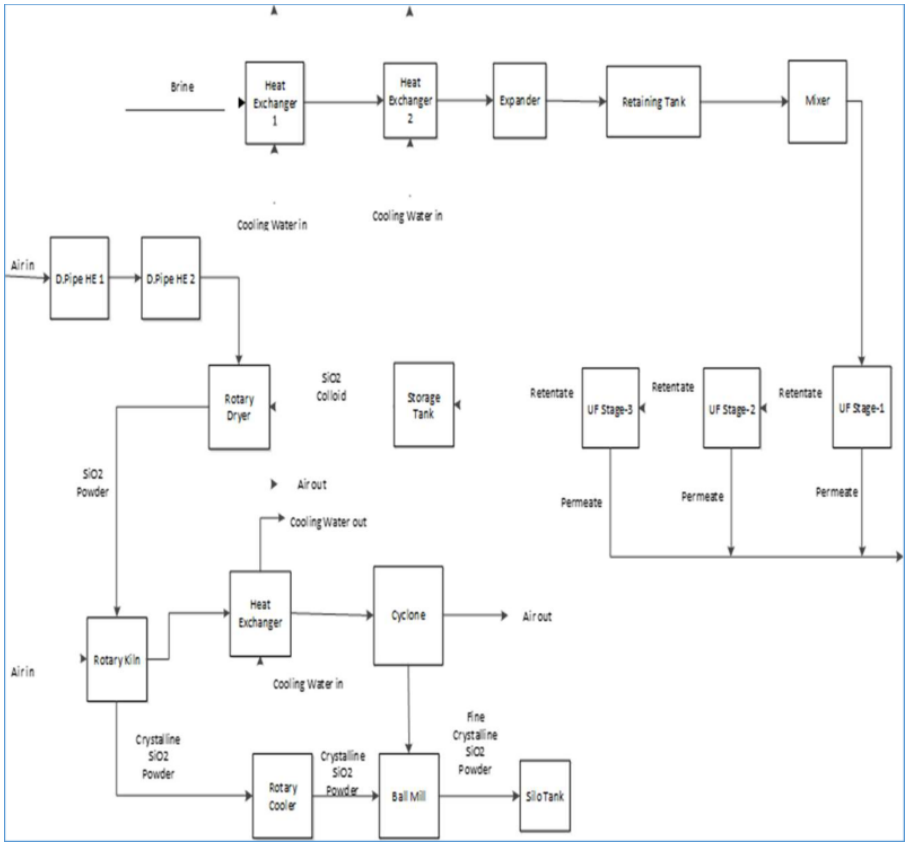

Figure 3: Block Flow Diagram of Silica Plant (Nursanto et l., 2023).

Table 2: Capital Expenditures (CAPEX) of Silica Factory.

	Component		Price
1	Purchased Equipment Cost	Rp	195,469,439,427
2	Delivery Equipment Cost	Rp	29,320,415,914
3	Equipment Installation	Rp	304,698,948,649
4	Piping	Rp	68,414,303,799
5	Instrumentation and Controls	Rp	20,313,263,243
7	Electrical Equipment	Rp	20,313,263,243
8	Building Including Services	Rp	29,975,550,512
9	Services Facilities	Rp	107,508,191,685
10	Land and Yard Improvement	Rp	77,143,679,746
Direct Plant Cost (DPC)		Rp	853.157.056.218
12	Engineering, Construction, and Supervision	Rp	81,253,052,973
13	Contractor's Fee	Rp	20,313,263,243
14	Contingency	Rp	50,783,158,108
15	Legal Expenses	Rp	10,156,631,622
INDIRECT PLANT COST (IDC)		Rp	162,506,105,946
Fixed Capital Invesment (FCI)		Rp	1,015,663,162,165
16	Raw materials inventory	Rp	27.145.690.727.97
17	Process inventory	Rp	20.132.441.217.10
18	Product inventory	Rp	50.783.158.108.23
19	Extended credit	Rp	97.002.823.975.20
Working Capital Cost		Rp	195,064,114,028.50
CAPITAL EXPENDITURE COST		Rp	1,210,727,176,193.19

Table 3: shows Operational Expenditures (OPEX) of Silica Factory.

A. VARIABLE PRODUCTION COST			
	Components	**Price**	
1	Raw materials	Rp	27,145,690,727.97
2	Labor	Rp	18,057,600,000.00
3	Maintenance	Rp	71,096,421,351.53
4	Operating Supplies	Rp	10,664,463,202.73
5	Utility	Rp	4,825,888,955.41
6	Laboratorium	Rp	1,805,760,000.00
7	Patent and Royalty	Rp	4,089,957,191.89
B. FIXED CHARGES			
1	Insurance	Rp	10,156,631,621.65
2	Property Tax	Rp	112,672,144.30
3	Bank Interest	Rp	48,126,409,228.68
4	Depreciation	Rp	92,171,327,786.04
C. PLANT OVERHEAD COST		Rp	332,829,832,885.96
GENERAL EXPENSES			
1	Administration	Rp	27,086,400,000.00
2	Marketing Distribution	Rp	40,899,571,918.86
3	Research and Development	Rp	8,179,914,383.77
OPERATIONAL EXPENDITURE COST		Rp	408,995,719,188.59

Silica Factory from geothermal brine (Assume $ 1 = Rp 15,000) for 5,000 ton/year CAPEX $ 80 million, OPEX $ 5,450/ton, and Working Capital $ 13 million.

By using decision support system like excel financial model, sizing and optimizing geothermal brines for Silica Factory can be done with sensitivity analysis.

3. CONCLUSION

By using decision support system like excel financial model, sizing and optimizing geothermal brines for Silica Factory can be done with sensitivity analysis. The financial model also can describe whether the lithium and silica factory are feasible to be built in Indonesia. The authors have researched that far for hybrid both Lithium and Silica extraction and manufacturing together are not yet successful to date. And as such the lithium factory and silica factory will be done each by different company.

REFERENCES

Eduardus Budi Nursanto et al., Chemical Department of University of Pertamina, Techno Analysis Study of Silica Factory from Geothermal Brine, Seminar Nasional TREnD, Technology of Renewable Energy Development, FTI Universitas Jayabaya, Juni 2023.

Goldman Sachs, Equity Research, Global Metals & Mining, Direct Lithium Extraction: A Potential Game Changing Technology, April 27, 2023.

Ian Warren, National Renewable Energy Laboratory (NREL), Techno-Economic Analysis of Lithium Extraction from Geothermal Brines, May 2021.

Geochemistry Monitoring During Drilling to Prevent Well Damage and Generation Loss in Darajat Geothermal Field

Yunia Syaffitri, Ngadi, Windu Hasta Bayu, and Hanna Melati Paramitasari

Star Energy Geothermal Salak and Darajat II, Ltd. Wisma Barito Pacific II, 23rd Floor
Jl. Let. Jend. S. Parman Kav. 60, Jakarta 11410, Indonesia

YSCL@starenergy.co.id, NNCX@starenergy.co.id,
winduhasta.bayu@starenergy.co.id, HPFW@starenergy.co.id

Keywords: Darajat, Well Monitoring, Drilling, NCG, Superheat, Steam Dominated Field, Throttling Scenario, Well Targeting

ABSTRACT

In a mature geothermal field with a dense well population, robust well targeting is essential to understand possible interference between make-up well targets with existing production wells during drilling. In a field with fewer production wells and ample steam buffer, production wells near the drilling area are often shut in temporarily to prevent adverse effects from drilling fluid. However, in a field with limited steam buffer, completely shutting in certain production wells is not always feasible due to the need to maintain steam supply for optimal power generation, therefore a specific well throttling scenario is required throughout the drilling of the reservoir section.

In Darajat Geothermal Field, a well throttling scenario is developed based on feed zone distance between new and existing well retrieved from 3D model. Monitoring of the nearby production well is conducted using real-time production data such as WHP and flowrate, meanwhile, daily geochemistry sampling is conducted to monitor other parameters like non-condensable gas (NCG) levels, superheat, pH, and total dissolved solids (TDS) in steam. Aside from the drilling impact on production wells, to avoids generation loss due to high NCG at power plant, geochemist also perform NCG monitoring at interface. Prior to drilling execution, the Geochemist also makes an estimation of the NCG content at power plant based on historical NCG increase trend, and the entry distance of the new well with existing production wells. These proactive approaches have been successfully implemented in multiple drilling campaigns at Darajat to prevent negative impacts on production wells and minimize disruption in power generation.

1. INTRODUCTION

Darajat geothermal fields are located within a mountain range of inactive andesitic volcanoes. They lie along the main trend of Sunda Volcanic Arc which extends from Sumatra to Flores (Hamilton, 1979; Hutchinson, 1989) (Figure 1). The field is located in the Kendang volcanic complex, which is a part of a Quaternary volcanic range in West Java that includes the active Gunung Papandayan (last eruption in 2002) and Gunung Guntur (last eruption in 1840) (Hadi et al., 2005; Rejeki et al., 2010). The Darajat geothermal field in West Java, about 230 km southeast of Jakarta (Figure 1), is the largest steam-dominated geothermal resource in Indonesia with an installed capacity of 271 MWe. Commercial production at Darajat commenced in 1994 with the commissioning of the 55 MWe Unit I. This was followed by Unit II (95 MWe) in 2000 and Unit III (110 MWe) in 2007. In 2009, the successful drilling campaign in 2007-2008 developed enough steam to allow Unit III to generate at 121 MWe; thus, increasing the installed capacity to the current 271 MWe. Under Joint Operation Contract ("JOC") with PT Pertamina Geothermal Energy ("PGE"), a subsidiary of PT Pertamina (Persero) (a state-owned oil and gas company), Star Energy Geothermal Darajat II, Limited ("SEGD") supplies steam to Unit I, owned by PT PLN (Persero) and operated by its subsidiary, PT Indonesia Power, and produces electricity from Unit II and III (Intani et al. 2021).

Continuous mass extraction from this field consequently promotes decline in well production due to pressure drawdown. Make-up well drillings are conducted periodically to maintain steam supply to the Darajat power plants. During well drilling, especially in the reservoir section, injection of drilling fluid to reservoir could foster adverse impact to nearby production well.

In a steam-dominated field like Darajat, an undesirable effect related to drilling fluid can be observed such as condensation due to low-temperature drilling fluid, scaling in nearby production well, and NCG increase related to air drilling. Permeability damage in a nearby well once observed during drilling with mud in the reservoir section. It occurred a long time ago, and now drilling of the reservoir section in Darajat only utilizes water / condensate.

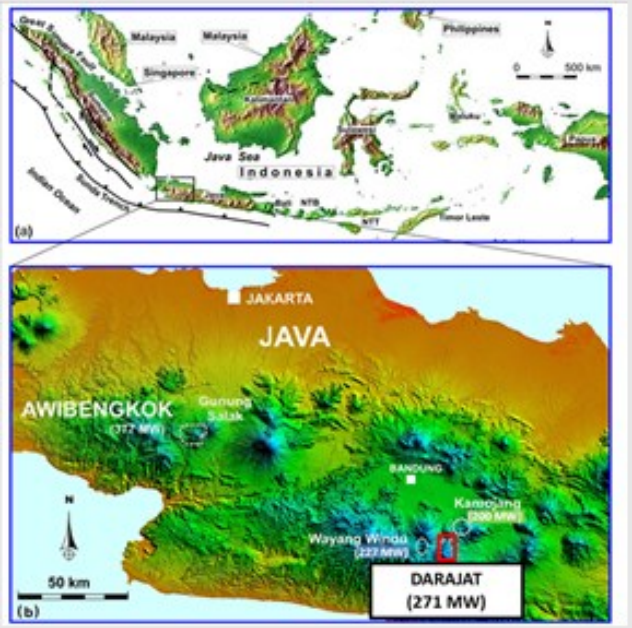

Figure 1: Location map shows Darajat contract area (red polygons).

To avoid the said effect above, most production wells near the new well trajectory are often shut in. However, shut in production wells could only proceed if sufficient steam buffer is available to support full generation. In cases of optimizing the steam buffer, sometimes completely shutting in certain production wells is not always feasible due to the need to maintain steam supply for optimal power generation.

This paper emphasizes more on the method to maintain existing well production, including minimize generation loss from increased non-condensable gas (NCG) and steam shortages due to wells shut in. The practice includes a detailed examination of a specific well throttling scenario, along with geochemical sampling and continuous production data monitoring.

2. METHODOLOGY

Monitoring activities during drilling can be divided into two distinct phases. The initial phase, termed preparation, or pre-drilling activity involves essential tasks completed prior to drilling commencement. This phase includes defining the well throttling strategy and planning the geochemistry sampling program. In contrast, the subsequent phase occurs during reservoir section drilling, primarily focusing on executing the monitoring program and setting up tactical strategies in response to any observed anomalies (see Figure 2).

To establish a dependable well throttling strategy and geochemistry monitoring program during drilling operations, it is crucial to have a robust well targeting framework as a foundational reference. In Darajat, the well targeting approach utilizes natural fracture modeling method for well placement, this method using fracture drivers to map the location of producing fractures (Intani et al., 2022) by using the natural fracture modelling method, which relies on specific criteria to identify optimal drilling locations and feed zone estimations within the well. This methodology ensures a clear trajectory and accurate estimation of the feed zone's location, essential for assessing proximity to existing wells.

In Darajat, a guideline based on historical data has been developed to determine the minimum separation distance between a new well target and the feed zones of existing offset wells. According to this guideline, the well throttling program is structured as follows:

200 - 250 m : Throttle offset production well to 25%
150 - 200 m : Throttle offset production well to 50%
< 150 m : Shut-in offset production well(s)

This throttling program were developed based on monitoring experience during drilling and have been calibrated through multiple drilling campaigns in Darajat to establish the most effective structure. However, these rules may vary by field depending on factors such as reservoir condition and fracture types.

For the geochemistry monitoring program, wells located within a 250-meter radius from the lateral distribution midpoint of the new target well are selected for sampling activities. Baseline geochemistry sampling is conducted

on these wells before reservoir section drilling begins, providing a reference for subsequent analyses. During reservoir section drilling, geochemical sampling focuses on several key parameters: NCG (Non-Condensable Gas), TDS (Total Dissolved Solids), pH, and Superheat. Monitoring NCG is particularly crucial because it often exhibits an increasing trend during drilling, attributed to air drilling or condensation in nearby wells. NCG, being a natural component of geothermal fluids, can have a significant impact on the operational efficiency of geothermal power plants (Özcan and Gökçen, 2010). Meanwhile, superheat value can indicate the arrival of drilling fluid in nearby production wells. At Darajat, additional parameters such as TDS and pH are also monitored. Since drilling fluid has higher TDS and pH compared to the steam condensate, these parameters provide further insight into the impact of drilling fluid on nearby production wells.

In estimating the increase in NCG in the well and power plant, historical data during normal production indicates that wells located closer to the midpoint production of the new target well (within 250 m) tend to exhibit a higher trend of NCG increase compared to those further away or with different trajectories. NCG levels typically show a gradual increase during drilling operations, peaking before stabilizing and potentially declining once the drilling concludes. Based on historical trends, NCG increases in wells with lateral distances less than 250 m can exceed five times the baseline data, highlighting the variability and importance of monitoring and strategic management during drilling operations

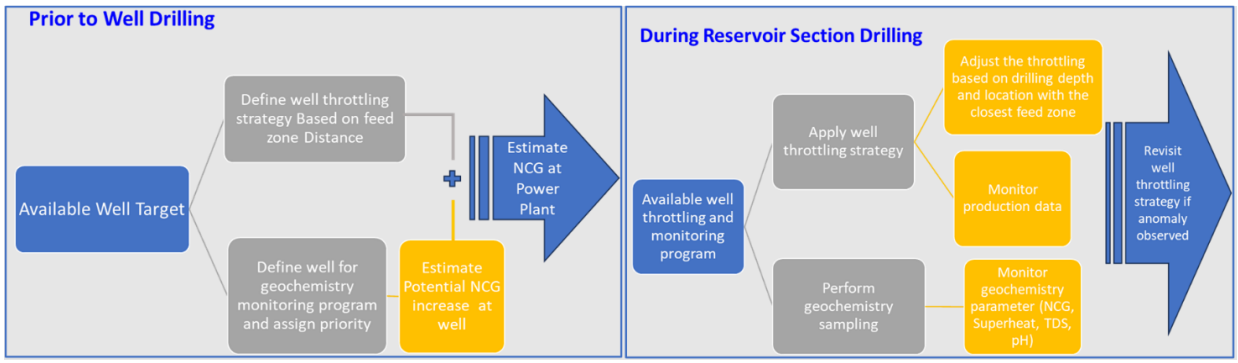

Figure 2: Flowchart of geochemistry monitoring program activity prior to well drilling and during reservoir section drilling.

Geochemists should create an NCG mass balance calculator to estimate the impact of NCG increase at production wells on each power plant. The NCG Mass balance is a simple spreadsheet which includes the mass flow rate and NCG from production wells supplying each unit. This NCG mass balance spreadsheet should include the adjusted mass flowrate resulted from the throttling program to calculate a better NCG estimation at the power plant. Accurate NCG estimation at power plants are needed to make sure NCG handling capacity at the power plant is sufficient to overcome the NCG increase, or else the unit might be degraded, and some adjustments should be made to the well throttling program or NCG removal system. During reservoir section drilling, geochemistry monitoring is conducted on the selected nearby well. Initially, wells with close distance (<250 m) should be monitored daily, meanwhile the wells with further distance (250 – 500 m) can be monitored every two days. Aside from geochemistry data, online production data of neighboring wells is also being monitored to see if any data anomalies appear. The frequency of geochemistry sampling can be adjusted according to the monitoring result. The well throttling strategy could also be adjusted if any anomaly occurs in the monitored well, which gives a bad sign to the production.

3. RESULT AND DISCUSSIONS

In the last couple of drilling campaign in Darajat, the well throttling strategy and well monitoring program during drilling have been carried out. This practice is essential to ensure optimum power generation and maintain well productivity during drilling.

3.1 Well Monitoring Result

An illustrative example of a well throttling program can be observed during the drilling of DRJ-DD in 2019, where nearby wells with feed zones less than 250 meters away were subject to specific operational adjustments. According to table in Figure 3, two such wells were throttled, while one located within less than 150 meters had to be shut in. To mitigate steam loss resulting from throttling, a dynamic strategy was implemented, adjusting throttling in response to the drilling progress. As the drilling depth moved away from the targeted zone, the throttling rates were modified to optimize flow from the affected wells.

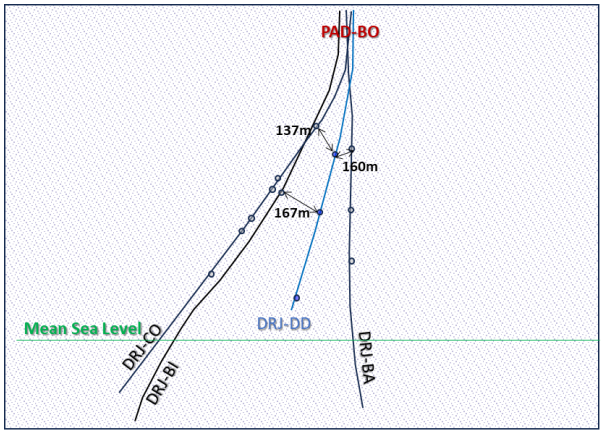

Offset Well	Min. Distance	Closest Target	Mitigation
DRJ-CO	137 m	Target 1	Shut in
DRJ-BA	160 m	Target 1	Throttling 50%
DRJ-BI	166 m	Target 2	Throttling 50%

Figure 3: 3D visualization depicting the distances between the new well target and identified feed zones in offset wells, alongside details of the implemented throttling strategy as shown in the accompanying table.

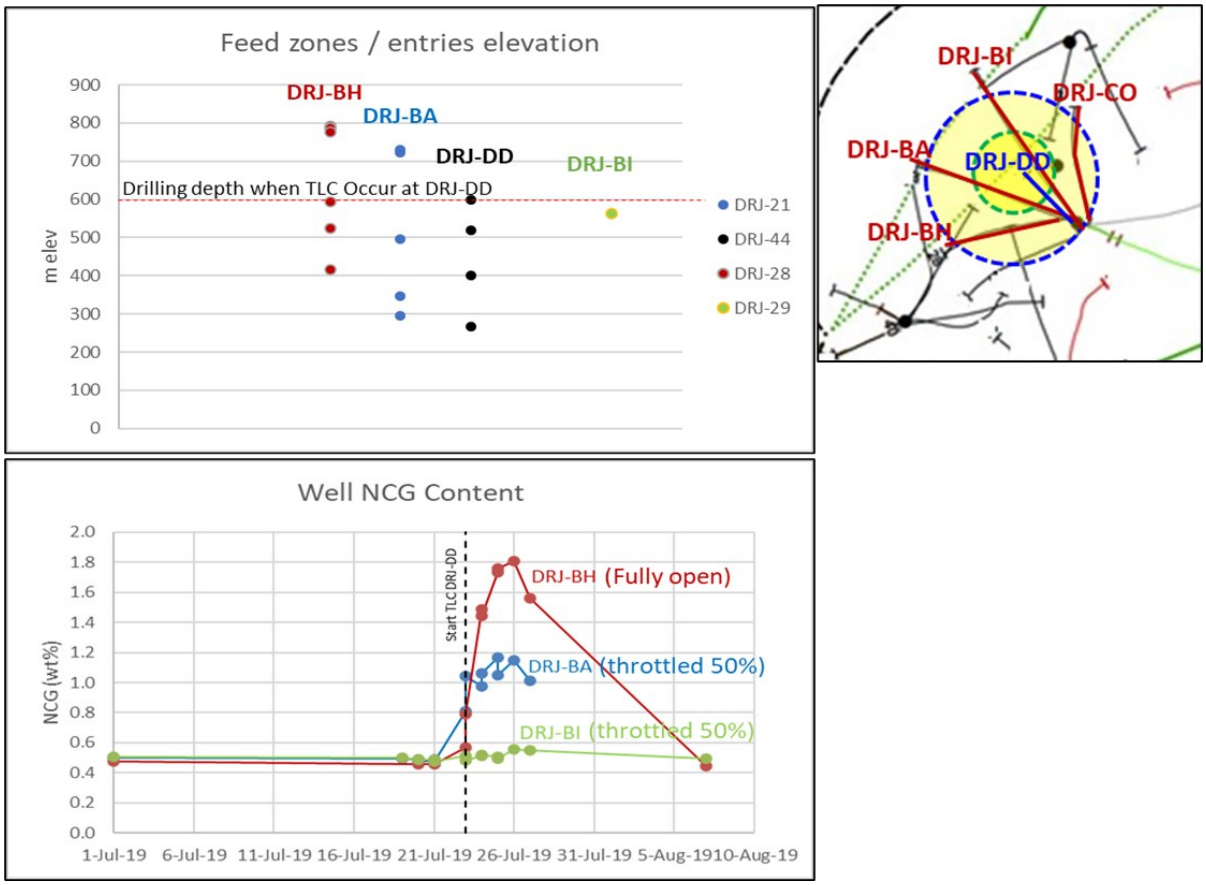

Figure 4: Graphic represents the correlation between well feed zones, TLC depths, and NCG increases observed in surrounding wells during DRJ-DD drilling.

During the DRJ-DD drilling, geochemistry monitoring revealed an increase in Non-Condensable Gas (NCG) coinciding with Total Loss Circulation (TLC) events. Significant NCG elevation was observed at offset wells located within a 250-meter radius from the midpoint production of DRJ-DD (see Figure 4), including DRJ-BI and DRJ-BA, which were among the throttled wells. Particularly, DRJ-BH, situated within a 500-meter radius from DRJ-DD, exhibited a significant NCG increase, peaking at 3.6 times the baseline value. This increase surpassed that of DRJ-BA and DRJ-BI, potentially influenced by factors such as similar entry elevations and higher mass extraction towards DRJ-BH compared to the closer wells.

Conversely, no significant changes in TDS (Total Dissolved Solids) or superheat were detected in these affected wells, suggesting that the NCG rise was likely associated with air drilling rather than condensation due to the

introduction of drilling fluid injection. Moreover, no production anomalies were reported from these wells during the NCG increase phase.

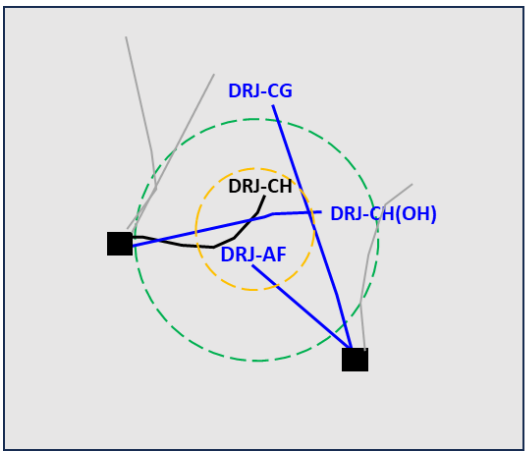

Offset Well	Min. Distance	Closest Target	Mitigation
DRJ-CH (OH)	55 m	Target 1	plugged
DRJ-AF	161 m	Target	Throttling 50%
DRJ-CG	225 m	Target 2	Throttling 25%

Figure 5: Lateral view depicting the distances between the new well target and identified feed zones in offset wells, complemented by details of the implemented throttling strategy as outlined in the accompanying table.

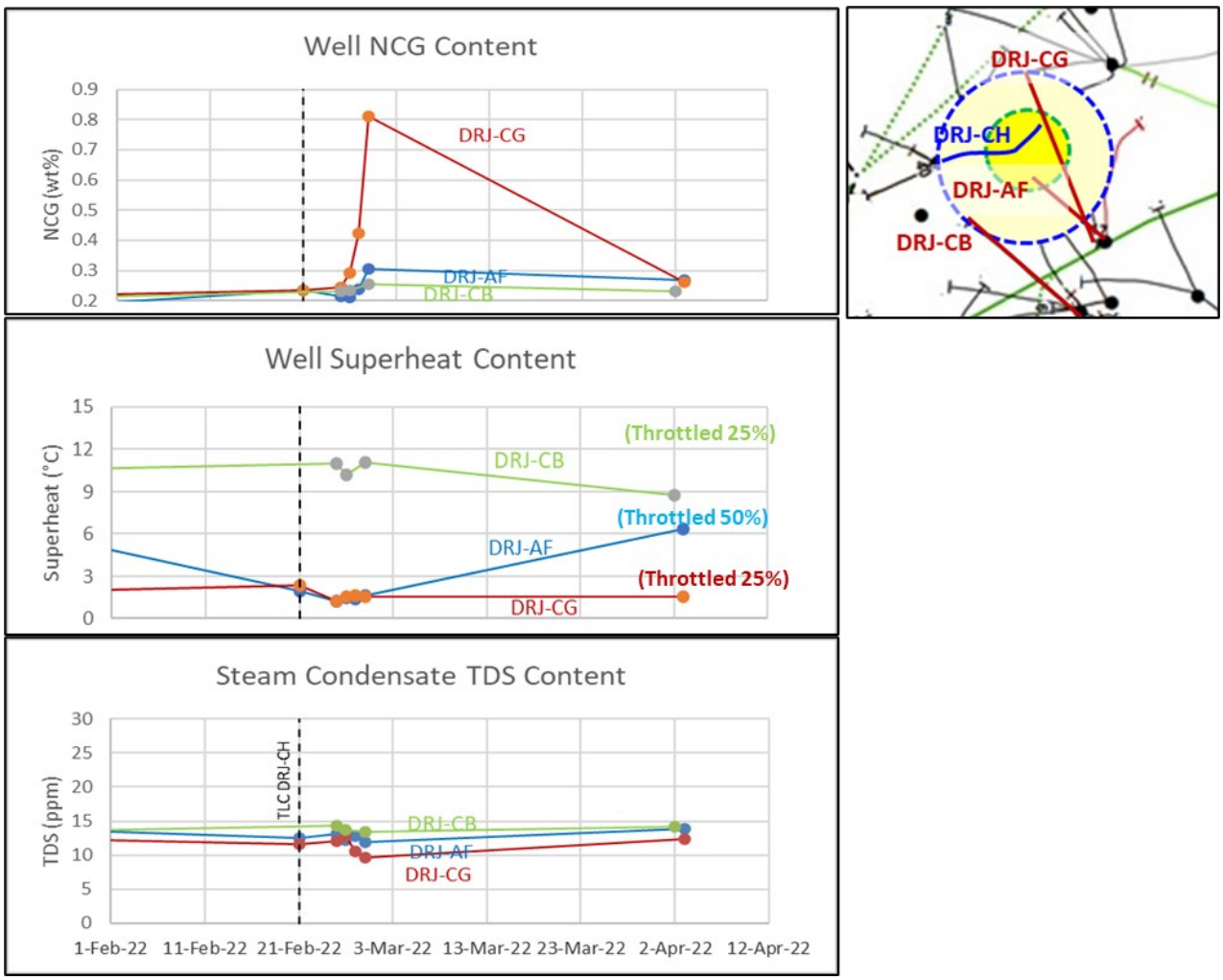

Figure 6: Graphic showing NCG increase and other observed geochemistry parameter in surrounding wells during DRJ-CH drilling.

Another example of effective throttling was applied during the DRJ-CH reservoir section drilling in 2022. Throughout this period, the DRJ-AF and DRJ-CG wells were operated at throttling rates of 50% and 25%, respectively. Significant increases in NCG were noted at the neighboring wells, DRJ-AF, and DRJ-AG, which are situated within a 250-meter radius of the midpoint production zone. Particularly noteworthy was the NCG increase at well DRJ-CG, where levels spiked up to four times higher than the baseline measurements, highlighting the complexities and impacts of operational adjustments during the drilling process. This finding again highlight correlation between higher mass extraction and flow streamline which affect NCG increase in the nearby well.

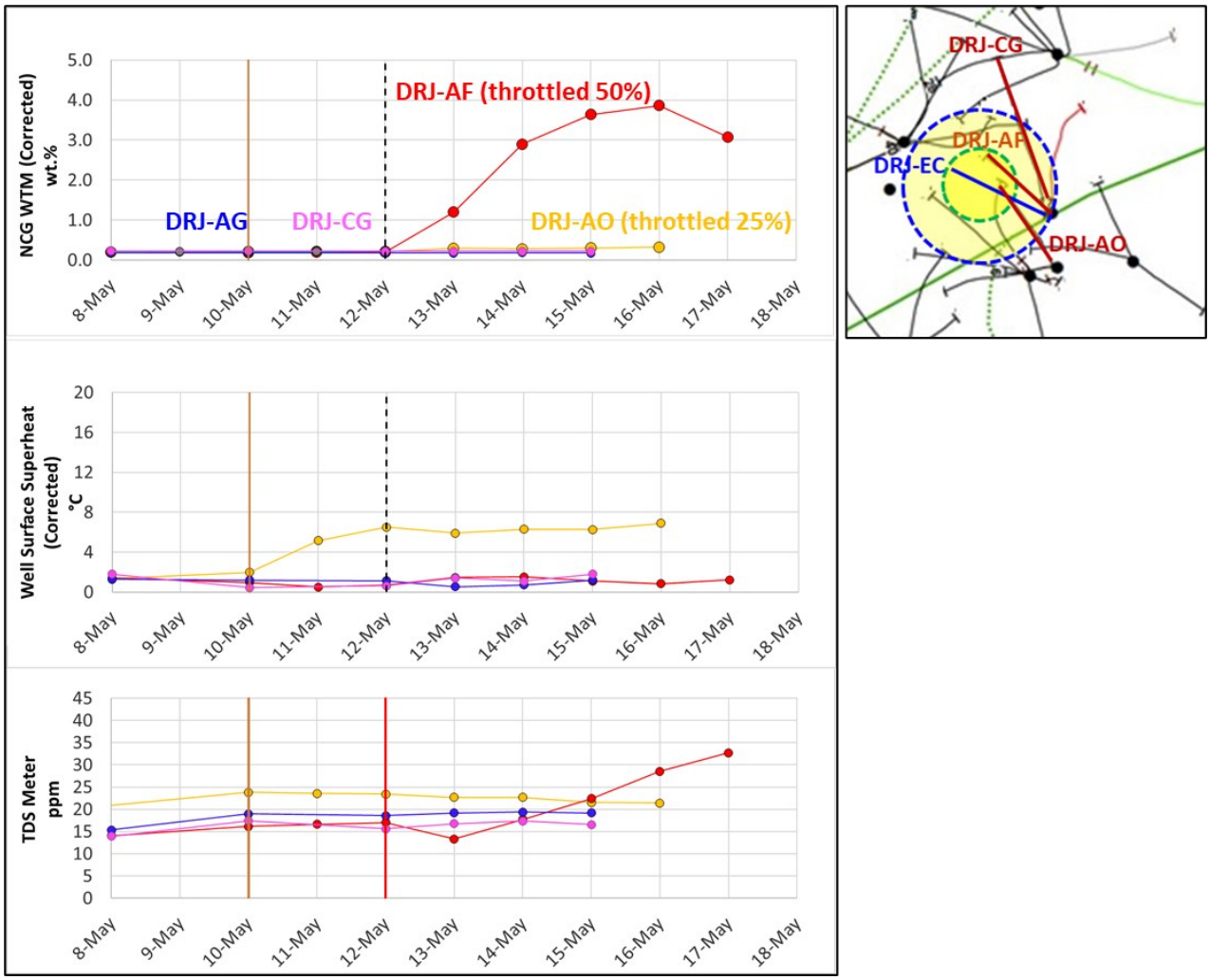

Figure 7: Graphic showing NCG increase at DRJ-AF and which was followed by TDS increase, suggesting drilling fluid effect in produced steam.

However, no pH and superheat change observed from these affected wells, suggesting the NCG increase was more related to air drilling instead of the condensation due to arrival of drilling fluid injection. The same condition as observed in nearby well during DRJ-BH drilling in 2019.

In the most recent drilling campaign, ongoing at present, a distinct trend in NCG increase has been noted compared to previous years. During DRJ-EC drilling, several nearby wells were temporarily offline due to unit shutdowns. Amid reservoir section drilling, DRJ-AF and DRJ-AO were throttled at rates of 50% and 25%, respectively. However, following TLC events at DRJ-EC, DRJ-AF experienced a significant NCG increase, rising up to 19 times the baseline value, exceeding recorded historical trends in Darajat. Conversely, DRJ-AO exhibited only a 1.3-fold NCG increase from baseline. The anomaly in DRJ-AF's NCG increase is attributed to surrounding wells' shut-in conditions, causing accumulated NCG from air drilling to be extracted at the nearest well, DRJ-AF. Despite the NCG increase, no production declines were observed from DRJ-AF (see Figure 8). However, the observed change in TDS and pH trends in DRJ-AF suggests the potential presence of drilling fluid reaching this well, in addition to air drilling components.

Geochemical monitoring is conducted not only at production wells but also at the power plant interface during reservoir section drilling. The primary objective of this monitoring at the power plant interface is to track the NCG

(non-condensable gas) content and ensure it remains within the handling capacity of the power plant. In recent drilling campaigns at Darajat, the implementation of a well throttling system has successfully kept the increase in NCG levels at the power plant below the capacity threshold of the Unit GRS system. Figure 9 below exhibits NCG increase at Darajat power plants during drilling in 2022. NCG increased significantly at Unit-B, but still below the NCG handling capacity of Unit-B at 1.5 wt.%.

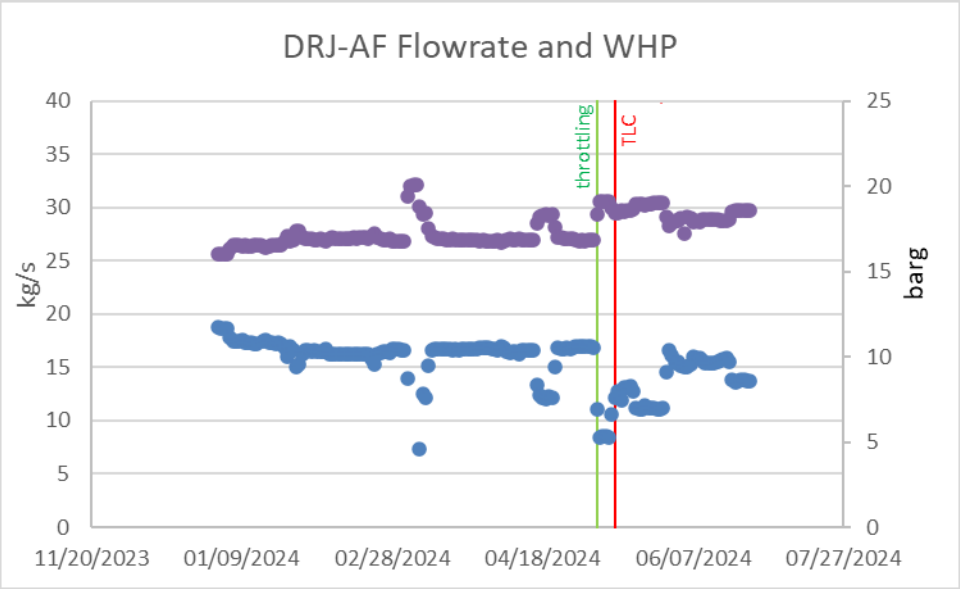

Figure 8: Production profile of DRJ-AF during drilling no indication of production anomaly observed during the high NCG increase in this well.

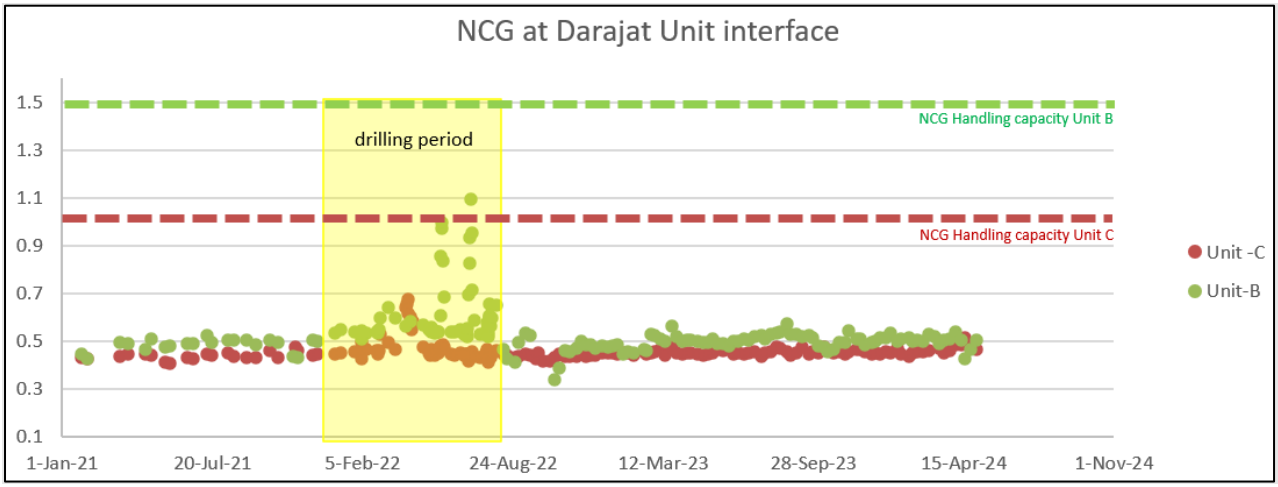

Figure 9: The NCG profile at the DRJ Unit-B interface during drilling in 2022 showed an increase up to 1.1 wt%. However, this remains below the handling capacity of Unit-B for NCG

3.2 Discussion

Observing the pattern of NCG increase in nearby production wells during drilling activities in Darajat reveals that beyond factors like feed zone distance, structure trend and well azimuth, mass extraction dynamics significantly influence the direction of NCG accumulation due to air drilling. Given the lower density of gas from air drilling compared to steam, it tends to accumulate in the shallower parts of the reservoir and migrates towards areas of lower pressure or higher mass production during specific operational phases, potentially shifting as operational conditions adjust. Interestingly, in Darajat, there appears to be no clear correlation between productivity of the drilled well and NCG increase in adjacent wells, suggesting that NCG elevation does not necessarily indicate a proportional impact on production.

Nevertheless, conducting thorough geochemistry monitoring provides substantial benefits on the production front, enabling preventive measures to mitigate any adverse effects on existing wells by promptly analyzing geochemistry data alongside production metrics. This proactive approach allows for timely mitigation strategies to be implemented upon identifying any indicators from the monitored data. Furthermore, having prior knowledge

of potential NCG increases in production wells and power plants facilitates readiness to manage higher NCG levels if they exceed operational thresholds, ensuring continuous and efficient power generation.

On top of that, the expense of deploying this monitoring program is considerably less than the potential hazards arising from inadequate well throttling strategies and monitoring. By integrating this program, the likelihood of production decline due to condensation or scaling in production wells during drilling is minimized, thereby safeguarding against revenue loss from reduced generation output.

ACKNOWLEDGEMENT

We thank Star Energy Geothermal Darajat II, Limited (SEGD) and for supporting this project and Pertamina Geothermal Energy (PGE) granting permission to publish this paper.

REFERENCES

Hadi, J., 2001, "The Darajat Geothermal Field Conceptual Model, A Vapor-dominated System," *Proceedings of the 5th INAGA Annual Scientific Conference and Exhibition*, Yogyakarta, Indonesia, March 7-10, 2001.

Hamilton, W..,1979, "Tectonics of the Indonesian Region," *United States Geological Survey Professional Paper 1078*, 45 pages.

Intani, R. G., Syaffitri, Y., Golla, G. U., Chrisnelson., Cita., F., Ginanjar., 2021, "The Darajat Geothermal Field, Indonesia, After 24 Years of Production," *Proceedings World Geothermal Congress 2020+1*, Reykjavik, Iceland, April - October 2021

Intani, R.G. et al., 2022, " Pioneering the use of natural fracture modeling for well placement at Darajat Field, Indonesia," *2022 Stanford Geothermal Workshop*, Stanford University, Stanford, (2022)

Özcan, Y.N, Gökçen, G., 2010, "Performance Analysis of Single-Flash Geothermal Power Plants: Gas Removal Systems Point of View," *Proceedings World Geothermal Congress 2010*, Bali, Indonesia, 25-29 April 2010

Rejeki, S., Rohrs, D., Nordquist, G., and Fitriyanto, A., 2010, "Geologic Conceptual Model Update of the Darajat Geothermal Field, Indonesia," *Proceedings World Geothermal Congress 2010*, Bali, Indonesia, 25-29 April 2010.

This page is intentionally left blank

Part 4:
Social, Politics, Economics, and Community

This page is intentionally left blank

Preliminary Study of Geothermal Separated Brine Utilization for District Heating at Dieng Plateau, Indonesia

Hendra Ardi Kurniawan[1], María Sigríður Guðjónsdóttir[2],
Málfríður Ómarsdóttir[3], Sarbeni Rangkut[1], and Herdian Ardi Febrianto[1]

[1]PT Geo Dipa Energi (Persero) Aldevco Octagon 2nd Floor,
Jl. Warung Jati Barat No. 75 Jakarta Selatan 12740 – Indonesia
[2]Department of Engineering, Reykjavik University, Menntavegur 1, 101 Reykjavik, Iceland
[3]GRÓ Geothermal Training Programme, Urðarhvarf 8 B (ÍSOR) · 203 Kópavogur · Iceland

hendra.ardi@geodipa.co.id

Keywords: geothermal, waste heat recovery, co-generation, direct utilization

ABSTRACT

The Dieng Plateau in the Central Java Province of Indonesia is known for its significant geothermal potential, particularly within the Dieng Geothermal Field. This paper presents a comprehensive analysis of the geothermal resources and heat demand in the area, focusing on the potential benefits of recovering separated brine as a heat source. The study includes an assessment of the local community's heat demand for bathing, with a survey indicating that 82.7% of respondents use hot water for bathing, primarily utilizing gas (LPG) for heating. Furthermore, the paper discusses the operational details of geothermal power plants in Dieng and highlights the significant amount of unused energy in the form of separated brine. The energy analysis demonstrates the potential for utilizing brine as a heat source, presenting advantages for the company, local communities, and the government. Based on the heat demand survey, every household's total energy consumption in one month was about 703 Gcal or 35,334 GJ/year. This amount of energy is equivalent to 18% of the annual energy consumed by each individual in Indonesia. Currently, PT Geo Dipa Energi uses a single flash system in which the separated brine is not utilized yet. It is potentially to recover the heat of 68.8 MW from this separated brine. The proposed recovery method involves using a counter-current heat exchanger made of stainless steel to prevent corrosion, with the separated brine flowing through the tube side and the groundwater flowing through the shell side. The calculated recovery energy is 28,190 kW, representing 40% of the total energy in the separated brine. Implementing separated brine heat recovery could bring various benefits, including creating a new revenue stream for the company, adopting a techno-social approach, ensuring a sustainable hot water supply, reducing carbon emissions, promoting education and tourism, and affecting the geothermal development. Moreover, there is potential for a reduction in government subsidies for providing natural gas, which could amount to Rp2,876,841,485 annually or lead to a decrease in gas consumption for providing heat in Dieng amounting to Rp4,018,581,255.

1. INTRODUCTION

Located in the regions of Wonosobo, Banjanegara, and Batang in the Central Java Province of Indonesia, the Dieng Plateau is an area of great geothermal interest. It is part of the Dieng Volcanic Complex (DVC) and is known for its diverse geothermal features, including fumaroles and hot springs. This region, referred to as the Dieng Geothermal Field, encompasses a high-temperature liquid-dominated reservoir spanning over 9.5 square kilometers. Studies have indicated that the Dieng geothermal field has the capacity to produce approximately 355 MW of power, primarily from the Sileri, Sikidang, and Pakuwaja sectors (Boedihardi et al., 1991 in Harijoko et al., 2016). Currently, geothermal energy is mainly utilized indirectly, with electricity generation sources being the primary form of utilization. PT Geo Dipa Energi (Persero) is a Special Mission Vehicle under the Indonesia Ministry of Finance, which is tasked to develop and operate a geothermal power plant in the Dieng Geothermal Field. Currently, two power plants produce geothermal energy in Dieng Geothermal Field: Dieng Unit-1 60 MW and Small-Scale Geothermal Power Plant (DSSGPP) 10 MW. The other utilization is direct utilization in the form of tourist attractions such as fumaroles and hot spring pools. Local communities mostly manage the hot spring pool, while the government owns the geothermal manifestation, such as fumaroles.

The Dieng plateau is situated 2000 meters above sea level, resulting in a temperature of around 16°C (see Figure 1). Compared to Jakarta, there is a 13°C temperature difference, making Dieng an attractive tourism destination for those who enjoy cooler weather. Based on weather measurements taken in 2023, the temperature is relatively high at the beginning and end of the year, while it reaches the lowest point around August. Sometimes in August-September, the temperature drops below 0°C, leading to "embun upas", a crystallized fog, formed in the surrounding area of Dieng (see Figure 2). This condition has led the local community to adapt by using hot water for household needs such as bathing. The research on energy demand focused on conducting an initial survey to

understand people's behavior regarding energy use for heating purposes. It is important to note that the research was limited to capturing the energy demand specifically for bathing. According to the survey, 82.7% of respondents use hot water for bathing, while the rest opt for other alternatives. Additionally, 95.3% of respondents utilize gas for heating water, while 4.7% use electricity for the same purpose.

In another perspective, PT Geo Dipa Energi operates a single flash steam geothermal power plant with a significant amount of unused energy in form of separated brine. Based on the first and second laws of the thermodynamics approach, Pambudi (2014) estimated exergy in the production well is at 59,518 kW and electrical generation at 21.71 MW with second law efficiency of around 36.48%. The separated brine value was 13.52 MW. Rudiyanto in 2021, another study showed that the exergy available in the production well was 106,515 kW, and electrical generation was at 40.68 MW with a second-law efficiency of 38.19%. This study showed that the amount of separated brine in the separator was 23.48 MW. A recent study, Hendra in 2023, the thermoeconomics in the Dieng geothermal field was studied using the same approach, and the result showed that the exergy available in the production well was 167,075 kW and electrical generation at 51.57 MW with second law efficiency of around 30.8%. The separated brine value was 51.7 MW. The summarized result of the previous study is presented in Table 1.

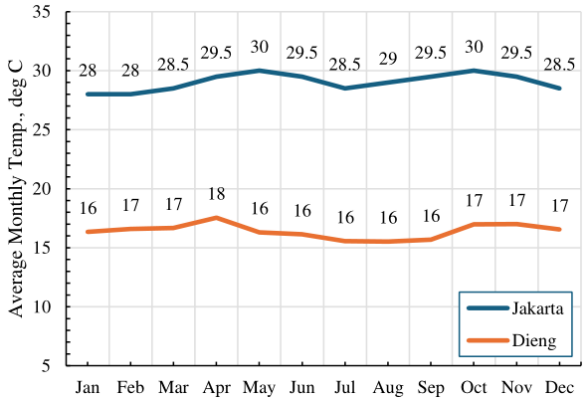

Figure 1: Average trend temperature comparison between Dieng and Jakarta over 2023 (Data: internal data measurement for Dieng, www.timeanddate.com for Jakarta).

Figure 2: "Embun upas" phenomenon in Dieng (Photo: travel.okezone.com).

Table 1: The summarized previous study related with thermodynamics in Dieng Geothermal Field.

Years	Available Exergy at Production Well (kW)	Electrical Generation (kW)	Exergy at Separated Brine in Separator (kW)	Overall Exergetic Efficiency (%)
2014[1]	59,518	21,710	13,523	36.5
2021[2]	106,515	40,680	23,481	38.2
2023[3]	167,075	51,570	51,771	30.8

Note: [1](Pambudi et al., 2014), [2](Bayu et al., 2021), and [3](Kurniawan et al., 2023)

The primary objective of this study is to comprehensively illustrate the potential benefits of harnessing brine as a heat source in the Dieng Plateau area. Utilizing brine as a heat source is one alternative that brings numerous advantages for the company, local communities, and government.

2. HEAT DEMAND

An initial survey has been conducted to understand the local community's behavior in using energy to provide hot water for daily activities within the Dieng Plateau. The survey's limitation is that it only captures the demand for heat for bathing. The survey was conducted by broadcasting a survey form through social media and an instant messaging app. The target of respondents is individuals who live in the Dieng Plateau area. 52 respondents filled out the survey. Although the number of respondents is small compared to the whole population, this number of respondents is sufficient for a pilot study (VanVoorhis, 2007). Figure 3 describes the number of respondents who use hot water for bathing, 82.7% of whom use hot water for bathing, while the rest opt for other alternatives. The next question is about how the respondents get the hot water. This question describes the type of energy that was used to generate heat to provide hot water. Based on the author's perspectives, there are three common energy sources to provide heat: solar water heaters, electrical water heaters, and natural gas water heaters. The survey

results show that respondents only use two energy resources, electrical and natural gas, with 4.7% and 95.3% for electrical and natural gas, respectively (see Figure 4).

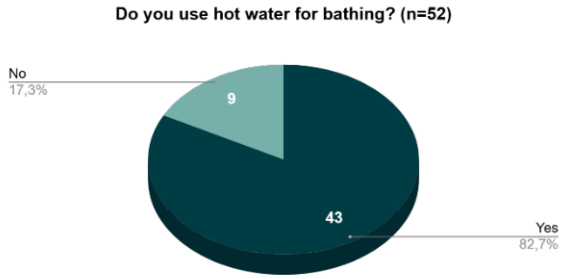

Figure 3: Respondents who use hot water for bathing.

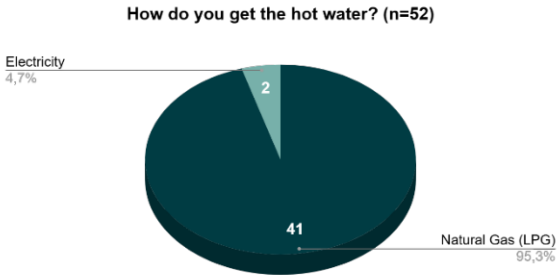

Figure 4: The energy source for providing heat for bathing.

The number of natural gas users is quite significant compared to gas. The author's hypothesis behind this phenomenon is that natural gas water heaters are more cost-competitive in operational cost and instant use compared to gas water heaters. The type of natural gas plays an essential role in operating the natural gas water heater since the price of natural gas is quite different. Natural gas in Indonesia is generally divided into subsidies and non-subsidies natural gas. The price of subsidies for natural gas is Rp4,250/kg (finance.detik.com), while for non-subsidies is Rp15,500/kg (bisnis.tempo.co). The survey result in Figure 5 also describes the type of gas used by respondents; the result shows that 90.2% of respondents use LPG 3 kg, which is a subsidized natural gas, while the rest of the ops use LPG 5.5 kg and 12 kg, which are non-subsidies.

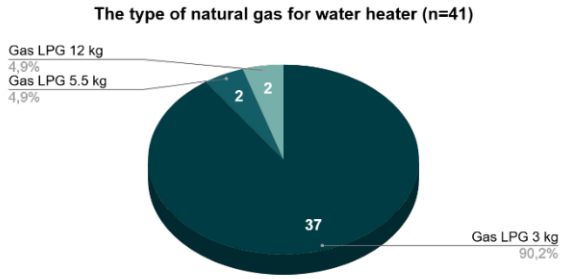

Figure 5: Natural gas types used by respondents who use gas water heater.

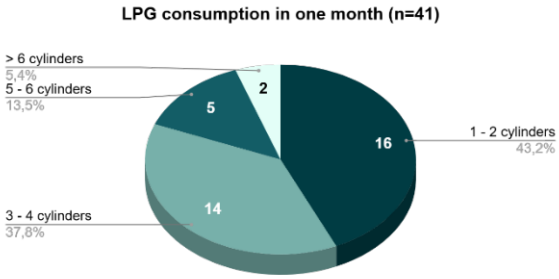

Figure 6: Respondents LPG consumption in one month for providing heat.

Figure 6 illustrates the monthly natural gas consumption in households, measured in cylinder units. The data reveals that 43.2% of households consume 1-2 cylinders, 37.6% consume 3-4 cylinders, 13.5% consume 5-6 cylinders, and 5.4% consume more than six cylinders. The size and the number of household members influence the quantity of cylinders used. Specifically, smaller cylinders lead to higher consumption, and households with more members have higher gas consumption. The relationship between Figure 5 and 6 is summarized in Table 2.

Table 2: Total natural gas (LPG) consumption in one month in Dieng Plateau area.

LPG Type (kg)	LPG Consumption in One Month (cylinders)	Respondents (1 respondents = 1 household)	Natural Gas Consumption (kg/month)
3	2	16	96
3	4	14	168
3	6	5	90
3	8	2	48
5.5	2	2	22
12	2	2	48
Natural Gas Consumption			**472**
Average LPG/Respondents (kg/month-household)			**11.5**

The average LPG consumption for one household is 11.5 kg per month. In terms of energy, 1 kg of LPG produces approximately 11,254 kilocalories (Kcal) of energy (www.esdm.go.id). The total energy required to provide heat for bathing is calculated to be 129,558 Kcal. This number is used as initial data to obtain the heat demand in the

Dieng Plateau area. The total number of households in the Dieng Plateau area is 6,889, distributed in two regencies and seven subdistricts.

Table 3: The number of households in the Dieng Plateau area (kemendagri.go.id).

Regency	Subdistrict	No. of households
Banjarnegara	Banjarnegara – Karangtengah	1,303
Banjarnegara	Batur – Dieng Kulon	1,056
Banjarnegara	Batur – Karangtengah	1,374
Banjarnegara	Batur – Kepakisan	1,044
Banjarnegara	Wanayasa – Karangtengah	600
Wonosobo	Kejajar – Dieng	783
Wonosobo	Kejajar – Sikunang	729
	Total	**6,889**

Based on the survey data and combined with the information from Table 3, the total energy consumption in one month was about 703 Gcal or 35,334 GJ/year. This amount of energy is equivalent to 18% of the annual energy consumed by each individual in Indonesia (Wong et al., 2024). Related to the subsidies given by the Government, the proportion of households who use subsidies and non-subsidies based on the survey is 90.2% and 9.8%, respectively. This proportion equals Rp239,736,790 and Rp95,144,981 for subsidies and non-subsidies in one month.

3. RESOURCE ASSESSMENT

The resource assessment begins with understanding the characteristics of the reservoir and production wells. As previously mentioned, Dieng has a geothermal potential of 355 MW from the Sileri, Sikidang, and Pakuwaja sectors. The fluid originates from a magmatic source and has a relatively high H2S/CO2 ratio in the central zone, with a low total gas content, which is uncommon for high-temperature geothermal systems. The reservoir temperature is around 300°C, and the geothermal fluid's enthalpy ranges from 1,163-1,860 kilojoules per kilogram (kJ/kg). It has a chloride content between 12,000 – 15,000 parts per million (ppm), gas content of 0.3-2.3 weight % of produced steam, steam fraction ranging from 30 – 50% (Layman et al., 2002), and silica content between 1,145-1,400 ppm in the discharge conditions (Pambudi et al., 2015).

Currently, PT Geo Dipa Energi generates electricity from Dieng Unit 1, which has a capacity of 60 MW, and a Small-Scale 10 MW unit with a total output of around 58.5 MW gross. The steam was collected from nine production wells located in the Sileri prospect area. Some of the well characteristics have already changed compared to the initial condition. Figure 7 shows that most production wells have characteristics closer to saturation liquid, with only two wells showing characteristics closer to saturation vapor. Wells closer to saturation liquid will produce more liquid than vapor. From an electrical production perspective, producing from wells with high steam fraction is more uncomplicated and relatively cost-economic than wells with low steam fraction. However, from a brine extraction viewpoint, producing from wells with a low steam fraction is more beneficial, as more energy from brine can be extracted.

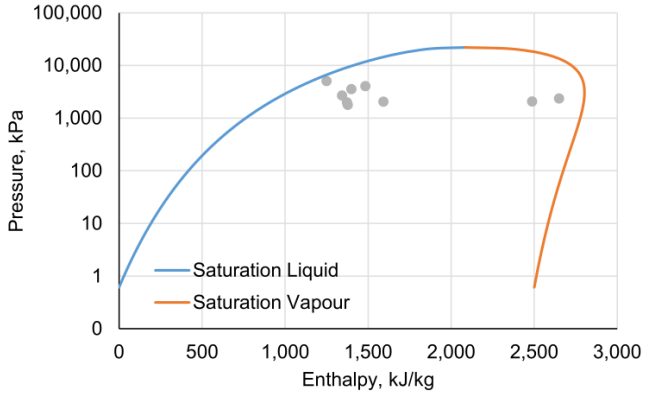

Figure 7: Production well in Dieng Geothermal Field characterized by pressure and enthalpy.

The total electrical generation is approximately 58.5 MW, resulting in a total brine production of around 314.2 tons per hour from all wellpads. The separator pressure at the wellpads ranges from 11 to 13 bar gauge. In this study, it is assumed to be 12 bar gauge for all wellpads. At this operating pressure, the brine temperature is 180°C,

with an enthalpy of approximately 787 kJ/kg. Therefore, the total energy available in the brine is approximately 68.8 MW.

4. DISTRICT HEATING BENCHMARKS

District heating powered by geothermal is not a new technology, especially for a four-season country with geothermal potential. China, Iceland, Turkey, France, and Germany are the leaders in district heating based on capacity and annual energy use. The total installed capacity is now 12,768 MWt, and the annual energy use amounts to 162,979 TJ/year (Lund et al., 2021). Geothermal energy as a source of district heating brings enormous benefits to the environment, economy, and lifestyle. The use of geothermal energy saved 100 million tons of CO2 emissions compared to emissions from using fossil fuels (Gunnlaugsson et al., 2015). In Indonesia, no report describes the direct use of geothermal energy for district heating. The only update about direct use is from WGC2015, where there was direct utilization for aquaculture in Lampung, palm sugar processing using brine in Lahendong, and mushroom cultivation in Pangalengan (Darma et al., 2021).

The author chose Iceland as a benchmark in this section since the same approach will be implemented in this paper. Geothermal district heating started in 1930 utilizing artesian flow from the shallow well in Iceland. Significant development started in 1950, as the demand for heat increased. Nowadays, two sources of district heating in Reykjavik are from low temperature geothermal and heated groundwater In low-temperature geothermal sources, hot water from geothermal wells flows to the surface and then to a deaerator to release the gas content in the fluids. Hot water production mainly uses submersible or vertical pumps to lift the water to the surface. The hot water flows to a tank before being distributed into the city. In another area of Iceland, low-temperature geothermal energy comes from springs, such as Deildartunga in the Reykholt geothermal field. Deildartunga Spring is the largest low-temperature hot spring in the world, producing 180 liters per second of boiling water. Deildartunga provides hot water for the district heating service of Akranes-Borgarnes in Western Iceland to approximately 10,000

residents of Akranes and Borgarnes. It distributes hot water across West Iceland via a 63-kilometer pipeline network from the Deildartunga hot spring (Gunnlaugsson et al., 2015).

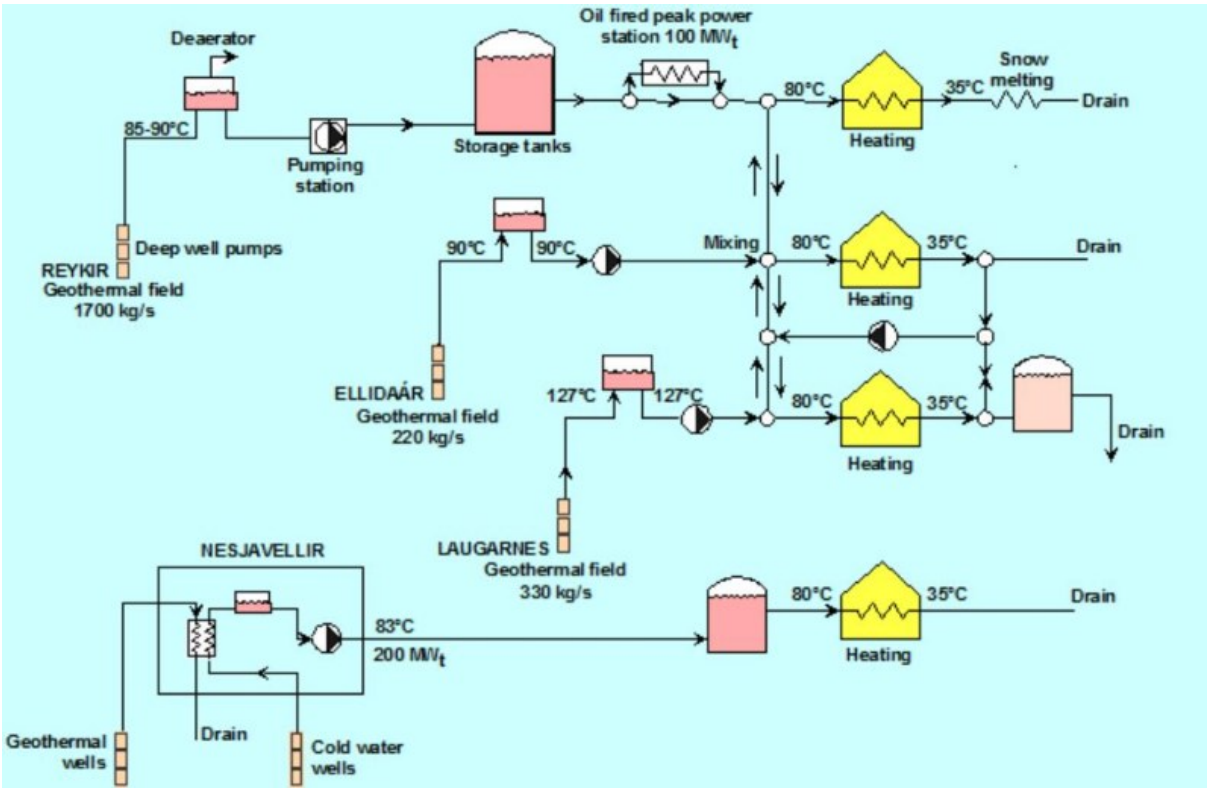

Figure 8: Simplify the district heating system in Reykjavik (Gunnlaugsson et al., 2015).

MW of hot water for district heating for Reykjavik and the surrounding area. Nesjavellir uses a heated groundwater system to produce hot water since the chemical composition in the geothermal water then the fluids cannot be used directly. The groundwater mainly acts as cooling waterfor condensing in the condenser (see Figure 9). The initial groundwater temperature is around 5 – 7°C with a flow rate of 1200 kg/s entering the condenser, and after

the condensing process, the groundwater temperature increases to about 55°C. In order to reach a sufficient temperature for district heating, the groundwater flows through a heat exchanger to increase the temperature to 87°C using separated brine from the separator at 192°C temperature (Gíslason, 2000). Then, the process continues to the deaerator to remove gas content, especially oxygen. The heated groundwater is injected with some geothermal steam, both to remove the last traces of dissolved oxygen by reacting with the hydrogen sulfide (H2S) in the steam and to adjust the water pH to 8.5 (Ballzus et al. 2000 in Gíslason, 2000).

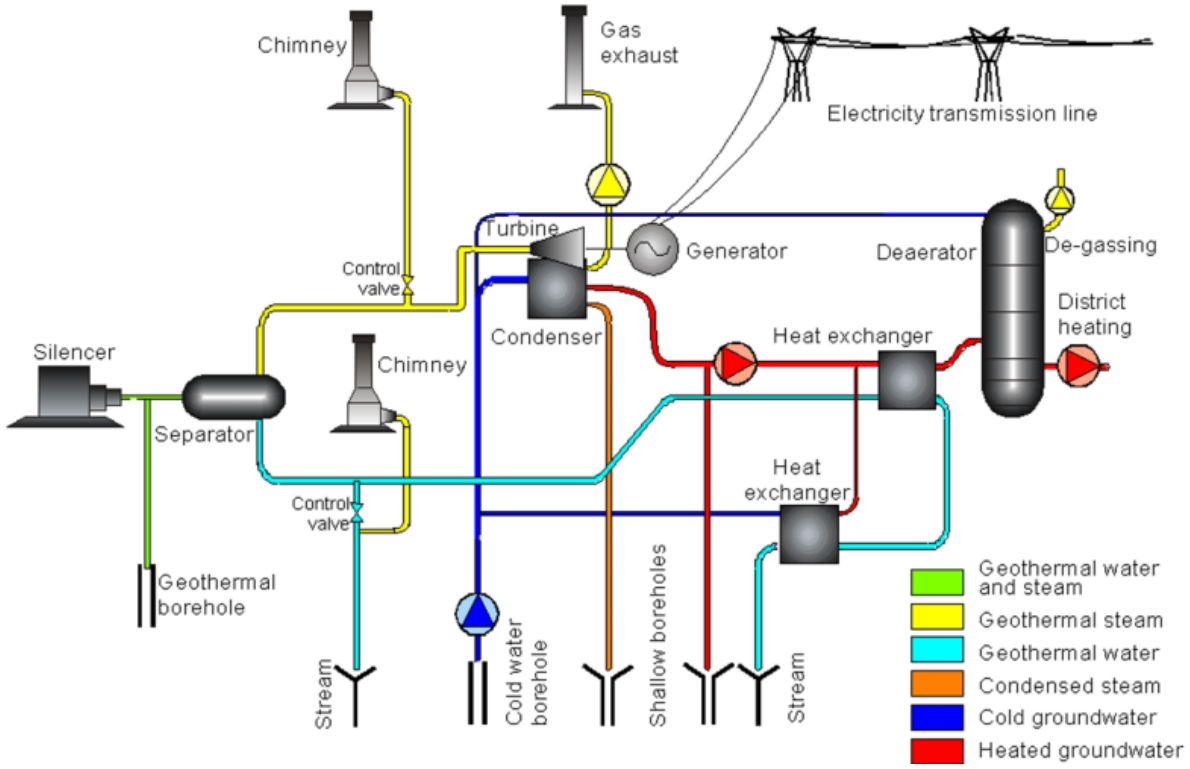

Figure 9: Schematic diagram of Nesjavellir Geothermal Power Plant (Gíslason, 2000).

Nesjavellir is one of the cogeneration power plants in Iceland, which produces 120 MW of electricity and 300

The shell and tube heat exchanger were used in Nesjavellir with brine in the tube and fresh water in the shell side. The heat exchanger has a counter flow of fluids direction and is made of stainless steel (Ballzus et al., 2000). This concept of heated groundwater in Nesjavellir is being tried to be adapted in the Dieng Geothermal Field with several adjustments due to the different fluid characteristics and flow process.

5. HEAT RECOVERY METHOD

In the typical process of geothermal production, the geothermal fluids flow from the reservoir to the surface under isenthalpic conditions and then to the separator for the separation process. The separation between steam and brine depends on the initial enthalpy from the well and the separation pressure, leading to variations in the steam fraction and thermodynamic conditions at different wells or wellpads. Figure 10 describes the process flow diagram in the steam field. The throttle valve controls the wellhead pressure and flow rate through adjustments to the valve opening. As the fluids are flushed, this leads to a decrease in pressure and temperature, eventually reaching a saturated state (1). The fluids are separated at the separator into steam and brine. The water level in the separator, regulated by the control valve (CV), influences the separation process. The separated steam (2) is directed to the power plant, while the separated brine (3) flows to the silencer to reduce noise when releasing the brine into the atmosphere. The pressure difference between the control valve and the silencer causes the brine to flash (4). Subsequently, the separated steam and brine are separated in the silencer. The steam is released into the atmosphere, and the brine is cooled in the open canal and cooling pond and then pumped to the injection well (5).

In this section, this study will outline the proposed considerations for recovering heat energy from separated brine. While similar heat recovery processes have been successfully implemented in Iceland, it is essential to note that adjustments are still necessary due to the uniqueness characteristics of each geothermal field. For example, at the Dieng power plants (Dieng Unit 1 60 MW and Small-Scale 10 MW), the condensing process relies on a circulating water system to condense the steam, thereby limiting groundwater consumption. As part of the proposed process, we plan to heat groundwater directly with separated brine from the separator at approximately 180°C.

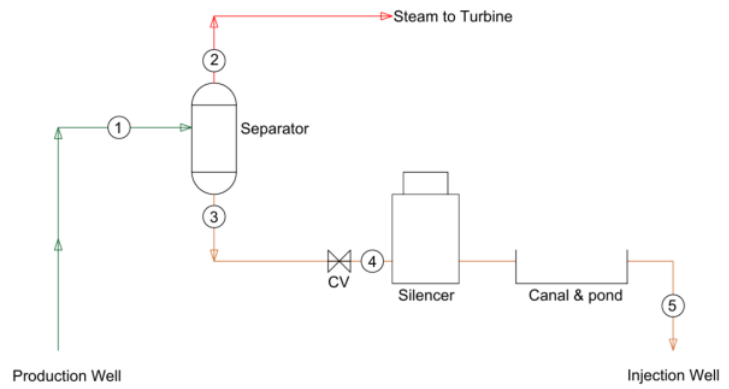

Figure 10: The process flow diagram in the wellpad of Dieng Geothermal Field.

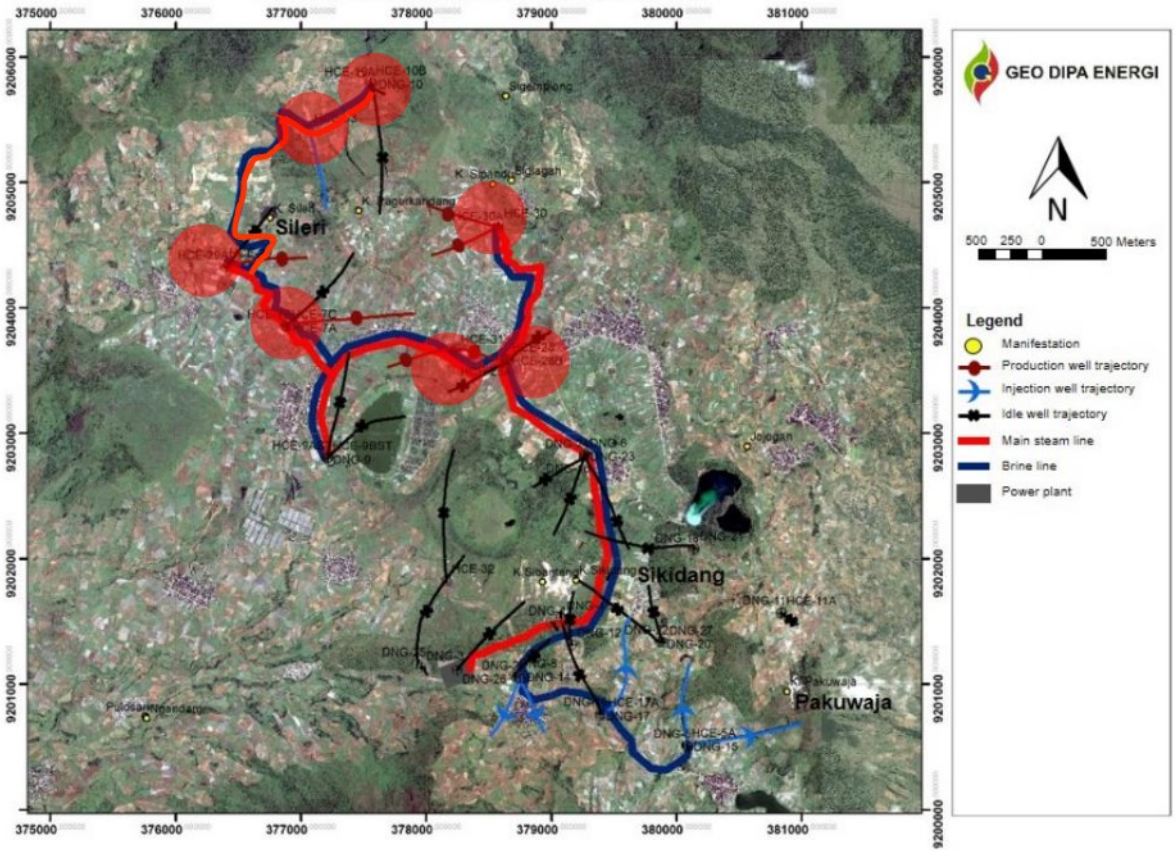

Figure 11: The map of the Dieng geothermal field (Modified from PT Geo Dipa Energi, 2018 in Sondakh, 2018).

5.1 Resource Management

The wellpad area in Dieng Geothermal Field is located separately and distributed in different locations. The red circle in Figure 11 figures out the location of the wellpad. The separation system is not centralized hence the separated brine is not collected in one area. In this particular scenario, it is essential to consider how resources can be effectively managed. This can be done by addressing various scenarios as below:

1. Separated brine is not collected into one area

Based on technical calculations, it is possible to collect brine from all wellpads in one area. However, this scenario is not a reliable solution due to the silica content in brine, which can cause silica deposition along distribution lines. Furthermore, this scenario needs high investment and maintenance costs.

2. Heat exchangers are installed on each wellpad

Installing heat exchangers on each wellpad provides a more reliable solution, even though the initial investment is high. This scenario offers a higher capacity factor, allowing for varying maintenance schedules for each wellpad.

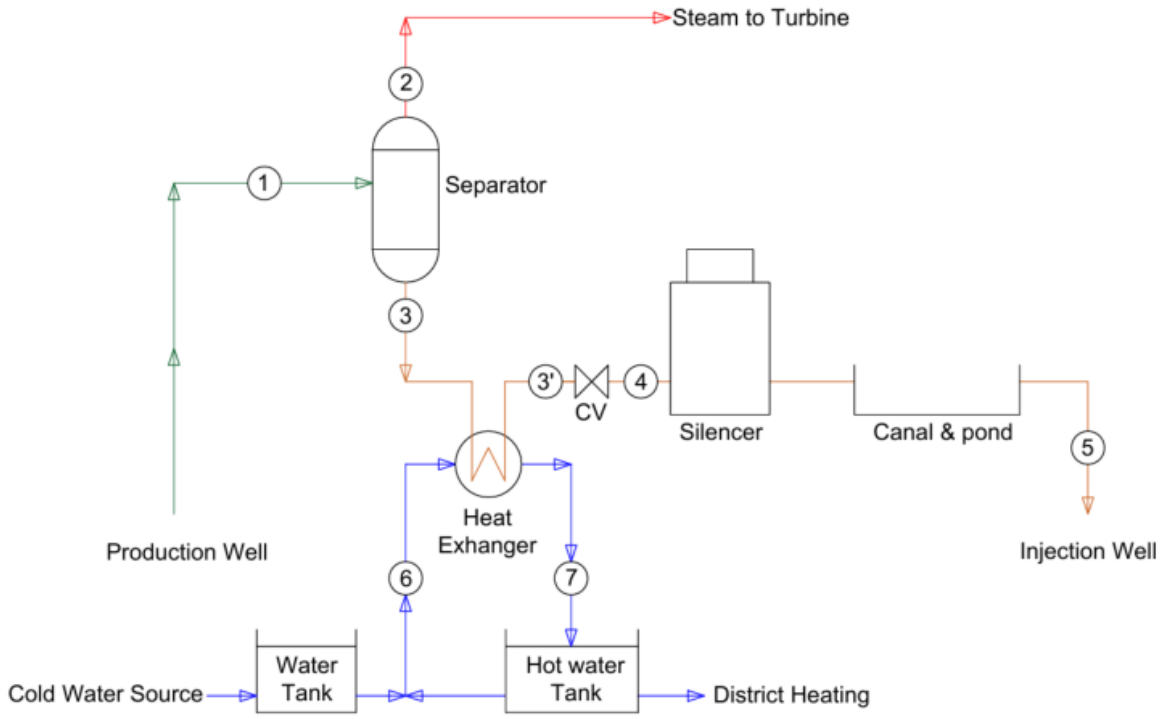

Figure 12: Proposed schematic of separated brine heat recovery.

5.2 Heat Exchanger

The heat exchanger plays a crucial role in energy extraction as a heat extractor of separated brine. In the proposed system, the type of heat exchanger is shell-and-tube, with separated brine on the tube side and groundwater on the shell side. The technical limitations considered in this study regarding heat exchanger selection are flow direction, surface area required, and material selection.

1. Flow direction

There are three common types of heat exchangers based on the flow direction: co-current, counter-current, and mixed (Learman, 2009). The proposed approach in this research is counter-current instead of parallel flow because running a parallel regime carries the potential for a temperature cross. This occurs when the temperatures of the streams are equal, whereas the objective of heat recovery is to ensure that the outlet temperature of the cold stream is higher than that of the hot stream (Welty et al., 2008 in Velasquez, 2020).

2. Surface area required

The selection of flow direction affects the surface area required. It is important to note that when designing the heat exchanger, the minimum required heat transfer surface area is often used to keep the cost down (Velasquez, 2020). The author compared the three types of heat exchangers, and the result shows that at the same heat exchanger duty (Q) required, counter-current heat exchangers have higher LMTD than other types with a lower heat transfer surface area required (see Table 12).

3. Material selection

The separated brine in the current condition is treated with 98% sulfuric acid to prevent scaling in the control valve (see Figure 10). This treatment lowers the pH of the separated brine to around 3 – 4. The proposed material will be stainless steel for both shell and tube.

5.3 Heat Recovery Process

As shown in Figure 10, the heat exchanger is intended to be positioned between the separator and the control valve. This arrangement prevents a significant pressure drop that could cause steam formation. If the heat exchanger is installed after the control valve, steam could be formed due to the pressure drop from the operating system to atmospheric pressure. In Figure 12, the heat recovery process begins with groundwater being transferred from any source to fill the cold-water tank and then piped to the heat exchanger (stream 6). The groundwater temperature increases due to heat transfer from the separated brine, while the temperature of the separated brine decreases due to heat transfer to the groundwater. A circulating line is proposed from the hot water tank to the

heat exchanger to accommodate demand fluctuations. When the demand is low, the groundwater will be circulated to the heat exchanger to maintain the temperature at the desired level. The detailed heat mass balance in this heat recovery process is detailed in Table 4.

According to thermodynamic calculations, the heat recovery from the brine at this circumstances is approximately 28,190 kW, which can produce 345 tons of hot water per hour. An interesting change in the system is the steam fraction formed in the silencer after heat recovery. In a previous study (Kurniawan et al., 2023), the steam fraction in the silencer was approximately 18%, whereas in this simulation, it dropped to 1%.

Table 4: The thermodynamic value of each stream in Figure 12.

Stream	Mass Flow (ton/hour)	Enthalpy (kJ/kg)	Steam Frac. (%)	Temp. (°C)	Pressure (bar a)
3	314.2	794	0	187	11.7
3	314.2	461	0	110	9.73
4	314.2	461	1	92	
6	345.2	84	0	20	
7	345.2	377	0	90	

6. THE BENEFITS OF DISTRICT HEATING

The implementation of district heating, a highly efficient system, benefits the company and the local community around the geothermal area. According to a previously mentioned study, the local community currently relies on the supply of natural gas (LPG), which involves a long distribution supply chain. The specific benefits of district heating are described below.

1. Stream revenue for the company

Currently, with the use of a single flash geothermal system, all separated brine is flashed to the atmosphere and then cooled down in the pond and open canal. However, by recovering the heat from this process, the company can add additional value to its current operation condition. This presents an opportunity to sell hot water, as there is a demand available for it. Therefore, the implementation of district heating allows the company to maximize the efficiency of its geothermal system and create a new revenue stream through the sale of hot water, thereby increasing its overall profitability.

2. Techno-social approach

The techno-social approach of district heating refers to the combination of technological and social factors in the implementation and operation of the heating system. This approach emphasizes the use of technological solutions for efficient energy production and distribution, while also considering the social impact and benefits for the local community. According to the survey results, 84.6% of the respondents want to use geothermal energy as a heat source for providing heat. By directly meeting the needs of the local community, the engagement between the company and the local community will increase, thereby reducing social problems or rejection. This, in turn, will increase the acceptance of geothermal development within the local community.

3. Sustainable supply of hot water

Using geothermal energy for district heating offers numerous benefits compared to traditional LPG heating. Geothermal energy provides a sustainable hot water supply using heat from the separated brine. It is an essentially unlimited resource. This means there is no concern about supply shortages or price fluctuations due to limited stock, as is often the case with LPG.

4. Carbon reducing

Moving from LPG to geothermal energy for district heating offers significant carbon reduction benefits. Geothermal energy produces much lower carbon emissions than traditional LPG heating. Utilizing geothermal energy for district heating can contribute to environmental sustainability and reduce our carbon footprint. This transition aligns with promoting sustainable and environmentally friendly practices, making it a positive step towards addressing climate change.

5. Education and tourism

Implementing geothermal district heating will bring significant educational and tourism benefits as it will be the first of its kind in the country. This pioneering initiative can serve as an educational model for students, researchers, and professionals interested in sustainable energy solutions. It can provide valuable insights into the practical application of geothermal technology, showcasing the environmental and economic advantages of

district heating systems. Furthermore, the unique nature of this proposed project can attract attention from domestic and international tourists. Visitors interested in sustainable energy and environmental initiatives may be drawn to witness the innovative geothermal district heating system. This can create opportunities for educational tours and workshops, fostering greater awareness and understanding of geothermal energy and its potential impact on addressing climate change.

6. Reducing the subsidies

The survey findings indicate that a significant proportion of respondents currently utilize natural gas, a predominantly subsidized resource. Making the switch to geothermal energy has the potential to significantly reduce the reliance on government subsidies for energy production and consumption.

7. CONCLUSION

According to the survey findings, a significant 82.7% of respondents depend on hot water for bathing, with 95.3% of them using natural gas (LPG) as the primary heat source. This reliance on natural gas amounts to 6.51 GJ/year, which equals 18% of the annual energy consumed per person in Indonesia. Additionally, in the Dieng area, PT Geo Dipa Energi is currently generating geothermal electricity using a single flash system, but the separated brine from this process is not being utilized. Calculations indicate a potential heat recovery of 68.8 MW from this separated brine. The proposed recovery method involves using a counter-current heat exchanger made of stainless steel to prevent corrosion, with the separated brine flowing through the tube side and the groundwater flowing through the shell side. The calculated recovery energy is 28,190 kW, representing 40% of the total energy in the separated brine. Implementing separated brine heat recovery could bring various benefits, including creating a new revenue stream for the company, adopting a techno-social approach, ensuring a sustainable hot water supply, reducing carbon emissions, and promoting education and tourism. Another important advantage of geothermal district heating is the potential reduction in government subsidies for providing natural gas. This reduction could amount to Rp2,876,841,485 annually or decrease total gas consumption (subsidies and non-subsidies) for heating in Dieng, amounting to Rp4,018,581,255 annually.

REFERENCES

Ballzus, C., Frimannson, H., Gunnarsson, G. I., & Hrolfsson, I. (2000). The Geothermal Power Plant at Nesjavellir, Iceland. *Proceedings World Geothermal Congress 2000*.

Darma, S., Imani, Y. L., Naufal, M., Shidqi, A., Riyanto, D., & Yunus Daud, M. (2021). Country Update: The Fast Growth of Geothermal Energy Development in Indonesia. *Proceedings World Geothermal Congress 2020+1*, 12, 1–9.

Gíslason, G. (2000). Nesjavellir Co-generation Plant, Iceland. Flow of Geothermal Steam and Non-condensable Gases. *Proceedings World Geothermal Congress 2000*.

Gunnlaugsson, E., Ívarsson, G., & Friðriksson, J. S. (2015). 85 Years of Successful District Heating in Reykjavík, Iceland. In *Proceedings World Geothermal Congress*.

Harijoko, A., Uruma, R., Wibowo, H. E., Setijadji, L. D., Imai, A., Yonezu, K., & Watanabe, K. (2016). Geochronology and magmatic evolution of the Dieng Volcanic Complex, Central Java, Indonesia and their relationships to geothermal resources. *Journal of Volcanology and Geothermal Research*, 310, 209–224. https://doi.org/10.1016/j.jvolgeores.2015.12.010

Kurniawan, H.A., 2023: *Thermoeconomic analysis of Dieng geothermal power plant*. Report 14 in: Geothermal Training in Iceland 2023, UNU-GTP, Iceland, 24 pp.

Layman, E. B., Agus, I., & Warsa, S. (2002). The Dieng Geothermal Resource, Central Java, Indonesia. *Geothermal Resources Council Transactions*, 26. https://www.researchgate.net/publication/289472019

Learman, S. (2009). *SIMPLE HEAT EXCHANGER SIZING CALCULATOR*. Blackmonk Engineering Ltd.

Lund, J. W., & Toth, A. N. (2021). Direct Utilization of Geothermal Energy 2020 Worldwide Review. *Proceedings World Geothermal Congress 2020+1*.

Pambudi, N. A., Itoi, R., Jalilinasrabady, S., & Jaelani, K. (2014). Exergy analysis and optimization of Dieng single-Flash geothermal power plant. *Energy Conversion and Management*, 78, 405–411. https://doi.org/10.1016/j.enconman.2013.10.073

Pambudi, N. A., Itoi, R., Jalilinasrabady, S., & Jaelani, K. (2015a). Performance improvement of a single-flash geothermal power plant in Dieng, Indonesia, upon conversion to a double-flash system using thermodynamic analysis. *Renewable Energy*, 80, 424–431. https://doi.org/10.1016/j.renene.2015.02.025

Pambudi, N. A., Itoi, R., Yamashiro, R., CSS Syah Alam, B. Y., Tusara, L., Jalilinasrabady, S., & Khasani, J. (2015b). The behavior of silica in geothermal brine from Dieng geothermal power plant, Indonesia. *Geothermics*, 54, 109–114.

PT Geo Dipa Energi (Persero). (2022). Annual Report 2022: *Transformation Towards a Geothermal Developer with the Implementation of Exploration & Production Well Drilling*. www.geodipa.co.id.

Rudiyanto, B., Bahthiyar, M. A., Pambudi, N. A., Widjonarko, & Hijriawan, M. (2021). An update of second law analysis and optimization of a single-flash geothermal power plant in Dieng, Indonesia. *Geothermics*, 96.

Sondakh, G.G., 2018: *Dieng geothermal project: Risk assessment for a decision on 60 MW expansion*. Report 26 in: Geothermal Training in Iceland 2018, UNU-GTP, Iceland, 29 pp.

VanVoorhis, C. R. W., & Morgan, B. L. (2007). *Understanding power and rules of thumb for determining sample sizes*. Tutorials in Quantitative Methods for Psychology, 3(2), 43-50.

Velasquez, B. (2020). *Thermoeconomic Analysis and Optimization of Geothermal Power Cycle Utilizing Aqueous Potassium Carbonate for Scrubbing Superheated Steam*. MSc. Thesis, University of Iceland, Reykjavik, Iceland, 84 pp.

Wong, R., & Dewayanti, A. (2024). *Indonesia's energy transition: Dependency, subsidies and renewables*. Asia & the Pacific Policy Studies, e391.

Subsurface Stochastic Integrated Workflows with Downhole Measurements for Preferred Field Development Strategy: Utah FORGE Case Study

Mulyani, S.[1], Khan, A.M.[2], Wisnubroto, B.[1],
Widiatmoko, W.[1], McLennan, J.[3], Trikukuh, J.S.[1], and Puspa, M.A[1]

[1]SLB, Jakarta, Indonesia
[2]SLB, Houston, Texas, USA
[3]University of Utah, Salt Lake City, USA

SMulyani@slb.com, Akhan813@slb.com, BWisnubroto@slb.com, WWidiatmoko@slb.com,
John.McLennan@slb.com, JTrikukuh@slb.com, MPuspa@slb.com

Keywords: fracture model, critically stressed fractures, geomechanics, enhanced geothermal

ABSTRACT

Stochastic techniques, when implemented with sufficient data, calibration, and quality control, enable us to build robust 3D geomodels. In this paper we present a multidomain geoscience approach integrating geology, geophysics, geomechanics, and fracture mechanics. The workflows include fracture characterization, fracture modeling, and geomechanics to comprehend overall geothermal reservoir conditions. Multiple data sources were deployed to reduce uncertainty and optimize lateral landing and field development in geothermal fields. Although natural fractures occupy a small volume of the subsurface formation, they often dominate fluid flow and solute transport in a geothermal system. One of the critical factors that dictate the ability of fractures to conduct fluid flow is their mechanical properties, which are dependent on their state of stress. We present a novel workflow that integrates a natural fracture permeability model that has been analyzed using critical stress prediction with other geological information to improve the delineation of favorable geothermal conditions or a "sweet spot" map as reference for well targeting at the Utah Frontier Observatory for Research in Geothermal Energy (FORGE) project site, Utah, USA. The reference field is classified as hot dry rock or an enhanced geothermal system (EGS); however, the workflow proposed in this study is applicable to other geothermal systems. The workflow starts with analyzing the open-source dataset of the Utah FORGE site to generate high-resolution 3D geological models, containing information such as lithology, geological structures, and temperature models. Openhole evaluation logs from six wells were consumed, including the injector and producer wells 16A-32 and 16B-32. Subsequently, the model is populated with a discrete fracture network (DFN) using a natural fracture prediction algorithm, which is a geomechanical inversion approach to model fracture networks (type, orientation, and spatial distribution) by calculating the stress distribution and rock failure criteria at the time of fracturing using available reservoir structure data, including faults, measured stress conditions, and tectonic settings. Once the fracture model is created, a critical stress analysis using a 3D mechanical earth model is performed on the fracture model to identify critically stressed/open fractures that contribute to fluid flow in the geothermal reservoir. Finally, the identified fracture planes that contribute to fluid flow are upscaled into a 3D fracture permeability model using the Oda method. The full 3D fracture permeability model is calibrated and tuned by using the laboratory core experiments elastic properties measurements, stress evaluation from fracture injection tests and fracturing treatments, microseismic and other downhole optic fiber measurements. The average map of the geomechanically analyzed fracture permeability model is statistically combined with temperatures maps to obtain the probability distribution or chance maps of favorable geothermal conditions with a high probability value, indicating a higher chance to have a geothermal area with excellent production potential. This strategy can be used in enhanced geothermal systems to enhance connection through fractures while mitigating thermal breakthroughs. The approach can also be used in field development of mature and green hydrothermal fields to maximize the power plant outputs.

1. INTRODUCTION

Geothermal systems aim at extracting heat from the Earth and transporting it to surface plants for power generation. Developing geothermal energy provides an alternate source of energy from oil and gas and is critical in diversifying the global energy mix today. A functional geothermal system, among other things, requires in-situ heat, carrier fluid (typically water), and system permeability (flow capacity). Based on these requirements, the energy developments within geothermal are broadly classified into three parts: (a) conventional hydrothermal systems (CHS) that have all three required elements. The source rock has permeability, either in the matrix or through large preexisting fractures; (b) EGSs that target the reservoirs where system permeability is not sufficient for flow. Hence large fracture networks are created through surface pumping of high-pressure fluid to hydraulically fracture the rock. These developments require an injector-producer doublet to be functional. The cold fluid is injected and circulated through the rock and benefits from the heat transfer from hot rock during its

transient travel from the injector to the producer; and (c) advanced geothermal systems (AGS) also target the same reservoirs as in EGS but here the network is created by the drilled wells instead of fractured rock. The heat transfer happens in the transient time of the circulating fluid through the network. Because these systems do not require the fluid to interact with the reservoir rock matrix, these are also known as closed-loop systems.

In this paper we try to address critical applications in the second development type above; i.e., EGS, using the detailed dataset of the US Department of Energy (DoE) -funded FORGE project. The success of an EGS project depends on a few things, such as (a) integrated life-cycle modeling of the geology, stratigraphy, natural fractures, hydraulic fracture propagation, geomechanical and geochemical dynamics during fracturing and circulation phases. A detailed review on this from the subsurface perspective is given by Kresse et al. (2024); (b) relative lateral placement of the doublet wells—this is critical because the cost efficiency of the project will depend on achieving a fine balance in well placement. The balance is required between close spacing between wells, which enables achieving a successful connection, at the same time with enough distance between them that enables sufficient transient time to achieve the required heat transfer; (c) thermal breakthroughs through highly conductive channels—these features can carry large amounts of circulation fluid compared to other parts of the network, limiting the capacity of EGS as a heat exchanger; (d) overall system conformance—similar to shale developments where maximizing cluster efficiency is critical, EGS also requires uniform fracture network generation. Cluster efficiency is defined as the ratio of effectively stimulated clusters and total clusters. This parameter dictates the production performance of shale completions. In EGS, similar nonuniformity in stimulating across the full lateral can lead to ineffective heat sweep efficiency.

Building a reliable 3D geomodel with accurate structural stratigraphy, geologic features, and geometry is a precursor to successful life-cycle modeling for EGS. The formation stratigraphy dictates the volumetrics and therefore the amount of energy that can be commercially produced from it (Wallis et al. 2017). In designing the EGS, we aim to artificially define this ultimate reservoir geometry, shape, and extent, and hence the preexisting geological structure and the stratigraphy is critical for consideration.

Also, constructing a reliable, realistic model of the existing discrete fracture adds to the previous step, serving the same purpose of assisting in an effective engineered design of the EGS. Fluid circulation depends on the density, orientation, and capacity of these fractures to interact with induced fractures to either reopen temporarily or for extended periods of time, thus adding to the system conductivity. For this reason, fracture characterization is equally critical in the overall design scheme.

In this paper, we attempt to construct a reliable geomodel with fractures based on multiple data sources such as image logs, injection-falloff test analysis, triaxial core test results, microearthquake data during phase1 stimulation of FORGE in 2022, openhole acoustic data, and calibrate elastic properties calculation from the doublet wells 16A(78)-32 and 16B(78)-32. In addition to the data, multiple stochastic property modeling techniques were used to come up with a model that addresses the four key challenges of EGS highlighted earlier in this section.

Even though the target for this study (from the perspective of the FORGE dataset) is EGS, the application spectrum can be implemented in CHS developments as well. Since reinjection of fluid through injection wells for pressure management is a critical element of CHS, structural modeling, and well placement patterns for production and injection wells are a high value task for geothermal operators. The work described here can efficiently be extended for applications history-matching processes and well placement to enhance field-development strategy.

2. REFERENCE FIELD

This research uses data originating from Utah FORGE in Utah, USA. This site is located around 322 km south of Salt Lake City and around 16 km north of Milford. The FORGE site is unpopulated and covers an area of about 5 km2. The site is situated within Utah's Renewable Energy Corridor, close to a wind farm, solar field, geothermal plant, and a biogas facility (Figure 1). The FORGE site is a field laboratory managed by the U.S. DoE, which provides a unique opportunity to develop and assess new technologies for characterizing, creating, and sustaining an EGS in a controlled environment. The main objective of the FORGE project is to demonstrate to the public, stakeholders, and the energy industry that EGS technologies have the potential to contribute significantly to future power generation (Moore et al., 2020).

The investigations for geothermal around the FORGE site have been ongoing since the late 1970s. Based on several science investigations, the geological condition of this field has been well defined. The lithology of this site consists of Tertiary plutonic rocks (granitoid), Paleozoic and Mesozoic sedimentary sequences, and Quaternary rhyolite lava flows. The geological structures in this field consist of four faults and fault systems, including the basin-bounding fault unconformity, Opal Mound fault, Negro Mag fault, and Mineral Mountain West fault system (Bartley, 2019; Kirby, 2019; Knudsen et al., 2019; Simmons et al., 2019). The basin-bounding fault unconformity marks the contact between the basin fills and the basement rocks, fault dips around 30°. Opal

Mound fault is a steep east-dipping fault, it is the hydrological barrier that prevents the westward hydrothermal flow of the Roosevelt Hydrothermal System (Allis and Larsen, 2012; Allis et al., 2016; Simmons et al., 2019). Black fault is a steeply dipping fault that strike in the E-W direction, it offsets old alluvial fan deposits in the Negro Mag wash area, and geomorphic evidence shows that most of the Pleistocene rhyolite bodies are located south of the fault. Mineral Mountains West fault system consists of parallel N-S trending and forming normal fault segments, these faults are rooted in the basin-bounding fault unconformity, with observable offsets exposed at the alluvium deposit's surface (Bartley, 2019).

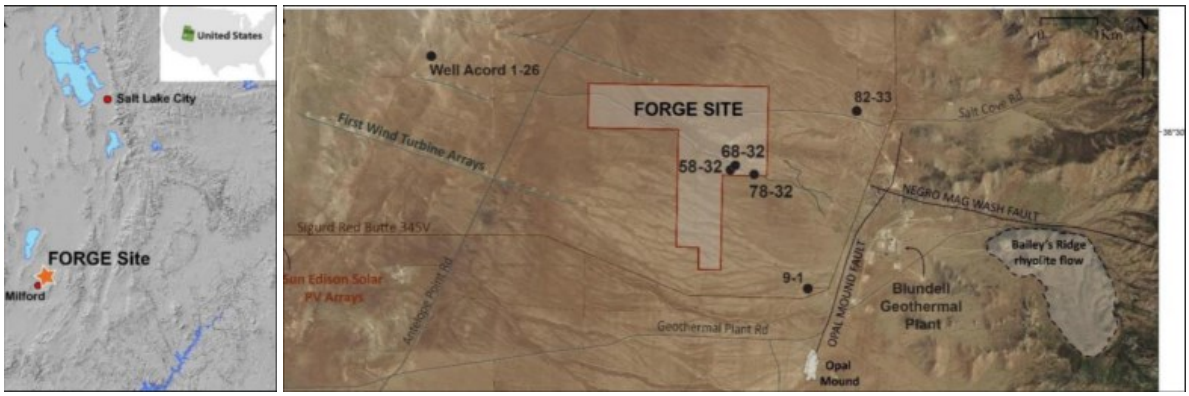

Figure 1: Location maps of the Utah FORGE site (left) and expanded view of the area surrounding the Utah FORGE site (right) (after Moore et al., 2020).

The Utah FORGE site is located within the Roosevelt Hot Springs geothermal area. The reservoir temperature of Roosevelt Geothermal Area that exceeds 250°C has a shallow cooling magma as the heat source (Moore et al., 2020). Suitable temperature range for EGS in the Utah FORGE site is found in the granitoid basement rock at a depth of at least 2,000 m with characteristically low permeability and consistent mechanical properties (Moore et al., 2020). In this field, the Opal Mound fault forms a hydraulic barrier separating the convective, permeable Roosevelt Hot Springs geothermal system from the low-permeability thermal regime to the west, beneath the FORGE site (Knudsen et al., 2019).

The FORGE site is located within a normal faulting regime, with a moderate contrast between the maximum and minimum horizontal stresses (McLennan, 2018). Induced fractures showed trend NNE-SSW as the direction of σHmax, while the stress gradient for σhmin, based on the results of the 2019 stimulations, range from 16.7 to 17.6 kPa/m. A gradient of 25.6 kPa/m (1.13 psi/ft) was calculated for σV. Three stimulations were conducted in 2019. The first stimulation was performed in the openhole section of the well, resulting slightly lower than the 2017 tests, suggesting the fracture system had developed some degree of permanence. Multiple stress signatures suggest closure of tensile fractures and dilated natural fractures (Moore et al., 2020).

3. DATA

Compared with earlier study, the only data that is different in this new study is the addition of data from new wells (16A-32 & 16B-32). The data from this well was then combined with the existing 3D model from the previous study. The structural, lithology, temperature, fracture, and geomechanics models are available within the same project modeling software. The novel value from this new study is added data from new wells. All the data and information usen in the study were obtained from the published website at the Energy and Geoscience Institute at the University of Utah (Energy and Geoscience Institute, 2021).

3.1 Existing Models

The existing models used to update the fracture and geomechanics models are the structural (faults) model, lithology model, temperature and fracture model. The faults model is a key input for the inversion process using a natural fracture prediction (NFP) fracture driver. This fracture driver is a geomechanical inversion approach to model fracture networks (type, orientation, and spatial distribution) by calculating the stress distribution and rock failure criteria at the time of fracturing based on the available reservoir fault model, measured stress conditions, and tectonic settings. The lithology model was used to filter the granitoid zone as the main lithology for the fracture modeling process. Moreover, the existing temperature model was used for the probability map. This model was built from the temperature log and temperature contour points, which distributed into the 3D model by using the kriging algorithm (Mulyani and Juandi, 2019). Previous research has been done to build a fracture model based on critical stress analysis to identify the effective fractures that contribute to fracture permeability (Mulyani et al., 2023). Four producer wells (Wells 58-32, 9-1, 52-21, and 14-2) were used to build this fracture model, with only one well (Well 58-32) that has the fracture point. With this limitation on the data availability, the uncertainty

level of the sweet spot generated based on fracture permeability is still high. The distribution of critically stressed fractures from the existing model can be seen in Figure 2.

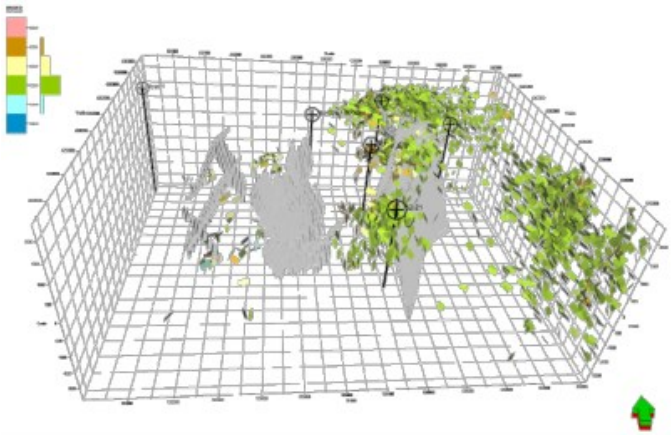

Figure 2: The distribution of critically stressed fractures based on the existing fracture model in the study area.

3.2 New Well Data

Two additional wells have been added to the previous study: Wells 16A-32 and 16B-32. These wells are an injector with borehole image data and a producer with modulus, elastic, and rock strength logs. Well 16A-32 has a maximum depth of 8,565 ft TVD located west of Well 58-32. Well 16B-32 is highly deviated like 16A-32, with a maximum depth of 8,352 ft TVD, as shown in Figure 3.

Figure 3: Satellite maps of the Utah FORGE site with location of existing Well 58-32 and new Wells 16A-32 and 16B-32 (left), and the cross section that parallels the trajectory of Well 16A-32 (right) (after Finnila and Jones, 2024).

Core data from Well 58-32 has also been obtained, to add the mechanical properties for the calibration of the previous study. A total of six wells (58-32, 9-1, 52-21, 14-2, 16A-32, and 16B-32) were used in this study to generate a more comprehensive fracture model.

The main input for the fracture model is well point fracture data, using all attributes such as dip angle, dip azimuth, and fracture classification. The fracture point data used for fracture modeling are the fracture data that are being defined as conductive-continuous fracture, conductive-noncontinuous fractures, conductive-partial resistive fractures, fault, and microfault. The original number for fracture data are 3.414 fractures; then after being filtered for fracture type, resulted in 2.966 fractures. These fracture data are located along the well trajectories at (-944 m) to 942 m depth. The main inputs for geomechanics analysis are well log data such as gamma ray, density, and sonic from Well 16A-32.

4. WORKFLOW

As a followup study to previous research, this research has a similar workflow including data preparation, fracture modeling process, critical stress analysis, fracture permeability upscaling, and creating the probability map. The next section gives the detailed explanation for each step of the process.

4.1 Data Preparation

During data preparation, added data from Well 16A-32 and 16B-32 were loaded into modeling software. All added data available in digital format can be imported directly without additional digitization process. The quality control was done by assessing the correct location of well data and the right content of well log information. The example of new data that have been loaded into modeling software are well path of 16A-32 and 16B-32, fracture point data along Well 16A-32, and microseismic data at the bottom of Well 16A-32 and 16B-32, as shown in Figure 4.

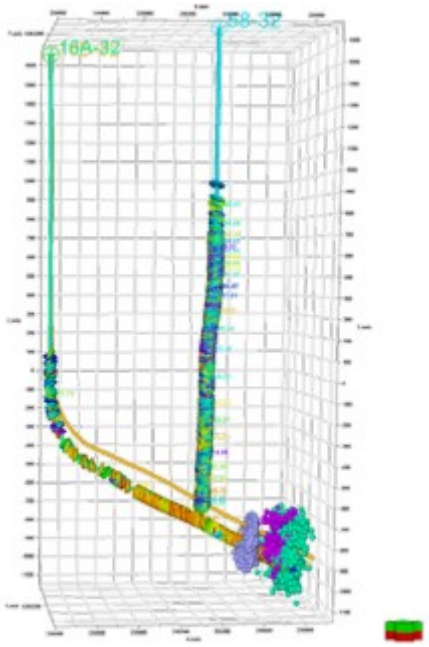

Figure 4: The additional data loaded into modeling software consist of well trajectories, fracture point, and microseismic.

4.2 Fracture Modeling Process

The purpose of modeling fractures is to create simulation properties with the power to predict the reservoir behavior. By modeling the fractures explicitly, one can honor the spatial relationships between properties in adjacent cells. Fracture modeling is a multistep process that involves the preparation of fracture well data, fault, and 3D grid model, followed by fracture driver generation and finally running the fracture model. Following the existing study done in 2022, in this study NFP was used as single fracture driver to create the DFN (Mulyani et al., 2022). NFP is a geomechanically based solution uses a geomechanics approach for computing maps of both natural fracture orientation and density trends, from observed major faults and observed fracture data along wells. To run the NFP process, fracture data with fracture characteristics information such as dip azimuth and dip angle should be classified into several fracture types. In this study the fracture classification is done using a cutoff dip angle of 70o to separate between fault (dip <= 70°) and joint (dip > 70°). The fracture data used as input were obtained from Wells 58-32 and 16A-32, with a total of 2,966 fracture data. The main process for NFP is creating the tectonic model. It was created by running multiple geomechanical simulations to acquire the best-fit stress parameters based on the present-day fault and fracture data. To improve accuracy, the tectonic model was subdivided into four tectonic events based on the prevailing major faults in the study area, from oldest to youngest: Fault Unconformity, Opal Mound fault, Negro Mag fault, and Mineral Mountain West fault system (Figure 5). The fracture data were used concurrently to model each tectonic event. For every running process, selected fracture data will be correlated to each tectonic event with the lowest fit cutoff of 0.7.

The result of all tectonic event modeling is consistent with the observed normal faulting regime with a different angle of principal stress and stress ratio. The unconformity fault used for tectonic event 1 has a stress ratio of 0.28 and angle 42°. The Opal Mound fault for tectonic event 2 has a stress ratio of 0.04 with angle 14°. The Negro Mag fault as tectonic event 3 has a stress ratio of 0.92 and angle 161°, and tectonic event 4, Mineral Mountain fault, has a stress ratio of 0 and angle 90°. The maximum fit of tectonic events 1 to 4 are as follows: 59.1%, 66%, 59%, and 66%. The maximum fit is a parameter showing how the match is the original well fracture data with calculated fracture data as the result of geomechanical inversion process. A higher maximum fit value will give a higher confidence for the geological accuracy of the tectonic model. This result is slightly higher than the existing study.

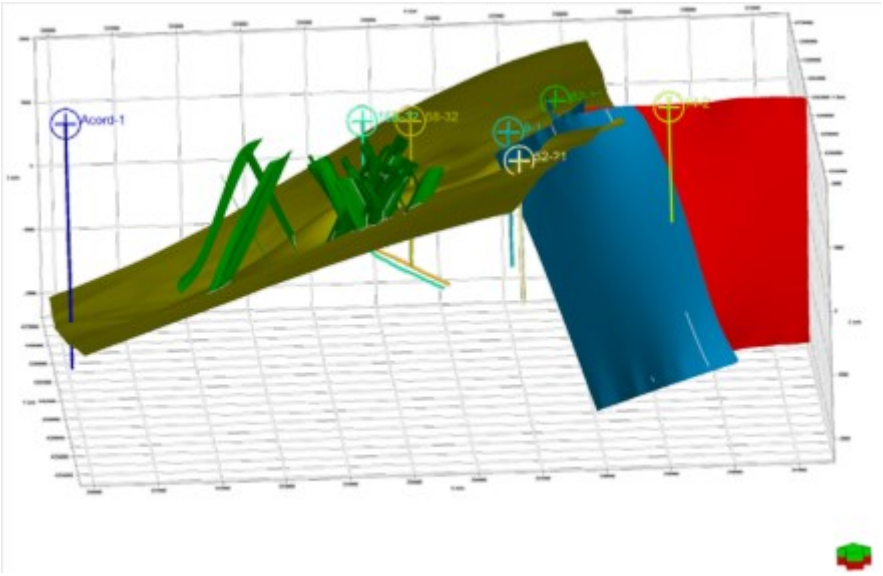

Figure 5: Fault model at the study area consisting of Fault Unconformity (yellow), Opal Mound fault (blue), Negro Mag fault (red), and Mineral Mountain West fault system (green).

Figure 6: The fracture model at microseismic location shown by fracture plane (blue) with fracture length around 460 m used for geometry input for DFN modeling.

The tectonic model process will create new attributes of fracture point well data, including fracture orientation of calculated fractures based on the geomechanics inversion for each tectonic event that was generated. The process will automatically compare the fracture orientation between observed data and calculated fracture data in the same position. In this case, if fracture data have a good match with tectonic model 1, then it will be classified as explained fracture by tectonic event 1. Meanwhile, the rest will be used for the next tectonic model and the fractures that could not be explained by any tectonic model will be classified as residual or unknown fractures. The sequences of tectonic events run for this study resulted in 317 fractures from original 2,966 fractures or around 11%. The total fractures that can be explained by those four tectonic events is around 89% higher than the previous study, which is around 82% of fractures that could be explained by NFP.

The next process is generating the fracture driver. This process used the final tectonic model and working 3D cellular grid as inputs. The results of this process are fracture properties driver set such as dip angle, dip azimuth, and intensity for each fracture type. The results are six fracture drivers set generated by all tectonic events for the fracture modeling process. In this study, the fracture model set that can be generated are tectonic model 1 (fault), tectonic model 1 (joint), tectonic model 2 (fault), tectonic model 2 (joint), tectonic model 3 (joint), and tectonic model 4 (joint). These new results are more comprehensive than the existing study because this one corresponds with all faults in study area, so each fault has representative fractures related to that fault.

The simulation method used in the fracture modeling process is stochastic and used granitoid for the zone in 3D grid, which was interpreted as a zone of interest in this reference study. For each fracture set, the parameter for fracture distribution, geometry, orientation, and aperture that will be modeled should be defined correctly. The fracture distribution and orientation used fracture intensity, dip angle, and dip azimuth from fracture driver

properties and the constant concentration value 10 to get more variation of fracture orientation. The parameter of fracture length for the fracture model following exponential algorithm which requires a mean value and a maximum value to be defined. The mean value of fracture length that is being used as input in the model is 25 m and maximum length of implicit fractures or the shortest discrete fracture is 250 m. To avoid the creation of large fractures, the maximum length of modeled fractures was defined as 460 m. The value of maximum length of fracture model was identified based on the available microseismic data. In this case, all microseismic data were used to create a deterministic fracture model resulting in three fracture planes with length around 460 m (Figure 6). For the fracture aperture model, log-normal was used as the method with an aperture mean of 0.000075 m and standard deviation of 0.0000015 m (Mulyani et al., 2022).

4.3 Critical Stress Analysis

The comprehensive geomechanics workflow for 3D critically stressed fracture analysis is implemented in this study by incorporating multidomain data from geology and geophysics (static model, magnetotelluric model, and fracture model) and new technology as a method during 3D mechanical property distribution (machine learning), as shown in Figure 7. The process begins with establishing a robust 1D geomechanics or 1D mechanical earth model (1D MEM) before conducting 3D geomechanics analysis. Initially, a 1D analysis was performed on the five offset wells available in the Utah FORGE area, adding one new offset well compared to the previous study in 2023. The 1D MEM was constructed and validated with rock mechanics testing data from another study from McLennan (2018). In the subsequent steps, the 1D MEM is scaled up to a 3D geomechanics grid and distributed across the entire 3D geomechanics model. Finally, the 3D geomechanics model undergoes simulation using a geomechanical simulator (finite element) to predict the stresses in the field. The simulated stresses output was used as one of the inputs for discontinuity stability analysis (critically stressed fracture) in the field.

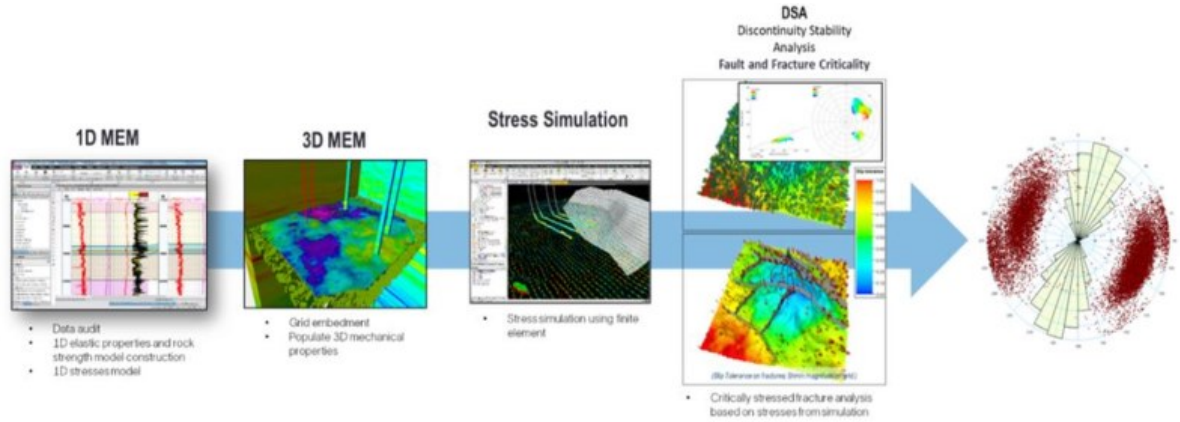

Figure 7: Workflow of 3D geomechanics for critically stressed fracture analysis.

4.4 Fracture Upscaling and Probability Map

The final stage of this study is combining the updated fracture permeability model with the available temperature model. Following the workaround from the earlier study, the updated fracture permeability model was obtained from a scale-up fracture network property from critically stressed fractures. This process converts the fracture attributes into dual-porosity or dual-permeability simulation properties. These are fracture porosity, fracture permeability, and sigma factor (the connectivity between the fractures and the matrix). In this study, the main output from the scale-up fracture network is the fracture permeability. The algorithm to calculate this property called the Oda method. It is a statistical calculation estimating permeability, based on the total area of fractures in each cell and their various parameters. This algorithm does not take the connectivity of fractures into account and can underestimate fracture permeability when the intensity is low (SLB, 2024).

The probability map is obtained through harmonic averaging of the fracture permeability for all directions; this way areas that feature poorly on at least one of the maps penalize the combined map (Figure 8). The harmonic mean works well with log-normal distributions and is commonly used for permeability because it is sensitive to lower values. After the permeability maps were calculated, the temperature model is then combined by using arithmetic averaging. This method can minimize the risks linked with uncertain data and geological interpretation. The resulting probability map is a combination of high potential zones based on identified permeability and temperature yields a synthetic view of the most favorable drilling locations (Mulyani et al., 2023).

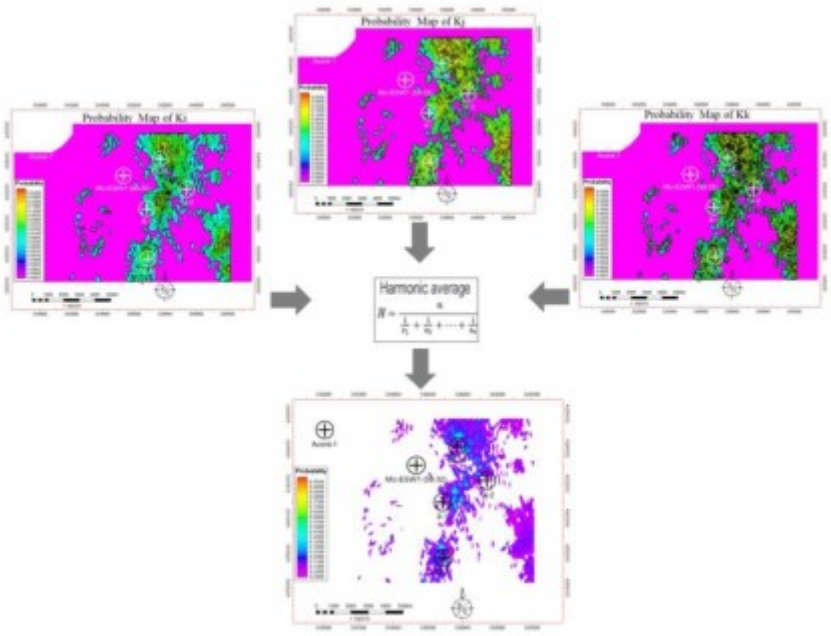

Figure 8: Harmonic averaging method to combine the parameters of fracture permeability ki, kj, and kk.

5. RESULTS AND DISCUSSION

In this study all results from the existing study were updated with new well data. The new results from this study consisting of updated fracture model, updated geomechanics model, updated critically stressed fractures, and updated probability map. The following is the detailed explanation for each result.

5.1 Updated Fracture Model

The existing fracture model was created by using the NFP fracture driver and fracture point data from a single well (58-32). Based on the tectonic model created by using the available faults data, four fracture driver sets were obtained: Tectonic model 1, related with Unconformity faults, resulting joint and fault type of fractures with high intensity in the southern part. Tectonic model 2 related with Opal Mound Faults resulting fault type of fractures with high intensity in the eastern part. Tectonic model 3 related with Negro Mag Fault and has a very small number of explained fractures data, therefore no intensity of fracture that can be calculated, while tectonic model 4 related with Mineral Mountains Faults resulting joint type and has highest intensity in the southwestern part. The total fracture model as a visible patch in this DFN is 104,438. Fracture orientations of all fractures in the model has two general orientations, including NW-SE and E-W (Figure 9). The NE-trending fractures are muted in the resulting model. The dip azimuth was dominated with fractures with a direction around N 300o E and the dip angle shows a normal trend (Mulyani and Aulia, 2022).

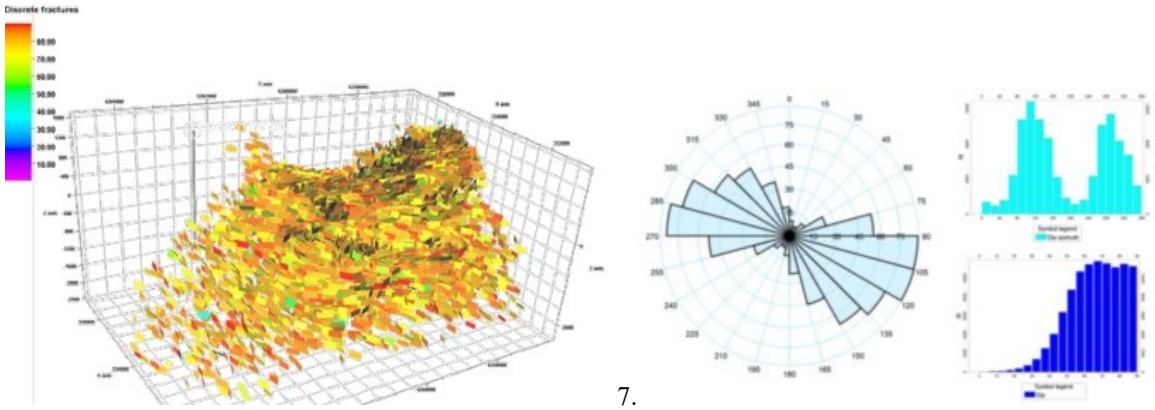

7.

Figure 9: Fracture model from one fracture set at existing fracture model (left), dip angle and azimuth of fracture model (right). Observed general orientations including NW-SE and E-W (after Mulyani and Aulia, 2022).

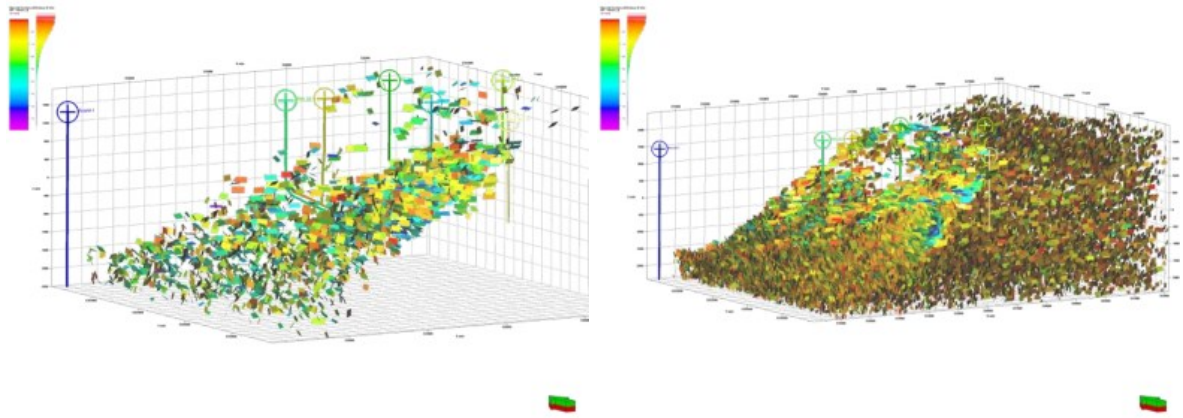

Figure 10: Fracture model generated from NFP of Unconformity Fault consist of fracture set 1 (fault) in the left and fracture set 2 (joint) in the right. The color of patches shows the dip angle of the fracture plane.

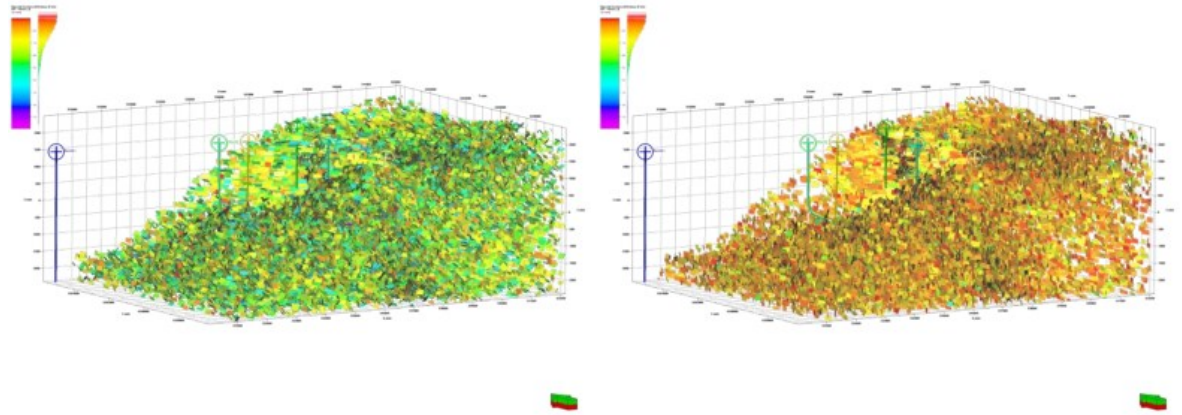

Figure 11: Fracture model generated from NFP of Opal Mound Fault consist of fracture set 3 (fault) in the left and fracture set 4 (joint) in the right. The color of patches shows the dip of fracture where fracture set 4 (joint) has igher value.

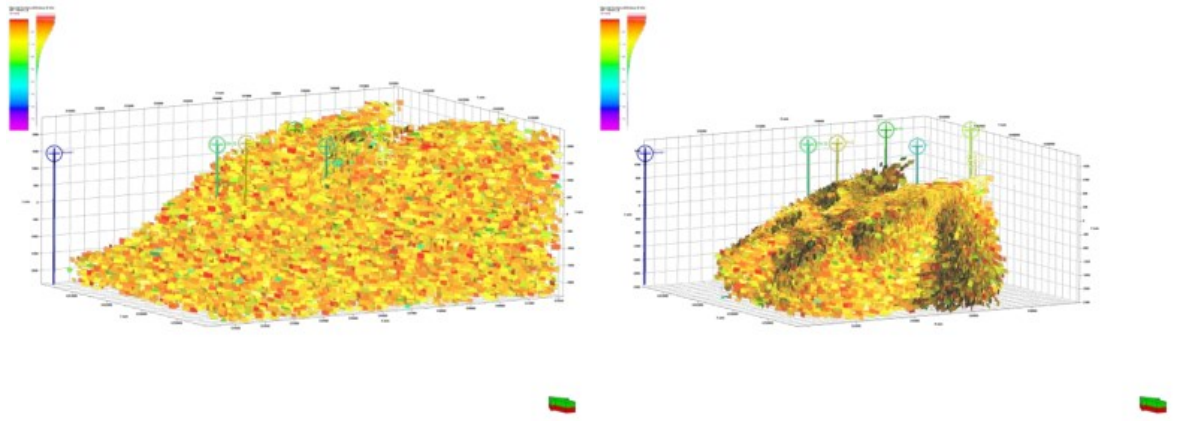

Figure 12: Fracture model generated from NFP of Negro Mag Fault consist of fracture set 5 (joints) on the left and fracture model generated from NFP of Mineral Mountain Fault System consist of fracture set 6 (joints) on the right.

The updated fracture model was created by using the same faults model to run NFP, with fracture point data from Well 58-32 and Well 16A-32. The DFN generated from fracture modeling consisting of six fracture sets based on NFP fracture drivers. There are two fracture sets corresponding to Unconformity Fault. The first fracture set defined as fractures related to faults shown in Figure 10 (left). This fracture model was distributed along the unconformity fault with more intensity on the lower part of the fault. The second fracture set defined as fracture

related to joints shown in Figure 10 (right). This fracture model has higher intensity compared with the fracture model related to fault and distributed in a whole granitoid zone.

There are two fracture sets corresponding to Opal Mound Fault. The first fracture set is defined as fracture related to faults, shown in Figure 11 (left). The second fracture set is defined as fracture related to joints, shown in Figure 11 (right). Both fracture sets have relatively high intensity with the fracture model distributed in a whole granitoid zone.

The fracture set corresponding to Negro Mag Fault consists of one fracture set related to joints. The fracture set distributed in a whole granitoid zone with relatively high fracture intensity in the eastern part as shown in Figure 12 (left), while the fracture set corresponding to Mineral Mountain Fault system consist of one fracture set related to joints. The fracture set concentrated in the central part is shown in Figure 12 (right). This fracture set is located under the Mineral Mountain Fault system, which is rooted to the Unconformity fault.

Each fracture patch from those fracture models has information about dip angle, dip azimuth, surface area, and fracture length. Therefore, we can see the fracture orientations for the entire model and the selected fractures crossed by the wells. The dip angle and dip azimuth of all fractures in the model can be seen in Figure 13. The orientation of the fault model is dominated with a N-S trend with dip angle ranging from 30° to 90°.

To validate the fracture model, fracture planes nearest the wellbore with a radius of 250 m were extracted to get their fracture orientations (Figure 14). The radius value was obtained based on the minimum length of fracture that will be generated as a discrete fracture in the model (Mulyani and Aulia, 2022).

The comparison between original fracture data from wells and fracture model's orientations are shown in Figure 15. Based on the trend of dip angle and dip azimuth in the histogram, the orientation of the fracture model has a good match with the fracture from well data. The orientation of the fracture model in the stereonet is relatively different than the one from well data; however, the results of the fault model have the same orientation with fracture data from Well 16A-32, which is relatively NE-SW. Overall, the fracture model was validated to be used for the next process in this study.

5.2 Updated Geomechanics Model

1D MEMs were developed to model pore pressure, rock mechanics properties, and in-situ stresses along the well trajectory. For this analysis, five wells were chosen as reference points to construct the 1D MEM within the Utah FORGE field: NU-ESW1 (58-32), 9-1, 52-21, 14-2, and 16B-32 (as additional offset well). Among these wells, 14-2 was specifically designated for blind testing during the 3D modeling phase. Rock mechanics properties, including Young's modulus, Poisson's ratio, unconfined compressive strength (UCS), and friction angle (FANG) were derived using density, compressional sonic, and shear sonic logs. These properties were calibrated against rock mechanics tests conducted by McLennan (2018), as illustrated in Figure 16.

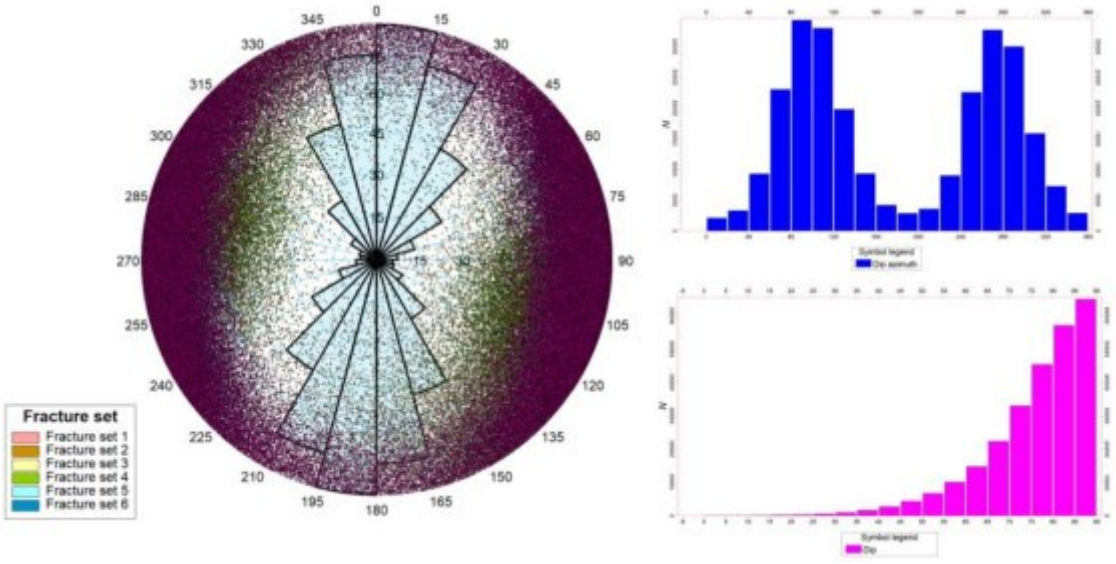

Figure 13: Dip angle and dip azimuth of updated fracture model with orientations relatively N-S.

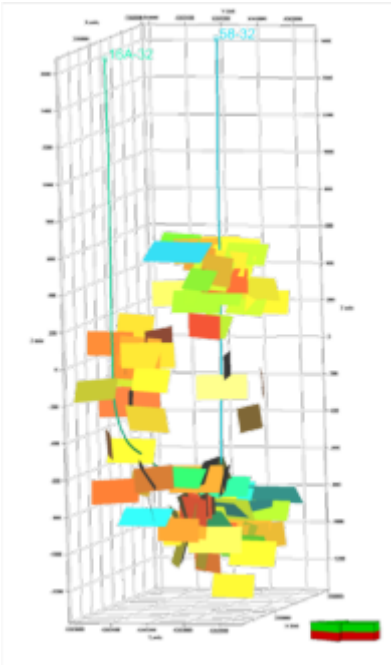

Figure 14: Selected fracture plane from fracture model near Wells 58-32 and 16A-32.

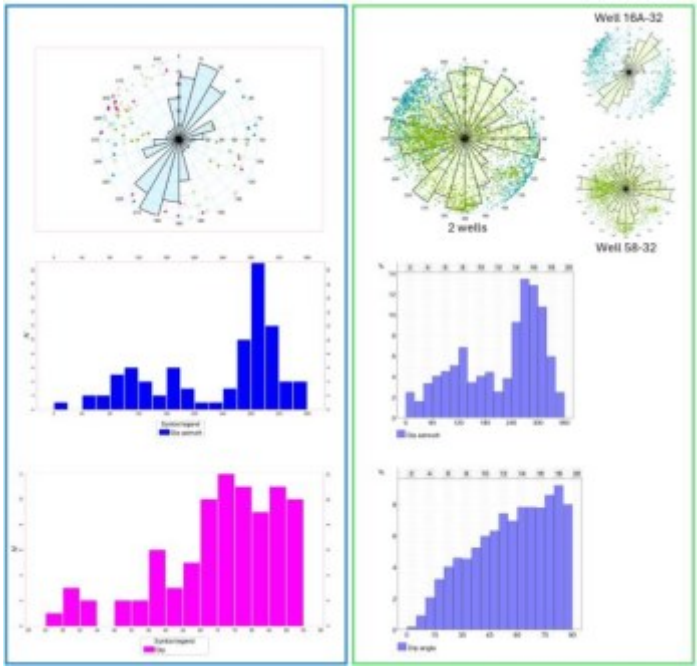

Figure 15: Comparison of fracture orientation from fracture model near well bore (left) and fracture orientation of fracture point data from well 58-32 and 16A-32 (right). The trend of dip angle and azimuth are match, while the orientation shown by stereonet has more similarity to well 16A-32 with trend Northeast-Southwest.

The temperature effect on mechanical properties must be considered as well (Blanton and Olson, 1999). Temperature measurements from Well MU-ESW1 (58-32) indicated a maximum of 266°F or 130°C. Li et al. (2021) conducted experimental tests on granite rock, indicating that mechanical properties (Young's modulus, UCS, tensile strength) do not notably change until temperatures reach 300°C, as depicted in Figure 17. Thus, given the maximum temperature recorded in Well MU-ESW1 (58-32) is 130°C, the study concluded that temperature effects on mechanical properties are negligible for this analysis.

Horizontal in-situ stresses were modeled based on the poroelastic method while honoring the overburden (vertical aspect) and tectonic process (horizontal). In this study, minimum horizontal stress was updated and calibrated with diagnostic fracture injection test (DFIT) interpretation report data from the field by Xing et al. (2020) with

the average value of 0.62 psi/ft and maximum horizontal stress average value of 0.77 psi/ft. Stress azimuth was taken from drilling-induced failure data from an image log in Well MU-ESW1 (58-32). Overall, the stress regime in this area is normal stress regime with the maximum horizontal stress direction being N30°E. The complete 1D MEM results are shown in Figure 16.

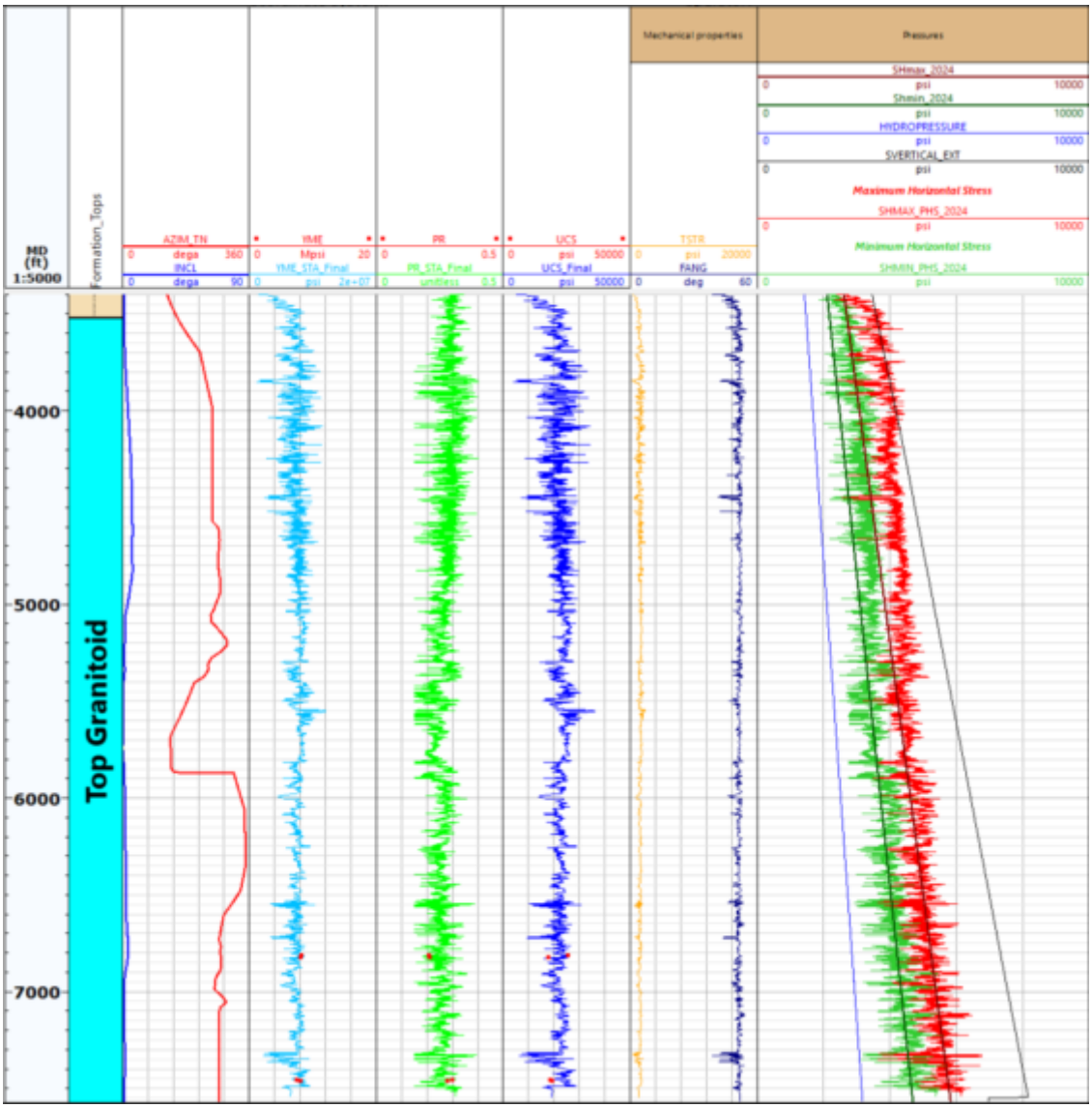

Figure 16: 1D MEM from Well MU-ESW1 (58-32). Red points in tracks 4 to 7 are rock mechanics test results from McLennan (2018). Dark green line in track 8 is average minimum horizontal stress value (0.62 psi/ft) and dark brown line in track 8 is average maximum horizontal stress value (0.77 psi/ft) from Moore et al. (2020).

The 3D static model is used as the foundation for constructing the 3D geomechanics model. However, the existing 3D static grid already encompasses the overburden area (approximately 2000 m above mean sea level). Therefore, an embedding process was undertaken to incorporate the lateral and subsurface burdens from the original 3D grid. This step was necessary to meet the requirements of the finite element method used in the geomechanical simulator, which relies on boundary stress conditions. The objective of this embedding process was to develop the 3D geomechanics model with a maximum 1:3 ratio, ensuring the effective transfer of constant stress/strain boundary loads applied on the surface to stress/strain dependent on the material properties. The original static grid consists of approximately 2.9 million cells, while the total number of cells after embedding increased to around 4.3 million (Figure 18).

The distribution of 3D mechanical properties was achieved using the machine-learning algorithm EMBER (embedded model estimator). EMBER integrates geostatistical models of spatial continuity and correlation into a decision forest-based framework for property modeling. Unlike methods that directly rely on geostatistics, EMBER embeds these models into a machine-learning approach, bridging the gap between geostatistical

techniques and other variables such as seismic data or, in this study, 3D magnetotelluric data. The results of the 3D mechanical properties are shown in Figure 19.

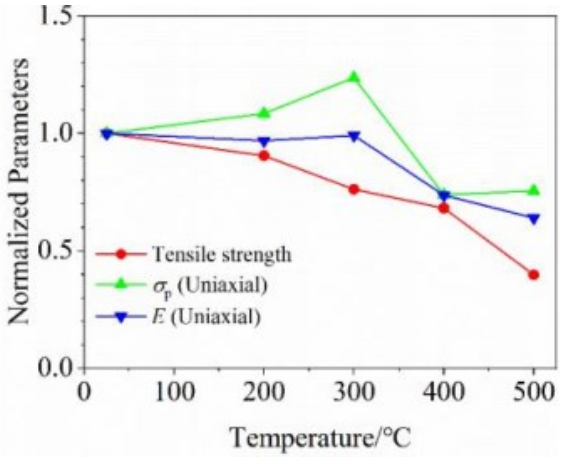

Figure 17: Temperature-dependency of granite under thermal treatment.

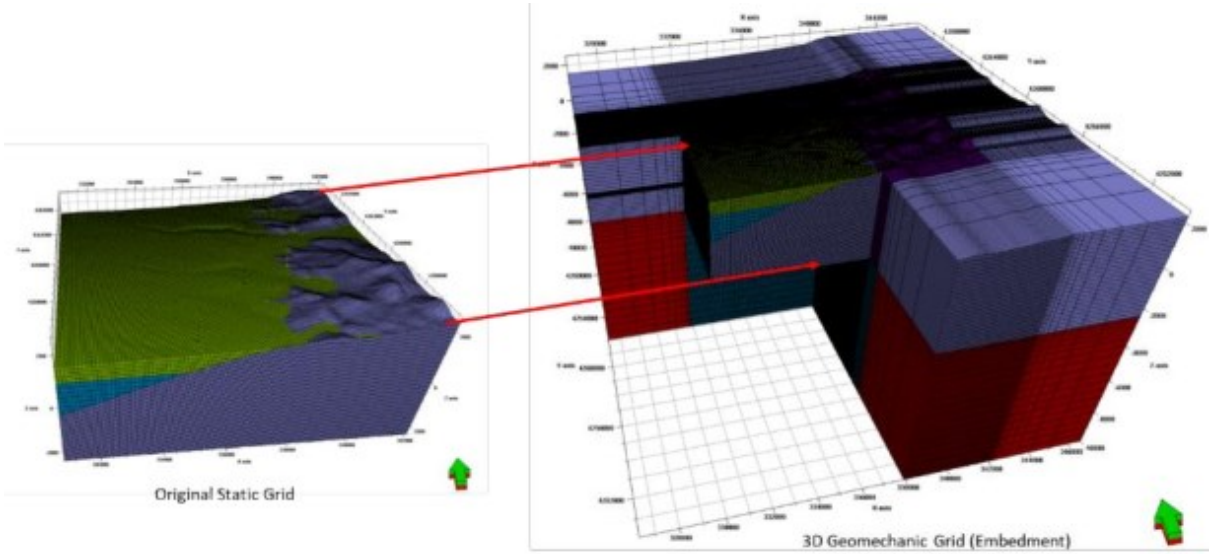

Figure 18: Grid embedment result.

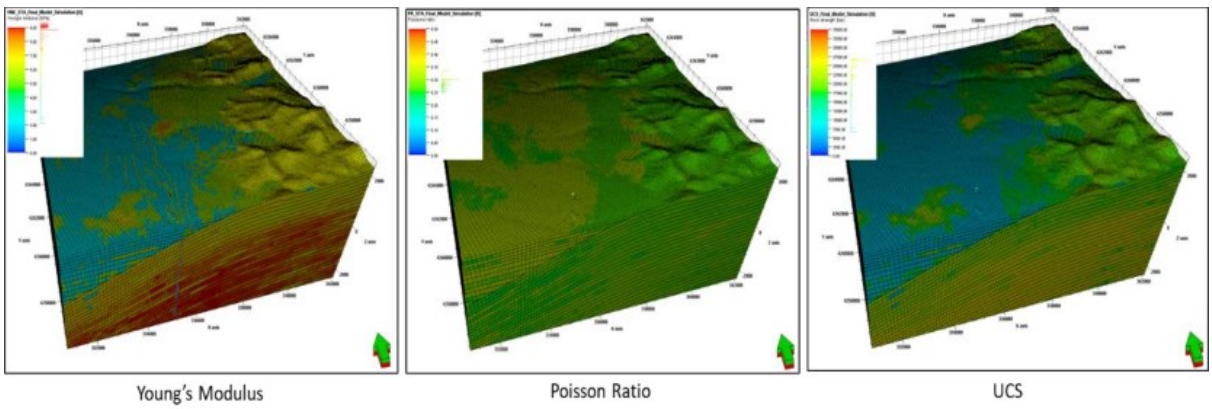

Figure 19: 3D mechanical properties.

The 3D stress simulation used strain parameters derived from previous 1D MEM analyses. Subsequently, the calculated 3D stress distribution was compared and validated against the 1D MEM stress profiles obtained from offset wells. The 3D geomechanical model was subjected to external far-field stresses along with internal vertical gravitational, pore pressure loads and distributed elastic properties of the model. An equilibrium stress condition was computed using a finite-element geomechanical simulator that incorporates plasticity. The variation of

minimum horizontal stress (Shmin) and maximum horizontal stress (SHMax) within the granitoid interval is illustrated in Figure 20.

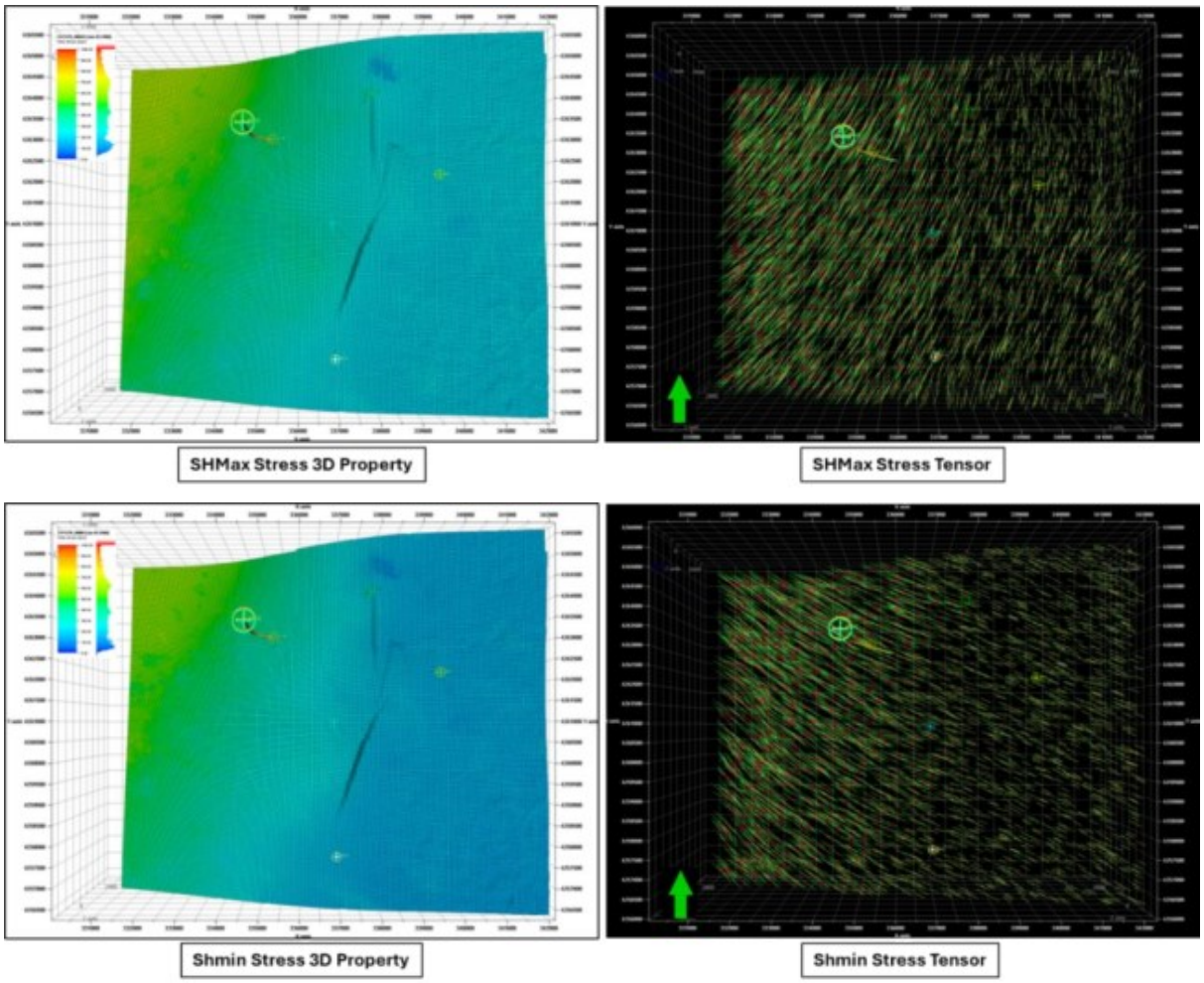

Figure 20: Variation of 3D horizontal stresses in granitoid interval.

5.3 Updated Critically Stressed Fractures

In this analysis, Discontinuity Stability analyzed the stability of fractures, specifically critically stressed fractures, using results from a geomechanical simulation conducted earlier in the study. Fracture stability was evaluated according to the Mohr-Coulomb criterion, which considers parameters such as the friction angle, cohesion of the discontinuity, dip angle, dip azimuth, and the 3D stress distribution provided by the geomechanical simulator. In this study, internal properties for the fracture were updated, and a friction angle of 22.5° (equivalent to a coefficient of friction of 0.41) was assumed for the fracture properties.

The discontinuity stability analysis for fractures shows that the fracture set 3 is more contributed in critically stressed fractures compared to the others fracture sets. The critically stressed fracture orientation predominantly with strike azimuth around North-South (175 deg and 355 deg) and with dip between 45° and 75° as shown in Figure 21. The 3D critically stress distribution in the field was shown in Figure 22.

5.4 Updated Probability Map

The fracture permeability model from updated critically stressed fractures consist of three sets in each direction (k_i, k_j, and k_k). According to the location of critically stressed fractures, the high fracture permeability was distributed intensively in the east of Opal Mound Faults as shown in Figure 23. Some regions in the west of Opal Mound Faults have relatively high fracture permeability at the lower part (from -1000 m to -1500 m) and concentrated at the intersection between the basin-bounding fault unconformity and the Mineral Mountain's fault system.

Aligned with the previous study, the average value for permeability in j and k directions (k_j and k_k) were higher than fracture permeability in i direction (k_i) (Mulyani et al., 2023). The average value of each fracture permeability

direction is k_i = 0.0044 md, k_j = 0.0106 md, and k_k = 0.0098 md. The average map of fracture permeability at three directions can be seen in Figure 24.

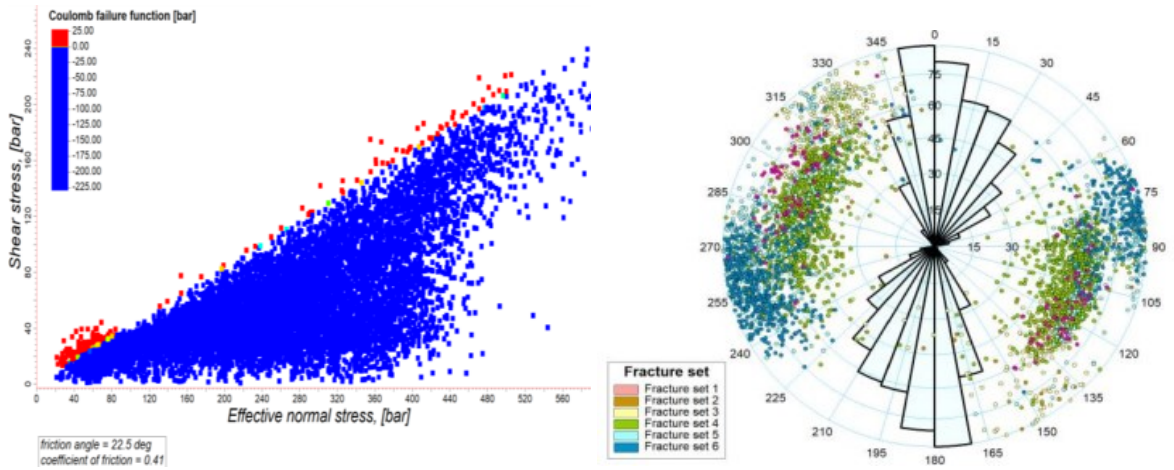

Figure 21: Critically stressed fracture orientation.

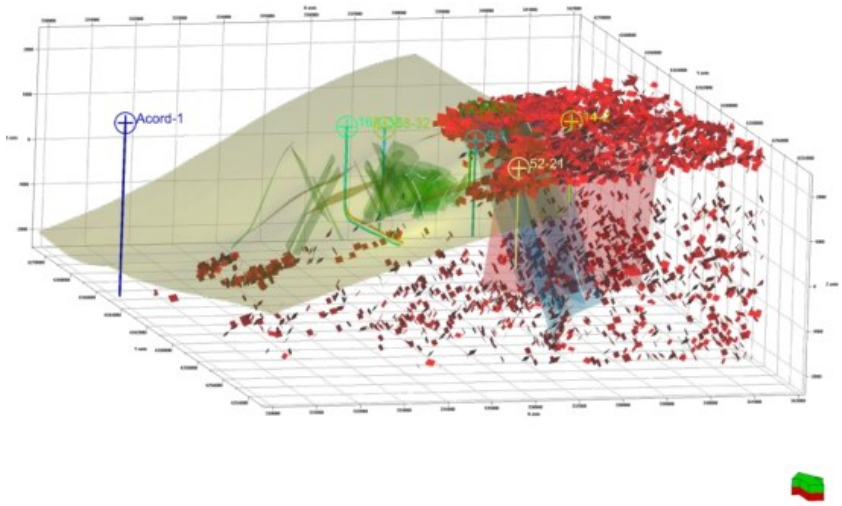

Figure 22: 3D critically stressed fracture distribution.

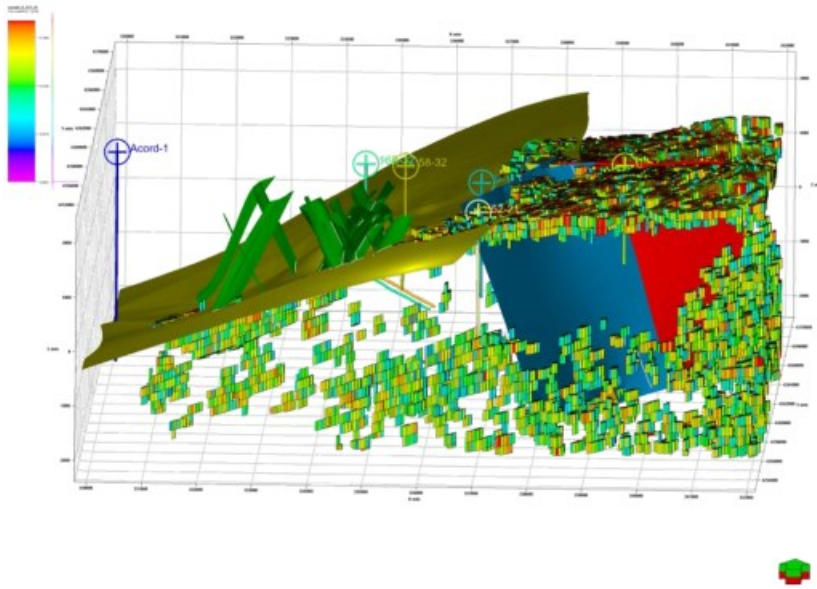

Figure 23: The distribution of high fracture permeability at *i* direction (k_i) based on updated critically stressed fractures and the faults model in the study area.

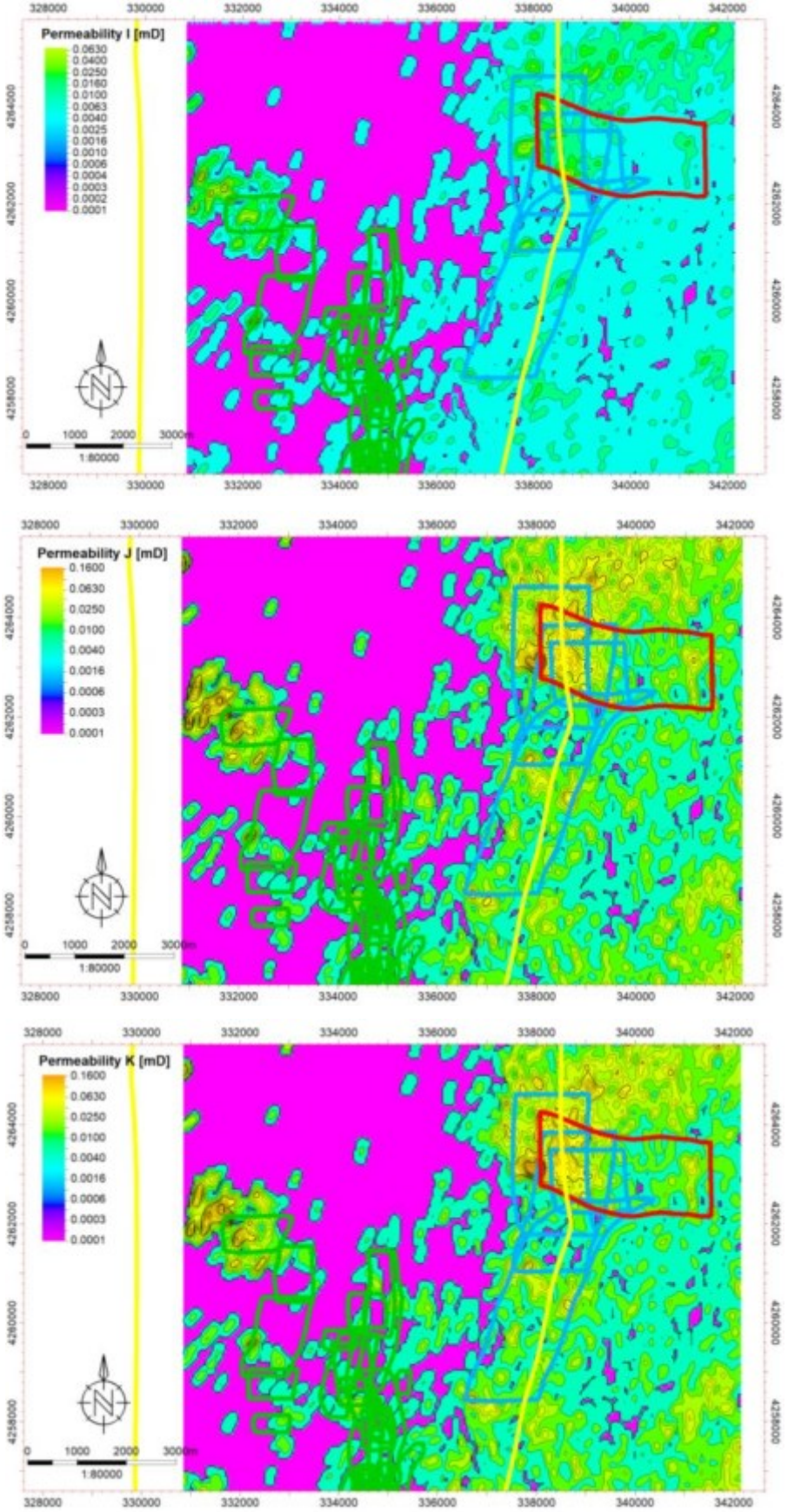

Figure 24: The average map of fracture permeability at *i* direction (k_i) (top), *j* direction (k_j) (middle) and *k* direction (k_k) (bottom) based on updated critically stressed fractures and the polygon of the faults model in the study area.

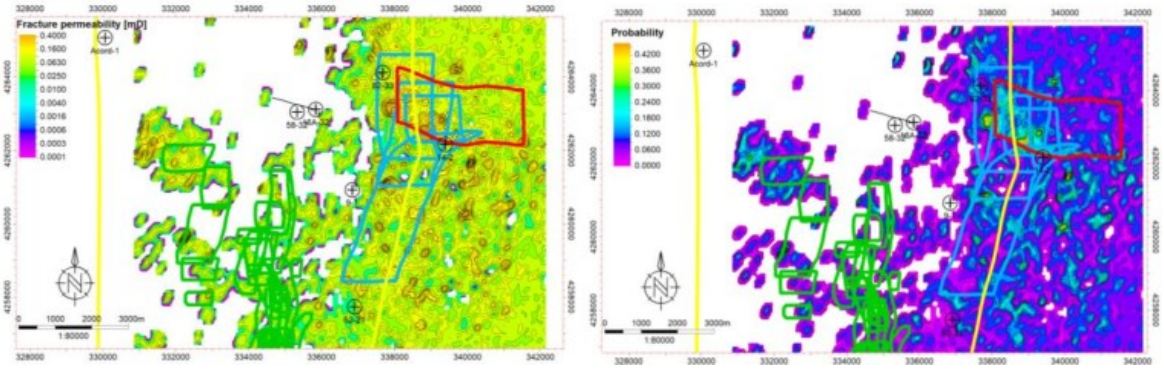

Figure 25: The result of harmonic averaging the fracture permeability k_i, k_j and k_k (left) and the probability map of fracture permeability equal to or greater than 0.95 m in the study area (right).

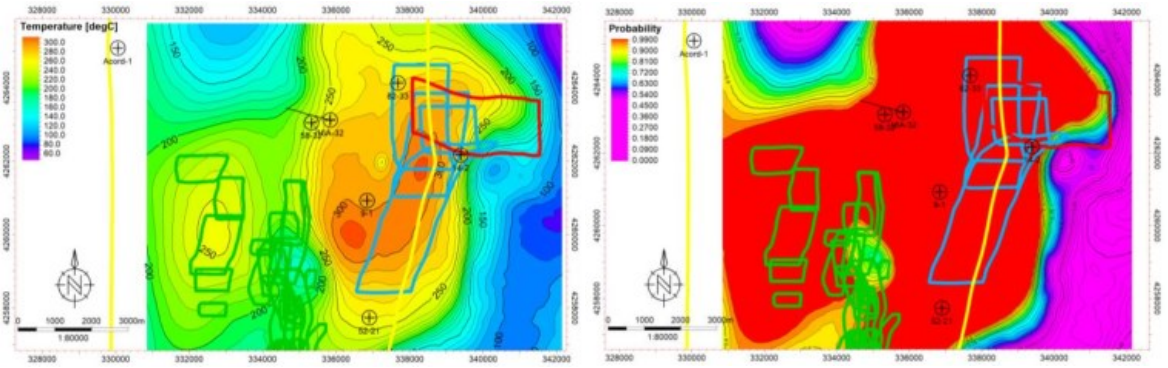

Figure 26: The average map of temperature model at the granitoid zone (left) and the probability map of the temperature equal to or greater than 200°C in the study area (right).

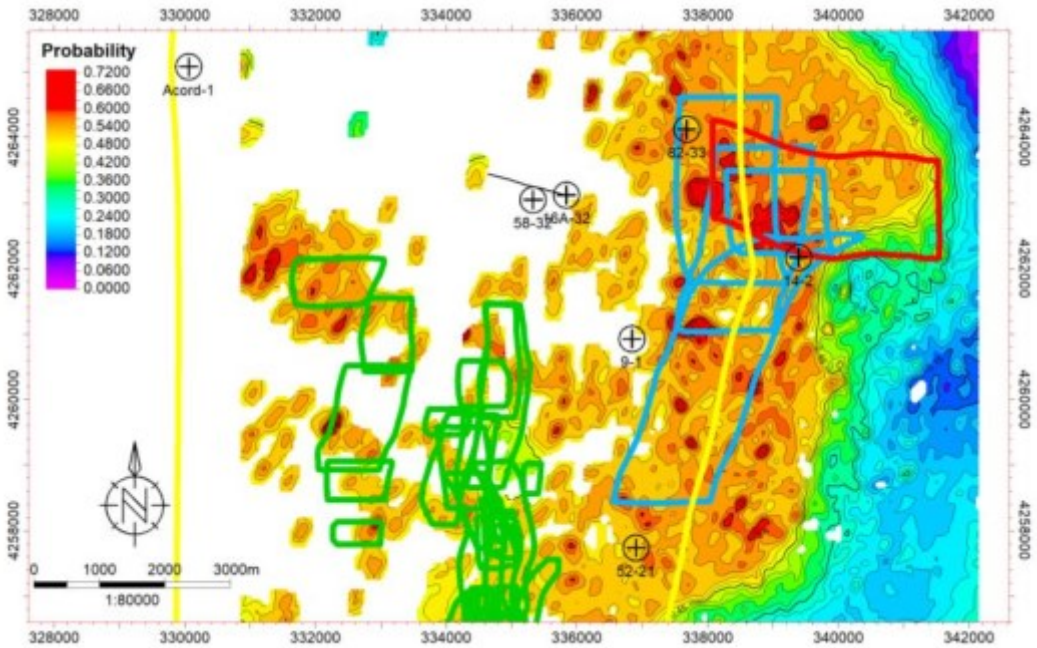

Figure 27: The final probability map of chance to get fracture permeability more than 0.95 md and temperature more than 200°C. The sweet-spot area identified with red color (high probability) is distributed close to the location of the faults model.

All those average maps extracted at the granitoid zone emphasize the region of interest. Overall, the fracture permeability has the same trend for all directions. Based on an average map of fracture permeability at k_j and k_k, the region with the highest value of fracture permeability is found at the area that overlaps with the Opal Mound Fault (blue polygon), Negro Mag fault (red polygon) and the base-bounding fault unconformity (yellow polygon).

The other region with the highest value of fracture permeability is found in the east, at the edge of the Mineral Mountain Faults system.

To obtain a probability map, the fracture permeabilities at three directions were combined by using the harmonic averaging shown in Figure 25 (left). After that, the value of fracture permeability was truncated with the threshold for the good permeability (probability=1) which is 0.95 md. The final fracture permeability then was normalized, with a range value of 0 to 1, as shown in Figure 25 (right).

The temperature map was used to generate a geothermal sweet spot probability map. In this study, the threshold for the hot temperature (probability=1) is 200°C. The temperature map that has been normalized with range value from 0 to 1 shows the probability of area with temperature greater than 200°C (Figure 26).

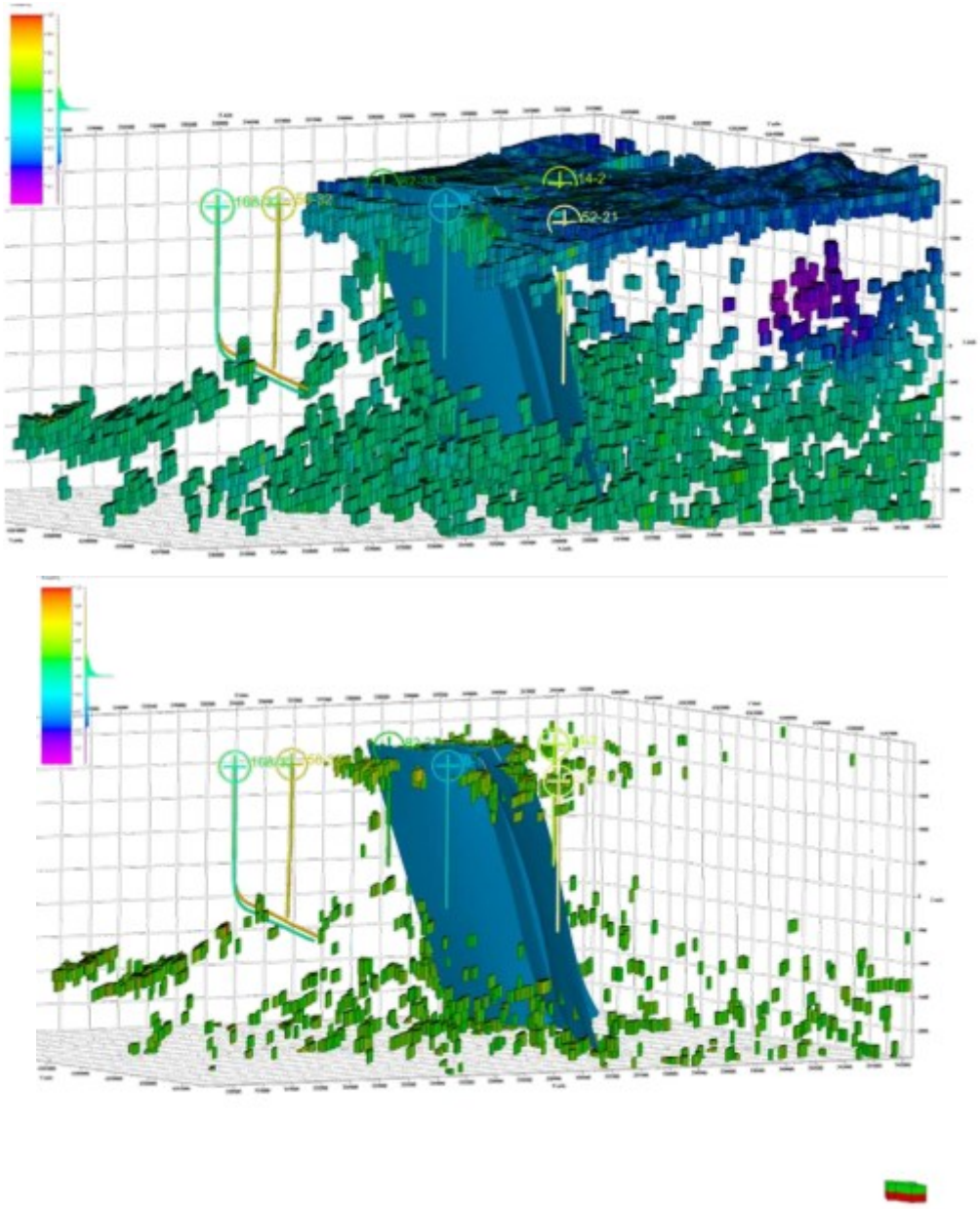

Figure 28: The 3D model of probability for the sweet-spot area (top) and the 3D model that has been filtered for the high value probability (> 0.6) (bottom). This visualization can give an overview for the next target for future development in this field.

The integration between harmonic average maps, which is the probability of effective permeability with the probability of temperature, represents the probability of the geothermal sweet-spot area. The arithmetic average of permeability and temperature probability map can be seen in Figure 27. The final probability map of the favorable area shows the higher chance of good permeability and good temperature region located between Well 82-33 and 14-2. The other location that is far from other wells can be found in the east, south of Well Acord 1.

This result is different from the earlier study, where the most favorable area was located in the central part of the study area or close to Well 9-1 (Mulyani et al., 2023).

Based on the literature study, the Opal Mound Fault is defined as the barrier between the hydrothermal system east of the faults and the low permeability west of the faults. This study aligns with those assumptions where the area with high probability for good temperatures and permeability more concentrated in the east. However, the area in the west can still be developed by having an enhanced process to increase the permeability. In this case, good fracture permeability from critically stressed fracture can be used as targets for the engineering process to get best results. Furthermore, the map of probability can give the picture of connectivity between critically stressed fractures in the western area. All the information can be extremely useful for a development plan in both the hydrothermal system region and the enhanced geothermal system part. The detailed visualization from the probability of a favorable geothermal area can be seen in a 3D view (Figure 28). In this study, a good potential reservoir exists mostly in the eastern part of the study area. However, the area with high probability (more than 60%) of good temperature and permeability occurs also in the western part, close to new Wells 16A-32 and 16B-32. Based on filtered values for high probability, some connecting regions with good reservoir potential can be identified as reference for the development target in the study area.

6. APPLICATION FROM RESULTS

The robust 3D modeling techniques demonstrated here present a spectrum of different applications to resolve existing challenges for EGS and CHS developments. Lateral landing for the producer in EGS requires a fine balance (detailed in the Introduction section). This requires optimizing the well placement along with the fracture geometry development. Having a reliable and calibrated initial model is only possible with an accurate 3D geomodel encompassing all the discrete fracture elements along with an accurate propagation model. Khan et al. (2024) demonstrates the criticality of the EGS network development, as shown in Figure 29. Even though their current work did not use this robust approach, the model presented in this paper will be integrated with a complex fracture propagation model in the near future. A sophisticated fracture model by itself will fail to accurately predict the producer lateral landing location and trajectory, if used without a robust geomodel with integrated geologic and geomechanical modeling.

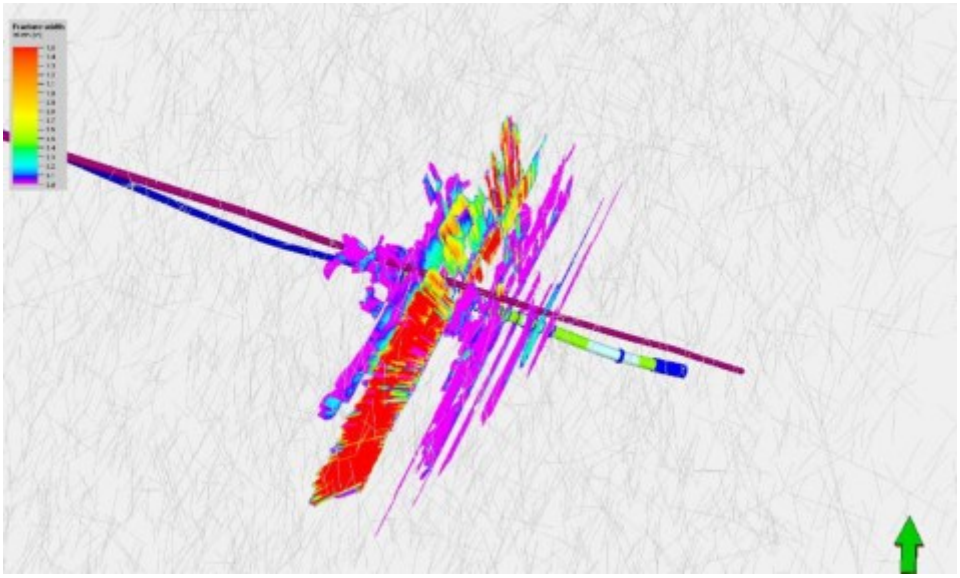

Figure 29: Stimulation fracture conductivity footprint with the DFN elements in grey plan view for fracture width showing the importance of hydraulic fracture interaction with natural fractures (after Khan et al., 2024).

In the context of EGS, understanding the locations of large faults or natural fracture elements with high aperture is critical to avoid connecting with these features and consequently mitigating thermal breakthroughs. This can be the next critical application of our approach here. Reasonable knowledge of reservoir shape, structure, and geometry, and the ability to predict (in probabilistic terms) a thermal breakthrough because of connecting the hydraulic fracture network with that feature is critical for our hydraulic fracturing design phase.

Extension of this modeling work can reap benefits for CHS projects as well. Loss of wells in terms of flow rate, enthalpy, and power generation because of a thermal breakthrough is equally critical for conventional systems as well. The consequences of these breakthroughs of unheated reinjection fluid to the production wells are a reduction

in discharge enthalpy and a reduction in total flow rate (due to the lower steam fraction and greater fluid column weight in the wellbore) (Horne, 1985). Figure 30 (from Inoue and Shimada, 1985) shows the loss of Well H-4 at Hatchobaru geothermal field in Japan due to thermal breakthrough. Despite once being one of the most immense producers in the field, the entire steam output of the well was lost over a period of about 2 1/2 years. If we implement a tight coupling between our probabilistic sweet-spot models with the dynamic reservoir models of the operators' field, such issues can be avoided.

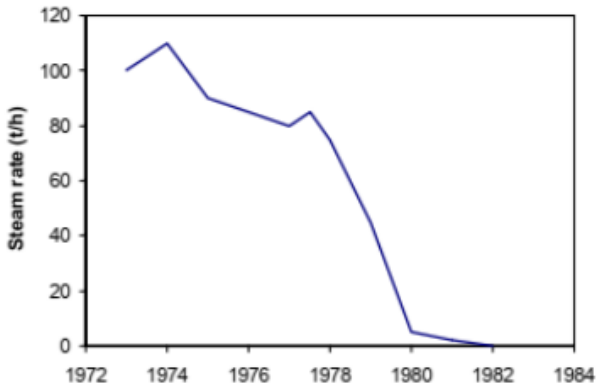

Figure 30: Thermal breakthrough occurrence in Well H-4 at the Hatchobaru geothermal field in Japan, causing complete loss of mass flow (after Inoue and Shimada, 1985).

Another possible application of this modeling work is aiding in history matching of CHS dynamic models. History matching of production data typically involves matching pressure, enthalpy, chemical ions, productivity index, etc. Typically, chemistry data aids in identifying connecting or boundary/barrier systems in the field between injectors and producers. In simple structured grid models, this exercise would not be appropriate as much as with a robust model presented here. The granular definition of geological and fracture features would enhance the experience of history matching, yielding accurate matches and changing the 3D model features in a more reliable way.

7. CONCLUSIONS

The integration workflow of critical stress prediction with other geological analyses resulted in the updated delineation of a favorable geothermal conditions map at the Utah FORGE project site. The calibration of this study was done by using added geomechanics parameters from the latest Wells 16 A and 16 B. The result showing the highest probability of sweet spot was found east of the Opal Mound Fault. The area west of Opal Mound Fault has some regions with good potential to be developed for enhancing connection through fractures while mitigating thermal breakthroughs. Detailed location of that region can be used as reference for the engineering process to develop the enhanced geothermal system at the project site. Overall, the results from this study show more comprehensive results than the earlier study due to added well information. This suggests the importance of updating the subsurface model for each new well dataset to get a better vision of the future development plan in the geothermal field.

ACKNOWLEDGEMENTS

The authors would like to thank the management of SLB who allowed us to use the exploration and production software, and the Energy and Geoscience Institute of University of Utah for permission to use the study data.

REFERENCES

Allis, R.G. and Larsen, G.: Roosevelt Hot Springs Geothermal Field, Utah—Reservoir Response After More Than 25 Years of Power Production. *Proceedings*, 37th Workshop on Geothermal Reservoir Engineering, Stanford University, Stanford, CA (2012).

Allis, R.G., Moore, J., Davatzes, N.C., Gwynn, M., Hardwick, C.L., Kirby, S.M., McLennan, J.D., Pankow, K.L., Potter, S., and Simmons, S.F.: EGS Concept Testing and Development at the Milford, Utah FORGE Site. *Proceedings*, 41st Workshop on Geothermal Reservoir Engineering, Stanford University, Stanford, California (2016).

Bartley, J.M.: Joint patterns in the Mineral Mountains intrusive complex and their roles in subsequent deformation and magmatism. *Utah Geological Survey Miscellaneous Publication*, 169-C (2019).

Blanton T.L., and Olson J. E.: Stress Magnitudes from logs – Effects of Tectonic Strains and Temperature. *SPE Reservoir Eval & Eng 2*, 01, (1999), 62–68. Paper Number: SPE-54653-PA.

Energy and Geoscience Institute at the University of Utah.: Utah FORGE: Well 58-32 (MU-ESW1) FMI Log Fracture Results [dataset] (2021). Retrieved from https://gdr.openei.org/submissions/1299, https://gdr.openei.org/submissions/1283, and https://utahforge.com/project-data-dashboard/

Horne, R.N.: Reservoir Engineering Aspects of Reinjection, *Geothermics*, 14, (1985), 449-458.

Finnila, A. and Jones, C.: Updated Reference Discrete Fracture Network Model at Utah FORGE. Proceedings, 49th Workshop on Geothermal Reservoir Engineering Stanford University, Stanford, California, February 12-14, 2024, SGP-TR-227 (2024).

Inoue, K., and Shimada, K.: Reinjection Experiences in the Otake and Hatchobaru Geothermal Fields, Japan, *Proceedings*, 7th New Zealand Geothermal Workshop, Auckland, New Zealand, p. 69-74 (1985).

Khan, A. M., Kresse, O., England, K., Xing, P., McLennan, J., Hobbs, B., and Deville, B.: Integrated Lifecycle Simulation for Utah FORGE: Part I – Fracture Geometry Calibration, *GRC Transactions*, 48, (2024).

Kirby, S. M.: Revised mapping of bedrock geology adjoining the Utah FORGE site. *Utah Geological Survey Miscellaneous Publication*, 169-A (2019).

Knudsen, T., Kleber, E., Hiscock, A., and Kirby, S.M.: Quaternary geology of the Utah FORGE site and vicinity, Millard and Beaver Counties, Utah. *Utah Geological Survey Miscellaneous Publication*, 169-B (2019).

Kresse, O., Khan, A. M., Gutierrez-Sosa, L., Hobbs, B., Sosio, G., Emelyanov, D., and Mehay, S.: A Review of Enhanced Geothermal Systems Sub-Surface Lifecycle Optimization, *GRC Transactions*, 48, (2024).

Li, N., Wang, H.B., Zhang, S.C., Zou, Y.S., Zhang, Z.P., and Zhou, T.: Effect of Cyclic Thermal Shock on Mechanical Properties and Brittleness of Granite. *Proceedings*, 55th U.S. Rock Mechanics/Geomechanics Symposium, Online, Paper Number: ARMA-2021-1581 (2021).

McLennan, John.: Utah FORGE: Well 58-32 Core Analyses, Energy and Geoscience Institute at the University of Utah. https://gdr.openei.org/submissions/1162. (2018).

McLennan, John.: Utah FORGE: Stress Measurements MU-ESW1 (Performed Sept 22-23, 2017), in Utah FORGE: Well 58-32 Core Analyses, Energy and Geoscience Institute at the University of Utah. https://gdr.openei.org/submissions/1162. (2018).

Moore, J., McLennan, J., Pankow, K., Simmons, S., Podgorny, R., Wannamaker, P., Jones, C., Rickard, W., and Xing, P.: The Utah Frontier Observatory for Research in Geothermal Energy (FORGE): A Laboratory for Characterizing, Creating and Sustaining Enhanced Geothermal Systems. *Proceedings*, 45th Workshop on Geothermal Reservoir Engineering Stanford University, Stanford, California (2020).

Mulyani, S., and Juandi, D.: Well Targeting based on Temperature and Structural Model in Geothermal Field by using Petrel Software. *Proceedings*, 7th Indonesia International Geothermal Convention and Exhibition (IIGCE), Jakarta, Indonesia (2019).

Mulyani, S. and Aulia, A.B.: Discrete Fracture Network Modelling Based on Natural Fracture Prediction Geomechanic Inversion Process. *Proceedings*, 8th Indonesia International Geothermal Convention and Exhibition (IIGCE), Jakarta, Indonesia (2022).

Mulyani, S., Aulia, A.B., Wisnubroto, B., Widiatmoko, W., Pradana, A., Trikukuh, J.S., and Puspa, M.A.: Comprehensive Study of Geology to Geomechanic for Delineating Sweet Spot Map in Geothermal Field. Study Case: Utah FORGE, USA, *GRC Transactions*, Vol. 47 (2023).

Simmons, S.F., Kirby, S.M., Bartley, J., Allis, R.G., Kleber, E.J., Knudsen, T.R., Miller, J.M., Hardwick, C.L., Rahilly, K., Fischer, T.P., Jones, C.G., and Moore, J.M. Update on the Geoscientific Understanding of the Utah FORGE Site. *Proceedings*, 44th Workshop on Geothermal Reservoir Engineering, Stanford University, Stanford, California (2019)

SLB. Petrel Help Version 2024.1. Build date March 7, 2024. Copyright © SLB (2024).

Wallis, I., Rowland, J., Cumming, W., and Dempsey, D.: The subsurface geometry of a natural geothermal reservoir. *New Zealand Geothermal workshop*, Rotorua, New Zealand (2017).

Xing, P., McLennan, J., Moore, J.: In-Situ Stress Measurements at the Utah Frontier Observatory for Research in Geothermal Energy (FORGE) Site. *Energies*, 13, 21(2020).

Using T2well for Simulating Tightly Coupled Wellbore-Reservoir Simulation in a Fully 3D Reservoir Model

Rony P. Nugraha[1,2], Ryan Tonkin[2], Theo Renaud[2],
John O'Sullivan[2], and Michael J. O'Sullivan[2]

[1]Geoenergi Solusi Indonesia (Geoenergis), Cibis Nine 11th Floor, Jakarta, Indonesia
[2]Department of Engineering Science, The University of Auckland, Private Bag 90210, Auckland, New Zealand

rony@geoenergis.com; rony.nugraha@auckland.ac.nz

Keywords: Welbore, Reservoir, 3D Model, Natural State, Production, Simulator, Tightly Coupled

ABSTRACT

Geothermal modelling plays a crucial role in the successful development of geothermal fields. It aids in the planning of resource utilization, as well as the assessment and management of geothermal fluid production to achieve optimal performance. A critical application of a wellbore/reservoir model is conducting future scenario simulations to make accurate forecasts using a well-calibrated reservoir model. To accurately simulate the future performance of geothermal wells, it is crucial to understand the coupling requirements and effectively integrate wellbore and reservoir simulators. T2Well is a simulator for non-isothermal and multiphase fluid flow that can model tightly coupled wellbore-reservoir flow. T2Well extends the capabilities of the numerical reservoir simulator TOUGH2 by integrating a wellbore sub-domain into the numerical grid, allowing it to compute flow in both the wellbore and the reservoir concurrently and efficiently. However, there are no published examples and no known projects where it has been applied to a full-scale 3D geothermal model.

This paper presents the construction of the 3D reservoir model following the standard practice in developing a dynamic model for a geothermal system. We utilized T2Well with Equation of State (EOS) 1 to identify the necessary model setup requirements for a convective hot geothermal reservoir system with temperature ranges from 250°C to 270°C. The initial conditions for the fully coupled wellbore-reservoir simulation are based on the results of the natural state simulation of a synthetic geothermal field. This research also provided insights from setting up the input data and model parameters within the T2Well environment.

1. INTRODUCTION

Geothermal modelling is pivotal for planning geothermal energy resources and evaluating and managing the production of geothermal fluids to ensure optimal performance. Traditionally, wellbore and reservoir models have been treated independently during simulations of future scenarios. The results from such simulations are typically derived from the reservoir conditions at the feedzones rather than from wellbore simulation results. While it is possible to manually convert the feedzone conditions to well production forecasts using a wellbore model at each reservoir simulation time step, this method is complex, time-consuming, and often results in extended simulation durations. Therefore, optimally coupled wellbore and reservoir models, along with a comprehensive understanding of the coupling requirements, are invaluable for accurately simulating the production forecasts of a geothermal field. This approach also aids in accurately simulating the future performance of geothermal wells using production history data derived from field surveys.

Several researchers have explored the integration of a geothermal reservoir simulator with a wellbore simulator. Hadgu et al. (1993) explicitly coupled TOUGH (Pruess, 1987) with the steady-state wellbore simulator WFSA (Hadgu and Freeston, 1990) using a bridging function named COUPLE, which facilitates the exchange of information between the simulators. Bhat et al. (2005) performed an explicit coupling of TOUGH2 (Pruess et al., 1999) with the HOLA simulator (Bjornsson, 1987) by integrating HOLA as a function/subroutine within TOUGH2. Gudmundsdottir (2012) utilized TOUGH2 and the steady-state wellbore simulator FloWell (Gudmundsdottir et al., 2012; Gudmundsdottir and Jonsson, 2015) to create a linked wellbore-reservoir simulator using the DELV type. However, no published examples or known projects have applied a tightly coupled wellbore reservoir simulation to a full-scale 3D geothermal model.

This paper presents a fully integrated wellbore-reservoir simulation applied to a full-scale 3D geothermal model using T2WELL (Pan and Oldenburg, 2014). The construction of the 3D reservoir model follows the modelling framework developed by the Geothermal Institute (O'Sullivan et al., 2023; Nugraha et al., 2022), which facilitates the generation of a dynamic model for a geothermal system. We employed T2Well with Equation of State (EOS)1, the same version used by Renaud et al. (2021a; 2021b; 2020; 2019a; 2019b) in their studies, to delineate the necessary model setup requirements for a convective hot geothermal reservoir system with temperature ranging

from 250°C to 260°C. Initially, we constructed the 3D numerical model with refinements in the main upflow and wellbore areas using PYTOUGH (Croucher, 2011; 2015) scripts. This research investigated the fully coupled wellbore-reservoir simulation with one vertical production well, referred to as WELL1. The initial conditions for the fully coupled wellbore-reservoir simulation are based on the results from the natural state simulation of a synthetic geothermal field. The production setup of the tightly coupled wellbore-reservoir simulation was executed using PYTOUGH scripts, and the fully coupled simulation results were visualized using TIM (Yeh et al., 2013).

2. T2WELL SIMULATOR

T2Well is a fully coupled simulator for non-isothermal and multiphase fluid flow, capable of modelling coupled wellbore-reservoir flow, and was first introduced by Pan et al. (2011). T2Well expands the functionalities of the numerical reservoir simulator TOUGH2 (Pruess et al., 1999; Finsterle et al., 2014) by incorporating a wellbore sub-domain within the numerical grid. This integration enables concurrent and efficient flow computation in the wellbore and the reservoir. The Drift Flux Model (Shi et al., 2005) is employed to seamlessly integrate the wellbore flow, applicable across a wide range of flow regimes, with the reservoir Darcy flow without resorting to any approximations such as single-phase flow, productivity index, or quasi-steady state (Pan and Oldenburg, 2014).

Initially, T2Well was deployed as a wellbore simulator for CO_2 and variable salinity water mixtures, simulating transient non-isothermal processes associated with CO_2 flow in deep wellbores. This included transitions from supercritical to gaseous phases, integrating the capabilities of the wellbore simulator T2Well and the reservoir simulator TOUGH2 (Pan et al., 2011). In this context, T2Well was utilized with the equation of state, ECO2N, to simulate CO_2 injection and leakage behavior via wellbores. Furthermore, T2Well has been applied in studies involving Enhanced Geothermal System (EGS) simulations with ECO2H (Pan et al., 2015), energy storage applications of compressed air with EOS7C (Oldenburg and Pan, 2013), and modelling the Macondo well blowout with EOIL (Oldenburg et al., 2011).

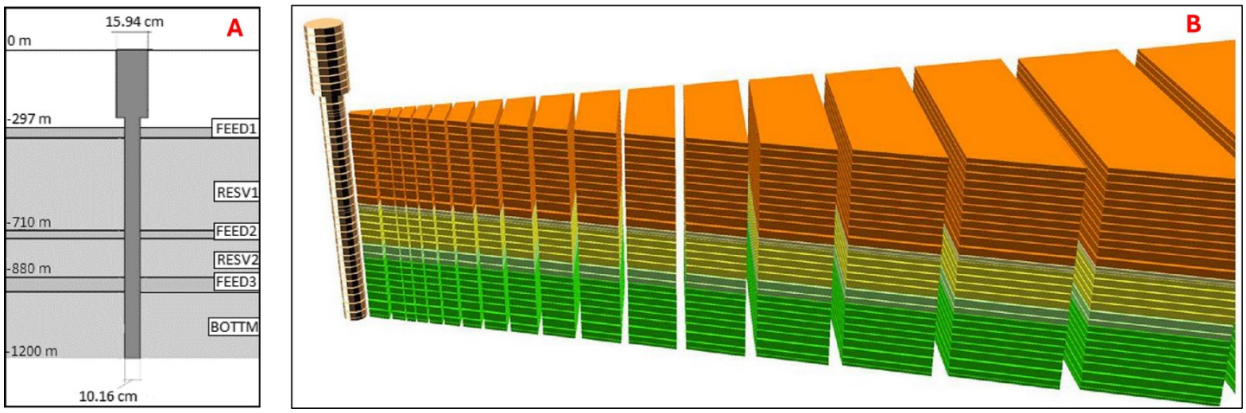

Figure 1: Conceptual model (A) and vertical cross-section of WW-01 wellbore-reservoir model (Vasini et al., 2018).

Vasini et al. (2018) employed T2Well and the EWASG Equation of State (EOS) to interpret a small production experiment in high-enthalpy geothermal reservoirs. The T2Well-EWASG was validated through a fully-coupled wellbore-reservoir simulation using their developed WW-01 wellbore-reservoir model (Figure 1). This model excluded the cap-rock's grid blocks; thus, the heat exchange between the wellbore and the cap-rock (area above 297 m depth) was simulated using T2Well's analytical function.

In subsequent work, Battistelli et al. (2020) integrated the new EOS2H module, suitable for subcritical and steam-like supercritical H2O-CO2 mixtures, into T2Well, the same version used by Vasini et al. (2018). The T2Well-EOS2H code was validated through simulations conducted with various supercritical reservoir simulators and steady-state subcritical and supercritical wellbore flow simulations. Battistelli et al. compared T2Well-EOS2H to T2Well-EWASG by modelling steady-state wellbore flow in two geothermal wells, W2 and KD13, referencing comparative literature (Barelli et al., 1982; James, 1975) used by Vasini et al. (2018).

3. 3D NUMERICAL MODEL DEVELOPMENT

The TOUGH2 model grid developed for this study (Figure 2) spans an area of 15 km x 13 km. It features large blocks set at 1 km x 1 km and is refined in the main upflow area to 500 m x 500 m. The depth of the model grid extends to 3.5 km, with vertical thicknesses ranging from 500 m for the last three bottom layers to 50 m near the

surface. The total number of blocks for this model is 6,580. This setup was conducted following best practices in constructing the 3D numerical model (O'Sullivan et al., 2023; Nugraha et al., 2022) to facilitate the simulation of a convective hot geothermal system.

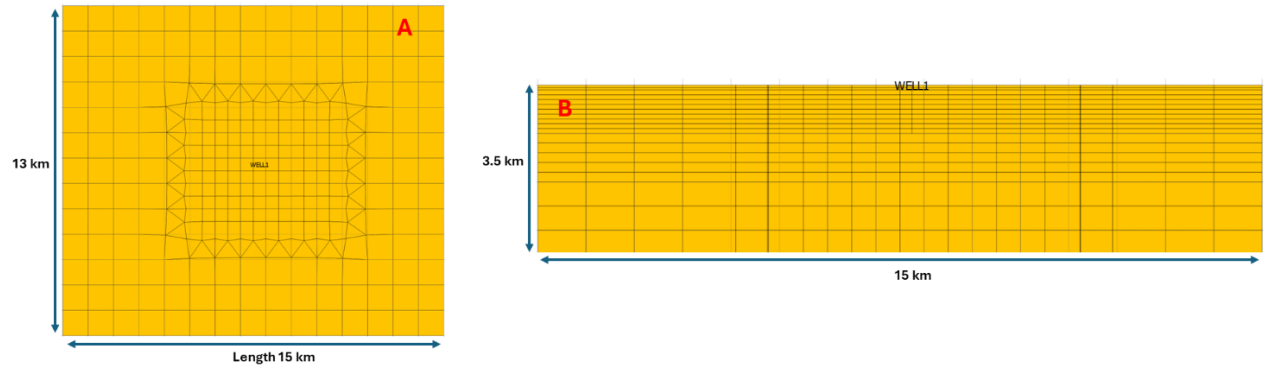

Figure 2: Top surface's plan view (A) and vertical cross-section (B) of the TOUGH2 model grid.

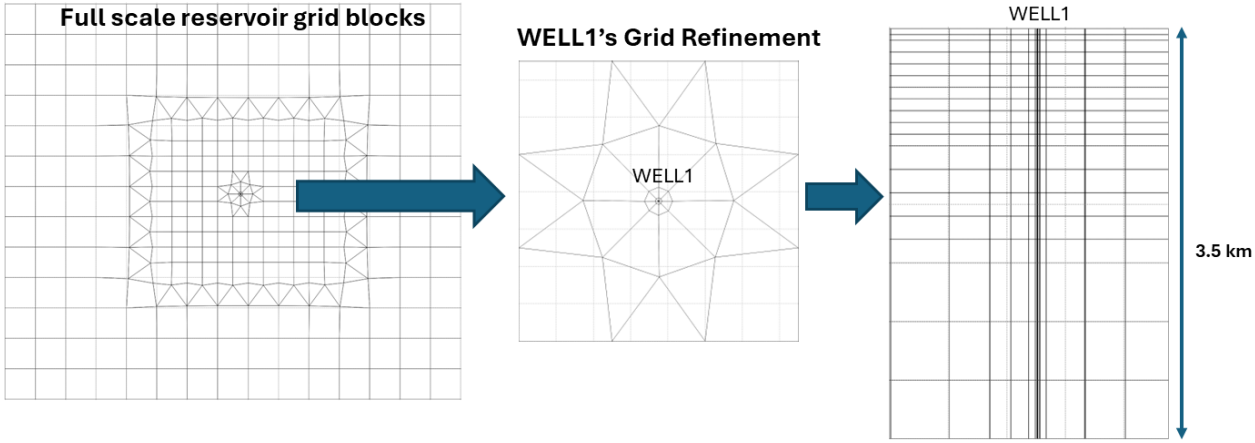

Figure 3: Local grid refinement surrounding the wellbore area WELL1 using optimized triangular refinement.

The trajectory of the planned production well (WELL1) is positioned at the center of the projected main upflow area. Utilizing the location of WELL1, we refined grid blocks surrounding the wellbore area through four stages of the optimal triangular scheme (Figure 3). This refinement was implemented to enable the radial flow of hot fluids during production scenario simulations and to ensure numerical stability by maintaining orthogonal connections among the refined blocks. As a result of this wellbore refinement, the total number of model grid blocks increased to 7,380.

As outlined in the previous chapter, T2Well is an extension of TOUGH2, equipped to conduct fully integrated wellbore-reservoir simulations. However, T2Well lacks the capabilities and computational efficiency of AUTOUGH2 (Yeh et al., 2012) for running a 3D model effectively. To ensure that the simulation process ran efficiently within a reasonable time frame, we aimed to keep the total number of model grid blocks under 10,000.

4. NATURAL STATE MODEL SETUP AND SIMULATION

4.1 Natural State Model Setup

Before utilizing the developed TOUGH2 model for natural state simulation, we categorized the model grid blocks into five distinct rock types, essential components of a convective geothermal system. As illustrated in Figure 4 below, we designated the last two bottom layers of the model as Basement (B0001), characterized by tight permeability. Adjacent to this, in the middle area of these two layers lies the Upflow (U0001), possessing vertical permeability to facilitate the upward flux of hot water to the reservoir zone. The Reservoir (R0001), located beneath the Claycap, exhibits high permeabilities in the X, Y, and Z directions, simulating the fractured zone. Above the reservoir zone and near the surface, the Claycap (R00A1) is defined by very tight permeability, indicative of the alteration zone. Surrounding the reservoir zone, the Outer zone (O0001) is typified by the permeability characteristics of volcanic rock. Detailed parameters of these five rock types are presented in Table 1.

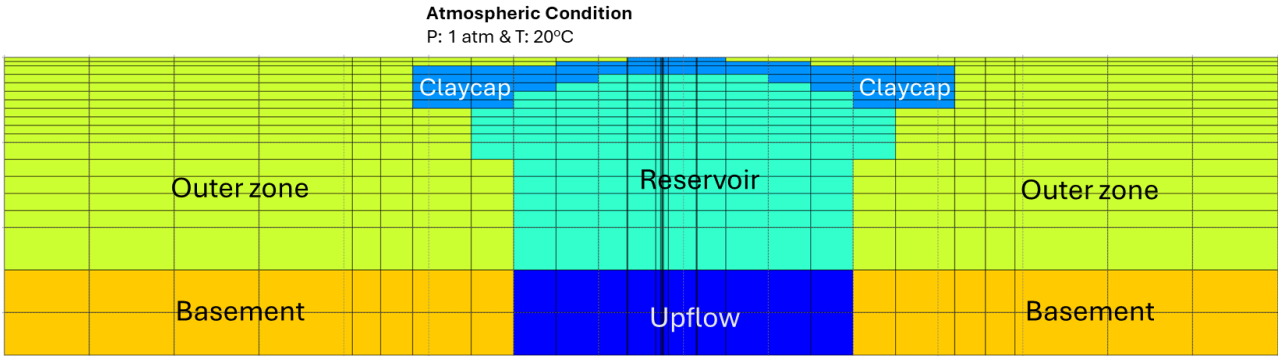

Figure 4: Rock type distribution within the TOUGH2 model and top boundary condition set up.

Table 1: Detailed parameters of the designated rock types.

	Name	DROK	POR	PER(1)	PER(2)	PER(3)	CWET	SPHT	FREQUENCY
1	0ATM1	2500	0.1	1.000000e-15	1.000000e-15	1.000000e-15	2.5	1000	368
2	O0001	2500	0.1	1.000000e-15	1.000000e-15	1.000000e-15	2.5	1000	4001
3	R00A1	2500	0.1	1.000000e-16	1.000000e-16	1.000000e-16	2.5	1000	785
4	B0001	2500	0.1	1.000000e-15	1.000000e-15	1.000000e-15	2.5	1000	538
5	R0001	2500	0.1	3.000000e-14	3.000000e-14	7.000000e-15	2.5	1000	1476
6	U0001	2500	0.1	1.000000e-15	1.000000e-15	5.000000e-15	2.5	1000	200

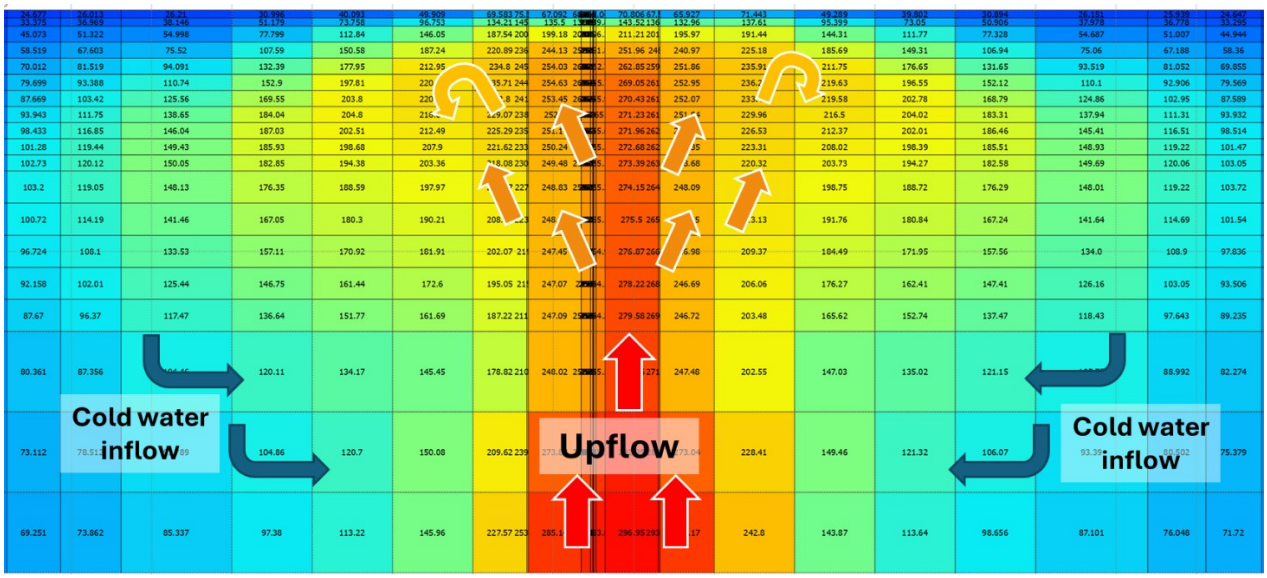

Figure 5: Simulated natural state temperature distribution of the synthetic geothermal model.

4.2 Boundary Condition Setup

Top boundary: At the top of the model, dry atmospheric conditions are assigned at the top surface blocks with a pressure of 1 atm and ambient temperature of 20°C. The equation of state, EOS1, is used in this model to describe pure water in its liquid, vapor, and two-phase states, which could simulate a convective hot geothermal system. An annual rainfall of 2,019.5 mm/year and an infiltration rate of 5% are used.

Side boundary: The side boundaries are presumed to be no-flow boundaries, i.e., no heat or mass entering or exiting the system. The side boundaries are far away (3 - 4 km) from the geothermal reservoir area.

Base boundary: The upflow of the geothermal system is represented by a hot water flux in the Upflow zone blocks, with a total constant mass input of 66.81 kg/s and an enthalpy ranging from 1,200 to 1,300 kJ/kg.

4.3 Natural State Simulation

The natural state model was executed over a simulated period of 3.17 x 10^6 years to achieve steady-state conditions. The simulation results (Figure 5) illustrate the temperature distribution within the reservoir zone, exhibiting a gradient from approximately 270°C in the deeper regions to about 250°C in the upper areas of the reservoir. The dynamics of the hot fluids are characterized by their upward movement from the Upflow blocks,

facilitated by the permeability structures embedded within the 3D model. Along their ascent, these fluids engage in thermal mixing with the saturated water, forming a characteristic convective plume of a liquid-dominated geothermal system. Subsequently, the hot fluids are redirected horizontally toward the periphery of the Reservoir zone, guided by the overlying Claycap's profile.

Over time, as the fluids traverse horizontally, they begin to cool and descend toward the deeper segments of the reservoir model. A cyclical process ensues where the cooling fluids mix anew with rising hot fluids from the Upflow blocks, effectively replenishing the Reservoir zone. Figure 6 depicts the static pressure and temperature around the wellbore location of WELL1, which is designated as the production target zone for the subsequent tightly coupled wellbore-reservoir simulation.

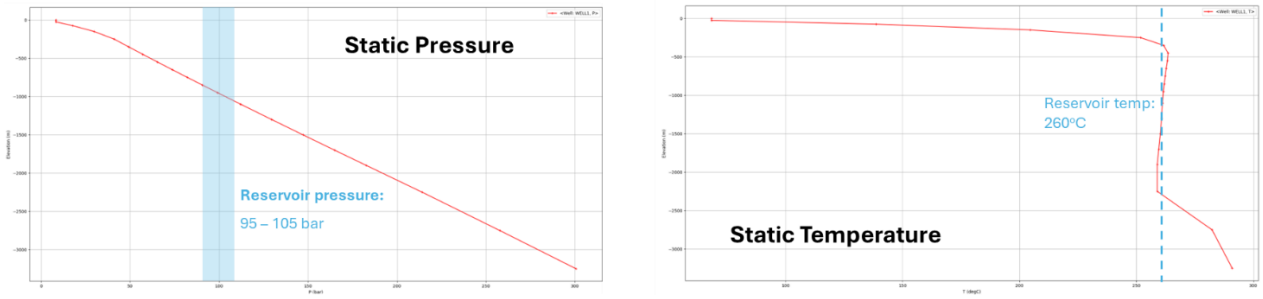

Figure 6: The profiles of static pressure (left) and temperature (right) around the wellbore location of WELL1.

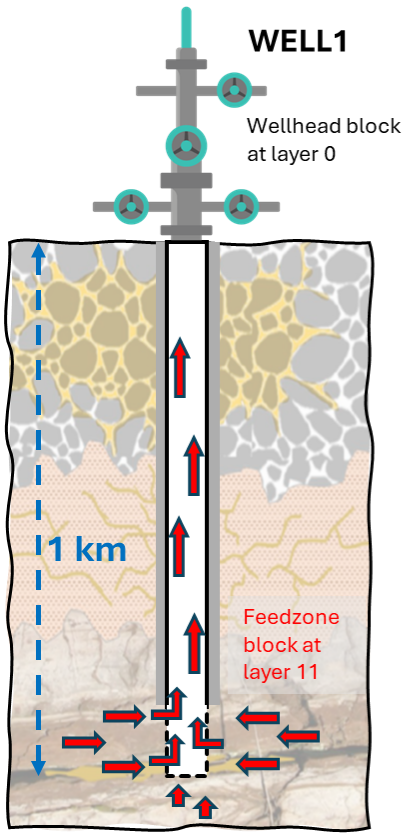

Wellbore Parameters

Parameter(s)	Value	Note
Length	1000 m	Vertical Wellbore
Diameter	9-5/8 inch	Production Casing
Wellhead Pressure	6.5 bar	
Atmospheric Temp	20°C	
Feedzone Depth	900 m - 1000 m	Single feedzone
Pipe Roughness	0.046 mm	Steel Pipe

Figure 7: Conceptual design (left) and wellbore parameters (right) of WELL1.

5. TIGHTLY COUPLED WELLBORE – RESERVOIR MODEL SETUP AND SIMULATION

5.1 Production Model Setup

WELL1 was designated as the production well in the production model by integrating specific wellbore parameters into the Natural State model. The conceptual design of WELL1, as depicted in Figure 7, targets the upper part of the reservoir at a depth of 1,000 meters. For WELL1, a 9 5/8 inch production casing is employed. The bottom block of WELL1, located at layer 11, is designated as the feedzone and features a thickness of 100 meters. A pipe roughness value of 0.046 mm was selected for this model, reflecting the typical roughness

associated with steel pipes. Furthermore, wellhead parameters are established at the surface block (layer 0) of WELL1, maintaining a constant pressure of 6.5 bar.

5.2 Tightly Coupled Wellbore-Reservoir Simulation

The production scenario was conducted over 3.156 x 10^7 seconds (approximately one year), during which the wellbore and reservoir were fully integrated. Figure 8 illustrates the simulation results across this one-year production period. Initially, WELL1 exhibited a high fluid flow rate of 271.56 kg/s. This rate rapidly decreased to 123.49 kg/s after just 132 seconds of production and diminished further to 42.19 kg/s after two hours. Beyond this point, the flow rate stabilized significantly, maintaining an average of 40.85 kg/s throughout the remainder of the year. Concurrently, the enthalpy profile of the produced fluids remained relatively consistent. The initial enthalpy was recorded at 1,148 kJ/kg, which only slightly decreased to 1,118 kJ/kg by the end of the year. This tightly coupled wellbore-reservoir simulation effectively captured the three distinct production phases of WELL1: transient, late transient, and pseudo-steady state conditions.

Furthermore, we can observe the detailed parameters of the fluids produced from this simulation, such as pressure, temperature, enthalpy, and mass flow profiles along the wellbore, as shown in Figure 9. The enthalpy profile slightly changes along the wellbore due to the thermal exchange between the wellbore blocks and the surrounding formations via conductive heat flow. This phenomenon is also in line with the temperature profile of the hot fluids along the wellbore, where the temperature is decreasing from initially 212°C in the feedzone to 164°C in the wellhead. The pressure along the wellbore is also declining from 19.2 bar in the feedzone to 6.5 bar in the wellhead due to the flow restriction inside the wellbore. From all those parameters, we can conclude that the condition of produced hot fluids is already two-phase when entering the wellbore through the feedzone, and it is expanding more due to the pressure decline while flowing upward to the surface, separating the steam and hot water.

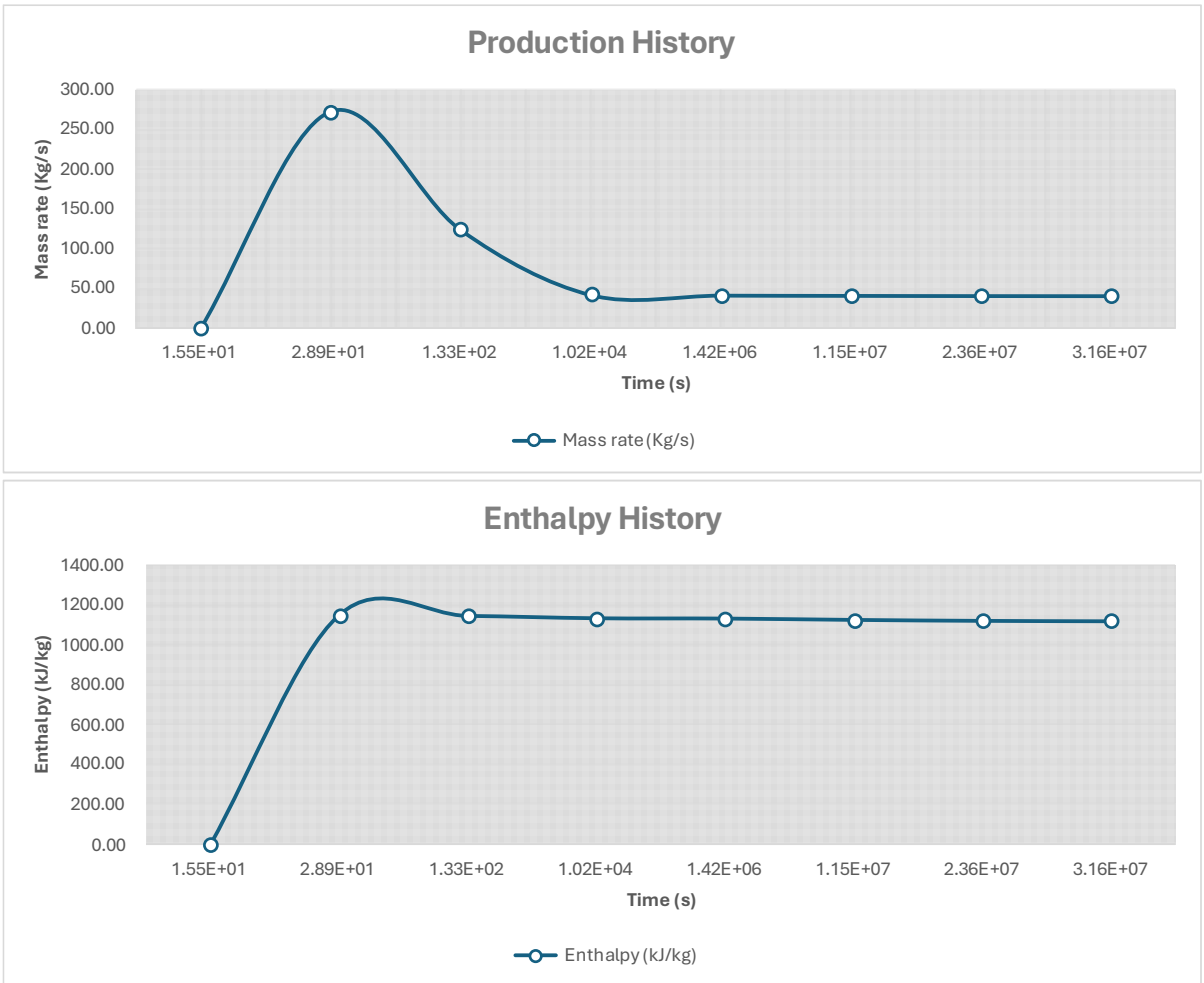

Figure 8: Simulation results for 1 year production period.

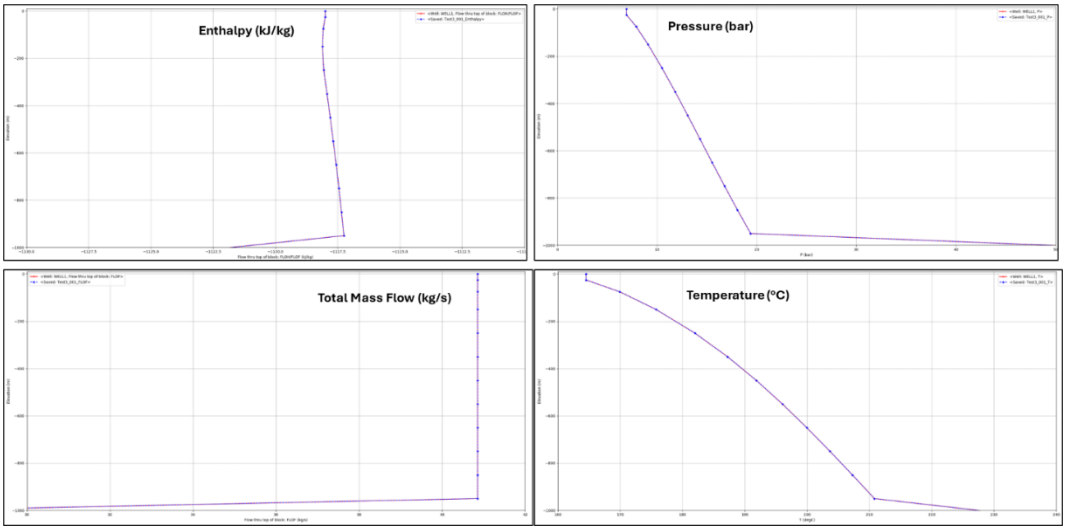

Figure 9: General workflow of the geothermal modelling process for resource assessment of an exploration field.

6. CONCLUSION

This project has successfully developed a full-scale 3D geothermal model for tightly coupled wellbore-reservoir simulations. The model's input setup requirements for a single vertical production well in a fully integrated wellbore-reservoir simulation have been addressed, yielding reliable simulation results. Through this fully integrated simulation using the T2WELL simulator, we were able to observe the common behavior of a geothermal production well. All produced fluid parameters along the wellbore can be visualized using the TIM tool. However, the historical production data need to be extracted and visualized using a different tool, such as an Excel spreadsheet. T2WELL also effectively simulated the three distinct production phases of WELL1: transient, late transient, and pseudo-steady state conditions.

The authors are planning further research to conduct various wellbore-reservoir coupling simulations using T2Well. These studies will explore how minimizing the reservoir grid meshes attached to the wellbore model impacts the simulation results and compare these results with those from the tightly coupled simulation in this project. The goal is to ensure that the simulation outcomes from other coupling methods are comparable in quality to those obtained from the fully coupled full-scale 3D reservoir model.

Some lessons learned in this research regarding the production model setup include:

1. Setting the volume of the Wellhead block at 1 x 10^{50} m^3 is crucial to ensure that the one-year production simulation runs smoothly until the end of the time steps.
2. The porosity and gas saturation of the wellhead element's initial conditions (incon) should be set at 99.99% and 0.99, respectively. The porosity parameter in the wellhead element represents the percentage of the wellbore aperture during the simulation, while the gas saturation represents the maximum allowable steam expansion in the wellhead block.
3. The incon temperature of the wellbore cells should align with the wellbore temperature derived from the Natural State simulation.

ACKNOWLEDGEMENTS

The authors thank our partner, Lawrence Berkeley National Laboratory (LBNL), for their collaboration and making research licenses available.

REFERENCES

Barelli, A., Corsi, R., Del Pizzo, G., & Scali, C. (1982). A two-phase flow model for geothermal wells in the presence of non-condensable gas. *Geothermics*, 11(3), 175-191.

Battistelli, A., Finsterle, S., Marcolini, M., & Pan, L. (2020). Modelling of coupled wellbore-reservoir flow in steam-like supercritical geothermal systems. *Geothermics*, 86, 101793.

Bhat, A., Swenson, D., & Gosavi, S. (2005). Coupling the HOLA wellbore simulator with TOUGH2. *Proc. 30th Workshop on Geothermal Reservoir Engineering*,

Bjornsson, G. (1987). *A multi-feedzone geothermal wellbore simulator*.

Croucher, A. (2011). PyTOUGH: A Python Scripting Library For Automating TOUGH2 Simulations. *Proceedings New Zealand Geothermal Workshop 2011*. Auckland.

Croucher, A. (2015). Recent Developments In The PyTOUGH Scripting Library For TOUGH2 Simulations. Proceedings 37th New Zealand Geothermal Workshop. Taupo.

Finsterle, S., Sonnenthal, E. L., & Spycher, N. (2014). Advances in subsurface modelling using the TOUGH suite of simulators. *Computers & Geosciences*, 2-12.

Guðmundsdóttir, H. (2012). *A coupled wellbore-reservoir simulator utilising measured wellhead conditions*

Gudmundsdottir, H., & Jonsson, M. T. (2015). The Wellbore simulator FloWell-model enhancement and verification. *Proceedings of the World Geothermal Congress*, Melbourne, Australia,

Gudmundsdottir, H., Jonsson, M. T., & Palsson, H. (2012). Coupling wellbore simulator with reservoir simulator. *Proceeding, 37th Workshop on Geothermal Reservoir Engineering*, Stanford University, Stanford, California,

Hadgu, T., & Freeston, D. H. (1990). A Multipurpose Wellbore Simulator. *Geothermal Resources Council Transactions*, 14 Part II, 1279-1286.

Hadgu, T., Zimmerman, R. W., & Bodvarsson, G. S. (1993). *Coupling of a reservoir simulator and a wellbore simulator for geothermal applications*.

James, R. (1975). Gas content of a hot-water reservoir estimated from downhole pressure and temperature measurements. *Proc. 2rid UN Syrup*. Development and Use of Geothermal Energy, 3, 1689-1691.

Nugraha, R. P., O'Sullivan, J., O'Sullivan, M. J., & Abdurachman, F. H. (2022). Geothermal Modelling: Industry Standard Practices. *Proceedings 47th Workshop on Geothermal Reservoir Engineering. Stanford*.

Oldenburg, C. M., Freifeld, B. M., Pruess, K., Pan, L., Finsterle, S., & Moridis, G. J. (2012). Numerical simulations of the Macondo well blowout reveal strong control of oil flow by reservoir permeability and exsolution of gas. *Proceedings of the National Academy of Sciences*, 109(50), 20254-20259.

Oldenburg, C. M., & Pan, L. (2013). Porous media compressed-air energy storage (PM-CAES): Theory and simulation of the coupled wellbore–reservoir system. *Transport in porous media*, 97(2), 201-221.

O'Sullivan, J., Popineau, J., Gravatt, M., Renaud, T., Riffault, J., Croucher, A., . . . O'Sullivan, M. (2023). An integrated, mesh-independent geothermal modelling framework. *Environmental Modelling & Software*, 163, 105666. doi:10.1016/j.envsoft.2023.105666.

Pan, L., Freifeld, B., Doughty, C., Zakem, S., Sheu, M., Cutright, B., & Terrall, T. (2015). Fully coupled wellbore-reservoir modelling of geothermal heat extraction using CO2 as the working fluid. *Geothermics*, 53, 100-113.

Pan, L., & Oldenburg, C. M. (2014). T2Well—an integrated wellbore–reservoir simulator. *Computers & Geosciences*, 65, 46-55.

Pan, L., Oldenburg, C., Wu, Y.-S., & Pruess, K. (2011). *T2Well/ECO2N Version 1.0: Multiphase and Non-Isothermal Model for Coupled Wellbore-Reservoir Flow of Carbon Dioxide and Variable Salinity Water*. Lawrence Berkeley National Laboratory.

Pruess, K. (1987). *TOUGH User's Guide. Report LBL-20700*, Lawrence Berkeley National Laboratory, Berkeley, California.

Pruess, K., Oldenburg, C., & Moridis, G. (1999). *TOUGH2 User's Guide Version 2.0*. Berkeley: University of California.

Shi, H., Holmes, J. A., Durlofsky, L. J., Aziz, K., Diaz, L., Alkaya, B., & Oddie, G. (2005). Drift-flux modelling of two-phase flow in wellbores. *Spe Journal*, 10(01), 24-33.

Vasini, E. M., Battistelli, A., Berry, P., Bonduà, S., Bortolotti, V., Cormio, C., & Pan, L. (2018). Interpretation of production tests in geothermal wells with T2Well-EWASG. *Geothermics*, 73, 158-167.

Yeh, A., Croucher, A. E., & O'Sullivan, M. J. (2012). Recent Developments In The AUTOUGH2 Simulator. *TOUGH Symposium 2012*. Berkeley: Lawrence Berkeley National Laboratory.

Yeh, A., Croucher, A., & O'Sullivan, M. (2013). TIM - Yet Another Graphical Tool For TOUGH2. *Proceedings 35th New Zealand Geothermal Workshop*. Rotorua.

The Design of COI (Cloud Control of Instrumentation) for Manpower Productivity and Carbon Credit Reduction Behavior at 55MW Geothermal Power Plant

Faris Abdillah, Nova Gandika and Mochammad Fa'iq Khasmadin

PT Geo Dipa Energi Unit Patuha, Bandung, Indonesia

faris@geodipa.co.id, nova@geodipa.co.id, faiq@geodipa.co.id

Keywords: Manpower Productivity, Carbon Credit Reduction, Cloud Control of Instrumentation

ABSTRACT

The geographical location of the PT Geo Dipa Energi Patuha geothermal field is located in an area that has extreme weather with a temperature range of 9-20^{o}C with predominantly rainy weather. However, the mobilization monitoring process to the steam field area requires fuel which will cause exhaust emissions. The duration of mobilization by the plant operator will require an accumulated time of around 18 hours in one day or an accumulated time of around 22 days (about 3 weeks) in one month. To ensure the availability of existing control equipment in the control room to work optimally. This situation is the best way to maximize the performance of monitoring in the control room with a fully automation and digitalization system for instrument equipment in the power plant and steam field area. That system is called "COI (Cloud Control of Instrumentation)". The COI will implement 5.0 technology and will be the first integrated system on a geothermal power plant in Indonesia. The work process of the COI (Cloud Control of Instrumentation) system is implementing Long Distance of Control Instrumentation. There are several devices synchronized to process instrumentation parameter readings in the steam field and power plant area. The input readings from the system come from the installed sensors and it is transferred in the form of data to the cloud, then the COI and DCS (distribution control system) controller will process the data to be displayed on each HMI (human machine interface). On the other hand, instrumentation devices will work automatically with remote control to carry out the data transfer processes, data acquisition, and initiate troubleshooting problems (parameter reading data will be stored in the cloud system to facilitate the analysis and troubleshooting process). This feature will make it easier to carry out the troubleshooting method, so that the work execution process in the field will be more efficient and exactly right. This method has proven effective in increasing work efficiency, human resource efficiency and reducing carbon emissions in the environment. The results of implementing this program can reduce carbon emissions by up to 98.35kg CO2 with fuel cost efficiency of up to 24 million. On the other hand, worker productivity will increase by around 84%. The savings from this program for the company reached 288 million IDR per year (fuel consumption).

1. INTRODUCTION

Indonesia is a country that has geothermal potential of 29.5 GW which will continue to increase along with exploration (Agency for the Assessment and Application of Technology, 2020). Patuha Geothermal is a power producer with a capacity of 60MW. The form of savings made is by making continuous improvement efforts. This plant has been operating since 2014 by relying on 10 active wells with a dry phase (PT Geo Dipa Energi - Patuha, 2019) and additional for another 2 wells of 7A and 7B (PT Geod Dipa Energi – Patuha, 2023).

The new GDE project for Patuha 2 will add mileage for the monitoring of instrument equipment in the well pad area carried out by the operator team, The COI was inspired by the existence of the Patuha project 2. At the GDE Patuha 1 mileage to the activity of 182,325 KM / Year requires a total of 14,025 liters of fuel / year, then the possible cost required for monitoring instrument equipment activities is IDR 204 million and generates CO2 as much as 91 Kg / year.

Referring to fuel consumption that requires 14,025 litter of fuel per year producing 91 kg per year, COI provides a solution to reduce solar usage and reduce carbon emissions, as much as 9,375 liters per year and 60.94 Kg CO2/year and save IDR 136 million per year. The efficiency of manpower can finally be better personalized with the COI which makes the monitoring activities of instrument equipment can be done from a distance (Control room) can also streamline the scope of work as an operator and integrated directly with the cloud technology that can be synergized with digitization technology 4.0. In other words, the free time of operators who are licensed with COI technology can be utilized for them to perform other activities such as deepening process understanding, improving skill and ability and making the latest innovations for the benefit of the company.

2. METHODS

2.1 Research Method

This research begins with raising issues that are happening at the Patuha Geo Dipa Energy unit. The issue is an effort to reduce vehicle exhaust gas emissions and optimize work productivity. After the issue is determined, observation work and research study are carried out. Data Schematic, Data Communication, Data Material, Data Fuel Consumption, Data Time Sheet. The function of the research and design of this tool is first to provide information related to the amount of material investment. Calculation and analysis of the relationship between COI and manpower productivity, as well as the number of emissions that can be reduced. The research flowchart was included in Figure 1.

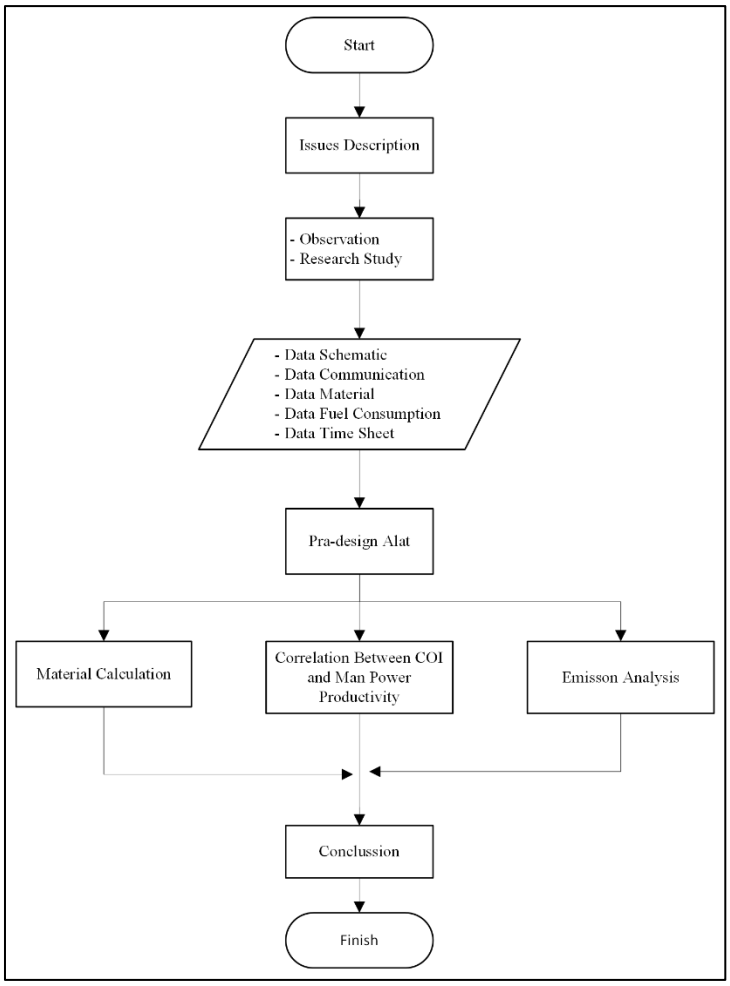

Figure 1: Research Flowchart.

2.2 Economic Analysis

The calculation of economic value in this research focuses on the cost savings used for purchasing fuel and the calculation of compensation and benefits for workers in relation to time and the annual electricity production value of the company. The analysis of fuel value calculation employs a simple analysis by determining the value of lost working hours and the price of fuel oil.

Potential Fuel Cost Savings = Lost working hours * fuel price.

Then, the calculation of lost time productivity value of manpower against electricity production can be analyzed simply by using the variable of lost time per hour, compensation value, and benefits per hour.

Lost Money and Time: lost work * hourly wage

The investment analysis calculation for COI equipment is conducted using the budget planning method adjusted with the self-assessment pricing method (HPS).

2.3 Emission Analysis

The method for calculating the reduction of emission values can be determined using variables X and Y, where variable X represents the accumulated value per km from fuel usage, while variable Y represents the emission content value from the vehicle's fuel. This company has been using fuel products from Pertamina under the brand "pertaminadex," a type of diesel fuel. Based on data from manufacturing, it shows that the content of that type of fuel is CO g/km (0.50); HC+Nox (0.30 g/km); Nox (0.25 g/km); and PM (0.025 g/km).

Emission: X * Y

X = accumulation

Y = rate

3. RESEARCH OF STUDY

3.1 COI Description of System

The COI (Cloud Control of Instrumentation) is a system that can be used to support works such as calibration and monitoring without requiring manpower coming directly to the field. It can help increases manpower productivity as well as help reduces the emissions. The COI is integrated into the system, i.e. 1. The engineering station is useful as a station that collects equipment data on the fields, configures the system and implements control algorithms. 2. The operation station is useful as a machine interface that provides feedback about what is being done or done, in addition to it can also display the command given by the control system, through this system also, by the operator is given the command to the instrument in the field. 3. The Cloud Control of Instrumentation workstation is a tool that is added and integrated with the engineering station used for: a. configuration management: - Remote configuration - User Security - Multiple Communication Protocols - Device Dashboards - Bulk Transfers - Smart Commissioning b. Diagnostic and Monitoring: - Comprehensive connectivity - Online Monitoring with Alert Monitor - DTM Launcher - Device viewer. c. Calibration Management: - calibration connections to field instrumentations. - Create test schemes -Create calibration routes - Calibrations reporting. d. Paperless Documentation: - Paperless Configuration - Paper without Calibrating Management - Paperless drawings and notes. 4. The field control system becomes the brain of the DCS, where control functions are performed, such as PID control, comparison control, ratio control, simple arithmetic operations and dynamic compensation. 5. Remote I/O is an input Output mechanism for measuring and controlling devices, allowing peripherals to communicate directly with the CPU, even remotely. 6. The field instruments, divided into sensors and final control elements.The sensors commonly used are flow meter, pressure, temperature, and level. Whereas final control elements can be controlling valve and on/off valve. The Topology of the COI has been included in Figure 2.

3.2 Description of Issues

The issues raised by this innovation start from the searches and facts in the field related to the use of motor vehicles for monitoring activities carried out by the operators of the team that is said to take a lot of time every day, then the emissions generated by the motor vehicles used in the monitoring activity above also became the issue of the COI technology that we poured on this innovation, in addition to the 2 things above is how much time can be better utilized by the team operators when realizing this technology COI for research and development time, improvement of individual skill and ability of each field operator. The distance and time it take to monitor instrument equipment on the ground is so far and long, so when there is an emergency moment it will slow down to conduct investigation and mitigation, with the COI technology related above can be the answer to facilitate and accelerate operations at the time.

3.3 Emission

Air pollution is the entry or introduction of living things, substances, energy and or other components into the air and or alteration of the order (composition) of the air by human activity or by natural processes so that the air quality becomes less or can no longer function according to its purpose. The transport sector associated with congestion generates emission gases in the air are 1. Carbon dioxide (CO2) Gases produced by perfect combustion of motor vehicles and plant fuels as well as gases from forest fires. 2. Carbon monoxide (CO) Gases that are colorless, odorless, and toxic. 4. PM (Material Particular) is the most visible and most dangerous air pollutant. This is a. aerosol: particles that fade and float in the air b. fog ‘mist’: aerosols that are fragments of water and are in the atmosphere c. smoke ‘smoke’: Aerosols which are mixtures of solid and liquid grains and flying fading in air d. dust ‘dust’: an aerosol of solid fragments and floating in air 5. Pb (Timbal) Heavy metals used by humans to increase combustion in motor vehicles. The result of such combustions is a lead oxide in the form of dust or particle that can be inhaled by human beings.

The number of emissions generated by the transport sector is influenced by the 1. speed of the vehicle. The flow of low-speed motor vehicles will lead to increased concentrations of carbon dioxide (CO) and hydrocarbon (HC) particles, which are more dangerous to health than high speed vehicles. These vehicles will also produce more emissions of exhaust gases containing Nitrogen Oxide (NOx). Provision of vehicle speed brakes in settlements or hallways, often referred to as "sleeping police," is a source of pollution. 2. Old vehicles age the machine is not functional/perfect due to maintenance and limited vehicle spare parts are no longer produced. Therefore, the age limitation of vehicles, especially for public transport, should be considered as one of the solutions. The older vehicles, especially those less wellined, the greater the potential to contribute air pollutants. 3. Traffic conditions High traffic volumes tend to give the largest proportion of air pollution. Moreover, the biggest potential pollution by motor vehicles is traffic congestion. Therefore, traffic regulation, traffic alarms, and strong measures against vehicle violations can help overcome traffic jams and thus reduce air pollution. 4. The road's geometry has resulted in increased fuel consumption of the vehicle, increasing air pollution due to the emissions of such vehicles. 5. The type of vehicle as well as the type of fuel used by each vehicle.

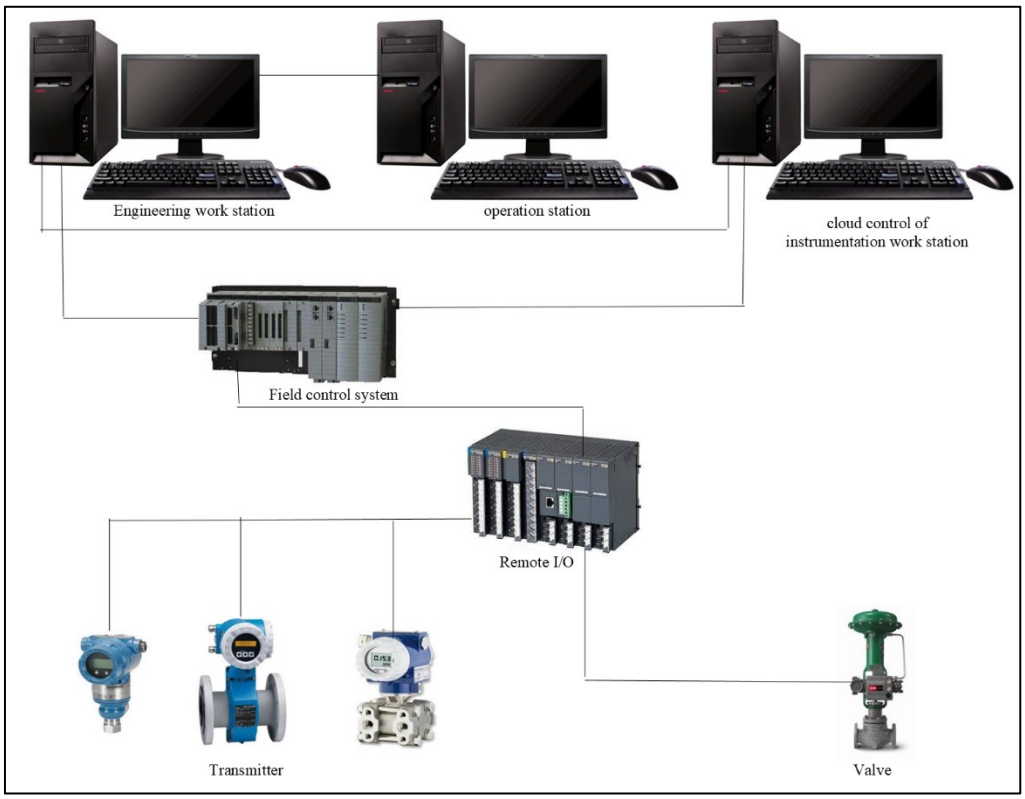

Figure 3: Topology of COI.

3.4 Working Efficiency

The routine monitoring of instrument equipment, which is usually performed by field operators six times a day, indicated has no impact on the increase in GWh and rather takes a lot of time at the time of mobilization to the production well area. By using it, the COI can help to perform routine monitoring of instrument equipment with a faster time flow without eliminating the accuracy of instrument readings because the COI can perform self-loop checks to ensure the reliability of the instruments. Meanwhile, 28 people divided into 4 groups also face the issue of long free time, which makes them standby without productivity. The free time gained after the COI can be used for continuous learning time or for conducting research for continuous improvement.

4. RESULT AND DISCUSSION

4.1 Emission Analysis

The type of vehicle used by this company is diesel, while the fuel used is Pertadex. (pertamina dex). The operational number of this vehicle is only one, and it is used repeatedly to monitor parameters in the steamfield. Although the company has chosen fuels with low carbon emissions, fossil energy still fundamentally has the potential to pollute the environment. The calculation of emission levels in this study is examined in terms of carbon monoxide, unburned fuel, NOx, and particulate matter. Based on the results of the emission value calculations presented in the graph shown in Figure 3. This calculation is carried out by comparing the emission values before and after the implementation of the program. There was a decrease in CO emissions of 60,938 g/km

from 91.163 g/km to 30,225 g/km after the implementation of the program. Meanwhile, the levels of HC+NOx experienced a decrease of 36,563 g/km from 54,698 g/km to 18,135 g/km. Then, the NOx levels decreased by 30,469 g/km from an initial 45,581 g/km to 15,112 g/km. Meanwhile, the particulate matter levels decreased by 3,047 g/km from 4,558 g/km to 1,511 g/km.

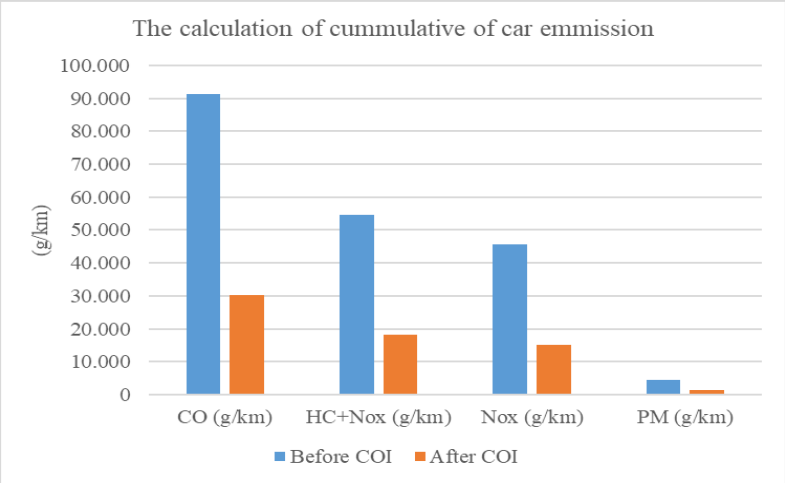

Figure 3: Comparison Chart of Emission Values Before and After COI Implementation.

The impact of the decrease in emission levels is a reduction in the mobility of vehicle operations. The implementation of COI affects the release of job tasks that can be monitored through the COI program features. A comparison of vehicle mobility before and after the implementation of the program is presented in Table 1. There is a decrease of 9,375 liters, from an initial 14,025 liters to 4,650 liters. The results of the COI program implementation are directly proportional to fuel savings and a reduction in carbon emissions.

4.2 Economic Analysis

4.2.1 Economic Analysis in Fuel Sector

The impact of the implementation of the COI program on fuel usage is inversely related. The greater the reduction in time and kilometers, the greater the savings, because the non-massive use of vehicles impacts fuel consumption. The comparison of annual fuel consumption values before and after the implementation of the COI program is presented in Table 1. The fuel consumption value before the COI program was implemented was 14,025 liters/year. Meanwhile, after the implementation of the COI program, it was around 4,650 liters/year. The total cost savings from fuel due to the implementation of the COI program is 136.4 million IDR.

Table 1: Vehicle Operational Data (Yearly).

No	Condition	Type of Vehicle	Fuel Category	Monitoring Time (h)	Fuel Consumption (liter)	Driving Range (km)	Price Fuel (million IDR)
1	Before COI	Double Cabin	Dexlite-Diesel	2,244	14,025	182,325	204,06
2	After COI	Double Cabin	Dexlite-Diesel	744	4,650	60,450	67,66

Before the implementation of the COI, based on a survey conducted among workers, it was found that the average work productivity value ranged from 36% with productivity levels reaching up to 80%, while the remaining 36% had productivity values below 60%, as shown in Figure 4. This shows a gap between the compensation and hourly benefits received by workers and their productivity value. The implementation of this program will increasingly affect workers' productivity, as the amount of leisure time increases. This will impact the relationship between the compensation received by employees and the productivity they deliver. To avoid a gap between compensation and productivity, based on a survey of workers, the implementation of COI has made employees more interested in participating in R&D and Continuous Learning and Improvement programs. This data was obtained from a survey presented in graphical form shown in Figure 5.

4.2.3 Economic Analysis COI Program

The investment amount for the COI program is around IDR 179,200,000. This figure is the result of calculations and surveys conducted in the marketplace. The total investment value includes the VAT. Details of the total investment value for this program are presented in Table 2. Meanwhile, the payback value of this program's investment refers to fuel savings, while the economic value from carbon credit sales and the savings on the human

resources side are disregarded. The Payback value is obtained by subtracting the investment value from the savings value in the fuel sector. Based on these calculations, the payback period for this system lasts only 17 months. The results of the payback value calculations are presented in Table 3.

4.2.2 Economic Analysis from Human Resources

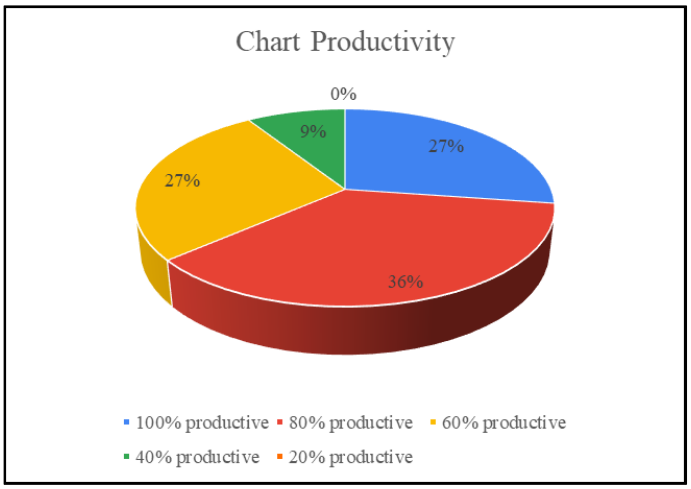

Figure 4: Worker Productivity Chart.

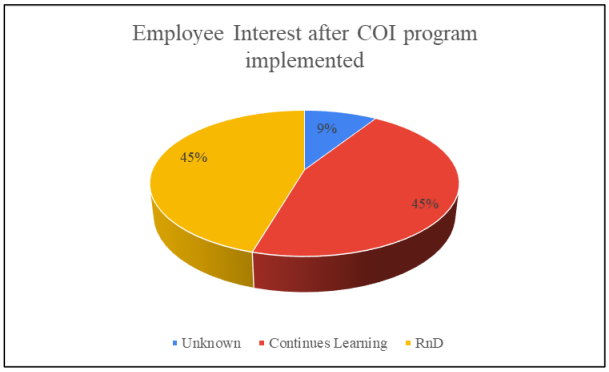

Figure 5: Chart of Employee Interest in Spending Free Time.

Table 2: Total Investment for COI.

No	Item	Qty	Unit	Price (IDR) /Unit	Total Price (IDR)
1	Software Management	1	Ea	80,000,000	80,000,000
2	PC COI	1	Ea	36,000,000	40,000,000
3	Communication Module	3	Ea	5,000,000	15,000,000
4	Kabel LAN	60	m	20,000	1,200,000
5	Installation Design and Risk Analysis (Technical Advisor)	1	Lot	30,000,000	30,000,000
6	Maintenance Cost	1	Lot	17,000,000	17,000,000
				Total	179,200,000
				PPN (11%)	19,712,000
				Grand Total	198,912,000

4.3 Manpower Productivity Analysis

The electricity production data at this plant tends to fluctuate over the course of a year, as seen in Figure 4. The average electricity production value is around 43.44 GWh. The lowest generation value is in February, while the highest generation value is in March. Compared to the lost time value, which remains constant in January, March, May, July, August, October, and December. The relationship between the productivity value of manpower and generation based on conditional data (adjusting to the generation value, the higher it is, the greater the lost time value, and if energy generation decreases, the lost time value becomes lower). The relationship between generation

and energy production is inversely proportional. Another comparison of the relationship between the COI program and manpower productivity is by reducing worker lost time. Based on the questionnaire from the employees, they are more interested in R&D and Continuous Learning and Improvement. Under the following conditions, the relationship between the implementation of the COI program and manpower is a win-win solution; workers can improve their skills and enhance their resilience for improvement and learning.

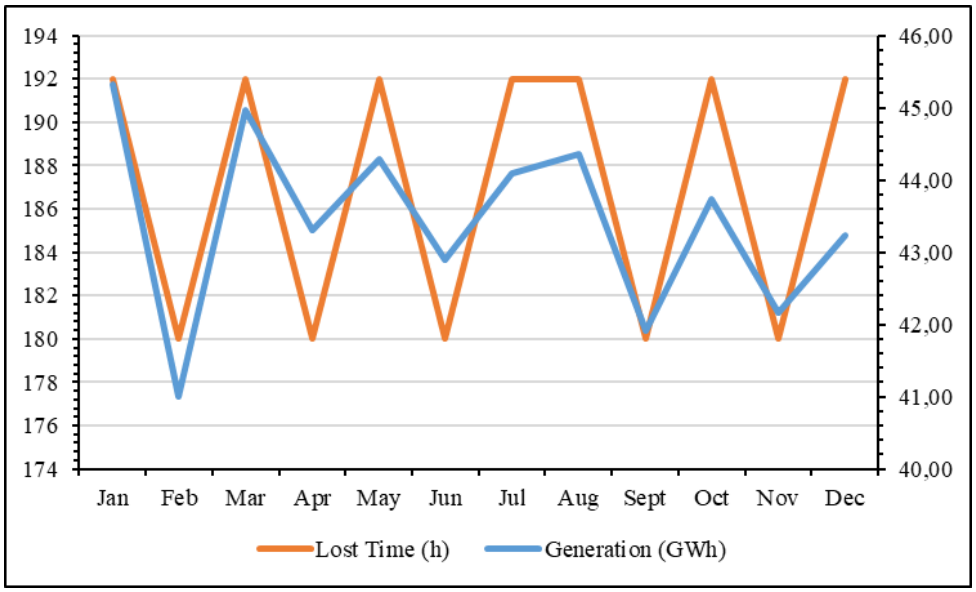

Figure 6: Comparison Chart of Generation (GWh) and Lost Time Productivity.

Table 3: The Scenario of Investment Return.

No	Month	Investment	Savings
1	January 25	198,912,000	187,545,333
2	February 25	187,545,333	176,178,667
3	March 25	176,178,667	164,812,000
4	April 25	164,812,000	153,445,333
5	May 25	153,445,333	142,078,667
6	June 25	142,078,667	130,712,000
7	July 25	130,712,000	119,345,333
8	August 25	119,345,333	107,978,667
9	September 25	107,978,667	96,612,000
10	October 25	96,612,000	85,245,333
11	November 25	85,245,333	73,878,667
12	December 25	73,878,667	62,512,000
13	January 26	62,512,000	51,145,333
14	February 26	51,145,333	39,778,667
15	March 26	39,778,667	28,412,000
16	April 26	28,412,000	17,045,333
17	May 26	17,045,333	5,678,667

5. CONCLUSION

Indonesia has a 29.5 GW geothermal potential, with Patuha Geothermal, a 60MW power producer, operating since 2014. The new GDE project for Patuha 2 will add mileage for monitoring instrument equipment in the well pad area. COI technology, inspired by Patuha 2, can reduce fuel consumption and carbon emissions by IDR 136 million per year. COI allows monitoring activities from a distance, streamlines operator scope, and integrates with cloud technology. This allows operators to focus on process understanding, skill improvement, and innovation for the company's benefit. The technology also allows operators to use their free time for other activities. The research

focuses on reducing vehicle exhaust gas emissions and optimizing work productivity at Patuha Geo Dipa Energy unit. It includes observation work and research on data schematics, communication, material, fuel consumption, and timesheets, aiming to calculate COI and reduce emissions. The Cloud Control of Instrumentation (COI) is a system that supports calibration and monitoring without requiring direct field manpower. It includes an engineering station for collecting equipment data, a machine interface for feedback, and a workstation for configuration management, diagnostic and monitoring, calibration management, and paperless documentation. The field control system functions as the DCS's brain, performing functions like PID control, comparison control, ratio control, and dynamic compensation. Remote I/O allows peripherals to communicate directly with the CPU. Field instruments are divided into sensors and final control elements, such as flow meters, pressure, temperature, and level. The COI can improve routine instrument equipment monitoring by ensuring faster time flow and accuracy without compromising reading accuracy. This method also allows for self-loop checks, reducing standby time for 28 people divided into 4 groups, allowing for continuous learning and research for improvement. The company uses diesel fuel, with a diesel engine and a dex fuel tank. The operational fuel tank is used for monitoring parameters in the steamfield. The study reveals a significant impact on carbon emissions from various sources, including carbon monoxide, unburned fuel, nox, and particulate meters. The implementation of the COI program significantly impacts the reduction of carbon emissions and the increase in fuel consumption. The study concludes that the COI program is crucial for environmental protection. The implementation of COI program has a significant impact on fuel consumption, with a decrease in consumption from 14,025 liters before COI implementation to 4,650 liters after. The cost of fuel from COI implementation is 136.4 million IDR. A survey showed that 36% of workers have a high productivity, while 60% have a low productivity. Implementing COI will also affect worker productivity, allowing for more time for R&D and continuous learning and improvement. The COI program's investment amount is IDR 179,200,000, based on market research and surveys. The program's payback is based on the reduction of waste, economic credit utilization, and human resource management. The payback period is only 17 months. The plant's production data is fluctuating, with a total output of 43.44 GWh. The COI program's productivity relationship with generation is based on the reduction of lost time workers. The program's implementation is a win-win solution, allowing employees to improve skills and increase learning opportunities.

REFERENCES

Emerson, AMS Device Manager. Accessed on 26 of August, from www.emerson.com

Yokogawa, Plant Resource Manager (PRM). Solutions and Asset Management and integrity. Accessed on 26 of Auguts 2024, from www.Yokogawa.com

Increasing the Attractiveness of Low-Medium Temperature Geothermal Resources Development in Indonesia: A Discussion from the Techno-Economic Perspective

Vincentius Adven Brilian[1,2], Daniel W. Adityatama[1], Triwening Larasati[1], M. Rizqi Al Asy'ari[1], Nadya Erichatama[1], Dorman P. Purba[3], and Khasani[2,4]

[1]Geoenergis (PT Geoenergi Solusi Indonesia), Cibis Nine 11th Floor, Jakarta, Indonesia
[2]Department of Mechanical and Industrial Engineering, Gadjah Mada University
[3]Enerka (PT Enerka Bhumi Pratama), Cibis Nine 11th Floor, Jakarta, Indonesia
[4]Geothermal Research Center, Faculty of Engineering, Gadjah Mada University

adven.brilian01@gmail.com

Keywords: geothermal, low-medium temperature, optimization, techno-economic

ABSTRACT

The development of geothermal power plants in Indonesia had reached an installed capacity of 2,413 MW by the end of 2023, which is equivalent to 11% of Indonesia's geothermal potential of 23 GW. However, the development of geothermal energy in Indonesia is still predominantly focused on high-temperature resources, with only 8.29 MW (0.3%) of the total installed capacity coming from low-medium temperature resources. Among the multidimensional challenges facing the Indonesian geothermal industry, the development of low-medium temperature geothermal resources is hindered by less attractive economic viability because these resources require the use of downhole pumps to discharge the fluid and the more expensive binary plant technology compared to flash plants. Despite this, 9 low-medium temperature geothermal fields with development plans totaling up to 430 MW are included in Indonesia's National Strategic Project (PSN) pipeline until 2030. Therefore, optimization from a techno-economic aspect is necessary to increase the economic attractiveness of developing low-medium temperature geothermal resources in Indonesia. This study aims to identify potential techno-economic optimization initiatives and to test the impact of these initiatives on reducing the levelized cost of electricity (LCOE) from low-medium temperature geothermal resources. Three potential initiatives, such as targeting shallow outflow wells, utilizing high-temperature electric submersible pumps (ESPs), implementing well stimulation, and employing modular plants, were identified through literature studies on the development of such resources in the United States. Thus, by applying these techno-economic optimization initiatives, it is hoped that the economic attractiveness of developing low-medium temperature resources can be enhanced and made competitive with the maturely developed high-temperature resources in Indonesia.

1. INTRODUCTION

Since its initiation during the first geothermal power plant (GPP) commissioning in Kamojang, West Java, in 1983, Indonesia's GPP development had achieved an installed capacity of 2,413 MW from 50 GPP units by the end of 2023, representing 11% of the country's geothermal potential of 23 GW. (ThinkGeoEnergy, 2024; Al Asy'ari, et al., 2023). However, the GPP development in Indonesia remains largely concentrated on high-temperature resources, with only 8.29 MW (0.3%) of the total installed capacity derived from low-medium temperature resources (GRG-Geoenergis, 2024b) despite having the potential of these resources of more than 9.6 GW (Putriyana, et al., 2022). The first commercial operation date (COD) of low-medium temperature resources GPP was achieved in 2013 at the Mataloko geothermal field with an installed capacity of 2.5 MW (EBTKE, 2020). The subsequent low-medium temperature resources GPP COD events were achieved after a decade, which were Sokoria GPP Unit 1 (5 MW) in 2022 and Sokoria GPP Unit 2 (3.29 MW) in 2023 (ThinkGeoEnergy, 2024). Nevertheless, 9 low-medium temperature GPP projects with a total planned development capacity of 430 MW have been identified as Indonesia's National Strategic Project (PSN) until 2030 (PLN, 2021).

The slow development of low-medium temperature geothermal resources in Indonesia is influenced by both general and specific causes. Generally, multi-dimensional challenges hinder geothermal development in Indonesia across all temperature ranges, as shown in Figure 1 (PLN, 2020). From a funding perspective, geothermal projects often face low bankability during high-risk exploration stages and licenses without fund access. Land and infrastructure present further obstacles, including time-consuming land acquisition, lack of existing infrastructure during early exploration, and remote locations. Additionally, social and environmental challenges such as community rejection, Environmental & Social Impact Assessments (ESIA), Land Acquisition & Resettlement Action Plans (LARAP), and forestry permit compliance add complexity. Project delays are further exacerbated by the slow awarding of Geothermal Working Area (WKP) licenses and the limited purchasing ability of Indonesia's sole electricity offtaker, PLN, necessitating prolonged negotiations between developers, PLN, and the government (Pambudi & Ulfa, 2024). Technical issues also play a significant role, including subsurface

uncertainties, low quality and availability of exploration data, and a shortage of skilled personnel. Specifically, low-medium temperature resources face challenges due to the lack of expertise in their exploration and development, as well as less attractive economic viability due to the higher costs of required technologies like binary plants and downhole pumps compared to those used for high-temperature resources (Yudha, et al., 2022). Consequently, techno-economic optimization initiatives are urgently needed to enhance the economic attractiveness of developing low-medium temperature geothermal resources in Indonesia.

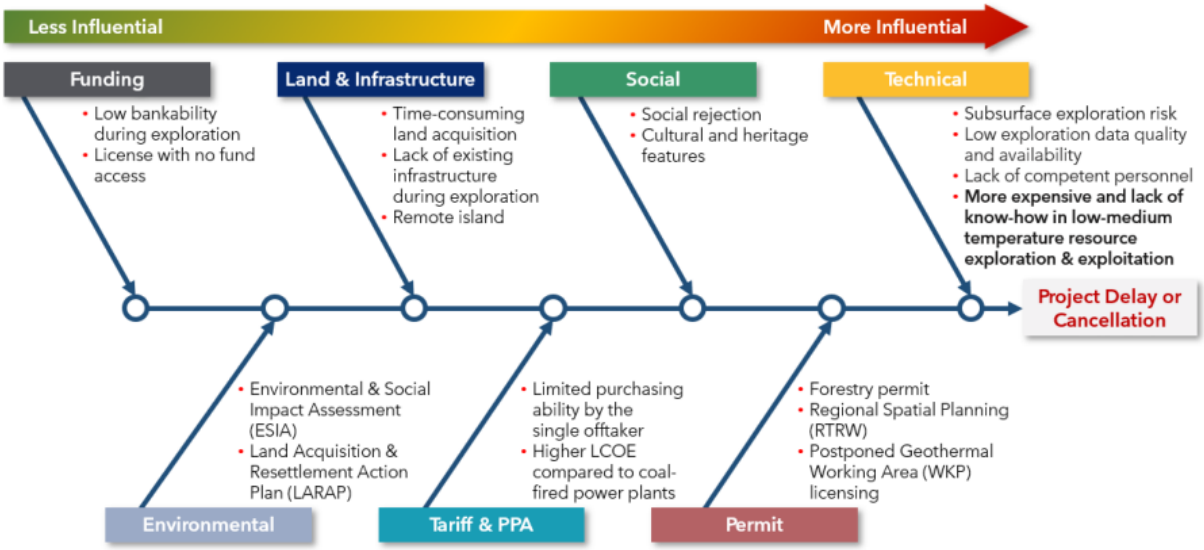

Figure 1: Challenges of Geothermal Development in Indonesia (Pambudi & Ulfa, 2024; Yudha, et al., 2022; PLN, 2020).

Some researchers have pioneered the technological or the techno-economic studies of low-medium temperature geothermal resources in Indonesia. (Febrianto, et al., 2019) summarized the experience on pumped geothermal well projects worldwide as well as improved the previous research by (IFC, 2013) about the effects of productivity index on the pumped geothermal well power output by performing an updated wellbore modeling with more appropriate technical assumptions for the conditions in Indonesia. (Prabowo, et al., 2021) delved more into the technical analyses of downhole pump engineering design for the application in the Tulehu geothermal field, Maluku, within the scope of the reservoir, production well, and the power plant through an analytical analysis of the well testing results to characterize the well's productivity, a calculation of the downhole pump system design, and a calculation of the binary plant's performance. The study revealed that the downhole pump is optimally set at 600 mMD with a potential to produce geothermal fluid at a rate of 173.8 t/h, equivalent to a binary plant net power output of 1.38 MW.

The first comprehensive evaluation of low-medium temperature geothermal resources development in Indonesia was attempted by (Ikhwan, et al., 2021) from the geoscience, technology, and social perspectives. The emphasis of the study was comparing the permeability control and characteristics of low-medium temperature resources in Indonesia and the U.S. with actual geothermal field case studies. A brief overview of pumped geothermal well technology and the potential social issues due to the proximity of such resources to the community settlement were also discussed. Another comprehensive evaluation of low-medium temperature geothermal resources in Indonesia was conducted by (Putriyana, et al., 2022), focusing on the use of statistical data to geologically characterize, locate the regional distribution, and quantify the resource potential of low-medium temperature geothermal resources in Indonesia. Additionally, the study reviewed the existing technologies for low-medium temperature resources, namely binary plant and downhole pump, by performing technical comparisons, such as comparing the organic Rankine cycles with the Kalina cycles for binary plants and comparing the lineshaft pumps with the electric submersible pumps for downhole pumps. Other technologies to optimize low-medium temperature geothermal resources' economic feasibility, such as well stimulation and modular power plant, are also mentioned in the study despite briefly.

The present study aims to identify potential techno-economic optimization initiatives and to test the impact of these initiatives on reducing the levelized cost of electricity (LCOE) from low-medium temperature geothermal resources. Therefore, byy achieving the aim of the study, the following research gaps on the previous studies on techno-economic aspects of low-medium temperature geothermal resources in Indonesia are expected to be fulfilled:

1. **United States experience in developing low-medium temperature resources**: the study by (Putriyana, et al., 2022) lacks the extraction of lessons learned of low-medium temperature geothermal resources development from the global experience. Meanwhile, the present study focuses on extracting the lessons learned from the United States since the U.S. have been developing low-medium temperature resources for more than 40 years with an installed capacity of 1,207 MW, accounting for 33% of the total U.S. installed capacity of 3,615 MW in 2023 (ThinkGeoEnergy, 2024; NREL, 2021).
2. **Transferrable knowledge from high-temperature resources development**: the study by (Putriyana, et al., 2022) lacks the evaluation of the geothermal field development experience that Indonesia have accumulated for the past 40 years, despite still focusing on high-temperature resources, which can be the stepping stones to develop low-medium temperature resources in the future. Meanwhile, the present study evaluates the initiatives from high-temperature resources development in Indonesia with actual field case studies, such as well stimulation in the Salak (Pasikki, et al., 2010) and Wayang Windu (Mulyadi, 2010) geothermal fields, outflow zone development in the Sibayak (Firanda, et al., 2024), Muara Laboh (Stimac, et al., 2019), and Ulubelu (Hochstein & Sudarman, 2015) geothermal fields, and modular power plant construction, to identify how these initiatives can be transferred to optimize low-medium temperature resources development.
3. **Emphasis on pumped geothermal well optimization**: the study by (Ikhwan, et al., 2021) did not correlate the permeability control and characteristics of low-medium temperature resources with the performance of downhole pumps reviewed in the study. Meanwhile, pumped well is a crucial element in the low-temperature geothermal power system to discharge the fluid due to the absence of the flashing process as the flow drive mechanism (Aydin & Merey, 2021; Sanyal, 2005). Therefore, the present study highlights the influence of permeability in controlling the performance of pumped geothermal wells based on the reservoir deliverability and well flow performance analyses.

Furthermore, to achieve the aim of the present study, the following research questions have to be addressed:

1. What is the current status of low-medium temperature geothermal resources development in Indonesia and the U.S.?
2. What are the techno-economic initiatives that can be learned from the low-medium temperature geothermal resources development experience in the U.S.?
3. What are the techno-economic initiatives that can be learned from the high-temperature geothermal resources development experience in Indonesia that can be transferred to optimize low-medium temperature geothermal resources development?
4. How is the impact of the identified techno-economic optimization initiatives on the LCOE of low-medium temperature geothermal resources?

2. POTENTIAL AND CURRENT DEVELOPMENT STATUS IN THE UNITED STATES AND INDONESIA

The potential and current development status of geothermal resources in the U.S. and Indonesia should be analyzed as a foundational knowledge that will provide a framework for identifying the techno-economic optimization initiatives for low-medium temperature geothermal resources. Nevertheless, the analysis is started by first understanding the classification of geothermal resources based on the temperature class and the system type hence the subsequent analysis throughout the paper can be made based on a consistent resource classification and thus an appropriate techno-economic analysis can be applied according to the resource characteristics.

2.1 Geothermal Resource Classification

Before delving into the techno-economic optimizations of low-medium temperature geothermal resources, understanding the classification of geothermal resources based on resource temperature and system type is crucial. This classification provides a clear framework for assessing the viability and potential of different geothermal projects. By categorizing resources according to their temperature, it becomes easier to determine the most suitable technologies and approaches for harnessing these resources efficiently. Additionally, knowing the type of geothermal system, whether it involves high-temperature or low-medium temperature resources, helps in planning and executing exploration, development, and operational strategies effectively for each resource class.

2.1.1 Based on the Resource Temperature

The classification of geothermal resources based on temperature, as depicted in Figure 2, reflects the evolving understanding of geothermal resources and technological advancements in geothermal resource exploitation. Historically, classifications by (Muffler & Cataldi, 1978; Hochstein, 1990; Hochstein, 1990; Bendritter & Cormy, 1990; Nicholson, 1993) primarily divided geothermal resources concerning their direct or indirect utilization capabilities, often based on their potential for exploitation. These classifications identified resource categories like "low," "intermediate," and "high" temperatures, with direct utilization typically involving lower temperatures and

indirect utilization involving higher temperatures. However, advancements in geothermal technology have shown that even low-medium temperature resources can now be effectively utilized for power generation, challenging earlier classifications. For example, binary power plants and the use of pumped wells have made it possible to generate electricity from resources previously considered suitable only for direct use.

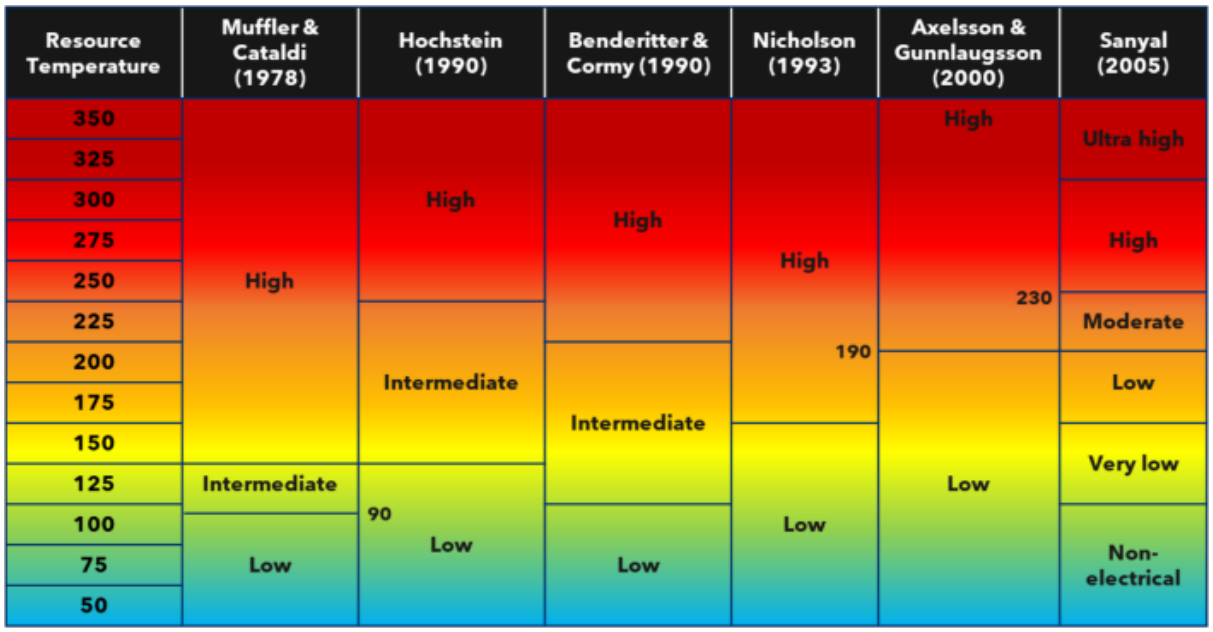

Figure 2: Geothermal Resource Classification Based on Temperature (Sanyal, 2005; Axelsson & Gunnlaugsson, 2000; Nicholson, 1993; Bendritter & Cormy, 1990; Hochstein, 1990; Muffler & Cataldi, 1978).

Meanwhile, (Sanyal, 2005) introduced a more comprehensive classification scheme that considers not only the resource temperature but also factors such as the steam fraction in the reservoir's mobile fluid phase, applicable power generation technology, production mechanisms, well productivity factors, and operational challenges. This new scheme enables a more precise and technology-suited division of temperature classes. For instance, Sanyal's classification acknowledges that "very low" temperature resources can be utilized for electricity generation using binary power plants and pumped wells, expanding the potential uses of geothermal resources beyond what was previously considered feasible. This shift in classification reflects the growing capability of modern geothermal technology to harness energy from a wider range of geothermal conditions, emphasizing the importance of considering technological advancements in resource assessment and utilization.

Due to the more comprehensive and technology-suited classification, the resource temperature classification in present study primarily refers to the Sanyal's classification. However, considering that the present study focuses on the low-medium temperature resources without needing the narrow temperature class range as in Sanyal's classification compared to the, the present study implements the following simplification in the resource temperature classification:

1. **Low-temperature**: 100 to < 190°C.
2. **Medium-temperature**: 190 to < 230°C.
3. **High-temperature**: higher than 230°C including steam-dominated fields.

Table 1: Geothermal Resource Classification by Sanyal (2005).

Temperature Class	Resource Temperature (ºC)	Mobile Fluid Phase in the Reservoir	Production Mechanism	Fluid Phase at the Wellhead	Well Power Output	Applicable GPP Type	Typical Operational Problem
Non-electrical grade	< 100	Compressed liquid	• Artesian self-flowing • Pumped	Compressed liquid	Depending on the reservoir flow capacity and static water level	Direct use	n/a
Very low	100 to < 150	Compressed liquid	Pumped	• Compressed liquid (if pumped) • Steam-liquid mixture (if self-flowing)	2-4 MWe	Binary	n/a
Low	150 to < 190	Compressed liquid	• Pumped • Self-flowing (at the higher temperature end of the range)	• Compressed liquid (if pumped) • Steam-liquid mixture (if self-flowing)	3-5 MWe	• Binary • Double-flash • Hybrid	• Calcite scaling in production wells • Stibnite scaling in binary GPPs
Medium	190 to < 230	Compressed liquid	Self-flowing	Steam-liquid mixture	3-12 MWe	• Single-flash • Double-flash • Hybrid	• Calcite scaling in production wells • Alumino-silicate scaling in injection wells
High	230 to < 300	Compressed liquid; liquid-dominated two-phase	Self-flowing	• Steam-liquid mixture • Saturated steam	Up to 25 MWe	• Single-flash • Hybrid	• Silica scaling in injection wells • Corrosion • High NCG content

Temperature Class	Resource Temperature (ºC)	Mobile Fluid Phase in the Reservoir	Production Mechanism	Fluid Phase at the Wellhead	Well Power Output	Applicable GPP Type	Typical Operational Problem
Very high	300+	Liquid-dominated two-phase	Self-flowing	• Steam-liquid mixture • Superheated steam	Up to 50 MWe	Single-flash	• High NCG content • Corrosion • Silica scaling in injection wells • Silica scaling in production wells at lower wellhead pressures
Steamfield	240 (33.5 bara pressure; 2800 kJ/kg enthalpy)	Steam	Self-flowing	• Saturated steam • Superheated steam	Up to 50 MWe	Dry steam	• High NCG content • Corrosion

2.1.2 Based on the Type of Systems

In addition to the geothermal resource classification based on the resource temperature, the classification of geothermal resources based on system type is crucial for understanding the geological and hydrogeological settings that influence the exploitation of geothermal energy. According to the classification by (Ormat, 2022), geothermal systems are broadly categorized into volcanic, waning volcanic, basinal, and hot sedimentary systems, as illustrated in Figure 3.

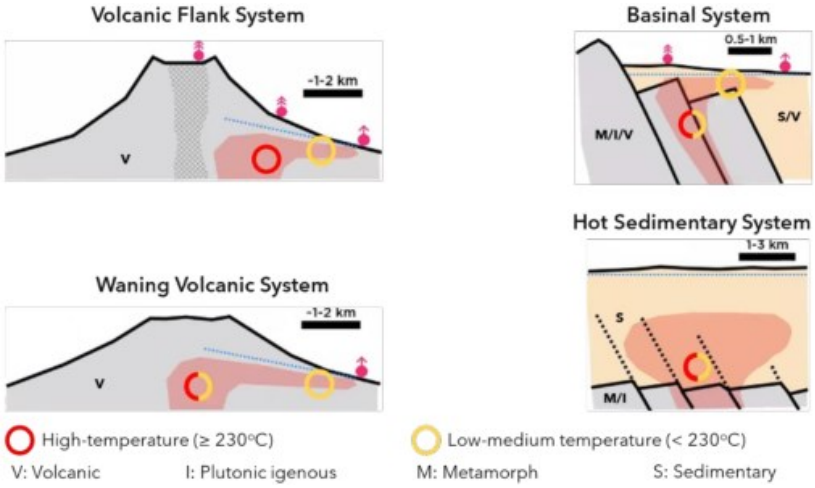

Figure 3: Geothermal Resource Classification Based on the Type of Systems (Ormat, 2022).

Volcanic systems, including arc volcanoes, shield volcanoes, and volcanic complexes, are typically associated with shallow magma bodies and volcanic rocks. These systems often feature steep terrains and upflow hydrogeology, with high-temperature resources, such as those found in Ulubelu and Dieng in Indonesia. In contrast, waning volcanic systems involve cooling intrusive bodies and similar steep volcanic terrains but are characterized by low to medium temperature classes, exemplified by fields like Danau Ranau in Indonesia. Furthermore, basinal systems, such as those found in the Basin and Range province, volcanic rift zones, and calderas, are influenced by amagmatic or magmatic bodies at varying depths. These systems, which can occur in volcanic, plutonic, igneous, metamorphic, or sedimentary rocks, typically feature flat to moderate terrains and upflow or outflow hydrogeology. High-temperature examples include Wairakei in New Zealand, while low to medium temperature examples include Tulehu in Indonesia and McGinness Hills in the U.S. Subsequently, hot sedimentary systems are characterized by amagmatic or deep magmatic bodies within plutonic, igneous, metamorphic, or sedimentary rocks in flat to moderate terrains with stratigraphic hydrogeology. These systems can host high-temperature fields like Salton Sea in the U.S. and low-temperature fields like Brawley in the U.S. The figures further illustrate the typical geological settings and temperature ranges for each system type, emphasizing the relationship between geothermal resource characteristics and their geological contexts. Table 2 summarizes the geothermal factors, host rock, terrain, hydrogeology, temperature class, and notable field examples of each geothermal system type.

2.2 Potential of Low-Medium Temperature Geothermal Resources in Indonesia

Indonesia possesses a considerable potential of low-medium temperature geothermal resources as much as 9,670 MW spread across 254 fields (Putriyana, et al., 2022), accounting for approximately 42% of Indonesia's total estimated geothermal potential of 23 GW (GRG-Geoenergis, 2024b). Furthermore, the regional distribution of these resources is illustrated in Figure 4. The majority of these resources are concentrated in Western Indonesia, amounting to about 5,834 MW, or 60% of the low-medium temperature resources, spread across Sumatra, Java, and Kalimantan. Notably, Sumatra alone harbors the largest share in this region with 3,419 MW, making up 36% of Indonesia's low-medium temperature geothermal resources. In contrast, Eastern Indonesia holds the remaining 3,836 MW, or 40% of the potential, which is distributed among regions like Bali and Nusa Tenggara, Sulawesi, Maluku, and Papua. Sulawesi stands out in this area, hosting the most numerous low-medium temperature geothermal fields in Indonesia with 85 fields and being the largest contributor in Eastern Indonesia with a capacity of 2,150 MW.

Table 2: Types of Geothermal Systems (Ormat, 2022; Moeck, 2014).

System Type	System Sub-Type	Geothermal Factor	Host Rock	Terrain	Hydrogeology	Temperature Class	Field Example
Volcanic system	Arc volcano, shield volcano, and volcanic complex	Shallow magma body	Volcanic	Steep	Upflow	High	• Ulubelu (Indonesia) • Dieng (Indonesia)
					Outflow	Low-medium	• Gunung Talang (Indonesia) • Gunung Sirung (Indonesia)
Waning volcanic system	-	Cooling intrusive body	Volcanic	Steep	Upflow	Low-medium	• Danau Ranau (Indonesia) • Jailolo (Indonesia) • Songa Wayaua (Indonesia) • Bittuang (Indonesia)
Basinal system	Basin and range, volcanic rift zone, and caldera	Amagmatic or shallow/deep/distal magmatic body	Volcanic, plutonic igneous, metamorph, or sedimentary	Flat-moderate	Upflow	High	• Wairakei (New Zealand) • Reykjanes (Iceland) • Olkaria (Kenya)
						Low-medium	• Bitung (Indonesia) • Tulehu (Indonesia) • McGinness Hills (U.S.)
					Outflow	Low-medium	• Salt Wells (U.S.) • San Emidio (U.S.) • Mammoth (U.S.) • Lower Steamboat (U.S.)
Hot sedimentary system	-	Amagmatic or shallow/deep/distal magmatic body	Plutonic igneous, metamorph, or sedimentary	Flat-moderate	Stratigraphic	High	• Salton Sea (U.S.) • Cerro Prieto (California)
						Low-medium	• Heber (U.S.) • Brawley (U.S.) • Unterhaching (Germany)

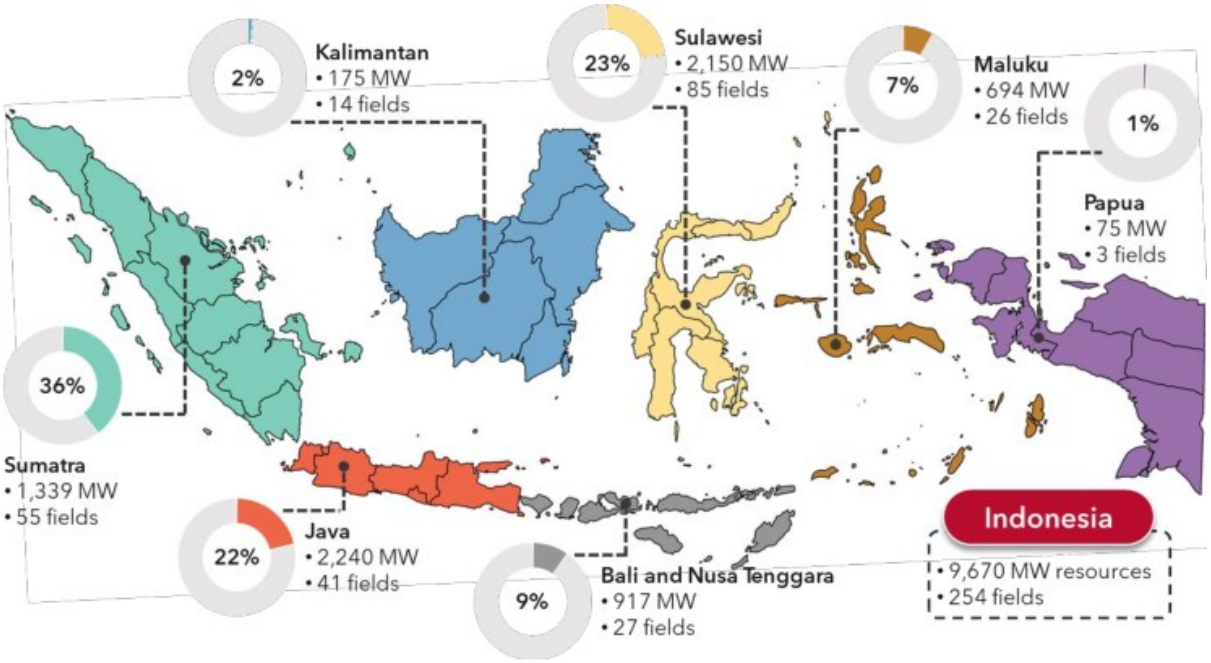

Figure 4: Low-Medium Temperature Geothermal Resources Distribution in Indonesia (Putriyana, et al., 2022). The Percentage Values Represent Each Region's Resource Portion to Indonesia's Total Low-Medium Temperature Resource.

These regional distributions align with the findings of (Kenyon & Beddoes, 1997), which linked geothermal gradients to oil well temperatures, and the heat flow gradient study by (Hamilton, 1973) that further indicated the geothermal potential in each region. The geothermal gradients, mostly ranging from 2–3°C/100 m in the Sumatra-Java outer-arc basin and typically around 3°C/100 m in East Kalimantan, are indicative of the varying geothermal activity across the regions. These gradients help in identifying potential areas for development and provide insights into the geothermal energy capacity that can be harnessed. In areas with higher gradients like the West Java and Madura Basins, where they often reach 4–5°C/100 m, and in the Barito Basin of Southeast Kalimantan, which exhibits gradients of about 3-4 °C/100 m, the potential for geothermal extraction is notably higher (Putriyana, et al., 2022).

2.3 Historical Geothermal Development in Indonesia

Since the commercial operation date (COD) of the first GPP in Indonesia at the Kamojang geothermal field in 1983, the focus on high-temperature resources has remained predominant in the country's geothermal development strategy. As of December 2023, high-temperature geothermal power plants contribute a significant 2,375 MW, which accounts for 99.5% of the total installed geothermal capacity in Indonesia, as shown in Figure 5. In contrast, low-medium temperature resources have seen a relatively limited development, with only 10.79 MW of installed capacity distributed across three units, which only accounts for 0.1% of the low-medium temperature geothermal resources potential. This includes a single unit at Mataloko with a capacity of 2.5 MW, which was the first medium-temperature geothermal power plant (GPP) commissioned in 2013, which is 30 years after the first GPP in Indonesia. Additionally, the Sokoria geothermal field in Eastern Nusa Tenggara saw the commissioning of two units in 2022 and 2023, adding a combined capacity of 8.29 MW. This situation underlines that despite having a considerable potential of low-medium temperature geothermal resources, Indonesia has yet to optimally develop these resources.

The evolution of GPP technology utilization in Indonesia over the years is illustrated in Figure 6, marking significant milestones and technological shifts. Initially, the geothermal sector in Indonesia, starting with the first power plant at Kamojang in West Java in 1983, primarily utilized dry steam and later, single-flash technology as the most dominant GPP technology in terms of the installed capacity and the number of units. It took over three decades after the first plant's commissioning for Indonesia to implement more complex technologies. The first double-flash unit began operation in 2021 at Rantau Dedap, and the combined flash-binary cycle was first adopted at Sarulla Unit 1 in North Sumatra in 2017. These later additions illustrate a move towards exploiting more efficient technologies. Binary GPP, the last GPP technology to be commercially utilized in Indonesia, was first used in 2022 as a bottoming cycle (0.5 MW) at the Lahendong GPP in North Sulawesi. However, it is important to note that binary technology had been part of combined flash-binary systems at the Sarulla and Sokoria GPPs integrated as a combined flash-binary cycle. Respectively, Units 1 (110 MW) and 2 (110 mw) of the combined

cycle Sarulla GPP was commissioned in 2017 and the Unit 3 (110 MW) was commissioned in 2018. Meanwhile, the Units 1 (5 MW) and 2 (3.29 MW) of the combined cycle Sokoria GPP were commissioned in 2022 and 2023, respectively.

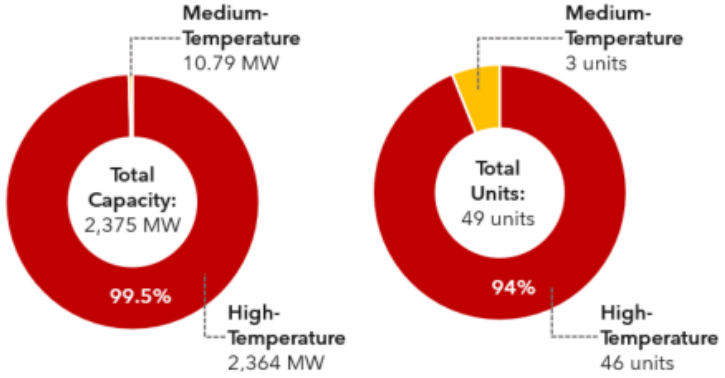

First GPP Based on Resource Temperature				
Temperature Class	GPP	Year	Capacity (MW)	Technology
High	Kamojang Unit 1	1983	30	Dry steam
Medium	Mataloko	2013	2.5	Single-flash

Figure 5: Current Geothermal Development in the Indonesia Based on Resource Temperature as of December 2023 (ThinkGeoEnergy, 2024; Al Asy'ari, et al., 2023; DiPippo, 2016).

First GPP Based on Technology			
Technology	GPP	Year	Capacity (MW)
Dry steam	Kamojang Unit 1	1983	30
Single-flash	Salak Unit 1	1994	60
Double-flash	Rantau Dedap Unit 1	2021	98.4
Combined	Sarulla Unit 1	2017	110
Binary	Lahendong Bottoming	2022	0.5

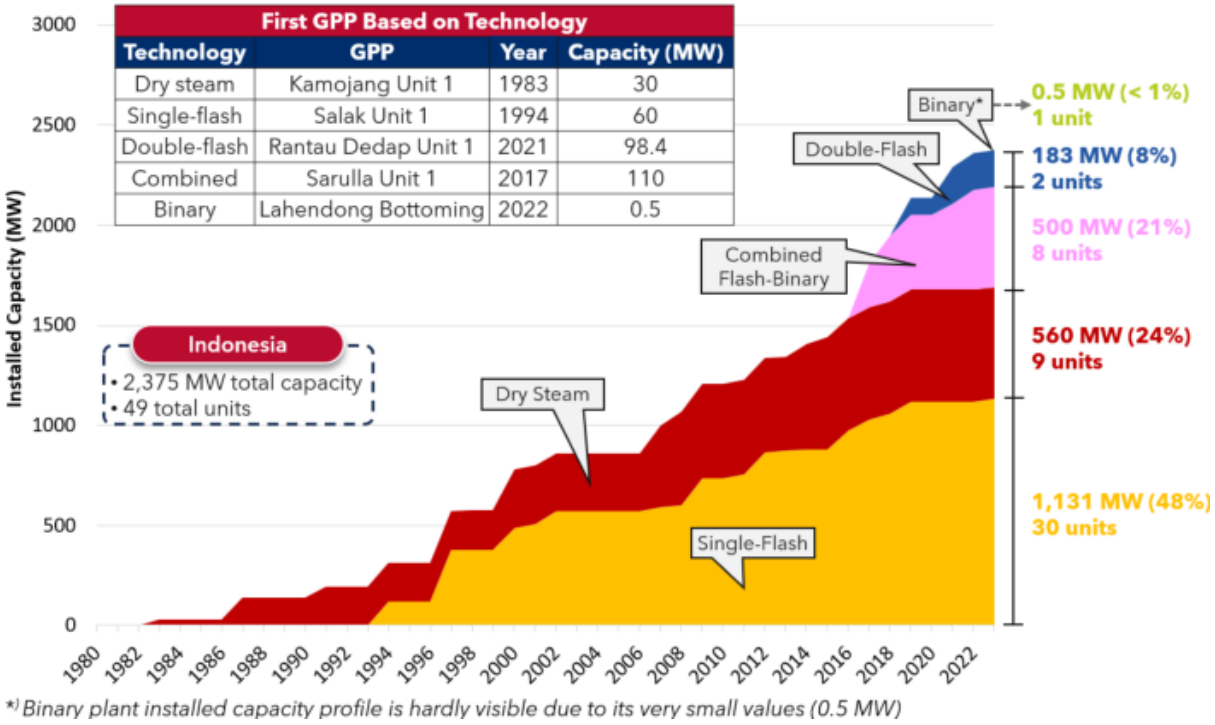

*) Binary plant installed capacity profile is hardly visible due to its very small values (0.5 MW)

Figure 6: Geothermal Development in the Indonesia Based on Power Plant Technology (ThinkGeoEnergy, 2024; Al Asy'ari, et al., 2023; DiPippo, 2016).

2.4 Future Geothermal Project Pipeline in Indonesia Based on Resource Temperature

In addition to the already developed geothermal fields, the Indonesian government has identified a list of fields requiring further analysis for potential future geothermal development. These prospects are outlined in the National Electricity Supply Business Plan (RUPTL) 2021 – 2030, in which the future geothermal project pipeline can be categorized into three ranks:

1. **Rank 1**: the projects identified as National Strategic Projects (PSN) which is already included in Neraca Daya or power grid so they supposedly become the most prioritized project to develop. There are about 22 fields included here that will supply about 1.5 GW power with expected COD year is already listed in RUPTL 2021 – 2030.
2. **Rank 2**: the projects that also already included in power grid, but no specific fields are assigned. The supply power is around 710 MW.
3. **Rank 3**: the potential projects that are not included in power grid and has no expected COD year stated in RUPTL 2021 - 2030. There are 80 fields included here with total capacity of around 4.3 GW.

By evaluating the RUPTL's Ranks 1, 2, and 3 project pipeline combined, as shown in Figure 7, most of the geothermal future pipeline projects in Indonesia are dominated by low-medium temperature resources development, amounting to 58 out of 94 fields (62%). Additionally, the region of Sumatera possess the highest amount of future pipeline project fields (30 fields) as well as the highest amount of low-medium temperature future pipeline project fields (16 fields). This strategic distribution indicates a significant role for Sumatra in Indonesia's geothermal expansion efforts, especially for low-medium temperature resources.

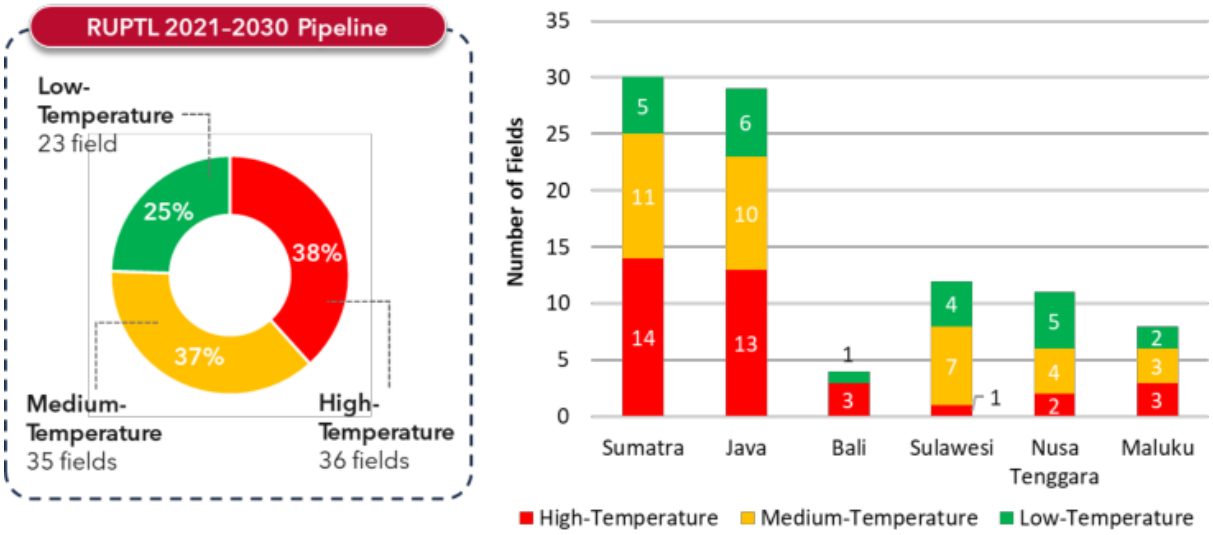

Figure 7: Indonesia's Geothermal Project Pipeline Based on RUPTL 2021 – 2030 (PLN, 2021; GRG-Geoenergis, 2024b).

Furthermore, Figure 8 shows that the Rank 1 pipeline projects in Indonesia are primarily focused on high-temperature fields, which constitute 13 out of the 22 fields (59%). However, when looking specifically at exploration projects within this ranking, there is a notable shift towards low to medium-temperature fields, which make up 9 out of the 16 exploration fields (62%). This trend indicates a growing interest in exploring and developing more low to medium-temperature green (undeveloped) fields in the future, reflecting a diversification in the types of geothermal resources being targeted for development in Indonesia. Notably, Sumatra has a significant focus on exploring high-temperature fields with 4 out of 6 fields to be explored and developed, while Java is prominent in medium-temperature exploration with 5 out of 8 fields to be explored. Most of the exploration projects will also be concentrated in Java, amounting to 8 (50%) out of the 16 Rank 1 exploration projects. Meanwhile, a low-temperature geothermal field is expected to be explored in the Nusa Tenggara region at the Oka Ile Ange geothermal field.

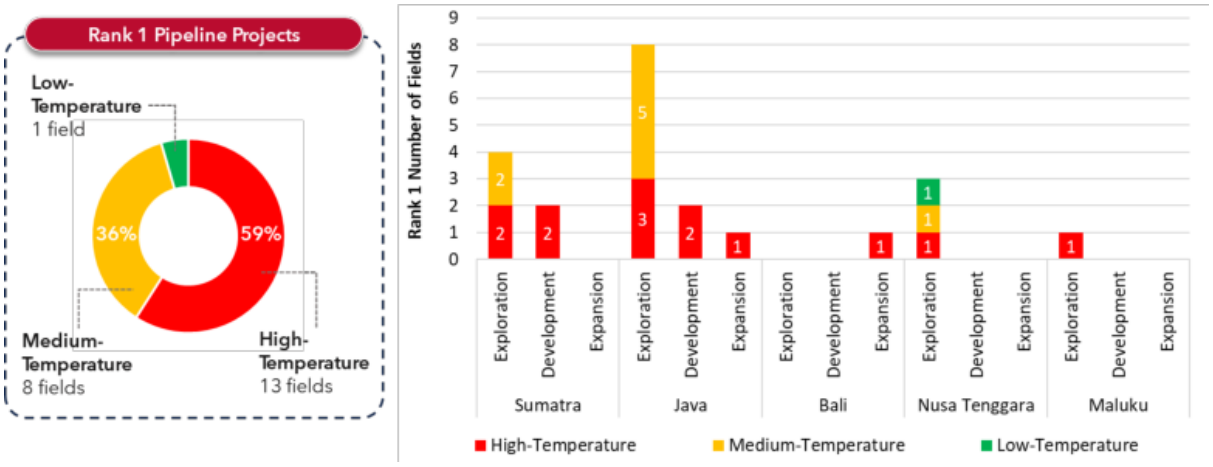

Figure 8: Indonesia's Rank 1 (National Strategic Project) Geothermal Project Pipeline Based on RUPTL 2021 – 2030 (PLN, 2021; GRG-Geoenergis, 2024b).

The 22 geothermal fields included in the Rank 1 pipeline projects in RUPTL 2021 – 2030 are classified further based on the geologic factor and the resource temperature, as shown in Table 3. The Sumatra region features projects in the Jaboi, Sungai Penuh, Danau Ranau, Hululais, Kepahiang, and Rajabasa geothermal fields, showcasing a range of medium to high temperatures due to the region's subduction and young volcanism.

Similarly, Java has numerous high-temperature projects such as those in the Rawa Danau, Cibuni, Candradimuka, Ungaran, Ijen, and Telaga Ngebel, with some medium and low-temperature fields like Tangkuban Perahu, Cisolok-Cisukarame, Tampomas, Baturaden, and Guci. The Bedugul project in Bali is another high-temperature field, while Maluku's Tulehu field is notable for its hybrid geologic setting combining young volcanism and fault systems. Nusa Tenggara includes fields like Atadei and Mount Sirung, with a mix of medium and high temperatures, and Oka Ile Ange, which represents a low-temperature field.

Table 3: Rank 1 Pipeline Projects Based on the Geologic Factor and Resource Temperature (GRG-Geoenergis, 2024b).

No	Region	Geothermal Field	Geologic Factor	Resource Temperature (°C)	Temperature Class	References
1	Sumatera	Jaboi	Hybrid (young volcanism and fault systems)	Min: 187 °C (sillica conductive) Max: 327 °C (gas geothermometry)	Medium	(Dwipa, et al., 2006; EBTKE, 2017; Nugraha & O'Sullivan, 2019)
2	Sumatera	Sungai Penuh	• Subduction • Young volcanism	250-280 °C (gas geothermometry)	High	(Hochstein & Sudarman, 2008; Sukhyar, et al., 2010; Darma, 2016; EBTKE, 2017)
3	Sumatera	Danau Ranau	• Subduction • Young volcanism	200-220 °C (Na-K-Mg)	Medium	(Afiat, et al., 2020; Idianto, et al., 2021; Rera, et al., 2021)
4	Sumatera	Hululais	• Subduction • Young volcanism	225-285°C (gas geothermometry from Kawah Biru and Kawah Hitam) >300oC (gas geothermometry from Kawah Belerang Atas)	High	(Kamah, et al., 2015; EBTKE, 2017; Nurseto, et al., 2021)
5	Sumatera	Kepahiang	• Subduction • Young volcanism	250 °C (gas geothermometer fumarole of Kaba Crater)	High	(EBTKE, 2017; Nurdyanto, et al., 2019; Nurseto, et al., 2021)
6	Sumatera	Rajabasa	• Subduction • Young volcanism	260-265 °C (Way Merak) 300-325 °C (gas geothermometry)	High	(Darmawan, et al., 2015; EBTKE, 2017)
7	Java	Rawa Danau	• Subduction • Young volcanism	260-270 °C (gas geothermometry)	High	(EBTKE, 2017; Syah, et al., 2019; Sumotarto, et al., 2019)
8	Java	Cibuni	• Subduction • Young volcanism	305 °C	High	(Layman & Soemarinda,2003)
9	Java	Tangkuban Perahu	• Subduction • Young volcanism	200-285 °C (Na-K geothermometry)	Medium	(Hochstein & Sudarman, 2015; Gaffar, 2018)
10	Java	Cisolok-Cisukarame	• Subduction Young volcanism	185-212°C (Na-K geothermometry)	Medium	(Mandradewi & Herdianita, 2010; Sumartha, et al., 2020)

No	Region	Geothermal Field	Geologic Factor	Resource Temperature (°C)	Temperature Class	References
11	Java	Tampomas	• Subduction • Young volcanism	187-208 °C (Silica geothermometry) (Direktorat Jendral EBTKE, 2017); 160-175 °C (silica geothermometry), 170 ± 10 °C (Na/K geothermometry)	Low	(EBTKE, 2017; Permadi, et al., 2022)
12	Java	Candradimuka	• Subduction • Young volcanism	250°C - 289°C (gas geothermometry)	High	(Bagaskara, et al., 2021)
13	Java	Ungaran	• Subduction • Young volcanism	>300 °C (gas geothermometry) Gradient temperature 10.4°C /100 m (thermal gradient well USL-1)	High	(Phuong, et al., 2012)
14	Java	Baturaden	• Subduction • Young volcanism	204-210 °C (Na-K-Mg geothermometry)	Medium	(EBTKE, 2017; Harijoko & Juhri, 2017; Iswahyudi, et al., 2020)
15	Java	Guci	• Subduction • Young volcanism	170-190 °C (K-Na-Ca and Na-K-Mg geothemometry); 331-382°C (Na/K geothermometer) 187-196°C (silica-enthalphy method)	Low	(Harijoko & Juhri, 2017; Iswahyudi, et al., 2020; Harijoko, et al., 2021)
16	Java	Ijen	• Subduction • Young volcanism	250-300 °C (in EBTKE, 2017)	High	(EBTKE, 2017; Daud, et al., 2019)
17	Java	Telaga Ngebel	• Subduction • Young volcanism	250-260 °C	High	(EBTKE, 2017; Yudiantoro, et al., 2020)
18	Bali	Bedugul	• Subduction • Young volcanism	280-320 °C	High	(Darma, et al., 2010)
19	Maluku	Tulehu	Hybrid (young volcanism and fault systems)	> 230 °C	High	(Daud, et al., 2022)
20	Nusa Tenggara	Atadei	Hybrid (young volcanism and fault systems)	~ 221°C (gas geothermometry)	Medium	(EBTKE, 2017; Prabata, 2018)
21	Nusa Tenggara	Oka Ile Ange	• Subduction • Young volcanism	148-173 °C	Low	(Nugraha, et al., 2018; EBTKE, 2017)
22	Nusa Tenggara	Mount Sirung	• Subduction • Young volcanism	260°C (H_2-CO_2 gas geothermometry)	High	(EBTKE, 2017; Putriyana, et al., 2021)

In contrast to Rank 1 projects, Figure 9 shows that Rank 3 pipeline geothermal projects in Indonesia primarily focus on low-medium temperature fields, which constitute 52 out of the 80 fields (65%). High-temperature fields still represent a significant portion, amounting to 28 out of 80 fields (35%). Sumatra has the highest number of low to medium-temperature Rank 3 fields, totaling 14, all in the exploration phase. Beyond Sumatra, other regions also feature prominently in the Rank 3 pipeline projects. Java has a balanced mix of high, medium, and low-temperature fields, with significant activity in both exploration and development phases. Bali's projects are mainly focused on medium-temperature fields, while Nusa Tenggara shows a substantial number of low and medium-temperature exploration projects. Sulawesi also has a diverse pipeline project resource temperature class, with a strong emphasis on low-medium temperature fields in the exploration phase. Maluku features a smaller number of projects, primarily in the exploration and development of low-medium temperature fields.

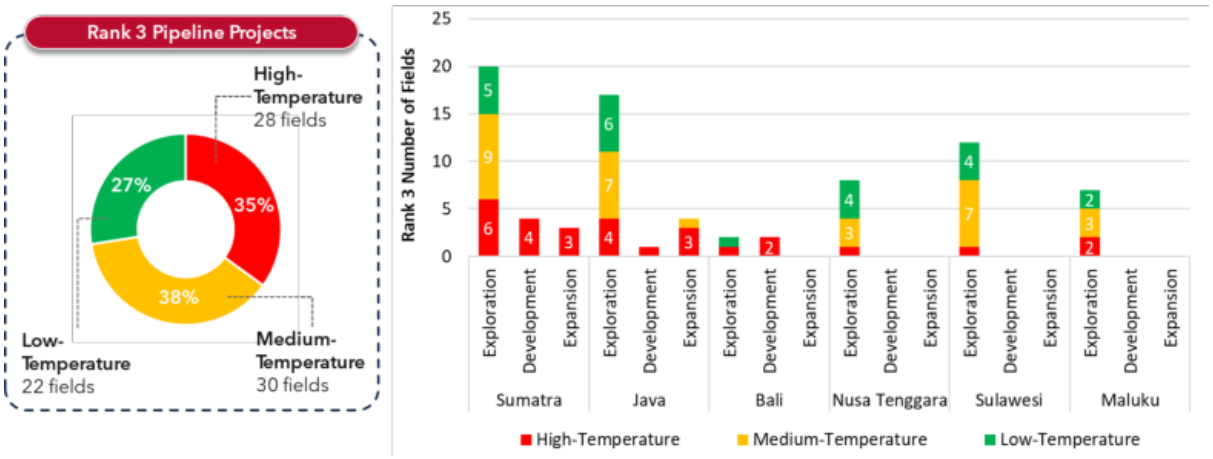

Figure 9: Indonesia's Rank 3 Geothermal Project Pipeline Based on RUPTL 2021 – 2030 (PLN, 2021; GRG-Geoenergis, 2024b).

2.5 Potential of Low-Medium Temperature Geothermal Resources in the United States

Figure 10 illustrates the distribution of low-medium temperature geothermal resources across the U.S. These resources, totaling 3.7 GW, represent 38% of the country's identified hydrothermal geothermal potential of 9.2 GW (USGS, 2008). The low-medium temperature resources are distributed across ten states, primarily in the west coast region (California, Oregon, and Washington), the Midwest (Nevada, New Mexico, Utah, Montana, Washington, and Colorado), and Alaska. Nevada stands out as the state with the largest low-medium temperature geothermal resources as much as 1,339 MW from 55 fields. In comparison, Indonesia has significantly larger identified low-medium temperature geothermal resources, totaling 9.7 GW. However, the number of identified fields is quite similar, with Indonesia having 254 fields compared to the 236 fields in the U.S. Despite Indonesia's greater resource potential, its utilization of these geothermal resources lags far behind that of the U.S.

2.6 Historical Geothermal Development in the United States

As of 2023, the installed geothermal power plant (GPP) capacity in the U.S. remains predominantly driven by high-temperature resources, which account for the majority of the 3,615 MW total capacity. Historically, the first high-temperature GPP commenced commercial operations in 1960 with the Geysers 1 plant in California, marking the beginning of geothermal energy utilization in the U.S., as shown in Figure 11. Over the decades, high-temperature resources have continued to be the backbone of geothermal energy production, contributing 2,408 MW across 45 plants, which represents 67% of the total installed capacity. In contrast, the development of geothermal power from low to medium-temperature resources began later, with significant advancements occurring in the mid-1980s. The first medium-temperature GPP was initiated with the Beowawe plant in Nevada in 1985, while the initial low-temperature plant started operations with the Wabuska 1 plant, also in Nevada, in 1984. These categories of geothermal resources have seen substantial growth over the last two decades, with low-temperature resources contributing 866 MW (24%) from 45 plants and medium-temperature resources adding 341 MW (9%) from 11 plants. This trend indicates a shift in the recent geothermal development in the U.S. in the last 20 years, focusing more on exploiting low to medium-temperature resources.

In terms of the GPP technology, as shown in Figure 12, the installed GPP capacity in the U.S. is predominantly driven by dry steam technology, which has been a cornerstone of geothermal energy production since the commissioning of the Geysers 1 plant in California in 1960. Dry steam plants currently contribute 1,477 MW across 18 plants, making up 40% of the total installed capacity.

However, in the last 20 years, there has been a significant shift towards binary technology, which now accounts for a substantial portion of the geothermal capacity. As of 2023, binary GPPs represent 1,298 MW, or 36% of the

total installed capacity, spread across 58 plants. The first binary GPP was commissioned in 1984 with the Wabuska 1 plant in Nevada. This technology has become more prevalent due to its ability to efficiently harness low-medium temperature geothermal resources. Flash plants, including single-flash, double-flash, and triple-flash technologies, collectively account for 27% of the installed capacity. Among these, double-flash plants are the most utilized, contributing 860 MW (24%) across 20 plants since the first double-flash GPP began operations in 1985 with the Heber 1 plant in California. Single-flash and triple-flash plants have smaller shares, with 60 MW (2%) from 4 plants and 55 MW (1%) from 1 plant, respectively. Overall, the GPP technology in the U.S. has seen a steady increase in the adoption of binary plants, while dry steam and double-flash technologies continue to play significant roles.

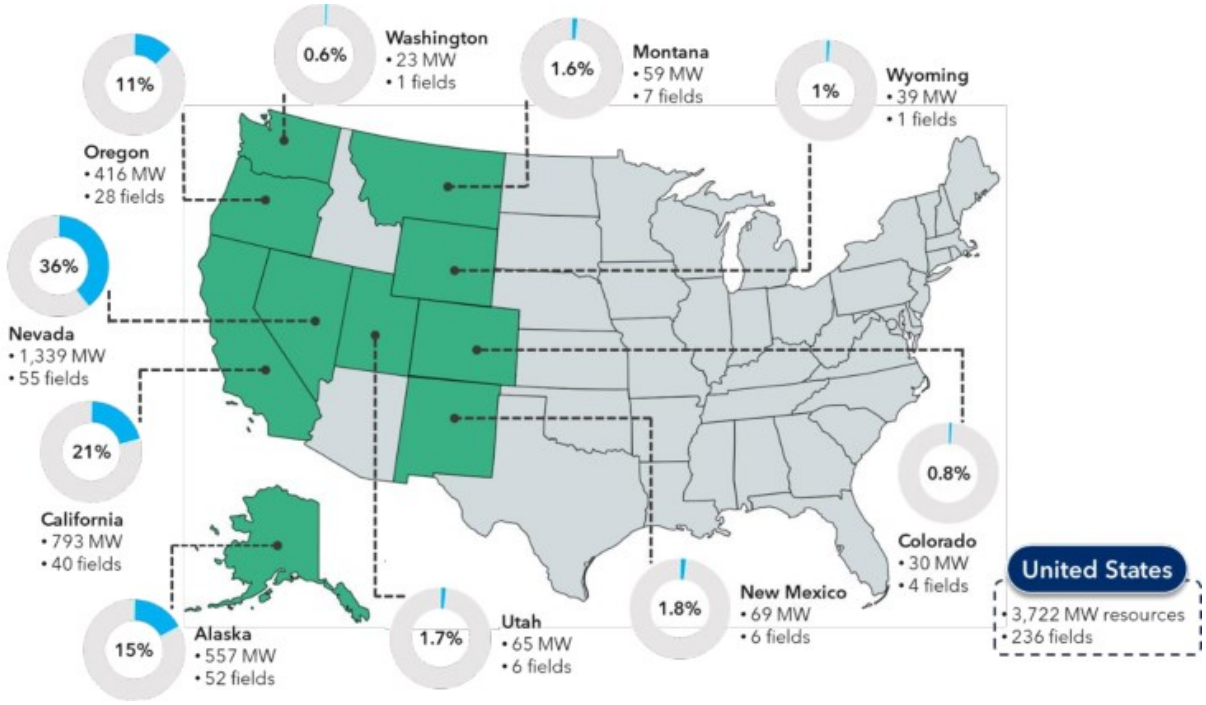

Figure 10: Low-Medium Temperature Geothermal Resources Distribution in the U.S. (USGS, 2008). The Percentage Values Represent Each State's Resource Portion to the Entire U.S. Resource.

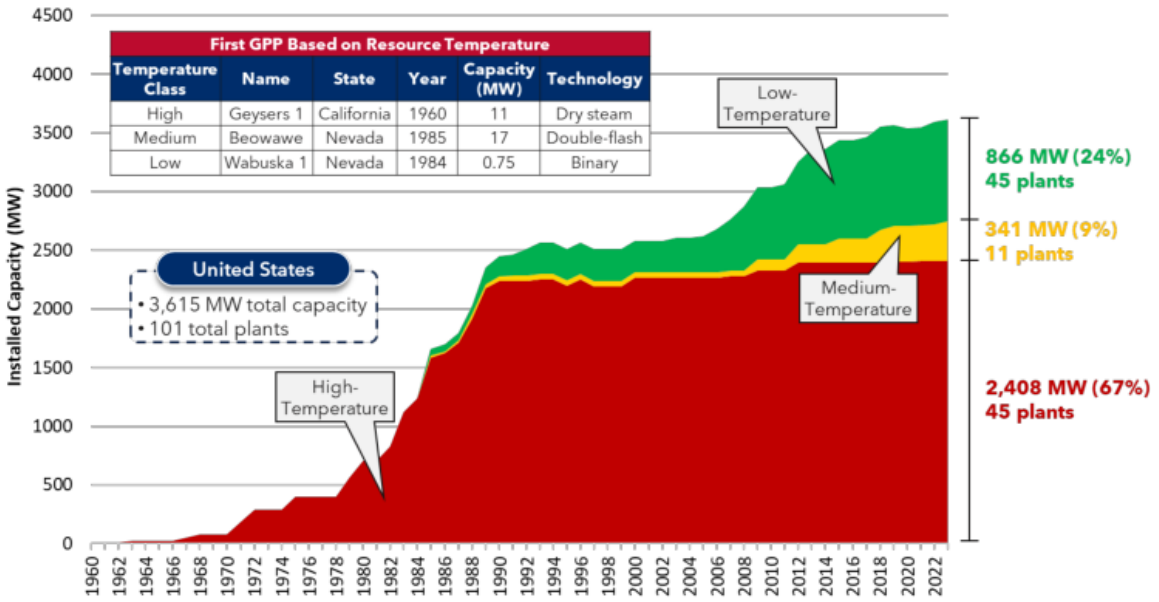

Figure 11: Geothermal Development in the U.S. Based on Resource Temperature (NREL, 2021; ThinkGeoEnergy, 2024).

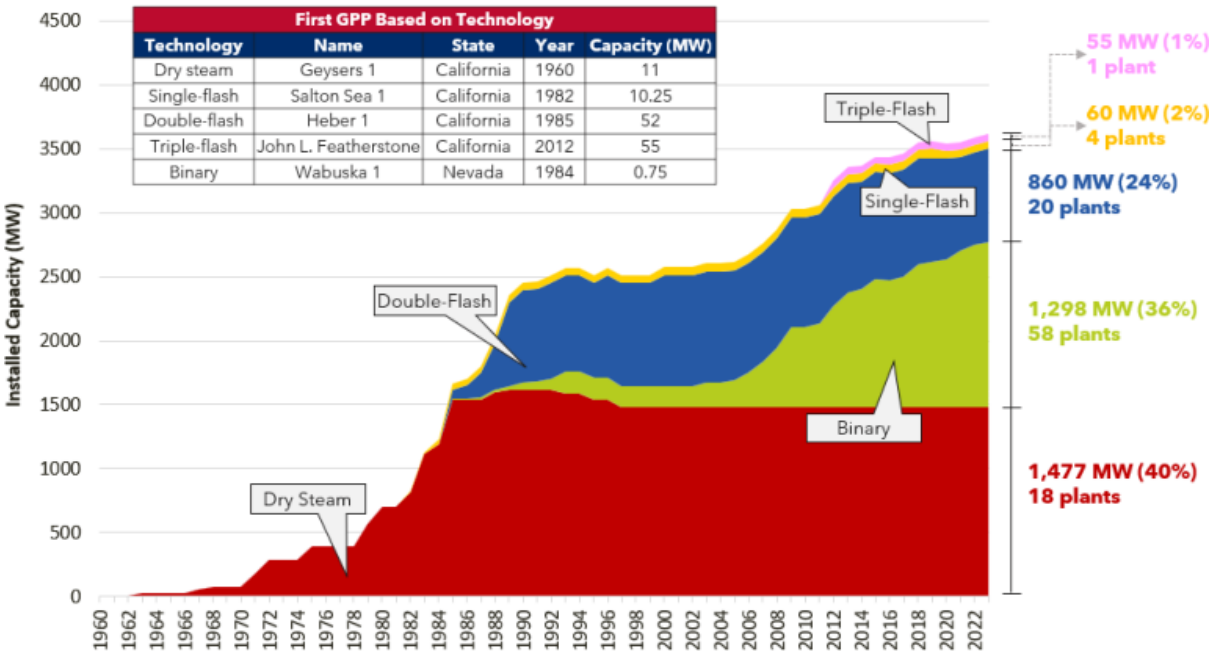

Figure 12: Geothermal Development in the U.S. Based on Power Plant Technology (NREL, 2021; ThinkGeoEnergy, 2024).

Furthermore, as shown in Figure 13, high-temperature GPPs are predominantly powered by dry steam technology, which accounts for 1,477 MW across 18 plants, making up 61% of the high-temperature capacity. In terms of the flash plants for high-temperature resources, double-flash technology is preferred over single-flash technology. Double-flash plants contribute 633 MW from 17 plants, while single-flash plants contribute 60 MW from 4 plants. This preference indicates the efficiency and effectiveness of double-flash technology for the high-temperature resources. Additionally, while mostly being used for low-medium temperature resources, binary plants are also utilized for high-temperature resources, contributing 182 MW from 5 plants, which include the binary plants in the Dixie Valley (Nevada), North Brawley (California), Puna (Hawaii), and Roosevelt (Utah) geothermal fields. For medium-temperature resources, binary technology is the dominant choice, representing 95% of the installed capacity with 324 MW from 10 plants. A small portion of double-flash technology is also utilized, contributing 17 MW from 1 plant. Similarly, in low-temperature geothermal fields, binary technology is the primary technology used, accounting for 92% of the installed capacity with 792 MW from 43 plants. Double- flash technology plays a minor role in these fields, with 74 MW from 2 plants. Overall, the distribution of geothermal power plant technologies in the U.S. reflects a strategic alignment with resource temperatures, optimizing the use of dry steam and double-flash technologies for high-temperature resources and binary technology for low to medium-temperature resources.

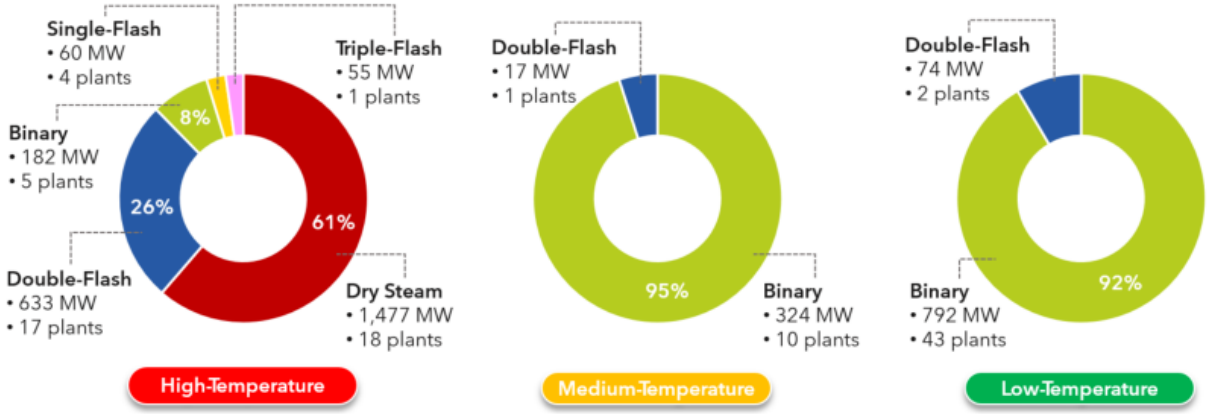

Figure 13: GPP Technology Installed Capacity Portion Based on Resource Temperature in the U.S. as of December 2023 (NREL, 2021; ThinkGeoEnergy, 2024).

Figure 14 illustrates the efficiency of geothermal power plants (GPP) based on reservoir temperature and enthalpy for different technologies: single-flash, double-flash, and binary (Zarrouk & Moon, 2014). Binary technology demonstrates its versatility across a wide range of temperatures, from low to medium. It maintains competitive

efficiency, starting at around 3% at 100°C and reaching nearly 8% at 230°C. This versatility makes binary plants an excellent choice for both low and medium-temperature resources. Double-flash technology can be applied to both the upper limit of low-temperature and the medium-temperature range. Its efficiency starts at about 5% at 190°C and approaches 7% at 230°C. While double-flash plants are efficient in these temperature ranges, binary plants generally exhibit higher efficiency at lower temperatures and remain competitive at medium temperatures, slightly lower than double-flash but higher than single-flash. Single-flash technology, represented by the yellow line, shows lower efficiency compared to both binary and double-flash technologies, particularly at higher temperatures. However, it is still a viable option for certain applications within the geothermal sector. This figure underscores the importance of selecting the appropriate GPP technology based on reservoir temperature to maximize efficiency, with binary plants demonstrating significant versatility across a broad temperature range.

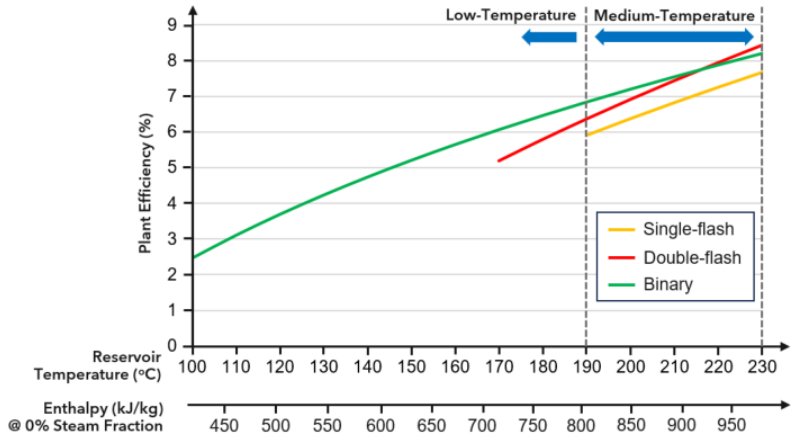

Figure 14: GPP Efficiency Based on Reservoir Temperature/Enthalpy for Different GPP Technologies (Zarrouk & Moon, 2014; Sanyal, 2005).

As of December 2023, the distribution of low-medium temperature binary GPP in the U.S. shown in Figure 15 reveals Nevada as the leader in installed capacity. Nevada holds the majority share, with a total installed capacity of 753 MW across 29 plants, accounting for 67% of the nation's total capacity. This dominance correlates with Nevada's abundant low-medium temperature geothermal resources compared to other states. California is the second-largest contributor, with 246 MW of geothermal capacity from 14 plants, representing 22% of the U.S. total for low-medium temperature binary plants. This significant contribution underscores California's role in the country's geothermal energy landscape. Other states also contribute to the overall geothermal capacity, albeit on a smaller scale. Utah has 45.3 MW from 2 plants, making up 4% of the total, while Oregon contributes 38.1 MW from 4 plants, accounting for 3%. Idaho adds 18 MW from 1 plant (2%), New Mexico provides 15 MW from 1 plant (1%), and Alaska has 1.1 MW from 2 plants, representing 0.01% of the national total. Overall, the total installed capacity for low-medium temperature binary GPPs in the U.S. is 1,116 MW, distributed across 53 plants. This figure highlights the varied contributions of different states, with Nevada and California playing the most significant roles.

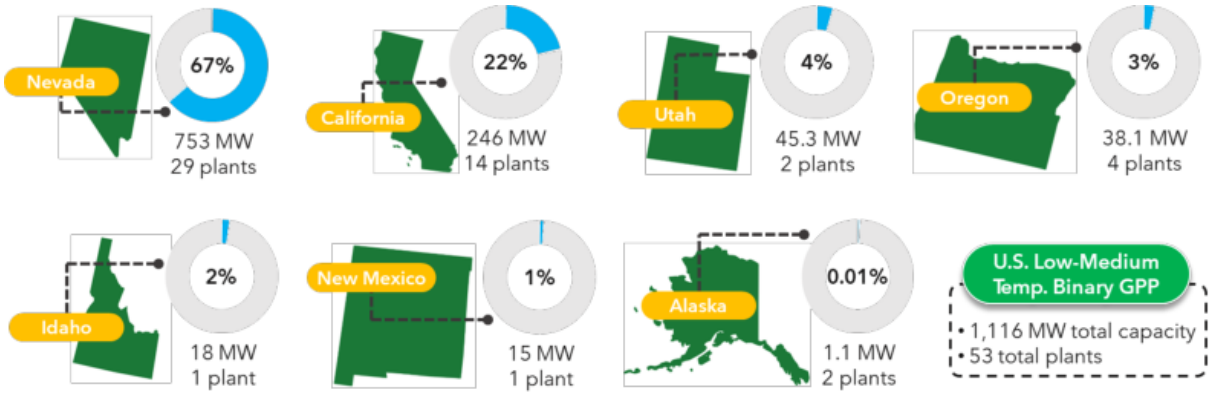

Figure 15: Low-Medium Temperature Binary GPPs' Installed Capacity Distribution in the U.S. as of December 2023 (NREL, 2021; ThinkGeoEnergy, 2024). The Percentage Values Represent Each State's Portion to the Entire U.S.

2.7 Comparison of Low-Medium Temperature GPP LCOE in the U.S. and Indonesia

The Levelized Cost of Electricity (LCOE) is a metric indicating the price at which electricity must be sold for the system to achieve break-even at the end of its operational lifetime (Papapetrou & Kosmadakis, 2021). It accounts for initial capital investment, ongoing operational and maintenance costs, and the expected energy output over the plant's lifetime and is formulated in Equation (1):

$$\text{LCOE}=\frac{\sum_{t=0}^{n}\frac{I_t+M_t}{1+r^t}}{\sum_{t=0}^{n}\frac{I_t+E_t}{1+r^t}} \quad (1)$$

where, t refers to the t-th year with t=0 means the start of the plant construction, n is the operational lifetime (year), It is the capital expenditures (USD) in year t, Mt is the fixed and variable operating expenditures (USD) in year t, r is the discount rate (or the weighted average cost of capital), and Et is the electricity generation (kWh) in year t. LCOE serves as an important tool for techno-economic analysis, helping stakeholders assess and compare the economic viability of low-medium temperature geothermal resources against other energy options. This aids in making informed decisions for techno-economic optimizations of low-medium temperature geothermal resources development. Figure 16 compares the LCOE for GPP between Indonesia and the U.S., focusing on both flash and binary technologies for low-medium temperature resources. In the U.S., the LCOE for flash technology is lower, ranging from 4.6 to 8.0 US¢/kWh, and for binary technology, it ranges from 6.2 to 11.9 US¢/kWh according to the 2023 Geothermal Annual Technology Baseline developed by (NREL, 2023). Meanwhile, the LCOE values for Indonesia are estimated using the LCOE calculator developed by (IESR, 2023) based on inputs such as capital expenditure (CAPEX), fixed operational expenditure (OPEX), capacity factor (CF), project life, and the weighted average cost of capital (WACC). The CAPEX for flash plants ranges from 4.7 to 8.0 million USD/MW , while for binary plants, it ranges from 7.1 to 10.0 million USD/MW (GRG-Geoenergis, 2024a). The fixed OPEX is set at 0.05 million USD/MW per year for flash plants and at 0.065 million USD/MW per year for binary plants. The capacity factor varies from 70% to 90%, with a project life of 30 years and a WACC of 10% (IESR, 2023). The calculation results show that, for Indonesia, the LCOE for flash technology ranges from 7.0 to 14.7 US¢/kWh, while for binary technology, it ranges from 10.5 to 18.4 US¢/kWh. Overall, the figure highlights that the LCOE for geothermal power is generally lower in the U.S. compared to Indonesia, particularly for binary technology. Furthermore, binary technology shows a wider range of costs in both countries, reflecting the variability in factors influencing the LCOE.

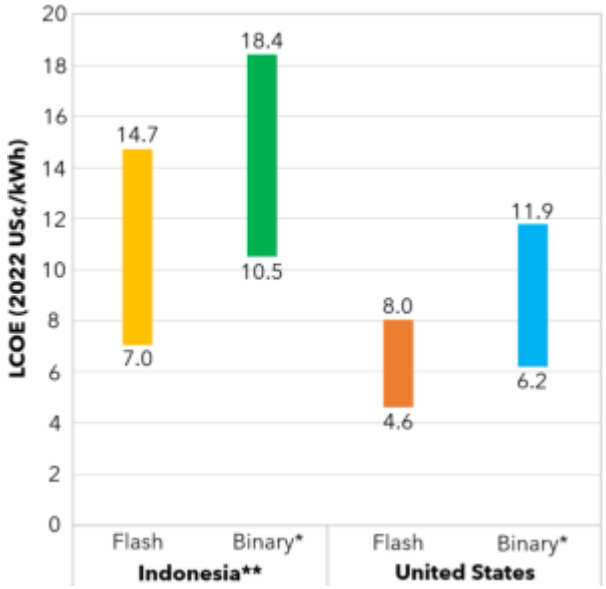

*) Only low-medium temperature binary GPP

**) Based on LCOE calculator (IESR, 2023) using the following inputs:

Input	Unit	Flash		Binary	
		Min	Max	Min	Max
CAPEX	MUSD/MW	4.7	8.0	7.1	10.0
Fixed OPEX	USD/MW/year	0.05	0.05	0.065	0.065
CF	-	70%	90%	70%	90%
Project life	Year	30	30	30	30
WACC	-	10%	10%	10%	10%

Figure 16: Geothermal LCOE Comparisons Between Indonesia and the U.S. (GRG-Geoenergis, 2024a; IESR, 2023; NREL, 2023).

Figure 17 illustrates a simplified structure of the LCOE and CAPEX for geothermal power projects. One significant factor that can reduce the LCOE is the offset provided by fiscal incentives. In the U.S., two prominent fiscal incentives are the Production Tax Credit (PTC) and the Investment Tax Credit (ITC) provided by the federal government in addition to the other incentives, such as accelerated depreciation, bonus depreciation, and the state-level incentives (NREL, 2021).

1. **Production Tax Credit**: it was first implemented in 2004 through the American Jobs Creation Act of 2004, allowing geothermal developers to offset their tax liability using a per-kilowatt-hour tax credit. Initially, the credit period was 5 years but was extended to 10 years in 2005 by the Energy Policy Act (Oregon Tech, 2012). The PTC base rate started at 1.8 cents/kWh in 2004 and increased to 2.75 cents/kWh in 2022, subject to annual inflation adjustments (IRS, 2022).
2. **Investment Tax Credit**: it was first implemented in 1978 through the Energy Tax Act of 1978 (Oregon Tech, 2012). This credit allows geothermal developers to offset a portion of their tax liability based on a percentage of the total project cost of qualified geothermal projects, with the current ITC rate being 6% or 30% of the project cost, depending on the conditions met by the geothermal developer as stipulated by the Inflation Reduction Act of 2022 (The White House, 2023).

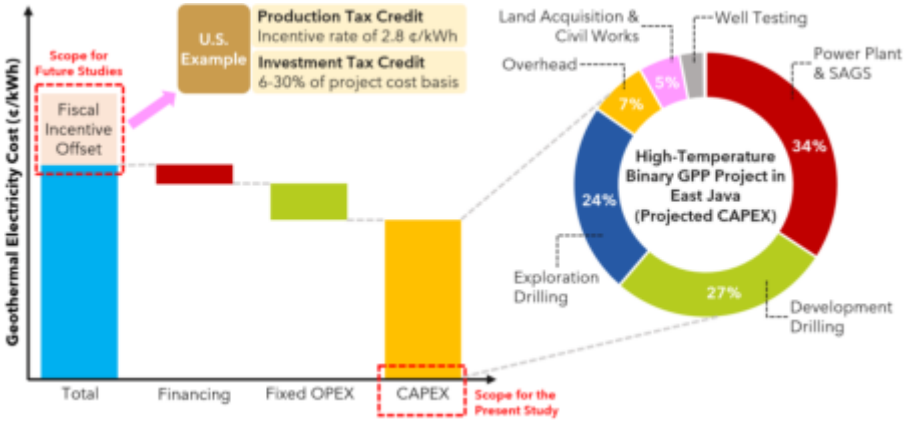

Figure 17: Simplified Geothermal LCOE and CAPEX Structure (IESR, 2023; GRG-Geoenergis, 2024a; NREL, 2021).

However, the current study does not include fiscal incentives, financing costs, and fixed OPEX within its scope. Instead, the focus of the current study is on optimizing the CAPEX to lower the LCOE for low-medium temperature geothermal resources, as CAPEX is the most significant component of the LCOE structure, as shown in Figure 17. Due to limited data availability, the authors faced challenges in breaking down the CAPEX for low-medium temperature geothermal resource development. Nevertheless, an example CAPEX breakdown from a high-temperature binary GPP project in East Java, Indonesia, provides valuable insights. It shows that the power plant, Steam Gathering System (SAGS), and drilling account for the majority of the CAPEX (GRG-Geoenergis, 2024a). Therefore, optimizing the costs associated with the power plant, SAGS, and drilling is crucial for improving the techno-economic feasibility of low-medium temperature geothermal resources. This focus on CAPEX optimization can significantly impact the overall techno-economic feasibility of low-medium temperature geothermal development projects.

3. LESSONS LEARNED FROM THE UNITED STATES AND THEIR POTENTIAL APPLICATION IN INDONESIA

Examining the lessons learned from the U.S. experience with low-medium temperature geothermal fields provides valuable insights into the potential techno-economic optimization initiatives that can be adopted into the Indonesian context. Additionally, Indonesia's experience with high-temperature fields also offers transferable knowledge that can be the foundation to adopt the initiatives from the U.S for the low-medium temperature fields. This section explores the lessons learned from the U.S. in developing low-medium temperature geothermal resources and how Indonesia can utilize their experience in developing high-temperature resources to adopt those lessons learned as potential optimization initiatives for Indonesia’s low-medium temperature resources.

3.1 Know-How in Utilizing Binary GPP and Pumped Well Technology

The development of low-medium temperature geothermal power plants (GPP) in the U.S. experienced two significant waves, with the first occurring in the 1980s-1990s and the second in the 2010s, in coincidence with the two significant waves of the overall GPP development in the U.S. Notably, the early involvement of leading developers such as Ormat, Cyrq Energy, Terra-Gen Power, and Open Mountain Energy, who commenced their initial operations during the first wave, played a crucial role in the resurgence of GPP development in the 2010s. Figure 18 indicates that by December 2023, these 4 developers collectively hold the majority of the installed capacity in the low-medium temperature GPP sector. The expertise and technological advancements accumulated by these companies during the first wave in the 1980s-1990s provided the know-how and experience for the subsequent development, especially during the second wave in the 2010s, thereby revitalizing the low-medium temperature GPP landscape in the U.S.

Developer	Low-Med Temp. GPP Capacity as of Dec 2023	First Low-Med Temp. GPP	Technology	COD Year
Ormat	886.9 MW (74%)	Steamboat 1	Binary	1985
Cyrq Energy	162.3 MW (14%)	Soda Lake 1	Binary	1987
Terra-Gen Power	91.5 MW (8%)	Beowawe	2-Flash	1985
Enel	26.8 MW (2%)	Salt Wells	Binary	2009
Open Mountain Energy	16.9 MW (1%)	Wabuska 1	Binary	1984
Others	14.5 MW (1%)	Wineagle	Binary	1988
Total	**1,198.9 (100%)**			

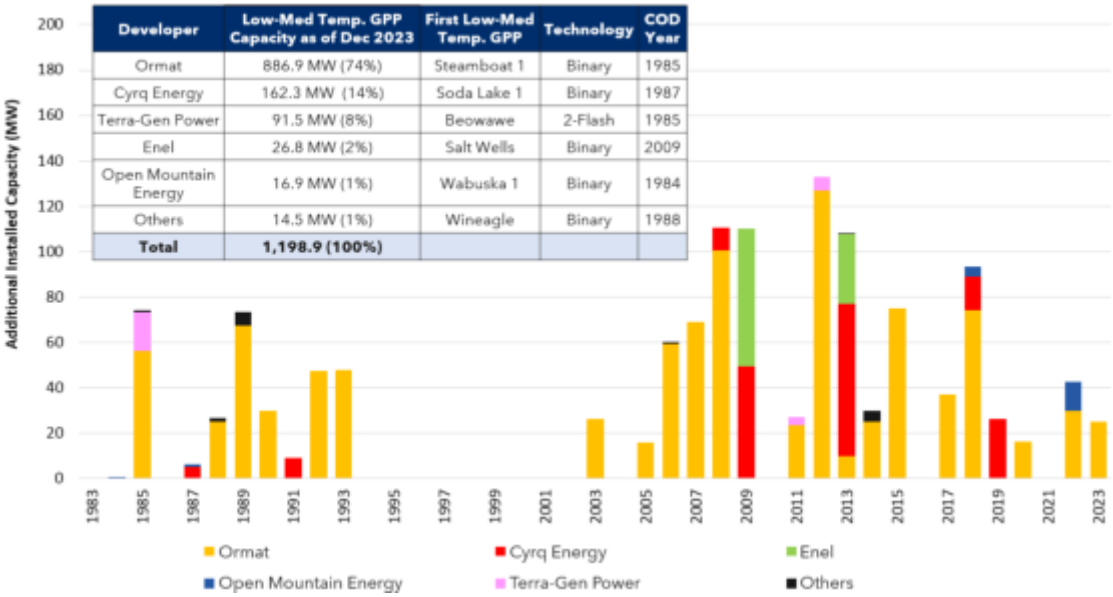

Figure 18: Low-Medium Temperature GPP Capacity Addition in the U.S. Based on the Developer Company (NREL, 2021).

Additionally, pumped geothermal wells are typically used to produce geothermal fluids from low-temperature resources due to the non-self-discharge characteristics of low-temperature geothermal wells excluding artesian wells and those with high NCG content, which might exhibit self-discharge (Sanyal, 2005). For a self-discharging geothermal well, the power output that can be achieved from that well is influenced by the well's productivity (flow rate and enthalpy) and the power plant's electric conversion efficiency. However, for a pumped geothermal well, the pumping power reduces the net power output that can be achieved from the well. Figure 19 illustrates the reservoir inflow performance relationship (IPR) and vertical lift performance (VLP) curves for a self-discharging well and a non-self-discharging well. IPR curve shows the reservoir's ability to deliver fluids to the wellbore under different bottomhole flowing pressure conditions. Meanwhile, VLP curve shows the required bottomhole flowing pressure to discharge the fluid from the bottomhole/feed zone to the wellhead at a given wellhead pressure (Kriptanto, 2024; Grant & Bixley, 2011). Well discharge occurs if the IPR curve intersects with the VLP curve (Guo, et al., 2017).

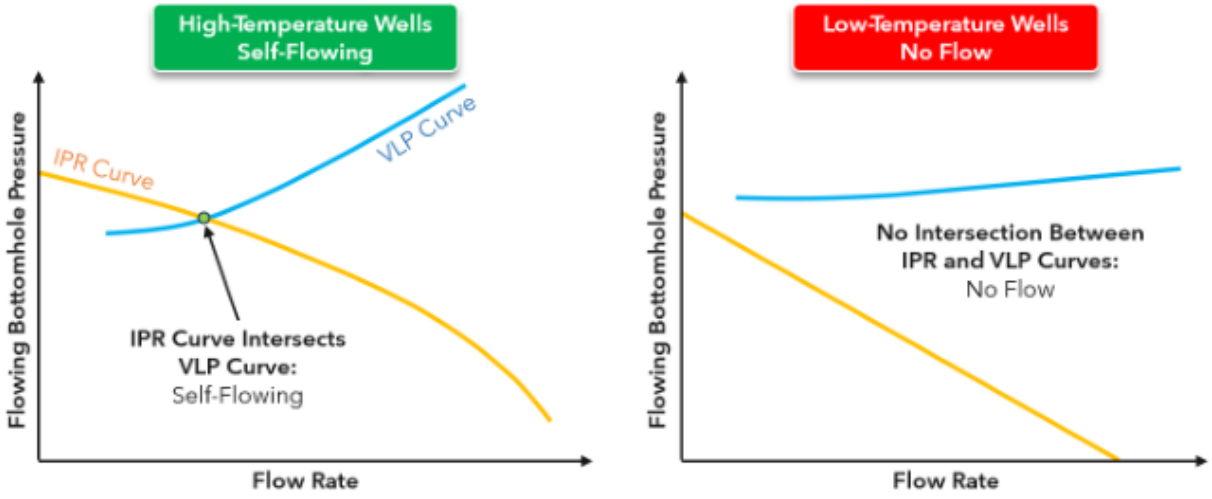

Figure 19: IPR and VLP Curves for High-Temperature Self-Flowing (Left) and Low-Temperature Non-Self-Flowing (Right) Geothermal Wells (Kriptanto, 2024; Zarrouk & McLean, 2019; Grant & Bixley, 2011).

It is possible that even in the reservoir's natural state, the IPR curve does not intersect with the VLP curve. It means that a well stimulation is needed since the beginning of the geothermal field's operation, such as using a downhole pump, implementing air compression or gas lifting methods, or performing permeability stimulations through fracturing or matrix acidizing (Mubarok & Zarrouk, 2017). Such case is typically found in low-temperature geothermal fields or high-temperature fields with a low natural permeability (Abrasaldo, et al., 2023).

Therefore, the drive mechanism of discharge from low-temperature geothermal wells is the pumping energy (Aydin & Merey, 2021; Sanyal, 2005). In another case, the IPR curve may intersect with the VLP curve during the early years of the field's operation, such as in high-temperature geothermal fields. The drive mechanism of discharge from high-temperature geothermal wells is the flashing process, which is the phase change of the geothermal fluid from liquid into a two-phase (steam and liquid mixture) due to a pressure drop causing the pressure to fall below the saturation pressure at the fluid's temperature (Budirianto, et al., 2020; Sanyal, 2005) However, as the reservoir pressure declines and a near-wellbore damage occurs, the IPR curve may "fall" until the IPR curve no longer intersects with the VLP curve, hence the well can no longer discharge fluids and well stimulations may be needed (Kriptanto, 2024; Marfo, et al., 2024). The net power output from a pumped geothermal well is formulated in Equations (2) and (3):

$$\dot{W}_{net,well} = \dot{W}_{gross,well} - \dot{W}_{pump} = \dot{m} \times h_{wh} \times \eta_{plant} - \frac{100 \times \dot{m} \times \rho \times \Delta P_{pumping}}{\eta_{pump}} \tag{2}$$

$$\Delta P_{pumping} = P_{wh} + \Delta P_{loss,elevation} + \Delta P_{loss,friction} - P_{suction} \tag{3}$$

where $\dot{m}$ is the fluid mass flow rate (kg/s), h_{wh} is the enthalpy at the wellhead (kJ/kg), η_{plant} is the power plant's electric efficiency (%), ρ is the fluid density (kg/m^3), $\Delta P_{pumping}$ is the dynamic pumping pressure (bar), η_{pump} is the pump efficiency (%), P_{wh} is the wellhead pressure (bar), $\Delta P_{loss,elevation}$ is the pressure drop due to elevation differences between the pump setting depth and the surface elevation (bar), $\Delta P_{loss,friction}$ is the pressure drop due to friction losses (bar), and $P_{suction}$ is the pump suction pressure (bar). It can be inferred from Equation (2) that a higher net power output from a pumped geothermal well can be achieved by enhancing the well productivity, plant efficiency, and pump efficiency while the reducing dynamic pumping pressure (and, if possible, fluid density by aiming for a hotter feed zone) (Tonkin, et al., 2023).

The dynamic pumping pressure informs how much pumping pressure is required to achieve the desired wellhead pressure at a given pump suction pressure to counter the pressure drop due to elevation differences and friction (Prabowo, et al., 2021). The elevation pressure drop, frictional pressure drop, pump suction pressure, and Fanning friction factor are respectively formulated in Equations (4), (5), (6), and (7):

$$\Delta P_{loss,elevation} = 0.0981 \times H_{set,pump} \tag{4}$$

$$\Delta P_{loss,friction} = \frac{124.8 \times f_F \times v^2 \times H_{set,pump}}{386.04 \times D_{well}} \tag{5}$$

$$P_{suction} = P_{wf} - 0.0981 \times (H_{FZ} - H_{set,pump}) \tag{6}$$

$$f_F = \frac{1}{4} \times \left(\frac{1}{1.74 - 2\log(2 \times \varepsilon)} \right)^2 \tag{7}$$

where $H_{set,pump}$ is the pump setting depth (m), f_F is the Fanning friction factor, v is the fluid flow velocity (m/s), D_{well} is the well inner diameter (m), P_{wf} is the flowing bottomhole pressure (bar) determined from the well's inflow performance relationship (IPR) curve, H_{FZ} is the feed zone depth (m), and ε is the wellbore roughness (m). It can be inferred from Equation (4) that minimizing the pump setting depth can contribute to reducing the elevation pressure losses, leading to a lower dynamic pumping pressure and thus a lower pumping parasitic load.

Furthermore, the fluid flow rate flowing into wellbore from the reservoir is determined by the reservoir permeability (often expressed as PI or permeability index in kg/s/bar). In other words, the downhole pump cannot increase the flow rate at a given flowing bottomhole pressure and thus cannot "elevate" the IPR curve since it depends on the reservoir deliverability (Kriptanto, 2024; Abrasaldo, et al., 2023). Instead, by providing external pressure support to the well, the downhole pump contributes in reducing the required flowing bottomhole pressure for the well to discharge fluid, hence "lowering" the VPL curve, with the given reservoir inflow performance (IPR) aimed to restore the intersection between the IPR and VLP curves (Kurniawan, 2021; Prabowo, et al., 2021). The fluid mass flow rate flowing into the wellbore is formulated in Equation (8):

$$\dot{m} = PI \times (P_{res} - P_{wf}) = \frac{2 \times k \times h \times (P_{res} - P_{wf})}{B \times \mu \times \left(\ln\left(\frac{r_{res}}{r_{well}} \right) + S \right)} \quad (8)$$

where P_{res} is the reservoir pressure (bar), k is the reservoir permeability (Darcy), h is the reservoir thickness (m), B is the reservoir fluid compressibility (dimensionless), μ is fluid viscosity (Pa-s), r_{res} is the reservoir drainage radius (m), r_{well} is the wellbore inner diameter (m), and S is the skin factor. The produced fluid's pressure drop from the reservoir to the wellbore and wellhead pumped geothermal wells is shown in Figure 20, which can illustrate that downhole pumps work on the principle of providing an external pressure support to the well so that the well can discharge fluid despite the reservoir inflow performance (deliverability) declines.

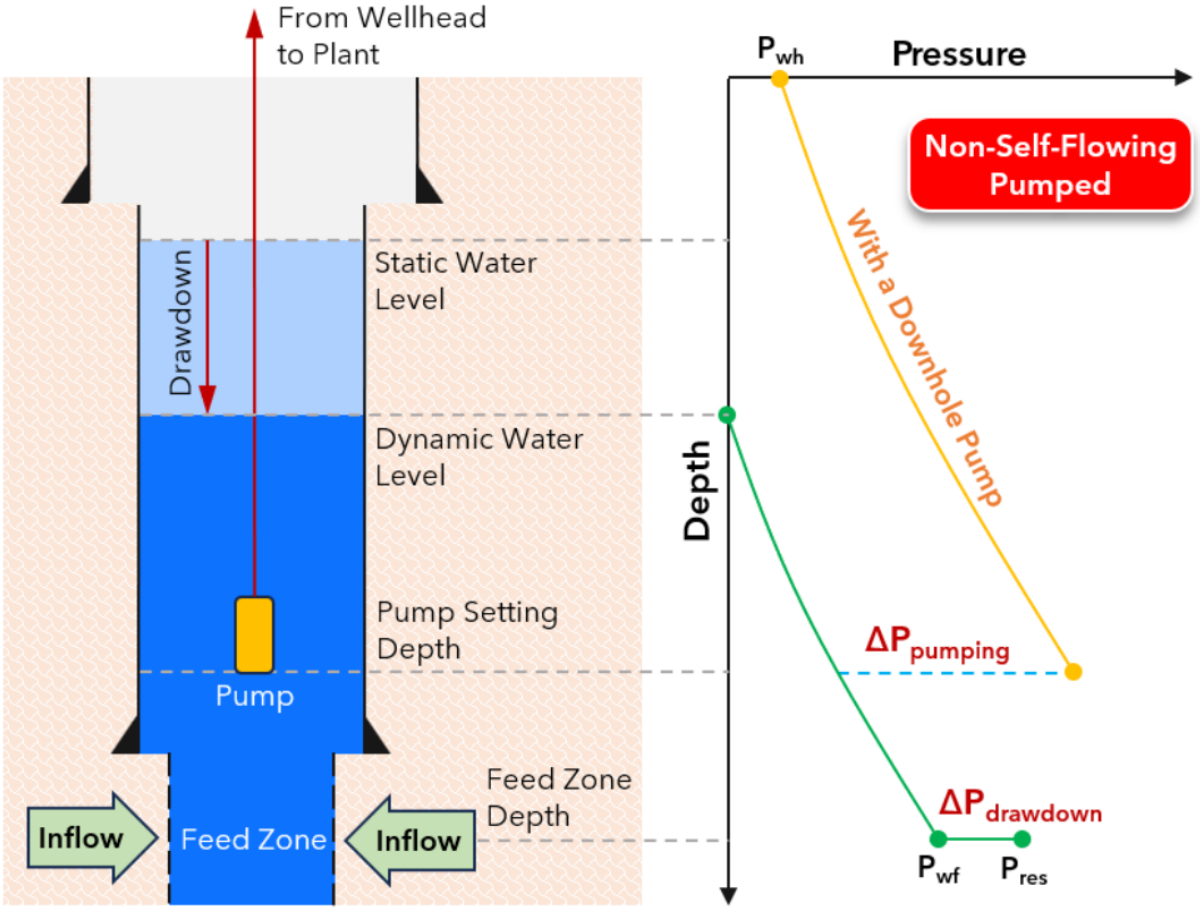

Figure 20: Pressure from the Reservoir to the Wellbore and Wellhead for Punped Liquid Geothermal Wells (Yearsley, 2023; Kurniawan, 2021).

Geothermal pumped-well power projects represent a growing niche within the broader geothermal industry, contributing around 1000 MW of installed generating capacity globally. Nevada, U.S., boasts the highest concentration of these projects, with approximately 15 fields totaling 724 MW of installed capacity, as shown in Table 4. The McGinness Hills project is the largest pumped-well facility globally, with an estimated capacity of 174 MW, followed by the Steamboat geothermal complex with 126.2 MW. Most projects in Nevada produce fluids within the 120-180°C range, though it also hosts the lowest reported resource temperature of about 100°C at Wabuska for any pumped-well geothermal power project worldwide. The prolific geothermal activity in Nevada's Basin and Range province is attributed to the region's high heat flow and extensional tectonic setting. Most geothermal activity in this area occurs along faults and is not associated with recent shallow magma sources. Extensional faulting is essential for creating productive geothermal systems, as fault zones facilitate the upflow of hot fluids and provide the high permeability for these systems. Generally, the productive feed zones are found at depths of 500-1500 meters.

There are two primary types of geothermal pumped wells, namely lineshaft pump (LSP) and electric submersible pump (ESP). The main difference between these two types lies in the location of their motors, as illustrated in Figure 21. In LSP systems, the motor is located at the surface, driving the pump impellers via a long shaft that extends down the well. This design allows for higher operational temperatures and lower wear due to the reduced rotational speed of the impellers. In contrast, ESP systems have their motors located downhole, directly connected

to the pump impellers. This configuration enables ESPs to handle higher pressures and flow rates and allows for more efficient directional drilling. However, ESPs are generally more expensive and require routine inspections due to their higher wear rates and operational complexities. Other than the motor equipment, the primary components, such as the pump impellers and screens, are similar between LSP and ESP systems.

Table 4: Operational Binary GPPs with Pumped Wells in Nevada (ThinkGeoEnergy, 2024; NREL, 2021; Febrianto, et al., 2019; Hernandez, et al., 2016; DiPippo & Kitz, 2015).

No	Field	GPP Name	COD Year	Resource Temp. (°C)	Avg. Prod. Well Depth (mMD)	Average MW/Well	Initial PPA Tariff (2022¢/kWh)	Operator	Capacity (MW)
1	Soda Lake	Soda Lake 2	1991	205	1,333	-	-	Cyrq Energy	9
		Soda Lake 3 Repower	2019	205		-	-	Cyrq Energy	26.3
2	Brady	Brady	1992	185	627	-	9.04	Ormat	21.5
		Desert Peak 2	2007	185		-	7.13	Ormat	26
3	Steamboat	Richard Burdette	2006	165	512	-	8.8	Ormat	30
		Galena 2	2007	165		-	6.84	Ormat	13.5
		Galena 3	2008	165		-	8.4	Ormat	30
		Steamboat 2	2008	165		-	9.04	Ormat	18.2
		Steamboat 3	2008	165		-	9.04	Ormat	18.2
		Steamboat Hills	2020	210		-	9.04	Ormat	16.3
4	Blue Mountain	Faulkner	2009	205	1,554	-	10.15	Cyrq Energy	49.5
5	Salt Wells	Salt Wells	2009	150	213	-	-	Enel	27.6
6	Stillwater	Stillwater	2009	160	648	-	-	Enel	33.1
7	Jersey Valley	Jersey Valley	2011	165	950	3.5	8.51	Ormat	23.5
8	Tuscarora	Tuscarora	2012	155	n/a	-	-	Ormat	32
9	San Emidio	San Emidio Repower	2012	190	806	3.5	11.5	Ormat	11.75
10	McGinness Hills	McGinness Hills I	2012	205	800	6.5	11.02	Ormat	50
		McGinness Hills II	2015	205		6.5	11.02	Ormat	50
		McGinness Hills III	2018	205		-	-	Ormat	74
11	Hazen	Patua	2013	155	2,700	-	-	Cyrq Energy	48
12	Don A. Campbell	Don A. Campbell I	2014	140	n/a	4	12.05	Ormat	25
		Don A. Campbell II	2015	140		-	9.83	Ormat	25
13	Tungsten Mountain	Tungsten Mountain	2017	125	n/a	-	9.04	Ormat	37
14	Wabuska	Whitegrass No. 1	2018	115	677	-	8.02	Open Mountain Energy	4.4
15	North Valley	North Valley	2023	190	n/a	-	-	Ormat	25
								Total	**724.8**

The comparison between LSPs and ESPs in geothermal applications reveals notable differences in their operational and environmental characteristics, as summarized in Table 5. LSPs can handle higher operating temperatures (up to 215°C) compared to conventional ESPs, which are typically limited to around 160°C, though the newer models by SLB, named Reda Thermal ESP, can handle up to 225° C (Kriptanto, 2024). LSPs operate at slightly lower pressures (⩽ 70 bar) and have a lower flow rate capacity (± 540 t/h) compared to ESPs, which can manage pressures (⩽ 75 bar) and higher flow rates (± 900 t/h). LSPs are limited to a maximum well depth of approximately 730 meters, whereas ESPs can be used in wells deeper than 1000 meters. Installation of LSPs is more time-consuming and requires surface-level motor drivers, while ESPs are quicker to install with downhole motors. LSPs are more efficient due to their lower rotational speeds, which also results in reduced wear compared to ESPs. However, ESPs are advantageous for directional drilling capabilities. In terms of cost, LSPs are less expensive in both capital and operational expenditures but require predictable maintenance schedules, whereas ESPs are more expensive and necessitate routine inspections. Additionally, LSPs pose an environmental risk due to the use of oil lubrication for shaft bearings, while ESPs do not have this impact. The choice between LSPs and ESPs depends on specific project needs, such as well depth, temperature, flow rate, and environmental considerations.

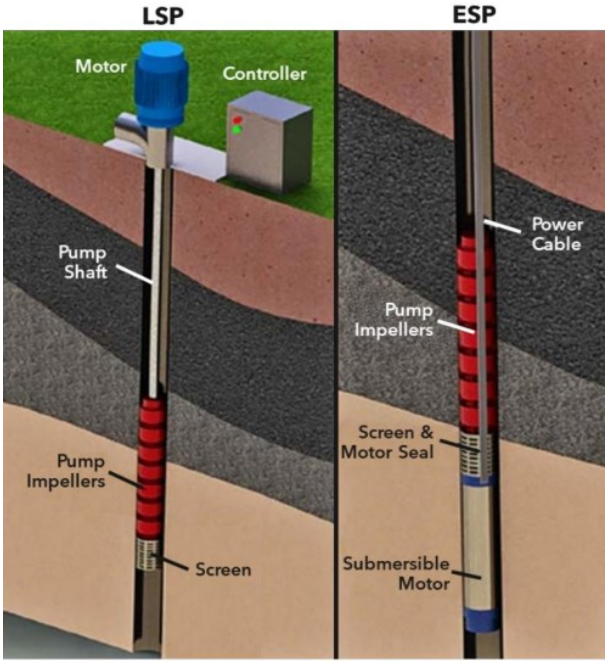

Figure 21: Primary Components of a Linesaft Pump (Left) and an Electric Submersible Pump (Right) (NREL, 2014).

Table 5: Comparison Between Lineshaft Pumps and Electric Submersible Pumps (Kriptanto, 2024; Febrianto, et al., 2019).

Parameter	Lineshaft Pump	Electric Submersible Pump
Operating temperature	High (≤ 215°C)	• Conventional: ≤ 160°C • SLB Reda Thermal ESP: ≤ 225°C
Operating pressure	Slightly lower (≤ 70 bar)	Slightly higher (≤ 75 bar)
Flow rate capacity	Lower (± 540 t/h)	Higher (± 900 t/h)
Maximum well depth	Limited to ≤ 730 m	Relatively deeper (> 1000 m)
Well deviation	Vertical well only	Directional well is possible
Installation time	Time-consuming	Relatively quick
Motor driver location	At the surface	Downhole
Pump and motor efficiency	Higher	Lower
Wear proneness	Lower (due to lower rotational speed)	Higher (due to higher rotational speed)
CAPEX and OPEX	Less expensive	More expensive
Maintenance schedule	Predictable	Routine inspection
Environmental impact	Present (due tue oil lubrication for shaft bearings)	None

To further compare the performance between LSP and ESP systems statistically, the empirical Mean Time Between Failures (MTBF) of LSPs is compared with the 17 geothermal ESPs summarized by (Lovekin, et al., 2021). MTBF, a reliability metric that estimates the average time a system or component operates before experiencing a failure, is a critical measure of reliability in LSP and ESP systems (Omrani, et al., 2021). The box plot in Figure 22 shows that, in general, ESPs tend to have shorter MTBF than LSPs. Specifically, the overall MTBF for LSPs is significantly higher, indicating greater reliability over time. The data further illustrate that as the operating temperature, flow rate, and depth increase, the MTBF for ESPs becomes shorter. ESPs used in low temperature environment (< 150°C), small flow rate (< 450 t/h), and shallow depth (< 300 m) conditions exhibit longer MTBF compared to those operating under higher temperature (≥ 150° C), larger flow rate (≥ 450 t/h), and greater depths (≥ 300 m). This trend suggests that more demanding operational conditions adversely affect the durability of ESPs.

Globally, the high-temperature high-flow rate Reda Thermal ESP developed by SLB has been installed in only one geothermal field, namely the Kizildere geothermal field in Turkey (Kriptanto, 2024). According to the case study information, the Reda Thermal ESP has been operating in the Kizildere geothermal field under challenging conditions, including temperatures up to 215°C and flow rates around 900 t/h. The ESP has successfully run for more than 600 days (almost 2 years) as of February 2024. However, this duration is still shorter than the mean and median MTBF for ESPs, which is 4.1 years. Consequently, while the Reda Thermal ESP has shown promising performance, its actual long-term durability remains uncertain.

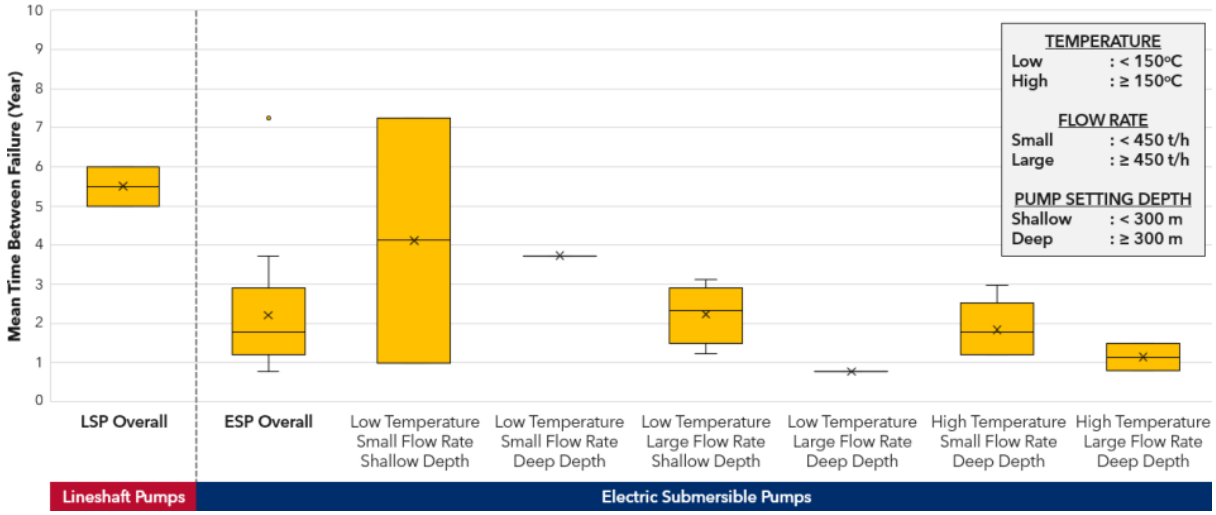

Figure 22: MBTF Comparisons Between LSP and ESP from 17 Geothermal Wells in the U.S. with an ESP Installed (Kriptanto, 2024; Lovekin, et al., 2021).

3.2 Developing the Shallow Outflow Zones

The development of low-medium temperature geothermal resources relies heavily on the downhole pump technology to discharge the non-self-discharging wells. As expressed in Equations (2) and (4), the net power output from a pumped geothermal well is influenced by the pump setting depth. The setting depth of a geothermal downhole pump is based on the principle that the pump inlet must be set sufficiently deep below the static water level so that the pump suction pressure is sufficiently high to prevent cavitation (boiling or the forming of bubbles) in the pump, which may damage the pump (Aydin & Merey, 2021; Prabowo, et al., 2021). To fulfill this principle, the following two parameters must be considered while determining the pump setting depth (Yearsley, 2023):

1. **Productivity index**: it determines the pressure drawdown (the difference between reservoir pressure and flowing bottomhole pressure), which influences the pump suction pressure value.
2. **Temperature**: it determines the saturation pressure of the geothermal fluid along the depth of the wellbore. Therefore, it becomes the crucial factor for limiting the allowable pressure drawdown. The higher the temperature, the higher the allowable pressure drawdown is for a particular depth throughout the wellbore.

The development of geothermal resources in Indonesia mainly focuses on producing from the reservoir at and around the hot upflow zone, aiming for a higher temperature and permeability (Firanda, et al., 2024; Stimac, et al., 2019; Hochstein & Sudarman, 2015). However, applying this approach for low-medium temperature resources may present drawbacks, such as the inability of the downhole pump's rating to meet the operating temperature and depth requirements as well as the smaller well power output due to the larger pump parasitic load because of the deeper hot upflow zone (Febrianto, et al., 2019). On the other hand, the peripheral outflow zone of a geothermal reservoir is typically not as hot as the central reservoir region around the upflow zone yet it is usually shallower especially in the volcanic geothermal systems (Ormat, 2022; Taborda, et al., 2022). Therefore, besides developing the hotter yet deeper upflow zone, developing the cooler yet shallower outflow zone in the low-medium temperature geothermal resources may provide the following benefits:

1. **Reduced drilling cost**: due to the shallower outflow zone, the required well depth can be reduced and thus the total drilling cost can be minimized (GRG-Geoenergis, 2024a; EBTKE, 2023; Purba, et al., 2020).
2. **Benign fluid**: fluids in upflow zones are typically more acidic and chemically aggressive due to high temperatures and pressure, which enhance mineral dissolution. In contrast, outflow zones have more benign fluids because they mix with cooler groundwater, leading to dilution and reduced chemical reactivity (Nayoan, et al., 2023; Pradipta, et al., 2023).
3. **Easier mobilization and demobilization**: since the outflow zone are usually located at lower elevation areas with a flatter terrain, mobilizing and demobilizing the equipment for drilling, power plant construction, and infrastructure preparation can become less challenging (GRG-Geoenergis, 2024c; Purba, et al., 2021).
4. **Allowing the use of downhole pump**: developing the shallower outflow zone allows for the use of LSPs, which performance is limited by the well depth (Putriyana, et al., 2022; Prabowo, et al., 2021).
5. **Increased well power output**: by lowering the depth of the static water level from the wellhead, the pump parasitic load can be minimized and thus the net power output can be maximized (Ormat, 2022;

Prabowo, et al., 2021). The possible well power output variations as a function of the static water level depth are illustrated in Figure 23.

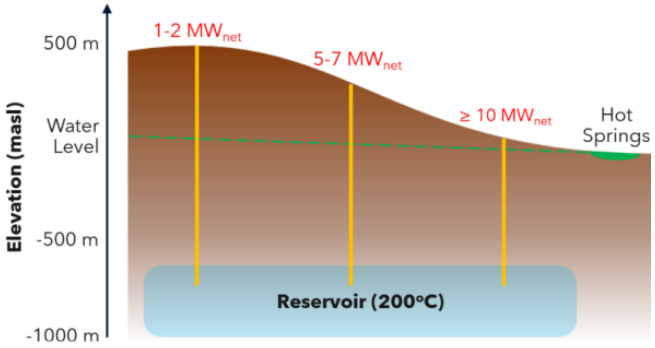

Figure 23: Pumped Well Output at Different Elevation Interval Between Wellhead and Static Water Level (Ormat, 2022).

Table 6: Examples of U.S. Experience in Developing the Outflow Zone in Low-Medium Temperature Geothermal Fields.

Parameter	Steamboat, Nevada	Mammoth, California
Resource Information		
Upflow temperature	175-200°C	180-200°C
Upflow temperature class	Low-medium temperature	Low-medium temperature
Main reservoir well depth	1,000-2,000 mMD	Not drilled due to mountaineous terrain
Developer	Ormat	Ormat
Development history	**1985:** Steamboat 1 (2 MW; binary; retired) Steamboat 1A (2.4 MW; binary; retired) **1988:** Steamboat Hills (16.3 MW; single-flash; retired) **2006:** Richard Burdette (30 MW; binary; online) **2007:** Galena 2 (13.5 MW; binary; online) Steamboat Hills Bottoming (5.5 MW; binary; online) **2008:** Galena 3 (30 MW; binary; online) Steamboat 2 (18.2 MW; binary; online) Steamboat 3 (18.2 MW; binary; online) **2020:** Steamboat Hills (16.3 MW; binary; online)	**1990:** MP-2 (15 MW; binary; online) PLES-1 (15 MW; binary; online) **2013:** MP-1 (10 MW; binary; online) **2022:** Casa Diablo IV (30 MW; binary; online)
Outflow Development		
Outflow temperature	150-175°C	130-200°C
Outflow temperature class	Low-temperature	Low-medium temperature
Outflow utilization	Production and reinjection areas	Production and reinjection areas
Outflow well depth	200-500 mMD	800-1,200
Literature source	(Ormat, 2022; NREL, 2021; Ayling, 2020)	(Ormat, 2022; Rutqvist, et al., 2021; NREL, 2021)

Table 6 summarizes the U.S. experience in developing the ouflow zone of low-medium temeprature geothermal fields. The advantages of developing shallower outflow zones, compared to deeper upflow zones, are apparent in the development experience gained in the Steamboat (Nevada) and Mammoth (California) geothermal fields. The depth of the outflow wells is evidently shallower than the upflow wells, which reduces drilling costs and allows reduction in downhole pump parastici load, optimizing operational efficiency and cost-effectiveness of low-medium temperature resources. The flatter terrain of outflow zones also eases drilling and equipment mobilization as well as the access to existing infrastructures.

3.2.1 Case Study #1: Steamboat, Nevada

The Steamboat geothermal field, located near Reno, Nevada, is geologically set within a complex of metamorphic rocks of sedimentary and volcanic origin, intruded by granitic rocks. These formations are further covered by younger volcanic rocks, approximately one million years old, which are believed to be the heat source for the geothermal system (Neupane, et al., 2015). The field is characterized by steep faults trending northeast and north, which contribute to the formation of a series of basins between the Carson Range and the Virginia Range. These

fault systems create conduits that control the geothermal fluid flow, resulting in a high-temperature resource with significant fracture permeability, particularly along the western and eastern sides of the reservoir (Klein, et al., 2007). The geothermal system at Steamboat features a conceptual model (Figure 24) where hot water ascends below the Upper Steamboat at about 200ºC, thus forming the upflow zone, then flows northeast at depths of 1,200-1,300 m into the outflow zone at the Lower Steamboat, where the fluids eventually discharge at the hot springs and into a shallow subsurface aquifer under Truckee Meadows (Ormat, 2022; Neupane, et al., 2015).

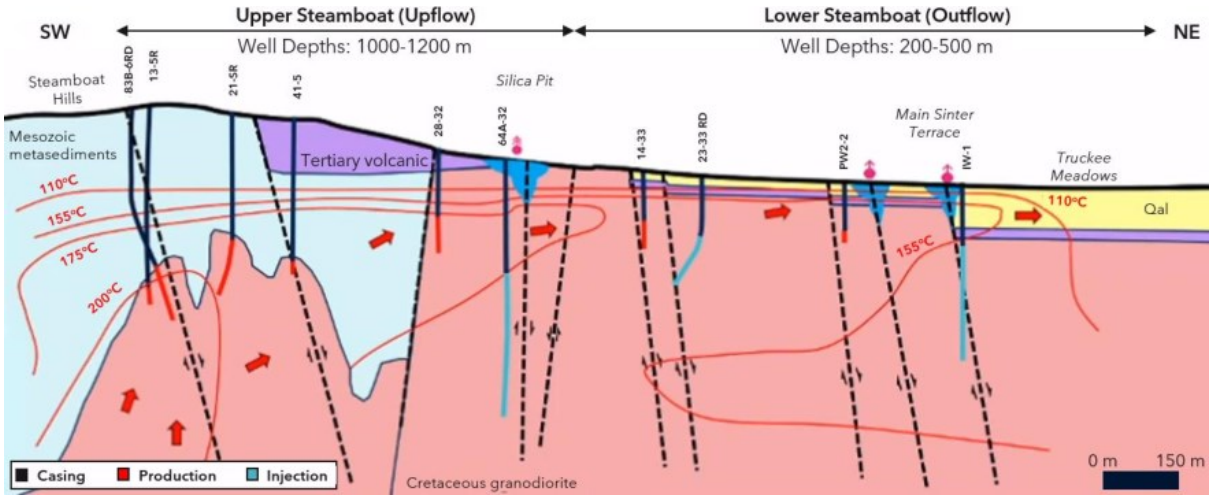

Figure 24: Conceptual Model of Steamboat Geothermal Field, Nevada (Ormat, 2022).

The Steamboat geothermal fields in Nevada have seen several development phases (ThinkGeoEnergy, 2024; NREL, 2021; Ayling, 2020). Initially, in 1985, the Steamboat 1 and Steamboat 1A binary plants were built with capacities of 2 MW and 2.4 MW, respectively, although these are now retired. Subsequently, the Steamboat Hills single-flash plant with the capacity of 16.3 MW was commissioned in 1988. Development picked up again in the mid-2000s: in 2006, the Richard Burdette plant (30 MW) became operational, followed by Galena 2 (13.5 MW) and Steamboat Hills Bottoming (5.5 MW) in 2007. The expansion continued in 2008 with Galena 3 (30 MW), Steamboat 2 (18.2 MW), and Steamboat 3 (18.2 MW). The most recent addition was Steamboat Hills (16.3 MW) in 2020 by retiring the existing Steamboat Hills single-flash plant and replacing it with a binary plant with pumped wells (Ormat, 2022). Furthermore, the well depths in the Steamboat fields vary between the upflow and outflow zones (Ormat, 2022). The upflow zone, located at Upper Steamboat, has wells that range from 1,000 to 1,200 meters deep, reaching temperatures of up to 200°C, as shown in Figure 24. Meanwhile, the outflow zone at Lower steamboat, which is used as both the production and reinjection areas, has shallower wells, ranging from 200 to 500 meters deep, with temperatures between 150 and 175°C.

3.2.2 Case Study #2: Mammoth, California

The Mammoth Geothermal Complex is strategically located at the base of a resurgent dome in the Long Valley Caldera. This dome formed due to the upward movement and swelling of the caldera floor, driven by activity in the magma chamber beneath it. The geothermal heat generated from this magma chamber causes groundwater to boil and turn to steam, resulting in fumaroles observable in areas like Fumarole Valley and Hot Creek, situated about 5 miles (8 km) to the northeast. The GPP development at the Mammoth geothermal field by Ormat has undergone significant development over the years (Robertson-Tait, et al., 2021; NREL, 2021). Initial developments began in 1990 with the installation of the MP-2 and PLES-1 binary plants, each with a capacity of 15 MW. Further expansion occurred in 2013 with the addition of the MP-1 plant, which has a capacity of 10 MW. The most recent development is the Casa Diablo IV plant, which came online in 2022, adding another 30 MW to the complex's capacity. The upflow zone in the West Moat area, characterized by low-medium temperature (180-200°C), has not been drilled due to the challenging mountainous terrain (Ormat, 2022). Consequently, development has been concentrated in the outflow zone at Casa Diablo, where production wells are drilled to depths ranging from 800 to 1200 meters, accessing reservoir temperatures between 130-200°C, as shown in Figure 25. The outflow zone also benefits from the use of pumped production wells, which help manage the calcite oversaturation conditions common in this area. Ormat is currently focusing on further expansion projects within the outflow zone, leveraging the existing infrastructure and favorable flatter terrain in the outflow zone (Ormat, 2022).

Meanwhile, Indonesia also has the experience in developing the outflow zone despite in high-temperature geothermal fields and the purpose of the development is currently limited to utilizing it as a reinjection area, as shown in Table 7, such as in the Muara Laboh (West Sumatra) and Sibayak (North Sumatra) geothermal fields

(Firanda, et al., 2015; Stimac, et al., 2019). Similar trends in the well depth can be observed, where the outflow wells are typically shallower than the upflow wells. However, the utilization of outflow zone for production can be expected in the future in the Ulubelu geothermal field, Lampung, in which the lower-temperature outflow zone, named Gunung Tiga, is currently being explored for future power generation (PGE, 2022).

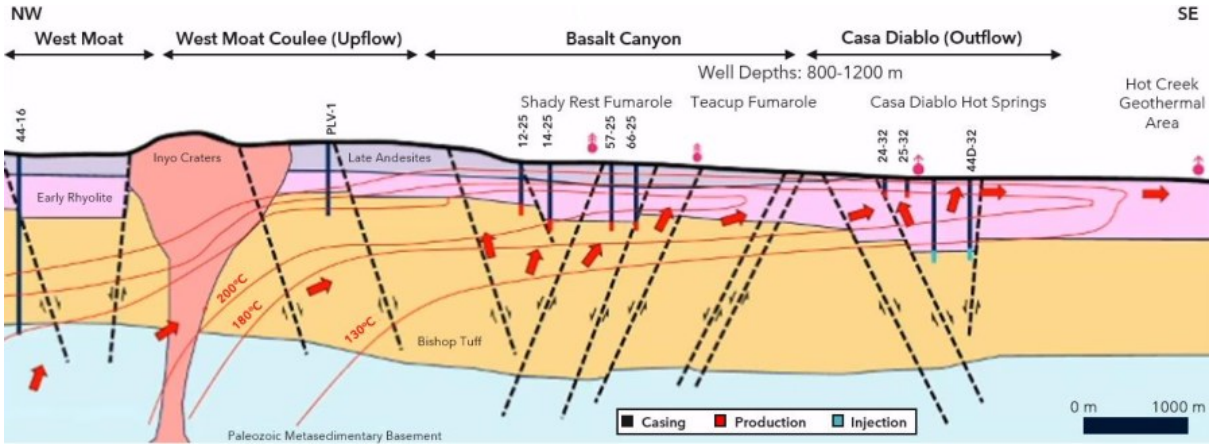

Figure 25: Conceptual Model of Mammoth Geothermal Field, California (Ormat, 2022).

Table 7: Examples of Indonesia's Experience in Developing the Outflow Zone in High-Temperature Geothermal Fields.

Parameter	Muara Laboh, West Sumatra	Ulubelu, Lampung	Sibayak, North Sumatra
Resource Information			
Upflow temperature	230-300°C	250-280°C	240-300°C
Upflow temperature class	High-temperature	High-temperature	High-temperature
Reservoir mobile fluid phase	Liquid-dominated	Liquid-dominated	Liquid-dominated
Terrain	Flat-moderate	Steep	Steep
Avg. main reservoir well depth	2,422 mMD	2,097 mMD	2,015 mMD
Developer	Supreme Energy	Pertamina Geothermal Energy	Pertamina Geothermal Energy
Development history	**2019:** Unit 1 (85 MW; double-flash) **Total capacity:** 85 MW	**2012:** Unit 1 (55 MW; single-flash) Unit 2 (55 MW; single-flash) **2016:** Unit 3 (55 MW; single-flash) **2017:** Unit 4 (55 MW; single-flash) **Total capacity:** 220 MW	**2008:** Unit 1 (10 MW; single-flash) **Total capacity:** 10 MW
Outflow Development			
Outflow temperature	160-220°C	150-240°C	150-230°C
Outflow temperature class	Low-medium temperature	Low-high temperature	Low-high temperature
Outflow utilization	Reinjection area	Still under exploration for future production	Reinjection area
Number of outflow wells	6 wells (reinjection)	None	3 wells (reinjection)
Avg. outflow well depth	1,925 mMD	None	1,690 mMD
Literature source	(GRG-Geoenergis, 2024b; EBTKE, 2020; Stimac, et al., 2019; Mussofan, et al., 2018)	(GRG-Geoenergis, 2024b; PGE, 2022; PGE, 2021; Hochstein & Sudarman, 2015)	(Firanda, et al., 2024; GRG-Geoenergis, 2024b; EBTKE, 2020; Atmojo, et al., 2001)

3.2.3 Indonesia's Experience #1: Muara Laboh, West Sumatra

The Muara Laboh geothermal field, located in a pull-apart basin along the Great Sumatera Fault (GSF), features a complex geological and structural setting. The system is hosted in a stratigraphic sequence ranging from Paleozoic metamorphic rocks to Quaternary volcanic deposits, with significant Middle Miocene granitic intrusions. Structurally, the field is characterized by fault segments like the Siulak and Suliti faults, with dominant N-S, NW-SE, and NE-SW fracture trends controlling permeability and fluid flow (Mussofan, et al., 2018). The geothermal reservoir, divided into SW and NE sectors, exhibits moderate to high temperatures (230-300°C). The SW sector, associated with the Patah Sembilan volcano, features deep upflow zones and high permeability along intrusion margins, while the NE sector, with its steam cap near the Idung Mancung fumarole, has secondary upflow along faults and fractures. The NNW outflow zone, originating from fluid flow parallel to the GSF, extends to the Sapan Malulong hot springs. The system's fluids are low in salinity and non-condensable gases, indicating

deep meteoric recharge and fault-controlled circulation (Stimac, et al., 2019). Figure 26 shows the conceptual model of the Muara Laboh geothermal field.

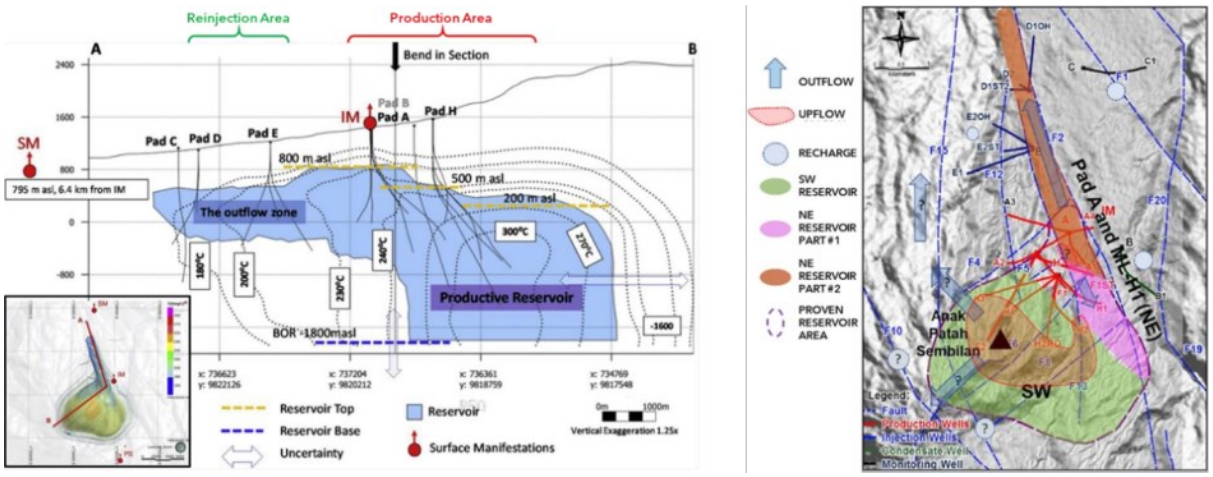

Figure 26: Conceptual Model of Muara Laboh Geothermal Field, West Sumatra (Stimac, et al., 2019).

The historical development of the Muara Laboh geothermal power plant began with the identification of its high potential during pre-feasibility studies conducted by Supreme Energy in 2008 (Stimac, et al., 2019). The first unit of the power plant, an 85 MW double-flash power station, was operational by 2019 (GRG-Geoenergis, 2024a; EBTKE, 2020). The NNW outflow zone of the field is currently utilized as the reinjection area, where six reinjection wells (D-1OH, D1ST2, D2, E1, E2OH, and E2ST) have been drilled in Pads D and E with a temperature of 160-220oC (Stimac, et al., 2019). The average outflow well depth of 1,925 mMD is shallower than the main reservoir wells, which average 2,422 mMD.

Furthermore, Muara Laboh is characterized by a geochemically compartmentalized reservoir (Alfiady, et al., 2021). The fluid chemistry in the outflow zone is characterized by low salinity, with chloride concentrations ranging from 400 to 1600 ppm and a benign chemical composition with low non-condensable gas (NCG) content of approximately 0.5 to 2 wt% in steam. The gas chemistry shows helium isotopic compositions (R/Ra) between 1.12 and 3.14, indicating contributions from near-surface crustal fluids and mixing between mantle and crustal fluid sources (Stimac, et al., 2019). Finally, despite not developing the outflow zone for production, the experience in drilling and developing the outflow zone for reinjection provides valuable experience and lessons learned about the permeability, hydrogeology, and fluid chemistry in the outflow zone for future development of low-medium temperature outflow zone in Indonesia.

3.2.4 Indonesia's Experience #2: Ulubelu Lampung

The Ulubelu geothermal field is known as a volcanic geothermal system with a large outflow structure, extending from the upflow zone near the dormant G. Rendingan stratovolcano to the south towards the Gunung Tiga outflow area and the further south Way Panas outflow area (Hochstein & Sudarman, 2015), as shown in Figure 27. The thermal manifestations are located on a steep terrain with a zonation pattern, with acidic SO4 springs found upstream, transitioning to neutral SO4-HCO3 springs mid-downstream, and finally to neutral Cl-SO4-HCO3 springs at the bottom where travertine deposits are present. The area was initially categorized as a caldera-type volcano or a volcano in a volcano-tectonic depression. This classification persisted into the early 1990s when detailed exploration surveys commenced in 1990, employing gravity, magnetic, DC- and MT resistivity methods. By 1995, three deep slim holes, each around 1.2 km, were drilled. The SL-3 slimhole well was presumed to be near the center of a volcano-tectonic depression reservoir. Although heat loss surveys were not conducted, the bottom hole temperatures in SL-3, showing an inverse profile with approximately 200°C at 0.95 km, did not indicate the presence of an 'upflow structure' for a high-temperature reservoir. Instead, the center of this structure is likely closer to the Rendigan stratovolcano.

The Ulubelu geothermal field has undergone significant development since 2012. Initially, two single-flash geothermal power plants (GPP) were established, each with a capacity of 55 MW. This was followed by the addition of two more units in 2016 and 2017, bringing the total capacity to 220 MW (ThinkGeoEnergy, 2024; GRG-Geoenergis, 2024a; EBTKE, 2020). All existing GPP developments are situated within the Ulubelu reservoir area, characterized by a high-temperature upflow (250-280°C) and steep terrain (GRG-Geoenergis, 2024b; Mubarok & Zarrouk, 2016). Meanwhile, the outflow zone in the Gunung Tiga area remains undeveloped. However, Pertamina Geothermal Energy is actively exploring this zone for future production potential. Based on the measured downhole temperature at a slimhole located at about 1 km from the Gunung Tiga prospect area, the subsurface temperature at the area can exceed 200°C (PGE, 2022). Meanwhile, the geoscience analysis suggests

that the outflow temperatur can range from 150 to 240oC (PGE, 2021) Therefore, the outflow zone has a wide temperature range class from low to high-temperature.

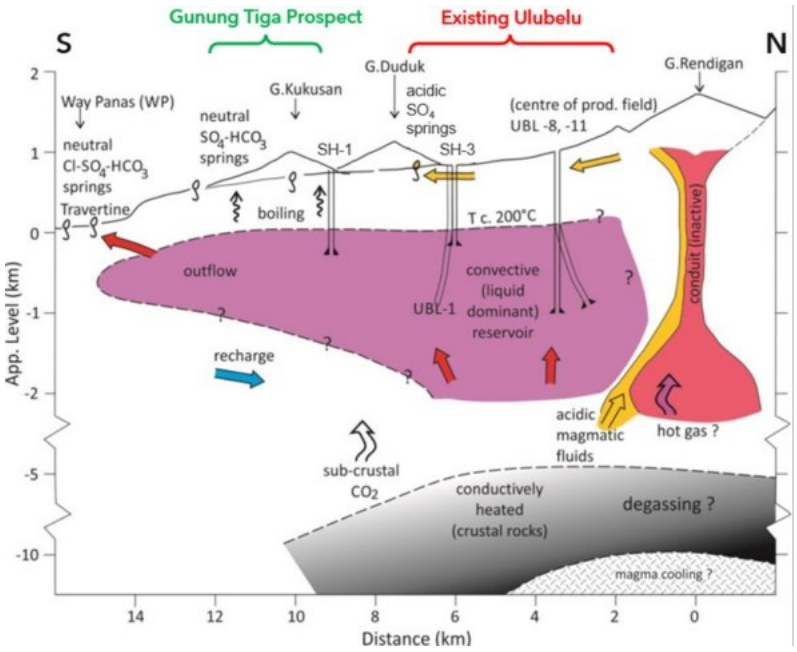

Figure 27: Conceptual Model of Ulubelu Geothermal Field, Lampung (Hochstein & Sudarman, 2015).

3.2.5 Indonesia's Experience #3: Sibayak, North Sumatra

The Sibayak geothermal field is located within the Singkut Caldera in North Sumatra, Indonesia, and is characterized by a volcanic-hosted geothermal system beneath Mount Sibayak (Firanda, et al., 2024; Atmojo, et al., 2001). The geological setting includes high temperatures ranging from 240ºC to 300ºC, primarily occurring in fractured zones of pre-Tertiary to Tertiary sedimentary rocks. The field's geothermal reservoir is dominated by hot liquid and is situated near the conduits of two small stratovolcanoes within the caldera. Extensive fractures and faults, such as the Tengkorak, Semangat Gunung, and Pariban Faults, enhance secondary permeability, contributing to the field's geothermal activity. The geothermal system's upflow zone is located directly beneath Mount Sibayak, while the outflow zone extends approximately 3 kilometers towards the E-SE direction, reaching the Karona hot springs. Furthermore, the field has a notable development history perfomed by Pertamina Geothermal Energy. In 2008, a 10 MW single-flash power plant (Unit 1) was commissioned, utilizing the field's high-temperature upflow zone with temperatures ranging from 240-300°C. The production wells reach an average depth of 2,015 meters measured depth (mMD), targeting the steeply terrained propylitic zone where the main geothermal resource is located. The outflow zon serves as a reinjection area, in which three reinjection wells, namely SBY-1, SBY-2, and SBY-9, are drilled to shallower depths, averaging around 1,690 mMD, compared to the deeper production wells near to the upflow zone shown in Figure 28 (Firanda, et al., 2015). The outflow zone is interpreted to have low-medium temperatures of 150-230°C based on the downhole measurements of the outflow wells and numerical modeling (Firanda, et al., 2024).

Furthermore, the permeability extent and depth distribution at Sibayak can be identified from the partial and total loss of circulation encountered during drilling as well as the feed zones identified from the water loss test. Most feed zones were found between -74 masl and -280 masl in many wells, while in SBY-5, they were identified at depths from -405 masl to -425 masl. The feed zones are likely controlled by local fractures and faults in the area, as well as the primary permeability of the metasediments. The injectivity index was highest in SBY-5 at 61.4 t/h/bar, and in SBY-6 at 55.4 t/h/bar, which are located in the central reservoir. The highest mass flow production was also observed in well SBY-5, with 173 t/h of brine and 35 t/h of steam. Meanwhile, the II values at the outflow wells (SBY-1, SBY-2, and SBY-9) are rather smaller compared to the central reservoir wells, each with an II of 4.3 t/h/bar, 5.4 t/h/bar, and 3.2 t/h/bar. Therefore, among these 3 wells, only SBY-2 that has the II value above the commercial II threshold of 5 t/h/bar. Nevertheless, it can be observed that the elevation of the major feed zone generally becomes higher (shallower feed zone) towards the outflow zone, as shown in Figure 29. The shallowest major feed zone and the second shallowest total lost circulation zone can be found at SBY-9 at the elevation of 360 masl and 490 masl, respectively (Firanda, et al., 2024).

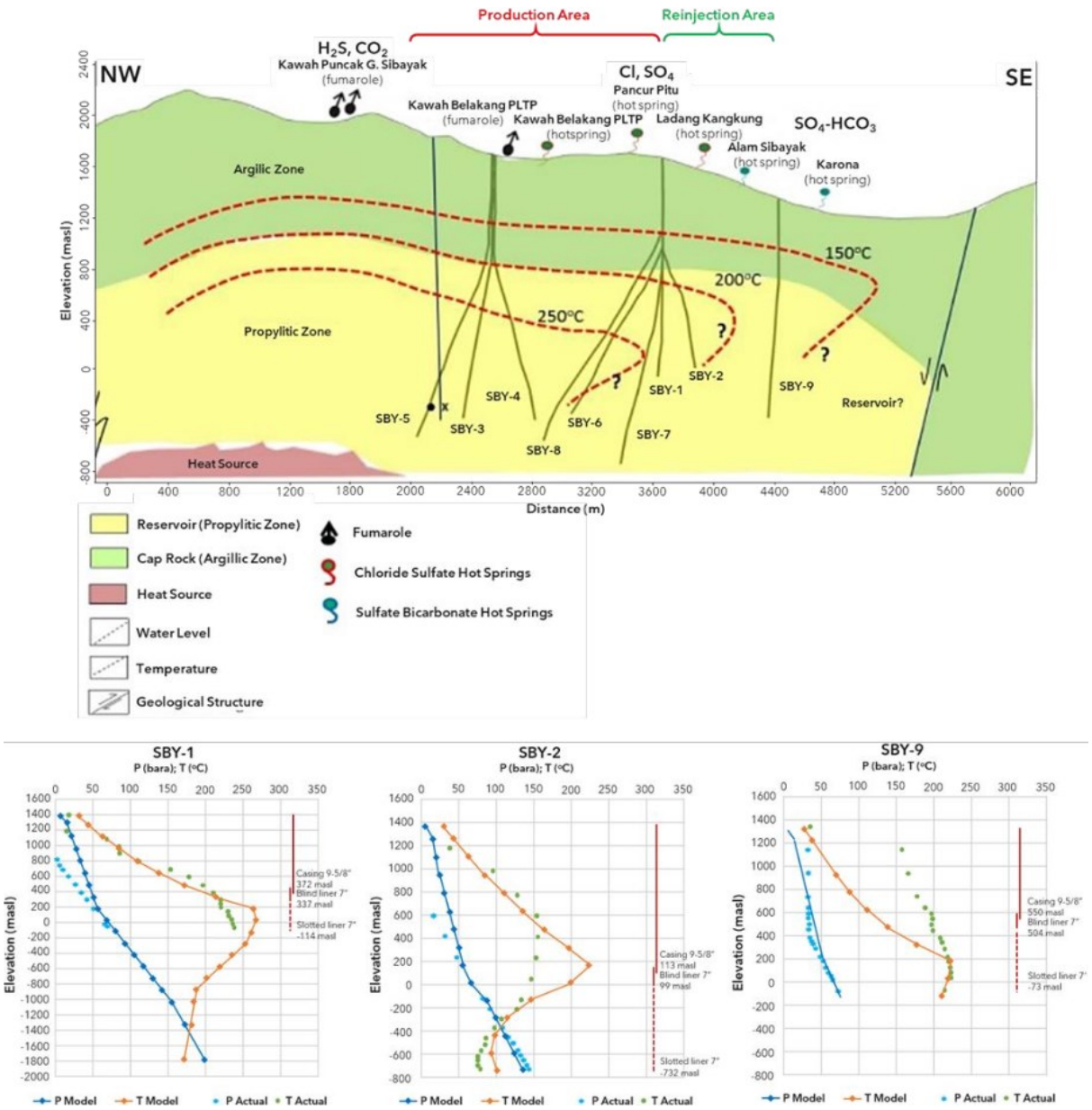

Figure 28: Conceptual Model of Sibayak Geothermal Field, North Sumatra (Top) and the Downhole Temperature & Pressure Profiles at Three Outflow Wells (Bottom) (Firanda, et al., 2024).

The permeability distribution at Sibayak provides the lessons learned that the development of low-medium temperature outflow may be challenged by the low permeability typically found at the boundary of a conventional hydrothermal reservoir in spite of the shallower feed zone depth. Consequently, the well targeting at the outflow zone has to consider the permeability target thoroughly to increase the probability of intersecting highly permeable zones. Otherwise, well stimulation techniques to improve the hydraulic connectivity to the main reservoir's permeable fracture networks might be needed.

3.3 Well Stimulation to Improve Permeability

Finding high permeability during drilling (well targeting) or improving permeability through well stimulation techniques is crucial to improve the techno-economic feasibility of low-medium temperature geothermal systems. The first reason why permeability is a significant parameter determining the techno-economic feasibility of a low-medium temperature geothermal systems is that permeability influences the net power output of a pumped geothermal well by determining the gross power output (determined by the mass flow of produced fluid) and parasitic load (determined by the pump energy required to discharge the well artificially). If a higher well power output can be achieved, a smaller number of wells is needed to support a certain GPP development capacity. Figure 30 illustrates how well output increases with higher operating temperatures and higher productivity indices (PI in L/s/bar). At lower temperatures (100-180°C), wells rely on pumped technology to achieve desired outputs. Beyond this temperature range, wells can transition to self-flowing mechanisms, especially with the utilization of

advanced downhole pumps like the SLB Reda Thermal ESP, which extends the operating temperature limit up to 215°C (Kriptanto, 2024). The productivity index indicates the reservoir's permeability, with higher values denoting more efficient fluid flow. For instance, wells with a PI of 30 l/s/bar exhibit significantly higher outputs compared to those with lower PIs. This relationship underscores the importance of both thermal and permeability characteristics in optimizing pumped well performance.

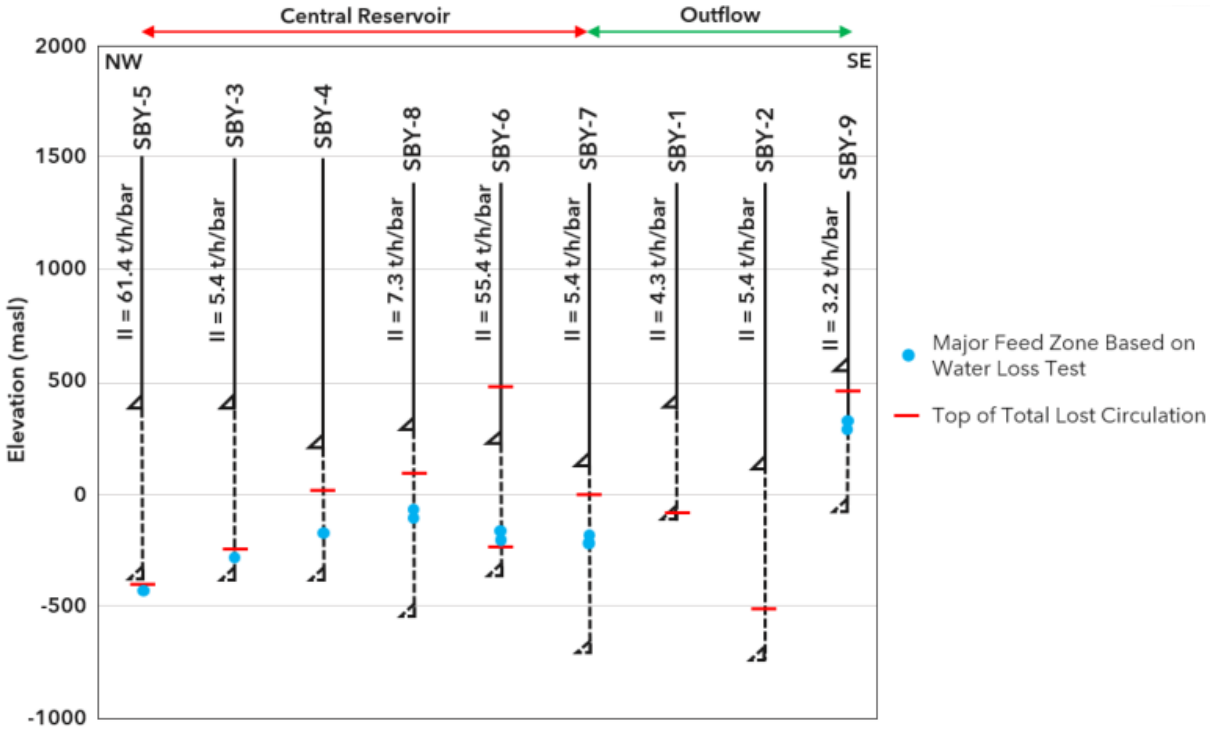

Figure 29: Major Feed Zones and Total Lost Circulation Zones at Sibayak Geothermal Wells (Firanda, et al., 2024).

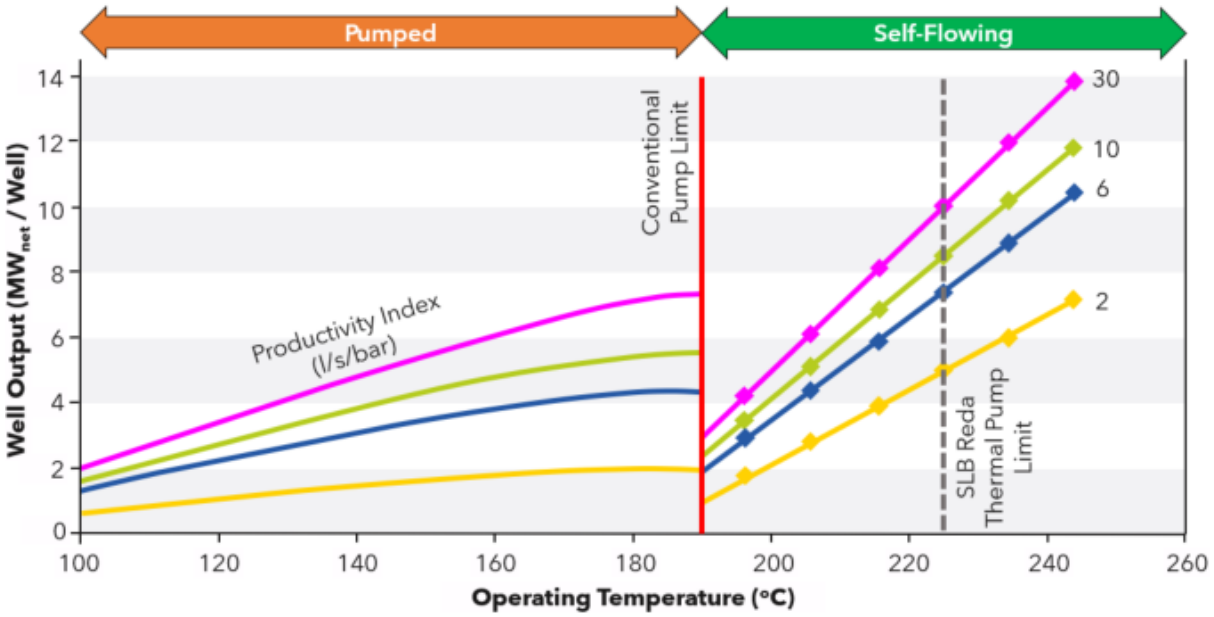

Figure 30: Well Power Output as a Function of Temperature and Productivity Index (Kriptanto, 2024; Febrianto, et al., 2019; IFC, 2013).

The influence of permeability and skin factor (due to the presence of permeable fractures) to the reservoir deliverability and the required pumping pressure by the downhole pump are illustrated in Figure 31. Given the PI correlation expressed by the Equation (8) and that the slope of a liquid-phase IPR curve is the negative of one over PI, the slope of the IPR curve becomes steeper as the permeability and/or skin factor decrease. Therefore, at a given flow rate inflow from the reservoir into the wellbore, the pumping pressure required to artificially

discharge the non-self-flowing well becomes higher as the reservoir permeability decreases due to the lower reservoir deliverability. In other words, wells with low permeability requires a higher pumping energy and thus results in a smaller well power output due to the higher pump parasitic load. Similarly, when the well intersects a permeable fracture zone (thus having a negative skin factor), the reservoir deliverability increases and thus the pumping pressure can be reduced. As a result, finding high permeability during drilling (well targeting) or improving permeability through well stimulation techniques is crucial to optimize the pumped well power output through an efficient artificial lift using downhole pumps.

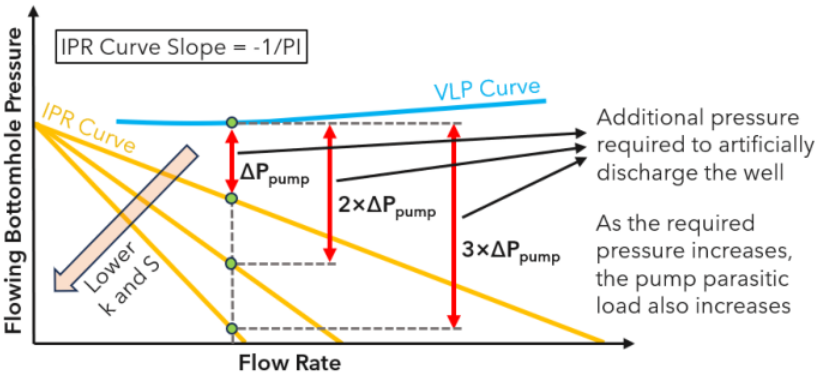

Figure 31: IPR Curve Variations as the Permeability (k) and Skin Factor (S) are Reduced for Liquid-Phase Geothermal Wells (Kriptanto, 2024; Zarrouk & McLean, 2019; Grant & Bixley, 2011).

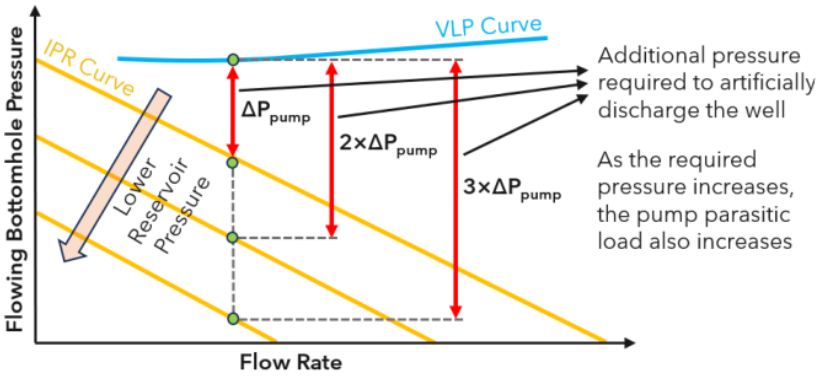

Figure 32: IPR Curve Variations as the Reservoir Pressure Decreases for Liquid-Phase Geothermal Wells (Kriptanto, 2024; Zarrouk & McLean, 2019; Grant & Bixley, 2011).

The second reason why permeability is important to improve the techno-economic feasibility of low-medium temperature geothermal systems is that permeability facilitates reservoir management by creating a sufficient injection capacity to provide reservoir pressure support and fluid replenishment. Therefore, the low-medium temperature geothermal resource can be sustainably extracted for a longer period and the downhole pump parasitic load can be minimized. As shown in Figure 32, as the reservoir pressure is depleted, the required pump energy to artificially discharge the well becomes higher, leading to a smaller well net power output. In this case, the IPR curve falls by not changing its slope since the reservoir deliverability decline is caused by reservoir pressure decline and the reservoir permeability and skin remain constant (constant PI value).

The binary geothermal power plant (GPP) system, as illustrated in Figure 33 (left), employs a closed-loop system at the surface to circulate the produced geothermal fluid. This system begins with hot brine being pumped from a production well to the surface, where it transfers heat to a secondary working fluid in a heat exchanger. The secondary fluid, typically an organic compound with a low boiling point, is vaporized and drives a binary turbine-generator to produce electricity. After passing through the turbine, the secondary fluid is condensed back into liquid form using an air-cooled condenser and recirculated back into the heat exchanger. Meanwhile, the cooled geothermal fluid is injected back into the reservoir through an injection well, ensuring that almost all of the produced fluid is reinjected, thereby minimizing environmental impact and sustaining the reservoir's pressure and thermal characteristics. Subsequently, Figure 33 (right) compares the fluid consumption per MW gross generated between low-medium temperature binary GPPs in the U.S. and high-temperature flash GPPs typically used in Indonesia. Binary GPPs, which operate at lower temperatures and utilize the binary cycle, consume a higher amount of geothermal fluid per MW gross generated compared to high-temperature flash GPPs. This difference underscores the importance of achieving sufficient injection capacity in binary GPPs through high permeability

reservoirs. High permeability ensures effective reinjection of geothermal fluids to maintain reservoir pressure and replenish the produced geothermal fluid.

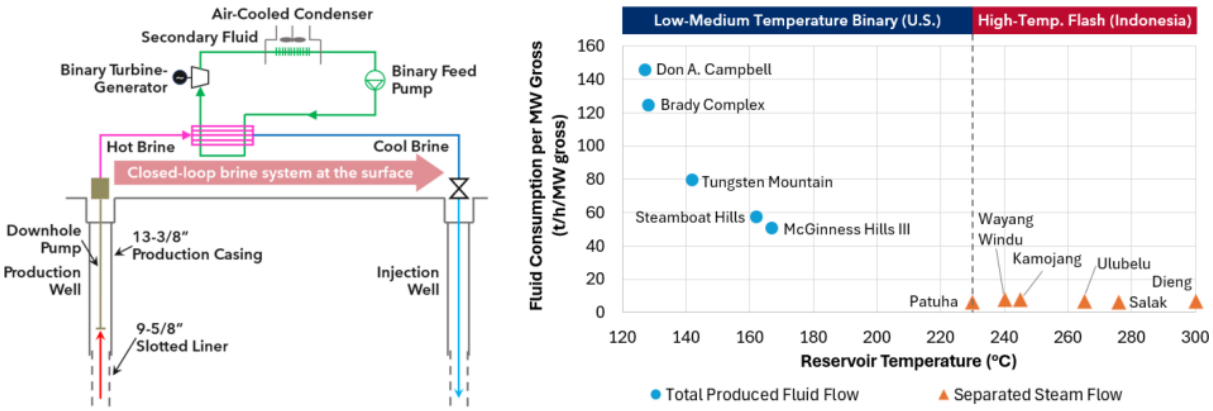

Figure 33: Binary Geothermal Plant with Pumped Well (Left); Comparison of Fluid Consumption of Geothermal Binary and Flash Plants (Right) (Ormat, 2022; NSA, 2020; Febrianto, et al., 2019).

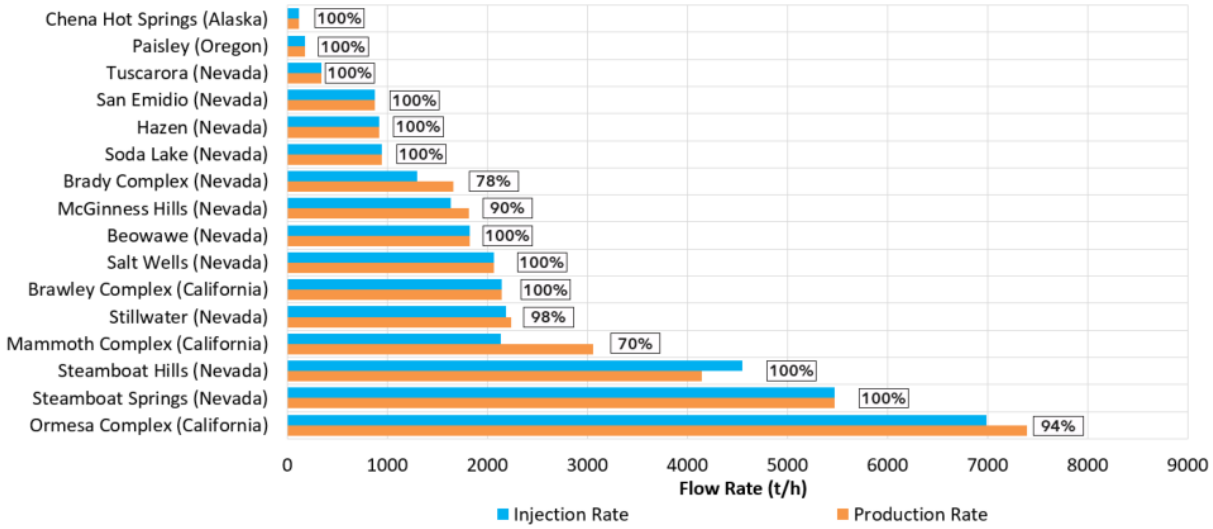

Figure 34: Injection-to-Production Flow Ratio in U.S. Low-Medium Temperature Geothermal Fields (Kamila, et al., 2021).

Furthermore, Figure 34 shows the ratio between the reinjected and produced geothermal fluid flow rates, denoted as the I/P ratio, for low-medium temperature geothermal fields in the U.S. According to (Kamila, et al., 2021), for low-medium temperature geothermal systems, maintaining a full reinjection or 100% I/P ratio is crucial for effective reservoir management by providing an adequate pressure support and fluid replenishment. This is evident as most of the low-medium temperature geothermal fields in the U.S., such as Brady Complex, McGinness Hills, and Steamboat Springs, achieve full reinjection (100% I/P ratio) due to the closed-loop system used in binary geothermal power plants (GPP). These systems ensure that the produced geothermal fluid is circulated and reinjected back into the reservoir, thereby sustaining reservoir pressure and preventing depletion. Therefore, achieving high permeability allows for a sufficient injection capacity to reinject 100% of the produced fluid, which is critical in preventing reservoir pressure decline and ensuring the continuous productivity of the geothermal system.

Injectivity index (II) is a measure of permeability that informs how much fluid flow rate that the well can accept at the given pressure differences between the reservoir pressure and the downhole pressure during injection expressed in t/h/bar (Luo, et al., 2023; Zarrouk & McLean, 2019). The II value can indicate the permeability of whether the geothermal well can be commercially utilized either as an injection well or a production well. The following II value classification can be used to evaluate the potential productivity of the well (Zarrouk & McLean, 2019)

1. **Poor (sub-commercial) producer**: < 5 t/h/bar injectivity.
2. **Moderate producer**: 5-50 t/h/bar injectivity.

3. **Excellent producer**: > 50 t/h/bar injectivity.

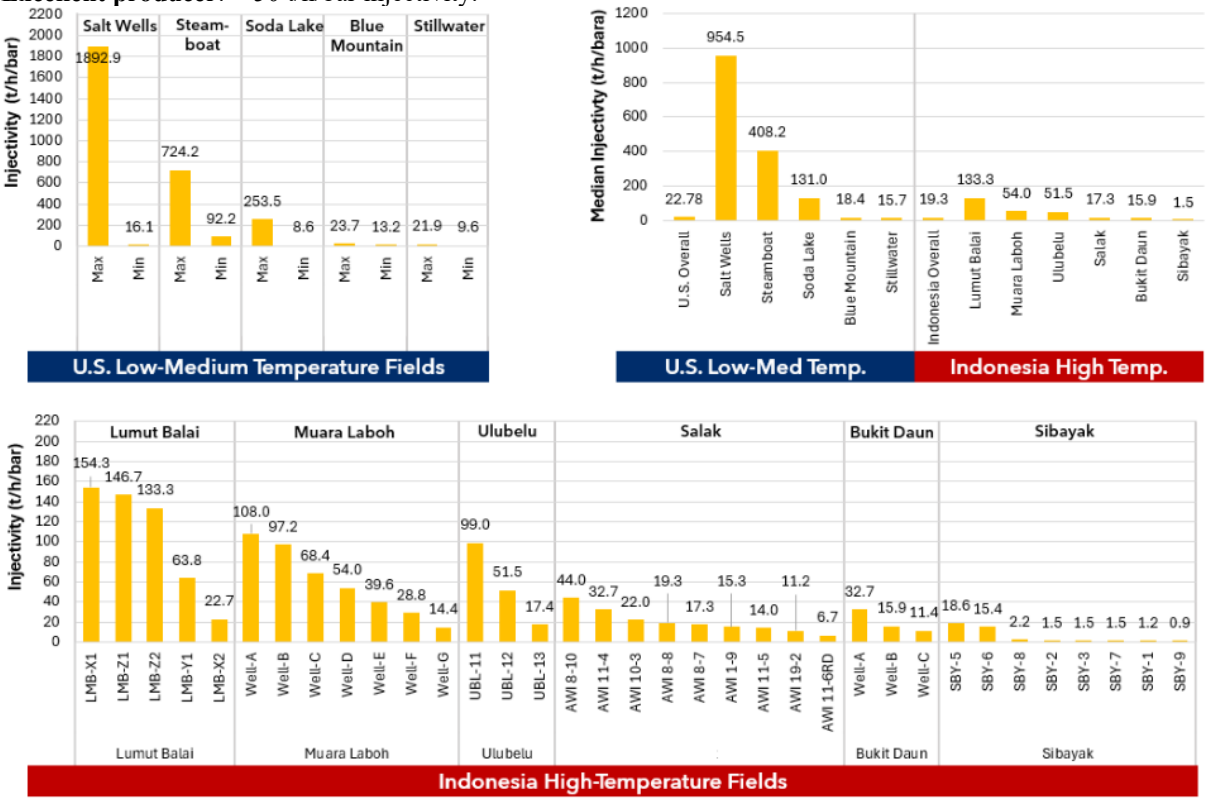

4.

5. **Figure 35: Permeability Comparisons Between Geothermal Fields in U.S. and Indonesia (Firanda, et al., 2024; Ikhwan, et al., 2021; Ikhwan, 2020; Mines, 2016; Mubarok & Zarrouk, 2016; Firanda, et al., 2015; Satya, et al., 2015; Rejeki, et al., 2010).**

Figure 35 compares the injectivity indices of geothermal fields in the U.S. and Indonesia. The injectivity index is significantly higher in U.S. low-medium temperature fields, such as Salt Wells and Steamboat, with maximum values reaching 1892.9 t/hr/bar and 724.2 t/hr/bar, respectively. In contrast, Indonesian high-temperature fields, like Lumut Balai and Muara Laboh, have much lower injectivity indices, with maximum values of 154.3 t/hr/bar and 108 t/hr/bar, respectively. This disparity in permeability is largely due to geological differences between the regions. The U.S. geothermal fields are often located in extensional tectonic settings, such as the Basin and Range province, where tectonic activity creates significant open fractures that enhance fluid flow (Ikhwan, et al., 2021). In contrast, Indonesian geothermal fields are primarily situated in compressional tectonic settings associated with subduction zones.

This geological environment tends to produce shear and strike-slip faults, which result in lower permeability compared to the extensional faults found in the U.S. The geological setting plays a critical role in determining the permeability of geothermal reservoirs. In the extensional regime of the U.S., tectonic activities create larger spatial displacements, leading to higher permeability magnitudes. Conversely, Indonesia's compressional regime results in more localized and less extensive faulting, limiting the permeability. This lower permeability in Indonesian geothermal fields poses challenges for an effective fluid reinjection for reservoir management and for an efficient artificial lift using the downhole pump.

Should the drilling fails to encounter sufficient permeability, one way to improve natural permeability is by creating man-made fractures through well permeability stimulation techniques, known as Enhanced Geothermal Systems (EGS). EGS span a range of resources, from low-permeability resources at existing conventional hydrothermal sites, known as "in-field" resources, to untapped, undeveloped deep (standalone) resources, as shown in Figure 36. The development and deployment of EGS technologies are expected to proceed in stages along this spectrum. Initially, EGS development will likely focus on in-field resources, converting sub-commercial wells into productive assets by applying EGS technologies, which create connections to productive conventional reservoirs and enhance heat recovery, reducing drilling costs and risks. The geothermal industry has experimented with in-field EGS with varying degrees of success, notably through innovative well stimulation and other improved EGS technologies. The U.S. Department of Energy's funded in-field EGS projects at low-medium temperature geothermal fields, such as Desert Peak, Brady's Hot Springs, Raft River, as well as commercial successes like Soda Lake, highlight the potential for further EGS improvements.

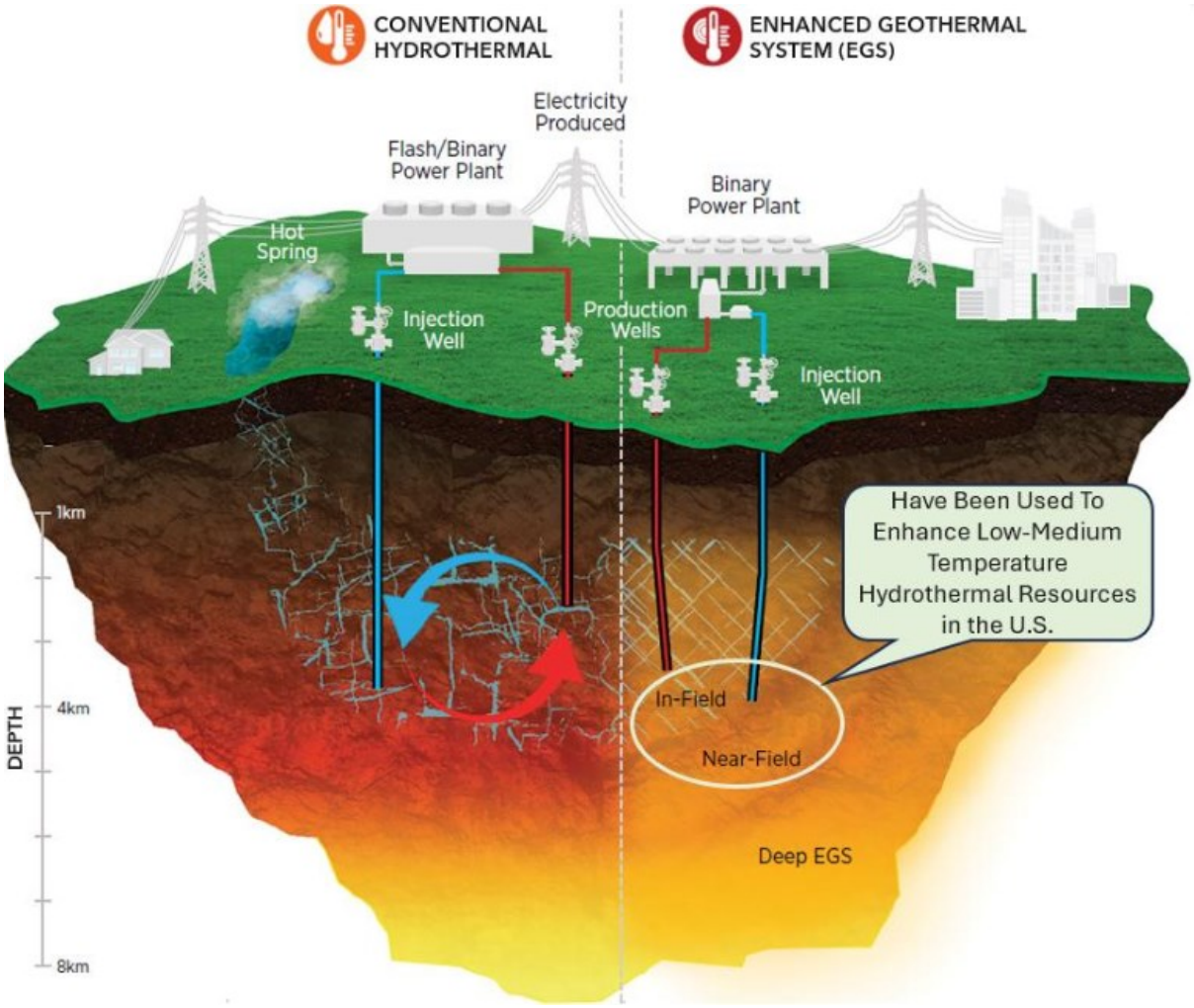

Figure 36: Types of Enhanced Geothermal Systems (U.S. DOE, 2019).

Once reliable in-field EGS resource capture is achieved, the next stage involves near-field EGS, targeting hot zones adjacent to conventional geothermal resources. These areas, typically hot due to nearby thermal anomalies but lacking permeability and fracture networks, can benefit from advanced EGS technology, expanding resource utilization beyond in-field environments and leveraging existing power-generating infrastructure. The final stage in EGS development focuses on deep standalone EGS resources. The progression from in-field to near-field to deep standalone EGS demonstrates a strategic approach to geothermal resource development, each stage building on the technological advancements and successes of the previous one. Table 8 summarizes the comparisons between in-field, near-field, and deep (standalone) EGS types.

Table 8: Comparison Between In-Field, Near-Field, and Deep (Standalone) EGS.

EGS Type	Description	Field/Project Example	Maturity
In-field	Creating permeability connections from sub-economic production or injection wells to a hydrothermal reservoir, thus enhancing heat sweep (for production wells) or pressure maintenance & fluid replenishment (for injection wells) from additional resource volumes.	**Low-medium temperature fields:** • Raft River, Idaho (Bradford, et al., 2015) • Soda Lake, Nevada (Lovekin, et al., 2017) **High-temperature fields:** n/a	Commercial
Near-field	Creating permeability connections between a hydrothermal reservoir and the low permeability yet hot & relatively well-characterized rock zones located in the margins of that hydrothermal reservoir.	**Low-medium temperature fields:** • Desert Peak, Nevada (Chabora, et al., 2012) • Brady's, Nevada (Drakos & Akerley, 2015) **High-temperature fields:** • Northwest Geysers, California (Garcia, et al., 2016)	Pilot
Deep (standalone)	Creating permeability and fluid circulation within hot dry rocks lacking natural permeability and reservoir fluid.	• Fervo Energy & Google, Nevada (Jiang, et al., 2023) • FORGE, Utah (Jiang, et al., 2023)	Pilot

The well stimulation techniques used for EGS are originally developed for the petroleum industry and have been adapted for geothermal applications as cost-effective alternatives to drilling new wells or re-drilling existing ones (Song, et al., 2023; Aqui & Zarrouk, 2011). In the petroleum sector, stimulation techniques have been utilized for over a century, primarily to enhance the economic viability of hydrocarbon resources by increasing the rate at which formations can deliver hydrocarbons (Gong, et al., 2023). Similarly, in geothermal applications, These techniques aim to enhance the connectivity between the wellbore and the natural fractures or faults within the reservoir, thereby improving the energy extraction efficiency, or creating a man-made reservoir in a hot dry rock lacking natural fractures or faults as a fluid flow pathway. Techniques such as hydraulic fracturing, acid fracturing, and thermal fracturing are the most commonly used to achieve these objectives besides the other techniques (Sharmin, et al., 2023; Li, et al., 2022). The available well stimulation techniques that can be used for EGS are as follows:

1. **Hydraulic fracturing**: it is used to create long, open, conductive fractures that extend deeper into the formation beyond the wellbore by applying hydraulic pressure to the rock formation until it surpasses the fracture breakdown pressure (Luo, et al., 2023; Aqui & Zarrouk, 2011). After the release of the hydraulic fracture, the fracture conductivity is maintained by either the proppant materials in the fracturing fluid, hydro-propping through a maintained injection above the fracture closure pressure, or the self-propping mechanism caused fracture surface roughness as a result of the shearing forces caused by a continuous injection below the fracture closure pressure (Lei, et al., 2023; Li, et al., 2021).
2. **Acid fracturing**: it is similar to hydraulic fracturing, sharing the same purpose of stimulating undamaged formations but by injecting acid at pressures higher than the formation fracture pressure to create or enhance fractures (Luo, et al., 2023; Aqui & Zarrouk, 2011). Its primary difference with the hydraulic fracturing is in the method of fracture creation and maintenance. To create fractures, acid fracturing relies on the dissolution and etching process performed above the formation fracture pressure. Meanwhile, to maintain fracture conductivity, it largely depends on the roughness formed on the fracture surfaces due to the etching process (Chen, et al., 2023; Deng, et al., 2022).
3. **Thermal fracturing**: it is a variation of hydraulic fracturing that, instead of using high hydraulic pressure to break the rock, uses cold fluid injection into the hot rock formation, causing thermal contraction and thus creating new fractures (Luo, et al., 2023; Peter-Borie, et al., 2019). The primary advantages of thermal fracturing over hydraulic or acid fracturing is the lower cost since the required pumping pressure is lower and it does not involve aggressive acid chemicals or chemically complex propped fracturing fluid. However, fracture closure is often a concern when designing a thermal fracturing treatment due to the restoration of thermal stress caused by the rock reheating after the well is put back into production since proppant is not utilized to maintain the fracture conductivity (Peter-Borie, et al., 2019). The mechanism of this reversible thermal contraction process is not fully understood yet the changes in rock strain seem to maintain the increased permeability (Li, et al., 2022; McLean, et al., 2016; Flores-Armenta & Alcalá, 2012).
4. **Shearing**: it involves injecting fluid at pressures lower than the minimum horizontal stress (Shmin) to reactivate or induce slip along existing fractures. This process does not create new fractures but rather reopens and allows movement along pre-existing fractures or faults (Mukuhira, et al., 2023). This technique is commonly used in scenarios where existing natural fractures can be reactivated to enhance fluid flow without creating new fractures (Bijay, et al., 2023; Luo, et al., 2023).
5. **Hydro-shearing**: it involves injecting fluid at pressures greater than the minimum horizontal stress (Shmin) to cause slip along existing fractures and potentially create new fractures (Li, et al., 2022). This process combines elements of both shearing and hydraulic fracturing, as it can activate existing fractures and also initiate new fractures. This technique can be used to reactivate existing fractures and create new fractures (Bijay & Ghazanfari, 2021).
6. **Deflagration (high energy gas fracturing)**: the near-wellbore formation damage is shattered and new small fractures are created using an intense gas wave generated by the vaporizing propellant, known as deflagration (Jiang, et al., 2023; McLean, et al., 2016; Aqui & Zarrouk, 2011).
7. **High-rate pulsed injection**: it involves the injection of fluid into the wellbore in rapid, high-pressure pulses rather than a continuous flow (Drakos & Akerley, 2015). The pulsed nature of the injection generates a series of pressure waves that propagate through the rock formation, creating or reactivating fractures (Zang, et al., 2024).
8. **Electric**: it employs electric current to stimulate the well, producing either electrothermal or electrodynamic effects. The electrothermal effect occurs in the near-wellbore zone, where heating with infrared, high frequency, or microwaves takes place. The electrodynamic effect cleans the bottom hole formation zone of clay particles, thereby restoring or enhancing the well's permeability (Ezzat, et al., 2022).
9. **Acoustic**: it utilizes a basic ultrasonic wave source, similar to those commonly used in everyday applications like descaling potable water filters or dental equipment. In geothermal applications, the

interaction between the acoustic field and the saturated porous rock can alter permeability or remove plugging materials (Covell, 2016).

Table 9: In-Field or Near-Field EGS Project Experience in the U.S. Low-Medium Temperature Geothermal Fields.

Parameter	Desert Peak, Nevada	Brady's Hot Springs, Nevada	Raft River, Idaho
Resource Information			
Average temperature	215°C	185°C	145°C
Temperature class	Medium-temperature	Low-temperature	Low-temperature
Developer	Ormat	Ormat	Ormat
Development history	**2007:** 26 MW (binary; online) **Total capacity in Dec 2023:** 26 MW	**1992:** 26.1 MW (double-flash; retired) **2018:** 21.5 MW (binary; online) **Total capacity in Dec 2023:** 21.5 MW	**2008:** 18 MW (binary; online) **Total capaciy in Dec 2023:** 18 MW
Well Stimulation Summary			
Project year	2010 – 2011	2013	2013 – 2014
EGS type	Near-field	Near-field	In-field
Stimulation technique	**Stage #1:** shearing **Stage #2:** matrix acidizing **Stage #3:** hydraulic fracturing	**Stage #1:** shearing **Stage #2:** hydro-shearing **Stage #3:** pulse injection	**Stage #1:** thermal fracturing **Stage #2:** hydraulic fracturing
Stimulation duration	**Stage #1:** 9 days **Stage #2:** 2.5 hours **Stage #3:** 24 days	**Stage #1:** 10 hours **Stage #2:** 9 hours **Stage #3:** 11 hours	**Stage #1:** 8 months **Stage #2:** 9 months
Initial injectivity	0.04 t/h/bar	0.15 t/h/bar	0.49 t/h/bar
Post-stimulation injectivity	**Stage #1:** 0.25 t/h/bar **Stage #2:** 0.07 t/h/bar **Stage #3:** 2.61 t/h/bar	**Stage #1:** 0.79 t/h/bar **Stage #2:** 1.48 t/h/bar **Stage #3:** 1.75 t/h/bar	**Stage #1:** 1.5 t/h/bar **Stage #2:** 5.52 t/h/bar
Post-stimulation commercial permeability as a producer well	Poor	Poor	Moderate
Literature source	(NREL, 2021; U.S. DOE, 2019; Zarrouk & McLean, 2019; ANL, 2014; Chabora, et al., 2012; USGS, 2008)	(NREL, 2021; U.S. DOE, 2019; Zarrouk & McLean, 2019; Drakos & Akerley, 2015; ANL, 2014; USGS, 2008)	(NREL, 2021; U.S. DOE, 2019; Zarrouk & McLean, 2019; Bradford, et al., 2015; ANL, 2014; USGS, 2008)

As the development of EGS continues to evolve, it is crucial to understand the practical applications and outcomes of various stimulation techniques in real-world scenarios. The following case studies provide insight into the in-field and near-field EGS project experiences within the U.S., particularly focusing on optimizing low-medium temperature fields, as summarized in Table 9. While the results summarized in Table 6 show that out of the three projects (Desert Peak, Brady's, and Raft River), only Raft River successfully achieved commercial permeability post-stimulation, all projects demonstrated significant improvements in injectivity and permeability. These outcomes highlight the potential for EGS techniques to optimize low-medium temperature resources and underscore the importance of the lessons learned from each project. The experiences gained from these projects offer valuable guidance for future EGS projects in both the low-medium and the high temperature geothermal fields.

3.3.1 Case Study #1: Desert Peak, Nevada (Hydraulic Stimulation)

Well 27-15 initially exhibited limited potential as a producer or injector, but its proximity to infrastructure, favorable bottomhole temperatures (180-195ºC), and demonstrated hydraulic connectivity to nearby injection wells made it a promising candidate for an EGS project (Akerley, et al., 2021). Located in the Desert Peak Geothermal Field in western Nevada and operated by Ormat Nevada Inc., this project received financial support from the U.S. Department of Energy's Geothermal Technologies Program (U.S. DOE, 2019). A multi-disciplinary team conducted a thorough investigation and identified the lower Tertiary Rhyolite unit (914-1,003 m deep) as the primary target for stimulation, as shown in Figure 37. The objectives of the EGS project were (Chabora, et al., 2012):

1. Develop and implement a site-specific EGS stimulation plan that showcases practical, cost-effective, and transferable techniques for other project settings.
2. Enhance hydraulic communication between well 27-15 and the existing production field to commercially acceptable levels.
3. Demonstrate the overall power plant production benefits achieved through this project.

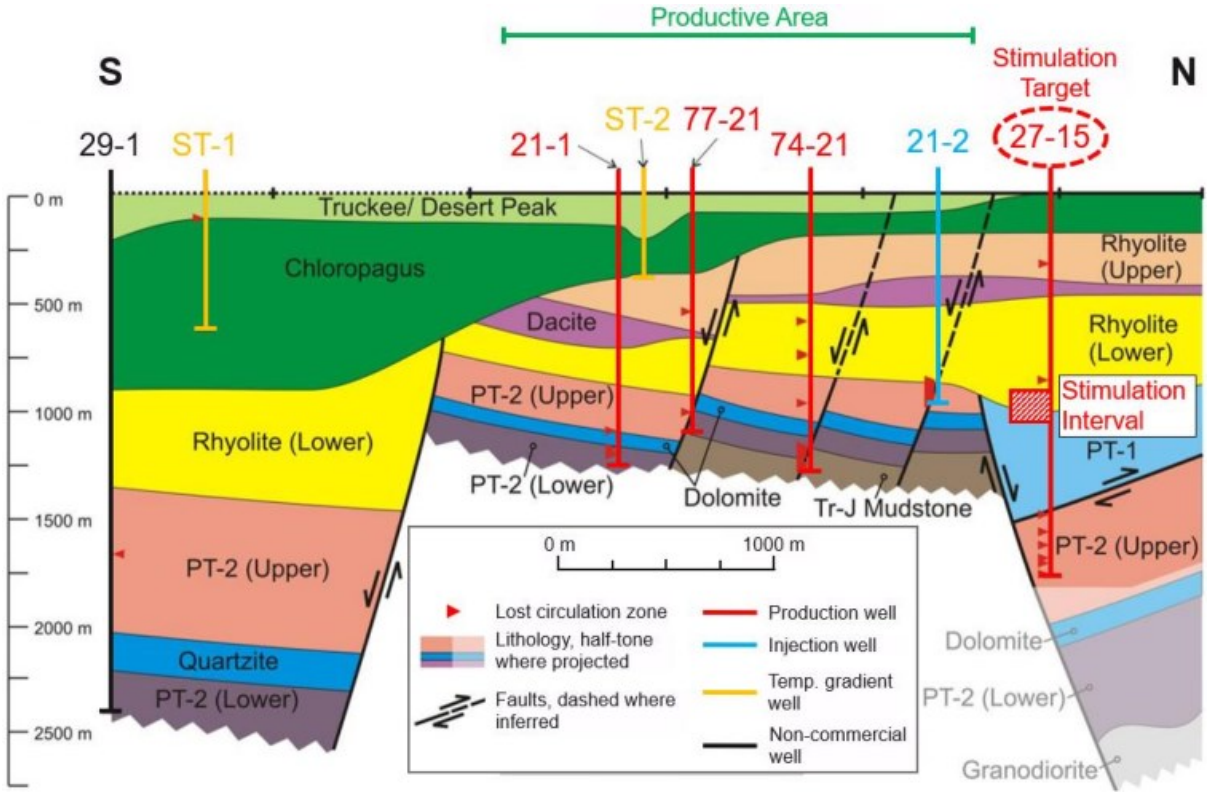

Figure 37: South-North Geological Cross Section Through Desert Peak Geothermal Field, Nevada and Well 27-15 as the Stimulation Target (Chabora, et al., 2012).

The well stimulation at Desert Peak involved a comprehensive multi-phase approach to enhance injectivity and permeability. This approach included shearing stimulation, matrix acidizing stimulation, and hydraulic fracturing, each contributing to the overall improvement of the well's performance. The operation and result of each stimulation stage (Akerley, et al., 2021; Chabora, et al., 2012) is summarized as follows:

1. **Stage #1 (shearing)**: this phase aimed to enhance permeability by promoting shear displacement along pre-existing fractures. This method involved low-pressure injection at fluid pressures below the least horizontal principal stress (Shmin). The initial injection pressures started at 17.2 bar (250 psi) and were incrementally increased by 6.9 bar (100 psi), reaching a maximum of 44.8 bar (650 psi). Each injection step lasted approximately one week, with pressure fall-off observations and Pressure-Temperature-Spinner (PTS) surveys conducted between steps. The results indicated a significant increase in injectivity, achieving approximately 0.79 t/h/bar (0.24 gpm/psi). However, this value was still below the threshold for commercial viability. The stimulation progress was primarily realized early in the process, suggesting that a shorter duration with higher pressures might have been equally effective and more efficient in terms of operational time and resources.
2. **Stage #2 (matrix acidizing)**: following the shearing phase, the chemical stimulation aimed to dissolve mineral precipitates and open partially sealed fractures to enhance injectivity. This phase consisted of a two-stage chemical treatment. In the first stage, 45,000 to 60,000 gallons of a 2-4% chelating acidic sodium sulfophthalate (SPA) solution were injected, followed by water displacement and a 48-hour reaction period. The second stage involved the injection of 12,000 gallons of a mixture of 12% hydrochloric acid (HCl) and 3% hydrofluoric acid (HF), followed by water displacement. The results showed temporary increases in injectivity to about 0.25 t/h/bar (0.076 gpm/psi), but the process led to wellbore instability. A subsequent wireline survey revealed that debris had filled the lower part of the well, necessitating a wellbore clean-out. This phase highlighted the need for controlled hydraulic fracturing to achieve more substantial and lasting permeability enhancements.
3. **Stage #3 (hydraulic fracturing)**: this final phase aimed to achieve substantial permeability improvements by injecting at high pressures and rates. This phase included two sub-phases: a medium flow-rate phase and a high flow-rate phase, as shown in Figure 38. During the medium flow-rate phase, the injection rate was fixed at 500 gpm using spent brine from the power plant. This resulted in an increase in injectivity to 1.86 t/h/bar (0.56 gpm/psi) and the detection of 33 microearthquake (MEQ) events (0.1-0.76 Mw). The high flow-rate phase saw the injection rate increase from 575 gpm to 725 gpm, achieving a maximum injectivity of 2.61 t/h/bar (0.79 gpm/psi), which is equivalent to a 60-fold

increase in injectivity from the pre-stimulation level, thus significantly enhancing the hydraulic connectivity between wells. The permanent gains in permeability were attributed to self-propping shear failure. Additionally, during the high injection rate phase, the gross output of the Desert Peak power plant temporarily increased by approximately 1.5 MW.

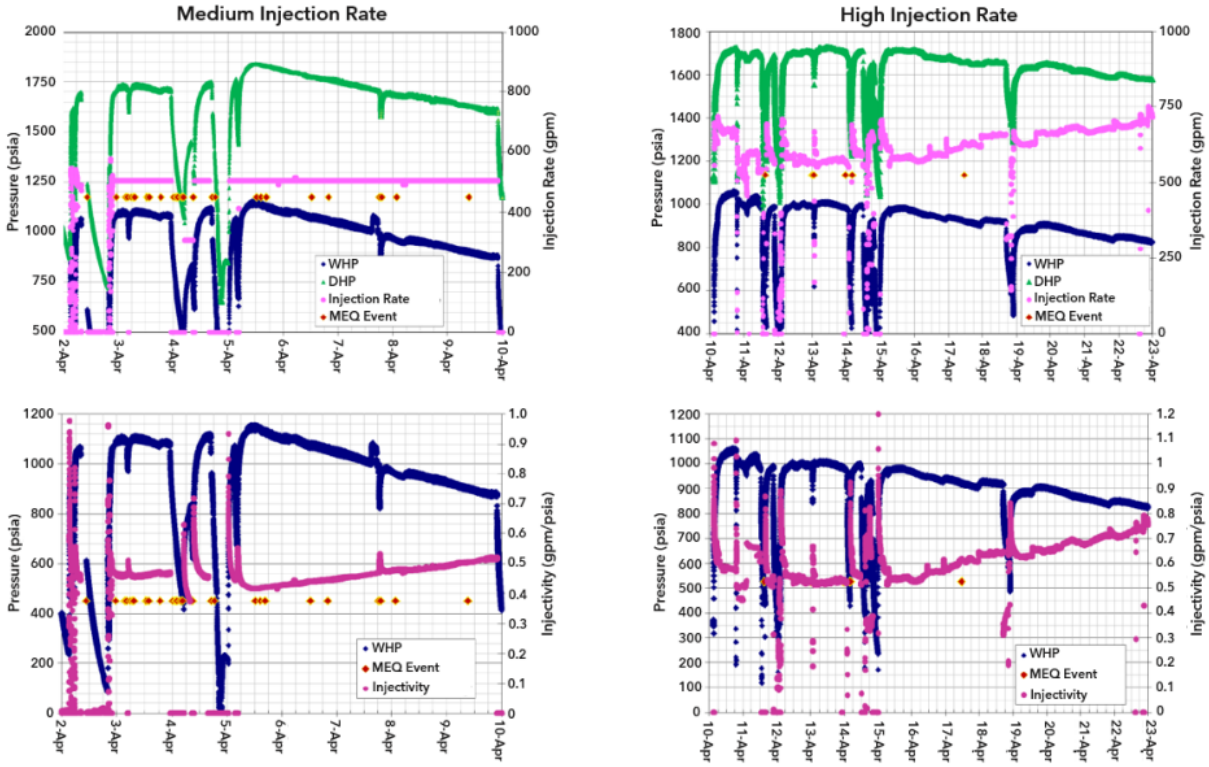

Figure 38: Measured Wellhead Pressure, Downhole Pressure, Injection Rate, Injectivity, and MEQ Events During the Medium (Left) and High (Right) Hydraulic Stimulation Injection Rates in the Desert Peak, Nevada (Chabora, et al., 2012).

These comprehensive well stimulation operations at Desert Peak collectively led to significant improvements in well injectivity and reservoir connectivity. Unfortunately, the post-stimulation permeability still fell short of the commercial permeability threshold of 5 t/h/bar. Nevertheles, the well stimulation at Desert Peak provided valuable insights and paved the way for future enhancements in geothermal stimulation projects.

3.3.2 Case Study #2: Brady's Hot Springs, Nevada (Shearing, Hydro-Shearing, and Pulsed Stimulation)

The Brady's geothermal field, situated approximately 50 kilometers northeast of Reno, Nevada, within the Hot Springs Mountains and Carson Sink, features a complex geological setting characterized by a Mesozoic metamorphic and plutonic basement overlaid with Cenozoic volcanic and sedimentary sequences. The primary geothermal reservoir, located between 600 and 1500 meters below the surface, lies within Oligocene ash-flow tuffs and Miocene lava flows (Akerley, et al., 2021). The Brady's Fault Zone, a prominent NNE-striking fault system, plays a crucial role in the field's geothermal activity, facilitating hydrothermal circulation. Well 15-12 ST1, which encountered high temperatures but low permeability, was selected for stimulation to enhance its hydraulic connectivity to more productive areas of the reservoir (Drakos & Akerley, 2015).

The 15-12 ST-1 well stimulation at Brady's involved a comprehensive multi-phase approach to enhance injectivity and permeability. This approach included shearing stimulation, hydro-shearing stimulation, and pulsed injection, each contributing to the overall improvement of the well's performance. The operation and result of each stimulation stage (Akerley, et al., 2021; Drakos & Akerley, 2015) is summarized as follows:

1. **Stage #1 (shearing)**: during this stimulation stage, the average injection rate was approximately 378 gpm, with an average injectivity of around 0.79 t/h/bar (0.24 gpm/psi). No microearthquakes (MEQs) were detected during this stage. The fall-off analysis showed that the closure pressure was uncertain, estimated at about 1058 psia, and the flow regime after closure was not certain.
2. **Stage #2 (hydro-shearing)**: during this stage, the maximum injection rate reached 650 gpm, with an average injectivity of approximately 1.48 t/h/bar (0.45 gpm/psi). Similar to Stage #1, no MEQs were detected. The fall-off analysis indicated an instantaneous shut-in pressure (ISIP) of around 935 psia

WHP. There were signs of pressure-dependent leak-off, which could be due to natural fractures or dilated fissures. The after-closure response suggested a radial flow pattern.

3. **Stage #3 (pulsed injection)**: this stage involved a maximum injection rate of about 1,100 gpm, with an average injectivity of around 1.75 t/h/bar (0.53 gpm/psi). As a result, an injectivity increase of 11-fold from the pre-stimulation level at 0.15 t/h/bar was achieved yet the commercial permeability threshold of 5 t/h/bar had not been met. Nevertheless, no MEQs were detected during this stage either. The fall-off analysis revealed a closure pressure of approximately 890 psia WHP, which was close to the minimum horizontal stress from the step-rate test. Similar to Stage #2, there were indications of pressure-dependent leak-off, likely from natural fractures or dilated fissures, and the after-closure response indicated radial flow.

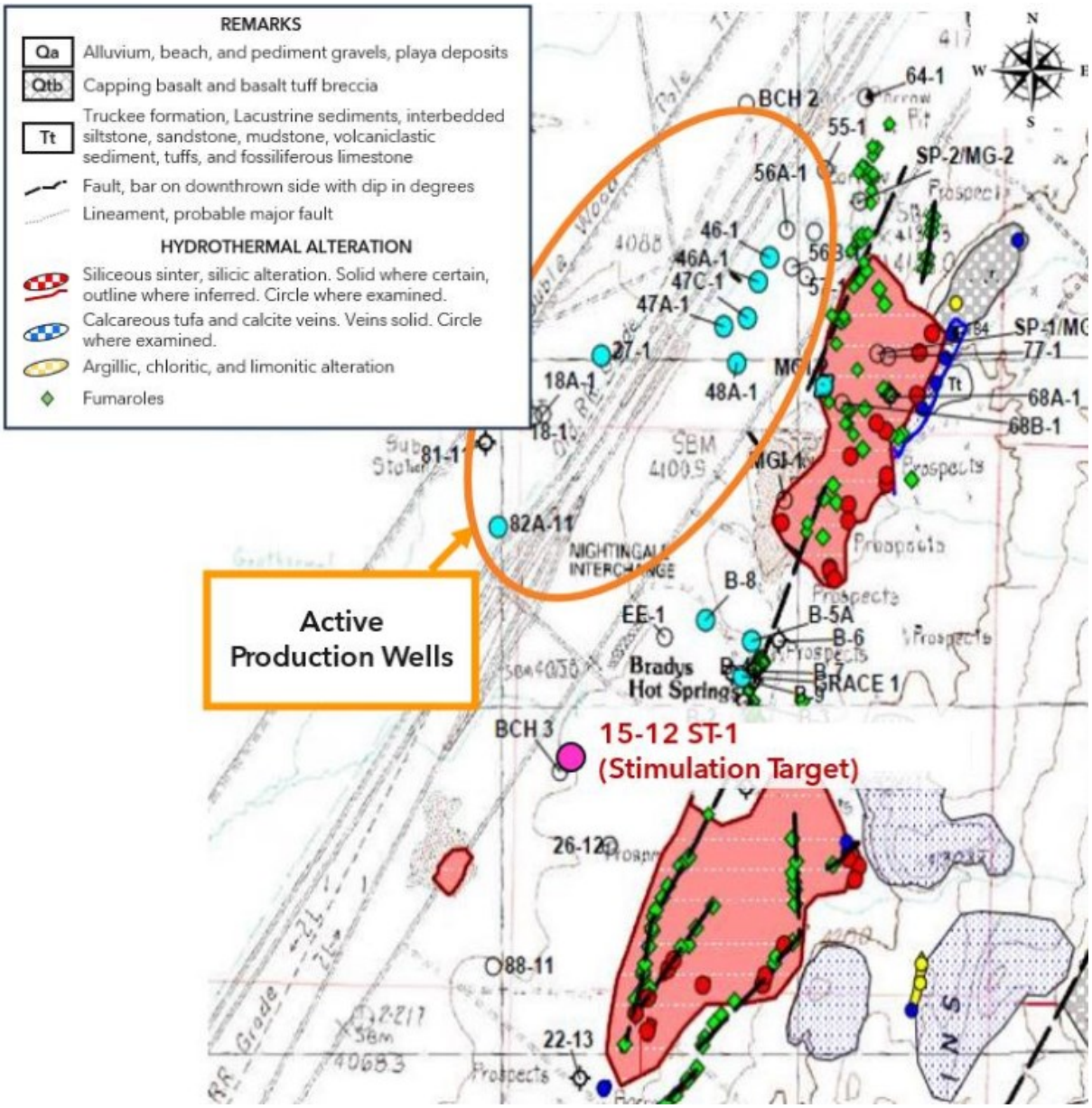

Figure 39: The Location of Well 15-12 ST-1 as the Stimulation Target in Brady's, Nevada (Drakos & Akerley, 2015).

3.3.3 Case Study #3: Raft River, Idaho (Thermal and Hydraulic Stimulation)

The Raft River geothermal field in Idaho is situated in a structurally complex terrain characterized by Cenozoic extension, Tertiary volcanism, and Precambrian rocks forming a metamorphic core complex. The field's geological setting includes approximately 1,524 meters of discontinuous Quaternary and Tertiary volcaniclastic and volcanic rocks overlying Precambrian basement rocks, primarily consisting of schist, quartzite, and quartz monzonite. The target formation for stimulation is the Elba Quartzite in the Precambrian basement, where fluid exits through a fracture zone at a depth of approximately 1,567 meters TVD. Well RRG-9 ST1 was selected for

stimulation due to its geologically strategic location within the Raft River field to target the Elba Quartzite formation effectively. From 2012 to 2014, this well underwent multiple stimulation campaigns, including hydraulic and thermal fracturing, with the main goals of developing and demonstrating practical, cost-effective EGS techniques and improving hydraulic communication between the well and the primary reservoir fracture networks. The location of RRG-9 ST1 in the field is shown in Figure 40.

The RRG-9 ST1 well stimulation at Raft River involved a combination of thermal and hydraulic fracturing techniques to enhance the permeability and injectivity of the geothermal reservoir. The operation and result of each stimulation stage (Xing, et al., 2024; Bradford, et al., 2015) is summarized as follows with the injectivity improvements is shown in Figure 41:

1. **Stage #1 (thermal fracturing)**: it began in June 2013 with low-rate stimulation using injectate from the geothermal plant at an average rate of 9.8 t/h (163 gpm), 34°C, and a wellhead pressure of 19.3 bar. This phase continued until late August 2013, at which point wellhead pressures were increased to 37.2 bar at an average rate of 32 t/h (534 Lpm). From September 12th to September 24th, 2013, cold water with an average surface temperature of approximately 12°C was injected to maximize thermal stress. This phase was followed by the resumption of warmer plant water injection on September 25th, 2013, which continued into 2014. The thermal fracturing managed to increase the well's injectivity from initially 0.49 t/h/bar (0.08 Lpm/kPa) to 1.5 t/h/bar (0.25 Lpm/kPa), equivalent to a 3-fold increase in injectivity.
2. **Stage #2 (hydraulic fracturing)**: it was conducted to further enhance permeability through high-pressure injection. This phase began in April 2014 by injecting cold water at 45°C at the rate of 71.76 t/h (1,196 Lpm) anf wellhead pressures of 17.93 bar. Furthermore, more than 20 microearthquakes (> 1 Mw) were recorded during the hydraulic fracturing phase. The modified Hall plot analysis showed that the hydraulic fracturing successfully increased fracture conductivity and/or a decreasing skin factor around the wellbore with the injectivity index rising significantly to 5.52 t/h/bara (0.9 Lpm/kPa) by December 2014, equivalent to an 11-fold increase in injectivity from the pre-stimulation level. The post-stimulation II has surpassed the commercial permeability threshold of 5 t/h/bar, hence can be utilized as a commercial production well.

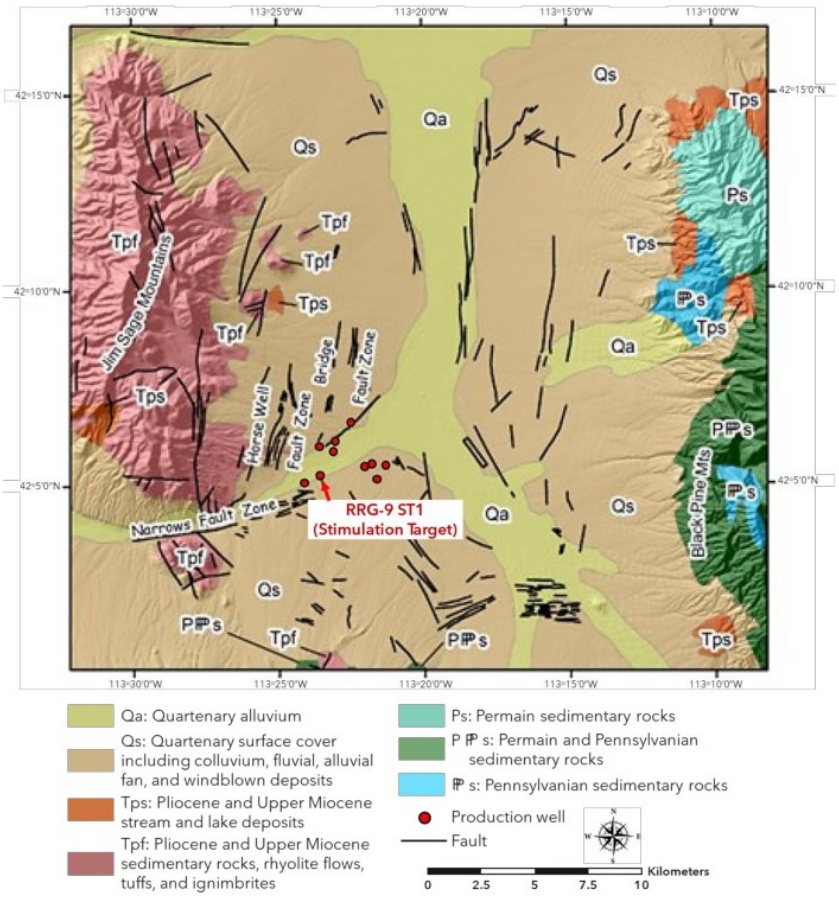

Figure 40: The Location of Well RRG-9 ST1 as the Stimulation Target in Raft River, Idaho (Bradford, et al., 2015).

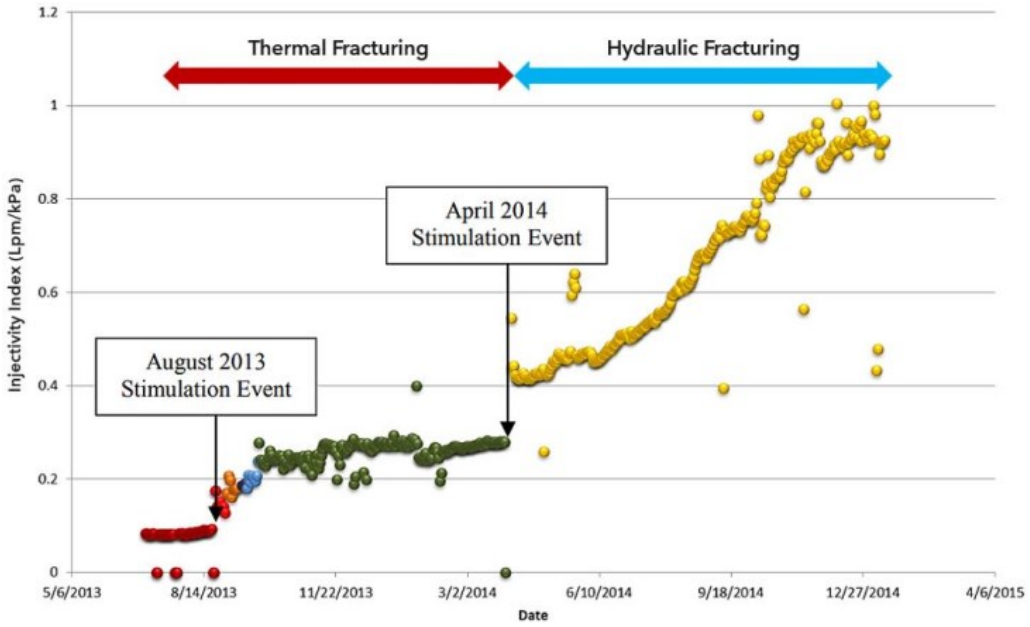

Figure 41: Injectivity Improvements During the Well Stimulation at Raft River, Idaho (Bradford, et al., 2015).

Table 10: Examples of Indonesia's In-Field EGS Project Experience in High-Temperature Geothermal Fields.

Resource Information						
Field	**Average Temperature**	**Temperature Class**	**Reservoir Mobile Fluid Phase**	**Developer**	**Developmernt History**	**Stimulation Year**
Salak, West Java (Golla, et al., 2020; EBTKE, 2020; Pasikki, et al., 2010)	240-312°C	High-temperature	Liquid-dominated	Chevron Geothermal (now Star Energy Geothermal)	**1994:** Unit 1 (60 MW) Unit 2 (60 MW) **1997:** Unit 3 (60 MW) **1997:** Unit 4 (65.6 MW) Unit 5 (65.6 MW) Unit 6 (65.6 MW) **Total capacity:** 376.8 MW	2004 – 2005
Wayang Windu, West Java (Mulyadi & Ashat, 2011)	280-300°C	High-temperature	Liquid-dominated	Chevron Geothermal (now Star Energy Geothermal)	**2000:** Unit 1 (100 MW) Unit 2 (117 MW) **Total capacity:** 227 MW	2007
Patuha, West Java (Ashat, et al., 2024)	230°C	High-temperature	Steam-dominated	Geo Dipa Enegi	**2014:** Unit 1 (55 MW) **Total capacity:** 55 MW	2022
Well Stimulation Summary						
Field	**Well**	**Technique**	**Stimulation Duration**	**Initial II (t/h/bar)**	**Post-Stimulation II (t/h/bar)**	**Post-Stimulation Commercial Permeability**
Salak, West Java (Golla, et al., 2020; Pasikki, et al., 2010)	AWI 11-5	**Stage #1:** Thermal fracturing **Stage #2:** Bullhead acidizing	**Stage #1:** 7 months **Stage #2:** 3 days	3.95	**Stage #1:** 14.45 **Stage #2:** n/a	Moderate
	AWI 11-6OH	**Stage #1:** Thermal fracturing **Stage #2:** Bullhead acidizing	**Stage #1:** 4 months **Stage #2:** 3 days	7.24	**Stage #1:** 14.45 **Stage #2:** 14.45	Moderate

	AWI 18-1	Hydraulic fracturing	13 months	2.96	7.95	Moderate
	AWI 20-1	Hydraulic fracturing	3 months	5.20	4.64	Poor
Field	**Well**	**Technique**	**Stimulation Duration**	**Initial Steam Prod. (t/h)**	**Post-Stimulation Steam Prod. (t/h)**	**Remarks**
Wayang Windu, West Java (Pizzocolo, et al., 2021; Mulyadi, 2010)	WWQ-2	Hydraulic fracturing	60 hours	14.4	28.9	✓ Open fracture ✓ Improved production ✓ Improved permeability
	WWQ-3	Hydraulic fracturing	n/a	n/a	n/a	✓ Open fracture X Improved production
	WWQ-4	Hydraulic fracturing	n/a	n/a	n/a	X Open fracture X Improved production
	WWA-2	Hydraulic fracturing	22 hours	14.4	21.8	✓ Open fracture ✓ Improved production ✓ Improved permeability
Field	**Well**	**Technique**	**Stimulation Duration**	**Initial Steam Prod. (t/h)**	**Post-Stimulation Steam Prod. (t/h)**	**Remarks**
Patuha, West Java (Lee, et al., 2023)	PPL-6	Hydraulic fracturing	22 hours	n/a	n/a	Injectivity test was not performed
	PPL-2	-	-	46.7	51.5	Affected by PPL-6 stimulation
	PPL-4	-	-	11.9	13.2	Affected by PPL-6 stimulation

Despite Indonesia not having optimally developed low-medium temperature resources like those in the U.S., the country has notable experience with EGS well stimulations in high-temperature geothermal fields. The application of EGS techniques s in Indonesia has been primarily focused on optimizing the productivity of these high-temperature resources. As summarized in Table 10, various well EGS stimulation techniques such as thermal fracturing and hydraulic fracturing have been employed with varying degrees of success across different geothermal fields. These efforts highlight Indonesia's potential to enhance geothermal production through EGS technologies, which can lay the foundational knowledge and provide lessons learned for future EGS applications in low-medium temperature geothermal fields.

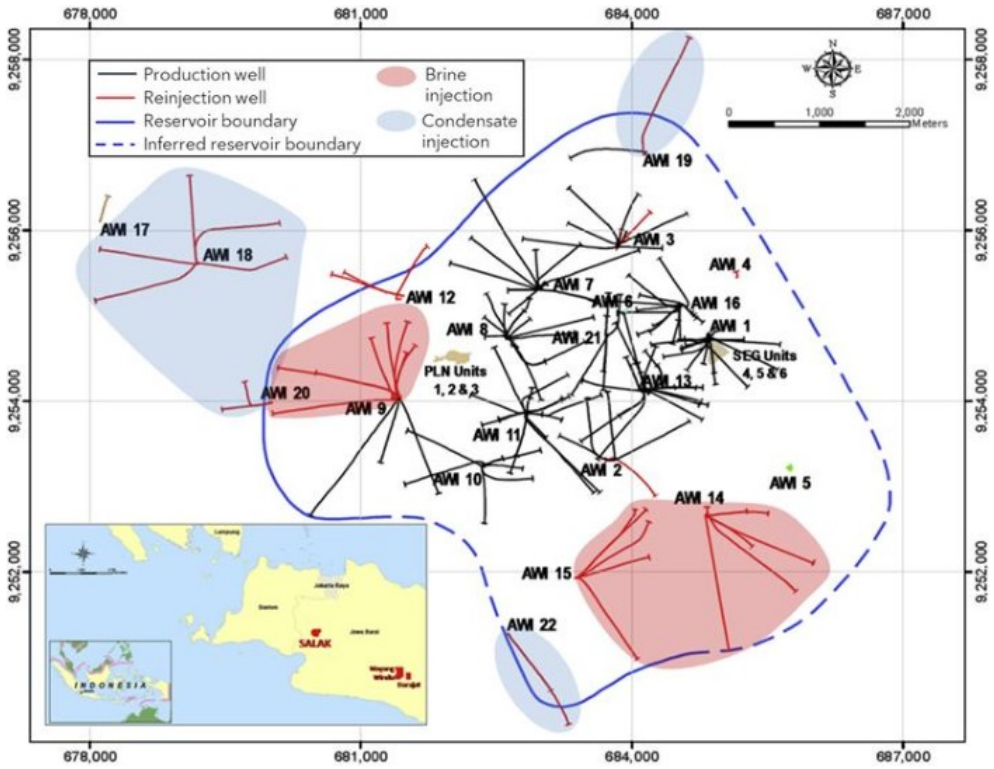

Figure 42: Well Trajectory at the Salak Geothermal Field, West Java (Golla, et al., 2020).

3.3.4 Indonesia's Experience #1: Salak, West Java (Thermal and Hydraulic Stimulation)

The Salak geothermal field is characterized by a high-temperature, water-dominated reservoir with temperatures exceeding 325°C and low-to-moderate non-condensable gas content (Stimac, et al., 2008). The reservoir is divided into four production cells (West, Central, East, and Far East) based on pressure measurements and the distribution of permeable zones identified in wells (Golla, et al., 2020). The primary fluid flow is controlled by northeast-trending surface and subsurface structures, contributing to the geothermal system's efficiency. Since the start of commercial production in 1994, the field has faced challenges such as injection breakthrough, wellbore scaling, and the influx of non-condensable gases, necessitating a series of well stimulation programs in 2005 to improve injectivity and sustain production levels (Pasikki, et al., 2010). Figure 42 shows the well trajectory within and around the reservoir boundary including the brine and condensate injection areas at the Salak geothermal field.

Two EGS wells stimulation techniques were impemented at the Salak geothermal field in 2005, namely thermal fracturing and hydraulic fracturing. The thermal fracturing was performed in addition to the subsequent bullhead acidizing at the AWI 11-15 and AWI 11-6OH wells. Meanwhile, the hydraulic fracturing was performed at the AWI 18-1 and AWI 20-1 wells. The II changes from those four wells due to the stimulations are displayed in Figure 43. Furthermore, the well stimulation operation and results at those wells (Pasikki, et al., 2010) are summarized as follows:

1. **AWI 11-5**: the well is first thermally stimulated by involving alternating injections of hot brine (165oC or 330°F) and cold condensate (38oC pr 100°F) at flow rates up to 892 t/h (2000 kph) for hot brine and 281 t/h (630 kph) for condensate. This was followed by a bullhead acid treatment using hydrochloric acid to address formation damage yet it failed to improve permeability due to low acid concentration and poor acid placement. The II increased from 3.95 t/h/bar (0.6 kph/psi) to 14.48 t/h/bar (2.2 kph/psi) over several cycles, indicating improved permeability. The injectivity improvement thus had met the commercial permeability threshold and the well was potential to be used as a production well.
2. **AWI 11-6OH**: similar to AWI 11-5, AWI 11-6OH first underwent thermal stimulation using hot brine and cold condensate. The II increased from 7.22 t/h/bar (1.1 kph/psi) to 14.45 t/h/bar (2.2 kph/psi) This process was followed by a slow acid stimulation (SAS) involving acidified cold water (HCl mixed with condensate) and later acidified hot water but it did not successfully improve the permeability further due to poor acid placement. Additionally, corrosion issues encountered during the acid treatment led to an early termination of the stimulation program.
3. **AWI 18-1**: the hydraulic stimulation at AWI 18-1 was conducted in two phases. The first phase involved continuous water injection using gravitational and positive displacement pumps, gradually increasing the injection rates. The second phase employed triplex pumps and a pressure cycling injection method. The injectivity significantly improved, with the II increasing by 180% from 2.96 t/h/bar (0.45 kph/psi) to 7.953 t/h/bar (1.21 kph/psi). Injection capacity increased tenfold, indicating successful stimulation and enhanced connectivity to fracture networks.
4. **AWI 20-1**: this multilateral well underwent hydraulic stimulation similar to AWI 18-1. Initial injectivity tests revealed low injectivities, leading to continuous and cycling injection operations with increasing condensate water rates. The post-stimulation II of 4.64 t/h/bar (0.7 kph/psi) was instead lower than the initial II of 5.2 t/h/bar (0.79 kph/psi). However, the injection flow rate at a given WHP was increased. Therefore, the improved injection performance was interpreted to be caused by the newly created connectivity to lower pressure fracture networks rather than enhanced permeability.

3.3.5 Indonesia's Experience #2: Wayang Windu, West Java (Hydraulic Stimulation)

The Wayang Windu geothermal field is characterized by a complex geological setting associated with the Sunda Volcanic Arc. The field features a transitional geothermal system with vapor-dominated and liquid-dominated zones, primarily hosted in andesitic volcanic rocks intruded by microdiorite-porphyry dikes (Mulyadi & Ashat, 2011). The northern part of the field, which provides over 90% of the steam production, consists of a vapor-dominated two-phase zone that overlies a deep liquid reservoir, as shown in Figure 44. In 2007, hydraulic fracturing was initiated as a well stimulation technique to address declining well productivity. This decision was informed by a micro earthquake (MEQ) survey conducted from May to July 2005, which provided detailed insights into the stress orientation and distribution within the field. The MEQ data indicated potential for hydraulic fracturing to enhance permeability and steam production by inducing fractures and improving fluid flow within the reservoir (Pizzocolo, et al., 2021; Mulyadi, 2010).

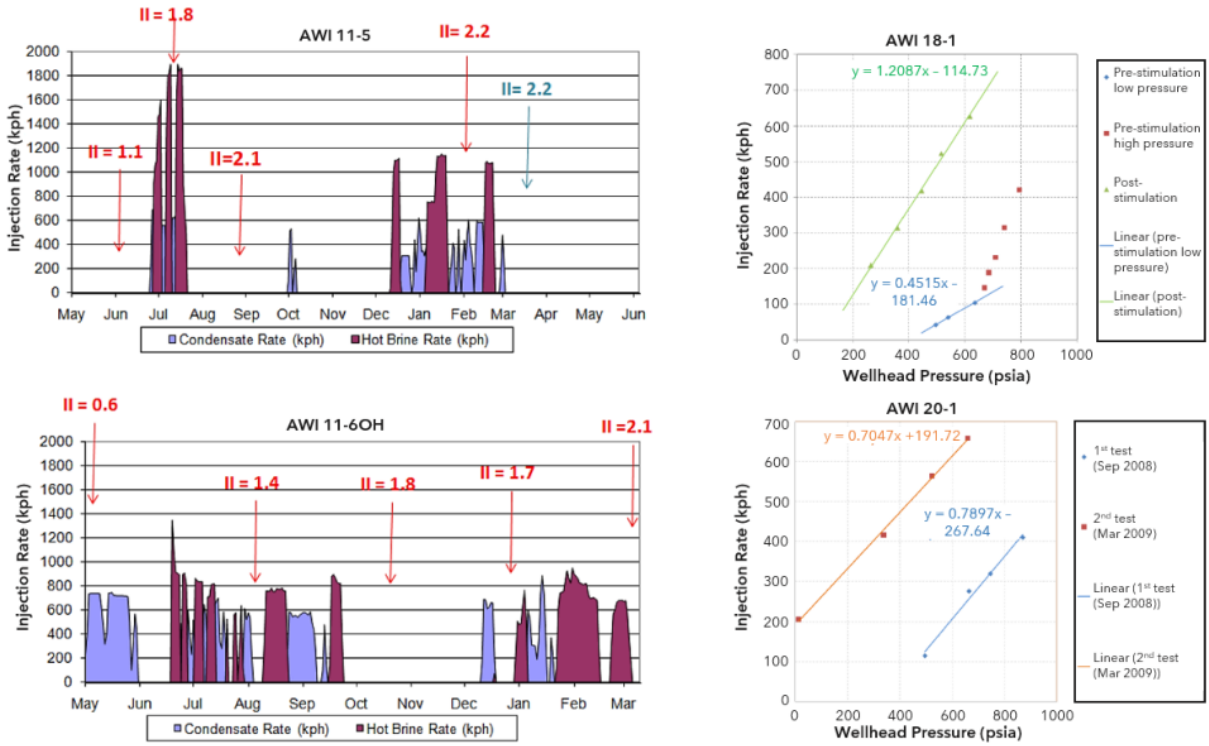

Figure 43: Injectivity Evolution During Thermal Fracturing (Left) and Hydraulic Fracturing (Right) at the Salak Geothermal Field, West Java (Pasikki, et al., 2010).

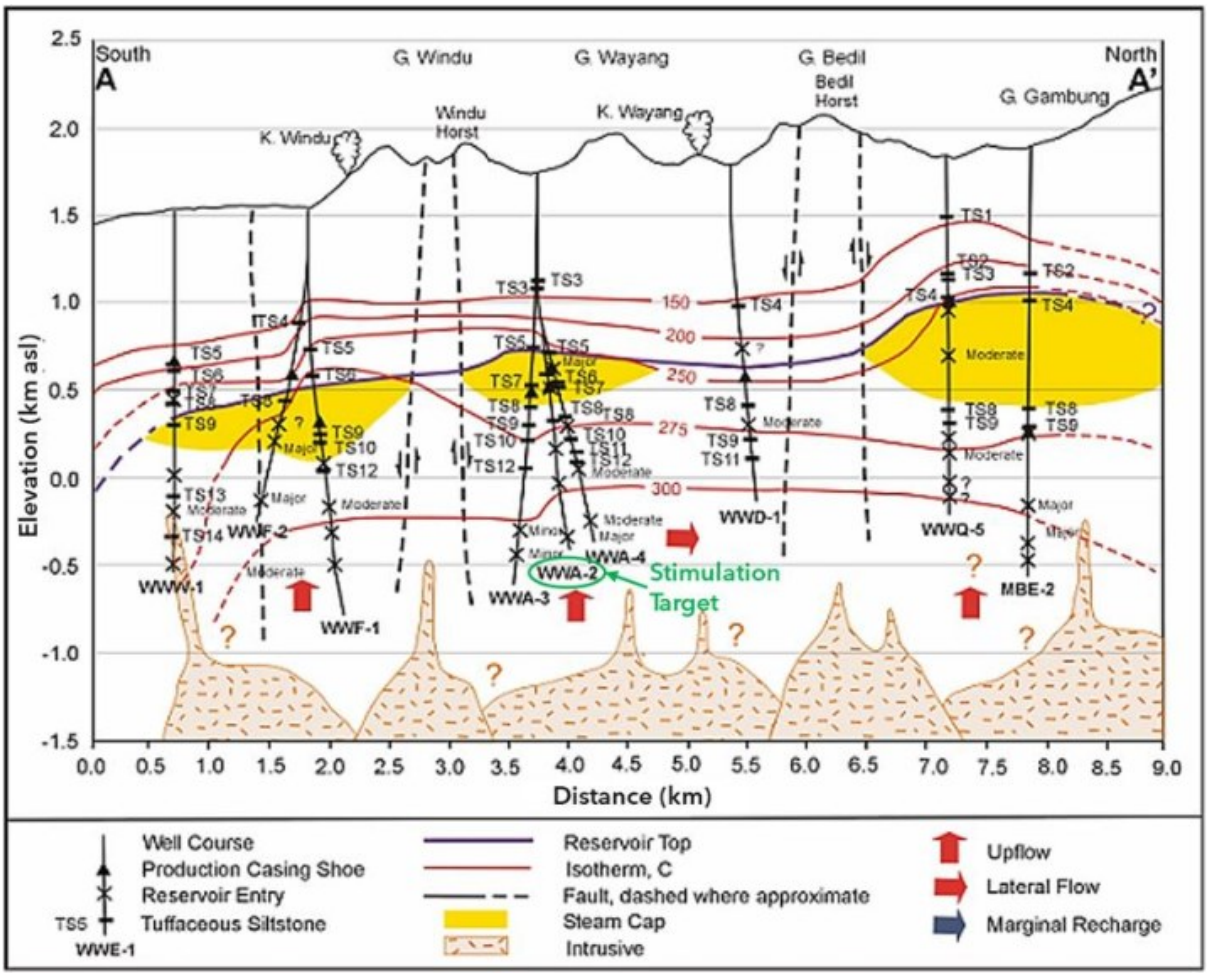

Figure 44: Conceptual Model of Wayang Windu Geothermal Field, West Java (Mulyadi & Ashat, 2011).

Four wells at Wayang Windu, namely WWQ-2, WWQ-3, WWQ-4, and WWA-2, were subjected to hydraulic fracturing techniques. The operations and results obtained from the hydraulic fracturing process applied to these wells, with a focus on their stimulation duration, initial and post-stimulation production, and specific observations (Mulyadi, 2010) are summarized as follows:

1. **WWQ-2**: hydraulic fracturing was performed at the WWQ-2 well with a stimulation duration of 60 hours. The bottomhole pressure (BHP) decreased from around 60 barg to a stable value after 3.5 hours, with fracture closure pressure observed at 47.6 barg during the fall-off test, as shown in Figure 45. The initial steam production was 14.4 t/h, which increased to 28.9 t/h post-stimulation, indicating a significant improvement in production and permeability. The well demonstrated an open fracture, which contributed to the increased productivity.
2. **WWQ-3**: the fracture closure pressure was noted at 51.2 barg after 1 hour during the fall-off test, as shown in Figure 45. Despite the presence of an open fracture, there was no observable improvement in production. This was attributed to the lower permeability of the well, which hindered the effectiveness of the hydraulic fracturing process.
3. **WWQ-4**: hydraulic fracturing failed to create an open fracture, and there were no improvements in production. The lack of fracture creation was due to the inability of the maximum injection rate to exceed the rock stress magnitude required for fracture initiation.
4. **WWA-2**: the hydraulic fracturing involved a stimulation duration of 22 hours. The initial steam production was 14.4 t/h, which increased to 21.8 t/h post-stimulation. The bottomhole pressure profile indicated successful fracture creation with improved permeability and production. The well showed an open fracture and demonstrated significant improvement in both production and permeability, similar to WWQ-2.

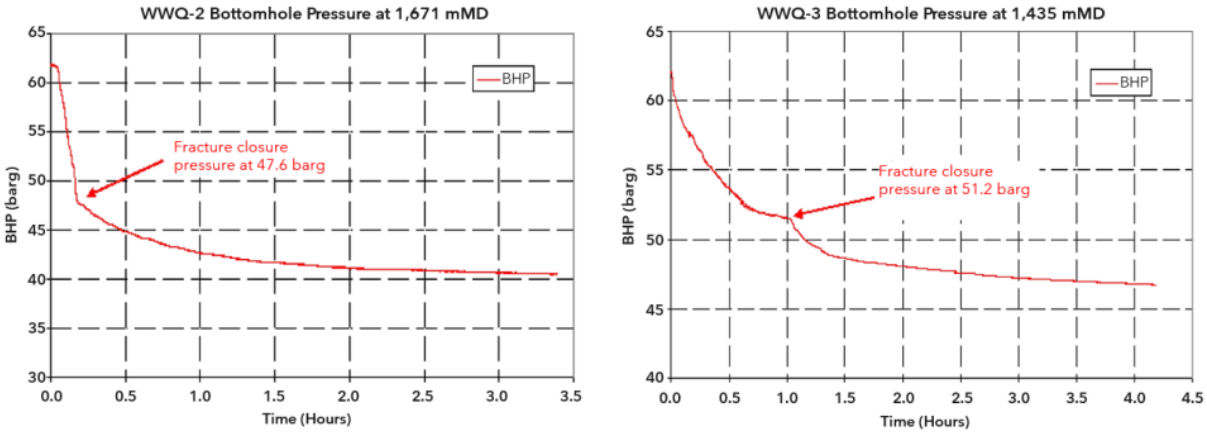

Figure 45: Bottomhole Pressure During the Fall-Off Test at WWQ-2 (Left) and WWQ-3 (Right) After Hydraulic Fracturing (Mulyadi, 2010).

The hydraulic fracturing operations at the Wayang Windu field yielded mixed results. Wells WWQ-2 and WWA-2 showed significant improvements in production and permeability due to the successful creation of open fractures. The fracture closure pressures observed at these wells were within the expected range, leading to enhanced steam production post-stimulation. However, wells WWQ-3 and WWQ-4 did not exhibit similar improvements. WWQ-3, despite having an open fracture, did not see production gains due to its lower permeability. WWQ-4 failed to create an open fracture, resulting in no improvement in production.

The study by (Pizzocolo, et al., 2021) further corroborates these mixed results by highlighting the technical and geological challenges associated with hydraulic fracturing in the Wayang Windu field. The long perforated liner and the dense natural fracture network in the wells pose significant obstacles to effective hydraulic fracturing. The study concludes that the Wayang Windu field is not suitable for hydraulic fracturing due to the following reasons:

1. **Long perforated liner**: the wells in the Wayang Windu field have long perforated liners, making it difficult to isolate short sections necessary for fracture location optimizations..
2. **High fluid leakoff rates**: the dense natural fracture network in the geothermal reservoir leads to high fluid leakoff rates, reducing the effectiveness of the hydraulic fracturing treatment. Hydraulic fracturing in Wayang Windu is also economically unviable due to he large volumes of fracture fluids and proppant required due to the high leakoff rates.
3. **Wellbore integrity issue**: significant variations in stress along the perforated sections increase the risk of wellbore integrity issues, such as plastic buckling and shear failure. Moreover, the absence of a

cemented annulus in the wells increases the likelihood of compromising wellbore integrity during hydraulic fracturing operations.

4. **Undesired fracture propagation pattern**: the induced fractures tend to propagate vertically to the clay cap zone, failing to penetrate the deeper parts of the reservoir that are crucial for improving connectivity with pre-existing fractures.

These factors compromise the economic feasibility and technical effectiveness of hydraulic fracturing, suggesting that alternative stimulation techniques, such as thermal and acid stimulations, may be more appropriate for this geothermal field.

3.3.6 Indonesia's Experience #3: Patuha, West Java (Hydraulic Stimulation)

The Patuha geothermal field is a volcano-hosted vapor-dominated geothermal system located in West Java, Indonesia, with high-temperature reservoirs ranging from 220°C to 260°C. The Patuha field's geological setting is influenced by the nearby volcanic activity of Mt. Patuha and other local volcanic structures such as Mt. Urug and Crater Putih. Surface manifestations like fumaroles and hot springs are indicative of the geothermal activity beneath (Ashat, et al., 2024). In the field, a geothermal power plant with an installed capacity of 55 MW was commissioned in 2014. However, the field has faced challenges such as declining steam production, prompting the need for well stimulation techniques like hydraulic fracturing to enhance permeability and sustain energy output (Lee, et al., 2023). Therefore, in 2022, a hydraulic stimulation was attempted at PPL-6, which eventually improved the productivity of the two nearby wells, namely PPL-2 and PPL-4, as shown in Figure 46.

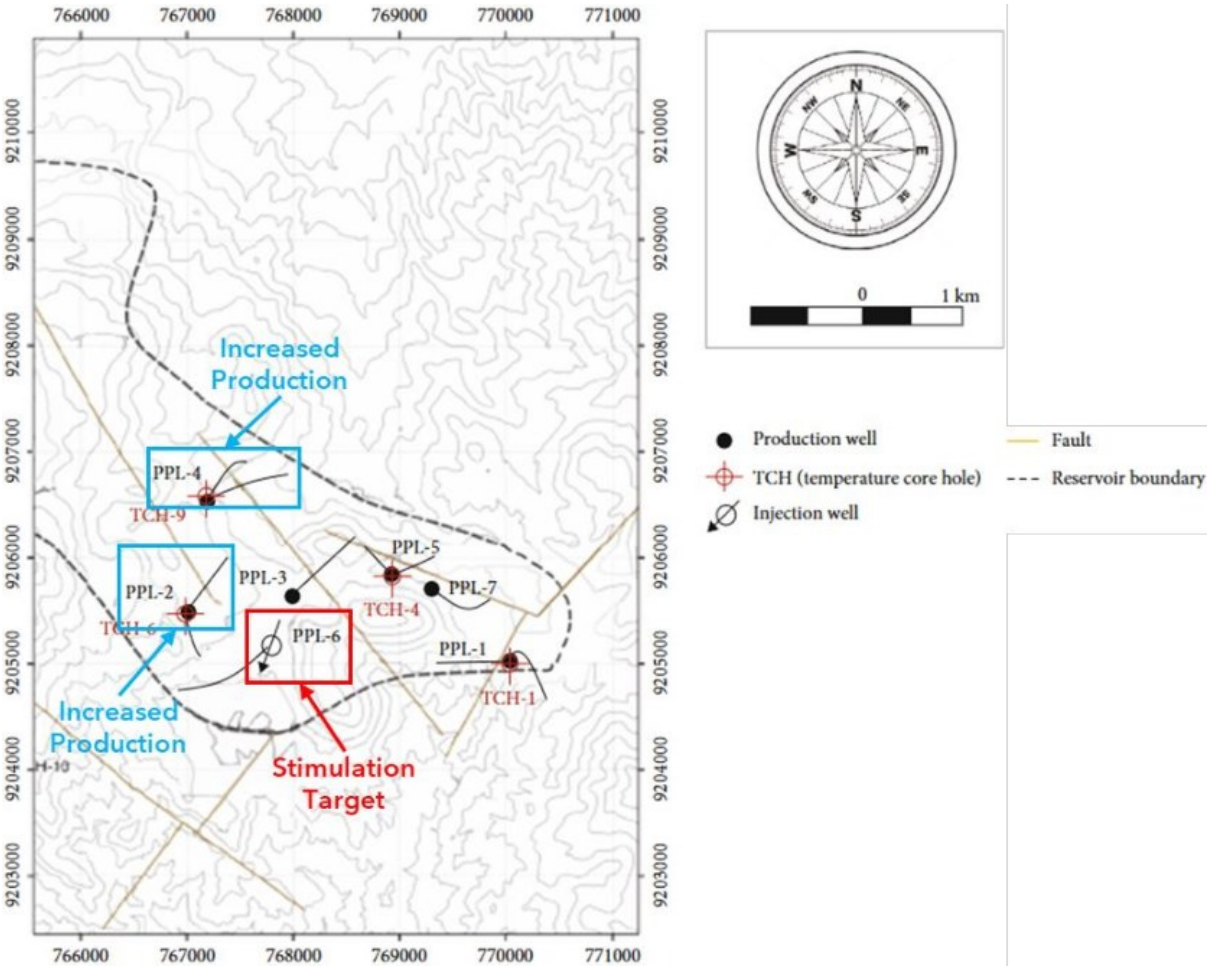

Figure 46: Well Trajectory and the Stimulated Wells at the Patuha Geothermal Field, West Java (Lee, et al., 2023).

The hydraulic fracturing process at PPL-6 involved the injection of 40,000 barrels of water through three distinct injection rate stages: step-up, plateau, and step-down. This operation was carefully monitored to assess its impact on reservoir pressure, temperature, and overall steam productivity. The measured injection rate and bottomhole pressure during each injection stage is shown in Figure 47. Furthermore, the observed injection behavior during each injections stage (Lee, et al., 2023) is summarized as follows:

1. **Step-up injection rate**: the water injection rate was gradually increased over a period of approximately 3.3 hours. The injection began at 3.18 m³/min (20 bbl/min) for the first 55 minutes, increased to 3.66 m³/min (23 bbl/min) for the next 90 minutes, and then to 4.93 m³/min (31 bbl/min) for the final 55 minutes. This phase was designed to carefully raise the bottom hole pressure and initiate fracture opening. The pressure response showed an initial sharp increase, indicating good permeability in the well, which accepted the injected water efficiently.
2. **Plateau constant rate injection**: water was injected at a constant rate of 4.13 m³/min (26 bbl/min) for 15 hours. During this period, the bottom hole pressure stabilized around 5.52 bar, with minor fluctuations, suggesting the reservoir's capacity to handle the sustained injection without significant disruption. The temperature profile indicated a slight decrease due to the cooler injected water, remaining below the saturation temperature, which was ideal for maintaining the liquid phase of the reservoir fluids.
3. **Step-down injection rate**: it involved gradually reducing the injection rate over 3.7 hours. The rates were decreased to 3.66 m³/min, 3.18 m³/min, 2.39 m³/min, 1.59 m³/min, and finally to 0.80 m³/min before stopping. This phase aimed to control the reactivation of steam inflow and prevent premature well reactivation. During this stage, fluctuations in pressure and temperature indicated phase changes as the steam and water mixed. The process required careful management to maintain stability and prevent excessive steam flow during the reduction of injection rates.

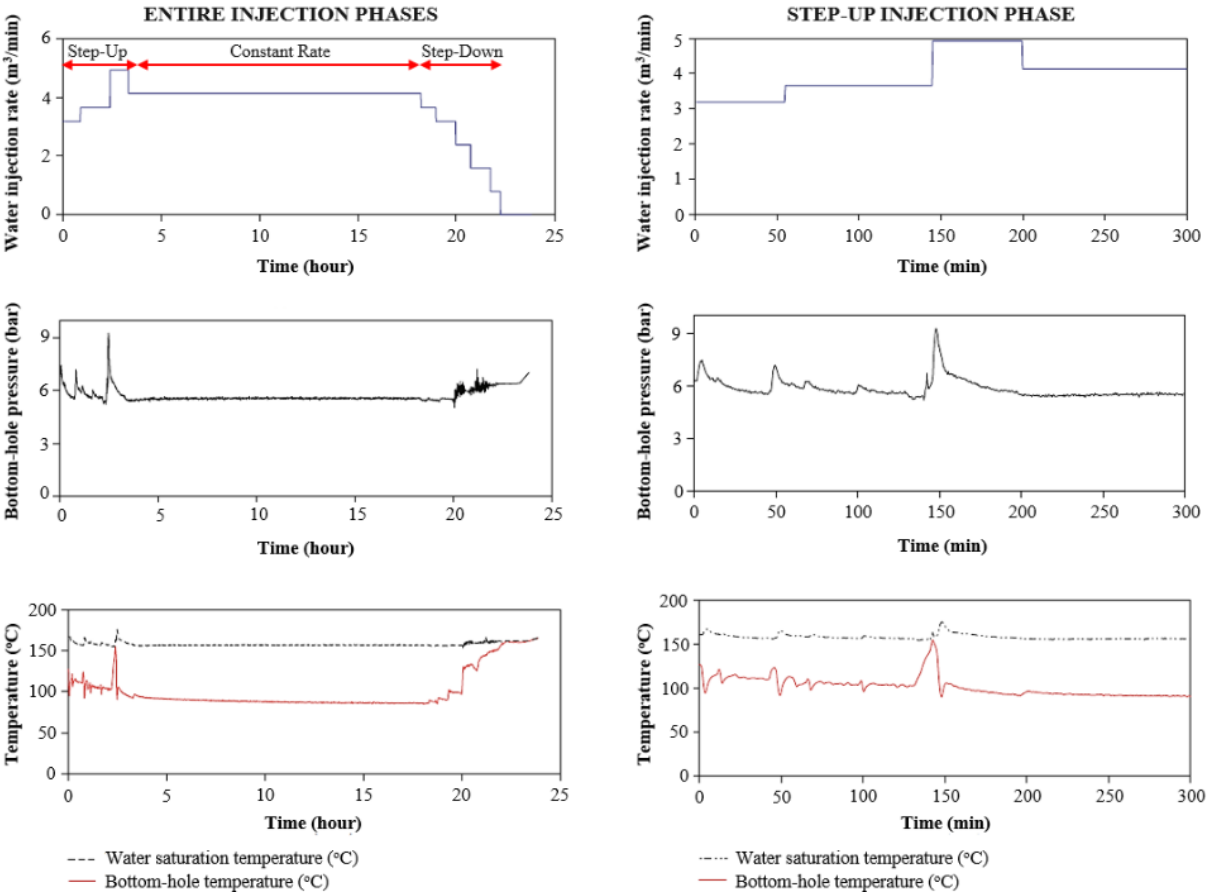

Figure 47: Measured Injection Rate and Bottomhole Pressure During the Three Injection Phases (Left) and During the Highlighted Step-Up Injection Phase (Right) During the PPL-6 Hydraulic Fracturing (Lee, et al., 2023).

The hydraulic stimulation at PPL-06 successfully increased the reservoir's permeability and steam production. The Hall plot analysis confirmed the formation was stimulated, with fractures opening after injecting approximately 4,000 barrels of water. This was evident as the Hall derivative tracked below the Hall integral, indicating reduced flow restriction, as shown in Figure 48. Furthermore, an increase in steam production was observed in the wells near to PPL-6, with PPL-2 showing a 9.6% increase from 46.7 t/h to 51.5 t/h and PPL-4 an 11.4% increase from 11.9 t/h to 13.2 t/h, as shown in Figure 48. Additionally, the overall power generation capacity of the Patuha field rose from 50.0 MWe to 56.3 MWe post-stimulation. This improvement was proportional to the volume of water injected, highlighting the efficiency of hydraulic stimulation in enhancing steam productivity in a vapor-dominated geothermalreservoir. However, the study emphasized the need for long-

term water injection to confirm the sustainability of these improvement effects and suggested further experimental analyses to optimize hydraulic fracturing designs (Lee, et al., 2023).

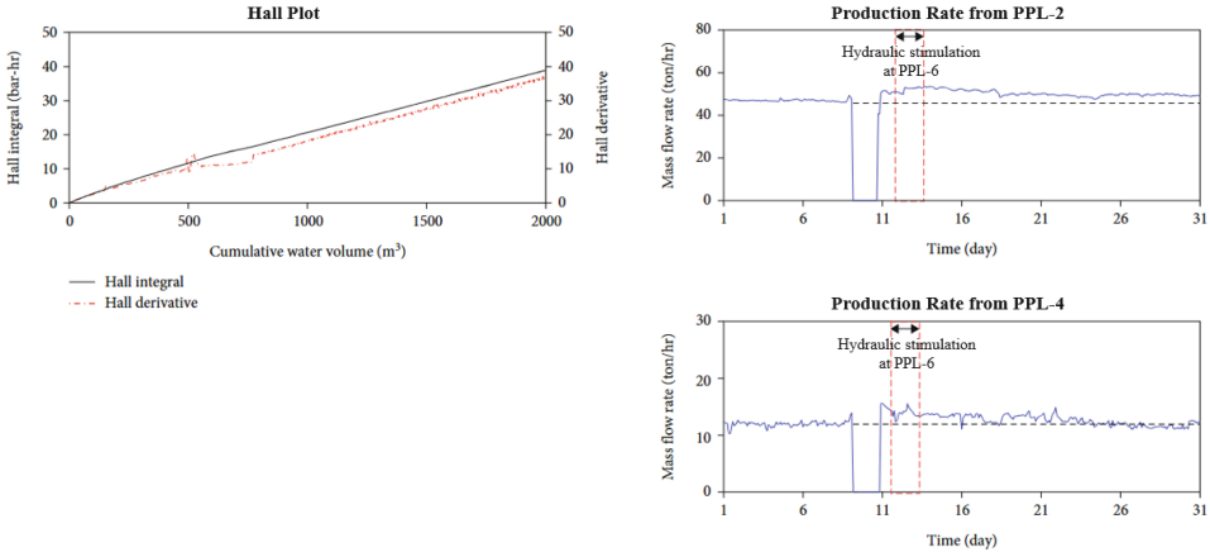

Figure 48: The Hall Plot (Left) and Production Rates at PPL-2 and PPL-4 (Right) In Response to the Hydraulic Stimulation at PPL-6 (Lee, et al., 2023).

Finally, the application of EGS in Indonesia's high-temperature geothermal fields, such as Salak, Wayang Windu, and Patuha, has provided valuable insights that can guide the optimization of low-medium temperature geothermal resources. The following lessons learned highlight key aspects that have proven crucial for the successful implementation of EGS technologies:

1. **Importance of selecting the appropriate stimulation technique**: the success of thermal stimulation in two wells and hydraulic stimulation in two other wells at the Salak field, combined with the increased steam production from hydraulic fracturing at Patuha, highlights the necessity of selecting the appropriate stimulation technique. However, the mixed results at Wayang Windu reveal that hydraulic stimulation may not be suitable for all fields due to factors such as geological setting, stress orientations, and fracture networks. These factors must be carefully evaluated to ensure the optimal selection of stimulation methods.
2. **Importance of detailed geological understanding**: the mixed results at Wayang Windu emphasize the necessity of a thorough geological understanding before applying hydraulic fracturing. Knowledge of stress orientations, fracture networks, and reservoir characteristics is crucial to predict the success of stimulation efforts accurately.
3. **Monitoring and adaptive management during stimulation operations**: continuous monitoring and adaptive management during stimulation operations, as practiced in all three fields, are essential to respond to real-time data and optimize stimulation parameters for better results.
4. **Importance of establishing a protocol to address EGS-induced seismicity**: Indonesia is highly tectonically active due to its location at the convergence of several major tectonic plates, including the Indo-Australian, Eurasian, Pacific plates. This positioning places Indonesia within both the Pacific Ring of Fire and the Alpide belt, leading to frequent and intense seismic and volcanic activity (Lu, et al., 2023; Hutchings & Mooney, 2021). The subduction of tectonic plates in this region generates significant volcanic and seismic activity, making Indonesia home to numerous active volcanoes. This geological setting necessitates the establishment of a protocol to address induced seismicity in EGS projects in Indonesia. The U.S. Department of Energy (DOE) launched an EGS-Induced Seismicity Protocol in 2012 to manage seismic risks and ensure public safety during EGS projects (U.S. DOE, 2012), driven by incidents like the magnitude 3.4 earthquake in Basel, Switzerland, in 2007 (Boyet, et al., 2023; Viganò, et al., 2021). (Kim, et al., 2018) proposed an EGS-induced seismicity protocol for the Pohang EGS project, Korea, by adopting U.S. DOE's protocol in response to the seismic events occurred in Pohang. The region is tectonically active, partly due to its proximity to the Yangsan fault, and there were more than 30 earthquakes recorded between 2005 and 2017 in Pohang (Kim, et al., 2018). These seismic events are interpreted to be caused by either natural, triggered, or EGS-induced mechanism (McGarr & Majer, 2023; Chang & Yoon, 2021). Similarly, Indonesia's EGS-induced seismicity protocol can be assembled by adopting the U.S. DOE's protocol and adjusting it into Indonesia's specific conditions. The U.S. DOE's procotol is comprised of seven steps summarized in Table 11.

These lessons emphasize the importance of carefully selecting and managing EGS techniques to improve geothermal production, especially in a tectonically-active region like Indonesia. Applying these insights can help unlock the potential of low-medium temperature geothermal resources, enhancing their permeability and optimizing the technical and economic feasibility of low-medium temperature geothermal resources in Indonesia.

3.4 Staging Development Using Modular Plants

Geothermal development projects can be performed using two approaches: 1) direct large-scale; or 2) staging. In the direct large-scale approach approach, as illustrated in Figure 49, development is performed in a single stage with a direct large-scale power plant installed capacity so that the Commercial Operation Date (COD) occurs only once. Developers who choose to use this approach generally aim to achieve:

1. **Lower CAPEX**: due to the economy of scale from the power plant capacity and the mobilization and demobilization of development drilling being carried out all at once.
2. **Higher revenue**: from the start of COD, developers immediately generate higher revenue due to the direct large-scale installed capacity since COD hence minimizing the value of revenue lost due to time value of money.

Table 11: Seven Protocol Steps Suggested by the U.S. DOE to Address EGS-Induced Seismicity (U.S. DOE, 2012).

Step	Description	Purpose	Recommended Approach
Step 1: Perform Preliminary Screening Evaluation	A rigorous initial screening to determine the overall feasibility of the EGS project and identify potential risks.	Evaluate the feasibility of an EGS project by assessing technical, socioeconomic, and financial risks. Identify potential show-stoppers and ensure public and regulatory acceptability.	Conduct a bounding analysis to categorize the likelihood of project approval. Review relevant laws, determine the radius of influence, identify potential impacts, and classify the overall risk.
Step 2: Implement and Outreach and Communication Program	Engage the community positively before and during project operations, addressing their concerns and demonstrating project benefits.	Ensure community acceptance by keeping public stakeholders informed and involved.	Develop and periodically update an outreach plan. Hold public meetings, site visits, and establish communication mechanisms to engage the community and stakeholders.
Step 3: Review and Select Criteria for Ground Vibration and Noise	Utilize existing criteria and standards to develop appropriate risk assessment criteria for EGS-induced seismicity.	Identify and evaluate existing standards and criteria for ground-borne noise and vibration impact assessment.	Assess existing conditions, review local ordinances, and evaluate criteria for building damage, human exposure, industrial activities, and ground-borne noise.
Step 4: Establish Local Seismic Monitoring	Continuous seismic monitoring throughout the project to ensure accurate data for operational decisions and mitigation strategies.	Gather baseline and operational seismic data to forecast and understand induced seismicity for mitigation and reservoir management.	Implement a comprehensive seismic monitoring program before and during project operations, ensuring data collection is unbiased.
Step 5: Quantify the Hazard from Natural and Induced Seismic Events	Compare natural and induced seismic hazards to understand the potential increase in hazard due to EGS activities.	Estimate the ground shaking hazard from natural and induced seismicity to assess potential damage or loss.	Perform Probabilistic Seismic Hazard Analysis (PSHA) and Deterministic Seismic Hazard Analysis (DSHA) for both natural and induced seismicity.
Step 6: Characterize the Risk of Induced Seismic Events	A higher resolution risk estimate for making informed decisions on project design and operations.	Develop a detailed estimate of the risk associated with the EGS project design, construction, and operation.	Conduct a rigorous risk assessment considering the variations in risk during future operations and evaluate alternative operational procedures.
Step 7: Develop Risk-Based Mitigation Plan	A proactive mitigation plan to address potential risks and ensure safe and effective EGS operations.	Create a mitigation plan based on the risk assessment to minimize negative impacts of induced seismicity.	Develop and implement mitigation strategies tailored to the specific risks identified in the risk assessment.

However, this approach presents the following drabwacks:

1. **Reservoir response uncertainty**: since the development is carried out directly with a large capacity, developers do not have the opportunity to evaluate reservoir response after COD. This leads to the risks of rapid reservoir decline and oversized power plant units, which can incur financial losses where actual generation levels are below the generation levels in the initial projected project value.

2. **Longer time to reach COD**: since the power plant capacity during COD is higher than in the staged development scheme, a higher steam power under wellhead is required. Therefore, more production and reinjection wells have to be drilled before COD, leading to a longer time to reach COD.

Meanwhile, in the staging development approach, as illustrated in Figure 50, the addition of installed capacity is carried out gradually through several CODs until finally reaching the desired total capacity. Developers who choose this approach generally aim to achieve:

1. **Earlier revenue generation**: because the power plant capacity at each COD is smaller compared to the direct large-scale scheme, the required steam power under the wellhead during COD is also reduced. Therefore, fewer production and reinjection wells need to be drilled before COD, resulting in an earlier COD and revenue generation.
2. **Reservoir sustainability**: because capacity expansion is done gradually, developers can evaluate reservoir response before deciding to increase installed capacity hence reducing the risks of reservoir overproduction.

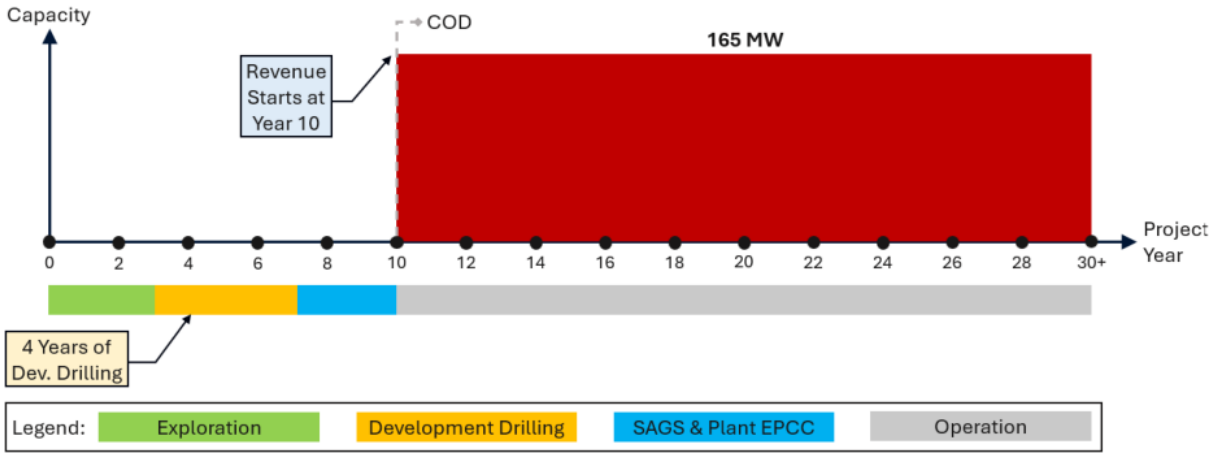

Figure 49: Direct Large-Scale Geothermal Power Plant Development Approach.

However, this approach presents the following drabwacks:

1. **Higher CAPEX**: due to the economy of scale from the power plant capacity and the mobilization and demobilization for the development drilling that are not performed at once, the CAPEX will be higher than the direct large-scale approach.
2. b: because the capacity of the power plant is added gradually, developers will lose more revenue due to the time value of money, altough the total power plant capacity will eventually be the same as the direct large-scale approach.

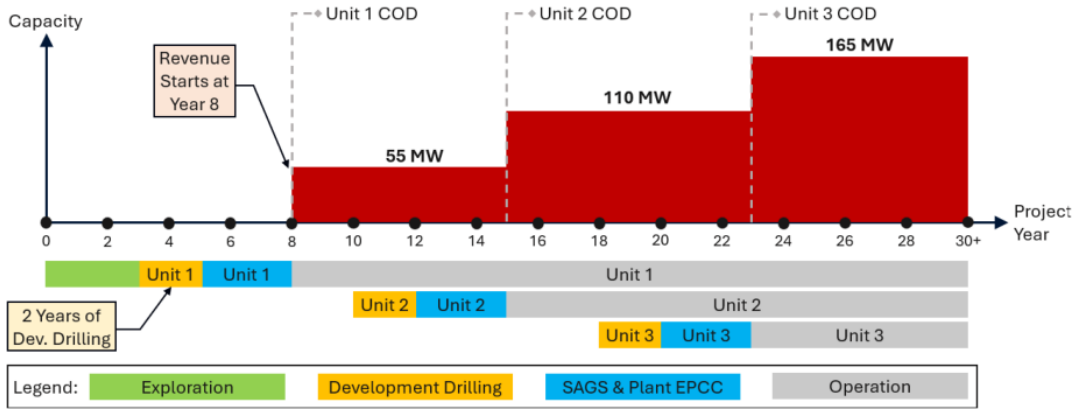

Figure 50: Staging Geothermal Power Plant Development Approach.

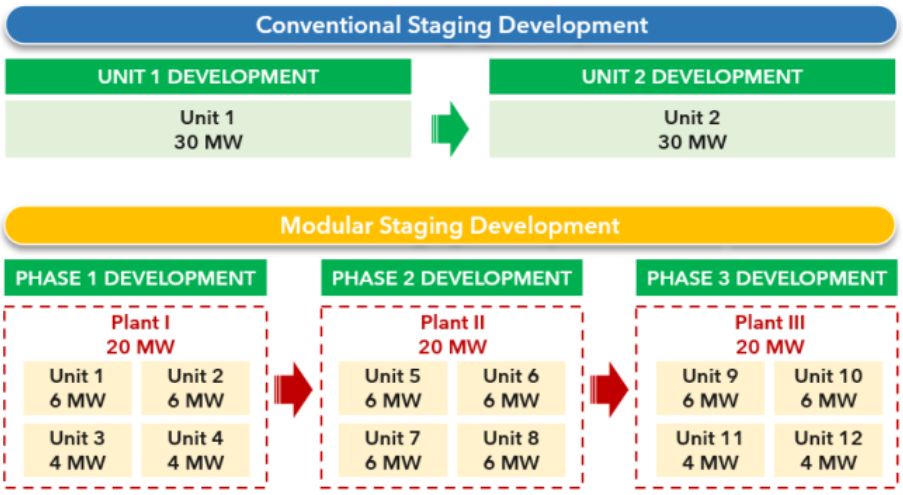

Figure 51: Staging Development Using Conventional Large Unit Plants (Top) and Modular Plants (Bottom).

3.4.1 Conventional and Modular Staging Development

Subsequently, the staging development approach can be classified further into the conventional staging and the modular staging development approach, as illustrated in Figure 51. The conventional staging development approach is straightforward, focusing on the sequential construction of large individual units, each representing a complete stage in the project's expansion. This method is linear, with each new unit signifying a substantial increase in overall capacity, typically employed in regions like Indonesia. In contrast, the modular staging development approach, commonly adopted in the United States, involves breaking down each phase into several smaller units within a single plant. This method allows for gradual and flexible scaling of the project. Each phase comprises multiple smaller units, which can be incrementally commissioned to match demand more closely and optimize resource use. This modular strategy facilitates phased investment and can adapt more dynamically to development needs and technological advancements.

In Indonesia, a conventional staging development approach is commonly used for geothermal power plant projects. Each stage of development is referred to as "Unit X," with the total capacity expressed as "[number of units] x [each unit's capacity]." By using the illustration in Figure 51 as an example, if Field ABC has two units of power plants, each with a 30 MW capacity, it is described as 2x30 MW. The development is staged into Unit 1 (30 MW) and Unit 2 (30 MW), facilitating a structured and phased approach to GPP capacity expansion. The conventional staging development offers the following advantages:

1. **Lower CAPEX**: the larger turbine unit capacity results in a cheaper unit plant CAPEX per megawatt of GPP installed capacity due to the economy of scale.
2. **Simpler operation & maintenance**: due to the less turbine units compared to the modular units, the plant's operation and maintenance are simpler and cheaper.

However, this approach may present the following disadvantages:

1. **Longer time to reach COD**: since each power plant unit possesses a larger capacity during COD compared to the smaller modular units, a higher steam power under wellhead is required. Therefore, more production and reinjection wells have to be drilled before COD, leading to a longer time to reach COD.
2. **Less flexibility during operation & maintenance**: if the turbine units need routine overhauls or unexpected shut-downs, the lost generation will be higher since a single turbine unit generates a larger capacity compared to a modular unit.

Meanwhile, in the United States, a modular staging development approach is commonly employed for power plant projects. Each stage of development is referred to as "Phase X." By using the illustration in Figure 51 as an example, in Field ABC, there are three plants: Plant I (20 MW), Plant II (20 MW), and Plant III (20 MW). Each plant consists of four units (turbines), with each unit having a capacity of 4 to 6 MW. This modular approach allows for flexible and scalable expansion of power generation capacity, enabling gradual increases in output as additional phases are developed and brought online. The conventional staging development offers the following advantages:

1. **Earlier revenue generation**: since modular units possess a smaller capacity compared to the conventional units, electricity generation and sales can be achieved after completing a single production

well drilling and a modular unit installation, which require significantly less time compared to drilling a large number of wells and constructing a larger plant.

2. **Higher flexibility during operation & maintenance**: if the turbine units need routine overhauls or unexpected shut-downs, the lost generation will be smaller since the other turbine units can remain operational.

However, this approach may present the following disadvantages:

1. **Higher CAPEX**: due to the economy of scale from the power plant capacity and the mobilization and demobilization for the development drilling that are not performed at once, the CAPEX will be higher than the direct large-scale approach.
2. **Complex operation & maintenance**: since the plant has a large number of modular turbine units (more equipment involved), conducting operation & maintenance activities becomes more challenging and costly.

3.4.2 Experience in the U.S.: McGinness Hills and Steamboat, Nevada

The McGinness Hills geothermal field has undergone three significant development stages (Robertson-Tait, et al., 2021; NREL, 2021). In 2012, the first phase was completed with the commissioning of three units, providing a capacity of 45 MW. This was followed by the second phase in 2015, which added another three units with the same capacity of 45 MW. The third phase, completed in 2018, introduced three more units, contributing an additional 48 MW. Altogether, the plant now operates nine units with a total installed capacity of 138 MW. Throughout these phases, the monitoring of reservoir response to development was crucial to ensure the sustainability of the resource during capacity expansions. It facilitated the updating of the conceptual model and the calibration of the numerical model, which guided the strategic expansion of the plant, ensuring sustainable and efficient development (Ormat, 2022). The historical development of McGinness Hills GPP is summarized in Figure 52.

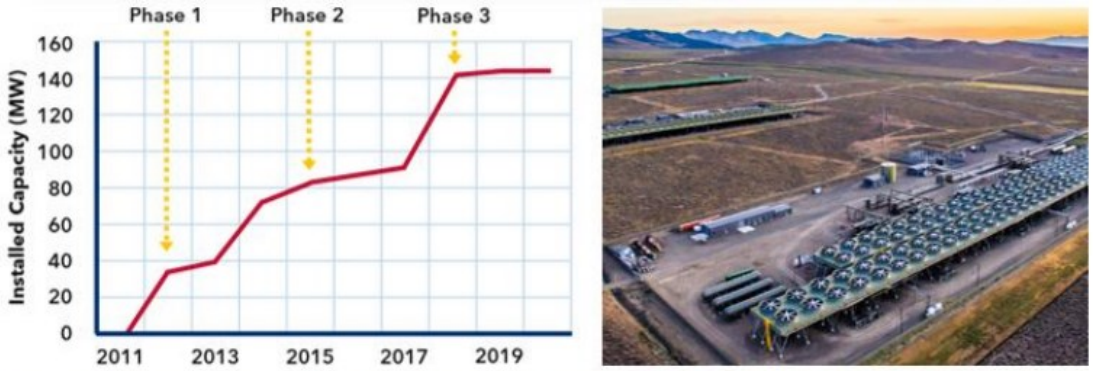

GPP Name	No. of Units	Capacity (MW)	COD Year
McGinness Hills 1	3	45	2012
McGinness Hills 2	3	45	2015
McGinness Hills 3	3	48	2018
Total	**9**	**138**	

Figure 52: McGinness Hills GPP Development History (Ormat, 2024; Robertson-Tait, et al., 2021; NREL, 2021).

Similarly, the Steamboat geothermal field has experienced a series of developments since its initial commissioning (Robertson-Tait, et al., 2021; NREL, 2021). Steamboat 1, the earliest installation in 1985, had the highest number of units, with seven turbines, contributing a modest 2 MW. That same year, Steamboat 1A added two more units, providing an additional 2.4 MW. In 1988, Steamboat Hills was developed with a single unit producing 16.3 MW. The early 2000s saw significant expansions, starting with Galena 1 and Galena 2 in 2006 and 2007, each adding 30 MW and 13.5 MW respectively. Additionally, the Steamboat Hills Bottoming plant added 5.5 MW in 2007. The trend of expansion continued with Galena 3 in 2008, which introduced another 30 MW, followed by Steamboat 2 and Steamboat 3, each adding two units with capacities of 18.2 MW in 2008. Over time, certain units were retired, notably Steamboat 1 and 1A, to optimize the overall capacity, which now stands at approximately 131.7 MW spread across 19 units. The historical development of Steamboat GPP is summarized in Figure 53.

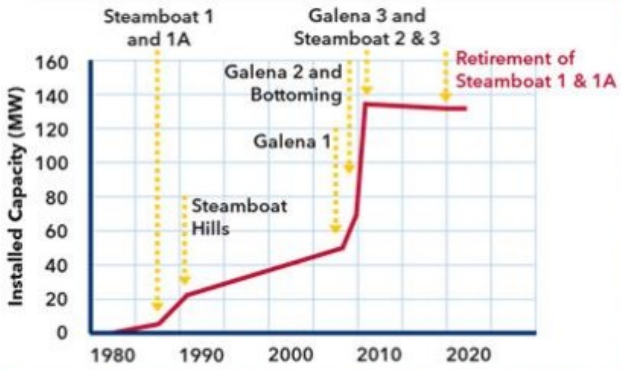

GPP Name	No. of Units	Capacity (MW)	COD Year
Steamboat 1	7	2	1985
Steamboat 1A	2	2.4	1985
Steamboat Hills	1	16.3	1988
Galena 1	2	30	2006
Galena 2	1	13.5	2007
Steamboat Hills Bottoming	1	5.5	2007
Galena 3	1	30	2008
Steamboat 2	2	18.2	2008
Steamboat 3	2	18.2	2008
Total	**19**	**131.7**	

Figure 53: Steamboat GPP Development History (Ormat, 2024; Robertson-Tait, et al., 2021; NREL, 2021).

4. CONCLUSION AND PATHFORWARD

The techno-economic optimization initiatives derived from the U.S. experience with low-medium temperature geothermal fields, combined with insights from Indonesia's high-temperature geothermal fields, provide a strategic pathway to enhance the economic attractiveness of low-medium temperature geothermal development in Indonesia. Currently, the development of these resources in Indonesia is sub-optimal compared to their potential and the advancements seen in high-temperature resources. By implementing advanced downhole pump technologies, such as electric submersible pumps (ESPs), and focusing on the development of shallower outflow zones, Indonesia can significantly reduce the levelized cost of electricity (LCOE). These strategies, along with lessons learned from successful high-temperature projects in Indonesia, such as well stimulation techniques and outflow zone optimization, can help mitigate the high initial costs and operational challenges typically associated with low-medium temperature fields.

Most future exploration pipeline projects (according to RUPTL 2021-2030) will be dominated by low-medium temperature resources. However, despite the availability and commercial success of technologies like binary plants, downhole pumps, and in-field enhanced geothermal systems (EGS) in the U.S. for over 40 years, Indonesia faces significant challenges. The lack of technological know-how and experience, coupled with hesitation to adopt these "new" technologies compared to the conventional high-temperature methods commonly used in Indonesia, hinders the development of low-medium temperature resources. Additionally, geological challenges such as deeper resources, lower permeability, and distinct host rock types (softer sedimentary rocks in the U.S. versus harder volcanic rocks in Indonesia) further complicate drilling operations and the discovery of commercial permeability, necessitating EGS stimulation in some cases.

To overcome these challenges and accelerate the development of Indonesia's vast low-medium temperature geothermal potential, the following steps are recommended:

1. **Resource Characterization**: Conduct detailed studies to characterize the resource depth and permeability of unexplored low-medium temperature geothermal fields. This will help identify resources that are technically and economically feasible to develop.
2. **Technology Transfer**: Enhance technology transfer from U.S. experts through technical training programs or business partnerships, such as joint ventures with experienced U.S. geothermal developers, including the induced seismicity mitigation for EGS projects.

3. **Adopt Best Practices**: Implement global best practices and foster technological innovation to create a more favorable investment climate and improve project bankability.
4. **Collaborative Efforts**: Encourage collaboration between the government, industry stakeholders, and international partners to drive advancements and achieve efficient, cost-effective development of low-medium temperature geothermal fields.

By adopting these optimization practices, Indonesia can diversify its energy portfolio, enhance energy security, and support sustainable economic growth. This collaborative approach will be crucial in realizing these advancements and achieving a more efficient and cost-effective low-medium temperature geothermal field development in Indonesia.

REFERENCES

Abrasaldo, P. M. B., Zarrouk, S. J. & Kempa-Liehr, A. W., 2023. Characterising and Predicting Low Discharge Pressure Events in Less Permeable Geothermal Production Wells. *Geothermics*, 112(102756).

Afiat, et al., 2020. Updated Conceptual Model and Resource Assessment using Numerical Reservoir Simulation of Danau Ranau Geothermal Field Indonesia. *IOP Conf. Series: Earth and Environmental Science*.

Akerley, J. H. et al., 2021. Near-Field EGS: *A Review and Comparison of the EGS Demonstration Projects at Desert Peak and Bradys*. Reykjavik, International Geothermal Association.

Al Asy'ari, M. R., Adityatama, D. W. & Purba, D., 2023. *Geothermal Field Management: Various Cases from Top Geothermal Producer Countries*. Stanford, Stanford University.

Alfiady, et al., 2021. *Geochemical Reservoir Compartmentalisation at Muara Laboh Geothermal Field, Indonesia*. Reykjavik, International Geothermal Association.

ANL, 2014. *Water Use in Enhanced Geothermal Systems (EGS): Geology of U.S. Stimulation Projects, Water Costs, and Alternative Water Source Policies*, Argonne: Argonne National Laboratory.

Aqui, A. R. & Zarrouk, S., 2011. *Permeability Enhancement of Conventional Geothermal Wells*. Auckland, The University of Auckland.

Ashat, A. et al., 2024. An Updated Numerical Model of Patuha Geothermal Field for Optimization and Sustainable Production. *Geothermics*, 121(103052).

Atmojo, J. P. et al., 2001. *Numerical Modeling Study of Sibayak Geothermal Reservoir, North Sumatra, Indonesia*. Stanford, Stanford University.

Axelsson, G. & Gunnlaugsson, E., 2000. *Long-Term Monitoring of High- and Low-Enthalpy Fields Under Exploitation*, Beppu-Morioka: World Geothermal Congress 2000 Short Course.

Aydin, H. & Merey, S., 2021. Design of Electrical Submersible Pump System in Geothermal Wells: A Case Study from West Anatolia, Turkey. *Energy*, 230(120891).

Ayling, B. F., 2020. *35 Years of Geothermal Power Generation in Nevada, USA: A Review of Field Development, Generation, and Production Histories*. Stanford, Stanford University, pp. 1-12.

Bagaskara, M. F. et al., 2021. Gas geochemistry analysis in Candradimuka Crater, Mount Lawu, Central Java, Indonesia. *IOP Conference Series: Earth and Environmental Science*.

Bendritter, Y. & Cormy, G., 1990. Possible Approach to Geothermal Research and Relative Cost Estimate. In: M. H. Dickson & M. Fanelli, eds. *Small Geothermal Resources*. Rome: UNITAR/UNDP Centre for Small Energy Resources, pp. 61-71.

Bijay, K. C. & Ghazanfari, E., 2021. Geothermal Reservoir Stimulation Through Hydro-Shearing: an Experimental Study Under Conditions Close to Enhanced Geothermal Systems. *Geothermics*, 96(102200).

Bijay, K. C., Ghazanfari, E. & Frash, L. P., 2023. Experimental Study of Fracture Slip due to Stress Perturbation in Fractured Geo-Resources. *Geomechanics for Energy and the Environment*, 33(100423).

Boyet, A., De Simone, S., Ge, S. & Vilarrasa, V., 2023. Poroelastic Stress Relaxation, Slip Stress Transfer and Friction Weakening Controlled Post-Injection Seismicity at the Basel Enhanced Geothermal System. *Communications Earth & Environment*, 4(104).

Bradford, J. et al., 2015. Recent Thermal and Hydraulic Stimulation Results at Raft River, ID EGS Site. Stanford, Stanford University.

Budirianto, E. et al., 2020. Stimulation Program of Air Compression and Nitrogen Injection in Geothermal Well. *International Journal of Smart Grid and Clean Energy*, 9(5), pp. 856-864.

Chabora, E. et al., 2012. *Hydraulic Stimulation of Well 27-15, Desert Peak Geothermal Field, Nevada, USA.* Stanford, Stanford University.

Chang, K. W. & Yoon, H., 2021. Mitigating Injection-Induced Seismicity Along Basement Faults by Extraction: Application to 2016–2018 Pohang Earthquakes. *JGR Solid Earth*, 126(4).

Chen, X. et al., 2023. Hydraulic, Acid, and Proppant-Carrying Acid Fracturing Stimulation of Volcanic Reservoirs in Sichuan Basin, China: an Experimental Study. *Petroleum Science and Technology*, 41(7), pp. 731-749.

Covell, C., 2016. *Hydraulic Well Stimulation in Low-Temperature Geothermal Areas for Direct Use* (Master's Thesis), Reykjavik: Master of Science in Energy Engineering - Iceland School of Energy.

Darma, S., 2016. *Indonesia: Vast geothermal potential, modest but growing exploitation*.

Darma, S. et al., 2010. *Geothermal Energy Update: Geothermal Energy Development and Utilization in Indonesia*. s.l., s.n.

Darmawan, I. G. B., Setijadji, L. D. & Wintolo, D., 2015. *Geology and geothermal system in Rajabasa Volcano South Lampung Regency, Indonesia* (Approach to field observations, water geochemistry and magnetic methods).

Daud, Y. et al., 2022. Investigation of the main reservoir of the Tulehu geothermal system (Indonesia) using 3-D inversion of MT data. *Geothermics*.

Daud, Y. et al., 2019. First horizontal derivative and Euler Deconvolution in application for reconstructing structural signature over the Blawan-Ijen Geothermal area. *IOP Conference Series: Earth and Environmental Science*.

Deng, L. et al., 2022. Physical and Mechanical Properties of Granite After High-Temperature and Acidic Treatment for the Enhanced Geothermal System. *Bulletin of Engineering Geology and the Environment*, 81(407).

DiPippo, R., 2016. *Geothermal Power Plants Principles, Applications, Case Studies, and Environmental Impact*.. Oxford: Elsevier.

DiPippo, R. & Kitz, K., 2015. Geothermal Binary Power Plants at Raft River, San Emidio, and Neal Hot Springs: Part 1 — Plant Descriptions and Design Performance Comparison. *GRC Transactions*, Volume 39, pp. 833-846.

Drakos, P. & Akerley, J., 2015. Bradys EGS Project, Washington, D.C.: U.S. Department of Energy.

Dwipa, S., Widodo, S., Suhanto, E. & Kusnadi, D., 2006. Integrated geological, geochemical and geophysical survey in Jaboi geothermal field, Nangro Aceh Darussalam, Indonesia. *Proceedings of the 7th Asian Geothermal Symposium*.

EBTKE, 2017. *Potensi Panas Bumi Indonesia Jilid 1*. Jakarta: Direktorat Panas Bumi Direktorat Jenderal EBTKE.

EBTKE, 2020. *Pedoman Investasi Pembangkit Listrik Tenaga Panas Bumi*, Jakarta: Directorate General of New Renewable Energy and Energy Conservation.

EBTKE, 2023. *Pedoman Efisiensi Biaya Pengeboran Panas Bumi*, Jakarta: Ministry of Energy and Mineral Resources.

Ezzat, M., Adams, B. M., Saar, M. O. & Vogler, D., 2022. Numerical Modeling of the Effects of Pore Characteristics on the Electric Breakdown of Rock for Plasma Pulse Geo Drilling. *Energies*, 15(1).

Febrianto, R. et al., 2019. Developing Low Temperature Geothermal Projects in Indonesia Using Pumped Well Technology. *IOP Conference Series: Earth and Environmental Science*, Volume 254, p. 012021.

Firanda, E. et al., 2024. *Updating Numerical Simulation Model of Sibayak Field, Indonesia*. Stanford, Stanford University.

Firanda, E., Saputra, M. B. & Silaban, M., 2015. *The Effect of Well Elevation on Production in Lumut Balai Field*. Melbourne, International Geothermal Association.

Flores-Armenta, M. & Alcalá, L. M., 2012. *How Much Stimulation We Can Afford?*, Santa Tecla: United Nations University Geothermal Training Programme (UNU-GTP).

Gaffar, E., 2018. The concept of geothermal exploration in west Java based on geophysical data. *IOP Conference Series: Earth and Environmental Science*.

Garcia, J. et al., 2016. The Northwest Geysers EGS Demonstration Project, California Part 1: Characterization and Reservoir Response to Injection. *Geothermics*, Volume 63, pp. 97-119.

Golla, G. U. et al., 2020. The Salak Field, Indonesia: On to the Next 20 Years of Production. *Geothermics*, 83(101715).

Gong, L. et al., 2023. Research Status and Development Trend of Key Technologies for Enhanced Geothermal Systems. *Natural Gas Industry B*, 10(2), pp. 140-164.

Grant, M. A. & Bixley, P. F., 2011. *Geothermal Reservoir Engineering (2nd Edition)*. Burlington: Elsevier.

GRG-Geoenergis, 2024a. *Geothermal Development Cost in Indonesia*, Jakarta: PT Sarana Multi Infrastruktur (Persero).

GRG-Geoenergis, 2024b. *Indonesia and Global Geothermal Resource*, Jakarta: PT Sarana Multi Infrastruktur (Persero).

GRG-Geoenergis, 2024c. *Geothermal Exploration Drilling Infrastructure Cost Review*, Jakarta: PT Sarana Multi Infrastruktur (Persero).

Guo, B., Lyons, W. C. & Ghalambor, A., 2017. *Petroleum Production Engineering: A Computer-Assisted Approach*. 2nd ed. Houston: Gulf Professional Publishing.

Hamilton, W., 1973. *Tectonics of the Indonesian Region*. Malaysia Bull, Volume 6, pp. 3-10.

Harijoko, A. & Juhri, S., 2017. Cl/B Ratio of Geothermal Fluid around Slamet Volcano, Jawa Tengah, Indonesia. *IOP Conference Series: Earth and Environmental Science*.

Harijoko, A. et al., 2021. Stratigraphy, chronology, and magma evolution of Holocene volcanic products from Mt. Slamet deposited in the Guci Valley, Central Java, Indonesia. *Journal of Volcanology and Geothermal Research*.

Hernandez, K., Richard, C. & Nathwani, J., 2016. *Estimating Project LCOE – an Analysis of Geothermal PPA Data*. Stanford, Stanford University.

Hochstein, M., 1990. *Classification and Assessment of Geothermal Resources*. In: Small Geothermal resource - A guide to Development and Utilization. Rome: UNITAR/UNDP Centre on small Energy Sources.

Hochstein, M. P. & Sudarman, S., 2015. *Indonesian Volcanic Geothermal Systems*. Melbourne, International Geothermal Association.

Hochstein, M. & Sudarman, S., 2008. History of geothermal exploration in Indonesia from 1970 to 2000. *Geothermics*, Volume 37, pp. 220-266.

Hutchings, S. J. & Mooney, W. D., 2021. The Seismicity of Indonesia and Tectonic Implications. Geochemistry, Geophysics, *Geosystems*, 22(9).

Idianto, O. et al., 2021. Updated conceptual model and resource assessment using numerical reservoir simulation of danau ranau geothermal field Indonesia. *IOP Conference Series: Earth and Environmental Science*.

IESR, 2023. *Making Energy Transition Succeed: A 2023's Update on The Levelized Cost of Electricity and Levelized Cost of Storage in Indonesia*, Jakarta: Institute for Essential Services Reform (IESR).

IFC, 2013. *Success of Geothermal Wells: A Global Review*, Pennsylvania: International Finance Corporation.

Ikhwan, M., 2020. *Geological Model and Permeability Framework of Bukit Daun Geothermal Field, Indonesia*. Waitanga, University of Auckland.

Ikhwan, M. et al., 2021. Initiation of Low-Temperature Geothermal System Development in Indonesia: The Potential Challenges. Jakarta, Proceedings, The 2nd Digital Indonesia International Geothermal Convention (DIIGC) 2021.

IRS, 2022. *Renewable Electricity Production Credit Amounts for Calendar Year 2022* , Washington, D.C.: Internal Revenue Service.

Iswahyudi, S., Attabik, L. W. & Saifrudin, N. A., 2020. Reservoir Temperature Calculation of Immature Geothermal Water from Hot Spring Around the Slamet Volcano. *IOP Conference Series: Earth and Environmental Science*.

Jiang, K., Deng, S., Jiang, X. & Li, H., 2023. Calculation of Fracture Number and Length Formed by Methane Deflagration Fracturing Technology. *International Journal of Impact Engineering*, 180(104701).

Jiang, S., Zhang, K., Moore, J. & McLennan, J., 2023. Lessons Learned from Hydrothermal to Hot Dry Rock Exploration and Production. Energy Geoscience, Volume 4, p. 100181.

Kamah, M. Y. et al., 2015. Succesful Exploration Campaign and to be Developed in Hululais Geothermal Field, Bengkulu Indonesia. s.l., *Proceedings World Geothermal Congress*.

Kamila, Z., Kaya, E. & Zarrouk, S. J., 2021. Reinjection in Geothermal Fields: An Updated Worldwide Review 2020. *Geothermics*, Volume 89, pp. 1-88.

Kenyon, C. S. & Beddoes, L. R., 1997. *Geothermal Gradient Map of Southeast Asia*, Singapore: Southeast Asia Petroleum Exploration Society.

Kim, K.-I.et al., 2018. Protocol for Induced Microseismicity in the First Enhanced Geothermal Systems Project in Pohang, Korea. *Renewable and Sustainable Energy Reviews*, Volume 91, pp. 1182-1191.

Klein, C. W., Johnson, S. & Spielman, P., 2007. Resource Exploitation at Steamboat, Nevada: What it takes to Document and Understand the Reservoir/Groundwater/Community Interaction. *GRC Transactions*, Volume 31, pp. 179-186.

Kriptanto, A., 2024. *Unleashing Geothermal Potential Maximizing Well Production with High-Temperature High-Flowrate Electrical Submersible Pump*, Jakarta: SLB.

Kurniawan, A., 2021. *Petroleum Production Engineering Lectures: Artificial Lift 1*, Yogyakarta: UPN "Veteran" Yogyakarta.

Layman, E. B. & Soemarinda, S., 2003. The Patuha vapor-dominated resource West Java, Indonesia. s.l., *Proceedings of the 28th Workshop on Geothermal Reservoir Engineering*, Stanford University.

Lee, S., Bae, W., Permadi, A. K. & Park, C., 2023. Hydraulic Stimulation of Enhanced Geothermal System: A Case Study at Patuha Geothermal Field, Indonesia. *International Journal of Energy Research*, 2023(9220337).

Lei, Z., Zhang, Y., Zhang, S. & Shi, Y., 2023. Numerical study of Hydraulic Fracturing Treatments and Geothermal Energy Extraction from a Naturally Fractured Granitic Formation. *Geothermics*, 111(102692).

Li, N., Xie, H., Hu, J. & Li, C., 2021. A Critical Review of the Experimental and Theoretical Research on Cyclic Hydraulic Fracturing for Geothermal Reservoir Stimulation. *Geomechanics and Geophysics for Geo-Energy and Geo-Resources*, 8(7).

Li, N. et al., 2022. Thermal-Shock-Induced Surface Softening and Conductivity Evolution of Hydraulic Fracture in Enhanced Geothermal System. *Geothermics*, 102(102405).

Li, S., Wang, S. & Tang, H., 2022. Stimulation Mechanism and Design of Enhanced Geothermal Systems: A Comprehensive Review. *Renewable and Sustainable Energy Reviews*, 155(111914).

Lovekin, J., Morrison, M., Champneys, G. & Morrow, J., 2017. Temperature Recovery after Long-term Injection: Case History from Soda Lake, Nevada. Geothermal Resources Council Transactions, Volume 41, pp. 2770-2779.

Lovekin, J. W. et al., 2021. *Geothermal Applications of Electric Submersible Pumps (ESPs) in the USA and Turkey*. Reykjavik, International Geothermal Association.

Luo, W. et al., 2023. Mechanisms Causing Injectivity Decline and Enhancement in Geothermal Projects. *Renewable and Sustainable Energy Reviews*, 185(113623).

Lu, Z., Li, J., Li, C.-F. & Du, X., 2023. Tectonic Controls on Effective Elastic Thickness of Lithospheres Around the Southeast Asian Subduction Zones. *Tectonophysics*, 863(229994).

Mandradewi, W. & Herdianita, N. R., 2010. Characteristics of Surface Manifestation, Cisolok, Sukabumi, West Java: With Relation to Cisolok Geothermal System. *Proceedings World Geothermal Congress*.

Marfo, S. A. et al., 2024. *Artificial Lift Design for Future Inflow and Outflow Performance for Jubilee Oilfield Using Historical Production Data and Artificial Neural Network Models*. In: D. A. Otchere, ed. Data Science and Machine Learning Applications in Subsurface Engineering. Boca Raton: CRC Press, pp. 261-285.

McGarr, A. & Majer, E. L., 2023. The 2017 Pohang, South Korea, Mw 5.4 Main Shock was Either Natural or Triggered, but not Induced. *Geothermics*, 107(102612).

McLean, K., Zarrouk, S. J. & Wilson, D., 2016. *Application of Numerical Methods for Geothermal Pressure Transient Analysis: a Deflagration Case Study from New Zealand*. Stanford, Stanford University.

Mines, G. L., 2016. GETEM User Manual, Idaho Falls: Idaho National Laboratory.

Moeck, I. S., 2014. Catalog of Geothermal Play Types Based on Geologic Controls. *Renewable and Sustainable Energy Reviews*, Volume 37, pp. 867-882.

Mubarok, M. H. & Zarrouk, S. J., 2016. *Steam-Field Design Overview of The Ulubelu Geothermal Project, Indonesia.* Auckland, s.n., pp. 1-6.

Mubarok, M. H. & Zarrouk, S. J., 2017. Discharge Stimulation of Geothermal Wells: Overview and Analysis. *Geothermics*, Volume 70, pp. 17-37.

Muffler, P. & Cataldi, R., 1978. Methods for Regional Assessment of Geothermal Resources. *Geothermics*, 7(2-4), pp. 53-89.

Mukuhira, Y., Ishibashi, T., Ito, T. & Asanuma, H., 2023. *Permeability Enhancement Process by Shear Slip on Existing Fractures from the Microseismic Perspective*. Stanford, Stanford University.

Mulyadi, 2010. Case Study: '*Hydraulic Fracturing Experience in the Wayang Windu Geothermal Field*'. Bali, International Geothermal Association.

Mulyadi & Ashat, A., 2011. *Reservoir Modeling of the Northern Vapor-Dominated Two-Phase Zone of the Wayang Windu Geothermal Field, Java, Indonesia*. Stanford, Stanford University.

Mussofan, W. et al., 2018. *Geothermal Resource Exploration along Great Sumatera Fault Segments in Muara Laboh: Perspectives from Geology and Structural Play*. Stanford, Stanford University.

Nayoan, A. G. P. et al., 2023. Upflow-outflow Zone Identification Based on Geochemistry Indicator and Fault Fracture Density Correlation Analysis in Mt. Gede Geothermal Case, West Java. *IOP Conference Series: Earth and Environmental Science*, 1159(012003).

Neupane, G. et al., 2015. *Validation of Multicomponent Equilibrium Geothermometry at Four Geothermal Power Plants*. Stanford, Stanford University.

Nicholson, K. N., 1993. *Geothermal Fluids. Chemistry and Exploration Techniques*. ISBN 3 540 56017 3 ed. Berlin: Springer Verlag.

NREL, 2014. *Electronic Submersible Pump (ESP) Technology and Limitations with Respect to Geothermal Systems*, Golden: National Renewable Energy Laboratory.

NREL, 2021. 2021 U.S. *Geothermal Power Production and District Heating Market Report*, Golden: National Renewable Energy Laboratory.

NREL, 2023. *Geothermal Annual Technology Baseline*, Golden: National Renewable Energy Laboratory.

NSA, 2020. SNI 6678:2020 *Conversion of Geothermal Fluid Flow Rate into Electricity*, Jakarta: National Standardization Agency.

Nugraha, H. S., Shiddiq, A. M. I., Agustin, F. & Surmayadi, M., 2018. Comparison of Application Faults and FractureDensity (FFD) Method using SRTM 90-m, SRTM 30-m, and Aster GDEM 30-m for Geothermal Exploration: a Case of Ile Ange Prospect. s.l., *7th ITB International Geothermal Workshop 2018*.

Nugraha, R. P. & O'Sullivan, J., 2019. A key process of natural state modeling: 3D Geological model of Jaboi Geothermal field, Nangro Aceh Darussalam, Indonesia. *IOP Conference Series: Earth and Environmental Science*.

Nurdyanto, B., Daud, Y. & Zarkasyi, A., 2019. Application of MT and Gravity Method to Potential Analysis of Kepahiang Geothermal, Bengkulu. s.l., *Proceeding Conference on Applied Electromagnetic Technology (AEMT)*.

Nurseto, S. T. et al., 2021. Structural Geology and Volcanism in Hululais Geothermal Area, Bengkulu, Indonesia. *IOP Conference Series: Earth and Environmental Science*.

Nurseto, S. T., Arifin, M. T., Pratama, G. R. & Nusantara, V. D., 2021. Structural Geology and Volcanism in Hululais Geothermal Area, Bengkulu, Indonesia. *IOP Conference Series: Earth and Environmental Science*.

Omrani, P. S. et al., 2021. *Overview of Opportunities and Challenges of Electrical Submersible Pumps ESP in the Geothermal Energy Production Systems*. Texas, Society of Petroleum Engineers.

Oregon Tech, 2012. *Geothermal Policy in the U.S., Klammath Falls*: Oregon Institute of Technology.

Ormat, 2022. *Introduction to Ormat, Lower Temperature Resources, and Ideas for Enhancing Geothermal in Indonesia*, Reno: Ormat Technologies, Inc..

Ormat, 2024. *Global Projects: Geothermal Power*, Reno: Ormat.

Pambudi, N. A. & Ulfa, D. K., 2024. The Geothermal Energy Landscape in Indonesia: A Comprehensive 2023 Update on Power Generation, Policies, Risks, Phase and the Role of Education. *Renewable and Sustainable Energy Reviews*, 189(114008).

Papapetrou, M. & Kosmadakis, G., 2021. *Resource, Environmental, and Economic Aspects of SGHE*. In: A. Tamburini, A. Cipollina & G. Micale, eds. Salinity Gradient Heat Engines. Cambridge: Elsevier, pp. 319-353.

Pasikki, R. G., Libert, F., Yoshioka, K. & Leonard, R., 2010. *Well Stimulation Techniques Applied at the Salak Geothermal Field*. Denpasar, International Geothermal Association.

Permadi, G. B. et al., 2022. *Hydrogeochemistry Model and Reservoir Compartment of Mount Tampomas Geothermal System Area in Sumedang Regency, West Java*.

Peter-Borie, M. et al., 2019. *Thermal Stimulation of the Deep Geothermal Wells: Insights from the H2020 - DEEPEGS project*. La Haye, European Geothermal Energy Council.

PGE, 2021. *Geology-Geophysics-Geochemistry (GGG) Materials for Gunung Tiga Prospect, Lampung*, Jakarta: PT Pertamina Geothermal Energy.

PGE, 2021. *Summary Geoscience Proyek Hululais Extension A (Bukit Daun)*, Jakarta: PT Pertamina Geothermal Energy.

PGE, 2022. *Feasibility Study of Gunung Tiga Prospect Exploration, Lampung*, Jakarta: PT Pertamina Geothermal Energy.

Phuong, N. K., Harijoko, A., Itoi, R. & Unoki, Y., 2012. Water geochemistry and soil gas survey at Ungaran geothermal field, central Java, Indonesia. *Journal of Volcanology and geothermal research*.

Pizzocolo, F. et al., 2021. *Feasibility Assessment of Hydraulic Fracture Stimulation Treatment in the Wayang Windu Geothermal Field (West Java, Indonesia)*. Reykjavik, International Geothermal Association.

PLN, 2020. *The Future is Now: Committing Geothermal Energy for Indonesia's Sustainable Development*, Jakarta: PT Perusahaan Listrik Negara (Persero).

PLN, 2021. Rencana Usaha Penyediaan Tenaga Listrik (RUPTL) 2021-2030, Jakarta: PT Perusahaan Listrik Negara (Persero).

Prabata, W., 2018. *Updating Conceptual Model Using Numerical Modelling for Geothermal Green Field Prospect Area in Atadei, East Nusa Tenggara*, Indonesia.

Prabowo, R., Saptadji, N. M., Maulana, D. T. & Nusiaputra, Y. Y., 2021. Study of Increase Geothermal Well Production Rate by Downhole Pump Installation for Utilization in Power Plant. *IOP Conference Series: Earth and Environmental Science*, 732(012023).

Pradipta, D. et al., 2023. Identification of Volcanic Geothermal Systems Based on Integrated Study of Volcanostratigraphy, Structural Geology, and Fluid Geochemistry in Southern Ngada Field, Indonesia. *IOP Conference Series: Earth and Environmental Science*, 1159(012002).

Purba, D. et al., 2020. *Geothermal Drilling Cost Optimization in Indonesia: A Discussion of Various Factors*. Stanford, Stanford University.

Purba, D. et al., 2021. *Drilling Infrastructure Construction Challenges in Geothermal Exploration Project in Eastern Indonesia*. Reykjavik, International Geothermal Association.

Putriyana, L., Daud, Y., Saha, B. B. & Nasruddin, N., 2022. A Comprehensive Data and Information on Low to Medium Temperature Geothermal Resources in Indonesia: A Review. Geomechanics and Geophysics for Geo-Energy and Geo-Resources, 8(58), pp. 1-29.

Putriyana, L., Ladiba, A. F. & Soekarno, H., 2021. *Simulasi Pengembangan Lapangan Panas Bumi Sirung Pantar, Kabupaten Alor, Nusa Tenggara Timur*. Ketenagalistrikan dan Energi Terbarukan.

Rejeki, S., Dave, R., Nordquist, G. & Fitriyanto, A., 2010. *Geologic Conceptual Model Update of the Darajat Geothermal Field, Indonesia*. Denpasar, International Geothermal Association.

Rera, G. F., Pratama, H. B. & Saptadji, N. M., 2021. Approach for Pre-Feasibility Study of Medium Enthalpy Geothermal Field, Case Study: Danau Ranau, Indonesia. *IOP Conference Series: Earth and Environmental Science*.

Robertson-Tait, A., Harvey, W., Hamm, S. & Boyd, L., 2021. *The United States of America Country Update 2020 – Power Generation*. Reykjavik, International Geothermal Association, pp. 1-15.

Rutqvist, J. et al., 2021. *Coupled Processes Analysis of Flexible Geothermal Production from a Liquid-Dominated Geothermal System: Impact on Wells*. Reykjavik, International Geothermal Association.

Sanyal, S. K., 2005. *Classification of Geothermal Systems - A Possible Scheme*. Stanford, Stanford University, pp. 85-88.

Satya, D. et al., 2015. *Geologic Modeling Workflow for Volcanic Hosted Geothermal Reservoirs: Case Study from Salak Geothermal Field*. Melbourne, International Geothermal Association.

Sharmin, T., Khan, N. R., Akram, M. S. & Ehsan, M. M., 2023. A State-of-the-Art Review on Geothermal Energy Extraction, Utilization, and Improvement Strategies: Conventional, Hybridized, and Enhanced Geothermal Systems. *International Journal of Thermofluids*, 18(100323).

Song, X. et al., 2023. Review of High-Temperature Geothermal Drilling and Exploitation Technologies. *Gondwana Research*, Volume 122, pp. 315-330.

Stimac, J. et al., 2019. An Overview of the Muara Laboh Geothermal System, Sumatra. *Geothermics*, Volume 82, pp. 150-167.

Stimac, J., Nordquist, G., Suminar, A. & Sirad-Azwar, L., 2008. *An overview of the Awibengkok geothermal system, Indonesia*. Volume 37, pp. 300-331.

Sukhyar, R., Soedibjo, A. W., Ganefianto, N. & Stimac, J., 2010. *Geothermal energy update: geothermal energy development and utilization in Indonesia*. s.l., World Geothermal Congress.

Sumartha, A. G. A. et al., 2020. Updating the Conceptual Model of Cisolok-Cisukarame Geothermal field, West Java, Indonesia. *IOP Conference Series: Earth and Environmental Science*.

Sumotarto, U., Hendrasto, F. & Triadi, W., 2019. Volcanostratigraphy of Batukuwung-Parakasak Geothermal Area, Serang Regency, West Java. *Journal of Physics: Conference Series*.

Syah, B. Y. C. S. S. et al., 2019. Hydrogeochemical and isotope characterization of geothermal waters from the Cidanau geothermal field, West Java, Indonesia. *Geothermics*.

Taborda, A. et al., 2022. Temperature Estimation of the Nevado del Ruiz Volcano Geothermal Reservoir: Insight from Western Hot Springs Hydrogeochemistry. *Journal of Geochemical Exploration*, 240(107049).

The White House, 2023. *Building a Clean Energy Economy: A Guidebook to the Inflation Reduction Act's Investments in Clean Energy and Climate Action*, Washington, D.C.: The White House.

ThinkGeoEnergy, 2024. *Global Geothermal Power Plant Map.* [Online] Available at: https://www.thinkgeoenergy.com/map/ [Accessed 9 May 2024].

Tonkin, R., O'Sullivan, J., Gravatt, M. & O'Sullivan, M., 2023. Simulation of Complex Transient Flows in Geothermal Wells. *Geothermics*, 108(102631).

U.S. DOE, 2012. *Protocol for Addressing Induced Seismicity Associated with Enhanced Geothermal Systems*, Washington, D.C.: U.S. Department of Energy.

U.S. DOE, 2019. *GeoVision: Harnessing the Heat Beneath Our Feet*, Washington, D.C.: United States Department of Energy.

USGS, 2008. *Assessment of Moderate- and High-Temperature Geothermal Resources of the United States*, Menlo Park: United States Geological Survey.

Viganò, A., Ranalli, G., Andreis, D. & Martin, S., 2021. Inversion for the static friction coefficient of Seismogenic Faults: Application to Induced Seismicity of the Basel Enhanced Geothermal System, Switzerland. *Journal of Geodynamics*, 145(101843).

Xing, P., Moore, J., Damjanac, B. & McLennan, J., 2024. Investigation of Thermal Cooling Effect of Long-Term Circulation in Raft River Enhanced Geothermal System. *Geothermics*, 120(103026).

Yearsley, E., 2023. *The Basics of Submersible Pumps in Geothermal Project*s, Heggedal: GeoExpro.

Yudha, S. W., Tjahjono, B. & Longhurst, P., 2022. Unearthing the Dynamics of Indonesia's Geothermal Energy Development. *Energies*, 15(14).

Yudiantoro, D. F. et al., 2020. Development of Ngebel Volcano as Geoheritage and Tourism Education of Volcano, Electric Energy and Geothermal, Ponorogo, East Java. *Proceeding of LPPM UPN "Veteran" Yogyakarta Conference Series 2020*–Engineering and Science Series.

Zang, A. et al., 2024. Comprehensive Data Set of In Situ Hydraulic Stimulation Experiments for Geothermal Purposes at the Äspö Hard Rock Laboratory (Sweden). *Earth System Science Data*, 16(1).

Zarrouk, S. J. & Moon, H., 2014. Efficiency of Geothermal Power Plants: A Worldwide Review. *Geothermics*, pp. 142-153.

Zarrouk, S. Q. & McLean, K., 2019. *Geothermal Well Test Analysis: Fundamentals, Applications and Advanced Techniques*. London: Elsevier.

Empowering Coffee Farmers: A Strategic CSR Approach for Climate Resilience and Market Positioning at Supreme Energy Rantau Dedap

Andri Muhamad Affandi and M. Pradikta F. R

Anwar Muhammad Foundation (AMF)

andri.affandi@amf.or.id, mohammad.pradikta@amf.or.id

Keywords: Climate Change Adaptability, Market Positioning, Livelihood Improvement Program (LIP), Post-Harvest Coffee Processing, Inclusive Financing, Aggregator Scheme

ABSTRACT

The Corporate Social Responsibility (CSR) initiative by Supreme Energy Rantau Dedap (SERD), in collaboration with the Anwar Muhammad Foundation (AMF) and other stakeholders, aims to enhance climate change adaptability and strengthen market positioning for coffee farmers in the SERD geothermal project area. This area encompasses the Lahat District, Muara Enim District, and Pagar Alam City in South Sumatra Province.

In developing this CSR program plan, the sustainability of the Livelihood Improvement Program (LIP) which has been implemented in 2019-2022 targeted 131 Project Affected Peoples (PAP), was taken into consideration. These PAP are divided into five Joint Business Groups (KUBE) located in two main villages, Tunggul Bute Village in Lahat District and Segamit Village in Muara Enim District. The LIP intervention aimed to strengthen six household livelihood assets of the PAP, namely human resources, natural resources, physical resources, financial resources, social resources, and intellectual resources. Evaluation results showed that the program successfully increased the PAP's income by 75% compared to their initial conditions, with the main source of income for the majority of PAP (approximately 90%) being coffee farming. Therefore, the primary target of CSR is coffee farmers, both those included in the PAP and other community members within the SERD geothermal project area.

The main problems faced by coffee farmers in the project area are: 1) unpredictable weather conditions affecting the quality and quantity of coffee harvests; 2) lack of skills and knowledge about good coffee farming practices; 3) lack of skills and knowledge about good post-harvest coffee processing; 4) limited access to capital for coffee farmers; and 5) low selling prices and limited market access. The implementation of the CSR program is expected to address these problems and ultimately improve the welfare of coffee farmers.

The scope of CSR activities for the 2023-2024 period includes data validation activities for 131 PAP, facilitation of coffee farmer institutional development, technical support for post-harvest coffee, support for coffee drying and storage infrastructure, facilitation of inclusive financing for coffee farmers through the Islamic Blended Finance (IBF) scheme, and facilitation of coffee marketing using the aggregator scheme. This period's CSR implementation is focuses on about 30 coffee farmers who belong to the Gunung Patah Farmer Group in Segamit Village. This is a new group formed by coffee farmers in the village and includes both PAP and non-PAP households.

The next stage of the CSR program intervention aims to increase coffee productivity, promote sustainable agroforestry practices, and improve market access for coffee products for the 2024-2025 timeframe The target beneficiaries of the CSR program in this period are approximately 250 coffee farmers. In order to improve market access, initial efforts have been made to open cooperation opportunities with the Swiss Import Promotion Programme (SIPPO) and local buyer partners. Some plans to carry out this cooperation will be implemented gradually and will be added to the CSR program for the 2024-2025 period.

1. INTRODUCTION

In South Sumatra Province, coffee farmers face significant challenges related to financial inclusion and climate change (Schroth, G., et al. 2015). The limited access to financial services exacerbates their vulnerability to climate-related impacts, resulting in suboptimal coffee production and market interactions. Supreme Energy Rantau Dedap (SERD) recognizes the need to address these challenges through a strategic Corporate Social Responsibility (CSR) approach aimed at empowering coffee farmers to achieve climate resilience and improve their market positioning.

1.1 Background

Coffee farmers in South Sumatra, particularly in remote areas, struggle with limited access to financial institutions. This lack of financial inclusion, coupled with the adverse effects of climate change, hampers their ability to invest in necessary adaptations, such as post-harvest processing improvements and sustainable farming practices (Sarvina, Y., et al. 2023). The region's coffee production is heavily impacted by changing rainfall patterns, which

can lead to decreased crop quality and yield (Schroth, G., et al. 2015). Additionally, the exploitation by intermediaries, or 'toke,' further diminishes farmers' income, creating an unsustainable market environment.

In developing this CSR program plan, it is also in the context of the sustainability of the Livelihood Improvement Program (LIP) which has been implemented from 2019 to 2022, directed towards 131 Project Affected Peoples (PAP). These PAP are divided into five Joint Business Groups (KUBE) located in two main villages, Tunggul Bute Village in Lahat District and Segamit Village in Muara Enim District. The LIP intervention aimed to strengthen six household livelihood assets of the PAP, namely human resources, natural resources, physical resources, financial resources, social resources, and intellectual resources. Evaluation results showed that the program successfully increased the PAP's income by 75% compared to their initial conditions, with the main source of income for the majority of PAP (approximately 90%) being coffee farming. Therefore, the primary target of CSR is coffee farmers, both those included in the PAP and other community members broadly in the SERD geothermal project area

1.2 Context and Objectives

The main problems faced by coffee farmers in the project area include unpredictable weather conditions affecting the quality and quantity of coffee harvests, lack of skills and knowledge about good coffee farming practices, lack of skills and knowledge about good post-harvest coffee processing, limited access to capital for coffee farmers, and low selling prices and limited market access.

The implementation of the CSR program is expected to provide solutions to these problems and ultimately improve the welfare of coffee farmers. The scope of CSR activities for the 2023-2024 period includes data validation activities for 131 PAP, facilitation of coffee farmer institutional development, technical support for post-harvest coffee, support for coffee drying and storage infrastructure, facilitation of inclusive financing for coffee farmers with the Islamic Blended Finance (IBF) scheme, and facilitation of coffee marketing with the aggregator scheme. The CSR implementation in this period focuses on about 30 coffee farmers who are members of the Gunung Patah Farmer Group in Segamit Village. This group is a new group formed based on the initiative of coffee farmers in the village, consisting of PAP and non-PAP households.

In the next stage for the 2024-2025 period, the target of the CSR program intervention is to increase coffee productivity, promote sustainable agroforestry practices, and improve market access for coffee products. The target beneficiaries of the CSR program in this period are approximately 250 coffee farmers. In order to improve market access, initial efforts have been made to open cooperation opportunities with the Swiss Import Promotion Programme (SIPPO) and local buyer partners. Some plans to realise this cooperation will be implemented gradually and will become part of the CSR program for the 2024-2025 period.

SERD's CSR program aims to enhance the livelihood of coffee farmers by addressing these critical issues. The primary objectives are:

1. Strengthening the farmers' capacity to adapt to climate change.
2. Improving their market positioning to ensure fair trade practices and sustainable income.

2. STRATEGIC FRAMEWORK

To achieve these objectives, SERD has adopted a comprehensive approach, incorporating the Sustainable Livelihoods Framework and the AMF Co-Transformative Enterprise Development (C-TED) model.

2.1 Sustainable Framework

The framework focuses on designing strategies to optimise available capital and assets in response to vulnerabilities (Krantz, L. 2001). A thorough analysis of assets and vulnerability factors is at the core of this approach (Serrat, O. 2017). Six Capitals of Sustainable Livelihood Framework:

1. Financial Capital: Enhancing farmers' access to inclusive financial services to support business development and climate-resilient practices.
2. Manufactured Capital: Providing necessary infrastructure and equipment for improved coffee processing and production.
3. Intellectual Capital: Building farmers' knowledge and skills through training and capacity-building initiatives.
4. Human Capital: Empowering farmers with competencies and motivation to innovate and improve their farming practices.
5. Social Capital: Strengthening community networks and stakeholder relationships to foster collective action and information sharing.
6. Natural Capital: Promoting sustainable use of natural resources to ensure long-term productivity and environmental conservation.

2.2 AMF Co-Transformative Enterprise Development (C-TED)

The framework is designed to foster collaborative growth between parties through mutual learning, mutual support, and co-innovation among local enterprises (Shen, W., et al 2022). This approach leverages collective strengths to address common challenges, promoting sustainable social and economic development (Liddle, J. 2018). Collaboration between public, private, and nonprofit sectors such as AMF is essential for social enterprises to address complex social challenges and foster innovation (Qi, L., et al 2024). Key components include Co-Create, Co-Execute, and Co-Operate, creating a dynamic ecosystem that benefits the entire community by:

1. Co-Create: Collaboratively generating innovative ideas and market-based solutions tailored to the farmers' needs.
2. Co-Execute: Implementing these solutions through inclusive partnerships and effective management practices.
3. Co-Operate: Ensuring continuous improvement and sustainability of the initiatives through iterative processes and stakeholder engagement.

3. KEY ACTIVITIES AND OUTCOMES

The CSR program encompasses several strategic initiatives aimed at addressing the climate and market challenges faced by coffee farmers. Program addresses factors necessary for farmers to face potential challenges presented by climate change and market challenges. According to (Wright, D. R., et al. 2024) these initiatives collectively aim to create a sustainable and prosperous future for coffee farming communities in South Sumatra Province, those strategies including:

Financial Inclusion Initiatives:

1. Facilitating access to microloans and other financial services to enable farmers to invest in necessary adaptations and improvements.
2. Providing financial literacy training to enhance farmers' ability to manage their finances effectively.

Climate Resilience Measures:

1. Supporting the installation of climate-resilient infrastructure, such as solar panels for post-harvest processing.
2. Promoting sustainable farming practices that improve soil health and water management.

Market Positioning and Fair Trade:

1. Establishing fair trade partnerships to ensure farmers receive equitable prices for their coffee.
2. Creating a cooperative model to aggregate coffee production, thereby enhancing bargaining power and market access.

Capacity Building:

1. Conducting training programs on best farming practices, quality control, and business management.
2. Facilitating knowledge exchange and collaboration among farmers to foster innovation and continuous improvement.

Environmental Conservation:

1. Implementing measures to protect and restore natural ecosystems, ensuring the sustainability of coffee production.
2. Promoting agroforestry and other practices that enhance biodiversity and ecosystem services.

These initiatives collectively aim to address the multifaceted challenges faced by coffee farmers in the SERD geothermal project area, ensuring their economic sustainability and environmental stewardship (Wright, D. R., et al. 2024). By providing financial tools, enhancing climate resilience, improving market access, building capacity, and conserving the environment, the CSR program seeks to create a sustainable and prosperous future for the coffee farming communities in South Sumatra Province.

The CSR program focuses on enhancing the capabilities of coffee farmers and strengthening agricultural markets through the 6 capital approach, stakeholder mapping, mentorship, and monitoring. Additional activities supporting the CSR program include the construction of a greenhouse (Dome) and storage warehouse, participation in the IIGCE, collaboration with the ADB mission, presenting at the Serelo CSR Award, and holding collaborative discussions with RIGSIS and the Directorate General of New, Renewable Energy, and Energy Conservation (EBTKE) of the Ministry of Energy and Mineral Resources (ESDM). The execution and outcomes of these activities are detailed below.

Figure 1: Training and Assistance in Post-Harvest Coffee Processing.

Figure 2: Coffee Farmers in Post-Harvest Coffee Processing Training.

Figure 3: Coffee Farmers in Post-Harvest Coffee Processing Training.

The first site visit took place from August 28-31, 2023, aiming to identify and analyze the conditions of coffee farmers to form the basis for the CSR program planning. Activities included sustainable livelihood surveys through in-depth interviews and discussions with various stakeholders. The agenda encompassed socializing the CSR program with KUBE members and coffee farmers in Tunggul Bute and Segamit villages, conducting questionnaires and FGDs, observing coffee plantations, and surveying potential locations for the greenhouse and storage warehouse. Key findings indicated financial unpreparedness among farmers due to dependency on harvest

income, unstable coffee prices, and reliance on middlemen for farming capital. The visit also identified the roles of local government and potential land for development in Talang Pisang.

The second site visit, held from November 15-19, 2023, focused on post-harvest training for coffee farmers and the presentation of post-harvest processing facilities. Activities included coordinating the training with the Gunung Patah Farmers Group, observing potential construction sites for post-harvest facilities, and conducting training sessions on both dry (natural) and wet (full wash) coffee processing methods. The training involved 25 participants from the Gunung Patah Farmers Group and featured discussions on facility development plans. Concurrently, the AMF team discussed the CSR program implementation and community empowerment criteria with the EBTKE team during their visit.

4. CROSS-CUTTING INITIATIVE

The CSR program is aligned with the International Finance Corporation (IFC) Environmental and Social Standards (ESS) Framework 2017 and the Sustainable Development Goals (SDGs) of Indonesia. It focuses on:

1. ESS1 - Assessment and Management of Environmental and Social Risks and Impacts: Ensuring comprehensive risk assessments and management plans to mitigate environmental and social impacts.
2. ESS6 - Biodiversity Conservation and Sustainable Management of Living Natural Resources: Promoting practices that support biodiversity conservation and sustainable use of natural resources.
3. ESS10 - Stakeholder Engagement and Information Disclosure: Maintaining transparent and inclusive stakeholder engagement throughout the program implementation.

The Corporate Social Responsibility (CSR) program in the SERD geothermal project area aligns with the International Finance Corporation (IFC) Environmental and Social Standards (ESS) Framework 2017 and Indonesia's Sustainable Development Goals (SDGs). It prioritises comprehensive risk assessments, biodiversity conservation, stakeholder engagement, and transparent information disclosure to address environmental and social challenges

The CSR initiatives also contribute to several SDGs, including:

1. Goal 1: Ending poverty by enhancing the economic resilience of coffee farmers.
2. Goal 5: Achieving gender equality by empowering women farmers.
3. Goal 8: Promoting sustained, inclusive, and sustainable economic growth.
4. Goal 13: Taking urgent action to combat climate change and its impacts.
5. Goal 15: Protecting, restoring, and promoting sustainable use of terrestrial ecosystems.

5. CONCLUSIONS

The strategic CSR approach of Supreme Energy Rantau Dedap aims to empower coffee farmers by addressing the dual challenges of climate change and market positioning. Through financial inclusion, capacity building, sustainable practices, and fair trade initiatives, the program seeks to enhance the resilience and livelihood of coffee farmers. By aligning with international standards and contributing to global sustainability goals, SERD demonstrates its commitment to fostering a sustainable and equitable coffee industry in South Sumatra.

REFERENCES

CSR SERD Progress Report. (2023). Anwar Muhammad Foundation

Krantz, L. (2001). The sustainable livelihood approach to poverty reduction. SIDA. *Division for Policy and Socio-Economic Analysis*, 44, 1-38.

Liddle, J. (2018). Aligning vertical structures and horizontal relationships: collaborative leadership and accountability mechanisms to enhance economic growth in England. *International Review of Administrative Sciences*, 84(4), 659-674.

Qi, L., Mito, H. R. B., & Akter, M. (2024). Social Enterprise Transformation and Its Effects on Socio-economic Development: A Comparative Case Study of Developed and Developing Countries. *Journal of the Knowledge Economy*, 1-20.

Sarvina, Y., June, T., Sutjahjo, S. H., Nurmalina, R., & Surmaini, E. (2023). Projection of Robusta Coffee's Climate Suitability for Sustainable Indonesian Coffee Production. *International Journal of Sustainable Development & Planning*, 18(4).

Schroth, G., Läderach, P., Blackburn Cuero, D. S., Neilson, J., & Bunn, C. (2015). Winner or loser of climate change? A modeling study of current and future climatic suitability of Arabica coffee in Indonesia. *Regional Environmental Change*, 15, 1473-1482.

Serrat, O. (2017). *The sustainable livelihoods approach*. Knowledge solutions: Tools, methods, and approaches to drive organizational performance, 21-26.

Shen, W., Nie, Y., Long, C., Song, Z., Zhang, Q., & Tang, D. (2022). Research on the mechanism of collaborative value Co-creation of enterprise–science community: a case study based on the green brand maoduoli. *Sustainability*, 14(22), 15439.

Wright, D. R., Bekessy, S. A., Lentini, P. E., Garrard, G. E., Gordon, A., Rodewald, A. D., ... & Selinske, M. J. (2024). *Sustainable coffee: A review of the diverse initiatives and governance dimensions of global coffee supply chains*. Ambio, 1 -18.

Preliminary Design of Waste Heat Recovery System Using Spiral Heat Exchanger from Geothermal Brine for Direct Use Utilization

Khasani[1,2], Shata Pramudya Ananda[1], Kevin Stephen Setiawan[1], and Andhika Putera Utama[3]

[1]Department of Mechanical and Industrial Engineering, Universitas Gadjah Mada
[2]Geothermal Research Center, Universitas Gadjah Mada
[3]PT Geo Dipa Energi (Persero)

khasani@ugm.ac.id, shatapramudya@mail.ugm.ac.id,
kevinstephen12@mail.ugm.ac.id, andhika.utama@geodipa.co.id

Keywords: Waste Heat Recovery, Geothermal brine, Spiral Heat Exchanger, Direct use, Dieng field

ABSTRACT

Most of the liquid dominated geothermal fields, such as Dieng, produce a significant quantity of hot brine that exits the separator. They still have enough pressure and temperature to be utilized to optimize the geothermal resource. However, most geothermal brines contain silica that may deposit in the brine pipelines and other equipment. The presence of silica deposition will afftect the operation and maintenance scenario including costs. The main component of a Waste Heat Recovery System is the heat exchanger. Since the main consideration of the study is the formation of deposited silica scale in the heat exchanger, the selection of heat exchanger type is crucial, hence the Spiral Heat Exchanger was chosen for ease of maintenance. The objective of this study is to evaluate the effectiveness of the designed heat transfer to extract heat from geothermal brines to the surface water to be utilized further, such as for water and space heating. This technology can be applied in locations like Dieng since hotels and homestays continue to use gas as their primary energy source, which is costly. The research project adopts analytical and computational studies using Ansys Fluent. From the given brine data and selected heat exchanger, the calculation indicated that the dimensions of the heat exchanger consist of a shell diameter of 563 mm, a spiral diameter of 543 mm and the number of spiral rotations of 10. Variations in mass flow rates of 0.25 kg/s, 0.5 kg/s, 1 kg/s, 1.4 kg/s, 2 kg/s, and 3 kg/s resulted in effectiveness values of 80.0%, 76.5%, 72.1%, 68.9%, 66.2% and 64%, respectively. The mass flow rate affects the total heat transfer rate, effectiveness, and pressure drop in the heat exchanger.

1. INTRODUCTION

One of the main concerns for most geothermal developers is to optimize their resources. It can be started from the very upstream subsurface side, i.e., monitoring reservoir performances to the downstream power plant side, such as utilizing “waste” brine leaving the separator. It is fortunate that most of geothermal systems in Indonesia are categorized as high enthalpy water dominated systems, so that they produce brines on the surface with large amount. Recently, many developers are utilizing this brine for electricity generation using Organic Rankine Cycle (ORC) binary power plant for additional power output. Hence, the power plant efficiency and revenue in the end will increase.

However, from the social point of view, the developers or companies have a mission that they are not only as business entities but also as social institutions, namely Corporate Social Responsibility (CSR) program. CSR program is not only in the form of charity but also empowering the community surrounding their working areas with their resource. One of the advantages by involving community directly or indirectly related to geothermal resource within their areas, it will help geothermal industry to promote geothermal also as their opportunity to get better live economically and environmentally. Hence, better acceptance for geothermal energy by the community or public can be achieved.

Dieng has been known as a tourist destination area where currently it does not need promotions to increase the level of tourist arrivals, both domestic and overseas. The required current situation is how to make tourists feel at home and comfortable staying longer in Dieng. One of the problems in Dieng is that it is very cold especially at night. Therefore, the facilities that are most needed are hot water for bathing and space heating in homestays. At present, in Dieng Kulon there are about 350 homestays, while overall in the Dieng area, which includes 7 villages, there are around 1500 homestays. Currently, to meet the need for hot water, all homestays use LPG as an energy source and only around 2% of homestays have installed space heating facilities. Meanwhile, Dieng is well known as one of the geothermal energy producers, which it can be utilized for this purpose. The benefits of using this energy are that apart from the wider use of green and clean energy from the environmental point of view, it is also expected that it will reduce the operational costs from economical consideration.

Meanwhile, in Dieng area there is an electricity producer company, namely PT. Geo Dipa Energi (Persero) which has operated the geothermal power plant for almost 20 years. In their operation, there is brine which still has sufficient heat with a ranging temperature of 160°C - 180°C. Considering this potential, it would be very beneficial if this brine is optimized by extracting this heat energy, including for bathing and space heating. However, since the implementation of this project involves many stake holders, all of them must be aware that all aspects of its development including partnership, social responsibility, business, and the final target is that the acceptance of geothermal energy by the community become crucial issues that must be handled. Another important activity that must be prepared is the preliminary design of the technology of the heat recovery from the technical point of view, particularly for Dieng.

2. PROPOSED TECHNOLOGY

2.1 Proposed System Configuration and Process

In this study, hotter geothermal brine leaving the separator is used to heat the colder surface ground water that will be utilized for some purposes, for example for bathing and/ or space heating as illustrated in Figure 1. To extract the heat from the brine, heat exchanger technology is used with ground water as the heat carrier medium for further utilization. The heated ground water is circulated through a closed piping system which is equipped with a flow rate, temperature and pressure measurement and control system, so that the performance of the waste heat recovery system can be achieved and operational safety is maintained. However, one of the problems faced in the utilization of brine from PT Geo Dipa Energi is the possibility of silica scaling deposition. For this reason, it is necessary to anticipate by preventive or corrective methods. The preventive method is carried out by adding inhibitors to prevent scaling with the consequence of additional operational costs. Meanwhile, the corrective method is carried out by designing equipment that are relatively easy to maintain. The colder brine leaving the heat exchanger then is transported to cooling pond or reinjection well.

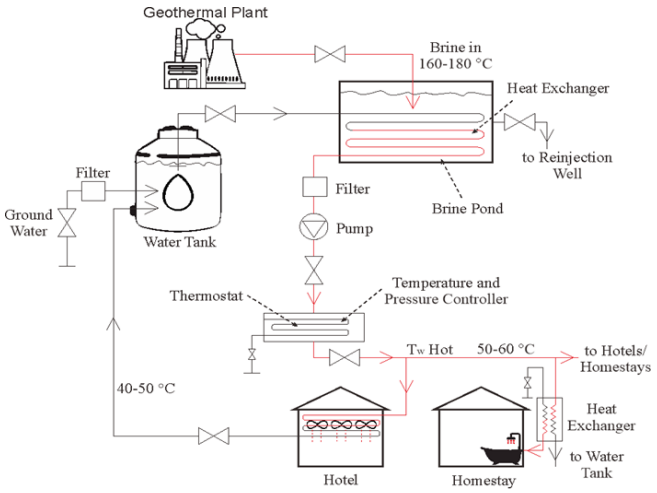

Figure 1: The proposed installation of waste heat recovery from geothermal brine for bathing and space heating.

2.2 Proposed Spiral Plate Heat Exchanger

In this study, we focus on the design and analysis of the proposed heat exchanger since it becomes the main and crucial component, especially in Dieng case. From the technical point of view, the main consideration of designing heat exchanger for heat recovery from brine in Dieng is its high potency of silica scaling formation inside the heat exchanger. For this reason, Spiral Plate Heat Exchanger (SPHE) is adopted since its easy maintenance. SPHE is a type of heat exchangers that use a spiral design to transfer heat between two fluids. It consists of two concentric spiral flow channels, one for each fluid, with the fluid flowing in the opposite direction. The channel is sealed and connects to a port on the cover, and its design optimizes effectiveness of transfer of heat and space. It also making it easier for manual cleaning. SPHE is very suitable for geothermal brine which tends to cause deposition due to high silica content. Due to its single channel geometry and continuously curved, this design creates high flow turbulence with high shear stress which reduces the risk of fouling. Channel geometry sole also creates a scrubbing effect that helps cleaning accumulation of deposits as they form. This effect will ensure that it remains high value of heat transfer that occurs in the heat exchanger. Figure 2 represents the proposed Spiral Plate Heat Exchanger.

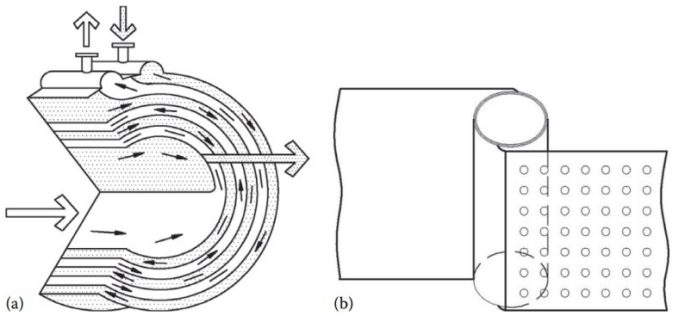

Figure 2: The schematic diagram of proposed Spiral Plate Heat Exchanger (a) unit and (b) two-plate design (with studs or plain). (Thulukkanam, 2013).

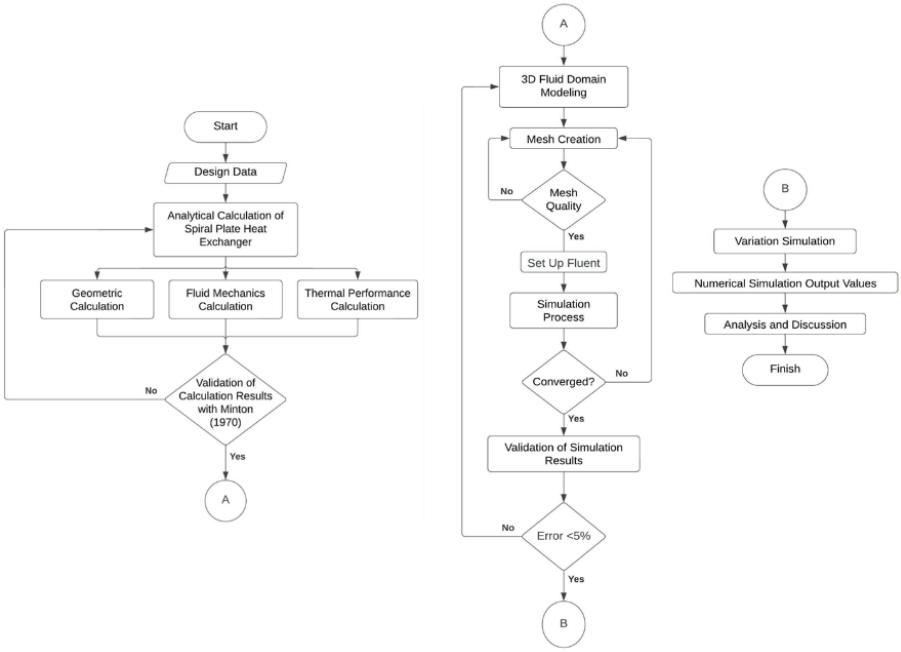

Figure 3: The flow chart of research steps and analysis.

3. METHODOLOGY

Both analytical and numerical methods are used for designing and evaluating the heat recovery system, particularly for the heat exchanger component as illustrated in Figure 3. Analytical method is adopted to design the geometry and dimension of heat exchanger, while the numerical (simulation) method is useful for understanding the physical phenomenon of the fluids from fluid mechanics and heat transfer point of views. We can also compare both results for validation of the calculation and the simulation at the same time.

3.1 Input Parameters

Input parameters for fluid and heat exchanger materials are presented in Table 1 and Table 2, respectively. In this study, the design of spiral plate heat exchanger is based on one proposed by Minton (1970).

Table 1: Input of fluid properties.

Properties	Value	Unit
Cold fluid inlet temperature ($T_{cold,in}$)	10	[°C]
Hot fluid inlet temperature ($T_{hot,in}$)	160	[°C]
Density (ρ)	998.2	[kg/m^3]
Specific heat (c_p)	4182	[J/kg K]
Thermal conductivity (k)	0.6	[W/m K]
Dinamic viscosity (μ)	0.001003	[kg/m s]

Table 2: Input of stainless-steel heat exchanger plate properties.

Properties	Value	Unit
Density (ρ)	8030	[kg/m^3]
Specific heat (c_p)	502.48	[J/kg K]
Thermal conductivity (k)	173073	[W/m K]

3.2 Analytical Approach

Analytical calculation refers to the basic governing heat transfer equation as well as the empirical equation introduced by Minton (1970). Furthermore, the basic dimensions of the spiral and plate dimensions follow the calculation results proposed by Shirazi et al. (2020) since it has the best thermal effectiveness. Then variations in the mass flow rate are carried out at the inlet of the two fluids, namely 0.25 kg/s, 0.5 kg/s, 1kg/s, 1.4 kg/s, 2kg/s, and 3 kg/s. With these six data variations, the values of the outlet temperature, pressure drop, total heat transfer rate and thermal effectiveness of the heat exchanger can be calculated using the log mean temperature difference (LMTD) method.

3.2.1 Geometrical Calculation

Geometrical calculations are the design basis for the size of the heat exchanger. In this study, only one type of geometrical design was used and then variations in the fluid mass flow rate were given. The plate sizes and basic geometries used in heat exchangers are presented in Table 3 that is proposed by Shirazi et al. (2020). These values are adopted with the consideration that this geometry is used for validation purpose with numerical study.

Table 3: Geometry of basic dimensions of proposed heat exchanger (Shirazi et al., 2020).

Properties	Value	Unit
Spiral inner diameter (D_i)	0.2032	[m]
Plate length (L)	11.55	[m]
Plate width (H)	0.5334	[m]
Plate thickness (x)	0.003175	[m]
Gap between plates for cold fluid (b_c)	0.00595	[m]
Gap between plates for hot fluid (b_h)	0.00476	[m]

By using the equations adopted from Dongwu (2003), Núñez et al. (2007) and Minton (1970) the parameters of spiral rotation, hydraulic diameter, outer diameter, free flow area, and heat transfer area can be obtained. These parameters are depicted in Table 4, while the calculated dimensions are illustrated in Figure 4.

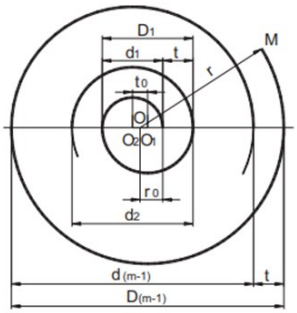

Figure 4: Schematic diagram of semi-circled spiral (Dongwu, 2003).

Table 4: Calculated parameters of proposed heat exchanger.

Parameters		Value	Unit
Spiral rotation (N)		10	[-]
Hydraulic diameter (L)	Cold fluid	0.0118	[m]
	Hot fluid	0.00944	[m]
Outer diameter (D_s)		0.5417	[m]
Free flow area (A_f)	Cold fluid	0.00317	[m]
	Hot fluid	0.00254	[m^2]
Heat transfer area (A)		12.3215	[m^2]

3.2.2 Thermofluids Calculation

Thermofluids parameters are affected by the fluid output from the heat exchanger. In this study, there are several variations in the mass flow rate to study its effects on thermofluids parameters. To give an overview the thermofluids design parameters, a mass flow rate value of 0.5 kg/s is used for cold fluids and hot fluids to demonstrate its effects. The values of the fluid properties used in the heat exchanger are presented in Table 1 while the calculated fluid mechanics parameters are listed in Table 5, while for thermal performances are presented in Table 6.

Table 5: Calculated fluid mechanics parameters for a given mass flow rate of 0.5 kg/s.

Parameters		Value	Unit
Reynolds number (Re)	Cold fluid	1848	[-]
	Hot fluid	1852	[-]
Critical Reynolds number (Re_{cr})	Cold fluid	5872	[-]
	Hot fluid	5471	[-]
Average velocity (V_f)	Cold fluid	0.158	[m/s]
	Hot fluid	0.197	[m/s]
Prandtl number (Pr)		6.99	[-]
Nusselt number (Nu)	Cold fluid	22.805	[-]
	Hot fluid	22.768	[-]
Pressure drop (ΔP)	Cold fluid	1807.3	[Pa]
	Hot fluid	2521.8	[Pa]

Table 6: Calculated thermal performances for a given mass flow rate of 0.5 kg/s.

Parameters		Value	Unit
Heat transfer coefficient (h)	Cold fluid	1160.77	[W/m^2 K]
	Hot fluid	1450.13	[W/m^2 K]
Total heat transfer coefficient (U)		576.52	[W/m^2 K]
Heat capacity rate ratio (C)		-1	[-]
Number of Transfer Units (NTU)		3.397	[-]
Temperature Difference Correction Factor (F_T)		0.962	[-]
Thermal effectiveness per Rotation (ε)		72.2	[%]
Total thermal effectiveness (ε_{tot})		76.5	[%]
Fluid outlet temperature (T_{out})	Cold fluid	124.86	[°C]
	Hot fluid	45.14	[°C]
Logarithmic Mean Temperature Difference (ΔT_{LM})		35.14	[K]
Total heat transfer rate (Q)		240.2	[kW]
Maximum total heat tranfer rate (Q_{max})		313.6	[kW]

3.2.3 Summary of Analytical Calculation

Analytical calculations were carried out on geometry, fluid mechanics and thermal performance by varying the independent variable mass flow rate at the heat exchanger inlet for both fluids. The calculated variations in mass flow rate are 0.25 kg/s, 0.5 kg/s, 1 kg/s, 1.4 kg/s, 2 kg/s, and 3 kg/s. The expected output from the calculation includes the outlet temperature and pressure drop of the cold fluid and hot fluid, the total heat transfer rate and the thermal effectiveness of the heat exchanger. A summary of the results of SPHE analytical calculations is presented in Table 7.

Table 7. Summary of analytical calculations for mass flow rate variation at the inlet.

Outputs	Inlet Mass Flow Rate [kg/s]					
	0.25	0.5	1	1.4	2	3
Flow Type	Laminar	Laminar	Laminar	Laminar	Turbulent	Turbulent
Re	925.29	1850.58	3701.16	5181.63	7402.33	11103.49
ΔP_{cold} [kPa]	1.194	1.807	2.793	3.481	16.075	33.087
ΔP_{hot} [kPa]	1.678	2.522	3.864	4.791	27.657	56.689
$T_{c,out}$ [°C]	130.1	124.9	118.2	114.3	109.5	103.1
$T_{h,out}$ [°C]	40	45.2	51.9	55.8	60.6	67.0
Q [kW]	125.48	240.17	452.42	610.24	831.51	1167.52
ε_{tot} [%]	80.0	76.6	72.2	69.5	66.3	62.1

3.3 Numerical Simulation Approach

From the analytical calculation described in Section 3.1 and the relevant data, the numerical simulation using Computational Fluid Dynamics (CFD) with Ansys 2023 R1to study the physical phenomenon of the fluids and the performance of the SPHE was carried out. The steps of numerical simulation are depicted in Figure 3, while in term of CFD the main activities consist of pre-processing, solving and post-processing (ANSYS, 2017).

3.3.1 Pre-Processing

In this sub-process, a three-dimensional geometry was created from two spiral plates as the basic geometry of the spiral plate heat exchanger. Then, the spiral plate geometry was transferred into .itp format to Ansys SpaceClaim to continue the 3D model creation process, namely creating the fluid domain as shown in Figure 5, the inter-fluid partition plate and the spiral plate heat exchanger cover. The next activities following this model creation included mesh independence test, and mesh arrangement that is illustrated in Figure 6.

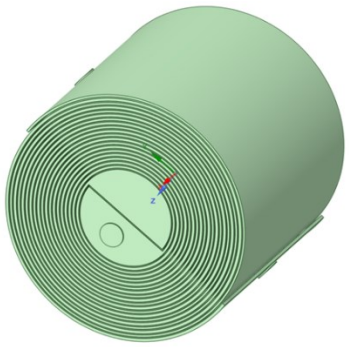

Figure 5: Fluid domain of 3D model of spiral plate heat exchanger.

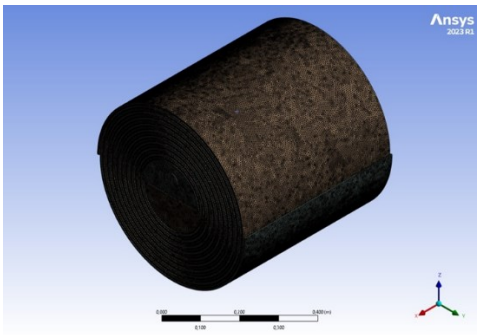

Figure 6: Result of fluid domain meshing of spiral plate heat exchanger.

3.3.2 Solving

This process was peformed in the set-up menu in Ansys Fluent that consisted of general set-up (steady or transient), model simulation (energy, viscous model, k-epsilon model, near-wall treatment), material of fluids (density, specific heat, thermal conductivity, viscosity), plate material (density, specific heat, thermal conductivity), cell zone conditions (water-liquid, stainless-steel), inlet-outlet boundary conditions (mass flow rate, turbulence specification, turbulent intensity, hydraulic diameter, temperature, thermal conditions), mesh interfaces (coupled wall), solution method (pressure velocity coupling, spatial discretization), solution controls (under-relaxation factors), initialization methods (hybrid inisialization), running (iteration calculation).

3.3.3 Post-Processing

After the solving process is carried out, the results of the simulation will be obtained. The simulation results can be visualized using Ansys CFD-Post software. In this study, the simulation results include temperature distribution, pressure distribution and flow field in the spiral plate heat exchanger.

4. RESULTS AND DISCUSSION

4.1 Validation

Simulated results were validated with analytical calculation on the spiral plate heat exchanger design that was made in the Ansys software. The validation stage was carried out based on simulations with fluid properties by Shirazi et al. (2020) compared with the results of analytical calculations. The properties of cold and hot fluids are shown in Table 8, while validation results are presented in Table 9.

Table 8: Properties of cold and hot fluids (Shirazi et al., 2020).

Properties	Cold Fluid	Hot Fluid
Mass Flow Rate [kg/s]	0.7465	0.7843
Inlet Temperature [°C]	60	200
Density [kg/m^3]	843	843
Specific Heat [J/kg K]	2763.288	2972.628
Thermal Conductivity [W/m K]	0.32339	0.34789
Dynamic Viscosity [kg/m s]	0.008	0.00335

Table 9: Validation result for SPHE simulation.

Output	Analytic	Simulation	Deviation [%]
Cold Fluid Outlet Temperature [°C]	150.46	154.06	2.4
Hot Fluid Outlet Temperature [°C]	120.25	119.06	0.99
Total Heat Transfer Rate [kW]	186.283	192.0	2.87
Total Thermal Effectiveness [%]	64.50	66.35	2.87

The difference between the analytical calculation and the simulation results shows a small deviation value and is within the deviation tolerance criteria. This shows that the simulation results are quite accurate and can describe the actual conditions of the spiral plate heat exchanger. Thus, the simulation process can be continued for simulations with variations in mass flow rate with water-liquid fluid properties.

4.2 Simulated Results

4.2.1 Contours for Main Parameters

After the simulations on the validation data that had been carried out, pictures of the temperature distribution contour, pressure distribution contour and streamline that occur in the heat exchanger were obtained as shown in Figure 7.

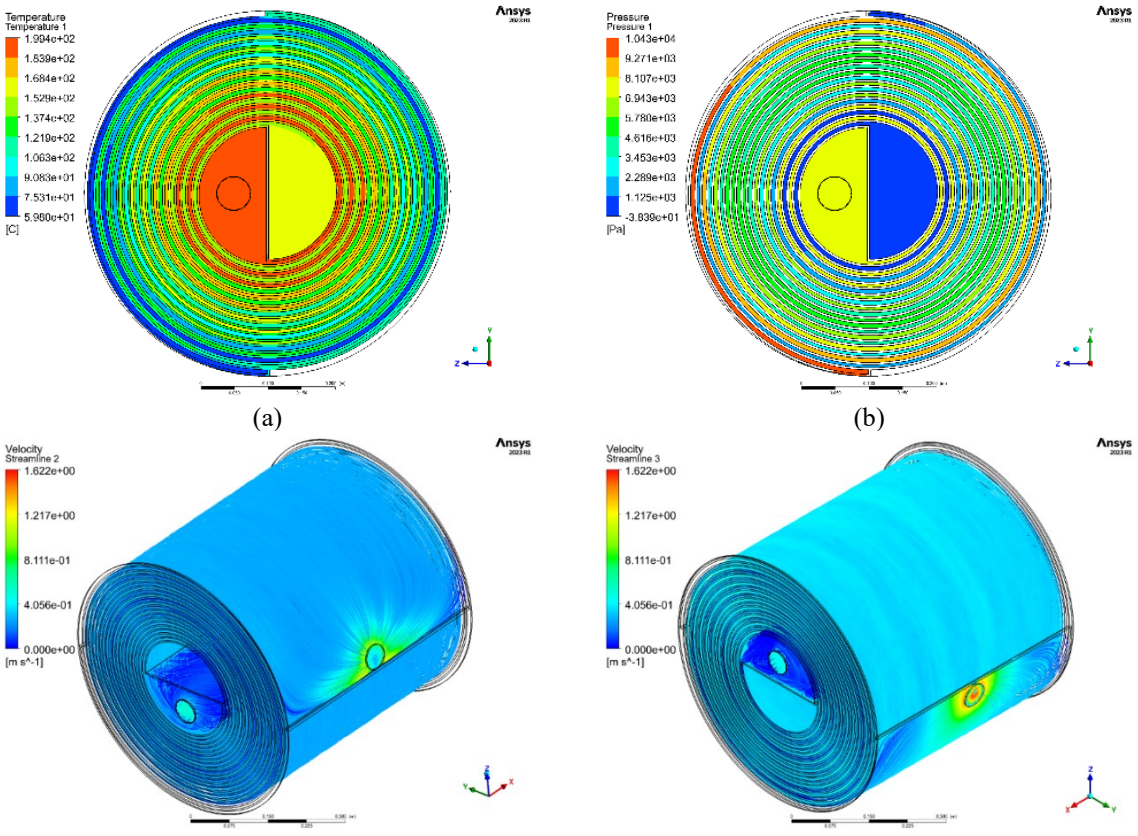

Figure 7: Main parameter contours: (a) temperature, (b) pressure, (c) cold streamline fluid, (c) hot streamline fluid.

The temperature distribution contour in Figure 7 (a) is taken from SPHE in the YZ Plane with a value of X = 0 m. It can be recognized the different color gradients in each fluid due to heat transfer between fluids, resulting in the

temperature of the stainless-steel plate changing, influenced by the temperature of the fluid. Based on the results of simulation data, the average temperature of the stainless-steel plate is 135.89°C. The pressure distribution contour in Figure 7 (b) is taken from SPHE in the YZ Plane with a value of X = 0 m. In can be noted the different color gradients in each fluid that represents pressure distribution gradient to consider the maximum pressure drop allowed in the SPHE. In the simulation, the outlet pressure value is determined by a gauge pressure of zero, so that the largest pressure will occur at the SPHE inlet section. Figure 7 (c) and (d) show the streamlines for cold and hot fluids, respectively. The average speed of hot fluid flow is faster than cold fluid, namely 0.303 m/s for hot fluid and 0.237 m/s for cold fluid, so the hot fluid is lighter than cold fluid. The maximum speed occurs at the outlet of both fluids, namely 0.95 m/s for the hot fluid and 0.485 m/s for the cold fluid.

4.2.2 Effects of Mass Flow Rate

After validation of the spiral plate heat exchanger simulation results was carried out, the heat exchanger simulation variations were continued with six different mass flow rates, i.e., 0.25 kg/s, 0.5 kg/s, 1 kg/s, 1.4 kg/s, 2 kg/s, and 3 kg/s to evaluate the differences in performance among these variations. No geometric changes were made to this variation of the simulation. Data on the properties of the water-liquid fluid and stainless-steel plates used in the Ansys Fluent software are in accordance with Tables 1 and 2. The results of simulation is depicted in Table 10.

Table 10: Summary of simulated results for different mass flow rates at the inlet.

Outputs	Mas Flow Rates at Inlet [kg/s]					
	0.25	**0.5**	**1**	**1.4**	**2**	**3**
$T_{cold,out}$ [°C]	134.43	131.49	126.71	122.57	120.01	113.36
$T_{hot,out}$ [°C]	36.33	40.72	46.47	49.36	54.18	59.78
ΔP_{cold} [kPa]	0.414	1.362	4.717	8.706	16.751	35.507
ΔP_{hot} [kPa]	0.669	2.169	7.586	14.023	27.122	57.762
Q [kW]	130.74	254.39	489.62	668.57	922.35	1313.99
ε_{tot} [%]	83.37	81.11	78.06	76.13	73.52	69.83
$T_{plate,avg}$ [°C]	78.56	79.52	79.65	78.97	80.06	79.76

4.2.3 Pressure Drop

The comparison between analytical calculation and simulation for pressure drops of the cold and hot fluids is shown in Figure 8.

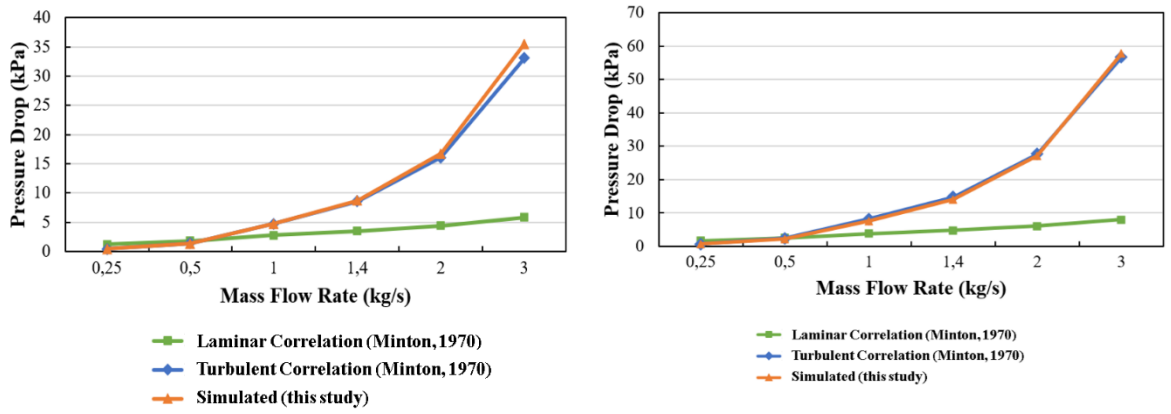

(a) (b)

Figure 8: Pressure drops in the fluids: (a) cold fluid, (b) hot fluid.

From Figures 8 (a) dan (b), it can be noted the higher the mass flow rate value, the higher the pressure drop value. Based on the results of analytical calculations, when the fluid speed reaches the critical Reynolds number, the laminar fluid flow will experience turbulence, causing a very high increase in pressure drop. Therefore, for spiral plate heat exchangers, the recommended mass flow rate value is below 1.4 kg/s with a Reynolds number below its critical value, because the type of flow is laminar which has a pressure drop below 10 kPa as recommended by Minton (1970). This will indirectly reduce heat exchanger manufacturing and maintenance costs. However, the pressure drops simulation results show a large percentage deviation from the results of analytical calculations for fluids with laminar flow. The reason for the difference is because the Ansys Fluent software with the standard viscous k-epsilon model can only determine that the flow acting on the spiral plate heat exchanger is turbulent, where the software uses a general calculation formula, whereas in the SPHE analytical calculation formula

presented by Minton (1970). There is an empirical pressure drop formula which is influenced by the value of the Reynolds number and its critical value of the fluid. It is proven that the trend of differences between simulation results and analytical calculation results is in line for cold and hot fluids, with an average error of only 4.53%.

4.2.4 Outlet Temperatures

The comparison between analytical calculation and simulation for outlet temperatures of the cold and hot fluids is shown in Figure 9.

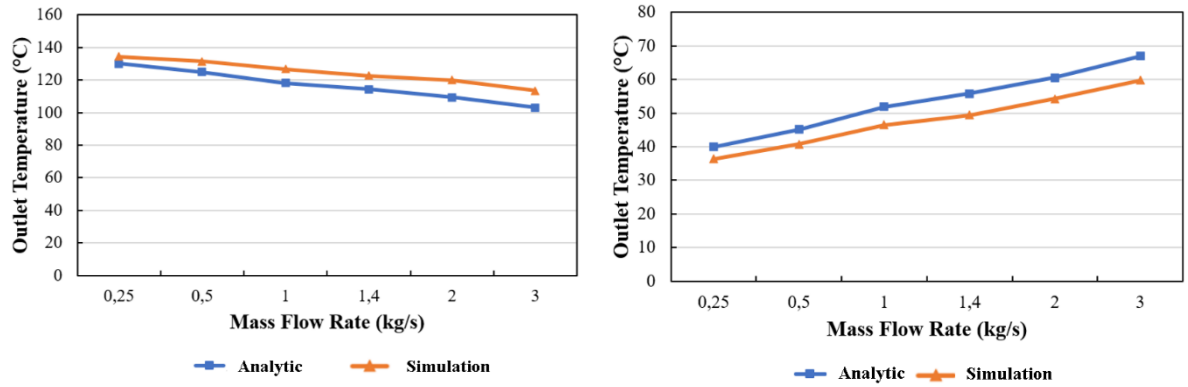

Figure 9: Outlet temperatures of the fluids: (a) cold fluid, (b) hot fluid.

From Figures 9 (a) and (b) it can be seen that variations in mass flow rate will affect cold fluids and hot fluids. The higher the mass flow rate, the cold fluid outlet temperature decreases, while the temperature of the hot fluid increases. This change trend is in line with the results of analytical calculations and simulations for both fluids, with an average error of 8.75%. External factors from fluid properties, such as fouling and scaling at a certain temperature will affect the selection of the appropriate mass flow rate.

4.2.5 Total Heat Transfer Rate and Total Thermal Effectiveness

Figure 10 shows the results of analytical calculations with simulation results for the total heat transfer rate and total thermal effectiveness with variations in the inlet mass flow rates.

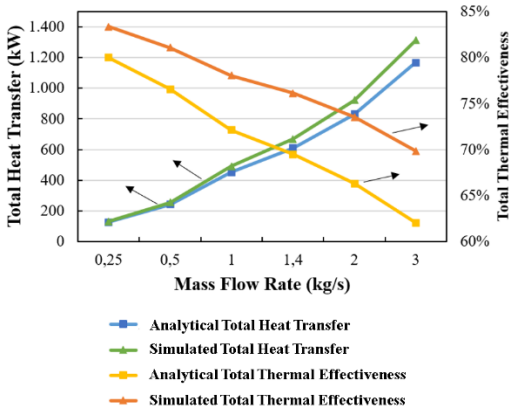

Figure 10: Total heat transfer and total thermal effectiveness for different mass flow rates.

From Figure 10, it can be observed that the mass flow rate greatly affects the total heat transfer rate that occurs in the heat exchanger. The higher the mass flow rate, the greater the total heat transfer rate. However, because a high mass flow rate causes a greater pressure drop, it will affect the total thermal effectiveness of the heat exchanger which decreases. It can also be noted that the analytical results and simulation results produce the same trend, with an average error of 8.57%.

5. CONCLUSIONS

From the discussion described in the previous sections, some of the important findings can be summarized as follows,

- Spiral Plate Heat Exchanger (SPHE) was adopted in this preliminary design study since its easy maintenance as the main consideration.
- The effect of mass flow rate on output results, an increase in mass flow rate will

    - lower the cold fluid outlet temperature, and increase the hot fluid outlet temperature,
    - increase the pressure drop and become more significant above a mass flow rate of 1.4 kg/s,
    - increase the total heat transfer rate and reduce thermal effectiveness.
- Thermal effectiveness of simulation results for mass flow rates of 0.25 kg/s, 0.5 kg/s, 1 kg/s, 1.4 kg/s, 2 kg/s, and 3 kg/s are 83.37%, 81.11%, 78.05%, 76.13%, 73.52%, and 69.82%, respectively.

ACKNOWLEDGEMENT

This research is funded by the Departement of Mechanical and Industrial Engineering, Faculty of Engineering, Universitas Gadjah Mada under the contract number of 1542901/UN1/FTK.1/III/PT/2024.

REFERENCES

ANSYS.: *ANSYS Fluent Users Guide*. SAS IP, (2017).

Dongwu, W.: Geometric Calculations for the Spiral Heat Exchanger, *Chem. Eng. Technol.*, **26**, (2003), 592–598.

Minton, P. E.: Designing spiral plate heat exchangers, *Chem. Eng.*, **77(4)**, (1970), 103–112.

Núñez, P.M., Dávalos, L. C., and Flores, M.: Alternative sizing methodology for compact heat exchangers of the spiral type. *Heat Transf Eng.*, **30**, (2009), 744–750.

Shirazi, A. H. S., Nasr, M. R. J., and Ghodrat, M.: Effects of Temperature Differences in Optimization of Spiral Plate Heat Exchangers, *Process Integration and Optimization for Sustainability*, **4**, (2020), 391–408.

Thulukkanam, K.: Heat Exchanger Design Handbook (2 ed.), CRC Press, (2013).

Studithermal: An Integrated Geothermal Learning

Vera Aprianti, Muhammad Sidqi, Victor Gomgom P.S,
Budiman Dwi Putra, M. Alzaid Ponka, Theresia Yolanda Sagala, Muchamad Harry,
Hendryansyah William, Bagus M. Iqbal, Welly Prabata, and Jantiur Situmorang

AILIMA, CIBIS Business Park, TB Simatupang, Jakarta, Indonesia

vera.aprianti@ailima.co.id

Keywords: geothermal education, learning, data management, data analytics, machine learning, cloud computing, JIWA

ABSTRACT

Given the importance of improving data quality to accelerate Indonesia's geothermal development in achieving Net Zero emissions, it is essential for current geothermal professionals to possess comprehensive geothermal literacy, technical expertise, industry insights, and sustainability awareness, combined with proficiency in the latest technology to optimize data value and mitigate risks. However, the accessibility of educational programs to thoroughly accommodate such criteria, particularly for undergraduates aiming for careers in the geothermal industry is unavailable. Furthermore, the gap between undergraduate students' knowledge and the geothermal industry's needs remains a challenge for the education sector. Studithermal, a learning program initiated by PT. Anugerah Indonesia Lima (AILIMA) in collaboration with Indonesia's Ministry of Education, Culture, Research, and Technology (MoECRT), is an innovative effort that aims to address this issue. It offers a comprehensive learning pathway via JIWA Cloud Computing System that combines advanced technology in collaborative data management, analytics, modeling, and machine learning with fundamentals and real-world experience in the industry to shape the future leaders of energy.

1. INTRODUCTION

1.1 Background

Geothermal energy presents a compelling solution for the global transition to clean energy. Indonesia, a country rich in geothermal potential, recognizes its strategic importance in achieving its Net Zero emissions goals. At the same time, geothermal can significantly contribute to a clean energy future alongside other renewables. However, the geothermal sector faces challenges related to data quality and the technical expertise of professionals. Improving data quality is crucial for developing and operating geothermal projects. Practicing data collection, entry, and governance by experts working together is essential in almost all work areas so it can be analyzed thoroughly for decision-making (Sidqi et al., 2024). Equally important is the quality of the human resources. A skilled workforce is essential for efficient geothermal development and operation. Therefore, investing in geothermal education is crucial for creating a competent workforce and unlocking Indonesia's full geothermal potential. By enhancing the skills of future workers, productivity in this sector is expected to increase.

Despite the recognized importance of geothermal energy, the lack of educational programs in local communities related to geothermal projects is one of the biggest challenges because it causes community resistance to this project in various regions (Umam et al., 2018). Moreover, no comprehensive educational programs are specifically designed for undergraduates aspiring to enter the geothermal industry. At the university level, undergraduate students still need to be provided with specific studies in geothermal energy. Those who pursue engineering studies such as geoscience or energy encounter geothermal topics in only one or two courses, which is insufficient to gain a complete understanding of geothermal literature and practices. While master's degree programs that offer comprehensive studies in geothermal science do exist, they may not be accessible to everyone to pursue further education at that level due to cost or individual circumstances.

Meanwhile, the reality is that the industry urgently needs a workforce. Increasing the geothermal workforce in Indonesia shows that the average workforce needs are around three people for every MW generated. Thus, with an average increase of 150 MW per year, 450 workers are needed per year. This increase should be the concern of the government and stakeholders in preparing this workforce (Umam et al., 2020). The workforce requirements include geologists, geophysicists, geochemists, reservoir engineers, production engineers, drilling engineers, project engineers, power plant engineers, drillers, technicians, and other skilled personnel. This calculation is for both the exploration phase and the operation and maintenance phase. Education plays a crucial role in meeting these needs, particularly at the university level. In Indonesia, the engineering majors that study renewable energy in the geothermal field are primarily mechanical engineering, chemical engineering, physical engineering, electrical engineering, petroleum engineering, geological engineering (geology), geophysics (geophysical

engineering), and energy conversion techniques (Umam et al., 2021). This gap hinders the development of a skilled workforce capable of addressing the challenges within the geothermal sector. To support geothermal development in Indonesia, geothermal-related courses must be integrated into the university curriculum, particularly in geology, geophysics, mining, petroleum, mechanical, or chemical engineering (Saptadji, 2010). It would be even better if undergraduate students in science, technology, engineering, and mathematics (STEM) programs could be introduced to geothermal science to increase their understanding and reduce the gap between graduates'knowledge and the practical needs of employers in the geothermal sector.

1.2 Objectives

The primary goal of the Studithermal program is to bridge the gap between academic knowledge and the practical needs of the geothermal industry. This program aims to develop a comprehensive learning pathway that equips undergraduates with the necessary geothermal literacy, technical expertise, industry insights, and sustainability awareness. To advance technological training, such as collaborative data management and machine learning, the program integrates advanced technology with fundamental education to enhance data management, analytics, and modeling skills using JIWA Cloud Computing System (Prabata et al., 2021), developed by PT. Anugerah Indonesia Lima (AILIMA). The specific objectives include:

- Improving geothermal literacy among students through a robust curriculum.
- Enhancing technical skills related to geothermal data management and analysis.
- Providing industry insights and real-world experience through collaborations with industry partners.
- Fostering sustainability awareness and the application of advanced technologies in geothermal projects.

By fostering a new generation of geothermal professionals equipped with advanced technical skills and industry insights, Studithermal aims to significantly contribute to Indonesia's goal of achieving Net Zero emissions through sustainable geothermal energy development and shape the future leaders of energy.

2. STUDITHERMAL

2.1 Program Design and Implementation

Studithermal is an intensive learning program designed to create synergy between understanding technology and practical applications in the geothermal industry. This program allows undergraduate students at universities in Indonesia under the Ministry of Education, Culture, Research, and Technology (MoECRT) to study outside their campus and earn up to 20 credits, equivalent to approximately ten subjects (assuming each subject is two credits) through the national curriculum policy called the Merdeka Belajar Kampus Merdeka (MBKM). This credit conversion is facilitated by the Ministry of Education, Culture, Research, and Technology (MoECRT) and participating universities where students are enrolled in the program, allowing students to apply their learning towards their degree requirements.

During the five months, students will have the opportunity to interact and learn with industry practitioners who will guide them and help bridge the gap between academic knowledge and industry needs. The program is conducted entirely online, allowing learners from various locations to participate and gain the same quality of education.

In the First batch, Studithermal takes on the learning topic of "Applied Data Management, Analysis, Modeling, and Machine Learning for Sustainable Geothermal Energy Development." This topic was chosen because it addresses the critical need for advanced technological training in the geothermal sector, ensuring that future professionals are equipped with the skills necessary to manage, analyze, and model geothermal data effectively. Furthermore, the integration of machine learning techniques enhances the ability to optimize geothermal energy development, contributing significantly to the sustainability and efficiency of geothermal projects. A capability assessment is conducted at the beginning to determine learners' prior knowledge and ensure the curriculum meets their current level of understanding.

2.2 Learning Module

The learning pathway is structured to enhance geothermal literacy, technical skills, and industry insights among undergraduate students. The First batch is from February 2024 to June 2024, The curriculum is divided into several key modules, each designed to cover a specific aspect of geothermal energy development.

The learning activities will focus on developing soft and hard skills through practical, real-world case studies in the industry, with hands-on project assignments for each module. The learning process is divided into 11 modules (shown in Figure 2). Each module includes hands-on project assignments, allowing students to apply theoretical knowledge to industry-relevant scenarios. The first ten modules serve as preparatory modules leading to the final module, the Final Project. These initial ten modules are designed to equip students with the foundational knowledge needed to complete the Final Project. Each learning material has been collaboratively developed with

Subject Matter Experts (SMEs) using extensive experience and competencies relevant to the studied topics. SMEs are practitioners actively working in the geothermal industry, bringing valuable real-world insights and expertise, with many having over a decade of in-depth experience. In the first batch, the contributed SMEs from both AILIMA and other prominent institutions and energy industries such as the Ministry of Energy and Mineral Resources Indonesia, Supreme Energy, Pertamina Geothermal Energy, Geo Dipa Energi, Medco Power Indonesia, Sumbawa Timur Mining, ENOWA, Pertamina Hulu Energi, ENI, Sarana Multi Infrastruktur, and more.

Figure 1: Learning Design of Studithermal.

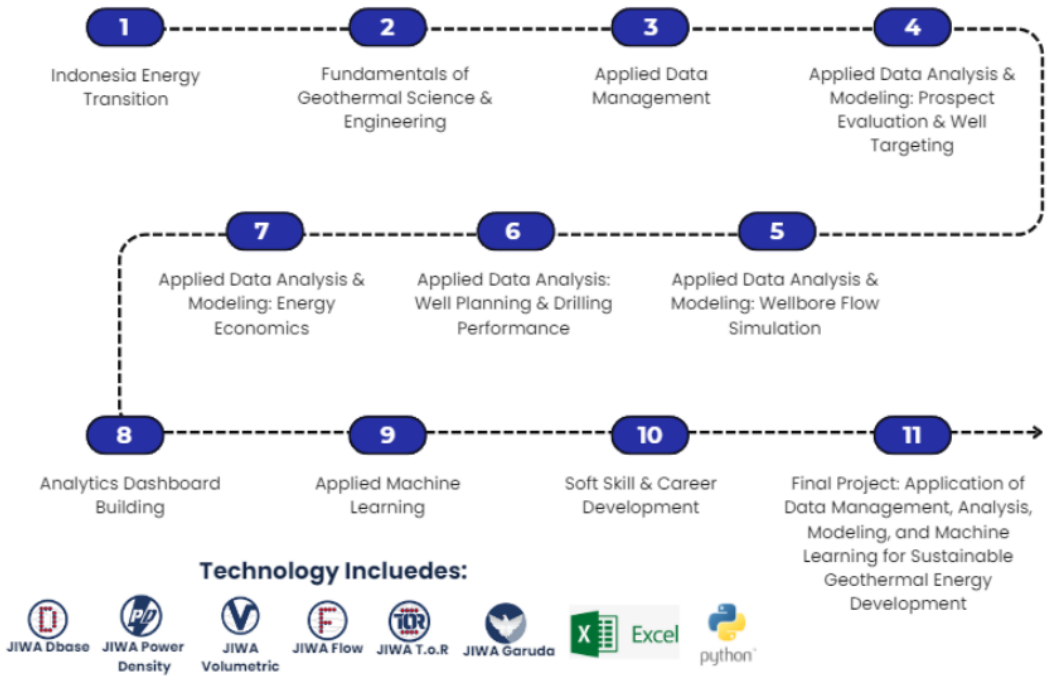

Figure 2: Curriculum Learning of Studithermal.

2.2.1 Technologies and tools

As a technology provider, particularly in the geothermal sector, AILIMA integrates specialized training into the curriculum for several of its technologies (JIWA Systems), as well as other relevant software. These technologies have already been used by various companies in the geothermal industry, making them essential skills for those beginning a career in this field. Throughout the program, students will leverage technologies, including:

2.2.2 Learning model

All learning activities in this program will be conducted fully online. The Learning Model will consist of synchronous sessions, where participants engage in real-time interaction with SMEs, mentors, and peers, as well as asynchronous sessions, where participants can access materials and complete tasks at their own pace, delivered through the JIWA Learning as a Learning Management System (LMS) developed by AILIMA. This format allows

participants from various cities in Indonesia to join the program and collaborate. Participants will have the opportunity to collaborate with others from diverse backgrounds, including different majors, hometowns, and universities.

Table 1: Software & Application usage.

Software and Application	Description
JIWA Dbase	Integrated geothermal data management and analysis in cloud system from preliminary survey, detail 3G, drilling and well testing, to operation and maintenance (O&M)
JIWA Power Density	Analytics tool to estimate geothermal resources in the early exploration stage
JIWA Volumetric	Resource and reserve estimation tool
JIWA Flow	An Artificial Intelegence to perform detail wellbore analysis for well characterization, well capacity estimation and optimization
JIWA ToR	Top of Reservoir (ToR) uncertainties estimation in the exploration stage with the probabilistic approach
JIWA Garuda	Multipurpose Machine Learning for everyone without coding
Microsoft Excel / Spreadsheet	Application for computation, organization, analysis and storage of data in tabular form
Python	An interpreted, object-oriented, high-level programming language with dynamic semantics

2.3 Participant Selection

In the first batch, a rigorous selection process was conducted to identify 100 participants from a pool of 3,489 applicants. The selection criteria included academic performance, interest in geothermal energy, personal growth and potential for future contributions to the industry. Each prospective participant will undergo a selection process involving the verification of administrative documents to ensure compatibility with the program and several initial tests. Several parameters are considered: students must be at least in their 5th semester of undergraduate program, and their major should be related to the program or come from a Science, Technology, Engineering, and Mathematics (STEM) discipline.

Figure 3: Participant Selection Process.

The selected participants come from 39 different universities across Indonesia, including both public and private institutions. They come from various study backgrounds that meet the selection criteria, ensuring a diverse cohort to promote inclusivity and a broad exchange of ideas.

This diversity in academic disciplines fosters a multidisciplinary approach, essential for addressing the complex challenges of geothermal energy development.

2.4 Project Based Learning

Project Based Learning stimulates students to actively participate in learning to maximize understanding and critical thinking capacity (Zulyusri at el., 2023). During the learning process, participants are grouped into teams and assigned mentors from AILIMA, who are geothermal engineers, to assist with day-to-day learning. Additionally, the instruction is provided by geothermal practitioners from both AILIMA and external collaborators, referred to as Subject Matter Experts (SMEs). These mentors offer continuous guidance and support throughout the program, helping to bridge the gap between academic learning and practical industry requirements. Team collaboration fosters a cooperative learning environment, encouraging participants to collectively share knowledge and tackle challenges.

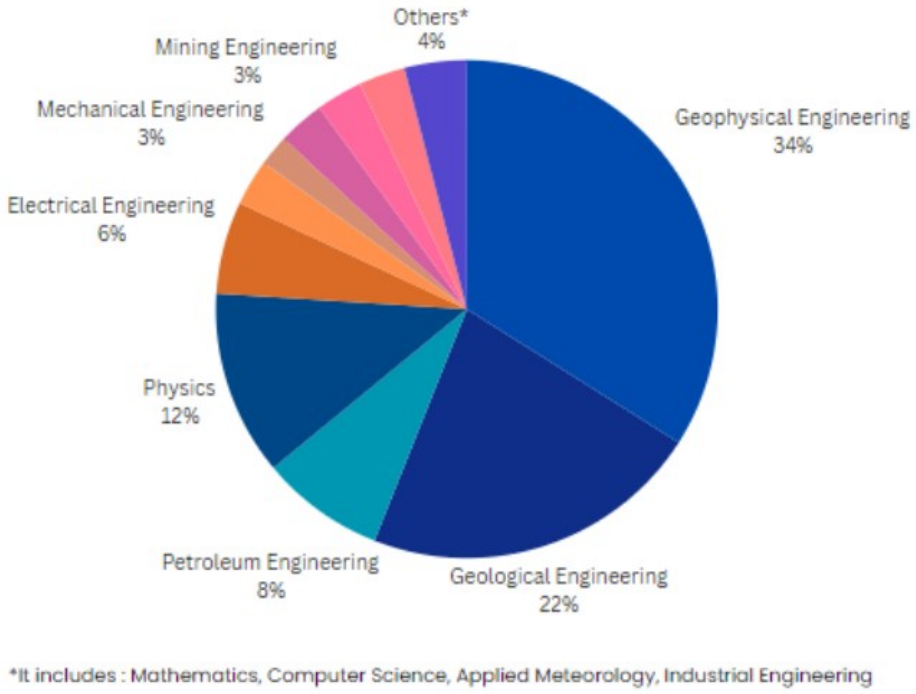

Figure 4: Pie Chart of Background Study Selected Participant batch 1.

This Approach allows participants to engage in individual hands-on project assignments related to each learning module, designed to reinforce theoretical knowledge through practical application. Towards the end of the program, participants collaborate on a final project focused on comprehensive geothermal prospect evaluation and proposing a sustainable development strategy. The project not only strengthens their technical knowledge but also cultivates key Skills: Digital Literacy, Citizenship, Working with Others, Problem-Solving & Decision Making, Self-Management, and Professionalism. The final project results are presented to a jury of experienced industry practitioners and AILIMA experts, showcasing the participants' analytical skills, collaborative problem-solving abilities, and innovative solutions. The judges evaluate the presentations based on technical accuracy, creativity, feasibility, and potential impact in the future development.

2.5 Knowledge and Skills Enhancement

Studithermal for batch 1 program concluded in June 2024, participants demonstrated significant improvements in several key competencies:

Table 2: Learning Outcomes of Studithermal.

Focus Areas	Learning Activities
Geothermal Literacy	Pre- and post-program assessments indicated a substantial increase in participants' understanding of geothermal energy principles, exploration techniques, and sustainability considerations
Technical Expertise	Practical assigments and project work led through hands-on project to enhance proficiency in data management, analysis, and modeling, as well as the application of machine learning techniques to geothermal data
Industry Insights	Collaboration with industry practioners was a critical component of the program's success. Mentorship and real-world case studies provided participants with invaluable industry insights and practical knowledge. This collaboration bridged the gap between academic learning and practical application, preparing participants for future careers in the geothemal industry

Moreover, participants who complete the program will possess extensive knowledge and skills essential for the geothermal industry, encompassing both technical and non-technical aspects critical in exploring and developing sustainable geothermal resources to support energy transition. Key roles covered included Geoscientist, Reservoir Engineer, Production Engineer, Drilling Engineer, Finance Analyst, and Project Engineer. Additionally, as digital talents, they can leverage their expertise and competencies in data analytics and machine learning. They can apply their skills as data analysts, data scientists, machine learning engineers, and/or similar roles to innovate new techniques for the geothermal industry, energy sector, or other domains.

3. GEOTHERMAL LEARNING AT AILIMA

AILIMA, as a leading learning provider focused on enhancing literacy in geothermal fields, currently offers a variety of learning programs for all audiences. The learning offerings are diverse and fullfield to participants' needs. AILIMA envisions a future where everyone has access to comprehensive, flexible, integrated, and job-relevant education in geothermal energy and technology. A systematic learning syllabus enables learners to study according to their needs, and access to learning is made easier through the JIWA Learning e-learning platform, allowing learners to study anytime and anywhere, thus ensuring that geothermal learning is accessible to everyone. There are plans to offer numerous courses with the hope of attracting even more participants to study geothermal sciences and energy, whether through the Studithermal program or other AILIMA learning initiatives.

4. SUMMARY AND RECOMMENDATION

The Studithermal program serves as a blueprint for future educational initiatives aimed at developing a skilled and knowledgeable workforce capable of advancing sustainable energy solutions. By integrating advanced technologies, practical industry experience, and comprehensive educational content, the program equipped participants with the skills and knowledge necessary to contribute to the sustainable development of geothermal energy. The collaboration with industry practitioners and the support from the MoECRT were instrumental in the program's success, providing participants with real-world insights and academic recognition. Through this initiative, AILIMA and MoECRT hope to significantly advance Indonesia's geothermal capabilities and support the country's ambition to achieve Net Zero emissions.

The success of the Studithermal program sets a precedent for future educational initiatives in the energy sector. The program's structure and methodology can be adapted and expanded to other areas of green and renewable energy, fostering a skilled workforce capable of driving sustainable development in Indonesia and beyond.

REFERENCES

Prabata, W., Situmorang, J., and Nainggolan, T.: JIWAFlow: A Cloud Computing Wellbore Simulator, *Proceedings*, 46th Workshop on Geothermal Reservoir Engineering, Stanford University, Stanford, CA (2021).

Saptadji, N. M.: Geothermal Education for Supporting Geothermal Development in Indonesia. *Proceedings World Geothermal Congress* (pp. 1-6), 2010.

Sidqi, M., Prabata, W., Situmorang, J., et al.: JIWA DBase: Integrated Geothermal Data Management and Analysis in Cloud System, *Proceedings*, 49th Workshop on Geothermal Reservoir Engineering, Stanford University, Stanford, CA (2024).

Umam, M. F., Muhammad, F., Adityatama, D. W., & Purba, D. P.: Tantangan Pengembangan Energi Panas Bumi Dalam Perannya terhadap Ketahanan Energi di Indonesia. *Swara Patra*, 8(3), (2018), 48-65.

Umam, M. F., D. W., & Purba, et al.: Renewable Energy Literacy in Supporting Geothermal Project in Indonesia: Where Are We Now?, *Proceedings*, 46th Workshop on Geothermal Reservoir Engineering Stanford University, Stanford, CA (2021).

Umam, M. F., Purnamasari, V., Nugraha, H. S., et al.: The Roadmap of Geothermal Human Resources Development: A Synergies between Agencies under the Ministry of Energy and Mineral Resources, *Proceedings*, 9th ITB International Geothermal Workshop, Bandung Institute of Technology, Bandung, Indonesia (2020).

Zulyusri, Z., Elfira, I. ., Lufri, L., & Santosa, T. A.: Literature Study: Utilization of the PjBL Model in Science Education to Improve Creativity and Critical Thinking Skills. Jurnal Penelitian Pendidikan IPA, 9(1), (2023), 133–14.

Overview of Future Geothermal Development Plan in Indonesia: Resource Characteristics and Challenges for Future Development

M. Ghassan J. Shalihin[1], Triwening Larasati[1], Dewi Gentana[1,3], Daniel Adityatama[1], Ferdino R. Fadhillah[2], Astri I. Mustika[2], Vicky Ray Chandra[1], Galih B. Permadi[1], and Serina A. Pongtuluran[1]

[1]PT. Geoenergi Solusi Indonesia (Geoenergis)
[2]PT. Sarana Multi Infrastruktur
[3]Universitas Padjadjaran

Keywords: Geothermal, high-temperature geothermal resource, low-temperature geothermal resource, medium-temperature geothermal resource, geothermal system, geothermal development strategies, Indonesia

ABSTRACT

Indonesia's geological landscape, predominantly shaped by subduction zone volcanoes, harbors high-temperature geothermal resources concentrated in areas such as Sumatra and Java. The study confirms that the majority of developed geothermal fields in Indonesia fall into the high-temperature category and are predominantly liquid-dominated. However, as Indonesia's government aims to tap into low to medium temperature resources in the future, challenges arise due to limited experience and success stories in this area. This necessitates innovative strategies and knowledge sharing to overcome obstacles in their future development. This study is part of our research to identify future geothermal projects in Indonesia and find the lessons learned and applicable feasible strategies for geothermal development in the country. The study is initiated by examining the current projection of geothermal energy development plans in Indonesia, tailored to the unique regional geological context. It underscores the considerable low-temperature geothermal prospects in the government's development plan, emphasizing the need for further study and exploration of low to moderate-temperature geothermal systems to build the necessary knowledge and strategies for successful development, including their discovery and utilization, is essential to unlocking the potential of these resources in Indonesia.

1. INTRODUCTION

The government of Indonesia is committed to support Net Zero Emission Target by 2060. One of its commitments is to increase the renewable energy capacity in the power generation mix, including geothermal energy. According to the Electricity Supply Plan of Indonesia (RUPTL), the utilization of Geothermal energy is expected to reach 5,799 MWe by 2030. As of mid-2024, the installed capacity in Indonesia is 2,418 MWe (ThinkGeoEnergy, 2024), leaving approximately 3,381 MWe needed to achieve the 2030 target.

Geothermal systems in Indonesia can be classified into low, medium, and high-temperature systems based on their temperatures. From an economic and feasibility perspective, high-temperature systems, particularly those associated with volcanic/magmatic systems, are still seen as the primary resource base for power generation in Indonesia. The most developed Indonesian geothermal fields, from the early 1980s to the present, fall into these 'volcanic-hosted' high-temperature systems (vide in Hochstein & Sudarman 2008 & 2015). The classification of reservoir temperature used in this study refers to the classification by Sanyal (2005). This classification is chosen because it has narrower temperature range compared to other classifications.

Nevertheless, to achieve the power generation mix and the net zero emission targets, low-medium temperature geothermal systems may need to be considered, especially since most high temperature systems in Indonesia have already been developed (e.g., Kamojang, Darajat, Dieng, Lahendong, etc). In fact, low to medium temperature systems offer more abundant prospects and are fairly distributed, as they do not necessarily have to be associated with volcanic setting (Wibowo, Hadi, & Risdianto, 2021; Putriyana L. , Daud, Saha, & Nasruddin, 2022). These resources can reach areas not located within volcanic regions, such as Kalimantan, parts of Sulawesi, and Papua.

Currently, low-medium temperature geothermal systems in Indonesia are still considered less attractive, partly due to their characteristics, which are not well understood. For example, the active thermal features (e.g., warm and hot springs) may not be as appealing as those in high temperature geothermal fields (e.g., fumarolic/solfataric steam discharge, boiling hot pool, etc). Additionally, some fields may lack surface thermal features, known as blind/hidden geothermal systems. Conventional exploration and extraction concepts used for high temperature system may not be fully applicable for these conditions, leading to very high resource risks and impacting their economic value. Therefore, understanding exploration and extraction strategies for low-medium temperature geothermal systems is critical to accelerate their development.

This study is part of our research to identify future geothermal projects in Indonesia and find the lessons learned and applicable feasible strategies for geothermal development in the country. The study is initiated by examining the current projection of geothermal energy development plans in Indonesia, tailored to the unique regional geological context. It underscores the considerable low-temperature geothermal prospects in the government's development plan, emphasizing the need for further study on low to medium temperature resources regarding their discovery and utilization.

2. GEOTHERMAL RESOURCES IN INDONESIA: REGIONAL SETTING

Indonesia is renowned for its abundant volcanic arcs, fault regimes, and sedimentary basins, all resulting from active tectonic processes. The subduction process has led to the formation of volcanic arcs extending from Sumatra to Nusa Tenggara and continuing to Sulawesi, endowing Indonesia with substantial geothermal energy resources. These regional settings play an important role to develop several geologic factors (i.e., topography, stress field, fault and fractures, lithology, etc.) which later controls several key parameters within the geothermal system such as permeability, reservoir characteristics and behaviour, fluid composition and flow, etc.

Additionally, fault regimes play a significant role in several geothermal fields, such as in Sumatra, where extensional regimes occur due to the influence of the Great Sumatran Fault (GSF). Similarly, in Sulawesi, several major regional faults, such as the Gorontalo graben zone and Palu-Koro fault zone, control several low-medium temperature geothermal prospects within the region.

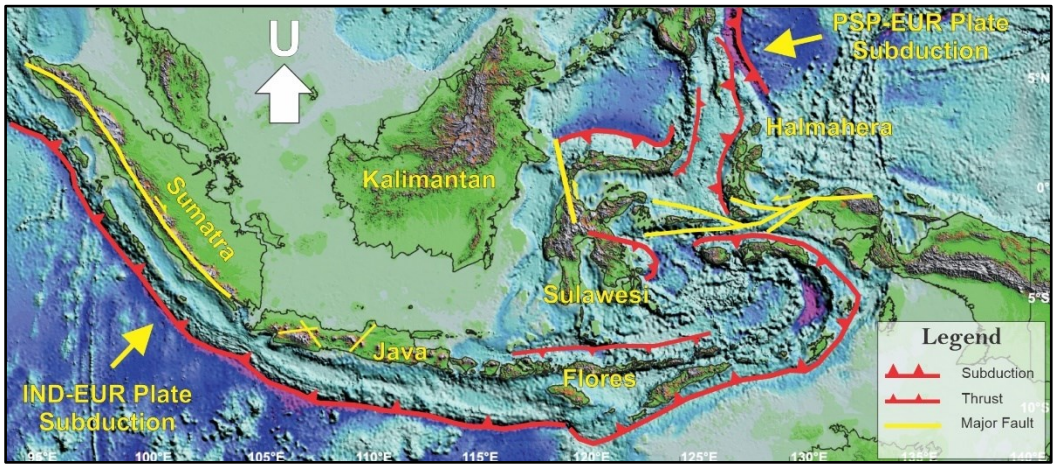

Figure 1: Major plate subduction zones and regional fault lines in Indonesia. IND-EUR: Indo-Australian Plate and Eurasian Plate. PSP-EUR: Philippine Sea Plate and Eurasian Plate (modified from Hall, 2009).

2.1 Tectonic setting

The present-day Indonesian archipelago has developed over a long period due to the region's complex plate tectonic setting (Hall, 2009). The archipelago is a product of several tectonic interactions, including the subduction of the Indo-Australian Plate (to the south and west) and the Philippine Plate (to the east) beneath the Eurasian Plate (to the north), as well as the subduction of the Pacific Plate (to the north) under the Indo-Australian Plate (to the south) along the northern margin of New Guinea Island. Figure 1 illustrates the Indonesian geological setting in relation to plate boundaries, highlighting regional fault lineaments across major islands resulting from these plate interactions. These tectonic movements have shaped Indonesia's geological features, including volcanic arcs, regional fault systems, and sedimentary basins.

Major geological features in Sumatra, such as the Barisan Mountain Range and the Great Sumatran Fault (GSF), are associated with the subducting Indo-Australian plate to the southwest. The Semangko Fault was an active fault in the mainland that divided the Sumatra Island, extending along the Bukit Barisan Mountains from Semangko Bay to Banda Aceh (McCaffrey, 2009). A large dextral fault of Sumatra Fault has active movement in Sumatra. The southern end of Sumatera Island cut by Semangko Fault (Siahaan, 2000; Gentana, et al., 2017) where the geothermal provenance with sufficient heat flow to power electricity generator was observed in the fault zone.

The volcanic arc in Sumatera is constructed on the continental crust, and the volcanoes sit on an uplifted pre-Tertiary basement terrane forming the Barisan Mountain Range (Simandjuntak & Barber, 1996). The region has experienced extension and subsidence, interpreted as a pull-apart basin formed by transtensional movement along the fault (Simandjuntak & Barber, 1996). This fault regime controls the occurrence of intrusions and volcanic activities within Sumatra (Hochstein & Sudarman, 1993; Simandjuntak & Barber, 1996). Several geothermal

fields, such as Namora I Langit and Silangkitang, are controlled by this regime, where the normal-fault boundary from pull-apart basins plays a crucial role as a fluid pathway, influencing reservoir structure and permeability (Hickman, et al., 2004; Muraoka, et al., 2010). Control of Neotectonic activity in Sumatra shows that there are various uplift and deformation processes in rocks, this causes variations in permeability which affects the distribution of manifestations in the prospect area (Gentana, et al., 2022).

In Java, the subduction of the Indo-Australian plate beneath the Eurasian plate to the south of the island has been occurring since the late Neogene (Sunda orogeny), forming geological features such as a forearc basin, a volcanic arc, Tertiary back-arc basins, and four main fault regimes across Java Island (Simandjuntak & Barber, 1996). This regime also controls several geothermal fields situated in Java. The major NW-SE oriented faults control West Java's volcanic arc and geothermal systems, such as Cisolok, Cilayu, and Cikundul. These faults act as a heat source and fluid pathway, as indicated by the alignment of volcanic edifices and surface thermal discharges (Purnomo & Pichler, 2014; Fauzi, et al., 2015). In Central Java, strike-slip faults with SW-NE and NW-SE trends significantly impact geological settings, resulting in subsidence, uplift, coastline indentation, and the shifting of the Quaternary volcanic arc (Satyana, 2007). The NW-SE lineament reflects some Quaternary volcanic chains in Central Java, such as Dieng-Sundoro-Sumbing and Telomoyo-Merapi-Merbabu. In Dieng, NW-SW trending faults are evident from the alignment of thermal manifestations, which are also spatially associated with the alignment of volcanic centers (Boedihardi, et al., 1991; Shalihin, et al., 2020). The depression between the Kendeng anticlinorium zone and the Southern Mountains (Pegunungan Selatan) in East Java controls the young volcanic arc within the area, which is favorable for developing volcano-hosted geothermal systems such as the Arjuno Welirang Volcanic Complex (van Bemmelen, 1949).

In Sulawesi, the tectonic setting is divided into four regions based on the lithotectonic province: (a) the Western and North Sulawesi Plutonic-Volcanic Arc; (b) the Central Sulawesi Metamorphic Belt; (c) the East Sulawesi Ophiolite Belt in the East Arm; and (d) the Banggai-Sula and Tukang-Besi continental fragments in the Southeast Arm (Soeria-Atmadja, et al., 1999; Baillie & Decker, 2022). The magmatic arc with Quaternary volcanoes is situated in the western and northern parts of Sulawesi, formed by the extensional tectonic movement of the Makassar Strait and the subduction of the Molucca Plate (Hartono, 1985; Zhang, et al., 2017). Geothermal prospects in the southern arm are more controlled by major faults; an example is the Bora Pulu geothermal field, primarily controlled by the Palu-Koro strike-slip fault (Abdullah, et al., 2020).

The Banda Arc in Eastern Indonesia is considered the product of the most recent continent collision in Indonesia. This arc is part of the Lesser Sunda-Banda Sector with double arc structures in the south and east (Von Der Borch, 1979). In the Lesser Sunda-Banda arc, Flores Island formed from the movement of the Pacific Block in the north and the subducting Australian continent in the south (Varekamp, et al., 1989; Muraoka, et al., 2005). Due to these tectonic movements, the geothermal system in the Bajawa Geothermal Field in Flores is controlled by lateral shear stress in the NNW-SSE trend (Muraoka, et al., 2005).

In Kalimantan, Sundaland extensional rifting in the Eocene age formed many thick sedimentary basins (Satyana, 1994). The rifting in Kalimantan led to the formation of numerous strike-slip and normal faults across the island. One regional strike-slip and normal fault is the Wonomulyo Fault, located in North Kalimantan. This fault system controls the fluid pathway of the Sajau geothermal prospect on the western side of the Tarakan Basin, while its geothermal fluid composition is influenced by intrusive rocks and the sedimentary basin environment (Kumalasari, et al., 2020).

2.2 Volcanism

Active plate tectonic interactions in Indonesia result in magmatic belts above the Benioff zone on the subducting plates. These features exist in active continental margins and island arcs across subduction lines (Hamilton W. , 1979). The magmatic belts bring magma to the surface, forming volcanic activities that host geothermal systems (Purnomo & Pichler, 2014). These areas are generally controlled by fault zones that serve as fluid pathways for surface manifestation discharges, with volcanic systems acting as the heat source (Hochstein & Sudarman, 2015).

Volcanism in Sumatra is controlled by the regional shear zone of the Sumatran Fault. Volcanic activities in Sumatra have an intermittent cycle, decreasing during the Eocene and becoming active again in the Late Miocene (Hochstein & Sudarman, 1993). Generally, geothermal prospects in Sumatra are located on the flank of volcanic edifices or pull-apart basins (Muraoka, et al., 2010). An example is the Sibayak geothermal field, situated within the Singkut Caldera, where geological structures controlled by volcanic activities enhance reservoir permeability (Atmojo, et al., 2000).

In Java, Tertiary magmatic activity occurred from the Late Eocene to Early Miocene and the Late Miocene to Late Pliocene, followed by Quaternary volcanism (Bellon et al., 1989 in Soeria-Atmadja et al., 1994). There are 17 volcano-hosted geothermal systems in Java, located on the Quaternary volcanic belt, with heat sources from intrusive rocks and magmatic activities (Purnomo & Pichler, 2014). One example is the Darajat geothermal field,

where the system is controlled by partially collapsed volcanic remnants, and the heat source is partial magma melt (Hadi, 2001).

Volcanic activity in the Banda Arc is associated with the subduction of the Indian-Australian plate towards the Eurasian plate, forming inner and outer volcanic arcs separated by the Savu forearc basin and Weber Deep (Bowin et al., 1977 in Von Der Borch, 1979). Geothermal prospects in the Eastern Banda Arc are linked to an active volcanic system formed by the mid-Tertiary collision of the Australian continent (Audley-Charles, 1975 in Nasution et al., 2002). An example is the Nage geothermal field, associated with the Inerie stratovolcano in the inner volcanic arc, notable for its high-volume manifestation discharge from magmatic sources (Nasution, et al., 2002).

The volcanic system in Kalimantan resulted from the subduction from Sumatra towards the Asiatic continent, emerging since the Cretaceous age (Katili, 1971). Late Cretaceous subduction in eastern Kalimantan led to mélange deposition associated with volcanic and granitic rocks in the southwest (Hartono, 1985). Currently, there is no active volcanism in Kalimantan. Most geothermal prospects are located in sedimentary basins and are less controlled by volcanism, categorized as low- to medium-temperature systems (Yushantarti, 2020).

Volcanism and plutonism in Sulawesi occurred with the subduction of the Molucca Slab. Late Quaternary volcanoes formed from the rifting in the Makassar Strait in western Sulawesi, extending to the northern arm of the Sangihe volcanic arc (Katili, 1971). This arc consists of Paleogene-Quaternary plutonic-volcanic rocks (Martosuwito, 2012). Unlike the southern arm, geothermal prospects in the northern arm are mainly controlled by Quaternary volcanism. The Lahendong geothermal system in northern Sulawesi is associated with Quaternary volcanic rocks, with its heat source from magma cooling beneath Mt. Lengkoan and Mt. Kasuratan (Siahaan, et al., 2005).

3. FUTURE GEOTHERMAL PROSPECTS IN INDONESIA

The Indonesian government has identified a list of fields for potential future geothermal development. These prospects are outlined in the National Electricity Supply Business Plan (RUPTL) 2021-2030 which can be categorized into three rankings (Figure 2):

- Rank 1: National Strategic Project (PSN) which already included in “Neraca Daya” or power grid so they supposedly become the most prioritized project to develop. There are about 37 projects included here that will supply about 1.5 GW power with expected COD year listed.
- Rank 2: project that also already included in power grid, but no specific fields are assigned. The supply power is around 710 MW.
- Rank 3: potential projects that are not included in power grid and has no expected COD year. There are 106 projects with total capacity of around 4.3 GW.

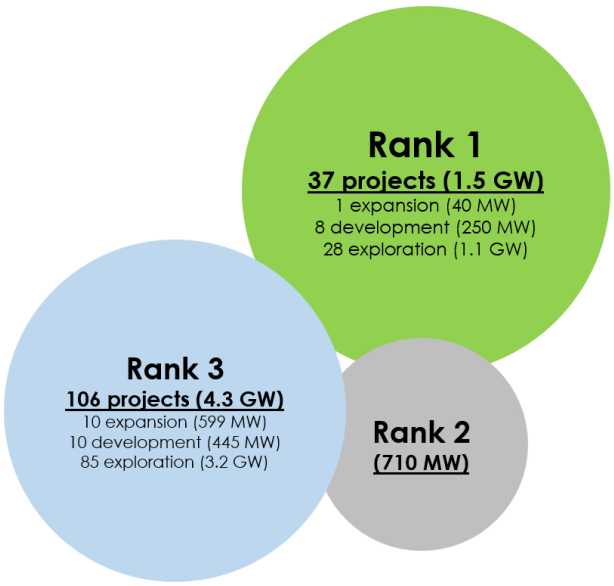

Figure 2: Priority distribution of Rank 1, Rank 2, and Rank 3 geothermal projects in RUPTL 2021-2030.

The geothermal fields listed in Ranking 1 are considered National Strategic Projects (PSN) and are included in the 'Neraca Daya' project list within the RUPTL 2021-2030. In contrast, the geothermal potential in Rank 2 is described as a general plan, which allocates one or several developers to supply a targeted quota of capacity by a specific year, without listing specific fields. Geothermal prospects in Ranking 3 have not yet been included in the 'Neraca Daya' and are currently not prioritized for immediate development, consisting of eighty fields. However, it is worth to note that geothermal prospects in Ranking 3 have considerable potential in low-medium temperature geothermal fields.

3.1 Rank 1 Indonesia's geothermal prospects in RUPTL 2021-2030

The geothermal fields listed in Ranking 1 are considered as National Strategic Projects and are included in the "Neraca Daya" project list in the RUPTL comprises twenty-three fields, mostly distributed along Sumatra, Java, Nusa Tenggara, and Maluku. Most of geothermal prospects listed here are often associated with arc volcanism linked to the subduction process of converging tectonic plates as seen in Tangkuban Perahu, Sungai Penuh, Ijen, Lawu, and Baturraden and others. The summary of these geothermal prospects characteristics categorized as Ranking 1 is presented in Table 1.

Based on their temperature, the fields listed in Rank 1 RUPTL 2021-2030 are predominantly categorized as high-temperature resources (14 of 22 fields). Most of them are in the exploration phase, such as Kepahiang, Rajabasa, Mount Sirung, while some fields have entered the development phase, including Ijen and Sungai Penuh. Additionally, some medium-temperature systems are also included in Rank 1, such as Danau Ranau, Cisolok, Baturaden, with a targeted production of about 350 MW much lower than the targeted production from the high temperature resource about ~1.1 GW.

Nevertheless, it is evident that medium to high-temperature resources still have a higher priority for future geothermal development in Indonesia (15 of 22 fields). However, it must be noted that temperature information from those listed fields still has some degrees of uncertainty as it derives from geochemical analyses, which may not fully represent the actual reservoir temperature in the subsurface. The distribution of the fields listed in rank 1 based on its temperature category are presented in Figure 3.

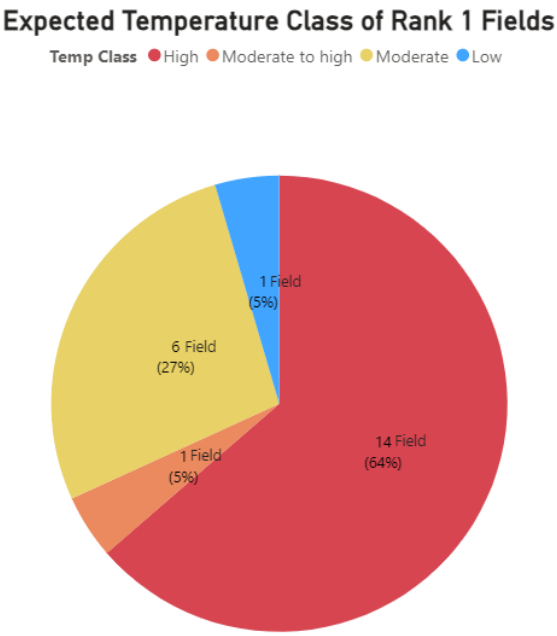

Figure 3: The distribution of the fields listed in rank 1 based on its interpreted reservoir temperature.

3.2 Rank 3 Indonesia's geothermal prospects in RUPTL 2021-2030

Unlike the fields listed in Ranking 1, the geothermal prospects listed in Ranking 3 have not yet been included in the 'Neraca Daya' and are currently not prioritized for immediate development, consisting of eighty fields. Based on their geological association, the fields listed in Rank 3 are more fairly distributed, situated in both magmatic and non-magmatic environments. The fields associated with volcanism generally share common characteristics with the currently developed geothermal fields. However, there are also fields situated in volcanic complexes without magmatic signatures (e.g., Candi Umbul-Telomoyo).

Table 1: Summary of geothermal fields characteristics categorized as Rank 1.

No	Geothermal field	Geologic factor	Reservoir temperature (°C)	Temperature category (Sanyal, 2005)	Reference(s)
1	Jaboi	Hybrid (young volcanism and fault systems)	327°C (gas geothermometry)	High	(Dwipa, et al., 2006; EBTKE, 2017; Nugraha & O'Sullivan, 2019)
2	Sungai Penuh	Subduction Young volcanism	250-280°C (gas geothermometry)	High	(Hochstein & Sudarman, 2008; Sukhyar, et al., 2010; Darma, 2016; EBTKE, 2017)
3	Danau Ranau	Subduction Young volcanism	200-220°C (Na-K-Mg)	Medium	(Afiat, et al., 2020; Idianto, et al., 2021; Rera, et al., 2021)
4	Hululais	Subduction Young volcanism	225-285°C (gas geothermometry from Kawah Biru and Kawah Hitam), >300°C (gas geothermometry from Kawah Belerang Atas)	High	(Kamah, et al., 2015; EBTKE, 2017; Nurseto, et al., 2021)
5	Kepahiang	Subduction Young volcanism	250°C (gas geothermometer fumarole of Kaba Crater)	High	(EBTKE, 2017; Nurdyanto, et al., 2019; Nurseto, et al., 2021)
6	Rajabasa	Subduction Young volcanism	260-265°C (Way Merak), 300-325°C (gas geothermometry)	High	(Darmawan, et al., 2015; EBTKE, 2017)
7	Rawa Danau	Subduction Young volcanism	260-270°C (gas geothermometry)	High	(EBTKE, 2017; Syah, et al., 2019; Sumotarto, et al., 2019)
8	Cibuni	Subduction Young volcanism	305°C	High	(Layman & Soemarinda, 2003)
9	Tangkuban Perahu	Subduction Young volcanism	200-285°C (Na-K geothermometry)	Medium to high	(Hochstein & Sudarman, 2015; Gaffar, 2018)
10	Cisolok-Cisukarame	Subduction Young volcanism	185-212ºC (Na-K geothermometry)	Medium	(Mandradewi & Herdianita, 2010; Sumartha, et al., 2020)
11	Tampomas	Subduction Young volcanism	187-208°C (Silica geothermometry) (Direktorat Jendral EBTKE, 2017), 160-175°C (silica geothermometry), 170 ± 10°C (Na/K geothermometry)	Low to Medium	(EBTKE, 2017; Permadi, et al., 2022)
12	Candradimuka	Subduction Young volcanism	250°C - 289°C (gas geothermometry)	High	(Bagaskara, et al., 2021)
13	Ungaran	Subduction Young volcanism	>300°C (gas geothermometry), Gradient temperature 10.4°C /100 m (thermal gradient well USL-1)	High	(Phuong, et al., 2012)

No	Geothermal field	Geologic factor	Reservoir temperature (°C)	Temperature category (Sanyal, 2005)	Reference(s)
14	Baturaden	Subduction Young volcanism	204-210°C (Na-K-Mg geothermometry)	Medium	(EBTKE, 2017; Harijoko & Juhri, 2017; Iswahyudi, et al., 2020)
15	Guci	Subduction Young volcanism	170-190°C (K-Na-Ca and Na-K-Mg geothemometry), 331-382°C (Na/K geothermometer) , 187-196°C (silica-enthalphy method)	Low to High	(Harijoko & Juhri, 2017; Iswahyudi, et al., 2020; Harijoko, et al., 2021)
16	Ijen	Subduction Young volcanism	250 - 300°C (in EBTKE, 2017)	High	(EBTKE, 2017; Daud, et al., 2019)
17	Telaga Ngebel	Subduction Young volcanism	250 - 260°C	High	(EBTKE, 2017; Yudiantoro, et al., 2020)
18	Bedugul	Subduction Young volcanism	280 - 320°C	High	(Darma, et al., 2010)
19	Tulehu	Hybrid (young volcanism and fault systems)	>230°C	High	(Daud, et al., 2022)
20	Atadei	Hybrid (young volcanism and fault systems)	~221°C (gas geothermometry)	Medium	(EBTKE, 2017; Prabata, 2018)
21	Oka Ile Ange	Subduction Young volcanism	148-173°C	Low	(Nugraha, et al., 2018; EBTKE, 2017)
22	Mount Sirung	Subduction Young volcanism	260°C (H2-CO2 gas geothermometry)	High	(EBTKE, 2017; Putriyana, et al., 2021)

The non-magmatic prospects listed in the Ranking 3 category are typically fault-controlled, with hydrology and resource distribution primarily confined by fault or fracture systems. Most of these prospects are located in Sumatra along the graben structure controlled by the GSF, such as Bonjol, Simisuh, Sumani, and Panti. In Sulawesi, the Palu-Koro fault zone also phosts several low-temperature geothermal prospects, including Bora Pulu, Marana, and Kadidia (EBTKE, 2017), while the Gorontalo graben zone hosts Suwawa and Pentadio prospects (Pasaribu, et al., 2023).

Some prospects are also associated with Tertiary volcanism, such as Cilayu and Ciseeng. According to the Geothermal Potential Book by EBTKE (2017), another type of geothermal resource in Indonesia is the hot sedimentary aquifer systems, exemplified by Sajau. However, this type of resource is not included in the RUPTL 2021-2030. A summary of geothermal prospects categorized as Ranking 3 is presented in Table 2.

Table 2: Summary of geothermal fields characteristics categorized as Rank 3.

Geologic Factor	Res. Temp. Classification (Sanyal, 2005)	Geothermal Field(s)	Reference
Young volcanism	High	Seulawah Agam[1]	[1] (EBTKE, 2017) [2] (Ikhwan, 2020) [3] (Stimac J. , Nordquist, Suminar, & Sirad-Azwar, 2008) [4] (Pratama, et al., 2015) [5] (Nasution, Widarto, Hutasoit, Yuliani, & Hadisoemarto, 2008) [6] (Purnomo & Pichler, 2015) [7] (Riogilang, et al., 2012) [8] (Iqbal, et al., 2016) [9] (Nasution, et al., 2000) [10] (Hidayatika, et al., 2015) [11] (Herdianita, et al., 2010) [12] (Hermawan, et al., 2012) [13] (Martadiastuti, et al., 2017) [14] (Makatita, 2018) [15] (Satrio, et al., 2020) 1[6] (Nurhadi & Sulaeman, 2010) [17] (Utami, Putra, & Dhia, 2019) [18] (Herdianita & Priadi, 2008) [19] (Azzam, et al., 2020) [20] (Rachmatika, et al., 2019) [21] (Pasaribu, et al., 2023) [22] (Kusnadi & Setiawan, 2009) [23] (Putriyana & Soekarno, 2015) [24] (Siombone, 2022) [25] (Yushantarti & Hermawan, 2022)
		Mt. Kembar[1]	
		Margabayur[1]	
		Tanjung Sakti[1]	
		Bukit Daun[2]	
		Cibeureum Parabakti[3]	
		Gede Pangrango[1]	
		Galunggung[4]	
		Papandayan[5]	
		Wilis[1]	
		Iyang Argopuro[1]	
		Krucil Trilis[1]	
		Batur[6]	
		Kotamobagu[7]	
		Telang Ranu[1]	
		Mt. Hamiding[1]	
		Mapos[8]	
		Nage[9]	
	Medium to high	Sekincau[10]	
		Way Ratai[1]	
	Medium	Geureudong[1]	
		Sipoholon Ria-ria[1]	
		Mt. Talang[1]	
		Songgoriti[14]	
		Ciremai[11]	
		Umbul-Telomoyo[12]	
		Jailolo[1]	
		Wae Sano[1]	
		Wae Pesi[1]	
	Low to medium	Lokop[1]	
	Low	Mt. Endut[1]	
		Mt. Pandan[1]	
		Arjuno Welirang[13]	
		Klabat-Wineru[1]	
		Akesahu[1]	
		Sembalun[15]	
		Gou-Inelika[1]	
		Lesugolo[1]	
		Hu'u[1]	
	No temperature data	Tambang Sawah	
		Sungai Tenang	
		Masigit	
		Bromo-Tengger	

Geologic Factor	Res. Temp. Classification (Sanyal, 2005)	Geothermal Field(s)	Reference
		Tabanan	
Tertiary volcanism	Low	Cilayu[18]	
		Ciseeng[18]	
Volcanism and fault system	High	Talamau[17]	
		Cubadak[1]	
		Wapsalit[16]	
		Sibual-buali[1]	
	Low	Simisuh[1]	
		Bonjol[1]	
		Sumani[1]	
		Panti[1]	
	No temperature data	Graho Nyabu	
Fault systems	Medium	Kadidia[1]	
		Puhuwato[1]	
		Bittuang[22]	
		Pincara[1]	
		Limbong[1]	
		Lainea[23]	
		Tehoru[24]	
	Low to medium	Marana[1]	
	Low	Bora-Pulu[1]	
		Suwawa[1]	
		Pentadio[1]	
		Banda Baru[25]	

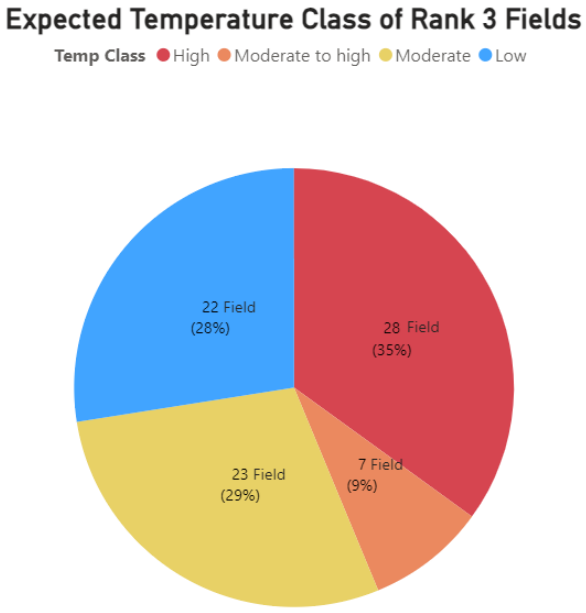

Figure 4: The distribution of the fields listed in rank 3 based on its interpreted reservoir temperature.

Slightly similar to the previously fields in Rank 1, several high-temperature fields are still included in Rank 3. However, a considerable amount of low to medium-temperature geothermal fields have already been included on this list (45 of 80 fields). It implies that after the fields listed in Rank 1 are already developed (which are mostly high temperature), the fields listed in this Rank 3 will become the next priority to be developed. Therefore, the

importance of further study on the exploration and utilization of the low-medium temperature systems in Indonesia should be initiated. The distribution of the fields listed in rank 3 based on its temperature category are presented in Figure 4.

4. RESOURCE CHARACTERISTICS OF FUTURE INDONESIA'S GEOTHERMAL PROSPECTS

4.1 Rank 1 Indonesia's geothermal prospects characteristics

Indonesia's geothermal prospects in Ranking 1 are predominantly influenced by arc volcanism associated with the subduction process. These areas are typically situated from the half-section to the active conduit-crater flanks of stratovolcanoes, exemplified by locations such as Tangkuban Perahu, Sungai Penuh, and Ijen (Danar & Syukar, 2010; Hochstein & Sudarman, Indonesian Volcanic Geothermal Systems, 2015; EBTKE, 2017), also within the crater such as Candradimuka prospect in Mt. Lawu (Bagaskara, et al., 2021). Meanwhile, prospects like Guci and Baturaden represent outflow systems from Mt. Slamet (Harijoko, et al., 2021), characterized by fumaroles and acidic hot springs in the upflow beneath the upper flank, with dilute chloride-bicarbonate discharges around the foothill as the outflow zone.

Developing geothermal resources in the magmatic environment requires consideration of the risk associated with acidic magmatic water, evident in fluid chemistry signatures. Several fields exhibit high non-condensable gas (NCG) content, such as Sungai Penuh with NCG around 0.5% and Bukit Daun reaching 6.83% near Kawah Belerang Atas (EBTKE, 2017). Lessons from developed geothermal fields in Indonesia like Lahendong, Dieng, and Sorik Marapi can inform strategies for managing high NCG contents in power plants.

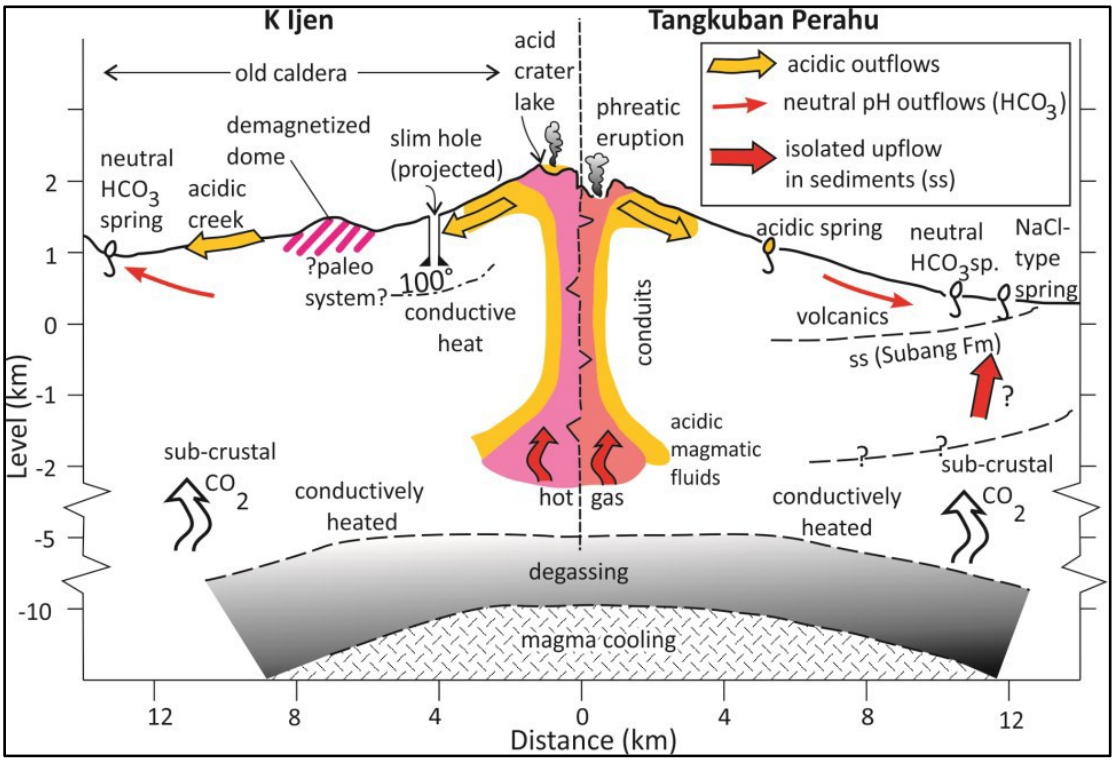

Figure 5: Illustration of volcanic-hosted geothermal systems at the Ijen and Tangkuban Perahu prospects typically associated with high-standing Quaternary volcanoes (conceptual model from Hochstein & Sudarman, 2015).

The absence of chloride hot springs and the prevalence of unequilibrated thermal manifestations—such as diluted and acidic condensate waters—in most prospects in this category limit the applicability of solute geothermometers. Gas geothermometers are often utilized for assessing reservoir temperatures (Hochstein & Sudarman, Indonesian Volcanic Geothermal Systems, 2015). Reservoir temperatures in Ranking 1 prospects generally range from moderate to high. Some intermediate to high temperature prospects, like Danau Ranau and Cisolok, indicate a cooling down process (Mandradewi & Herdianita, 2010; Rera, et al., 2021). The example of volcanic-hosted geothermal systems for some prospects in in Indonesia is illustrated in Figure 5.

Additionally, there are prospects in Indonesia that are expected to exhibit a hybrid nature, influenced by both magmatic activity and fault systems. For example, Jaboi on Weh Island is controlled by the Great Sumatran Fault (GSF), occurring within the graben zone formed by the stretching of faults like Leumo Matee (NNW-SSE) and

Ceunohot (NE-SW) as part of the GSF on the western side of Sumatra. Jaboi's heat source is likely associated with the Leumo Matee and Seumeureguh volcanoes; however, the occurrence of the Ceunohot fault likely controls the highest temperature zones in Jaboi. This is indicated by gradient thermal well data, which shows that wells situated closer to the fault tend to have higher temperature conditions than those located farther away (Dwipa, Widodo, Suhanto, & Kusnadi, 2006; Soetoyo & Widodo, 2010; Sumintadireja, Kasbani, & Suhanto, 2010; Nugraha & O'Sullivan, 2019). Conceptual model of Jaboi geothermal systems is presented in Figure 6.

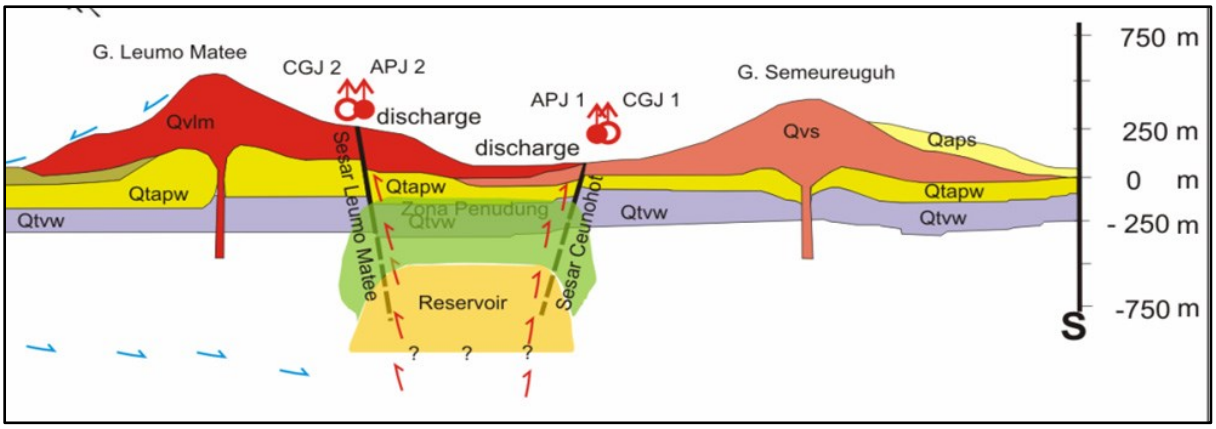

Figure 6: The Jaboi geothermal system might be categorized as a hybrid. Although Mount Leumo Matee and Seumeuregeu likely provide the heat sources, drilling data indicates that faults control the high-temperature zones within the system (conceptual model from Sumintadireja, et al., 2010).

Hybrid systems also might be seen for several prospects in Eastern Indunesia such as Tulehu (Molucca) and Atadei (East Nusa Tenggara). Tulehu, situated along NE-SW normal faults, is governed by Mt. Eriwekang as a potential heat source, supported by age dating indicating Quaternary eruptions around 413±6 kA (Daud et al., 2022). Na-Cl waters discharge along the northeastern shore and within the Tulehu peninsula, exemplified by undiluted geothermal liquid at Pulau Batulompa, characterized by high SiO2, K, and Li contents typical of deep, high-enthalpy geothermal reservoirs with temperature around 230°C (Marini & Susangkyono, 1999; Daud, et al., 2022). Meanwhile, Atadei, situated in the Watuwawer Caldera complex within the Quaternary Stratovolcano system comprising Mt. Ile Ape, Mt. Ile Werung, and Mt. Ile Hobal, relies on an intrusive magma chamber beneath Watuwawer Caldera as its heat source. This system is influenced by deep leakage along the Watuwawer and Lewo-Kebingan faults, allowing upwelling of hot geothermal fluid to Watuwawer Caldera and lateral flow through Mauraja Fault. Atadei is characterized by medium reservoir temperatures (Prabata, 2018).

4.2 Rank 3 Indonesia's geothermal prospects characteristics

Several geothermal prospects listed in Ranking 3 are influenced by magmatism associated with Quaternary stratovolcanoes. Thermal manifestations from magmatic influence include fumaroles (e.g., Seulawah Agam, Margabayur, Bukit Daun), solfataras (e.g., Bukit Daun), and sulfate hot springs (e.g., Tujuh Warna Crater in Bukit Daun). Some prospects lack gas or magmatic signatures, like Candi Umbul-Telomoyo, where thermal manifestations are primarily dilute chloride-bicarbonate springs (Hermawan, et al., 2012). Some of these prospects are expected to have high reservoir temperatures, including Seulawah Agam, Margabayur, Gede Pangrango, Papandayan and others. Additionally, some prospect exhibit medium to high temperature systems, such as Sekincau, Way Ratai, Mt. Ciremai, Jailolo, and Wae Sano. Hybrid systems are expected to occur in some low to medium geothermal prospects in Sumatra, including Simisuh, Bonjol, Sumani, and Panti.

Additionally, many of geothermal prospects in Rank 3 can be categorized as fault-controlled geothermal systems, where the heat source is unrelated to Quaternary magmatism, with hydrology systems and resource distribution primarily constrained by fault systems. In Central Sulawesi, prospects like Kadidia, Bora-Pulu, and Marana are influenced by the Palu-Koro sinistral strike-slip fault, creating graben zones with transtensional regimes (Figure 7). The heat source here is predicted to be deep Miocene to Pliocene granitic intrusions, with reservoir rocks comprising Pre-Tertiary to recent metamorphic and sedimentary rocks (EBTKE, 2017; Rachmatika, Haryanto, Hutabarat, Hermawan, & Mustofa, 2019). In Gorontalo, prospects like Suwawa, Pohuwato, and Pentadio are governed by the Gorontalo graben zone within the Limboto-Bone rift (Pasaribu, et al., 2023), featuring dyke systems beneath the graben zone as heat sources. In South Sulawesi, Bituang, Pincara, and Limbong are controlled by normal faults, heating through Tertiary volcanism (EBTKE, 2017). In Southeast Sulawesi, Lainea is influenced by the NW-SE Boro-boro fault, arising from the collision zone of the Australia Microcontinent, with fluids infiltrating through fault planes heated by metamorphism (EBTKE, 2017).

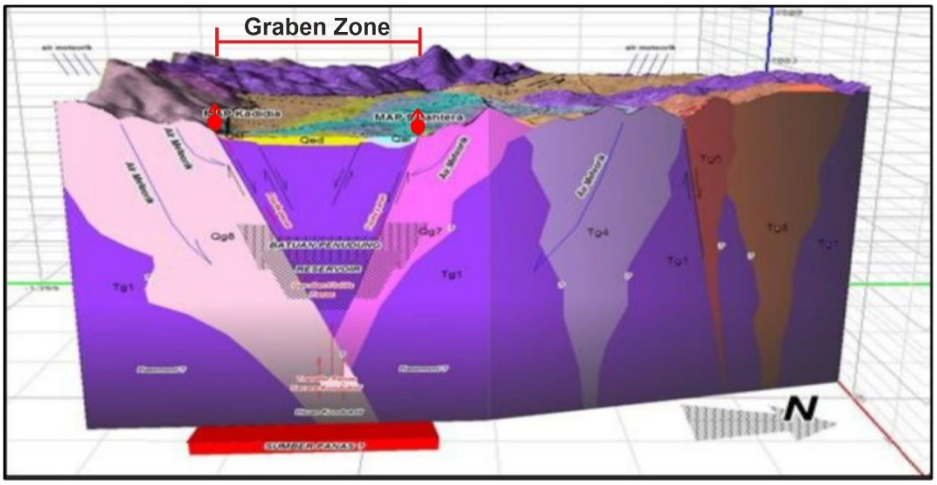

Figure 7: The Kadidia prospect in Sulawesi can be categorized as a fault-controlled system. This prospect is located within the graben zone created by the Palu-Koro fault systems. The faults allow deep fluid circulation within the graben, forming a geothermal system characterized by the presence of several warm springs in proximity of the faults (conceptual model was modified from EBTKE, 2017).

In Java, there are geothermal prospects associated with Tertiary volcanism such as Cilayu and Ciseeng, which are hosted by Middle Miocene diorite intrusions uplifted along fault planes, influencing thermal anomalies and fluid hydrology (Herdianita & Priadi, 2008; Azzam, et al., 2020). In the Moluccas, some geothermal prospects such as Tehoru and Badar Baru are interpreted to be influenced by metamorphic complexes (Siombone, 2022; Yushantarti & Hermawan, 2022). All of these Tertiary and metamorphic-influenced geothermal systems are interpreted to have low to medium temperature reservoirs.

5. CONCLUDING REMARKS AND PATH FORWARD

Currently, most of the developed geothermal fields in Indonesia are volcano-hosted high-temperature resources, providing abundant lessons learned for developing potential high-temperature resources in the future. However, it is worth noting that Indonesia also has considerable potential in low-temperature geothermal prospects, none of which have been developed yet.

High-temperature resources still have a higher priority for future geothermal development in Indonesia, as many high-temperature fields are listed in the RUPTL 2021-2030 as National Strategic Projects (Rank 1 category). However, a significant number of low to moderate-temperature geothermal fields are also listed, though with a lower priority (Rank 3 category). Despite their current low priority, many low to moderate-temperature resources are expected to be part of Indonesia's future development pipeline.

Geothermal developers and investors in Indonesia face challenges in developing low to moderate-temperature geothermal resources due to a lack of experience or success stories to draw from. This underscores the critical need for further study and exploration of these geothermal systems. Building the necessary knowledge and strategies for successful development, including their discovery and utilization, is essential to unlocking the potential of these resources in Indonesia.

To optimize geothermal development strategies in Indonesia, implementing development strategies, technologies, and utilization methods used in developed low to medium geothermal fields worldwide, such as those in the USA, Turkey, and other countries, could serve as an initial step to initiate development of low to medium geothermal prospects in Indonesia. This study represents our next path forward, building on the findings of our initial study.

To analyze comparable development strategies and practices that can be applied in the Indonesian context, it is crucial to acknowledge the unique characteristics of each geothermal field worldwide. Factors such as geologic conditions, fluid characteristics, and power generation technology selection can significantly influence geothermal development strategies. Therefore, categorizing similar geothermal fields into distinct categories and comparing fields within the same category offers the best methodology for analysis, considering the diverse factors that influence development strategies. This approach will guide our future research efforts in optimizing geothermal development strategies in Indonesia.

REFERENCES

Abdullah, A., Puspita, R. & Hamad, H., 2020. Review of Regional Geological Structures on the Appearance of Geothermal Manifestations in the "Neck" Region of Western Sulawesi Island. *MATEC Web of Conferences* 331.

Afiat, et al., 2020. Updated Conceptual Model and Resource Assessment using Numerical Reservoir Simulation of Danau Ranau Geothermal Field Indonesia. *IOP Conf. Series: Earth and Environmental Science*.

Atmojo, J. et al., 2000. Modeling Studies of Sibayak Geothermal Reservoir, Northern Sumatra, Indonesia. Tohoku, Japan, *World Geothermal Congress 2000*.

Azzam, I., Hendrasto, F. & Sumotarto, U., 2020. *Hydrogeochemical Study Of Ciseeng Thermal Springs, West Java Province, Indonesia*.

Bagaskara, M. F. et al., 2021. Gas geochemistry analysis in Candradimuka Crater, Mount Lawu, Central Java, Indonesia. IOP Conference Series: Earth and Environmental Science.

Bagaskara, M. F. et al., 2021. Gas geochemistry analysis in Candradimuka Crater, Mount Lawu, Central Java, Indonesia. *IOP Conference Series: Earth and Environmental Science*.

Baillie, P. & Decker, J., 2022. Enigmatic Sulawesi: The Tectonic Collage. *Berita Sedimentologi*, 48(1).

Boedihardi, M., Suranto & Sudarman, S., 1991. Evaluation of the Dieng Geothermal Fields: Review of development strategy. s.l., *Proceedings 20th Indonesian Petroleum Association*.

Danar, A. & Syukar, R., 2010. *Energi Panas Bumi di Indonesia: Kebijakan Pengembangan dan Keputusan Investasi*. Geological Agency of the Ministry of Energy and Mineral Resources.

Darma, S., 2016. *Indonesia: Vast geothermal potential, modest but growing exploitation*.

Darma, S. et al., 2010. *Geothermal Energy Update: Geothermal Energy Development and Utilization in Indonesia*. s.l., s.n.

Darmawan, I. G. B., Setijadji, L. D. & Wintolo, D., 2015. *Geology and geothermal system in Rajabasa Volcano South Lampung Regency, Indonesia (Approach to field observations, water geochemistry and magnetic methods)*.

Daud, Y. et al., 2022. *Investigation of the main reservoir of the Tulehu geothermal system (Indonesia) using 3-D inversion of MT data. Geothermics*.

Daud, Y. et al., 2019. First horizontal derivative and Euler Deconvolution in application for reconstructing structural signature over the Blawan-Ijen Geothermal area. *IOP Conference Series: Earth and Environmental Science*.

Dwipa, S., Widodo, S., Suhanto, E. & Kusnadi, D., 2006. Integrated geological, geochemical and geophysical survey in Jaboi geothermal field, Nangro Aceh Darussalam, Indonesia. *Proceedings of the 7th Asian Geothermal Symposium*.

EBTKE, 2017. *Potensi Panas Bumi Indonesia Jilid 1*. Jakarta: Direktorat Panas Bumi Direktorat Jenderal EBTKE.

Fauzi, A., Permana, H., Indarto, S. & Gaffar, E., 2015. Regional Structure Control on Geothermal Systems in West Java, Indonesia. Melbourne, Australia, *Proceedings World Geothermal Congress*.

Gaffar, E., 2018. The concept of geothermal exploration in west Java based on geophysical data. *IOP Conference Series: Earth and Environmental Science*.

Gentana, D. et al., 2017. *Determination of Tanggamus Geothermal Prospect Area, Lampung Province, South Sumatra Based on Remote Sensing and 3D Micromine Software*. Helsinki, Finland, FIG Working Week.

Gentana, D. et al., 2022. *Aplikasi Geomorfologi Kuantitatif dalam Eksplorasi Pendahuluan Panas Bumi (in Indonesian)*. Bandung: UNPAD Press.

Hadi, J., 2001. The Darajat Geothermal Field Conceptual Model, A Vapor Dominated System. s.l., *Proceedings 5th INAGA Annual Scientific Conference and Exhibitions*.

Hall, R., 2009. *Indonesia, Geology. In: Encyclopedia of Islands*. s.l.:University of California Press, pp. 454-460.

Hamilton, W., 1979. *Tectonics of the Indonesian Region*, US: US Geological Survey Profesional Paper 1078.

Harijoko, A. & Juhri, S., 2017. Cl/B Ratio of Geothermal Fluid around Slamet Volcano, Jawa Tengah, Indonesia. *IOP Conference Series: Earth and Environmental Science*.

Harijoko, A. et al., 2021. Stratigraphy, chronology, and magma evolution of Holocene volcanic products from Mt. Slamet deposited in the Guci Valley, Central Java, Indonesia. *Journal of Volcanology and Geothermal Research*.

Hartono, 1985. Summary of Tectonic Development of Kalimantan and Adjacent Areas. *Energy*, 10(3-4), pp. 341-352.

Herdianita, N. R., Julinawati, T. & Amorita, I. E., 2010. Hydrogeochemistry of Thermal Water from Surface Manifestation at Gunung Ciremai and Its Surrounding, Cirebon, West Java–Indonesia. *Proceedings World Geothermal Congress 2010*.

Herdianita, N. R. & Priadi, B., 2008. *The chemical compositions of thermal waters at Ciarinem and Cilayu, Pameungpeuk, West Java—Indonesia*.

Hermawan, D., Widodo, S. & Mulyadi, E., 2012. Sistem Panas Bumi Daerah Candi Umbul-Telomoyo Berdasarkan Kajian Geologi Dan Geokimia. *Buletin Sumber Daya Geologi*.

Hickman, R. G. et al., 2004. Tectonic and stratigraphic evolution of the Sarulla graben geothermal area, North Sumatra, Indonesia. *Journal of Asian Earth Sciences*, Volume 23(3), pp. 435-448.

Hidayatika, A., Utami, P., Suharno, S. & Amukti, R., 2015. *Analysis of Thermal Manifestation in Suoh West Lampung Indonesia*.

Hochstein, M. & Sudarman, S., 1993. Geothermal Resources of Sumatra. *Geothermics*, pp. 181-200.

Hochstein, M. & Sudarman, S., 2008. History of geothermal exploration in Indonesia from 1970 to 2000. *Geothermics*, Volume 37, pp. 220-266.

Hochstein, M. & Sudarman, S., 2015. Indonesian Volcanic Geothermal Systems. s.l., *Proceedings World Geothermal Congress 2015*.

Idianto, O. et al., 2021. Updated conceptual model and resource assessment using numerical reservoir simulation of danau ranau geothermal field Indonesia. *IOP Conference Series: Earth and Environmental Science*.

Ikhwan, M., 2020. *Geological Model and Permeability Framework of Bukit Daun Geothermal Field, Indonesia*.

Iqbal, M., Herdianita, N. R. & Risdianto, D., 2016. Characteristic of geothermal fluid at East Manggarai, Flores, East Nusa Tenggara. *IOP Conference Series: Earth and Environmental Science*.

Iswahyudi, S., Attabik, L. W. & Saifrudin, N. A., 2020. Reservoir Temperature Calculation of Immature Geothermal Water from Hot Spring Around the Slamet Volcano. *IOP Conference Series: Earth and Environmental Science.*

Kamah, M. Y. et al., 2015. Succesful Exploration Campaign and to be Developed in Hululais Geothermal Field, Bengkulu Indonesia. s.l., *Proceedings World Geothermal Congress 2015*.

Katili, J., 1971. A review of the geotectonic theories and tectonic maps of Indonesia. *Earth-Science Reviews*, 7(3), pp. 143-163.

Kumalasari, D. I. et al., 2020. Geochemical Prospecting Investigation in Non-Volcanic Geothermal Area: A Case Study of Sajau, East Tanjung Palas, Bulungan, North Kalimantan. ITB International Geothermal Workshop.

Kusnadi, D. & Setiawan, D. I., 2009. *Penyelidikan Geokimia Daerah Panasbumi Bittuang Kabupaten Tana Toraja, Provinsi Sulawesi Selatan*. Geological Agency, Ministry of Energy and Mineral Resources.

Layman, E. B. & Soemarinda, S., 2003. The Patuha vapor-dominated resource West Java, Indonesia. s.l., *Proceedings of the 28th Workshop on Geothermal Reservoir Engineering*, Stanford University.

Makatita, W. D. C., 2018. *GEOLOGI DAN TINJAUAN KEPROSPEKAN PANASBUMI BERDASARKAN ANALISIS DATA GEOKIMIA DAERAH SONGGORITI, KABUPATEN MALANG, PROVINSI JAWA TIMUR*.

Mandradewi, W. & Herdianita, N. R., 2010. Characteristics of Surface Manifestation, Cisolok, Sukabumi, West Java: With Relation to Cisolok Geothermal System. s.l., *Proceedings World Geothermal Congress 2010*.

Mandradewi, W. & Herdianita, N. R., 2010. Characteristics of Surface Manifestation, Cisolok, Sukabumi, West Java: With Relation to Cisolok Geothermal System. s.l., *Proceedings World Geothermal Congress 2010*.

Marini, L. & Susangkyono, A., 1999. Fluid geochemistry of Ambon Island (Indonesia). *Geothermics*.

Martadiastuti, V., Harijoko, A., Warmada, I. W. & Yonezu, K., 2017. Hydrogeochemical Characterization of Geothermal Water in Arjuno-Welirang, East Java, Indonesia. *J Appl Geol*.

Martosuwito, S., 2012. Tectonostratigraphy of the Eastern Part of Sulawesi, Indonesia, in Relation to the Terrane Origins. *Jurnal Sumber Daya Geologi*, 22(4).

McCaffrey, R., 2009. *The Tectonic Framework of the Sumatran Subduction Zone*. Annual Review of Earth and Planetary Sciences.

Muraoka, H. et al., 2005. Geology and Geothermal Systems in the Bajawa Volcanic Rift Zone, Flores, Eastern Indonesia. *Proceedings World Geothermal Congress 2005*.

Muraoka, H. et al., 2010. Geothermal Systems Constrained by The Sumatran Fault and Its Pull-Apart Basins in Sumatra, Western Indonesia. Bali, Indonesia, *Proceedings World Geothermal Congress 2010*.

Nasution, A. et al., 2002. Geothermal prospects of Flores Island in Indonesia viewed from their volcanism and hot water geochemistry. *Bulletin of the Geological Survey of Japan*, 53(2/3), pp. 87-97.

Nasution, A., Takashima, I. & Muraoka, H., 2000. The geology and geochemistry of Mataloko-Nage-Bobo geothermal areas, central Flores, Indonesia. *Proceedings of World Geothermal Congress 2000*.

Nasution, A. et al., 2008. Geothermal Geophysical Study Of Mt. Papandayan, Garut District, West Java Indonesia. *Proceedings of the 8th Asian Geothermal Symposium*.

Nugraha, H. S., Shiddiq, A. M. I., Agustin, F. & Surmayadi, M., 2018. Comparison of Application Faults and FractureDensity (FFD) Method using SRTM 90-m, SRTM 30-m, and Aster GDEM 30-m for Geothermal Exploration: a Case of Ile Ange Prospect. s.l., *Proceedings 7th ITB International Geothermal Workshop*.

Nugraha, R. P. & O'Sullivan, J., 2019. A key process of natural state modeling: 3D Geological model of Jaboi Geothermal field, Nangro Aceh Darussalam, Indonesia. *IOP Conference Series: Earth and Environmental Science*.

Nurdyanto, B., Daud, Y. & Zarkasyi, A., 2019. Application of MT and Gravity Method to Potential Analysis of Kepahiang Geothermal, Bengkulu. s.l., *Proceedings Conference on Applied Electromagnetic Technology (AEMT)*.

Nurhadi, M. & Sulaeman, B., 2010. *Surface Manifestation in Wapsalit Geothermal Area, Buru Island, Indonesia*.

Nurseto, S. T. et al., 2021. Structural Geology and Volcanism in Hululais Geothermal Area, Bengkulu, Indonesia. *IOP Conference Series: Earth and Environmental Science*.

Nurseto, S. T., Arifin, M. T., Pratama, G. R. & Nusantara, V. D., 2021. Structural Geology and Volcanism in Hululais Geothermal Area, Bengkulu, Indonesia. *IOP Conference Series: Earth and Environmental Science*.

Pasaribu, A. H., Pratama, A. B. & Pramudityo, D., 2023. Heat Source Identification by Reprocessing Geoscience Data to Update Conceptual Model of Pentadio Geothermal Prospect Area. *IOP Conference Series: Earth and Environmental Science*.

Permadi, G. B. et al., 2022. *Hydrogeochemistry Model and Reservoir Compartment of Mount Tampomas Geothermal System Area in Sumedang Regency, West Java*.

Phuong, N. K., Harijoko, A., Itoi, R. & Unoki, Y., 2012. Water geochemistry and soil gas survey at Ungaran geothermal field, central Java, Indonesia. *Journal of Volcanology and geothermal research*.

Prabata, W., 2018. *Updating Conceptual Model Using Numerical Modelling for Geothermal Green Field Prospect Area in Atadei, East Nusa Tenggara, Indonesia*.

Pratama, A. et al., 2015. Groundwater and river water interaction at Ciromban and Cibeureum riverbank, Tasikmalaya: Can we solve water shortage?. *AIP Conference Proceedings*.

Purnomo, B. J. & Pichler, T., 2014. Geothermal systems on the island of Java, Indonesia. *Journal of Volcanology and Geothermal Research*, Volume 285, pp. 47-59.

Purnomo, B. J. & Pichler, T., 2015. Geothermal systems on the island of Bali, Indonesia. *Journal of Volcanology and Geothermal Research*.

Putriyana, L., Daud, Y., Saha, B. B. & Nasruddin, N., 2022. A comprehensive data and information on low to medium temperature geothermal resources in Indonesia: a review. *Geomechanics and Geophysics for Geo-Energy and Geo-Resources*, 8(58).

Putriyana, L., Ladiba, A. F. & Soekarno, H., 2021. *Simulasi Pengembangan Lapangan Panas Bumi Sirung Pantar, Kabupaten Alor, Nusa Tenggara Timur. Ketenagalistrikan dan Energi Terbarukan*.

Putriyana, L. & Soekarno, H., 2015. *THE DEVELOPMENT SIMULATION OF LAINEA GEOTHERMAL FIELD*. Ketenagalistrikan dan Energi Terbarukan.

Rachmatika, D. et al., 2019. *CHARACTERISTICS OF MINERAL ALTERATION ZONES IN KADIDIA GEOTHERMAL FIELD, SIGI DISTRICT, CENTRAL SULAWESI PROVINCE*.

Rera, G. F., Pratama, H. B. & Saptadji, N. M., 2021. Approach for Pre-Feasibility Study of Medium Enthalpy Geothermal Field, Case Study: Danau Ranau, Indonesia. *IOP Conference Series: Earth and Environmental Science*.

Riogilang, H., ITOI, R. & TAGUCHI, S., 2012. Origin of hot spring water in the Kotamobagu geothermal field, northern Sulawesi, Indonesia. *Journal of the Geothermal Research Society of Japan*.

Sanyal, S. K., 2005. Classification of geothermal systems - a possible scheme. California, *Proceedings, 30th Workshop on Geothermal Reservoir Engineering*, Stanford University.

Sanyal, S. K., 2005. *Classification of geothermal systems - a possible scheme. Stanford*, California, Stanford University.

Satrio, S. et al., 2020. Isotope and Geochemistry Characterization of Hot Springs and Cold Springs of Sembalun–Rinjani Area, East Lombok, West Nusa Tenggara–Indonesia. *Indonesian Journal of Chemistry*.

Satyana, A. H., 1994. The northern massifs of the Meratus Mountains, South Kalimantan: nature, evolution, and tectonic implications to the Barito structures. *Proceedings 23rd IAGI Annual Convention*, pp. 457-470.

Satyana, A. H., 2007. CENTRAL JAVA, INDONESIA – A "TERRA INCOGNITA" IN PETROLEUM EXPLORATION: NEW CONSIDERATIONS ON THE TECTONIC EVOLUTION AND PETROLEUM IMPLICATIONS. *Proceedings 31st IPA Annual Convention and Exhibition*.

Shalihin, M., Utami, P. & Nurpratama, M., 2020. The Subsurface Geology and Hydorthermal Alteration of the Dieng Geothermal Field, Central Java: A Peogress Report. *IOP Conf. Series: Earth and Environmental Science*, Volume 417.

Siahaan, E. E., 2000. Overprinting Events from Crosscutting Veins and Mineral Assemblages in Ulubelu Geothermal Field, Indonesia. Japan, *Proceedings World Geothermal Congress 2000*.

Siahaan, E. E. et al., 2005. Tectonism and Volcanism Study in the Minahasa Compartment of the North Arm of Sulawesi Related to Lahendong Geothermal Field, Indonesia. Antalya, Turkey, *Proceedings World Geothermal Congress 2005*.

Simandjuntak, T. & Barber, A., 1996. Contrasting tectonic styles in the Neogene orogenic belts of Indonesia. *Geological Society Special Publications*, pp. 185-201.

Siombone, S. H., 2022. ANALISIS SUHU PERMUKAAN DAN KONDISI GEOMORFOLOGI KAWASAN GEOTERMAL TEHORU MENGGUNAKAN LANDSAT-8 DAN DEM. *Jurnal Geofisika Eksplorasi*.

Soeria-Atmadja, R. et al., 1994. Tertiary magmatic belts in Java. *Journal of Southeast Asia Earth Sciences*, 9(1/2), pp. 13-27.

Soeria-Atmadja, R., Priadi, B., van Leewen, T. & Kavalieris, I., 1999. *Tectonic setting of porphyry Cu-Au, Mo and related mineralization associated with contrasted Neogene magmatism in the Western Sulawesi Arc*. The Island Arc, pp. 47-55.

Soetoyo & Widodo, S., 2010. Pengaruh sesar normal Ceunohot terhadap landaian temperatur sumur JBO-1 dan JBO-2 di lapangan panas bumi Jaboi, Sabang, Nangroe Aceh Darussalam. *Buletin Sumber Daya Geologi*, 5(3), pp. 182-192.

Stimac, J., Nordquist, G., Suminar, A. & Sirad-Azwar, L., 2008. *An overview of the Awibengkok geothermal system, Indonesia*. Volume 37, pp. 300-331.

Sukhyar, R., Soedibjo, A. W., Ganefianto, N. & Stimac, J., 2010. Geothermal energy update: geothermal energy development and utilization in Indonesia. s.l., *Proceedings World Geothermal Congress 2010*.

Sumartha, A. G. A. et al., 2020. Updating the Conceptual Model of Cisolok-Cisukarame Geothermal field, West Java, Indonesia. *IOP Conference Series: Earth and Environmental Science*.

Sumintadireja, P., Kasbani & Suhanto, E., 2010. Jaboi Geothermal Field Boundary, Nangroe Aceh Darussalam, Based on Geology and Geophysics Exploration Data. Bali, Indonesia, *Proceedings World Geothermal Congress 2010*.

Sumotarto, U., Hendrasto, F. & Triadi, W., 2019. Volcanostratigraphy of Batukuwung-Parakasak Geothermal Area, Serang Regency, West Java. *Journal of Physics: Conference Series*.

Syah, B. Y. C. S. S. et al., 2019. Hydrogeochemical and isotope characterization of geothermal waters from the Cidanau geothermal field, West Java, Indonesia. *Geothermics*.

ThinkGeoEnergy, 2024. [Online] Available at: https://www.thinkgeoenergy.com/thinkgeoenergys-top-10-geothermal-countries-2023-power-generation-capacity/ [Accessed 15 July 2024].

Utami, Z. D., Putra, A. & Dhia, H., 2019. *The estimation of geothermal reservoir temperature using geothermometer equation in Cubadak area, Pasaman regency, West Sumatra, Indonesia*.

van Bemmelen, R., 1949. *The Geologi of Indonesia*. s.l.:The Hague.

Varekamp, J. C. et al., 1989. Volcanism and Tectonics in The Eastern Sunda Arc, Indoneisa. *Netherlands Journal of Sea Research*, 24(2/3), pp. 313-322.

Von Der Borch, C. C., 1979. Continent-Island arc collision in the Banda Arc. *Tectonophysics*, 54(3-4), pp. 169-193.

Wibowo, A., Hadi, M. & Risdianto, D., 2021. Sistem Panas Bumi Temperatur Rendah-Sedang pada Cekungan Kutai dan Rekomendasi Pemanfaatannya. *Buletin Sumber Daya Geologi*, 16(2), pp. 133-151.

Yudiantoro, D. F. et al., 2020. Development of Ngebel Volcano as Geoheritage and Tourism Education of Volcano, Electric Energy and Geothermal, Ponorogo, East Java. *Proceedings of LPPM UPN "Veteran" Yogyakarta Conference Series 2020–Engineering and Science Series*.

Yushantarti, A., 2020. Thermal Fluids Characteristics of Low Temperature Geothermal Systems at Kalimantan Island, Indonesia. California, *Proceeding 45th Workshop on Geothermal Reservoir Engineering*, Stanford University.

Yushantarti, A. & Hermawan, D., 2022. *An Early Geothermal Fluids Characteristics Interpretation at Nif Warm Springs at Bula Basin, East Seram Regency, Maluku, Indonesia*.

Zhang, Q., Guo, F., Zhang, L. & Wu, Y., 2017. Geodynamics of divergent double subduction: 3-D numerical modeling of a Cenozoic example in the Molucca Sea Region, Indonesia. *Journal of Geophysical Research: Solid Earth*.

Preliminary Assessment on the Hot Sedimentary Aquifer Geothermal System in the Midyan Basin in the Kingdom of Saudi Arabia

Vicky Rai Chandra[1], Triwening Larasati[1], M. Ghassan Jazmi Shalihin[1], Astri Indra Mustika[1], Ferdino R Fadhillah[2], Galih Bayu Permadi[1], and Serina Andiani Pongtuluran[1]

[1]PT. Geoenergi Solusi Indonesia (Geoenergis)
[2]PT Enerka Bhumi Pratama

Keywords: Hot Sedimentary Aquifer, Midyan, Saudi Arabia, Low-medium Enthalpy, Geothermal

ABSTRACT

The hot sedimentary aquifer geothermal system is believed to be well-developed in the west coastal region of the Arabian Peninsula, particularly in the Midyan area, located in the northwestern part of the Kingdom of Saudi Arabia. Numerous efforts have been undertaken to conduct geoscientific exploration in this area, including geological mapping through remote sensing and ground-truthing activities, geophysical studies involving aeromagnetic surveys, regional gravity measurements, active seismic surveys, and the evaluation of pre-existing hydrocarbon exploratory wells. These efforts, involving the evaluation of combined public domain data and direct acquisition of field data, aim to assess the geothermal energy potential of the area.

The Midyan Basin exhibits elevated heat anomalies in the basin depocenter, primarily hosted in the pre-salt formation reservoir. This reservoir is intensely fractured due to the Red Sea rifting and the movement of the Gulf of Aqaba strike-slip fault. The heat source is interpreted to originate from the deep mantle, combined with radiogenic heat production from radioactive minerals in the granite basement. The presence of the salt formation also contributes to the elevated heat in this area, acting as a cap rock that seals hot water within the pre-salt reservoirs. The pre-salt formations, likely the Al Wajh, Burqan, or Magna formations, are interpreted to be the reservoir of the system, capped by the Mansiyah salt formation and intra-silt, mud, and claystone layers within each formation.

The next challenges in developing this energy source include drilling deep enough to prove the conceptual model while considering the potential of intersecting hydrocarbon prospective reservoirs and associated geohazards. Additionally, the hot water in the reservoir may not be sufficient for self-discharge to generate power, necessitating the use of downhole heat pumps to extract this energy. However, direct-use applications should also be considered for this energy source, given the high demand. These factors will significantly impact the economic viability of this geothermal prospect area.

1. INTRODUCTION

Geothermal resource province in Saudi Arabia particularly lies on the western coast and is associated with the Red Sea. The distinguished geothermal resource potential is commonly in accordance with volcanic fields (called Harrat) and was inferred by the presence of hot springs, specifically in Jizan and Al Lith. However, there are potential areas that might host the hot sedimentary aquifer system within the basin along the west coast, including in the Midyan area at the northwestern.

In Midyan area, however, there is no surface thermal manifestation identified. Despite the lack of surface manifestations, several studies have shown the presence of high heat flow in Midyan area (e.g., in Aboud, et al., 2023). This absence of surface indicators could be due to several factors: there may be no hydrothermal activity present, or the heat could be confined within a sedimentary basin, forming a confined aquifer. The latter condition is particularly relevant in the context of the Midyan region due to its subsurface geology condition.

In this paper, we present the results of our surface geoscientific investigations in the Midyan Area, providing insights into the geothermal characteristics of this region. We discuss the geological and geophysical data collected, analyze the potential for a hot sedimentary aquifer system, and propose further steps for geothermal exploration and development. By understanding the geothermal potential in this area, Saudi Arabia can diversify its energy portfolio and contribute to global efforts in sustainable energy utilization.

2. GEOLOGICAL SETTING

The Midyan basin (Figure 1) is geologically influenced by the development of the Red Sea Rifting and the Strike Slip movement of the Gulf of Aqaba. The Red Sea Rifting is part of the triple junction in the Afar region that spreads the Arabian Plate, Nubian Plate, and Somali Plate, then it creates the Red Sea Rift, Gulf of Aden Rift, and

Main Ethiopian Rift. The main Ethiopian rift is well known as the main heat provider of the geothermal system in the East Africa region.

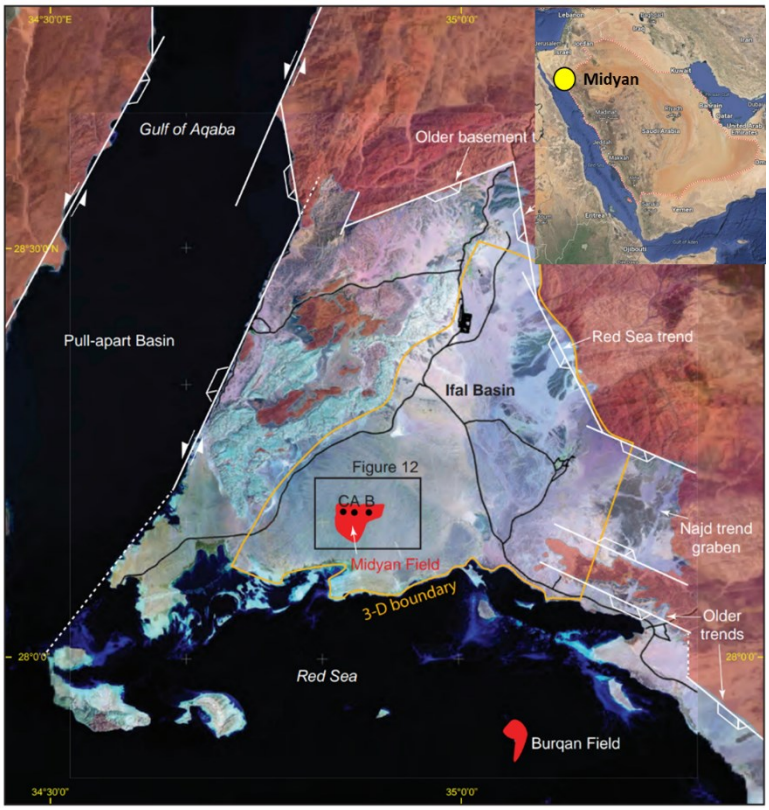

Figure 1: Tectonic framework of the Midyan Area (modified from Tubbs, 2014).

The Red Sea rift stretched out from the Afar region, at the south to the Gulf of Suez, towards the north. In the early stages of the rift, the Gulf of Suez was part of the Red Sea, sharing its geological history and structural patterns. The Red Sea basin features several zones of half-grabens that dip towards either the Arabian or African plates, with accommodation zones in between. These structures have been extensively studied in the Gulf of Suez and observed throughout the main Red Sea area.

2.1 The Red Sea Rift Development

The Red Sea Rift initiated 30-32 million years ago by the depression of the Afar plume, rifts the African-Arabian continental plate, and eventually developed into an oceanic rift. Prior to the beginning of the Red Sea Rift periods, the pre-Miocene formations existed with the Cretaceous formations being the oldest. These formations are thickest at the Gulf of Suez and become thinner towards the south, disappearing offshore and in outcrops in the northern areas of the Red Sea. Some Cretaceous outcrops are preserved within grabens along the Saudi western coast, extending towards the Yemen border.

- **Early Rift Stage (31-27 Ma)**

  During the early rift stage, characterized by normal extension, the entire 2,200 km long Red Sea opened simultaneously (Figure 2 left and Figure 2 right). At this time, the Early Oligocene deposits consisted of continental sands from the Al Wajh formation, present as continental red beds and lacustrine deposits up to 2200 meters thick. This period was followed by a marine incursion that deposited deep marine turbidites of the Burqan formation in tectonically active regions (Bosworth, et al., 2005).

- **Mid-Rift Stage**

  During 18-17.5 Ma, a significant environmental change occurred, marked by mid-clysmic unconformity during the Burqan sedimentary deposition. This event ended the deposition of the Maqna group, which showed low tectonic activity and basin-wide restriction (Figure 3 left and Figure 3 right), leading to the formation of regional anhydrite layers and the extensive Mansiyah halite (Bosworth, et al., 2005).

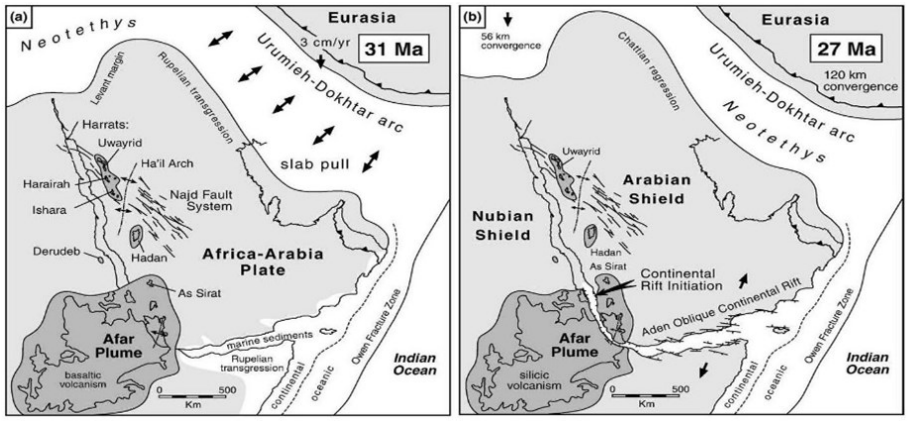

Figure 2: The early stage of the Red Sea rifting (Bosworth, et al., 2005).

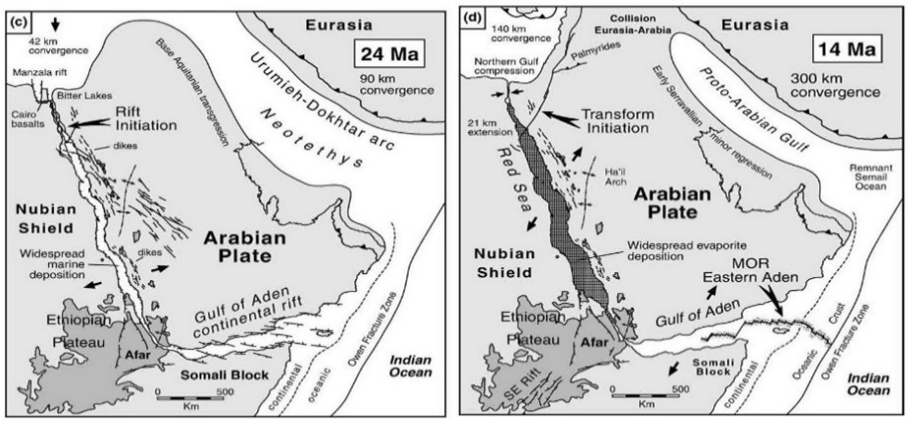

Figure 3: The mid-Clysmic unconformity occurred (Bosworth, et al., 2005).

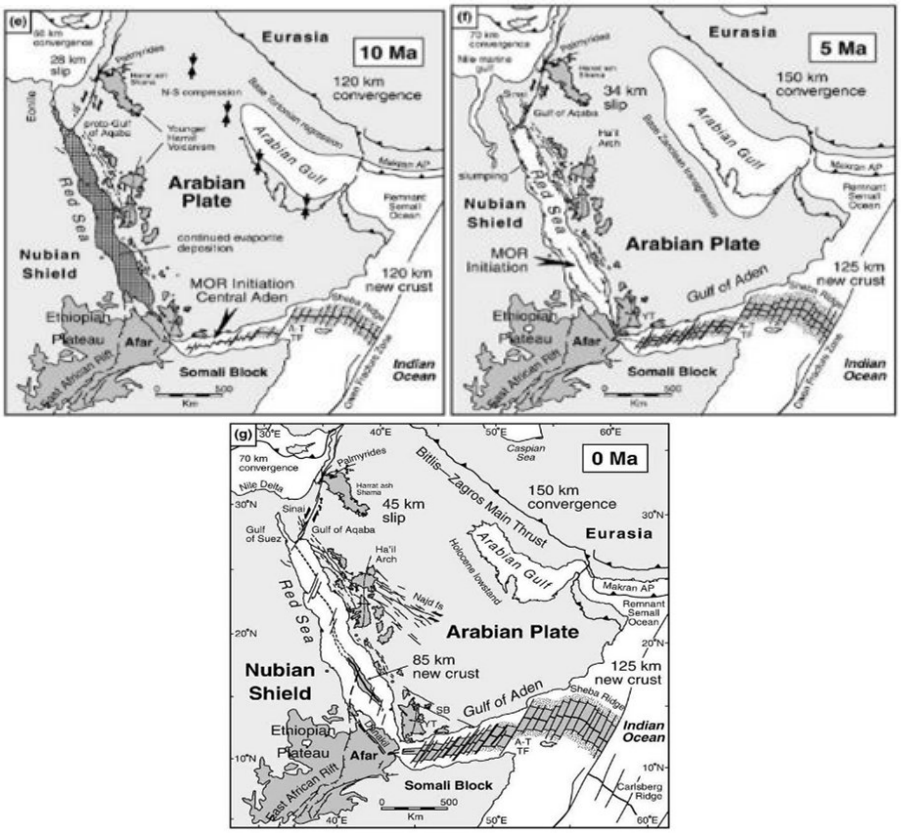

Figure 4: The late rift sequence and the opening of the Gulf of Aqaba (Bosworth, et al., 2005).

- **Late Rift Stage (14-12 Ma)**

  The Gulf of Aden rift evolved into an oceanic ridge with seafloor spreading. The collision between the Arabian and Eurasian plates rotated the Arabian plate counterclockwise, shifting the Red Sea to a rift-oblique extension (Figure 4 upper left, Figure 4 upper right, and Figure 4 bottom). This reactivated faults and caused strike-slip deformation, particularly in the northern Red Sea and the Midyan peninsula (Bosworth, et al., 2005).

2.2 The Gulf of Aqaba Opening

The counterclockwise rotation of the Arabian plate causes the opening of the Gulf of Aqaba, halting extension along the Gulf of Suez. This created strike-slip deformation across the basin, along the Gulf of Aqaba, and extended to the Dead Sea at the further north (Figure 5). This is also altering subsalt topography and causing the Mansiyah halite to move towards the center of the Red Sea. This process formed accommodation zones filled by the post-salt Ghawwas and Lisan formations.

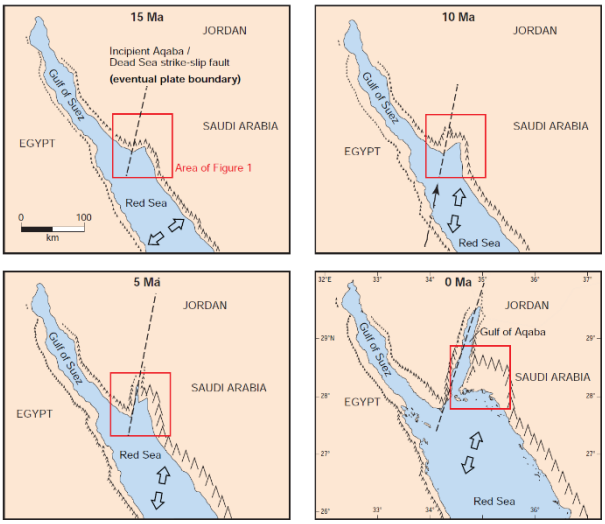

Figure 5: The opening of the Gulf of Aqaba (Tubbs, et al., 2014).

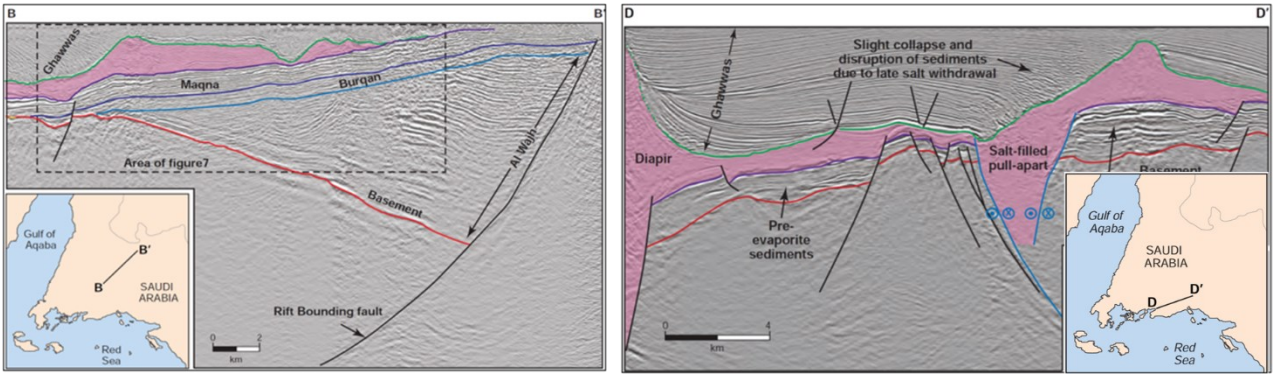

Figure 6: The Midyan basin structures (vertically exaggerated) described by Tubbs, et al. (2014)., Rift-basin structure is shown on the left side while pull-apart basin structure is shown on the right side.

3. MIDYAN BASIN MODEL AND STRATIGRAPHY LAYERS

The Basin model of Midyan area has been constructed comprehensively while doing hydrocarbon exploration by some parties. 2D and 3D seismic lines cover this area evenly and help to understand the basin structures, including the stratigraphic layers in it. Tubbs, et al. (2014), shows six seismic profiles and the interpretation across the area (Figure 6). Additionally, during the geothermal exploration, some other parties have added the 2D seismic lines to investigate the depocenter of the basin further where it is extended to Al Bad' at the north and Ras Shaik Humaid at the west.

The Midyan Basin is primarily characterized as a half-graben structure, formed due to extensional tectonics during the Miocene. The structural framework of the basin is defined by a series of normal faults, which are crucial for

the deposition and preservation of sedimentary layers. Additionally, the area is influenced by the strike-slip movement of the Gulf of Aqaba and the Dead Sea fault. This is evidenced by the presence of strike-slip faults observed in surface rock scarps and pull-apart structures within the region.

The basin fill comprises thick sequences of syn-rift siliciclastic rocks, which are primarily deposited during periods of tectonic activity. The pre-rift section comprised by **Neoproterozoic basement** that consists of commonly granitic, also metasediments, metavolcanics, and gabbro, with noticeable pockets of Cretaceous Adaffa Sandstones (Clark, 1987 in Tubbs, et al., 2014). The syn-rift section is comprised of Al Wajh formation, Burqan formation, Magna group, and Mansiyah formation. The post-rift section consists of Lisan group, Ghawwas formation, and post-Ghawwas formation (Beydoun, 1991; Hughes & Beydoun, 1992).

- **The Al Wajh formation** represents the earliest rift deposition of continental red beds that form sand wedges on top of the basement, generally within rotated half grabens. The Al Wajh sediment is expected to be composed of high porosity sandstone with the possibility of layers of tight facies in shales that were deposited along lacustrine beds in the basin.
- **The Burqan formation** signifies the first basin-wide marine incursion, marking the organized rift propagation across the Red Sea basin and its connection with global oceans. It consists of marine turbidites and is generally composed of interbedded sandstones and mudstones/shales, creating vertically stacked reservoir-seal pairs.
- During the formation of **the Maqna group**, rift kinematics started to slow down onshore, and there is evidence of basin-wide restrictions. The Maqna group comprises formations of siliciclastic/carbonate layers and anhydrite layers, resulting in vertically stacked reservoir-seal pairs, with the two anhydrite formations acting as seals.
- **The Mansiyah formation** is characterized by massive halite deposits, marking the peak of basin-wide restriction and a period of slow subsidence. This formation is correlated with the end of the active rift phase of the Red Sea faults and the activity along the Gulf of Aqaba strike-slip. The Mansiyah salt acts as the ultimate regional seal, capping the Maqna group, and is effective unless rift faults offset the base of the salt by more than the remaining salt thickness.
- Finally, **the Ghawwas formation** is a post-salt formation that is heavily influenced by salt evacuation, which controls both accommodation space and formation structures. This formation's characteristics are shaped by the dynamics of salt movement and the resultant geological features

4. GEOTHERMAL CONCEPTUAL MODEL

Currently, there are no geothermal drilling explorations conducted in the Midyan area to explore the subsurface parameters that were used to construct the geothermal conceptual model. Thus far, the conceptual model has been constructed by the surface geoscience data and the addition of the oil and gas wells data.

Extensive geoscience surveys have been conducted in the area, including comprehensive 2D and 3D seismic surveys. Regional magnetic data has been utilized to identify basement anomalies and determine the Curie depth. Additionally, regional gravity data from the Saudi Geological Survey has been used to enhance the interpretation of basement distribution and inferred faults. Surface geological mapping has also been performed to document the variety of lithologies, faults, and fractures. However, the absence of surface geothermal manifestations in the region makes the interpretation quite challenging.

The geothermal system in the Midyan area is identified as a hot sedimentary aquifer type. The critical resource parameters of this system include the temperature, permeability, reservoirs, and cap rocks. The primary heat source is thought to originate from deep below the region, linked to a thinning crust. Additionally, radiogenic heat from the decay of radioactive minerals in the granite basement contributes to the area's heat anomaly. Heat is conducted through the basement rock and ascends via faults and fractures, while convective heat transfer is likely present in the sedimentary layers. The temperature contour in Figure 7 does not accurately represent the actual heat distribution in the system, as it is influenced by the variety of lithologies and local fractures.

The heat convects through the sandstone reservoir of the pre-salt formation, potentially originating from the Al Wajh, Burqan, or Magna formations. These sandstone formations share similar characteristics, including porosity, permeability, and anomalous overpressure pores. The reservoir's thickness ranges from 1-2 km and can reach up to 4-5 km at the basin's depocenter. The reservoir is capped by siltstone and claystone within the formation and by the Mansiyah salt layer. However, while the salt layer effectively caps fluid movement, it does not impede heat transfer due to its excellent thermal conductivity.

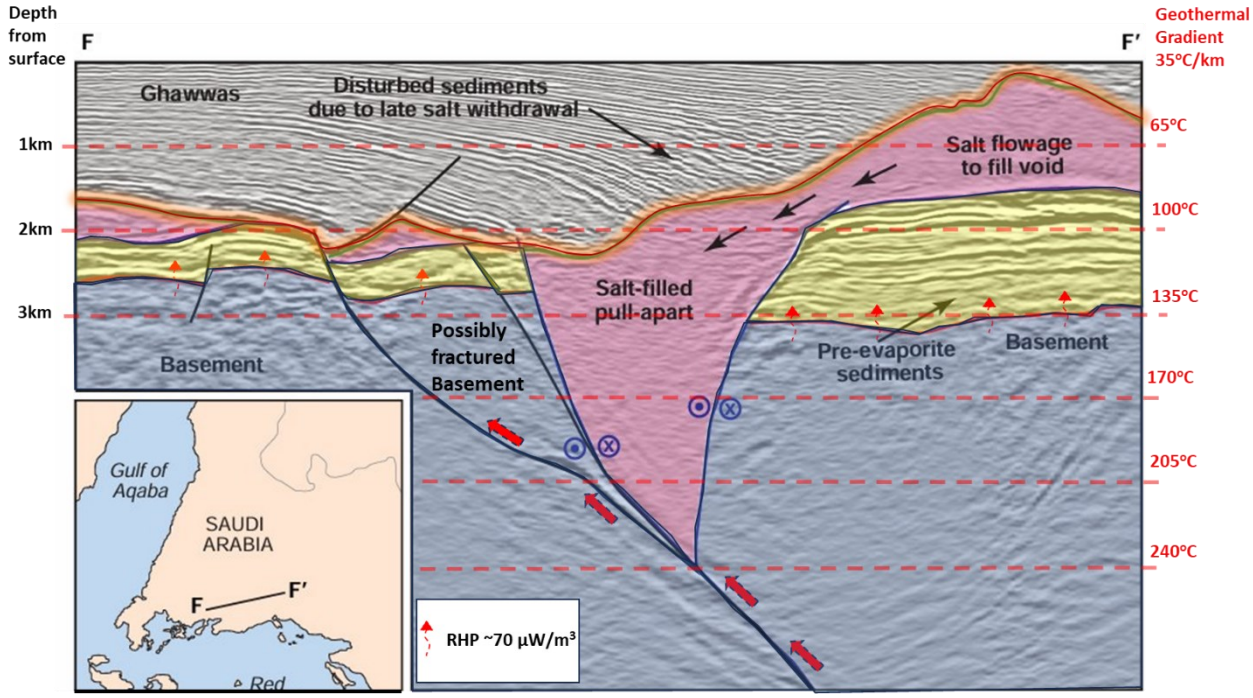

Figure 7: Proposed resource conceptual model in Midyan area (modified from Tubbs, et al., 2014). The geothermal gradient is inferred from the curie depth; The radiogenic heat production is analog from the closest surface granite analysis; Basement rocks are in dark gray, potential reservoir rocks in yellow, and the massive impermeable salt layer in pink.

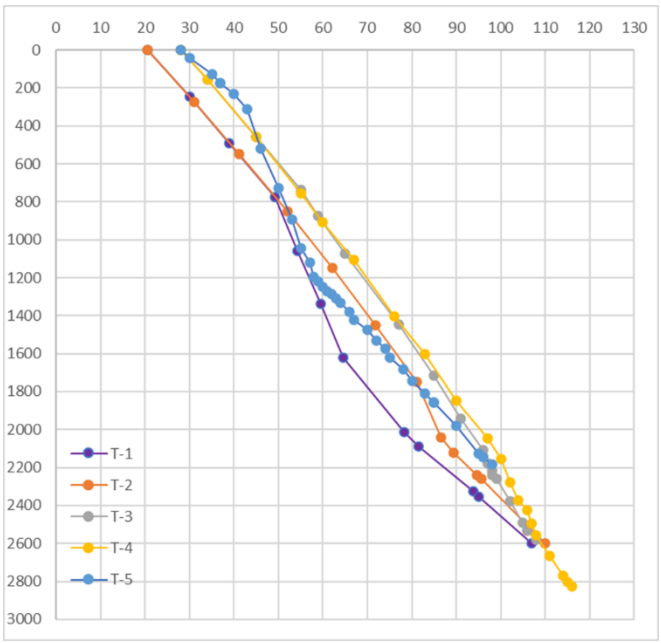

Figure 8: Temperature profile from several deep wells in the area.

4.1 Elevated Heat Anomaly

Heat exploration in the Midyan area is extremely challenging due to the absence of typical thermal signatures such as hot or warm springs, fumaroles, steaming ground, or altered ground that are usually found in conventional geothermal fields. The elevated heat in this region is theoretically interpreted from the regional geological setting associated with the thinning crust from the Red Sea rifting, which brings the hot mantle closer to the surface. This interpretation is supported by the curie temperature profile derived from regional magnetic data. Additionally, radioactive minerals from the granitic body bounding the basin could be a potential heat source for this system. The presence of a salt layer further aids in elevating heat along the body of the salt, allowing access to significant heat at shallower depths

4.1.1 Temperature Data from Deep Wells

There is limited subsurface data available in this area, sourced only from several deep wells (Figure 8). The quality of this data is uncertain, as the actual conditions of the wells are unknown. Additionally, the details regarding the measurement procedures, tool specifications, and the times at which measurements were taken are absent, making it impossible to conduct a data quality check. Furthermore, the locations of these wells are concealed to meet confidentiality protocols. From the deep wells, it is observed that the maximum temperature can reach 110°C at a depth of 2600 m, suggesting a temperature gradient of about 33-35°C/km for the deep formation.

4.1.2 Currie Point Depth

Curie temperature is a point at which magnetic minerals lose their magnetization due to high temperature (580ºC). It can be the bottom of the basement surface or the Moho surface (Aboud, et al., 2023). The curie point depth analysis was carried out by Aboud, et al. (2023) to image the subsurface of NEOM area, specifically the Midyan basin area. The data used in the analysis are collected worldwide from various magnetic surveys (ground, airborne, marine surveys) and compiled/merged into one magnetic model called World Digital Magnetic Anomaly Map (WDMAM). The result shows that the Curie point depth of the Midyan area is variously calculated at 12.9km to 15.4km at the promising area.

The curie point then can be used to calculate the regional temperature gradient of the area, considering the heat transfer mechanism is homogeneous to the surface. Simplified formula adapted to measure the geothermal gradient, Geothermal Gradient (GG) = 580ºC / Curie depth. The temperature gradient of the Midyan area is calculated at 37-44ºC/km at the promising area. To compare with the actual temperature data from the deep wells, at the depth of 3000m, it is calculated the temperature would be at 140-160ºC respectively with the average atmospheric temperature of 30ºC.

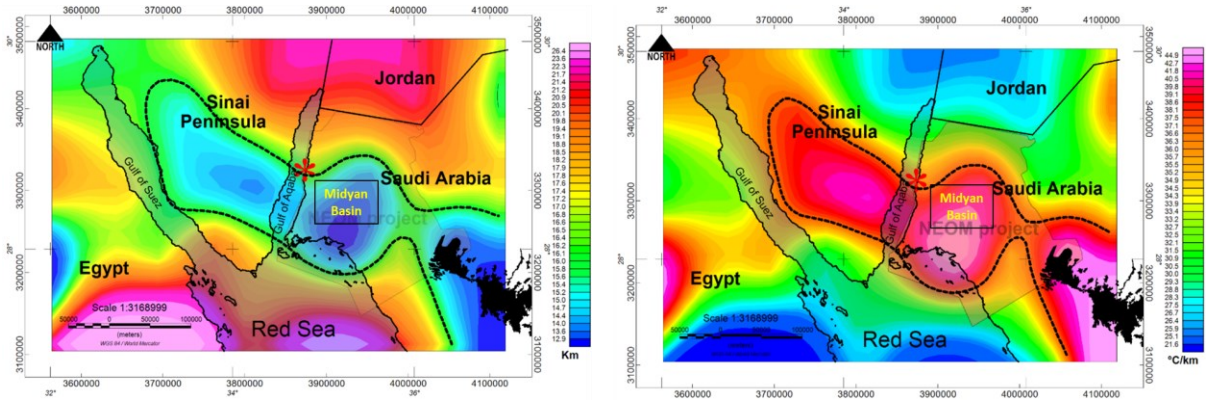

Figure 9: Currie depth map (left) and geothermal gradient map (right) from Aboud, et al. (2023).

4.1.3 Radiogenic Heat Source

Many studies have been conducted to assess the Radiogenic Heat Production (RHP) from the felsic plutonic rock within the Arabian Shield, particularly surrounding the Midyan area. Despite there being no sample directly taken from the subsurface basement of the Midyan area, the closest samples from Ghurayyah and the Gulf of Aqaba rocks could be the analog for the Midyan area (Figure 10). The amount of radioactive minerals is uniquely high, specifically in the veins of the rocks (see Table 1). During the radioactive decay, mass is converted to energy, and an important part of this energy is converted to heat. All natural radioactive isotopes generate heat to a certain extent but only the contributions of the decay series of 238U, 232Th, and the isotope 40K are geologically significant.

The same granite type is considered to exist as the basement of the Midyan basin. It appears in the seismic profiles that the basement spread evenly within the Midyan area with the top of the basement at 6 km at the depocenter, getting shallower towards the edge of the basin.

Table 1: Radioactive minerals from Felsic rocks taken from the surrounding Midyan area (modified from Harris & Marriner, 1980).

Sample	U (ppm)	Th (ppm)	K (wt%)	RHP (μW/m^3)
Ghurayyah Granite 1	104	625	2.59	70.2
Ghurayyah Granite 2	88	160	2.63	33.9
Gulf of Aqaba Granite (Vain)	363	590	1.65	134.2

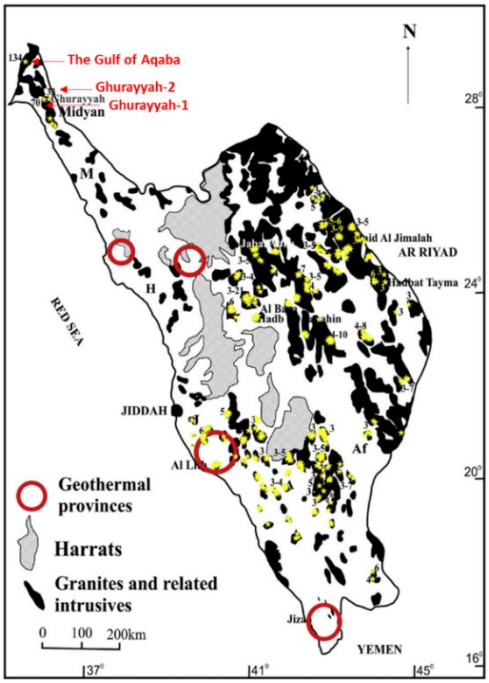

Figure 10: The location of Ghurayyah and The Gulf of Aqaba Granite samples (modified after Chandrasekharam, et al., 2015). The numbers indicate heat generated by the granites in µW/m3 calculated based on U, Th, and K values.

The radioactive heat production of granite rocks (RHP in μWm^{-3}) can be calculated by considering the heat generation constant (amount of heat released per gram U, Th and K per unit time) and from the uranium, thorium and potassium concentrations CU, CTh, CK present in rock (Cermak, Huckenholz, Rybach, & Schmid, 1982; Rybach, 1988 in Abbady & Al-Ghamdi, 2018):

$$RHP = \rho\,(9.52\,CU + 2.56\,CTh + 3.48\,CK)10^{-5} \quad (1)$$

where ρ is the bulk density of rock; Cu and CTh are in weight ppm; Ck is in weight %.

4.2 Salt Layer

The temperature gradient within sedimentary stacks in basin settings can be unusually high due to the increased thermal conductivity of salt layers. An analysis conducted in Eemshaven, Netherlands, reveals a temperature increase of between 17°C and 25°C at the same depth when comparing locations with normal stratigraphic salt thickness to those at the top of the salt structure (Daniilidis & Herber, 2017). Similarly, a study in the Pripyat Trough, Belarus, concludes that the highest heat flow density values, reaching up to 80-100 mW/m², occur at the crest of salt domes and caprocks, with a significant decrease at the base of the salt dome (Zui, et al., 2016). In the Midyan area, the presence of Mansiyah Salt locally affects the geothermal gradient and heat flow density within the basin. However, the proposed conceptual model does not yet reflect the final isothermal contour that accommodates the presence of the Mansiyah Salt.

Due to their high thermal conductivity, salt layers can act as efficient channels for heat, creating local positive thermal anomalies in the overburden of salt accumulations (Moeck & Breadsmore, 2014; Moeck, 2014). This unique property makes the areas above these formations are attractive targets for geothermal exploration, as the heat is channeled through the salt, creating a distinct temperature change in salt topography. Daniilidis & Herber (2017) demonstrated a 40% increase in energy extraction and a 25°C temperature rise within a salt formation in the north of the Netherlands, emphasizing the influence of salt thickness variations on heat gradients and thermal conductivity scenarios. Additionally, the geometric shape of salt domes affects heat accumulation, with narrower domes leading to less concentrated heat compared to elongated, conical structures (Daniilidis & Herber, 2017).

The presence of salt formations in the Midyan area can be identified through seismic line profiles published by Tubbs, et al. (2014). Modeling efforts of this salt formation are critical for geothermal resource modeling, as it influences heat flow direction within the reservoir. A study by Zui, et al. (2016) concludes that in the Pripyat field, Belarus, the salt layer controls heat flow density and direction. Additionally, the salt formation is impermeable; while it can conduct heat, it cannot allow fluid flow within the formation, thus acting as a cap rock for the underlying reservoirs. Understanding the Mansiyah Salt formation is essential for identifying where heat accumulates and how it is directed. This knowledge can help target resource areas, as it provides a substantial

amount of heat at both the top and bottom of the salt formation. By accessing this heat, drilling operations can avoid intersecting the salt formation, thereby reducing risks.

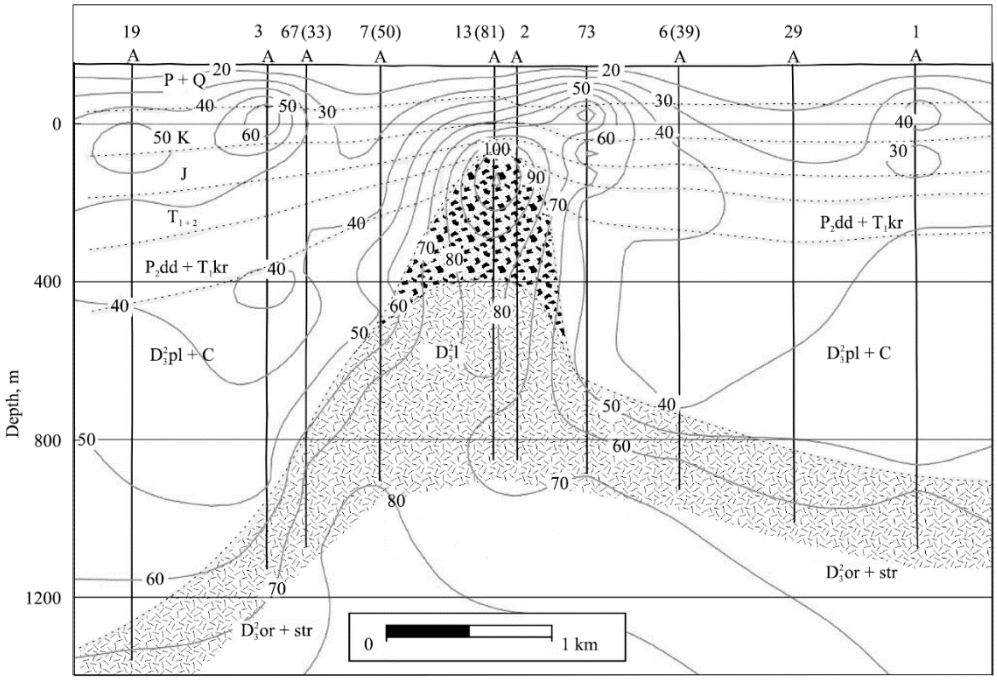

Figure 11:Salt dome profile versus heat flow in Pripyat Trough, Belarus (Zui, et al., 2016).

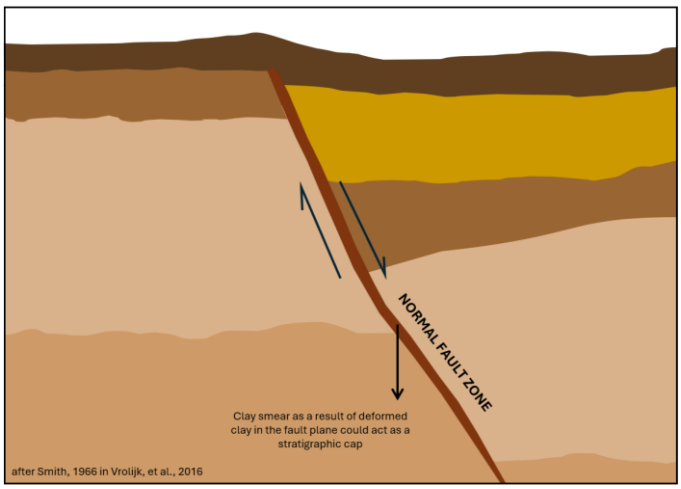

Figure 12: Illustration of clay smear concept (modified after Smith, 1966 in Vrolijk, et al., 2016).

4.3 Capping Mechanism

The presence of a clay cap, similar to that in conventional geothermal systems, is unlikely in the Midyan area. Instead, the impermeable rocks within the formation, originally deposited, are more likely to control the cap mechanism. This type of capping mechanism is akin to that found in hydrocarbon traps. For example:

- The red and green mudstones in the Al Wajh formation (Hughes & Johnson, 2005) potentially act as caps for the porous sandstones below.
- The calcareous mudstone of the Subayti member and the mud-dominated succession of the Nutaysh member of the Burqan formation (Hughes & Johnson, 2005).
- The deep marine mudstone of the Magna formation (Hughes & Johnson, 2005).

The tectonic evolution of this area has facilitated the development of stratigraphic caps, often combined with faults, which may be filled by clay (clay smear). Clay smears form in normal faults that deform layered sedimentary sequences, typically clastic sequences. They develop through mechanical processes alone and include the entire fault zone, from the most highly deformed clay to stratigraphically coherent fault lenses of shale. This

results in a lithologically and structurally heterogeneous fault zone, becoming significant once beds are completely offset from each other (Vrolijk, et al., 2016). Although no previous studies specifically address clay smears along the faults in the Midyan area, the area's stratigraphic layers and salt formations suggest the potential presence of this phenomenon.

Furthermore, the pre-salt reservoir rocks are significantly capped by the massive salt layer of the Mansiyah formation. This impermeable salt layer covers the entire Al Wajh, Burqan, and Magna reservoirs. However, due to its irregular distribution, variations in salt layer thickness are expected within the same area.

4.4 Reservoir Targets

The hot water reservoir in the Midyan area is influenced by the distribution of stratigraphic layers and is stored in porous sedimentary rocks and sharp formation contacts. Due to the presence of both permeable and impermeable strata, the water primarily moves laterally through the formations rather than vertically. The most promising formations for hosting hot water are the pre-salt formations, including the Al Wajh, Burqan, and Magna formations, as well as the contacts between these formations. Additionally, the bottom of the Ghawwas formation (post-salt) could also serve as a reservoir target, though the temperature there may be lower.

These promising formations are significantly influenced by the structural characteristics of the Midyan basin. The basin's prominent structures include the rift-bounding faults created by the Red Sea spreading and the pull-apart fault system caused by the Dead Sea strike-slip movement. These structures are believed to connect with the heat supply from below. The heat from the thinning crust moves upward primarily through conductive processes in the basement rock and convective processes along the faults. Reservoirs located closer to these faults can be expected to have higher temperatures. However, these faults are less likely to host large volumes of hot water. In addition, the basement contacts with the above formations are also expected to be permeable due to their sharp and disconformity nature. The heat generated from the decay of radioactive minerals in the basement moves upward and is primarily stored in these permeable basement contacts.

In summary, the reservoir and permeability targets of this hot sedimentary aquifer system include:

- **Top Basement Unconformity:** The top basement in the Red Sea, often heavily fractured and overlain by continental sands of the Al Wajh formation, offers significant reservoir potential.
- **Al Wajh Sands:** These sands, capped by an intra-Al Wajh facies seal or the Burqan formation seal, are another viable target.
- **Burqan Formation Sandstones:** These sandstones, capped by inter-formation seals, present promising reservoir prospects.
- **Maqna Group Reservoirs:** Capped by the anhydrites within the group or the Mansiyah salt, these reservoirs are attractive geothermal targets.
- **Bottom of Ghawwas Formation:** Located at the contact with the Mansiyah salt, this formation benefits from the salt's good thermal conductivity, efficiently transferring heat from below to above the salt layer. This allows access to the thermal properties without intersecting the salt layer, which is known to complicate drilling operations.
- **Major Rift-Bounding and Pull-Apart Faults:** These faults play a crucial role in heat distribution and can enhance the geothermal potential of adjacent reservoirs.

By understanding the distribution and movement of hot water in relation to both stratigraphic layers and structural features, we can better target potential reservoirs and optimize geothermal exploration efforts in the Midyan area.

5. UNCERTAINTY AND RECOMMENDATION

The proposed conceptual model requires validation due to its construction based on limited data. Although the geological framework of the area is extensively documented from numerous studies primarily targeting oil and gas exploration, the understanding of its geothermal potential remains inadequately explored. To maximize exploration efforts, a comprehensive approach involving detailed structural mapping, high-resolution 3D seismic surveys, advanced magnetic surveys (airborne or ground), precision gravity surveys, and ultimately, exploratory drilling is recommended.

The uncertainties inherent in the conceptual model are substantial and encompass several key parameters:

1. **Heat Source**: Despite the existence of temperature profiles from multiple wells in the area, the specific conditions of these wells are not fully understood, complicating the interpretation of temperature data. The curie depth inferred from regional magnetic data (Aboud, et al., 2023) does not necessarily represent the actual isotherm contour of the area, as it primarily indicates the depth of the demagnetized zone within the mantle. Furthermore, the radiogenic heat production calculated from surface granite samples

may not accurately reflect the characteristics of the Midyan basement, which could comprise Neoproterozoic granite with potentially diminished radioactive mineral content over time.

2. **Salt Layer**: The presence of the Mansiyah salt layer, as interpreted from 3D seismic profiles, necessitates corroboration through direct lithological sampling to ascertain the mineral composition and measure the thermal conductivity of the salt body. Detailed 3D modeling of the salt body is crucial for a more precise understanding of the geological and geothermal context of the area.
3. **Cap Rocks**: The potential cap rocks, including siltstone, mudstone, and claystone, cannot be precisely identified through current 3D seismic profiles, which lack the resolution to distinguish between sand and clay formations. These profiles rely on analogs from oil and gas exploration in the Suez and Sinai Peninsula. Additionally, the presence of smear clay along faults must be verified through direct exploration drilling.
4. **Reservoirs**: The pre-salt reservoirs, currently interpreted solely based on 3D seismic data, leave open the possibility of various underlying formations such as the Al Wajh, Burqan, or Magna formations. Each of these formations exhibits distinct lithological characteristics, pressure regimes, and permeability, which may significantly influence reservoir properties.

Deep geothermal drilling is essential to substantially reduce these uncertainties. Although advanced geoscience exploration techniques are available and can mitigate some of the system's uncertainties, the Midyan area is presently characterized as a hot sedimentary geothermal system with no evident surface manifestations. Consequently, it is improbable to resolve all uncertainties entirely without drilling. We recommend transitioning to deep exploration drilling, as the current geothermal system interpretation, while adequate, can be significantly enhanced with additional data.

REFERENCES

Abbady, A. G. E. & Al-Ghamdi, A. H.: Heat production rate from radioactive elements of granite rocks in north and southeastern Arabian shield Kingdom of Saudi Arabia, *Journal of Radiation Research and Applied Sciences*, 11(4), (2018), 281-290.

Aboud, E. et al.: Geothermal Imaging of the Saudi Cross-Border City of NEOM Deduced from Magnetic Data, *Sustainability*, 15(4549), (2023).

Beydoun, Z. R.: Arabian Plate Hydrocarbon Geology and Potential - A Plate Tectonic Approach, American Association of Petroleum Geologists, *Studies in Geology*, 334, (1991), 77.

Bosworth, W., Huchon, P. & McClay, K.: The Red Sea and Gulf of Aden Basins, *Journal of African Earth Sciences*, 43, (2005), 334-378.

Chandrasekharam, D. et al.: The potential of high heat generating granites as EGS source to generate power and reduce CO2 emissions, western Arabian shield, Saudi Arabia, *Journal of African Earth Sciences*, 112, (2015), 213-233.

Daniilidis, A. & Herber, R.: Salt intrusions providing a new geothermal exploration target for higher energy recovery at shallower depths, *Energy*, (2017).

Harris, N. B. W. & Marriner, G. F.: Geochemistry and petrogenesis of a peralkaline granite complex from the Midian Mountains, Saudi Arabia, *Lithos*, 13(4), (1980), 325-337.

Hughes, G. W. a. G. & Johnson, R. S.: Lithostratigraphy of the Red Sea Region, *GeoArabia*, 10(3), (2005), 49-126.

Hughes, G. W. & Beydoun, Z. R.: The Red Sea-Gulf of Aden: Biostratigraphy, Lithostratigraphy and Paleoenvironments, *Journal of Petroleum Geology*, 15(2), (1992), 135-156.

Moeck, I. S.: Catalog of geothermal play types based on geologic controls, *Renewable and Sustainable Energy Reviews*, (2014), 867-882.

Moeck, I. S. & Breadsmore, G.: A new 'geothermal play type' catalog: Steamlining exploration decision making, Proceedings, 39th Workshop on Geothermal Reservoir Engineering, Stanford University, Stanford CA (2014).

Nagihara, S.: Three-dimensional inverse modeling of the refractive heat-flow anomaly associated with salt diapirism, *AAPG Bulletin*, 87(7), (2003), 1207-1222.

Tubbs, R. E. et al.: Midyan Peninsula, northern Red Sea, Saudi Arabia: Seismic imaging and regional interpretation. *GeoArabia*, 19(3), (2014), 165-184.

Vrolijk, P., Urai, J. & Kettermann, M.: Clay Smear: Review of Mechanism and Applications, *Journal of Structural Geology*, 86, (2016), 95-152.

Zui, V. I., Dubanevich, M. A. & Vasilionak, E. A. Salt Domes of the Pripyat Trough as Heat Accumulators, *Вестник БГУ*, 2(2), (2016), 85-90.

Numerical Study on The Effects of Nanofluids on Heat Transfer Enhancement of a Closed Loop Geothermal Co-Axial System in an Unproductive-Idle Geothermal Well

Marcellinus Davinci[1], Khasani[1], Vincentius Adven Brilian[1],
Budi Santoso Wibowo[1], and Fefria Tanbar[2]

[1]Department of Mechanical and Industrial Engineering, Universitas Gadjah Mada, Yogyakarta, Indonesia
[2]Research Institute, PT PLN (Persero), South Jakarta, Indonesia 12760

davincimarcellinus7@gmail.com, khasani@ugm.ac.id, adven.brilian01@gmail.com,
budisantosowibowo@mail.ugm.ac.id, fefria.t@pln.co.id

Keywords: closed-loop geothermal system, idle geothermal well, heat transfer, pump power

ABSTRACT

Many geothermal fields experience derating or decreased power output. This can be caused by the decline in well productivity or, in the worst case scenario, the wells stop flowing. They can be idle and not used as production wells for a period of time, while still maintaining sufficient heat to be utilized. A tubing system may be inserted into the idle wells while working fluid is pumped through it, extracing heat from the surrounding formation through conduction and convection whenever geothermal fluid is available in the wellbore. The hotter working fluid leaving the tubing system can be used direcetly generate electricity. The purpose of this study is to conduct numerical analysis of heat extraction by using a closed loop system in an unproductive geothermal well. This research uses four different working fluids, namely water, carbon nanotubes, graphene, and titanium oxide, each with a mass flow rate of 1 kg/s. Numerical simulations using COMSOL Multiphysics software are conducted to determine the outlet temperature of the working fluid and the pump power required to move the fluid. The results showed that the carbon nanotube (CNT) working fluid yields a superior outlet temperature compared to the other fluids, while water produces the lowest outlet temperature. The highest outlet temperature recorded reaches 156°C, while the lowest outlet temperature is at 140°C. The pump power required to move the graphene fluid is relatively low at 3.048 kW, whereas the carbon nanotube fluid requires the highest pump power at 3,398 kW.

1. INTRODUCTION

The primary advantage of closed-loop geothermal heat extraction is its ability to operate effectively regardless of reservoir permeability and the nature of the fluid present (Yuan et al., 2021). Currently, most geothermal exploitation still adopts the traditional approach, namely by extracting geothermal fluid, in the form of steam or hot water, directly from reservoirs. However, this approach can cause a number of problems. For example, production fluids can contain chemical solutions from rocks that can damage wells and surface equipment due to their corrosive properties. Additionally, production fluids may carry hazardous chemicals, such as acid gases, from reservoirs to the surface, which should be considered hazardous pollutants. The reservoir fluid itself may be hazardous and require special handling. The reaction between the injected working fluid and the rock can also cause formation damage. Additionally, reservoir permeability may be insufficient to inject or recover working fluid at adequate flow rates. One solution to overcome this problem is to isolate the reservoir fluid from the geothermal energy extraction infrastructure using a downbore heat exchanger (DBHX) circulation system. In this system, the working fluid does not come into direct contact with the hot rock, and this method is currently generally applied to closed-loop systems. Closed-loop systems are systems that are installed in idle and existing wells and do not require subsurface permeability because they use closed pipes that are specially designed to deliver heat transfer fluids through rock layers and then up to the surface. In closed loop systems, it is possible to use alternative heat transfer fluids that are superior to water in certain conditions. Closed loop systems can take heat from temperature resources (when permeability is generally very limited), where there is more efficient power generation. In addition, this technology is very suitable for use in hot dry rock conditions where water is not naturally available at that location. Magma only heats the dry rock above it. Therefore, a closed loop system is needed to capture heat in the dry rock.

In a closed-loop system, the fluids used are water and supercritical carbon dioxide (sCO_2). These two fluids are quite good in closed loop systems, but still have many shortcomings in heat transfer. Therefore, many methods have been developed to increase heat transfer. There are two ways to increase heat transfer, namely active and passive methods. The active method is an increase in heat transfer influenced by external factors, such as the use of geothermal pumps and the use of efficient heat exchangers. Meanwhile, passive methods refer to efforts to increase heat transfer efficiency without involving the use of external resources or additional energy, such as increasing thermal conductivity by injecting nanofluids as working fluids. Nanofluids are liquid suspensions in which nanomaterials are dispersed into a base fluid. Nanoscale additives produce superior thermophysical

properties compared to base fluids. In general, nanofluids are used to increase the thermal conductivity of fluids, which can be useful in a variety of applications, including cooling or heating systems (Wang et al., 2023). Some characteristics of nanofluids involve very small particles and good dispersion in the carrier fluid. According to several researchers, nanofluids that are often used are TiO_2 (Abbasi et al., 2015), CuO (Du et al., 2020), $CNTs$ (Ali et al., 2021), Al_2O_3 (Kapicioglu et al., 2020), Graphene (Ali, 2022), Fe_3O_4 (Cobanoglu et al., 2022).

2. NUMERICAL MODELING

Numerical modeling of closed-loop geothermal systems in idle geothermal wells is studied using numerical simulations using COMSOL software. The well is modeled in 2D axisymmetric space dimensions which will later be revolved to reflect the original condition of the well. This calculation uses the nonisothermal flow multiphysics package which combines the laminar flow physics package with heat transfer in the solid and liquid physics packages. The simulation in this research is in steady conditions and in this section the equations used, the domain model, and the boundary conditions of the numerical simulation are presented.

2.1. Governing Equations

In COMSOL software, mass, energy and momentum conservation parameters can be solved. The equations that govern the laminar flow physics package are stated in Equations (1), (2), and (3).

$$\rho(\boldsymbol{u}\cdot\nabla)\boldsymbol{u} = \nabla\cdot[-\rho\boldsymbol{I} + \boldsymbol{K}] + \boldsymbol{F} \quad (1)$$

$$\rho\nabla\cdot(\boldsymbol{u}) = 0 \quad (2)$$

$$\boldsymbol{K} = \mu(\nabla\boldsymbol{u} + (\nabla\boldsymbol{u})^T) \quad (3)$$

The equations that govern heat transfer in solid and fluid physics packages are expressed in Equations (4), (5), and (6) as follows (COMSOL, 2018):

$$\rho c_{\boldsymbol{p}}\boldsymbol{u}\cdot\nabla T + \nabla\cdot\boldsymbol{q} = Q + Q_{ted} \quad (4)$$

$$\rho c_p\,\boldsymbol{u}\cdot\nabla T + \nabla\cdot\boldsymbol{q} = Q + Q_p + Q_{vd} \quad (5)$$

$$\boldsymbol{q} = -k\nabla T \quad (6)$$

where **ρ** is the density of the fluid (kg/m^3), **u** is the fluid flow velocity vector (m/s), **I** is the unit matrix, **F** is the object force vector (N/m^3), **μ** is the dynamic viscosity of the fluid (Pa s) , **T** is the absolute temperature (K), $\mathbf{c_p}$ is the specific heat at constant pressure (J/kg-K), $\dot{\mathbf{q}}$ is the heat flux by conduction (W/m^2), $\dot{\mathbf{Q}}$ is the heat source other than viscous heating (W/m^3), $\dot{\mathbf{Q}}_{\mathbf{ted}}$ is the thermoelastic damping heat source (/m^3), $\dot{\mathbf{Q}}_{\mathbf{p}}$ is the heat source due to pressure changes (W/m^3), and $\dot{\mathbf{Q}}_{\mathbf{vd}}$ is the viscous dissipation (W/m^3).

2.2. Model Description

Figure 1 models a closed loop geothermal system for an inactive geothermal well which is the numerical simulation domain in this research. This inactive geothermal well was created to approach original conditions in the Mataloko MT-3 well in eastern Indonesia with a depth of 613 meters with a temperature of 170°C in the reservoir section. This well has a mass flow rate of 1 kg/s with a pressure of 6.5 bar. A coaxial borehole heat exchanger is inserted into the well to extract nanofluid heat by inserting water as a working fluid into the annulus space of the borehole heat exchanger. The inner tubing in the borehole heat exchanger is isolated to prevent heat energy loss and, in this study, the inner tubing is assumed to be completely isolated. The outer tubing is made of thermally conductive material, allowing maximum heat transfer. In addition, inactive geothermal wells are assumed to be surrounded by homogeneous rock and the rock layers are impermeable and non-porous. This rock is assumed to have a conductive base with a temperature of 170°C and a surface temperature of 25°C (Wahyuningsih, 2004).

Table 1: Properties of Materials (Hu et al,. 2020).

Parameter	Unit	Casing Pipe	Insulation Pipe	Cement	Rock
Thermal conductivity	W/m-K	44.5	0.26	Comsol	Comsol
Specific heat	J/kg-K	475	1700	2000	1000
Density	kg/m^3	7850	1150	2300	2600

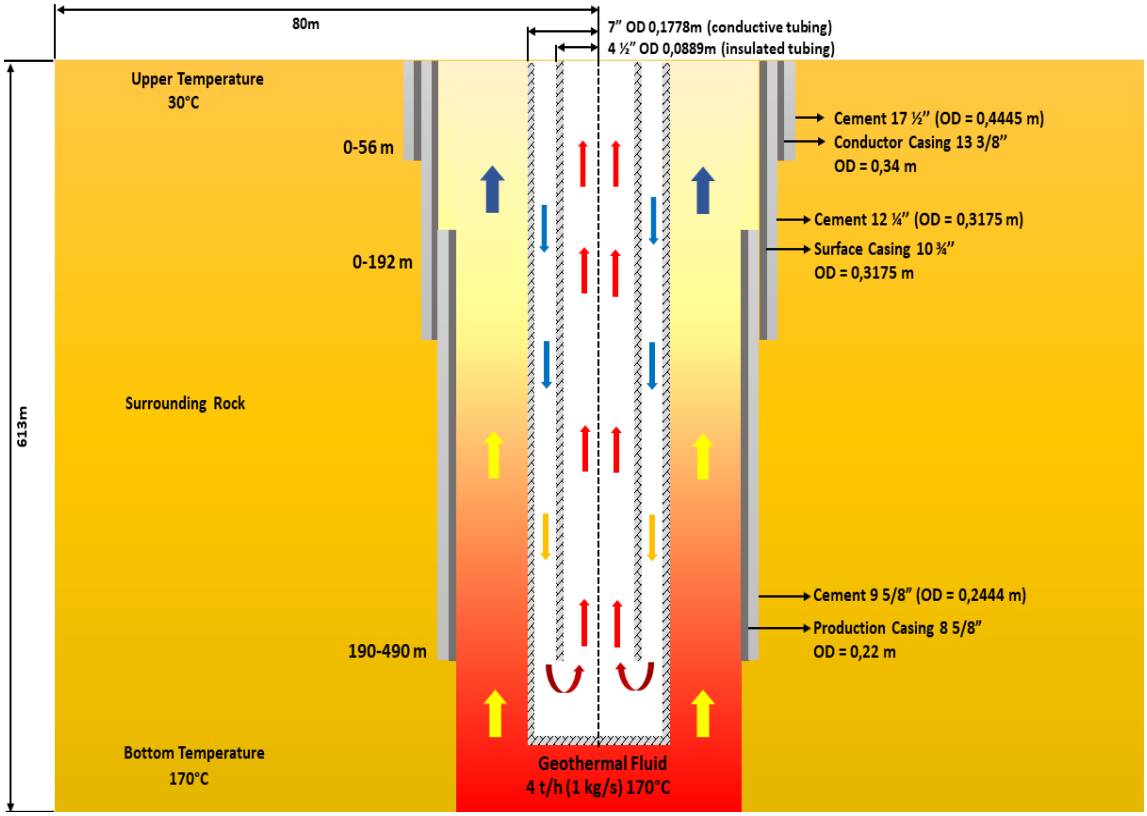

Figure 1: Schematic of the simulated Closed-Loop Geothermal system in an idle geothermal well.

2.3. Boundary Conditions

To enable closed-loop geothermal system simulation model on the inactive Matalako MT-3 geothermal well described in Section 2.2, the boundary conditions used are listed in Table 2. These values were obtained from several literatures and conditions in the field.

Table 2: Boundary conditions of the numerical simulation.

Parameter	Unit	Value	References
Nanofluida mass flow rate	kg/s	1	(James & Gould, 1987)
Nanofluida inlet temperature	^oC	28	(Wahyuningsih, 2004)
Nanofluida inlet pressure	bar	1	(Hu et al., 2020)
Working fluid injection flow rate	kg/s	1	(Hu et al., 2020)
Working fluid injection temperature	^oC	28	(Wahyuningsih, 2004)
Working fluid inlet pressure	bar	1	(Hu et al., 2020)
Working fluid outlet pressure	bar	1	(Hu et al., 2020)
Reservoir temperature	^oC	170	(Wahyuningsih, 2004)
Ambient temperature	^oC	25	(PT. PLN, 2019)

3. RESULTS AND DISCUSSION

Before carrying out simulations related to closed-loop geothermal system, the numerical model of inactive geothermal wells must be validated by matching the shut-in pressure and temperature conditions, then compared with inactive geothermal wells without a closed-loop system. From this step, then we can find out whether the results of this numerical simulation can describe real conditions in the field or not. Apart from that, to see an increase in heat transfer, variations in the given nanofluids were used.

3.1. Natural State Validation

This well flow simulation is needed to validate the actual conditions of the well using a simulated well that has not been added with tubing by comparing temperature profiles at various depths. In Figure 2, the actual temperature profile from Well MT-03 is compared with the temperature profile from the simulated well (in yellow) with the same mass flow rate, namely 4 tonnes per hour or 1 kilogram per second (in red). From this

graph, the temperature profile of the well flowing at a rate of 4 tons per hour has a similar pattern to the temperature profile from the simulation, but there is a temperature difference at a depth of 200 meters. This is because the definition of rocks around the well is different from the conditions that occur in the field. However, it can be concluded that the simulated well is able to reflect the conditions of the actual well.

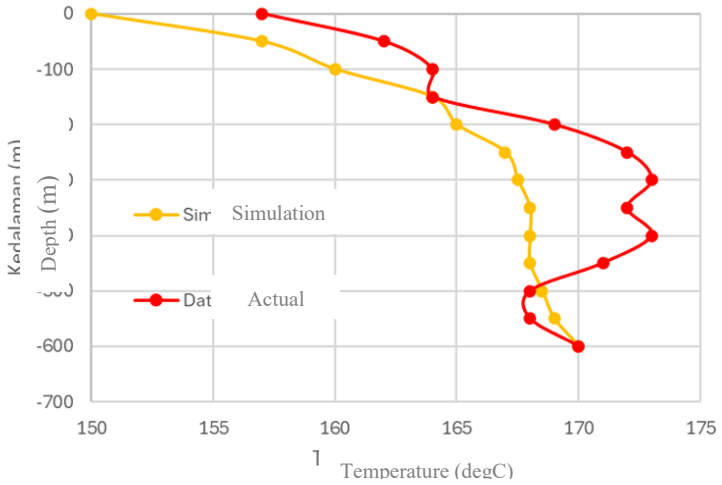

Figure 2: Comparison between Closed-Loop Geothermal System and Actual Well.

3.2. Temperature Profile and Contour in Well MT-03 Model with Nanofluid Variations

The simulation results show that there is a relationship between the temperature gradient in the well wall area and the properties of the working fluid used. From the simulation results, an analysis process can be carried out to determine the heat distribution that occurs in each fluid used.

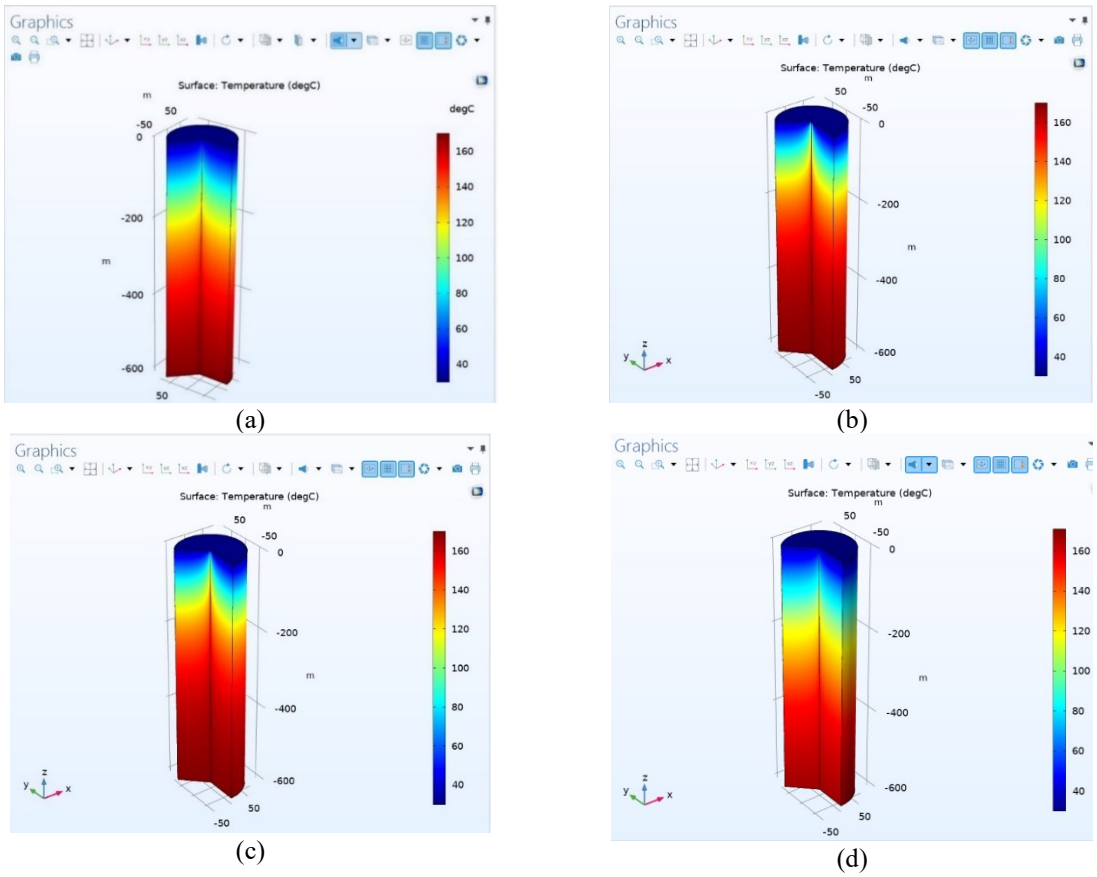

Figure 3: Temperature profile: (a) Graphene nanofluid (b) CarbonNanotube nanofluid (c) Titanium Oxide nanofluid (d) Water fluid.

From Figure 3, it can be seen that the temperature gradient is linear from 170°C at the bottom of the well which indicates the reservoir temperature, and the ground surface temperature is 30°C as the environmental temperature.

In this research, a model was used with an inflow velocity of 1 kg/s. This can be seen in Figure 3 that the simulation results show a temperature profile that forms a cone shape around the geothermal well due to geothermal extraction. Geothermal energy production causes a sharp upward curve along with the nanofluid's good ability to conduct heat. When using graphene and water, the temperature profile shows the depressions that occur are not too sharp compared to the other two nanofluids, namely CarbonNanoTube and Titanium Oxide. In addition, at a depth of ± 200 meters, based on the temperature profile, the use of CarbonNanotube and Titanium Oxide nanofluids can reach 120°C, while graphene nanofluids and water at that depth only produce temperatures of 100°C. This shows that graphene and water nanofluids have a worse ability to conduct heat than other nanofluids.

3.3. Temperature Distribution and Working Fluid Performance

The simulation results show a uniform well model using a variety of working fluids, namely water, graphene, titanium oxide and carbon nanotubes. From the simulation results, an analysis process was carried out to determine the heat distribution in each nanofluid used. The difference in the temperature increases of the working fluid as it enters in annulus and as it flows out of the well is clearly illustrated in Figure 4. When the working fluid enters the well, its temperature will increase with the depth of the well. The temperature reaches its peak as it approaches the bottom of the well because at that point, the working fluid first interacts with the reservoir or surrounding hot rock. The heat energy carried by the working fluid is maintained when it exits the well to prevent heat energy loss to the environment during its journey to the surface. When using graphene as a working fluid, the output temperature of 140°C increases by 110°C compared to the inlet temperature of the well, which is 30°C. As a comparison, using titanium oxide as a working fluid, it produces an output temperature of 154°C with an increase of 124°C from the well inlet temperature and carbon nanotubes produce 156°C and an increase of 126°C.

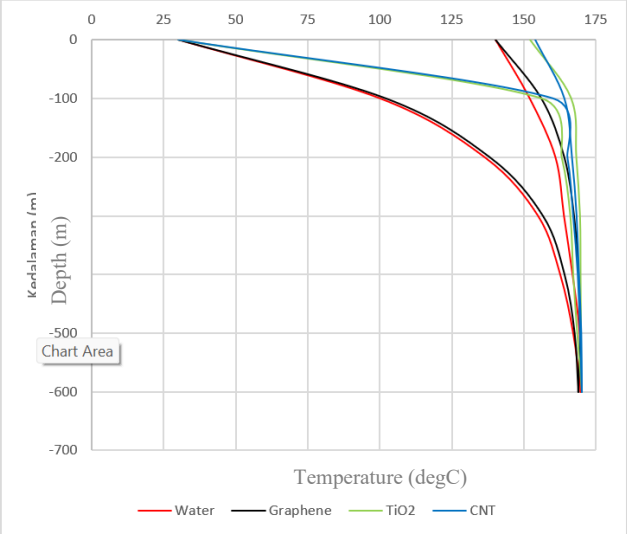

Figure 4: Temperature distribution profile at the inlet and outlet holes in the tubing.

Figure 4 shows the temperature increase profile with variations in each fluid used. The fluid enters with a temperature of 30°C to the end of the well and returns to the ground surface. Carbon nanotube and titanium oxide fluids are easier to conduct heat when they are at the initial depth. This is because the properties of these two fluids are almost the same. Apart from that, carbon nanotubes and titanium oxide have a lower specific heat than water and graphene, which is around 700-1000 J/kg.K, while water and graphene have almost the same specific heat of 4100-4200 J/kg.K. With a lower specific heat, carbon nanotube and titanium oxide fluids can heat up more quickly because the heat required to raise one degree of temperature is less and fluids that have a high specific heat have better temperature stability. In Figure 4, it can also be seen that the graph of the increase in fluid temperature of water and graphene is more stable. Meanwhile, carbon nanotube and titanium oxide fluids have high specific heat, therefore the temperature increase is very significant.

Figure 5 shows the pump power needed to move fluid from the bottom of the well to the surface. The pump power produced is caused by the large pressure drop that occurs in the tube. The greater the pressure drop that occurs in the tube, the greater the pump power required to move the fluid. The pressure drop that occurs is influenced by several factors such as fluid speed, friction that occurs, and the density of the fluid itself.

3.4. Required Pump Power

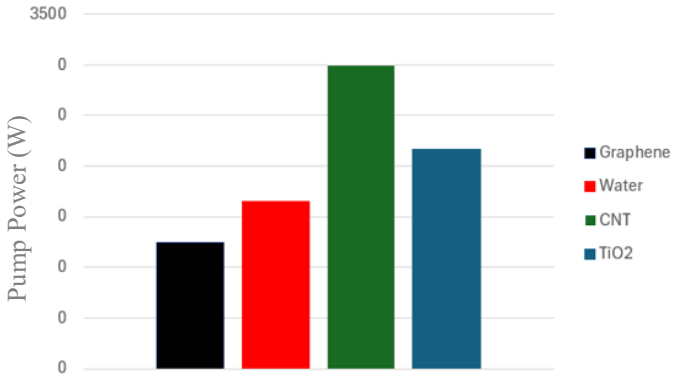

Figure 5: Nanofluids Pump Power.

Carbon nanotube fluid is a fluid that requires the greatest power among other fluids. Carbon nanotube fluid has a greater speed compared to other fluids, namely it has a speed of ±0.1725 m/s. The relatively large fluid velocity in the pipe will increase the friction between the fluid and the walls of the pipe channel will be even greater. In addition, the energy required to overcome this friction will increase and there will be an increase in energy consumption. Meanwhile, water fluid and titanium oxide almost have the same speed results, it's just that the density of the water fluid is lower than titanium oxide so the power used to move the graphene fluid is less than the titanium oxide fluid. This is because low density will also produce low hydrostatic pressure, so that when the hydrostatic pressure is low, the pump will provide less energy to the fluid to overcome the lower hydrostatic pressure. Graphene fluids tend to require a small force to move the fluid from one location to another. This fluid has a speed of 0.161 m/s and a density of ±937.66 kg/m^3. This factor influences the power to move graphene fluid because the speed tends to be low and the density is not too high when the fluid reaches a temperature of 170°C at the bottom of the tubing.

4. CONCLUSIONS

Based on research that has been carried out using COMSOL Multiphysics 6.1 software and analyzing the results of the simulation process, and also from the simulation and calculation results it is found that:

1. The thermal properties of the working fluid influence the fluid's ability to conduct heat. Carbon NanoTube and Titanium oxide nanofluids produce higher exit fluid temperatures than Graphene and water. This is because graphene and water have a higher specific heat capacity than these two fluids. Therefore, the amount of heat used to increase 1 degree of temperature per unit mass becomes higher. Carbon NanoTube nanofluid has more significant heat transfer results because it has a lower specific heat than other nanofluids.
2. The speed of fluid flow and the density of the fluid affect the power capacity of the pump used to move fluid from one location to another. Carbon NanoTube nanofluid has a higher speed than other nanofluids. The higher the speed, the greater the pressure drop and pump power required, causing energy loss. Carbon NanoTube nanofluid has a pump power of 3.398 kW. Meanwhile, Titanium Oxide and Graphene nanofluid have almost the same speed during the simulation process, but Graphene nanofluid has a lower density value. This affects the pressure drop and friction force because the greater the density, the more molecules will interact with the walls. Graphene has the lowest pump power for moving fluid, namely 3.048 kW.

ACKNOWLEDGEMENT

This research is funded by the Indonesian Endowment Fund for Education (LPDP) on behalf of the Indonesian Ministry of Education, Culture, Research and Technology and managed under the INSPIRASI Program (Grant No. 2924/E3/AL.04/2024 and 4809/UN1.P/HK.08.00/2024).

REFERENCES

Abbasi, S., Zebarjad, S. M., NoieBaghban, S. H., Youssefi, A., & EKRAMI, K. M.: *Thermal conductivity of water based nanofluids containing decorated multi walled carbon nanotubes with different amounts of TiO2 nanoparticles*. (2015).

Ali, N., Bahman, A. M., Aljuwayhel, N. F., Ebrahim, S. A., Mukherjee, S., & Alsayegh, A.: Carbon-based nanofluids and their advances towards heat transfer applications—a review. *Nanomaterials*, *11*(6), 1628, (2021).

Ali, N.: Graphene-based nanofluids: production parameter effects on thermophysical properties and dispersion stability. *Nanomaterials*, *12*(3), 357, (2022).

Cobanoglu, N., Banisharif, A., Estelle, P., Karadeniz, Z.H.: The developing flow characteristics of water-ethylene glycol mixture based $Fe3O4$ nanofluids in eccentric annular ducts in low temperature applications, *Int. J. Thermofluids* 14 (2022). http://dx.doi.org/10.1016/j.ijft.2022.100149.

COMSOL: *CFD Module User's Guide*, COMSOL, Stockholm, (2018).

COMSOL: *Heat Trasfer Module User's Guide*, COMSOL, Stockholm, (2018).

Du, R., Jiang, D., Wanga, Y., & Shah, K.W.: An experimental investigation of CuO/water nanofluid heat transfer in geothermal heat exchanger, *Energy Build*. 227. 1–13, (2020). http://dx.doi.org/10.1016/j.enbuild.2020.110402.

Duangthongsuk, W., & Wongwises, S.: Measurement of temperature-dependent thermal conductivity and viscosity of TiO2-water nanofluids. *Experimental thermal and fluid science*, *33*(4), 706-714, (2009).

Feng, T., Li, L., Shi, Q., Zhang, Y., & Li, G.: Heat capacity and thermodynamic functions of TiO2 (h). *The Journal of Chemical Thermodynamics*, *145*, 106040, (2020).

Hu, X., Banks, J., Wu L., and Liu, W.V.: Numerical Modeling of a Coaxial Borehole Heat Exchanger to Exploit Geothermal Energy from Abandoned Petroleum Wells in Hinton, Alberta, *Renewable Energy,* vol. 148, pp. 1110-1123, (2020).

James, R., and Gould, T.: "Bleeding Characteristics of Geothermal Wells," in *Proceedings of the12th Workshop on Geothermal Reservoir Engineering*, Stanford, (1987).

Kapıcıoğlu, A., Esen, H.: Experimental investigation on using $Al2O3$/ethylene glycol-water nano-fluid in different types of horizontal ground heat exchangers, *Appl. Therm. Eng.* 165 (2020) http://dx.doi.org/10.1016/j.applthermaleng.2019. 114559.

PT PLN (Persero): "*Profil Unit Layanan Pusat Listrik Mataloko*" PT PLN (Persero), Jakarta, (2019).

Wahyuningsih, R., and Sitorus, K.: "Evaluasi Lapangan Panas Bumi Mataloko Pasca Pengeboran dan Uji Alir Sumur MT-3 dan MT-4," in *Proceedings of the 33rd Annual Convention & Exhibition 2004*, Bandung, (2004).

Wang, J., Yang, X., Klemeš, J. J., Tian, K., Ma, T., & Sunden, B.: A review on nanofluid stability: preparation and application. *Renewable and Sustainable Energy Reviews*, *188*, 113854, (2023).

Yuan, W., Chen, Z., Grasby, S.E., and Little, E.: Closed-Loop Geothermal Energy Recovery from Deep High Enthalpy Systems, *Renewable Energy*, vol. 177, pp. 976-991, (2021).

Lean Project Exploration Drilling Organization

Seto Tanimo, Tommy Souvanir, and Rifqi Alfaizi

1Ormat Geothermal Indonesia, DEA Tower II, Jl. Mega Kuningan Barat no.1, Jakarta Selatan, Indonesia

tanset@gmail.com

Keywords: Lean project drilling, project drilling organization, geothermal exploration, geothermal project

ABSTRACT

The number of Geothermal exploration drilling projects over the last decade has been relatively low, with a significant gap between the stages and a very low success ratio, resulting in a lack of learning curve for geothermal exploration projects. With a limited number of geothermal explorations in Indonesia and only a few companies performing the exploration, almost all geothermal companies in Indonesia are not prepared for an experienced project organization to handle the geothermal drilling exploration project, which faces the challenge of a large volume of work while staying within budget and exploration time window. The majority of geothermal project tasks were carried out by a separate team for each stage, and they finished when their work was accomplished. With a transition time between stages, there was a gap of and unsynchronized information, which most of the time resulted in remedial and additional work in each stage. Having a reliable exploration team is one of the most critical factors in the success of geothermal exploration project drilling execution. Because exploratory projects are typically short in duration, have a wide range of work scopes, and are cost sensitive, the project team must be small, multitasking, problem solvers, quick learners, collaborative, and have expanded roles and responsibilities. This paper will discuss some innovative approaches to build a reliable project drilling execution team that has proven to complete project on time and within budget.

1. INTRODUCTION

The geothermal prospects are distributed across Indonesia from west to east, however only the western part of Indonesia is actively developed compared to the eastern part of Indonesia. Most of the highest reserves that has more than 100 Mwe are in the western part of Indonesia, many of these high-reserve fields are already developed or in the progress of development, while the other remaining fields are being delayed due to permitting issues, regulatory hurdles, land-use conflict, or low project's economic due to reserve capacity size and location.

The eastern part of Indonesia relatively has medium to low reserves which are spread across many islands, these medium and low reserves are suitable with the demography and electricity demands of eastern Indonesia that is relatively lower compared to the western part of the country. The peculiarity of geothermal in eastern region could be the best answer for mid-term electricity deficit while also providing regional energy security for long-term growth.

2. GEOTHERMAL EXPLORATION CHALLENGES

Despite the region's significant potential, developing geothermal projects in eastern Indonesia presents a number economic and logistical challenges, including scarcity of skilled workers, transportation and logistics, accommodation and living conditions, material and equipment costs, services and support, fuel availability and higher tariffs. These issues resulted in the project execution unable to operate 24/7, necessitating more transportation time and costs, and making it difficult to stay under budget. Despite having stronger infrastructure than the eastern region, exploration in the western region also has its own challenge such as protected natural forest and remote location with limited access.

The Preliminary Survey and Exploration License (PSPE) scheme legislation in recent geothermal exploration, combined with current geothermal exploration trends are more toward low-medium enthalpy, adds the exploration hurdles such as constrained budget, minimum number of wells, short exploration time windows, no room for error, with Zero Incident as the ultimate goal.

With all the hurdles and complexity issues, having a reliable project drilling execution team is essential for getting the project started and keeping it on track in terms of the schedule and budget. The project drilling execution team need at minimum to have competences of geothermal exploration exposure with a proven knowledges and experiences, working with the limited support and resource, be innovative and problem solver, good coordination and collaborative, good Individual soft and hard skill, multi-tasking and discipline and strong leadership.

Those competencies are very desirable and nearly impossible to obtain, yet they are required to ensure that the goal is met. In the recent geothermal exploration at the eastern Indonesia, the project team has innovated

approaches in a reliable exploration project drilling execution team, as shown in Figure 1, breaking the common practices in the exploration project and successfully meeting the objectives, and with their competencies, some achievements have been extraordinary.

Project Drilling Execution Team \ PROJECT PHASE	Civil Work Preparation	Civil Work	Pre Mob Preparation	Rig Mobilization	Rig Up	Drilling	Rig Down & Demob	Well Testing	Heavy Equipment Demob
Project Drilling Engineer	✓	✓	✓	✓	✓	✓	✓	✓	✓
EHS Coordinator	✓	✓	✓	✓	✓	✓	✓	✓	✓
Civil Manager	✓	✓	✓	-	-	-	-	-	-
Civil Site Supervisor	✓	✓	✓	✓	-	-	-	-	-
EHS Officer	✓	✓	✓	✓	✓	✓	✓	✓	✓
QAQC	✓	✓	✓	✓	✓	✓	✓	✓	✓
Company Man	-	-	-	-	✓	✓	✓	-	-
Wireline & Well Testing Supervisor	-	-	-	-	-	✓	✓	✓	-

Figure 1: Project Drilling Execution Team.

2.1 A Small Project Drilling Execution Team with Extensive Role and Responsibilities

Given the limited budget and tight schedule of the exploration project, a small project drilling execution team is required to be agile and adaptable for rapid changes and complex problems. With a small project drilling execution team, there will be insufficient resources to manage simultaneous tasks, therefore the project team need to establish an extended role and responsibilities to keep the project drilling execution team lean while also providing cross-functional assistance.

During the civil construction, starting from preparation to commissioning, the civil site supervisor is assisted by QA/QC and EHS Officer for daily supervision on site. With this assistance, simultaneous activity in different areas may be closely monitored to assure the execution as per plan, and at the same time, it gave a new exposure for the drilling team members with the civil work activities, which will be an advantage when needed for maintaining civil infrastructure such as water intake, water supply system, well pad, access road, etc.

When the drilling rig started mobilization most of the civil work has been completed, the Drilling Team assisted by the Civil Site Supervisor to supervise the unloading process, mobilization from the port to stagging and from stagging to the site, this additional supervisor helped the drilling team to have 24/7 supervision on mobilization activities to ensure it's performed efficiently and safely. The Civil Site Supervisors also received a new exposure in supervising massive mobilization of drilling equipment continuously and time sensitive.

After drilling commenced, the drilling team also supported the Wireline Supervisor in operating the in-house wireline unit. Wireline supervisors were assisted in setting up the unit, performed logging operations and storing it. After drilling is completed, to conduct well testing, Well Testing Supervisor also help by the Drilling Team to mobilize the testing equipment to the site, set up and commission the equipment, inspection by regulator, perform well testing, moving from one pad to next pad, and storing the equipment.

2.2 A Professional with Demonstrated Exploration and Multidisciplinary Experiences

To enable a lean team to begin work immediately and efficiently after it is formed, each project execution team should be a professional with demonstrated exploration and multidisciplinary experience, capable of preparing and executing the detail execution plan in collaboration and synergy with the team's other disciplines. Hiring a professional with specific exploration experience, paired with project's short timeline, task complexity, and site location, proved to be a difficulty, but the project was successfully addressed by offering an extensive time frame combined with appealing benefits in compensation of extended role and responsibility.

2.3 Project Team Synergy Improves Work Efficiency

Fostering synergy within the project drilling execution team is beneficial for collaborative problem solving, effective communication and smooth information sharing, as well as work efficiency, but it is difficult to achieve, especially when the project drilling execution team is just getting started, there is little time for introductions, and there are different expertise and professional backgrounds. To achieve synergy, best practice for effective communication and coordination in drilling operation was introduce to project drilling execution team, along with reporting and work techniques.

2.4 Single Communication Channel

One communication channel for the project drilling execution team, assisting quick information alignment, which is powerful for work progress integrated monitoring and raise team awareness and initiative for collaboration, problem solving, and prompt corrective action.

3. A LEAN PROJECT DRILLING EXECUTION TEAM EFFECTIVELY MET OBJECTIVE WITH AN EXCEPTIONAL ACHIEVEMENT AND TEAM LEARNING (A SUCCESS STORY)

Effective communication and good cross functional collaboration in a lean project drilling execution team have successfully met project objective of completing the project ahead of schedule, within budget, with an exceptional performance, and providing good experience for the team members to learn new skills. The very first challenge for the project team was to begin the civil work immediately in order to have the first well spud before end of July 2023, as per the exploration time frame commitment with the regulator. The project execution team successfully build three (3) well pads, 2.8 kilometers access road, a laydown area, a drilling camp, a water intake, and water supply system within six (6) months, starting from December 2022 until June 2023.

Rig mobilization commenced after the major civil work has been completed, and it took seventy-three (73) days from the first day of mobilization at Cirebon – West of Java Island to spud-in at Wapsalit – Buru island, which is 17 days faster than the target days. Before the first shipment arrived at Namlea port at Buru island, local road and bridge authorities notified that two (2) out of thirty-two (32) bridges along the road from Namlea port to Wapsalit site are not capable to support the maximum load of the rig equipment. To address the bridges issues, the project drilling execution team successfully constructed two (2) sixty tons (60 T) temporary bridges with lengths of 12 meters and 18 meters in less than a month as shown in Figure 2 for both the bridges. The 12 meters bridges installation was completed in seven (7) days and the 18 meters was completed in ten (10) days with the installation cost less than USD 190,000 for both bridges. Both bridges were successfully tested and safely supported the rig equipment mobilization with maximum load of fifty-four (54) tons.

Figure 2: Wapsalit Temporary Bridge Installation.

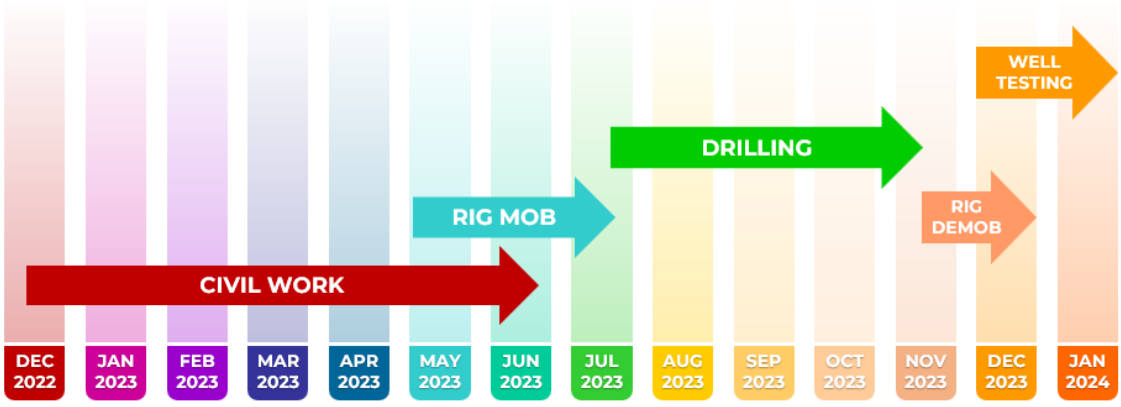

Figure 3: Project Timeline.

The first well was successfully spudded two (2) weeks before the end of commitment date, which was a significant accomplishment for the entire exploration activities. The first well was completed drilled safely to the target depth within the budget, while the second well drilled 513 meters deeper than first well with meter per day doubled than the first well and dollar per meter fifty percent lower than the first well. During drilling, in house wireline unit

was operated to run down hole tool and execute logging task, resulting in significant cost saving on wireline unit rentals. After drilling was completed, the drilling team aided the well testing supervisor with aerated package operation and heavy equipment supervision to mobilize, set up, move, and store well testing equipment, which was extremely beneficial in conducting the well testing job cost and time efficiently.

4. CONCLUSION

The innovation of a lean and collaborative project drilling execution team has effectively break away from a traditional method of geothermal project execution in Indonesia, resulting in project execution that not only satisfied the project objectives of time and cost efficiency but also a safe operation.

The efficient time and cost performance delivered by the project drilling execution team easily justifies the project team's outstanding compensation benefit. In addition, a lean project drilling execution team also provides an opportunity for the team to gain new skills. This lean project organization will help to accelerate the geothermal exploration by addressing the lack of skilled individuals and project continuity.

REFERENCES

Indonesia project drilling team, Wapsalit project drilling lookback, Ormat Geothermal Indonesia, Jakarta (2023).

Komite teknis 27-05, Panas Bumi : SNI 6009 : 2017 Klasifikasi sumber daya dan cadangan energi panas bumi Indonesia, BSNI, Jakarta (2017).

Riza, and Berry, B : Slimhole drilling experience at Darajat Geothermal Field, West Java, Indonesia, Proceeding, 20*th* NZ Geothermal Workshop 1998, Amoseas Indonesia Inc, Jakarta (1998).

Enhancing the Added Value of Organic Waste and Brine as a Secondary Geothermal Product Through COMBINE (Compost Brine) Innovation at PGE Karaha Area

Muhammad Sabdian Harwanda, Yanuaris Dwi Cahyono, Awaludin, and Muhamad Taufik

PT Pertamina (Persero)

Muhammad.harwanda@pertamina.com, Yanuarisdwic@pertamina.com,
Awaludin.01@pertamina.com, Muhamad.taufik2@pertamina.com

Keywords: Organic Fertilizer, Compost, Geothermal Energy, Direct Use Geothermal, Nutrients

ABSTRACT

The Karaha Geothermal area has two-phase steam characteristics, which is a flowing fluid consisting of steam and brine (water produced from geothermal sources). The steam is used to generate electrical energy, while the brine is reinjected back into the reservoir. Based on laboratory analysis, the brine contains many minerals with relatively high concentrations. The test results of brine sample from Pond KRH 4 at the Quality Testing Laboratory in the Kamojang area indicate that the brine contains minerals needed by plants, such as macro nutrients and micronutrients. To support operations in the Karaha area, routine grass cutting activities are carried out throughout the Geothermal Power Plan Area and geothermal well clusters. The grass cutting work can generates waste from wild grass cuttings amounting to 110 tons per year, which can cause various environmental issues. These issues include creating habitats for snakes that can endanger workers conducting patrol checks or causing blockages in water flow paths within the drainage system.

Currently, the utilization of geothermal energy in the PGE Karaha area is only in the form of indirect use, which is the conversion of geothermal energy into electricity. The absence of derivative products from geothermal energy becomes one fact that needs to be resolved, as it aligns with the directive from the President Director of Pertamina Persero, Vision and Mission of PT PGE company, and KPI of President Director PT PGE related to secondary revenue initiative. One effort to solve this problem is to create an innovation by utilizing cut wild grass combine with geothermal hot water (brine) to produce a marketable product in the form of solid organic fertilizer for plants. COMBINE (Compost Brine) fertilizer is answer for the solid organic fertilizer produced, which contains macro and micronutrient elements that meet the requirements of the Indonesian National Standard (SNI) for compost quality standards 19-7030-2004. The production of COMBINE fertilizer is carried out using a formula consisting of 150 ml of EM-4 solution, 150 grams of molasses, 15 liters of brine, and 80 kg of waste from wild grass cuttings, with a composting time period of 1-2 months.

The innovation of the COMBINE fertilizer has been implemented in farmer groups around the area as a corporate social responsibility (CSR) program, and this innovation can also be replicated to other geothermal areas. The positive impacts of the COMBINE fertilizer innovation for the company and the community around the geothermal working area of the Karaha are as follows: Minimizes the accumulation of organic waste from wild grass cuttings, thus eliminating habitats for venomous snakes that could endanger workers, COMBINE fertilizer has the potential to increase company revenue if commercialized, With using of COMBINE fertilizer provides positive impacts on soil compared to the use of chemical fertilizers, Provides a solution regarding the lack of fertilizer supply to local farmers around the Karaha area, and Establishes mutually beneficial cooperation between the community and company related to the development of COMBINE fertilizer.

1. INTRODUCTION

PT Pertamina Geothermal Energy Tbk (PGE) manages a part of the geothermal working areas in Indonesia. One of the geothermal working areas managed by PGE is the Karaha Chakrabuana geothermal working area. PGE Karaha Area operates a Geothermal Power Plant (PLTP) with an installed capacity of 30 MW. Currently, PGE Karaha Area manages 6 production wells, 1 injection well, 3 injection wells under study status, and 1 well under recovery status. These wells are located in several clusters: production well KRH 4-1 and injection study well KRH 4-3 are located in cluster KRH 4; production well KRH 5-1, injection study well KRH 5-3, and recovery well KRH 5-2 are located in cluster KRH 5; injection well KRH 2-1 is located in cluster KRH 2; injection study well KRH 6-1 is located in cluster KRH 6; and production wells TLG 3-1, TLG 3-2, TLG 3-3, TLG 3-4 are located in cluster TLG 3. The Karaha geothermal area covers a vast region, consisting of the Fluids Collection and Reinjection System (FCRS) and the Geothermal Power Plant (PLTP), with a geothermal working area of 55400 hectares in a mountainous region.

With such a vast geothermal working area, it is necessary to pay attention to and treat environmental aspects. For example, grass that grows in the work area must be regularly cut to prevent it from becoming a habitat for venomous animals such as snakes which could endanger workers as shown in Figure 1. To support operations in the Karaha area, routine grass cutting activities are carried out throughout the geothermal power plan area and geothermal well clusters. The grass cutting work can generates waste from wild grass cuttings amounting to 110 tons per year which can cause various environmental issues. The accumulation of organic waste presents both a problem and an opportunity if managed properly. The opportunity that can be taken with organic waste in the form of wild grass cuttings is to use it as a raw material for compost fertilizer.

Figure 1: The condition of wild grass in the separator area of Cluster KRH 4.

Figure 2: The condition of Pond Cluster KRH 4.

The Karaha Geothermal Area has two-phase steam characteristics, which is a flowing fluid consisting of steam and brine (water produced from geothermal sources). Steam and brine are first separated in the separator, with the steam directed to the geothermal power plant (PLTP) to generate electrical energy, while the brine is reinjected back into the reservoir. There are two types of reinjection systems in Karaha area it is the hot reinjection system and the cold reinjection system. In the hot reinjection system, the brine from the separator is directly channeled to the reinjection well located in the same cluster, such as in clusters Karaha 5 and Karaha 6. In contrast, the cold reinjection system involves directing the brine from the separator to a pond as shown in Figure 2 for cooling before it is reinjected into the reinjection well, as seen in cluster Karaha 4.

Based on laboratory analysis in Figure 3, the brine contains many minerals with relatively high concentrations. The test results of brine sample from Pond KRH 4 at the Quality Testing Laboratory in the Kamojang area indicate that the brine contains minerals needed by plants, such as macro nutrients (potassium 1154.76 ppm, calcium 773.8 ppm, magnesium 0.45 ppm), and micronutrients (sodium 4547.96 ppm, silica 366.49 ppm, chloride 9540.22 ppm, boron 185.10 ppm, lithium 19.08 ppm). The brine water can be utilized as an additional raw material in the production of compost fertilizer, thereby enhancing the macro and micronutrient content.

Currently, the utilization of geothermal energy in the PGE Karaha area is only in the form of indirect use, which is the conversion of geothermal energy into electricity. The absence of derivative products from geothermal energy becomes one fact that needs to be resolved, as it aligns with the directive from the President Director of Pertamina Persero, Vision and Mission of PT PGE company, and KPI of President Director PT PGE related to secondary

revenue initiative. One effort to solve this problem is to create an innovation by utilizing cut wild grass combine with geothermal hot water (brine) to produce a marketable product in the form of solid organic fertilizer for plants.

PERTAMINA GEOTHERMAL ENERGY

LABORATORIUM UJI MUTU - AREA KAMOJANG
PERTAMINA GEOTHERMAL ENERGY
Jln. Raya Kamojang Kab. Bandung
PO Box 120 Garut 44151
Telp. 022-780 6882
Email : lab.pgekmj@pertamina.com

KAN

LAPORAN HASIL PENGUJIAN
LHU-23048/LUM/2023

NO. URUT : 9
IDENTITAS SAMPEL : 23048-9
NAMA SAMPEL : POND 4
TANGGAL SAMPLING : 31 Maret 2023
JENIS SAMPEL : INJ
METODE SAMPLING : TKI C-020/PGE142/2019-S9

NO	PARAMETER ANALISIS	SATUAN	HASIL	METODE
1	Konduktivitas pada suhu 25°C	µS/cm	24450,00	TKI No. C-007/PGE240LAB/2019-S9 (Conductivity meter)
2	pH pada suhu 25°C	-	6,92	TKI No. C-010/PGE240LAB/2019-S9 (pH Meter)
3	TDS kalkulasi*	ppm	16464,26	TKI No. C-011/PGE240LAB/2019-S9 (Kalkulasi)
4	Natrium (Na^+)	ppm	4547,96	TKI No. C-001/PGE240LAB/2019-S9 (ICP-OES)
5	Kalium (K^+)	ppm	1154,76	TKI No. C-001/PGE240LAB/2019-S9 (ICP-OES)
6	Kalsium (Ca^{2+})	ppm	773,80	TKI No. C-001/PGE240LAB/2019-S9 (ICP-OES)
7	Magnesium (Mg^{2+})	ppm	0,45	APHA edisi 23 tahun 2017, Metode 3111 B (AAS)
8	Litium (Li^+)	ppm	19,08	APHA edisi 23 tahun 2017, Metode 3111 B (AAS)
9	Besi total (Fe^{2+3+})**	ppm	0,93	APHA edisi 23 tahun 2017, Metode 3111 B (AAS)
10	Bikarbonat (HCO_3^-)**	ppm	39,33	TKI No. C-015/PGE240LAB/2019-S9 (Titrasi Asam Basa)
11	Klorida (Cl^-)	ppm	9540,22	TKI No. C-016/PGE240LAB/2019-S9 (Titrasi Argentometri)
12	Sulfat (SO_4^{2-})	ppm	60,58	TKI No. C-017/PGE240LAB/2019-S9 (Turbidimetri)
13	Boron (B)	ppm	185,10	TKI No. C-001/PGE240LAB/2019-S9 (ICP-OES)
14	Silika (SiO_2)	ppm	366,49	TKI No. C-001/PGE240LAB/2019-S9 (ICP-OES)

*Hasil penjumlahan konsentrasi unsur/senyawa non-volatil Na, K, Ca, Mg, Li, Fe, Cl, SO4, dan SiO2
** Parameter belum terakreditasi ISO/IEC 17025:2017

Figure 3: Result The Quality Testing Brine Sample Laboratory in the Kamojang Area.

2. LITERATURE

2.1 Compost

Compost can be defined as the result of the decomposition of organic matter, while composting is the process which organic matter undergoes biological decomposition, particularly by microbes that utilize organic matter as an energy source (Adewumi et al., 2005; Hansen et al., 2006). The composting process is a natural one, where organic matter biologically decomposes through microorganisms that convert organic material into an energy source. During compost process production, a balanced mixture of materials is combined, sufficient water is added, ensuring good aeration, and adding activators to accelerate the composting process (Isroi, 2008).

2.1.1 Composting Time

The duration of composting depends on the characteristics of the materials being composted, the composting method used, and whether composting activators are added. Naturally, composting can take from several weeks to two years for the compost to be fully mature (Rynk et al., 1992). Mature compost feels soft when crushed because during the composting process, organic matter undergoes decay and decomposition, resulting in changes from fresh material to amorphous, dark-colored microbial substances. This substance is akin to soil material (Sutedjo et al., 1991). Compost maturity is influenced by various factors during the composting process. After composting is complete, the raw materials will change color to a dark brown (Indriani, 1999).

2.1.2 Quality of Compost

The quality of compost is greatly determined by its maturity level, in addition to its heavy metal content. Organic material that isn't fully decomposed can have detrimental effects on plant growth. Generally, mature compost exhibits the following characteristics: Dark brown to black color and crumbly texture; Insolubility in water, although some parts of the compost can form a suspension; Highly soluble in alkaline solvents, sodium pyrophosphate, or ammonium oxalate solution with producing a dark extract that can be further fractionated into humic, fulvic, and humic substances; a carbon to nitrogen ratio ranging from 20 to 40, depending on the raw materials and degree of humification; high cation exchange capacity and water absorption capability; beneficial effects on soil and plant growth when applied to soil; a temperature almost the same as the ambient air temperature; absence of volatile fatty acids and odorless (Sutanto, 2002).

The carbon to nitrogen (C/N) ratio is an important parameter, which will relate the composting reactions to the relative concentrations of essential chemical constituents required for the growth and metabolic reactions of the microbial population. Compounds such as carbohydrates, in addition to being sources of carbon for the microbial biomass, will generate energy required for the microbial metabolic activity. Nitrogen is an essential component of proteins and amino acids required for the growth of the microbial biomass. Generally, it is recommended that, to maintain an active microbial population in a composting operation, the available carbon to nitrogen ratio should be kept at appropriate levels. Lower ratios will result in losses of nitrogenous compounds, while higher ratios will retard the composting reactions (Inbar *et al.,* 1991).

2.1.3 Functions of Compost

Compost has properties that improve soil structure, increase the binding capacity of sandy soil, enhance soil binding capacity, promotes better drainage and air circulation in the soil, aid in the decomposition of mineral materials, provide nutrients for microbes, and reduce the activity of harmful microorganisms (Yovita, 2001). According to Isroi and Yuliarti (2009), the way to restore soil fertility is by using organic fertilizers such as compost, which is believed to enhance soil fertility. Organic fertilizers can mitigate the adverse effects of chemical fertilizers and also restore soil fertility to its original state. Mayadewi (2007) also supports this view, who asserts that organic fertilizers are among the types of fertilizers that contain nutrients supporting soil fertility and the growth of soil organisms. Organic fertilizers have natural properties that do not harm the soil and provide macro elements such as nitrogen, phosphorus, and potassium, as well as micro elements such as iron, zinc, boron, cobalt, and molybdenum.

2.1.4 Benefits of Organic Fertilizer

According to Primantoro (2001) and Sutanto (2002), the benefits of using organic fertilizer are as follows:

1. Organic fertilizer functions as a granulator, thereby can improving soil structure. The presence of organic matter can bind soil particles in larger aggregates, making the soil looser. In sandy-textured soil, organic matter will increase the binding between particles.
2. The soil's water absorption capacity can be increased with the application of organic fertilizer, as it can biding more water and for a longer period.
3. Organic fertilizer can improve the living conditions within the soil. Soil microorganisms play a crucial role in organic matter transformation. With the presence of organic fertilizer, microorganisms actively decompose the organic matter because it provides them with energy, allowing nutrients in the soil to be absorbed by plants. Soil rich in organic matter will accelerate the proliferation of fungi, bacteria, microflora, and microfauna.
4. The nutrients in organic fertilizer are a food source for plants. Although present in smaller quantities, organic fertilizer contains a complete range of nutrients and serves as a source of essential elements such as nitrogen (N), phosphorus (P), and sulfur (S).

2.2 Macro and Micronutrients

The nutrient content in compost is quite comprehensive, encompassing both macro nutrients (N, P, K, Ca, Mg, S) and micronutrients (Fe, Cu, Mn, Zn, Mo, B, Cl) that are essential for plants growth. Although the nutrient content in compost is not as high as in chemical fertilizers, it still plays a crucial role. Consequently, compost is usually applied in larger quantities compared to chemical fertilizers (Isroi and Yuliarti, 2009).

Another advantage of compost lies in its organic matter content, including humic and fulvic acids, which are beneficial for stimulating plant growth. In the short term, compost usage can improve the physical properties of soil and increase soil biological activity by supplying some of the plants' nutrient needs. In the long term, compost application can restore soil fertility and productivity (Isroi and Yuliarti, 2009).

To determine the quality of compost, it is necessary observations of its physical properties such as color, odor, and texture. Generally, successful composting is categorized as complete or effective when the physical quality

of compost meets the quality criteria specified in the Indonesian National Standard (SNI). The Indonesian National Standard (SNI) refers to international compost quality standards such as the British Colombia Class I Compost Regulation dan Standard of Canada (CAN/BHQ 0413-200), especially regarding heavy metal micro-nutrient quality with permissible maximum values and also refers to compost products produced by various compost producers in Indonesia. Indicators used to assess organic fertilizers include pH and organic carbon content. The pH according to the Indonesian National Standard (SNI) 19-7030-2004 ranges from 6.80 to 7.46, potassium (K_2O) in organic fertilizers has a minimum value of 0.20%, and phosphorus (P_2O_5) has a minimum value of 0.01% (SNI, 2004).

2.3 Geothermal Brine

Geothermal brine or water of geothermal is the hot water product resulting from the geothermal separation process at a separator equipment. Typically, brine is directly reinjected into the reservoir as part of reservoir management efforts to prepare it for re-accommodating geothermal heat. This practice helps mitigate potential risks associated with utilizing the brine. The contents of brine include carbon dioxide (CO_2), hydrogen sulfide (H_2S), ammonia (NH_3), methane (CH_4), sodium chloride (NaCl), bBoron (B), arsenic (As), and mercury (Hg), which also pose a high potential for environmental damage.

3. DISCUSSION

3.1 COMBINE (Compost Brine) Production Process

The raw materials used in the process of making compost brine consist of the main raw materials, which are wild grass clippings and geothermal water. Additional materials such as EM-4 solution and molasses, which are used in the decomposition process of the main raw materials. The EM-4 solution is a type of liquid that contains various bacteria, including decomposers, Lactobacillus sp., lactic acid bacteria, photosynthetic bacteria, Streptomyces, cellulose-decomposing fungi, and phosphate-solubilizing bacteria, which function as natural decomposers of organic matter (Akmal, 2004). The wild grass cuttings collected from cluster areas and the geothermal power plan (PLTP) are first chopped to obtain uniform uniform-sized raw materials, into accelerate the decomposition process of the organic materials. During the composting process, the additional materials undergo decay and decomposition, resulting in changes to the fresh materials, the formation of microbial cell substances, and transformation into a dark amorphous form. This substance is referred to as “soil-like matter” (Sutedjo et al., 1991).

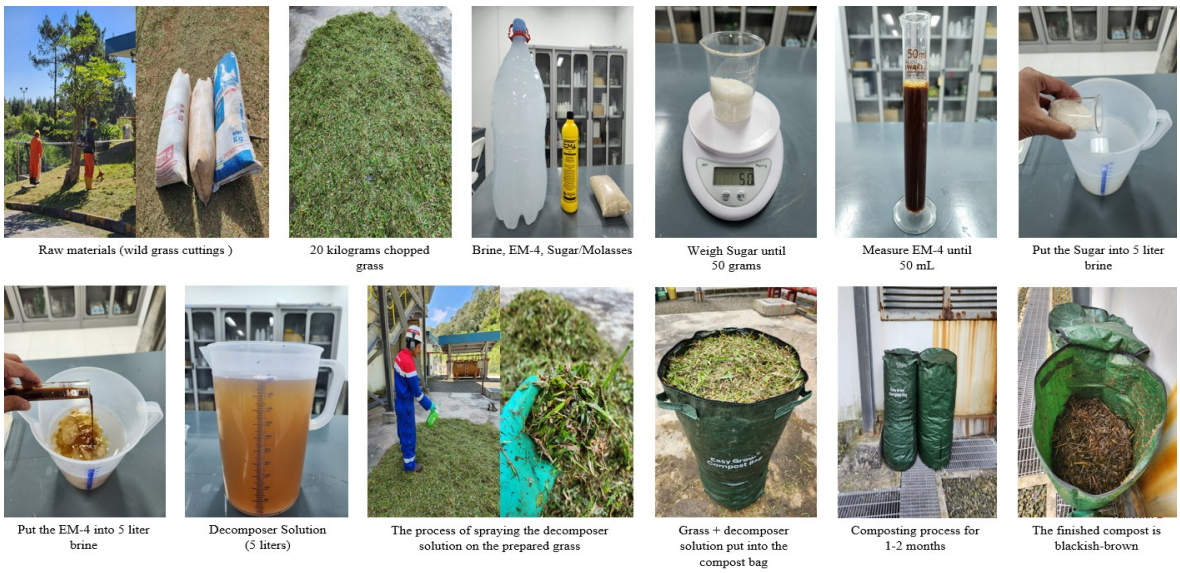

Figure 4: Diagram process of making compost brine fertilizer.

The production process of COMBINE fertilizer starts by cutting the grass into small, uniform pieces. Next, a decomposer solution is made by mixing 150 ml of effective microorganism solution (EM-4), 150 grams of molasses/sugar, and 15 liters of geothermal water (brine). This decomposer solution is evenly sprayed into 60 kg of shredded grass and placed into a compost bag for composting, which takes 1-2 months as shown in Figure 4. According to SNI 19-7030-2004 standards, compost maturity is indicated by a volume reduction of approximately 30%-40%, a dark color of compost, an earthy smell, and a C/N ratio of 10-20. Sutedjo *et. al* (1991), mature compost will feel soft when crushed because the organic materials undergo decomposition and transformation on fresh materials during composting, the formation of microbial cell substances, and transformation into a dark amorphous form. This substance is referred to as soil-like matter. After the composting process is complete, the

raw materials change color to a dark brown. The color change is caused by the activity of microorganisms working during the decomposition process. The color produced in this study has met the standard (SNI 19-7030-2004), which specifies that compost should be dark brown.

3.2 Quality Test of COMBINE (Compost Brine) Fertilizer

The produced COMBINE fertilizer has been subjected to sample testing at the Ministry of Industry's laboratory to observe the content of macro nutrients and micronutrients. Based on the analysis results in Figure 5, COMBINE fertilizer contains macro nutrients such as nitrogen 2.36%, phosphorus 10.87%, and potassium 23.32%, calcium 311.8 ppm, magnesium 3181 ppm, and contains micronutrients including sodium 6837 ppm, iron 4176 ppm, chloride 10515 ppm, copper 1.28 ppm, zinc 155 ppm, manganese 134.2 ppm, silica 366.49 ppm, boron 185.1 ppm, cobalt 1.02 ppm, and lithium 19.08 ppm.

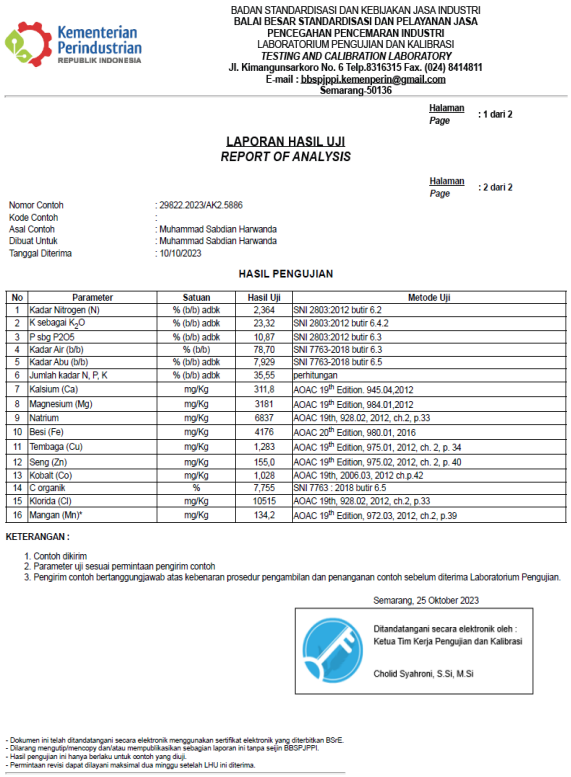

Kementerian Perindustrian
REPUBLIK INDONESIA

BADAN STANDARDISASI DAN KEBIJAKAN JASA INDUSTRI
BALAI BESAR STANDARDISASI DAN PELAYANAN JASA PENCEGAHAN PENCEMARAN INDUSTRI
LABORATORIUM PENGUJIAN DAN KALIBRASI
TESTING AND CALIBRATION LABORATORY
Jl. Kimangunsarkoro No. 6 Telp.8316315 Fax. (024) 8414811
E-mail : **bbspjppi.kemenperin@gmail.com**
Semarang-50136

Halaman / *Page* : 1 dari 2

LAPORAN HASIL UJI
REPORT OF ANALYSIS

Halaman / *Page* : 2 dari 2

Nomor Contoh : 29822.2023/AK2.5886
Kode Contoh :
Asal Contoh : Muhammad Sabdian Harwanda
Dibuat Untuk : Muhammad Sabdian Harwanda
Tanggal Diterima : 10/10/2023

HASIL PENGUJIAN

No	Parameter	Satuan	Hasil Uji	Metode Uji
1	Kadar Nitrogen (N)	% (b/b) adbk	2,364	SNI 2803:2012 butir 6.2
2	K sebagai K_2O	% (b/b) adbk	23,32	SNI 2803:2012 butir 6.4.2
3	P sbg P2O5	% (b/b) adbk	10,87	SNI 2803:2012 butir 6.3
4	Kadar Air (b/b)	% (b/b)	78,70	SNI 7763-2018 butir 6.3
5	Kadar Abu (b/b)	% (b/b) adbk	7,929	SNI 7763-2018 butir 6.5
6	Jumlah kadar N, P, K	% (b/b) adbk	35,55	perhitungan
7	Kalsium (Ca)	mg/Kg	311,8	AOAC 19th Edition. 945.04,2012
8	Magnesium (Mg)	mg/Kg	3181	AOAC 19th Edition, 984.01,2012
9	Natrium	mg/Kg	6837	AOAC 19th, 928.02, 2012, ch.2, p.33
10	Besi (Fe)	mg/Kg	4176	AOAC 20th Edition, 980.01, 2016
11	Tembaga (Cu)	mg/Kg	1,283	AOAC 19th Edition, 975.01, 2012, ch. 2, p. 34
12	Seng (Zn)	mg/Kg	155,0	AOAC 19th Edition, 975.02, 2012, ch. 2, p. 40
13	Kobalt (Co)	mg/Kg	1,028	AOAC 19th, 2006.03, 2012 ch.p.42
14	C organik	%	7,755	SNI 7763 : 2018 butir 6.5
15	Klorida (Cl)	mg/Kg	10515	AOAC 19th, 928.02, 2012, ch.2, p.33
16	Mangan (Mn)*	mg/Kg	134,2	AOAC 19th Edition, 972.03, 2012, ch.2, p.39

KETERANGAN :

1. Contoh dikirim
2. Parameter uji sesuai permintaan pengirim contoh
3. Pengirim contoh bertanggungjawab atas kebenaran prosedur pengambilan dan penanganan contoh sebelum diterima Laboratorium Pengujian.

Semarang, 25 Oktober 2023

Ditandatangani secara elektronik oleh :
Ketua Tim Kerja Pengujian dan Kalibrasi

Cholid Syahroni, S.Si, M.Si

- Dokumen ini telah ditandatangani secara elektronik menggunakan sertifikat elektronik yang diterbitkan BSrE.
- Dilarang mengutip/mencopy dan/atau mempublikasikan sebagian laporan ini tanpa seijin BBSPJPPI.
- Hasil pengujian ini hanya berlaku untuk contoh yang diuji.
- Permintaan revisi dapat dilayani maksimal dua minggu setelah LHU ini diterima.

Figure 5: Result The Quality Testing Nutrients COMBINE.

The COMBINE fertilizer is answer for the solid organic fertilizer produced, which contains macro and micronutrient elements that meet the requirements of the Indonesian National Standard (SNI) for Compost Quality Standards 19-7030-2004.

3.2.1 Nitrogen Nutrient (N)

Based on laboratory analysis results, the COMBINE fertilizer sample contains 2.36% nitrogen, which is higher compared to the Indonesian National Standard (SNI, 2004) in minimum requirement of 0.40% nitrogen content for compost. Yuwono (2005), states that organic materials with excessively high carbon content cause a prolonged decomposition process. Conversely, if the carbon content is too low, there will be an excess of nitrogen, resulting in the formation of ammonia (NH_3). Excessive ammonia content can poison bacteria and cause the necessary nitrogen to be lost. Additionally, according to Outerbridge (1991), the population of microorganisms increases or decreases according to environmental conditions in relation to the substrate.

3.2.2 Phosphorus Nutrient (P)

Based on laboratory analysis results, the COMBINE fertilizer sample contains 10.87% phosphorus, which is higher compared to the Indonesian National Standard (SNI, 2004) in minimum requirement of 0.1% phosphorus content for compost. According to Miftahul (2003), suggests that the high or low phosphorus content in compost may be due to the amount of phosphorus contained in the raw materials used and the number of microbes involved in the composting process.

3.2.3 Potassium Nutrient (K)

Based on laboratory analysis results, the COMBINE fertilizer sample contains 23.32% potassium, which is higher compared to the Indonesian National Standard (SNI, 2004) in minimum requirement of 0.2% potassium content for compost. The high potassium content in the COMBINE fertilizer is indicated to be due to the raw material from geothermal brine, which already contains a significant amount of potassium (1154.76 ppm). Sutedjo et al. (1991) state that potassium used by microorganisms in the substrate material acts as a catalyst, and their presence activity of microorganisms greatly influence the increase in potassium content. Potassium bound and stored within cells by bacteria and fungi can become available again upon decomposition. This statement is supported by Hardiani et al. (2011), who assert that potassium is used by microorganisms in the substrate material as a catalyst, and the presence of bacteria and other microorganisms significantly affects the increase in potassium content.

3.3 Implementation of COMBINE (Compost Brine) fertilizer

After the laboratory analysis of COMBINE fertilizer, it was tested on chili with three sample variations: sample 1 (chili without fertilizer), sample 2 (chili with chemical fertilizer), and sample 3 (chili with COMBINE fertilizer). Five chile were planted in each sample, measuring 30 cm by 30 cm in polybags. Ten weeks were dedicated to the collecting of data, with weekly measurements. The height of the chili, the quantity of leaves, and the quantity of fruits were among the information gathered. Chili peppers were used as samples in the trial because they have a growth period from planting to harvest of approximately 80-90 days, and the process of measuring height and counting the number of leaves is relatively easier.

3.3.1 Comparison Height of Chili

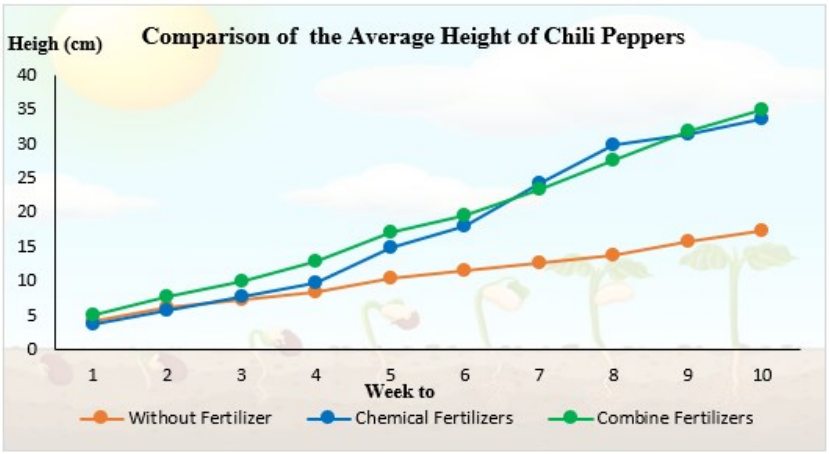

Figure 6: Comparison Height of Chili.

Based on the growth comparison height of chili in Figure 6, those without any fertilizer showed very slow and stunted growth, indicating a lack of essential macro and micronutrients which disrupted their growth process. According to Dwidjoseputro (1983), if all nutrients are available in sufficient amounts and in an absorbable form, the chili will thrive. Chili that are deficient in nitrogen grow stunted, their leaves turn yellowish-green, and if the deficiency is severe, older leaves turn yellow from the tips to the veins, then brown and dry, ultimately leading to a significant yield reduction. Conversely, if the chili have excess nitrogen, they will develop larger stems, delayed maturity, and reduced fruit quality (Hardjowigeno, 1995).

In the sample where chili was given NPK 16 16 16 chemical fertilizer in Figure 6, the growth of the chili appeared normal because all essential macro nutrients were adequately provided in high amounts. The addition of nitrogen (N) through fertilization stimulates root growth and increases root weight. Roots growing in soil with sufficient N are larger and relatively short, while roots in soil lacking N are longer, smaller, and more abundant (Marscher, 1986). The N absorbed by chili is crucial for the formation of stems, leaves, and branches. The differences in the number of branches observed reflect the varying N nutrient supply from each type of compost. The taller the chili, the more branches it forms (Nurmayulis et al., 2014).

Based on Figure 6, in the sample variation where chili was given COMBINE fertilizer, they exhibited faster, and taller growth compared to those treated with chemical fertilizer. This suggests that the macro nutrients required by the chili were well met, and the micronutrients in the COMBINE fertilizer also played a key role in their growth. Sutejo (1991) stated that adding organic matter to the soil can increase microorganism activity, such as bacteria and fungi, which function as granulators to improve soil structure. Organic matter is also used as an energy source for microorganisms, allowing them to develop and become more active (Suripin, 2002). Organic fertilizers like compost contain both macro and micronutrients, providing nutrition to chili and influencing the

number of branches per chili (Khandaker et al., 2017). Taller chili can easily access sunlight for photosynthesis. The products of photosynthesis are distributed throughout the chili to stimulate both vegetative and generative growth.

3.3.2 Comparison Number of Chili Leaves

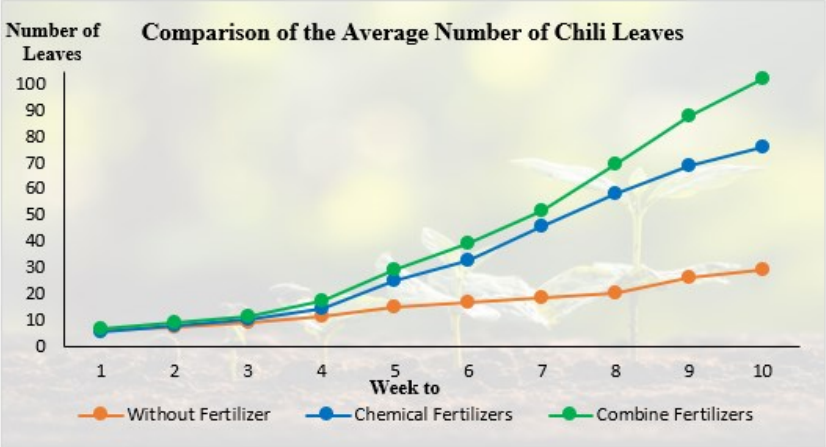

Figure 7: Comparison Number of Chili Leaves.

Based on the growth comparison number of chili leaves in Figure 7, chili that were not given any fertilizer had very few leaves, and the leaves were curled. This indicates that these chili lacked essential macro nutrients needed for leaf growth. According to Dobermann and Fairhurst (2000), nitrogen (N) can stimulate the overall growth of chili, including the leaves. The nitrogen content in chili leaves is closely related to the rate for photosynthesis, affecting the formation of biomass that serves as a food reserve for the chili, and the excess of these food reserves is stored in the fruit. Leaves that lack calcium nutrients will become curled, which aligns with Fageria et al. (1991), who stated that newly formed young leaves appear white, the growing points die (apical dieback), and the leaves curl.

In the sample variation where chili received NPK 16 16 16 chemical fertilizer in Figure 7, the chili showed many numbers of leaves due to the adequate supply of macro nutrients N, P, and K. The increased number of leaves allows the chili to maximize photosynthesis, thereby supporting their growth. Nitrogen is crucial for chlorophyll formation, which is important for photosynthesis (Pranata, 2004). However, by the 7th week, some chili leaves started to curl, which is a sign of calcium nutrient deficiency. This observation is in line with Fageria et al. (1991), who found that newly formed young leaves become white, the growing points die (apical dieback), and the leaves curl. Therefore, dolomite lime was applied in the 9th week, and leaf growth began to improve gradually. Leaf appearance can also be a significant indicator of nitrogen sufficiency in chili tissues, as nitrogen is essential for chlorophyll production, which imparts the green color to leaves (Mangel and Kirby, 1987).

Based on Figure 7, in the chili samples treated with COMBINE fertilizer, there was a higher number of leaves compared to those treated with chemical fertilizer, and there was no curling of leaves observed during the growth process. This indicates that both macro and micronutrients essential for leaf development were effectively supplied. Organic fertilizers, such as compost, provide both macro and micronutrients necessary for chili nutrition, which impacts the number of branches per chili (Khandaker et al. 2017). A greater number of leaves also facilitates more effective photosynthesis, supporting the growth of the chili. According to Surtinah (2007), good vegetative growth can also have a positive impact on the generative growth of chili.

3.3.3 Comparison Number of Chili Fruits

Based on the growth comparison number of chili fruits in Figure 8, the chili that received no fertilizer at all produced very few fruits, and fruiting only began in the 10th week. This indicates that these chilies suffered from a deficiency of macro nutrients essential for fruit development. Haryatini and Santoso (2000) state that having adequate nutrients during growth causes more active chili metabolism, which improves cell differentiation processes and ultimately leads to increased fruit weight and length. In addition to nitrogen for supporting vegetative growth, phosphorus and potassium in the growing medium also contribute to fruit development and enhance fruit quality, including fruit diameter (Gardner et al. 1991).

In the variation of chili samples treated with NPK 16-16-16 chemical fertilizer in Figure 8, the first fruits appeared in week 7, but the number of fruits was relatively low. On week 12, a fruit booster fertilizer, KNO3 and MKP, which are high in phosphorus (P) and potassium (K), was applied to accelerate the generative phase of the chilis growth. Following the application of the fruit booster fertilizer, there was a significant increase in the number of

chili fruits compared to before the booster was applied. This is supported by Nurlenawati and Nimih (2010), who state that phosphorus is essential for the generative phase of chili, especially for flower, fruit, and seed formation. High phosphorus absorption aids in cell core formation and plays a crucial role in meristematic tissue development. High levels of phosphorus in the soil solution due to phosphorus fertilization enable better nutrient absorption by chili. Lakitan (1993) also notes that potassium acts as an activator for various essential enzymes involved in photosynthesis and respiration, as well as enzymes responsible for protein and starch synthesis.

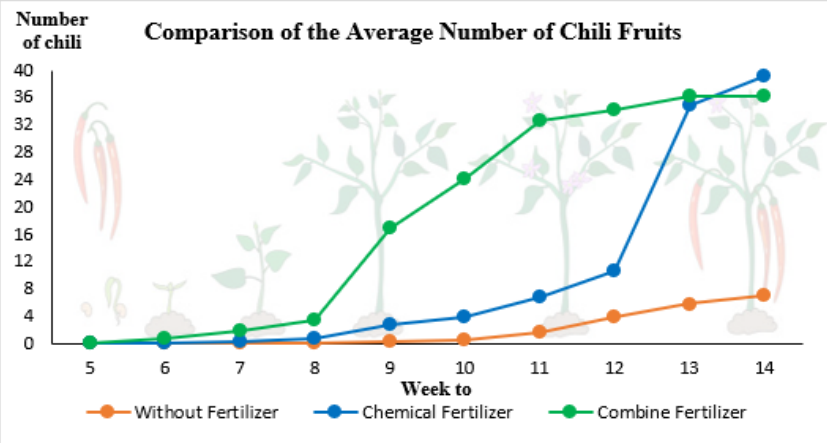

Figure 8: Comparison Number of Chili Fruits.

Based on Figure 8, in the chili variation treated with COMBINE fertilizer, the first fruits appeared in week 6, which is one week earlier compared to the chili that received chemical fertilizer. This difference can be attributed to the higher nutrient content of phosphorus (P) at 10.87% and potassium (K) at 23.32% in COMBINE fertilizer compared to the chemical fertilizer. Additionally, the increase in the number of fruits on the COMBINE fertilizer treated chili was relatively more consistent each week, indicating that both macro and micronutrients required by chili during the generative phase were effectively met. The application of organic fertilizers like compost can enhance phosphorus availability, with phosphorus playing a crucial role in flower formation and fruit maturation (Hapsoh et al. 2019). According to Harjadi (1979), fruit formation and filling are significantly influenced by nutrients such as N, P, and K, which are involved in photosynthesis processes for the synthesis of carbohydrates, fats, proteins, minerals, and vitamins, which are then translocated to the fruit storage areas. Nurhayati (2006) states that chili can be produced well if the nutrients required are available in sufficient quantities.

4. CONCLUSION

The comparison graphs of chili growth height, number of leaves, and number of fruits show that chili plants fertilized with COMBINE fertilizer have a faster growth rate, more leaves, and earlier fruit development compared to those with no fertilizer or chemical fertilizer, and they are also more resistant to pests. This demonstrates that the macro and micronutrients in COMBINE fertilizer can optimally support the nutritional requirements of chili plants throughout both the vegetative and generative stages. During the trial, COMBINE fertilizer was used only once in a 1:1 ratio of soil to COMBINE fertilizer at the planting media preparation stage.

The innovation of COMBINE fertilizer has been implemented in farmer groups around the area as a corporate social responsibility (CSR) program, and this innovation can also be replicated to other Geothermal Areas. The positive impacts of the COMBINE fertilizer innovation for the company and the community around the geothermal working area of the Karaha area are as follows:

- Minimizes the accumulation of organic waste from wild grass cuttings, thus eliminating habitats for venomous snakes that could endanger workers.
- The COMBINE fertilizer has the potential to increase company revenue if commercialized.
- With using of COMBINE fertilizer provides positive impacts on soil compared to the use of chemical fertilizers.
- Provides a solution regarding the lack of fertilizer supply to local farmers around the Karaha area.
- Establishes mutually beneficial cooperation between the community and company related to the development of COMBINE fertilizer.

REFERENCES

Adewumi, I.K., M.O., J.A. Adeptu, & Y.L. Fabiyi. (2005). Planning of organic fertilizer industries for municipal solid waste management. *J. App. Sci. Res.* 1(3):285-291.

Akmal. S. 2004. Fermentation of Rice Straw with Probiotics as Ruminant Animal Feed. *Agrista Journal*.

Doberman, A., & Fairhust, T. (2000). *Rice Nutrient Disorders and Nutrient Managemant*. Potash and Phospate Institute of Canada and International Rice Reseach Institute. Oxford Georaphic Printers Pte Ltd. Canada, Philipines. 192P.

Dwidjoseputro. (1983). *Introduction to Plant Physiology*. Jakarta: Gramedia Pustaka.

Fageria, N. K., V.C. Baligar, & C.A. Jones (1991). *Growth and mineral nutrition of filed crops*. Marcel Dekker, Inc., New York.

Gardner, F.P., R.B. Pearce, & R.L. Mitchell. (1991). *Physiology of Crop Plants*. Ul-Press. Jakarta.

Hansen, T.L., G.S. Bhander, & T.H. Christensen. (2006). Life cycle modelling of environmental impacts of application of processed organic municipal solid waste on agricultural land (EASEWASTE). *Waste Manage*. Res. 24: 153166.

Hapsoh, Z. Leyna Z & Murniati. (2019). Effect of TKKS Compost, Rice Straw, and NPK fertilizer on the Growth and Yield of Chili Pepper Plants (Capsicum annuum L.). *J. Horti. Indo*. 10(1): 20-26.

Hardiani. (2011). Bioremediation of Lead (Pb) in Soil Contaminated with Deinking Process Paper Industry Sludge Waste. *Cellulose Journal*, Vol. 1, No. 1, Juni 2011: 31 – 41. Accessed March 16, 2015.

Hardjowigeno, S. (1995). *Geology*. Jakarta: Akademika Pressindo.

Harjadi, S.S. (1979). *Introduction to agronomy*. Gramedia. Jakarta.

Haryatini, B.A., & M. Santoso. (2000). *Growth and Yield of Red Chili Pepper (Capsicum annuum) on Andisol with Mycorrhiza, Phosphorus fertilizer, and Plant Growth Regulators*. Thesis. Plant Science Study Program. Graduate School, Brawijaya University. Malang.

Inbar, Y., Chen, Y., & Hoitink, H. A. J. (1991). *Properties for establishing standards for utilization of composts in container media*. In P. L. Bishop & W. D. Gunther (Eds.), Compost production, quality, and use (pp. 287-301). Elsevier Science Publishers

Indriani, H.Y. (1999). *Making Compost in a Nutshell*. PT. Penebar Swadaya. Jakarta.

Isroi. (2008). Granular Organic fertilizer: A Practical Guide by Researchers at the Indonesian Plantation Biotechnology Research Center. Bogor.

Khandaker, M.M.F., Rohani, T., Dalorima, & Mat, N. (2017). Effects of Different Organic fertilizers on Growth, Yield and Quality of Capsicum annuum L. var. Kulai (Red Chilli Kulai). *Biosci. Biotech. Res. Asia*. 14(1): 185-192.

Lakitan, B. (1993). *Plant Physiology and Plant Development*. PT. Raja Grafindo Persada. Jakarta.

Mangel, K., & Kirby, EA. (1987). *Principles of Plant Nutrition*. 4th Edition. International Potash Institute. Worblaufen-Bern, Switzerland.

Marschner, H. (1986). *Mineral Nutrition of Higher Plants*. Institute of Plant Nutrition Univ. Hohenheim. Fed. Rep. of Jerman.

Mayadewi, A. (2007). The Effect of Manure Type and Planting Distance on Weed Growth in Sweet Corn. *Agritrop*, 26 (4): 153 – 159 ISN: 02158620.

Mifathul. (2003). *Evaluation of Compost Quality from Various Cities as a Basis for Developing Composting SOPs*. IPB. Bogor.

Nurhayati, H.M.Y. (2006). *Fundamentals of Soil Science*. Universitas of Lampung.

Nurlenawati, N., Jannah, A., & Nimih. (2010). Growth and Yield Response of Prabu Variety Red Chili Pepper (Capsicum annuum L.) to Various Doses of Phosphate fertilizer and Rice Straw Bokashi from Oyster Mushroom Waste. *Jurnal Agrika*. 4(1):9-15.

Nurmayulis, A.A., Fatmawati, & Andini, D., (2014). Growth and Yield of Pole Beans (Phaseolus vulgaris L.) in Response to Animal Manure and Various Organic fertilizers. *J. Agro*. 3(2): 91-96.

Outerbridge, Thomas (ed). (1991). *Solid Waste in Indonesia: Problem or Resource*. Yayasan Obor Indonesia. Jakarta.

Parnata, Ayub, S. (2004). Liquid Organic fertilizers: Applications and Benefits. Agromedia Pustaka 112. Jakarta.

Rynk, R.M., Van de Camp, G. B., Wilson, T. L,. Richard, J. J., Kolega, F.R., Gouin, L., Liberty, Jr., D. Kay, D. W. Murphy, H.A J. Hoitink, & W.F. Brinton. (1992). On-farm Composting Handbook. Editor R. Rynk. Northeast Regional Agricultural Engineering Servise, U.S. Departement of Agricultural. Ithaca, N. Y., Pp. 1-13.

SNI (Standar Nasional Indonesia). (2004). Specifications of Compost from Domestic Organic Waste. SNI 19-7030-2004. Badan Standar Nasional Indonesia. Jakarta.

Suripin. (2002). Conservation of Soil and Water Resources. Yogyakarta: Penerbit Andi.

Surtinah. (2007). Study on the Relationship Between Vegetative Growth and Tomato (Lycopersicum esculentum Mill.) Production. Agronomy Study Program, Faculty of Agriculture, Lancang Kuning University, Vol.4 No 1.

Sutanto, Rachman. (2002). Application of Organic Farming (Dissemination and Development). Kanisius. Yogyakarta.

Sutedjo, M.M., A.G. Kartasapoetra, & RD. S. Sastroatmodjo, (1991). *Soil Microbiology*. First Edition. Rineka Cipta. Jakarta.

Yuwono, D. (2005). *Compost*. Penebar Swadaya. Jakarta.

Yovita. (2001). *Quick Composting*. Penebar Swadaya. Jakarta.

Upstream Digitalization and Software in Research Department of Pertamina Part I : PertaGAMANT

Taufiq[1], Irnaka, T.M.[2], Suryanto, W.[2], Koestono, H.[1], and Mujihardi, B.[1]

[1]Technology Development I, PT. Pertamina (Persero)
[2]University of Gadjah Mada

taufiqgeophysics76@gmail.com

Keywords: upstream digitalization, non-seismic processing, noise tomography method, ground-aeromagnetic method

ABSTRACT

In the geoscience study, we require software as a data processing tool which is an important part of the Company's operational activities. In meeting these needs, Pertamina with the Research and Technology Department developed several innovations in the field of digitalization and software to assist in the processing of geoscience data, one of which is PertaGAMANT. PertaGAMANT is geophysical data processing software used to process Ambient Noise Tomography (ANT), Spatial Auto Correlation (SPAC), Gradient Density from Time-Lapse Microgravity Data, Ground Magnetic, and Aeromagnetic data. This software can be run real-time with cloud-based system, so operator or user can operate the software wherever and whenever they are with licensing system (Single Sign On) to protect confidentiality of the data.

1. INTRODUCTION

PertaGAMANT or we called Pertamina Gadjah Mada New Technology is a software to process non-seismic geophysical data processing with several module such as Ambient Noise Tomography (ANT), Spatial Auto Correlation (SPAC), Gradient Density from Time-Lapse Microgravity Data, Ground Magnetic, and Aeromagnetic data.

This software has been developed by the Research & Technology Department of Pertamina from 2020 until 2024 and has entered version 3. With this software, workers can process geophysical data to help in exploration, monitoring and field development activities.

2. METHOD

2.1 Noise Tomography Method

On noise tomography method, we have three techniques to record ambient noise data, which is pairing technique, clustering technique, and ring creation. Especially in pairing techniques, seismogram is arranged based on grid with spatial distance r so that in the cross-correlation process, one station will be correlated to all installed seismometer or station to obtain a group velocity. An illustration of the station configuration scheme (Ambient Noise Tomography method) can be seen in Figure 1.

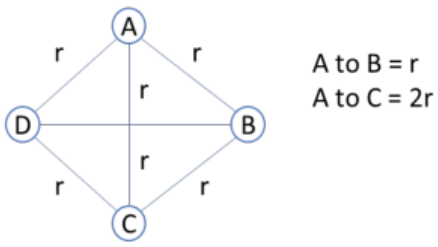

Figure 1: illustration of pairing technique on station configuration to get ambient noise data.

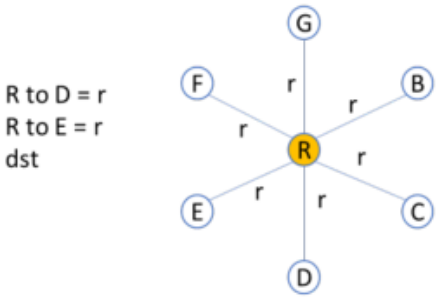

Figure 2: illustration of ring creation technique with reference station to get ambient noise data.

Clustering technique is the same as pairing techniques, but the cross-correlation process separates into several clusters, which then results from the cross-correlation will be combined in one map.

On Ring Creation Technique (Spatial Autocorrelation method), seismogram is arranged based on double triangular (north and south) like a hexagonal grid with spatial distance r. the spatial distance represents the depth penetration of subsurface velocity. An illustration of the station configuration scheme can be seen in Figure 2.

2.2 Time-Lapse Microgravity Method

Time-lapse microgravity method is the development of gravity method (x,y,z) by adding the 4th dimension of time (t). The principle of this method is to repeat gravity measurement either daily, weekly, monthly, or yearly by using a gravimeter which has an accuracy in the order of micro-Gal (Taufiq, 2015).

2.3 Geomagnetic Method

Geomagnetic Method is one of geophysical methods that used a potential field (this case a magnetic field) parameter that produced by the earth to determine a magnetic variation of rock on subsurface. Magnetic acquisition on Land is a geophysical method that measures the Earth's magnetic field anomaly on surface to determine the susceptibility variation of rocks on subsurface (derived on inversion process). In this technique can be measure with spatial distance per point on 300 meters until 1 kilometer (called detailed acquisition technique) (Taufiq, 2023).

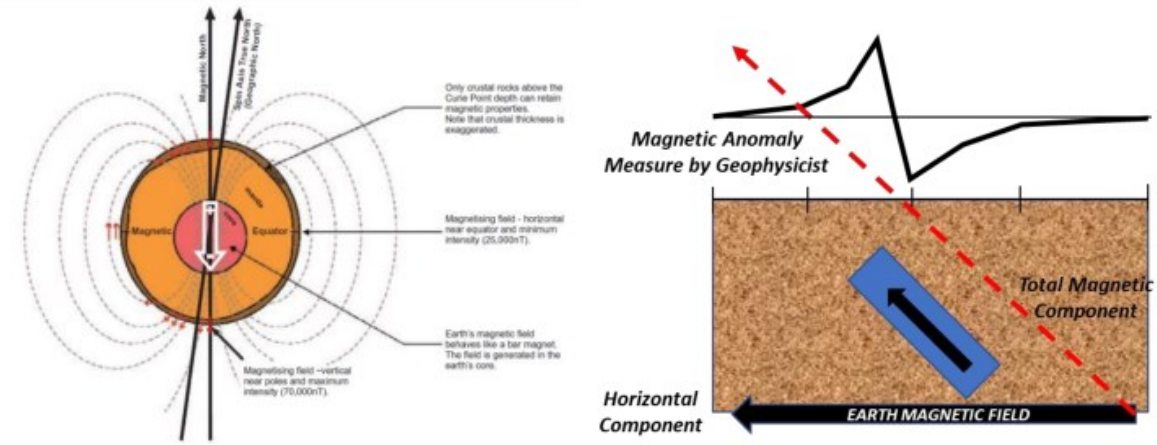

Figure 3: Illustration of Earth Magnetic Field (left) and Magnetic Anomaly measure by Geophysicist on Surface to identify subsurface condition (modified from Blakely, 1995 and Isles, 2014).

3. DISCUSSION

PertaGAMANT software can process geoscience data as in the method described above in real time because this software is operated on a cloud-based system so that users can operate the software wherever and whenever they are. Users can log in by entering the username and password (see Figure 4) that they created previously. This software is also equipped with a licensing feature which makes users feel safe when operating the software on a single-account system.

3.1 Module of Noise Tomography (ANT and SPAC) Processing

After acquisition, the data will be checked to know the quality of waveform based on threshold, event detection, and noise. Then, the data will be processed with splitting and windowing techniques to get a good condition of data. Data (after waveform preparation) is then processed with several steps as in the flowchart below (Figure 5). The differences of pairing and clustering technique are about station pairing configuration, first, the clustering technique used station pairing around measurement station with control of spatial distance. Second, the pairing technique used all the stations in the area to pair with measurement station. Last, on ring creation technique, we used reference station or central station to measure with minimum 6 station pair on grid spatial distance to process cross-correlation.

Based on the flowchart (Figure 5), with PertaGAMANT software, we can process the ambient noise data with pairing technique (see on Figure 6) and with ring creation technique (see on Figure 7). Then proses cross-correlation (Figure 8), Dispersion Curve (Figure 9), and Inversion with MCMC method (Figure 10).

3.2 Modul Gradient Density from Microgravity Processing

In this module (see Figure 11), we can create gradient (vector) density from time-lapse microgravity data to know the distribution of fluid flow direction on reservoir. This module in 2024, is still under development to adding new feature to process gravity monitoring data by time (monthly or yearly).

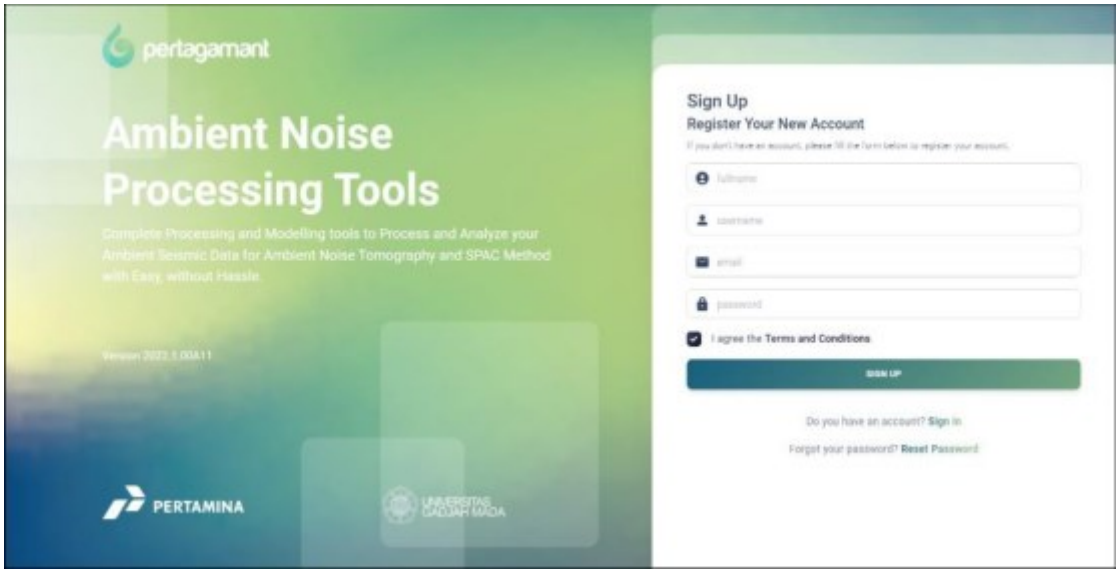

Figure 4: User Interface of software PertaGAMANT log-in system.

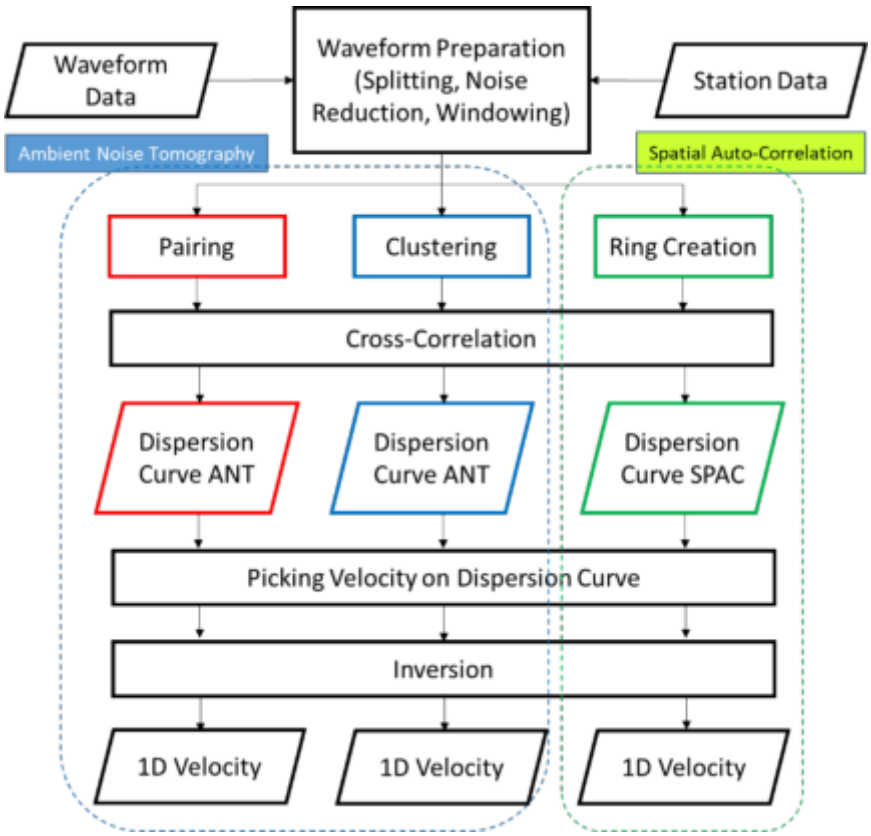

Figure 5: Flow chart to process Ambient Noise data with pairing (left), clustering (mid), and ring creation technique (right).

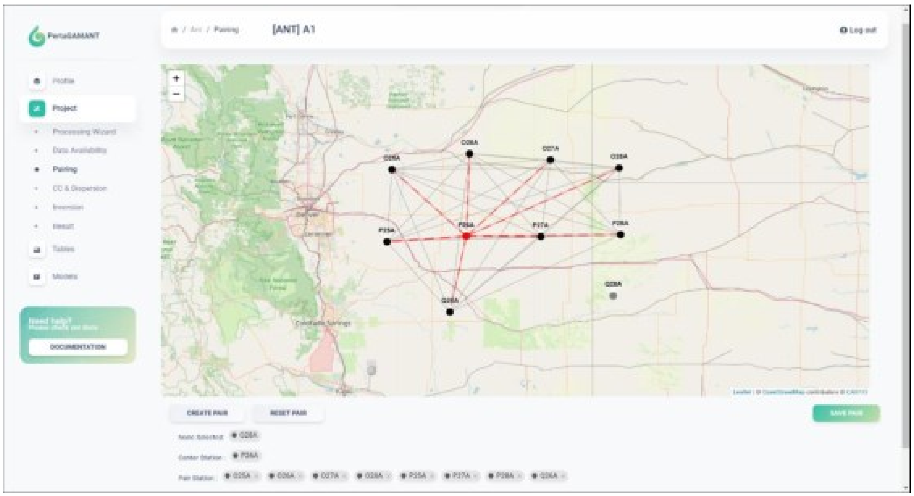

Figure 6: User Interface of software PertaGAMANT to process Noise Tomography with Pairing Technique.

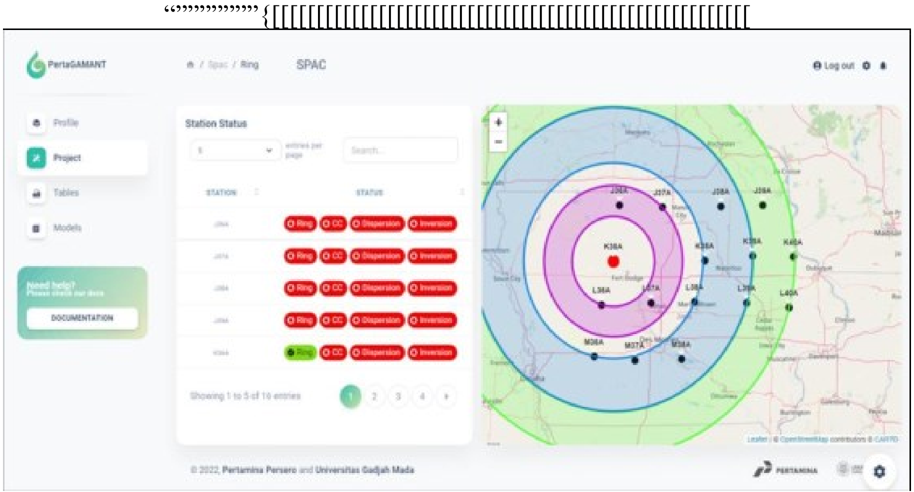

Figure 7: User Interface of software PertaGAMANT to process Noise Tomography with Ring Creation Technique.

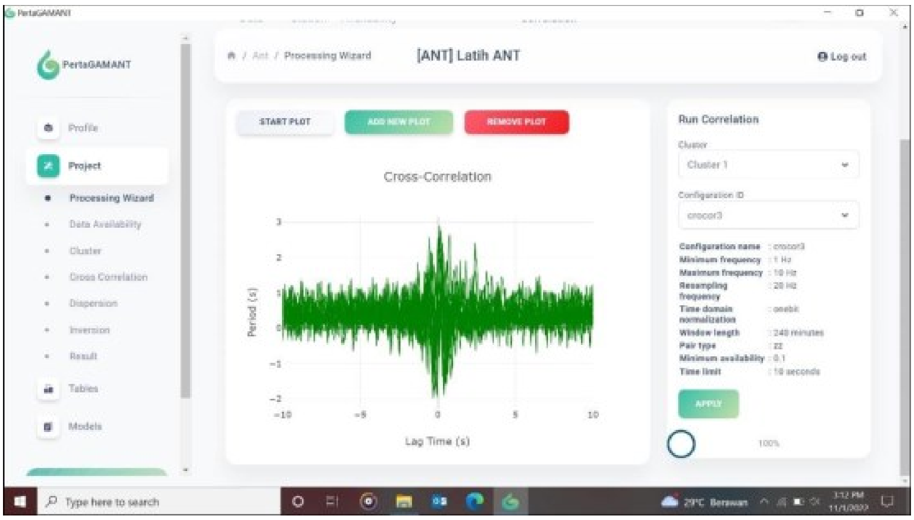

Figure 8: User Interface of software PertaGAMANT on process Cross-Correlation.

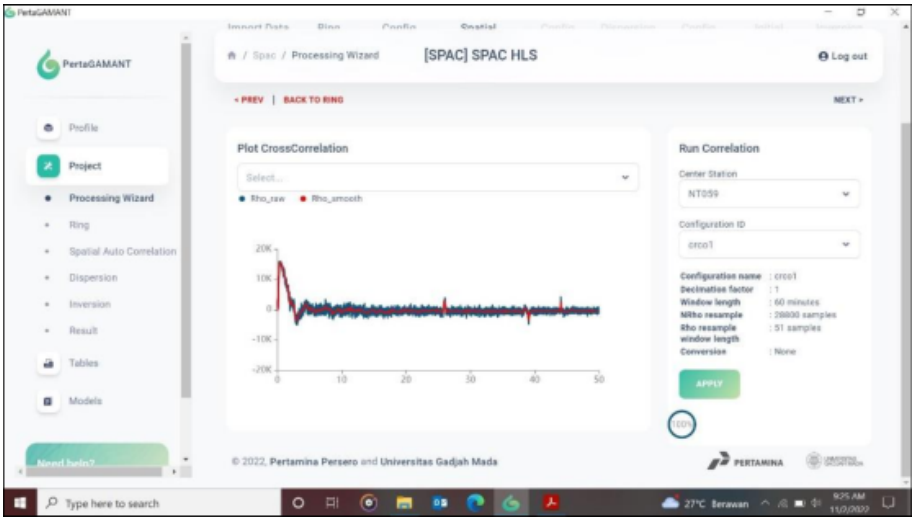

Figure 9: User Interface of software PertaGAMANT on process Picking Dispersion Curve (on SPAC).

Figure 10: User Interface of software PertaGAMANT on process Inversion.

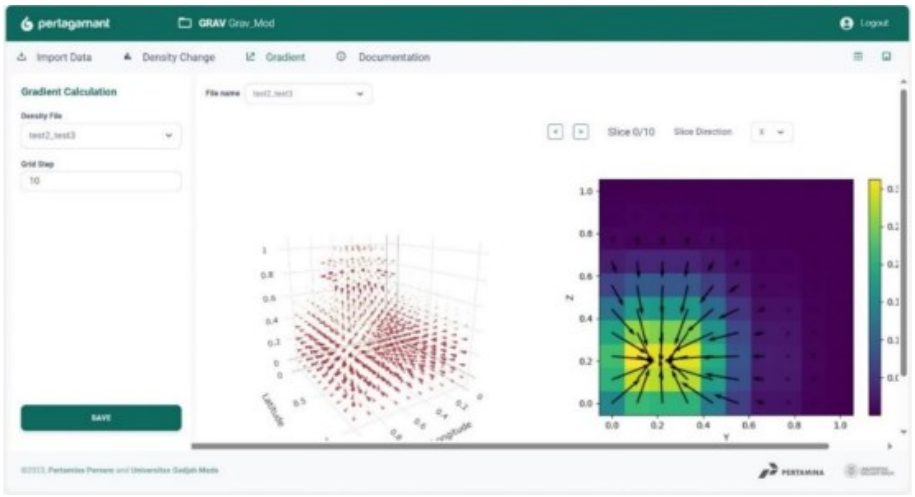

Figure 11: Simulation of gradient density from microgravity data on software PertaGAMANT.

3.3 Modul Ground Magnetic and Aeromagnetic Processing

On PertaGAMANT, we can process geomagnetic data and aeromagnetic data with flowchart below (Figure 12). The difference between ground and aeromagnetic data is located on additional correction such as effect of height variation (combination with UAV or Drone can eliminate this factor) and leveling (using micro-levelling and tie-line levelling) data (see Figure 13).

PertaGAMANT can also carry out forward and inverse modelling processes from ground and aero magnetic data to describe the initial conditions of the subsurface as an initial reference in determining reservoir boundaries along with other supporting data. An illustration of making a model based on magnetic data can be seen in Figure 15.

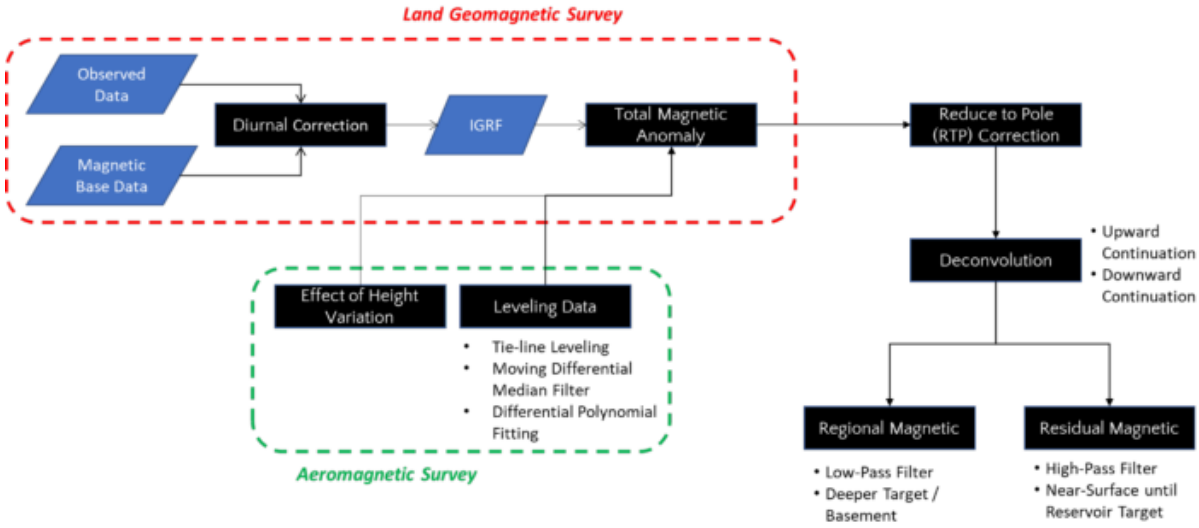

Figure 12: Flow chart to process Land Geomagnetic and Aeromagnetic Data.

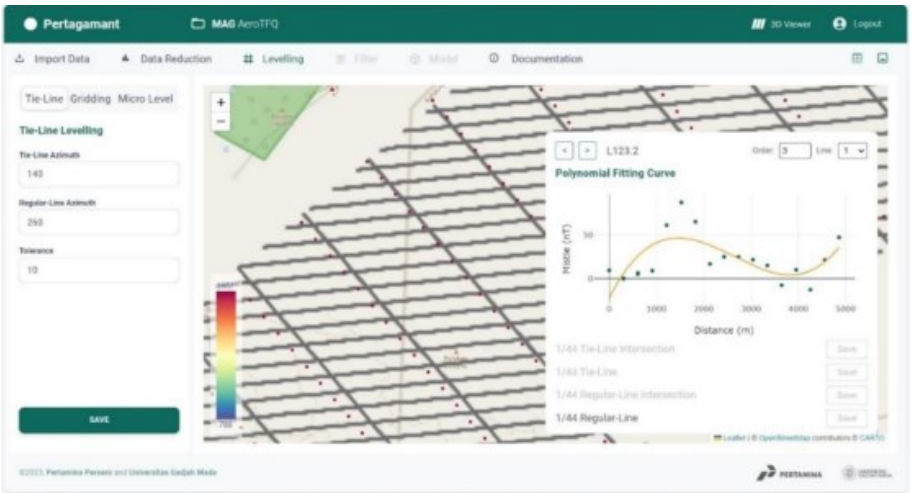

Figure 13: User Interface of software PertaGAMANT to process tie-line levelling on Aeromagnetic.

4. DISCUSSION

The conclusion from this research that:

1. PertaGAMANT software can process geoscience data in Real-Time on Cloud-Based Systems with Licensing and Log-In System Features, so users feel safe when operating this software.
2. PertaGAMANT can process geoscience data such as Ambient Noise Tomography (ANT), Spatial Auto-Correlation (SPAC), Gradient Density from Time-Lapse Microgravity Data, Ground Magnetic, and Aeromagnetic Data.

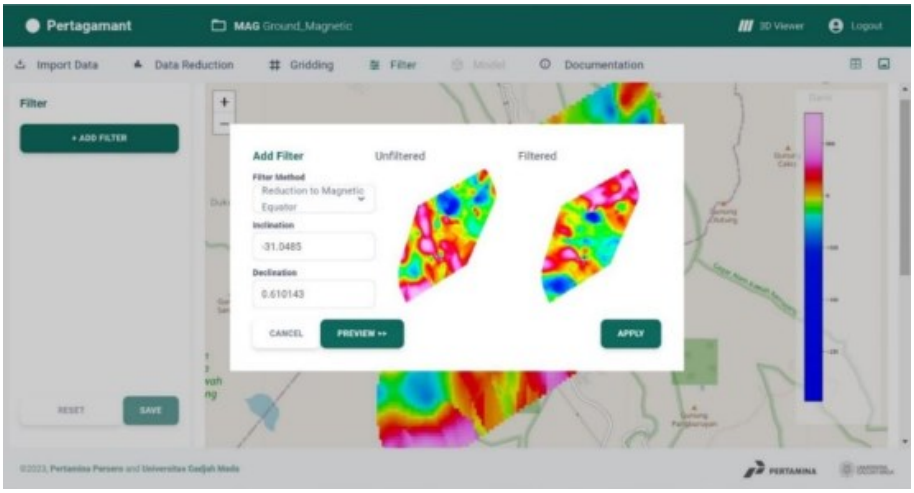

Figure 14: User Interface of software PertaGAMANT to process reduce to equator on magnetic data.

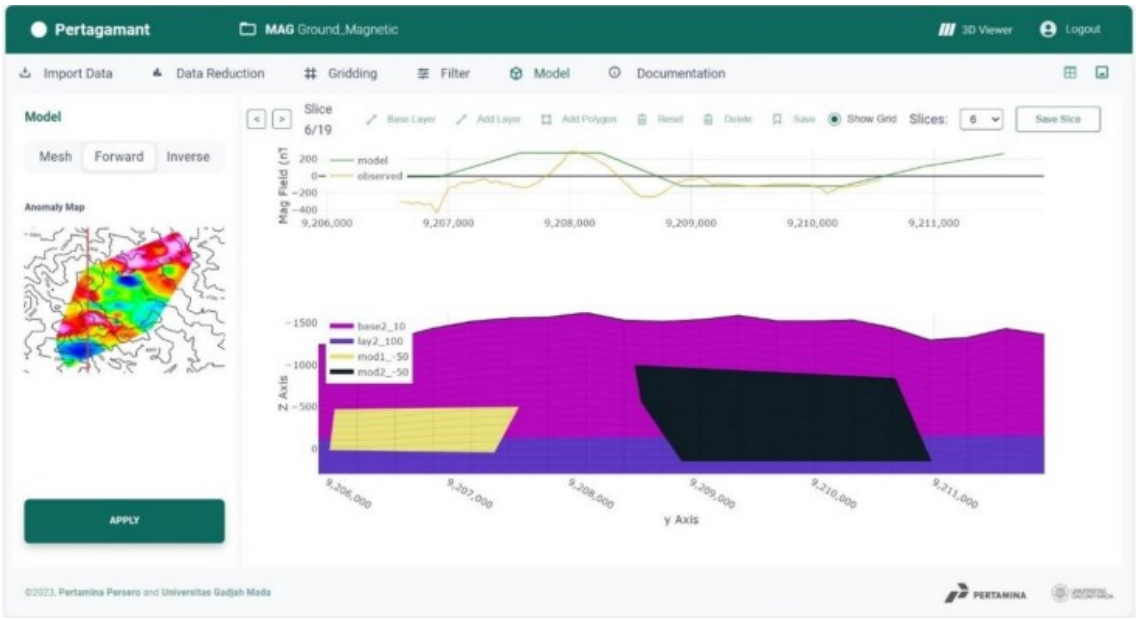

Figure 15: Example of 2D forward modelling from magnetic data on software PertaGAMANT.

REFERENCES

Blakely, R.J.: *Potential Theory in Gravity and Magnetic Application*. Cambridge University Press, (1995).

Isles, D.J. and Rankin, L.R.: Geological Interpretation of Aeromagnetic Data, *Economic Geology*, 109 (2014), 1495-1496.

Saygin, E., dan Kennett.: Ambient Noise Tomography of Australian Continent, Ambient Seismic Noise Tomography of Australia Continent, *Tectonophysics*, 481 (2010), 116-125.

Srigutomo, W., Handayani, G., Pribadi, A.R., Nugraha, A.M.: Investigation of 1D Shear Wave Velocity Profile using the Spatial Autocorrelation (SPAC) method: Case Study at West Park ITB Campus Bandung Indonesia, *ARPN Journal of Engineering and Applied Sciences*, 13 (2018), 2096-2107.

Taufiq, Retnowati, E. Zaenudin, A.: Time-Lapse Microgravity to monitor Fluid Movement Estimation, Water Saturation, Pressure, and Density Changes in Reservoir (Case Studies on Field "TFQ", Sumatera). *Indonesian Petroleum Association Proceedings*, 39 (2015), IPA15-SE-045.

Taufiq, T.: The Comparison of Land, Drone, and Aeromagnetic on Geothermal Investigation. *EAGE Conference on the Future Energy-Role of Geoscience in Energy Transition*, 1 (2023), 1-5.

Enhancing Geothermal Resource Development in Indonesia: The Role of Personnel Certification and Capacity Building

Daniel Adityatama[1], M. Rizqi Al Asyari[1], Ferdino R. Fadhillah[2], Nadya Erichatama[1], Dorman Purba[3], and Desak Nyoman Inten Apriani[2]

[1]PT Geoenergi Solusi Indonesia, Jakarta, Indonesia
[2]PT Sarana Multi Infrastruktur (Persero), Jakarta, Indonesia
[3]PT Enerka Bhumi Pratama, Jakarta, Indonesia

daniel.adityatama@geoenergis.com

Keywords: geothermal, project, Indonesia, capacity building, competency assessment

ABSTRACT

The development of Indonesia's geothermal resources could be improved by enhancing the skills and expertise of its workforce. This paper looks at findings from a study by PT SMI and GRG-Geoenergis, supported by EBTKE, which suggests that better training for workers might support the initiatives to lower costs in geothermal exploration. One major issue identified is the lack of standardized certification for personnel in geothermal exploration, which may lead to less efficient operations and higher chances of project failures.

The research supports the idea of creating a national certification system specifically for the geothermal sector, along with targeted training programs. These efforts aim to improve the skills of both current and future geothermal workers, possibly leading to better project management and technical execution. The paper also explores the potential role of PPSDM KEBTKE in expanding its educational and certification services to more directly support the geothermal industry.

By making these changes, there is a chance to not only cut exploration costs but also to boost the success and sustainability of geothermal projects in Indonesia. These improvements could help build a more skilled and certified workforce, thus strengthening Indonesia's position in the global geothermal market and making better use of its vast geothermal potential.

1. INTRODUCTION

At present, Indonesia does not have a dedicated national certification scheme to verify the specialized competencies required for key personnel in geothermal exploration projects, specifically in pivotal areas like geosciences (including geology, geochemistry, and geophysics), drilling, and reservoir management. This lack of a structured certification framework poses a significant risk, as it allows for the potential involvement of individuals who may not possess the essential experience or minimum skill level required to secure the success of geothermal exploration projects. Such a scenario not only jeopardizes the project's goals but also compromises human safety, environmental sustainability, and cost-effectiveness.

In Indonesia's geothermal sector, especially during exploration, it's common for new entrants to recruit key personnel from the oil, gas, or mining industries due to perceived similarities. This trend is likely to continue as more companies unfamiliar with the unique aspects of Indonesia's geothermal environment enter the market.

Yet, geothermal resources exhibit distinct geological, geochemical, and geophysical characteristics that diverge significantly from those in oil, gas, or mining contexts. The unique challenges of geothermal exploration, such as understanding complex geothermal systems, dealing with high-temperature and corrosive fluids, and managing more variable resource parameters, requiring specific expertise and approaches.

In the absence of a national competency certification (Figure 1), individuals without geothermal backgrounds may enter key roles in geothermal exploration projects in Indonesia. Each geothermal company in Indonesia has unique recruitment procedures, which without a standardized certification, leaves room for professionals with no previous backgrounds in geothermal projects to assume critical positions.

Geothermal companies face numerous exploration challenges and must form teams with diverse backgrounds and competencies to address the risks. One of the examples is shown in Figure 2, which illustrates a typical organizational structure of a geothermal company operating drilling projects. The key personnel must manage the team from various backgrounds (and even various companies) for a safe and successful drilling operation.

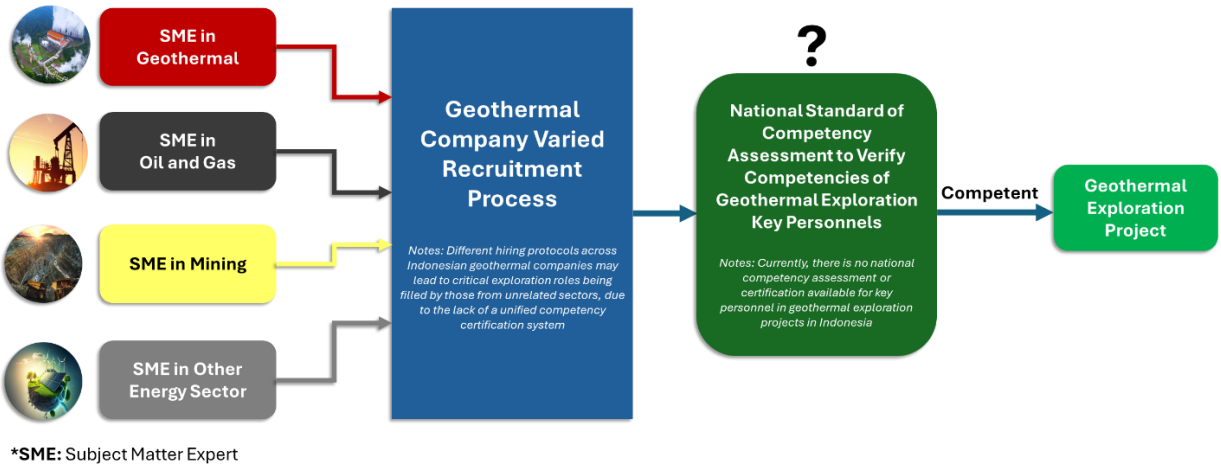

Figure 1: The current situation in Indonesia regarding the recruitment of experts or key personnel to manage exploration projects lacks a vital competency assessment process necessary to ensure project outcomes.

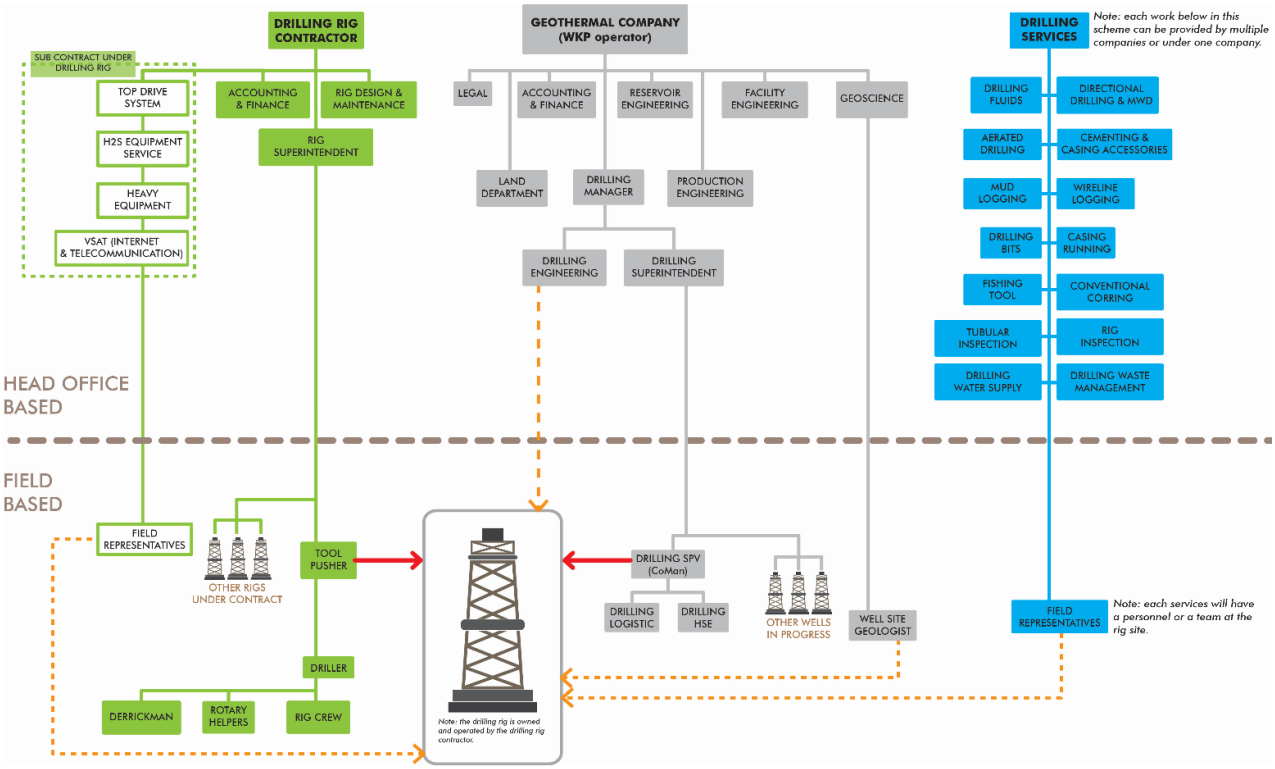

Figure 2: Typical organization structure in geothermal drilling project in Indonesia (modified from Purba et al., 2020).

2. SIGNIFICANCE OF HAVING KEY PERSONNEL WITH THE RIGHT COMPETENCIES IN GEOTHERMAL PROJECT

Given the complex and detailed nature of geothermal exploration, the lack of properly trained and experienced professionals can lead to a variety of negative outcomes, escalating both financial and operational risks:

1. **Operational Failures and Safety Incidents**: Personnel who lack experience or qualifications may not fully understand the complex geological formations involved in geothermal drilling. This can result in the use of unsuitable drilling techniques, leading to operational failures. For example, an incorrect evaluation of the pressure and temperature conditions in geothermal reservoirs might result in poorly designed wells, increasing the risk of well failures, blowouts, or even catastrophic accidents that could compromise worker safety and harm the environment.

2. **Financial Consequences**: The absence of skilled personnel carries significant financial risks. Drilling is a major expense in geothermal projects, and errors due to insufficient expertise can produce non-productive wells, requiring more investment to fix these errors or to abandon the wells completely. Drilling at incorrect locations because of inaccurate geological assessments can create dry wells that yield no geothermal fluids, thus inflating investment losses and exploration costs.
3. **Project Delays**: Inadequate expertise can significantly delay project timelines. Teams lacking the necessary qualifications might take longer to conduct drilling operations, encounter technical problems, or need multiple attempts to succeed. These delays not only increase costs but also push back the timeline for generating revenue from the geothermal resource. For instance, if a drilling team inadequately manages well casing and cementing due to a lack of knowledge about geothermal-specific practices, it might cause issues with well integrity that require extensive and costly repairs or workover.
4. **Reputational Damage**: The inability to employ skilled personnel can damage the reputation of the companies and the wider Indonesian geothermal sector. Technical failures and inefficiencies may make international investors and partners reluctant to participate in projects, leading to a decline in investor confidence and potentially hampering the sector's growth. Public incidents resulting from incompetence could foster widespread doubt and negatively impact the sector's reputation.

There is a risks associated with personnel not familiar with geothermal project. Introducing personnel from related industries who are not familiar with geothermal projects into geothermal exploration introduces considerable risks. These extend beyond operational inefficiencies to include safety issues, environmental compliance, and the financial sustainability of exploration efforts. Personnel who are not familiar with the intricacies of geothermal exploration may make strategic errors and costly mistakes that impact both immediate operations and the long-term development of the sector.

a. **Challenges with Inaccurate Well Targeting**: Precise well location targeting is crucial in geothermal exploration to effectively access heat reservoirs. This task requires a deep understanding of the geological, geochemical, and geophysical attributes of geothermal systems. Personnel from sectors like oil and gas may lack the detailed knowledge needed for successful well targeting in a geothermal setting.
b. **Overlooking Environmental and Social Impacts**: Those not familiar with geothermal exploration may not fully grasp the environmental complexities involved, nor anticipate the potential ecological impacts. This oversight can result in conflicts with protected areas, leading to environmental harm, disruptions to local ecosystems, and possible legal consequences, along with delays and extra costs for environmental mitigation and conservation.
c. **Failures in Drilling Infrastructure Construction**: Personnel inexperienced with the unique conditions of geothermal sites may struggle with setting up infrastructure in the challenging environments typical of these locations, such as areas with high-relief terrain, water scarcity, close to residential zones, or landslide-prone areas. Their lack of familiarity can cause infrastructure failures, posing safety risks and environmental issues, and leading to significant project delays and additional costs.
d. **Lack of Stuck-Pipe Prevention Measures**: The causes of stuck-pipe incidents in geothermal drilling are often different from those in oil and gas, involving specific geological challenges like fractured formations and reactive soils that are not typically found in other drilling contexts. Using inappropriate strategies can exacerbate problems, causing costly delays and equipment damage.
e. **Unsuitable Well Control Methods**: Well control practices in geothermal drilling need to address the unique properties of subsurface fluids and pressures found in these environments, which differ markedly from those in oil and gas. Conventional well control methods may not be adequate for managing the high-temperature fluids and potential phase changes encountered in geothermal wells.
f. **Increased Risk of Cost Overruns and Project Delays**: The absence of specialized expertise in geothermal exploration significantly raises the likelihood of cost overruns. This issue can manifest in various ways throughout a project's lifecycle, from poor initial planning and resource misallocation to delays in project timelines, increased chances of technical failures, and failures to meet regulatory and environmental standards.

3. LACK OF PERSONNEL COMPETENCY ASSESSMENT AND CERTIFICATION

Indonesia currently faces a significant challenge due to the absence of a formal certification system to verify the competencies of personnel in geothermal exploration. This gap allows professionals from oil, gas, and mining industries to transition into geothermal roles without fully understanding the sector's specific demands. While this cross-industry movement diversifies the talent pool, it raises concerns about project effectiveness and safety due to the lack of a dedicated competency framework for geothermal activities.

The Indonesian Ministry of Energy and Mineral Resources has established PPSDM KEBTKE, an entity tasked with delivering targeted education, training, and competency assessments to produce qualified professionals in fields such as electricity, renewable energy, and energy conservation. However, currently, PPSDM KEBTKE and the government only require safety certifications, for example, for operational supervisors. Certifications for key positions, such as geology, geochemistry, and geophysics experts at PPSDM KEBTKE, are not mandatory, which means there is no requirement for personnel to be certified in these areas. Additionally, for drilling, the only mandatory certification is well control, provided at PPSDM Migas in Cepu, Central Java. However, this well control certification primarily targets the oil and gas industry, where the mechanisms for well control and kicks differ significantly from those in geothermal drilling and can greatly impact operational safety. The full list of geothermal-related training and certification provided by PPSDM KEBTKE is shown in Table 1.

Table 1: List of geothermal-related training and certification topic conducted by PPSDM KEBTKE.

Course/Training/ Certification	Learning Method	Average Course Duration
PPSDM KEBTKE: CERTIFICATION		
Pengawas Operasional Pertama (POP) Panas Bumi	Online Training & Hybrid	5 days
Pengawas Operasional Madya (POM) Panas Bumi	Online Training & Hybrid	5 days
Pengawas Operasional Utama (POU) Panas Bumi	Online Training & Hybrid	5 days
Ahli Geologi Panas Bumi	Online Training & Hybrid	5 days
Ahli Geokimia Panas Bumi	Online Training & Hybrid	5 days
Introduction Energy Management System ISO 50001:2018	Online Training	1 day
Manajer Energi pada Industri	Online Training	5 days
Audit Energi pada Industri	Online Training	6 days
PPSDM KEBTKE: TRAINING (*PELATIHAN/BIMBINGAN TEKNIS*)		
Pemanfaatan langsung panas bumi (Geothermal Direct use)	Online Training	2 days
Desain Pembangkit berbasis ORC pada Panas Bumi	Online Training	2 days
Pembangkit Listrik Tenaga Panas Bumi Berbasis Binari (Geothermal Binary Power Plant)	Online Training	2 days
Penyusunan Tingkat Komponen Dalam Negeri (TKDN) Bidang Panas Bumi	Information Not Available	Information Not Available
Penyusunan Rencana Pemanfaatan dan Pengelolaan Limbah Lumpur	Information Not Available	Information Not Available
Pemanfaatan Panas Bumi untuk Pembangkit Skala Kecil	Information Not Available	Information Not Available
Kegiatan Survei Pendahuluan Panas Bumi	Information Not Available	Information Not Available
Evaluasi Kelayakan EBT	Information Not Available	Information Not Available
Monitoring dan Evaluasi Pembangunan EBT	Information Not Available	Information Not Available

*Note that the certification for specific geothermal exploration positions are only for operational supervisors and certain technical roles such as geology, geochemistry, and geophysics experts, but they are not mandatory for all key positions in geothermal exploration.

Understanding the nature of geothermal projects, which is distinct from other power generation projects (where geothermal requires exploration that may not find any resources), is also crucial. If geothermal projects, especially exploration phases, are run or led by project managers lacking sufficient knowledge, it is likely that these managers will not fully appreciate the associated risks and uncertainties. This lack of understanding can lead to inappropriate exploration strategies, making the exploration phase disproportionately expensive when uncertainties are still high.

Understanding the nature of geothermal projects, which is distinct from other power generation projects (where geothermal requires exploration that may not find any resources), is also crucial. If geothermal projects, especially exploration phases, are run or led by project managers lacking sufficient knowledge, it is likely that these managers

will not fully appreciate the associated risks and uncertainties. This lack of understanding can lead to inappropriate exploration strategies, making the exploration phase disproportionately expensive when uncertainties are still high.

Furthermore, the lack of capacity building and competency assessment threatens the future success of projects. Without adequate preparation and verification of skills, future geothermal initiatives may face escalated risks, inefficiencies, and potentially failed outcomes, undermining the sector's growth and development.

4. CURRENT AVAILABLE GEOTHERMAL TRAINING AND CERTIFICATION

4.1 New Zealand Support for Training in the Indonesian Geothermal Sector (NZSTIGS)

The New Zealand Support for Training in the Indonesian Geothermal Sector (NZSTIGS) is a collaborative effort between New Zealand and Indonesia aimed at enhancing the geothermal sector's capabilities in Indonesia through education and training (Douglas, Stuart, & Dwiyudha, 2021; Kantor Berita Antara, 2023; Umam, et al., 2021). his initiative has led to the creation of specialized training curricula and programs that are delivered to Indonesian trainers and technicians, with a strong emphasis on enhancing the skills of local personnel in both the private and public sectors of the geothermal industry.

NZSTIGS includes a variety of training programs aimed at improving skills at various levels within the geothermal industry in Indonesia. The training offered under this initiative includes:

a. Train-the-Trainer Programs: These programs are designed to provide Indonesian instructors with the skills and knowledge necessary to effectively teach geothermal technology and operations, focusing on enhancing teaching methods and practical skill application.
b. Technical Training for Operators and Technicians: Tailored courses that aim to increase the technical skills of those directly involved in the operations of geothermal plants, covering the operation and maintenance of equipment, safety protocols, and methods to optimize efficiency.
c. Capacity Building and Leadership Training: These programs focus on developing management skills and leadership capabilities among senior geothermal sector personnel, ensuring that operations are technically adept and efficiently managed.
d. Curriculum Development: This involves working with local educational institutions to develop and refine curricula tailored to the specific needs of Indonesia’s geothermal industry, ensuring alignment with current industry standards and requirements.

4.2 Other Geothermal Training, Education, and Certification in Indonesia

Beyond international collaborations, Indonesia has a range of domestic training and certification programs focused on enhancing geothermal expertise. Apart from PPSDM KEBTKE, various local institutions offer specialized training and certification in geothermal energy, as outlined below:

a. ITB Geothermal Master Program: Beyond its master’s program, the Institut Teknologi Bandung (ITB) also hosts the annual ITB International Geothermal Workshop (IIGW), which features practical field trips and post-event courses focused on topics like geothermal reservoir simulation and 3D modeling.
b. UGM – Geothermal Research Center: The Geothermal Research Center at Universitas Gadjah Mada (UGM) provides a variety of geothermal training and courses aimed at professionals and government personnel. These include professional short courses that are interactive and comprehensive, incorporating lectures, lab/field exercises, and group projects. Developed in collaboration with international institutions such as The University of Auckland and GNS Science, these courses are updated annually to reflect the changing needs of the geothermal market. UGM also offers specialized training tailored for government staff and customizable in-house training for companies, covering a wide range of geothermal development topics.
c. Enerka: Enerka delivers a diverse set of educational programs through its digital platform, designed to foster collaboration among industry professionals, students, and academics. This platform includes webinars and online courses that focus on geothermal drilling, reservoir management, and the challenges of energy transition. Enerka also offers offline training sessions conducted by experts, addressing various topics related to energy, including geothermal, to enhance skills and provide continuous learning opportunities.
d. AILIMA: Through its JIWA Learning platform, AILIMA provides a selection of online courses centered on geothermal energy, likely covering areas such as geothermal drilling, resource assessment, and wellbore simulation.

These training and certification initiatives are essential for cultivating the necessary expertise within Indonesia’s expanding geothermal sector, offering both theoretical knowledge and practical skills vital for the growth of this

renewable energy source. Additional details regarding potential geothermal education and training providers in Indonesia are shown in Table 2 and Figure 3.

Table 2: List of geothermal informal education provider in Indonesia (modified from Ayuningtyas et al., 2023).

Institution/Provider	Programs	Topics	Learning Method	Course Duration (Avg.)
PT Enerka Bhumi Pratama (ENERKA)	Free Webinar	Drilling, reservoir, production, geoscience, surface facilities, social, finance	E-Learning	1-2 hours
	Training	Drilling, reservoir, production, geoscience, surface facilities, social, finance, procurement	Online Training & Hybrid	8-12 hours
	Online Courses	Drilling, geosciences	E-Learning	10 hours
PT Anugerah Indonesia Lima (AILIMA)	Free Webinar	Drilling, Production, Reservoir	E-Learning	1-2 hours
	Online Courses	Drilling, geosciences, production, reservoir, finance	E-Learning	3 hours
Gemilang Training	Training	Introduction of Geothermal	Offline Training	2 days
PT Vyntech Multi Solutions	Training	Introduction of Geothermal	Offline & Online Training	2 days
Institut Teknologi Bandung (Geothermal Master Program)	Training	Geothermal Exploration & Development	Online	Tentative
Universitas Gadjah Mada	Training	Geothermal Exploration	Offline Training	Tentative

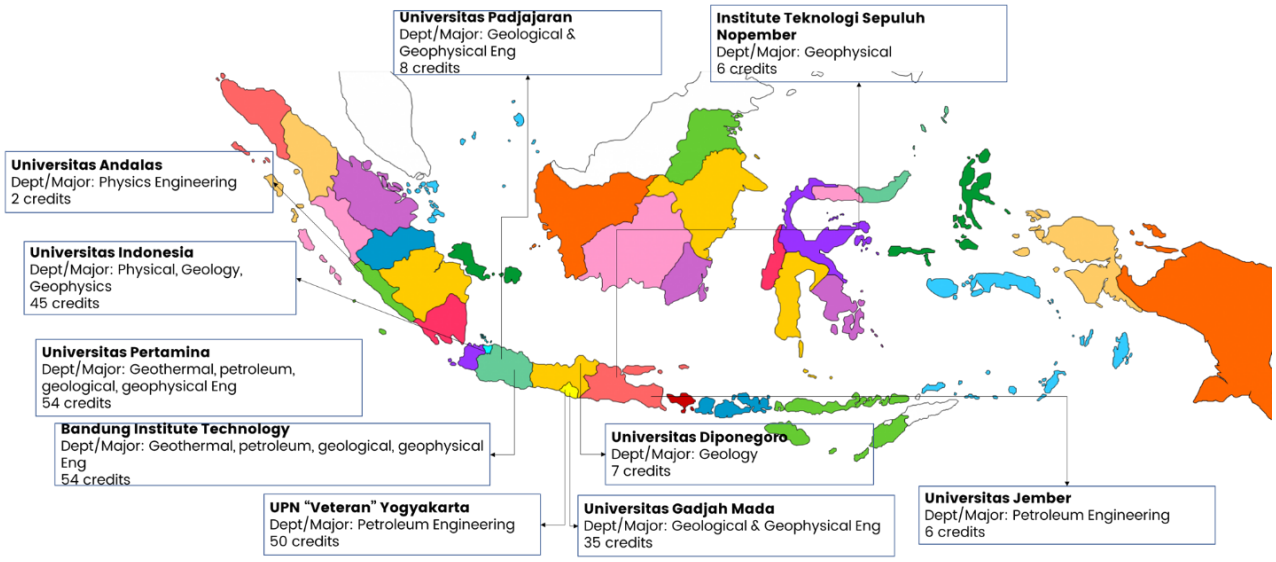

Figure 3: Geothermal formal education provider or universities in Indonesia (modified from Ayuningtyas et al., 2023).

5. OPPORTUNITY TO OPTIMIZE PPSDM KEBTKE FOR GEOTHERMAL TRAINING AND CERTIFICATION

5.1 History of PPSDM KEBTKE

EBTKE recognizes the potential to enhance the roles of its existing training and certification bodies, such as the Center for Human Resource Development in Electricity, New Energy, Renewable Energy, and Energy Conservation (PPSDM KEBTKE). This center is primarily responsible for developing human resources in the sectors of electricity, new energy, renewable energy, and energy conservation. There is an opportunity for PPSDM KEBTKE to expand its training and certification offerings, particularly for personnel involved in Indonesia's geothermal projects.

Historically, the development of PPSDM has been in step with the introduction of Regional Autonomy, aiding developmental activities in the Energy and Mineral Resources sector. This alignment was formalized with the issuance of Presidential Decree No. 165 of 2000, establishing an Energy and Mineral Resources Education and Training Agency that included the Center for Electricity and New Renewable Energy Training (Ketenagalistrikan dan Energi Baru Terbarukan / KEBT). The formation of this institution was further detailed in the Minister of Energy and Mineral Resources Decree No. 150 of 2001 and defined by Ministerial Decree No. 30 of 2005 concerning the Organization and Work Procedure of the Ministry of Energy and Mineral Resources. Following organizational restructuring under the Regulation of the Ministry of Energy and Mineral Resources No. 18 of 2010 regarding the Organization and Work Procedure of the Ministry, the KEBT Training Center was rebranded as KEBTKE (Ketenagalistrikan, Energi Baru Terbarukan dan Konservasi Energi / Electricity, New and Renewable Energy, Energy Conservation). In 2016, with Ministerial Regulation No. 13 concerning the Organization and Work Procedure, KEBTKE was renamed PPSDM KEBTKE, tasked with the development of human resources in the specified fields.

5.2 Improvement Opportunities for PPSDM KEBTKE to Support Geothermal

As of a recent workshop held on April 30, 2024, with participation from PT SMI, EBTKE, and GRG-Geoenergis, it has been observed that PPSDM KEBTKE still offers a limited range of training and certification programs specifically for the geothermal industry. Currently, the certifications primarily focus on operational supervisor certifications (Pratama, Madya, and Utama) with an emphasis on Occupational Safety and Health to safeguard individuals and the environment during geothermal project operations in Indonesia. These certification programs for Pengawas Operasional are considered well-established and are strictly monitored by EBTKE, mandatory for the Head of Geothermal (Kepala Teknis Panas Bumi - KTPB) and recommended for several key roles in geothermal companies.

However, certifications for technical personnel, particularly in geoscience fields such as geology, geochemistry, and geophysics, are still not strictly implemented. Currently, key geoscience personnel in geothermal companies or consultants are not required to have these certifications to participate in geothermal exploration or development projects in Indonesia.

Furthermore, there appears to be a lack of alignment between the training courses and the certification list offered by PPSDM KEBTKE. Typically, individuals should undergo relevant training before attempting certification. For instance, PPSDM KEBTKE could enhance geoscience training programs to better prepare candidates for certifications in Geothermal Geology, Geochemistry, or Geophysics.

There is also a notable opportunity to expand the certification offerings for drilling personnel, considering drilling projects are major cost contributors in geothermal ventures. Ensuring that personnel managing these projects possess the necessary competencies is crucial. Currently, no certifications for drilling personnel are evident, although the training list includes a course on "Development of Plans for the Utilization and Management of Mud Waste." This course, while common in the market, seems ambiguously placed on the training list and might be more relevant for HSE drilling personnel than for drilling engineers. PPSDM KEBTKE could collaborate with the geothermal team at EBTKE to identify essential skills and competencies required for geothermal drilling personnel, such as drilling managers, engineers, superintendents, and supervisors.

6. POTENTIAL IMPLEMENTATION FRAMEWORKS FOR GEOTHERMAL CAPACITY BUILDING AND COMPETENCY ASSSESSMENT

6.1 Capacity Building and Competency Assessment Process

Capacity building and competency assessment are two interconnected processes that must continuously evolve as Indonesia develops and utilizes geothermal energy. Figure 4 illustrates a simple flowchart detailing how capacity building and competency assessment fit into the broader human resource development strategy, aimed at ensuring that key personnel are equipped to oversee geothermal exploration projects effectively in Indonesia.

Indonesia might consider two approaches Figure 4): the first scenario presumes that the proposed key personnel already meet the required competence levels, making them likely candidates to successfully complete the certification process. The second scenario, suitable for candidates with experience in the broader energy sector but lacking specialization in geothermal, suggests that they engage in a capacity-building program prior to competency assessment. This approach is not only designed to prepare them for certification but also to enhance their capabilities to manage upcoming exploration projects efficiently.

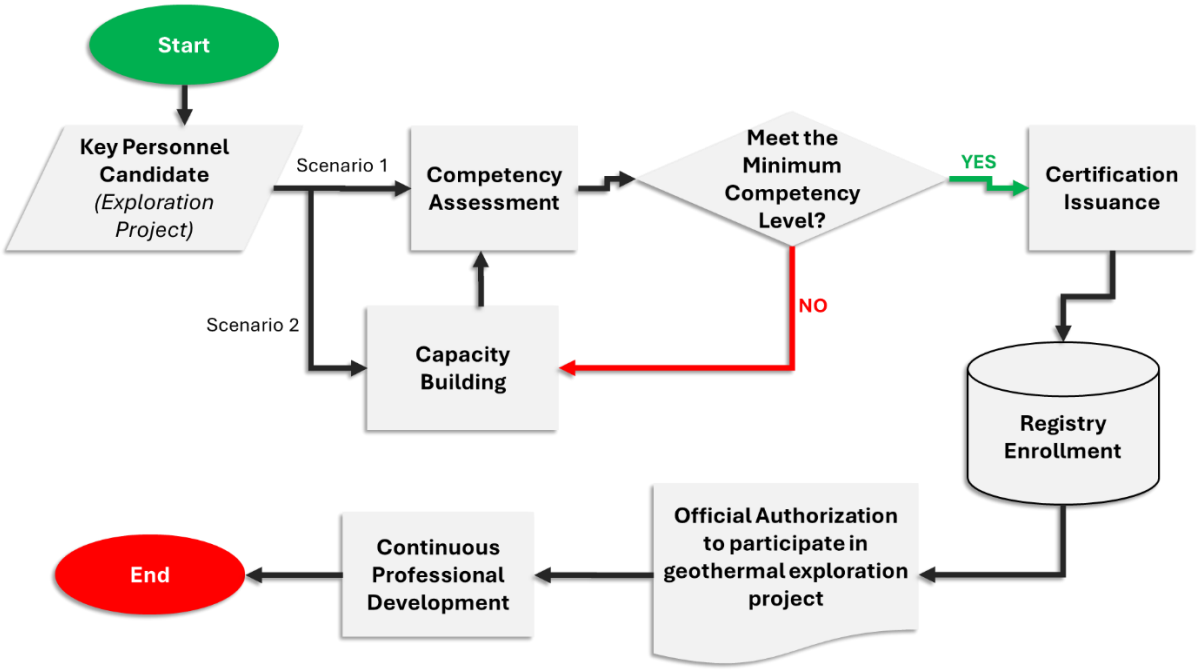

Figure 4: High-level flowchart depicting the capacity building and competency assessment process to ensure skilled management of geothermal projects in Indonesia.

When considering personnel applications, including international candidates without Indonesian certification, the following scenarios may be applied:

a. International experts are required to obtain Indonesian certification. This practice mirrors that of Indonesia's oil and gas sector, where every international expert must secure well control certification at PPSDM Migas Cepu. The certification program is offered in both Indonesian and English to accommodate international participants.
b. International experts with significant experience in Indonesia's geothermal sector or who have attained a certain educational level in geothermal studies might be considered as alternatives to undergoing certification.

The specifics of this mechanism will be further developed by a task force charged with shaping the certification program.

6.2 Proposed Implementation Framework

To outline the path forward for the Indonesian Government in addressing these Policy Opportunities, this sub-chapter proposes an Implementation Framework. This framework is designed to bolster the competencies of Indonesia's geothermal workforce and provides a structured roadmap for the government to effectively implement policy recommendations:

1. Establish a cross-sectoral task force:
    a. Form a task force with representatives from the Ministry of Energy, educational institutions, industry associations, and international experts to oversee policy implementation.
    b. The task force's main function would be to coordinate activities, track progress, and align initiatives with strategic national energy objectives.
    c. The urgency and focus of this task force are crucial for catalyzing immediate progress.
2. Develop and approve competency standards:
    a. Collaborate with international experts to establish competency standards for key geothermal roles that reflect both local requirements and global best practices.

   b. Organize a thorough review and approval process with multi-sectoral stakeholder involvement to ensure broad industry support and government ratification.
   c. Promptly allocate funding and initiate program development to meet current and future competency needs in the sector.

3. Establish certification and accreditation bodies, or utilize the existing bodies (BNSP):
   a. Designate authoritative bodies to manage the certification process, equipped with the necessary expertise and resources.
   b. Develop accreditation criteria for training programs to maintain consistency and quality across educational and professional development initiatives.
   c. Engage potential certification partners listed in Table 2 and Figure 3, positioning PPSDM KEBTKE as a potential leader under EBTKE supervision.

4. Roll out training and certification program:
   a. Launch targeted training programs to address identified competency gaps, utilizing both local and international resources.
   b. Introduce a certification process that is accessible and mandatory for key personnel in the geothermal sector, with potential providers as shown in Table 2 and Figure 3.

5. Foster industry-academia partnership:
   a. Promote collaborations between geothermal companies and educational institutions to tailor academic programs to industry needs and provide practical experience.
   b. Support joint R&D projects that focus on cutting-edge geothermal technologies and methods.

6. Monitor, evaluate, and iterate:
   a. Set up systems for continuous monitoring and evaluation of the implementation process, using performance indicators to measure progress and impact.
   b. Regularly refine competency standards and training programs based on feedback, technological advancements, and changing industry demands.

As an initial action, the Government of Indonesia could expand PPSDM KEBTKE's certification offerings to include specialized programs across various geothermal disciplines such as exploration, geoscience, drilling, reservoir, and power plant management. This expansion would not only enhance the competency of the geothermal workforce but also position PPSDM KEBTKE as a leader in capacity building and competency assessment within Indonesia's geothermal industry, laying a strong foundation for sectoral growth.

REFERENCES

Ayuningtyas, R., Purba, D., Adityatama, D., Erichatama, N., & Asyari, M. (2023). A Mapping of Various Geothermal Education in Indonesia to Ease Geothermal Personnel Gain Comprehensive Knowledge. World Geothermal Congress 2023. Beijing: International Geothermal Association.

Direktorat Panas Bumi. (2022). Buku Pintar Umum Panas Bumi.

Douglas, J., Stuart, C., & Dwiyudha, H. (2021). Supporting Sustainability in the Indonesian Geothermal Sector Through New Training Methods for Technician and Operators. Proceedings World Geothermal Congress 2020+1. Reykjavik, Iceland.

EBTKE, 2023b. PENGEMBANGAN PANAS BUMI, Jakarta: Direktorat Panas Bumi.

GRG-Geoenergis. (2024). Geothermal Drilling Costs in Indonesia: Statistics, Influencing Factors, Benchmark, and Industry Practices. Jakarta: PT Sarana Multi Infrastruktur (Persero), , GRG, and PT Geoenergi Solusi Indonesia (Geoenergis).

IGA. (2014). Best practices guide for geothermal exploration. Bochum, Germany: International Geothermal Association.

Kantor Berita Antara. (2023, July 13). Indonesia, New Zealand agree to continue geothermal cooperation. Retrieved from en.antaranews.com: https://en.antaranews.com/news/288246/indonesia-new-zealand-agree-to-continue-geothermal-cooperation

Purba, D., Adityatama, D., Asyari, M., Christiantoro, B., Brilian, V., Erichatama, N., Mustika, A., Apriani, D.N.I., Siregar, R. (2024). Drilling Rig Selection for Geothermal Exploration: Evaluating Factors and

Decision-making Criteria. 49th Stanford Geothermal Workshop on Reservoir Engineering. Stanford, California. Retrieved from https://pangea.stanford.edu/ERE/pdf/IGAstandard/SGW/2024/Purba.pdf

Purba, D., Adityatama, D., Fadhillah, F., Asyari, M., Ivana, J., Tiyana, R., Larasati, T., Nugraha, R. (2022). A Discussion on Oil & Gas and Geothermal Drilling Environment Differences and Their Impacts to Well Control Methods. 47th Stanford Geothermal Workshop Reservoir Engineering. Stanford, California. Retrieved from https://pangea.stanford.edu/ERE/pdf/IGAstandard/SGW/2022/Purba.pdf

Purba, D.P., Adityatama, D.W., Nugraha, R. P., Ayuningtyas, R. R., Chandra, V. R., Al-Hassan, M. A., Ramadhan, R. F., Rizqy, M. M. (2021a). Resource Assessment Methods Selection for Geothermal Exploration Project in Indonesia: What Are the Considerations? Proceedings, 46th Workshop on Geothermal Reservoir Engineering, Stanford University, Stanford, California, United States.

Purba, D., Adityatama, D., Siregar, F., Solehudin, M., Asyari, M., Wicaksana, A., Umam, M., Alamsyah, D., Asokawaty, R. (2021). Integrated Stuck-Pipe-Prevention Campaign in Geothermal Drilling Project in Indonesia: A Proactive Approach. World Geothermal Congress 2020+1. Reykjavik: International Geothermal Association. Retrieved from https://www.geothermal-energy.org/pdf/IGAstandard/WGC/2020/21102.pdf

Purba, D.P., Adityatama, D.W., Agustino, V., Fininda, F., Alamsyah, D., and Muhammad, F. (2020). Geothermal Drilling Cost Optimization in Indonesia: A Discussion of Various Factors, Proceedings, 45th Workshop on Geothermal Reservoir Engineering, Stanford University, Stanford, California, United States.

Purba, D.P., Adityatama, D.W., Umam, M.F., and Muhammad, F. (2019). Key Considerations in Developing Strategy for Geothermal Exploration Drilling Project in Indonesia, Proceedings, 44th Workshop on Geothermal Reservoir Engineering, Stanford University, Stanford, California, United States.

Purba, D.P (2018).: Energy 785 Research Project Report: Investigation on Geothermal Resource Assessment Methods in Reducing Exploration Risk in Indonesia Geothermal System. The University of Auckland, New Zealand. Unpublished manuscript.

Poernomo, A. S. (2015). An overview of Indonesia Geothermal Development – Current Status and Its Challenges. Pp. 1 – 11. In: Proceedings of World Geothermal Congress, Melbourne, Australia

ThinkGeoEnergy. (2023). Top 10 Geothermal Countries 2022 – Power Generation Capacity (MW). https://www.Thinkgeoenergy.Com/Thinkgeoenergys-Top-10-Geothermal-Countries-2022-Power-Generation-Capacity-Mw/Amp/. 11 January 2023.

Umam, M., Adityatama, D., & Purba, D. (2018). Tantangan Pengembangan Energi Panas Bumi Dalam Perannya terhadap Ketahanan Energi di Indonesia. Swara Patra, 8(3), 48-65.

Umam, M., Purba, D., Yanuarizky, R., Selia, S., Napitu, A., Hendinata, L., & Ramadhani, I. (2021). Renewable Energy Literacy in Supporting Geothermal Project in Indonesia: Where Are We Now. PROCEEDINGS, 46th Workshop on Geothermal Reservoir Engineering. Stanford, California.

Utami, P. (2010). High-temperature Geothermal Area and its Challenges for Civil Engineering Works. PERTEMUAN ILMIAH TAHUNAN XIV HATTI. Indonesia.

A Framework for Geothermal Drilling Data Integration for Preparing the Development of Geothermal Drilling Database in Indonesia

Dorman Purba[1,3], Desak Nyoman Inten Apriani[1], M. Rizqi Al Asyari[2], Nadya Erichatama[2], Daniel W. Adityatama[2], Ferdino R. Fadhillah[1], and Astri Indra Mustika[1]

[1]PT Sarana Multi Infrastruktur (Persero), Sahid Sudirman Centre, Indonesia
[2]PT Geoenergi Solusi Indonesia (GEOENERGIS), Jakarta, Indonesia
[3]PT ENERKA Bhumi Pratama, Cibis Park, Indonesia

dorman.kons.dpb@ptsmi.co.id; dorman.purba@enerklaz.com

Keywords: geothermal, NPT, database, exploration, regulation, policy, stakeholders, drilling, stuck-pipe, cost, resource, risk, derisking, feasibility, economic, financial, Indonesia

ABSTRACT

In Indonesia, assessing drilling costs and performance is challenging due to the absence of a centralized geothermal drilling database. This stands in contrast to the oil and gas sector, which benefits from established databases like IHS Rushmore. The lack of similar resources in the geothermal sector underscores the need for a more structured approach to data collection and management to better inform decisions and improve operational efficiencies.

This study proposes adopting models like IHS Rushmore from the oil and gas industry, which promote standardized data collection and transparent operational insights. By requiring systematic data submission and encouraging data sharing, this framework aims to improve planning accuracy, reduce drilling costs, and facilitate smoother project execution.

Implementing this system would involve establishing a robust regulatory framework for mandatory data sharing, as well as developing a digital platform accessible to government agencies, developers, and researchers. This platform would enable real-time data analysis, supporting proactive adjustments in drilling operations and strategic decision-making. Furthermore, the database is envisioned as an essential tool for capacity building among governmental bodies and stakeholders, thereby enhancing Indonesia's competitiveness in the global geothermal market.

1. INTRODUCTION

1.1 Geothermal Development Challenges in Indonesia

Indonesia possesses approximately 40% of the world's geothermal reserves, making it one of the most promising countries globally for geothermal energy, with an estimated potential of around 18,000 megawatts (MWe). Despite this significant potential, only about 13% of it is currently utilized, translating to an installed capacity of 2,356 MWe (ThinkGeoEnergy, 2023). This utilization rate is comparatively low when measured against countries like New Zealand, which uses 38% of its potential, and the United States, which utilizes 21% (Asokawaty et al., 2020). To improve this rate, the Government of Indonesia (GoI) aims to achieve 5,486 MWe of geothermal power plant installations by 2030 (Direktorat Panas Bumi, 2022).

Numerous studies and papers have outlined the various challenges faced by the Indonesian government and geothermal developers in advancing geothermal projects (Ibrahim et al., 2005; IGA, 2014; Poernomo, 2015; Darma, 2016; Purba, 2018; Umam et al., 2018; Purba et al., 2019; Purba et al., 2020a; Utami, 2010; Purba et al., 2021a). The exploration phase stands out as the most critical stage in achieving the national geothermal targets.

Achieving Indonesia's geothermal energy goals necessitates collaboration among all stakeholders, including government bodies, geothermal development companies, investors, off-takers, academics, researchers, local communities, and various institutions involved in these projects.

The primary challenges in developing geothermal energy in Indonesia stem from two main factors:

1. The high level of uncertainty about the presence of economically viable geothermal resources (resource risk).
2. The substantial costs associated with drilling activities required to confirm these resources.

Geothermal drilling is widely recognized as a complex and expensive endeavor due to subsurface uncertainties, surface-level challenges, and the involvement of multiple stakeholders, organizations, and equipment (Bodley, 2018; Gul and Aslanoglu, 2018). Poor project management can lead to project failures (Discenza and Forman,

2007). Experts such as Southon and Gorbachev (2003), Kipsang (2015), Bodley (2018), and Otieno (2016) emphasize the critical importance of the planning phase and a thorough understanding of all drilling activities to manage costs effectively. Additionally, Hole (2008) categorizes the cost-driving factors into those that are beyond control and those that can be managed.

1.2 Geothermal Drilling Cost in Indonesia

Geothermal drilling represents a significant portion of total project costs, influenced by geological complexity, drilling depth, and the availability of infrastructure and expertise. Indonesia's geothermal drilling costs are among the highest in the world, primarily due to challenging geological conditions and inadequate local infrastructure for deep drilling operations.

These high drilling costs impact both the economic viability and the overall pace of geothermal development in Indonesia. Reducing these costs through improved efficiency, technology, and data analysis is essential for accelerating geothermal energy development. Given Indonesia's substantial geothermal energy potential, understanding the dynamics of drilling costs is crucial. This section compares Indonesia's geothermal drilling costs with global practices to identify actionable insights for cost optimization.

1.2.1 Global Context of Geothermal Drilling Cost

Geothermal drilling costs vary widely across the globe due to geological, geographical, and market factors. Countries like the Philippines and Indonesia face some of the highest drilling costs per meter, largely due to challenging geological conditions and less developed local supply chains. These variations highlight the need for context-specific cost management strategies and a detailed understanding of each country's unique challenges.

Figure 1 summarizes average drilling costs per meter for geothermal wells in various countries. The Philippines has the highest drilling cost at 4586 USD per meter, followed by Indonesia at 3432 USD per meter. The USA ranks third at 3032 USD per meter. Kenya's costs are 2667 USD per meter, while New Zealand and Iceland have lower costs at 2597 USD and 2376 USD per meter, respectively.

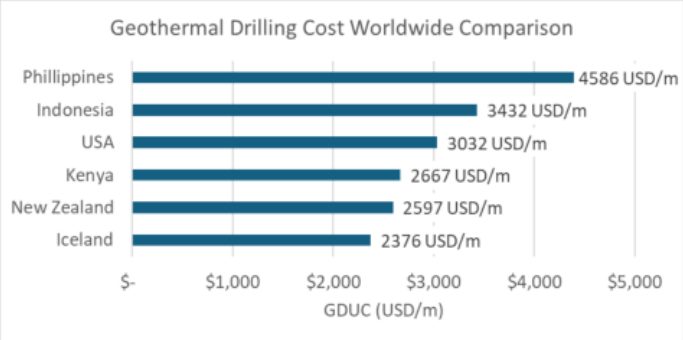

Figure 1: Bar Chart of Average Geothermal Drilling Cost Worldwide (GRG-Geoenergis, 2024).

1.2.2 Indonesia Geothermal Drilling Cost Landscape

In Indonesia, high geothermal drilling costs are driven by well depth, geological complexity, and logistical challenges. Costs increase with well depth due to higher complexity and risk. This relationship underscores the critical nature of well depth in drilling operations.

Geothermal Drilling Unit Cost (GDUC), proposed by Zuhro and Arif (2015), measures drilling performance in USD per meter, allowing cost comparison between wells of different depths. Figure 2 illustrates the GDUC distribution in Indonesia, ranging from 1,300 to 22,000 USD per meter per well. Wells exceeding 7,000 USD per meter are rare outliers. Using the median as a more stable measure, typical drilling costs in Indonesia fall within the interquartile range of 2,733 to 4,549 USD per meter, with a median of 3,432 USD per meter.

The varied well depths in Indonesia reflect a complex drilling landscape where decisions on well depth must balance technical requirements and cost implications. The significant variability in costs highlights diverse operational efficiencies and geological challenges across projects.

Geological hazards, particularly stuck-pipe incidents, contribute to high drilling costs. A PT SMI (2023) study shows these incidents can triple normal drilling costs. Table 1 details the highest drilling costs in Indonesia, with the most expensive well at 29.4 million USD for a 2,160-meter depth, which was non-productive. High costs were largely due to 311.5 hours of Non-Productive Time (NPT) caused by stuck pipes, constituting 27% of the drilling duration and leading to cost overruns. Similar incidents caused the second and third highest costs of 28.4 million USD and 24.1 million USD, respectively.

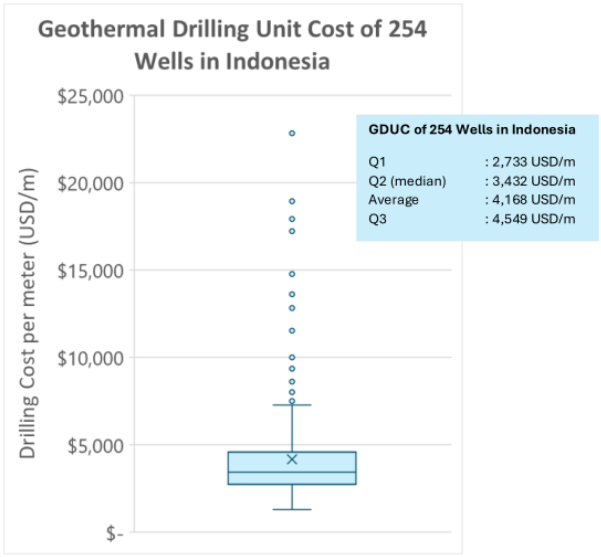

Figure 2: Box Plot of Geothermal Drilling Unit Cost in Indonesia (GRG-Geoenergis, 2024).

Table 1: Outlier Data of the Highest Drilling Cost in Indonesia (GRG-Geoenergis, 2024).

No	Well Name (De-identified)	Well Location	Well Depth (mMD)	Total Drilling Cost (USD)	Drilling Cost per meter (USD/m)	Well Status
1	Highest Well Cost-1	Sumatra	2,160	$29,408,487	$13,615	Non-productive
2	Highest Well Cost-2	Sumatra	1,654	$28,441,465	$17,196	Non-productive
3	Highest Well Cost-3	Sumatra	2,941	$24,110,166	$8,198	Productive
4	Highest Well Cost-4	East Java	2,770	$22,904,286	$8,269	Productive
5	Highest Well Cost-5	Sumatra	3,014	$21,352,215	$7,084	Productive
6	Highest Well Cost-6	Sumatra	2,272	$19,824,782	$8,725	Non-productive
7	Highest Well Cost-7	Sumatra	3,006	$17,559,075	$5,841	Productive
8	Highest Well Cost-8	Sumatra	1,503	$17,335,170	$11,534	Non-productive
9	Highest Well Cost-9	Sumatra	1,253	$17,323,032	$13,825	Non-productive
10	Highest Well Cost-10	Sumatra	2,133	$15,988,860	$7,494	Non-productive
11	Highest Well Cost-11	Sumatra	1,829	$15,938,855	$8,716	Non-productive
12	Highest Well Cost-12	Sumatra	1,668	$15,605,100	$9,356	Productive
13	Highest Well Cost-13	Sumatra	2,500	$15,563,587	$6,225	Non-productive

This data underscores the high-risk nature of geothermal drilling in Indonesia, frequently encountering substantial cost overruns and the risk of no steam production. Preventing stuck-pipe incidents is crucial to managing costs in geothermal projects.

1.3 Problem Statement and Findings

Indonesia holds about 40% of the world's geothermal reserves, with an estimated potential of 18,000 megawatts (MWe). However, only 13% of this potential is currently utilized. High geothermal drilling costs, driven by geological complexity, well depth, and logistical challenges, hinder the economic viability and pace of development. These costs are among the highest globally, worsened by the lack of a standardized, integrated drilling database, which hold back effective cost analysis, strategic planning, and operational efficiency.

There are two significant gaps that geothermal stakeholders in Indonesia need to address for drilling cost optimization:

1. *Lack of Integrated Database and Standardization*: Indonesia's geothermal sector lacks a centralized, integrated database to compile and standardize drilling data across various projects and locations. This absence hinders effective cost analysis, obscures sector-wide performance metrics, and impedes the identification of cost-saving opportunities. Without standardized costing structures, benchmarking against both national and international standards become inaccurate and inefficient.
2. *Data Confidentiality and Publication Scarcity*: The confidential nature of drilling data complicates the landscape, as developers often hesitate to share data due to competitive concerns or proprietary considerations. This results in a scarcity of publicly available information. Additionally, the lack of comprehensive publications on geothermal drilling costs limits the sector's access to valuable insights and learnings. Existing reports often lack detailed cost breakdowns, failing to provide a robust foundation for thorough analysis and informed decision-making.

Drilling constitutes a major portion of the overall cost in geothermal projects, and its optimization is crucial given the high risks associated with operational uncertainties The absence of a centralized database prevents benchmarking, cost optimization, and knowledge sharing among developers, further stalled by the confidential nature of existing data. Geological hazards like stuck-pipe incidents lead to significant cost overruns, underscoring the need for robust data to improve drilling practices and risk management.

To overcome these challenges, a comprehensive framework for geothermal drilling data integration is essential. Establishing a centralized, accessible database will facilitate detailed cost analysis, enhance efficiency through data-driven insights, and promote transparency and collaboration among stakeholders, thereby accelerating the utilization of Indonesia's geothermal potential.

1.4 Study Objectives

This study aims to offer actionable recommendations for establishing standardized regulations for the collection and management of geothermal drilling data. Standardizing these practices will increase data accessibility and transparency, aligning Indonesia with global data management standards such as the IHS Rushmore platform. This alignment will enhance project planning, reduce costs, and improve competitiveness in the global geothermal energy market.

2. ENHANCING DRILLING EFFICIENCY WITH STRATEGIC DATA MANAGEMENT

2.1 Differentiating Data, Information, and Knowledge

Adityatama et al. (2021) provide insights into the definition of data, highlighting that its meaning can vary depending on the source or context. Essentially, data consists of facts, numbers, or other entities that, in isolation, lack context or purpose. To become useful, data must be organized into a coherent format, transforming it into information. This information can then be interpreted, analyzed, and utilized for various purposes such as decision-making and evaluation, thereby evolving into knowledge, as depicted in Figure 3. Without systematic organization into databases or documents, data remains practically unusable.

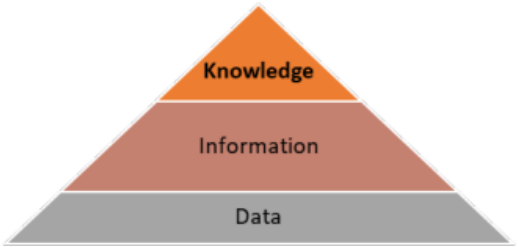

Figure 3: Illustration of data, information, and knowledge (modified from Damski, 2014).

Oracle (2019) defines data management as "the practice of collecting, keeping, and using data efficiently and cost-effectively." However, the scope of data management in drilling operations often remains ambiguous. Some might consider streaming real-time mud logging data from a drilling site to headquarters or storing various data types on company servers as sufficient forms of data management. Damski (2014), however, argues that such practices are insufficient from a business standpoint, as they incur costs without direct returns on investment (ROI). True value from data management emerges only when the information derived from the data informs decisions that enhance the company's business processes, thereby justifying the initial investment.

Moreover, the potential for business intelligence relies on data being readily available and accessible. When data is processed and accessible, the quality of business intelligence or data interpretation can lead to improved drilling programs and more accurate drilling cost estimations. However, learning from past drilling operations is often compromised by the lack of a robust database or data management system, which discourages engineers from

seeking out valuable data. According to Johnson (2002) and Sokovic, Pavletic, & Pipan (2010), the PDCA (Plan, Do, Check, Act) cycle is a vital approach to quality management and continuous improvement in capturing and leveraging drilling data across all stages of a well's lifecycle.

Figure 4: Optimizing Drilling Operations - Leveraging the Lessons Learned Cycle from Historical Drilling Data (Adityatama et al., 2021).

2.2 Utilizing the Lessons Learned Cycle from Historical Drilling Data

Drilling represents a significant portion of the overall costs in geothermal projects, making its optimization crucial due to the high risks associated with operational uncertainties. Enhancing the planning and execution of drilling operations through detailed analysis of historical drilling data is essential (Figure 4).

However, as Iyoho et al. (2004) point out, such analysis is often not conducted as rigorously as it should be. A significant barrier to consistent drilling analysis is the lack of a comprehensive knowledge-based data management system that can effectively integrate and analyze relevant drilling and geological data.

The issue of knowledge retention in the oil and gas industry, particularly within drilling operations, is significant (Sumbal, Tsui, See-to, & Barendrecht, 2017). There exists a notable generation gap among drilling engineers, underscoring the necessity of documenting lessons learned and ensuring knowledge transfer between generations (Damski, 2014). Given these challenges in a well-established sector like oil and gas, it is reasonable to anticipate similar issues in the less-developed geothermal industry. Without detailed records of lessons learned, process descriptions, field knowledge, and comprehensive analyses of previous drilling operations, optimizing or enhancing future drilling plans in the geothermal sector will be challenging, if not unfeasible.

2.3 Learning Curve in Geothermal Drilling

In geothermal drilling, new fields often show less efficient performance, with longer drilling durations, increased Non-Productive Time (NPT), and higher costs. This inefficiency usually decreases as operations continue. The learning curve concept varies significantly by site and operator. Expertise and experience from one location may not transfer effectively to another, even with the same operator. This is especially true when drilling extends to new or unexplored areas with unexpected challenges.

Figure 5 illustrates this pattern at Pertamina Geothermal Energy (PGE) from 2007 to 2011, where an upward trend in the rate of well completion (ROWC) shows growing efficiency. However, the ROWC dropped between 2012 and 2013 due to expansion into new areas and using an unfamiliar contractor.

Understanding the learning curve is crucial for reducing drilling costs. Familiarity with the team's capabilities and equipment, combined with insights from previous drilling in the same area, can reduce NPT, leading to better performance and cost optimization.

2.4 What Is Non-Productive Time (NPT)?

GRG-Geoenergis (2024) defines Non-Productive Time (NPT) as periods when drilling operations are unexpectedly halted or when drilling rates are critically low (Emhanna, 2018). NPT not only affects the timeline but also significantly increases operational costs, making the reduction of NPT crucial for enhancing drilling efficiency and reducing expenses. Originating in the 1960s, various studies and methodologies have since been developed to manage and minimize NPT to acceptable levels (Barakat, et al., 2021). NPT is a primary factor in project delays and cost overruns in drilling projects due to standby charges and penalties related to equipment and personnel (Hsieh, 2010). Figure 6 illustrates a typical NPT breakdown, commonly included in the Final Well Report or End of Well Report.

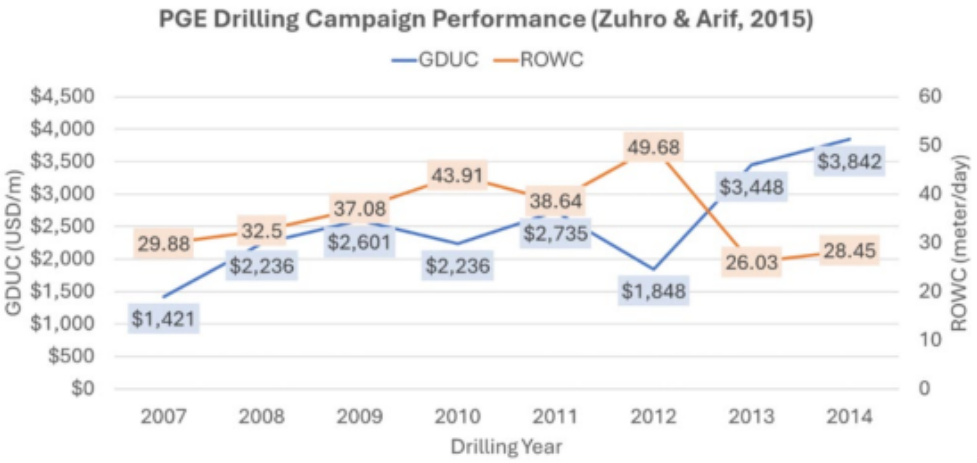

Figure 5: PGE Drilling Campaign Performance (Zuhro & Arif, 2015).

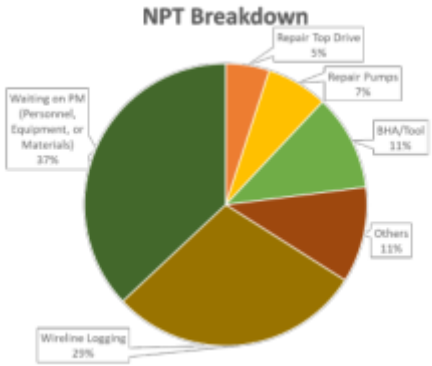

Figure 6: Example of NPT Breakdown in one of Geothermal Field in Indonesia (GRG-Geoenergis, 2024).

Interviews conducted by GRG-Geoenergis (2024) revealed that the highest drilling costs in Indonesia were primarily due to repeated stuck pipe incidents. One well experienced 311.5 hours of Non-Productive Time (NPT), constituting 27% of the total drilling duration, significantly extending the schedule and causing substantial cost overruns. Similar issues contributed to the second and third most expensive wells, costing 28.4 million USD and 24.1 million USD, respectively. These frequent occurrences underscore the inherent risks and high costs in geothermal drilling, highlighting the urgent need for effective stuck pipe prevention strategies to minimize financial losses and improve operational efficiency.

2.5 Potential Problems of Lacking a Standardized Geothermal Drilling Database in Indonesia

The absence of a standardized geothermal drilling database in Indonesia presents several significant potential problems:

1. *Inefficient Cost Management*: Without a centralized database, accurate cost analysis and benchmarking are difficult, leading to higher exploration and development costs as opportunities for cost reduction are harder to identify and implement.
2. *Limited Benchmarking Capabilities*: The lack of standardized and accessible data makes it problematic to compare performance, costs, and best practices across different projects or against international standards, limiting the ability to learn from past projects and improve future operations.
3. *Impaired Strategic Planning*: Strategic decision-making relies heavily on robust data. The absence of a comprehensive database hinders effective planning by the government and developers, potentially delaying new projects and the optimization of existing ones.
4. *Barrier to Research and Development*: Researchers and developers need detailed historical data to innovate and improve geothermal drilling technologies. Without access to such data, the pace of technological advancement and environmental studies in the geothermal sector may slow down.
5. *Regulatory and Policy Challenges*: The government's ability to formulate and enforce regulations that promote efficient and environmentally sustainable geothermal development is compromised without detailed and reliable data.

6. *Transparency and Accountability Issues*: A comprehensive database would enhance transparency by making information available to all stakeholders, including the public. Its absence can lead to accountability issues, making it difficult to trace problems or inefficiencies back to their sources.
7. *Competitive Disadvantage*: On an international scale, the lack of a centralized data system can place Indonesia at a competitive disadvantage compared to countries with robust data infrastructures, potentially affecting foreign investment and collaboration opportunities in the geothermal sector.

2.6 IHS Rushmore: An Oil and Gas Industry Standard in Peer-To-Peer Performance Data Sharing

IHS Markit's Rushmore Reviews, known as IHS Rushmore, is a leading service in the oil and gas industry, offering benchmarking and analysis. Its Drilling Performance Review (DPR) is a global platform, used by over 170 operators from 100 countries for sharing and analyzing drilling data. Known for its accuracy and independent quality control, the DPR includes around 120 data fields. It offers metrics, charting options, and tools like the Rushmore Estimated Drilling Days (REDD) and Rushmore Drilling Index (RDI), covering aspects such as:

1. Well identification.
2. Drilling technical details and methods.
3. Drilling fluid and coring / logging.
4. Hole size, mud, and casings.
5. Time durations including Non-Productive Time (NPT).
6. NPT codes.
7. Costs.
8. Time-depth chart.

The IHS Markit Rushmore Drilling Database (Figure 7) functions as a collaborative, data-driven tool that helps oil and gas companies benchmark their performance, gain insights into industry trends, and make informed decisions to optimize their drilling and completion operations. It has been proven to enhance operational efficiency and strategic planning with its comprehensive data and insights.

Figure 7: Snippet of IHS Rushmore Dashboard (S&P Global, 2022).

3. ESTABLISHING INDONESIA'S GEOTHERMAL DRILLING DATA SYSTEM

3.1 Analyzing the Current State of Indonesia's Geothermal Drilling Costs and Performance

In the pursuit of establishing a standardized framework for geothermal drilling cost structure and performance reporting in Indonesia, it is imperative to scrutinize the prevailing impediments that hinder process efficiency and industry transparency. Several challenges that currently faced by Government of Indonesia (GoI) and related stakeholders for developing drilling database is summarized as follows:

a. The Drilling cost reports submitted by developers have Various Format.
Based on discussion with EBTKE, the format of drilling cost reports/structures submitted by developers to EBTKE is varied. Some cost reports combine several cost/line items, complicating the input into drilling cost databases and hindering consistent, apple-to-apple cost comparisons.

b. Benchmarking and Lesson Learn Extraction Might be Challenging.
The heterogeneity of report formats further presents a challenge in the extraction of lessons learned and the establishment of industry-wide benchmarks. The capacity for a sector to evolve and optimize is contingent upon the systematic collation and analysis of historical data. Due to these inconsistencies in cost reporting, extracting lessons learned or identifying optimal practices by apple-to-apple comparison is more challenging.

c. Lack of a Standardized Costing Structure for Geothermal Drilling in Indonesia.
Indonesia currently doesn't have a standardized way of breaking down the costs of geothermal drilling. Currently, there is no regulation or policy that obligates developers to use a uniform/standard format for submitting drilling cost reports to EBTKE. Unlike the oil and gas sector in Indonesia, which benefits from established Budget Schedules (BS) 19 and 20 as provided and enforced by SKK Migas, the geothermal industry currently lacks a standardized cost structure for drilling. This absence of standardization not only hinders accurate cost estimation for future projects but also complicates comprehensive cost evaluations and analyses. Moreover, not all the BS-19 and BS-20-line item can be applicable with geothermal drilling project. Without a uniform costing framework that is enforced by the government, developers will most likely use their own cost structures when reporting to the government, leading to challenges in comparing costs and performance across various projects from different companies in Indonesia. A consistent framework would enable a detailed breakdown of various costs such as rig and equipment expenses, supporting services, materials, labor, and infrastructure. This level of detail is vital for optimizing costs, effectively managing risks, and developing a more accurate cost estimate. It also facilitates prudent resource allocation and allows for benchmarking against industry standards, which is essential for maintaining project viability and competitiveness.

d. Absence of Obligatory Policy for Cost and Performance Reporting in Geothermal Drilling.
Though the Directorate General of New, Renewable Energy, and Energy Conservation (EBTKE) has recommended the adoption of BS-19 and BS-20 standards for geothermal drilling, developers have not uniformly followed these guidelines. This indicates an absence of obligatory policy or regulation governing such standardizations of cost reporting within the geothermal sector. Additionally, align with WB's concern that not only drilling performance reporting is required to be submitted by geothermal developer, but also it requires to submit supporting information such as well pressure and temperature (P&T) and well output

3.2 Adopting Drilling Cost Reporting Format from Indonesia's Oil and Gas Industry

Indonesia has established standard costing for oil and gas drilling, detailed in Budget Schedules (BS) 19 and 20, as regulated in document PTK-063/SKKMA0000/2017/S (SKK Migas, 2017). These reports are specifically utilized for documenting and reporting drilling costs by the Cooperation Contract Contractors (KKKS) to the Special Task Force for Upstream Oil and Gas Business Activities (SKK Migas). These formats are crucial to the industry's cost recovery mechanism, allowing KKKS to be reimbursed for operational costs incurred in upstream oil and gas activities. Utilization of BS 19 and BS 20 is explained as follow:

1. BS 19 (Budget Schedule 19): This schedule is used to report both tangible and intangible costs associated with drilling, workover, or well services in oil and gas operations. It includes a wide array of costs such as:
    a. Tangible Costs: Expenses on physical items like casing, casing accessories, tubing, and surface and subsurface well equipment.
    b. Intangible Costs: Costs related to non-physical aspects such as drilling preparation and termination, drilling service operations, formation evaluation, completion, and general expenses like project management, permits, and overhead costs.
2. BS 20 (Budget Schedule 20): This schedule complements BS 19 by detailing the material lists that constitute the tangible and intangible costs reported in BS 19. Essentially, BS 20 provides a breakdown of the components that make up the total drilling costs.

These schedules are instrumental in maintaining transparency and accountability in financial reporting within Indonesia's oil and gas sector. By standardizing the cost reporting process, BS 19 and BS 20 ensure that all relevant expenses are duly recorded and reported, facilitating the cost recovery process, and aiding in the efficient financial management of upstream oil and gas activities. Figure 8 show the snippets of BS 19 and BS 20 used in the Indonesian oil and gas industry.

Currently, EBTKE, as the Indonesian government's representative in regulating the geothermal industry, has advised developers to adopt the BS 19 and BS 20 forms from the oil and gas industry for reporting drilling costs, both in the planning and realization stages. However, as discussed in previous sub-section, interviews with EBTKE reveal that not all developers use or submit drilling costs using these formats. One reason EBTKE cannot enforce this practice is that, unlike the oil and gas industry, the geothermal industry in Indonesia does not operate on a cost recovery scheme. In the case of SKK Migas, if an oil company fails to submit cost reports in the prescribed format, SKK Migas has the authority to reject the company's cost recovery requests.

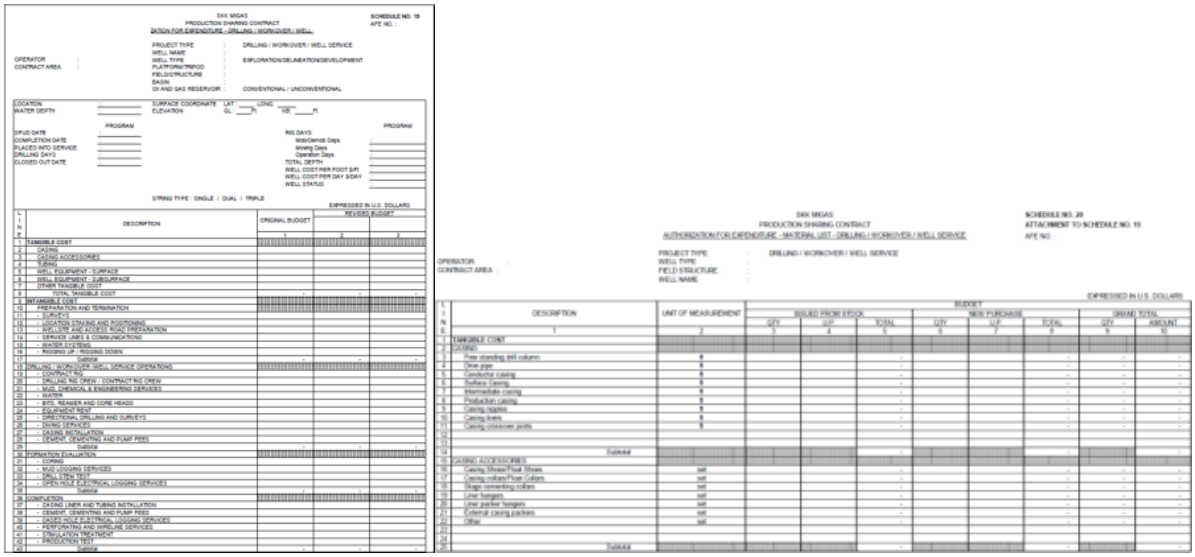

Figure 8: Snippet of Budget Schedule and Report 19 (BS 19) (left) and Budget Schedule and Report 20 (BS 20) (right) (SKK Migas, 2017).

Subsequently, the standard of drilling costing structure of Indonesia's geothermal industry is synthesized according to the geothermal drilling cost components that illustrated in Appendix 1. Proposed Geothermal Drilling Cost Structure Reporting The proposed geothermal drilling cost reporting form is derived from the BS 19 and B20 in the oil and gas industry, the geothermal drilling cost components that have been identified in this study, drilling cost reporting experience from several geothermal developers in Indonesia, and EBTKE's work and budget plan.

3.3 Adopting Drilling Performance Reporting Format from Indonesia's Oil and Gas Industry

In oil and gas industry, after the well is already completely drilled and tested, the oil and gas companies usually are obligated to submit several documents to Special Task Force for Upstream Oil and Gas Business Activities (SKK Migas) for project close-out.

Based on Interview with oil and gas developer company, several drilling-related documents that are obligated to be submitted to SKK Migas after well completely drilled are as follows:

1. End of Well Report (EOWR) / Final Well Report (FWR)
2. Well Post Mortem (excel and pdf document)
   The well memo/postmortem report generally contains the well basic information (well name, AFE number, rig used, spud and complete date, total drilling days, well depth plan vs actual, total planned vs realization well cost), casing program vs actual, time distribution summary, well operation summary, well schematic and completion diagram).
3. Well Form 19-I (excel and pdf document)
   Several contents of this document are like well memo / postmortem report. The Well Form 19-I is the complete version of postmortem report. This document contains such as the breakdown of drilling times (moving days, operation days, and completion days), rig contract name, well cost per foot ($/ft), well cost per day ($/day), breakdown of planned and actual well cost (tangible and intangible cost), summary of bit record, summary of drilling fluid and cement record, well equipment surface and subsurface information, summary of logging tools used and result, documentation of wellhead after completion, non-productive time (NPT) analysis and budget impact, also program changes during operation and budget impact.
4. Recapitulation of Daily Drilling Report (DDR) (excel and pdf document).
5. Final Time Distribution (Final Time Vs Depth Vs Cost) (excel and pdf document).
6. Budget and Realization of Drilling Authorization for Expenditure (AFE) (excel and pdf document).
   The example of well memo/postmortem report, form 19-I, recapitulation of daily drilling report, final time distribution, also budget and realization of drilling authorization for expenditure (AFE) can be found in Appendix 2. Example of Drilling Project Close-out Performance Reporting.

The adoption of such a thorough reporting structure ensures meticulous record-keeping and performance analysis. The well postmortem and form 19-I, for example, provide detailed breakdowns of drilling activities, costs, and

equipment used, allowing for a deep dive into operational efficiencies and financial accountability. Such documents also enable a transparent review of time distribution, operational summary, and a comprehensive comparison of planned versus actual well depth and costs.

By integrating these oil and gas industry practices, geothermal stands to benefit from enhanced project evaluations, facilitating the identification of cost-saving opportunities and efficiency improvements. Moreover, these reports can aid in minimizing non-productive time (NPT) through a detailed analysis of past projects, which can directly lead to a more economically robust and technically sound approach to future drilling endeavors.

The adoption of the drilling performance reporting format used in Indonesia's oil and gas industry signifies a strategic shift towards more disciplined, transparent, and efficient operations within the geothermal sector. It underscores a commitment to continuous improvement, fostering an environment where data-driven decision-making propels the industry forward. The rigorous analysis made possible by these reports will not only bolster the performance of individual projects but also contribute to the broader goal of sustainable and responsible energy development in Indonesia. Thus, this practice is not merely an administrative change but a cornerstone for the future of energy resilience and the optimization of geothermal resources in the country.

3.4 Strategies for Developing Indonesia's Geothermal Drilling Database

Based on the discussion above, several potential ways forward for developing Indonesia's geothermal drilling database can be drawn as follows:

1. **Develop a Standardized Drilling Cost Reporting Format.**
   EBTKE is recommended to establish a standardized reporting format regarding the geothermal drilling cost reporting. Developing standardized drilling cost structure can be done by adopt and modify the established cost structure in Indonesian oil and gas industry (BS 19 and BS 20) and previous drilling cost structure that already submitted by geothermal developers. It will enable a quick cost and performance analysis using common metrics such as: Days per 10k feet drilled (days/10k); USD per meter (US$/m), total NPT (days) and any related analytics that are usually used in geothermal drilling cost analysis.
2. Develop a Standardized Drilling Performance Reporting Format.
   EBTKE is recommended to establish a standardized reporting format for drilling performance benchmarks. Learning from oil and gas industry in Indonesia that already well-established, EBTKE can consider obligating performance reporting for supporting geothermal drilling database with document as follows:
   a. Lesson learns and best practice extraction from:
      - Time Distribution (Drilling Time vs. Depth vs. Cost),
      - Productive Time and Non-Productive (PT & NPT) Time Distribution and Breakdown,
      - Recapitulation of Daily Drilling Report
   b. Summary of Operation in shape of Postmortem Report and Form 19-I document that adjusted for geothermal drilling project.
   c. Additional well information such as well pressure & temperature (P & T), also well output (MW)
3. **Government Enforcement on Cost and Performance Submission**
   There is an alternative that EBTKE can revise or amend current Regulation to mandate/obligate geothermal developers to adhere to the drilling cost and performance reporting format established by EBTKE. It is aimed to ensure transparency and consistency in drilling cost and performance reporting.
4. **Socialization to Key Role of Drilling Team of Geothermal Developers**
   Socialization related to the drilling cost structure and reporting format that is already standardized to geothermal developer is important. Proper socialization will increase geothermal developers' awareness of the new policy. Several key roles that must be invited during the socialization are Drilling Manager, Drilling Engineer, Drilling Cost Control, Performance Engineer, and any other related role that manages drilling data reporting and analysis in geothermal developer.
5. **Annual analysis and public disclosure.**
   Perform deep analysis on the drilling data annually using independent consultants and release to public according to the current regulation.
6. **Annual Geothermal Drilling Best Practice Sharing Session**
   The annual geothermal drilling best practice sharing session plays a crucial role in facilitating knowledge exchange and collaboration between regulators, geothermal developers, and service companies. It serves as a vital platform for sharing experiences, addressing recent drilling experiences, and promoting

innovation and efficiency in drilling practices. Such collaboration is essential for enhancing operational safety, reducing risks, and optimizing drilling cost.

Moreover, these sessions contribute significantly to the sustainable development of the geothermal sector by fostering the adoption of environmentally responsible drilling practices. They aid in skill development, ensure compliance with regulatory standards, and support the industry's commitment to sustainable energy development, benefiting not only the companies involved but also the broader community and environment.

The impact of the proposed way forward to geothermal drilling industry can lead to the cost and drilling performance reports submitted by geothermal developers to EBTKE will have a uniform/ standardized format. A standardized drilling cost structure format and performance reporting format used and followed by developers for reporting to EBTKE might be led to easier database entry and enable apple-to-apple analysis for performance benchmarking of each drilling project.

The standardized drilling cost and performance reporting also can be useful for extracting the lesson learn and best practices to optimize drilling preparation and operation among geothermal developers in Indonesia.

3.5 Implementation Framework

The development of a comprehensive geothermal drilling database is a multifaceted endeavor requiring thorough planning and execution. The following steps outline a strategic approach to creating this vital resource, ensuring it meets the industry's needs and adheres to best practices in data management.

3.5.1 Technical Specifications and Data Collection Protocols

To initiate the project for developing a geothermal drilling data database in Indonesia, the first step is to create a repository where this data will be stored. This can be done as follows:

1. Database Architecture: Develop a robust database architecture that can handle large volumes of data, ensuring scalability and ease of access. Define the technical specifications based on industry standards and specific requirements of the Indonesian geothermal sector. Figure 9 presents a simplified flowchart illustrating how drilling data is integrated into the database.

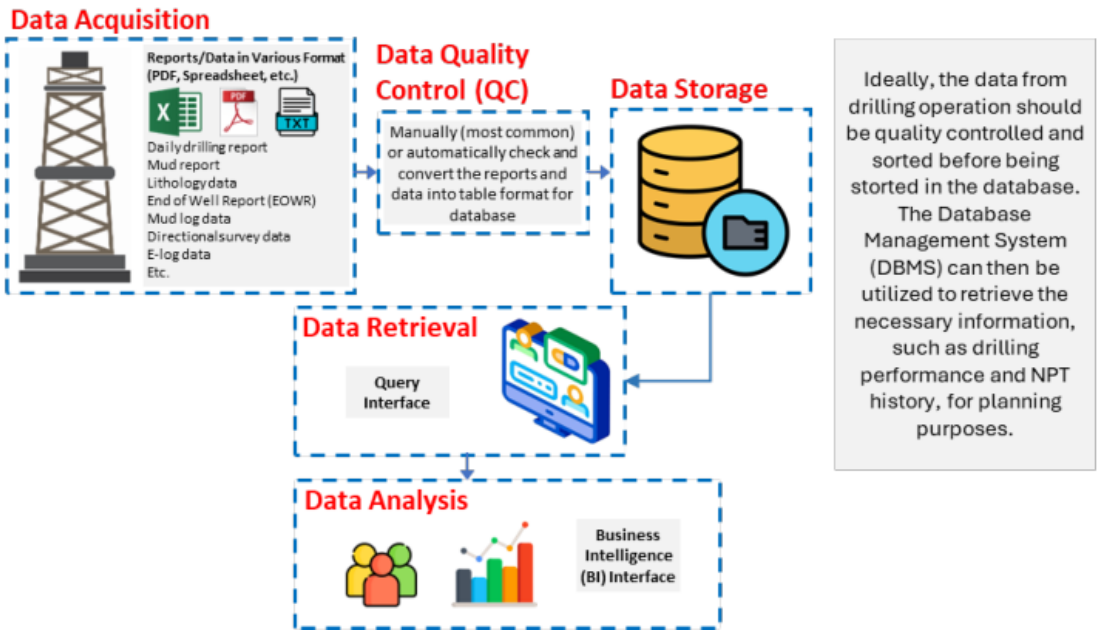

Figure 9: Illustration of Drilling Data Management (modified from Adityatama, 2021).

2. Data Standardization: Establish standardized formats and protocols for data submission to ensure consistency and comparability across different data sets.
    a. This includes defining key data fields, units of measurement, and classification schemes. The types of data that must be standardized and submitted to the Government of Indonesia can be agreed upon by forming a special Task Force comprised of representatives from geothermal developers, academia, drilling contractors, and drilling consultants.
    b. For the implementation of the pilot project database, where the actual cost is low, uncomplicated, and does not require extensive resources, we can utilize simple existing software such as Excel and Power BI (Figure 10).

c. Regarding data cleansing, it can be delegated to developers using a standardized data submission format provided by EBTKE. Consequently, developers are responsible for cleansing and formatting their drilling data before submission to EBTKE. Subsequently, an independent consultant can periodically (twice a year or annually) check the data accuracy through random sampling.

3. Data Collection and Submission: Implement secure and user-friendly mechanisms for data collection and submission. Encourage geothermal developers to contribute data by demonstrating the mutual benefits of shared insights and sector-wide improvements.

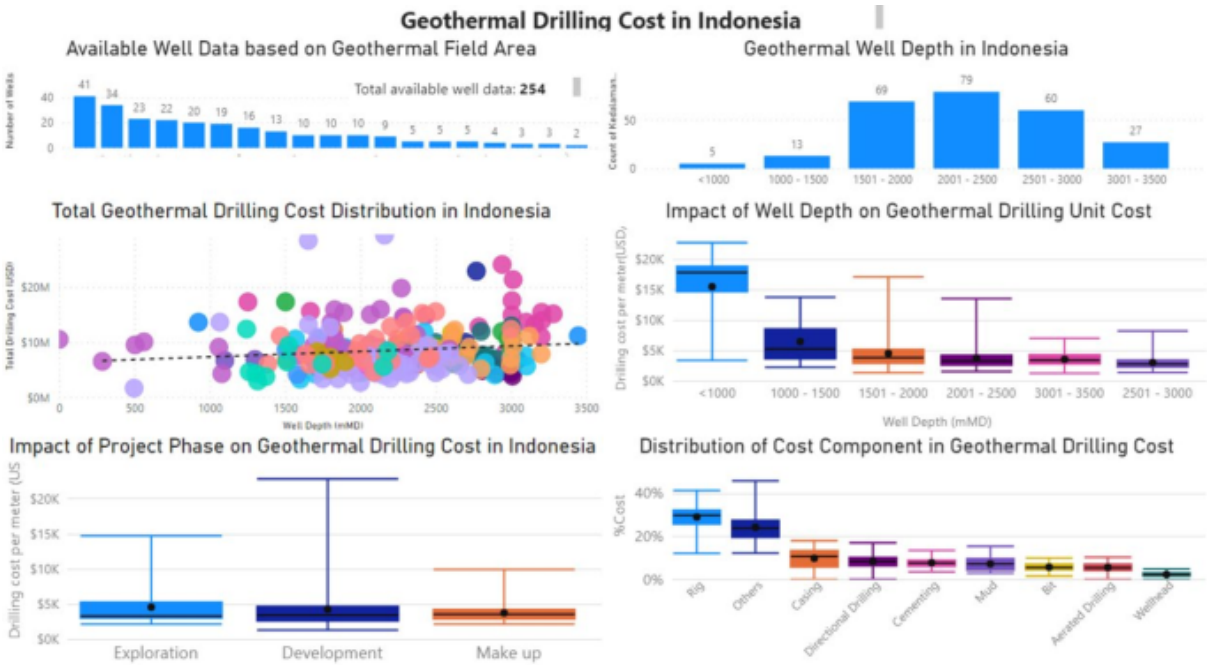

Figure 10: Example of utilization of simple existing software such as Excel and Power BI for geothermal drilling database pilot project.

3.5.2 Phased Integration Approach

Once the repository for data storage and retrieval is available, a small-scale pilot program should be conducted to test the system. This can then be gradually scaled up to involve more data incrementally:

1. Pilot Program: Initiate database development with a pilot program focusing on a specific region or subset of geothermal projects. This approach allows for the identification of potential issues and enables iterative improvements based on user feedback and initial outcomes.
2. Expansion and Scale-Up: Following the successful implementation of the pilot program, gradually expand the database to include additional regions and projects. This phased expansion facilitates continuous learning and adaptation, ensuring the database evolves to meet the sector's changing needs.

3.5.3 Government Leadership and Stakeholder Engagement

Given that all drilling data collected in the integrated database will be owned by the Government of Indonesia, the government will assume the role of coordinator for this initiative:

1. Government Coordination: Emphasize the crucial role of government bodies, particularly EBTKE, in leading and coordinating this initiative. Government leadership is essential for setting policy directions, mobilizing resources, and fostering collaboration across different stakeholders.
2. Stakeholder Engagement: Engage a broad spectrum of stakeholders, including geothermal developers, regulatory bodies, academic institutions, and industry associations, to ensure the database reflects diverse perspectives and needs. Active stakeholder engagement is key to building consensus, encouraging data sharing, and maximizing the database's utility and impact.
3. Resource Allocation: Advocate for the allocation of necessary resources, including funding, technical expertise, and administrative support, to facilitate the successful development and operation of the database.

3.5.4 Training and Capacity Building

1. Training Programs: Implement targeted training programs for all stakeholders involved in data submission and usage to ensure they are proficient in utilizing the database effectively. This includes training on how to input data, how to interpret the data outputs, and how to use the data for decision-making.
2. Capacity Building: Develop workshops and seminars that help build the necessary skills for database management, data analysis, and strategic use of data in geothermal development.

3.5.5 Legal and Regulatory Framework

1. Data Privacy and Security Protocols: Establish clear guidelines on data privacy, focusing on the protection of sensitive information and compliance with international data protection regulations.
2. Regulatory Support: Work with legislative bodies to create supportive policies that mandate data sharing among geothermal developers and define penalties for non-compliance, ensuring that data collection becomes a routine practice in the industry.

3.5.6 Continuous Improvement and Adaptation

1. Feedback Mechanism: Set up a structured feedback mechanism that allows users to report issues, suggest improvements, and adapt the database to better meet their needs over time.
2. Regular Updates and Maintenance: Ensure the database is regularly updated with new data, features, and security measures to keep it relevant and useful.

3.5.7 Marketing and Communication Strategy

1. Promotion Plan: Develop a comprehensive plan to promote the benefits and successes of the database to encourage wider adoption and utilization across the industry.
2. Stakeholder Communication: Maintain regular communication with all stakeholders through newsletters, updates, and forums to keep them informed about the database's progress, benefits, and ways to contribute.

4. DISCUSSION

Indonesia's geothermal energy development faces significant delays due to the absence of an integrated drilling data database, which severely impacts cost analysis, strategic planning, and operational efficiency. The lack of standardized data collection and the confidential nature of existing data restrict public access and detailed analysis. This situation delays collective learning among geothermal developers, especially new entrants, as they cannot benefit from the challenges and experiences of established developers in similar projects.

This lack of shared knowledge leads to inefficient planning and execution of drilling projects, inflating costs detrimentally for Indonesia. Unlike global practices where platforms like IHS Rushmore enable data sharing and foster innovation, the absence of a similar system in Indonesia stifles benchmarking and internal efficiencies. Establishing a unified database is essential to enhance transparency, enable effective cost management, and boost the competitiveness of Indonesia's geothermal industry.

This paper has provided actionable recommendations to establish standardized regulations for the collection and management of geothermal drilling data. Such standardization would increase data accessibility and transparency, aligning Indonesia with global data management practices like the IHS Rushmore platform, thereby enhancing project planning, reducing costs, and boosting competitiveness in the global geothermal energy market.

The proposed integrated data framework is designed to resolve data access challenges and harmonize data reporting, thus enabling robust cost analysis and sector-wide benchmarking.

By institutionalizing these measures within the geothermal sector, Indonesia can significantly enhance its geothermal drilling cost analysis and optimization, reinforcing its position as a leader in global geothermal energy development. This initiative calls for a united front from all sector stakeholders to champion data-driven improvements, leveraging Indonesia's geothermal potential to its fullest in a sustainable and economically viable manner.

Implementing this integrated data framework presents several challenges that need to be addressed. Firstly, establishing standardized data collection protocols across various stakeholders requires significant coordination and agreement, which can be time-consuming and complex. Secondly, ensuring data confidentiality while promoting transparency and data sharing poses a delicate balance that must be carefully managed to maintain trust among developers. Thirdly, the initial costs of setting up the database infrastructure and training personnel may be substantial, requiring strong financial and institutional support. Lastly, there may be resistance to change from stakeholders accustomed to existing practices, necessitating effective communication and advocacy to

demonstrate the long-term benefits of the new system. Overcoming these challenges will be crucial for the successful implementation and sustainability of the geothermal drilling database in Indonesia.

In conclusion, addressing the current gaps in data integration and standardization is crucial for Indonesia to fully realize its geothermal potential. A collaborative effort among government bodies, developers, academia, and industry professionals is necessary to implement a robust and transparent geothermal drilling database. This will not only streamline operations and reduce costs but also foster innovation and ensure Indonesia's competitive edge in the global geothermal market. By committing to these improvements, Indonesia can pave the way for a more efficient, cost-effective, and sustainable geothermal energy sector.

REFERENCES

Adityatama, D., Purba, D., Marza, S., Muhammad, F., Asokawaty, R., Kusumawardani, R., & Mukti, A. (2021). The Significance of Drilling Data Management to Improve Geothermal Drilling Planning and Operation in Indonesia. *World Geothermal Congress 2020+1*. Reykjavik. Retrieved from https://www.geothermal-energy.org/pdf/IGAstandard/WGC/2020/21082.pdf

Asokawaty, R. F., Purba, D. P., Adityatama, D. W., Muhammad, F., & Umam, M. (2020). Indonesia's Geothermal Development Comp are to World Top Geothermal Producers. *45th Workshop on Geothermal Reservoir Engineering*.

Barakat, M., Ela, M. A. E. & Khalaf, F., 2021. Integrating risk management concepts into the drilling non-productive time, s.l.: *J Petrol Explor Prod Technol* 11, 887–900.

Bodley, C., 2018. *Project Planning for Geothermal Exploration Drilling in Saint Lucia*, Reykjavik: United Nations University Geothermal Training Programme (UNU-GTP).

Damski, Carlos. 2014. *Drilling Data Vortex: Where the bits meet the bits*. Australia: Genesis Publishing and Services Pty Ltd.

Darma, S. (2016). *Indonesia: Vast geothermal potential, modest but growing exploitation*. In Geothermal Power Generation: Developments and Innovation (pp. 609–643). Elsevier Inc. https://doi.org/10.1016/B978-0-08-100337-4.00021-8

Direktorat Panas Bumi. (2022). *Buku Pintar Umum Panas Bumi*.

Discenza, R. & Forman, J. B., 2007. *Seven Causes of Project Failure: How to Recognize Them and How to Initiate Project Recovery*, Atlanta: PMI® Global Congress 2007.

Emhanna, S., 2018. Analysis of Non-Productive Time (NPT) in Drilling Operations- A Case Study of the Ghadames Basin, s.l.: *Second Scientific Conference of Oil and Gas* Feb 5-7 / 2018 Ajdabiya - LibyaAt: Ajdabiya – Libya.

GRG-Geoenergis. (2024). *Geothermal Drilling Costs in Indonesia: Statistics, Influencing Factors, Benchmark, and Industry Practices*. Jakarta: PT Sarana Multi Infrastruktur (Persero)

Gul, S. & Aslanoglu, V. (2018). *Drilling and Well Completion Cost Analysis of Geothermal Wells in Turkey*. Stanford, s.n., pp. 1-20.

Halliburton (2021). Halliburton. s.l., *Halliburton Project Management (HPM)*.

Hsieh, L., 2010. Rig NPT – *The Ugly Truth*, s.l.: Drilling Contractor Magazine, International Association of Drilling Contractors (IADC).

Ibrahim, R. F., & Fauzi, A, Suryadarma. (2005). The progress of geothermal energy resources activities in Indonesia. Paper presented at the *Proceeding World Geothermal Congress 2005*, 1-7.

IGA. (2014). *Best practices guide for geothermal exploration*. Bochum, Germany: International Geothermal Association.

Iyoho, A. W., K. K. Millheim, B. K. Virginillo, A. R. Adeleye, and M. J. Crumrine. (2004). "Methodology and Benefits of a Drilling Analysis Paradigm." IADC/SPE *Drilling Conference 2004*. Dallas, Texas: SPE International.

Iyoho, A. W., R. A. Meize, K. K. Millheim, and M. J. Crumrine. (2005). "Lessons from Integrated Analysis of GOM Drilling Performance." *Offshore Technology Conference* 200. Houston: SPE International.

Johnson, C. N. 2002. "*The benefits of PDCA*." Quality Progress (Proquest) 35 (5). https://search.proquest.com/openview/6fb24b731a9c0c8bafd90096fd751e76/1?pq-origsite=gscholar&cbl=34671.

Kipsang, C.: Cost Model for Geothermal Wells, *PROCEEDINGS World Geothermal Congress*, (2015).

ORACLE. 2019. "*What is Data Management?*" ORACLE. Accessed June 5, 2019. https://www.oracle.com/database/what-is-data-management/.

Otieno, P. K. O.: Impact of Drilling Equipment Quality Condition and Expertise Availability on Well Drilling Cost – A Case Study of Olkaria Geothermal Field. *Proceedings 6th African Rift Geothermal Conference in Ethiopia*, (2016).

Poernomo, A. S. (2015). An overview of Indonesia Geothermal Development – Current Status and Its Challenges. Pp. 1 – 11. In: *Proceedings of World Geothermal Congress*, Melbourne, Australia

Purba, D., Adityatama, D., Asyari, M., Christiantoro, B., Brilian, V., Erichatama, N., Mustika, A., Apriani, D.N.I., Siregar, R. (2024). Drilling Rig Selection for Geothermal Exploration: Evaluating Factors and Decision-making Criteria. *49th Stanford Geothermal Workshop on Reservoir Engineering. Stanford, California*. Retrieved from https://pangea.stanford.edu/ERE/pdf/IGAstandard/SGW/2024/Purba.pdf

Purba, D., Adityatama, D., Fadhillah, F., Asyari, M., Ivana, J., Tiyana, R., Larasati, T., Nugraha, R. (2022). A Discussion on Oil & Gas and Geothermal Drilling Environment Differences and Their Impacts to Well Control Methods. *47th Stanford Geothermal Workshop Reservoir Engineering. Stanford, California*. Retrieved from https://pangea.stanford.edu/ERE/pdf/IGAstandard/SGW/2022/Purba.pdf

Purba, D.P., Adityatama, D.W., Nugraha, R. P., Ayuningtyas, R. R., Chandra, V. R., Al-Hassan, M. A., Ramadhan, R. F., Rizqy, M. M. (2021a). Resource Assessment Methods Selection for Geothermal Exploration Project in Indonesia: What Are the Considerations? *Proceedings, 46th Workshop on Geothermal Reservoir Engineering*, Stanford University, Stanford, California, United States.

Purba, D., Adityatama, D., Siregar, F., Solehudin, M., Asyari, M., Wicaksana, A., Umam, M., Alamsyah, D., Asokawaty, R. (2021). Integrated Stuck-Pipe-Prevention Campaign in Geothermal Drilling Project in Indonesia: A Proactive Approach. *World Geothermal Congress 2020+1*. Reykjavik: International Geothermal Association. Retrieved from https://www.geothermal-energy.org/pdf/IGAstandard/WGC/2020/21102.pdf

Purba, D.P., Adityatama, D.W., Agustino, V., Fininda, F., Alamsyah, D., and Muhammad, F. (2020). Geothermal Drilling Cost Optimization in Indonesia: A Discussion of Various Factors, *Proceedings, 45th Workshop on Geothermal Reservoir Engineering*, Stanford University, Stanford, California, United States.

Purba, D.P., Adityatama, D.W., Umam, M.F., and Muhammad, F. (2019). Key Considerations in Developing Strategy for Geothermal Exploration Drilling Project in Indonesia, *Proceedings, 44th Workshop on Geothermal Reservoir Engineering*, Stanford University, Stanford, California, United States.

Purba, D.P (2018).: Energy 785 Research Project Report: *Investigation on Geothermal Resource Assessment Methods in Reducing Exploration Risk in Indonesia Geothermal System*. The University of Auckland, New Zealand. Unpublished manuscript.

SKK Migas. (2017). *Pedoman Tata Kerja Tentang Financial Budget and Reporting Manual of Production Sharing Contract dan Chart of Account*. Jakarta, Indonesia: PTK-063/SKKMA0000/2017/S0.

Sokovic, M., D. Pavletic, and K. K. Pipan. 2010. "Quality Improvement Methodologies - PDCA Cycle, RADAR Matrix, DMAIC and DFSS." *Journal of Acheivements in Materials and MAnufacturing Engineering* (International OCSCO World Press) 43 (1).

Sumbal, M. S., E. Tsui, E. See-to, and A. Barendrecht. 2017. "Knowledge retention and aging workforce in the oil and gas industry: a multi perspective study." *Journal of Knowledge Management* (Emerald) 21 (4): 907-924. doi:10.1108/JKM-07-2016-0281.

ThinkGeoEnergy. (2023). *Top 10 Geothermal Countries 2022* – Power Generation Capacity (MW). https://www.Thinkgeoenergy.Com/Thinkgeoenergys-Top-10-Geothermal-Countries-2022-Power-Generation-Capacity-Mw/Amp/. 11 January 2023.

Umam, M., Adityatama, D., & Purba, D. (2018). Tantangan Pengembangan Energi Panas Bumi Dalam Perannya terhadap Ketahanan Energi di Indonesia. *Swara Patra*, 8(3), 48-65.

Utami, P. (2010). *High-temperature Geothermal Area and its Challenges for Civil Engineering Works*. PERTEMUAN ILMIAH TAHUNAN XIV HATTI. Indonesia.

Zuhro, A. A. & Arif, G. R. (2015). Pertamina Geothermal Energy Drilling Campaign. s.l., *World Geothermal Congress 2015*.

Thermoelectric Generator Application for Low-Temperature Geothermal Resources in Steam Field

Mochammad Ibrahim Agam, Alfian Rangga, Dyah Intan, and Hafid Agil

PT Star Energy

mochammad.ibrahimagam@starenergy.co.id, alfian.ranggapradhivatama@starenergy.co.id, dyah.intanartika@starenergy.co.id, hafid.agilnugroho@starenergy.co.id

Keywords: sump pit, lighting, thermoelectric generator (TEGs), condensate, low enthalpy resources, steam field, waste heat, energy efficiency

ABSTRACT

Geothermal power plant uses steam to generates power, the steam was exploited from steam field around the power plant, and because of the long distance piping system, steam tends to lose it temperature gradually and undergo phase changes to water, this water will usually be collected automatically from automatic drain pot (ADP) and will be streamed directly into sump pit located in well pad area. Collected condensate still has low enthalpy, and usually this heat is wasted through the air, heat also wasted at flange through which is not covered by pipe isolation to cover the heat. Applying Thermoelectric generation technology provides a solid-state solution for the direct conversion of thermal energy into electricity. This approach stands in contrast to traditional methods that rely on mechanical work, offering a unique advantage with thermoelectric power converters (TEG) that are devoid of moving parts. This results in a compact, silent, reliable, and eco-friendly power solution. This idea is to harness the potential of thermoelectric generators to tap into the low-enthalpy thermal energy present in each sump pit within a steam field. This power generation system employs TEG modules, fabricated using cost-effective methods, to achieve superior efficiency in converting thermal energy to electricity. The electricity generated from this system is intended for lighting in local well pad, and public street. Our findings underscore the promise of thermoelectric generation technology in enhancing energy efficiency and sustainability.

1. INTRODUCTION

In the realm of renewable energy, geothermal power plants have long been recognized for their potential to generate electricity using the Earth's natural heat. However, the efficiency of these systems is often compromised by the loss of thermal energy during the transportation of steam from the steam field to the power plant. This paper aims to address this issue by introducing an innovative approach that harnesses the wasted thermal energy to generate electricity. The focus of our study is the application of Thermoelectric Generation (TEG) technology, a solid-state solution that directly converts thermal energy into electricity. Unlike traditional methods that rely on mechanical work, TEG offer a unique advantage as they are devoid of moving parts, resulting in a compact, silent, reliable, and eco-friendly power solution. Our research explores the potential of TEG to tap into the low-enthalpy thermal energy present in each sump pit within a steam field, and uncovered flange along the existing main steam piping. We employ TEG modules, fabricated using cost-effective methods, to achieve superior efficiency in converting thermal energy to electricity. The electricity generated from this system is intended for lighting in local well pad and public streets, thereby enhancing energy efficiency and sustainability. This paper presents our findings and underscores the promise of thermoelectric generation technology in enhancing energy efficiency and sustainability in geothermal power plants. We believe that our research will contribute significantly to the ongoing efforts to optimize the use of renewable energy sources and pave the way for more sustainable and efficient power generation systems.

2. MATERIALS AND METHOD

This experiment uses a simple method to demonstrate the potential for generating electricity from TEG. The test is carried out directly by placing the TEG module on the waste heat source that has been collected in the sump pit to simulate the generation potential, using three TEG panels connected in series. The waste heat source is hot water condensate collected in the sump pit from the steam line, the hot side of the module will be installed directly around the condensate pipe, and for cooling will use cold air directly from the surrounding environment, which will pass through the cold side of the module through the heat sink. Thermal paste is used to ensure that the hot and cold temperatures in the module are evenly distributed. The TEG panel will convert ΔT from both sides of the module into DC voltage that can be used to charge the battery, and also to light the lights through the inverter. It is hoped that it can reduce electricity infrastructure bills in the future. This TEG has three main parts, including: 1. TEG Module, 2. Heat Sink, 3. Spacer.

2.1 TEG Module

The module used in this experiment is made of ceramic/Bismuth Telluride (Bi2Te3) as shown in Figure 1. This module was chosen because it is easily available on the market and its price is quite affordable. The specifications of this module can be seen in Table 1. These modules will be arranged in series, with a distance between modules of 20 mm and a distance between the module and the heat source of 0.2 mm which will be limited by using an aluminum spacer.

Table 1: TEG Module Spesification.

Specification	Value
Material	Ceramic / Bismuth Telluride (Bi_2Te_3)
Model Number	SP1848-27145
Maximum Temperature (°C)	150
Open Circuit Voltage (v)	4.8
Color (mm)	White
Width (mm)	40
Length (mm)	40
Height (mm)	4
Weight (gm)	30

Figure 1: TEG Module.

Figure 2: Heat Sink.

2.2 Heat sink

The material of the heat sink is aluminum which possessed light weight and good thermal conductivity. This heat sink was cut according to the TEG module size, to properly mount at the surface of module cold side. Thermal paste was applied between the heat sink and module cold side to insure cooling distribution spread evenly.

2.3 Spacer

The spacer is an aluminum component which is used to maintain the gap between TEG module hot side and the heat source, so the TEG does not directly stick to the heat source. It also will help to distribute the heat spread evenly on the hot side by applying thermal paste.

This TEG panel has a simple construction and has aluminum material that can transfer heat easily to the heat sink on the cold side, and the spacer on the hot side. this will simplify maintenance and the relocation process if necessary.

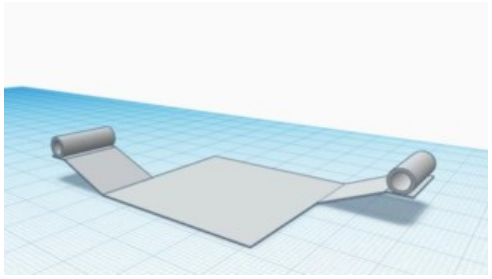

Figure 3: Spacer.

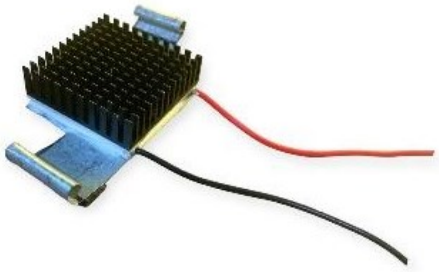

Figure 4: TEG Panel Assembly.

2.4 Proposed 3 TEG Panel

As in figure 5. The TEG panels will be connected in series. The heat source comes from the zero discharge condensate pipe, while for cooling it will use passive cooling from the surrounding air that will pass through the heat sink. On the hot and cold sides of the module will use thermal paste to help even out the temperature distribution.

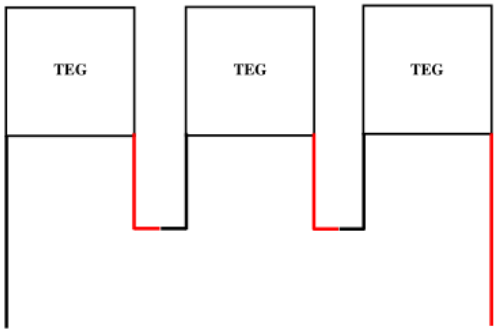

Figure 5: Schematic diagram of 3 TEG panel.

2.5 TEG System Efficiency

The Seebeck effect uses temperature differences to generate electricity in thermoelectric devices built from the junction of two materials. Temperature differences can be converted into other types of energy through several technologies (Esen et al., 2012). Any device that converts temperature differences into energy has a Carnot efficiency as a fundamental limit. Using the Carnot efficiency which can be calculated using equation (1) below (G. Kumar et al., 2017). With Th and Tc, respectively, representing the hot and cold temperatures that form the temperature difference.

$$\eta c = \frac{\mathrm{Th} - \mathrm{Tc}}{\mathrm{Th}} \tag{1}$$

3. RESULTS AND DISCUSSION

3.1 Effect of Passive Cooling and Heating Method on The Temperature Difference of 3 TEG Panel

Heating and cooling of the appropriate thermoelectric material will increase the efficiency, the method is passive or active (B. Pfeiffelmann et al., 2021). In this experiment, passive cooling is used which utilizes the surrounding air directly, but the results of this passive cooling have large thermal resistance and have a negative impact on the power output. From the three TEG panels that were tested experimentally starting at 17:00 and lasting for 2 hours, it can be seen that at the beginning of the experiment (Tc) was at 16^{o}C, which then increased due to the influence

of (Th), after some time and reached a stable condition at 56 °C. The hot side (Th) and cold side (Tc) temperatures are in Figure 6.

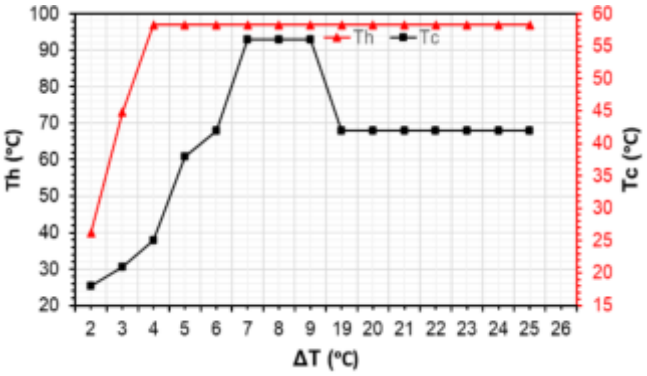

Figure 6: ΔT, Th, Tc of a 3 TEG panel.

3.2 Performance of 3 TEG Panel

The voltage generated at the terminal with ΔT across the TEG module is shown in Figure 7. From this figure it can be seen, at the beginning of the experiment, the open circuit (Voc) is 0 v, and rises to 9.81 v, then stabilizes at 5.73 v. This shows that the output voltage is proportional to ΔT.

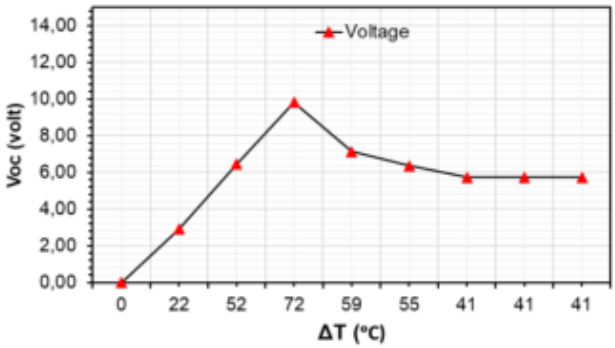

Figure 7: Open circuit voltage of 3 TEG panel.

3.3 Carnot Efficiency of TEG Panel

TEG shows the Carnot efficiency at various values of ΔT determined using equation (1) the results of which can be seen in figure 9. The Carnot efficiency (ηc) of the TEG module depends on the temperature of the hot and cold sides of the module which has an average of 1.29%.

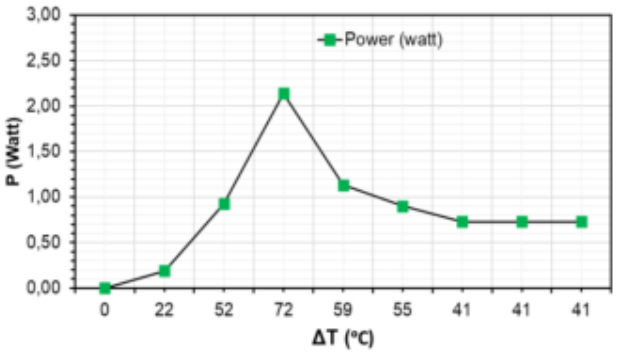

Figure 8: Power of 3 TEG panel vs ΔT.

3.4 System Implementation Cost Estimation and Economic Analysis

Economic analysis and cost assessment for system installation are two important considerations of the project (Awan et al., 2022). This section estimates the cost of a 3 TEG panel from its key component, as shown in table 2.

This experimental TEG panel was built with cheap material because it only aims to show potential of opportunities for power generation from low enthalpy resource in steam field that could be used as an option for future electrical infrastructure.

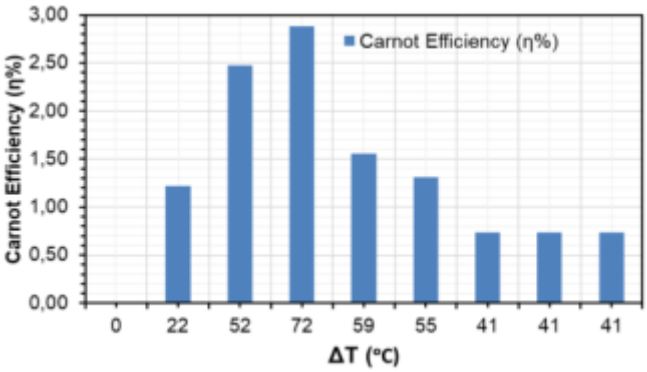

Figure 9: Carnot Efficiency of 3 TEG panel.

Table 2: Component costs of TEG Panel.

Component	Cost (idr)
TEG Module	35.000
Heat Sink	12.000
Spacer	5000

4. CONCLUSION AND FUTURE WORK

From this experiment, it can be concluded that the TEG panel is able to produce power and voltage that can be utilized later for lighting purposes in the local area and can also be used as an option to cut the cost of pulling cables for electricity needs in the local area. With low implementation costs, this approach can be recommended for a cheap and efficient electrical system. In the future, to generates more power, applying active cooling and heating method to increase and control ΔT, and use larger number of TEG modules is recommended. Furthermore, applying ten check algorithms might help to improve the performance of TEG panel (Awa Afzal et al., 2018).

REFERENCES

Awa Afzal Awan, Muhammad M., and Tahir Mahmood. 2018. "A Novel Ten Check Maximum Power Point Tracking Algorithm for a Standalone Solar Photovoltaic System" Electronics 7, no. 11: 327. https://doi.org/10.3390/electronics7110327

Awan, Muhammad M.A., Muhammad Y. Javed, Aamer B. Asghar, Krzysztof Ejsmont, and Zia-ur-Rehman. 2022. "Economic Integration of Renewable and Conventional Power Sources—A Case Study" Energies 15, no. 6: 2141. https://doi.org/10.3390/en15062141.

B. Pfeiffelmann, A.C. Benim, F. Joos, "Water-Cooled Thermoelectric Generators for Improved Net Output Power: A Review", Energies, Vol. 14, pp. 1-29, 2021.

Esen, Dilek Ozlem, Elif Balta, and Aykut Kaman. "An experimental investigation of thermoelectric cooling with solar panel." In 2012 International Conference on Renewable Energy Research and Applications (ICRERA), pp. 1-6. IEEE, 2012.

G. Kumar, and S.K. Pandey, "Efficiency calculation of thermoelectric generator by extracting waste heat, for practical applications", Journal of Renewable and Sustainable Energy, Vol. 7, No. 1, pp. 1-4, 2017.

The Impact of Geothermal Coffee Process (GCP) As an Empowered Community of PT. Pertamina Geothermal Energy Tbk. AG Kamojang On the Development of Renewable Energy Discourse Among the Society

Ovinda Hariyesa, Muhammad N. Fauzan, Andre Mathew, and Dyah H. Kinanthi

PT Pertamina Geotherma Energy Tbk. Area Kamojang, West Java, Indonesia 40383

Ovinda.hariyesa@pertamina.com

Keywords: Empowered Community, Renewable Energy, Geothermal Development, Society

ABSTRACT

This research aims to investigate the influence of Geothermal Coffee Process (GCP) as a community development initiative by PT. Pertamina Geothermal Energy Tbk. Area Geothermal Kamojang on the education and awareness enhancement of the public regarding renewable energy, specifically in the context of geothermal business and its benefits to society. GCP serves as a tangible manifestation of the company's Corporate Social Responsibility (CSR) program, wherein direct utilization of geothermal energy as a source of heat energy in processing the coffee products produced, especially the process of drying coffee beans. This presents a potential new avenue for expanding public education on geothermal energy. Therefore, this research seeks to examine whether the direct utilization of geothermal heat by the Geothermal Coffee Process (GCP) community group can contribute to the development of education on renewable energy or if its focus remains limited as a form of the company's CSR program. The study is conducted around Kamojang, Laksana Village, Bandung Regency, utilizing a qualitative methodology. Data collection involves observation, interviews, and documentation to gather both qualitative and measurable quantitative data. The research findings indicate that GCP has a significant impact on the development of education regarding renewable energy and its utilization by the community through the activities undertaken by the empowered community.

1. INTRODUCTION

PT Pertamina Geothermal Energy Tbk AG Kamojang Area is situated between two regencies, with the majority of the area located in Bandung Regency and the remainder in Garut Regency. The history of geothermal energy exploration in Indonesia began at Kamojang, Bandung. Exploration of geothermal energy at Kamojang commenced in 1918 under Dutch colonial government. In 1974, the government assigned PT Pertamina the task of surveying geothermal sources and conducting exploration and exploitation for electricity generation. In 1983, the Kamojang Geothermal Power Plant Unit I officially commenced operations, capable of generating 30 MegaWatts (MW) of electricity. PGE AG Kamojang Area has continuously increased its electricity production capacity utilizing geothermal energy. Currently, PGE AG Kamojang produces 235 MW of electricity.

Development Stages:
a. Drilling 1 : 1926
b. COD PLTP Unit-1 : 1983
c. COD PLTP Unit-2 & 3 : 1987
d. COD PLTP Unit-4 : 2008
e. COD PLTP Unit-5 : 2015

PGE AG Kamojang produces electricity to supply Java, Madura, and Bali. The average annual electricity production reaches 1,752 GWh. PGE AG Kamojang has successfully reduced emissions by 1.23 million tCO_2e per year, equivalent to 4.057 million Barrels of Oil Equivalent (BOE). The establishment of PGE AG Kamojang has enabled annual foreign exchange savings of 264,000,000 US dollars. Assuming a household electricity requirement of 450 V, PGE AG Kamojang can supply electricity to approximately 522,000 homes in Java, Madura, and Bali.

PT Pertamina Geothermal Energy Tbk, as a publicly listed company, adheres to the Environment, Social, and Governance (ESG) Risk Rating, achieving a top-tier ranking of 1 in the categories of renewable energy companies and manufacturing companies, and ranking within the top 10 overall. This ESG assessment was conducted by Sustainalytics, receiving a score of 8.4, categorized as negligible risk, and a score of 2.0 for Good ESG Performance from Sustainable Fitch. In terms of achievements, PGE AG Kamojang stands as the sole power generation company to receive the PROPER Gold Award 13 times consecutively since 2011. In addition to the PROPER Gold awards, PGE AG Kamojang has also garnered 146 awards across various levels, spanning local, national, and international recognition.

As part of its corporate social and environmental responsibility to the community, PGE AG Kamojang has contributed to various community development programs based on the company's 5 pillars of CSR: empowerment, education, environment, health, social, and infrastructure. In an effort to create new innovations in the field of CSR, PGE AG Kamojang has developed a program using direct-use geothermal known as the Geothermal Coffee Process (GCP). This program aims to use residual steam from steam traps for drying coffee through a Geothermal Dryhouse. Through this innovation, there are significant impacts for both the company and the community.

2. METHODOLOGY

In conceptualizing how the discourse on geothermal energy as renewable energy is developed within the community through the Geothermal Coffee Process (GCP), this research is accompanied by a capacity building mechanism for a deeper examination.

The empowered community of PGE AG Kamojang, namely the Geothermal Coffee Process (GCP), serves as a medium in developing the discourse on geothermal energy as renewable energy, adding a new dimension to this discourse. Through the capacity building mechanism, a further investigation will be conducted on how the Geothermal Coffee Process (GCP), as a empowered community of PGE AG Kamojang, actively plays a role in expanding the discourse on geothermal energy as renewable energy to the community. According to Chelminski (2018), the capacity building mechanism is described as the provision of resources for developing human capacity, either through training and education. In this research, the capacity building mechanism may take the form of training coffee farmers, benchmarking by external parties in exploring direct-use geothermal in the CSR Program through the Geothermal Coffee Process (GCP), coffee exhibitions, and other informal activities of the GCP group.

3. DISCUSSIONS

Innovation through the direct-use of geothermal in the field of CSR also creates a new approach to developing community knowledge about geothermal discourse. Through the Geothermal Coffee Process (GCP), educational tools for the community become more extensive by showcasing the benefits of geothermal energy beyond its use for electricity generation. This research is focused on examining the impact of the Geothermal Coffee Process (GCP) as an empowered community initiative by PT. Pertamina Geothermal Energy Tbk. AG Kamojang on the development of renewable energy discourse among the society.

3.1 New Innovation through Geothermal Coffee Process (GCP)

Kamojang is located in a mountainous region that is administratively part of Laksana Village, Ibun District, Bandung Regency. The hilly terrain of Kamojang results in the majority of its residents being farmers, including coffee farmers, vegetable farmers, and others. In the farming profession, unpredictable weather is one of the issues that can hinder agricultural processes, especially coffee farming, which requires a drying period of up to 45 days. Unstable weather conditions can obstruct the drying process and lead to ineffective coffee production.

The unstable weather conditions that hinder coffee farming, particularly in the areas surrounding the company's operations, have prompted PGE AG Kamojang to create a new innovation that addresses the problems faced by coffee farmers. After extensive research and trials, a new innovation was developed to tackle this issue: the Geothermal Dry House. This device is a coffee drying house that utilizes direct geothermal energy in its drying process by using residual steam from the blowdown line, which is channeled through pipes to heat the coffee drying house. This innovation is utilized by the company's empowered community, who are part of the Geothermal Coffee Process (GCP), consisting of coffee farmers from the areas around the company.

In community empowerment activities around the company, the empowered community acts as a subject collaborating with the company to achieve common goals. Community empowerment itself aims to provide independence and positive change amidst existing problems. Broadly, these activities are divided into four aspects that promote the creation of an independent and prosperous empowered community.

These four aspects are infrastructure, charity, capacity building, and community assistance. The Geothermal Coffee Process has implemented and developed these four aspects. The GCP Group consists of three coffee groups from Ibun District, namely Akkar Kopi and Ecovill Kopi, and one group from Samarang District, namely Penyoe Kakopi. Each member of the GCP collaborates with the company to achieve common goals in developing coffee products processed through the Geothermal Dry House, branded as Canaya Geothermal Coffee.

3.1.1 Geothermal Dryhouse Innovative Infrastructure

The innovation of the Geothermal Dryhouse, as a form of direct use of geothermal energy, can have a direct impact on the community. This direct utilization not only assists coffee farmers and processors in addressing issues in coffee processing but also provides positive economic, social, and environmental value. The technological innovation in the form of the dry house encourages farmers to learn how to use the equipment and

disseminate information about direct use geothermal to the broader community. Supporting infrastructure for production benefits farmers as the geothermal dry house brings values of efficiency and effectiveness in drying coffee cherries. This infrastructural innovation accelerates actors in expanding the utilization of geothermal energy more broadly. The slow pace of innovation, adoption, and development of clean technology innovations in developing countries is largely attributed to market and institutional failures such as lack of information, transaction costs, weak financing institutions, and poor technological adaptability to the developing country's absorptive capacity or technological sophistication (Acemoglu et al., 2012; Dechezleprêtre et al., 2012; Stoneman and Diederen, 1994 in Chelminski, 2018).

The advantage of the Geothermal Dryhouse is that it can dry coffee 75% faster than conventional sun-drying methods. Previously, drying coffee would take 30-45 days, but now it takes only 3-10 days around Kamojang, where the weather is often foggy and rainy. Drying in the dry house can occur 24 hours a day with fluctuating temperatures between 26 to 50 degrees Celsius. The temperature dynamics, which are made as natural as conventional drying, can maintain the distinctive characteristics and flavors of Kamojang Arabica coffee.

The market potential for geothermal dry house technology within the next 5 years in the coffee industry appears promising. The efficiency, quality assurance, and extended drying capabilities through expansion of the geothermal dry house can attract more coffee farmers and buyers, leading to potential growth and market expansion:

a. Increased Efficiency: The geothermal dry house can accelerate drying time significantly, up to 75% faster than conventional methods. This increased efficiency can lead to higher productivity and throughput in coffee drying processes.
b. Extended Drying Season: The ability to dry coffee beans regardless of the season can provide a competitive advantage to coffee farmers, allowing them to operate year-round and be less affected by seasonal variations. This extended drying season could attract more farmers to adopt this technology.
c. Stable Drying Conditions: The stability of drying temperature and humidity in geothermal dry houses can help maintain the quality of coffee beans, ensuring that the flavor is not compromised. This quality assurance can be a crucial selling point in the market.
d. Contamination Reduction: By reducing the risk of contamination from dust, dirt, and insects, the geothermal dry house method ensures higher-quality coffee beans. This assurance of quality can be a key factor in attracting buyers who prioritize cleanliness and quality standards.
e. Consumer Preference: The positive testimonies from local coffee farmers regarding the taste and absence of smell issues in the dried coffee could lead to increased consumer trust and preference for dried coffee using geothermal technology.

With its array of advantages, geothermal dry house technology presents promising potential for significant market growth and expansion in the coffee industry over the next five years. By enhancing efficiency, extending drying seasons, ensuring stable drying conditions, reducing contamination risks, and garnering increased consumer preference, this technology opens new opportunities for coffee farmers and stakeholders across the coffee supply chain to optimize quality and productivity, while expanding their market share.

In addition, the limitation of this tool lies in its restricted area of use. Direct use can only be accessed in the area around the company's operations, meaning that only the community partners can directly utilize the dry house. Communities from outside the area can also benefit from the dry house, but in a limited system. One way is by drying coffee cherries in the dry house under a makloon system, which is also managed by the GCP Group. Nevertheless, the broader use of the dry house directly promotes the development of geothermal energy to be more widely recognized. The replication of the dry house and its increasing capacity usage requires monitoring and supervision by the company's maintenance, operation, and HSE teams. To ensure that the infrastructure is safe and functions properly, periodic technical descriptive reviews of the Geothermal Dryhouse are necessary. Below is a technical overview of the design and the steam trap system that channels steam inside the dry house.

The existing Geothermal Dryhouse has a width of 6 m, length of 8 m, and height of 4.5 m, as shown in Figure 1. The heating pipe utilizes the blowdown from the main pipeline as the heat source so that the geothermal steam flows from the blowdown towards the dryhouse to transfer its heat to the dry house air. The total length of the existing heating pipe is 43.5 m.

The actual documentations of the existing geothermal dryhouse and heating pipe connection to the main pipeline's blowdown are shown in Figure 2. The dryhouse has three coffee tables with a single U-loop heating pipe under each table. The heating pipe is made of carbon steel with the specification code of SMLS Pipe CS API 5L Gr B 1" SCH 40.

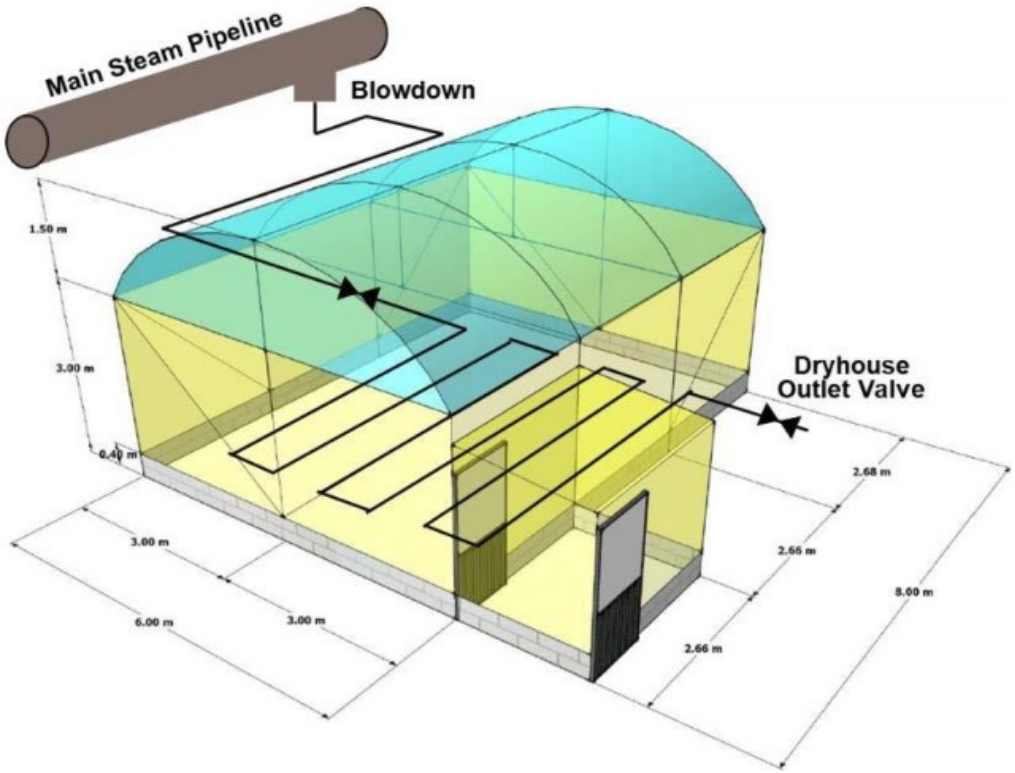

Figure 1: Existing Geothermal Dryhouse Dimensions and Heating Pipe Schematic.

Figure 2: Existing geothermal dryhouse dimensions and heating pipe connection to the blowdown.

In order to maintain the dry house temperature at a desired value, the heating load must be equal to the rate of heat loss and the rate of trapped radiation. The geothermal steam flows inside the heating pipe and transfers its heat to the dry house air. This involves convection heat transfer on the inner and outer pipe walls, conduction heat transfer at the pipe wall, and radiation heat transfer on the outer pipe walls. The thermal circuit of the heat transfer process.

The geothermal steam flowing inside the heating pipe is at saturated vapor phase. Therefore, film condensation occurs as the steam transfers heat to the dry house air. The heating pipe is operated by opening the blowdown valve hence the geothermal steam from the main pipeline could flow inside the heating pipe towards the dry house. Meanwhile, the outlet valve at the end of the heating pipe remains closed. During the pipe operation, the dry house temperature is measured using a thermo hygrometer. Therefore, the dry house air temperature during the heating pipe operation could be evaluated. After a minimum 24 hours of operation, the blowdown valve is closed again to shut down the heating pipe.

Geothermal Dryhouse has the advantages of being weather-independent, available heat around the clock, and naturally-controlled temperature and humidity. Based on technical evaluation the results indicated that the heating pipe was able to increase the dry house temperature. However, the condensate builds up inside the heating pipe reduces the dry house temperature minutes after the heating pipe operation. Therefore, it is responded by installing two stream traps, each installed at the inlet and outlet of the drying house to reduce condensate in the steam

entering the drying house and remove the condensate formed while the steam is in the drying house. The actual operation hours for geothermal dry house entail a continuous cycle of work, with operations spanning 24 hours each day. This setup results in a substantial cumulative working time of 5,760 hours annually.

Maintenance Scheme of Geothermal Dryhouse conducts proactive and preventive maintenance with regular schedules to avoid production failures. These plans are maintained based on manual machine operation data, predictive maintenance principles, and machine degradation level analysis. In line with the concept of sustainable power plant operations, socio-ecological safety is ensured through social inclusion practices in the Geothermal Coffee Process program, and monitored through annual Social License Index (for social safety) and annual geophysical surveys (for steam resource sustainability).

The heightened interest of the community in the Geothermal Dryhouse has boosted the productivity levels of the Geothermal Coffee Process. To meet this rising demand, replication of the Geothermal Dryhouse is being undertaken to further enhance the productivity of the Geothermal Coffee Process.

Figure 2: Geothermal Dryhouse Replication.

3.2 Geothermal Coffee Process (GCP) impacts on the Discourse Development of Renewable Energy Among the Society

As an empowered community of PGE AG Kamojang's CSR Program, the Geothermal Coffee Process (GCP) serves as an example of how geothermal energy can be utilized not only for electricity generation but also for direct community empowerment. Through the capacity building mechanism, the impact of the Geothermal Coffee Process (GCP) on the development of the discourse on geothermal energy as a renewable energy source is explained as follows.

3.2.1 Capacity Building Through Geothermal Coffee Process (GCP) and PGE AG Kamojang

In an effort to develop geothermal energy through educational initiatives, the first approach undertaken by the GCP Group involves activities such as training, workshops, and capacity building. The initial activity is a workshop for the GCP Group, aimed at enhancing the capacity of coffee farmers as an empowered community benefiting from the company's CSR program through direct use of geothermal energy.

The next step is the coffee training provided by the GCP Group to raise awareness among the community, particularly coffee farmers, about the innovative Geothermal Dryhouse. This innovation has a positive impact on coffee farming by introducing a more efficient coffee processing method compared to conventional methods. Through this training, approximately 42 coffee farmers gain knowledge about utilizing geothermal energy for coffee farming. They participate in practical sessions on harvesting, seedling, and fertilizing coffee plants at Mr. Nono's farm. Some farmers bring tools such as hoes, soil perforation pipes, commonly used fertilizers, and special cutters or scissors for coffee plant cuttings. The farmers actively listen and ask questions to the instructor. Among the questions are how to increase coffee productivity or yield, the spacing for planting coffee seedlings, the criteria

for sustainable coffee seedlings that do not harm future harvest growth, and alternative fertilizers and their appropriate quantities to enhance the growth rate of coffee plants.

Figure 3: Coffee Training with Coffee Farmers.

Figure 4: Field Coffee Training with Coffee Farmers.

Farmers have also expressed several challenges in maintaining the supply of coffee cherries to downstream actors. One of the main challenges is the unpredictable annual fluctuation in coffee cherry prices, which is usually influenced by the quality of the coffee harvest each year, including the quantity of coffee produced in each harvest season.

The obstacles faced by coffee farmers also stem from the inadequacies in the infrastructure used to cultivate and develop coffee plantations. The equipment used by farmers significantly impacts their ability to care for their crops, highlighting the need for adequate materials and methods to support farmers in increasing the productivity of their coffee harvests. Collaboration with various stakeholders and benchmarking in different locations were suggested by several coffee enthusiasts participating in the training.

Increased coffee productivity will lead to higher harvest quantities each season. Therefore, several factors directly influence or encourage farmers to be interested in utilizing the Geothermal Dry House's direct-use services. The more farmers educated on improving coffee farm management and coffee cherry processing, the higher the coffee productivity, impacting farmers' ability to meet market demand. Additionally, farmers and the broader community will become more aware of geothermal energy as a clean and environmentally friendly energy source that can support existing local business processes.

3.2.2 External Visitors to Geothermal Coffee Process (GCP)

Figure 5: External Benchmarking.

PGE AG Kamojang frequently receives visits from schools, universities, companies, and various other groups. The purpose of these visits varies depending on the needs of the guests, whether for education, benchmarking, or other reasons. Each visit includes materials related to the CSR Program of PGE AG Kamojang, which encompasses the Geothermal Coffee Process (GCP). Additionally, there are visits to the Geothermal Dryhouse to observe the coffee processing conducted by the Geothermal Coffee Process (GCP). This serves as a new learning medium for visitors to study the direct use of geothermal energy for coffee drying. The total number of visitors over the past two years has reached approximately 10,000 people from diverse backgrounds.

3.2.3 Geothermal Coffee Process through Exhibitions

The Geothermal Coffee Process (GCP) has had the opportunity to participate in various exhibitions at regional, national, and international levels. For example, West Java Festival 2023, IIGCE 2023, IIGW 2023, Coaching Clinic PROPER Exhibition 2023, Forum CSR Jawa Barat 2024, Dekranas 2024,Global Geothermal Impact Summit 2024, Clean Energy Ministerial Senior's Official Meeting & Gathering 2024 and other exhibitions. These opportunities have been maximized to serve as a medium for expanding the discourse on the direct utilization of geothermal energy. Additionally, these occasions have been used to showcase the excellence of PGE AG Kamojang in the direct utilization of geothermal energy through its CSR Program, featuring the Geothermal Dryhouse and its product, Canaya Geothermal Coffee, which has become a hallmark of PGE AG Kamojang and the Geothermal Coffee Process group.

Figure 6: Geothermal Coffee Process on Exhibitions.

Exhibitions provide an opportunity for the Geothermal Coffee Process to expand its network across various groups, including the general public, coffee enthusiasts, coffee entrepreneurs, and others. Thus, this medium not only serves to broaden the discourse on geothermal energy but also aims to increase public interest in directly experiencing coffee produced using geothermal energy.

3.2.4 Geothermal Coffee Process Other Activities

Capacity building agendas and bootcamps are planned and partially realized to recruit outstanding talents that contribute to the sustainability of the Geothermal Coffee Group. At least 1,540 customers enjoy the GCP coffee products. Furthermore, the group strives to expand its business and market through both B2C and B2B models. Through The Canaya Geothermal Coffee, local community awareness of coffee cultivation potential increases, and with the presence of The Canaya Geothermal Coffee, it also supports the following beneficiaries: 6 main managers of The Canaya Geothermal Coffee, 15 Coffee Farmers, 4 Baristas, 2 Coffee Sorters, 1.537 coffee enthusiasts, and business partnerships with 35 B2B and B2C partners. In general, the Community Satisfaction Index (CSI) for the overall program of PT. Pertamina Geothermal Energy Tbk. Area Kamojang including The Canaya Geothermal Coffee scored 82.7, which falls under the A category for service quality, which is classified as very satisfied.

Figure 7: Drying Process in Geothermal Dryhouse.

Above is an activity of the coffee drying process inside the Geothermal Dryhouse. Several farmers are seen turning over coffee beans spread on tables, with steam flowing underneath through installed pipes. An 8 x 6-meter dry house can dry at least 4 tons of coffee beans per month. Meanwhile, the second dry house, measuring 16 x 4 meters, has a maximum capacity five times greater than the first dry house. This demonstrates that direct use of geothermal energy can significantly enhance productivity, effectiveness, and efficiency in achieving dried coffee bean quantities. Therefore, opportunities for coffee exports are wide open with broader stakeholder collaboration.

4. CONCLUSION

The community empowered through the Geothermal Coffee Process is a pioneer in the development of geothermal energy at local, national, and international levels. The compelling testimonials from this empowered society, experiencing direct benefits from geothermal direct use, provide broad access to narratives about geothermal energy for the wider community. The activities of the Geothermal Coffee Process (GCP), supported by corporate collaboration in infrastructure, capacity building, and facilitation of activities with external stakeholders, not only yield economic, social, and environmental benefits but also position the Geothermal Dryouse as an innovative tool in geothermal direct use that fosters significant opportunities in education and the advancement of renewable energy use in the future. As more people become educated about the positive benefits of geothermal direct use, there is an increasing likelihood that future geothermal development will be recognized and chosen by communities at local, national, and international levels.

REFERENCES

Attwood, C., Bridle, R., Gass, P., Halimanjaya, A. S., Laan, T., Lontoh, L., Sanchez, L., & Toft, L. (2017). Renewable Energy and Subsidies in Indonesia. In *Financial Supports for Coal and Renewables in Indonesia* (pp. 29–34). International Institute for Sustainable Development (IISD). http://www.jstor.org/stable/resrep14780.8

Berg, R. C., Cohen, K., Rubio, J., & Guzman, A. (2023). *Turning Up the Heat on Geothermal Energy Development in Latin America: Varying Scenarios for Costa Rica, El Salvador, and Peru*. Center for Strategic and International Studies (CSIS). http://www.jstor.org/stable/resrep48465

Chelminski, K. (2018). *Harnessing the Ring of Fire: Political economy of clean energy development finance on geothermal development in Indonesia and the Philippines*. Energy Policy Research Group, University of Cambridge. http://www.jstor.org/stable/resrep30435

Fan, K., & Nam, S. (2018). Accelerating Geothermal Development in Indonesia: A Case Study in the Underutilization of Geothermal Energy. *Consilience*, 19, 103–129. http://www.jstor.org/stable/26427715

Farouq, C.U., et al., (2023). Technical and Business Evaluation of Geothermal Dryhouse for Coffee in Kamojang, West Java, Indonesia. *PROCEEDINGS*, 12th ITB International Geothermal Workshop 2023. Institut Teknologi Bandung, Indonesia, June 6–7, 2023

Hamilton, T. (2015). AN UNDERGROUND ECONOMY WE WANT TO ENCOURAGE. *Corporate Knights*, 14(3), 67–69. http://www.jstor.org/stable/44149878

IWAKI, T. (1983). Development Trends of Geothermal Energy Resources in Japan. *Energy Exploration & Exploitation*, 2(4), 357–360. http://www.jstor.org/stable/43753490

Petroski, H. (2013). Engineering: Geothermal Energy. *American Scientist*, 101(4), 251–255. http://www.jstor.org/stable/43707717

W.G., NASA, USGS, DOE, & EPA. (2019). ENERGY & SUSTAINABILITY NEWS. *The Military Engineer*, 111(722), 30–35. https://www.jstor.org/stable/26699532

Harnessing Low Enthalpy Energy: Innovatave Solutions for Sustainable Development

Fariz Alfarizi, Haris Mubarok, and Muhammad Farras Zahran Al-baihaqi

parisalfa09@gmail.com, harismubarok05@gmail.com, farrasbaihaqi7@gmail.com

Keywords: Low Enthalpy Geothermal, ORC, Kalina Cycle System, Renewable Energy

ABSTRACT

Indonesia has great potential in the development of geothermal energy, especially widespread low enthalpy geothermal resources. However, its utilization is still not optimal due to the limitations of existing technology. This paper introduces the innovation of merging two geothermal cycles, namely the merger of two main cycles in geothermal power plants, the Organic Rankine Cycle (ORC) and the Kalina Cycle System (KCS-34), which are designed to improve efficiency and flexibility in the utilization of low-temperature geothermal sources. Analysis of the merging system shows that this innovation is able to maximize the use of waste heat, resulting in higher energy output than conventional systems.

The simulation results show that this system has the potential to produce about 5,972 kW of power, with higher thermal efficiency than the stand-alone ORC and Kalina KCS-34. From an economic perspective, the system has a competitive Return on Investment (ROI), with an estimated payback period of around 8-10 years. In addition, this innovation has also succeeded in significantly reducing carbon emissions, making it a more environmentally friendly energy solution.

The potential application of this technology is not only limited to power plants, but also in various other sectors such as the processing industry, agriculture, fisheries, tourism, and construction. The paper concludes that with adequate regulatory and infrastructure support, this innovation can be the key to the sustainable development of renewable energy in Indonesia.

1. INTRODUCTION

Indonesia has tremendous geothermal energy potential because it is located along the Pacific Ring of Fire, which is a region with high volcanic and tectonic activity. According to data from the Geological Agency of the Ministry of Energy and Mineral Resources (EMR), the total potential of geothermal energy in Indonesia is estimated to reach 29,215 Megawatts (MW). This makes Indonesia one of the countries with the largest geothermal energy reserves in the world, which is even estimated to account for around 40% of the global geothermal potential. This figure is often referred to in various international reports, including those compiled by the World Bank.

In the context of the global energy transition to reduce dependence on fossil fuels, Indonesia has set ambitious targets to increase the contribution of renewable energy in the national energy mix. The government targets that by 2025, renewable energy will account for 23% of the total energy mix, and increase to 31% by 2050. Meanwhile, the use of petroleum is projected to be significantly reduced. However, the utilization of the great potential of geothermal energy in Indonesia is still far from optimal.

The Kalina cycle is a geothermal power generation system developed by Dr. Alexandre Kalina. The system is specifically designed to utilize low-temperature geothermal sources, which conventional power generation systems cannot use. One of the main advantages of the Kalina Cycle is the use of an ammonia-water mixture as a working fluid. This mixture has unique thermal properties that allow for higher energy efficiency than other similar systems.

Kalina Cycle System 34 (KCS-34) is a more advanced version of the traditional Kalina Cycle. This design aims to improve efficiency in utilizing residual heat from energy sources with low temperatures. The KCS-34 can operate at lower temperatures than traditional Rankine cycles, with operating temperatures typically ranging from 100°C to 180°C. By using an ammonia-water mixture, KCS-34 can regulate the mass fraction to maximize thermal efficiency, allowing this system to work more effectively in a variety of operating conditions. The use of KCS-34 in the geothermal context in Indonesia is very relevant, considering the large number of geothermal sources with low to medium temperatures spread throughout the country.

On the other hand, the Organic Rankine Cycle (ORC) is a thermodynamic cycle similar to the conventional Rankine Cycle , but it uses an organic working fluid with a low boiling point. ORC is very effective in utilizing heat sources with low to moderate temperatures, such as those often found in geothermal energy sources in

Indonesia. The ORC can operate at lower temperatures than traditional Rankine cycles, with operating temperatures typically ranging from 80°C to 150°C. Flexibility in the selection of working fluids allows the ORC to be optimized according to the conditions of the available heat source. ORC is also known for its high efficiency in converting heat from energy sources with temperatures below 150°C into electrical energy, making it an excellent choice for geothermal applications in Indonesia.

However, the development of low-enthalpy geothermal energy in Indonesia still faces major challenges due to the limitations of available technology. Although the potential of this low-enthalpy energy is large, the technology needed to utilize it is still not widely developed, even though this potential can be a significant solution to the needs of renewable energy in Indonesia. The combination of the Kalina KCS-34 Cycle and the Organic Rankine Cycle (ORC) offers an opportunity to overcome this challenge, by leveraging the advantages of each technology to maximize the efficiency of geothermal resource utilization in Indonesia. In an effort to answer the challenge of developing geothermal energy, especially for low enthalpy energy in Indonesia, we are developing an innovation that combines two cycles, namely the Kalina KCS-34 Cycle and the Organic Rankine Cycle (ORC). This innovation aims to overcome technological barriers that currently limit the exploration and utilization of geothermal resources in Indonesia. This innovation is designed to maximize the potential of low enthalpy geothermal energy through a more efficient, economical, and environmentally friendly approach. With the application of advanced technology and innovative approaches, this innovation is expected to be able to increase the use of geothermal energy more widely and sustainably in Indonesia, as well as support the national target of increasing the portion of renewable energy in the energy mix.

2. THERMODYNAMIC ANALYSIS

Equipment such as turbines, pumps, compressors, and heat exchangers are examples of open systems. An open system is a system in which there is an exchange of energy (in the form of heat and work) as well as mass with the surrounding environment. In this system, both mass and energy can cross the boundaries of a permeable system. In other words, an open system allows the masses to enter and exit the system. As a result, the system volume remains unchanged, so it is often referred to as the control volume. This control volume is an area set to facilitate the analysis of the flow of mass and energy that occurs. Thus, in this system, the volume of the system does not change so it is also called volume control. Volume control is a restriction of the review area on a component to facilitate calculations in more detail. The energy transfer at the volume control limit occurs in the form of work and heat. In Figure 1. It can be seen that in the inlet (i) is the flow of mass into the control volume and exit (e) is the flow of mass out of the control volume. In the control volume, two laws apply, namely mass conservation and energy conservation.

$\frac{dE_{cv}}{dt}$ =A<a0>i – Áe ṁe ..... (1.1)

$$\frac{de_{cv}}{dt} = \dot{Q} - \dot{w} + \dot{m}_i\left(u_i + \frac{V_i^2}{2} + gz_i\right) - \dot{m}_e\left(u_i + \frac{V_e^2}{2} + gz_e\right) \quad \text{..... (1.2)}$$

Assuming that the work of the incoming fluid is considered negative and the work of the outgoing fluid is positive, the notation Ẇ in equation 1.2 indicates the force affected by the work of the incoming fluid (Ẇi) and the outgoing fluid (Ẇe) passing through the control volume. The power of Ẇ can also be described as the product of force (F) and velocity (V). This force itself is the result of the multiplication between the pressure (p) and the surface area that receives the pressure (A). In addition, Ẇ is also affected by the conditions around the control volume, such as shaft rotation, mass and energy transfer from the control volume limit, as well as electrical effects, denoted as Ẇcv. Thus, Ẇ can be formulated as shown in equation 1.3.

$$\dot{w} = \dot{w}_{cv} + \dot{w}_e - \dot{w}_i$$

$$\dot{w} = \dot{w}_{cv} + (p_e A_e)V_e - (p_i A_i)V_i \quad \text{..... (1.3)}$$

With AV = ṁv, then equation 1.3 becomes equation 1.4.

$$\dot{w} = \dot{w}_{cv} + \dot{m}_e(p_e v_e) - \dot{m}_i(p_i v_i) \quad \text{..... (1.4)}$$

Equation 2.4 is substituted in equation 1.2 so that it becomes equation 2.5.

$$\frac{de_{cv}}{dt} = \dot{Q}_{cv} \text{ -) -)} \quad \text{..... (1.5)} \dot{W}_{cv} + \dot{m}_i(u_i + p_i v_i + \frac{V_i^2}{2} + gz_i \dot{m}_e(u_e + p_e v_e + \frac{V_e^2}{2} + gz_e$$

The subscript "cv" is added to Q̇ to emphasize that the rate of heat transfer occurs at the boundary of the control volume. Equation 1.5 can be written using the specific enthalphy (h) where h = u + pv. Then equation 1.5 becomes equation 1.6.

$\frac{de_{cv}}{dt} = \dot{Q}_{cv}$ -) -) ..... (1.6) $\dot{W}_{cv} + \dot{m}_i(h_i + \frac{V_i^2}{2} + gz_i \dot{m}_e(h_e + \frac{V_e^2}{2} + gz_e$

In the actual state there may be several locations around the boundary that are traversed by the flow of incoming or outgoing mass, thus equation 1.6 becomes equation 1.7.

$\frac{de_{cv}}{dt} = \dot{Q}_{cv}$ -) -) ..... (1.7) $\dot{W}_{cv} + \sum_i \dot{m}_i (h_i + \frac{V_i^2}{2} + gz_i \sum_e \dot{m}_e (h_e + \frac{V_e^2}{2} + gz_e$

The volume control condition is assumed to be steady state to make the calculation process easier. A steady state is an ideal state which means that all properties do not change with time. Likewise, the rate of mass flow, the rate of thermal energy transfer, and work also do not change with time. Therefore, in the principle of the law of mass conservation in equation 1.1 can be equation 1.8.

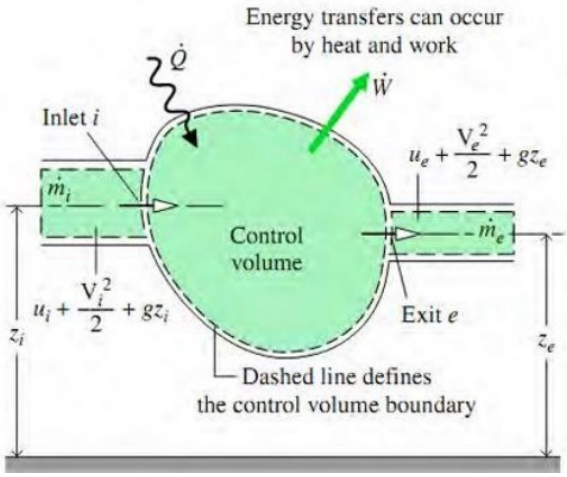

Figure 1: Volume Control Illustration.

$\frac{dE_{cv}}{dt}$ =Ai ṁi – Σe ṁe ..... (1.8)
0 = Σi ṁi – Σe ṁe
Ci = Ṁi = Σe ṁe

As well as on the principle of energy conservation in a steady state, equation 1.2 can be equation 1.9.

$\frac{dE_{cv}}{dt} = \dot{Q}_{cv} - \dot{W}_{cv} + \dot{m}_i(h_i + \frac{V_i^2}{2} + gz_i)$ - Σe ṁe (he + + gz$\frac{V^2_e}{2}$e) ..... (1.9)

$0 = \dot{Q}_{cv} - \dot{W}_{cv} + \dot{m}_i(h_i + \frac{V_i^2}{2} + gz_i)$ - Σe ṁe (he + + gz$\frac{V^2_e}{2}$e)

Qcv – Wcv + Σi ṁi (hi + + gz$\frac{V^2_i}{2}$i) = Σe ṁe (he + + gz$\frac{V^2_e}{2}$e)

3. DISCUSSION

In the midst of the global climate crisis, the world is increasingly shifting to renewable energy with low carbon emissions, with geothermal energy being one of the solutions. Indonesia, thanks to its position at the confluence of tectonic plates, has abundant geothermal reserves. According to the Geological Agency of the Ministry of Energy and Mineral Resources, Indonesia has a geothermal energy potential of 29,215 MW, or around 40% of the global geothermal potential. High enthalpy geothermal, with temperatures above 200°C, is commonly found in active volcanic regions such as West Java and North Sumatra, suitable for large-scale power plants using technologies such as Flash Steam Power Plants. Meanwhile, the enthalpy geothermal medium, with temperatures between 100°C to 200°C, is often utilized for cogeneration, with significant potential in areas such as Dieng, Central Java. Low enthalpy geothermal, with temperatures below 100°C, is distributed in non-volcanic areas such as South Sumatra and Nusa Tenggara, and can be optimized for small-scale power plants using technologies such as Organic Rankine Cycle (ORC) and Kalina Cycle System (KCS).

Geothermal energy is also classified based on the depth of its heat source. Shallow geothermal, which comes from the earth's layers closer to the surface, is often used for heating and cooling systems through Ground Source Heat Pumps (GSHP) technology. While deep geothermal, from a deeper layer, is more suitable for power plants with high temperatures to drive turbines. Geothermal applications in Indonesia vary, ranging from power plants with technologies such as Flash Steam, Binary Cycle, and Dry Steam Power Plants to direct applications such as space

heating, drying agricultural products, and heating fish ponds. With its wealth of geothermal resources, Indonesia has a great opportunity to develop renewable energy and reduce carbon emissions, optimizing the potential spread throughout the region, both volcanic and non-volcanic.

3.1. 2-Cycle Merger

In the world of geothermal energy generation, the two most well-known and frequently used cycles are the Organic Rankine Cycle (ORC) and the Kalina Cycle System (KCS) 34. Although both are designed to efficiently utilize the heat energy from the low enthalpy source, these two cycles usually operate separately due to the differences in the characteristics of the working fluid and its operational principles. However, in the midst of the need for innovation in the use of renewable energy, the idea of combining the advantages of these two cycles into one new system has emerged. This innovation is designed to optimize efficiency and flexibility in the utilization of low enthalpy geothermal resources, by integrating the best aspects of ORC and Kalina KCS 34. The merger aims to create a more adaptive and effective power generation system, which can make better use of the variety of heat sources and generate greater energy output. This innovation is a step forward in geothermal technology, offering innovative solutions to the energy challenges of the future.

3.1.1. Integrated System Design

ORC uses organic fluids with a lower boiling point than water, so it can operate efficiently at lower temperatures. The integration of the ORC with the KCS 34 allows for more effective heat recovery from low-enthalpy geothermal sources. The design of an integrated system must take into account the thermal properties of both cycles. A good heat exchanger network is essential to ensure efficient heat transfer between the two cycles. This requires detailed thermal analysis and simulation to optimize system configuration.

3.1.2. Practical Analysis

This paper presents innovative solutions to utilize low enthalpy energy using a combined Kalina and ORC system including its practical applications. Geothermal power plants in regions with low- to medium-temperature heat sources (120-150°C) can benefit from the combined Kalina-ORC system. For example, in Indonesia, which has many geothermal sources with these temperatures, this combined system allows for higher efficiency in electricity generation, so that it can generate more energy by utilizing existing resources.

Case Study: In Wayang Windu, Indonesia, the implementation of the Kalina-ORC joint system allowed for an increase in electricity output without major investment in new infrastructure. Total efficiency increased by up to 18%, which significantly reduces the cost per kWh of electricity generated by wind power with wildlife detection, wind power with wildlife detection, offshore wind power, where underwater structures and wind farms function as artificial reefs.

3.2. Merge System Analysis

Equipment such as turbines, pumps, compressors, and heat exchangers are examples of open systems. An open system is a system in which there is an exchange of energy (in the form of heat and work) as well as mass with its environment. In this system, both mass and energy can cross the boundaries of a permeable system. In other words, an open system allows the flow of mass in and out of the system. Therefore, the volume of the system remains constant, so it is also called the control volume. This volume control is a boundary area that is set to facilitate the analysis of the flow of mass and energy that occurs.

3.2.1. Modeling and Simulation Results

Figure 2 shows a process flow diagram of a thermal energy generation system involving a combination of components such as gas turbines, pumps, heat exchangers, and cooling systems.

Here is a brief description of the components and energy flows in the system:

Compressor (K-100): Air (Air Feed) is compressed by this compressor with an energy input of Q comp The high-pressure air is then flowed to the turbine components for the combustion process. Combustor: Fuel gas is mixed with high-pressure air in the combustion chamber (Combustor). The heat generated from this combustion is used to rotate the turbine. Gas Turbine (CRV-100): The gas turbine produces a power of 5972 kW with a heat flow of 2,150 × 107 kJ/h This energy is the main output of the generation system.

Heat Exchangers (K-101, K-102, E-101): After passing through the turbine, the hot exhaust gases are passed through several heat exchangers to heat the water and produce steam that will be used for additional work, or for further processing. The system is designed to optimize the use of heat from gaseous fuel and harness that energy to generate electricity. The system is designed to optimize the use of heat from gaseous fuel and harness that energy to generate electricity. The thermal efficiency of the gas turbines used is one of the main focuses in this analysis

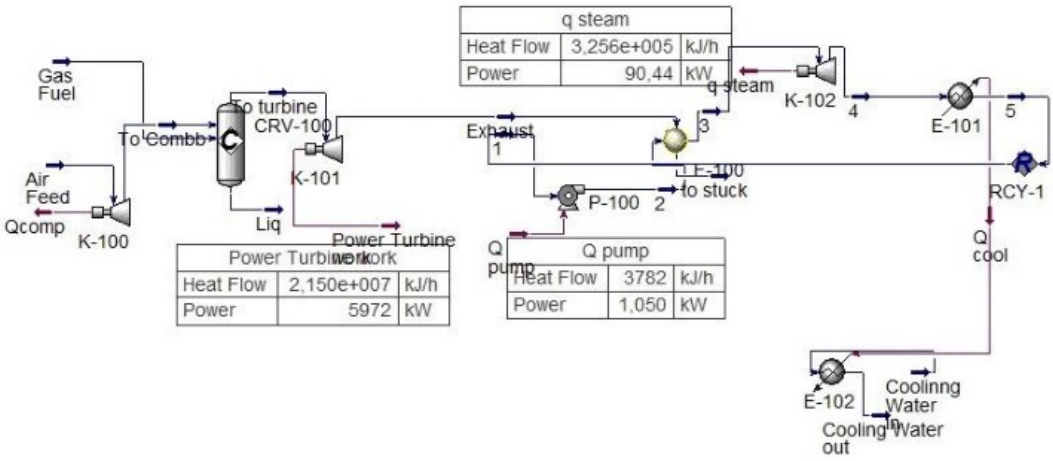

Figure 2: Results and Simulations.

The system demonstrates the efficient distribution of energy between power production through turbines and residual heat management. The measured heat flow at multiple points shows how thermal energy is processed and distributed along the system The Cooling System helps to remove excess heat from the working fluid, ensuring that the system remains in safe and efficient operating conditionsBy using fuel gas as the main energy source and utilizing efficient gas turbine and heat exchanger technology, the system has the potential to reduce carbon emissions. The utilization of residual heat also helps in reducing the need for additional fuel, which directly reduces the carbon footprint of the plant's operations. A combined system involving a gas turbine, heat exchanger, and cooling system as shown in the image is an effective solution for efficient and low-emission energy generation. With the optimal utilization of residual heat and energy distribution, these systems can provide significant power output while minimizing environmental impact. However, to achieve maximum results, these systems require careful design and careful maintenance.

3.2.2. Pressure Analysis on Turbines

The cycle modeling of KCS 34 and ORC that has been simulated with no errors and waring is coupled with the simulation of various variations. This variation was carried out at the fluid pressure at the turbine inlet with a pressure of 2 bar, 5 bar, 7 bar, 9 bar, and 11 bar at an ammonia-water mass fraction of 85.8%. From these variations the power generated by each variation and the quality of the steam coming out of the turbine from each pressure. The following is a table of data resulting from the variation in pressure obtained:

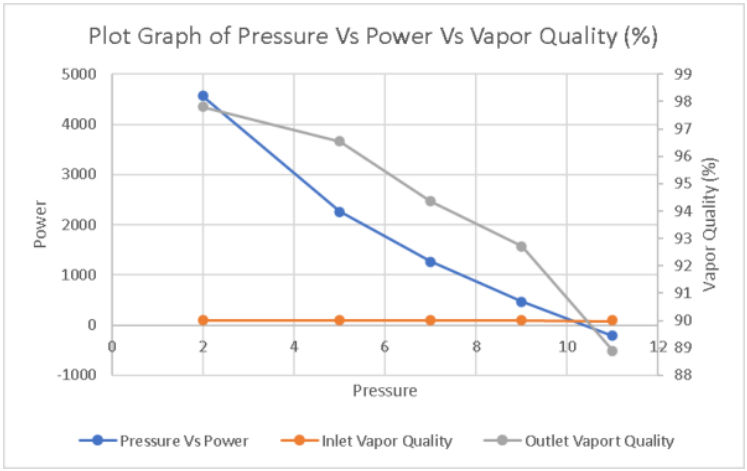

Figure 3: Pressure vs Power vs Steam Quality Chart Plot (%).

The graph shows that there is a negative correlation between pressure and power generated by the geothermal system. At lower pressures, the power produced reaches a maximum figure of around 5000 MW. However, as the pressure increases to 12 MPa, the power decreases significantly to near zero.

This decrease can be explained by thermodynamic theory where an increase in pressure in a geothermal system leads to a decrease in turbine efficiency. This is due to the fact that at higher pressures, the steam produced tends

to be more saturated with water. This saturated steam has a higher density and a smaller specific volume, thus reducing the ability of the steam to perform mechanical work on the turbine

The graph also displays two lines that show the quality of the steam at the inlet and outlet points of the system. The quality of the steam inlet is relatively stable at around 90%, indicating that the condition of the steam entering the system is quite consistent. However, the quality of the outlet steam has decreased significantly along with the increase in pressure.

At low pressure, the steam quality of the outlet reaches about 98%, but decreases to about 90% at the highest pressure measured. This decrease in quality indicates that some of the steam turns into water as the pressure increases, which in turn can decrease the efficiency of the system and increase the potential for damage to the turbine due to erosion and corrosion.

From the graph, it can be concluded that pressure has a significant influence on the power generated and steam quality in geothermal systems with low enthalpy energy. To achieve maximum efficiency, the system must be operated at optimal pressure, where the power generated is high enough and the quality of the steam is maintained above a certain threshold to prevent damage to the system components.

The system design also needs to consider pressure control and steam quality management to maximize the efficiency and longevity of the equipment. In addition, the use of steam separation or steam drying technology may be necessary to maintain high steam quality at various operating pressures.

3.2.3. Analysis of Variation in Fluid Mass Fraction at 22 Bar Pressure

In the table below there are seven variations of the mass fraction with the power produced and the quality of the turbine output steam from each variation of the mass fraction. Then from the table above, Figure 4 is obtained, which is a graph of the influence of mass fraction on the power and quality of turbine output steam at a pressure of 22 bar. Figure 4 is a trend of the cyclic power graph of Kalina KCS 34 and ORC of the quality of turbine output steam due to the influence of the fluid mass fraction at a pressure of 22 bar.

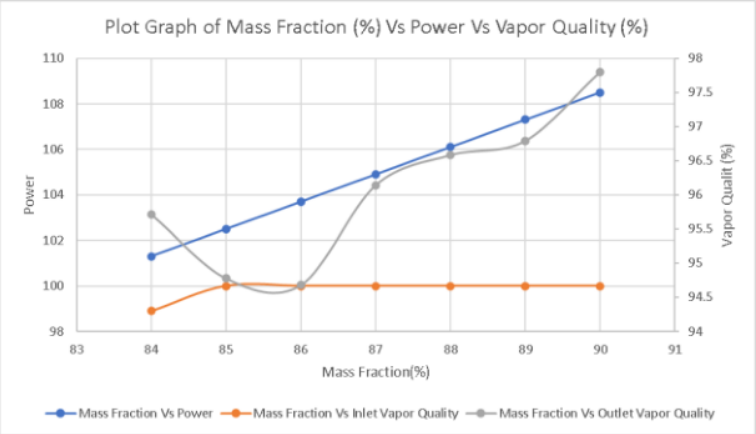

Figure 4: Mass Fraction Chart (%) vs Power vs Steam Quality (%).

The graph above shows the relationship between fraction, power, and steam quality at inlets and outlets in a thermodynamic system. This analysis refers to how changes in fractions affect system performance, especially on the power generated and steam quality. The blue line in the graph shows the relationship between fractions and power. Along with the increase in fraction from about 84 to 90, there is a consistent increase in power. This signifies that an increase in fraction, which may be related to the amount of fuel or the mass of the flow of the working fluid, results in greater power. This significant increase in power indicates better energy conversion efficiency, where energy stored in fuel or working fluid is converted into more effective mechanical work. This is in line with the principle of thermodynamics that an increase in energy input (in this case a fraction) can result in a higher energy output, depending on the efficiency of the system (Cengel & Boles, 2015). The orange line depicts the relationship between the fraction and the quality of the steam on the inlet. Interestingly, this line is almost flat, indicating that the increase in fraction does not significantly affect the quality of the steam at the inlet, which is stable at around 95.4% to 95.5%. This stability may be due to the operating conditions of the system that remain constant on the inlet section, so that the quality of the steam does not change much even though the fraction increases (Moran & Shapiro, 2010). This suggests that other variables such as temperature or inlet pressure may be more dominant in determining steam quality at this point, while fractions have a more minimal impact.

The gray line shows the relationship between the fraction and the quality of the steam at the outlet. It can be seen that in the fraction of about 85, the quality of steam decreases slightly, but then increases as the fraction increases.

The overall steam quality at the outlet improved from about 95% to almost 98% when the fraction increased from 84 to 90. This increase can be due to improvements in heat transfer or increased efficiency of the vapor change phase as the fraction increases. The temporary decline in fraction 85 may be due to changes in suboptimal operating conditions, but the general trend continues to show an improvement in steam quality indicating an improvement in thermodynamic efficiency (Incropera et al., 2007). From the analysis of this graph, it can be concluded that the increase in fraction has a positive impact on the power generated and the quality of steam at the outlet. The steam quality at the inlet tends to be stable and is not much affected by fractional changes, which signals the need for further analysis on other variables that may further affect the steam quality at that point. These findings support the importance of fraction optimization in the system to achieve better overall performance.

3.3. Economic Analysis

To evaluate the financial feasibility of the application of the low enthalpy geothermal heat pump technology shown in the figure, we will conduct an economic analysis that includes the calculation of initial costs, operational costs, and energy savings generated. In addition, we will also calculate the Return On Investment (ROI) and potential savings in the long term.

3.3.1. Financial Analysis

The initial cost includes the purchase and installation of the main equipment in the system, such as compressors, turbines, heat exchangers, pumps, and cooling systems. These cost estimates can vary depending on the scale of the project and geographic conditions. Here are the main components of the initial cost:

- Compressor (K-100): The cost for an industrial compressor with the capacity as shown in the figure can range from USD 200,000 to USD 500,000, depending on its capacity and efficiency.
- Gas Turbine (CRV-100): A gas turbine with a capacity of about 5 MW can require an investment cost of around USD 1.5 million to USD 2.5 million.
- Heat Exchanger (K-101, K-102, E-101): The cost for a heat exchanger ranges from USD 100,000 to USD 300,000 per unit, depending on the design and material.
- Pump (P-100): A pump with the indicated capacity can cost around USD 50,000 to USD 150,000.
- Refrigeration System (E-102, RCY-1): An efficient refrigeration system can cost an investment of around USD 100,000 to USD 300,000.

If we take the highest cost estimate for each component, the total initial cost can reach around USD 3.95 million to USD 4.75 million.

3.3.2. Cost Estimation Analysis

Operational costs include energy costs, routine maintenance, and replacement of necessary components during the operational period. Here is an estimate of the annual operating costs:

- Energy for Compressor and Pump Operation: Assuming the energy consumption of the compressor and pump corresponds to the given power value (5972 kW for turbines and 1050 kW for pumps), and with an average commercial electricity tariff of USD 0.10 per kWh, the annual energy cost can be calculated as follows:

  Annual Energy Cost = ((5972+1050) kW × 8760 hours/year) × $0.10/kWh
  Annual Energy Cost = 7,022,160 kWh × $0.10/kWh
  Annual Energy Cost = $702,216/year
  Annual Energy Cost=7,022,160kWh×0.10USD/kWh=702,216USD/year

- Maintenance and Replacement of Components: This cost can be about 2-3% of the initial cost per year, so it is about USD 100,000 to USD 150,000 per year.
- Estimated Total Annual Operating Costs are approximately USD 802,216 to USD 852,216 per year.

3.3.3. Energy Savings

Assuming that this system produces energy with 45% higher efficiency compared to conventional systems, and that a comparable conventional system requires an energy cost of USD 1.2 million per year, the annual energy savings can be calculated as follows:

Annual Energy Savings = $1.2 million × 0.45

Annual Energy Savings = $540,000/year

Annual Energy Savings = $1.2 million × $0.45 = $540,000/year

3.3.4. Return On Investment (ROI)

ROI = Annual Savings / Total Initial Investment × 100%

ROI = $540,000/year /$4.75 million ×100% = 11.37%

3.3.5. Payback Period

The payback period is the time it takes to recoup the initial investment through energy savings. This can be calculated as:

Payback Period = Total Initial Investment/Annual Savings

Payback Period = 4.75 million USD = 540,000 USD/year ≈ 8.8 years

However, if we take into account annual operating costs, the actual payback period may be longer, around 9-10 years, depending on the actual operating costs and savings achieved.

3.4. Application in Various Sectors

To compare the thermodynamic performance of the combined system shown in the figure above with the Kalina KCS 34 cycle and the Organic Rankine Cycle (ORC), we will perform an analysis based on energy efficiency, thermal output, and carbon emissions. Here is a detailed comparison of the three systems.

3.4.1. Energy Efficiency

- Combined System

  The combined system shown in the figure uses a combination of thermal cycles, which involves a gas turbine, a heat exchanger, and a cooling system. The energy efficiency of these systems depends on the optimization of heat transfer and turbine performance. With a turbine producing around 5972 kW of power and a heat exchanger that utilizes waste heat to generate additional energy, the efficiency of this system is quite high, mainly due to the reuse of waste heat.

- Kalina KCS 34

  The Kalina KCS 34 cycle is a thermodynamic cycle that utilizes an ammonia-water mixture as a working fluid. This allows for heat utilization at various temperature levels with higher efficiency than conventional ORC. Kalina cycles typically achieve higher thermal efficiency, about 10-15% more efficient than ORCs, especially in applications with heat sources ranging from medium to low temperatures. In the case of Kalina KCS 34, thermal efficiency can reach up to 50-55%, depending on the conditions of the heat source.

- Organic Rankine Cycle (ORC)

  ORC uses an organic fluid with a low boiling point to generate power from a heat source that is not high enough for a standard Rankine cycle. ORC is often used in low to medium temperature heat sources and is known to have lower thermal efficiency than the Kalina cycle, with a range of

- Comparison

  Energy Efficiency: Kalina KCS 34 > ORC > Combined System

  The Kalina KCS 34 cycle has the highest energy efficiency due to its ability to utilize various temperature levels, followed by a combined system that reuses waste heat, and finally an ORC that has lower efficiency.

3.4.2. Output Termal

- Combined System

  This system shows the thermal output of various components such as turbines and heat exchangers. With a waste heat value of 2.15 kJ/h from the turbine and a heat output of 3,256 kJ/h from the heat exchanger, the system makes optimal use of the waste heat to generate additional thermal output, which can be used for heating applications or additional energy production.

- Kalina KCS 34

  The Kalina cycle can produce significant thermal output due to its ammonia-water working fluid which allows the utilization of heat energy at various temperature points. The thermal output of the Kalina KCS 34 cycle is often greater than that of ORC due to the more flexible and efficient nature of the working fluid in utilizing the heat source.

- Organic Rankine Cycle (ORC)

  ORC tends to have a lower thermal output compared to combined and Kalina cycle systems due to limitations in the utilization of heat sources at low temperatures. Nonetheless, ORC is more commonly used in applications where simplicity and low cost are a priority, even if the thermal output is not as large as other systems.

- Comparison

  Thermal Output: Kalina KCS 34 > > Combined System

  Combined systems, with the utilization of waste heat from multiple sources, tend to produce greater thermal output than Kalina KCS 34 and ORC cycles

3.4.3. Carbon Emissions

- Combined System

  By reusing waste heat, this system has the potential to reduce carbon emissions compared to systems that rely solely on fossil fuels. With high energy efficiency, the carbon emissions from these systems are relatively low, especially when compared to fossil fuel-based systems that do not utilize waste heat.

- Kalina KCS 34

  The Kalina cycle is known to have lower carbon emissions due to its higher efficiency in utilizing thermal energy. Thus, the energy use per unit of output is lower, which directly reduces carbon emissions. The Kalina cycle is commonly used in power plants that want to maximize efficiency while minimizing environmental impact.

- Organic Rankine Cycle (ORC)

  Although ORCs have lower thermal efficiency, carbon emissions from ORCs can also be minimized if these systems are combined with renewable heat sources, such as waste heat from industrial processes or geothermal sources. However, compared to the Kalina KCS 34 and the combined system, the carbon emissions from the ORC can be higher due to the lower efficiency.

- Comparison

  Carbon Emissions: Kalina KCS 34 < Combined System < ORC

  The Kalina KCS 34 cycle has the lowest carbon emissions due to higher energy efficiency, followed by the combined system, and finally the ORC.

3.4.4. Comparison Results

In terms of thermodynamics, the Kalina KCS 34 cycle shows superior performance with the highest energy efficiency and lowest carbon emissions, especially in applications with medium to low temperature heat sources. The combined system, as depicted in the image above, offers a good balance between energy efficiency and thermal output, as well as a reduction in carbon emissions through the reuse of waste heat. ORCs, despite their lower efficiency, remain a viable option in situations where design simplicity and low cost are preferred.

For applications where energy efficiency and carbon emission reduction are top priorities, the Kalina KCS 34 cycle is more recommended. However, if flexibility in the utilization of waste heat and large thermal output are required, a combined system can be the best option. ORC can be selected for small-scale applications with renewable heat sources.

3.5. Application in Various Sectors

Indonesia, with its abundant geothermal potential, is at the forefront of efforts to utilize renewable energy sources for future energy needs. In particular, low enthalpy geothermal, known for its low temperatures, presents a great opportunity for the development of innovative technologies that can address renewable energy challenges in various sectors. This innovation, as we have developed through an integration system that combines the advantages of the ORC cycle and Kalina KCS is one of the breakthrough efforts to improve efficiency and flexibility in the utilization of geothermal energy.

This innovation opens the door to a wider range of applications of geothermal low enthalpy, not only in small-scale power plants, but also for direct applications in the industrial, agricultural and tourism sectors. By optimizing this technology, we can be more efficient in using geothermal resources scattered throughout the country, both in volcanic and non-volcanic regions. These innovations allow the use of energy for drying agricultural produce,

heating fish ponds, and even spa facilities in the tourism industry, at lower costs and minimal environmental impact.

In the following sections, it will be explained in more detail how this technology can be applied in Indonesia's key sectors, as well as how the integration of these innovations can provide solutions to sustainable energy needs. This discussion will cover the technical aspects of the implementation of the integrated system, as well as its impact on energy efficiency and contribution to the national renewable energy target. Thus, we can see the whole picture of how innovation in low enthalpy geothermal can be the answer to Indonesia's future energy challenges.

3.6. Implementation Strategy

In an effort to utilize technology low enthalpy geothermal Effectively, it is important to develop a comprehensive implementation strategy. This strategy should include adequate technical planning, supportive regulatory arrangements, and identification of challenges that may arise. Technical needs involve the selection and installation of appropriate technologies, while regulations must ensure policy support and incentives. Challenges that may be faced include technical constraints, adaptation to local conditions, and harmonious arrangements with existing energy regulations. With a planned strategy, this technology can be effectively integrated to support sustainable energy growth in Indonesia.

3.6.1. Technical Requirements

The application of low enthalpy geothermal technology in Indonesia requires the right selection of technology and efficient system design, such as ORC that is effective at low temperatures and KCS that uses ammonia-water mixtures to improve efficiency. Supporting infrastructure is also crucial, including geothermal wells designed for heat extraction efficiency, power distribution networks to connect plants with end-users, and processing and maintenance facilities to maintain optimal operations. Given Indonesia's varied geological conditions, the design of the system must be adapted to geothermal potential and local challenges, such as accessibility and environmental impacts, to ensure maximum benefits from these technologies.

3.6.2. Regulation

To ensure that the application of geothermal low enthalpy technology runs effectively and in accordance with the provisions of the law in Indonesia, an understanding of the regulations governing the geothermal sector is very important. Law Number 21 of 2014 concerning Geothermal and Government Regulation Number 7 of 2017 are the main legal basis that includes sustainable management, efficiency, and support for technological innovation. Articles in this law, such as Article 3 which establishes national energy development goals and Article 4 which emphasizes sustainable management, support the development of this technology, which integrates ORC and KCS-34 to improve energy efficiency. Government regulations also provide incentives and ease of licensing for research and development of geothermal technology. Support from local regulations and local government policies further facilitates the application of geothermal technology in areas with high potential. Overall, the regulatory framework in Indonesia provides a strong foundation for the development and implementation of efficient and environmentally friendly geothermal innovations.

3.7. Analysis of possible challenges at the time of implementation

The implementation of low enthalpy geothermal technology in Indonesia faces several main challenges, both technical, infrastructive, social, and environmental. Technically, geological variability and technological adaptations such as ORC and KCS 34 to local conditions require accurate geothermal evaluation and system adjustment. In terms of infrastructure, the construction of drilling wells and electricity distribution systems in remote areas requires complex costs and logistics. In addition, electricity grid connectivity is also an obstacle, especially in areas with inadequate infrastructure. Social challenges include the acceptance of local communities, which requires effective socialization to gain support and reduce conflict. On the environmental side, although geothermal energy is relatively clean, large projects still have the potential to cause environmental impacts that require careful mitigation. Facing and responding to these challenges with the right strategy will ensure that the implementation of this technology runs efficiently and provides significant benefits for the development of renewable energy in Indonesia.

4. STUDY CASE

To reinforce the thermodynamic analysis that has been carried out previously, we will add relevant case studies regarding the application of the Kalina KCS 34 system, ORC, and combined system as shown in the figure. This case study will provide insight into how these technologies are applied in real-world situations and how they perform under various operational conditions.

4.1 Case Study 1: Geothermal Power Plant with Kalina KCS 34 Cycle in Chena, Alaska

Background:

The Geothermal Power Plant in Chena, Alaska, is one of the most well-known examples of the use of the Kalina KCS 34 cycle to utilize low-temperature geothermal sources. Chena Hot Springs, with a heat source temperature of around 74°C, is an ideal location for the testing and application of Kalina KCS 34, which is designed for high efficiency with a low-temperature heat source.

Implementation and Results:

The power plant uses the Kalina KCS 34 cycle, which is capable of converting low-temperature geothermal heat into electricity with significant efficiency. The system is capable of achieving thermal efficiency of about 45%, much higher compared to standard ORC under similar conditions, which typically has an efficiency of around 20-30%. With an electrical output of around 400 kW, the plant has proven that the Kalina KCS 34 can be operated stably and efficiently in extreme environmental conditions, such as the one in Alaska. In addition, because these systems reduce reliance on fossil fuels, carbon emissions are significantly reduced.

Lessons to Take:

This case study shows that Kalina KCS 34 is very effective in utilizing low-temperature heat sources, and can be used in remote locations with limited infrastructure. Its high efficiency and reduced carbon emissions make it an excellent solution for regions looking to maximize the use of renewable energy sources while minimizing environmental impact.

4.2 Case Study 2: ORC Implementation in a Geothermal Power Plant in Neustadt-Glewe, Germany

Background:

The power plant in Neustadt-Glewe is another example of the use of ORC technology to utilize low- to medium-temperature geothermal sources. The plant uses ORC to utilize a heat source with a temperature of around 98°C.

Implementation and Results:

The ORC system applied here uses organic fluids as a working medium that has a low boiling point, allowing the conversion of geothermal energy into electricity with an efficiency of about 10-20%, depending on the operating conditions. The electricity output from this plant is about 210 kW. Although the efficiency is lower compared to the Kalina cycle, the ORC system has advantages in terms of simple design, lower initial cost, and the ability to be easily integrated into existing systems.

Lessons to Take:

ORCs are ideal for small to medium-scale applications, especially in locations that require energy solutions with lower initial costs. However, the lower efficiency means that in the long run, ORC may result in smaller energy savings and a greater environmental impact compared to the Kalina cycle.

4.3 Case Study 3: Combined Systems at an Industrial Plant in California

Background:

An industrial plant in California has implemented a combined system similar to the one shown in the image above. The system utilizes the exhaust heat from the gas turbine to improve the overall efficiency of the plant.

Implementation and Results:

In this case, the plant uses a gas turbine with an output of 5 MW for the industrial process, and the waste heat from the turbine is used in the heat exchanger system to heat additional working fluids which are then used to generate more energy or for further heating processes in the plant. The system has successfully increased the thermal efficiency of the entire plant by up to 55%, higher than the use of separate gas turbines. In addition, the plant's carbon emissions are also reduced by around 25% thanks to the reuse of waste heat.

Lessons to Take:

Combined systems are particularly beneficial in industrial applications where exhaust heat is often not utilized to its full potential. By using waste heat to improve energy efficiency, the system not only reduces energy consumption but also reduces carbon emissions, making it a highly effective solution in energy saving and environmental protection efforts.

4.4 Conclusion of the Case Study

These three case studies show that each technology has its own advantages and disadvantages:

- Kalina KCS 34 is most effective in utilizing low to medium temperature heat sources with high efficiency and low carbon emissions. It is the best choice for applications in remote locations or places where energy efficiency and carbon emission reduction are prioritized.
- ORC is a more economical option for small to medium-scale applications with a low heat source. Despite their lower efficiency, ORCs offer lower upfront costs and ease of integration with existing systems.
- The Combined System offers high thermal efficiency and optimal utilization of waste heat, making it an ideal choice for industrial applications looking to optimize energy use and reduce carbon emissions.

5. CONCLUSION

The innovation of combining two cycles, namely the Organic Rankine Cycle (ORC) and the Kalina Cycle System (KCS-34), offers a significant solution to utilize low enthalpy geothermal energy in Indonesia. The combination of these two cycles in one integrated system, results in a more efficient and flexible power generation system compared to conventional systems that only use one of the cycles separately.

The analysis of the merging system shows that the integration of ORC and KCS-34 provides higher energy efficiency by making optimal use of waste heat. This combined system is able to maximize the use of heat from geothermal sources with a low to moderate temperature range, so that it can produce a greater thermal output than using an ORC or KCS-34 system independently. Simulations show that the system can operate with about 5,972 kW of power from the turbine and harness the waste heat to generate additional energy.

From economic analysis, this combined system offers promising financial profit potential. The initial cost of the investment may be higher than that of conventional systems, but the Return on Investment (ROI) and Payback Period show that with higher energy savings and better efficiency, the investment can return in a shorter period of time, which is about 8-10 years. In addition, with significant annual savings, the system can provide long-term economic benefits.

Comparative analysis with conventional systems confirms that this combined system has better thermal efficiency compared to the stand-alone ORC and Kalina KCS-34 systems. Additionally, the system has lower carbon emissions thanks to its more effective utilization of waste heat, making it a more environmentally friendly option when it comes to generating electricity from geothermal sources.

The results and simulations show that the design of this system not only improves energy efficiency but also reduces environmental impact and provides more optimal performance under various operating conditions. With more efficient energy distribution and optimal waste heat management, the system has significantly reduced fuel consumption and carbon emissions, which is in line with Indonesia's goal of developing renewable energy sustainably.

The innovative combination of two cycles of ORC and Kalina KCS-34 through this system presents an efficient and environmentally friendly solution for geothermal power generation in Indonesia. With simulation results showing improved energy efficiency and reduced carbon emissions, this innovation has great potential to support the national energy transition towards sustainable renewable resources. The merger of these two cycles is a step forward in geothermal technology that can bring Indonesia closer to the clean and efficient energy target.

REFERENCES

Agus Noor Sidiq. (2008). *Energy Analysis and Allergy of Kalina Cycle System (Kcs) 11 with Variation in the Mass Fraction of Ammonia-Water Mixture*. FT UI.

Borsukiewicz-Gozdur, A., & Nowak, W. (2007). Comparative Analysis of Natural and Synthetic Refrigerants in Application to LowTemperature Clausius–Rankine Cycle. *Energy Conversion and Management*, 48(9), 2393-2401.

Cengel, Y. A., & Boles, M. A. (2015). *Thermodynamics: An Engineering Approach*. McGraw-Hill Education.

D'Agostino D., Minichiello F., Petito F., Renno C., Valentino A. (2022). *Retrofit Strategies To Obtain A NZEB Using Low Enthalpy Geothermal Energy Systems*. ScienceDirect.

De León-Ruiz J.E., Beltrán-Chacón R., Carvajal-Mariscal I., Zacarías A., Rodríguez-Maese R. (2022). *A data-driven approach to low-enthalpy shallow geothermal energy extraction: A case study on indoor heating for precision agriculture applications*. ScienceDirect.

Glassley, W. E. (2014). *Geothermal Energy: Renewable Energy and the Environment*. CRC Press.

Gonzalo, Chiriboga. (2020). *Harnessing of geothermal energy for a greenhouse in Ecuador employing a heat pump: design, construction, and feasibility assessment*. PMC.

Hettiarachchi, H. D. M., Golubovic, M., Worek, W. M., & Ikegami, Y. (2007). The Performance of the Kalina Cycle System 34 with Low-Temperature Heat Sources. *Journal of Energy Resources Technology*, 129(3), 243-247.

Incropera, F. P., DeWitt, D. P., Bergman, T. L., & Lavine, A. S. (2007). *Fundamentals of Heat and Mass Transfer*. John Wiley & Sons.

Johnson, I., Choate, W. T., & Davidson, A. (2008). *Waste Heat Recovery: Technology and Opportunities in U.S. Industry*. U.S. Department of Energy.

Lund, J. W. (2003). Direct Application of Geothermal Energy: Worldwide Review. *Geothermics*, 32(4-6), 471-481.

Lund, J. W., & Freeston, D. H. (2010). World-Wide Direct Uses of Geothermal Energy 2010. *Geothermics*, 39(3), 143-160.

Moran, M. J., & Shapiro, H. N. (2010). *Fundamentals of Engineering Thermodynamics*. John Wiley & Sons.

Ngoc Tran, James Fross, Kaitlyn Mykleby, John Roff, Catalin Teodoriu. (2020). *The Economics of Low Enthalpy Geothermal Resources: A Case Study for Small Heat Harnessing Concept in Oklahoma*. Stanford University.

Noh, Y., Jafarinejad, S., Anand, P. (2024). *A Review on Harnessing Renewable Energy Synergies for Achieving Urban Net-Zero Energy Buildings: Technologies, Performance Evaluation, Policies, Challenges, and Future Direction*. MDPI.

OJP LP2M UIN Jambi. 2023. *View of HOW IS ESD (Education for Sustainable Development) Integrated with Renewable Energy Systems*. OJP LP2M UIN Jambi.

Rahmat Widodo and Fanny Leestiana. (2023). Study on the Utilization of the Kalina 11 and 34 Cycle System as PLTP. I *JURNAL TEKNIK ITS* Vol. 12(2), ISSN: 2337-3539 (2301-9271 Print).

Rizky Agassy Sihombing, Muslim Muslim, Taufik Rahman, Amir Karimi. (2024). Literature Study of the E-book Based on Education for Sustainable Development (ESD) as the Main Solution to Improving Sustainability Awareness. *Jurnal Insecta*.

Rybach, L., & Mongillo, M. (2006). Geothermal Sustainability - A Review with Identified Research Needs. *Geothermal Resources Council Transactions*, 30, 1083-1090.

Solano-Arguedas A.F., Vargas-Azofeifa I., Barrantes-Jiménez K., Carmona-Villalobos G., Solís-Ramírez K., Rodríguez-Mora K., Álvarez-Saborío Y., Casanova-Treto P. (2022). *Exploring low enthalpy geothermal energy in Costa Rica: A pilot project to improve tourism energy matrix efficiency*. Eurogeologists.

Yose Ardhani Farasi, Dr. -Ing. Sihana; Dr. Khasani, S.T., M.Eng. (No publication date found). *Thermodynamic Analysis of the Kalina Cycle System (Kcs) 11 in the Jailolo - Halmahera Geothermal Field*. ETD Repository UGM.

Zhang X, Li Z, Wang J, Wu Y and Ma C. (2021). Performance Improvement of KCS (Kalina Cycle System) 34 by Replacing Throttle Valve With Single-Screw Expander. *Frontiers in Energy Research*, 9:741704. doi: 10.3389/fenrg.2021.741704.

Digitalization of Geothermal Plant Facilities

Wasis Hartono

BB (PT ABB Sakti Industri), Jl. Margomulyo No. 44 Kav. E 1-2, Surabaya, Indonesia

wasis.hartono@id.abb.com

Keywords: Geothermal plant, power plant, digitalization, digital solutions, geothermal plant facilities, asset performance management, energy management and optimization, operation optimization, advanced process control, cyber security

ABSTRACT

Bridging the shift from automation to autonomous operation, ABB's integrated digital solutions address key objectives related to assets, operations, and people. While digital transformation enables autonomy in the energy industry, achieving autonomous operations involves managing various complexities, such as extended operation, remote operation, integrated analytics, and augmented operation. Geothermal power generation plants have a complex configuration, with large steam consumption, multiple production wells, multiples turbines and significant variability in steam production due natural variability of the geothermal process.

ABB's Asset Performance Management (APM) solutions help ensure the reliability of geothermal assets, which involves applying latest technologies such as AI/ML to predict equipment issues, and to predict asset or component life more accurately, so that predictive maintenance and future capital investment can be planned further in advance. Part of this approach, ABB addresses critical geothermal assets like heat exchangers, pumps, pipeline, filter or geothermal wells related issues and corresponding failure modes.

The control and optimization of the multiple power generation and steam networks in geothermal production field, especially with multi-sites, is challenging due to the inherent complexity of the field, the significant interactions between process equipment and the continuous disturbances caused by variability in steam generation by the well. Optimization of energy export and minimization of production costs can be achieved consistently through adaptation of digital solution that manage and optimize the energy and processes. The solution is capable of continuously adapting power generation and steam networks operations to the variability in steam production to maximize power generation efficiency and profits. ABB's OPTIMAX-Advanced Process Control for example offers stabilization of steam in the headers and transfer lines and improve ability to manage disturbances with minimal manual intervention. Also, the solution aim is to optimize the operation and improve the benefit, such as via optimal load allocation on steam generation and turbines, reduction of venting and use of pressure reduction valves, automatic minimization or maximization of internal power production considering daily power prices. One key part of whole digital transformation ecosystem is the exchange of data internally as well externally and to ensure the data transfer is safe and secure, where the relevant Cyber Security practices must be in place. ABB's Cyber Security Workplace (CSWP) addresses the cybersecurity aspects of OT/IT convergence, ensuring secure integration. This comprehensive software ecosystem enhances the reliability, efficiency, and intelligence of geothermal facilities. As a technology leader in electrification and automation, ABB is at the core of propelling the energy transition forward. It's range of solutions optimizes power consumption and processes, crucial for stabilizing renewables and mitigating new energy market risks and effective data management provides transparency and actionable insights, driving efficiency and sustainability gains.

1. INTRODUCTION

Geothermal plays important role in considerably emerging part of Indonesia's power generation, particularly from new and renewable energy sources. Indonesia's investment plan for the $20 billion Just Energy Transition Partnership (JETP) calls for rapid growth in renewable energy of all kinds, including geothermal energy.

Geothermal and hydro can supply the grid with steadier and more predictable forms of electricity generation. According to the JETP scenario, by 2030 geothermal (268 projects) and hydro (470 projects) will produce 22% of Indonesia's electricity. To achieve these goals (which are, it must be said, wildly optimistic) both variable and dispatchable renewables need to grow rapidly over the next seven years.

Huge potential success given the experience and involvement from geothermal developer Geo Dipa (government and PLN owned), PERTAMINA, and PLN.

ABB's integrated solutions in automation, excitation, and turbine control as well as instrumentation, electrical systems and advanced optimization packages ensure flexibility and availability for the customer. Digital solutions such as predictive maintenance solutions reduce O&M costs and insights for operational strategies. Another digital

solution for plant performance, especially in steam and power networks, optimizes the energy export and processes.

Example of ABB's works are retrofit and replace Darajat geothermal plant control, through digital technologies and turbine control systems to improve flexibility, reliability, availability and reduce maintenance cost at the two geothermal plants.

Geothermal power generation plants have a complex configuration, with large steam consumption, multiple production wells, multiples turbines and significant variability in steam production due natural variability of the geothermal process.

Bridging the shift from automation to autonomous operation, ABB's integrated digital solutions address key objectives related to assets, operations, and people. While digital transformation enables autonomy in the energy industry, achieving autonomous operations involves managing various complexities, such as extended operation, remote operation, integrated analytics, and augmented operation.

The paper will give brief overview on ABB digital solutions from Asset Performance Management (APM), Energy Management and Optimization OPTIMAX®-Advanced Process Control, and Cyber Security point of views.

2. MANAGING ASSETS THROUGH ABB ABILITY™ ASSETS PERFORMANCE MANAGEMENT (APM)

ABB's Asset Performance Management (APM) solutions help ensure the reliability of geothermal assets, which involves applying latest technologies such as AI/ML to predict equipment issues, and to predict asset or component life more accurately, so that predictive maintenance and future capital investment can be planned further in advance. Part of this approach, ABB addresses critical geothermal assets like heat exchangers, pumps, pipeline, filter or geothermal wells related issues and corresponding failure modes.

2.1 ABB Ability™ Assets Performance Management

ABB Ability™ Asset Performance Management is a scalable enterprise solution that reduces unscheduled maintenance costs by helping the user better understand and predict asset performance. Higher reliability and production efficiency can be achieved by minimizing or eliminating costly, unplanned downtime. It helps the user extract the most value from the assets by avoiding the uncertainties, risks, and costs of ineffective maintenance approaches. Using data-driven decision making, asset performance and maintenance across the entire enterprise can be optimized.

ABB's Asset Performance Management solutions help ensure the reliability of geothermal assets, which involves applying latest technologies such as AI/ML to predict equipment issues, and to predict asset or component life more accurately, so that predictive maintenance and future capital investment can be planned further in advance. Part of this approach, ABB addresses critical geothermal assets like heat exchangers, pumps, pipeline, filter or geothermal wells related issues and corresponding failure modes.

ABB Ability™ Asset Performance Management is next generation AI-Based Asset Performance Management with vendor agnostic, enterprise-grade, and flexible deployments feature. In Condition Monitoring feature (through AssetInsight or APM Predict solution), adding Condition Monitoring on the Edge into existing OT landscape becomes easier as the solution will start prioritizing maintenance activities based on data. It can provide condition monitoring of electrical, rotating, instruments and IT through OT data/sensors and pre-built asset models to monitor known failure modes. It will provide maintenance workplace with detailed real-time information.

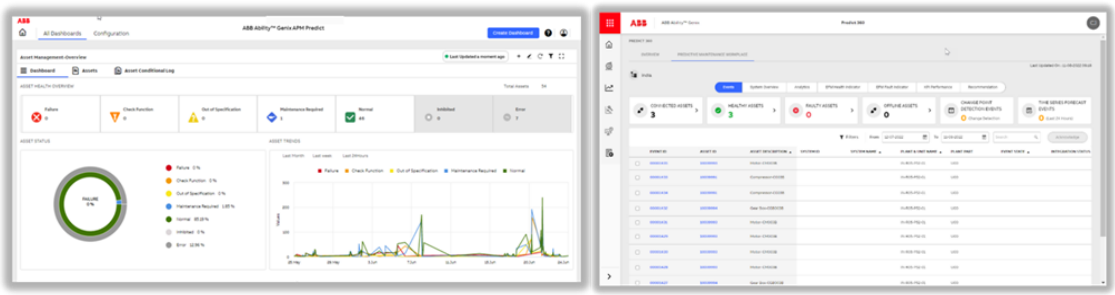

Figure 1: Sample of ABB APM Predict and APM 306 dashboards.

In Advanced Prediction feature (through APM 360), testing, training, and deploying advanced predictive & prescriptive models becomes collaborative by capturing & codifying the knowledge of experts to increase

outcomes. The solution is working with OT/IT/ET contextualized data + derived or predicted parameters, self-service fault modeling throughout asset life cycle, rule-based and AI/ML, library of configurable asset models with pre-built dominant failure modes, and events management, fault monitoring tools with recommendations and automated work order creation.

In Maximum Performance feature (through APM 360), a holistic view of asset performance, health, maintenance schedules, lifecycle cost becomes possible as all it will connect APM, work, operations, and management to realize more value. It works with parametrized asset templates (pre-built performance models), Digital Twin, and 360° view on Performance – Asset Performance, Asset Health, Maintenance Strategy Execution, and Life Cycle Cost.

2.2 Prebuilt asset models

The prebuilt asset models (rule-based or custom logic) in APM built-in library (see Figure 2) are key for conditioning monitoring with real-time fault detection and performance monitoring, single variable threshold monitoring, as well as derived/calculated monitoring. Further the advance predictions are provided by advanced fault modeling and prediction using hybrid modeling techniques. Typically, the 1st Principles physics-based performance models and self-service data driven models using AI/ML algorithms (multi-variate) are incorporated. The Maximum Performance will give asset insights across performance, health, maintenance schedules and life cycle cost by combined & contextualized OT/ET/IT data, Predictive Maintenance Workplace including analytics with CMMS data (as applicable).

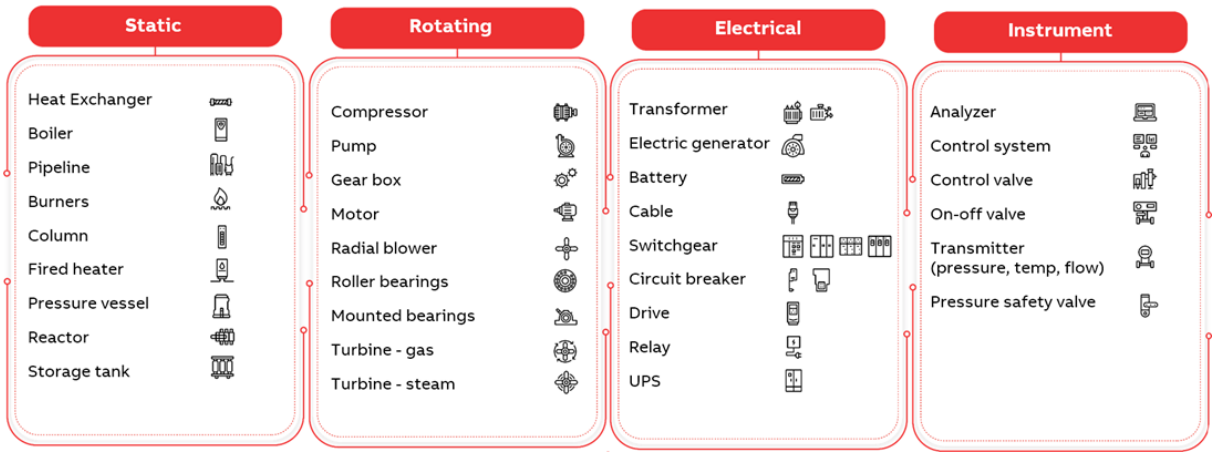

Figure 2: ABB APM's library of pre-built asset models based on domain experience.

In today's rapidly evolving industrial landscape, the integration of advanced analytics and enhanced Asset Performance Management solutions has become paramount for organizations seeking to optimize operational efficiency, reduce costs, and enhance asset performance.

2.3 Data-driven recommendations and actions for asset maintenance.

ABB's cutting-edge technology of ABB Ability™ Asset Performance Management provides advanced analytics and management of asset performance, which play a pivotal role in driving cost reduction, increasing production efficiency, and optimizing resource utilization. There are various showcases success stories where early alerts from ABB's solutions prevented unplanned equipment failures and optimized operational costs, underscoring the tangible benefits of proactive maintenance strategies. Moreover, the transition from reactive to proactive maintenance, facilitated by ABB's solutions, highlights the importance of leveraging the Industrial Internet of Things (IIoT) revolution to revolutionize asset performance monitoring.

By harnessing advanced Machine Learning and Artificial Intelligence capabilities, ABB's APM solutions continuously monitor asset health, detect potential issues, and trigger alerts for timely intervention. This proactive approach empowers organizations to make data-driven decisions, optimize maintenance schedules, and minimize downtime, ultimately enhancing overall operational efficiency (see Figure 3). The transformative potential of advanced analytics and digital tools in driving industrial transformation, optimizing maintenance strategies, and paving the way for a sustainable and efficient future in the industrial sector is evident.

From a practical standpoint, even the best asset management systems do not rely on equipment and data communications systems alone. They depend on human involvement in a culture of continuous improvement among plant operators, maintenance crews, and plant management derived from statistics, data science, heuristic learning, and other expert knowledge. Some perspective on how to make the transition to digital solutions realistically to be respected as there are issues regarding human acceptance of predictive maintenance and asset

management systems which need to be addressed. Something as small as giving users the ability to tweak automated predictive analytics approaches with their own personal experience can be key to successful initial adoption.

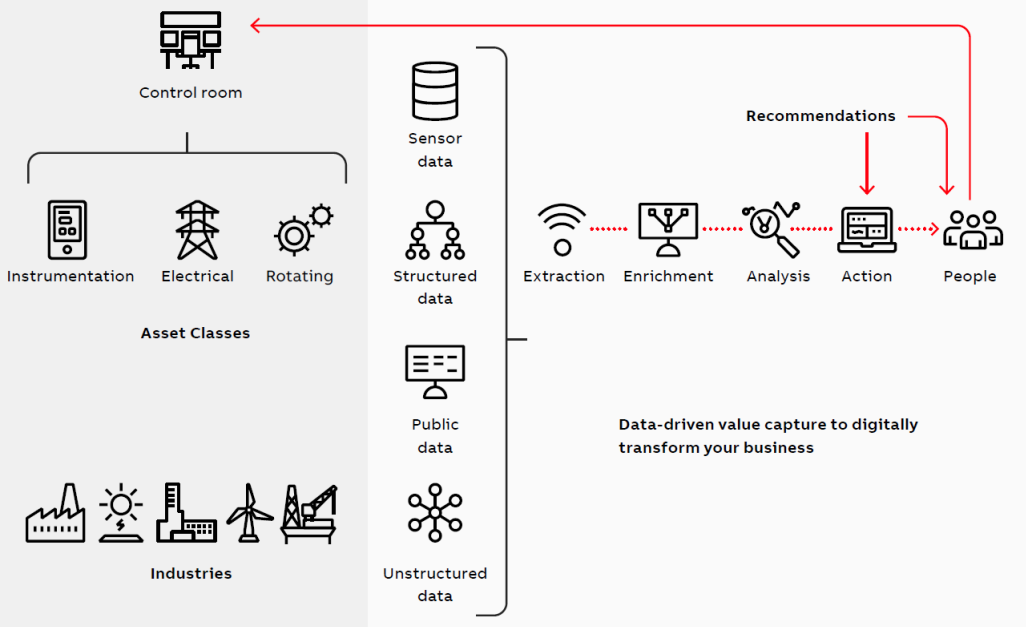

Figure 3: Data driven recommendations and actions in ABB Asset Performance Management application.

The integration of advanced analytics and enhanced Asset Performance Management solutions offered by ABB represents a paradigm shift in industrial operations. By embracing data analytics, artificial intelligence, and digital technologies, organizations can unlock new levels of efficiency, reliability, and sustainability. The journey towards digitalization and enhanced asset performance is not just a technological evolution but a strategic imperative for organizations looking to thrive in the competitive industrial landscape. ABB's commitment to driving innovation and industrial transformation underscores the company's role as a global leader in electrification and automation, shaping a more sustainable and resource-efficient future for industries worldwide, including in geothermal power segment.

3. PERFORMANCE OPTIMIZATION THROUGH ABB ABILITY™ ENERGY MANAGEMENT AND OPTIMIZATION - OPTIMAX® AND ADVANCED PROCESS CONTROL (APC)

The control and optimization of the multiple power generation and steam networks in geothermal production field, especially with multi-sites, is challenging due to the inherent complexity of the field, the significant interactions between process equipment and the continuous disturbances caused by variability in steam generation by the well.

Optimization of energy export and minimization of production costs can be achieved consistently through adaptation of digital solution that manage and optimize the energy and processes.

3.1 ABB Ability™ Energy Management and Optimization – OPTIMAX®-Advanced Process Control

The solution is capable of continuously adapting power generation and steam networks operations to the variability in steam production to maximize power generation efficiency and profits. ABB's OPTIMAX®-Advanced Process Control offers stabilization of steam in the headers and transfer lines, implement optimal load allocation and resulting steam transfer, and improve ability to manage disturbances and balance variability with minimal manual intervention.

The solution is also aimed to optimize the operation and improve the benefit, such as via optimal load allocation on steam generation and turbines, reduction of venting and use of pressure reduction valves, automatic minimization or maximization of internal power production considering daily power prices.

In case of steam turbine optimization, steam turbine efficiency curves can be considered or adopted in the configuration, as well as other parameters such as transfer line losses and equipment constraints. The solution will favor the most favorable load allocation, allowing production maximization and optimization of power revenues and stabilize pressure across all headers and transfer lines, reducing metal stresses, steam losses and variability in operations liked to personnel experience.

Additional benefits from the solution, such as the ability to stabilize operations, reduce manual, actions and standardize operations are also obvious.

3.2 Advanced Process Control underlying technology

The digital solution will be covering the Power Generation and Steam Networks in its application configuration. It will manage the relevant equipment and will operate so to optimize operations and referred here as the "power generation optimization" or "steam and power optimization". It applies the Advanced Process Control (APC) and Energy Optimization application covering the coordination of the geothermal power generation plant.

Advanced Process Control (APC) is a Model-based Predictive Control (MPC) which both actually have a slightly different technical meaning. In a simplified view, MPC describes the technology more accurately while APC is a term often describing a broader set of technologies, which could range from Advanced Regulatory Control in the DCS to full-blown Model Predictive Control technologies. However, in industrial context the APC and MPC acronyms are very often considered equivalent or close to equivalent.

Traditionally, Advanced Process Control relies on Model Predictive Control technology and moving horizon estimation strategies that use either a linear or non-linear mathematical model of the industrial plant and smart algorithms to estimate control-related process in the future.

In terms of modeling process, APC has always been focused on a data-driven approach, where models are built out of process data, either with dedicated step-tests or via a careful selection of historical data. This provides significant benefit in terms of engineering effort compared to model development considering first principles and equipment data.

The basic concept behind the APC technology is to use Model Predictive Control (MPC) as control synthesis technology, representing the plant and process units under consideration as a dynamic system, reacting according to continuous dynamics. This technology allows to map system response to known changes in variables, like setpoints, normally handled by plant personnel, to key variables in the process that are linked to production quality, production load and key constraints. This mapping is performed to the extent of identifying a dynamic model, linking the first variables, known as independent variables or inputs, to the latter ones, known as dependent or output variables.

ABB Model Predictive Control software, named Predict & Control, uses a modern and, at the same time, a very robust technology, based on state-space formulation and use of an explicit state estimation via a Predictor based on Kalman filter (Figure 4).

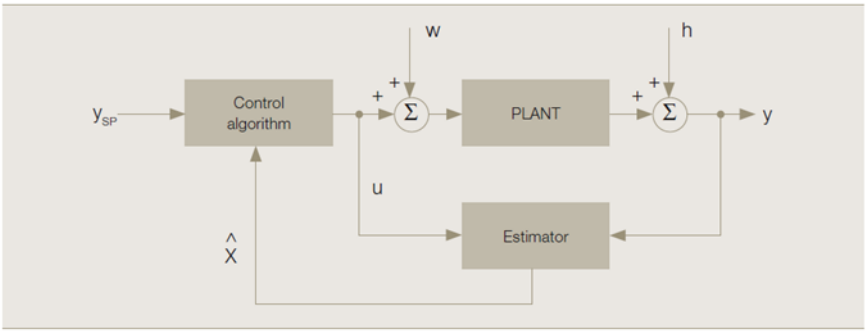

Figure 4: Basic principle of ABB's Predict & Control.

3.3 Plant Performance Optimization

The quantifiable process benefits achieved with this technology are often exceeded as a result of the addition of process expertise from APC application engineers and of the interaction between these engineers and the Clients specialists. These benefits will include reduced energy consumption, improved quality control, and increased throughput.

In addition to that, MPC delivers further benefits that are tangible but whose value is difficult to quantify, such as process stabilization and reduction in variability due personnel experience and operation style.

Illustration on how the MPC improve performance and moving operation to new optimized point are shown in Figure 5 below.

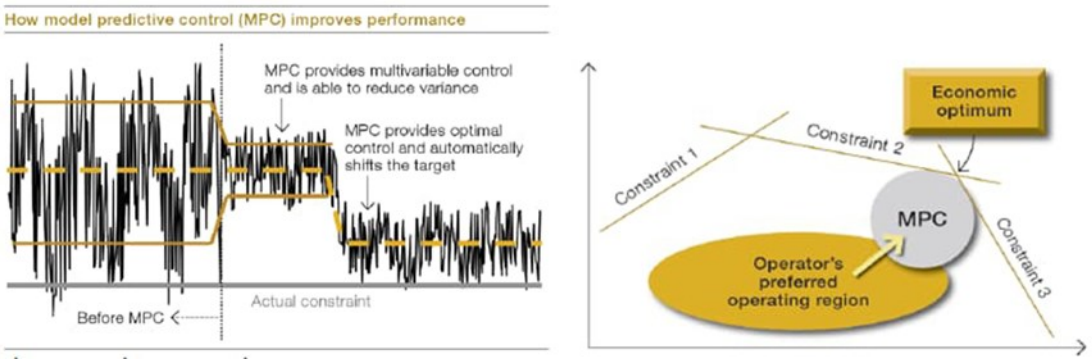

Figure 5: Illustration of MPC impact on variance and moving operation to optimized point.

An additional control layer (as Real-Time Optimization module) may be needed in cases where the economics of the process units or plant are complex and can change significantly over time.

In geothermal plant with steam network, the optimizer covers balancing steam over the various steam sources so to minimize production costs and calculating the optimal load allocation for the relevant equipment by considering actual steam production, equipment efficiency curves, equipment limits and relevant constraints, and transfer lines losses.

The optimizer then dispatches these orders to an APC control layer, which provides coordinated, decoupled control of pressure and power generation, which will stabilize steam headers and steam transfer lines, implement optimal load allocation and resulting steam transfer as computed by the Real Time Optimizer, and reject disturbances, balance variability in the steam production.

The base control level modulates the actuators affecting the plant to maintain the measured process quantities at their setpoints (see Figure 6).

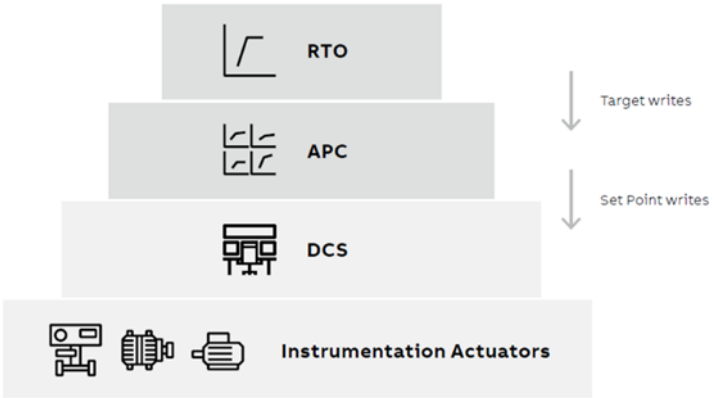

Figure 6: Real-Time Optimizer and Advanced Process Control integrated solution.

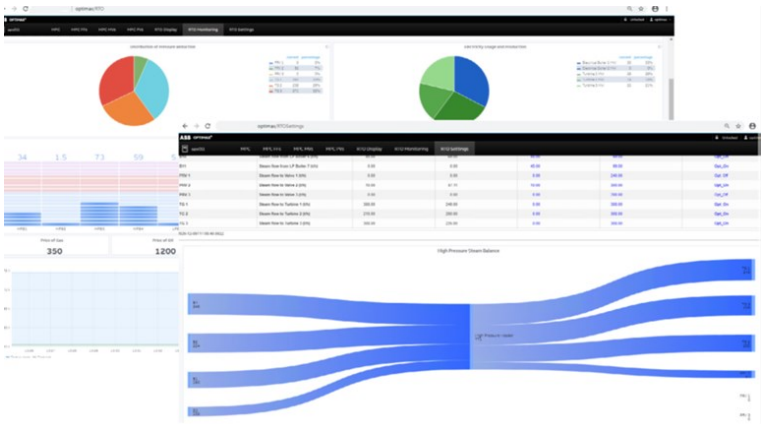

Figure 7: Sample of advanced dashboards providing insights on Steam Network economics and efficiency.

Steam & Power Optimization has a very modular, scalable software configuration based on ABB OPTIMAX and Predict & Control multivariable controller software. The same architecture and same software modules can be applied to small and very large steam networks, including the ones in geothermal power plants. Sample of advanced dashboards providing insights on Steam Network economics and efficiency is shown in Figure 7.

4. SECURING CYBER THROUGH ABB ABILITY™ CYBER SECURITY WORKPLACE (CSWP)

One key part of whole digital transformation ecosystem is the exchange of data internally as well externally and to ensure the data transfer is safe and secure, where the relevant Cyber Security practices must be in place. ABB's Cyber Security Workplace (CSWP) addresses the cybersecurity aspects of OT/IT convergence, ensuring secure integration. This comprehensive software ecosystem enhances the reliability, efficiency, and intelligence of geothermal facilities.

4.1 Cyber Security

Cyber-attacks against industrial plants are growing in frequency, level of sophistication, and degree of harm inflicted. Today's advanced threats need advanced cyber security solutions designed for industrial users protecting your systems without compromising reliability. Staying ahead of cyber criminals and keeping your production secure requires a new simplified approach to managing foundational security.

The situation of where the cyber disaster in the industrial plant is typical. Thousands of distributed assets, multiple control loops, hundreds of controllers, and next to no cyber security.

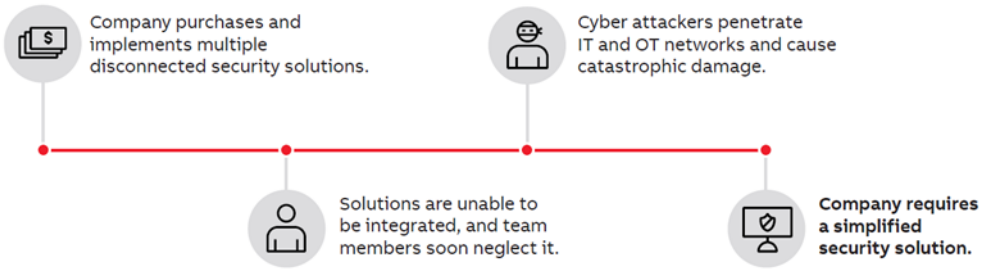

Figure 8: Typical sequence of events of cyber-attack.

A common misconception is that both cyber-attacks and cyber security controls are sophisticated and complex. In fact, the methods criminals use to infiltrate industrial networks are often relatively straightforward. When cyber security controls are perceived to be complex or intimidating to operate and manage, one of two things happens:

1. Implemented security controls get neglected, significantly reducing their efficiency.
2. Security is viewed as a hassle and is never implemented.

A customer's investment in security controls is wasted if those tools are not implemented, operated, and maintained correctly.

4.2 ABB Ability™ Cyber Security Workplace (CSWP)

ABB Ability™ Cyber Security Workplace automates security insights and defense. It gives security teams complete visibility of their security controls by providing a consolidated view of all security controls in a simple and intuitive user interface.

ABB Ability™ Cyber Security Workplace collects security-relevant data from ABB and third-party cyber security solutions and forwards it into a consolidated native application. Operators can seamlessly monitor the status of their security controls, perform maintenance activities to increase resiliency, and receive alerts with actionable insights to remediate threats and reduce risks.

As one simplified platform for security operations, the solution will shift from multiple siloed security tools and take charge of your security program. It will manage security updates, malware protection, and system backups, provide set alarms and get notified when increased risk exists, provide risk root cause analysis and remediation playbooks to identify and neutralize risks, manage remote access by setting remote access time limits, temporary passwords, and audit history tracking, and provide configurable reports to quickly show compliance.

ABB Ability™ Cyber Security Workplace was designed to quickly identify increased risk in your control system environment, such as with checkmarks to signify there are no cases of increased security risk, stop-light like KPIs to identify and prioritize risks, or intuitive actions to remediate risk, e.g., start a backup job when a backup fails.

When a cyber threat is present in the IT network, it may be best to isolate systems from the network to protect critical systems to prevent production loss or harm to personnel. Cyber Security Workplace enables system

administrators to isolate the control system network at the click of a button to keep critical assets safe and production online.

In addition, ABB Ability Cyber Security Workplace's risk root cause analysis was built to provide the cyber expertise by identifying the node(s) and reason that increased risk exists, detailing the potential impact of the risk, as well as providing remediation steps to return risk to an acceptable level.

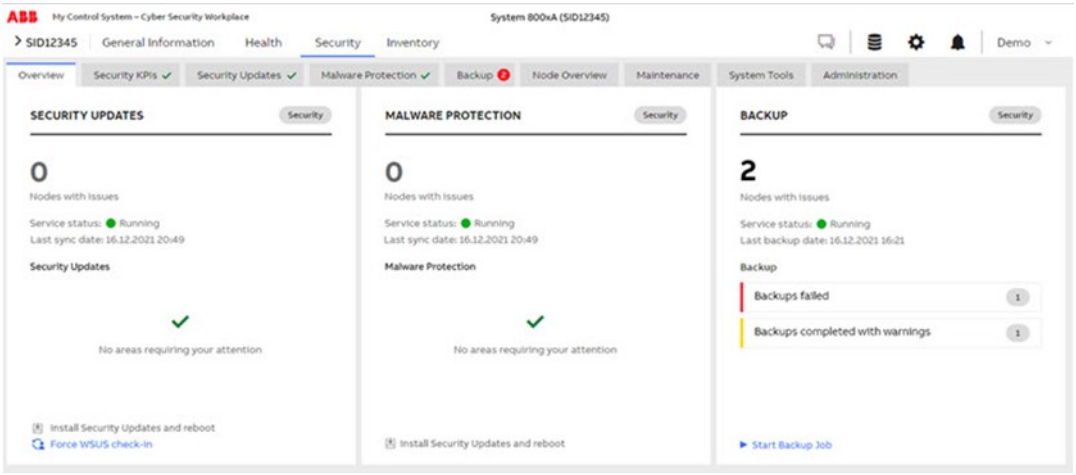

Figure 9: Sample of ABB Cyber Security Workplace dashboard providing simple and intuitive user interface.

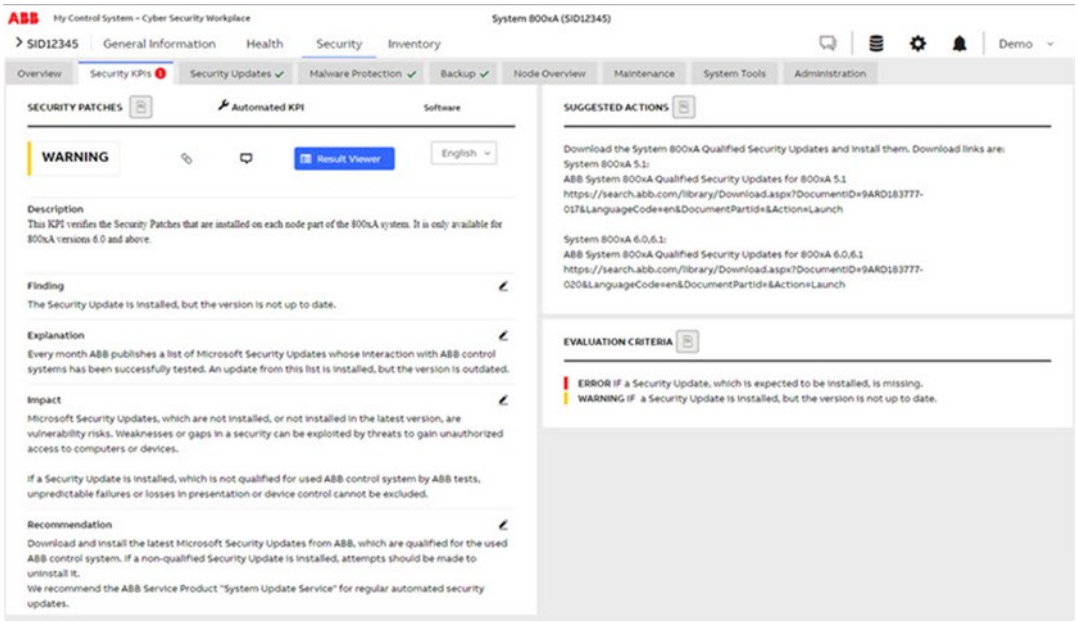

Figure 10: Sample of Risk Root Cause analysis dashboard.

4.3 The implementation

ABB Ability™ Cyber Security Workplace connects to implemented security controls, such as Microsoft WSUS or McAfee ePO, to gather pertinent information about the performance and status of those controls. The collected data is transformed to easy-to-understand KPIs and presented to the user. The user can also interact with some of the controls to perform basic cyber security related tasks e.g. reboot a node.

The workplace fits into the Reference Architecture and can be integrated with the control systems and security controls of ABB Ability™ System 800xA, ABB Ability™ Symphony Plus; and Microsoft WSUS, McAfee ePO, Symantec SEPM, Acronis Backup, and Quest Netvault.

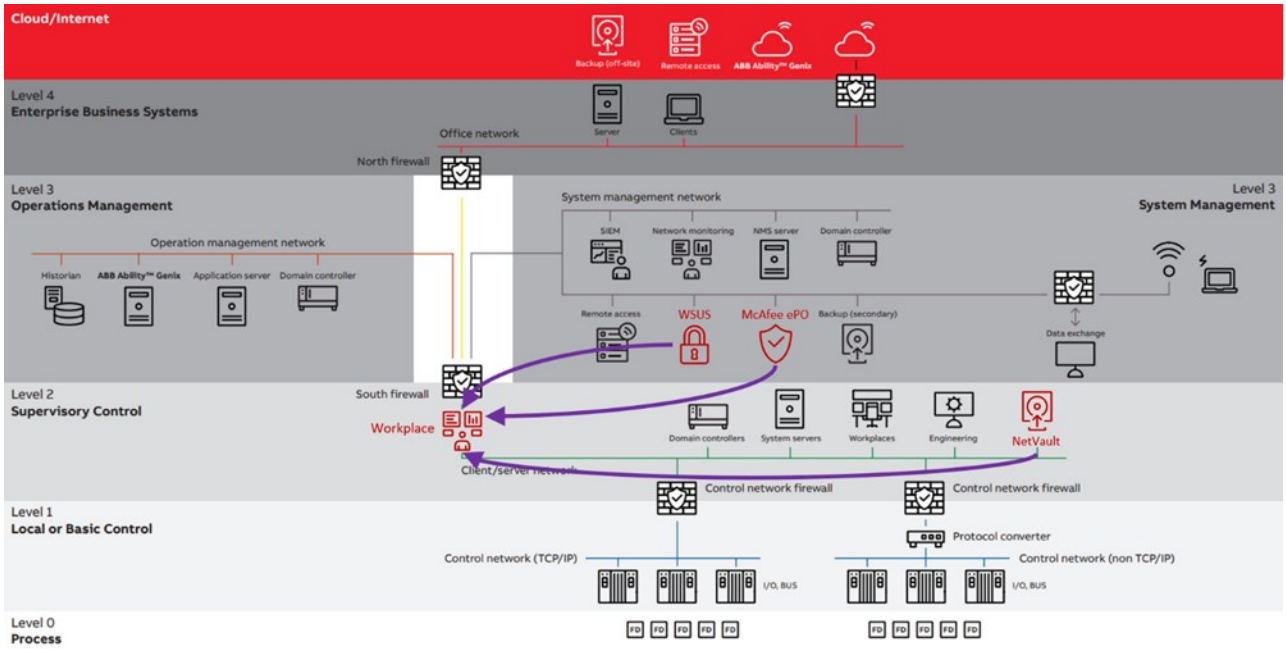

Figure 11: Typical implementation of ABB Cyber Security Workplace.

5. CONCLUSION

As a technology leader in electrification and automation, ABB is at the core of propelling the energy transition forward. This includes the ABB digital solutions with its range of solutions that optimizes asset operation and maintenance, power consumption and processes, as wells cyber security of the system. This is crucial for stabilizing renewables and effective data management provides transparency and actionable insights, driving efficiency and sustainability gains, including in geothermal power segment.

REFERENCES

Jones, Stacey: ABB brings Advanced Analytics and Enhanced Asset Performance into Reach, *ABB Whitepaper* (2023).

Asset Performance Management – APM software | ABB – https://new.abb.com/industrial-software/asset-performance-management.

Capitalizing on A New Mindset for Asset Management, *ABB Article on Water Online* – www.wateronline.com.

Plotting The Quickest Route to Better Asset Maintenance, *ABB Article on Water Online* – www.wateronline.com.

Steam and Power Optimization: Superior management of steam network complexity, *ABB Brochure* (2021).

Power Generation Optimization for Geothermal Production Field, *ABB Internal Technical Writeup* (2024).

ABB Ability™ Cyber Security Workplace, *ABB Brochure* (2021).

ABB Ability Cyber Security Workplace: Security simplified – https://new.abb.com/process-automation/process-automation-service/advanced-digital-services/cyber-security/abb-cyber-security-services/abb-ability-cyber-security-workplace.

My Control System (on-premise) Operation, *ABB User Manual* (2022).

The Canaya Geothermal Coffee Process Revolutionizing Signature of Arabica Coffee Production with Geothermal Dryhouse in Kamojang, West Java, Indonesia

Muhammad N. Fauzan[1], Cecep U. Farouq[2], Adi Rahmadi[3],
Aan Taryana[1], Syalva T.M. Yusuf[1], Ovinda Hariyesa[1], and Dyah H. Kinanthi[1]

[1]PT Pertamina Geothermal Energy Area Kamojang, West Java, Indonesia, 40383
[2]PT Pertamina Geothermal Energy Area Ulubelu, Lampung, Indonesia, 35387
[3]PT Pertamina Geothermal Energy Tbk, Jakarta Pusat, Indonesia, 10110

muhammad.fauzan4@pertamina.com

Keywords: Geothermal Dryhouse, Coffee Drying, Sustainable Energy, Heat Transfer,Economic Benefits

ABSTRACT

The coffee farmers in Kamojang currently rely on conventional sun-drying methods, facing challenges due to the area's cold ambient temperatures and unpredictable weather. To address this, PT PGE Area Kamojang constructed a geothermal dry house utilizing a heating pipe connected to an existing geothermal steam pipeline. In this comprehensive study, the existing geothermal dry house undergoes evaluation from both technical and business perspectives. The technical assessment focuses on the thermal performance of the heating pipe, determining the heating load, required pipe length, and the impact of pipe operation on dry house temperature. Analytical methods reveal a required heating load of 10.94 kW, necessitating a 41.79 m pipe length. Subsequently, experimental trials conducted on multiple occasions show enhancements through technical adjustments, such as steam trap installation and valve rearrangement, resulting in improved heating pipe performance, maintaining temperatures above 40°C for extended periods.

On the business front, qualitative analysis examines the potential for profit enhancement stemming from reduced drying durations. By substituting conventional methods with the geothermal dry house, drying times could potentially decrease from 2-3 weeks to 1-2 weeks, while preserving coffee flavour and minimizing odor issues. The business evaluation anticipates significant benefits for farmers, correlating shorter drying times with increased profitability. This integrated approach, blending technical optimization with business insights, underscores the promising solution offered by the geothermal dry house, addressing operational challenges and driving economic gains for coffee farmers in Kamojang.

1. INTRODUCTION

Indonesia has a geothermal energy potential of 23.9 GW of which only 10% of the geothermal potential is utilized (Ayuningtyas et al., 2021). The utilization of geothermal potential can be divided into two methods, namely direct and indirect utilizations (Lukmana & Helmy, 2020). The main example of indirect utilization is for electricity generation. Meanwhile, examples of direct use are hot water baths, room heaters, and dryers for plantation and fishery products. However, currently the use of geothermal energy in Indonesia is still dominated by indirect use for electricity generation (Darma et al., 2021).

Kamojang is a region in Bandung Regency, West Java, Indonesia, area which produces a primary plantation commodity, namely Arabica coffee (Coffea arabica L.). According to the local coffee farmers, the production rate of Kamojang coffee green beans usually reaches 8-9 tons per year. The optimal temperatures for coffee drying are in the range of 35-45°C (da Costa et al., 2021). However, currently Kamojang coffee farmers still rely on natural drying using the sun's radiation. The frequently changing weather and low temperatures in the Kamojang region make coffee drying take 2-3 weeks. Therefore, PT Pertamina Geothermal Energy (PGE) Area Kamojang, through the Corporate Social Responsibility (CSR) scheme, took the initiative to create a geothermal steam-powered coffee dryer machine named Geothermal Coffee in 2018 with the hope that coffee drying will no longer depend on weather and climate so that drying can be done more efficiently. However, (Badan Perencanaan Pembangunan Daerah Kabupaten Bandung, 2021) stated that this method was not optimal because coffee has a sensitivity to absorb the smell of sulfur from geothermal steam, which affects the taste of coffee and the large number of coffee beans that are damaged due to overly high temperatures. Responding to this, PT PGE Area Kamojang is looking for an alternative method of drying coffee, namely using a dryhouse. Currently, PT PGE Area Kamojang has built a trial dryhouse with heating pipes which is connected to blowdown on the main pipeline that distributes geothermal steam to the Kamojang Geothermal Power Plant (GPP). Geothermal dryhouse has the advantages of being weather independent, available heat around the clock, and naturally-controlled temperature and humidity. This method is similar to conventional drying method but relying on geothermal as a constant heat supply instead

of the fluctuative sun radiation. Moreover, the existing dryhouse has been improved to mitigate sulfur smell issues by using double door access and a distant steam exhaust.

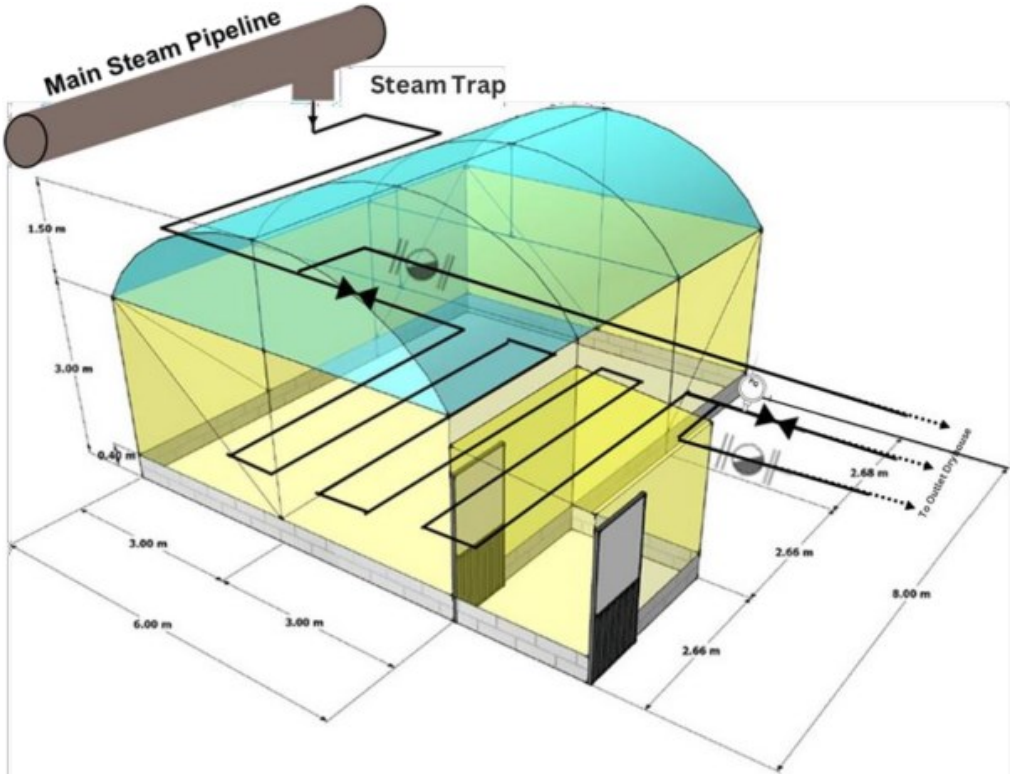

Figure 1: Geothermal Dry House Design.

Figure 2: Geothermal Dry House Construction.

2. GEOTHERMAL DRYHOUSE DESIGN

The existing geothermal dryhouse has a width of 6 m, length of 8 m, and height of 4.5 m, as shown in Figure 1. The heating pipe utilizes the blowdown from the main pipeline as the heat source so that the geothermal steam flows from the blowdown towards the dryhouse to transfer its heat to the dryhouse air. The total length of the existing heating pipe is 43.5 m.

3. METHODOLOGY

3.1 Technical Section

The technical evaluation studies the thermal performance of the heating pipe to calculate the dryhouse heating load, the required heating pipe length, the effect of heating pipe operation on the dryhouse temperature, and the suggested technical improvements. The technical evaluation is performed through analytical and experimental methods explained in the following.

3.1.1 Analytical Method

The analytical method is used to evaluate the dry house technically based on the necessary governing equations. In order to maintain the dry house temperature at a desired value, the heating load must be equal to the rate of heat loss and the rate of trapped radiation. The energy balance equation of dry house is expressed in Equations (1) and (2) as follows:

$$Q_{load} = Q_{loss} - Q_{rad} \quad (1)$$

$$Q_{loss} = (Q_{str} + Q_{air}) \cdot C_{cond} \cdot C_{cli} \quad (2)$$

where Q_{load}, Q_{loss}, Q_{str}, Q_{inf}, Q_{rad}, C_{con}, C_{cli}, and are heating load, structural heat loss rate (kW), heat loss rate through air infiltration (kW), heat gain through trapped radiation (kW), construction factor, and climate factor, respectively. The structural heatloss rate is calculated using Equation (3) as follows:

$$Q_{str} = U \cdot A \cdot (T_{\infty,dh} - T_{\infty,amb}) \quad (3)$$

where U, A, $T_{\infty,dh}$, and $T_{\infty,amb}$ are structural overall heat transfer coefficient (kW/m2·K), wall and roof area (m^2), dry house temperature (°C), and ambient temperature (°C) respectively. The heat loss rate through air infiltration is calculated using Equation (4) as follows:

$$Q_{air} = N \cdot V_{dh} \cdot \rho_{a,dh} \cdot c_{pa,dh} \cdot (T_{\infty,dh} - T_{\infty,amb}) \quad (4)$$

where N, V_{dh}, $\rho_{a,dh}$, $c_{p,a,dh}$, $T_{\infty,dh}$, and $T_{\infty,amb}$ are air exchange rate (s^{-1}), dry house inner volume (m^3), density of air inside dry house (kg/m^3), isobaric specific heat of air inside dry house (kJ/kg·K), dry house temperature (°C), and ambient temperature (°C) respectively.

$$Q_{rad} = F \cdot (A_{dh} I_h + A_{roof} I_{dn}) \quad (5)$$

where F, A_{dh}, A_{roof}, I_h, and I_{dn} are fraction of trapped radiation energy (%), wall and roof area (m^2), roof area (m^2), horizontal irradiation intensity (kW/m^2), and direct normal irradiation intensity (kW/m^2), respectively.

The geothermal steam flows inside the heating pipe and transfer its heat to the dry house air. This involves convection heat transfer on the inner and outer pipe walls, conduction heat transfer at the pipe wall, and radiation heat transfer on the outer pipe walls. The thermal circuit of the heat transfer process is shown in Figure 3.

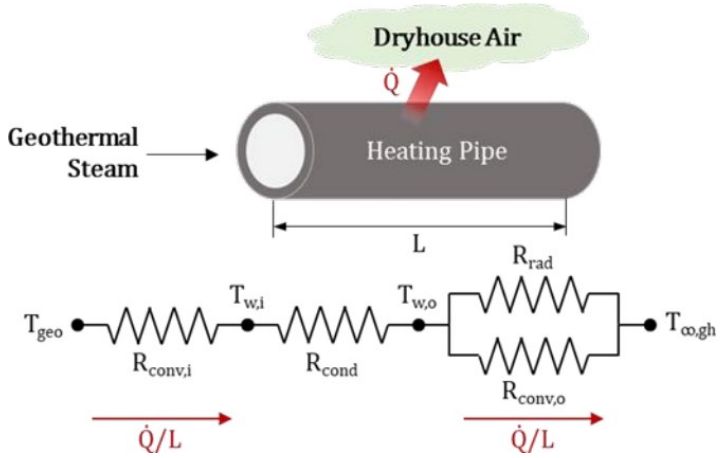

Figure 3: Thermal resistance of heat transfer from geothermal steam to dry house air.

The geothermal steam flowing inside the heating pipe is at saturated vapor phase. Therefore, film condensation occurs as the steam transfers heat to the dry house air. The forced convection heat transfer coefficient and thermal resistance with film condensation for internal flow inside a horizontal cylindrical pipe are expressed in Equations (6) and (7), respectively, according to Bergman et al. (2017) and Berian and Khusaini (2022) as follows:

$$h_{conv,i} = 0.555\left[\frac{g\rho_l(\rho_l-\rho_v)k_l^3}{\mu_l(T_{sat}-T_{w,i})D_i}\left(h_{fg}+\frac{3}{8}c_{p,l}(T_{sat}-T_{w,i})\right)\right]^{0,25} \quad (6)$$

$$R_{conv,i} = \frac{1}{h_{conv,i}\,\pi D_i\,L} \quad (7)$$

where $h_{conv,i}$, $R_{conv,i}$, g, ρ_l, ρ_v, k_l, μ_l, D_i, L, h_{fg}, $c_{p,l}$, T_{sat}, and $T_{w,i}$ are convection heat transfer coefficient on inner pipe wall (kW/m^2·K), convection thermal resistance on inner pipe wall (m·K/kW), gravitational acceleration (m/s^2), condensate density (kg/m^3), steam density (kg/m^3), condensate thermal conductivity (kW/m·K), condensate viscosity (Pa·s), inner pipe diameter (m), pipe length (m), condensate isobaric specific heat (kJ/kg·K), saturation temperature (°C), and inner pipe wall temperature (°C), respectively.

The outer pipe wall is exposed to the dry house air flowing across the pipe. The natural convection heat transfer coefficient and thermal resistance of external flow across a cylindrical pipe are expressed in Equations (8) and (9), respectively, according to Bergman et al. (2017) and Berian and Khusaini (2022) as follows:

$$h_{conv,o} = \frac{k_f}{D_o}\left[0{,}6+\frac{0{,}387Ra_D^{\frac{1}{6}}}{\left[1+\left(\frac{0{,}559}{Pr}\right)^{\frac{9}{16}}\right]^{\frac{8}{27}}}\right]^2 \quad (8)$$

$$R_{conv,o} = \frac{1}{h_{conv,o}\pi D_o L} \quad (9)$$

where $h_{conv,o}$, $R_{conv,i}$, k_f, Ra_D, Pr, D_i, and L are convection heat transfer coefficient on outer pipe wall (kW/m^2·K), convection thermal resistance on outer pipe wall (m·K/kW), fluid thermal conductivity (kW/m·K), Rayleigh number, Prandtl number, outer pipe diameter (m), and pipe length (m), respectively.

The heating pipe also emits radiation to the surrounding. The radiation heat transfer coefficient and thermal resistance are expressed in Equations (10) and (11), respectively, as follows:

$$h_{rad} = \sigma\epsilon\left(T_{w,0}^2+T_\infty^2\right)\left(T_{w,o}-T_{\infty,dh}\right) \quad (10)$$

$$R_{rad} = \frac{1}{h_{rad}\,A_{w,o}} \quad (11)$$

where h_{rad}, R_{rad}, σ, ϵ, $A_{w,o}$, $T_{w,o}$, and T_∞ are radiation heat transfer coefficient (kW/m^2·K), radiation thermal resistance (m·K/kW), emissivity, Stefan-Boltzmann constant, outer pipe wall area (m^2), outer pipe wall temperature (K), and dryhouse temperature (K), respectively.

The values of the parameters needed in the analytical heat transfer calculations in heating pipes are obtained through field data and assumptions using literature studies as shown in Table 1.

3.1.2 Experimental Methode

The heating pipe is operated by opening the blowdown valve hence the geothermal steam from the main pipeline could flow inside the heating pipe towards the dryhouse. Meanwhile, the outlet valve at the end of the heating pipe remains closed. During the pipe operational, the dryhouse temperature is measured using a thermohygrometer. Therefore, the dryhouse air temperature during the heating pipe operation could be evaluated. After minimum 24 hours of operation, the blowdown valve is closed again to shut down the heating pipe.

Geothermal Dry House has the advantages of being weather-independent, available heat around the clock, and naturally-controlled temperature and humidity. Based on technical evaluation the results indicated that the heating pipe was able to increase the dry house temperature. However, the condensate builds up inside the heating pipe reduces the dry house temperature minutes after the heating pipe operation. Therefore, it is responded by installing two stream traps, each installed at the inlet and outlet of the drying house to reduce condensate in the steam entering the drying house and remove the condensate formed while the steam is in the drying house.

Table 1: Values of parameters in the analytical calculations.

Parameter	Value	Source
Geothermal steam mass flow rate	0.114 kg/s	Field data
Geothermal steam temperature	187.2°C	Field data
Geothermal steam pressure	11.8 bara	Field data
Geothermal steam phase	Saturated vapor	Field data
Heating pipe segment length inside dry house	43.5 m	Field data

Parameter	Value	Source
Dry house inner volume	200.55 m^3	Field data
Dry house wall and roof area	156.27 m^2	Field data
Dry house wall area	55.64 m^2	Field data
Average daily dry house temp. without heater	36.8°C	Field data
Dryhouse design temperature	40°C	Interview with local farmer; da Costa (2021)
Ambient temperature	19°C	Rudiyanto et al. (2022)
Ambient pressure	0.85 bara	Rudiyanto et al. (2022)
Dry house overall heat transfer coefficient	0.5 kW/m²·K	ASHRAE (2019)
Air exchange rate due to infiltration	0.0004167/s	ASHRAE (2019)
Fraction of trapped radiation	75%	Ahamed et al. (2018)
Horizontal irradiation intensity	0.00122 kW/m²	Solargis (2019)
Direct normal irradiation intensity	0.001277 kW/m²	Solargis (2019)
Construction factor	1.02	ASHRAE (2019)
Climate factor	0.41	ASHRAE (2019)
Heating pipe thermal conductivity	0.0567 kW/m·K	

3.2 Operation Hours (Day/Month/Year) & Maintanance Scheme (In-House, Contracted Out Service, Government, Others

3.2.1 Operation Hours (Day/Month/Year)

The actual operation hours for geothermal dry house entail a continuous cycle of work, with operations spanning 24 hours each day. This setup results in a substantial cumulative working time of 5,760 hours annually.

Actual operation hours:
Working hours 24 hours per day
Working days 240 days per year
Total working hours 5,760 hours per year

3.2.2 Maintanance Scheme (In-House, Contracted Out Service, Government, Others)

The Geothermal Dry House conducts proactive and preventive maintenance with regular schedules to avoid production failures. These plans are maintained based on manual machine operation data, predictive maintenance principles, and machine degradation level analysis. In line with the concept of sustainable power plant operations, socio-ecological safety is ensured through social inclusion practices in the Geothermal Coffee Process program, and monitored through annual Social License Index (for social safety) and annual geophysical surveys (for steam resource sustainability).

3.2.3 Other Maintanance Measures (Training, After-Sales Service)

In the realm of geothermal coffee processing, additional maintenance measures are essential for seamless operations and maximizing technology efficiency.

1. Regular Training Programs

Figure 4: Coffee Training for Community.

Training programs are essential not only for personnel involved in operating and maintaining complex machinery but also for coffee farmers. These programs equip farmers with the knowledge and skills needed to effectively manage their coffee farms in conjunction with geothermal technology. Additionally, operators and technicians receive training on the operation, maintenance, and troubleshooting of geothermal coffee processing equipment.

2. Preventive Maintenance Plans
   Developing and implementing preventive maintenance plans for Canaya Geothermal Dry house, including regular inspections, cleaning, calibrations of machinery to prevent potential breakdowns and extend the lifespan of the dry house.
3. Scheduled Monitoring Systems
   Scheduled monitoring systems in Canaya Geothermal Dry house ensure ideal conditions for drying coffee beans by continuously tracking temperature and humidity levels. This critical oversight maintains quality and enhances efficiency.

3.3 Bussiness Section

This project was 100% fully funded by PT. Pertamina Geothemal Energy Tbk – Area Kamojang. The CSR scheme provides financial support for capital expenditure needs and working capital requirements.

The market potential for geothermal dry house technology within the next 5 years in the coffee industry appears promising. The efficiency, quality assurance, and extended drying capabilities through expansion of the geothermal dry house can attract more coffee farmers and buyers, leading to potential growth and market expansion:

1. Increased Efficiency: The geothermal dry house can accelerate drying time significantly, up to 75% faster than conventional methods. This increased efficiency can lead to higher productivity and throughput in coffee drying processes.
2. Extended Drying Season: The ability to dry coffee beans regardless of the season can provide a competitive advantage to coffee farmers, allowing them to operate year-round and be less affected by seasonal variations. This extended drying season could attract more farmers to adopt this technology.
3. Stable Drying Conditions: The stability of drying temperature and humidity in geothermal dry houses can help maintain the quality of coffee beans, ensuring that the flavor is not compromised. This quality assurance can be a crucial selling point in the market.
4. Contamination Reduction: By reducing the risk of contamination from dust, dirt, and insects, the geothermal dry house method ensures higher-quality coffee beans. This assurance of quality can be a key factor in attracting buyers who prioritize cleanliness and quality standards.
5. Consumer Preference: The positive testimonies from local coffee farmers regarding the taste and absence of smell issues in the dried coffee could lead to increased consumer trust and preference for dried coffee using geothermal technology.

With its array of advantages, geothermal dry house technology presents promising potential for significant market growth and expansion in the coffee industry over the next five years. By enhancing efficiency, extending drying seasons, ensuring stable drying conditions, reducing contamination risks, and garnering increased consumer preference, this technology opens new for coffee farmers and stakeholders across the coffee supply chain to optimize quality and productivity, while expanding their market share.

As for the calculation for forecasting the market size for geothermal dry house technology in the coffee industry in Indonesia over the next 5 years based on value creation by 2023:

Table 2: Value Creation by 2023.

No.	Description	Value
1	Revenue of Geothermal Coffee Management	Rp. 182.613.999
2	Cost saving of geothermal coffee process	Rp. 36.855.632
	Total Real of Value Creation by 2023	Rp. 182.613.999

Value Creation in 2023 : Rp. 182.613.999 Production per Month in 2023 : 2 tons Value Creation per Ton :

Value Creation per Ton = Value Creation / Production per Month (12)
= Rp. 182.613.999 / 2 tons
= Rp. 91.306.999 per ton

Production Growth = 5% per year (assumed) Projected Annual Value Creation:

Projected Annual Value Creation :

Table 3: Projected Annual Value Creation (per ton).

2024	2025	2026	2027	2028
Rp. 95,872,349	Rp 100,665,967	Rp 105,699,266	Rp 111,000,230	Rp 116,598,242

These calculations show the expected yearly value created by the geothermal dry house technology in the coffee industry from 2024 to 2028. Each year, the value created per ton of coffee is determined by multiplying the previous year's value by a 5% growth rate. This could estimate of how much value the technology is likely to generate annually over the five-year period.

Projected Market Size:
Multiply the value creation per ton by the total annual coffee production
Year 2024: Rp. 95,872,349 per ton * (production per month * 4 months)
= Rp. 95,872,349 per ton * (2 tons * 4 months)
= Rp. 95,872,349 per ton * 8
= Rp. 766,978,792

Table 4: Projected Market Size.

2024	2025	2026	2027	2028
Rp. 766,978,792	Rp. 1,207,991604	Rp. 1,691,188,256	Rp. 2,220,004,600	Rp. 2,798,357,808

*estimated increase of 1 ton in production per year compared to the previous year.

This calculation shows the market size for geothermal dry house technology in Indonesia's coffee industry by multiplying the value created per ton with total annual coffee production. It gives an idea of the market opportunity for this technology.

3.4 Resources

3.4.1 Local Manufacturing/Content of System

The equipment and machines of Canaya Geothermal Dry house were realized by PT. Pertamina Geothermal Energy Tbk in collaboration with local groups.

Table 5: Equipment & Service Project Items.

No.	Equipment & Service Project Items	% (Est. Cost Invesment)	Local Community Involvement
1	Outer pipe wall	15%	provided by local/domestic suppliers
2	Steam trap dry house	20%	provided by local/domestic suppliers
3	Dry house construction	30%	Local labour in technical and general skill in collaboration with PGE team
4	Construction and Modification	35%	Local labour in technical and general skill in collaboration with PGE team

3.4.2 Local Service Content

- Raw material: 100% has been supplied from within 50 kilometres from the power plant, with 70% coming form local industries or farmers and 30% coming from the shareholders
- Spare Parts and Services: 100% of spare parts and services are supplied or provided by local/domestic manufacturers or suppliers (within Indonesia region), thus the maintenance/service costs are low, as well as emergency shutdowns
- The workforce comes from within the company in collaboration with local workers with appropriate competencies and skills

4. RESULT AND DISCUSSION

4.1 Technical Evaluation : Analytical Method

Based on the calculation results, the total heat loss in the dryhouse is 11.14 kW involving the construction factor coefficient and climate factor coefficient of 1.02 and 0.41 respectively. Most of the heat losses occur through the structure of the dryhouse walls and roof as much as 9.35 kW. Meanwhile, the rest was caused by air infiltration of 1.79 kW. Since the dryhouse obtains heat through trapped radiation of 0.2 kW, the heating power required to keep the dryhouse air temperature constant is 10.94 kW, as shown in Table 6 .

Table 6: Geothermal dryhouse heat loss and heat load.

Parameter	Value	Unit
Structural heat loss	9.35	kW
Air infiltration heat loss	1.79	kW
Construction factor	1.02	-
Climate factor	0.41	-
Total heat loss	11.41	kW
Radiation heat gain	0.2	kW
Heat load	10.94	kW

The convection heat transfer coefficient with film condensation on the inner wall of the pipe is 27 kW/m2·K. Convection heat transfer involving a phase change has a higher heat transfer coefficient than convection without a phase change. The total thermal resistance from convection, conduction and radiation is 561.26 m·K/kW. Thus, the heat transfer rate per unit pipe length is 0.2618 kW/m and the required length of heating pipe to meet the heating power requirement (10.94 kW) is 41.79 m, as shown in Table 7. Therefore, the existing pipe length (43.5 m) has met the required pipe length.

Table 7: Results of analytical heating pipe heat transfer calculation.

Parameter	Value	Unit
Convection heat transfer coeff. on the inner pipe wall	27.0	kW/m^2·K
Convection heat transfer coeff. on the outer pipe wall	0.0075	kW/m^2·K
Radiation heat transfer coefficient	0.0095	kW/m^2·K
Convection thermal resistance on the inner pipe wall	0.44	m·K/kW
Pipe wall conduction thermal resistance	0.63	m·K/kW
Convection thermal resistance on the outer pipe wall	0.0013	m·K/kW
Radiation thermal resistance	1,004.1	m·K/kW
Total thermal resistance	561.26	m·K/kW
Inner pipe wall temperature	186.99	^{o}C
Outer pipe wall temperature	186.72	^{o}C
Heat transfer rate per unit length	0.2618	kW/m
Required heating pipe length	41.79	m

Since the geothermal steam is in the saturated vapor phase when it enters the inlet of the dryhouse, the heat transfer from the steam to the air of the dryhouse causes the formation of condensate from the steam. Based on the results of the calculation of the heat transfer parameters in Table 2, the rate of condensate formation per unit pipe length is 0.000235 kg/s·m or 0.8462 L/h·m. With an existing pipe length of 43.5 m, the total condensate formation rate is 0.010224 kg/s or 36.81 L/h, as shown in Table 8.

Table 8: Results of condensatiozszn rate calculation.

Parameter	Value	Unit
Saturation temp. at the geothermal steam pressure	187.2	^{o}C
Existing heating pipe length	43.5	m
Condensation rate per unit length	0.000235	kg/s·m
	0.8462	L/h·m
Total condensation rate	0.010224	kg/s
	36.81	L/h

4.2 Experimental Method: First Trial (16-18 January 2023)

The trial operation of the heating pipe was performed twice. The first trial was on 16-18 January 2023, while the second trial was on 27 April – 4 May 2023. During the first trial, the blowdown valve from the main pipeline was opened on 16 January 2023 at 02:00 p.m. The valve at the end of the heating pipe at the outlet of the dryhouse remains closed. The dryhouse temperature profile after heating pipe operation on Trial 1 is shown in Figure 4. The initial dryhouse temperature when the blowdown valve was opened was 33°C. After the blowdown valve was opened, the dryhouse temperature gradually increased until reaching the maximum temperature of 36.5^{o}C was achieved 28 minutes after operation started (at 02.28 p.m.). Afterwards, the dryhouse temperature showed a declining trend. Therefore, the heating pipe could not reach the dryhouse design temperature of 40°C. During the night, the dryhouse temperature declined to as low as 23°C before increasing again in the morning. The failure to

reach the design temperature was caused by the condensate buildup in the heating pipe which cannot be removed because the end valve is closed. With an inner heating pipe diameter of 0.02664 m and a length of existing heating pipe of 43.5 m, the volume of the cavity in the heating pipe is 0.024 m^3 or 24 L. If the rate of condensate formation based on Table 3 is 36.81 L/h, then the condensate will fill all the cavities in the pipe within 40 minutes after the heating pipe is operated.

Based on the evaluated results of the first trial, three technical improvements are suggested:

1. Two steam traps are needed, each installed at the inlet and outlet of the dryhouse. The steam trap at the inlet reduces condensate in geothermal steam that flows into the dryhouse. Meanwhile, the steam trap at the outlet removes the condensate that forms while the steam is in the dryhouse. Based on the results of calculating the rate of formation of condensate in Table 4 of 0.03681 tph and by providing an allowance factor of 50%, the required capacity of each steam trap is 0.055 tph of condensate.
2. The geothermal steam will experience a pressure drop when flowing in the heating pipe. While the steam pressure at the main pipeline blowdown can be known from the operational data of Kamojang GPP, a pressure gage should be installed at the dryhouse outlet to calculate the pressure drop experienced by the steam inside the heating pipe.
3. Before the heating pipe enters the drying house, there is a 15 meter-long heating pipe segment between the main pipeline blowdown and the drying house inlet. To reduce heat loss in this pipe segment and maximize the heat transferred to the dryhouse, this heating pipe segment should be insulated.

4.3 Experimental Method: Second Trial (27 April – 4 May 2023)

In response to the suggested technical improvements based on the first trial, two steam traps, a pressure gauge, thermal insulation were installed before the second trial. During the second trial, the blowdown valve from the main pipeline was opened on 27 April 2023 at 09:00 a.m. The dryhouse temperature profile after heating pipe operation on Trial 2 is shown in Figure 4. The initial dryhouse temperature when the blowdown valve was opened was 39°C. After the blowdown valve was opened, the dryhouse temperature gradually increased until surpassing the dryhouse design temperature of 40°C at 09:03 a.m. The dryhouse temperature kept increasing until reaching the maximum temperature of 43°C at 10:42 a.m. (1 hour and 42 minutes after heating pipe operation). The dryhouse temperature remained higher than 40°C until 11:19 a.m. and then was followed by a declining trend with a slight increase between 00:44 p.m. and 01:27 p.m. On Trial 2, the dryhouse temperature during the night was maintained higher than on Trial 1. This indicates that the technical improvements managed to improve the heating pipe's performance on maintaining the dryhouse temperature. However, the presence of condensate buildup inside the heating pipe suggests that the newly installed steam traps did not work properly.

Based on the evaluated results of the second trial, two technical improvements are suggested:

1. To discover why the condensate buildup still occurred, recheck the newly installed steam traps by exchanging the inlet and outlet steam traps.
2. To improve the air circulation and minimize the sulfur's smell, two access doors and distant air exhaust should be added into the dryhouse.

4.4 Experimental Method: Third Trial (31 May – 5 June 2023)

In response to the suggested technical improvements based on the second trial, the inlet and outlet steam traps' were exchanged to discover whether the condensate buildup issue was caused by the steam traps themselves or by a systemic issue. During the second trial, the blowdown valve from the main pipeline was opened on 31 May 2023 at 11:00 a.m. The dryhouse temperature profile after heating pipe operation on Trial 3 is shown in Figure 5. The initial dryhouse temperature when the blowdown valve was opened was 39°C. After the blowdown valve was opened, the dryhouse temperature gradualy increased until surpassing the dryhouse design temperature of 40°C at 11:18 a.m. The dryhouse temperature kept increasing until reaching the maximum temperature of 43°C at 00:01 p.m (1 hour and 1 minute after heating pipe operation). The dryhouse temperature remained higher than 40°C until 02:39 p.m. and then was followed by a declining trend. On Trial 3, the dryhouse temperature during the night was maintained higher than on Trial 2. This indicates that the technical improvements managed to improve the heating pipe's performance on maintaining the dryhouse temperature.

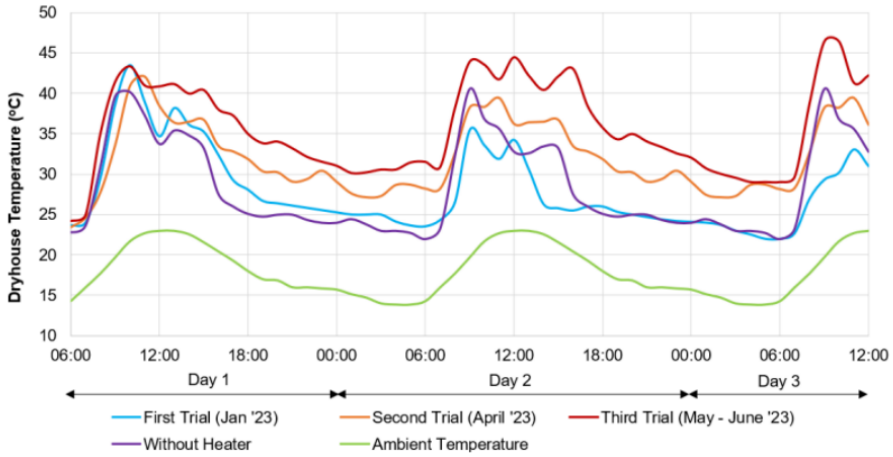

Figure 5: Dryhouse temperature after heating pipe operation from Trials 1, 2, and 3.

4.5 Business and Social Evaluation

4.5.1 Benefits (User, Community, Country)

Benefits to Project Owners (PT. Pertamina Geothermal Energy Tbk.)

- Direct-use of company's raw material to Corporate Social Responsibility Program
- Creates good image for the company and relevant shareholders

Benefits to the community and surrounding

- Helps in economic growth in the community by increasing revenue by around IDR 182.6 million Rupiah per year.
- Saves around IDR 36.8 million Rupiah per year in operational costs for local economic activities.
- Enhances the value of the local community through the originality of Kamojang's signature Canaya Geothermal Coffee
- Creates 35 partner B2B & B2C
- Contributes to organic waste recycling by up to 419.2 kg/year

Benefits to the Country

- Contributes to reduce greenhouse gas emission from using geothermal energy instead of fossil fuel for dry house approximately 21,949 tons CO2 per year.
- Promotes Kamojang's signature product, "The Canaya Geothermal Coffee" to the wider community, which can become a regional to international tourism attraction.

Figure 6: Canaya Geothermal Coffee.

4.5.2 Corporate Social Responsibility Program

The Geothermal Coffee Group, as one of PGE Kamojang's CSR programs, consists of a coalition of 3 coffee groups from Kamojang and its surroundings. This group aims to improve the welfare of local farmers by applying green processing principles in coffee processing. The members of the group are also often referred to as the Geothermal Coffee Process or GCP group, comprising 6 core members from Penyoe Kakopi, Ecovill, and the

Akkar Kamojang. This group utilizes geothermal dry house for drying coffee cherries, making it 75% more effective compared to sun drying. Initially, drying required a duration of 1 to 1.5 months, but with the geothermal dry house, drying can be accomplished in just 3-7 days. Additionally, group members can enhance their capacities based on their skills, whether as coffee farmers, processors, or baristas. Capacity building agendas and bootcamps are planned and partially realized to recruit outstanding talents that contribute to the sustainability of the Geothermal Coffee Group. At least 1,540 customers enjoy the GCP coffee products. Furthermore, the group strives to expand its business and market through both B2C and B2B models.

4.5.3 Community/People Awareness, Participation, and Acceptence

Through The Canaya Geothermal Coffee, local community awareness of coffee cultivation potential increases, and with the presence of The Canaya Geothermal Coffee, it also supports the following beneficiaries: 6 main managers of The Canaya Geothermal Coffee, 15 Coffee Farmers, 4 Baristas, 2 Coffee Sorters, 1.537 coffee enthusiasts, and business partnerships with 35 B2B and B2C partners. In general, the Community Satisfaction Index (CSI) for the overall program of PT. Pertamina Geothermal Energy Tbk. Area Kamojang including The Canaya Geothermal Coffee scored 82.7, which falls under the A category for service quality, which is classified as very satisfied.

4.6 Replicability Evaluations

4.6.1 Relevance, Impact, Efficiency

The implementation of coffee drying methods using geothermal dry house by PT Pertamina Geothermal Energy Tbk Area Kamojang (PGE Kamojang) holds significant relevance in terms of replicability. This is due to several factors:

1. Available Technology: Geothermal heating technology has proven to be effective and available in many regions with geothermal potential. Therefore, this method can be easily replicated in other areas with similar geothermal potential.
2. Scalability: The coffee drying method using geothermal heaters can be adapted to different production scales. It can range from small-scale for local coffee farmers to large-scale for larger coffee processing industries.
3. Potential Environmental Impact Reduction: By reducing reliance on fossil fuels or wood for coffee drying, the use of geothermal heaters can help reduce negative environmental impacts, such as greenhouse gas emissions and deforestation.

Furthermore, in term of impact and efficiency, the replication of this geothermal dry house provides significant impact and enhances efficiency in the production process.

1. Positive Environmental Impact: The use of geothermal heaters in the coffee drying process has a positive environmental impact. By reducing the use of fossil fuels or wood, this method helps reduce greenhouse gas emissions and alleviate pressure on forests as a source of fuelwood.
2. Operational Efficiency: Compared to conventional drying methods that rely on weather conditions, the use of geothermal heaters can enhance operational efficiency. The availability of stable and controllable heat energy accelerates the coffee drying process without significantly affecting its quality.
3. Social and Economic Impact: Increased efficiency in the coffee drying process can have positive social and economic impacts on coffee farmers and stakeholders in the coffee sector. Simplifying the drying process can enhance productivity and product quality, which in turn can increase income and competitiveness for local coffee farmers.

Thus, the implementation of coffee drying methods using geothermal dry house is not only relevant in terms of replicability but also has significant positive impacts on the environment, operational efficiency, and socio-economic well-being of local communities. This makes it a promising solution in efforts to enhance sustainability and efficiency in the coffee industry.

4.6.2 Cost Effectiveness (No, Low, High Cost)

The Canaya Geothermal Coffee's sustainability hinges on the harmonization of various elements, including equipment, steam provision, and community backing. While no specific equipment issues are highlighted, challenges persist concerning steam resources and social support, common hurdles in geothermal endeavors. Hence, establishing a green living ecosystem serves as a savvy strategy to mitigate the eco-social quandary that could undermine operational stability if neglected.

Securing a sustainable and dependable steam supply is paramount for The Canaya Geothermal Coffee's long-term prosperity. This entails efficient resource management, routine well upkeep, and continuous reservoir health monitoring. Furthermore, fostering social backing from the local community is vital for ensuring project

sustainability. Cultivating robust community bonds and addressing their concerns are crucial steps toward garnering support and fostering trust.

4.6.3 Sustainability of Project

The integration of the green living ecosystems concept into The Canaya Geothermal Coffee's business process marks a pivotal breakthrough in both project development and dry house operation. It is advisable to initiate this process during the inception phase. However, it's worth noting that introducing these sustainable practices during the operational phase of an existing geothermal dry house is never too late. Given the significant threat of declining well performance in geothermal operations, efforts to mitigate this risk by sustaining the ecosystem surrounding the geothermal reservoir are prudent measures.

4.6.4 Others

Geothermal dry house has the advantages of being weather-independent, available heat around the clock, and naturally controlled temperature and humidity. This method is similar to the conventional drying method but relies on geothermal as a constant heat supply instead of the fluctuating sun radiation. Moreover, the existing dry house has been improved to mitigate sulfur smell issues by using double door access and a distant steam exhaust. In this study, the existing geothermal dry house for coffee drying in Kamojang is evaluated from the technical and business aspects. The implementation of geothermal Dry house offers a sustainable, efficient, and cost-effective alternative to conventional heating and cooling systems, with the potential to reduce carbon emissions, enhance energy independence, and stimulate economic development. Additionally, this approach can serve as a strong defense for the company against social problems.

4.7 Amount of Fossil Energy Avoided

The Geothermal Dry House using geothermal steam as dry house or equivalent to 25,229 MW and reducing greenhouse gasses 21,949 tCO2/year.

5. CONCLUSION

Geothermal dryhouse has the advantages of being weather-independent, available heat around the clock, and naturally-controlled temperature and humidity. This method is similar to conventional drying method but relying on geothermal as a constant heat supply instead of the fluctuative sun radiation. Moreover, the existing dryhouse has been improved to mitigate sulfur smell issues by using double door access and a distant steam exhaust. In this study, the existing geothermal dryhouse for coffee drying in Kamojang is evaluated from the technical and business aspects. Based on technical evaluation, the required heating power is 10.94 kW with a heat transfer rate per unit length of heating pipe is 0.2618 kW/m. Thus, the required length of heating pipe is 41.79 m which has been fulfilled by the length of the existing heating pipe with a length of 43.5 m. The results indicated that the heating pipe was able to increase the dryhouse temperature. However, the condensate buildup inside the heating pipe reduces the dryhouse temperature minutes after the heating pipe operation. Therefore, it is responded by installing two stream traps, each installed at the inlet and outlet of the drying house to reduce condensate in the steam entering the drying house and remove the condensate formed while the steam is in the drying house. Subsequently, the heating pipe was tested operational twice on 16-17 January and 27-28 April 2023. On Trial 1, the heating pipe performance was not optimal due to condensate buildup inside the heating pipe. Therefore, steam traps were installed to reduce the condensate buildup. As a result, on Trial 2, the heating pipe performance was better, which was indicated by the higher and stable dryhouse temperature during the night. On Trial 3, the dryhouse temperature during the night was maintained higher than on Trial 2. This indicates that the technical improvements managed to improve the heating pipe’s performance on maintaining the dryhouse temperature. After all, the geothermal dryhouse can accelerate drying time significantly, up to 75% faster than conventional methods. This increased efficiency can lead to higher productivity and throughput in coffee drying processes.

REFERENCES

Ahamed, M. S., Guo, H., Tanino, K. (2018): A quasi-steady state model for predicting the heating requirements of conventional dryhouses in cold regions. *Information Processing in Agriculture*, 5, 33-46.

Ayuningtyas, R. R., Purba, D., Adityatama, D. W. (2021): Geothermal Role as Renewable Energy in Energy Mix Indonesia During and Post COVID-19 Pandemic. In *Proceedings of the 46th Workshop on Geothermal Reservoir Engineering*. Stanford University, Stanford, CA.

Badan Perencanaan Pembangunan Daerah Kabupaten Bandung. (2021): Perencanaan Pengembangan Potensi Wisata Geothermal Tahun Angaran 2021. Kabupaten Bandung

Berian, Z. Y., Khusaini, R. D. (2022): Preliminary Study on Geothermal Direct Utilization: A Case Study of Dryhouse Optimization at Wayang Windu Geothermal Area. *IOP Conference Series: Earth and Environmental Science*, 1-14.

da Costa, F. O., Alvarenga, T. F., de Mesquita, T. V., Júnior, I. P. (2021): Hybrid drying of pulped arabica coffee cherry beans using a hexagonal microwave dryer designed by numerical simulations. *Journal of Food Process Engineering*, 1-13

Darma, S., Imani, Y. L., Shidqi, M. N., Riyanto, T. D., Daud, M. Y. (2021): Country Update: The Fast Growth of Geothermal Energy Development in Indonesia. In *Proceedings of the World Geothermal Congress 2020+1*. International Geothermal Association, Reykjavik.

Farouq, C. U. et al. (2024): Technical and Business Evaluation of Geothermal Dryhouse for Coffee in Kamojang, West Java, Indonesia. In *IOP Conf. Ser.: Earth and Environmental Science*. 1293. 012007. IOP Publishing Ltd. England.

Lukmana, A. H., & Helmy, M. F. (2020): A Techno-Economic Analysis of Geothermal Energy in West Java. In *LPPM UPN "Veteran" Yogyakarta Conference Series Proceeding on Engineering Science Series*. LPPM UPN "Veteran Yogyakarta", Yogyakarta.

Rudiyanto, B., Illah, I. A., Pambudi, N. A., Cheng, C.-C., Adiprana, R., Imran, M., ... Handogo, R. (2017): Preliminary analysis of dry-steam geothermal power plant by employing exergy assessment: Case study in Kamojang geothermal power plant, Indonesia. *Case Studies in Thermal Engineering*, 10, 292-231.

Solargis. (2019): *Solar Resource Map Direct Normal Irradiation Indonesia*. The World Bank, Washington, D.C.

Solargis. (2019): *Solar Resource Map Horizontal Irradiation Indonesia*. The World Bank, Washington, D.C.

The American Society of Heating, Refrigerating, and Air-Conditioning Engineers. (2019): *Heating, Ventilation, and Air-Conditioning Applications*. ASHRAE, Atlanta.

Part 5:
General

This page is intentionally left blank

Optimizing Geothermal Investment in Indonesia: Adopting US Tax Credit Mechanisms

Nadya Erichatama[1], Vincentius Adven Brillian[1],
Ferdino R. Fadhillah[2], M. Rizqi Al Asy'ari[1], Daniel Adityatama[1],
Desak Inten Nyoman Apriani[2], and Dorman Purba[2]

[1]PT Geoenergi Solusi Indonesia, Jakarta, Indonesia
[2]PT Sarana Multi Infrastruktur (Persero), Jakarta, Indonesia

nadyaerichatama@geoenergis.com, erichatamanadya@gmail.com

Keywords: geothermal, tax incentives, tax allowance, tax holiday, tax credit, production tax credit, investment tax credit

ABSTRACT

Geothermal projects require substantial initial investments, largely due to costly exploration and infrastructure development. This capital-intensive nature not only extends the payback period but also increases financial risk, making external funding crucial. Tax incentives such as credits and deductions can significantly lower the investment threshold by reducing tax liabilities and enhancing the project's appeal to investors. Currently, Indonesia offers tax incentives for the geothermal industry through mechanisms such as tax holidays and tax allowances, primarily applying tax deduction methods. In contrast, the United States has implemented tax credit mechanisms, notably the Production Tax Credit (PTC) and Investment Tax Credit (ITC), which provide a more advantageous financial benefit. Tax credits are inherently more beneficial than deductions because they offer dollar-for-dollar tax savings, directly reducing tax liability. Furthermore, the United States also utilizes tax credit monetization, including tax credit transfers and tax equity financing. These mechanisms convert non-cash tax benefits into immediate capital, enhancing project cash flows—a critical advantage for geothermal projects with high capital costs.

Implementing a similar tax credit and monetization framework in Indonesia could provide substantial benefits over the current tax reduction incentives. This paper aims to explore the lessons learned from the US tax credit mechanism and assess its applicability in Indonesia to enhance the effectiveness of tax incentives for the geothermal sector.

1. INTRODUCTION

The development of geothermal projects can be divided into several phases: the preliminary survey, exploration and delineation drilling, development drilling and EPC (Engineering, Procurement, and Construction) for the power plant, followed by steam production and maintenance. Figure 1 illustrates the typical stages of a geothermal project along with its associated risk profile and investment cost. It highlights the high risk and substantial investment required to develop a geothermal project.

Despite the substantial capital needed for geothermal project development, investment in Indonesia's geothermal sector showed a decreasing trend from 2016 to 2021. This decline can be attributed to both internal and external factors related to project conditions. Internally, the significant capital requirement during the EPC phase is a major obstacle. Externally, aspects such as market trends, regulatory frameworks, economic stability, and fiscal incentives significantly influence the investment landscape for geothermal projects.

This paper aims to explore new fiscal incentives to boost geothermal investment in Indonesia by learning from the success of the US tax credit mechanism. Specifically, the study investigates the US Production Tax Credit (PTC) and Investment Tax Credit (ITC) models, seeking to identify key elements that could be adapted to enhance Indonesia's fiscal policies. The goal is to propose a tax incentives alternative that can effectively reduce the financial risks and barriers faced by geothermal developers in Indonesia.

2. TAX INCENTIVES BENCHMARK FROM US GEOTHERMAL INDUSTRY

As of 2023, the United States has reached an installed geothermal capacity of 3,771 MW, marking its initiation with the first geothermal power plant (GPP) operational at the Geysers in 1971. This positions the United States as a global leader in geothermal energy. The growth of the U.S. geothermal sector has been significantly influenced by two main factors: supportive federal and state-level policies and the economic dynamics shaped by natural gas prices and the development of the oil and gas industry.

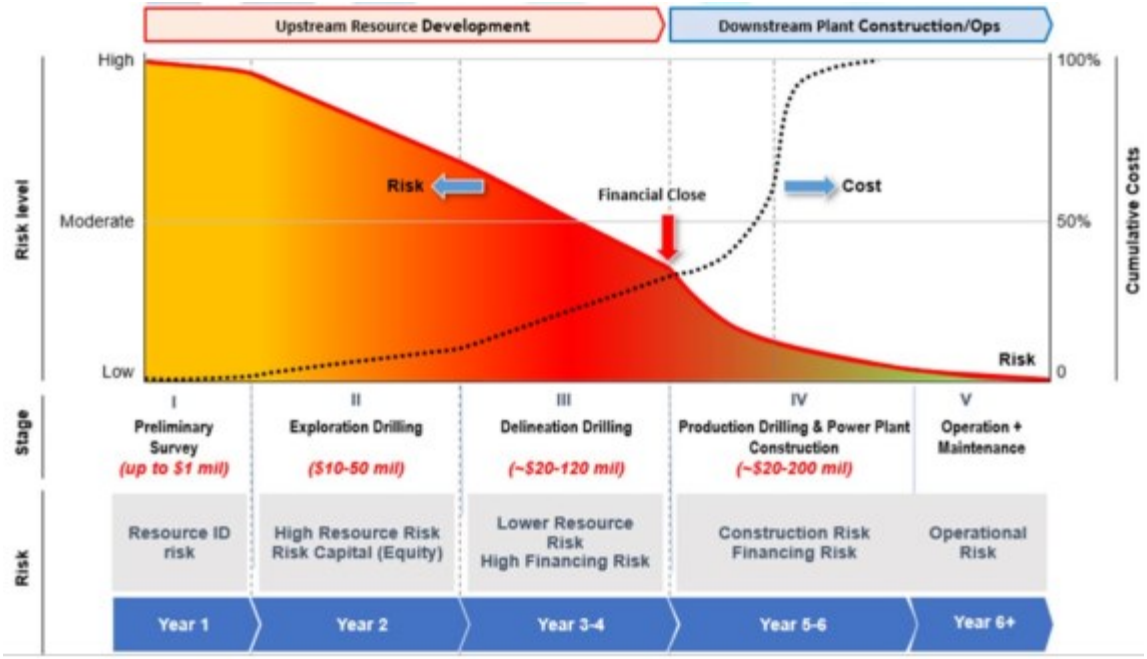

Figure 1: Geothermal development project phases and typical risk profile (modified from World Bank, 2019).

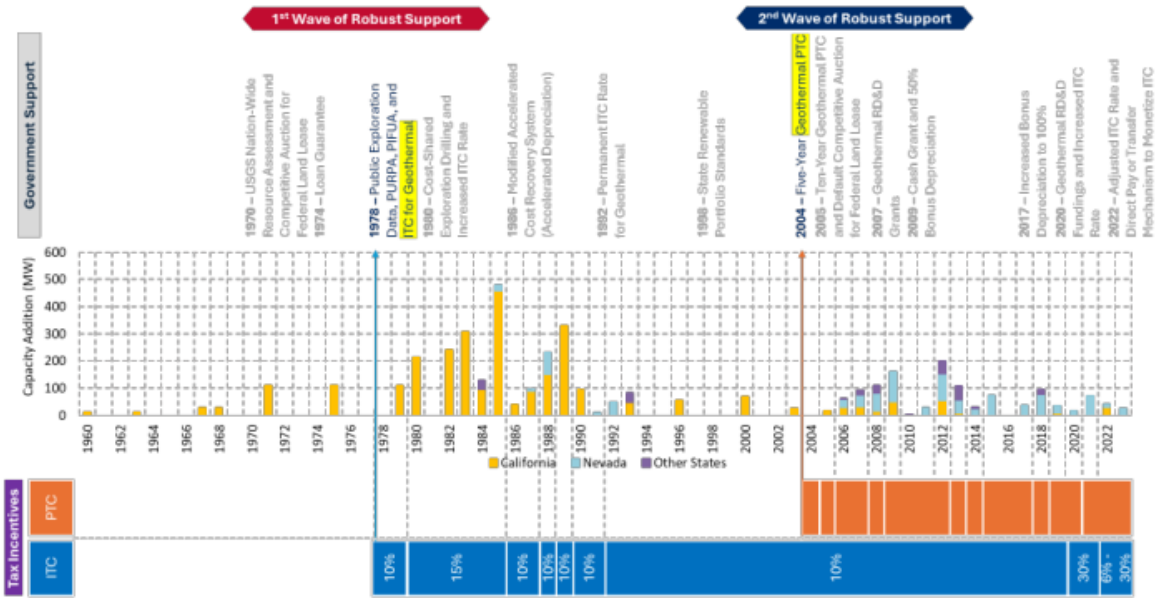

Figure 2: Annual Installed Geothermal Capacity and Key Federal Policy Milestones.

Federal and state policies have played a crucial role in fostering geothermal development through two major policy waves. The first wave, initiated in the 1970s, featured the introduction of federal land leasing regulations tailored for geothermal developments, exploration de-risking programs, and open access to exploration data. This period also saw the introduction of an investment tax credit (ITC) and the establishment of markets for investor-operated GPPs. The second wave, starting in the 2000s, implemented royalties, cash grants, a production tax credit (PTC), and other state-level incentives aimed at supporting geothermal power producers. These policies further mandated that utility companies procure a specified portion of their electricity from renewable sources.

One of the federal policies applied to geothermal energy in the U.S. is the use of tax incentives, particularly the ITC and PTC. The ITC, which offers a 10% credit for geothermal projects, was first enacted in 1978, while the PTC was introduced in 2005 specifically for geothermal energy. These federal renewable tax credits have undergone numerous extensions, modifications, and renewals, with significant changes introduced by the Inflation Reduction Act of 2022 (IRA 2022). This act expanded eligible technologies, extended the expiration date, modified the scheduled step-down in value, provided new bonus credits, and established new criteria to qualify for the full credit (DSIRE, 2023; U.S. Department of Energy, 2024).

Figure 1 illustrates the annual installed geothermal capacity alongside key federal policy milestones, including cash grants, loan guarantees, and tax incentives. The observed growth in the U.S. geothermal installed capacity, which aligns with the implementation of the Investment Tax Credit (ITC) and Production Tax Credit (PTC), highlights the potential effectiveness of these tax credit mechanisms. This connection prompts a compelling opportunity to study these frameworks in detail to assess their applicability in Indonesia. By examining the mechanisms and benefits of the ITC and PTC, Indonesia can consider adopting similar strategies to attract investment and accelerate the development of its geothermal sector.

2.1 Investment Tax Credit (ITC)

The Investment Tax Credit (ITC) reduces the tax liability by a percentage of the eligible investment cost during the tax year. It is an upfront tax credit that does not vary by system performance. For geothermal electricity, the ITC is given in the year of the Commercial Operation Date (COD) of the geothermal power plant.

Under the IRA 2022, the base ITC rate for geothermal is 6% of the eligible investment cost. The ITC rate can increase to 30% if the geothermal developer meets the "Labor Requirements1". Additionally, there are bonus credits that can be accessed to maximize the ITC rates, such as:

1. **Domestic content bonus**: an additional 10% of ITC rates.
2. **Energy community bonus**: an additional 10% of ITC rates.

Labor requirements including: 1) Prevailing wages requirements: for the first five years of the project for the ITC must be paid at the prevailing rates of that location; 2) Apprenticeship requirements: projects must ensure that 10-15% of total labor hours are performed by qualified apprentices (DSIRE, 2023).

The ITC is determined based on the plant's investment cost, making it crucial to understand which expenses qualify for inclusion to accurately calculate the project's eligible tax credit. The eligible investment cost for ITC includes equipment used to produce, distribute, or utilize energy derived from a geothermal source. This includes all equipment involved in the generation and distribution of geothermal energy within the plant. However, it excludes equipment used for the transmission of electricity from the plant to the grid, such as transmission lines.

2.2 Production Tax Credit (PTC)

The Production Tax Credit (PTC) is a per kilowatt-hour (kWh) tax credit for electricity generated by geothermal power plant for the first 10 years of a system's operation. It reduces federal income tax liability and is adjusted annually for inflation based on the GDP implicit price deflator from 1992.

Under the IRA 2022, the base PTC rate for geothermal is 0.55 cents USD per kWh, which can increase to 2.75 cents USD per kWh if the "Labor Requirements" are met. Additionally, bonus credits can further enhance the PTC rates:

1. **Domestic content bonus**: an additional 0.1 cents USD per kWh.
2. **Energy community bonus**: an additional 0.1 cents USD per kWh.

2.3 Enhancement Features for ITC and PTC

In addition to maximizing ITC or PTC rates by meeting labor requirements and obtaining bonus credits, geothermal developers can also enhance their tax credit benefits through the use of carryforward or tax credit transfer mechanisms. These mechanisms are designed to ensure that any unused tax credits from the current tax year can be fully utilized.

2.3.1 Tax Credit Carry-forward

The ITC and PTC can be carried forward if the tax liability is lower than the credit earned within the tax year. This mechanism allows taxpayers to apply unused tax credits from the current tax year to offset tax liabilities in future years, ensuring they can fully benefit from the credits even when their current-year tax liability is insufficient to utilize the entire amount.

The carryforward period for these credits typically ranges from 20 to 22 years after the tax credit is earned. The specific duration and rules governing the application of these credits may vary based on the particular tax credit and jurisdiction. At the end of the carryforward period, one-half of any unused credit can be deducted, with the remaining amount expiring. However, carryforward credits are not eligible for transferability, meaning it cannot be sold or transferred to another taxpayer.

2.3.2 Tax Credit Transfer

In the United States, geothermal developers with ITC or PTC are eligible to monetize their unused tax credits through a tax credit transfer mechanism. This mechanism allows developers with unused tax credits to sell or transfer all or a portion of these credits to an unrelated eligible taxpayer. This process enables the developer to

monetize their unused tax credits, while the purchasing taxpayer can utilize the acquired credits to offset their own tax liabilities.

Figure 3: Illustration of Tax Credit Carryforward Mechanism.

Terms and conditions for geothermal developers with ITC/PTC looking to monetize their tax credits are as follows:

1. The seller may sell the tax credit at a discounted price.
2. The benefit of the depreciation bonus from the tax credit cannot be transferred.
3. These payments are not considered gross income for federal tax purposes.
4. The carried forward credits are not eligible for credit transfer.
5. The portions of credits can be sold to multiple buyers within the same years.
6. The transfer of only the bonus credit amount of a tax credit is not permitted.

Payments for the credit transfer must be made in cash and are not considered gross income for federal purposes, meaning no federal taxes are owed on receiving the payment, and no deduction is available to the tax credit buyer for making the payment.

3. EXISTING GEOTHERMAL TAX INCENTIVES IN INDONESIA

The Government of Indonesia has introduced corporate income tax incentives specifically targeted at the geothermal industry, including tax holidays and tax allowances. These incentives are designed to enhance the attractiveness of geothermal projects by reducing the financial burden on companies, thereby promoting increased investment and improving profitability within the sector.

This section aims to examine the current geothermal corporate income tax incentives, focusing on the effectiveness of these incentives for geothermal project in Indonesia.

3.1 Tax Holiday

A tax holiday is one of the investment incentives provided by the Government of Indonesia, regulated by PMK No. 35 of 2018. This incentive offers a corporate income tax exemption for a period ranging from 5 to 20 years. The duration of the tax holiday is determined based on the amount of investment costs, as shown in Table 1.

Table 1: Tax Holiday Period based on the Total Investment Cost.

No	Total Investment Cost	Tax Holiday Period
1	IDR 0.5 to 1 trillion	5 years
2	IDR 1 to 5 trillion	7 years
3	IDR 5 to 15 trillion	10 years
4	IDR 15 to 30 trillion	15 years
5	More than IDR 30 trillion	20 years

For geothermal project with an investment exceeding IDR 0.5 trillion, developers are eligible for a 50% tax reduction for two years during the transition period following the initial tax holiday. Additionally, geothermal developers with an investment of more than IDR 0.1 trillion can receive a 50% tax reduction for the first five years of operation, followed by a 25% tax reduction for the subsequent two-year transition period.

3.2 Tax Allowance

Government Regulation No. 78 of 2019 (GR 78/2019) in Indonesia includes a tax allowance as one of its incentives to promote investment in various sectors, including geothermal energy. This tax allowance provides an investment tax deduction equivalent to 30% of the fixed capital investment, which is applied at a rate of 5% per

year over six years. Additionally, geothermal projects benefit from an eight-year depreciation period for both tangible and intangible assets. The geothermal industry is also eligible for a loss carryforward for up to five years, which can be extended to a maximum of ten years under certain conditions.

3.3 Study Literature on Effectiveness of Tax Holiday and Tax Allowance for Geothermal Project

While the government of Indonesia has attempted to attract investment in geothermal energy through tax holidays and tax allowances, numerous studies have highlighted the drawbacks of these incentives in attracting long-term investments, particularly for capital-intensive projects like geothermal energy development.

3.3.1 Limitations of Tax Holidays for Geothermal Project

The idea of a tax holiday is quite appealing as it provides a 100% reduction in corporate income tax for several periods, effectively serving as a tax exemption for those periods. However, tax holidays have several shortcomings as incentives to promote investments. According to several studies, the limitations of tax holidays are as follows:

1. Stotsky (2024) argues that tax holidays tend to attract short-term projects that yield quick returns rather than long-term investments. These long-term projects, which may offer greater value over time but do not generate profits in the early years, often find tax holidays less appealing as they do not benefit immediately from the tax exemption period.
2. Holland and Vann (1998) noted that tax holidays are less beneficial for significant capital-intensive projects, such as geothermal developments, which typically do not achieve profitability in the initial years. This misalignment between the tax holiday period and the financial realities of geothermal projects limits the effectiveness of such incentives.
3. Fadhillah et al. (2023) provide a case study that underscores the ineffectiveness of the current tax holiday structure for geothermal projects in Indonesia. The study demonstrates that the timing and design of these tax incentives do not align with the financial realities faced by geothermal developers. Without sufficient tax liabilities in the initial years, the tax holiday fails to provide the intended financial relief, thereby not enhancing project attractiveness or significantly reducing electricity generation costs.

These findings suggest that while tax holidays may be effective for certain types of investments, they are not well-suited for long-term, capital-intensive projects like geothermal energy development. To improve their efficacy, it is crucial to adjust the structure of tax incentives to better match the financial timelines and needs of these projects. This could potentially attract more sustainable investments and enhance the development of the geothermal sector in Indonesia.

3.3.2 Limitations of Tax Allowance for Geothermal Project

In the context of geothermal projects that do not have sufficient tax liabilities during the initial years of operation, tax allowance facilities become ineffective. Although tax allowances can be carried over, the carryover period of only five years is insufficient to accommodate the cash flow conditions of geothermal projects.

For example, Company A has a geothermal power plant with a capacity of 30 MW and a capital expenditure (capex) of 204 million USD. Company A plans to use a tax allowance at a rate of 6% for five years. Table 2 shows a simple simulation of the tax calculation for this project.

Table 2: Simplified Example of Tax Allowance in a Geothermal Project.

	Years of operation					
	1	**2**	**3**	**4**	**5**	**6**
Profit before tax	$-814	$-6,289	$-5,814	$-5,246	$-5,678	$-5,726
Tax allowance	$12,244	$12,244	$12,244	$12,244	$12,244	-
Tax amount	-	-	-	-	-	-

	Years of operation					
	7	**8**	**9**	**10**	**11**	**12**
Profit before tax	$-4,748	$-3,995	$-3,299	$-1,834	$-1,184	$1,088
Tax allowance	-	-	-	-	-	-
Tax amount	-	-	-	-	-	$266.21

The example above indicates that Company A does not have sufficient taxable income until the 12th year of operation, while the tax allowance period ends in the fifth year after COD. This underscores that the tax allowance cannot be utilized at all for the geothermal project developed by Company A. This observation aligns with Stotsky (2024), who noted that tax allowances are most beneficial to firms with existing income. Such firms can use the

incentives from new investments to shelter a portion of their income from tax. In contrast, firms with low income cannot benefit from the incentive until the investment starts generating income.

This finding suggests that the implementation of tax allowances for geothermal projects in Indonesia requires adjustments, such as extending the tax allowance period and/or extending the loss carryover period of the tax allowance itself.

4. DISCUSSION

4.1 Comparison of tax incentive mechanisms in Indonesia and the United States

There are notable contrasts in the tax incentives applied in the United States and Indonesia, particularly in the methods of taxation employed. Indonesia utilizes the tax exemption method for tax holidays and the tax deduction method for tax allowances, whereas the United States employs the tax credit mechanism. Essentially, a tax deduction is an amount that can be subtracted from a taxpayer's gross income, thereby reducing the amount of income subject to tax. Deductions lower taxable income, and their value depends on the taxpayer's marginal tax rate. A tax exemption, on the other hand, excludes certain income from being taxed altogether. This means that the exempted income is not considered part of the taxable income. For instance, in Indonesia, geothermal projects which applied for tax holiday might be granted tax-exempt status for a specified period, thus encouraging investment in those areas by completely removing the tax burden on that income. In contrast, a tax credit is a direct reduction of the tax owed, rather than a reduction of taxable income. It reduces the tax liability dollar-for-dollar, making it potentially more beneficial than a deduction or exemption, as it directly lowers the amount of tax that needs to be paid. The summary of differences between tax deductions, tax exemptions, and tax credits is shown in Table 3.

Table 3: Summary of The Difference between Tax Deduction, Tax Exemption, and Tax Credit.

Aspects	Tax Exemption	Tax Deduction	Tax Credit
Definition	Specific income excluded from being taxed	An amount subtracted from gross income to reduce taxable income	A direct reduction in the amount of tax owed
Function	Reduces gross income, hence lowering taxable income	Lowers taxable income; value depends on taxpayer's marginal tax rate	Reduces tax liability dollar-for-dollar
Impact	Excludes certain types of income from taxation entirely	Reduces the amount of income subject to tax, thereby lowering tax liability	Directly decreases the total tax owed, potentially resulting in a refund
Examples	Tax Holiday	Tax Allowance	1. Investment Tax Credit 2. Production Tax Credit

To better understand the difference between a tax deduction and a tax credit, consider two companies, Company A and Company B, each with a taxable income of $1,000,000. Both are eligible for a $100,000 benefit, but Company A receives a tax deduction, while Company B receives a tax credit. Table 4 shows the simplified calculation for each case.

Table 4: Simplified Example of Tax Deduction and Tax Credit Mechanism.

Company	Tax Incentive	Original taxable income	Tax deduction	Taxable income after tax deduction	Income tax rate	Tax liability	Tax credit	Tax owed
Company A	Tax deduction	$ 1,000,000	$ 100,000	$ 900,000	25%	$ 225,000	-	$ 225,000
Company B	Tax credit	$ 1,000,000	-	$ 1,000,000	25%	$ 250,000	$ 100,000	$ 150,000

The example above demonstrates that tax credits are generally more advantageous than deductions because they provide a dollar-for-dollar reduction in tax liability, directly decreasing the amount of tax owed. This is in contrast to tax deductions, which merely reduce the taxable income upon which the tax liability is calculated. As shown, while both deductions and credits offer tax benefits, tax credits typically have a more substantial and straightforward impact on lowering the overall tax burden.

4.2 Potential Benefits in Adopting Tax Credit Transfer Mechanism

In addition to tax credit mechanisms such as ITC and PTC, another beneficial approach that can be adopted from U.S. tax incentives is the tax credit transfer mechanism. This mechanism allows developers to fully utilize the tax

facilities. Furthermore, several potential benefits can be achieved through the implementation of tax credit transfers:

1. **Increased Liquidity for Developers**: Tax credit transfers allow developers to sell unused tax credits to other entities,providing immediate capital that can be reinvested in their projects. This is particularly beneficial for geothermal projects,which require substantial upfront investment.
2. **Attracting New Investors**: Tax credit transfers can attract a wider range of investors, including those who may not bedirectly involved in geothermal energy but are interested in purchasing tax credits to offset their own tax liabilities.
3. **Boosting Project Viability**: The ability to transfer tax credits can make geothermal projects more financially viable byreducing the effective cost of capital and improving project economics.
4. **Enhanced Return on Investment**: Developers can achieve a better return on investment by converting non-cash taxbenefits into actual cash flow, thus making projects more attractive to stakeholders.

4.3 Challenges and Opportunities in Adopting US Tax Credit Mechanisms in Indonesia

Adopting tax credits for geothermal energy projects in Indonesia offers significant opportunities but also presents several challenges that need to be addressed for successful implementation.

The potential opportunities of adopting US tax credit mechanisms are as follows:

1. Direct Reduction in Tax Liability: Tax credits are more advantageous than deductions because they provide a dollar-for-dollar reduction in tax liability, directly decreasing the amount of tax owed. This makes tax credits a powerful tool for improving the financial attractiveness of geothermal projects.
2. Enhanced Utilization of Tax Facilities: Developers can fully utilize tax facilities through several enhancement features as follows:
    a. Tax Credit Transfer: Allows developers to sell unused tax credits to other entities, providing immediate capital that can be reinvested in their projects. This improves liquidity and project cash flow, crucial for the capital-intensive nature of geothermal projects.
    b. Carryforward Provisions: Enable developers to use tax credits that exceed their current tax liability in future years, ensuring that the benefits of the credits are not lost due to initial non-profitability.
    c. Credit Bonus: Additional incentives can be provided for meeting specific criteria, such as using local resources or achieving certain production milestones, further enhancing the attractiveness of investments.
3. Boosting Investment and Economic Growth: The introduction of tax credits can attract a broader range of investors, including those not directly involved in geothermal energy but interested in purchasing tax credits to offset their tax liabilities.

Despite the significant opportunities presented by adopting U.S. tax credit mechanisms for geothermal projects in Indonesia, several challenges must be addressed to implement such a new tax incentive effectively. These challenges include:

1. Defining Eligible Expenditures: One of the major technical issues in adopting the Investment Tax Credit (ITC) is defining eligible expenditures. Achieving a precise definition is crucial to direct the incentive to the desired activities and minimize revenue "leakage." At the same time, it is essential to provide taxpayers with certainty regarding the applicability of the incentive (Holland & Vann, 1998).
2. Setting the Appropriate Rate: Determining the appropriate rate for the tax credit is complex. The rate must be attractive enough to incentivize investment without causing significant revenue loss for the government. Striking this balance is crucial to ensure the effectiveness of the tax credit.
3. Policy and Regulatory Changes: Implementing a new tax credit system requires changes to existing policies and regulations. Ensuring policy stability and consistency is vital to maintaining investor confidence. Frequent changes or uncertainties in tax policy can deter long-term investments.
4. Administrative Implementation: Introducing tax credits involves setting up robust administrative systems to manage, monitor, and enforce the new policies effectively. This includes handling applications, ensuring compliance, and processing claims, all of which can be resource-intensive.

While the adoption of tax credits for geothermal energy in Indonesia presents notable opportunities to stimulate investment and advance renewable energy goals, it also involves significant challenges that need to be carefully managed. Addressing these challenges through clear definitions, appropriate rates, robust administration, and policy stability can help maximize the benefits of tax credits and support the sustainable development of Indonesia’s geothermal sector.

5. CONCLUSION AND PATH FORWARD

Currently, the implementation of tax holidays and tax allowances as incentives in Indonesian geothermal projects exhibits several shortcomings that hinder developers from fully utilizing these benefits. Numerous studies have highlighted the need for adjustments, such as extending both the tax holiday and the loss carryover periods for tax allowance facilities.

Additionally, this study proposes adopting the U.S. tax credit mechanism, which includes ITC and PTC, along with enhancement features such as bonus credits and credit transferability. Tax credits offer a dollar-for-dollar reduction in tax liability, directly reducing the amount of tax owed. According to the authors, this makes the tax credit scheme a more advantageous option compared to the tax deduction scheme used in tax allowances. Furthermore, implementing the enhancement feature of credit transfer could allow developers to maximize the use of the tax facility during the early operational phase of geothermal power plants, which typically do not yet have sufficient tax liabilities. This tax credit transfer mechanism could also provide an alternative for developers to generate revenue during the initial operational phase.

Moreover, it is essential to conduct further assessments to evaluate the impact of utilizing tax credits on the financial feasibility of projects. Such analysis will provide a clearer understanding of both the benefits and the drawbacks associated with this form of tax incentive. There is also a need for more comprehensive studies aimed at developing a policy brief and a framework to facilitate the implementation of tax credits in Indonesia, ensuring that these incentives effectively support the development of the sector.

REFERENCES

Abidin, M., Rosdiana, H., & Salomo, R. (2020). Tax Incentive Policy for Geothermal Development: A Comparative Analysis in ASEAN. *Int. Journal of Renewable Energy Development* (IJRED), 53-61.

Azhgaliyeva, D., Kapsaplyamova, Z., & Low, L. (2018). *Implications of Fiscal and Financial Policies for Unlocking Green Finance and Green Investment*. Tokyo: Asian Development Bank Institute. Retrieved from https://www.adb.org/publications/implications-fiscal-financial-policies-unlocking-green-finance-and-green-investment

BKPM. (2018). *Pedoman dan Tata Cara Pemberian Fasilitas Tax Holiday dan Tax Allowance*. Jakarta.

DJEBTKE-KESDM. (2021). *Pedoman Investasi Pembangkit Listrik Tenaga Panas Bumi*. Jakarta: Direktorat Jenderal Energi Baru, Terbarukan, dan Konservasi Energi, Kementerian Energi dan Sumber Daya Mineral.

DSIRE. (2023, August 29). *Business Energy Investment Tax Credit (ITC)*. Retrieved from programs.dsireusa.org: https://programs.dsireusa.org/system/program/detail/658

DSIRE. (2023, August 29). *Renewable Electricity Production Tax Credit (PTC)*. Retrieved from programs.dsireusa.org: https://programs.dsireusa.org/system/program/detail/734

Fadhillah, F., Tjendarsa, K., Damayanti, S., Adityatama, D., & Purba, D. (2023). *Economic Evaluation of Bravo Geothermal Prospect in Participating Green Energy Effort*. Gema Ekonomi.

Holland, D., & Vann, R. (1998). Income Tax Incentives for Investment. In *Tax Law Design and Drafting (volume 2)*. International Monetary Fund.

IRENA. (2022). *Indonesia Energy Transition Outlook*. Abu Dhabi: International Renewable Energy Agency.

IRENA and CPI. (2023). *Global Landscape of Renewable Energy Finance 2023*. Abu Dhabi: International Renewable Energy Agency.

Mai, T., Cole, W., Lantz, E., Marcy, C., & Sigrin, B. (2016). *Impacts of Federal Tax Credit Extensions on Renewable Deployment and Power Sector Emissions*. Colorado: National Renewable Energy Laboratory.

Owens, B. (2002). *An Economic Valuation of a Geothermal Production Tax Credit*. Colorado: National Renewable Energy Laboratory.

Pivot Energy. (2024, April 2024). *Clean Energy Financing: Unlocking Renewable Energy Growth with Transferable Tax Credits*. Retrieved from pivotenergy.net: https://www.pivotenergy.net/blog/clean-energy-financing-unlocking-renewable-energy-growth-with-transferable-tax-credits

PT SMI, GRG, Geoenergis. (2024). *Government Support to Indonesia Geothermal: A Review of Fiscal Incentives*. Jakarta.

Rosdiana, H. (2008). Rekonstruksi Konsepsi Supply Side Tax Policy. *Jurnal Ilmu Administrasi dan Organisasi, Bisnis & Birokrasi*, vol. 15, 202-205.

Speer, B. (2012). *Geothermal Brief: Market and Policy Impacts Update*. Colorado: National Renewable Energy Laboratory.

Stotsky, J. (2024). Tax Incentives and Investment. *The Governance Brief*, Issue 54, 1-15.

U.S. Department of Energy. (2024). *Federal Solar Tax Credits for Business*. United States.

UNCTAD. (2000). *Tax Incentives and Foreign Direct Investment: A Global Survey*. Geneva, United Nations: ASIT Advisory Studies No. 16.

United States Environmental Protection Agency. (2023, December 18). *Renewable Electricity Production Tax Credit Information*. Retrieved from epa.gov/lmop: https://www.epa.gov/lmop/renewable-electricity-production-tax-credit-information

Geothermal Drilling Cost Landscape in Indonesia: Cost Trend, Outlier Cost, and Drilling Cost Component

Nadya Erichatama[1], Dorman Purba[1], Daniel Adityatama[2], and M. Rizqi Al Asy'ari[2]

[1]PT Enerka Bhumi Pratama, Cibis Nine 11th Floor, Jakarta, Indonesia
[2]PT Geoenergi Solusi Indonesia, Jakarta, Indonesia

nadya.e@enerklaz.com, erichatamanadya@gmail.com

Keywords: Geothermal drilling cost in Indonesia, geothermal drilling unit cost (GDUC), geothermal drilling cost component

ABSTRACT

The development of geothermal energy as a clean and sustainable energy source in Indonesia faces significant challenges due to the high costs associated with drilling. This paper provides a detailed analysis of geothermal drilling costs in Indonesia by examining actual and historical data from various projects. The study addresses the difficulties in accessing comprehensive cost data due to the absence of an integrated database, the confidential nature of drilling costs, and the lack of standardized reporting and costing structures. Despite these challenges, the study compiles data from 254 drilling records between 2011 and 2023, normalizing costs to 2023 values using the Producer Price Index (PPI). This study indicates a wide cost range from 1,300 to 22,000 USD per meter, with most costs clustering between 2,733 and 4,549 USD per meter and a median of 3,432 USD per meter.

The study also highlights the impact of drilling difficulties and failures on cost outliers, providing insights into the highest and lowest drilling costs recorded. The findings underscore the need for improved data management and standardization in geothermal drilling in Indonesia to enhance cost efficiency and support the sustainable development of geothermal energy.

1. INTRODUCTION

The development of geothermal energy, a clean and sustainable energy source, is often impeded by the substantial costs involved in drilling. This paper presents a detailed analysis of geothermal drilling costs in Indonesia, aiming to provide a comprehensive understanding of these expenses by examining the actual and historical drilling costs of various projects.

1.1 Challenges in Accessing Geothermal Drilling Cost Data in Indonesia

One method to identify these costs in Indonesia is through a database that includes data from all developers. However, no such geothermal drilling database currently exists in Indonesia, presenting a significant challenge in gathering accurate data. Consequently, the quality of our analysis depends on the data we can access. Accessing geothermal drilling cost data in Indonesia is notably challenging. Several factors contribute to this difficulty:

1. **Absence of a Geothermal Drilling Database**: No integrated database currently exists for geothermal drilling, complicating the collection of comprehensive data.
2. **Confidential Nature of Drilling Costs**: Developers rarely disclose geothermal drilling costs due to their confidential nature, hindering the free flow of information necessary for effective data gathering, benchmarking, and analysis. Interviews suggest there is no clear rationale for this secrecy, given that drilling data are specific to each field and operator.
3. **Scarcity of Publications**: There is a noticeable lack of comprehensive publications on geothermal drilling costs, which may be linked to the confidential nature of such data. This scarcity limits the availability of publishable drilling cost data. Additionally, some existing publications offer cost estimates for hypothetical wells, which are unsuitable for this analysis.
4. **Incomplete Data in Reports**: Many reports do not provide a complete breakdown of total drilling costs, resulting in an inadequate dataset for detailed cost analysis. This issue stems from the absence of a standard reporting requirement enforced by the Indonesian government for documenting geothermal drilling activities.
5. **Lack of Standardized Costing Structure**: The Indonesian government has not mandated developers to collect and submit drilling data in a standardized format, complicating the task of conducting accurate cost component analysis.

1.2 Available Geothermal Drilling Data

Despite the challenges in obtaining comprehensive geothermal drilling cost data, this study has made a concerted effort to compile information from various sources. A total of 254 drilling records from Indonesia, spanning the years 2011 to 2023, were acquired. To ensure consistency and relevance, all data was normalized to 2023 values using the Producer Price Index (PPI) from the US Department of Labor's Bureau of Labor Statistics.

Of the 254 Indonesian drilling data records collected, only 51 wells have a detailed cost breakdown. The cost breakdown presented in this study includes only rig costs, tangibles, and drilling services. It does not cover mobilization and demobilization costs, nor site preparation expenses. Given that approximately 825 geothermal wells have been drilled in Indonesia from 1970 to 2023 (Purwanto et al., 2021; Geoenergis, 2023), the dataset used in this study is relatively limited. This limitation highlights the urgent need for improvements in the storage and management of geothermal drilling data in Indonesia.

2. GEOTHERMAL DRILLING WELL DEPTH TREND IN INDONESIA

To accurately assess the baseline costs of geothermal drilling in Indonesia, this study begins with understanding the typical well depths within the country is essential. This knowledge is key, as the depth of the well is a critical factor that significantly impacts the overall drilling costs.

Figure 1 shows the well depth distribution of 254 geothermal wells in Indonesia. The distribution shows a wide variation in well depths, stretching from below 500 meters to over 3,000 meters. However, the frequency of wells noticeably diminishes as the depth surpasses 2,500 meters, suggesting that wells within this range are less common. Additionally, wells that are deeper than 3,000 meters are relatively rare. Overall, 70% of geothermal well depth in Indonesia ranging from 1,600 – 2,800 meters with average depth of 2,254 meters.

Figure 1 also reveals that there are several wells with depths less than 1,200 meters measured depth (mMD), which are considered shallow and shallower than the typical depth of the top of the geothermal reservoir in Indonesia, approximately 1,200-2,000 meters. Further analysis of drilling and chronological data indicates that all these wells failed to reach their target depth due to various reasons, such as stuck pipes, or running out of budget that prevented them from reaching the target depth. These unsuccessful wells can impact the statistical analysis of drilling costs, for instance, in USD/m analysis, as they may inflate the USD/m value due to their shallow depth.

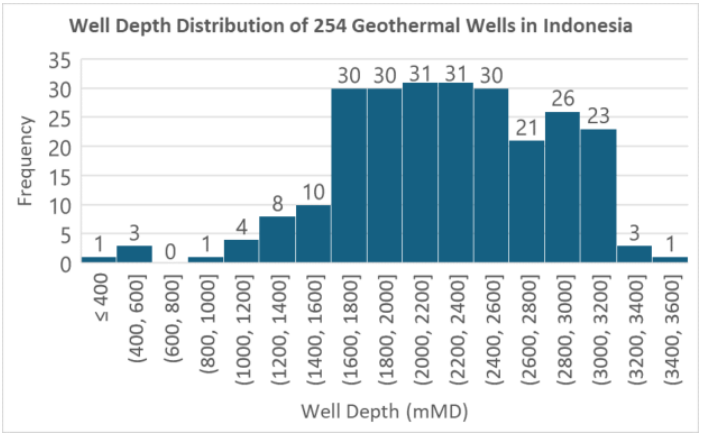

Figure 1: Histogram of Well Depth from 254 Geothermal Wells in Indonesia.

According to (Sanyal, et al., 2011a), depth is considered the primary determinant of the drilling cost of a geothermal well, with the cost typically increasing exponentially as depth increases in any country. Therefore, to understand the baseline trend of total geothermal drilling costs in Indonesia, a statistical analysis was conducted on the distribution of these costs in relation to well depth. Additionally, Lukawski (2016) found that, with increasing depth, drilling problems escalate, not in a linear fashion, but significantly at specific depths within the reservoir zone. Therefore, the addition of drilling depth must be carefully considered in terms of risk, cost, and benefit.

3. GEOTHERMAL DRILLING COST TREND IN INDONESIA

Figure 2 illustrates the distribution of total drilling costs of 254 geothermal wells in Indonesia. The drilling cost data distribution presented reveals a scattered trend with a wide range of total drilling costs for geothermal wells in Indonesia, varying significantly from 1 million to 25 million USD per well. This extensive variability poses challenges for drilling engineers in establishing a definitive baseline for drilling costs for planning purposes.

Concurrently, this significant fluctuation suggests that there are opportunities for Indonesia to enhance the efficiency of its geothermal drilling expenses.

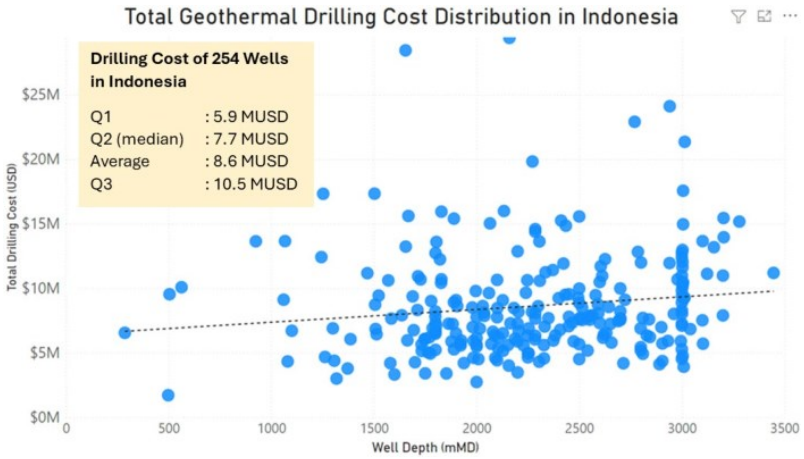

Figure 2: Scatter Chart of Total Geothermal Drilling Cost of 254 Wells in Indonesia.

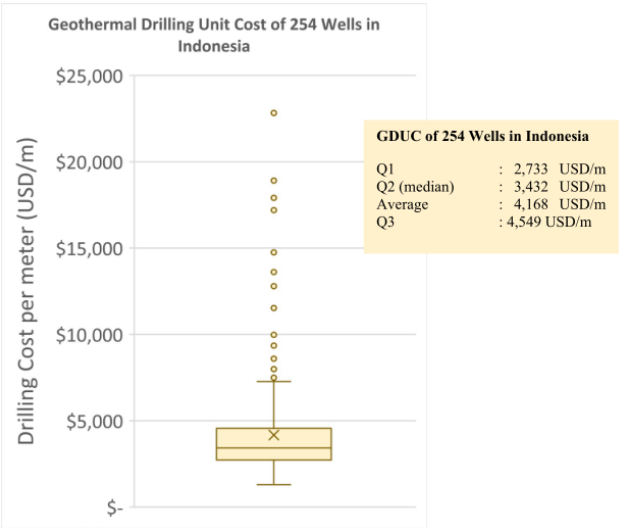

Figure 3: Box Plot of Geothermal Drilling Unit Cost in Indonesia.

One way to measure geothermal drilling performance is by using Geothermal Drilling Unit Cost (GDUC) as suggested by Zuhro and Arif (2015). The GDUC measures geothermal drilling performance in USD/m, with the intention to be able to compare the drilling cost between wells with different depth. Figure 3 shows the distribution of Geothermal Drilling Unit Cost (GDUC) in Indonesia. The box plot reveals a wide variation in the distribution of GDUC, with figures ranging from 1,300 to 22,000 USD per meter per well. It is also noted that wells costing more than 7,000 USD per meter are rare, representing outliers in this dataset. Given the dataset's susceptibility to outliers, the median is utilized as a more suitable measure to represent the drilling cost data, as it is less affected by these extreme values. Overall, the typical drilling cost range in Indonesia is fall within the interquartile range of 2,733 to 4,549 USD per meter with median of 3,432 USD per meter.

4. GEOTHERMAL DRILLING COST COMPONENT

In addition to understanding the trends in drilling costs per well, it is important to understand the specific components of these costs. Analyzing these cost components is crucial for identifying which components have the largest share and the most significant impact on geothermal drilling projects.

This section examines the recent trends in geothermal drilling costs, focusing on key contributors and their influence on overall project budgets. By analyzing these trends, geothermal companies can better manage costs and improve operational efficiency, leading to more successful drilling projects.

In this study, an analysis of the cost component distribution was conducted using data from 51 drilling projects. It was found that each company has different systems for classifying cost components. Therefore, this study attempts to classify drilling cost components based on major drilling elements, as follows:

1. Rig.
2. Bit.
3. Wellhead.
4. Casing.
5. Drilling fluid.
6. Cementing.
7. Directional drilling.
8. Aerated drilling.
9. Fuel.
10. Other costs, which include expenses other than the eight cost components mentioned above. These expenses consist of various smaller cost items, each of which contributes a relatively low percentage (ranging from less than 1% to no more than 3%) to the total drilling cost. Together, these "other costs" make up around 20% of the total drilling cost.

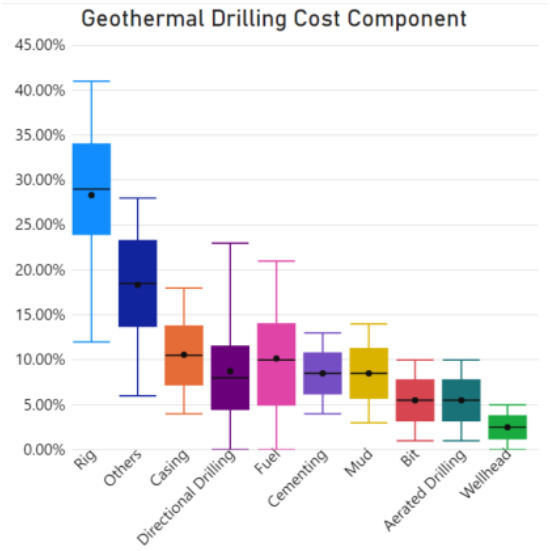

Figure 4: Percentage Distribution in Geothermal Drilling Cost Component.

Figure 4 presents a box plot showing the percentage distribution of drilling cost components based on data from 51 wells. The analysis indicates that the most substantial contributors to drilling costs are the drilling rig, casing, directional drilling, cementing, and drilling fluid. "Other costs" are not considered as substantial contributors to the drilling cost component, as they consist of a group of different services and/or materials.

Table 1: Summary of Percentage Distribution in Geothermal Drilling Cost Component.

No	Cost Component	Percentage of Cost Contribution (%)			
		Q1	Q2	Average	Q3
1	Rig	24	29	28	34
2	Casing	7	10	10	14
3	Directional drilling	4	8	9	11
4	Fuel	5	10	10	14
5	Cementing	6	8	8	10
6	Drilling fluid (mud)	5	8	8	11
7	Aerated drilling	3	5	5	7
8	Bit	3	5	5	7
9	Wellhead	1	2	2	3
10	Other costs	13	18	18	23

Table 3 summarizes the distribution of drilling cost components in Indonesian projects. The data reveals that the largest cost components are rig costs (24 – 34%), casing (7 – 14%), directional drilling (4 – 11%), fuel (5 – 10%), and cementing (6 – 10%). Collectively, these top five components account for approximately 80% of the total drilling cost. This observation is consistent with Pareto's Principle, often summarized as "80% of the effects arise from 20% of the causes." Should this pattern of cost distribution persist across various geothermal drilling operations in Indonesia, it would imply that drilling teams ought to prioritize the management of principal service

contracts that account for over 80% of the drilling costs. This approach suggests a strategic focus on key areas of expenditure rather than an equal distribution of resources and efforts across all contracts.

5. DRILLING COST OUTLIER

Figure 5 shows the distribution of geothermal drilling costs in Indonesia and highlights the presence of outlier data. The outlier data were identified using the 1.5 * IQR rule, a common statistical method that considers a data point an outlier if it is more than 1.5 times the interquartile range (IQR) above the third quartile or below the first quartile. Applying this rule to our dataset helps pinpoint unusually high costs in drilling operations. The analysis identified 13 wells with excessively high drilling costs, with a total expenditure of 176.5 million USD for these wells alone.

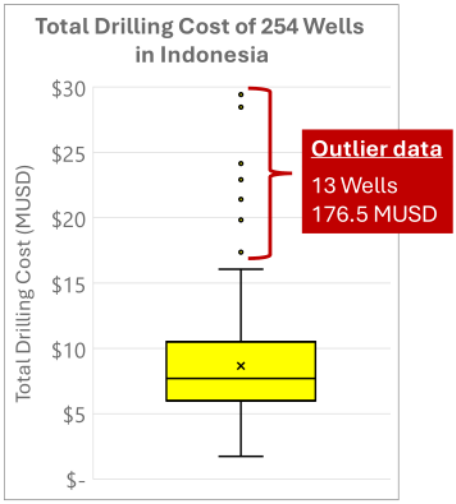

Figure 5: Outlier Data in the Box Plot of Geothermal Drilling Cost in Indonesia.

A further examination of the outliers reveals that the exceptionally high GDUC values are caused by several factors, such as:

1. **Recorded failed wells**. In the data presented, there are several wells that do not reach the total depth (TD) or reservoir depth, resulting in wells with very shallow depths. These wells are usually failed and non-productive ones, which are then decided to be abandoned before reaching the TD. This shallow well depth then influences the GDUC value or drilling cost per meter, where the smaller the well depth, the smaller the divisor of the total drilling cost, resulting in a high GDUC value.
2. **Drilling difficulties or drilling problems**. Some wells with high GDUC values are also influenced by drilling difficulties encountered during drilling, such as stuck pipes and blow-outs. These drilling difficulties then lead to Non-Productive Time (NPT) and additional drilling days. The longer the duration of drilling due to various drilling issues, the higher the well cost becomes, primarily due to the increasing rental costs of drilling rigs.

This subsection aims to analyze the causes of outlier data in the distribution of geothermal drilling costs in Indonesia, focusing on both the lowest and highest costs. The objective of this analysis is to gain a deeper understanding of the nature of geothermal drilling costs in Indonesia and to identify potential areas for improvement in cost efficiency.

5.1 Analysis on Excessively High Drilling Cost

In this study, the outlier data for excessively high drilling costs were identified using the 1.5 * IQR rule. This commonly used statistical rule states that a data point is considered an outlier if it is more than 1.5 times the interquartile range (IQR) above the third quartile or below the first quartile. Applying this rule to our dataset helps pinpoint unusually high costs in drilling operations.

Table 1 shows the outlier data for the highest total drilling cost in Indonesia. The data reveal that the most expensive drilling instance was recorded at 29.4 million USD for a well reaching a depth of ~2100 meters MD. Despite this significantly high cost, the well turned out to be not productive.

According to interviews, this highest drilling cost in Indonesia was attributed to multiple incidents of stuck pipes. The well accounted for 311.5 NPT (Non-Productive Time) hours or equal to 27% of the total drilling duration due to stuck pipe alone. This high NPT subsequently affected the addition of drilling days and caused a cost overrun.

Similarly, the second and third highest costs, at 28.4 million USD and 24.1 million USD respectively, were also due to multiple stuck pipe incidents in each well.

Table 2: Outlier Data of the Highest Drilling Cost in Indonesia.

No	Well Name	Well Depth (mMD)	Total Drilling Cost (USD)	Drilling Cost per meter (USD/m)	Well Status
1	Well A	~2100	$29,408,487	~$13,600	Non-productive
2	Well B	~1600	$28,441,465	~$17,100	Non-productive
3	Well C	~2900	$24,110,166	~$8,100	Productive
4	Well D	~2700	$22,904,286	~$8,200	Productive
5	Well E	~3000	$21,352,215	~$7,000	Productive
6	Well F	~2200	$19,824,782	~$8,000	Non-productive
7	Well G	~3000	$17,559,075	~$5,000	Productive
8	Well H	~1500	$17,335,170	~$11,500	Non-productive
9	Well I	~1200	$17,323,032	~$13,800	Non-productive
10	Well J	~2100	$15,988,860	~$7,400	Non-productive
11	Well K	~1800	$15,938,855	~$8,700	Non-productive
12	Well M	~1600	$15,605,100	~$9,300	Productive
13	Well N	~2500	$15,563,587	~$6,200	Non-productive

The data above further explains that geothermal drilling represents a high-risk venture, often encountering substantial cost overruns and even the possibility of no steam production. The analysis indicates that a significant contributor to these overruns is incidents of stuck pipes. Thus, the prevention of stuck pipes becomes important in drilling operations in geothermal projects to avoid these cost overruns.

5.2 Analysis on the Lowest Drilling Cost

In addition to observing outlier data with the highest drilling costs in Indonesia, observations were also made on the lowest drilling costs. The lowest value in this study was determined using a sorting method, where the collected dataset was sorted to identify the three lowest drilling costs. The objective of analyzing the three lowest drilling costs in Indonesia is to investigate the underlying factors contributing to these reduced expenses. This analysis seeks to identify any effective cost-saving strategies employed by the operators, with the intention of applying similar practices in future operations to achieve cost efficiency.

Table 3 shows a summary of the three lowest drilling costs in Indonesia. From this data, it is known that the cheapest drilling cost in Indonesia is 1.7 million USD for a depth of ~500 mMD. Given this very shallow depth, it can be ascertained that this well is a failed well that did not reach Total Depth (TD). This is further supported by the fact that the well is not producing, and interview findings indicate that it has been permanently plug and abandonment (P&A).

Table 3: Top 3 of the Lowest Drilling Cost in Indonesia.

No	Well Name	Well Depth (mMD)	Total Drilling Cost (USD)	Drilling Cost per meter (USD/m)	Well Status
1	Well O	~500	$1,709,100	~$3,430	Non-productive
2	Well P	~2000	$2,733,380	~$1,300	Productive
3	Well Q	~1300	$2,998,551	~$2,200	Non-productive

To understand the cost efficiency tips for the cheapest well, this study conducted interviews with related stakeholders involved in the drilling operation of Well P. From these interviews, it was found that this cost efficiency was achieved with several strategies as follows:

1. Long-term contracts and/or high quantities allowed for extensions without requiring a tender process. The high number of wells or extended contract durations incentivizes contractors to offer lower contract values.
2. Extensive and ongoing drilling campaigns mean that drilling services or rigs remain in the working area of the developer, reducing the costs associated with multiple mobilizations and demobilizations. While this lowers the total drilling cost, the cost per MW is higher due to more wells being required to achieve a certain electricity output, given the low success rate of drilling. As the drilling contractors drill more wells in the same area, they will accumulate lessons learned and leave the learning curve phase, ultimately leading to better performance and cost optimization.

3. The Developer owns and operates drilling rigs and several drilling services, including aerated drilling and cementing. Aerated drilling can be notably costly in Indonesia due to the scarcity of contractors, which allows them to dictate terms to geothermal developers.

However, these strategies may not necessarily be applicable to all developers, considering that each field has its own unique characteristics, and each developer has different operating strategies. Overall, this observation of the highest and lowest geothermal drilling cost data underscores the significant range in both expenses and outcomes associated with geothermal drilling in Indonesia.

6. CONCLUSION AND PATH FORWARD

The study reveals that geothermal drilling costs in Indonesia exhibit significant variability, ranging from 2 million to 29 million USD per well. This wide range underscores the diverse challenges and conditions encountered in geothermal drilling operations. High-cost outliers, such as the instances of wells costing up to 29 million USD per well, highlight specific challenges like incidents of stuck pipes, which can drastically increase costs. These findings point to the critical need for detailed analysis and effective management strategies to address these high-cost cases.

This study has also identified the components that contribute to 80% of the total drilling cost: rig, casing, directional drilling, fuel, and cementing. If this pattern of cost distribution persists across various geothermal drilling operations in Indonesia, it implies that drilling teams should prioritize the management of these principal service contracts, which account for the majority of the drilling costs. This approach suggests a strategic focus on key areas of expenditure rather than an equal distribution of resources and efforts across all contracts.

To further enhance the understanding and management of geothermal drilling costs in Indonesia, the following steps are recommended:

1. **Regular Updates to the Study**: Continuously update the study with new drilling data on an annual basis to capture trends and advancements in drilling technology. Regular updates will ensure that the analysis remains relevant and reflective of the current state of geothermal drilling in Indonesia.
2. **Enhanced Data Transparency and Sharing**: Encourage developers to disclose drilling cost data by addressing confidentiality concerns and demonstrating the collective benefits of data sharing for the industry. Promote the publication of comprehensive reports and studies on geothermal drilling costs to build a robust body of knowledge.
3. **Standardization of Reporting Requirements**: Collaborate with the Indonesian government to establish standardized reporting requirements for geothermal drilling activities. This will ensure consistency and completeness in the data collected, enhancing the reliability of the database.
4. **Development of a Geothermal Drilling Database**: Establish an integrated database for geothermal drilling costs in Indonesia. This database should include comprehensive data from all developers, ensuring that drilling engineers can access up-to-date information across the country. The database should standardize the collection and reporting of drilling cost components, facilitating accurate cost comparisons and benchmarking.

By implementing these steps, the geothermal industry in Indonesia can achieve greater cost efficiency and support the sustainable development of geothermal energy. The creation of an integrated database will play a crucial role in ensuring that drilling engineers can make better-informed decisions, ultimately contributing to the overall success and growth of the geothermal sector.

REFERENCES

Adityatama, D. et al., 2021. *The Significance of Drilling Data Management to Improve Geothermal Drilling Planning and Operation in Indonesia*. Reykjavik, s.n.

EBTKE, 2019. *Geothermal Drilling Regulation*, Jakarta: Ministry of Energy and Mineral Resources.

EBTKE, 2023b. *PENGEMBANGAN PANAS BUMI*, Jakarta: Direktorat Panas Bumi.

EBTKE, 2023c. *FORUM GROUP DISCUSSION GEOTHERMAL DRILLING DAYS*, s.l.: s.n.

EBTKE, 2023. *Pedoman Efisiensi Biaya Pengeboran Panas Bumi,* Jakarta: Ministry of Energy and Mineral Resources.

ESMAP, 2012. *Geothermal Handbook: Planning and Financing Power Generation*, Washington, D.C.: Energy Sector Management Assistance Program.

Gul, S. & Aslanoglu, V., 2018. *Drilling and Well Completion Cost Analysis of Geothermal Wells in Turkey*. Stanford, California, s.n.

Hartono and Ashadi, 2020. *The Economical Way to Drill Geothermal*, s.l.: s.n.

LPPM FEB UI, 2023. *Buku Putih: Analisis Bisnis dan Kebijakan untuk Mendorong Investasi Pembangkit Listrik Tenaga Panas Bumi (PLTP) di Indonesia*, s.l.: LPPM FEB UI.

ORACLE, n.d. *What Is a Database?*. [Online] Available at: https://www.oracle.com/id/database/what-is-database/ [Accessed 12 March 2023].

Purba, D. et al., 2020. *Geothermal Drilling Cost Optimization in Indonesia: A Discussion of Various Factors*. Stanford, Stanford University.

Purba, D. et al., 2021. *Integrated Stuck-Pipe-Prevention Campaign in Geothermal Drilling Project in Indonesia: A Proactive Approach*. Reykjavik, Indonesian Geothermal Association, pp. 1-11.

Purba, D. P., Adityatama, D. W., Umam, M. F. & Muhammad, F., 2019. *Key Considerations in Developing Strategy for Geothermal Exploration Drilling Project in Indonesia*. Stanford, s.n., pp. 1-12.

Purwanto, E. H., Suwarno, E., Lukman, R. F. & Herdiyanto, B., 2018. *Geothermal Drilling in Indonesia: A Review of Drilling Operation, Evaluation of Well Cost and Well Capacity*. Jakarta, s.n., pp. 1-9.

Sanyal et al, 2011. An Investigation of Drilling Success in Geothermal, s.l.: *GRC Transactions*, Vol. 35, 2011.

Sanyal, S. et al., 2011a. Geothermal Resource Risk in Indonesia - A Statistical Inquiry. s.l., *Thirty-Sixth Workshop on Geothermal Reservoir Engineering*.

Zuhro, A. A. & Arif, G. R., 2015. Pertamina Geothermal Energy Drilling Campaign. s.l., *World Geothermal Congress 2015*.

Proposing Corporate Work Plan and Budget (WP&B) Based on Risk Management to Ensure the Sustainability of Business Operations in the Kamojang Geothermal Area

Darussalam, Harahap. R., and Iman. A.S.

PT Pertamina Geothermal Energy Tbk

darussalam_1@pertamina.com, rahmad.h@pertamina.com, ahmad.iman@pertamina.com

Keywords: Work Plan and Budget (WP&B), Risk Management, Geothermal, Sustainability, Business Operations

ABSTRACT

The Kamojang Geothermal Area is an area that has been operating for quite a long time and continues to produce within the Kamojang-Darajat Geothermal Working Area (GWA). Kamojang Geothermal Power Plant (GPP) Unit 1, the first unit, began operations in 1983 and its production continuity has been maintained to this day. The sustainability of business operations needs to be supported by a comprehensive operation and maintenance budget. Every year, the operational and maintenance costs are proposed in the Work Plan and Budget (WP&B) Operating Cost Budget (OCB) submitted by the Kamojang Geothermal Area to the Head Office of PT Pertamina Geothermal Energy Tbk. To propose a comprehensive operation and maintenance budget, an appropriate basis is required as a reference. In this case, the Kamojang Geothermal Area will submit the WP&B OCB based on risk management so that the proposed budget truly aligns with the risk mitigation plan for the existing risks.

Risk management is an effort to manage risks based on the results of identifying potential hazards and everything that can impact a business operation. To address existing risks, mitigation is necessary to maintain the risks at a desired condition by reducing the level of residual risk from the inherent risk level. In determining the level of risk, a Risk Tolerance Limit (RTL) will be established and calculated based on the planned profit for the proposed WP&B year. The risk itself will be assessed based on the impact and probability of uncertainties that will affect business operations.

Considering the aging condition of assets and equipment in the Kamojang Geothermal Area, it is necessary to record potential risks based on the actual condition of these assets and equipment. The steps for proposing a risk-based WP&B include:

1. Risk identification (examining potential costs, accident history, and benchmarking similar equipment)
2. Calculating probability, impact, and risk weight
3. Recording the mitigation plan to be implemented and comprehensively calculating the mitigation costs
4. Determining the appropriate Cost Center/Work Breakdown Structure (WBS) and General Ledger (GL) account
5. Summarizing the WP&B OCB proposal based on risk management
6. Proposing and conducting a challenge session for the WP&B OCB with the Head Office of PT Pertamina Geothermal Energy Tbk

Therefore, it is expected that the proposed WP&B OCB will be a comprehensive risk management-based budget, and its use can be accounted for as a risk mitigation effort to ensure the sustainability of the Kamojang Geothermal Area business operations.

1. INTRODUCTION

The Kamojang Geothermal Area is one of the geothermal fields belonging to PT Pertamina Geothermal Energy Tbk and the first geothermal field to have been operating in Indonesia since 1983 when the first Kamojang Geothermal Power Plant (GPP) Unit 1 commenced operation. Nowadays, the Kamojang Geothermal Area has 5 (five) GPPs, with the latest unit commercialized in 2015 and a total installed capacity of around 235 MW.

The Kamojang Geothermal Area is an area that has been operating for quite a long time and continues to produce within the Kamojang-Darajat Geothermal Working Area (GWA). The sustainability of Kamojang Geothermal Area's business operations is about maintaining the reliability of its GPPs and production facilities. In order to keep the business operations running smoothly, the Kamojang Geothermal Area needs the Operating Cost Budget (OCB) to support the availability of tools, equipment, and services needed in operation and maintenance activities.

On the other hand, the sustainability of Kamojang Geothermal Area business operations should be ensured to meet the contracted production amounts for supplying steam and electricity to PLN as stated in the purchase agreement.

Figure 1: Kamojang Geothermal Power Plant.

2. METHOD

Every year, the operational and maintenance costs are proposed in the Work Plan and Budget (WP&B) Operating Cost Budget (OCB) submitted by the Kamojang Geothermal Area to the Head Office of PT Pertamina Geothermal Energy Tbk. To propose a comprehensive operation and maintenance budget, an appropriate basis is required as a reference. In this case, the Kamojang Geothermal Area will submit the WP&B OCB based on risk management so that the proposed budget truly aligns with the risk mitigation plan for the existing risks.

Risk management is an effort to manage risks based on the results of identifying potential hazards and everything that can impact a business operation. To address existing risks, mitigation is necessary to maintain the risks at a desired condition by reducing the level of residual risk from the inherent risk level. In determining the level of risk, a Risk Tolerance Limit (RTL) will be established and calculated based on the planned profit for the proposed WP&B year. The risk itself will be assessed based on the impact and probability of uncertainties that will affect business operations.

Considering the aging condition of assets and equipment in the Kamojang Geothermal Area, it is necessary to record potential risks based on the actual condition of these assets and equipment. The steps for proposing a risk-based WP&B include:

1. Risk identification (examining potential costs, accident history, and benchmarking similar equipment). For example, risk identification based on equipment failure is as follows:

Table 1: Historical Equipment Failure Data.

Date	GPP	Disturbance Status	Start Time	End Time	Duration (Hours)	Derating (Mw) (Based on URC)	Energy Lost (kWh)	Location	Cause	Remarks
02/10/21	Unit 5	FO1 (Forced Outage Immediate)	16:24	10:00	17.6	35.07	529,363.3	GPP	Main Steam System	Scrubber Leak
03/10/21	Unit 5	FO1 (Forced Outage Immediate)	10:00	10:00	24	35.07	841,566.7	GPP	Main Steam System	Scrubber Leak

2. Calculating probability, impact, and risk weight. Probability is measured by the criteria of frequency level. For the example above, the risk probability is “likely” or a score of 4 based on the company risk management guidance. Next, the impact is calculated in Table 2.

Table 2: Risk Event and Calculation of Its Impact.

7	**Unplanned Shutdown & Derating at GPP Unit 5**			
No	***Inherent Risk Financial Impact:***	***Value (Thousand USD)***	***Description***	
1	Loss Production Benchmark damage to Bottom Scrubber Unit-5 2021	>2000	30-day shutdown	
	Total Inherent Risk Financial Impact Value	**>2000**	**% Impact of Vavlue/RTL**	**Impact Score based on Impact Index (1= 0%-20%, 2=20%-40%, 3=40%-60%, 4=60%-80%, 5=80%-100%)**
			89.00%	5

After that, calculate the risk weighting as probability multiplied by impact, which equals 4 x 5 = 20, categorizing it as “high risk” based on the company's risk management guidance

3. Recording the mitigation plan to be implemented and comprehensively calculating the mitigation costs Calculate the mitigation costs to prevent the risk of Unplanned Shutdown & Derating events at GPP Unit 5

Table 3: Risk Mitigation Plan.

7	**Unplanned Shutdown & Derating at GPP Unit 5**		
No	***Risk Mitigation Plan:***	***Value (Thousand USD)***	***Description***
1	Maintenance costs, replacement of spare parts, repair of tools and equipment	>200	OCB for Non Rotating, Rotating, Instrument, and Electrical work centers

4. Determining the appropriate Cost Center/Work Breakdown Structure (WBS) and General Ledger (GL) account Based on the calculation of mitigation costs above, input and allocate those costs to the appropriate Cost Center/WBS and General Ledger (GL) account, for example:

Table 4: Cost Center and GL Account.

Cost Center	***Cost Center Description***	***GL Account***	***GL Account Description***	***Description in the WP&B OCB***	***Value (Thousand USD)***
C0121002	Maintenance KMJ - Joint Cost	6001013110	PLANT & MACHINERY MATERIAL & EQUIPMENT CONSUMED	OCB for Non Rotating, Rotating, Instrument, and Electrical work centers	>200

5. Summarizing the WP&B OCB proposal based on risk management. All calculations from the risk mitigation plan are then summarized on the worksheet of WP&B OCB
6. Proposing and conducting a challenge session for the WP&B OCB with the Head Office of PT Pertamina Geothermal Energy Tbk.

3. DISCUSSION

The relationship between the cost of risk mitigation and the comprehensive WP&B OCB submission is that the cost of risk mitigation provides a strong foundation for determining the budget required for business operations of Kamojang Geothermal Area. On the other hand, a good WP&B will be in line with the WP&B of the Directorate General of New, Renewable Energy, and Energy Conservation (NREEC), also known as the Rencana Kerja dan Anggaran Biaya (RKAB), which is mandatory to be submitted and approved by the Directorate General of New, Renewable Energy and Energy Conservation (NREEC), representing the Ministry of Energy and Mineral Resources (MEMR). By understanding and calculating the mitigation costs needed to reduce or avoid the impacts of potential risks, the Kamojang Geothermal Area can develop a more accurate and comprehensive budget. This enables Kamojang to allocate resources more effectively and minimize potential disruptions or additional costs that may arise from unexpected risk events.

Comprehensive WP&B submission based on the cost of risk mitigation is crucial in business operations for several key reasons:

1. Better Planning, by considering the costs of risk mitigation, companies can better plan for potential risks that may affect their projects or business operations. Resources can be allocated more strategically, ensuring that high-risk areas receive the necessary attention and funding.
2. More Effective Risk Management, identifying and evaluating mitigation costs helps in more effectively managing risks. This allows companies to anticipate potential issues and take necessary preventive or recovery measures. Risk management allows for proactive measures to be put in place, reducing the likelihood of risks materializing and impacting operations.
3. Financial Stability, including mitigation costs in the budget ensures that companies have adequate resources to handle potential risks. This helps maintain financial stability and reduces the risk of funding shortages during projects. Financial stability is maintained as resources are set aside to handle potential risks, preventing disruptions in operations.
4. Improved Decision-Making, a comprehensive budget submission based on mitigation costs provides a strong foundation for better decision-making. Management can prioritize projects with reasonable mitigation costs and avoid projects with uncontrolled risks. By showing that risks are managed proactively, the company can build trust with stakeholders, enhancing its reputation and credibility.

4. CONCLUSION

Proposing a Corporate Work Plan and Budget (WP&B) based on risk management involves integrating risk assessment and mitigation strategies into the financial and operational planning processes of a business is important. This approach ensures that potential risks are identified, evaluated, and addressed within the budget and work plan, leading to more resilient and sustainable business operations.

Therefore, it is expected that the proposed WP&B OCB will be a comprehensive risk management-based budget, and its use can be accounted for as a risk mitigation effort to ensure the sustainability of the Kamojang Geothermal Area business operations.

In summary, integrating the costs of risk mitigation into WP&B OCB submissions helps ensure that companies can manage their operations better, reduce uncertainty, and increase the likelihood of long-term success. This approach enhances planning, risk management, financial stability, decision-making, stakeholder confidence, and long-term sustainability, ultimately leading to more resilient and successful business operations.

REFERENCES

PT Pertamina Geothermal Energy Tbk.: 2023 Annual Report, *Elevate*, (2024).

PT Pertamina Geothermal Energy Tbk.: Enterprise Risk Management, *Guidance No. A-001/PGE310/2023-S9*, (2023).

PT Pertamina Geothermal Energy Tbk.: *Operational Risk Management*, Organizational Procedure No B-002/PGE244/2016-S0, (2016).

PT Pertamina Geothermal Energy Tbk.: *Asessment and Mitigation Risk*, Organizational Procedure No B-001/PGE113/2018-S9, (2018).

PT Pertamina Geothermal Energy Tbk.: *Proposing the Corporate Work Plan and Budget*, Organizational Procedure No B-004/PGE112/2018-S9, (2018).

Cendrowski, H., and Mair, W.C.: *Enterprise Risk Management and Coso, A Guide for Directors, Executives, and Practitioners*, (2009), 13.

Challenges in Meeting International Standards for Impact Assessments in Indonesia Geothermal Projects

Ni Putu Wulan Romianingsih[1], Suyud Warno Utomo, and Udi Syahnoedi Hamzah[2]

[1]Jacobs
[2]University of Indonesia

Wulan.Romianingsih@jacobs.com, suyudwarno@gmail.com, udi.syahnoedi@ui.ac.id

Keywords: Environmental impact assessment, geothermal, Indonesia, stakeholder engagement

ABSTRACT

Geothermal energy, recognized for its potential as a sustainable and low-emission power source poses a substantial environmental and social risks. Therefore, the importance of conducting comprehensive environmental and social impact assessment (ESIA) cannot be overstated. With the strategic importance of geothermal energy in supporting nationwide growth, it is imperative that good industry practice and internationally-compliant environmental and social impact assessment (ESIA) would need to be connected. The alignment and conduct of the local permitting requirements and the international ESIA standards can be challenging and consequently impede the process. However, there are only a few studies that examine procedural and process challenges for Indonesia and how these affect the ESIA process for geothermal projects. Drawing on the analysis of completed ESIAs and the semi-structured interview with stakeholders and ESIA experts, this paper identifies key challenges which include: (1) insufficient understanding of international standards and practice, (2) discrepancies between national and international requirements, (3) differences in risk appetite, and (4) challenges in integrating national and international assessment processes. The authors aim to raise awareness of these issues to foster improvements in ESIA practices in Indonesia and worldwide, especially concerning geothermal projects.

1. INTRODUCTION

Geothermal energy exploitations and productions present significant environmental and social risks and because they can alter the physical, biological, and social environments (Rahman et al., 2022). Therefore, the integration of environmental impact assessment and social impact assessment is crucially becoming part of project approval process (Dendena & Corsi, 2015; Ortiz et al., 2018) to prevent and/or mitigate negative environmental impacts, social conflicts, and financial losses. The concept and practice of ESIA are well-established and extensively developed at the international level (Glasson et al., 2019; Gulakov et al., 2020; Quigley, 2021), with agreed-upon values, principles, and guidelines for implementation (Asian Development Bank, 2009; International Finance Corporation, 2012a; International Union for Conservation of Nature, 2020; Vanclay et al., 2015). ESIA is widely used by private lending institutions that adhere to the Equator Principles, multilateral development banks, and other international financial institution (Corsi et al., 2015; Dendena & Corsi, 2015; Romianingsih et al., 2023; Vanclay, 2020).

Romianingsih et al. (2023) have studied the discrepancies between ESIA based on international standards and *Analisis Mengenai Dampak Lingkungan* (Indonesia Environmental Impact Assessment or Amdal) which follows national regulations. This issue is common in developing countries and countries in transition (Gulakov & Vanclay, 2018; Omenge et al., 2020). However, the article is fully based on document analysis, excluding the perspective of the key stakeholders. This proceeding paper aims to address the gaps by exploring the challenges of implementing international ESIA standards in Indonesia, particularly for geothermal projects, through document analysis and semi-structure interviews with key stakeholders and leading ESIA experts in Indonesia.

2. LITERATURE REVIEW

2.1 ESIA versus Amdal

Environmental Impact Assessment (EIA) is a systematic, holistic, and multidisciplinary process used to identify and evaluate the potential environmental consequences of proposed development plans, thereby facilitating informed decision-making and sound environmental management (Glasson et al., 2019; Loomis & Dziedzic, 2018; Roos et al., 2020). The EIA (called Amdal in Indonesia) was formally introduced in Indonesia in 1982 through the enactment of Law No. 4 of 1982 on Basic Provisions for Environmental Management. However, its implementation was initially limited due to the lack of detailed guidelines and the limited understanding of key stakeholders. During this period, some Amdal studies were conducted to meet foreign aid requirements and donor agency requests (Purnama, 2014). It was not until 1986, with the enforcement of Government Regulation No. 29

of 1986 on Environmental Impact Analysis, that EIA began to be systematically and extensively implemented (Purnama, 2014).

Social impact assessment (SIA), health impact assessment (HIA), and strategic environmental assessment (SEA) have also developed under the umbrella of the EIA due to dissatisfaction with previous assessments that had been implemented (Hacking, 2019; Harris et al., 2018; Vanclay, 2020). A growing body of literature has been published on Amdal in the past five years which criticize the weakness of regulatory enforcement of Amdal. The regulation is supposedly weak with ineffective penalties for non-compliance (Zahroh & Najicha, 2022), the lack of accountability of public participation process (Kurniawan et al., 2020; Lai & Hamilton, 2021), and the absence of climate change discussion, biodiversity offset, and analysis of alternative (Swangjang, 2018). These feedback and evaluation would justify the requirement for ESIA which follow the international standards to close those gaps identified in Amdal. ESIA provides a more comprehensive approach for integrated assessments that encompasses evaluation of the biophysical and social impacts of projects, programs, and policy initiatives (Dendena & Corsi, 2015).

The commitment of financial institutions to adopt voluntary regulations aims to ensure their activities contribute positively to sustainable development (Contreras et al., 2019). In the last decade, development projects funded by international institutions have been required to meet environmental and social standards established by these institutions while also complying with Indonesia's national regulations and standards. These environmental and social safeguards form the foundation for the formulation of Environmental and Social Impact Assessments (ESIA).

2.2 International Standards for ESIA

Geothermal projects in Indonesia heavily involve foreign investors due to their substantial investment requirements (Chelminski, 2022; Rakhmah, 2023). This trend reflects developed countries' commitment to supporting developing nations in transitioning to renewable energy sources (Mori, 2020). It has become standard practice for project developers to prepare ESIA as a prerequisite for securing loans from international financial institutions. Depending on the preferences of the lenders or donors involved, one or more of the followings would typically be applicable in Indonesia:

a. International Finance Corporation Performance Standards on Environmental and Social Sustainability (IFC PS);
b. Asian Development Bank Safeguard Policy Statement (ADB SPS);
c. Guidelines for Confirmation of Environmental and Social Considerations by Japan Bank for International Cooperation (JBIC);
d. Equator Principles 4 (EP4); and
e. The World Bank Environmental and Social Framework. (World Bank ESF) including the World Bank Group Environmental, Health, and Safety (EHS) Guidelines for Geothermal Power Generation

The aforementioned detail the requirements for the preparation of ESIA documents which the project sponsor shall adhere to in order to ensure environmental and social aspects are addressed with the process, including meaningful public participation, assessment and management of projects impacts across its project phases. Among these standards, the IFC PS often serves as primary benchmark. While internationally recognized, the Principles and Guidelines on Business and Human Rights have seen limited reference in Indonesia thus far (Götzmann et al., 2016). The IFC Performance Standards ensure comprehensive consideration of labor and working conditions (PS2); resource efficiency and pollution prevention (PS3); community health, safety, and security (PS4); involuntary resettlement (PS5); biodiversity conservation (PS6); indigenous peoples (PS7); and cultural heritage (PS8). These are generally in alignment with all 17 United Nations Sustainable Development Goals (UN SDGs). Emphasis must be placed on addressing the needs and aspirations of vulnerable communities. The IFC Performance Standards also provide definitions for project area of influence (AOI), associated facilities, and cumulative effects (International Finance Corporation, 2012a). After conducting the impact assessments, project proponents are required to establish ongoing monitoring processes and effective systems for managing social and environmental impacts for the whole lifecycle of the project.

3. METHODOLOGY

The methodology from Gulakov et al. (2020) was adapted for this study with minor modifications. This paper primarily analyzed two completed geothermal ESIAs in Indonesia as case studies. As part of triangulation to mitigate potential bias, the study also incorporated semi-structured interviews with nine stakeholders (as presented on Table 2) and two ESIA experts based in Indonesia All interviews were conducted in accordance with social research ethics (Vanclay et al., 2013), with each interviewee signing a consent form prior to participation. Table 2 presents the breakdown of the interviewees based on their role and/or institution.

Table 1: SDG Mapping of IFC Performance Standards (International Finance Corporation, 2023).

IFC Performance Standards	SDG Alignment
Performance Standards 1 Assessment and Management of Environmental and Social Risks and Impacts	
Performance Standards 2 Labor and Working Conditions	
Performance Standards 3 Resource Efficiency and Pollution Prevention	
Performance Standards 4 Community Health, Safety, and Security	
Performance Standards 5 Land Acquisition and Involuntary Resettlement	
Performance Standards 6 Biodiversity Conservation and Sustainable Management of Living Natural Resources	
Performance Standards 7 Indigenous Peoples	
Performance Standards 8 Cultural Heritage	

Table 2: List of Interviewees.

Institution/Role	Number of Interviewees
Project sponsors (private corporations)	2
Ministry of Environment and Forestry	1
Local Environmental Agency	1
Financial institutions	2
Consultants	2
Academia	1
ESIA experts based in Indonesia	2

The discrepancy between procedural features of Amdal and ESIA as well as national requirements and international requirements for impact assessment formed the basis of the interviews with the stakeholders and experts. These interviews were conducted either in person or via MS Teams or Zoom between January and April 2023. The language of the interviews, Indonesian or English, was chosen based on the preference of the interviewees. Each interview lasted between 60 to 90 minutes, and interviewees were informed in advance about the topics and the outline of the questions. Following the interviews, the authors employed simple coding techniques to analyze the qualitative data, aiming to capture the key themes and synthesize the overall findings from the interviews.

4. RESULTS AND DISCUSSION

Based on the document analysis and interviews, four key challenges were identified: (1) insufficient understanding of international standards and practice, (2) discrepancies between national and international requirements, (3) difference in risk appetite, and (4) challenges in integrating national and international assessment processes.

4.1 Insufficient understanding of international standards and practice

Typically, in Indonesia, performance standards and requirements are perceived as regulations to be complied by a project. The specificcompliance requirements are presented in a checklist and/or template that a project must accomplish. This approach is shaped by the conventional nature of Amdal requirements. Similar to an ESIA screening and scoping, the local Amdal process is initiated by a screening process that identifies the project type, compliance requirements, and reporting threshold set in the regulations. Should the project exceed a certain threshold, usually for environmentally critical projects, an EIA becomes mandatory. Another example is Government Regulation No. 22 of 2021 and its appendices that specify the stakeholders to be engaged, procedures for public disclosure of the project, the template for Amdal document, among others. These guidelines are highly

detailed and straightforward, making them easy to follow, but they also indirectly suggest that anything beyond the prescribed requirements is excessive and unnecessary, thus discouraging the adoption of best practices during the impact assessment process.

Geothermal companies, familiar with these national requirements and experienced in their application, often adopt an Amdal approach to ESIA. However, such approach is fundamentally flawed when applied to international standards, as it contradicts their intended purpose. Unlike prescriptive national regulations, international standards offer a framework for managing potential social impacts of a project. They do not provide the same threshold screening requirements as local Amdal but require the project developer to screen the project with defining project magnitude, boundary, emissions, and scientific rationale which are often beyond the requirements and review scope of the local ministry. Other challenges include the lack of alignment between Amdal and ESIA on stakeholder engagements wherein the international requirement is vaguer on procedural steps but does require comprehensive stakeholder identification and consultations. It is up to the project proponent and their consultants to choose and adapt methods for effective information sharing and engagement. Four interviewees noted that international standards focus on principles, while Indonesian requirements specify detailed processes and template. Overemphasis on detailed national regulations can cause company personnel to focus on ticking the box and meeting the minimum requirement, hence, losing sight of the broader objectives (Gulakov et al., 2020).

However, one interviewee raise a contradictive opinion: the lack of understanding and limited practical application of international standards in Indonesia can be attributed to the disconnect between these global frameworks and the local context. While the principles underlying these standards are universally applicable, their implementation requires a nuanced understanding of the unique cultural, political, and socioeconomic factors that shape the Indonesian business landscape. For example, the flexibility inherent in the non-prescriptive nature of the IFC Performance Standards and the ADB Safeguard Policy Statement can be both a strength and a challenge. This flexibility allows for the tailoring of the standards to local needs, but many studies suggest that it also creates ambiguity that can be exploited by companies seeking to minimize their compliance efforts (ADB, 2014; Cahyandito & Pau, 2017; Thanh et al., 2020).

It is also observed from interviews that smaller companies in particular often struggle to understand the nuances and practical applications of international standards while multinational enterprises operating in Indonesia recognized the importance of these international standards and platforms in informing their scoping practices. This is consistent with what has been studied by Borgert et. al. (2018) but the recognition did not necessarily translate to a deep understanding or consistent application of the requirements.

This lack of understanding, coupled with the time and budget constraints faced by project sponsors, has led to a tendency to prioritize speed over the comprehensive analysis necessary for a meaningful impact assessment. The rush to complete the assessment process, driven by these external pressures, often compromises the integrity of the findings and the ability to effectively address potential environmental, social, and economic implications.

4.2 Discrepancies between national and international requirements

Project developers must comply with national laws when planning for geothermal projects. If they are seeking international funding, they must also adhere to the IFC PS requirements (International Finance Corporation, 2012a). However, the document analysis and the interviews identified discrepancies between national law and the IFC requirements. One of the primary differences lie in the stakeholder engagement procedures. IFC PS and ADB SPS mandate meaningful public consultation, requiring project developers to actively seek input from affected communities, including marginalized or vulnerable groups. However, the national regulations in Indonesia are not as comprehensive as international standards, leading to limitation in the depth and breadth of stakeholder engagement. For instance, indigenous communities in Indonesia are not always clearly defined, and the recognition of their rights and the need for their free, prior, and informed consent (FPIC) is not consistently applied across all geothermal projects. This can create issues between the project developers' obligations under national standards and their ability to comply with international standards, potentially leading to conflicts.

Another area of divergence relates to the definitions and thresholds used in assessing environmental and social impacts. International frameworks often have more comprehensive and stringent criteria for determining the significance of impacts, such as the IFC's requirements around the assessment of ecosystem services (Borgert et al., 2018). In contrast, Indonesian regulations may rely on less rigorous impact assessment methodologies, leading to discrepancies in the identification and mitigation of potential adverse effects (Borgert et al., 2018). The treatment of ecosystem services for the local impact assessment often miss the key assessment and mitigations for biodiversity values critical for livelihood, natural capital, and climate resilience. Additionally, the local definition of “critical habitat” is limited to the definition from national legislation which significantly differs from international guidance documents that include ecologically sensitive areas, key biodiversity areas, and others resulting in the underestimation or overlooking of sensitive ecological areas that warrant special protection measures (Semedi et al., 2017).

This disconnect between international and national standards can also manifest in the approach to managing resettlement and livelihood restoration. While international guidelines emphasize the need for comprehensive compensation, support for livelihood restoration, and the prevention of impoverishment, national regulations in Indonesia may not always mandate such comprehensive measures, potentially leaving affected communities inadequately supported (Borgert et al., 2018). Moreover, international guidance notes (International Finance Corporation, 2012b) recognize the rights of informal settlers and stakeholders without formal proof of authority/ownership of land and assets while the local regulations often do not consider these for compensation.

In terms of indigenous peoples and indigenous cultural communities, the lack of a clear and unified definition of "indigenous peoples" in the Indonesian context can create ambiguity and a failure to recognize the unique rights and needs of these communities, which are often central to international standards (Ferrol-Schulte et al., 2015). This can lead to the exclusion of important stakeholders from

the consultation and decision-making processes, potentially exacerbating existing vulnerabilities and tensions. The international standards, such as the IFC Performance Standards, require a more rigorous assessment of the environmental and social impacts, as well as stronger protections for indigenous rights and community livelihoods. However, the national regulations may not have provided sufficient safeguards, leading to conflicts between the project developers' obligations and their ability to comply with local requirements. This disconnect can undermine the intended benefits and leave affected communities insufficiently supported.

The other key difference is in the determination of project area of influence (AOI). International standards mandate that the ESIA takes into account the impacts of associated facilities, whereas Indonesian regulations do not. Associated facilities are described as “facilities that are not funded as part of the project and that would not have been constructed or expanded if the project did not exist, and without which the project would not be viable” (International Finance Corporation, 2012). Examples of such facilities often include pipelines, utilities, warehouses, and logistics terminals. Moreover, Amdal process has primarily concerned with the direct, immediate effects of a project on surrounding environment and communities while ESIA process emphasizes the ongoing management and monitoring of environmental and social impacts throughout a project's lifecycle, with a stronger emphasis on overall positive outcomes and community engagement (Vanclay, 2020). Additionally, under international performance standards, the AOI may be amended or expanded based on the verification and magnitude of impacts during project construction and operations based on results of modeling exercises (e.g., air dispersion, thermal plume, etc). The local regulation definition of AOI remains constant throughout project implementation.

4.3 Differences in risk appetite

The interviewees from financial intuitions and the ESIA experts stressed that there are the differing risk appetites between the government as the reviewer and approver of Amdal, and the financial institutions as the reviewer and approver of ESIA. Amdal embodies the project's environmental management, whereas ESIA serves as risk management documentation mandated by lenders. The government, as the entity responsible for the overall development and economic growth of the country, often has a higher risk tolerance when it comes to environmental and social impacts, as they may prioritize economic considerations over strict environmental and social safeguards. This can lead to the approval of projects with relatively higher environmental and social risks, as long as they are deemed economically beneficial for the country.

In contrast, financial institutions, particularly those that have adopted the IFC Performance Standards, have a low-risk appetite when it comes to environmental and social impacts. These institutions are primarily concerned with the financial and reputational risks associated with financing projects with significant environmental and social risks, and they are often more stringent in their evaluation and approval of projects. This difference in risk appetite can result in situations where a project that has been approved by the government under the Amdal process may not meet the requirements set forth by the international standards.

4.4 Challenges in integrating Amdal and ESIA processes

When a project is in its early stages and the proponent seeks international financing, both Amdal and ESIA are generally required. This raises the question of whether these two processes can be combined as the timeline for execution and approvals for Amdal impact the ESIA schedule and would have schedule and commercial effects to the proponent’s project Are their differences so substantial that they should be performed separately or in parallel rather than as a combined process?

While both assessment frameworks aim to ensure environmental and social sustainability, their differences in principles, requirements, reporting formats, and decision-making processes present significant challenges for integration. As one interviewee noted, some consultants have attempted to combine them, but often decide later that keeping them separate is more practical. The complexity of merging the two processes necessitates that project developers invest considerable time and resources in collecting, analyzing, and presenting data to meet both

national and international standards. This can lead to delays, increased costs, and potential conflicts among stakeholders.

To simplify the process, the case study projects completed the Amdal according to national requirements and then prepare a Supplementary ESIA to address issues not covered by Amdal, such as labor conditions, livelihood restoration, involuntary resettlement, biodiversity, cultural heritage, indigenous peoples, and cumulative impacts. Further, to save time and budget during the early stages of a project, project sponsors and consultants usually map the differing national and international requirements and develop a strategy for conducting stakeholder engagement of Amdal and ESIA as a joint process. The same approach applies to baseline studies. Efforts must be made to ensure these studies meet both national and international standards. It is noteworthy that representatives from the case study company are cooperative and hence made this approach doable. However, if company staffs are not cooperative or do not understand the need for more extensive ESIA consultations, it is advisable to conduct EIA and ESIA stakeholder engagement and baseline studies in parallel.

5. CONCLUSION

Implementing international standards for impact assessment in Indonesia is typically challenging. A significant issue arises from the differences between the requirements of Amdal and international ESIA procedures. It can be problematic when company personnel accustomed to the national EIA framework apply the same approach to the international ESIA process. Since the results of Amdal and ESIA undergo different review processes with varying risk appetites, combining them is difficult. The most practical and pragmatic approach is to complete Amdal according to national requirements and then prepare a Supplementary ESIA to address any issues not covered by Amdal.

Addressing these challenges requires a multi-pronged approach. Strengthening the regulatory framework for environmental and social impact assessment, while also enhancing stakeholder engagement and awareness, can help bridge the gap between theory and practice. Investing in capacity-building initiatives that enhance the project sponsors' understanding of the assessment process and the importance of adhering to global best practices. This may involve targeted training programs, knowledge-sharing workshops, and the establishment of collaborative networks that facilitate the exchange of expertise and lessons learned across geothermal projects. Additionally, project sponsors must be willing to allocate adequate resources, both in terms of time and funding, to support a thorough and rigorous impact assessment process that aligns with international norms and requirements.

ACKNOWLEDGEMENT

We extend our appreciation to the representatives of the case study projects and all interviewees for their cooperation during the data collection. We thank Ardi Hartanto, Claire Aitkenhead, and Katherine Gavile for their constructive feedback on this paper.

REFERENCES

Asian Development Bank (ADB): *Safeguard Policy Statement*, (2009).

Asian Development Bank (ADB): *ASEAN corporate governance scorecard: country reports and assessments*, (2014).

Borgert, T., Donovan, J D., Topple, C., & Masli, E K.: Determining what is important for sustainability: scoping processes of sustainability assessments. *Impact Assessment and Project Appraisal*, 37(1), (2018), 33-47

Chelminski, K: Climate Finance Effectiveness: A Comparative Analysis of Geothermal Development in Indonesia and the Philippines. *The Journal of Environment & Development*, 31(2), (2022), 136–167.

Corsi, S., Oppio, A., & Dendena, B.: ESIA (Environmental and Social Impact Assessment): A tool to minimize territorial conflicts, *Chemical Engineering Transactions*, 43, (2015), 2215–2220.

Dendena, B., & Corsi, S.: The Environmental and Social Impact Assessment: A further step towards an integrated assessment process. *Journal of Cleaner Production*, 108, (2015), 965–977.

Ferrol-Schulte, D., Gorris, P., Baitoningsih, W., Adhuri, D.S., & Ferse, S.C.A.: Coastal livelihood vulnerability to marine resource degradation: A review of the Indonesian national coastal and marine policy framework. *Marine Policy*, 52, (2015), 163-171.

Glasson, J., Therivel, R., & Chadwick, A.: *Introduction to environmental impact assessment 4th Edition*. Book, Routledge, London (2019).

Götzmann, N., Vanclay, F., & Seier, F.: Social and human rights impact assessments: what can they learn from each other?, *Impact Assessment and Project Appraisal*, 34(1), (2016), 14–23.

Gulakov, I., & Vanclay, F.: Social impact assessment in the Russian federation: Does it meet the key values of democracy and civil society? *Impact Assessment and Project Appraisal*, 36(6), (2018), 494–505.

Gulakov, I., Vanclay, F., Ignatev, A., & Arts, J.: Challenges in meeting international standards in undertaking social impact assessment in Russia, *Environmental Impact Assessment Review*, 83(April), (2020), 106410

Hacking, T.: The SDGs and the sustainability assessment of private-sector projects: theoretical conceptualisation and comparison with current practice using the case study of the Asian Development Bank, *Impact Assessment and Project Appraisal*, 37(1), (2019), 2–16.

Harris, P., Riley, E., Sainsbury, P., Kent, J., & Baum, F.: Including health in environmental impact assessments of three mega transport projects in Sydney , Australia : A critical , institutional , analysis. *Environmental Impact Assessment Review*, 68(August), (2018), 109–116.

International Finance Corporation (IFC): *IFC Performance Standards on Environmental and Social Sustainability*, (2012a).

International Finance Corporation (IFC): *Guidance Notes to Performance Standards on Environmental and Social Sustainability*, (2012b)

International Finance Corporation (IFC): *Advancing UN Sustainable Development Goals through IFC's Environmental, Social, and Governance Standards*, (2023).

International Union for Conservation of Nature (IUCN): *Environmental and Social Impact Assessment (ESIA)* (Issue March), (2020).

Kurniawan, A. R., Murayama, T., & Nishikizawa, S.: A qualitative content analysis of environmental impact assessment in Indonesia: a case study of nickel smelter processing, *Impact Assessment and Project Appraisal*, 38(3), (2020), 194–204.

Lai, J. Y., & Hamilton, A.: For whom do NGOs speak? Accountability and legitimacy in pursuit of just environmental impact assessment, *Environmental Impact Assessment Review*, 86(1), (2021), 106468.

Loomis, J. J., & Dziedzic, M.: Evaluating EIA systems' effectiveness : A state of the art, *Environmental Impact Assessment Review* 68, (2018), 29–37.

Mori, A.: Foreign actors, faster transitions? Co-evolution of complementarities, perspectives and sociotechnical systems in the case of Indonesia's electricity supply system, *Energy Research and Social Science*, 69(April), (2020), 101594.

Omenge, P. M., Obwoyere, G. O., Eshiamwata, G. W., Makindi, S. M., & Nathwani, J.: Environmental and social impact assessment procedural steps that underpin conflict identification: Reference to renewable energy resource development in Kenya. *International Journal of Energy Production and Management*, 5(2), . (2020), 157–174.

Ortiz, G., Domínguez-Gómez, J. A., Aledo, A., & Urgeghe, A. M.: Participatory multi-criteria decision analysis for prioritizing impacts in environmental and social impact assessments, *Sustainability: Science, Practice, and Policy*, 14(1), (2018), 6–21.

Purnama, D. (2014). AMDAL dan Pengelolaan Lingkungan. Modul, 1–46. Quigley, G. T. (2021). *The evolution of Environmental and Social Impact Assessments in Hydropower*. https://nmbu.brage.unit.no/nmbu-xmlui/handle/11250/2835650

Rahman, A., Farrok, O., & Haque, M. M. (2022). Environmental impact of renewable energy source based electrical power plants: Solar, wind, hydroelectric, biomass, geothermal, tidal, ocean, and osmotic. *Renewable and Sustainable Energy Reviews*, 161(March), 112279. https://doi.org/10.1016/j.rser.2022.112279

Rakhmah, T. (2023). *Addressing investment challenges to foster capital mobilization into geothermal power projects in Indonesia and New Zealand*. In H. Phoumin, F. Taghizadeh-Hesary, & F. Kimura (Eds.), Green Finance and Renewable Energy in ASEAN and East Asia (1st Edition). Routledge.

Romianingsih, N.P.W; Utomo, S.W.; and Hamzah, U.S.:a comparative study of different practices in environmental impact assessment, *Journal of Environmental Science and Sustainable Development*, 6(1), (2023), 50-69.

Roos, C., Cilliers, D. P., Retief, F. P., Alberts, R. C., & Bond, A. J.: Regulators' perceptions of environmental impact assessment (EIA) benefits in a sustainable development context. *Environmental Impact Assessment Review*, 81, (2020), 106360.

Semedi, J M., Willemen, L., Nurlambang, T., Meer, F V D., & Koestoer, R H.: Developing a framework for assessing the impact of geothermal development phases on ecosystem services, *Proceedings, IOP Publishing*, (2017).

Swangjang, K.: Comparative review of EIA in the Association of Southeast Asian Nations, *Environmental Impact Assessment Review*, 72(March), (2018), 33–42.

Vanclay, F. Baines, J.T., Taylor, C.N.: Principles for ethical research involving humans: ethical professional practice in impact assessment Part I, *Impact Assessment and Project Appraisal*, 31(4), (2013), 243-253.

Vanclay, F. Reflections on Social Impact Assessment in the 21st century. *Impact Assessment and Project Appraisal*, 38(2), (2020), 126–131.

Vanclay, F., Esteves, A. M., Aucamp, I., & Franks, D. M.: Social Impact Assessment: Guidance for assessing and managing the social impacts of projects, *International Association for Impact Assessment*, (2015).

Zahroh, U. A., & Najicha, F. U.: Problems and Challenges on Environmental Law Enforcement in Indonesia : AMDAL in the Context of Administrative Law, *Indonesian State Law Review (ISLRev)*, 5(2), (2022), 53–66.

Coexistence Study Between Wildlife Keystone Species and Darajat Geothermal Power Plant in West Java, Indonesia

Muhammad Riyadhi[1], Iqbal Abi Yaghsyah[1], and Toni Ahmad Slamet[2]

[1]Star Energy Geothermal Darajat II, Limited,
[2]BKSDA JABAR Seksi Konservasi Wilayah V Garut

m.riyadhi@starenergy.co.id

Keywords: Keystone Species, Wildlife, Coexistence, Geothermal Power Plant, Eco-Friendly

ABSTRACT

Human activity is inevitably impacting the environment in every environment component including air, water and soil which potentially affect biodiversity. Considered as renewable and eco-friendly, geothermal power plant would still potentially impact the environment including the biodiversity that lives in it. The objective of this paper is to study whether the wildlife could possibly coexist with Darajat Geothermal Power Plant which is located within Taman Wisata Alam Gunung Papandayan (Nature Park), Garut Regency, West Java, Indonesia. The objects for this study are the keystone species at Gunung Papandayan Nature Park which is Javan leopard (Panthera pardus melas). Javan leopard is reported to be elusive and rarely seen near the power plant. To confirm the existence of Javan leopard near Darajat Geothermal Power Plant facilities, Star Energy Geothermal Darajat II, Limited (SEGD) initiated wildlife monitoring around the facilities with cruising method and camera traps. The result of this study shows that Javan leopard was able to adapt and uses geothermal facilities such as steam pipeline inspection pathway, inactive well pad and roads. This study indicates that the keystone species at Gunung Papandayan Nature Park can adapt and coexist with Darajat Geothermal Power Plant.

1. INTRODUCTION

The trends of increasing temperature due to global warming are keep growing up. The main cause of global warming is the emission of greenhouse gasses produced by anthropogenic activities specifically activity that uses huge amount of fossil fuel (Mukhopadhyay, 2013). Therefore, the development of renewable energy has become global concern. Geothermal power is a renewable energy resource that has attracted significant and continued investment with a forecasted growth of 28% power generation capacity (approx. 4GW) between 2018 and 2023 (IEA, 2018; Ng et al., 2021). However, increases in renewable energy infrastructure can also be associated with negative impacts on habitats and species (Ng et al., 2021). There is a numerous overlap between renewable energy facilities and important conservation areas that potentially compromise the goals of biodiversity conservation (Rehbein et al, 2020).

In this modern era, it is more difficult to maintain biodiversity and function of forests. This is caused by the increasing needs of humans require more land for production. In fact, forests have various functions both directly and indirectly utilized. Some functions that usually getting overlooked are weather control, carbon storage, water storage and aesthetic functions (Pearce,2017). These functions do not directly impact the economy of the community, but their absence will affect human life in general.

Indonesia is a mega biodiversity country, blessed with abundant geothermal energy potential. With great potential to utilize renewable geothermal energy there is also potential threat of negative impact on biodiversity. A geothermal power plant in Darajat as an example is located at Gunung Papandayan Nature Park area that has high biodiversity. The latest research suggests that at least 101 species of birds, 15 species of herpetofauna and 24 species of mammals including endangered species such as Javan surili, dhole and Javan leopard found in this area (Junaid and Fariz, 2021). Biodiversity is a comprehensive umbrella term for the extent of nature's variety or variation within the natural system; both in number and frequency. Biodiversity exists as a complex web of life forms that interact with each other in an ecosystem, in a region or globally. Biodiversity drives the functioning of ecosystems through countless reciprocal interactions with the physical and chemical components of the environment (The Royal Society, 2003). Humans' activity near wildlife habitat will likely trigger a conflict between them.

Animals with remarkable adaptation ability might be able coexist with humans despite the rapid changes in their habitat. Coexistence is defined as a dynamic but sustainable state in which humans and wildlife co-adapt to living in shared landscapes, where human interactions with wildlife are governed by effective institutions that ensure long-term wildlife population persistence, social legitimacy, and tolerable levels of risk (Mekonen, 2020). The survival of the keystone species is the most important among the other species. Keystone species are those whose

existence affects the ecosystem (Payton et al., 2002). They include organisms that control potential dominants, provide critical resources, act as mutualists and act as ecosystem engineers. The absence of the keystone species may trigger the ecosystem to collapse.

The goal of this paper is to study the possibility of sensitive keystone species to coexist with geothermal power plant facility. This paper will represent how geothermal activity could potentially impact wildlife which later can be used to develop conservation plan to manage the potential impact. The subject of this research is Javan leopard (*Panthera pardus melas*). Javan leopard act as top predator to control the population of its prey and stabilize the ecosystem.

2. METHOD

2.1 Study Site

Research was conducted from 22 February 2022 to 27 February 2024 in a Darajat Geothermal Power Plant located in Pasirwangi Village, Garut, West Java, Indonesia (coordinate 07°11'09"- 07°15'40"S and 107°41'54"-107°45'40"E). Darajat Power Plant is located within Taman Wisata Alam (Nature Park), Hutan Lindung (Protected Forest) and private land around 1740-2200 above sea level in a valley near Mount Kendang which is part of Papandayan Mountains. The location study is narrowed to Nature Park area around geothermal facilities such as well pads, steam pipeline and biodiversity essential area (e.g., water hole).

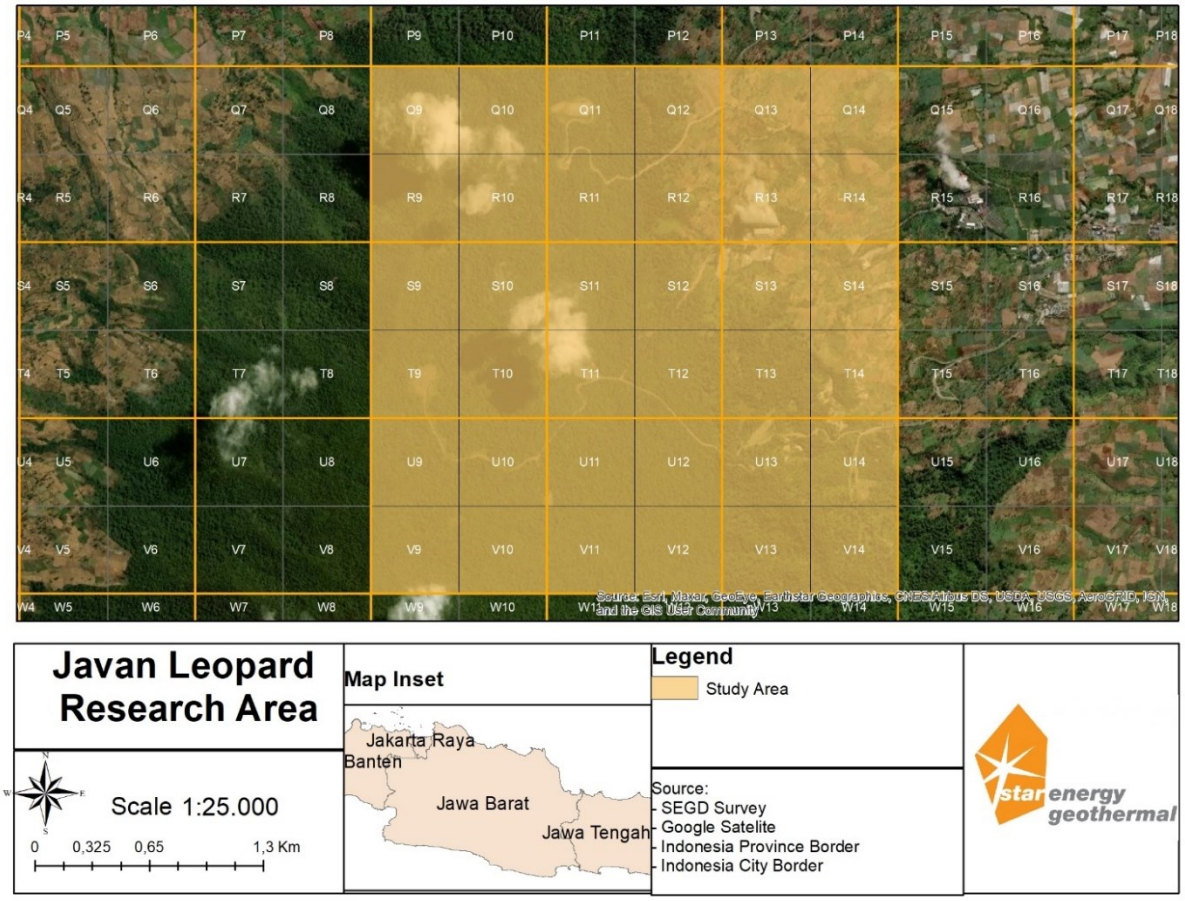

Figure 1: Study location map.

2.2 Procedure

Research Data were collected through direct and indirect data collection methodology. Direct data were collected using Visual Encounter Survey (VES) method and camera traps installation. VES data collected by cruising through footpath available at the area (large mammals will be more likely to use these footpath). Indirect data such as carcasses, footprints, feces, claw marks and other sign that prove the existence of Javan leopard were recorded simultaneously with VES method. Javan leopard footprints were identified referring to a guidebook (Van Strien, 1983). Camera traps were installed using line transect method, measuring about 1 kilometre in length. 2 camera traps were installed in each transect. The distance between camera depends on the observation of Javan leopard signs and their potential tracks in the area. Camera traps installation location were based on signs found in the area. Total of six camera traps were being used in the study, and all cameras are set to record video. The

camera surveillance period was set for three month per location and being checked monthly for maintenance and data collection. Camera traps were installed near a track that potentially used by wildlife. Camera traps were mounted on a tree 15-30 cm above the ground depending on the contour of the installation location and camera properties (Molloy, 2018). Field guide is used as a reference to identify species of animals observed or their existence signs (Shepherd & Shepherd 2018).

Due to the increase in the spread of covid-19 cases, data collection was carried out by following the covid-19 protocol issued by the Indonesian government and the Star Energy Geothermal Darajat company. Before conducting the study, all participants were required to take an antigen test. The number of participants was also limited to the minimum. After all participant candidates are declared covid-free, the research is carried out. During the research, contact between participants was limited to a minimum and risky contact such us borrowing cutlery was not allowed. The camera traps method makes it possible for this research to be held for a long period of time with less contact of the researcher team.

2.3 Data Analysis

2.3.1 Number of individuals

The Javan leopard number of individuals is calculated by identifying Javan leopard recorded by camera traps. Face and flank spot pattern were used to identify the individual. Individual's gender was identified from their physical appearances. The home range size of Javan leopard and physical barrier were also considered (e.g., farmland, cliff, roads) to determine the individual.

2.3.1 Encounter rate

The data were analysed by estimating encounter rate of the species. Encounter rate was calculated by dividing number of captured pictures of Javan leopard with total days the cameras were active, multiplied by 100 (O'Brien et al. 2003; Shahida et al. 2018). Encounter were considered distinct events if occurred more than 30 minutes apart or if the next encounter is different individual.

3. RESULT AND DISCUSSION

Camera traps data collection was conducted from February 2022 to February 2024 and successfully identified 9 Javan leopards. The leopards were recorded 131 times during the research. The population are consisted of two adult males, four adult females, one juvenile and two cubs. Some leopards were interested in camera traps that they tried to sniff them especially when the camera traps were just installed or getting moved to other location. Their curiosity made it possible for the camera to capture spot pattern of their faces and flanks. This facial and body spot features was used to identify each of Javan leopard individuals. Javan leopard population is shown in table 1.

Javan leopards were captured at several locations around Geothermal field site.Within the observation area, there are several signs that indicate leopard's existence such as feces, footprints, and claw marks. These signs show that leopards were passing these locations frequently. There are nine individuals captured by camera traps.

Table 1: Leopard's population structure.

Individuals	Age Class	Sex
Leopard A	Adult	Female
Leopard B	Adult	Female
Leopard C	Adult	Male
Leopard D	Adult	Male
Leopard E	Adult	Female
Leopard F	Juvenile	Not identified
Leopard G	Adult	Female
Leopard H	Cubs	Not identified
Leopard I	Cubs	Not identified

One of the most frequently used pathways is a path near well pad W1 and well pad SF. There was several individual that uses this path but the most often is leopard D. Leopard D is considered an alpha male in the area due to his wide range of area in Darajat geothermal field site and frequent record. Several female individuals also sighted using this track which is overlapping of female's and male's home range is common in leopard (Snider et al., 2021, Muller et al., 2022). This track is located in the far end of geothermal field site, making this location is rarely visited. Although there are signs that showing these track is often used by animals and human. These condition makes this location a suitable track for Javan leopard since they prefer a spacious footpath rather than vegetation dense track.

SEGD archives show that leopard monitoring has been conducted in Darajat geothermal field site. In the biodiversity report, it was noted that in 2016 four leopard individuals were found in Darajat Geothermal field site. A total of four leopard individuals were found again in 2022. In 2022, SEGD began to conduct routine and intensive biodiversity monitoring. In 2023, two new adults and one juvenile were identified. two cubs were found, bringing the total number of new individuals to nine in 2024. This finding is a good sign that the javan leopards population is regenerating.

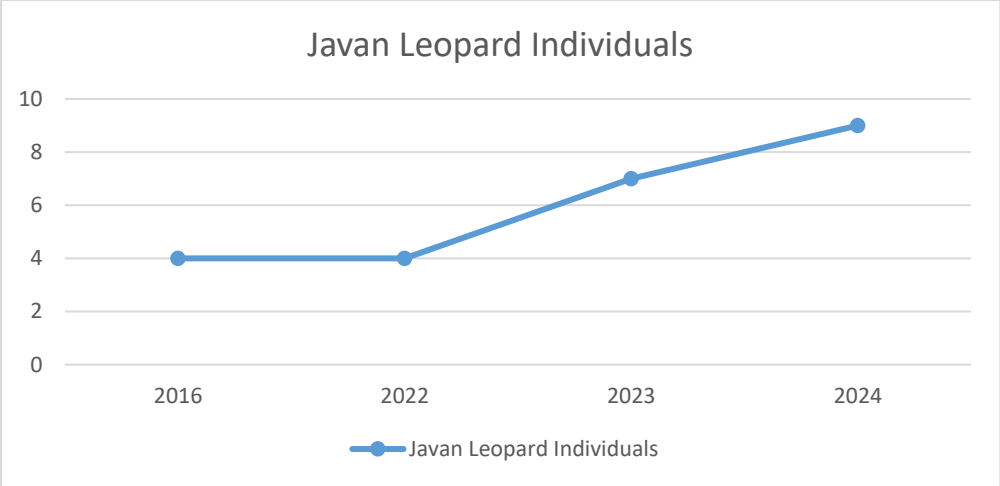

Figure 2: Leopard encounter rate.

Encounter rate analysis shows that javan leopard in Darajat has ER value of 17,8%. Camera traps were able to capture 131 picture based on 735 trap days. W1 & SF site is the most visited site among the site sampling areas. According to the encounter rate of each individual Leopard D has the highest encounter rate which indicate that Darajat geothermal field site is indeed its homerange area and possibly its core area. Core area is an area which is used more often than the rest of the homerange area and it is morelikely is an area that used to sleep/rest, find shelter and an area with abundant food sources (Burt, 1943). Leopard C has the second highest encounter rate. Though Leopard C's encounter keeps getting lower each year. It is possible that Leopard C was a young male adult looking for its own teritory. It's possible that it has already established its own homerange making his appeareance getting rare.

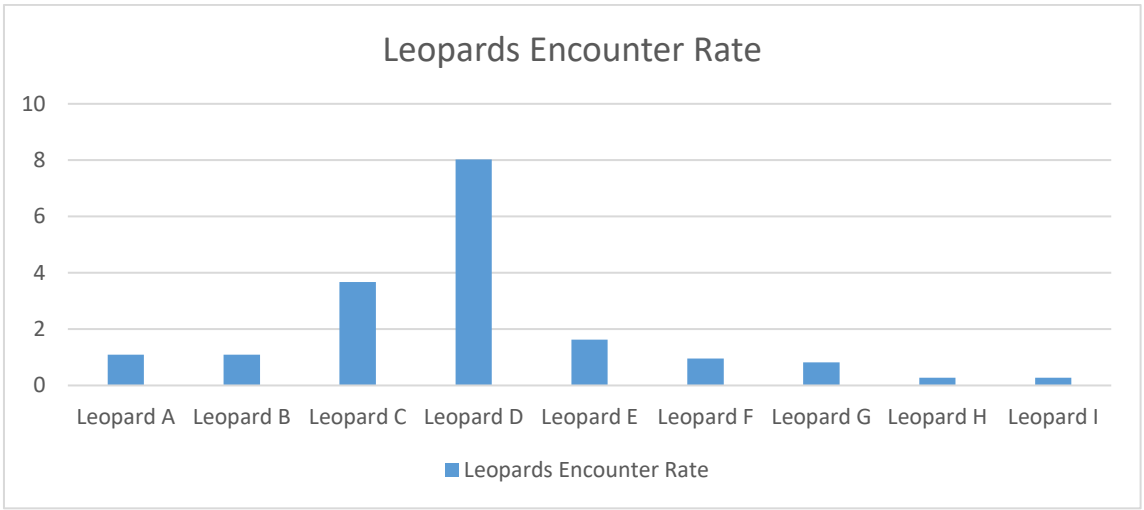

Figure 3: Leopard's encounter frequency.

Javan leopard captured in relatively remote area and far from humans activity. Geothermal steam extraction operation most of the time operate automatically. The company staff only visit wellpad and steampipe once in a while for inspection and maintenance. Wellpad area will be busy and produce high intensity noises only when there is a drilling project or a maintenance program. For example the data collected from SF wellpad. Camera traps were installed near drilling activity project area for two months but no animals passes by the area. Only small mammals such as tree shrew and birds were captured. It is most likely due to disturbance caused by well drilling process conducted in wellpad SF. Seeing how geothermal production works with its low maintenance and low humans activity it seems javan leopard was able to adapt and live alongside geothermal company activity.

Figure 4: Example of javan leopard sign.

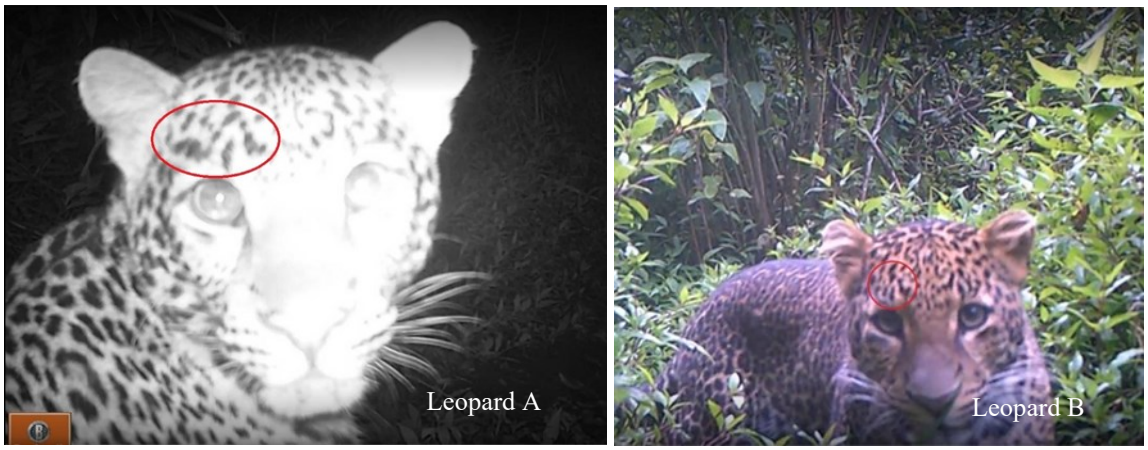

Javan leopards can adapt and live near a geothermal powerplant is because the area is a habitat for its potential prey. There are at least 18 identified potential prey found near geothermal activity. The abundance of prey species allows the javan leopard to survive. The primary prey for javan leopard is ungulates and primates (Gunawan et al., 2012). Primates such as javan surili (Presbytis comata) and ebony leaf monkey (Trachypithecus auratus) are frequently seen in various location near geothermal facilities.

Table 2: Potential prey.

No	Family	Latin Name	Local name
1.	Bovidae	Bubalus bubalis	Water Buffalo
2.	Canidae	Canis lupus familiaris	Domesticated dog
3.	Cercopithecidae	Presbytis comata	Javan surili
4.	Cercopithecidae	Trachypithecus auratus	Ebony leaf monkey
5.	Cervidae	Muntiacus muntjak	Barking deer
6.	Hystricidae	Hystrix javanica	Sunda porcupine
7.	Manidae	Manis javanica	Sunda pangolin
8.	Mephitidae	Mydaus javanensis	Sunda skunk
9.	Muridae	Rattus tiomanicus	Malayan field rat
10.	Mustelidae	Herpestes javanicus	Javan mongoose
11.	Mustelidae	Martes flavigula	Yellow throated marten
12.	Mustelidae	Melogale orientalis	Javan ferret badger
13.	Mustelidae	Mustela lutreolina	Indonesia mountain weasle
14.	Phasianidae	Arborophila javanica	Chestnut-bellied partridge
15.	Phasianidae	Gallus Gallus	Red junglefowl
16.	Sciuridae	Callosciurus notatus	Plantain squirrel
17.	Suidae	Sus scrofa	Wild boar
18.	Tupaiidae	Tupaia javanica	Horsefield's treesrew
19.	Viverridae	Paradoxurus hemaproditus	Javan civet
20.	Viverridae	Prionodon linsang	Linsang

No	Family	Latin Name	Local name
21.	Viverridae	Viverricula indica	Small indian civet
22.	Sciuridae	Petaurista petaurista	Red giant flying squirrel

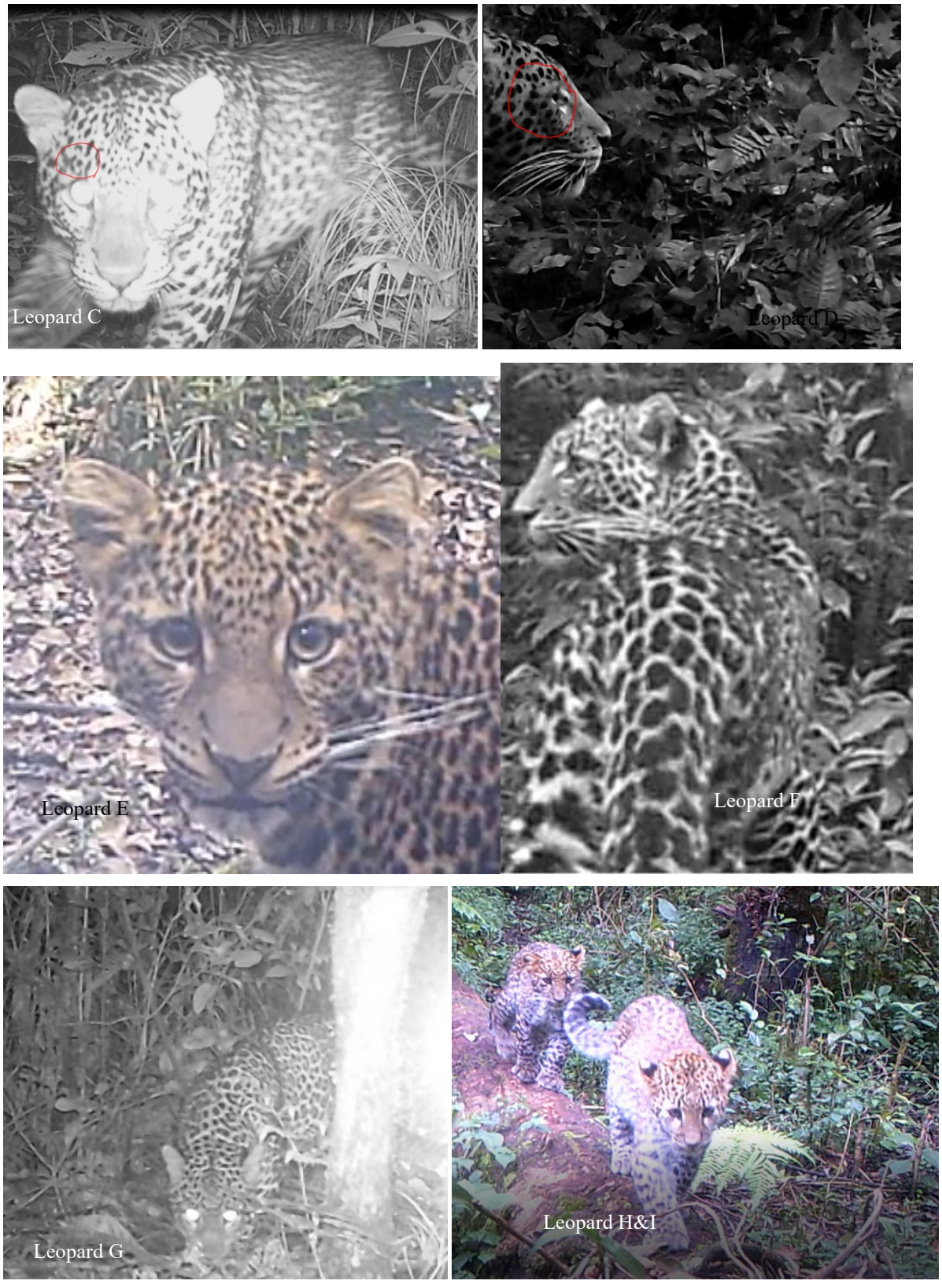

Figure 5: Leopard facial spot.

Potential prey species in Darajat mostly from family Mustelidae. Overall leopard species prefer to hunt large prey weighting 10-40 kg (Hayward et al., 2006). In Darajat the only prey that fits into this category is wild boar and barking deer. When these prey is hard to find or in difficult times Javan leopard may depend heavily on locally abundant small prey which is abundant in Darajat. Abundant prey option species in Darajat is one of the reasons javan leopard succeeded to adapt in geothermal project area.

4. CONCLUSION

Javan leopard as one of the keystone species within Papandayan Nature Park is proven to be able to coexist with Darajat Geothermal operation. They can adapt to various type of land including brushwood, natural forest, forest patch around geothermal power plant facilities such as well pad and steam pipeline. The reason Javan leopard was able to adapt in geothermal site is the nature of geothermal operation with low maintenance and low human activity, healthy ecosystem and abundance of prey species option. Geothermal power plant operation has potential to operate in-sync with biodiversity conservation. Javan leopard existence as keystone species around geothermal operation is a sign that the ecosystem is healthy and could provide their needs to survive. It is expected that the existence of geothermal operations can positively influence efforts to maintain forest functions and biodiversity due to geothermal operation dependence to ecosystem services which is water and geothermal.

ACKNOWLEDGEMENTS

We would like to thank Star Energy Geothermal Darajat II, Limited for supporting this research by providing necessary equipment for the research and financial support for the research and publication. We would also like to thank Garut BKSDA wilayah V for supporting this research by sharing valuable information of the research field site, provided permit to enter and conducted the research within the Gunung Papandayan Nature Park, and supervised the activities. This research was conducted during the covid-19 pandemic. The success of this study is due to the compliance of the parties involved with the covid-19 protocol.

REFERENCES

Burt, W.H. (1943). Territoriality and Home Range Concepts as Applied to Mammals. *Journal of Mammalogy, 24*, 346-352.

Gunawan, H., 2019. *Live in harmony, human and javan leopard : an approach to mitigation and conflict management*, Bogor, Indonesia: IPB Press.

Gunawan, Hendra & Prasetyo, Lilik & Mardiastuti, Ani & Kartono, Agus. 2012. HABITAT MACAN TUTUL JAWA (Panthera pardus melas Cuvier 1809) DI LANSEKAP HUTAN TANAMAN PINUS. *Jurnal Penelitian Hutan dan Konservasi Alam*. 9. 049-067. 10.20886/jphka.2012.9.1.049-067

Gunawan, Hendra & Sihombing, Vivin S. 2017. Habitat Preference of the Javan Leopard (Panthera pardus melas Cuvier 1809) in Western Java. *Jurnal Penelitian Hutan dan Konservasi Alam*. Vol 1:35-43

Hayward, M. W., Henschel, P., O'Brien, J., Hofmeyr, M., Balme, G., & Kerley, G. I. H. (200*6). Prey preferences of the leopard (Panthera pardus). Journal of Zoology, 0(0), 060606025751008–??? doi:10.1111/j.1469-7998.2006.00139.x*

Junaid, Achmad R. and Fariz Muladi. 2021. Report: *Hasil Survey Keanekaragaman Fauna Cagar Alam Papandayan, Jawa Barat*. (Report no. BI-Report-Java-II-21)

Mekonen, Sefi. (2020). Coexistence between human and wildlife: The nature, causes and mitigations of human wildlife conflict around Bale Mountains National Park, Southeast Ethiopia. *BMC ecology*. 20. 51. 10.1186/s12898-020-00319-1.

Molloy, Shaun. (2018). *A Practical Guide to Using Camera Traps for Wildlife Monitoring* in Natural Resource Management Projects.. 10.13140/RG.2.2.28025.57449.

Mukhopadhyay, Sumit & Hou, Zhangshuan & Gosink, Luke & Bacon, D. & Doughty, C. & Li, Jun & Wei, Lingli & Gasda, Sarah & Bacci, Giacomo & Govindan, Rajesh. (2013). Model Comparison and Uncertainty Quantification for Geologic Carbon Storage: The Sim-SEQ Initiative. *Energy Procedia*. 37. 3867-3874. 10.1016/j.egypro.2013.06.284.

Müller, L., Briers-Louw, W. D., Seele, B. C., Stefanus Lochner, C., & Amin, R. 2022. *Population size, density, and ranging behaviour in a key leopard population in the Western Cape, South Africa*. *PLOS ONE*, *17*(5). https://doi.org/10.1371/journal.pone.0254507

Ng, Cheryl & White, Thomas & Katariya, Vineet & Pollard, Edward. (2021). *Geothermal power generation and biodiversity: the business case for managing risk and creating opportunity*.

Payton, Ian & Fenner, M. & Lee, W.G.. (2002). *Keystone Species: The Concept and its Relevance for Conservation Management in New Zealand*. Science for Conservation. 5-29.

Pearce, D.W. (2017) *The economic value of biodiversity*. New York: Earthscan from Routledge.

Rehbein, José Andrés & Watson, James & Lane, Joe & Sonter, Laura & Venter, Oscar & Atkinson, Scott & Allan, James. (2020). Renewable energy development threatens many globally important biodiversity areas. *Global Change Biology*. 26. 10.1111/gcb.15067.

Shanida, Sya Sya & Partasasmita, Ruhyat & Husodo, Teguh & Parikesit, Pampang & FEBRIANTO, PUPUT & Megantara, Erri. (2018). The existence of javan leopard (Panthera pardus melas cuvier, 1809) in the non-conservation forest areas of Cisokan, Cianjur, West Java, Indonesia. *Biodiversitas*. 19. 42-46. 10.13057/biodiv/d190107.

Shepherd, C. R., Shepherd, L. A., & Duckworth, W. 2018. *A naturalist's guide to the mammals of Southeast Asia: Brunei, Cambodia, Indonesia, Laos, Malaysia, Myanmar, the Philippines, Singapore, Thailand and Vietnam*

Snider, M. H., Athreya, V. R., Balme, G. A., Bidner, L. R., Farhadinia, M. S., Fattebert, J., Gompper, M. E., Gubbi, S., Hunter, L. T., Isbell, L. A., Macdonald, D. W., Odden, M., Owen, C. R., Slotow, R., Spalton, J. A., Stein, A. B., Steyn, V., Vanak, A. T., Weise, F. J., … Kays, R. (2021). Home range variation in Leopards living across the human density gradient. *Journal of Mammalogy*, 102(4), 1138–1148. https://doi.org/10.1093/jmammal/gyab068

The Royal Society. 2003. *Measuring biodiversity for conservation*. London, United Kingdom.

van Strien NJ. 1983. *A Guide to the Tracks of Mammals of Western Indonesia. School of Environmental Conservation Management*. Ciawi, Indonesia.

Marketing Innovation and Utilization of Geothermal Coffee Products through Commercial Coffeeshop Schemes

Erwandi Yanto[1], Dian Pratomo[1], Mahmud Khairi[1], Teresia Maririsky[1],
Ahmad Indra Sakti Harahap[2], Adi Rahmadi[2], Dewi Sri Utami[2], and Fajriyah Usman[2]

[1]PT Pertamina Geothermal Energy
[2]Rumah BUMN Riau

erwandi.yanto@pertamina.com

Keywords: Pertamina-mentored SMEs, Geothermal Coffee, Canaya, Liberica, Kampar, Commercial Coffeeshop Scheme, Marketing Innovation

ABSTRACT

This study aims to develop innovative marketing strategies for coffee products utilizing geothermal energy, produced by Pertamina-mentored SMEs under the Canaya, Liberica, and Kampar brands, through a commercial coffeeshop scheme for the public with the brand "KabarBaik RB Coffeeshop". Pertamina-mentored SMEs often face challenges in marketing and branding their coffee products in domestic or global.

The big concept and road map of the study will be about sustainability where all the product and residu will be re-used without harming the environment within the program of Rumah BUMN Riau as one of CSR program of PT Pertamina Geothermal Energy. Therefore, this study will be a pilot project to SME's of Pertamina to optimize the marketing and support the ESG and SDG implementation internally. On the other hand, this coffeeshop is operated by the person with disabilities as the effort to create more jobs for handicapped or disabilities communities.

The research expects to identify marketing innovations to increase sales of Pertamina-mentored SME coffee products. These innovations may include: Developing strong branding, creating unique and appealing logos, taglines, and brand identities, designing attractive packaging, Utilizing high-quality materials and creative designs, leveraging social media, promoting coffee products to a wider consumer base with the tagline as "Simplicity in Silence" means that , participating in coffee exhibitions and festivals, increasing brand awareness and reaching new customers, developing partnerships with coffeeshops, expanding the distribution network for coffee products. By implementing these marketing innovations, the study hopes to increase sales of Pertamina-mentored SME coffee products and enhance their competitiveness within the Indonesian coffee market.

1. INTRODUCTION

MSMEs (Micro, Small and Medium Enterprises) according to Ministry of State Owned Entreprise and Ministry of Cooperatives and Small and Medium Enterprises are types of businesses that have certain criteria, such as number of employees, turnover and limited capital.

Classification :

- Micro business: employees <10 people, capital/assets <50 million, turnover <300 million/year
- Small Businesses: employees 10-49 people, capital/assets 50 million – 500 million, turnover >300 million – 2.5M/year
- Medium Businesses : 50-200 employees, capital/assets 500 million – 10 billion, >2.5M – 50 M/year

Beneficiaries: Individuals, groups or business entities who directly or indirectly receive benefits from programs, services or initiatives from Rumah BUMN, while the beneficiaries are MSMEs, cooperatives, or individuals who want to start business.

- Direct: Individuals, groups or entities that directly benefit from programs, services and initiatives of Rumah BUMN, for example training participants, guidance, or assistance with access to markets.
- Indirect: Individuals, groups or entities that are not directly involved in participating in the Rumah BUMN program but receive impacts or benefits from program implementation as a domino effect or changes that occur in the surrounding environment.

Types of benefits to SME's community or individuals including Technical, Training, Business Assistance, Market Access, Financing etc. to help improve prosperity, growth and competitiveness in the business world.

2. RUMAH BUMN

Rumah BUMN is a forum for CSR accountability Pertamina (Persero) and its subsidiaries against Ministry of State Owned Entreprise of Indonesia. Rumah BUMN can be a forum for synergy and collaboration in the CSR program for all PT Pertamina (Persero) business units and its subsidiaries, especially in Riau region. Rumah BUMN views the need for synergy and collaboration in the CSR program, especially in terms of developing Pertamina-assisted MSMEs so that there is no overlapping of programs. CSR and funding for MSMEs assisted by Pertamina in Riau Region.

Rumah BUMN has sufficient capacity to support assisted MSMEs in Riau is including registration, guidance, development, and certification which can make the MSMEs that are fostered rise to a higher class and be able to compete on the global stage. Rumah BUMN needs support from all Pertamina business units in the Riau region to improve portfolio in order to achieve operational independence and increase innovation for assisted MSMEs.

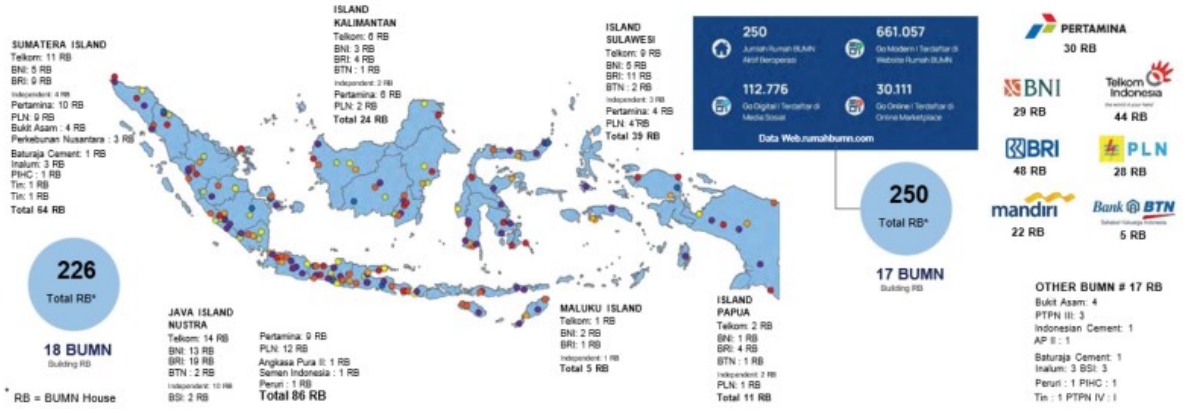

Figure 1: The Distribution Map of Rumah BUMN in Indonesia.

Rumah BUMN distribution map in Figure 1, a program by Pertamina to support micro, small, and medium enterprises (MSMEs), has a wide distribution across Indonesia. While I can't provide the exact number of locations due to privacy concerns, here's what I can tell you:

- Extensive Network: There are over 500 Rumah BUMN locations spread throughout Indonesia.
- Nationwide Presence: Rumah BUMN aims to be present in every major city and province.
- Targeted Locations: They prioritize establishing locations in areas with a high concentration of MSMEs.

PT Pertamina Geothermal Energy as one of the subsidiary of PT Pertamina (Persero) had already assigned by Ministry of State Owned Entreprise of Indonesia to develop and empower SME's as the proof of its existence to the SME communities all around Indonesia. Pertamina's Rumah BUMN program empowers micro, small, and medium enterprises (MSMEs) across Indonesia. The program boasts a presence in various regions, including Aceh Timur, Aceh Tamiang, Kepulauan Meranti, Dumai, Pekanbaru, Bengkulu, Rejang Lebong, Serdang Bedagai, Ogan Ilir, Kerinci, Lampung Tengah, Kepulauan Seribu, Purbalingga, Temanggung, Mojokerto, Situbondo, Klungkung, Sumbawa Barat, Dompu, Lombok Timur, Banjarmasin, Balikpapan, Berau, Palangkaraya, Seruyan, Sanggau, Bone Bolango, Parigi Moutong, Minahasa Selatan, and Tojo Una-una (Shown in Figure 1).

Standardization of Rumah BUMN MSMEs capabilities:

- Product Standards: technical specifications, production methods, raw materials, and manufacturing processes according to quality standards, security, applicable regulations.
- Process Standards: procedures and business practices for MSMEs in carrying out operations including quality management, risk, environment, etc.
- Service Standards: service quality related to response time, reliability, customer satisfaction, and internal ethical standards service
- Management Standards: standards of general management practices such as strategic planning, HR, finance, marketing, and operations for the sustainability of MSME businesses.

2.1 Rumah BUMN Riau

Rumah BUMN Riau has a mission in empowering MSMEs in Pekanbaru Rumah BUMN Riau is a non-profit organization, plays a vital role in supporting the growth of micro, small, and medium enterprises (MSMEs) in Pekanbaru. Their program operates like a well-oiled machine, fostering MSME development through a series of interconnected initiatives.

2.1.1 The Role of Rumah BUMN Riau

Rumah BUMN creates a comprehensive program that empowers MSMEs to flourish while fostering a spirit of social responsibility within the business community of Pekanbaru. These are several roles of Rumah BUMN Riau as follows :

- **Cultivating the Next Generation of Entrepreneurs**
  The program begins with a focus on millennials. Rumah BUMN establishes a "Millennials Activity Center" – a dedicated space for young people to learn and grow as future business leaders. This center offers resources for studying business, internship opportunities, and participation in specially designed millennial programs organized by BUMNs (State-Owned Enterprises).

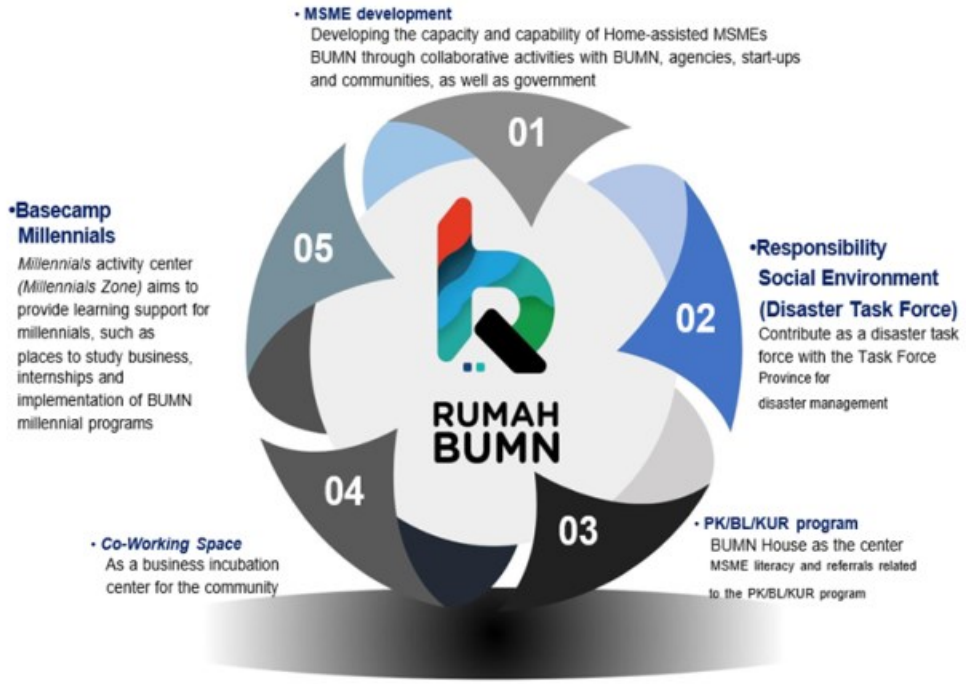

Figure 2: The Role of Rumah BUMN Riau in Indonesia.

- **Building Capacity and Capability**
  At the core of the program lies MSME development. Rumah BUMN works collaboratively with BUMNs, government agencies, startups, communities, and the government itself to empower MSMEs. Through these collaborations, they provide resources and training programs that enhance the capacity and capability of local businesses.
- **Nurturing Businesses within a Supportive Environments**
  The program offers a dedicated "Co-Working Space" that functions as a business incubator. This space fosters MSME literacy by providing resources and guidance. Additionally, the Co-Working Space acts as a referral center, connecting entrepreneurs with relevant government credit programs like PK/BL/KUR, which can provide crucial financial support for business growth.
- **Extending a Helping Hand**
  The program goes beyond just business development. Rumah BUMN recognizes the importance of social responsibility. The final stage emphasizes "Responsibility (Social Environment)" and participation in a "Disaster Task Force." This initiative encourages MSMEs to contribute to the community by working alongside the Provincial Task Force during disaster relief efforts.

2.1.2 The Ecosystem of Rumah BUMN Riau

Rumah BUMN Riau acts as a vital hub for empowering micro, small, and medium enterprises (MSMEs) across the Riau province in Indonesia. It fosters a comprehensive ecosystem that equips MSMEs with the tools and resources they need to thrive.

- **A Multi-Layered Approach to Supporting MSMEs**

Figure 4 depicts a diagram outlining the key components of Rumah BUMN's program to support micro, small, and medium enterprises (MSMEs) in Indonesia. The diagram uses a circular structure with arrows indicating the interconnectedness of the various program elements.

- **Central Hub: Rumah BUMN Riau**
  At the center of the circle sits the text "RUMAH BUMN" with the organization's logo. This central placement emphasizes Rumah BUMN as the core entity facilitating MSME development.
- **Empowering the Next Generation**
  Rumah BUMN Riau become the center provides millennials with resources for business education, internship opportunities, and participation in specific programs designed by BUMNs (State-Owned Enterprises) to cultivate young entrepreneurial talent.
- **Strengthening MSME Capacity**
  Rumah BUMN's collaborative efforts to enhance MSME capabilities. They achieve this by working with various stakeholders, including BUMNs, government agencies, startups, local communities, and the government itself. Through these partnerships, Rumah BUMN creates and delivers programs that strengthen the capacity and capabilities of MSMEs in the region. On the other hand, Rumah BUMN Riau provide all the SME's products to be displayed in the outlet gallery as shown in Figure 3 to support the sales and marketing of their products.

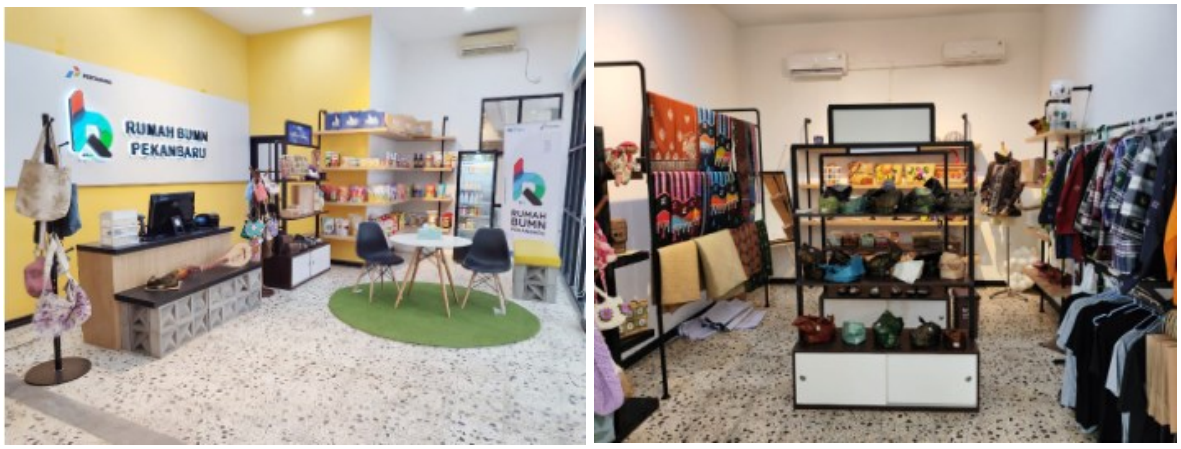

Figure 3: Outlet Gallery of Rumah BUMN Pekanbaru to Display SME's Products.

Figure 4: The Ecosystem of Rumah BUMN in Indonesia.

- **Providing a Supportive Ecosystem**
  Rumah BUMN Riau as The Co-Working Space functions as a business incubator, offering resources and guidance specifically geared towards MSME literacy. It further emphasizes the role of the Co-Working Space as a referral center, connecting entrepreneurs with relevant government credit programs (PK/BL/KUR) that provide financial aid crucial for business growth.
- **Fostering Social Responsibility**
  Represented by an icon of people helping people, delves into Rumah BUMN's initiative beyond pure business development. The text describes "Responsibility (Social Environment)" with a focus on participation in a "Disaster Task Force." This program element highlights Rumah BUMN's commitment to social responsibility. It encourages MSMEs to give back to the community by working alongside the Provincial Task Force during disaster relief efforts.

3. RESULT

KabarBaik RB coffeeshop is one of the business innovation from Rumah BUMN Riau which is located in Pekanbaru to optimize the sales and marketing of geothermal coffee product from PT Pertamina Geothermal Energy CSR program, where some of them produced using the direct heat of geothermal fluids from the geothermal production. The following are social business model canvas of KabarBaik RB Coffeeshop.

A. Social Project Objective:

To empower Pertamina Geothermal Energy SMEs through "KabarBaik RB Coffee" in Figure 5, creating jobs for people with disabilities, promoting sustainable practices, and building a collaborative ecosystem with various stakeholders to drive social and economic impact.

Figure 5. The Appearance and Existence of KabarBaik RB Coffeeshop in Pekanbaru (Canaya Coffee from Kamojang, Latif Coffee from Lumut Balai, and Brown Sugar from Lahendong).

B. Problem:

In addition to previous challenges, address the need for innovative marketing strategies and collaborative partnerships to ensure the coffee shop's sustainability and maximize its social impact. The other problem and challenges are the existing of established and fancy coffeeshop surroung this coffeeshop which can be a big deal for visitor to consider to come and buy at this coffee-shop with its simplicity and their socio-preneur scheme.

C. Proposed Solution:

- Implement a multi-faceted marketing strategy focusing on ESG and sustainability:
  This strategy will integrate environmental, social, and governance aspects into all marketing efforts. It will highlight the coffee shop's use of locally-sourced, sustainable coffee beans, waste reduction initiatives, and eco-friendly practices. Social impact will be showcased through stories of deaf employees and local SME partners. The governance aspect will be addressed through transparent communication of decision-making processes and regular impact reports. Sustainability will be promoted through educational content, workshops, and a themed menu, all designed to engage customers in the shop's mission and encourage responsible consumption.

- Develop partnerships with state-owned enterprises, government agencies, private sector, and youth communities:
  KabarBaik RB Coffee will forge strategic partnerships across various sectors to expand its reach and impact. For state-owned enterprises and private sector companies, it will offer corporate packages, employee discounts, and collaborative CSR initiatives. Government partnerships will involve participation in social and environmental programs, hosting policy discussions, and supporting local SME initiatives. Youth community engagement will focus on providing internship opportunities, hosting entrepreneurship workshops, and collaborating on social media campaigns. These partnerships will not only drive business growth but also create a supportive ecosystem for the coffee shop's social and environmental mission..

- Create a social media presence that highlights social impact and sustainability efforts:
  The coffee shop will develop a robust social media strategy across platforms like Instagram, TikTok, Facebook, and LinkedIn, each tailored to the platform's strengths. Content will focus on showcasing the shop's social impact and sustainability efforts through visually appealing posts, short-form videos, and longer-form content. Regular features will include a "Meet the Maker" series highlighting local SME products, "Sustainability Tip of the Week", and "Impact Spotlight" showcasing the shop's initiatives. Engagement will be fostered through user-generated content campaigns, interactive polls, and live Q&A sessions. Collaborations with local eco-influencers, social activists, and youth community leaders will help expand reach and credibility, creating a dynamic and impactful social media presence that aligns with the shop's values and mission.

D. Target Beneficiaries:

- Local youth communities:
  KabarBaik RB Coffee will actively engage and support local youth communities in Pekanbaru and the surrounding Riau region. This group includes students, young professionals, and budding entrepreneurs aged 18-35. The coffee shop will serve as a hub for youth-oriented activities, offering a space for networking, skill-building workshops, and collaborative projects. By providing internship opportunities, hosting youth-led events, and showcasing young local talent, the coffee shop aims to empower this demographic. The goal is to nurture a new generation of socially and environmentally conscious leaders who can drive sustainable development in the region, while also cultivating a loyal customer base that aligns with the shop's values and vision for the future.

- Environmentally and socially conscious consumers
  This target group comprises individuals who prioritize sustainability and social impact in their purchasing decisions. These consumers, ranging from young adults to seniors, are willing to pay a premium for products and experiences that align with their values. KabarBaik RB Coffee will cater to this group by offering ethically sourced coffee, eco-friendly packaging, and a menu that includes plant-based and locally sourced options. The shop's commitment to employing deaf individuals and supporting local SMEs will resonate with these consumers' desire for social impact. By providing a space that not only serves quality coffee but also educates about sustainability and facilitates community engagement, the coffee shop aims to become a preferred destination for this growing segment of mindful consumers, fostering loyalty and word-of-mouth promotion.

- Corporate and government partners looking for CSR opportunities
  KabarBaik RB Coffee will position itself as an attractive partner for corporations and government agencies seeking meaningful Corporate Social Responsibility (CSR) initiatives. This group includes local and national companies, state-owned enterprises, and government departments interested in demonstrating their commitment to social and environmental causes. The coffee shop will offer these partners unique opportunities to engage in impactful CSR activities, such as sponsoring skills training for deaf employees, supporting local SME product showcases, or collaborating on sustainability workshops. By aligning with KabarBaik RB Coffee's mission, these partners can enhance their public image, engage their employees in meaningful volunteer work, and contribute to local community development. The coffee shop will benefit from increased visibility, potential funding, and expanded networks, creating a win-win situation that amplifies its social and environmental impact.

E. Forms of Activities:

Marketing and Partnerships:

- Develop and maintain an engaging social media presence; KabarBaik RB Coffee will create and curate compelling content across various social media platforms, showcasing its products, sustainability initiatives, and social impact to build brand awareness and foster community engagement.

- Organize sustainability-themed events and workshops; The coffee shop will host regular events and workshops focused on sustainability topics, such as eco-friendly living, responsible consumption, and social entrepreneurship, to educate and inspire its customers and the wider community.
- Collaborate with youth communities for events and promotions; By partnering with local youth organizations and student groups, KabarBaik RB Coffee will co-create events, campaigns, and promotional activities that resonate with young audiences and promote the shop's mission.
- Establish partnership programs with state-owned enterprises, government agencies, and private companies; The coffee shop will develop tailored partnership programs offering corporate packages, collaborative CSR initiatives, and co-branded products to engage larger organizations and expand its reach and impact.
- Create loyalty programs for corporate partners and regular customers; KabarBaik RB Coffee will implement a multi-tiered loyalty program that rewards both individual customers and corporate partners for their purchases, participation in sustainability initiatives, and engagement with the shop's social mission.

F. Stakeholders/Partners:

- State-owned enterprises in Pekanbaru and surrounding areas:
  KabarBaik RB Coffee will engage with state-owned enterprises to create mutually beneficial partnerships, offering corporate packages, employee engagement programs, and collaborative CSR initiatives that align with both parties' social and environmental goals.
- Local and regional government agencies:
  The coffee shop will collaborate with government agencies to support local economic development, participate in public-private partnerships, and contribute to policy discussions on sustainability and social inclusion.Youth communities and organizations in Pekanbaru
- Private sector companies interested in CSR:
  KabarBaik RB Coffee will partner with socially responsible businesses to develop joint initiatives, such as employee volunteer programs, co-branded sustainable products, and sponsored events that amplify both parties' positive impact on the community.
- Youth communities and organizations in Pekanbaru:
  By fostering relationships with local youth groups, the coffee shop will create opportunities for young people to engage in sustainability projects, gain work experience, and contribute to community development initiatives.
- Social media influencers and content creators
  KabarBaik RB Coffee will collaborate with local influencers and content creators who align with its values to produce authentic, engaging content that promotes the shop's mission, products, and impact to a wider audience.

G. Project Duration:

Remains 8 months for the initial phase, with long-term operation plans

H. Challenges:

- Building and maintaining effective partnerships with diverse stakeholders; Forge strong, collaborative relationships with a variety of groups to achieve shared objectives.
- Consistently creating engaging content for social media; Regularly develop content that captures attention and sparks interaction on social media platforms.
- Balancing commercial success with social and environmental goals; Strive for profitability while also considering positive social impact and environmental responsibility.

I. Required Budget:

Increase to Rp. 150,000,000 to account for additional marketing and partnership development efforts

J. Project Social Outcomes:

- Increased awareness of sustainable and inclusive business practices; Educating and motivating people to adopt business models that benefit both society and the environment. This can involve showcasing success stories, highlighting the positive social and environmental impact of sustainable practices, and offering resources for businesses to implement them.

- Stronger collaborative ecosystem among businesses, government, and communities: Fostering a network where all parties work together to achieve shared goals for economic and social development. This can involve encouraging open communication and collaboration between businesses, government agencies, and community organizations, allowing for joint initiatives that address local needs and create a more supportive environment for business growth.
- Enhanced visibility and support for local SMEs and their products; Elevating the profile and providing resources to empower small and medium-sized enterprises in a specific location. This might involve creating platforms for SMEs to showcase their products and services, offering training and mentorship programs to help them develop their business skills, and advocating for policies that support the growth of local businesses.

K. Impact of Activities:

- Community Engagement: Fostering a sense of community and shared purpose among diverse stakeholders. This impact strengthens social bonds and collaboration by creating opportunities for people from various backgrounds to connect, build trust, and work together towards common goals that benefit the entire community.
- Sustainable Consumption: Promoting environmentally and socially responsible consumer behavior. This impact encourages people to make conscious choices when purchasing goods and services, prioritizing products that minimize environmental damage and support ethical labor practices. This can lead to a more sustainable and responsible consumer culture.
- Youth Empowerment: Engaging and inspiring local youth through collaborative initiatives. This impact provides young people with opportunities to participate in decision-making processes, develop their skills, and contribute to their communities. It fosters a sense of agency and empowers them to become active and responsible citizens who shape the future.

L. Post-Project Sustainability Plan:

- Develop a robust partner management system to maintain and grow collaborations; This system would streamline communication, track progress on joint initiatives, and ensure clear roles and responsibilities for each partner. This fosters long-term, mutually beneficial partnerships that contribute to achieving shared goals.
- Create a content calendar and strategy for ongoing social media engagement; A well-defined content calendar helps plan and publish engaging content regularly, keeping audiences informed and interested. The strategy component ensures the content aligns with overall goals, resonates with target audiences, and drives desired actions on social media platforms.
- Establish an advisory board including representatives from key stakeholder groups; An advisory board offers valuable insights, expertise, and connections from diverse perspectives. Including representatives from key stakeholder groups like businesses, government, and community organizations fosters a more inclusive approach and ensures initiatives address the needs of all involved.
- Implement a data-driven approach to measure and communicate social and environmental impact; By collecting and analyzing data, this approach allows for a more accurate assessment of the program's effectiveness. It enables the program to demonstrate the positive change it creates in terms of social and environmental outcomes, fostering transparency and accountability.

Marketing Strategy Highlights:

- Social Media Engagement: Develop a strong presence on platforms like Instagram, TikTok, and Facebook, showcasing the coffee shop's social impact, sustainability efforts, and unique offerings.
    - Platforms: Develop a strong presence on Instagram, TikTok, and Facebook, reaching a wider audience through the most popular social media channels.
    - Content Strategy: Showcase the coffee shop's social impact through engaging content (e.g., employee stories, community events), highlight sustainability efforts (e.g., sourcing, waste reduction), and promote unique offerings (e.g., signature drinks, limited-edition merchandise).
    - Goal: Build brand loyalty, attract customers who value social responsibility, and generate excitement about the coffee shop's offerings.
- ESG and Sustainability Theming: Center all marketing materials and in-store experiences around environmental, social, and governance (ESG) principles and sustainability practices.
    - Marketing Materials: Center all marketing materials around environmental, social, and governance (ESG) principles. This can include using recycled or sustainable packaging, incorporating eco-friendly themes in visuals, and highlighting ethical sourcing practices.

- In-Store Experience: Extend the ESG focus to the in-store experience. Offer reusable cups for discounts, display information about sustainability initiatives, and create a welcoming atmosphere that reflects the coffee shop's values.
- Goal: Attract environmentally and socially conscious customers, differentiate from competitors, and reinforce the brand's commitment to positive change.

Collaborative Partnerships:

- BUMN (State-Owned Enterprises): Develop corporate packages, host events, and create special promotions for employees.
- Government: Engage in public-private partnerships for social programs, host policy discussions, and participate in government-led initiatives.
- Private Sector: Offer corporate social responsibility (CSR) opportunities, create co-branded products, and develop employee engagement programs.
- Youth Communities: Organize youth-focused events, provide internship opportunities, and collaborate on social media campaigns.

Community Events: Host regular workshops, talks, and networking events centered around sustainability, entrepreneurship, and social impact.

Loyalty Program: Implement a points-based system that rewards not only purchases but also participation in sustainability initiatives and community events.

Impact Reporting: Regularly publish and promote impact reports highlighting the coffee shop's contribution to local SMEs, job creation for people with disabilities, and environmental sustainability.

Influencer Collaborations: Partner with local influencers and content creators who align with the brand's values to expand reach and credibility.

This enhanced strategy aims to create a vibrant ecosystem around "KabarBaik RB Coffee", positioning it not just as a coffee shop, but as a hub for sustainable business practices, community engagement, and social impact in Pekanbaru and the broader Riau region.

4. CONCLUSION

- KabarBaik RB Coffeeshop is a shining example of how a business can use geothermal product coffee as a force for good. By empowering local businesses, creating jobs for people with disabilities, promoting sustainable practices, and fostering a collaborative community, they're brewing a brighter future for Pekanbaru.
- Their innovative marketing strategies engage socially conscious customers, while their commitment to community engagement fosters a sense of shared purpose. By measuring their impact and continuously adapting their approach, KabarBaik RB Coffeeshop ensures long-term sustainability and maximizes their positive influence.
- KabarBaik RB Coffeeshop serves as a model for social entrepreneurship, inspiring others to use business as a tool for positive change. Their success story demonstrates the power of collaboration, environmental responsibility, and community engagement. In the end, they're not just brewing delicious coffee – they're brewing a better future, one cup at a time.
- KabarBaik RB Coffeeshop isn't just about serving delicious coffee; it's a social enterprise brewing a brighter future for Pekanbaru. They empower local businesses, create jobs for people with disabilities, promote sustainable practices, and foster a collaborative community through coffee. Their innovative marketing strategy is key to their success. Engaging social media content on platforms like Instagram, TikTok, and Facebook showcases their social impact stories, sustainability efforts, and unique offerings, attracting customers who value their mission. KabarBaik RB Coffeeshop integrates ESG principles into their marketing, using recycled materials, highlighting eco-friendly practices, and offering reusable cups, resonating with environmentally conscious consumers.

ACKNOWLEDGEMENT

KabarBaik RB Coffeeshop would like to express its sincere gratitude to Pertamina Geothermal Energy, a subsidiary of PT Pertamina Persero, for their invaluable support in supplying our coffee shop with high-quality coffee beans and brown sugar sourced directly from their geothermal fields. We would also like to extend our appreciation to the Ministry of State Owned Entreprise of Indonesia for establishing Rumah BUMN and providing the necessary funding through Rumah BUMN Riau, which serves as the mother institution for KabarBaik RB Coffeeshop.

REFERENCES

Adie, G., Guimarães, L., & Freire, N. (2019). The impact of training and mentoring on the internationalization of small and medium-sized enterprises (SMEs). *Journal of Small Business & Entrepreneurship*, 27(2), 223-242.

Adomako, S., & Amoah, A. Y. (2016). The impact of training and development on small and medium enterprises' performance in Ghana. *International Journal of Entrepreneurial Development*, 17(3), 232-250.

Al-Shami, S. S., & Anis, Z. (2020). The role of training and development programs in enhancing the performance of small and medium enterprises (SMEs). *International Journal of Entrepreneurship and Management*, 24(2), 119-134.

Amelia, R. (2023, July 10). *Dukung Kemajuan UMKM, Rumah BUMN Kolaborasi dengan PT Pos Indonesia* [Supporting the Advancement of MSMEs, Rumah BUMN Collaborates with PT Pos Indonesia]. Detik Indonesia. Retrieved from https://www.detakindonesia.co.id/

Amran, A., & Devi, S. S. (2016). The impact of training and development on the performance of small and medium enterprises (SMEs) in Malaysia. *International Journal of Business and Management*, 11(2), 136-143.

Bosma, N., Chowdhury, J., & Díaz-García, C. (2019). The role of business incubation programs in fostering SME internationalization: A systematic review and research agenda. *International Small Business Journal*, 37(7), 1183-1210.

Celia, L., & Rialp, A. (2017). The impact of training and development on the innovation performance of SMEs. *Journal of Small Business & Entrepreneurship*, 25(1), 71-92.

Colombini, M., Gatti, P., & Molino, L. (2016). *The effect of training on human capital and firm performance: Evidence from Italian SMEs. Research Policy*, 45(9), 1718-1732.

Cordoba-Rodríguez, R., López-García, M. C., & López-Carmona, E. S. (2017). Training and development for family businesses: A review of the literature and future research avenues. *Family Business Review*, 30(1), 101-120.

Crisan, V., Grigore, C., & Purcărea, A. (2019). The role of training and development in fostering innovation in small and medium-sized enterprises (SMEs). *Sustainability* (Switzerland), 11(17), 4520.

Davidsson, P., Klofsten, M., & Wennekers, A. (2002). How do entrepreneurs learn? A revised model of small firm learning. *Entrepreneurship Theory and Practice*, 26(3), 339-358.

De Fátima Lima, J., Fernandes, J. M., & Adie, G. (2020). The impact of training and mentoring on the development of entrepreneurial competencies in small and medium-sized enterprises. *Journal of Small Business & Entrepreneurship*, 28(4), 527-548.

De Fretes, R., & Van der Meer, R. B. (2005). Using the resource-based view to explain why SMEs outsource training. *Journal of Small Business Management*, 43(4), 438-454.

National Standardization Agency of Indonesia. (n.d.). Home. Retrieved July 13, 2024, from https://www.bsn.go.id/

Ministry of Cooperatives and Small and Medium Enterprises of the Republic of Indonesia. (n.d.). Home. Retrieved July 13, 2024, from https://www.kemenkopukm.go.id/

Ministry of Cooperatives and Small and Medium Enterprises of the Republic of Indonesia. (n.d.). Smesta. Retrieved July 13, 2024, from https://smesta.kemenkopukm.go.id/

Nabi, G., Liñán, P., & Fayolle, A. (2017). The role of training and human capital development in SME performance: A meta-analysis of the empirical literature. *Journal of Business Research*, 70(11), 4344-4354.

Organisation for Economic Co-operation and Development (OECD). (2017). *SME and Entrepreneurship Policy: A framework for Boosting Job Creation and Growth*. OECD Publishing.

Prihatiningtyas, D. A., & Soetrisno, I. (2013). An Investigation into the Factors Affecting the Success of Training Programs for Micro and Small Enterprises (MSME) Owners in Indonesia. International *Journal of Business and Management*, 8(2), 101-108.

Wong, V. S., Mohamed, M. H., & Ibrahim, A. H. (2015). Training and development for SMEs in Malaysia: A review of the literature. *International Journal of Business and Management*, 10(2), 90-100.

Yuliana, & Siswanto. (2017). Exploring and Designing Employee Training and Development Programs for SMEs in Jabodetabek and Bandung. *Journal of Economics and Sustainable Development*, 8(14), 189-195.

Yulianingsih, E., Siswanto, Mulyono, & Sutarto. (2018). The Influence of Entrepreneurship Training on the Productivity of SMEs in Semarang City, Indonesia. *The Journal of People's Social Sciences* (PEOPLE: International Journal of Social Sciences), 23(2), 229-238.

Lifecycle Environmental Evaluation of Fossil and Renewable Energy Sources: Insights from Coal-fired and Geothermal Power Plant

Irhan Febijanto[1], Yudistian Yunis[2], Nadirah Nadirah[1], Ahmad Ismed Yanuar[1], Hismiaty Bahua[1], A. L. S. M. Sihombing[1], I. M.A.D. Susila[1], and Kris Pudyastuti[3]

[1]National Research and Innovation Agency
[2]PT Geo Dipa Energi (Persero)
[3]PT CDM Indonesia Jaya

irhan.febijanto@gmail.com, yudistian@geodipa.co.id, kris.pudyastuti12@gmail.com

Keywords: Geothermal Power Plant, Coal-Fired Power Plant, Comparison, Life Cycle Assessment, Environmental Impacts

ABSTRACT

Indonesia has 40% of the world's geothermal potential, equivalent to 28,617 MW. However, this potential has yet to be fully utilized, with only about 4.5% used for electricity generation. Despite the government's encouragement to build more geothermal power plants (GPPs) to support the energy mix and achieve net zero emissions targets, most of Indonesia's power generation still comes from coal-fired power plants (CFPPs), which make up 47.3% of the total generating capacity in the country, with a total capacity of 20.8 GW. Increasing the number of operating GPPs can help in reducing greenhouse gas emissions. On the other hand, adding more geothermal power generation units will have the opposite effect. However, there has not been comprehensive research comparing the environmental impacts of GPP with CFPP, which is the most common type of generator in Indonesia. In this study, we use the life cycle assessment (LCA) method to evaluate the environmental impact of existing GPP units, and then compare the results with existing CFPP units. This comparison aims to provide valuable insight into the environmental impacts of these two types of plants to help decision-makers and stakeholders make informed choices regarding the development and operation of GPPs and CFPPs in Indonesia, contributing to the development of a comprehensive net zero emissions strategy.

1. INTRODUCTION

Geothermal Power Plant (GPP) is an environmentally friendly power plant with a low environmental impact. Research comparing the environmental impact of GPP and CFPP-related environmental impacts, such as acidification and global warming potential (GWP), needs to be quantitatively assessed to ensure the advantages of CFPP in terms of environmental impact. Life Cycle Assessment (LCA) analyzes the environmental impact of a product, process, or system, such as a power plant, from fuel extraction to final disposal. Several methodologies, including ISO standards, TRACI, ReCiPe, CML, Ecoinvent, and ILCD, are used in this analysis process. Product Category Rules (PCR) (EPD International, 2021) were used to standardize the comparison of the LCA for specific products or product categories, enabling consistent comparisons of environmental impact categories. The product categories in this study were both types of CFPP and GPP.

Research on LCA of Geothermal Power Plants (GPP) in Indonesia is quite limited. Generally, the research still focuses on the environmental impacts of GPP operation. In a small-scale geothermal plant, Tampubolon (2023) found that the release of non-condensable gas (NCG) into the air from cooling towers contributes to acidification, which is the primary environmental impact at geothermal power plants. This finding was supported by a similar study at Wayang Windu GPP (Annisa & Rahardyan, 2018). Additionally, an LCA analysis at Kamojang GPP (Alfian Ardyansyah & Maya Sopha, 2018) revealed that the operational phase of GPP has the most significant environmental impact, particularly in terms of global warming potential (GWP) emissions and acidification. Another study at Patuha GPP also found that GWP and accidification impacts were more significant compared to other environmental impacts (Sondakh, 2022). To support Indonesia's net-zero emission strategy, it is essential to compare the environmental impacts of GPP using LCA with those of CFPP utilizing the same boundary system. Therefore, a research initiative was undertaken wherein LCA calculations using PCR were employed to analyze the environmental impact of a GPP unit in West Java and a CFPP unit in Banten. A quantitative comparison of the impacts in this category can offer new insights regarding quantitative environmental impacts.

2. MATERIAL AND METHODS

2.1 Power plant overview

This study used operational data from a 315 MW capacity CFPP in Banten and a 55 MW capacity GPP in West Java, Indonesia. Both power plants are base-load power plants connected to the Jawa-Madura-Bali (JAMALI)

grid. The chimney emissions from the CFPP, including CO_2, CO, SO_2, O_2, NOx, and PM2.5 from both units, were measured hourly by the continuous emission monitoring system (CEMS). The emissions data for the GPP were obtained from the Environmental Report. The environmental impacts of both types of PP were compared and assessed simultaneously using the LCA method. The data encompassed various inputs and outputs of both units' energy, materials, and emissions. The environmental impact of GPP was assessed and compared to that of CFPP.

Table 1: Operational Parameter of GPP and CFPP.

Parameter	Unit	GPP	CFPP
Operation days	days	365	276
Operation time	h	8760	6,624
Capacity factor	%	100	75.6
Fuel Consumption	t	-	1,063,232.2

2.2 LCA method

The LCA study referred to the guidelines for ISO14040:2006/Amd1:2020 and ISO 14044:2006/Amd2:2020. These guidelines outline four phases of LCA: goal and scope definition, inventory analysis, impact assessment, and interpretation. The study also considered the MOEF's LCA report preparation guidelines from 2021. It evaluated the environmental impact of GPP and CFPP operations, including fuel, chemicals, products, air, soil, and water emissions. To assess these impacts, the study used the openLCA data processing software with the Ecoinvent 3.8 database, which contains life cycle inventory data and emission factors. The study used the default impact categories and calculation methods specified in the Product Category Rules for Electricity, Steam, and Hot/Cold Water Generation and Distribution systems. It considered impact categories like GWP, Abiotic depletion (ADP) elements and Abiotic depletion (ADP) fossil, Acidification Potential (AP), Eutrophication (EP), Ozone layer depletion (ODP), Photochemical oxidation POFP, Water Use (WU). The study used various methodologies for assessing these categories, such as IPCC 100-year GWP for GWP assessment, CML-IA baseline (World 2000) methodology for EP, ADP elements and ADP fossil, AP and ReCiPe Midpoint (H) (2008) methodology for POFP. The AWARE approach was used for WU.

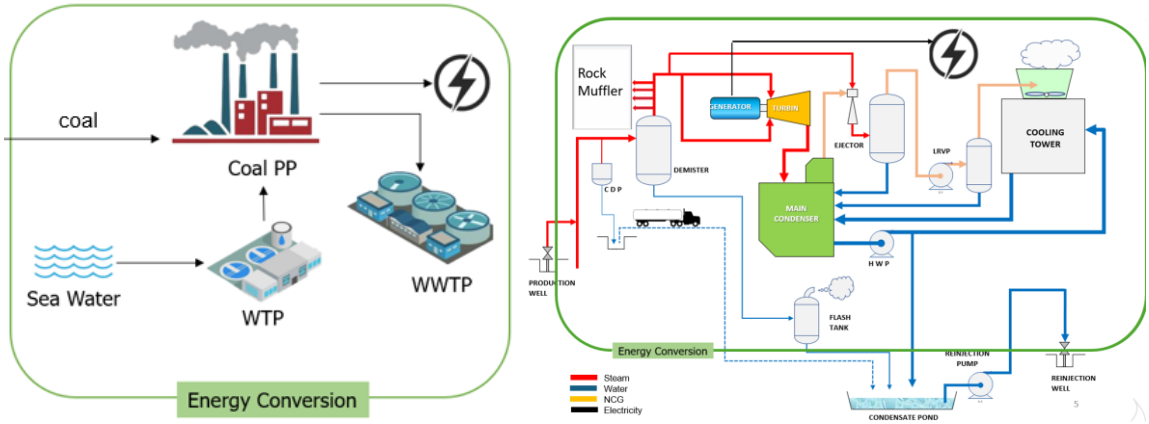

Figure 1: Boundary System (gate to gate) for CFPP and GPP.

2.1.1 Goal and scope definition

The first step in the Life Cycle Assessment (LCA) process is to define the objectives and scope. This stage determines the overall plan for conducting the LCA analysis. The objective is to calculate the amount of environmental impact during the operational process of procuring raw materials for coal and geothermal steam, as well as PP operation, based on the functional unit of 1 kWh of electricity produced. The functional unit is the main element that needs to be considered when comparing two different systems to normalize them, defining the environmental impact point of view related to the function of the identified system (Sala and Garcia, 2016). Both systems are from transportation fuel for the CFPP in Banten and piping transportation of geothermal steam for the GPP in West Java (gate to gate). The study acquired primary data from CFPP (Febijanto et al., 2024) and secondary data from GPP. The collected data for both power plants included geothermal steam, coal fuel, chemicals, water requirements, internal electricity usage, emissions, and waste. The background data was obtained from the literature and the Ecoinvent 3.8 dataset. Figure 1 illustrates the boundaries of the GPP and CFPP from gate to gate.

The coal supply chain starts with the receipt of coal at the power plant (PP), followed by the combustion of coal and processing of water at the water treatment plant (WTP) and wastewater treatment plant (WWTP) stages. Meanwhile, geothermal power plants focus on the operation of power plants to generate electricity by utilizing steam derived from geothermal heat. Overall, this study offers a thorough and detailed analysis of the supply chains involved in the CFPP and GPP operations. The data obtained from both primary and background sources help to illuminate the different environmental impacts of both types of power plants and provide valuable insights for comparing them as part of the national renewable energy development strategy and for future research and development in this field.

2.2.2 Life cycle inventory

The second step of LCA is known as life cycle inventory (LCI) analysis. It is a technique used to measure the amount of energy used, raw materials used, and environmental effects at every stage of a system's evaluation (EPD International, 2021). According to ISO14040:2006/Amd1:2020, the LCI considers the product's input and output at every stage of its life cycle. This section explains the system boundary for each scenario, as well as the data sources and underlying presumptions. During the inventory stage of the LCA process, the energy flow from fuel consumption, mass balance at each stage, and operational processes, including steam flow from wellheads and the combustion of coal to produce electricity, WTP, and WWTP, were all analyzed.

2.2.3 Impact analysis

When evaluating the environmental impact of inventory data, it is called life cycle impact analysis (LCIA). During this process, the identified environmental flows (inventory analysis) and the defined impact categories (goal and scope definitions) are used to assess potential impacts. The evaluation of each scenario's possible environmental effects utilized the specifications outlined in the PCR for Electricity Generation) (EPD International, 2021). Impact categories considered in this study included GWP, AP, EP, ODP, POFP, ADP elements, ADP fossil, WS, and LU.

2.3 Construction of the scenario

The comparison of environmental impacts in the GPP and CFPP operational phases was carried out based on the GPP scenario operating for 8760 hours in 2023, while the CFPP was based on actual operations in 2022.

3. RESULT AND DISCUSSION

The results of calculating environmental impact categories for CFPP and GPP are shown Table 2.

Table 2: LCIA results for GPP compared to CFPP.

Impact categories	Methodology	Unit	CFPP	GPP
ADP, elements	cml baseline	kg Sb eq	3.40×10^{-10}	0
ADP, fossil fuels	cml baseline	MJ	2.13×10^{-4}	0
EP	cml baseline	kg PO4--- eq	2.66×10^{-4}	0.12×10^{-4}
ODP (optional)	cml baseline	kg CFC-11 eq	3.25×10^{-12}	0
POFP	ei Recipe midpoint H vs 1.3	kg NMVOC	2.17×10^{-3}	0.018×10^{-3}
WU	AWARE	m^3 eq	5.18×10^{-3}	0.07×10^{-3}
GWP $_{100a}$	IPCC 2021 GWP 100	kg CO_2 eq	1.19	8.42×10^{-3}
AP (fate not incl.)	CML non baseline	kg SO_2 eq	1.41×10^{-3}	3.92×10^{-3}

Table 3: LCIA results for GPP compared to CFPP in the different methodology (kWh).

Impact categories	Methodology	Unit	CFPP	GPP
AP	Tracy 2.1	kg SO_2 eq	3.44×10^{-3}	3.92×10^{-3}
AP	Recipe midpoint H	kg SO_2 eq	2.76×10^{-3}	0.01×10^{-3}
AP	Cml baseline	kg SO_2 eq	1.00×10^{-3}	0.052×10^{-3}
AP (fate not incl.)	Cml non baseline	kg SO_2 eq	1.41×10^{-3}	3.92×10^{-3}

The overall environmental impact per electricity production from GPP is lower than CFPP, except for AP. Regarding the AP results, this result strongly supports the results of previous research (Alfian Ardyansyah & Maya Sopha, 2018; Annisa & Rahardyan, 2018; Pangihutan Christian Tampubolon et al., 2022; Sondakh, 2022), that the biggest environmental impact of GPP was AP. The AP mainly was caused by non-condensable gas released into the air from the cooling tower.

The selection method in LCA is the important point, Table 3 indicates AP result from several methodologies in LCA analysis. Each LCA methodology is a combination of several different factors and processes, which will influence the results. The CML Non-Baseline (Guinee J.B, 2002) and Tracy 2.1 (Bare et al., 2003) methodologies consider hydrogen sulfide (H_2S) as an AP contributor, while the ReCiPe Midpoint H (Goedkoop et al., 2009) and CML Baseline (Guinee J.B, 2002) methodologies do not consider H_2S as an AP contributor. The inclusion of H_2S will provide the result with higher AP potential, especially for power plants with high H_2S emissions such as in GPP. From the data obtained, the results of the AP impact were not caused by H_2S (98.38%) alone but by NH_3 (1.31%) and NOx (0.30%). For comparison, the AP impact on CFPP originated from Nitrogen Oxide, NOx which emitted from the combustion process in boiler furnace (Sigal et al., 2022). As shown in Table 2, the GWP impact in CFPP was 1.19 kgCO2eq/kWh, and in GPP was 0.00842 kgCO2eq/kWh. In this study, the H_2S emissions intensity in GPP was 2.05 gr/kWh. According to the previous study, the intensity in the others GPP was as follows, Wayang Windu GPP produced 2.54 gr/kWh, Kamojang GPP 0.14 gr/kWh, and Ulubelu GPP 1.68 gr/kWh (Edhi Budhi Soesilo & Heviati, 2015).

Naturally occurring gases (NCGs) found in geofluids are typically released into the atmosphere, except for hydrogen sulfide. Before releasing hydrogen sulfide, it must be scrubbed. However, due to growing concerns about greenhouse gas (CO_2) emissions, NCGs are now being compressed and reinjected into the reservoir along with the used geofluid. NCGs in geofluids can contribute to environmental AP, particularly if they contain gases such as carbon dioxide (CO_2) and hydrogen sulfide (H_2S) (Finster et al., 2015). When CO_2 dissolves in water, it can create carbonic acid (H_2CO_3), which lowers the pH of the water and causes AP. Meanwhile, H_2S can be oxidized to sulfuric acid (H_2SO_4), which can also lead to AP.

To mitigate the AP produced by GPP, several steps can be taken (Bošnjaković et al., 2019): 1) Use of Scrubber Technology: Scrubbers can reduce emissions of acid gases such as SO_2 by absorbing harmful gases and converting them into less dangerous substances before releasing them into the atmosphere. 2) Geothermal Fluid Reinjection: Returning used geothermal fluid into the reservoir can help reduce acid gas emissions into the atmosphere, maintain reservoir pressure, and reduce the risk of subsidence. 3) Emission Monitoring and Control: Installing a sophisticated real-time emissions monitoring system can measure and control acid gas emissions, allowing operators to take immediate corrective action if emissions exceed permitted limits. 4) Use of Neutralizing Chemicals: Adding neutralizing chemicals to geothermal fluids before release can help reduce acidity levels and prevent environmental AP.

4. CONCLUSION

The study results indicated that the influence of AP from GPP operations was more notable than the impact of AP from CFPP operations. Even though nearly all environmental impacts from GPP operations were lower, when comparing environmental impacts using the same methodology and boundary system, it becomes evident that we should focus more on the impact of AP from GPP.

REFERENCES

Alfian Ardyansyah, F., & Maya Sopha, B. (2018). The 6 th Indonesia International Geothermal Convention & Exhibition (IIGCE) 2018 Cendrawasih Hall-Jakarta Convention Center Indonesia. *Th 6th Indonesia International Geothermal Convention & Exhibition (IIGCE)* .

Annisa, R., & Rahardyan, B. (2018). Life Cycle Assessment Applications To The Dry Steam Geothermal Power Generation (Case Study: Star Energy Geothermal Wayang Windu, Ltd, Indonesia). In */ IjoLCAS* (Vol. 2, Issue 2).

Bare, J. C. , Norris, G. A. , Pennington, D. W., & McKone, T. (2003). The Tool for the Reduction and Assessment of Chemical and Other Environmental Impacts. *Journal of Industrial Ecology*, 6(3–4), 49–78.

Bošnjaković, M., Stojkov, M., & Jurjević, M. (2019). Environmental impact of geothermal power plants. *Tehnicki Vjesnik*, 26(5), 1515–1522. https://doi.org/10.17559/TV-20180829122640

Edhi Budhi Soesilo, T., & Heviati, E. (2015). Geothermal Power Plant Emissions in Indonesia. In *Proceedings World Geothermal Congress*.

EPD International. (2021). *Product Category Rules* (PCR).

Febijanto, I., Rosmeika, R., Nadirah, N., Yanuar, A. I., Sihombing, A. L., Susila, I. M. A. D., Bahua, H., Kurniawati, I. Z., Barkah, A., Santoso, A. D., Herdioso, R., Rustianto, B., Oktaufik, M. A. M., Suryana, Y., Syamsudin, E., Aditiyawan, A., Gazali, N., Soedjati, D., & Soleh, M. (2024). The environmental perspective on biomass co-firing operations at coal-fired power plants in the Banten region, Indonesia: a life cycle approach. Energy, *Ecology and Environment*. https://doi.org/10.1007/s40974-024-00329-5

Finster, M., Clark, C., Schroeder, J., & Martino, L. (2015). Geothermal produced fluids: Characteristics, treatment technologies, and management options. In *Renewable and Sustainable Energy Reviews* (Vol. 50, pp. 952–966). Elsevier Ltd. https://doi.org/10.1016/j.rser.2015.05.059

Goedkoop, M., Heijungs, R., Huijbregts, M., De Schryver, A., Struijs, J., & Van Zelm, R. (2009). *A Life Cycle Impact Assessment Method which Comprises Harmonised Category Indicators at the Midpoint and the Endpoint Level*. Report I.

Guinee J.B. (2002). *Handbook on Life Cycle Assessment: Operational Guide to the* (Guinee J.B, Ed.). Springler.

Pangihutan Christian Tampubolon, A., Hadiyanto, H., & Kusdiyantini, E. (2022). *Impact of Small-Scale Geothermal Power Plant Replenishment with A Life Cycle Assessment* (Vol. 12, Issue 2).

Sigal, I. Ya., Smikhula, A. V., Marasin, O. V., Gurevich, M. O., & Lavrentsov, E. M. (2022). METHODS TO REDUCE NOX FORMATION DURING GAS COMBUSTION IN BOILERS. *Energy Technologies & Resource Saving*, 4, 62–72. https://doi.org/10.33070/etars.4.2022.06

Sondakh, G. G. (2022). *Life Cycle Assessment of the Geothermal Power Plant in the Patuha Geothermal Field, Indonesia*.

Tampubolon, J. V., & Dalimi, R. (2023). Impact of Electric Vehicles toward Energy Reliability of the Jawa-Madura-Bali Electrical Power System. *IOP Conference Series: Earth and Environmental Science*, 1199(1). https://doi.org/10.1088/1755-1315/1199/1/012005

PROPER Implementation in Star Energy Geothermal Darajat II, Limited

Muhammad Riyadhi and Micia Zaputi Rohimah

PT Star Energy

m.riyadhi@starenergy.co.id

Keywords: Cost efficiency, environmental performance, geothermal energy, innovation, PROPER

ABSTRACT

Operational processes are the backbone of every company. They are carefully planned out and carried out to maximize production and meet the company's objectives. However, these operational activities can exert significant impacts on the environment, yielding both beneficial and detrimental effects. From resource extraction and production processes to waste generation and emissions, every stage of industrial production entails environmental implications. Therefore, effective environmental management is crucial to preserve natural functions and minimize potential environmental impacts. In response to these challenges, the Indonesian Government has implemented various initiatives, including Program Penilaian Peringkat Kinerja Perusahaan dalam Pengelolaan Lingkungan (PROPER) as a public disclosure program for environmental compliance. This program was initiated to enhance active participation and company performance in environmental monitoring and management. Under PROPER, companies are categorized into five-color tiers—gold, green, blue, red, and black—based on their environmental performance. The program evaluates companies' compliance with environmental regulations, as well as its further initiatives to improve their overall environmental performance. The adoption of PROPER is also expected to promote diverse innovations within the production process. A company's dedication to environmental stewardship may stimulate the establishment of novel innovations for reducing environmental impacts. Through optimal resource utilization, companies can minimize raw material consumption and mitigate waste generation, thus realizing operational cost efficiency. This integrated approach not only improves environmental sustainability but also highlights the economic benefits of responsible environmental management. One of the companies actively engaging in the implementation of PROPER is Star Energy Geothermal Darajat II, Limited (SEGD). Specializing in geothermal power plant operations, SEGD has an installed power generation capacity of 274,5 MW, which is then distributed to the Java-Madura-Bali (JAMALI) interconnection system. Through its active participation in PROPER, SEGD consistently aims to improve its environmental performance. The company's effort in environmental management can be proven by the achievement of the gold PROPER award in 2022-2023, the highest tier award. This recognition emphasizes the company's dedication to conduct geothermal operations in harmony with environmental and social aspects, setting a commendable standard for the industry. This study aims to analyze the influence of PROPER implementation on SEGD's environmental performance and operational cost efficiency. The research was carried out using a descriptive method with a quantitative approach. This study shows that the implementation of PROPER in SEGD positively influences the company's environmental performance, resulting in reductions of energy use, water consumption, water pollutant load, CO_2 emissions, non-hazardous waste, hazardous waste, and preservation of biodiversity, including trees and animals. This study further shows that the implementation of PROPER reduces the operational costs of SEGD.

1. INTRODUCTION

The presence of a company in an area can have both negative and positive impacts. Industry can boost the regional economy by creating jobs for various skill levels, thereby increasing the employment rate and income level of the local community over the long term (Samsul et al., 2018). However, industry presence in a region can also pose challenges alongside their role in driving economic growth. From resource extraction and production processes to waste generation and emissions, every stage of industrial processes has the potential to generate environmental impacts, including on water, soil, and air. This impact is generally caused by waste produced, and its form can be liquid, gas, or particulate. Improper waste management can degrade environmental quality and have widespread impacts on humans, animals, and plants. For example, the discharge of industrial wastewater that is not adequately treated directly into water bodies can pollute the water and disrupt the aquatic ecosystem, making the water unsuitable for aquatic biota to live. Moreover, in the short term, exposure to polluted water can cause various human health problems, including skin irritation and diarrhea (Shultana & Khan, 2022). Some pollutants can accumulate in the human body over time, and in the long term, this will result in more severe health problems.

Therefore, effective environmental management is crucial to preserve natural functions and minimize potential environmental impacts. When a company implements environmental management strategies, it sets a series of practices and policies to prevent and reduce its environmental footprint. These strategies typically include

minimizing resource consumption, reducing waste generation, optimizing energy efficiency, and mitigating pollution emissions. Companies can significantly improve their environmental performance metrics by adhering to environmental regulations and adopting best practices (Nugrahani & Handono, 2023). Moreover, environmental management practices in companies are driven by standardization, regulations, and programs regarding environmental management. The Ministry of Environment and Forestry initiated a system to encourage corporate environmental management practices, namely the Company Performance Rating Assessment Program in Environmental Management (PROPER), as a public disclosure program for environmental compliance.

PROPER is an evaluation of company performance in environmental management by assessing compliance with applicable environmental regulations. PROPER's existence is hoped to increase business actors' awareness of complying with laws and regulations. Then, after this awareness is formed, the company is expected to improve its performance in managing and preserving the environment. Under PROPER, companies are categorized into five-color tiers based on their environmental performance: gold, green, blue, red, and black. The program evaluates companies' compliance with environmental regulations, as well as its further initiatives to improve their overall environmental performance (MoEF, 2021).

On the other hand, adopting PROPER also aims to promote diverse innovations within companies' production processes. A company's dedication to environmental stewardship may stimulate the development and implementation of novel innovations to reduce potential environmental impacts. These innovations often focus on optimizing resource utilization, which helps minimize raw material consumption and waste generation. This integrated approach improves environmental sustainability and highlights the economic benefits of responsible environmental management from upstream to downstream. For example, implementing new initiatives on waste management not only reduces the amount of waste generated by the company but also creates cost efficiencies related to the disposal of this waste (Wahyudianto & Boedisantoso, 2018).

One of the companies actively involved in the PROPER implementation is Star Energy Geothermal Darajat II, Limited (SEGD). SEGD operates a geothermal field that spans Garut Regency and Bandung Regency in West Java. The location of SEGD's wells falls within Natural Recretion Parks, Nature Reserves, Protection Forests, and residential areas. Specializing in geothermal power plant operations, SEGD has an installed power generation capacity of 274.5 MW, which is integrated into the Java-Madura-Bali (JAMALI) interconnection system. Through its active participation in PROPER, SEGD consistently aims to improve its environmental performance. The company's commitment to environmental management is highlighted by its achievement of the gold PROPER award in 2022-2023, the highest recognition in the program. This study aims to analyze the influence of PROPER implementation on SEGD's environmental performance and operational cost efficiency.

2. METHOD

The method used in this research is descriptive with a quantitative approach. In this method, variables are described as they are, supported by data in the form of numbers generated from the actual situation. The data obtained will be summarized and analyzed to provide a clear and detailed picture of the data that has been collected as it is (Sudirman et al., 2020). This research was conducted using secondary data in the form of PROPER implementation data at the Company in the 2022-2023 period obtained from reports or documents with the company's permission. Literature was also used to support this research, including regulations, publications, and papers related to the topic under study.

3. RESULT AND DISCUSSION

According to Putri (2018), the company's compliance assessment is based on fulfilling environmental documents, reporting requirements, and compliance with required environmental management. Apart from its activities having to fall under environmental management documents, the company must also report all environmental monitoring and management activities carried out to fulfill this criterion. Environmental management in question includes water pollution control, air pollution control, hazardous waste management, and non-hazardous waste management. After a company is temporarily declared to have fully complied with environmental regulations, the assessment will continue against criteria beyond compliance. The beyond compliance criteria look at the company's commitment to managing the environment beyond regulatory compliance. This includes integrating environmental management system practices, in a form of Life Cycle Assessment (LCA), energy efficiency, emission reduction, reduce, reuse, and recycle of hazardous waste and non hazardous waste, water and water pollution load reduction. Moreover, the company also has to integrate biodiversity protection, community development, and social innovation in the company's environmental management efforts (MoEF, 2021).

Beyond Compliance, in the context of PROPER, refers to companies not only meeting the minimum standards set by environmental regulations and laws but also proactively adopting practices that surpass these legal requirements. This demands a commitment to positively impacting the environment beyond mere regulatory

obligations. When a company seeks to exceed compliance standards, it can generate a broader and more positive environmental impact. During the 2022-2023 PROPER assessment period, SEGD implemented various eco-innovation programs across its operational activities as part of its commitment to improve their environmental performance. These initiatives included enhancing energy efficiency, reducing emissions, and implementing strategies for the reduction, reuse, and recycling of both hazardous and non-hazardous waste. Additionally, SEGD focused on reducing water consumption and water pollution loads as part of its comprehensive approach to environmental protection.

3.1 Energy Efficiency

Over time, production wells or steam supplies at geothermal power plant facilities often experience a decline in production. These issues arise due to various factors, such as blockages in drilling channels or accumulation of mineral deposits. To improve production, maintenance and repairs need to be carried out regularly, including cleaning the well and removing blockages. This ensures tha the quantity of steam flow will return to normal levels. Previously, was typically addressed by checking and repairing the well using acid and water. However, in 2022, SEGD initiated an innovative application aimed at enhancing steam production called "ANTI GUSUR BUMI."

Initially, geothermal wells experiencing decreased production are thoroughly evaluated. The condition of each production well is assessed and analyzed by the technical team. This assessment includes visual inspections, measurement of operational parameters, and analysis of production data before and after the production decline, aiming to pinpoint the root causes of the issues. If the main cause is identified as blockage or mineral deposits accumulation, cleaning the well becomes necessary. ANTI GUSUR BUMI addresses this by changing the wellhead pressure through repeated open-close cycles.

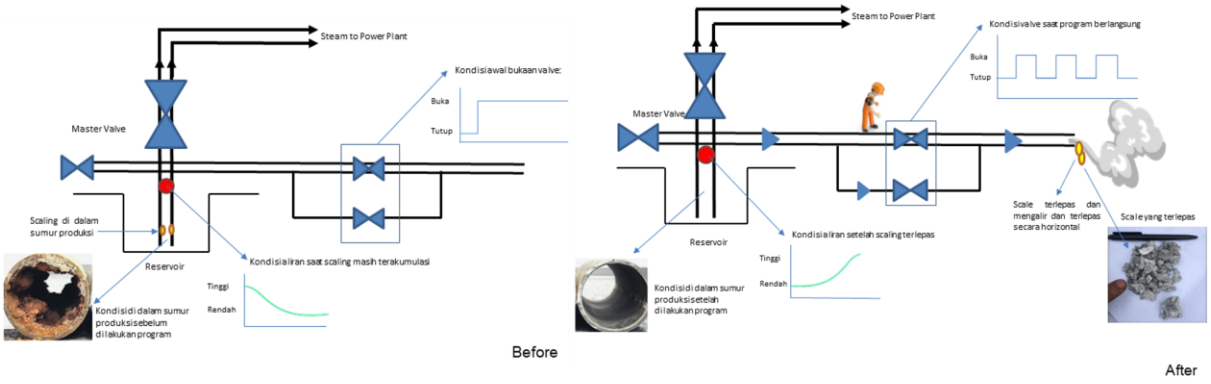

Figure 1: Scheme of ANTI GUSUR BUMI program.

This method was first implemented in Indonesia's geothermal energy sector by SEGD. From January 2022 to June 2023, this method was successfully applied to one of SEGD's production wells. This innovation successfully re-optimized the steam production rate of the DRJ-37 production well, increasing it from 14.5 kg/s to 19.9 kg/s and consequently, steam reserves from the well increased in absolute terms by 5.4 kg/s or equivalent to 3.2 MWe /well. Additionally, through the use of this innovation, SEGD achieved savings equivalent to the potential fuel use required for drilling one well, totaling 1,747 GJ per well. The implementation of this method enabled the company to achieve an energy efficiency of 34,266.71 GJ, equivalent to a cost efficiency of IDR 10,642,190,026.

3.2 Emission Reduction

In 2022, SEGD launched the SIAP TEMPUR innovation program aimed at resolving the issue of declining steam production in geothermal wells. This decline is primarily caused by scale buildup in the production well pipes, which reduces the steam supply needed to rotate turbines. Without proper cleaning and maintenance, this problem worsens, with steam production decreasing by 8% annually in geothermal facilities, potentially leading to daily generation losses of US$ 21,289.

Previously, high-pressure fluids were used with the Coiled Tubing Unit (CTU) to address this issue. However, this method involved lengthy preparation processes, including equipment mobilization and demobilization. Moreover, this method posed risks to the integrity of the well pipe casing. Apart from that, several significant health and safety hazards could potentially arise, such as exposure to toxic hydrogen sulfide gas, falling from heights, and exposure to condensate spills.

The SIAP TEMPUR program utilizes a descaling system employing an internally developed grinding tool pulled upwards through a wireline intervention technique, using mechanical force in a hammering action to remove scale. By implementing this program, SEGD optimizes steam production rates and increases steam reserves using simpler and more cost-effective equipment compared to traditional methods. SEGD leads this innovation in

Indonesia's geothermal energy sector, achieving an additional steam production of 21,518.04 MWh annually and reducing emissions by 18,720.69 tons of CO_2e, resulting in cost savings equivalent to IDR 23,653,216,826.

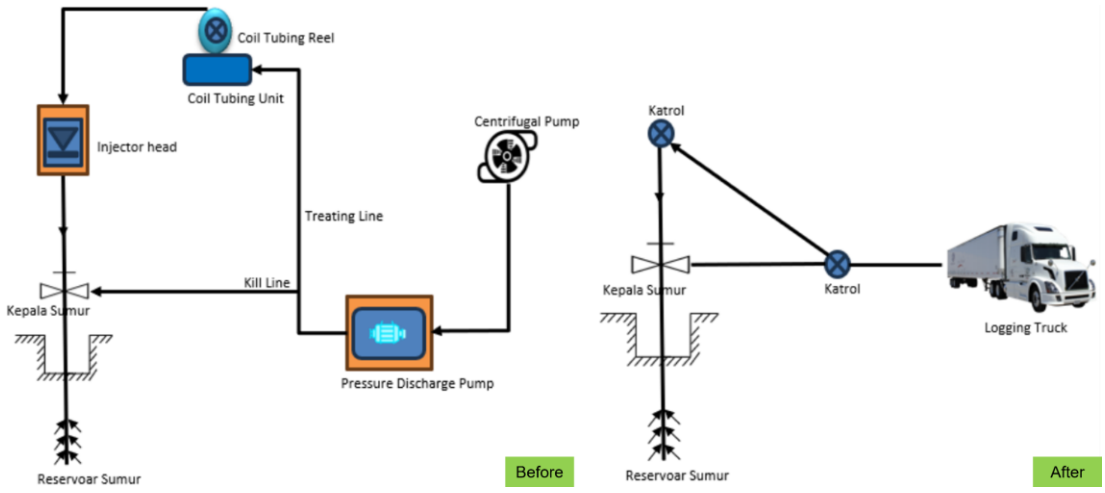

Figure 2: Scheme of SIAP TEMPUR program.

3.3 Reduce, Reuse, and Recycle of Hazardous Waste

To clean machine equipment, chemical cleaning products containing hazardous substances like grease and rust cleaners are often utilized. However, continuous use of these products contributes to an increase in hazardous waste and contaminated materials generation, including packaging, cleaning residues, and oil contaminated rag. Manual cleaning with these chemicals is suboptimal and time-consuming. Furthermore, their use increases the need for personal protective equipment for worker since the exposure to hazardous substances is higher.

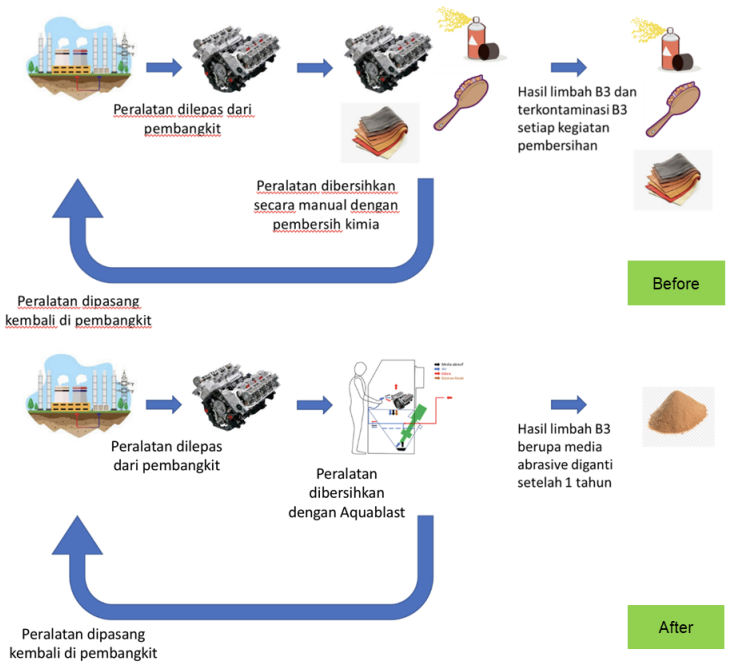

Figure 3: Scheme of PERAK LOGAM AMAN program.

In 2022, SEGD introduced an innovative approach called PERAK LOGAM AMAN for cleaning machine equipment and components using water-based solutions and abrasive materials. This pioneering method is the first of its kind in Indonesia's geothermal energy sector. The machine operates by combining compressed air with closed circulating water and abrasive materials. Using this system significantly reduces cleaning time by up to 14 hours per job. Moreover, it ensures effective equipment cleaning, enhancing reliability and preventing potential Lost Production Opportunity (LPO) losses totaling 20,800 per year. This method has proven effective in reducing hazardous waste generation by 0.575 tons, equivalent to cost savings to IDR 300,105,934.

3.4 Reduce, Reuse, and Recycle of Non-Hazardous Waste

In 2022, there was an upward trend in coffee consumption trends in Darajat, SEGD's operational area, leading to an increase in coffee residue generated by local cafes. Improper management of this waste can potentially clog waste channels and degrade wastewater quality. However, with appropriate processing, coffee residue waste can be turned into a valuable resource. Recognizing this opportunity, SEGD developed the PENIPU SUHU innovation program to repurpose non-hazardous waste, specifically coffee residue, for community benefit.

Figure 4: Scheme of PENIPU SUHU program.

Under the PENIPU SUHU program, coffee residue waste from SEGD's operational area is processed into a substrate supplement for maintaining Black Soldier Fly Larvae (BSFL). To enhance its nutrient content, the coffee residue undergoes fermentation to degrade phenolic compounds. Once its completely fermented, the coffee residue is added to containers where BSFL grow. This method has proven to accelerate BSF growth by only 10 days compared to conventional methods using fruit or vegetable waste. Through this initiative, the program successfully reduced non-hazardous waste generation by 0.81 tons, achieving a total cost efficiency of IDR 73,631,348.

3.5 Efficiency and Water Pollution Load Reduction

SEGD initiated the SIRSAK program to prevent drilling stuck by utilizing condensate water as a drilling fluid. Prior to this program, surface water from around the drilling site was used. However, drilling stuck often still occurs because the quality and availability of surface water were inconsistent and can not be guaranteed, leading to frequent drilling issues and increased costs. In response, SEGD introduced the innovative approach of utilizing condensate water flow as a drilling fluid. This switch ensures drilling operations remain uninterrupted because the fluid parameters can be closely monitored, maintaining quality consistently. Consequently, drilling schedules are adhered to and costs are controlled as planned. Through this program, SEGD has reduced water usage by 446,267.57 m^3, resulting in cost savings equivalent to IDR 10,932,216,697.

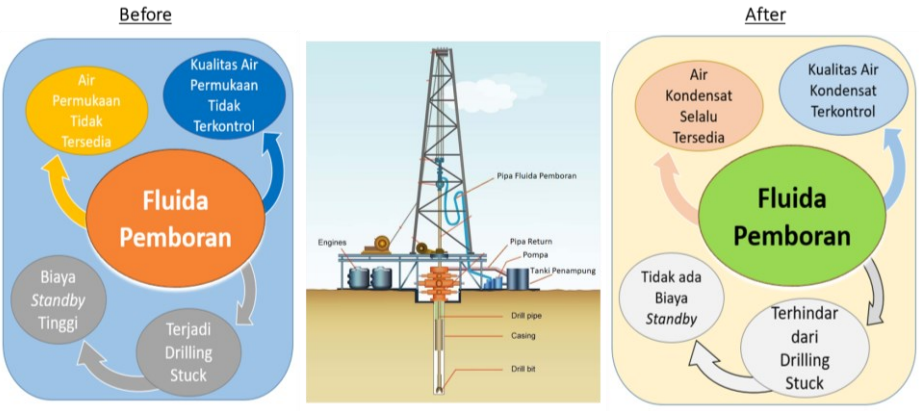

Figure 5: Scheme of SIRSAK program.

3.6 Biodiversity Protection

The Cikupakan area, situated within a river basin, faces erosion risks due to high river flows. The Darajat geothermal field is located in the Protected Forest area and the Mount Papandayan Nature Recreation Park. Within the Darajat Protected Forest, there is a noticable absence of hardwood trees, dominated instead by annual plants harvested every three months. This absence of hardwood trees in areas like Cigupakan, Well Pad S4, and Well Pad 18 results in insufficient canopy cover to mitigate the impact of rainwater on the soil. Additionally, the absence of varied plant species with soil-binding root systems and the lack of barriers contribute to soil erosion and increase the risk of landslides. Previous planting programs in the Darajat geothermal fields had low success rates because extensive annual plantations require sufficient sunlight, often disturbing and displacing newly planted vegetation.

In 2022, SEGD initiated the ASEP RESTO program, which builds upon previous efforts in planting on critical and conservation lands. Earlier plantings focused solely on endemic species found in the Darajat geothermal field area. However, the challenge with endemic plants lies in their slow growth rate, extending their vulnerable period and necessitating ongoing monitoring. To address this, the program integrates fast-growing plants like the Alder trees alongside endemic species. These endemic plants are planted alternately with fast-growing plants. Before the program, SEGD's planting efforts had a low success rate, with only about 25% of plants surviving. Hardwood plants, due to their slow growth, reached heights of 3-4 meters since planting in 2019, but recent plantings in 2021 saw minimal height increases of 5-10 cm due to low canopy cover around 10%.

Figure 5: Before and after the implementation of ASEP RESTO program.

Post-program implementation, the success rate rise up to 80%, achieving a 40% canopy cover. By using this method, the vegetation planted are more disease resistant and their growth is more sustainable. Notably, Alder trees saw a height increase, with seedlings growing from an average of 30 cm at planting to 2-3 meters within a year—a growth up to 1000%. This initiative also increase urban sustainability by contributing 0.6% of the required Green Open Space (RTH), filling a deficit of 613 hectares in Garut Regency. Furthermore, this program led to increase in the biodiversity index to 1.6118 H'Shannon-Wiener and the planting of 9,334 trees by 2023. This innovation has successfully contributed to improvements such as a potential reduction of 5,600 tons of CO_2 emissions and conservation of 162,692 m^3 of water.

3.6 Community Development

In Garut, flash floods often occur, and one of the factors causing this is the degradation of the upstream Cimanuk watershed area. The conversion of forest land that occurs reduces the soil's ability to absorb rainwater, thus causing erosion and flooding in the area. To overcome these challenges, SEGD introduced the Insan Smart initiative (Inovasi Sahabat Hutan Sinergi Menjaga Alam Darajat), which integrates environmental conservation with community economic interests. This initiative focuses on sustainable forest management involving local communities within SEGD's operational area. The goal is to improve the quality of the upstream forest in the Cimanuk watershed while enhancing community welfare.

Under Insan Smart, vulnerable groups, previously engaged in illegal land clearing for plantation within conservation area and wildlife hunting, have been transformed into conservation agents. They now actively participate in planting, maintaining, and patrolling forest areas. Additionally, to boost community income, these agents are involved in beekeeping activities for honey production in SEGD's forested areas. This economic incentive motivates the community to protect the Cimanuk watershed forest further more, showing a symbiotic relationship between sustainable forest management and community prosperity.

Figure 6: Community's active participation in Insan Smart program.

Previously, from 2016 to 2018, the community played a passive role in SEGD's conservation efforts, resulting in low tree survival rates. However, since the Insan Smart initiative launched in 2020, the community's role has evolved into proactive participation across all program stages, increasing tree survival rates to over 90%. This high survival rate not only indicates the success of community engagement but also correlates with increased carbon sequestration, erosion control, and water infiltration. The utilization of forest land for honey cultivation has provided alternative economic opportunities, reducing the need for illegal land clearing and hunting in the Darajat Forest area.

As of July 2023, the KTH Madu Darajat Berkah's average income is projected to reach IDR 22,100,000 for the year. Insan Smart strengthens community relationship with conservation targets, resulting in a greater responsibility and commitment awareness to environmental preservation and natural resource management. This innovation promotes social and economic development by offering sustainable livelihoods through environmentally-friendly economic activities, such as honey production and sustainable forest product harvesting. Moreover, the Madani Wangi program have an impact on the environment in the form of additional carbon reserves of 2,464.32 kg, potential water captured of 58.65 m^3, nutrient loss control of 150.18 kg, and CO_2 absorption of 7,290.3 tons/year.

By integrating environmental management programs and considerations into its core business strategy, SEGD effectively mitigates environmental risks. This approach not only increases operational efficiency and decreases costs but also strengthens relationships with local communities in its operational areas. Prioritizing environmental conservation and participating in initiatives like PROPER enables companies to contribute to sustainable development goals and ensure long-term environmental sustainability.

Table 1: Absolute value and cost efficiency from the implementation of eco-innovation programs.

Criteria	Absolute Value	Unit	Cost Efficiency
Energy Efficiency	34,266.71	GJ	Rp10,642,190.03
Emission Reduction	18,720.69	ton CO_2eq	Rp23,653,216.83
Reduse, Reuse, and Recycle of Hazardous Waste	0.58	ton	Rp300,105,934.00
Reduse, Reuse, and Recycle of Non-Hazardous Waste	0.81	ton	Rp73,631,348
Water and Water Pollution Load Reduction	446,267.57	m^3	Rp10,932,216,697
Biodiversity Protection	1.61	H'Shannon-Wiener	
	9,334.00	tree	
	31.00	species	
	2.97	Ha	
	5,600.00	ton CO_2	
	162,692.00	m^3	
Total			**Rp11,340,249,385.85**

In 2023, SEGD implemented environmental management innovations through PROPER, resulting in reductions across various metrics such as energy consumption, water use, water pollutant loads, CO_2 emissions, non-hazardous waste, hazardous waste, and preservation of biodiversity, including trees and wildlife. These efforts not only showcase SEGD's commitment to exceeding compliance standards but also led to substantial cost savings amounting to IDR 11,340,249,385.85. As a result of these achievements, SEGD earned the highest rating— the gold award—indicating its excellence for environmental performance and compliance to environmental regulations.

4. CONCLUSION

This study shows that the implementation of PROPER in SEGD positively influences the company's environmental performance, resulting in reductions of 34,266.71 GJ in energy use, 18,720.69 tons of CO_2eq emissions, 466,267.57 m^3 in water consumption, 0.575 tons of hazardous waste, 0.81 tons of non-hazardous waste, and preservation of biodiversity, including increase in the biodiversity index to 1.6118 H'Shannon-Wiener, planting of 9,334 trees, penyediaan ruang terbuka hijau seluas 613 Ha, serta potential reduction of 5,600 tons of CO_2 emissions and conservation of 162,692 m^3 of water. This study further shows that the implementation of PROPER in SEGD reduces the operational costs by IDR 11,340,249,385.85.

REFERENCES

Ministry of Environmental and Forestry (MoEF).: Peraturan Menteri Lingkungan Hidup dan Kehutanan Republik Indonesia Nomor 1 Tahun 2021 tentang *Program Penilaian Peringkat Kinerja Perusahaan dalam Pengelolaan Lingkungan Hidup*, (2021).

Nugrahani, T. S. and Handono, W. S.: Determinants of Firm Value: The Role of Environmental Disclosure Practices, *Proceeding of International Conference on Accounting and Finance*, **1**, (2023), 230-240.

Putri, B. A. N.: *Penerapan PROPER (Program Penilaian Peringkat Kinerja Perusahaan dalam Pengelolaan Lingkungan Hidup) dalam Kinerja Lingkungan di PLTGU Tanjung Batu*, Universitas Brawijaya, Malang (2018).

Samsul, Budiman, A. A., and Anshariah: Analisis Dampak Positif Industri Terhadap Masyarakat, *Jurnal Geomine*, **6**, (2018), 54-59.

Shultana, S., and Khan, R. A.: Water QUality Assessment, Reasons of River Water Pollution, Impact on Human Health and Remediation of Polluted River Water, *GSC Advanced Research and Reviews*, **10**, (2022), 107-115.

Sudirman, Kondolayuk, M. L., Sriwahyuningrum, A., Cahaya, I. M. E., Astuti, N. L. S., Setiawan, J., Tandirerung, W. Y., Rahmi, S., Nusantari, D. O., Indrawati, F., Fittriya, N. L., Aziza, N., Kurniawati, N., Wardhana, A., and Hasanah, T.: *Metodologi Penelitian 1: Deskriptif Kuantitatif* in Metodologi Penelitian 1, CV. Media Sains Indonesia, Bandung (2020).

Wahyudianto, F. E., and Boedisantoso, R.: Penerapan PROPER sebagai Alat Pemicu Inovasi Teknologi Industri Berkelajutan, *IPTEK Journal of Proceedings Series*, **2**, (2018), 59-64.

Gender Action Plan: An Approach to Mitigate Risks and Impacts of Geothermal Projects

Maya Ryandita[1], Desak Nyoman Inten Apriani[1], Afandi[1], Eviyanti[1], Astri Indra Mustika[1,2], Dorman Purba[1,2], and Ferdino R Fadhillah[1,2]

[1]PT Sarana Multi Infrastruktur (Persero), Sahid Sudirman Center 49th floor, Jakarta, Indonesia
[2]ENERKA Bhumi Pratama, Cibis Park, Jakarta, Indonesia

maya.pmugeothermal@ptsmi.co.id

Keywords: gender action plan, gender and geothermal energy, social impacts and risks, safeguard instruments

ABSTRACT

Geothermal projects in Indonesia have been pivotal in advancing sustainable energy goals. However, these projects can pose significant risks and adverse impacts on local communities, particularly on women. Issues such as gender inequality in employment, health and safety concerns, displacement and loss of livelihoods, social and cultural impacts, and limited participation in decision-making are among those affecting women, who play crucial roles in their communities. If these issues are not addressed, the long-term success and acceptance of geothermal energy projects will be difficult to achieve. Drawing on existing literature, this paper provides a comprehensive overview of the various impacts of geothermal projects in Indonesia using a gender lens. This paper highlights the significance to identify and reduce gender gaps and risks of geothermal projects, through the development of a Gender Action Plan (GAP). This paper suggests developers to develop and implement GAP as a strategy to mitigate the risks of geothermal projects. It explores how preparation and implementation of GAP, which has become one of funding proposal requirements for the Geothermal Resource Risk Mitigation Program (GREM), could be potential to promote gender equity and better manage the risks of the projects. It examines GAP as a roadmap to address the gender issues by planning and implementing gender-informed health and safety procedures, gender-sensitive community engagement, inclusive employment practices, and fair compensation and resettlement policies, with a focus on restoring livelihoods for women. Based on good practices and lesson learned, it introduce steps to develop GAP so that it could effectively reduce gender gaps and mitigate the risks of geothermal project, which is essential for promoting gender equity and ensuring the sustainability of geothermal energy initiatives.

1. INTRODUCTION

1.1 Indonesia Geothermal Utilization

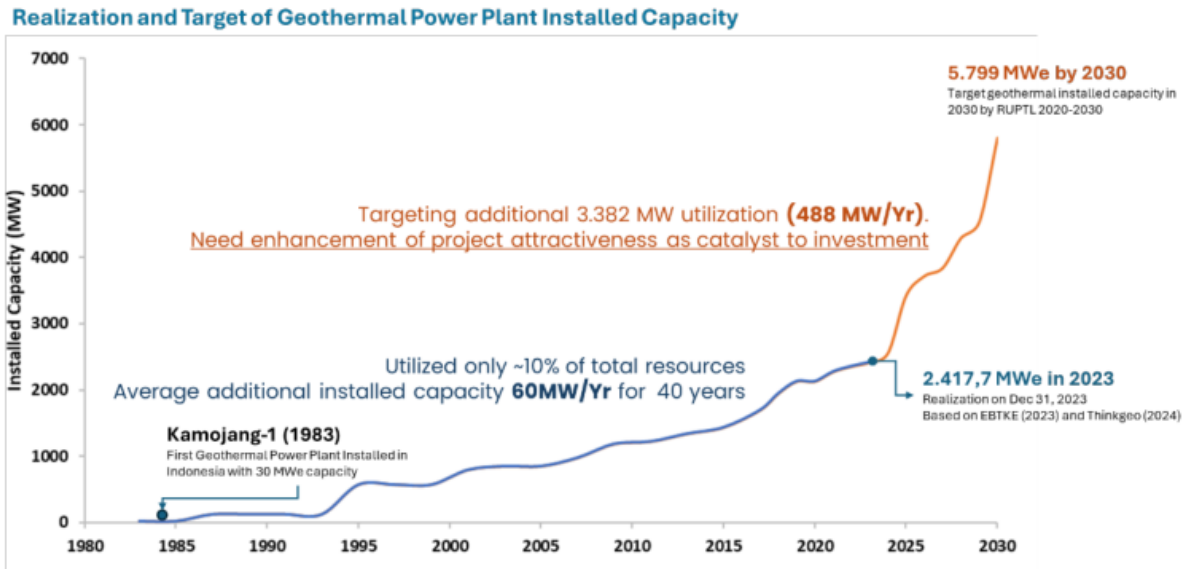

Figure 1: The utilized and target for Indonesia installed geothermal power plant.

Indonesia possesses vast potential for untapped renewable energy sources, including geothermal, wind, hydro, biomass, and solar. Renewable energy provides a local and reliable energy supply, with demand expected to rise in the future. The country has a firm plan to accelerate the utilization of renewable energy as the primary source

to support energy growth and achieve its net zero carbon emissions target (IRENA, 2022). Geothermal energy, as a form of green energy, is a critical component of Indonesia's strategy to achieve 23% renewable energy by 2025 and an additional 21% of renewable power generation by 2030.

Indonesia ranks second globally in geothermal capacity, with 2,417 MW installed out of an estimated 23 GW total potential. This means the country has utilized only about 10% of its total potential, with an average annual capacity increase of around 60 MW from first commercial geothermal power plan in Kamojang operated in 1983. The current state of geothermal development presents significant challenges to meeting the government's targets by 2030. To expedite geothermal development, it is essential to promote exploration activities and address associated risks to enhance investment attractiveness.

1.2 Exploration Risk, Indonesia De-Risking Facility, and Gender Requirements

The primary objective of an exploration program is to identify and characterize geothermal resources that can be economically developed using an appropriate plan of development based on the exploration results.During the exploration stages, geothermal developers and investors frequently face dilemmas when making investment decisions. This is because they must invest significant upfront capital while relying on limited and uncertain information about the geothermal resource potential.

Cost-wise, drilling activities and the construction of supporting infrastructure, such as access roads and well pads, represent the most significant expenses in an exploration project. The main challenges of geothermal exploration in Indonesia can be summarized as follows (IGA, 2014; Poernomo, 2015; Darma S. , 2016; Umam, Adityatama, & Purba, 2018; Siahaan, Purba, Septiani, & Paripurna, 2023):

1. Difficulty in locating the "hottest area": Geothermal resources could not directly be manifested at the surface, necessitating detailed geological, geochemical, and geophysical (3G) surveys and test well drilling. The lack of clear surface indications or thermal manifestations can make it challenging to identify the most promising areas for exploration, leading to an increased risk of drilling dry wells.
2. High exploration costs: The expenses for 3G surveys, developing a reliable conceptual model, and drilling test wells can be substantial. There is always a risk that geothermal projects may not yield viable resources, making it challenging for developers to secure funding for exploration activities due to the high upfront capital and uncertainties involved.
3. Complex geology: Geothermal resources in Indonesia are mainly located in a volcanic area with complex geological environments, making it difficult to understand the subsurface conditions and identify the most promising areas for exploration.
4. Lack of direct and reliable data: In some cases, there may be a need for more data on the geology and geochemistry of an area, making it challenging to identify potential resources and plan the exploration activities.
5. Environmental impacts: Exploration activities can have various environmental impacts, such as air and surface water pollution, soil degradation, hazardous noise, release of hazardous gases, landslides, deforestation, and the potential for groundwater contamination. Mitigating these impacts can be costly and time-consuming.
6. Social and community impacts: Exploration activities can also have social and community impacts, such as displacement of local communities and land-use conflicts. Developers need to address these impacts and engage with local communities to ensure their support and minimize the risk of project delays or cancellations.
7. Uncertain regulations: Geothermal exploration is subject to various national, regional, and local regulations. The uncertainty can make it difficult for developers to navigate the regulatory environment and can increase the risk of project delays or cancellations.

A geothermal exploration de-risking scheme is a strategic approach designed to mitigate the financial risks inherent in geothermal exploration projects. The primary objective of this scheme is to create efficient exploration programs that enhance the success ratio of exploration (Siahaan, Septiani, Purba, & Paripurna, 2023). ESMAP (2016) and Nur (2023) emphasize the significance of exploration de-risking programs as critical pathways to accelerate and enhance the development and utilization of geothermal resources.

Geothermal Resource Risk Mitigation (GREM) is a de-risking facility for geothermal exploration projects developed by PT Sarana Multi Infrastruktur (SMI) and the World Bank. The main objective of this facility is to accelerate geothermal development investment in Indonesia by providing financing for upstream resource development, particularly exploration and delineation drilling, which are crucial for resource confirmation. The facility offers geothermal developers, who have already obtained working areas and performed preliminary surveys, a debt package for exploration and delineation drilling (Apriani, Amorini, Suseno, & Purba, 2023; PT SMI, 2021).

This is critical because commercial debt and financing facilities are often reluctant to fund exploration drilling due to the high uncertainty and risk involved. In contrast, GREM provides support by funding exploration drilling to confirm the presence of a sufficient productive steam resource for power generation. If the resource is confirmed to be sufficient, the developer can proceed with the project using commercial project finance for exploitation drilling and power plant development. This process increases the confidence of other financing institutions, encouraging them to fund the subsequent development stages of the pertinent Working Area (Apriani, Amorini, Suseno, & Purba, 2023). Since the facility is developed in collaboration with the World Bank, the requirements for safeguard instruments must adhere to World Bank standards, including the Gender Action Plan (GAP).

The World Bank recognizes that geothermal projects need strategies that address social issues, including gender disparities, and that overlooking gender gaps can jeopardize the projects' effectiveness, efficiency, and sustainability. Thus, in implementing GREM, it is expected that geothermal projects seek to integrate gender-responsive designs by: i) including gender perspectives in geothermal workplace health and safety standards, ii) increasing the employment of women in technical roles, and iii) facilitating plans to reduce gender gaps in activities funded under GREM (The World Bank, 2019). This involves a thorough analysis of various aspects of gender gaps and the consideration of targeted interventions outlined in a gender action plan, developed and implemented by the developers, with supervision by PT SMI.

1.3 Research Objectives and Methodology

Using a gender perspective, this paper aims to explore how developing and implementing a Gender Action Plan (GAP) can help developers better manage project risks and improve development outcomes, leading to a more sustainable project path. It is argued that GAP can be a practical approach to reduce gender gaps, mitigate risks, and improve the development outcomes of geothermal projects. This research is based on a literature review that examined reports, publications, research articles, and guidelines on gender aspects in geothermal exploration projects and relevant regulations. It addresses the following question:

1. What are the potential gender risks of geothermal projects in Indonesia?
2. How can GAP support the project to mitigate the gender risks and impacts of geothermal projects?
3. What are the challenges and lesson learned in developing GAP?

The paper is structured as follows: section 2 will explain the significance of a gender perspective and gender action plan in the geothermal context; section 3 will discuss the risks of geothermal projects associated with three major pathways of impact: (i) changes in land and natural resource use, (ii) changes in employment and economic patterns, and (iii) changes to the environment and health; section 4 will explore how to mitigate these risks through GAP; section 5 will describe the challenges and lessons learned in developing GAP. The paper will conclude with suggestions on how developers can effectively develop and implement GAP to reduce gender gaps, mitigate risks, and improve development outcomes.

2. UTILIZING A GENDER LENS: WHY IT MATTERS

2.1 Gender perspective in geothermal energy context

Gender, as defined by UN Women (n.d.), refers to the roles, behaviors, activities, and attributes that a society considers appropriate for men and women at a given time. It encompasses the social attributes and opportunities linked to being male or female, the relationships between men and women, and the relationships among women and among men. These characteristics, opportunities, and relationships are socially constructed and learned through socialization processes. They are specific to context and time, and they are changeable. Gender dictates what is expected, allowed, and valued in a man or woman in a given context. In most societies, there are differences and inequalities between men and women in terms of responsibilities, activities, access to and control over resources, and decision-making opportunities. Gender is part of a broader socio-cultural context, which also includes factors such as class, race, poverty level, ethnic group, sexual orientation, disability, and age (UN Women, n.d.).

Adopting a gender perspective means recognizing and addressing the different needs, experiences, and challenges faced by men and women. It involves integrating gender considerations into policies and practices to promote equality and ensure that both genders benefit equally from development initiatives (UN Women, n.d.). Like other renewable energy projects, while geothermal energy projects have the potential for broad and far reaching benefits, they are found to be more effective when gender equality is taken into account (Rojas et al., 2011). For instance, in cases where a project involves community resettlement, local social norms may unfairly disadvantage women during compensation procedures. Moreover, sociocultural norms or legal constraints within a country may deter women from pursuing employment in the geothermal sector, potentially resulting in resistance that undermines broader development outcomes, such as sustainable economic growth and poverty alleviation (ESMAP, 2019).

Furthermore, using a gender perspective can advocate for collecting sex-disaggregated data and implementing monitoring and evaluation (M&E) processes that specifically address gender disparities. The geothermal sector currently lacks comprehensive collection and analysis of sex-disaggregated data concerning the socioeconomic, environmental, and health risks associated with projects, as well as access to project benefits (Schomer, 2019). Without systematic collection and analysis of data disaggregated bysex and demographic factors, there is a risk that geothermal project designs may neglect the need for targeted interventions tailored to the specific requirements of men and women. This oversight could hinder the project's ability to achieve its development goals (Schomer, 2019). For example, at the community level, sex-disaggregated data are crucial for areas such as compensation distribution, outcomes of livelihood restoration efforts, and reported grievances, including insights gathered from community consultations that involve women. At the industry level, such data are essential for understanding workforce demographics, wage disparities, and job satisfaction levels (ESMAP, 2019).

By applying a gender lens, it becomes evident that the geothermal sector is traditionally male-dominated, with men holding the majority of technical and leadership roles (ESMAP, 2019). While new investments in geothermal infrastructure create new employment opportunities, experience shows that increases in labor force participation typically occur first among men, compared to women. In the Indonesian context, nationwide data from the Geothermal Resources Directorate (MEMR) shows that, from a survey of the 12 leading developers in the sector, the total number of employees is 1,408. Of these, only 202 are female, making up about 14 percent of the workforce. The majority of these women (over 70 percent) are in administrative and support roles rather than managerial or technical positions. At the site level, the number of women in technical and managerial roles is even lower, with just 15 women in such positions across all 12 companies surveyed by MEMR.

The gender disparity can be attributed to various factors, including historical biases, educational barriers, and workplace cultures that may not be conducive to gender equality (ILO, 2019). Based on focus group discussions with recent female geosciences graduates, inadequate accommodation and bathroom facilities at certain sites discourage women from pursuing field-based work, including those who have yet to take on domestic responsibilities at home (World Bank, 2019). Moreover, given the remote locations of most geothermal resource areas, educated women with degrees in relevant fields face significant barriers to entering higher-level professional positions such as geologist and engineer. These roles often require spending extended periods in the field on a fly-in, fly-out basis, which poses a challenge for women who are also likely balancing domestic care responsibilities for young children or the elderly. Although there is little discrimination, many women choose to opt out for this reason. Another key reason these jobs are predominantly held by men is the relatively low proportion of women in remote areas who have access to the education needed to meet the minimum qualifications.

Additionally, neglecting gender concerns casts doubt on a company's commitment to sustainable development (Hill, C, Madden, C & Collins, N, 2017). Companies that overlook gender equality and women's rights risk violating human rights, including the principles outlined in the Convention on the Elimination of All Forms of Discrimination Against Women (CEDAW) and may disregard the importance of adhering to government regulations on gender mainstreaming throughout all stages of development in Indonesia.

2.2 Gender-related regulations pertinent to geothermal projects in Indonesia

Indonesia lacks robust regulations addressing gender aspects in land and natural resource use, as well as environmental and health changes related to extractive industries. However, Indonesia has issued Presidential Instruction Number 9 of 2000, mandating gender mainstreaming at all stages of development, which requires gender analysis and the inclusion of women's perspectives in all sectors. Additionally, the government has made significant progress in developing gender regulations in the workplace. According to the Global Business Guide (in Sosa, 2019), Indonesia has a set of laws and sector-specific regulations that prohibit discrimination and promote equality. The most notable is the Labor Law (Manpower Act No.13 of 2003), which stipulates that everyone has the same opportunity to get a job without discrimination (Art. 5), and all workers have the right to equal treatment from their employer without discrimination based on sex, ethnicity, race, religion, skin color, or political orientation (Art. 6). The Labor Law also states that termination of employment is not allowed if it is based on ideology, religion, political inclination, ethnic group, race, social group, gender, physical condition, or marital status (Art. 153i). Additionally, the Labor Law (Manpower Act No.13 of 2003, Art. 86 and 87) includes provisions for occupational safety and health management, ensuring that every worker has the right to protection against safety and health hazards, immorality, and indecency, and is treated with respect for human dignity and religious values. The Manpower Act also covers annual, sick, maternity, and other types of leave that employers must provide. Below are the relevant Indonesian regulations concerning gender and other intersectional issues1:

- Presidential Instruction Number 9 of 2000 concerning Gender Mainstreaming
- National Strategy for Acceleration of Gender Mainstreaming in Planning and Gender-Responsive Budgeting 2012

- Law No. 7 of 1984 concerning the ratification of Convention on the Elimination of All Forms of Discrimination against Women/CEDAW.
- Law No. 8 of 2016 concerning Persons with Disabilities;
- Law No. 35 of 2014 on Amendments to Law No. 23 of 2002 on Child Protection
- Regulation of Ministry of Environment and Forestry no. 17/2012 on Guideline for Community Involvement in the Process of Environmental and Social Impact Analysis
- Regulation of Ministry of Home Affairs no. 52/2014 concerning Guidelines for Recognition and Protection of Indigenous People;
- Manpower Act No.13 of 2003: same opportunity to get a job without discrimination
- Manpower Act No.13 of 2003: the right to receive protection against safety and health hazards, protection against immorality and indecency, and treatment that shows respect to human dignity and religious values
- Manpower Act No.13 of 2003 regulates annual, sick, maternity, and other types of leave that must be offered by employers.

Without considering intersectionality, efforts to promote gender equality may be inadequate or could even worsen conditions for the most disadvantaged women. It is important to acknowledge and understand that different forms of discrimination—based on gender, age, race, class, disability, and sexuality—can interact to create social oppressions. This concept is crucial for gender equality as it highlights how overlapping forms of discrimination can intensify inequality (UNDP, 2023).

3. MITIGATING THE GENDER RISKS AND IMPACTS THROUGH GAP

3.1 The process of developing GAP

A GAP serves as a roadmap to promote gender equality in the design, implementation, operations and maintenance as well as monitoring and evaluation of projects. It is tailored to the project's intended outcomes and activities and is developed based on a gender analysis or assessment of the projects, including the gender impacts and risks (UN Women/ UNOPS, 2019; ESMAP, n.d.). It will serve as a critical guide for activities that protect, engage and empower women and socially-excluded groups in diverse roles including beneficiaries, workers, including construction and contract workers, advisors, managers, and political decision makers (UNDP, 2023). Generally, in developing the GAP, developers need to (UNDP, 2023):

- Involve both men and women.
- Seek tailored technical assistance (e.g., from gender advisers or specialists) to identify and addresses the specific needs of women and vulnerable groups through conducting gender analysis, trainings, and developing implementation manuals.
- Maintain regular stakeholder engagement and communication to ensure participatory decision-making throughout implementation processes. This includes conducting gender-sensitive trainings for men, involving women's organizations, local NGOs, and community-based organizations (CBOs), and making necessary adjustments to the GAP.
- Promote diversity and equality in the sector by increasing women's participation in the workforce, enhancing their employability, and addressing gender pay gaps where they exist.

Based on PT SMI's Gender Action Plan Manual (2024), the process of developing the GAP (Figure 2) broadly encompasses the following:

1. Analysis: This involves utilizing disaggregated data by sex, conducting gender assessments by applying gender analysis tools, and identifying gender gaps. This process begins during the project's preparation stage and continues throughout all phases of development activities, extending to post-implementation monitoring and evaluation (M&E) and reporting. During project design, the analysis aims to identify the specific needs, values, opportunities, and constraints experienced by men and women within the community affected by the project.
2. Actions: The GAP should outline actions or measures to address gender gaps identified through the analysis and the application of gender analysis tools.
3. Monitoring & Evaluation: Developers must regularly monitor, evaluate, improve, and report on the implementation of the GAP to PT SMI. The GAP should include SMART indicators to measure progress in closing gender gaps and achieving development outcomes.

3.2 Gender impacts and risks of geothermal projects

It has been noted in the growing literature that men and women can be affected differently by the risks posed by geothermal energy and other renewable energy projects (Nelson & Kuriakose, 2017; ESMAP, 2019). A publication by ESMAP (2019) discusses how these risks affect women differently than men in relation with three major pathways of impact:

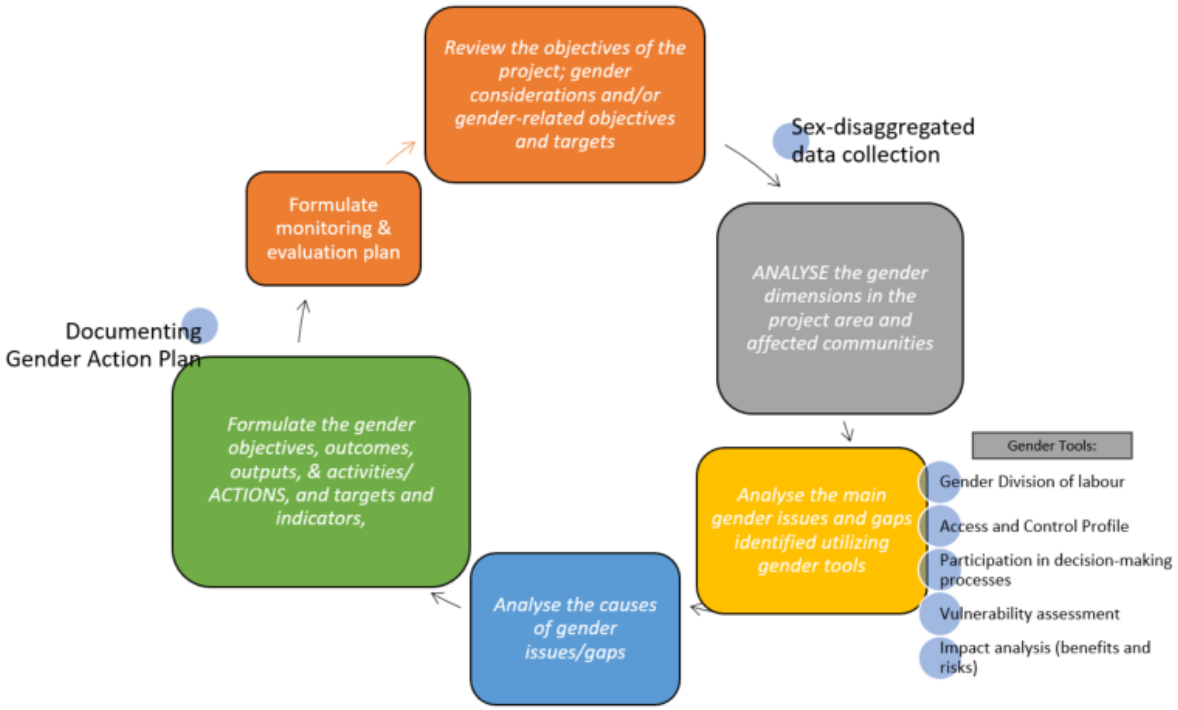

Figure 2: The stages of developing GAP.

3.2 1 Changes in Land and Natural Resource Use

- Decrease in Land Availability: The reduction in land available for small-scale agricultural activities and livestock grazing disproportionately affects women, who often rely on these resources for their families' livelihoods. In many communities, women play a critical role in food production and household nutrition. Limited access to land not only threatens their economic stability but also increases their vulnerability to poverty and food insecurity.
- Decrease in Water or Fuelwood Availability: Women are typically responsible for collecting water and fuelwood for their households. A decrease in the availability of these resources can result in women spending additional time and effort to gather them, which often comes at the expense of other productive activities. This increased burden can lead to physical exhaustion and diminished economic opportunities. Furthermore, the increased time spent collecting resources may expose women to risks, including gender-based violence, as they may have to travel longer distances alone.
- Limited Rights to Land Ownership: Despite constitutional guarantees of equality, many women face significant barriers to land ownership due to customary laws and practices. In regions where traditional norms prevail, women's rights to land are often subordinate to those of men, which limits their ability to secure a stable source of income or collateral for loans. This inequity can perpetuate a cycle of dependence and disadvantage, making it difficult for women to improve their economic standing in the face of geothermal development.

3.2.2 Changes to Employment and Economic Patterns

- Work Culture Limitations: The geothermal sector often has a work culture that can be unwelcoming to women. This environment may include implicit biases, a lack of supportive policies, and a predominantly male workforce, all of which can hinder women's engagement and retention in these jobs. As a result, women may feel isolated or undervalued, leading to higher turnover rates and fewer opportunities for career advancement.
- Intra-Household Bargaining and Power Dynamics: Women frequently face intra-household dynamics that limit their participation in the geothermal sector. Traditional gender roles often dictate that women bear the primary responsibility for domestic chores and caregiving, which can restrict their ability to pursue employment opportunities. Travel constraints, due to societal expectations or safety concerns, further exacerbate these barriers, making it difficult for women to engage in the workforce fully.
- Social Gender Norms and Expectations: Social norms often dictate the roles and behaviors expected of men and women, influencing women's access to employment in the geothermal sector. Women may be discouraged from pursuing technical or leadership roles due to these expectations, resulting in a workforce that lacks diversity and underrepresents female perspectives in decision-making processes.

- Lack of Professional Networks and Mentorship: The absence of established professional networks and mentors for women in the geothermal sector can create significant obstacles. Without access to guidance and support from experienced female professionals, women may struggle to navigate their careers, limiting their opportunities for advancement and professional growth.
- Unwelcoming Work Environment: A lack of supportive infrastructure, such as sanitary facilities and appropriate personal protective equipment (PPE) for women, can create a hostile work environment. Additionally, the absence of policies aimed at preventing harassment and gender-based violence can further deter women from entering or remaining in the workforce. This environment not only affects job satisfaction but also impacts women's health and safety at work.

3.2.3 Changes to the Environment and Health

- Sex-Specific Reproductive Health Issues: Geothermal projects can lead to environmental contamination that affects reproductive health differently for men and women. Men may experience sperm DNA fragmentation due to exposure to pollutants, potentially impacting fertility. Women, on the other hand, may face serious risks during pregnancy, such asintrauterine growth restriction, which can result from contaminated air and water. These health challenges highlight the need for gender-sensitive health assessments in geothermal development.
- Increase in Gender-Based Violence and Human Trafficking: The influx of predominantly male construction workers into local communities can exacerbate social tensions and lead to a rise in gender-based violence (GBV) and human trafficking. Women in these communities may become more vulnerable to exploitation and violence, often feeling unsafe due to the increased presence of transient workers. This situation calls for comprehensive safety measures and community support systems to protect women's rights and well-being.
- Rise in Substance Abuse and Health Issues: Geothermal projects can also contribute to social instability, leading to increased substance abuse and criminality. Communities may experience a rise in sexually transmitted infections (STIs) as a result of changing social dynamics and increased risks associated with transient workforces. Women may bear the brunt of these health issues, as they often have less access to healthcare and face stigmatization related to sexual health.

3.3 Measures to mitigate the risks

To effectively manage the risks and opportunities associated with each identified pathway, developers in the geothermal sector may include the following measures2 in the GAP (Based on good practices by USAID, 2019 and ESMAP 2019):

3.3.1 Changes in Land and Natural Resource Use

- Engage Local Stakeholders: Initiate discussions with local communities, including both men and women, before drilling begins to understand their cultural connections to the land and its uses. This helps in identifying suitable sites.
- Analyze Land Ownership: Conduct assessments of land ownership rates, titling occurrences, and natural resource usage patterns.
- Adjust Negotiations and Compensation: Modify sale negotiations, compensation, and resettlement strategies to address the differences between men and women, ensuring fair outcomes.
- Consider Land Management Structures: Evaluate the suitability of various land ownership and management models involving local men and women, considering the cultural significance of the geothermal resource.
- Ensure Equitable Land Improvements: Make sure that essential land improvements required by the project, as well as additional voluntary enhancements (like providing clean water or promoting tourism), benefit the affected communities equitably.

3.3.2 Changes to Employment and Economic Patterns

- Establish a Safe and Inclusive Work Environment: Create a workplace that prioritizes safety and inclusivity, ensuring that protocols are respectful of both men and women.
- Implement Hiring and Training Quotas: Consider introducing quotas for hiring and training, as well as preferential scoring in procurement and tendering. To mitigate potential backlash, clearly communicate the rationale and positive impacts of these measures to all stakeholders.
- Enhance Women's Employment: Develop a strategy aimed at increasing women's employment across all direct job offerings. Analyze worker categories and career development paths to improve recruitment, retention, and promotion opportunities for women.

- Identify Job Creation Opportunities: From the project's inception, seek out opportunities associated with the direct and indirect uses of geothermal resources to create jobs for women entrepreneurs, boost women's agricultural productivity, and enhance overall working conditions for women.

3.3.3 Changes to Environment and Health

- Increase Community Awareness: Educate the community about the known toxins present in traditionally utilized geothermal resources, and seek culturally appropriate solutions in collaboration with local stakeholders.
- Conduct Inclusive Consultations: Engage both men and women in affected communities to gather their diverse perspectives on environmental and health risks associated with the project. Regularly share monitoring data with them to address concerns and foster trust.
- Design Beneficial Projects: Structure project benefits from direct-use applications of geothermal energy and water supply systems to alleviate women's time burdens, improve livelihoods, and promote better health outcomes for families.
- Sensitize Stakeholders: Raise awareness among contractors and the local community about the potential risks linked to the influx of male construction workers. Ensure that codes of conduct are established for workers and support ongoing monitoring and reporting of safeguards, alongside a gender-sensitive grievance redress mechanism (GRM). Consider partnering with service providers to offer health and counseling services.

4. CHALLENGES AND LESSON LEARNED IN DEVELOPING GAP

Creating a Gender Action Plan (GAP) in the geothermal sector can present several notable challenges. One primary issue is the lack of awareness and understanding regarding the importance of gender mainstreaming. Many stakeholders do not recognize how gender dynamics can impact project outcomes, leading to missed opportunities for promoting equity and enhancing project effectiveness. This gap in awareness can hinder the integration of gender considerations into project planning and execution, ultimately affecting both the community and project success.

Another challenge lies in the limited knowledge and experience among team members responsible for developing the GAP. The exploration team often lack the necessary expertise to conduct thorough gender analyses, which are crucial for identifying gender gaps within the project area. This deficiency can lead to ineffective strategies that fail to address the unique needs and contributions of different gender groups.

To address these challenges, it is evident that engaging gender specialists and conducting regular capacity-building sessions for developers, Environmental and Social Impact Assessment (ESIA) consultants, and other involved parties is essential. Training programs can equip team members with the skills needed to effectively integrate gender considerations into their work. By fostering a deeper understanding of gender issues, these initiatives can help create a more inclusive and equitable project environment.

Additionally, the scarcity of gender-disaggregated data poses a significant barrier to effective gender analysis. Without sufficient data, it becomes difficult to identify and address gender gaps at the project level. The dynamic nature of gender situations necessitates ongoing reassessment and validation of these gaps through primary data collection. This emphasizes the importance of establishing robust data collection mechanisms to ensure informed decision-making throughout the project lifecycle.

5. CONCLUSION

Using a gender lens in the context of geothermal energy is crucial for several reasons. Firstly, it helps to identify and address disparities in access to opportunities and benefits between men and women within the sector. This approach ensures that development initiatives are inclusive and equitable, promoting the full participation of both genders in decision-making processes and economic activities. Secondly, applying a gender perspective facilitates the collection of sex-disaggregated data, which is essential for accurately assessing the impact of geothermal projects on different segments of the population. By understanding how men and women are affected differently by project activities, stakeholders can tailor interventions to mitigate risks and maximize positive outcomes for all. Thirdly, incorporating gender considerations supports sustainable development by fostering environments where women can contribute effectively to the sector's growth, thereby enhancing overall project effectiveness and long-term success. Lastly, integrating gender lens will contribute to fulfil company's commitment in supporting sustainable development. Thus, applying a gender perspective and addressing gender gaps are crucial for the effectiveness, efficiency, and sustainability of geothermal projects.

This paper highlights that a GAP serves as a practical strategy to narrow gender disparities, reduce risks, and improve the results of geothermal projects. Developing a GAP in the geothermal sector involves navigating

significant challenges, including lack of awareness, limited experience, and data constraints. However, through targeted capacity building, comprehensive data collection, and stakeholder engagement, it is possible to overcome these hurdles and foster a more inclusive approach to project development. Emphasizing the importance of gender mainstreaming will not only enhance project outcomes but also promote greater equity and sustainability within the sector.

REFERENCES

ESMAP. (2019). *Gender Equality in the Geothermal Energy Sector: Road to Sustainability*. Energy Sector Management Assistance Program (ESMAP) Knowledge Series 028/19. Washington, DC: World Bank.

Hill, C, Madden, C & Collins, N. (2017*). A Guide to Gender Impact Assessment for the Extractive Industries*. Oxfam: Melbourne.

Nelson, S., & Kuriakose, A.T. (2017). *Gender and Renewable Energy: Entry Points for Women's Livelihoods and Employment*.

PT Sarana Multi Infrastruktur. (2022). *Indonesia Geothermal Resources Risk Mitigation Project*: Developer Manual

PT Sarana Multi Infrastruktur. (2024). *Indonesia Geothermal Resources Risk Mitigation Project: Manual for Gender Action Plan Development, Gender-based Violence and Violence against Children*.

USAID. (2019, May). *Engendering utilities: Delivering gender equality*: A best practices framework for utilities.

UN Women.(n.d). *Gender Mainstreaming - Concepts and definitions*.

United Nations Development Programme. (2023). *What is intersectionality? And why is it important for gender equality?*. Retrieved from https://www.undp.org/bosnia-herzegovina/blog/what-intersectionality-and-why-it-important-gender-equality

Sosa, Diana Ortiz. (2020). *Best Practices on Gender Inclusion Relevant to the Geothermal Industry*.

World Bank. (2024). *Accelerate Gender Equality for A Sustainable, Resilient, and Inclusive Future*. Retrieved from https://documents1.worldbank.org/curated/en/099013107142345483/pdf/SECBOS04cf7b650208a5e08b784c0db6a4.pdf

World Bank. (2023). *Gender Aspects for GREM*.

World Bank. (2019). *Report-International Bank for Reconstruction and Development Project Appraisal Document*. Retrieved from https://document.worldbank.org/

Indonesia Country Update 2024: Historical and Future Geothermal Development

Muchsin Chasani Abdul Qadir[1], Desak Nyoman Inten Apriani[2], Dorman Purba[2,3], Ferdino R Fadhillah[2,3], Andreas Suseno[2], and Astri Indra Mustika[2]

[1]World Bank Indonesia, Indonesia Stock Exchange Building, Jakarta, Indonesia
[2]PT Sarana Multi Infrastruktur (Persero), Sahid Sudirman Center 49th floor, Jakarta, Indonesia
[3]Enerka Bhumi Pratama, Jakarta, Indonesia

mqadir@worldbank.org

Keywords: Geothermal Development; Exploration Risk; Regulatory Framework; Binary Technology; Investment Attractiveness

ABSTRACT

Indonesia possesses a large potential of geothermal resources that has only been utilized by around 10 percent. As one of the top two geothermal countries in the world, exploration started in 1926 during the Dutch colonial era with the first commercial geothermal power plant operated 40 years ago. The Government of Indonesia plans to accelerate geothermal utilization as a baseload for green electricity generation in the future. To achieve this national target, a deep understanding related to the current status and upcoming conditions for Indonesia geothermal is needed to formulate a better development strategy.

The authors conducted literature reviews to understand the current and future Indonesia geothermal development trend from resource-technology, regulatory, and economic-financing perspectives. The study result shows that most of the developed geothermal fields in Indonesia within Sumatera and Java regions are categorized as high-temperature and associated with volcanic systems. For those developed fields, the geothermal developers predominantly employed flash power plants for power generation, while the dry steam power plants are utilized for steam-dominated conditions. The Government of Indonesia has set a clear regulatory framework for geothermal utilization through the geothermal law, national energy mix target, and presidential regulation promoting renewable energy tariffs. The government also deploys several fiscal incentives in terms of tax incentives and exploration supports to attract investment for geothermal development. Unfortunately, the geothermal sector investment climate still needs further improvement to provide a more impactful approach to increase investment attractiveness.

With most high-temperature geothermal fields having been developed, the remaining undeveloped geothermal fields are low to moderate-temperature systems. The shifting of resource conditions is also affecting the adoption of binary technology for plant effectiveness. There are challenges for geothermal investors in Indonesia to develop this kind of resource due to a lack of experience and a necessary period of learning curve. This condition creates another higher investment risk in addition to the exploration risk that could be supported by an exploration de-risking program. The current strategy from the exploration phase to the development phase and incentives for development needs to be improved to tackle these risks.

1. INTRODUCTION

The geothermal development in Indonesia started in 1926 during the Dutch colonial era with a commercial utilization remarked through Kamojang Geothermal Power Plant (30MW) in 1983. Nowadays, Indonesia is the top two geothermal country in the world with a 2.417 MW installed capacity from approximately 23 GW total potential. This means that Indonesia only utilized around 10 percent of its total potential with an average additional capacity of around 60 MW per annum. The Government of Indonesia has a plan to utilize geothermal energy as a baseload to replace coal/diesel power plants and set the target of utilization to reach 5.799 MW in 2030. The government target emphasizes the significant increase in the average additional installed capacity toward 488 MW per annum from 2024 to 2030. This is a big target that needs to be achieved and requires catalyzes for geothermal development through a better investment condition. Figure 1 shows the historical and target for geothermal power utilization based on EBTKE (2023) and ThinkGeoEnergy (2024).

There are 46 geothermal power plants, including the expansion unit, developed by State-Owned Enterprises (SOE) and private Independent Power Producer (IPP) in 17 geothermal working areas, which are dominantly located in Sumatera and Java Islands. From existing conditions as shown in Figure 2, the top three geothermal power producers in Indonesia are dominated by the IPP sector with the Joint Operating Contract (JOC) Star Energy Geothermal Ltd. owning the biggest total capacity (Figure 2) of 874 MW coming from only 3 geothermal fields.

Meanwhile, PT Pertamina Geothermal Energy (Persero) (PT PGE) is in second place with a total capacity of 677 MW coming from 6 geothermal fields. The total geothermal capacity from these two developers is 64 percent of the total installed capacity in Indonesia while the remaining capacity is contributed by the JOC Sarulla Operation Ltd., PT Supreme Energy, KS Orka Renewables, PT Geo Dipa Energi (Persero) (PT GDE), and PT Perusahaan Listrik Negara (Persero) (PT PLN). These two major developers seem to have different strategies in their geothermal portfolio development. The JOC Star Energy Geothermal Ltd. tends to maximize the development with a limited number of fields whereas PT Pertamina Geothermal Energy (Persero) develops more sites and scattered fields with lesser potential capacity in each field.

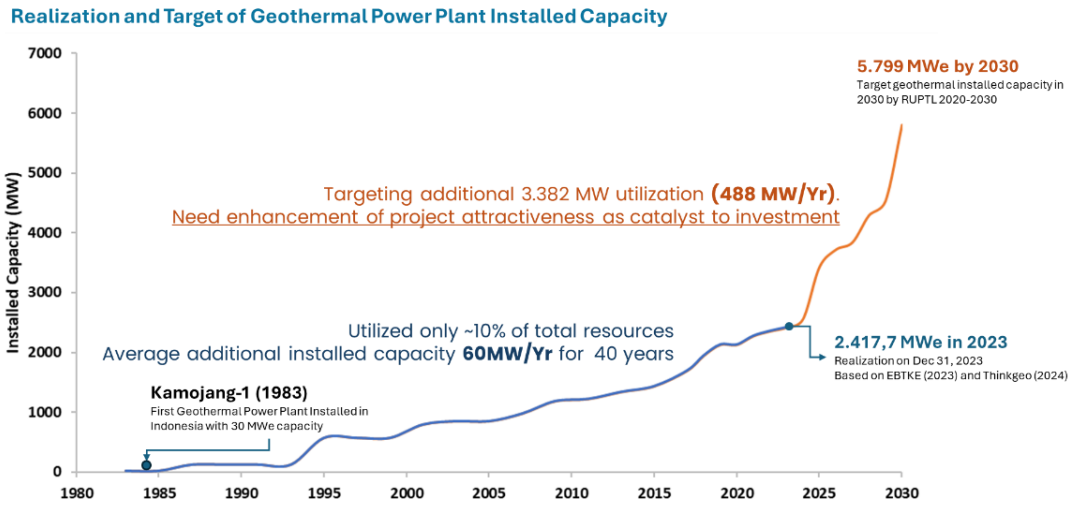

Figure 1: Indonesia geothermal power plant installed capacity and target for 2023 based on EBTKE (2023) and ThinkGeoEnergy (2024).

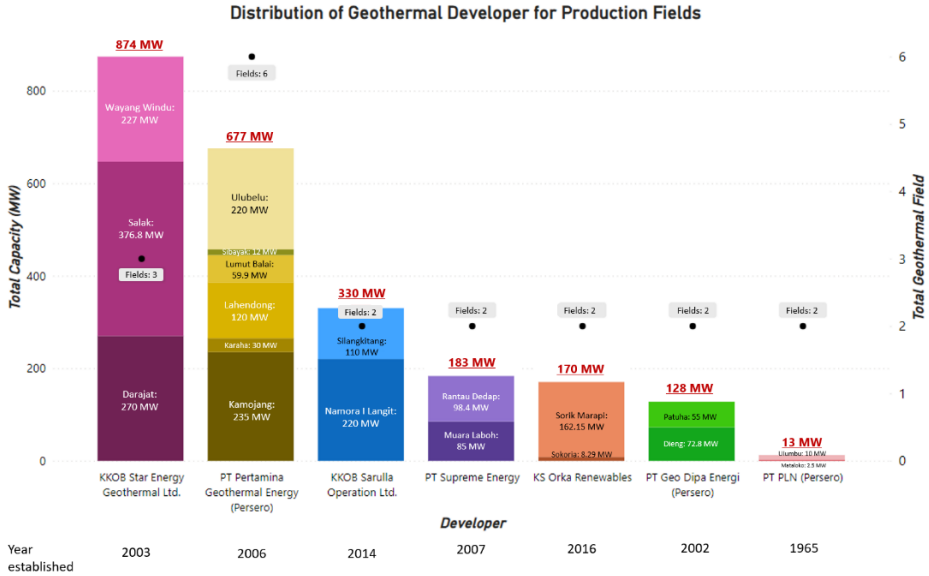

Figure 2: Operating geothermal developers in Indonesia.

1.1 Research Objective

The research in this paper aims to provide an update on the geothermal development trend in Indonesia and to understand better Indonesia's geothermal development trend from resource-technology, regulatory, and economic-financing perspectives. The research question is How is the landscape of regulatory, economic-finance, technical, and social environmental in developing Indonesia geothermal?

1.2 Research methods

The authors conducted literature reviews and discussions with several experts to understand the landscape of Indonesia's geothermal. The information then being analyzed using PESTEL framework to determine the trend, including the opportunities and challenges for future Indonesia geothermal development.

2. GEOTHERMAL BUSINESS OVERVIEW

2.1 Geothermal Business Model and Project Stages

Geothermal industry products are mainly in the form of steam-heat to be used for electricity generation. This utilization is the most common primary stream of revenue for geothermal projects in Indonesia. The business-as-usual condition for geothermal business is that the generated steam/electricity would be off-taken by PT PLN as the electricity single buyer in Indonesia. Afterward, the electricity is then transmitted and distributed by PT PLN to consumers from various sectors, including industries, commercials, offices, and households. PT PLN's position as a single buyer has created a strong negotiation power for PT PLN and it becomes the strongest external parameter influencing the geothermal business through tariff determination that gives an advantage to PT PLN. The geothermal power business process, particularly for electricity generation, encompasses several key phases: preliminary survey, surface exploration, exploration test drilling, project review, field development, power plant construction, commissioning, and production (ESMAP, 2012; IGA, 2014). Under the existing regulations in Indonesia, a geothermal project is given a maximum duration of seven years from preliminary surveys until the start of electricity production. If a company successfully reaches the commercial operation date (COD), it will be granted a utilization license for 30 years. However, if a company fails to reach a COD, they are required to return the working area to the government (Purba, et al., 2021; GoI, 2014). Figure 3 shows the typical project stages in Indonesia.

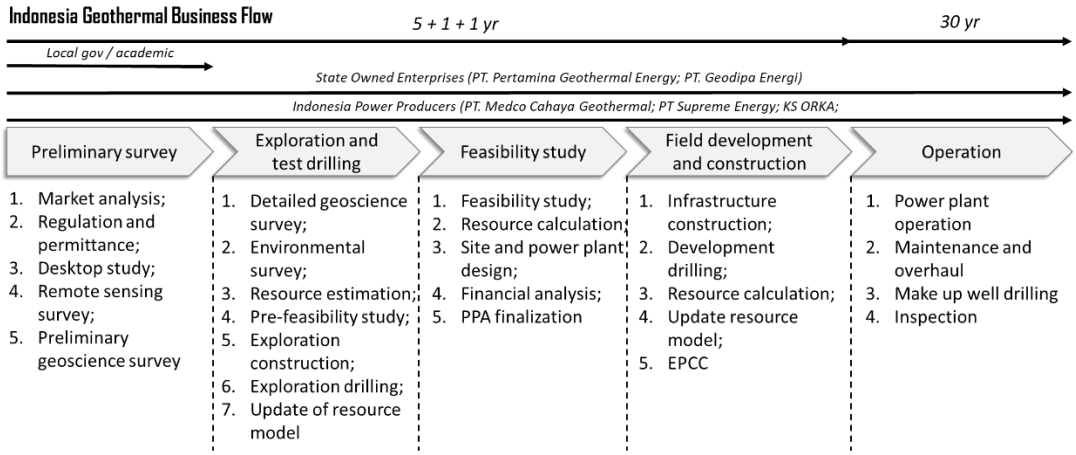

Figure 3: Typical geothermal project stages in Indonesia.

Furthermore, other derivative products also may be in the forms of district heating, plantation drying, tourism, and balneology, which is called geothermal direct use. Indonesia's geothermal industry lacks direct use business scheme and is utilized mainly as corporate social responsibility programs to increase the social acceptance of the projects, not as additional revenue to the projects. It contrasts with practice in Iceland and New Zealand that utilize the direct utilization as commercial products that could generate additional revenues for the project (IRENA, 2017; Lund & Toth, 2021; MEMR, 2019).

Brillian (2024) explained that the geothermal business owners in Indonesia also currently exercise the innovative geothermal energy sales scheme through off-grid or captive use. This approach sells electricity or steam directly to industrial consumers expecting to gain more competitive tariffs compared with PT PLN's tariff and streamline the negotiation process. Developers would negotiate the Power Purchase Agreement (PPA) or steam sales contract directly with potential buyers following the Notification of Resource Confirmation (NORC), which provides an option for the developers to choose the geothermal energy buyer.

2.2 Indonesia Geothermal Fiscal Regime

The geothermal fiscal regime in Indonesia is characterized by two primary utilization regimes outlined by the Indonesia Geothermal Law No. 21/2014, which are the net operating income scheme for the existing working area under the Joint Operating Contract (*Wilayah Kerja Eksisting*) prior to the Geothermal Law enactment and the royalty system for the geothermal areas with business license working area after issuance of the law (*Wilayah Kerja Panas Bumi / Izin Panas Bumi*). The royalty scheme uses deductions from gross revenue consisting of production fees, fixed fees, and production bonuses for the government (2024) as shown in Figure 4. The central government takes consists of royalties fees and corporate income tax. The local government receives part of production fees (at the province and regent levels) and production bonus (at the regent level). In comparison, the developer takes revenue deducted from government take, operating expenses, and interest expenses. Although the royalty scheme calculation is like a concession, this mechanism still holds the entitlement of resources belonging to the state. Figure 5 shows the schematic of the royalty "IPB" scheme (MEMR, 2022) .

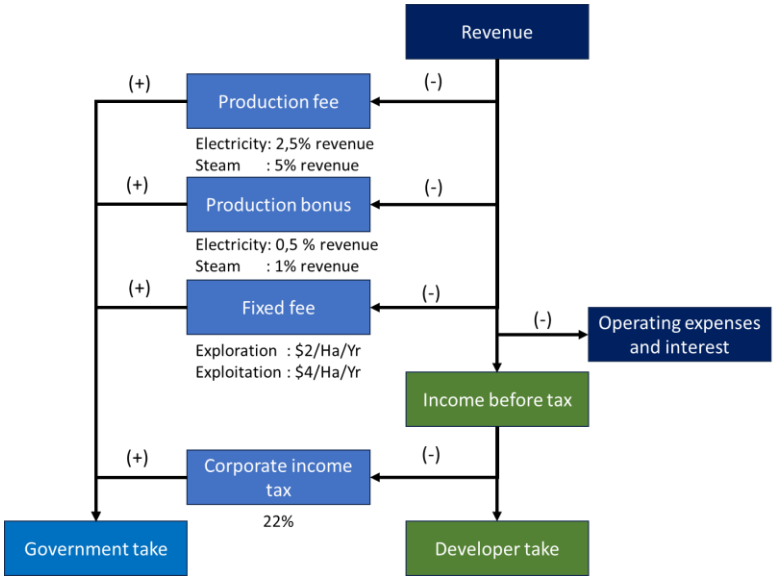

Figure 4: Royalty scheme for Indonesia geothermal.

2.3 Geothermal Financing Structure

Geothermal power development involves substantial risks of investment and exploration, especially geological exploration upholding uncertainty of unproven resources. The loss during the initial project phase due to these risks affects the projects' funding options for the developers.

The pre-operation period typically utilizes a combination of funding sources, including shareholder equity and external financing (such as loans or grants), as described by the ASEAN Center for Energy (2022) and Yescombe (2014). Fuentes (2022) summarize the suitable capital options for geothermal power projects as shown in Table 1.

Table 1: Suitable geothermal project funding option based on Fuentes (2022).

Project Phase		Type of Capital	Financial Risk	Capital Required	Suitable (Alternative) Finance Methods
1.Project Definition		Risk-absorbing, Risk-sharing	High	Low	Subsidies/grants/donations, crowdfunding (E/R), direct lending combined with governmental guarantee, governmental lease
2. Exploration		Risk-absorbing, Risk-sharing	High	Medium	Subsidies/grants/donations, crowdfunding (E/R), direct lending combined with governmental guarantee, governmental lease
3. Drilling	(A) First Well	Risk-absorbing, Risk-sharing	High	High	Subsidies/grants, crowdfunding (E/(L)/R), governmental lease, direct lending combined with governmental guarantee, green bonds, regular loan, regular bond, equity
	(B) Resource Development	Debt	High/ Medium	High	Crowdfunding ((E)/L/R), governmental lease, direct lending, green bonds, regular loan, regular bond, equity
4. Construction		Debt	Low	High	Crowdfunding (L/R), direct lending, leasing
5. Operation		Debt	Low	Medium	Crowdfunding (L/R), direct lending, leasing
6. Decommissioning and Post-Closure		Reserves, Risk-absorbing. (Government)	Medium	Low	Retained profits, governmental funds

The highest risk is imposed on the developers at the preliminary stage which usually uses the equity, government grant, or de-risking facility to fund the project at this stage. Only after the geothermal reserve is proven - around 50 - 65 percent of steam capacity is confirmed under well head from drilling stages, development phase begins by using financing options from an external institutions (i.e loans) (Siahaan, et al., 2022; Siahaan, et al., 2023; ADB&WB, 2015). Siahaan (2022) and Fadhillah (2023) explains the funding sources for geothermal power project development as follows:

1. **Shareholder equity**. Through equity, project capital is financed by the company's internal stakeholders. The developers raise this equity using various approaches such as company loans - shareholder loans

before proven reserves, bonds, or shares after proven reserves. Typically, the exploration phases of a geothermal project are financed through equity (Yescombe, 2014; Siahaan, et al., 2022; Fadhillah, et al., 2023).

2. **Grants and de-risking facility**. These are other sources of funding for project developers, particularly during the exploration drilling phase provided by various stakeholders, including the government, international financial institutions, donors, and others (ACE, 2022). Since funding comes from different sources, risk and cost are shared through multiple stakeholders avoiding full loss on one party (Siahaan, et al., 2022; Siahaan, et al., 2023).
3. **Loans**. It is a widely common type of funding in which capital comes from external financial institutions under specific terms and conditions for repayment. Loans commonly support 70 percent of project capital that could be accessed after the exploration phases are completed when certainty for proven reserves is higher (GT Management, 2020). Obtaining loans from external financial institutions enables geothermal developers to secure the necessary funds for project development and construction. This type of funding provides a wide range of options for developers apart from relying on limited internal equity or shareholder funding. The loan in general could be diversified into:
    a. Soft loan. This type of loan offers extended repayment periods and lower interest rates, with sometimes requiring a government sovereign guarantee. These elements look more appealing to manage a developer's cash flow in high investment type of project. Soft loans are often provided by governments, development banks, and international financial institutions with the aim of promoting sustainable and socially beneficial projects, such as renewable energy initiatives. The soft loan could encourage investment in projects, especially those that may not be economically viable under commercial loan conditions. While the soft loans are mostly accessible for public geothermal developers, it is not the case for private developers.
    b. Commercial loans. This type of loan takes debt with a regular interest rate and tenor period. The general approach for Indonesia's geothermal investment would assume the interest of 7 percent with 15 years of tenure (DJEBTKE-KESDM, 2021).

3. THE LANDSCAPE OF INDONESIA GEOTHERMAL

3.1 Regulatory

The Government of Indonesia has set a clear direction and target to support the development of renewable energy, including geothermal. This condition creates an opportunity for the geothermal business to grow and accelerate. Geothermal energy, with hydropower, is expected to be the primary baseload of electricity generation to substitute coal/diesel power plants since the Government of Indonesia plans to implement early phase-out coal power plants as part of its Long-Term Strategy for Low Carbon and Climate Resilience 2050. Refer to PT PLN's Business Plan / RUPTL 2021, geothermal power is targeted to support 16.9 percent of renewable energy power generation, equal to 7.56 percent of the total national electricity demand, with the increasing pattern over the year (PLN, 2021). The utilization of geothermal as green energy is important in Indonesia's efforts to achieve 23 percent renewable energy by 2025 and another additional 21percent of renewable power generation by 2030 (DEN, 2022a). While the 2025 target is no longer realistic to be achieved, the official revised target has not been announced by the government.

Vakulchuk, Overland, & Suryadi (2022) emphasize that the Government of Indonesia's commitment is the leading condition in renewable energy policies in ASEAN. The government of Indonesia has already set a clear energy roadmap under energy law to support the renewable energy effort, as shown in Figure 5 (IRENA, 2022). However, many works need to be done since the latest 2022 version of the Regulatory Indicator for Renewable Energy (RISE) index by the World Bank (2018) has scored Indonesia an average of 56 of the maximum 100 scores (71 for electricity access, 66 for clean cooking, 53 for renewable energy, and 32 for energy efficiency).

The Indonesian government is actively engaged in formulating a new regulatory framework under the upcoming new and renewable energy law, which is crucial for the future trajectory of the country's energy sector. This legislative update is anticipated with keen interest by industry stakeholders, particularly for its potential to introduce clear regulations concerning the power-wheeling scheme. Such a scheme, including specific provisions for off-grid or captive use mechanisms, is expected to significantly enhance the attractiveness of renewable energy projects. By allowing electricity producers to sell power directly to end-users through a wheeling scheme or to use it for their own consumption without having to rely solely on the national grid, these provisions could open up new opportunities for energy projects.

Additionally, the Indonesian government is involved in inter-ministerial discussions aimed at further incentivizing investments in the renewable sector. One of the pivotal regulatory adjustments under consideration is the waiver of local content requirements for projects financed by multilateral/bilateral financing institutions. This potential regulatory relaxation is seen as a strategic move to attract more foreign investment and global financial

participation in Indonesia's renewable energy projects. By reducing the mandate for locally sourced materials and services, the government aims to lower the barriers to entry and operation for projects backed by international banks and financial entities, which often face challenges in meeting stringent local content stipulations.

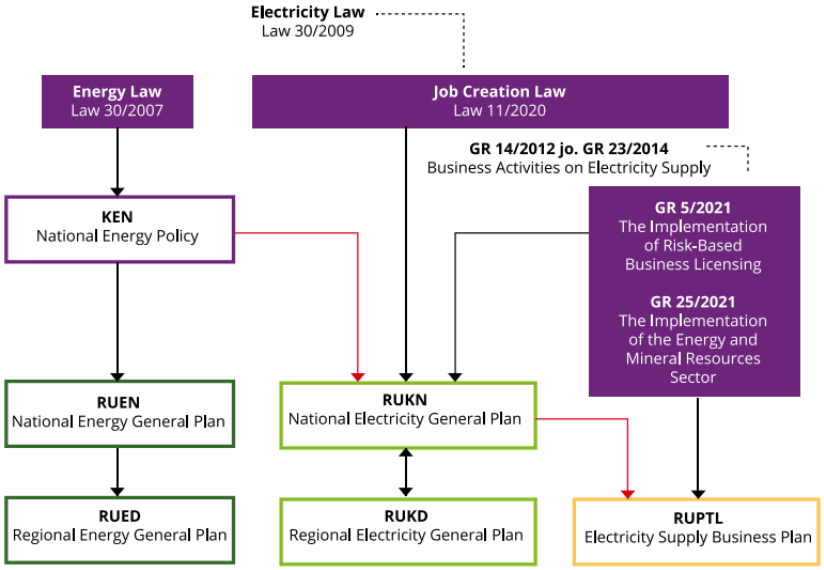

Figure 5: The regulatory framework for national energy target.

Table 2: The financing source for several geothermal projects in Indonesia.

Bank	Developer	Project	Loan agreement year	Grace period	Repayment period	Debt amount (MUSD)	Base rate	Fixed spread
BNI	PT Geo Dipa Energi (Persero)	Development-Patuha 1	2009	3	8	103.06	6.25%	
ADB	PT Geo Dipa Energi (Persero)	Development-Patuha 2-Dieng 2	2020	5	15	300.00	SOFR	0.50%
SMI	PT Geo Dipa Energi (Persero)	Development-Dieng small scale	2019		7,5	19.00	LIBOR	2.00%
SMI	PT Medco Cahaya Geothermal	Development Ijen	2023	3,25	15	100.00	SOFR-3M	2.00%
MLA	PT Pertamina Geothermal Energy Tbk	General purpose	2021	-	1	800.00	LIBOR-3M	0.70%
JICA	PT Pertamina Geothermal Energy Tbk	Development-Lumut balai	2012	10	30	192.87	0.30%	0.30%
JICA	PT Pertamina Geothermal Energy Tbk	Development-Lumut balai	2012	10	30	10.46	0.01%	0.01%
IBRD	PT Pertamina Geothermal Energy Tbk	Development Ulubelu 3 4-Lahendong 5 6	2014	6	15	129.04	LIBOR	0.45%
CTF	PT Pertamina Geothermal Energy Tbk	Development Ulubelu 3 4-Lahendong 5 6	2014	7	30	124.31	0.25%	0.25%

3.2 Economic-Financing

3.2.1 Financing Facility

Geothermal developers, including those in the private sector, often struggle to access financing for the exploration drilling stage due to the perceived high risks associated with the industry, which is characterized by its capital-intensive nature, extended investment periods, and significant uncertainties. Financial institutions, cautious due

to a limited track record in renewable energy financing, tend to demand higher interest rates and enforce stringent credit risk mitigations such as strict covenants and collateral requirements. This prudence is exacerbated by inconsistent government policies, which contribute to a volatile regulatory environment, and a lack of competition among financial institutions in the renewable energy funding market, leading to less advantageous loan conditions for geothermal projects (ADB, 2019).

Soft loan as one of the financing options has challenges to be accessed by private geothermal developers since development banks or other institutions may require a sovereign guarantee and stringent social and environmental requirements which could add financial burden to the developers. With no possibility to obtain a sovereign guarantee, this mismatch in environmental and social requirements may make it more challenging for private developers to access soft loans from these institutions.

Development banks play a crucial role in financing Indonesia's geothermal projects, providing necessary support for their development and expansion. Table 3 shows the list of financing institutions for several geothermal projects in Indonesia that shows the average fixed spread is 1.25 percent. Notable contributions include:

a. International Bank for Reconstruction and Development (IBRD) of the World Bank: It has supported the Ulubelu unit 3-4 and Lahendong unit 5-6 geothermal projects. These initiatives expand geothermal capacity, contributing to sustainable energy solutions.
b. Asian Development Bank (ADB): ADB has been instrumental in funding several geothermal projects, including Rantau Dedap, Muara Laboh, Dieng-2, Patuha-2, and Sarulla. These projects enhance the geothermal energy infrastructure in their respective locations.
c. Japan International Cooperation Agency (JICA) / Japan Bank for International Cooperation (JBIC): They have provided support for projects like Lumut Balai, Lahendong, Tulehu, Kamojang, and Ulubelu. This support reflects Japan's commitment to renewable energy and international cooperation in sustainable development.

3.2.2 De-risking Facility

A geothermal exploration de-risking scheme is a strategic approach designed to mitigate the financial risks inherent in geothermal exploration projects. The primary objective of this scheme is to create an efficient exploration program that enhances the ratio of successful exploration (Siahaan, Septiani, Purba, & Paripurna, 2023). ESMAP (2016) and Nur (2023) strengthen the significance of the exploration de-risking program as a critical path to accelerate and enhance the development and utilization of geothermal resources.

1. The Geothermal Energy Upstream Development Program (GEUDP) is a joint initiative between the Government of Indonesia and the World Bank with the primary goal of promoting the development of greenfield geothermal areas that have not yet been tendered, particularly in remote regions of Indonesia. The program aims to support and facilitate exploration and drilling activities in order to assess the geothermal potential in untapped areas and promote the development of clean and sustainable geothermal energy resources. However, most of these projects are still in the early stages of exploration activities (Siahaan, Septiani, & Purba, 2023). Under the GEUDP, the Indonesian government assumes full responsibility for the risk of exploration drilling if the geothermal resource is not proven or deemed economically viable. In cases where the geothermal resource is found to be feasible for electricity generation, the relevant Working Areas (WKP) will be tendered, along with the geothermal data package acquired during the exploration drilling process. The winner of the tender has an obligation to repay the exploration cost with a certain margin (Siahaan, Purba, Septiani, & Paripurna, 2023).
2. The Geothermal Resource Risk Mitigation Program (GREM) The GREM Project is a geothermal exploration financing initiative operated by the World Bank in collaboration with the Government of the Republic of Indonesia. Managed by PT Sarana Multi Infrastruktur (Persero), this program is designed to address exploration risks associated with geothermal exploration stages. This program offers a risk-sharing mechanism with a de-risking scheme to tackle exploration. One of the key features of this facility is its ability to reduce payments by up to 50 percent of the total facility costs for each project that encounters unsuccessful exploration drilling. Thus, GREM provides significant support for geothermal development in Indonesia by reducing the financial burden and risks for developers in this sector. The aim of the program is to encourage broader participation from business entities in the geothermal sector, particularly by reducing exploration risks, which are known as one of the greatest risks in geothermal project development.
3. Government Drilling by the Geological Agency is a geothermal exploration campaign under the Ministry of Energy and Mineral Resources (MEMR) that is funded by the state budget. The government bears all of the exploration risk and is responsible for exploration costs. The activities carried out by the Geological Agency include preliminary surveys, land acquisition, obtaining necessary permits, infrastructure construction work,

drilling, well testing, and updating the pre-feasibility study (pre-FS) document (Siahaan, Septiani, Purba, & Paripurna, 2023).

3.2.3 Tariff Setting

Since 2017, Indonesia's MEMR has aimed to make electricity more affordable by setting the electricity generation Basic Cost of Provision (BPP) as a benchmark for renewable energy pricing from Independent Power Producers (IPPs) to PLN. MEMR Regulation 50/2017 and its revision under MEMR Regulation 4/2020 defined pricing based on BPP, setting prices higher or lower based on regional costs compared to the national average. However, using BPP as a benchmark for geothermal tariffs has significant drawbacks due to its heavy influence from the coal-dominated power sector, in particular for Java and Sumatra regions where the most geothermal potential sites are located. As of January 2023, coal-fired plants accounted for 66.01 percent of Indonesia's total capacity, distorting the BPP and affecting geothermal pricing. These factors suggest that the BPP model needs adjustments to incorporate external costs and provide a fairer comparison between coal and geothermal power, thus supporting more balanced and sustainable energy policies. Three key issues make BPP inappropriate for geothermal pricing:

1. Inequitable Incentives: Coal plants benefit from subsidies like the Domestic Market Obligation (DMO), keeping their costs artificially low. Without these subsidies, coal tariffs could be much higher and could fluctuate following its international price.
2. External Costs: BPP does not account for the environmental and health costs associated with coal power, such as emissions and pollutants, which have substantial social costs.
3. Supply Risks: Coal supply is unreliable, as seen in 2001 when PT Indonesia Power had to reduce its geothermal power plant operations due to coal shortages.

Geothermal Power Plant – electricity price

Capacity (MW)	Ceiling Price (HPT)							
	s.d 10 MW		>10 MW s.d. 50 MW		>50 MW s.d 100MW		>100 MW	
	Stg thn 1-10	Stg thn 11-30	Stg thn 1-10	Stg thn 11-30	Stg thn 1-10	Stg thn 11-30	Stg thn 1-10	Stg thn 11-30
Staging Price (cent $/kWh)	9,76 x F	8,30	9,41 x F	8,00	8,64 x F	7,35	7,65 x F	6,50
Levelized Price (cent $/kWh)	9,25		8,92		8,19		7,25	

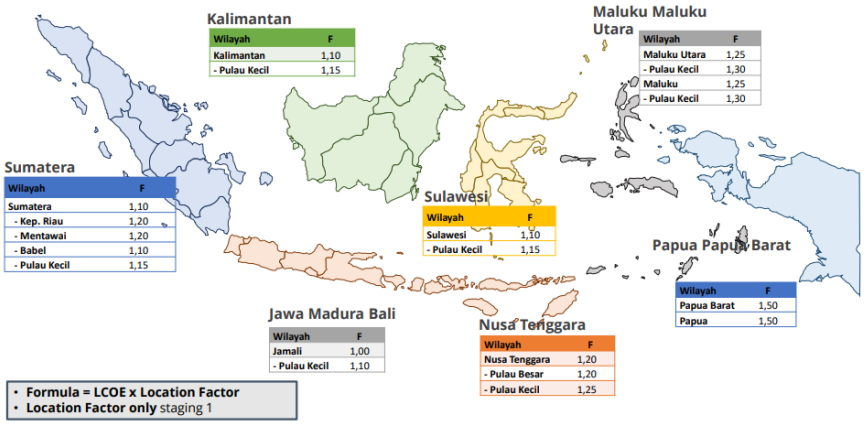

Figure 6: The base tariff and location factor of geothermal tariff under presidential regulation 112/2022.

Indonesia's geothermal tariff introduced a new ceiling with a staging tariff system in 2022, determined by the power plant's location and capacity. This method is specified in Presidential Regulation 112/2022, which updates the earlier ceiling tariff structure. The staging system splits the operational lifespan of a geothermal power plant into two phases: Stage 1 (years 1 to 10) and Stage 2 (years 11 and beyond). Each phase has a separate ceiling for the base tariff that developers can negotiate with PLN (GoI, 2022). Additionally, the location factor serves as a multiplier index for the base tariff during Stage 1. This adjustment accounts for the variation in development costs resulting from differing infrastructure conditions across regions (MEMR, 2022b). Figure 6 shows the distribution of base tariff and location factor. The calculation of the applied base tariff is below.

Tariff stage 1 =a greed tariff x location factor

Tariff stage 2 = agreed tariff

In recent discussions with stakeholders in the geothermal sector, several critical insights have been gathered regarding the new tariff scheme implemented for geothermal projects. Including:

1. Clarity on tariff for expansion of an existing project. A significant concern raised by stakeholders is the ambiguity surrounding tariffs for the expansion of existing geothermal projects. Currently, the regulatory framework does not clearly stipulate how tariffs are adjusted for additional units within existing projects. Developers argue that allowing expansion projects to secure the maximum tariff rate, akin to that of the first unit, would not only simplify financial planning but also maximize profitability. Stakeholders collectively suggest that a more effective regulatory approach would incentivize operational units immediately upon development, rather than deferring financial benefits until subsequent units are constructed. This immediate incentive could accelerate project expansion and contribute to more rapid scaling of geothermal capacity.
2. Staging Down Tariffs, the unique and complex nature of geothermal development, characterized by variable field conditions and decline rates, necessitates continual investment in make-up wells to maintain power output. However, the existing tariff staging poses a significant challenge. As stakeholders pointed out, the practice of reducing tariffs in later stages undermines project economics at critical phases when substantial investments are needed for maintenance and expansion. This reduction in tariffs can lead to diminished cash flows during periods that are crucial for the sustained operation and growth of the facility.

3.2.4 Fiscal Incentives

Indonesia's government has already launched several incentives for geothermal such as tax holiday/tax allowance, import tax exemption, and land tax exemption as shown in Figure 7. EBTKE (2022) emphasizes that the tax facility could reduce the levelized cost of electricity (LCOE) by 0.07-0.19 US cents/kWh. The explanation of each tax facility as below:

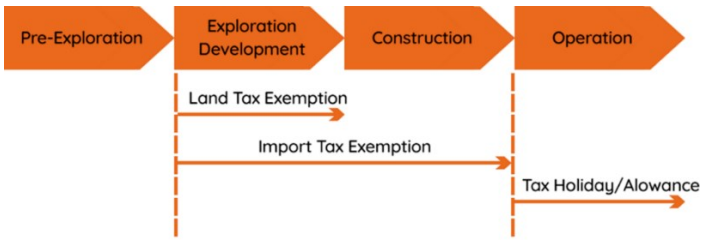

Figure 7: The effective period of Indonesia geothermal tax incentives per project period modified from EBTKE (2021).

The Government of Indonesia offers various fiscal incentives to promote investment and profitability in the geothermal industry. These incentives aim to create a favorable investment climate by reducing business costs and risks for investors. The incentives are provided through different government programs, encouraging businesses to invest in geothermal projects to maximize benefits (Chalk, 2001) (UNCTAD, 2000). Based on EBTKE (2022; 2021), Lesmana et al (2020), Winofa et al (2020), Abidin (2020), and Fadhillah (2023), current fiscal incentives implemented for the geothermal industry as shown in Table 3.

Table 3: Current fiscal incentives for geothermal.

Fiscal incentives	Remarks	Effective period of project stage
Tax holiday (PMK 130 / 2020)	The geothermal industry with an investment of more than IDR500 billion would be eligible to obtain 5 years tax holiday. The details of the tax holiday period as below: - 5 years for IDR500 billion to IDR1 trillion investments - 7 years for IDR1 to 5 trillion investments - 10 years for IDR5 to 15 trillion investments - 25 years for IDR15 to 30 trillion investments - 20 years for > IDR30 trillion investments the developer also would get a 50 percent reduction (for > IDR500 billion investments) for 2 years during the transition period after the facility. The geothermal developer with > IDR0.1 trillion investments is also eligible to obtain a 50 percent tax reduction in the first five years of operation, continued by two years transition period that obtains a 25 percent tax reduction (EBTKE, 2021)	Operation

Fiscal incentives	Remarks	Effective period of project stage
Tax allowance (GR 78/2019)		
- Investment Allowance	Reduction of taxable income equals 5 percent per year of the total investment for the 6-year period and 30 percent of the total investment for the full period. The investment should be owned by the main business entity and not transferred during the period (Abidin, et al., 2020; Lesmana, et al., 2020)	Operation
• Accelerated depreciation amortization	The Geothermal industry classified as "class 3" uses the double declining balance method with the 8-year period for tangible and intangible asset	Operation
• Loss carry over	The geothermal industry is eligible to perform loss carry forward for 5-year period with a maximum of no longer than 10 years. The geothermal as new and renewable energy is also eligible to obtain 1 year additional of the facility.	Operation
Land tax exemption (PMK 172/2019)	The land tax for the geothermal industry is exempted during the exploration phases (MoF, 2016). The land tax is charged during production phases with guidance from the directorate general of tax regulations No. PER-45/PJ/2013.	Exploration
Import tax and value-added tax exemption (PMK 172/2016)	The geothermal industry is 100 percent exempted from import tax for equipment that is not available / adequately produced in Indonesia (Abidin, et al., 2020; Lesmana, et al., 2020). The geothermal industry is not imposed VAT (Abidin, et al., 2020)	Exploration and development

As indicated by Kristina (2018) and Nugraha et al. (2017), the current tax incentives for geothermal projects in Indonesia have not demonstrated a significant impact in enhancing project attractiveness or reducing the cost of electricity generation. The incentives, as per IRENA (2022) and IESR (2022), include a tax holiday that allows for a 100 percent tax reduction for corporate income tax (PPh) for a period of 5 to 20 years. However, this incentive has not been effectively utilized, mainly because most renewable energy (RE) developers do not generate taxable profits during the initial five years of project implementation. Therefore, Fadhillah (2023) provide the case example of ineffective tax holiday period.

3.3 Technical

3.3.1 Resource

Indonesia is a region with the largest conventional convective geothermal resource potential in the world with 80 percent of the geothermal fields being spatially associated around volcanic areas. (ADB, 2018; Darma, et al., 2021). Geothermal fields in Indonesia are mostly situated within moderate to steep mountainous terrain. This geographical feature presents challenges in terms of accessibility and conducting geothermal survey activities in these areas (Hochstein & Sudarman, History of geothermal exploration in Indonesia from 1970 to 2000, 2008; Hochstein & Sudarman, Indonesian Volcanic Geothermal Systems, 2015). Steep terrain conditions present several challenges because they lead to extended times and higher infrastructure costs for drilling equipment mobilization, given that the roads are often uphill and winding. Moreover, finding flat and stable areas for constructing drilling well pads and power plants can be a challenge (Umam et al., 2018; Purba et al., 2020). The steep condition may also require many turns and greater lengths to reach target elevations for the pads. In such situations, many of the currently developed fields have resorted to directional drilling, which can increase costs and risks (Hole, 2006; Umam et al., 2018).

Based on the temperature classification by Sanyal (2005), it is confirmed that most of the developed geothermal fields in Indonesia fall in the high-temperature category. Making Indonesia have abundant lessons learnt to be applied for developing any potential high-temperature resource in the future.

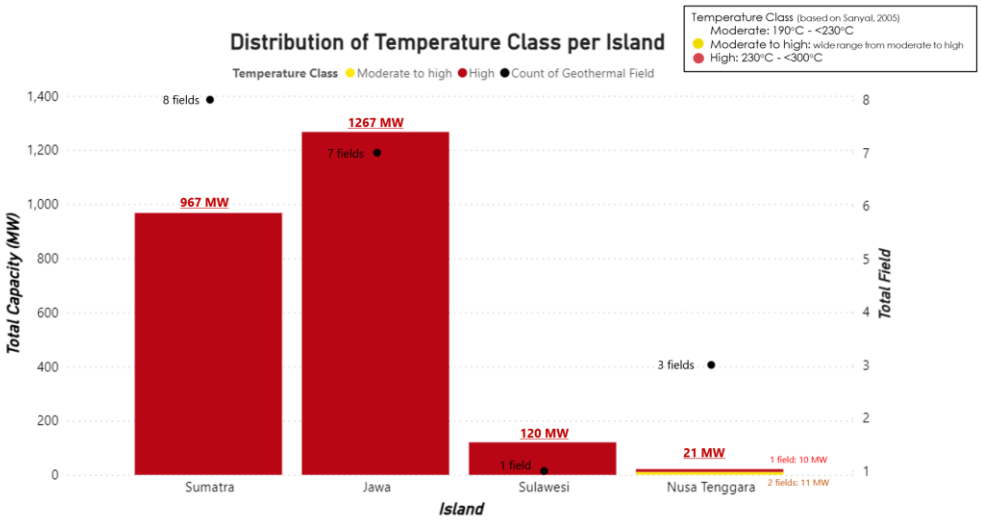

Figure 8: The distribution of resource temperature for geothermal projects in operation per island.

The Indonesian government has identified a list of fields requiring further analysis for potential future geothermal development. These prospects are outlined in the National Electricity Supply Business Plan (RUPTL) 2021-2030. The geothermal prospects in the future pipeline can be categorized into three rankings (Figure 9):

- Rank 1: National Strategic Project (PSN) which is already included in "Neraca Daya" of PLN RUPTL so they supposedly become the most prioritized project to develop.
- Rank 2: projects that are also already included in the PLN RUPTL, but no specific fields are assigned. The supply power is around 710 MW.
- Rank 3: potential projects that are not included in the PLN RUPTL and have no expected COD year. There are 106 projects with a total capacity of around 4.3 GW.

Based on their temperature, the fields listed in Rank 1 RUPTL 2021-2030 are predominantly categorized as high-temperature resources (13 of 22 fields). Most of them are in the exploration phase, such as Kepahiang, Rajabasa, Mount Sirung, while some fields have entered the development phase, including Ijen and Sungai Penuh. Additionally, some moderate-temperature systems are also included in Rank 1, such as Danau Ranau, Cisolok, Baturaden, with a targeted production of about 350 MW much lower than the targeted production from the high-temperature resource of about ~1,1 GW. Figure 9 shows the distribution Rank 1 project per area per temperature classification.

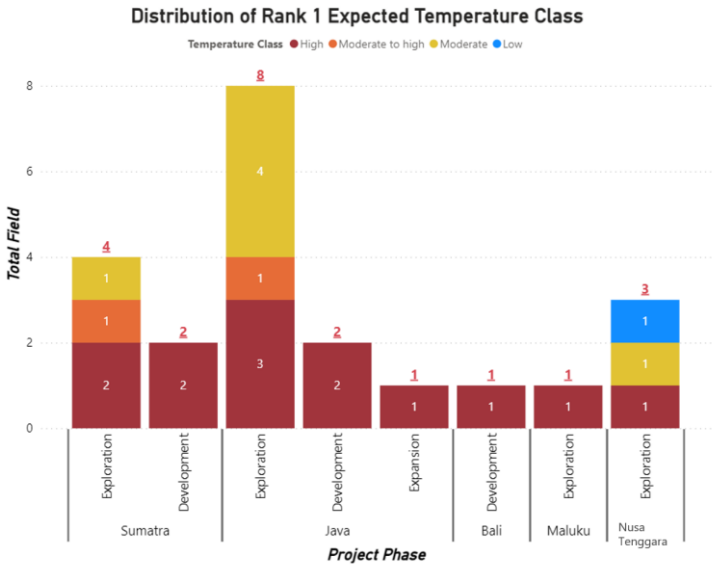

Figure 9: The rank 1 expected temperatures per area.

Slightly similar to the previous fields in Rank 1, several high-temperature fields are still included in Rank 3 (28 of 80 fields). However, a considerable amount of low to moderate-temperature geothermal fields have already been included on this list. It implies that after the fields listed in Rank 1 are already COD or developed (which are mostly high temperature), the fields listed in Rank 3 will become the next priority to be developed. Figure 10 shows the Rank 3 projects per area per temperature classification.

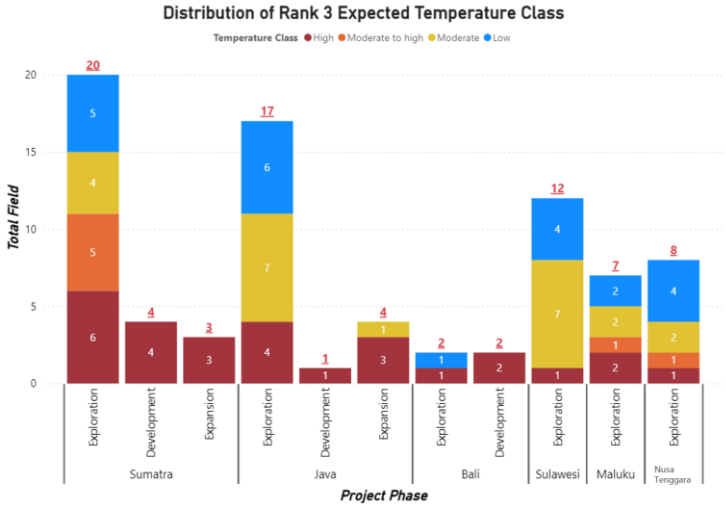

Figure 10: The rank 3 expected temperatures per area.

3.3.2 Power Plant Technology

Geothermal resources are utilized for electrical generation by extracting geothermal fluids from the reservoir and utilizing the resulting steam to drive a turbine connected to a generator (Ameri, et al., 2006). The following power plant technologies have been utilized in various Indonesia geothermal projects:

1. Single flash plants only use a single-pressure separator to separate vapor from the liquid. The separation occurs at constant pressure and temperature. The vapor generated is sent to a steam turbine, while the liquid is reinjected back to the ground (Assad, et al., 2017). This type of power plant is commonly employed in Indonesia, with utilization identified in 14 geothermal production fields, including Salak Awibengkok, Wayang Windu, Lahendong, Dieng, and Karaha Bodas (Siregar, 2004; Sulistyardi, 2010; Pambudi, Itoi, Jalilinasrabady, & Jaelani, 2014; Harvey & Wallace, 2016; Pambudi N. A., Geothermal power generation in Indonesia, a country within the ring of fire: Current status, future development and policy, 2018; Rachmat, Wibowo, & Surachman, 2018; Gunawan, 2021; Pratama, Widiatmo, & Ashat, 2021).
2. Multiple flash plants are a natural extension of the single-flash process. They employ two or three sequential separators, resulting in high, moderate, and low-pressure steam flows that drive the steam turbine. The use of the double-flash system has been explored in Muara Laboh (Oya & Takamiya, 2020).
3. *Dry-steam plants* are primarily used in vapor-dominated reservoir systems. In such reservoirs, most of the geothermal fluid has already reached the vapor phase due to conductive heat transfer from the surrounding water-saturated rocks (White, et al., 1971). In Indonesia, geothermal fields that employ these types of power plants include Patuha, Kamojang, and Darajat geothermal fields (Mendive et al., 2014; Setyawan et al., 2019).
4. *Binary power plant* is implemented for low-enthalpy geothermal systems. However, with advances in chemical technology, they can now operate at temperatures up to 200°C by using various secondary fluids (Redko A, et al., 2016). In addition, binary plants are occasionally employed in higher enthalpy fields that require additional pressure support, such as the Ngatamariki geothermal field in New Zealand (Assad, et al., 2017). Up until now, there is no solely binary power plant system installed for the power grid in Indonesia. A combined flash plant and binary plants have been utilized by Sarulla geothermal projects with a total 330 MW capacity. However, in the near future, a two-phase binary power plant will be commenced in Ijen field to fill an additional 31.4 MW capacity to the Java-Bali power grid.

Power plant units that are preferred to be used in Indonesia are predominantly single flash, comprising more than 50 percent of the total units in Indonesia, and supplying almost 50 percent of the total capacity (Figure 11). The dry steam plant, even though it is specifically used for vapor-dominated resources, is placed second in terms of used technology in Indonesia, showing a large development of vapor-dominated resources. It is followed by a combined cycle flash-binary plant and later a double flash plant. The single flash plant is predominantly used by fields developed before 2013, while from 2013 up to recent development, combined cycle flash-binary and double

flash started to commence. Combined cycle flash-binary, especially, is gaining popularity in recent development. As for the development trend, medium to large capacity development (51-100 MW) seems to be preferred. Developers, notably the JOC Sarulla Operation Ltd., tend to develop their resources on a large scale per unit (>100 MW) using combined cycle flash-binary.

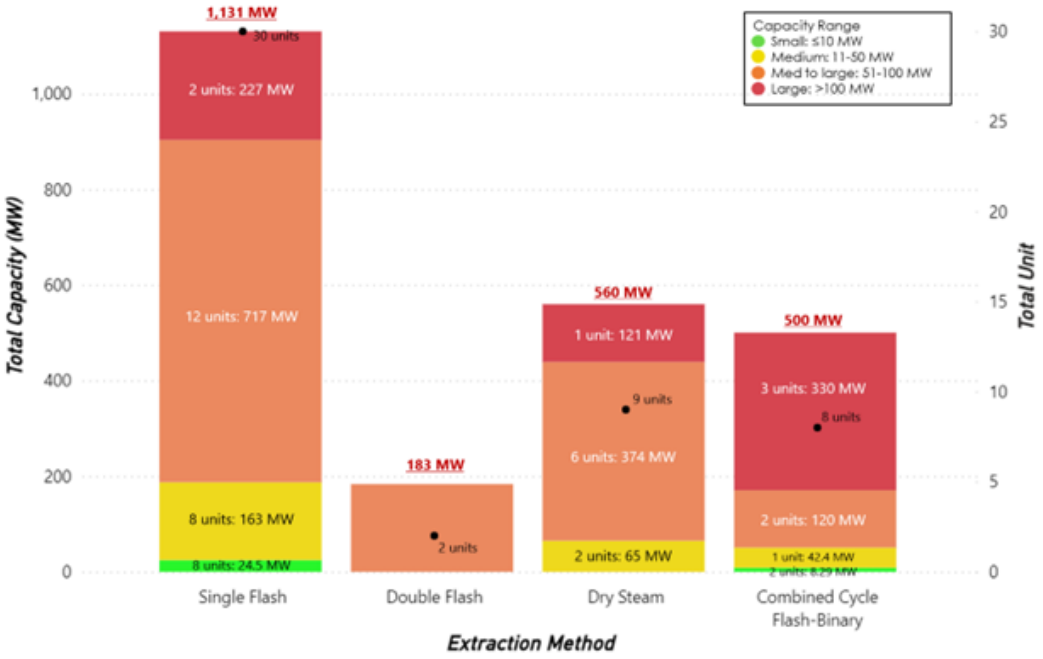

Figure 11: The installed capacity of power plant technology in Indonesia.

3.4 Social-Environmental

Geothermal energy is considered as sustainable and clean for the community (Cataldi, 1999). However, several geothermal projects faced social rejections due to a lack of public understanding of geothermal projects, lack of instant benefit to the community, and disturbance to the landscape. The significant scale rejection becomes a major issue that leads to the delay and cancellation of the geothermal projects (i.g Mt Lawu, Tampomas, Tangkuban Parahu). Social conflict could negatively impact projects/corporate reputation and financial perspective since the social rejection could lead to project delay and nonproductive time (Fadhillah, et al., 2022).

Fadhillah (2022) emphasizes that environmental issues as the most significant aspect of the geothermal projects involved almost in all the rejections (Figure 12). The environmental concerns are water sources such as scarcity and contamination, soil fertility, natural disasters (floods, landslides, and earthquakes), and accidents during drilling and well testing. The economic concerns related to the community anti-trust with land acquisition mechanisms, disruption to mass agricultural areas, and natural tourist attractions as a local occupation. Furthermore, cultural issues are related to the concern that project activity would disturb historical-sacred places, traditional houses, and communities.

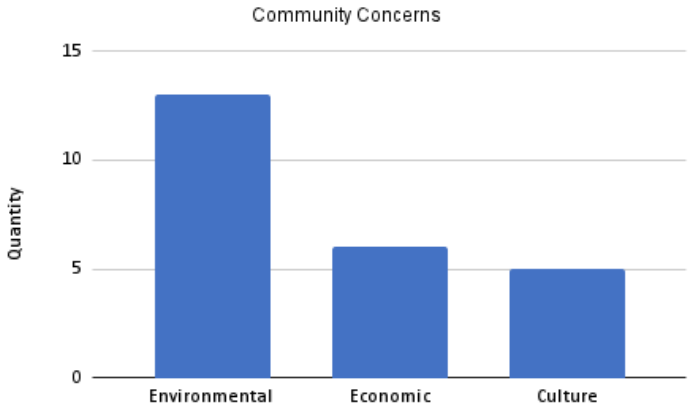

Figure 12: Community concerns to geothermal projects where each rejection may derive from more than one concern.

4. FUTURE OF INDONESIA GEOTHERMAL: SHIFTING RESOURCE PARADIGM

Indonesia's geothermal landscape is undergoing a significant transition with an increasing focus on low to moderate-temperature geothermal systems. Traditionally, high-temperature systems have dominated the exploration efforts; however, recent developments indicate a promising potential in low-enthalpy systems that have yet to be fully tapped. Despite the inclusion of numerous such fields—like Gunung Endut, Tampomas, Sembalun, and Galunggung—in Indonesia's Geothermal Development Pipeline as per the Electricity Supply Business Plan (Rencana Usaha Penyediaan Tenaga Listrik 2021-2030), no low-temperature fields have been developed so far (Putriyana L., Daud, Saha, & Nasruddin, 2022). The challenges in developing low to moderate-temperature in Indonesia, including:

1. **This shift necessitates a deeper understanding of appropriate exploration and production methods** tailored to the unique characteristics of these lower-temperature resources. One of the primary challenges is the limited experience and historical data regarding the successful exploitation of low to moderate-temperature geothermal systems. Unlike high-temperature systems, which have been extensively developed and studied, these lower-temperature fields lack documented methodologies and success stories that can guide developers and reduce perceived risks. Some development strategies and technologies are applied for several low-temperature geothermal fields worldwide, such as Brady in the USA and Flúdir-Midfell in Iceland. Although their condition (e.g., geologic setting, geothermal characteristic) is very different from in Indonesia, however, studying development strategies and technologies implemented in low-temperature geothermal fields worldwide could serve as a first step to initiate particularly low geothermal prospects development in Indonesia.
2. **Technology innovation and adaptation**, the need for specialized technology and approaches tailored to effectively explore and exploit these systems adds another layer of complexity. The current geothermal technology, flash system, is predominantly designed for higher temperature resources, necessitating adaptation of new technology, binary power plant, to produce the resource effectively.
3. **De-risking method and investment incentives**, the gap in expertise not only elevates the risk associated with these projects but also influences the expected returns as higher risk requires higher return, potentially deterring investment attractiveness. To address these challenges, the role of de-risking facilities becomes crucial. There is a critical need for the government to enhance current de-risking measures to better share and mitigate project risks associated with these geothermal prospects.

Additionally, the Indonesian government is urged to adapt and evolve its regulatory frameworks to support more innovative approaches to revenue streams. These could include off-grid/captive use mechanisms, power wheeling arrangements, and direct utilization of derivative products like green hydrogen and minerals extraction. Such regulatory adaptations would not only foster the development of low to moderate-temperature geothermal resources but also align with global trends toward more sustainable and versatile energy solutions. By doing so, Indonesia can secure its position as a leader in geothermal energy while promoting sustainable development within the sector.

5. CONCLUSION

In conclusion, Indonesia's geothermal resources offer vast potential, yet the exploration and development processes still face significant challenges that must be addressed to optimize utilization. While the government has established a robust regulatory framework and provided fiscal incentives to spur investment, these measures require enhancement to fully capitalize on the evolving geothermal resource conditions. As Indonesia transitions from high to lower-temperature geothermal systems, there is a pressing need for adaptation in technology and strategies. The shift towards binary technology to accommodate moderate temperature resources necessitates a strategic response to mitigate the risks associated with the learning curve and inexperience in this area. Strengthening exploration de-risking programs and refining development strategies are critical steps towards fostering a conducive investment environment and achieving Indonesia's ambitions for green electricity generation. This paper underscores the importance of an integrated approach that encompasses technological adaptation, regulatory support, and financial incentives to drive the future of geothermal energy in Indonesia.

REFERENCES

Abidin, M. Z., Rosdiana, H., & Salomo, R. V. (2020). Tax Incentive Policy for Geothermal Development: A Comparative Analysis in ASEAN. *Int. Journal of Renewable Energy Development*.

ACE. (2022). *Impact Analysis and Review on Governance of Renewable Energy Financing Scheme in ASEAN*. Jakarta: ASEAN Center for Energy.

ADB. (2014). *Unlocking Indonesia's geothermal potential*. Asian Development Bank.

ADB. (2019). *Renewable Energy Financing Scheme for Indonesia. Manila*: Asian Development Bank.

ADB&WB. (2015). *Unlocking Indonesia Geothermal Potential*. Asian Development Bank.

Brilian, V. A., Adityatama, D. W., Mukti, A. W., Asy'ari, M. R., Purba, D., Fadhillah, F. R., & Erichatama, N. (2024). Geothermal Captive Use to Support Industrial Activities: Applicable Industry Sectors, Worldwide Experience, and Its Potential and Challenges in Indonesia. *Workshop on Geothermal Reservoir Engineering*. California: Standord University.

Cataldi, R. (1999). Social acceptance: a sine qua non for geothermal. *Bulletin d'Hydrogiologie* No 17.

Chalk, N. A. (2001). *Tax Incentives in The Philippines: A Regional Perspective.* IMF Working Paper.

DEN. (2022a). *Indonesia Energy Outlook 2022-2032*. Jakarta: Ministry of Energy and Mineral Resources.

DJEBTKE-KESDM. (2021). *Pedoman Investasi Pembangkit Listrik Tenaga Panas Bumi*. Jakarta: Direktorat Jenderal Energi Baru, Terbarukan, dan Konservasi Energi, Kementerian Energi dan Sumber Daya Mineral.

EBTKE. (2021). *Pedoman Investasi Pembangkit Listrik Tenaga Panas Bumi. Jakarta*: Direktorat Jenderal Energi Baru, Terbarukan, dan Konservasi Energi, Kementerian Energi dan Sumber Daya Mineral.

EBTKE. (2022). *Pengembangan Panas Bumi di Indonesia*. Jakarta: Ministry of Energy and Mineral Resources.

Fadhillah, F. R. (2023). *Economic Evaluation of Bravo Geothermal Prospect*. Jakarta: ITB School of Business and Management-Thesis.

Fadhillah, F. R., Asyari, M. R., Bagaskara, A., Vanda, D. V., Adityatama, D. W., & Purba, D. (2022). Challenges in Getting Public Acceptance on Geothermal Project in Indonesia. *Indonesia International Geothermal Conference*. Jakarta: IGA.

Fadhillah, F. R., Tjendarsa, K., Damayanti, S. M., Adityatama, D., & Purba, D. (2023). *Economic Evaluation of Bravo Geothermal Prospect in Participating Green Energy Effort*. Gema Ekonomi.

Fuentes, F., Isabel, A. B., Baisch, C., Bodo, B., Elíasson, O., Falcone, G., . . . Ioannou, A. (2022). *The CROWDTHERMAL Project: Creating Public Acceptance of Geothermal Energy and Opportunities for Community Financing. Energies*.

GoI. (2022). Presidential Regulation 112/2022: *Percepatan Pengembangan Energi Terbarukan untuk Penyediaan Tenaga Listrik. Jakarta*: Government of Indonesia.

GT Management. (2020). *Cost of Production from Geothermal Project in Indonesia*. Jakarta: GT Management.

Gunawan, I. W. (2021). Overview Potensi Panas Bumi di Provinsi Jawa Barat. *Jurnal Energi Baru dan Terbarukan*, 2(2), 60-73.

Harvey, W., & Wallace, K. (2016). *Flash steam geothermal energy conversion systems: single-, double-, and triple-flash and combined-cycle plants. Geothermal Power Generation*. Woodhead Publishing, 249-290.

Hochstein, M., & Sudarman, S. (2008). History of geothermal exploration in Indonesia from 1970 to 2000. *Geothermics*, 37, 220-266.

Hochstein, M., & Sudarman, S. (2015). Indonesian Volcanic Geothermal Systems. *World Geothermal Congress 2015*.

IESR. (2022). *Indonesia Energy Transition Outlook*. Jakarta: Institute for Essential Services Reform.

IRENA. (2017). *Geothermal power: technology brief*. Abu Dhabi: International Renewable Energy Agency.

IRENA. (2022). *Indonesia Energy Transition Outlook*. Abu Dhabi: International Renewable Energy Agency.

Lesmana, A., Winofa, N. C., Pratama, H. B., Ashat, A., & Saptadji, N. M. (2020). Preliminary Financial Modelling with Probabilistic Approach for Geothermal Development Project in Indonesia. *ITB International Geothermal Workshop*. Bandung: IOP Conferences.

Lund, J. W., & Toth, A. N. (2021). Direct Uttilization of Geothermal Energy 2020 Wordwide Review. *World Geothermal Congress 2020+1*. Reykjavik: World Geothermal Congress.

MEMR. (2019, 04 12). *Potensi Pemanfaatan Langsung Panas Bumi di Perhotelan dan Industri*. Retrieved from Berita: https://litbang.esdm.go.id/index.php/news-center/arsip-berita/potensi-pemanfaatan-langsung-panas-bumi-di-perhotelan-dan-

industri#:~:text=Pemanfaatan%20langsung%20panas%20bumi%20di%20Indonesia%20sudah%20mulai%20digunakan%20untuk,%2C%20industri%2C%20dan%20k

MEMR. (2022). Presentasi: *Pengembangan Panas Bumi di Indonesia*. Jakarta: KESDM.

MEMR. (2022b). Presidential Regulation 112/2022 *Percepatan Pengembangan Energi Terbarukan untuk Penyediaan Tenaga Listrik. MEMR*.

MoF. (2016). Peraturan Menteri Keuangan No 172/2016 Tentang *Pengurangan Pajak Bumi dan Bangunan Untuk Kegiatan Usaha Pertambangan/Pengusahaan Panas Bumi Pada Tahap Eksplorasi*. Jakarta: Ministry of Finance Republic Indonesia.

Oya, N., & Takamiya, A. (2020). Introduction of EPC Project for Muara Laboh Geothermal. *GRC Transactions*, 44.

Pambudi, N. A. (2018). Geothermal power generation in Indonesia, a country within the ring of fire: Current status, future development and policy. Renewable and Sustainable Energy Reviews, 81, 2893-2901.

Pambudi, N. A., Itoi, R., Jalilinasrabady, S., & Jaelani, K. (2014). Exergy analysis and optimization of Dieng single-flash geothermal power plant. *Energy Conversion and Management*, 78, 405-411.

PLN. (2021). *Rencana Usaha Penyediaan Tenaga Listrik. Jakarta: Perusahaan Listrik Negara*.

Pratama, H. B., Widiatmo, J. S., & Ashat, A. (2021). Numerical investigative modeling of changes within the Patuha geothermal reservoir and its production sustainability under two different conversion technologies. *Natural Resources Research*, 30(4), 2969-2987.

Rachmat, A., Wibowo, A. S., & Surachman, A. (2018). Exergoeconomic analysis and optimization of a combined double flash–binary cycle for Ulubelu geothermal power plant in Indonesia. IOP Conference Series: *Earth and Environmental Science*, 105, No. 1, p. 012087. IOP Publishing.

Siahaan, M. F., Purba, D., Septiani, G. A., & Paripurna, A. (2022). Preparing Technical and Commercial Documents for Geothermal Exploration Project Financing in Indonesia. *Stanford Geothermal Workshop*. California: Stanford University.

Siahaan, M. F., Septiani, G. A., Purba, D., & Paripurna, A. (2023). Geothermal Exploration Project De-risking: Discussion on Various Scheme. *Stanford Geothermal Workshop*.

Siregar, P. (2004). *Optimization of Electrical Power Production Process for the Sibayak Geothermal Field, Indonesia*. Reykjavic, Iceland: The United Nations University.

Sulistyardi, H. B. (2010). *Basic Design of Lumut Balai 2x55 MW Geothermal Power Plant, Indonesia*. Geothermal Training Program, 615-624.

UNCTAD. (2000). *Tax Incentives and Foreign Direct Investment: A Global Survey*. Geneva: United Nation.

Vakulchuk, R., Overland, I., & Suryadi, B. (2022). ASEAN's *Energy Transition: How to Attract More Investment in Renewable Energy*. Elsevier.

Winofa, N. C., Lesmana, A., Pratama, H. B., Saptadji, N. M., & Ashat, A. (2020). The Application of Numerical Simulation Result for Geothermal Financial Model with Probailistic Approach: A Comprehensive Study. Bandung: *IIGW*.

World Bank. (2018). *Regulatory indicators for sustainable energy*. Jakarta: World Bank.

Yescombe, E. (2014). *Principles of Project Finance*. London: Elsevier.

Yudha, S. W., & Tjahjono, B. (2019). *Stakeholder mapping and analysis of the renewable energy industry in Indonesia*. MDPI.

Navigating Indonesia's Energy Transition: Comparative Advantages of Geothermal, Solar, and Wind Resources

Chandra Hasudungan, Desak Nyoman Inten Apriani, Dorman Purba,
Andreas Suseno, Ferdino R Fadhillah, and Astri Indra Mustika

PT Sarana Multi Infrastruktur (Persero), Sahid Sudirman Center 49th floor, Jakarta, Indonesia

chandra.pmugeothermal@ptsmi.co.id

Keywords: Indonesia Energy Transition, Geothermal Energy, Renewable Energy Potential, Solar and Wind Power, Net-Zero Emissions 2060

ABSTRACT

As Indonesia navigates its ambitious journey towards net-zero emissions by 2060, understanding the role and potential of renewable energy sources becomes imperative. This study presents a rigorous comparative analysis of geothermal, solar, and wind energies, emphasizing their capacity, environmental impact, economic benefits, and feasibility for scale-up within the Indonesian archipelago.

This study findings reveal that Indonesia possesses substantial untapped geothermal potential, with key sites located along the Pacific Ring of Fire. Geothermal energy, capable of providing stable baseload power, is identified as the most viable option for immediate scale-up due to its consistent energy output and lower environmental footprint compared to solar and wind. While solar and wind energy offer significant potential, their intermittent nature and higher land use requirements necessitate robust energy storage solutions and strategic siting to minimize ecological impacts. Indonesia's geothermal resources, estimated at 23,060 MW, are primarily concentrated in Sumatra and Java, offering a stable baseload power with over 16,676.94 GWh produced annually. In contrast, solar and wind energies, despite having a combined potential exceeding 3,400 GW, currently deliver less than 1,000 GWh per year. This underutilization underscores significant scalability opportunities, especially for geothermal energy, which currently operates at only 10.48% of its potential.

The economic analysis reveals that geothermal energy not only supports substantial direct and indirect employment but also contributes robustly to government revenues through fixed and production-based contributions, significantly more than solar and wind. Geothermally enhanced areas witness substantial infrastructural and community development, catalyzing local economic growth.

1. INTRODUCTION

Indonesia has large potential for untapped renewable energy sources, including geothermal, wind, hydro, bio, and solar. Renewable energy provides local and reliable energy supply that increases demand in the future. Indonesia has a rigid plan to accelerate renewable energy utilization the primary source to support energy growth and achieve the country's net zero carbon emissions target (IRENA, 2022). Figure 1 shows Indonesia’s energy demand projection from 2021 to 2032 based on the Ministry of Energy and Mineral Resources-MEMR (2021). The business-as-usual (BaU) scenario shows 4.8% growth per year, while the optimistic (OPT) scenario shows 6% growth yearly. The graph emphasizes electricity as the most significant growing energy demand in ten years.

The significant increase in electricity demand is aligned with the projected power plant supply from 2021-2032 based on MEMR (2022) as shown in Figure 2. The power supply from renewable energy will support 21%-28% of electric power generation in 2032. It has the most increasing pattern over the year, with a detailed breakdown in Figure 3. It is aligned with regulated national energy mix that emphasizes enhancing renewable energy utilization to replace fossil energy. The Government of Indonesia (GoI) set the renewable energy contribution to 23% of the energy mix in 2025, increasing to 31% in 2030.

The more detailed percentages of renewable electricity energy are shown in Figure 3 Indonesia energy mix for power generation in 2021-2030 (modified from PLN, 2021). It emphasizes geothermal as the second largest power generation from renewable energy by 2025. It targeted to support 16.9% of renewable energy power generation, equal to 7.56% of the total national electricity demand, with the increasing pattern over the year (PLN, 2021). Geothermal is also expected to be baseload of electricity that replaces coal’s primary power generation in Indonesia (World bank, 2011).

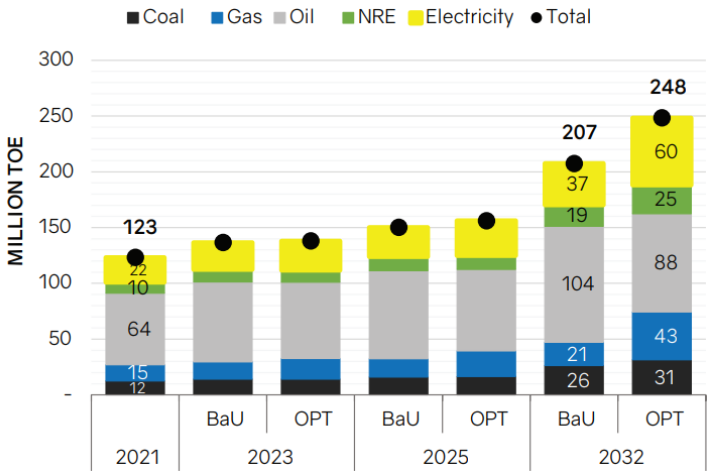

Figure 1: Indonesia energy demand projection 2022-2032 (MEMR, 2022).

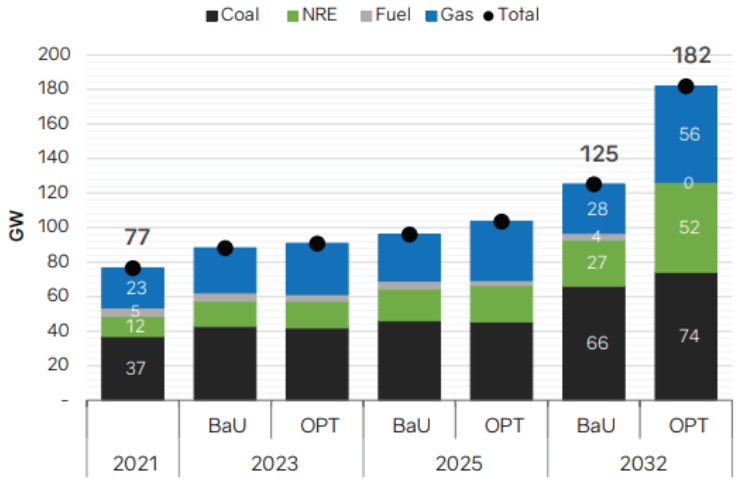

Figure 2: The power plant capacity projection for 2021 – 2032 (DEN, 2022).

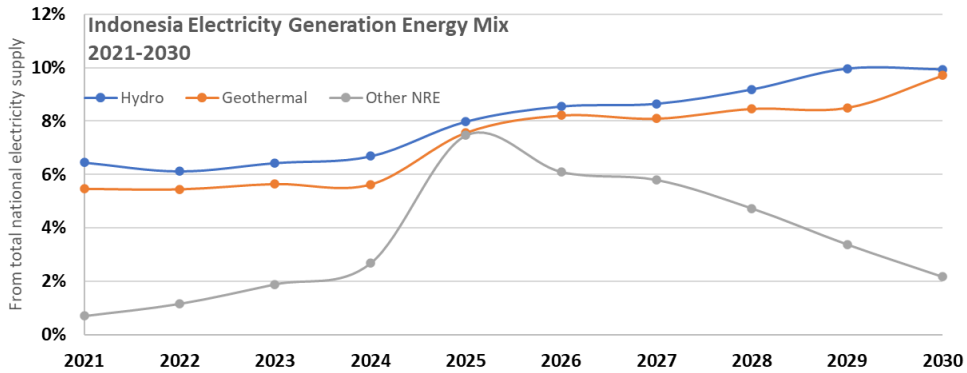

Figure 3: Indonesia energy mix for power generation in 2021-2030 (modified from PLN, 2021).

The primary objective of this study is to conduct a comprehensive comparative analysis of geothermal, solar, and wind energy sources in Indonesia, evaluating their capacity, environmental impacts, economic benefits, and scalability. This analysis aims to identify the most viable renewable energy source for immediate scale-up within the Indonesian archipelago to aid in achieving the nation's ambitious net-zero emissions target by 2060. The central research question of this study is: What are the comparative of geothermal, solar, and wind energy in contributing to Indonesia's renewable energy landscape?

2. INDONESIA GEOTHERMAL LANDSCAPE

The geothermal development in Indonesia has started from colonized era with commercial utilization remarked through Kamojang Geothermal Power Plant (30MW) in 1983. Nowadays, Indonesia is top two geothermal country

in the world with 2,417 MW installed capacity from approximately 23 GW total potential. It means that Indonesia only utilized around 10% of total potential with average additional capacity around 60 MW per annum. Government of Indonesia has plan to utilize geothermal as baseload to replace coal power plant and set the target of utilization to reach 5,799 MW in 2030. The government target emphasizes the significant increase in average of additional installed capacity toward 488 MW per annum from 2024 to 2030. This bold target needs to be achieved by catalyzing geothermal development though better investment condition. Figure 4 shows the historical and target for geothermal power utilization based on EBTKE (2023) and Thinkgeo (2024).

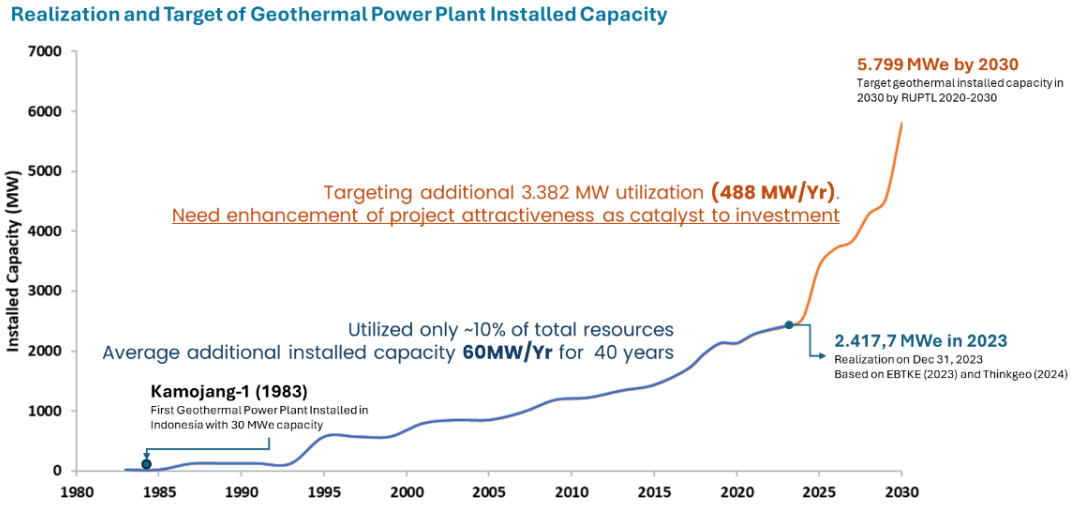

Figure 4: Indonesia geothermal power plant installed capacity and target for 2023 based on EBTKE (2023) and Thinkgeo (2024)

There are 46 geothermal power plants, including the expansion unit, developed by State-Owned Enterprises (SOE) and Independent Power Producer (IPP) in 17 geothermal working areas with dominantly located in Sumatera and Java. From existing conditions as shown in Figure 5, the top-3 of geothermal producers in Indonesia is dominated from IPP sector with KKOB Star Energy Geothermal Ltd. owns the highest capacity among other developers (Figure 5) with the total of 874 MW coming from only 3 geothermal fields. Meanwhile, PT Pertamina Geothermal Energy (Persero) is in second place with the total of 677 MW coming from 6 geothermal fields. These two developers owning half of the total installed capacity in Indonesia while the remaining half is supplied from KKOB Sarulla Operation Ltd., PT Supreme Energy, KS Orka Renewables, PT Geo Dipa Energi (Persero), and PT PLN (Persero). These two majority developers seem have a different development strategy. KKOB Star Energy Geothermal Ltd. tends to maximize the development of a few fields while PT Pertamina Geothermal Energy (Persero) owns more fields with lesser capacity supply.

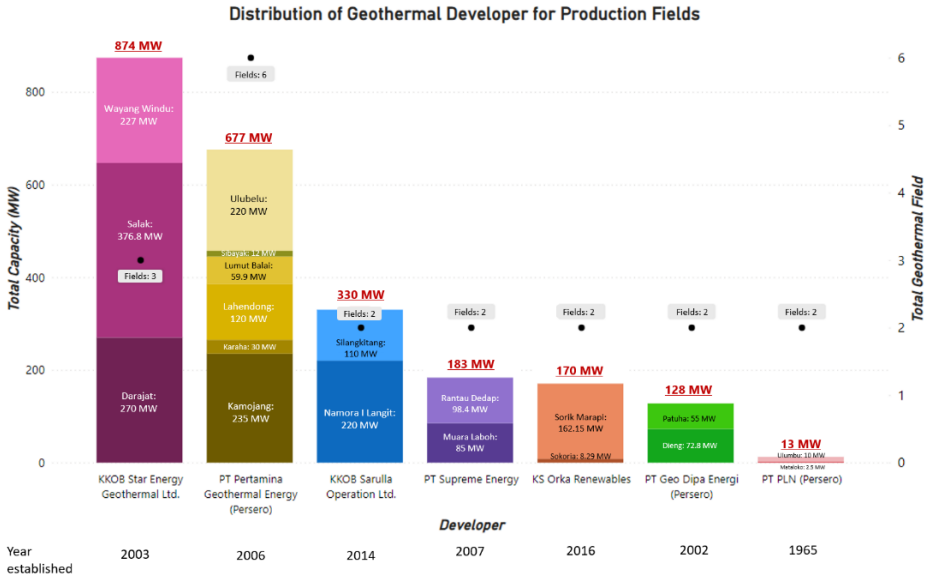

Figure 5: Geothermal player in Indonesia.

3. INDONESIA RENEWABLE ENERGY OVERVIEW

3.1 Geothermal

Geothermal power is energy derived from the natural heat of the earth, captured from hot springs, geysers, volcanic activity, or other processes occurring beneath the Earth's surface. This heat is used to produce steam that drives turbines to generate electricity. Indonesia, with its position along the Pacific 'Ring of Fire', has access to numerous geothermal sites where the Earth's crust is thin and volcanic activity is high, facilitating easier access to geothermal energy.

Geothermal energy is harnessed by extracting natural heat, typically in the form of steam or hot water, from reservoirs via production wells. This steam is then directed to turbines, where its mechanical energy is converted into electricity. The remaining fluid is reinjected back into the subsurface. The mechanism is illustrated in Figure 6. Consequently, geothermal energy utilization is limited to its locations due to its site-specific nature. Additionally, geothermal plants necessitate ongoing monitoring and maintenance to address scaling and corrosion issues in equipment. Geothermal energy, with its high energy density, can generate more power from a smaller footprint compared to solar or wind energy sources. This characteristic makes it a compelling option for renewable energy production, particularly in regions where land availability is limited.

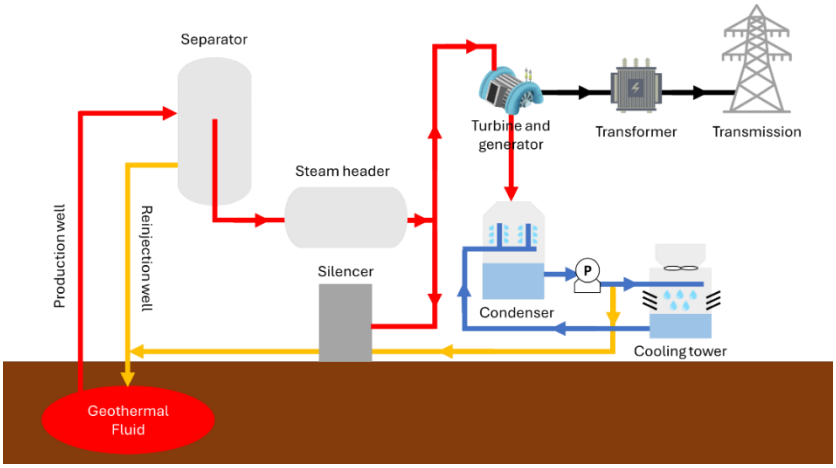

Figure 6: Schematic illustration of geothermal power generation mechanism. Modified design from Yokogawa (2024).

Geothermal technology, well-established and continually innovating, focuses on improving efficiency and reducing costs, particularly for low-medium enthalpy systems (EBTKE, 2023b). Ongoing research aims to enhance resource exploration, optimize drilling techniques, and develop enhanced geothermal systems (EGS) technologies to expand accessible resources. With stable and reliable power generation, unaffected by weather conditions or time of day, geothermal energy can serve as baseload power, typically without the need for storage due to its constant output (Dipayana & Ramadhan, 2022a; IESR, 2022a). In periods of reduced availability, hybrid systems with biomass or conventional backup can maintain supply, with minimal integration challenges compared to intermittent renewables (IESR, 2022a).

Geothermal is currently used widely as an energy source. In Indonesia, the utilization of geothermal energy contributes to government revenues through various tax and non-tax streams. Tax streams including Income Tax (PPh), Value Added Tax (VAT or PPN), Land and Building Tax (PBB), Import Duties, Taxes in the Framework of Import (PDRI), and local taxes and regional levies contribute significantly to state coffers (EBTKE, 2023b). Conversely, the non-tax revenues (PNBP) are sourced from state levies, with 20% allocated to the Central Government and 80% to the Regional Government. These levies consist of fixed contributions for exploration and exploitation, set at $2 and $4 per hectare per year, respectively, alongside production contributions calculated at 5% of the selling price for steam and 2.5% for electricity. Furthermore, production bonuses, following the same 20:80 distribution between the Central and Regional Governments, are also part of the revenue generation scheme (EBTKE, 2023b).

Indonesia ranks among the world's leading geothermal energy producers, securing second place after the USA in terms of generated power capacity, contributing to 14% of the total world installed capacity (ThinkGeoEnergy, 2024). With a current installed capacity of 2.4 GW as of 2024, the nation is actively tapping into its estimated 23 GW potential. Despite this progress, approximately 90% of the total geothermal potential remains untapped, including low-medium temperature resources, indicating ample room for further exploration and development. Geothermal projects are widespread across the archipelago, with significant operations concentrated on Java and

Sumatra, complemented by emerging ventures in less developed regions like Sulawesi and East Nusa Tenggara. Nonetheless, a substantial portion of Indonesia's geothermal potential remains unexplored, underscoring significant opportunities for future expansion. This potential growth is further highlighted in the targets outlined in the RUPTL 2021-2030 (PLN, 2021a; EBTKE, 2023b), aiming for significant additional capacity by 2030.

The Indonesian government, alongside companies like PT Pertamina Geothermal Energy (Persero), is keen on expanding geothermal capacity. This effort is in alignment with the country's $20 billion Just Energy Transition Partnership (JETP) aimed at accelerating the adoption of renewable energy sources and reducing reliance on fossil fuels. In accordance with this effort, the Fast Track Program for geothermal projects also exists to expedite project development. Such initiatives underscore Indonesia's commitment to sustainable energy development and position the country as a key player in the global transition towards cleaner and more sustainable energy sources.

Despite Indonesia's significant progress in harnessing geothermal energy, several challenges persist that hinder further expansion of this renewable resource, notably the high initial cost investment required for geothermal development. Geothermal exploration and development involve substantial upfront investment and geological risk, impacting project finance and insurance rates. Moreover, the development phase of geothermal projects demands expensive capital and entails high upfront investment, ranging from 4.5 to 9 million USD/MW (GRG-Geoenergis, 2024). These costs are offset by moderate to low operational costs and a high-capacity factor over time. The levelized cost of electricity (LCOE) for geothermal energy in Indonesia ranges from 3.56 to 12.06 cUSD/kWh, with capital expenditures (CAPEX) accounting for 6.65 cUSD/kWh and operational expenditures (OPEX) comprising 0.74 cUSD/kWh according to the latest updates by IESR (2024a; 2024b). Additionally, the high-risk, high-cost nature of investment in the exploration stage of geothermal projects poses a significant challenge. Exploratory drilling and reservoir assessments entail substantial financial commitments and technical uncertainties, making it a daunting prospect for investors. Moreover, the development phase of geothermal projects also demands expensive capital and entails high upfront investment notably in the SAGS and power plant construction, contributing to the overall risk profile of such ventures (ESMAP, 2012). Furthermore, geothermal projects often have long development times due to the exploration and drilling phase, typically spanning 5-10 years from exploration to operation (EBTKE, 2023b). Despite these challenges, integrating geothermal energy with other renewables and storage can optimize the energy mix and enhance grid stability despite the high initial costs with addition of stable output of energy so it is not reliant on storage.

Several initiatives have been implemented in Indonesia to promote geothermal energy through de-risking schemes, particularly in the exploration stage. Risk mitigation strategies, including government incentives and international funding, are employed to attract investment in the geothermal sector (World Bank, 2021). One notable initiative is government drilling performed by the Geological Agency to gather essential subsurface information and reduce exploration risks for potential developers. Additionally, Indonesia's geothermal sector has attracted international investment, supported by government policies and international funding (ADB, 2020). Investment rates are influenced by resource risk and high upfront costs, but initiatives like the Geothermal Exploration Risk Mitigation Program (GEUDP) and Geothermal Resource Risk Mitigation (GREM) aim to mitigate these financial risks associated with geothermal exploration activities by providing funding support for exploration drilling.

3.2 Wind

Wind power harnesses the kinetic energy from the wind to turn blades connected to an electric generator to produce electricity. The rotor blade in the wind turbines will rotate when the wind blows following the wind direction for efficiency, and drives a generator inside the turbine housing (Figure 7). The rotational energy is then converted into electrical energy and transmitted to the grid. Optimal performance would be achieved by regular maintenance of the wind turbines, especially for offshore installations.

Modern wind turbines are installed on land or offshore and come in various sizes to serve different needs, from small turbines for individual homes to large wind farms that contribute to the grid. Offshore wind projects offer substantial scalability but at higher costs (GWEC, 2021; GWEC, 2022) while onshore projects are limited by site suitability and land availability.

The wind energy technology is considered mature already with current improvements focused in turbine technology and efficiency. As technology matures and costs decrease, wind energy promises long-term price stability, particularly in regions with strong and consistent wind resources (Wiser, et al., 2011; US DOE, 2021; IEA, 2023), such as coastal regions or open plains. Advances in turbine technology, including larger rotor diameters for lower wind speed sites and floating offshore wind turbines, are expanding feasible locations.

The wind energy in general is intermittent with variable energy density which is highly dependent on local wind conditions. As it is influenced by the weather, location, and altitude, wind energy is considered cannot be a baseload supplier. To manage short-term intermittency, wind energy often utilizes battery storage and it also

necessitates advanced grid management and hybrid systems with other energy sources to maintain grid stability (IESR, 2022a; IRENA, 2022a).

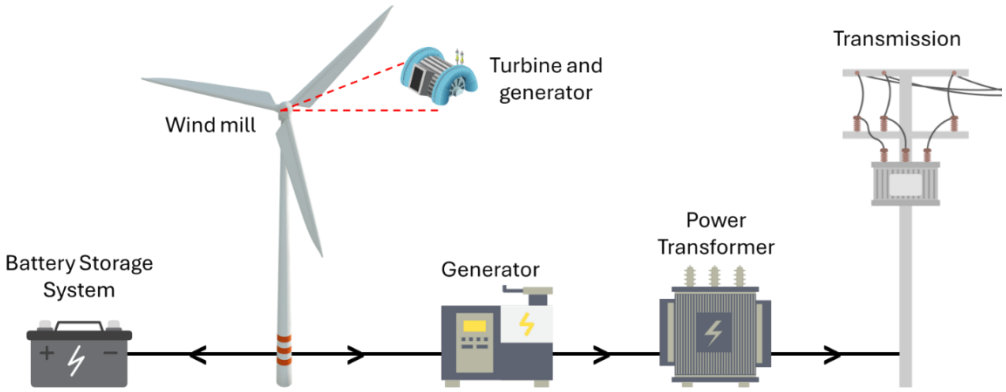

Figure 7: Wind energy power generation from the turbine to the grid and storage.

Wind energy in Indonesia is in a nascent stage. With its long coastline and hilly terrain, Indonesia has pockets of high wind potential, especially in the East and in coastal areas facing the open sea such as East Nusa Tenggara, South Kalimantan, West Java, South Sulawesi, Aceh, and Papua where the wind velocity could reach more than 6 m/s. There have been several pilot projects and studies to evaluate the feasibility of wind farms in the country. As technology advances and investment increases, wind power has the potential to become a more significant part of Indonesia's renewable energy mix, complementing the existing geothermal and solar resources.

Indonesia's wind energy potential is estimated at 155 GW coming from offshore potential for 94.231 GW and onshore for 60.647 GW. The current installation is only 154.3 MW, indicating the underutilization of substantial untapped resources (AEAI, 2022; MEMR, 2022; EBTKE, 2023b; BAPPENAS, 2024). A strategic partnership that aims to develop this sector further, reflecting a growing interest in wind energy despite its current early development stage. Areas like Nusa Tenggara Timur showcase the highest wind energy potential, with the government providing supportive policies and incentives for growth.

The levelized cost of electricity (LCOE) for Onshore Wind in Indonesia ranging from 3.92 to 18.77 cUSD/kWh. According to the latest updates by IESR, the refined LCOE stands at 7.47 cUSD/kWh, with capital expenditures (CAPEX) accounting for 5.45 cUSD/kWh and operational expenditures (OPEX) comprising 2.01 cUSD/kWh (IESR, 2024a; IESR, 2024b). The wind energy project has a moderate development time, ranging from about 3-5 years from site selection to operation but it is subject to permitting and construction timelines.

The development cost for wind project is influenced by site-specific factors and the cost of turbines. The development will be more cost-effective when developed at suitable sites. The onshore wind is among the lowest-cost sources of new electricity generation (Lazard, 2023). The relatively higher cost is usually due to the nascent stage of wind energy development in the country as a result of high initial investments and complex logistics. Offshore wind, not yet developed in Indonesia, would entail higher costs than onshore wind due to the complexities of working in marine environment (GWEC, 2020).

The wind power sector contributes to governmental financial inflows via a dual revenue framework encompassing taxes and non-tax avenues. Taxation revenue from wind power includes Income Tax (PPh), Value Added Tax (VAT/PPN), Land and Building Tax (PBB), Import Duties, and PDRI taxes, in addition to local taxes and regional levies. On the non-tax front (PNBP), the government collects land lease fees and various licensing fees, such as those for business and environmental licenses. Moreover, wind power projects may incur royalty fees when utilizing state-owned resources, further enhancing the sector's fiscal contribution.

Similar to solar, wind projects increasingly incorporate storage to mitigate intermittency. Large-scale batteries and hybrid systems offer long-term solutions but require significant investment. The financial viability of the development improves with advancing storage technologies, decreasing costs, supportive policies, and increasing market competitiveness resulting in significant growth globally in the industry (GWEC, 2021; IRENA, 2021a). Additionally, wind energy, particularly onshore, has seen significant cost reductions, making it competitive with traditional and other renewable energy sources. Robust investment is also seen in offshore wind, facilitated by financial instruments like green bonds and power purchase agreements (GWEC, 2021; GWEC, 2023).

3.3 Solar

Solar power technology captures energy from the sun and converts it into electricity through photovoltaic (PV) cells. These cells allow photons to knock electrons free from atoms, generating electricity directed to the grid or

stored in batteries. The overall mechanism is illustrated in Figure 8. Solar installations range from small rooftop setups to large utility-scale farms, offering scalability. The solar power technology is already mature with ongoing advancements in efficiency and cost reduction. Recent innovations include using higher efficiency PV materials, building-integrated photovoltaics (BIPV), usage of emerging technologies like perovskite solar cells, and floating solar panels on reservoirs and lakes (IRENA, 2019; NREL, 2021; Sharma, 2023). The modular nature of solar technology facilitates rapid deployment (IESR, 2019; IESR, 2021a).

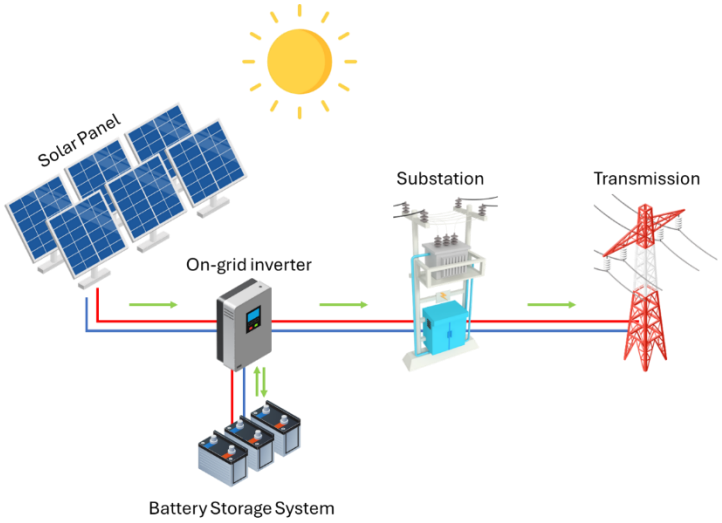

Figure 8: Illustration of solar power generation flow from radiation capture to electricity grid and storage. Modified design from Avenston (2024).

Solar panels require minimal maintenance, primarily cleaning to maintain efficiency. However, solar provides low energy density and requires expansive areas to generate significant power output. Additionally, the intermittent nature of solar energy necessitates the implementation of energy storage solutions to ensure reliability, often complemented by battery systems to enhance flexibility in power distribution. In addressing the storage challenge, solutions such as pumped hydro and flow batteries are commonly employed for larger-scale storage. Furthermore, the integration of solar power with other renewable energy sources and advanced grid management technologies is crucial to bolster reliability and optimize energy production. However, achieving consistent reliability is contingent upon overcoming daily and seasonal variations influenced by factors like weather conditions, geographic location, temperature fluctuations, and daylight duration (IESR, 2022a; IRENA, 2022a). Despite these complexities, solar energy remains a sustainable and progressively cost-effective solution for power generation, playing a pivotal role in meeting global energy demands while mitigating environmental impacts.

The solar energy usage is virtually unlimited and applicable worldwide with particularly strong growth in regions with high solar irradiance. The solar energy potential is widely accessible in Indonesia, scalable for residential to industrial utility scale. The abundant sunshine across the tropical region offers a theoretical potential of over 200 GW peak. Rural electrification programs have been particularly successful in using solar power, and there is a growing trend in urban areas to adopt solar energy for residential and commercial use. Indonesia has a solar potential of 3,294 GW, yet only 317 MW of capacity is currently utilized. Solar resources are abundant across the nation, especially in regions like Nusa Tenggara Timur (NTT), West Kalimantan, and Riau where they experience higher levels of radiation. Indonesia's solar energy sector is burgeoning, with the government actively promoting solar panel installations through incentives and programs. The Indonesia Solar Energy Outlook 2023 underscores solar PV's role in the energy transition, highlighting ongoing projects and future plans. With an average generation potential of 4.8-5.1 kWh/m^2/day, solar energy presents a low-cost and flexible option, supported by investments and initiatives like those from East Ventures into companies such as Xurya, which focuses on expanding rooftop solar power plants. However, compared to its potential, solar power remains underutilized in Indonesia, with opportunities for expansion particularly in decentralized (notably eastern regions) and off-grid areas (PLN, 2021a; PLN, 2021b).

Solar projects typically entail lower upfront costs and shorter development timelines, mitigating investment risk, although policy and regulatory uncertainties can introduce additional challenges (IESR, 2021b; IRENA, 2023a). Development timelines are relatively short, ranging from 1 to 2 years for utility-scale projects and even shorter for residential and commercial installations. Solar energy requires significant investment in storage to manage intermittency (IESR, 2022a). The cost-effectiveness of solar investments depends on the scale of storage and advancements in battery technology (IRENA, 2022b).

Currently, the global photovoltaic (PV) price is declining and battery costs are decreasing, enhancing the feasibility of solar technology (IESR, 2022a; IRENA, 2022b; IRENA & ACE, 2022). It fueled the expansion of the technology although challenges persist in distribution and installation (IRENA & ACE, 2022). Supportive policies such as government incentives also have made solar investments more attractive (IESR, 2022a; BNEF, 2023). Innovative financing models like solar leasing and power purchase agreements (PPAs) have broadened access to capital (SEIA, 2024). In the global case, this results in rapid growth of solar energy market, attracting both local and international investment propelled by cost reductions and efficiency improvements.

The levelized cost of electricity (LCOE) for solar PV utility scale in Indonesia ranges from 4.09 to 10.09 cUSD/kWh, with a refined LCOE of 5.79 cUSD/kWh (4.92 cUSD/kWh for CAPEX and 0.87 cUSD/kWh for OPEX), as per the latest updates by IESR (2024a; 2024b). There has been a 78% decline in solar PPA prices from 2015 to 2022. The current interests in Indonesia's renewable energy industry also emphasize the potential of utility-scale and floating solar power plants. Clear auction mechanisms, transparent local content requirements, and stable policies are advocated to foster the solar industry's growth and meet Indonesia's solar targets (IESR, 2022b).

Utilizing solar energy in Indonesia presents an opportunity for revenue generation through various channels. Within the solar energy sector, the government can generate revenue through both taxation and non-tax mechanisms. Tax revenues are sourced from Income Tax (PPh), Value Added Tax (VAT/PPN), Land and Building Tax (PBB), Import Duties, Taxes related to Imports (PDRI), and a variety of local taxes and levies. Additionally, non-tax revenues (PNBP) can be derived from land lease fees, licensing fees such as business and environmental licenses, and potentially royalties, particularly in cases where solar power projects utilize state-owned resources. These revenue streams contribute to the financial sustainability of solar energy initiatives while supporting government budgets and public services.

3.4 Comparison of geothermal, wind, and solar

Indonesia stands at the forefront of renewable energy, boasting a landscape rich in geothermal, solar, and wind resources. These abundant sources each contribute significantly to the nation's energy transition, showcasing Indonesia's commitment to sustainable development and environmental stewardship. Geothermal energy serves as a cornerstone due to its vast and stable output. Geothermal energy, deriving from subsurface reservoirs primarily found in volcanic areas, offers stable output but requires high initial investment costs. Despite high initial costs, geothermal's consistent base-load capacity offers a predictable financial model.

Conversely, solar and wind are rapidly emerging as key components for the country’s energy transition, supported by technological advancements and favorable government policies. Open-spaced areas provide ideal conditions for the expansive development of these renewable sources. Both solar and wind energy rely on surface factors such as weather and climate and offer lower initial costs, albeit with challenges related to energy storage and grid integration. Managing the intermittency of solar and wind power is crucial for their financial viability, necessitating the implementation of energy storage systems and improved grid integration. However, advancements in technology and changing market dynamics, including decreasing costs for energy storage, hold promise for enhancing the competitiveness of these renewable sources.

The load curve of a power system represents the variation in demand for electricity over time, typically across a 24-hour period. The provided illustration delineates how different fuel sources contribute to meeting this demand (Figure 9), focusing on renewable sources such as geothermal, solar, and wind energy. Geothermal energy, characterized by its ability to provide a constant output, forms the base layer of the load curve, indicating its role as a reliable and stable energy source. Above it, solar and wind energies fluctuate, filling in the mid to peak demand spaces, mirroring their variable nature and dependency on environmental factors.

The capacity factor is a critical measure of the efficiency of power plants, reflecting the actual output over a period relative to the maximum possible output under continuous operation. Geothermal power plants typically have high capacity factors due to the consistency of heat supply from the earth’s core, making them highly reliable for base-load power generation. In contrast, solar and wind energies exhibit lower capacity factors, as they are subject to the variability of weather and time of day. The Figure 9 demonstrates the varying capacity factors of energy sources, with geothermal energy maintaining a steady presence, while solar and wind peak during certain periods.

The load curve and capacity factor analysis underscore the complementary roles of geothermal, solar, and wind energy in an integrated power generation system. Geothermal energy's consistent output is crucial for meeting the continuous baseline demand. It is less affected by climate variability, offering a stable and reliable energy source under changing climate conditions (IPCC, 2023a; IPCC, 2023b). Solar energy's effectiveness can be impacted by changes in weather patterns, cloud cover, and temperature (IPCC, 2011). It peaks during daylight hours, providing substantial energy during midday peaks. Similar to solar energy, wind energy is also affected by weather changes. A shift in the wind pattern may occur due to climate change, affecting wind farm efficiency (Kara & Sahin, 2023).

Wind energy also can offer significant contributions, especially during periods when solar power is reduced. Together, these renewable sources can create a balanced and sustainable energy mix, capable of responding to the grid's demands while reducing reliance on fossil fuels.

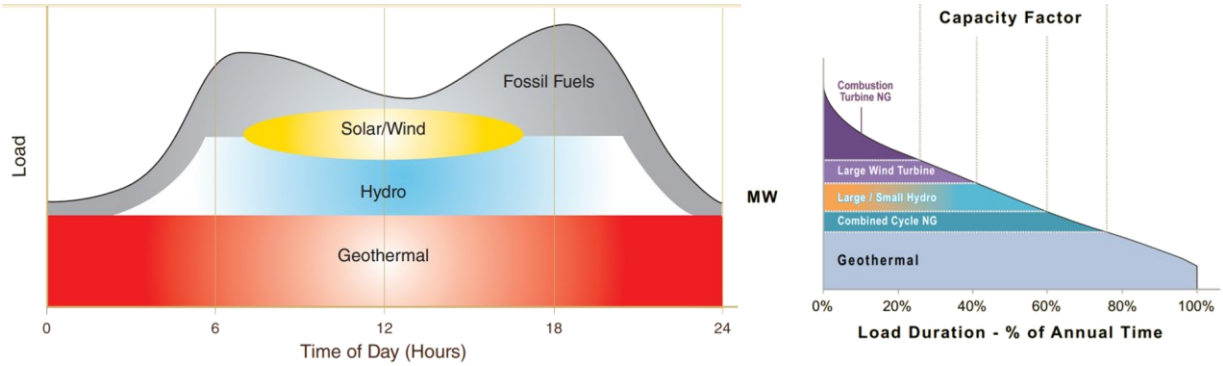

Figure 9: Simplified Load Curve vs Typical Fuel Sources. Modified from Gehringer & Lokhsa (2012).

The analysis of the load curve in conjunction with typical fuel sources highlights the importance of a diversified energy portfolio, with geothermal, solar, and wind energy playing distinctive yet complementary roles. Geothermal energy's reliability, coupled with the targeted contributions of solar and wind, provides a clear pathway toward a more sustainable and resilient energy future. As the world progresses towards cleaner energy solutions, the strategic integration of these renewable sources will be paramount in shaping an efficient and sustainable power generation landscape.

Furthermore, all three technologies present significant opportunities to reduce carbon emissions. Geothermal has a relatively low environmental footprint per MW of electricity generated with emissions primarily from construction and drilling activities, not from operational (Bošnjaković et al, 2019). However, it has potential local environmental impact, including land subsidence and water resources. Geothermal development project utilizes high water usage, primarily during drilling and workover operation, and it is also required for cooling tower in geothermal power plant. Geothermal energy stands out for its efficient land use compared to solar and wind installations of similar capacity, but the exploration area can be extensive (DiPippo, 2008). Sustainable resource management practices are essential to mitigate these impacts (IPCC, 2023a).

Meanwhile, solar and wind projects necessitate careful siting to mitigate impacts on land use and biodiversity. While they require significant land areas for utility-scale projects, which could pose challenges in densely populated regions, wind farms often offer dual land use opportunities for agriculture or grazing, minimizing their actual footprint (Goodale, 2018). However, landscape and wildlife can also be affected. Offshore wind has less visual impact and further reduces land use, but raises concerns about marine habitats (Goodale, 2018). Operational emissions are low in wind project (World Bank, 2011; Farr, H et al, 2021). The emissions come mainly from turbine manufacturing and installation and mitigation strategies are being developed (ESA, 2019). Once in the operational stage, wind farms produce no direct emissions, offering significant environmental benefits (GWEC, 2021). Wind energy installations also have a lower water usage, primarily used for cleaning panels and some in the manufacturing process.

Solar energy has a low emission during operation and contributes significantly to carbon emission reduction. Solar energy's modular or rooftop installations for residential use also have minimal footprints (NREL, 2022a; Silalahi & Gunawan, 2022). However, concerns regarding land use and lifecycle environmental impacts, including manufacturing, transportation, and disposal, are emerging in solar projects, prompting efforts to increase solar panel recycling (PVPS, 2021; NREL, 2022b; Bošnjakovic´, Santa, Crnac, & Bošnjakovi´c, 2023; EPA, 2023). Solar energy installations have a low water usage, mainly for turbine cooling in some designs and maintenance.

4. COST OF DEVELOPMENT BETWEEN GEOTHERMAL, WIND, AND SOLAR

The initial investment costs for renewable energy projects in Indonesia vary significantly depending on the technology. Geothermal projects, for instance, require substantial upfront investment primarily due to the high costs associated with exploration and drilling. However, once operational, geothermal plants benefit from relatively low operational and maintenance costs, and a high-capacity factor due to the consistent availability of geothermal resources.

In contrast, solar power projects demand a lower initial investment, largely due to the decreasing cost of photovoltaic panels and associated equipment. Solar projects can be deployed relatively quickly and are scalable,

allowing for incremental investments aligned with demand growth. Nonetheless, the operational costs, while lower than geothermal, include regular maintenance and potential panel replacement over time.

Wind power projects fall between geothermal and solar in terms of initial investment. The cost of wind turbines and the complexity of site development contribute to the initial costs. Operational expenses are moderate but can be higher in offshore settings due to the challenging environment and accessibility for maintenance.

When comparing the cost-effectiveness of these renewable energy sources, several factors are considered. Geothermal energy, despite its high initial cost, often delivers the best long-term returns due to its consistent base-load power generation capability. Solar energy is increasingly cost-competitive, with declining hardware costs and improving efficiency making it an attractive option, especially for distributed energy solutions. Wind energy's cost-effectiveness is highly site-dependent; in areas with consistent wind patterns, it can offer competitive long-term value.

5. CONCLUSION

The study conclusively identifies geothermal energy as the most viable option for immediate scale-up within Indonesia's renewable energy portfolio, due to its ability to provide stable baseload power and its relatively lower environmental footprint. The findings highlight Indonesia's substantial untapped geothermal potential, particularly along the Pacific Ring of Fire, with an estimated capacity of 23,060 MW. Despite this high potential, the current utilization is just over 10%, signaling a significant opportunity for expansion. Geothermal energy not only promises stable energy output but also brings considerable economic benefits, such as substantial employment opportunities and contributions to government revenue, surpassing those offered by solar and wind energies. The intermittent nature and higher land use requirements of solar and wind energies underscore the need for enhanced storage solutions and careful site planning to optimize their deployment without extensive ecological impacts. The conclusion drawn from this analysis is that, while all three renewable sources hold considerable potential, geothermal energy stands out as the most strategically advantageous for Indonesia, given its current capability and readiness for scale-up.

Table 1: Comparison of Development Costs and Levelized Cost of Electricity (LCOE) for Geothermal, Solar, and Wind Energy in Indonesia.

POINT OF COMPARISON	GEOTHERMAL	SOLAR	WIND
Global Trend Cost	**Slightly increasing,** IRENA (2022b) reports that LCOE for geothermal energy has increased by +6% from 2010 to 2022.	**Significantly decreasing,** IRENA (2022b) reports that Solar PV and Concentrated Solar Power (CSP) was decreased approximately -89% and -69% respectively from 2010 to 2022	**Significantly decreasing,** IRENA (2022b) reports that onshore wind and offshore wind was decreased approximately -69% and -59% respectively from 2010 to 2022
Trend Cost in Indonesia	**Slightly decreasing,** IESR (2023a) reports a slight increase in the LCOE range for geothermal energy, moving from **5.47 – 10.26** in 2019 to **3.56 – 12.06** in 2022.	**Slightly decreasing** IESR (2023a) reports a slight increase in the LCOE range for utility scale solar PV, moving from **5.84 – 12.34** in 2019 to **4.09 – 10.09** in 2022.	**Slightly decreasing,** IESR (2023a) reports a slight increase in the LCOE range for wind onshore, moving from **8.62 – 16.10** in 2019 to **3.92 – 18.77** in 2022.
Levelized Cost of Electricity (LCOE) Global	5.6 USDc/kWh in 2022	**Solar PV:** 4.9 USDc/kWh in 2022 **CSP:** 11.8 USDc/kWh in 2022	**Onshore Wind:** 3.3 USDc/kWh in 2022 **Offshore Wind:** 8.1 USDc/kWh in 2022
Levelized Cost of Electricity (LCOE) Indonesia	The levelized cost of electricity (LCOE) for geothermal energy in Indonesia ranging from 3.56 to 12.06 USDc/kWh.	The levelized cost of electricity (LCOE) for Solar PV Utility Scale in Indonesia ranging from 4.09 to 10.09 USDc/kWh.	The levelized cost of electricity (LCOE) for Onshore Wind in Indonesia ranging from 3.92 to 18.77 USDc/kWh.

POINT OF COMPARISON	GEOTHERMAL	SOLAR	WIND
	According to the latest updates by IESR, the refined LCOE stands at **6.79 USDc/kWh**, with capital expenditures (CAPEX) accounting for 6.65 USDc/kWh and operational expenditures (OPEX) comprising 0.74 USDc/kWh (IESR, 2024a; IESR, 2024b).	According to the latest updates by IESR, the refined LCOE stands at **5.79 USDc/kWh**, with capital expenditures (CAPEX) accounting for 4.92 USDc/kWh and operational expenditures (OPEX) comprising 0.87 USDc/kWh (IESR, 2024a; IESR, 2024b).	According to the latest updates by IESR, the refined LCOE stands at **7.47 USDc/kWh**, with capital expenditures (CAPEX) accounting for 5.45 USDc/kWh and operational expenditures (OPEX) comprising 2.01 USDc/kWh (IESR, 2024a; IESR, 2024b). Then, the offshore wind has LCOE around 11.31 USDc/kWh in 2022
Major Cost Component	In a geothermal project, the major cost components include the **EPC power plant**, which accounts for approximately 34-48% of the total project cost, and **drilling activities**, which represent about 33-51% of the total expense.	For solar PV project in utility-scale, the major cost components are the **PV Modules** that accounts are approximately 35 – 44% of the total project cost, followed by **Balance of System (BOS)** and **Installation labor cost** that account 12 – 26% and 15 -26% respectively	Both in onshore wind and offshore project, the largest cost component is the **Wind Turbine** component that accounts approximately 27.6 – 55.4% from the total project cost. The second largest cost component is typically **substructure and foundation** that account 13 – 27.7% of the total project cost.

REFERENCES

ADB. (2020). *ADB Approves $300 Million Loan to Increase Indonesia's Geothermal Electricity Generation*. https://www.adb.org/news/adb-approves-300-million-loan-increase-indonesias-geothermal-electricity-generation.

AEAI. (2022). *Indonesia Wind Power Potential & Challenges*.

Avenston. (2024). *Solar PV On Grid*. Retrieved from Avenston: https://avenston.com/en/services/commercial-pv/types/on-grid/)

BAPPENAS. (2024). *Bahan Diskusi: Mendorong Investasi Pembangkit Listrik Tenaga Panas Bumi (PLTP)*.

BNEF. (2023). *Cost of Clean Energy Technologies Drop as Expensive Debt Offset by Cooling Commodity Prices*. https://about.bnef.com/blog/cost-of-clean-energy-technologies-drop-as-expensive-debt-offset-by-cooling-commodity-prices/.

Bošnjaković et al. (2019). *Environmental Impact of Geothermal Power Plants*. Tehnicki vjesnik - Technical Gazette.

Bošnjakovic´, M., Santa, R., Crnac, Z., & Bošnjakovi´c, T. (2023). *Environmental Impact of PV Power Systems.* Sustainability 2023, 15, 11888. https://doi.org/10.3390/su15151188.

Dipayana, G. F., & Ramadhan, R. A. (2022a). *Geothermal Energy in Indonesia*. BRIN.

DiPippo, R. (2008). *Geothermal Power Plants: Principles, Applications, Case Studies and Environmental Impact*. Elsevier.

EBTKE. (2023b). *Pengembangan Panas Bumi Indonesia Update Oktober 2023*.

EPA. (2023). *End-of-Life Solar Panels: Regulations and Management*. https://www.epa.gov/hw/end-life-solar-panels-regulations-and-management.

ESA. (2019). *Impacts to Wildlife of Wind Energy Siting and Operation in The United States*.

ESMAP. (2012). *Geothermal Handbook: Planning and Financing Power Generation*.

Farr, H et al. (2021). *Potential environmental effects of deepwater floating offshore wind energy facilities*. Ocean and Coastal Management 207 (2021) 105611.

Gehringer & Lokhsa. (2012). *Geothermal Handbook: Planning and Financing Power Generation*. ESMAP Technical Report.

Goodale, M. (2018). *Cumulative adverse effects of offshore wind energy development on wildlife*.

GRG-Geoenergis. (2024). *Overview of Geothermal Development in Indonesia: Current Update and Upcoming Projects*.

GWEC. (2020). *Global Wind Offshore Report 2020*.

GWEC. (2021). *Global Offshore Wind Report*.

GWEC. (2022). *Global Offshore Wind Report 2022*.

GWEC. (2023). *Global Wind Report 2023*.

IEA. (2023). *Why is wind power important?* https://www.iea.org/energy-system/renewables/wind.

IESR. (2019). *Harnessing Indonesia's Solar Potential: Yellow is The New Black*. https://iesr.or.id/harnessing-indonesias-solar-potential-yellow-is-the-new-black.

IESR. (2021a). *Beyond 207 Gigawatts: Unleashing Indonesia's Solar Potential. Nationwide solar potential assessment based on geographic information system (GIS) mapping* .

IESR. (2021b). *Indonesia Energy Transition Outlook 2022*.

IESR. (2022a). *Indonesia Energy Transition Outlook 2023. Tracking Progress of Energy Transition in Indonesia: Pursuing Energy Security in the Time of Transition*.

IESR. (2022b). *Having Slow Solar PV Development in 2022, Indonesia Needs to Push the Implementation of Supporting Policies*. https://iesr.or.id/en/having-slow-solar-pv-development-in-2022-indonesia-needs-to-push-the-implementation-of-supporting-policies.

IESR. (2023a). *Making Energy Transition Succeed: A 2023's Update on the Levelized Cost of Electricity and Levelized Cost of Storage in Indonesia*. IESR.

IESR. (2024a). *Indonesia Energy Transition Outlook (IETO)*.

IESR. (2024b). *Indonesia LCOE Calculator by IESR*.

IPCC. (2011). *Renewable Energy Sourcecs and Climate Change Mitigation*.

IPCC. (2023a). *Geothermal Energy*.

IPCC. (2023b). *Climate Change 2023 Synthesis Report*.

IRENA & ACE. (2022). *Renewable Energy Outlook for ASEAN Towards a Regional Energy Transition*.

IRENA. (2019). *Future of Solar Photovoltaic: Deployment, investment, technology, grid integration and socio-economic aspects*.

IRENA. (2021a). *Renewable Energy and Jobs: Annual Review 2021*.

IRENA. (2022). *Indonesia Energy Transition Outlook*. Abu Dhabi: International Renewable Energy Agency.

IRENA. (2022a). *Indonesian Energy Transition Outlook*.

IRENA. (2022b). *Renewable Power Generation Costs*.

IRENA. (2023a). *World Energy Transitions Outlook 2023*.

Kara, T., & Sahin, A. D. (2023). *Implications of Climate Change on Wind Energy Potential*.

Lazard. (2023). *Levelized Cost of Energy*.

MEMR. (2022). *Wind Energy Potential per Province*.

NREL. (2021). *New Perovskite Design Shows Path to Higher Efficiency*. https://www.nrel.gov/news/program/2021/new-perovskite-design-shows-path-to-higher-efficiency.html.

NREL. (2022a). *Environmental and Circular Economy Implications of Solar Energy in a Decarbonized U.S Grid*.

NREL. (2022b). *Environmental and Circular Economy Implications of Solar Energy in a Decarbonized U.S. Grid* .

PLN. (2021). *Rencana Usaha Penyediaan Tenaga Listrik. Jakarta: Perusahaan Listrik Negara*.

PLN. (2021a). *Rencana Umum Penyediaan Tenaga Listrik (RUPTL) 2021 - 2030*. PLN.

PLN. (2021b). *Optimizing Strategy in Realizing Sustainable Energy Transition*.

PVPS. (2021). *Annual Report 2021*.

SEIA. (2024*). Solar Industry Research Data*. https://www.seia.org/solar-industry-research-data.

Sharma, V. (2023). *COMPARATIVE ANALYSIS OF CURRENT SOLAR TECHNOLOGIES AND PEROVSKITE SOLAR TECHNOLOGY*.

Silalahi, D. F., & Gunawan, D. (2022). *Solar Energy Potentials and Opportunity of Floating Solar PV in Indonesia*.

ThinkGeoEnergy. (2024, January 8). *ThinkGeoEnergy's Top 10 Geothermal Countries 2023 – Power Generation Capacity*. Retrieved from ThinkGeoEnergy: https://www.thinkgeoenergy.com/thinkgeoenergys-top-10-geothermal-countries-2023-power-generation-capacity/

US DOE. (2021). *Offshore wind market report: 2021 edition*.

Wiser, R., Z. Yang, M., Hand, O., Hohmeyer, D., Infi eld, P. H., Jensen, V., . . . Sinden. (2011). *Wind Energy*. In IPCC Special Report on Renewable Energy Sources and Climate Change.

World Bank. (2011). *Greening the Wind: Environmental and Social Considerations for Wind Power Development*.

World bank. (2011). *Penggunaan energi panas bumi Indonesia akan naik secara signifikan*. Retrieved from World Bank: https://www.worldbank.org/in/news/feature/2011/07/26/indonesia-expand-geothermal-power-alternative-coal

World Bank. (2021). *Indonesia Geothermal Resource Risk Mitigation Project (GREM).*

Yokogawa. (2024). *Geothermal Power*. Retrieved from Yokogawa: https://www.yokogawa.com/eu/industries/renewable-energy/geothermal-power/#Challenges

INSAN SMART - APIForestry and Natural Forest Succession Approach to Achieve Sustainable Community-Based Forest Restoration

Muhammad Riyadhi, M. Panji Pranadikusumah, and Iqbal Abi Yaghsyah

Star Energy Geothermal Darajat II, Limited

m.riyadhi@starenergy.co.id

Keywords: biodiversity, forest conservation, geothermal energy, social innovation

ABSTRACT

Geothermal Power Plant is one of the Power Plants that embraced forest to maintain the power supply sustainability. Located partly in Taman Wisata Alam Gunung Papandayan (Nature Park) and Darajat Protected Forest in Garut Regency, West Java, Indonesia, Star Energy Geothermal Darajat (SEGD) has always been in effort in maintaining the forest surrounding the facilities. The objective of this study is to descrobe the performance of INSAN SMART, a sustainable community-based forest restoration project at Cigupakan Area with apiforestry approach and by simulating natural forest succession. The study shows high level of trees survival rate and biodiversity while providing livelihood to the community.

1. INTRODUCTION

Forest encroachment is a global issue that has yet to be solved. Rapid industrial development causes land clearing for conversion to other uses to occur at an alarming pace. The loss of forests can lead to the loss of ecological services such as clean water, clean air and flood prevention. Forest lost also affect ecological services provided by biodiversity such as natural pollination, natural pest control and resources provider. These ecological services often forgotten and deemed not important, although in fact it is as much important as the industrial development itself. Without the services and the resources provided by nature, it is impossible for the industrial activity to run.

Although forest restoration effort always being promoted, the forest area that were lost doesn't get better in fact it keeps getting worse. This is because ecosystem recovery takes a long time which cause forest lost rate is always faster than forest recovery rate. In addition, social issues contribute to the obstruction of the ecosystem recovery process. People with low economies tend to live with nature and take resources from nature directly. The local often utilize natural resources from nearby forest, resources taken include clean water, goods such as wildlife and woods, etc. In addition, the community is also encroaching forest areas to be used as agricultural land. Even though the government already made a regulation on land usage the locals won't budge. Efforts to educate the community to leave the protected areas alone or adopt agroforestry farming systems have been fruitless. The community believes that vegetable crops are more profitable and has faster capital turnover. Therefore, there is a need for an innovative planting system that generates profits but does not damage the forest.

INSAN SMART is an ecosystem restoration program conducted by Star Energy Geothermal Darajat II, Limited. This program adopts an apiforestry system, which is a combination of bee cultivation (*Apis cerana*) with production crop cultivation in the form of stands. Some types of plants planted are pioneer plants, fruit plants and native plants of Mount Papandayan. Honey cultivation was chosen because the process does not require land clearing, on the contrary, honey cultivation requires a lot of flowering plants as food for bees to produce honey. In the process, this program is in collaboration with the Darajat Honey Forest Farmer Group and is supported by BKSDA.

The purpose of this paper is to describe the results of the INSAN SMART program. This paper will describe the efficiency of the apiforestry program and its implementation in the field. Hopefully this program will encourage successful reforestation program all around the globe.

2. METHOD

2.1 Study Site

Research was conducted from August 2022 to March 2024 in a Darajat Geothermal Power Plant located in Pasirwangi Village, Garut, West Java, Indonesia (coordinate 07°11'09"- 07°15'40"S and 107°41'54"-107°45'40"E). The study location is specified to piece of land within an area called Cigupakan. This 1.8 ha area is part of Star Energy Geothermal Darajat operation area which the company decide to use this land as a reforestation zone. Darajat Power Plant is located within Taman Wisata Alam (Nature Park), Hutan Lindung (Protected Forest) and private land with elevation around 1740-2200 above sea level in a valley near Mount Kendang which is part of Papandayan Mountains.

Figure 1: Forest Restoration Site.

2.2 Procedure

Participant observation method with action research approach were used to collect the Data. Data were collected directly while the observer themselves participated on the event. The subjects are not aware that they are being watched (Ugwu et al, 2023). The program is consisted of planting trees, trees maintenance and beehive installation. All activities are being observed and recorded.

2.3 Data Analysis

Data were analyzed using Interpretative phenomenological analysis. Data then presented using qualitative descriptive approach. The presentation of data from a qualitative descriptive study involves a straight forward descriptive summary of the informational contents of the data that is organized in a logical manner (Jiggins et al., 2016).

3. RESULT AND DISCUSSION

One of the environmental problems in Darajat is the shrinking forest area. The depletion of forest area occurs mostly in protected forest areas. Although protected forest regulation requires the land utilization to use an agroforestry system by combining production crops with tree stands, in practice there are many garden areas that use a homogeneous plantation system. Some types of crops grown by the community include cabbages, potatoes, carrots, chillies and other annual crops.

Homogeneous planting systems cause many environmental problems. This is because homogeneous planting systems cannot accommodate many diverse types of fauna that are useful for maintaining environmental balance (Vellend et al., 2007). The lack of canopy cover in the plantation area results in a lack of water infiltration and increases soil erosion by water (Yücesan et al., 2019). The steep slope adds to the high runoff rate of rainwater that causes erosion in the plantation area and increases the potential for flooding in the Garut City.

Efforts have been made to replant the plantation to restore its function as a protected forest. However, these efforts have been fruitless. The reason is that every time planting is carried out in the plantation area, the plant seeds that have been planted will be plucked after a few days of planting. Some of the factors that cause the loss of these seedlings are the lack of care and supervision of the seedlings. It is not uncommon for seedlings to be deliberately uprooted because it is considered that they will block the sunlight from the vegetable plants and cause the quality of the harvested vegetables to be less than optimal. The slow-growing nature of tree species makes it difficult to monitor tree growth.

Based on these problems, it can be concluded that innovative reforestation efforts are needed that use fast-growing tree species, intensive supervision and care of seedlings and agroforestry systems that provide profit for the locals. The Apiforestry system was chosen for the implementation of the reforestation programme in the Darajat

Geothermal area. The Apiforestry system is a combination of a beekeeping system with an agroforestry system. In the implementation of the INSAN SMART programme, the community, namely the Kelompok Tani Hutan (KTH) Madu Darajat Berkah and the government agency, namely the West Java BKSDA Seksi Konservasi Wilayah (SKW) V, ensure the success of the programme.

3.1 Reforestation Program

The reforestation programme in this study uses a system that replicates the natural succession process in nature and accelerates it. Succession is a process of change in ecological and environmental aspects that continues regularly over a period of time and forms new biodiversity communities. Succession is a long process that takes a long time. Natural succession couldn't keep up with the rate of forest destruction, where the forest recovery rate is slower than the forest destruction rate. It is hoped that accelerating the succession process can increase the success rate of forest reforestation programmes.

Succession replication is carried out by planting local plants in the Mount Papandayan Nature Reserve combined with fast-growing plants we called pioneer plant. The planting distance used is 4x4 meters where endemic plants planted in the middle (figure 2). The type of fast-growing plant used is Kibadak (*Alnus* sp). Kibadak plants were chosen because they have a fast growth rate. Kibadak will provide shade and protection to local plants that require longer growing time. Kibadak's shade cover will maintain soil moisture in the dry season and inhibit the growth of weeds that could potentially inhibit the growth of local plants (Isaac et al., 2024). After planting, the saplings are cared for by watering during the dry season, fertilizing and weeding. Plant growth is always monitored and recorded. In addition to local plants, production plants are planted that will become bee food for honey bee cultivation.

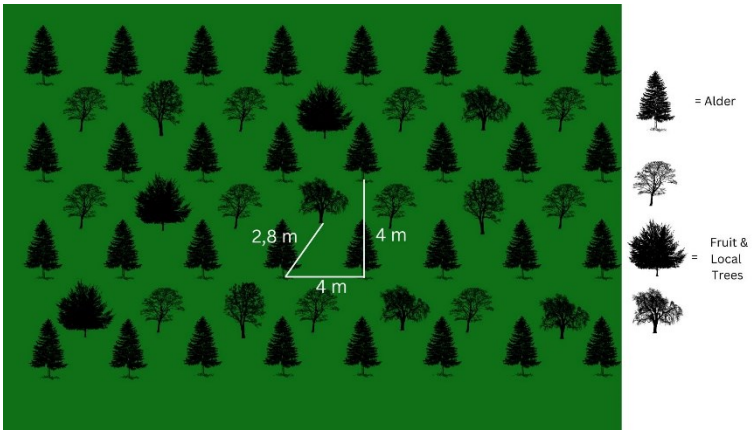

Figure 2: Planting model.

Restoration activity was carried out by SEGD together with KTH Madu Darajat Berkah, which is an organization assisted by BBKSDA West Java SKW V. This community organization deeply aware of the importance of protecting the environment. Members of KTH Madu Darajat Berkah often conduct reforestation and tree planting activities around Mount Papandayan. The restoration project was guided and supervised by BKSDA officers. Planting is carried out in the Darajat Geothermal Field area which is part of the SEGD Right of Way (RoW). Thus this restoration program is a collaboration of three institution.

The restoration program shows promising results. After 22 months after planting, the kibadak plants have reached an average height of 3 meters. Kibadak trees that were planted grows really well and there are no indications of plant uprooting by irresponsible parties. The presence of buffaloes grazing in the planting area did not hinder the growth and development of the kibadak plants. The fast-growing kibadak plants provide shade and shelter to the slower-growing local plants. The thick trunk and dense canopy make it difficult for buffalo herds to pass through the planting area. The dense canopy cover is also expected to inhibit the growth of grasses that require a lot of sunlight. Eventually the grasses in the planting area will disappear and reduce the buffalo's interest in visiting the planting area.

Some local plants have been planted in the Cigupakan area. Local plants were planted simultaneously with pioneer plants. Local plants continue to be added throughout the year. Local plants couldn't be planted in abundance number. This is because the availability of local plant seedlings is difficult to obtain. Because local seedlings have not been widely cultivated and most types of forest plants cannot be cultivated, planting local plants is mostly done by moving plant seeds from protected forest areas around the plantation. Currently, 30 types of local plants have been planted with the number as in the table 1.

Figure 3: Buffalo grazing at plantation area.

Table 1: List of plants.

No	Species	Amount
1	Babasaran	150
1	Beleketebe	4
1	Cantigi	3
4	Caringin	400
5	Cerem	128
6	Dayang	150
7	Huru bentol	9
8	Huru bodas	261
9	Huru cabe	1
10	Huru katulampa	154
11	Huru leueur	12
12	Huru sintok	3
13	Jamuju	1
14	Kaliandra Merah	0
15	Kalimorot	100
16	Karika	50
17	Ki amis	1
18	Ki badak	6000
19	Ki beuruem	162
20	Ki honje	1
21	Ki hujan	170
22	Ki jambe	1
23	Ki jeruk	255
24	Ki putri	75
25	Ki sapu	50
26	Ki Sireum	150
27	Ki tembaga	13
28	Larapuyan	2
29	Puspa	102
30	Ramogencel	200
31	Santos lemon	15
Total		8623

3.2 Bee keeping Program

In addition to the reforestation program, SEGD collaborated with KTH Madu Darajat Berkah and BBKSDA Jabar SKW V to develop a honey farm based on sustainability by combining it with an agroforestry system. This

program is carried out with the same institution as the reforestation program because this activity is part of a series of activities.

Honey cultivation is one of the activities of the Darajat community that has been carried out for a long time. There are two types of honey that are utilized by the Darajat local community, namely Odeng (*Apis dorsata*) & Nyiruan (*Apis cerana*). Odeng is a wild forest honeybee that cannot be cultivated. This honey bee has a large size nests placed in high branches. While nyiruan is a bee that comes from the forest, but this species has the characteristics of a smaller body size, likes to nest in weathered wood or in the ground and is more docile so that it is possible to be cultivated (Niem & Trung, 1999).

Honey farming was chosen because honey is one of the natural resources of non-timber forest products. Honey farming does not require large tracts of open land to operate, instead honey farming requires lush, overgrown land with food plants (flowering plants). In addition, pure honey has a high economic value, so honey cultivation is a business opportunity that generates high income but does not damage the forest. Members of KTH Madu Darajat Berkah understand this very well, therefore they are determined to carry out reforestation activities, especially by planting flowering plants such as red calliandra (*Calliandra calothyrsus*), *Xanthostemon Chrysanthus* and fruit plants.

KTH Madu Darajat Berkah is tasked with making bee boxes and finding bee colonies for cultivation. The honey box is made from wooden boards with a length of 30 cm, a width of 26 cm and a height of 40 cm. The top of the box can be opened to harvest honey and conduct colony checks. Inside the box, frames are placed as a place for bees to build nests that will later be used to store honey. In one honey box, 8-12 frames are placed. The honey bee used for honey cultivation is the A. cerana (Nyiruan) species.

The process of taking bee colonies is carried out by removing colonies from nature (such as in tree branches, dead wood and from the ground). Taking bee colonies begins with finding bee colonies in nature. The type of bee colony must be confirmed that the type is A. *cerana* and not A. *dorsata* which is a type of bee that cannot be cultivated. Once the bee colony is found, fumigation is carried out. Fogging is done to reduce attacks from bee colonies. Then the queen bee of the target bee colony is identified. Queen bees have a different morphology from worker bees. The queen bee is bigger in size . After identification, the queen bee is separated from the colony by putting the queen bee into a special container to avoid the escape of the queen bee. Then the queen bee is put into the box. Instinctively, worker bees will follow where the queen bee goes, so that when the queen bee is stored in the box, the colony will automatically enter the box. Then transfer the honeycomb containing honey, pollen and bee pupae into the box. Honey and Pollen serve as a food source for bee colonies. After the entire bee colony follows the queen into the box, the box is closed and moved to the beekeeping area.

During bee harvesting, KTH members will use safety equipment in the form of a bee veil to cover the head and face. Honeybee safety standards require honey harvesters to wear special clothing that covers the entire body of the person harvesting the honey. Bee stings can cause allergic reactions that cause hives and even shortness of breath (Rayamane et al., 2014). However, KTH members who do honey harvesting are used to bee stings. They often do not use special clothing to protect their bodies. If stung by bees, they will show mild allergic reactions such as rashes and inflammation around the sting marks.

Bee colonies can be harvested after two to four weeks, depending on feed availability. At the change of seasons, honey production is very high. This is because at the turn of the season many plants start to flower so the bees can produce a lot of honey. Honey is harvested by smoking the bee colonies first to reduce the stinging potential of the bee colonies. Then the honey box is opened while still being smoked. The frames inside the box are taken out and the honeycomb built on the frames by the bees is taken using a knife and placed into a container. Only half of the frames in the bee box are harvested. Over-harvesting can cause the bee colony to stress and leave the hive box.

In addition to relying on honey from cultivation, the group also collects honey from people who have honey boxes. In addition to A. cerana honey, the group also receives A. dorsata forest honey purchased from forest honey hunters. The profession of forest honey hunter is a side job that still exists in the Darajat area, this is because the Darajat area still has many beautiful forest areas. So it is possible for forest bee colonies to develop.

The honey collected will then be packaged into several products. The products sold are honey that has been separated from the hive and honey that is sold together with the hive. The collected honey will be stored in a large plastic overnight. The honey will flow out of the hive and gather at the bottom of the plastic. The separated honey will then be filtered using a 60 mesh filter cloth. The filtered honey is then packed into plastic bottles of various sizes. The packaging sizes used include 100 ml and 250 ml. Beehives that have been taken honey are sold as honey with hives.

The honey produced from the cultivation process has a variety of different flavor notes depending on the type of forage eaten by the honeybees. Forest honey and honey collected from other places have taste notes of coffee,

chayote and forest plants. Group-produced honey generally has a taste note of calliandra. The taste note of calliandra has a sweet, floral aroma and a very sweet taste and not too thick viscosity. It is generally bright yellow in color and clear.

Honey cultivation has many challenges in its implementation. Some of the problems faced are extreme weather changes, animal disturbances and human disturbances. Various efforts have been made to anticipate and overcome the impact of these challenges.

The Apiforestry activity program is an example of the implementation of 3 P (People, Profit & Planet) sustainability. The implementation of the 3 P's is in line with the Company's vision and mission of renewable energy, namely the sustainable use of natural resources. This is because renewable energy is highly dependent on renewable resources generated by ecosystem services.

4. CONCLUSION

Apiforestry activities are forest restoration activities that involve local communities. This program implements the 3 P concept, namely People, planet and profit. The implementation of the 3 P's allows forest restoration efforts to run sustainably. Some of the factors that led to the success of this program are as follows:

1. Planting is done in SEGD areas where intensive monitoring is possible.
2. Activities are carried out in collaboration with state institutions engaged in conservation and also community organizations that are passionate about forest reforestation efforts.
3. Planting uses a planting model that combines pioneer and local plants.
4. The apiforestry model generates economic benefits so that the community sees the benefits in forest management efforts.

REFERENCES

Cropley, Arthur. (2023). Qualitative Research Methods: A Practice-Oriented Introduction.

Isaac, M.E. *et al.* (2024) 'Shade tree trait diversity and functions in agroforestry systems: A review of which traits matter', *Journal of Applied Ecology*, 61(6), pp. 1159–1173. doi:10.1111/1365-2664.14652.

Jiggins Colorafi, Karen & Evans, Bronwynne. (2016). Qualitative Descriptive Methods in Health Science Research. HERD: Health Environments Research & Design Journal. 9. 10.1177/1937586715614171. Interpretative phenomenological analysis

NIEM, N.V. and TRUNG, L.Q. (1999) 'Morphological comparison of three Asian native honey bees (apis cerana, A. Dorsata, A. Florea) in northern Vietnam and Thailand', *BIOTROPIA* [Preprint], (14). doi:10.11598/btb.1999.0.14.153.

Rayamane, Anand & P, kumar & G, kishor & R, Dayayanada & Saraf, Ashish. (2014). HONEY BEE STINGS AND ANAPHYLAXIS: REVIEW. Journal of Forensic Medicine, Science and Law. 23.

Ugwu, Chinyere & Eze, Val. (2023). Qualitative Research. 8. 20-35.

VELLEND, M. *et al.* (2007) 'Homogenization of forest plant communities and weakening of species–environment relationships via agricultural land use', *Journal of Ecology*, 95(3), pp. 565–573. doi:10.1111/j.1365-2745.2007.01233.x.

Yücesan, Zafer & Hacisalihoglu, Sezgin & Kezik, Ugur & Karadag, H.. (2019). Effects of canopy on soil erosion and carbon sequestration in a Pedunculate Oak (Quercus robur L. subsp. robur L.) coppice stand during the conversion process into high forest. Austrian Journal of Forest Science. 45-66.

Hill, Deborah & Webster, Thomas. (1995). Apiculture and forestry (bees and trees). Agroforestry Systems. 29. 313-320. 10.1007/BF00704877.

Analysis of CO_2 Emission Intensity of Geothermal Power Plant: Case Study Star Energy Geothermal Darajat II, Limited

Muhammad Riyadhi and Micia Zaputi Rohimah

Star Energy Geothermal Darajat II, Limited

m.riyadhi@starenergy.co.id

Keywords: CO_2 emission intensity, geothermal energy, JAMALI, sustainability performance, sustainable energy

ABSTRACT

The renewable energy sector has developed in recent years, marking a turning point toward a greener energy future. Among other options, geothermal energy stands out as a promising solution, particularly for Indonesia. Geothermal energy utilizes natural energy sources, geothermal fluid, that are present within geothermal reservoirs. With its abundant geothermal potential reserves, Indonesia has the opportunity to utilize this resource to meet the nation's energy demand while simultaneously reducing the dependence on fossil fuels. The reliability of geothermal energy further enhances its appeal as a sustainable solution, offering consistent and dependable power over a long time. Geothermal energy generates minimal environmental impacts since it requires less land areas relative to other power plants. Since geothermal power plants only utilize geothermal steam, they emit less emissions during the process relative to fossil fueled power plants. Geothermal power plants generate minimal CO_2 because there is no fossil fuel-based combustion during the electricity generation. The primary emission contributors of geothermal energy are carbon dioxide (CO_2), hydrogen sulfide (H_2S), and ammonia (NH_3) since they are naturally present in the steam as Non-Condensable Gas (NCG). However, these emissions are lower compared to those from fossil-fueled power plants. Star Energy Geothermal Darajat power plant (SEGD) is a prime example of geothermal energy utilization in Indonesia. With a combined capacity of 274.5 MW, SEGD provides continuous electricity to the communities connected to the Java, Madura, and Bali (JAMALI) interconnection system. This study aims to analyze SEGD's CO_2 emission intensity and evaluate the company's sustainability performance. Utilizing a quantitative method, the study shows that SEGD has a CO_2 emission intensity that is lower than the JAMALI interconnection system, thus providing more sustainable energy.

1. INTRODUCTION

According to Ministry of Energy and Mineral Resources (2022), Indonesia is facing an increase in electrical energy demand, currently reaching 40 GW, with the highest demand coming from the Java, Madura, and Bali regions, accounting for 72.4% of this total in 2020. This growing demand is driven by economic growth, with annual projections indicating an increase of 5% to 6% in the years ahead. However, Indonesia still relies heavily on fossil fuels, predominantly coal and oil, to meet these energy demands. This situation is still likely to happen in the following years. Coal accounts for 61.5% of total electricity generation in Indonesia, while oil and biofuel contribute 6.20%. Gas makes up 16.8%, whereas new and renewable energy sources, despite their potential, currently represent a share of 15.5% (PwC, 2023). This new and renewable sector includes hydropower, geothermal, solar, wind, and other energy, all of which hold the potential to support a clean energy transition for the nation. Expanding new and renewable energy utilization represents a promising approach to growing energy demands while reducing the demand for and dependency on fossil fuels.

Indonesia's energy sector still relies heavily on fossil fuels as the primary source of electricity generation, a trend expected to persist well into the following years. As outlined by PLN (2021), coal-fired power plants are projected to increase by 35% from 134 TWh in 2021 to 264 TWh in 2030. Moreover, coal will contribute approximately 60% of the country's electricity generation mix by 2030. In the same period, gas utilization as an electricity generation source is also predicted to increase by almost half while oil use plummeted. Indonesia's dependence on fossil fuels will continue, reinforced by the planning and development of new fossil-fueled plants. This significant dependence on fossil fuel is primarily driven by its cost-effectiveness relative to alternative electricity generation methods. Besides that, the availability of fossil fuels within Indonesia and their compatibility with existing transportation infrastructure also contribute to their popularity in the energy sector.

The dominance of fossil fuels in Indonesia's energy sector has environmental consequences, including air emissions. Currently, the energy sector ranks as the nation's second-largest emitter of greenhouse gas emissions, with electricity generation alone accounting for over 40% of these emissions. Projections indicate this percentage could escalate to 58% by 2030 if the current situation continues. The main contributor of emissions emitted from the energy sector is coal power plants, particularly carbon dioxide. Among other power plants, coal-fired plants emit the highest proportion of emissions, accounting for up to 84.2% of the total emissions generated within the

sector. Oil and gas contributed roughly 11.3% and 4.5% of the emissions, respectively (IEA, 2023).

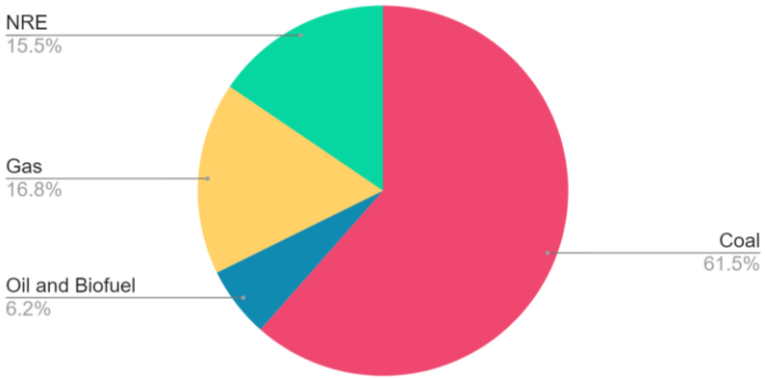

Figure 1: Indonesia's Electricity Mix Percentage in 2022.

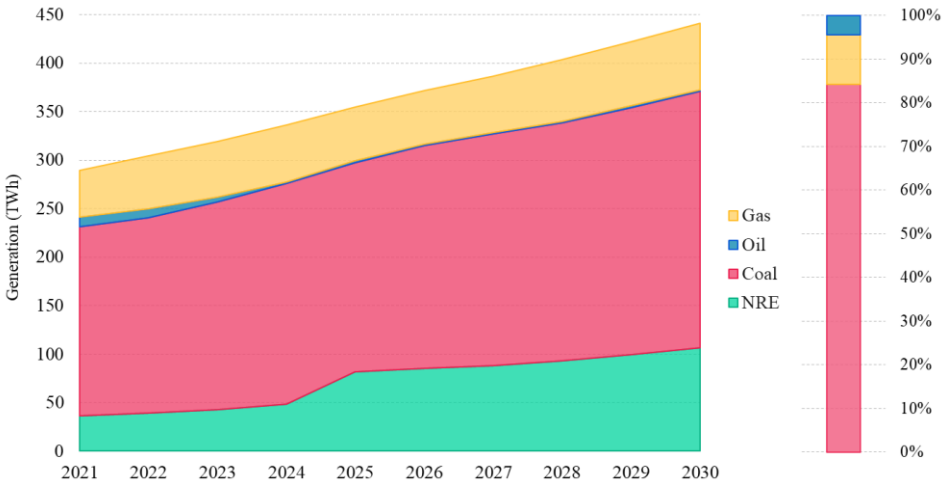

Figure 2: Indonesia's Electricity Projection and Percentage Share by Types.

Indonesia must accelerate its transition initiatives to cleaner energy to overcome this situation. Despite the nation's opportunity, new and renewable energy, including geothermal energy, is still underutilized in Indonesia. Indonesia has the largest geothermal potential globally, at 40% of the world's total reserves. Indonesia's geothermal resources and reserves are estimated at 23.6 GW, highlighting the country's immense capacity for geothermal energy production. It is composed of 5,714 MW speculative resources, 3,467 MW hypothetical resources, 9,575 possible reserves, 1,494 probable reserves, and 3,341.5 proven reserves, which spread on Sumatera, Jawa, Bali, Nusa Tenggara, Kalimantan, Sulawesi, Maluku, and Papua. Despite the big numbers, the actual utilization of geothermal energy in Indonesia currently stands at only 2,597.51 MW of installed capacity (MEMR, 2024). This shows that Indonesia has a lot of room to utilize its potential for further development of geothermal energy and reduce its reliance on fossil fuels.

According to Bertani and Thain (2002), geothermal power plants emit up to 7.5 times less carbon dioxide than fossil-fueled plants. This is because the electricity generation process does not involve fossil fuel combustion. Emissions from geothermal power plants mainly come from the steam, the raw material used for electricity generation, not from the process itself. This steam naturally contains carbon dioxide, along with a small amount of hydrogen sulfide (H2S) and ammonia (NH3). These gases are called Non-Condensable Gases (NCGs) because they are dissolved in steam and cannot be condensed. NCGs are typically vented from the power plant system since their presence affects the efficiency. However, the emissions released are lower than the greenhouse gases released during fossil fuel combustion (Fridriksson, 2016).

Star Energy Geothermal Darajat II, Limited (SEGD) is one of the leading players in the geothermal energy sector, focusing on sustainable energy production. SEGD's operational area covers two areas in West Java: Pasirwangi District, Garut Regency and Kertasari District, Bandung Regency. The company operates two power plants, Unit II and Unit III, with a combined capacity to generate 271 MW of electricity. SEGD operates under a joint operation contract with PT Pertamina Geothermal Energy. This collaboration involves supplying steam to the Unit I power plant, managed by PT Indonesia Power, and generating electricity from Unit II (95 MW) and Unit III (110 MW). The electricity produced is distributed through an interconnection system to reliably meet the energy demands of

communities in the Java, Madura, and Bali (JAMALI) regions. This study aims to analyze SEGD's CO_2 emission intensity and evaluate the company's sustainability performance.

2. METHOD

This research was conducted in two stages: first, calculation of SEGD's CO_2 emission intensity, and second, comparison of this intensity with the JAMALI interconnection system's CO_2 emission intensity. The emission intensity of SEGD was calculated using the methodology specified in Ministry of Environment and Forestry Regulation No. 21 of 2008, Attachment IX, regarding the reporting requirements for monitoring and measuring emissions from stationary sources such as geothermal power plants. Moreover, the calculation followed the guidelines agreed upon by the Indonesia geothermal power plant association for determining emission loads. The equation for calculating CO_2 emission intensity is as follows:

$$EI = \frac{Ms \times \%\, NCG \times \%\, CO_2}{MW} \quad (1)$$

where *EI, MW, %NCG, %CO_2* are emission intensity, generation (MW), steam flowrate (ton/hours), composition NCG in steam (%weight), and CO_2 fraction in NCG (%weight), respectively.

Subsequently, the obtained emission intensity of SEGD was compared with the CO_2 emission intensity of the JAMALI interconnection system, as reported by the Ministry of Energy and Mineral Resources (MEMR) in 2019. This comparison evaluates the company's sustainability performance. The data used in this study is secondary data with the permission of SEGD, including the amount of steam consumption, operational time, percent weight of NCG, total generated electricity, and percent weight of CO_2 emissions in NCG for unit II and unit III, averaged from 2020 to 2023.

3. RESULT AND DISCUSSION

SEGD is a geothermal energy company that operates two power plants, unit II and unit III, that utilizes steam as its primary energy source. Steam from the production well is first directed to a separator, which removes any remaining water. The high-pressure, dry steam from the separator is then channeled into the turbine, where it rotates the turbine blades to drive a generator and produce electrical power. A small portion of the generated electricity—4%—is used to operate the plant's equipment and for internal purposes, while the majority—96%—is supplied to the National Electricity Company (PLN) distribution network.Unit II and unit III each have a complete production setup, including a production well, scrubber, steam header, turbine, generator, main transformer, household transformer, condenser, gas removal system (GRS), cooling tower, and reinjection well.

The amount of greenhouse gas emissions produced by each geothermal power plant can vary depending on several factors, including the amount of steam consumed and the composition of the geothermal gases contained in the steam. In the context of geothermal power production, these gases are commonly referred to as non-condensable gases (NCGs) because they do not condense under the same physical conditions as water vapor but remain in the gas phase (Fridriksson, 2016). Generally, the composition of NCGs is dominated by CO_2. Other gases are typically present in low concentrations, ranging from a few percent to a fraction of a percent. Steam produced from the Dajat geothermal field contains approximately 0.45 to 0.5 percent NCGs. Of these NCGs, CO_2 constitutes, on average, about 94 percent of the total, according to sampling results conducted by SEGD. To determine the weight percent of CO_2 in the NCGs, the weight percent of NCGs and the weight percent of CO_2 are multiplied, as shown in Table 1.

In the context of calculating the CO_2 emission intensity of geothermal power plants, an assumption made is that all CO_2 present in the geothermal steam that enters the generation system is eventually released into the atmosphere through the cooling tower, along with water vapor. This assumption is made due to the process of simplifying emission calculations and focusing attention to the major emission parameter in geothermal power generation, which is CO_2 . It is important to note that this approach excludes certain minor sources of CO_2 emissions that might be present during the production process. For instance, fugitive CO_2 emissions that may occur during well testing activities, or small amounts of CO_2 that might be lost from the wells themselves, are not considered in this calculation. These sources are regarded as negligible in the context of this specific calculation, meaning they are considered to have a minimal impact on the overall CO_2 emission intensity (Fridriksson, 2016).

One method to calculate CO_2 emissions from geothermal power plants is through the analysis of steam flowrate data. The steam flowrate, expressed in tons per hour, represents the quantity of steam generated and supplied to the power plant for electricity production. This data is important in calculating the CO_2 emissions from the power plant. Steam contains trace amounts of CO_2 and by multiplying the steam flowrate by the percentage of CO_2 by weight in the steam, we the amount of CO_2 emitted can be known. Based on the calculation results, it is known

that the CO_2 flow rate emitted from SEGD's power plant facility ranges from 2.72 to 3.18 tons per hour. The CO_2 flowrate calculation results can be seen in Table 4.

Table 1: Percent weight of NCG in steam.

Year	%NCG (%weight)		
	Unit II	Unit III	Average
2020	0.463%	0.437%	0.450%
2021	0.483%	0.438%	0.461%
2022	0.556%	0.463%	0.510%
2023	0.502%	0.454%	0.478%

Table 2: Percent weight of CO_2 in NCG.

Year	%CO_2 (%weight)		
	Unit II	Unit III	Average
2020	94.99%	92.67%	93.83%
2021	95.00%	92.89%	93.94%
2022	95.21%	93.03%	94.12%
2023	95.41%	92.87%	94.14%

Table 3: Percent weight of CO_2 in steam.

Year	%CO_2 in steam		
	Unit II	Unit III	Average
2020	0.44%	0.40%	0.42%
2021	0.46%	0.41%	0.43%
2022	0.53%	0.43%	0.48%
2023	0.48%	0.42%	0.45%

Table 4: CO_2 flowrate.

Year	CO_2 Flowrate (ton/h)		
	Unit II	Unit III	Average
2020	2.51	2.90	2.72
2021	2.70	2.95	2.84
2022	3.08	3.07	3.12
2023	2.59	2.98	2.81

Table 5: Emission intensity of SEGD.

Year	Emission Intensity (ton CO_2/MWh)	
	Unit II	Unit III
2020	0.027	0.025
2021	0.029	0.026
2022	0.036	0.026
2023	0.028	0.026
Average	**0.030**	**0.026**

Emission intensity is an indicator used to assess the environmental impact of various production processes, including the electricity generation process. It is quantified by dividing the total carbon dioxide (CO_2) by the total amount of electricity generated over a specific period of time. Emission intensity is typically expressed in units of tons of CO_2 per megawatt-hour (tons CO_2/MWh) which represents the amount of CO_2 emissions emitted for each megawatt-hour of electricity generated. For instance, in the case of SEGD, the emission intensities of SEGD are 0.026 tons CO_2/MWh for Unit II and 0.034 tons CO_2/MWh for Unit III, respectively. Overall, when considering the emissions from both Unit II and Unit III combined, the emission intensity is calculated to be 0.056 tons of CO_2 per megawatt-hour of electricity generated. This combined emission intensity value provides an aggregate measure of the CO_2 emissions associated with the total electricity generation from these two units.

Emission intensity is a measure of how much greenhouse gas is emitted per unit of electricity generated. it is useful for comparison between different types of power plants, as it is independent of the source (McLean & Richardson, 2016). By offering a uniform unit of measurement, emission intensity enables a straightforward comparison across a range of power generation technologies and energy sourcesIt translates diverse emission profiles into a common unit, making it easier to evaluate and compare the environmental impacts of various

technologies and methods. Furthermore, we can better understand how effectively different energy sources contribute to greenhouse gas emissions relative to the amount of electricity they produce. Moreover, emission intensity serves as a tool for stakeholders, including policymakers, energy producers, and consumers, to evaluate the sustainability aspect of their electricity generation.

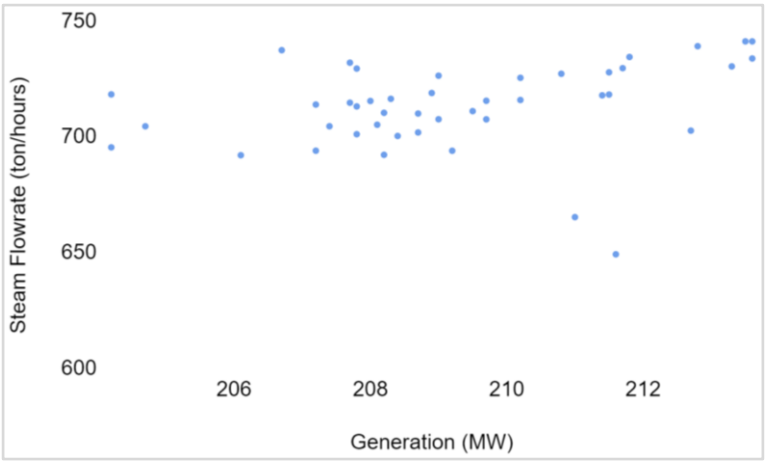

Figure 3: Steam flowrate and generation of SEGD.

To evaluate the company's sustainability performance, the value of the emission intensity of SEGD that has been obtained is then compared with the emission intensity of JAMALI interconnection system. This comparison can provide a clear understanding of the relative contribution of SEGD's CO_2 emissions to the overall emissions of the JAMALI electricity network. It also helps to understand whether the electricity produced by SEGD is a more or less sustainable option compared to others. According to the electricity system greenhouse gas emission factors in 2019, it is stated that the CM ex-ante emission intensity for JAMALI is 0.83 CO_2/MWh. ex ante refers to planning, forecasting, or decision-making activities carried out in advance of actual events. This approach helps optimize resources and manage risks. After comparison, overall, SEGD only shares 6.75% CO_2 emissions of the JAMALI interconnection system.

4. CONCLUSION

This study revealed that the overall CO_2 emission intensity of SEGD from unit II and unit III power plant is 0.056 ton CO_2/MW. With that, SEGD only share 3.36% CO_2 emission of the JAMALI interconnection system, thus providing more sustainable energy.

REFERENCES

Bertani, R., and Thain, I.: Geothermal power generating plant CO_2 emission survey, *IGA News*, **49**, (2002), 1-3.

Fridriksson, T., Mateos, A., Audinet, P., and Orucu, Y.: Greenhouse Gases from Geothermal Power Production Interim Technical Note, The World Bank, Washington DC (2016).

International Energy Agency (IEA): World Energy Balances 2023 Edition, France (2023).

McLean, K., and Richardson, I.: Greenhouse Gas Emissions From New Zealand Geothermal Power Generation in Context, *Proceedings*, 38th New Zealand Geothermal Workshop, (2016)

Ministry of Energy and Mineral Resources Republic of Indonesia (MEMR): Data Colelction Survey on Power Sector in Indonesia for Decarbonization Final Report, (2022).

Ministry of Energy and Mineral Resources Republic of Indonesia (MEMR): Handbook of Energy & Economic Statistics of Indonesia 2023, (2023).

Ministry of Environment and Forestry (MoEF): Peraturan Menteri Negara Lingkungan Hidup Nomor 21 Tahun 2008 tentang Baku Mutu Emisi Sumber Tidak Bergerak Bagi Usaha dan/atau Kegiatan Pembangkit Tenaga Listik Termal, (2008).

Perusahaan Listrik Negara (PLN): Rencana Usaha Penyediaan Tenaga Listrik (RUPTL) 2021-2030, (2021).

PwC: Power in Indonesia Investment and Taxation Guide, (2023).

Assessing Cost-Effective Exploration Methods: A Comparative Study for the Financial Viability of Indonesia's Geothermal Future

Dorman Purba[1,2], Ferdino R. Fadhillah[2], Desak Nyoman Inten Apriani[2], Daniel W. Adityatama[3], M. Rizqi Al Asyari[3], Nadya Erichatama[1,3], V. Adven Brilian[3], and Astri Indra Mustika[2]

[1]PT ENERKA Bhumi Pratama, Cibis Park, Indonesia
[2]PT Sarana Multi Infrastruktur (Persero), Sahid Sudirman Centre, Indonesia
[3]PT Geoenergi Solusi Indonesia (GEOENERGIS), Jakarta, Indonesia

dorman.purba@enerklaz.com, dorman.kons.dpb@ptsmi.co.id

Keywords: Slimhole Drilling, Big Hole Drilling, Exploration Cost Management, Internal Rate of Return (IRR), Walkaway Costs – A unique concept analyzed in geothermal project risks

ABSTRACT

Indonesia, home to one of the world's largest geothermal reserves, is trying to expand its geothermal capacity to meet national energy demands and achieve sustainable development goals. The exploration phase, which serves as the foundation for subsequent project stages, remains critical to unlocking Indonesia's geothermal potential. However, high exploration costs and uncertainties present significant barriers to the financial viability of many geothermal projects. This paper examines the impact of these exploration costs on the economic feasibility of geothermal projects in Indonesia, focusing on the financial inefficiencies caused by varying cost management practices.

The paper presents a comparative analysis of two key exploration strategies: slimhole and bighole drilling. Using a hypothetical "Alpha" geothermal project case study, we simulate the financial outcomes of each strategy, highlighting their respective success rates, cost implications, and impacts on project cash flow and internal rate of return (IRR). The results show that slimhole drilling offers more favorable financial outcomes, reducing upfront costs and mitigating risks through incremental learning, though it presents trade-offs in data accuracy.

This paper identifies the key factors contributing to cost overruns and provides evidence-based recommendations for optimizing exploration expenditures, such as the use of reservoir numerical modeling during the exploration phase. Several strategies for planning drilling operations are also briefly discussed in this paper. These findings aim to guide policymakers and industry stakeholders in adopting standardized, cost-effective exploration practices to improve the financial viability and sustainability of Indonesia's geothermal projects.

1. INTRODUCTION

1.1 Geothermal Overview in Indonesia

Indonesia, gifted with one of the world's largest geothermal resources, is positioned as a potential global leader in geothermal energy development. Currently, the country has an installed geothermal capacity of approximately 2.4 gigawatts (GW), making it the second-largest geothermal producer in the world. However, this represents only a fraction of its estimated geothermal potential of 23.7 GW. The Indonesian government has recognized the strategic importance of geothermal energy in its energy transition efforts, aiming to diversify its energy mix and reduce greenhouse gas emissions. To this end, the government has set an ambitious target to increase geothermal capacity to 5.7 GW by 2030. Achieving these targets is crucial for meeting the rising energy demand sustainably and reducing reliance on fossil fuels.

1.2 Importance of Exploration Projects

Geothermal exploration projects are pivotal in realizing Indonesia's geothermal development targets. Most of the additional megawatts required to meet these targets are expected to come from newly explored prospect areas. Exploration is the critical phase in geothermal project development, where subsurface conditions are assessed to confirm the presence of exploitable geothermal resources. Proper management of exploration projects is essential for minimizing risks and costs, thereby enhancing the feasibility of subsequent development phases. Effective exploration practices can significantly reduce uncertainties, leading to more accurate resource assessments and better-informed investment decisions. Thus, optimizing exploration cost management is vital for all geothermal stakeholders, including government agencies, state-owned enterprises (SOEs), and private developers, to ensure the economic viability of geothermal projects.

Many published studies and papers have discussed the challenges the Indonesian government and the geothermal developers will face in developing geothermal projects in Indonesia (Ibrahim et al., 2005; IGA, 2014; Poernomo, 2015; Darma, 2016; Purba, 2018; Umam et al., 2018; Purba et al., 2019; Purba et al., 2020). Despite those challenges, the exploration phase is currently the most critical phase that Indonesia needs to take into action to seriously achieve the national geothermal target. Figure 1 shows that Indonesia has only been developing a few geothermal areas for geothermal power generation despite Indonesia's vast potential.

Figure 1 (Pusdatin ESDM, 2020) also shows Indonesia's distribution of geothermal areas according to each area's progress. Areas colored green, light green, and yellow indicate areas that have been through a preliminary survey, commonly the 3G survey. In some areas, the government, academic institutions, and geothermal developers have conducted surveys such as the temperature gradient hole or deep slim hole. Pink indicates the areas ready for development, whereas red indicates areas that have already been developed.

While Table 1 shows the list of the 22 geothermal prospect areas or concession areas still in the exploration stage and is expected to contribute to achieve the national geothermal target.

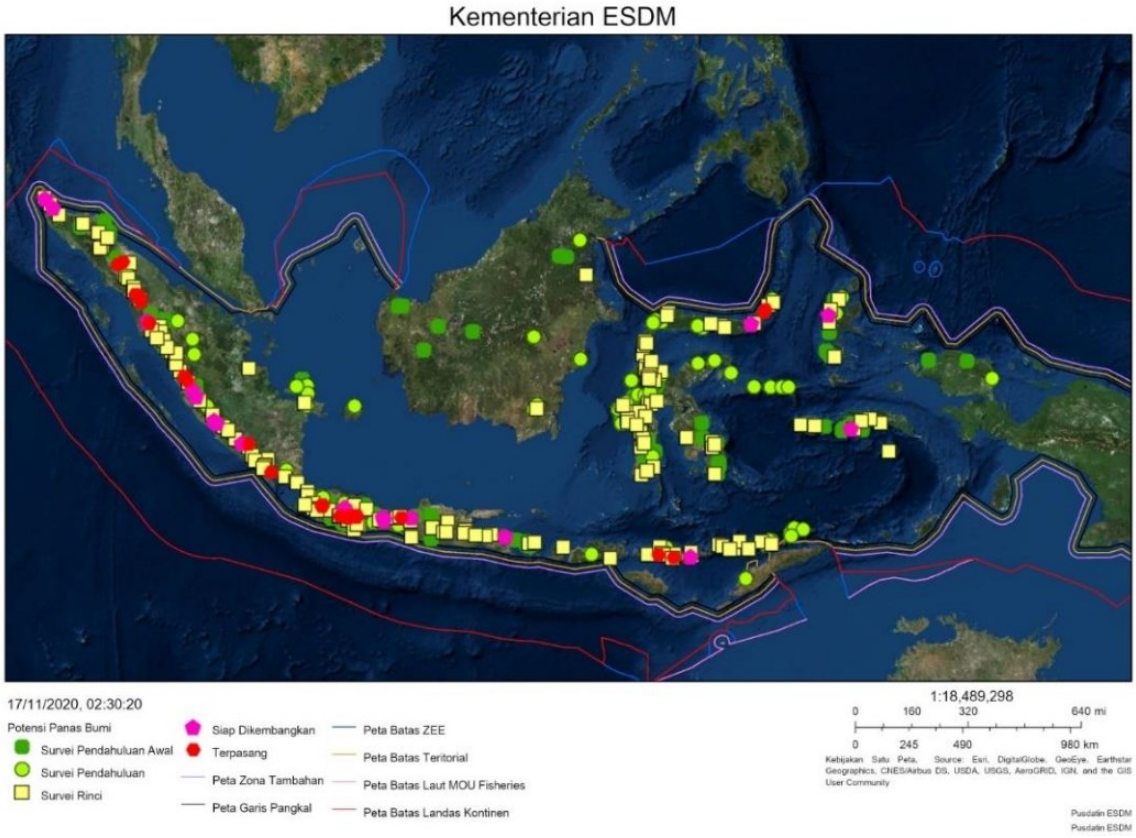

Figure 1: Maps of geothermal potential area in Indonesia with its status (Pusdatin ESDM, 2020).

The megawatt electricity (MWe) figures for each prospective geothermal area listed in Table 1 are estimates provided by the Indonesian government, typically based on initial exploration activities that rely on limited surface studies. These figures will be updated as more data becomes available, whether from more detailed surface surveys or drilling data. Table 1 also shows that even if geothermal stakeholders are only 50% successful in developing the areas listed, an additional 2,000 MWe could be achieved. When combined with the 2,400 MWe already installed, this would result in a total installed capacity of 4,400 MWe. While this still falls short of the national target, it brings the country significantly closer to meeting its goals.

1.3 Problem Statement

Understanding the importance of exploration in Indonesia, as discussed in the previous sub-section, the authors began to investigate deeper into why many exploration projects in Indonesia fail to meet expectations in terms of timeline and cost. One of the initial findings is that geothermal exploration projects are managed by various entities, including government agencies, SOEs, and private developers. However, there are clear indications of significant disparities in how these entities manage exploration costs. These differences stem from varying levels of expertise, resources, and strategic approaches to exploration. Some entities may lack the technical expertise or

financial discipline necessary for efficient cost management, resulting in overspending and economic inefficiencies. This inconsistency in managing exploration costs presents a major obstacle to the overall progress of geothermal development in Indonesia, potentially hindering the country's ability to achieve its ambitious geothermal targets.

Table 1: List of Indonesia's Geothermal Prospect Areas/ Concession Areas in the Exploration Stage (modified from Direktorat Panas Bumi, 2022; Siahaan et al., 2023).

No.	Name of the Prospect Area / Concession Area	Location	Estimated Potential Capacity (MWe)	Developer
1.	Tulehu	Maluku	31	PT PLN (Persero)
2.	Gn. Ungaran	Central Java	150	PT PLN (Persero)
3.	Atadei	East Nusa Tenggara	40	PT PLN (Persero)
4.	Songa Wayaua	North Maluku	42	PT PLN (Persero)
5.	Danau Ranau	South Sumatera	210	PT PLN (Persero)
6.	Oka Ile Ange	East Nusa Tenggara	50	PT PLN (Persero)
7.	Kepahiang	Bengkulu	254	PT PLN (Persero)
8.	Gn. Sirung	East Nusa Tenggara	152	PT PLN (Persero)
9.	Tangkuban Perahu	West Java	375	PT PLN (Persero)
10.	North Patuha (WKP Patuha)	West Java	55	PT Geo Dipa Energi
11.	Candradimuka (WKP Dieng)	Central Java	50	PT Geo Dipa Energi
12.	Candi Umbul Telomoyo	Central Java	92	PT Geo Dipa Energi
13.	Gn. Arjuno Welirang	East Java	302	PT Geo Dipa Energi
14.	Gn. Rajabasa	Lampung	283	PT Supreme Energy Rajabasa
15.	Rawa Dano	Banten	385	PT Sintesa Banten Geothermal
16.	Baturaden	Central Java	258	PT Sejahtera Alam Energy
17.	Telaga Ngebel	East Java	120	PT Bakrie Darmakarya Energi
18.	Seulawah Agam	Aceh	223	PT Geothermal Energi Seulawah
19.	Gn. Lawu	Central Java & East Java	332	PT Pertamina Geothermal Energy
20.	Kotamobagu	North Sulawesi	410	PT Pertamina Geothermal Energy
21.	Jaboi	Aceh	107	PT Sabang Geothermal Energy
22.	Gn. Talang – Bukit Kili	West Sumatera	90	PT Hitay Daya Energy
		TOTAL	4,011	

This study then identifies several cases where high exploration costs have significantly undermined the economic feasibility of geothermal projects. It is hoped that this paper will encourage the geothermal community in Indonesia to take more serious steps toward formulating a comprehensive guide for developing exploration strategies tailored to the country's current geothermal prospects. Unlike the easier-to-explore fields of previous generations, today's geothermal areas present more complex challenges, requiring innovative approaches and strategic planning to ensure project viability.

1.3.1 Exploration Cost Challenges

By default, geothermal exploration in Indonesia presents significant financial challenges, with exploration costs being among the highest globally. This is primarily due to the complexity of drilling operations, the increasing difficulty of targeting viable well locations, and social and environmental hurdles. The high upfront capital required for exploration, combined with the financial risks associated with uncertain outcomes, often deters investment. These cost challenges can halt geothermal projects before they even reach the development phase, making it crucial to explore cost-effective strategies that can ensure the economic viability of such projects.

Indonesia's current geothermal prospects present far greater exploration challenges compared to earlier, more accessible fields. Unlike the geothermal areas previously explored, many of the remaining prospects exhibit minimal or no surface manifestations, making it harder to detect viable geothermal resources. Additionally, these fields are characterized by smaller resource sizes and low to medium enthalpy, further complicating exploration efforts. The difficulty in targeting optimal well locations is exacerbated by social and environmental issues, such as land use conflicts and community resistance, which can delay projects and increase costs. The relatively "easy" geothermal fields have been largely exhausted, and the conventional exploration approaches that worked in the past are no longer relevant for Indonesia's remaining prospects. In this evolving landscape, a shift in exploration strategy is essential, requiring more innovative, cost-effective, and adaptive methods to unlock Indonesia's remaining geothermal potential.

1.3.2 Current Exploration Strategies and Dilemmas

Choosing the appropriate exploration strategy is one of the key dilemmas faced by geothermal stakeholders in Indonesia. The decision between slimhole and bighole drilling, both widely used in the industry, presents a complex trade-off:

a. *Slimhole drilling* offers a lower-cost option, allowing developers to test multiple areas with limited upfront investment.However, the data obtained from slimholes may lack the depth and accuracy needed to fully assess the resource.
b. *Bighole drilling*, while providing more comprehensive and reliable data, comes with significantly higher costs and greater financial risk, especially in the exploration phase where success rates are uncertain.

Adding to the complexity, slimhole drilling remains relatively underutilized in Indonesia due to a long hiatus in exploration using this method and the limited availability of experienced contractors. This situation puts further pressure on developers to opt for bighole drilling, despite its higher costs, to ensure faster results that satisfy investor, and shareholder demands for early revenue and project completion.

1.3.3 The Need for Advanced Exploration Techniques

With the rapid advancement of computer technology, there is potential to enhance exploration accuracy and reduce costs by integrating advanced numerical modeling into the exploration phase. By combining static and dynamic models, stakeholders can improve the well-targeting process, quantify resource uncertainties, and optimize exploration strategies. However, the adoption of such technologies remains slow, largely due to perceptions of high upfront costs and long lead times. The need to incorporate more cost-effective exploration techniques, while managing financial risks, is critical for Indonesia to scale up its geothermal energy production.

At the time this study was conducted, the authors found that very few exploration projects in Indonesia, whether managed by private developers, SOEs, or government entities, were utilizing reservoir numerical modeling as part of the decision-making process. Unfortunately, many geothermal players are still stuck in an outdated mindset, believing that reservoir numerical modeling is difficult, expensive, and time-consuming. In reality, with advancements in technology, reservoir numerical modeling can now be completed in a matter of weeks or even days if the data is available in a standardized format.

1.3.4 Financial Inefficiencies and Walkaway Costs

Another major problem or dilemma in geothermal exploration is the financial inefficiency stemming from inconsistent cost management practices across different stakeholders—government agencies, state-owned enterprises (SOEs), and private developers. These inefficiencies can lead to excessive expenditure and unproductive wells, increasing the overall "walkaway costs" in cases of exploration failure. For example, bighole drilling failures carry significantly higher walkaway costs, sometimes amounting to hundreds of millions of dollars, which can severely impact the financial feasibility of a project.

Walkaway costs are often overlooked or underestimated by stakeholders in Indonesia because they require projects to be executed in stages rather than all at once. Considering walkaway costs is frequently interpreted by decision-makers as prolonging the project timeline to reach Commercial Operation Date (COD), which is seen as reducing the overall economic value of a project.

In summary, the high costs, strategic dilemmas, and technological gaps in geothermal exploration in Indonesia create a significant barrier to achieving the country's geothermal energy goals. Addressing these challenges requires careful planning, effective cost management, and the adoption of advanced exploration strategies to reduce financial risks and improve the likelihood of successful project outcomes.

1.4 Study Objectives

The authors' motivation for conducting this study and publishing this paper is to trigger discussions around the differences between the exploration and development phases, particularly in terms of resource uncertainties and

the importance of keeping CAPEX as low as possible from the earliest stages. The authors observed that, at the time of writing this paper, there was a tendency among geothermal exploration project implementers in Indonesia to overlook exploration cost planning in their rush to proceed quickly. Therefore, this paper aims to achieve several key objectives, as outlined in Table 2.

2. GEOTHERMAL EXPLORATION OVERVIEW

Understanding the criticality of the exploration stage is essential as it determines the feasibility and potential success of geothermal projects. This phase involves identifying viable resources, assessing their quality and quantity, and evaluating economic feasibility. Proper execution during exploration reduces risks, optimizes costs, and enhances project success. Without a solid foundation from thorough exploration, subsequent phases face increased uncertainties and higher costs. Recognizing this importance ensures stakeholders prioritize careful planning and resource allocation early in geothermal development.

2.1 Geothermal Exploration Regulation in Indonesia

Geothermal development in Indonesia follows a structured framework outlined in Law (Undang-undang/UU) No. 21/2014 and Government Regulation (Peraturan Pemerintah/PP) No. 7/2017. A comprehensive understanding of the regulatory framework governing the geothermal industry in a specific country, such as Indonesia, is essential as it directly influences project strategies, cost estimations and economic analysis.

Table 2: The study objectives.

No.	Objectives	Description
1.	To analyze the impact of exploration costs on the overall financial viability of geothermal projects through simulation of various scenarios.	This objective involves simulating both actual and hypothetical cases, such as the "Alpha Project," to explore the financial outcomes of different drilling strategies (e.g., slimhole vs. bighole). The study aims to assess how exploration expenditures, success ratios, and well targeting influence cash flow, internal rate of return (IRR), and other key financial metrics in geothermal projects.
2.	To identify the key drivers behind high exploration costs in Indonesia's geothermal sector.	This objective seeks to pinpoint specific factors that contribute to elevated exploration costs, such as technical challenges (e.g., difficult well targeting, low enthalpy resources), and inefficiencies in project execution. Additionally, it will examine the challenges posed by limited contractor availability and the financial implications of social and environmental issues.
3.	To compare slimhole and bighole drilling strategies and evaluate their cost-effectiveness in exploration and project development.	This objective focuses on providing a comparative analysis of slimhole and bighole drilling, as demonstrated in the "Alpha Project" simulation. It aims to identify the trade-offs between the two approaches in terms of cost, data accuracy, success rates, and risk mitigation, while highlighting the potential of slimhole drilling to reduce walkaway costs and improve project economics.
4.	To develop actionable strategies for reducing exploration costs and improving the financial feasibility of geothermal projects in Indonesia.	Based on the findings, this objective will outline evidence-based recommendations and best practices to help stakeholders—government agencies, SOEs, private developers—optimize exploration expenditures. The strategies will include integrating advanced modeling technologies, improving exploration planning, and adopting standardized cost management practices to enhance the overall economic viability of geothermal investments.

Table 3 summarizes these regulations that delineate the various stages involved in the development process. Familiarity with these regulations is vital to promptly identify any potential conflicts between local regulations and the guidelines established by international financial institutions. Such early recognition ensures alignment with the prescribed regulatory requirements, enabling smooth project implementation and adherence to international standards.

Table 3: Geothermal development stages in Indonesia (modified from Adityatama et al., 2020; Siahaan et al., 2023; Direktorat Panas Bumi, 2022).

Geothermal Development Stage	Description	Eligible institution conducting the activity	Duration
Preliminary Survey	Identify areas with potential geothermal resources and conductsurveys to gather information on the geology, geochemistry, and geophysics of the area. The result from the survey is then being integrated to develop conceptual model, resource assessment, and well targeting.	Government/Business Entity/State-Owned Enterprise	1 year
Exploration and Feasibility Study	Proving a geothermal resource exists and proving/delineating sufficient reserves for development. Once a viable resource has been identified, the resource assessment phase begins. This includes determining the size of the resource and the potential for energy production. Engineers will also conduct various studies such as environmental impact assessment, social impact assessment, and feasibility study.	Government/Business Entity/State-Owned Enterprise	5 + 1 + 1 years
Development and Construction	Proving that development of the resource is technically and economically feasible by drilling production and injection wells. Constructing the geothermal facility on specification, on time and on budget.	Business Entity/State-Owned Enterprise	2-4 years
Operation and Maintenance	After the construction of the power plant is finished, it will be operated and maintained. The operators will monitor the power plant's performance, make repairs and improvements as necessary, and ensure that it is operating in compliance with relevant regulations.	Business Entity/State-Owned Enterprise	30 years

2.2 Geothermal Exploration Objectives

Geothermal exploration projects are integral to the development of geothermal energy resources. They are designed to assess the viability of a site for geothermal energy production, ensuring that subsequent development phases are based on solid scientific data and economic analyses. The primary objectives of a geothermal exploration project can be categorized into three main areas: identification of geothermal resources, resource assessment, and feasibility evaluation.

1. **Identification of Geothermal Resources**. The foremost objective of any geothermal exploration project is the identification of geothermal resources. This involves confirming the presence and extent of subsurface heat sources, which are typically located in areas with volcanic activity or tectonic plate boundaries. During this phase, exploration teams employ various geophysical and geochemical methods to detect anomalies that indicate geothermal activity. Techniques such as remote sensing, seismic surveys, magnetotelluric (MT) surveys, and soil gas sampling are used to gather preliminary data about the geothermal potential of a site. The goal is to delineate areas with high temperature gradients, which suggests the presence of significant geothermal reservoirs. Accurate identification is crucial as it lays the foundation for more detailed studies and reduces the risk of unsuccessful drilling.
2. **Resource Assessment**. Once a geothermal resource is identified, the next objective is to assess the quality and quantity of the resource. This involves a detailed evaluation of the geothermal reservoir, including its temperature, pressure, permeability, volume, and fluid chemistry. Exploratory drilling is a key activity during this phase, where test wells are drilled to obtain direct measurements from the reservoir. The data collected from these wells, including temperature logs, fluid samples, and pressure readings, are analyzed to estimate the potential energy output of the geothermal resource. The assessment also involves reservoir modeling and simulation to predict the behavior of the reservoir over time under various production scenarios. This comprehensive evaluation helps in determining the sustainability of the resource and its capacity to support long-term energy production.
3. **Feasibility Evaluation**. The final objective of a geothermal exploration project is to evaluate the economic feasibility of developing geothermal resources. This involves a thorough cost-benefit analysis, considering both the capital expenditure required for development and the potential revenue from energy production. Key factors in this evaluation include the costs of drilling, construction of power plants, infrastructure development, and ongoing operational and maintenance expenses. The feasibility study

also examines the potential market for geothermal energy, including electricity prices, demand forecasts, and potential off-take agreements. Environmental and regulatory considerations are also factored into the economic analysis, as compliance with environmental regulations and obtaining necessary permits can impact project timelines and costs. Ultimately, the feasibility evaluation aims to determine whether the geothermal project can deliver a satisfactory return on investment, guiding decision-makers on whether to proceed with development.

2.3 Risks in Exploration Phase

Geothermal exploration can be challenging, as it involves identifying and assessing the potential for geothermal resources in a specific area. The fundamental objective of a geothermal exploration program is to identify and characterize a geothermal resource that can be economically developed by applying an optimized design based on the exploration results.

Therefore, it is common for geothermal developers or investors to face dilemmas with making investment decisions in the exploration stage. The difficulty is created by the requirement to spend high upfront capital but relying on information that is still very minimal and has a very high level of uncertainty. Additionally, the most significant cost component of an exploration project comes from the drilling activities and the construction cost of supporting infrastructures such as access roads, well pads, and other supporting facilities. This portion could significantly impact on the total project costs if not planned and managed correctly.

The main challenges of geothermal exploration in Indonesia are summarized as follows (IGA, 2014; Poernomo, 2015; Darma, 2016; Purba, 2018; Umam et al., 2018; Purba et al., 2019; Adityatama, 2020; Purba et al., 2020; Purba et al., 2021a; Purba et al., 2021b; ADB, 2015; Utami, 2010):

1. **Difficulty in locating the "hottest area"**: Geothermal resources are not always visible at the surface and can be challenging to locate without conducting detailed geological, geochemical, and geophysical (3G) surveys and drilling test wells. The unclear indications or thermal manifestations from surface studies can make it challenging to identify the most promising areas for exploration and increase the risk of drilling "dry" wells.
2. **High exploration costs**: Conducting 3G surveys, developing a reliable conceptual model, and drilling test wells can be expensive, and there is always the risk that a project will not yield a viable resource. The high upfront capital and resource uncertainties can make it difficult for developers to secure funding for exploration activities. Indonesia is currently known as one of the most expensive countries for geothermal drilling, with costs ranging from 2,900 to 4,000 USD per meter. In the exploration phase, drilling costs per well are generally higher than during the development phase.
3. **Complex geology**: Geothermal resources in Indonesia are mainly located in a volcanic area with complex geological environments, making it difficult to understand the subsurface conditions and identify the most promising areas for exploration. The difficulty of assessing geological and subsurface conditions is further compounded by the shortage of experienced geoscience personnel with strong foundational knowledge of Indonesia's geothermal geology.
4. **Lack of direct and reliable data**: In some cases, there may be a need for more data on the geology and geochemistry of an area, making it challenging to identify potential resources and plan the exploration activities. Currently, an increasing number of geothermal prospects in Indonesia are considered "blind systems," meaning there are little to no surface indications or manifestations that provide information about the reservoir. This greatly increases the exploration risk, as project license holders must proceed with exploration drilling based on very limited data.
5. **Environmental impacts**: Exploration activities can have various environmental impacts, such as air and surface water pollution, soil degradation, hazardous noise, release of hazardous gases, landslides, deforestation, and the potential for groundwater contamination. Mitigating these impacts can be costly and time-consuming.
6. **Social and community issues**: Exploration activities can also have social and community impacts, such as displacement of local communities and land-use conflicts. Developers need to address these impacts and engage with local communities to ensure their support and minimize the risk of project delays or cancellations. This aspect is often overlooked during exploration drilling planning, where project owners assume that all the land needed for drilling can be easily acquired. As a result, they often fail to prepare proper contingency or mitigation plans.
7. **Uncertain regulations**: Geothermal exploration is subject to various national, regional, and local regulations. The uncertainty can make it difficult for developers to navigate the regulatory environment and can increase the risk of project delays or cancellations. One of the long-standing issues is the regulation of geothermal electricity tariffs and the risk-sharing mechanism between the government and private or state-owned developers in the exploration phase.

Given the high uncertainty and risks involved in the exploration stage, most commercial lenders are still reluctant to provide financing facilities for this purpose. Even international financial institutions (IFI) are reluctant to fund up-front exploration and typically will provide financing only once 50% or more of the steam resource is proven (Asian Development Bank and The World Bank, 2015). With this consideration, exploration drilling generally requires the sponsor's equity, which may only be recovered if the drilling reveals that the resource is technically sufficient and economically viable for exploitation. Meanwhile, from the developers' point of view, to mobilize the up-front equity needed for exploration, they will also consider the adequacy of the tariff, which adds to the challenges faced by the developers given the single buyer model applied in Indonesia.

One way that GoI has taken to tackle the challenges in the exploration stage is by launching the Infrastructure Financing for Geothermal Sector fund / Pembiayaan Infrastruktur Sektor Panas Bumi ("PISP Fund") through PT Sarana Multi Infrastruktur (Persero), as stipulated in the Minister of Finance Regulation No. 80 in 2022. This solution can be an alternative funding scheme that the developers may consider financing their exploration program, of which the typical funding application process will be described in sub-section 5.4 in this paper.

2.4 Cost of Geothermal Exploration in Indonesia

The cost of geothermal exploration in Indonesia can vary significantly, as it is contingent upon project-specific factors and the chosen exploration drilling strategy. An estimate of exploration costs is presented in Table 4, providing an overview of the anticipated expenses associated with conducting geothermal exploration drilling.

Table 4 illustrates the sequential stages involved in the execution of an exploration project, encompassing a range of activities that are conducted progressively, beginning with low-cost data collection attempts. Following the initial data collection, developers can proceed with activities that entail more significant investments if the results exhibit positive indications of geothermal potential. Notably, Table 4 provides a distinct representation of the climax of all exploration activities, which is the drilling of deep wells. This activity incurs the highest costs within the exploration stage.

It is important to note that the costs outlined in Table 4 are subject to variations based on multiple factors, including the depth and complexity of drilling, geological conditions, logistical considerations, and local context. Therefore, the figures provided should be regarded as approximate and indicative rather than absolute values. Additionally, the cost estimates in the rightmost column of Table 4 show a wide range, primarily due to the lower costs of slimhole drilling and the higher costs of bighole drilling, especially when infrastructure is required in areas with challenging terrain and logistics. Furthermore, incidents such as stuck pipe during bighole drilling can cause significant cost increases.

The tabulated information underscores the systematic progression of exploration efforts, whereby preliminary activities with relatively lower expenses pave the way for more resource-intensive undertakings. The delineation of cost variations among the stages underscores the significance of cautious financial planning and decision-making in geothermal exploration initiatives. By comprehending the cost implications associated with each stage, developers can effectively allocate resources and assess the financial feasibility of progressing further in the exploration process.

2.5 Differences between Exploration and Development Stages

2.5.1 Resource risk levels and drilling success criteria in the exploration and development stages

Managing a geothermal exploration project with a development mindset is risky because exploration aims to confirm resource viability with minimal costs. Prematurely adopting a development approach can lead to excessive financial waste, as significant infrastructure and operational investments may be made before confirming the resource's adequacy. This approach can jeopardize the project's economic feasibility, inflate costs, and lead to substantial financial losses. Prioritizing cautious, cost-effective exploration is crucial to avoid overcommitting resources and encountering unforeseen challenges, ensuring the project's long-term success and sustainability.

Therefore, it is crucial for decision-makers in geothermal energy development projects to understand the differences between the exploration and development phases from various perspectives. Table 5 illustrates the distinctions between geothermal projects in the exploration phase and those in the development phase.

2.5.2 Comparison of Drilling and Power Plant Construction Difficulties

As discussed in Table 4 and Table 5, drilling activities, particularly during the exploration phase, account for a significant portion of costs and are associated with high uncertainties. Figure 2 illustrates the comparison between the cost portions of drilling and power plant construction relative to their difficulty levels, helping decision-makers understand the nature of risks associated with these activities.

Table 4: Cost estimate of geothermal exploration drilling (modified from IGA, 2014; GeothermEx, 2010; Purwanto et al., 2018; Purba et al, 2019; Purba et al., 2020; Adityatama, 2020; Purba et al., 2021a; Purba et al., 2021b; Kristianto, 2018; Jacobs, 2022; Utami, 2010; GGGI, 2023).

Activity	Geology survey	Geochemistry survey	Geophysical survey	Initial conceptual integration and well targeting	Exploration drilling
Activity Description	Geological mapping on an area of 400 km^2. The work package including pre-field-work study, rock sampling and identification, structural mapping, and reporting.	Work package including a pre-field-work study, liquid and gas sampling from 30 locations, laboratory analysis and reporting.	Work package including pre-field-work study, 100 MT stations and 150 Gravity stations, interpretations, and reporting.	Integrate all report from 3G surveys to create several scenarios of conceptual models, including peer review.	Using 3 (three) standard/big hole type or 5 (five) slimhole type or combination of 2 (two) slimholes and 1 (one) full-size well. The cost estimate includes infrastructure construction cost to support the drilling operation. The duration estimate includes procurement process, preparation, equipment mobilization, drilling, well testing and demobilization.
KrisEstimated Duration	4-8 months	4-8 months	4-8 months	3-6 months	18 - 36 months
Cost Estimate (USD)	300,000 – 700,000	200,000 – 400,000	1,000,000 – 2,000,000	100,000 – 200,000	15,000,000 – 50,000,000
Considerations	Accuracy might be affected by terrain, weather, and field personnel experiences.	Accuracy might be affected by sampling method (minimize contamination) and laboratory competences.	Accuracy might be affected by noise during data acquisition anddata processing method, including personnel interpretation.	Accuracy might be affected by 3G data accuracy and personnel experiences and interpretation.	Deep wells, whether slimhole or bighole, allow the exploration team to acquire direct downhole data from the reservoir, providing valuable insights for more accurate resource assessment. However, this approach requires significantly more time and higher costs compared to 3G surveys.

Table 5: Distinctions between geothermal projects in the exploration phase and those in the development phase (GGGI, 2023; IGA, 2014; Purba et al., 2019; Purba et al., 2021a; Purba et al., 2021b).

Aspect	Exploration Stage	Development Stage
Primary Objective	The primary objective of the exploration phase is to prove the existence of a geothermal resource by gathering comprehensive information on the reservoir's characteristics, including temperature, pressure, permeability, geology, and chemistry. This phase typically begins by identifying and drilling in the most promising areas, or "sweet spots," to maximize the chances of success.	The primary objective of the development phase is to develop and exploit the confirmed geothermal resource for energy production. This involves drilling sufficient wells to meet the project's megawatt (MW) target and achieving the Commercial Operation Date (COD).

Aspect	Exploration Stage	Development Stage
Level of the Resource Risk	Very high due to: 1. The possibility of not finding a viable geothermal resource despite significant investment 2. Uncertainty about the reservoir's capacity, temperature, permeability, pressure, and sustainability.	Low to medium, with several points of considerations: 1. Over-extraction of the geothermal fluid can deplete the resource faster than anticipated, affecting the long-term viability of the project. 2. Proper reinjection of the spent geothermal fluid is crucial to maintain reservoir pressure and sustainability. Challenges in reinjection, such as blockage or inadequate reinjection wells, can affect resource longevity. 3. Improperly managed reinjection can lead to thermal breakthrough, where cooler reinjected fluids prematurely reach production wells, reducing overall thermal efficiency.
Typical Activities	Preliminary survey, surface studies / 3G surveys, preliminary environmental and social assessment, exploration drilling, resource assessment.	Additional surface studies after exploration drilling, Feasibility Study, Financial Close, Appraisal and Development Drilling, Power Plant and SAGS construction, COD, Further Resource Assessment, Reservoir Management
Well / Drilling Success Definition	Success for an exploration well is defined by obtaining positive outcomes, specifically identifying a viable geothermal resource with indicators that suggest it has development potential.	Success for development wells is defined by the establishment of suitable production and injection wells that can be effectively utilized in the production and injection strategy of a geothermal development project.

This is important to discuss in this paper because the authors observed that some geothermal investors in Indonesia still view power plant construction as riskier than drilling activities. This might be true if the power plant is procured and built before the geothermal resource beneath the surface is confirmed. In such cases, there is a risk that the plant's installed capacity may exceed the geothermal reservoir's ability to supply sufficient hot water or steam to the surface.

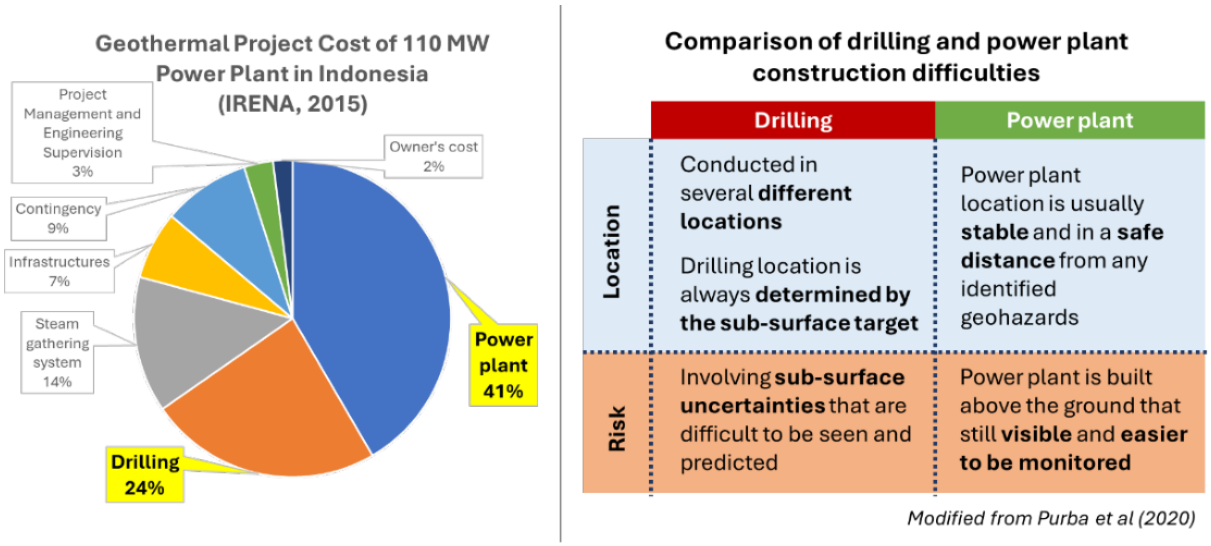

Figure 2: Comparison of Costs and Difficulty Levels Between Drilling Activities and Power Plant Construction in Geothermal Projects (IRENA, 2015; Purba et al., 2019; Purba et al., 2020; Purwanto et al., 2018; Utami, 2010).

3. IMPORTANCE OF CAPEX IN GEOTHERMAL PROJECTS

Capital Expenditure (CAPEX) is a critical component in the financial planning and economic assessment of all projects, including geothermal. Understanding its importance is essential for evaluating the feasibility and sustainability of these projects. The key reasons why CAPEX is vital in geothermal projects are:

1. Initial Investment and Project Feasibility

a. High Upfront Costs: Geothermal projects require significant initial investments, particularly during the exploration and drilling phases. CAPEX covers the cost of land acquisition, drilling exploratory wells, infrastructure development, and setting up geothermal plants.
b. Financial Risk: The high CAPEX associated with geothermal projects introduces substantial financial risks. Investors and developers must secure considerable funding before the project can commence, making it imperative to manage these costs effectively.

2. Impact on Economic Viability
   a. Return on Investment (ROI): The economic viability of geothermal projects heavily depends on the initial CAPEX. Lowering CAPEX can improve the ROI by reducing the payback period and enhancing profitability.
   b. Internal Rate of Return (IRR): As shown in the sensitivity analysis, CAPEX has a significant impact on the IRR of geothermal projects. A high CAPEX can lower the IRR, making the project less attractive to investors and financiers.

3. Operational Efficiency and Cost Management
   a. Operational Costs: While CAPEX primarily focuses on initial costs, it also influences long-term operational efficiency. Investments in high-quality infrastructure and technology can reduce maintenance and operational costs over the project's lifespan.
   b. Cost Overruns: Effective management of CAPEX is crucial to avoid cost overruns, which can derail the project timeline and budget. Accurate estimation and control of CAPEX ensure that the project stays within financial constraints.

4. Financing and Investment Decisions
   a. Attracting Investment: A well-managed CAPEX profile makes geothermal projects more appealing to investors and financial institutions. Transparent and realistic CAPEX estimates build confidence among stakeholders and facilitate funding.
   b. Financing Terms: The ability to control and justify CAPEX can influence the terms and conditions of financing. Lower CAPEX may lead to more favorable loan terms and interest rates, reducing the financial burden on the project.

5. Regulatory and Environmental Considerations
   a. Compliance and Permitting: CAPEX includes costs related to regulatory compliance and environmental permitting. Ensuring that these aspects are adequately funded is essential for project approval and sustainability.
   b. Sustainability Investments: Allocating CAPEX towards sustainable practices and technologies can enhance the environmental profile of geothermal projects, aligning them with national and international sustainability goals.

3.1 CAPEX Components

Understanding the CAPEX component in geothermal projects is critical for effective financial planning, risk management, securing investment, and ensuring long-term operational efficiency. It enables stakeholders to make informed decisions, optimize costs, and enhance the overall feasibility and sustainability of geothermal energy projects. By comprehensively analyzing CAPEX, project developers can better navigate the complexities of geothermal project development and contribute to the successful expansion of geothermal energy capacity. The typical CAPEX component in a geothermal project is show in Table 6. In the following chapter, this study will present a project economic simulation with different CAPEX levels during the exploration phase. The first case involves slimhole drilling with lower CAPEX, compared to the second case, which uses bighole drilling with higher CAPEX.

Table 6: The list of CAPEX component in a geothermal project..

CAPEX component	Remarks
Preliminary survey	The cost related to 3G Survey, permittance, and desk study
Exploration	Cost related to the permittance, ESIA study, land acquisition, infrastructure work, and exploration well to confirm the presence of geothermal resource.
Appraisal	Cost related to the additional permittance, land acquisition, infrastructure work, and appraisal well to provide required steam under well-head for FID purpose. The appraisal cost in project November is higher than exploration cost since this stage has more well to drill.
Development	Cost related to the additional permittance, land acquisition, infrastructure work, drilling, and EPC SAGS-power plant.

CAPEX component	Remarks
De-risking and GREM	Cost related to the payment of GREM or other de-risking facility (i.e. commitment fee, interest, and success premium).
Finance cost	Cost related to financing activity for development phase (i.e. interest during construction, and commitment fee)
Reinvestment	Cost related to the make-up well drilling activities after COD.

3.2 Impact of Various Cost Components on the Internal Rate of Return (IRR) of Geothermal Projects

Understanding which cost components most impact Internal Rate of Return (IRR) and the role of IRR in geothermal projects is essential for effective financial planning, risk management, and strategic decision-making. By focusing on the most influential cost drivers, stakeholders can enhance project viability, attract investment, and ensure sustainable development. The insights gained from analyzing the impact of exploration costs on IRR are critical for optimizing the economic feasibility of geothermal projects in Indonesia, ultimately contributing to the country's energy security and sustainable development goals.

The IRR is a crucial metric for assessing the profitability and efficiency of geothermal projects. A higher IRR indicates a more financially attractive project, making it easier to attract investors and secure funding. IRR serves as a benchmark for comparing geothermal projects with alternative investments, helping stakeholders choose projects with the best potential returns. It boosts investor confidence by reflecting the project's potential for adequate returns, which is essential for securing both private and institutional investments. Financial institutions often use IRR as a criterion for funding approval, with strong IRRs leading to more financial support.

IRR also provides a quantitative measure of project performance over its lifecycle, aiding in evaluating whether the project meets financial goals. It assists in long-term planning and forecasting, guiding future project developments and expansions. Furthermore, IRR helps assess financial risk, with lower IRRs indicating higher financial risks and the need for risk mitigation strategies. By setting investment thresholds based on IRR, projects can ensure that only financially viable projects are pursued, optimizing resource use and enhancing project success.

Figure 3 provided offers a sensitivity analysis that highlights the impact of various cost components on the Internal Rate of Return (IRR) of geothermal projects. The primary takeaway from this analysis is the significant influence of Capital Expenditure (CAPEX) on the economic viability of geothermal projects. This insight is crucial for understanding the broader context of exploration costs in the geothermal sector.

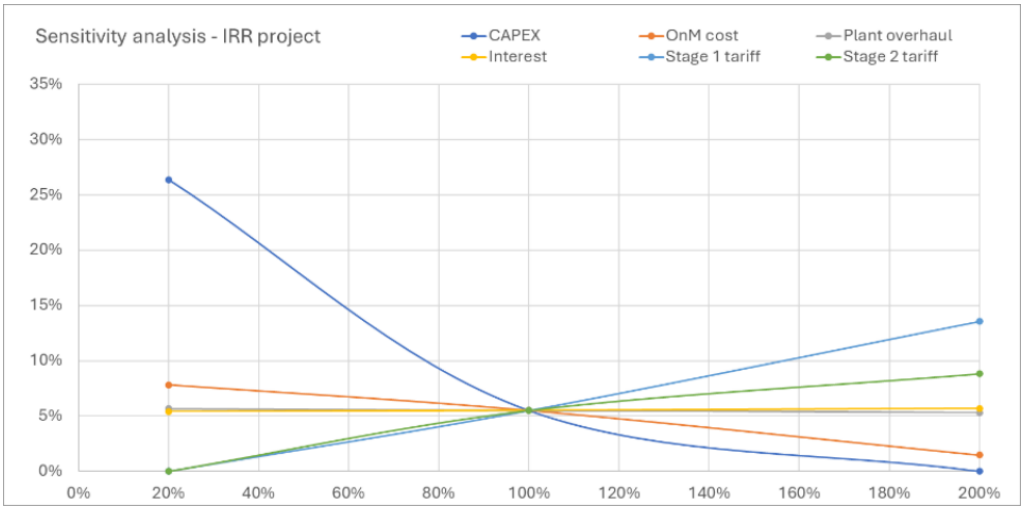

Figure 3: The Significancy of Capital expenditure (CAPEX) to the Geothermal Project Economics (GRG-Geoenergis, 2024).

Additionally, Figure 4 presents a sensitivity analysis of a geothermal project to identify the most influential parameters on the project's return. This analysis is crucial as additional project efforts are required to ensure a fair return on equity. The NPV-IRR sensitivity analysis includes parameters such as CAPEX, OPEX, and tariffs.

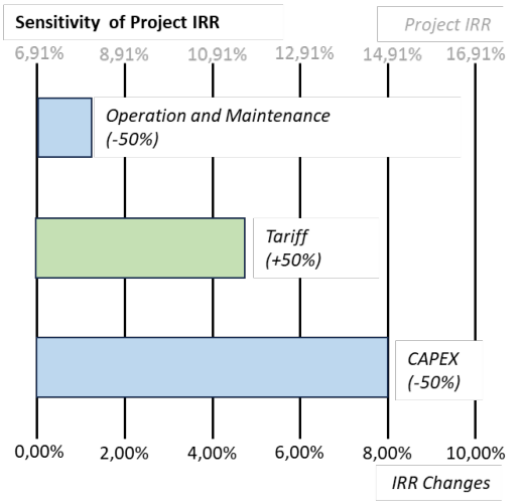

Figure 4: The Tornado Chart of Sensitivity analysis of Project IRR (GRG-Geoenergis, 2024).

Key Observations from Figure 3 and Figure 4 are:

1. Dominance of CAPEX:
    a. CAPEX emerges as the most influential factor affecting the IRR of geothermal projects. The sensitivity analysis demonstrates that changes in CAPEX have a more pronounced impact on the IRR compared to other cost components.
    b. The IRR's sensitivity to CAPEX underscores the critical nature of managing capital costs effectively to ensure project feasibility. High CAPEX can severely undermine the financial attractiveness of geothermal projects, leading to potential financial inefficiencies.
2. Comparison with Other Cost Components:
    a. While Operation and Maintenance (OnM) costs, plant overhaul expenses, and interest rates also influence the IRR, their impact is relatively less significant compared to CAPEX.
    b. The analysis indicates that changes in tariffs (both Stage 1 and Stage 2) also affect the IRR, particularly the Stage 2 tariff, which shows a substantial impact. However, CAPEX remains the dominant factor.
3. Implications for Exploration Costs:
    a. Exploration costs, as a component of overall CAPEX, play a crucial role in determining the financial feasibility of geothermal projects. The variability in exploration cost management practices can lead to significant discrepancies in CAPEX, thereby affecting the IRR.
    b. The high sensitivity of IRR to CAPEX highlights the need for standardized and efficient exploration cost management practices among stakeholders, including government agencies, SOEs, private developers, and new entrants.

4. CASE ANALYSIS: ALPHA GEOTHERMAL PROJECT

At the beginning of this study, the authors planned to conduct a financial simulation using data from actual exploration projects in Indonesia, selecting two sample projects with exploration costs under 50 MUSD and two sample projects with costs exceeding 50 MUSD. Unfortunately, due to concerns over data confidentiality and the fact that the sampled exploration projects were still ongoing, the authors decided to use hypothetical data so that the study could proceed and be published.

4.1 Assumptions

“Alpha Geothermal” Project is hypothetical 55MW net geothermal power plant that is in Java area. The 55MW capacity is selected based on the most projected geothermal power plant in RUPTL 2021-2030 (Figure 5). The Java area is projected to have the highest additional installed geothermal power plant capacity (Figure 6). Alpha project has 20.000 Ha working area. Figure 5 shows the distribution on expected power plant capacity on RUPTL 2020-2030, while Figure 6 emphasize Java area as highest region of planned geothermal power plant.

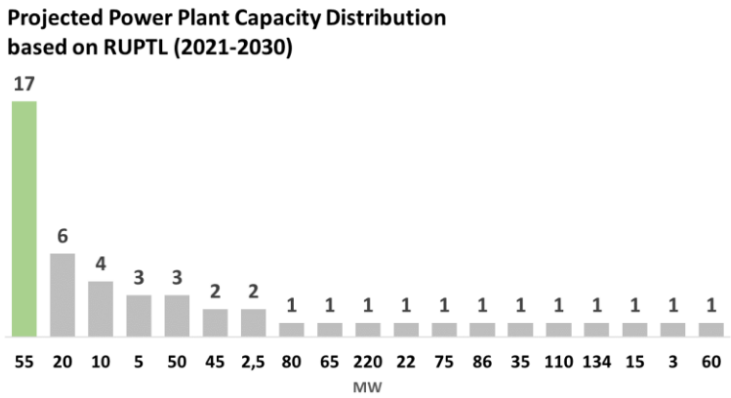

Figure 5: The Distribution of Projected Geothermal Power Plant Capacity per Number of Units.

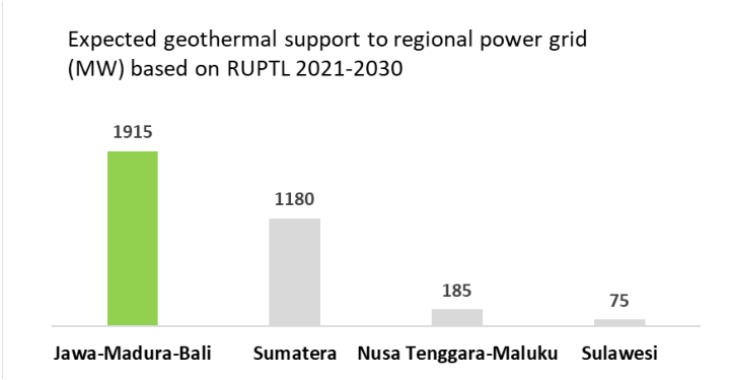

Figure 6: The Distribution of Expected Geothermal Power Support for Each Region.

This "Alpha Geothermal" project addresses the conditions necessary to determine the appropriate drilling strategy from a financial perspective. Four scenarios (Table 7 and Table 8) were simulated in this study, comparing two teams using different approaches. The slimhole scenario assumes a team with a mindset focused on phased and cautious development, while the bighole scenario assumes a team aiming for rapid development.

Table 7 outlines the assumptions used in each scenario, with all four cases progressing through three project phases: exploration, appraisal, and development. The cost and success rate assumptions were made by the authors, based on various references (IGA, 2014; IRENA, 2015; IFC, 2013; Adityatama et al., 2020; Purba et al., 2021b) and interviews with several geothermal experts in Indonesia conducted during this study.

Table 7: Assumptions explanation of each scenario assessed in this study.

Cases / Scenarios	Exploration	Appraisal	Development
Slimhole	A total of five slimhole wells were drilled, considering the relatively low cost of slimhole drilling (USD 2M per well). The costs already account for drilling infrastructure and mobilization-demobilization expenses. The objective was to cover a wider tested area to provide the exploration team with more data for resource assessment and planning for the next drilling phase. At this stage, the drilling success ratio is assumed to be only 40%, meaning that out of the five wells drilled, only 2	After successfully confirming the resource with two slimhole wells out of the 5 (five) drilled, the team had sufficient data to proceed with field development using bighole wells. However, recognizing the remaining risks, the team decided to adopt a phased strategy for the 10 wells to be drilled. They would first drill five wells, evaluate the results, and proceed with the next five wells if deemed feasible. The drilling success rate increased to 70%, as the five initial drilling points could serve as valuable references. As a	With the availability of data from five slimhole wells and ten bighole wells, where a total of 9 (nine) wells provided information confirming the presence of the resource and its characteristics, the success rate at this stage can be assumed to be 80%. This means that to achieve the remaining 30 MW, only 8 (eight) more wells are needed, assuming six of them will successfully produce 5 MW per well. The total capacity achieved would be 65 MW, which includes a buffer for the utilization of 55 MW.

Cases / Scenarios	Exploration	Appraisal	Development
	(two) successfully confirmed the presence of the resource.	result, there will be 7 (seven) wells that can serve as production wells, providing a total of 35 MW at the wellhead.	
Slimhole Overrun	The same assumptions as the slimhole case above apply; however, in this scenario, one slimhole well encountered operational issues, resulting in a cost overrun of up toUSD 3M.	The same assumptions as the slimhole case above apply.	The same assumptions as the slimhole case above apply. The difference is that due to the cost overrun during the explorationphase, there is an additional cost of USD 1M compared to the previous slimhole scenario.
Bighole	In this scenario, the exploration team chose to use bighole drilling, with a total of three wells costing USD 9M per well, including mobilization-demobilization and infrastructure. The team opted for bighole drilling as they were more familiar with full-size wells and wanted the option for directional drilling and sidetracking when needed. The drilling success ratio is 40%, meaning that out of the three wells drilled, only one will confirm the presence of the resource. The team also hoped that if a well was successful, it could be directly used as a production well, with the assumption that one successful well could yield 5MW per well.	Since only one well in the exploration phase successfully confirmed the presence of a subsurface resource, the risk during the appraisal phase remains high, with the drilling success ratio only increasing to 60%. With this success ratio, only six wells out of the ten drilled will successfully produce 5 MW per well, providing 30 MW at the wellhead, which totals 35 MW when combined with the 5 MW already obtained during the exploration phase. In this scenario, it is assumed that the team opted to drill all 10 bighole wells without conducting an evaluation after the first five wells.	Since there is data from only 13 wells, and only seven of those wells provided information on the presence and characteristics of the resource, the success rate at this stage increases to only 75%. This means that nine additional wells are needed to obtain six wells with a capacity of 5 MW per well, equivalent to an additional 30 MW at the wellhead. This would result in a total of 65 MW when combined with the capacity achieved during the exploration and appraisal phases.
Bighole Overrun	The same assumptions as the bighole case above apply; however, in this scenario, one bighole encountered operational issues, resulting in a cost overrun of up to USD 20M. This cost increase is based on actual data, where a stuck pipe incident during bighole drilling can reach up to USD 29M in Indonesia.	The same assumptions as the bighole case above apply.	The same assumptions as the bighole case above apply. The difference is that due to the cost overrun during the exploration phase, there is an additional costof USD 11M compared to the previous bighole scenario.

Table 8 presents the key assumptions outlined in Table 7 that are ready to be incorporated into the financial model for simulation. The figure of 14.5 MUSD per well for failed bighole cases in the exploration phase is derived from the average of two failed wells in the bighole case. The first well experienced an overrun, reaching up to 20 MUSD, while the second well, although it failed to confirm the resource, remained within the 9 MUSD/well budget. This gives a total of 29 MUSD, which, when divided between the two wells, results in an average of 14.5 MUSD per well.

Each case will aim for a target of 65 MW gross total well capacity, considering a buffer of 10-30% from the net target of 55 MW. A middle value is assumed, with approximately 10 MW considered sufficient as a buffer to account for various issues that may arise during production.

4.2 The "Walkaway" Cost

The walkaway cost in geothermal project represents the cumulative financial loss incurred if the project is terminated before reaching the production stage, typically due to poor resource quality, technical challenges or significant unresolved issues during project. Analyzing walkaway costs is crucial for assessing the financial viability and risk exposure of geothermal projects, particularly during the early stages of exploration and appraisal that financed by equity. The understanding of walkaway cost is important to provide crystal view of the worst-case financial scenario. It serves as indicator to take necessary action to safeguard the investment through appropriate project strategy and risk mitigation.

Exploration teams might overlook walkaway costs in project planning due to a focus on success, where failure scenarios are seen as unlikely. Pressure to meet tight deadlines and financial targets can lead to skipping detailed risk assessments. Estimating walkaway costs is complex, and many decision-makers underestimate or ignore these costs, seeing them as low-probability risks. Additionally, financial planning tends to prioritize upfront costs and potential returns, leaving walkaway costs underemphasized.

Table 8: The key assumptions on the exploration drilling aspect for financial model input.

	Slimhole	Slimhole overrun	Big hole	Big Hole overrun
Exploration Phase				
Exploration success ratio	40%			
-Exploration drilled well				
--Slimhole	5 wells	5 well	-	-
--Big hole	-	-	3 wells	3 wells
Well cost				
-- Success slimhole	2 MUSD/well		-	-
-- Failed slimhole	2 MUSD/well	3 MUSD/well	-	-
-- Success big hole			9 MUSD/well	
-- Failed big hole			9 MUSD/well	14.5 MUSD/well
Appraisal Phase				
-Appraisal success ratio	70%		60%	
-Appraisal drilled well				
-- Big hole	5 +5 wells	5 +5 wells	10 wells	10 wells
Well cost				
-- Success big hole	9 MUSD/ Well			
-- Failed big hole	9 MUSD/ Well			
Development Phase				
-Development success ratio	80%		75%	
-Development well				
-- Big hole	8 wells	8 wells	9 wells	9 wells
Well cost				
-- Success big hole	9 MUSD/ Well			
-- Failed big hole	9 MUSD/ Well			

The authors have obtained data from at least two geothermal projects in Indonesia that are still in the exploration phase. However, this data is confidential and cannot be published in this paper. Both projects have spent over 50 MUSD on exploration costs without reaching any significant conclusions about the resources in the prospective areas. This puts the investors in a difficult position, as a substantial amount of money has already been spent, making it hard to abandon the project due to the large sunk costs. However, they also lack sufficient data to move forward, meaning further expensive drilling activities are still required. This situation arose because the decision-makers in charge of the exploration projects did not consider walkaway costs in their planning.

In the simulation of "Alpha Geothermal" project, the slimhole case demonstrates lower walkaway cost compared to the bighole scenario. If developer decides to exit the project after the exploration phase, the financial loss in the slimhole scenario is estimated at 10-11 million USD (Figure 7), whereas the big hole scenario could result in a loss of up to 27-38 million USD (Figure 8). Utilizing slimholes provides a cost-effective method for resource confirmation, as it allows for more efficient allocation of capital during the high-risk exploration phase. This approach enables developers to assess multiple areas for better evaluation and decision making with similar investment levels required for single bighole well, which typically only tests one location.

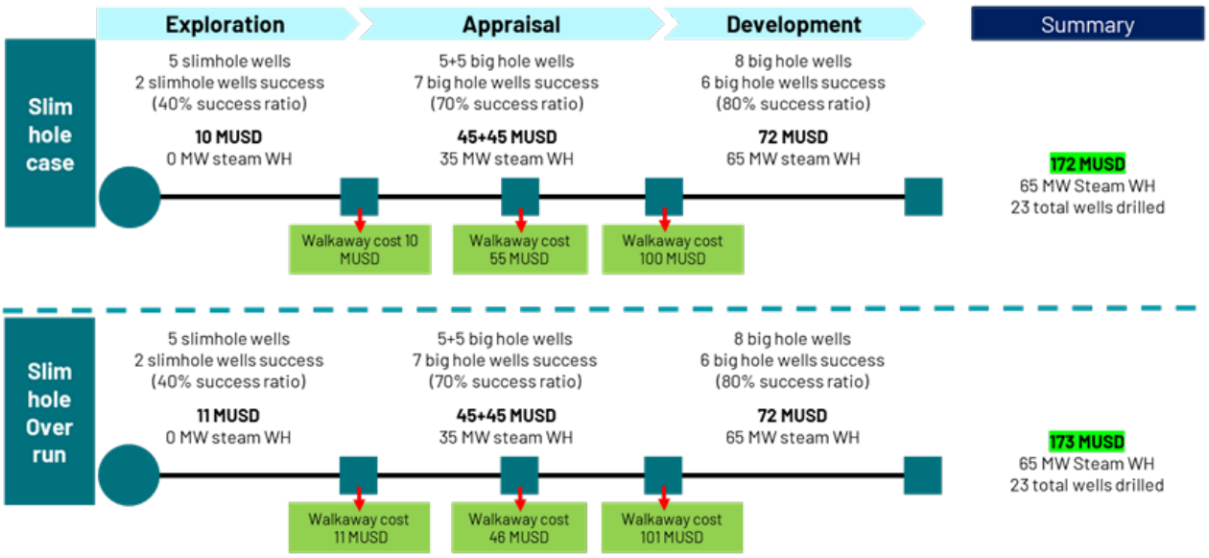

Figure 7: Walkaway Illustrations of Slimhole Cases: Normal and Overrun.

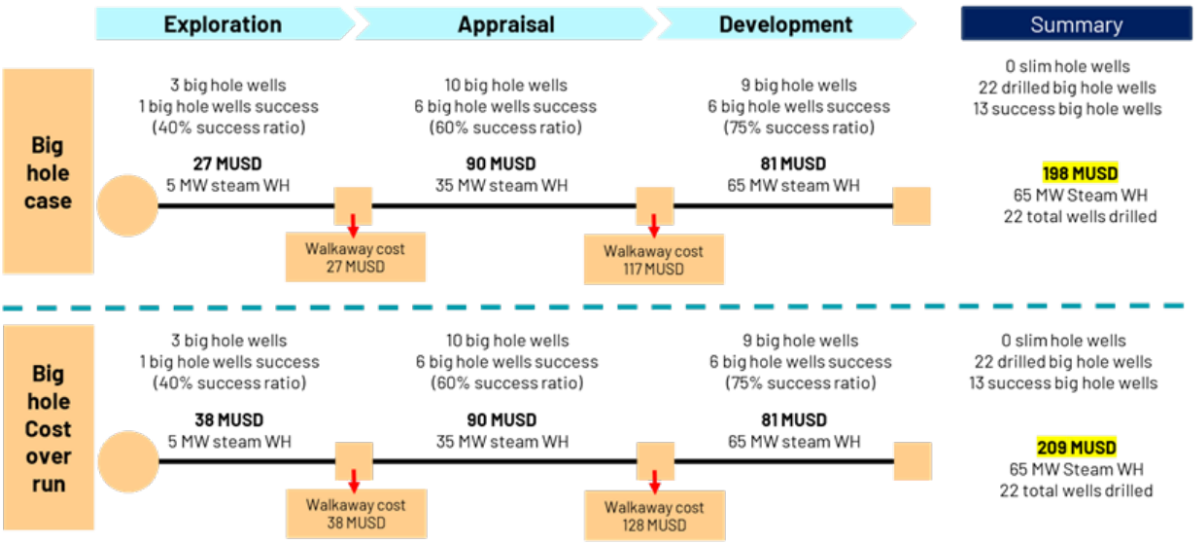

Figure 8: Walkaway Illustrations of Bighole Cases: Normal and Overrun.

4.3 Net Cashflow and Equity Return

Figure 9 shows the cash flow graph for the hypothetical 55 MW Alpha Project comparing the financial trajectories of big hole and slim hole drilling scenarios. During the early exploration and appraisal stages, which are typically financed entirely by equity with no external debt involvement, the slimhole scenario shows a clear financial advantage. The lower initial capital required for slim hole drilling results in smaller negative cash flow, reducing the burden on equity funding.

The bighole scenario, with its substantial equity cash requirements, poses a greater financial risk during these early stages. In contrast, the slim hole approach not only mitigates this risk but also provides greater financial flexibility by preserving equity capital. This reduced financial exposure allows for a more phased investment approach, enabling the developer to better manage uncertainties and adapt to changing project dynamics without jeopardizing the overall financial performance of the project.

Lowering CAPEX during exploration and appraisal stages improves net cash flow and boosts equity returns. With reduced upfront costs, especially through slimhole drilling, the project requires less capital, leading to smaller cash flow deficits and faster equity break even point. This strengthens the project's financial position, making future financing easier and reducing reliance on additional equity or costly debt. Additionally, lower CAPEX enhances the internal rate of return (IRR), as lower investment yields the same future revenue, resulting in higher overall equity returns and making the project more financially attractive.

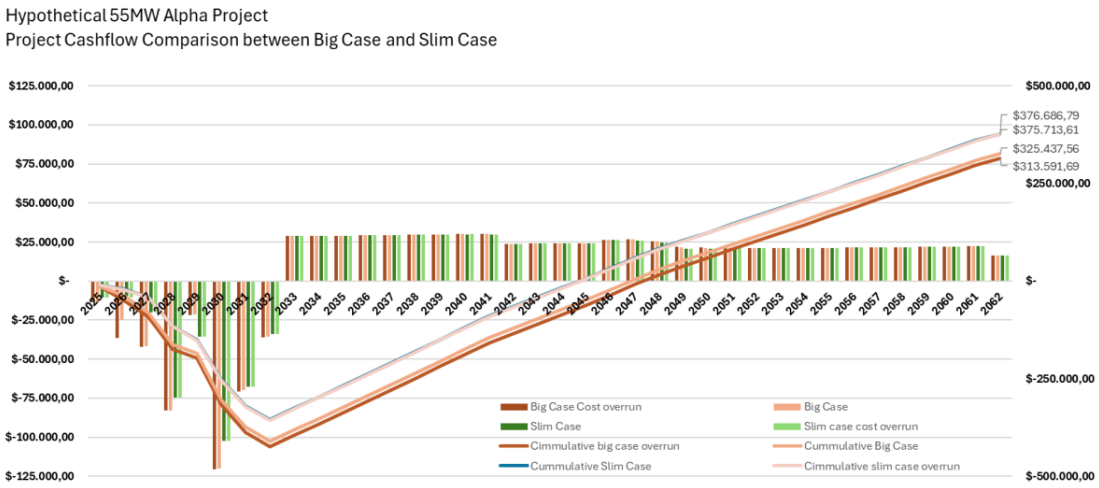

Figure 9: The Cashflow Graph for The Hypothetical 55 MW Alpha Project Comparing the Financial Trajectories ff Bighole and Slimhole Drilling Scenarios.

Table 9 illustrates the Internal Rate of Return (IRR) for equity under both base and cost overrun conditions for slim hole and big hole drilling scenarios. In the base condition, the slimhole scenario achieves an IRR of 6.48%, compared to just 4.17% for the big hole case. This suggests that slimhole drilling provides more favorable return on equity due to its lower upfront costs and reduced financial exposure during the high-risk exploration phase, which is typically funded solely by equity.

When cost overruns occur, the IRR for the slimhole scenario shows only a slight decline, indicating minimal impact on equity returns despite unforeseen cost increases. In contrast, the bighole scenario experiences a significant decline in IRR, highlighting its risk to cost escalations during the exploration stage. This is particularly critical because any failure in the bighole scenario can severely impact the overall project's financial viability, placing a substantial burden on equity investors.

Table 9: Comparison of IRR Equity between slim case and big case.

IRR Equity	Base condition	Cost overrun condition	Changes
Slim case	6.48%	6.44%	-0.04%
Big case	4.17%	3.52%	-0.65%

4.4. Discussion on Slimhole vs Bighole Based on the Simulation Result

The financial simulations in sub-sections 4.2 and 4.3 show that slimhole drilling offers several advantages over bighole drilling, especially if a significant cost overrun occurs during bighole operations. Numerous papers have already discussed the technical aspects of why slimhole drilling is much more cost-effective and worth considering for exploration in Indonesia (GRG-Geoenergis, 2024; Purba, 2018; Purba et al., 2021a; Purba et al., 2021b; Apriani et al., 2018; Adityatama et al., 2020; Adityatama et al., 2021; Purba et al., 2019; Sumardi, 2022a; Sumardi 2022b; Wiharlan, 2021). In this sub-section, the authors will briefly discuss the comparison between slimhole and bighole drilling in terms of resource assessment during the exploration phase.

4.4.1 Wider coverage of testing area with lower cost using slimhole

Slimhole drilling offers significant advantages in geothermal exploration, particularly in terms of cost efficiency and maximizing subsurface data collection. With unit costs ranging from approximately 1.5 to 3 MUSD per well, slimhole wells are considerably more affordable than bighole wells, which typically cost between 7 and 10 MUSD per well. This substantial cost difference allows for a higher number of wells to be drilled with the same budget. For example, the cost of drilling one bighole well can be used to drill between three to five slimhole wells. By drilling more wells, exploration teams can cover a larger geographical area, providing a more comprehensive understanding of the subsurface.

The increased number of wells drilled through slimhole techniques significantly enhances the quality and quantity of data collected. Each additional well provides crucial information about the geothermal reservoir's characteristics, such as fluid flow, pressure, and temperature. This data is essential for reservoir numerical modeling, allowing for more accurate predictions of resource potential and reducing the uncertainties that typically accompany geothermal exploration. As a result, slimhole drilling not only offers cost savings but also improves

the overall reliability of resource assessments, helping to optimize the subsequent development phases and reduce financial risks.

4.4.2 Overall project economics enhancement

Slimhole drilling not only reduces costs during the exploration phase but also significantly increases the likelihood of success in the appraisal and development phases. By testing more areas with slimhole wells, exploration teams can gather a much deeper understanding of the subsurface characteristics, such as fluid distribution, temperature gradients, and reservoir boundaries. This improved understanding helps to identify the most promising drilling locations, leading to a higher success rate when transitioning to the appraisal and development stages. As a result, the overall project risks are reduced, increasing the chances of securing productive wells in subsequent phases.

Additionally, the higher success rates during appraisal and development due to slimhole data reduce the need for unnecessary drilling activities, which directly translates to lower total drilling costs. This cost reduction improves the economic feasibility of the project, making it more attractive to investors and lenders. The time gained by using slimholes for early-stage exploration also allows project developers to thoroughly analyze the data, prepare more accurate project proposals, and engage potential investors or lenders with greater confidence, further boosting the project's financial prospects.

4.4.3 Minimizing Walkaway Costs

One of the significant advantages of slimhole drilling in geothermal exploration is its ability to drastically reduce walkaway costs in the event of a failed exploration. In any exploration activity, there is always a risk that the wells drilled may not yield the desired sub-surface geothermal resource, leading to financial losses. With bighole wells, which can cost between 7 and 10 MUSD per well, or 20 MUSD if major incidents happened, the financial impact of a failed well can be substantial, leading to large sunk costs that investors must absorb. In contrast, slimhole wells cost considerably less—typically between 1.5 and 3 MUSD per well—so the financial impact of a failed exploration is much lower. This reduction in walkaway costs makes slimhole drilling a more attractive option, especially in high-risk areas where the likelihood of failure is uncertain.

For investors, reducing the financial risk associated with exploration is a key factor in decision-making. Slimhole drilling provides a safety net by lowering the potential losses in case a well does not produce viable geothermal resources. This makes it easier for investors to commit to exploration projects, as their financial exposure is minimized.

4.4.4 The risk of bighole overrun cost

In geothermal drilling, particularly with bighole wells, the risk of cost overruns due to major incidents like stuck pipe is a significant concern. Data from Indonesia shows that such incidents can increase costs by as much as 29 MUSD (Table 10). Stuck pipe occurs when the drill string becomes stuck and trapped in the wellbore, often due to challenging subsurface conditions. This issue is not uncommon, especially in exploration phases, where the subsurface is largely unknown. Even during the development phase, stuck pipe remains a frequent problem, as Indonesia's volcanic systems are highly heterogeneous, making it difficult to create accurate geoscientific predictions. This unpredictability adds to the operational risks and often leads to costly delays and additional drilling efforts.

Table 10: Actual drilling cost from 13 wells of bighole drilling in Indonesia (GRG-Geoenergis, 2024).

No.	Well Name	Project Location	Well Depth (mMD)	Total Drilling Cost (USD)	Drilling Cost per meter (USD/m)	Well Status
1.	Well 1	Sumatera	2,160	$29,408,487	$13,615	Non-productive
2.	Well 2	Sumatera	1,654	$28,441,465	$17,196	Non-productive
3.	Well 3	Sumatera	2,941	$24,110,166	$8,198	Productive
4.	Well 4	East Java	2,770	$22,904,286	$8,269	Productive
5.	Well 5	Sumatera	3,014	$21,352,215	$7,084	Productive
6.	Well 6	Sumatera	2,272	$19,824,782	$8,725	Non-productive
7.	Well 7	Sumatera	3,006	$17,559,075	$5,841	Productive
8.	Well 8	Sumatera	1,503	$17,335,170	$11,534	Non-productive
9.	Well 9	Sumatera	1,253	$17,323,032	$13,825	Non-productive
10.	Well 10	Sumatera	2,133	$15,988,860	$7,494	Non-productive
11.	Well 11	Sumatera	1,829	$15,938,855	$8,716	Non-productive
12.	Well 12	Sumatera	1,668	$15,605,100	$9,356	Productive
13.	Well 13	Sumatera	2,500	$15,563,587	$6,225	Non-productive

The challenge of avoiding drilling surprises is heightened by the fact that exploration drilling is typically planned with very limited subsurface data. This lack of comprehensive information increases the likelihood of encountering unforeseen subsurface hazards, such as unstable formations or high-pressure zones, which can result in stuck pipe or other major incidents. Additionally, the cost implications of such incidents are exacerbated by the high daily rental rates of rigs used for drilling slimhole wells, which generally require 1,000 to 2,000 horsepower, depending on the well design, drilling trajectory, and rig availability. When stuck pipe or other significant issues occur, the rig rental costs can skyrocket, as the downtime needed to resolve the problem directly translates into higher expenses. With daily rig rental costs being substantial, a delay of just a few days can quickly inflate overall project costs, adding to the financial risks already inherent in geothermal exploration.

These risks make cost management critical in geothermal projects, particularly during the exploration phase. While slimhole drilling offers a lower-cost alternative to bighole wells, the potential for cost overruns remains high due to Indonesia's complex geological conditions. Therefore, thorough planning, real-time monitoring, and flexible mitigation strategies are essential to minimize the financial impact of such incidents and ensure that geothermal exploration remains economically viable.

5. MANAGING EXPLORATION COST

5.1 High Level Strategy in Managing Exploration Cost

After reviewing the analysis in Figure 3 and Figure 4, it is evident that managing exploration costs is critical for maintaining a favourable IRR and ensuring the economic feasibility of geothermal projects. Based on the sensitivity analysis, these are several key considerations to optimize exploration expenditures and enhance project feasibility:

1. *Implement Standardized Cost Management Practices*: Develop and enforce standardized practices for managing exploration costs across different stakeholders. This can help reduce financial inefficiencies and ensure more predictable CAPEX outcomes.
2. *Adopt Best Practices from Successful Case Studies*: Analyse and adopt cost management strategies from successful geothermal projects that have managed to control exploration costs effectively. Sharing these best practices can help other projects achieve similar efficiencies.
3. *Policy Support for Cost Reduction*: Advocate for supportive policies that facilitate cost reductions in exploration. This includes providing financial incentives, streamlining regulatory processes, and promoting technological innovations that can lower exploration costs.
4. *Focus on Cost-Effective Exploration Techniques*: Invest in research and development of cost-effective exploration techniques. Utilizing advanced geophysical surveys, drilling technologies, and data analytics can help reduce the overall cost burden of exploration.

5.2 Role in Advanced Reservoir Numerical Modelling to Optimize Exploration Strategy

A study by O'Sullivan et al. (2024) demonstrated that reservoir numerical modelling has played a critical role in assessing the potential of six undeveloped geothermal fields in Indonesia: Ciremai, Kepahiang, Kotamobagu, Maritaing, Massepe, and Papandayan. These fields present complex geological conditions, and traditional exploration methods would have faced significant challenges in providing accurate resource estimates due to the uncertainties associated with subsurface characteristics.

Table 11: Summary of reservoir numerical modeling on six undeveloped geothermal fields in Indonesia (O'Sullivan et al., 2024).

Field	Geological Features	Modeling Outcome	Main Challenges	Potential Power Output Estimate	Numerical Modeling Remarks
Ciremai	Volcanic-type system, deep water table, complex stratigraphy	Identified need for highly deviated wells due to deep water table	Deep water table affecting well discharge pressure	55.1 MWe	Developed a highly deviated well scenario due to deep water table, improving well placement strategy.
Kepahiang	Thick clay cap, volcanic nature, fault-controlled fluid movement	More conservative estimate of potential due to deep reservoir	Thick clay cap complicating access to geothermal resource	63.1 MWe	Refined the resource potential estimate with a focus on the deep reservoir beneath the clay cap.

Field	Geological Features	Modeling Outcome	Main Challenges	Potential Power Output Estimate	Numerical Modeling Remarks
		beneath clay cap			
Kotamobagu	Complex geological setting with multiple volcanic formations, uncertain reservoir size	Refined target reservoir size, smaller than initial interpretations	Uncertainty in target reservoir size based on MT data	270 MWe	Provided a more accurate target reservoir size, addressing the uncertainties from initial geophysical surveys.
Maritaing	Fault-controlled fluid system with volcanic and sedimentary formations	3D geological model improved understanding of fault-controlled fluid movement	Complex interaction of volcanic and sedimentary formations	22.9 MWe	Created a 3D geological model to clarify fault-controlled fluid movement, enhancing reservoir understanding.
Massepe	Upflow zone identified through resistivity anomalies, fault-controlled	Resistivity anomalies mapped the upflow zone, optimizing well placement	Identifying optimal drilling locations in upflow zone	43.4 MWe	Mapped resistivity anomalies and identified upflow zones for optimal well placement.
Papandayan	Volcanic-type system with complex fault structures and a clay cap dome	Identified feasible drilling locations and clarified the impact of fault structures	Navigating fault systems and clay cap to determine drilling feasibility	28.4 MWe	Assessed fault structures and the clay cap to identify feasible drilling locations and refine power output estimates.

In all six cases, numerical modelling provided more realistic resource assessments, helping to identify the challenges and opportunities unique to each geothermal field. By integrating real-world data and simulating production scenarios, these models offered insights that traditional methods could not, ultimately aiding in the decision-making process for developing Indonesia's geothermal resources efficiently.

In short, the study (O'Sullivan et al., 2014) presents six case studies showcasing a new framework for assessing the resource potential of geothermal systems. The framework utilizes early-stage exploration data to calibrate numerical reservoir models and estimate the potential power output of geothermal systems. This approach offers a more realistic estimate of geothermal resource potential compared to traditional methods, such as stored heat calculations, as it better accounts for the complex dynamics within the reservoir that influence energy extraction. By applying advanced numerical models, researchers were able to generate more reliable data on each field's potential power output, helping stakeholders make informed decisions regarding project feasibility.

5.3 Cost Reduction Options in Drilling

Implementing initiatives to reduce geothermal development costs in Indonesia is essential for enhancing the feasibility and efficiency of geothermal projects. Based on an evaluation of development cost data from three fields in Indonesia between 2019 and 2024 (GRG-Geoenergis, 2024), drilling is one of the components have the highest costs among the other cost components. Therefore, initiatives to reduce the overall development cost through optimization of drilling costs may be critical.

Employing initiatives to reduce geothermal drilling costs in Indonesia is crucial for enhancing the overall feasibility and efficiency of geothermal projects. Based on an evaluation of drilling cost data, drilling issues related to stuck pipes and well control (blowouts) can significantly inflate costs, sometimes exceeding 10 million USD per well. Therefore, initiatives to reduce the likelihood of such problems with stuck pipes and well control are critical. By addressing these issues, drilling costs can be kept within a reasonable threshold, as determined by expert interviews. In general, the authors identify two opportunities for project owners to optimize drilling costs, which are in the planning phase and operation phase, as outlined in Table 12.

To clarify the points outlined in Table 12 and provide specific examples, a study by GRG-Geoenergis (2024) has identified a range of initiatives for reducing geothermal drilling costs, drawing from various efforts by geothermal

developers both in Indonesia and globally. A detailed explanation of these initiatives and strategies is provided in the GRG-Geoenergis (2024) report, while a brief illustration of the initiatives is presented in in Figure 10.

5.4 Geothermal De-risking Scheme

Several approaches could also play a role in optimizing development costs, including geothermal de-risking scheme, soft loan application, and the optimization of derivative geothermal products. One of the initiatives by the Indonesian government to promote geothermal exploration projects is the creation of exploration financing schemes that include de-risking features, or in some cases, the government directly taking over exploration activities in a prospective area. A geothermal exploration risk mitigation scheme involves a set of strategies and measures aimed at reducing the financial risks associated with geothermal resource exploration. Common exploration methods encompass various techniques, such as conducting surface studies, drilling test wells, and constructing a conceptual model of the geothermal system. Typically, geothermal developers fund these activities using their company's equity (Siahaan, Septiani, & Purba, 2023).

Financial institutions often hesitate to finance geothermal exploration projects due to their lack of familiarity with such ventures and the inherent risks linked to geothermal resource viability. To address this challenge, government bodies and donor organizations have established programs to mitigate or significantly reduce the financial risks associated with geothermal exploration projects. These risk reduction programs may encompass government-led exploration initiatives, loan guarantees, grants, cooperative agreements, drilling failure insurance, and cost-sharing arrangements. Currently, there are several risk mitigation schemes for geothermal exploration projects. Table 13 provides a summary of the available facilities aimed at de-risking geothermal exploration in Indonesia.

Table 12: Areas of opportunities to optimize exploration drilling cost.

Phase	Typical cost-optimization areas / opportunities	Implementation Challenges
Planning phase	1. **Key personnel recruitment**: Prioritize hiring highly competent personnel over those with less experience to ensure the ability to design a cost-effective drilling plan. 2. **Well type selection and well design**: Conduct a proper assessment to ensure that the well type and design align with the exploration objectives, meaning they should not be too minimal, but also not excessive ("overkill"). 3. **Rig selection**: Perform rig sizing and market surveys to ensure you acquire a fit-for-purpose rig at the best price, based on current market availability. 4. **Peer-review**: If conducted properly, this process can help project owners identify gaps or potential cost overruns that may not have been adequately mitigated by the exploration drilling planning team. 5. **Collective risk assessment process**: Conduct various meetings and workshops, such as risk assessments, DWOP (Drill-Well-on-Paper), and stuck-pipe prevention campaigns, to ensure that all personnel involved in the exploration drilling project, including consultants and contractors, contribute to the identification and mitigation of drilling risks. This will ultimately help reduce the likelihood of cost overruns during operations due to stuck-pipe incidents, for instance. 6. **Rig, equipment, tool and material inspection**: Ensure that all equipment, tools and materials to be used have been inspected by certified personnel to verify that everything on-site is in proper working condition and ready for use.	1. The geothermal industry in Indonesia is currently facing an expertise gap due to the irregularity of geothermal drilling projects. This makes it difficult to find drilling experts in Indonesia who have both planning experience and a deep understanding of geothermal-specific risks. 2. Rigs used for bighole drilling typically come from the oil and gas industry, while rigs for slimhole drilling are sourced from the mining industry. This means that the geothermal industry is dependent on market conditions in both the oil and gas and mining industries when looking for rigs to use in geothermal exploration projects. 3. The authors found that many Drilling Engineers in Indonesia's geothermal industry are not yet accustomed to or skilled in acting as workshop facilitators. As a result, processes like risk assessments or stuck-pipe prevention campaigns are oftenconducted in a less effective manner.
Operation phase	1. **Key personnel recruitment**: Prioritize hiring highly competent personnel over those with less experience to ensure the ability to execute and supervise operations according to the plan. Additionally, emphasize strong communication skills to ensure the	1. Drilling Supervisors and drilling contractors in Indonesia typically come from the oil and gas industry, meaning geothermal companies often must compete to secure skilled and

Phase	Typical cost-optimization areas / opportunities	Implementation Challenges
	operations and planning teams can collaborate effectively during the execution phase, helping to prevent cost overruns. 2. **Regular monitoring and inspection during operation**: Ensure that critical equipment, tools, and materials are consistently monitored and inspected at regular intervals according to applicable standards, such as inspecting drill strings after drilling one or two wells. 3. **SOP and mitigation plan in place**: Ensuring that the operations team has and fully understands all SOPs and mitigation plans for potential incidents during drilling can lead to smoother operations and reduce the likelihood of cost overruns.	reliable personnel for drilling operations. 2. Operations teams are often hired just as drilling operations are about to begin, leaving them with insufficient time to familiarize themselves with the drilling program. As a result, they may not contribute to improving the planning, which can lead to operations not proceeding according to the initial plan.

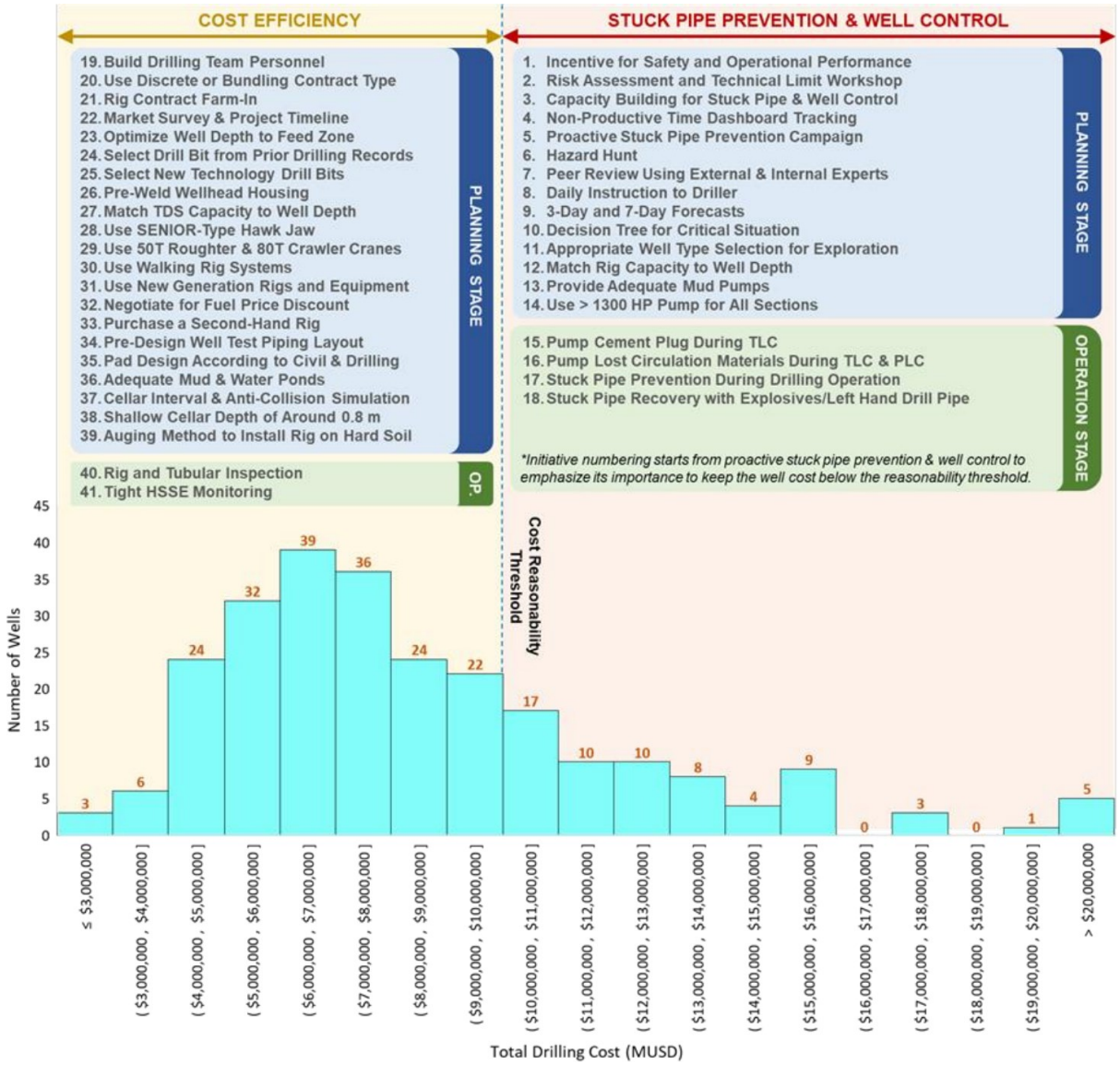

Figure 10: Drilling Cost Reduction Initiatives (GRG-Geoenergis, 2024).

Table 13: Geothermal exploration de-risking facilities in Indonesia (modified from Siahaan, et al., 2023; Apriani et al., 2018).

De-Risking Scheme	Name of Program	Brief Description
Government-led exploration (until exploration drilling)	Geothermal Energy Upstream Development Project (GEUDP)	The GEUDP is a government-sponsored exploration drilling through a collaboration between the Indonesian government and the World Bank. Its primary goal is to develop previously untendered greenfield geothermal areas in remote regions of Indonesia. In this program, the government assumes full responsibility for exploration drilling risks if the resource is either unproven or lacks economic viability.
	Government Drilling Performed by the Geological Agency	The funding for this scheme is sourced from the State Budget (APBN), and the government assumes full responsibility for covering all associated risks. The scope of activities encompasses preliminary surveys, land acquisition, permit procurement, infrastructure construction, drilling operations, well testing, and the updating of pre-feasibility study documents. If the results from the Governments' drilling activities cannot confirm the presence of economically viable geothermal resources, the subsequent phases will be financed through the GEUDP program.
Loan and risk-sharing	Geothermal Resource Risk Mitigation Project (GREM)	The GREM facility consists of two main components, namely: **Component 1:** Referred to as Geothermal Resource Risk Mitigation which introduces a risk-sharing mechanism, wherein developers may be eligible for partial repayment of the facility (up to 50% of the total facility limit) if their exploration efforts prove unsuccessful. **Component 2:** Dedicated to providing technical assistance and enhancing the capacity of SMI and relevant stakeholders.
	State-Owned Enterprise (SOE) Drilling	The SOE drilling program closely resembles the GREM, but it is exclusively funded through the PISP (Geothermal Sector Infrastructure Financing Fund) funds. This facility offers a combination of blended loans and de-risking support.

The various schemes in Table 13, while aimed at sharing the risk between the government and geothermal investors, do not clearly explain how to effectively manage the costs of geothermal exploration projects. This means that the possibility of cost overruns remains high, even when utilizing the available funding facilities. These facilities are designed to share risk, but they lack guidelines for cost-effective exploration project management to ensure the project's feasibility.

6. DISCUSSION AND POTENTIAL WAY FORWARD

This paper dedicates significant discussion to exploration activities, even though the primary focus is on cost aspects. The authors have done this to provide context for readers who may not be familiar with the geothermal industry in Indonesia. The hope is that this paper will trigger further discussions on how to optimize exploration costs in Indonesia. Below is the concluding discussion of this paper.

6.1 Impact of Exploration CAPEX

Geothermal exploration is crucial for Indonesia's energy targets, as most new capacity will come from newly explored areas. Proper exploration management reduces risks and costs, enhancing project feasibility and leading to better resource assessments and investment decisions. Effective exploration practices are vital for government agencies, SOEs, and private developers to ensure economic viability.

Despite challenges, the exploration phase is key to meeting national geothermal targets. The limited development despite Indonesia's vast potential, indicating the need for more exploration efforts. Various entities manage geothermal projects, but disparities in cost management exist due to differences in expertise, resources, and strategies. These inefficiencies lead to overspending and economic challenges, hindering geothermal development.

High exploration costs negatively impact project feasibility, as excessive spending inflates overall costs and reduces economic returns. Aligning cost management practices among stakeholders is essential for maintaining project viability and achieving renewable energy goals. Adopting a development mindset during exploration is

risky and can lead to financial waste. Effective, cost-conscious exploration is crucial to avoid overcommitting resources and ensure long-term project success.

This study emphasizes that CAPEX is a cornerstone of geothermal project development. It affects every aspect of the project, from initial feasibility and financial risk to operational efficiency and investment attractiveness. Effective management of CAPEX is essential for ensuring the economic viability and long-term success of geothermal projects. Stakeholders must prioritize accurate estimation, strategic allocation, and diligent management of CAPEX to optimize project outcomes and contribute to the sustainable development of geothermal energy.

By addressing the critical issue of exploration costs and their impact on CAPEX, stakeholders can enhance the economic viability and attractiveness of geothermal investments in Indonesia. This will ultimately contribute to the country's energy security and sustainable development goals.

Identifying which cost components most significantly impact the Internal Rate of Return (IRR) is vital for effective resource allocation, risk management, strategic decision-making, and financial planning. By understanding the key cost drivers, project managers can allocate resources more effectively, implement better cost control measures, and develop targeted risk mitigation strategies. This knowledge also informs strategic decisions, prioritizing investments that optimize IRR, thereby enhancing the project's financial attractiveness. Additionally, detailed CAPEX analysis can lead to more favourable financing terms, securing better funding conditions.

These insights, derived from the sensitivity analysis, provide a robust foundation for the paper's arguments and recommendations, guiding policymakers, industry stakeholders, and investors towards more effective practices and supportive policy interventions. Furthermore, this paper briefly explores current options identified in the Indonesian geothermal industry that stakeholders might consider for managing their geothermal exploration projects. These options aim to optimize costs and achieve attractive project economics. The authors plan to discuss the details of each option in a separate paper.

6.2 Challenges in Implementing Slimhole Drilling in Geothermal Exploration

Implementing slimhole drilling in geothermal exploration in Indonesia presents several challenges, despite its appeal on financial models. One significant issue is that slimhole drilling is relatively "new" to the current geothermal industry due to the long hiatus in its use. Slimhole drilling was more commonly employed in the 1980s and 1990s, but its utilization largely stopped after the 1998 monetary crisis. It wasn't until 2016 that slimhole drilling re-emerged, leaving a gap of around 20 years without substantial exploration using this method. As a result, much of the current geothermal workforce lacks experience and familiarity with slimhole drilling, making it a less attractive option for many project owners.

Another challenge is the limited availability of reliable slimhole drilling contractors in Indonesia. At the time this study was conducted, only one contractor stood out in the market, but unfortunately, this contractor struggled with poor management. This led to several incomplete drilling projects, leaving many project owners dissatisfied and hesitant to consider slimhole drilling in future endeavours. The lack of trust in slimhole contractors has made it difficult for the method to gain traction, despite its potential cost-saving benefits.

Additionally, the rigs used for slimhole drilling in Indonesia are often sourced from the mining industry. While these rigs can be adapted for geothermal use, the standards and specifications required for geothermal projects are different from those in the mining sector. This necessitates modifications to the rigs, which can add complexity and additional costs to the process. These challenges highlight the need for better contractor management, increased technical expertise, and the development of rigs specifically suited for geothermal exploration if slimhole drilling is to become a more viable and widely accepted method in Indonesia's geothermal industry.

6.3 Policy and Industry Recommendations

To support the development of geothermal projects in Indonesia, both policymakers and industry stakeholders should focus on creating a more favourable environment for cost-efficient exploration. First, the government can enhance its risk-sharing mechanisms to reduce the financial burden on developers, particularly during the high-risk exploration phase. Policies that provide more structured financial support, such as grants or exploration cost guarantees, can incentivize developers to pursue slimhole drilling and other cost-effective techniques without the fear of significant sunk costs.

Secondly, government need to regulate the standardized cost management practices across different stakeholders to minimize financial inefficiencies and ensure predictable capital expenditure (CAPEX) outcomes. Regulations should mandate the adoption of standardized practices for cost estimation, budgeting, and reporting. Establishing regulatory framework that enforces best practices for cost management, including regular audits and financial transparency, will help align project costs with planned budgets and reduce the likelihood of cost

under/overestimate. Additionally, regulatory frameworks should be updated to streamline the permitting process, reducing delays and lowering administrative costs for developers.

From an industry perspective, there is a need for more collaboration among geothermal developers, contractors, and financial institutions to standardize best practices for exploration cost management. Industry-wide initiatives, such as peer reviews and shared databases of exploration results, could help reduce inefficiencies and avoid repeating costly mistakes. Furthermore, investment in workforce training and development is crucial, particularly to address the gap in slimhole drilling expertise. The geothermal stakeholder should put attention in capacity-building programs that focus on specialized geothermal drilling techniques, reservoir modelling, and risk management. These programs can be developed in collaboration with academic institutions and international organizations. This would help to accelerate the learning curve and avoid excessive exploration costs. Finally, by fostering a culture of collaboration and continuous improvement, both policy and industry can contribute to making geothermal exploration in Indonesia more financially viable and sustainable in the long term.

6.4 Future Research Directions

As geothermal exploration continues to evolve in Indonesia, future research should focus on further refining cost-effective exploration techniques, particularly in relation to slimhole drilling. There is a clear need for studies that compare the long-term performance and data reliability of slimhole versus bighole wells beyond the initial exploration phase. Additionally, research should explore innovative ways to integrate advanced reservoir numerical modelling earlier in the exploration process to enhance decision-making and reduce uncertainties. These studies would provide valuable insights for improving well-targeting, minimizing drilling risks, and enhancing resource assessments, thus contributing to a more efficient exploration strategy.

Moreover, future research should examine the potential for new financing mechanisms tailored to support geothermal exploration projects in high-risk areas. Current funding schemes, while helpful, often lack a structured approach to managing cost overruns and walkaway costs. Investigating risk mitigation strategies such as insurance-based solutions, and examining their impact on project feasibility, could significantly reduce financial risks for investors. By advancing research in these areas, the geothermal community can create more resilient and financially viable exploration strategies to help Indonesia achieve its ambitious energy targets.

REFERENCES

Adityatama, D.: *Mengenal Tahapan Proyek Panas Bumi di Indonesia*. www.enerklaz.com. (2020).

Adityatama, D., Purba, D., Muhammad, F., Agustino, V., Wiharlan, H., & Pasmeputra, K..: Slimhole Drilling Overview for Geothermal Exploration in Indonesia: Potential and Challenges, *Proceedings*, 45th Workshop on Geothermal Reservoir Engineering, Stanford University, Stanford, CA (2020).

Adityatama, D., Agustino, V., Wiharlan, H., Muhammad, F., Alamsyah, D., Purba, D.: Assessing Drilling Rig Options for Conducting Geothermal Exploration Slimhole Drilling in Indonesia, *Proceedings*, 46th Workshop on Geothermal Reservoir Engineering, Stanford University, Stanford, CA (2021).

Apriani, D. N. I., Randle, J. B., & Paripurna, A.: *Government Drilling Program for Geothermal Exploration in Indonesia*. 14–16, (2018).

Asian Development Bank (ADB), & The World Bank.: *Unlocking Indonesia's Geothermal Potential*. ASIAN DEVELOPMENT BANK, (2015).

Asokawaty, R. F., Purba, D. P., Adityatama, D. W., Muhammad, F., & Umam, M.: Indonesia's Geothermal Development Compared to World Top Geothermal Producers. *45th Workshop on Geothermal Reservoir Engineering*, (2020).

Darma, S.: Indonesia: *Vast geothermal potential, modest but growing exploitation. In Geothermal Power Generation: Developments and Innovation* (pp. 609–643). Elsevier Inc. https://doi.org/10.1016/B978-0-08-100337-4.00021-8, (2016).

Direktorat Panas Bumi.: *Buku Pintar Umum Panas Bumi*, (2022).

GeothermEx.: *An assessment of geothermal resource risks in Indonesia*, (2010).

GGGI.: *A Guideline to Differentiate Cost Type in Geothermal Development Project in Indonesia: Blawan-Ijen Geothermal Prospect Area Case*. Global Green Growth Institute report to PT SMI (unpublished), (2023).

GRG-Geoenergis: *Study of Geothermal Development Cost Reduction*. An unpublished report developed for PT SMI and EBTKE. (2024)

Ibrahim, R. F., & Fauzi, A., Suryadarma.: The progress of geothermal energy resources activities in Indonesia. *Proceeding World Geothermal Congress 2005*, 1-7, (2005).

IFC: *Success of Geothermal Wells: A Global Study*, International Finance Corporation with input from GeothermEx, Inc., (2013).

IGA.: *Best practices guide for geothermal exploration*. Bochum, Germany: International Geothermal Association, (2014).

IRENA: *Renewable Power Generation Costs in 2014*, International Renewable Energy Agency, Abu Dhabi (2015).

Jacobs, & PT SMI.: *GREM Evaluation Framework Criteria*, (2022).

Kristianto, B.: *Discussion on 3G surveys cost and duration in geothermal exploration in Indonesia*. Personal communication, (2018).

O'Sullivan, J., Alia, W., Aloanis, A., Dekkers, K., Fuad, A., Gravatt, M., Nagoro, B., Nugraha, R., Popineau, J., Pratama, A., Rahmansyah, F., Renaud, T., Riffault, J., Syahrul, A., Takodama, I., Tonkin, R., O'Sullivan, M.: Towards a New Framework for the Systematic Assessment of Indonesia's Undeveloped Geothermal Resources *PROCEEDINGS*, The 10th Indonesia International Geothermal Convention & Exhibition (IIGCE) (2024).

PT SMI.: *Indonesia Geothermal Resource Risk Mitigation Project Developer Manual*. https://ptsmi.co.id/strategiccooperation/grem, (2022a).

PT SMI.: *De-risking of Geothermal Exploration from Lender's Perspective*, (2022b).

Purba, D.P.: Energy 785 Research Project Report: *Investigation on Geothermal Resource Assessment Methods in Reducing Exploration Risk in Indonesia Geothermal System*. The University of Auckland, New Zealand. Unpublished manuscript, (2018).

Purba, D.P., Adityatama, D.W., Umam, M.F., and Muhammad, F.: Key Considerations in Developing Strategy for Geothermal Exploration Drilling Project in Indonesia, *Proceedings*, 44th Workshop on Geothermal Reservoir Engineering, Stanford University, Stanford, California, United States, (2019).

Purba, D.P., Adityatama, D.W., Agustino, V., Fininda, F., Alamsyah, D., and Muhammad, F.: Geothermal Drilling Cost Optimization in Indonesia: A Discussion of Various Factors, *Proceedings*, 45th Workshop on Geothermal Reservoir Engineering, Stanford University, Stanford, California, United States, (2020).

Purba, D.P., Adityatama, D.W., Nugraha, R. P., Ayuningtyas, R. R., Chandra1, V. R., Al-Hassan, M. A., Ramadhan, R. F., Rizqi, M. M.: Resource Assessment Methods Selection for Geothermal Exploration Project in Indonesia: What Are the Considerations? *Proceedings*, 46th Workshop on Geothermal Reservoir Engineering, Stanford University, Stanford, California, United States, (2021a).

Purba, D., Adityatama, D. W., Nugraha, R. P., Rizkiani, G. P., Izzat, R., Chandra, V. R., Kristianto, B.: Expediting Geothermal Exploration in Indonesia: Should We Consider Slimhole Drilling? *Proceedings*, 46th Workshop on Geothermal Reservoir Engineering, Stanford University, Stanford, CA (2021b).

Pusdatin ESDM: Ministry of Energy and Mineral Resources Media Center (2020).

Poernomo, A. S.: An overview of Indonesia Geothermal Development – Current Status and Its Challenges. Pp. 1 – 11. In: *Proceedings of World Geothermal Congress,* Melbourne, Australia, (2014).

Purwanto, E. H., Suwarno, E., Lukman, R. F., and Herdiyanto, B.: Geothermal Drilling in Indonesia: A Review of Drilling Operation, Evaluation of Well Cost and Well Capacity, *Proceedings*, 6th Indonesia International Geothermal Convention & Exhibition, Jakarta, Indonesia, (2018).

Siahaan, M. F., Septiani, G. A., Purba, D., Paripurna, A.: Geothermal Exploration Project De-risking: Discussion on Various Schemes. *Proceedings*, 48th Workshop on Geothermal Reservoir Engineering, Stanford University, Stanford, CA (2023).

Sumardi, J. A., Al Asy'ari, M. R., Wigati, T. S., Pinandito, F. S., Adityatama, D. W., Purba, D.: Summary of Geothermal Slimhole Drilling Operation in the Last 10 Years: Lessons Learned for Geothermal Exploration in Indonesia, *Proceedings*, 47th Workshop on Geothermal Reservoir Engineering, Stanford University, Stanford, CA (2022a).

Sumardi, J. A., Al Asy'ari, M. R., Ramadhan, R.F, Pinandito, F. S., Purba, D., Adityatama, D., Siregar, S., Hafly, M. N., Fadhillah, F. R.: Indonesia Geothermal Drilling History: What We Can Learn from It? *Proceedings*, 47th Workshop on Geothermal Reservoir Engineering, Stanford University, Stanford, CA (2022b).

ThinkGeoenergy.: *Top 10 Geothermal Countries 2022 – Power Generation Capacity (MW)*. https://Www.Thinkgeoenergy.Com/Thinkgeoenergys-Top-10-Geothermal-Countries-2022-Power-Generation-Capacity-Mw/Amp/, (2023).

Umam, M., Adityatama, D., & Purba, D.: Tantangan Pengembangan Energi Panas Bumi Dalam Perannya terhadap Ketahanan Energi di Indonesia. *Swara Patra*, 8(3), 48-65, (2018):

Utami, P.: High-temperature Geothermal Area and its Challenges for Civil Engineering Works. *PERTEMUAN ILMIAH TAHUNAN XIV HATTI*. Indonesia, (2010).

Wiharlan, H., Agustino, V., Chaerudin, D., Adityatama, D., Pratiwinda, R., Mawajaya, .: Hydraulic Rig and Its Challenge to Conduct Slimhole Geothermal Exploration Drilling, *Proceedings*, 43rd New Zealand Geothermal Workshop 23-25 November 2021 Wellington, New Zealand ISSN 2703-4275 (2021).

Insights for Developer Compliance to Lender Procurement Guidelines in Geothermal Exploration Financing

Aryani Amir[1], Desak Nyoman Inten Apriani[1], Ery Surandaru[1],
Muchsin Qadir Jailani[2], Dorman Purba[1], and Astri Indra Mustika[1]

[1]PT Sarana Multi Infrastruktur (Persero), Sahid Sudirman Center 49th floor, Jakarta, Indonesia
[2]World Bank Indonesia, Indonesia Stock Exhchange Building, Jakarta, Indonesia

Aryani.pmugeothermal@ptsmi.co.id

Keywords: geothermal, exploration, GREM, SMI, resource, risk, drilling, cost, procurement, budget, finance, fund, market, developer, lender

ABSTRACT

Navigating the challenges of geothermal exploration financing in Indonesia, developers encounter significant obstacles due to the limited availability of financing facilities that address exploration risks. The Government of Indonesia, the World Bank, and PT Sarana Multi Infrastruktur (PT SMI) are crucial in enhancing the sustainable geothermal energy projects by offering exploratory financing and risk mitigation through the Geothermal Resource Risk Mitigation (GREM) program. Developers aiming to utilize this facility must comply with rigorous international financing guidelines, including specific procurement guidelines for public developers.

This paper reviews lender documentation and publications to elucidate the GREM procurement guidelines and the advantages that compliance brings to developers. Additionally, it addresses the complexities and administrative challenges developers encounter in adhering to these guidelines. The author proposes several measures to streamline the procurement process, enhancing collaboration between lenders and borrowers.

In conclusion, this paper delineates a comprehensive strategy for geothermal developers to effectively navigate lender procurement guidelines. By clarifying these processes and suggesting methods to alleviate administrative burdens, it aims to enhance project viability and promote the wider adoption of geothermal energy exploration in Indonesia.

1. INTRODUCTION

Indonesia's ambitious plan to significantly expand its geothermal power plant installed capacity is illustrated by the country's target of reaching 5,799 MW by 2030. As of 2023, the installed capacity stands at 2,417.7 MW, highlighting the need for a substantial increase of 3,382 MW over the next seven years. This translates to an average annual addition of 488 MW, a considerable leap from the historical average of 60 MW per year over the past four decades.

The first geothermal power plant in Indonesia, Kamojang-1, was installed in 1983 with a capacity of 30 MW (Darma, Imani, Shidqi, Riyanto, & Daud, Country Update: The Fast Growth of Geothermal Energy Development in Indonesia, 2021; Mansoer & Idral, 2015). Since then, the growth has been steady but slow, utilizing only about 10% of the total geothermal resources. The current pace of development underscores the necessity for massive exploration activities to identify and develop new geothermal resources. Figure 1 shows the historical and target for geothermal power utilization based on EBTKE (2023) and Thinkgeo (2024).

To meet the 2030 target, Indonesia should enhance its exploration efforts and adopt comprehensive de-risking measures. Exploration involves identifying viable geothermal resources, which requires significant investment and technological expertise. De-risking strategies, such as the Geothermal Resource Risk Mitigation (GREM) program, are essential to reduce the financial risks associated with exploration and early-stage development.

These efforts will not only accelerate the development of new geothermal projects but also ensure that the projects are financially viable and sustainable. By addressing the exploration and risk challenges, Indonesia can unlock its vast geothermal potential, contributing significantly to the country's renewable energy goals and sustainability target.

1.1 Opportunity and Challenges of Geothermal Business

The geothermal sector in Indonesia holds significant market potential, particularly due to the concentration of current reserves in Sumatra and Java, regions with substantial electricity demand. These areas are heavily reliant on coal-fired power plants, which are being phased out under a program initiated by the Government of Indonesia (GoI). This strategic move to reduce coal dependency presents an opportunity for geothermal electricity generation

to emerge as a viable substitute (Fadhillah, et al., 2023). Geothermal energy, capable of providing baseload power, is expected to replace coal as the primary source of power generation in Indonesia (World bank, 2011).

Despite its promising potential, the geothermal industry in Indonesia faces significant challenges in attracting investors. The high risks associated with geothermal projects are not adequately compensated by returns, deterring investment. Development projects frequently encounter obstacles during the transition to the production phase, including unfavorable economic conditions, limited resource availability, and social concerns. The industry's progression is influenced by a complex interplay of political, economic, social, and technical (Komendantova, et al., 2012; IRENA, 2022). Figure 2 shows the general problem of Indonesia geothermal project based on Fadhillah (Fadhillah F. R., Economic Evaluation of Bravo Geothermal Prospect in Participating Green Energy Effort, 2023).

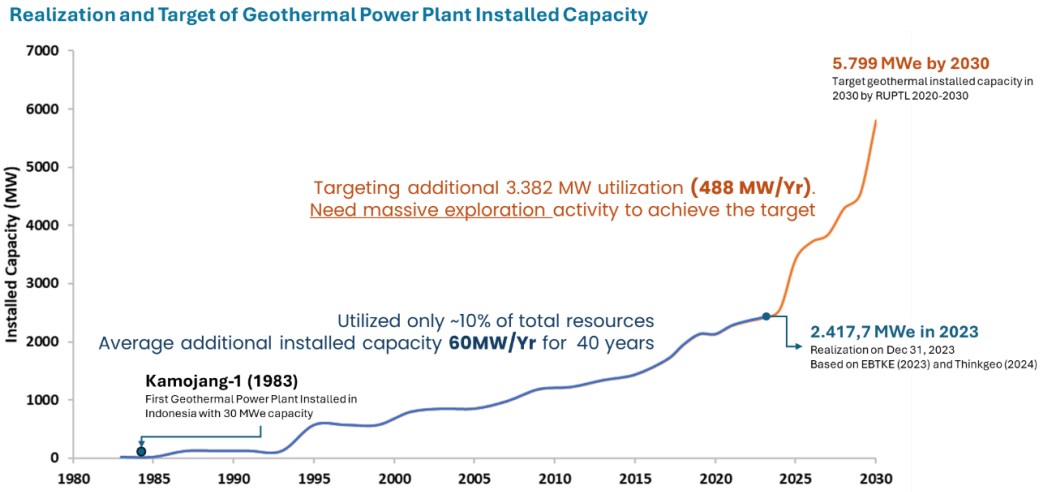

Figure 1: Target for geothermal power utilization based on EBTKE (2023) and Thinkgeo (2024).

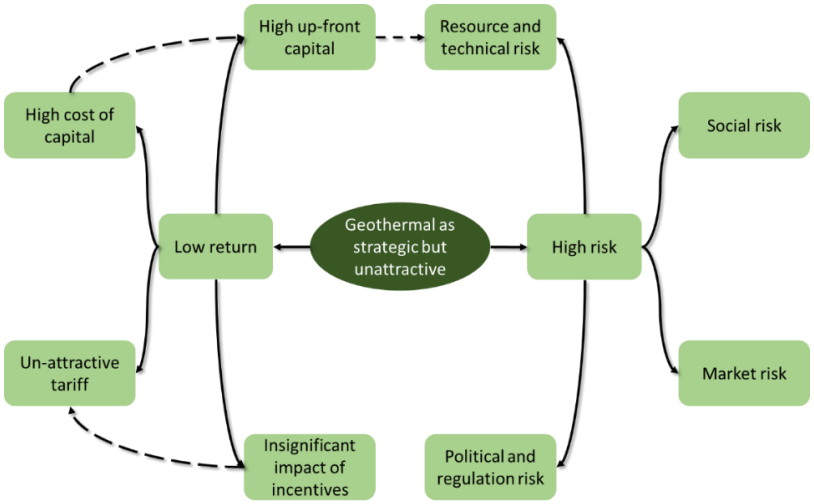

Figure 2: The problem tree of general Indonesia geothermal project.

1.2 Research Objective

The primary objective of this research is to provide geothermal developers with review to navigate and comply with lender procurement guidelines. This strategy is aimed at enhancing project viability and promoting the wider adoption of geothermal energy exploration in Indonesia by clarifying the processes involved and suggesting methods to alleviate administrative burdens associated with these processes.

2. INDONESIA GEOTHERMAL BUSINESS OVERVIEW

2.1 Geothermal Project Stage

The geothermal business process, especially for electricity generation, mainly consisted of preliminary survey, exploration, test drilling, project review, field development, power plant construction, commissioning, and production phases (ESMAP, 2012; IGA, 2014). A geothermal company in Indonesia is eligible to perform

preliminary survey until feasibility study for 7 years maximum. The company that successfully reaches commercial operation date (COD) would obtain 30 years of license, Conversely, in cases where an area is found unpromising for geothermal development during the preliminary survey and feasibility study phase, the company is obliged to relinquish the rights to that specific area to the government (Purba, et al., 2021; GoI, 2014). The summary of Indonesia geothermal project stages shown in Figure 3 based on (Fadhillah F. R., Economic Evaluation of Bravo Geothermal Prospect in Participating Green Energy Effort, 2023).

In the exploration phase of geothermal development in Indonesia, the government has launched several initiatives and introduced specific terminologies to support the process. These measures are intended to reduce exploration risks and encourage a favorable investment climate (Apriani, et al., 2023). Below are some of the key government-implemented schemes and terminologies (Table 1):

In Indonesia's geothermal industry, electricity generation is the primary product and main revenue source. Under common business practices, steam or electricity is sold to Perusahaan Listrik Negara (PLN), the state-owned electricity company, which is the exclusive buyer. This gives PLN considerable influence in the market, particularly in setting tariffs, which often benefits the company (Fadhillah F. R., 2023). Subsequently, PLN also transmits and distributes electricity to consumers across various sectors, including industrial, commercial, and residential users (Brilian, et al., 2024). This arrangement is known as the on-grid model.

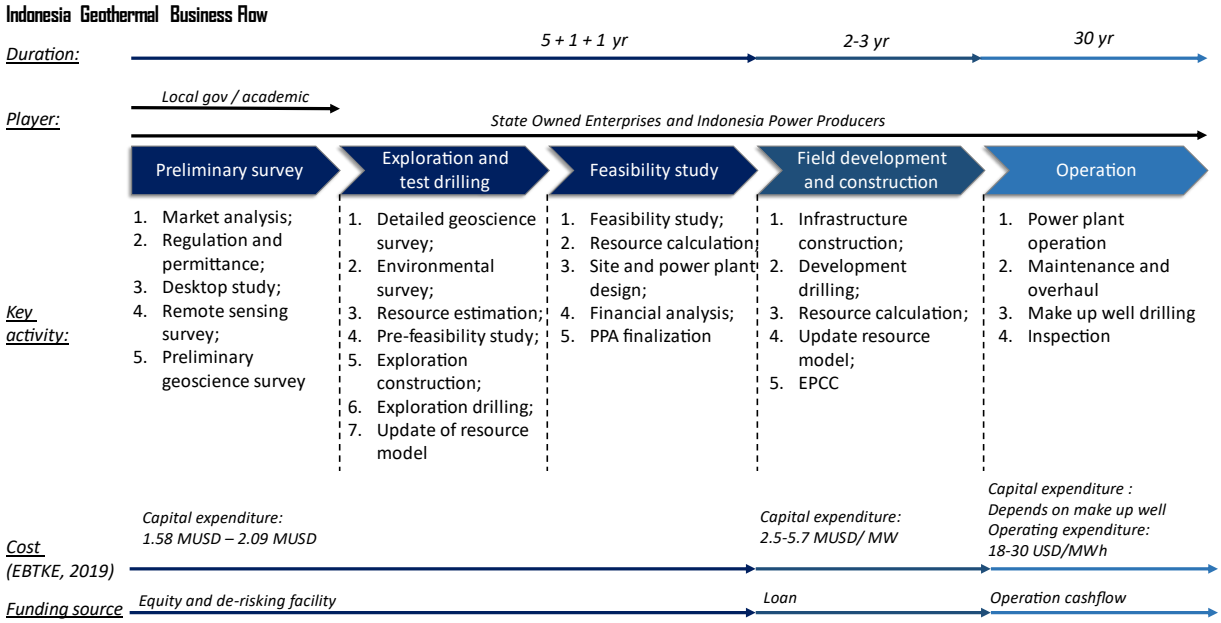

Figure 3: Indonesia geothermal business flow modified from GoI (2014), Purba (2021), and ESDM (2022).

Table 1: Geothermal exploration schemes and terminologies in Indonesia.

***Wilayah Terbuka* (Geothermal Open Area)**	An area suspected of having geothermal potential outside the coordinate boundaries of a Geothermal Working Area
Assignment Area	A Geothermal Open Area with certain coordinate boundaries offered to an Other Party for PSP or PSPE
WKP (Geothermal Working Area)	An area with defined coordinate boundaries used for the exploitation of Geothermal for Indirect Use (power)
***Penugasan Survei Pendahuluan*/PSP (Preliminary Survey Assignment)**	The assignment given by the Ministry of Energy and Mineral Resources to carry out the Preliminary Survey activity
***Penugasan Survei Pendahuluan dan Eksplorasi/PSPE* (Preliminary Survey and Exploration Assignment)**	The assignment given by the Ministry of Energy and Mineral Resources to carry out the activities of the Preliminary Survey and Exploration
***Izin Panas Bumi/IPB* (Geothermal License)**	Permit to conduct exploration and/or exploitation of Geothermal for Indirect Utilization in certain working areas
Government Drilling	Scheme for government to conduct the early stage of geothermal development (preliminary survey and exploration drilling)

2.2 Goods and Services in Geothermal Exploration Procurement

Understanding the goods and services essential for a geothermal exploration project holds pivotal significance for successful project outcomes. Precise comprehension aids in meticulous project planning by accurately assessing required resources for tasks like drilling and geological assessments. This knowledge is crucial for effective budgeting, preventing financial constraints and ensuring optimal allocation of funds for procurement, equipment rental, and specialized services (Amir Aryani, 2023).

Additionally, recognizing the required goods and services enhances procurement planning, encouraging early engagement with suppliers and fostering robust competition among them. This profound understanding also facilitates better communication and collaboration within project teams, aligning efforts with project objectives, reducing miscommunications, and boosting project management effectiveness. In essence, knowing precisely what goods and services are needed for geothermal exploration is crucial for efficient resource management, transparent procurement activities, and strong team cohesion, all of which play a pivotal role in the success of the project.

3. LENDER PROCUREMENT GUIDELINE IN GREM FACILITY

Lender procurement guidelines comprise standardized protocols and principles formulated by financial institutions to regulate procurement activities across diverse projects and initiatives. These guidelines strive to promote transparency, fairness, and efficiency in selecting suppliers, contractors, and service providers for projects financed by these institutions. Crafted to address a broad spectrum of procurement operations on an international scale, these rules are crucial for maintaining integrity throughout the procurement cycle. Additionally, these guidelines take into account several critical aspects specific to geothermal projects during the procurement process.

The initial financing mechanism for geothermal energy projects typically relies solely on support from international financial institutions. This form of backing is crucial, especially given the substantial costs associated with geothermal exploration and development. Institutions such as the International Bank for Reconstruction and Development (IBRD), the Asian Development Bank (ADB), the Japan Bank for International Cooperation (JBIC), the World Bank (WB), and the Japan International Cooperation Agency (JICA) play significant roles in this sector by providing financial backing that underpins many of the early and capital-intensive stages of geothermal projects, ensuring that such renewable energy initiatives can get off the ground.

Lender procurement guidelines, established by these institutions, are essential for governing how funded projects proceed with acquiring goods, services, and works. These guidelines are designed to foster a procurement process that is transparent, fair, and efficient, helping to prevent corruption and ensuring that contractors and service providers are selected based on merit and capability, which is vital for the successful completion of any project. Consideration factors within lender procurement guidelines encompass several key areas:

First, adherence to lender procurement guidelines ensures compliance with the standardized instructions and principles established by lending institutions. This adherence fosters transparency, fairness, and efficiency in the procurement process, specifically tailored to address needs unique to the geothermal sector such as drilling equipment, geophysical surveys, resource assessment, and environmental considerations.

Risk mitigation strategies are also pivotal, focusing on addressing geological uncertainties and the technical complexities inherent in geothermal exploration projects. These strategies include conducting thorough background checks on vendors, suppliers, contractors, and other involved parties to mitigate risks associated with fraud, corruption, or conflicts of interest, and implementing penalties, sanctions, or legal actions if fraudulent activities are detected.

Compliance with global issues is critical, involving the evaluation of borrower countries based on factors like gender equality, environmental concerns, social impact, and stability in conflict-prone areas. Contractors failing to meet these global issues requirements, including those related to gender-based violence and discrimination, are subject to disqualification.

Counterterrorism measures require screening contractors and consultants to ensure they are not involved in any terrorist activities and verifying that winning bidders or recommended consultants are not on the lenders' debarred lists before contract signatures.

Lastly, procurement process monitoring is conducted through the use of online systems that track every step from the identification of needs to contract management. This includes uploading relevant procurement documentation for lender review, especially for packages that require prior approval. These measures collectively ensure a robust, secure, and compliant procurement process aligned with international standards and lender expectations.

3.1 Requirements and Implications for Project Developers

Lenders typically impose a set of requirements on developers managing geothermal exploration projects, which serve as prerequisites for securing funding and ensuring efficient procurement processes. One such requirement is the preparation of a comprehensive procurement strategy that details the developers' analysis to identify the most suitable procurement method. This strategy allows for flexibility in designing approaches that maximize cost-effectiveness and align with project objectives, thus providing a strong foundation for successful project implementation. The implications of this include giving developers insight into the project's procurement needs and potential challenges, allowing for tailored procurement strategies that align with project objectives, enhancing the likelihood of achieving cost-effectiveness, and providing a framework for effective project management and risk mitigation.

Furthermore, developers are required to ensure that contractors and consultants are not on the lenders' debarred list. Engaging only qualified parties helps maintain the integrity of the procurement process and trust with lenders, ensures compliance with lender requirements, and minimizes legal and financial risks. This process is crucial in facilitating the selection of competent contractors and consultants for efficient project execution.

Another critical aspect is adherence to the principle of fairness in procurement processes, often challenging local content requirements that favor local manufacturers. This adherence ensures impartiality and transparency and may lead to conflicts between government regulations and lender requirements. Developers are challenged to balance compliance with local regulations and international procurement standards, highlighting the importance of addressing regulatory conflicts early in project planning to minimize delays and complications.

Finally, general terms and conditions of contracts are stipulated, requiring that contracts awarded through International Competitive Bidding (ICB) be in English, and that international arbitration takes precedence over national arbitration. This requirement aligns with international procurement and contract management standards and ensures consistency and clarity in contractual agreements. It also facilitates international cooperation and trade by standardizing contractual language and arbitration procedures, promotes adherence to internationally recognized procurement and contract management best practices, and encourages developers to familiarize themselves with global standards and regulations, enhancing their competitiveness in international markets. These collective measures help developers navigate the complex landscape of geothermal project financing effectively..

3.2 Impact of Lender Procurement Guidelines on Geothermal Project Exploration Planning

Developers to meticulously align their exploration planning with lender procurement guidelines. These guidelines profoundly impact the planning stages of geothermal projects, which are inherently capital-intensive and complex. The influence of these guidelines manifests in several critical areas:

1. **Project Viability Assessment**: Lenders require a detailed viability assessment of geothermal projects before providing financing. This assessment includes geological, technical, and economic evaluations to determine if the project is financially viable. Exploration plans must, therefore, align with these stringent assessment criteria to ensure the project is deemed financially sound.
2. **Technical Expertise**: Lenders often stipulate that the project team must possess the necessary expertise in geothermal exploration and development. This requirement impacts exploration planning by necessitating the involvement of skilled geologists, engineers, and other specialists right from the project's inception, ensuring that all technical aspects are handled by experts.
3. **Environmental and Regulatory Compliance**: Stringent compliance with environmental and regulatory standards is a common requirement from lenders. Exploration plans must include detailed environmental impact assessments and ensure all necessary permits are obtained. Compliance with local, state, and federal regulations is crucial, as failure to meet these standards can lead to the denial of financing.
4. **Resource Assessment**: Lenders seek assurances that the geothermal resource is well-defined and sustainable. A comprehensive resource assessment is critical, providing detailed data on the resource's size, temperature, and productivity. Such assessments must adhere to industry standards and best practices to meet the stringent requirements set by lenders.
5. **Risk Mitigation**: Given the risk-averse nature of lenders, exploration plans must include thorough risk assessments and mitigation strategies. These strategies should address potential issues such as drilling risks, reservoir performance uncertainties, and equipment reliability to assure lenders of the project's feasibility and security.
6. **Cost Estimation**: Accurate and detailed cost estimation is essential for lenders to evaluate the financial requirements and economic feasibility of a project. Exploration planning should encompass detailed cost estimates covering all aspects of the project, from exploration activities and drilling to equipment procurement and infrastructure development. These estimates must align with lender criteria and industry standards to ensure accuracy and reliability.

7. **Project Timeline**: Lenders typically have specific expectations for project timelines, from exploration to resource confirmation and overall project development. Delays in any phase of exploration can adversely affect financing and the project's economic prospects. Hence, realistic and carefully considered timelines are crucial components of exploration planning.

Providing comprehensive and precise information in a funding proposal is vital. This includes details about the project's goals, technical specifications, expected outcomes, budget, timeline, and procurement plans. Information about the management team's experience, market demand, and competitive landscape also plays a crucial role. Such detailed submissions not only build trust with lenders but also enhance the likelihood of securing necessary funding by demonstrating the project's potential for success and capacity to meet financial obligations.

4. CHALLENGES TO FOLLOW THE LENDER PROCUREMENT GUIDELINE

The procurement process is a structured and strategic approach for acquiring goods, services, or works from external suppliers or contractors. This process generally unfolds through several key steps: identifying procurement needs and specifications, selecting suppliers, negotiating contracts, and managing these contracts. The sequence includes conducting market research, prequalifying suppliers, issuing requests for proposals or bids, evaluating these proposals, and overseeing supplier relationships.

Effective procurement processes are designed to ensure transparency, foster competition, achieve value for money, and comply with legal and regulatory standards. While the specifics of the process can vary by organization, industry, or project, the primary aim is to acquire the appropriate goods and services, at the right time and cost, in the correct quantities, all while maintaining quality and managing risks.

The procurement process, however, is fraught with challenges and risks. Key issues include identifying reliable suppliers capable of meeting the demands for quality, quantity, and timing—failures here can lead to project delays, subpar products, and increased costs. Legal and regulatory compliance is critical to avoid disputes, penalties, and potential damage to reputation. Additionally, procurement timelines may need extensions, especially for packages requiring prior lender review, to accommodate the time needed to receive no objections from the lender.

The process is also vulnerable to unethical practices such as bid rigging, bribery, and kickbacks, which can result in financial losses and tarnish an organization's integrity. Managing risks related to supplier reliability, delivery delays, and market fluctuations requires proactive risk mitigation strategies and comprehensive contingency planning. Balancing ethical considerations, such as environmental and social impacts within the supply chain, presents its own set of challenges. Ensuring responsible practices while maintaining cost efficiency demands a careful balance.

Moreover, navigating the complex web of domestic and international legal and regulatory frameworks is a significant challenge that requires meticulous attention to detail. Promoting transparency and fairness in procurement is crucial to preventing favoritism, bias, and corruption, ensuring that evaluations are consistent and objective, and mitigating conflicts of interest.

Understanding procurement guidelines is vital for all project stakeholders, as these guidelines provide a framework for adhering to legal and ethical standards and fostering an environment of transparency and impartiality during supplier selection. This understanding not only facilitates efficient decision-making but also enhances communication, allowing stakeholders to synchronize their efforts effectively. It also plays a crucial role in preemptively addressing potential risks through well-defined risk management strategies, establishing a system of accountability, and optimizing resource allocation. This collective comprehension fosters trust among stakeholders and is essential for the successful completion of projects, aligning efforts with project objectives and timelines.

5. CONCLUSION

The conclusion of the document emphasizes the vital role of procurement in the geothermal business process, particularly under the Geothermal Resource Risk Mitigation (GREM) facility in Indonesia. It highlights the necessity for geothermal developers to thoroughly understand the procurement demands dictated by their selected financial sources. A lack of comprehension regarding these procurement requirements can lead to extended delays, inflated costs, and diminished value of project revenues.

Despite the GREM facility's goal to fast-track the utilization of geothermal energy in Indonesia, its deployment faces notable challenges, especially in the procurement aspect. The paper addresses these issues with the intent to enhance stakeholder awareness of the challenges posed by procurement guidelines required by donors and International Financial Institutions (IFIs). This discussion is meant to foster deeper dialogues to discover an

optimal balance between Donor Requirements, Indonesian Government Regulations, and Company Internal Policies, ensuring that procurement guidelines support rather than hinder project progression.

Looking forward, the paper signals the authors' intention to delve into specific challenges in future discussions. These will focus on two prevalent topics within Indonesian geothermal forums: the implementation of local content requirements (*Tingkat Kandungan Dalam Negeri* / TKDN) in geothermal projects funded by International Donors / IFIs, and the difficulties related to conducting precise market surveys for the development of reliable procurement plans. By concentrating on these particular issues, the authors aim to offer more detailed insights and practical solutions, thereby enriching the ongoing discourse on geothermal development in Indonesia.

REFERENCES

Amir Aryani [et al.] Exploring the Impact of Lender Procurement Guidelines on Geothermal Project Exploration Planning: Indonesia's GREM Perspective [Conference] // IIGCE 2023. - Jakarta : [s.n.], 2023.

Apriani Desak Nyoman Inten [et al.] Addressing Geothermal Exploration Resource Risk in Indonesia: Introducing GREM as a Pioneer De Risking Facility [Conference] // IIGCE 2023. - Jakarta : [s.n.], 2023.

Brilian Vincentius A. [et al.] Geothermal Captive Use to Support Industrial Activities: Applicable Industry Sectors, Worldwide Experience, and Its Potential and Challenges in Indonesia [Conference] // Workshop on Geothermal Reservoir Engineering. - California : Standord University, 2024.

Darma Surya [et al.] Country Update: The Fast Growth of Geothermal Energy Development in Indonesia [Conference] // World Geothermal Congress 2020+1. - Reykjavik : WGC, 2021.

ESMAP Geothermal Handbook [Report]. - [s.l.] : World Bank, 2012.

Fadhillah Ferdino R [et al.] Economic Evaluation of Bravo Geothermal Prospect in Participating Green Energy Effort [Journal] // Gema Ekonomi. - 2023.

Fadhillah Ferdino R Economic Evaluation of Bravo Geothermal Prospect in Participating Green Energy Effort [Report]. - Jakarta : Institute Teknologi Bandung, 2023.

GoI Law 14/2014 : Geothermal Law [Book]. - Jakarta : Government of Indonesia, 2014.

IGA Best Practice Guide for Geothermal Exploration [Report]. - Jakarta : World Bank, 2014.

IRENA Indonesia Energy Transition Outlook [Report]. - Abu Dhabi : International Renewable Energy Agency, 2022.

Komendantova Nadejda [et al.] Perception of risks in renewable energy projects: The case of concentrated solar power in North Africa [Journal] // Elsevier. - 2012.

Mansoer W. Resmiasih and Idral Alanda Geothermal Resources Development in Indonesia: A History [Conference] // World Geothermal Congress. - Melbourne : WGC, 2015.

Purba Dorman [et al.] Resource Assessment Methods Selection for Geothermal Exploration Project in Indonesia:What Are the Considerations? [Conference] // Stanford Geothermal Workshop. - Stanford : Stanford University, 2021.

ThinkGeo ThinkGeoEnergy's Top 10 Geothermal Countries 2023 – Power Generation Capacity [Online] // Webinar. - 2024. - https://www.thinkgeoenergy.com/thinkgeoenergys-top-10-geothermal-countries-2023-power-generation-capacity/.

World bank Penggunaan energi panas bumi Indonesia akan naik secara signifikan [Online] // World Bank. - 2011. - https://www.worldbank.org/in/news/feature/2011/07/26/indonesia-expand-geothermal-power-alternative-coal.

Impact of Tax Facility Incentives to Geothermal Project Bankability: Comparison between National and Worldwide Practice

Andreas Adi Suseno[1], Desak Nyoman Inten Apriani[1], Muchsin Qadir Jailani[2], Aulia Pratama[3], Bogy Ariyanto[4], Dorman Purba[1], and Ferdino R Fadhillah[1]

[1]PT Sarana Multi Infrastruktur (Persero), Sahid Sudirman Center 49th floor, Jakarta, Indonesia
[2]World Bank, Indonesia Stock Exchange Building, Jakarta, Indonesia
[3]Ministry of Energy & Mineral Resources, Jakarta, Indonesia
[4]Ministry of Finance, Jakarta, Indonesia

andreas.pmugeothermal@ptsmi.co.id

Keywords: tax facility, tax incentives, geothermal, geothermal project bankability, tax holiday, tax allowance, renewable energy, fiscal incentive

ABSTRACT

Indonesia, a top two global leader in geothermal utilization, has set ambitious targets to maximize its utilization of this renewable resource. To achieve these goals, substantial investment is essential, and one of the primary strategies employed by the Indonesian government is the provision of tax fiscal incentives aimed at enhancing the investment climate by reducing costs and risks for investors.

This study conducts a comprehensive literature review to evaluate the effectiveness of global tax incentive approaches for renewable energy development, with a focus on comparing the strategies of Indonesia and the USA—two leading countries in geothermal energy utilization. In Indonesia, the government's support includes tax holidays, tax allowances, import tax exemptions, and land tax exemptions, which are designed to ease financial burdens throughout the exploration and operational phases of geothermal projects. In contrast, the USA utilizes a combination of federal tax credits, specifically the Production Tax Credit (PTC) and the Investment Tax Credit (ITC), to stimulate investments in geothermal energy.

This paper also undertakes an economic evaluation of projects to assess the financial impacts of these tax facilities on project bankability. Using scenario analysis based on published economic data of geothermal projects, the study compares the effects of tax incentives in both countries on project returns and debt repayment capabilities. The findings suggest potential improvements for Indonesia, such as extending the tax holiday period to 10 years post-operation, enhancing land tax exemptions, and better aligning incentives with the phases of positive taxable profit generation. Additionally, the adoption of production tax credit scheme, similarto that of the USA, is recommended to significantly enhance the bankability of geothermal projects in Indonesia. This research provides valuable insights into optimizing tax incentive strategies to attract greater investment and ensure the sustainable development of geothermal energy.

1. INTRODUCTION

The geothermal development in Indonesia has started from colonized era with commercial utilization remarked through Kamojang Geothermal Power Plant (30MW) in 1983. Nowadays, Indonesia is top two geothermal country in the world with 2.417 MW installed capacity from approximately 23 GW total potential. It means that Indonesia only utilized around 10% of total potential with average additional capacity around 60 MW per annum. There are 46 geothermal power plants developed by State-Owned Enterprises (SOE) and Independent Power Producer (IPP) in 17 geothermal working areas.

Government of Indonesia has plan to utilize geothermal as baseload to replace coal power plant and set the target of utilization to reach 5.799 MW in 2030. The government target emphasizes the significant increase in average of additional installed capacity toward 488 MW per annum from 2024 to 2030. This bold target needs to be achieved by catalyzing geothermal investment though better project attractiveness, including from fiscal incentive perspective. Figure 1 shows the historical and target for geothermal power utilization based on EBTKE (2023) and Thinkgeo (2024).

1.1 Opportunity and Challenges of Geothermal Business

Indonesia, as a leading nation for renewable energy potential in ASEAN, faces unattractive conditions for renewable investment, including geothermal. Based on ESDM (2022), the geothermal investment realization shows declining pattern during 2016-2021 (Figure 1). The situation contradicts the target to increase geothermal utilization, which requires USD 27 billion additional investment based on SMI (2018). Furthermore, Indonesia is positioned at rank 63 from 132 of the worlds and rank 5 of 10 ASEAN countries related renewable regulation

rank, including the assessment of regulation-incentives support and attribute of the financial incentives for the geothermal (Table 1).

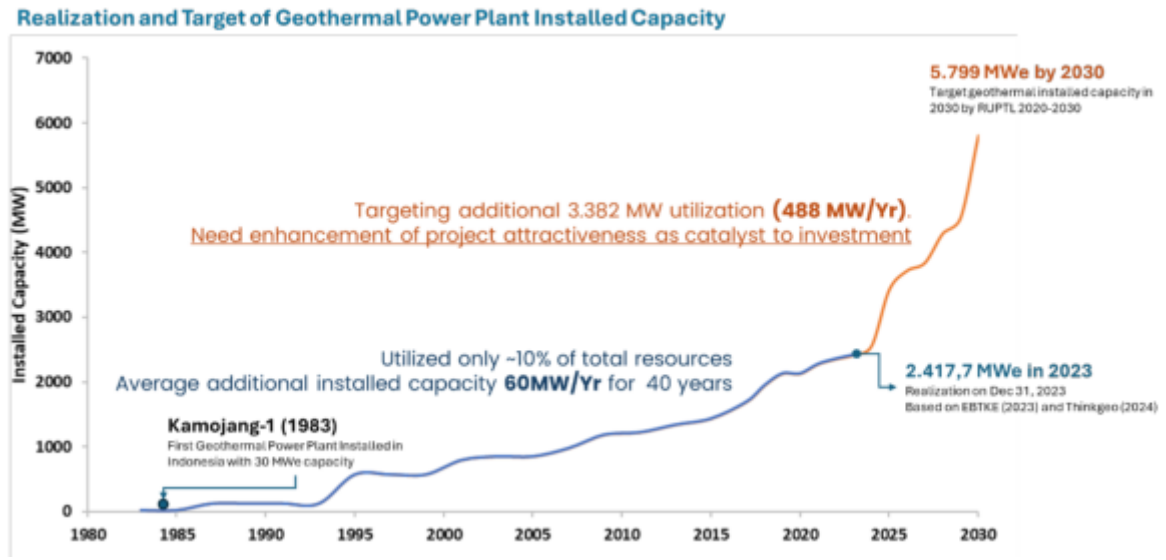

Figure 1: Indonesia geothermal power plant installed capacity and target for 2023 based on EBTKE (2023) and Thinkgeo (2024).

Table 1: The world regulation in sustainable energy rank for ASEAN countries (Vakulchuk, et al., 2022).

Country	Total score	(1) Legal framework for RE	(2) Planning for RE expansion	(3) Incentives and regulatory support	(4) Attributes of financial and regulatory incentives	(5) Network connection and use	(6) Counterparty risk	(7) Carbon pricing and monitoring
Vietnam	467	100	98	79	58	66	66	0
Philippines	437	100	59	77	83	53	65	0
Malaysia	404	100	71	70	58	32	73	0
Singapore	377	100	64	19	67	60	67	0
Indonesia	376	100	66	31	33	13	83	50
Thailand	329	50	56	56	67	20	80	0
Cambodia	289	100	15	18	0	30	76	50
Laos	214	100	55	27	8	7	17	0
Myanmar	195	50	48	34	17	6	40	0

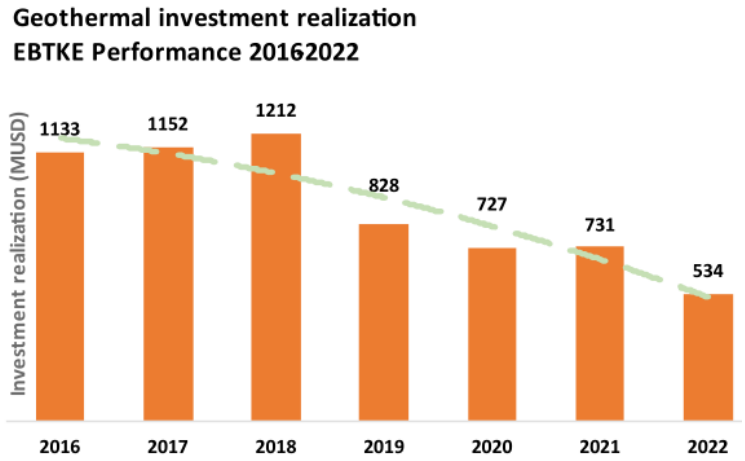

Figure 2: Indonesia geothermal investment realization from 2016 to 2022 (modified from EBTKE, 2022).

The trend of declining geothermal investment realization can be attributed to both internal and external factors concerning project conditions. Internally, the nature of geothermal projects is such that the bulk of investment is typically required during the development phase, particularly during the Engineering, Procurement, and

Construction (EPC) stage. This phase demands significant capital as it involves the construction of infrastructure and power plant necessary for the project's operation.

After the completion of the EPC phase and the onset of the Commercial Operation Date (COD), investment levels generally decline. This pattern could be observed in the substantial investments made in 2016, 2017, and 2018 by major players such as Pertamina Geothermal Energy, Sarulla Operation, and Sorik Marapi Geothermal, which were all in the process of conducting EPC activities in their respective fields.

In 2019, a marked reduction in investment was observed, coinciding with several fields beginning operation, including Lumut Balai, Sorik Marapi, Muara Laboh, Sarulla (2018), and Karaha (2018). As these projects transitioned from the capital-intensive development phase to operational status, the requirement for heavy investment subsided, leading to an overall decrease in the investment figures for the sector.

External factors, including market trends, regulatory environments, economic stability, and fiscal incentives, plays significant role in shaping the investment landscape for geothermal projects, alongside the internal project life cycle dynamics. The country's renewable incentives are underperforming due to the lax enforcement of regulations, which stands in contrast to the more effective incentive structures in Vietnam, Malaysia, and the Philippines. This disparity influences Indonesia's attractiveness to investors and shapes its investment patterns within the renewable sector (Vakulchuk, et al., 2022).

1.2 Problem Statement

The Alpha project, a hypothetical geothermal project in Indonesia, encounters difficulties in providing acceptable return to shareholder. This situation presents significant barrier to project advancement, given the high upfront costs required for resource confirmation and production, alongside the need for commercial financing for development. Author is considering utilizing the government fiscal facility in form of tax holiday to enhance the economic return.

The implementation of fiscal incentives for renewable energy across the world is also assessed to formulate more impactful fiscal incentive from project economic perspective. Author use US tax facility as benchmark since US is nation with most installed geothermal capacity globally.

1.3 Research Question and Objective

The objective of this paper is to provide project economic analysis with recommendations by assessing whether tax facilities provide more significant impact to enhance project return. The research questions are:

1. How is the practice of fiscal incentives practiced across the world?
2. How is the project economic comparison between Indonesian tax facility or US tax facility? Which scenario provides better return?

2. GLOBAL AND REGIONAL PRACTICE FOR FISCAL INCENTIVES

Renewable energy promotion has been performed in various ways, including fiscal-financial, policy-regulatory, researchdevelopment, and voluntary programs (ADB Institute, 2018). Fiscal incentives aim to enhance the investment climate by increasing the business profit with less cost/risk to investors. The incentives provided through several government programs influence the business decision to encourage investment, profitability, and benefits (Chalk, 2001; UNCTAD, 2000). Although government and investors are interested in obtaining more excellent take from the business, Afandi (2017) notes the fiscal incentive should balance the government value (e.g., project acceleration, increasing production) and investor reward (e.g. promising return and risk sharing). Furthermore, the government also aims to boost exploration activity and increase production.

REN21 (2023) analyse the fiscal incentives and investment practices across the nation as shown in figure below. The high-income countries lead in implementing most incentives, with the most common being public investment, loans, grants, capital subsidies, or rebates, observed in 41 countries. This is followed by investment or production tax credits, used by 35 countries, and reductions in sales, energy, CO2, VAT, or other taxes, adopted by 39 countries. Feed-in tariffs or premium payments are also popular, especially in high and upper-middle-income countries, indicating a preference for guaranteed price mechanisms to encourage renewable energy production. In contrast, upper-middle-income countries show a strong preference for net metering or billing, used by 23 countries, allowing consumers to sell surplus energy back to the grid, effectively reducing their energy costs. However, as income levels decrease, the adoption of these incentives generally declines, highlighting the challenges lower-income countries face in funding extensive renewable energy policies. For instance, lower-income countries have lesser engagement with complex fiscal tools like feed-in tariffs and tax credits, primarily using public investments and tax reductions more modestly. This pattern underscores the correlation between a country's economic capacity and the breadth of its renewable energy incentives.

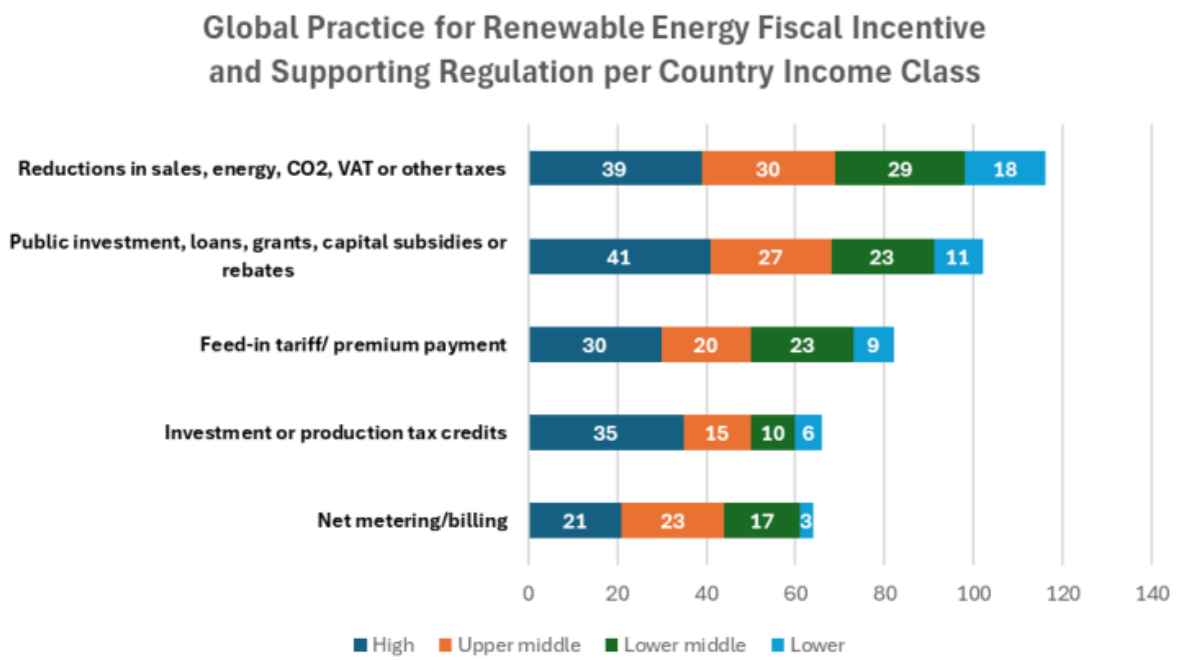

Figure 3: Global Practice for Renewable Energy Fiscal Incentive and Supporting Regulation per Country Income Class.

Asian Development Bank (2018), highlights the recommended strategy of employing fiscal and financial incentives to promote renewable energy, encompassing geothermal resources. This includes mechanisms such as Feed-in Tariffs (FITs), grants, soft loans, and tax incentives:

- Feed-in Tariff (FIT) are policy mechanisms designed to promote the deployment of renewable energy technologies by providing adequate compensation above the electricity market price. This compensation incentivizes investors to accelerate their investments in renewable energy technologies and reduce uncertainties associated with their deployment. FITs have significantly deployed renewable energy technologies in Europe, especially in Germany, Spain, and France. The policy mechanism has accelerated investment in renewable energy technologies and boosted their development in these countries. The compensation provided by FITs has provided investors with the necessary financial incentives to invest in renewable energy technologies. It accommodates the high upfront costs associated with renewable energy technologies.
- Grants have emerged as a critical mechanism for promoting the deployment of renewable energy technologies, particularly in developing countries. Othman, et al. (2019) and Hemphill (2015) emphasizes that grants provided by international organizations (e.g. World Bank, the International Finance Corporation (IFC), and the Global Environment Facility) have played a significant role in promoting the deployment of renewable energy in developing countries. Grants used to enhance the profitability by providing additional cash flow to the project through the investment grant program. The grants also could be utilized to enhance project deliverability by providing technical assistance in the preparation of bankable resource assessment, environmental-social impact assessment, technical design, financial model, and supporting document (ADB, 2019).
- Soft loans have become an increasingly alternative financing mechanism for renewable energy projects, particularly in developing countries. IRENA (2020) mention that soft loan positively reduces the cost of capital for renewable energy projects, enhancing financial viability and investment attractiveness. Soft loans also reduce investment risks by providing more extended repayment periods, lower interest rates, and more flexible repayment terms. It would be critical in bridging the financing gap for renewable energy projects, enabling greater access to capital for developers, and facilitating the deployment of renewable energy in the developing country (Bhusal, et al., 2021).
- Tax incentives, such as tax credits, deductions, and exemptions, have significantly encouraged the development of renewable energy projects in the United States. Hemphill & Sampson (2015) emphasizes that tax incentives have impact to increasing the attractiveness of renewable energy projects to investors.

According to Rio (2014), the fiscal incentives for renewable energy generally launched to boost the utilization of renewable energy using collaborative approach between instruments. Vakulchuk, Overland, & Suryadi (2022)

summarize the fiscal incentives that applied for renewable energy in ASEAN that emphasize the practice of multi-instrument deployment to support renewable energy development as shown in Figure 4.

Type of policy		Philippines	Vietnam	Indonesia	Malaysia	Thailand	Singapore	Myanmar	Laos	Brunei	Cambodia
Regulatory policies	1. Renewable energy targets	•	•	•	•	•	•	•	•	•	•
	2. Renewable energy in INDC or NDC	•	•	•	•	•	•	•	•	•	
	3. Feed-in tariff/auctions/premium payment	•	•	•	•	•					
	4. Electric utility quota obligation/RPS	•	•	•	•						
	5. Net metering/billing/direct consumption-supply	•	•	•	•		•				
	6. Biofuel blend obligation/mandate/target	•	•	•	•	•					
	7. Renewable heat obligation/mandate										
	8. Tradable REC		•								
Fiscal incentives and public financing	9. Tendering	•		•	•		•				
	10. Tax incentives	•	•	•	•	•		•	•		•
	11. Investment or production tax credits	•	•	•							
	12. Reductions in sales, CO2, VAT or taxes	•	•	•	•	•		•			
	13. Energy production payments	•				•					
	14. Public investment/loans/grants/capital subsidies/rebates	•	•	•	•	•	•		•		
	Total	12	11	11	10	8	5	4	3	2	2

Sources REN21 (2019, 2022), ACE (2020)

Figure 4: The renewable energy incentives application in ASEAN (Vakulchuk, et al., 2022).

ASEAN Center for Energy (2022) emphasizes several incentives seems be success program to boost renewable energy in ASEAN. The success program, such as:

- Attractive Feed in Tariff (FITs) applied in the Philippines, Malaysia, and Vietnam. The attractive FIT enhances the renewable energy project attractiveness through fair margin for the developer. In Vietnam, the development of renewable energy is accelerated after the implementation of FIT. While the Philippines used the FIT schemes to provide the abovemarket tariff certainty to renewable energy investors for 20 years project period.
- Tax exemption applies to Vietnam, Malaysia, Indonesia, and the Philippines. The tax exemption is applied to reduce the government's take for better rewards to renewable energy investor.
- Private investment in transmission lines was applied in Vietnam to enhance the connectivity of green power plants to the national electricity grid. The transmission line is essential to distribute the produced electricity to the off taker.
- Net metering applied in Malaysia. The implementation of net metering success in accelerating the investment for solar panels allows consumers to install rooftop solar systems, generate electricity for their consumption, and sell any excess electricity to the government.

3. COMPARISON BETWEEN US AND INDONESIA FISSCAL INCENTIVES

3.1 United States Practice

The United States' geothermal installed capacity as of 2023 have reached 3,771 MW after the first GPP COD back in 1971 at the Geysers, putting United States as the nation with the largest geothermal installed capacity globally. There are two key enablers to geothermal development in the United States:

1. Federal and state-level policy support;
2. Fluctuating natural gas prices; and
3. Oil and gas industry maturity.

The policy support is embodied in the form of two waves of policies enactment. The first wave occurred in the 1970s by providing federal land leasing regulation for geothermal developments, exploration de-risking programs, open-access exploration data, investment tax credit, and the market creation for GPPs operated by investors. Meanwhile, the second wave came in the 2000s through royalties, cash grants, production tax credit, and other state-level incentives provided to geothermal power producers as well as mandating a certain amount of renewable electricity that must be sold by utility companies at the state-level. The federal budget for geothermal activities during these two periods was also increased, hence stimulating geothermal development. Furthermore, these two periods of policy support coincided with the spiking natural gas prices during these periods, hence making geothermal electricity more competitive

3.1.1 Production tax credit

The Production Tax Credit (PTC) is a significant financial incentive designed to promote the generation of electricity from renewable energy sources, including geothermal energy, in the United States. The PTC offers a per kilowatt-hour (kWh) tax credit for electricity produced during the first 10 years operation, effectively reducing the tax expenses of the project and enhancing its financial viability.

The PTC rates range from 0.55 to 2.75 cents per kWh of electricity produced. Additionally, there are supplementary bonuses available to further incentivize the use of domestic content and support energy communities. Specifically, a domestic content bonus provides an additional 0.1 cents per kWh, and an energy community bonus offers an extra 0.1 cents per kWh, enhancing the overall value of the tax credits available to geothermal projects.

Eligibility for the PTC requires annual claims for the first 10 years following the commercial operation date (COD). The formula for calculating the PTC is:

PTC = generation capacity per year (kWh)
× (PTC rates + domestic content bonus + energy community bonus)

3.1.2 Investment tax credit

The Investment Tax Credit (ITC) is a crucial financial mechanism aimed at incentivizing investment in renewable energy projects, including geothermal energy, by reducing the tax liability for a percentage of eligible investment costs during the tax year. Unlike the Production Tax Credit (PTC), the ITC is an upfront tax credit that does not depend on the system's performance but rather on the initial capital expenditure.

The ITC rates range from 6% to 30% of the eligible investment cost, with additional bonuses to further enhance its value. Specifically, projects can receive a domestic content bonus and an energy community bonus, each adding an additional 10% of the eligible investment cost. These bonuses are designed to promote the use of domestic materials and support the economic development of energy communities.

Eligible expenses for the ITC include:

1. Labor Costs: Expenses related to onsite preparation, assembly, and original installation of the geothermal system.
2. Equipment Costs: Costs associated with necessary equipment such as heat pumps, piping, and other components directly linked to the geothermal heat pump system.
3. Onsite Preparation Costs: Costs incurred to prepare the site for installing the geothermal system.

3.2 Indonesia Practice

Indonesia's government has already launched several incentives for geothermal such as tax holiday/tax allowance, import tax exemption, and land tax exemption as shown in Figure 5. EBTKE (2022) emphasizes that the tax facility could reduce the levelized cost of electricity (LCOE) by 0.07-0.19 US cents/kWh. The explanation of each tax facility as below:

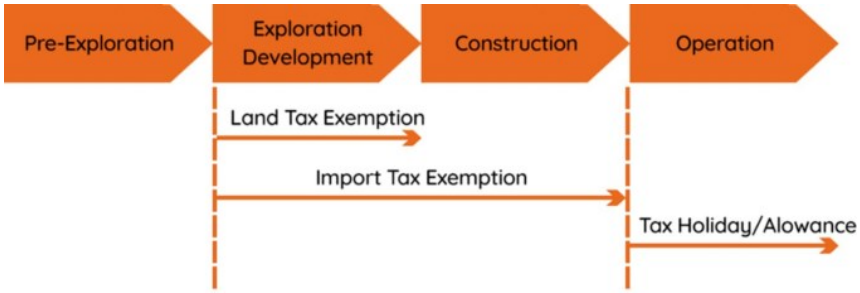

Figure 5: The effective period of Indonesia geothermal tax incentives per project period modified from EBTKE (2021).

The Government of Indonesia offers various fiscal incentives to promote investment and profitability in the geothermal industry. These incentives aim to create a favorable investment climate by reducing business costs and risks for investors. The incentives are provided through different government programs, encouraging businesses to invest in geothermal projects to maximize benefits. (Chalk, 2001) (UNCTAD, 2000). Based on EBTKE (2022; 2021), Lesmana et al (2020), Winofa et al (2020), Abidin (2020), and Fadhillah (2023), current fiscal incentives implemented for the geothermal industry as shown in Table 2.

As indicated by Kristina (2018) and Nugraha et al. (2017), the current tax incentives for geothermal projects in Indonesia have not demonstrated significant impact in enhancing project attractiveness or reducing the cost of electricity generation. The incentives, as per IRENA (2022) and IESR (2022), include a tax holiday that allows for 100% tax reduction for corporate income tax (PPh) for a period of 5 to 20 years. However, this particular incentive has not been effectively utilized, mainly because most renewable energy (RE) developers do not generate taxable profits during the initial five years of project implementation. Fadhillah (2023) provide the case example of ineffective tax holiday period.

Table 2: Current fiscal incentives for geothermal.

Fiscal incentives	Remarks	Effective period of project stage
Tax holiday (PMK 130 / 2020)	The geothermal industry with an investment of more than USD 0.5 trillion would be eligible to obtain 5 years tax holiday. The detail of the tax holiday period as below: - 5 years for IDR 0.5 to 1 trillion investment - 7 years for IDR 1 to 5 trillion investment - 10 years for IDR 5 to 15 trillion investment - 25 years for IDR 15 to 30 trillion investment - 20 years for more than IDR 30 trillion investment The developer would also get the 50% reduction (for more than IDR 0.5 trillion investment) for 2 years during the transition period after the facility. The geothermal developer with more than IDR 0.1 trillion investment is also eligible to obtain 50% tax reduction in the first five years of operation, continued by 2 years transition period that obtain 25% tax reduction (EBTKE, 2021)	Operation
Operation Tax allowance (GR 78/2019)		
• Investment allowance \	Reduction of taxable income equals 5% per year of the total investment for the 6-year period and 30% of the total investment for the full period. The investment should be owned by the main business entity and not transferred during the period (Abidin, et al., 2020; Lesmana, et al., 2020).	Operation
• Accelerated depreciation amortization	Geothermal classified as “class 3” use the double declining balance method with the 8-year period for tangible and intangible asset.	Operation
• Loss carry over	Geothermal industry is eligible to perform loss carry forward for 5-year period with maximum no longer than 10 years. Geothermal as new and renewable energy also eligible to obtain 1 year additional of the facility.	Operation
Land tax exemption (PMK 172/2019)	The land tax for geothermal industry is exempted during the exploration phases (MoF, 2016). The land tax is charged on production phases with guidance to directorate general of tax regulations No. PER-45/PJ/2013.	Exploration
Import tax and value added tax exemption (PMK 172/2016)	Geothermal industry is 100% exempted from import tax for the equipment that not available / adequately produced in Indonesia (Abidin, et al., 2020; Lesmana, et al., 2020). Geothermal industry is not imposed to VAT (Abidin, et al., 2020)	Exploration and development

4. DISCUSSION

Despite the various tax incentives available for geothermal projects in Indonesia, their effectiveness in enhancing project attractiveness and reducing the cost of electricity generation remains questionable. Studies by Kristina (2018) and Nugraha et al. (2017) highlight that these incentives have not significantly impacted the geothermal sector's development.

The current tax incentives, as outlined by IRENA (2022) and IESR (2022), include a tax holiday that provides a 100% reduction in corporate income tax (PPh) for a period ranging from 5 to 20 years. In theory, this should make geothermal projects more financially viable by lowering the tax burden on developers during the early years of project implementation. However, the practical application of this incentive has proven to be less effective.

A key reason for the ineffectiveness of the tax holiday is that most renewable energy developers, including those in the geothermal sector, do not generate taxable profits during the initial years of project implementation. This period is typically marked by depreciation expenses, as non cash and tax deductible expenses. Consequently, the

tax holiday, while generous on paper, offers limited real-world benefits since there are minimal profits to offset with the tax reduction.

Fadhillah (2023) provides a case example illustrating the ineffectiveness of the current tax holiday period. The case demonstrates that the timing and structure of the tax incentives do not align well with the financial realities faced by geothermal developers. Without taxable income in the initial years, the tax holiday does not provide the intended financial relief, thereby failing to improve project attractiveness or significantly reduce electricity generation costs.

Stakeholder feedback on Indonesia tax facility

From the sectoral regulator perspectives, acknowledges the significance of the tax holiday in attracting geothermal developers to Indonesia. However, it is suggested that the current tax holiday could be improved by extending the period, especially for renewable projects. This is particularly crucial for geothermal power plants located in eastern Indonesia, where smaller power plants require more incentives to create an attractive investment climate. The disparity in investment size between eastern and western areas means that the current tax holiday period may not be sufficient for the former. However, ideal government incentives should not overly burden the state budget but should significantly expedite geothermal development. Properly utilized incentives are expected to reduce the need for subsidies allocated to PLN through tariff reductions. Proposals for additional incentives should be well-supported with comprehensive justifications and demonstrate a strong commitment to accelerating geothermal projects affordably.

While the business player views that fiscal incentives like tax holidays need better alignment with the unique financial lifecycle of geothermal projects, which typically start generating positive taxable income around seven years after the commercial operation date (COD). Assuming a project obtains a 10-year tax holiday, the benefits are predominantly realized only during the last three years of the holiday period. Therefore, adjusting the timing of these incentives to coincide with the period when developers begin to generate positive taxable profits would enhance their effectiveness.

5. CONCLUSION

Indonesia has introduced various fiscal incentives to reduce financial barriers and promote the growth of the geothermal energy sector. These incentives include tax holidays/allowances, import tax exemptions, and land tax exemptions. The goal is to make geothermal projects more financially viable and attractive to developers. While stakeholders recognize that these incentives are competitive compared to global standards, they also point out significant bureaucratic inefficiencies that hinder their effectiveness. To further enhance Indonesia's fiscal incentives, the country can draw insights from the US schemes of Production Tax Credit (PTC) and Investment Tax Credit (ITC).

REFERENCES

Abidin Mohammad Zainul, Rosdiana Haula and Salomo Roy Valiant Tax Incentive Policy for Geothermal Development: A Comparative Analysis in ASEAN [Journal] // Int. Jour nal of Renewable Energy Development. - 2020.

ACE Impact Analysis and Review on Governance of Renewable Energy Financing Scheme in ASEAN [Report]. - Jakarta : ASEAN Center for Energy, 2022.

ADB Institute Implication of Fiscal and Financial Policies for Unlocking Green Finance and Green Investment [Report]. - Tokyo : Asian Development Bank, 2018.

ADB Renewable Energy Financing Scheme for Indonesia [Report]. - Manila : Asian Development Bank, 2019.

ADB Unlocking Indonesia’s geothermal potential [Report]. - [s.l.] : Asian Development Bank, 2014.

Afandi Maruf Proposed Deep Water Fiscal Term To Attract Oil and Gas Investment in Indonesia [Report]. - Jakarta : ITB School of Business and Management, 2017.

Bhusal M.R and Krishna C.R Sustainability in Financial Management: An Analysis of Soft Loan Financing of Renewable Energy in India. [Journal] // International Journal of Energy Economics and Policy. - 2021.

Chalk N. A Tax Incentives in The Philippines: A Regional Perspective [Report]. - [s.l.] : IMF Working Paper, 2001.

EBTKE Laporan Kinerja Tahunan 2021 [Report]. - Jakarta : Ditjen EBTKE, 2022.

EBTKE Pedoman Investasi Pembangkit Listrik Tenaga Panas Bumi [Report]. - Jakarta : Direktorat Jenderal Energi Baru, Terbarukan, dan Konservasi Energi, Kementerian Energi dan Sumber Daya Mineral, 2021.

EBTKE Pengembangan Panas Bumi di Indonesia. [Report]. - Jakarta : Ministry of Energy and Mineral Resources, 2022.

Fadhillah Ferdino R [et al.] Economic Evaluation of Bravo Geothermal Prospect in Participating Green Energy Effort [Journal] Gema Ekonomi. - 2023.

GoI Presidential Regulation 112/2022: Percepatan Pengembangan Energi Terbarukan untuk Penyediaan Tenaga Listrik [Book]. Jakarta : Government of Indonesia, 2022.

Hemphill T.A and Sampson E Renewable Energy Finance: Powering the Future. [Book]. - London : Imperial College Press, 2015.

IRENA Renewable Energy Finance: Institutions and Mechanisms [Report]. - [s.l.] : IRENA, 2020.

Lesmana Ade [et al.] Preliminary Financial Modelling with Probabilistic Approach for Geothermal Development Project in Indonesia [Conference] // ITB International Geothermal Workshop. - Bandung : IOP Conferences, 2020.

MEMR Presidential Regulation 112/2022 Percepatan Pengembangan Energi Terbarukan untuk Penyediaan Tenaga Listrik [Report]. - [s.l.] : MEMR, 2022b.

MoF Peraturan Menteri Keuangan No 172/2016 Tentang Pengurangan Pajak Bumi dan Bangunan Untuk Kegiatan Usaha Pertambangan/Pengusahaan Panas Bumi Pada Tahap Eksplorasi [Book]. - Jakarta : Ministry of Finance Republic Indonesia, 2016.

Othman N., Jafari Y and Adnan The Role of International Grants in Renewable Energy Deployment in Developing Countries [Journal] // Journal of Renewable Energy. - 2019.

REN21 Renewables 2023 Global Status Report Collection Global Overview. - Paris : REN21 Secretariat, 2023.

UNCTAD Tax Incentives and Foreign Direct Investment: A Global Survey [Report]. - Geneva : United Nation, 2000.

Vakulchuk Roman, Overland Indra and Suryadi Beni ASEAN's Energy Transition: How to Attract More Investment in Renewable Energy [Journal] // Elsevier. - 2022.

Winofa Nevi Cahya [et al.] The Application of Numerical Simulation Result for Geothermal Financial Model with Probailistic Approach: A Comprehensive Study [Conference]. - Bandung : IIGW, 2020.

Pertamina Geothermal Energy Kamojang Restoration Management and Potential Carbon Sequestration from the Biomass Value

Syalva Taskia, Fauzi Ariq, and Hendrik K. Sinaga

PT Pertamina Geothermal Energy

syalva.muhamad@pertamina.com, fauziariq13@gmail.com

Keywords: biodiversity, biomass, carbon, climate change,forest restoration, ecosystem, geothermal, kamojang, landscape ecology, project management, sequestration

ABSTRACT

Geothermal areas and power plants are frequently surrounded by forests or conservation areas, necessitating careful environmental management to mitigate the impact of energy production on these ecosystems. Since 2008, PT. Pertamina Geothermal Energy (PGE) Kamojang has initiated a comprehensive tree-planting program around well sites and power plants. This program includes the planting of endemic species such as Ki Bereum (Saurauia cauliflora), Lame (Alstonia scholaris), and Ki Honje (Pittosporum ferrugineum), among others, as part of their environmental restoration efforts. The initiative involves stakeholders and the local community in the planning, implementation, and evaluation processes, ensuring a collaborative approach to ecological conservation. Natural forests play a crucial role in regulating greenhouse gas concentrations in the atmosphere, making them integral to a comprehensive response to climate change. According to Brown (1997), plants absorb CO2 from the atmosphere and convert it into organic matter through photosynthesis, a process essential for their growth. This biological function allows plants to capture carbon dioxide and store it in their biomass. To quantify the carbon sequestration potential of the planted trees, measurements are conducted using allometric equations derived from regression analysis for specific tree types or groups, following the guidelines outlined in SNI 7725:2011. These measurements are crucial for understanding the carbon dynamics within the reforested areas and for assessing the effectiveness of the reforestation efforts. The results from planting sites Well KMJ-41 and Well KMJ-32 indicate a total carbon absorption capacity of 2.111 tons CO2 per year. Among the various species, Ki Honje demonstrated the highest potential for carbon absorption, with a value of 0.044 tons CO2. This significant potential is particularly noteworthy given the young age of the plants in these areas, suggesting that their carbon sequestration capacity will increase as they mature. The role of natural forests extends beyond carbon sequestration. Protecting these forests is essential not only for mitigating climate change but also for maintaining the sustainability of the water cycle and supporting geothermal operations. By preserving natural forests and enhancing reforestation efforts, it is possible to create a synergistic relationship that benefits both the environment and energy production. PGE Kamojang's tree-planting program exemplifies how operational activities can be aligned with environmental sustainability goals. By involving local communities and stakeholders, the program ensures that the reforestation efforts are grounded in local ecological and social aspects.

1. INTRODUCTION

PT Pertamina Geothermal Energy in Kamojang, West Java, Indonesia, serves as a critical site for both geothermal energy production and environmental restoration. The restoration management at Kamojang aims to expedite the recovery of former commercial forests to their natural states, introducing elements such as decaying wood, charred wood, deciduous trees, and varied forest structure, which are essential for supporting rare and threatened species. The approach to habitat restoration involves controlled burning and enhancing the quality and continuity of decaying wood, thereby fostering diverse, productive, and multifunctional landscapes resilient to economic fluctuations and climatic changes.

A significant aspect of this restoration effort is its potential for CO2 absorption through tree planting. As a major contributor to global warming, CO2 levels are rising due to industrial activities, motorized vehicle use, power plant emissions, and forest fires. Plants play a crucial role in mitigating these effects by absorbing CO2 during photosynthesis and converting it into organic matter. According to Brown (1997) and Maiti et al. (2015), this process allows plants to capture and store carbon in their biomass, contributing significantly to carbon sequestration. The Intergovernmental Panel on Climate Change (IPCC, 2007) identifies five carbon sources: above-ground biomass, below-ground biomass, dead trees, litter, and soil. The Kamojang area, managed by PGE, possesses substantial vegetation assets that can effectively absorb and store CO2 from these sources. The successful management of vegetation in this area offers a viable solution to combating global warming by maximizing the potential for carbon sequestration and storage.

The primary aim of this research is to determine effective restoration management and forest landscape restoration (FLR) strategies that enhance the ecological and carbon sequestration functions of reforested areas. By focusing on the Kamojang area managed by PGE, the research seeks to develop and implement restoration techniques that promote biodiversity, improve habitat conditions for rare and threatened species, and create resilient forest ecosystems. A key component of this research is quantifying the carbon sequestration potential of the planted trees. This involves conducting precise measurements using allometric equations derived from regression analysis for specific tree types or groups, in accordance with the guidelines outlined in SNI 7725:2011. These measurements are essential for understanding carbon dynamics within the reforested areas and for evaluating the success of reforestation efforts. Accurately quantifying carbon sequestration enables researchers to assess the effectiveness of various restoration strategies and provides valuable data for optimizing future restoration projects to maximize both ecological and climate mitigation benefits.

2. METHODS

2.1 Data Collection

The data collection for this study includes both primary and secondary data. Primary data were obtained by measuring the diameter, height, anwood density of the plants cultivated by PGE Kamojang. Secondary data were gathered from the company's records such as environmental management data including biodiversity conservation.

2.1.1 Determining Plot Size and Number of Plot

Plot size and nu mber of plot determine based on SNI 7724:2011, with a 10% sampling intensity, resulting in a total plot area of about 7,000 m². Seventeen plots of 20m x 20m were established for trees, with sub-plots of 10m x 10m for poles, 5m x 5m for saplings, and 2m x 2m for seedlings, litter, and understory vegetation.

2.1.2 Measurement of Tree

Tree Diameter at Breast Height (DBH) was measured by wrapping a measuring tape around the tree to obtain the circumference, which was then converted to diameter using the formula :

$$d = k / \pi \quad (1)$$

Where k is circumference of the tree and π (3.1416).

Wood Density Wood density was determined by cutting a branch, measuring its volume, and weighing it before and after drying in an oven at 105°C for 48 hours. Tree height was measured using a clinometer, utilizing the concept of similar triangles to calculate the tree height based on the angle of elevation.

2.2. Data Calculation: Biomass and Carbon Sequestration

Biomass was calculated using the allometric equation (Chave,20..), suitable for Kamojang forest condition using the formula :

$$Y = 0.0509 \times \rho \times DBH2 \times T \quad (2)$$

Where Y is a total biomass (g), DBH is diameter at breast height (cm), ρ is wood density (g/cm³), and T is tree height (cm).

Carbon storage was then estimated by converting biomass to stored carbon using a factor of 0.46. Approximately 46% of the biomass content in a tree is carbon. This result is obtained from laboratory results and applies to all types of trees, SNI (2011). The equation is as shown in equation below :

$$\text{Stored Carbon} = Y \times 0.46 \quad (3)$$

After obtaining the value of the carbon stored in a tree, the potential carbon absorption of a tree can be calculated by multiplying it by the ratio of the relative molecular mass of CO2, which is 44, to the relative atomic mass of carbon, which is 12.. Therefore, equation 3 is obtained as follows:

$$\text{CO2 Sequestration} = \text{Stored Carbon} \times \text{Carbon Conversion Factor} \quad (4)$$

Where Carbon Conversion Factor is 3.67.

2.3. Restoration Management

This study utilizes qualitative data to evaluate the restoration management of PGE Kamojang through the Forest Landscape Restoration (FLR) approach and examines adherence to national guidelines. Specifically, it references the Regulation of the Minister of Environment and Forestry of the Republic of Indonesia No. 23 of 2021, which pertains to the Implementation of Forest and Land Rehabilitation, and the Regulation of the Minister of Environment and Forestry of the Republic of Indonesia No. 4 of 2019, which governs the Utilization of

Geothermal Environmental Services in National Parks, Grand Forest Parks, and Nature Tourism Parks, where part of the PGE Kamojang area is designated as a Nature Tourism Park (Taman Wisata Alam).

Table 1: Forest Landscape Restoration (FLR) Strategies.

Category		Principles
Project Management and Governance		
1	Landscape Scale	FLR should target areas larger than a single site but smaller than an ecoregion
2	Prioritization	Optimize ecological and human outcomes, considering social, economic, political, and ecological factors
3	Legal and Normative Compliance	Programs must comply with applicable laws and local norms (good governance)
4	Participation	Active collaboration with local communities and stakeholders
5	Adaptive Management	Continuous monitoring of ecological and human outcomes
Social Aspects		
6	Enhance Livelihoods	Improving local livelihoods through financial outcomes, poverty alleviation, food security, and non-material benefits like landscape beauty and recreation.
7	Inclusiveness and Equity	Programs should benefit all stakeholders, emphasizing gender equality and support for marginalized groups.
8	Capacity Building	Local stakeholders should be provided with scientific and technical information, and programs should build capacities for active participation, informed by local and indigenous knowledge
Ecological Aspects		
9	Biodiversity Conservation	Protect native ecosystems and species
10	Landscape Heterogeneity and Connectivity	Programs should enhance landscape functionality,
11	Provision of Ecosystem Goods and Services	Ensure the provision of ecosystem services such as carbon storage, natural pest control, pollination, ecotourism, and the supply of water, food, timber, and non-timber products, while minimizing trade-offs.

2.3.1 Forest Landscape Restoration (FLR)

The effectiveness of forest landscape restoration (FLR) is evaluated based on principles encompassing project management, human aspects, and ecological aspects. These principles guide the assessment of FLR's ability to regain ecological integrity and enhance human well-being. This table summarizes the key principles under each category for Project Management and Governance, Human Aspects, and Ecological Aspects relevant to Forest Landscape Restoration (FLR) initiatives.

2.3.2 National Law

The holders of the IPJLPB Exploitation and Utilization permit, as referred to the Regulation of the Minister of Environment and Forestry of the Republic of Indonesia No. 4 of 2019 in Article 35 paragraph (3) letter b, that shown in Table 2.

Table 2: Indonesia National Law Requirements.

No	Requirement	Description
1	Area Protection	Conduct protection and security activities in the permitted area, including preventing illegal logging, wildlife hunting, encroachment, settlement, and forest fires.
2	Tree Replacement	Do not cut down trees; if cutting is necessary, replace the trees at a ratio of 1:100 with seedlings to be planted in locations designated by the local UPT and maintained until the end of the permit.
3	Replanting	Plant and maintain vegetation for five years in utilized areas that are no longer in use.
4	Compliance with Environmental Permits	Follow the requirements stated in the Environmental Permit (AMDAL) documents.

3. RESULT AND DISCUSSION

3.1. Forest Landscape Restoration (FLR) Analysis

PGE Kamojang restoration program meets all the criteria for effective project management and governance through the application of the Forest Landscape Restoration (FLR) approach. The project targets areas that are larger than a single site but smaller than an ecoregion, ensuring comprehensive restoration efforts through GIS mapping and land use checking. Prioritization is given to sites that promise increased ecological benefits and fast-growing tree species such as Kihonje. Compliance with legal and normative requirements is strictly adhered to, supported by policies, law enforcement, and land tenure governance. Ecological and socio-economic monitoring is conducted through environmental-social mapping, and a Biodiversity Action Plan (BAP) is implemented alongside environmental studies. Active participation from local communities and stakeholders is encouraged through inclusion in planning, management, and monitoring processes, as well as environmental workshops and multi-sectoral collaboration with stakeholders and NGOs. Adaptive management practices are employed, with continuous monitoring of ecological and human outcomes, ensuring the project's sustainability and effectiveness.

Figure 1: Implementation of Project Management & Governance in PGE Kamojang Forest Landscape Restoration (FLR).

Restoration strongly emphasizes biodiversity conservation, aiming to restore the populations of endemic species within the geothermal operation area. To accelerate plant growth and enhance biodiversity, the project employs the Miyawaki planting method, which is known for its ability to create dense, native forests in a short period. This approach not only promotes rapid vegetation growth, but also contributes to the resilience of the ecosystem in the geothermal area. In terms of promoting ecosystem services, the restoration efforts focus on several critical functions. Natural recharge for water resources is enhanced, ensuring the sustainability of water supplies that are used for geothermal operations. The project also plays a significant role in carbon storage, helping to mitigate climate change by sequestering carbon dioxide. Soil protection is another key benefit, as the restored vegetation helps prevent soil erosion and degradation. Additionally, the restoration project contributes to disaster management, specifically by mitigating the risk of landslides through improved vegetation (vetiver) cover and root systems that stabilize the soil. From an ecological perspective, the project aims to increase landscape heterogeneity. By utilizing various restoration and planting methods, including the cultivation of multiple tree species, the project enhances the structural diversity of the landscape. This heterogeneity is crucial for creating a robust and resilient ecosystem capable of withstanding environmental stresses and supporting a wide range of wildlife species.

Workers in the restoration activities receive monetary income, providing direct financial support to the individuals involved. Additionally, the project promotes economic diversification by encouraging the production and sale of organic fertilizer, offering an alternative source of income for local farmers. Further, the provision of seeds for the restoration project creates another stream of monetary income, helping to sustain the economic well-being of the community. Capacity building is a central component of the project, empowering local communities and stakeholders to actively implement and monitor the restoration program. Through workshops and training sessions, participants gain valuable skills and knowledge in conservation techniques, environmental management, and sustainable practices. Conservation education is also emphasized, raising awareness about the importance of biodiversity and ecological health. From a social perspective, the project prioritizes inclusiveness and equity. Gender equality is promoted by involving women local farmers in nursery plantation activities, ensuring that

women have equal opportunities to benefit from the project. The restoration project fosters local empowerment by opening up job opportunities, thereby strengthening the community's economic resilience and social cohesion.

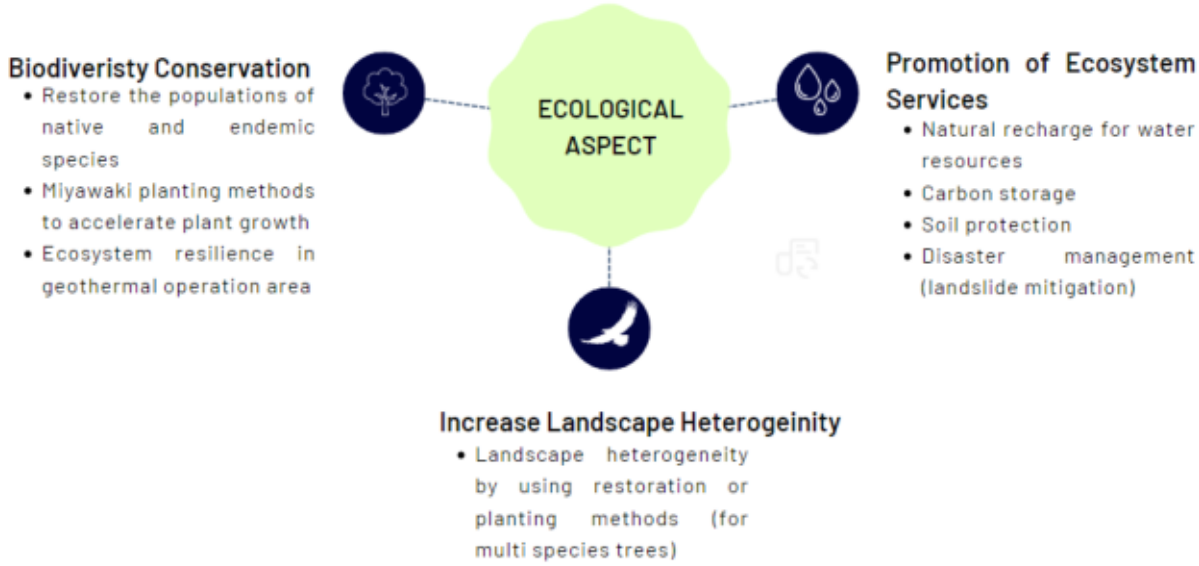

Figure 2: Implementation of Ecological Aspect in PGE Kamojang Forest Landscape Restoration (FLR).

Figure 3: Implementation of Social Aspect in PGE Kamojang Forest Landscape Restoration (FLR).

Table 3: Indonesia National Law Compliance Analysis.

No	Requirement	Description	Analysis
1	Area Protection	Conduct protection and security activities in the permitted area, including preventing illegal logging, wildlife hunting, encroachment, settlement, and forest fires.	PGE Kamojang have implemented comprehensive protection and security measures in the designated area. These activities include regular patrols to deter illegal logging and wildlife hunting every shift, monitoring systems (CCTV & security portals), and fire prevention strategies such as firebreak and community awareness programs
2	Tree Replacement	Do not cut down trees; if cutting is necessary, replace the trees at a ratio of 1:100 with seedlings to	PGE Kamojang adhere strictly to the no-cutting policy. This tree replacement strategy effectively

No	Requirement	Description	Analysis
		be planted in locations designated by the local UPT and maintained until the end of the permit.	compensates for any loss of trees, promoting reforestation and ecological balance.
3	Replanting	Plant and maintain vegetation for five years in utilized areas that are no longer in use.	PGE Kamojang consistently replant and maintain vegetation in areas that have been utilized and are no longer in active use. This replanting process is carried out over a five-year period, ensuring that the restored areas achieve a stable and self-sustaining ecosystem. Tofal replantation from 2008-2023 are 632,052 trees with success growth ratio > 85%.
4	Compliance with Environmental Permits	Follow the requirements stated in the Environmental Permit (AMDAL) documents.	The permit holders fully comply with all the stipulations outlined in the Environmental Permit (AMDAL) documents. This includes conducting regular environmental impact assessments, adhering to mitigation measures, and ensuring that all activities within the permitted area align with the environmental standards and regulations specified in the AMDAL. Regular audits and reporting ensure transparency and accountability, demonstrating the permit holders' commitment to environmental stewardship.

3.2. National Law Compliance Analysis

PGE Kamojang as the holders of the IPJLPB Exploitation and Utilization permit, as specified in the Regulation of the Minister of Environment and Forestry of the Republic of Indonesia No. 4 of 2019 in Article 35 paragraph (3) letter b, are mandated to fulfill several key requirements to ensure sustainable and responsible management of the permitted area.

PGE Kamojang as the holders of the IPJLPB Exploitation and Utilization permit have successfully complied with all key requirements specified by the Regulation of the Minister of Environment and Forestry of the Republic of Indonesia No. 4 of 2019 in Article 35 paragraph (3) letter b.

3.2. Carbon Sequestration Analysis

3.2.1 Biomass

The wood density, DBH (diameter at breast height), and height values for each Kamojang endemic tree species were meticulously gathered through precise calculations. These values are critical for understanding the structural properties and biomass of the trees. By obtaining accurate measurements of these parameters, the project can better assess the ecological benefits provided by each species, presented in Table 4.

Table 4: Kamojang Endemic Tree Calculation Result.

Tree Species	Average DBH (cm)	Average Height (cm)	Wood Density (g/cm³)	Average Biomass Value (g)
Ki Bereum (*Distylum stellare*)	1.3	238.89	0.75	14.89
Lame (*Distylum stellare*)	1.68	147.08	0.48	10.13
Ki Honje (*Pittosporum ferrugineum*)	1.86	290	0.51	25.97
Ki Sireum (*Syzygium lineatum*)	1.60	215	0.815	22.69
Salam (*Syzygium polyanthum*)	1.80	235	0.558	21.63
Peutag (*Syzygium densiflorum*)	1.80	200	0.66	21.77

3.2.2 Correlation of Parameters with Biomass Values

According to the research by Uthbah et al. (2017) and Yuliasmara et al. (2009), tree biomass geometrically correlates parallelly with tree diameter and height. In this study, Ki Bereum plants were sampled to determine the correlation between tree diameter and height with their biomass values. The correlation between diameter and biomass can be seen in Figure 4. In the figure, the diameter of Ki Bereum plants shows a parallel correlation with the biomass value contained. With an R2 value of 0.8473, indicating that 84.73% of the biomass value is influenced by the diameter of the plant. Meanwhile, the correlation of tree height with the contained biomass value can be seen in Figure 4. Correlation of tree height with biomass value of Ki Bereum plants shows a reasonably

parallel correlation, but height has a smaller correlation compared to diameter. In the allometric biomass equation, biomass is proportional to the square of the diameter, hence height correlates less with biomass compared to diameter. Tree height has an R2 value of 0.8339, indicating that 83.39% of the biomass value is influenced by the height of the tree.

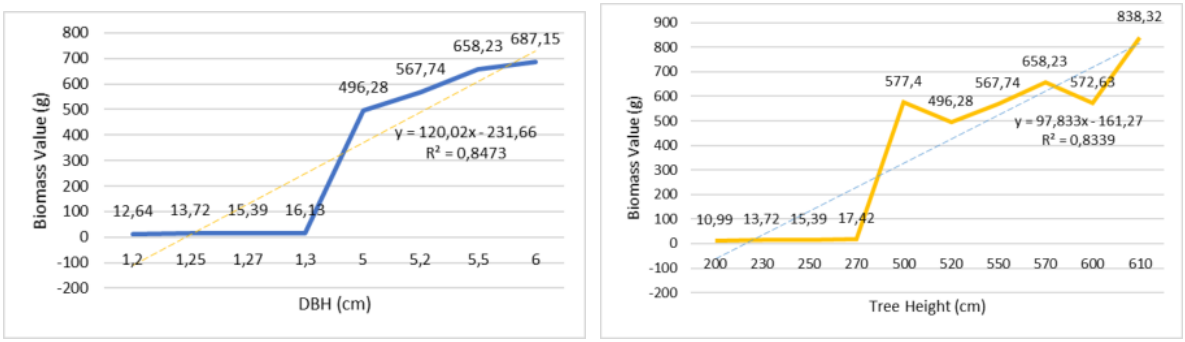

Figure 4: Correlation of DBH (left) and Tree Height (right) with Biomass Value of Ki Bereum.

3.2.3 Carbon Sequestration

Carbon sequestration in each plot is calculated to determine the carbon sequestration potential of the plants cultivated by PGE Kamojang. Carbon sequestration is calculated based on the stored carbon value in each plot, which is then divided by the age of the plants in that area (KMJ-41, 3 years and KMJ-32, 5 years). The average carbon sequestration value in the planting area of well KMJ-41 is approximately 0.218 tCO2/ha/year, with a land area of 5 hectares for the planting area of well KMJ-41, the carbon sequestration capacity in this area is approximately 1.088 tCO2/ha/year.

Table 5: Carbon Sequestration of KMJ-41.

Plot	Total Biomass (g)	Stored Carbon (Kg)	Stored Carbon (Ton/Ha)	Stored Carbon (Ton/Ha/year)	Carbon Sequestration (Ton/Ha/year)
1	150.50	0.069	0.173	0.058	0.212
2	141.58	0.065	0.163	0.054	0.199
3	165.18	0.076	0.190	0.063	0.232
4	158.36	0.073	0.182	0.061	0.223
5	157.78	0.073	0.181	0.061	0.222
				Average	0.218

Carbon sequestration values correlate directly with the biomass of the plants. Therefore, factors influencing biomass values will enhance the carbon sequestration potential of the plants. According to the table above, plants with the highest carbon sequestration values are Salam and Ki Honje plants. This is because these plants have the highest biomass values, which are influenced significantly by their larger diameters compared to other plant species, as indicated in the Table 6.

Table 6: Carbon Sequestration of Kamojang Endemic Tree Species.

Tree Species	Average Biomass Value (g)	Stored Carbon (Kg)	Carbon Sequestration (Ton)
Ki Bereum (*Distylum stellare*)	14.89	0.007	0.025
Lame (*Distylum stellare*)	10.13	0.005	0.017
Ki Honje (*Pittosporum ferrugineum*)	25.97	0.012	0.044
Ki Sireum (*Syzygium lineatum*)	22.69	0.010	0.038
Salam (*Syzygium polyanthum*)	21.63	0.009	0.037
Peutag *(Syzygium densiflorum*)	21.77	0.010	0.037

Carbon sequestration capacity in the planting area of well KMJ-32 is approximately 0.633 tCO2/ha/year. Plot 6 contains Ki Bereum plants, with a land area of approximately 2 hectares the carbon sequestration potential approximately 1,266 tCO2/year. This value is higher compared to the research plot in the KMJ-41 well area., due to the older age of the plants, resulting in greater height and diameter compared to the planting area in the KMJ-41 well area. Therefore, the carbon sequestration potential of both planting areas totals approximately 2,111 tCO2/year.

Figure 5: Kamojang Endemic Trees.

Table 7: Carbon Sequestration of KMJ-32.

Plot	Total Biomass (g)	Stored Carbon (Kg)	Stored Carbon (Ton/Ha)	Stored Carbon (Ton/Ha/year)	Carbon Sequestration (Ton/Ha/year)
6	4669.74	4.752	0.859	0.172	0.633

4. CONCLUSION

The Kamojang restoration management program, utilizing the Forest Landscape Restoration (FLR) approach, has effectively restored biodiversity and ecological health in the geothermal operation area. By targeting areas larger than a single site but smaller than an ecoregion, the program ensures comprehensive restoration through GIS mapping and prioritization of ecologically beneficial sites. Strict adherence to legal requirements, inclusive stakeholder participation, and adaptive management practices have facilitated sustainable project implementation. The use of the Miyawaki planting method has accelerated vegetation growth and biodiversity, enhancing ecosystem resilience. The program also contributes to water resource sustainability, soil protection, and disaster risk mitigation, promoting a robust and diverse landscape.

In terms of carbon sequestration, the Kamojang project has demonstrated significant potential. Detailed measurements of tree species' diameter, height, and wood density have enabled precise biomass and carbon storage calculations. The project shows a direct correlation between biomass and carbon sequestration, with species like Ki Honje and Salam showing the highest values. The calculated carbon sequestration rates for planting areas indicate a substantial capacity to sequester carbon dioxide, totaling approximately 2,111 tCO2/year across different plots. This underscores the project's role in mitigating climate change, enhancing carbon storage, and supporting sustainable environmental practices within the geothermal operation area.

REFERENCES

Badan Standarisasi Nasional. 2011. SNI 7724:2011. Pengukuran dan Penghitungan Cadangan Karbon – Pengukuran Lapangan untuk Penaksiran Cadangan Karbon Hutan (*ground based forest carbon accounting*). Badan Standarisasi Nasional: Jakarta

Badan Standarisasi Nasional. 2011. SNI 7725:2011. Penyusunan Persamaan Alometrik untuk Penaksiran Cadangan Karbon Hutan Berdasar Pengukuran Lapangan (*ground based forest carbon accounting*). Badan Standarisasi Nasional: Jakarta

Baharuddin, B. 2013. Analisis Potensi Tegakan Bambu Parring (Gigantochloa atter) Sebagai Penyerap Dan Penyimpan Karbon (Studi Kasus Pengelolaan Hutan Bambu Rakyat Di Tanralili Kabupaten Maros. *The Fifth International Symposium Indonesian Wood Research Society* (IWoRS).

Chave, J., Andalo, C., Brown, S., Cairns, M. A., Chambers, J. Q., Eamus, D., & Yamakura, T. 2005. Tree allometry and improved estimation of carbon stocks and balance in tropical forests. *Oecologia*, 145, 87-99.

César, R.G.; Belei, L.; Badari, C.G.; Viani, R.A.G.; Chazdon, R.L.; Gutierrez, V.; Brancalion, P.H.S.; Morsello, C. Forest and Landscape Restoration: A Review EmphaSizing Principles, Concepts, and Practices. *Land* 2021, 10, 28. https://doi.org/10.3390/land 1001002

IPCC. 2006. *IPCC Guidelines for National Greenhouse Gas Inventories*. OECD.

Kaleka, Y. U., Anggraeni, D. M., Garung, E. R., Deke, O. 2023. Emisi Gas Rumah Kaca (GRK) on Road dengan Tier-2 Di Sumba Barat Daya. *Borneo Journal of Science and Mathematics Education*, 3(1), 16-25.

Kuncoro, D. D., Husodo, T., Kusmoro, J., Hendrawan, R., Afriyanti, F., Megantara, E. N. 2020. Above-ground carbon stock at Kamojang Regions, West Java, Indonesia. *Biodiversitas Journal of Biological Diversity*, 21(4), 1749-1754

Labiba, D., Pradoto, W. 2018. Sebaran emisi CO2 dan implikasinya terhadap penataan ruang area industri di Kabupaten Kendal. *Jurnal Pengembangan Kota*, 6(2), 164-173.

Laksminingpuri, N., Martinus, A. 2014. Studi Kandungan Dan Temperatur Gas Panas Bumi Kamojang Dengan Diagram Grid. Beta Gamma. Majalah Ilmiah Aplikasi Isotop dan Radiasi, 4(2), 69-79

Mamentu, f. T., Laloma, a., Londa, V. 2020. Manajemen Pengelolaan Sumber Daya Alam (Tenaga Uap) Pada PT. Pertamina Geothermal Energy Area Lahendong Kota Tomohon. *Jurnal Administrasi Publik*, 6(92), 1-12.

McPherson, E. G., van Doorn, N. S., Peper, P. J. 2016. *Urban Tree Database and Allometric Equations* (Vol. 253). Albany, CA, USA: US Department of Agriculture, Forest Service, Pacific Southwest Research Station.

Pandit, I. K., Nandika, D., Darmawan, I. W. 2011. Analisis sifat dasar kayu hasil hutan tanaman rakyat. *Jurnal Ilmu Pertanian Indonesia*, 16(2), 119-124.

Passal, A.I., Gun Mardiatmoko, Fransina Latumahina. 2019. Estimasi Karbon Tersimpan Skala Plot Pada Agroforestry Pola Dusung di Negeri Hutumuri, Kecamatan Leitimur Selatan, Kota Ambon. *Jurnal Hutan Tropis*, 7(2), 131-144.

Septiawan, W., Indriyanto, I., Duryat, D. 2017. Jenis Tanaman, Kerapatan, dan Stratifikasi Tajuk Pada Hutan Kemasyarakatan Kelompok Tani Rukun Makmur 1 di Register 30 Gunung Ranggamus, Lampung. *Jurnal Sylva Lestari*, 5(2), 88-101.

Tihurua, E. F., Sulistyawati, E. 2019. *Keragaman Kerapatan Kayu Batang Dan Cabang Komunitas Pohon Di Hutan Gunung Papandayan, Jawa Barat*. BERITA BIOLOGI, 18(2), 145-154.

Tuyor, J. B., de Jesus, A. C., Medrano, R. S., Garcia, J. R. D., Salinio, S. M., & Santos, L. S. 2005. Impact of geothermal well testing on exposed vegetation in the Northern Negros Geothermal Project, Philippines. *Geothermics*, 34(2), 252-265.

Umroni, A. 2012. Metode Inventarisasi Model-Model Pengelolaan Hutan Rakyat di NTT. *Jurnal Warta Cendana*, 6(1), 12-18.

Wibowo, A., Samsoedin, I., Nurjahjawilasa, S., Muttaqin, Z. 2013. *Petunjuk Praktis Menghitung Cadangan Karbon Hutan* (Practical Guide to Calculating Forest Carbon Reserves). Bogor: Pusat Penelitian dan Pengembangan Perubahan Iklim dan Kebijakan Badan Penelitian dan Pengembangan Kehutanan. Kementerian Kehutanan, Republik Indonesia Kerjasama dengan United Nations Educational, Scientific and Cultural Otganization (UNESCO)

Yamani, A. 2013. Studi kandungan karbon pada hutan alam sekunder di Hutan Pendidikan Mandiangin Fakultas Kehutanan Unlam. *Jurnal Hutan Tropis*, 1(1), 86-91

Yuliasmara F, Wibawa A, Prawoto AA. 2009. Karbon tersimpan pada berbagai umur dan sistem pertanaman kakao : Pendekatan Allometrik. *Pelita Perkebunan*. 25(2),86-100.

Zanne, A.E., Lopez-Gonzalez, G., Coomes, D.A., Ilic, J., Jansen, S., Lewis, S.L., Miller, R.B., Swenson, N.G., Wiemann, M.C., Chave, J. 2009. *Global wood density database*. Dryad

Comparative Analysis of Geothermal PPPs: International Insights and Indonesia's Cases

Candra Sri Sutama, Ali Ashat, Suardi Nur, and Desti Alkano

candra.sutama@outlook.com, labgeothermal@gmail.com,
suardinur.fst@ar-raniry.ac.id, d.alkano@ecadin.org

Keywords: Public-private partnership, PPP, developing countries, energy, Indonesia, geothermal

ABSTRACT

Public-private partnerships (PPP) is a collaborative agreement between a public authority and a private or semi-private entity to deliver a public service and in which part of the risks and investments are transferred outside of the public entity's hands, leading generally to long-term agreements. These partnerships can potentially leverage the strengths of both sectors: the public sector's ability to provide regulatory oversight and the private sector's experience, expertise, and efficiency. By sharing risks and responsibilities, PPP can accelerate project timelines, improve service delivery, and foster innovation while reducing the financial burden on the public sector.

Indonesia possesses one of the world's largest geothermal potentials, but only around 10% of it has been utilized. The challenges to further develop geothermal in Indonesia are multi-faceted, including in financing, technical expertise, innovation, and social-ecological concerns. Public-private partnership (PPP) presents a promising development model that can leverage private sector expertise, innovation, and financing, potentially accelerating the advancement of geothermal projects in the country.

The study begins with an introduction to PPP, the potential benefits, and the implementation of PPP, particularly in developing countries. The second part examines geothermal financing in various countries, including Kenya, Turkey, and the US, public and private roles, as well as existing PPP models. These cases are analyzed to identify success, challenges, and the role of government policies and incentives in fostering effective collaborations. Key aspects such as risk allocation, financing structures, and regulatory frameworks, are reviewed to understand their impacts.

The next part of the paper shifts focus to the geothermal landscape in Indonesia. The current state of Indonesia's geothermal sector is reviewed, highlighting the regulatory landscape, the role of government initiatives, and private sector involvements, followed by existing PPP frameworks, and experiences in the geothermal projects. Subsequently, the public and private involvement models and cases are compared with other countries analyzed previously, with different conditions highlighted accordingly. An empirical analysis is performed to identify opportunities for improving the effectiveness of PPP and future potentials of PPP applications, in considerations where international best practices can be adapted. Recommendations are provided to enhance policy frameworks, improve risk management, and streamline project approval processes, including focusing on the importance of creating a conducive investment environment and consistent regulatory policies.

The final part concludes that strategically integrating the best practices of public-private partnerships, customized to Indonesia's unique socio-economic and geological context, can significantly advance its geothermal sector. By drawing on global experiences and developing frameworks tailored to Indonesia's specific conditions, the country can optimize its geothermal potential, thereby enhancing national energy security and achieving sustainable development goals. This comparative analysis provides valuable insights not only for Indonesia but also for other emerging economies aiming to develop their geothermal resources through effective public-private partnerships.

1. INTRODUCTION TO PUBLIC-PRIVATE PARTNERSHIP (PPP)

Significant infrastructure investments are needed worldwide, especially in many developing and emerging economies, to stimulate economic growth and meet environmental goals. According to a report by the Global Infrastructure Hub (2017), the global demand for infrastructure investment, which encompasses energy, telecommunications, transportation (including airports, ports, railways, and roads), and water, is expected to reach $94 trillion by 2040, represents 3.55% of global GDP. An extra $3.5 trillion will also be necessary to fulfill the United Nations' Sustainable Development Goals for electricity and water.

Governments are ultimately responsible for providing public services and the infrastructure required for their delivery. Infrastructure investment is often part of the social contract between a government and its citizens (The World Bank, 2017), and it is probably universally agreed that the state has to play a role in providing public

infrastructure (Yescombe, 2007). However, when the government is faced with pervasive challenges to provide them, considering infrastructures involve huge amounts of capital investment, private investments are often mobilized through public-private partnership (PPP). The capital-intensive nature of basic infrastructure and competition for limited government budgetary resources have prompted governments to invite private investors to fulfill the widening demand-supply gap for infrastructure while the governments are endeavoring to meet the social commitments within the fiscal constraints (Yurdakul et al., 2022).

1.1 Definition, Core Characteristics, and Types

Saussier et al. (2009) defined PPP broadly as an agreement between a public authority (whether at the state or local level) and a private or semi-private entity to deliver a public service and in which part of the risks and investments are transferred outside of the public entity's hands, leading generally to long-term agreements. This definition aligns with Alfen et al. (2009), which describes PPP as "a wide range of arrangements whereby government responsibilities are outsourced to commercial partners, and risk is shared between the public and private sectors to bring about desired outcomes in areas associated with public policy". Alfen et al. (2009) observed various PPP implementation methods as each country adapts the process as appropriate for its own culture, economy, political climate, and legal system. Despite those variations, Iossa & Saussier (2017) identified four primary characteristics of PPPs: (1) task bundling, (2) risk transfer, (3) medium-long-term contracting, and (4) private finance. Table 1 presents a list of various institutions and government agencies' definitions of PPPs, which generally encompass these core characteristics.

Based on the nature of the service and the degree of risk transfer involved in the contracts, PPP contracts can be categorized into two distinct types (Yescombe, 2007; Iossa & Saussier, 2017):

1. "Concession" or also called the financially freestanding project: this is when the private sector's main source of income comes from the user. In these contracts, the private sector revenue is linked to the level of usage or demand for the service. Toll road projects very commonly fall under the concession type.
2. "Availability-based contract" is when the private-sector party mainly sells the service to the public-sector party. In this type of contract, the private sector is partially or all responsible for designing, building, and maintaining the infrastructure and services, but payment from the public sector party is based on the availability of the infrastructure and services, regardless of the level of usage. This model is often used for projects such as hospitals, schools, prisons, waste-water treatment plants, and waste incinerators.

As mentioned in the previous section, one of the common and defining feature of PPP is that it bundles multiple task or phases of a project into a single agreement. The specific responsibilities assigned to the private sector vary depending on the nature of the asset and service involved. Common functions typically include (1) **Design:** developing the project from initial concept and output requirements to construction-ready design specifications, (2) **Build** (when PPPs are used for new infrastructure assets and a private party is required to construct them) or **Rehabilitate** (where PPP involve existing assets and private party is responsible for rehabilitating or extending the asset), (3) **Finance**, (4) **Maintain**, and (5) **Operate** (The World Bank, 2017).

Table 1: Definition of PPP by various institutions and governments.

Institution	Definition
The World Bank (2017)	A long-term contract between a private party and a government entity for providing a public asset or service, in which the private party bears significant risk and management responsibility, and remuneration is linked to performance
Asian Development Bank/ ADB (2008)	A range of possible relationships among public and private entities in the context of infrastructure and other services; present a framework that—while engaging the private sector—-acknowledge and structures the role of government in ensuring that social obligations are met and successful sector reforms and public investments achieved
European Commission (2003)	A partnership between the public sector and the private sector for the purpose of delivering a project or a service traditionally provided by the public sector
UK Government (UK Trade & Investment, 2013)	General term for partnerships that involve everything from operating facilities and providing services on behalf of the public to flexible methods of financing these services
Indonesia Government (Presidential Regulation 38, 2015)	Cooperation between the Government and Business Entity on Infrastructure Provision for the best interest of the Public, in accordance with the pre-determined specifications (by the Minister / Head of Institution / Head of Region/ State-owned Enterprise (SOE) / Regional-owned Enterprise (ROE)), partially or fully uses the resources from the Business Entity while considering risks allocation among Parties.

Based on the above, several types of PPP exist. The most traditional is **BOT (build-operate-transfer)**, in which, as the name suggests, the private sector is responsible for building and operating the asset. The private sector undertakes the investment in capital assets, though the financing comes from the public sector, which also holds the financial risk. When the contract ends, asset ownership is transferred to the public sector according to the terms initially agreed upon unless an extension or renewal of the contract is later approved. Other models include **DBFO (design-build-finance-operate)**, in which the private partner is responsible for the whole stages of the project (Iossa & Saussier, 2017). Table 2 provides a detailed overview of various infrastructure provision models, highlighting the differing public and private sector involvement levels. It illustrates the spectrum from fully public to fully private projects.

Build-Own-Operate (BOO) contract is viewed by some scholars as privatized project (Engel et al., 2020; Trebilcock & Rosenstock, 2015; Yescombe, 2007). Trebilcock and Rosenstock (2015) argue that asset ownership is the key distinction between PPPs and privatization; thus, any arrangement wherein the asset remains with the private entity at the end of the contract period would not fall into the PPP category. However, BOO is classified as PPP by several literatures (Azarian et al, 2022, Cheng et al., 2019; Grimsey & Lewis, 2004;). Additionally, legislation in various countries including Vietnam, the Philippines, India, Kenya, and Indonesia, also recognize BOO as a form of PPP. Therefore, in those countries, BOO model may benefit from state's financial incentives such as tax-exempt status (DPI HCMC PPP Division, 2017; Republic of the Philippines PPP Center, 2012; India Department of Economic Affairs, 2023; ADB, 2020).

From the perspective of asset ownerships, BOO arrangement that resembles privatization highlights contractual structure disadvantages for public entity (Akhtar, et al 2023 ; William, 2023). To address these disadvantage issues, the BOOT arrangement has therefore emerged that make the asset ownerships to public entity at the end of contractual period is possible (Akhtar, et al 2023).

Table 2: Public and private provision of infrastructure classified by the involvement of public and private sector (ADB, 2021; Yescombe, 2007).

	Strong public participation ←					→ Strong private participation
			← Public private partnership →			
Contract Type	**Public-sector procurement**	**Franchise *(Affermage)***	**Design – Build – Finance – Operate (DBFO)**	**Build – Transfer – Operate (BTO)**	**Build – Operate – Transfer (BOT)**	**Build – Own – Operate (BOO)**
Construction	Public sector	Public sector	Private sector	Private sector	Private sector	Private sector
Operation	Public sector	Private sector	Private sector	Private sector	Private sector	Private sector
Ownership	Public sector	Public sector	Public sector	Private sector during construction, the public sector	Private sector during the contract, then the public sector	Private sector
Who pays?	Public sector	Users	Public sector or users	Public sector or users	Public sector or users	Private sector off-taker, public sector, or users
Who is paid?	n/a	Private sector	Private sector	Private sector	Private sector	Private sector

1.2 Potential benefits of PPP

While a range of diverse potential positive outcome promises have been made in the context of reforms leading to PPP implementation, its fiscal and financial benefits are consistently mentioned (Alfen, 2009; Estache, 2006; Liu & Love, 2014; Than Nguyen et al. 2020; Yurdakul et al., 2022). The expected fiscal benefits of reforming to PPP, especially in the short term, were often seen as PPP's main advantage. The anticipated gains came from three sources: (i) income from asset sales, leases, or rentals; (ii) reduced public sector operational and capital expenditures due to shifting responsibilities to private operators; and (iii) a net increase in tax and non-tax revenues (Estache, 2006). However, this has to be considered very carefully, and several studies challenged this view. Engel et al. (2020) argued that, independently of the type of procurement, whether it is PPP or traditional procurement, the fiscal impact of a project in present value is the same. For example, in the case of a toll road project, the government may initially save by not having to pay upfront for the construction. But, subsequently, these savings are equal to the toll revenues that will go to the hands of private partners during the duration of the PPP contract. The study concluded that PPPs would be more credible if their effects on the intertemporal fiscal constraint were acknowledged, meaning investments in PPPs should be accounted for as public investments in public accounts, given their equivalent effect on the intertemporal fiscal constraint.

Literature suggests vast potential benefits of PPP other than the fiscal benefit discussed above. The PPP concept has been widely proposed to overcome the public sector's limitations as it is believed that it has many advantages, such as potentially using the private sector's resources, stirring up innovation, improving productivity, providing better risk allocation, promoting value for money and delivering cost-effectiveness (Ng et al., 2012). These benefits reveal the main objective and justification, which is the economic case of PPP: efficiency gain (Engel et al., 2020). Most governments are drawing their decisions for PPP based on the greater efficiency the private promoter delivers compared to traditional public procurement (Alfen et al., 2009). PPP comes with the promise of higher productive efficiency, a possible trade-off between productive and allocative efficiency, and higher costs, some of which are real resource costs to society, others not (Valila, 2020).

The following section discusses further the potential advantages of PPP based on a wide number of literature (Alfen et al., 2009; Engel et al, 2020; Estache, 2006; Saussier & de Brux, 2018; Valila, 2020):

1. **Leveraging the expertise and experience of private sector:** Private sector often offer extensive expertise and experience, which the public sector may lack of. This includes better management techniques, latest technology adoptions, and optimized solutions that can significantly enhance the effectiveness and efficiency of public services. This expertise is critical in complex projects where specialized knowledge significantly influences outcomes. Further, creating a Special Purpose Vehicle (SPV) for PPP execution allows a clearly defined scope and dedicated management team that reports to the firm's board.
2. **Introducing competition:** Traditionally, the public sector lacks market pressure that drives efficiency and innovation. By opening the public sector to private participation, it encourages companies to compete for obtaining contracts through offering better values, solutions, and service delivery. The competition can benefit the public, as it can lead to higher quality service at lower costs.
3. **Innovation**: The private sector's drive for profit and competitive advantage fosters innovation. In a PPP model, this can translate into innovative ways of managing public services that improve quality, efficiency, and user satisfaction. Innovation can range from new technological implementations to advanced management practices that streamline operations and reduce costs.
4. **Risk sharing:** PPP allows the distribution of risks between public entities to private operators, such as production risks, demand-related risks, and operating costs, according to which party can manage them best. This optimal risk allocation leads to better project management and lower life-cycle costs, hence higher efficiency. In some cases, private operators, with their broader range of activities and risk management expertise, can diversify and handle these risks more effectively than public organizations. In other cases, risk sharing can attract private investment to sectors where risk is a significant barrier. In summary, the ideal level of risk-sharing depends on several factors: how much risk the private contractor is willing to take on, the costs they incur to manage these risks, and the relationship between their unobserved efforts and the results that can be seen.
5. **Restructuring public sector services:** by embracing private sector capital and practices, reducing political interference. PPPs allow public sector services to be restructured by leveraging the operational expertise of the private sector, potentially leading to efficiency and better service quality. Additionally, minimizing political interference can result in more stable and predictable project management, allowing to building of an environment where long-term planning and strategic making is possible (Hodge & Greve, 2007). In the concession model, PPP enables users to pay the firm responsible for building and operating the infrastructure asset directly, thereby eliminating the inefficiency costs associated with government bureaucracy.
6. **Project bundling minimizes total life-cycle cost**: The reasoning is that because the concessionaire will operate and maintain the project, it will design and build the project to minimize life-cycle costs. Moreover, if there is strict monitoring of compliance with the conservation standards, it is in the concessionaire's interest to design and build the project to maintain the infrastructure at minimum life-cycle costs.
7. **Economic of scale:** Private partners in PPP are often specialists who serve multiple customers in the same business, allowing them to reduce average costs and pass these savings through competitive pricing. This particularly applies when substantial fixed costs must be spread over large production volumes. Thus, this benefit only applies in conditions where the assets involved are very specialized or if the public entity retains a monopoly.

2. PPP IN DEVELOPING COUNTRIES

2.1 Overview

PPP has been practiced and utilized extensively around the globe for some time now, in both developing and developed countries (Osei-Kyei and Chan, 2017; Abdel Aziz, 2007). According to Fabre & Straub (2023), in

terms of their contribution to investments in physical and social infrastructure, estimates indicate that PPPs represent approximately 3 percent of global infrastructure spending. In addition, a number of PPPs attract a significant share of public financing, both directly or indirectly, through guarantees. PPP is, globally, seen as a valuable tool for mobilizing private sector resources and addressing infrastructure gaps. Several multilateral development institutions, including the World Bank, Asian Development Bank, Inter-American Development Bank, and European Bank for Reconstruction and Development, have drawn strategic directions to better support PPP, including institutional arrangements, product offerings, focused interventions, and knowledge management. Further highlighting PPP's importance globally to foster development, PPP is also explicitly mentioned in the United Nations 2030 Agenda for Sustainable Development, specifically under Sustainable Development Goal 17: Strengthen the means of implementation and revitalize the Global Partnership for Sustainable Development (UN, 2015) Lately, the implementation of PPP financing model is also extended to de-risk high risk projects particularly in developing countries (Sastoque et al, 2024 ;). PPP financing model provides a partnerships framework to incentivize the essential projects that can reduce the risks and project costs borne by private partners (Hou et al, 2024).

While there has been a long history of private sector provision of public goods and services, the PPP model has re-emerged in developed economies since the beginning of the 1990s and even earlier in the 1980s (Grimsey & Lewis, 2004; Vining et al, 2004; Zwalf, 2020). However, PPP started to be used in developing countries much later than that. For example, Wang et al. (2022) observed that the Chinese government began to promote PPP projects only in 2014. Another emerging economy, Brazil, started to see PPP projects become a reality only in 2007, even though it has enacted the PPP Law since 2004 (Barral & Haas, 2007). India started earlier by marking the onset of several PPP projects in the transport and power sector in mid-1990 (Sharma et al., 2021); however, it was only in 2004 that India formed an infrastructure committee to promote and supervise PPP policies formulations and project implementations (Cheng et al, 2019). Within a similar timeframe to others, Indonesia starts to develop PPP after decentralization reform in the 2000s (Yaya, 2014).

According to data from the World Bank (2024), as shown in Figure 1, 2023 saw total private sector commitments in infrastructure (including all types of private sector investments from PPP to full privatization) in low- and medium-income countries reached US$ 86 billion, indicating a bounce back after a significant drop in private sector investments in infrastructure following Covid 19 pandemic. However, this is merely equivalent to 0.2% of these countries' GDP. This amount is also very far from the average infrastructure investment required in those countries, which is estimated at US$ 1.5 trillion per year (Rozenberg & Fay, 2019).

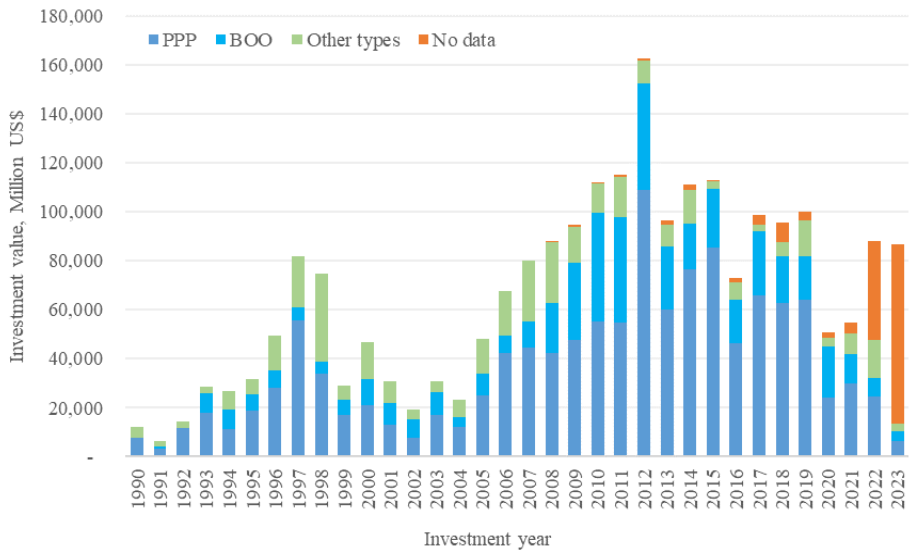

Figure 1: Private Investment in Infrastructure Projects, including PPP (Build-Lease-Transfer, Build-Rehabilitate-Operate-Transfer, Rehabilitate-Operate-Transfer, and Build-Operate-Transfer), Build-Own-Operate, Other Types (Lease contract, Merchant, Rental, etc.), and Projects with No Data, in Low and Mid-Income Countries, 1990-2023 (data from The World Bank, 2024).

In recent years, data from the World Bank Private Participation in Infrastructure indicated well how much of the total private investments could be categorized as PPP (Build-Lease-Transfer, Build-Rehabilitate-Operate-Transfer, Rehabilitate-Operate-Transfer, and Build-Operate-Transfer). Between 1999 and 2021, on average, 56% of total private investments could be classified as PPP. However, it is important to note that the majority of private investment types in 2022-2023 were not categorized (no data), and only a small proportion were clearly classified

as PPP categories. This does not necessarily mean that PPP investment dropped significantly, as the investment types are not clearly categorized.

2.2 PPP in Energy Sector of Developing Countries

Governments usually use PPP for economic infrastructure, such as energy, electricity, roads, airports, ports, railways transport, or social infrastructure, includes education, health, water and sanitation and urban or rural development (Grimsey & Lewis, 2004). In industrialized countries, PPPs are used in areas of public service provision including education, health services, waste management and public buildings. In the other side, in developing countries with enormous needs for basic infrastructure, PPPs are often seen in the power, water, or road sectors in order to sustain the countries' rapid economic growth (Alfen et al., 2019).

PPP in the power generation sector is typically established to develop a specified amount of power capacity or a particular project. The power purchase agreement (PPA) and/or concession agreement outline the obligations, benefits, and risk allocations. In a standard PPP for power generation, private investors construct a power plant and agree to sell the electricity produced to a publicly owned utility. The public authority assumes the demand risk by guaranteeing a minimum payment for the plant's availability or capacity, regardless of whether its output is needed. Additionally, a usage payment is made to cover the fuel costs for the plant. (ESMAP, 2012)

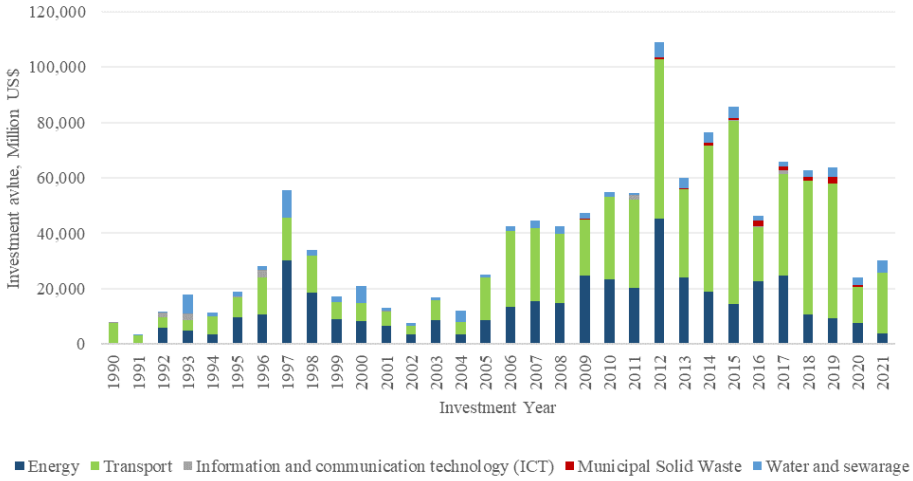

Figure 2: Investment Values of PPP Projects (Build-Lease-Transfer, Build-Rehabilitate-Operate-Transfer, Rehabilitate-Operate-Transfer, and Build-Operate-Transfer) by Sector, in Low and Mid-Income Countries, 1990-2021 (data from The World Bank, 2024).

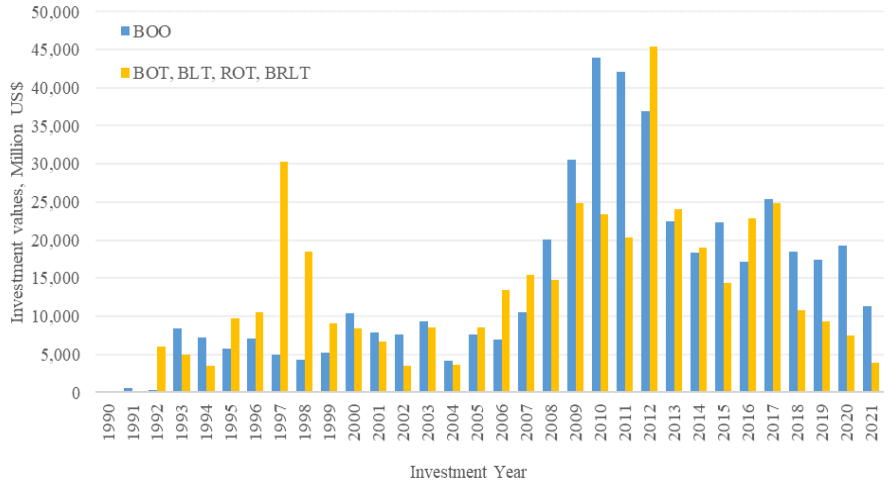

Figure 3: Investment Values of BOO Projects in Energy Sector compared to PPP Projects (Build-Lease-Transfer, Build-Rehabilitate-Operate-Transfer, Rehabilitate-Operate-Transfer, and Build-Operate-Transfer) in Energy Sector, in Low- and Mid-Income Countries, 1990-2021 (data from The World Bank, 2024).

Indeed, data extracted from the World Bank PPI database shows that, over the period from 1990 to 2021, nearly 90% of investments in PPP projects (Build-Lease-Transfer, Build-Rehabilitate-Operate-Transfer, Rehabilitate-

Operate-Transfer, and Build-Operate-Transfer) in low and middle-income countries were predominantly in the transport and energy sectors. Over those years, in average, investment in energy sector represents 36% of all PPP investments. As a note, in this dataset, transport sector consists of airport, road, port, and railway, while energy sector consists of electricity generation, transmission, distribution, natural gas transmission and distribution. The third largest sector is water and sewerage sector, but the average share, by far, only represents 9% of total investment (Figure 2). Authors do not include the numbers of PPP investments in year 2022-2023 because of the inadequacy of accurate categorization, as mentioned in section 2.1 above.

An interesting aspect of energy projects is that many were executed using the Build-Operate-Own (BOO) model, which is classified as PPP by several institutions, including the Indonesian government (see section 1.1). Figure 3 illustrates that the BOO model is widely used in energy projects, with total investment values slightly higher (6% larger) than all other PPP models combined over the years. In fact, more than 93% of BOO projects in The World Bank's database from 1990-2021 are in the energy sector. More importantly, the bulk of those projects (75%) are in electricity generation.

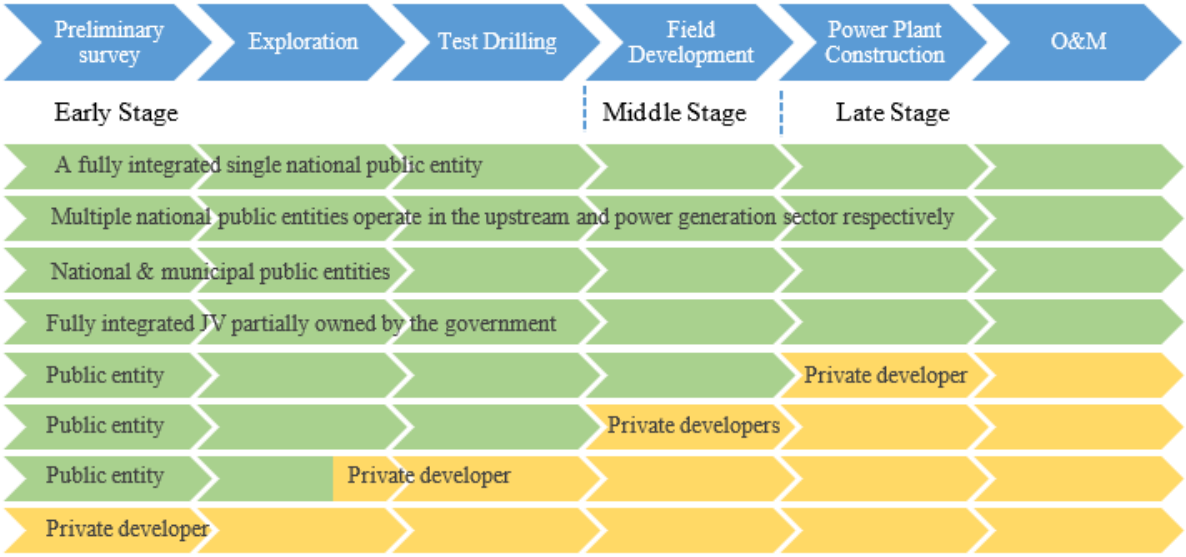

Figure 4: Models of Geothermal Power Development in International Practice (based on ESMAP, 2012)

3. PPP IN GEOTHERMAL KENYA, TÜRKIYE, AND THE US

Geothermal energy is the energy contained as heat in the earth's interior. For decades, natural steam and hot water from geothermal sources have been used to generate electricity, as well as for space heating and industrial processes (Barbier, 2002). The discussions forward exclusively refer to geothermal for power generation, unless otherwise specified.

By the end of 2023, the global geothermal capacity has reached 16,355 MW. The top 10 geothermal countries are the **United State**s (3,900 MW), **Indonesia** (2,418 MW), **Philippines** (1,952 MW), **Türkiye** (1,691 MW), **New Zealand** (1,042 MW), **Kenya** (985 MW), **Mexico** (976 MW), Italy (916 MW), **Iceland** (754 MW), and **Japan** (576 MW). Those countries represent 93% of total installed capacity globally. Note that different calculation methods can affect the total reported capacity, resulting in variations in the numbers presented by different countries and organizations (Cariaga, 2024).

Although geothermal is unique amongst other renewable energy sources as it provides baseload power, adopting geothermal energy has lagged significantly behind solar and wind. While many of the risks involved in geothermal projects are similar to other power or electricity generation projects, including: completion or delay risk, off-take risk, market demand or price risk, as well as operational and regulatory risks, they also involve additional complexities. Those are mainly attributable to (i) uncertainties over resource availability in poorly-explored reservoirs and (ii) the concentration of full-lifetime costs into early-stage capital expenditure (capex). The early stage of geothermal projects is subject to a high degree of unpredictability, with the risk involved decreasing progressively as investments advance (Nur et al., 2023; Younger, 2015).

The initial phases of greenfield geothermal project development (surface-based exploration, discovery, and exploration drilling to confirm the availability and viability of the resource) carry the highest risks and require financial investments. Private parties are often unwilling to invest at this stage due to the potential for

inadequate/unviable resource findings, resulting in substantial sunk costs that cannot be recovered. Test drilling alone can account for up to 15% of the overall capital cost. Therefore, one of the main issues for countries to develop geothermal resources is similar: the ability of the private sector to take on the high risks associated with the exploration and development of geothermal resources. Indeed, these early phases typically depend on public sector investment, while private investors tend to enter the project at more mature phases (Nyokabi et al, 2023; Oliver & Stadelmann, 2015).

In the next sections we will go through the overview geothermal development in select top geothermal countries, the financing mechanism to develop geothermal in each country, including PPP, as well as the electricity market which form the downstream segment of geothermal power industry.

3.1 Geothermal in Kenya

3.1.1 Overview

Kenya, an East African nation, is particularly notable for its renewable energy development. In 2021, around 90% of its total electricity generation are from renewable sources. Further, geothermal constitutes the largest share of the total renewable electricity at 45%, and the rests come from hydro (33%), wind (18%), and a little bit from solar and biofuel (IEA, 2024a).

Kenya can be considered one of the most advanced African electricity markets in terms of policy and regulatory effectiveness. Since the 1990s, the governance of its power sector has continuously evolved to reflect market fundamentals, ensure reliable electricity for its growing economy as well as to attract new investments, improve competition, and progressively open the electricity market. In 1997, the government has unbundled the electricity subsectors to enhance efficiency, with KenGen (Kenya Electricity Generating Company) mandated to generate power and KPLC (Kenya Power and Lighting Company) mandated to transmit and distribute power. Since then, geothermal power developed by the public sector, through KenGen, has increased from 45 MWe in 1997 to 706 MWe in 2019 (IRENA, 2020). Further, the 2019 Energy Act liberalized the electricity supply industry, opening private sector participation in generation, transmission, distribution, and off-grid. Another decisive step in attracting private sector investments has been the 2021 Public-Private Partnership Bill, which established a framework for public-private cooperation in infrastructure and services (UNECA, 2022). Electricity pricing is determined by the Energy and Petroleum Regulatory Authority (EPRA), which sets tariffs for residential and commercial consumers and determines the prices for electricity generated. Electricity prices are set with the aim of attaining sufficient revenue to meet generation, transmission, and distribution requirements, reflective of the cost of power generation, which forms the base, pass-through charges, system losses, taxes, and levies (KIPPRA, 2023)

Geothermal development in Kenya started in the Olkaria field in the 80s with 45 MW capacity and only restarted again in the same field in the year 2000 to total 58 W capacity (Omenda et al., 2023). At the end of 2023, Kenya has an installed geothermal capacity of 985 MW, an impressive increase of 24-fold over 24 years. There are three geothermal fields in operation in Kenya by the beginning of 2024: **Olkaria field** (where 99% of the geothermal electricity is generated), **Eburru field**, and **Menengai field**. The government is targeting installed generation of 5,000 MW by 2030, with additional capacity from Olkaria and Eburru field (Gutiérrez-Negrín, 2024)

3.1.2 Financing geothermal, including PPP, in Kenya

Financing of geothermal projects in Kenya has relied on private, public and grant financing. Public finance was used for most of the early stages of geothermal exploration in Kenya through government-owned companies: KenGen (Kenya Electricity Generating Company) and GDC (Geothermal Development Company). GDC was established to accelerate geothermal development by derisking geothermal projects through the undertaking the early stage of geothermal development. It channels funding from exchequer and concessionary finance guaranteed by the government (Kiptanui & Kipyego, 2021; Omenda et al, 2023). The cumulative government financial support for the two institutions was more than USD 5 billion between 2003 and 2016. Most of the financial support to GDC was for resource evaluation, exploration, appraisal and production drilling while concessionary loans lent to KenGen were for power plant developments (IRENA, 2020).

All the successful projects so far in Kenya are those that benefitted from public financing at some stage of their development:

- Public finance was used in all the successful projects starting with the development of **Olkaria's 45 MWe, Olkaria II, Olkaria IV, Olkaria V and Olkaria I Units 4, 5, 6** projects developed by KenGen through concessionary finance. Whereas **Olkaria III** project is being undertaken by private investor, the initial stages from surface exploration to appraisal drilling was undertaken by KenGen through public finance before the field was licensed to Orpower4 Inc. by the Government of Kenya through PPP arrangement. Subsequent projects that include production drilling, steam field and power plant development were financed by the IPP (Independent Power Producer) through equity and loans.

- In **Menengai field**, GDC undertook exploration, appraisal and production drilling, steam field development and has then entered into a steam sales agreement with three IPPs for the development of 105 MWe. GDC will be steam supplier while the IPPs will use private finance to setup the power plants and enter into PPAs with off-taker.

The Government of Kenya also recently licensed IPPs to explore and develop geothermal resources for power generation using their own financial resources. Only Akiira and Barrier geothermal prospects are the only ones so far funded by private investors for exploration drilling and detailed surface studies, respectively (Omenda et al., 2023).

According to the Kenya Public Partnership Act No. 14/2021, the PPP arrangements recognized several models including the most common schemes such as BOOT (Build-Own-Operate-Transfer), BOO (Build-Own-Operate), BOT (Build-Own-Transfer), and BLT (Build-Lease-Transfer) (PPP Directorate, 2021). Table 3 shows the list of PPP models of several geothermal projects in Kenya.

Table 3: PPP Models of Several Geothermal Projects in Kenya (Kiptanui & Kipyego, 2021; Nyokabi, 2020; Richter, 2020).

No	Project	Contracting Authority	PPP Model
1	155 MWe Olkaria III	Gov. Kenya	BOO
2	35 MWe Sosian Menengai Geothermal Power Plant Project	GDC	BOO
3	35 MWe QPEA GT Menengai Geothermal Power Plant Project	GDC	BOO
4	35 MWe OrPower 22 Menengai Geothermal Power Plant Project	GDC	BOO
5	140 MWe Olkaria VI	KenGen	BOOT

3.2 Geothermal in Türkiye

3.2.1 Overview

Türkiye has garnered attention for its impressive geothermal power capacity's growth, which has increased tremendously from just 20 MW in 2005 to more than 1.6 GW by the end of 2023 (Gutiérrez-Negrín, 2024; Cariaga, 2024). Besides its gigawatt geothermal capacity for electricity generation, Türkiye is also the world's second-largest user of geothermal heating, surpassed only by China (Mertoğlu et al., 2020).

Türkiye has liberalized the electricity sector to a good extent. Both public and private companies, as well as organized industrial zones, can generate electricity with a license from the Energy Market Regulation Authority (EMRA). Transmission remains a state monopoly through Turkish Electricity Transmission Company (TEİAŞ). In 2013, a new type of market was introduced under the Electricity Market Law, leading to the establishment of EPİAŞ. This entity, jointly owned by TEİAŞ, Borsa Istanbul, and private companies, responsible for the operations of energy market and is tasked with operating the day-ahead market, the intraday market, and the newly created YEK-G green certificate market. In the downstream side, electricity distribution and supply are legally unbundled, operated, and carried out by both private and public companies (Somay et al, 2021; PwC, 2023).

3.2.2 Financing geothermal, including PPP, in Türkiye

Although geothermal research and investigations in Türkiye have been ongoing since the 1960s, and in 1984 Europe's second largest geothermal plant (after Italy) was constructed at Denizli-Kizildere, the country's geothermal power generation activities progressed very slowly thereafter (Tut Haklidir, 2015). According to study by Korucan et al. (2024), the critical milestones that accelerated geothermal developments in Türkiye were (1) the adoption of the Law on Geothermal Resources and Natural Mineral Waters in 2007 which set the rules for the exploration and exploitation of geothermal resources, and (2) the amendment in 2010 to Renewable Energy Law offering a feed-in tariff mechanism (*YEKDEM*) that was 105 US$/MWh and for ten years from the commissioning date. Additional incentives were also provided to the plants for their locally produced equipment, up to 27 US$/MWh for 5-year period.

Aside from the feed-in tariff, there is a Risk Sharing Mechanism (RSM) funded by the World Bank, established in 2016. The RSM program assesses the location of the planned project site, providing grants that cover either 40% or 60% of the well's cost, depending on the site's rating (Saltuk et al., 2023). Given that geothermal development in Türkiye relies heavily on the private sector, the RSM supports investors during the riskiest development stages. This is crucial as private license holders must bear full exploration risks in areas with minimal or no government backing. Historically, geothermal development in Türkiye was driven by the General Directorate of Mineral Research and Exploration (MTA). MTA has started geothermal exploration since 1962, discovered over 190 geothermal fields, of which around 20 were deemed suitable for electricity production.

However, its capacity for extensive geothermal exploration drilling has diminished, significantly slowing exploration activities and leaving potential regions remain largely unexplored. RSM reduced private investors' exposures to significant capital expenditures and exploration risks in the early development phases (The World Bank, 2016).

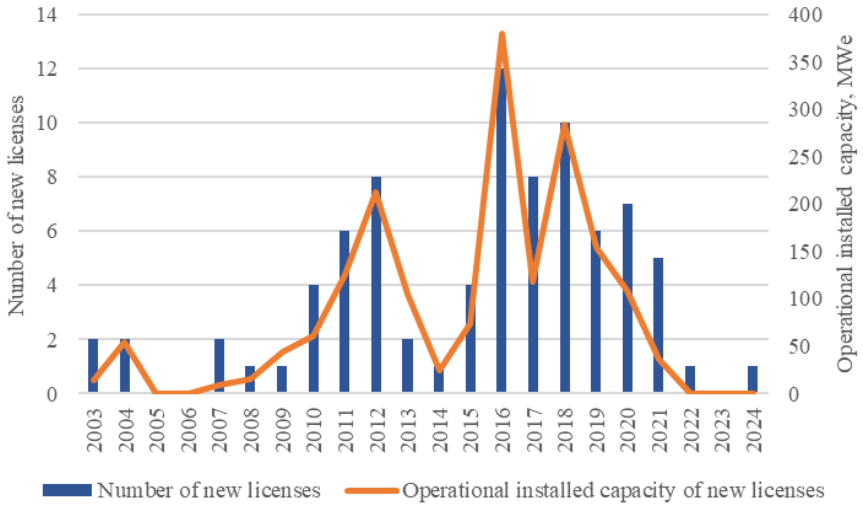

Figure 5: Number of new licenses and their installed capacity in Türkiye, 2003-2024 (based on data by Korucan et al., 2024).

With those mechanisms, the geothermal market became very attractive for investors, even those from non-energy sectors such as construction, textile, and real-estate. However, after 2021, as can be seen in Figure 5. Number of new licenses and their installed capacity in Türkiye, 2003-2024 (based on data by Korucan et al., 2024)the geothermal growth has stalled. Among many issues observed, the change in the YEKDEM mechanism in 2021, which switched incentives from USD to Turkish Lira, was a significant obstacle to new investments. Due to the depreciation of the domestic currency against USD, the incentives are not any more attractive and discouraging investment. On the other hand, the costs related to the feed-in tariff system are reflected in the invoices that people regularly pay. Therefore, the devaluating Turkish Lira was a part of the main reasons for the clash of interests among the renewable energy investors, the state, the people, and other relevant actors (Can Sever, 2021; Korucan et al., 2024). To address these issues, YEKDEM was recently updated in May 2023, and the results will be seen in the succeeding years. The new regulation retains the Turkish Lira for the application price in the support scheme but also introduces monthly US$-indexed adjustment. The system also includes an escalation process by adopting the floor and ceiling price principles in payments (Cariaga, 2023).

PPP in geothermal is not widely discussed in Türkiye. One notable PPP case is Gümüşköy Geothermal Project, developed a Build-Own-Transfer scheme. The private partner, BM Holding, undertook early-stage exploration and invested up to US$ 12 M in exploration and development, when finally debt financing, 70% of the total cost, was secured. The Government of Turkey's provision of a ten-year feed-in tariff (10.5 USD¢/kWh) ensured the project was financially viable (Oliver & Stadelmann, 2015).

According to the World Bank PPFI database (2024), there are only five PPP geothermal projects (Build-Lease-Transfer, Build-Rehabilitate-Operate-Transfer, Rehabilitate-Operate-Transfer, and Build-Operate-Transfer) listed in Türkiye from 1990-2023 and all are brownfield projects: Zorlu Kizildere projects. There is only one is greenfield project, Efeler Geothermal Project (170 MW, year 2015) which was executed in BOO scheme.

3.3 Geothermal in the United States of America

3.3.1 Overview

The United States (US) remains the leader in installed geothermal capacity for power generation with nearly 4 GW of electricity-generating capacity installed, representing around 24% of the world's total capacity. More than 90% of the U.S. geothermal capacity is in the states of California and Nevada. Beside geothermal for electricity, the US also has 20.7 GW_{th} installed geothermal capacity for direct use (IEA Geothermal, 2024). The capacity growth in the past decade is only approximately 10%, as the addition of new plants has been offset by the retirement or decommissioning of others. The GeoVision study, initiated by US Department of Energy, sees that with business as usual scenario and using current technology, geothermal capacity in the US can grow to 6 GW in 2050, but with regulatory reform this can reach 13 GW. The GeoVision TI scenario, which models the most optimistic assumptions and cost reductions, indicates significant potential for geothermal deployment, especially

for Enhanced Geothermal Systems (EGS) resources. The scenario projects more than 60 GW of geothermal power generation after 2030, with a substantial portion coming from deep-EGS resources (US Department of Energy, 2019).

Electric utilities in the United States operate under a variety of market structures, depending upon the states in which they operate. Some states adopt deregulation/restructuring, allowing market competition for retail energy supply to electricity customers. Utilities in deregulated markets are prohibited from generation and transmission ownership and are only responsible for distribution, operations, maintenance from the point of grid interconnection to the meter, and billing ratepayers. On the other hand, regulated markets feature vertically integrated utilities that own or control the total flow of electricity from generation to meter (US Environmental Protection Agency, 2024). Around 30% of US states are deregulated, including some of the most populous such as California, Texas, New York, and Pennsylvania, but not Florida (American Public Power Association, 2021). In deregulated areas, electricity customers have the option of selecting an electric supplier rather than being required to purchase electricity from their local electric utility. This introduces competition for retail electricity prices. Some states also support geothermal development by enforcing Renewable Portfolio Standard, by requiring a certain amount of electricity sold by utilities to come from renewable energy sources (NREL, 2021).

Geothermal operators typically sell electricity through power purchase agreements (PPA) which provide long-term financial stability, but also to the wholesale markets which include day-ahead and real-time markets.

Table 4: Public Geothermal PPA Pricing (NREL 2024).

Project	State	Size (MW)	Pricing (US$/MWh)	Term (years)
Hell's Kitchen	California	40	74.00	25
Whitegrass	Nevada	3	67.50	25
Star Peak	Nevada	125	70.25	25
Casa Diablo	California	16	68.00	20
Puna	Hawaii	46	70.00	30

3.3.2 Financing geothermal in the US

In the US, geothermal projects are predominantly developed through private investments. Nevertheless, there are several mechanism to support geothermal developments over the year, with the followings, among others, currently in place (NREL, 2021):

- **Tax-Based Incentives:** Investment Tax Credit (ITC) offers up to 30% of qualifying capital cost in tax credits and Production Tax Credit (PTC) offers tax credit proportional to power plant's electricity generation (adjusted annually for inflation, PTC was 2.5 cents per kWh in May 2020).
- **Cash Grant (1603 Grant):** in 2009, the government allowed geothermal developer to claim 30% cash grant in lieu of the PTC. However, this grant closed for application in 2011.
- **Depreciation Acceleration & Bonus Depreciation:** the depreciation acceleration scheme allows geothermal projects for a 5-year depreciation schedule, therefore the operators can use the total depreciation value of the asset for tax deduction sooner. The bonus depreciation allows geothermal companies to deduct between 50-100% of their qualifying assets in the first year of the operation.
- **Federal Funding and Grants:** Through Energy Act 2020, DOE is authorizes annual budget authorized at $170 million for research and development activities, including advanced hydrothermal resource tools, demonstration projects, oil and gas, technology transfer, and co-production of geothermal energy and minerals.
- DOE also initiated **User-Coupled Confirmation Drilling Program (UCDP)** designed to financially assist geothermal power developers in the initial stages of confirming hydrothermal reservoirs. UCDP takes 20% of the cost if the project was successful in the confirmation of geothermal resources, and 90% from UCDP if not, with limited fund of US$ 3 M per application.
- **State level incentives:** vary widely among states with the following examples: in Nevada, owners of geothermal power systems of at least 10-MW capacity are eligible for a 55% property tax abatement for 20 years. Alaska offers Renewable Energy Fund Grant, which includes geothermal, values up to US$ 2 M per project.

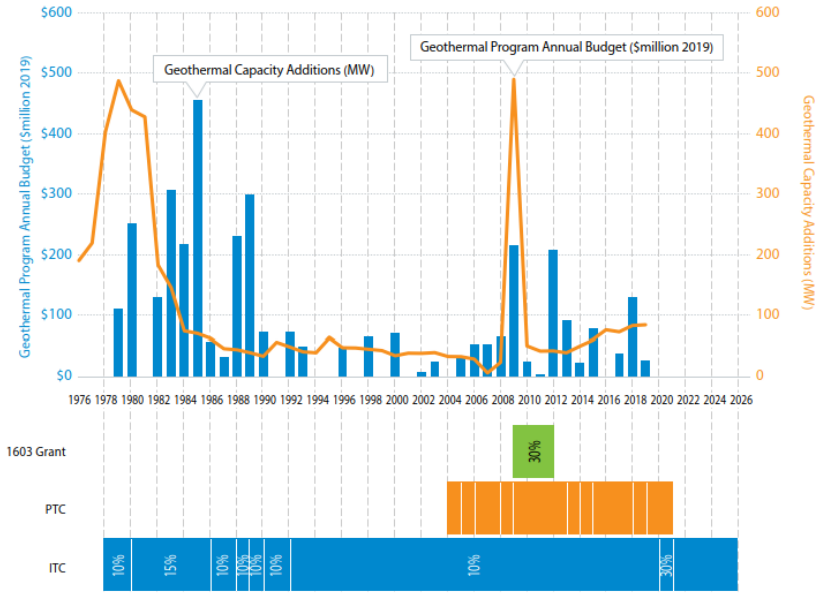

Figure 6:Timeline showing annual data for federal fundings for geothermal program (1603 Grant, PTC, ITC) and geothermal capacity addition (NREL, 2021).

4. GEOTHERMAL IN INDONESIA

4.1 Overview

Indonesia holds approximately 40% of global geothermal potential or 23.7 GW, with the largest potentials lie in the islands of Java and Sumatra (Indonesia Ministry of Energy and Mineral Resources, 2024). Nevertheless, in 2021, geothermal energy only represents 5.2 % of Indonesia's electricity mix (IEA, 2024b). By the end of 2023, the total geothermal installed capacity in the country is 2.4 GW or only around 10% of the total potential. The Government of Indonesia initially aimed to achieve a geothermal installed capacity of 7.2 GW by 2025. However, due to slow progress, this target was revised to 2030 (Hakim, 2023).

4.2 Financing geothermal in Indonesia

Currently, there are more than 8 geothermal operators in Indonesia, three of them are state-owned: Pertamina Geothermal Energy (PGE), Perusahaan Listrik Negara (PLN; the state electricity company), and Geo Dipa Energi. Operators are responsible to undertake and finance the total project, i.e. starting from the very early project stage (initial survey and/or exploration), development, until power plant construction, to operation and maintenance.

To mitigate the risks associated with early project development, the government is undertaking government exploration drilling through MEMR. As of May 2024, the Nage field in East Nusa Tenggara is the only site successfully explored under the government drilling scheme and ready for tender. Additionally, since 2019, the Geothermal Resource Risk Mitigation (GREM) program offers loans with a provision for 50% forgiveness if the exploration drilling results deem the resource uneconomic. The total commitment of GREM funding is USD 651.25 million which comes from a combination of multilateral funds (International Bank for Reconstruction and Development, Green Climate Fund, Clean Technology Fund) and Geothermal Sector Infrastructure Development (*Pembiayaan Infrastruktur Sektor Panas Bumi*, PISP) funds. However, by early 2024, no geothermal operator has yet utilized the GREM fund (Amir et al., 2024; Cariaga, 2024b; Indonesia MEMR, 2020; PT SMI, 2024).

Indonesia is a single-buyer electricity market, where the state, through the National Electricity Company (Perusahaan Listrik Negara, PLN), buys all the electricity generated in the country and resells it to the electricity consumers at regulated price. Indonesian regulations do not allow independent power producer (IPP) to enter into direct power purchase agreement (PPA) with customers. This limits the ability of consumers to procure power produced from renewable sources directly. This is especially true for commercial and industrial consumers who are increasingly setting ambitious clean energy procurement targets (WEF, 2022). The private sectors can only participate in electricity generation as IPP with a PPA in place for performance-based payments from the public sector party over a long-term concession period. This PPA structure is consistent with the general principles of PPPs. (Atmo et al., 2016). Accordingly, IPPs in a single buyer market models have been classified as PPP power generation projects (Voelker et al., 2008). Previously, the PPP model for renewable energy is limited to Build-Own-Operate-Transfer (BOOT) scheme, but with the Indonesia MEMR Regulation 4/2020, Build-Own-Operate

(BOO) model is allowed (Indonesia MEMR, 2020). This revision was based on the difficulties for private developers in terms of land ownership and the ability to obtain finance with the BOOT scheme.

The Government of Indonesia does not set a feed-in tariff for electricity for renewable energy, but sets highest benchmark price for electricity from renewable energy through Presidential Regulation 112/2022. The values depends on the source of energy, plant capacity, and is adjusted for each region (Table 5 and Table 6).

Table 5: Electricity from Geothermal Buying Price based on Presidential Regulation 112/2022.

No	Capacity	Highest Benchmark Price (cent USD/kWh)	
		Year 1-10 (F= location factor)	Year 11-30
1.	Up to 10 MW	9.76 x F	8.30
2.	>10 MW to 50 MW	9.41 x F	8.00
3.	50 MW to 100 MW	8.64 x F	7.35
4.	> 100 MW	7.65 x F	6.50

Table 6: Electricity Price Location Factor (F) based on Presidential Regulation 112/2022.

No	Region	Location Factor (F)
1	Java, Madura, Bali	1.00
	Small islands	1.10
2	Sumatra	1.10
	Riau Archipelago & Mentawai	1.20
	Bangka Belitung	1.10
	Small islands	1.15
3	Kalimantan	1.10
	Small islands	1.15
4	Sulawesi	1.10
	Small islands	1.10
5	Nusa Tenggara	1.20
	Small islands	1.25
6	South Maluku and Maluku	1.25
	Small Islands	1.30
7	Papua, including West Papua	1.50

4.3 PPP Frameworks and Institutional Setup in Indonesia

Indonesia's first official legislation on PPP, Presidential Decree 7/1998, focused on Government Cooperation with Private Business Entities in Infrastructure Development and/or Management, was specifically designed to stimulate private investment in infrastructure development following the monetary crisis (Permatasari et al., 2019). Since then, the government has made several efforts to enhance the attractiveness of PPPs by refining policies and regulatory frameworks, including updating the presidential decree with new regulations in 2015 (**Error! Reference source not found.**) and the most recent operational regulation relating PPP implementation i n Indonesia is stipulated in Indonesia Ministry of National Development Planning Regulation No. 7/2023 concerning Implementation of Government and Business Entity Cooperation in Infrastructure Provisions.

The policies developed over the years include several frameworks to support PPP implementations. Indonesia now has in place several government-support mechanisms (Indonesia Ministry of Finance, 2024; Indonesia Ministry of National Development Planning, 2023):

- **Project development facility (PDF)**: a facility provided by the Ministry of Finance to prepare pre-feasibility study, bidding documents, and assist in the PPP project transaction until it reaches the financial close.
- **Infrastructure guarantee facility**: this facility guarantees the financial obligations of a government contracting agency to compensate the project company in the event of infrastructure risks, as stipulated by the risk allocations agreed upon in the PPP agreement.
- **Viability gap fund (VGF)**: this government support, in the form of a contribution of some of the construction cost, given in cash to a PPP project that is already economically viable but has not had financial feasibility. VGF can be given when there is no other alternative to make the PPP Project financially feasible. It would only be given to infrastructure projects that are unable to deliver large

profits or with too long a turnaround time to attract investors to participate in the tender and does not include costs related to land acquisition and tax incentives

- **Land acquisition process**: One of the major impediments of PPP projects has been the land acquisition process. To address this, the government has issued revision of the land acquisition law under Presidential Regulation No. 148 of 2015. The law limits the land acquisition procedure to approximately 512 days and allows for the revocation of land rights in the public interest. To expedite the process further, the regulations enable private sector entities to acquire land on behalf of a government contracting agency and to seek subsequent reimbursement from the government. For example, in 2015, the Ministry of Finance established a bridging finance mechanism to facilitate the timely reimbursement of land acquisition costs to investors.

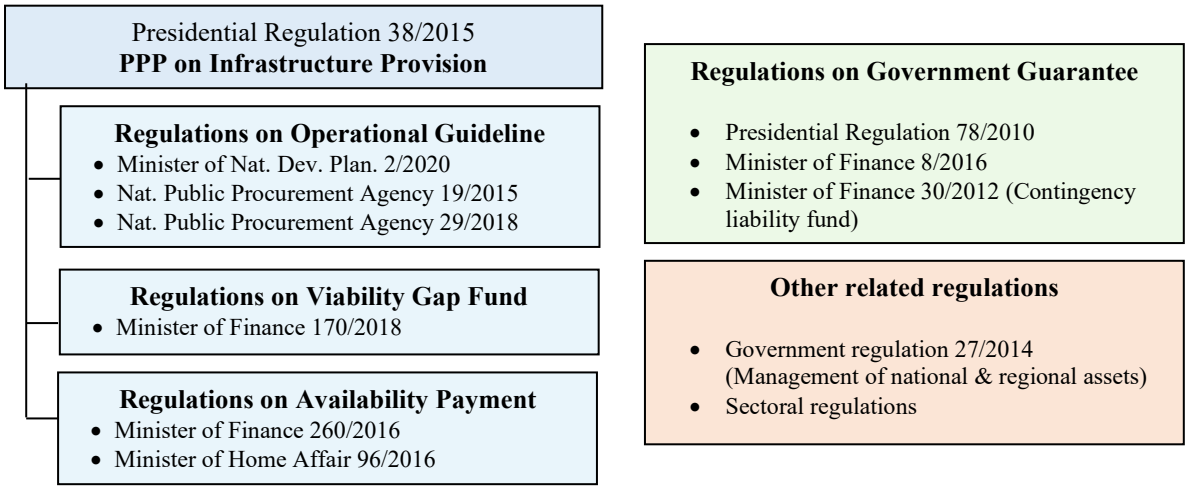

Figure 7: PPP Regulations in Indonesia (Indonesia Ministry of Finance, 2024).

According to Indonesia Ministry of National Development Planning (2023), PPP in Indonesia is driven by the following entities:

- the Ministry of National Development Planning/National Development Planning Agency/ Bappenas,
- the PPP Unit under the ministry of Finance, and
- the PPP Joint Office: formed in 2017 to accelerate the implementation of PPP, serving as central coordination body for those projects. The office consists of several ministries, including (1) Coordinating Ministry of Economic Affairs, (2) Coordinating Ministry of Maritime and Investment Affairs, (3) Ministry of Finance, (4) Ministry of Home Affairs, (5) Ministry of National Development Planning/National Development Planning Agency (Bappenas) (6) Ministry of Investment/Indonesia's Investment Coordinating Board (BKPM), and (7) National Public Procurement Agency (LKPP).

In addition, there are companies that play an active role in facilitating PPP (ADB, 2020):

- **Indonesia Infrastructure Guarantee Fund (IIGF)** or PT Penjaminan Infrastruktur Indonesia: a state-owned enterprise under the Ministry of Finance responsible for providing government guarantees for infrastructure projects developed under PPP,
- **PT Sarana Multi Infrastruktur (PT SMI)**: a special mission vehicle under the Ministry of Finance which is engaged in financing and preparing infrastructure projects,
- **PT Indonesia Infrastructure Finance (PT IFF)**, a private non-banking finance corporation providing infrastructure financing and advisory services, established by the Indonesia Ministry of Finance and other multi-/bi-lateral institutions. Ownership is shared by PT SMI (30%), Asian Development Bank (20%), IFC (20%), KfW (15.1%), and Sumitomo Mitsui Banking Corporation (14.9%).

Since 2009, the Ministry of National Development Planning/National Development Planning Agency/Bappenas annually publishes a document known as the "PPP Book", officially titled "PPP Infrastructure Projects Plan in Indonesia". It contains comprehensive updates on regulatory landscape, operational frameworks, and registered projects. Projects are divided into several groups based on the progress: ready-to-offer projects, projects currently under preparation, tendered projects, and a list of "success stories" or projects that are already closed financially.

Interestingly, the only power/electricity generation project listed in PPP Books, from all the years 2016 up to the latest in 2023, is the construction of Central Java Power Plant 2x1000 MW. Obviously, **there is no geothermal project listed in the registered PPP Projects**. It therefore means that geothermal projects currently do not benefit from the PPP supports provided by the government.

For eligible power projects in Indonesia, a different scheme is offered to address the concern on PLN creditworthiness and default risk: they are entitled to apply for Business Viability Guarantee Letter (BVGL) issued by Ministry of Finance (Rakhmadi and Sutiyono, 2015). In geothermal energy projects, Sarulla was the first project that received BVGL and followed by Muara Laboh, later on.

5. DISCUSSION AND RECOMMENDATIONS

The comparative analysis of geothermal public-private partnership (PPP) frameworks and cases from Kenya, Türkiye, and the United States reveals distinct approaches and outcomes in developing geothermal energy projects, providing valuable insights for Indonesia. The international cases in this study represent three countries with varying degrees of public and private involvements in developing geothermal projects:

- **Kenya** cases show projects with significant both public and private involvements, supported with well-institutionalized PPP schemes and frameworks in the country's regulations. Geothermal Development Company (GDC), as government arm, has played a crucial role in mitigating early-stage project risks, which has been instrumental in achieving a 24-fold increase in geothermal capacity over just two decades, nearing 1 GW installed capacity. The Kenyan model benefits from strong public financing at critical early stages, effectively derisking projects for private investors.
- **Türkiye** case highlights the importance of attractive feed-in tariff mechanism (YEKDEM), on top of a risk-sharing mechanism (RSM) to derisk the early riskiest stage of geothermal project. Public participations in the early and riskiest stage of the project through Directorate of Mineral Research and Exploration (MTA) also exist but recently decline and are compensated with RSM. Those combinations have catapulted Türkiye to stands out as one of countries with fastest growing geothermal capacity. However, in 2021, without significantly changing the model of public involvement, a change in feed-in tariff scheme had decreased the attractiveness of incentives and therefore reduced significantly the numbers of project being initiated. Türkiye government hence introduced a 2023 revision of the feed-in tariff mechanism to attract back private investments.
- **The United States** showcases very dominant private sector involvements in geothermal development, supported by various government supports including tax incentives and grants for early-stage exploration. This model underscores the importance of consistent government support throughout all project phases, contributing to steady geothermal development.

The empirical analysis of these international cases identifies several opportunities and recommendations for enhancing the effectiveness of PPPs in Indonesia's geothermal sector:

1. **Enhancing policy framework of risk-sharing mechanisms in the early stages of geothermal projects**
   Currently, the risks in the earliest stages of Indonesia's geothermal projects are borne solely by the operators. The existing derisking schemes, such as Government Drilling and the Geothermal Resource Risk Mechanism (GREM), are still in their infancy and have not yet been utilized by any operator. Indonesia can learn from Kenya, where the Geothermal Development Company (GDC), a dedicated public entity responsible for exploration activities, has been crucial for geothermal growth. Additionally, Indonesia can adopt the approach used in the US, where the government provides grants to share early-stage development risks instead of assigning a public entity for exploration.

2. **Enhancing policy frameworks to attract more investment by providing incentives and supports throughout all phases of geothermal projects**
   Turkey's case demonstrates that an attractive feed-in tariff significantly influences private sector participation in geothermal projects. In the US, the government offers innovative incentives across all project phases, both at federal and state levels. These include grants during the exploration phase, various tax incentives, attractive depreciation schemes, and funding for research and development (R&D). Implementing similar comprehensive support structures in Indonesia could attract more private investment in geothermal projects.

3. **Establishing a clearly-defined PPP frameworks for geothermal activities**
   Building on the recommendations from points (1) and (2), Indonesia can establish a comprehensive PPP framework specifically for geothermal activities. Although Indonesia already has a robust PPP framework, as detailed in Section 3.3, the energy sector, including geothermal, has not been a primary focus. By formally incorporating geothermal projects into the institutional PPP framework, these projects can leverage the various supports and incentives currently available for PPP initiatives in Indonesia, such as the viability gap fund and project preparation fund. This inclusion will ensure that geothermal projects benefit from the same level of support and regulatory clarity as other infrastructure projects.

4. **Deregulation of electricity market**
   In all those countries discussed, electricity market deregulations and liberalizations play important roles in building geothermal growth and renewable energy in general. Electricity market deregulations and liberalizations support geothermal growth by fostering a competitive environment that attracts private investment, which is essential for the capital-intensive nature of geothermal projects. By allowing geothermal operators to sell electricity through Power Purchase Agreements (PPAs) and on wholesale markets, deregulated markets provide long-term financial stability and access to diverse revenue streams, thereby encouraging more geothermal projects. Additionally, these reforms introduce market-based pricing mechanisms, enhancing the viability of geothermal energy compared to other energy sources and driving innovation and cost reductions in the sector. While implementing such deregulation in Indonesia may be challenging due to the current market structure, gradually introducing some level of deregulation over time will ultimately benefit the country's energy sector and its citizens.

6. CONCLUSION

Strategically integrating the best practices of public-private partnerships, customized to Indonesia's unique contexts, can significantly advance its geothermal sector. By drawing on global experiences and developing frameworks tailored to Indonesia's specific conditions, the country can optimize its geothermal potential, thereby enhancing national energy security and achieving sustainable development goals. This comparative analysis provides valuable insights for Indonesia and other emerging economies aiming to develop their geothermal resources through effective public-private partnerships. Implementing these strategies can lead to a more resilient and sustainable energy future for Indonesia and similar nations.

REFERENCES

Abdel Aziz, A.M. (2007) Successful delivery of public–private partnerships for infrastructure development. J. Constr. Eng. Manag. 133 (12), 918–931.

ADB (2020) Public-Private Partnership Monitor Indonesia. ISBN 978-92-9262-109-4 (print); 978-92-9262-110-0 (electronic); 978-92-9262-111-7 (ebook) Publication Stock No. SGP210069-2 . DOI: http://dx.doi.org/10.22617/SGP210069-2

ADB (2021) Public–Private Partnerships in Developing Asian Countries: Practical Suggestions for Future Development Assistance. Asian Development Bank Institute Policy Brief no.2021-5 (September)

Akhtar, M. et al. (2023) Identification of Various Execution Modes and Their Respective Risks for Public–Private Partnership (PPP) Infrastructure Projects. *Buildings* **2023**, *13*, 1889. https://doi.org/10.3390/buildings13081889

Alfen, H.W., et al. (2009) Public-Private Partnership in infrastructure development: Case studies from Asia and Europe, Schriftenreihe der Professur Betriebswirtschaftslehre im Bauwesen, No. 7, Verlag der Bauhaus-Universität, Weimar, https://nbn-resolving.de/urn:nbn:de:gbv:27-20100922-160114-1American Public Power Association (2021) Retail Electric Rates in Deregulated and Regulated States: 2021 UPDATE. Virginia.

Amir, A., et al. (2024) Exploring the Impact of Lender Procurement Guidelines on Geothermal Project Exploration Planning: Indonesia's GREM Perspective. PROCEEDINGS, 49th Workshop on Geothermal Reservoir Engineering Stanford University, Stanford, California, February 12-14, 2024

Atmo, G.U., et al.(2016) Comparative performance of PPPs and traditional procurement projects in Indonesia. International Journal of Public Sector Management Vol. 30 No. 2, 2017. pp. 118-136.Azarian et al, 2022

Barbier.E. (2002) Geothermal energy technology and current status: an overview, Renewable and Sustainable Energy Reviews Volume 6, Issues 1–2, 2002, Pages 3-65

Barral, W., & Haas, A., (2007) Public-Private Partnership (PPP) in Brazil, 41 International Law. 957 (2007). https://scholar.smu.edu/til/vol41/iss3/7

Can Sever, B. (2021) Turkey's Feed-In Tariff System of the Renewable Energy Sources Support Mechanism (YEKDEM), Turkey News Brief and Action Alert, Climate Scorecard, 11 April 2021, accessed July 2024 < https://www.climatescorecard.org/2021/04/turkeys-feed-in-tariff-system-of-the-renewable-energy-sources-support-mechanism-yekdem/>

Cariaga, C. (2023) JESDER Chair shares thoughts on the new YEKDEM scheme in Türkiye, . ThinkGeoEnergy, 17 May 2023, accessed July 2024, <https://www.thinkgeoenergy.com/thinkgeoenergys-top-10-geothermal-countries-2023-power-generation-capacity/>

Cariaga, C. (2024a) ThinkGeoEnergy's Top 10 Geothermal Countries 2023 – Power Generation Capacity. *ThinkGeoEnergy*, 8 January 2024, accessed July 2024 <https://www.thinkgeoenergy.com/thinkgeoenergys-top-10-geothermal-countries-2023-power-generation-capacity/>

Cariaga, C. (2024b) Tender announced for 46-MW Nage geothermal working site in Indonesia. ThinkGeoEnergy, 2 May 2024. Accessed July 2024 < https://www.thinkgeoenergy.com/tender-announced-for-46-mw-nage-geothermal-working-site-in-indonesia/>

Cheng, Z. et al. (2019) Diversification or convergence: An international comparison of PPP policy and management between the UK, India, and China. Engineering, Construction and Architectural Management, Vol. 27 No. 6, pp. 1315-1335. https://doi.org/10.1108/ECAM-06-2019-0290

DPU HCMC PPP Division (2017), "PPP Contracts", Department of Planning and Investment Public-Private Partnership Division, accessed May 2024 < https://ppp.tphcm.gov.vn/en/hinh-thuc-doi-tac-cong-tu.html>

Engel, E., et al. (2020) "When and How to Use Public-Private Partnerships in Infrastructure: Lessons From the International Experience". NBER Working Paper No. 26766, February 2020. JEL No. H11,H42,H83

ESMAP (2012) Geothermal Handbook: Planning and Financing Power Generation. Energy Sector Management Assistance Program. The World Bank, Washington DC.

Estache, A., (2006) PPI Partnerships vs. PPI Divorces in LDCs, Review of Industrial Organization (2006) 29:3–26, DOI 10.1007/s11151-006-9107-7

European Commission (2003) Guidelines for Successful Public-Private Partnerships. Accessed July 2024 <https://www.ebrd.com/what-we-do/sectors/legal-reform/ppp-concessions/international-standards.html>

Fabre, A., and Straub, S. (2023) The Impact of Public-Private Partnerships (PPPs) in Infrastructure, Health and Education. Journal of Economic Literature 2023, 61(2), 1–61, https://doi.org/10.1257/jel.20211607

Global Infrastructure Hub (2017). Global Infrastructure Outlook, accessed February 2024 <https://outlook.gihub.org/>

Grimsey, D., & Lewis, M. K. (2004). Public-Private Partnerships – the worldwide revolution in Infrastructure Provision and Project Finance. UK: Edward Elgar Publishing Limited. Cheltenham

Gutiérrez-Negrín, L.C.A.(2024) Evolution of worldwide geothermal power 2020–2023. Geothermal Energy, 2024, 12:14

Hakim, L.N. (2023) Target Panas Bumi 7,2 GW Sulit Tercapai, ESDM Pertimbangkan Tambah Insentif. Bisnis.com, 19 September 2023, accessed July 2024, <https://ekonomi.bisnis.com/read/20230919/44/1696524/target-panas-bumi-72-gw-sulit-tercapai-esdm-pertimbangkan-tambah-insentif>

Hou et al. (2024) Government subsidy and benefit distribution mechanisms for transportation PPP projects: An evolutionary game perspective, Journal of Environmental Management, Volume 359, 2024, 120981, ISSN 0301-4797, https://doi.org/10.1016/j.jenvman.2024.120981.

IEA (2024a) Kenya, Sources of electricity generation, International Energy Agency, Countries & regions, accessed July 2024 https://www.iea.org/countries/kenya/electricity

IEA (2024b) Indonesia, Sources of electricity generation, International Energy Agency, Countries & regions, accessed July 2024 <https://www.iea.org/countries/indonesia/electricity>

IEA Geothermal (2024) 2022 United States Country Report. U.S. Department of Energy Geothermal Technologies Office, February 2024.

India Department of Economic Affairs (2023). Glossary of Terms. Accessed May 2024, <https://www.pppinindia.gov.in/glossary#:~:text=Build%20Own%20Operate%20(BOO)%3A,such%20as%20tax%2Dexempt%20status>

Indonesia Ministry of Finance, 2024, Public Private Partnership. Accessed June 2024 <https://kpbu.kemenkeu.go.id//>

Indonesia Ministry of National Development Planning (2023) Public Private Partnership Infrastructure Projects Plan Indonesia 2023. National Development Planning Minister Decree Number KEP.67/M.PPN/HK/06/2023.

Indonesia MEMR (2020). Pengembangan Panas Bumi Indonesia. Direktorat Jenderal Energy Baru Terbarukan dan Konservasi Energi, Direktorat Panas Bumi. Juli 2020.

Iossa, E., and Saussier, S. (2017) "Public-private partnerships in Europe for building and managing public infrastructures: An economic perspective", EPPP DP No. 2017-6, September 2017

IRENA (2020), Geothermal Development in Eastern Africa: Recommendations for power and direct use, International Renewable Energy Agency, Abu Dhabi.

KIPPRA (2023), Addressing High Electricity Prices to Improve Kenyan Households' Welfare. Kenya Institute for Public Policy Research and Analysis, 5 July 2023, accessed July 2024 < https://kippra.or.ke/addressing-high-electricity-prices-to-improve-kenyan-households-welfare/>

Kiptanui, S.K., and Kipyego, E. (2021) Estimating the Optimal Levelized Geothermal Steam Tariff for Kenya. Proceedings World Geothermal Congress 2020+1. Reykjavik, Iceland, April - October 2021

Korucan, A., et al. (2024) Opportunities and challenges of geothermal energy in Türkiye. Energy for Sustainable Development 79 (2024) 101417

Liu, J., and Love, P.E.D, (2014). " Public-Private Partnerships: a review of theory and practice of performance measurement". International Journal of Productivity and Performance Management Vol. 63 No. 4, 2014 pp. 499-512

Mertoglu, O., Şimşek, Ş., and Basarir, N. (2020) Geothermal energy use: Projections and country update for Turkey , Proceedings World Geothermal Congress 2020, Reykjavik, Iceland, April 26 - May 2, 2020

Ng, S.T., et al. (2012) Factors influencing the success of PPP at feasibility stage – a tripartite comparison study in Hong Kong, Habitat International, Vol. 36 No. 4, pp. 423-432.

NREL (2021) 2021 U.S. Geothermal Power Production and District Heating Market Report. National Renewable Energy Laboratory, Golden, CO

Nur, S., et al. (2023) Determining optimal incentives for geothermal projects procured within PPP framework under the tariff constraints. Renewable Energy Focus 45 (2023) 21–39

Nyokabi, J. et al. (2022) Reinvigorating Geothermal Project Finance in Kenya through Public-Private Partnership. Proceedings, 9th African Rift Geothermal Conference. Djibouti, 3rd November – 5th November 2022

Oliver, P., and Stadelmann., M.. (2015) Public Finance and Private Exploration in Geothermal: Gümüşköy Case Study, Turkey, A Climate Policy Initiative Series: The Role of Public Finance in Deploying Geothermal, March 2015, Climate Investment Funds

Omenda P, et al. (2023) Country update report for Kenya 2020—2022. In: Proceedings of the world geothermal congress 2023, Beijing, China, 15–17 September 2023.

Osei-Kyei, R., and Chan, A.P.C. (2017) Comparative Study of Governments' Reasons/Motivations for Adopting Public-Private Partnership Policy in Developing and Developed Economies/Countries. International Journal of Strategic Property Management. 2018 Volume 22 Issue 5: 403–414. https://doi.org/10.3846/ijspm.2018.5223

Permatasari, Y., et al. (2020) Institutional Transformation of Public Private Partnership to Ensure Low Transaction Costs: Case Study of Infrastructure Provision at the Ministry of Public Works and Housing of the Republic of Indonesia. Systemic Practice and Action Research (2020) 33:149–165

PPP Directorate (2021) The Public Private Partnership Act no.14 of 2021. Republic of Kenya National Treasury and Planning. https://www.pppunit.go.ke/thepublicprivatepartnershipsact_no-14of2021/

PT SMI (2024) Geothermal Resource Risk Mitigation (GREM). Strategic Cooperation. Accessed July 2024. < https://ptsmi.co.id/strategic-cooperation/grem>

PwC (2023) Overview of the Turkish Electricity Market. September 2023, accessed July 2024. https://www.pwc.com.tr/tr/sektorler/enerji/2024/overview-of-the-turkish-electricity-market-2023.pdf

Rakhmadi, R., and Sutiyono, G. (2015) Using Private Finance to Accelerate Geothermal Deployment: Sarulla Geothermal Power Plant, Indonesia, Climate Policy Initiative, June 2015.

Republic of the Philippines PPP Center (2012) PPP Contractual Arrangements. Accessed May 2024 <https://ppp.gov.ph/wp-content/uploads/2015/01/List-of-PPP-Modality.pdf>

Richter, A. (2020) Five groups shortlisted for 140 MW PPP Olkaria VI project with KenGen, Kenya. 12 May 2020. Accessed July 2024. https://www.thinkgeoenergy.com/five-groups-shortlisted-for-140-mw-ppp-olkaria-vi-project-with-kengen-kenya/

Saltuk, F., et al. (2023) isk Sharing Mechanism (RSM) Program in Türkiye: Methodology and Lessons Learned. Proceedings World Geothermal Congress 2023, Beijing, China, April 17 – 21, 2023

Saussier,S., et al. (2009) Public–Private Agreements, Institutions, and Competition. Review of Industrial Organization (2009) 35:1–18,DOI 10.1007/s11151-009-9226-z

Saussier, S., and de Brux, J. (eds.), (2018) The Economics of Public-Private Partnerships, https://doi.org/10.1007/978-3-319-68050-7_2

Sastoque, et al. (2016) A Proposal for Risk Allocation in Social Infrastructure Projects Applying PPP in Colombia, Procedia Engineering, Volume 145, Pages 1354-1361, 2016, ISSN 1877-7058, https://doi.org/10.1016/j.proeng.2016.04.174

Sharma, R.K., et al. (2021). Investigating critical factors that encourage public-private partnership in infrastructure projects in emerging economies: Evidence from the Republic of India. Journal of Public Affairs, 22(4), e2713. https://doi-org.ezproxy.hec.fr/10.1002/pa.2713

Somay et al. (2021) Electricity Regulation in Turkey: Overview. Thomson Reuters Practical Law. 01 September 2021, accessed July 2024. https://uk.practicallaw.thomsonreuters.com/

Than Nguyen, P., et al. (2020) "Success Factors for Public-Private Partnership Infrastructure Projects in Vietnam". International Journal on Advanced Science Engineering Information Technology. Vol.10 (2020) No. 2

The World Bank (2017) PPP Reference Guide - PPP Basics. Public-Private Partnership Legal Resource Center [https://ppp.worldbank.org/public-private-partnership/library/ppp-reference-guide-ppp-basics] Accessed February 2024

The World Bank (2016) Republic of Turkey Geothermal Development Project. International Bank for Reconstruction and Development Project Appraisal Document. Energy and Extractives Global Practice Turkey Country Management Unit Europe and Central Asia Region, October 13, 2016.

The World Bank (2024) PPI Data. Private Participation in Infrastructure, Infrastructure Finance, PPPs and Guarantees, accessed July 2024 < https://ppi.worldbank.org/en/ppidata>

Trebilcock, M., & Rosenstock, M., (2015) Infrastructure Public–Private Partnerships in the Developing World: Lessons from Recent Experience, The Journal of Development Studies, 51:4, 335-354, DOI: 10.1080/00220388.2014.959935

Tut Haklidir, F. S. (2015). Geothermal energy sources and geothermal power plant technologies in Turkey. In Energy Systems and Management (pp. 115–124). Springer International Publishing. https://doi.org/10.1007/978-3-319-16024-5_11.

UK Trade & Investment (2013) Healthcare UK: Public Private Partnerships. Accessed May 2024 < https://assets.publishing.service.gov.uk/media/ 5a7c7835e5274a559005a152/07_PPP_28.11.13.pdf>

UN (2015) General Assembly, Transforming Our World: the 2030 Agenda for Sustainable Development, Resolution adopted by the General Assembly on 25 September 2015. United Nations.

UNECA (United Nations Economic Commission for Africa) (2022) Regulatory Review of the Electricity Market in Kenya: Towards Crowding-in Private Sector Investment. Addis Ababa:. © UN. ECA, https://hdl.handle.net/10855/49979

United States Environmental Protection Agency (2024). Understanding Electricity Market Frameworks & Policies. June 30,2024. Accessed July 2024. < https://www.epa.gov/greenpower/understanding-electricity-market-frameworks-policies>

US Department of Energy (2019) GeoVision: Harnessing the Heat Beneath Our Feet. http://www.osti.gov/scitech

Välilä, T., (2020) An overview of economic theory and evidence of public-private partnerships in the procurement of (transport) infrastructure. Utilities Policy 62 (2020) 100995

Vining, A. et al. (2004). PUBLIC-PRIVATE PARTNERSHIPS IN THE U.S. AND CANADA: CASE STUDIES AND LESSONS. International Public Procurement Conference Proceedings, Volume3. 2004.

Voelker, C., et al. (2008) Political risk perception in Indonesian power projects. Journal of Financial Management of Property and Construction. VOL. 13 NO. 1 2008, pp. 18-34

Wang, F., et al. (2022) The Effects of Investment in Major Construction Projects on Regional Economic Growth Quality: A Difference-In-Differences Analysis Based on PPP Policy. Sustainability, 2022, 14, 6796. https://doi.org/10.3390/su14116796

WEF (World Economic Forum) (2022) Policy Opportunities to Advance Clean Energy Investment in Indonesia. Policy Paper, November 2022. Geneva, Switzerland.

Williams, T.P. (2003) Moving to Public-Private Partnerships: Learning from Experience around the World. IBM Endowment for The Business of Governmen7. Arlington, VA.

World Bank. Beyond the Gap: How Countries Can Afford the Infrastructure They Need while Protecting the Planet. Sustainable Infrastructure Series. Washington, DC: World Bank. doi:10.1596/978-1-4648-1363-4.

Yaya, R., (2014) Public-Private Partnerships: an International Development vis a vis Indonesia Experience. Journal of Government and Politics 5(2):209. August 2014. http://dx.doi.org/10.18196/jgp.2014.0020

Yescombe, E.R. (2007) Public Private Partnerships: Principles of Policy and Finance. Elsevier, Oxford, UK.

Younger, P.L. (2015) Geothermal Energy: Delivering on the Global Potential, Energies 2015, 8(10), 11737-11754; https://doi.org/10.3390/en81011737

Yurdakul, H., et al. (2022), Macroeconomic drivers of Public Private Partnership (PPP) projects in low income and developing countries: A panel data analysis, Borsa Istanbul Review 22-1 (2022) 37e46

Zwalf, S., (2022) From turnpikes to toll-roads: a short history of government policy for privately financed public infrastructure in Australia, Journal of Economic Policy Reform, 25:2, 103-120, DOI: 10.1080/17487870.2020.1716754

Safeguard Requirements for Indonesia Geothermal Exploration Financing and De-Risking Facility

Eviyanti, Desak Nyoman Inten Apriani, Afandi, Dorman Purba, Maya Ryandita, Ferdino R Fadhillah, and Astri Indra Mustika

PT Sarana Multi Infrastruktur (Persero), Sahid Sudirman Center 49th floor, Jakarta, Indonesia

eviyanti.pmugeothermal@ptsmi.co.id

Keywords: GREM, GEUDP, De-Risking, World Bank, Geothermal, Exploration, Safeguard, ESMF, environmental, social

ABSTRACT

Geothermal exploration projects face significant challenges with high capital and high-risk conditions. The challenges also entail substantial environmental and social risks, necessitating rigorous safeguard measures to ensure sustainable development. During the exploration stage, the developer faces a limited financing option since the commercial financers hesitate to tackle exploration risk. The Government of Indonesia, the World Bank, and PT Sarana Multi Infrastruktur (Persero) ("SMI") launched an exploration financing and de-risking scheme called the Geothermal Resource Risk Mitigation (GREM) program.

This paper provides an in-depth analysis of safeguard requirements from the perspective of lenders, who play a critical role in financing these projects. Initially, the introduction delineates the importance of safeguard measures, setting forth the research objectives and offering a synopsis of international standards and guidelines that shape lender policies.

From the lender's perspective, the author examines the reasons for prioritizing safeguard requirements, their role in ensuring compliance, and the challenges and benefits of incorporating these requirements into financing decisions. Real-world insights are provided through case studies, including one from a geothermal field that applied for funding from a financial institution.

Evaluating the effectiveness of safeguard requirements is essential for continual improvement. The paper discusses monitoring and evaluation mechanisms and stresses the importance of assessing the impact of safeguard requirements on project outcomes. It also identifies areas for improvement in safeguard implementation.

In conclusion, this paper provides valuable insights into safeguard requirements in geothermal exploration projects from lenders' perspectives, enriched by lessons from a specific geothermal field's application to financial institutions. By understanding the key aspects and challenges of safeguard implementation, project stakeholders, including lenders, developers, and policymakers, can better navigate and enhance the sustainability of geothermal exploration projects.

1. INTRODUCTION

The geothermal development in Indonesia started from the colonized era with commercial utilization remarked through Kamojang Geothermal Power Plant (30MW) in 1983 (Darma, Imani, Shidqi, Riyanto, & Daud, 2021; Mansoer & Idral, 2015). Nowadays, Indonesia is top two geothermal countries in the world with a 2.417 MW installed capacity from approximately 23 GW total potential. It means that Indonesia only utilized around 10% of its total potential with an average additional capacity of around 60 MW per annum (ThinkGeo, 2024). There are 46 geothermal power plants developed by State-Owned Enterprises (SOE) and Independent Power Producer (IPP) in 17 geothermal working areas (Pambudi, 2023).

The government of Indonesia has a plan to utilize geothermal as a baseload to replace coal power plants and set the target of utilization to reach 5.799 MW in 2030 (Fadhillah, Tjendarsa, Damayanti, Purba, and Adityatama, 2024). The government target emphasizes the significant increase in the average of additional installed capacity toward 488 MW per annum from 2024 to 2030. This bold target needs to be achieved by catalyzing geothermal investment through better project attractiveness, including from a project economic perspective. Figure 1 shows the historical and target for geothermal power utilization based on PLN (2021), EBTKE (2023), and ThinkGeo (2024).

1.1 Challenges of Geothermal Project

Several challenges in the geothermal project derive from the lag of current utilization and the challenging target in 2030. Geothermal as reliable and sustainable energy to become baseload energy is well known as a high-risk project with long phases to reach the commercial operation date (COD). However, this reliability has several

challenges that might be faced and need to be solved by the company and government. Setiawan (2014) proposed the limiting factor of geothermal development that can be divided into three categories as explained in Table 1 below:

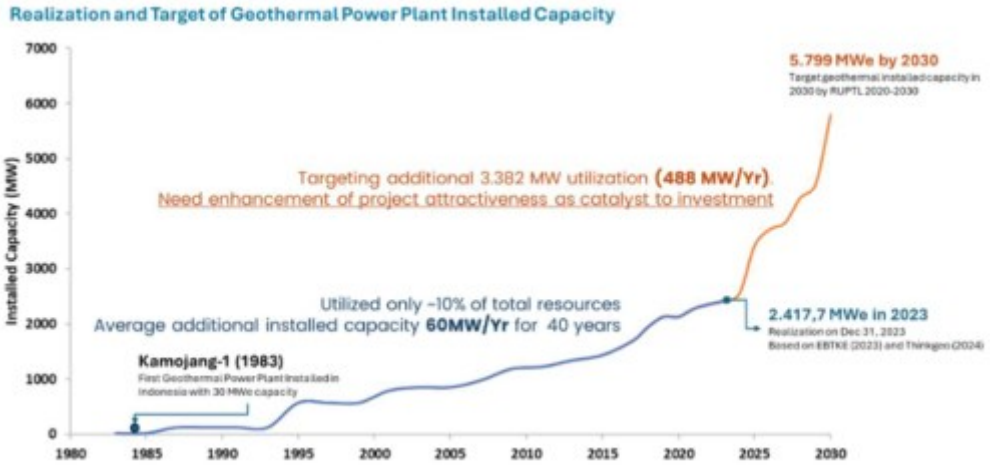

Figure 1: Indonesia geothermal power plant installed capacity and target for 2023 based on EBTKE (2023) and ThinkGeo (2024).

Table 1: Typical geothermal challenges in Indonesia.

Categories	Challenges	Remarks
Upstream challenges	High resource risk and complex uncertainty	Limiting factors in the upstream development stage cover the activity of geothermal exploration. The first limiting factor in the upstream stage is the lack of available reserve data for the auction process, resulting in unattractive investment. Many investors are concerned about the data and report quality, which does not briefly explain geothermal resource's extraction and development strategy and only focuses on the geoscience aspect without social and environmental considerations (Asian Development Bank, 2015 in Fan & Nam, 2018). It commonly needs long phases to develop geothermal energy, from 5–10 years until the commercial operation to mitigate the risk.
	High upfront/initial construction cost	The second limiting factor on the upstream side is high investment in the initial period, where the exploration phase is estimated to cost about 12 to 28 million USD, with an average of 7.6 million USD per exploration well (Purba et al., 2021b; Purwanto, 2019)
	Overlap with conservation/protected forests	The third problem is the location of geothermal working areas that overlap with production forests, conservation areas, and protected forests. Meijaard et al. (2019) found that there is a total of 13,025 MW of electricity potential from geothermal prospects in Indonesia, which are located within the protected forest (5,736 MW), production forest (2,416 MW), and conservation areas (4,873 MW)
	High relief terrain	Geothermal systems in Indonesia are mainly found along high-relief volcanic arcs and can be detected by surface manifestations that release water or steam at boiling temperatures at ground level (Hochstein & Sudarman, 2015). Due to the unique characteristics of volcanic locations where heat, rocks, and liquids interact dynamically, organically, and actively, Utami (2010) describes the various obstacles encountered when executing civil works in geothermal zones in Indonesia.
	Land acquisition issues	In general, the local community uses the flat area in Indonesia's volcanic area for agriculture or housing. Providing the acquisition cost for a family's livelihood in rural Indonesia is often tricky, especially if the land is their only asset. One mitigation strategy is allowing enough time for the landowner to move from one source of livelihood to another. Negotiation is frequently tough if the property buyer (geothermal developer or local government) demands a strict timeline for the landowner to leave the land they have worked on for years (Purba, 2021b).

Categories	Challenges	Remarks
	Poor existing	infrastructure condition The challenge of equipment inter-island mobilization in Indonesia is heavily influenced by infrastructure circumstances such as road access, transportation modes, and high-voltage electrical networks that would be utilized to drain electricity generated by PLTP. Furthermore, Indonesia's geothermal prospects are often located in high terrain forest areas that are distant from primary road access, both provincial and district highways. It makes mobilization of drilling equipment problematic. The existing infrastructure generally needs to be upgraded before equipment mobilization (Purba, 2021b).
Downstream challenges	Offtake market	The main factor limiting the downstream side of the geothermal development stage in Indonesia is the geothermal electricity market. According to Widiatmoro and Nusiaputra (2020), geothermal energy is considered environmentally friendly and has good security of supply and accessibility, but it is less affordable compared to other forms of energy. Moreover, in several area in Indonesia was already oversupplied and has limited grid system to absorb the generated electricity from geothermal energy.
	Single buyer	The first problem downstream is that there is only a single buyer for geothermal electricity in Indonesia: PT PLN (Persero). Lesmana et al. (2020) and Ministry of Energy and Mineral Resources Decree No. 37/2018 PT PLN (Persero) acted as the single buyer of electricity generated from geothermal power plants. Furthermore, the tariff of geothermal electricity is also regulated by the government by Ministry Decree No. 169.K/HK.02/MEM.M/2021, where the price depends on the location of geothermal prospects and is reviewed again by a price matrix based on exploration and development results (Widiatmoro & Nusiaputra, 2020). This regulation is resulting the weak bargaining process between the developer companies and PT PLN (Persero) in Indonesia's geothermal electricity business. Another problem on the downstream side is that geothermal power is not cost competitive with hydro or coal-fired energy generation, at least in the western Indonesia region (Purwanto, 2019).
Additional challenges	Local personnel competencies	Based on (Purba et al, 2021c; Umam et al, 2018), there is a lack of adequate competency in developing geothermal project since some current geothermal practitioners come from oil and gas industry that need several training and workshops before involved in geothermal project.
	Lack of public understanding on geothermal energy	The public's lack of understanding of the importance of geothermal projects frequently leads to rejection, resulting in delays in geothermal development initiatives. This circumstance is most common when geothermal projects are still in the discovery stage and local governments, development corporations, and local communities still recognize each other and have not yet created trust between each side—social dynamic condition and public acceptance issues that can be stopper of geothermal project.

1.2 Research Objective

The objective of this research is to offer insight related to safeguard requirements from lenders for the geothermal exploration project financed by the International Financing Institution and to provide general guidelines for investors of the geothermal developers to be eligible for funding and for supporting sustainable development. This research is based on a literature study that involved a review of reports on geothermal exploration projects, relevant provisions, publications, research articles, and guidelines on the Environmental, Health and Safety.

1. What is the significance of safeguard requirements in lending decisions?
2. What are the safeguard requirements for the geothermal exploration financing and de-risking facility?
3. What are the challenges to comply with safeguards requirements for the geothermal exploration projects under GREM facility?

2. ENVIRONMENTAL AND SOCIAL RISKS IN GEOTHERMAL EXPLORATION PROJECTS

The majority of geothermal potential is located in or close to forest areas has raised societal concerns about environmental and social impacts, especially in forests that play an important role in supplying fresh water, harbor

endangered wildlife, or have high cultural or religious values. The degree to which these social and environmental risks and impacts vary between geothermal power projects is not well understood. (PROFOR and the World Bank, 2019). Geothermal energy is a clean and sustainable source of power, however, major concerns or issues of environmental and particularly social are challenging. The developers are required to identify environmental, social, health and safety potential impacts or risks properly and comprehensively.

Geothermal exploration projects, while offering significant potential for renewable energy generation, are not without environmental and social risks. These risks can arise at various stages of the project, from exploration and development to operation and closure. Here's an elaboration on the environmental and social risks associated with geothermal exploration projects (Table 2).

Table 2: The environmental and social risks associated with geothermal exploration projects.

Environmental Risks	Social Risks
1. **Impacts due to Land Disturbance**: The construction of access roads, drilling pads, and infrastructure can result in habitat disruption and land degradation. This may impact local ecosystems, biodiversity, and soil stability. 2. **Water Resource Depletion**: Geothermal projects require large amounts of water for drilling, reservoir stimulation, and cooling. Over-extraction of water can lead to reduced groundwater levels, affecting local water sources, ecosystems, and agriculture. 3. **Water Pollution**: Chemicals used in drilling and well stimulation, as well as naturally occurring elements brought to the surface through geothermal fluids, can contaminate surface and groundwater. This pollution can harm aquatic life and pose risks to local communities relying on water sources. 4. **Induced Seismicity**: Injection and extraction of fluids into and from the geothermal reservoir can induce seismic activity. While most induced earthquakes are minor, there's a risk of larger events that could damage infrastructure and raise safety concerns. 5. **Air and Noise Pollution**: Drilling, machinery operation, and the release of gases like hydrogen sulfide can lead to air and noise pollution, affecting air quality and local communities' well-being.	1. **Land Acquisition and Resettlement**: Geothermal projects often require land acquisition, which can result in the displacement of local communities, affecting their livelihoods and traditional way of life. Inadequate compensation and resettlement processes can lead to social tensions. 2. **Cultural Heritage Impact**: Geothermal projects might encroach upon culturally significant sites or areas of historical importance to local communities. Disruption to cultural heritage can lead to social discontent. 3. **Community Health and Safety**: Potential exposure to geothermal gases and the industrial activities associated with exploration and power plant operation can pose health and safety risks to nearby communities. 4. **Employment Impact**: While geothermal projects can create job opportunities, there's a risk that local communities might not benefit as expected due to a lack of required skills or preference for outside expertise. 5. **Lack of Consultation and Participation**: Failing to involve local communities in decision-making and not seeking their input can lead to misunderstandings, opposition, and conflicts.

3. OVERVIEW OF GEOTHERMAL EXPLORATION FINANCING AND DE-RISKING FACILITY

Financing the geothermal exploration project is still considered a high-risk business for lenders as the resource uncertainty is still high. This section will further discuss the funding options for the geothermal exploration project that is currently available in Indonesia. Geothermal exploration is the riskiest phase of geothermal energy development and is challenging for developers. Thus, to scale up investment in geothermal energy by reducing the risks of early-stage exploration, the World Bank approved a loan in September 2019, accompanied by grants from the Green Climate Fund (GCF) and the Clean Technology Fund (CTF), two institutions supporting climate-friendly development.

There are two geothermal exploration de-risking facilities in Indonesia financed by the World Bank as follows:

1. **Geothermal Energy Upstream Development Project (GEUDP)**
   Geothermal Energy Upstream Development Project (GEUDP) is a government-sponsored exploration drilling collaboration program between the Government of Indonesia and the World Bank. The program aims to develop geothermal areas that have yet to be tendered, especially in eastern Indonesia, where the area's electrification ratio is low compared to the other parts of Indonesia (Apriani et al., 2018). The source of funds for the GEUDP program comes from the PISP Fund of USD 49 million, with matching grants from the Clean Technology Fund (CTF) of USD 49 million and the Global Environment Facility of USD 6.25 million. The

program also received grants from the New Zealand Ministry of Foreign Affairs and Trade (NZ MFAT) in the form of technical assistance that equals the amount of NZD 2.13 million.

MEMR, as the beneficiary of this program, will propose a geothermal prospect area to MoF to seek exploration support under the GEUDP program. Then, as the technical implementing agency, PT Geo Dipa Energi ("GDE") will conduct a preliminary assessment to see whether the proposed area is feasible to continue exploration drilling. Suppose the result shows that the proposed prospect area is viable, MoF will issue an assignment letter to GDE as the technical implementing agency and PT SMI as the financial manager to conduct the exploration drilling activities, which is supported under the GEUDP scheme.

The data acquired in the exploration drilling will be assessed by an independent party and discussed in the Joint Committee meeting to decide if the geothermal resource in the prospect area is proven and sufficient to be tendered by MEMR. Assuming that the resource is now de-risked, then MEMR will proceed with the tender process of WKP. In this stage, the participation of both public and private sector geothermal developers in the tender process is expected to increase as the geothermal resource risk has significantly reduced.

2. **Geothermal Resources Risk Mitigation (GREM) Project**
The GREM Project was initiated by the Government of Indonesia (GoI) through PT SMI in collaboration with the World Bank with the objective of accelerating the development of geothermal power generation projects in Indonesia. The ultimate objective is to further stimulate the development of a clean energy source in Indonesia by de-risking it through up-front avoidance of high-risk areas and effectively mitigating social and environmental impacts through good operational management. (The World Bank Group, 2019). Under the Indonesia Geothermal Resource Risk Mitigation (GREM) project, the financing will help public and private sector developers mitigate risks in the exploration of geothermal resources, including covering a part of the cost in case of unsuccessful exploration. The GREM project will also finance technical assistance and capacity building of key stakeholders in the geothermal sector.

   Under the GREM Project, a new Geothermal Resource Risk Mitigation Facility will be established. The new facility shall enable early-stage financing of geothermal projects for public and private developers to enable the increase of geothermal power generation capacities in the country. The Facility is envisaged to include three windows:

   a. Public developer window; and
   b. Private developer window.

   In regard to the GREM facility, it is designated to support the exploration drilling undertaken by geothermal developers who already hold the license or concession of geothermal working areas. The GREM facility is intended for SOE developers/subsidiaries of SOEs ("GREM Public Window") and private developers ("GREM Private Window"). One of the prerequisites for the geothermal developers to access this facility is that they already have the preliminary data of the prospect area/WKP. The unique feature of GREM is the availability of a de-risking facility or a risk-sharing scheme at which, in the event of an exploration failure, the developer does not fully bear the risks and costs of exploration.

The overview of geothermal exploration de-risking facilities available in Indonesia that just discussed is illustrated in Figure 2.

4.SAFEGUARD REQUIREMENTS FOR FINANCING DECISION

4.1 Lender Safeguard Requirements for Sustainability Development

Geothermal exploration projects carry inherent environmental and social risks that must be managed effectively. Safeguard requirements are crucial in mitigating these risks and ensuring sustainable project development. To ensure the success of a project, it is crucial to identify both the positive and negative impacts of its activities at the earlier stage of the project cycle. Therefore, a strategic approach and management plan can be developed to avoid, minimize, and mitigate or compensate for adverse risks and impacts of a project as well as enhance its positive impacts in compliance with the National laws, safeguard policies and standards.

The World Bank Group is deeply committed to fostering sustainable development globally, emphasizing the long-term preservation of the planet, social inclusivity, and reducing economic impacts on future generations. To align with this mission, World Bank-funded projects aim to enhance opportunities for inclusive participation, particularly among vulnerable groups such as women, children, individuals with disabilities, youth, and minorities, while promoting the responsible management of natural resources.

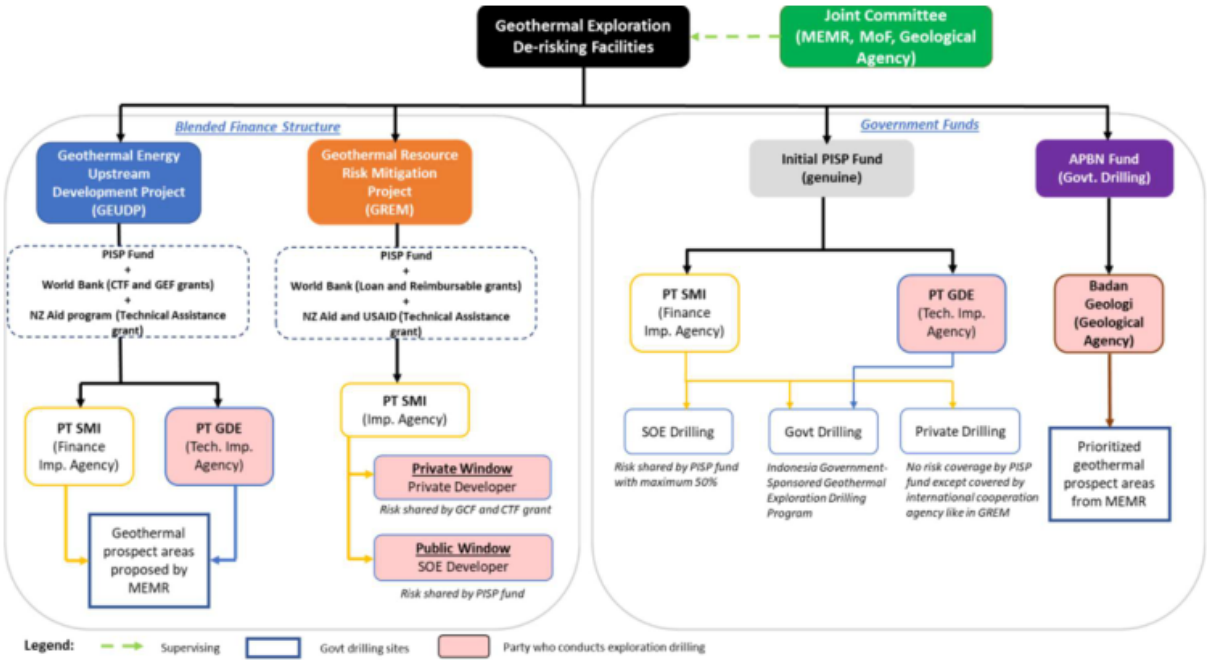

Figure 2: Overview of Geothermal Exploration De-Risking Facilities in Indonesia (PT SMI, 2022a).

The core tool for managing environmental and social concerns within these projects is the World Bank's Safeguard Policies. These policies establish a comprehensive system for assessing and managing risks and impacts, embedding environmental and social considerations into the decision-making process. They facilitate development through specific tools and participatory methods that ensure transparent and inclusive project design, which is crucial for engendering local community ownership.

These Safeguard Policies mandate the early identification and assessment of potential adverse environmental and specific social impacts during the project cycle. They also require that any unavoidable adverse effects be mitigated or minimized as much as possible, and they ensure that relevant information is disseminated in a timely manner to stakeholders, allowing for feedback on the impact assessments and mitigation proposals.

In August 2016, the World Bank introduced a more expansive set of guidelines known as the Environmental and Social Framework (ESF), which has been applicable to all new World Bank investment projects since October 1, 2018. The ESF broadens the scope of addressing environmental and social risks, offering a more comprehensive approach compared to the traditional Safeguard Policies.

Nevertheless, projects initiated before the ESF's implementation date, such as the Geothermal Resource Risk Mitigation (GREM) facility, continue to operate under the older World Bank Operational Policies (OPs) and Bank Procedures (BPs). To optimize these projects' approaches to environmental and social governance, it is recommended that they reference the Environmental and Social Standards (ESS) outlined in the ESF alongside the existing OPs/BPs. This integrated approach can enhance the projects' strategies for managing environmental and social issues, ensuring they adhere to the most current and effective sustainability practices.

As a financial intermediary, PT SMI has ten elements of the Environmental and Social Safeguard (ESS) Procedures that are commensurate with the World Bank policies, consist of 1)ESS-1: Assessment and management of environmental and social risks and impacts; 2) ESS-2: Labor and working conditions; 3) ESS-3: Pollution prevention and abatement; 4) ESS-4: Safety, health and security; 5)ESS-5: Land acquisition and resettlement; 6) ESS-6: Biodiversity conservation and natural resources management; 7) ESS-7: Indigenous peoples and local community; 8) ESS-8: Cultural heritage; 9) ESS-9: Energy conservation and environment-friendly energy; and ESS-10: Consultation and grievance mechanism.

4.2 The World Bank Safeguards Policies for the GREM Facility

World Bank safeguard policies are designed to prevent and mitigate undue harm to people and their environment in the development process. As the Bank's environmental and social agendas have evolved, its safeguard policies have also shifted from focusing on mitigating the potential environmental and social damage toward a more comprehensive focus on the sustainability of projects (a shift from do no harm towards do good). As such, the Bank's social and environmental safeguard policies seek to ensure that relevant measures, capacities and processes are in place, and that their application helps the Bank's borrowers decide what actions and programs need to be

taken to ensure the environmental and social soundness of projects. Safeguard policies also provide a platform for the participation of stakeholders in project design and selection and have been an important instrument for building ownership among local populations.

Table 3: The World Bank ESS, Safeguard Policies (OPs/BPs) and the New Key Elements of the Standards (Modified from The World Bank Environmental and Social Framework, Implementation Update, September 2020).

The ESF	OPs/BPs	New Key Elements
ESS1: Assessment and Management of Environmental and Social Risks and Impacts	OP/BP4.01(Environmental Assessment)	Integrates Environmental and Social Assessment; includes requirements related to non-discrimination and social inclusion; proportionality and adaptive management; use of the ESCP
ESS2: Labor and Working Conditions	OP/BP4.01 (Environmental Assessment) and EHS Guidelines	Prohibits child labor and forced labor, heightened focus on OHS, grievance mechanisms
ESS3: Resource Efficiency and Pollution Prevention and Management	OP4.09 (Pest Management) and EHS Guidelines	Promotes efficient management of energy, water, and other resources and materials; hazardous materials management; pesticides; GHG assessment mandate
ESS4: Community Health and Safety	OP/BP4.37 (Safety of Dams) and EHS Guidelines	Assess risks and impacts on communities; Design of safe and resilient infrastructure, equipment operation, products, services, road safety, hazardous materials; emergency preparedness
ESS5: Land Acquisition, Restrictions on Land Use and Involuntary Resettlement	OP/BP4.12 (Involuntary Resettlement)	Greater clarity on treatment of state land, land titling, access to common resources, voluntary transactions, forced evictions
ESS6: Biodiversity Conservation and Sustainable Management of Living Natural Resources	OP/BP4.04 (Natural Habitats) and OP/BP4.36 (Forests)	More detail and descriptive definition of habitat; expanded requirement to assess and mitigate impacts on biodiversity including in primary supply chains; biodiversity offsets; management of living resources in additional sectors (e.g. agriculture)
ESS7: Indigenous Peoples/Sub-Saharan African Historically Underserved Traditional Local Communities	OP/BP4.10 (Indigenous Peoples)	Clearer definitions of IP, requires FPIC in specified circumstances
ESS8: Cultural Heritage	OP/BP4.11 (Physical Cultural Resources)	Enhanced consultation with affected communities, intangible heritage
ESS9: Financial Intermediaries	OP/BP 4.01 (Environmental Assessment)	Establish E&S procedures commensurate with FI nature, risk level and impact
ESS10: Stakeholder Engagement and Information Disclosure	Consolidates WB Engagement Provisions	Meaningful consultation, access to information and grievance redress through the life of project

Each of the World Bank's policies plays a crucial role in ensuring that World Bank-financed projects not only meet strict environmental and social standards but also engage positively with affected communities, thereby supporting the overarching goals of sustainable development and social inclusiveness.

The World Bank environmental and social safeguard policies triggered by the geothermal exploration project are follow:

OP/BP 4.01 known as the Umbrella Safeguards Policy, delineates the environmental assessment process essential for compliance with other safeguard policies. This policy is crafted to enhance the environmental and social soundness and sustainability of investment projects by integrating environmental and social aspects into decision-

making processes. Essentially, the Environmental Assessment (EA) evaluates a project's potential environmental risks and impacts in its area of influence, examines project alternatives, and identifies ways to improve project selection, siting, planning, design, and implementation. It also encompasses mitigating and managing adverse environmental impacts throughout project implementation. A vital component of the EA is the screening process, initiated as early as possible, to determine the necessary scope of environmental assessment appropriate to the potential impacts and risks. Geothermal exploration projects typically fall into Category A or B, with Category A for projects with broader significant impacts and Category B for those with localized, manageable impacts.

OP/BP 4.04 focuses on the preservation of natural habitats, aiming to support environmentally sustainable development by promoting the conservation and rehabilitation of natural habitats and their functions. This policy protects habitats that are legally protected, officially proposed for protection, recognized by local communities, necessary for maintaining viability of protected areas, or recognized as having high conservation value. It mandates a stringent assessment of potential impacts on biodiversity and restricts significant conversion or degradation of critical natural habitats, ensuring any intervention is justifiable by substantial net benefits and includes appropriate mitigation measures.

OP/BP 4.36 addresses the strategic utilization of forests to reduce poverty sustainably while integrating forest management into economic development and preserving essential environmental services and values of forests. This policy restricts financing projects that may cause significant conversion or degradation of critical forest areas or habitats, ensuring forest conservation and sustainable management.

OP/BP 4.11 outlines the measures for protecting physical cultural resources (PCR) that might be affected by project activities. This is particularly relevant in regions like Indonesia, where geothermal manifestations may be considered sacred by local communities. The policy requires the development of PCR Management Plans and procedures for chance findings as part of the ESIA and ESMP processes.

OP/BP 4.10 emphasizes the importance of engaging with Indigenous peoples through free, prior, and informed consultations, especially where projects affect areas with Indigenous presence or collective attachment. It necessitates obtaining broad community support and implementing culturally appropriate benefits and mitigation strategies through an Indigenous Peoples Plan (IPP) or Framework (IPPF).

OP/BP 4.12 tackles involuntary resettlement, aiming to minimize direct economic and social impacts that cause displacement or loss of livelihood. Projects must be sited to avoid or minimize these impacts, and where unavoidable, comprehensive resettlement plans must be developed and consultations with affected communities conducted.

OP/BP 4.37 pertains to the safety of dams, requiring that any dam construction associated with a project meet stringent safety standards overseen by competent professionals. This includes specific safety measures for design, construction, operation, and maintenance, integrated into legal agreements and monitored for compliance.

4.3 Environmental and Social Management Framework (ESMF) of The GREM Facility

The World Bank designed environmental and social safeguard policies for supporting borrowers in the development and implementation of projects that are environmentally and socially sustainable. PT SMI as a Financial Intermediary in collaboration with the World Bank has prepared the GREM Environmental and Social Management Framework (GREM ESMF). The document details the environmental and social safeguard policies, principles, procedures, institutional arrangements, and workflows in avoidance, minimization, or mitigation of any adverse environmental or social impacts of infrastructure projects supported by the Geothermal Resource Risk Mitigation Project (GREM).

Table 4: The Key Safeguard Instruments and Permits Requirements for the GREM Facility.

Stage	Safeguard Instrument/Permit	Remarks
GREM Facility Application (Proposal)	Approved UKL – UPL	Has been approved by the authority. To comply with the applicable GoI laws and regulations
	ESIA and ESMP (Approved Final Draft)	To comply with the World Bank policies and GREM ESMF. ESMP is specifically prepared for managing the impacts and risks of the project.
	Environmental Permit/Approval	Has been issued by the Ministry of Environment and Forestry
	Forest Area Use Permit, if applicable	If the permit is not yet issued, the developer is required to provide details

Stage	Safeguard Instrument/Permit	Remarks
		on the current status of the permitting process
Financing Approval Process	Final ESIA and ESMP	To be approved by PT SMI and the World Bank. Finalization and disclosure of the UKL-UPL, ESIA, and ESMP documents are minimum requirements for financing approval by the Financing Committee.
Before Construction and Drilling Activities Commence	Sub-plans and procedures of the project ESMP	Sub-plans and procedures that need to be prepared are subject to the results of Environmental and Social Due Diligence (Corrective Action Plan).
	Final Stakeholder Engagement Plan (SEP) and Grievance Redress Mechanism (GRM)	These documents shall be prepared in project preparation from the outset of the ESIA study. Involve stakeholders at the early stage of the project cycle to ensure their participation and input.
	Land Acquisition and Resettlement Action Plan (LARAP) and Livelihood Restoration Plan (LRP)	If any land /assets and/or any loss of income (livelihood) are affected by the project. No work begins until land acquisition and resettlement has been completed.
	Indigenous People Plan (IPP)	If triggered in the ESIA and ESMP
	Physical Cultural Heritage Management Plan (PCHRMP) and Chance Find Procedure (CFP)	Despite the physical cultural heritage is not triggered, the Chance Find Procedure is still required.
	Gender Action Plan (GAP) and Gender Based Violence (GBV) Risk Management	This is an instrument as required by the World Bank policy for proposing gender equality in the design and implementation of projects, and to protect women in the project area from gender-based violence
	Forest area Use Permit (PPKH)	Issued by the MoEF or the authority in accordance with the applicable related regulation
	Surface Water Extraction Permit (SIPPA)	Issued by the Ministry of Public Works and Housing or the authority in accordance with the applicable related regulation
	Contractor – ESMP (C-ESMP) and Standard Operation Procedures	The C-ESMP is detailed Project ESMP that shall be prepared by an awarded Contractor and approved/cleared by PT SMI and the World Bank before site work begins

To qualify for financing under the Geothermal Resource Risk Mitigation (GREM) facility and ensure compliance with World Bank policies, developers must meticulously implement their projects in line with the provisions outlined in the GREM Environmental and Social Management Framework (ESMF). This includes adherence to all mitigation plans specified in each safeguard instrument and any supplemental instruments to the satisfaction of the overseeing bodies.

As a fundamental condition of eligibility for GREM facility financing, developers are required at an early stage to submit several critical documents. These include the Environmental Management Effort and Environmental Monitoring Effort (Upaya Pengelolaan Lingkungan - Upaya Pemantauan Lingkungan, or UKL-UPL) along with the Environmental Permit/Approval. Additionally, an approved final draft of the Environmental and Social Impact Assessment (ESIA) and the Environmental and Social Management Plan (ESMP) must be included as integral parts of their proposal documents.

The essential safeguard instruments and permits necessary for obtaining and maintaining eligibility under the GREM facility are comprehensively listed and described in Table 4. This table serves as a crucial reference for developers to ensure they meet all the required environmental and social compliance standards, thereby facilitating a smooth and compliant project development process under the GREM facility.

The key safeguard instruments and permits that are required for the GREM facility are summarized in Table 4.

5. THE CHALLENGES AN LESSONS-LEARNED OF SAFEGUARD COMPLIANCE FOR THE GREM FINANCING

5.1 The Challenges in the Safeguard Compliance in Geothermal Exploration Project

For projects under the Geothermal Resource Risk Mitigation (GREM) facility, adherence to both the applicable national laws and regulations of Indonesia (GoI regulations) and the World Bank Safeguard Policies is required. A crucial element of project compliance involves identifying and addressing any discrepancies between these two sets of guidelines. Discrepancies are documented in a comparison detailed in Table 5, which presents key features of both the GoI regulations and the World Bank's policies.

In instances where conflicts arise between the national laws/regulations and the World Bank Policies, the principle of applying the highest standard is adopted. This approach mandates that the project should adhere to the more stringent standards with regard to minimizing social and environmental impacts. Essentially, wherever there is a difference in requirements, the project must default to the regulations that offer the greatest level of protection for the environment and social welfare. This ensures that the project not only fulfills its legal obligations but also aligns with best practices in sustainable and socially responsible development.

Table 5: Comparison between GOI Laws/Regulation and the World Bank Policy.

No.	Topic	Indonesian Regulation	The World Bank Policy
1.	Applicable Safeguard Instrument	Geothermal exploration requires only an Environmental Management Plan and Monitoring Plan (UPL-UKL), regardless of potential impacts, according to GOI Regulation No. 5 of 2021 Appendix I in the Energy and Mineral Resources Sector.	OP4.01 requires an assessment of safeguard instruments depending on the classification of activity based on risk
2.	Associated Facilities	The GOI laws and regulations consider project activities discretely – consider each phase as a separate environmental permit process, and thus require separate application and obtainment of approvals accordingly (GOI Regulation No. 22 of 2021 Appendix III)	OP4.01 Environmental Assessment requires an assessment of associated facilities where they are considered part of the Project (either geographically, or over time),
3.	Utilization of Forest Area	Remove barriers to carrying out geothermal exploration and exploitation activities in forests and protected areas - take into account the low-impact use of ecosystem services and that geothermal is accepted and increasingly considered as a nationally strategic activity (Geothermal Law No. 21 of 2014, Article 5, Section 2)	The World Bank policies (OP 4.36 and 4.04) have maintained their requirements and standards regardless of the activities and require full impact assessment / significant mitigation before sub-project appraisal, or not funding certain exploration activities – that may result in degradation or removal of critical habitats
4.	Involuntary Resettlement	Land acquisition plan based on a feasibility study, the project suitability to the spatial plan.	Different planning instruments must be prepared to achieve the objectives of the policy and must cover all aspects of the proposed resettlement (LARAP)
5.	Eligibility of Indigenous People	Indigenous Peoples are covered by the land acquisition and resettlement legislation once they have been legally recognized	IPs are covered when screening identifies the presence of IPs as per characteristics in OP4.10 policy (which does not require any legal recognition).

In addition to the regulations gaps as a challenge, the case study for the safeguard issue is the geothermal exploration project in Wae Sano village, Sano Nggoang District, West Manggarai Regency, East Nusa Tenggara Province. The Wae Sano Geothermal Exploration Project under GEUDP was established in 2017 with funding

from the World Bank. The full broad community support from the community as the World Bank requirements were not achieved. The local people opposed the project, because the Wae Sano geothermal exploration is in people's living space and will have a significant environmental and social impact on them. Consultations with stakeholders from local government, community leaders and the community had been conducted, but the community's stance has not changed. Following consultation with the stakeholders in Wae Sano village on December 2022, the World Bank canceled financing for a geothermal exploration project.

According to Raffaele Cataldi (2001) and Afandi et.al (2023) Social acceptance is an important requisite for the smooth implementation of geothermal projects, especially at the exploration phase. It is known that in several geothermal exploration projects in Indonesia are still facing Societal Challenges due to the presence of negative stigma towards geothermal exploration projects.

Another challenge relates to land use. Most geothermal potential in Indonesia is in or close to forest areas. This has raised societal concerns about environmental and social impacts, especially in forests that play an important role in supplying fresh water, harbor endangered wildlife, or have high cultural or religious values. Environmental and social impacts and risks associated with geothermal power development are complex and significant and the degree to which these risks and impacts vary between geothermal power projects is not well understood.

5.2 Lessons Learned of Safeguard Compliance for the GREM Financing

From the lender's perspective, adherence to safeguard requirements, national regulations, and World Bank safeguard policies, including those outlined in the Environmental and Social Management Framework (ESMF), enhances a geothermal developer's eligibility for funding and demonstrates a commitment to sustainable practices. During the preparation of a geothermal exploration project, PT Sarana Multi Infrastruktur (PT SMI) identified several areas where developers encountered significant challenges with these safeguards requirements. The key findings are summarized below:

1. Safeguard Instruments Preparation (ESIA, ESMP, and others):
    - The scope of the Environmental and Social Impact Assessment (ESIA) required by international standards is broader than the national requirements (UKL-UPL or AMDAL). Developers need to prepare safeguard instruments that comply with the GREM ESMF to align with World Bank policies, the Resettlement Policy Framework (RPF), and Indigenous Peoples Planning Framework (IPPF).
    - The project area of influence was inadequately defined in the ESIA documents, failing to include project footprints, ancillary, and associated facilities.
    - The screening and scoping processes were improperly conducted, which failed to appropriately categorize the document and define the ESIA's scope. Engaging subject matter experts in this process is crucial.
    - Baseline data collection was inaccurate and did not reflect the actual conditions of sensitive receptors for both dry and wet seasons.
    - Information on project activities was limited, making it difficult to assess potential impacts and risks comprehensively. The initial project design was unavailable during the ESIA preparation, and design alternatives necessary for impact assessment and mitigation were not considered.
2. Project Organization and Team Capacity:
    - There was a notable lack of dedicated Environmental, Health, and Safety (EHS) personnel to manage the project, coupled with limited knowledge and experience in geothermal development, which are crucial for implementing and monitoring safeguards.
3. Stakeholders Engagement and Consultation:
    - There was insufficient engagement and consultation with stakeholders, as well as inadequate dissemination of information regarding the potential impacts and risks of the proposed geothermal activities.
4. Land-related Issues:
    - Developers faced challenges in the permitting process to secure areas within protected forests, unclear land ownership, and issues related to communal and social forestry lands. The effort required for land acquisition was compounded by community reluctance to sell or lease land, especially productive agricultural land.

Effectively preparing a project by incorporating safeguard instruments and engaging stakeholders comprehensively will bring numerous benefits. Meeting safeguard requirements not only increases local community acceptance but also ensures smoother implementation for geothermal exploration and contributes to sustainable development goals.

6. MONITORING AND EVALUATION OF THE SAFEGUARD COMPLIANCE

Evaluating the effectiveness of safeguard requirements is essential for continual improvement. The monitoring and evaluation of safeguard compliance are divided into two stages during the GREM duration, namely monitoring and evaluation of all safeguard-related requirements prior to the exploration financing agreement signing, and monitoring the implementation of the actions plan in the safeguard instruments during construction, exploration drilling, well testing activities.

The safeguard instruments of UKL-UPL, ESIA and ESMP including Gender Action Plan are mandatory documents for the proposal of the GREM facility. Before submitting the proposal, the Project Management Unit of PT SMI as a Financial Intermediary will advise the sub-borrower during the safeguard instruments preparation to comply them with the World Bank policies and standards.

After proposal submission, there will be an Environmental and Social Due Diligence (ESDD) process from the financing division of PT SMI supported by an Independent ESDD Consultant to indicate any red flags and find any gaps that need to be fulfilled by the sub-borrower before financing agreement signing.

At minimum, the list of requirements for the environmental, social, health, and safety due diligence process for the GREM facility to be taken into account by the sub-borrower is presented in Table 6.

Table 6: List of Requirements for the Environmental, Social, Health and Safety Due Diligence Process for GREM Facility.

Aspect	Remarks
HSE Policies and Organization	HSE organization capacity and competency to manage environmental and social risks. Show responsibilities and any relevant company policies.
Environmental Aspect Summary	Summary of the main environmental context, and key issues that may be faced. Summary of studies completed to date. The environmental aspect summary must covering the AMDAL or UKL-UPL document and environmental baseline, the developers also need to present potential impacts and planned mitigation that need to be included but not limited to: matrix of impacts on the environment, air quality and odor, noise, groundwater, surface water quality, surface hydrology and hydraulics, biohazard potential/terrestrial ecology flora and fauna, visual impact, sustainability and climate change, drilling waste management process, domestic waste management, potential geohazard and geotechnical issues, borrow to use permit/PPKH status, and other necessary permits.
Environmental and Social risks	Description of the environmental and social context and identification of any sensitive receptors, issues, risks.
Baseline data	Detail the data parameters for impact environmental and social assessment of geothermal exploration drilling activities in accordance with National Regulations, PT SMI's ESS Procedures and WB policies. Description/scope of baseline studies completed, underway or planned and who is undertaking the studies.
Project Area of Influence	Define the Project Area of Influence (AOI), and cumulative impacts. Describe the basis and show its map.
Safeguard instruments	List the safeguard instruments in accordance with GREM ESMF, SMI's ESS procedures, and the World Bank Policies. Provide status and plans for completion.
Enviro and social permits (e.g. UKL- UPL)	Status of the permits that relate directly to drilling, their scope (and match with drilling plans). Identify any issues or gaps. Summary of required environmental and social permits and approvals as per legislation that have been obtained or in the process of being obtained or will be obtained in the future.
Standard Operating Procedures (SOPs)	List and status of Environmental and Social SOPs required during construction, drilling and well testing
Social acceptance	The level of acceptance of the main project with the community. Summarize any community engagement made to date, key issues and possible barriers to the project. Describe plans for any mitigations and ongoing social engagement and CSR activities. The summary of social impact assessment that needs to be covered but not limited to socio-cultural, socio-economic, geothermal education, traffic, transport, and community safety, community displacement, community health and safety, stakeholders' response, and other related impact.
Social engagement	Status of community engagement, level of acceptance, plans for further engagement before, during and after drilling. The information can be presented not only using paragraphs but also using a table with include social engagement activity type, date, time, location, number of local people involved, name of the leader from the

Aspect	Remarks
	community, name of representative from the company, key takeaway from each engagement, etc.
Land status & ownership	Ownership of the land required for the drilling, facilities and access roads. Public / private, forestry or protected or heritage areas. Maps, aerial photography, commentary on status. Commentary on the plan for land acquisition as may be required for the project. Status of land ownership over the areas required for water supply, access road and well pad upgrade or construction. Plans for land acquisition or lease.
Compensation	Compensation that may be required for land acquisition or use, or for general nuisance to community. Scope of compensation, methods for distribution.
Direct heat use Projects	Identify any direct heat use projects that may be associated with the project (if applicable)

7. CONCLUSION AND DISCUSSIONS

The conclusion of the paper emphasizes the critical role of safeguard requirements in the financing and sustainable development of geothermal exploration projects. It highlights the intricate challenges and substantial risks associated with these projects, particularly in terms of environmental and social impacts, and the necessity for robust safeguard measures to manage these risks effectively. This approach is crucial for improving safeguard implementation practices and enhancing the overall sustainability and success of geothermal exploration projects.

For the effectiveness of safeguard implementation, it is imperative to consider but not limited to the followings:

1. A comprehensive ESIA and ESMP will help the developers to identify, avoid, minimize, and mitigate for adverse impacts and risks as well as enhancing the positive impacts of project to achieve project sustainable development. The capacity building on the World Bank safeguard requirements to the developers and their ESIA consultant is beneficial to enable them in assessing the impacts and the mitigation plans thoroughly and comprehensively to avoid, minimize, and mitigate or compensate for adverse impacts to comply with the World Bank policies and Good International Industry Practice (GIIP) standards. This also will make the ESIA a reliable basis for decision-making;
2. ESMP shall be reviewed regularly during its implementation for any improvement on the mitigation measures of impacts due to new or non-anticipated impacts. The developers shall ensure effective implementation of the ESMP, which the potential environmental and social impacts being managed and mitigated effectively for sustainable development;
3. Consultations should be held with key stakeholders to determine potential concerns and issues associated with the project as early as possible in the project cycle and through the life of the project. The proposed project activities and its potential impacts shall be socialized to stakeholders including local communities transparently;
4. Capacity building to communities and other stakeholders on the geothermal development project is important to enhance their knowledge on geothermal energy as a renewable energy in comparison with other renewable energy sources. The public's lack of understanding of the importance of geothermal projects frequently leads to rejection, resulting in delays in geothermal development initiatives. This circumstance is most common when geothermal projects are still in the discovery stage and local governments, development corporations, and local communities still recognize each other and have not yet created trust between each side—social dynamic conditions and public acceptance issues that can be stopper of geothermal project. (Fadhillah et all , 2022 and 2023);
5. Multi-stakeholder collaboration and partnerships play an important role in the success of a project. The early involvement of the community and other stakeholders will build their participation towards the project. With continuous, transparent and effective communication about the project and its potential impacts and an approach that takes into account local culture, any concerns from the community can be discussed and solutions sought as early as possible. With this approach, It is expected that there will be no rejection of the project.

REFERENCES

ADB. (2014). Unlocking Indonesia’s geothermal potential. Asian Development Bank.

Afandi, Purba.D, Apriani, DNI, Fadhillah,FR, Mustika, Astri Indra (2024). Social Safeguard Measures in Geothermal Exploration: Fulfilling Requirements for the Geothermal Resource Risk Mitigation Program. Proceedings, 49th Workshop on Geothermal Reservoir Engineering. California: Stanford University, Stanford, California

ESMAP. (2021). Preparing Feasibility Studies For Financing of Geothermal . Washington DC: World Bank.

Fadhillah, F. R. (2023). Economic Evaluation of Bravo Geothermal Prospect in Participating Green Energy Effort. Jakarta: Institute Teknologi Bandung.

Fadhillah, F. R., Tjendarsa, K., Damayanti, S. M., Purba, D., & Adityatama, D. (2024). Economic Evaluation of Bravo Geothermal Project as Effort for Green Energy Transition.

GoI. (2022). Presidential Regulation 112/2022: Percepatan Pengembangan Energi Terbarukan untuk Penyediaan Tenaga Listrik. Jakarta: Government of Indonesia.

Himberg. H: Comparative Review of Multilateral Development Bank Safeguard Systems. Consultant, Operations Policy and Country Services (May 2015).

Kasimbazi, E.: Compliance with Safeguard Policies of The World Bank and African Development Bank, Proceedings, 29th Annual Conference of the International Association for Impact Assessment Accra International Conference Center, Accra, Ghana (2009).

MEMR. (2022b). Presidential Regulation 112/2022 Percepatan Pengembangan Energi Terbarukan untuk Penyediaan Tenaga Listrik. MEMR.

PLN. (2021). RUPTL 2021-2030. Jakarta: Perusahaan Listrik Negara.

Prasetya.M.,Nurdin, Muhammad.,Kushendratno, Agus.W. : Forest Area Boundary Situation Survey: A National Land Strategic Program to Support Land Tenure Security in Indonesia, FIG e-Working Week, Smart Surveyor Land and Water Management-Challenges in a New Reality Virtually, Netherlands, 21-25 June 2921.

PROFOR and the World Bank Group.: Rapid Environmental and Social Assessment of Geothermal Development in Conservation Forest Areas In Indonesia (August 2019)

PT SMI.: Indonesia Geothermal Resource Risk Mitigation Project Developer Manual. (2022).

PT SMI. Indonesia Geothermal Resource Risk Mitigation Project GREM (P166071) Environmental and Social Management Framework. (2019).

Siahaan, M., Septiani,G., Purba,D: Geothermal Exploration Project De-risking: Discussion on Various Schemes, Proceedings, 48th Workshop on Geothermal Reservoir Engineering, Stanford University, Stanford, California, February 6-8, 2023

The World Bank.: Environmental and Social Policies. https://www.worldbank.org/en/projects-operations/environmental-and-social-policies (Accessed on 31 August 2023)

The World Bank Group.: The World Bank Group Strategy. Washington, DC: World Bank Group (October 2013).

The World Bank.: Preparing Feasibility Studies for the Financing of Geothermal Projects. ESMAP. An Overview of Best Practices. Washington, DC.(2021)

The World Bank.: The World Bank Environmental and Social Framework, World Bank Environmental and Social Policy for Investment Project Financing (2017).

The World Bank.: Geothermal Handbook: Planning and Financing Power Generation. ESMAP. Technical Report 002/12.Washington DC(2012).

The World Bank.: Safeguards and Sustainability Policies in a Changing World. IEG Study Series. An Independent Evaluation of World Bank Group Experience.Washington, DC (2010)

The World Bank.: Scaling Up Renewable Geothermal Energy in Indonesia. ESMAP. Washington DC (2014)

World Bank. (2018). Regulatory indicators for sustainable energy. Jakarta: WB.

World Bank Group. Design and Implementation: Safeguards (2013). https://www.worldbank.org/en/topic/communitydrivendevelopment/brief/cdd-fiduciary-issues (assessed on 10 September 2024)

Implementing FPIC Stakeholder Engagement in Geothermal Projects

Satoshi Ishihara, Greg Guldin, Adi Prasetijo, Muchsin Qadir, and Annye Simbolon

World Bank Group

sishihara@worldbank.org, greg@crossculturalconsult.com,
prasetijo@gmail.com, mqadir@worldbank.org, asimbolon@worldbank.org

Keywords: FPIC, stakeholder engagement, Indonesia, geothermal

ABSTRACT

There is a growing recognition, bolstered by research and experience, that good stakeholder engagement helps reduce social risk and negative impacts while providing superior developmental outcomes to local communities, and overall lowers project costs to the developers, the financiers, and the government. Good stakeholder engagement is particularly important to identify social groups vulnerable to shocks due to the project and identify their distinctive needs and concerns. Among other stakeholders, Indigenous Peoples (IP) are particularly vulnerable to the loss of, alienation from, or exploitation of their land and access to natural and cultural resources. In recognition of this vulnerability, an increasing number of International Financial Institutions (IFIs) require their clients to obtain the Free, Prior, and Informed Consent (FPIC) of the affected Indigenous Peoples when such circumstances occur under the projects they finance. Projects often struggle though with precisely how to engage with a broad range of stakeholders, including importantly Indigenous and local communities, for lack of clear technical guidance.

This paper summarizes a recommended Technical Guidelines which will provide step-by-step procedures and concrete actions as pathways toward carrying out meaningful stakeholder engagement and achieving their FPIC where required, under the "Participation and Partnership Framework (PPF)" as the overarching conceptual framework. The PPF also suggests that this approach be made available not only for Indigenous communities but for any project when significant community risks are present. The Technical Guidance discusses how to do this by laying out three basic approaches that the project can use depending on the scale of risks and impacts as well as the characteristics of the affected people: FPIC- Standard, FPIC-Lite, and FPIC-Like.

1. INTRODUCTION

Indonesia has enormous potential and challenges in terms of development and renewable energy. Emerging global standards and IFIs have committed to supporting renewable energy and collaborating to speed the development of energy transition initiatives. Significant developments will necessitate using new energy sources such as solar, water, wind, and geothermal. However, renewable energy production and transition affect, and are affected by, the surrounding population throughout the project's operational life, including particularly Indigenous Peoples who retain deep cultural ties and rely on the natural resources of their home territories.

Meaningful stakeholder engagement (SE) is becoming more widely acknowledged as an essential component of social risk management. This is because it assists projects in obtaining a "social license to operate" and reduces the potential risk of rejection from affected people or criticism from civil society. In Indonesia, where experience is minimal, particularly in the public sector, stakeholder participation is frequently considered merely a consultation meeting or two for a safeguard document. Weak engagement from stakeholders often results in resistance from local communities, which can be avoided or minimized through meaningful stakeholder interaction.

Meaningful stakeholder engagement and processes to achieve and maintain community support are particularly important if the project affects Indigenous Peoples (IP) and will go a long way toward achieving the enhanced consultation standard of Free, Prior and Informed Consent (FPIC) that is required under many international standards such as the World Bank's Environmental and Social Framework (ESF) and IFC's Performance Standards (PS). A good understanding of how enhanced meaningful stakeholder engagement can lead to FPIC and what additional activities and documentation are needed to meet FPIC requirements will help renewable energy projects overcome potential social risks while minimizing compliance risks. A heightened awareness of international good practice on stakeholder engagement and FPIC in the renewable energy sector will also have a spill-over effect in other sectors since many principles, processes, and procedures on meaningful stakeholder engagement and FPIC are similar across sectors.

These Technical Guidelines (TG) also follow up on the "Stakeholder Engagement & FPIC 101" workshop held in February 2023 by the World Bank Indonesia which had these key takeaways:

1. Practitioners need guidance on clear processes to reach consent and criteria to recognize it, and which is acceptable to all parties including international financiers. All stakeholders need to agree upfront on processes to reach and confirm consent, including who will give consent.
2. Convincing a project's senior management of the value of meaningful SE and FPIC with concrete case examples, especially to secure necessary budget, is key.
3. SE should start early and continue throughout project preparation and into implementation, but the challenge is that SE and FPIC are typically seen as a matter of compliance. As a result, SE including that with Indigenous Peoples, is often limited to a public consultation meeting to meet policy requirements just before project approval.
4. It is important to embed FPIC processes in legally binding assessment processes such as Environmental and Social Impact Assessment (ESIA) to enhance the legitimacy of FPIC and ensure it is conducted as a process. Agreements made between the project and the community (and the local government as relevant) when prepared as a condition of consent should be in legally binding documents.
5. Significant legacy issues including pre-existing discontents and intra-community tensions should be assessed upfront and addressed if they could negatively affect the project before the project initiates an FPIC process on project specific matters. Experience shows that unresolved legacy issues can negatively affect FPIC processes that may otherwise be adequate and make it difficult for the project to obtain a "social license to operate."

Lastly, all users of these TG need to consider them as one part of a broad range of social and environmental safeguard policy document guidance. The ten Environmental and Social Standards of the World Bank, like their cousin policy documents of the other IFI and affiliated entities, need to be seen in conjunction with those policies along with the myriad national, regional, and sectoral guidance that have emerged these recent years.

2. WHAT'S FPIC?

"Free, Prior and Informed Consent," like the term "Indigenous Peoples", has no universally agreed upon definition. For the World Bank, consent refers to the collective support of affected Indigenous Peoples' communities…for the project activities that affect them reached through a culturally appropriate process. It may exist even if some individuals or groups object to such project activities....(Environmental and Social Standard 7, ESS7, para. 26).

In both international and national use, FPIC has heretofore been applied exclusively to Indigenous Peoples. FPIC is an approach of involving Indigenous Peoples in the discussion and decision-making of projects that will affect them. It is grounded on the recognition by international legal instruments of the collective rights of Indigenous Peoples and it is considered a substantive framework and integral component of the Indigenous People's exercise of their right of self-determination and to their rights to land, territories, and resources. It allows Indigenous Peoples to give or withhold their consent to any project design, implementation arrangements, and/or matter impacting them or their customary lands, territories, and resources. Importantly, "consent" does not merely mean saying "yes." It also means saying "No" or delaying a "No" or "Yes" until the affected Indigenous Peoples are informed appropriately and accurately on all project-related matters which will impact their lives and lifeways. The FPIC process thus builds on and expands ESS10's emphasis on "meaningful consultation." FPIC refers to both (i) a process of seeking consent, and (ii) an outcome in terms of a decision and should include documented proof of both.

These Technical Guidelines recognize the positive benefits that FPIC bestows on both the affected communities and the projects that are projected to be implemented in, on, or near their lands and proffers such benefits to non-Indigenous communities as well as those communities recognized as Indigenous. The Participation and Partnership Framework thus is not limited in application solely to Indigenous-affecting projects but to all those projects either Indigenous or facing significant environmental or social risks. FPIC can be a boon to them all.

It is important furthermore to note that FPIC is an agreement that continues in full validity past the decision point of any positive consent approval following good faith negotiations (see below). FPIC agreements may be suspended or withdrawn if the agreements achieved are seen not to be followed. Also, we should recognize that FPIC concerns group collective rights not individual rights and so the consent process does not require unanimity of opinion nor grant any individual or community a veto over the collective domains and collective will of the people participating in the FPIC process or of the communities and peoples in question.

Under the IFI Indigenous Peoples' policies, FPIC is generally required under any one of three circumstances as described by the World Bank:

a) have adverse impacts on land and natural resources subject to traditional ownership or under customary use or occupation;

b) cause relocation of Indigenous Peoples…from land and natural resources subject to traditional ownership or under customary use or occupation; or

c) have significant impacts on Indigenous Peoples'…cultural heritage that is material to the identity and/or cultural, ceremonial, or spiritual aspects of the affected Indigenous Peoples'…lives.

(ESS7, para.24)

And what does each of the four "FPIC" components mean?

- **Free**—without coercion, intimidation, manipulation, threat, or bribery; an independent process of decision-making.
- **Prior**—the right to follow their own decision-making process—accurate and full information is received, consent has been sought sufficiently in advance, before any project activities have been authorized or commenced, and that the time requirements of the indigenous community's consultation/consensus processes have been respected.
- **Informed**—information is provided in a language and form that are easily understood by the community, covering the nature, scope, purpose, duration and locality of the project or activity as well as information about areas that will be affected; potential economic, social, cultural, and environmental impacts--both positive and negative—as well as all involved actors, and the procedures that the project or activity may entail. It is the right to have accurate, accessible, sufficient information on matters for decision-making in a culturally compatible manner.
- **Consent** — a collective and independent decision of affected Indigenous Peoples after following their own process of decision-making. It is the right of Indigenous Peoples to give or withhold their consent to any decision that will impact their lands, territories, resources, and lifeways (From: United Nations Permanent Forum on Indigenous Issues (UNPFII), Report of the International Workshop on Methodologies Regarding Free Prior and Informed Consent, Document E/C.19/2005/3, endorsed by the UNPFII at its Fourth Session).

The four different components, "Free," "Prior," "Informed," and "Consent," add substantial meaning to the FPIC approach. Each of these elements has its own meaning, principles and processes, and manner of implementation. They are, however, interrelated and should be applied in an integrated and holistic manner. The first three components (Free, Prior, and Informed) qualify and set the conditions of "consent" as a decision- making process. Therefore, "consent" is required before any action takes place (Prior), is independently decided (Free), and is based on accurate and sufficient information, and full understanding (Informed) for it to be a valid outcome of a collective decision. Experience has also taught that these attributes of FPIC—and their allied principles of transparency, inclusion, and mutual respect—best also carry over into the post-FPIC decision period of FPIC agreement implementation. An Indigenous Peoples Plan (IPP) composed of mitigation measures, compensation and benefit-sharing measures reached in agreement with local Indigenous Peoples should--like the FPIC process itself--be guided by the principle of upholding the collective rights of Indigenous Peoples.

From this perspective, although a positive "consent decision" takes place at a certain time and cannot be simply revoked, FPIC operational principles of transparency and collaboration can serve as a gateway to ongoing engagement for the life of the project and any FPIC agreements approved by that consent decision must be carried out in good faith.

3. THE PARTICIPATION AND PARTNERSHIP FRAMEWORK (PPF)

The FPIC-compliant "Participation and Partnership Framework" (PPF) recasts project-affected communities as partners in project design and implementation, rather than as a group of external stakeholders to consult or negotiate with. As is described in more detail below, the PPF seeks to apply the FPIC principles and the Good Faith Negotiations (GFN) approaches throughout the project life and treat project affected communities as partners in project design, implementation, monitoring and discussions on course corrections, to help the project gain and maintain a social license to operate. The PPF aims to do so by building and maintaining positive relationships among stakeholders including the Affected Communities, contractors, governments, civil society organizations and the project proponents, based on transparency, inclusion, and mutual respect, while applying a risk-based approach to avoid overwhelming any stakeholder unnecessarily. Project experience upon which the PPF was based includes that garnered by Indigenous Peoples Organizations and international development specialists such as the Nepal Federation of Indigenous Nationalities (NEFIN) and the Regional Council of Authorized [Indigenous] Representatives ([RCAR] of Sakhalin, RF) and secondly by the firm Cross-Cultural Consulting Services (CCCS) working in Indonesia, Tanzania, Ethiopia, Russia, and Nepal

Consistent with the principles of the GFN provided in the Guidance Notes of the World Bank's ESS7 and IFC's PS7, the PPF serves as the overarching framework for these TG by:

a) Providing detailed guidance on how to apply the principles of FPIC and GFN during the project implementation (FPIC Implementation) phase, in addition to the project preparation (FPIC Negotiation) phase.
b) Treating Indigenous and local communities as partners in project design and implementation rather than external entities to negotiate with.
c) Fashioning a three-sided alliance of partners composed of Indigenous/local communities, local governments and the project as critical partners in key discussions and long-term planning.
d) Allowing both Indigenous and local communities to participate in decision-making processes to develop and implement risk mitigation and benefit generation measures, including monitoring, evaluation, and grievance redress, as part of the IPP or Social Impact Management Plan (SIMP) governance.

The Project Office (PO), through FPIC Coordinator who coordinates with relevant units within the PO, will implement and fund project activities including risk mitigation, benefit generation and FPIC processes. They will report to the relevant government agencies and their own financiers on project performance including compliance on E&S matters and stakeholder engagement. Importantly, a senior management, ideally the project director or deputy director, should represent the project and participate in discussions and decision making at the Working Group (WG)/Governing Board (GB) on matters that concern affected Indigenous and non-Indigenous communities (hereafter, called "FPIC Communities").

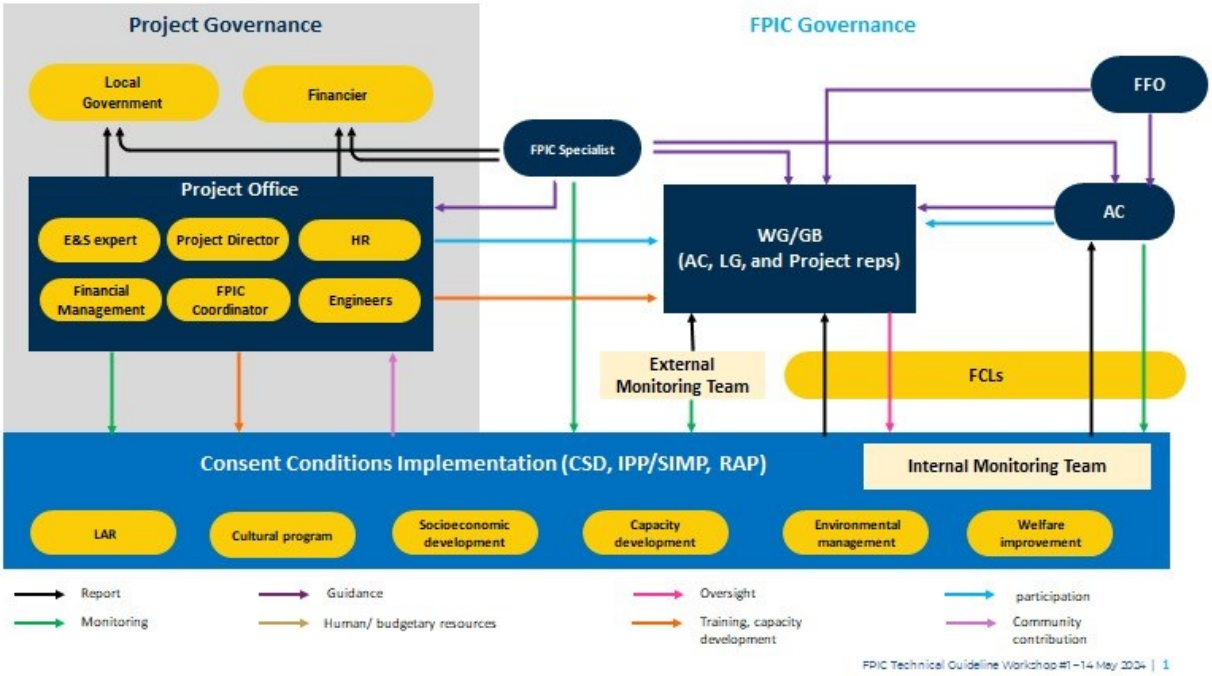

Figure 1: Project - FPIC Governance, both on the project side (left) and the community side (right).

The Advisory Council (AC) consists of representatives from the FPIC Communities and leads their discussion on FPIC processes and project matters that concern them. The AC will participate in the WG which is a tripartite decision body (communities, local governments, the project) that negotiates FPIC, and the GB is its successor that oversees FPIC implementation if FPIC is obtained. FPIC Community Liaisons (FCL) "connect" the AC and members of the FPIC Communities, facilitate discussions in-between consultation meetings and flag issues to the AC, so that the AC can make decisions based on broad-based and inclusive deliberative processes. The Working Group (WG)/ Governing Board (GB) serves as the "decision body" on project matters that concern affected communities while the AC served as the "consent body", independent of the WG/GB.

In between both sides there is the FPIC Specialist who will bridge the project and the community and facilitate their negotiations and who might also serve as the independent External Monitor (EM) during FPIC implementation to monitor adequate implementation of consent conditions including risk mitigation and benefit

generation measures. As will be mentioned below, the FPIC Specialist will play the role of the FFO where risks are not significant and having an independent FFO does not justify the cost; this would most likely occur only when the FPIC-Lite approach is followed.

At the bottom there are Program Committees (PC) responsible for overseeing the implementation of consent conditions including risk mitigation and benefit enhancement measures. The PCs consist of community representatives, and report to WG and/ or GB. An internal monitoring team will monitor progress and performance of activities agreed upon as consent conditions including risk mitigation, benefit generation and capacity development. and report to the WG/GB, AC, and the project.

Detailed roles and responsibilities of respective players will differ between the FPIC Negotiation and Implementation Phases.

4. ADJUSTING FPIC TO PROJECT RISK LEVEL

As a form of stakeholder engagement, FPIC can take different forms and styles. Not all projects must pursue the full FPIC process--its scale and extent can differ depending on project circumstances. FPIC strategies should be responsive to the needs of the Affected Communities as well as the requirements of the financier and the regulator, so that rounds of consultations and other aspects of an FPIC effort can be calibrated to match likely project impacts and avoid overwhelming any stakeholder unnecessarily.

Depending on project circumstances, the scope of FPIC could be expanded or reduced. For example, when Indigenous and neighboring non-Indigenous communities are both affected by the same project, or when some Indigenous communities are subject to one of the three FPIC-requiring circumstances, but others are not, all members of the project-affected communities could be incorporated into the same FPIC process. A possible expansion of FPIC scope, including the pros and cons of such an approach, should be carefully evaluated in the context of FPIC planning.

Conversely, the scope of FPIC may also be limited to certain project aspects, such as when a linear project passes through multiple administrative units and requires FPIC only for a specific component. As stated in the World Bank's GN7 (para. 25.2): "In some projects, FPIC may be required only in relation to specific portions of land or aspects of a project. Examples include: (a) linear projects that pass through multiple human habitats, which may require FPIC for the component that traverses [indigenous peoples'] lands; (b) projects comprising multiple subprojects, some of which are located on [indigenous peoples'] lands, which may require FPIC for the subprojects located on those lands; and (c) projects involving an expansion of ongoing activities, which may require FPIC for the new project activities."

Experience has taught that there are at least three broad approaches to FPIC application:

a) FPIC-Standard: the aim is to achieve FPIC for a project which will significantly affect an IP community in full compliance with applicable IP standards requiring FPIC. These Technical Guidelines will set out this full and robust approach in the chapters following Part One while also touching on how the other approaches below can be utilized.

b) FPIC-Lite: for those FPIC-triggering projects likely resulting in more modest effects on the IP communities, less intensive consultations, studies, and documentation, while keeping the core principles of FPIC, can be sufficient to meet the applicable IP standards. An FPIC-inspired Indigenous Peoples Plan (IPP) may or may not be prepared depending on the requirement of the financier, or an FPIC-inspired SIMP may substitute the IPP together with a Stakeholder Engagement Plan (SEP) to document consultation processes that led to FPIC.

c) FPIC-Like: those projects that do not affect an IP community, but which involve significant stakeholder risks can apply parts of the FPIC Standard approach to build collaborative relationships with key stakeholders toward resolving their concerns in mutually acceptable ways that benefit all, thereby giving the project a "social license to operate. A formal consent statement—while desirable--may or may not be prepared because for this type of project, FPIC is typically not required by financiers or regulators. An FPIC-inspired SIMP would be the operational equivalent of an FPIC-inspired IPP.

From this perspective, FPIC can become a guideway to good stakeholder engagement for most projects. Oxfam (2024:5) has recognized—and endorsed--this emerging global trend of applying FPIC to projects affecting a broad swath of communities Indigenous and non-Indigenous alike:

"The safeguard provided by the principles of FPIC is increasingly interpreted as a best practice standard for affected local communities who do not fit the international legal definitions of rights-holding Indigenous peoples. Many land-connected or frontline communities share similar socioeconomic and political characteristics and long-standing customary connections to land.…In this way, the principles of FPIC represent a best practice for a just

transition and sustainable development, and a crucial project safeguard that can increase the legitimacy of a project in the eyes of all rights holders and reduce the risk of social conflict. For this reason, it is one of the most important legal rights and safeguards for protecting human rights and fighting inequality."

The PPF recognizes this continuing value of the FPIC process and extends the principles and practices from the FPIC Negotiation Phase past a positive consent decision into the equally important FPIC Implementation Phase.

5. FPIC STAKEHOLDER ENGAGEMENT FOR GEOTHERMAL PROJECTS

Geothermal energy, while part of the renewable energy category, is somewhat distinct from other industries and so FPIC stakeholder engagement must take the industry's peculiarities into account when approaching project and community interactions. Its unique aspects that cause distinctive stakeholder risks and affects the outcomes of stakeholder management should be well considered, and detailed guidance be provided on stakeholder engagement and FPIC processes for geothermal development stages:

1. Preliminary and 3G Surveys (geological, geophysical, geochemical): Focus 2A
2. Infrastructure Preparation and Exploration Drilling: Focus 2A
3. Construction (of well pads, access roads, piping system, power plant, etc.): Focus 3A
4. Operation: Focus 4A

Throughout the long period of project preparation and implementation, the project needs to be careful to ensure that FPIC is implemented consistently with all ESS, and particularly with the ESIA process. This will enable affected communities to engage in the FPIC process with a good understanding of potential risks and benefits.

5.1 Long Time Frame

Geothermal project development commonly needs between five and ten years to fully move to commercial operation—and sometimes even longer. While this may be technically necessary, it raises some complications regarding local community engagement:

a) **Personnel turnover**: Contractors, developers, government and project staff, and community leaders in the latter stages of project development are usually not the ones that had initial discussions and reached initial agreements. Lack of awareness and lack of commitment to others' promises can cause a breakdown in communication and trust. The original individuals involved in negotiations or discussions may have been committed to any agreements made or understood, but these can be easily forgotten or ignored as the individuals who represent their parties change. Without documented records of initial understandings memories get hazy and misunderstandings are born.

b) **Legacy issues**: Personnel turnover is exacerbated at a larger scale when different developers and contractors carry out geothermal operations at various phases and stages of development, depending on the investment program that has been approved. In the case of private investment schemes, for instance, in which the developer changes between the preparation/exploration and construction stages based on the tender results, this presents the question of continuity of completion from the preparation/exploration stage to the construction stage and beyond into operation. Legacy problems at each step need to be reviewed and steps taken to resolve them.

c) **Unmet promises and unrealistic expectations**: During early contacts and consultations unauthorized or implicit promises may be made to deliver benefits (such as connecting the affected communities to the electrical grid or to provide energy free of charge) or that the project will be implemented soon. When these things don't materialize promptly due to unavoidable circumstances such as delays in bidding processes, time needed for the developer to secure funding, etc., the initial positive or at least neutral attitude to the project begins to turn negative.

d) **Community "Consultation Fatigue"**: Repeated meetings with the community over years leads to community cynicism and boredom especially during early phases when community consultations discuss the project in vague terms and the project cannot take on many of the concrete inputs from community members. The risk is particularly large when the same old issues get discussed each time new staff get on board or new developers get hired to start engaging with affected communities newly.

e) **Regulatory Changes**: Regulatory frameworks can change over time, affecting project permits, compliance, and financial incentives. These also may affect communities.

5.2 Negative Public Perception of Geothermal Projects

There is a negative perception of drilling activities for exploration due to frequently circulated stories which claim serious negative effects. Community fears are multiple and mainly environmentally focused:

a) Geothermal projects will lower the groundwater supplies and pollute the water with poisonous chemicals.
b) Geothermal projects will cause poisonous gases like H2S (hydrogen sulfide) to be released into adjoining communities.
c) Geothermal projects will all generate dust and noise due to the construction machinery itself and truck movement.
d) Geothermal projects will generate unpleasant odors, noise, or visual disturbances that can lead to mental health issues in people living near the project.
e) Geothermal projects will trigger landslides and earthquakes, and possibly floods as well.
f) Geothermal projects expose local employees to a range of safety hazards.

Economic and cultural risks also loom large:

a) Agricultural productivity will be harmed.
b) Tourist industry will be damaged as natural resources are harmed or tourists scared away.
c) Historical and sacred places will be damaged.
d) Local communities will not likely benefit from the project, especially in the early stages of the project as land is taken out of production to build project infrastructure.

As Adityatama, et al 2018; Umam, et al, 2018; Purba, et al (2020) indicate, such community concerns should be taken as genuine to avoid unnecessary community pushback. Geothermal projects should seek to bring affected communities along by honestly and transparently informing them as to the true nature, risks, and benefits in ways that are easy to understand for them, instead of explaining project risks and benefits in overly technical terms.

5.3 Informational and Compensatory Efforts are Critical

A significant informational and compensatory effort needs to be undertaken early on in project planning and initiation. The project needs to address community fears while not shying away from realistic and accurate risk assessments (along with planned mitigation measures). Yet highly complex technical issues are not easily conveyed in local community meetings, even if facilitated by skilled community workers; how to present them to the affected communities in an accessible format needs to be seriously considered (see Chapter Four, Focus 2A and Box 1 below). Extensive consultations with information sharing needs to take place from the start.

Communities should be entitled to:

a) Receive fair and objective information on risks and benefits of geothermal operations, including project risk management systems and emergency response mechanisms.
b) Benefit from geothermal operations through the corporate social responsibility (CSR) and/or community development programs.
c) Receive fair compensation for damages due directly to geothermal operations.
d) Participate in ESIA process and Environmental and Social Management Plan (ESMP) design and implementation.
e) Use fair and accessible Grievance Redress Mechanisms including judicial systems.

Information sharing and consultation process should go beyond community members directly or indirectly affected by the project. Developers in some countries—including Indonesia—are typically not too concerned with Non-Government Organizations (NGOs) and may not engage them from the start. Outreach to NGOs and Civil Society Organization (CSOs) is a critical part of the entire stakeholder engagement process. Neglecting such stakeholders can cost the project dearly during a later stage.

5.4 FPIC in Stages?

Geothermal projects are broadly classified into two phases: exploration and exploitation phases. The direct footprint of the first exploration drilling phase is typically limited to a few hectares of land for drilling locations, storing materials and drilling employee camps. This differs from the construction stage, which impacts larger areas, directly and indirectly. The FPIC process should be conducted differently at different phases given the different scale and scope of impact.

During the exploration phase, project impacts on local communities are typically limited other than loss of a limited size of land. Compensation should be paid for land loss at the fair replacement value per SPI 204. Those

community members outside the drilling site will not lose land or non-land assets and will thus not receive compensation. While this is legally compliant, it often frustrates many community members whose land will not be acquired as they feel they need to bear various, non-land risks from inadequate wastes and wastewater treatment to potential Hydrogen Sulfide (H2S) leakages including during the exploration phase.

Also, community members will unlikely make neat distinctions between the exploration and exploitation phases of a geothermal project. Pointing out that the main risks and benefits will only occur if the project progresses past the exploration stage may do little to assuage concerns of the local community who may well consider that the exploration phase is just the early phase of an exploitation phase that will come inevitably. They may just become "concerned" from the moment they hear the word "geothermal" which they may associate with some incidents that occurred in another island. Addressing impacts that will occur during the exploration phase only may well not satisfy them.

It may therefore make sense that FPIC-Lite approach is applied during the exploration phase, even though the size of impact and the characteristics of affected people may not require FPIC. It would involve extensive information-sharing and consultations with the community at large in addition to those whose assets would be directly affected. It would set out an agreement as to how the project and the community would engage during the initial exploration stage including exploratory drilling and prior to a decision as to whether to develop the project was made. While the focus will be on activities during the exploration phase, the potential scale and scope of impact that may occur during the exploitation phase, and possible time lag between the two phases, should also be discussed so that community members can make an informed decision based on a good understanding of the full spectrum of the project.

If it is decided that the project would move to the exploitation phase, a new and second FPIC process should begin. Firstly, where there is a significant time gap between the two phases, or different agents are hired to do the exploitation than the one who did the exploration, FPIC achieved at the exploration phase need to be renewed. This time the affected communities would be asked prior to construction beginning to give their FPIC for the project and the measures which would affect them. Similarly, any documents such as an IPP prepared during the first FPIC process would need to be updated as would any comparable SEP. This second FPIC process would best follow guidelines for a full FPIC-Standard process, the scale and scope of which would be adjusted depending on the nature and scale of impacts.

6. INITIAL ENGAGEMENT DURING SURVEYS AND EXPLORATION STAGE IN GEOTHERMAL PROJECTS

Initial stages of stakeholder engagement and FPIC preparation for geothermal projects are affected greatly by the particular nature of these projects as discussed above. As was noted therein, it's probably best to use the "FPIC-lite" approach when working with local and/or Indigenous communities affected by a geothermal project during the survey and exploration phase. Yet even so, there remains a need for extensive consultations since there is much misunderstanding of this type of project and it's best to have a neutral entity such as an FFO to serve as a mediator in discussions between developers and the host community. Also, as mentioned above, local community members, Indigenous or not, may not differentiate between the exploration and exploitation phases, requiring the FPIC process to consider more than the limited impacts that may occur during the exploration phase and refer to the potentially more significant risks that may occur during the exploitation phase.

This need for an added effort stands in contrast to the absence of statutorily required consultations since an Environment Impact Assessment (EIA) and its mandatory consultation process would not typically be invoked for the relatively small exploratory geothermal area. The consultation requirements for the lower UKL/UPL standard may not be sufficient to address community concerns.

During this stage, therefore, projects need to establish community outreach programs to inform about the project as it might be challenging to explain to the community in a clear and easy-to-understand way about the technology to be employed and how it would affect the community. The focus of such extensive consultations should be on education on geothermal risks and mitigation measures and possible benefits from the project. Such outreach efforts can include an overview of geothermal development in general, geothermal development in Indonesia, technical and environmental aspects of geothermal development, and potential impacts/risks of geothermal development and its mitigation measures.

The FPIC-lite approach must also tease out what promises might have been made or implied by the project and the community and clear and honest clarifications made at this point (dealing with "legacy" issues).

Yet even at this early stage, fears may emerge, and accidents occur. Stories will undoubtedly circulate of poisonous gas leaks, but policy lacks specific regulations discussing safe boundaries between drilling locations and residential areas. Furthermore, national health and safety guidelines are often not properly enforced, adding to the

doubts and confusion. For this reason, any initial FPIC-lite agreement should include specification of such distances and a system to monitor such—preferably with community co-participation. Furthermore, the developer can offset community perceived risks with a CSR benefits program even before a decision is made to fully develop the geothermal field. However, projects must be leery of overpromising jobs in this early stage since the need for technical skills will mean that few local jobs will be actually available at that time.

7. ACHIEVING SOCIAL LICENSE & FPIC IN GEOTHERMAL PROJECTS

Once the decision is made to move to the exploitation phase, a new phase of FPIC Process must begin. Whereas the initial survey and exploration phases might have sufficed with an FPIC-Lite approach, the full FPIC approach is probably necessary in this exploitation phase because the impacts are bigger:

- Drilling production wells and injection equipment
- A piping system
- A power plant
- An access road

At this point, community attitudes often begin to turn negative as a large external workforce is brought in and local cultural norms come under stress. They often become concerned about environmental risks (noise pollution, water pollution, induced earthquakes/landslides), foreign workers' influences, and diminishing skilled and non-skilled job opportunities.

Mass land clearance and associated loss of forests to build the access road, well pads, and basecamps often trigger community concerns related to loss of ecosystem services including clean water and agro-forestry opportunities, fears of wild animals' entering villages, and so on. Heavy equipment mobilization and massive soil movements often induce soil and water contamination, dirty roads, dust, or even injuries and fatalities. An extensive use of local water sources can induce contamination and loss of water resources. Health and safety risks related to H2S gas and blowout events can be a source of significant concerns (Adityatama, Purba, & Kristianto, 2018). Presence of large external work often forces raises local concerns about the different cultures and social values between local and non-local workers in daily interaction.

The FPIC process must consider all these fears honestly and transparently through an inclusive ESIA process. A well-crafted and facilitated FPIC process can keep affected communities informed of potential project environmental and social risk and impacts while also inform the project and the ESIA process of their needs and concerns in return. Potential benefit generation measures can also be discussed and agreed upon, including through the establishment of community development fund to which the project can contribute parts of the operating revenues to fund initiatives identified by community members themselves. As a result, affected communities will be able to gain a deeper understanding of project effects and mitigation measures and receive long-term benefits that may more than compensate potential residual risks, helping the project gain a social license to operate and become better able to manage risks that may unexpectedly occur despite all the management measures.

5. CONCLUSION: FPIC-COMPLIANT STAKEHOLDER ENGAGEMENT AS A PROJECT BONUS

While some projects have dreaded carrying out an FPIC process, experience shows that projects benefit by embracing the FPIC principles to build positive and long-lasting relations with affected communities and local governments in a spirit of participation and partnership. What might have been previously resisted as a project-complicating turn of events can develop into a multi-stranded bonus for the project that:

- **Deals with the Past**: through multiple rounds of stakeholder engagement, the FPIC process provides an opportunity to "press a reset button" by addressing any outstanding project "legacy issues" during the negotiations leading to an agreement.
- **Deals with the Present**: allows the project to come to an understanding with the local communities as to the impacts of the project, risk mitigation, benefits-sharing, and resolution of outstanding concerns/grievances culminating in an FPIC agreement.
- **Deals with the Future**: By building in an ongoing project-communities governance structure into the IPP/SIMP and similar instruments, the project can carry over the good will and trust that the FPIC process might engender into long-lasting collaboration with local communities.

Although, per international safeguards standards, "consent" can be granted or determined at only one point in time, any significant change to the project design, implementation arrangements, and/or expected outcomes may require the project to obtain FPIC for such changes. Project designs, and implementation schedules and arrangements, often change during implementation. Also, many unexpected incidents occur during implementation. It is therefore a prudent risk management strategy to establish a constructive partnership with

affected communities based FPIC principles without regard to compliance requirements. Doing so requires unpacking compliance requirements with regard to FPIC in light of strategic risk management and apply FPIC principles flexibly based on the needs of all key stakeholders including the project, affected communities and local governments. The results are sustainable outcomes that benefit all: stable financial return with good market reputation for (private) project proponents; the achievement of policy goals and the expansion of economic base for (local) governments; and the enhanced welfare level and voice for affected communities.

REFERENCES

Adityatama, D., Purba, D., & Kristianto, B. Integrated Geothermal Direct Use Facility as An Alternative Approach In Community Engagement at Early Exploration Phase in Indonesia. IIGCE. Jakarta. (2018).

EBRD (European Bank for Reconstruction and Development). Performance Requirement 7 (2018).

Ibrohim, Prasetyo, & Rekinagara, "Understanding Social Acceptance of Geothermal Energy: A Case Study from Mt. Lawu, Indonesia", In IOP Conf. Ser.: Earth Environ. Sci. 254 01200. (2019).

Purba, D., Adityatama, D. W., Agustino, V., Fininda, F., Alamsyah, D., & Muhammad, F. "Geothermal Drilling Cost Optimization in Indonesia: A Discussion of Various Factors." Proceedings, 45th Workshop on Geothermal Reservoir Engineering. California: IGA. (2020).

Umam, M. F., Muhammad, F., Adityatama, D. W., & Purba, D. P. Tantangan Pengembangan Energi Panas Bumi Dalam Perannya Terhadap Ketahanan Energi di Indonesia. Swara Patra. (2018).

United Nations Permanent Forum on Indigenous Issues (UNPFII). "Bringing Companies into The New Indigenous Peoples Participation & Partnership Paradigm For FPIC-Inclusive Development," In Implementing FPIC In the Context of Indigenous-Corporate Dialog, UNPFII Side-Event, April 2023.

World Bank. Environmental And Social Framework (ESF) (Worldbank.Org). ESS10

World Bank. Environmental And Social Framework (ESF) (Worldbank.Org). ESS7

Unlocking the Socioeconomic Opportunities of Geothermal Project Development and Operation

Stephanie A. Pinnington, Kavita Rai, Elin Hallgrimsdottir, and Muchsin Abdul Qadir

World Bank Group
1818 H Street, N.W., Mail Stop MC 13-1302, Washington, DC 20433 U.S.A.

Spinnington@worldbank.org

Keywords: Geothermal Energy, Socioeconomic Benefits, Value Chain, Localization, Employment, Skill Development, Benefit Sharing, Gender Equality, Social Inclusion

ABSTRACT

Geothermal energy projects, encompassing both electricity generation and direct use of geothermal heat, offer significant opportunities for national and local socioeconomic development. One tangible economic gain is the creation of new direct employment opportunities in construction and operation. Additionally, geothermal projects generate indirect jobs in upstream industries that supply and service the geothermal sector, such as equipment manufacturing. A vast number of induced jobs also emerge from the spending by those directly and indirectly employed in the geothermal industry, as well as from new economic activities enabled by improved access to electricity or heat, such as jobs in geothermal spas or geothermal-supported agricultural processes. The availability of reliable, stable, and affordable energy (both heat and electricity) can have a far-reaching economic impact by attracting industrial players to establish local operations and fostering the growth of small and medium enterprises. While economic benefits are more readily quantifiable, social benefits are equally important. These include enhanced educational opportunities, skill development and diversification, and the introduction of new services and infrastructure by geothermal developers. This paper summarizes key findings and recommendations from a recent report by the World Bank Energy Sector Management Assistance Program (ESMAP), titled "Geothermal Energy: Unveiling the Socioeconomic Benefits." The socioeconomic benefits are analyzed across four categories: participation of domestic companies in the geothermal value chain; geothermal employment and skill development; local development and benefit sharing; and gender equality and social inclusion.

1. INTRODUCTION

Geothermal energy offers a sustainable and reliable solution for many regions, providing a constant power source that can complement variable renewable energy sources and drive the energy transition forward. Unlike intermittent renewable sources like solar and wind, geothermal energy is available 24/7, making it a vital component in achieving energy security and grid stability. Geothermal energy is harnessed in two primary ways:

- Electricity Generation: Geothermal resources are utilized to generate electricity through technologies such as flash steam plants and binary cycle power plants. Flash steam plants use high-pressure hot water from the ground to produce steam that drives a turbine, while binary cycle plants transfer the heat from geothermal water to a secondary fluid with a lower boiling point, which then vaporizes to drive the turbine.
- Direct Use: Geothermal heat is directly applied in various sectors, including thermal baths, greenhouses, aquaculture, industrial processes, and district heating systems. This direct use of geothermal energy can significantly reduce energy costs and carbon emissions in these applications.

Additionally, there is potential to develop integrated systems that combine geothermal electricity generation with direct use applications. These cascading systems utilize geothermal effluent—fluid that has already been used for electricity generation—for lower-temperature applications, such as heating buildings or greenhouses. The versatility of geothermal energy in providing both direct heating solutions and electricity generation, and its ability to provide baseload power, makes it a crucial element in the transition to a sustainable and low-carbon future.

IRENA's World Energy Transitions Outlook provides a strategic roadmap to limit the global temperature increase to 1.5° Celsius. To achieve this target, the roadmap estimates that the installed capacity of geothermal energy must nearly double from 2020 levels by 2030 (IRENA 2023). This ambitious goal highlights the significant role geothermal energy can play in global climate mitigation efforts. Beyond its environmental benefits, expanding geothermal capacity presents a substantial opportunity to generate socioeconomic benefits for local communities and nations. These benefits include the creation of new business opportunities, job growth, skill development, and improved access to essential infrastructure, which can foster economic growth and enhance social inclusion. By

investing in geothermal energy, it is possible for governments to address climate change while simultaneously driving sustainable development and improving quality of life for communities.

This report delves into the socioeconomic benefits that can be actively shaped and significantly enhanced during project development and operation, across both electricity generation and direct use projects. Though important socioeconomic outcomes, this report does not explore broader sectoral advantages, such as the societal and economic benefits attributed to improved energy security, low-cost supply, and reduced greenhouse gas emissions.

In the context of this report, the explored socioeconomic benefits are grouped into the following four categories, as derived from the World Bank Sustainable Renewables Risk Mitigation guidelines (World Bank 2022):

1. *Participation of domestic companies in the geothermal value chain*: Developing and operating geothermal projects creates opportunities for domestic companies to offer goods and services, positively impacting economies. Contracts, varying in size, contribute to fiscal revenues, gross domestic product, and job growth.
2. *Geothermal employment and skill development*: Projects generate direct, indirect, and induced jobs and promote on-the-job learning and formal education opportunities. This results in new skills and greater diversity in the national workforce, promoting domestic employment.
3. *Local development/benefit sharing*: Developers collaborate with local communities to ensure lasting benefits and gain community acceptance. Approaches range from infrastructure improvements and skill development programs to revenue-sharing mechanisms.
4. *Gender equality and social inclusion*: Carefully designed geothermal projects can advance gender equality and social inclusion, addressing disparities based on social identity factors.

This article covers the first three categories in sequence, while gender equality and social inclusion are addressed throughout the paper, recognizing their intersectional nature and impact on achieving equity. The four categories are illustrated in Figure 1.

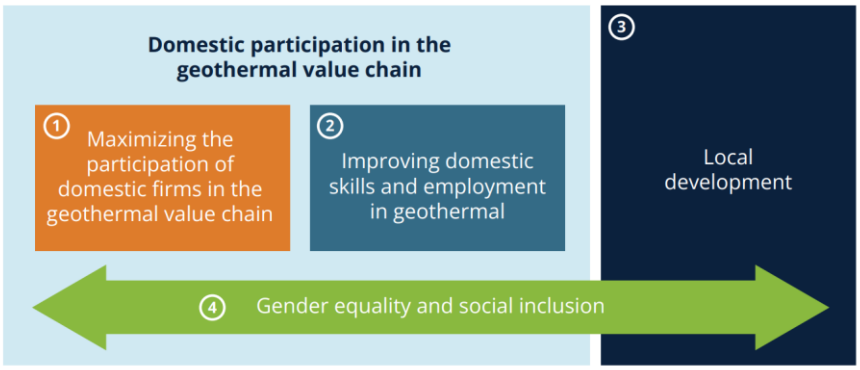

Figure 1: Socioeconomic categories.
(Figure source: ESMAP 2023)

2. LEVERAGING THE GEOTHERMAL VALUE CHAIN TO GENERATE SOCIOECONOMIC BENEFITS

Mapping the geothermal value chain is a crucial first step toward maximizing the potential socioeconomic benefits of geothermal projects. Localization opportunities can be created by identifying where goods, services, and labor can be sourced domestically, thereby adding value and bolstering a country's gross domestic product. Recognizing gaps in domestically available goods, services, and labor presents an opportunity to develop support programs to enhance the domestic industry's capabilities over the medium to long term. Figure 2 illustrates the geothermal value chain at a high level.

It should be noted that in Figure 2, manufacturing sits outside the value chain, as many components are produced outside the project countries. Geothermal turbines, condensers, cooling towers, and generators are highly specialized pieces of equipment, manufactured in only a handful of countries. However, some components, such as heat exchangers, pumps, valves, piping, and cladding, may be manufactured domestically.

Specific value chain activities that require highly specialized expertise and are less likely to be localized. In contrast, many countries present significant potential to localize activities within the value chain's construction and operation and maintenance (O&M) segments. Even when international companies are engaged, it is feasible and advantageous to employ local labor or subcontract portions of the work to domestic firms (ESMAP 2023).

It is important to acknowledge that each country will have a distinct level of domestic capacity in the geothermal value chain. This capacity is highly influenced by factors such as market maturity, availability of skilled labor, policies and regulations, and experience in related industries.

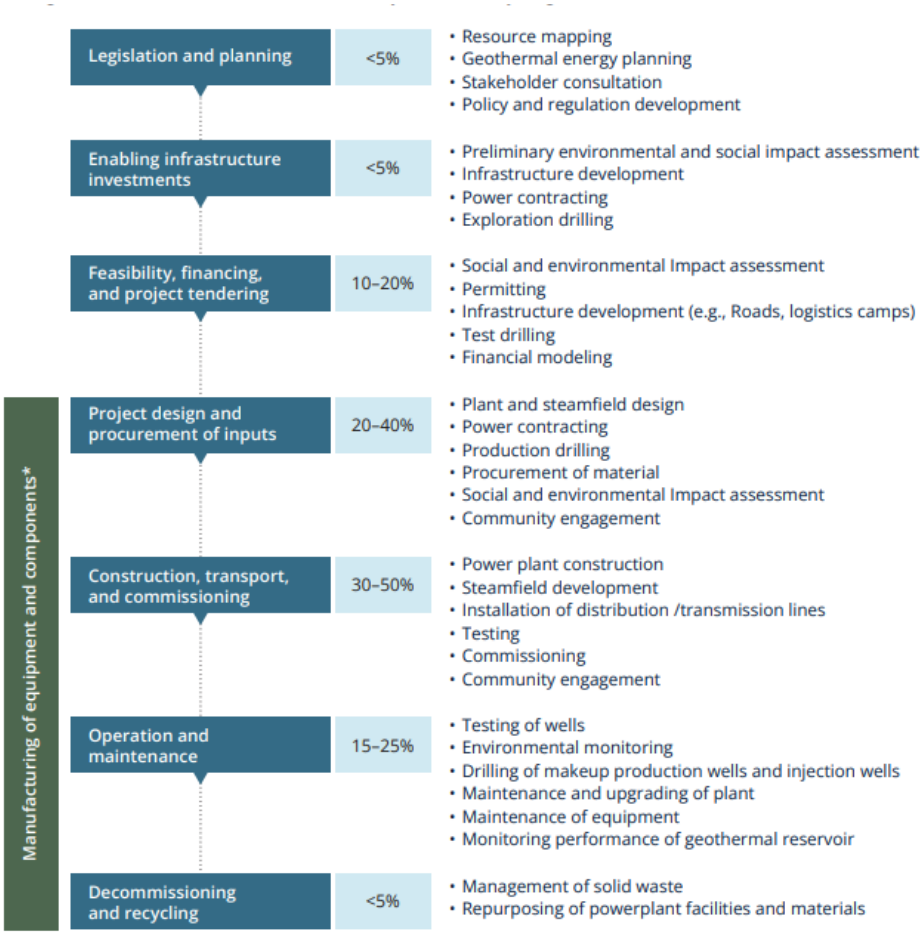

Source: World Bank 2022b and World Bank market sounding 2022.
Note: Figure assumes a 25-year project life cycle.

Figure 2: Localization potential for services along the geothermal value chain. (Figure source: ESMAP 2023)

Governments can leverage project procurement to promote localization within the geothermal value chain. They can help domestic companies grow and develop by incentivizing domestic procurement of certain components and services by developers. However, such procurement practices should be carefully balanced to ensure they do not adversely affect project viability and tariffs.

For example, Türkiye and Indonesia have implemented policies to encourage domestic procurement in their renewable energy sectors. In Türkiye, the renewable energy law supports geothermal generation through a feed-in tariff program. This law included a support scheme called the Renewable Energy Resources Support Mechanism, offering a tariff top-up to power producers who use domestic mechanical and/or electromechanical components (ESMAP 2023). This incentivizes the procurement of domestic components.

In Indonesia, a less flexible approach has been adopted to nurture local manufacturing capacity. Geothermal developers are required to procure a set percentage of components and services domestically, with the exact percentage depending on the project's size. While this measure has successfully incubated local capacity, developers have noted that it limits flexibility and motivation to exceed the established requirements (ESMAP 2023).

Some governments have tailored procurement policies to favor women and disadvantaged groups. The Government of Kenya, for example, has tailored procurement requirements to favor women and disadvantaged groups. Initially, in 2005, Kenya mandated that all government entities procure at least 25 percent of goods and services from small and medium-sized enterprises (SMEs) to address unemployment. However, recognizing that some groups were still being left behind, the government introduced new legislation in 2013 requiring that 30

percent of all goods and services be procured from SMEs owned by youth, women, and disabled individuals. This regulation applies to geothermal entities like the Geothermal Development Company and the majority state-owned power utility KenGen (ESMAP 2023).

Clusters and industry associations also play a pivotal role in enhancing the capacities of the domestic industry. These entities contribute significantly to industry growth through activities such as training, facilitating stakeholder collaboration, and fostering an environment conducive to technology transfer and research and development. For example, Iceland's Renewable Energy Cluster is a nonprofit organization that unites 34 members from across the country. This includes educational and research organizations, energy companies, engineering and consultancy firms, and start-ups, all working together to create a platform that supports entrepreneurship and the export of geothermal knowledge and technology. In Indonesia, the Indonesian Geothermal Association (INAGA) plays a crucial role in supporting industry development by actively participating in the creation and review of geothermal regulations and offering continuous input to the government on related issues. Additionally, INAGA fosters industry collaboration and knowledge sharing through seminars, panel discussions, and conventions.

Crafting specialized financial products can help domestic companies access the capital they need to participate in the geothermal value chain and achieve scale. For example, they may require financing to adapt their business operations, acquire equipment, or hire and train new staff. Such tailored financial solutions help to overcome financing barriers and facilitate greater participation in the industry (ESMAP 2023).

Türkiye has scaled up the participation of domestic companies in the geothermal value chain through strategic financial incentives, particularly in geothermal greenhouses. The Turkish government worked with financial institutions like Ziraat Bank and the Agricultural Credit Cooperative to offer low-interest loans with flexible terms, including a principal grace period of up to two years. Investors can also access grants from the Ministry of Agriculture and Forestry and a national rural development program to further bolster their business case (IRENA 2022).

These financial supports have greatly increased participation in the geothermal sector, particularly through geothermal-heated greenhouses, leading to substantial downstream socioeconomic benefits. For instance, a 71.7-hectare project in Aydin produces 20,000 tons of tomatoes annually and employs 750 people, while another greenhouse in Kütahya produces 35,000 tons of tomatoes and employs 1,100 people. These targeted financial incentives have fostered economic growth and job creation in local communities (ESMAP 2023).

3. EMPLOYMENT CREATION AND SKILLS DEVELOPMENT

In 2021, the geothermal sector provided direct employment to approximately 196,000 individuals globally, more than doubling from 2020 (IRENA and ILO 2022). China leads with 78,000 jobs, followed by the European Union with 60,000, and the United States with 8,000.

Construction and O&M generate the most direct employment across a geothermal project's life cycle. While construction roles are more abundant, they tend to be short-term. Conversely, O&M positions, although fewer, offer employment over the entire lifespan of a geothermal plant. For example, a 50 MW project would create about 155 person-years of construction jobs and 35-60 permanent O&M jobs over 30-50 years, the equivalent of up to 3,000 person-years (ESMAP 2023). Note that the definition of a person-year can vary based on different contexts. A person-year is calculated by dividing the total number of hours worked by all employees on a project by the typical number of hours worked in a year. The creation of induced jobs, although challenging to quantify, can be substantial for geothermal projects. These jobs may arise from greater energy access, availability of heat to scale agricultural or industrial applications, or increased growth of domestic industries due to greater energy reliability.

As of 2022, women held only 22 percent of the jobs in the geothermal sector (ESMAP 2019). The gender disparity is even more pronounced in on-site geothermal jobs and skills roles, including those in construction and operations & maintenance (O&M), where an ESMAP survey found that female participation ranged from zero to 20 percent at most (ESMAP 2023). These roles have traditionally been male-dominated due to the requirement of technical STEM (science, technology, engineering, and mathematics) education, where women have historically been underrepresented.

Over the past four decades, the percentage of women in the geothermal workforce has indeed risen. In 1980, it was only 10 percent. However, this figure also suggests that without intervention, the geothermal sector will not achieve gender equality until 2100 (ESMAP 2023).

Organizations such as Women in Geothermal (WING), along with forward-thinking governments and companies, are working to change these trends. Proactive programs and policies to bring more women into STEM education,

recruit and retain female talent, narrow the gender pay gap, and showcase female leaders are making concrete differences. For example, LaGEO, a government-owned entity responsible for geothermal development in El Salvador, has taken significant steps to improve female employment. LaGEO operates two geothermal plants: one in Ahuachapán with an installed capacity of 95 MW, and another in Berlin with a capacity of 109.4 MW. Currently, 25 percent of LaGEO's staff are women, encompassing both administrative and technical roles (ESMAP 2023).

To further enhance this ratio, LaGEO has implemented policies such as flexible working hours and remote working options, and created female-friendly facilities, including a dedicated nursing room for new mothers. A notable achievement has been increasing female participation in traditionally male-dominated technical roles. By prioritizing women for short-term maintenance roles during major overhauls of the geothermal generation units, LaGEO has boosted female participation in these roles by 30 percent, from 22 women in 2016 to 83 in 2022 (ESMAP 2023).

Geothermal direct use projects hold immense potential for local job creation across various sectors such as agriculture, tourism, and industry. These projects can be stand-alone or complement power generation projects by utilizing excess heat. The types of jobs created depend on the specific end use of geothermal heat. In Poland, a study comparing 10 municipalities with geothermal projects to a control group showed significant employment growth, particularly in the trade and service sectors. Geothermal spas and recreational centers were key drivers of this growth, especially in smaller municipalities, highlighting the potential of geothermal projects to catalyze rural tourism and economic development (Kurek et al. 2021). Industrial uses like district heating improved residents' quality of life but had a lesser impact on employment structures.

Geothermal applications in agriculture, such as geothermal-heated greenhouses and food drying, offer significant yet underexploited potential for job creation. These applications can boost production, reduce food wastage, and create a variety of skilled and unskilled jobs, especially in developing countries where agriculture is the largest employer. Geothermal projects can contribute to gender equity and support women, who play a central role in food production. Opportunities for women in geothermal direct use projects are considered greater than in power production due to the diverse job types available. For instance, in Iceland's Blue Lagoon spa, 58% of jobs are held by women, while in Mexico's Deshidratador Geotermico de Alimentos de Nayarit food drying project and Türkiye's Caldiran Geothermal greenhouse project, women hold 80% and 75% of jobs, respectively (ESMAP 2023).

Despite over a century of using geothermal resources for electricity production, many countries still lack the necessary human resources to support the industry's growth, limiting the potential for domestic employment.

Recruiting highly skilled individuals is the greatest challenge. An ESMAP survey found that 72% of developers reported difficulties in hiring high-skilled labor domestically, with 29% facing this challenge often and 43% occasionally. The hardest roles to fill include geoscientists, geothermal modelers, production and reservoir engineers, drilling specialists, and plant engineers. Medium-skilled roles present occasional recruitment challenges for 43% of developers, while low-skilled roles are the easiest to fill, with 93% of respondents finding local community members who can be trained on the job (ESMAP 2023).

Governments and developers are addressing skill shortages by introducing new geothermal curricula and sending individuals abroad for training in established geothermal markets. For example, Iceland and El Salvador have implemented programs to address the education gap in geothermal expertise for international and regional audiences. Iceland's Geothermal Training Program (GTP), launched in 1979 under the Centre for Capacity Development, Sustainability, and Societal Change (GRÓ), provides intensive hands-on training and tailored programs to strengthen geothermal expertise in developing countries. Since many countries lack geothermal-specific education, the GRÓ GTP has trained 766 fellows from 65 countries, with some advancing to master's or doctorate degrees (ESMAP 2023).

In El Salvador, a partnership between GRÓ GTP, LaGeo, and the University of El Salvador established a five-month geothermal diploma program. In 2022, the program attracted 29 students from various Latin American countries, focusing on gender equality with 44 percent female participants (ESMAP 2023). This initiative provides geothermal training in the native language of participants, making El Salvador a growing hub for geothermal education in Latin America. These programs demonstrate how international collaboration can meet educational needs in countries without sufficient demand for their own geothermal training programs.

Additionally, developers often hire individuals lacking geothermal-specific experience and provide on-the-job training. For example, Indonesia-based Supreme Energy and PT Geo Dipa Energy offer training programs for community members to become plant operators, technicians, field chemists, and well testing officers. PT Geo Dipa Energy also provided welding training to 40 villagers, offering both theory and practical classes, along with certification (ESMAP 2023).

Supreme Energy, founded in 2007, is an Indonesia-based independent power producer. The company has two operational plants, with a total of 170 megawatts of installed capacity, and another site in development. It employs 187 staff; of these, 117 work at the two operational geothermal plants. The team at Supreme Energy has had a strong focus on acquiring and retaining quality talent, and the company has grown quickly over the past 15 years. Although Indonesia's geothermal industry benefits greatly from the wealth of expertise in the country's well-developed domestic oil and gas industry, there are still skills unique to the geothermal industry that require time and effort to develop.

Early in their operations, companies working in geothermal energy struggled to retain experts in the geosciences field, such as geologists, geoscientists, and geophysicists. Given the limited number of qualified subsurface specialists, and the high demand for their skills, employees were often recruited by other companies. High turnover rates presented a business challenge. Rather than recruit talent from abroad, as many companies do when talent is not easily available domestically, Supreme Energy's human resources team devised a strategy to grow talent in house. They decided to hire a cohort of 10 new graduates with geoscience backgrounds and put into action a plan to provide on-the-job learning and an array of professional development opportunities. Most of the new recruits were given the opportunity to study abroad, either in New Zealand or Iceland, to further develop their specialized knowledge. The strategy proved successful, and the company now has a competent geoscience team.

The company has also recognized the opportunity to recruit experienced staff from the oil and gas sector—including electrical and mechanical engineers, environmental engineers, biodiversity specialists, health and safety experts—who can then receive specialized geothermal knowledge once they step into their new roles. The company's induction training program complements classroom learning and on-the-job training with job shadowing, whereby a new hire conducts day-to-day work with an experienced peer in a similar role.

At the power plant level, it has also been a top priority for Supreme Energy to hire members of the local community. Since the specific skills required are not always easily available within the communities surrounding project sites, the company launched a geothermal development program for outstanding associate's and bachelor's degree holders from surrounding communities. Those selected enter a yearlong program, which includes four months of in-class learning, conducted in cooperation with a local university. They then transition to eight months of on-the-job training, after which the trainees are assigned to various roles, including power plant operator, mechanical and electrical technician, field chemist, and well testing officer.

Figure 3: New personnel training at Supreme Energy facility in Cepu, Indonesia. Photo Source: Supreme Energy. (ESMAP 2023).

To expand the geothermal workforce, it is important to disseminate information about job opportunities. Initiatives such as student competitions, mentorship programs, internships, and apprenticeships are instrumental in introducing individuals to career paths in the sector. For example, the US Department of Energy's Geothermal Technologies Office runs an annual student competition called the Geothermal Collegiate Competition. This competition engages students from across the country in solving real-world problems related to geothermal energy. It serves a dual purpose: inspiring a new generation of geothermal scientists and stakeholders, and contributing to research and innovation for the expansion of geothermal energy.

In 2022, the competition focused on planning a direct use project, requiring teams to conduct site identification, resource and demand assessments, conceptual design, and stakeholder engagement. The winning team from the University of Oklahoma was awarded $10,000 for designing a system to repurpose six abandoned oil and gas wells to provide geothermal energy for educational and municipal buildings, including those operated by the

Absentee Shawnee Tribe and Citizen Potawatomi Nation (ESMAP 2023). As a result of this in-depth exposure to the geothermal industry, several team members, originally enrolled in the oil and gas program, chose to pursue advanced studies focusing on geothermal energy. This competition highlights how student competitions can open students' eyes to potential career prospects and pathways in the geothermal sector.

Some governments have successfully integrated incentives into the project procurement process to encourage developers and subcontractors to train and hire domestic or local labor. Jobs created at the local level within communities surrounding geothermal project sites can have extensive socioeconomic benefits and greatly enhance social acceptance of these projects (as detailed in the following section). Roles that can be readily filled by local community members include construction laborers, drivers, security personnel, cooks, cleaners, community engagement liaisons, and administrative staff. With appropriate training, individuals can also be hired for field and pipeline maintenance, as well as plant technician and operator positions.

For example, governments can incentivize domestic hiring in geothermal projects through several strategies. One effective approach is to request developers to produce a plan detailing how they will employ domestic and local workers. This plan ensures that developers design a strategy for recruiting domestic staff and encourages subcontractors to hire locally. It outlines the types of roles that could be filled by the local population and may include plans for training the local workforce to upskill individuals to employable levels.

Another strategy involves providing incentives for developers to meet specified targets for local or domestic employment. For instance, developers could earn additional points during the proposal evaluation stage for committing to these targets, which may become contractual obligations, such as in power purchase agreements. These incentives can be further refined to encourage the hiring of women and socially disadvantaged groups.

Additionally, developers may be required or incentivized to implement and fund education, apprenticeships, and training programs for the domestic workforce. This could involve contributing to the establishment of higher education programs, supporting existing or developing new vocational training programs in welding, electrical work, plumbing, and masonry, and offering apprenticeships or on-the-job training. By providing practical, hands-on training specific to the geothermal industry, developers can ensure that trainees receive employment post-training. These training and education programs can also be tailored to target women and socially disadvantaged groups, further promoting inclusive workforce development.

4. LOCAL DEVELOPMENT AND BENFIT SHARING

Nurturing a positive and enduring relationship with local communities is crucial for developers to gain trust and secure a social license to operate in the geothermal sector. Establishing such a relationship typically involves contributing to lasting benefits within these communities and exceeding the requirements of legal social and environmental frameworks to compensate for losses incurred during project development. Developers have many motivations to share benefits beyond gaining acceptance for project development. Sometimes, benefit sharing is driven by a need to attain favorable environmental, social, and governance ratings or to secure financing, while in other cases, it is driven by the desire to create a positive company image.

To effectively share benefits with local communities, developers must prioritize timely and transparent communication, conduct detailed consultations, and implement collaborative programmatic interventions. It is imperative for developers to strike the right balance between their realistic capabilities and communities' aspirations.

Three primary categories for benefit sharing can be explored:

Improvements or additions to local infrastructure and services: This could include building or improving local infrastructure, or assessing how geothermal resources can be shared for general community purposes, such as heating or agricultural applications. This type of benefit is commonly provided by developers. For example, nearly all developers contribute to community infrastructure, such as building roads, which are often necessary for site access. A survey conducted for this study revealed that out of 15 developers, 13 (87 percent) invested in local infrastructure (ESMAP 2023). Examples of such contributions include constructing schools, plants for processing local agricultural products, wells and water distribution systems, sports areas, roads and bridges, traditional markets, renovations to places of worship, and health clinics. Exploring the potential for community members to utilize geothermal heat through the development of a direct use project is less common, but it would offer numerous benefits to the community, including new jobs and additional sources of income.

Enhancing skills and capability at the community level: Education and training programs are essential to ensure that local community members can easily access new job opportunities created by geothermal projects. These training programs may focus on geothermal-related skills or other sectors, such as improving agricultural practices for local farmers, or building computer or literacy skills. According to a survey of developers, 73 percent offer

training to prepare for geothermal employment, 53 percent provide training to improve performance in other areas like literacy and computer use, and 80 percent focus on enterprise development (EMSAP 2023). For example, in Nicaragua, Polaris Renewable Energy supports educational opportunities for children, youth, and adults, including women. The company provides computer training for teachers and supplies tablets and computers to schools. Additionally, Polaris enhances farmers' technical capacity, including assistance with product commercialization (ESMAP 2023).

Revenue-/ownership-sharing arrangements: Revenue and ownership-sharing arrangements in geothermal projects can involve offering equity stakes, establishing beneficial taxation systems, or directing a portion of revenue to community-controlled entities. Of the 15 developers surveyed, only 33 percent had set up some form of revenue-sharing arrangement (ESMAP 2023). Several examples are provided below:

- In New Zealand, the Māori owned entity Tauhara North No. 2 Trust holds equity stakes in multiple geothermal developments, directing revenue from these operations, estimated at NZ$6 million per year, to grants and programs supporting Māori people (ESMAP 2023).
- In Kenya, the Energy Act 2019 mandates that geothermal licensees pay royalties on the extracted resources' value, with royalties apportioned to the national government (75 percent), county government (20 percent), and local community (5 percent). The community's share is managed through a trust fund established by local community regulations (ESMAP 2023).
- In El Salvador, LaGEO has established a nonprofit foundation called FundaGeo to support community development activities. LaGEO contributes 20 percent of its budget annually to the foundation, with the option to adjust the budget if more funds are needed to support communities (ESMAP 2023).

Including benefit-sharing elements in procurement documents ensures developers fulfill their commitments to communities and allows governments to align project objectives with their local development plans. In some countries, constitutional or macro-level legal frameworks already facilitate benefit distribution at the regional and/or local level, such as through royalty and licensing frameworks. Similarly, government-implemented policies promoting gender equality and social inclusion have bolstered the participation of women and vulnerable groups in benefit-sharing activities.

For example, Indonesia mandates that all geothermal electricity generation permit holders implement corporate social responsibility (CSR) programs focused on local community development and empowerment through the regional government. These costs are included in the annual work program and budget of the permit holders (ESMAP 2023).

In Kenya, proposed regulations require that revenue from energy resource exploitation be shared equitably among government levels and that investments benefit local communities through profits, training, employment, technology transfer, and CSR programs. However, a clear framework for benefit-sharing mechanisms is still needed (ESMAP 2023). Both KenGen and the Geothermal Development Company have multiple programs benefiting communities.

In Türkiye, all licensees must pay the state a yearly fee equivalent to 1 percent of their income, with 20 percent of this fee allocated to the budget of the local municipality where the project site is located (ESMAP 2023).

Above all, cultivating enduring trust with local communities is paramount. Sustained engagement and transparent information mitigate the risk of costly delays or litigation and may ultimately lead to fruitful partnerships. For example, Baseload Capital has created new revenue streams for rural communities in Japan by partnering with local businesses to enhance economic resilience. Japan has a long history of onsens, or natural hot springs, often accompanied by inns called ryokans. In recent years, many small rural businesses operating these onsens have struggled financially, leading to closures.

Baseload Capital initiated a small-scale pilot project with local business owners eager to continue their traditions. The project utilizes heat from the hot springs to generate electricity. After the hot water is used for power generation, it is supplied to the onsens at a temperature suitable for bathing. This innovative approach not only provides a stable supply of clean electricity and hot water but also creates a new long-term revenue source for onsen owners. Baseload Capital and community members hope that this model of pairing rural tourism with electricity generation can be replicated elsewhere, fostering economic sustainability in rural areas (ESMAP 2023).

Countries with varying levels of geothermal development can benefit from each other’s experiences in project management. A recent successful example involves the exchange of lessons in community engagement between Kenya and New Zealand. Recognizing the opportunity to learn from New Zealand’s successes in engaging communities and respecting sacred geothermal sites, Power Africa, the United States Energy Association, and the Geothermal Energy Association facilitated a partnership between Kenya's state-owned utility KenGen, New Zealand's Contact Energy, and two trusts: the Tauhara North No. 2 Trust and the Ngati Tahu Tribal Lands Trust.

This partnership included four exchange missions, where representatives from New Zealand and Kenya visited geothermal sites in both countries to share ideas and best practices in community engagement and partnership models. Inspired by the lessons learned from New Zealand, KenGen developed a new state-of-the-art community engagement program. Additionally, New Zealand counterparts assisted Maasai community leaders in developing strategic visions, including commercial ventures and social development goals (ESMAP 2023).

Focusing on long-term, high-impact outcomes in benefit sharing is essential for fostering sustainable community development. While infrastructure projects like the construction of a football field may be in high demand and provide immediate benefits, they do not yield the same lasting impact as training or enterprise development programs. These programs build local capacities, enhancing community resilience and independence over time.

For example, in the Philippines, the Energy Development Corporation (EDC), the largest geothermal producer in the country and the third largest globally, has significantly evolved its CSR strategy. Initially, EDC's CSR activities were broad, encompassing health, infrastructure, and education, focusing on what could be given to communities. This approach led to a growing reliance on the company.

Recognizing the need for more sustainable outcomes, EDC shifted its philosophy from transactional philanthropy to transformative empowerment. According to EDC's CSR Lead, the company now prioritizes long-term strategies that protect natural resources while simultaneously contributing to community livelihoods and breaking intergenerational poverty cycles. The focus of CSR activities was narrowed to environmental conservation, education, and social enterprise development. Instead of providing handouts, EDC now equips communities with the tools and capacity to improve themselves.

A prime example of this shift is EDC's environmental conservation program, which has planted over six million trees and restored over 10,000 hectares of land. Beyond environmental benefits, this program has empowered community members to become social entrepreneurs, raising and selling tree seedlings, producing forest-friendly coffee, and leading ecotourism ventures. EDC has supported communities in organizing 121 peoples' organizations, three of which have formalized as cooperatives. These organizations receive business training, assistance in securing operating permits, and initial capital for start-up expenses. This strategic approach underscores the importance of focusing on high-impact, sustainable outcomes in benefit sharing to achieve lasting positive effects (ESMAP 2023).

5. CONCLUSION

When planned effectively, all geothermal projects, regardless of size, can be designed to maximize positive socioeconomic outcomes. These outcomes are critical to all stakeholders, including governments, developers (public and private), operators, and the citizens of the project country, both broadly and at the project site level.

Governments can strategically harness geothermal projects as powerful instruments for economic growth, development, poverty reduction, and social justice. Developing new geothermal projects presents a valuable opportunity to cultivate local industry. There is potential to nurture the growth of domestic companies capable of providing essential goods and services for project development, operation, and maintenance, depending on market readiness. Such companies can often grow to cater to multiple industries. Governments can reap fiscal gains from this industrial growth through income taxes levied on those directly or indirectly engaged in the geothermal sector, and taxes on businesses and goods and services required by the sector. Additionally, the availability of reliable and affordable energy has extensive economic implications. It can act as a catalyst for industrial players to establish local operations and further nurture the growth of small and medium enterprises.

Projects can also be designed to effectively align with local, regional, and national priorities for socioeconomic development, reducing the burden on governments to deliver on these plans independently. For example, the infrastructure developed for a project, such as improved road access, can benefit communities. Developers often pledge to bring additional benefits to communities through other infrastructure projects (e.g., schools, health centers, and drinking water) and socioeconomic development programs (e.g., literacy training and agriculture development programs). With proactive policies in place, governments can ensure the equitable distribution of these benefits among their populations, fostering inclusive prosperity for all.

Optimizing socioeconomic benefits within the project country, particularly the project community, is a pivotal strategy for developers and operators to achieve desired project outcomes. Delivering tangible advantages to the project country, especially to local communities, is a potent risk mitigation tool. It reduces the likelihood of opposition, minimizes conflict management costs, and mitigates the risk of valuable investment opportunities being overlooked. Benefits can include a share of the project's profit and local initiatives to improve the livelihoods of people adjacent to the project.

Collaborating with appropriately consulted local communities offers an opportunity to tap into their knowledge and foster trust and partnerships. This collaborative approach increases the feasibility of projects and helps them remain sustainable in the long term. Publicly listed companies, which are constantly striving to increase their environmental, social, and governance ratings, acknowledge the strategic significance of a robust corporate social responsibility strategy, enhancing their appeal to retail and institutional investors and contributing significantly to their public image.

There are also advantages for developers in developing local supply chains, which will benefit the domestic industry and country. Developing local supply chains can reduce project costs and lead to improved operation and maintenance for geothermal plants over the long term.

Geothermal projects hold the potential to empower citizens. Research estimates underscore the employment impact of geothermal projects. Beyond direct employment, geothermal projects generate indirect jobs in upstream industries and create additional induced jobs through the spending habits of those directly and indirectly involved in the industry. For instance, workers contribute to the local economy during construction by spending a portion of their income within the project community. This, in turn, stimulates additional jobs in the restaurant, retail, transportation, and hospitality industries. The emergence of new employment prospects, particularly in rural and low-income communities, holds the potential for substantial social transformations.

While economic benefits are often more easily quantified, equally significant social benefits encompass new educational opportunities and achievements, skill development, and diversification. Through ongoing community consultations, local communities are given the voice and agency to direct local development and benefit-sharing activities that they feel are needed and most beneficial to their way of life.

At the project site and community levels, infrastructure improvements introduced by developers and/or operators, along with development programs, wield far-reaching socioeconomic impacts, including enhanced mobility, improved health care and education, and increased income generation prospects.

In summary, geothermal projects offer a unique blend of economic, social, and environmental benefits that can drive substantial progress in development and poverty reduction. However, these projects also present challenges that require careful planning and community engagement. By strategically harnessing geothermal energy, governments and developers can foster local industry, create jobs, and improve infrastructure, aligning projects with broader socioeconomic goals. Effective collaboration with local communities ensures that the benefits are equitably distributed, enhancing the sustainability and acceptance of these projects. Ultimately, geothermal energy stands as a powerful tool for achieving inclusive prosperity and long-term development, making it a vital component of a sustainable future.

REFERENCES

Energy Sector Management Assistance Program (ESMAP): Geothermal Energy: Unveiling the Socioeconomic Benefits, World Bank, Washington, DC (2023).

Energy Sector Management Assistance Program (ESMAP): Gender Equality in the Geothermal Energy Sector: Road to Sustainability, ESMAP Knowledge Series 028/19, World Bank, Washington, DC (2019).

International Renewable Energy Agency (IRENA): Powering Agri-Food Value Chains with Geothermal Heat: A Guidebook for Policy Makers, International Renewable Energy Agency, Abu Dhabi (2022).

International Renewable Energy Agency (IRENA): World Energy Transitions Outlook 2023: 1.5°C Pathway, International Renewable Energy Agency, Abu Dhabi (2023).

International Renewable Energy Agency (IRENA) and International Labor Organization (ILO): Renewable Energy and Jobs: Annual Review 2022, International Renewable Energy Agency, Abu Dhabi, (2022).

Kurek, A. K., Heijman, W., Ophem, J., Gedek, S., and Stroiny, J.: The Contribution of the Geothermal Resources to Local Employment: Case Study from Poland, Energy Reports, 7, (2021), 1190-1202.

World Bank: A Sure Path to Renewable Energy: Maximizing Socioeconomic Benefits Triggered by Renewables, World Bank, Washington, DC (2022).

Role of Exploration Financing Program to De-risk Indonesia Geothermal

Ferdino R Fadhillah[1], Desak Nyoman Inten Apriani[1], Andreas Suseno[1], Muchsin Qadir Jailani[2], Dorman Purba[1], and Astri Indra Mustika[1]

[1]PT Sarana Multi Infrastruktur (Persero), Sahid Sudirman Center 49th floor, Jakarta, Indonesia
[2]World Bank Indonesia, Indonesia Stock Exchange Building, Jakarta, Indonesia

ferdino@ptsmi.co.id, rfferdino@gmail.com

Keywords: Geothermal Exploration, Risk Mitigation, GREM Program, Indonesia Geothermal Development, Exploration Financing

ABSTRACT

Indonesia is committed to the significant goal of maximizing geothermal energy utilization, necessitating extensive exploration activities. To address the inherent risks, the Indonesian government, in partnership with the World Bank, introduced the Geothermal Resource Risk Mitigation (GREM) program. This facility supports the exploration phase by providing financial mechanisms that de-risk projects.

This study conducts a literature review to assess the challenges confronting geothermal exploration projects in Indonesia. It introduces the key objectives, financing structure, and opportunities provided by the GREM facility. GREM offers risk assessments, technical assistance, and financial support to mitigate the inherent risks of geothermal exploration. This mitigation not only makes geothermal investments more attractive but also improves the bankability of projects and facilitates easier access to financing. The economic analysis is based on published data related to project capital and operational expenditures, revenue projections, financing strategies, and tax treatment.

The paper also includes a project finance analysis to highlight the benefits of utilizing the GREM facility. By employing decision tree with expected monetary value approach, the study evaluates the walk away cost with considering success rate of exploration in hypothetical Indonesian project, comparing scenarios with and without de-risking initiatives.

Our findings indicate that targeted de-risking efforts significantly lower walkaway costs by sharing risks with financiers or the government. The use of de-risking schemes during the exploration stage also reduces the required return from investors, as the associated risks are distributed broader. This study underscores the importance of exploration de-risking application in enhancing geothermal investment. It provides insights for stakeholders aiming to optimize their investment strategies and enhance the resilience of geothermal projects.

1. INTRODUCTION

Indonesia's ambitious plan to significantly expand its geothermal power plant installed capacity is illustrated by the country's target of reaching 5,799 MW by 2030. As of 2023, the installed capacity stands at 2,417.7 MW, highlighting the need for a substantial increase of 3,382 MW over the next seven years. This translates to an average annual addition of 488 MW, a considerable leap from the historical average of 60 MW per year over the past four decades.

The first geothermal power plant in Indonesia, Kamojang-1, was installed in 1983 with a capacity of 30 MW (Darma, Imani, Shidqi, Riyanto, & Daud, Country Update: The Fast Growth of Geothermal Energy Development in Indonesia, 2021; Mansoer & Idral, 2015). Since then, the growth has been steady but slow, utilizing only about 10% of the total geothermal resources. The current pace of development underscores the necessity for massive exploration activities to identify and develop new geothermal resources. Figure 1 shows the historical and target for geothermal power utilization based on EBTKE (2023) and Thinkgeo (2024).

To meet the 2030 target, Indonesia should enhance its exploration efforts and adopt comprehensive de-risking measures. Exploration involves identifying viable geothermal resources, which requires significant investment and technological expertise. De-risking strategies, such as the Geothermal Resource Risk Mitigation (GREM) program, are essential to reduce the financial risks associated with exploration and early-stage development.

These efforts will not only accelerate the development of new geothermal projects but also ensure that the projects are financially viable and sustainable. By addressing the exploration and risk challenges, Indonesia can unlock its vast geothermal potential, contributing significantly to the country's renewable energy goals and sustainability target.

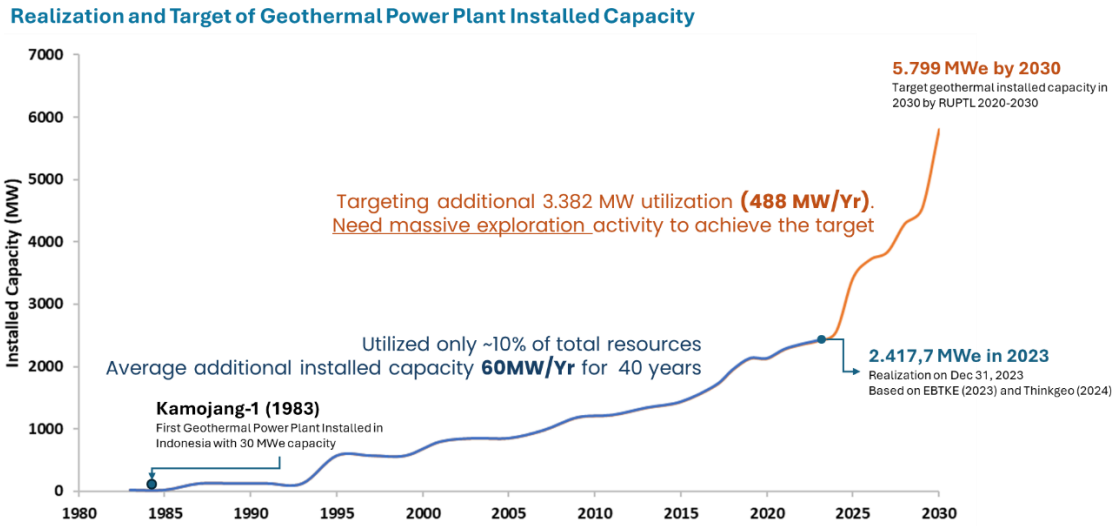

Figure 1: target for geothermal power utilization based on EBTKE (2023) and Thinkgeo (2024).

1.1 Opportunity and Challenges of Geothermal Business

The geothermal sector in Indonesia holds significant market potential, particularly due to the concentration of current reserves in Sumatra and Java, regions with substantial electricity demand. These areas are heavily reliant on coal-fired power plants, which are being phased out under a program initiated by the Government of Indonesia (GoI). This strategic move to reduce coal dependency presents an opportunity for geothermal electricity generation to emerge as a viable substitute (Fadhillah, et al., 2023). Geothermal energy, capable of providing baseload power, is expected to replace coal as the primary source of power generation in Indonesia (World bank, 2011).

Despite its promising potential, the geothermal industry in Indonesia faces significant challenges in attracting investors. The high risks associated with geothermal projects are not adequately compensated by returns, deterring investment. Development projects frequently encounter obstacles during the transition to the production phase, including unfavorable economic conditions, limited resource availability, and social concerns. The industry's progression is influenced by a complex interplay of political, economic, social, and technical (Komendantova, Patt, Barras, & Battaglini, 2012; IRENA, 2022). Figure 2 shows the general problem of Indonesia geothermal project based on Fadhillah (Fadhillah F. R., Economic Evaluation of Bravo Geothermal Prospect in Participating Green Energy Effort, 2023).

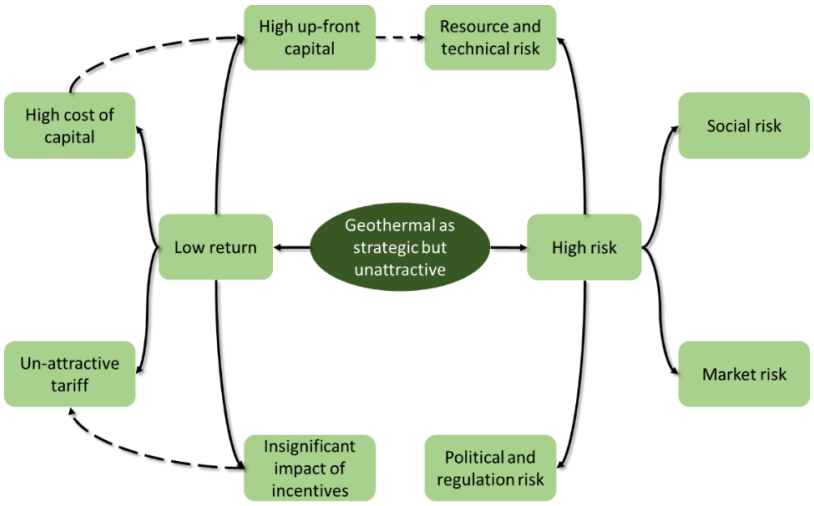

Figure 2: The problem tree of general Indonesia geothermal project.

1.2 Research Question and Objective

The main goal of this study is to assess exploration de-risking program affects the financial viability and attractiveness of geothermal exploration projects in Indonesia. Additionally, the paper introduces the Geothermal Resource Risk Mitigation Program (GREM) as a de-risking facility in Indonesia through a literature review. The research addresses the following questions:

1. What are the major risks encountered by geothermal projects during the exploration stage in Indonesia?
2. How does the mechanism of Geothermal Resources Risk Mitigation program (GREM)?
3. What is the impact of the geothermal de-risking program on project attractiveness from a financial perspective?

2. INDONESIA GEOTHERMAL BUSINESS OVERVIEW

2.1 Indonesia Geothermal Player

Indonesia has 46 geothermal power plants, including expansion units, developed by both State-Owned Enterprises (SOE) and Independent Power Producers (IPP) across 17 geothermal working areas, primarily in Sumatra and Java (Fadhillah F. R., Economic Evaluation of Bravo Geothermal Prospect in Participating Green Energy Effort, 2023; Brilian, et al., 2024). The top three geothermal producers in the country are mainly from the IPP sector. KKOB Star Energy Geothermal Ltd. leads with the highest capacity, totaling 874 MW from just three geothermal fields. PT Pertamina Geothermal Energy (Persero) ranks second, with 677 MW from six fields. Together, these two developers account for half of Indonesia's total installed geothermal capacity. The other half is provided by KKOB Sarulla Operation Ltd., PT Supreme Energy, KS Orka Renewables, PT Geo Dipa Energi (Persero), and PT PLN (Persero).

Notably, KKOB Star Energy Geothermal Ltd. and PT Pertamina Geothermal Energy (Persero) employ different development strategies. KKOB Star Energy focuses on maximizing output from a limited number of fields, whereas PT Pertamina Geothermal Energy manages a larger number of fields, each with relatively smaller capacities.

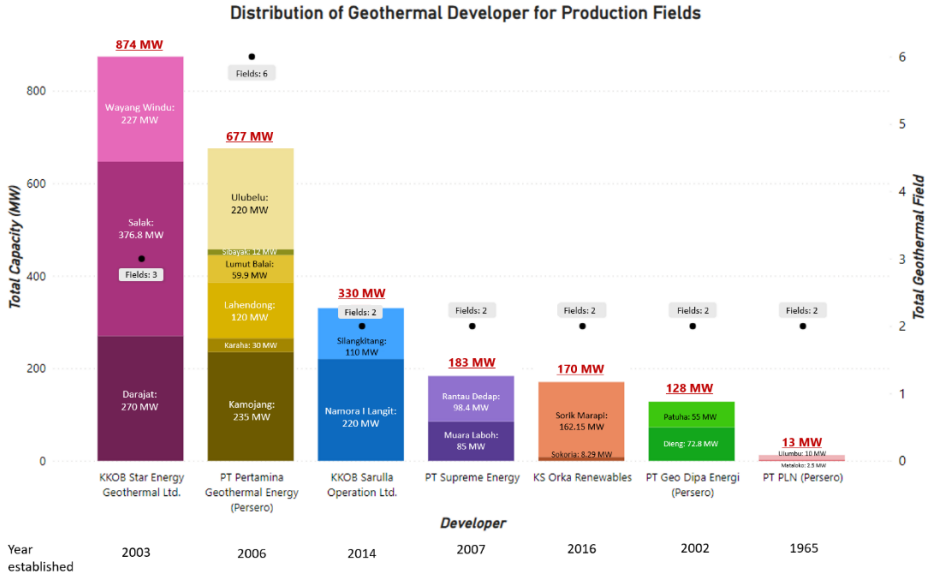

Figure 3: Geothermal player in Indonesia.

2.2 Geothermal Project Stage

The geothermal business process, especially for electricity generation, mainly consisted of preliminary survey, exploration, test drilling, project review, field development, power plant construction, commissioning, and production phases (ESMAP, 2012; IGA, 2014). A geothermal company in Indonesia is eligible to perform preliminary survey until feasibility study for 7 years maximum. The company that successfully reaches commercial operation date (COD) would obtain 30 years of license, Conversely, in cases where an area is found unpromising for geothermal development during the preliminary survey and feasibility study phase, the company is obliged to relinquish the rights to that specific area to the government (Purba, et al., 2021; GoI, 2014). The summary of Indonesia geothermal project stages shown in Figure 4 based on (Fadhillah F. R., Economic Evaluation of Bravo Geothermal Prospect in Participating Green Energy Effort, 2023).

In the exploration phase of geothermal development in Indonesia, the government has launched several initiatives and introduced specific terminologies to support the process. These measures are intended to reduce exploration risks and encourage a favorable investment climate (Apriani, et al., 2023). Below are some of the key government-implemented schemes and terminologies (Table 1):

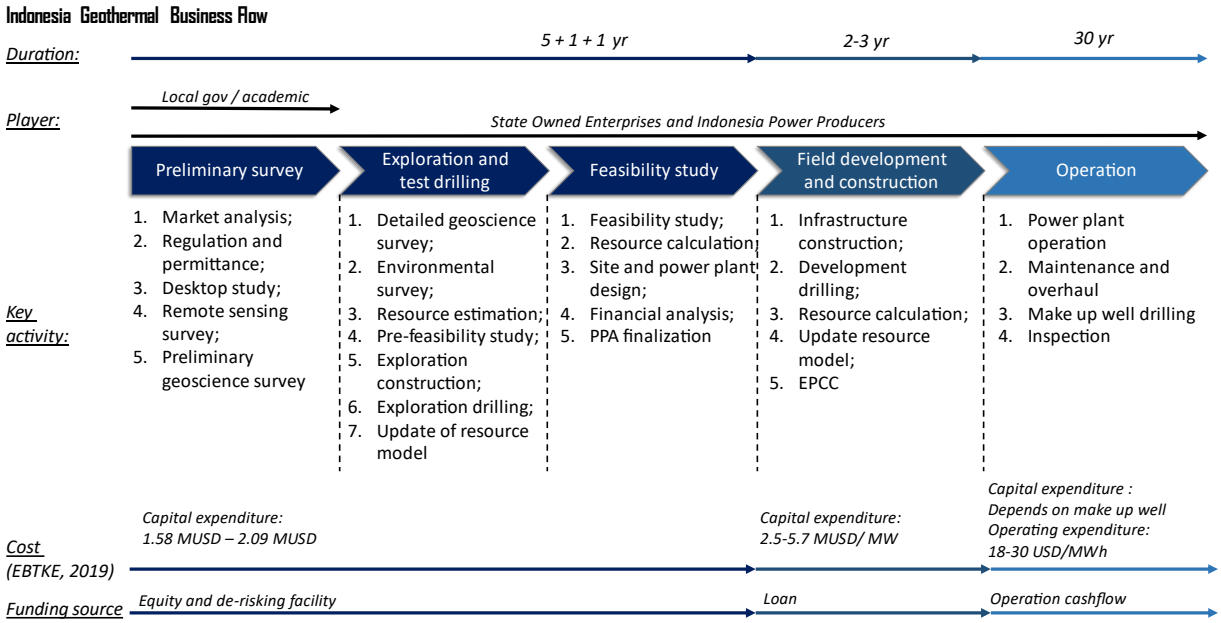

Figure 4: Indonesia geothermal business flow modified from GoI (2014), Purba (2021), and ESDM (2022).

Table 1: Geothermal exploration schemes and terminologies in Indonesia.

***Wilayah Terbuka* (Geothermal Open Area)**	An area suspected of having geothermal potential outside the coordinate boundaries of a Geothermal Working Area
Assignment Area	A Geothermal Open Area with certain coordinate boundaries offered to an Other Party for PSP or PSPE
WKP (Geothermal Working Area)	An area with defined coordinate boundaries used for the exploitation of Geothermal for Indirect Use (power)
***Penugasan Survei Pendahuluan*/PSP (Preliminary Survey Assignment)**	The assignment given by the Ministry of Energy and Mineral Resources to carry out the Preliminary Survey activity
***Penugasan Survei Pendahuluan dan Eksplorasi/PSPE* (Preliminary Survey and Exploration Assignment)**	The assignment given by the Ministry of Energy and Mineral Resources to carry out the activities of the Preliminary Survey and Exploration
***Izin Panas Bumi/IPB* (Geothermal License)**	Permit to conduct exploration and/or exploitation of Geothermal for Indirect Utilization in certain working areas
Government Drilling	Scheme for government to conduct the early stage of geothermal development (preliminary survey and exploration drilling)

In Indonesia's geothermal industry, electricity generation is the primary product and main revenue source. Under common business practices, the steam or electricity is sold to Perusahaan Listrik Negara (PLN), the state-owned electricity company, which is the exclusive buyer. This gives PLN considerable influence in the market, particularly in setting tariffs, which often benefits the company (Fadhillah F. R., 2023). Subsequently, PLN also transmits and distributes electricity to consumers across various sectors, including industrial, commercial, and residential users (Brilian, et al., 2024). This arrangement is known as the on-grid model.

2.3 Geothermal Exploration Challenges

The main objective of geothermal exploration programs is to identify and assess resources that can be economically developed based on exploration findings (Apriani, et al., 2023). However, developers and investors frequently face dilemmas during this stage due to the need for significant upfront capital investment and the reliance on limited, uncertain information about geothermal potential.

Drilling activities and the construction of essential infrastructure, such as access roads and well pads, represent the most substantial costs in an exploration project. The primary challenges in Indonesia's geothermal exploration are summarized below (IGA, 2014; Poernomo A. S., 2015; Darma S. , Indonesia: Vast geothermal potential, modest but growing exploitation, 2016; Umam, Adityatama, & Purba, 2018; Siahaan, Purba, Septiani, &

Paripurna, Preparing Technical and Commercial Documents for Geothermal Exploration Project Financing in Indonesia, 2023):

1. Difficulty in locating the "hottest area": Geothermal resources could not directly be manifested at the surface, necessitating detailed geological, geochemical, and geophysical (3G) surveys and test well drilling. The lack of clear surface indications or thermal manifestations can make it challenging to identify the most promising areas for exploration, leading to an increased risk of drilling dry wells.
2. High exploration costs: The expenses for 3G surveys, developing a reliable conceptual model, and drilling test wells can be substantial. There is always a risk that geothermal projects may not yield viable resources, making it challenging for developers to secure funding for exploration activities due to the high upfront capital and uncertainties involved.
3. Complex geology: Geothermal resources in Indonesia are mainly located in a volcanic area with complex geological environments, making it difficult to understand the subsurface conditions and identify the most promising areas for exploration.
4. Lack of direct and reliable data: In some cases, there may be a need for more data on the geology and geochemistry of an area, making it challenging to identify potential resources and plan the exploration activities.
5. Environmental impacts: Exploration activities can have various environmental impacts, such as air and surface water pollution, soil degradation, hazardous noise, release of hazardous gases, landslides, deforestation, and the potential for groundwater contamination. Mitigating these impacts can be costly and time-consuming.
6. Social and community impacts: Exploration activities can also have social and community impacts, such as displacement of local communities and land-use conflicts. Developers need to address these impacts and engage with local communities to ensure their support and minimize the risk of project delays or cancellations.
7. Uncertain regulations: Geothermal exploration is subject to various national, regional, and local regulations. The uncertainty can make it difficult for developers to navigate the regulatory environment and can increase the risk of project delays or cancellations.

Sanyal et al. (2011) provided statistical data from the Kamojang field in Indonesia, showing an initial drilling success rate of 20-50% for the first six wells. The study highlighted significant fluctuations in success rates as additional wells were drilled, which gradually stabilized during the development phase and exceeded 70% in the operational phase. This data underscores the inherent challenges and uncertainties of geothermal exploration drilling, emphasizing the necessity of effective risk mitigation strategies to improve the overall success rate of geothermal projects.

IFC (2013) reported an average success rate of 50% across 2,613 wells. Notably, success rates improved with subsequent drilling activities, starting at 59% for the first five wells and rising to 71% for the first 30 wells, with this upward trend continuing beyond the 50th well. The dataset for this analysis included both publicly available information and confidential data shared by individual geothermal developers with GeothermEx, Inc. over four decades.

The exploration stage of geothermal development is characterized by the primary risk associated with the uncertainty of identifying economically viable geothermal resources. Recognizing this challenge, institutions within the global geothermal industry have undertaken efforts to develop schemes aimed at mitigating risks for geothermal developers during the exploration phase. Subsequent chapters will delve into an in-depth examination of the various schemes presently employed in the geothermal industry.

2.4 Geothermal Exploration Cost

The cost associated with geothermal exploration in Indonesia can differ widely, depending on the specific aspects of the project and the exploration drilling approach employed. Table 2 offers an estimate of the costs expected for carrying out geothermal exploration drilling, giving a broad view of the financial expenses involved.

This table describes the step-by-step process of an exploration project, highlighting various phases that are undertaken sequentially, starting with attempts to gather data at a lower cost. After the initial collection of data, if the findings suggest a viable geothermal presence, developers may move forward with more substantial investment activities. Noteworthy in Table 2 is the emphasis on the peak of exploration endeavours—the drilling of deep wells, which stands as the most expensive phase of exploration.

The information laid out in the table illustrates a strategic approach to exploration, where early-stage activities with lower costs set the stage for subsequent, more intensive investments. Highlighting the cost differences between phases emphasizes the importance of careful financial planning and decision-making in geothermal

exploration projects. Understanding the financial implications at each phase allows developers to manage their resources and evaluate the economic viability of advancing through the exploration stages.

It is crucial to recognize that the costs presented in Table 2 can vary based on a variety of factors, such as drilling depth and complexity, geological conditions, logistical challenges, and the specific circumstances of the local area. As such, the costs should be viewed as estimates that provide a general guide rather than definitive figures.

Table 1: Cost estimate of geothermal exploration drilling (modified from IGA, 2014; GeothermEx, 2010; Purwanto et al., 2018; Purba et al, 2019; Purba et al., 2020; Adityatama, 2020; Purba et al., 2021).

Activity	Geology survey	Geochemistry survey	Geophysical survey	Initial conceptual integration and well targeting	Exploration drilling
Activity Description	Geological mapping on an area of 400 km^2. The work package including pre-field-work study, rock sampling and identification, structural mapping, and reporting.	Work package including a pre-field-work study, liquid and gas sampling from 30 locations, laboratory analysis and reporting.	Work package including pre-field-work study, 100 MT stations and 150 Gravity stations, interpretations, and reporting.	Integrate all report from 3G surveys to create several scenarios of conceptual models, including peer review.	Using 3 standard/big hole type or 5 slim hole type or combination of 2 slimholes and 1 full-size well. The cost estimate includes infrastructure construction cost to support the drilling operation. The duration estimate includes procurement, preparation, mobilization, drilling, well testing and demobilization.
Duration	4-8 months	4-8 months	4-8 months	3-6 months	18 - 36 months
Cost Estimate (USD)	300,000 – 700,000	200,000 – 400,000	1,000,000 – 2,000,000	100,000 – 200,000	15,000,000 – 50,000,000
Considerations	Accuracy might be affected by terrain, weather, and field personnel experiences.	Accuracy might be affected by sampling method (minimize contamination) and laboratory competences.	Accuracy might be affected by noise during data acquisition and processing method, including personnel interpretation.	Accuracy might be affected by 3G data accuracy and personnel experiences and interpretation.	Allow the exploration team to acquire downhole data directly from the reservoir, which is valuable for more accurate resource assessment but requires higher cost and time than the 3G survey.

3. GLOBAL AND INDONESIA EXPLORATION DE-RISKING SCHEME

A geothermal exploration de-risking scheme is a strategic approach designed to mitigate the financial risks inherent in geothermal exploration projects. The main objective of this scheme is to develop efficient exploration programs that increase the success ratio of exploration activities (Apriani, et al., 2023). ESMAP (2016) and Nur (2023) highlight the importance of exploration de-risking programs as crucial for accelerating and enhancing the development and utilization of geothermal resources.

Government agencies and entities play a pivotal role in mitigating risks associated with geothermal projects, particularly during the exploration phase. This can be achieved through various mechanisms, such as providing financial support, technical assistance, and regulatory oversight. In some instances, governments may act as the sole developer of a geothermal project, assuming all associated risks. Even when development financing is available, the sovereign guarantees typically required mean that the government ultimately bears the risk of project failure. For a government-led exploration program to be effective, it requires an entity with strong in-house expertise, access to appropriate technology, and sufficient financial resources (ESMAP, 2016)

1. **Government drilling** through various mechanisms, such as financial support, technical assistance, and regulatory oversight. In certain instances, governments may even take on the role of the sole developer of a geothermal project, thereby assuming all associated risks. Additionally, when development financing is provided, the requirement for sovereign guarantees often means that the government ultimately bears the risk of project failure. For a government-led exploration program to be successful, it must involve an entity with strong in-house expertise, access to appropriate technology, and sufficient financial resources. (ESMAP, 2016). ESMAP (2016) emphasizes the government led exploration program already executes in 12 countries with 31 projects that equals to 3.613 MW capacity.

2. **Grants and loans, along with cost-sharing arrangements**, play crucial roles in supporting geothermal projects. rants, which are non-repayable funds provided by governments, organizations, or agencies, are often used to fund exploration, feasibility studies, and early-stage development, thereby mitigating financial risks. In contrast, loans are funds borrowed by geothermal developers from financial institutions or governments to cover project expenses. Unlike grants, loans must be repaid with interest over a specified period, increasing the overall costs of the project. (Fadhillah, 2023).

   Cost-sharing arrangements involve distributing project expenses among various stakeholders, such as government entities, private investors, and development agencies. These arrangements help to spread the financial burden and incentivize collaboration, promoting sustainable geothermal development (ESMAP, 2016). effective cost-shared exploration can be achieved through the following strategies:
   a. Government Commitment to Geothermal Expansion: When the government is dedicated to rapidly increasing geothermal generation capacity, it can encourage private-sector involvement by implementing supportive policies.
   b. Attracting Private Investment and Expertise: In situations where the government lacks sufficient geothermal expertise, it is vital to attract private investment and technical knowledge to tap into the country's geothermal resources.
   c. Experience and Selection of Developers: The effectiveness of cost-shared drilling relies on selecting experienced developers through a transparent process with clear criteria, including their willingness and capability to invest risk capital in exploration drilling.
   d. Ensuring Project Continuity: Beneficiaries of cost-sharing funds should be committed to fully developing the project through all subsequent stages until it becomes operational, rather than transferring development rights to other investors after receiving cost-sharing benefits. This ensures the project's continuity and successful completion.

3. **Loan guarantees** serve as a form of financial assurance for lenders, ensuring that if a project encounters unforeseen difficulties or defaults, the guaranteed portion of the loan will be covered by the government or specific financial institutions. This mechanism reduces perceived risks for lenders and encourages them to offer more favorable lending terms to project developers (Apriani, et al., 2023).

Table 3 provides a comparison of various exploration financing facilities utilized in different countries around the world. A detailed comparison of each of these facilities will be presented in a separate table at the end of this paper based on Apriani (2023).

3.1 Indonesia Practice

Indonesia has implemented four geothermal resource risk mitigation schemes. These include government-sponsored exploration drilling (GEUDP), government-led exploration drilling, cost-sharing funding facilities for both public and private developers (GREM), and specific SOE drilling facilities.

a. **The Government-sponsored exploration drilling, executed in partnership with the World Bank through the Geothermal Energy Upstream Development Project (GEUDP),** utilizes funds from both the World Bank and the Indonesian government (via the PISP fund) to finance from 3G surveys to exploration drilling. Initially, SMI led these activities, later transitioning to PT Geo Dipa Energi (Persero) or GDE as the executing body. Once an exploration area is proven viable for geothermal development,

it is to be put up for tender, along with the geothermal data package acquired during exploration drilling. If a developer wins the bid for the geothermal working area explored under GEUDP, they will be required to pay some form of fee or reimbursement.

b. **Government-led exploration drilling, which is implemented by Geological Agency**. In contrast with the GEUDP, where the government only sponsors the exploration activity through the funding via PISP fund, in this scheme the Government through Geological Agency (Badan Geologi) also conduct the exploration surveys and drilling. The Government Drilling by Geological Agency is fully funded by State Budget (APBN), in contrast with GEUDP which has some funding from the World Bank. Should the result be promising, the geothermal working area is then put up for tender. However, unlike the GEUDP scheme, the developer winning the concession is not required to reimburse or pay success fee for the exploration drilling.

c. **The Exploration drilling funding facility for public developers and private developers, facilitated by the World Bank's Geothermal Resource Risk Mitigation (GREM) project**, is designed to reduce financial risks in geothermal exploration. It supports both public and private entities by offering up to USD 30 million per project, with a distinctive feature of risk-sharing that allows for partial repayment for unproductive exploration. In addition to financial support, GREM includes a component for technical assistance and capacity building, enhancing the competencies of key stakeholders in geothermal development.

d. **Exploration drilling funding facility for SOE (SOE Drilling Facility).** The SOE Drilling Facility mirrors the GREM Public Window in structure but relies solely on PISP funding. It also caps funding at USD 30 million per project, offering a mix of loans and risk mitigation support exclusively for SOEs.

These aforementioned schemes are at various stages of implementation, with ongoing projects but no final outcomes yet, making it challenging to assess their effectiveness fully from actual results. The summary of the current risk mitigation schemes in Indonesia and the impact on geothermal development in Indonesia is shown in Table 4.

Table 3: Comparison of Various Exploration Financing Support in Various Countries.

Country	Government led exploration	Grants / loan and cost sharing	Loan guarantee
Turkiye	Government led exploration	Risk sharing mechanism	-
New Zealand	Government led exploration	-	-
East Africa	-	1. East Africa Rift Geothermal Development Program 2. Africa Geothermal Risk Mitigation Program	-
United States	US DOE through national laboratories.	1. User Coupled Confirmation Drilling Program (UCDP) 2. American Recovery and Reinvestment Act (ARRA)	1. Geothermal Loan Guarantee Program (GLGP) 2. Loans for Geothermal Reservoir Confirmation Program
Indonesia	1. Geothermal Energy Upstream Development Project (GEUDP) 2. Government Drilling through Geological Agency	1. Geothermal Resource Risk Mitigation Project (GREM) 2. State Owned Enterprise (SOE) Drilling	1. Sovereign guarantee

Table 4: Summary of the current resource risk mitigation scheme in Indonesia.

Risk Mitigation Scheme	Main Features / Benefit	Current Progress	Impact on Geothermal Development in Indonesia
GEUDP **Year starts of the program: 2017**	Increase success rate for developer's exploration as the bidders can use real	WB withdrew its financing for the geothermal exploration in Wae Sano due to lack of community acceptance in the area. This happened prior any	Due to indefinite delays in the drilling at Wae Sano and the recent commencement at Jailolo, it is currently not possible to assess the actual impact of the GEUDP on

Risk Mitigation Scheme	Main Features / Benefit	Current Progress	Impact on Geothermal Development in Indonesia
	resource information obtained by drilling. Reduces the number of wells to be drilled to reach required MW. Shorten the developer's exploration duration. Reduce cost of equity. Increases the successful of concession tender on resource proven project.	wells have been drilled in Wae Sano. The Government of Indonesia then decided to continue Wae Sano outside the GEUDP program. The current project ongoing under GEUDP program is Jailolo, in which the 3G survey has been done and currently in progress of exploration drilling preparation.	geothermal development in Indonesia. The theoretical impact of the GEUDP program on geothermal tariffs will be discussed in later sections.
Government Drilling by Geological Agency **Year starts of the program: 2019**	Increase success rate during further exploration drilling by developer if the Geological Agency's drilling success to find economic geothermal resource. Potentially reduces the exploration duration. Increases the successful of concession tender on resource proven project.	Drilling in Cisolok failed to reach the targeted 2,000 mMD depth well, and was only able to reach 806 mMD in CKK-1A. The second well (CKK-2) was not drilled due to the significant cost overrun in drilling in the first well. Drilling in Nage was significantly longer than initial plan. NGE-01A reached 1,500 mMD after 175 days, while the NGE-02 only reached 600 mMD before experiencing stuck pipe and then abandoned. NGE-01A drilling result shows high temperature (260 degC), but no permeability. To date, only Nage that has been put to tender by EBTKE.	Although Nage was put up for tender in 2022 and retendered in 2023, the response has been lackluster, with Pertamina Geothermal Energy (PGEO) withdrawing from the tender process. Interviews with several geothermal developers revealed that some companies believe the resource areas in Cisolok and Nage have not been sufficiently derisked. This is attributed to the failure to reach total depth (TD) and to identify economically viable geothermal reservoirs in both areas.
GREM **Year starts of the program: 2020**	Provides loan for exploration and delineation. Reduce walkaway cost or cost of failure. Reduce cost of equity.	The application for GREM facility is currently ongoing for two Public Window exploration projects. The technical proposals from the developers are currently being reviewed prior deciding whether to continue the process or not. From the Private Window, so far there are three developers that have signed the NDA. There are a total of four geothermal fields that are in Preliminary Assessment by SMI from the Private Window application.	So far, no drilling has been funded by GREM, but four developers (one SOE and three private) have signed NDAs with SMI to initiate GREM funding applications for seven exploration fields. This suggests that the funding facility's partial repayment or forgiveness options are appealing to developers, potentially boosting private investment in Indonesia's geothermal exploration.
SOE Drilling	Similar to GREM.	GDE has submitted the technical proposal for SOE Drilling funding facility for	Currently, only one exploration field owned by a state-owned enterprise has begun the application

Risk Mitigation Scheme	Main Features / Benefit	Current Progress	Impact on Geothermal Development in Indonesia
Year starts of the program: 2020	Provide loan for exploration. Reduce walkaway cost or cost of failure. Reduce cost of equity.	Candradimuka field. The technical proposal is currently being reviewed by SMI.	process for SOE drilling funding. The process is still in its early stages, making it premature to evaluate its overall impact on Indonesia's geothermal development.

4. GEOTHERMAL RESOURCE RISK MITIGATION PROGRAM (GREM) IMPLICATION TO PROJECT

4.1 GREM Mechanism

The Geothermal Resource Risk Mitigation (GREM) facility, established by Sarana Multi Infrastruktur (SMI) in collaboration with the World Bank, is designed to mitigate risks associated with geothermal exploration projects. The primary objective of GREM is to expedite investment in Indonesia's geothermal sector by providing financial support for upstream resource development. This support is particularly focused on exploration and delineation drilling, which are essential for resource confirmation. The facility offers a debt package to geothermal developers who have already secured a working area and conducted preliminary surveys, thereby facilitating critical exploration and delineation drilling activities.

This facility is crucial because conventional debt and financing sources are typically reluctant to fund exploration drilling due to the high levels of uncertainty and risk involved. In contrast, GREM provides the necessary financial support for exploration drilling to confirm the presence of sufficient productive steam resources for power generation. Once the resource is confirmed as sufficient, developers can proceed with the project using commercial project finance for exploitation drilling and power plant development. Consequently, GREM not only facilitates the initial stages of geothermal development but also boosts confidence among other financial institutions, making them more likely to fund subsequent development stages of the pertinent working area. (Siahaan, Purba, Septiani, & Paripurna, 2023; Siahaan, Septiani, Purba, & Paripurna, 2023; SMI, 2021).

Siahaan et al (2023) emphasize the unique feature of GREM, which is the availability of a de-risking facility in the event of exploration failure. This feature ensures that the developer does not fully bear the risks and costs associated with exploration. According to SMI (2021), this facility provides a form of “forgiveness” for each project, allowing the developer to repay only a portion (up to 50%) of the total facility in the event of exploration and/or political risk:

1. Exploration Risk: This involves the possibility that despite completing all drilling activities and adhering to the exploration cost budget as specified in the work plan, an independent assessment of the geothermal data and information concludes that the exploitation and/or utilization stage in that area is not feasible.
2. Political Risk: This occurs when government actions, based on applicable laws and regulations, halt the implementation of activities specified in the work plan and exploration cost budget.

Based on MoF Regulation No. 80/2022 Article 34, financing provided by PT SMI to public developers may include a risk-sharing mechanism that allows for forgiveness of up to 50% of the total facility in the event of exploration and/or political risks. GREM incorporates this risk-sharing mechanism, enabling developers to receive partial repayment of the facility (up to 50% of the total facility limit) in the case of unsuccessful explorations. Consequently, the GREM facility offers crucial early-stage support, helping to mobilize downstream financing from commercial and other financiers on a larger scale.

Table 5 provides a comparison of various exploration financing support in Indonesia and other countries particularly facility supports that are intended to the public and private geothermal developers as explained above. Due limited information on the geothermal de-risking facility, the comparison will not include United States and New Zealand geothermal exploration de-risking scheme based on Apriani (2023).

4.2 GREM IMPACT TO PROJECT ATTRACTIVENESS

4.2.1 Reduction in walkaway cost

The program significantly reduces the walkaway cost for developers in the event of failed exploration, thereby mitigating one of the primary financial risks associated with geothermal projects. Walkaway cost refers to the sunk costs that developers must absorb when an exploration project does not yield viable geothermal resources, often leading to substantial financial losses.

By reducing the walkaway costs, GREM effectively lowers the financial risks associated with unsuccessful geothermal exploration. This encourages more developers to enter the geothermal sector, knowing that their potential losses are mitigated through the risk-sharing mechanism. Furthermore, this reduction in financial risk makes geothermal projects more attractive to investors.

Figure 5 shows the simulation using decision tree with economic monetary value for GREM facilities. Under the GREM program, developers receive partial forgiveness of up to 50% of the exploration costs in the event of failure. For instance, in a typical exploration project with a total cost of 40 million USD, GREM covers 30 million USD of this amount. If the exploration is unsuccessful, GREM forgives 15 million USD of the drilling costs, significantly lowering the financial burden on developers. This significant reduction means that developers are more likely to undertake geothermal exploration, knowing that their potential financial losses are mitigated by the GREM facility. This not only makes geothermal projects more financially viable but also more attractive to investors who are typically risk-averse.

Table 52: Comparison of Various Exploration Financing Support in Various Countries (Siahaan et al, 2023).

Parameter	GREM Public Window (Indonesia)	GREM Private Window (Indonesia)	RSM (Turkey)	GRMF (East Africa)
Source of Funding	A combination of Multilateral Funds (channeled through the IBRD) and Geothermal Fund from the Indonesian Government	Multilateral Funds (channeled through the IBRD)	Clean Technology Fund (CTF)	German Federal Ministry for Economic Cooperation and the European Union (EU) - Africa Infrastructure Trust Fund through KfW Entwicklungsbank (KfW)
Eligible Beneficiary	Public geothermal developers (SOE/ majority owned by SOE developers)	Private geothermal developers	Private geothermal developers	Public developers, private developers, and Public Private Partnership (PPP)
Type of Facility Support	Loan with de-risking feature	Loan combined with subscription of Financial Instrument(s) issued by the private developers	Reimbursable Grant	Grant
Facility Limit	75% of the approved Total Drilling Program Costs with cap at maximum USD 30 million per project	75% of the approved Total Drilling Program Costs with cap at maximum USD 30 million per project	Maximum USD 4 million per project	- Infrastructure grants: up to 20% of the costs for infrastructure required for surface studies and drilling programs. - Surface study grants: up to 80% of eligible costs for surface study (excluding infrastructure costs). - Drilling grants: up to 40% of cost of exploration drilling and testing programs for reservoir confirmation wells (excluding infrastructure costs). - Continuation Premium: up to 30% of the approved costs of continuation activities or up to 30% of the developer's share of

Parameter	GREM Public Window (Indonesia)	GREM Private Window (Indonesia)	RSM (Turkey)	GRMF (East Africa)
				the eligible costs incurred. during the initial drilling, whatever is lower.
Eligible Expenditures	- Surface Studies (only for legacy financing) - Exploration drilling - Well-Testing	- Exploration drilling - Well-Testing	Exploration drilling (infrastructure costs shall not be included). Depending on the project location, exploration study costs may be eligible	- Surface studies - Exploration drilling and well testing
Facility Disbursement Scheme	- The disbursement schedule is discussed and agreed between PT SMI and the beneficiary during loan negotiation. - Every disbursement request will require the beneficiary to qualify that they are within an acceptable bound of the pro-forma budgets. - All disbursements must result in debt-to-equity ratio being maintained of not more than 75:25	- The disbursement schedule is discussed and agreed between PT SMI and the beneficiary during loan negotiation. - Every disbursement request will require the beneficiary to qualify that they are within an acceptable bound of the pro-forma budgets. - All disbursements must result in debt-to-equity ratio being maintained of not more than 75:25	Reimbursement of actual Acceptable Well Cost (AWC) incurred by the license holder.	Disbursement of grant funding based on project milestones and achievement of specified targets.
Repayment Obligation of the Beneficiary	Principal and interest with potential principal forgiveness if the exploration is unsuccessful	Principal and interest with potential principal forgiveness if the exploration is unsuccessful	5 (five) percent of success fee of the Acceptable Well Cost (AWC) if the exploration is successful	Grant funding, no repayment obligation

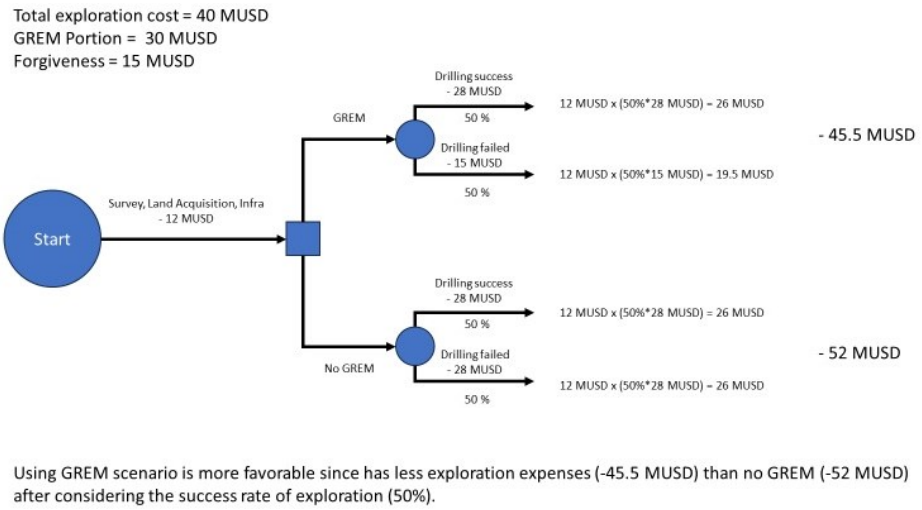

Figure 5: simulation using decision tree with economic monetary value for GREM facilities.

4.2.2 Risk sharing led to lower required return

The reduced risk associated with GREM-backed projects directly impacts the cost of equity. Typically, geothermal projects face high costs of equity due to the inherent uncertainties and risks involved, especially during the early exploration stages. However, with the GREM program sharing these risks, the perceived risk by investors is lower, which leads to a decrease in the required return on equity. According to GT Management (2020), the cost of equity is assumed to decrease to 12.5% for State-Owned Enterprise (SOE) developers and 15% for Independent Power Producers (IPP) developers, as opposed to higher rates typically associated with greenfield projects.

This reduction in the cost of equity translates into a lower discount rate used in Net Present Value (NPV) calculations, thereby enhancing the project's NPV. A lower discount rate means future cash flows are valued higher, which improves the overall financial attractiveness of the project. Investors are more likely to commit funds to projects with higher NPVs, which makes GREM-backed geothermal projects more competitive in the market.

5. CONCLUSION

The Geothermal Resource Risk Mitigation (GREM) program, introduced by the Indonesian government in partnership with the World Bank, plays a crucial role in enhancing geothermal energy utilization in Indonesia by addressing the significant risks associated with exploration activities. This study highlights the challenges faced by geothermal exploration projects and demonstrates how the GREM facility provides comprehensive support through risk assessments, technical assistance, and financial mechanisms. The economic analysis and project finance evaluation reveal that targeted de-risking efforts significantly reduce walkaway costs and lower the required return from investors by distributing risks more broadly. These findings emphasize the importance of de-risking initiatives in making geothermal investments more attractive and bankable. The study provides valuable insights for stakeholders to optimize their investment strategies and improve the resilience and financial viability of geothermal projects in Indonesia.

REFERENCES

Apriani Desak Nyoman Inten [et al.] Addressing Geothermal Exploration Resource Risk in Indonesia: Introducing GREM as a Pioneer De Risking Facility [Conference] // IIGCE 2023. - Jakarta : [s.n.], 2023.

Brilian Vincentius A. [et al.] Geothermal Captive Use to Support Industrial Activities: Applicable Industry Sectors, Worldwide Experience, and Its Potential and Challenges in Indonesia [Conference] // Workshop on Geothermal Reservoir Engineering. - California : Standord University, 2024.

Darma S Indonesia: Vast geothermal potential, modest but growing exploitation [Journal] // Geothermal Power Generation: Developments and Innovation. - 2016.

Darma Surya [et al.] Country Update: The Fast Growth of Geothermal Energy Development in Indonesia [Conference] // World Geothermal Congress 2020+1. - Reykjavik : WGC, 2021.

EBTKE Pedoman Investasi Pembangkit Listrik Tenaga Panas Bumi [Report]. - Jakarta: Direktorat Jenderal Energi Baru, Terbarukan, dan Konservasi Energi, Kementerian Energi dan Sumber Daya Mineral, 2021.

EBTKE Pengembangan Panas Bumi di Indonesia. [Report]. - Jakarta: Ministry of Energy and Mineral Resources, 2022.

ESMAP Comparative Analysis of Approaches to Geothermal Resource Risk Mitigation [Report]. - [s.l.] : ESMAP, 2016.

ESMAP Geothermal Handbook [Report]. - [s.l.] : World Bank, 2012.

Fadhillah Ferdino R [et al.] Economic Evaluation of Bravo Geothermal Prospect in Participating Green Energy Effort [Journal] // Gema Ekonomi. - 2023.

Fadhillah Ferdino R Economic Evaluation of Bravo Geothermal Prospect in Participating Green Energy Effort [Report]. - Jakarta : Institut Teknologi Bandung, 2023.

GoI Law 14/2014 : Geothermal Law [Book]. - Jakarta: Government of Indonesia, 2014.

IGA Best Practice Guide for Geothermal Exploration [Report]. - Jakarta: World Bank, 2014.

IRENA Indonesia Energy Transition Outlook [Report]. - Abu Dhabi: International Renewable Energy Agency, 2022.

Komendantova Nadejda [et al.] Perception of risks in renewable energy projects: The case of concentrated solar power in North Africa [Journal] // Elsevier. - 2012.

Mansoer W. Resmiasih and Idral Alanda Geothermal Resources Development in Indonesia: A History [Conference] // World Geothermal Congress. - Melbourne: WGC, 2015.

Nur S [et al.] Determining Optimal Incentives for Geothermal Project Framework Under Tariff Constraint [Journal] // Elsevier. - 2023.

Poernomo A. S An overview of Indonesia Geothermal Development – Current Status and Its Challenges. [Conference] // Proceedings of World Geothermal Congress. - Melbourne: [s.n.], 2015.

Purba Dorman [et al.] Resource Assessment Methods Selection for Geothermal Exploration Project in Indonesia: What Are the Considerations? [Conference] // Stanford Geothermal Workshop. - Stanford: Stanford University, 2021.

Siahaan Maria F. [et al.] Preparing Technical and Commercial Documents for Geothermal Exploration Project Financing in Indonesia [Conference] // Stanford Geothermal Workshop. - 2023.

ThinkGeo ThinkGeoEnergy's Top 10 Geothermal Countries 2023 – Power Generation Capacity [Online] // Webinar. - 2024. - https://www.thinkgeoenergy.com/thinkgeoenergys-top-10-geothermal-countries-2023-power-generation-capacity/.

Umam M., Adityatama D and Purba D Tantangan Pengembangan Energi Panas Bumi Dalam Perannya terhadap Ketahanan terhadap Ketahanan Energi di Indonesia. [Journal] // Swara Patra. - 2018.

World bank Penggunaan energi panas bumi Indonesia akan naik secara signifikan [Online] // World Bank. - 2011. - https://www.worldbank.org/in/news/feature/2011/07/26/indonesia-expand-geothermal-power-alternative-coal.

A Multi-Actor Analysis and Policy Analysis for Geothermal Development in Indonesia

Andi Susmanto[1,2] and Akhmad Hidayatno[1]

[1]Department of Industrial Engineering Universitas Indonesia, Depok 16424, Indonesia
[2]Ministry of Energy and Mineral Resources, Jakarta 10320, Indonesia

andi.susmanto21@ui.ac.id, akhmad.hidayatno@ui.ac.id

Keywords: multi-actor analysis, PESTLE, policy; geothermal energy, Indonesia

ABSTRACT

The Indonesian government has prepared a road map for Net Zero Emissions (NZE) in the energy sector by 2060. The government is committed internationally to reducing greenhouse gas emissions as part of its Nationally Determined Contributions. This paper presents a comprehensive analysis of geothermal development through multi-actor analysis and a political, economic, social, technological, legal, and environmental (PESTLE) analysis and policy analysis approach by reviewing the most up-to-date relevant literature. This study focuses on multi-actor analysis in geothermal development through the actors, interests, authorities, and regulations in regulating the geothermal activities of each actor. The results show that geothermal energy development involves stakeholders, policies or regulations, institutions, technology, and other interconnected and changing elements. Based on the results of stakeholder analysis and policy analysis, the Ministry of Environment and Forestry (MEF) and the Ministry of Finance (MF) are key stakeholders in geothermal development. To encourage geothermal development to achieve the NZE 2060 target, MEF can do this by facilitating Environmental Approval and licensing in conservation forest areas and encouraging geothermal development in conservation forest areas by changing the function of the Nature Reserve Forest Area into a Nature Conservation Area with utilization zones/blocks. Meanwhile, MF can encourage geothermal development by providing fiscal and non-fiscal facilities to improve the economics of geothermal projects.

1. INTRODUCTION

Geothermal energy development is a dynamic and complex process involving stakeholders, policies or regulations, institutions, technology, and other interconnected and changing elements (Vidal & Marle, 2015; Yudha et al., 2021). This complexity increases the challenges for the government in achieving these goals. A systematic and holistic approach is needed to understand the complexity of geothermal energy development. Understanding the relationship between the elements involved in developing the geothermal energy sector is becoming increasingly important and necessary to develop long-term strategies to encourage the development of the geothermal energy sector (Yudha et al., 2022). Geothermal development is a complex matter because it is surrounded by many external factors which often create uncertainty and hinder its development. Project scale, interrelationships, regulations, context, permits, and project stage contribute to the complex nature of geothermal development (Vidal & Marle, 2015).

ESMAP divides geothermal development into several stages: preliminary survey, exploration, well testing, project planning and review, field development and drilling of production and injection wells (exploitation), construction, start-up, commissioning, and operation and maintenance. Full-scale geothermal development projects typically take 5 to 10 years to complete. Due to the long development cycle of these projects, GPP is not a quick fix to a country's electricity supply problems. However, it must be part of a long-term electricity generation strategy (Gehringer & Loksha, 2012). Geothermal has advantages compared to other power plants, namely that it is a clean, environmentally friendly, and renewable energy source, does not require large areas of land, and does not have a significant impact on the environment because it implements a closed cycle, namely that geothermal fluid that has been utilized into electrical energy will be injected back into the in the bowels of the earth. Apart from that, geothermal energy has other advantages, namely that it is free from the risk of fluctuations in primary energy prices, does not depend on the weather, and can only be used to provide local energy so that it can be used as capital for national energy security.

Therefore, this research is interested in examining multi-actor and PESTLE research as an approach to developing a Geothermal Power Plant (GPP) in Indonesia. This literature review will map the challenges and opportunities in developing sustainable GPP. The study began by mapping stakeholders in geothermal development, studying the literature on mapping regulations and stakeholder authority from a sustainable perspective, and identifying indicators used to measure the interest or performance of stakeholders in geothermal development in Indonesia.

3. RESEARCH METHODOLOGY

3.1 Case Study: Geothermal Development in Indonesia

Identifying, mapping, and analyzing the dynamic relationships between each level are essential pillars of a multi-level perspective framework in Indonesia's geothermal energy development transition process. The actors involved in the geothermal energy transition in Indonesia are energy providers, the Indonesian National Electricity Company, and consumers (Wisaksono et al., 2018). Geothermal resource development projects in Indonesia can be categorized as public-private partnerships, where business relationships are formed between private companies and government institutions to implement electricity supply projects. The problem of geothermal development in Indonesia is also greatly influenced by infrastructure conditions, such as road access, transportation modes, and high-voltage electricity transmission that will be used to supply electricity produced by GPP (Yudha et al., 2022).

The Indonesian Government has committed to contributing to preventing climate change and rising global temperatures through the 21st Conference of Parties (COP) of the United Nations Framework Convention on Climate Change (UNFCC) in 2015, better known as the Paris Agreement to reduce emissions by 29% by own efforts and become 41% with international cooperation by 2030. The Indonesian Government's commitment was later ratified by the Paris Agreement on the United Nations Framework Convention Concerning Climate Change. This commitment to climate change aligns with the Indonesian Government's commitment to the seventh Sustainable Development Goal (SDGs), namely ensuring access to affordable, reliable, sustainable, and modern energy for all. The global target for 2030 for renewable energy is to substantially increase the proportion of renewable energy in the worldwide energy mix. As a national energy policy guideline to provide direction for national energy management to realize energy independence and national energy security to support sustainable national development, the Indonesian Government sets a renewable energy mix of 23% of the primary energy mix in 2025 and 31% in 2050.

To increase the electrification ratio, support the achievement of renewable energy mix targets, and reduce greenhouse gas emissions, it is necessary to develop electricity infrastructure, especially power plants sourced from renewable energy. In the PLN Electricity Supply Business Plan (RUPTL) for 2021-2030, electricity generation sourced from renewable energy is targeted at 20,923 megawatts or the equivalent of 51.6% of the total electricity generation and renewable energy mix for electricity generation in 2025 is targeted at 23%. The additional capacity of the GPP in the PLN RUPTL 2021-2030 is targeted at 3,355 megawatts. The Indonesian government has prepared a road map for NZE in the energy sector by 2060. It is hoped that GPP capacity can increase significantly from 2,200 megawatts in 2021 to 5,500 megawatts in 2030 and 22,000 megawatts in 2060. Indonesia has enormous potential geothermal resources, and their locations are spread along the active volcanic route (ring of fire) starting from Sumatra, Java, Bali, Nusa Tenggara, North Sulawesi, and Maluku. Based on the Regional Distribution Map and Indonesian Geothermal Resources in 2023, Indonesia's geothermal resources are 23,591.8 megawatts. However, the use of geothermal energy for electrical energy in 2024 will only reach 2,597.51 megawatts or 11% of the total geothermal resources.

Even though the potential is enormous, there are still many obstacles that hinder the optimal use of geothermal energy, both from technical and non-technical aspects, including high-risk geothermal exploration, geothermal locations in conservation areas, pricing mechanisms, infrastructure that has not yet been built which affects geothermal development, power wheeling, and community resistance. One of the biggest obstacles in developing geothermal energy lies in the early stages of upstream geothermal projects, namely the exploration stage. Geothermal resource development projects in Indonesia can be categorized as public-private partnerships (PPP), where business relationships are formed between private companies and government institutions to implement electricity supply projects. The problem of geothermal development in Indonesia is also greatly influenced by infrastructure conditions, such as road access, transportation modes, and high-voltage electricity transmission that will be used to supply electricity produced by GPP (Yudha et al., 2022).

3.2 Methodology

Several methods are available to support actor analysis. The basic procedure covers six steps: formulation of a problem, inventory of the actors involved, exhibiting the formal chart, determining the actors' interests, mapping out the interdependencies between actors, and determining the consequences of these findings (Enserink et al., 2022). PESTLE analysis is often used to uncover problems and discourses that are primarily qualitative, making them difficult or unsuitable to be resolved quantitatively. In particular, it can be used to holistically analyze and describe various problems. PESTLE analysis has recently been applied to specific industrial sectors, such as the conventional energy industry, fossil fuels (Climent Barba et al., 2016; Yudha et al., 2018), and renewable energy (Islam & Mamun, 2017; Mytilinou et al., 2017).

Using PESTLE analysis, new strategic policies can be developed to replace and update policies that are no longer effective or efficient. PESTLE analysis can also be used to monitor macro or external environmental factors that play a role in impacts on the environment. Political analysis looks at the extent and impact of state power on the

economy. For example, specific environmental policies may impose sanctions on companies that cannot comply. Economic factors directly impact economic capacity, organizations, industrial/market sectors, and nation-states. Social factors examine the social context of these institutions, including, but not limited to, population analysis, demographics, and cultural trends. Technological factors relate to technological progress, including research and development (R&D), specialized technology, and automation. Legal factors consider laws and policies, including consumer protection laws, safety standards, and employment laws. Environmental factors are all critical factors conditioned or influenced by environmental problems, geographical location, global climate change, weather, et cetera (Yudha & Tjahjono, 2019). This research uses multi-actor analysis and PESTLE as the approach. Stakeholder analysis is a simple tool whose proper use may be expected to develop in accuracy and value as analysts gain experience, especially learning to recognize stakeholders and stakes from having seen the like before in other projects. PESTLE analysis is a framework or tool commonly used in business management to analyze the environment in which they operate or plan to launch new operations.

The geothermal project development for the case study was mapped, and the actors for various stages were analyzed. An actor analysis covering six steps was performed to characterize the development of the geothermal project. As shown in Figure 1 and Figure 2, one of the preliminary steps is the literature review.

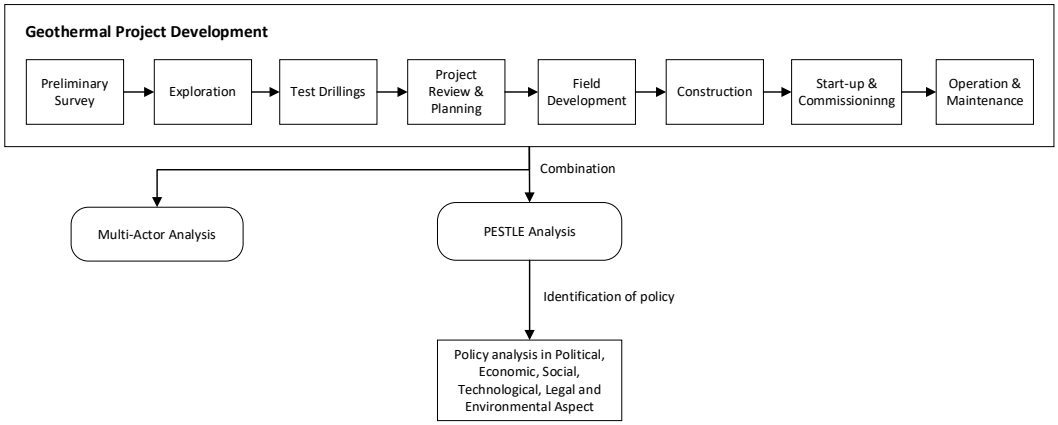

Figure 1: Concept of multi-actor analysis and policy analysis for the geothermal development.

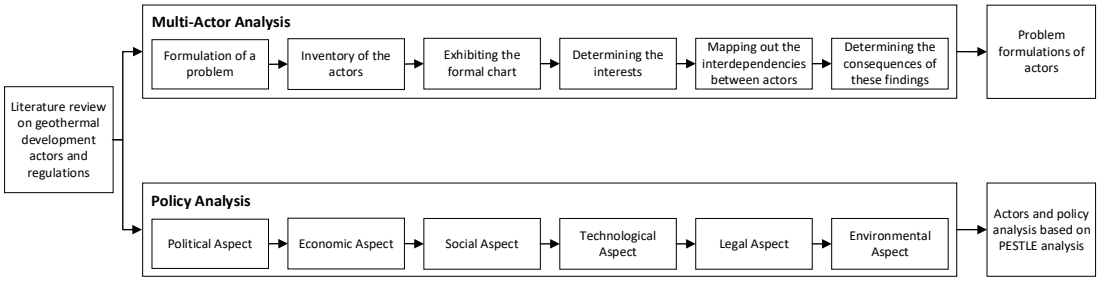

Figure 2: Research methodology.

4. RESULT AND DISCUSSION

4.1 Multi-Actor Analysis

A complex policy structure surrounds the geothermal industry, with multiple actors holding conflicting powers and agendas. The stakeholder structure consists of ministries, local governments, PLN, IPP, and PT SMI, a state-owned enterprise that the Ministry of Finance has assigned to manage PISP funds. The policy structure surrounding the geothermal industry in Indonesia is shown in Figure 3.

Based on the multi-actor concept seen from various points of view, namely perceptions of problems, goals, interests, root causes, resources, and positions based on policies in geothermal development in Indonesia, there is a perspective of perception and goals of each actor who has different interests. Ministries or institutions involved in geothermal development have different perceptions and points of view, so it needs to be mapped out from the policy aspects of each ministry or institution so that geothermal development in Indonesia can be encouraged to achieve the energy sector's NZE target by 2060, a multi-actor analysis of geothermal development is shown in Table 1. From various actors' perceptions of existing problems, it turns out that all actors related to the geothermal industry have a common interest, namely joint efforts to optimize geothermal utilization and encourage the achievement of the target of increasing the installed capacity of GPP.

Table 1: Multi-actor analysis of geothermal development in Indonesia.

Actor	Problem Perception	Objective(s)	Interest(s)	Cause of Problem	Resources	Position
Ministry of Energy and Mineral Resources (MEMR)	Increasing the contribution of GPP to the national energy mix in the energy transition of the electricity sector.	Increasing the development of GPP to support Indonesia's NZE target in 2060.	Accelerating the development of GPP to reduce carbon emissions.	GPP is renewable energy that can be used as a baseload in the electricity system and contribute to reducing carbon emissions.	Authority to regulate geothermal business activities and determine electricity rates from GPP.	Ensure that the percentage of geothermal utilization for the national energy mix increases and reduces carbon emissions.
Ministry of Finance (MF)	The increasing need for incentives is due to the capital-intensive nature of geothermal projects with high risks.	Encourage geothermal project investment programs to increase national geothermal production.	Attracting investors in GPP to encourage national economic growth.	Investing in GPP projects requires high capital and uncertainty at the exploration stage.	Authority to regulate exemption from import duties and non-collection of taxes on import goods for geothermal operations.	Ensure support for fiscal incentives to increase geothermal utilization to reduce carbon emissions.
Ministry of Agrarian Affairs/Land and Spatial Planning (MAA/LSP)	Spatial planning to create a sustainable space for geothermal business activities.	Suitability of national, provincial, district/city spatial planning that accommodates detailed spatial planning for constructing GPP.	Providing legal certainty in implementing spatial planning, including business and geothermal business activities.	The spatial plan is the basis for the Environmental Approval requirements for geothermal business plans and activities.	Authority to prepare and determine detailed national spatial planning plans as a reference for provincial/ regency/city plans and permits in the rural/land and spatial planning sectors.	Ensure spatial planning support for the construction of GPP.
Ministry of Environment and Forestry (MEF)	We are increasing the need for environmental protection and management for geothermal activities.	Suitability of geothermal business plans and activities to mitigate impacts on the environment.	Use of renewable energy and GPP to reduce carbon emissions in Indonesia	GPPs are renewable energy that have low carbon emissions and are environmentally friendly	The authority to determine Environmental Approval for geothermal activities is an activity that requires an analysis of environmental impacts (AMDAL) or environmental management efforts and ecological monitoring efforts (UKL-UPL).	Ensure the achievement of greenhouse gas emission reduction in the energy sector by using renewable energy, especially GPP.
	Increasing carbon emissions, deforestation rates, and the need to develop renewable energy from	Regulate the use of some forest areas for development outside forestry activities, which have inevitable	Encourage using environmentally friendly GPP in protected forests, production forests, and	There is an increased need for forestry land to construct GPP projects whose prospect areas are in	Authority to determine Forest Area Use Approvals for geothermal business activities located in protected forests, production forests, and	Ensure the use of protected forest areas or production forests for geothermal power generation activities

Actor	Problem Perception	Objective(s)	Interest(s)	Cause of Problem	Resources	Position
	environmentally friendly GPP.	strategic objectives, including constructing GPP.	conservation forest areas.	protected forests, production forests, and conservation forest areas.	conservation forest areas through the Online Single Submission (OSS) system.	without changing the primary function of the forest area by considering specific area and time limits as well as environmental sustainability.
Ministry for Public Works and Human Settlements (MPWHS)	Increased allocation of regional road infrastructure needs to overcome constraints and obstacles in supporting the development of GPP.	Accelerate the improvement of regional road connectivity to provide maximum benefits and encourage infrastructure activities for GPP.	Providing accessible regional road infrastructure with good road conditions to support GPP infrastructure activities.	The GPP developer's site is in a remote area with inadequate infrastructure that requires increased road stability.	Authority to carry out regional road construction activities and help improve the stability of roads for constructing GPP infrastructure.	Improving the quality of roads and bridges to support GPP infrastructure activities.
	Allocation of water resources to support geothermal exploration and exploitation activities.	Realizing the orderly implementation of permits for using water resources for exploration well drilling and geothermal exploitation activities.	Providing water resources for geothermal exploration and exploitation activities by establishing priorities.	When exploration well drilling and geothermal exploitation activities take place, there is an increased need to use water resources as a medium and material.	Authority to determine technical recommendations and permits to use water resources for geothermal exploration and exploitation activities.	Ensure that water resources can be used for geothermal exploration and exploitation activities.
Ministry of Internal Affairs (MIA)	The initial stages of geothermal development at GPP project locations in the region and the local community present many obstacles.	Encourage orderly support for the implementation of geothermal activities within the regional government.	Encourage ease of licensing, incentives, and guaranteed land availability for geothermal business activities within the local government.	The construction of a GPP requires the support of the local government so that it can contribute to regional income.	The authority to formulate policies to support the development of GPP within the regional government and prepare regional income and expenditure budgets from geothermal profit-sharing funds and geothermal production bonuses.	Ensure the implementation of policies and licensing processes in the regions for constructing GPP.
Ministry of State-Owned Enterprises (MSOE)	Increasing renewable energy in the electricity mix is a goal of the general plan for electricity supply at	Fulfilling the installed capacity target for GPP in the PLN Electricity Supply Business Plan.	Encourage PLN to prioritize renewable energy, including GPP.	Increased demand for renewable energy, including GPP, to reduce carbon emissions.	Authority to set targets for additional installed renewable energy capacity in PLN performance indicators.	Ensure the target for adding renewable energy installed capacity is achieved according to the PLN Electricity Supply Business Plan.

Actor	Problem Perception	Objective(s)	Interest(s)	Cause of Problem	Resources	Position
	PLN Electricity Supply Business Plan.					
Ministry of Industry (MI)	Increased need for domestically produced goods and services for developing GPP infrastructure.	Meet domestic component and service levels for GPP infrastructure.	Increasing domestic production capabilities, including design and engineering, that invest and produce in Indonesia for GPP infrastructure.	Encourage investment in the electricity industry in Indonesia to meet the needs for GPP infrastructure using domestically produced goods and services with quality that can operate according to the planned technical life.	Authority to determine the value of domestic component levels of goods and services for GPP.	Increase the level of domestic components with technical specifications by domestic production requirements and quantities to meet GPP infrastructure needs.
Ministry of Investment/ Head of the Investment Coordinating Board (MI/HICB)	Increased investment in renewable energy from GPP to reduce greenhouse gas emissions in the energy sector.	Meeting the need to accelerate and increase capital investment for GPP.	Encourage the implementation of geothermal energy exploitation through the Online Single Submission (OSS) system.	The increasing need for GPP is due to the policy prioritizing purchasing electricity that utilizes renewable energy sources.	Authority for issuing business permits in the form of Indonesian Standard Industrial Classification (ISIC) 06202 Geothermal Permit and Preliminary Survey and Exploration Assignments.	Ensure the implementation of the geothermal energy business through business licensing through ISIC 06202 Geothermal Permit, Preliminary Survey and Exploration Assignments through the OSS system.
	There is an increasing need to utilize space for geothermal environmental services in national park conservation forest areas, grand forest parks, and natural tourism parks to construct GPP.	Fulfilling the need to accelerate and increase capital investment for Suitable Space Utilization Activities (SSUA) for geothermal power generation business activities	Encourage implementation of SSUA for geothermal power generation business activities through the OSS system.	Increased spatial planning requirements for geothermal power generation business activities.	Authority to issue SSUA for the development of a GPP.	Ensure SSUA is implemented for geothermal power generation business activities through the OSS system.
	There is an increasing need to construct GPP using geothermal environmental services	Fulfilling the need to accelerate and increase capital investment for constructing GPP	Encourage the implementation of the utilization of geothermal	The increasing need for GPP is due to the policy prioritizing purchasing electricity	Authority to issue Business Licensing - Geothermal Environmental Services Utilization Permit Exploration	Ensure the use of national park areas, grand forest parks, and natural tourism parks for geothermal

Actor	Problem Perception	Objective(s)	Interest(s)	Cause of Problem	Resources	Position
	in national park conservation forest areas, grand forest parks, and natural tourism parks.	through geothermal environmental services in national park areas, grand forest parks, and natural tourism parks.	environmental services through electronically integrated business licensing.	that utilizes renewable energy sources.	Phase and Business Licensing - Geothermal Environmental Services Utilization Permit Exploitation and Utilization Phase ISIC 02209 in utilization zones or blocks in national park areas, grand forest parks and natural tourism parks.	power generation business activities without changing the primary function of forest areas by taking into account specific area and time limits and environmental sustainability through the principles of conservation of natural resources and ecosystems through the OSS system.
Local Government	Increase income from profit-sharing funds from geothermal business activities through production bonuses for the regions.	Increasing regional development and community welfare around GPP projects.	Supporting the sustainability of GPP projects to improve community health welfare and regional development.	The geothermal power generation industry is a high-investment project that will meet the local grid system's electricity needs over a long and sustainable period.	The authority to provide licensing facilities, incentives, and guarantees of land availability by its designation.	Ensure support for project sustainability and handling of social issues in the context of developing GPP.
PLN	The target for utilizing renewable energy from GPP in the renewable energy mix should be increased based on the general national electricity plan.	To increase the electrification ratio, support the achievement of renewable energy mix targets, reduce greenhouse gas emissions, and prioritize the development of power plants sourced from renewable energy from GPP.	Fulfil and increase the realization of electric power loads and completion of GPP projects by IPP.	Electricity sales projections and other indicators, such as economic growth, influence the condition of electricity supply and demand.	Authority to allocate GPP projects by IPP by signing a Power Purchase Agreement/Letter of Intent	Ensure electricity is purchased through the pre-transaction agreement (PTA) when bidding for hot work areas after the IPP has completed exploration activities and proven geothermal reserves.
IPP	There is uncertainty regarding the timeline for negotiating the purchase price of	Providing legal certainty in implementing electricity purchase	Accelerate the development of GPP after completing exploration activities	Limited economics of the purchase price of electricity from GPP by PLN.	Authority to explore feasibility studies, exploitation, and utilization, as well as accelerating the implementation	Ensure that the sale of electricity to PLN is by PTA when offering hot work areas after

Actor	Problem Perception	Objective(s)	Interest(s)	Cause of Problem	Resources	Position
	geothermal electricity after completing exploration activities and having proven geothermal reserves.	and sale agreements so that power plants in the electric power system meet the required system obligation	and having proven geothermal reserves.		of the Commercial Operation Date (COD).	completing exploration activities and having proven geothermal reserves.
SMI	Increasing need for incentives to support the use of GPP.	Support for geothermal development takes the form of financing and funding facilities provided to mitigate risks (de-risking facilities) that hinder the participation of business entities in delivering infrastructure for the geothermal sector.	Carry out assignments for exploration support and financing and exploration financing to increase the involvement of business entities in providing infrastructure for the geothermal industry.	Increasing funding and financing needs by business entities to mitigate risks (de-risking facilities) in providing geothermal infrastructure.	Authority to determine fees and levies, provide funding and infrastructure financing, and provide fiscal facilities in the form of exemption from import duties and no tax for geothermal operations.	Ensure funding support, financing, and fiscal facilities to increase national geothermal production.

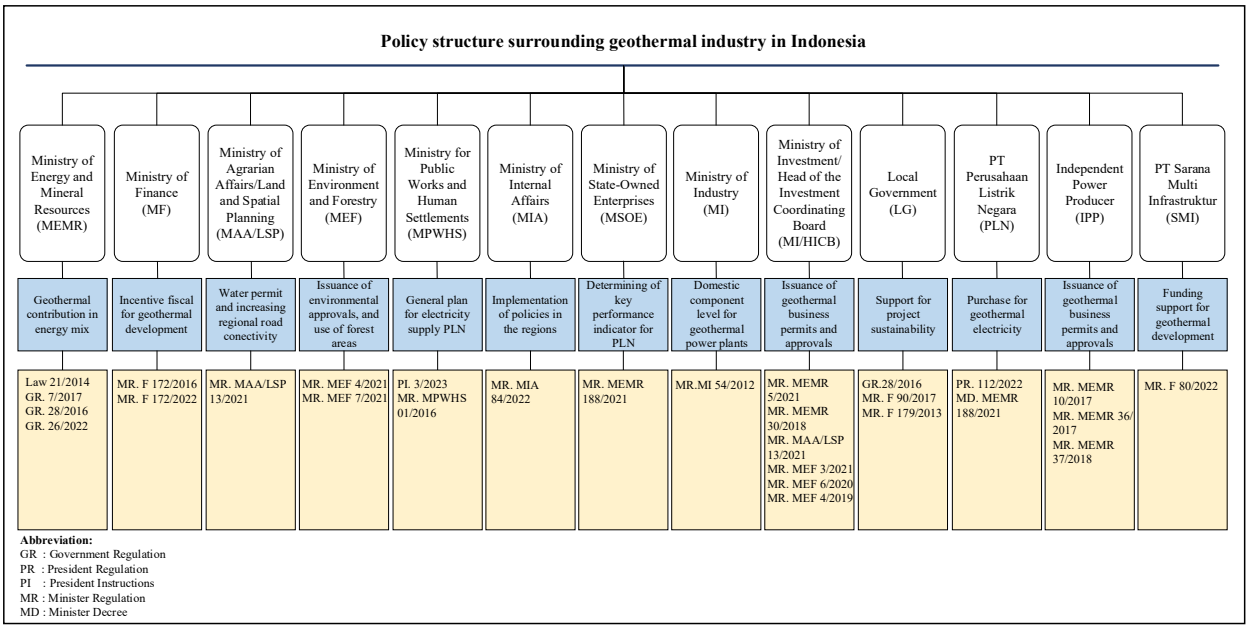

Figure 3: Policy structure surrounding the geothermal industry in Indonesia.

4.2 PESTLE Analysis

Conducting a PESTLE analysis is essential to identify the various stakeholders involved in the geothermal industry. These stakeholders include actors, institutions, and other related parties who have a vested interest in geothermal energy development in Indonesia and may be impacted by the policies and activities of the organizations involved in the industry. By identifying these stakeholders, organizations can better understand their needs and concerns and work to develop strategies that benefit all parties involved.

4.2.1 Politic

The Energy Law plays a crucial role in governing and regulating the energy sector in Indonesia. It provides a legal framework for managing and developing various energy resources in the country, including oil, gas, coal, and renewable energy sources. This law aims to ensure sustainable and efficient use of energy resources, promote energy security, and attract investment in the energy sector. Therefore, the Energy Law is vital for Indonesia's energy industry (Yudha et al., 2018). The Geothermal Law is designed to regulate and supervise geothermal activities conducted for business purposes. Its main objective is to ensure that companies involved in geothermal energy generation adhere to specific guidelines and standards regarding exploration, exploitation, and utilization of geothermal resources. The policy of the geothermal business is shown in Figure 4.

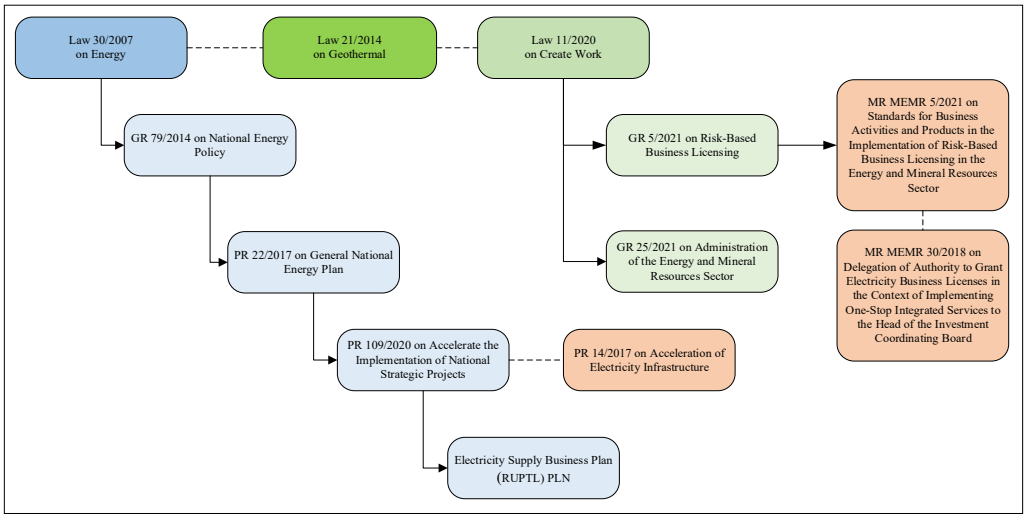

Figure 4: Geothermal business policy.

4.2.2 Economic

To accelerate renewable energy development for electricity supply, the Indonesian Government has set renewable energy price tariffs, including GPP price tariffs with a ceiling price reference. The electricity purchase price policy from GPP has undergone several changes (Setiawan et al., 2022), most recently through Presidential Regulation 112/2022 on the Acceleration of Renewable Energy Development for the Supply of Electric Power. The ceiling price for geothermal electricity is based on location factors (F), as shown in Figure 5.

In the arrangement, the purchase price of electricity from GPP by PLN is determined based on development capacity using the highest benchmark price. The highest benchmark price is the price after being multiplied by a location factor. The purchase price of GPP electricity from IPP by PLN is shown in Tables 2 and 3.

The purchase of electricity from GPP by PLN is determined based on a price matrix, the amount of generation capacity, and the enthalpy value of geothermal exploration results. This pricing matrix can be categorized as a feed-in-tariff (FIT) model based on complex generation capacity and enthalpy variations. Here is an example of a GPP price matrix with a location factor of 1. The price matric of GPP is shown in Tables 4 and 5.

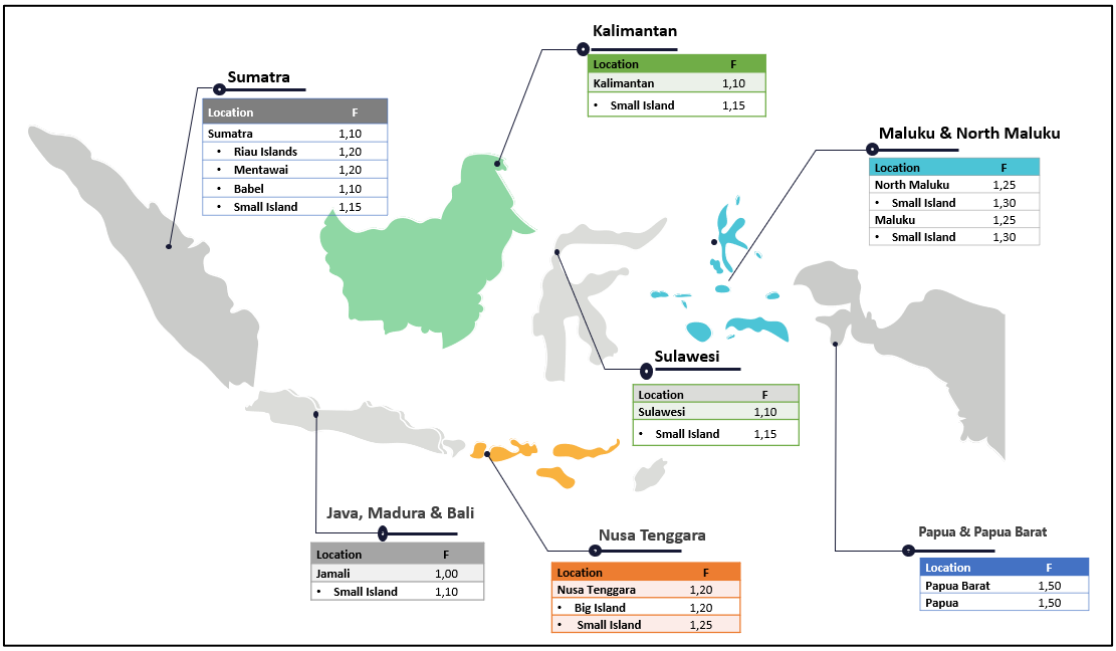

Figure 5: The ceiling price for geothermal electricity is based on location factors.

Table 2: Electric power purchase from the geothermal energy.

Capacity	Ceiling Price Tariff (cent USD/kWh)	
	1st to 10th Year	11st to 30th Year
up to 10 MW	(9.76 x F)*	8.30
>10 MW up to 50 MW	(9.41 x F)*	8.00
>50 MW up to 100 MW	(8.64 x F)*	7.35
>100 MW	(7.65 x F)*	6.50

Table 3: The purchase price of the geothermal steam power equivalent to electricity.

Capacity	Ceiling Price Tariff (cent USD/kWh)	
	1st to 10th Year	11st to 30th Year
up to 10 MW	(6.60 x F)*	5.60
>10 MW up to 50 MW	(6.25 x F)*	5.31
>50 MW up to 100 MW	(5.48 x F)*	4.65
>100 MW	(4.48 x F)*	3.81

Table 4: Price Matrix of GPP Base Price 1.

Base Price 1 (c/kWh)		Development Capacity							
		10	20	30	45	50	55	80	100
Enthalpy (kJ/k	950	9.76	9.41	9.41	9.41	9.41	8.64	8.64	8.64
	1,000	9.76	9.41	9.41	9.41	9.41	8.64	8.64	8.64

	1,050	9.76	9.41	9.41	9.41	9.41	8.64	8.64	8.64
	1,100	9.76	9.41	9.41	9.41	9.41	8.64	8.64	8.64
	1,150	9.76	9.41	9.41	9.41	9.41	8.64	8.64	8.64
	1,200	9.76	9.41	9.41	9.41	9.41	8.64	8.64	8.63
	1,250	9.76	9.41	9.41	9.41	9.41	8.64	8.64	8.43
	1,300	9.76	9.41	9.41	9.41	9.31	8.64	8.64	8.13
	1,350	9.76	9.41	9.41	9.41	9.17	8.64	8.31	7.83
	1,400	9.76	9.41	9.41	9.41	9.32	8.64	8.23	7.74
	1,450	9.76	9.41	9.41	9.31	8.97	8.64	8.13	7.63

Table 5: Price Matrix of GPP Base Price 2.

Base Price 2 (c/kWh)	Development Capacity							
	10	**20**	**30**	**45**	**50**	**55**	**80**	**100**
	8.30	8.00	8.00	8.00	8.00	7.35	7.35	7.35

The following provision applies base price 1 is defined as a base price for years 1 to 10, and base price 2 is defined as a base price for years 11 to 30. Power price (P) can be calculated as base price with the escalation of components fixed operating and maintenance costs (B) and variable operating and maintenance costs (D) maximum of 25%, multiplied by the index which was agreed upon later (United States Principal Party of Interest/USPPI or 2%), added by transmission price (TPC) if applicable.

As can be formulated as follows:

$$P = Pb \times I$$

Pb = Base price that is determined by points 1 and 2 above
I = maximum (1 + 0.25 x Y)
Y = USPPI or 2% according to agreement

4.2.2.1 Financial Obligation from the MF

Financial obligations from the MF include Value Added Tax (PPN), Land and Building Tax (PBB), and Income Tax (PPh). Based on data from four geothermal permit holders who have been operating, the land and building tax rate for land bodies for business entities holding geothermal permits ranges from 0.77% - 1.47%, with an average of 1.36% of revenue. Meanwhile, the land and building tax for onshore land bodies for business entities holding geothermal permits ranges from 0.41% - 1.83%, with an average of 0.52% of revenue. The analysis of taxation for the geothermal development charged by the IPP by the provisions of the statutory regulations is shown in Table 6.

Table 6: The taxation for the geothermal development.

Financial Obligation	Tariff	Regulation
Value Added Tax	11%	Law 7/2021
Land and Building Tax		
Land Bodies	1.36%	MR MF 172/PMK.010/2016
Onshore	0.52%	MR MF 137/PMK.03/2017 The Director General of Taxes Regulation PER-45/PJ/2013
Income Tax	22%	Law 7/2021

4.2.2.2 Financial Obligation from the MEMR

Financial obligations from the MEMR are non-tax state revenues, including geothermal fixed fees and geothermal production fees (royalties). Another financial obligation is the production bonus, which the geothermal holding business entity pays directly to the district/city in the producing area. Costs imposed on IPPs at the geothermal exploitation stage are in the form of fixed exploration and exploitation fees, production fees and production bonuses in the amount of 2 USD/hectare per year for exploration and exploitation fixed fees before COD and 4 USD/hectare for exploration fixed fees and exploitation after COD, a production bonus of 1% on gross income from sales of geothermal steam or 0.5% on gross income from sales of electricity. The financial obligation of the business geothermal energy from the MEMR is shown in Table 7.

Table 7: Financial obligation of the business geothermal energy from the MEMR.

No.	Financial Obligation	Amount of value (USD/IDR)	Explanation	Regulation
1.	Geothermal fixed fees			
	a. Fixed fees of exploration and exploitation before the COD	USD 2/hectare	Per year	GR 26/2022 MR MEMR 5/2023
	b. Fixed fees of exploitation after COD	USD 4/hectare		
2	Geothermal production fees			
	a. Steam	5% x geothermal steam power purchase price	After COD	GR 26/2022 MR MEMR 5/2023
	b. Electricity	2.5% x electric power purchase price		
3.	Production Bonuses			
	a. Steam	0.5% x revenue from steam sales	After COD	GR 28/2016 MR MEMR 23/2017
	b. Electricity	1% x revenue from electricity sales		

4.2.2.3. Financial Obligation from the MEF

Utilization of forest areas for development purposes outside of forestry activities is carried out based on the Forest Area Use Approval (PPKH) and is granted by MEF based on application. Approvals for the use of forest areas in provinces that do not have sufficient forest areas are required to pay PNBP for the use of forest areas, pay compensation for PNBP, and carry out planting in the context of rehabilitating River Watersheds (DAS). Meanwhile, in conservation areas, the non-tax state revenue rate is in the form of fees and levies for Geothermal Environmental Services Utilization Permit. Fees are charged once when the permit is issued, while levies are charged annually. The financial obligation of the business geothermal energy from the MEF is shown in Table 8.

Table 8: Financial obligation of the business geothermal energy from the MEF.

No.	Financial Obligation	Amount of value (IDR)	Explanation	Regulation
1.	Protected Forest and Production Forest Area	Non-tax state revenues: (L1x1xtariff) + (L2x4xtariff)		
	a. Protected Forest	IDR 2,000,000/hectare	Per year	GR 33/2014
	b. Production Forest	IDR 1,600,000/hectare	Per year	
2.	Conservation Area			
	a. Fees for Utilization of Geothermal Environmental Services	IDR 50,000,000/hectare	One time	Revised GR 12/2014
	b. Levies for Utilization of Geothermal Environmental Services	IDR 9,000,000/hectare	Per year	

4.2.3 Social

The socio-cultural aspect is critical in the public acceptance of the project and overcoming social resistance. Understanding citizen's preferences towards the development of geothermal energy leads to a greater understanding of what shapes of strategies and policies should be taken in the project (Ibrohim et al., 2019). When a geothermal project is not managed properly, the social political, and cultural conditions of the community can be a failure factor in geothermal development. Political support was obtained from the regional government and village government (Setiyono et al., 2019). The geothermal business entity has social and environmental responsibilities. This responsibility is an obligation for business entities that carry out business activities in the field of natural resources both inside and outside the business entity environment that are carried out by the Board of Directors based on the company's annual work plan which contains activity plans and budgets needed to implement social and environmental responsibilities. In preparing and determining activity plans and budgets, business entities must pay attention to appropriateness and fairness. Business entities that do not carry out social and environmental responsibilities are subject to sanctions by statutory provisions. Meanwhile, business entities that have played a role and carried out social responsibility can be given awards by the authorized agencies. Social and environmental responsibilities must be implemented by business entities at the exploration stage. Geothermal permit holders are also required to develop development and empowerment programs for local communities around the work area. Local community development and empowerment programs must be implemented by business entities at the exploitation and utilization stages. The social obligation in geothermal development is shown in Figure 6.

4.2.4 Technological

To accelerate the development of electricity infrastructure while still prioritizing the use of domestic products, the MEMR has issued the Ministry Regulation MEMR 11/2024 on the use of domestic products for the development of electricity infrastructure and derivative regulations as shown in Figure 7 and Figure 8. The electricity infrastructure for electricity generation originating from renewable energy sources starts from activities survey to obtain renewable energy sources.

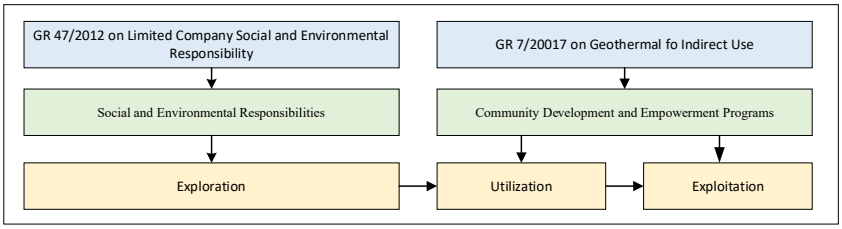

Figure 6: Social obligations in geothermal development.

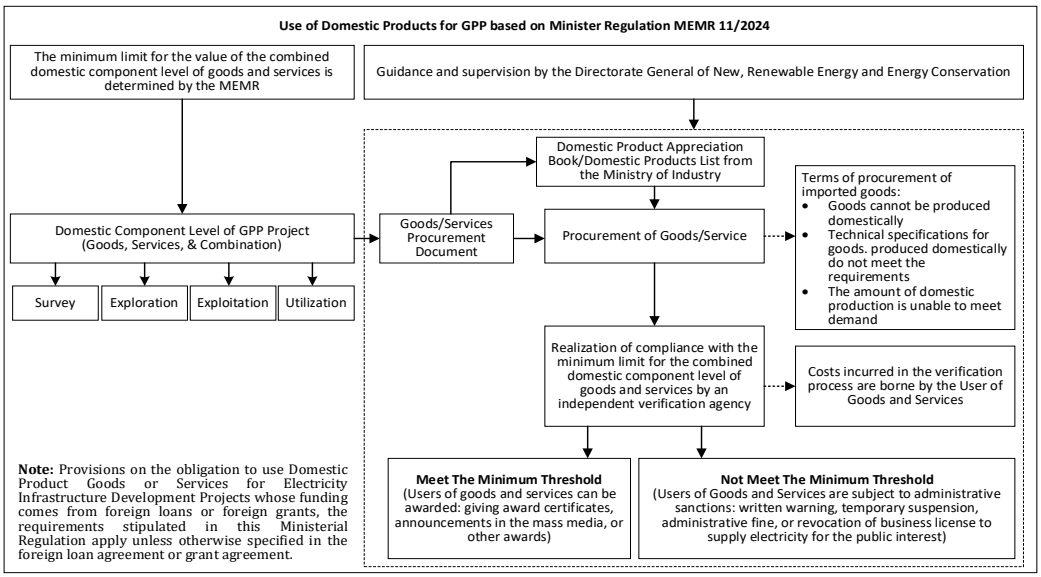

Figure 7: Domestic component level for GPP.

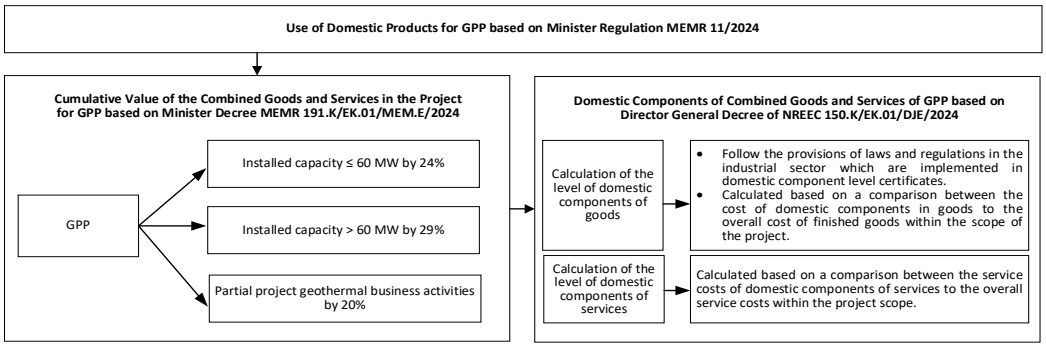

Figure 8: Minimum domestic component level threshold for GPP.

4.2.4 Legal

Geothermal development in Indonesia is regulated by Geothermal Law and its derivative regulations. The utilization of geothermal energy for electricity is the authority of the central government. Meanwhile, direct use of geothermal energy is under the regional government's authority. Regulations in the geothermal sector in Indonesia are the most complete compared to other renewable energy regulations; regulations in the geothermal sector are shown in Figure 9.

4.2.5 Environmental

Environmental Approval documents generally use UKL-UPL at the geothermal exploration stage, but for exploration activities that change the shape of the land and landscape, an AMDAL is required. Meanwhile, at the geothermal exploitation stage, Environmental Approval documents use AMDAL. Based on Ministerial Regulation MEF 4/2021, the types of mandatory activities/businesses that require AMDAL on a scale/scale are infrastructure development with earthworks that have a volume of > 500,000 m3 or a road construction length of > 5 km.

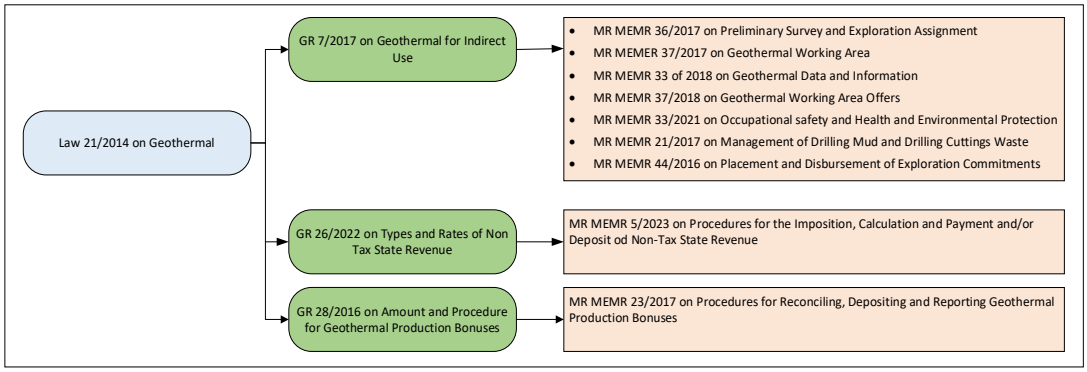

Figure 9: Regulation of geothermal for electricity.

Geothermal activities in protected forest areas or production forests are priority activities outside of forestry activities without being limited by zones/blocks. Meanwhile, for geothermal utilization in conservation forest areas (national parks, grand forest parks, and nature tourism parks). Geothermal environmental services in national parks, grand forest parks, and nature tourism parks mandate that geothermal utilization can be carried out in utilization zones through a conservation area environmental services mechanism. Nazif et al. (2021) studied land status of geothermal resources distribution are 46% private land, 18% conversation forest, 28% protected forest, 4% limited production forest, 3% protected forest, and 1% conservation production forest. The regulation of geothermal utilization in forest areas is shown in Figure 10.

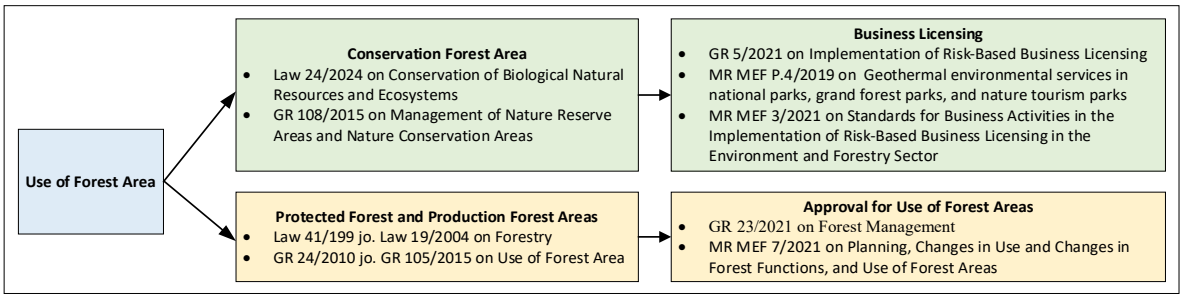

Figure 10: Regulation of geothermal utilization in forest area.

4. DISCUSSION AND RESULT

Based on the multi-actor analysis and PESTLE analysis, there are quite a lot of stakeholders in geothermal development in Indonesia, including Ministries/Agencies, Regional Government, PLN, IPP, SMI, and other stakeholders who need synergy so that obstacles in geothermal development can be overcome. resolved easily. We can see more holistically how certain aspects of PESTLE dynamically impact each other. Although the economic aspect of the geothermal industry is one of the most pressing problems, this aspect can also be considered the starting point for geothermal development in Indonesia.

The regulation of geothermal energy, taking into account political, economic, social, technological, legal, and environmental aspects, is highly comprehensive. It is important to encourage and facilitate the Environmental Approval permits that are currently being processed at the Ministry of Environment and Forestry, including permits in conservation areas. Moreover, providing fiscal and non-fiscal incentives through the Ministry of Finance and imposing state revenue levies from non-taxes by the MEMR can increase the involvement of business entities in developing geothermal energy.

In order to reach the target for geothermal development, MEF can facilitate environmental approval and licensing in conservation forest areas. Additionally, MEF can encourage geothermal development in these areas by changing the function of the Nature Reserve Forest Area into a Nature Conservation Area with utilization zones or blocks. Meanwhile, MF can support geothermal development by providing fiscal and non-fiscal facilities to enhance the economics of geothermal projects. In addition, through PESTLE analysis, we can further highlight the intersecting and overlapping sectoral interests in the geothermal sector. Through PESTLE, a better understanding of the interrelationships of these various aspects is juxtaposed and discussed through stakeholders. In this actor analysis and PESTLE analysis, various stakeholders have been identified who contribute to the development and utilization of geothermal energy, and their relationships are shown in Table 9.

Table 9: Actor Analysis and PESTLE analysis of the geothermal energy industry in Indonesia.

Actors	Political	Economic	Social	Technology	Environment	Legal
MEMR	√	√	√	√	√	√
MF	√	√		√	√	√
MAA/LSP		√			√	√
MEF	√	√	√		√	√
MPWHS		√	√		√	√
MIA			√			√
MSOE		√				√
MI		√		√		√
MI/HICB		√				√
Local Government		√	√		√	√
PLN		√		√	√	√
SMI		√	√			√
IPP		√	√	√	√	√

5. CONCLUSION

The development and utilization of GPP are assessed from the stakeholder aspect using actor analysis to identify and link overlapping and cross-sectoral stakeholder interests in the renewable energy sector in Indonesia. The current policy is still in its initial stages and requires significant improvement, considering that the geothermal industry needs to grow. The need for appropriate policies has made GPP stakeholders and actors face various risks, including economic and technological. The ability of policymakers in Indonesia to identify and mitigate these risks is the key to success in developing geothermal energy.

In the future, it is hoped that the government can formulate breakthrough policies to advance the geothermal sector, such as providing convenience to investors in the geothermal industry and providing fiscal incentives, thereby enabling the management of the geothermal energy supply chain effectively and efficiently. Apart from that, it should be noted that Indonesia's GPP target of 22,000 MW of primary energy mix in 2060 can be achieved. The actor analysis for stakeholders in the geothermal sector will also help strengthen the starting point for formulating a comprehensive national supply chain management framework for geothermal energy.

ACKNOWLEDGEMENT

Author Contribution: A.S. and A.H. established the review topic and chose the classification approach; A.S. planned the methodology and collected data; A.S. and A.H. jointly analyzed the data and wrote the paper.

Funding: This research received no external funding.

Conflict of Interest: The authors declare no conflict of interest.

REFERENCES

Climent Barba, F., Martínez-Denegri Sánchez, G., Soler Seguí, B., Gohari Darabkhani, H., & Anthony, E. J. (2016). A technical evaluation, performance analysis and risk assessment of multiple novel oxy-turbine power cycles with complete CO2 capture. *Journal of Cleaner Production*, 133, 971–985. https://doi.org/10.1016/j.jclepro.2016.05.189

Enserink, B., Bots, P., Van Daalen, E., Hermans, L., Kortmann, R., Koppenjan, J., Kwakkel, J., Ruijgh, T., Slinger, J., & Thissen, W. (2022). *Policy Analysis of Multi-Actor Systems Second Edition*.

Gehringer, M., & Loksha, V. (2012). *Geothermal handbook: Planning and Financing Power Generation*.

Ibrohim, A., Prasetyo, R. M., & Rekinagara, I. H. (2019). Understanding Social Acceptance of Geothermal Energy: A Case Study from Mt. Lawu, Indonesia. *IOP Conference Series: Earth and Environmental Science*, 254(1). https://doi.org/10.1088/1755-1315/254/1/012009

Islam, F. R., & Mamun, K. A. (2017). Possibilities and challenges of implementing renewable energy in the light of PESTLE & SWOT analyses for island countries. *Green Energy and Technology*, 0(9783319501963). https://doi.org/10.1007/978-3-319-50197-0_1

Mytilinou, V., Kolios, A. J., & Di Lorenzo, G. (2017). A comparative multi-disciplinary policy review in wind energy developments in Europe. *International Journal of Sustainable Energy*, 36(8), 754–774. https://doi.org/10.1080/14786451.2015.1100194

Nazif, H., Purwanto, H., Susmanto, A., & Paradigma, D. (2021). *Sustainable Geothermal Utilization for Outstanding Universal Value Sustainability*.

Setiawan, A. D., Dewi, M. P., Jafino, B. A., & Hidayatno, A. (2022). Evaluating feed-in tariff policies on enhancing geothermal development in Indonesia. *Energy Policy*, 168. https://doi.org/10.1016/j.enpol.2022.113164

Setiyono, B., Setyawan, A., Susanto, H., Punto, E., Abdulrahman, W., Edi Susangkiyono, A., Chandra Budiman, R., & Delfa, Z. (2019). *Considering Social Aspects of Geothermal Project: The Case of Social Mapping of Geothermal Project on Mount Ungaran*. https://doi.org/10.1051/e3sconf/201

Vidal, L.-A., & Marle, F. (2015). *Understanding project complexity Implications on project management*.

Wisaksono, A., Murphy, J., Sharp, J. H., & Younger, P. L. (2018). The multi-level perspective analysis: Indonesia geothermal energy transition study. *IOP Conference Series: Earth and Environmental Science*, 106(1). https://doi.org/10.1088/1755-1315/106/1/012114

Yudha, S. W., & Tjahjono, B. (2019). Stakeholder mapping and analysis of the renewable energy industry in Indonesia. In *Energies* (Vol. 12, Issue 4). MDPI AG. https://doi.org/10.3390/en12040602

Yudha, S. W., Tjahjono, B., & Kolios, A. (2018). A PESTLE policy mapping and stakeholder analysis of Indonesia's fossil fuel energy industry. In *Energies* (Vol. 11, Issue 5). MDPI AG. https://doi.org/10.3390/en11051272

Yudha, S. W., Tjahjono, B., & Longhurst, P. (2021). Stakeholders' recount on the dynamics of indonesia's renewable energy sector. *Energies*, 14(10). https://doi.org/10.3390/en14102762

Yudha, S. W., Tjahjono, B., & Longhurst, P. (2022). Unearthing the Dynamics of Indonesia's Geothermal Energy Development. *Energies*, 15(14). https://doi.org/10.3390/en15145009

A 20 Year Retrospective: Analysis the Impact of Star Energy's Scholarship Program to Pangalengan Community Using MSC Technique

Mila Puspita, Firman Hidayat, Rahmat Hidayat, and Ismail Hidayat

PT Star Energy

mila.puspita@starenergy.co.id, firman.hidayat@starenergy.co.id, rahmat.hidayat@starenergy.co.id, ismail.hidayat@starenergy.co.id, carolina.magdalena@polban.ac.id

Keywords: Scholarship impact, Corporate social responsibility, Community empowerment

ABSTRACT

This study evaluates the transformative impact of the Star Energy Geothermal Wayang Windu, Limited (SEGWWL) scholarship program, spanning from 2005 to 2024, on its recipients using the Most Significant Change (MSC) technique. The research reveals that the scholarship has significantly influenced the educational achievements, personal and professional growth, also social contributions of the recipients, many of whom have received support since elementary school. By removing financial barriers and fostering a sense of responsibility and community engagement, the scholarship has enabled recipients to pursue higher education and successful careers. The scholarship has solidified Star Energy's reputation as a catalyst for social change, building unshakable trust and goodwill within the community. Discontinuing this program would risk unraveling these gains, jeopardizing both the social fabric of the community and the company's legacy. The study underscores the imperative to not only maintain but expand this critical initiative, positioning it as a cornerstone of Star Energy's commitment to sustainable and impactful corporate social responsibility.

1. INTRODUCTION

1.1 The Background of the Study

The significance of corporate social responsibility (CSR) has grown substantially in recent years, with companies increasingly recognizing the need to balance economic performance with social and environmental contributions. This is particularly relevant in developing countries, where CSR initiatives can play a vital role in addressing socio-economic challenges. Star Energy Geothermal Wayang Windu, Limited (SEGWWL), a major player in Indonesia's geothermal sector, has integrated CSR into its business model, focusing on community development through education, economic empowerment, social, environment and health. The community development program is based on the results of social mapping carried out by academics. This is an implementation of the collaboration hexahelix concept. The hexa-helix concept is a development of penta-helix concept with addition in the role of law and regulation (Zakaria, 2019).

The SEGWWL scholarship program, initiated in 2005, is a key component of this strategy, aimed at improving educational access and outcomes for underprivileged and high achieving students in the Pangalengan area, thereby fostering sustainable community development (Silvius & Schipper, 2014). This is in line with statistical data that shows that in 2004 the percentage of continuing school from elementary school to junior high school was 16% while in 2019 it increased to 39% as well as the percentage of continuing school from junior high school to senior high school which increased from 39% to 62% (Badan Pusat Statistik, 2004 dan 2020).

Scholarship programs, particularly those funded through CSR initiatives, have been shown to significantly impact students' academic achievements and socio-economic status. Previous studies have demonstrated that financial aid and scholarships not only increase college attendance rates but also enhance academic persistence and completion (Dynarski, 2003; Castleman & Long, 2016). In the context of SEGWWL, the scholarship program targets students across various educational levels, from elementary school to university, with the aim of bridging educational gaps and empowering the community. This study seeks to evaluate the broader impact of this program especially scholarship in university level, focusing on both the personal and social outcomes for the recipients.

1.2 Main Research Problem and General Solution

Despite the well-documented benefits of scholarships, there is a need for more nuanced evaluations that capture the full range of impacts, particularly in the context of CSR-driven programs. Traditional metrics such as graduation rates and academic performance, while important, may not fully reflect the broader social and personal changes brought about by such scholarships. Research indicates that scholarships can influence not only educational outcomes but also long-term career success and community involvement (Erickson et al., 2021; Greene et al., 1997). However, there remains a gap in understanding how these programs impact the recipients beyond the immediate academic environment.

To address this research gap, this study employs the Most Significant Change (MSC) technique, a qualitative evaluation method that collects and analyzes personal stories from scholarship recipients. This technique is particularly effective in capturing the complex and often subjective changes experienced by individuals as a result of educational support. By focusing on the narratives of the scholarship recipients, this study aims to provide a deeper understanding of the personal and social impacts of the SEGWWL scholarship program, offering insights that go beyond traditional quantitative assessments (Dart & Davies, 2003).

2. OBJECTIVE

The objective of this study is to evaluate the impact of the Star Energy Geothermal Wayang Windu, Limited (SEGWWL) scholarship program 2005 to 2024, using the Most Significant Change (MSC) technique to capture both personal and social changes experienced by the recipients. This research is novel in its application of the MSC technique to a CSR-driven scholarship program within the Indonesian context, offering a unique perspective on the role of corporate initiatives in educational and community development. By focusing on the qualitative experiences of scholarship recipients, this study provides a deeper understanding of the program's impact beyond traditional academic metrics.

The scope of this research is centered on analyzing the narratives of scholarship recipients from the Pangalengan area, who have benefited from the SEGWWL program. Data were collected through in-depth interviews with un-structure question, allowing for a comprehensive assessment of the scholarship's impact on personal development, academic success, and community involvement. The findings are expected to contribute to the broader discourse on corporate social responsibility and education, offering valuable insights for both academic researchers and corporate policymakers on the effectiveness of scholarship programs in promoting sustainable development.

3. METHODOLOGY

3.1 The Most Significant Change for Evaluating Program

The Most Significant Change (MSC) technique is widely recognized for its ability to capture qualitative data that reflects the real-life impacts of programs, especially in contexts where outcomes are varied and non-linear. Originally developed for use in international development projects, MSC has since been applied in various fields to evaluate the effectiveness of complex interventions. The technique involves collecting stories from program participants and then analyzing these stories to identify the most significant changes brought about by the program (Dart & Davies, 2003). This approach allows evaluators to understand the diverse ways in which programs influence participants, making it ideal for assessing the impact of the SEGWWL scholarship program.

In evaluating educational interventions, the MSC technique has been praised for its participatory nature, which involves stakeholders in the process of identifying significant changes. This participatory approach ensures that the evaluation reflects the perspectives of those directly affected by the program, thereby providing a more comprehensive understanding of its impact. Research on similar scholarship programs has demonstrated that this method can uncover insights that might be overlooked by more traditional evaluation techniques, particularly regarding the personal and community-level changes that occur as a result of educational support (Mills & Wolf, 2017; Erickson et al., 2021).

The MSC technique's application in this study is further supported by its adaptability to different contexts, making it suitable for analyzing the diverse impacts of the SEGWWL scholarship program across different educational levels and socioeconomic backgrounds. By focusing on the most significant changes, this study aims to provide a rich, nuanced understanding of how the scholarship program has influenced recipients' lives, contributing to both their personal growth and the development of their communities.

3.2 Materials

The materials used in this study primarily consisted of qualitative data collected from scholarship recipients of the SEGWWL program. This data included detailed personal narratives and transcripts from interviews conducted with selected recipients. The study also utilized records and documents related to the SEGWWL scholarship program, such as recipient lists, educational outcomes, and background information on the scholarship administration. The use of the Most Significant Change (MSC) technique required careful selection of respondents who could provide comprehensive and reflective accounts of their experiences, thus serving as the primary source of data (Davies & Dart, n.d.).

3.3 Sample Preparation

The sample preparation involved identifying and selecting scholarship recipients from the Pangalengan area who had received scholarships between 2005-2024. The selection criteria were based on the willingness of recipients to participate and the significance of their achievements as determined by the scholarship's impact on their educational and professional development. Once identified, respondents were contacted and briefed on the study's

purpose, and informed consent was obtained. Data collection was facilitated through structured interviews, which were designed to elicit detailed accounts of the recipients' experiences with the scholarship program, using guidelines established by the MSC technique (Dart & Davies, 2003).

3.4 Experimental Set-up

The experimental setup for this study centered around the application of the MSC technique to evaluate the qualitative impact of the SEGWWL scholarship program. The process involved collecting and analyzing stories from the scholarship recipients, which were then reviewed to identify the most significant changes in their lives attributed to the scholarship. This technique required an iterative approach where respondents' narratives were collected, categorized, and analyzed in multiple stages to ensure comprehensive data interpretation. The structured interviews served as the primary data collection tool, allowing for in-depth exploration of personal and professional changes experienced by the respondents (Davies & Dart, n.d.).

3.5 Specific Literature Review that Led to Research Gaps

A review of existing literature highlights the positive impact of scholarships on students' educational attainment and socio-economic mobility. Studies have consistently shown that scholarships increase college attendance and completion rates, particularly among disadvantaged groups (Gleason & Dynarski, 2002; Bettinger, 2004). Furthermore, research suggests that scholarships can lead to improved academic performance and long-term career success, providing recipients with the financial support and motivation needed to pursue higher education (Dynarski, 2003; Castleman & Long, 2016). However, much of this research has focused on scholarships provided by government and private entities, with relatively little attention given to CSR-driven scholarship programs.

Moreover, while the academic and professional benefits of scholarships are well-documented, there is a lack of studies examining the broader social impacts of such programs, particularly in developing countries. The existing literature does not fully address how scholarships influence recipients' personal development, social integration, and community involvement, aspects that are critical to understanding the full impact of educational support programs (Goldrick-Rab et al., 2009; Deming & Dynarski, 2009). This gap is particularly evident in the context of Indonesia, where the intersection of corporate social responsibility and educational development has not been extensively explored.

This study aims to fill these gaps by applying the MSC technique to evaluate the personal and social impacts of the SEGWWL scholarship program. By focusing on the experiences of scholarship recipients, this research seeks to provide new insights into how CSR-driven scholarships contribute to both individual and community development, thereby expanding the understanding of the role of education in sustainable development.

4. FINDING AND DISCUSSION

4.1 Personal and Professional Growth

The impact of the SEGWWL scholarship program on its recipients has been profound and multifaceted, as evidenced by the narratives of Aji Muharam Somantri, Shandra Ufa Dewi Nugraha, Risye Nuroctaviani Lausi, and Vieska Rofianissa. These individuals have highlighted significant changes in their personal, academic, and professional lives attributable to the scholarship support. Aji Muharam Somantri, who graduated from Bandung State Polytechnic, attributes his current role as a Senior Engineer at Toyota Motor Corporation to the comprehensive support received during his studies, including full tuition coverage and additional financial aid for living expenses. His involvement in various academic and extracurricular activities further facilitated his career development.

Shandra Ufa Dewi Nugraha, a graduate of Padjadjaran University, emphasizes the economic relief and opportunities the scholarship provided, enabling her to continue her education without financial burden. Her active participation in university organizations and committees significantly contributed to her personal growth and the establishment of her current business, Homestay Shavira. Similarly, Risye Nuroctaviani Lausi, who pursued a midwifery degree at Padjadjaran University, experienced enhanced academic focus and professional maturity through the support provided by the scholarship, which included full tuition and accommodation costs. Her role as a Coordinator Midwife at KPBS General Hospital reflects the practical application of her education and the scholarship's impact on her career trajectory.

Vieska Rofianissa, a chemical engineering graduate from Bandung State Polytechnic, underscores the critical financial support received, which allowed her to focus on her studies and eventually secure a position at the National Research and Innovation Agency (BRIN). Her journey illustrates the challenges and successes faced by scholarship recipients, highlighting the significant role of the SEG scholarship in facilitating access to higher education and subsequent professional opportunities.

4.2 Social Impact of Scholarship Program

The social impact of the SEGWWL scholarship program is evident in the way it has influenced not only the recipients' lives but also their families and communities.

The scholarship has empowered recipients to contribute to their communities in meaningful ways. For instance, Aji Muharam Somantri, in addition to his professional achievements, has shared his knowledge with his community by offering advice on electricity efficiency and safety, extending the benefits of his education to others. This form of community involvement indicates that the scholarship program fosters a sense of responsibility and civic engagement among its recipients, encouraging them to give back to their communities.

4.3 Discuss by Comparing and Contrasting from Literature Data

The findings from the SEGWWL scholarship program align with existing research that highlights the transformative impact of financial aid on student outcomes. Studies such as those by Greene et al. (1997) and Mills & Wolf (2017) demonstrate that scholarships significantly improve students' academic achievements and increase college attendance and completion rates. The scholarship recipients in this study experienced similar benefits, using the financial support to access higher education and achieve notable professional successes. The SEGWWL scholarship's non-binding nature, which allows recipients the freedom to choose their career paths post-graduation, further enhances its positive impact by supporting individual autonomy and career development.

However, the SEGWWL program's broader social implications, such as recipients financing their siblings' education, suggest a ripple effect that is less commonly discussed in the literature. This aspect of the scholarship's impact, where the benefits extend to the recipients' families and communities, echoes findings by Erickson et al. (2021), who noted similar patterns in the Louisiana Scholarship Program. This broader impact highlights the potential of scholarships to contribute to community development and social mobility, beyond the immediate academic achievements of the recipients.

4.4 Discuss the Importance of the Findings and Their Scientific and Practical Implications

The findings from this study underscore the importance of CSR-driven scholarship programs like the SEGWWL scholarship in fostering educational attainment and socio-economic mobility. By providing financial support, these programs remove significant barriers to higher education for underprivileged and high achieving students, enabling them to achieve their academic and professional potential. The transformative personal development reported by the recipients, such as the shift in character and enhanced self-confidence, is a testament to the scholarship's role in not only supporting education but also in shaping resilient, responsible, and ambitious individuals.

Scientifically, this study contributes to the understanding of the broader social impacts of scholarship programs, particularly in developing countries. It demonstrates that the benefits of scholarships extend beyond the individual recipients to their families and communities, suggesting a potential for long-term socio-economic development. Practically, the insights gained from this study can inform the design and implementation of future scholarship programs, emphasizing the need for comprehensive support that includes not only financial aid but also opportunities for personal and professional development. The study’s findings support the expansion of such programs to reach more students and suggest that involving multiple stakeholders in the process can enhance the overall impact of these educational initiatives.

4.5 Highlight Findings

1. **Scholarship Recipients had been Awarded the Scholarship since Elementary School**
   Among the interviewees, it was found that 3 out of 4 scholarship recipients had been awarded the scholarship since elementary school as a recognition of their academic achievements. This early support has significantly motivated these students to maintain and improve their academic performance. Beyond benefiting the recipients, this initiative has also generated a positive impact for the company in the form of goodwill, as Star Energy has become a well-known and trusted name within the community. The company’s contribution is directly felt by the public, enhancing trust in Star Energy, particularly when families consider higher education opportunities for their children supported by these scholarships.

2. **Increase Social Mobility with More Confidence**
   This scholarship also plays an important role in increasing social mobility for its recipients. By providing the financial resources necessary to access higher education, scholarship programs for outstanding students from various levels of education, the program has enabled recipients from economically disadvantaged backgrounds to gain more confidence for continue a higher education and secure professional roles that would otherwise have been inaccessible. This upward social mobility is a testament to the scholarship’s role in reducing socio-economic disparities and promoting equality of opportunity within the community.

3. **Breaking the Cycle of Educational Disadvantage**
   The scholarship has had a significant impact on breaking the cycle of low educational attainment in the Pangalengan area. Many recipients, like Shandra Ufa Dewi Nugraha and Vieska Rofianissa, are now supporting their siblings' education, effectively using their own educational advancement to elevate the educational status of their families. This cascading effect illustrates how the scholarship program not only benefits individual recipients but also extends its impact to future generations, contributing to a gradual upliftment of the community's educational level.

5. CONCLUSION

This study highlights the significant impact of the Star Energy Geothermal Wayang Windu (SEGWWL) scholarship program on its recipients, both in terms of personal development and broader social influence. The scholarship has been instrumental in providing educational opportunities to underprivileged and high achieving students, enabling them to achieve academic success and professional growth.

The Star Energy Geothermal Wayang Windu (SEGWWL) scholarship program has proven to be a transformative force, not only in the lives of its recipients but also in the reputation and social responsibility of the company. To maximize its impact, the SEGWWL scholarship program should consider expanding its reach to include more students, particularly at the undergraduate level, and partnering with additional universities. By investing in the education of underprivileged and high achieving students, the program has unlocked pathways to higher education, professional success, and personal growth that would otherwise remain inaccessible. The Most Significant Change (MSC) technique has revealed that this scholarship is more than financial aid—it is a catalyst for change, fostering resilience, leadership, and a commitment to giving back to the community. The positive ripple effects of this program extend beyond the individual recipients, enhancing the educational standards of entire families and strengthening the social fabric of the community. For Star Energy, the program is not just a philanthropic endeavor but a strategic investment in building long-term goodwill and trust within the community. To dismantle or diminish this program would be to undermine a vital bridge between corporate responsibility and community development, risking both the company's reputation and its connection with the people it serves. Therefore, maintaining and expanding this scholarship program is not just advisable—it is essential for sustaining the positive legacy that Star Energy has built.

REFERENCES

Silvius, A. J. G., & Schipper, R. P. J. (2014). Sustainability in project management: A literature review and impact analysis. *Social Business*, 4(1), 63–96. https://doi.org/10.1362/204440814X13948909253866

Greene, J. P., Howell, W. G., & Peterson, P. E. (1997). *Lessons from the Cleveland Scholarship Program*.

Erickson, H. H., Mills, J. N., & Wolf, P. J. (2021). The Effects of the Louisiana Scholarship Program on Student Achievement and College Entrance. *Journal of Research on Educational Effectiveness*, 14(4), 861–899. https://doi.org/10.1080/19345747.2021.1938311

Mills, J. N., & Wolf, P. J. (2017). *The Effects of the Louisiana Scholarship Program on Student Achievement After Three Years. School Choice Demonstration Project*. https://scholarworks.uark.edu/scdp/12

Byantoro, G.A., Wardoyoe, D.T.W., Karwanto, Khamidi, A., Nursalim, M., et al. (2024). The Impact of Scholarships on Student Achievement: A Mix Methods Study. *Jurnal Pendidikan dan Pembelajaran*, 5(1), 1371-1378. https://jurnaledukasia.org/index.php/edukasia/article/view/1036/659

Erwin., Abbas, M.J., Syakhrani, A.W. (2024). The Role of Education Management in Managing the Scholarship Programme and Its Impact on Student Achievement. *Indonesian Journal of Education*, 4(2), 530-544. https://injoe.org/index.php/INJOE/article/view/120/158

Dart, J., & Davies, R. (2003). A Dialogical, Story-Based Evaluation Tool: The Most Significant Change Technique. *The American Journal of Evaluation*, 24(2), 137–155. https://doi.org/10.1016/S1098-2140(03)00024-9

Davies, R., & Dart, J. (n.d.). *The "Most Significant Change" (MSC) Technique: A Guide to Its Use Acronyms*.

Dynarski, S. (2003). Does Aid Matter? Measuring the Effect of Student Aid on College Attendance and Completion. *American Economic Review*, 93(1), 279-288.

Angrist, J. D., & Pischke, J. S. (2008). *Mostly Harmless Econometrics: An Empiricist's Companion*. Princeton University Press.

Castleman, B. L., & Long, B. T. (2016). Looking Beyond Enrollment: The Causal Effect of Need-Based Grants on College Access, Persistence, and Graduation. *Journal of Labor Economics*, 34(4), 1023-1073.

Cabrera, A. F., & La Nasa, S. M. (2001). On the Path to College: Three Critical Tasks Facing America's Disadvantaged. *Research in Higher Education*, 42(2), 119-149.

Turner, S. E. (2004). *Going to College and Finishing College: Explaining Different Educational Outcomes*. University of Michigan Press.

Gleason, P., & Dynarski, M. (2002). Do We Know Whom to Help? Implementation of the Upward Bound Math-Science Program Evaluation. *Journal of Education for Students Placed at Risk*, 7(1), 53-80.

Bettinger, E. P. (2004). *How Financial Aid Affects Persistence*. National Bureau of Economic Research.

Deming, D., & Dynarski, S. (2009). *Into College, Out of Poverty? Policies to Increase the Postsecondary Attainment of the Poor*. National Bureau of Economic Research.

Goldrick-Rab, S., Harris, D. N., & Trostel, P. A. (2009). *Why Financial Aid Matters (or Does Not) for College Success: Toward a New Interdisciplinary Perspective*. Higher Education: Handbook of Theory and Research, 24, 1-45.

Zakaria, (2019). *The Hexa-Helix Concept for Supporting Sustainable Regional Development (Case Study: Citatah Area, Padalarang Subdistrict, West Java, Indonesia)*. Earth and Environmental Science

Badan Pusat Statistik. (2004) *Kabupaten Bandung dalam Angka 2004*. Retrieved from https://bandungkab.bps.go.id/publication/2009/01/01/98ec8474fbbf4acb3606e7ab/kabupaten-bandung-dalam-angka-2004.html

Badan Pusat Statistik. (2004) *Kecamatan Pangalengan dalam Angka 2020*. Retrieved from https://bandungkab.bps.go.id/publication/2020/09/28/9aaedf5c49ced530de62be46/kecamatan-pangalengan-dalam-angka-2020.html

Geothermal Beyond Electricity: A Study on Leveraging Various Geothermal Value Chain as Innovative Additional Revenue Option for Implementation in Indonesia

M. Rizqi Al Asy'ari[1], Daniel W. Adityatama[1], Nadya Erichatama[1], Vincentius Adven Brilian[1], Ferdino R Fadhillah[2], Desak Nyoman Inten Apriani[2], Dorman Purba[2], Astri Indra Mustika[2], and Triwening Larasati[1]

[1]GEOENERGIS, Cibis Nine 11th Floor, Jakarta Selatan 12560, Indonesia
[2]PT Sarana Multi Infrastruktur (Persero), Sahid Sudirman Center 49th floor, Jakarta, Indonesia

rizqialasyari21@gmail.com, rizqialasyari@geoenergis.com

Keywords: geothermal, derivative product, secondary product

ABSTRACT

Globally, the development of geothermal projects is not only for electricity generation, but also for its other value chain and derivative product for increasing revenue beyond ceiling tariff. This research explores the expansive realm of geothermal energy derivative products, drawing vital insights from the United States to propose strategic implementations for Indonesia. The research commences with an in-depth examination of the U.S. geothermal business model, emphasizing electricity generation and the integral role of the electricity grid. It addresses the market's challenges and opportunities, focusing on how geothermal derivative products are interwoven into U.S. business strategies.

The paper delineates various geothermal value chain and derivative products prevalent in the U.S., including direct use, and groundbreaking methods for extracting lithium, silica, and hydrogen. Each product is scrutinized for its economic viability, market potential, environmental benefits, and the existing policy framework that supports its development. This examination unveils the multifaceted value these derivatives add to the traditional geothermal energy spectrum, highlighting their potential to enhance energy sustainability and economic growth. Looking forward, the study delves into the future landscape of geothermal derivatives in the U.S., spotlighting research initiatives, innovative technologies, and pilot projects that promise to redefine geothermal energy utilization. This forward-looking perspective not only signifies growth in the U.S. but also sets a benchmark for Indonesia.

The core of the research encapsulates a comparative analysis, extracting lessons from the U.S. to envisage a tailored geothermal derivative implementation strategy for Indonesia. By dissecting successful U.S. practices, the study identifies transferable strategies, policy recommendations, and technical prerequisites tailored to Indonesia's geothermal context. It underscores the necessity for a supportive policy environment, strategic investment, and technological adaptation to foster a robust geothermal derivative market in Indonesia.

In its culmination, the paper synthesizes key insights, offering a strategic roadmap for Indonesia to harness the untapped potential of geothermal derivatives. By integrating lessons from the U.S., it advocates for a holistic approach that aligns economic, environmental, and technological objectives, thereby propelling Indonesia towards a sustainable energy future and positioning it as a frontrunner in geothermal energy innovation. This research stands as a pivotal reference for stakeholders in the geothermal energy sector, policy-makers, and the academic community, providing a comprehensive framework to guide the strategic expansion of geothermal derivative products in Indonesia and beyond.

1. INTRODUCTION

The utilization of geothermal energy has predominantly centered around electricity generation, yet the potential of geothermal resources extends far beyond this conventional application. Globally, there is a growing interest in exploring geothermal derivative products as a means to enhance revenue streams and promote sustainable energy practices. This study delves into the diverse realm of geothermal energy derivative products, drawing pivotal insights from the United States, a leader in geothermal innovation, to propose strategic implementations for Indonesia. By examining the U.S. geothermal business model, this research aims to identify transferable strategies that can bolster Indonesia's geothermal industry, thereby fostering economic growth, energy sustainability, and environmental benefits.

1.1 Research Background

In the quest for sustainable energy solutions, geothermal energy emerges as a pivotal player within the renewable energy landscape. With its ability to provide baseload power and minimal environmental footprint, geothermal energy stands out as a particularly resilient and reliable source. This paper explores the expanded role of

geothermal energy beyond conventional electricity generation, delving into its derivative products as innovative revenue streams.

Geothermal energy, a renewable and sustainable resource, has long been harnessed for electricity generation. However, as the global energy landscape evolves, there is an increasing emphasis on maximizing the value of geothermal resources by leveraging derivative products. These secondary products, such as district heating and cooling systems, and the extraction of valuable minerals like lithium, silica, and hydrogen, present significant opportunities for enhancing the economic viability and sustainability of geothermal projects.

The United States has been a pioneer in geothermal electricity generation, leveraging its rich geothermal resources to produce reliable, renewable energy which currently become 1st rank of top geothermal producer country by installed capacity (see Figure 1) (Thinkgeoenergy, 2024; Al Asy'ari, Adityatama, Brilian, Erichatama, & Purba, 2024; Richter, 2023). As the largest producer of geothermal power, the U.S. harnesses the earth's heat, primarily concentrated in the western states such as California and Nevada, to generate electricity. This process involves using steam produced from natural geothermal reservoirs to power turbines. The technology has evolved over decades, with the U.S. continuously expanding its capacity through both traditional hydrothermal plants and innovative approaches like Enhanced Geothermal Systems (EGS).

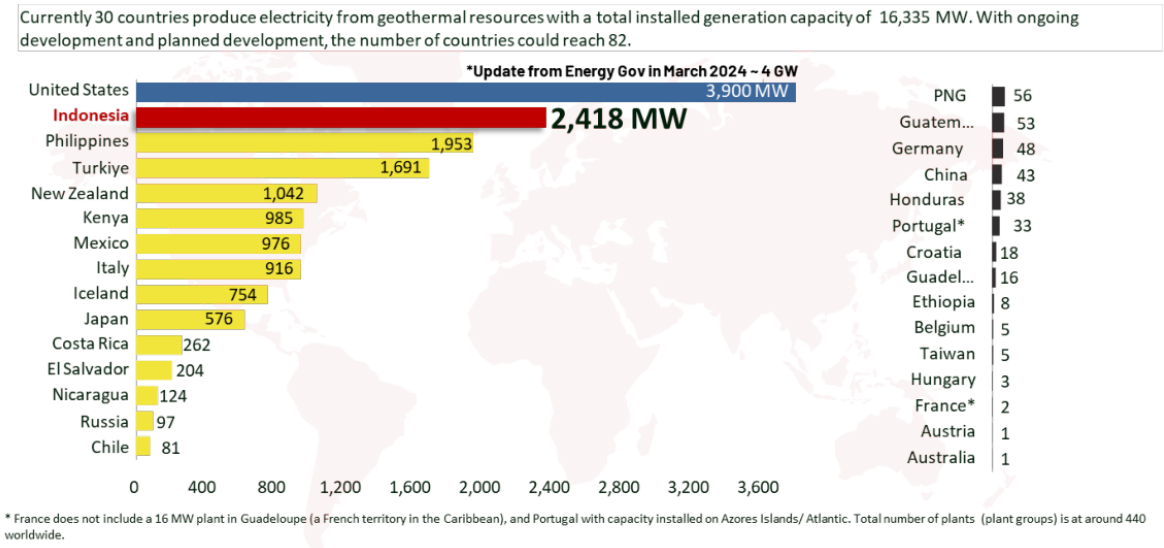

Figure 1: Global update of geothermal power plant installed capacity as per update January 2024. Modified from (Thinkgeoenergy, 2024; Al Asy'ari, Adityatama, Brilian, Erichatama, & Purba, 2024; Richter, 2023)

In the United States, the integration of geothermal derivative products into business models has been instrumental in overcoming market challenges and capitalizing on new opportunities. The U.S. experience provides a rich repository of knowledge on the economic, environmental, and policy dimensions of geothermal derivatives. By drawing lessons from the U.S., this study aims to inform the development of a robust geothermal derivative market in Indonesia, a country with vast untapped geothermal potential.

1.2 Research Objectives and Method

The primary objective of this research is to explore and evaluate the potential of geothermal derivative products in the United States and propose strategic implementations for Indonesia. This objective is pursued through a comprehensive examination of the U.S. geothermal business model, focusing on electricity generation and the integral role of the electricity grid. The study seeks to address the following specific objectives:

1. *Identify and analyze geothermal value chain and derivative products prevalent in the United States*, including district heating and cooling systems, and methods for extracting lithium, silica, and hydrogen. This analysis will cover the economic viability, market potential, environmental benefits, and policy frameworks that support these products.
2. *Assess the future landscape of geothermal value chain and derivatives in the U.S*, highlighting ongoing research initiatives, innovative technologies, and pilot projects. This forward-looking analysis will provide insights into potential growth areas and technological advancements in the geothermal sector.
3. *Conduct a comparative analysis to extract lessons from the U.S. experience*, develop a tailored geothermal value chain and derivative product implementation strategy for Indonesia. This will involve

identifying transferable strategies, policy recommendations, and technical prerequisites suited to Indonesia's geothermal context.

4. *Develop Key Insights for Indonesia*, synthesizing key insights from the U.S. and advocating for a holistic approach that aligns economic, environmental, and technological objectives to foster a sustainable geothermal energy future in Indonesia.

To achieve these objectives, the research adopts a multi-method approach, encompassing a holistic review of existing literature on geothermal energy and derivative products, with a focus on U.S. practices and experiences. Then, Detailed case studies of successful geothermal derivative projects in the United States, providing practical insights and lessons learned. This study also conducts a systematic comparison of the geothermal sectors in the U.S. and Indonesia, identifying similarities, differences, and areas for potential adaptation. Moreover, the authors engage with key stakeholders in the geothermal industry, including policymakers, industry experts, and academic researchers, to gather qualitative insights and validate findings.

By integrating these methods, the research aims to provide a comprehensive framework for leveraging geothermal derivative products in Indonesia, thereby contributing to the country's energy diversification and sustainability goals.

2. OVERVIEW OF GEOTHERMAL ELECTRICITY GENERATION IN THE UNITED STATES

The United States holds the prestigious position of being the leading producer of geothermal electricity globally, largely attributed to its extensive and well-managed geothermal resources concentrated in the western states such as California and Nevada. The foundation of geothermal energy utilization in the U.S. is built upon decades of technological advancements and strategic policy frameworks that have cultivated a robust infrastructure capable of leveraging the earth's heat effectively. This heat is primarily harnessed through hydrothermal power systems, where naturally occurring steam and hot water from the earth's crust drive turbines to generate electricity.

Geothermal power plants in the U.S. have evolved through three main technological stages: dry steam, flash steam, and binary cycle. Each technology corresponds to the specific characteristics of geothermal reservoirs, optimizing energy extraction based on steam quality and temperature. For instance, the Geysers in California, the largest geothermal complex globally, utilizes dry steam directly emitted from the earth to power turbines, showcasing one of the oldest and most efficient forms of geothermal electricity generation.

The integration of Enhanced Geothermal Systems (EGS) marks a significant technological shift, aimed at expanding geothermal applications beyond natural hydrothermal resources. EGS involves artificially creating reservoirs in hot dry rock formations, which are abundant but previously inaccessible for energy production. This innovation not only broadens the geographical scope of geothermal energy production but also enhances its reliability and output, ensuring a consistent energy supply regardless of natural hydrothermal availability. The economic viability of these systems has seen continuous improvement, supported by both governmental incentives and private investments. Initiatives such as the Geothermal Technologies Office (GTO) under the U.S. Department of Energy focus on advancing technologies that reduce costs and risks associated with geothermal development. Such policies not only reinforce the operational capacities of geothermal facilities but also stimulate research and development in next-generation geothermal technologies.

By meticulously harnessing these advanced technologies and supportive policies, the U.S. continues to enhance its geothermal electricity generation capacity, setting a formidable benchmark in both technological innovation and sustainable energy practices. This comprehensive approach underpins the U.S. geothermal sector’s success, providing valuable lessons and adaptable strategies for countries like Indonesia, aiming to escalate their geothermal development to a similar echelon of energy efficiency and economic profitability.

Figure 2 presents a detailed overview of the organizational and regulatory framework of the U.S. electricity market. The map segment delineates the various electricity regions managed by independent system operators (ISOs) and regional transmission organizations (RTOs), which are instrumental in coordinating, controlling, and monitoring the electrical grid as well as facilitating electricity market operations. These entities play a critical role in ensuring the reliability of electricity supply and the integration of diverse power sources, including renewable energies like geothermal, into the grid. The figure also encapsulates the three-tier regulatory structure that governs the U.S. electricity market, consisting of federal, state, and municipal levels. At the federal level, entities like the Department of Energy (DOE) and the Federal Energy Regulatory Commission (FERC) set broad policies and regulations that ensure an open and non-discriminatory transmission grid, promoting competition and enhancing the economic efficiency of the electricity market. State regulators, such as the Public Utilities Commission of Nevada, tailor these policies to local contexts, addressing state-specific energy needs and conditions. At the municipal level, agencies manage local energy services and regulatory compliance, ensuring that the federal and state policies are effectively implemented in urban and rural communities alike.

This comprehensive structure supports a stable, reliable, and adaptable energy system, crucial for integrating sustainable energy practices. Such a framework is particularly relevant when considering the expansion of geothermal energy usage in the United States, as it highlights the critical role of regulatory bodies and market operators in facilitating the growth of renewable energy within an established grid infrastructure. The figure underscores the necessity for robust governance and coordinated management in fostering a sustainable and efficient energy market, serving as a model for other countries aiming to enhance their energy systems.

Transitioning from a general overview of the electricity models and regulatory frameworks in the United States, it is essential to examine how demographic factors, specifically population density, influence the structuring and efficiency of these models. Figure 3 delves into the relationship between population density and the U.S. electricity market, highlighting the disparity in retail competition across various states.

Figure 3 illustrates the significant impact of population density on the electricity market model in the United States, categorizing states into those with dense and sparse populations. The map color-codes states according to their level of retail electricity competition—full, partial, or none—which correlates strongly with population density. States with high population densities, such as those in the Northeast and parts of the West Coast, are marked in green, indicating full retail competition. This competition is viable due to high electricity demand and the economic efficiency of shorter distribution networks in these areas, making them attractive for energy providers.

Conversely, states with low population densities, primarily located in the Midwest and parts of the Rocky Mountain region, are depicted with striped patterns. These areas have partial or no retail competition, attributed to lower electricity demand and the logistical challenges posed by longer distribution lines required to connect dispersed consumers. The pie charts adjacent to the map further quantify this distribution, showing that only a small fraction of states have fully embraced retail competition, with the majority having partial or none, reflecting the logistical and economic constraints in less populated areas.

This visualization underscores the complexities and regional variations in the U.S. electricity market, influenced by demographic factors. The analysis reveals that while densely populated areas can support a competitive market due to their infrastructure and demand, sparsely populated areas face inherent challenges that deter competitive retail electricity markets. Understanding these dynamics is crucial for policymakers and market designers aiming to enhance energy efficiency and market competitiveness across diverse geographic and demographic landscapes.

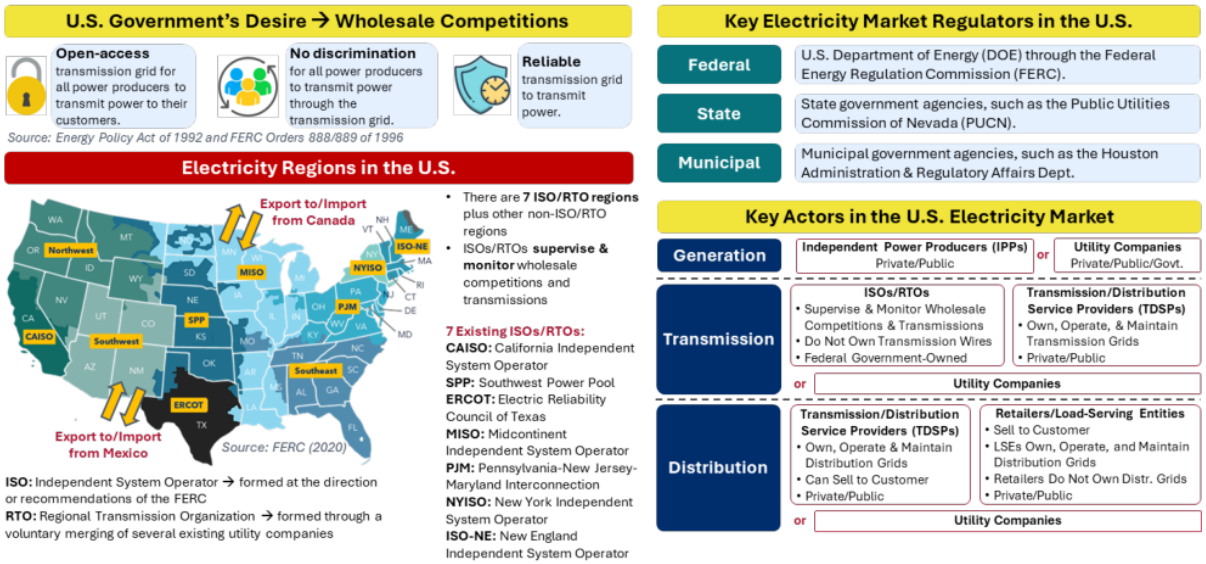

Figure 2: United States Electricity Model Highlight Modified from (Geoenergis, 2024a).

Building on the discussion of how population density influences the structure of electricity markets, it is essential to delve deeper into the various models of electricity market structures that are employed across the United States. These models reflect different approaches to regulation, competition, and service provision, shaped by historical, economic, and demographic factors. Figure 4 presents an overview of four distinct electricity market models operating within the United States, each characterized by different levels of integration and competition.

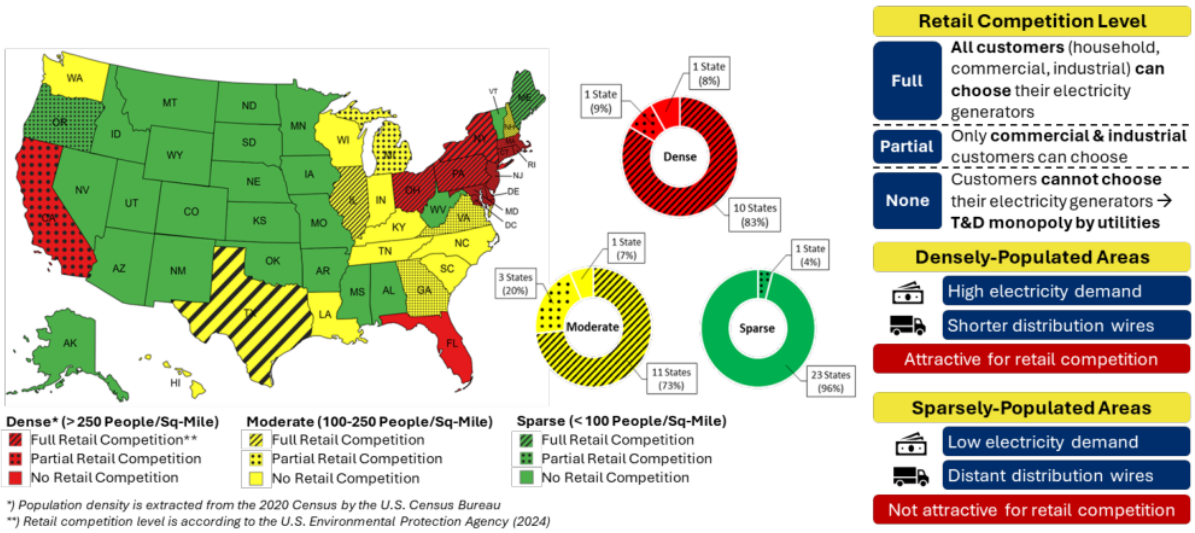

Figure 3: Influence of Population Density to the U.S. Electricity Market Model Modified from (Geoenergis, 2024a).

Model 1: Vertically Integrated In the traditional vertically integrated model, a single monopoly utility is responsible for all stages of electricity production, from generation to transmission and distribution, ending with customer billing. This model is prevalent in areas where a single utility company controls the entire process, often regulated by state agencies to ensure service provision and price control. This setup is common among state-owned utilities and investor-owned utilities (IOUs), which manage extensive infrastructure and serve a large customer base. Despite the potential for conflicts of interest between utility owners and customers, this model benefits from streamlined operations and centralized control.

Model 2: Vertically Integrated with a Single Buyer The single buyer model introduces a limited level of competition by allowing independent power producers (IPPs) to sell electricity to a centralized purchasing agency, which then manages transmission and distribution to end consumers. This model is typically found in restructured markets where the vertically integrated utility remains, often state-owned, and aims to introduce competition at the generation level while maintaining a monopoly over transmission and distribution. This approach seeks to leverage competitive pricing from IPPs while ensuring stable and regulated delivery to consumers.

Model 3: Wholesale Competition without Retail Competition The wholesale competition model allows for greater market dynamics by enabling multiple generators to sell electricity directly to distribution companies (Discos) or load-serving entities (LSEs) through an open transmission network managed by an independent system operator (ISO) or regional transmission organization (RTO). While Discos or LSEs may still hold monopolies over local distribution, the open access to transmission lines encourages competitive pricing and efficient generator dispatch. This model is common in several restructured markets globally, including parts of the U.S., the UK, and Australia.

Model 4: Wholesale Competition with Full/Partial Retail Competition In the most competitive model, both wholesale and retail electricity markets are open to competition. Customers have the freedom to choose their electricity suppliers from a variety of retail providers, who purchase electricity from competing generators through an open transmission network. This model supports a fully competitive environment, fostering innovation and customer-centric services. Regulatory oversight ensures that transmission and distribution remain reliable and fair, often through separate entities such as Transmission Service Providers (TSPs) and Distribution Service Providers (DSPs). The Electric Reliability Council of Texas (ERCOT) is a prominent example, offering extensive retail choice and competitive market dynamics.

Each of these models represents different strategies for managing the balance between regulation and competition, reflecting the unique needs and circumstances of various regions. Understanding these models is crucial for designing effective policies and frameworks that can enhance the efficiency, reliability, and sustainability of electricity markets.

Having explored the general electricity market models and their regulatory frameworks, it is pertinent to examine specific examples of how these models are implemented across various states in the U.S., particularly those with significant geothermal resources. Figure 5 focuses on prominent electricity market models in key geothermal states, highlighting how different regulatory and market structures support the integration and utilization of geothermal energy within these states.

Each state's approach to integrating geothermal energy within its electricity market model demonstrates the diverse strategies employed across the U.S. These models reflect the varying degrees of market competition and regulatory oversight, tailored to each state's specific needs and resources. Understanding these different implementations provides valuable insights into how geothermal energy can be effectively managed and expanded within various regulatory frameworks.

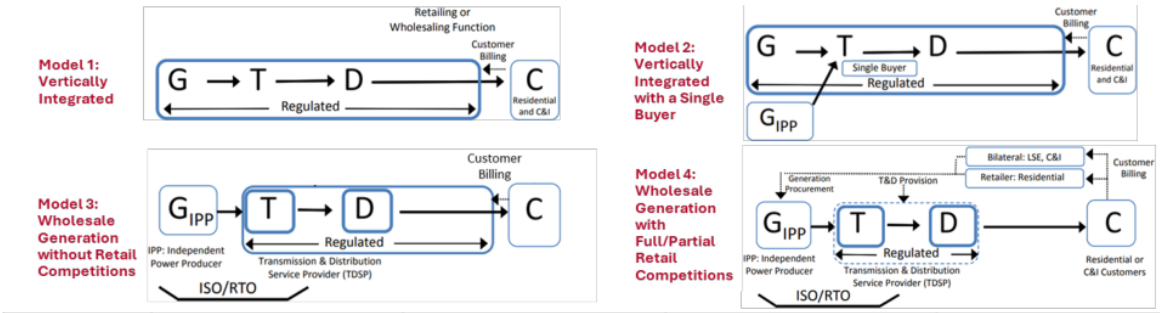

Parameter	Model 1	Model 2	Model 3	Model 4
Generation actor	Utility companies (private/public/government)	• Utility companies (private/public/government) • IPPs (private/public)	IPPs (private/public)	IPPs (private/public)
Transmission actor	Utility companies (private/public/government)	Utility companies (private/public/government)	• ISOs/RTOs (federal government) • TDSP (private/public)	ISOs/RTOs (federal government)
Distribution actor	Utility companies (private/public/government)	Utility companies (private/public/government)	• TDSP (private/public) • LSEs (private/public)	• Retailers (private/public) • LSEs (private/public)
Generation pricing mechanism	None (due to vertical monopoly by utility companies)	Fixed price → future market	• Wholesale price → spot market (minute-basis) • Fixed price → future market	• Wholesale price → spot market (minute-basis) • Fixed price → future market
Customer pricing mechanism	Fixed price (daily/monthly/ seasonal) → future market	Fixed price (daily/monthly/ seasonal) → future market	Fixed price (daily/monthly/ seasonal) → future market	Fixed price (daily/monthly/ seasonal) → future market
Customer billing	To utility companies	To utility companies	To TDSPs	• Residential → to retailers • C&I → to LSEs

Figure 4: Electricity Market Model in United States Modified from (Geoenergis, 2024a).

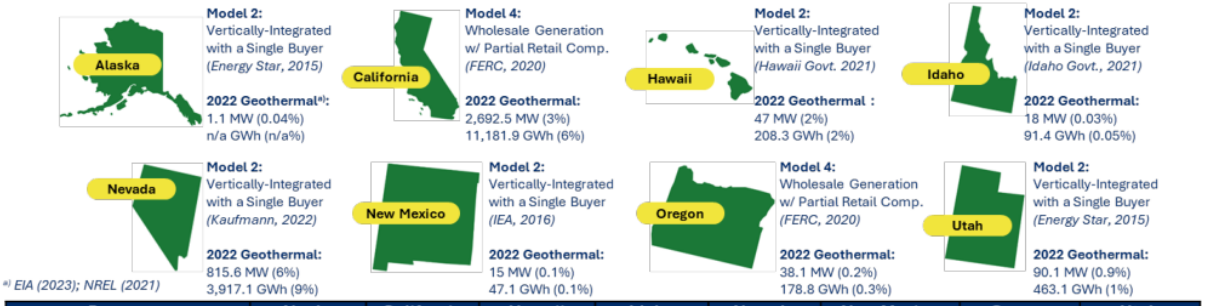

[a] EIA (2023); NREL (2021)

Parameter	Alaska	California	Hawaii	Idaho	Nevada	New Mexico	Oregon	Utah
Regulatory Body	Regulatory Commission of Alaska (RCA)	California Public Utilities Commission (CPUC)	Hawaii Public Utilities Commission (HPUC)	Idaho Public Utilities Commission (IPUC)	Public Utilities Commission of Nevada (PUCN)	New Mexico Public Regulation Commission (NM-PRC)	Oregon Public Utilities Commission (OPUC)	Utah Public Service Commission (UPSC)
2020 Population[b]	733,391	39,538,223	1,455,271	1,839,106	3,104,614	2,117,522	4,237,256	3,271,616
2020 Population Density (per Square Mile)[b]	1.3 (Sparse)	253.7 (Dense)	226.6 (Moderate)	22.3 (Sparse)	28.3 (Sparse)	17.5 (Sparse)	44.1 (Sparse)	39.7 (Sparse)
2022 Total Generation (GWh)[c]	6,694	203,384	9,337	16,278	42,492	40,889	61,318	39,386
2022 Imported (GWh)[c]	0	71,503	0	11,883	0	0	0	0
2022 Total Supply (GWh)[c]	**6,694**	**274,804**	**9,337**	**28,161**	**42,592**	**40,889**	**61,318**	**39,386**
2022 Total Demand (GWh)[c]	**6,002**	**251,869**	**9,039**	**26,201**	**39,320**	**27,156**	**56,327**	**33,366**

[b] U.S. EIA (2023) [c] U.S. Census Bureau (2020)

Figure 5: Prominent Electricity Market Model in the U.S. "Geothermal States" Modified from (Geoenergis, 2024a).

3. CURRENT UNITED STATES PLAN FOR INCREASING GEOTHERMAL EXPOSURE TOWARDS NET ZERO FUTURE

As the global community intensifies its efforts to combat climate change, the United States has embarked on an ambitious journey to achieve a net-zero carbon future by mid-century. Central to this initiative is the strategic expansion of geothermal energy, a versatile and sustainable resource with the potential to provide continuous, reliable power while significantly reducing greenhouse gas emissions. This section explores the current plans and strategies employed by the U.S. to enhance geothermal energy utilization, examining the roles of technological innovation, policy support, and market incentives in driving this transition.

The United States' plan to increase geothermal exposure as part of its strategy to achieve a net-zero carbon future is multifaceted, involving advancements in technology, supportive policy frameworks, and targeted market incentives. One of the key components of this plan is the development and deployment of Enhanced Geothermal Systems (EGS). EGS technology allows for the extraction of geothermal energy from dry, non-porous rocks by artificially creating reservoirs through hydraulic stimulation. This innovation significantly expands the geographic and geological scope of geothermal energy production, making it viable in regions previously considered unsuitable for traditional hydrothermal plants.

Federal initiatives, such as those spearheaded by the U.S. Department of Energy (DOE), play a crucial role in advancing geothermal technologies. The DOE's Geothermal Technologies Office (GTO) focuses on research, development, and demonstration projects aimed at reducing the costs and risks associated with geothermal energy deployment. Programs like the Frontier Observatory for Research in Geothermal Energy (FORGE) are at the forefront of testing and validating EGS technologies, providing a blueprint for future large-scale implementations. Also, various geothermal value chain and derivative product is increasing the exposure of geothermal energy in the United States.

In addition to technological advancements, policy support is pivotal in fostering an environment conducive to geothermal energy growth. The extension of federal tax credits, such as the Investment Tax Credit (ITC) and Production Tax Credit (PTC), provides significant financial incentives for geothermal projects. These credits lower the capital costs for developers, making geothermal projects more economically attractive. Furthermore, state-level policies and renewable portfolio standards (RPS) mandate utilities to include a certain percentage of renewable energy in their supply mix, further driving the demand for geothermal power.

Market incentives also play a vital role in promoting geothermal energy. The establishment of competitive power purchase agreements (PPAs) ensures stable revenue streams for geothermal developers, encouraging investment in new projects. Additionally, the integration of geothermal energy into state and regional grid systems enhances grid reliability and resilience, supporting broader energy market stability.

The U.S. geothermal strategy also includes efforts to streamline regulatory processes and reduce permitting times, addressing one of the significant barriers to geothermal development. Collaborative initiatives between federal and state agencies aim to harmonize regulations and simplify the approval process for geothermal projects, thus accelerating their deployment.

By leveraging these technological, policy, and market mechanisms, the United States aims to significantly expand its geothermal energy capacity, contributing to its overarching goal of a net-zero carbon future. This strategic approach not only supports the transition to a sustainable energy system but also positions geothermal energy as a cornerstone of the U.S. renewable energy portfolio.

To understand the current landscape and future potential of geothermal energy in the United States, it is crucial to examine the historical trends in geothermal capacity expansion. This historical perspective provides insights into the growth patterns, technological advancements, and regional developments that have shaped the U.S. geothermal industry. Figure 6 illustrates the installed geothermal capacity in the U.S. from 1960 to 2023, highlighting contributions from major geothermal fields and key periods of deployment.

Figure 6 provides a comprehensive overview of the historical installed geothermal capacity in the United States, segmented by field location and spanning from 1960 to 2023. The graph delineates significant growth phases and the contribution of various geothermal fields to the overall capacity.

From 1960 to 1990, the U.S. geothermal industry experienced a rapid deployment rate of 81.3 MW per year, primarily driven by the development of major fields such as The Geysers in California. The Geysers, the largest geothermal field in the world, played a pivotal role during this period, significantly boosting the national capacity. This early growth phase was characterized by pioneering

technological advancements and substantial investments in geothermal infrastructure. Post-1990, the deployment rate slowed to 35.7 MW per year, reflecting a period of consolidation and strategic expansion. The development of additional fields such as Salton Sea, Coso, McGinness Hills, and Heber contributed to this growth. Notably, these top five fields collectively account for 70% of the total installed capacity as of 2023, underscoring their critical importance to the U.S. geothermal landscape.

The graph also highlights the cumulative contributions of these fields:

- **The Geysers**: With a total capacity of 1,634 MW, it constitutes 43% of the national total, illustrating its dominance in the sector.
- **Salton Sea**: Contributing 448 MW (12%), this field has been instrumental in maintaining steady capacity growth.

- **Coso**: With a capacity of 270 MW (7%), it has been a significant player in the geothermal market.
- **McGinness Hills**: Adding 174 MW (5%) to the total capacity, this field represents the continued expansion into Nevada's geothermal resources.
- **Heber**: With a contribution of 162 MW (4%), it underscores the role of diversified geographic development.

The right side of the figure provides a summary of the capacity contributions and average deployment rates. Out of the 37 geothermal fields, the top five fields contribute 41% of the total capacity, highlighting their strategic importance. The average deployment rate reflects the periods of rapid initial growth and subsequent steady expansion.

By analyzing these historical trends, we gain valuable insights into the factors that have driven geothermal development in the U.S., including technological innovation, resource availability, and policy support. This historical context is crucial for shaping future strategies to enhance geothermal energy deployment, aiming towards the ambitious goal of a net-zero carbon future.

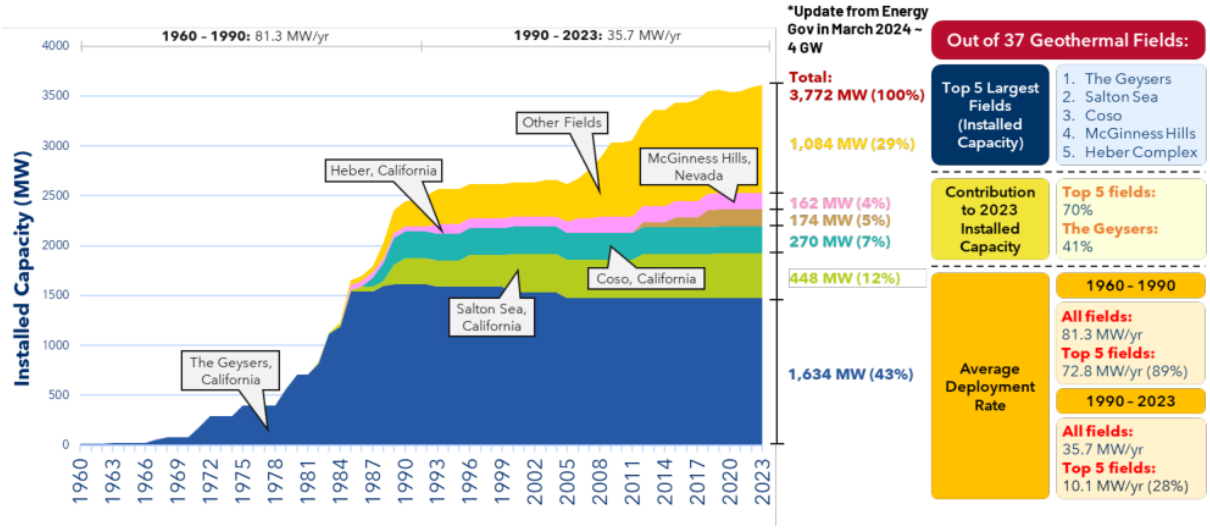

Figure 6: Historical Installed Capacity Based on Field Location.

As the global energy landscape continues to evolve, the role of geothermal energy is expanding beyond traditional electricity generation. Innovative business models are emerging that leverage the full potential of geothermal resources, offering diverse applications and revenue streams.

Figure 7 showcases the diverse business models for geothermal energy that have emerged globally, emphasizing both conventional and innovative applications. The diagram is divided into two primary segments: Power Generation and Beyond Electricity Generation, each encompassing various strategies and technologies to maximize the utilization of geothermal resources. By embracing these innovative business models, geothermal energy can significantly contribute to global energy sustainability goals. The diverse applications highlight the potential for geothermal energy to not only provide reliable electricity but also to drive economic growth through its varied and adaptable uses. This multifaceted approach ensures that geothermal energy remains a vital component of the global transition to a sustainable energy future.

As the geothermal industry evolves, it has become imperative to explore and implement next-generation technologies that can tap into a broader spectrum of geothermal resources. These advancements aim to overcome the limitations of conventional hydrothermal systems, thereby expanding geothermal energy's reach and potential. Figure 8 illustrates the three primary categories of geothermal power generation: conventional hydrothermal, Enhanced Geothermal Systems (EGS), and closed-loop geothermal systems. Each category represents a step towards achieving greater scalability and efficiency in geothermal energy production.

The integration of these next-generation technologies marks a paradigm shift in geothermal energy utilization, allowing for a broader and more efficient exploitation of geothermal resources. By overcoming the limitations of conventional systems, EGS and closed loop technologies pave the way for geothermal energy to become a cornerstone of sustainable energy systems worldwide. These advancements support the strategic expansion of geothermal energy, contributing significantly to the goal of achieving a net-zero carbon future.

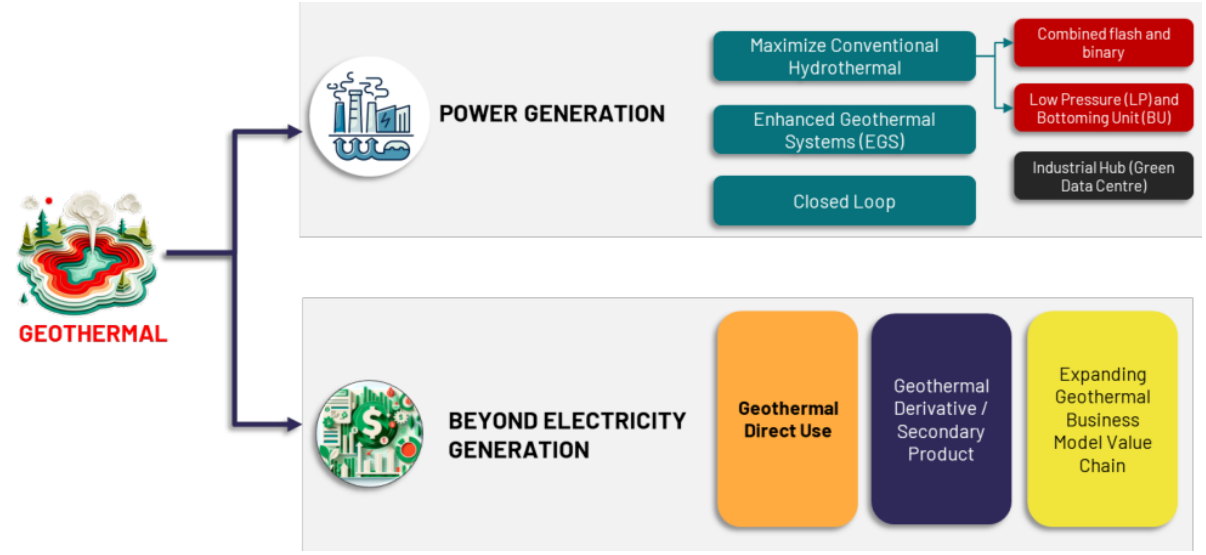

Figure 7: Geothermal Business Model Option that Currently Emerged Globally.

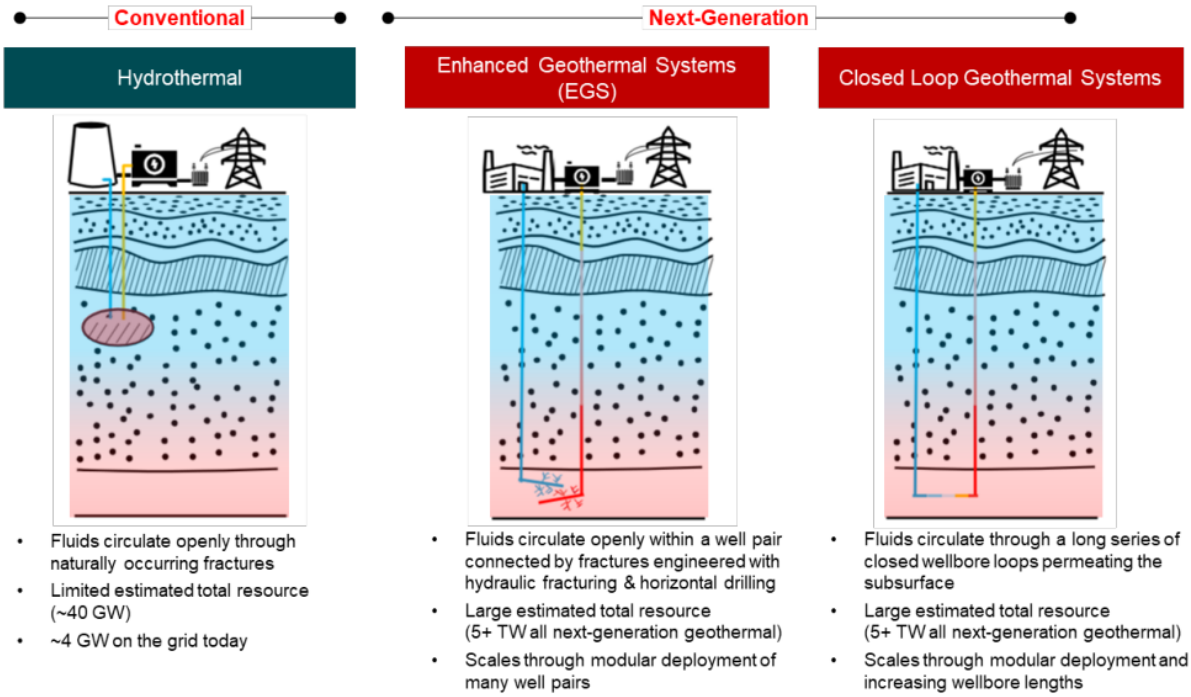

Figure 8: Next-generation geothermal technologies engineer their own resources (Achieving Scale) Modified from (US DOE, 2024).

Having discussed the technological advancements in geothermal energy, it is crucial to consider the strategic roadmap that the United States has outlined to scale these innovations across the country. The following section delves into the phased approach planned for expanding the geographic reach of next-generation geothermal technologies. Figure 9 outlines a strategic roadmap for the large-scale deployment of next-generation geothermal technologies in the United States, structured in two major stages: "Reaching Liftoff" and "Achieving Scale." This phased approach aims to systematically prove the market potential and expand the geographical reach of geothermal energy, ensuring a comprehensive and sustainable integration into the national energy mix.

4. CURRENT OPTION FOR GEOTHERMAL BEYOND ELECTRICITY

While geothermal energy is traditionally associated with electricity generation, its potential extends far beyond this conventional application. Innovative technologies and business models are emerging that exploit geothermal resources for a variety of direct-use applications, creating new revenue streams and enhancing sustainability. This section explores the current options for utilizing geothermal energy beyond electricity production, highlighting

the diverse ways in which geothermal resources can be harnessed to provide heating, cooling, and valuable by-products such as minerals and industrial applications.

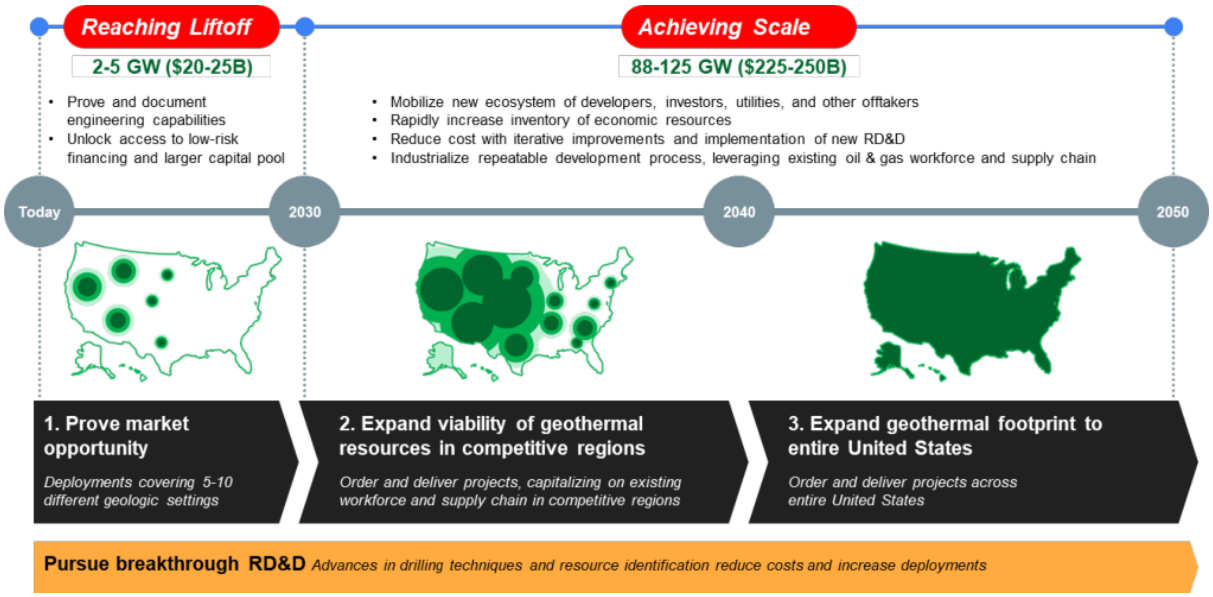

Figure 9: Scale for next-generation geothermal can proceed in two stages with increasing geographic reach in United States Modified from (US DOE, 2024).

The utilization of geothermal energy beyond electricity generation encompasses a wide range of direct-use applications that capitalize on the inherent thermal properties of geothermal resources. These applications provide significant economic and environmental benefits, contributing to the diversification and resilience of energy systems. One of the primary direct-use applications of geothermal energy is district heating, where hot water from geothermal sources is distributed through a network of pipes to heat residential, commercial, and industrial buildings. This method is highly efficient, reducing the need for fossil fuel-based heating systems and lowering greenhouse gas emissions. Countries such as Iceland and New Zealand have successfully implemented extensive geothermal district heating networks, demonstrating the feasibility and benefits of this approach.

In addition to district heating, geothermal energy can be used for greenhouse heating, aquaculture, and industrial processes. Greenhouse heating with geothermal energy allows for year-round agricultural production, even in cold climates, by maintaining optimal growing temperatures. Similarly, geothermal aquaculture supports the farming of fish and other aquatic species by providing a stable and warm water environment, enhancing growth rates and productivity.

Innovative technologies are also being developed to extract valuable minerals from geothermal brines, such as lithium, silica, and other elements. The extraction of lithium from geothermal brines, for example, presents a sustainable method to meet the increasing demand for this critical component in batteries for electric vehicles and renewable energy storage. The Salton Sea geothermal field in California is a notable example, where projects are underway to develop commercial-scale lithium extraction facilities.

Geothermal energy can also power industrial applications and support the development of eco-industrial parks. These parks integrate multiple industrial processes that utilize geothermal heat, creating synergies and reducing overall energy consumption. Examples include using geothermal energy for drying agricultural products, pasteurizing dairy products, and other heat-intensive industrial activities. This approach not only enhances the efficiency of individual processes but also promotes the sustainable development of industrial activities.

As geothermal energy continues to gain traction as a sustainable and versatile resource, its applications are expanding beyond traditional electricity generation. Innovative uses of geothermal energy are emerging worldwide, offering additional revenue streams and enhancing the overall economic viability of geothermal projects. Figure 10 illustrates the diverse array of applications for geothermal energy beyond electricity generation, highlighting how these innovations can create new revenue opportunities for geothermal companies. The figure is divided into three main categories: Geothermal Direct Use, Geothermal Derivative Products, and Expanding Geothermal Business Model Value Chain. By exploring these diverse applications, geothermal companies can tap into new markets and revenue streams, enhancing their economic resilience and contributing to global sustainability goals.

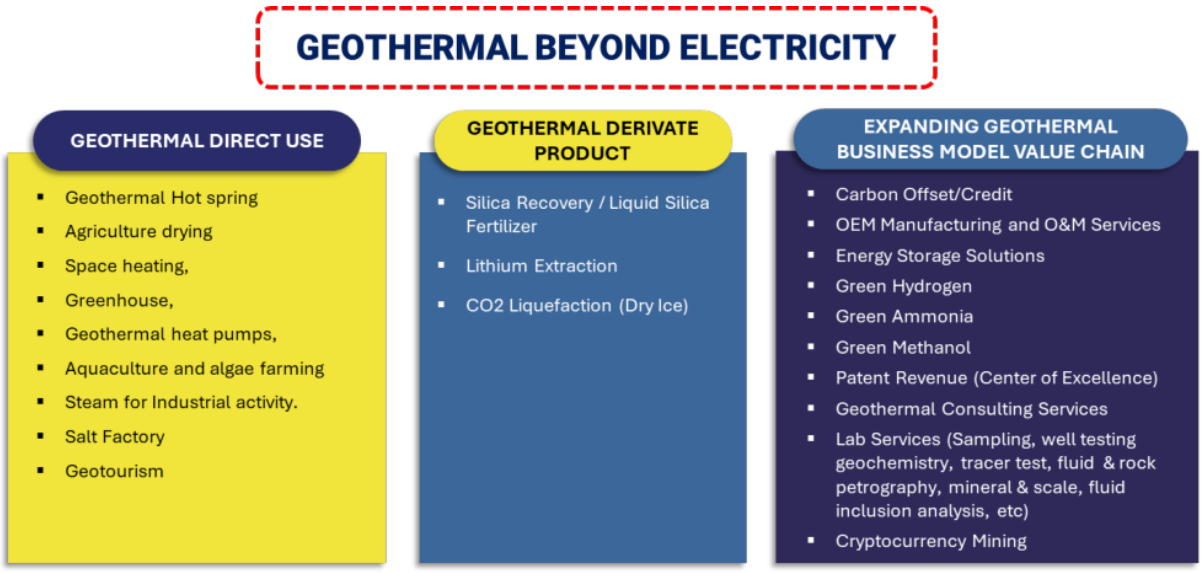

Figure 10: Identified Beyond Electricity Innovation Worldwide for Adding Additional Revenue for Geothermal Company

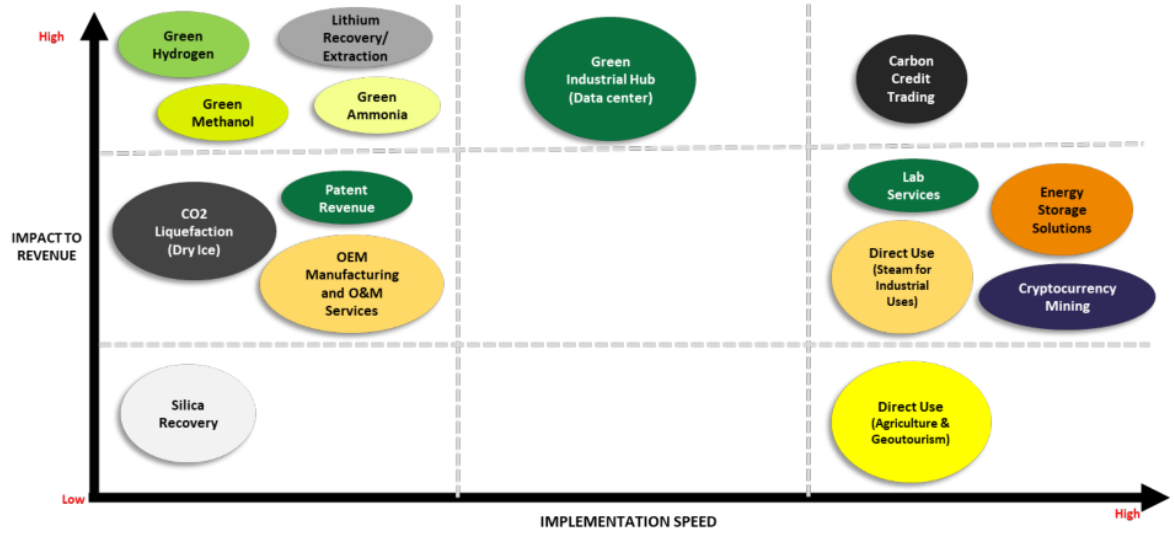

Figure 11: Preliminary Assessment on Geothermal Beyond Electricity Option.

Beyond electricity generation, geothermal energy in the U.S. has given rise to a variety of geothermal value chain and derivative products that offer additional economic and environmental benefits. These include direct heating applications, such as district heating systems, greenhouse heating, and aquaculture, which utilize the heat directly from geothermal sources. Innovative technologies are also being developed to extract valuable minerals like lithium from geothermal brines, presenting new revenue streams and contributing to the sustainability of geothermal operations. The development of these derivative products reflects a growing recognition of the multifaceted value of geothermal resources, expanding the industry's potential beyond mere power production.

By understanding these elements of the geothermal business model in the U.S., this section sets the stage for discussing the potential applications and strategies for Indonesia, leveraging the insights and successes from a well-established geothermal market to foster similar growth and sustainability in a different geographic and economic context.

After examining the diverse applications of geothermal energy beyond electricity generation, it is essential to assess these options in terms of their potential impact and feasibility. Figure 11 offers a preliminary assessment of various geothermal applications beyond electricity generation, plotted on a matrix that considers both feasibility and potential impact. This visual representation aids in understanding which applications are most viable and impactful, guiding strategic decision-making for stakeholders in the geothermal industry.

This assessment highlights the diverse opportunities for utilizing geothermal energy beyond electricity generation. By identifying applications with the highest feasibility and impact, stakeholders can prioritize investments and development efforts, maximizing the benefits of geothermal resources and contributing to sustainable energy and economic growth.

The expansion of geothermal applications beyond electricity generation represents a significant opportunity to diversify and strengthen the geothermal business model. By integrating direct-use applications and derivative products into the geothermal value chain, stakeholders can create new revenue streams and enhance the overall economic viability of geothermal projects. This holistic approach aligns with global trends towards sustainable and circular economies, where maximizing resource efficiency and minimizing waste are paramount.

In short, the current options for geothermal energy beyond electricity offer a multitude of benefits and opportunities. By leveraging these diverse applications, geothermal energy can play a pivotal role in achieving sustainability goals, reducing reliance on fossil fuels, and fostering economic growth through innovative and efficient use of natural resources.

4.1 The Position of Geothermal Derivative Products in the U.S. Geothermal Business Models

The integration of geothermal derivative products into the U.S. geothermal business models marks a strategic evolution from traditional electricity generation to a broader, more diversified utilization of geothermal resources. This shift not only enhances the economic viability of geothermal projects but also aligns with broader environmental and sustainability goals.

Geothermal derivative products represent a significant economic opportunity. These applications directly utilize the thermal energy from geothermal sources without the intermediary step of electricity generation, reducing energy loss and increasing efficiency. In regions like the Pacific Northwest and parts of California where geothermal activity is high, these uses have been integrated into local economies, providing heat for homes, businesses, and agricultural operations.

The expansion into derivative products enhances the environmental appeal of geothermal energy. By using geothermal heat directly, these applications avoid the emissions associated with burning fossil fuels for heating purposes. Moreover, the extraction of minerals such as lithium from geothermal brines presents an opportunity to support the growing renewable energy sector, particularly in battery production for electric vehicles, without the extensive environmental impact associated with traditional mining processes.

U.S. policy frameworks have increasingly recognized and supported the development of geothermal derivative products. Initiatives and incentives aimed at reducing carbon footprints and promoting renewable energy use have facilitated the growth of this sector. Policies that streamline permitting processes and provide financial incentives for the development of both geothermal power and its derivatives are crucial for the sector's growth.

The technological innovation surrounding geothermal derivative products is a key aspect of their position in U.S. business models. Advanced technologies that allow for the efficient extraction of heat and minerals from geothermal fluids are being developed and refined, further expanding the potential applications of geothermal energy. Research and development efforts supported by both government and private sectors are vital in overcoming the technical challenges associated with these innovations.

The strategic importance of geothermal derivative products in U.S. business models cannot be overstated. By diversifying the applications of geothermal energy, businesses can reduce risk, increase resilience, and tap into new markets. This diversification also aligns with global trends towards sustainability and the circular economy, where maximizing resource efficiency is key.

In short, geothermal derivative products are positioned as both a complement and a significant enhancement to the traditional geothermal business model in the United States. They provide a pathway to not only economic diversification but also to achieving sustainability and environmental goals, thereby reinforcing the strategic value of geothermal energy in the renewable energy landscape. This multifaceted approach not only solidifies the role of geothermal energy in the current market but also ensures its relevance and expansion in the future energy scenarios.

5. LESSON LEARNED FROM UNITED STATES FOR IMPLEMENTATION IN INDONESIA

The United States has long been a pioneer in geothermal energy development, not only for electricity generation but also for a multitude of direct-use applications and derivative products. These innovative approaches have demonstrated significant economic and environmental benefits, providing valuable lessons for other countries with geothermal potential, such as Indonesia. This section focuses on the key lessons learned from the U.S. experience in geothermal applications beyond electricity generation and explores how these strategies can be effectively implemented in Indonesia to maximize the value of its geothermal resources.

The U.S. has successfully harnessed geothermal energy for a range of applications beyond electricity generation, offering a wealth of insights that can be adapted for Indonesia's geothermal sector. Key lessons from the U.S. experience highlight the importance of technological innovation, supportive policy frameworks, and strategic market development.

- **Market Development and Diversification**: The U.S. has already diversified its geothermal market by integrating geothermal energy into various sectors, creating multiple revenue streams. Direct-use applications such as district heating, aquaculture, and industrial heating have proven economically viable and environmentally beneficial. Indonesia can adopt a similar approach by promoting the integration of geothermal energy into non-electrical applications. Encouraging the development of geothermal greenhouses, aquaculture farms, and industrial parks can create new economic opportunities and enhance the sustainability of energy use.
- **Geothermal Derivative Products**: The extraction of valuable minerals from geothermal brines, such as lithium and silica, has emerged as a significant revenue stream in the U.S. The Salton Sea geothermal field in California exemplifies how geothermal operations can be coupled with mineral extraction to enhance economic viability. Indonesia, with its rich geothermal resources, can explore the potential for extracting minerals from geothermal fluids, adding value to geothermal projects and supporting the growth of related industries, such as battery production for electric vehicles.
- **Community and Environmental Benefits**: Geothermal direct-use applications provide substantial community and environmental benefits. The U.S. experience shows that geothermal district heating can significantly reduce greenhouse gas emissions and provide affordable heating solutions for communities. In Indonesia, implementing geothermal district heating systems can improve air quality and reduce reliance on fossil fuels, contributing to national sustainability goals and enhancing the quality of life for local populations.

By learning from the U.S. experience, Indonesia can develop a comprehensive strategy for utilizing geothermal energy beyond electricity generation. Adopting advanced technologies, creating supportive policy frameworks, diversifying market applications, exploring derivative products, and emphasizing community and environmental benefits will enable Indonesia to maximize the value of its geothermal resources. These efforts will not only support economic growth but also contribute to Indonesia's commitment to sustainable development and climate change mitigation.

6. CONCLUSION AND PATH FORWARD

The utilization of geothermal energy beyond electricity generation offers Indonesia a valuable opportunity to harness its geothermal resources for diverse applications. By learning from the U.S. experience and implementing strategic measures, Indonesia can unlock the full potential of its geothermal resources, fostering sustainable economic development and contributing to a resilient and low-carbon energy future. The path forward requires coordinated efforts, strategic investments, and a commitment to exploring and developing geothermal applications that extend beyond traditional power generation.

Based on the study results, several paths forward that can be drawn are summarized as follows:

- *Policy and Regulatory Support*: Establishing supportive policies and regulations that encourage investment in geothermal beyond electricity applications. This includes incentives for research and development, financial support for pilot projects, and streamlined permitting processes.
- *Collaboration and Partnerships*: Building partnerships between government agencies, industry stakeholders, and research institutions to advance geothermal technologies and applications. Collaborative efforts can facilitate knowledge sharing, resource pooling, and the development of innovative solutions.
- *Investment in Research and Development*: Prioritizing research and development to advance geothermal technologies and geothermal beyond electricity generation option. Investment in R&D will drive technological advancements and enhance the viability of new applications.
- *Public Awareness and Education*: Raising awareness about the benefits of geothermal energy beyond electricity generation through public education campaigns and community engagement. This will help garner support for geothermal projects and promote broader acceptance of geothermal technologies.

It is important to note that this study is preliminary, and a more detailed analysis of each aspect is required before proceeding to pilot implementation or commercial-scale application in Indonesia. Additionally, this study is still in the drafting stage; further elaboration, revisions, and additional explanations will be incorporated as the work progresses.

REFERENCES

Al Asy'ari, M., Adityatama, D., Brilian, V., Erichatama, N., & Purba, D. (2024). *Beyond Electricity: Geothermal Direct Use Business Models and Potential Applications in Indonesia*. Stanford, California: *PROCEEDINGS*, 49th Workshop on Geothermal Reservoir Engineering.

Geoenergis. (2024a). *Comparison Study of Geothermal Energy Utilization Development in the US for Indonesia's Acceleration of Geothermal Power Plant Development*.

Richter, A. (2023). *Low enthalpy geothermal an attempt to positioning*. Thinkgeoenergy.

Thinkgeoenergy. (2024). *ThinkGeoEnergy's Top 10 Geothermal Countries 2023 – Power Generation Capacity*. https://www.thinkgeoenergy.com/thinkgeoenergys-top-10-geothermal-countries-2023-power-generation-capacity/.

US DOE. (2024). *Pathways to Commercial Liftoff: Next-Generation Geothermal Power*. U.S Department of Energy.

Utilizing Geothermal Resources for Green Ammonia Production: A Techno-Economic Analysis for Decarbonizing Coal Power Plants in Indonesia

Annisa N Hidayah[1], Danny Kusuma[1], Yudithia Prastika[2], and Koichi Yamashita[3]

[1]Aarunya Mitra Optima
[2]PT Sarana Multi-Infrastuktur (Persero)
[3]Global Challenge

Keywords: Geothermal, Green Ammonia, Ammonia Co-firing, CFPP Early Retirement

ABSTRACT

Indonesia boasts abundant geothermal potential, with estimates exceeding 20GW, as per data from the Ministry of Energy and Mineral Resources (MEMR). However, current exploitation remains relatively modest, with only around 2GW utilized, highlighting a significant untapped resource, particularly in Eastern Indonesia. Yet, in remote areas, where geothermal potential is rich, electricity demand often falls below the typical capacity of geothermal plants, rendering development economically infeasible or leading to oversized installations with excess capacity.

This paper explores an innovative solution to this challenge by leveraging geothermal energy not solely for electricity generation but also for the production of secondary products, notably green energy carriers, i.e., green ammonia for this study. Recent technological advancements have enabled the utilization of green ammonia as a clean alternative fuel, suitable for co-firing in coal power plants, offering a pathway to decarbonize Indonesia's energy mix.

On the other hand, Indonesia's Net Zero Emissions (NZE) plan not only to develop more new and renewable energy, but also to include an early retirement program for Coal Fired Power Plants (CFPPs). The paper investigates the comparative merits of two decarbonization strategies.

Firstly, it examines the conventional approach of CFPP early retirement, which aims to reduce emissions from the power sector. However, some analyses have raised concerns about the economic viability and substantial costs associated with this strategy. Under this paper, the CFPP retirement age is assumed mid-range around 15-20 years and the DCF method is used to understand the remaining value estimation.

In comparison, the paper proposes an alternative approach: utilizing excess geothermal capacity to produce green ammonia for co-firing in existing CFPPs. Excess electricity of the geothermal power plant could be utilized in an ammonia plant where the product, green ammonia, is then transported to the target CFPPs for co-firing.

By conducting a comprehensive techno-economic analysis, the study seeks to provide stakeholders with insights into the comparative cost-effectiveness of these strategies. The anticipated findings not only offer guidance on the most economically viable pathway for decarbonizing CFPP but also stimulate discussions on maximizing geothermal utilization by improving financial viability of geothermal project, especially in Eastern Indonesia. Furthermore, the paper will propose policy implications derived from the analysis results, which could serve as a foundation for informed decision-making in the power and geothermal sectors, aligning with Indonesia's broader sustainable development goals.

1. INTRODUCTION

The global shift towards sustainable energy has sparked a significant interest in hydrogen, particularly green hydrogen, which is produced through the electrolysis of water using renewable energy (RE) sources (IEA, 2019). Indonesia, with its vast RE potential, especially in geothermal energy estimated at around 29 gigawatts (GW) (Darma, 2021), stands at the forefront of this transition. However, in eastern Indonesia, many energy reservoirs remain unutilized or underutilized due to low demand.

Indonesia's power generation is predominantly coal-based, contributing to around 61.55 percent of the nation's electricity mix as of 2022 (Statista, 2022). To align with the Net Zero Emissions (NZE) target, the Government of Indonesia (GoI) has initiated an early retirement program for coal-fired power plants (CFPPs), phaseout of CFPP by 2056 and no coal usage beyond 2030 (Cui & Tumiwa, 2022). This transition, while environmentally crucial, comes with substantial costs. Retiring young assets before the end of their operational lifetime leads to lost revenue and potential legal complexities, especially in cases where Independent Power Producers (IPPs) are

bound by Power Purchase Agreements (PPAs) with take-or-pay clauses. In addition, it is estimated that around USD 4.6 billion is required for Indonesia to fund and meet the cost of CFPPs retirement by 2030 (IESR, 2022).

In response to these challenges, Indonesia is exploring innovative technologies such as ammonia co-firing in CFPPs. Ammonia, when burned, does not produce CO_2, making it an attractive option for co-firing with coal and reducing the carbon footprint of existing power plants (Yamashita & Urakata, 2023). For instance, a 20% co-firing ratio means ammonia replaces 20% of coal by energy content. Mitsubishi Heavy Industries, Ltd. (MHI) is among the companies developing technologies to enable ammonia co-firing in both circular firing and opposed firing systems of coal-fired boilers (Yamashita & Urakata, 2023). In addition, JERA, Japan's biggest power generator, recently completed a groundbreaking three-month 20% ammonia co-firing with coal trial at its Hekinan Thermal Power Station in central Japan with promising outcomes. Notably, nitrogen oxide (NOx) levels remained unchanged compared to coal-only firing, sulfur oxide emissions decreased by 20%, and nitrous oxide—a potent greenhouse gas—was undetectable (Obayashi, 2024). While this technology is still in its nascent stages, it represents a promising step towards Indonesia's commitment to a cleaner, more sustainable energy future.

Ammonia can be produced in many ways resulting in the different colors of ammonia, such as grey, blue and green ammonia. Grey ammonia is produced from natural gas without any carbon capture and storage (CCS) while blue ammonia incorporates CCS for its by-products. At the same time, green ammonia is produced using green hydrogen generated by water electrolysis, powered by renewable energy. Geothermal energy is aimed to be used for this purpose as the source of renewable energy. Currently, Pertamina NRE collaborates with Tokyo Electric Power Company Holdings (TEPCO HD) on green hydrogen and green ammonia development using geothermal (Pertamina, 2022). The remaining heat from separated geothermal brine from Ulubelu Geothermal Power Plant Unit 1-4 is used to an integrated geothermal bottoming Organic Rankine Cycle (ORC) Binary Plant and electrolysis (Brilian, Khasani, Mubarok, Ruliandi, & Firmansyah, 2022). Interestingly, the usage of excess power (during nighttime) from the geothermal power plants in eastern Indonesia could be a game-changer due to very low demand while literature on this specific case is scarce, the potential impact is immense. If successful, this unique case could demonstrate the viability of geothermal-based ammonia production and contribute to cleaner energy solutions. Therefore, the objective of this study is to assess the economic feasibility of producing green ammonia from geothermal sources and apply it to reduce emissions by co-firing it to existing CFPPs.

2. CASE COMPARISON

Under this study, we assume that the CFPP is owned by PT PLN (Persero) or its subsidiaries. The assumed capacity for the CFPP is 400 MW. This number is selected based on the averaged capacity of some CFPPs that are ranging between 100 – 800 MW (see Table below) which were also identified to be easily achievable plants for swift shutdown, contributing to the GoI's plan reach NZE (Cui & Tumiwa, 2022). The potential CFPP age to be phased out by the GoI is 15 years old and assumed remaining period to operate is 25 years.

Table 1: List of CFPPs equipped with sub-critical technology.

Plant	Area	Capacity (MW)	COD Year	Technology
Bukit Asam Muara Enim	South Sumatera	260	1987	Subcritical
PLN Paiton	East Java	800	1994	Subcritical
Ombilin	West Sumatera	200	1996	Subcritical
Asam-asam	South Kalimantan	260	2000	Subcritical
Cilacap Sumber	Central Java	600	2006	Subcritical
Tarahan	Lampung	100	2007	Subcritical
Bangka Baru	Bangka-Belitung	60	2014	Subcritical
Merak	Banten	120	2014	Subcritical
Cikarang	West Java	280	2017	Subcritical
Tabalong	South Kalimantan	200	2019	Subcritical

2.1 Technology Comparison

For case comparison, we designed two hypothetical cases to compare the economic impacts:

2.1.1 Case 1 - Early Retirement of CFPP and Replacement with Renewable Energy (RE) Power Plant

This study replicates the Asian Development Bank's (ADB) Energy Transition Mechanism (ETM) initiative, focusing on the premature decommissioning of Cirebon-1, Coal-Fired Power Plant (CFPP) in Indonesia, slated for retirement 7 years ahead of schedule (ADB, 2023). Alongside the cessation of operations at the CFPP, PT PLN is urged to facilitate the establishment of a Renewable Energy (RE) power facility to offset the resultant

electricity deficit. To facilitate comparative analysis, the RE power plant's annual electricity generation must be commensurate with that of the CFPP.

2.1.2. Case 2 - Retrofitting Existing CFPP into Co-firing with Green Ammonia

In this scenario, the CFPP undergoes retrofitting to enable cofiring with green ammonia produced using the Haber-Bosch and electrolysis processes, powered sustainably by a geothermal plant. To ensure emissions comparability, the green ammonia production capacity is designed to match the energy output equivalent of one unit of CFPP, with cofiring at 20% of its Lower Heating Value (LHV). Consequently, the produced ammonia is sufficient to supply five units of CFPPs, each cofiring at 20%.

The ammonia production facility is assumed to be situated near the port, with electricity sourced from a geothermal plant delivered via PT PLN's existing transmission infrastructure. The ammonia, produced in liquid form, is then transported by shipping to the designated CFPP. Upon arrival at the port of destination, the ammonia is stored, regasified, and piped to the CFPP. The CFPP's boiler is modified to accommodate ammonia gas combustion, which necessitates retrofitting with flue gas treatment to ensure NOx emissions remain within permissible environmental standards.

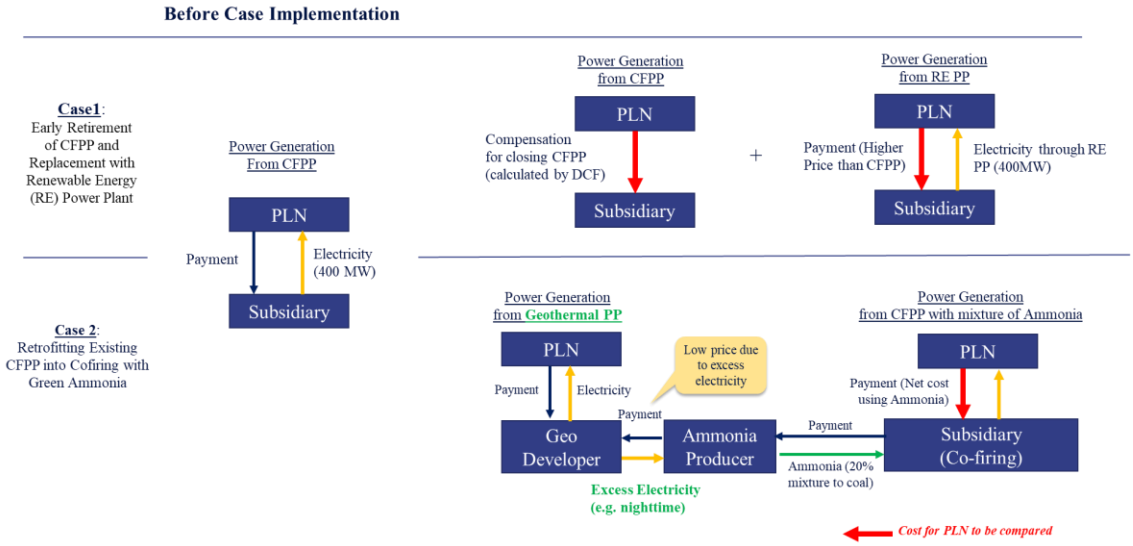

Figure 1: Money flow of hypothetical case comparison.

2.2 Cash Flow Comparison

Based on above case comparison, the cash flow is as follows

2.2.1 Case 1 - Early Retirement of CFPP and Replacement with Renewable Energy (RE) Power Plant

The premature closure of a power plant entails forfeiting potential future cash flows equivalent to the remaining economic value of the plant. The cash flow analysis for the operation of a CFPP assumes revenue derived from electricity sales, calculated as the Power Purchase Agreement (PPA) tariff multiplied by annual electricity generation. For the CFPP, a PPA tariff of USD 60/MWh is assumed. During operation, expenses include the cost of coal supply and operating expenditures (OPEX). The delivered price of coal is assumed to be USD 50/ton for sub-bituminous coal with an energy density of 20 MJ/kg LHV. Additionally, at year zero, costs associated with plant removal are incurred.

In parallel, PT PLN incurs costs related to the development of a Renewable Energy (RE) power plant as a replacement. For simplicity, this cost is assumed to align with the Levelized Cost of Electricity (LCOE) of a solar PV and battery system, set at USD 90/MWh.

2.2.2. Case 2 - Retrofitting Existing CFPP into Co-firing with Green Ammonia

In the case of co-firing, PT PLN incurs costs associated with retrofitting the CFPP to enable ammonia cofiring. Limited cost data is available due to the evolving nature of the technology. An analysis by IEEJ estimates a capital expenditure (CAPEX) of USD 224 million for achieving 20% co-firing capacity in a 700 MW plant (IEEJ, 2022). Conversely, operational expenditures (OPEX) for the retrofitted plant are assumed to remain comparable to those of a non-retrofitted plant for simplicity and are thus excluded from the cash flow calculations.

Another significant aspect of the cash flow analysis for the co-firing scenario is the procurement cost of green ammonia. The delivered cost of ammonia is assumed to encompass production and transportation expenses. For

instance, transportation costs for ammonia over a distance of 2000 km from eastern Indonesia to CFPPs in Java and Sumatra are estimated at USD 15.43/ton (Nayak-Luke, et al., 2021).

Moreover, ammonia production involves costs associated with hydrogen electrolysis and the Haber-Bosch process. According to the International Energy Agency (IEA), the cost of electrolysis-based hydrogen and subsequent ammonia production is influenced by electricity prices and plant operating hours. Utilizing geothermal electricity ensures high plant utilization during peak hours, potentially reducing the levelized production cost. Assuming nighttime geothermal electricity costs of USD 10/MWh due to low demand, hydrogen production costs could decrease to approximately USD 1/kg, making ammonia production competitive with grey hydrogen derived from natural gas. Consequently, the production cost of ammonia is estimated at USD 200/ton (IEA, 2019).

As a consequence of co-firing with ammonia, the CFPP owner reduces coal consumption by 20%. However, due to ammonia's lower energy density of 19 MJ/kg LHV, the quantity of ammonia required for co-firing is slightly greater than the reduction in coal mass.

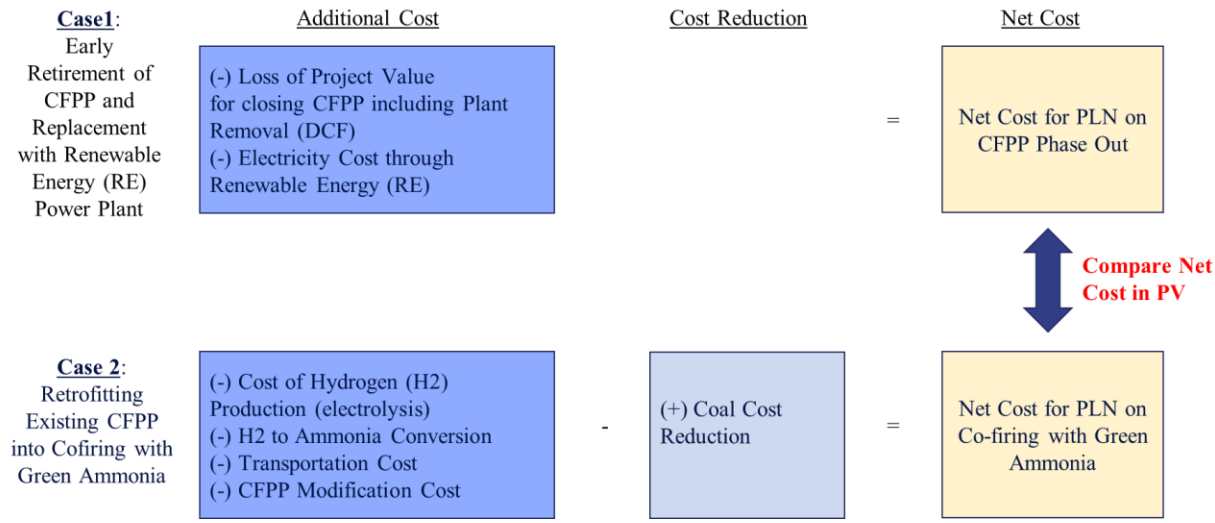

Figure 2: Cash flow comparison of the hypothetical cases.

3. METHODOLOGY AND ASSUMPTIONS

3.1 Economic Analysis Methodology

The lifecycle net cost of Case 1 and 2 was evaluated and the viewpoint of PT PLN was compared. The lifecycle net costs of Case 1 and 2 were converted into present value by using discount rate. For Case 1, the loss of project value for closing CFPP including plant removal was estimated by using Discounted Cashflow (DCF) method. DCF method is typically used to assess corporate value considering future free cash flow of the company with the following formula.

$$\text{DCF} = \frac{(\text{Year 1 FCF})}{(1+\text{discount rate})} + \frac{(\text{Year 2 FCF})}{(1+\text{discount rate})^2} + \frac{(\text{Year 3 FCF})}{(1+\text{discount rate})^3} + \cdots$$

$$\text{Free cash flow (FCF)} = \text{Operating Cash Flow} + \text{Investing Cash Flow}$$

3.2 Assumptions

3.2.1 Parameter Value

Table 2 summarizes the key assumptions and settings for the projects.

4. RESULT AND ANALYSIS

4.1 Calculation Result

By calculating the parameter value described in Section 3.2 using the methodology outlined in Section 3.1, it was found that the total Net Present Value (NPV) for the total cost of implementing Case 2 (retrofitting an existing CFPP to co-fire with green ammonia) is lower than that of Case 1 (early retirement of CFPP and replacement with RE Power Plants). This result is based on the assumption that the ammonia used for co-firing is produced using excess electricity from a geothermal power plant, with an assumed very low price of 1 cent/kWh. Additionally, Case 2 assumes the use of RE from solar power plants, with a current average PPA price of approximately 6

cents/kWh. The results may vary if these assumptions are adjusted. Therefore, a sensitivity analysis is performed in Section 4.2 to understand the effect of changing these parameters.

Table 2: List of assumptions.

Parameters	Value	Assumptions and References
CFPP		
Capacity	400 MW	-
Age	25 years	-
Remaining lifetime	15 years	-
Plant efficiency	35%	-
Coal price	USD 50/ton	Coal ceiling price for PLN
Plant capacity factor	85%	-
Plant retrofit (cofiring) cost	USD 224 million/700 MW	(IEEJ, 2022)
Plant decommissioning cost	USD 10,000/MW	(Malley, 2016)
Plant fixed OPEX	USD 40,000/MW/year	(EIA, 2020)
Plant variable OPEX	USD 4.5/MWh	(EIA, 2020)
LCOE of RE replacement powerplant	USD 90/MWh	(IESR, 2021)
Ammonia production and transportation		
Electricity supply price	USD 10/MWh	Excess electricity from geothermal power plant, e.g., low demand at night nighttime
Ammonia production cost	USD 200/ton ammonia	(IEA,2019)
Ammonia transport cost	USD 15.4 / ton ammonia	Distance 2000 – 3000 km, assuming transporting from Eastern Indonesia to Java Island (Nayak-Luke, et al., 2021)
Financial		
Discount rate	10%	-

3.2.2 Timeline

Table 3: Case timeline assumptions.

Case 1	**Year Implemented**	**Total Year**
Operation of CFPP	Year 16	1 Year
Decommissioning of CFPP	Year 17	1 Year
Construction of RE as replacement for CFPP	Year 16	1 Year
Operation of RE	Year 17 – Year 40	24 Years
Decommissioning of RE	Year 40	1 Year
Case 2	**Year Implemented**	**Total Year**
Operation of Geothermal Power Plant	Year 16 – Year 40	25 Years
Operation of CFPP	Year 16 – Year 40	25 Years
Construction of Electrolysis & Haber Bosch	Year 16	1 Year
Construction of Cofiring Equipment at CFPP	Year 16	1 Year
Operation of Cofiring Equipment at CFPP	Year 17 – Year 40	24 Years
Decommissioning of CFPP	Year 40	1 Year

The analysis further examines the cost breakdown associated with each scenario. In the case of early retirement, the predominant cost factor is the expense incurred in substituting power supply with RE sources. It is noteworthy, however, that this cost element is expected to diminish over time concurrent with advancements in RE technology and the maturation of its market. Additionally, a significant portion of costs are attributed to the loss of FCF of existing CFPP assets. The imposition of carbon taxes may exert downward pressure on this asset value, as CFPP operators would be compelled to absorb additional expenses associated with carbon emissions during operational phases. Alternatively, installation of carbon capture technologies presents another avenue for CFPP operators, albeit at an added cost.

Conversely, the examination of the co-firing scenario reveals that the primary cost driver is the procurement of green ammonia, significantly outweighing the savings derived from reduced coal expenditures by more than fivefold. Given their comparable LHV, this implies that the cost per ton of green ammonia is five times greater

than that of coal. Furthermore, this situation is exacerbated by the assumption of a low-cost geothermal electricity supply for ammonia production at USD 10/MWh by the author. This figure starkly contrasts with the typical electricity supply prices in Indonesia, which generally range between USD50 to 100/MWh.

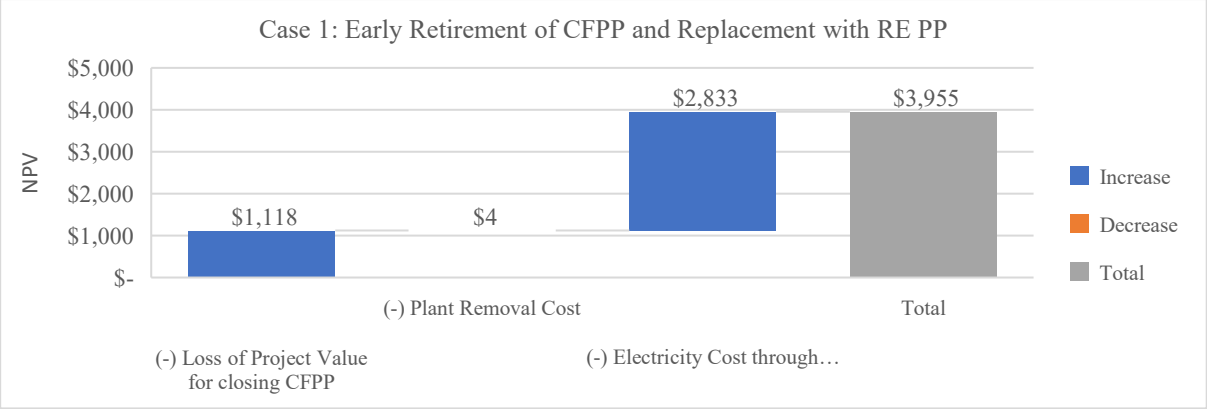

Figure 3: Cost NPV of early retirement case.

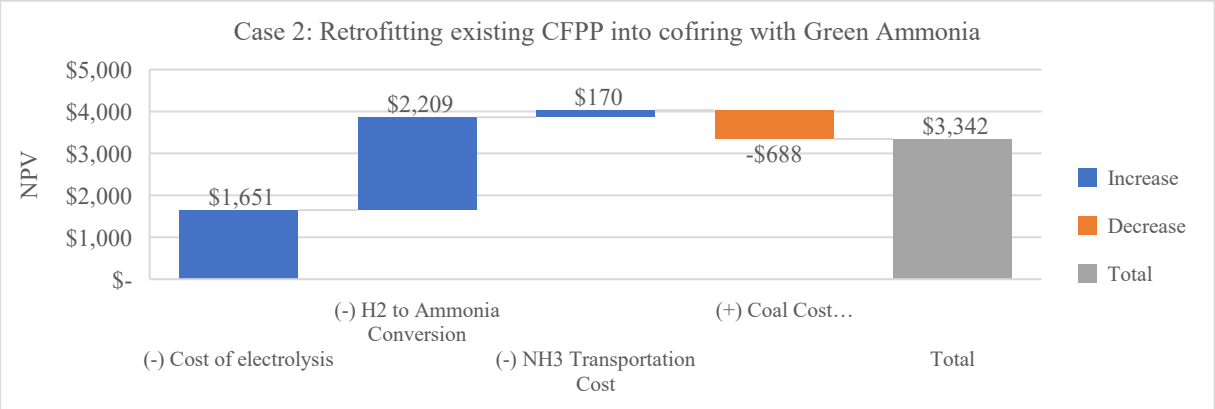

Figure 4: Cost NPV of co-firing case.
(Number shown is in Million USD)

4.2 Sensitivity Analysis

A sensitivity analysis was performed on two parameters, as summarized in the following table:

Table 4: Sensitivity analysis assumptions.

Case	Parameter Analyzed	Low	Mid	High
Case 1 - Early Retirement of CFPP and Replacement with RE Power Plant	LCOE of RE replacement powerplant	6 cents/kWh[1]	9 cents/kWh[2]	12 cents/kWh[3]
Case 2 - Retrofitting Existing CFPP into Cofiring with Green Ammonia	Electricity supply price *(from geothermal power plant)* for Ammonia Production	1 cent/kWh[4]	7 cents/kWh[5]	9.76 cents/kWh[6]

Note:
The price presented in the table above is based on the following assumptions:
[1]Indonesia's historical solar Power Purchase Agreements (PPAs) and bid prices in 2020 ranged from 5.5 to 6.3 cents per kWh (IESR, 2021).
[2]An auction for one of the first significant solar plus storage projects revealed a winning bid of 9.075 cents per kWh (IESR, 2022).
[3]The highest ceiling price for solar power plants, as stipulated by Presidential Regulation No. 112/2022, without considering location factors, is 11.5 cents per kWh.
[4]There is an assumption regarding the price of excess electricity during periods of low demand, such as nighttime (see Figure 5).
[5]The Basic Production Price (BPP) stated in the Ministry of Energy and Mineral Resources (MEMR) Decree 169.K/HK.02/MEM.M/2021 is 7.05 cents per kWh.

[6]The highest geothermal ceiling price, as outlined in Presidential Regulation No. 112/2022, without considering location factors, is 9.76 cents per kWh.

Based on the parameters set above, 9 (nine) scenarios were developed, and the results are summarized in table below.

Table 5: Sensitivity analysis result.

Scenarios	Assumptions on Parameter Value		NPV Comparison (in Million USD)	
	LCOE of RE replacement powerplant	Electricity price for Ammonia Production (From Geothermal PP)	Case 1	Case 2
Scenario A	6 cents/kWh	1.0 cent/kWh	$ 3,011	$ 3,342
Scenario B		7.0 cents/kWh	$ 3,011	$ 10,648
Scenario C		9.7 cents/kWh	$ 3,011	$ 13,936
Scenario D	9 cents/kWh	1.0 cent/kWh	$ 3,955	$ 3,342
Scenario E		7.0 cents/kWh	$ 3,955	$ 10,648
Scenario F		9.7 cents/kWh	$ 3,955	$ 13,936
Scenario G	12 cents/kWh	1.0 cent/kWh	$ 4,900	$ 3,342
Scenario H		7.0 cents/kWh	$ 4,900	$ 10,648
Scenario I		9.7 cents/kWh	$ 4,900	$ 13,936

4.3 Discussion

From the calculation results of the 9 (nine) scenarios, it can be observed that Case 2 (Retrofitting Existing CFPP to Co-fire with Green Ammonia) is only feasible when the geothermal electricity price for ammonia production is low, such as when utilizing excess power from a geothermal power plant, which is reflected in Scenarios D and G. When the geothermal electricity price for ammonia production approaches the BPP of PT PLN at 7 cents/kWh or higher, the total cost increases significantly. In such cases, it becomes more sensible to implement Case 1 (Early Retirement of CFPP and Replacement with RE PP) as a strategy for power sector decarbonization.

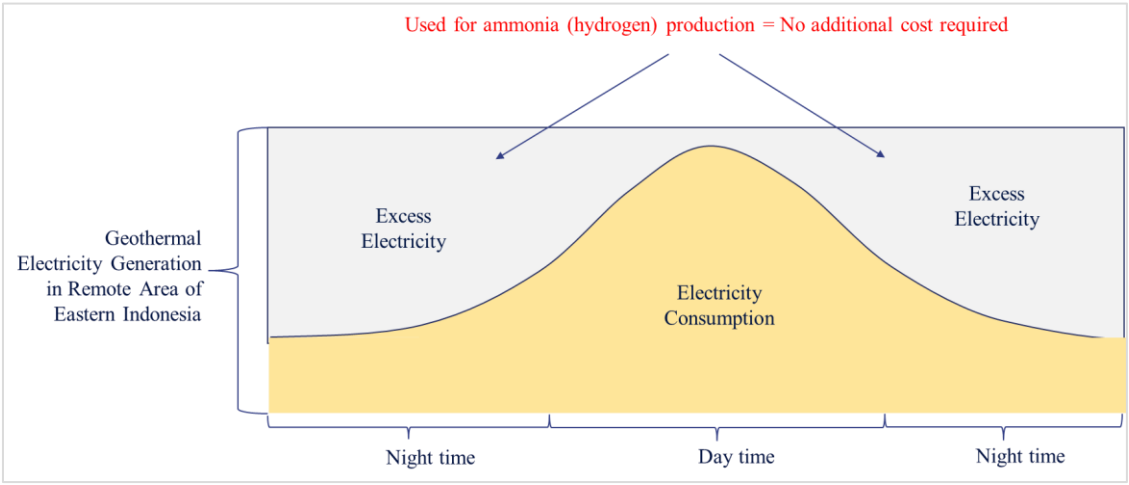

Figure 5: Geothermal powerplant electricity output profile in low demand areas.

The low geothermal electricity price for ammonia production can be achieved by utilizing excess electricity from geothermal power plants, such as during nighttime when the demand is low, as illustrated in Figure 5. Typically, geothermal power plants are set as the baseload power source, providing electricity to meet the minimum demand nearly 24 hours a day. However, if the geothermal power plant is located in sparsely populated areas with very low demand, such as in Eastern Indonesia, electricity generation may still exceed demand even after supplying the minimum nighttime load. We assume that this excess electricity would otherwise be curtailed by the power plant. Therefore, it is plausible that the owners of the power plants would be willing to sell this excess electricity at a very low price.

Utilizing excess geothermal electricity for ammonia production is also expected to maximize geothermal utilization, thereby increasing the revenue of the geothermal power plant. Therefore, the implementation of Case 2 could also contribute to improving the financial viability of geothermal projects, especially in Eastern Indonesia.

In addition, based on the sensitivity analysis results, it is determined that Case 2 exhibits increased competitiveness when the price of RE required to replace CFPP**S** exceeds 7 cents per kilowatt-hour (kWh). Consequently, Case 2 is recommended over Case 1 for regions with limited RE resource potential, which may lead to relatively higher RE prices.

5. CONCLUSION

There is a high demand for green ammonia (or hydrogen) under the net zero carbon emission policy target in Indonesia. Green ammonia production requires a large amount of electricity generated from RE (e.g., solar, wind, hydro, geothermal), which is more costly compared to electricity generated from fossil fuels. In the remote area of Eastern Indonesia, there exists considerable potential for geothermal resources. However, due to the limited demand and lack of connection to the major grid, the electricity generation capacity from geothermal resources must be set lower than the actual geothermal resource capacity. Additionally, since geothermal power plants generate a constant amount of electricity over a 24-hour period, some of this electricity cannot be fully utilized during nighttime hours.

By utilizing excess electricity generated from geothermal power plants located in remote areas that are not connected to the major grid, green ammonia (or hydrogen) could be produced at a lower cost. This approach could also address the mismatch between electricity demand and geothermal resource capacity in the remote regions of Eastern Indonesia. With such potential for low-cost green ammonia production utilizing geothermal, the current coal phaseout scenario could be further examined because ammonia co-firing may present a more economical solution for some types of CFPP in comparison with a phaseout scenario.

The findings of this study offer valuable insights for shaping policies aimed at transitioning the power sector, particularly in decarbonizing CFPPs. Co-firing with green ammonia emerges as a viable strategy for mitigating emissions from CFPPs. Specifically, sourcing green ammonia from geothermal sources presents a potentially economically competitive alternative to early retirement of CFPPs, particularly in regions where geothermal power plants are currently operating below capacity. The necessity of affordable electricity supply for green ammonia production serves as a critical benchmark for policymakers in designing pricing mechanisms for future projects in this domain.

REFERENCES

ADB (2023). New Agreement Aims to Retire Indonesia 660-MW Coal Plant Almost 7 Years Early. Retrieved July 2024, from https://www.adb.org/news/new-agreement-aims-retire-indonesia-660-mw-coal-plant-almost-7-years-early

Brilian, V. A., Khasani, Mubarok, M. H., Ruliandi, D., & Firmansyah, W. (2022). Techno-Economic Study of Green Hydrogen Production Using Integrated Bottoming Organic Rankine Cycle and Electrolysis Systems in Ulubelu Geothermal Power Plant. *The 8th Indonesia International Geothermal Convention & Exhibition (IIGCE).* Jakarta, Indonesia: Research Gate.

Cui, R., & Tumiwa, F. (2022). Financing Indonesia's Coal Phase-out: A Just and Accelerated Retirement Pathway to Net-Zero. IESR.

Darma, S. (2021). Country Update: The Fast Growth of Geothermal Energy Development in Indonesia. *Proceedings World Geothermal Congress.* Reykjavik, Iceland.

IEA. (2019). *The Future of Hydrogen*. (IEA) Retrieved June 2024, from https://www.iea.org/reports/the-future-of-hydrogen

IEEJ. (2022). Co-firing of Clean Ammonia for Decarbonization in Asia, from https://www.icfa-conference.org/archive/2022/doc/2-3_IEE.pdf

IESR. (2022, November). *APLSI Declares Just Energy Transition, Supports Acceleration of Green Energy Mix*. (IESR) Retrieved June 2024, from https://iesr.or.id/en/tag/cfpp-early-retirement

Malley, Ed. (2016). Coal Power Plant Post-Retirement Options. Retrieved from Power Magazine: https://www.powermag.com/coal-power-plant-post-retirement-options/

Nayak-Luke, R. M., Forbes, C., Cesaro, Z., Bañares-Alcántara, R., & Rouwenhorst, K. H. R. (2021). Techno-Economic Aspects of Production, Storage and Distribution of Ammonia. In A. Valera-Medina, & R. Banares-

Alcantara (Eds.), Techno-Economic Challenges of Green Ammonia as an Energy Vector (pp. 191-207). Elsevier. https://doi.org/10.1016/B978-0-12-820560-0.00008-4

Obayashi, Y. (2024, June 26). *JERA ends ammonia co-firing trial at coal power station with positive results.* Retrieved from Reuters: https://www.reuters.com/business/energy/jera-ends-ammonia-co-firing-trial-coal-power-station-with-positive-results-2024-06-26/

Pertamina. (2022, October 19). *Pertamina NRE - TEPCO HD Joint Study on The Development of Green Hydrogen and Green Ammonia*. Retrieved from Pertamina: https://www.pertamina.com/en/news-room/news-release/pertamina-nre-tepco-hd-joint-study-on-the-development-of-green-hydrogen-and-green-ammonia

Statista. (2022). *Energy mix for power generation in Indonesia in 2022*. (Statista) Retrieved June 2024, from https://www.statista.com/statistics/993362/indonesia-energy-mix-for-power-generation-by-source/

Yamashita, T., & Urakata, Y. (2023, September). *Mitsubishi Heavy Industries.* Retrieved June 2024, from https://www.mhi.co.jp/technology/review/pdf/e603/e603060.pdf

Application Hydrogeochemical Studies in The Development of Geomedicine: A Lesson Learned of Mount Tampomas Geothermal Area as Geothermal Energy and Balneology Resource

Galih Bayu Permadi[1,2], Triwening Larasati[1], Zefanya Mesakh Dwi Cahya Wirya Putra[2], Andri E.A. Wibowo[3], Vicky Rai Chandra[1], and M. Ghasan Jazmi Shalihin[1]

[1]PT Geoenergi Solusi Indonesia (Geoenergis), Indonesia
[2]Geological Engineering, Faculty of Exploration and Production Technology, Universitas Pertamina, Indonesia
[3]Pusat Sumber Daya Mineral Batubara dan Panas Bumi (PSDMBP), Bandung, West Java

galihbayup@gmail.com

Keywords: Geomedicine, Tampomas, Balneology, Geothermal, Surface Thermal Manifestation

ABSTRACT

Geomedicine is a branch of earth science that combines spatial information with its relevance to public health. Not only merely explain the benefits of surface geological features for health purposes, but this field also mitigates the risks posed by specific geological conditions. Geothermal manifestations are among the geological features that can be utilized in geomedicine. For decades, Indonesian communities have used the warm water from geothermal manifestations as an alternative treatment, an example includes the local community living in the vicinity of Mount Tampomas Geothermal Area. Fluid geochemistry analysis of surface thermal manifestations can deepen our understanding of the use of geomedicine.

The geothermal area of Mount Tampomas consists of warm springs and pools with temperatures ranging from 35°C to 50°C and pH levels from 6.67 to 7.93 with a Cl-HCO_3 type and Immature Water. There is Ciuyah warm spiring which contains high Total Dissolved Solid (TDS) and EC with 19,976 mg/L and 22,000 µs/cm, respectively. Local communities believe that the content of this warm water can serve as an alternative treatment. However, different conditions arise during geothermal exploration activities, where communities still misunderstand the definitions of potential benefits and risks of geothermal resources.

Instead of solely presenting geochemical analyses of Mount Tampomas, this study showcases variations in geothermal fluid geochemistry from various regions in Indonesia and provides an introductory framework for utilizing them in balneology practices. This study is also expected to serve as a means to properly enhance the public's understanding of geothermal resources.

1. INTRODUCTION

The concept of geomedicine varies significantly between geographical and geological perspectives. In geography, geomedicine is concerned with how spatial data can be used to describe and analyze the medical information of populations. This might include studying the distribution of health outcomes and healthcare resources across different regions (Davenhall, 2012). Conversely, the geological perspective of geomedicine involves examining the influence of natural elements and conditions derived from geological environments (Bowman, Bobrowsky and Selinus 2003). This perspective includes assessing the health impacts of naturally occurring elements in the soil, which can vary with the local geology and affect food grown in these soils. Additionally, it involves studying the health effects of geological events like volcanic eruptions, landslides, and earthquakes, as well as human activity resulting from specific geological conditions.

Though the concept was acknowledged just recently, it has been unconsciously applied ever since ancient times. Early civilizations recognized that an excess or deficiency of natural elements could cause diseases, and they used various elements for healing purposes. They also observed the negative impact of mining on human health (Rodriguez, Torres and Favas 2016, Bowman, Bobrowsky and Selinus 2003). Despite its long history of application, it is only in recent times that the field has been systematically studied, leading to the development of geomedicine as a formal discipline.

Understanding the interplay between geological factors and human health can lead to significant advancements in public health. By exploring how natural elements and conditions influence diseases, geomedicine helps identify health risks and develop targeted interventions. This approach also enhances the effectiveness of treatments utilizing natural resources like mineral-rich soils and waters. Bridging the gap between geology and medicine, this field has the potential to improve health outcomes and resource allocation, ultimately enhancing the quality of life for many.

One prominent aspect of geomedicine is the utilization of geothermal manifestations. Natural geothermal features, such as hot springs, have been used for therapeutic purposes for centuries due to their mineral-rich waters and unique properties. Beyond their relaxing warmth, understanding the chemistry of these waters offers insights into the geothermal activity and the overall geothermal system, as well as the health benefits of the elements contained in the water. Essential minerals for the human body can naturally derive from rock-forming minerals, which dissolve in water through physical and chemical processes, resulting in mineral-enriched water (Javed, et al. 2009). Geothermal manifestations effectively store these minerals in hot water, mud, or emitted gases (Galvez, Torres-Piles and Ortega-Rincon 2018, Shoedarto, et al. 2016, Javed, et al. 2009).

Balneology, a branch of geomedicine, studies the properties of geothermal water and its therapeutic use beyond recreation (Lazarowicz and Michalowski 2015). It emphasizes using mineral content and water temperature for relaxation and anti-inflammation. Despite its global application, the potential of balneology in Indonesia needs further exploration and study. Simultaneously, balneology addresses health risks by analyzing the release of harmful substances, enabling the development of strategies to mitigate these risks. By integrating geological insights with medical knowledge, balneology not only harnesses natural resources for health benefits but also ensures the safety and sustainability of these practices, providing a holistic approach to health and wellness that is deeply rooted in the natural environment.

In advance, this study is focused on the Mount Tampomas geothermal prospect area. Mount Tampomas is a Quaternary type B volcano located in Sumedang Regency, West Java, Indonesia, approximately 42 km northeast of Bandung city (Figure 1). Mount Tampomas is one of the areas included in the exploration zone, and a detailed 3G survey has been conducted by the Geological Agency for geoscience data acquisition as part of the government drilling program. Previous studies have described the Tampomas Geothermal system as a medium enthalpy system with an estimated reservoir temperature of 170°C ± 10°C and a liquid-dominated system (Permadi G. B., Herdianita, Amanda, Wibowo, & Putra, 2022; Iskandar, Demawan, Sianipar, Suryantini, & Notosiswoyo, 2018; Rahayudin, et al., 2018). However, social issues arose during the exploration as residents opposed the development of the geothermal project for power generation. Despite this, the local community has been utilizing the hot water around Mount Tampomas for hot spring baths or balneotherapy for several decades.

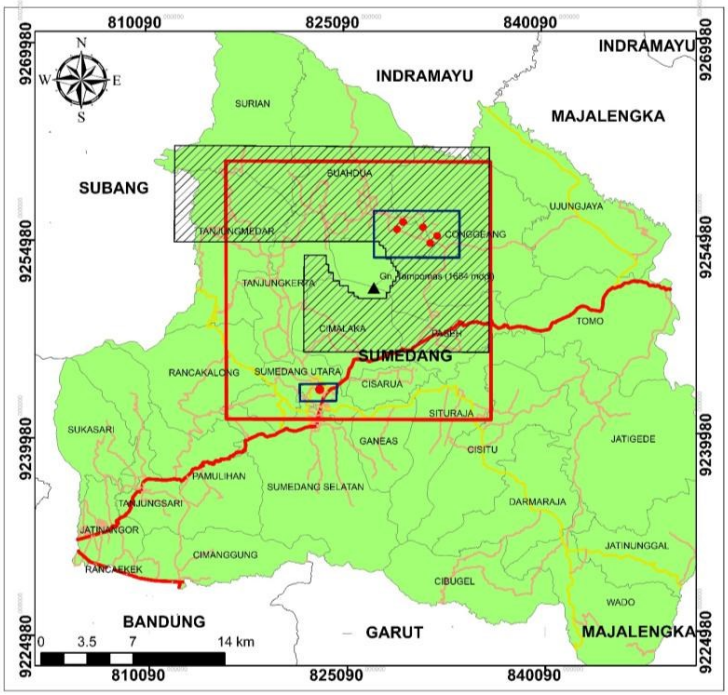

Figure 1: Location map of Tampomas geothermal area, the thermal surface manifestations distributed on the north and south of Mt Tampomas.

The primary objectives of this paper are to identify potential balneology resources at Mount Tampomas based on geochemical analysis of the water, this information will serve as a foundational reference for developing balneotherapy, specifically in Indonesia.

2. METHODOLOGY

The primary data for this research is based on geological and geochemical exploration data conducted by the Geological Agency during the 2021 survey. Using this primary data, geological analysis was carried out, producing a geological map that includes the distribution of lithology, and geological structures. The geochemical analysis of water in the study area includes basic hydrogeochemical analysis, which involves the assessment of physical parameters (pH, EC, TDS), observation of dissolved element concentrations using a Schoeller diagram, determination of water type using a Cl-SO_4-HCO_3 ternary diagram, and water equilibrium analysis based on a Na-K-Mg ternary diagram.

Based on the information obtained from the geological and geochemical conditions of the Mount Tampomas geothermal system, an analysis of the potential benefits and risks was conducted based on the total concentration of each dissolved chemical element in the geothermal fluid. The results of this analysis are used to determine whether the current use of hot water around Mount Tampomas is appropriate or not. The final section of this paper discusses the key points that can be drawn and potentially applied to other geothermal fields in Indonesia to develop balneology resources based on hydrogeochemical analysis.

3. GEOLOGICAL RESOURCES OF MOUNT TAMPOMAS

3.1 Geological setting

Physiographically, Mount Tampomas is located in the Quaternary Mountain Zone (van Bemmelen 1949). Based on remote sensing analysis using DEM imagery, a circular feature was identified surrounding the current Tampomas Cone. This circular feature is interpreted as the result of the ancient volcanic activity of Old Tampomas (Lumbanbatu, et al. 2005). The presence of this circular feature is also believed to separate the geothermal reservoir compartments beneath Mount Tampomas (Permadi G. B., Herdianita, Amanda, Wibowo, & Putra, 2022). In addition to the circular feature, the lineaments of geological structures in and around Mount Tampomas have NE-SW and NW-SE orientations, which align with the primary stress direction of Java Island, which is N-S.

Based on the geological regional map, the earliest volcanic product, originating from the ancient Mount Sumedang, is represented by volcanic breccia (Qob) found to the south of Mount Tampomas. This was followed by the evolution of Mount Cimalaka, which later underwent a collapse, forming the Cimalaka Caldera (Lumbanbatu, et al. 2005). The younger volcanic products are believed to result from eruptions of Mount Tampomas and its parasitic cones, producing undifferentiated materials (Qyu) scattered around the mountain. Additionally, pumice tuff (Qyt) deposits extend from the south to the west of Mount Tampomas, succeeded by breccia and agglomerate (Qyb) on the lower slopes, and lava (Qyl) shaping the current volcanic cone of Mount Tampomas (Silitonga 1973). The appearance of warm water is located on Quaternary undifferentiated volcanic products (Qyu).

3.2 Geothermal Fluid Characteristics

The geothermal potential area of Mount Tampomas has geothermal manifestations in the form of hot springs and warm water pools. The residents have utilized some of these warm water pools as public bathing places, while others remain as natural discharges. These hot springs and warm water pools are located in the northeastern foothills of Mount Tampomas, namely Ciuyah hot springs (APCU), Cilendre hot springs (APCLD 1,2), Conggeang hot springs (APC 1,2), Cileuncang hot spring (APCLC), Cileungsing (APCL), and there is one warm spring located south of Mount Tampomas in the city of Sumedang, namely Ciseupan warm spring (APCS 1,2). The surface manifestations of Mount Tampomas extend to the north and south, primarily featuring warm springs and pools with temperatures ranging from 34.7°C to 50.7°C.

A Schoeller diagram (Figure 3) describes the pattern of anion and cation contents of 9 geothermal water samples from Mount Tampomas. The diagram also shows a similarity of chemical patterns among the geothermal waters, with comparable levels of Na^+, K+, Ca^{2+}, Mg^{2+}, NH_4^+, Cl^-, and HCO^{3-} ions. However, it indicates that the concentrations of Li^+ and $SO4^{2-}$ in the Ciseupan area (APCS-1 & 2) are lower than in other hot waters. Meanwhile, the highest concentrations of Ca^{2+} and Cl^- are found in the Ciuyah Hot Spring (APCU), which correlates with its physical parameters, having the highest TDS (Total Dissolved Solids) with 19,976 mg/L. In addition, it appears that the NH_4^+ content in the Mount Tampomas geothermal system is indicated to be relatively high.

All physical properties of surface thermal manifestations can be seen in the Table 1. The hydrogeochemical characteristics can be assessed through the analysis of Cl-SO_4-HCO_3 and Na-K-Mg ternary diagrams (Figure 4), which indicates the hydrothermal fluid characteristics based on the primary dissolved elements. Although focused on major anions and cations, these analyses can explain the relationship between the emergence of warm water and the subsurface lithological conditions, which in turn helps identify the occurrence of other trace elements that may appear in specific areas.

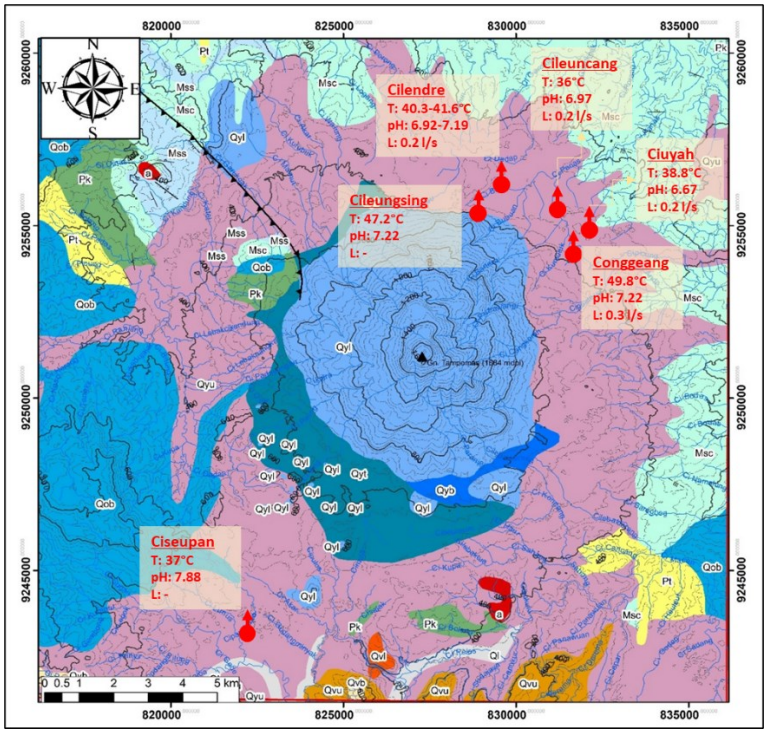

Figure 2: The geological map of Mount Tampomas Geothermal Area and its surface thermal manifestations distribution (modified from Silitonga, 1973).

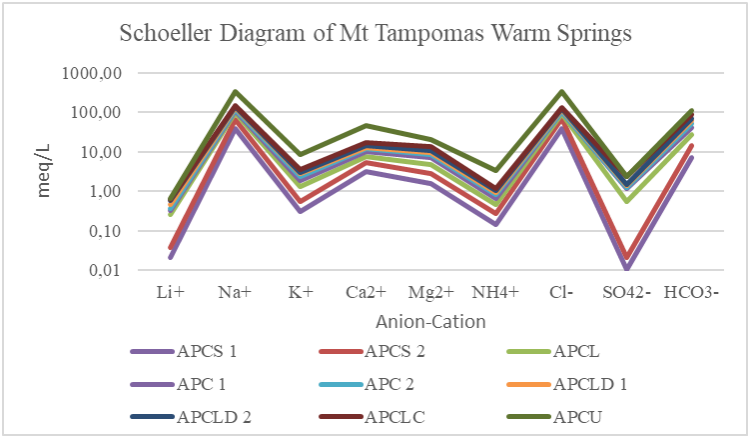

Figure 3: The Schoeller Diagram of chemical constituents within the Mount Tampomas Area.

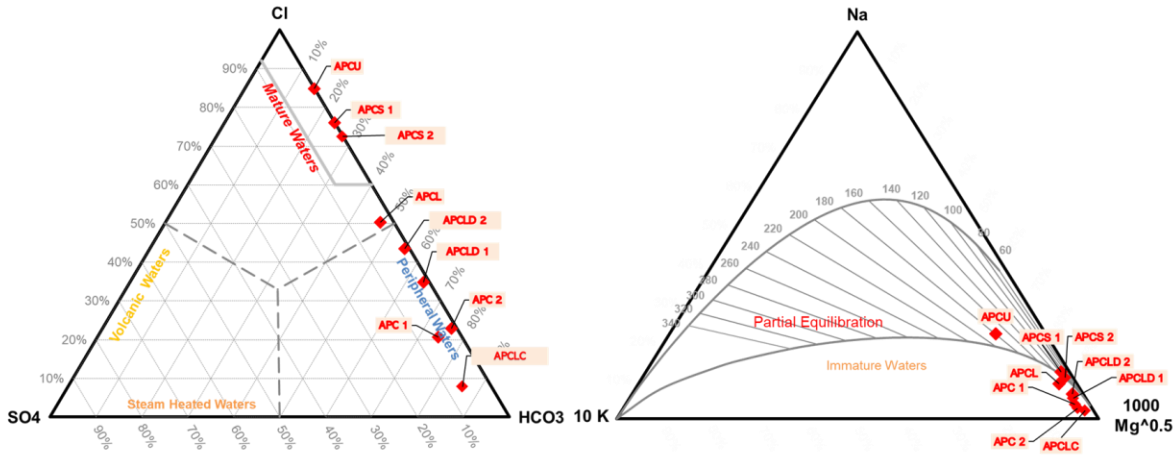

Figure 4: Cl-SO_4-HCO_3 and Na-K-Mg ternary diagrams of warm springs in Mount Tampomas Geothermal Area.

The characteristics of warm water around Mount Tampomas, based on the Cl-SO_4-HCO_3 ternary diagram, can be categorized into three types: chloride water, chloride-bicarbonate water, and bicarbonate water with neutral pH. According to the Na-K-Mg ternary diagram, only Ciuyah Hot Spring (APCU) exhibits partial equilibrium with the rocks of the deep geothermal reservoir, while the other warm waters are characterized as immature water due to mixing with surface water.

Table 1: The physical parameters of warms springs in Mount Tampomas and its surroundings (Geological Agency, 2021).

No	Warm Spring Code	pH	Temp (°C)	EC (μs/cm)	TDS (mg/L)	Remarks
1	APCS 1	7.88	37	4,640	3,560	Carried out from an abandoned public bath pool
2	APCS 2	7.93	34.7	3,610	2,752	The sample was taken from a resident's pump well located not far from APCS 1, with a well depth of approximately 7 meters.
3	APC 1	7.22	49.8	2,350	1,752	Abandoned public warm spring bath, near the main road, residents usually called it Sekarwangi Warm Spring.
4	APC 2	7.06	50.7	1,446	940	A natural warm spring, discharging from a fracture, can be classified as seepage due to its occurrence in the riverbed.
5	APCLD 1	6.92	40.3	1,173	896	A natural warm pool in the middle of the rice field has been utilized as a warm spring bath.
6	APCLD 2	7.19	41.6	1,315	1,028	A natural warm pool in the middle of the rice field, near APCLD 1, has been utilized as a warm spring bath.
7	APCLC	6.97	36	1,277	1,277	A natural warm spring, discharging from a fracture on the riverside, has been utilized as a warm spring bath.
8	APCU	6.67	38.8	2,200	19,976	A natural warm spring that discharges from a fracture has led residents to construct public bathrooms to collect the spring water flow.
9	APCL	7.22	47.2	2,350	1,752	The only hot spring bathing pool that has been commercially utilized.

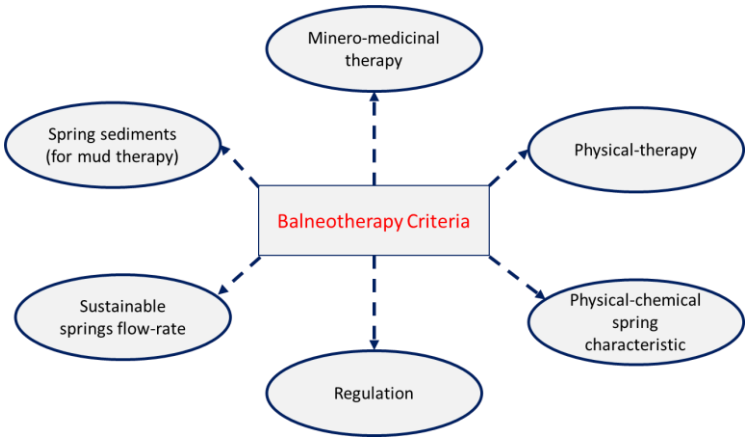

Figure 5: Key criteria in utilizing thermal-water for balneology resource (adopted from Al Dulaymie, et al., 2013).

4. BALNEOLOGY RESOURCE OF MOUNT TAMPOMAS

Through detailed hydrogeochemical analysis, it is inferred that the geothermal manifestations at Mount Tampomas possess characteristics that make them ideal for balneology, the therapeutic use of mineral-rich waters (Sukenik, et al. 1990). The presence of dissolved elements in these geothermal waters aligns with the essential criteria for balneotherapy, which requires water to contain specific minerals to be effective for therapeutic purposes. Such mineral-rich waters are believed to offer various health benefits, including improved circulation, relief from skin conditions, and relaxation of muscles. Given these properties, the geothermal resources at Mount

Tampomas have significant potential for development as a natural source of healing and wellness, attracting interest in both health tourism and local therapeutic use.

A deeper explanation of the supporting criteria for balneotherapy development goes beyond just the dissolved minerals in hydrothermal fluids. At least six criteria need to be considered when utilizing balneotherapy (Al Dulaymie, et al. 2013), in addition to dissolved minerals for therapy, including the physical benefits it can provide, the benefits arising from the chemical and physical properties of the fluid, dissolved sediments (for areas where mud deposits are present), the sustainability of thermal water flow, and, of course, local regulations that distinguish between warm water and regular groundwater (Figure 5).

A summary of the warm water conditions around Mount Tampomas, including its physical and chemical characteristics, is provided in the following section.

1. Ciseupan Warm Spring

   Ciseupan warm spring is the only warm water that is located to the south of Mt Tampomas, Sumedang City. This warm water source is situated amidst rice fields, near residential areas. Ciseupan warm water was formerly a public hot spring bath, which is no longer in use. Observations and field measurements indicate that this warm water has a temperature of 37°C with a neutral pH of 7.88. The discharge water from this source can no longer be identified, with only a few gas bubbles appearing at the bottom of the pool (Figure 6).

   Not far from the Ciseupan warm pool, there is a community-owned borehole with a depth of approximately 7 meters. The owner of the borehole reported that the water from this borehole is warm, which is supported by field measurements showing a water temperature of 34.7°C with a neutral pH of 7.32. The borehole owner uses this water for daily needs such as bathing, washing, drinking, and cooking. The presence of warm water in this borehole is likely due to a perched aquifer located in this area, which has been influenced by hydrothermal fluids. This is an important observation, as not all thermal waters are suitable for use as drinking water or for cooking.

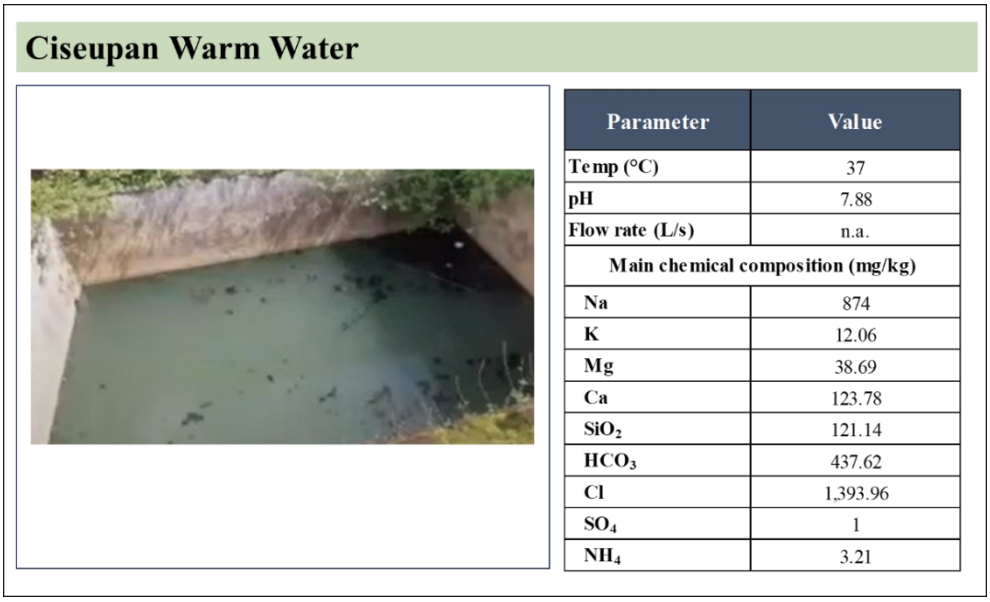

Parameter	Value
Temp (°C)	37
pH	7.88
Flow rate (L/s)	n.a.
Main chemical composition (mg/kg)	
Na	874
K	12.06
Mg	38.69
Ca	123.78
SiO_2	121.14
HCO_3	437.62
Cl	1,393.96
SO_4	1
NH_4	3.21

Figure 6: The location of the Ciseupan warm pool and its physical and chemical parameters (adopted from PSDMBP, 2021).

2. Conggeang/Sekarwangi Warm Spring

   Conggeang warm water, also known as Sekarwangi warm water, has the highest temperature among the warm water manifestations around Gunung Tampomas, at 49.9°C, with a pH of 7.22 and a measured flow rate of 0.3 l/s. Similar to the Ciseupan warm water pool, the Conggeang warm water pool was initially a public hot spring bath created by the residents to accommodate the flow of warm water from beneath the surface. This warm water pool now appears to be seldom used by the community, with only an outlet channel from the pool being used by some residents for bathing (Figure 6).

Conggeang/Sekarwangi Warm Water

Parameter	Value
Temp (°C)	49.8
pH	7.22
Flow rate (L/s)	0.3
Main chemical composition (mg/kg)	
Na	290.09
K	24.11
Mg	55.07
Ca	88
SiO_2	226.40
HCO_3	871.45
Cl	242.76
SO_4	60
NH_4	4.81

Figure 7: The location of Conggeang/Sekarwangi warm pool with its physical and chemical parameters (adopted from PSDMBP, 2021).

Cilendre Warm Water

Parameter	Value
Temp (°C)	40.3
pH	6.92
Flow rate (L/s)	0.2
Main chemical composition (mg/kg)	
Na	280.04
K	14.01
Mg	24.35
Ca	43.65
SiO_2	149.81
HCO_3	485.18
Cl	264.54
SO_4	10
NH_4	2.70

Figure 8: The location of Cilendre warm pool and its physical and chemical parameters (adopted from PSDMBP, 2021).

3. Cilendre Warm Spring

Cilendre warm water is located in a rice field area, with two warm water pools nearby. However, only one pool is used by residents as a public hot spring bath (Figure 8). Field observations indicate that the warm water here appears clearer compared to other thermal waters, which are generally oxidized and contain salt deposits. Field measurements show a water temperature of 40.3°C, a neutral pH of 6.92, and a flow rate of 0.2 l/s.

4. Cileuncang/Bojong Warm Spring

Cileuncang/Bojong warm water is a thermal manifestation that emerges at the riverbank through rock fractures (Figure 9). Residents have constructed an artificial channel to direct the warm water, which is then used as a public hot spring bath. The rocks around this warm water have undergone intensive oxidation. Field measurements indicate that this warm water has a temperature of 36°C, a neutral pH of 6.97, and a flow rate of 0.2 l/s emerging from the rock fractures.

Cileuncang/Bojong Warm Water

Parameter	Value
Temp (°C)	36
pH	6.97
Flow rate (L/s)	0.2
Main chemical composition (mg/kg)	
Na	182.18
K	15.82
Mg	73.76
Ca	123.09
SiO_2	186.15
HCO_3	1,091.02
Cl	99.75
SO_4	80
NH_4	3.54

Figure 9: The location of the Cileuncang/Bojong warm pool and its physical and chemical parameters (adopted from PSDMBP, 2021).

Ciuyah Warm Water

Parameter	Value
Temp (°C)	38.8
pH	6.67
Flow rate (L/s)	0.1
Main chemical composition (mg/kg)	
Na	4,108
K	194.46
Mg	162.08
Ca	1,127.28
SiO_2	173.26
HCO_3	1,365.47
Cl	7,688.74
SO_4	10
NH_4	49

Figure 10: The location of the Ciuyah warm pool and its physical and chemical parameters (adopted from PSDMBP, 2021).

5. Ciuyah Warm Spring

As its name suggests, Ciuyah warm water, derived from the word "*uyah*" which means salt, is associated with salt deposits found around its thermal spring discharge (Figure 10). The spring emerges through fracture with a low flow rate of 0.1 l/s. Additionally, this warm water has a temperature of 38.8°C and a pH that is close to neutral at 6.67. Nearby, residents have constructed a public toilet to collect the warm water from this spring, which is used as a public bath.

The uniqueness of this warm spring is that it contains several dissolved elements which based on laboratory analysis, have higher concentrations compared to other thermal waters. These elements include Na, K, Mg, Ca, HCO_3, Cl, and NH_4. The high concentrations of these dissolved elements are suspected to be related to the host rocks of this warm water, which are associated with marine sedimentary rocks that also serve as the reservoir for this thermal water (Iskandar, Demawan, Sianipar, Suryantini, & Notosiswoyo, 2018; Rahayudin, et al., 2018; Permadi G. B., Herdianita, Amanda, Wibowo, & Putra, 2022).

6. Cileungsing Warm Spring

Cileungsing warm water is located in the Buah Dua area and has been commercially used as a public hot spring pool (Figure 11). The natural warm water output at Cileungsing cannot be observed because the residents have constructed artificial pools and channels. This warm water has a temperature of 47.2°C and a pH of 7.22.

Cileungsing Warm Water

Parameter	Value
Temp (°C)	47.2
pH	7.22
Flow rate (L/s)	n.a.
Main chemical composition (mg/kg)	
Na	700.53
K	28.36
Mg	45.83
Ca	92.08
SiO_2	194.24
HCO_3	786.20
Cl	848.45
SO_4	50
NH_4	4.16

Figure 11: The location of the Cileungsing warm pool and its physical and chemical parameters (adopted from PSDMBP, 2021).

In addition to considering the dissolved elements, the temperature range of the warm waters at Mount Tampomas, currently used for public baths such as Conggeang/Sekarwangi, Cilendre, Cileungsing, Cileuncang, and Ciuyah, also supports their suitability for public bath. The water temperature, ranging from 36 to 49.8°C, falls within the ideal range for hot spring baths, making it comfortable and beneficial for bathers. This temperature range is not only pleasant for relaxation but is also effective in promoting blood circulation, relieving muscle tension, and providing therapeutic benefits. Therefore, the warm water sources at these locations are well-suited for development as hot spring facilities, offering both recreational and health benefits to visitors.

The therapeutic benefits of spring water primarily stem from the chemical action of minerals, which are absorbed into the skin and bloodstream through osmosis, supporting skin health. The physical impact of spring water is attributed to its temperature, which helps widen the skin's pores, allowing oxygen to flow more easily into the treated tissues. The thermal and mechanical effects of water not only increase blood flow to tissues but also reduce vasoconstriction. The absorption of mineral elements through the skin depends on factors such as skin thickness, blood circulation, exposure method, contact duration, application rate, skin absorption conditions, pressure, temperature, pH, osmotic properties, ion exchange capacity, particle size, chemical form, and environmental conditions. These factors influence processes like osmosis, diffusion, surface tension, cell charge, and metabolism (Morales 2004).

In addition to the presence of dissolved minerals in geothermal water, physical parameters such as temperature and pH can also influence the optimization of hot water utilization for balneotherapy. Temperature variations will affect the recommended duration for the community to soak in the water. The following is an example of a study conducted on the utilization of balneotherapy in warm water around Mount Tampomas. The elements studied include essential elements beneficial to the body, such as Na, K, Mg, and Ca. Additionally, other elements that specifically describe the characteristics of the geothermal system of Mount Tampomas were also examined in this case study, including the main anions Cl, SO_4, HCO_3, and NH_4, which are compounds found in the warm water of Mount Tampomas due to the influence of formation fluids/connate water.

The chemical and physical parameters found in the warm water of Mount Tampomas were compared to the minimum values of Balneological Active Components (BAC) according to Lazzerini and Cardoso da Silva (2020). It can be seen that some of the measured ranges in the Mount Tampomas area are below the minimum BAC values. Further evaluation highlights the high presence of NH_4 in Ciuyah, which may potentially be toxic to the body if used regularly, especially considering that Ciuyah is currently utilized as a water source by local bathhouses. Additionally, it should be noted that while some warm water may be suitable for balneotherapy, it

may not be appropriate for other purposes, such as everyday activities like cooking and washing, which could form the basis for the application of warm water from Ciseupan, as found in local boreholes.

Table 2: The summary of concentration and range of value chemical and physical characteristics of warm water at Mount Tampomas area compared to Balneological Active Components (BAC), red highlights indicate the value is below the minimum BAC (adopted from Lazzerini, et al., 2020; Minister of Health Regulation No.1205/Menkes/Per/X/2004).

Parameter	Unit	BAC	Range of Value	Remarks
Temperature	°C	33	36 - 49.8	**Too hot (>43.3°C)**, thermal water is only for partial body soak: arms, hands, feet, local wraps/compresses. **Hot (37.7-40.5°C), generally** tolerable for most soak therapies: soak duration 15-25 minutes. **Warm water (36.6-37.7°C)**, Slightly above body temperature. Ideal for mineral soak absorption: soak duration 15-30 minutes. **Neutral (32.2-36.6°C)**, Cooling that can be tolerated, used for short-term soaking of less than 5 minutes: for warming reflex.
TDS	mg/kg	444	896-19,976	High TDS contributes give freshness, lightness, softness, malleability, and skin comfort
Flow rate	L/s	1	0.2 - 0.3	The water flow rate affects the sustainability of the appearance of warm water.
pH		8.5	6.67 - 7.88	The pH of the warm water at Mount Tampomas appears to be lower than the BAC (<8.5). Still, in general, all pH levels are categorized as neutral, which has the potential not to cause skin irritation, especially when the therapy is performed over a long period.
Na	mg/kg	725	182.18 - 4108	Sodium in balneotherapy helps maintain Cell renewal and moisturizing
K		20	12.06 - 194.46	Potassium in balneotherapy helps maintain electrolyte balance, improves blood circulation, relieves muscle pain, supports skin health, and aids in detoxification.
Mg		121.6	24.35 - 162.08	Major aqueous dermal absorption rate
Ca		256	43.65 - 1127.28	Sedative, dermatitis, rheumatology
SiO2		25.3	121.14 - 226.40	Anti-inflammatory, adsorption potentiate, sedative, skincare
HCO3		196.6	437.62 - 1365.47	Antioxidant effects, skincare, rheumatology, sedative
Cl		1171	99.75 - 7688.74	Exciting and resolute action, cellular stimulants blood and lymphatic circulation, skincare, rheumatology
SO4		408	20 - 80	Under the BAC
NH4		n.a.	2.70 - 49	There is no specific BAC for NH4 since this content is considered toxic; however, the normal concentration of NH4 in hydrothermal fluids is generally 0.5 mg/kg.

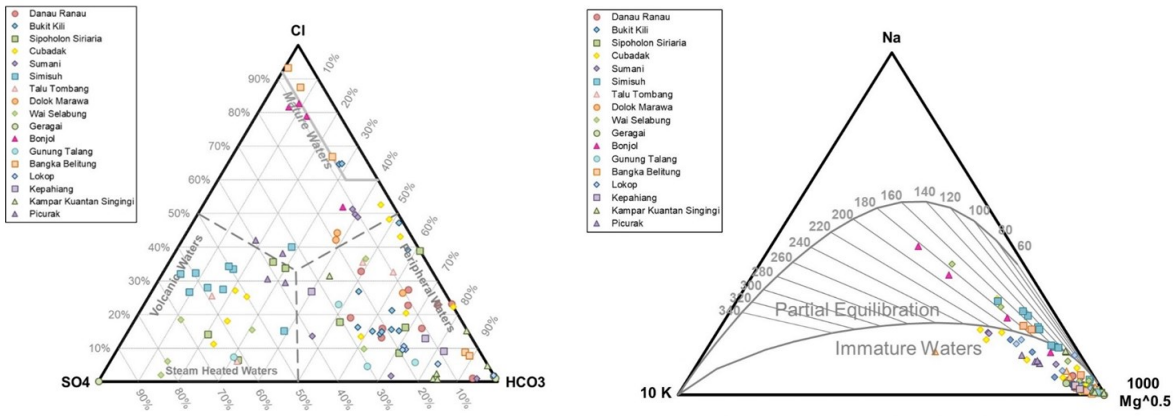

Figure 12: Compilation of Cl-SO_4-HCO_3 and Na-K-Mg ternary diagram of various geothermal systems in Sumatra that may contribute the initial hydrothermal fluid characteristics (Chenchen, et al. 2020).

5. INITIAL ANALYSES OF GEOTHERMAL FLUID GEOCHEMISTRY

For comparison, detailed exploration data from geothermal fields in Indonesia can serve as an initial reference in identifying balneotherapy resources in the country. Figure 12 shows the results of an analysis of major anions and cations in geothermal fluids from fields located on the island of Sumatra. Although this analysis is still quite general, the fluid types and their equilibrium levels can provide an initial indication of whether the thermal fluid

is directly associated with the geothermal reservoir or not. This can also help enhance the initial understanding of the hydrogeochemical system in a geothermal area.

Thermal water associated with geothermal reservoirs will naturally be more effective as a balneology resource compared to thermal water that has undergone near-surface processes, such as steam-heated water or water that has been heavily diluted. This is related to the content of dissolved elements and mineral compounds in thermal water and the level of effectiveness of thermal water absorption by the skin. Nevertheless, the next step is to conduct an in-depth hydrogeochemical analysis to identify the dominant tracers in a given area and their implications for balneotherapy.

6. LOCAL COMMUNITY PERCEPTIONS

The geothermal prospects of Mount Tampomas are well-known, particularly regarding the local community's opposition to any geothermal exploration activities for electricity generation. It has been openly stated that residents reject all surface survey activities and geothermal exploration drilling (Figure 13). However, the local community seems highly enthusiastic about utilizing geothermal energy for public bathing, which is believed to provide health benefits. We believe optimizing geothermal energy should not be limited to electricity generation alone. The direct use of geothermal energy for balneotherapy is a simple example that the community can easily accept.

Figure 13: Several banners from residents around Mount Tampomas expressing opposition to geothermal exploration survey activities.

Moreover, utilizing geothermal energy for balneotherapy can provide an opportunity to increase the local community's knowledge of Mount Tampomas regarding the basic understanding of geothermal systems. In the last survey, several opinions from the community tended to lack understanding of what a geothermal system is. This was evident from several banners stating that geothermal drilling activities could trigger the release of chemical elements from beneath the earth to the surface. In fact, without realizing it, these geothermal chemical elements can naturally dissolve in hot water and are not entirely harmful to humans. Thus, this balneotherapy study can help bridge the knowledge gap in the local community.

7. CONCLUSION AND PATH FORWARDS

Here is the conclusion of the lessons learned from the utilization of balneotherapy in the Mt Tampomas Geothermal Area:

- Balneotherapy is an alternative direct-use application that can be implemented in the Mt Tampomas geothermal area, which faces community rejection issues during the exploration phase.
- Hydrogeochemical analysis can bridge the characteristics and uniqueness of the fluids in a particular geothermal field, as the dissolved chemical content in hydrothermal fluids may offer benefits or even be toxic at certain levels.
- In addition to dissolved chemical elements, other physical parameters such as manifestation temperature, pH, and flow rate are also considered in optimizing balneotherapy.

- A key lesson learned from the balneology resources in Mount Tampomas, particularly in the Ciseupan area, is that not all warm water suitable for balneotherapy can be used for other purposes. This highlights the need for careful evaluation of water properties to ensure safe and appropriate use, considering that water fit for therapeutic purposes may not always meet the standards required for daily activities such as cooking and washing.

In addition to technical aspects, the utilization and study of balneotherapy in Indonesia can specifically involve several key stakeholders necessary to develop balneotherapy systematically. The following is a summary of the stakeholders that should at least play a role in the development of balneotherapy in Indonesia. Naturally, this must also be accompanied by the development of regulations that will serve as a reference for future balneotherapy development in the country.

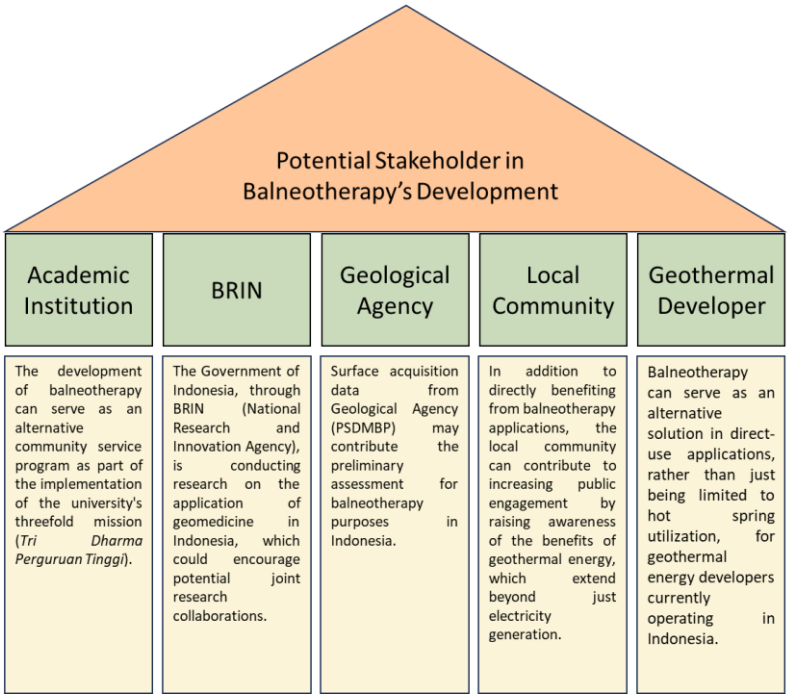

Figure 14: Potential stakeholder for developing balneotherapy as a geothermal direct-use utilization in Indonesia.

REFERENCES

Al Dulaymie, Abed S, Bayan M Hussien, Moshtaq A Gharbi, and Husam N Mekhlif. 2013. "Balneological Study Based on The Hydrogeochemical Aspects of the Sulfate Springs Water (Hit-Kubaiysa Region), Iraq." *Arab Journal Geoscience* 801-816.

Bowman, C.A, P.T. Bobrowsky, and O Selinus. 2003. "Medical Geology: New Relevance in the Earth Sciences." *Episodes* 26(270).

Chenchen, Yuniar Zhafira Abdillah, M Firdaus Al Hakim, Suryantini, and Nurhadi M. 2020. "The Application of Geochemical Ternary Diagram to Analyze Characteristics of Geothermal Waters in Sumatera Island, Indonesia." *Proceedings World Geothermal Congress*. Reykjavik, Iceland.

Davenhall, Bill. 2012. "*Geomedicine: Geography and Personal Health*." ESRI.

Galvez, I, S Torres-Piles, and E Ortega-Rincon. 2018. "Balneotherapy, Immune System, and Stress Response: A Hormetic Strategy?" *International Journal of Molecular Sciences* 19 (1687).

Iskandar, Irwan, Fikri A Demawan, Juni Y Sianipar, Suryantini, and Sudarto Notosiswoyo. 2018. "Characteristic and Mixing Mechanism of Thermal Fluid at the Tampomas Volcano, West Java, using Hydrogeochemistry, Stable Isotope, and 22Rn Analyses." *Geosciences* 8 (103).

Javed, A, J Iqbal, U Asghar, Farooq A Khan, Alia B Munshi, and I Sddiqui. 2009. "A Study to Evaluate Therapeutic Properties of Minerals of Manghopir Hot Springs, Karachi." *J. Chem. Soc. Pak* 31 (3): 396-401.

Lazarowicz, K, and M Michalowski. 2015. "Analyze the Balneotherapeutic Properties of Thermal Springs in Poland." *Journal of the Polish Mineral Engineering Society* 277-281.

Lazzerini, Fabio T, and Paulo S Cardoso da Silva. 2020. "*Guarani Aquifer System (GAS): Geothermal Spa Balneology Assessment*." 33-59.

Lumbanbatu, K, S Bronto, M.H Dirk, and S Sulistyono. 2005. *Laporan Akhir Penelitian Petrologi dan Geokimia Batuan Gunung Api Tampomas-Kareumbi-Mandalawangi dan Sekitarnya, Tepi Timur Cekungan Bandung, Jawa Barat*. Bandung: Puslitbang Geologi (Unpublished).

Morales. 2004. "*SPAs and Health Center*." Index Enfermeria 281-295.

Permadi, Galih B, Niniek R Herdianita, Fajar F Amanda, Andri E A Wibowo, and Zefanya M D C W Putra. 2022. "Hydrogeochemistry Model and Reservoir Compartment of Mount Tampomas Geothermal System Area in Sumedang Regency, West Java." Makassar: *Proceedings PIT IAGI* 51st 2022.

Putra, Zefanya M.D.C.W. 2022. *Studi Petrografi, Geokimia Unsur Utama, dan Dating Thermoluminescence (TL) Batuan Daerah Panas Bumi Gunung Api Tampomas, Kabupaten Sumedang, Provinsi Jawa Bara*t. Jakarta: Universitas Pertamina.

Rahayudin, Yudi, Koki Kashiwaya, Andi Susmanto, Yohei Tada, Irwan Iskandar, and Katsuki Koike. 2018. "Estimation of Fluid-Rock Interaction Process and Recharge Area of the Tampomas Geothermal Field, West Java, Indonesia by Water Chemistry." Stanford, California: *Proceedings, 43rd Workshop on Geothermal Reservoir Engineering*.

Rodriguez, I, J Torres, and P Favas. 2016. "Geomedicine and History of Science: A Contribution to Scientific Culture. In: Vasconelos, C (eds)." *Geoscience Education* (16) 207-223.

Shoedarto, Riostantieka, M, Ferry R Aries, D Irawan, F Perdana, I Arisbaya, and Indrawan B. 2016. "Raising Public Acceptance of Geothermal Utilization Through Direct Application in Indonesia." Stanford: Proceedings 41st Workshop on Geothermal Reservoir Engineering, Stanford University.

Silitonga. 1973. *The Geological Map of Lembang, Bandung, West Java*. Bandung: Geological Research and Development Center (GRDC).

Sukenik, S, D Buskila, L Neumann, A Kleiner-Baumgarten, S Zimlichman, and J Horowitz. 1990. "*Sulphur Bath and Mud Pack Treatment for Rheumatoid Arthritis at the Dead Sea Area.*" Annals of the Rheumatic Disease 99-102.

van Bemmelen, R.W. 1949. *The Geology of Indonesia*. The Hague: Government Printing Office.

Enhancing Indonesia Geothermal Project Bankability Through Off-Grid Utilization

Desak Nyoman Inten Apriani[1], Muchsin Qadir Jailani[2], Dorman Purba[1], Andreas Suseno[1], Ferdino R Fadhillah[1], and Astri Indra Mustika[1]

[1]PT Sarana Multi Infrastruktur (Persero), Sahid Sudirman Center 49th floor, Jakarta, Indonesia
[2]World Bank Indonesia, Indonesia Stock Exchange Building, Jakarta, Indonesia

desak@ptsmi.co.id

Keywords: Geothermal Energy Investment, Off-Grid Power Solutions, Renewable Energy Economics, Mining Industry Electrification, Regulatory Challenges in Geothermal

ABSTRACT

Indonesia is recognized as the world's second-largest producer of geothermal energy, yet it has exploited only approximately 10% of its estimated 23.9 GW capacity, utilizing merely 2,418 MW. The Indonesian government has ambitious plans to increase geothermal power generation to 5,799 MW by 2030, which necessitates an acceleration in geothermal development. However, the acceleration of these investments is hindered by the low bankability of geothermal projects, primarily due to insufficient returns for investors and limited debt repayment capacities for lenders. This is exacerbated by high initial investments and unfavorable tariffs influenced by the unattractive regulated ceiling tariffs and substantial bargaining power of on-grid buyers.

This study aims to evaluate the economic viability of off-grid geothermal sales through off-grid sales to industry/mining compared to conventional on-grid electricity sales. The study also identifies potential challenges and opportunity for off-grid geothermal Utilization in Indonesia. The research uses the Political, Economic, Social, Technological, Environmental, and Legal (PESTEL) framework to analyze the general external condition of the geothermal business in Indonesia. The project finance data sourced from published reports and publication is used to perform capital budgeting and scenario analysis to determine which business scheme provides better bankability. The project bankability assessment is performed from both the investor's and lender's perspectives, focusing on returns (Net Present Value-Internal Rate of Return) and debt repayment ability (Debt Service Coverage Ratio).

The result indicates off-grid geothermal sales have promising bankability rather than the conventional on grid electricity sales since have higher return and stronger repayment ability. It is supported by the opportunity from mining industry appetite to enhance business sustainability and increasing demand of green electricity. The key challenges derived from legal perspective since Indonesia does not establish clear regulation related to off grid geothermal utilization. This research also suggest government to develop clear regulation framework for geothermal off-grid utilization in Indonesia.

1. INTRODUCTION

The geothermal development in Indonesia has started from colonized era with commercial utilization remarked through Kamojang Geothermal Power Plant (30MW) in 1983 (Darma, Imani, Shidqi, Riyanto, & Daud, Country Update: The Fast Growth of Geothermal Energy Development in Indonesia, 2021; Mansoer & Idral, 2015). Nowadays, Indonesia is top two geothermal country in the world with 2.417 MW installed capacity from approximately 23 GW total potential. It means that Indonesia only utilized around 10% of total potential with average additional capacity around 60 MW per annum (ThinkGeo, 2024). There are 46 geothermal power plants developed by State-Owned Enterprises (SOE) and Independent Power Producer (IPP) in 17 geothermal working areas (Pambudi, 2023).

Government of Indonesia has plan to utilize geothermal as baseload to replace coal power plant and set the target of utilization to reach 5.799 MW in 2030 (Fadhillah, Tjendarsa, Damayanti, Purba, & Adityatama, 2024). The government target emphasizes the significant increase in average of additional installed capacity toward 488 MW per annum from 2024 to 2030. This bold target needs to be achieved by catalyzing geothermal investment though better project attractiveness, including from project economic perspective. Figure 1 shows the historical and target for geothermal power utilization based on PLN (2021), EBTKE (2023) and ThinkGeo (2024).

1.1 Opportunity and Challenges of Geothermal Business

Government of Indonesia emphasizes geothermal as the second largest power generation from renewable energy by 2025. It targeted to support 16.9% of renewable energy power generation, equal to 7.56% of the total national electricity demand, with the increasing utilization over the year (PLN, 2021). The utilization of geothermal as

green energy is important in Indonesia's efforts to achieve 23% renewable energy by 2025 and another additional 21% of renewable power generation by 2030. The regulatory indicator for renewable energy (RISE) index by the world bank (2018) placed Indonesia in high-rank performance related to the renewable energy legal framework. The government of Indonesia has already set clear energy roadmap under energy law to support the renewable energy effort, including the fiscal incentives, government drilling programs, and risk mitigation programs (ESMAP, 2016).

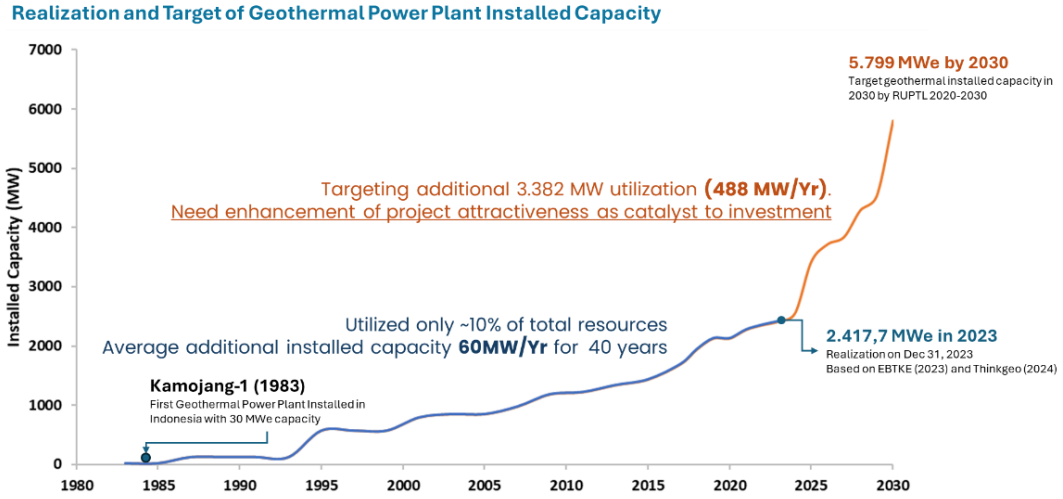

Figure 1: Indonesia geothermal power plant installed capacity and target for 2023 based on EBTKE (2023) and Thinkgeo (2024).

Research by Geothermex (2010) and Castlerock (2010) emphasizing that the main barrier to geothermal development in Indonesia lies in the significant risk involved during extensive investments. Indonesia's geothermal sector possesses significant potential, yet it remains unattractive to investors due to the high risks and low returns involved. Geothermal projects often face substantial hurdles in achieving adequate returns and satisfactory repayment capabilities due to a mismatch between regulated ceiling tariffs and project costs and risk profiles. Many projects fail to progress to the production phase because of unfavourable economic conditions, challenging resource characteristics, and social issues, all of which are influenced by political, economic, social, and technical factors.

Geothermal electricity sales face high power of the buyer since it only allowed by regulation to sell for Perusahaan Listrik Negara (PLN) as single buyer through power purchasing agreement (PPA). The high power of buyer could impact the cashflow of the business since buyer has stronger position put lower price. It regulates the sales contract for 30 years with tariff mechanisms per presidential regulation 112/2022. The PLN has the right to negotiate the geothermal tariff with the developer in business to business (B to B) approach with their primary objective to obtain efficient as low as possible electricity tariff which may not be attractive for investor. Table 1 shows the key challenges of geothermal project by ESMAP (2021).

Table 1: The general challenges of geothermal project.

Aspect	Challenges
Political - Legal	• Geothermal projects can be influenced by political instability, changes in government, or shifts in energy policies. Political instability can lead to delays in decision-making and project execution, affecting the project's financial performance and overall viability. • Uncertainties due to changes in government policies, regulations, or permitting processes. Delays in obtaining necessary approvals or unexpected changes in regulatory requirements can lead to project disruptions, increased costs, and uncertainty in project timelines
Economic	• Potential discrepancy between the expected revenue of the project and the actual realization, not necessarily due to lower production, but rather the possibility that the developer may not receive the payments for the production as initially anticipated. • One of the primary risks is cost increases, which can occur due to factors such as inflation, fluctuations in material prices, or unforeseen expenses during construction and operation. These cost overruns can strain the project's budget and affect its economic feasibility. Furthermore, changes in financing conditions, including fluctuations in interest rates or currency exchange rates, can expose the project to financial volatility. Higher interest rates

Aspect	Challenges
	can increase borrowing costs, while currency changes may affect debt repayment obligations and project revenue.
Social-Environmental	• Social environment risks in geothermal projects include community opposition, land rights and displacement issues, environmental impacts, concerns about cultural heritage, health and safety risks, and challenges in equitable benefit sharing.
Technical	• The risk that the production drilling campaign may fail to achieve the required capacity or do so with cost overruns. This pertains to the possibility of encountering challenges during the drilling process that could impede reaching the intended capacity or result in unforeseen expenses. • Risk of resource depletion due to exploitation, making it unsustainable for the planned duration. In this scenario, the geothermal resource may not perform as initially estimated, leading to difficulties in maintaining production at the power plant in accordance with the intended capacity. • Risks related to technical issues that may arise during drilling, plant construction, or plant operation. The challenges may lead to adverse impacts, including escalated costs, delays in project timelines, or revenue losses due to reduced energy generation. • Risks related to natural hazards such as earthquakes, floods, and volcanoes, which could impact the project's operations and infrastructure. Additionally, security risks in the area may pose challenges and uncertainties that need to be considered. • Risks include delays, management issues, inadequate budgeting, and procurement challenges. Proactive strategies and effective planning are crucial to address these risks and achieve project objectives.

1.2 Problem Statement

The Alpha project, a hypothetical geothermal project in Indonesia, encounters difficulties in providing acceptable return to shareholder and securing external funding due to inadequate cash flow to meet liquidity requirements. This situation presents significant barrier to project advancement, given the high upfront costs required for resource confirmation and production, alongside the need for commercial financing for development. Furthermore, the project struggles with negotiating tariffs and securing Power Purchase Agreement (PPA) a critical requirement for obtaining project financing from lenders, with single state off-taker.

Project owner is considering the option of selling steam directly to a nearby mining operator, which also demand this supply to support electricity for its operations. The project is evaluating two potential sales scenarios: selling electricity to the state off-taker (Business as Usual) or direct sales to a nearby mining operator (off-grid sales). To determine the most advantageous scenario for the project, shareholders, and potential external financiers, the project owner needs a comprehensive economic analysis through this study.

1.3 Research Question and Objective

The objective of this paper is to provide project economic analysis with recommendations to geothermal project in determining the sales scenario to provide better return and repayment ability. The research questions are:

1. How is the project economic comparison between Business as Usual and off grid sales? Which scenario provides better return and repayment ability?
2. If the off-grid scheme is more attractive, where are the potential area in Indonesia to apply similar scheme?

2. GEOTHERMAL BUSINESS OVERVIEW

2.1 Geothermal Business Model: On Grid versus Off Grid

In the geothermal industry, the primary product is steam that used for electricity generation. This utilization represents the main revenue stream for geothermal projects in Indonesia. Under typical business conditions, the generated steam or electricity is purchased by Perusahaan Listrik Negara (PLN), the state-owned electricity company, which acts as the sole buyer. PLN's position as the single buyer serves it significant power in the market, particularly in determining tariffs, that often supports its advantage (Fadhillah, 2023). Subsequently, PLN also transmits and distributes electricity to consumers across various sectors, including industrial, commercial, and residential users (Brilian, et al., 2024). This arrangement is known as the on-grid model.

The off-grid utilization concept aims to bypass PLN and sell electricity or steam directly to industrial consumers. This approach is intended to offer more competitive tariffs and streamline the negotiation process. Developers would negotiate the Power Purchase Agreement (PPA) or steam sales contract directly with potential buyers

following the Notification of Resource Confirmation (NORC), which provides option for developer to choose the buyer. In an electricity sales scheme, the project stages remain similar to the business-as-usual model, including survey, exploration drilling, development drilling, and the construction of a Steam Above Ground System (SAGS) and a power plant. In contrast, under a steam sales contract, the developer can avoid the expense and effort of constructing the SAGS and power plant, as these would be prepared by the off taker. Figure 2 illustrates the business model of on-grid and off-grid, while Table 2 summarizes the difference between both schemes.

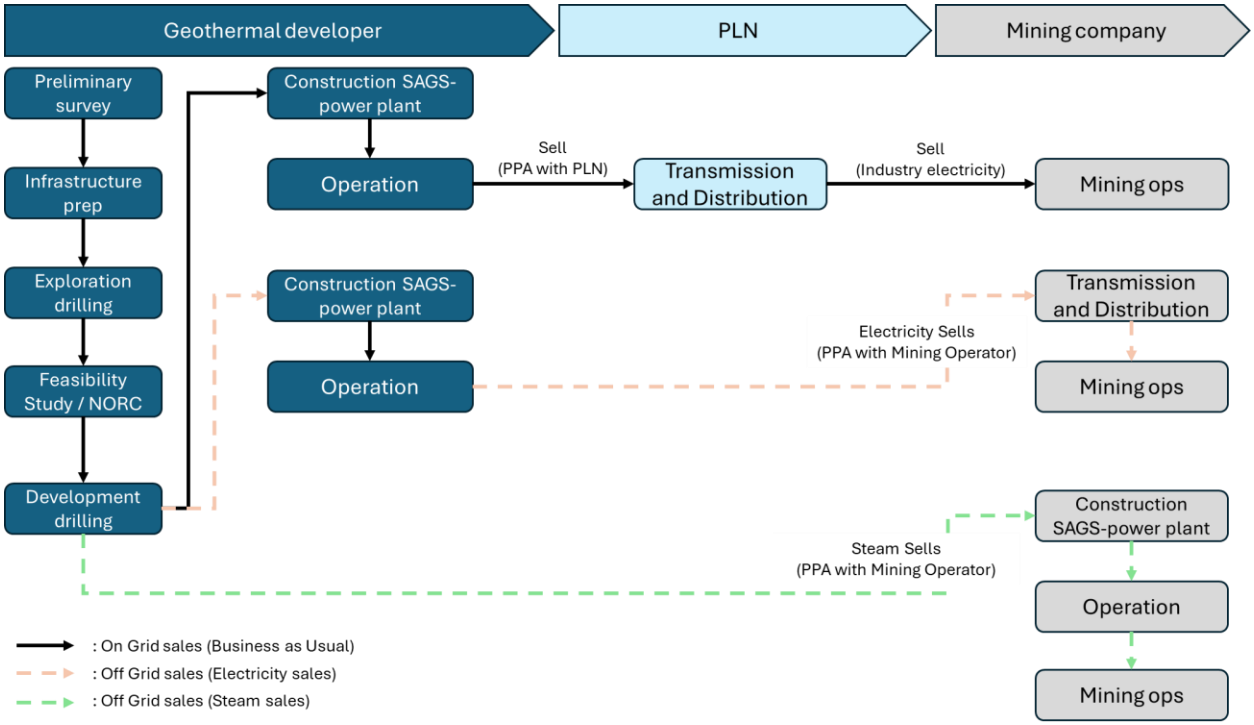

Figure 2: The differences between conventional geothermal power generation and geothermal captive use business models for the industrial sector.

Table 2: The differences between On Grid and Off Grid.

Parameter	On grid (electricity sales)	Off grid (electricity/steam sales)
Buyer	PLN, (single offtaker, the amount will be dependent to PLN roadmap)	Private or SOE, (potential for multiple buyers based on industry demand and resource condition)
Developer's power for negotiation	Very low, developer face no option of buyer.	Moderate, Developer may have several potential buyer(s)
Negotiation process	Prolong negotiation since PLN also encounter many projects and need calculation related to state subsidy for electricity.	Expected for more efficient process since the buyer usually need the power in certain date.

2.2 Indonesia Regulated Tariff Scheme

Indonesia's geothermal tariff framework uses ceiling with staging system, determined by the power plant's location and capacity. This method is specified in Presidential Regulation 112/2022, which updates the earlier ceiling tariff structure. The staging system splits the operational lifespan of a geothermal power plant into two phases: Stage 1 (years 1 to 10) and Stage 2 (years 11 and beyond). Each phase has a separate ceiling for the base tariff that developers can negotiate with PLN (GoI, 2022). Additionally, the location factor serves as a multiplier index for the base tariff during Stage 1. This adjustment accounts for the variation in development costs resulting from differing infrastructure conditions across regions (MEMR, 2022b). Figure 3 shows the distribution of base tariff and location factor. The calculation of the applied base tariff as below.

$$Tariff\ stage\ 1 = agreed\ tariff\ x\ location\ factor$$

$$Tariff\ stage\ 2 = agreed\ tariff$$

Geothermal Power Plant – electricity price

Capacity (MW)	Ceiling Price (HPT)							
	s.d 10 MW		>10 MW s.d. 50 MW		>50 MW s.d 100MW		>100 MW	
	Stg thn 1-10	Stg thn 11-30	Stg thn 1-10	Stg thn 11-30	Stg thn 1-10	Stg thn 11-30	Stg thn 1-10	Stg thn 11-30
Staging Price (cent $/kWh)	9,76 x F	8,30	9,41 x F	8,00	8,64 x F	7,35	7,65 x F	6,50
Levelized Price (cent $/kWh)	9,25		8,92		8,19		7,25	

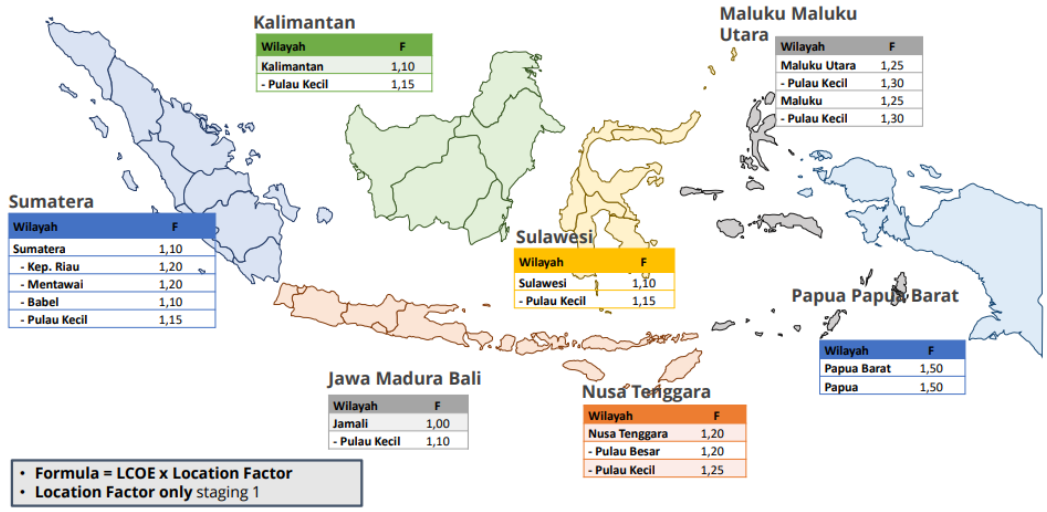

Figure 3: The base tariff and location factor of geothermal tariff under presidential regulation 112/2022.

ADB (2014) explained that Indonesia's geothermal tariff adopts an escalation approach over the years, utilizing a partial percentage of the tariff (α) to adjust the tariff values. The escalation factor used for this adjustment is based on the United States Producer Price Index (US PPI), as the contracts are denominated in USD. The calculation is as follows:

$$P(t) = [(1 - \alpha)P(0)] + [\alpha P(0)USPPI(t)/USPPI(0)]$$

where

P(t) = Tariff in year t, in US¢/kWh

P(0) = (base) tariff at COD = Tariff bid at time of tender, in year (0)

USPPI(t) = United States Producer Price Index for year (t)

USPPI(0) = United States Producer Price Index for year (0)

α = Coefficient (determined by ad-hoc discussion with range 0.25-0.4)

3. METHODOLOGY

The study gathers secondary data through an extensive literature review, concentrating on the financial parameters of geothermal projects within the on-grid scheme. This involves examining previous studies, reports, and relevant regulations to understand the cost structures, revenue models, and financial performance of on-grid geothermal projects. Key financial parameters analyzed include capital expenditure (CAPEX), operational and maintenance (O&M) costs, tariffs, and projected revenues.

To evaluate the economic outcomes of both on-grid and off-grid scenarios, the author develops and simulates a comprehensive financial model. This model incorporates various economic parameters such as initial investment costs, ongoing operational expenses, expected revenues, discount rates, and potential financing structures. The simulation helps determine key financial metrics like net present value (NPV), internal rate of return (IRR), and Debt Service Coverage Ratio (DSCR), providing a clear picture of the project's economic feasibility under different scenarios.

Furthermore, the author conducts a literature review to identify the potential challenges associated with off-grid utilization. This includes examining issues such as regulatory barriers, technical challenges, market demand uncertainties, and social acceptance. The review also explores potential geographic areas where off-grid geothermal projects could be most viable, considering factors like proximity to industrial users, resource availability, and infrastructure conditions.

By combining data from literature reviews, expert consultations, and financial simulations, the study aims to provide a thorough analysis of the economic feasibility and potential challenges of both on-grid and off-grid geothermal project utilization in Indonesia.

4. DISCUSSION

4.1 Project Economic Analysis

4.1.1 On Grid Scenario

The cashflow is discounted to determine the project feasibility through NPV and IRR. The applied discount rate for project cashflow is equal to WACC (7.12%), while the equity cashflow use discount rate on cost of equity (11%). Although cumulative cashflow shows positive condition, the result of Alpha project economic calculations shows infeasible condition for equity. The NPV for project and equity cashflow shows negative condition, where NPV project equals -14.12 MUSD and NPV equity equals -41.22 MUSD. The IRR calculation for project and equity falls below the discount rate. The IRR project is 6.52%, while the IRR equity is 6.39%. The result of NPV and IRR indicates the project does not provide fair return to the equity.

The calculation of Debt Service Coverage Ratio (DSCR) reveals that the XYZ project fails to meet the lender's requirements regarding the minimum DSCR. The lender stipulates that the minimum DSCR should not fall below 1.2 throughout the project's duration. However, the XYZ project's minimum DSCR is recorded at 1.07, indicating a deficiency in meeting the lender's specified threshold. The low DSCR of 1.07 signals to the lender that the project may struggle to generate sufficient cash flow to service its debt obligations. As a result, the lender may view the project as higher risk and may be hesitant to extend the requested funding or impose more stringent loan conditions to mitigate potential risks.

4.1.2 Off Grid Scenario

The cash flow analysis for the off-grid utilization of geothermal energy to support mining operations in Indonesia indicates promising returns with improved repayment capabilities. The enhanced project cash flow stems from achieving more favorable tariffs in agreements with mining operators. The determination of these tariffs has undergone a more efficient process, accelerating the project's operational start date. Consequently, this efficiency boost positively impacts the project's Net Present Value (NPV) and Internal Rate of Return (IRR).

The improved tariff arrangements not only expedite the project's operational timeline but also contribute to a stronger financial outlook. Higher tariffs result in increased revenue, which, in turn, enhances the project's cash flow stability. This financial improvement significantly bolsters the Debt Service Coverage Ratio (DSCR), reflecting the project's strengthened ability to meet its debt obligations.

4.2 Geothermal Energy Utilization to Support Mining Electricity

High-temperature geothermal systems are often linked to volcanism and tectonic activity, with many high-enthalpy geothermal resources also associated with high concentrations of hydrothermal alteration minerals such as gold and copper, this is due to the tendency of precious metals to precipitate and deposit as a result of the boiling and mixing of deep geothermal fluids. When managed effectively, this condition can benefit mining operations, as geothermal energy can provide a sustainable energy source that aligns with the goals of many mining companies (Patsa, Zyl, Zarrouk, & Arianpoo, 2015).

Mining industries typically prefer gas turbines or diesel generators for captive energy use due to their low upfront costs, compact equipment, quick installation, and short ramp-up periods (IRENA, 2019). However, these energy sources pose significant operational challenges, such as expensive fuel requirements and an insecure fuel supply chain, particularly in rural areas or remote islands. Additionally, the use of fossil fuels creates high greenhouse gas (GHG) emissions which does not align with global target and management direction towards sustainable mining operation.

The presence of geothermal potential near industrial sites presents a promising option for a relatively inexpensive and clean energy source for captive use, as shown in Table 2 and Figure 4. The levelized cost of electricity (LCOE) for geothermal energy is significantly lower than that of diesel generators and is comparable to that of gas turbines. Additionally, geothermal energy produces negligible greenhouse gas (GHG) emissions compared to diesel and natural gas.

The alignment of geothermal energy with sustainable mining operations is particularly noteworthy. Sustainable mining practices prioritize reducing environmental impact and minimizing carbon footprints, goals that geothermal energy supports effectively. By providing a stable and reliable energy source with low operational costs, geothermal energy can help mining companies achieve their sustainability targets while ensuring energy security.

Moreover, the LCOE values in Table 2 and Figure 4 do not account for externalities such as carbon taxes on fossil fuel power generation. If these externalities were included, the LCOE for geothermal power plants (GPP) would likely be even more favorable. This further enhances the appeal of geothermal energy for mining operations, as it not only offers cost savings but also aligns with regulatory trends toward carbon pricing and environmental accountability. It supports the industry's move toward greener practices by significantly lowering GHG emissions and providing a more stable and sustainable energy source. This alignment with sustainable mining goals makes geothermal energy a strategic choice for companies looking to enhance their environmental stewardship while maintaining economic viability.

Brillian (2024) compares various energy source that utilized in mining operation to geothermal and potential area of mining that adjacent to geothermal in Indonesia. Geothermal energy offers several advantages, making it an attractive option for sustainable industrial operations, particularly in sectors like mining. One of its primary benefits is the low levelized cost of electricity (LCOE), which ranges from 3.6 to 13.4 USD¢/kWh, significantly lower than diesel generators and comparable to gas turbines. Additionally, geothermal energy boasts a high-capacity factor of 80-95%, ensuring a reliable and consistent energy supply. It also produces minimal greenhouse gas emissions (0.02-0.24 kg CO2e/kWh), making it a much cleaner option compared to diesel and gas turbines. Unlike these fossil fuel-based energy sources, geothermal energy requires no fuel, eliminating supply chain issues and reducing operational costs. Furthermore, geothermal projects are exempt from carbon taxes, providing a financial advantage.

However, geothermal energy also presents several challenges. The initial capital expenditure is high, ranging from $4-6 million per MW, significantly more than the $0.5-0.8 million per MW for diesel generators and $0.8-0.9 million per MW for gas turbines. Geothermal projects also require substantial land (5,000-20,000 m²/MW), which can be a limiting factor in densely populated or land-scarce areas. The installation duration for geothermal projects is long, typically taking 5-7 years to complete, compared to less than a year for diesel generators and 2-4 years for gas turbines. Additionally, geothermal plants have a moderate ramp-up time of 10-20 minutes, longer than the less than 1-minute ramp-up time for diesel generators, though similar to gas turbines.

4.3 Challenges of Geothermal Off Grid Utilization

The off-grid or captive use of geothermal energy to support mining operations in Indonesia presents a unique set of challenges that must be addressed to realize its full potential. One of the primary challenges is the high cost associated with geothermal as source of energy, especially compared to gas plants. For mining operations, this can be particularly daunting, as they must balance these costs against the economic benefits of using a reliable and sustainable energy source.

Regulatory and policy frameworks also pose challenges to the off-grid use of geothermal energy for mining. In Indonesia, the regulatory environment for geothermal development is complex, with multiple permits and approvals required from various government agencies. This can lead to delays and increased costs for mining companies seeking to adopt geothermal energy. Furthermore, the current regulatory framework may not adequately address the specific needs and circumstances of off-grid geothermal projects, particularly those that serve captive users like mining operations. There is a need for more streamlined and supportive policies that facilitate the development of off-grid geothermal projects.

The regulatory and policy landscape further complicates the adoption of off-grid geothermal energy for mining in Indonesia. The regulatory framework governing geothermal development is multifaceted, involving numerous permits and approvals from various governmental agencies. This complexity can result in delays and increased costs for mining companies pursuing geothermal energy solutions. Furthermore, the current regulatory framework may not fully address the unique requirements of off-grid geothermal projects, particularly those catering to captive users like mining operations. There is a pressing need for more streamlined and supportive policies to facilitate the development of off-grid geothermal initiatives.

Logistical and operational challenges also play a critical role. Mining operations are frequently situated in remote, difficult-to-access areas, complicating the transportation and installation of geothermal equipment. The absence of existing infrastructure, such as roads and power lines, exacerbates these challenges, making it difficult to establish and maintain geothermal facilities. Moreover, the intermittent nature of mining operations, which often experience fluctuating energy demands, necessitates flexible and adaptive geothermal energy solutions capable of efficiently meeting varying load requirements.

A significant concern is the financial risk related to the purchasing power of the off-taker, particularly when the off-taker is a private entity such as a mining operator. The reliance on a single private off-taker introduces a degree of financial uncertainty. The purchasing power of the mining operator can be influenced by various factors, including fluctuations in commodity prices, operational challenges, and overall market conditions. Should the

mining operator encounter financial difficulties, this could adversely affect their ability to honor long-term power purchase agreements, thereby impacting the project's revenue stream and financial stability.

5. CONCLUSION

The off-grid utilization of geothermal shows promising potential since it may provide better tariff for geothermal developer with fair negotiation process. The scheme needs further preparation to tackle various challenges and optimize its potential in Indonesia. The regulator, business owners, mining operators, and financers is recommended to held through discussions to formulate excellence scheme for off grid geothermal utilization.

REFERENCES

ADB. (2014). *Unlocking Indonesia's geothermal potential. Asian Development Bank*.

Brilian, V. A., Adityatama, D. W., Mukti, A. W., Asy'ari, M. R., Purba, D., Fadhillah, F. R., & Erichatama, N. (2024). Geothermal Captive Use to Support Industrial Activities: Applicable Industry Sectors, Worldwide Experience, and Its Potential and Challenges in Indonesia. *Workshop on Geothermal Reservoir Engineering*. California: Stanford University.

Darma, S., Imani, Y. L., Shidqi, M. N., Riyanto, T. D., & Daud, M. Y. (2021). Country Update: The Fast Growth of Geothermal Energy Development in Indonesia. *World Geothermal Congress 2020+1*. Reykjavik: WGC.

ESMAP. (2016). *Comparative Analysis of Approaches to Geothermal Resource Risk Mitigation*. ESMAP.

ESMAP. (2021). *Preparing Feasibility Studies for Financing of Geothermal*. Washington DC: World Bank.

Fadhillah, F. R. (2023). *Economic Evaluation of Bravo Geothermal Prospect in Participating Green Energy Effort*. Jakarta: Institute Teknologi Bandung.

Fadhillah, F. R., Tjendarsa, K., Damayanti, S. M., Purba, D., & Adityatama, D. (2024). *Economic Evaluation of Bravo Geothermal Project as Effort for Green Energy Transition*.

GoI. (2022). Presidential Regulation 112/2022: *Percepatan Pengembangan Energi Terbarukan untuk Penyediaan Tenaga Listrik*. Jakarta: Government of Indonesia.

Mansoer, W. R., & Idral, A. (2015). Geothermal Resources Development in Indonesia: A History. World Geothermal Congress. Melbourne: WGC.

MEMR. (2022b). Presidential Regulation 112/2022 *Percepatan Pengembangan Energi Terbarukan untuk Penyediaan Tenaga Listrik*. MEMR.

Pambudi. (2023). *Renewable Energy in Indonesia: Current Status, Potential, and Future Development. Sustainability*.

Patsa, E., Zyl, D. V., Zarrouk, S. J., & Arianpoo, N. (2015). Geothermal Energy in Mining Developments: Synergies and Opportunities Throughout a Mine's Operational Life Cycle. *World Geothermal Congress*. Melbourne: WGC.

PLN. (2021). *RUPTL 2021-2030*. Jakarta: Perusahaan Listrik Negara.

ThinkGeo. (2024). *ThinkGeoEnergy's Top 10 Geothermal Countries 2023 – Power Generation Capacity*. Retrieved from Webinar: https://www.thinkgeoenergy.com/thinkgeoenergys-top-10-geothermal-countries-2023-power-generation-capacity/

World Bank. (2018). *Regulatory indicators for sustainable energy*. Jakarta: WB.

Geothermal Beyond Energy: Total Extraction and Circular Economy of Valuable Elements from Geothermal Brine

Himawan Tri Bayu Murti Petrus[1], Vincent Sutresno Hadi Sujoto[1], Chandra Edward Suryanaga[1], Dewa Putu Agus Sudarmaja[1], Sutijan[1], Agus Prasetya[1], Ferian Anggara[2], Siti Nurul Aisyiyah Jenie[3], Widi Astuti[4], Andhika Putera Utama[5], Syamsumin[5], Supremlehaq Taqwim[5], Delvirah Elisa Sabatini Singkuang[5], and Ayu Gracia Ade Sumartha[5]

[1]Department of Chemical Engineering (Sustainable Mineral Processing Research Group), Faculty of Engineering, Universitas Gadjah Mada, Jl. Grafika No.2, Kampus UGM, Yogyakarta, 55281, Indonesia
[2]Department of Geological Engineering (Sustainable Mineral Processing Research Group), Faculty of Engineering, Universitas Gadjah Mada, Jl. Grafika No.2, Kampus UGM, Yogyakarta, 55281, Indonesia
[3]Research Center for Mineral Processing, National Research and Innovation Agency (BRIN), Jalan Ir. Sutami Km.15, Tanjung Bintang, Sindang Sari, Lampung Selatan, Kabupaten Lampung Selatan, Lampung, 35361, Indonesia
[4]Research Center for Advanced Chemical, National Research and Innovation Agency (BRIN), Jl. Puspiptek Serpong, Kec. Setu, Kota Tangerang Selatan, Banten, 15314, Indonesia
[5]PT. Geo Dipa Energi (Persero), Jl. Dieng RT 01 RW 01, Area Industri, Sikunang, Banjarnegara, Kabupaten Wonosobo Jawa Tengah, 56354, Indonesia

bayupetrus@ugm.ac.id

Keywords: circular economy, environmental conservation, geothermal resource management, sustainable mining, valuable mineral recovery

ABSTRACT

Geothermal energy, a significant form of renewable energy, has conventionally been employed for generating electricity and heating purposes. This study presents a novel approach to geothermal use by investigating the comprehensive extraction and circular economy of essential elements from geothermal brine. In this study, we introduce novel methodologies that enable the retrieval of valuable minerals, such as lithium and silica, from geothermal brine. Consequently, this process effectively converts geothermal brine into a reservoir of valuable resources. This method not only enhances the exploitation of geothermal sites in a more diversified manner but also corresponds with the fundamental principles of the circular economy. The circular economy model effectively reduces waste and enhances resource efficiency by implementing sustainable extraction methods and recycling procedures. This study thoroughly examines the extraction procedures, assessing their viability, effectiveness, and ecological consequences. Moreover, adopting this comprehensive methodology mitigates the environmental impact by diminishing the reliance on conventional mining practices and fostering conscientious resource stewardship. This study makes a valuable contribution to sustainable practices by proposing a change in geothermal operations from single-purpose energy production to multifunctional resource recovery. By doing so, it aims to enhance the long-term viability of geothermal resources. This study represents a significant advancement in reevaluating the function of geothermal energy within the framework of a circular economy, with a focus on fostering environmental conservation, stimulating economic development, and ensuring the sustainable utilization of resources.

1. INTRODUCTION

Geothermal energy has long been recognized as a valuable renewable source, mainly used for electricity generation and direct heating. Historically, the primary focus has been on using thermal energy from geothermal reservoirs to generate electricity. However, the geothermal business is on the verge of a paradigm revolution fueled by the demand for more sustainable and diverse resource utilization strategies. Geothermal brine, a byproduct of geothermal energy extraction, comprises a diverse range of dissolved minerals and elements, including lithium, silica, and other vital compounds (Kusumastuti et al., 2018; Qurrahman et al., 2021). Historically, these ingredients have been neglected, with brine frequently being re-injected into the reservoir or disposed of without fully realizing its potential. This mistake represents a missed opportunity to pursue a more sustainable and efficient resource management approach.

In light of the expanding global need for essential minerals such as lithium for electric car batteries and silica for various industrial applications, extracting these elements from geothermal brine appears to be a feasible alternative (Goldberg et al., 2023). This strategy not only complies with the ideas of the circular economy but also reduces the environmental impact of typical mining practices. The geothermal business can transition from a model of

single-purpose energy generation to a multifunctional resource recovery paradigm by using geothermal brine as a source of valuable minerals (Kölbel et al., 2023). The circular economy paradigm strongly emphasizes encouraging sustainable activities, improving resource efficiency, and cutting waste. By incorporating these ideas into geothermal operations, more sustainable and eco-friendly procedures may be developed. These principles are realized by the complete extraction of valuable elements from geothermal brine, which reduces the environmental impact of energy production and converts waste into resources.

One significant challenge in utilizing geothermal brine is silica deposition, which can clog pipes and equipment. This issue necessitates effectively managing and using silica to prevent operational disruptions (Setiawan et al., 2019). The potential to convert this byproduct into a valuable resource further underscores the importance of comprehensive mineral extraction from geothermal brine. In addition to silica, other valuable minerals such as lithium can be harnessed, adding economic value and promoting resource efficiency within the geothermal industry.

This study investigates novel approaches to extracting silica, lithium, and other necessary components from geothermal brine. It evaluates various extraction processes' effects on the environment, economy, and technical viability. The results are intended to offer a solid basis for reframing the function of geothermal energy in a circular economy, encouraging environmental conservation, and advancing sustainable economic growth. The long-term sustainability and viability of geothermal resources are enhanced by this research, which refocuses the emphasis from energy generation to resource recovery. It emphasizes how crucial it is for the geothermal business to include cutting-edge extraction methods and circular economy ideas to pave the path for a more resource-efficient and sustainable future.

2. GEOTHERMAL BRINE

Geothermal brine refers to a high-temperature solution of salts that flows through solid rock and becomes enriched with solutes from the surrounding rock (Kabay et al., 2018). A multitude of chemical constituents are dissolved within geothermal brines in the various strata of the Earth. Lithium is an extractable constituent found in geothermal brines. Seawater is the primary source of lithium, but the amount of lithium found in seawater is relatively tiny, specifically 0.1-0.2 mg/dm^3. Geothermal brine technology offers significant potential, with concentrations ranging from 10 to 500 mg/dm^3 (Siekierka, Tomaszewska, and Bryjak, 2018).

Indonesia has numerous geothermal brine sources, primarily located in the region stretching from the island of Sumatra to the islands of Nusa Tenggara. There are a minimum of 62 geothermal sites situated on Java Island that can be utilized for their thermal resources. These fields are distributed across the entire island (Setijadji, 2010). Geothermal regions can be classified into fault-hosted and volcano-hosted geothermal systems based on their underlying geology. Seven geothermal developments are located in volcanoes, and out of these, five can generate power (Purnomo and Pichler, 2014). Geothermal faults that are hosted are often not well-developed and are hardly investigated because the energy produced is negligible.

As previously stated, geothermal systems in Java are categorized into volcanic and fault hosts. Out of the twenty-five researched geothermal systems, only eight are classified as fault-hosted, while the rest are volcano-hosted. The eight fault-hosted systems are Pacitan, Maribaya, Batu Kapur, Pakenjeng, Cilayu, Cikundul, Cisolok, and Parangtritis. Segaran, Arjuna-Welirang Volcano, Mount Lawu, Mount Ungaran, Dukuh Temple, Dieng, Kalianget, Slamet Volcano, Ciawi, Sumur Village, Tampomas, Cipanas, Ciater, Darajat, Kamojang, Pangalengan, and Patuha are significant landmarks in the region. (Purnomo and Pichler, 2014). In contrast, the Tertiary volcanic belt is the primary location of fault-hosted geothermal systems. Volcanoes in the Quaternary volcanic belt are the exclusive locations for geothermal systems.

Figure 1 illustrates the authors' advanced approach to transforming geothermal resources into valuable minerals. The process strongly emphasizes silica recovery, which utilizes cutting-edge technologies like forward osmosis (FO), electrodialysis (ED), and ion sieve adsorption. This comprehensive strategy is carefully formulated to maximize the efficiency of extracting silica and lithium from geothermal brines while reducing environmental impact. FO is notable for its capacity to properly handle high-silica solutions, resulting in efficient separation and reduced energy usage compared to traditional processes. After the recovery of silica, the process of concentrating lithium ions is carried out by utilizing selective ion transport across membranes with the help of an applied electric field. This process improves the quality and strength of lithium in the brine. In addition, the process of ion sieve adsorption enhances the quality of the lithium product, resulting in a high level of purity that is well-suited for a range of industrial uses, such as battery production. The combined employment of these cutting-edge technologies enhances the efficiency of mineral recovery rates and promotes the sustainable utilization of resources by minimizing waste output and optimizing energy efficiency. The authors' approach emphasizes their dedication to sustainable development in the geothermal industry, which aligns with worldwide environmental objectives and standards while ensuring the effective extraction of rich minerals from geothermal brines.

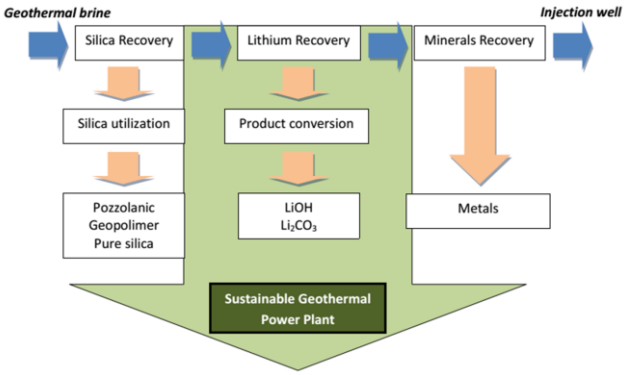

Figure 1: Processing concept of converting geothermal resources into valuable minerals.

3. SILICA RECOVERY

A significant obstacle in harnessing geothermal brine is the accumulation of silica, which can obstruct pipes and machinery, leading to operational complications (Figure 2). Efficient management and exploitation of silica are essential for avoiding these disturbances. The significance of thorough mineral extraction from geothermal brine is shown by converting this byproduct into a valuable resource. In addition to silica, precious minerals such as lithium can be mined, increasing economic value and promoting resource efficiency in the geothermal industry.

Extracting silica from geothermal brine is challenging but potentially fruitful in commercial settings. Geothermal brines include substantial amounts of dissolved silica, a naturally occurring mineral that, if not carefully controlled, can cause scaling problems in processing equipment and pipelines. Scaling is the process in which silica separates from the brine due to temperature, pressure, or chemical composition changes. This phenomenon leads to the formation of deposits that can impede flow, decrease heat transfer efficiency, and raise operational expenses.

Figure 2: Silica Deposition Clogging in Geothermal Power Plants.

An integrated strategy efficiently extracts silica from geothermal brines while addressing scaling issues. Initially, thorough pre-treatment operations are essential. The methods entail using filtration and sedimentation techniques to eliminate particles and impurities from the brine, decreasing the initial silica content and reducing fouling in subsequent equipment. Consistent surveillance and preemptive upkeep are crucial for a prosperous silica retrieval plan. By regularly analyzing the silica levels in the brine and closely monitoring scaling tendencies, operators may predict possible problems and promptly apply cleaning and anti-scaling treatments. This strategy extends the operating lifespan of equipment and guarantees continual production efficiency.

3.1 Nanosilica

Nanosilica is extensively utilized in various fields, including but not limited to thermal and electrical insulation, humidity sensing, chromatography, and catalysis (Hessien et al., 2009). Techniques for generating nanosilica include chemical precipitation, gas phase agglomeration, and the sol-gel technique. The sol-gel method and the chemical precipitation method are the two generally employed techniques. Hence, for this investigation, the chemical precipitation approach was selected. The chemical precipitation method involves the formation of a solid precipitate in a solution due to a chemical reaction. Precipitation typically happens when the amount of dissolved ions approaches the maximum level at which they may remain dissolved, causing the creation of a salt. The precipitation method is commonly performed concurrently, where the silicate solution and H2SO4 solution are combined simultaneously during the operation. Despite its limited usage, nanosilica has versatile applications

across multiple industries. Its applications include its utilization as a catalyst precursor, absorbent, and composite filter. In addition, nanosilica substantially impacts the structural strength of HVFA, which will be further elaborated on in the following section. Nanosilica materials use epoxy resin composites due to their advantageous qualities, including tensile, compressive, and shear strength.

Figure 3: Nanosilica product from geothermal silica.

By optimizing influential parameters such as pH and reactant ratios, the synthesis of nanosilica has been successfully achieved (Figure 3). The nanosilica achieved a maximum yield above 75% through thorough investigation and optimization of process parameters. Accurate pH regulation and appropriate proportions between the silicate solution and H_2SO_4 are crucial in attaining maximum effectiveness in nanosilica manufacturing. The results indicate that the chemical precipitation method employed in this work successfully generates nanosilica with a high yield, hence facilitating its extensive utilization across diverse industrial sectors. Particle size analysis is conducted using transmission electron microscopy (TEM) and particle size analysis (PSA) tests. The transmission electron microscopy (TEM) test is performed to examine the morphology of the product. The TEM test might be utilized in this scenario to verify the suitability of the PSA test conducted (Figure 4).

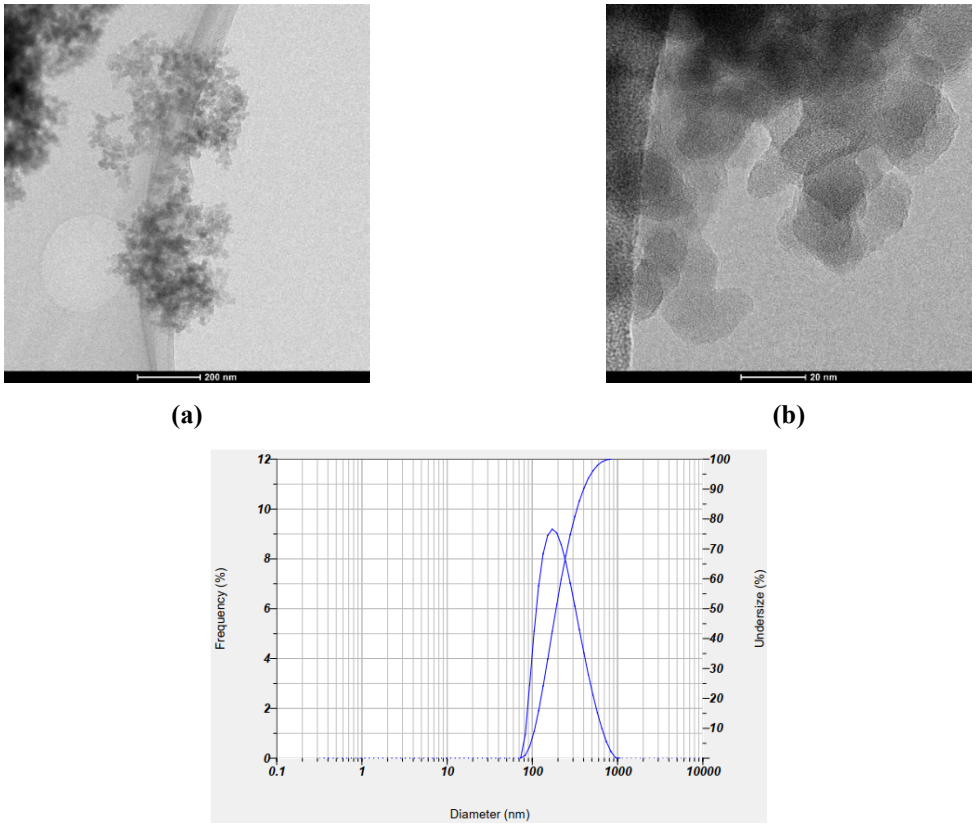

(a) **(b)**

(c)

Figure 4: TEM and PSA analysis, (a) TEM 200nm, (b) TEM 20nm, and (c) PSA.

The PSA test was conducted to ascertain the particle size of the nanosilica product that was produced. A product is classified as a nanoparticle if its size is less than 100 nm. According to the PSA nano silica test conducted under different working conditions, it can be concluded that the product obtained is not in the form of nanoparticles, as its size ranges from 181.1 nm to 280.1 nm. Nevertheless, upon TEM examination conducted on the identical

product, it is evident that the particles are still not represented at a size of 200 nm. The newly developed silica nanoparticles are visible at 20 nm, indicating that the end product can be categorized as a nanoparticle. According to estimates, the nanosilica particles are believed to form agglomerates, which means that the size measured by PSA analysis does not include the nanoparticles. Therefore, considering the various factors discussed earlier, it may be inferred that the product is a nanoparticle.

3.2 Silica gel

Indonesia is a significant consumer of silica gel, a highly coveted product globally. The demand for silica gel in Indonesia has been consistently growing and is expected to continue to rise, fueled by the country's robust consumer buying power. Indonesia has the potential to significantly increase the production of silica gel, which might lead to a reduction or complete elimination of the requirement for imports. It can potentially establish itself as a country that sells goods to other nations. This product is essential due to the extensive global need for silica gel in many industries.

Silica gel is a granular substance that resembles glass and has a very porous structure. It is created by synthesizing sodium silicate. The creation reaction of silica gel can be categorized into two distinct stages specifically (Ciriminna et al., 2013):

Hidrolisis: $Na_2SiO_3 + H_2O + 2HCl \rightarrow Si(OH)_4 + 2NaCl$ (1)

Kondensasi: $Si(OH)_4 + (OH)_4 Si \rightarrow (OH)_3 Si{-}O{-}Si(OH)_3 + H_2O$ (2)

Despite its name containing "gel," it is still categorized as solid silica. Silica gel is a preventative measure against excessive moisture by inhibiting its occurrence. Silica is a secure substance that helps retain moisture in various items such as food, medications, delicate materials, electronics, and even films. This product is frequently encountered in packages and shipments containing films, cameras, binoculars, computer equipment, leather shoes, clothing, food, pharmaceuticals, and other products. This hygroscopic compound absorbs moisture without changing its composition. Silica is a hygroscopic substance that can adsorb moisture and liquid particles from the surrounding air or spaces. Silica additionally aids in the prevention of harm to stored commodities. This hygroscopic substance also functions as a rust inhibitor for metals, mitigating the potential for short circuits in microelectronics and reducing the oxidation and degradation of chemicals due to elevated atmospheric humidity.

Figure 5: Silica gel product from geothermal silica.

The production of silica gel from geothermal brine has been effectively achieved by considering many factors, such as the concentration of the acid solution and the dilution of sodium silicate (Figure 5). This procedure produces silica gel with a high capacity for absorbing water vapor. Using geothermal energy to produce silica gel is cost-effective and environmentally sustainable, as it repurposes industrial waste for moisture management and protecting delicate items.

Silica gel was characterized using Fourier Transform Infrared (FTIR) spectroscopy to analyze its absorption bands. The FTIR analysis results (Figure 6) indicate a high degree of similarity in curve intensity with the silica gel white/SiO2 database, achieving a score of 851. This score surpasses other databases that may exhibit a similar infrared absorption intensity to the sample. This investigation presents data regarding the effective production of silica gel from geothermal silica utilizing the sol-gel technique.

The FTIR analysis results also provide information about the functional groups in the silica gel sample. Several peaks are observed in the frequency spectrum of the silica gel sample, as shown in Figure 6. At a frequency of 1055.86 cm^{-1}, it indicates the Si-O group, which signifies the vibration characteristics of SiO_4 and indicates the polymerization of Si-O-Si. The bending vibration at 1633.87 cm^{-1} also shows the presence of siloxane (Si-O) groups (Nuryono and Narsito, 2010). The broad band at the frequency of 3385.06 cm^{-1} represents the vibration of -OH groups (hydroxyl) originating from silanol (Si-OH) or hydrated water. Generally, the absorption bands appearing in the silica gel spectrum indicate that the functional groups present in silica gel produced from geothermal silica include silanol (Si-OH) and siloxane (Si-O-Si) groups (Sdiri et al., 2014).

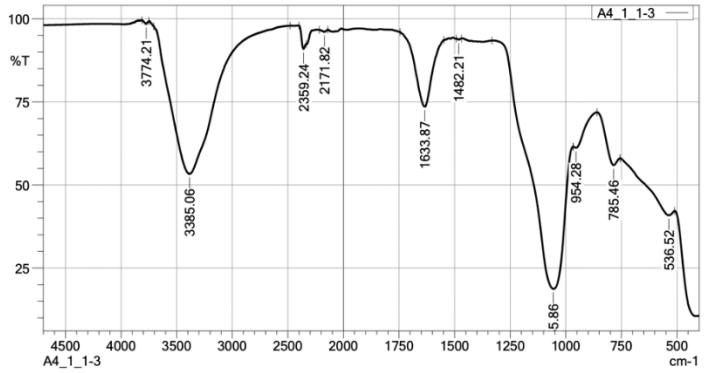

Figure 6: FTIR analysis result of silica gel.

3.3 Material Construction

The massive infrastructure development in the past decade has led to a continuous growth in demand for construction materials, including concrete. This fact has prompted various companies, both government-owned and private, to compete in creating high-quality concrete at competitive prices. According to data from the Indonesian Precast and Prestressed Concrete Association (AP3I), concrete production has shown an increasing trend each year. In 2015, the production capacity of concrete reached 25.30 million tons per year, and it further increased in 2017 to 35 million tons per year. It is estimated that these numbers will continue to grow in the future, considering that Indonesia is one of the countries that may still develop its infrastructure.

Concrete construction materials utilizing HVFA (High Volume Fly Ash) can be produced by combining coal fly ash with silica and incorporating a base activator like sodium hydroxide (NaOH). HVFA concrete is a composite material composed of pozzolan and activator. Pozzolan is a substance that consists of silica and alumina. Aluminum and silicon-containing materials are treated with very concentrated alkaline solutions to activate them (Palomo, Grutzeck, and Blanco, 1999). The reference is from Palomo, Grutzeck, and Blanco's work published in 1999. Fly ash waste is utilized as a binding agent in concrete compositions. Sodium hydroxide and sodium silicate are commonly employed as activators. Sodium silicate acts as a catalyst to speed up the polymerization reaction.

In contrast, sodium hydroxide reacts with the aluminum (Al) and silicon (Si) atoms present to form robust polymer bonds (Hardjito, 2005). Increasing the molarity leads to a corresponding increase in compressive and splitting strength. Nevertheless, it has been discovered that HVFA concrete exhibits more brittleness compared to standard concrete (Ekaputri and Triwulan, 2013). Like cement, fly ash mixed with alkali activators requires time to react and eventually harden. The testing of setting time in cement is influenced by the type of cement used and the amount of water used. In the case of fly ash, the setting time is greatly influenced by the grade of fly ash used, the ratio of fly ash to alkali activator, and the level of molarity of the alkali activator used.

Criado et al. (2007) demonstrated that a high amount of reactive silica triggers the formation of a higher quantity of geopolymer gel, which in turn enhances the mechanical strength of concrete (Criado et al., 2007). On the other hand, the distribution of particle size has a significant impact on the reactivity of fly ash. A higher number of fine particles will result in a larger surface area and a higher reactivity, leading to a greater compressive strength (Diaz, Allouche, and Eklund, 2010). The addition of nanosilica in Portland cement concrete systems has been extensively investigated, and it has been found that nanosilica can be used as an additive. Nanosilica has a positive influence on the mechanical properties of concrete (Phoo-ngernkham et al., 2014). It is expected that the addition of nanosilica will also have a positive impact on extreme environmental conditions.

Concrete production with nanosilica has been successfully achieved by including many contributing components, such as the fly ash-to-cement ratio (Figure 7). The analysis has achieved optimal circumstances, leading to a compressive strength of 26.9 MPa and a 2547 kg/m³ density for High Volume Fly Ash (HVFA) concrete. This achievement significantly exceeds the quality standard established by SNI DT 91-0008-2007 for K225 concrete, which mandates a compressive strength of 19.3 MPa. The findings suggest that including nanosilica in the concrete mixture can significantly enhance its mechanical characteristics, broadening its construction applicability through increased strength and density.

FTIR analysis was also conducted in this study. In Figure 8, FTIR spectra of HVFA concrete samples exhibit peaks in the wavenumber regions of 900 – 1300 cm^{-1}, 1650 cm^{-1}, and 3400 – 3650 cm^{-1}, resembling groups typically found in zeolites. The Si-O-T group observed at wavenumbers of 900 – 1300 cm^{-1} indicates the presence of copolymerization reactions. These peaks suggest the existence of silica-alumina bonds characteristic of zeolite-like structures within the HVFA concrete matrix. The FTIR analysis offers detailed insights into the chemical bonding and structure of the concrete, emphasizing the incorporation of nanosilica and its role in forming these

distinctive functional groups. This characterization highlights the potential enhancement of concrete properties through nanosilica addition, thereby improving performance and durability in various construction applications.

Figure 7: Material construction product from geothermal silica.

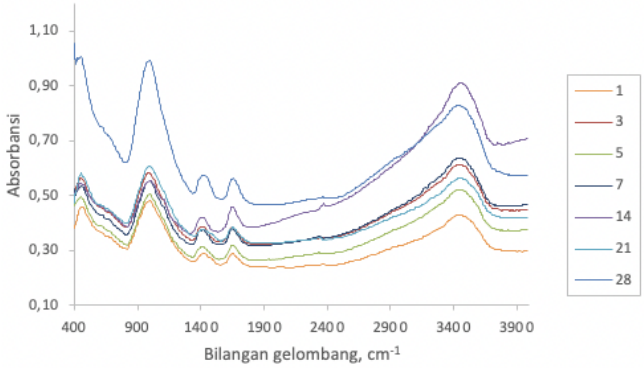

Figure 8: FTIR analysis result.

4. LITHIUM RECOVERY

Lithium can be acquired from two distinct sources: natural sources, including minerals, salt lakes, subterranean water, and seawater, as well as artificial ones, such as recycling operations involving electronic trash and lithium batteries (Siekierka dkk., 2018). Lithium is an element that is not commonly discovered, although it can be found in certain rocks and certain sea waters. However, its presence is always in tiny amounts. The average concentration in the Earth's upper crust has been calculated to be approximately 60 parts per million (ppm) and is ranked 27th in element abundance (Garrett, 2004). The lithium concentration process commonly relies on solar evaporation as the primary technique. Despite its simplicity, the conventional method of salt manufacture from brine, as practiced by salt farmers, remains highly susceptible to weather conditions. Solar radiation is the primary catalyst for saltwater vaporization, resulting in salt formation (Flexer dkk., 2018). Developed countries have started designing membrane technology to extract essential minerals like lithium. A pressure-driven membrane separation method involves the application of a pressure difference across a membrane. This pressure difference might take the form of microfiltration (MF), ultrafiltration (UF), nanofiltration (NF), or reverse osmosis (RO).

4.1 Forward osmosis

In osmosis, water diffuses through a selectively permeable membrane from a region of higher chemical potential to a lower chemical potential. This phenomenon arises from the gradient in solute concentration across the membrane, which generates a driving force. There are various well-known applications of this phenomenon, such as reverse osmosis (RO), pressure retarded osmosis (PRO), and forward osmosis (FO). Water treatment technologies have generally widely employed reverse osmosis (RO). The utilization of reverse osmosis (RO) for treatment purposes is often accompanied by notable economic drawbacks, including elevated membrane fouling rates and substantial operational energy expenses resulting from the requirement of external pressure to traverse the permeable membrane. On the other hand, the forward osmosis (FO) process, which is also a type of osmotic process, has benefits that are not present in reverse osmosis (RO) (Cath et al., 2006).

In the process of forward osmosis (FO), the draw solution (DS) serves as the driving force to counterbalance the osmotic pressure, enabling water to flow through the permeable membrane without requiring external pressure, as is the case in the reverse osmosis (RO) process. The features of the DS substantially determine the effectiveness of the FO process, and there are numerous crucial criteria for selecting it. Initially, the DS should possess a

comparatively elevated osmotic pressure. The DS must also be easily reconstructable after surgery. Finally, the DS must reduce the focused pressure on a single membrane side (Zhao et al., 2012). In Forward Osmosis (FO), the Draw Solution (DS) undergoes two stages: initial dilution and subsequent concentration. During the initial phase, a substance with elevated osmotic pressure absorbs water from the feed. The diluted substance is reconcentrated in the following phase using alternative methods (Long et al., 2018). After a more thorough analysis, it has been shown that the second stage plays a pivotal role in improving the operation's energy efficiency.

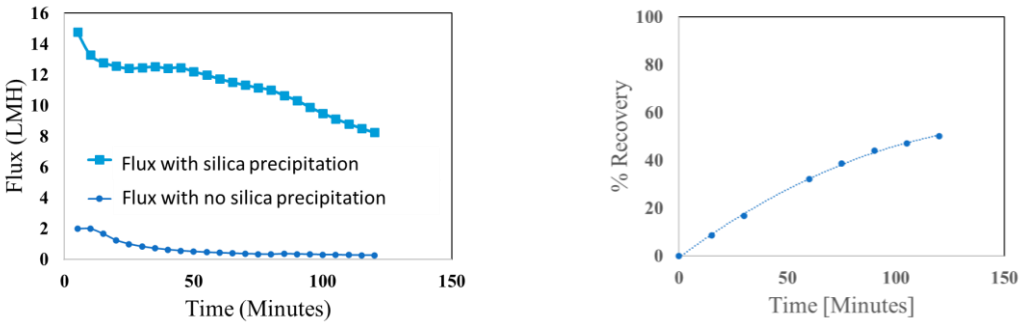

(a) (b)

Figure 9: Graphical insights from optimized lithium recovery study results using forward osmosis technology for (a) flux and (b) recovery percentage (Mustika et al., 2022; Sutijan et al., 2022).

The investigation of forward osmosis (FO) for the purification of geothermal brines with lithium has yielded encouraging findings (Figure 9), namely in terms of achieving a lithium recovery rate of roughly 50% and attaining a greater flux (around 38 LMH) compared to alternative membrane approaches. Nevertheless, there are substantial obstacles that must be confronted during the implementation of this technology. Before the forward osmosis (FO) procedure, it is necessary to eliminate silica present in geothermal water. It is essential to take this step because silica can create fouling and the buildup of material on the membrane surface, which decreases process efficiency and requires frequent membrane cleaning for maintenance purposes.

Forward osmosis (FO) has been determined to have a higher propensity for fouling in comparison to other membrane technologies, such as nanofiltration (NF) and reverse osmosis (RO). Fouling is commonly ascribed to the presence of suspended particles and organic matter in geothermal solutions. Hence, FO systems should incorporate efficient tactics to reduce and control fouling, such as careful membrane selection and effective pretreatment techniques. However, FO's benefits in extracting lithium and its ability to handle more significant amounts of fluid flow have great potential in treating geothermal water. Forward osmosis (FO) may offer a more energy-efficient and environmentally sustainable alternative to existing technologies such as reverse osmosis (RO), particularly considering the growing scarcity of water resources and the increasing demand for lithium in batteries and electronic industries. Future research endeavors could enhance the efficiency of forward osmosis (FO) by optimizing operational conditions, enhancing fouling resistance, and minimizing total operational expenses. This endeavor will bolster the competitiveness of forward osmosis (FO) technology in geothermal water treatment and lithium extraction in the coming years.

4.2 Electrodialysis

Electrodialysis (ED) is a method that involves the movement of ions across a membrane as a result of an applied electrical potential difference and the flow of electric current (Mulder, 2003). Typically, ED experiments are conducted using an electrodialysis stack consisting of a cation exchange membrane (CEM), an anion exchange membrane (AEM), an anode electrode (e.g., iridium-coated titanium), and a cathode electrode (e.g., stainless steel) (Nie et al., 2017). Multiple investigations have demonstrated that Li^+ ions can permeate the monovalent ion exchange membrane, moving from the brine (feed) to the concentrate (purified solution) due to an electric driving force during the process. Conversely, ions like Mg^{2+} and Ca^{2+} cannot pass through the monovalent ion exchange membrane and remain in the feed solution (Zhang et al., 2020). Hence, electrochemical deposition (ED) demonstrates significant promise in lithium extraction, particularly in brine separation.

According to various research, the electrodialysis (ED) approach offers several benefits in comparison to alternative techniques for separating membranes (Van Der Hoek et al., 1998; Post et al., 2007; Walha et al., 2007). Electrodialysis significantly benefits conventional membrane separation technologies by requiring minimal feed preparation. This result is achieved through reverse polarity operation, which minimizes membrane fouling and scaling. Furthermore, electrodialysis allows far greater brine concentrations due to the absence of any restrictions

imposed by osmotic pressure. The ion exchange membrane's chemical and mechanical stability ensures a prolonged lifespan, especially when exposed to harsh and oxidizing components in the feed water.

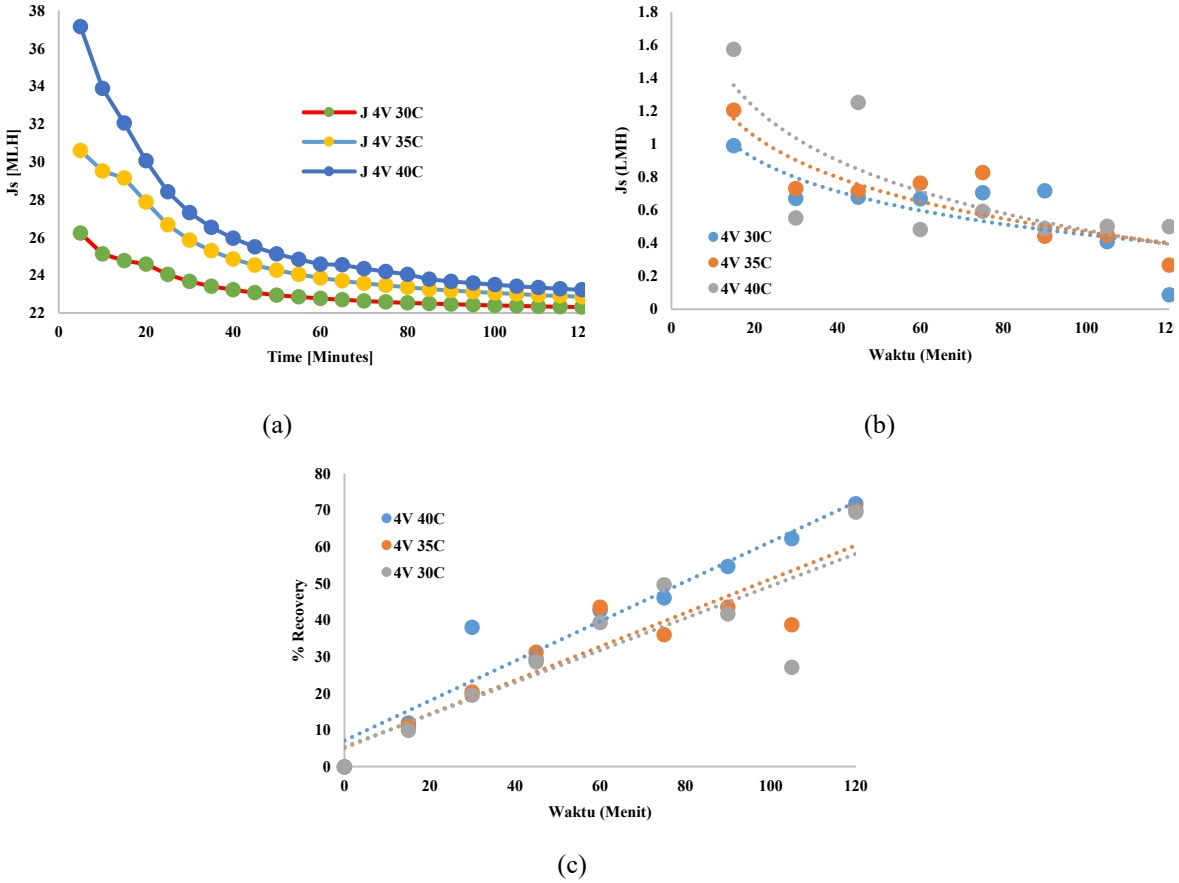

Figure 10: Graphical insights from optimized lithium recovery study results using electrodialysis technology for (a) solution flux, (b) ionic flux, and (c) recovery percentage (Jati et al., 2023; Sujoto et al., 2022).

Electrodialysis for lithium extraction has demonstrated considerable promise within the industry. Electrodialysis employs an electric field to segregate lithium ions from the solution using ion-selective membranes. While the flux generated may not be as substantial as that of alternative membrane technologies, the recovery percentage surpasses 70%, as evidenced in Figure 7. These findings render electrodialysis a compelling substitute for traditional separation technologies. An essential benefit of electrodialysis is its notable separation efficiency. The electric field employed in this procedure can efficiently extract lithium ions from the solution, enabling a remarkably effective separation. The high accuracy of ion-selective membranes guarantees the precise separation of lithium ions from other ions in the solution, improving the end product's quality. This phase is essential for industrial and battery applications where the purity of lithium is of utmost importance.

Moreover, electrodialysis has excellent scalability and may be seamlessly combined with other separation technologies to enhance the overall efficiency of the extraction process. This method is scalable and may be adapted to suit the requirements of various sectors. It can also serve as a final step following initial separation processes utilizing alternative membrane technologies. The adaptability of electrodialysis makes it highly suitable for usage in diverse environmental situations and with varied brine sources. Electrodialysis offers the benefit of consuming less energy compared to alternative separation technologies. Although this method necessitates using an electric field that consumes energy, the technology has advanced to function with improved energy efficiency. Electrodialysis minimizes waste production, which is crucial in mitigating the environmental consequences of lithium extraction.

In general, while the flow generated by electrodialysis is not as substantial as that of other membrane technologies, this approach has great potential due to its high recovery rate, energy efficiency, and capability to manufacture lithium products with excellent purity. Research findings suggest that electrodialysis has the potential to play a significant role in future lithium extraction methods. It offers a practical and eco-friendly option for the fast-growing lithium sector.

4.2 Ion sieve adsorption

A sieve ion adsorbent is an inorganic substance that utilizes redox reactions, ion exchange, or heating processes to incorporate template ions into inorganic compounds, forming oxide compounds. These processes can be conceptualized as a fusion of oxidation and reduction. Subsequently, the eluent will displace the template ion from its crystalline location, while the vacant crystal sites will remain intact. Consequently, traditional crystal sites can only accommodate ions with ionic radii equal to or smaller than the target ion's structure when forming inorganic materials. This constraint guarantees that inorganic materials are incapable of incorporating additional ions. These chemicals are inclined to attract template ions and tend to create the most favorable crystal structures.

Consequently, the template ion exhibits both a memory effect and a reliable filtering function, allowing it to adsorb the target ion even in the presence of numerous ions. The phenomenon is referred to as the ion sieve effect. An ion sieve technology selectively permits the passage of just lithium ions because it possesses the smallest ionic radius among all metal ions.

The adsorbent is a crucial component of the adsorption process. Therefore, the selection of the adsorbent is also vital in this study. The categorization of adsorbents for the lithium recovery process, as described by Safari et al. (2020), can be classified into (Safari, Lottermoser, and Alessi, 2020):

- Ion-imprinted polymer sorbent is made from functional polymerized hydrophilic monomers whose target is to capture the expected or taken ion.
- Metal oxide sorbent is made of metal and divided into manganese, titanium, and aluminum.

Unlike ion-imprinted polymer sorbents, metal oxide sorbents provide several advantages. They are easy to synthesize, highly selective for lithium, and may be easily extracted from the adsorbent (Safari, Lottermoser, and Alessi, 2020). Nevertheless, the metal oxide sorbent is not yet considered the optimal adsorbent material for lithium recovery from brine due to existing challenges in enhancing chemical degradation and sorbent lifecycle. These improvements are necessary for achieving better performance and enabling widespread commercial production. This study will utilize a titanium-based adsorbent due to its specific lithium affinity. Theoretically, the titanium basis has a maximum adsorption capacity of 127 milligrams per gram, but the manganese base can only retain up to 68 milligrams per gram (Lawagon et al., 2016).

The choice of ion sieve adsorption was based on its favorable characteristics, including low toxicity, low cost, excellent chemical stability, and high lithium adsorption capacity. This adsorbent is usually the most promising choice (Weng et al., 2020). The ion sieve adsorption procedure necessitates the use of an adsorbent material. This material has undergone thorough investigation on a global scale to identify the most effective adsorbent for lithium recovery. A highly favored adsorbent is metal oxide due to its exceptional affinity for lithium and its efficient absorption during manufacturing. Ion sieve adsorption can be categorized into lithium manganese oxide (LMO) and lithium titanium oxide (LTO). This investigation will utilize LTO. Current research on ion sieve adsorption continues to prioritize the usage of manganese-based ion sieves. This approach has limitations: the structure is susceptible to breakage and has substantial solute loss. Titanium-based ion sieve adsorption effectively addresses the drawbacks of manganese-based ion sieve adsorption, including reduced loss and a stable structure (Shi et al., 2013).

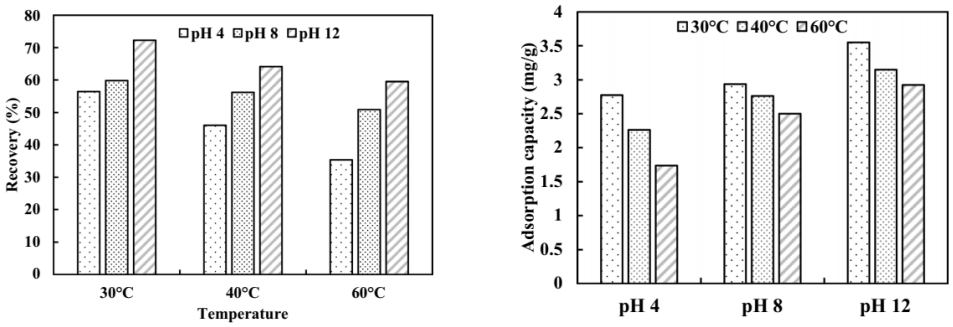

Figure 11: Graphical insights from optimized lithium recovery study results using ion-sieved adsorption technology (Tangkas et al., 2023).

The study aimed to examine the impact of temperature and pH fluctuations on the adsorption capacity of a lithium adsorbent (Figure 11). Under optimum temperature and pH settings, the analysis revealed a lithium adsorption capacity of 3.55 mg/g and a recovery efficiency above 70%. This work holds great importance because of the substantial significance of lithium in lithium-ion battery applications and other energy-related businesses.

Enhancing the effectiveness of the lithium adsorption and recovery process can be achieved by improving adsorption conditions, such as temperature and pH.

Regarding future advancements, there are possibilities to investigate improving the stability and augmenting the adsorption capacity of the adsorbent. To enhance stability, one can change the structure of the adsorbent or include functional groups to improve endurance under different pH and temperature circumstances. One can pursue material changes or surface engineering approaches to increase the surface area or introduce specialized binding sites for lithium ions to enhance the adsorption capacity. These developments aim to improve lithium recovery techniques' effectiveness and long-term viability, supporting the broader objectives of expanding sustainable energy systems that depend on lithium resources. Subsequent investigations could prioritize expanding these enhanced adsorption methods for use in industrial settings, thus tackling the increasing need for lithium while mitigating ecological consequences.

4. ECONOMIC POTENTIAL OF MINERAL EXTRACTION FROM GEOTHERMAL RESOURCES

The economic viability of mining minerals from geothermal resources has emerged as a prominent subject in the worldwide discussion on energy and resources. Due to the rising market value of essential minerals like silica and lithium, the renewable energy sector emphasizes the economic opportunities associated with developing and utilizing these resources. PT. Geo Dipa Energi, a prominent participant in this sector, demonstrates the potential for substantial financial gains by using cutting-edge technologies to extract and purify minerals from geothermal brines. In addition to the financial advantages, these initiatives can improve energy self-sufficiency and decrease carbon emissions, fostering new economic prospects and facilitating the shift towards a more sustainable economy based on natural resources.

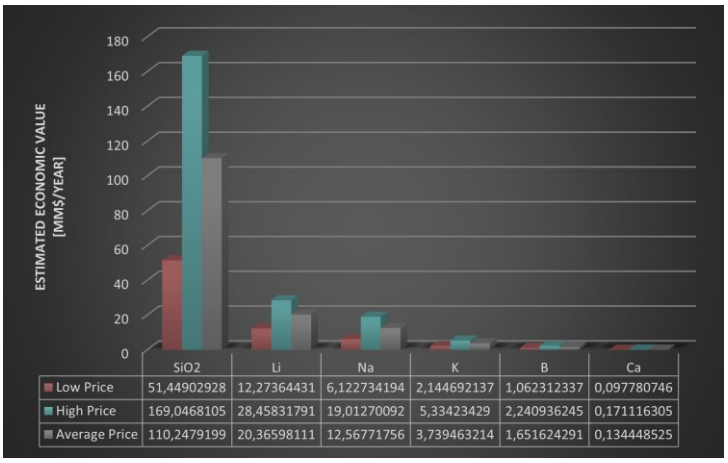

	SiO2	Li	Na	K	B	Ca
Low Price	51,44902928	12,27364431	6,122734194	2,144692137	1,062312337	0,097780746
High Price	169,0468105	28,45831791	19,01270092	5,33423429	2,240936245	0,171116305
Average Price	110,2479199	20,36598111	12,56771756	3,739463214	1,651624291	0,134448525

Figure 12: Potential annual profits from each valuable element by PT. Geo Dipa Energi.

Figure 12 presents a comprehensive summary of PT. Geo Dipa Energi's anticipated yearly earnings from extracting precious components from geothermal resources. Silica is the top performer in profitability, with an expected annual profit of almost $169 million. The prominence of silica recovery in their processing method emphasizes its strategic importance due to its strong market demand and economic worth in diverse industries such as glass manufacture, electronics, and construction materials. Advanced techniques such as forward osmosis, electrodialysis, and ion sieve adsorption are used to extract and purify silica. These technologies ensure efficient use of resources and minimize environmental impact.

Lithium is expected to generate approximately $28 million in annual sales, making it a significant source of income after silica. The growing need for lithium in batteries for electric vehicles and renewable energy storage systems enhances its economic importance. Advanced extraction methods are utilized to concentrate and purify lithium from geothermal brines, improving its quality and making it more suitable for the market. In addition, Figure 12 illustrates the possible financial gains from additional precious minerals, including sodium (Na), potassium (K), boron (B), and calcium (Ca), all of which play a substantial role in determining the economic viability of the project. These minerals are used in several industries, including agriculture (as fertilizers), pharmaceuticals, and industrial operations. Thorough extraction and processing methods are employed to optimize the retrieval of these precious materials and guarantee the implementation of sustainable resource management techniques.

The anticipated financial gains depicted in Figure 12 highlight the dedication to utilizing geothermal resources for economic benefit while upholding principles of environmental sustainability. The objective is to become a prominent player in sustainable mineral extraction from geothermal brines by concentrating on valuable minerals

such as silica and lithium. This result will be achieved through advanced technologies and efficient processing methods. Doing so aims to positively contribute to economic growth and environmental stewardship in the energy sector.

5. CONCLUSION

This study investigates an innovative method for harnessing geothermal energy by collecting minerals from geothermal brine to promote a circular economy. The technologies described for extracting lithium and silica from geothermal brine show great promise in converting waste into valuable minerals. The study focuses on novel extraction techniques and assesses the environmental consequences of these methods. This work significantly adds to the advancement of geothermal operations' sustainability by transitioning from a single-purpose energy production model to a multifunctional resource recovery approach. This approach is anticipated to decrease dependence on traditional mining methods and improve the effectiveness of utilizing natural resources.

Furthermore, adopting the concepts of the circular economy has the potential to broaden the economic advantages of geothermal energy beyond just energy generation. This research highlights the positive economic prospects of incorporating geothermal energy into a circular economy framework. The goal is to not only safeguard the environment but also to promote local economic growth and ensure sustainable resource management for the long term.

ACKNOWLEDGEMENTS

The authors thank Universitas Gadjah Mada (UGM) for providing the necessary facilities. The study of extracting rich minerals from geothermal brines has been dramatically advanced by UGM's essential contributions. In addition, the authors express gratitude to the Indonesian Ministry of Research and Technology/National Research and Innovation Agency (BRIN) for providing their facilities. The facility support offered by BRIN has been crucial in promoting the progress of this project. The authors would like to express their appreciation to PT. Geo Dipa Energi for their valuable support in supplying geothermal brine waste and silica.

CONFLICT OF INTEREST

The authors declare that they have no conflict of interest.

REFERENCES

Cath, T.Y., Childress, A.E., and Elimelech, M.: Forward Osmosis: Principles, Applications, and Recent Developments , *Journal of Membrane Science* , 281, (2006), 70–87.

Ciriminna, R., Fidalgo, A., Pandarus, V., Béland, F., Ilharco, L.M., and Pagliaro, M.: The Sol-Gel Route to Advanced Silica-Based Materials and Recent Applications , *Chemical Reviews* , 113, (2013), 6592–6620.

Criado, M., Fernández-Jiménez, A., de la Torre, A.G., Aranda, M.A.G., and Palomo, A.: An XRD Study of the Effect of the SiO2/Na2O Ratio on the Alkali Activation of Fly Ash , *Cement and Concrete Research* , 37, (2007), 671–79.

Diaz, E.I., Allouche, E.N., and Eklund, S.: Factors Affecting the Suitability of Fly Ash as Source Material for Geopolymers , *Fuel* , 89, (2010), 992–96.

Ekaputri, J.J. and Triwulan: The Efforts to Use Porong Mud as an Additive Material for Geopolymer Concrete , Seminar Nasional Tentang Usaha Pemanfaatan Lumpur Porong sebagai Bahan Bangunan, KLH, ITS, Surabaya (2013).

Flexer, V., Baspineiro, C.F., and Galli, C.I.: Lithium Recovery from Brines: A Vital Raw Material for Green Energies with a Potential Environmental Impact in Its Mining and Processing, *Science of The Total Environment*, 639, (2018), 1188–1204.

Garrett, D.E.: *Handbook of Lithium and Natural Calcium Chloride Their Deposits, Processing, Uses, and Properties*.

Goldberg, V., Dashti, A., Egert, R., Benny, B., Kohl, T., and Nitschke, F.: *Challenges and Opportunities for Lithium Extraction from Geothermal Systems in Germany—Part 3: The Return of the Extraction Brine, Energies*, 16, (2023), 5899.

Hardjito, D.: *Studies on Fly Ash-Based Geopolymer Concrete* Perth: Curtin's Institutional Research Repository.

Hessien, M.M., Rashad, M.M., Zaky, R.R., Abdel-Aal, E.A., and El-Barawy, K.A.: Controlling the Synthesis Conditions for Silica Nanosphere from Semi-Burned Rice Straw, *Materials Science and Engineering*: B, 162, (2009), 14–21.

Van Der Hoek, J.P., Rijnbende, D.O., Lokin, C.J.A., Bonné, P.A.C., Loonen, M.T., and Hofman, J.A.M.H.: Electrodialysis as an Alternative for Reverse Osmosis in an Integrated Membrane System, *Desalination*, 117, (1998), 159–72.

Jati, A.D., Sujoto, V.S.H., Sutijan, Petrus, H.T.B.M., and Mulyono, P.: Lithium Extraction from Geothermal Brine Using Electrodialysis Method in *IOP Conference Series: Earth and Environmental Science*, 12018.

Kabay, N., Sözal, P.Y., Yavuz, E., Yüksel, M., and Yüksel, Ü.: Geothermal Water Management eds. Jochen Bundschuh and Barbara Tomaszewska (2018).

Kölbel, L., Kölbel, T., Herrmann, L., Kaymakci, E., Ghergut, I., Poirel, A., and Schneider, J.: Lithium Extraction from Geothermal Brines in the Upper Rhine Graben: A Case Study of Potential and Current State of the Art, *Hydrometallurgy*, 221, (2023), 106131.

Kusumastuti, Y., Kobayashi, M., Purwaningtyas, F.Y., Najmina, M., Murti Petrus, H.T.B., Putri, N.R.E., Budhijanto, and Tanihara, M.: Characterization of Three-Dimensional Scaffolds from Local Chitosan/Alginate/Geothermal Silica for Potential Tissue Engineering Applications, *Journal of Engineering Science and Technology*, 13, (2018), 3500–3515.

Lawagon, C.P., Nisola, G.M., Mun, J., Tron, A., Torrejos, R.E.C., Seo, J.G., Kim, H., and Chung, W.J.: Adsorptive Li+ Mining from Liquid Resources by H2TiO3: Equilibrium, Kinetics, Thermodynamics, and Mechanisms, Journal of Industrial and Engineering Chemistry, 35, (2016), 347–56.

Long, Q., Jia, Y., Li, J., Yang, J., Liu, F., Zheng, J., and Yu, B.: Recent Advance on Draw Solutes Development in Forward Osmosis, *Processes*, 6, (2018), 165.

Mulder, M.: *Basic Principles of Membrane Technology* (1996).

Mustika, P.C.B.W., Astuti, W., Sumardi, S., Petrus, H.T.B.M., and Sutijan: Separation Characteristic and Selectivity of Lithium from Geothermal Brine Using Forward Osmosis, *Journal of Sustainable Metallurgy*, 8, (2022), 1769–84.

Nie, X.Y., Sun, S.Y., Sun, Z., Song, X., and Yu, J.G.: Ion-Fractionation of Lithium Ions from Magnesium Ions by Electrodialysis Using Monovalent Selective Ion-Exchange Membranes, *Desalination*, 403, (2017), 128–35.

Nuryono, N. and Narsito, N.: EFFECT OF ACID CONCENTRATION ON CHARACTERS OF SILICA GEL SYNTHESIZED FROM SODIUM SILICATE, *Indonesian Journal of Chemistry*, 5, (2010), 23–30.

Palomo, A., Grutzeck, M.W., and Blanco, M.T.: Alkali-Activated Fly Ashes, *Cement and Concrete Research*, 29, (1999), 1323–29.

Phoo-ngernkham, T., Chindaprasirt, P., Sata, V., Hanjitsuwan, S., and Hatanaka, S.: The Effect of Adding Nano-SiO2 and Nano-Al2O3 on Properties of High Calcium Fly Ash Geopolymer Cured at Ambient Temperature, *Materials & Design*, 55, (2014), 58–65.

Post, J.W., Veerman, J., Hamelers, H.V.M., Euverink, G.J.W., Metz, S.J., Nymeijer, K., and Buisman, C.J.N.: Salinity-Gradient Power: Evaluation of Pressure-Retarded Osmosis and Reverse Electrodialysis, *Journal of Membrane Science* , 288, (2007), 218–30.

Purnomo, B.J. and Pichler, T.: Geothermal Systems on the Island of Java, Indonesia , *Journal of Volcanology and Geothermal Research* , 285, (2014), 47–59.

Qurrahman, A.H., Wilopo, W., Susanto, S.P., and Petrus, H.T.B.M.: Energy and Exergy Analysis of Dieng Geothermal Power Plant , *International Journal of Technology* , 12, (2021), 175.

Safari, S., Lottermoser, B.G., and Alessi, D.S.: Metal Oxide Sorbents for the Sustainable Recovery of Lithium from Unconventional Resources , *Applied Materials Today* , 19, (2020), 100638.

Sdiri, A., Higashi, T., Bouaziz, S., and Benzina, M.: Synthesis and Characterization of Silica Gel from Siliceous Sands of Southern Tunisia , *Arabian Journal of Chemistry* , 7, (2014), 486–93.

Setiawan, F.A., Rahayuningsih, E., Petrus, H.T.B.M., Nurpratama, M.I., and Perdana, I.: Kinetics of Silica Precipitation in Geothermal Brine with Seeds Addition: Minimizing Silica Scaling in a Cold Re-Injection System , *Geothermal Energy* , 7, (2019), 22.

Setijadji, L.D.: Segmented Volcanic Arc and Its Association with Geothermal Fields in Java Island, Indonesia , *Proceedings World Geothermal Congress* (2010), 25–29.

Shi, X.C., Zhang, Z.B., Zhou, D.F., Zhang, L.F., Chen, B.Z., and Yu, L.L.: Synthesis of Li+ Adsorbent (H2TiO3) and Its Adsorption Properties , *Transactions of Nonferrous Metals Society of China* (English Edition) , 23, (2013), 253–59.

Siekierka, A., Tomaszewska, B., and Bryjak, M.: Lithium Capturing from Geothermal Water by Hybrid Capacitive Deionization , *Desalination* , 436, (2018), 8–14.

Sujoto, V.S.H., Sutijan, Astuti, W., Sumardi, S., Louis, I.S.Y., and Petrus, H.T.B.M.: Effect of Operating Conditions on Lithium Recovery from Synthetic Geothermal Brine Using Electrodialysis Method , Journal of Sustainable Metallurgy , 8, (2022), 274–87.

Sutijan, S., Wahyudi, S., Ismail, M.F., Mustika, P.C.B., Astuti, W., Prasetya, A., and Petrus, H.T.B.M.: Forward Osmosis to Concentrate Lithium from Brine: The Effect of Operating Conditions (PH and Temperature) , *International Journal of Technology* , 13, (2022), 136.

Tangkas, I.W.C.W.H., Sujoto, V.S.H., Astuti, W., Jenie, S.N.A., Anggara, F., Utama, A.P., Petrus, H.T.B.M., and Sutijan: Synthesis of Titanium Ion Sieves and Its Application for Lithium Recovery from Artificial Indonesian Geothermal Brine *, Journal of Sustainable Metallurgy* , 9, (2023), 613–24.

Walha, K., Amar, R. Ben, Firdaous, L., Quéméneur, F., and Jaouen, P.: Brackish Groundwater Treatment by Nanofiltration, Reverse Osmosis and Electrodialysis in Tunisia: Performance and Cost Comparison , *Desalination* , 207, (2007), 95–106.

Weng, D., Duan, H., Hou, Y., Huo, J., Chen, L., Zhang, F., and Wang, J.: Introduction of Manganese Based Lithium-Ion Sieve-A Review , *Progress in Natural Science: Materials International* , 30, (2020), 139–52.

Zhang, Y., Wang, L., Sun, W., Hu, Y., and Tang, H.: Membrane Technologies for Li+/Mg2+ Separation from Salt-Lake Brines and Seawater: A Comprehensive Review , *Journal of Industrial and Engineering Chemistry* , 81, (2020), 7–23.

Zhao, S., Zou, L., Tang, C.Y., and Mulcahy, D.: Recent Developments in Forward Osmosis: Opportunities and Challenges *, Journal of Membrane Science* , 396, (2012), 1–21.

Utilizing Geothermal Fluid By-products from Lahendong Geothermal Area for Liquid Nanosilica Geothermal Booster to Support Sustainable Farming in Tompaso, Minahasa Regency, North Sulawesi

Muhammad Gilang Madiantara[1], Muhamad Didih[1], Abdi Rayhan Garniwan[1], Navilia Hanin Pradipta[1], Pri Utami[2,5], Ronny Martien[3,5], and Ngadisih[4,5]

[1]PT Pertamina Geothermal Energy Tbk Area Lahendong
[2]Dept. of Geological Engineering, Faculty of Engineering, UGM
[3]Dept. of Pharmaceutics, Faculty of Pharmacy, UGM
[4]Dept. of Agricultural and Biosystem Engineering, Faculty of Agricultural Technology, UGM
[5]Geothermal Research Centre, Faculty of Engineering, UGM

muhammad.gilang@pertamina.com, p.utami@ugm.ac.id

Keywords: Lahendong Geothermal Area, Nanosilica, Geothermal By-products, Sustainable agriculture

ABSTRACT

The Minahasa volcanic field is blessed with significant geothermal potential, demonstrated by the operational success of the 120 MWe Lahendong Geothermal Power Plants. Within the Minahasa Regency, Tompaso stands out as a sub-district characterized by an agrarian lifestyle deeply rooted in cultural heritage. Situated at an elevation of 800 meters above sea level, the fertile soils of Tompaso provide an ideal environment for agriculture.

The sustainability of geothermal operations hinges on a delicate balance of social harmony, environmental stewardship, and effective governance. PT Pertamina Geothermal Energy Tbk Area Lahendong endeavors to foster this balance by repurposing deposits from geothermal brine, previously regarded as waste. Collaborative research conducted by Universitas Gadjah Mada and PT Pertamina Geothermal Energy Tbk Area Lahendong reveals that the interaction between fluids and rocks within the Lahendong geothermal system yields deposit rich in approximately 60 elements and compounds, mirroring those found in volcanic ash. Through nanotechnology processing, these deposits are transformed into liquid booster, offering a promising alternative to chemical fertilizers and pesticides, as well as organic manure, which can pose long-term environmental challenges. The diverse array of compounds and elements presents in the geothermal deposit, including those from the oxide group, alkali metals, alkaline earth metals, basic metals, semi-metals, non-metals, lanthanides, actinides, and transition metals, are all vital for plant growth and development, with silica playing a particularly crucial role in reinforcing plant structures. Drawing inspiration from the traditional Minahasan couple dance known as "Katrili," the booster, applied through alternating pouring and spraying methods, is aptly named "Katrili." Developed as a fusion of Minahasan and European arts, the Katrili dance originally served as a celebration of gratitude for agricultural abundance and successful trade.

In Indonesia's agricultural sector, fertilizer scarcity poses a significant challenge. Thus, the innovation of repurposing geothermal by-products into a liquid booster does not only address the welfare of farmers but also enhance the environmental sustainability of geothermal energy production.

1. INTRODUCTION

1.1 Minahasa Volcanic Field

Minahasa district is situated in a volcanic field (Figure 1) in the northern arm of Sulawesi, which is part of the Sangihe volcanic arc (Hamilton, 1979). This NE-SW trending volcanic arc includes Mts. Ambang, Soputan, Lokon, Mahawu, Tangkoko, Ruang, Karangetang, and Mt. Awu, extending to the volcanic islands in the north (Hamilton, 1979).

The prominent volcanic structure in the area is the structurally controlled, 20 X 10 km2 Tondano Caldera (Lecuyer et al., 1997), within which the Lahendong Geothermal Working Area (GWA/WKP) is situated. Recent volcanic activity in Minahasa includes the eruptions of Mts. Soputan, Lokon, and Mahawu, providing fertile volcanic soils.

The Lahendong Geothermal Working Area (GWA/WKP), determined based on the Decree of the Minister of Mineral Resources Number 2067 K/30/MEM/2012 is partly located in the Minahasa Regency. The Tompaso sector of the Lahendong GWA is water-dominated, with the reservoir temperatures ranging from 260°C to 300°C. The heat source is believed to be igneous rock bodies beneath the Sempu volcano and other smaller volcanic cones. The development of the geothermal energy sector in Lahendong runs side-by-side in harmony with agricultural activities in the Minahasa Volcanic Field.

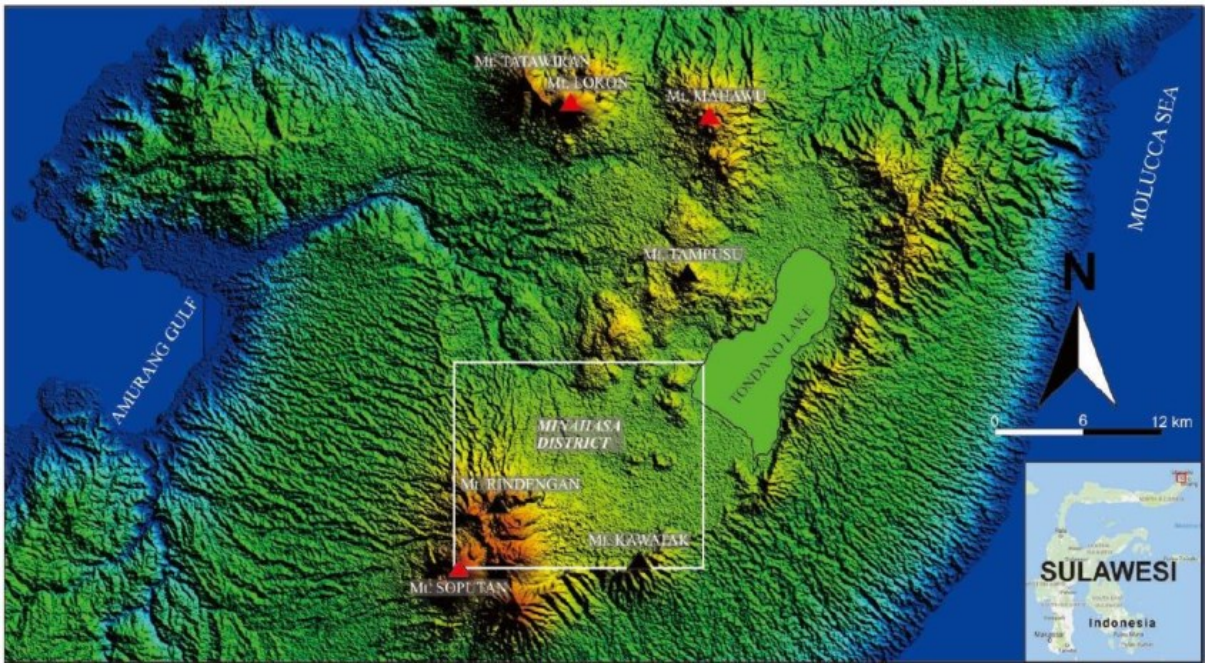

Figure 1: Location of the Lahendong Geothermal Area (outlined by the white curve) in the Digital Elevation Model base map (Badan Informasi Geospasial, 2024) showing its spatial association with the Tondano Lake and the volcanoes.

Figure 2: Brine canals with silica deposits in the Tompaso sector of the Lahendong GWA.

1.2 Geothermal Deposit

The natural fluid-rock interaction processes in the subsurface enrich the geothermal fluids in parts of the Lahendong geothermal field with silica and other compounds and elements (Utami et al., 2015; Utami et al., 2021). Consequently, some geothermal wells operated by PT Pertamina Geothermal Energy Tbk Area Lahendong produce fluids containing these dissolved components, which gradually deposit upon cooling. In a closed-loop system, before the geothermal fluid is reinjected into the reinjection well, it passes through the brine canals (Figure 2), leading to a buildup white sludge over time. This white sludge, generally referred to as silica deposit, was previously considered to have no added value and potentially harmful to geothermal production equipment if not removed regularly. However, our research shows that the deposits from Lahendong geothermal fluids contain numerous elements and compounds similar to volcanic ash. These elements and compounds are essential for supporting plant growth.

1.3 Minahasa Agricultural Activity

Most of the population in Minahasa district earns a living as farmers. The agricultural products in Minahasa Regency include lowland rice, corn, shallots, chilies, cayenne peppers, tomatoes, coconuts, and cloves. They are economically attractive and hence serve as the main source of income for the region.

Like other regions, North Sulawesi is experiencing a fertilizer shortage, leading to hardship for farmers due to the high price of the fertilizer in the market. This condition is predicted to persist for a long time due to the Russian-Ukrainian war, which has been causing shortage of chemical supplies for chemical fertilizer and pesticide industries.

The above situation provides a way for the geothermal industry to contribute to helping the agricultural sector. We process Lahendong geothermal fluid by-products into liquid fertilizers and plant enhancers/boosters by applying nanotechnology. This approach transforms silica deposits into a product with strategic and economic value that help meet farmers' needs and introduces a new perspective: "geothermal by-products are a blessing for farmers".

1.4 Naming the Product

To introduce the liquid booster developed from geothermal by-products from Lahendong GWA by PT Pertamina Geothermal Energy Tbk Area Lahendong in collaboration with Universitas Gadjah Mada, we and the local farming community name it "Katrili". This name reflects the method of applying the fertilizer and booster simultaneously, involving both watering and spraying, which can be compared to a pair of Katrili dancers moving in unison to the rhythm (Figure 3). The Katrili dance, an acculturation of European and Minahasa cultures, is deeply embedded in the social life of the community. It was introduced by the Portuguese traders, who came to North Sulawesi to buy agricultural products from the locals. Even in modern times, the Katrili dance is performed at various events, including “Pengucapan Syukur” (Thanksgiving) celebrations for abundant harvests (Wenas, 2007).

Figure 3: An illustration of the Katrili dance.

2. KATRILI FERTILIZER/BOOSTER

2.1 Geochemical Analysis of Geothermal Deposits

Deposits taken from the cooling ponds of Geothermal Power Plant units 1-4 (Lahendong sector) and units 5&6 (Tompaso sector), were analyzed. XRD analyses indicate that the deposits are dominated by amorphous silica and some salts. Geochemical analyses show that they contain about 60 elements and compounds including oxides, alkali metals, alkaline earth metals, and rare earth metals, essential for plant growth and development. Synthetic fertilizers available in the market do not have such a complete set of important constituents. The concentrations of the oxides in the geothermal deposit from Lahendong are comparable to the composition of volcanic ashes from Soputan (Budi et al., 2019) and Ibu (Saing et al., 2014) as presented in Figure 4.

2.2 Formulation and Composition of the Liquid Booster

"Katrili" fertilizer/booster is formulated and processed by applying nanotechnology such that the particle is so small and will not clog the nozzle of the sprayer. Particle size characterization is conducted using a Particle Size Analyzer (PSA) as a measure of quality control. The "Katrili" resulted liquid booster was diluted and analyzed. The ready to use liquid contains silica and bicarbonate as the dominant constituents, and other essential and trace elements. No harmful elements present within the threshold permitted for application to plants.

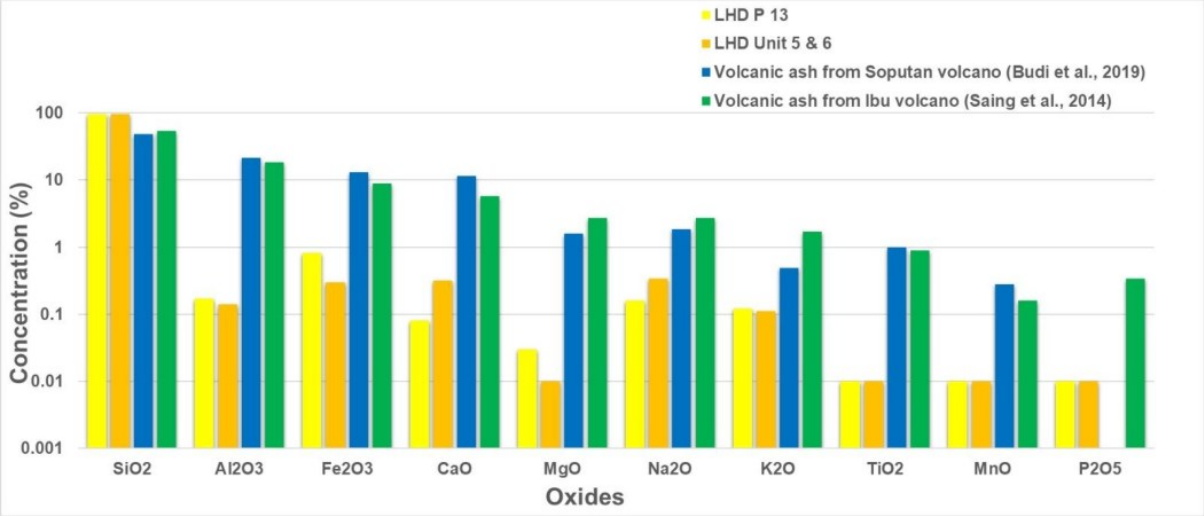

Figure 4: Bar chart showing the oxide compositions of the samples of the Lahendong geothermal deposits and volcanic ashes from Soputan and Ibu volcanoes.

2.3 Application

Each hectare of horticultural plants requires 10 liters of liquid fertilizer and booster for each application. As a fertilizer, the "Katrili" is poured into the soil once a month during the planting period, using a dose of 1 liter of fertilizer diluted with water to reach a total volume of 100 liters. As a plant strengthener, the "Katrili" is sprayed on plants every other week during the growing period, using a dose of 1 liter diluted with water to reach a total volume of 20 liters.

3. DEMONSTRATION PLOTS

Three demonstration plot (demplot) or designated area of land used as a model for agricultural practices, are prepared to showcase various planting and treatment designs. The planning and establishment of demonstration plots are crucial to exemplify environmentally friendly planting systems to the community. The locations and the design of each demonstration plot, as well as the preferred plant and planting patterns were established during focus group discussions (FGD) conducted beforehand with the partner farmers. The demonstration plots utilize the participating farmers' land located within the geothermal operation area in the Tompaso sector (Figure 5). Every plot is divided into 2 m X 2 m compartments, each is designated for specific treatment.

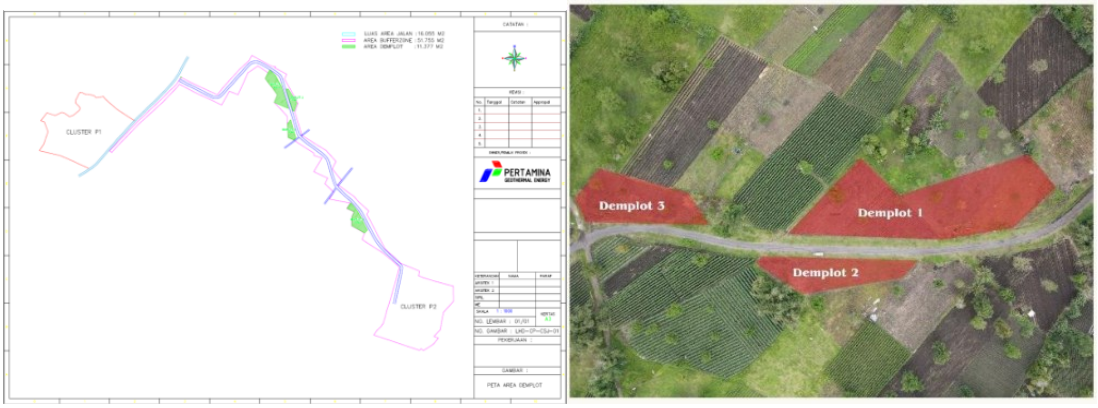

Figure 5: (Left) Map showing the location of the demonstration plots with respect to the clusters of geothermal wells P1 and P2. (Right) Aerial photograph of the demonstration plots.

The plant chosen for testing the effectiveness of Katrili fertilizer and booster is tomato, as the Tompaso Farming Community has been planting it during the time of our experiment. We distributed the “Katrili” liquid booster to two groups of participating farmers (example in Figure 6) who belong to the local church organizations, namely the Gereja Masehi Injili Minahasa (GMIM) and the Kerapatan Gereja Protestan Minahasa (KGPM).

Figure 6: Distribution of the "Katrili" liquid booster to the partner farmers in Tompaso.

The treatment using the "Katrili" booster is outlined in Table 1. Each treatment has been applied to a 2 m X 2 m plot and repeated 3 times, resulting in 18 experimental plots. Soil and plant samples will be collected from both the demonstration plots on farmers' existing land and the 2 m X 2 m plots before being treated, and during harvest, to analyze macro-nutrient (NPK) content, microorganisms, and heavy metal levels.

Table 1: Summary of the treatments applied to the demonstration plots in Tompaso.

No	Description	Symbol
1	Without Fertilizers and Pesticides	K
2	Existing Fertilizer + Pesticide	P1
3	Fertilizer + Existing Pesticides + Katrili	P2
4	Organic Fertilizer	P3
5	Organic Fertilizer + Katrili	P4
6	Chemical Fertilizer + Organic Fertilizer + Katrili	P5

4. FUTURE PLANS

The Tompaso farming community has shown interest in adopting the "Katrili" booster in their agricultural practices. The success of "Katrili" will meet their need for a locally available and environmentally friendly fertilizer and plant booster. Moving forward, we plan to work on large-scale production to commercialize geothermal by-products, utilizing both business-to-customer (B2C) and business-to-business (B2B) models to diversify the direct use of these by-products. We will explore opportunities for collaborative research and development between PT Pertamina Geothermal Energy Tbk Area Lahendong and Universitas Gadjah Mada to advance the production line.

ACKNOWLEDGEMENTS

The authors thank the management of PT Pertamina Geothermal Energy Tbk Area Lahendong and Universitas Gadjah Mada for their support of our research. We also express our gratitude to our partner farmers for their enthusiastic participation. Special thanks to Mr. Fatih Fauzi for his assistance in conditioning the samples prior to laboratory analyses and for drafting Figure 4. Additionally, we thank Mr. Tegar Narendra for creating the illustration of the Katrili dance used in the product labels and shown in Figure 3.

REFERENCES

Badan Informasi Geospasial. https://tanahair.indonesia.go.id/portal-web. Accessed in July 2024.

Budi, S., Fajri, R., Santoso, N.A., and Bijaksana, S., 2014. Multimethod Characterization of Volcanic Ashes from The Sunda Island Arc. *IOP Conf. Series: Earth and Environmental Science* 318 (2019) 012011. 6 p. doi:10.1088/1755-1315/318/1/012011.

Hamilton, W.B., 1979, *Tectonics of the Indonesian Region* (Geological Survey Professional Paper 1078): Washington, United States Government Printing Office, 345 p.

Lécuyer, F., Bellier, O., Gourgaud, A., and Vincent, P.M., 1997, Tectonique Active du Nord-Est de Sulawesi (Indonésie) et Contrôle Structural de la Caldeira de Tondano (Active Tectonics of North-East Sulawesi (Indonesia) and Structural Control of the Tondano Caldera: *Earth and Planetary Sciences*, v. 325, p. 607-613.

Saing, U.B., Bani, P., and Kristianto, 2014. Ibu volcano, a center of spectacular dacite dome growth and long-term continuous eruptive discharges. *Journal of Volcanology and Geothermal Research* 282 (2014), p. 36–42.

Utami, P., Widarto, D.S., Atmojo, J.P., Kamah, Y., Browne, P.R.L., Warmada, I.W., Bignall, G., and Chambefort, I., 2015. Hydrothermal Alteration and the Evolution of the Lahendong Geothermal System, North Sulawesi, *Proc. World Geothermal Congress 2015 Melbourne*, 19-25 April 2015, 10 p.

Utami, P, Sidqi, M, Siahaan, Y, Shalihin, M.G.J, Siahaan, E.E, and Silaban, M. 2021. Geothermal Prospects in Lahendong Geothermal Field of the Tomohon – Minahasa Volcanic Terrain (TMVT), North Sulawesi, Indonesia, *Proc. World Geothermal Congress 2020+1 Reykjavik*, Iceland, April - October 2021, 9 p.

Wenas, J. 2007. *Sejarah dan Kebudayaan Minahasa*. Institut Seni Budaya Sulawesi Utara, 187 p.

The Utilization Scheme of Geothermal Brine for Balneotherapy Facilities in Dieng, Central Java

Danu Ari Wibowo, Muhammad Syakhis Qomaruddin, Azaria Dian Khoirunnisa, Dwi Ayu Kurniasih, Aafiansyah Su'daa, and Arief Putra Pratama

Gadjah Mada University

danuariwibowo@mail.ugm.ac.id

Keywords: Dieng, Geothermal, Balneology, Health, Tourism

ABSTRACT

Central Java has the only high-enthalpy Geothermal Power Plant complex located in Dieng. The geothermal reservoir stretches across Sileri in the northwest, Sikidang, and Pakuwaja in the southeast. The Dieng area possesses tremendous geothermal energy potential, However, only 10.3% or around 60 MW of its potential is utilized. From the test results, hydrothermal in the Dieng area has mineral content that includes several elements, such as lithium 77.31-99.4 mg/l, silica 1,109.25 to 1,220.9 mg/l, boron 404.16-589.4 mg/l, potassium 2,532.2-4536.5 mg/l, and manganese 5.49-15.82 mg/l. At the moment, there is still a resource that has not been utilized, namely waste heat. Waste heat appears in the form of liquid-phase hydrothermal (brine) with a pH range of 6-7 and a temperature value of 180°C. The energy from the brine has the potential to be a source of water heating in hot spring facilities (balneology) with the help of heat exchanger technology. The process of flowing brine from geothermal production wells to heat exchanger machines around balneology facilities is carried out using pipes. The high mineral content in the brine causes scaling. Scaling on the pipe occurs due to the formation of deposits that can hinder the distribution of water and reduce the thermal conductivity and heat transfer coefficient. Therefore, PAC (Poly Aluminum Chloride) coagulant was used with a PAC concentration of 10 ppm, a pH value of 8, and the addition of Polyamide flocculant of 1 ppm. Then, the neutralized brine is used in the heat exchange system for balneology. The enthalpy of the geothermal working fluid is transferred to the heat pump working fluid (refrigerant) through the heat exchanger coil, causing the refrigerant to vaporize. Afterward, the refrigerant vapor is compressed to increase pressure and temperature. This high-temperature refrigerant is passed through the condenser pipe to warm the water in the balneology. As a result, the hot water from the heat exchange process has a temperature of less than 40°C and can be for hot baths. Hot baths can have physiological effects on the human body by inducing significant improvements in macro and microvascular functions. Hot baths can also trigger the release of endorphins, hormones that induce relaxation and sedation effects to resist drowsiness. Previous research also states that sleep quality becomes 100% better after a hot shower. The habit of taking a hot bath has a good impact on health, giving adequate sleep quality, lowering stress levels, and increasing happiness. The scheme of utilizing brine for balneological facilities can also enrich the tourism aspect of Dieng, open doors to economic activity, and improve social standards for the surrounding community.

1. INTRODUCTION

Tourism is one of the sectors that affect the development and increase of a country's income. Tourism is one of the world's most significant and fastest-growing economic sectors (Yakup, 2019). Dieng Plateau is a highland tourism area in Central Java located in Banjarnegara Regency and Wonosobo Regency, which is one of the leading tourist areas that has attractions offered in the form of natural and artificial tourism (Priyanto, 2016). The development of the tourism industry in this area is increasing, it can be seen from the increase in tourist attractions, in addition to natural tourism there is also artificial tourism or culinary tourism. Tourism is one of the sectors that affect the development and increase of a country's income. Tourism is one of the world's most significant and fastest-growing economic sectors (Yakup, 2019). Dieng Plateau is a highland tourism area in Central Java located in Banjarnegara Regency and Wonosobo Regency, which is one of the leading tourist areas that has attractions offered in the form of natural and artificial tourism (Priyanto, 2016). The development of the tourism industry in this area is increasing, it can be seen from the increase in tourist attractions, in addition to natural tourism there is also artificial tourism or culinary tourism. Tourism is one of the sectors that affect the development and increase of a country's income. Tourism is one of the world's most significant and fastest-growing economic sectors (Yakup, 2019). Dieng Plateau is a highland tourism area in Central Java located in Banjarnegara Regency and Wonosobo Regency, which is one of the leading tourist areas that has attractions offered in the form of natural and artificial tourism (Priyanto, 2016). The development of the tourism industry in this area is increasing, it can be seen from the increase in tourist attractions, in addition to natural tourism there is also artificial tourism or culinary tourism.

Figure 1: Dieng Tourism Region.

Hot springs or balneology is one type of tourism offered by Dieng. Currently, several places serve hot spring tourism in Dieng, including D'Qiano Hot Spring Waterpark, Toyabira, Sendang Sipandu, and Segar Asri (Aristyan, 2023). These hot springs come from the direct utilization of hot springs located around the tour, due to geothermal activity that occurs in the area. Dieng is an active volcanic area, whose heat from within the earth heats groundwater which then comes to the surface as hot springs. Direct utilization has the challenge that filtration needs to be done first so that the hot water used is safe and free from harmful substances (Herlambang, 2022). The location of hot springs is also influenced by geological factors, which are not available everywhere.

In addition, the Dieng area has great geothermal energy potential, although until now it has only been utilized by 10.3% of its total reserves or around 60 MW of the total geothermal energy potential of 580 MW in the region (Nurrochim, 2021). Currently, the Dieng geothermal field is managed by PT Geo Dipa Energi (Persero) which was established in 2002 to manage the assets of Himpurna California Energy Ltd (consisting of 1 unit of 55 MW geothermal power plant certified in 1998 and 27 wells) which were taken over by the government (Mazaya & Kurniawan, 2022). The Dieng geothermal field consists of 5 areas namely Sikidang area, Sileri area, Siglagah area, Sipandu area, and Bitingan area. The Sikidang area manifestation has an estimated temperature of 90°C with a pH of 2-3, the Sileri area has an estimated temperature of 80°C with a pH of 6, the Siglagah area has an estimated temperature of 70°C with a pH of 6-7, the Sipandu area has an estimated temperature of 80°C with a pH of 6-7, and the Bitingan area has an estimated temperature of 65°C with a pH of 6-7. In addition, Dieng geothermal also releases waste heat which is channeled through the separator outlet in the form of brine (Wisnu et al, 2020).

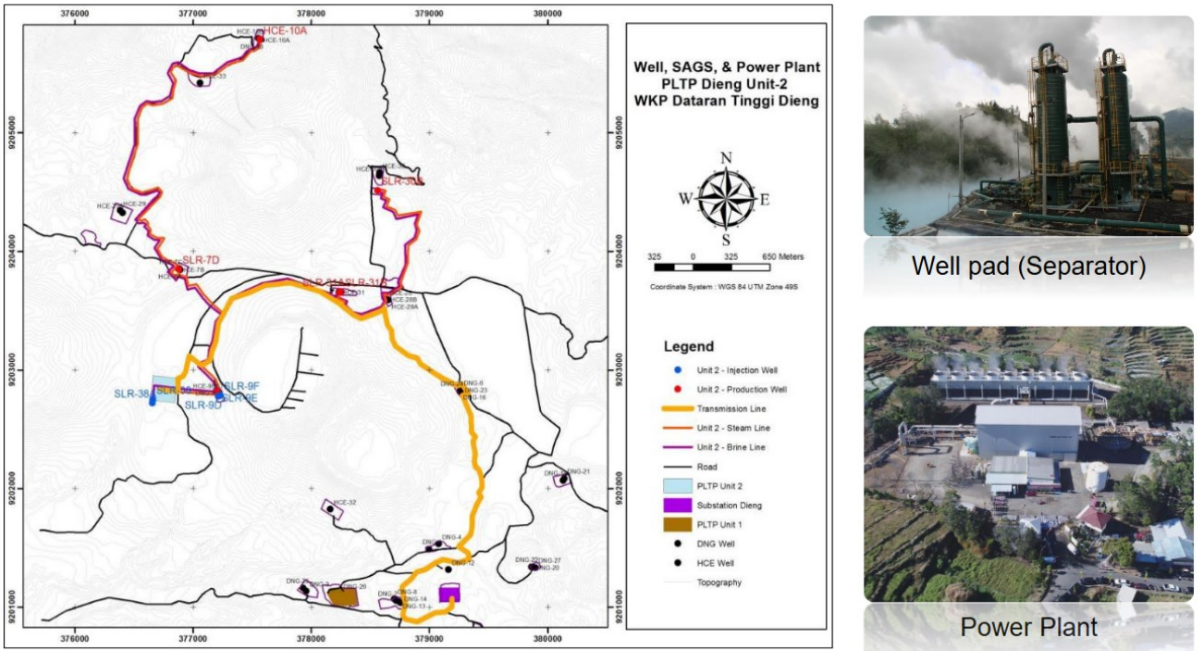

Figure 2: Location of Dieng Geothermal Field (Wisnu et al., 2020).

The challenges and obstacles faced in utilizing hot springs can be overcome through waste heat from the Dieng Geothermal Power Plant (PLTP). This paper focuses on how waste heat from the Dieng Geothermal Power Plant

can be utilized as an energy source for hot spring tourism (balneology), including the technical aspects and processes involved. In addition, this paper also includes economic and social analyses related to the application of this technology.

2. FIELD OVERVIEW

2.1 Trends in Balneology Usage

Balneology refers to the use of geothermal water for bathing and therapy. It is a long-established tradition that has existed for thousands of years. The Romans were perhaps the first to practice balneology as they already differentiated bathing for leisure and establishments for healing purposes (balneology). In Xiaotangshan Sanitarium, China, balneology has existed as a means of muscular and skeletal therapy for more than five centuries (Saptadji, 2019). Balneology presents in many forms as depicted below.

Figure 3: (a) Balneology for open-communal bathing, (b). Balneology as Mud-bathing, (c) Balneo-based Spa (Balneology Association of North America).

Most balneology presents in the form of open-communal bathing and, on some occasions, is developed for spas. Mud/ peat therapy commonly exists when geothermal water can mix with volcanic mud, creating a healing and mineral-rich source of balneotherapy (Smith and Puczkó, 2016). The Czech Republic classifies balneology as a central branch of rehabilitative treatment combined with a certain health regimen. Some other countries even include balneotherapy as an insurance-covered health service. However, there has been a shift in the intention of balneology site visitation due to the growing rate of tourism. In Hungary, the locals visit balneology sites for health and medical purposes. On the other hand, international tourists strive to visit the sites for pleasure and satisfaction. Germany, a place with strong-cultured balneology spas, has also changed the labeling of "spa for health" to "spa for wellness". In Indonesia, a glimpse of balneology can be seen in the picture below.

Figure 4: (a) Communal Bathing in Dieng, (b) Balneology-base Waterpark (Shoedarto et al., 2016).

Balneology may present as a medium to gain public acceptance of geothermal energy in Indonesia. Promoting a friendly and economically interesting way for the community to utilize the potential of geothermal energy (Shoedarto et al., 2016).

2.2 Balneology in terms of Health

The role of balneotherapy as a geothermal bathing area has various benefits to human health, especially for interconnected immune and psychological responses. The effects of hot baths on immunity are directly anti-inflammatory and immunosuppressive at the cellular level. In patients with induced atopic dermatitis, serum levels

of pro-inflammatory cytokines such as IL-1β, IL-13 and TNF-α decreased significantly after treatment with high concentrations of spring water. Treated patients also experienced modulation of inflammatory cytokines through an increase in anti-inflammatory IGF-1, while serum levels of pro-inflammatory cytokines TNF-α and IL-1β decreased. Patients with rheumatic diseases experienced reduced concentrations of prostaglandin E2 and leukotriene B4, and C-reactive protein after balneotherapy. Sulfur-containing hot baths can increase the level of Foxp3+ Treg cells that play a role in immunosuppressive activity. In addition, balneotherapy gives a positive influence to the oxidant/antioxidant system by reducing the production of reactive oxygen (ROS) and nitrogen which then impacts immunosuppressive activity (Maccarone et al., 2020).

Balneotherapy using iron-rich hot water and sulfuric acid chloride is ideal at 38-40 ℃, especially for cardiovascular responses. The correlation between balneotherapy and the ideal temperature is closely related to the difference in the body's response during hot and cold seasons. Balneotherapy in summer is only needed for a short time so as not to increase heart pressure excessively, while in winter balneotherapy activities need to be considered for duration to prevent a significant decrease in blood pressure (Wang et al., 2023).

The physiological effects on cardiovascular health were proven through case study-based research on 98 patients with musculoskeletal diseases. The treatment given was physiotherapy referral with balneotherapy. The results of the application of the method showed that diastolic pressure decreased and pulse rate increased, leading to good changes such as decreased pulse pressure and cardiac stress, and increased vascular elasticity (Sas et al., 2016). Thus, balneotherapy has the potential to reduce cardiac workload and increase vasodilation. However, the application of this therapy still requires attention to the risks that may be posed to certain body conditions. Individuals with potential chronic cardiovascular and lung diseases are recommended to perform balneotherapy in 1 cycle under 20 minutes (Wang et al., 2023).

2.3 Fluid Characteristics in Geothermal Dieng

The production fluids in the Dieng geothermal field are different from those in other geothermal fields in Indonesia. In addition to mostly being water, the fluids in Dieng have a high concentration of silica, about ± 900 mg/L. The Dieng Geothermal Reservoir has an installed capacity of 60 MW, divided into the Sileri and Sikidang areas (Wahyudityo et al., 2013). The Sileri area has neutral fluids, although there is a chance for magmatic fluids to mix in. Neutralization happens due to strong water-rock interactions within the reservoir. Temperatures here range from 283-338°C, with a chloride content of 69.22 mg/L. The fluid source is rainwater that has been heated, mixed with degassed magmatic fluids, boiled, and interacted with sedimentary or meta-sedimentary rocks (Kencana et al., 2024). The Sileri reservoir is characterized by high chloride content and a boron concentration of 3.84 mg/L, indicating interaction with sedimentary rock formations. Additionally, this reservoir has SiO2 and Fe concentrations of 41.09 mg/L and 0.12 mg/L, respectively. Other mineral contents include K at 21.3 mg/L, Ca at 13.69 mg/L, and Mg at 58.97 mg/L (Ramadhan et al., 2013). Hydrothermal fluids in the Sileri reservoir move vertically to the upflow zones in Pagerkandang Crater and Merdada Crater. The Sileri area also has a steam cap zone, characterized by excess enthalpy, high non-condensable gas (NCG) content, and a low water-to-steam ratio, which affects the overall efficiency of energy extraction. The presence of high NCG levels, primarily composed of CO_2 with traces of H_2S and CH_4, influences the steam chemistry and can lead to operational challenges such as scaling and corrosion in power plant equipment. These factors necessitate careful monitoring and management to optimize geothermal production and maintain reservoir sustainability.

The Sikidang area has more acidic fluids with a pH of 3.88, influenced by the dominance of magmatic fluids. This reservoir has two phases, with most wells reaching the steam cap zone and some wells reaching the liquid zone. A boiling zone is estimated between the liquid and steam reservoirs. Fluid temperatures in this reservoir range from 260-324°C, with high non-condensable gas (NCG) content, between 2-21%. Fluid flow in the Sikidang area comes from upflow zones around Pangonan Crater, Sikidang, and Sibanteng manifestations. These upflow zones are linked to acidic fluid zones, indicating potential acidic fluids deep within the reservoir (Kencana et al., 2024). The Sikidang reservoir has lower chloride and boron contents compared to the Sileri reservoir, with concentrations of 27.48 mg/L and 0.69 mg/L, respectively. Additionally, this reservoir contains SiO2 at 58.68 mg/L, Fe at 11.44 mg/L, K at 51.6 mg/L, Ca at 43.5 mg/L, and Mg at 58.94 mg/L (Ramadhan et al., 2013).

2.4 Balneology Scheme in General

The balneological process begins with the identification and utilization of mineral or hot water sources that have therapeutic potential. Once the source is found, the next stage is water extraction and processing. This process involves a series of methods to purify and optimize the mineral content of water, thereby maximizing its therapeutic benefits (Gianfaldoni et al., 2017). The treated water then enters the storage and distribution phases. This stage is crucial to ensuring water quality is maintained and consistently available for various therapeutic applications.

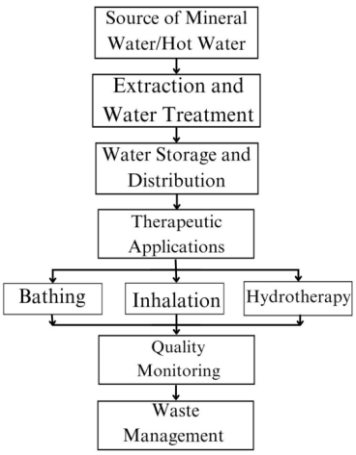

Figure 5: Balneology Scheme.

The therapeutic application of mineral water or hot water is divided into three main methods: soaking, inhalation, and hydrotherapy. Soaking involves immersing the body in mineral water, allowing the absorption of minerals through the skin, and providing a relaxing effect (Nasermoaddeli and Kagamimori, 2005). Inhalation uses mineral water vapor for respiratory therapy, potentially treating respiratory tract problems. Hydrotherapy includes a variety of techniques for using water for healing, including pressurized water massage and temperature contrast therapy. Each of these methods is designed to optimize the therapeutic benefits of mineral water, tailored to the specific needs of the patient or user.

After therapeutic application, the balneological process continues with two important stages, namely quality monitoring and waste management. Quality monitoring is a vital step to ensure the consistent effectiveness and safety of the use of mineral water in therapy. This includes regular testing of mineral composition, pH, and other water quality parameters. The final stage, waste management, is a sustainable aspect of balneology. This process involves treating used water to minimize its environmental impact, including recycling or safe disposal. Thus, the balneological cycle not only focuses on health benefits but also pays attention to aspects of environmental sustainability, creating a holistic approach to the use of mineral water resources for health (Gutenbrunner et al., 2010).

3. METHODOLOGY

This research uses a descriptive research approach to provide an actual picture of the geothermal conditions, potentials, and challenges that will be researched and planned. According to Faridi et al. (2021) Descriptive research is research that aims to describe existing phenomena, namely natural phenomena or man-made phenomena, or which is used to analyze or describe the results of a subject, but is not intended to provide broader implications. The methods used in the preparation of this scientific work are literature studies from books, journals, and relevant articles.

Data collection in this research was conducted through literature studies. According to Danial and Warsiah (2009), literature study is a form of research conducted by researchers by collecting a number of books, magazines, or other sources of information relevant to the research problem and objectives. In this study, secondary data used was obtained from literature journals. Data analysis was carried out using qualitative methods, namely by categorizing the raw data obtained as needed, presenting data interpretation, and narrated data analysis in accordance with the topic of discussion. Then, conclusions are drawn based on the data that has been processed. This research will identify and analyze waste heat from the Dieng geothermal power plant, existing potential, and challenges to formulate appropriate solutions

4. RESULT AND DISCUSSION

4.1 Brine Waste Processing

The process of flowing hot water from geothermal production wells to balneological facilities is carried out using pipes. The pipes used must be strong against corrosion, high pressure and temperature, and salinity. According to Nogara & Zarrouk (2018), several types of materials help prevent corrosion, such as carbon steel, stainless steel, and other corrosion-resistant alloys (CRA) which contain iron, nickel, chromium, and molybdenum in varying amounts. The salinity of geothermal hot water is very high which causes scaling to occur. Scaling in pipes occurs due to the formation of deposits which can hinder the water distribution process, besides that scaling reduces thermal conductivity and all heat transfer coefficients (Baba and Ármannsson, 2006). The common scaling is

amorphous silica scale (SiO2) (Agustinus et al, 2018). The following is an example of an image of scaling occurring.

Figure 6: Amorphous Silica Scale on Re-injection Pipes (PT. Geodipa Energi, 2009).

It is necessary to prevent scaling from occurring in order to reduce obstacles to the hot water flow process. There are 3 methods studied to prevent scaling in pipes, below is an explanation of each method.

1. PAC (Poly Aluminium Chloride)
   Research from Syafri and Rosana (2018) on preventive techniques to minimize scaling in the Dieng geothermal area using PAC (Poly Aluminum Chloride) coagulant is considered effective. The optimum dose required is a PAC concentration of 10 ppm, pH conditions of 8, and the addition of a Polyamide flocculant concentration of 1 ppm. Mixing or stirring treatment can increase the effectiveness of preventing scaling because the added coagulants and flocculants can be homogeneous so they work optimally. Flocculant is polyelectrolyte such as Polyamide compounds which serves to accelerate the larger formation of the floc core. The floc-floc density becomes greater than the density of water so that the floc-floc will form a precipitate sludge. The rate of deposition takes place gradually through the settling hindered phase, transition phase, and compacting phase (Kawamura, 1991).

Figure 7: Comparison of the Effectiveness of Coagulant Types on Precipitation (Agustinus et al, 2018).

2. pH Modification
   pH modification system has been adopted as an alternative scale prevention method since 2003. The purpose of this method is to reduce the silica-scaling rate by adjusting brine pH with sulfuric acid. Concentrated H2SO4 is injected into the brine in Hatchobaru, Japan, and at pH 5-6, the silica scaling rate was reduced significantly (Kiyota and Uchiyama, 2011). Because most geothermal liquids have extremely large buffer capacity, even for a small decrease, a large amount of acid is required (Topçu et al., 2019). For the mitigation of amorphous silica and metal silicates, pH modification with concentrated sulphuric acid (H2SO4) has been used in the Mak-Ban (Bulalo, Philippines) geothermal field (Gallup, 2011). Moreover, H2SO4 application contributes to the reduction of hazardous hydrogen sulfide emission from geothermal power stations that produced hydrogen sulfide gas was converted to H2SO4 with the help of a sulfur-oxidizing bacteria Thiobacillus thioparus (Hirowatari, 1996). To reduce the scaling rate, the pH was modified to slightly lower, but it was difficult to lower the pH in terms of corrosion problems of equipment. Corrosion is a serious issue, particularly in the elbow part of the pipeline, when such inorganic acids are dosed in the system. Apart from that, the hazards of sulfuric acid are also a factor in considering the use of this method.
3. Carbon dioxide (CO2) Injection
   Moreover, CO2 injection is another approach to prevent metal silicate scaling. Topçu et al. (2019) injected CO2 gas into the TGPP with various flow rates, and the results emphasized that 20.6 m3 /s CO2 injections showed a better performance than 55 ppm formic acid injection, and less corrosion is observed in CO2 gas injection (Topçu et al., 2019). In this way, a sustainable route can be achieved in geothermal systems by capturing the released CO2 from the system and injecting it through the wells. As a new perspective on the pH modification and antiscalant application in geothermal systems, there is a patent

application for the usage of CO2 as an antiscalant (Baba et al., 2020). The need for high capital and complex machine systems are challenges in implementing CO2 injection.

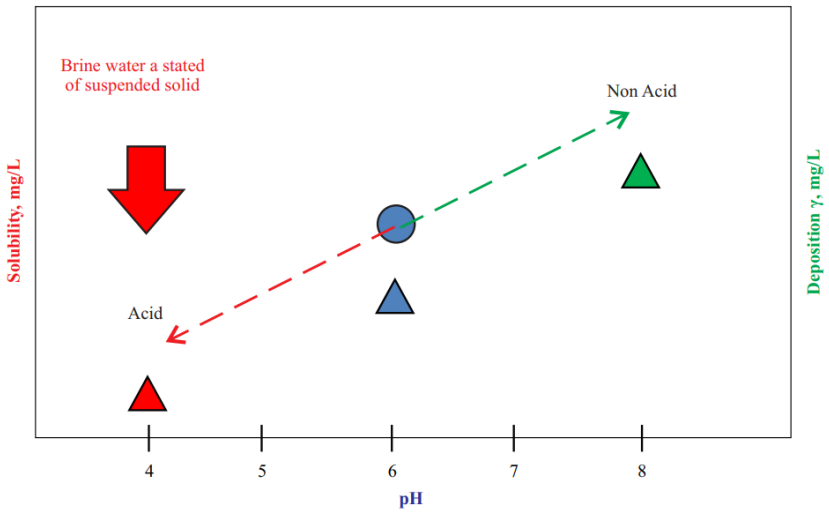

Figure 8: Graph of the Relationship between pH with Solubility and Deposition (Agustinus et al, 2018).

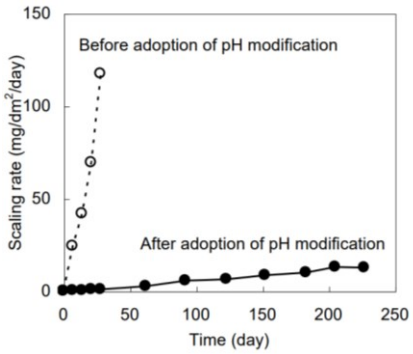

Figure 9: Effect of pH Modification on the Scaling Rate (Kiyota & Uchiyama, 2011).

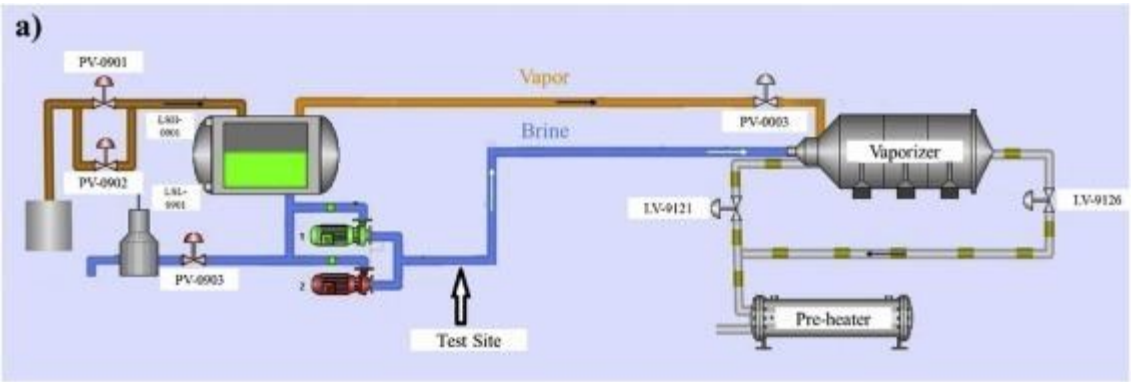

Figure 10: Scheme of The System CO2 Injection (Topcu et al, 2019).

Each method has its own advantages and disadvantages, so it needs to be considered in terms of economics, sustainability, and level of hazards. Below is a table of comparison levels between parameters and scaling prevention methods.

Of the three methods, taking into account the existing aspects, the recommended method to use is PAC coagulant, because it is seen from the side effects and costs required. As for the optimum conditions dose required is a PAC concentration of 10 ppm, pH conditions of 8, and the addition of a Polyamide flocculant concentration of 1 ppm.

Table 1: Comparison Levels Between Parameters and Scaling Prevention Methods.

Parameter	Methods of Scaling Prevention		
	PAC	pH Modification	CO2Injection
Complexity	Medium	Low	High
Corrosion Tendency	Low	High	Low
Environmental Hazard	Low	High	Low
Investment	Medium	Low	High
Sustainability	Medium	Medium	High

4.2 Balneology Scheme of Brine Waste

The brine temperature from the separator's outlet in Dieng geothermal reaches 180°C (Wisnu et al., 2020). In this temperature range, Dieng geothermal can be utilized through direct geothermal use, such as space heating or domestic hot water supply, as shown in the Lindal diagram (Chiasson, 2016). Therefore, the geothermal utilization of Dieng can be done by using a Geothermal Heat Pump (GHP) system.

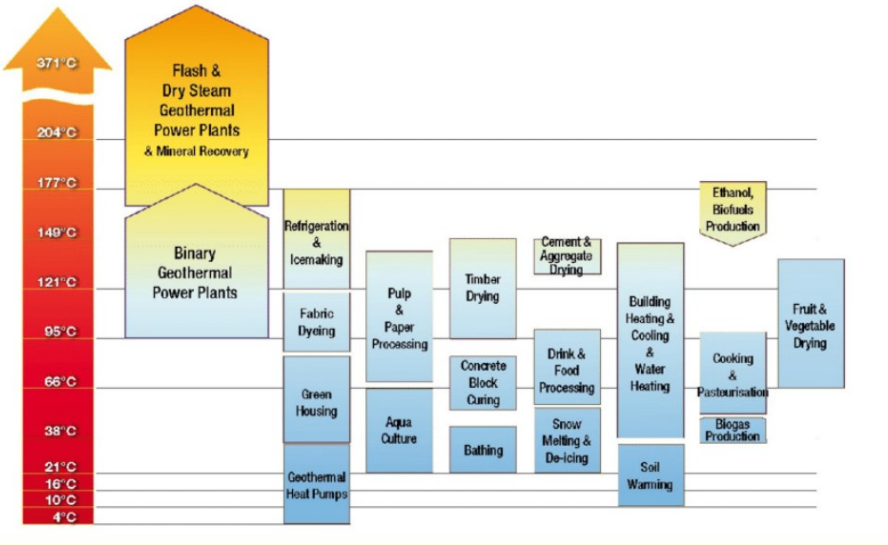

Figure 11: Lindal Diagram (Climo et al., 2015).

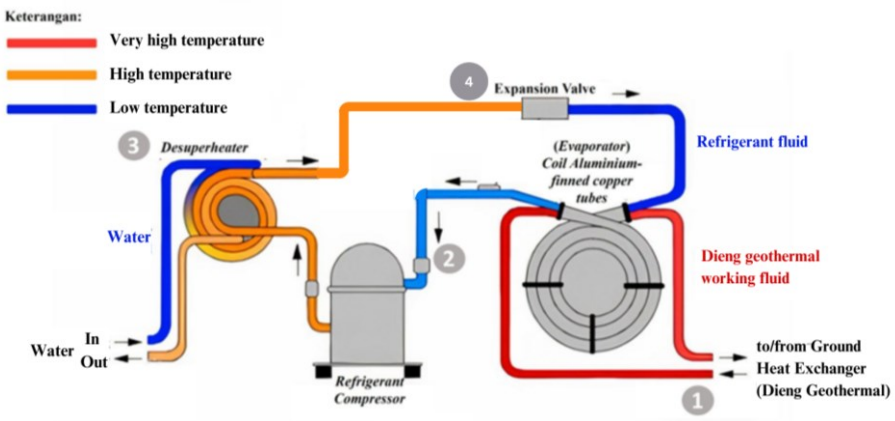

Figure 12: Geothermal Heat Pump (GHP) system in geothermal Dieng (Modified from Lund et al., 2004).

The heat exchange process in the Geothermal Heat Pump starts by transferring enthalpy from the Dieng geothermal working fluid to the heat exchanger working fluid in the evaporator. At this stage, the aluminum-finned copper tubes of the refrigerant heat exchanger act as a medium for heat exchange between the geothermal working fluid and the refrigerant (Chiasson, 2016).

Proper refrigerant selection in aluminum-finned copper tube coils is critical to ensure optimal performance and heat exchange efficiency in heat exchangers (Greco et al., 1997). Some common refrigerant types used in

geothermal heat pump applications are R-410A and R-407C (Kim et al., 2011). Factors considered in refrigerant selection include thermal efficiency, chemical stability, environmental impact, and safety.

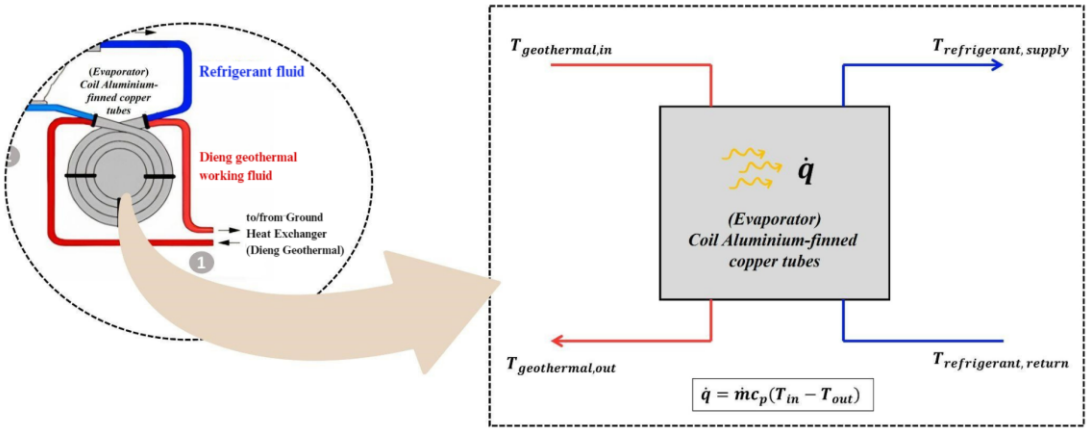

Figure 13: Displacement arrow of aluminum-finned copper tubes coil.

Table 2: Characteristics of refrigerant types R410A & R407C.

Refrigerant Type	Key Properties	Physical Properties	(GWP*)	Source
R410A (R32 and R125 hydrofluorocarbon (HFC) mixtures)	– Non-flammable – Non-toxic – Used in home air conditioning systems	– Critical Pressure: 4.92 MPa (713 psi) – Critical Temperature: 72.8°C (163.0°F) – Liquid Density: 1.21 kg/L	2.088	Kim, W., Kang, D., Lee, Y., & Jung, D. (2011)
R407C	– Non-flammable – Non-toxic – Used in home air conditioning systems	– Critical Pressure: 4.62 MPa (669 psi) – Critical Temperature: 87.3°C (189.1°F) – Liquid Density: 1.16 kg/L	1.774	Greco, A., Mastrullo, R., & Palombo, A. (1997)

*GWP (Global Warming Potential) is a number that measures the impact of these gases on global warming compared to CO_2 over a given period.

After the refrigerant working fluid undergoes vaporization in the evaporator, the resulting vapor enters the compressor to be increased in pressure and temperature. The compressor is responsible for increasing the pressure and temperature of the refrigerant to increase the heat exchange efficiency in the condenser. The high temperature of the compressed refrigerant is then flowed to the desuperheater to absorb excess heat from the refrigerant which is in a superheat condition after passing through the compressor (Hengel et al., 2016). Desuperheaters are effectively used as a heat source in domestic hot water supply by transferring excess heat from the refrigerant into domestic water. The hot water produced is around 50.43°C (Chahartaghi et al., 2019), which is utilized for hot springs or balneology.

Next, the refrigerant will enter the expansion valve. Inside the expansion valve, the temperature and pressure of the refrigerant will be lowered significantly. This process causes the refrigerant to experience a drastic drop in temperature and pressure, preparing it to return to the evaporator. After passing through the expansion valve, the refrigerant which is now in its initial low-pressure and low-temperature state, will then enter the evaporator to absorb heat from the geothermal fluid again. This process will continue to repeat in the cycle.

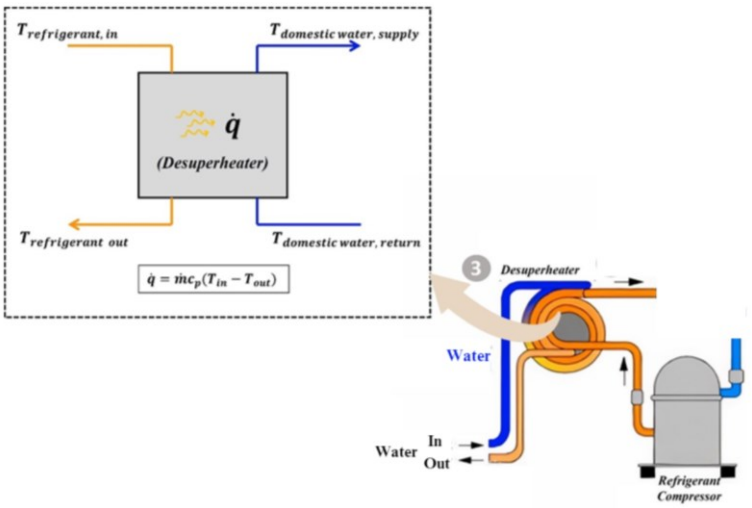

Figure 14: Heat transfer from Desuperheater.

4.3 Biological Analysis

Warm bath therapy through balneotherapy can cause dilation vessels blood, reducing viscosity blood and reduces tension resulting muscle improve blood circulation, so that can help lower blood pressure. This is also the best way and hassle-free side effects after use so it can be used as an alternative for reducing blood pressure (Fembi et al., 2019). The effects of balneotherapy generally appear as thermal, mechanical or chemical effects. Balneotherapy can be an alternative treatment method for treating health problems such as respiratory, cardiovascular, endocrine and neurological problems (Galvez et al., 2018). The thermal effect produced by the body is in the temperature range of 35-40 degrees Celsius. In this temperature range, blood flow in the body will increase, causing increased blood flow to the heart, lungs and brain (An et al., 2019). Hot water therapy in this temperature range can cause the body's rectal temperature to increase, namely to 38 degrees Celsius, and also cause the pulse rate to increase to 127 ± 18 beats/minute (Brunt et al., 2016).

4.4 Socio-economic Analysis

The application of brine waste in balneology in the Dieng area has complex social impacts, especially given the characteristics of the area as a tourist destination and geothermal site. One of the main problems that arises is the tension between the use of geothermal resources for electricity generation and their potential for balneological development. Local communities that have long relied on tourism as a source of income may feel threatened by changes in the economic landscape brought about by large-scale geothermal projects (Sukhyar et al., 2016). The problem that needs to be resolved concerns the use of brine waste for balneology in order to bridge this gap, create new jobs in the health and tourism sectors, and still utilize the potential of geothermal energy.

Another social aspect that needs to be considered is changes in land use patterns and community access to natural resources. The development of balneological facilities that utilize brine waste changes the dynamics of land ownership and management around geothermal sources (Yuniar et al., 2019). This problem has the potential to cause conflict if not managed well, especially if there is a perception that local communities are marginalized in the development process. A concrete case can be seen in complex negotiations between geothermal companies, regional governments, and local communities regarding land use rights and the sharing of economic benefits from balneological projects.

Social acceptance of geothermal projects is a key factor. Experience in various regions of Indonesia shows that community acceptance of geothermal projects often depends on perceptions regarding the direct benefits that can be felt by local communities (Nugroho, 2019). In Dieng, the integration of balneology in geothermal utilization could be a catalyst for increasing social acceptance. By demonstrating that brine waste can be used to create health and tourism facilities that benefit local communities, geothermal projects have the potential to gain wider support. However, the success of implementing brine waste-based balneology depends on transparent communication, involving the community in decision-making, and implementing a fair and sustainable benefit sharing program. If managed well, the development of brine waste-based balneology in Dieng can become a model for harmonization between the interests of the energy industry, tourism, health, and the aspirations of local communities (Oktavia et al., 2021).

A balneological review from an economic aspect in the Dieng area needs to consider the existence of several operating hot springs, such as D'Qiano Hot Spring Waterpark, Tegalsari, Sendang Sipandu, Legok Munggang, and Segar Asri. These facilities have become an integral part of Dieng's tourism landscape, attracting local visitors

as well as tourists from outside the area. The existence of hot springs shows that there is a market being formed for balneological services in the region, which is a positive indicator for the potential development of brine waste-based balneology (Oktavia et al., 2021).

In the context of balneological development using a brine waste system, economic analysis is crucial for assessing the feasibility and sustainability of the project. The initial investment costs to implement a brine waste processing system in balneological facilities can be quite substantial, including water treatment infrastructure, the construction of bathing facilities, and the development of supporting amenities (Lund, 2006). Utilizing brine waste, which is a by-product of geothermal power plants, can produce long-term cost efficiencies compared to conventional hot springs, which require natural hot water sources or artificial heating.

To assess the economic feasibility of this project, several economic indicators need to be considered. Break Even Point (BEP) is achieved within 3-5 years, depending on the scale of investment and level of tourist visits (Shortall et al., 2015). Levelized Cost of Energy (LCOE), to calculate the cost per visitor or per balneology session by considering the total cost over the life of the project divided by the number of visitors served (Yasukawa et al., 2018). The payback period is estimated to be between 5-7 years, considering the existing market potential and added value from the use of brine waste (Lund and Boyd, 2016). The project's internal rate of return (IRR) reaches 15-20%, making it attractive for investors (Lund, 2006). The benefit-cost ratio (BCR) is expected to be greater than 1, around 1.3–1.5, indicating that the economic benefits exceed the costs (Shortall et al., 2015).

The application of the brine waste system in balneology in Dieng not only has the potential to create long-term operational cost efficiencies, but the application of the brine waste system in balneology can open up opportunities for product differentiation. Balneological facilities that utilize brine waste can promote themselves as eco-friendly destinations, attracting market segments that care about the environment and health. Through this balneology, economic value will be increased through premium pricing and increased occupancy. In addition, integration with the geothermal energy sector can create economic synergies, where waste processing costs from power plants can be offset by income from balneological facilities. This holistic approach has the potential to create a business model that is more sustainable and resilient to fluctuations in the conventional tourism market (Oktavia et al., 2021).

5. CONCLUSION

The integration of geothermal heat pump technology with Dieng's geothermal energy source not only provides a clean and efficient solution for hot springs (balneology), but also has the potential to improve the overall health of Dieng communities and tourists and support sustainable tourism growth. With the active involvement of the younger generation in encouraging the utilization of clean and sustainable energy, Dieng can become a pioneer in maintaining a balance between economic growth and environmental preservation. By taking concrete action in utilizing Dieng's geothermal energy as a source of hot springs (balneology), we can realize easy access to clean energy to support sustainable tourism.

REFERENCES

Agustinus, E. T. S., Syafri, I., Rosana, M. F., & Zulkarnain, I. 2018. Scale prevention technique to minimized scaling on re-injection pipes in Dieng geothermal field, Central Java Province, Indonesia. *Indonesian Journal on Geoscience*. 5(2) : 129-136.

An, J., Lee, I & Yi, Y. 2019. The thermal effects of water immersion on health outcomes : an integrative review. *International Journal of Environmental Research and Public Health*. 16(1280) : 1-21

Aristyan, A. 2023. *4 Pemandian Air Panas Di Dieng Ini Cocok Untuk Relaksasi Tubuh, Wisatawan Harus Kesini!*. https://www.wonosobozone.com/berita/4679585699/4-pemandian-air-panas-di-dieng-ini-cocok-untuk-relaksasi-tubuh-wisatawan-harus-kesini?page=3. Diakses pada 5 Juli 2024.

Baba, A., Demir, M. M., Koç, G., Avcı, İ. 2020. *Geothermal power plant system used as a line inhibitor to prevent the scaling of greenhouse gases emitted from the system*. Patent number: WO2021145839A3

Brunt V.E., Jeckell, A.T., Ely, B.R., Howard, M.J., Thijssen, D.H.J., and Minson, C.T. 2016. Acute hot water immersion is protective against impaired vascular function following forearm ischemia-reperfusion in young healthy humas. *Am J Physiol Regul Integr Comp Physiol*. 311(2016) : 1-8

Chahartaghi, M., Kalami, M., Ahmadi, M.H., Kumar, R. and Jilte, R. 2019. Energy and exergy analyses and thermo-economic optimization of geothermal heat pump for domestic water heating. *International Journal of Low-Carbon Technologies*. 14(2) : .108-121.

Chiasson, A. D. (2016). *Geothermal heat pump and heat engine systems: Theory and practice*. John Wiley & Sons.

Climo, M., Hall, J., Coyle, F., Seward, A., Bendall, S., Carey, B. and White, B., 2015. Direct Use: Opportunities and Development Initiatives in New Zealand. In *Proceedings World Geothermal Congress*.

Danial, E, & Warsiah, N 2009, *Metode Penulisan Karya Ilmiah*, Bandung, Laboratorium Pendidikan Kewarganegaraan.

Faridi, A, Susilawaty, A, Rahmiati, B.F, Sianturi, E, Adiputra, I, M, S, Budiastutik, I, Oktaviani, N, P, W, Trisnadewi, N, W, Tania, P, O, A, Ramdany, R, & Fitriani, R, J, 2021. '*Metodologi Penelitian Kesehatan*'.

Fembi, P.N., Pora, Y.D., Vianiatiz P & Zale, Z. 2017. Pengaruh terapi mandi air hangat terhadap penurunan tekanan darah pada penderita hipertensi di RW 10 kelurahan waioti kecamatan alok timur kabupaten sikka. *Jurnal Keperawatan dan Kesehatan Masyarakat*. 4(2) : 99-124

Gallup, D. L. 2011. Brine pH modification scale control technology. A review Mercury contamination in the oil and gas industry. *GRC Transactions* 35.

Galvez, I., Piles, S.T and Rincon, E.O. 2018. Balnotherapy, immune system, and stress response : a hormetic strategy. *International Journal of Molecular Sciences*. 19(6) : 1-19

Gianfaldoni, S., Tchernev, G., Wollina, U., Roccia, M. G., Fioranelli, M., Gianfaldoni, R., & Lotti, T. (2017). History of the baths and thermal medicine. *Journal of Medical Sciences*. 5(4) : 566-568.

Gutenbrunner, C., Bender, T., Cantista, P and Karagülle, Z. 2010. *A proposal for a worldwide definition of health resort*

Hengel, F., Heinz, A., & Rieberer, R. 2016. Performance analysis of a heat pump with desuperheater for residential buildings using different control and implementation strategies. *Applied Thermal Engineering*. 105(2016) : 256-265. https://doi.org/10.1016/J.APPLTHERMALENG.2016.05.110.

Herlambang, D. 2022. *PENGOLAHAN AIR TERKONTAMINASI FLUIDA PANAS BUMI UNTUK KEBUTUHAN AIR DOMESTIK DI DUSUN DARUM, DESA CANDI, KECAMATAN BANDUNGAN, KABUPATEN SEMARANG, PROVINSI JAWA TENGAH* (Doctoral dissertation, UPN'Veteran" Yogyakarta)

Hirowatari, K. 1996. Scale prevention method by brine acidification with biochemical reactors. *Geothermics* 25.

Kawamura, S. 1991. *Integrated Design of Water Treatment Facilities*, John Wiley & Sons, Inc, New York.

Kencana, A. Y., Elfina, J. S. A., Fajri, R. J., Supijo, M. C., & Nurpratama, M. I.,2024, *Initial State Fluid Geochemistry of the Dieng Geothermal Field, Indonesia*: New Constraints for Conceptual Model.

Kim, W., Kang, D., Lee, Y., & Jung, D. 2011. Performance of HFC32/HFC125 Mixtures for Heat Pumps. Korean *Journal of Air-Conditioning and Refrigeration Engineering*. 23 (2011) : 791-798.

Kiyota, Y., Uchiyama, N. 2011. Silica scale prevention effects of brine pH modification at Hatchobaru power station, Japan. *Proceedings International Workshop on Mineral Scaling*.

Lichti, K. A., Brown, K. L. 2013. *Prediction and Monitoring of Scaling and Corrosion in pH Adjusted Geothermal Brine Solutions*. Corrosion

Lund, J. W. (2006). Geothermal spas in the Czech Republic and Slovakia. *GHC Bulletin*. 27(3) : 25-29.

Lund, J. W., & Boyd, T. L. (2016). Direct utilization of geothermal energy 2015 worldwide review. *Geothermics*, 60, 66-93.

Maccarone, M. C., Magro, G., Solimene, U., & Masiero, S. (2020). The effects of balneotherapy on human immune function: should baths and mud applications have a role during covid-19 pandemic? *Bulletin of Rehabilitation Medicine*. 3(97): 22-24. DOI: 10.38025/2078-1962-2020-97-3-22-24.

Mazaya, A. and Kurniawan, T. 2022. COLLABORATIVE GOVERNANCE PEMANFAATAN ENERGI PANAS BUMI SEBAGAI SUMBER PEMBANGKIT LISTRIK (Studi Kasus Pembangkit Listrik Tenaga Panas Bumi Dieng, Jawa Tengah). *Jurnal Inovasi Penelitian*. 3(4).

Nasermoaddeli, A., & Kagamimori, S. 2005. Balneotherapy in medicine: A review. *Environmental Health and Preventive Medicine*, 10(4), 171-179.

Nogara, J., & Zarrouk, S. J. 2018. Corrosion in geothermal environment Part 2: Metals and alloys. *Renewable and Sustainable Energy Reviews*, 82, 1347-1363.

Nugroho, C. (2019). Social acceptance of geothermal energy: A case study from Mt. Lawu, Indonesia. *Geothermics*, 82, 288-296.

Nurrochim, W. F., & Harmoko, U. 2021. Analisa Optimalisasi "Abandoned Well Production" Menggunakan "Downhole Heat Exchanger (DHE)" Sebagai Sumber Energi Baru di Lapangan Panas Bumi Dieng. *Jurnal Energi Baru dan Terbarukan*, 2(1), 14-26.

Oktavia, J., Mulyani, R., & Supriatna, J. 2021. Sustainable geotourism development in Dieng Plateau: Balancing conservation, community empowerment, and economic benefits. *Journal of Environmental Management*, 292, 112730.

Priyanto, P., & Safitri, D. 2016.. Pengembangan Potensi Desa Wisata Berbasis Budayatinjauan Terhadap Desa Wisata Di Jawa Tengah. Jurnal Vokasi Indonesia, 4(1), 7. Wahyudi, J. (2017). Potensi Produksi Biogas dan Mitigasi Emisi Gas Rumah Kaca di Industri Tahu. *Prosiding Sains Nasional dan Teknologi*, 1(1).

PT. Geodipa Energi, 2009. *Rencana Pengelolaan Lingkungan dan Rencana Pemantauan Lingkungan* (RKL-RPL) Triwulan II, Laporan Pelaksanaan, Dieng, Jawa Tengah.

Ramadhan, et al. 2013. *Hotwater Geochemistry for Interpreting The Condition of Geothermal Reservoir, Dieng Plateau Case, Banjarnegara-Wonosobo Regency, Central Java*

Saptadji, N. M.2019. *Teknik Geotermal* (2nd ed.). ITB Press.

Sas, S., Celenay, S. T., & Kaya, D. O. 2016. The effects of balneotherapy on acute, process-related, and cumulative peripheral cardiac responses and pulmonary functions in patients with musculoskeletal disorders. *Turk J Med Sci*. 46(6): 1700-1706. DOI: 10.3906/sag-1505-31.

Shoedarto, R., Aries, F., Perdana, D., Arisbaya, I. and Indrawan, B. 2016. Raising Public Acceptance of Geothermal Utilization Through Direct Application in Indonesia. *PROCEEDINGS, 41st Workshop on Geothermal Reservoir Engineering*.

Shortall, R., Davidsdottir, B., & Axelsson, G. 2015. Geothermal energy for sustainable development: A review of sustainability impacts and assessment frameworks. *Renewable and Sustainable Energy Reviews*, 44, 391-406.

Smith , M., & Puczkó, L. 2017. *The Rouletdge Handbook of Health Tourism* [Review of The Rouletdge Handbook of Health Tourism]. Taylor & Francis Grou.

Sukhyar, R., Priadi, B., & Sudarman, S. 2016.. The development of geothermal energy in Indonesia: An overview of industry status and future growth. *Proceedings World Geothermal Congress*.

Topcu, G., Koç, G. A., Baba, A., & Demir, M. M. 2019. The injection of CO2 to hypersaline geothermal brine: A case study for Tuzla region. *Geothermics*. 80 (2019) : 86-91.

Valizadeh, L., Seyyedrasooli, A., Zamanazadeh, V & Nasiri, K. 2015. Comparing the effects of reflexology and footbath on sleep quality in the elderly: a controlled clinical trial. *Iran red Crescent Med J*. 17(11) : 1-8.

Wahyudityo, R., Harto, A. W., & Suryopratomo, K. 2013. Analisis Scaling Silika pada Pipa Injeksi Brine di Lapangan Panas Bumi Dieng dengan Studi Kasus di PT. Geo Dipa Energi. *Teknofisika*, 2(1), 7-14.

Wang, P. C., Song, Q. C., Chen, C. Y., & Sun, T. C. 2023. Cardiovascular physiological effects of balneotherapy: focus on seasonal differences. *Hypertens Res*. 46(7): 1650-1661. DOI: 10.1038/s41440-023-01248-4.

Wisnu, Agung., Marza, Supriadinata., Lory Phil., Shannon Cowlin., 2020. *Geothermal Direct Use in Dieng, Indonesia*. Asian Clean Energy Forum 2020

Yakup, A. P. 2019. *Pengaruh Sektor Pariwisata terhadap Pertumbuhan Ekonomi di Indonesia* (Doctoral dissertation, Universitas Airlangga).

Yasukawa, K., Kubota, H., Soma, N., & Noda, T. 2018. Integration of natural and social environment in the implementation of geothermal projects. *Geothermics*, 73, 111-123.

Yuniar, D., Wibowo, A., & Kurniawan, F. 2019. Analyzing the impact of geothermal power plant development on community livelihood assets in Dieng Plateau, Central Java, Indonesia. *Geothermics*, 82, 44-51.

The Sustainable Impact of Patuha Geothermal Power Plant Project: A Carbon Trading Mechanism Case Study

Delvirah Elisa Sabatini Singkuang[1], Rosana Pribadi[2], Gina Lisdiani[2], Wien Pratama Abi Wicaksono[3], Agung Soni[3], Saltsa Prehtina Muryani[3], and Saktiyo Tri Nugroho[1]

[1]PT Geo Dipa Energi (Persero), Gedung Aldevco Octagon, Jakarta, Indonesia
[2]ecosecurities, Rue de la Faïencerie 2, 1227 Geneva, Switzerland
[3]PT Geo Dipa Energi (Persero) Unit Patuha

delvirah@geodipa.co.id

Keywords: geothermal, carbon trading, Indonesia, Patuha, carbon pricing policy, CDM

ABSTRACT

Climate change is a critical issue that has become a major global focus, with its primary cause being the accumulation of greenhouse gas emissions, particularly carbon dioxide (CO_2). Through the Kyoto Protocol and later the Paris Agreement, world leaders strive to anticipate the impacts of climate change through various methods. One of them is the implementation of renewable energy that emits none or very little CO2 to replace fossil fuels. Among these renewable energy sources, geothermal energy stands out due to its potential as a baseload energy source. The stability that geothermal energy provides is crucial to meet the global Net Zero Emission (NZE) target, as it would maintain a steady supply of electricity and ensure that energy demands are met without interruption. However, this requires key enablers, such as regulations and policies, to support the transition towards sustainable development.

A policy that economists consider highly effective is carbon pricing. As the name suggests, carbon pricing puts a price for carbon reduction to encourage industries and even countries to reduce their carbon emission. It comprises of two instruments, namely trading and non-trading instruments. By involving carbon trading as one of the instruments in the development of renewable energy, it can encourage the reduction of carbon emission, thus helping the world move closer to the NZE target.

Indonesia has an estimated total potential of 23 GW geothermal energy source, which amounts to 40% of the world's resource, making it a key player and a significant participant in the carbon trading mechanism. One of the major geothermal power plants in Indonesia is Patuha Unit-1, which is located in West Java and has the capacity of 55 MW. Operated by PT Geo Dipa Energi (Persero), it has been registered under the UNFCCC Clean Development Mechanism (CDM) since 2012. By implementing this mechanism, it is estimated that the project could reduce approximately 263,851 tCO_2e annually. Not only that, the project also estimated to experience an increase of IRR from 6.73% to 7.96%, making it essential for the viability of the project. This study analyses the multifaceted impact that CDM has on Patuha Unit-1 geothermal power plant project, including economic, environmental, and social aspects, while also contributing to the global decarbonisation goal.

1. INTRODUCTION

Since the 1960s, global temperature warming due to human activities has increased drastically. Compared to the pre-Industrial Revolution era, the global average temperature has risen by up to 1.1°C and is estimated to reach or exceed 1.5°C in the next 20 years, unless immediate actions towards reducing greenhouse gas (GHG) emissions are taken. With the expiration of the Kyoto Protocol at the end of 2020, global climate policy now refers to the Paris Agreement, which aims to prevent the global average temperature from increasing by more than 2°C and to limit the increase even further to 1.5°C. While the Kyoto Protocol bound developed countries to set joint commitments, the Paris Agreement has every country, including developing countries, determine their own commitments independently. These contributions are outlined in the Nationally Determined Contributions (NDCs).

Article 6 in the Paris Agreement is highlighted as embracing the business sector and leveraging the global market to support each country's government efforts to reduce carbon emissions. Through various cooperative approaches, the private sector is also encouraged to contribute to reducing carbon emissions and invest in green energy. One mechanism for achieving these ambitious goals is carbon pricing. Carbon pricing is an instrument that captures the external costs of GHG emissions—such as damage to crops and loss of property from man-made natural disaster—and ties them to their sources through a price, usually in the form of a price on the carbon dioxide (CO_2) emitted (World Bank, 2024). This carbon pricing assigns a price to GHG emissions that negatively impact

the environment. Economists believe that carbon pricing is one of the most efficient methods to encourage the reduction of GHG emissions. Several Scandinavian countries have implemented it since the 1990s; as of 2019, there are 56 carbon pricing policies implemented worldwide (Pérez & Rhode, 2020).

Indonesia has also strengthened their climate commitment by pledging to reduce their GHG emissions by 31.89% through own efforts and 43.20% with international assistance by 2030 under the Enhanced Nationally Determined Contribution (NDC). To achieve this, the government is undertaking several efforts in many sectors, including promoting renewable energy sources through policies and incentives. The government has set an ambitious target of generating 23% of its energy from renewable sources by 2025. The country itself is blessed with a significant geothermal resource of approximately 23.36 GW spread across 356 geothermal locations. However, it has only utilised less than 10% of its geothermal potential. In 2021, only 2.3% of Indonesia's primary energy mix came from the geothermal sector, while in 2023 only 13.1% of Indonesia's primary energy mix is from renewable energy.

The development of geothermal power plants ties into carbon pricing as it represents a shift towards low-carbon energy production. By investing in geothermal energy, a country reduces their GHG emissions, thereby lowering its carbon footprint. As a renewable and technically emission-free energy source, geothermal becomes more economically attractive under carbon pricing mechanisms. As the cost of carbon emissions rises, the cost-effectiveness of geothermal energy improves, encouraging further investment and development. This will help countries, like Indonesia, meet its emission reduction targets more efficiently while benefiting from the economic advantages provided by carbon pricing mechanism. This paper presents the importance of carbon pricing, in particular the carbon trading mechanism, to further the development of renewable energy, specifically geothermal sector in Indonesia, and the need for suitable policies to encourage this process by doing a case study on the sustainable impacts of the CDM on Patuha Unit-1 geothermal power plant project.

2. CARBON TRADING COMPONENTS

Looking back on the implementation of the Kyoto Protocol, it was often criticised for its perceived inequity, primarily due to its differentiated approach between developed and developing countries. Under which the obligation to reduce the emission were divided into two groups: Annex I countries, mainly developed nations required to reduce emissions, and Non-Annex countries, mainly developing nations that only had to report their emissions, but could also help reduce the emissions by cooperating with Annex I countries. A more progressive and ambitious emission reduction strategy necessitating equal contributions from all nations was seen as crucial. Thus, the Paris Agreement was established at the end of 2015, adopting a universal applicability approach. All participating countries committed to reducing their GHG emissions based on the principles of equity and common but differentiated responsibilities, as well as respective capabilities, considering their unique national circumstances. It was considered a turning point in international climate policy. The main goal is to keep the increase in global temperatures below 2°C above pre-Industrial Revolution levels and to limit the increase even further to 1.5°C. In contrast to the Kyoto Protocol, in Paris Agreement every country has the same opportunity to participate and is encouraged to submit their commitments for climate change efforts.

2.1 Carbon Project

Carbon project, an initiative designed to reduce, remove or avoid GHG emissions, with the goal of generating carbon credit, is one of the efforts to reduce the GHG emissions that is well connected to the carbon trading mechanism. One of the market-based mechanism under the Kyoto Protocol was CDM, and numerous carbon projects were developed under this mechanism. The CDM allows emission-reduction (or emission removal) projects in developing countries to earn certified emission reduction (CER) credits, each equivalent to one tonne of CO_2. These CERs can be traded and sold, and used by industrialized countries to meet a part of their emission reduction targets under the Kyoto Protocol (Kyoto Protocol Article 12). With the CDM market collapsing due to a combination of several factors, including oversupply of carbon credits, the economic downturn following the 2008 financial crisis, regulatory uncertainties, lack of new commitment under the Kyoto Protocol, resulted in credits from CDM projects prices dropped. Hence, with the emerging of voluntary market, which later strengthen by the adoption of the Paris Agreement in 2015, projects were shifting and operating under the voluntary market. Although carbon projects are operating under different market and mechanism, there are main requirements that those projects need to fulfil in order to be considered as eligible carbon projects. These requirements are set under the CDM and voluntary market standards which cover the principles, rules, requirements, as well as methodology to quantify the emission reduction for different kind of projects. To be eligible as carbon projects, a project must proof that it is reducing any of the GHG emission because of its activity. However, not all projects that reduced its emissions can be considered as a carbon project because it also needs to prove its additionality.

Carbon projects can be developed using different kind of technologies, including renewable energy, energy efficiency, methane avoidance, landfill gas, fuel switching, and other technologies that in principle will reduce

GHG emissions. Any carbon projects using technologies that prevent additional GHG emissions to enter the atmosphere by reducing the sources of emissions are categorised as carbon avoidance, which will become the main focus of this paper. Additionally, there are also carbon projects focusing on the nature-based solutions which will not be discussed in this paper.

2.1.1 Baseline Emissions, Project Emissions, Leakage and Emission Reduction

The concept of calculating emission reduction in a potential carbon project is determined by the value of the baseline emissions, project emissions, and leakage when applicable. A baseline emission is the GHG emissions that would occur in the baseline scenario meaning emissions that occur when the project activity is not implemented. For power generation projects, a baseline emission would be the existing emissions coming from the electricity network where a new renewable power plant will be connected to. This baseline emission is calculated based on the grid emission factor resulting from a mix of power plants that are supplying its electricity to that network.

A project emission is the GHG emissions that would occur as a result of the project activity. For power generation projects, a project emission comes from any activities under the overall project that emit the GHG, such as the use of steam in the geothermal project or the use of diesel fuel during power plant's shutdown period. Those emissions are to be monitored and included as project emissions.

A leakage from a carbon project is defined as GHG emission which occurs outside the project boundary, and which is measurable and attributable to the project activity. As an example, emissions from the transportation of diesel fuel to the project boundary can be considered as a leakage, as well as electricity consumption for a certain type of project. Determination of leakage for each type of project is different and is specific following the applicable methodology.

2.1.2 Additionality

Additionality is a crucial factor that determines whether a project is eligible to be considered as a carbon project or not. The definition of additionality under the CDM is the effect of the project activity to reduce anthropogenic GHG emissions below the level that would have occurred in the absence of the project activity. It implies that the project would not proceed without the CDM's intervention. To determine its additionality, a project must apply tools from UNFCCC that would demonstrate the additionality of a project. These tools will be able to show the extent to which carbon revenues bridge the viability gap for a project to be implemented and actually reduce GHG emissions. If a project can be implemented without the revenues or the push from carbon market or because it is a business-as-usual activity, then the project is not additional and is not eligible as carbon project. Three types of additionalities are recognised:

a) Project Additionality: This indicates that the project would likely not occur without CDM registration.
b) Environmental Additionality: This suggests that in the absence of the CDM project, a less GHG-friendly activity would likely be undertaken.
c) Technological Additionality: This requires that project activities involve the transfer of clean technologies that were previously unavailable in the project's region.

Thus, CDM project activities, and carbon projects in general, must demonstrate both additionality and contributions to sustainable development to be eligible. This eligibility check is conducted through the validation process which determine whether a proposed project meets the requirements to be registered as carbon project. Once a carbon project is registered and in operation, it must implement the monitoring plan that has been approved during the registration process. This monitoring activity will measure parameters that determine the actual reduction of GHG emission. This monitored emission reduction will then undergo a verification process to get it certified according to the standards that it is registered to. Only certified emission reductions will be able to be traded in the carbon market.

2.2 Carbon Trading

Pérez and Rhode (2020) noted that global CO_2 emissions have reached their highest level in 2017, with an increasing trend for the last 250 years and an average annual growth rate of 3%. Currently, China and the United States are the biggest polluter, followed by India and Russia (Figure 1). As a response, carbon pricing initiatives have emerged as vital tools for both the public and private sectors, as these assign a cost to carbon or GHG that negatively impacts the environment. By internalising the cost of carbon emissions, the societal burden is shifted to the polluters themselves, adhering to the polluter-pays principle. When polluters are made to pay for their emissions, they are discouraged from emitting as much, and the products they manufacture become relatively more expensive. This leads to reduced demand for their products and incentivises innovation to develop greener methods of providing goods and services. This rationale underscores the need for deliberate policy measures to price pollution. For the purpose of clarity, this paper will only focus on carbon trading instruments.

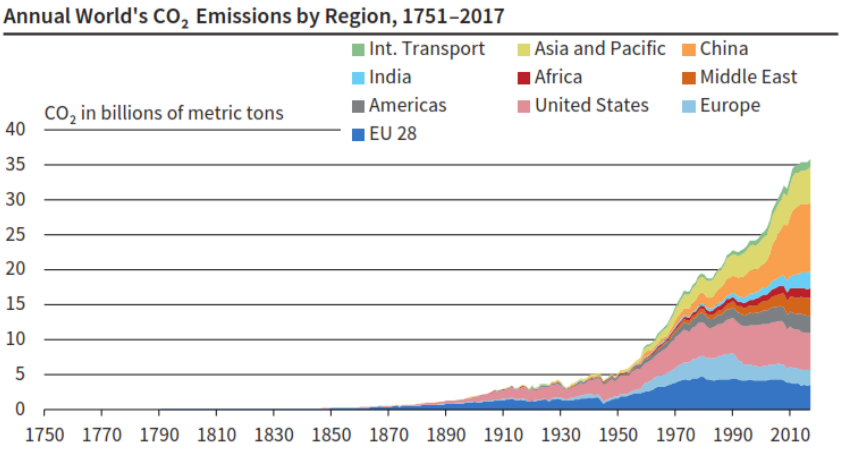

Figure 1: Annual world's CO_2 emissions by region (1751-2017). (Pérez & Rhode, 2020).

The carbon trading instrument, commonly known as cap-and-trade, involves trading certificates allocated in limited quantities in the carbon market. If the party generating carbon credits has a surplus of credits beyond what it needs, then it can sell the surplus on the market. On the other hand, if any party is lacking credits, then it can purchase from those with a surplus or from the market. This creates a carbon market situation determined by supply and demand, making the carbon price subject to market conditions. Generally, there are two types of trading instruments: emission trading schemes (ETS) and the crediting mechanism, which trade emission permits and carbon credits, respectively. Although this scheme mitigates overall carbon emissions and ensures flexibility, especially for businesses, the market-determined price implies higher uncertainty.

2.2.1 International Carbon Market

In general, the global carbon market is separated into two categories: regulatory market and voluntary market. The regulatory market was initiated under the Kyoto Protocol through three mechanisms, including the CDM, which will be highlighted in this paper. The voluntary market, born to capture those eligible carbon project that could not be implemented under CDM, was later strengthened by the Paris Agreement. The regulatory carbon market, i.e. CDM, is mandatory, involves host country government support and sometimes government-to-government (G2G) transactions. Annex I countries, that have ratified the Kyoto Protocol, have carbon credit quota per annum. Those that exceed their quota (credit deficit) have options to buy carbon credits from registered CDM projects in the developing countries. The voluntary carbon market, or offset emission, involves business-to-business (B2B) transactions and is generally supported by private entities with high attention to climate change. Awareness of their carbon footprint in their business activities drives the private sectors to participate in the market to reduce their emissions.

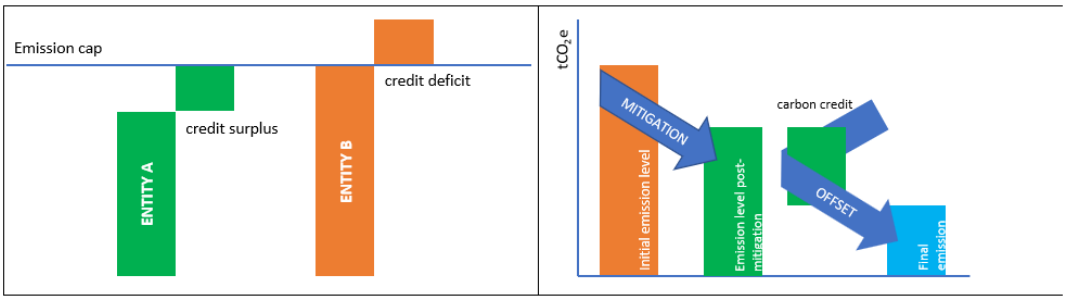

Figure 2: Regulatory and voluntary carbon schemes.
(Source: Fiscal Policy Agency of the Ministry of Finance of the Republic of Indonesia, 2021)

Based on IGES CDM Project Database (2024), as of February 2023, the majority of CDM projects globally in the pipeline are renewable energy projects, accounting for 68% of the total with the majority of this comes from wind and hydro power project. The total issued CERs up to the year 2020 is approximately 2,351 million tonnes of CO_2. Under Article 12 of the Kyoto Protocol, the CDM allows projects to earn Certified Emission Reduction (CER) credits, each equivalent to one ton of CO_2, which count towards meeting a country's Kyoto Protocol targets. As explained above, it is only limited to Annex I countries. In contrast, Article 6 of the Paris Agreement defines a carbon market driven by supply and demand for international cooperation and the exchange of emission reductions between countries. This allows all governments to engage in voluntary cooperation in implementing their NDCs. While similar to its predecessor, Article 6 introduces greater flexibility, enabling both businesses and countries to participate voluntarily in achieving their NDC targets, which enhances the potential for broader

engagement and innovation in carbon reduction efforts, making the Paris Agreement's carbon market a more inclusive and dynamic mechanism for addressing climate change.

Separately, UNDP Voluntary Carbon Market Report (2024) noted that an approximate of 352 million tCO_2e of volume have been issued from the voluntary carbon market in 2021. There are several prominent carbon standards which companies have used to engage in international carbon market transactions, including American Carbon Registry (ACR), Climate Action Reserve (CAR), Gold Standard (GS), Verified Carbon Standard (VCS), Global Carbon Council (GCC), Plan Vivo (PV), and Climate Forward (CF). VCS holds the largest share of carbon credits, followed by GS. Climate Focus (2023) noted that South Asia region holds the largest share in voluntary carbon market, followed by East and South Africa in terms of total projects registered (19%) and Latin America and the Carribean in terms of credits issued (19.3%). Southeast Asia and Developing Pacific only accounts for 6.2% of projects registered and 11.8% of credits issued.

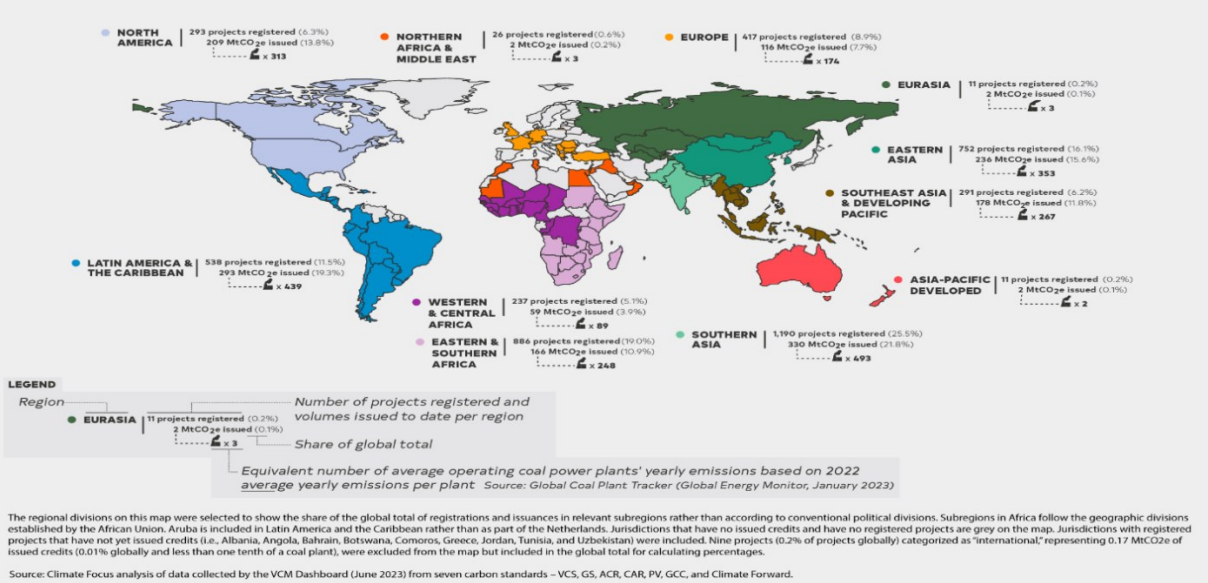

Figure 3: VCM credits issuance and registered projects. (UNDP Voluntary Carbon Market Report, 2024)

2.2.2 Indonesia Domestic Carbon Market

In 2021, the Government of Indonesia issued Presidential Regulation 98/2021 on Carbon Pricing, which requires businesses to reduce their emissions by adhering to an emission cap to meet the country's NDC targets. Only after achieving these targets businesses are allowed to monetize their credits in the market. This regulation represents a significant step in aligning Indonesia's climate action with economic value and international economic benefits. Consequently, the Government of Indonesia has identified carbon pricing as a key instrument to fulfill its GHG emission reduction commitments under the NDC while also incentivizing or commercializing the outcomes of these actions. Investors and businesses entering Indonesia's carbon market must understand the underlying principles of carbon pricing, which will be further clarified in the implementing regulations.

The Presidential Regulation explicitly delegates coordination authority across various ministerial sectors. Mulyana (2023) noted that through the Minister of Environment and Forestry (MoEF) Regulation 21/2022, the MoEF heads the general procedures for the implementation of carbon pricing. Delegation of authorities to different sectors has led to the establishment of a comprehensive carbon pricing regulatory framework. Multiple sector ministries, such as the Ministry of Energy and Mineral Resources (MEMR), have the authority to regulate carbon quota at the ministerial level. For instance, MEMR Regulation 16/2022 is crucial for Indonesia's energy sector as it sets the roadmap and cap for the power plant subsector.

Much like its international counterpart, the traded carbon credits in Indonesia's domestic carbon market are referred to as *Sertifikat Pengurangan Emisi Gas Rumah Kaca* (SPE GRK). All carbon projects are registered in the *Sistem Registri Nasional Pengendalian Perubahan Iklim* (SRN PPI), an Indonesian government-mandated carbon registry platform. SRN PPI serves as a comprehensive data policy tool for GHG emissions, accessible to the public, and containing detailed information on carbon projects, such as the account holder, the issued credit, the corresponding mitigation activity, and the credit status (whether retired or available).

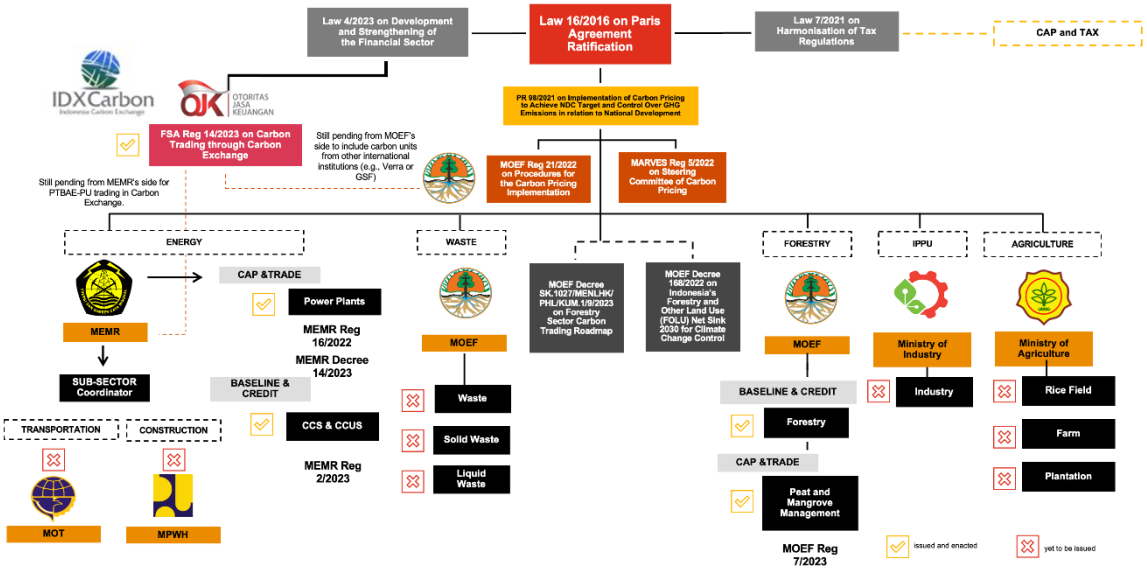

Figure 4: Current Indonesia's carbon pricing regulatory framework. (Mulyana, Fifiek and Indra Allen, 2023)

SRN PPI is anticipated to align with IDX Carbon, an Indonesian official carbon exchange, which was launched in September 2023 and operates under the supervision of the Financial Services Authority (Otoritas Jasa Keuangan, OJK). The Government of Indonesia currently uses IDX Carbon to focus on domestic carbon trading, prioritising its 2030 commitment. OJK Regulation 14/2023 underscores the necessity for traded carbon credits to be registered in SRN PPI beforehand. Although IDX Carbon appears to open opportunities for international carbon trading, this provision will be subject to further implementing regulations to be discussed with the MoEF.

2.3 Carbon Buyers and Sellers

The carbon market will not be alive if there is no buyers and sellers who conducted transactions in the market. In this market, sellers are project owners or project developers that initiate renewable energy projects which in and of itself generates carbon credits by reducing their GHG emissions. Buyers are businesses, organisations, even governments that wish to offset their carbon emissions by purchasing carbon credits from the sellers to meet their emission reduction target.

The Patuha Unit-1 project is developed by GDE and is registered under CDM with two project participants, GDE and Ecosecurities International Limited. Under the CDM, the buyers are Annex I countries, as it is within the Kyoto Protocol timeline, while the registered project participants are the sellers of CERs. Today, the market adopts the Paris Agreement in meeting their NDC and NZE plan, hence GDE upcoming GDE's units have the chance to be registered in the voluntary carbon market. Under the Paris Agreement, buyers are not limited to Annex I countries, making the carbon market driven by supply and demand, as well as the need for each country to meet their NDC targets. As a project owner, GDE already has PPAs for both Dieng and Patuha Geothermal Concession Areas, each with a planned 8 units to be developed. Therefore, GDE, with its significant potential still abundant in its geothermal areas to develop more geothermal power plants, has the chance to participate in the voluntary market.

Considering current carbon pricing regulations and policies in Indonesia, the carbon credits from these future projects should be traded within SRN PPI framework. Fossil-fuel based power plants or other companies aiming to offset their carbon emissions should be able to purchase these newly issued credits. Looking at the bigger picture of Indonesia's carbon policy, it is shown that international carbon market has proven significant demand for carbon credits. Hence it would be an opportunity for all the stakeholders in Indonesia to participate and collaborate with the international carbon market as it could leverage the country's targets to meet NDC, while at the same time invite investments to come into the country.

3. GEOTHERMAL POTENTIAL FOR EMISSION REDUCTION IN INDONESIA

Located in the Pacific Ring of Fire among three active tectonic plates, Indonesia boasts approximately 127 active volcanoes, resulting in a substantial geothermal resource potential of about 23.36 GW and making it one of the top three countries with the largest geothermal reserve alongside the United States and Japan (JFS Japan, n.d.). The capacity factor of geothermal power plants can reach 90% per year, allowing them to serve as a reliable baseload in electricity systems with higher capacity utilisation compared to other energy sources. Unlike wind

and solar energy, geothermal energy's productivity is relatively unaffected by climate change, offering a consistent and stable energy supply throughout the year. The utilisation of geothermal energy can significantly reduce dependence on fossil fuels. Guttiérez-Negrin (2024) noted a global increase in geothermal installed capacity from 15,414 MW to 16,318 MW between 2018 and 2021, with Indonesia contributing 246 MW to this growth. In 2020-2021, Indonesia held the second highest geothermal installed capacity globally, as shown in Figure 5.

Table 1: Geothermal Resources in Indonesia. (Geological Agency, 2021)

No.	Island	Points of Location	Resources (MW)					Total Installed Capacity
			Speculative	Hypothetic	Reserves			
					Probable	Possible	Proven	
1	Sumatera	101	2,167	1,567	3,624	976	1,126.4	949.75
2	Java	75	1,259	1,191	3,260	377	1,820	1,253.8
3	Bali	6	70	21	104	110	30	0
4	Nusa Tenggara	34	215	146	783	121	12.5	19.08
5	Kalimantan	14	151	18	6	0	0	0
6	Sulawesi	90	1,352	342	989	180	120	120
7	Maluku	33	560	91	485	6	2	0
8	Papua	3	75	0	0	0	0	0
Total Location		**356**						
Subtotal Potential Resource			**5,849**	**3,376**	**14,131.9**			
Total Potential Resource			**23,356.9**					

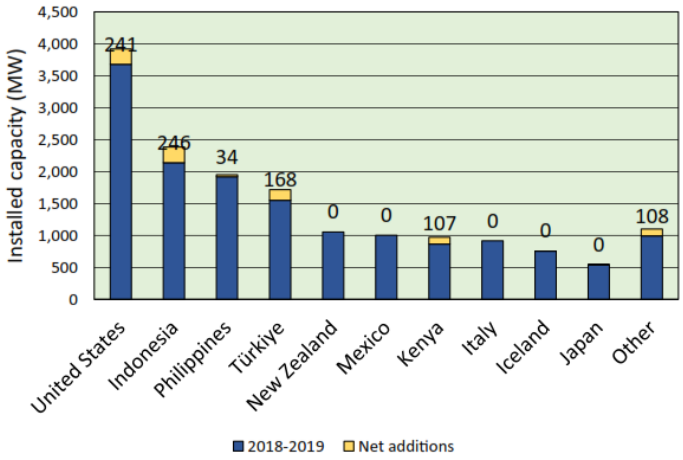

Figure 5: Top ten countries with the highest geothermal installed capacity in 2020-2021, and net additions in MW over the last 3 years. (Guttiérez-Negrin, 2024)

Indonesia's geothermal industry has a long history, with the first major project established in Kamojang, West Java, in 1983. The largest individual field by installed capacity is Gunung Salak in West Java, with 376.8 MW across six single-flash power plants, followed by Sarulla in North Sumatra, with 330 MW in three binary ORC power plants. These fields are operated by JOCC Star Energy Geothermal Salak, Ltd., and JOCC Sarulla Operations Ltd., respectively (Susmanto et al., 2023). As of 2022, there are 18 operational geothermal fields in Indonesia, including Dieng and Patuha, each with a net capacity of 55 MW, owned by PT Geo Dipa Energi (Persero) (GDE).

3.1 The Challenges to Indonesia's Geothermal Development

The Government of Indonesia's energy strategy focuses on diversification, environmental sustainability, and maximising the use of domestic energy resources. The National Energy Policy (Kebijakan Energi Nasional, KEN) 2014 targets a primary energy mix of 23% new and renewable energy (NRE), with 3% from geothermal, by 2025. Indonesia is also committed to achieving NZE by 2060 or earlier. Geothermal power is pivotal in reaching these targets, given Indonesia's status as the country with the largest potential geothermal capacity. However, the country currently utilises only about 9.81% of its geothermal potential. Development of geothermal power projects is prioritised in both the State-Owned Electricity Company's (PLN) Electricity Business Plan (Rencana Usaha Penyediaan Tenaga Listrik, RUPTL) and the Government's National Energy General Plan (Rencana Umum Energi Nasional, RUEN) to meet Indonesia's NRE target. However, the overall pace of development has been slow.

Despite being commercially viable, geothermal power projects in Indonesia face significant sector-specific challenges that deter investments. Setiawan (2014) categorises these challenges into upstream side problems, downstream side problems, and supporting side problems.

3.1.1 Upstream Side Problems

The lack of information on available reserves leads to investor uncertainty, which results in high upfront capital requirements. The risk of exploration failure further hinders project bankability and complicates financing efforts. Additionally, geothermal sites sometimes overlap with conservation and protected forests, posing environmental and regulatory challenges.

3.1.2 Downstream Side Problems

Inadequate incentives and pricing mechanisms fail to reflect the environmental benefits of geothermal technology and do not provide investors with a return commensurate with the higher risks associated with developing green geothermal fields. The presence of only one buyer in the geothermal market weakens the sellers' bargaining position, further deterring investment.

3.1.3 Supporting Side Problems

Indonesia's complex bureaucracy poses significant obstacles to realising the country's ambitious climate targets, with too many business permits as well as inconsistent rules and regulations. This bureaucratic complexity indicates a lack of commitment and awareness among consumers and society about renewable energy development.

Given the slow pace of geothermal power project development and the sector-specific challenges, policymakers in Indonesia should emphasise the importance of carbon trading as a strategic tool to realise the country's domestic and international climate and renewable energy goals. By prioritising carbon trading, Indonesia can leverage market mechanisms to attract investment in geothermal energy, stimulate innovation in green technologies, and ensure a cost-efficient and transparent path to achieve its NDC and NZE targets by 2060.

3.2 Analysis of Carbon Trading on Geothermal Projects in Indonesia

As explained previously, an eligible carbon project must meet additionality requirements as well as proving its sustainable impact. Thus, engaging a geothermal project as carbon project in carbon trading mechanism can significantly enhance the financial viability of geothermal projects in Indonesia. It should be noted that geothermal projects are heavily dependent on government support, such as subsidies or tax incentives, to make it bankable. By incentivising geothermal projects with carbon trading, it not only boosts the economic attractiveness of renewable energy projects as a whole, but also drives higher demand for geothermal energy. Companies will strive to meet emission reduction targets; increased demand can lead to more favorable power purchase agreements (PPAs) or feed-in tariffs for geothermal electricity, which will provide a stable revenue stream for developers (Indonesia Carbon Trading Handbook, 2022). This should also be supported by a solid policy from the government of Indonesia, as transparent carbon market further enhances market efficiency and competitiveness (Saputra et al., 2022).

Pongtuluran et al. (2024) conducted a hypothetical case study to analyse the effect of carbon trading in a geothermal project by comparing two scenarios: one without carbon trading (Baseline Case) and one with carbon trading (Optimised Case). The Baseline Case relies solely on electricity sales to PLN, while the Optimised Case includes revenue from both electricity sales and carbon trading. The study, focusing on Project ABC located on Java island with a capacity of 55 MW and a capital cost of USD 243 million, employs standard geothermal power plant parameters, such as a 90% capacity factor and major plant overhauls every five years. The economic feasibility assessment compares project revenue, net present value (NPV), and internal rate of return (IRR) between the two scenarios, as illustrated in Figure 6.

In the assessment for a 30-year operational period, the Baseline Scenario generates cumulative revenue of USD 1.088 million but results in a negative NPV of USD -31 million for the project and USD -43 million for equity. With a weighted average cost of capital (WACC) of 7.73% and a cost of equity of 13.5%, the project's IRR of 6.24% and equity's IRR of 6.47% fall short. Conversely, the Optimised Scenario yields greater cumulative revenue of USD 1.122 million, and while the NPV and IRR remain unfavorable, they show improvement. The project's NPV is USD -24 million and the equity's NPV is USD -40 million, with a project IRR of 6.59% and an equity IRR of 7%. Although both still below the desired rate, the hypothetical case shows the benefits of carbon trading inclusion in a geothermal project by enhancing the project's financial performance, demonstrating increased revenue as well as improved NPV and IRR compared to the Baseline Scenario.

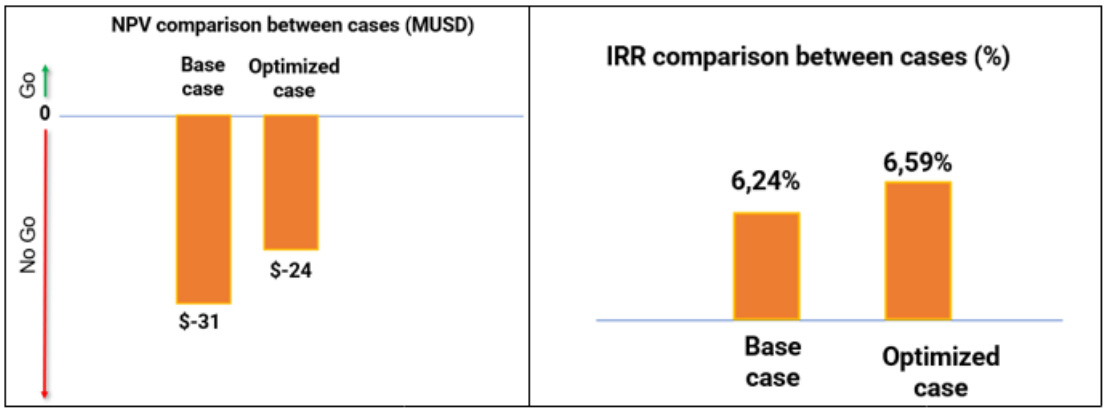

Figure 6: NPV and IRR Projections of Baseline Scenario and Optimised Scenario of Project ABC. (Pongtuluran, 2024)

4. SUSTAINABLE IMPACT OF CDM ON PATUHA UNIT-1 GEOTHERMAL PROJECT

Patuha Unit-1 is one of the major geothermal power plants in Indonesia, having its 55 MW capacity in operation and generating electricity for the Jawa-Madura-Bali (JAMALI) grid, which serves as the biggest grid in Indonesia. This power plant activity has been registered under the CDM since 2012 using CDM methodology ACM0002 of Consolidated Baseline Methodology for Grid-Connected Electricity Generation from Renewable Sources, version 12.2. The activity has proven its additionality by showing that the inclusion of carbon mechanism could increase the Patuha Unit-1's IRR from 6.73% to 7.96% and bridging the viability gap of the project at the time of decision making. During those times, its registration as a CDM project also played a role in the push for the project to be realised and in operation starting September 2014.

In its CDM registered documents, the power plant was expected to reduce an estimate amount of 263,851 tCO_2e annually, taking into account the latest grid emission factor at the time of project registration. The power plant's actual emission reduction certified under CDM has not yet been determined as the power plant is still undergoing verification process when this paper is written. However, the sustainable impact of the power plant can be acknowledged.

Since its start of operation in September 2014, the power plant has supplied an average of annual electricity generation of 446.43 GWh to the JAMALI grid. Hence, it supports the reduction of GHG emissions in the grid. Taking the latest grid emission factor value issued by the Ministry of Energy and Mineral Resources of 0.83 tCO_2e/MWh for JAMALI, those generations can be estimated to quantify as a gross reduction of 370,536 tCO_2e GHG emissions per year. Although the net value of the reduction will be lower as it needs to consider the detailed annual steam production and diesel fuel usage during any shutdown period in the power plant, this reduction of over 0.3 million tCO_2e of GHG per year is equivalent to the amount of CO_2 emissions absorbed around by 463 hectares of Indonesia's average primary dryland forest. This clearly illustrates how the power plant is contributing directly to the environment with positive impact and help the country to achieve its net zero emission and NDC target.

In addition to its support related to SDG 13 for climate action through its direct effort in reducing GHG emissions, the power plant has also been providing positive impact for the communities in four villages who live around its location. The impact includes environmental impact, social impact, and economic impact.

In the environmental aspect, the power plant always prioritised environmental sustainability so that the ongoing operational processes do not disturb the surrounding environment. The power plant also minimises any potential disturbances that may arise, such as equipment noise/noise inside the power plant and wells, by installing silencer walls, planting trees around the guardrail and using rock mufflers. They also collaborate with the communities around the operational area to carry out conservation programs so that the communities improve their awareness of environmental sustainability concerns. The conservation programme includes flora and fauna species where they conserve land orchids (*Goodyera viridiflora* and *Anoectochilus spp*), Javanese primate Surili (*Presbytis comata*) and Lutung *(Trachypithecus auratus*).

To ensure that the power plant operation also gives positive social impacts to the community, the power plant implements many programmes, such as the scholarship programme for bright young students, book donations to improve literacy and reading interest in the village communities, and vocational training to improve skills. During the COVID-19 pandemic period, the power plant supported the local communities in the health and economic sector by providing training for healthcare for collaborative COVID-19 treatment and management, improving

communities' awareness on sanitation and health issues, and providing staple food package to ensure food security for the communities.

Through construction or investment of infrastructure in the surrounding area where Patuha Unit-1 is operated, the power plant provides indirect economic impacts to the communities. One example is the program to improve the electricity network as the villages are in the remote area that is very far from the main road and thus not yet well connected to the grid. With more reliable electricity, children in the villages can study well during the night and the birth process that happens during nighttime in the villages can be done with ease. Further example is the collaboration of the power plant with Village-Owned Enterprise *(BUMDes)* by providing training and education to improve local workforce's competency and expertise that help their income source.

Ideally, when a carbon project's emissions reduction has been certified, this certified emission reduction can be sold in the carbon market and thus adding revenue to the power plant. This additional revenue will help the power plant operational cost and can also improve the environmental, social and economic impact that the power plant has been giving to the communities. Currently, the power plant is undergoing a verification process with one of its aims is to be able to take some benefit of the certified emission reduction sales to the community by ensuring continuous improved impact to the community.

5. CONCLUSION

With the Global CO_2 emissions showing an increasing trend overtime, i.e. average annual growth rate of 3%, urgent action and intensified efforts to tackle the climate change impact are required. The world now strives to limit the rise of global average temperature to 1.5°C, which means immediate action is crucial. The transition from the Kyoto Protocol to the Paris Agreement underscores the collective responsibility of all nations to mitigate climate change through independently determined commitments, more commonly known as NDC. It marked a significant shift in international climate policy, emphasising universal participation and equal contributions from all nations to mitigate GHG emissions.

Furthermore, the carbon trading mechanism as one of carbon pricing instruments plays an important role, especially in Indonesia, to reach the country's NDC. It is a flexible, market-drive solution for reducing emissions, with both regulatory and voluntary markets playing pivotal roles. A well-established carbon trading mechanism ensure transparency and provide options for buyers, which enhances the appeal of carbon projects that employ various technologies to reduce GHG emissions. Indonesia's domestic carbon market, regulated by Presidential Regulation 98/2021, encourages businesses to meet the country's NDC target while enables the monetisation of carbon credits. Compared to other Asian countries, Indonesia is ahead in their carbon market initiatives. Many renewable energy project developers are eager to learn more about Indonesia's domestic carbon market process, as well as available options for buyers and sellers. This clarity can help carbon credits from Indonesia to be traded internationally and domestically through the approved mechanisms by the government.

Being one of the top three countries with the highest geothermal potential and installed capacity, Indonesia would be amiss to not utilise their geothermal resources to help the development of renewable energy and to support the country's decarbonization goals. Geothermal's characteristics of high capacity factor, reliability, and the fact that it is not affected by climate variability makes it a consistent and a key player in reducing dependence on fossil fuels. However, geothermal is not without its challenges; its development has long been plagued with high upfront costs, regulatory hurdles, and inadequate incentives. Carbon trading has the potential to enhance the economic feasibility and viability of geothermal projects by providing additional revenue through carbon credits sales. It also encourages investment and innovation, which in turn supports Indonesia's NDC and NZE targets. A hypothetical geothermal project case study simulated by Pongtuluran et al. (2024) shows that the addition of carbon credit sales increased the project's revenue, IRR, and NPV, as compared to scenario without carbon credit sales.

As one of Indonesia's major geothermal power plants, Patuha Unit-1, with a capacity of 55 MW, has been pivotal in reducing GHG emissions and supporting the JAMALI grid. Registered under the CDM since 2012, it demonstrated additionality by increasing its IRR from 6.73% to 7.96%, making the project viable. The power plant, operational since September 2014, has supplied an average of 446.43 GWh annually, reducing an estimated 370,536 tCO_2e GHG emissions per year. This impact is equivalent to CO_2 absorption by 463 hectares of primary dryland forest and it aids Indonesia's NDC and NZE targets. The project also fulfils SDG 13 for climate action through its direct effort in reducing GHG emissions. The additional revenue that the power plant receives from carbon trading will help the operational cost as well as improve the welfare of its environment and social landscape. Since operating, the plant has positively impacted local communities, particularly the four nearby villages. It improves the energy mix in the JAMALI grid (SDG 7), provides training to improve local workforce's

competency, and scholarships for students in the village communities (SDG 4). It also collaborates with the communities around the operational area to carry out conservation programs for local flora and fauna (SDG 15) (Department of Economic and Social Affairs, United Nations, 2024).

As such, while Indonesia embraces the change towards a sustainable future, there is still more work that can be done to encourage more participants, particularly in the carbon market. Indonesia still has rooms of improvements, including enhancing the carbon market framework, providing more clarity and transparency on the implementation of carbon market, as well as participating and collaborating with the international carbon market. More international collaborations would speed up the country's road to net zero emission and fulfill their NDC goals.

REFERENCES

Alhusni et al.: Geothermal Business Outlook in Indonesia, *Proceedings*, 48th Workshop on Geothermal Reservoir Engineering, 6-8 February 2023, Stanford University, USA, (2023).

Asian Development Bank: From Kyoto to Paris – Transitioning the Clean Development Mechanism, *Asian Development Bank*, (2021).

Bisore, Simon and Walter Hecq: Regulated (CDM) and voluntary carbon offset schemes as carbon offset markets: competition or complementary?, *Centre Emile Bernheim*, 12, **16**, (2012).

Bowen, Alex: The case for carbon pricing, Grantham Research Institute on Climate Change and the Environment & Centre for Climate Change Economics and Policy, (2011).

Criqui, P., et al: Carbon Taxation: A Tale of Three Countries, *Sustainability*, **11**, (2019).

Department of Economic and Social Affairs, United Nations, 2024. *Sustainable Development, The 17 Goals*. Available at: https://sdgs.un.org/goals

Geo Dipa: *Yearly Production Data*, (2023).

Geo Dipa, *Sustainability Report*, (2020-2023).

GoI, 2022. *Government of Indonesia*, *National Forest Reference Level for Deforestation, Forest Degradation and Enhancement of Forest Carbon Stock*, 2022, p.15-16, Available at: https://redd.unfccc.int/media/2nd_frl_indonesia_final_submit.pdfGutiérrez-Negrin, Luis: Evolution of worldwide geothermal power 2020-2023, Geothermal Energy, 12, **14**, (2024).

IPCC: Summary for Policymakers" in Global Warming of 1.5°C. *An IPCC Special Report on the impacts of global warming of 1.5°C above pre-industrial levels and related global greenhouse gas emission pathways, in the context of strengthening the global response to the threat of climate change, sustainable development, and efforts to eradicate poverty*, in Press, (2018).

JFS Japan, n.d., Geothermal power: *Japan has world's third largest geothermal reserves, 60 percent of which can be Developed* | JFS Japan for sustainability. (n.d.). JFS Japan for Sustainability. Available at: https://www.japanfs.org/en/news/archives/news_id035043.html

Kazunari Kainou, CEPR: *Collapse of the Clean Development Mechanism scheme under the Kyoto Protocol and its spillover: Consequences of 'carbon panic'*, (2022). (Available at: https://cepr.org/voxeu/columns/collapse-clean-development-mechanism-scheme-under-kyoto-protocol-and-its-spillover)

Liverman, Diana: *Carbon offsets, the CDM, and sustainable development*, (2009), 130-141.

Ministry of Energy and Mineral Resources of the Republic of Indonesia: *Ministerial Decree on Electricity Grid Emission Factor No. 163.K/HK.02/MEM.S/2021, (2021).* (Available at: https://jdih.esdm.go.id/index.php/web/result/2183/detail ESDM)

Mulyana, Fifiek and Indra Allen: *Indonesia's Carbon Pricing: Understanding the Basic Regulatory Framework, PWC*, (2023).

Net-Zero Asset Owner Alliance (Alliance): Discussion paper on governmental carbon-pricing, *UN Environment Programme Finance Initiative*, (2022).

Pérez, Maria Hofbauer and Carla Rhode: Carbon Pricing: International Comparison, *ifo DICE Report*, **18**, (2020), 49-58.

Pongtuluran et al.: Assessing the Impact of Carbon Trading to Indonesia Geothermal Project Economic, *Proceedings*, 49th Workshop on Geothermal Reservoir Engineering, 12-14 February 2024, Stanford University, USA, (2024).

Pramudianto, Andreas: Dari Kyoto Protocol 1997 hingga Paris Agreement 2015: Dinamika Diplomasi Perubahan Iklim Global dan ASEAN Menuju 2020, *GLOBAL*, **18**, (2016), 76-93.

Rijal, Neelam: Voluntary Carbon Market (VCM) Report: Landscape, Opportunities and Challenges for Private Sector Engagement in Nepal, *United Nations Development Programme*, (2024).

Setiawan, Hadi: Geothermal Energy Development in Indonesia: Progress, Challenges and Prospect, *International Journal on Advanced Science Engineering and Information Technology*, 4, **4**, (2014).

Susmanto et al.: Update on geothermal development status and working areas potential in Indonesia, *Proceedings*, World Geothermal Congress, 15-17 September 2023, Beijing, China, (2023).

Tim Penyusun: Indonesia Carbon Trading Handbook, *Katadata Insight Center*, (2022).

Tsukui et al.: IGES CDM Project Database, *Institute for Global Environmental Strategies*, Hayama, Japan, (2024).

United Nation Framework Convention on Climate Change (UNFCCC): *Glossary of CDM Terms*, (2022). (Available at: https://cdm.unfccc.int/Reference/Guidclarif/glos_CDM.pdf)

Webb, C., & Zakir, Z.: *What the Paris Agreement means for carbon pricing and natural climate solutions: A business guide*, The Nature Conservancy, (2019).

World Bank, *What is Carbon Pricing*, Accessed 2024. Available at: https://carbonpricingdashboard.worldbank.org/what-carbon-pricing

SMART Heating System: IoT-Enhanced Geothermal Brine Utilization for Efficient Space and Water Heating in Dieng Tourism Areas

Yoga Sanjaya[1], Bintang Putra Megantara[2], Farhan Izzat[3],
M. Ihsan Fadhlurahman[2], and Sevilla Maharani[4]

[1]Department of Mechanical and Industrial Engineering, Faculty of Engineering, UGM
[2]Department of Nuclear Engineering and Engineering Physics, Faculty of Engineering, UGM
[3]Department of Geological Engineering, Faculty of Engineering, UGM
[4]Department of Archeology, Faculty of Social Science, UGM

yogasanjaya@mail.ugm.ac.id, bintangputramegantara2004@mail.ugm.ac.id, farhanizzat2004@mail.ugm.ac.id, mihsanfadhlurahman@mail.ugm.ac.id, sevillamaharani2004@mail.ugm.ac.id

Keywords: Geothermal Brine Utilization, Heating System, Internet of Things, Energy Efficiency, Tourism Facilities

ABSTRACT

Popularly referred to as the Land Above the Clouds, Dieng is a highland in Central Java, Indonesia, that offers stunning natural beauty and rich culture. In recent years, Dieng has developed into one of Indonesia's most popular tourist destinations, attracting thousands of domestic and foreign tourists each year. This success is not only caused by its natural and cultural beauty, but is also supported by developing accessibility, improved tourism services, and comfortable accommodation facilities. In providing accommodation facilities, spaces and water heating for tourists become indispensable. Apart from its tourism aspects, Dieng also possesses electricity-producing geothermal fields (power plants) in Central Java. However, the power plant only utilizes steam-phase geothermal fluids, resulting in waste in the form of liquid-phase geothermal fluids (brine). The brine has tremendous potential as its temperature reaches 180°C. This indicates potential utilization of geothermal brine to provide comfortable accommodation facilities, especially for space and water heating. In the proposed scenario, the brine from the separator outlet will be transmitted through pipes to the tourism areas. This energy will be utilized for the space heating and water heating systems in villas. Based on analysis, assuming a heat loss of 5°C per kilometer on the pipes and a brine flow rate of 0.5 kg/s, the energy carried by this brine reaches 304.5 kW. The brine will flow through an aluminum-finned copper tube coil to transfer heat to the refrigerant. Subsequently, the refrigerant will pass through a compressor to increase its pressure and temperature; thus, transforming the liquid phase of the refrigerant into a superheated phase. This superheated phase of the refrigerant will be utilized for water heating through a desuperheater and for space heating through a condenser. In the space heating mechanism, cold air from outside will be drawn into the space by a blower fan, making direct contact with the condenser. Consequently, the heat from the refrigerant in the condenser will be transferred to the air, producing warm air suitable for space heating in the villas. To maximize energy usage and efficiency in space heating, a SMART heating system is proposed. The SMART heating system integrates the concept of IoT (Internet of Things) to carry out automatic control and monitoring of space and water heating systems. The system utilizes a temperature sensor for data acquisition of space conditions. Then, the control unit reads the data for processing. If the control unit detects the space temperature is below 20°C, it activates a reversing valve to heat the refrigerant with brine. Afterwards, the control unit activates the blower fan to warm the space. The SMART heating system regulates the opening of valves, as well as the performance of the blower so that the space temperature is ideal (20-22°C). Besides that, the water-heating scenario operates as the user's instruction. The hot water is stored in the storage tank for supply. The embedded IoT within the SMART heating system enables a more efficient energy management process, reduces greenhouse gas output from refrigerants, and reduces operational expenses.

1. INTRODUCTION

Dieng, a popular tourist spot situated in Central Java, Indonesia, has garnered favor among both domestic and international travelers. The breathtaking natural landscapes, vibrant cultural heritage, and diverse array of attractions have solidified Dieng's status as one of the top tourist destinations. The Dieng Plateau stands out as one of the main draws, renowned for its striking mountain vistas and refreshing climate, providing a distinct contrast to the typical tropical setting found in most parts of Indonesia. Additionally, sites such as the active Sikidang Crater offer visitors a unique opportunity to witness geothermal phenomena firsthand. Dieng has not only natural and cultural charm, but it is also enhancing its tourist amenities, such as accommodation and infrastructure, to enhance the overall tourist experience. These initiatives have effectively boosted the annual tourist footfall. Data from the Central Java Tourism Office shows that the number of tourist visits to Dieng increases consistently every year. In 2021, Dieng recorded more than 1.5 million tourist visits, and this number

continued to increase in subsequent years. In 2022, the number of visits increased to around 1.8 million tourists, and it is estimated that in 2023, visits will reach more than 2 million tourists.

Travelers who visit Dieng often seek comfort, particularly due to the cold temperature in the area. The use of geothermal energy for room and water heaters can offer additional comfort for tourists. Dieng is known for its significant geothermal potential and the utilization of geothermal steam phase for electricity generation. This process results in the production of liquid phase geothermal fluid (brine) with a temperature of up to 180°C. This brine holds great potential as an alternative energy source, particularly for providing comfortable accommodation facilities, including heating rooms and water in lodgings. The incorporation of brine for both room heating and water heating purposes has the potential to enhance the comfort of tourists while simultaneously decreasing reliance on environmentally harmful fossil energy sources. A research study focusing on the resource consumption patterns of guests residing in self-contained B&B accommodations was conducted. Data was gathered through a smart metering system spanning across four different seasons. The study revealed that the adoption of renewable energy sources, alterations in guest behavior, and emphasis on environmental preservation can significantly enhance resource utilization efficiency. Guests who were provided with sustainability guidance and information managed to achieve savings of 27% in electricity consumption, 22% in gas consumption, 22% in water usage, and 10% in firewood consumption (Warren, 2018).The substantial growth in tourism awareness and the increasing preference for sustainable accommodations among tourists, which prioritize renewable energy, effective waste management, and eco-friendly facilities, presents a lucrative opportunity for utilizing brine for space and water heating. Additionally, it can enhance tourism activities by providing unique and attractive amenities for visitors.

2. FIELD OVERVIEW

2.1 Reservoir Characterization

The Dieng geothermal field is a 63 km2, liquid dominated reservoir geothermal field located in Central Java, approximately 80 kilometers to the northwest of the Special Province of Yogyakarta. Currently, the Dieng field is operated by PT. Geo Dipa Energi with a total installed capacity of 60 MW as of 2019, though a resource estimation by West JEC (2006) using numerical methods indicate that the resource size is 240 MW.

From a geological perspective, the Dieng field has three main prospect areas; Sikidang, Sileri, and Pakuwaja. These prospect areas are separated by low permeability and low temperature barriers, defined by a gravity high and a low conductivity. Thus, a barrier separates the Sileri sector and Sikidang sector in the north and the Pakuwaja sector in the southeast. This study focuses mainly on the Sileri sector as the heating lines mainly utilize brine from wellsite 28, 30, and 31 which are located in the Sileri sector. The geothermal system of the Sileri sector is expressed by the surface discharge in the form of fumarolic discharges in Mt. Sipandu and hot spring discharge in Bitingan and Sileri Crater. These discharges indicate the location of an upflow zone in the Sileri sector. Based on analysis conducted by Shalihin et al., 2022, these findings indicate a mature hydrothermal system.

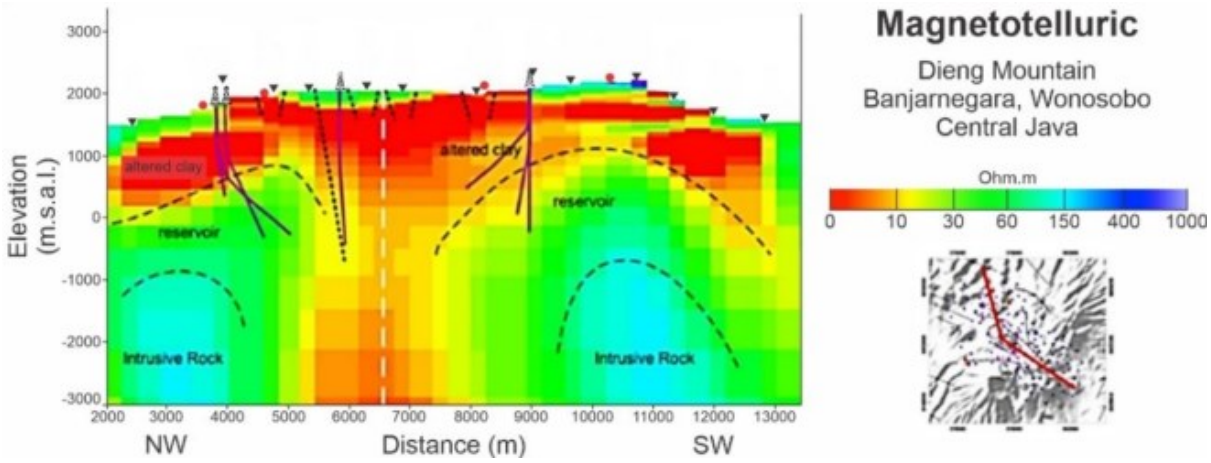

Figure 1: Cross-sectional 2D MT Inversion model of the Dieng Geothermal Field, Sileri sector is to the NW, Sikidang is to the SW. (PT. Geo Dipa Energi in MEMR, 2017)

2.2 Fluids Characterization

Sileri sector The subsurface hydrothermal mineral assemblage in the Sileri Crater consists of epidote, wairakite, calcite, quartz, albite, and clays (smectite, chlorite, illite), indicating the interactions of the rocks with near neutral pH-alkali chloride waters (Shalihin et al., 2022). The fluid originates from meteoric water which experiences slight mixing with magmatic fluid, water-rock interaction with sedimentary or meta-sedimentary rocks, and intensive boiling. Furthermore, the fluid is known to be two-phase (liquid-dominated) with neutral pH,

temperature ranging from 283 to 338 °C, low NCG (<1 wt%), enthalpy value 379.7 kJ/kg (Kencana et al., 2024; Pambudi et al., 2015). The elemental composition of geothermal fluid in Sileri Crater is as shown in Table 1.

Table 1: Fluid composition of Sileri Crater.

Element (ppm)	Sampling 1	Sampling 2
SiO2	1400	1145
Cl	21,499	25,400
SO4	-	-
Li	40	60
Na	8340	11,460
K	2520	3340
Mg	-	-
Ca	440	860

2.3 Silica Scaling Analysis

Silica scaling analysis is conducted to determine whether silica deposition will occur in the pipeline transmission for district heating. Silica scaling can affect the mass flow rate of the brine produced. The presence of silica scaling can be assessed by the Silica Saturation Index (SSI) of the geothermal fluid well. SSI can be calculated from the ratio of the saturated pressure of silica to the wellhead pressure according to equation (1).

$$SSI = \frac{P_{sat}(Silica)}{WHP} \quad (1)$$

According to data from PT Geo Dipa Energi, the saturated pressure values of silica and the wellhead pressure are as follows:

Table 2: SSI value at wellsite in Dieng area, PT Geo Dipa Energi (2023).

Wellsite	P_{sat}(Silica) (barg)	Well Head Pressure (barg)	SSI	Silica Scaling
HCE-29	24.9	45.6	0.54	Impossible
HCE-7B	22.2	23	0.96	Impossible
HCE-7C	27.5	33.4	0.82	Impossible
HCE-28A	20.	20	1	Saturated
HCE-28B	21.9	28	0.78	Impossible
HCE-30	23.4	34.1	0.68	Impossible
HCE-31	17	18.6	0.91	Impossible
HCE-10A	15.3	36.3	0.42	Impossible

SSI parameters can be used to estimate the amount of silica scaling with the following criteria, (Sofyan et al., 2021):

- If SSI > 1, the fluid is supersaturated and silica deposition is possible.
- If SSI = 1, the fluid is saturated.
- If SSI < 1, the fluid is undersaturated, so silica precipitation is impossible.

Based on Table 2, it can be concluded that there is a need to consider measures for handling potential silica scaling at wellsite HCE-28A before installing the pipeline transmission for district heating.

3. RESULTS AND DISCUSSION

3.1 Heat Transfer Analysis in the SMART Heating System

Heat transfer analysis is conducted using several mathematical models in accordance with thermodynamic processes. The parameter considered in the calculations is the temperature of the brine from the outlet separator. The parameters of the brine are shown in Table 3.

Based on Table 3, it can be seen that the brine temperature is 182 °C and it carries an enthalpy of 772.3 kJ/kg. The heat transfer analysis is conducted by considering three aspects: the pipe transmission system, the heat exchanger system, and the space heating system. The analysis evaluates the energy transfer efficiency and the energy losses that occur.

Table 3: Parameters of the brine from outlet separator of the single flash power plant (Pambudi et al., 2015).

Parameter	Value	Unit
Enthalpy h	772.3	kJ/kg
Entropy s	2.159	kJ/kg K
Pressure P	10.5	bar
Temperature T	182	$°C$
Mass flow $\dot{m}$	110.6	kg/s
Energy	77,077	kW
Exergy	16,143	kW

3.1.1 Pipeline Transmission System

Transmission line to distribute the brine will be installed in the Sikadang area, considering the large number of homestays in the area. The transmission pipeline will be connected to the brine line from then channeled to the homestay area and will be returned to the south brine pipeline to maintain the stability of the mass flow rate at the injection well.

Brine from the outlet separator will be channeled to the homestay facilities through a pipeline transmission system. The installation of the pipeline starts from wellpad #28 and leads to the brine channel to the pond and injection well. Figure 3 shows the pipeline route scheme for district heating in the Dieng tourist area.

Estimated length of the pipeline obtained from calculations using Google Maps is 2.86 km. From this length, it is necessary to consider the pressure drop produced to determine the heat loss that occurs due to the pipeline. To calculate the pressure drop produced by the pipeline transmission, equation (2) can be used.

$$\Delta P_f = 1.75\times10^{-4}\frac{fL\dot{m}^2}{\rho D^5} \quad (2)$$

$$f = \frac{0.25}{\left\{log\left[\frac{\epsilon}{3.7D}+\frac{5.74}{Re^{0.9}}\right]\right\}^2} \quad (3)$$

$$Re = \frac{4}{\pi}\frac{\dot{m}}{\mu D} \quad (4)$$

where L, $\dot{m}$, ρ, D, f, Re, ϵ, μ are the pipe length (ft), mass flow rate (lbm/s), brine density (lbm/ft3), inside diameter of pipe (in), friction factor given by the Swamee-Jain equation (3), Reynolds number, pipe roughness (ft), and absolute viscosity (lbm/ft s).

To consider the magnitude of the pressure drop generated in pipeline transmission, it is essential to select the pipe diameter and determine the desired mass flow rate. This selection utilizes commercial pipes made of ASTM A106 Gr B material. Analysis involves choosing pipe dimensions that result in the lowest pressure drop by adjusting the dependent variables: mass flow rate and inside pipe diameter. Figure 4 illustrates the analysis results of pipe diameter and brine mass flow rate's impact on pressure drop.

Based on Figure 4, it can be considered to choose a larger pipe diameter and reduce the mass flow rate of brine. Under optimal conditions, a pipe with an 80 cm diameter and a mass flow rate of 0.5 kg/s results in a pressure drop of 8×10^{-10} kPa, which corresponds to a temperature decrease as calculated in Table 4 and 5.

According to the calculations based on the change in brine enthalpy, the temperature drop due to pressure drop is not significant, with $\Delta T = 0.03°C$. Because of this minimal temperature drop, the transmission pipe does not require insulation coating. Therefore, brine from the brine line at 182°C will enter the district heating transmission pipe with an estimated temperature of 181.97°C after covering 2.86 km. Alternatively, we can estimate it to be 181°C, considering the thermal conductivity of the pipe which can cause heat loss.

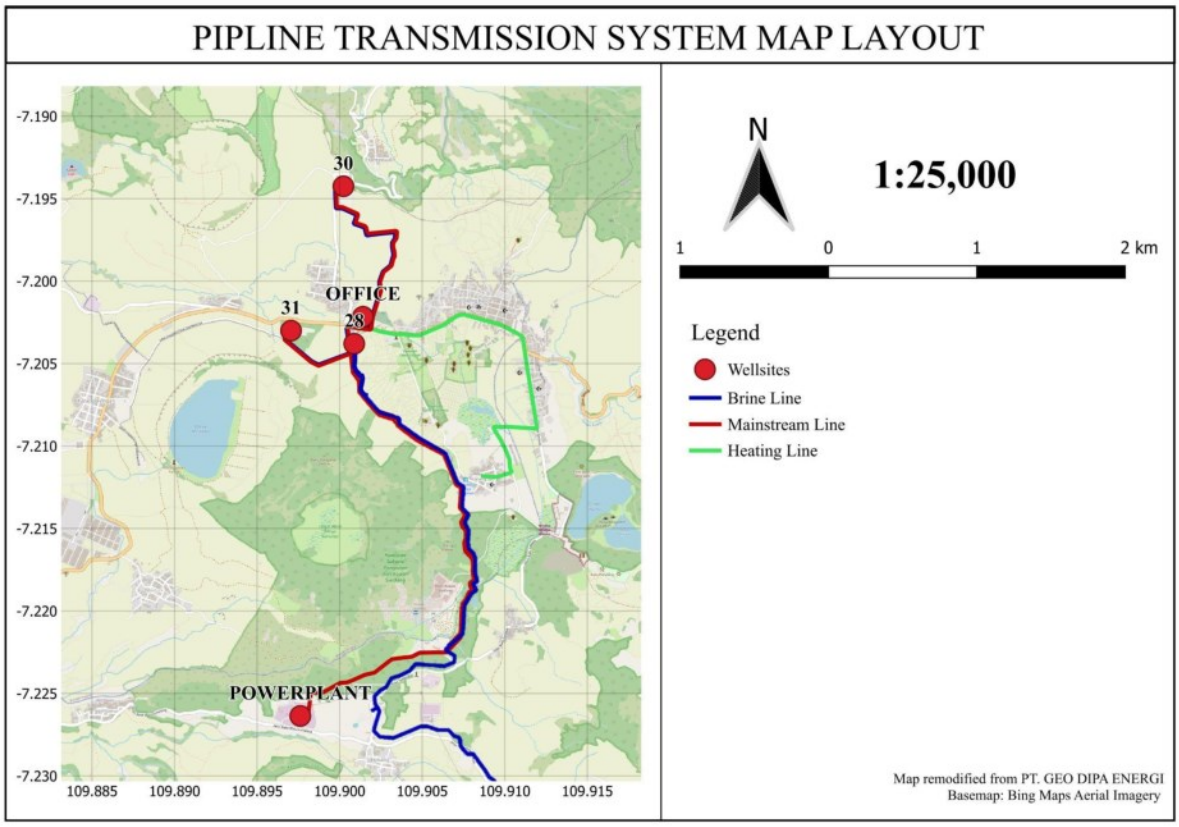

Figure 2: Pipeline Transmission System Map Layout (PT. Geo Dipa Energi in MEMR, 2017).

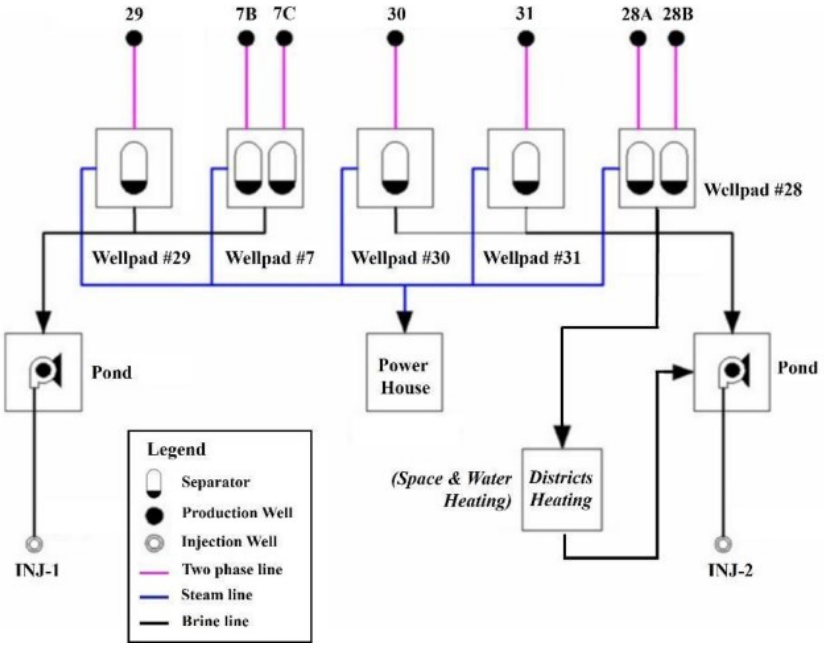

Figure 3: Scheme of brine extraction through pipeline transmission from well pad #28 for district heating (Modified from Pambudi et al., 2015).

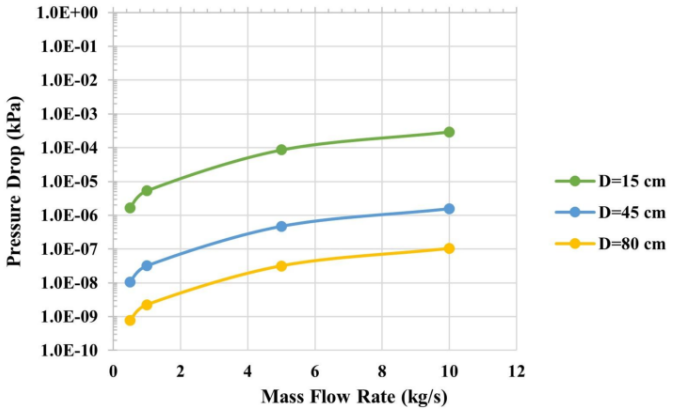

Figure 4: Relationship of changes in mass flow rate and pipe diameter to the pressure drop generated on a logarithmic scale for the selection of district heating transmission pipe dimensions.

Table 4: Interpolation of pressure data with enthalpy from pipeline transmission system due to pressure drop.

Pressure Table (Cengel et al., 2011)	Value (kPa)	Enthalpy (kJ/kg)
P1	1000	762.51
P(2.86 km)	1050 - 8×10^{-10}	**771.77**
P2	1100	781.03

Table 5: Interpolation of temperature data with enthalpy from pipeline transmission system due to pressure drop.

Temperature Table (Cengel et al., 2011)	Value (°C)	Enthalpy (kJ/kg)
T1	180	763.05
T(2.86 km)	**181.97**	771.77
T2	185	785.19

To determine the necessary refrigerant temperature change in the heat exchanger, we can follow the 'rule of thumb' (Lund, 2010). The rule of thumb for determining the temperature in a water heating system heat exchanger is 10/5/5. This rule indicates that 10 is the temperature difference between the water supplied to the water tank and the water temperature, 5 is the temperature difference between the refrigerant entering the heat exchanger and the water supplied to the water tank, and the last 5 is the temperature difference between the refrigerant leaving the heat exchanger and the water temperature. For determining the temperature in a heat exchanger for space heating, the 15/10/10 rule is used. The rule for space heating indicates that 15 is the temperature difference between the air supplied to the space and the air temperature, 10 is the temperature difference between the refrigerant entering the heat exchanger and the air supplied to the space, and the last 10 is the temperature difference between the refrigerant leaving the heat exchanger and the air temperature.

In practice, to achieve a water temperature of 45°C and a room temperature of 20°C, which are the average temperatures at which most people feel comfortable, the temperature design shown in Figure 6 is required.

After the temperatures at the heat exchanger are established, the temperature changes occurring at the compressor and expansion valve can be determined using the T-s diagram shown in Figure 7. Once the temperatures of each component are known, the temperature change of the brine in this condition is calculated by determining the amount of heat required to change the phase of the refrigerant to gas, or Q_L(kJ/kg).

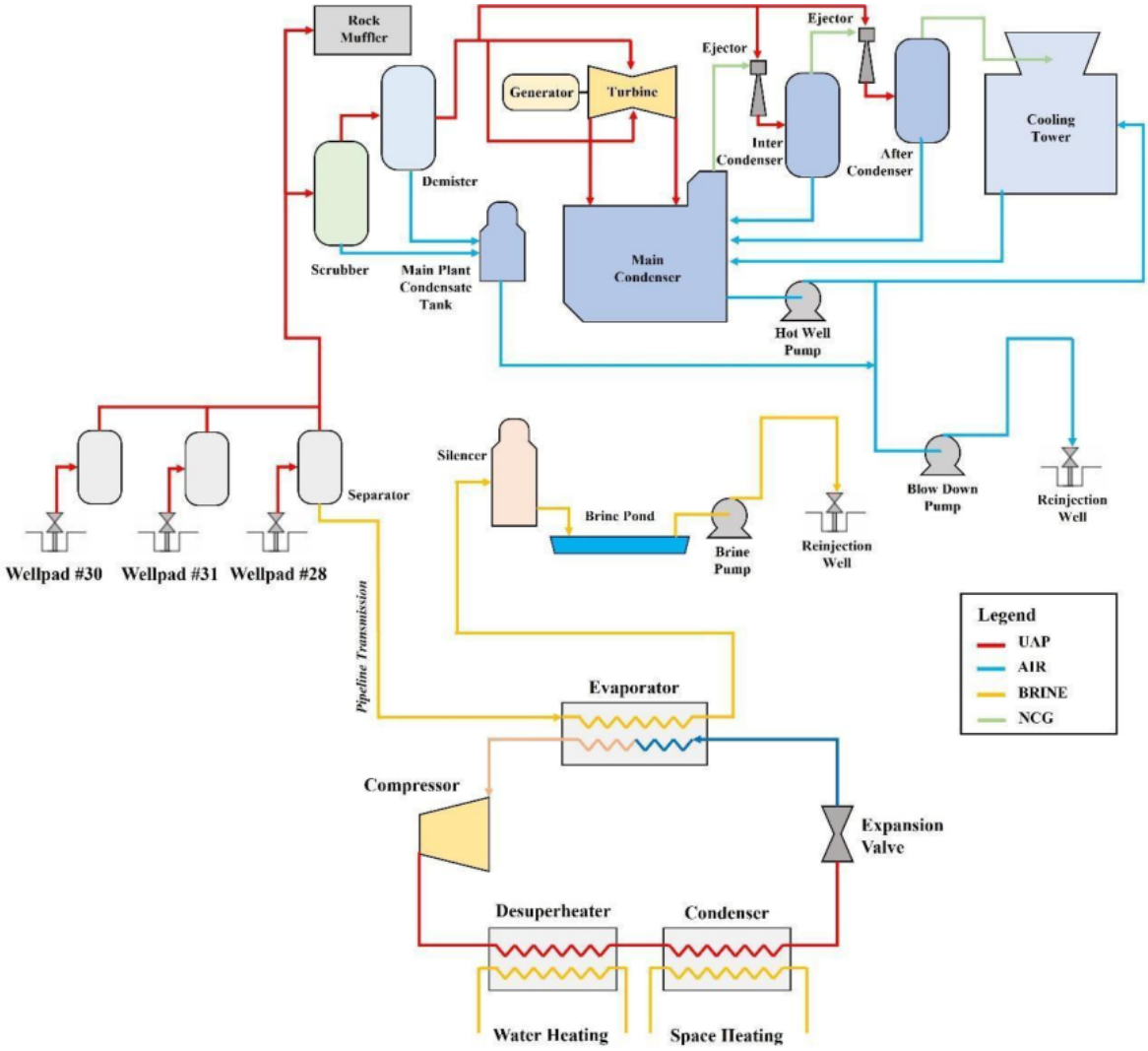

Figure 5: Scheme of district heating system from geothermal power plant.

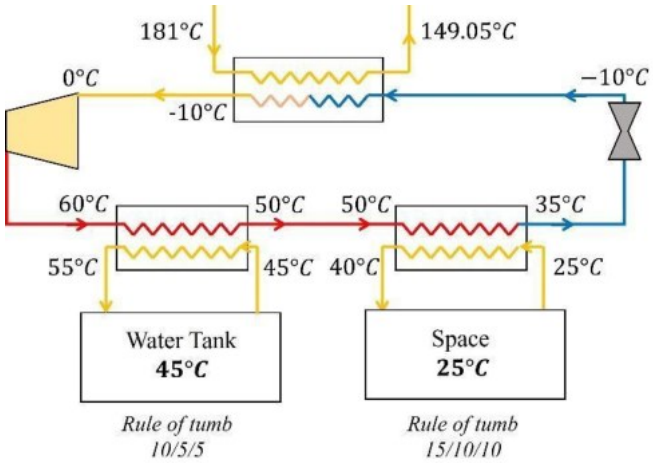

Figure 6: Temperature design of water heating and space heating heat exchanger.

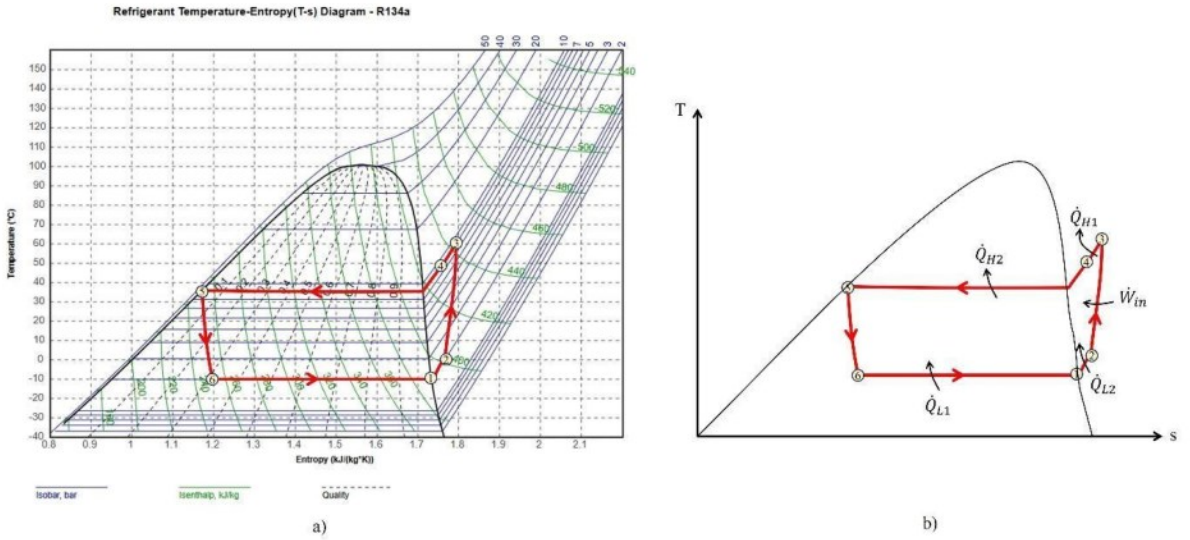

Figure 7: a) T-s diagram for heat pump system cycle,
b) Cycle energy conservation in heat pump system for water and space heating.

Energy conservation equation for the heat pump system is as follows:

$$Q_{H1} + Q_{H2} = Q_{L1} + Q_{L2} + W_{in} \text{ (kJ/kg)} \quad (5)$$

where Q_{H1}, Q_{H2}, $QL1$, Q_{L2} dan W_{in} are the heat transferred to the water heating system, the heat transferred to the space heating system, the heat absorbed from the brine, the heat absorbed from the sub-heating process, and the work input to the compressor.

To calculate the heat and work produced or required, equations (6), (7), and (8) can be used. Once the energy values for each process are determined, Coefficient of Performance (COP) can be calculated according to equation (9) for the actual cycle and equation (10) for the Carnot cycle.

$$Q_L(1 \rightarrow 2) = (h_2 - h_1) \quad (6)$$

$$W_{in}(2 \rightarrow 3) = (h_3 - h_2) \quad (7)$$

$$Q_H(3 \rightarrow 4) = (h_3 - h_4) \quad (8)$$

$$COP_{HP} = Q_H / W_{in} \quad (9)$$

$$COP_{HP,\,Carnot} = 1 / (1 - (T_L/T_H)) \quad (10)$$

After calculating according to Table 6 and 7, it is found that the heat pump COP has a value of 4.62, which means that this heat pump can transfer 4.62 units of heat to the space heating and water heating system for each unit of electrical energy consumed. Meanwhile, the COP of the Carnot heat pump has a value of 5.57. This value is higher because the Carnot cycle is based on ideal conditions, which is a reversible thermodynamic cycle. Thus, the COP Carnot indicates the maximum efficiency limit of this heat pump system is 5.57.

Table 6: parameter values of each heat pump cycle condition.

State	Temperature		Pressure (kPa)	Enthalpy (kJ/kg)	Phase
	°C	K			
1	-10	263	200	392.9	gas
2	0	273	200	401.4	superheated
3	60	333	900	443.5	superheated
4	50	323	900	433.2	superheated
5	35	308	900	249.2	fluid
6	-10	263	200	249.2	x =0.317
Brine in	181	454	1050	771.77	fluid
Brine out	149.05	422.05	1050	628.07	fluid

Table 7: Value of heat transferred and absorbed by each heat pump process.

Process	Heat Transfer	Value (kJ/kg)
6 - 1 (evaporation)	QL1	143.7
1 - 2 (sub-heating)	QL2	8.5
2 - 3 (isentropic)	Win	42.1
3 - 4 (water heating)	QH1	10.3
4 - 5 (space heating)	QH2	184
5 - 6 (throttling)	-	-

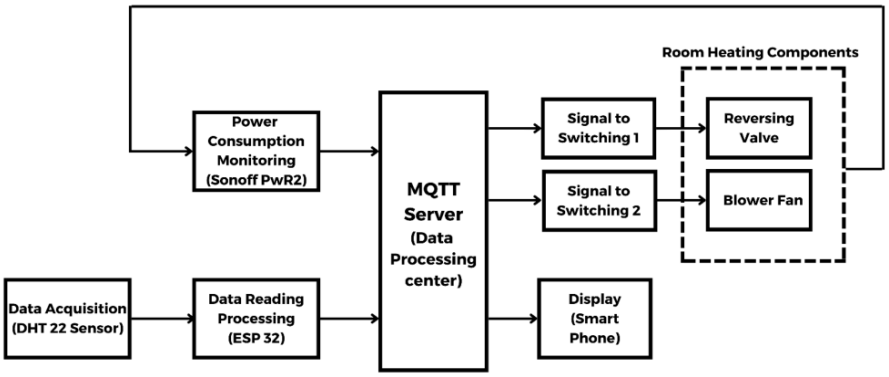

Figure 8: IoT Architecture of the SMART Heating System for Room Heating.

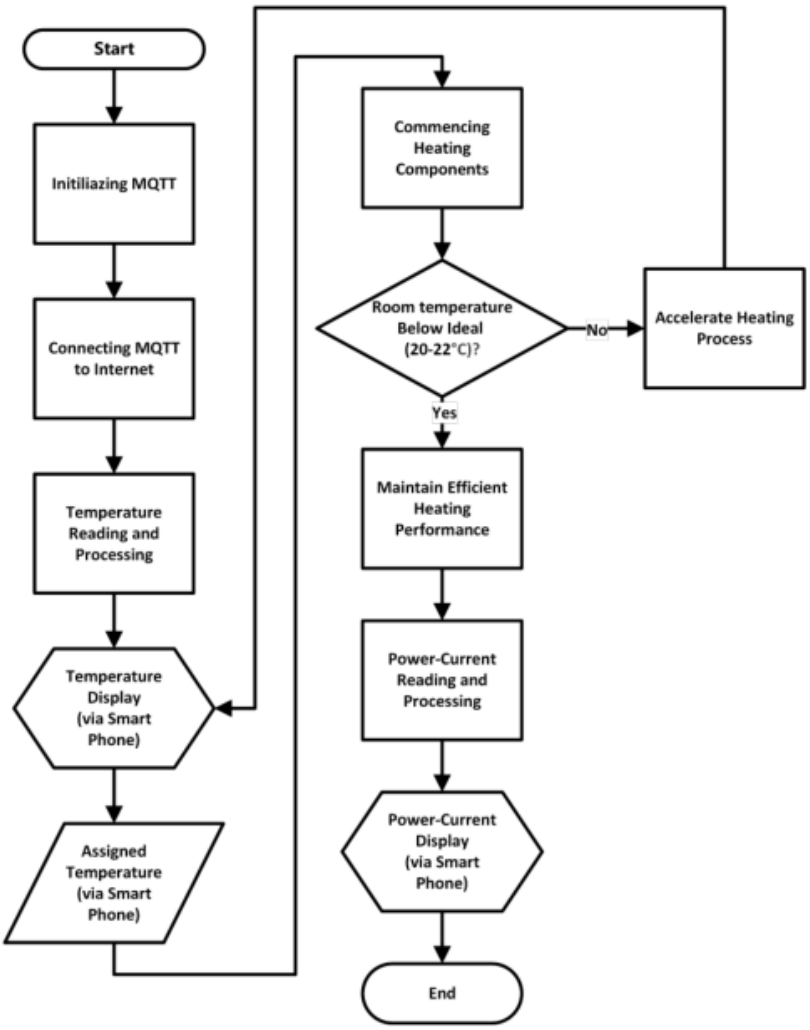

Figure 9: Flow Diagram of the SMART Heating System for Room Heating.

3.2 Automation Scheme in The SMART Heating System

3.2.1 The SMART Heating System for Room Heating

The IoT architecture of the SMART heating System, specifically for room heating, centers around an MQTT (Message Queuing Telemetry Transport) which runs on TCP/IP protocol transport. The MQTT is a broker (server) to which clients are registered. Clients compromise publishers (message or information transferring elements) and subscribers (message or information receiving elements) are registered. The schematic architecture of the SMART Heating System for room heating is as depicted by Figure 8.

Figure 8 shows that temperature data is acquired by DHT 22 sensor and transported to ESP 32 for reading and processing. Then, ESP 32 will publish the information (data processing output) to the server. MQTT will give instructions to other components in accordance with the processing result; the result will be subscribed to the smartphone. To be more specific, the flow diagram, demonstrating how the SMART Heating System operates, is as shown in Figure 9.

Figure 9 shows that the system begins with MQTT initialization. Afterward, the initial room temperature data is acquired and displayed on the smartphone. The user (human input) can assign the desired temperature via mobile phone and the heating components will perform accordingly. If the room temperature is below the desired temperature, then the heating process will be accelerated. When the desired temperature is achieved, the system will maintain its stability; thus, minimizing the inefficient use of energy.

3.2.2 The SMART Heating System for Water Heating

The IoT architecture of the SMART Heating System for water heating utilizes MQTT as the center of data processing. The schematic architecture of the SMART Heating System for water heating is as depicted by Figure 10.

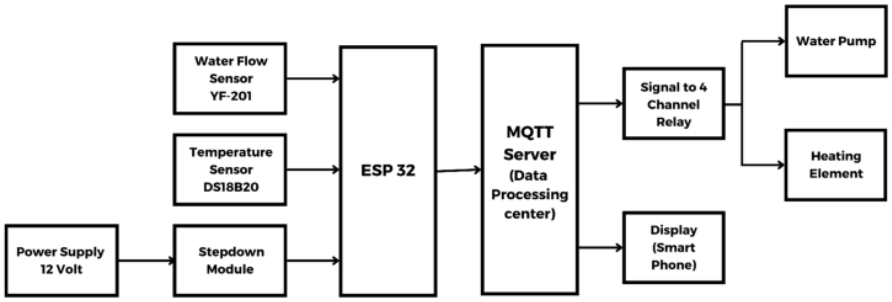

Figure 10: IoT Architecture of the SMART Heating System for Water Heating.

As Shown in Figure 10, the water flow sensor (YF-201) and the temperature sensor (DS18820) acquire the data for ESP 32 to process. Then, the result will be published on the MQTT server. Afterward, the broker will instruct the water pump and heating element (via 4 4-channel relay) to function accordingly. To be more precise, the workflow diagram of the SMART Heating System for water heating is as depicted in Figure 11.

As shown by Figure 11, the system starts with MQTT initialization. Subsequently, the desired temperature and volume will be assigned via smartphone. Pump and heating components will operate accordingly to produce hot water as instructed. Through this mechanism, the system will be able to produce hot water through the efficient use of energy.

3.3 Social Aspect of The SMART Heating System

The implementation of the SMART Heating System, which incorporates the Internet of Things (IoT) concept in the Dieng region, presents significant prospects for improved efficacy and management in the utilization of geothermal energy. Nevertheless, the effectiveness of this technology is heavily reliant on the reception from the local community. This is due to the fact that a technology may satisfy technical criteria, but it may not always be embraced socially. Acceptance of technology is not simply divided into two, but is a continuum that can change over time, either in a positive or negative form (Wolfe et al., 2002).

Based on previous research on the acceptance of geothermal energy advancement in Dieng, it is evident that the community has a high level of knowledge about the benefits of geothermal energy. Specifically, 83% of the community agrees that geothermal energy can be used for electricity production, and 53% believe that this energy will be utilized in the future (Wibowo et al., 2021). The integration of the SMART Heating System with IoT has the potential to be well received by the community. Additionally, the 32% belief that geothermal technology can help prevent global warming indicates a level of environmental awareness that can be further strengthened through additional education on the efficiency and sustainability of this system.

Moreover, the SMART Heating System not only provides an effective and eco-friendly heating solution, but also delivers a variety of important social advantages to the local community and tourism industry in Dieng.

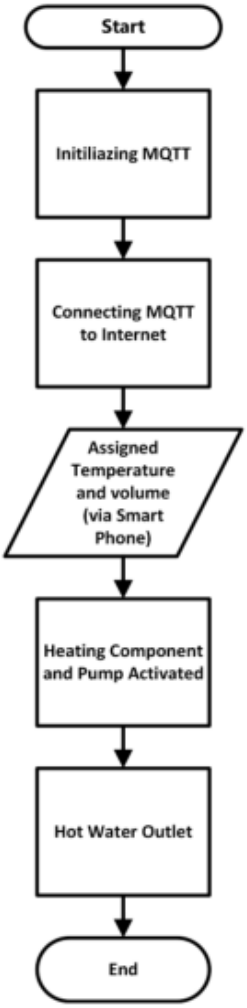

Figure 11: Flow Diagram of the SMART Heating System for Water Heating.

3.3.1 Improved Quality of Life for Local Communities

The integration of IoT technology into the SMART heating system not only grants local residents access to cutting-edge technology but also plays a crucial role in enhancing their comprehension and proficiency in utilizing advanced technology. Through the incorporation of IoT technology, residents will become more adept at utilizing smart devices and automation, consequently enhancing their technical skills. Furthermore, receiving training and education, particularly in the field of renewable energy technology and management, will equip them with practical knowledge on how to operate and maintain the system. Witnessing firsthand the integration of IoT technology with renewable energy sources like geothermal energy will help individuals realize that environmentally friendly energy is not merely a theoretical concept but something that can be put into practice and utilized daily. Therefore, the utilization of IoT technology in renewable energy-based water and space heating systems can serve as a significant catalyst for fostering more environmentally conscious behavior among local communities.

3.3.2 Environmental Impact Reduction

This technology aims to enhance energy efficiency through the utilization of geothermal waste, which has not been fully utilized until now. By decreasing reliance on fossil fuels, the system will contribute to the reduction of greenhouse gas emissions, thereby supporting initiatives to mitigate climate change. Furthermore, the integration of IoT allows for more efficient monitoring and management, which in turn promotes improved and sustainable waste management practices.

3.3.3 Safety of Use

IoT systems facilitate the automated monitoring and regulation of heating systems, which can enhance safety and minimize the chances of fire or malfunction. Through sensors and interconnected devices, issues can be identified and addressed promptly. Additionally, remote control functionality allows for swift responses to emergencies, thereby improving user and property safety.

3.3.3 Tourism Attraction Enhancement

The implementation of the SMART Heating System will have a significant positive impact on travelers in Dieng. Through the utilization of this innovative technology, tourists will enjoy enhanced lodging standards, resulting in heightened comfort levels due to the provision of steady and dependable heating. This enhancement not only boosts tourist contentment but also bolsters Dieng's reputation as a contemporary and environmentally conscious tourist spot. Furthermore, the system serves as an extra draw for environmentally and sustainability-conscious travelers, thereby promoting sustainable tourism.

REFERENCES

Abad, J., Romero, D., Dolalas, J., Parocha, R., and Macabebe, E.: MQTT Based Appliance Control and Automation with Room Occupancy Monitoring Using YOLO, *Proceedings*, Intelligent Computing, 283, (2021).

Cengel, Y. A., Boles, M. A., & Kanoğlu, M.: *Thermodynamics: an engineering approach* (Vol. 5, p. 445). New York: McGraw-hill (2011).

Chandrasekaran, G., Neelam Sanjeev Kumar, Chokkalingam A, Gowrishankar V, Neeraj Priyadarshi, and Khan, B.: IoT enabled smart solar water heater system using real time ThingSpeak IoT platform, *IET Renewable Power Generation*, (2023).

DiPippo, R.: *Geothermal power plants: principles, applications, case studies and environmental impact*. Butterworth-Heinemann (2012).

Flynn, R. *Risk and the Public Acceptance of New Technologies*. In: Flynn, R., Bellaby, P. (eds) Risk and the Public Acceptance of New Technologies, Palgrave Macmillan, London, (2007), https://doi.org/10.1057/9780230591288_1.

Kencana, A., Elfina, Alibazah, J., Fajri, R.,Supijo, C., and Nurpratama, M.: Initial State Fluid Geochemistry of the Dieng Geothermal Field, Indonesia: New Constraints for Conceptual Model, *Proceedings*, , 49th Workshop on Geothermal Reservoir Engineering, Stanford University, Stanford, (2024).

Lund, J. W.: Direct heat utilization of geothermal resources worldwide 2005. *ASEG Extended Abstracts*, 1, (2006), 1-15.

Lund, J., Sanner, B., Rybach, L., Curtis, R., & Hellström, G.: Geothermal (ground-source) heat pumps: a world overview. *Geo-Heat Center Quarterly Bulletin*, 25(3), (2004).

Mburu, M.: Feasibility Study on Direct Utilisation of Energy from Geothermal Brine – A Case Study of Olkaria Geothermal Power Plant, Kenya. *Proceedings World Geothermal Congress* 2010.

Ministry of Energy and Mineral Resources, Republic of Indonesia.: Potensi Panas Bumi Indonesia Jilid 1. Directorate of Geothermal Mineral Resource, (2017).

O'Halloran, R. (2023, May). *Eco-friendly & sustainable lodging practices and possibilities*. Hospitality Net. https://www.hospitalitynet.org/opinion/4116433.html

Pambudi, N. A., Itoi, R., Yamashiro, R., CSS Syah Alam, B. Y., Tusara, L., Jalilinasrabady, S., & Khasani, J.: The behavior of silica in geothermal brine from Dieng Geothermal Power Plant, Indonesia, *Geothermics*, 54, (2010), 109–114.

Pambudi, N. A., Itoi, R., Jalilinasrabady, S., & Jaelani, K.: Performance improvement of a single-flash geothermal power plant in Dieng, Indonesia, upon conversion to a double-flash system using thermodynamic analysis. *Renewable Energy*, 80, (2015), 424–431.

Park, C.-H., Shim, B. O., and Park, J.-W.: Open-source IoT monitoring system of a shallow geothermal system for heating and cooling year-round in Korea. *Energy*, 250, (2022).

Rahayuningsih, M., & Wati, Y. H. (2023). Strategi Pengembangan Pariwisata Kawasan Dieng Kejajar Wonosobo. *Jurnal Geosains West Science*, 1, 17–22.

Shalihin, M. G. J., Darmawan, D., Tiyana, R. A., and Chandra, V. R.: The Geology and Geothermal System of the Dieng Geothermal Field, Central Java, Indonesia, *Proceedings*, 47th Workshop on Geothermal Reservoir Engineering, Stanford University, (2022).

Sihono, Yunanto, B., Kusuma, M., Munawaroh, S., Suryono, Wisaksono, A., Krishna, B., and Utomo, K.: Monitoring Room Temperature and the Use of Cooling Power Based on IoT, *Proceedings*, International Conference on Innovation in Science and Technology 2020, 208, (2020).

Shalihin, M., Darmawan, D., Tiyana, R., and Chandra, V.: The Geology and Geothermal System of the Dieng Geothermal Field, Central Java, Indonesia, *Proceedings*, 47th Workshop on Geothermal Reservoir Engineering, Stanford University, Stanford, (2022).

Sofyan, A., Aka, H. S., Suranta, B. Y., & Ratasya, S. M. A.: Analysis of Silica Saturation Index (SSI), Scale Formation Rate, and Scale Formation Time Based on Geothermal Production Well Head Pressure at Well" X. Indonesian Journal of Petroleum and Mineral, 1(1), (2021).Susanti, H., Musyafiq, A., Purnata, H., and Ilahi, N.: Automated Water Heating Management with Internet of Things, *Jurnal Jartel Jurnal Jaringan Telekomunikasi*, 13, (2023), 128-134.

Warren, C., Becken, S., Nguyen, K., & Stewart, R. A. (2018). Transitioning to smart sustainable tourist accommodation: Service innovation results. *Journal of Cleaner Production*, 201, 599–608. https://doi.org/10.1016/j.jclepro.2018.08.063.

Widjaja, M., Halim, D., and Andarini, R.: The Development of an IoT-based Indoor Air Monitoring System Towards Smart Energy Efficient Classroom, Ultima Computing : *Jurnal Sistem Komputer*, 14, (2022), 28-35.

Wisnu, Agung., Marza, Supriadinata., Lory Phil., Shannon Cowlin.: *Geothermal Direct Use in Dieng, Indonesia*. Asian Clean Energy Forum (2020).

West JEC.: *Feasibility Study for Dieng No. 4, 5, and 6 Unit Geothermal Power Development.* (2006)

Wibowo, K. M., Hadi, S., & Pambudi, N. A.: Acceptance analysis of the progress of geothermal energy in Dieng Indonesia. *THE 3RD INTERNATIONAL CONFERENCE ON SCIENCE EDUCATION AND TECHNOLOGY (ICOSETH 2021)*, (2021), https://doi.org/10.1063/5.0150713

THE 10th INDONESIA INTERNATIONAL GEOTHERMAL CONVENTION & EXHIBITION 2024

For more information, please contact to:

SPONSORSHIP, EXHIBITION, CONVENTION & REGISTRATION

Ms. Nadya
M: +62 818-0620-6445
E: marketing@iigce.com

Ms. Rahma
M: +62 811-858-160
E: convention@iigce.com

Ms. Winda
M: +62 896-8256-1354
E: registration@iigce.com

Ms. Elsya
M: +62 815-3931-4953
E: technicalpaper@iigce.com

On Us Asia
Plaza Asia 18th Floor - Zone D
Jl. Jend. Sudirman Kav. 59
Jakarta Selatan 12190 - Indonesia
P: +62 21 5151 2477
F: +62 21 5151 2478
E: info@iigce.com

@inaga_iigce
@inaga_iigce
IIGCE 2024
IIGCE Convention and Exhibition
www.iigce.com

©2024 PT Energi Kreatif Dinamika. All Rights Reserved.

ISSN 2986-1268

Asosiasi Panasbumi Indonesia (API)
Apartemen Menteng Square, BR-9 Tower B
Jl. Matraman No 30 E, Jakarta Pusat - 10320 Indonesia
Email: api.inaga@yahoo.co.id